A total synthesis of (±)-triophamine

EDWARD PIERS, J. MICHAEL CHONG, KIRK GUSTAFSON,[1] AND RAYMOND J. ANDERSEN[1]

Department of Chemistry, University of British Columbia, 2036 Main Mall, University Campus, Vancouver, B.C., Canada V6T 1Y6

Received June 10, 1983

EDWARD PIERS, J. MICHAEL CHONG, KIRK GUSTAFSON, and RAYMOND J. ANDERSEN. Can. J. Chem. **62**, 1 (1984).

Treatment of ethyl 2-pentynoate (**14**) with lithium (phenylthio)(tri-*n*-butylstannyl)cuprate (**12**) afforded, in 76% yield, ethyl (*Z*)-3-(tri-*n*-butylstannyl)-2-pentenoate (**15**). On the other hand, when compound **14** was allowed to react with the (tri-*n*-butylstannyl)copper reagent **13**, ethyl (*E*)-3-(tri-*n*-butylstannyl)-2-pentenoate (**21**) was produced in 83% yield. Reduction (diisobutylaluminum hydride, ether) of the esters **15** and **21** gave the alcohols **16** and **22**, respectively. Treatment of each of the latter substances with pyridine − sulfur trioxide complex, followed by further reduction of the resultant intermediates with lithium aluminum hydride, provided the geometrically isomeric alkenylstannanes **17** and **23**. Conjugate addition of (*E*)-3-lithio-2-pentene (**18**) (formed by transmetalation of **17**) to compound **19** produced the olefinic trimethylhydrazide **20**, which was converted (diisobutylaluminum hydride, ether; pyridinium dichromate, dimethylformamide) into the corresponding carboxylic acid **2**. Subjection of compound **23** to a sequence of reactions identical with that used for the conversion of **17** into **2** provided the isomeric acid **3**, which was identical (infrared, ^{1}H nmr) with the natural acid derived from triophamine (**1**). Conversion of **3** into the *p*-nitrophenyl ester **26**, followed by condensation of the latter substance with guanidine, afforded a chromatographically separable mixture of (±)-triophamine (**1**) and the corresponding diastereomer.

EDWARD PIERS, J. MICHAEL CHONG, KIRK GUSTAFSON et RAYMOND J. ANDERSEN. Can. J. Chem. **62**, 1 (1984).

Le pentyne-2 oate d'éthyl (**14**) réagit avec le (phénylthio)-(tri-*n*-butylstannyl)cuprate de lithium (**12**) pour donner, avec un rendement de 76%, le (*Z*)-(tri-*n*-butylstannyl)-3 pentène-2 oate d'éthyle (**15**). Par ailleurs, quand on fait réagir le composé **14** avec le réactif (tri-*n*-butylstannyl)cuivre (**13**), on obtient avec un rendement de 83%, le (*E*)-(tri-*n*-butylstannyl)-3 pentène-2 oate d'éthyle (**21**). Par réduction des esters **15** et **21** (par l'hydrure de diisobutylaluminium dans l'éther), on obtient respectivement les alcools **16** et **22**. Ces alcools, par une réaction avec le complexe de pyridine − trioxyde de soufre suivie de la réduction des intermédiaires résultants par l'alanate de lithium, conduisent aux alkénylstannates **17** et **23** qui sont des isomères géométriques. L'addition conjuguée du (*Z*)-lithio-3 pentène-2 (**18**) (formé par la transmétallation du composé **17**) sur le composé **19** conduit au triméthylhydrazide oléfinique **20** que l'on transforme (hydrure de diisobutylaluminium, éther; dichromate de pyridium, diméthylformamide) en l'acide carboxylique correspondant (**2**). Le composé **23**, soumis à la suite de réaction qui permet de transformer le composé **17** en composé **2**, donne l'acide isomère **3** que l'on a identifié (ir et rmn du ^{1}H) à l'acide naturel provenant de la triophamine (**1**). La transformation du composé **3** en ester *p*-nitrophényle (**26**), suivie de la condensation de l'ester sur la guanidine, donne un mélange de (±)-triophamine (**1**) et du diastéréoisomère correspondant que l'on peut séparer par chromatographie.

[Traduit par le journal]

Introduction

The skin extracts of many dorid nudibranchs contain novel metabolites, some of which are believed to function as chemical antifeedants (1). Recently, two of us reported the isolation of triophamine from the dorid *Triopha catalinae* and showed that this metabolite possesses the unique diacylguanidine structure shown in **1** (2). Although the stereochemistry of the

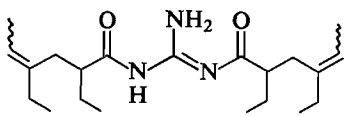

1

carbon−carbon double bonds present in triophamine was not defined by the structural elucidation work (2), it is pertinent to note that the structurally interesting carbon skeleton of the acyl residues of this substance has not been encountered previously in natural products and cannot be derived readily from "standard" biosynthetic pathways. We describe herein a total synthesis of (±)-triophamine which confirms the structural assignment and establishes the geometry about the alkene linkage in the acyl moieties.

Results and discussion

(a) *General considerations*

It seems clear that the final stages of a total synthesis of (±)-triophamine (**1**) would involve condensation of guanidine with a suitable functional derivative of one of the carboxylic acids **2** or **3** (see Scheme 1). Therefore, the first synthetic task was the stereoselective synthesis of one (or both) of the latter substances. Although many different routes for the preparation of **2** and **3** can be envisaged, our projected syntheses were

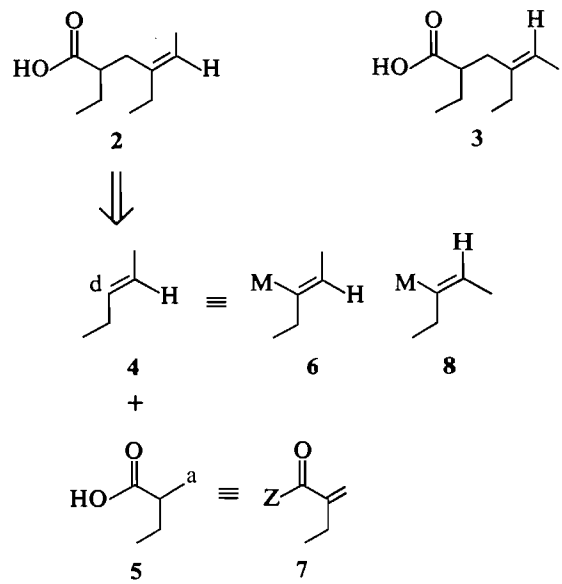

SCHEME 1

[1]Also from the Department of Oceanography.

Can. J. Chem. Downloaded from www.nrcresearchpress.com by 210.87.254.5 on 09/06/12
For personal use only.

based on the retrosynthetic plan shown in Scheme 1. Thus, heterolytic disconnection of the C-3—C-4 bond in **2** provides, as one possibility, the donor synthon **4** and the acceptor synthon **5**. From a synthetic point of view, then, the acid **2** could be prepared by conjugate addition of a stereochemically homogeneous organometallic reagent **6** (M = Li, (CuY)Li, etc.) to a suitable derivative of 2-ethylpropenoic acid **7** (Z = OR, NR_2, etc.). Similarly, 1,4-addition of an organometallic reagent **8** to the substrate **7** would produce, after appropriate functional group manipulation, the olefinic acid **3**.

The synthetic plan outlined above was prejudiced by the results of some recent studies carried out in our laboratories. Explicitly, it had been shown (3, 4) that the reaction of α,β-acetylenic esters **9** with (trimethylstannyl)copper reagents can be controlled experimentally to produce, stereoselectively, either of the geometrically isomeric products **10** or **11**. For example, when **9** is allowed to react with lithium (phenylthio)(trimethylstannyl)cuprate under the conditions shown in eq. [1], the product consists very largely of the β-trimethylstannyl α,β-unsaturated ester **10**. On the other hand, reaction of **9** with (trimethylstannyl)copper at −78°C affords exclusively the geometrically isomeric olefinic ester **11**

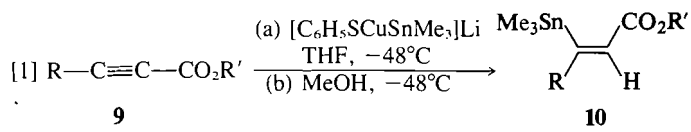

9 **10**

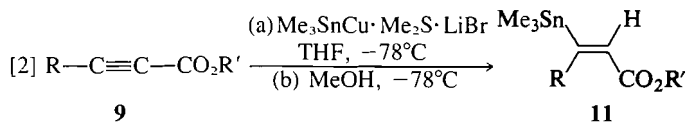

9 **11**

(eq. [2]). Since the transmetalation (RLi) of trialkylvinylstannanes to produce vinyllithium reagents is a well-known process, it appeared that compounds **10** and **11** (R = C_2H_5) would serve as convenient precursors of the required reagents **6** and **8** (M = Li, (CuY)Li, etc.), respectively.

(b) *Preparation of (Z)-(2) and (E)-2,4-diethyl-4-hexenoic acid (3)*

In our work involving the use of (trialkylstannyl)copper reagents, we have employed nearly exclusively trimethylstannyl compounds. However, since some of the projected trimethylstannyl intermediates necessary for the present work (for example, compounds **6** and **8**, M = $SnMe_3$) would probably be quite volatile, we chose to carry out this study with the corresponding tri-*n*-butylstannyl derivatives.

Treatment of a cold (−20°C) solution of (tri-*n*-butylstannyl)-lithium (5) in tetrahydrofuran (THF) with 1 equivalent of phenylthiocopper (6) provided a deep red solution of lithium (phenylthio)(tri-*n*-butylstannyl)cuprate (**12**)[2] (see Scheme 2). On the other hand, when (tri-*n*-butylstannyl)lithium (5) was allowed to react (THF, −78°C) with 1 equivalent of copper bromide − dimethyl sulfide complex (7), a solution (also dark red) of the (tri-*n*-butylstannyl)copper reagent **13**[2] (8) was

[2]The actual constitutions of reagents **12** and **13** are unknown. However, the formulations shown in **12** and **13** are used for the sake of convenience and on the basis of analogy with the usual representations of corresponding alkylcopper reagents.

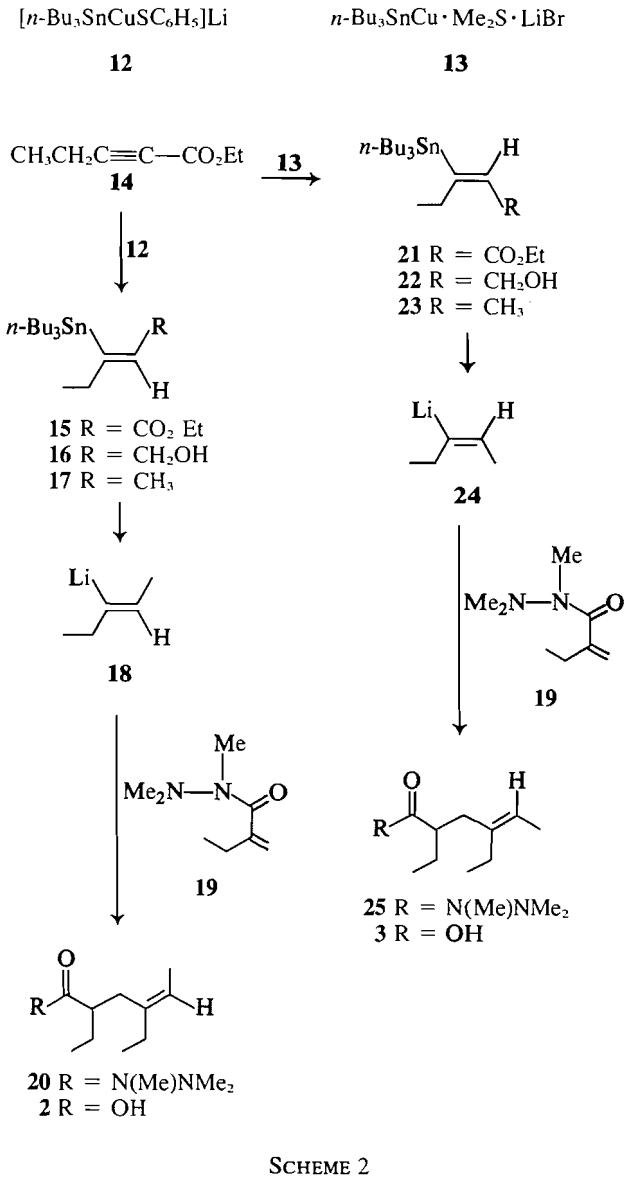

SCHEME 2

produced.

Reaction of ethyl 2-pentynoate (**14**) with each of the reagents **12** (THF, −48°C) and **13** (THF, −78°C), followed in each case by appropriate work-up and chromatographic purification of the crude product, afforded, respectively, ethyl (*Z*)-3-(tri-*n*-butylstannyl)-2-pentenoate (**15**) (76%) and the corresponding geometric isomer **21** (83%). The proton nuclear magnetic resonance (^{1}H nmr) spectra of the latter substances fully corroborated the stereochemical assignments. Thus, the C-4 methylene protons of compound **15** give rise to a doublet of quartets (J = 7.5, 1.5 Hz) at δ 2.42 while the analogous signal for the corresponding protons of **21** is found at δ 2.88. It seems clear, therefore, that the ethyl group of the pentenoate chain is *cis* to the ester function in the latter isomer. Furthermore, in compounds such as **15** and **21**, the magnitude of the coupling constants associated with the coupling of the alkene proton with the tin nuclei (^{117}Sn and ^{119}Sn isotopes) is stereochemically diagnostic. It is known (9) that when the trialkylstannyl group and the vicinal alkene proton are in a *trans* relationship, $|J_{Sn-H}|$ is much larger than when these groups are *cis* to one another. In compounds **15** and **21**, the values of $|J_{Sn-H}|$ are 109 and 65

Can. J. Chem. Downloaded from www.nrcresearchpress.com by 210.87.254.5 on 09/06/12
For personal use only.

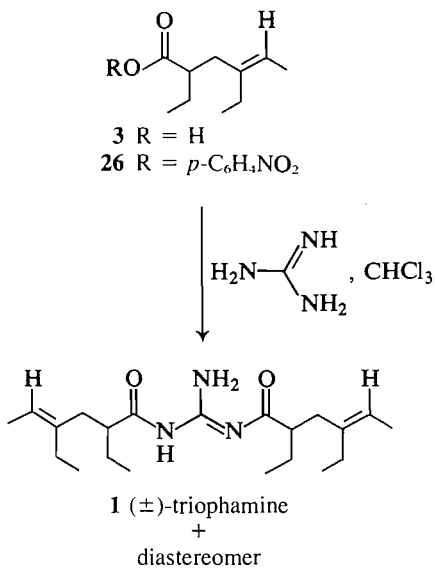

SCHEME 3

Hz,[3] respectively.

Reduction of the ester **15** with diisobutylaluminum hydride in ether afforded the alcohol **16**. When this material was allowed to react with pyridine − sulfur trioxide complex in THF, and the resultant intermediate was reduced directly with lithium aluminum hydride (10), (*Z*)-3-(tri-*n*-butylstannyl)-2-pentene (**17**) was produced in 87% yield. Transmetalation (*n*-butyllithium, THF, −20°C) of compound **17**, followed by conjugate addition (THF, −78°C) of the resultant vinyllithium species **18** to the *N*,*N*′,*N*′-trimethylhydrazide derivative of 2-ethylpropenoic acid (**19**)[4] (11), provided, in addition to small amounts of the starting materials **17** and **19**, the olefinic trimethylhydrazide **20** (42% yield).

Trimethylhydrazides are known to be very resistant to hydrolysis. It was, therefore, somewhat surprising to find that treatment of compound **20** with hot dilute hydrochloric acid for only 2 h totally converted this substrate into a single product (78% yield). However, spectral data showed that the product was 2,4,4-triethylbutyrolactone and it was thus clear that the carbon−carbon double bond had participated in the hydrolysis process.

It was found eventually that the desired conversion of the trimethylhydrazide **20** into the corresponding acid **2** could be effected by treatment of the former substance with 1.1 equivalents of diisobutylaluminum hydride (ether, 0°C), followed by direct oxidation of the resultant crude product with pyridinium dichromate in dimethylformamide (12). The purified product, (*Z*)-2,4-diethyl-4-hexenoic acid (**2**), was obtained in 50% yield based on unrecovered **20**, and provided spectra (infrared, ^{1}H nmr) which were very similar to, but clearly different from, those of the olefinic carboxylic acid obtained from natural triophamine. Presumably, therefore, the olefinic linkage of the acyl residues of triophamine possesses an (*E*) rather than a (*Z*) configuration.

[3]These coupling constants represent the average of the ^{117}Sn—H and ^{119}Sn—H values.

[4]This material was prepared from 2-ethylpropenoic acid via the corresponding acid chloride. See the experimental section for details.

The synthesis of the required carboxylic acid **3** was accomplished via a route which paralleled that described for the isomeric acid **2**. Thus, conversion of the ester **21**, via the intermediates **22** and **23**, into (*Z*)-3-lithio-2-pentene (**24**), followed by conjugate addition of the latter reagent to compound **19**, afforded the olefinic trimethylhydrazide **25**. The corresponding carboxylic acid **3**, obtained from **25** via a procedure identical with that used for the conversion of **20** into **2**, gave spectra (infrared, ^{1}H nmr) identical with those of the natural acid derived from triophamine.

(c) *Synthesis of triophamine (**1**) and its diastereomer (Scheme 3)*

Treatment of the carboxylic acid **3** with *p*-nitrophenol in the presence of N,N′-dicyclohexylcarbodiimide afforded in excellent yield the crystalline *p*-nitrophenyl ester **26**. Condensation of this material with guanidine under carefully monitored conditions provided a chromatographically separable mixture of (±)-triophamine (**1**) and the expected diastereomer. The former product gave spectra (infrared, ^{1}H nmr) identical with those of the natural product.

In summary, the synthetic work described herein corroborates the conclusions of structural work done on triophamine (2) and establishes the configuration of the olefinic double bonds present in this interesting natural product.

Experimental

General

Melting points and distillation temperatures are uncorrected. Infrared (ir) spectra were recorded on Perkin−Elmer model 710B spectrophotometers. Proton nuclear magnetic resonance (^{1}H nmr) spectra (deuterochloroform solution) were measured using Bruker spectrometers, models WP-80 and/or WH-400. Tetramethylsilane was employed as the internal standard for all compounds except those containing the tri-*n*-butylstannyl group. In these cases, the chemical shifts were measured relative to that of the chloroform proton (δ 7.25). High resolution mass spectrometric measurements were recorded on a Kratos MS-50 mass spectrometer. Gas−liquid chromatography (glc) was carried out with a Hewlett−Packard model 5832 A gas chromatograph.

*Ethyl (Z)-3-(tri-*n*-butylstannyl)-2-pentenoate (**15**)*

To a cold (−20°C) stirred solution of hexa-*n*-butylditin (6.96 g, 12.0 mmol) in 100 mL of dry THF under an atmosphere of argon was added a solution of *n*-butyllithium in hexane (7.14 mL, 1.68 *M*, 12.0 mmol). The resultant yellow solution was stirred at −20°C for 20 min. Phenylthiocopper (2.06 g, 12 mmol) was added and the deep red solution which formed within 1 min was stirred (−20°C) for an additional 20 min. After the reaction mixture had been cooled to −78°C, a solution of ethyl 2-pentynoate (**14**) (1.26 g, 10 mmol) in 5 mL of dry THF was added and the resulting solution was stirred at −78°C for 15 min and at −48°C for 4 h. Ethanol (1 mL) and ether (100 mL) were added and the mixture was allowed to warm to room temperature. During this time a flocculent yellow precipitate formed. The slurry was treated with anhydrous magnesium sulfate and then was filtered through a short column of Florisil. The column was washed with further volumes of ether. Removal of the solvent from the combined eluate gave a pale yellow oil which contained, on the basis of glc analysis, tetra-*n*-butyltin, hexa-*n*-butylditin, and a mixture of ethyl (*Z*)- (**15**) and (*E*)-3-(tri-*n*-butylstannyl)-2-pentenoate (**21**), in a ratio of 97:3, respectively. Subjection of this material to column chromatography on silica gel (150 g, elution with 1:100 ether − petroleum ether) provided a clear oil which upon distillation (air-bath temperature 128−135°C/0.3 Torr) gave 3.18 g (76%) of the unsaturated ester **15** as a colorless liquid; ir (film): 1700, 1595, 1200, 880 cm^{-1}; ^{1}H nmr δ: 0.7−1.8 (diffuse m, 33H), 2.42 (d of q, 2H, J = 7.5, 1.5

Can. J. Chem. Downloaded from www.nrcresearchpress.com by 210.87.254.5 on 09/06/12
For personal use only.

Can. J. Chem. Downloaded from www.nrcresearchpress.com by 210.87.254.5 on 09/06/12
For personal use only.

Hz, with satellite peaks indicating $J_{Sn-H} \approx 53$ Hz), 4.17 (q, 2H, J = 7 Hz), 6.38 (t, 1H, J = 1.5 Hz, with satellite peaks indicating J_{Sn-H} = 109 Hz). *Exact Mass* calcd. for $C_{15}H_{29}O_2{}^{120}Sn$ ($M^+ - C_4H_9$):[5] 361.1190; found: 361.1187.

Ethyl (E)-3-(tri-n-butylstannyl)-2-pentenoate (21)

To a cold (−20°C) stirred solution of hexa-*n*-butylditin (15.1 g, 26 mmol) in dry THF (200 mL) under an atmosphere of argon was added a solution of *n*-butyllithium in hexane (15.9 mL, 1.63 *M*, 26 mmol). The yellow solution was stirred at −20°C for 20 min and then was cooled to −78°C. Cuprous bromide − dimethyl sulfide complex (5.34 g, 26 mmol) was added and the mixture was stirred at −78°C for 30 min. To the resulting dark red solution was added a solution of ethyl 2-pentynoate (**14**) (2.52 g, 20 mmol) in 10 mL of dry THF and stirring was continued at −78°C for a further 3 h. Ethanol (1 mL), saturated aqueous ammonium chloride (pH 8, 20 mL), and ether (200 mL) were added successively and the mixture was allowed to warm to room temperature. The layers were separated and the aqueous phase was extracted thoroughly with ether. The combined extracts were washed with saturated aqueous ammonium chloride (pH 8) and dried over anhydrous magnesium sulfate. Removal of the solvent afforded a yellow oil which was subjected to column chromatography on silica gel (250 g, elution of the column with 1:50 ether − petroleum ether). Distillation (air-bath temperature 130°C/0.3 Torr) of the material obtained from the appropriate fractions gave 6.92 g (83%) of the unsaturated ester **21** as a colorless oil; ir (film): 1710, 1585, 1180, 870 cm^{-1}; ^1H nmr δ: 0.7−1.8 (diffuse m, 33H), 2.88 (d of q, 2H, J = 7.5, 1.2 Hz, with satellite peaks indicating $J_{Sn-H} \approx 56$ Hz), 4.16 (q, 2H, J = 7 Hz), 5.92 (t, 1H, J = 1.2 Hz, with satellite peaks indicating J_{Sn-H} = 65 Hz). *Exact Mass* calcd. for $C_{15}H_{29}O_2{}^{120}Sn$ ($M^+ - C_4H_9$): 361.1190; found: 361.1207.

(Z)-3-(Tri-n-butylstannyl)-2-penten-1-ol (16)

To a cold (−78°C) stirred solution of the ester **15** (418 mg, 1.0 mmol) in dry ether (12 mL) under an atmosphere of argon was added a solution of diisobutylaluminum hydride in hexane (2.5 mL, 1 *M*, 2.5 mmol). The colorless solution was stirred at −78°C for 1 h and at 0°C for 2 h. After 0.5 mL of saturated aqueous ammonium chloride had been added, the mixture was allowed to warm to room temperature. The resultant slurry was treated with anhydrous magnesium sulfate and then was filtered through a short column of Florisil. The column was washed with ether. Removal of the solvent from the combined eluate, followed by distillation (air-bath temperature 120−125°C/0.3 Torr) of the residual oil, furnished 339 mg (90%) of the alcohol **16** as a clear oil; ir (film): 3320, 1460, 1010 cm^{-1}; ^1H nmr δ: 0.8−1.7 (diffuse m, 31H), 2.22 (broad q, 2H, J = 7 Hz), 4.04 (d after addition of D_2O, 2H, J = 7 Hz), 6.22 (t of t, 1H, J = 6.5, 1.3 Hz, with satellite peaks indicating J_{Sn-H} = 128 Hz). *Exact Mass* calcd. for $C_{13}H_{27}O^{120}Sn$ ($M^+ - C_4H_9$): 319.1084; found: 319.1085.

(E)-3-(Tri-n-butylstannyl)-2-penten-1-ol (22)

This material was prepared by diisobutylaluminum hydride reduction of the unsaturated ester **21**, via a procedure identical with that described above. From 338 mg (0.81 mmol) of **21** there was obtained 286 mg (94%) of the alcohol **22** as a clear, colorless oil; ir (film): 3270, 1460, 1020 cm^{-1}; ^1H nmr δ: 0.7−1.1 (diffuse m, 31H), 2.31 (broad q, 2H, J = 7 Hz, with satellite peaks indicating $J_{Sn-H} \approx 56$ Hz), 4.25 (d after addition of D_2O, 2H, J = 6 Hz), 5.72 (broad t, 1H, J = 6 Hz, with satellite peaks indicating J_{Sn-H} = 70 Hz). *Exact Mass* calcd. for $C_{13}H_{27}O^{120}Sn$ ($M^+ - C_4H_9$): 319.1084; found: 319.1082.

(Z)-3-(Tri-n-butylstannyl)-3-pentene (17)

To a cold (0°C) stirred solution of the alcohol **16** (2.45 g, 6.52 mmol) in 20 mL of dry THF under an atmosphere of argon was added in one portion 1.56 g (9.77 mmol) of pyridine − sulfur trioxide complex. The resulting suspension was stirred at 0°C for 3 h. A solution-slurry of lithium aluminum hydride (1.1 g) in 20 mL of dry THF was added and the reaction mixture was stirred at 0°C for 1 h and at room temperature for 3 h. After the mixture had been recooled to 0°C, sodium sulfate decahydrate was added in portions until noticeable reaction ceased. The mixture was allowed to warm to room temperature, was treated with anhydrous magnesium sulfate, and then was filtered through a short column of Florisil. The inorganic salts were washed thoroughly with ether. Removal of the solvent from the combined filtrate, followed by distillation (air-bath temperature ~150°C/12 Torr) of the residual material afforded 2.04 g (87%) of the alkene **17** as a pale yellow oil; ir (film): 1620, 1460, 1080 cm^{-1}; ^1H nmr δ: 0.8−1.6 (diffuse m, 30H), 1.70 (broad d, 3H, J = 6.5 Hz), 2.17 (broad q, 2H, J = 7 Hz, with satellite peaks indicating $J_{Sn-H} \approx$ 48 Hz), 6.10 (q of t, 1H, J = 6.5, 1.3 Hz, with satellite peaks indicating J_{Sn-H} = 138 Hz). *Exact Mass* calcd. for $C_{13}H_{27}{}^{120}Sn$ ($M^+ - C_4H_9$): 303.1135; found: 303.1135.

(E)-3-(Tri-n-butylstannyl)-2-pentene (23)

Conversion of the unsaturated alcohol **22** into the alkene **23** was accomplished via a procedure identical with that described above. From 336 mg (0.93 mmol) of **22** there was obtained 278 mg (83%) of **23** as a pale yellow oil; ir (film): 1580, 1440, 1060 cm^{-1}; ^1H nmr δ: 0.7−1.6 (diffuse m, 30H), 1.70 (d, 3H, J = 6.6 Hz), 2.27 (broad q, 2H, J = 7.3 Hz, with satellite peaks indicating $J_{Sn-H} \approx 56$ Hz), 5.58 (broad q, 1H, J = 6.6 Hz, with satellite peaks indicating J_{Sn-H} = 71 Hz). *Exact Mass* calcd. for $C_{13}H_{27}{}^{120}Sn$ ($M^+ - C_4H_9$): 303.1135; found: 303.1132.

Preparation of the N,N',N'-trimethylhydrazide of 2-ethylpropenoic acid (19)

A solution of 2-ethylpropenoic acid (4.1 g, 41 mmol) and oxalyl chloride (11 mL, 3 equiv.) in 180 mL of hexanes was heated (reflux) for 1 h. The solvent and excess oxalyl chloride were removed by distillation (atmospheric pressure) and the residue was taken up in 10 mL of dry dichloromethane. This solution was added to a cold (−78°C) solution of trimethylhydrazine (6.1 g, 82 mmol) and triethylamine (17 mL, 123 mmol) in 150 mL of dichloromethane. The reaction mixture was stirred at −78°C for 1 h and then was allowed to warm to room temperature. Saturated aqueous ammonium chloride was added and the layers were separated. The organic layer was washed with 1 *N* hydrochloric acid and then was dried over anhydrous magnesium sulfate. Removal of the solvent (distillation at atmospheric pressure), followed by distillation (air-bath temperature 108−112°C/12 Torr) of the residual material, furnished 2.2 g (34%) of the trimethylhydrazide **19**; ir (film): 1650, 1450, 1380, 905 cm^{-1}; ^1H nmr δ: 1.05 (t, 3H, J = 7 Hz), 2.31 (broad q, 2H, J = 7 Hz), 2.47 (s, 6H), 2.88 (s, 3H), 4.95−5.10 (m, 2H). *Exact Mass* calcd. for $C_8H_{16}N_2O$: 156.1262; found: 156.1231.

Preparation of the N,N',N'-trimethylhydrazide of (Z)-2,4-diethyl-4-hexenoic acid (20)

To a cold (−20°C) stirred solution of the tri-*n*-butylstannane **17** (366 mg, 1.02 mmol) in 5 mL of dry THF was added a solution of *n*-butyllithium in hexane (0.6 mL, 1.62 *M*, 0.97 mmol). The solution was stirred at −20°C for 1 h and then was cooled to −78°C. A solution of the unsaturated trimethylhydrazide **19** (159 mg, 1.02 mmol) in 2 mL of dry THF was added dropwise and the reaction mixture was stirred at −78°C for 1 h. Saturated aqueous ammonium chloride and ether were added successively and the layers were separated. The aqueous layer was extracted with ether and the combined extracts were washed with saturated aqueous ammonium chloride and dried over anhydrous magnesium sulfate. Removal of the solvent provided an oil which, on the basis of the analysis by glc, consisted of a mixture of the desired product **20**, the two starting materials **17** and **19**, and tetra-*n*-butyltin. This material was subjected to column chromatography on silica gel (25 g, elution with 1:1 ether − petroleum ether). Evaporation of the solvent from the appropriate fractions gave 97 mg (42%) of the trimethylhydrazide **20**; ir (film): 1645, 1458,

[5]In accord with previous observations (13, 14) regarding mass spectrometry of trialkylstannyl compounds, the mass spectra of the tri-*n*-butylstannyl derivatives reported herein did not exhibit molecular ion peaks. Therefore, in each case, the high resolution measurement was carried out on the $m/e = M^+ - C_4H_9$ fragment.

Can. J. Chem. Downloaded from www.nrcresearchpress.com by 210.87.254.5 on 09/06/12
For personal use only.

1380, 1180, 1155 cm^{-1}; ^1H nmr δ: 0.82 (t, 3H, J = 7 Hz), 0.98 (t, 3H, J = 7 Hz), 1.17–2.33 (diffuse m, 9H), 2.48 (s, 6H), 2.88 (s, 3H), 3.25–3.73 (m, 1H), 5.25 (broad q, 1H, J = 7 Hz). *Exact Mass* calcd. for $C_{13}H_{26}ON_2$: 226.2045; found: 226.2046.

Preparation of the N,N′,N′*-trimethylhydrazide of* (E)*-2,4-diethyl-4-hexenoic acid (25)*

This substance was prepared from (*E*)-3-(tri-*n*-butylstannyl)-2-pentene (**23**) and the trimethylhydrazide **19** via a procedure essentially identical with that described above. Column chromatography (silica gel, 55 g; 1:1 ether – petroleum ether) of the crude material obtained from 900 mg (5.77 mmol) of the trimethylhydrazide **19** provided 534 mg (41%) of the desired product **25**; ir (film): 1640, 1450, 1380, 1180, 1150 cm^{-1}; ^1H nmr δ: 0.82 (t, 3H, J = 7 Hz), 0.98 (t, 3H, J = 7 Hz), 1.17–2.35 (diffuse m, 9H), 2.46, 2.50, 2.88 (s, s, s, 3H each), 3.25–3.75 (m, 1H), 5.20 (broad q, 1H, J = 7 Hz). *Exact Mass* calcd. for $C_{13}H_{26}ON_2$: 226.2045; found: 226.2046.

(Z)-2,4-Diethyl-4-hexenoic acid (2)

To a cold (−78°C) stirred solution of the trimethylhydrazide **20** (24 mg, 0.11 mmol) in 3 mL of dry ether was added a solution of diisobutylaluminum hydride in hexane (0.12 mL, 1 *M*, 0.12 mmol). The reaction mixture was stirred at −78°C for 30 min and at 0°C for 2 h. A few drops of saturated aqueous ammonium chloride were added and the mixture was allowed to warm to room temperature. After anhydrous magnesium sulfate had been added to the resultant slurry, it was filtered through a short column of Florisil. The column was washed with ether and the solvent was removed from the combined eluate. The residual mixture was taken up in dimethylformamide (2 mL), the resultant solution was treated with 200 mg of pyridinium dichromate, and the mixture was stirred overnight at room temperature. Water (10 mL) was added and the resultant mixture was extracted thoroughly with ether. The combined extract was washed successively with brine and 2 × 15 mL of 0.1 *N* aqueous sodium hydroxide (these extracts were retained, see below), and then dried over anhydrous magnesium sulfate. Removal of the solvent, followed by bulb-to-bulb distillation of the residual oil, provided 12 mg of the starting material **20**.

The above-mentioned basic extracts were acidified (1 mL of 3 *N* hydrochloric acid) and the resulting mixture was washed with dichloromethane (3 × 15 mL). The combined organic solution was dried over anhydrous magnesium sulfate. Removal of the solvent, followed by distillation (air-bath temperature ~ 100°C/12 Torr) of the residual oil gave 4.5 mg (50% based on unrecovered **20**) of the acid **2**; ir (film): 3300–2550, 1700 cm^{-1}; ^1H nmr (400 MHz) δ: 0.99 (t, 3H, J = 7 Hz), 1.02 (t, 3H, J = 7 Hz), 1.55–1.79 and 1.66 (m, 2H and d, 3H, J = 6 Hz), 2.09 (q, 2H, J = 7 Hz), 2.28–2.40 (m, 1H), 2.49–2.63 (m, 2H), 5.05 (q, 1H, J = 6 Hz). *Exact Mass* calcd. for $C_{10}H_{18}O_2$: 170.1307; found: 170.1309.

(E)-2,4-Diethyl-4-hexenoic acid (3)

This compound was obtained from the trimethylhydrazide **25** via a procedure identical with that described above. From 516 mg of **25** there was obtained, in addition to 180 mg of the starting material **25**, 177 mg (70% based on unrecovered **25**) of the unsaturated acid **3**; ir (film): 3400–2400, 1700 cm^{-1}; ^1H nmr (400 MHz) δ: 0.95 (t, 3H, J = 7 Hz), 0.97 (t, 3H, J = 7 Hz), 1.51–1.65 and 1.58 (m, 2H and d, 3H, J = 6.5 Hz), 2.04 (q, 2H, J = 7 Hz), 2.15 (d of d, 1H, J = 14, 6 Hz), 2.35 (d of d, 1H, J = 14, 8 Hz), 2.42–2.52 (m, 1H), 5.24 (q, 1H, J = 6.5 Hz). *Exact Mass* calcd. for $C_{10}H_{18}O_2$: 170.1307; found: 170.1308.

p-*Nitrophenyl* (E)*-2,4-diethyl-4-hexenoate (26)*

To a stirred solution of the carboxylic acid **3** (120 mg, 0.71 mmol) and *p*-nitrophenol (150 mg, 1.08 mmol) in 3 mL of dry acetonitrile was added 300 mg (1.47 mmol) of *N,N′*-dicyclohexylcarbodiimide, and the resultant mixture was stirred at room temperature for 12 h. Removal of the solvent under reduced pressure provided a solid which was triturated with chloroform. Filtration of the mixture, followed by removal of the solvent from the filtrate, gave a solid which was purified by flash chromatography (15) on 28 g of silica gel. Elution of the column with 1:3 hexane–chloroform afforded 180 mg (87%) of the desired ester **26**. A small sample of this material, obtained from methanol, exhibited mp 45–46°C; ir ($CHCl_3$): 1755 cm^{-1}; ^1H nmr δ: 1.01 (t, 3H, J = 7 Hz), 1.04 (t, 3H, J = 7 Hz), 1.42–1.86 and 1.62 (m, 2H and d, 3H, J = 7 Hz), 2.13 (q, 2H, J = 7 Hz), 2.28–2.85 (m, 3H), 5.33 (q, 1H, J = 7 Hz), 7.23 (d, 2H, J = 9 Hz), 8.31 (d, 2H, J = 9 Hz). *Exact Mass* calcd. for $C_{16}H_{21}NO_4$: 291.1471; found: 291.1496.

(±)-Triophamine (1) and its diastereomer

Subjection of guanidine hydrochloride to ion-exchange chromatography on a column of Dowex 1-X8 (HO^- form) provided free guanidine. Small amounts of the latter material were added at 1 h intervals to a stirred solution of the *p*-nitrophenyl ester **26** (34 mg, 0.12 mmol) in 2mL of chloroform. The progress of the reaction was monitored by thin-layer chromatography (silica gel, 1:1 hexane–ether). It was found that if the reaction was allowed to proceed to completion (disappearance of **26**), appreciable quantities of side product(s) were formed and the yield of desired material was low. Therefore, after approximately 50–75% of the starting material **26** had reacted, the reaction mixture was filtered and the collected solid was washed with 4 × 5 mL of chloroform. Removal of the solvent from the combined filtrate gave a yellow oil which was subjected to preparative thin-layer chromatography. There was thus obtained 9.1 mg of the ester **26** and 7.4 mg (48% based on unrecovered **26**) of a mixture of (±)-triophamine (**1**) and its diastereomer. This mixture of diastereomers was separated by repeated preparative thin-layer chromatography on silica gel 60 PF-254 (19:1 hexane – isopropyl alcohol). (±)-Triophamine (4.0 mg) exhibited infrared and ^1H nmr spectra identical with those of the natural product (2), while the diastereomer exhibited ir ($CHCl_3$): 3323, 1700, 1630, 1160 cm^{-1}; ^1H nmr δ: 0.91 (t, 3H, J = 7 Hz), 0.95 (t, 3H, J = 7 Hz), 1.46–1.67 and 1.56 (m, 2H and d, 3H, J = 7 Hz), 2.03 (q, 2H, J = 7 Hz), 2.11 (d of d, 1H, J = 6, 13 Hz), 2.28–2.37 (m, 1H), 2.37–2.47 (m, 1H), 5.20 (q, 1H, J = 7 Hz). *Exact Mass* calcd. for $C_{21}H_{37}N_3O_2$: 363.2885; found: 363.2883.

Acknowledgements

We are grateful to the Natural Sciences and Engineering Research Council of Canada for financial support and a Postgraduate Scholarship (to J.M.C.), and to the University of British Columbia for a Graduate Fellowship (to K.G.).

1. G. R. SCHULTE and P. J. SCHEUER. Tetrahedron, **38**, 1857 (1982); J. E. THOMPSON, R. P. WALKER, S. J. WRATTEN, and D. J. FAULKNER. Tetrahedron, **38**, 1865 (1982); J. HELLOU, R. J. ANDERSEN, and J. E. THOMPSON. Tetrahedron, **38**, 1875 (1982); S. W. AYER and R. J. ANDERSEN. Tetrahedron Lett. **23**, 1039 (1982).
2. K. GUSTAFSON and R. J. ANDERSEN. J. Org. Chem. **47**, 2167 (1982).
3. E. PIERS and H. E. MORTON. J. Org. Chem. **45**, 4263 (1980).
4. E. PIERS, J. M. CHONG, and H. E. MORTON. Tetrahedron Lett. **22**, 4905 (1981).
5. W. C. STILL. J. Am. Chem. Soc. **100**, 1481 (1978).
6. G. H. POSNER, D. J. BRUNELLE, and L. SINOWAY. Synthesis, 662 (1974).
7. H. O. HOUSE, C. Y. CHU, J. M. WILKENS, and M. J. UMEN. J. Org. Chem. **40**, 1460 (1975); P. G. M. WUTS. Synth. Commun. **11**, 139 (1981).
8. D. E. SEITZ and S.-H. LEE. Tetrahedron Lett. **22**, 4909 (1981).
9. A. J. LEUSINK, H. A. BUDDING, and J. W. MARSMAN. J. Organomet. Chem. **9**, 285 (1967).
10. E. J. COREY and K. ACHIWA. J. Org. Chem. **34**, 3667 (1969).
11. S. KNAPP and J. CALIENNI. Synth. Commun. **10**, 837 (1980).
12. E. J. COREY and G. SCHMIDT. Tetrahedron Lett. 399 (1979).
13. J. L. OCCOLOWITZ. Tetrahedron Lett. 5291 (1966).
14. H. G. KUIVILA, K.-H. TSAI, and D. G. I. KINGSTON. J. Organomet. Chem. **23**, 129 (1970).
15. W. C. STILL, M. KAHN, and A. MITRA. J. Org. Chem. **43**, 2923 (1978).

Cellulose organic solvents: V. Conformational aspects of *N*,*N*-dimethyl ethanolamine *N*-oxide in its crystalline and diluted states

E. R. MAIA,[1] A. PÉGUY, AND S. PÉREZ[2]

Centre de Recherches sur les Macromolécules Végétales, C.N.R.S. B.P. 68, 38402 St Martin d'Hères Cédex, France[3]

Received January 18, 1983

E. R. MAIA, A. PÉGUY, and S. PÉREZ. Can. J. Chem. **62**, 6 (1984).

N,*N*-Dimethyl ethanolamine *N*-oxide (DMEAO) belongs to the class of tertiary amine oxide molecules that are good solvents for cellulose, although not being cyclic. Crystallographic investigation shows that anhydrous DMEAO is monoclinic, space group *Cc*, $a = 25.725(9)$, $b = 7.023(4)$, $c = 9.483(5)$ Å, $\beta = 101.16(10)°$, $Z = 12$. The crystal structure has been solved by direct methods and refined to a final *R* value of 0.063 for 575 observed reflexions. Three independent molecules are found within the asymmetric unit; one of these displays a pseudo-cyclic form dictated by the occurrence of a strong intramolecular hydrogen bond. Conformational investigation of DMEAO in solution, using ir and nmr spectroscopy shows that this pseudo-cyclic form is more likely to occur in diluted states. These findings are related to the ability of this tertiary amine oxide to act as a good solvent, up to a water content of one water molecule per DMEAO molecule.

E. R. MAIA, A. PÉGUY et S. PÉREZ. Can. J. Chem. **62**, 6 (1984).

Bien que ne possédant pas de structure cyclique, le *N*-oxyde de *N*,*N*-diméthyl ethanolamine (DMEAO) appartient à cette nouvelle classe de solvants organiques de la cellulose, que constituent les oxydes d'amines tertiaires. A l'état cristallin, la forme anhydre du DMEAO cristallise dans le groupe d'espace *Cc* du système monoclinique, caractérisé par les paramètres suivants: $a = 25.725(9)$, $b = 7.023(4)$, $c = 9.483(5)$ Å, $\beta = 101.16(10)°$, $Z = 12$. La structure cristalline a été résolue par méthodes directes et affinée jusqu'à un facteur de reliabilité final $R = 0.063$ calculé pour 575 réflexions indépendantes. La résolution de cette structure permet de mettre en évidence l'existence de 3 molécules cristallographiquement indépendantes, parmi lesquelles apparait une molécule dans une conformation pseudo-cyclique stabilisée par une forte liaison hydrogène intramoléculaire. Les études de spectroscopie ir et rmn en milieu dilué permettent de conclure que l'existence de cette conformation est aussi privilégiée en solution. Ces différents éléments permettent d'expliquer pourquoi cet oxyde d'amine tertiaire non cyclique agit comme un bon solvant de la cellulose et ce jusqu'à une valeur limite correspondant à un état monohydraté du DMEAO.

Can. J. Chem. Downloaded from www.nrcresearchpress.com by 210.87.254.40 on 09/06/12
For personal use only.

Introduction

In the search for new cellulose organic solvents, tertiary amine oxide molecules have particularly attracted attention (1–5). In the patents, a claim for tertiary amine oxide to be a solvent is to be cyclic, as for example *N*-methylmorpholine *N*-oxide (abbreviated MMNO). However, some examples have been found where a non cyclic molecule could exhibit good solvent properties; as in the case of *N*,*N*-dimethyl ethanolamine *N*-oxide (abbreviated DMEAO). For this particular molecule, the occurrence of a pseudo-cyclic form, stabilized by an intramolecular hydrogen bond, has been speculated (3). Such a conformation would meet the spatial requirements postulated (3, 4) for the ring dimension (5.15 Å) to fit into the hydrophobic portion of the cellulose macromolecule. Moreover, detailed crystallographic investigations on MMNO (6–8) coupled with computer simulation (9) have underlined that the solvent molecule should possess an hydrophobic end, in order to prevent any segmental recombination of the cellulose chains. Again this would tend to indicate a pseudo-ring shape for DMEAO. In order to ascertain the conformational behaviour of DMEAO, solid state and solution properties have been investigated using X-ray diffraction and infrared and nuclear magnetic resonance respectively. Among other parameters, cellulose dissolution in tertiary amine oxides is found to depend on the water content of the mixture. It was therefore of interest to investigate whether or not DMEAO was complexed with water molecules in the solid state.

Experimental

Material

N,*N*-Dimethyl ethanolamine *N*-oxide (DMEAO) was a gift from Dr. R. N. Armstrong, American Enka (U.S.A.). The starting material was dissolved in anhydrous acetone at 50°C. The solution was cooled to 35°C where nucleation occurred. A further lowering of the temperature of about 1°C a day, over a week, yielded single crystals. Crystals suitable for X-ray investigation ($0.2 \times 0.2 \times 0.15$ mm) were mounted in capillaries, all operations being performed in a drybox.

Infrared and nuclear magnetic resonance spectroscopy

Infrared spectra were recorded on a 598 Perkin Elmer spectrometer using KBr discs. A cell of about 2 cm path was used. CS_2 was used as a solvent, and checked into the cell in order to ascertain the lack of any absorption between 3000 and 4000 cm^{-1}.

The ^1H nmr spectra were run at 60, 100, and 250 MHz, respectively, on a Bruker WP60, on a Bruker WP100 and on a Cameca superconducting spectrometer. The spectra were recorded in dimethylsulfoxide D6 in 5 mm tubes at room temperature. Theoretical spectrum calculations were performed using the BNC12 ITRCAL computer program.

Crystal structure determination

The space group was determined from precession photographs. The unit-cell dimensions were obtained as part of the alignment process on an automatic diffractometer by a least-squares fit to the settings of 18 well-centered reflexions. The density was measured by flotation in a mixture of anhydrous CCl_4 and cyclohexane. The crystal data are as follows

$C_4O_2NH_{11}$ mw = 105.2

Monoclinic, space group *Cc* ($h\,k\,l$): $h + k \neq 2n$; ($h\,0\,l$): $l \neq 2n$, $h \neq 2n$; ($0\,k\,0$): $k \neq 2n$; $a = 25.725(9)$ Å, $b = 7.023(4)$ Å, $c = 9.483(5)$ Å, $\beta = 101.16(10)°$, $V = 1680.9$ Å^3, $Z = 12$, $d_c = 1.247$ Mg m^{-3}, $d_{obs} = 1.21$ Mg m^{-3}, μ(CuKα) = 0.66 mm^{-1}, λ(CuKα) = 1.54178 Å, F (000) = 696 e.

Intensity data were collected on a Philips PW1100 diffractometer using Ni-filtered Cu radiation and the 0–2θ scan mode, up to $\theta = 55°$.

[1] Present address: Departamento de Quimica, Univ. Federal de Alagoas, Maceio, Alagoas, Brasil.

[2] To whom correspondence should be addressed.

[3] Laboratoire Propre du C.N.R.S., associé à l'Université Scientifique et Médicale de Grenoble, France.

TABLE 1. Final atomic coordinates: fractional coordinates ($\times 10^4$; for H $\times 10^3$) and isotropic thermal parameters (Å^2). For non-hydrogen atoms: $B_{eq} = (4/3) \sum_i \sum_j \beta_{ij} a_i a_j$

Atom	x/a (σ)	y/b (σ)	z/c (σ)	B_{eq}	Atom	x/a (σ)	y/b (σ)	z/c (σ)	B_{ii}
O(1)	9845(5)	5401(14)	5711(15)	4.0	H(C2,1)	1034(8)	548(28)	432(21)	7.0
C(2)	10361(7)	5775(27)	5361(20)	3.5	H(C2,2)	1046(8)	712(30)	555(20)	7.0
C(3)	10746(7)	4428(24)	6318(18)	2.6	H(C3,1)	1080(7)	477(27)	734(22)	7.0
N(4)	11289(6)	4388(16)	5982(15)	2.6	H(C3,2)	1060(7)	311(31)	623(21)	7.0
C(5)	11549(8)	6342(26)	6171(20)	3.5	H(C5,1)	1135(7)	724(28)	561(21)	7.0
C(6)	11622(8)	3048(28)	6944(21)	3.0	H(C5,2)	1158(7)	687(31)	712(22)	7.0
O(7)	11270(5)	3818(14)	4551(12)	2.6	H(C5,3)	1195(8)	627(27)	591(19)	7.0
					H(C6,1)	1166(7)	332(29)	796(22)	7.0
					H(C6,2)	1150(8)	179(32)	690(20)	7.0
					H(C6,3)	1204(8)	307(27)	674(19)	7.0
O(1′)	10979(6)	9824(15)	9169(14)	3.3	H(O1′)	1101(8)	861(27)	912(23)	7.0
C(2′)	10507(7)	10027(29)	8148(21)	3.5	H(C2′,1)	1040(8)	1133(27)	801(20)	7.0
C(3′)	10076(7)	9038(23)	8677(18)	2.5	H(C2′,2)	1054(7)	944(28)	718(20)	7.0
N(4′)	9514(6)	9283(17)	7732(15)	2.8	H(C3′,1)	1009(7)	943(28)	967(20)	7.0
C(5)	9326(8)	11336(23)	7687(21)	3.6	H(C3′,2)	1014(7)	768(31)	873(20)	7.0
C(6′)	9148(8)	8101(30)	8343(23)	4.1	H(C5′,1)	957(8)	1208(28)	729(22)	7.0
O(7′)	9533(5)	8714(15)	6315(12)	3.2	H(C5′,2)	932(7)	1167(29)	863(22)	7.0
					H(C5′,3)	897(7)	1147(28)	708(20)	7.0
					H(C6′,1)	913(8)	853(29)	934(21)	7.0
					H(C6′,2)	923(7)	674(30)	830(20)	7.0
					H(C6′,3)	876(8)	819(27)	778(20)	7.0
O(1″)	7905(6)	10157(14)	6035(14)	3.8	H(C5″,1)	712(8)	578(27)	464(20)	7.0
C(2″)	7896(12)	9587(28)	4570(21)	4.7	H(C5″,2)	740(7)	461(28)	354(21)	7.0
C(3″)	7903(22)	7884(3)	4231(25)	6.1	H(C5″,3)	743(8)	387(31)	518(22)	7.0
N(4″)	7903(6)	6151(16)	5153(17)	3.5	H(C6″,1)	836(7)	464(26)	395(22)	7.0
C(5″)	7432(9)	5041(4)	4539(26)	5.4	H(C6″,2)	868(8)	571(28)	553(21)	7.0
C(6″)	8371(12)	4965(47)	5049(27)	6.2	H(C6″,3)	838(8)	373(31)	570(21)	7.0
O(7″)	7891	6625(14)	6555	3.2					

The intensities of two reference reflexions, measured every 2 h, decrease by about 8% of their initial values over the duration of the data collection. This decrease was taken into account during the data reduction which was performed using the usual manner. Of the 841 independent reflexions measured, only 575 ($I > 2.5\sigma(I)$) were employed for the structure determination and refinement. Because of the small size of the crystals and the low value of the absorption coefficient ($\mu = 0.66$ mm^{-1}), no absorption correction was applied. The atomic scattering factors used for the hydrogen and non-hydrogen atoms were taken from Stewart *et al.* (10) and Cromer and Waber (11), respectively.

The systematic absences are compatible with both *Cc* and *C*2/*c* space groups. It was decided to solve the structure in the non-centrosymmetric space group *Cc*. From the observed density 1.21 Mg m^{-3}, it can be deduced that the asymmetric unit may contain up to three independent DMEAO molecules.

A set of normalized structure factors $|E|$ was obtained after isotropic temperature factor correction. Analysis of the $|E|$ statistics indicated a non-centrosymmetric space group. The structure was solved by a straightforward application of the MULTAN (12). The *E*-map computed with the best set of phases revealed first seven non-hydrogen atoms defining one DMEAO molecule. A second DMEAO molecule was revealed after two least-squares refinement cycles. Two more cycles of full-matrix least-squares refinement ($R = 0.16$) followed by a difference Fourier map, indicated the location of non-hydrogen atoms revealing the presence of a third DMEAO molecule. Therefore three crystallographically independent molecules were found; such an asymmetric unit content yields a calculated density of 1.25 Mg m^{-3} that compares well with the observed value. Several cycles of full-matrix least-squares refinement led to a conventional *R* value of 0.10. Thirty H atoms were located on successive Fourier difference synthesis and included in the refinement with isotropic temperature factors. Six H atoms (H(O1), H(O1″), H(C2″,1), H(C2″,2), H(C3″,1), and H(C3″,1)) could not been located. The final *R* values for the observed reflexions only and for all the measured reflexions were 0.063 and 0.079 respectively. The quantity minimized was $\Sigma w(F_o - F_c)^2$, each reflexion being assigned a unit weight. A final electron density map showed no significant residual peaks, the extreme fluctuations being -0.30 and 0.35 e$^-$ Å^3.

Results and discussion

The positional parameters are presented in Table 1.[4] A schematic diagram of the molecule along with the numbering of the atoms is shown in Fig. 1. In the following discussion, the atoms belonging to the three independent entities in DMEAO are labelled as unprimed, primed, and double primed.

Solid state

The interatomic distances, bond angles, and torsion angles are given in Tables 2, 3, and 4. For bond distances and bond angles, the estimated standard deviations are about 0.02 Å and 0.03°, respectively. For the unprimed and primed molecules the estimated standard deviations on torsion angles are about 1.7° and amount to 6.4° for the double primed residue. Thus the reliability of geometrical information is greatly reduced. This low accuracy is attributed to the paucity of the number of observed reflexions compared with the number of parameters being refined. Another puzzling structural feature is the intolerable C(2″)—C(3″) distance which is accompanied by a strong anisotropy of the associated thermal parameters that could re-

[4] The structure factor table is available upon request, at a nominal charge, from the Depository of Unpublished Data, CISTI, National Research Council of Canada, Ottawa, Ont., Canada K1A 0S2.

Can. J. Chem. Downloaded from www.nrcresearchpress.com by 210.87.254.40 on 09/06/12
For personal use only.

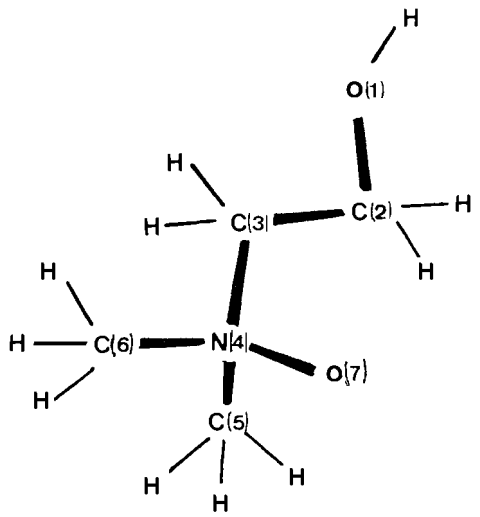

FIG. 1. Numbering of the atoms in the molecule of *N*,*N*-dimethyl ethanolamine *N*-oxide (DMEAO).

TABLE 2. Bond distances (Å), the standard deviations are indicated in parentheses

Bonds	Distance with residues		
	Unprimed	Primed	Double primed
O(1)—C(2)	1.45(2)	1.41(2)	1.44(2)
C(2)—C(3)	1.53(2)	1.48(2)	1.24(3)
C(3)—N(4)	1.49(2)	1.56(2)	1.50(2)
N(4)—C(5)	1.52(2)	1.52(2)	1.46(3)
N(4)—C(6)	1.47(2)	1.46(2)	1.48(3)
N(4)—O(7)	1.41(1)	1.41(2)	1.38(2)

TABLE 3. Bond angles (°), the standard deviations are indicated in parentheses

Bonds	Angles with residues		
	Unprimed	Primed	Double primed
O(1)—C(2)—C(3)	106(1)	109(1)	121(2)
C(2)—C(3)—N(4)	114(1)	115(1)	129(2)
C(3)—N(4)—C(5)	112(1)	112(1)	107(2)
C(3)—N(4)—C(6)	110(1)	108(1)	109(2)
C(3)—N(4)—O(7)	111(1)	109(1)	112(1)
C(5)—N(4)—C(6)	108(1)	109(1)	107(2)
C(5)—N(4)—O(7)	108(1)	108(1)	110(1)
C(6)—N(4)—O(7)	109(1)	111(1)	112(1)

sult from disorder. However, since the primary goal of this study was an investigation of the conformational behaviour of DMEAO, no other refinement approaches were tried to solve this anomaly. Within these restrictions, bond distances and angles conform to values tabulated for already solved *N*-oxide containing structures (9).

Without any doubt the more interesting aspect is the occurrence of three crystallographic independent molecules among which two different stable conformers are found. The overall conformation of DMEAO can be described by two torsional angles: τ1 (O(1)—C(2)—C(3)—N(4)) and τ2 C(2)—C(3)—N(4)—O(7)). With respect to these angles, two molecules occur in a *trans–gauche* form (Fig. 2), whereas a *cis–cis* arrangement is found for the third one (Fig. 2). This arrangement that results in a short non-bonded C(2″) . . . . O(7″) distance is stabilized by the strong intramolecular hydrogen bond between O(1″) and O(7″), the distance being 2.56 Å. When the H(O1″) hydrogen atom is considered, the resulting scheme is a planar system, made up of the six following atoms: H(1″), O(1″), C(2″), C(3″), N(4″), O(7″).

TABLE 4. Torsion angles (deg)

Bonds	Torsion angles with residues		
	Unprimed	Primed	Double primed
O(1)—C(2)—C(3)—N(4)	172(1)	175(1)	2(8)
C(2)—C(3)—N(4)—C(5)	61(2)	−65(2)	121(6)
C(2)—C(3)—N(4)—C(6)	−179(2)	176(2)	−124(6)
C(2)—C(3)—N(4)—O(7)	−59(2)	55(2)	0(7)

FIG. 2. Stereoscopic views (PITMOS) of the molecule of DMEAO as occurring in the *trans–gauche* and *cis–cis* conformation.

A projection of the structure (13) onto the plane (0 1 0) is shown in Fig. 3, whereas Table 5 lists the hydrogen bond characteristics. Both primed and unprimed molecules that occur in a *trans–gauche* conformation are linked through hydrogen bonding in which the N—O site acts as the receptor, the donor being the alcohol group. The resulting feature is a propagation of molecules along the *c* axis in a polymer-like fashion. In contrast, the *cis–cis* conformer does not exhibit any strong intermolecular bonding, its surrounding being only weak van der Waals forces. Hence the overall packing feature is a layer type structure.

Conformation in solution

Typical infrared spectra obtained for a 0.005 *M* and 0.001 *M* concentration of DMEAO in CS_2 are shown in Fig. 4*a* and 4*b*, respectively; the occurrence of a peak at 3410 cm^{-1} can be clearly shown. This occurrence is independent of the concentration and can be assigned to the OH stretching frequency involved in an intramolecular hydrogen bonding, since it occurs at lower level than a free hydroxyl which absorbs at about 3625 cm^{-1}. At very low concentration (Fig. 4*b*) there is no peak at 3625 cm^{-1} thereby indicating that no free hydroxyl group is present. Moreover, the frequency of the absorption band remains concentration independent; this being a crucial test for intrabonding.

Further evidence for the occurrence of intramolecular hydrogen bonding can be inferred from nmr spectroscopy. ^1H spectra of DMEAO and dimethyl ethanolamine (abbreviated as DMEA) have been obtained. The coupling constants and $\Delta\nu_{AB}$ values corresponding to DMEAO and DMEA, along with those of *N*-methylmorpholine (abbreviated as NMM) are listed in Table 6. A four spin system involving protons of the two following types, either A_2X_2 or AA′BB′, yields spectrum symmetrical about its midpoint. In the case of A_2X_2 pattern, a further symmetry about the midpoint of each half of the pattern is disclosed. This is the case for dimethylethanolamine which exhibits a double triplet. This is an A_2X_2 type giving a first-order spectrum because A and X are equally coupled (un-

Can. J. Chem. Downloaded from www.nrcresearchpress.com by 210.87.254.40 on 09/06/12
For personal use only.

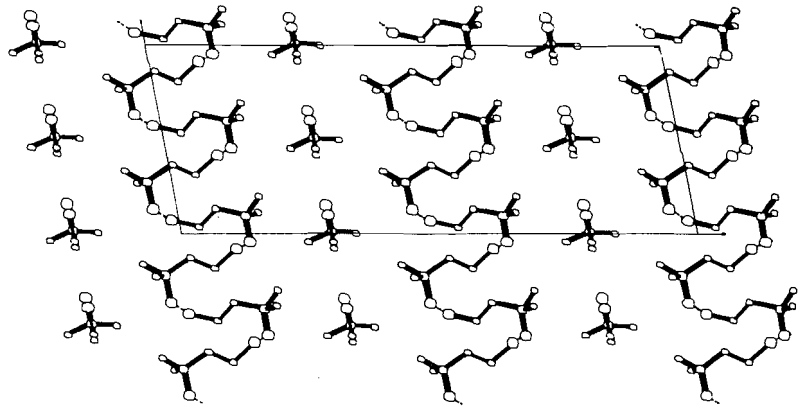

FIG. 3. View of the packing (PITMOS). The hydrogen bonds are shown as dashed lines. The H atoms of the DMEAO molecules are omitted.

TABLE 5. Hydrogen bonding in DMEAO*

i j k	D_{jk}(Å)	D_{ik}(Å)	θ_{ijk}(deg)
O(1) . . . . . O(7′)$_{I}$		2.56(2)	
O(1′)—H(01′) . . . O(7)$_{II}$	1.85(20)	2.67(2)	159(20)
O(1″) . . . . . O(7″)$_{I}$		2.53(2)	

*With O(1′)—H(O1′) = 0.86(20) Å, N(4)—O(7) . . . H(O1′) = 115(7)°; I = x, y, z; II = x, $(-y + 1)$, $(1/2 + z)$.

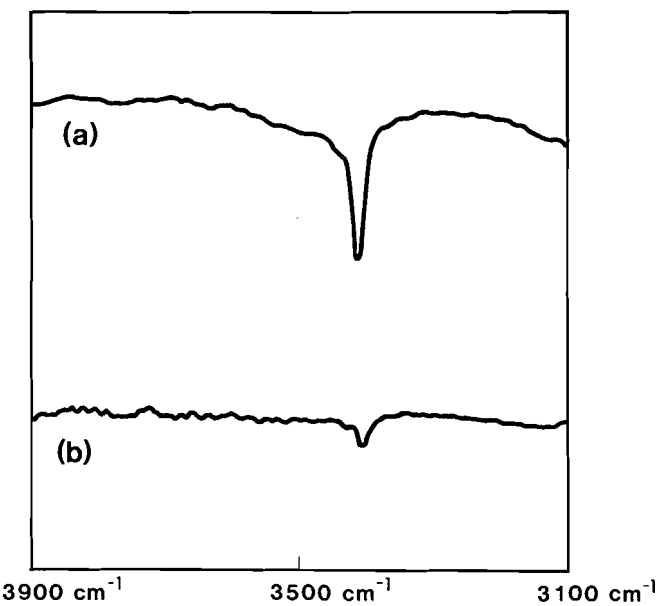

FIG. 4. Infrared spectrum of DMEAO in CS_2: (*a*) 0.005 *M* concentration, (*b*) 0.001 *M* concentration.

primed) ($J_{A,X}$ = 5.7 Hz and $\Delta\nu_{AX}$ = 1.18 ppm) and obey the simple multiplicity rules. Conversely, the ^{1}H DMEAO spectrum can be analyzed as a AA′BB′ system. Such a conclusion also arises from the coupling constant values (Table 6) which compare well with those derived from another AA′BB′ system displayed by *N*-methymorpholine (14). Dimethyl ethanolamine does not have any N—O bond and cannot exhibit any intramolecular hydrogen bond and its resulting "pseudo-cyclic" form. On the other hand, DMEAO in its diluted state, exhibits such an intramolecular cyclization. Indeed a *trans* conformation of the molecule should have yielded a double triplet due to the equally coupled hydrogen atoms. An intramolecular hydrogen bond involving N(4) instead of O(1) cannot be possible due to the magnitude of $J_{2e,3a}$ of about 6.8.

TABLE 6. Coupling constants (Hz) for the methylene protons of DMEAO and *N*-methylmorpholine (NMM)

Molecule	$J_{2e,2a}$	$J_{2e,3e}$	$J_{2e,3a}$	$J_{3e,3a}$	$\Delta\nu_{AB}$
DMEAO	−13.2	3.2	6.8	−13.0	0.57
NMM(14)	−13.2	3.05	6.65	−13.4	0.30

Conclusion

The present work shows that DMEAO can exhibit several stable conformers, among which a pseudo-cyclic structure may be expected to occur in diluted states. The overall geometrical shape of the pseudo-cyclic molecule is a ring, having dimension less than 5.15 Å, which seems to be the upper limit that tertiary amine oxide molecules can have in order to penetrate the cellulose structure and act as a good solvent. Moreover this cyclic structure results in a strong disparity between its polar N—O bond and the apolar end; this was shown to be an essential feature for the solvent molecules in order to prevent any segmental recombination of the cellulose chains (9). Therefore, it appears that the search for new solvents for cellulose should not be restricted to the consideration of molecules exhibiting cyclic moieties, as long as pseudo-cyclic forms can occur.

In a way similar to MMNO, the dissolving power of DMEAO depends on the temperature of the solution, the water content of the mixture, the concentration and the degree of polymerization of the cellulose. As the water content increases, the ability of DMEAO to dissolve cellulose decreases. No cellulose can be dissolved when the molecular ratio of water to DMEAO reaches 1, unless the water content is reduced by application of vacuum (15). In the case of MMNO, this nonsolvent character is reached for a water content equal to or greater than 2. Such a behaviour can be rationalized by the fact that in MMNO the oxygen atom of the N—O bond can interact through its two available lone-pairs, with either water molecules or hydroxylic oxygen atoms of cellulose. In contrast, the oxygen atom of the N—O bond in the pseudo-cyclic conformation of DMEAO has only one lone-pair available, through which strong intermolecular hydrogen bonding is possible. Therefore only one water molecule per DMEAO molecule is sufficient to saturate the hydrogen bond possibility of the N—O linkage to cellulose, and would hamper any solvent character.

Acknowledgements

The authors thank Pr. D. Gagnaire and Dr. H. Chanzy for

Can. J. Chem. Downloaded from www.nrcresearchpress.com by 210.87.254.40 on 09/06/12
For personal use only.

their continuous interest in this work. The data collection was performed within the "Groupe Grenoblois de Diffractomètrie".

1. D. L. JOHNSON. Br. Pat. No. 1144084, 1969; U.S. Pat. No. 3447939 (1969).
2. N. E. FRANKS and J. K. VARGA. U.S. Pat. No. 4145532 (1979).
3. N. E. FRANKS and J. K. VARGA. U.S. Pat. No. 4196282 (1980).
4. N. E. FRANKS and J. K. VARGA. U.S. Pat. No. 4247688 (1981).
5. H. CHANZY, B. CHUMPITAZI, and A. PÉGUY. Carbohydr. Polym. **2**, 35 (1982).
6. E. MAIA, A. PÉGUY, and S. PÉREZ. Acta Crystallogr. B**37**, 1858 (1981).
7. E. MAIA and S. PÉREZ. Acta Crystallogr. B**38**, 849 (1982).
8. H. CHANZY, E. MAIA, and S. PÉREZ. Acta Crystallogr. B**38**, 852 (1982).
9. E. MAIA and S. PÉREZ. Nouv. J. Chim. **7**, 89 (1983).
10. R. F. STEWART, E. R. DAVIDSON, and W. T. SIMPSON. J. Chem. Phys. **42**, 3175 (1965).
11. D. T. CROMER and J. T. WABER. Acta Crystallogr. **18**, 104 (1965).
12. P. MAIN, L. LESSINGER, M. M. WOOLFSON, G. GERMAIN, and J. P. DECLERC. MULTAN 77. A system of computer programs for the automatic solution of crystal structures from X-ray diffraction data. (1977). Universities of York, England and Louvain, Belgium.
13. M. L. DHEU and S. PÉREZ. PITMOS. Programmes Interactifs de Tracés de Molécules et de Structures. CERMAV; CNRS, Grenoble, France. 1980.
14. W. B. SMITH and B. A. SHOULDERS. J. Phys. Chem. **69**, 579 (1965).
15. P. NOÉ. Thèse de Docteur Ingénieur. CERMAV; USMG, Grenoble, France. 1982.

Can. J. Chem. Downloaded from www.nrcresearchpress.com by 210.87.254.40 on 09/06/12
For personal use only.

Permanganate peroxidation of cyclohexene.I. The unusual effect of turbulent stirring and dilution upon glycol yields

JAY E. TAYLOR, DAVID WILLIAMS, KENNETH EDWARDS, DONALD OTONNAA, AND DAVID SAMANICH
Department of Chemistry, Kent State University, Kent, OH 44242, U.S.A.

Received May 31, 1983

JAY E. TAYLOR, DAVID WILLIAMS, KENNETH EDWARDS, DONALD OTONNAA, and DAVID SAMANICH. Can. J. Chem. **62**, 11 (1984).

Yields of *cis*-1,2-cyclohexanediol formed by the reaction of methanol–water solutions of potassium permanganate with cyclohexene varied from nearly zero to a high of 84% as a function of stirring efficiency and dilution. This unusual effect is attributed to the formation of an intermediate hypomanganate ester ion which after formation may undergo reaction [1] with water to form the glycol or [2] with excess MnO_4^- to form higher oxidation products. The factor of increased stirring and dilution reduced localized excess of MnO_4^- and, thereby, minimized the contribution of reaction [2]. Addition of modest concentrations of methanol increased the yield, and this is attributed to enhanced solubilization and dispersion of the insoluble cyclohexene. Sodium hydroxide was beneficial to the reaction but only in low concentrations.

JAY E. TAYLOR, DAVID WILLIAMS, KENNETH EDWARDS, DONALD OTONNAA et DAVID SAMANICH. Can. J. Chem. **62**, 11 (1984).

Les rendements en cyclohexanediol-1,2-*cis* formé lors de la réaction du cyclohexène avec du permanganate de potassium dans des solutions aqueuses de méthanol varient de 0 à près de 84% en fonction de l'efficacité de l'agitation et de la dilution. On attribue cet effect inhabituel à la formation d'un intermédiaire, un ion hypomanganique, qui après sa formation, peut subir soit la réaction [1] avec l'eau conduisant au glycol, soit la réaction [2] avec un excès de MnO_4^- pour former des produits plus oxydés. L'effet combiné d'une meilleure agitation et d'une plus grande dilution réduit la présence localisée d'excès de MnO_4^- et diminuent ainsi la contribution de la réaction [2]. L'addition de faibles quantités de méthanol augmente le rendement; on attribue ce résultat à une meilleure solubilisation et une plus grande dispersion du cyclohexène qui est insoluble. L'addition d'hydroxyde de sodium est bénéfique à la réaction mais uniquement à de faibles concentrations.

[Traduit par le journal]

Can. J. Chem. Downloaded from www.nrcresearchpress.com by 210.87.254.5 on 09/06/12
For personal use only.

The conversion of cyclic alkenes to stereospecific glycols has been the subject of a number of investigations. Whereas performic acid quite generally gives good yields (60–90%) of *trans*-glycols (1) and is both easy to use and applicable to a wide variety of alkenes, the various reagents which have been used for the preparation of *cis*-glycols are each beset with serious disadvantages. Osmium tetroxide (2) and thallium acetate (3) are costly and poisonous and the procedures are quite involved. The iodine – silver acetate procedure (4) has been reported not to be dependably stereospecific (5) and is expensive for larger preparations as is the iodine – potassium iodate technique (6).

Potassium permanganate solutions (7, 8) have been used alone and with a variety of additives including sodium hydroxide, magnesium sulfate, acetone, various alcohols, and phase transfer reagents. Potassium permanganate solubilized in anhydrous dichloromethane has been reported to give good yields with several more complex alkenes (9), but other permanganate procedures have generally been characterized by yields often under 50% and commonly in the range of 10–30% for simple alkenes. Significantly higher yields have been obtained from only a very limited number of alkenes (8, 10, 11) which are generally substituted by negative and/or solubilizing groups. For certain glycols, the necessity of recovery of a highly soluble product from dilute aqueous solution has provided a further difficulty.

In view of the several advantages of permanganate peroxidations, a search for procedures to overcome the indicated disadvantages was initiated. This paper reports excellent success for *cis*-1,2-cyclohexanediol, both with respect to improvement of yields and ease of recovery of the glycol. In addition, some further insights concerning the mechanism of the reaction have evolved.

Experimental

cis-*1,2-Cyclohexanediol*

The apparatus used and a typical preparation are described for each of two reactor volumes. Variations on each of these procedures are defined in Table 1.

Procedure A (5-L reactor)

A solution containing 1 g NaOH (1.7 mL 50% solution) in 450 mL water was placed in a 5-L flanged reaction flask (Ace Glass Co.) with a 10-cm id neck. A fabricated 1/2-in. thick Plexiglas cover sheet, clamped to the flask, accommodated a thermometer, inlet tube, and stirrer whose shaft rotated inside a copper tube acting also as a condenser. The necessity of a sealed stirring unit was thereby eliminated.

The thermometer and addition tube were inserted through holes in the cover using rubber tubing to make gas tight seals. The addition tube consisted of a short length of 0.5-mm capillary tubing connected to a 2-L addition funnel, or equivalent, by 1.5–2.5-mm id capillary glass tubing. The lengths of capillary tubing and overall height of flow were selected to insure an addition time of 2–3 hours at a very consistent flow rate. The tip of the addition tube extended into the top of the reaction flask so that the $KMnO_4$ solution dripped with small droplets into the area of *maximum* turbulence. Both rapidity of dispersion and consistency of addition were highly essential for optimum yields.

The flask and stirrer were tipped at an angle of 45° to effect increased turbulence. The 3-prong, 5-cm diameter stirrer with 45° angle blades was activated by a 1/30 hp motor turning at ~1750 rpm. The 5/16-in. stirring shaft extended 40 cm below the motor and rotated inside the 1.3-cm id, 10.5-cm long copper tube. This tube is threaded through the Plexiglas cover and is located parallel to and as near as feasible to the lower edge of the neck of the flask. Since the flask and tube were at a 45° angle, a trough of Dry Ice supported outside the Cu tube provided cooling to make the Cu tube a condenser. (Note: an ice water condenser was later shown to be preferable.) The stirrer was extended sufficiently near the bottom of the flask so as to be immersed in the initial volume of liquid. The thrust of the stirrer was parallel to the shaft and angled off the bottom of the flask. Minimum circular

TABLE 1. Formation of *cis*-1,2-cyclohexanediol by $KMnO_4$ peroxidation of cyclohexene

Expt. No.	Initial conditions, cyclohexene slurry: Volume, L	C_6H_{10} *m*	NaOH, g	CH_3OH vol%	$KMnO_4$ solution: *m*/vol (L)	Addition time, h	Product glycol, g	Melting point °C	Yield %	Procedure
1	0.54	0.0492	1.0	15	0.0492/1.6	2.0	4.86	97–98	84[a]	A
2	0.475	0.0492	1.0	4	0.0492/1.5	2.7	4.17	97–98	73	A
3	0.555	0.0492	[b]	18	0.0492/1.5	1.8	0.4	90–95	7[c]	A
4	0.550	0.303	1.0	18	0.303/1.55	1.3	23.83 2.46	96–97.5 91.5–94	75	A[d]
5	0.550	0.453[e] 0.038[f]	1.0	18	0.303/1.55	1.1	27.4	96.5–97.5	59[g]	A[d]
6	0.055	0.049[e] 0.034[f]	0.2	—	0.05/0.14	0	Trace	—	>0	Hand stirred
7	0.555	0.303	1.0	14	0.304/1.55	3.4	23.7	97–98	68	A[d]
8	0.57	0.453[e] 0.026[f]	1.0	14	0.304/1.55	3.5	24.7	97–98	50[g]	A[d]
9	0.555	0.304	1.0	14	0.304/1.55	2.1	25.1	96.5–97.5	71	A
10	0.59	0.339	1.0	10	0.35/1.8	3.5	23.3	—[h]	57	A[i]
11	0.59	0.50[e] 0.02[f]	1.0	10	0.35/1.8	3.4	31.0	96–97.5	55[g]	A[i]
12	1.75	0.5	20.0	11	0.5/2.5	2.0	22.0	94–95	38	A(12L)[d]
13	1.84	0.5	4.0	11	0.49/2.5	3.5	24.5 10.5	97–98 92–94.5	72	A(12L)[d]
14	0.56	0.257[j]	0.7	14	~0.26/1.6[k]	2.0	20.0	97–98	67	A
15	0.22	0.0985	0.4	—	0.0985/0.5	1.8	6.01 0.40	96.5–97.5 92–94	56	B
16	0.21	0.0985	0.4	14	0.0985/0.5	1.7	8.40	97–98	73	B
17	0.21	0.0985	0.4	14	0.0985/0.5	2.4	7.69	94–96	67	B[l]
18	~0.05	0.098	—	—	0.04/0.1	~1	0.70	[m]	15	[n]
19	~0.05	0.196	—	—	0.04/0.1	~1	1.24	[m]	27	[n]
20	~0.05	0.294	—	—	0.04/0.1	~1	1.84	[m]	40	[n]

[a]This yield has been repeated.
[b]$MgSO_4 \cdot 7H_2O$ (25.5 g, 0.103 *m*) was added to the $KMnO_4$ solution to maintain neutrality.
[c]An additional 0.6 g of high melting nonacidic product was also isolated.
[d]Addition of $KMnO_4$ from dropping funnel.
[e]Initial charge.
[f]Alkene recovered.
[g]Yield based on initial charge less alkene recovered.
[h]Melting point was in the same range as in the preceding diols.
[i]Submerged jet addition.
[j]Disodium maleate (0.054 *m*) was added.
[k]This represents the approximate concentration of $KMnO_4$ remaining after reaction with the sodium maleate.
[l]Somewhat irregular addition of $KMnO_4$.
[m]Early experiment in which the SO_2 treated solution was not neutralized with $NaHCO_3$. The mp was low (85–90°C) due to adipic acid. Crystalline appearance was excellent. The yield was based on $KMnO_4$, assuming 1 $KMnO_4 \equiv 1$ alkene.
[n]A small reactor (~500 mL) was used with less efficient stirring than is described under procedures A or B.

motion of the liquid was necessary to provide maximum turbulence.

Freshly distilled cyclohexene, 24.9 g, 0.303 *m*, was added, followed by 100 mL methanol. The mixture was cooled to ~0°C using a Dry Ice – methanol bath or a methanol–ice bath maintained at −10 to −5°C. A filtered solution containing 48 g (0.3 *m*) $KMnO_4$ in 1.55 L solution was added over a period of 2–3 hours through the previously described addition tube. After completion of the addition, stirring was continued for 10–15 min, and then SO_2 gas was bubbled into the reactor to *just* dissolve the MnO_2. The cover and stirrer were then removed and solid $NaHCO_3$ was added with partial precipitation of $MnCO_3$ and $MnSO_3$ and neutralization of adipic acid. After a period of settling, at pH 7.5–8, the solution was filtered. The clear or slightly turbid solution was then extracted with CH_2Cl_2 continuously with a Wehrli type (12) extractor until no more product was obtained. The reflux time required was 5 days using a 2-hole rubber stoppered 2-L bottle extractor or two days with three 700-mL (48 mm × 40 cm) vertical tube extractors. The time depends on the rapidity of reflux and minimization of CH_2Cl_2 globule size. The globule size may be minimized by allowing the CH_2Cl_2 to pass through a perforated test tube underneath the water surface. Completion was indicated by extending the extraction period for one or two days.

The resulting CH_2Cl_2 solution was distilled to a volume of roughly 6 times the product weight and then was allowed to crystallize first at room temperature and finally at 4–7°C. The crystals were filtered and washed twice with CH_2Cl_2 previously cooled to −15°C. The filtrate was then concentrated to about 1/10 its volume and the above procedure repeated. Additional recoveries from the filtrates were continued if needed. Yield, 23.84 g; mp 95.5–97°C, plus 2.46 g, mp 91.5–94°C; total, 26.30 g, 75% yield.

The general procedure was also used with a 12-L flask.

Procedure B (One-liter reactor)

The reactor, a rectangular bottle, 8 × 12 cm base, top ground flat, was covered with a flat Plexiglas sheet, 1/4 in. thick, having entry ports for the identical stirrer and same accommodations as in Procedure A.

A solution containing 10 mL 1 *M* NaOH and 160 mL water was added to the covered reactor flask. The solution was cooled to ~0°C

Can. J. Chem. Downloaded from www.nrcresearchpress.com by 210.87.254.5 on 09/06/12
For personal use only.

Can. J. Chem. Downloaded from www.nrcresearchpress.com by 210.87.254.5 on 09/06/12
For personal use only.

in a methanol – Dry Ice bath, and 10 mL (8.09 g, 0.0895 *m*) freshly distilled cyclohexene was added followed by 30 mL methanol. The stirring was started and, with the temperature maintained between 0 and 3°C, a filtered solution of 15.57 g (0.0985 *m*) $KMnO_4$ in 500 mL water (0.097 *M*) was added in 1.7 hours using a calibrated capillary tube to control the rate of addition. The $KMnO_4$ was added in the form of a stream of small droplets impinging upon the area of maximum turbulence near the stirring shaft.

The product recovery procedure corresponds with that described under A, yield 8.40 g, 73%, mp 97–98°C.

The data

Since oxidation of an alkene by an aqueous solution of permanganate ion produces a variety of products, it may be assumed that each of the products is formed in separate subreactions as part of the overall oxidation. Accordingly, if the peroxidation step can be maximized and the other oxidations minimized, then greatly improved yields of glycols can be obtained. This appears to have been accomplished for cyclohexene via the simple expedients of turbulent mixing and dilution.

The yields of *cis*-1,2-cyclohexanediol formed by permanganate peroxidation of cyclohexene may vary from nearly zero to as high as 84% depending solely upon the nature of the imposed conditions of stirring and dilution. In expt. 6, Table 1, the entire amount of $KMnO_4$ was rapidly mixed with the cyclohexene, and the mixture was hand-stirred erratically over a period of about 30 min. After work-up of the product as in Procedure A, roughly 0.3 g of solid product, which included only a few scattered characteristic crystals of *cis*-1,2-cyclohexanediol, was obtained.

In complete contrast, the slow addition of dilute $KMnO_4$ to a slurry of cyclohexene under conditions of highly turbulent stirring gave a yield of 84%. See expt. 1, Table 1. Also, yields in the range of 71–75% were routinely obtained with less dilution under otherwise optimum conditions.

Minor alterations in procedure significantly affected the reaction. Yields could be markedly decreased if the $KMnO_4$ solution was not added in the area of maximum turbulence. Erratic addition of the $KMnO_4$ solution reduced yields as demonstrated in comparing expts. 16 and 17. In the latter experiments, occasional spurts of $KMnO_4$ altered the smoothness of flow, and the yield was lowered by about 6%. When the $KMnO_4$ solution was injected underneath the surface, there resulted an ~18% reduction in yields. Compare expt. 4 with expt. 10. Presumably there was a localized excess of $KMnO_4$ which was not as rapidly dispersed as in topside addition. The effect was not as pronounced, however, in the presence of excess alkene, as seen in comparing expts. 5 and 11. The addition of the $KMnO_4$ solution in the form of more numerous smaller droplets (expt. 9) as compared to fewer larger droplets (expts. 7 or 4) did not significantly affect yields.

Due to the difficulty in reproducing stirring efficiency in different experiments, it must be emphasized that there can be considerable variation in observed yields. Thus, the data are best interpreted qualitatively.

Similar yields were obtained upon employing Procedures A and B, i.e., 75 versus 73% yield. Compare expt. 4 with expt. 16.

A slower rate of addition of $KMnO_4$ did appear to decrease yields. Compare expts. 4 and 5 with 7 and 8. Possibly, this could have been due to loss of cyclohexene vapor during the elongated time of addition.

Under conditions of less than adequate stirring and low product yields, addition of excess alkene promoted a marked increase in yield. In expts. 18, 19, and 20 to crude yields increased from 15 to 40%, based on $KMnO_4$, as the $KMnO_4$–alkene ratio was varied from 1:2.45 to 1:7.35. With initial higher yields there was, in contrast, a lowering of the yield (based on cyclohexene used) upon increasing the alkene–$KMnO_4$ ratio from 1:1 to 3:2. Compare expt. 4 with 5, 7, with 8, and 10 with 11. Note, however, that in each of these cases, the gross product recovery was greater with excess alkene. Thus, the lowered overall yield was most probably due to solubility and vapor losses of alkene during the recovery process.

A variety of additives was tested for effectiveness on the peroxidation reaction. Very low concentrations of sodium hydroxide appeared to enhance yields and were used routinely on nearly all peroxidations. Mildly acidic conditions were particularly disastrous. The substitution of mangesium sulfate for sodium hydroxide reduce the glycol yield to ~7%. Compare expts. 1 and 3. In turn, higher basicity also reduced yields. The addition of 20 g NaOH instead of 4 g effected a decrease from 72 to 38%. See expts. 12 and 13.

Methanol appeared to be beneficial in lower concentrations. Compare expts. 15 and 17, where a 17% increase in yield occurred upon adding methanol in 15% initial concentration.

The additions of 0.1 *M* $CuSO_4$, 0.1 *M* NH_4OH, and saturated $NaHCO_3$ were all deleterious to the peroxidation reaction whereas adding 0.1–0.2 *M* Na_3PO_4 had no significant effect. The $NaHCO_3$ gave particularly poor results. The specific data are not included herein.

Due to the inconvenience of recovery of larger amounts of *cis*-1,2-cyclohexanediol from very dilute solutions, the more concentrated solutions as in expt. 4 are recommended for a preparative procedure.

The possibility of a synergistic affect by a second alkene on cyclohexene was considered. In expt. 14, a solution of 0.31 mol of $KMnO_4$ (0.19 *M*) was added to a slurry of 0.26 mol cyclohexene with 0.054 *m* sodium maleate. The maleate was oxidized rapidly forming tartrates, etc.; these products were retained in solution upon neutralization with $NaHCO_3$. The yield was lowered slightly but not to a significant extent.

A simple procedure for quantitative recovery of the glycols from dilute aqueous solutions has also been developed. The solution of the glycol is first made basic with $NaHCO_3$ and then extracted continuously for 2–7 days with CH_2Cl_2. The purpose of the $NaHCO_3$ is to prevent extraction of any organic acids.

Discussion

The data of the paper clearly indicate that the yields of *cis*-1,2-cyclohexanediol are extraordinarily sensitive to turbulent mixing and presumably to dilution. Thus, it appears that minimization of localized excesses of permanganate ion enhances glycol yields. The changes in yields due to variations on the basic procedures, e.g., injection under the surface, etc., also support this general concept. Obviously, permanganate ion is essential for the initial reaction, but secondary oxidations by that same ion lead to other undesirable (for this work) oxidation products.

The marked increase in yields with decreased localized excesses of MnO_4^- suggests further implications in the presently described mechanism (13). There is the possibility of reaction of excess permanganate ion with the product glycol, but this

Can. J. Chem. Downloaded from www.nrcresearchpress.com by 210.87.254.5 on 09/06/12
For personal use only.

reaction appears to be quite slow and, therefore, of minor importance. Excellent evidence has been presented for the existence of an unstable intermediate hypomanganate ester ion (13–16) which forms rapidly and decomposes to various products.

The following mechanism, proposed to explain the data of this paper, is an adaptation of the hypomanganate ester concept specifically for glycol formation. The complex forms rapidly as follows:

[1] $MnO_4^- + -\overset{|}{C}=\overset{|}{C}- \rightarrow$ 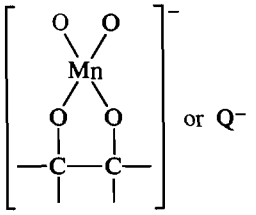 or Q^-

Once formed, Q^- may then undergo either of two alternative decompositions, one with excess MnO_4^- and the other with solvent water

[2] Q^- to $MnO_4^- \rightarrow$ diacid and other oxidation products

[3] $Q^- + H_2O \rightarrow MnO_3^- +$ 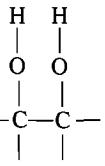

[3*a*] $2MnO_3^- \rightarrow MnO_4^{2-} \rightarrow MnO_2$

[3*b*] $2H_2O + 3MnO_4^{2-} \rightarrow 2MnO_4^- + MnO_2 + 4OH^-$

Any conditions which reduces excess permanganate ion also reduces the probability of continued oxidation by reaction [2].

Reaction [1] depends on the efficiency of dispersion of the insoluble cyclohexene, which is greatly enhanced by turbulent stirring. Under the most ideal conditions of stirring, the cyclohexene globules are minimized in size, and surface contact with the MnO_4^- is maximized. The interaction between MnO_4^- and the double bond of cyclohexene, reaction [1], then becomes extremely rapid. Once the intermediate hypomanganate ester is formed, it may react with water, reaction [3]. Or, if a significant excess concentration of MnO_4^- is present, the more rapid reaction [2] occurs, forming products more highly oxidized than the glycol. Any condition which decreases the excess permanganate ion also reduces the probability of further oxidation by reaction [2]. Thus with efficient stirring the undesired oxidation products are minimized.

References in the literature concerning the obvious mechanical effects of stirring on the rates of reactions are extensive (17). In this paper an unusual mechanistic effect due to stirring is presented. More recently Bourne and co-workers (18) have made extensive studies of mixing upon a system of competitive consecutive reactions involving a diazo coupling of the type

[4] $A + B \rightarrow R$

[5] $R + B \rightarrow S$

The impact of the effect of stirring appears to be much greater in the permanganate reaction since there is a third reaction

[6] $R + H_2O \rightarrow T$

which provides an additional alternative and reaction [5] is highly sensitive to MnO_4^- (B) concentrations. The heterogeneity of the cyclohexene–water system precludes a more rigorous treatment of this reaction.

Methanol was selected as a cosolvent with water since it does not form oxidation or condensation products which interfere with the purification of the *cis*-1,2-cyclohexanediol. The beneficial effect of methanol at lower concentrations may be attributed to increased solubility of the alkene, permitting more efficient contact between MnO_4^- and alkene. Also the methanol may act as a mild dispersant to decrease size and increase stability of the cyclohexene globules. However, due to activity effects which may enhance reaction [2] and inhibit reaction [3], much larger amounts of methanol could have an adverse effect.

Since ionic strength also has a marked effect on ionic activity, added salts should significantly increase the rate of reaction [2] at the expense of reaction [3]. Accordingly, it is possible that the adverse effects of added NaOH (expt. 12), added $MgSO_4$ (expt. 3), or an excess of $NaHCO_3$ may be, at least in part, due to an ionic strength or activity effect.

In expts. 18–20, glycol yields increased as the alkene-to-$KMnO_4$ ratio was increased. This suggests the possibility that eq. [1] is reversible and Q^- increases with increasing alkene. This effect would be evident only at lower yield conditions as seen in expts. 4 and 5, etc. Obviously, further work is needed to affirm or deny the above suggestion.

Studies of permanganate peroxidations of various alkenes under high efficiency stirring conditions are being continued. Glycol yields in the range 50–60% have been obtained for cyclopentene, 1-methylcyclohexene, cycloheptene, and cyclooctene with minor adaptations in the procedure. These and certain other alkenes are under further investigation to determine if additional improvements in yields are possible.

1. A. ROEBUCK and H. ADKINS. Organic Syntheses. Vol. III. Wiley, New York. 1955. p. 217.
2. V. VAN RHEENEN, D. Y. CHA, and W. M. HARTLEY. Org. Synth. **58**, 43 (1978).
3. R. C. CAMBIE and P. S. RUTLEDGE. Org. Synth. **59**, 169 (1979).
4. R. B. WOODWARD and F. V. BRUTCHER, JR. J. Am. Chem. Soc. **80**, 209 (1958); K. B. WIBERG and K. A. SAEGEBARTH. J. Am. Chem. Soc. **79**, 6256 (1957).
5. C. A. BUNTON and M. D. CARR. J. Chem. Soc. 770 (1963).
6. L. MANGONI, M. ADINOLFI, G. BARONE, and M. PARRILLI. Tetrahedron Lett. 4485 (1973).
7. D. G. LEE. The oxidation of organic compounds by permanganate ion and hexavalent chromium. Open Court, La Salle, IL. 1980. Chapt. 1.
8. F. D. GUNSTONE. Advances in organic chemistry. Vol. 1. Interscience, New York. 1960. pp. 103–110.
9. T. OGINO and K. MOCHIZUKI. Chem. Lett. 443 (1979).
10. E. J. WITZEMANN, W. L. EVANS, H. HASS, and E. F. SCHROEDER. Organic syntheses. Vol. II. Wiley, New York. 1943. p. 307.
11. J. E. COLEMAN, C. RICCIUTI, and D. SWERN. J. Am. Chem. Soc. **78**, 5342 (1956).
12. A. WEISSBERGER. Technique of organic chemistry. 2nd ed. Separations and purifications. Part I. Interscience, New York. 1966. p. 230.
13. R. STEWART. *In* Oxidation in organic chemistry. Part A. *Edited by* K. B. Wiberg. Academic Press, New York. 1965. pp. 41–46.
14. D. G. LEE and J. R. BROWNRIDGE. J. Am. Chem. Soc. **96**, 5517 (1974).
15. K. B. WIBERG, C. J. DEUTSCH, and J. ROCEK. J. Am. Chem. Soc. **95**, 3034 (1973).
16. D. G. LEE and J. R. BROWNRIDGE. J. Am. Chem. Soc. **95**, 3033 (1973).

17. A. WEISSBERGER. Technique of organic chemistry. Vol. III. 2nd. ed. Laboratory engineering. Part II. Interscience, New York. 1957. p. 238.

18. W. ANGST, J. R. BOURNE, and R. N. SHARMA. Chem. Eng. Sci. **37**, 1259 (1982), and preceding publications.

Can. J. Chem. Downloaded from www.nrcresearchpress.com by 210.87.254.5 on 09/06/12
For personal use only.

Uracil analogues of the acyclonucleoside 9-[[2-hydroxy-1-(hydroxymethyl)ethoxy]-methyl]guanine (BIOLF-62)[1]

KELVIN K. OGILVIE,[2] RAYMOND G. HAMILTON, MICHAEL F. GILLEN, and BRUNO K. RADATUS
Department of Chemistry, McGill University, Montreal, P.Q., Canada H3A 2K6

AND

KENDALL O. SMITH and KAREN S. GALLOWAY
Department of Microbiology, The University of Texas, San Antonio, TX 78284, U.S.A.

Received March 7, 1983

KELVIN K. OGILVIE, RAYMOND G. HAMILTON, MICHAEL F. GILLEN, BRUNO K. RADATUS, KENDALL O. SMITH, and KAREN S. GALLOWAY. Can. J. Chem. **62**, 16 (1984).

A series of substituted uracil analogues of the antiviral agent 9-[[2-hydroxy-1(hydroxymethyl)ethoxy]methyl]guanine (BIOLF-62) has been synthesized and characterized. The uracil analogues show little activity against herpesviruses.

KELVIN K. OGILVIE, RAYMOND G. HAMILTON, MICHAEL F. GILLEN, BRUNO K. RADATUS, KENDALL O. SMITH et KAREN S. GALLOWAY. Can. J. Chem. **62**, 16 (1984).

On a synthétisé et caractérisé une série d'uraciles substitués qui sont des analogues de l'agent antiviral [[hydroxy-2 (hydroxyméthyl)-1 éthoxy]methyl]-9 guanine (BIOLF-62). Les analogues uraciles montrent peu d'activité vis-à-vis des virus de l'herpès.

[Traduit par le journal]

Can. J. Chem. Downloaded from www.nrcresearchpress.com by 210.87.254.40 on 09/06/12
For personal use only.

Introduction

Nucleoside analogues have gained increasing importance through their biological activity, particularly as antiviral and anticancer compounds (1). While many such analogues have an intact but modified furanose ring, others can be considered as ring-open nucleoside analogues (2–4). We have introduced a novel ring-open nucleoside structure **1** (5–7) which possesses all of the chemical functionality of deoxyribonucleosides but which lacks the rigid furanose ring structure. The purine derivatives of structure **1** have shown remarkable activity against herpesviruses (8–10). In this report we wish to describe the synthesis of a series of pyrimidine analogues of structure **1**.

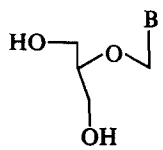

1

A number of pyrimidine bases have conferred activity to nucleoside analogues. Halogens present at the 5-position of uracil (e.g. 5-fluorouracil and 5-iodouracil) have induced antitumor and antiviral activity to nucleoside analogues (11–15). 5-Methyluracil arabinonucleosides have been reported to selectively inhibit HSV-1 and HSV-2 (16). 5-Propyluracil nucleosides have been reported to possess antiviral activity (17, 18). The (*E*)-5-(2-bromovinyl)uracil nucleosides have significant inhibitory activity against HSV-1. 3-Deazauracil nucleosides inhibit replication in bacteria and RNA viruses (1). 5-Nitrouracil nucleosides show potent cytotoxic activity (21). We have prepared derivatives of our general structure **1** containing these and other modifications of the uracil ring and tested them for activity against herpesviruses.

Results and discussion

Compounds **4***a*–*e* were prepared (Scheme 1) by condensing the persilylated base (**2***a*–*e*) with the chloromethyl ether **3** (6). Both mercuric cyanide and tetra-*n*-butylammonium iodide (TBAI) were used as catalysts in the coupling reaction. While both are effective catalysts, TBAI has the advantage of lower toxicity, is required in smaller quantities, and the reactions are generally easier to manipulate during work-up. The 6-azauracil and 3-deazauracil derivatives **6***a* and **7***a* were also prepared by TBAI catalyzed coupling reactions.

The removal of the benzyl groups from **4** to give the unprotected compounds **5** generally proceeded smoothly in both direct or phase transfer catalytic hydrogenation. However, for the 5-bromo derivative **4***d* and the 5-nitro derivative **4***e* alternate routes were required. PdO catalyzed hydrogenation led to the removal of the 5-bromine atom from **4***d* and conversion of the 5-nitro to the 5-amino derivative **5***f*. Fortunately, the boron-trichloride cleavage (22) of the benzyl groups proceeded smoothly without effect on either the 5-bromo or 5-nitro substituents.

The synthesis of the 5-allyl and 5-*n*-propyl derivatives **8** and **9** (Scheme 2) was modelled after that of Ruth and Bergstrom (23) using organopalladium intermediates. The uracil derivative **5***a* was treated first with mercuric acetate followed by condensation with allyl chloride in the presence of Li_2PdCl_4. The 5-allyl derivative **8** was obtained in 62% yield and was hydrogenated to the 5-*n*-propyl derivative **9** in 97% yield.

The 5-iodouracil derivative **5***g* was of interest in its own right and as an intermediate to the bromovinyl derivative **13**. The method of Robins *et al.* (24) was used to introduce the iodine into position C-5 of the uracil ring. The treatment of **5***a* with iodine monochloride led to numerous unidentified products. However, the diacetyl derivative (**10**, Scheme 3) was smoothly converted into the 5-iodo derivative **11** using this procedure. Compound **11** was deacylated to **5***g* using potassium carbonate in methanol.

Compound **11** also served as the starting point for the introduction of the bromovinyl side chain at C-5. The general procedure of Dieck and Heck (25) as applied to nucleosides (26)

[1]Part III in a series on antiviral and acyclonucleosides. Part II is ref. 6.

[2]Author to whom correspondence may be addressed.

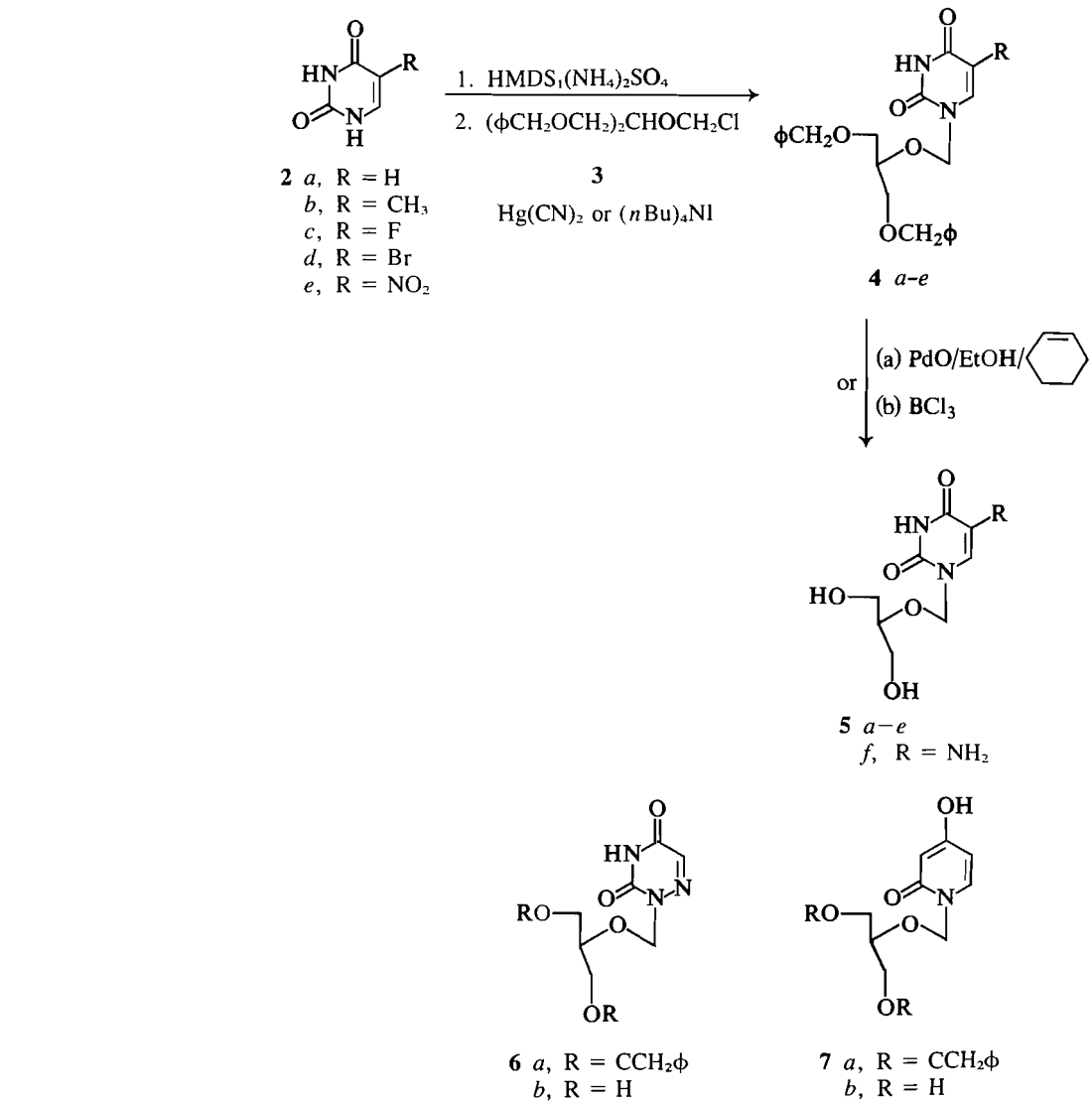

2 *a*, R = H
b, R = CH_3
c, R = F
d, R = Br
e, R = NO_2

4 *a–e*

5 *a–e*
f, R = NH_2

6 *a*, R = $CCH_2\phi$
b, R = H

7 *a*, R = $CCH_2\phi$
b, R = H

SCHEME 1

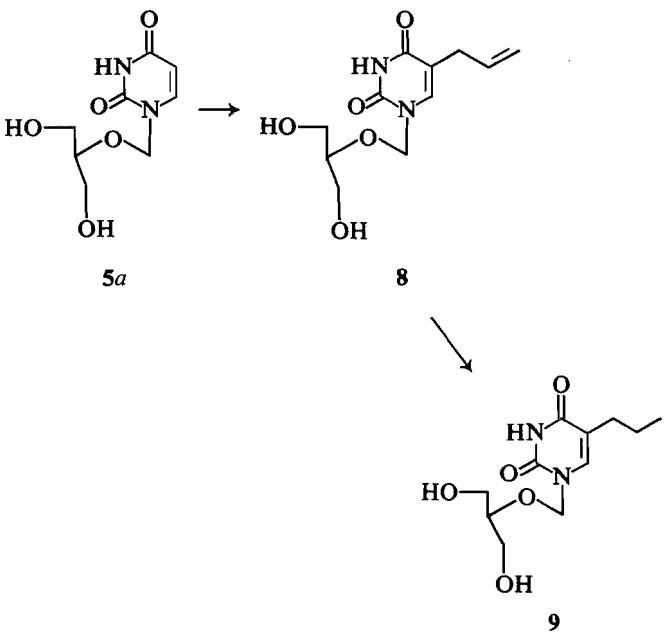

5*a* **8** **9**

SCHEME 2

was used. This procedure involves the conversion of the 5-iodo to the 5-methyl propenoate (**12**). The *trans* assignment arises from the 16 Hz coupling constant between the vinylic hydrogens (23). The ester groups on **12** were hydrolyzed and the bromine was introduced using *N*-bromosuccinimide (27), giving **13** in 55% yield.

The properties of these compounds are collected in Tables 1 to 4. These compounds were tested for activity against HSV-1. None of the compounds tested showed significant activity, all having ED_{50} values equal to, or greater than, 32 μg/mL.

Experimental

General methods

Thin-layer chromatographic data (R_f values) are recorded from Merck Kieselgel 60F254 analytical sheets. Column chromatography was performed using Merck silica gel 60 (230–400 mesh) packed in glass columns (1.5 cm diameter up to 1 g of material, 5 cm diameter for over 1 g of material) using 15 g of silica per gram of crude material.

Uracil bases were purchased from Sigma Chemical Co. Compound **3** was prepared as previously described (6).

Ultraviolet spectra were recorded on a Cary 17 spectrometer. Nuclear magnetic resonance spectra were recorded using a Bruker WH-90, a Varian XL-200, and a Varian T60A spectrometer.

Can. J. Chem. Downloaded from www.nrcresearchpress.com by 210.87.254.40 on 09/06/12
For personal use only.

Can. J. Chem. Downloaded from www.nrcresearchpress.com by 210.87.254.40 on 09/06/12
For personal use only.

TABLE 1. Physical properties of acyclonucleosides

Compound	Melting point (°C)	R_f^*	Ultraviolet (λ_{max}, nm(ε)) EtOH	0.1 *N* HCl	H_2O	0.1 *N* NaOH
4*a*	Oil	0.27[a]	257			
4*b*	96–97.5	0.20[b]	264			
4*c*	87.5–88.5	0.33[b]	265			
4*d*	Oil	0.40[b]	274			
4*e*	Oil	0.33[b]	300			
6*a*	Oil	0.33[b]	260			
7*a*	67–69	0.81[c]	282			
10	106–108	0.10[a]	256			
11	Oil	0.30[a]	283			
12	126–127	0.24[a]	296			
5*a*	120–122	0.31[c]		258(10700)	258(10400)	259(7300)
5*b*	155–156	0.19[c]	264	264(8400)	264(8100)	263(5900)
5*c*	130–131	0.33[c]		265(7600)	266(7500)	266(5700)
5*d*	145–147	0.43[c]		276(7900)	276(7400)	274(5500)
5*e*	167–169	0.32[c]		299(11000)	307(9700)	321(12000)
5*f*	146–147	0.17[c]		261(7300)	291(5700)	286(4700)
5*g*	148–149	0.43[c]		283(6800)	283(6300)	275(4800)
6*b*	128–129	0.40[c]		261(5400)	259(5400)	252(6000)
7*b*	120–122	0.28[c]		275(3700)	275(4500)	267(5600)
8	99–101	0.49[c]		265(7600)	265(7300)	264(5400)
9	105–106	0.48[c]		265(7700)	265(7100)	266(5300)
13	142–143	0.48[c]		290(9600)	289(8950)	282(7600)

*Solvents (a) ethyl acetate – hexane (7:3); (b) ethyl acetate – hexane (3:2); (c)dichloromethane – methanol (4:1).

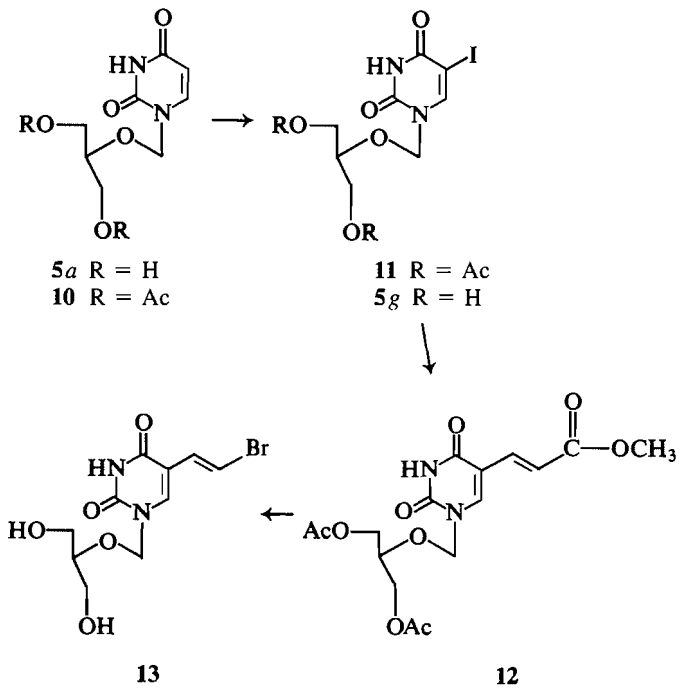

5*a* R = H
10 R = Ac
11 R = Ac
5*g* R = H
13
12

SCHEME 3

Preparation of 1,3-dibenzyloxy-2-chloromomethoxypropane (3)

1,3-Dibenzyloxy-2-propanol (95.9 g, 0.35 mol) and trioxymethylene (paraformaldehyde, 11.2 g) were added to 1,2-dichloroethane (250 mL, distilled from P_2O_5). The mixture was cooled in an ice-water bath and dry HCl was bubbled through the stirred mixture for 8 h (care is taken to exclude moisture). Anhydrous calcium chloride was added and after a few minutes the solution was collected by filtration. The solution was concentrated at reduced pressure (bath temperature 40°C) to a syrup. An ^{1}Hmr spectrum of this material indicated that it contained 87% of **3** and 13% unreacted 1,3-dibenzyloxy-2-propanol which does not interfere in subsequent condensations. 1,3-Dichloroethane was added to bring the weight of material to 306 g (which contains 306 mmol of **3**). This stock solution can be stored under refrigeration without deterioration for several months. The ^{1}Hmr spectrum of **3** shows signals at δ (ppm vs. TMS in $CDCl_3$): 3.70 (d, —CH_2—), 4.13 (m, —CH—), 4.58 (s, —CH_2—ϕ), 5.70 (s, —CH_2—Cl), and 7.38 (m, aromatic).

General procedure for the preparation of 1-[[2-hydroxy-1-(hydroxymethyl)ethoxy]methyl] derivatives 4, 6, and 7

5-Fluorouracil (4.0 g, 20 mmol) and ammonium sulfate (1 g) were added to hexamethyldisilazane (70 mL). The mixture was heated at reflux under the exclusion of moisture until the solution became clear (1 h in this example). The solvent was removed at reduced pressure and the residue was dried under vacuum. The residue was dissolved in benzene (50 mL) and mercuric cyanide (10.1 g, 40 mmol) was added. The mixture was heated below reflux temperature and chloromethyl ether **3** (9.6 g, 30 mmol) was added. The mixture was heated at reflux under a nitrogen atmosphere for 2.5 h. The solution was collected by filtration and concentrated to a gum at reduced pressure. Dichloromethane (150 mL) was added and the solution was extracted first with 30% potassium iodide solution (aqueous) followed by saturated sodium chloride solution. The solution was dried over sodium sulfate, collected by filtration, and concentrated to leave 13 g of material. This material was purified by chromatography on silica gel using ethyl acetate – hexane (6:4). Compound **4***c* was obtained (19.5 mmol) in 65% yield. Properties of **4***c* are collected, together with all compounds **4** as well as **6***a* and **7***a*, in Tables 1 to 4.

This procedure was used for the preparation of **4***b*–**4***d*. The solvent used for silica gel purification was ethyl acetate – hexane (6:4) in each case. Yields were **4***b*, 57%; **4***c*, 65%; and **4***d*, 60%.

Compounds **4***a*, **4***e*, **6***a*, and **7***a* were prepared in a similar fashion except that 0.16 mmol of tetra-*n*-butylammonium iodide was used in place of mercuric cyanide (30 mmol) as catalyst. The coupling reaction was carried out in dichloromethane instead of benzene. After heating at reflux for 1.5 h, the solution was cooled to room tem-

TABLE 2. ^{13}C nuclear magnetic resonance data (δ, ppm) for acyclonucleosides*†

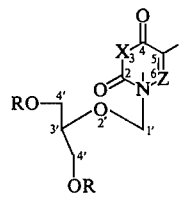

Compound	C-2	C-4	C-5	C-6	C-1′	C-3′	C-4′	—CH_2ϕ
4*b*[a]	151.2	164.2	110.9	139.2	76.0	77.0	69.9	73.1
4*c*	149.8	157.2	140.4	127.3	76.7	77.9	70.0	73.3
		($J_{C,F}$ 26.9)	($J_{C,F}$ 238.0)	($J_{C,F}$ 31.7)				
4*d*	150.6	159.4	97.0	143.1	76.9	78.2	70.1	73.5
4*e*	149.0	154.2	125.7	147.9	78.2	79.7	70.1	73.6
7*a*[b]	165.2	169.5	103.5	138.1	77.0	76.5	70.1	73.3
11[c]	150.9	160.3	69.1	147.9	76.0	75.1	63.0	
12[d]	150.2	161.7	110.8	145.3	76.5	75.5	63.2	
5*a*	151.1	163.8	101.5	145.1	76.0	80.7	61.0	
5*c*	150.0	157.8	139.9	129.4	75.3	81.1	61.2	
		($J_{C,F}$ 25.6)	($J_{C,F}$ 229.5)	($J_{C,F}$ 33.0)				
5*d*	150.5	159.7	95.2	144.7	76.3	81.0	61.0	
5*e*	149.5	155.2	125.3	150.0	77.6	82.2	61.1	
5*f*	149.7	161.3	119.2	123.0	75.6	80.0	60.9	
5*g*	152.3	162.9	70.0	148.7	76.1	80.4	60.9	
6*b*	148.5	157.1	135.7	—	78.7	81.0	61.0	
7*b*[e]	163.5	167.5	100.6	139.2	75.8	80.3	61.0	
8[f]	151.2	163.8	111.8	141.2	76.0	80.6	61.1	
9[g]	151.1	164.1	113.1	140.8	75.8	80.4	61.0	
13[h]	149.9	162.1	109.5	143.8	76.2	81.0	60.9	

*Assignments are based, where possible, by analogy to base assignments in ref. 28, by heteronuclear correlated 2D spectra, or from the off-resonance decoupled spectra. (a) δ 5-CH_3 at 11.9 ppm (b) C-3 at 99.2 ppm (c) $CH_3C(=O)$— at 20.7 and 170.5 ppm (d) $CH_3OC(=O)$—CH=CH— assigned as 51.7, 167.8, 120.0, and 135.7 ppm respectively; $CH_3C(=O)$— at 20.7 and 170.6 ppm (e) C-3 at 98.4 ppm (f) CH_2=CH—CH_2 assigned as 116.5, 135.6, and 30.1 ppm respectively (g) $CH_3CH_2CH_2$— assigned as 13.5, 21.3, and 21.8 ppm respectively (h) BrCH=CH— assigned at 129.5 and 106.6 respectively.

†Spectra for compounds **4***b*–**4***e*, **7***a*, **11**, and **12** were obtained in $CDCl_3$. All others were obtained in DMSO-d_6. Normal spectra were recorded on a Bruker WH90 spectrometer. The heteronuclear correlated spectra were obtained on a Varian XL200 spectrometer.

perature and diluted with water (10 mL) and methanol (40 mL). After stirring for 2 min the solvents were removed at reduced pressure and the residue was dissolved in dichloromethane (75 mL). The solution was washed with saturated sodium chloride solution and water and then dried over sodium sulfate. The solvent was removed at reduced pressure and the product obtained by chromatography over silica gel. Compounds **4***a* and **4***e* were obtained using ethyl acetate – hexane (6:4) while ethyl acetate – hexane (1:1) was used for **6***a*. Compound **7***a* was obtained pure by direct crystallization from diethyl ether. Yields were **4***a*, 60%; **4***e*, 60%; **6***a*, 63%; and **7***a*, 94%. Properties are collected in Tables 1 to 4.

Procedures for the removal of benzyl groups

A. *Palladium oxide – ethanol – cyclohexene*

To 1 g of the dibenzyl derivative in a 25 mL flask was added ethanol (10 mL), cyclohexene (3 mL), and freshly prepared palladium oxide (200 mg). The reaction mixture was stirred until tlc showed only product material (usually 15–20 h). The solution was collected by filtration and evaporated to dryness at reduced pressure. Products were obtained pure after crystallization from ethanol. Products obtained in this manner and the observed yields are as follows: **5***a* (100%); **5***b* (77%); **5***c* (100%); **6***b* (100%); and **7***b* (96%). Compound **4***e* was converted into the 5-aminouracil derivative **5***f* (40%) by this procedure. Properties of the products are collected in Tables 1 to 4.

B. *Boron trichloride in dichloromethane*

To 2 g of the dibenzyl compound in dry dichloromethane (25 mL) was added boron trichloride in dichloromethane (5 mL, 1 *M* solution). The mixture was stirred under nitrogen at −78°C for 2 h. An additional 5 mL of the boron trichloride solution was added and stirring was continued for 1 h. At this point a solution (50 mL) of methanol and dichloromethane (1:1) was added and the solution was allowed to warm to room temperature. The solution was collected by filtration and the solvents were removed at reduced pressure. The dry residue was generally crystallized from ethanol to give the pure product. Products and yields obtained by this route were: **5***d* (87%) and **5***e* (85%). Properties are collected in Tables 1 to 4.

Preparation of the 5-allyluracil derivative 8

To a solution of **5***a* (760 mg, 2.5 mmol) in water (6 mL) was added a solution of mercuric acetate (1.27 g, 3.9 mmol) in water (7 mL). The mixture was stirred at 60°C for 21 h, whereupon the precipitate was collected by filtration and washed successively with 0.1 *N* sodium chloride in water (60 mL), ethanol (20 mL), and diethyl ether (30 mL). After drying, 1.15 g of white powder was obtained. Of this

Can. J. Chem. Downloaded from www.nrcresearchpress.com by 210.87.254.40 on 09/06/12
For personal use only.

TABLE 3. Proton magnetic resonance data for acyclonucleosides*

Compound	δ ppm (*J*, Hz)≠ H-5	H-6	C-1′	C-3′	C-4′	—CH_2—ϕ	Other
4*a*	5.6(d, 8)	‡	5.2(s)	4.0(m)	3.5(d, 5)	4.5(s)	
4*b*	—	7.1(s)	5.2(s)	4.0(m)	3.5(d, 5)	4.5(s)	CH_3—, 1.8(s)
4*c*	—	‡	5.2(s)	4.0(m)	3.5(d, 5)	4.5(s)	
4*d*	—	7.7(s)	5.3(s)	4.0(m)	3.5(d, 5)	4.5(s)	
4*e*	—	9.2(s)	5.5(s)	4.1(m)	3.6(d, 5)	4.5(s)	
6*a*	‡	—	5.5(s)	4.2(m)	3.6(d, 5)	4.5(s)	
7*a*	6.0(d, d)	‡	5.4(s)	4.1(m)	3.6(d, 5)	4.5(s)	H-3, 6.0(d, d)
10	5.7(d, 8)	7.3(d, 8)	5.2(s)	4.1(b)	4.1(b)		CH_3CO—, 2.1(s)
11	—	7.8(s)*	5.2(s)	4.2(b)	4.2(b)		CH_3CO—, 2.1(s)
12	—	7.7(s)	5.3(s)	4.2(b)	4.2(b)		CH_3CO—, 2.1(s); CH_3 CO—, 3.8(s); HC=CH, 6.9, 7.4 (d, *J* = 16)
5*a*	5.60(d, 7.8)	7.69(d, 7.8)	5.18(s)	δ 3′ and 4′, complex at 3.45 ppm			
5*b*	—	7.57(s)	5.18(s)	4.0(m)	3.47(d)		CH_3—, 1.7(s)
5*c*	—	8.09(d, 6.6)	5.16(s)	δ 3′ and 4′, complex at 3.42 ppm			
5*d*	—	8.24(s)	5.20(s)	complex at 3.45 ppm			
5*e*	—	9.29(s)	5.35(s)	complex at 3.45 ppm			
5*f*	—	6.87(s)	5.12(s)	complex at 3.45 ppm			$—NH_2$, 4.18(bs)
5*g*	—	8.12(s)	5.14(s)	complex at 3.41 ppm			
6*b*	7.48(s)	—	5.29(s)	complex at 3.43 ppm			
7*b*	5.94(d, d, $J_{5,6}$ = 7.5, $J_{5,3}$ = 2.4)	7.58(d, 7.5)	5.30(s)	complex at 3.41 ppm			H-3, 5.64(d, 2.4)
8	—	7.49(s)	5.19(s)	complex at 3.44 ppm			H, C=C, 5.1 (c); H, C=C, H, 5.84(ddt, 17, 10, 6.2); —CH_2—, 2.97 (d, 6.2)
9	—	7.51(s)	5.18(s)	complex at 3.44 ppm			CH_3—, 0.87(t, 7.2) CH_3CH_2—, 1.45(c); —CH_2—C=, 2.17(t, 7.5)
13	—	8.0(s)	5.2(s)	complex at 3.4 ppm			HC=, 6.84, 7.28(d, 13.5)

*4*a*–4*e*, 6*a*, 7*a*, **10**–**12** were at 60 MHz in $CDCl_3$, all other spectra were run at 200 MHz in DMSO-d_6.
‡These signals were hidden under the aromatic signals.
≠Numbering system is as described in Table 2.

material, 760 mg was stirred with methanol (10 mL) for 10 min. Allyl chloride (1.28 g, 16.8 mmol), followed by a 0.1 *N* methanolic solution (3.6 mL, 0.37 mmol) of dilithium palladium tetrachloride (Li_2PdCl_4), was added to the milky white solution. The solution turned black and was stirred at room temperature for 16 h. Hydrogen sulfide was bubbled through the mixture for 45 s. The solution (yellow) was collected by filtration. The desired product **8** was obtained pure after silica gel chromatography (methanol–dichloromethane; 1:9). The yield was 62%. Properties are collected in Tables 1 to 4.

(a) *Conversion of **8** to the 5-propyluracil derivative **9***

Compond **8** (211 mg, 0.82 mmol) was dissolved in dry methanol (10 mL) and subjected to hydrogenation at 1 atm in the presence of 10% palladium on carbon. After 1.5 h the solution was collected by filtration through Celite. Compound **9** was obtained as a white crystalline compound, mp 105–106°C, in 97% yield. Properties are collected in Tables 1 to 4.

(b) *Preparation of the diacetyluracil derivative **10***

Compound **5***a* (600 mg, 2.7 mmol) was dissolved in pyridine (2 mL). Acetic anhydride (2 mL) was added and the solution was stirred at room temperature for 3 h. Solvents were removed at reduced pressure and the product was obtained after chromatography on silica gel (ethyl acetate – hexane; 7:3). Compound **10** was obtained as a crystalline compound in 96% yield. Properties are collected in Tables 1 to 4.

*Preparation of the 5-iodo derivatives **11** and **5**g*

To a solution of **10** (710 mg, 2.3 mmol) in dry dichloromethane (30 mL) was added a solution of iodine-monochloride, (780 mg, 4.8 mmol) in dichloromethane (10 mL). The mixture was heated at reflux for 2 h, cooled to room temperature, and washed successively with a 2% sodium bisulfite solution (aqueous, 7 mL), water, and finally, saturated sodium chloride solution. The solution was dried over sodium sulfate. The solvents were removed at reduced pressure and the product **11** was obtained in 87% after chromatography on silica gel using ethyl acetate – hexane (7:3).

The acetyl groups were removed from **11** to give **5***g* in 100% yield using anhydrous potassium carbonate in methanol (2.5 mg K_2CO_3/mL methanol/100 mg of **11**) for 65 h, followed by neutralization with Dowex 50XW-XH (H^+ form) resin.

Properties of **5***g* and **11** are collected in Tables 1 to 4.

Can. J. Chem. Downloaded from www.nrcresearchpress.com by 210.87.254.40 on 09/06/12
For personal use only.

TABLE 4. Elemental analyses*

Compound	Molecular formula	Calculated			Found		
		C	H	N	C	H	N
5*a*	$C_8H_{12}N_2O_5$	44.45	5.59	12.96	44.46	5.28	12.81
5*b*	$C_9H_{14}N_2O_5$	46.95	6.13	12.17	47.08	6.25	12.18
5*c*	$C_8H_{11}FN_2O_5$	41.03	4.73	11.96	41.20	4.74	11.82
5*d*	$C_8H_{11}BrN_2O_5$	32.56	3.75	9.49	32.63	3.69	9.60
5*e*	$C_8H_{11}N_3O_7$	36.79	4.24	16.09	36.84	4.21	15.84
5*f*	$C_8H_{13}N_3O_5$	41.56	5.66	18.17	41.10	5.52	17.48
5*g*	$C_8H_{11}IN_2O_5$	28.09	3.24	8.19	28.11	3.03	8.05
6*b*	$C_7H_{11}N_3O_5$	38.71	5.10	19.35	38.80	5.20	19.30
7*b*	$C_9H_{13}NO_5$	50.23	6.08	6.51	50.60	6.12	6.66
8	$C_{11}H_{16}N_2O_5$	51.56	6.29	10.93	51.34	6.20	10.75
9	$C_{11}H_{18}N_2O_5$	51.16	7.02	10.85	50.87	7.01	10.73
13	$C_{10}H_{13}BrN_2O_5$	37.38	4.08	8.72	37.09	4.21	8.50

*Analyses performed by Canadian Microanalytical Service, Vancouver, B.C.

(a) *Conversion of **11** into the propenoate derivative **12***

Dry *N,N*-dimethylformamide (10 mL) was added to a 25 mL round-bottom flask containing compound **11** (467 mg, 1.1 mmol), palladium acetate (11.2 mg, 0.05 mmol), methyl acrylate (172 mg, 2 mmol), and triethyl amine (121 mg, 1.2 mmol). The resulting solution was heated at 70°C for 5 h. The solvent was removed at reduced pressure and the product **12** was obtained in 68% yield after chromatography on silica gel using ethyl acetate – hexane (7:3). Properties of **12** are collected in Tables 1 to 4.

(b) *Conversion of **12** into the bromovinyluracil derivative **13***

Compound **12** (286 mg, 0.75 mmol) was dissolved in a 0.5 *N* sodium hydroxide solution (20 mL, aqueous) and the solution was stirred at room temperature for 2 h. The solution was neutralized with Dowex 50 W-XH (H^+ form) and the solvent was then removed at reduced pressure. The solid residue was redissolved in water (15 mL). Potassium acetate (134 mg) was added and the solution was heated to 70°C. *N*-Bromosuccinimide (121 mg, 0.68 mmol) was added to the hot solution which was then stirred for 2 h without external heating. The solvent was removed at reduced pressure and the residue was applied to a silica gel column which was eluted with dichloromethane–methanol (9:1). The product collected and crystallized from methanol (with ether) to give pure **13** in 55% yield. Properties are collected in Tables 1 to 4.

Acknowledgements

We gratefully acknowledge financial assistance from Bio Logicals Inc. and the Natural Sciences and Engineering Research Council of Canada. We are also indebted to Dr. Françoise Sauriol for assistance with ^{13}C spectral assignments.

1. R. J. WALKER, E. DECLERCQ, and F. ECKSTEIN. (*Editors*). Nucleoside analogues: chemistry, biology, and medical applications. Plenum Press, New York. 1979.
2. P. M. KELLER, J. A. FYFE, L. BEAUCHAMP, C. M. LUBBERS, P. A. FURMAN, H. J. SCHAEFFER, and G. B. ELION. Biochem. Pharmacol. **30**, 3071 (1981).
3. A. C. SCHROEDER, R. G. HUGHES, and A. BLOCH. J. Med. Chem. **24**, 1078 (1981).
4. E. DECLERCQ and A. HOLY. J. Med. Chem. **22**, 510 (1979).
5. K. K. OGILVIE and M. F. GILLEN. Tetahedron Lett. **21**, 327 (1980).
6. K. K. OGILVIE, U. O. CHERIYAN, B. K. RADATUS, K. O. SMITH, K. S. GALLOWAY, and W. L. KENNELL. Can. J. Chem. **60**, 3005 (1982).
7. M. F. GILLEN. Ph.D. Thesis, McGill University, Montreal, 1980.
8. K. O. SMITH, K. S. GALLOWAY, W. L. KENNELL, K. K. OGILVIE, and B. K. RADATUS. Antimicrob. Agents Chemother. **22**, 55 (1982).
9. K. O. SMITH, K. S. GALLOWAY, K. K. OGILVIE, and U. O. CHERIYAN. Antimicrob. Agents Chemother. **22**, 1026 (1982).
10. K. O. SMITH, S. L. HODGES, K. S. GALLOWAY, K. K. OGILVIE, and U. O. CHERIYAN. J. Infect. Dis. In press.
11. A. F. COOK, M. J. HOLMAN, M. J. KRAMER, and P. W. TROWN. J. Med. Chem. **22**, 1330 (1979).
12. A. ROSOWSKY, S-H. KIM, D. TRITES, and M. WICK. J. Med. Chem. **25**, 1034 (1982).
13. C. HEIDELBERGER. Cancer Res. **30**, 1549 (1970).
14. P. H. FISCHER, M. S. CHEN, and W. H. PRUSOFF. Biochem. Biophys. Acta, **606**, 236 (1980).
15. B. GOZ. Pharmacol. Rev. **29**, 249 (1978).
16. W. E. G. MALLER, R. K. ZAHN, A. MAIDHOF, R. BEYER, and J. ARENDES. Chem. Biol. Interact. **23**, 141 (1978).
17. E. DECLERCQ, J. DESCHAMPS, and D. SHUGAR. Antimicrob. Agents Chemother. **13**, 545 (1978).
18. J. L. RUTH and Y-C. CHENG. J. Biol. Chem. **257**, 10261 (1982).
19. E. DECLERCQ, J. DESCAMPS, P. DESOMMER, P. J. BARR, A. S. JONES, and R. T. WALKER. Proc. Natl. Acad. Sci. U.S.A. **76**, 2947 (1979).
20. A. S. JONES, S. G. RAHIM, and R. T. WALKER. J. Med. Chem. **24**, 759 (1981).
21. W. L. WASHTIEN and D. V. SANTI. J. Med. Chem. **25**, 1252 (1982).
22. F. SEELA and S. MENKHOFF. Justus Liebigs Ann. Chem. 813 (1982).
23. J. L. RUTH and D. E. BERGSTROM. J. Org. Chem. **43**, 2870 (1978); J. Carbohydr. Nucleosides Nucleotides, **4**, 257 (1977).
24. M. J. ROBINS, P. L. BARR, and J. GIZIEWICA. Can. J. Chem. **60**, 554 (1982).
25. H. A. DIECK and R. F. HECK. J. Am. Chem. Soc. **96**, 1133 (1974).
26. D. E. BERGSTROM and M. K. OGAWA. J. Am. Chem. Soc. **100**, 8106 (1978).
27. A. S. JONES, G. VERHELST, and R. T. WALKER. Tetrahedron Lett. 4415 (1979).
28. J. B. STOTHERS. Carbon-13 NMR spectroscopy. Academic Press, New York. 1972.

Can. J. Chem. Downloaded from www.nrcresearchpress.com by 210.87.254.40 on 09/06/12
For personal use only.

Complexes des ions Hg^{2+} avec le monomère et le dimère de la thymine: 5-methyl-2,4 (1*H*, 3*H*) pyrimidinedione[1]

M. M. PETIT-RAMEL et G. THOMAS-DAVID

Laboratoire de Chimie Analytique II, Université Claude Bernard, Lyon I, 43 Boulevard du 11 novembre 1918, 69622 Villeurbanne Cedex, France

ET

G. PERICHET et P. POUYET

Laboratoire de Photochimie, Université Claude Bernard, Lyon I, 43 Boulevard du 11 novembre 1918, 69622 Villeurbanne Cedex, France

Reçu le 1 novembre 1982[2]

M. M. PETIT-RAMEL, G. THOMAS-DAVID, G. PERICHET et P. POUYET. Can. J. Chem. **62**, 22 (1984).

Les constantes d'association relatives aux complexes des ions Hg^{2+} avec les formes monomère (TM) et dimère (TD) de la thymine sont calculées à partir de mesures protométriques effectuées dans un large domaine de pH: $2 < pH < 11$. Le traitement des données de chacun des systèmes est conduit par une méthode de pit-mapping et l'on peut donner la répartition des diverses espèces complexes en fonction du pH.

En ce qui concerne le monomère, les ions Hg^{2+} ayant une coordinence de degré deux, traduite par la configuration linéaire d'espèces non chélatées, on peut mettre en évidence les complexes $[Hg(TM)]^+$ (log $\beta_{101} = 10{,}65$) et $[Hg(TM)_2]$ (log $\beta_{102} = 20{,}70$). Les photodimères (TD) obtenus par irradiation de la thymine monomère (TM) à 260 nm, en solution dans l'eau gelée à −10°C sont du type (*méso*) *cis*, *syn*. Il donnent des complexes avec Hg^{2+} de type $[Hg(TD)]$ (log $\beta_{101} = 13{,}55$), $[HgH_{-1}(TD)]^-$ (log $\beta_{1-11} = 6{,}73$) et $[HgH_{-2}(TD)]^{2-}$ (log $\beta_{1-21} = -1{,}69$). Le complexe $[Hg(TD)]$ a un spectre d'absorption nettement déplacé vers les grandes longueurs d'onde ($\lambda = 280$ nm), alors que le dimère (TD) n'absorbe qu'en dessous de 240 nm. Une irradiation à 280 nm provoque l'apparition du complexe $[Hg(TM)_2]$, donc la rupture du cycle cyclobutane au niveau du dimère.

M. M. PETIT-RAMEL, G. THOMAS-DAVID, G. PERICHET, and P. POUYET. Can. J. Chem. **62**, 22 (1984).

The association constants for Hg^{2+}-complexes involving monomeric (TM) and dimeric (TD) forms of thymine are determined by pH-titration measurements made over a wide pH range $2 < pH < 11$. In both systems, the experimental data have been analyzed by a pit-mapping method and the concentration distribution of the various complex species is plotted versus a pH gradient.

Because of the tendency of Hg^{2+} to form two bonds in a linear configuration, non-chelate complexes $[Hg(TM)^+]$ (log $\beta_{101} = 10.65$) and $[Hg(TM)_2]$ (log $\beta_{102} = 20.70$) are formed with the monomer thymine.

Photodimers, obtained after irradiation of monomer thymine at 260 nm in frozen water (−10°C), are the (*meso*)-*cis*, *syn* forms and can be complexed by the Hg^{2+} ions in $[Hg(TD)]$ (log $\beta_{101} = 13.55$), $[HgH_{-1}(TD)]^-$ (log $\beta_{1-11} = 6.73$), and $[HgH_{-2}(TD)]^{2-}$ (log $\beta_{1-21} = 1.69$) species. $[Hg(TD)]$ complex shows an absorption spectrum shifting towards 280 nm, whereas the free dimer ligand absorbs lower than 240 nm only. An irradiation at 280 nm provides the formation of the $[Hg(TM)_2]$ complex and consequently the breaking of the cyclobutane cycle in the dimer molecule.

Introduction

Beukers et Berends (1) ont montré que la thymine se dimérisait réversiblement en solution aqueuse par irradiation à 280 nm et pour une température voisine de 0°C. Le dimère obtenu, isolé sous forme cristalline présentait une absorption uv très différente de celle du monomère. En outre, L. Wulff et coll. (2, 3) ont précisé que la photosensibilisation de l'ADN "in vivo", à 280 nm, se produisait entre deux molécules adjacentes situées sur le même brin de l'hélice, les molécules de thymine passant ainsi d'un "état monomère" à un "état dimère".

Dans la mesure où il semble directement lié au blocage des virus et des bactéries et à l'activation des microorganismes, l'importance de l'interprétation biologique de ce phénomène de dimérisation a été soulignée par de nombreux auteurs (4−7). En ce qui concerne la réversibilité de la réaction photochimique, l'équilibre de conversion thymine-dimère en thymine-monomère peut être envisagé sous deux aspects complémentaires: (*i*) par irradiation, à une longueur d'onde voisine de 250 nm, de la molécule de thymine-dimère isolée (8); et (*ii*) par utilisation d'enzymes (E) de photoréactivation agissant selon le schéma:

[1] ADN bloqué (abs. <300 nm) + E (abs. <300 nm) → ADNE complexe (abs. >400 nm)

$$\xrightarrow[\text{visible}]{\text{irradiation}} \text{ADN} + \text{E}$$

Nous avons essayé de "modéliser" cette réaction au niveau de la thymine en utilisant les ions Hg^{2+}. Schématiquement, les réactions peuvent s'écrire de la façon suivante dans la mesure où une seule espèce complexe se formerait respectivement avec les thymines monomère et dimère:

[2] $H(TM) + H(TM) + h\nu \rightarrow H_2(TD)$

[3] $H_2(TD) + Hg^{2+} \rightarrow [Hg(TD)] + 2H^+$

[4] $[Hg(TD)] + h\nu' \rightarrow [Hg(TM)_2]$

La première irradiation $h\nu$, dimérisant normalement la thymine ligand monomère H(TM), le ligand dimère $H_2(TD)$ peut se complexer éventuellement en $[Hg(TD)]$. Une seconde irradiation $h\nu'$, favorise la décomposition du complexe dimérisé en complexe monomère $[Hg(TM)_2]$.

Notre contribution porte donc sur l'identification et le calcul des stabilités thermodynamiques de toutes les espèces complexes formées avec les oligomères de rang 1 et 2 de la thymine

[1]Avec la collaboration technique de C. Perret.

[2]Revision reçu le 18 mai 1983.

Can. J. Chem. Downloaded from www.nrcresearchpress.com by 210.87.254.105 on 09/06/12
For personal use only.

Can. J. Chem. Downloaded from www.nrcresearchpress.com by 210.87.254.105 on 09/06/12
For personal use only.

et nous tenterons de dégager une interprétation analytique des réactions précédentes.

Nous définirons par β_{pqr} la constante de stabilité globale d'une espèce complexe de formule générale $M_pH_qA_r$ où M représente l'atome métallique central, H l'atome d'hydrogène et A le ligand, dont la formation est régie par l'équilibre:

$$[5] \quad pM + qH + rA \rightleftarrows M_pH_qA_r$$

où

$$[6] \quad \beta_{pqr} = \frac{[M_pH_qA_r]}{[M]^p[H]^q[A]^r}$$

avec p et $r > 0$, $q > 0$ pour les espèces protonées, et $q < 0$ pour les espèces hydroxydées avec $[OH^-] = [H_{-1}]K_w$.

Lors de la neutralisation, nous pouvons définir un nombre moyen de protons neutralisables par mole de ligand:

$$[7] \quad \bar{q} = \frac{C_H - [H] + [OH]}{C_A}$$

où C_A est la concentration totale en ligand; [H] et [OH] sont respectivement les concentrations en H^+ et OH^- à l'équilibre; C_H est la concentration en protons telle que:

$$[8] \quad C_H = qC_A - B$$

B est la concentration de l'hydroxyde ajouté.

Les systèmes, dans lesquels interviennent les formes protonnées des coordinats et les espèces mono ou polynucléaires des complexes métalliques ont été résolus à l'aide d'un programme-type issu du Letagrop (9), modifié et testé dans notre laboratoire sur de multiples équilibres (10–12). Ce programme permet l'affinement des paramètres par la méthode du pit-mapping dont nous rappelons brièvement le principe.

Les transformées des courbes de titration $\bar{q} = f(\text{pH})$ sont rendues linéaires par un développement en série de Fourier et les équations issues de cette nouvelle expression sont dérivées jusqu'à une minimisation convenable de la somme $\gamma = \Sigma(\bar{q}_{exp} - \bar{q}_{calc})^2$. Cette dernière fonction dépend d'un nombre n de paramètres et est représentée dans un espace à $(n + 1)$ dimensions par une "nappe". Cette technique permet d'extrapoler les valeurs des paramètres β_{pqr} vers des valeurs voisines de celles rendant minimum l'expression γ. Cette méthode se justifie théoriquement dans la mesure où les écarts $(\bar{q}_{exp} - \bar{q}_{calc})$ sont des variables aléatoires de même écart-type, σ, et il est alors possible, compte tenu de l'erreur systématique expérimentale sur $\bar{q}_{exp}$, de calculer les déviations standards afférentes à chaque constante β_{pqr}.

Resultats

1. *Interactions Hg^{2+}—thymine monomère*

Les bases puriques et pyrimidiques, composantes des acides nucléiques, sont généralement faibles et bien qu'elles puissent complexer de nombreux cations tels Cu^{2+}, Ni^{2+}, Zn^{2+}, Co^{2+}, Mg^{2+} et Ca^{2+} (13–16), il existe des interactions métal-coordinat privilégiées avec les ions Hg^{2+} dont l'influence a été notée au niveau de la molécule de thymine, soit isolée (17), soit replacée dans une séquence d'ADN (18–20).

En ce qui concerne particulièrement la thymine monomère isolée, les travaux de Davidson et coll. (17) font état d'une liaison stable avec les ions Hg^{2+} par formation d'un seul complexe de type $[Hg(TM)_2]$.

Pour assurer un maximum d'homogénéité à notre étude, nous avons recalculé dans un premier temps, la constante de stabilité protonique β_{011}, de la thymine monomère H(TM), dont la valeur concorde parfaitement avec les références ci-dessus (tableau 1). Bien qu'il y ait, dans chaque molécule de monomère, deux possibilités d'échange relatives à chaque hydrogène porté par les fonctions amines en N_1 et N_3 (fig. 3), une seule déprotonation est observée dans le domaine de pH envisagé (fig. 1*a*). Les mesures protométriques se révélant inopérantes pour une telle différenciation, nous pouvons cependant supposer que le fort effet inductif des groupements C=O, portés par les C_2 et C_4 encadrant la fonction amine, activent préférentiellement la déprotonation en N_3, la seconde déprotonation de l'hydrogène porté par N_1 se situant vers pH 12 (13).

En présence des ions mercuriques, le choix des rapports ligand/métal > 4 dépend de deux phénomènes: (*i*) une hydrolyse importante, dès les faibles pH, par formation des espèces $[HgH_{-1}]$ soluble et $[HgH_{-2}]$ peu soluble; et (*ii*) une dismutation des ions Hg^{2+} (21), en présence d'un excès de métal:

TABLEAU 1. Constantes de formation des complexes Hg^{2+}—thymine monomère $\mu = 0{,}1$ ($NaClO_4$); $t^0 = 25°C$

Espèces	p	q	r	log β_{pqr}	Références 17	29	13	22
H(TM)	0	1	1	9,80(0,01)*	9,8	9,65(0,01)	9,1	
$[Hg(TM)]^+$	1	0	1	10,65(0,02)				
$[Hg(TM)_2]$	1	0	2	20,70(0,03)	21,2			
$[HgH_{-1}]^+$	1	−1	0	−3,10(0,03)				3,68

*Ecarts-types correspondant aux constantes.

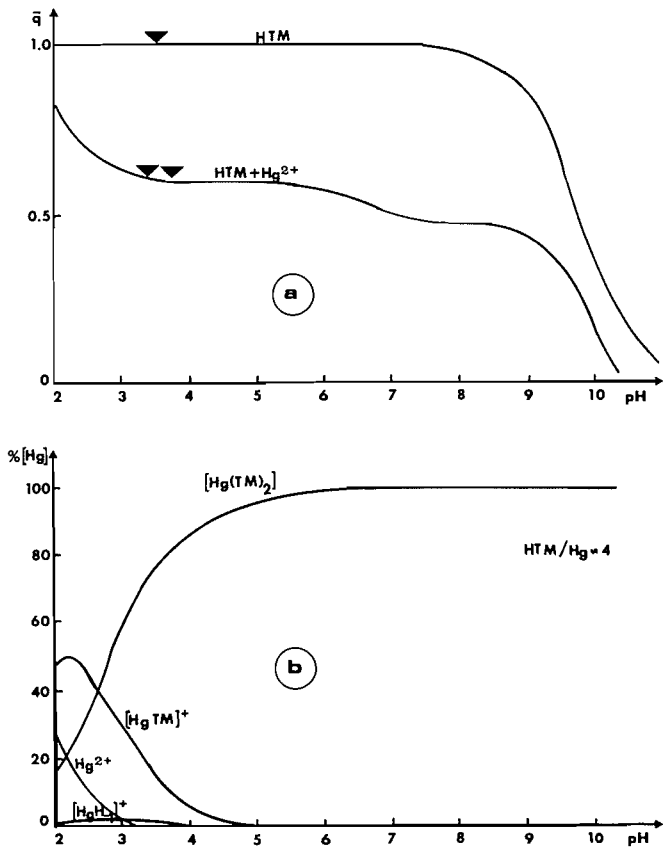

FIG. 1. Système Hg^{2+}—thymine monomère. (*a*) $\bar{q} = f(\text{pH})$; ▼[HTM] = 2×10^{-3} *M*; ▼▼[HTM] = 2×10^{-3} *M*; $[Hg^{2+}] = 4{,}750 \times 10^{-4}$ *M*. (*b*) Répartition des espèces: [HTM] = 2×10^{-3} *M*; $[Hg^{2+}] = 4{,}750 \times 10^{-4}$ *M*.

Can. J. Chem. Downloaded from www.nrcresearchpress.com by 210.87.254.105 on 09/06/12
For personal use only.

[9] $Hg^{2+} + Hg \rightleftarrows Hg_2^{2+}$

En ce qui concerne la mise en évidence des espèces complexes et le calcul de leurs constantes de stabilité, la démarche que nous suivrons découle directement de l'examen des courbes de formation $\bar{n} = f(p(TM))$ — où $\bar{n}$ représente le nombre moyen de ligand libre déprotoné — qui permettent d'identifier deux espèces complexes successives répondant aux équilibres:

[10] $H(TM) + Hg^{2+} \rightleftarrows [Hg(TM)]^+ + H^+$

[11] $2H(TM) + Hg^{2+} \rightleftarrows [Hg(TM)_2] + 2H^+$

A partir de solutions 2×10^{-3} *M* en thymine-monomère et avec quatre rapports ligand/métal sensiblement égaux à 1, 2, 4 et 10, totalisant 240 points expérimentaux, la méthode d'affinement par pit-mapping sur le nombre moyen $\bar{q}$ de protons neutralisables (fig. 1*a*) de la molécule conduit aux valeurs rassemblées dans le tableau 1. L'introduction, dans le cycle d'affinement, de la constante $\beta_{1\text{-}10}$, relative à la formation de l'espèce hydroxydée soluble $[HgH_{-1}]$ n'améliore pas sensiblement la convergence bien que la valeur obtenue soit en bon accord avec nos références bibliographiques (22–24). Le tracé des courbes de distribution (fig. 1*b*) qui permet de suivre l'évolution des espèces formées en fonction du pH, montre en effet que dans nos conditions expérimentales (ligand/métal > 4) la quantité d'espèces hydroxydées reste négligeable.

Quant au complexe $[Hg(TM)]^+$, non signalé dans la littérature, il faut souligner que son domaine d'existence se situe vers les faibles pH, sa disparition étant presque totale à pH 4.

2. Interactions Hg^{2+}—thymine dimère

Le dimère étant beaucoup moins soluble que le monomère en solution aqueuse, la concentration utilisée ne peut excèder 10^{-4} *M*. Nous ne disposions d'aucune donnée bibliographique chiffrant les stabilités protoniques et a fortiori les stabilités des complexes et nous avons suivi le même protocole d'étude que pour le monomère.

La transformée des courbes de neutralisation $\bar{q} = f(pH)$ (fig. 2*a*) correspond bien à la présence de deux protons neutralisables $H_2(TD)$ relatifs aux constantes β_{021} et β_{011} du tableau 2.

La faible solubilité du dimère, impliquant de faibles concentrations en ions mercuriques a pour conséquence directe d'augmenter l'hydrolyse et de restreindre le rapport ligand/métal au voisinage de 1 et les calculs d'affinement ont porté sur deux valeurs de rapport $H(TD)/Hg^{2+} = 0{,}90$ et 1 soit environ 120 points expérimentaux. Selon le domaine de pH considéré, le traitement des données potentiométriques fait apparaître la formation simultanée du complexe simple [Hg(TD)] et d'espèces hydroxydées.

$3 < pH < 9$

[12] $H_2(TD) + Hg^{2+} \rightleftarrows [Hg(TD)] + 2H^+$

$3 < pH < 6$

[13] $Hg^{2+} + HH_{-1} \rightleftarrows [HgH_{-1}]^+ + H^+$

$6 < pH < 9$

[14] $\begin{cases} TD^{2-} + Hg^{2+} + HH_{-1} \rightleftarrows [HgH_{-1}(TD)]^- + H^+ \\ TD^{2-} + Hg^{2+} + 2HH_{-1} \rightleftarrows [HgH_{-2}(TD)]^{2-} + 2H^+ \end{cases}$

L'ensemble des constantes β_{101}, $\beta_{1\text{-}11}$ et $\beta_{1\text{-}21}$ correspondant respectivement aux équilibres de formation des espèces [Hg(TD)], $[HgH_{-1}]^+$, $[HgH_{-1}(TD)]^-$ et $[HgH_{-2}(TD)]^{2-}$ (tableau 2) conduit à une convergence rapide du processus d'affinement, la valeur recalculée de l'espèce $[HgH_{-1}]^+$ déjà prise en compte dans l'étude de la thymine monomère restant parfaitement concordante. La courbe de distribution des espèces en fonction du pH (fig. 2*b*) permet de situer précisément leurs domaines de formation, dans nos conditions expérimentales.

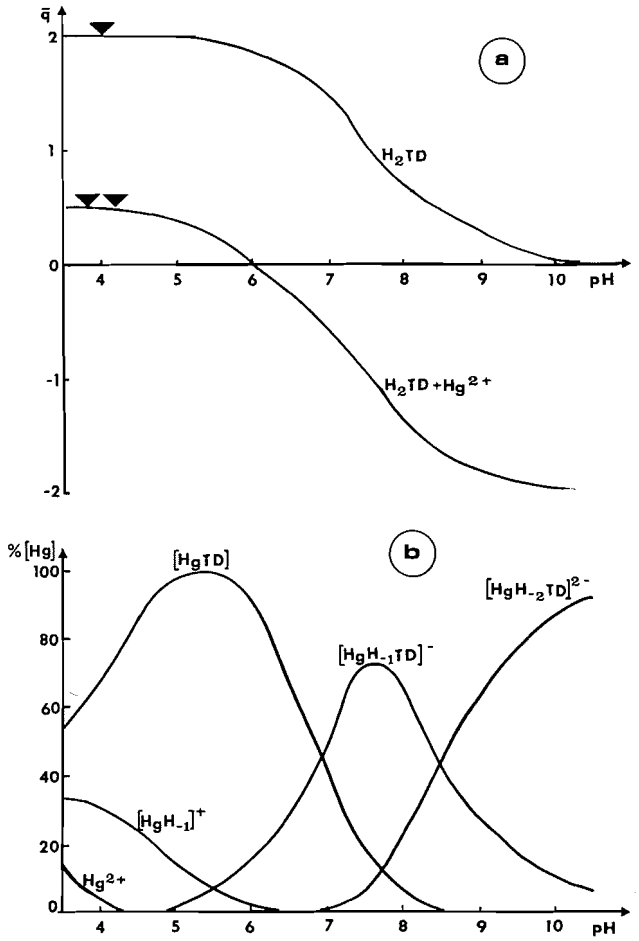

FIG. 2. Système Hg^{2+}—thymine dimère. (*a*) $\bar{q} = f(pH)$; ▼$[H_2TD] = 9{,}96 \times 10^{-5}$ *M*; ▼▼$[H_2TD] = 9{,}96 \times 10^{-5}$ *M*; $[Hg^{2+}] = 9{,}5 \times 10^{-5}$ *M*. (*b*) Répartition des espèces: $[H_2TD] = 9{,}96 \times 10^{-5}$ *M*; $[Hg^{2+}] = 9{,}5 \times 10^{-5}$ *M*.

TABLEAU 2. Constantes de formation des complexes Hg^{2+}—thymine dimère $\mu = 0{,}1$ ($NaClO_4$) $t^0 = 25°C$

Espèces	*p*	*q*	*r*	log β_{pqr}
H(TD)	0	1	1	8,60(0,01)*
$H_2(TD)$	0	2	1	15,54(0,02)
[Hg(TD)]	1	0	1	13,55(0,02)
$[HgH_{-1}(TD)]^-$	1	−1	1	6,73(0,03)
$[HgH_{-2}(TD)]^{2-}$	1	−2	1	−1,69(0,04)
$[HgH_{-1}]^+$	1	−1	0	−3,10(0,03)

*Ecarts-types correspondants aux constantes.

Discussion

L'examen comparé des complexes mercuriques obtenus avec la thymine monomère et la thymine dimère appelle plusieurs remarques.

1. Ions mercuriques

Les interactions Hg^{2+}-coordinat sont généralement accom-

Can. J. Chem. Downloaded from www.nrcresearchpress.com by 210.87.254.105 on 09/06/12
For personal use only.

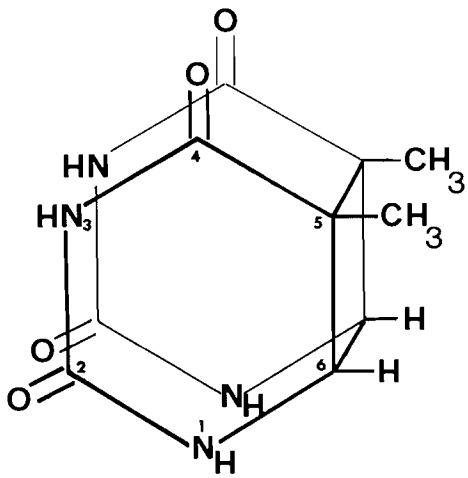

FIG. 3. Thymine dimère (isomère *cis-syn*).

pagnées de phénomènes secondaires: (*i*) Réaction d'hydrolyse simple sur les ions métalliques et formation, dès pH 2, de l'espèce soluble $[HgH_{-1}]^+$, qui, si elle reste négligeable pour le système monomère, atteint une valeur relative de 30% de la concentration totale en métal dans le cas du système dimère, les espèces supérieures $[HgH_{-n}]^{2-n}$ avec $n > 1$, n'étant pas retenues dans nos conditions expérimentales. (*ii*) Formation d'espèces complexes hydroxydées $[HgH_{-1}(TD)]^-$ et $[HgH_{-2}(TD)]^{2-}$, la dilution importante des solutions du système dimère favorisant la permanence des ions hydroxydes. (*iii*) Equilibre de dismutation des ions $[Hg_2^{2+}]$ dont nous nous sommes affranchis en travaillant à des concentrations $[Hg^{2+}] < 10^{-3}$ *M*.

2. Coordinats et complexes

Le monomère H(TM) et le dimère $H_2(TD)$ se comportent respectivement comme un mono et un diacide très faibles et les valeurs des tableaux 1 et 2 recoupent la règle générale de stabilité protonique plus élevée dans un cycle comportant une double liaison (monomère) que lorsque cette dernière est rompu (dimère).

Une étude systématique, à de faibles valeurs de pH, a permis de mettre en évidence un nouveau complexe: la première espèce du monomère $[Hg(TM)]^+$, la seconde $[Hg(TM_2]$, plus stable, ayant déjà été signalée (17).

Parmi les quatre formes isomériques de la thymine dimère décrites par Wulff et Fraenkel (2), le dimère (*meso*) *cis-syn* apparait comme la configuration la plus probable, que ce soit après irradiation d'une solution de thymine monomère gelée ou après photodimérisation des molécules adjacentes de thymine, situées sur chaque hélice d'ADN (fig. 3).

En présence d'ions Hg^{2+}, la formation de complexes du type [Hg(TD)], comme les espèces hydroxydées correspondantes, accrédite encore la configuration "*meso*" par liaison systématique du métal sur les atomes d'azote N_3.

En outre, l'absence d'espèces condensées en thymine dimère telles que $[Hg_2(TD)_2]$ et $[Hg_2(TD)_4]$ dont l'introduction dans l'affinement ne modifie en aucune manière la variance, trouve une justification normale au vu de nos conditions expérimentales. L'intervalle de variation des rapports ligand/métal, impérativement voisin de 1 pour raison d'hydrolyse, ne permet pas d'accréditer ces espèces polynucléaires de rang 2, dans la mesure où nous n'observons pas sur les courbes de formation $\bar{n} = f(p(TD))$, le déplacement caractéristique $\Delta p(TD)$ consécutif à une variation, Δm, de la concentration en métal (25), et que nous avons souvent mis en évidence dans d'autres systèmes (26, 27).

Partie expérimentale

Deux chaînes de mesure, convenablement étalonnées permettent de mesurer conjointement le pH et le pM dans un large domaine de pH: $2 < pH < 11$.

pH: électrode en verre / solution à 25 ± 0,1°C / NaCl saturé / électrode au calomel

pM: électrode de mercure en J / solution à 25 ± 0,1°C / Na_2SO_4 saturé / électrode au sulfate mercureux Hg_2SO_4/Hg

Chaque jeu d'électrodes est relié à un potentiomètre ISIS 20 000 TACUSSEL et les mesures sont effectuées sur des solutions aqueuses, thermostatées à 25 ± 0,1°C, dont la force ionique est maintenue constante à l'aide d'une solution de $NaClO_4$ 0,1 *M*.

Les solutions d'acide perchlorique Prolabo R.P. et de soude Merck sont dosées par des solutions étalons de biphtalate de potassium Merck. L'ajustement de la force ionique est effectuée par une solution de titre connu en perchlorate de sodium Merck. Le perchlorate de mercure est préparé par attaque à chaud d'hydroxyde mercurique par l'acide perchlorique jusqu'à neutralisation, puis dosé par l'EDTA à l'aide d'une électrode de mercure en J.

La thymine monomère utilisée provient des laboratoires Merck.

La thymine dimère est préparée par irradiation de solutions de thymine monomère dans l'eau (10^{-3} *M*) gelée à −10°C. L'irradiation a lieu à l'aide d'une lampe à vapeur de mercure haute pression. Les solutions sont évaporées à sec. Le résidu est ensuite dissous dans l'eau bouillante et filtré. Le filtrat est concentré et les cristaux de thymine dimère cristallisent avant ceux de monomère et Wang (28) a montré que seule la forme "*meso*" isomère *cis-syn* est obtenue.

1. R. BEUKERS et W. BERENDS. Biochim. Biophys. Acta, **41**, 573 (1960).
2. D. L. WULFF et G. FRAENKEL. Biochim. Biophys. Acta, **51**, 332 (1961).
3. D. L. WULFF. J. Mol. Biol. **7**, 431 (1963).
4. K. C. SMITH. *In* Photobiology: action of light on living materials. *Edited by* A. G. GIESE. New York. 1963.
5. A. WACKER. *In* Progress in nucleic acid research Vol. 1. *Edited by* J. N. Davidson and W. E. Cohn, New York. 1963.
6. R. BEUKERS, J. IJLSTRA et W. BERENDS. Rec. Trav. Chim. Pays-Bas, **79**, 101 (1959).
7. A. WACKER, H. DELLWEG et D. WEINBLUM. Naturwissenschaften, **47**, 477 (1960).
8. R. BEUKERS, J. IJLSTRA et W. BERENDS. Rec. Trav. Chim. Pays-Bas, **78**, 833 (1959).
9. L. G. SILLEN. Acta Chem. Scand. **18**, 1085 (1964).
10. R. P. MARTIN. Rev. Pure Appl. Chem. **19**, 171 (1969).
11. E. MICHAUD, G. PIVERT, G. DUC, M. PETIT-RAMEL et G. THOMAS-DAVID. Can. J. Chem. **60**(9), 1063 (1982).
12. M. PETIT-RAMEL et L. MOSONI–FRESENIUS. Z. Anal. Chem. **313**, 544 (1982).
13. M. M. TAQUI KHAN et C. R. KRISHNAMOORTY. J. Inorg. Nucl. Chem. **36**, 711 (1974).
14. W. LOHMANN, M. HILLERBRAND et M. KLENERT. Z. Naturforsch. **29**, 667 (1974).
15. L. G. MARZILLI et T. J. KISTENMACHER. Acc. Chem. Res. **10**, 146 (1976).
16. L. G. MARZILLI. *In* Progress in inorganic chemistry. Ed. Wiley, New York. 1977.
17. R. FERREIRA, E. BEN-ZVI, T. YAMANE, J. VASILEVSKIS et N. DAVIDSON. *In* Advances in coordination compounds. Ed. S. Kirschner, New York. 1961.
18. T. YAMANE et N. DAVIDSON. J. Am. Chem. Soc. **83**, 2599 (1961).
19. R. O. RAHN, J. K. SETLOW et L. C. LANDRY. Photochem. Pho-

tobiol. **18**, 39 (1973).
20. D. DING et F. S. ALLEN. Biochim. Biophys. Acta, **610**, 72 (1980).
21. A. JONSSON, I. QVAFORT et L. G. SILLEN. Acta Chem. Scand. **1**, 461 (1947).
22. S. HIETANEN et L. G. SILLEN. Acta Chem. Scand. **6**, 747 (1952).
23. R. W. SCHMID et L. N. REILLEY. J. Am. Chem. Soc. **78**, 5513 (1956).
24. G. ANDEREGG, G. SCHARZENBACH, M. PADMOYO et Ö. BORG. Helv. Chim. Acta, **41**, 988 (1958).
25. L. C. VAN POUCKE et H. F. DE BRABANDER. Talanta, **20**, 733 (1973).
26. I. KHALIL et M. M. PETIT-RAMEL. Bull. Soc. Chim. Fr. **11–12**, 1127 (1977).
27. I. KHALIL, M. M. PETIT-RAMEL et C. CHAPELET-BARBIER. Can. J. Chem. **56**, 1919 (1978).
28. S. Y. WANG. Photochem. Photobiol. **3**, 395 (1964).
29. A. M. FISKIN et N. BEER. Biochemistry, **4**, 1289 (1965).

Can. J. Chem. Downloaded from www.nrcresearchpress.com by 210.87.254.105 on 09/06/12
For personal use only.

Ab initio studies of complexes between SiF_4 and ammonia

J. M. CHEHAYBER, S. T. NAGY,[1] AND C. S. LIN[2]

Department of Chemistry, University of Windsor, Windsor, Ont., Canada N9B 3P4

Received June 6, 1983

J. M. CHEHAYBER, S. T. NAGY, and C. S. LIN. Can. J. Chem. **62**, 27 (1984).

Ab initio minimal basis set STO-6G calculations show axial-$SiF_4 . NH_3$ and *trans*-$SiF_4 . 2NH_3$ to be energetically more stable with respect to SiF_4 and ammonia. All other geometrical isomers are 1.0–2.0 eV higher.

Our calculation results rule out the steric hindrance between ligands as the reason $SiF_4 . 2NH_3$ is, according to experimental evidences, *cis* while complexes of bulkier ligands are *trans*.

Since the *cis*-$SiF_4 . 2NH_3$ has a large electric dipole moment and a suitable charge arrangement it is conceivably the favoured form in the solid phase. The *cis* → *trans* rearrangement may take place under conditions where the advantages of the *cis* are not operative.

Although there is some degree of covalency in the Si—N bond it remains largely electrostatic, with the lone pair of ammonia attracted to the positively charged Si atom. The lone pair does not appear to be extensively altered by the complex formation.

J. M. CHEHAYBER, S. T. NAGY et C. S. LIN. Can. J. Chem. **62**, 27 (1984).

Les calculs *ab initio* utilisant l'ensemble minimal de base STO-6G montrent que le $SiF_4 . NH_3$ axial et le $SiF_4 . 2NH_3$ *trans* sont, du point de vue énergétique, plus stables que le SiF_4 et l'ammoniac. Tous les autres isomères géométriques sont plus élevés de 1,0 à 2,0 eV.

Les résultats de nos calculs suggèrent que l'encombrement stérique entre les ligands n'explique pas pourquoi le $SiF_4 . 2NH_3$ est expérimentalement en position *cis* alors que des complexes impliquant des ligands plus encombrants sont en position *trans*.

Puisque le $SiF_4 . 2NH_3$ *cis* a un grand moment dipolaire électrique et un arrangement de charge convenable, on concoit que cette forme soit favorisée à l'état solide. La transposition *cis* → *trans* peut se produire dans des conditions où les avantages du composé *cis* n'interviennent pas.

Bien que la liaison Si—N soit covalente dans une certaine mesure, elle demeure principalement électrostatique avec le doublet libre de l'ammoniac attiré par l'atome de Si chargé positivement. Le doublet libre ne semble pas être fortement altéré par la formation du complexe.

[Traduit par le journal]

Introduction

Complexes of the type $MX_4 . nL$, with n = 1,2, M standing for Group IV metals (Si, Ge, Sn, Pb), X for halogen and L being uni- or bidentate ligands, e.g. Me_3N, Me_3P, NH_3, BiPy etc. have been known for a long time. Synthesis of the complex $SiF_4 . 2NH_3$ was first reported by Davy in 1812 (1) and various chemical and physical properties of the complex were subjects of several early studies (2–5).

For the 1:1 adducts, $MX_4 . L$, there are two plausible geometrical isomers, with the ligand L in the axial or equatorial positions. (Henceforth a complex will be labelled according to the position of the ligand; a for axial and e for equatorial.) Likewise, the octahedral 1:2 adducts, $MX_4 . 2L$, have two geometrical isomers, *trans* and *cis*.

The few studies on the complex $SiF_4 . L$ where L is NH_3 (6) or a strong base $(CH_3)_3N$ (7, 8) agreed on the axial configuration as the favoured isomer. As for the 1:2 adduct, $MX_4 . 2L$, the results are more contentious.

In 1960 Muetterties (9) reported ^{19}F nmr spectra of some soluble octahedral $SiF_4 . 2L$ complexes. A single resonance line was observed in each case, strongly indicative of the *trans* arrangement. Furthermore, several Group IV complexes are also shown by X-ray diffraction to favour the *trans* form in the solid state. These include $SiF_4 . 2Py$ (10), $GeCl_4 . 2Py$ (11), $SnCl_4 . 2HMPT$ and $SnBr_4 . 2HMPT$ (12). $SiF_4 . 2N(CH_3)_3$ was also known (7, 8) to be *trans*.

On the contrary, in their study of the ir spectra of $SiF_4 . 2NH_3$, Aggarwal and Onyszchuk (13) assigned the doublet, at 905 and 935 cm^{-1}, to the Si—N stretching and a broad peak centred on 725 cm^{-1} as the result of coupling among four bands attributable to the Si—F stretching modes. They thus concluded that the *cis* form was favoured.

These apparently conflicting experimental results suggest intriguing situations. For example, the geometrical preference of the complexes may depend very sensitively on their natures, e.g., electronegativities and/or bulkiness of the ligands. The energies of the complexes can be such that equilibria between the two geometrical isomers may shift from one form to the other under suitable conditions. It is also possible that the reaction pathways to 1:2 adducts lead to one form which subsequently transforms into the other as conditions change.

These studies are an attempt to clarify these questions. In the first part, we calculated the electronic structures of five complexes: *trans* and *cis* isomers of $SiF_4 . 2NH_3$ and a-, e-, and square pyramidal, sp-$SiF_4 . NH_3$. The results are described in this report.

Calculation and results

Since one of our purposes is to look into the pathways to $SiF_4 . 2NH_3$ calculations on the sp-$SiF_4 . NH_3$ is done as well.

A QCPE program based on the minimal basis set *ab initio* MO theory, GAUSSIAN 70 (14) was used in this work. In all cases optimal geometries were first determined by using a simpler basis set, STO-3G.

Molecular parameters of primary importance in these complexes are $r_{Si—N}$, ∠F—Si—N, and ∠F—Si—F′, followed by $r_{Si—F}$, and least crucial are the orientation of ammonia molecules and $r_{N—H}$. For *cis*-$SiF_4 . 2NH_3$ the angle ∠N—Si—N′ also belongs to the first group.

We first varied ∠F—Si—N and ∠F—Si—F′ for several values of $r_{Si—N}$ with the geometry of NH_3 frozen at its isolated state and $r_{Si—F}$ about 5–10% longer than in SiF_4. After the

---

[1]1982 summer student.

[2]C.S.L. thanks the Natural Sciences and Engineering Research Council of Canada for a grant.

Can. J. Chem. Downloaded from www.nrcresearchpress.com by 210.87.254.42 on 09/06/12
For personal use only.

Can. J. Chem. Downloaded from www.nrcresearchpress.com by 210.87.254.42 on 09/06/12
For personal use only.

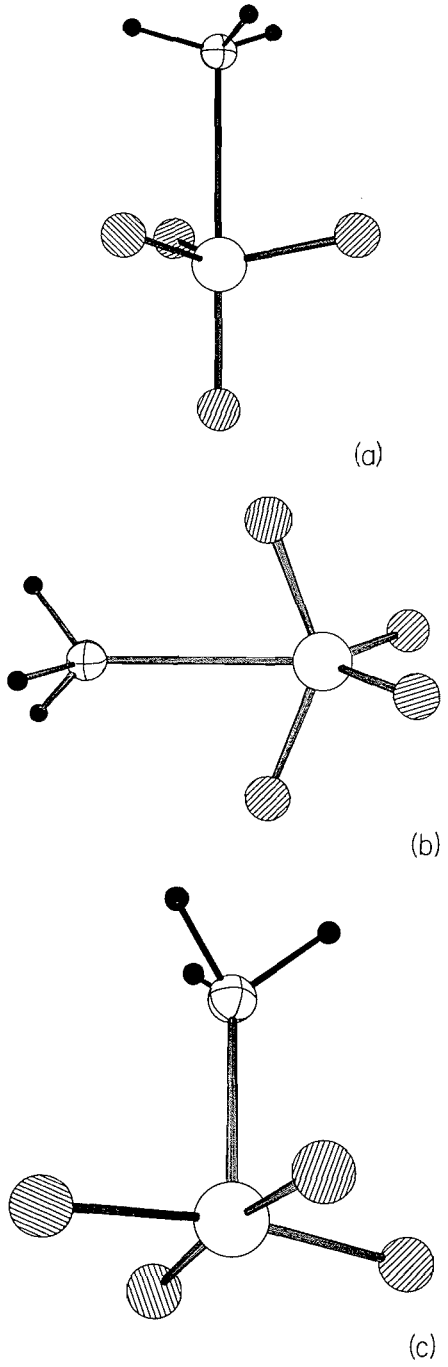

FIG. 1. (*a*) Axial $SiF_4.NH_3$. Bond lengths (Å): Si—N, 2.392; N—H, 1.007; Si—F_e, 1.573; Si—F_a, 1.621. Bond angles (deg): N—Si—F_e, 78.5; F_a—Si—F_e, 101.5; F_e—Si—F_e, 116.1. (*b*) Equatorial $SiF_4.NH_3$. Bond lengths (Å): Si—N, 2.439; Si—F_e, 1.609; Si—F_a, 1.604; N—H, 1.008. Bond angles (deg): N—Si—F_e, 109.9; N—Si—F_a, 69.4; F_a—Si—F_a, 101.6. (*c*) Square pyramidal $SiF_4.NH_3$. Bond lengths (Å): Si—N, 2.012; Si—F, 1.619; N—H, 1.007. Bond angles (deg): N—Si—F, 95.3; F—Si—F, 89.5. ○, Si; ⊕, N; ▨, F; ●, H.

primary group was optimized, r_{Si-F} was optimized and the same procedure was repeated once. Afterwards, the same was applied to the third and last group. These geometries were then used as the input for the optimization with the STO-6G. Since the total energies of these complexes are in the high hundreds of atomic units optimization was terminated when the total energy has converged to the fourth decimal place, 0.0001.

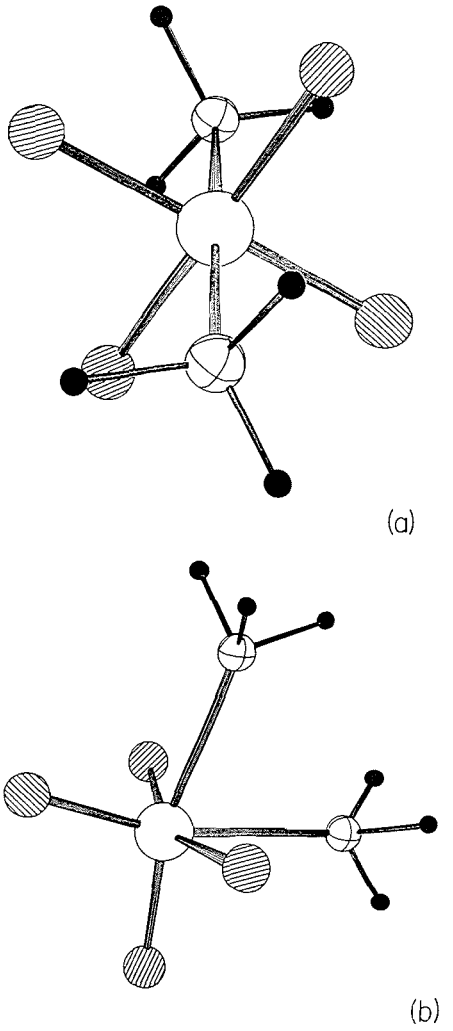

FIG. 2. (*a*) *trans*-$SiF_4.2NH_3$. Bond lengths (Å): Si—N, 2.041; N—H, 1.008; Si—F, 1.632. (*b*) *cis*-$SiF_4.2NH_3$. Bond lengths (Å) Si—N, 2.112; N—H, 1.007; Si—F_e, 1.638; Si—F_a, 1.640. Bond angles (deg): F_e—Si—F_a, 98.1; N_e—Si—F_e, 79.6; N—Si—F_e, 89.3; N—Si—N, 76.5.

Optimal geometries determined by the STO-6G are generally not significantly different from those from the STO-3G. Figures 1 and 2 give sketches of these molecules and their primary bond lengths and angles.

Energies and charge distributions are given in Table 1. For ease of comparison SiF_4 and NH_3 are also included.

Discussion

(A) Energy and molecular geometry

From Table 1 it is obvious that relative to the dissociation limit $SiF_4 + NH_3$ the most stable of the 1:1 adducts is the axial. This is in agreement with the consensus shown by experimental observations (6–8).

The equatorial form is 1.343 eV above the axial. Although this energy difference is not large considering all the internal degrees of freedom of a complex of this size, the 1:1 adduct is stable only at low temperature and it is not likely that the complex would exist in an equilibrium between the axial and equatorial forms. There has been no report of the experimental observation of e-$SiF_4.NH_3$.

Various bond lengths in the two isomers are very close and

TABLE 1. Calculated total energy, dissociation energy, charge distributions, charge transfer, and dipole moment of $SiF_4 . nNH_3$, n = 1, 2

Molecule	E_T (au)	ΔE (eV)[a]	Charge distributions[b] Si	N	F_a	F_e	H	CT[c]	μ_{el} (D)
$SiF_4 . NH_3$									
Axial	−739.8365	0.433	1.470	−0.531	−0.397	−0.385	0.205	0.084	4.19
Equatorial	−739.7872	−0.910	1.433	−0.496	−0.365	−0.380	0.185	0.057	4.81
Square pyramidal	−739.7508	−1.90	1.456	−0.519	−0.415		0.241	0.204	6.19
$SiF_4 . 2NH_3$									
trans	−795.8187	0.359	1.463	−0.533	−0.463		0.243	0.196	0.0
cis	−795.7620	−1.184	1.450	−0.467	−0.428	−0.421	0.197	0.124	8.94
SiF_4	−683.8357		1.434		−0.358				0.0
NH_3	−55.9849			−0.509			0.169		1.52

[a]ΔE is the difference between E_T and the energies of appropriate component molecules.
[b]F_a and F_e refer, respectively to F atoms on the axial and equatorial positions.
[c]CT stands for charge transfer per NH_3.

the charge distributions are also within a few percent of each other. It is shown below that the net electrostatic interactions in these two isomers are the same and their Si—N bond orders are also very similar. Hence, to explain why the axial is more stable one must look at other factors.

Repulsion between two covalent bonds is a concept well accepted at all levels of chemistry. From Fig. 1(*a*) and 1(*b*) one can see that Si—F bonds fall into two categories. One has its axis perpendicular to, and the other parallel with, that of the lone pair of ammonia. Obviously they exert different repulsion against the lone pair. The axial has three Si—F bonds roughly perpendicular (79°) to the axis of the lone pair and one Si—F bond supplementary to the Si—N bond. In the equatorial, two Si—F bonds are at 70° to the lone pair and two are in the equatorial plane. The difference may explain the relative stabilities of these two isomers.

It is interesting to look at the molecular geometries of these isomers from the viewpoint of perturbation to the tetrahedral structure of SiF_4 due to the complex formation with NH_3.

With respect to the N atom, the four F atoms can be divided into two groups. Those F atoms on the same side of the Si atom as the N are the primary neighbours, F_p, of the N atom while those on the opposite side are the secondary neighbours, F_s. For example, all three F atoms on the equatorial position of the axial, Fig. 1(*a*) are three F_p's and the only axial F atom is the sole F_s.

One then observes in Fig. 1 that the angle $\angle F_s—Si—F_s$ is hardly perturbed from the tetrahedral angle of 109° 28′. On the other hand, $\angle F_p—Si—F_s$ of both axial and equatorial and $\angle F_p—Si—F_p$ of the axial show deviations of approximately −8° and +7°, respectively.

Thus, formation of a complex with NH_3 does not cause very large changes to the geometry of SiF_4 except in the sp-isomer. A more severe deviation from the tetrahedral structure is accompanied by a higher energy.

In these complexes the bond Si—N between NH_3 and SiF_4 is a coordinate covalent bond which essentially is a lone pair of N pointed to the positively charged Si because of the electrostatic effect. Optimal geometries of the axial and equatorial show the angle between a coordinate covalent bond and an ordinary covalent bond, $\angle F_p—Si—N$, to be smaller than the angle between two covalent bonds, $\angle F_p—Si—F_s$. Since repulsion between two bonds is an important factor in determining the bond angle, this can be construed as an indication of a weaker repulsion exerted by a lone pair. This observation agrees with the notion that a coordinate covalent bond is not a full-fledged covalent bond.

Of the two isomers of $SiF_4 . 2NH_3$ the *trans* form is found to be energetically lower than the *cis* by 1.54 eV. That those complexes which are experimentally observed to be *trans* (7−12) all have ligands much bulkier than NH_3 may prompt one to speculate that the steric effect is the dominating factor in the *cis*−*trans* question. Our calculation results clearly show this not to be the case.

Table 1 shows that while the total energy of *trans*-$SiF_4 . 2NH_3$ is 0.359 eV lower than the total dissociation products, $SiF_4 + 2NH_3$, the following equations are also true:

$$\text{a-}SiF_4 . NH_3 + NH_3 \rightarrow \textit{trans}\text{-}SiF_4 . 2NH_3 - 0.074 \text{ eV}$$

$$\text{e-}SiF_4 . NH_3 + NH_3 \rightarrow \textit{cis}\text{-}SiF_4 . 2NH_3 - 0.274 \text{ eV}$$

In both cases the total energy of the 1:2 adduct is higher by a small amount than that of the reactants.

Most certainly inclusion of CI and probably of 3*d* atomic orbitals on Si are likely to lower the calculated energy of the 1:2 adducts more than that of the 1:1, making the former energetically more stable since the differences are so small. In any event, the possibility of the 1:1 adduct, upon formation, to proceed to its 1:2 counterpart can not be ruled out. Thus, 1:1 and 1:2 adducts may establish an equilibrium unless other factors intervene.

Complexes $SiF_4 . L$ with a highly electronegative ligand are known (7, 8) to exist in equilibrium with the 1:2 adducts but for those of other ligands, e.g. NH_3, 1:1 adducts are chemically stable only at low temperatures and under specific conditions (13). Our calculation results generally agree with these observations.

In the course of calculations it was noticed that while the use of the STO-6G basis set lowered the total energy of these complexes by a sizable amount from those of STO-3G calculations the relative stabilities of the five complexes remained the same, although small changes in the detail were inevitable.

(B) Charge distributions

Going over Table 1 from the left to the right one finds that the very substantial positive charge on the Si atom of these complexes changes very little from the value of 1.434 in SiF_4. It is interesting to notice, however, that in all cases but the equatorial, the Si atom becomes even more positive, albeit only slightly, upon formation of complexes with the electron donor, NH_3.

Can. J. Chem. Downloaded from www.nrcresearchpress.com by 210.87.254.42 on 09/06/12
For personal use only.

Can. J. Chem. Downloaded from www.nrcresearchpress.com by 210.87.254.42 on 09/06/12
For personal use only.

The negative charge on N varies more widely in terms of % change. That the charge in the *cis* is significantly smaller than that in all other complexes and than that in ammonia is perhaps due to the proximity of two ammonia molecules in the *cis* arrangement.

Charges on the F atoms clearly fall into two groups. Those of axial and equatorial 1:1 adducts are around 0.385, or about 10% higher than in SiF_4. F atoms of the sp-$SiF_4.NH_3$ have a considerably larger negative charge and belong to the second group with 1:2 adducts where the charges range up to 30% greater than in SiF_4.

The large negative charges on the N and F atoms are reflected in the positive charge on the H atoms. Although the 1:2 adduct has twice as many H atoms per SiF_4 compared to the 1:1 complexes, the positive charge of the H atoms in the *trans* is nonetheless the largest of all, 0.243, or more than 40% larger than that of NH_3! Charge distributions in e-$SiF_4.NH_3$ come closest to those of component molecules. One also notices that the charges on all atoms of ammonia are always smaller in the *cis* than in the *trans*.

More interesting is the charge transfer from NH_3 to SiF_4. Table 1 shows the charge transfer (CT) in the axial and equatorial to be quite small. Thus, although these two complexes are all strongly polar, as the charges on each atom indicate, they are hardly ionic and the polarity is strictly an internal property of the component molecules SiF_4 and NH_3.

In contrast, sp-$SiF_4.NH_3$ and both 1:2 adducts are considerably more ionic. It must be noted that the charge transfer of 0.196 and 0.124 for the *trans*- and *cis*-$SiF_4.2NH_3$, respectively, are values per NH_3 molecule. Undoubtedly the drastic distortions from the tetrahedral structure of SiF_4 in these complexes led to this more extensive rearrangement of the electron density.

Net electrostatic interactions between SiF_4 and the ligand clearly reflect the degree of the charge transfer. The values are -0.25 eV for each of a- and e-$SiF_4.NH_3$, -0.56 for sp-$SiF_4.NH_3$, -1.13 eV and -0.80 eV, respectively, for *trans*- and *cis*-$SiF_4.2NH_3$.

Albeit with some variations, the exterior of these complexes is basically an ellipsoid where the major axis is not much longer than the minor axes. Referring to Figs. 1 and 2 and Table 1 it becomes evident that in all complexes, except *trans*-$SiF_4.2NH_3$, one end of the ellipsoid is spanned by the positively charged H atoms while the opposite half of the ellipsoid is defined by the four negatively charged F atoms. Enveloped inside this shell are the Si and N atoms.

This overall exterior polarity enables these four complexes to form an ionic solid with a head-to-tail arrangement, providing a further stabilization. This facility is most pronounced in the *cis* 1:2 adduct due to the larger charges on the atoms and the higher number of H atoms compared to the 1:1 adducts. Thus, although the total energy of the isolated *cis* isomer is 1.543 eV higher than that of the *trans*, when all factors are considered, it is highly possible that the *cis* arrangement becomes sufficiently stable in the solid phase to co-exist with the *trans* isomer or even become the favoured form. This is essentially the point Aggarwal and Onyszchuk (13) made in explaining their ir spectra.

The *trans* form of the 1:2 adduct is different. Because of its axial symmetry both ends of the ellipsoid are positively charged and only at the mid-section is a ring of negative charges composed of four F atoms. Despite its large charge transfer, 0.196 per NH_3, and high internal polarity, its overall exterior charge arrangements are not conducive with the additional stabilization mentioned above.

Is $SiF_4.2NH_3$ *trans* or *cis*? The answer seems to depend on the physical state of the complex. In the solid phase it is conceivably in the *cis* form. On the contrary, the *trans* arrangement should be favoured whenever the added stabilization from condensation is not in effect. This includes the gaseous and solution phases and when the complex is dispersed into solid matrices. This may explain the conflicting experimental observations on the 1:2 adducts. Since all bonds around the Si atom are single bonds, transformation between *cis* and *trans* isomers may not involve a very high barrier.

We rule out the size of the ligands as the deciding factor but its electronegativity may play a crucial part. We are presently looking into these questions.

(C) Si—N bonding

Being molecular complexes, the mode whereby the component molecules are linked together is of utmost interest. Bond angles are used above as a circumstantial evidence to assert that the Si—N bond is not a full-fledged covalent bond. It is also shown that the net electrostatic interaction is to hold the complexes together. In general, the more severe the distortion from the tetrahedral shape of SiF_4, the larger the magnitude of the net attraction is. While the ionicity of the complexes increases from 1:1 adducts to 1:2 adducts, the Si—N bond still has some covalent character. For example, a-$SiF_4.NH_3$ has a bond energy of 0.433 eV but its net electrostatic effect is only -0.25 eV. Obviously there must be covalency in the Si—N bond to account for the bond energy.[3]

The bond order is an approximate gauge of the covalency of a bond. It ranges from the value of ± 1.0 for purely covalent bond to 0.0 for a purely ionic bond. In the 1:1 complexes the Si—N bond has the highest bond order of 0.22 in the axial, followed by 0.15 in the equatorial, and -0.03 in the square pyramidal. The small charge transfer in the axial and the equatorial and their moderately low bond orders can be taken to indicate that the bonding between the ammonia and SiF_4 molecules is mainly electrostatic, involving the lone pair of ammonia. While some measure of covalency is established in the bond its bond order is low, even in comparison with a highly polar bond such as CO. Hence it seems safe to say that no fundamental change has been inflicted onto the lone pair of the ammonia molecule, despite the complex formation. For the square pyramidal the lone pair is even less affected and the bonding is exclusively electrostatic.

The *trans* isomer of the 1:2 adduct has a bond order of 0.12 and the *cis* is moderately antibonding at -0.15. Other than one being bonding and the other being antibonding, the nature of the Si—N bond in these two complexes should be quite similar to that of a- and e-$SiF_4.NH_3$.

1. J. DAVY. Philos. Trans. R. Soc. London, 352 (1812).
2. W. MIXTER. Am. Chem. J. **2**, 153 (1881).
3. J. GIERUT, F. SOWA, and J. NIEULAND. J. Am. Chem. Soc. **58**, 786 (1936).
4. T. S. PIPER and E. G. ROCHOW. J. Am. Chem. Soc. **76**, 4318 (1954).

[3]In fact the bond Si—N accounts for more than just the difference 0.183 eV (+0.433 − 0.25) since the value 0.433 eV is in reference to the neutral $SiF_4 + NH_3$ while -0.25 eV is in reference to $(SiF_4)^{-q} + (NH_3)^{+q}$, with $q = 0.084$.

5. D. M. MILLER and H. H. SISLER. J. Am. Chem. Soc. **77**, 4998 (1955).
6. B. AULT. Inorg. Chem. **20**, 2817 (1981).
7. I. R. BEATTIE and G. A. OZIN. J. Chem. Soc. A, 370 (1970).
8. J. E. FERGUSSON, D. K. GRANT, K. HICKFORD, and C. J. WILKINS. J. Chem. Soc. 99 (1959).
9. E. L. MUETTERTIES. J. Am. Chem. Soc. **82**, 1082 (1960).
10. E. L. MUETTERTIES. Acta Crystallogr. B**25**, 156 (1969).
11. R. HULME, G. J. LEIGH, and I. R. BEATTIE. J. Chem. Soc. 366 (1960).
12. R. HULME, G. J. LEIGH, and I. R. BEATTIE. J. Organomet. Chem. **144**, 39 (1978).
13. R. C. AGGARWAL and M. ONYSZCHUK. Can. J. Chem. **41**, 876 (1963).
14. W. J. HEHRE *et al.* QCPE, **11**, 236 (1973).

Can. J. Chem. Downloaded from www.nrcresearchpress.com by 210.87.254.42 on 09/06/12
For personal use only.

Crystal structure of diethylammonium tetrachloro(*p*-phenoxyphenyl)tellurate

RAJ K. CHADHA, JOHN E. DRAKE, and MASOOD A. KHAN
Chemistry Department, University of Windsor, Windsor, Ont. Canada N9B 3P4

Received May 18, 1983

RAJ K. CHADHA, JOHN E. DRAKE, and MASOOD A. KHAN. Can. J. Chem. **62**, 32 (1984).

The crystal structure of diethylammonium tetrachloro(*p*-phenoxyphenyl)tellurate has been determined by the heavy atom method. The crystals are monoclinic, space group $C2/c$, with unit cell dimensions $a = 19.675(5)$, $b = 7.634(3)$, $c = 28.716(6)$ Å, $\beta = 105.58(2)°$, and $Z = 8$. For 2636 "observed" reflections ($I > 3\ \sigma(I)$), $R = 0.030$. The primary geometry about tellurium is based on a square pyramid with a secondary interaction on the vacant side of the tellurium coordination octahedron. The ions are apparently linked by weak interionic hydrogen bonding along the crystallographic *b* axis.

RAJ K. CHADHA, JOHN E. DRAKE et MASOOD A. KHAN. Can. J. Chem. **62**, 32 (1984).

On a déterminé la structure du cristal de tétrachloro(*p*-phénoxyphényl)tellurate de diéthylammonium par la méthode de l'atome lourd. Les cristaux appartiennent au groupe d'espace monoclinique $C2/c$ avec $a = 19,675(5)$, $b = 7,634(3)$, $c = 28,716(6)$ Å, $\beta = 105,58(2)°$ et $Z = 8$ pour 2636 réflexions observées avec ($I > 3\sigma(I)$) et $R = 0,030$. La géométrie primaire autour du tellure est une pyramide carrée avec une interaction secondaire du côté libre de la coordination octaédrique du tellure. Les ions sont apparemment liés par une faible liaison hydrogène interconique le long de l'axe cristallographique *b*.

[Traduit par le journal]

Introduction

The preparation and spectroscopic properties of a series of dialkylammonium tetrachloroaryltellurates have been reported by Miller and Chadha (1). It was suggested on the basis of vibrational spectroscopy and on ^1H nmr data recorded at various temperatures and dilutions that weak hydrogen bonding existed between the hydrogen atoms of the cations and chlorine atoms of the anions. To establish the nature of interionic interactions in the solid state, we present the crystal structure of diethylammonium tetrachloro(*p*-phenoxyphenyl)tellurate. A further reason for this study is the general lack of detailed structural investigations of penta-coordinated ionic salts of tellurium. Studies of these are of particular interest in terms of the question of the importance of a stereochemically active lone pair and of secondary tellurium–halogen interactions.

Experimental section

The compound was prepared by the method already described (1). Two recrystallisations of the crude product from CH_2Cl_2 afforded plate like colourless crystals of the title compound. The density was measured by the flotation method in CCl_4/CH_3I.

A crystal with approximate dimensions (0.06 × 0.1 × 0.2 mm) was mounted along the largest dimension, subsequently shown to be the *b* axis, and data were collected on a Syntex $P2_1$ diffractometer following the procedure described previously (2). The intensities of three monitor reflections did not change significantly during data collection. The systematic absences (hkl, $h + k = 2n + 1$; $h0l$, $l = 2n + 1$), are consistent with $C2/c$ and Cc space groups. The former was used and later assumed correct because of successful refinement of the structure. The data were corrected for Lorentz and polarisation effects and the analytical absorption correction was applied. Details of the X-ray data are given in Table 1.

The position of the tellurium atom was obtained from a sharpened Patterson synthesis and the positions of the remaining non-hydrogen atoms were determined from a difference Fourier map. The structure was refined anisotropically by the full-matrix least-squares methods. The refinement converged to $R = (\Sigma||F_o| - |F_c||/\Sigma|F_o|) = 0.040$. A difference map at this stage showed peaks at plausible hydrogen positions. Hydrogen atoms were included in subsequent refinement in ideal positions (C—H = N—H = 0.95 Å, ∠CCH = 120.0°, and ∠CNH = 109.5°) with isotropic values assigned 0.01 greater than the atoms they are attached to. Hydrogen atoms attached to the carbon atoms of the cation, $Et_2NH_2^+$, were not included in calculations because the cation was disordered, as reflected by high thermal parameters for the carbon atoms. Fixing the C—C bond length did not yield better refinement. Finally, it was decided to refine all the atoms anisotropically in order to allow the model which is closest to the real structure. Fortunately, the nitrogen atom is not disordered; therefore, this problem has little or no effect on the anion, which is the main theme of this work. Refinement gave final values of $R = 0.030$ and $R_{WF} = [\Sigma\omega\Delta^2/\Sigma\omega F_o^2]^{1/2} = 0.033$. In the final two cycles of refinement the largest shift/error ratio was 0.05, and the final difference map had no feature of chemical significance with the largest peak 0.5 e Å^{-3}. The function $(|F_o| - |F_c|)^2$ was minimized during least-squares refinement. Unit weights were used in the initial stages and in the final cycles, a weighting scheme of the form $\omega = 1/[\sigma^2(F) + \rho F^2]$ was employed with a final ρ value of 0.002. A few low-angle reflections were found to be affected by secondary extinction. An empirical

TABLE 1. Crystallographic data

a (Å)	19.675(5)
b (Å)	7.634(3)
c (Å)	28.716(6)
β (°)	105.58(2)
V (Å^3)	4154.6(10)
Crystal system	Monoclinic
Space group	$C2/c$
Mol. wt.	512.6
Z	8
ρ_c (g cm^{-3})	1.64
ρ_o (g cm^{-3})	1.63
Radiation	MoKα, $\lambda = 0.71069$ Å
Monochromator	Highly oriented graphite
T (°C)	21
Abs. coeff. μ (cm^{-1})	18.12
Min. abs. corr.	1.247
Max. abs. corr.	1.490
2θ angle (deg)	4–50
Scan type	coupled θ (crystal)/2θ (counter)
Scan width	$K_{\alpha 1} - 1°$ to $K_{\alpha 2} + 1°$
Scan speed (deg min^{-1})	variable, 2.02–4.88
Bkgd time/scan time	0.5
Total reflcns measd	4074 (+h, +k, ±l)
Unique data used	2636 with [I > 3σ(I)]
No. of parameters (NP)	208
R	0.030
R_{WF}	0.033

Can. J. Chem. Downloaded from www.nrcresearchpress.com by 210.87.254.40 on 09/06/12
For personal use only.

Can. J. Chem. Downloaded from www.nrcresearchpress.com by 210.87.254.40 on 09/06/12
For personal use only.

TABLE 2. Final fractional coordinates and isotropic thermal parameters for non-hydrogen atoms of $[(C_2H_5)_2NH_2]^+$ $[p\text{-}C_6H_5OC_6H_4TeCl_4]^-$ with standard deviations in parentheses

Atom	x	y	z	U^*_{eq} (Å^2 × 10^3)
Te	0.20135(2)	0.26220(4)	0.42919(1)	42.7
Cl(1)	0.0745(1)	0.2366(2)	0.4263(1)	63
Cl(2)	0.1809(1)	0.5453(2)	0.3874(1)	65
Cl(3)	0.2239(1)	−0.0447(2)	0.4687(0)	58
Cl(4)	0.3324(1)	0.2814(2)	0.4323(1)	67
O	0.1512(2)	−0.1200(6)	0.2296(2)	86
N	0.1502(3)	0.2275(7)	0.0534(2)	79
C(1)	0.1373(8)	0.2999(12)	0.0985(5)	158
C(2)	0.1608(8)	0.2279(17)	0.1401(4)	181
C(3)	0.0790(11)	0.1810(24)	0.0166(9)	118
C(4)	0.0479(9)	0.2713(27)	−0.0159(5)	235
C(11)	0.1821(2)	0.1342(6)	0.3610(2)	99
C(12)	0.1314(3)	0.0034(7)	0.3495(2)	54
C(13)	0.1188(3)	−0.0809(7)	0.3052(2)	62
C(14)	0.1595(3)	−0.0413(8)	0.2743(2)	60
C(15)	0.2086(3)	0.0922(8)	0.2858(2)	67
C(16)	0.2197(3)	0.1806(7)	0.3287(2)	57
C(21)	0.1080(3)	−0.2642(9)	0.2167(2)	68
C(22)	0.0556(3)	−0.2567(9)	0.1741(3)	85
C(23)	0.0139(4)	−0.4042(12)	0.1589(3)	96
C(24)	0.0240(4)	−0.5486(11)	0.1862(3)	97
C(25)	0.0758(4)	−0.5571(9)	0.2278(3)	87
C(26)	0.1193(3)	−0.4132(9)	0.2437(2)	76

*U_{eq} for the non-hydrogen atoms is calculated from the refined anisotropic thermal parameters (deposited) ($U_{eq} = (1/3)\sum_{i=1}^{3}(\text{RMSD})_i^2$, RMSD values are taken from ORTEP output).

isotropic extinction parameter, x, was used employing the equation $F_c = F[1 - 0.0001x(F^2/\sin\theta)]$ and refined to a value of 0.00040.

Scattering factors for all non-hydrogen atoms, including the anomalous dispersion correction for Te and Cl were obtained from Ibers and Hamilton (3) and for hydrogen atoms from Stewart *et al.* (4). Programs used include SHELX, XANADU, ORTEP, and ABSORB (5).

The final atomic coordinates for non-hydrogen atoms are given in Table 2 and important distances and angles in Table 3.[1]

Results and discussion

The tellurium atom in the $[p\text{-PhOPhTeCl}_4]^-$ anion has an approximate square pyramidal coordination with the organic group in the apical position (Fig. 1). The square plane is slightly distorted with the chlorine atoms alternatively above and below their mean plane by 0.030(2) Å and with the tellurium atom positioned above the plane by 0.040(1) Å. The structure of the anion is similar to the $[MeTeI_4]^-$ anion in the compound β-Me_2TeI_2 (6) and the structural unit, $CTeCl_4$, of organotellurium trichlorides (7–9). It is generally assumed that these arrangements reflect a tendency for the tellurium atom to adopt octahedral geometry with the non-bonding electron-pair occupying the sixth position.

However, this sixth position also provides the site for a secondary-bonding interaction between the tellurium atom and a chlorine atom, Cl(3′), $(1/2 - x, 1/2 - y, -z)$ on an adjacent molecule at a distance of 3.619 Å. Such a distance is typical of Cl---Te secondary bonds and is significantly shorter than the sum of the van der Waals radii (4.0 Å)(5). The bond angle C(11)—Te---Cl(3′) is 162.2(2)° rather than the 180° that might be expected if in fact the tellurium lone-pair was stereochemically totally inactive. The two anions joined together by these secondary interactions constitute centrosymmetric dimers in which the $RTeCl_4$ units are associated base to base (Fig. 2).

Other examples in which secondary interactions have been noted on the vacant site of the coordination octahedron are $SeOCl_2.2Py$ (10), $C_9H_8NO^+SeOCl_3^-$ (11) and most notably in β-Me_2TeI_2 (6). In the latter case, which has been shown to be correctly formulated as $[Me_3Te]^+[MeTeI_4]^-$, the $[MeTeI_4]^-$ anions can also be described as made up of centrosymmetric dimers and the C—Te---I angle of 166° is very close to the value of the C—Te---Cl angle in $[p\text{-PhOPhTeCl}_4]^-$. For $[MeTeI_4]^-$ it was argued that the secondary interaction probably involved donation from the lone-pair on tellurium into vacant *d*-orbitals on iodine. However, such bonding seems improbable for chlorine atoms and the similarity in the structures suggests that in both cases the donation is more probably from halogen lone-pairs towards the more electro-positive tel-

TABLE 3. Interatomic distances (Å) and angles (deg)*

Bond	Distance	Bonds	Angle
Te—Cl(1)	2.482(1)	Cl(1)—Te—Cl(2)	91.2(1)
Te—Cl(2)	2.451(1)	Cl(1)—Te—Cl(3)	89.8(1)
Te—Cl(3)	2.589(1)	Cl(1)—Te—Cl(4)	178.8(1)
Te—Cl(4)	2.558(1)	Cl(2)—Te—Cl(3)	176.7(1)
Te—C(11)	2.127(5)	Cl(2)—Te—Cl(4)	90.0(1)
C(11)—C(12)	1.384(6)	Cl(3)—Te—Cl(4)	89.1(1)
C(11)—C(16)	1.379(6)	Cl(1)—Te—C(11)	90.2(1)
C(12)—C(13)	1.391(7)	Cl(2)—Te—C(11)	89.4(1)
C(13)—C(14)	1.375(7)	Cl(3)—Te—C(11)	87.4(1)
C(14)—C(15)	1.385(7)	Cl(4)—Te—C(11)	89.3(1)
C(15)—C(16)	1.373(7)	Te—C(11)—C(12)	119.2(1)
C(14)—O	1.386(6)	Te—C(11)—C(16)	120.2(3)
O—C(21)	1.378(7)	C(12)—C(11)—C(16)	120.6(5)
C(21)—C(22)	1.372(9)	C(11)—C(12)—C(13)	119.3(5)
C(21)—C(26)	1.358(8)	C(12)—C(13)—C(14)	120.1(5)
C(22)—C(23)	1.386(9)	C(14)—C(15)—C(16)	120.5(5)
C(23)—C(24)	1.337(10)	C(11)—C(16)—C(15)	119.6(5)
C(24)—C(25)	1.352(10)	C(13)—C(14)—C(15)	119.7(5)
C(25)—C(26)	1.400(8)	C(13)—C(14)—O	124.2(5)
N—C(1)	1.49(1)	C(15)—C(14)—O	116.0(5)
N—C(3)	1.54(2)	C(14)—O—C(21)	120.3(4)
C(1)—C(2)	1.30(1)	O—C(21)—C(22)	118.3(6)
C(3)—C(4)	1.19(2)	O—C(21)—C(26)	121.0(6)
H(1)---Cl(3″)	2.368	C(22)—C(21)—C(26)	120.6(6)
H(2)---Cl(4)	2.646	C(21)—C(22)—C(23)	119.6(7)
H(2)---Cl(2)	2.857	C(22)—C(23)—C(24)	119.8(7)
Te---Cl(3′)	3.619	C(23)—C(24)—C(25)	121.2(7)
Te---Te′	4.007	C(24)—C(25)—C(26)	120.1(7)
		C(21)—C(26)—C(25)	118.6(6)
		C(1)—N—C(3)	110.2(11)
		N—C(1)—C(2)	123(1)
		N—C(3)—C(4)	124(2)
		N—H(1)---Cl(3″)	151.7(2)
		N—H(2)---Cl(4)	143.0(3)
		N—H(2)---Cl(2)	135.7(2)
		Te′—Cl(3′)---Te	78.5(3)
		C(11)—Te---Cl(3′)	162.2(3)

*Symmetry equivalent positions: primes are $1/2 - x$, $1/2 - y$, $-z$; double primes are x, $1 + y$, z.

[1]Tables of fractional coordinates for hydrogen atoms, lists of structure factors, and anisotropic thermal parameters (18 pages) are available, at a nominal charge, from the Depository of Unpublished Data, CISTI, National Research Council of Canada, Ottawa, Ont., Canada K1A 0S2.

Can. J. Chem. Downloaded from www.nrcresearchpress.com by 210.87.254.40 on 09/06/12
For personal use only.

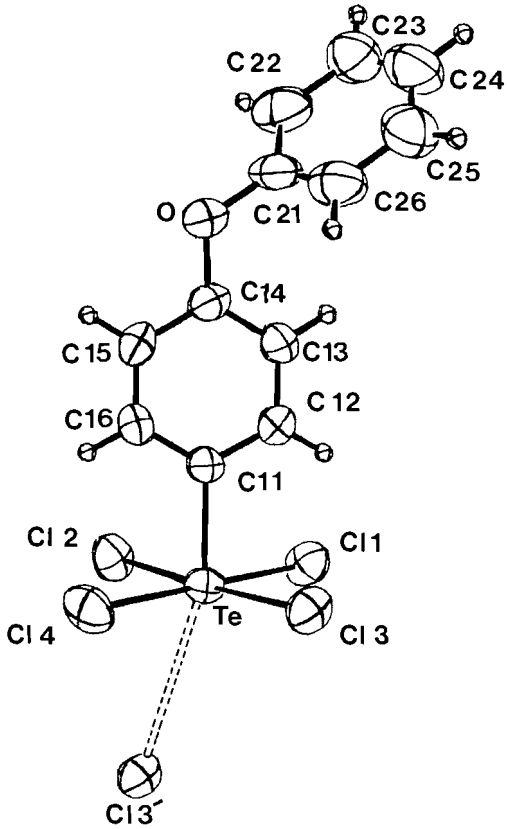

FIG. 1. ORTEP plot of the anion $[p\text{-}C_6H_5OC_6H_4TeCl_4]^-$. The non-hydrogen atoms are drawn with 50% probability ellipsoids. Hydrogen atoms are drawn arbitrarily small.

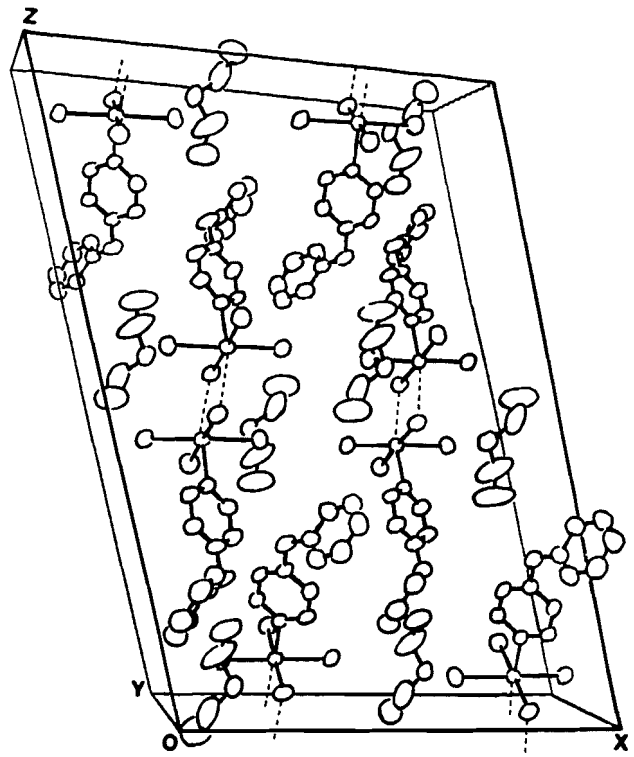

FIG. 2. Unit cell packing of $[(C_2H_5)_2NH_2]^+[p\text{-}C_6H_5OC_6H_4TeCl_4]^-$. Hydrogen atoms are omitted for clarity.

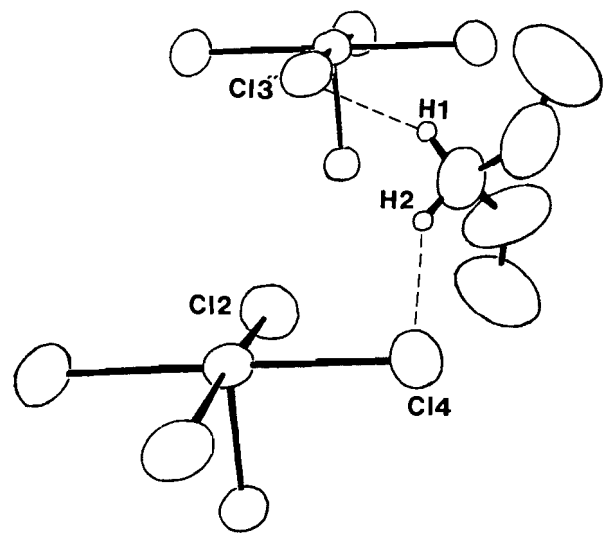

FIG. 3. Interionic hydrogen bonding parallel to the *y* axis.

lurium atom. With the chlorine atom essentially occupying the sixth coordination site, the stereochemical activity of the tellurium lone-pair, which is inactive in $[TeCl_6]^{2-}$ (12), is called into question. In both $[MeTeI_4]^-$ and $[p\text{-}PhOPhTeCl_4]^-$, there is a similar deviation from 180° so it is hard to believe the distortion arises from packing effects of the bulky *p*-PhOPh group or the counter-ion. The Te—Cl---Te′ angle is 78.5(3)°, rather than 90°, which results in the Cl(3) and Cl(3′) atoms in the bridge being moved further apart and the tellurium atoms closer together. On a model assuming stereochemically active lone-pairs on tellurium, any distortion would surely be expected to place the Te atoms further apart rather than closer together. The Te---Te′ distance of 4.007 Å is similar to that found in $TeCl_4$ which also has a distorted octahedral environment in the solid state (13).

In addition to the Te---Cl secondary interactions, the packing suggests that there are also some weak interionic hydrogen-bond interactions as had been suggested in studies on solutions (1). The closest H---Cl (2.368 Å) contact (Fig. 3) occurs between the H(1) atom of the cation $Et_2NH_2^+$ and Cl(3″) (x, $1 + y$, z) of the anion. Crystal growth is apparently most rapid along the crystallographic *y* axis as the longest dimension of the crystal is parallel to the *b* axis.

The Te—Cl primary bond lengths have significant differences and can be related to the involvement of the chlorine atoms in the interionic interactions. The longest bond (2.589 (1) Å) is formed by Cl(3), the chlorine atom involved in the secondary interaction with the tellurium atom of the adjacent molecule as well as in a weak hydrogen bond. The bond Te—Cl(4) is 2.558(1) Å. The atoms Cl(1) and Cl(2) are not involved in any significant secondary interactions, and the bond lengths Te—Cl(1) (2.482(1) Å) and Te—Cl(2) (2.451(1) Å) are shorter. The average Te—Cl bond of 2.52(1) Å is comparable to the Te—Cl bond length of 2.54 Å in $TeCl_6^{2-}$ (12), which adopts regular octahedral geometry.

Acknowledgement

We wish to thank the Natural Sciences and Engineering Research Council of Canada for financial support.

1. J. M. MILLER and R. K. CHADHA. J. Organomet. Chem. **216**, 177 (1981).
2. M. KHAN, R. C. STEEVENSZ, D. G. TUCK, J. G. NOLTES, and

P. W. R. CORFIELD. Inorg. Chem. **19**, 3407 (1980).
3. J. A. IBERS and W. C. HAMILTON (*Editors*). International tables for X-ray crystallography. Vol. IV. Kynoch Press, Birmingham, England. 1974.
4. R. F. STEWART, E. R. DAVIDSON, and M. T. SIMPSON. J. Chem. Phys. **42**, 3175 (1965).
5. R. K. CHADHA, J. E. DRAKE, and W. KHAN. Acta Crystallogr. C **39**, 45 (1983).
6. F. EINSTEIN, J. TROTTER, and C. WILLISTON. J. Chem. Soc. A, 2018 (1967).
7. P. H. BIRD, V. KUMAR, and B. C. PANT. Inorg. Chem. **19**, 2487 (1980).
8. N. W. ALCOCK and W. D. HARRISON. J. Chem. Soc. Dalton Trans. 251 (1982).
9. D. KOBELT and E. F. PAULUS. Angew. Chem. Int. Ed. Engl. **10**, 74 (1971).
10. I. LINDQVIST and G. NAHRINGBAUER. Acta Crystallogr. **12**, 638 (1959).
11. A. W. CORDES. Inorg. Chem. **6**, 1204 (1967).
12. A. HAZELL. Acta Chem. Scand. **20**, 165 (1966).
13. B. BUSS and B. KREBS. Inorg. Chem. **10**, 2795 (1971).

Can. J. Chem. Downloaded from www.nrcresearchpress.com by 210.87.254.40 on 09/06/12
For personal use only.

L'électrodissolution du cuivre dans les solutions bromurées

ROBERT-LOUIS BROSSARD
Institut de recherche d'Hydro-Québec, C.P. 1000, 1800 Montée Ste-Julie, Varennes (Qué.), Canada J0L 2P0

Reçu le 24 mai 1983

ROBERT-LOUIS BROSSARD. Can. J. Chem. **62**, 36 (1984).

La dissolution de l'anode de cuivre a été étudiée en solution aqueuse de pH égal à 4 dont la concentration en NaBr dissous varie de 0,1 *M* à 1,2 *M*. Dans la zone où l'accumulation du produit de corrosion sur le cuivre est inexistante ou marginale, le courant de dissolution est décomposable en un phénomène de surface, d'une part, et en un phénomène de diffusion des ions dans la solution, d'autre part. Le courant associé à chacune de ces étapes lentes a été déterminé à partir des relations linéraire i^{-1} vs. $\omega^{-1/2}$.

Par ailleurs, les principales caractéristiques du comportement de l'anode de cuivre sont en termes de dérivées partielles: $(\partial E/\partial \log_{10} i)_{25°C,\ Br^-} \simeq 60$ mV/décade, $(\partial i_d/\partial\omega^{1/2})_{E,\ Br^-}$ = constante, $(\partial E/\partial \log_{10} (i_d\cdot\omega^{-1/2}))_{25°C,\ Br^-} \simeq 59$ mV/décade alors que l'ordre de la réaction par rapport aux ions bromures est égal à 2. De plus, la relation E vs. $\log_{10} i_\infty$ est assimilable à une droite, ce qui est la conséquence d'un phénomène de surface limité par un transfert électronique. Un modèle de dissolution est présenté à partir duquel on retrouve les principales caractéristiques de la dissolution du cuivre. Selon ce modèle, le terme i_d est entièrement attribuable à la diffusion d'un bromocomplexe de cuivre, le $CuBr_2^-$, depuis la surface de l'électrode jusqu'au sein de la solution. Pour sa part, le calcul de l'énergie d'activation apparente en considérant le modèle proposé est de 7 kcal/mol alors que la valeur expérimentale est de 6,5 kcal/mol.

Enfin, la vague d'oxydation observée lorsque la tension d'électrode devient suffisamment anodique par rapport à la tension réversible de la réaction Cu + Br^- = CuBr + e, est associée à la passivation du cuivre par le CuBr γ.

ROBERT-LOUIS BROSSARD. Can. J. Chem. **62**, 36 (1984).

The dissolution of a copper anode has been studied in aqueous solutions, at pH 4, for a range of concentrations varying from 0.1 *M* to 1.2 *M* in NaBr. Where the accumulation of the corrosion product on the copper was nonexistent or negligible, two phenomena account for the dissolution current: a surface phenomenon and a phenomenon of diffusion of the ions into the solution. The current associated with each of these slow steps has been determined from the linear relationship i^{-1} vs. $\omega^{-1/2}$.

The main characteristics of the copper anode behavior are expressed as partial derivatives: $(\partial E/\partial \log_{10} i)_{25°C,\ Br^-} \simeq 60$ mV/decade, $(\partial i_d/\partial\omega^{1/2})_{E,\ Br^-}$ = constant, $(\partial E/\partial \log_{10} (i_d\cdot\omega^{-1/2}))_{25°C,\ Br^-} \simeq 59$ mV/decade, while the reaction order for the bromide ions is equal to 2. Furthermore, the linearity of the relationship E vs. $\log_{10} i$ arises as a direct consequence of a surface phenomenon limited by an electron transfer. A dissolution model that describes the main characteristics of the copper dissolution is presented. According to this model, the term i_d is entirely ascribable to the diffusion of a copper bromide complex, $CuBr_2^-$, from the surface of the electrode into the solution. The apparent activation energy calculation is 7 kcal/mol according to the model, while the experimental value is 6.5 kcal/mol.

Finally, the observed oxidation wave when the electrode potential becomes sufficiently anodic compared to the reversible potential of the reaction Cu + Br^- = CuBr + e, is associated with the passivation of the copper by γ-CuBr.

[Journal translation]

Introduction

Un nombre relativement restreint de chercheurs se sont penchés sur l'étude de la dissolution du cuivre en présence des ions Br^- (1 à 6). Il a été établi que la valence de dissolution du cuivre est de +1 dans le domaine de dissolution active (1) alors que le cuivre a tendance à se recouvrir de CuBr lorsque la tension devient suffisamment anodique (2 à 4).

Le présent travail se propose d'élucider le procédé d'électrode durant la dissolution active du cuivre en solution aqueuse légèrement acide dont la concentration en Br^- est comprise entre 0,1 et 1,2 *M*.

Partie expérimentale

2.1 *La cellule et ses accessoires*

Les détails relatifs à la cellule et ses accessoires ainsi qu'aux électrodes de travail sont donnés dans un article précédent (7). L'électrode de cuive se présente sous la forme d'un fil de 0,64 cm de diamètre, d'une plaque de 1 cm × 2 cm ou d'un disque de 0,5 cm de diamètre, les surfaces de l'échantillon sont respectivement de 0,4 cm^2, 2 cm^2 et 0,196 cm^2.

2.2 *La préparation des essais*

Un barbottage d'azote de 6 h précède l'immersion de l'électrode de cuivre dans la solution. Les solutions contiennent entre 0,1 et 1,2 *M* de NaBr dissous. Un tampon à base de phtalate de potassium est utilisé pour stabiliser le pH à 4.

La méthode employée par Shoesmith et Lee (8, 9) a été retenue pour le polissage du cuivre: l'échantillon est d'abord poli mécaniquement par abrasion avec du papier au carbure de silicium, le polissage se termine avec de l'alumine de 1 μ. L'échantillon est alors rinçé à l'alcool, à l'acétone puis à l'eau distillée avant son immersion.

2.3 *Les techniques expérimentales utilisées*

Les courbes tension−courant ont été obtenues en balayage linéaire de la tension. L'électrode à disque tournant a été utilisée en imposant une tension d'électrode constante alors que la vitesse de rotation (ω) varie de 25,12 rad s^{-1} jusqu'à 628,3 rad s^{-1}. On obtient ainsi le courant en fonction ω. Le disque de cuivre est poli à chaque changement de tension. Un bain thermostatique a servi au contrôle de la température qui est comprise entre 22°C et 80°C.

Enfin, les valeurs de la tension sont données par rapport à l'électrode au calomel saturée.

Résultats expérimentaux

3.1 *Apparition du produit de corrosion*

L'enregistrement obtenu en balayage linéaire de la tension, reproduit à la fig. 1, et qui correspond à une vitesse de balayage en tension de 5 mV s^{-1}, est représentatif du comportement de l'anode de cuivre. La courbe montre une vague d'oxydation bien définie dont le maximum a comme coordonnées 20 mA cm^{-2} (i_{pl}) et −92 ± 4 mV_{ecs} (E_{pl}). D'après les travaux réalisés dans les solutions bromurées acides (1), la valence de dissolution du cuivre est égale à 1.

Par ailleurs, la relation E vs. $\log_{10} i$ est linéaire dans la partie

Can. J. Chem. Downloaded from www.nrcresearchpress.com by 210.87.254.6 on 09/06/12
For personal use only.

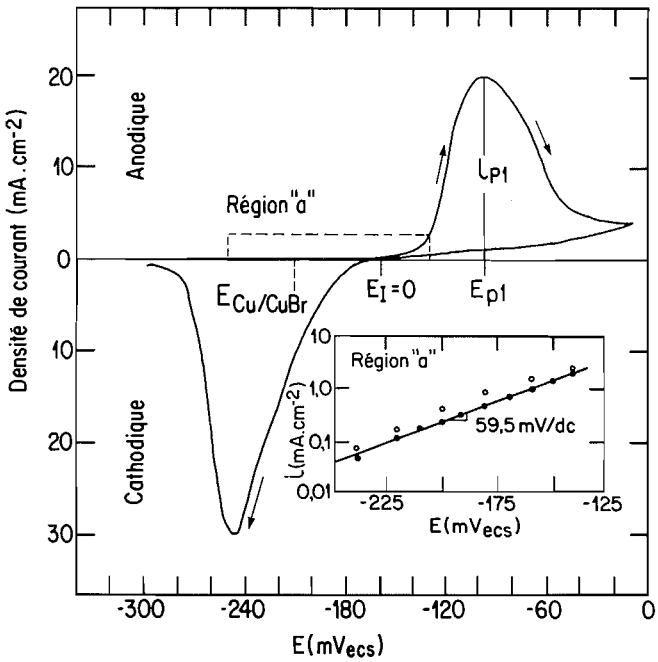

FIG. 1. Courbe de polarisation en balayage linéaire de la tension sur un fil de cuivre. Balayage à 5 mV s^{-1}. NaBr: 0,5 *M*. $E_{i=0}$: tension à courant nul. L'électrode est en position stationnaire. La région "a" en médaillon correspond à la première portion de la partie ascendante de la vague d'oxydation; ● sans agitation; ○ avec un barbottage d'azote de 87 mL min^{-1}.

ascendante de la vague d'oxydation, appelée région "a", sur la fig. 1. L'examen de la surface de l'anode par le microscope à balayage a permis d'observer que le cuivre reste à nu dans cette région. L'accumulation du produit de corrosion sur l'électrode est perceptible dès que la tension imposée dépasse de 70 mV environ (Figs. 1, 2) la tension réversible ($E_{Cu/CuBr}$) de la réaction:

[1] $Cu + Br^- = CuBr + e$

qui est donnée par (10, 11)

[2] $E_{Cu/CuBr} = -0{,}239 - 0{,}059 \log_{10} (Br^-)$

où $E_{Cu/CuBr}$ est en volt par rapport à l'électrode au calomel saturé. Pour sa part, E_{pl} dépasse de 115 mV environ $E_{Cu/CuBr}$.

Dans le cas illustré à la fig. 2, le produit de corrosion est présent d'une façon très discrète sur la surface pour des tensions de −170 mV et −140 mV; l'échantillon est alors dans la région "a" (Fig. 1). La présence du produit de corrosion est de plus en plus importante en dehors de la région "a" quand la tension augmente (−110 mV, −80 mV et 0 mV). On remarque que la surface n'est pas uniformément recouverte par le produit de corrosion alors que la vague d'oxydation est compatible avec la passivation de la surface par le produit de corrosion i.e. −80 mV et 0 mV. Pour sa part, la relation *E* vs. $\log_{10} i$ cesse d'être linéaire lorsque le produit de corrosion est présent sur le cuivre. Ce changement au niveau de la relation *E* vs. $\log_{10} i$ laisse croire à un changement au niveau du mécanisme de dissolution.

La diffraction aux rayons X a permis l'identification du produit de corrosion. Il est constitué d'un seul composé qui est le bromure cuivreux gamma (CuBr γ).

Enfin, la vague cathodique (Fig. 1) correspond à la réduction du CuBr γ.

3.2 *Comportement du cuivre dans la zone de dissolution active (région "a" (Fig. 1))*

L'anode de cuivre, polarisée à des tensions pour lesquelles le produit de corrosion est totalement absent ou présent d'une façon très discrète sur la surface de l'électrode, a les particularités suivantes:

(a) la relation *E* vs. $\log_{10} i$ est linéaire avec une pente voisine de 60 mV/décade (Fig. 3)

$$\left(\frac{\partial E}{\partial \log_{10} i}\right)_{25°C,\ Br^-} = 60 \text{ mV/décade};$$

(b) il y a élévation du courant de dissolution lorsque la vitesse de rotation de l'électrode (ω) augmente (Fig. 4); cependant que la pente ($\partial i/\partial \omega^{1/2}$) diminue avec ω croissant;

(c) l'ordre de la réaction par rapport aux ions Br^- est voisin de 2 (Fig. 5);

(d) la valence de dissolution est égale à 1;

(e) une augmentation de la température se traduit par une élévation significative du courant de dissolution (Fig. 6).

Discussion

4.1 *Analyse des courbes* i *vs.* $\omega^{1/2}$

L'allure des courbes *i* vs. $\omega^{1/2}$ est caractéristique d'un procédé d'électrode mixte (12), c'est-à-dire que le courant mesuré résulte de ce procédé d'électrode qui a deux étapes lentes. Ces étapes lentes sont la diffusion des ions dans la solution, d'une part, et un phénomène de surface comme le transfert électronique, d'autre part. Dans le cas où ces deux étapes lentes sont en série, le courant global est décomposable en deux courants selon (10):

[3] $i^{-1} = i_\infty^{-1} + i_d^{-1}$

où *i* est le courant global, i_∞ est le courant de dissolution indépendant de la vitesse de rotation de l'électrode alors que i_d est le courant attribué à la diffusion. D'après Levich (13), l'expression qui lie le courant de diffusion à la vitesse de rotation de l'électrode est

[4] $i_d = B\omega^{1/2}$

où *B* est une constante et ω est la vitesse de rotation de l'électrode en rad s^{-1}. Les relations [3] et [4] donnent:

[5] $i^{-1} = i_\infty^{-1} + B^{-1}\,\omega^{-1/2}$

Ainsi, i^{-1} exprimé en fonction de $\omega^{-1/2}$ doit donner une droite dont les valeurs de i_∞^{-1} et de B^{-1} sont déterminables à partir de la pente et de l'ordonnée à l'origine (Fig. 7) (9, 12). L'inverse de la pente $\partial(i^{-1})/\partial(\omega^{-1/2})$ correspond à *B*, c'est-à-dire au produit $i_d \cdot \omega^{-1/2}$ alors que i_∞^{-1} est obtenu par extrapolation de la droite jusqu'à $\omega^{-1/2}$ égal à zéro. Dans l'exemple reproduit à la figure 7, *B* est égal à 0,14 mA cm^{-2} $rad^{-1/2}$ $s^{1/2}$ alors que i_∞ est de 1,7 mA cm^{-2}. Les valeurs de *B*, i.e. de $i_d \cdot \omega^{-1/2}$, ont été déterminées pour différentes valeurs de la tension imposée dans 0,5 *M* NaBr (Fig. 8). La relation *E* vs. $\log_{10} (i_d \cdot \omega^{-1/2})$ est linéaire avec une pente de 60 mV/décade approximativement.

Par ailleurs, les valeurs calculées pour i_∞ sont données en fonction de la tension d'électrode à la figure 9 pour 0,5 *M* en NaBr. La relation *E* vs. $\log_{10} i_\infty$, assimilable à une droite dont la pente est de 100 ± 10 mV/décade, suggère que le phénomène de surface est contrôlé par un transfert électronique.

4.2 *Mécanisme de dissolution*

L'augmentation du courant de dissolution avec la vitesse de

Can. J. Chem. Downloaded from www.nrcresearchpress.com by 210.87.254.6 on 09/06/12
For personal use only.

Can. J. Chem. Downloaded from www.nrcresearchpress.com by 210.87.254.6 on 09/06/12
For personal use only.

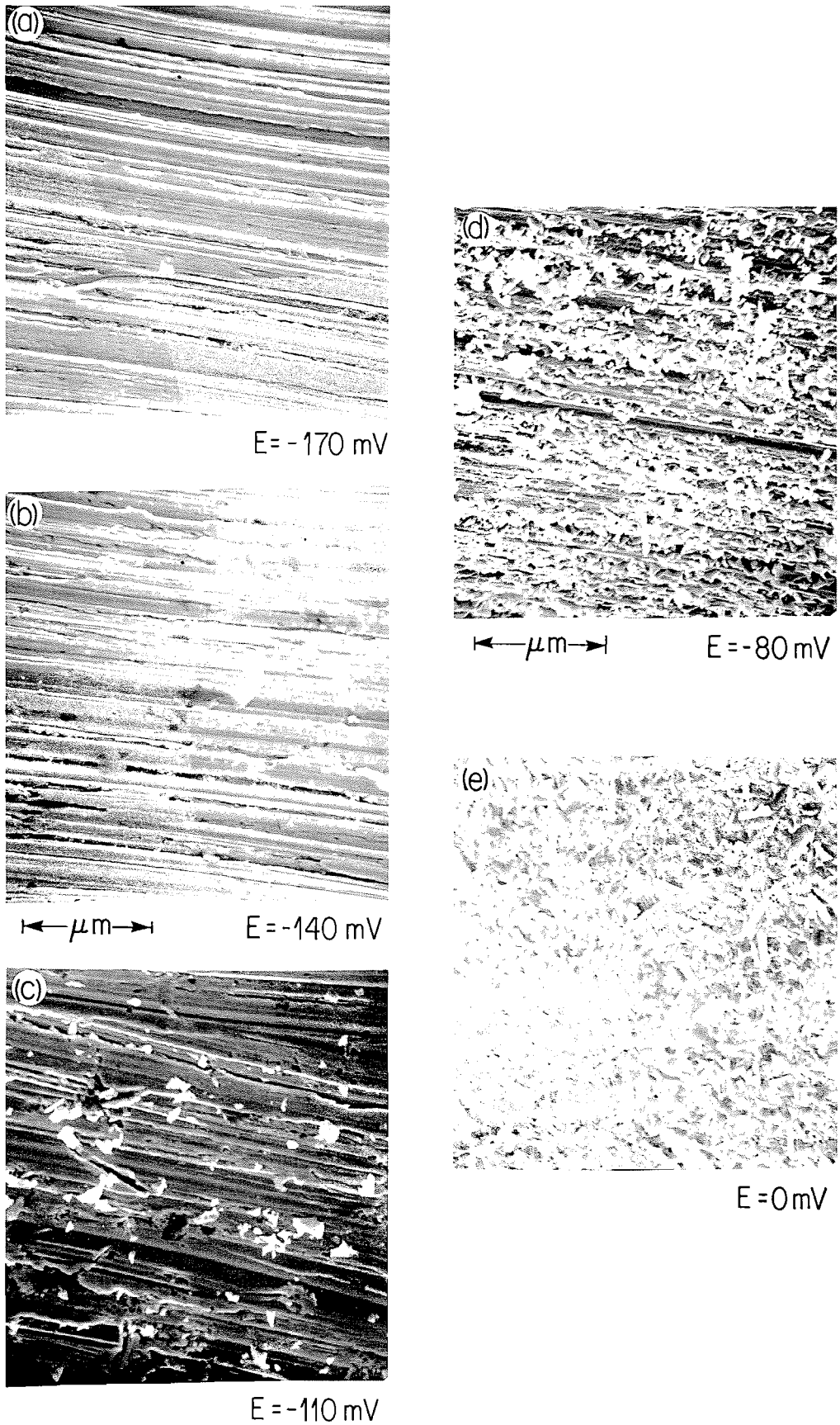

FIG. 2. Aspect de la surface durant l'oxydation anodique. Les conditions expérimentales sont celles de la fig. 1 alors que la solution était non agitée. La tension pour laquelle l'échantillon a été retiré de la solution est donnée au bas de chaque figure.

Can. J. Chem. Downloaded from www.nrcresearchpress.com by 210.87.254.6 on 09/06/12
For personal use only.

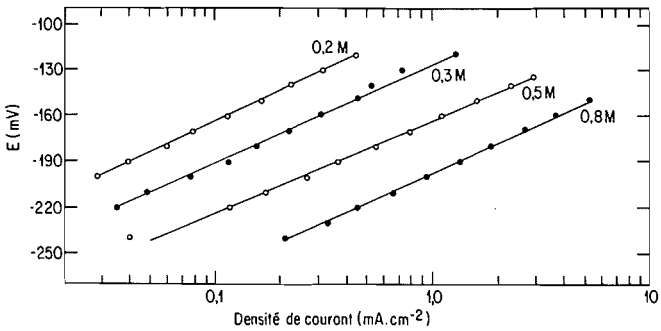

FIG. 3. Tension d'électrode en fonction du courant de dissolution anodique pour différentes concentrations en Br^-. Balayage à 5 mV s^{-1} sur un fil de cuivre en position stationnaire et en solution non agitée.

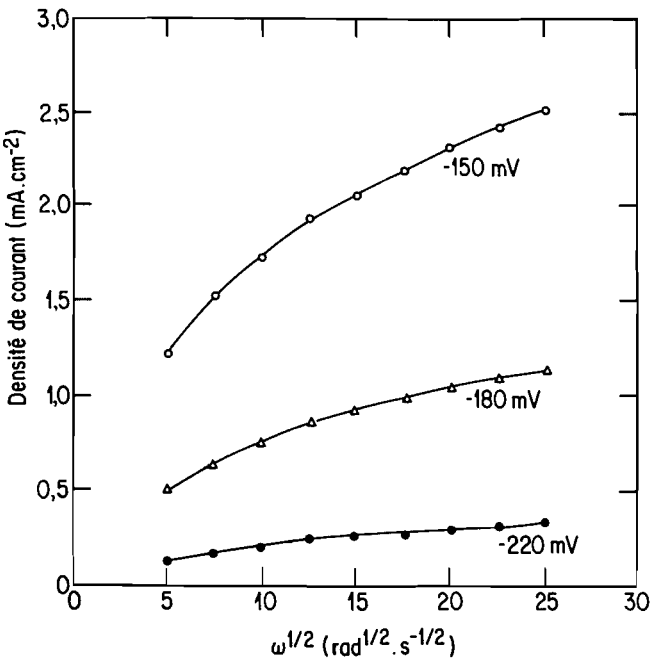

FIG. 4. Courant de dissolution anodique en fonction de $\omega^{1/2}$ à différentes valeurs de la tension imposée. NaBr: 0,5 *M*. La dissolution du cuivre est active.

rotation de l'électrode (Fig. 4), la linéarité de la relation i^{-1} vs. $\omega^{-1/2}$ (Fig. 7) et, enfin, le fait que la relation E vs. $\log_{10} i_\infty$ soit assimilable à une droite (Fig. 8) suggère que la réaction est contrôlée par deux étapes en série. La première est attribuable au transfert électronique à l'interface électrode–électrolyte, l'autre à la diffusion d'une espèce ionique en solution. Par ailleurs, l'espèce la plus stable pour le cuivre dissous est le $CuBr_2^-$ (14) dans la gamme de concentration en Br^- considérée. Ainsi, lorsque la dissolution du cuivre sous forme de $CuBr_2^-$ est envisagée, les étapes les plus probables sont:

[6] $\quad Cu + 2Br^- \rightarrow (CuBr_2^-)_i + e$

qui est suivie de

[7] $\quad (CuBr_2^-)_i \rightarrow (CuBr_2^-)_s$

où les indices i et s représentent la concentration à la surface de l'électrode et au sein de la solution. La première réaction, qui est une étape globale, correspond à l'oxydation du cuivre en $CuBr_2^-$; elle peut être décomposée en deux étapes dont l'une

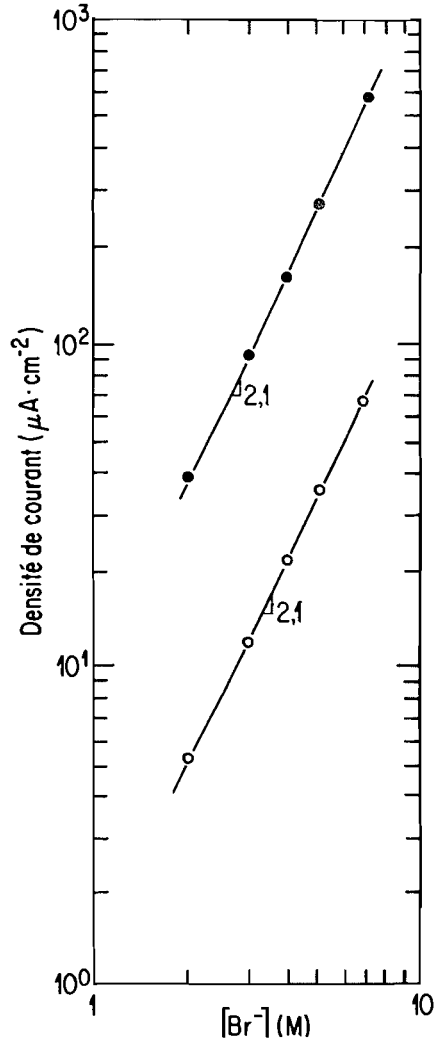

FIG. 5. Influence de la concentration en ions Br^- sur le courant de dissolution anodique. Balayage à 5 mV s^{-1} sur un fil de cuivre en position stationnaire et en solution non agitée; ● pour $E = -150$ mV; ○ pour $E = -200$ mV.

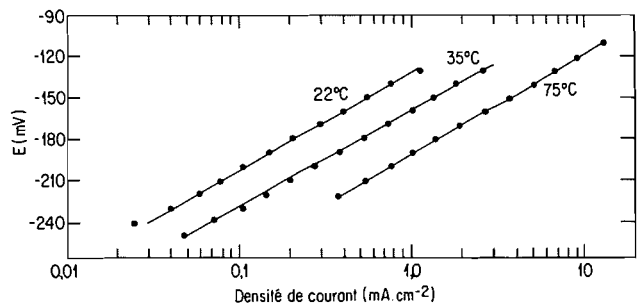

FIG. 6. Influence de la température sur le courant de dissolution. Balayage à 5 mV s^{-1}. NaBr = 0,4 *M*. L'échantillon est un fil de cuivre en position stationnaire et en solution non agitée.

d'entre elles correspond au transfert électronique. La deuxième étape coincide avec la diffusion du $CuBr_2^-$ depuis la surface de l'anode jusqu'au coeur de la solution.

4.2.1 *Cas des vitesses de rotation lente*

Pour sa part, la relation entre le courant qui traverse l'électrode et la vitesse de rotation de l'électrode (relation [5])

Can. J. Chem. Downloaded from www.nrcresearchpress.com by 210.87.254.6 on 09/06/12
For personal use only.

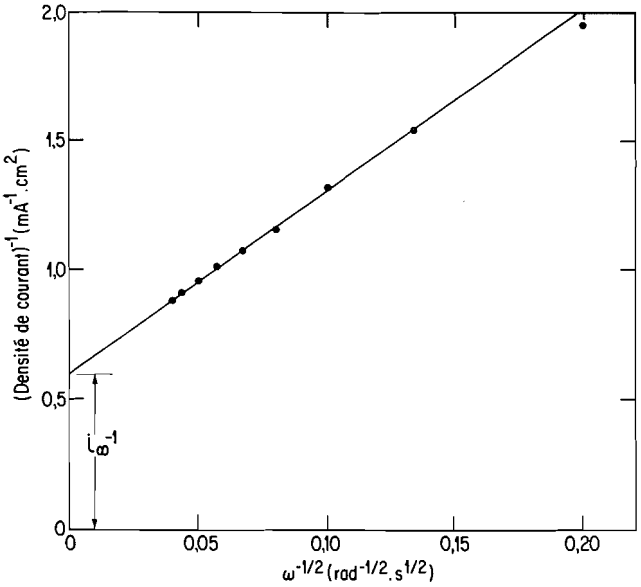

FIG. 7. Inverse du courant de dissolution anodique en fonction de $\omega^{-1/2}$ avec $E = -180$ mV et NaBr 0,5 M. i_∞ est le courant à vitesse de rotation infinie.

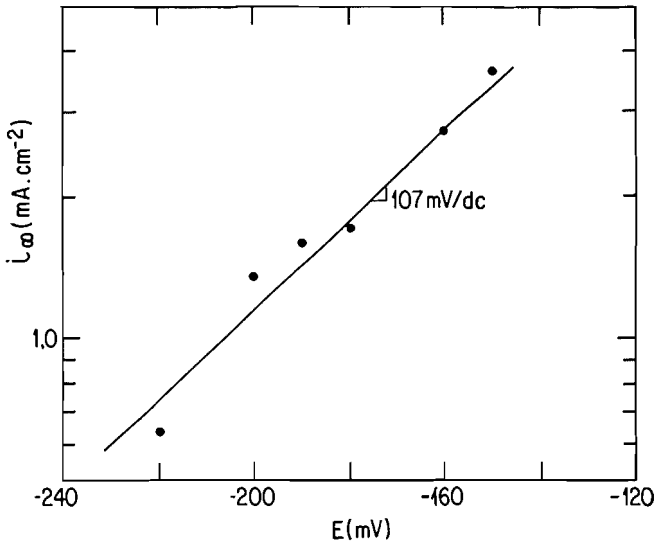

FIG. 9. Courant à vitesse de rotation infinie en fonction de la tension imposée pour NaBr égal à 0,5 M.

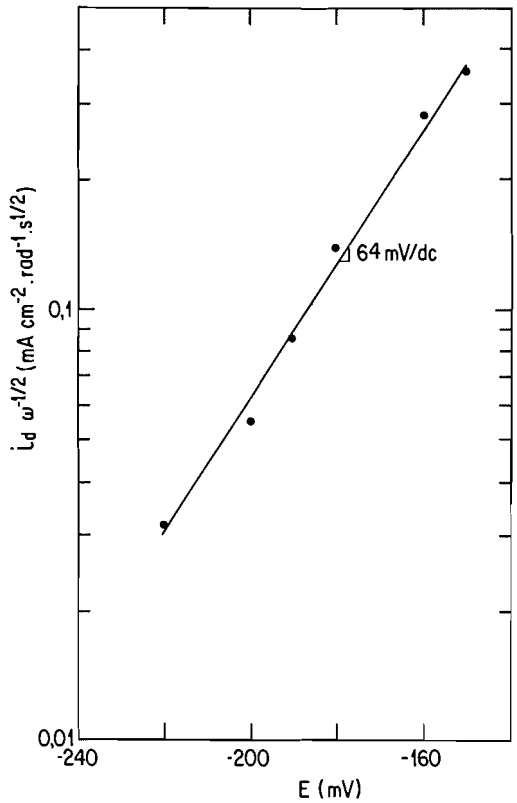

FIG. 8. $i_d \cdot \omega^{-1/2}$ en fonction de la tension imposée pour NaBr égal à 0,5 M.

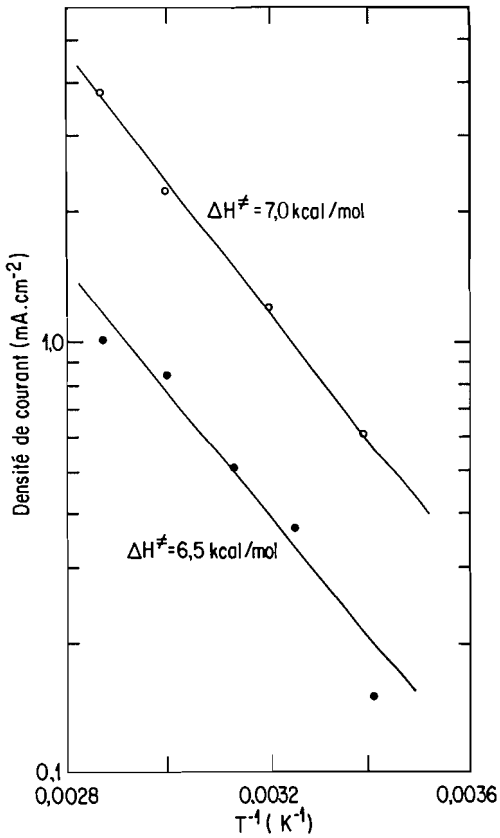

FIG. 10. Densité de courant anodique en fonction de l'inverse de la température; ● valeurs expérimentales du courant déduites des courbes E vs. $\log_{10} i$, représentées à la fig. 6, et qui correspondent à $E = -190$ mV; ○ valeurs relatives du courant calculées à partir de la relation [20].

indique que le terme $B^{-1}\omega^{-1/2}$ tend à devenir le terme dominant en présence d'une agitation peu intense, donc, le courant est contrôlé par la diffusion, c'est-à-dire que $i \sim i_d$ lorsque ω est petit. Dans ces conditions, il est raisonnable de considérer la réaction [6] comme l'étape rapide, et la réaction [7] comme l'étape déterminante. L'étape [6] est alors dans un état voisin de l'équilibre; ce qui autorise à utiliser l'équation de Nernst:

$$[8] \quad E = E^0_{Cu/CuBr_2^-} + \frac{RT}{F} \ln \frac{[CuBr_2^-]_i}{[Br^-]^2}$$

Le réarrangement des termes donne:

$$[9] \quad [CuBr_2^-]_i = [Br^-]^2 \exp \frac{F}{RT}(E - E^0_{Cu/CuBr_2^-})$$

Can. J. Chem. Downloaded from www.nrcresearchpress.com by 210.87.254.6 on 09/06/12
For personal use only.

Rappelons que l'étape lente est une étape de diffusion. Par conséquent, la vitesse de la réaction est donnée par la première loi de Fick:

$$[10] \quad i_d = \frac{ZFD}{\delta}[CuBr_2^-]_i$$

La combinaison des relations [8], [9] et [10] donne:

$$[11] \quad i_d = \frac{ZFD}{\delta}[Br^-]^2 \exp\frac{F}{RT}(E - E^0_{Cu/CuBr_2^-})$$

Pour un fil de cuivre en l'absence d'agitation imposée, l'écriture de la relation [11] se simplifie:

$$[12] \quad i_d = k_l[Br^-]^2 \exp\left(\frac{F}{RT}\right)(E - E^0_{Cu/CuBr_2^-})$$

où k_l est une constante de proportionnalité. L'utilisation de l'électrode à disque tournant permet d'écrire (13) selon Levich:

$$[13] \quad \delta = 1{,}63\, D^{1/3}_{CuBr_2^-}\, \nu^{1/6}\, \omega^{-1/2}$$

La substitution de δ dans la relation [11] donne:

$$[14] \quad i_d = 0{,}62\, ZF\, \nu^{-1/6}\, D^{2/3}_{CuBr_2^-}\, \omega^{1/2}\, [Br^-]^2 \exp\frac{F}{RT} \times (E - E^0_{Cu/CuBr_2^-})$$

où Z, la charge de l'espèce qui diffuse, est égale à 1; ν, la viscosité cinématique, est voisine de $0{,}96 \times 10^{-2}$ cm^2 s^{-1} (15); $D_{CuBr_2^-}$ est le coefficient de diffusion de l'espèce $CuBr_2^-$; ω est la vitesse de rotation de l'électrode en radians par seconde; E est la tension d'électrode alors que $E^0_{Cu/CuBr_2^-}$ est la tension d'équilibre standard pour la réaction [1].

Les dérivées partielles de la relation [12] sont:

$$[15] \quad \left(\frac{\partial E}{\partial \log_{10} i_d}\right)_{295\text{ K},\ Br^-} \simeq 59 \text{ mV/décade}$$

$$[16] \quad \frac{\partial i_d}{\partial [Br^-]_E} = 2$$

alors que les dérivées partielles de la relation [14] sont:

$$[17] \quad \left(\frac{\partial i_d}{\partial \omega^{1/2}}\right)_{E,\ Br^-} = \text{constante}$$

$$[18] \quad \left(\frac{\partial E}{\partial \log_{10}(i_d \cdot \omega^{-1/2})}\right)_{295\text{ K},\ Br^-} \simeq 59 \text{ mV/décade}$$

Les équations [15] et [16] sont semblables aux caractéristiques (a) et (c) trouvées pour la dissolution active du cuivre (Figs. 3, 5). De plus, la relation [17] est conforme à la relation [4], qui est la relation de Levich alors que la relation [18] correspond à la caractéristique observée à la fig. 8. Ainsi, le mécanisme de dissolution formé par les étapes [6] et [7] est en harmonie avec les caractéristiques du comportement de l'anode de cuivre. La formation du $CuBr_2^-$, proposée dans ce mécanisme, tend à confirmer le fait que le cuivre dissous a une tendance marquée à être associé aux ions Br^- pour former des complexes (14).

Pour sa part, le coefficient de diffusion est calculable à partir de l'équation [19] obtenue par transformation de la relation [14]:

$$[19] \quad D^{2/3}_{CuBr_2^-} = \frac{7{,}702 \times 10^{-6} \times (i_d \cdot \omega^{-1/2})}{[Br^-]^2 \exp[(38{,}92)(E - E^0_{Cu/CuBr_2^-})]}$$

Les termes Z, F, ν et F/RT ont été remplacés par leur valeur respective. $E^0_{Cu/CuBr_2^-}$ égal à -54 mV$_{ecs}$ a été calculée à partir des valeurs des enthalpies libres de formation standard pour les ions Br^- (11) alors que $-44{,}750$ cal mol^{-1} a été utilisé dans le cas du $CuBr_2^-$.[1] Il est donc suffisant de connaître $i_d \cdot \omega^{-1/2}$, pour des valeurs de Br^- et de E données (Fig. 5), pour que le coefficient de diffusion soit calculable à partir de la relation [19]. C'est ainsi que les valeurs du coefficient de diffusion, données au Tableau 1 pour 0,5 M Br^-, ont été déterminées; ces valeurs voisines de $1{,}4 \times 10^{-5}$ cm^2 s^{-1} sont indépendantes de la tension imposée. Elles sont tout à fait en accord avec celles de la littérature (réf. 15, p. 80 et réf. 16).

TABLEAU 1. Valeurs expérimentales du coefficient de diffusion pour 0,5 M NaBr

E (mV$_{ecs}$)	D (10^{-5} cm^2/s)[a]
−220	1,55
−200	1,11
−190	1,71
−180	1,40
−160	1,74
−150	1,39

[a]Déterminée à partir de la relation [19] et des valeurs données à la fig. 8.

Par ailleurs, l'appauvrissement de la solution en ions Br^- à la surface de l'électrode, $[Br^-]_i$, est envisageable d'après la réaction [6] lorsque le courant de dissolution est suffisamment élevé. Lorsque $[Br^-]_i$ est voisin de zéro, il est prévisible qu'un courant limite (i_l) soit atteint qui dépend de la diffusion des ions Br^- depuis le coeur de la solution jusqu'à la surface de l'électrode et en conséquence, i_l doit être directement proportionnel à la concentration en ions $[Br^-]$ dans la solution. Comme le montre l'enregistrement reproduit à la figure 1, un courant limite (i_{pl}) est effectivement observé, mais en dehors de la zone de dissolution active, i.e. de la région "a", alors que le courant dans la région "a" ne dépasse pas 0,14 i_{pl} environ. De plus, toujours dans la région "a", l'ordre de la réaction par rapport aux ions Br^- est voisin de 2 (Fig. 5).

Il est donc raisonnable de considérer que la concentration en ions Br^- est la même à la surface de l'électrode et au coeur de la solution dans la zone de dissolution active.

C'est ainsi que le courant de diffusion est entièrement explicable à partir de la diffusion de l'espèce $CuBr_2^-$ dans la solution.

L'énergie d'activation apparente, $\Delta H^{\ddagger}$, a été déterminée à partir de la pente de la droite donnée par le courant de dissolution en fonction de T^{-1} (Fig. 10). L'électrode était en position stationnaire et la solution n'était pas agitée. Le courant a été obtenu à partir des courbes E vs. $\log_{10} i$ (Fig. 6) dans une gamme de températures comprises entre 22°C et 75°C. Les densités de courant correspondent à une tension de -190 mV. La valeur expérimentale de $\Delta H^{\ddagger}$ est de 6,5 kcal/mol.

Pour leur part, les valeurs relatives du courant de dissolution (i_r) ont été calculées en fonction de la température pour une tension de -190 mV. La relation [20], dérivée de la relation [14], a été utilisée:

$$[20] \quad \log_{10} i \propto \frac{2}{3}\log_{10} D + \frac{F}{2{,}303\, RT}(E - E^0_{Cu/CuBr_2^-}) - \frac{1}{6}\log \nu$$

[1]L. Brossard et G. Larochelle. Résultats expérimentaux non publiés.

Rappelons que $i \sim i_d$ pour une électrode en présence d'une agitation peu intense. La variation de D (17) et de ν (18) avec la température a été pris en considération pour le calcul de i_r. D a été choisi égal à $1{,}4 \times 10^{-5}$ cm^2/s à 22°C (Tableau 1). Ainsi, la valeur de $\Delta H^{\ddagger}$, déduite de la droite $\log_{10} i_r$ vs. T^{-1}, est de 7,0 kcal/mol. Cette valeur est en harmonie avec 6,5 kcal/mol déterminée expérimentalement.

4.2.2. *Cas des vitesses de rotation rapide*

Enfin, la relation [5] suggère que le phénomène de surface devient prédominant lorsque ω est grand alors que le phénomène de diffusion est marginal. Selon le modèle de dissolution envisagé, la réaction [6] devient l'étape déterminante alors que la réaction [7] devient l'étape rapide. Dans ce cas, le phénomène de surface doit être caractéristique d'un transfert électronique; ce qui est confirmé expérimentalement (Fig. 8). En s'inspirant des travaux de Moreau (19) relatifs à la dissolution du cuivre dans les solutions concentrées en HCl, la réaction [6] est capable d'être décomposée en deux nouvelles étapes qui sont:

$$[21] \quad Cu + Br^- = (CuBr^-)_{ads}$$

$$[22] \quad (CuBr^-)_{ads} + Br^- \rightarrow (CuBr_2^-) + e$$

C'est l'étape [22], le transfert électronique, qui serait l'étape déterminante en présence d'une agitation intense. Néanmoins, l'utilisation de techniques transitoires combinées à l'utilisation de l'électrode à disque tournant avec anneau (réf. 12, chap. 8) devrait permettre de préciser davantage la nature de la réaction [6]. Des travaux de laboratoire sont actuellement en cours.

Conclusions

1. Les courbes du courant de dissolution en fonction de la racine carrée de la vitesse de rotation de l'électrode ont une allure qui est caractéristique d'un procédé d'électrode qui est mixte. Le procédé d'électrode est dominé par la diffusion des ions dans la solution lorsque ω est petit ou par un phénomène de surface lorsque ω est grand.

2. Le courant associé à chacune de ces étapes lentes est déterminable à partir des relations i^{-1} vs. $\omega^{-1/2}$. La linéarité entre la tension d'électrode et le logarithme de i_∞ suggère que le phénomène de surface est limité par un transfert électronique. Pour sa part, le terme i_d est entièrement imputable, selon le modèle considéré, à la diffusion d'un bromo-complexe de cuivre, le $CuBr_2^-$, depuis la surface de l'électrode jusqu'au coeur de la solution. Le modèle est valide dans le domaine de dissolution pour lequel l'accumulation du produit de corrosion sur la surface de l'électrode est inexistante ou marginale.

3. L'énergie d'activation apparente, $\Delta H^{\ddagger}$, est de 6,5 kcal/mol. Cette valeur est en accord avec la valeur de 7 kcal/mol déduite de l'expression générale du courant en fonction des différents paramètres expérimentaux.

4. Une vague d'oxydation est observée lorsque la tension d'électrode devient suffisamment anodique par rapport à la tension réversible $E_{Cu/CuBr}$. Cette vague est associée à la passivation de la surface du cuivre par le CuBr γ.

Remerciements

L'auteur tient à remercier Monsieur G. Larochelle qui a effectué une partie du travail expérimental ainsi que Messieurs A. Joly et R. Dubuc pour l'examen des surfaces.

1. L. F. KOZIN, E. E. KOBRAND et K. K. LEPESOV. Izv. Akad. Nauk Kaz. SSR, Ser. Khim. **24**, 31 (1974).
2. J. FRANCO et N. K. PATEL. J. Electrochem. Soc. India, **22**, 172 (1973).
3. J. FRANCO et N. K. PATEL. J. Inst. Chemists (India), **50**, 243 (1978).
4. S. NAGESWAR et T. H. SETTY. Proc. Indian Acad. Sci. Sect. A, **71**, 282 (1972).
5. E. D. MOR et A. M. BECCARIA. Br. Corros. J. **12**, 243 (1977).
6. S. M. MAYANNA et T. H. V. SETTY. Indian J. Chem. **12**, 1083 (1974).
7. R. L. BROSSARD. Can. J. Chem. **60**, 616 (1982).
8. D. W. SHOESMITH, T. E. RUMMERY, D. OWEN et W. LEE. J. Electrochem. Soc. **123**, 790 (1976).
9. D. W. SHOESMITH et W. LEE. Electrochim. Acta, **22**, 1411 (1977).
10. W. LATIMER. Oxidation potentials. 2e éd. Prentice–Hall, New York. 1952.
11. C. E. WICKS et F. E. BLOCK. Bulletin 605, U.S. Bureau of Mines, Washington. 1963. p. 43.
12. A. J. BARD et L. R. FAULKNER. Electrochemical methods. J. Wiley & Sons, New York 1980. Chap. 6.
13. V. G. LEVICH. Physiochemical hydrodynamics. Prentice–Hall, Englewood Cliffs, NJ. 1962.
14. P. PASCAL. Nouveau traité de chimie minérale. Tome III. Masson et Cie, Paris. 1957. p. 274.
15. R. PARSONS. Handbook of electrochemical constants. Butterworths Scientific Publ. London. 1959. p. 77.
16. I. A. SEMENOV, V. F. LAZAREV et A. I. LEVIN. Sov. Electrochem. **11**, 1013 (1975).
17. J. G. PERRY. Chemical engineers handbook. 4e éd. McGraw–Hill, New York. 1963.
18. R. B. BIRD, W. E. STEWART et E. L. LIGHTFOOT. Transport phenomena. John Wiley & Sons, New York. 1960. p. 8.
19. A. MOREAU. Electrochim. Acta, **26**, 497 (1981).

Can. J. Chem. Downloaded from www.nrcresearchpress.com by 210.87.254.6 on 09/06/12
For personal use only.

Cyclotétra(λ^3-phosphazanes) dérivant de diamines-1,2. Précurseurs de composés du phosphore dicoordonné

CHRISTIAN MALAVAUD, THÉOPHILE N'GANDO M'PONDO, LUCIEN LOPEZ et JEAN BARRANS
E.R.A. C.N.R.S. 926. Synthèse, Réactivité et Structure de molécules phosphorées, Université Paul Sabatier, 31062 Toulouse Cédex, France

ET

JEAN-PIERRE LEGROS
Laboratoire de Chimie de coordination du C.N.R.S., 205 route de Narbonne, 31400 Toulouse, France

Reçu le 27 janvier 1983[1]

CHRISTIAN MALAVAUD, THÉOPHILE N'GANDO M'PONDO, LUCIEN LOPEZ, JEAN BARRANS et JEAN-PIERRE LEGROS. Can. J. Chem. **62**, 43 (1984).

Les cyclotétraphosphazanes **2** et **5**, obtenus à partir de diamines-1,2 sont des oligomères de diazaphospholes-1,3,2 susceptibles de se dépolymériser par voie thermique, ou par complexation avec le trifluorure de bore. La présence du cycle orthophénylène stabilise la forme dicoordonnée et permet d'expliquer la réactivité des benzo-4,5 diazaphosphole-1,3,2 **3** vis-à-vis des composés à hydrogène mobile; ces réactions se font par une addition de type 1.2 tandis qu'avec les diazaphospholes complexés **4** et **8**, le butanol conduit à une addition du type 1.1.

CHRISTIAN MALAVAUD, THÉOPHILE N'GANDO M'PONDO, LUCIEN LOPEZ, JEAN BARRANS, and JEAN-PIERRE LEGROS. Can. J. Chem. **62**, 43 (1984).

Cyclotetraphosphazanes **2** and **5** obtained from 1,2-diamines are 1,3,2-diazaphosphole oligomers leading to the monomeric form by either thermal equilibrium or by complexing with boron trifluoride. The dicoordinated form stabilized by an orthophenylene ring could explain the reactivity of 4,5-benzo 1,3,2-diazaphosphole **3** with compounds having a mobile hydrogen; these reactions were a 1.2 type addition while butanol led to a 1.1 type addition with complexed 1,3,2-diazaphospholes **4** and **8**.

La chimie des composés du phosphore dicoordonné s'est beaucoup développée ces dernières années. Cependant, si de nombreux composés à liaison —P=C< ont été signalés (1), peu de composés à liaison —P=N— ont été isolés (2–5). Cette difficulté provient sans doute de la facilité de polymérisation des phosphazènes —P=N— en cyclophosphazanes: $(—\underset{|}{P}—\underset{|}{N}—)_n$ (n = 2, 3, 4) (6).

Néanmoins un équilibre thermique, monomère $P^{II} \rightleftarrows$ oligomère P^{III} a été observé pour la première fois dans le cas des diazadiphosphétidines par Scherer et Glässel (2*c*) et dans notre laboratoire dans le cas de tétramères (7); nous avons également montré que cette dépolymérisation était possible en complexant les benzocyclophosphazanes par des acides de Lewis (BF_3, $AlCl_3$, $ZnCl_2$. . .), réaction [1]:

[1] 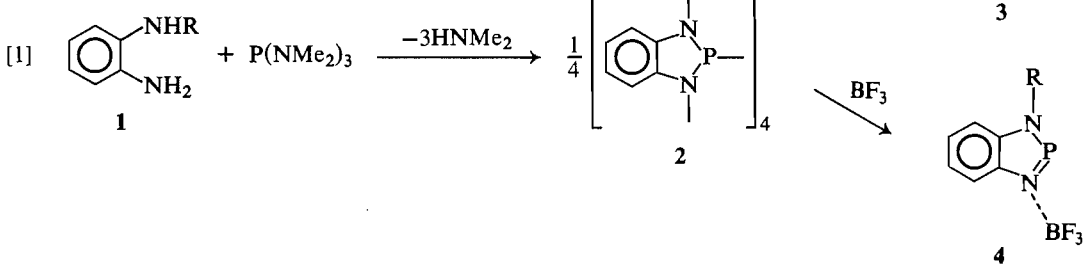

1 2 3 4

Dans le présent travail nous avons préparé des cyclophosphazanes **5** dérivant de *N*-alkyléthylènediamines et comparé leur stabilité à celle des cyclotétraphosphazanes **2** dérivant des *N*-alkylorthophénylènediamines, afin de dégager l'influence du reste phénylène-1,2 et celui des substituants de l'atome d'azote sur l'équilibre monomère $P^{II} \rightleftarrows$ oligomère P^{III}.

Pour mettre en évidence la présence du monomère, nous avons étudié l'addition de composés à hydrogène mobile, à la température ordinaire, sur ces dérivés (8) et sur leurs complexes **4** et **8** avec le trifluorure de bore.

Résultats et discussion

I. Réaction générale de synthèse

La tris(diméthylamino)phosphine, par réaction avec les

[1]Révision reçue le 7 juillet 1983.

Can. J. Chem. Downloaded from www.nrcresearchpress.com by 210.87.254.5 on 09/06/12
For personal use only.

Can. J. Chem. Downloaded from www.nrcresearchpress.com by 210.87.254.5 on 09/06/12
For personal use only.

TABLEAU 1. Cyclophosphazanes dérivant de l'orthophénylènediamine $C_6H_5(NH_2)NHR^2$

No	R^2	$\delta^{31}P$ (ppm)	F(°C)		Analyses pondérales C	H	N	P
2*a*	H	80	145	calc.	52,94	3,68	20,59	22,79
				tr.	53,05	4,44	19,07	19,71
2*b*	Et	84	251		58,53	5,49	17,07	18,90
					58,40	5,48	17,03	18,95
2*c*	nPr	86	194		60,67	6,18	15,73	17,42
					59,73	6,18	15,10	16,76
2*d*	iPr	84	255		60,67	6,18	15,73	17,42
					60,72	6,05	15,48	17,41
2*e*	sBu	81	218		62,5	6,77	14,58	16,15
					62,28	6,83	14,58	16,07
2*f*	iPent	80	262		64,08	7,28	13,59	15,05
					63,91	7,34	13,72	15,02
2*g*	$PhCH_2$	86	204		69,03	4,87	12,39	13,71
					67,98	5,06	12,65	13,07
2*h*	Ph(ref. 7)	Insol.	>350					

TABLEAU 2. Cyclophosphazanes dérivant de l'éthylènediamine $R^2HN—CHR^1CH_2—NH_2$

No	R^1	R^2	$\delta^{31}P$ (ppm)	F(°C)		Analyses pondérales C	H	N	P
5*a*	Me	H	99,25	128	calc.	35,29	6,86	27,45	30,39
					tr.	36,76	6,84	24,02	26,58
5*b*	H	Me	99,40	187		35,29	6,86	27,45	30,39
						35,12	7,32	26,85	29,32
5*c*	H	Et	98,50	118		41,38	7,75	24,13	26,72
						41,24	7,83	23,53	25,71
5*d*	H	nPr	99,7	75		46,1	8,46	21,5	23,85
						45,77	8,48	21,11	23,36
5*e*	H	iPr	95	148		46,1	8,46	21,5	23,85
						45,95	8,50	21,17	23,65
5*f*	H	Ph	91,7	108		58,53	5,48	17,07	18,90
						58,26	6,56	17,58	17,14

diamines-1,2, conduit à des oligomères tant pour les dérivés de l'orthophénylènediamine (tableau 1, composés **2***a*–*h*) que pour les dérivés de l'éthylènediamine (tableau 2, composés **5***a*–*f*).

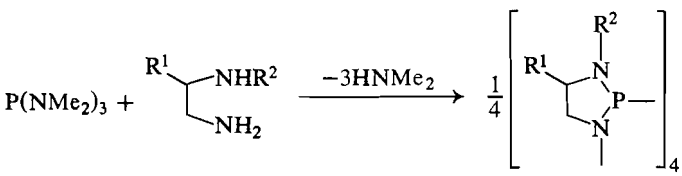

5

Par spectrométrie de masse par désorption de champ nous avons montré (7) que $n = 4$ pour tous les dérivés **2** de l'orthophénylènediamine; il en est de même pour les dérivés **5** de l'éthylènediamine.

Une étude structurale par diffraction des rayons X du composé **5***d* confirme ces résultats: la structure cristalline est en effet constituée d'entités tétramères indépendantes. La molécule (Fig. 1) possède un centre de symétrie cristallographique; il en résulte que, contrairement à l'octaméthylcyclotétraphosphazane (6*b*), le cycle central à huit chainons ne présente pas la forme couronne; sa conformation (Fig. 2) s'apparente à la

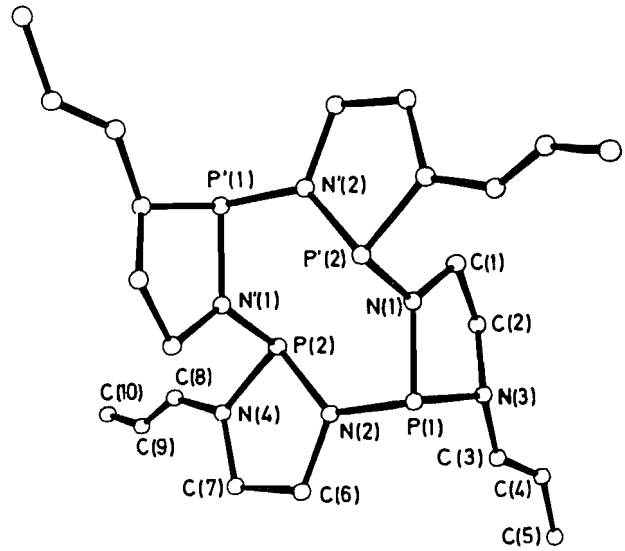

FIG. 1. Représentation perspective de la molécule tétramère **5***d*. L'opération d'inversion par rapport au centre de symétrie est indiquée par ' (apostrophe). Les atomes d'hydrogène sont omis. Distances et angles dans le cycle à huit chaînons: P(1)—N(1) = 1,711(4), P(1)—N(2) = 1,703(5), P(2)—N(2) = 1,714(5), P(2)—N'(1) = 1,694(5) Å; N(1)—P(1)—N(2) = 100,7(2), N'(1)—P(2)—N(2) = 103,6(2), P(1)—N(1)—P'(2) = 119,9(3), P(1)—N(2)—P(2) = 127,8(3)°.

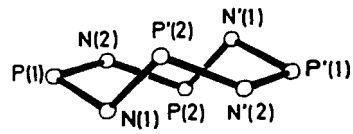

FIG. 2. Conformation du cycle à huit chaînons du tétramère **5***d*.

forme canonique "twisted chair" du cyclooctane (9).

Dans le tableau 3 sont consignés les distances et angles interatomiques. Les liaisons P—N du cycle central sont très voisines avec une longueur moyenne de 1,705(5) Å. Dans les cycles à cinq chaînons les liaisons P(1)—N(3) et P(2)—N(4) sont significativement plus longues que dans des molécules monomères analogues telles que les triazaphospholes (10). Les angles sur le phosphore N(1)—P(1)—N(3) et N(2)—P(2)—N(4) sont aussi plus fermés. La somme des angles ayant pour sommet un même atome de phosphore est en moyenne égale à 299(1)°. L'environnement des atomes d'azote N(1) et N(2) est rigoureusement plan, tandis que pour les atomes N(3) et N(4) il ne s'écarte que peu de la planéité (somme des angles = 353(2)° en moyenne). Cette dernière remarque doit d'ailleurs être tempérée à cause de l'existence d'un phénomène de désordre qui affecte les atomes de carbone; ce désordre, non résolu, est aussi responsable des valeurs anormales des distances C—C et des angles (N, C)—C—C (cf. partie expérimentale).

Les caractéristiques géométriques du tétramère **5***d* sont finalement très proches de celles observées pour un tétramère de triazaphosphole-1,2,4,3 complexé par $Cr(CO)_5$ (11).

Les spectres de masse par impact électronique du composé **5***d* montrent, outre les pics correspondants aux masses $\frac{M^+}{4}$ (130), $\frac{M^+}{2}$ (260), $\frac{3M^+}{4}$ (390) et M^+ (520), les ions $\left(\frac{M^+}{4} - 85\right)$, $\left(\frac{M^+}{2} - 85\right)$ et $(M^+ - 85)$, résultant du départ d'un groupe-

Can. J. Chem. Downloaded from www.nrcresearchpress.com by 210.87.254.5 on 09/06/12
For personal use only.

TABLEAU 3. Distances (Å) et angles (°) interatomiques pour le composé **5***d*. Les écarts standards sont indiqués entre parenthèses. L'apostrophe désigne la position équivalente $1 - x$, $1 - y$, $-z$

Atomes	Distance (Å)	Atomes	Angle (°)
P(1)—N(1)	1,711(4)	N(1)—P(1)—N(2)	100,7(2)
P(1)—N(2)	1,703(5)	N(2)—P(1)—N(3)	107,8(3)
P(1)—N(3)	1,671(6)	N(1)—P(1)—N(3)	90,9(3)
P(2)—N'(1)	1,694(5)	N'(1)—P(2)—N(2)	103,6(2)
P(2)—N(2)	1,714(5)	N'(1)—P(2)—N(4)	104,2(3)
P(2)—N(4)	1,699(5)	N(2)—P(2)—N(4)	90,6(2)
N(1)—C(1)	1,464(7)	P(1)—N(1)—C(1)	114,1(4)
N(2)—C(6)	1,462(7)	P(1)—N(1)—P'(2)	119,9(3)
N(3)—C(2)	1,441(9)	P'(2)—N(1)—C(1)	125,9(4)
N(3)—C(3)	1,44(1)	P(1)—N(2)—P(2)	127,8(3)
N(4)—C(7)	1,422(8)	P(1)—N(2)—C(6)	118,5(4)
N(4)—C(8)	1,364(9)	P(2)—N(2)—C(6)	113,7(4)
C(1)—C(2)	1,511(9)	P(1)—N(3)—C(2)	111,3(5)
C(3)—C(4)	1,12(1)	P(1)—N(3)—C(3)	119,1(7)
C(4)—C(5)	1,43(1)	C(2)—N(3)—C(3)	116,0(7)
C(6)—C(7)	1,42(1)	P(2)—N(4)—C(7)	114,6(5)
C(8)—C(9)	1,19(1)	P(2)—N(4)—C(8)	122,5(5)
C(9)—C(10)	1,25(1)	C(7)—N(4)—C(8)	123,0(6)
		N(1)—C(1)—C(2)	105,4(5)
		N(3)—C(2)—C(1)	107,3(6)
		N(3)—C(3)—C(4)	136(2)
		C(3)—C(4)—C(5)	135(2)
		N(2)—C(6)—C(7)	109,3(6)
		N(4)—C(7)—C(6)	111,5(6)
		N(4)—C(7)—C(9)	141(1)
		C(8)—C(9)—C(10)	142(2)

ment CH_2—CH_2—N—Pr; on observe aussi un pic correspondant au fragment $\left[\begin{matrix}\diagup\text{NHPr}\\ \diagdown\text{NH}_2^+\end{matrix}\right.$. Dans le cas des benzocylophosphazanes **2**, on observe seulement la présence du monomère $\left(\frac{M^+}{4}\right)$ ainsi que les fragments de cet ion dont les pics principaux correspondent à:

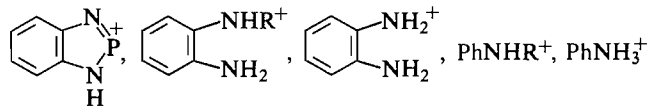

II. Réactivité des phosphazanes 2 et 5

1. *Réaction des composés à hydrogène mobile*

Parmi les réactifs à hydrogène mobile testés (alcool, phénol, amine), seuls les composés hydroxylés réagissent de façon notable à la température ordinaire.

Le phénol rompt les liaisons P—N des cycles phosphazanes **2** et **5**, pour donner des phénoxy-2 diazaphospholanes-1,3,2 qui, par élimination d'une molécule de phénol sous vide, redonnent les cyclophosphazanes selon la réaction [2]:

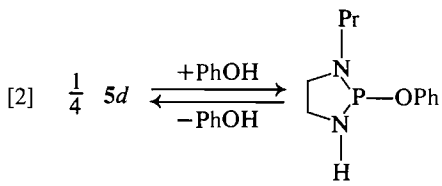

6*a* $\delta^{31}P = 124$

Le n-butanol par une réaction comparable, mais plus lente, donne avec les composés **2**, des butoxy-2 diazaphospholane-1,3,2 (réaction [3]):

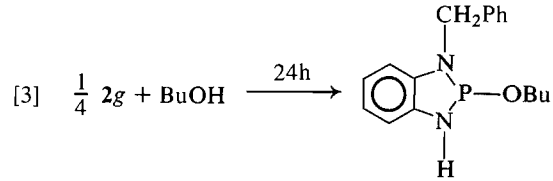

7*a*

On n'observe aucune réaction du butanol avec les composés **5**.

2. *Stabilité thermique*

Par rmn de ^{31}P à température variable (60 à 150°C), nous avons pu mettre en évidence un équilibre [1] entre une forme dicoordonnée **3** et les cyclotétraphosphazanes **2** (7) (à l'exception du composé **2***a*, R = H, qui se décompose lorsqu'on le chauffe).

L'emploi de solvant polaire permet de déplacer cet équilibre. C'est ainsi que le pourcentage de **3***e* qui est de 30% dans le xylène à 130°C passe à 57% dans le nitrobenzène à cette même température. La pyridine qui est un bon solvant des cyclophosphazanes permet aussi d'obtenir l'équilibre précedent à sa température d'ébullition.

Variation de l'équilibre **2***e* ⇆ **3***e* dans le nitrobenzène

T(°C)	60	90	110	130	150
% **3***e*	0	0	2	57	100
% **2***e*	100	100	98	43	0

Il faut toutefois noter que lorsqu'on revient à la température ordinaire, le retour vers la forme cyclophosphazane **2** n'est pas instantané. On peut observer pendant plusieurs dizaines de minutes en rmn de ^{31}P, le signal correspondant à la forme dicoordonnée **3**.

Des équilibres thermiques monomère ⇌ dimère ont déjà été observés pour des composés du phosphore dicoordonné acycliques. La dimérisation se produit par une cyclo addition (2 + 2) (2*c*, 12) ou (2 + 1) (5):

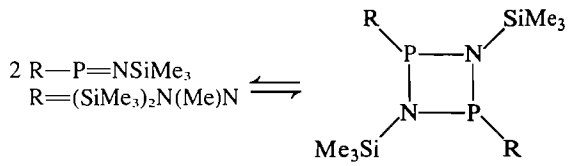

(réf. 2*c*)

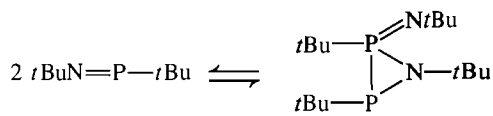

(réf. 5)

La dimérisation (2 + 2) thermodynamiquement favorisée n'a pas lieu pour nos dérivés, probablement pour des raisons de contraintes de cycle. En effet à notre connaissance il n'a pas été signalé de diazadiphosphétidines du phosphore tricoordonné dont les atomes de phosphore et d'azote font partie d'un cycle à cinq chainons tel que A, alors que des diazadiphosphétidines B du phosphore pentacoordonné ont été isolées (13, 14).

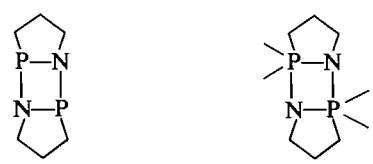

(A) (B)

Can. J. Chem. Downloaded from www.nrcresearchpress.com by 210.87.254.5 on 09/06/12
For personal use only.

TABLEAU 4. Déplacement chimique et point de fusion des diazaphospholes

		3	4		8		
No	R	$\delta^{31}P$	$\delta^{31}P$	F(°C)	R	$\delta^{31}P$	F(°C)
a	H	238	222				
b	Et	232					
c	nPr	236	226	145			
d	iPr	228	225,6	132	nPr	285	78
e	sBu	225,8	226,7	104	iPr	284	
f	iPent	232	226		Ph	280	
g	$PhCH_2$	228	224,8	122			
h	Ph		205,9				

Les déplacements chimiques $\delta^{31}P$ des benzodiazaphospholes-1,3,2 **3** (tableau 4) sont comparables à ceux observés pour d'autres diazaphospholes (15*a*) (**4***c*).

Avec les cyclo(λ^3-phosphazanes) **5**, nous n'avons jamais pu observer, par rmn de ^{31}P, un équilibre thermique comparable à [1], quel que soit le solvant utilisé.

La possibilité de conjugaison de la liaison P=N— avec le reste phénylène semble donc être un facteur de stabilisation de la forme dicoordonnée, rendant possible son observation par rmn de ^{31}P. Notons que la présence d'une double liaison dans le cycle augmente la possibilité de conjugaison, et c'est ainsi que des triazaphospholes-1,2,4,3 et des diazaphospholes-1,3,2 stables ont pu être isolés (3, 4*c*).

3. Complexation dépolymérisante

L'addition de trifluorure de bore sur les composés **2** donne instantanément les dérivés du phosphore dicoordonné **4***a*–*h* (tableau 4). Avec les phosphazanes **5**, la réaction plus lente (24 h) conduit également à des composés du phosphore dicoordonné **8***a*–*f* (tableau 4).

Le trifluorure de bore (acide dur) présentera une plus grande affinité pour les atomes d'azote (base dure) que pour l'atome de phosphore (base molle) (16, 17).

L'examen des spectres de rmn de ^{31}P montre que la complexation ne se fait pas sur l'atome de phosphore; en effet, si l'on compare le déplacement chimique de ^{31}P du diazaphosphole monomère obtenu par dépolymérisation thermique avec celui du diazaphosphole obtenu par complexation avec BF_3 (tableau 4) on remarque qu'ils sont très voisins; si la complexation avait lieu sur l'atome de phosphore on aurait d'une part des valeurs de $\delta^{31}P$ très différentes (blindage de l'ordre de 50 à 100), d'autre part un couplage bore–phosphore facilement observable (150 à 200 Hz) (18).

Pour déterminer sur quel atome d'azote se fait la complexation nous avons examiné plus particulièrement le complexe du trifluorure de bore et du benzyl-1 benzo-4,5 diazaphosphole-1,3,2 par rmn de ^{31}P, ^1H, ^{13}C et relevé les caractéristiques suivantes pour le groupement CH_2:

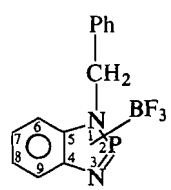

4*g*

rmn de ^{13}C δ = 50,54 $^2J_{P^{13}C}$ = 13,7 Hz
rmn de ^{31}P $^3J_{PH}$ = 8 Hz
rmn de ^1H δ = 4,4

Le groupement méthylénique du phosphazane initial **2***g* a pratiquement le même déplacement chimique δ^1H = 4,32. On peut remarquer aussi que ce signal est large ($\Delta\nu_{1/2}$ = 12 Hz) alors que dans le spectre de rmp du complexe la structure fine apparait bien puisque l'on peut mesurer la constante de couplage $^3J_{HP}$, ce ne serait pas le cas si BF_3 était fixé sur l'azote 1: on aurait d'une part un déblindage du signal CH_2 et apparition d'un couplage $^3J_{HF}$ (10 à 20 Hz) ou au moins élargissement du signal.

On peut donc raisonnablement penser que la complexation s'effectue sur l'azote 3; on note également le déblindage élevé ($\Delta\delta^1H$ = 1,5 ppm) du signal d'un noyau hydrogène du cycle benzénique (probablement le proton 9) dû à la proximité de BF_3 fixé sur l'azote en position 3.

La complexation d'un triazaphosphole par le trifluorure de bore amène un blindage du signal du déplacement chimique de ^{31}P de quelques ppm (3*b*) comme nous l'observons entre les composés **3** et **4**. La grande stabilité des composés **8**, le déplacement chimique de ^{31}P et l'absence d'observation de la forme dicoordonnée libre correspondante ne nous permettent pas d'exclure la contribution d'une forme chargée (B) isoélectronique des cations diazaphosphenium (15*b*–*e*) dont on a montré la grande stabilité (15*f*).

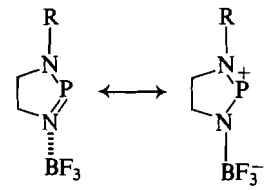

(A) (B)

III. Réactivité des complexes du phosphore dicoordonné ***4*** *et* ***8***

1. Action de la triéthylamine NEt_3

L'addition de triéthylamine sur **4** et **8** permet de revenir aux cyclotétraphosphazanes **2** et **5**. On doit remarquer que cette oligomérisation n'est pas instantantée, dans le cas des benzo-4,5 diazaphospholes-1,3,2 on voit persister pendant quelques dizaines de minutes le signal de rmn de ^{31}P du monomère libre (identique à celui observé dans la dépolymérisation thermique, tableau 4).

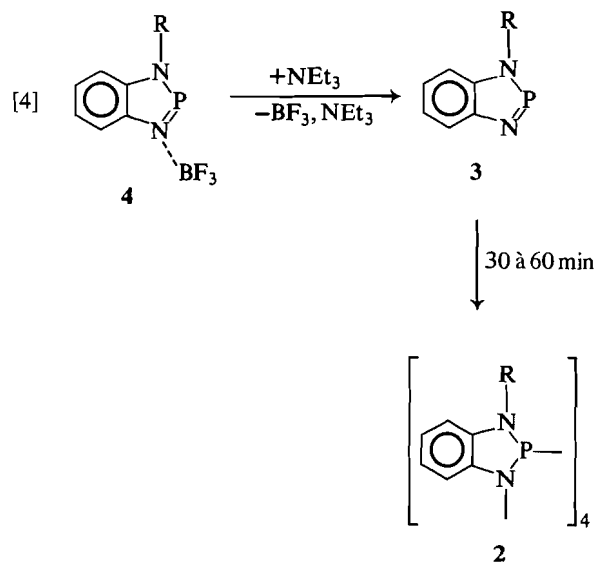

Dans le cas des diazaphospholes **8**, l'oligomérisation est instantanée et nous n'avons pas détecté de composé du phosphore dicoordonné intermédiaire analogue à **3**.

Can. J. Chem. Downloaded from www.nrcresearchpress.com by 210.87.254.5 on 09/06/12
For personal use only.

2. *Action de la diéthylamine $NHEt_2$*

L'addition d'une amine secondaire (proportion 2:1) souligne la différence de réactivité des composés **4** et **8**. Alors que les composés **4** conduisent aux diéthylamino-2 diazaphospholane-1,3,2 par l'intermédiaire du composé du phosphore dicoordonné libre **3** (réaction [5]), les composés **8** ne donnent que les cyclotétraphosphazanes **5** (réaction [6]).

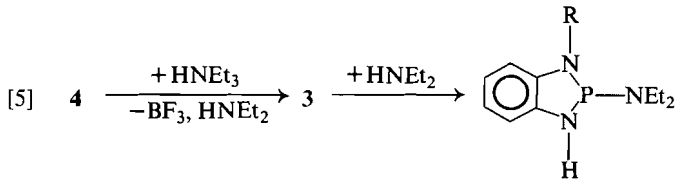

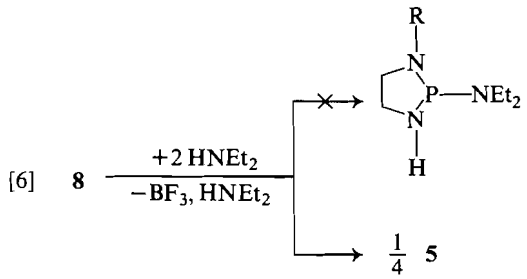

La réaction [6] s'explique si l'on admet que la vitesse d'oligomérisation du composé du phosphore dicoordonné libre est plus grande que la vitesse d'addition de la diéthylamine sur ce dérivé.

3. *Réaction des alcools en présence de base*

En présence d'une base tertiaire les composés **4** réagissent avec les alcools pour donner des alkoxy-2 diazaphospholane-1,3,2 résultant d'une addition 1.2 sur le composé du phosphore dicoordonné libre **3**.

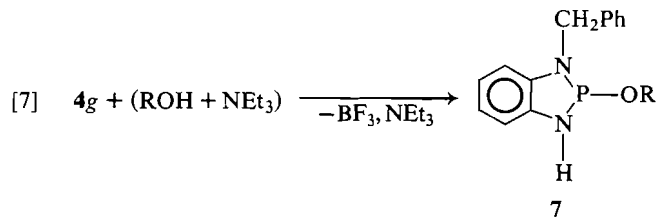

7

	R	$\delta^{31}P$ (ppm)	J_{PH} (Hz)
7*a*	nBu	101	30
7*b*	Me	101	25
7*c*	Et	101	30
7*d*	$PhCH_2$	104	

Les produits obtenus ont été identifiés par rmn de ^{31}P, par comparaison avec ceux que l'on obtient par action directe de Cl_2POR sur la diamine correspondante **1**.

Les diols en présence de base réagissent comme les alcools avec les composés **4**, mais conduisent, cette fois, à des spirophosphoranes à liaison PH **9** (réaction [8]).

Ces produits ont été identifiés par comparaison de leurs spectres avec ceux de produits authentiques obtenus par action de diméthylamino-2 dioxaphospholane-1,3,2 sur les diamines correspondantes **1** (19).

En présence de base tertiaire, les composés **8** réagissent avec les alcools pour donner deux composés: le cyclotétraphosphazane **5** et l'alcoxy-2 diazaphospholane-1,3,2 (réaction [9]).

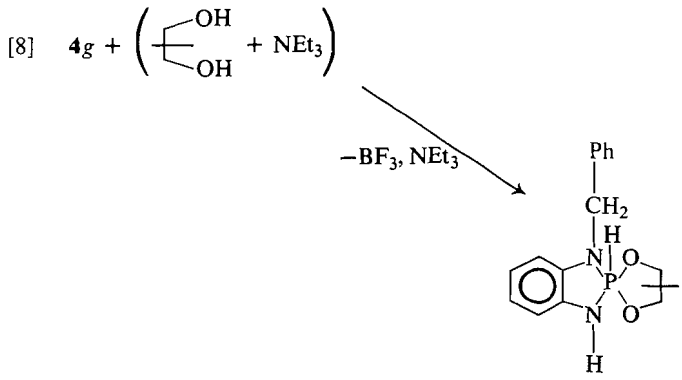

9

		$\delta^{31}P$ (ppm)	$^2J_{PH}$ (Hz)
9*a*	$(CH_2)_2$	−45,5	744
9*b*	$(CMe_2)_2$	−53	748
9*c*		−41	800

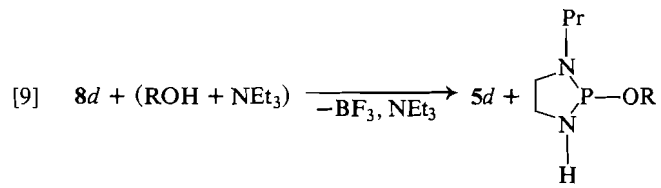

6

	R	$\delta^{31}P$
6*b*	Me	117,4
6*c*	nBu	118
6*d*	*t*Bu	117,8

4. *Réaction des alcools suivie de la neutralisation des complexes*

En l'absence de base tertiaire les alcools réagissent différemment sur les complexes **4** et **8**. C'est ainsi que l'addition de butanol sur le composé **4***g* conduit par une réaction lente (4 jours) à la formation d'un dérivé du phosphore tétracoordonné **10** (δ ^{31}P = 9 ppm; J_{PH} = 725 Hz). L'addition ultérieure de triéthylamine modifie peu le spectre de rmn de ^{31}P (**11**: δ

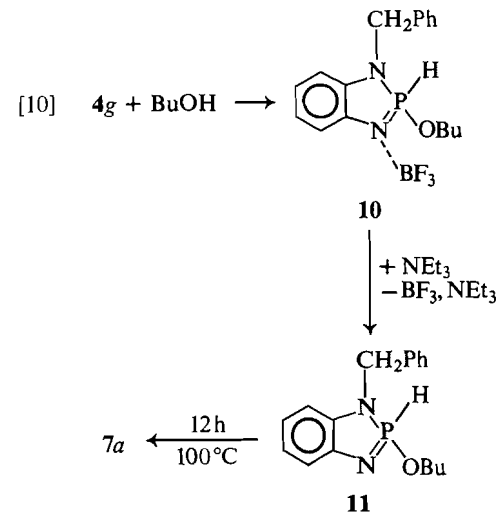

^{31}P = 9,5 ppm, J_{PH} = 687 Hz). Quand on chauffe 12 h à 100°C, on obtient un composé du phosphore tricoordonné **7***a* (δ ^{31}P = 101, J_{PNH} = 30 Hz) identique à celui de la réaction [3].

On observe également un composé du phosphore tétracoordonné **12** (δ ^{31}P = 39, J_{PH} = 698 Hz) par addition de n-butanol sur **8***d*; mais dans ce cas la réaction est immédiate, l'addition de triéthylamine fait disparaitre instantanément le dérivé tétracoordonné au profit de l'alcoxyphospholane **6***c* (118 ppm) et du tétracyclophosphazane **5***d*.

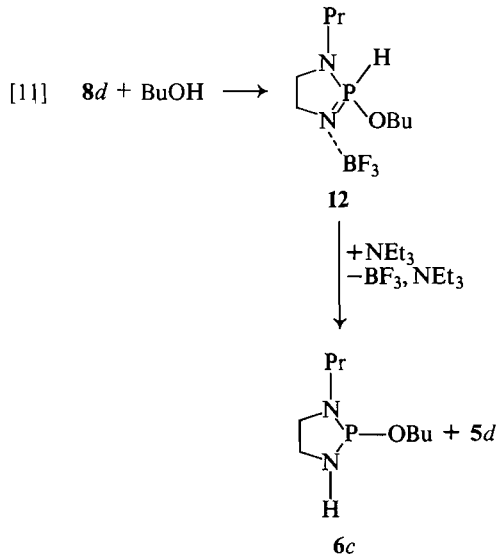

Le comportement de **4***g* et **8***d* vis-à-vis des alcools peut s'expliquer par une addition 1.1 des alcools, suivie d'un réarrangement (réactions [10] et [11]). Ici encore la stabilité du composé **11** serait dûe aux possibilités de conjugaison de la double liaison P=N avec le cycle benzo. Dans la réaction [11], on obtient les mêmes produits finals que dans la réaction [9], ce qui pourrait s'expliquer en admettant la libération de diazaphosphole libre et de butanol, puis leur réaction, lors de l'addition de triéthylamine sur **12**.

Des réactions d'addition 1.1 sur des composés du phosphore dicoordonné ont déjà été mentionnées dans la littérature (2*a*, 20). Très récemment nous avons observé au laboratoire un autre exemple d'addition 1.1 suivie d'un réarrangement 1.2 (réaction [12] (8)).

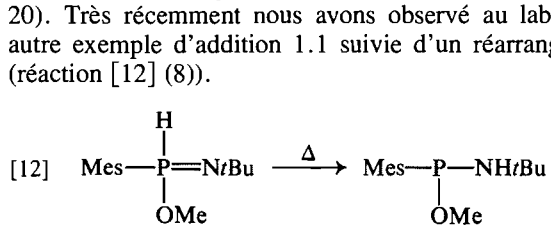

Conclusion

Ce travail montre que les cyclophosphazanes **2** et **5** dérivant des diamines-1,2 sont des tétramères, composés du phosphore tricoordonné qui, par chauffage ou par complexation dépolymérisante avec le trifluorure de bore, donnent des composés du phosphore dicoordonné possédant une liaison —P=N. On peut en outre faire les remarques suivantes.

1. La présence d'un cycle orthophénylène est un facteur de stabilisation des diazaphospholes **3**, et permet leur observation en rmn de ^{31}P; soit à partir de l'équilibre thermique [1] monomère $P^{II} \rightleftarrows$ tétramère P^{III} (excepté R = H), soit lors de la neutralisation des diazaphospholes complexés **4** (réaction [4]).

2. L'addition de réactifs à hydrogène mobile HX sur les diazaphospholes **3** se fait suivant une réaction de type 1.2 (réactions [2] [5] [7] [8]).

3. La complexation de l'atome d'azote de la double liaison P=N (diazaphospholes **4** et **8**) nous a permis, dans le cas des alcools, d'obtenir des additions 1.1, suivies d'un réarrangement (réactions [10] et [11]).

Partie expérimentale

Les analyses (C, H, N, P, B, F) ont été effectuées par le service central de microanalyse du C.N.R.S.

Les spectres de rmn de ^{1}H, ^{31}P et ^{13}C ont été respectivement enregistrés sur les spectromètres suivants: ^{1}H, Varian HA 100 (100 MHz) référence interne TMS; ^{31}P, Perkin–Elmer R32 (36,43 MHz) référence externe H_3PO_4, solution aqueuse à 85%; ^{13}C, Cameca (62,86 MHz) référence interne TMS.

Les spectres de masse par desorption de champ ont été réalisés avec un appareil Varian mat 311 A.

Les modes opératoires suivants sont typiques de la préparation de ces composés.

Cyclotétraphosphazanes **2**a–h *et* **5**a–f

Un mélange de tris(diméthylamino)phosphine 6,24 g (0,04 mol) et de 5,5 g (0,04 mol) de N-iPr(*o*)phénylènediamine dans 20 cm^3 de xylène est chauffé au reflux; la diméthylamine formée, entrainée par un courant d'azote sec, est titrée par une solution normale d'acide sulfurique. On neutralise 85% de la quantité théorique d'amine en une heure; le cyclophosphazane **2***d* cristallise au refroidissement, le précipité est lavé à l'hexane et séché sous vide sur anhydride phosphorique.

Diazaphospholes-1,3,2 complexés **4**a–h *et* **8**d–f

Trifluoro(butyl-1 benzo-4,5 diazaphosphole-1,3,2-N^3) bore **4**e

On ajoute en refroidissant 0,44 cm^3 d'éthérate de trifluorure de bore (0,0036 mol) à 0,69 g (0,009 mol) de *N*-butylcyclotétraphosphazane en suspension dans 4 cm^3 de benzène anhydre. Après une heure à la température ambiante, on concentre sous vide la solution jaune clair obtenue, et on isole les cristaux formés. On recristallise dans le benzène anhydre, Rdt, 96%, *F* = 104°C. *Poids Moléc.*: 260. *Anal.* calc.: C 46,19, H 5,04, N 10,91, P 11,92, F 21,92; tr.: C 45,58, H 5,13, N 10,54, P 11,70, F 20,89.

Trifluoro(n-propyl-1 dihydro-4,5 diazaphosphole-1,3,2-N^3) bore **8**d

A 3 g de *N*-propylcyclotétraphosphazane **5***d* dissous dans 10 cm^3 de CH_2Cl_2 anhydre, refroidi à 0°C, on ajoute sous atmosphère inerte 2,85 cm^3 de $BF_3 \cdot Et_2O$. Après 24 h, on concentre la solution et isole des cristaux blancs qui sont lavés deux fois à l'hexane anhydre, et séchés sur P_2O_5 sous vide, Rdt, 80%, *F* = 76–78°C. *Poids Moléc.* 198. *Anal.* calc.: C 30,30, H 5,56, N 14,14, P 15,66, B 5,56, F 28,79; tr.: C 30,3, H 5,30, N 13,56, P 15,47, B 5,21, F 26,98.

Spirophosphoranes à liaison PH **9**a–c

On chauffe au bain d'huile, un mélange équimoléculaire de diméthylamino-2 dioxaphospholane-1,3,2 et de *N*-benzylorthophénylènediamine (3×10^{-2} mol) dans 20 cm^3 d'acétonitrile; après réaction, on ajoute 10 cm^3 de toluène et évapore l'acétonitrile sous vide. La solution est abandonnée jusqu'à cristallisation (24 h). Les cristaux, filtrés sous vide, sont lavés avec Et_2O anhydre et séchés sur P_2O_5.

				Analyse			
No	Rdt	*F*(°C)		C	H	N	P
9*a*	60	80	calc.	62,5	5,90	9,72	10,76
			tr.	61,08	6,11	9,87	10,17
9*b*	40	98	calc.	66,28	7,26	8,14	9,01
			tr.	65,98	7,44	8,25	9,01
9*c*	70	108	calc.	67,86	5,06	8,33	9,23
			tr.	67,90	5,17	8,51	9,02

Can. J. Chem. Downloaded from www.nrcresearchpress.com by 210.87.254.5 on 09/06/12
For personal use only.

TABLEAU 5. Coordonnées fractionnaires finales ($\times 10^4$) des atomes autres que l'hydrogène pour le composé **5***d*[a]

Atome	*x*	*y*	*z*	Atome	*x*	*y*	*z*
P(1)	6512(2)	3561(1)	0008(1)	P(2)	4633(2)	4857(1)	−1630(1)
N(1)	6483(5)	4834(4)	0621(4)	N(2)	5331(5)	3685(4)	−1083(4)
N(3)	7931(6)	3825(5)	−0593(5)	N(4)	3790(6)	4137(4)	−2692(5)
C(1)	7453(7)	5579(5)	0170(6)	C(6)	4853(9)	2699(6)	−1683(7)
C(2)	8075(8)	4971(7)	−0825(7)	C(7)	3920(10)	2989(6)	−2589(8)
C(3)	8400(12)	3100(11)	−1481(12)	C(8)	3074(13)	4627(7)	−3585(9)
C(4)	9374(13)	2870(11)	−1804(14)	C(9)	2552(17)	4429(10)	−4523(11)
C(5)	9830(11)	2104(9)	−2648(10)	C(10)	2061(20)	4871(13)	−5431(11)

[a]Les écarts standards sont indiqués entre parenthèses.

Réactivité du trifluoro(benzyl-1 benzo-4,5 diazaphosphole-1,3,2-N^3) bore **4**g

Addition de $HNEt_2$ (réaction [5])

Dans un tube de rmn on introduit 0,175 g ($5,8 \times 10^{-4}$ mol) de **4***g* dissous dans 0,5 cm^3 de toluène, on enregistre le spectre de rmn ($\delta^{31}P = 226$), on ajoute alors, à 0°C, 0,086 g ($11,7 \times 10^{-4}$ mol) de diéthylamine fraichement distillée sur potasse; après quelques minutes d'agitation on enregistre à nouveau le spectre ($\delta^{31}P = 99$).

Addition des alcools en présence de triéthylamine (réactions [7] et [8])

Le mode opératoire est analogue à celui décrit précédemment mais on replace la diéthylamine par un mélange équimoléculaire d'alcool et de triéthylamine.

Addition de n-butanol (réaction [10])

A une solution de 0,0659 g de **4***g* dans 0,5 cm^3 de CH_2Cl_2, maintenue à 0°C ($\delta^{31}P = 226$), on ajoute 0,0255 g de n-BuOH. L'avancement de la réaction est suivi, à la température ordinaire, en enregistrant les spectres de rmn de ^{31}P: on observe une diminution du signal de **4***g* (226) au profit du signal de **10** ($\delta^{31}P = 9$, $J_{PH} = 725$ Hz); la réaction est terminée en quatre jours. On ajoute à 0°C un équivalent de triéthylamine en solution dans un cm^3 de toluène. Le chlorure de méthylène est évaporé sous vide; la solution toluénique, filtrée et concentrée sous vide, est spectrographiée (**11**: $\delta^{31}P = 101$, $J_{PNH} = 30$ Hz).

Réactivité du trifluoro(propyl-1 dihydro-4,5 diazaphosphole-1,3,2-N^3) bore **8**d

Les additions d'amine (réaction [6]), d'alcool en présence d'amine (réaction [9]) et d'alcool (réaction [11]) ont été effectuées d'une façon analogues aux réactions [5], [7], [8], [10] avec pour solvant le chlorure de méthylène.

Détermination de la structure cristalline de **5**d

$P_4N_8C_{20}H_{44}$ $M = 520,5$

Monoclinique, $a = 10,332(2)$, $b = 12,288(2)$, $c = 11,258(3)$ Å, $\beta = 92,34(2)°$, $V = 1428,1$ Å^3, $\rho_o = 1,19(3)$, $\rho_c = 1,21$ g cm^3 pour $Z = 2$, groupe spatial: $P2_1/C$, $F(000) = 560$, $\mu = 2,4$ cm^{-1} (MoKα, $\lambda = 0,71069$ Å).

Le groupe spatial a été déterminé photographiquement par la méthode de précession. Un diffractomètre automatique CAD4 Enraf−Nonius a été utilisé pour l'affinement des paramètres cristallins (sur 25 réflexions) et pour les mesures d'intensité. Les intensités des réflexions *hkl* et $\bar{h}kl$ ont été collectées pour $2° < \theta < 25°$ dans le mode de balayage $\theta/2\theta$. Sur les 2508 réflexions indépendantes mesurées, 1537 satisfaisant au critère $I > 2\sigma(I)$ ont été considérées comme observées et utilisées pour la détermination et l'affinement de la structure. La correction de Lorentz polarisation a été apportée mais aucune correction d'absorption n'a été appliquée en raison de la faible valeur de μ et de la forme parallélépipédique du cristal (0,6 × 0,4 × 0,4 mm).

La structure a été déterminée par les méthodes directes (21) et affinée avec inversion de la matrice complète en utilisant le système SHELX (22). Tous les atomes autres que l'hydrogène ont été affinés anisotropiquement tandis que les atomes d'hydrogène ont été placés en position calculée (C—H = 0.97 Å) et affectés d'un facteur de température isotrope fixe $U = 0,1$ Å^2. Après convergence les facteurs d'accord sont $R = \Sigma(k|F_o| - |F_c|)/\Sigma\, k|F_o| = 0,069$ et $R' = [\Sigma(k|F_o| - |F_c|)^2/\Sigma\, k^2|F_o|^2]^{1/2} = 0,065$.

La synthèse de Fourier différence finale ne présente aucun pic significatif. Cependant les valeurs anormalement élevées des facteurs de température des atomes de carbone, les liaisons C—C trop courtes, ainsi que les angles (N, C)—C—C trop grands (cf. tableau 3) révèlent un phénomène de désordre affectant principalement les groupes propyles. Ce désordre n'a pu être résolu. Les coordonnées finales des atomes autres que l'hydrogène figurent au tableau 5; leurs facteurs de température anisotropes (tableau 6) ainsi que la liste des amplitudes des facteurs de structure observés et calculés ont été confiés au dépôt des données non publiées.[2]

1. (*a*) E. FLUCK. *Dans* Topics in Phosphorus Chemistry. Vol. 10. *Edité par* M. Grayson et E. J. Griffith. Interscience. 1980. p. 193. (*b*) R. APPEL, F. KNOLL et I. RUPPERT. Angew. Chem. Int. Ed. Engl. **20**, 731 (1981); (*c*) V. G. ANDRIANOV,, YU. T. STRUCHKOV, N. Z. SHVETSOV-SHILOVSKII, N. P. IGNATOVA, R. G. BOBKOVA et N. N. MEL'NIKOV. Dokl. Akad. Nauk SSSR, **211**, 1101 (1973).
2. (*a*) E. NIECKE et W. FLICK. Angew. Chem. Int. Ed. Engl. **13**, 585 (1973); (*b*) O. J. SCHERER et K. KUHN. Chem. Ber. **107**, 2113 (1974); (*c*) O. J. SCHERER et W. GLÄSSEL. Chem. Ber. **110**, 3874 (1977).
3. (*a*) Y. CHARBONNEL et J. BARRANS. C.R. Acad. Sci. Sér. C, **278**, 355 (1974); (*b*) Y. CHARBONNEL et J. BARRANS. Tetrahedron, **32**, 2039 (1976).
4. (*a*) A. SCHMIDPETER, J. LUBER et H. TAUTZ. Angew. Chem. Int. Ed. Engl. **16**, 546 (1977); (*b*) A. SCHMIDPETER et H. TAUTZ. Z. Naturforsch. Teil B, **35**, 1222 (1980); (*c*) A. SCHMIDPETER et K. KARAGHIOSOFF. Z. Naturforsch. Teil B, **36**, 1273 (1981).
5. E. NIECKE, R. RÜGER et W. W. SCHOELLER. Angew. Chem. Int. Ed. Engl. **20**, 1034 (1981).
6. (*a*) R. A. SHAW. Phosphorus Sulfur, **4**, 101 (1978); (*b*) W. ZEISS, W. SCHWARZ et H. HESS. Angew. Chem. Int. Ed. Eng. **16**, 407 (1977);' (*c*) W. ZEISS et K. BARLOS. Z. Naturforsch. Teil B, **34**, 423 (1979); (*d*) W. ZEISS, A. POINTNER, C. ENGELHARDT et H. KLEHR. Z. Anorg. Allg. Chem. **475**, 256 (1981).
7. C. MALAVAUD, M. T. BOISDON, Y. CHARBONNEL et J. BARRANS. Tetrahedron Lett. **20**, 447 (1979).
8. C. LEHOUSSE, M. HADDAD et J. BARRANS. Tetrahedron Lett. **23**, 4171 (1982).
9. F. A. L. ANET et J. KRANE. Tetrahedron Lett. 5029 (1973).
10. S. POHL. Chem. Ber. **112**, 3159 (1979); J. P. LEGROS, Y. CHARBONNEL, J. BARRANS et J. GALY. C.R. Acad. Sci. Ser. C,

[2]On peut les obtenir à un prix nominal en s'adressant au dépôt des données non publiées, ICIST, Conseil National de Recherches du Canada, Ottawa, Canada K1A 0S2.

Can. J. Chem. Downloaded from www.nrcresearchpress.com by 210.87.254.5 on 09/06/12
For personal use only.

286, 319 (1978); J. P. LEGROS, Y. CHARBONNEL et J. BARRANS. C.R. Acad. Sci. Ser. C, **291**, 271 (1980).
11. A. SCHMIDPETER, H. TAUTZ, J. VON SEYERL et G. HUTTNE. Angew. Chem. Int. Ed. Engl. **20**, 408 (1981).
12. O. J. SCHERER. Nachr. Chem. Tech. **28**, 392 (1980).
13. A. E. KALININ, V. G. ANDRIANOV et YU. T. STRUCKHOV. Zhur. Strukt. Khim. **15**, 1132 (1974.
14. A. SCHMIDPETER et J. LUBER. Chem. Ber. **108**, 820 (1975).
15. (*a*) A. F. VASIL'EV, L. V. VILKOV, N. P. IGNATOVA, N. N. MEL'NIKOV, V. V. NEGREBETSKII, N. I. SHVETSOV-SHILOVSKII et L. S. KHAIKIN. Dokl. Akad. Nauk SSSR, **183**, 95 (1968). (*b*) S. FLEMING, M. K. LUPTON et K. JEKOT. Inorg. Chem. **11**, 2534 (1972); (*c*) R. W. KOPP, A. C. BOND et R. W. PARRY. Inorg. Chem. **15**, 3042 (1976); (*d*) M. G. THOMAS, R. W. KOPP, C. W. SCHULTZ et R. W. PARRY. J. Am. Chem. Soc. **96**, 2646 (1974); (*e*) M. G. THOMAS, C. W. SCHULTZ et R. W. PARRY. Inorg. Chem., **16**, 994 (1977); (*f*) B. E. MARYANOFF et R. O. HUTCHINS. J. Org. Chem. **37**, 3475 (1972).
16. R. G. PEARSON et J. SONGSTAD. J. Am. Chem. Soc., **89**, 1827 (1967).
17. J. B. COLLINS, P. VON R. SCHLEYER, J. S. BINKLEY et J. A. POPLE. J. Chem. Phys. **64**, 5142 (1976).
18. J. P. TUCHAGUES. Thèse Doctorat d'Etat no 725, Toulouse (1976).
19. C. MALAVAUD. Thèse Doctorat d'Etat no 944, Toulouse (1980).
20. (*a*) M. R. MARRE, M. T. BOISDON et M. SANCHEZ. Tetrahedron Lett. **23**, 853 (1982). (*b*) L. N. MARKOVSKII, V. D. ROMANENKO et A. V. RUBAN. Phosphorus Sulfur, **9**, 221 (1980); (*c*) V. D. ROMANENKO, A. V. RUBAN, N. N. KALIBABCHUK, S. V. IKSANOVA et L. N. MARKOVSKII. Zh. Obshch. Khim. **51**, 1726 (1981).
21. P. MAIN, S. E. HULL, L. LESSINGER, G. GERMAIN, J. DECLERCQ, et M. M. WOOLFSON. MULTAN 78. A system of computer programs for the automatic solution of crystal structures from X-ray diffraction data. Universities of York, England, and Louvain, Belgium. 1978.
22. G. M. SHELDRICK. SHELX 76. A program for crystal structure determination. University Chemical Laboratories, Cambridge, England. 1976.

Can. J. Chem. Downloaded from www.nrcresearchpress.com by 210.87.254.5 on 09/06/12
For personal use only.

Separation of U(VI) from aqueous solutions by precipitate flotation with 8-quinolinol and surfactants

KAMAL SHAKIR AND KAMAL BENYAMIN
Nuclear Chemistry Department, Nuclear Research Centre, Atomic Energy Establishment, Cairo, Egypt
AND
MOURAD AZIZ
Radiation Protection Department, Nuclear Research Centre, Atomic Energy Establishment, Cairo, Egypt

Received December 16, 1982[1]

KAMAL SHAKIR, KAMAL BENYAMIN, and MOURAD AZIZ. Can. J. Chem. **62**, 51 (1984).

Foam separation investigations over the 2.5–10.5 pH range show that U(VI) can be successfully separated from aqueous solutions by precipitation with oxine and subsequent flotation of the precipitate, either in absence or in presence of surfactant collectors. Collectors tested were: cetyl trimethyl ammonium bromide (CTAB) and sodium lauryl sulphate (NaLS). The extent of removal depends on many factors and removals as high as 98% could be achieved when uranyl oxinate precipitate was floated, under certain controlled conditions, in the presence of CTAB. Factors affecting the percentage removal were investigated and the best conditions were selected. The results obtained are discussed in terms of the hydrolytic behaviour of U(VI).

KAMAL SHAKIR, KAMAL BENYAMIN et MOURAD AZIZ. Can. J. Chem. **62**, 51 (1984).

Des études sur la séparation des mousses dans l'intervalle de pH allant de 2,5 à 10,5 révèlent que le U(VI) peut être séparé avec succès des solutions aqueuses par précipitation avec l'oxine et une flottation subséquente du précipité en présence ou non de collecteurs surfactants. Les collecteurs étudiés sont: le bromure de cétyltriméthylammonium (BCTA) et le sel de sodium du sulfate de lauryle (NaLS). Le taux de séparation dépend de plusieurs facteurs et on peut réaliser une séparation à 98% lorsqu'on fait flotter le précipité d'oxinate d'uranyle dans certaines conditions contrôlées en présence de BCTA. On a étudié les facteurs qui influencent le pourcentage de séparation et on a choisi les meilleurs conditions. On discute des résultats obtenus en fonction du comportement hydrolytique de l'U(VI).

[Traduit par le journal]

Can. J. Chem. Downloaded from www.nrcresearchpress.com by 210.87.254.105 on 09/06/12
For personal use only.

Introduction

The increasing use of nuclear energy has stimulated the search for new simple processes to separate uranium from dilute solutions for either the metal recovery or solution decontamination. For these purposes, precipitate flotation seems to offer many advantages.

Two kinds of precipitate flotation are known (1). (*i*) In the first kind, the ion to be separated is precipitated, usually as hydroxide. A surface-active collector is then added to the dispersion and well stirred, whereby the collector is adsorbed on the surfaces of the precipitate particulates rendering them hydrophobic (2). (*ii*) In the second kind (3), precipitates with hydrophobic surfaces are obtained by allowing the metal ion to react with a suitable organic reagent (not a surfactant) to form an insoluble product with hydrophobic surface.

The separation of hexavalent uranium by precipitate flotation has received little attention. Few publications (4–7) which deal with separation of uranium by precipitate flotation processes of the first kind, and only one (8) which deals with its removal by a process of the second kind, have appeared in the literature. The aim of the present work was, therefore, to investigate the separation of U(VI) from aqueous media by precipitate flotation of the first and second kinds as well as by a process which combines both techniques. The surfactants sodium lauryl sulphate (NaLS) and cetyl trimethyl ammonium bromide (CTAB) were used as collectors for flotation of the first kind, while 8-hydroxyquinoline (oxine) was used as a precipitant in precipitate flotation of the second kind. Oxine was chosen because it has been sucessfully used in extraction of metal ions and in separation of uranium for analytical, recovery, and decontamination purposes (9–14).

[1] Revision received July 15, 1983.

Experimental

Apparatus and reagents

The flotation system and cell used were exactly similar to those previously described (15, 16).

A stock solution of 0.01 *M* uranyl chloride in 0.01 *M* HCl was prepared. The exact concentration of U(VI) in this stock solution was determined gravimetrically by the 8-hydroxyquinoline method (17).

Solutions of reagent grade sodium chloride, hydrochloric acid, and CO_2-free sodium hydroxide were used to adjust the ionic strength and/or the pH.

The collector solutions were freshly prepared daily. Absolute ethanol was used as a solvent as well as a frother, at a dose of two mL of alcohol per 450 mL of UO_2Cl_2 solution.

The solution of oxine was prepared weekly by dissolution in absolute ethanol and was preserved in dark bottles.

General procedure of flotation

Uranyl chloride solutions (1×10^{-4} *M*) were prepared in 500 mL volumetric flasks and were adjusted to 0.02 ionic strength and the desired pH. The solutions were then left to age for 10 minutes, shaken well, and 450 mL were transferred to the flotation cell. The pH of the solution in the cell was measured and recorded.

Flotation was started by passing pure N_2 gas at a rate of 55 cm^3/min. At the end of each experiment samples of the bulk solution were withdrawn, while the gas was still bubbling, for uranium analysis. Oxine was found to shift the pH of uranyl solutions to higher values. Therefore, unless otherwise specified, in experiments where oxine was used, 1 mL of oxine solution of the proper concentration was added dropwise to the uranyl solution in the volumetric flask prior to the pH adjustment. Collectors, when used, were injected into the bulk solution in the flotation cell.

In experiments with oxine alone, the removal was fast and reached its limit within a few minutes, whereas in the presence of collectors the ultimate removal was reached within one hour. Therefore, in the accompanying figures a time interval of 20 minutes was chosen for presenting the flotation results obtained with oxine. For results with

surfactants or with oxine plus surfactant, a time interval of 60 minutes was selected.

Analysis

For uranium analysis the samples were acidified with nitric acid to dissolve the precipitate, if any, then evaporated and heated on a bare flame to destroy the organic matter. Depending on the uranyl ion concentration, uranium was determined spectrophotometrically with either Thoron (18) or Aresenazo III (19) as the colorimetric reagent.

Results and calculations

1. Effect of pH

(a) Flotation of the first kind

Figure 1 shows the effect of pH on the percentage removal of U(VI) using different concentrations of either the anionic collector, NaLS, or the cationic collector, CTAB. For comparison, the figure also shows the theoretical precipitate flotation curve, that is, the precipitate formation curve as calculated from the data published for U(VI) hydrolysis.

In calculating the precipitate flotation curve it was assumed that insoluble hydrolysis products of U(VI) are completely removed by flotation and hence the percentage removal (% M) of the metal ion would be (20):

$$[1] \quad \% \text{ M} = 100\,(1 - C_s/C_a)$$

where C_a is the analytical U(VI) concentration, and C_s is the maximum concentration of soluble U(VI) species and can be related to the hydrogen ion activity by the equation:

$$[2] \quad C_s = H^*K_{so}[H + {}^*\beta_{1,1} + 2H^*\beta_{2,2}\,{}^*K_{so} + 3^*\beta_{5,3}\,{}^*K_{so}^2 + 3H^*\beta_{4,3}\,{}^*K_{so}^2]$$

where $^*K_{so}$ is the solubility or dissociation constant $[UO_2^{2+}]/[H]^2$ and $^*\beta_{1,1}$, $^*\beta_{2,2}$, . . . etc. are the overall formation constants of the hydrolysis products: $UO_2(OH)^+$, $(UO_2)_2(OH)_2^{2+}$; . . . etc.

The values of the various constants used to calculate the precipitate flotation curve were taken from ref. 21 and were corrected to our experimental ionic strength by eq. [3] (21):

$$[3] \quad \log {}^*\beta' = \log {}^*\beta + a\mu^{1/2}/(1 + \mu^{1/2}) + bm_x$$

where μ is the ionic strength and m_x is the molality of the chloride ion. The coefficients a and b were obtained from ref. 21.

The theoretical precipitate flotation curve (Fig. 1) shows that U(VI) starts precipitation at pH 5.7. The fraction of each of the hydrolysis species found in solution at the lower pH values could be calculated from the formation constants. The results obtained are presented in Fig. 2.

As shown from Fig. 1, the experimental flotation curves obtained with CTAB agree with the calculated precipitate flotation curve, indicating that the cationic collector, CTAB, can readily float uranyl precipitates but cannot remove the UO_2^{2+} ion or its polynuclear hydrolysis products. The anionic collector NaLS, on the other hand, cannot float uranyl precipitates though it can partially remove soluble uranyl species. Under our experimental conditions, optimum removals of about 46% and 95% were obtained with NaLS and CTAB respectively.

(b) Flotation of the second kind

Results of experiments on the UO_2^{2+}–HOx flotation systems investigated are summarized in Fig. 3. Removals are seen to increase and the effective pH range is extended towards both sides with increased HOx concentration; apparently the flotation process is very sensitive to this parameter. With the highest HOx concentration tested (2×10^{-3} *M*), removals greater than 92% could be achieved. The effective pH range of U(VI) removal lies in the range 4.2 to 8.2, but the curve shows a significant drop in the pH region 4.5–5.2 with a minimum at about pH 4.7.

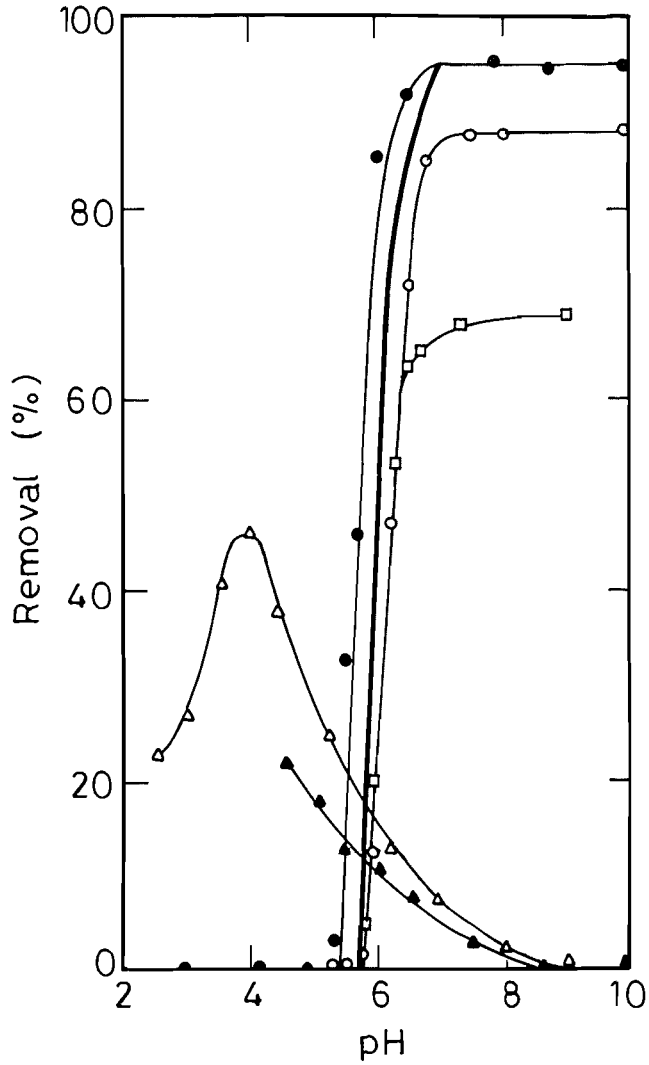

FIG. 1. Theoretical precipitate flotation curve and percentage removals obtained for 1×10^{-4} *M* UO_2Cl_2 solutions of various pH values using different concentrations of either NaLS or CTAB. (—) Theoretical precipitate flotation curve; NaLS: (△) 8×10^{-4} *M*; (▲) 3×10^{-4} *M*; CTAB: (●) 8×10^{-4} *M*; (○) 2×10^{-4} *M*, (□) 5×10^{-5} *M*.

(c) Combined flotation of the first and second kinds

Flotation experiments using HOx as precipitant and either NaLS or CTAB as collector were performed. The results are plotted in Fig. 4. When these are compared with those plotted in Fig. 3, it becomes obvious that CTAB significantly improves the flotation results though it does not affect the removal pattern. At the optimum pH, removals greater than 98% could be achieved. NaLS, on the other hand, slightly increases the percentage removal in the pH range ~5–6.5 but affects it adversely at higher pH values.

In the flotation experiments described in this work the uranyl solutions used to prepare the flotation systems had pH 3.9. When HOx was added to these solutions, the pH values of the resulting systems were found to increase to about 4.3, 4.6, and 5.35 for HOx concentrations of 3×10^{-4} *M*, 8×10^{-4} *M*, and

Can. J. Chem. Downloaded from www.nrcresearchpress.com by 210.87.254.105 on 09/06/12
For personal use only.

Can. J. Chem. Downloaded from www.nrcresearchpress.com by 210.87.254.105 on 09/06/12
For personal use only.

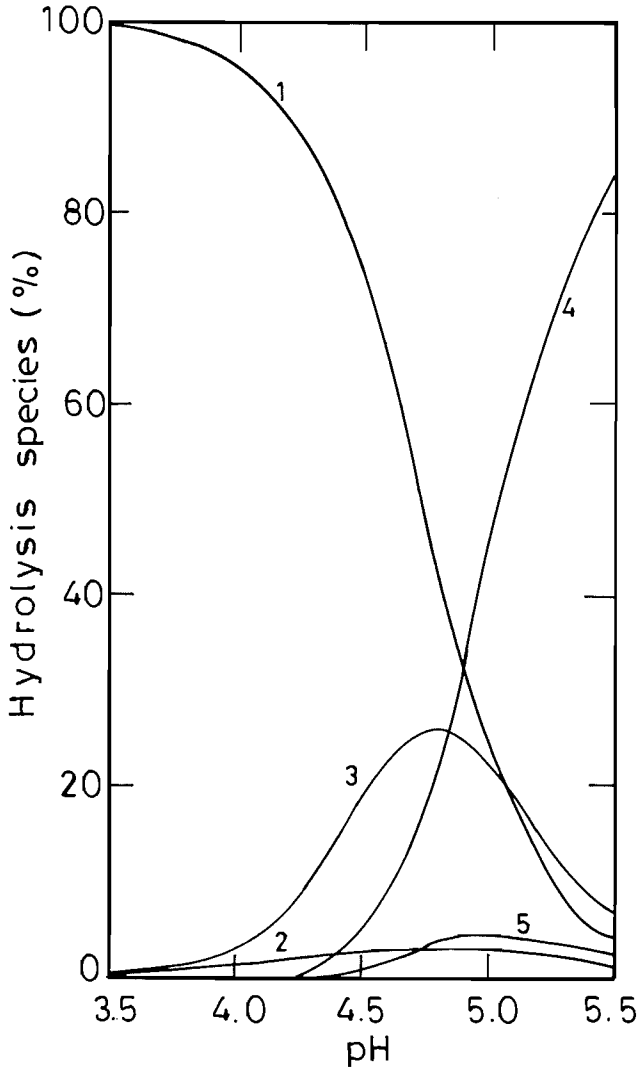

FIG. 2. Distribution of hydrolysis species in 1×10^{-4} *M* UO_2Cl_2 at $\mu = 0.02$ *M* (Cl^-) and 25°C. 1. UO_2^{2+}; 2. $UO_2(OH)^+$; 3. $(UO_2)_2(OH)_2^{2+}$; 4. $(UO_2)_3(OH)_5^+$, 5. $(UO_2)_3(OH)_4^{2+}$.

2×10^{-3} *M* respectively. These (original) pH's of the systems were then brought to the required values by adding either an acid or an alkali. However, when such systems were subjected to flotation, sharp drops in the percentage removals were observed at about pH 4.7 (Fig. 3 and Fig. 4, curves 2, 3, and 4). This defect could be amended by adding the oxine solution to uranyl solutions of pH values so low as not to allow the pH's of the resulting systems to exceed 3.5, the pH at which polynuclear hydrolysis species start formation (Fig. 2).

2. *Effects of HOx, CTAB, and HOx–CTAB concentrations on the percentage removal of U(VI)*

Figure 5 shows the percentage removals of U(VI) using: (*i*) varying concentrations of HOx, (*ii*) different CTAB concentrations, (*iii*) initial constant CTAB concentration (8×10^{-4} *M*) and different HOx concentrations, and (*iv*) initial constant HOx concentration (8×10^{-4} *M*) and varying CTAB concentrations.

As shown from the figure (curve No. 1), the percentage removal obtained with HOx sharply increases with increasing initial HOx concentration until an oxine – metal ion molar ratio of 7.0 is reached where the curve tends to level off. The addition of CTAB to the UO_2–HOx system significantly increases the percentage removal, especially when the proper

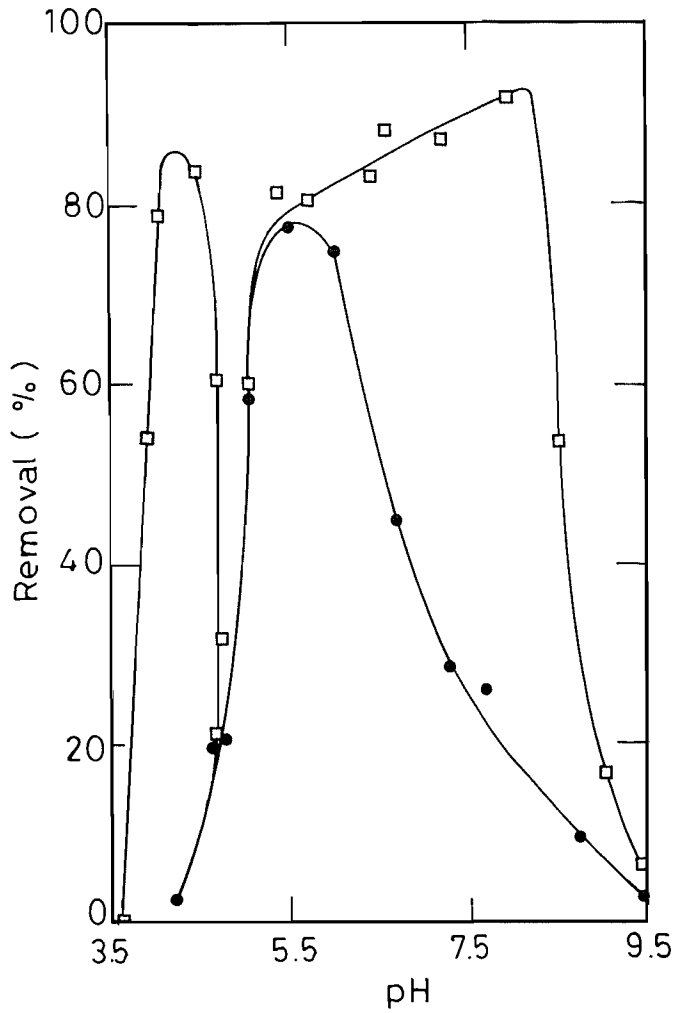

FIG. 3. Removals obtained for 1×10^{-4} *M* UO_2Cl_2 solutions of various pH values using different concentrations of oxine. HOx: (●) 8×10^{-4} *M*, (□) 2×10^{-3} *M*.

amounts of HOx and CTAB are used (curves No. 3 and 4). With improper ratios of the reagents, the percentage removal decreases from the maximum.

Discussion

Results obtained for the U(VI) flotation systems under investigation can be best interpreted in terms of the hydrolytic behaviour of the element and the complexing properties of oxine.

As shown from Fig. 1, with the strong anionic collector NaLS, maximum removal was obtained at pH 3.8 where the soluble UO_2^{2+} species predominates (Fig. 2) and decreased upon either decreasing or increasing the pH; that is, removal took place by only an ion flotation mechanism. In all our experiments, the initial ionic strength was kept constant, i.e., the sum of the initial concentrations of the sodium ions plus hydrogen ions was fixed and hence the sodium ion concentration decreased as the acidity was increased. Removals decreased from the maximum with decreasing pH (Fig. 1), apparently because the metal ion species could not compete against hydrogen ions for the collector anions as successfully as against sodium ions. This is readily explainable since H^+ has a higher charge density than Na^+ and is therefore harder to displace from the laurylsulphate anion.

Can. J. Chem. Downloaded from www.nrcresearchpress.com by 210.87.254.105 on 09/06/12
For personal use only.

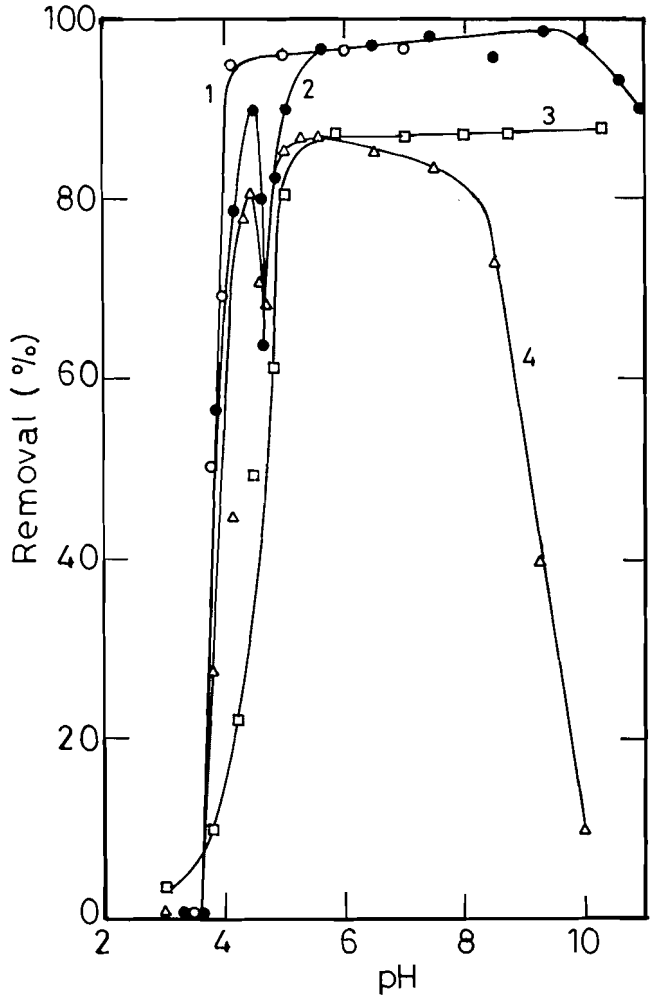

FIG. 4. Percentage removals obtained with either NaLS or CTAB for UO_2Cl_2–HOx systems adjusted to various pH values.

Curve No.	Collector (M)	HOx (M)	Original pH of the UO_2–HOx system
1	5×10^{-4} CTAB	2×10^{-3}	3.2
2	5×10^{-4} CTAB	2×10^{-3}	5.35
3	5×10^{-4} CTAB	3×10^{-4}	4.3
4	5×10^{-4} NaLS	2×10^{-3}	5.35

The decrease of removal with increasing pH can be attributed to the formation of polynuclear uranyl species. As the pH is increased towards the precipitation point, the concentration of the polynuclear hydrolysis species also increases (Fig. 2). Apparently, soluble polynuclear species do not compete as well for the collector anions as does UO_2^{2+} which has a higher charge density.

With CTAB, the soluble uranyl species could not be removed but insoluble species could be successfully floated. The soluble uranyl species are all positively charged and hence, from electrostatic considerations, these species would not be expected to be floated by the cationic collector, CTAB. The removal of the insoluble uranyl species with cationic collectors indicates that these species are negatively charged. However, the removal is not a simple function of the collector concentration since removals of about 70%, 88%, and 95% are obtained with collector – metal ion molar ratios of 0.5, 2, and 8 respectively (Fig. 1). This suggests that the precipitate is not

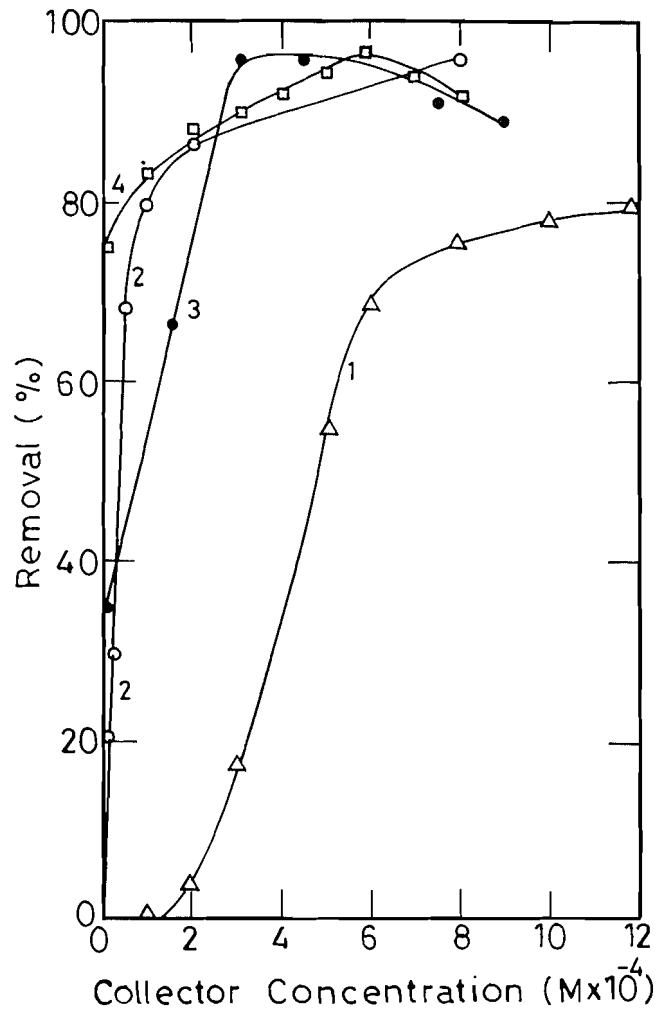

FIG. 5. Percentage removals obtained for 1×10^{-4} M UO_2Cl_2 solutions using different concentrations of oxine, CTAB, or mixtures of both. 1. HOx, pH 5.5; 2. CTAB, pH 8.5; 3. [CTAB] 8×10^{-4} M + [HOx] variable, pH 5.5; 4. [HOx] 8×10^{-4} M + [CTAB] variable, pH 5.5.

homogeneous in structure, i.e., species of various structures and charge densities and, consequently, of different flotation tendencies are present. This seems to be consistent with the literature (21–23) according to which uranyl hydroxide, owing to its pronounced amphoteric properties, can readily form uranates in neutral and basic media. Since uranates are solid solutions of various polyuranates (21, 22), they would be expected to have different flotation tendencies.

Precipitate flotation of the second kind was investigated using oxine. Under basic or weakly acidic conditions, oxine precipitates U(VI) quantitatively as a dark red adduct, $UO_2 \cdot Ox_2 \cdot HOx$ (24, 25). The theoretical precipitate flotation curve of this adduct could not be calculated owing to the lack of data on its equilibrium constants, but the effect of HOx and hydrogen ion concentrations on the formation and, consequently, removal of the adduct can be qualitatively shown by the equation:

$$[4] \quad UO_2^{2+} + 3HOx \rightleftharpoons UO_2Ox_2 \cdot HOx + 2H^+$$

for which the equilibrium constant would be:

$$[5] \quad K = \frac{[H^+]^2}{[UO_2^{2+}][HOx]^3}$$

Can. J. Chem. Downloaded from www.nrcresearchpress.com by 210.87.254.105 on 09/06/12
For personal use only.

In agreement with the above equilibrium, it is found experimentally that the percentage removal of uranium highly depends on the HOx concentration and increases as the quantity of oxine added is increased (Fig. 3). At the lowest HOx concentration tested, 8×10^{-4} *M*, the optimum removal is attained at pH 5.7. The sharp decrease from the optimum removal with decreasing pH is attributed to the increased tendency of the precipitant (HOx) to be protonated, whereas the decrease of the removal from the maximum with increasing pH is caused by the increased competition of OH^- for U(VI) and the consequent formation of hydrolytic uranyl precipitates. As shown from Fig. 3, increasing the oxine concentration results not only in a higher percentage removal but also in a wider effective pH range of U(VI) flotation. With the highest oxine concentration tested, 2×10^{-3} *M*, the optimum pH for uranium removal lies in the range 4.2–8.2. This range agrees with that, 4.1–8.8, reported (26) for uranyl oxinate precipitation.

U(VI) separation by combined precipitate flotation of the first and second kinds was also investigated. On comparing the results (Fig. 4) with those obtained with oxine alone (Fig. 3), it is noticed that NaLS does not significantly affect the percentage removal whereas CTAB markedly improves it at pH values greater than 5. These results are readily explainable since, except around pH 3.8, NaLS cannot significantly remove U(VI) but CTAB can successfully remove uranyl hydroxide and uranates from neutral and alkaline media (Fig. 1). Therefore the increased removal which is observed when CTAB is added to the UO_2^{2+}–HOx system can be attributed to the simultaneous removal of hydrolytic uranyl precipitates by CTAB and the self-flotation of uranyl oxinate. CTAB cannot remove soluble uranyl species (Fig. 1) and it therefore does not affect the removal results obtained by oxine at pH values below that of U(VI) precipitation. At relatively high hydroxyl ion concentrations (pH >10) the removal decreases due to the high competitive effect of OH^-, against both oxine and CTAB, for U(VI).

The effects of reagent (CTAB and HOx) concentration on the percentage removal is summarized in Fig. 5 which suggests that uranium removal depends, among other factors, on the molar ratio of oxine/CTAB. With the initial concentration of one of these reagents held constant, the percentage of uranium removal increases with increasing concentration of the other reagent until an optimum is attained; then it tends to decrease. It was experimentally found that HOx can be removed with CTAB but hydrolytic uranyl products and the insoluble $UO_2 \cdot Ox_2 \cdot HOx$ appear to be removed in preference to HOx. Therefore, at the region of maximum uranium removal there should be a judicious balance between the ratios of free oxine, uranyl adduct, hydrolytic uranyl precipitates, and CTAB. Increasing the oxine concentration to values above that required for the balance results in increased competition of the excess oxine against the hydrolytic uranyl precipitates for CTAB. On the other hand, increasing the CTAB concentration to values higher than that of the balance results in removal of free oxine from the system by flotation, and consequently the adduct tends to dissociate. Besides, high CTAB concentrations can decrease the gas surface area available for the attachment of the uranyl adduct by reason of the increased competitive effect of CTAB for the surfaces of gas bubbles.

For recovery purposes, oxine and CTAB can be removed from the foam phase by the method suggested elsewhere (10).

1. T. PINFOLD. *In* Adsorptive bubble separation techniques. *Edited by* R. Lemlich. Academic Press, New York. 1972. Chapt. 5. p. 75.
2. R. E. BAARSON and C. L. RAY. Precipitate flotation, a new metal extraction and concentration technique. Am. Inst. Mining, Metall. and Pet. Eng. Symposium, Dallas, Texas. 1963.
3. E. J. MAHNE and T. A. PINFOLD. Chem. Ind. (London) **30**, 1299 (1966).
4. K. SHAKIR. Sep. Sci. **8**, 345 (1973).
5. L. D. SKRYLEV and S. G. MAKRUSHIN. Zh. Prikl. Khim. **34**, 2403 (1961); Nucl. Sci. Abstr. **16**, 12799 (1962).
6. K. SHAKIR. Chem. Scr. **6**, 70 (1974).
7. Z. ZIVANOV, D. MISKOVIC, and E. KARLOVIC. Zb. Prir. Nauke Matica Srp. **52**, 239 (1977); Chem. Abstr. **89**, 15008 l (1978).
8. E. J. MAHNE and T. A. PINFOLD. J. Appl. Chem. **19**, 57 (1969).
9. J. KORKISCH. Modern methods for the separation of rarer metal ions. Pergamon Press, London. 1969, and references cited.
10. K. SHAKIR and S. SAMY. J. Less Common Metals, **71**, 265 (1980).
11. R. D. WEED. HW-76867(1963); Nucl. Sci. Abstr. **17**, 40682 (1963).
12. W. E. CLIFFORD, E. P. BULLWINKEL, L. A. MCCLAINE, and P. NOBLE, JR. J. Am. Chem. Soc. **80**, 2959 (1958).
13. K. L. CHENG and H. Y. GUH. Mikrochim. Acta, **1**, 55 (1978).
14. K. MOTOJIMA, E. TACHIKAWA, H. KAMIYAMA, and T. IMAHASHI. Ann. Nucl. Energy, **5**, 5 (1978); Chem. Abstr. **89**, 32707 q (1978).
15. K. SHAKIR and M. AZIZ. J. Appl. Chem. Biotechnol. **27**, 1 (1977).
16. K. SHAKIR and M. AZIZ. Radiochim. Acta, **26**, 113 (1979).
17. A. I. VOGEL. Quantitative inorganic analysis. 2nd ed. Longmans Green, London. 1953. p. 471.
18. S. P. SANGAL. Microchem. J. **7**, 331 (1963).
19. A. A. NEMODRUK and L. P. GLUKHOVA. J. Anal. Chem. (USSR) **18**, 85 (1963).
20. A. J. RUBIN and J. D. JOHNSON. Anal. Chem. **39**, 298 (1967).
21. C. F. BAES, JUN, and R. E. MESMER. The hydrolysis of cations. Wiley–Interscience Publishers, New York. 1976. pp. 176–182.
22. J. E. RICCI and F. J. LOPREST. J. Am. Chem. Soc. **77**, 2119 (1955).
23. A. I. BUSEV, V. G. TIPTSOVA, and V. M. IVANOV. Analytical chemistry of rare elements. Translated from the Russian by A. Rosinkin. Mir Publishers. 1981. p. 124.
24. F. HECHT and W. REICH-ROHRWIG. Monatsh. Chem. **53**, 596 (1929).
25. F. J. FRERE. J. Am. Chem. Soc. **55**, 4362 (1933).
26. H. GOTO. Sci. Rep. Tohoku Imp. Univ. Ser. 1, **26**, 391 (1937).

Nuclear magnetic resonance studies of microemulsions and related systems: 2-butoxyethanol in water

O. DESROSIERS, T. VAN DINTER,[1] AND J. K. SAUNDERS
Department of Chemistry, Université de Sherbrooke, Sherbrooke, P.Q., Canada J1K 2R1

Received November 4, 1982[2]

O. DESROSIERS, T. VAN DINTER, and J. K. SAUNDERS. Can. J. Chem. **62**, 56 (1984).

The ^{13}C chemical shift, T_1, and ^2H T_1 data for 2-butoxyethanol (BE) in D_2O as a function of concentration are presented. The nmr parameters are consistent with thermodynamic data for the same system in that it appears that 2-butoxyethanol in water undergoes a pseudo phase transition at about 1.2 *M*. The chemical shift for each carbon is different in the microphase relative to either aqueous solution or pure BE. The shift differences are due to a combination of factors, conformer population changes, changes in the polarity of the oxygen, and a solvent effect on chemical shift. The more organic the medium, the higher the population of *trans* relative to *gauche* conformers. The motion of BE is more restricted in the microphase than in either dilute aqueous solution or in the pure liquid. The number of adsorbed D_2O molecules per molecule of BE is less in the microphase than in aqueous solution.

O. DESROSIERS, T. VAN DINTER et J. K. SAUNDERS. Can. J. Chem. **62**, 56 (1984).

On rapporte des déplacements chimiques du ^{13}C et des données de T_1 et ^2H T_1 relatives au butoxy-2 éthanol (BE) dans le D_2O en fonction de la concentration. Les paramètres de la rmn s'accordent avec les données thermodynamiques de ce système dans lequel il semble que le butoxy-2 éthanol dans l'eau subit une pseudotransition de phase à environ 1,2 *M*. Le déplacement chimique de chaque carbone est différent dans la microphase par rapport à la solution aqueuse de BE ou par rapport au BE pur. Les différences de déplacement chimique sont provoquées par une combinaison de facteurs: variation de la population du conformère, variation de la polarité de l'oxygène et l'effet du solvant sur le déplacement chimique. Plus le milieu est organique plus la population de conformère *trans* sera élevée par rapport à celle du conformère *gauche*. Le mouvement du BE est plus restreint dans la microphase que dans la solution aqueuse diluée ou dans le liquide pur. Le nombre de molécules de D_2O absorbées par molécule de BE est plus faible dans la microphase que dans la solution aqueuse.

[Traduit par le journal]

Can. J. Chem. Downloaded from www.nrcresearchpress.com by 210.87.254.105 on 09/06/12
For personal use only.

The high solubilizing capacity of microemulsions (1), in particular in their application in tertiary oil recovery processes (2), has prompted extensive studies of their physicochemical properties (3, 4). Of particular interest is the role of the cosurfactant (5) and detection of microphase transitions if they occur. Nuclear magnetic resonance (nmr) can be of considerable value in these studies as the local environment of the various components can be ascertained from chemical shift data and the molecular dynamics can be determined from relaxation times (4) and pulsed gradient spin echo measurements (6).

As part of an nmr study of microemulsions we have examined the chemical shift (δ) and relaxation time (T_1) data of the system 2-butoxyethanol (BE) in D_2O. The study is restricted to the water-rich region. This system was chosen because BE has interesting properties as a cosurfactant (7) in microemulsions and thermodynamic data (8) have shown that it undergoes a microphase transition in the region of 0.02 to 0.04 mole fraction. Since this concentration corresponds to approximately 1.5 *M*, it was felt that it would be an excellent system to study the effect of pseudo phase transitions on nmr parameters. Also, a study of a relatively simple system should aid in the interpretation of the more complex microemulsion results. The most common microphase transition in binary aqueous systems is the formation of micelles. Chemical shift data (9–12) have been employed to detect the cmc, the concentration at which micellization occurs. From a ^{13}C relaxation time standpoint, this transition occurs at such low concentration that it is extremely difficult to detect (13). It is also difficult to detect the cmc by studying the relaxation data of the solvent, water, since the mole fraction of water at the cmc is virtually that of water itself and thus any changes in solvation are masked by the large proportion of nonsolvating water molecules.

Results and discussion

The ^{13}C chemical shifts at 32°C for C(2) (see Table 1) are plotted as a function of concentration in Fig. 1. The chemical shift dependence on concentration is not linear and an inflection occurs at 1.2 *M*, the concentration at which the microphase transition was detected by thermodynamic data (8). If follows therefore that the chemical shift in this system is sensitive to some form of phase transition and that the new microphase might be something resembling an ill-defined micelle or patches of relatively unsolvated BE molecules, as suggested by Iwasaki and Fujiyama (14). In the case of micelle formation, the number of monomers which associate to form the micelle has been determined (9, 10) by assuming the simple model $n\mathrm{M} \rightleftarrows \mathrm{M}_n$. The average aggregate number n can then be estimated using eq. [1]

$$[1] \quad \ln (C_t\, \delta_{obs}) = n \ln [C_t(\delta_{ag} - \delta_{obs})] + \ln K + \ln n - (n - 1) \ln \delta_{ag}$$

where C_t is the total concentration of solute, δ_{ag} the chemical shift in the micelle relative to aqueous solution, δ_{obs} the observed chemical shift relative to aqueous solution, and K is the equilibrium constant given by $K = [\mathrm{M}_n]/[\mathrm{M}]^n$. The value of δ_{ag} may be estimated from extrapolation of plots of δ_{obs} versus $1/C_t$ (9). Application of this model to the results for BE is given in Fig. 2 where a plot of $\ln (C_t\, \delta_{obs})$ versus $\ln [C_t\, (\delta_{ag} - \delta_{obs})]$ for C(3) at 32°C is given. The average value of n is found to be 8 ± 4, which corresponds to the value of 9 ± 3 obtained from thermodynamic data (15).

BE has the advantage relative to surfactants in that the chemical shift of pure BE can be determined directly. Table 4 con-

[1] Present address: Department of Chemistry, McMaster University, Hamilton, Ontario.

[2] Revision received July 7, 1983.

TABLE 1. Chemical shift[a] and relaxation time[b] data for 2-butoxyethanol in D_2O at 32°C

Concentration	Parameter	Carbon-13 C-1	C-2	C-3	C-4	C-5	C-6	^2H T_1
0.2 *M*	δ	61.20	72.00	71.67	31.58	19.43	13.96	0.38
0.3 *M*	T_1	2.5	2.8	2.9	3.3	4.4	4.7	
	δ	61.20	72.00	71.68	31.59	19.44	13.97	
0.4 *M*								0.36
0.5 *M*	T_1	2.5	2.7	3.1	3.5	4.6	5.1	
	δ	61.21	72.03	71.69	31.62	19.46	14.00	
0.6 *M*								0.33
0.7 *M*	T_1	2.3	2.4	2.8	3.3	4.4	5.1	
	δ	61.21	72.04	71.69	31.63	19.48	14.02	
0.8 *M*								0.30
0.9 *M*	δ	61.22	72.08	71.69	31.68	19.51	14.07	
1.0 *M*	T_1	2.2	2.3	2.6	3.0	3.8	4.6	0.29
	δ	61.22	72.10	71.67	31.71	19.52	14.04	
1.2 *M*	T_1	2.1	2.2	2.4	2.8	3.6	4.6	0.29
	δ	61.22	72.16	71.66	31.78	19.57	14.12	
1.5 *M*	T_1	1.9	2.0	2.2	2.7	3.6	4.9	0.28
	δ	61.23	72.22	71.63	31.85	19.61	14.16	
1.7 *M*	δ	61.23	72.25	71.61	31.89	19.63	14.17	0.28
2.0 *M*	T_1	1.9	2.0	2.2	2.6	3.4	4.6	0.26
	δ	61.24	72.29	71.59	31.94	19.66	14.20	
2.5 *M*	T_1	2.0	2.0	2.1	2.5	3.6	4.6	0.24
	δ	61.24	72.34	71.56	32.00	19.68	14.22	
3.0 *M*	T_1	1.9	1.9	2.2	2.6	3.8	4.8	0.22
	δ	61.25	72.37	71.53	32.03	19.70	14.22	
	T_1[c]	1.8	1.9	2.3	2.8	3.6	4.9	
4.0 *M*	T_1	1.9	1.9	2.2	2.5	3.7	4.6	0.19
	δ	61.27	72.43	71.50	32.10	19.73	14.24	
5.0 *M*	T_1	1.8	1.8	2.1	2.6	3.5	4.4	0.16
	δ	61.27	72.48	71.46	32.14	19.74	14.24	
Liquid	T_1	2.2	2.3	3.0	3.5	4.3	4.6	0.10[d]
	δ	62.19	73.32	71.85	32.85	20.21	14.77	

[a] In ppm relative to TMS; measured relative to dioxane and corrected using $\delta_{TMS} = \delta_{dioxane} + 67.4$; estimated error ±0.02 ppm.
[b] In seconds; estimated error ±5% for ^{13}C (22.6 MHz) and ±5% for ^2H (13.8 MHz).
[c] Measured at 100 MHz.
[d] Measured for OD deuterium of liquid 2-butoxyethanol at 46 MHz.

tains a comparison of pure BE chemical shifts with those obtained by extrapolation from a plot of δ_{obs} versus $[\text{concentration}]^{-1}$. For each carbon, the measured value is significantly undeshielded from that obtained by extrapolation. The most striking difference is that observed for C-3, which appears to be heading for higher field with increasing BE concentration but which is in fact deshielded in the neat liquid relative to that observed at infinite dilution in aqueous solution. Obviously then, from a chemical shift point of view, the environment for each carbon in the microphase differs from that in liquid BE.

The factors which influence ^{13}C chemical shift variations can be classified as (1) changes in conformer populations, (2) polarity changes, and (3) solvent effects. To illustrate the effect of conformer population changes, Table 3 contains the various conformations and the chemical shift increments (17) due to the *gauche* interactions in these conformations for butanol. The effect of changes in polarity and solvent effects are difficult to ascertain (18). One example where a polar effect is documented is the deprotonation of a protonated amine which deshields the β carbon by 5 ppm and the α, γ, and δ carbons by about 1 ppm (19).

The carbons of surfactants are all more deshielded when in a micelle than in aqueous solution. This has been interpreted in terms of an increase in the population of *trans* relative to the *gauche* conformations in the micelle (16). Similar results are obtained for alcohols solubilized in micelles (16) in the water-rich region. For BE, all carbons are more deshielded in the neat liquid than in the microphase. All carbons, with the exception of C-3, are more deshielded in the microphase than in aqueous solution. It appears, therefore, that more than one factor causes the chemical shift variations in BE. In order to reduce the number of factors, the chemical shifts of both 4-methylcyclohexanols, cyclohexanol, and butanol have been studied. Cyclohexanol was measured as a neat liquid and then at a relatively low concentration in water. The latter contained

Can. J. Chem. Downloaded from www.nrcresearchpress.com by 210.87.254.105 on 09/06/12
For personal use only.

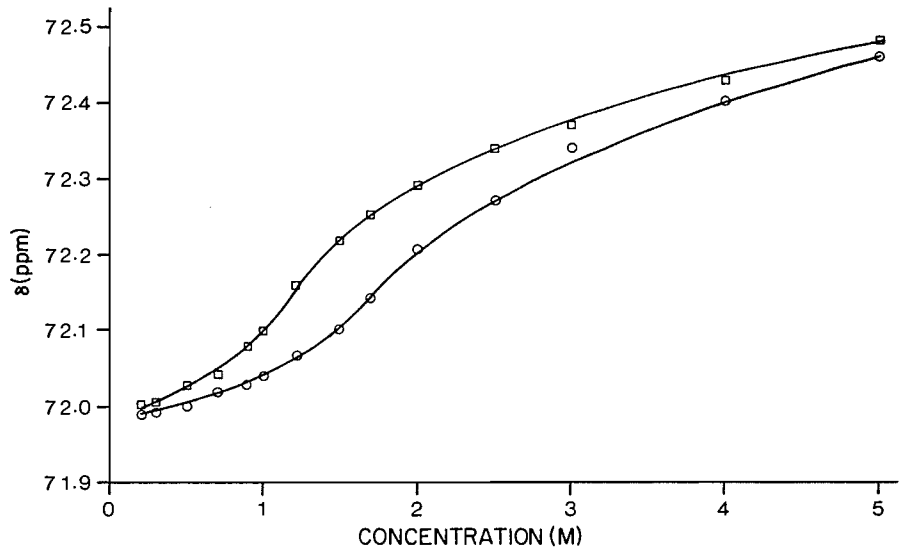

FIG. 1. Plot of chemical shifts as a function of concentration for C(2) of BE at 32°C (□) and 8°C (○).

TABLE 2. Chemical shift[a] and relaxation time[b] data for 2-butoxyethanol in D_2O at 8°C

		Carbon-13						
Concentration	Parameter	C-1	C-2	C-3	C-4	C-5	C-6	^2H T_1
0.2 *M*	T_1	1.0	1.0	1.2	1.5	2.0	2.5	0.24
	δ	61.10	71.99	71.72	31.56	19.45	13.96	
0.3 *M*	δ	61.11	71.99	71.72	31.59	19.48	14.00	
0.4 *M*	T_1	1.0	1.0	1.1	1.4	1.8	2.4	0.21
0.5 *M*	δ	61.11	72.00	71.73	31.61	19.49	14.02	
0.6 *M*	T_1	1.0	1.0	1.2	1.3	1.8	2.3	0.20
0.7 *M*	δ	61.12	72.02	71.74	31.63	19.51	14.06	
0.8 *M*	T_1	1.0	1.0	1.1	1.3	1.7	2.3	0.19
0.9 *M*	δ	61.12	72.03	71.74	31.64	19.52	14.07	
1.0 *M*	T_1	0.94	0.93	1.1	1.2	1.7	2.2	0.17
	δ	61.13	72.04	71.74	31.65	19.53	14.08	
1.2 *M*	T_1	0.97	0.97	1.1	1.3	1.6	2.2	0.16
	δ	61.14	72.07	71.75	31.69	19.56	14.13	
1.3 *M*	T_1	0.79	0.83	0.93	1.1	1.4	2.1	0.16
1.5 *M*	T_1	0.74	0.73	0.86	1.0	1.4	2.1	0.15
	δ	61.14	72.10	71.70	31.73	19.56	14.18	
1.6 *M*								0.16
1.7 *M*	T_1	0.74	0.76	0.83	1.0	1.4	2.1	0.15
	δ	61.14	72.14	71.66	31.78	19.60	14.16	
1.8 *M*								0.15
2.0 *M*	T_1	0.76	0.72	0.82	1.0	1.4	2.1	0.15
	δ	61.14	72.21	71.65	31.85	19.65	14.21	
2.2 *M*								0.13
2.5 *M*	T_1	0.77	0.78	0.86	1.1	1.5	2.2	0.12
	δ	61.13	72.27	71.60	31.92	19.68	14.26	
3.0 *M*	T_1	0.71	0.72	0.80	1.0	1.3	2.1	0.11
	δ	61.15	72.34	71.59	32.00	19.72	14.31	
3.5 *M*	T_1	0.71	0.76	0.80	1.1	1.4	2.1	0.10
4.0 *M*	T_1	0.77	0.78	0.87	1.0	1.4	2.2	0.085
	δ	61.16	72.40	71.53	32.07	19.75	14.32	
5.0 *M*	T_1	0.73	0.74	0.88	1.1	1.5	2.2	0.074
	δ	61.17	72.46	71.48	32.14	19.78	14.32	

[a] In ppm relative to TMS (measured as for 32°C).
[b] In seconds (errors as for 32°C).

cyclohexanol both in solution and as a separate phase.

The resonances in both phases were observable and hence the exchange rate must be slow on the nmr time scale. Dilution afforded a spectrum with only the resonances for dissolved

Can. J. Chem. Downloaded from www.nrcresearchpress.com by 210.87.254.105 on 09/06/12
For personal use only.

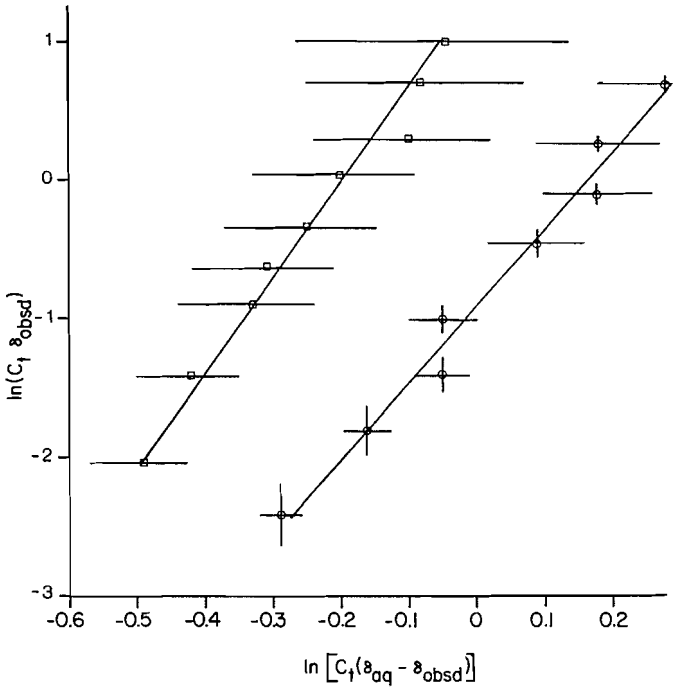

FIG. 2. Plot of ln (C_t δ_{obsd}) versus ln $C_t(\delta_{ag} - \delta_{obsd})$ for C(3) of BE at 32°C (□) and 8°C (○). The error bars for the results at 32°C represent an error of ±0.04 ppm in the estimation of δ_{ag}. The error bars for the plot at 8°C represent an error of ±0.02 ppm in δ_{obs}.

cyclohexanol present. Further dilution (factor of 5) resulted in an identical spectrum being recorded. The 4-methylcyclohexanols were measured under the same conditions. The δ values for n-butanol as a very dilute aqueous solution and as a neat liquid were also determined. The results from this study are given in Table 4.

The cyclohexanol derivatives can exist in two conformations. The preferred conformation of *trans*-4-methylcyclohexanol is estimated to be more stable by 2.6 kcal/mol (20). The energy difference for *cis*-4-methylcyclohexanol is 1 kcal/mol and for cyclohexanol it is 0.8 kcal/mol (20). Thus, for the *trans* compound, any chemical shift differences should be due to factors other than conformational population changes. The carbon carrying the hydrophilic group is more shielded in the organic than in the aqueous phase, whereas the reverse is observed for the other carbons. In light of the uniformity of the effect on the β, γ, and δ carbons, it appears unlikely that these differences represent differences in the polarity of the polar group. The differences will therefore be assigned to a direct solvent effect on chemical shift. The *cis* compound shows the same trends although the numerical values are different. The trend for the difference in Δδ values between *cis* and *trans* is consistent with an increase in the high energy conformer in aqueous solution. This corresponds to an increase in the *gauche* conformation for the methyl group. For cyclohexanol, the Δδ values are similar to those obtained for the *trans* compound. The small differences probably are a result of a conformational population change. All carbons are more deshielded in the neat liquid than when in the organic phase in water. The most significant effect is at C(2).

All carbons in butanol are deshielded in the organic relative to the aqueous phase. Inspection of Table 3 shows that a conformational population change affects all carbons in the same direction or has zero effect. The most logical interpretation of

TABLE 3. Conformations[a] and predicted chemical shift increments[b] for butanol

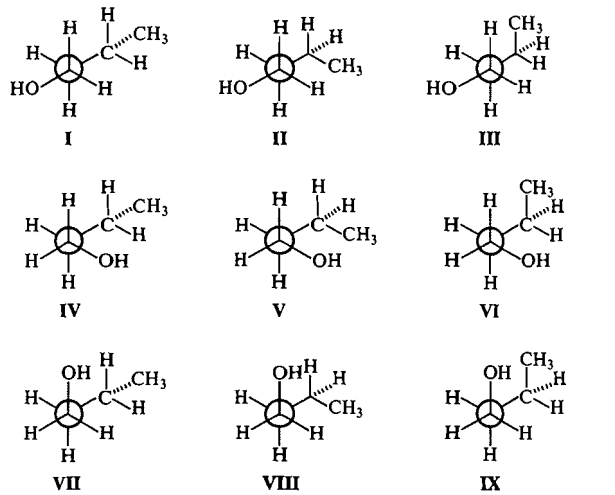

	Predicted shift increments			
Conformation	C-1	C-2	C-3	C-4
I	10	20	10	10
II	5	17	7	5
III	5	17	7	5
IV	7	17	5	10
VI	2	14	2	5
VII	7	17	5	10
VIII	2	14	2	5

[a] Conformations V and IX are neglected as they contain the high energy δ *syn* axial interaction.

[b] See ref. 25 for discussion of the various interactions. Since trends are required, each *gauche* interaction involving a C—H bond is incremented by 5 ppm and each C—C—C—C or O—C—C—C *gauche* interaction is incremented by 2 ppm.

the Δδ values is an increase in the *trans* conformations in the organic phase and a smaller direct solvent effect on chemical shift than that observed in *trans*-4-methylcyclohexanol.

Comparison of Δδ values for the appropriate carbons of BE with butanol suggest that the factors influencing the hydrophobic portion of BE are those which cause the Δδ values in butanol. The difference in Δδ values obtained by extrapolation relative to those recorded for a neat liquid are all in the same direction and of similar magnitude. This suggests that these differences are due mainly to changes in conformer populations, with *trans* conformations being more populated in the neat liquid. In view of the relative shielding of C(3) in the microphase relative to aqueous solution, one must conclude that these Δδ values must be due mainly to solvent effects on chemical shift. From inspection of Table 3,[3] it is obvious that conformer population changes cannot result in the relative shielding of one carbon and deshielding of all others.

Inspection of the data in Table 4 shows that the largest shift difference between pure liquid and aqueous solution occurs at the carbon β to the oxygen. From Table 3 it is evident that this cannot be ascribed to changes in conformer populations. As mentioned earlier, one factor which has a more pronounced

[3] The predicted effect on chemical shift for BE will be similar to those for butanol except that the numerical values for carbons 2–4 will show a larger variation.

Can. J. Chem. Downloaded from www.nrcresearchpress.com by 210.87.254.105 on 09/06/12
For personal use only.

TABLE 4. Chemical shifts[a] of 2-butoxyethanol, butanol, and cyclohexanol derivatives as liquids and in dilute aqueous solutions

Compound	Phase[b]	C-1	C-2	C-3	C-4	C-5	C-6
2-Butoxyethanol	Aqueous	61.19	71.97	71.66	31.55	19.40	13.94
	Organic (1)	61.32	72.68	71.34	32.33	19.82	14.28
	Organic (2)	62.19	73.32	71.85	32.85	20.21	14.57
	Δδ (1)	0.13	0.69	−0.32	0.78	0.42	0.34
	Δδ (2)	1.00	1.35	0.19	1.30	0.81	0.63
Butanol	Aqueous	61.57	33.46	18.37	13.06		
	Organic (2)	61.82	35.07	19.25	13.72		
	Δδ (2)	0.25	1.61	0.88	0.66		
Cyclohexanol	Aqueous	70.29	34.29	23.81	24.94		
	Organic (1)	69.43	35.04	24.31	25.65		
	Organic (2)	69.51	35.40	24.42	25.86		
	Δδ (1)	−0.86	0.75	0.50	0.71		
	Δδ (2)	−0.78	1.11	0.61	0.92		
cis-4-CH_3-cyclohexanol[c]	Aqueous	67.54	30.79	28.67	29.97	20.58	
	Organic (1)	66.09	31.84	29.14	31.08	21.34	
	Δδ	−1.45	1.05	0.47	1.09	0.76	
trans-4-CH_3-cyclohexanol	Aqueous	70.79	32.84	34.32	31.20	21.26	
	Organic (1)	69.98	33.55	35.02	31.84	21.89	
	Δδ	−0.81	0.71	0.70	0.64	0.63	

[a] Chemical shifts in ppm relative to TMS. Shifts of butanol and cyclohexanol measured relative to TMS in a capillary.
[b] Organic (1) phase represents organic phase in D_2O either by extrapolation or direct measurement (see text). Organic (2) phase is as a pure liquid.
[c] For the methylcyclohexanols, C-5 refers to the methyl group carbon.

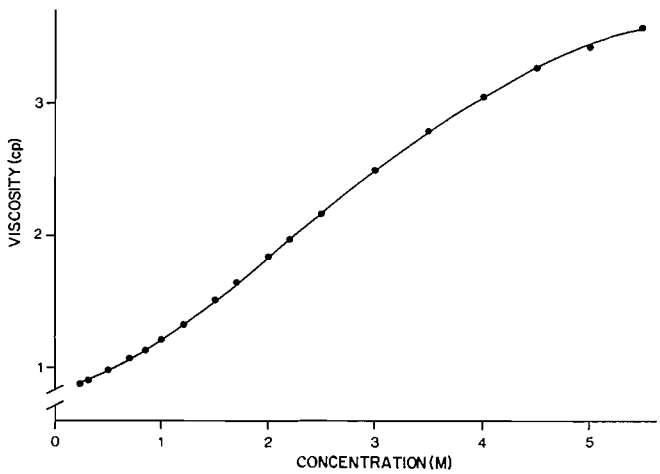

FIG. 3. Plot of viscosity as a function of concentration.

effect on the β carbon than any other carbon is a change in charge on the polar group. Thus by analogy with amines, the increased shielding at β carbons when dissolving the alcohol in water is the result of a decrease of effective negative charge on the oxygen in water. Using the amine results (19), one would expect C(2) of cyclohexanol to be shielded by about 5 ppm in the neutral species relative to the anion.

The chemical shift data at 8°C (see Table 2) show a similar dependence on concentration to that obtained at 32°C. Figure 1 contains a plot of δ as a function of concentration for C(2) at 8°C and Fig. 2 a plot of ln C_t δ_{obs} versus ln $C_t(\delta_{ag} - \delta_{obs})$ for C(3) at this temperature. The microphase transition as detected by this technique occurs at about 1.6 *M*, a higher concentration than at 32°C consistent with the thermodynamic data (8).

The relaxation rate, T_1^{-1}, is given by $T_1^{-1} = \bar{H}^2 \tau_c$ where τ_c is the correlation time and $\bar{H}$ represents the interaction responsible for the relaxation, in the present case either dipolar or quadrupolar. The correlation time according to the Stokes–Einstein equation is given by $\tau_c = 4\pi a^3\eta/3kT$, where a is the effective molecular radius and η the viscosity. Thus, in principle, the relaxation rate should depend on viscosity although in many cases this is not so. The viscosity of BE as a function of concentration is given in Fig. 3. There are 3 main points from this curve. First of all, there is an inflection at about 1.2 *M* which corresponds to the pseudo phase transition. Secondly, the viscosity at concentrations above 3.5 *M* is higher than that of liquid BE. Finally, there is no correlation between viscosity and relaxation rates.

The microphase transition is detected to be about 1.0 *M* at 32°C and 1.2 *M* at 8°C from T_1 data. Figure 4 illustrates the effect of concentration on the relaxation rate for C(1) at both temperatures. The curves for the other carbons are similar although the effect of concentration on carbons towards the end of the chain is less pronounced. Unlike surfactants in micelles (13) and microemulsions and alcohols in microemulsions (4), the relaxation rate is independent of spectrometer frequency. The nOe at 100 MHz for each carbon is 3 ± 0.1. The relaxation is therefore controlled by the dipolar interaction and the rotation can be characterized by one correlation time, τ_{eff}. The value of τ_{eff} can, however, have more than one component.

The observed relaxation rate $(1/T_1)_{obs}$ is given by eq. [2]

$$[2] \quad \left(\frac{1}{T_1}\right)_{obs} = \left[C_{ag}\left(\frac{1}{T_1}\right)_{ag} + C_m\left(\frac{1}{T_1}\right)_m\right][C_t]^{-1}$$

where the subscripts ag and m refer to BE in the microphase and as a monomer in aqueous solution respectively. This equation presumes that the T_1 values in the two phases remain constant with concentration. In view of the effect of concentration on δ values and on T_1 values in micelles (13), it would be expected that $(T_1)_{obs}$ would decrease with increasing concentration since the curve in Fig. 3 implies that $(T_1)_{ag}$ is greater than $(T_1)_m$. The fact that $(T_1)_{obs}$ remains constant after 1.7 *M* is

Can. J. Chem. Downloaded from www.nrcresearchpress.com by 210.87.254.105 on 09/06/12
For personal use only.

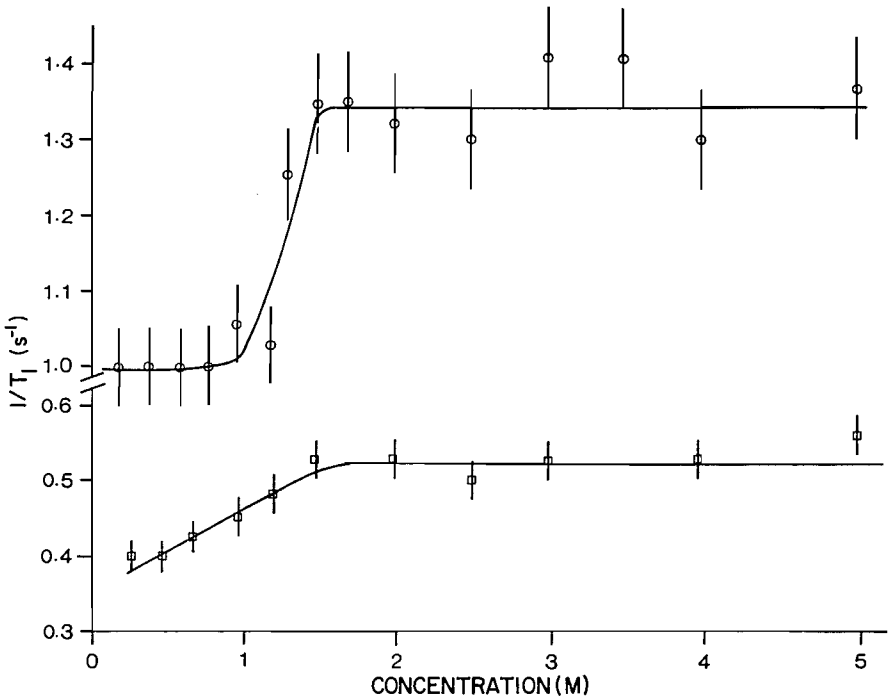

FIG. 4. Plot of $(1/T_1)_{obs}$ as a function of concentration for C(3) of BE at 32°C (□) and 8°C (○). Error bars correspond to an error of ±5%.

a consequence of either $(T_1)_m$ decreasing or $(T_1)_{ag}$ increasing as concentration increases or a combination of both.

The ^2H relaxation rates as a function of concentration are shown in Fig. 5 for the data obtained at 32°C and at 8°C. The curves have the same profile[4] at both temperatures but, again, the effect of concentration is more pronounced at the lower temperature. Since only one deuterium resonance is observed, there must be rapid exchange process between D_2O and the OD group of BE. The overall rate is then given by eq. [3]

$$[3]\quad \left(\frac{1}{T_1}\right)_{obs} = \left[2C_{D_2O}\left(\frac{1}{T_1}\right)_{D_2O} + C_{BE}\left(\frac{1}{T_1}\right)_{BE}\right][2\,C_{D_2O} + C_{BE}]^{-1}$$

where C_{D_2O} and C_{BE} are the concentrations of D_2O and BE respectively and $(T_1)_{BE}$ is the relaxation time of the deuterium of BE. The relaxation rate of the deuterium of the OD group of BE should be proportional to C(1) of BE provided the rotation rate about the C(1)—O bond remains constant and provided the quadrupolar coupling constant is independent of concentration. It has been shown (21) that the quadrupolar coupling constant of deuterium is proportional to the stretching frequency of the O—D (or O—H) bond. A study of overtones of this vibration as a function of concentration showed that ν_{O-D} was invariant within the concentrations of interest. Since the C(1) and C(2) T_1 values vary virtually identically with concentration, we have assumed that the OD does also, and have thus calculated $(T_1)_{D_2O}$ as a function of concentration using eq. [3], the C(1) T_1 values as a function of concentration, and the observed T_1 value of the OD group in BE. A plot of $(T_1^{-1})_{D_2O}$ versus concentration at 32°C is given in Fig. 6.

The relaxation rate of D_2O involved in solvation in which the D_2O is in rapid exchange between bulk liquid and being adsorbed is given by eq. [4] (22)

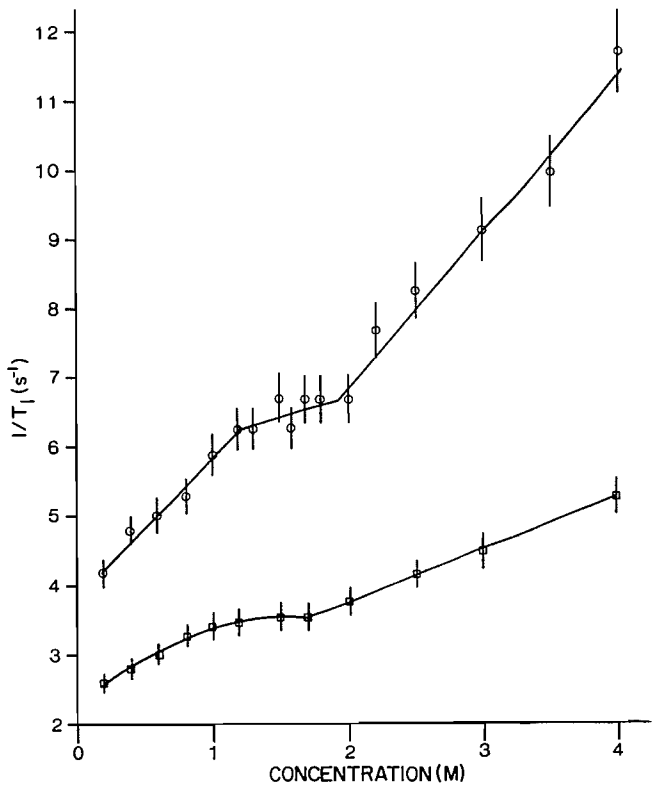

FIG. 5. Plot of ^2H $(1/T_1)_{obs}$ as a function of concentration at 32°C (□) and 8°C (○). Error bars correspond to an error of ±5%.

$$[4]\quad \left(\frac{1}{T_1}\right)_{obs} = \left(\frac{1}{T_1}\right)_{bulk}\left(1 - \frac{n_D C}{50}\right) + K^2\frac{n_D C}{50}\tau_c$$

where n_D is the number of adsorbed molecules, C the concentration of solute, $K = e^2qQ/h$ with the symbols having their usual significance, and τ_c is the correlation time of adsorbed D_2O. The relaxation rate thus increases with concentration

[4] At first glance it may appear that this curve could be represented by a straight line. We believe, however, that the curve drawn is a true representation of the effect of concentration on the deuterium relaxation rates (see experimental section for details).

Can. J. Chem. Downloaded from www.nrcresearchpress.com by 210.87.254.105 on 09/06/12
For personal use only.

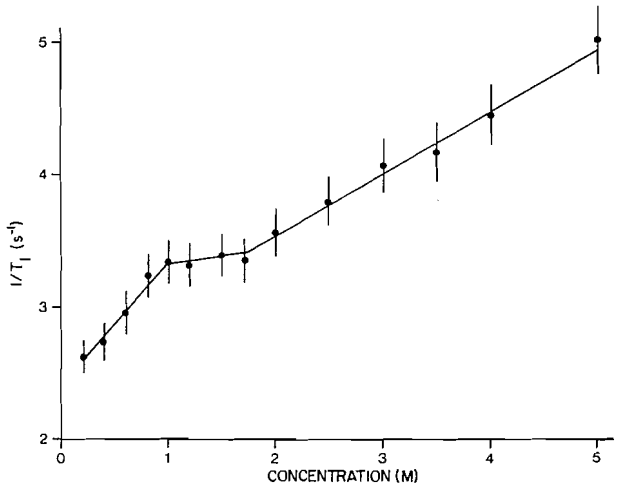

FIG. 6. Plot of $(1/T_1)_{D_2O}$ as a function of concentration at 32°C. Error bars correspond to an error of ±5%.

(23). The pseudo phase transition, then, from Fig. 6 is at about 1.25 *M*. From eq. [5] $d(1/T_1)dC$ is equal to $K^2 n_D \tau_c/50$ when $n_D c < 50$ (22). The initial slope of Fig. 5 gives, basically, $d(1/T_1)dC$ for the monomer. After the microphase transition, eq. [4] is no longer valid, since the solute is present both as a monomer and in the microphase. The second term of eq. [4] must be replaced by $K^2/50\ (n_{D_{ag}} \tau_{c_{ag}} C_{ag} + n_{D_m} \tau_{c_m} C_m)$. Extrapolation to zero concentration of the straight line in Fig. 6 obtained as a function of concentration above 1.7 *M* gives the same value of $(T_1^{-1})_{bulk}$ as the first part of the curve. The slope is less than that obtained for the first straight line. This implies that $n_{D_{ag}} \tau_{c_{AG}} < n_{D_m} \tau_{c_m}$ (n_D corresponds to the number of D_2O molecules per molecule of BE). The increase in τ_c for adsorbed D_2O relative to bulk D_2O is assumed to be due to the decreased motion of the solute causing decreased motion of the solvent rather than an increase in the structure of the water (23). In fact, $d(1/T_1)/dC$ is roughly proportional to molecular size (23) and it would therefore be expected that $\tau_{c_{ag}} > \tau_{c_m}$. We may then conclude that $n_{D_m} > n_{D_{ag}}$, which intuitively appears logical.

Conclusion

The intepretation of the effect of BE concentration on the nmr parameters employed herein is consistent with a microphase transition occuring at about 1.2 *M*, as had been detected by thermodynamic measurements. The nmr chemical shifts and thermodynamic data can satisfactorily be interpreted in terms of the simple model $n\text{BE} \rightleftarrows \text{BE}_n$. However, unlike the thermodynamic data which showed essentially BE properties after the transition, the nmr data of BE in the microphase differ from pure BE. The BE carbon relaxation rates suggest more restricted motion in the microphase than in the pure liquid. In micelles, the relaxation rates can also be interpreted in terms of the simple model $n\text{M} \rightleftarrows \text{M}_n$ which is not the case here. This may be due to failure of the model or, more likely, concentration-dependent relaxation rates of BE in the microphase, in the aqueous phase, or both. The chemical shifts for BE in the microphase differ from those observed in pure liquid. It is proposed that this difference is mainly due to conformer population changes.

The structure of the microphase from the nmr results can be rationalized better in terms of the model proposed by Iwasaki and Fujiyama (14) than in terms of some micelle-like structure. The behaviour of carbons 3–6 of BE with respect to chemical shift parallel those of cyclohexanol. For the latter, chemical shifts corresponding to cyclohexanol, both aqueous and organic phases, could be observed. For BE solutions, there is obviously rapid exchange between the aqueous and microphases such that on the nmr time scale only the average is observed. The D_2O relaxation rates are also in agreement with the model since it appears that the number of adsorbed D_2O molecules per molecule of BE is less in the microphase.

Experimental

2-Butoxyethanol, obtained from Baker Chemicals, was distilled and kept over 4 Å molecular sieves. Densities were measured with a commercial version (SODEV, Sherbrooke, Quebec) of a flow densimeter. Viscosities were measured using a standard Ostwald viscometer. Most of the nmr measurements were made on a Bruker HX-90 spectrometer. Chemical shifts were measured relative to dioxane in a central capillary and corrected to TMS. Generally such widths of 2000 Hz were employed using 8 K of data points. Shifts are estimated to be accurate to ±0.02 ppm. No corrections for bulk magnetic susceptibility were made. The T_1 measurements were obtained by use of the standard inversion recovery technique as described previously (24). Results were treated using both an exponential three-parameter fit and a logarithmic plot. The T_1 values are assumed accurate to ±5%.

These errors refer to absolute errors. The relative errors, particularly for ^2H, are significantly less. The signal-to-noise ratios for the ^2H spectra were very high and therefore many measurements could be recorded in a short time. The ^2H relaxation times at each concentration were measured several times (at least 6) and the results were reproducible to within ±2%. To verify that the curves given in Fig. 5 represent the true effect of concentration on the relaxation rates, measurements were performed at other temperatures. In each case the profile was the same, i.e. with increasing concentration T_1 decreased, then remained essentially constant, and then decreased again. Temperatures were measured by use of a thermocouple placed in an nmr tube in the magnet and are presumed accurate to ±2°C. The 100 MHz spectra were recorded at the NMR Regional Centre in Montreal.

Acknowledgements

The authors express their appreciation to Professor J. E. Desnoyers for extremely helpful discussions and to the Natural Sciences and Engineering Research Council of Canada for financial support.

1. L. M. PRINCE. Microemulsions. Academic Press, New York. 1977.
2. (*a*) V. K. BANSAL and D. O. SHAH. Micellization, solubilization, microemulsions. Vol. 1. Plenum Press, New York. 1976. p. 87; (*b*) D. O. SHAH. J. Colloid Interface Sci. **37**, 744 (1971).
3. J. BIAIS, B. CLIN, P. LALANNE, and B. LEMANCEAU. J. Chim. Phys. Phys. Chim. Biol. **74**, 1197 (1977); A. M. BELLOCQ, J. BIAIS, B. CLIN, P. LALANNE, and B. LEMANCEAU. J. Colloid Interface Sci. **70**, 524 (1979).
4. Y. TRICOT, J. KIWI, W. NIEDERBERGER, and M. GRATZAL. J. Phys. Chem. **85**, 862 (1981).
5. L. M. PRINCE. J. Colloid Interface Sci. **23**, 165 (1967); R. A. MACKAY, K. LETTS, and C. JONES. Micellization, solubilization, microemulsions. Vol. 2. Plenum Press, New York. 1977. p. 1976; E. RUCKENSTEIN and J. C. CHI. J. Chem. Soc. Faraday Trans. 2, **71**, 1960 (1975).
6. P. STILBS, M. E. MOSELEY, and B. LINDMAN. J. Magn. Reson. **40**, 401 (1980).
7. J. E. DESNOYERS, F. QUIRION, D. HÉTU, and G. PERRON. Can. J. Chem. Eng. **61**, 672 (1983).
8. G. ROUX, G. PERRON, and J. E. DESNOYERS. J. Phys. Chem. **82**, 966 (1978).
9. B. O. PERSSON, T. DRAKENBERG, and B. LINDMAN. J. Phys. Chem. **80**, 2124 (1976); **83**, 3011 (1979).

Can. J. Chem. Downloaded from www.nrcresearchpress.com by 210.87.254.105 on 09/06/12
For personal use only.

10. N. MULLER. J. Magn. Reson. **28**, 203 (1977).
11. G. KRESHECK and C. JONES. J. Colloid Interface Sci. **77**, 278 (1980).
12. N. MULLER and R. H. BIRKHAHN. J. Phys. Chem. **71**, 957 (1967).
13. H. WENNERSTROM, B. LINDMAN, O. SODERMAN, T. DRAKENBERG, and J. B. ROSENHOLM. J. Am. Chem. Soc. **101**, 6860 (1979).
14. K. IWASAKI and T. FUJIYAMA. J. Phys. Chem. **81**, 1908 (1977).
15. G. ROUX, G. PERRON, and J. E. DESNOYERS. J. Solution Chem. **7**, 639 (1978).
16. J. B. ROSENHOLM, T. DRAKENBERG, and B. LINDMAN. J. Colloid Interface Sci. **63**, 538 (1978).
17. H. BEIERBECK and J. K. SAUNDERS. Can. J. Chem. **58**, 1258 (1980).
18. J. B. STOTHERS. Carbon-13 NMR spectroscopy. Academic Press, New York, NY. 1972.
19. K. F. KOCH, J. A. RHOADES, E. W. HAGAMAN, and E. WENKERT. J. Am. Chem. Soc. **96**, 3300 (1974).
20. N. L. ALLINGER and M. A. MILLER. J. Am. Chem. Soc. **83**, 2145 (1961); E. L. ELIEL, N. L. ALLINGER, S. J. ANGYAL, and G. A. MORRISON. Conformational analysis. John Wiley and Sons, New York, NY. 1965.
21. H. H. MANTSCH, H. SAITO, and I. C. P. SMITH. Prog. Nucl. Magn. Reson. Spectrosc. **11**, 211 (1977).
22. G. ENGEL and H. G. HERTZ. Ber. Bunsenges. Physik. Chem. **72**, 808 (1968).
23. J. A. GLASEL. J. Am. Chem. Soc. **92**, 372 (1970).
24. H. BEIERBECK, R. MARTINO, and J. K. SAUNDERS. Can. J. Chem. **58**, 102 (1980).
25. H. BEIERBECK, J. K. SAUNDERS, and J. W. APSIMON. Can. J. Chem. **55**, 2813 (1977).

Can. J. Chem. Downloaded from www.nrcresearchpress.com by 210.87.254.105 on 09/06/12
For personal use only.

Comparison of photoconductivity and optical absorption spectra of trapped electrons in γ-irradiated 2,2,4-trimethylpentane/2,2-dimethylbutane/2-methyltetrahydrofuran mixture glasses at 77 K

TOYOAKI KIMURA, KAZUNOBU HIRAO, NAOTO OKABE, and KENJI FUEKI

Department of Synthetic Chemistry, Faculty of Engineering, Nagoya University, Chikusa-ku, Nagoya 464, Japan

Received April 20, 1983

TOYOAKI KIMURA, KAZUNOBU HIRAO, NAOTO OKABE, and KENJI FUEKI. Can. J. Chem. **62**, 64 (1984).

Optical absorption and photoconductivity spectra of trapped electrons in γ-irradiated 2,2,4-trimethylpentane (TMP)/2,2-dimethylbutane (DMB)/2-methyltetrahydrofuran (MTHF) mixture glasses at 77 K have been measured. It is found that the magnitude of the photocurrent increases with decreasing MTHF concentration, which is ascribed to the increase in electron mobility with decreasing MTHF concentration in TMP/DMB/MTHF systems. It is also found that the photoconductivity spectra shift to the lower energy side with decreasing MTHF concentration. Although the photoconductivity spectrum in the neat MTHF system is separated from the corresponding optical absorption spectrum, the spectrum becomes closer to the latter with decreasing MTHF concentration in TMP/DMB/MTHF systems. This result indicates that the extent of bound–free transitions increases relative to bound–bound transitions with decreasing MTHF concentration for the photon absorption process of trapped electrons in TMP/DMB/MTHF systems.

TOYOAKI KIMURA, KAZUNOBU HIRAO, NAOTO OKABE et KENJI FUEKI. Can. J. Chem. **62**, 64 (1984).

On a mesuré à 77 K les spectres d'absorption optique et de photoconductivité des électrons piégés dans un mélange vitreux de triméthyl-2,2,4 pentane (TMP)/diméthyl-2,2 butane (DMB)/méthyl-2 tétrahydrofuranne (MTHF) irradié aux rayons γ. On a trouvé que l'intensité du photocourant augmente lorsque la concentration du MTHF diminue, ce qui l'on attribue à une augmentation de la mobilité de l'électron lorsque diminue la concentration du MTHF dans le système TMP/DMB/MTHF. On a également trouvé que les spectres de photoconductivité glissent du côté de faible énergie lorsque la concentration de MTHF diminue. Bien que le spectre de photoconductivité du système MTHF pur soit séparé du spectre correspondant d'absorption optique, ces deux spectres se rapprochent beaucoup lorsque la concentration de MTHF du système TMP/DMB/MTHF diminue. Ce résultat indique que le taux de transitions liaison–libre augmente par rapport aux transitions liaison–liaison lorsque la concentration de MTHF diminue dans le processus d'absorption du photon pour les électrons piégés dans le système TMP/DMB/MTHF.

[Traduit par le journal]

Introduction

It is well known that ionizing radiations produce trapped electrons in organic glasses. Trapped electrons in γ-irradiated organic glasses at low temperatures, usually 77 or 4 K, have been widely investigated by various methods. Organic glasses used so far are such that excess electrons can be localized in them. Recently, we have found that a mixture of 2,2,4-trimethylpentane (TMP) and 2,2-dimethylbutane (DMB) makes a clear and crack-free glass at 77 K and that electrons are not stably trapped in this mixture glass (1). Previously we have used this TMP–DMB glassy matrix to investigate the mechanism of electron trapping and obtained some interesting results on trapped electrons in γ-irradiated TMP–DMB–3-methylhexane (3MHx) systems (1) and TMP–DMB–alcohol systems (2) at 77 K. Since TMP, DMB, and 3MHx are nonpolar substances, it is expected that the TMP–DMB–3MHx systems form homogeneous mixtures. On the other hand, it has been recognized that alcohol molecules aggregate and make clusters in hydrocarbon matrices (3). This implies that alcohol–hydrocarbon systems form inhomogeneous mixtures consisting of polar regions, namely, alcohol clusters and nonpolar regions surrounding the alcohol clusters. This is supported by the fact that trapped electrons in γ-irradiated alcohol–hydrocarbon systems show two separated optical absorption bands, each of which is nearly the same as that in γ-irradiated hydrocarbons or that in γ-irradiated alcohols (4). Because of such inhomogeneity, the nature of electrons trapped in alcohol clusters and in a hydrocarbon matrix is not basically affected by the concentration of added alcohol except at very low concentrations of alcohol (4). However, it has been suggested from an optical absorption study on trapped electrons in 2-methyltetrahydrofuran (MTHF)/3-methylpentane (3MP) mixture glasses that the MTHF/3MP systems are nearly homogeneous at 77 K (5). By analogy we may expect that MTHF and TMP/DMB make nearly homogeneous mixtures at 77 K. Then we could also expect that the nature of electrons trapped by polar MTHF molecules would be affected by the addition of TMP/DMB, in which electrons are not stably trapped.

In order to investigate the nature of trapped electrons in TMP/DMB/MTHF systems at 77 K, we have measured both optical absorption and photoconductivity spectra over the MTHF concentration range of 5 to 100 mol%. A number of studies have been made on the optical absorption spectra of trapped electrons in a neat MTHF glass (6), but there have been only a few photoconductivity studies of trapped electrons in this matrix (7, 8).

Experimental

Tokyo Kasei 2-methyltetrahydrofuran (guaranteed reagent) was passed through an activated alumina column under argon atmosphere and the middle portion was used for the next step of purification. This process was repeated twice. MTHF was degassed on a vacuum line and vacuum-distilled into a glass bulb with molecular sieve (13X) which had been activated at 550 K *in vacuo* for 12 h before use. After purification by the molecular sieve three times, MTHF was stored over a Na–K alloy. Nakarai Chemicals 2,2-dimethylbutane (guaranteed reagent) and Kishida Chemical 2,2,4-trimethylpentane (spectrograde) were purified using molecular sieve 13X by the same procedure as above. A mixture of TMP and DMB was made in 1:1 volume ratio at room temperature. The desired amount of sample was taken by a volumetric flask under vacuum and transferred into a conductivity cell (described below) and sealed off the vacuum line. The schematic view of the conductivity cell is shown in Fig. 1. Electrodes were made of Supracil quartz coated with In–Sn so that both conductivity and

Can. J. Chem. Downloaded from www.nrcresearchpress.com by 210.87.254.40 on 09/06/12
For personal use only.

Can. J. Chem. Downloaded from www.nrcresearchpress.com by 210.87.254.40 on 09/06/12
For personal use only.

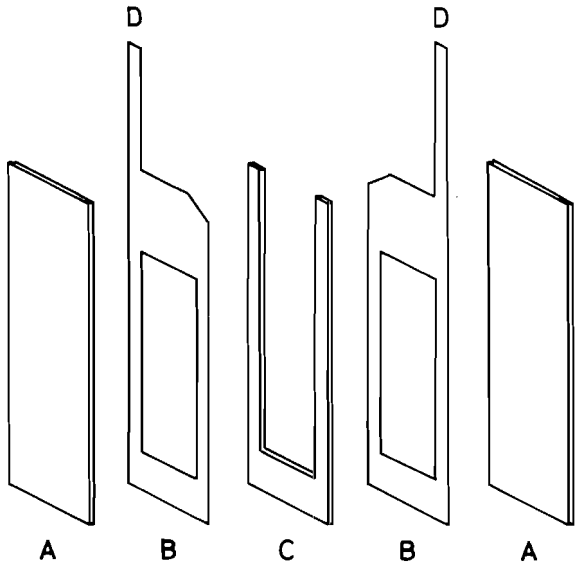

FIG. 1. Schematic view of photoconductivity cell. *A*, spracil quartz electrode coated with In−Sn; *B*, copper foil; *C*, Teflon spacer; and *D*, connection to tungsten wire (see text).

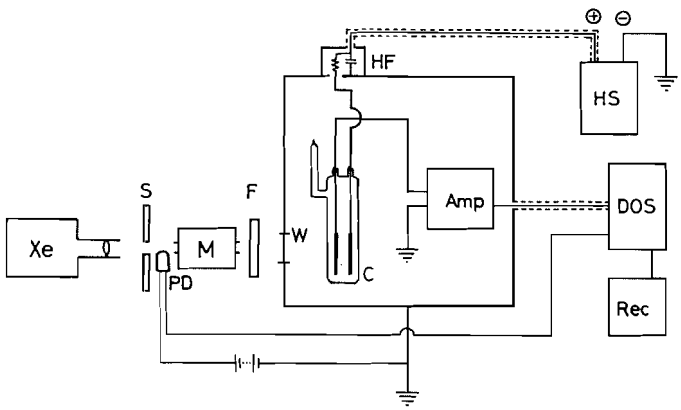

FIG. 2. Block diagram of photoconductivity measurement. Xe, xenon lamp; S, mechanical shutter; PD, photodiode; M, monochromator; F, optical filter; W, spracil quartz window coated with In−Sn; C, photoconductivity cell; HF, highvoltage filter; Amp, current amplifier; HS, high voltage supply; DOS, digital oscilloscope; Rec, recorder.

optical measurements can be made. The distance between the electrode (50 mm × 9 mm) was 0.6 mm. The block diagram of the photoconductivity measurement is shown in Fig. 2. γ-Irradiated samples in a liquid nitrogen Dewar were photoexcited by monochromatic light from a 1 kW xenon lamp (Xebex UXL 1000D-0) through a mechanical shutter, a monochromator (Ritsu MC-10N), and a glass filter. A dc voltage (500 V) from a power supply (Watanabe PH-8A) was applied to electrodes through an electrical filter. Photocurrents were amplified by a current amplifier (Keithley 427) and recorded on a digital oscilloscope (Nicolet 2090-204) which was triggered by a photodiode set behind the mechanical shutter. The photoconductivity cell unit and amplifier were shielded by a copper box which was connected to ground. Cable from the output connector of the amplifier to the oscilloscope, that from the high voltage supply to the filter, and the AC power line for the amplifier were shielded. Beside electrical noises, mechanical vibrations cause serious noises even when they are small. In order to minimize such noises from the vibrations, the copper box was mounted on a polystyrene foam and helium gas was introduced into liquid nitrogen in the Dewar before measurement. This can eliminate the noises arising from bubbling of liquid nitrogen during the measurement.

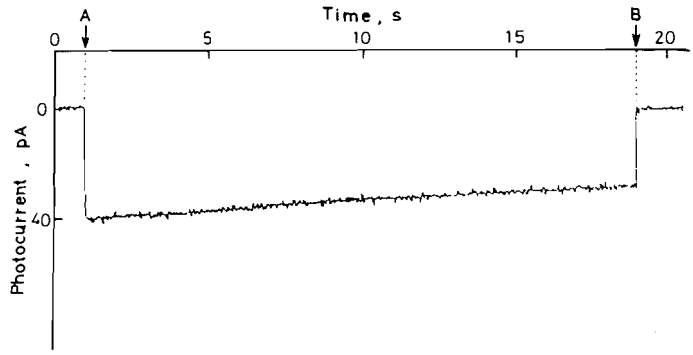

FIG. 3. Time profile of photocurrent in TMP − DMB − 5 mol% MTHF system. A, shutter opened; B, shutter closed.

For the photoconductivity measurement in the visible region, the monochromator with a bandwidth of <30 nm combined with a Toshiba UV-39 glass filter, which cuts off light shorter than 390 nm, was used. For the ir region the monochromator with a bandwidth of ~60 nm combined with either a Toshiba IR-D1A glass filter or a silicone filter, which cuts off light shorter than 900 nm or 1100 nm, respectively, was used. Light intensities were measured by a radiometer (YSI model 65A). We have made a device by which light intensities at the same position as that for the conductivity cell can be measured.

γ-Irradiation was made by γ-rays from a ^{60}Co source. The irradiation dose was 2.8×10^5 rad for photoconductivity measurements and 0.93×10^5 rad for optical absorption measurements. The optical absorption measurements were carried out with a Hitachi 323 spectrophotometer.

Results and discussion

1. Photocurrents in TMP/DMB/MTHF glasses

We have observed that photocurrents in a γ-irradiated neat MTHF glass are quite low compared with those in nonpolar hydrocarbons such as 3MP or 3MHx. The photocurrent per incident photon per unit time[1] in a neat MTHF glass was at most $\sim 10^{-31}$ C/photon, whereas those in 3MP and 3MHx are $\sim 10^{-27}$ (9) and $\sim 10^{-26}$ C/photon,[2] respectively. It is noted that the photocurrent in the neat MTHF glass is lower by five orders of magnitude than that in 3MHx. This contrasts with the published data (10) which report that the photocurrent in 3MHx is much smaller than that in MTHF, although the photocurrents are not measured with monochromatic light but by the differential filter method (8). This discrepancy might arise partly from the difference in the ways of purification. Purification in ref. 8 uses no activated alumina column with inert gas atmosphere. In a γ-irradiated MTHF glass, previously purified by an alumina column as described above, photobleaching of trapped electrons causes an esr radical signal to decrease in intensity, but a MTHF sample without such purification[3] does not show a decrease.

The time profiles of photocurrents in γ-irradiated TMP−DMB−MTHF glasses exhibit generally a flat shape. Figure 3 illustrates the time profile of the photocurrent in TMP − DMB − 5 mol% MTHF glass. It is seen that the photocurrent rises instantaneously when the shutter is opened and falls to zero

[1]The photocurrent per incident photon per unit time is expressed in units of A/(photons/s) or (C/s)/(photon/s) ≡ C/photon. Hereafter we simply call this quantity as the photocurent per incident photon.

[2]N. Okabe, T. Kimura and K. Fueki, unpublished results.

[3]The esr measurement was done at the Department of Chemistry, University of Wisconsin, in 1975.

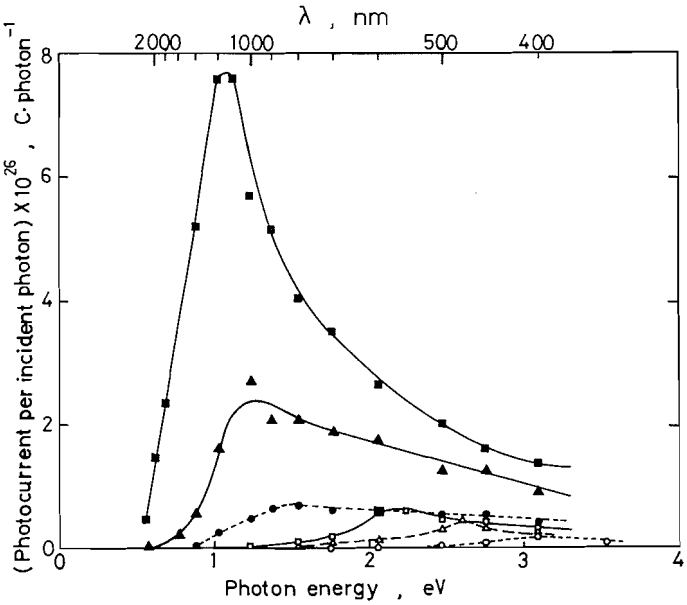

FIG. 4. Photocurrent per incident photon vs. photon energy in TMP–DMB–MTHF systems. ○, neat MTHF; △, TMP – DMB – 90 mol% MTHF; □, TMP – DMB – 75 mol% MTHF; ●, TMP – DMB – 50 mol% MTHF; ▲, TMP – DMB – 25 mol% MTHF; ■, TMP – DMB – 5 mol% MTHF.

when it is closed. In every case throughout this work neither a large decrease nor a slow rise of photocurrents such as those reported in the literature (7, 8) is observed.The flat profile of photocurrents seems reasonable because our monochromatic light cannot be expected to bleach out a significant fraction of trapped electrons within a second. It is also hard to understand the slow rise of photocurrents on a time scale of seconds unless the incident light causes a MTHF glass to increase in temperature leading to the thermal release of trapped electrons.

Since we confirm that the time profile is flat with a time constant (10 ms) of the amplifier, we use a time constant of 300 ms for the photoconductivity measurement in order to increase the S/N ratio when the photocurrent is low.

2. Photoconductivity spectra in TMP/DMB/MTHF glasses

Photocurrents per incident photon, observed at the start of light irradiation, in the TMP/DMB/MTHF systems are shown in Fig. 4. The photoconductivity spectrum for the neat MTHF glass in Fig. 4 shows that the photocurrent is maximum at a photon energy of 3.1 eV (λ_{max}^{ph} = 400 nm). This is somewhat higher than those reported in refs. 7 and 8. The photoconductivity threshold in the neat MTHF glass is obtained to be 1.5 eV (λ_{th}^{ph} = 800 nm) from the photoconductivity spectrum displayed on an enlarged scale (which is not shown here). The following facts can be seen from Fig. 4: (*1*) the maximum photocurrent in a specified TMP/DMB/MTHF system increases with decreasing MTHF concentration; and (2) the energy of the incident photons at which the photocurrent in a specified TMP/DMB/MTHF system is a maximum shifts to the lower energy side with decreasing MTHF concentration.

The photocurrent is proportional to the product of $\mu_e \cdot \tau \cdot \phi$, where μ_e is the electron mobility, τ is the lifetime of electrons in the conduction band, and ϕ is the probability of transition of the ground-state trapped electron to the conduction band induced by the incident photon (11). The values of electron mobilities in TMP and DMB at 77 K are not available at present. Tezuka *et al.* have reported the Arrhenius plot of μ_e in solid TMP in the temperature range down to 125 K (12). Extrapolating these data to 77 K leads to a value of 0.01 $cm^2\ V^{-1}\ s^{-1}$ for μ_e in TMP at 77 K, which is slightly lower than that in 3MP (13) and MTHF (14) at 77 K.[4] On the other hand, it is known that μ_e in DMB increases with decreasing temperature in the temperature range from 189 to 170 K (15). The reported value of μ_e in DMB at 170 K is ~20 $cm^2\ V^{-1}\ s^{-1}$. Thus it is expected that μ_e in DMB at 77 K would be higher than 20 $cm^2\ V^{-1}\ s^{-1}$ by simple extrapolation. The value of μ_e in MTHF is reported to be 0.055 $cm^2\ V^{-1}\ s^{-1}$ (14). However, Rice and Kevan have criticized this value later (16) and supported Ogasawara and Kevan's results, in which the lower limit of μ_e in MTHF is given to be 0.005 $cm^2\ V^{-1}\ s^{-1}$ (17). Clearly, μ_e in a 1:1 mixture of TMP and DMB would be considerably higher than that in MTHF at 77 K. Thus, the value of μ_e in TMP/DMB/MTHF systems at 77 K is expected to increase with decreasing MTHF concentration. As is shown in Fig. 4, the maximum photocurrent in TMP/DMB/5 mol% MTHF system is higher by two orders of magnitude than that in the neat MTHF system. The increase in the maximum photocurrent in the TMP/DMB/MTHF system with decreasing MTHF concentration may be explained in terms of the increase in μ_e. Another factor responsible for the increase in the maximum photocurrent would be an increase in τ with decreasing MTHF concentration, because electrons cannot be trapped in the TMP/DMB system at 77 K (1). Comparing the photocurrent in the TMP/DMB/5 mol% MTHF system with that in the neat MTHF system, the former is higher than the latter by more than one order of magnitude over the entire range of incident photon energies studied. Therefore it is unlikely that a large increase in the photocurrent in the TMP/DMB/5 mol% MTHF system is ascribed mainly to an increase in ϕ.

The V_0 values in MTHF, TMP, and DMB at 77 K are reported to be 1.15, 0.57, and 0.59 eV, respectively (18). The addition of TMP and DMB to MTHF therefore leads to lower V_0 values in the TMP/DMB/MTHF systems than that in the neat MTHF system at 77 K. The shift of the photoconductivity threshold and photocurrent maximum to the lower energy side with decreasing MTHF concentration in the TMP/DMB/MTHF systems can then be explained in terms of the decrease in the V_0 value.

3. Optical absorption spectra of trapped electrons in TMP–DMB–MTHF systems

Optical absorption spectra of trapped electrons in γ-irradiated TMP/DMB/MTHF systems at 77 K are shown in Fig. 5. Optical absorption maxima are observed around 1300 nm, indicating that electrons are trapped in MTHF aggregates. As is shown in Fig. 5, the optical absorption spectrum of trapped electrons decreases in the intensity with decreasing MTHF concentration. Two separated absorption peaks are observed over the MTHF concentration range from 50 to 100 mol%. The intensity of the peak at the shorter wavelength is higher than that at the longer wavelength in the neat MTHF system. The former is almost equal to the latter at the MTHF concentrations of 90 and 75 mol%, and the former is lower than the latter when the MTHF concentration is 50 mol%. Only one peak is observed at the MTHF concentrations of 25 and 5 mol%. Such a change in the absorption band structure perhaps indicates a change in the structure of the electron's

[4]Recent work (16) has shown that these electron mobility values (13, 14) were due to experimental artifacts.

Can. J. Chem. Downloaded from www.nrcresearchpress.com by 210.87.254.40 on 09/06/12
For personal use only.

Can. J. Chem. Downloaded from www.nrcresearchpress.com by 210.87.254.40 on 09/06/12
For personal use only.

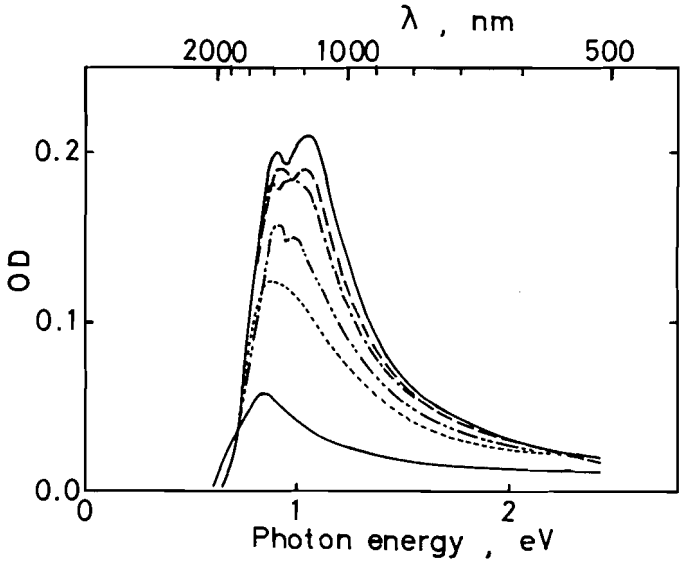

FIG. 5. Optical density of trapped electron absorption in TMP–DMB–MTHF systems vs. photon energy. — (top), neat MTHF; – – –, TMP – DMB – 90 mol% MTHF; –•–•–, TMP – DMB – 75 mol% MTHF; –••–, TMP – DMB – 50 mol% MTHF; ---, TMP – DMB – 25 mol% MTHF; — (bottom) TMP – DMB – 5 mol% MTHF.

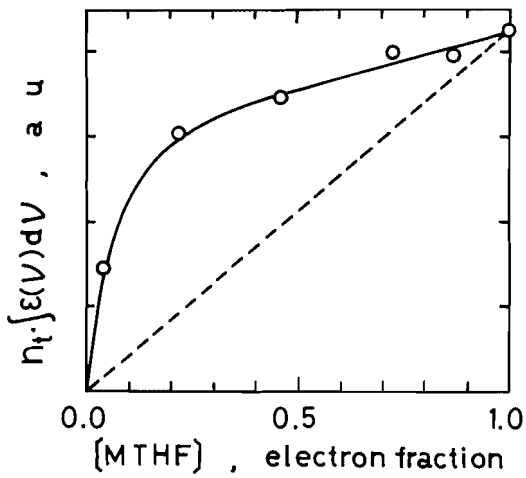

FIG. 6. Integrated optical absorption of trapped electrons vs. electron fraction of MTHF. The ordinate is given in an arbitrary unit.

solvation layer with MTHF concentration.

The tails of the optical absorption spectra on the shorter and longer wavelength sides converge to common curves within experimental errors over the MTHF concentration range from 25 to 100 mol% (Fig. 5). However, the curve of the spectrum for the TMP/DMB/5 mol% MTHF system lies above those for other systems at wavelengths longer than 1700 nm (0.72 eV). It should also be noted that the absorption maximum for the TMP/DMB/5 mol% MTHF system is shifted slightly to a longer wavelength compared with the remainder. The shift of the absorption maximum and the change in the relative intensities at wavelengths longer than the absorption maximum has also been reported for TMP/DMB/3MHx systems at 77 K (1).

In order to see the effect of MTHF concentration on the yield of trapped electrons in the TMP/DMB/MTHF systems, we have integrated the optical absorption spectra as displayed by OD vs. ν over the energy range from 3.65 eV (340 nm) to the thresholds of the spectra, which are obtained by extrapolating the absorption curves to zero OD. Let the number of trapped electrons per unit volume and the molar extinction coefficient of trapped electrons at ν be n_t and $\epsilon(\nu)$, respectively. The values of $n_t \int \epsilon(\nu)d\nu$ in an arbitrary unit thus obtained are shown as a function of electron fraction of added MTHF in Fig. 6. Unfortunately, no data are available for $\epsilon(\nu)$ of trapped electrons in the TMP/DMB/MTHF systems. Thus, we assume here that $\int \epsilon(\nu)d\nu$ is constant over the MTHF concentration range studied. If this assumption holds, the trapped electron yields in the TMP/DMB/MTHF systems will be higher than those expected from the contribution of direct radiolysis of MTHF added, because the experimental points lie above the dotted line in Fig. 6. Results similar to that in Fig. 6 have been previously obtained for alcohol–hydrocarbon systems in the liquid (19) and glassy states (4), but not in TMP/DMB/3MHx (1) and TMP/DMB/alcohol systems (2) at 77 K, where trapped electron yields are not higher than those expected from the contribution of direct radiolysis of 3MHx or alcohols added. Therefore it should be pointed out that the mechanism for electron trapping is different in TMP/DMB/MTHF systems and in TMP/DMB/3MHx or TMP/DMB/alcohol systems. Such difference in the electron trapping mechanism can be explained as follows: in TMP–DMB–3MHx systems, 3MHx is expected to mix homogeneously with TMP and DMB. High concentrations of TMP and DMB hinder the formation of 3MHx layers, which comprise several 3MHx molecules and are capable of trapping electrons, thus leading to a decrease in trapped electron yield. When one or two 3MHx molecules in a layer are replaced by one or two DMB molecules, the layer could lose its ability to trap an electron. On the other hand, in TMP/DMB/alcohol systems, the addition of alcohol does not appear to change substantially the property of the region outside the alcohol aggregate. Electrons generated in the TMP/DMB region outside the alcohol aggregate may preferentially react with geminate positive ions in the TMP/DMB region but not with the alcohol aggregate. Recently, we have found that some electron scavengers have considerably less efficiency for electron scavenging in the TMP/DMB systems than in other hydrocarbon systems at 77 K in which electrons can be localized.[5] The fact that the trapped electron yields lie above the dotted line in Fig. 6 can be explained if we assume that the property of TMP/DMB/MTHF systems is in between that of TMP/DMB/3MHx systems and that of TMP/DMB/alcohol systems. When MTHF is mixed with TMP and DMB, the recombination between electrons and positive ions mentioned above may be moderated by the MTHF molecules dispersing in the TMP/DMB region. In other words, since the MTHF molecule has a stronger affinity for electrons than the 3MHx molecule, it is capable of trapping electrons even when the MTHF concentration is relatively low. An alternative explanation for the difference in trapped electron yields between TMP/DMB/MTHF and TMP/DMB/alcohol systems may be the difference in the extent of aggregation of the polar component between these two systems.

It should also be noted that, as is seen from Fig. 6, the yield of trapped electrons varies by less than a factor of three over the MTHF concentration from 5 mol% to 100 mol%, but it is in the opposite direction to the change in magnitude of photocurrent.

4. Comparison between optical and photoconductivity spectra in the TMP/DMB/MTHF systems

As is already described, the photoconductivity spectra in the

[5]T. Kimura, T. Yoshida, and K. Fueki. Unpublished results.

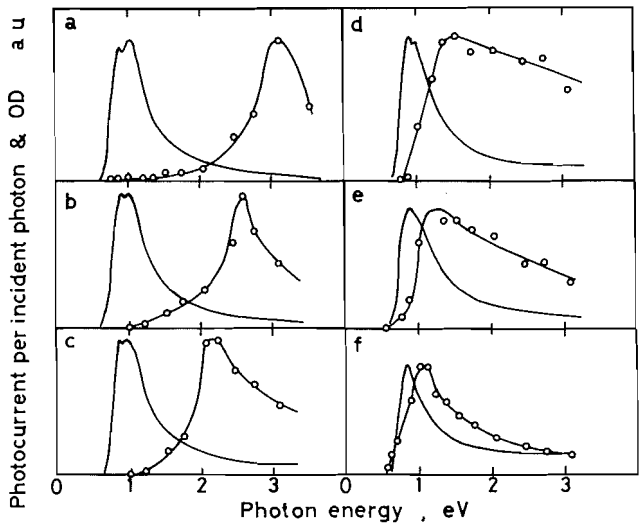

FIG. 7. Photoconductivity per incident photon and optical density of trapped electron absorption in TMP–DMB–MTHF systems vs. photon energy. *a*, neat MTHF; *b*, TMP – DMB – 90 mol% MTHF; *c*, TMP – DMB – 75 mol% MTHF; *d*, TMP – DMB – 50 mol% MTHF; *e*, TMP – DMB – 25 mol% MTHF; *f*, TMP – DMB – 5 mol% MTHF.

TABLE 1. Transition energies, E^{ph}_{max}, E^{ph}_{th}, and E^{ab}_{max} corresponding to λ^{ph}_{max}, λ^{ph}_{th}, and λ^{ab}_{max}, respectively, for trapped electrons in TMP–DMB–MTHF systems at 77 K

MTHF, mol%	E^{ph}_{max}, eV	E^{ph}_{th}, eV	E^{ab}_{max}, eV
100	3.1	1.5	0.92, 1.05
90	2.6	1.4	0.92, 1.03
75	2.3	1.2	0.89, 0.98
50	1.5	0.9	0.89, 0.98
25	1.4	0.7	0.89
5	1.1	0.5	0.84

TMP/DMB/MTHF systems shift towards the lower energy side with decreasing MTHF concentration, although the optical absorption spectra in these systems do not shift as significantly as the photoconductivity spectra. In order to demonstrate this clearly we have shown optical absorption and photoconductivity spectra in the TMP/DMB/MTHF system at the specified MTHF concentration in Fig. 7. The optical absorption and photoconductivity spectra in Fig. 7 are normalized to give the same value on the ordinate at each maximum. As is shown in Fig. 7, the optical absorption maximum, λ^{ab}_{max}, and photoconductivity maximum, λ^{ph}_{max}, in the neat MTHF system are separated by ~2 eV. However, λ^{ph}_{max} comes closer to λ^{ab}_{max} with decreasing MTHF concentration. In the TMP/DMB/5 mol% MTHF system the difference between λ^{ph}_{max} and λ^{ab}_{max} is ~0.2 eV. It is easy to visualize that the photoconductivity spectrum will be even closer to the optical absorption spectrum when the MTHF concentration is less than 5 mol%. The values of transition energies corresponding to λ^{ph}_{max}, λ^{ab}_{max}, and the photoconductivity threshold, λ^{ph}_{th}, for trapped electrons in the TMP/DMB/MTHF systems are listed in Table 1.

The optical absorption of trapped electrons is interpreted in terms of bound–bound and bound–free transitions (7–11, 20–22), although some workers have ascribed the entire spectrum to bound–free transitions (23). The present results also support the existence of bound–bound transitions. As is shown in Fig. 7*a*, bound–bound transitions dominate at the photon energy of ~1 eV and bound–free transitions at ~3 eV. When only bound–free transitions are allowed, photoconductivity and optical absorption spectra should be superimposable (11). Therefore, the fact that the photoconductivity spectrum in the TMP/DMB/MTHF system becomes closer to the corresponding optical absorption spectrum with decreasing MTHF concentration indicates that the extent of bound–free transitions increases with decreasing MTHF concentration. The V_0 value is expected to be lowered with decreasing MTHF concentration. The mean depth of electron traps in the TMP/DMB/MTHF system is also expected to be shallower with decreasing MTHF concentration. Thus, it seems plausible that the extent of bound–free transitions increases with decreasing MTHF concentration.

1. T. KIMURA, N. OGAWA, and K. FUEKI. Bull. Chem. Soc. Jpn. **54**, 3854 (1981).
2. T. KIMURA, K. YASUDA, S. FUKUDA, and K. FUEKI. Can. J. Chem. **61**, 553 (1983).
3. G. A. KENNEY-WALLACE and C. D. JONAH. J. Phys. Chem. **86**, 2572 (1982).
4. M. ITO, T. KIMURA, and K. FUEKI. Can. J. Chem. **59**, 2803 (1981).
5. T. ITO, N. UJIKAWA, and K. FUEKI. J. Phys. Chem. **79**, 2479 (1975).
6. L. KEVAN. *In* Advances in radiation chemistry. Vol. 4. *Edited by* M. Burton and J. L. Magee. Wiley-Interscience, New York. 1974. p. 248.
7. K. F. BAVERSTOCK and P. J. DYNE. Can. J. Chem. **48**, 2128 (1970).
8. T. HUANG, I. EISELE, D. P. LIN, and L. KEVAN. J. Chem. Phys. **56**, 4702 (1972).
9. T. FUNABASHI, N. OKABE, T. KIMURA, and K. FUEKI. J. Chem. Phys. **75**, 1576 (1981).
10. T. HUANG and L. KEVAN. J. Am. Chem. Soc. **95**, 3122 (1973).
11. S. A. RICE and L. KEVAN. J. Phys. Chem. **81**, 847 (1977).
12. T. TEZUKA, H. NAMBA, Y. NAKAMURA, M. CHIBA, K. SHINSAKA, and Y. HATANO. Radiat. Phys. Chem. **21**, 199 (1983).
13. Y. MARUYAMA and K. FUNABASHI. J. Chem. Phys. **56**, 2342 (1972).
14. T. HUANG and L. KEVAN. J. Chem. Phys. **61**, 4660 (1974).
15. J.-P. DODELET and G. R. FREEMAN. Can. J. Chem. **55**, 2264 (1977).
16. S. A. RICE and L. KEVAN. Radiat. Phys. Chem. **15**, 353 (1980).
17. M. OGASAWARA and L. KEVAN. Bull. Chem. Soc. Jpn. **51**, 2762 (1978).
18. D. GRAND and A. BERNAS. J. Phys. Chem. **81**, 1209 (1977).
19. J. R. BRANDON and R. F. FIRESTONE. J. Phys. Chem. **78**, 792 (1974).
20. S. A. RICE, G. DOLIVO, and L. KEVAN. J. Chem. Phys. **70**, 18 (1979).
21. N. KATO, K. AKIYAMA, and K. FUEKI. J. Phys. Chem. **85**, 3087 (1981).
22. T. SHIDA, S. IWATA, and T. WATANABE. J. Phys. Chem. **76**, 3683 (1972).
23. T. ICHIKAWA and H. YOSHIDA. J. Chem. Phys. **73**, 1540 (1980).

Can. J. Chem. Downloaded from www.nrcresearchpress.com by 210.87.254.40 on 09/06/12
For personal use only.

O-Methylation of a sulfone with methyl fluoride – antimony pentafluoride – sulfur dioxide. Preparation and properties of tetrahydro-1-methoxythiophenium 1-oxide hexafluoroantimonate[1]

MAGDY MALAK ABDEL-MALIK, PHILIP ARTHUR WOODWORTH DEAN, AND JAMES FREDERICK KING
Department of Chemistry, University of Western Ontario, London, Ont., Canada N6A 5B7

Received July 5, 1983

MAGDY MALAK ABDEL-MALIK, PHILIP ARTHUR WOODWORTH DEAN, and JAMES FREDERICK KING. Can. J. Chem. **62**, 69 (1984).

Reaction of sulfolane (tetrahydrothiophene 1,1-dioxide) (**1**) with methyl fluoride – antimony pentafluoride in liquid sulfur dioxide gives crystalline tetrahydro-1-methoxythiophenium 1-oxide hexafluoroantimonate (**2**), thereby providing the first characterized example of an alkoxysulfoxonium salt. This salt (**2**) is also formed, but more slowly, by reaction of methyl fluoride with the crystalline 1:1 complex of sulfolane and antimony pentafluoride. Reaction of **2** with nucleophiles leads to transfer of the methyl group, a facile process even with such weak nucleophiles as nitrobenzene and phenyl *N*,*N*-dimethylsulfamate. Spectroscopic evidence has been obtained for *O*-methylation of other sulfones, either by reaction with $MeF \cdot SbF_5 \cdot SO_2$, or via the sulfone $\cdot SbF_5$ complex and methyl fluoride, or by transmethylation with **2**.

MAGDY MALAK ABDEL-MALIK, PHILIP ARTHUR WOODWORTH DEAN et JAMES FREDERICK KING. Can. J. Chem. **62**, 69 (1984).

La réaction du sulfolane (tétrahydrothiophènedioxyde-1,1) (**1**) avec le fluorure de méthyle/pentafluorure d'antimoine dans du bioxyde de soufre liquide donne l'antimoine hexafluoro de tétrahydrométhoxy-1 thiophéniumoxyde-1 (**2**) cristallin fournissant ainsi le premier exemple caractérisé d'un sel d'alkoxysulfoxonium. Ce sel (**2**) se forme également, mais plus lentement, par la réaction du fluorure de méthyle avec le complexe cristallin 1:1 de sulfolane et de pentafluorure d'antimoine. Le composé **2** réagit avec les nucléophiles et conduit à un transfert de méthyle ce qui se produit très facilement même avec des nucléophiles faibles, tels le nitrobenzène et le *N*,*N*-diméthylphénylsulfamate. On a obtenu des preuves spectroscopiques pour la *O*-méthylation d'autres sulfones, soit par réaction avec le $MeF \cdot SbF_5 \cdot SO_2$ ou par l'intermédiaire du complexe sulfone $\cdot SbF_5$ et du fluorure de méthyle, soit par une trans-méthylation impliquant le composé **2**.

[Traduit par le journal]

Sulfones are notoriously weak nucleophiles, being protonated only by very strong acids and forming stable complexes only with powerful Lewis acids (1, 2, and refs. cited). The low reactivity of sulfolane[2] (**1**) has, in fact, led to its use as a solvent

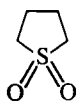

1

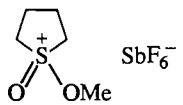

2

for such powerful alkylating agents as methyl trifluoromethanesulfonate and trimethyloxonium tetrafluoroborate (4, 5). Whiting and co-workers (6) have shown that *O*-arylation of sulfones to form aryloxysulfoxonium salts can be effected with aryldiazonium salts, a reaction which apparently proceeds by way of the exceedingly reactive aryl cation. Alkoxysulfoxonium species, formed both by *O*-alkylation of sulfones (5, 7) and by other pathways (8–11), have been postulated as intermediates on a number of occasions. The only report known to us in which any property of an alkoxysulfoxonium salt has been described, however, is that of Jackman and co-workers (4) who mention briefly in a footnote that "treating anhydrous solutions of silver tetrafluoroborate or silver hexafluoroantimonate in sulfolane with methyl iodide" gives solutions showing a singlet at 4.45 ppm in the ^{1}Hmr spectrum; the solutions were described as "unstable at room temperature", decomposing in respectively 1 h and 24 h.

In connection with a collaborative study of the genotoxic effects of powerful alkylating agents, it has been found that sulfolane is an unreactive, water-miscible solvent suitable for the examination of the mutagenic activity of alkylating agents by the Ames test.[3] A particular focus of this study has been the use of very powerful alkylating agents not requiring any kind of potentiation *in situ* but which are added to the biological system in the form that actually delivers the alkyl group to the biological receptor. It is evident that in any such investigation the product of the alkylation of the solvent holds a unique position, since it is likely to be the most powerful alkylating agent that can reliably be added using the solvent as diluent. Any more potent alkylating agent than this will probably alkylate the solvent in the time taken to make up a solution and introduce it to the biological testing medium.[4] Accordingly, we set out to obtain a very simple *O*-alkylated derivative of sulfolane, viz. tetrahydro-1-methoxythiophenium 1-oxide hexafluoroantimonate (**2**). Its preparation and characterization, along with a preliminary study of its reactions with nucleophiles, form the basis of this paper; its behaviour in biological systems will be described elsewhere.

Results and discussion

Methyl fluoride – antimony pentafluoride in sulfur dioxide is an extremely powerful methylating agent which has been

[1]Part 25 in the series Organic Sulfur Mechanisms; for part 24, see ref. 23.

[2]In this paper we use the trivial name "sulfolane" in preference to the clumsier alternatives "tetramethylene sulfone" and "tetrahydrothiophene 1,1-dioxide"; the last is preferred by Chemical Abstracts, but the first – in its overseas form, "sulpholane" – is the entry name in the most recent edition of the Dictionary of Organic Compounds (3).

[3]J. E. Cummins, K. Rochefort, J. D. Lock, and J. F. King. Unpublished observations.

[4]As we have noted elsewhere (12), failure to take account of this possibility can give highly misleading results.

Can. J. Chem. Downloaded from www.nrcresearchpress.com by 210.87.254.5 on 09/06/12
For personal use only.

Can. J. Chem. Downloaded from www.nrcresearchpress.com by 210.87.254.5 on 09/06/12
For personal use only.

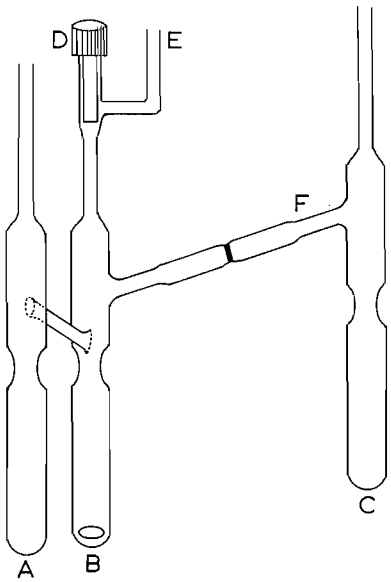

FIG. 1. Apparatus for preparation of **2**.

shown to contain $MeOSO^+$ $Sb_nF^-_{5n+1}$ (13–15). The reaction of sulfolane (**1**) with this methylating agent appeared, from preliminary experiments in conventional round-bottomed flasks, to lead to the *O*-methylated product (**2**). The ^{1}Hmr spectrum showed a sharp peak around 4.5 ppm along with complex signals centred around 3.9 and 2.6 ppm. This procedure generally gave the product as a yellowish syrup, though on one occasion white crystals were obtained; in all cases, however, the nmr spectrum of the product showed unreacted sulfolane. Use of dry box – vacuum line techniques with the apparatus shown in Fig. 1, as described in detail in the experimental section, led to a procedure in which premixed $MeF \cdot SbF_5 \cdot SO_2$ was added to a slight excess of **1** in SO_2, and which consistently gave **2** as a white crystalline solid. The identity of this material was established by elemental analysis, nmr spectroscopy, and its chemical reactions. The ^{13}Cmr spectrum of **2** (in liquid sulfur dioxide) showed resonances at δ 61.4, 50.4, and 22.7; sulfolane (**1**) itself under these conditions shows signals at 51.5 and 22.8 ppm. Comparison of the ^{13}Cmr spectrum of **2** with that of **1** and with those of other methylated sulfones (see below) allows the assignment of the signal at 61.4 ppm in the spectrum of **2** to the $\diagdown\overset{+}{\mathrm{S}}\mathrm{O}\text{—}\mathrm{O}Me\diagup$ group. The ^{1}Hmr spectrum of **2** (in CD_2Cl_2) consisted of a sharp singlet at 4.49 ppm and a pair of multiplets in the ranges 3.6 to 4.2 and 2.5 to 2.7 ppm; on decoupling (by irradiating at 2.6 and 3.9 ppm, respectively) the latter signals were in turn transformed into an AB quartet (δ 4.04 and 3.81, J_{AB} 15 Hz) and an apparent singlet (δ 2.58 ppm).

The ^{1}Hmr spectrum of a mixture of **1** and **2**, in CD_2Cl_2 or in neat **1**, is simply a superimposition of the spectra of **1** and **2**. When **2** is dissolved in sulfolane-d_8 (about 10 equiv.) and the spectrum run as soon as possible (<10 min), the multiplets around 3.9 and 2.6 ppm almost disappear, the strong signals at 3.0 and 2.2 ppm characteristic of sulfolane (**1**) appear, while the singlet at 4.49 ppm is unaltered; the spectrum remains unchanged on standing for at least one week. These observations clearly indicate that under our conditions the transfer of the methyl group from **2** to **1** is fast on the chemical time-scale ($t_{1/2}$ < 2 min), but slow on the nmr time-scale ($t_{1/2}$ > 0.025 s, as shown by the absence of coalescence of the methylene signals of **1** and **2** in CD_2Cl_2 or neat **1**).

In a sealed tube the alkoxysulfonium salt (**2**) keeps indefinitely as the crystalline solid or a solution in liquid sulfur dioxide; solutions of **2** in sulfolane showed no significant decomposition in one week but gradually turned brown over longer periods. As noted above, however, Jackman and coworkers (4) reported that **2** in sulfolane decomposes to methyl fluoride and SbF_5 in 24 h. It seems likely from the absorption they observed at 4.45 ppm in the ^{1}Hmr spectrum that they indeed had **2** in the solution, and in the absence of further information we ascribe the relatively rapid decomposition of their sample to the action of impurities.

We have also looked into the possibility of making **2** by reacting a preformed sulfolane·SbF_5 complex with methyl fluoride in the hope that, once formed, handling an easily prepared, stable isolable complex might avoid some of the experimental difficulties attendant upon frequent quantitative transfer of antimony pentafluoride. Sulfolane and SbF_5 gave a solid product which gave correct elemental analyses for a 1:1 complex and which showed ^{1}Hmr multiplets centered at 2.1 and 3.3 ppm and ^{13}Cmr lines at 53.3 and 22.6 ppm. Reaction of this complex with excess MeF in liquid SO_2 in an nmr tube showed a clean conversion to **2** which required, however, a number of hours at room temperature to go to completion.

Methylene chloride-d_2 solutions of **2**, though sufficiently stable for the determination of nmr spectra, gradually decompose ($t_{1/2}$ ~ 5 h) with formation of sulfolane and a peak at 3.0 ppm ascribed to methyl chloride; the same peak appears, but more slowly, with chloroform-*d*. These observations point to the following scheme involving initial formation of a dialkylchloronium ion (16) which then cleaves to methyl chloride and the unstable halocarbenium species (17).

$$\mathbf{2} + \mathrm{ClCD}_n\mathrm{Cl}_{(3-n)} \rightarrow \mathbf{1} + [\mathrm{CH_3}\text{—}\overset{+}{\mathrm{Cl}}\text{—}\mathrm{CD}_n\mathrm{Cl}_{(3-n)}] \rightarrow \mathrm{CH_3Cl} + [\overset{+}{\mathrm{C}}\mathrm{D}_n\mathrm{Cl}_{(3-n)}]$$

These observations, of course, imply that **2** is a very powerful methylating agent, and we have carried out some preliminary experiments using nmr to make a brief survey of its methylating capabilities. As expected, **2** reacts instantly with water, the ^{1}Hmr spectrum (in D_2O) showing a methanol resonance at 3.35 ppm and the two multiplets of sulfolane at 2.2 and 3.1 ppm. Table 1 summarizes a number of nmr experiments, which show that **2** rapidly methylates sulfoxides, diphenyl sulfide, and sulfones, and reacts rather more slowly with nitrobenzene and phenyl *N*,*N*-dimethylsulfamate. This last reaction allows a very rough comparison of **2** with methyl fluorosulfate. Whereas the reaction with **2** in CD_2Cl_2 solution (~0.1 *M* in substrate and ~0.05 *M* in **2**) was about two-thirds complete after about 40 min at room temperature, even neat methyl fluorosulfate was unreacted after 12 h at room temperature and required heating at 50°C for several hours to achieve the same extent of methylation (18); one may thus conservatively estimate that **2** is at least three orders of magnitude more reactive than methyl fluorosulfate. The reactions of **2** with dimethyl and diethyl sulfones were, like that with sulfolane-d_8, complete in less than the time required to observe the nmr spectrum. The spectra showed peaks appropriate to equilibrium mixtures (in CD_2Cl_2) with equilibrium constants, *K*, of roughly 0.3 and 0.6, respectively.

$$R_2SO_2 + \mathbf{2} \overset{K}{\rightleftharpoons} R_2\overset{+}{\mathrm{S}}(=\mathrm{O})\mathrm{OMe}\ \ SbF_6^- + \mathbf{1}$$

TABLE 1. Methylations[a] with tetrahydro-1-methoxythiophenium 1-oxide hexafluoroantimonate (**2**)

Substrate	^{1}Hmr peaks[b]	Assignment	Reaction extent and time
$PhNO_2$	4.84(s), 7.8–8.8.0(m), 8.6–8.7("d")	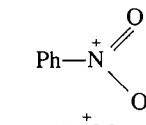	>60% in 40 min
Ph_2S	3.58(s), 7.8(s)	$Ph_2\overset{+}{S}Me$	Complete in <10 min
Me_2SO	3.31(s), 4.15(s)	$Me_2\overset{+}{S}$—OMe[d]	Complete in <10 min
Ph_2SO	4.30(s), 7.86("s")	$Ph_2\overset{+}{S}OMe$	Complete in <10 min
Me_2SO_2	3.86(s), 4.45(s)	Equilibrium mixture (see text)	Complete in <10 min
Et_2SO_2	1.58(t), 3.90(q), 4.42(s)	Equilibrium mixture (see text)	Complete in <10 min
$PhOSO_2NMe_2$	3.71(s), 7.4–7.6(m)	$PhOSO_2\overset{+}{N}Me_3$[e]	>70% in 40 min
	4.66(s), 3.76(s), 3.56(s), 2.7–3.5(m) 2.0–2.5(m)	plus unidentified material	Complete in <10 min

[a]In CD_2Cl_2 at room temperature.
[b]XL-100 spectra.
[c]Reported: 4.65 and 7.6–8.2 ppm in liquid SO_2 (16).
[d]J. D. Lock (unpublished observations in this laboratory) found 3.23 and 4.02 ppm (in CD_3CN).
[e]Reported: 3.70 and 7.56 ppm (in CD_3CN) (18).
[f]Reported: 4.86, 3.18, 2.24 ppm in liquid SO_2 (16).

We have also explored the preparation of other *O*-methylated sulfones by reaction of the sulfone with $SbF_6 \cdot MeF \cdot SO_2$. The ^{13}Cmr spectrum of the product from dimethyl sulfone showed peaks at 60.9 and 39.9 ppm along with a signal for the unreacted sulfone (at 42.8 ppm). Upon washing with Freon 21 we obtained a solid material which appeared to be a 60:40 mixture of $Me_2\overset{+}{S}O$—OMe SbF_6^- and Me_2SO_2, but we were unable to remove the remaining sulfone. The peaks at 60.9 and 39.9 ppm also appeared when dimethyl sulfone was mixed with **2** in liquid SO_2, with the signal amplitudes corresponding to $K \sim 0.4$. Reaction of the solid $Me_2SO_2 \cdot SbF_5$ complex with methyl fluoride in liquid SO_2, overnight at room temperature, gave a material which showed strong ^{13}Cmr resonances at 60.7 and 39.8 ppm (from $Me_2\overset{+}{S}O_2Me$ and $Me_2\overset{+}{S}O_2$Me respectively) with only a weak signal (at 42.6 ppm) due to unreacted Me_2SO_2, thereby evidently providing the cleanest specimen of $Me_2\overset{+}{S}O$—OMe SbF_6^- that we have observed to date.

Attempts to methylate diethyl sulfone with $MeF \cdot SbF_5 \cdot SO_2$ gave only intractable oily products, while transmethylation with **2** in liquid SO_2 gave a mixture showing ^{13}Cmr lines due to unreacted diethyl sulfone (δ_C = 46.6 and 5.4 ppm), unreacted **2**, and the expected $Et_2\overset{+}{S}O_2$Me (δ_C = 61.0, 46.6, and 5.4 ppm); we estimate $K \sim 0.8$ in liquid SO_2. Similar reactions of diphenyl sulfone showed largely unreacted starting materials with small peaks at 62.3, 129.2, 132.0, and 139.3 ppm, reasonably attributable to $Ph_2\overset{+}{S}O$—OMe SbF_6^- ($K < 0.1$).

This study shows that alkoxysulfoxonium salts are stable, isolable materials with interesting potential as alkylating agents. We hope to exploit this potential in future work.

Experimental

Sulfolane (tetramethylene sulfone; Aldrich Chemical Co.) was purified as described in the literature (19) and stored over 3 Å molecular sieves at 40°C. Antimony pentafluoride (PCR Research Chemicals, Inc.) was distilled twice in a dry nitrogen atmosphere before use, then stored in a sealed container in a dry box. Sulfur dioxide (Canadian Liquid Air Ltd; anhydrous grade) and dichlorofluoromethane (Freon 21; Matheson of Canada Ltd.) were allowed to stand over 3 Å molecular sieves, in the gas and liquid phases, respectively, for at least 12 h before use. Neither methyl fluoride (Pfaltz and Bauer, Inc.) nor dimethyl sulfone (Aldrich Chemical Co.) showed any significant impurity by ^{1}Hmr spectroscopy; they were used as received, as were diphenyl sulfone (Aldrich), which showed no impurity by ^{13}C nmr, and sulfolane-d_8 (Merck Sharp and Dohme Canada Ltd.). Diethyl sulfone was prepared by oxidation of diethyl sulfide with hydrogen peroxide – acetic acid; mp 73°C (lit. (20) mp 70°C).

The reaction vessel for the reactions with methyl fluoride – antimony pentafluoride (Fig. 1) consisted of three 18-mm od glass tubes, A, B, and C, each with constriction, as shown, and of roughly 20-mL capacity. The upper part of tubes A and C was made of 9-mm od (ca. 6-mm id) special-wall glass tubing (which is particularly easy to flame seal) while tube B was topped by a 6-mm Rotaflo Teflon stopcock, D. The A–B connection was of 9-mm od special-wall tubing and sloped upwards at ca. 30° above horizontal from B to A while the C–B connection similarly sloped from B to C but had in it a 10-mm medium sinter; the A–B and B–C connections were mutually at right angles. Tube B, the principal reaction vessel, contained a Teflon-covered magnetic stirrer bar. The dimensions of the apparatus were determined in large part by the necessity of having it pass through the 30-cm diameter port of the glove box (see below).

The apparatus was baked out at 140°C (50°C for the Teflon stopcock) and then transferred to an N_2-filled dry box in which the dry atmosphere was maintained by circulation through liquid nitrogen cooled copper coils.

Reaction of sulfolane with methyl fluoride – antimony pentafluoride

In the glove box, antimony pentafluoride (4.2 g; 19 mmol) was added to tube B from an all-glass syringe. The stopcock D was closed and the openings on A and C were sealed with serum caps before the apparatus was removed from the dry box. Using standard N_2-vacuum techniques, warm liquid sulfolane (2.5 mL, 26 mmol) was injected into the tube A under nitrogen. The apparatus was then attached to a glass and Teflon vacuum line at E using a 3/8-in. Ultratorr fitting, evacuated, and, with A and B cooled in liquid nitrogen, the 9-mm tubes attached to A and C were flame sealed. On the calibrated

Can. J. Chem. Downloaded from www.nrcresearchpress.com by 210.87.254.5 on 09/06/12
For personal use only.

Can. J. Chem. Downloaded from www.nrcresearchpress.com by 210.87.254.5 on 09/06/12
For personal use only.

vacuum line, SO_2 (ca. 75 mmol) was metered into tube B by gaseous volume and a similar amount was condensed onto the sulfolane. Methyl fluoride (25 mmol) was similarly condensed into tube B, before closing D. The apparatus was moved from the vacuum line and allowed to warm to room temperature (**with care!** the vessel being under ca. 3 atm pressure).

The mixture of SbF_5 and CH_3F in SO_2 was stirred for 15 min at room temperature, then poured into the sulfolane solution in tube A; the addition was noticeably exothermic and was accompanied by the appearance of a slight yellow colour. The total reaction mixture was returned to tube B and stirred for a further 15 min. Excess CH_3F and SO_2 were removed by slow cooling of tube A over a few hours. Finally A was frozen in liquid N_2 before flame sealing the arm between A and B. After reattachment to the vacuum line, dichlorofluoromethane (ca. 10 mmol) was condensed through D onto the oily, yellow viscous residue in tube B using liquid nitrogen cooling. The apparatus was once more removed from the vacuum line and allowed to warm to room temperature. The Freon–product mixture was stirred for 5–10 min before decanting the upper (Freon) layer (which contains unreacted sulfolane) from B into C. The Freon was returned to tube B by cooling and this washing process repreated twice. Finally, the Freon was returned to B and the heterogeneous mixture of the product with Freon kept in an ice bath for about 30 min. During this time, white crystals of the product formed. The mother liquor was decanted into C and the product washed twice with Freon before cooling C in liquid N_2 and flame sealing at F.

The rest of the apparatus (tube B) containing the pure product was reattached to the vacuum line and pumped for several hours to remove any residual Freon. In the dry box, the apparatus was broken at the constriction. The product (5.8 g, 82% yield) was transferred to a sealable glass container and stored in the dry box at room temperature. Under these conditions little deterioration was noticed over a period of several months. *Anal.* calcd. for $C_5H_{11}O_2SSbF_6$: C 16.19, H 2.99, S 8.64, Sb 32.82; found: C 16.05, H 3.09, S 8.66, Sb 33.13.

Preparation of antimony pentafluoride – sulfolane 1:1 adduct

A two-armed H-shaped glass reaction/filtration vessel of a type described earlier (21) was used for this synthesis. In the glove box, antimony pentafluoride (4.0 g, 18 mmol) was added from an all-glass syringe to the arm with no stirrer. The 9-mm od outlet of each tube was capped with a serum cap for removal of the apparatus from the dry box. Outside the glove box, liquid sulfolane (1.9 mL, 20 mmol) was added to the arm with the stirrer under a flow of dry nitrogen. The apparatus was attached to the vacuum line at the sulfolane side, evacuated, and flame sealed at the unattached outlet. Sulfur dioxide (ca. 75 mmol) was introduced with liquid nitrogen cooling prior to separation from the vacuum line by flame sealing at the 9-mm outlet. With care (see above), the apparatus was allowed to warm to room temperature, some SO_2 was condensed onto the SbF_5 by gentle cooling, and the SbF_5 solution was slowly added to the well-stirred sulfolane solution. Slow reduction of the solution volume by cooling the opposite arm, with the concomitant cooling effect on the product solution, resulted in crystallization of the product which was filtered off, washed with small portions of SO_2, and isolated in the general manner reported previously (21). *Anal.* calcd. for $C_4H_8O_2SSbF_5$: C 14.26, H 2.39; found: C 14.03, H 2.56.

Nuclear magnetic resonance samples and spectra

Samples for proton nmr spectroscopy, except those involving liquid SO_2 as solvent, were prepared in standard 5-mm od capped nmr tubes. The experiments in Table 1 were carried out by transferring **2** (~20 mg, ~0.05 mmol) to the nmr tube in the dry box and adding the substrate (~0.1 mmol), CD_2Cl_2 (1 mL), and TMS. The spectra (XL-100) were run within 5 min, with subsequent spectra to follow the course of slow reactions run on the T-60 at appropriate intervals.

For samples in liquid SO_2 the procedure was as follows: a 5-mm od medium-walled nmr tube sealed onto ca. 8-cm lengths of 9-mm od special-walled glass tubing was baked out at 140°C; under an atmosphere of dry nitrogen (in the dry box for solid materials or a flow of H_2SO_4-dried N_2 for liquids) an appropriate mass of each solid reactant or volume of liquid sulfolane was added to the tube; the tube was attached to the calibrated vacuum line via the 9-mm tubing and 3/8-in. Ultratorr union and evacuated; with liquid N_2 cooling, appropriate amounts of SO_2 and MeF, when needed, were metered into the tube before flame sealing at the top of the 5-mm od section. Samples for ^{13}C nmr spectroscopy of SO_2 solutions were made up in an analogous manner in flame-sealed handmade tubes of 10-mm od standard-wall glass tubing.

Samples contained in capped tubes were used immediately. Similarly the solutions in flame-sealed tubes were used fresh or stored in liquid nitrogen until used.

Proton nmr spectra were measured using a Varian T-60, Varian EM-360, or Varian XL-100-12 spectrometer. All the ^{13}C nmr spectra were obtained at 308 K using the XL-100-12 spectrometer system operating at 25.2 MHz in the FT mode; the 10-mm sample tubes were held coaxially in a 12-mm od standard nmr tube and a 10% (v/v) solution of dioxane in D_2O in the outer annulus was used as an external ^2D lock and ^{13}C reference, as described earlier (22). For this reference, δ_C (TMS in SO_2, int) = δ_C (dioxane in D_2O, ext) + 67.8 ppm (22). Typically, satisfactory ^{13}C nmr spectra of ca. 0.15 *m* solutions were obtained in several thousand transients with a 5 kHz spectra window, 3.3 s acquisition time, 3.5 s cycle time, and 35° (8.5 μs) tip angle (pulse width) (28° (7 μs) for samples containing Ph_2SO_2).

Acknowledgments

This work was supported by NSERC Strategic Grant G0506. We are grateful to the co-holders of this grant, Professors J. E. Cummins (Department of Plant Sciences, principal investigator), J. V. Frei (Department of Pathology), and B. G. Boyes (Department of Anatomy), for their collaboration in the larger investigation, which made the present study possible.

1. G. A. OLAH, A. T. KU, and J. A. OLAH. J. Org. Chem. **35**, 3904 (1970).
2. R. C. PAUL, D. S. DHILLON, D. KONWER, and J. K. PURI. J. Inorg. Nucl. Chem. **39**, 1011 (1977).
3. Dictionary of organic compounds. 5th ed. Chapman and Hall, New York and London. 1982. Entry S-00998.
4. C. P. WONG, L. M. JACKMAN, and R. G. PORTMAN. Tetrahedron Lett. 921 (1974).
5. E. S. LEWIS, S. KUKES, and C. D. SLATER. J. Am. Chem. Soc. **102**, 1619 (1980).
6. G. R. CHALKLEY, D. J. SNODIN, G. STEVENS, and M. C. WHITING. J. Chem. Soc. (C), 682 (1970).
7. S. BRAVERMAN and D. REISMAN. Tetrahedron Lett. 1753 (1977).
8. G. R. CHALKLEY, D. J. SNODIN, G. STEVENS, and M. C. WHITING. J. Chem. Soc. Perkin Trans. 1, 1580 (1978).
9. T. DURST and K. C. TIN. Can. J. Chem. **49**, 2374 (1971).
10. F. JUNG and T. DURST. J. Chem. Soc. Chem. Commun. 4 (1973).
11. F. JUNG, N. K. SHARMA, and T. DURST. J. Am. Chem. Soc. **95**, 3420 (1973).
12. J. E. CUMMINS and J. F. KING. Chem. Br. **15**, 329 (1979).
13. P. E. PETERSON, R. BROCKINGTON, and D. W. VIDRINE. J. Am. Chem. Soc. **98**, 2660 (1976).
14. G. A. OLAH, D. J. DONOVAN, and H. C. LIN. J. Am. Chem. Soc. **98**, 2661 (1976).
15. R. J. GILLESPIE, F. G. RIDDELL, and D. R. SLIM. J. Am. Chem. Soc. **98**, 8069 (1976).
16. G. A. OLAH, J. R. DE MEMBER, Y. K. MO, J. J. SVOBODA, P. SCHILLING, and J. A. OLAH. J. Am. Chem. Soc. **96**, 884 (1974).
17. G. A. OLAH and Y. K. MO. *In* Carbonium ions. *Edited by* G. A. Olah and P. v. R. Schleyer. Wiley–Interscience, New York. 1976. Chapt. 36. p. 2135, esp. p. 2146.
18. J. F. KING and T. M. L. LEE. Can. J. Chem. **59**, 356 (1981).
19. L. F. FIESER and M. FIESER. Reagents for organic synthesis.

Vol. 1. John Wiley and Sons, New York. 1968. p. 1144.
20. S. F. BIRCH and W. S. G. P. NORRIS. J. Chem. Soc. **127**, 1934 (1925).
21. T. BIRCHALL, P. A. W. DEAN, and R. J. GILLESPIE. J. Chem. Soc. (A), 1777 (1971).
22. P. A. W. DEAN, D. G. IBBOTT, and J. B. STOTHERS. Can. J. Chem. **54**, 166 (1976).
23. J. F. KING and J. H. HILLHOUSE. Can. J. Chem. **61**, 1583 (1983).

Can. J. Chem. Downloaded from www.nrcresearchpress.com by 210.87.254.5 on 09/06/12
For personal use only.

Vinyl ether hydrolysis. XVII. Oxacyclonon-2,8-diene and the question of the unorthodox reaction mechanism for 9-methoxyoxacyclonon-2-ene[1]

R. A. BURT, Y. CHIANG, A. J. KRESGE,[2] AND S. SZILAGYI

Department of Chemistry and Scarborough College, University of Toronto, Scarborough, Ont., Canada M1C 1A4

Received June 1, 1983

R. A. BURT, Y. CHIANG, A. J. KRESGE, and S. SZILAGYI. Can. J. Chem. **62**, 74 (1984).

The acid-catalyzed hydrolysis of the nine-membered ring cyclic vinyl ether, oxacyclonon-2,8-diene, occurs with a normal isotope effect, $k_{H^+}/k_{D^+} = 1.94$, which indicates that this reaction proceeds by the conventional vinyl ether hydrolysis mechanism involving rate-determining proton transfer to carbon. The specific rate of this reaction, $k_{H^+} = 3.9 \times 10^{-3} M^{-1} s^{-1}$, may then be used to show that there is no significant ring-size effect on the rate of hydrolysis of a vinyl ether group in a nine-membered ring. The previously noted unusually great reactivity of the vinyl ether group in 9-methoxyoxacyclonon-2-ene, for which an unorthodox reaction mechanism has been claimed, must therefore be due to some other cause.

R. A. BURT, Y. CHIANG, A. J. KRESGE et S. SZILAGYI. Can. J. Chem. **62**, 74 (1984).

L'hydrolyse de l'éther vinylique cyclique à 9 chaînons, oxacyclononedième-2,8, catalysée par un acide, se produit avec un effet isotopique normal $k_{H^+}/k_{D^+} = 1,94$ qui indique que cette réaction se fait selon le mécanisme conventionnel d'hydrolyse d'un éther vinylique qui implique comme étape déterminante le transfert du proton au carbone. On peut utiliser la vitesse spécifique de cette réaction $k_{H^+} = 3,9 \times 10^{-3} M^{-1} s^{-1}$ pour montrer alors que la dimension du cycle n'a pas un effet significatif sur la vitesse d'hydrolyse d'un éther vinylique dans un cycle à 9 chaînons. La grande réactivité d'un groupe éther vinylique dans le méthoxy-9 cyclononène-2 rapportée antérieurement, et pour laquelle on a proposé un mécanisme peu orthodoxe doit donc être dû à d'autres causes.

[Traduit par le journal]

The acid-catalyzed hydrolysis of simple vinyl ethers is known to occur by rate-determining protonation of the β-carbon atom of the double bond system [1], followed by rapid steps which convert the ensuing alkoxycation to a

$$[1]\quad CH_2{=}CHOR \xrightarrow[slow]{HA} CH_3\overset{+}{C}HOR$$

$$[2]\quad CH_3\overset{+}{C}HOR \xrightarrow[fast]{H_2O} CH_3\underset{OH}{C}HOR \xrightarrow[fast]{} CH_3\underset{O}{C}H + HOR$$

hemiacetal intermediate and then transform the latter into saturated alcohol plus aldehyde or ketone products [2] (1). The sole exception to this reaction mechanism appears to be the hydrolysis of the vinyl ether functional group in 9-methoxyoxacyclonon-2-ene, **1** (2).[3] Evidence obtained for this substrate

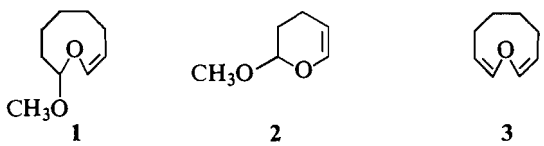

1 **2** **3**

suggests that, in dilute hydrochloric acid solution, it reacts by slow proton transfer to carbon, but that in acetic acid buffers some subsequent step becomes rate determining and carbon protonation therefore is reversible.[4]

We have tried, so far with no success, to induce a similar change in rate-determining step in the hydrolysis of other vinyl ethers (7). In the course of this work, however, we learned that **1** appears to be unusually reactive, even under conditions where its hydrolysis mechanism seems to be normal: the six-membered ring homolog of **1**, 2-methoxy-2,3-dihydropyran, **2**, is 500 times less reactive (7*b*). In order to detemine whether this unexpected reactivity is a consequence of the difference in ring size between **1** and **2**, or is caused by some further peculiarity in the mechanism of hydrolysis of **1**, we have now examined the reaction of oxacyclonon-2,8-diene, **3**, a cyclic vinyl ether whose ring contains the same number of atoms as **1**.

Experimental

Materials

Oxacyclonon-2,8-diene was prepared from 1,3-cyclooctadiene (Chemical Samples Co.) via the monoepoxide (8) by a modification of the thermolysis method of Crandall and Watkins (9), using a higher temperature and shorter reaction time plus diphenyl ether as a diluent to suppress polymerization. Maximum yields of the divinyl ether (48%) were obtained by heating the epoxide plus an equal amount of diphenyl ether at 255°C for 60 min in a Pyrex vessel, which had been washed with aqueous sodium hydroxide, water, and then carefully dried. The product was separated from diluent and unconverted starting material by hplc; its nmr spectrum was consistent with its structure.

All other materials were best available commercial grades. Solutions in H_2O were prepared using deionized water which was purified further by distillation from alkaline permanganate, and those in D_2O using heavy water (Merck, Sharpe, and Dohme) as received.

Kinetics

Rates of reaction were determined spectroscopically by monitoring the strong end absorption of oxacyclonon-2,8-diene at 200 nm. Measurements were made using a Cary Model 118C spectrometer with cell compartment thermostatted at 25.1 ± 0.05°C. Absorbance readings were generally taken to about 90% reaction and endpoints were measured after 10 half-lives. The latter were stable, and the data conformed to the first-order rate law precisely.

Results

First-order rate constants for the hydrolysis of oxacyclonon-2,8-diene catalyzed by dilute hydrochloric acid were deter-

[1]For Part XVI, see ref. 14.

[2]Author to whom correspondence may be addressed.

[3]The names of **1** and **2** in the Hantzsh–Widman system of nomenclature for heterocyclic compounds are 2-methoxy-2,3,4,5,6,7-hexahydrooxonin and 2,3,4,5-tetrahydrooxonin respectively.

[4]Reversible carbon protonation is known to occur in the hydrolysis of vinyl amines under some conditions (3), and it has also been demonstrated recently in the hydrolysis of certain vinyl selenides (4), ketene dithioacetals (5), and ketene diselenoacetals (6).

Can. J. Chem. Downloaded from www.nrcresearchpress.com by 210.87.254.40 on 09/06/12
For personal use only.

Can. J. Chem. Downloaded from www.nrcresearchpress.com by 210.87.254.40 on 09/06/12
For personal use only.

TABLE 1. Rates of hydrolysis of oxacyclonon-2,8-diene in dilute hydrochloric acid solutions at 25°C[a]

[Acid], M	$10^4\ k_{obs}$, s^{-1}
H_2O solution	
0.0098	0.372, 0.372
0.0200	0.751, 0.735, 0.762
0.0400	1.57, 1.56, 1.56
0.0700	2.72, 2.71, 2.71
0.100	3.85, 3.91
$k_{H^+} = (3.90 \pm 0.02) \times 10^{-3}\ M^{-1}\ s^{-1}$	
D_2O solution	
0.0227	0.402, 0.402
0.0469	0.843, 0.849
0.0690	1.36, 1.35
0.0929	1.77, 1.79
0.118	2.30, 2.32
$k_{D^+} = (2.01 \pm 0.03) \times 10^{-3}\ M^{-1}\ s^{-1}$	

[a]Ionic strength = acid concentration; error limits are standard deviations of mean values.

TABLE 2. Rates of hydrolysis of oxacyclonon-2,8-diene in concentrated perchloric acid solutions at 25°C[a]

Wt.% $HClO_4$	$10^3\ k_{obs}$, s^{-1}
4.70	2.75, 2.75, 2.77
9.20	8.14, 7.85, 8.17
13.45	18.1, 18.4, 18.2
17.45	37.2, 36.5, 36.0
21.21	68.4, 67.3, 68.2

[a]Ionic strength = acid concentration.

mined in H_2O and in D_2O solution; the data are summarized in Table 1. In both solvents the reaction rate proved to be exactly proportional to acid concentration with no detectable uncatalyzed component. Linear least-squares analysis gave the following second-order rate constants: $k_{H^+} = (3.90 \pm 0.02) \times 10^{-3}\ M^{-1}\ s^{-1}$ and $k_{D^+} = (2.01 \pm 0.03) \times 10^{-3})\ M^{-1}\ s^{-1}$; these provide the isotope effect $k_{H^+}/k_{D^+} = 1.94 \pm 0.03$.

Rates of reaction were also measured in concentrated perchloric acid in H_2O only, in the range 5–20 wt.% acid; these data are summarized in Table 2. In this medium, first-order rate constants increased with acidity more rapidly than in direct proportionality to the first power of acid concentration, and an acidity function had to be used to correlate the data. The X_0 function (10), which appears to be the best currently available measure of acidity in aqueous perchloric acid (11), gave a good linear relation (Fig. 1), but the second-order rate constant obtained from the intercept of this plot, $k_{H^+} = (4.71 \pm 0.11) \times 10^{-3}\ M^{-1}\ s^{-1}$, is some 20% higher than that measured directly in dilute hydrochloric acid solutions; this exemplifies the difficulty of making accurate extrapolations from concentrated to dilute aqueous acids.

Discussion

The isotope effect determined here for the hydrolysis of oxacyclonon-2,8-diene catalyzed by the hydronium ion is in the normal direction and of appreciable magnitude: $k_{H^+}/k_{D^+} = 1.94$. This indicates that proton transfer from this acid to the substrate occurs in the rate-determining step of this reaction, and that the hydrolysis of this vinyl ether takes place by the normal slow proton transfer mechanism of eqs. [1] and [2].

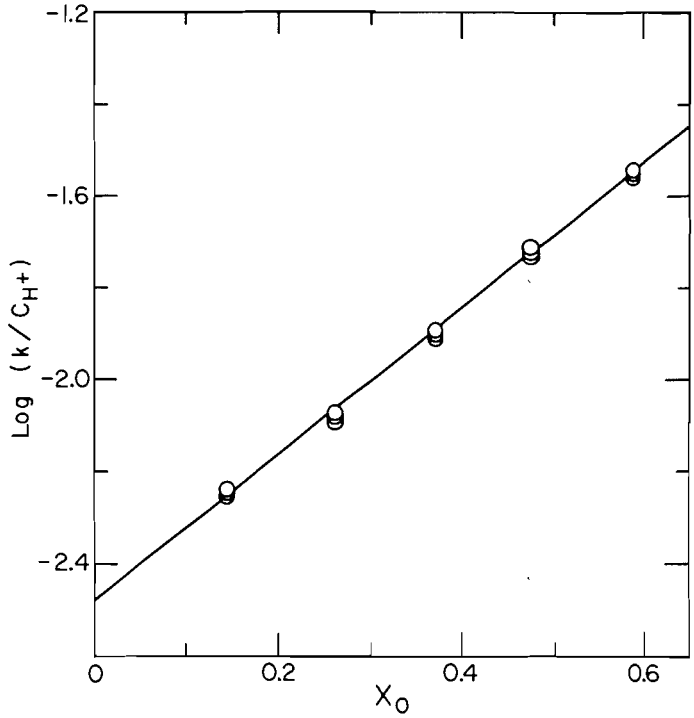

FIG. 1. Rates of hydrolysis of oxacyclonon-2-8-diene measured in concentrated aqueous perchloric acid correlated by the Cox–Yates X_0 function.

This mechanistic conclusion is reinforced by the very close correspondence of this isotope effect to the value predicted, $k_{H^+}/k_{D^+} = 1.97$, from a correlation of isotope effects with free energies of activation for a group of some 30 vinyl ethers known to react by this mechanism (1*c*).

With this mechanistic assignment in hand, an estimate of the effect of ring size upon the reactivity of the vinyl ether functional group in 9-methoxyoxacyclonon-2-ene, **1**, and 2-methoxy-2,3-dihydropyran, **2**, may be made. The fact that the presently studied substrate has two vinyl ether groups sharing the same oxygen atom, and will consequently be less reactive than a simple single vinyl ether, must be taken into account. This may be done by introducing the factor 210, which is the ratio of specific rate constants for the hydrolysis of ethyl vinyl ether, $k_{H^+} = 1.75\ M^{-1}\ s^{-1}$ (1*b*) and divinyl ether, $k_{H^+} = 8.3 \times 10^{-3}\ M^{-1}\ s^{-1}$ (12). This treatment gives $k_{H^+} = (3.9 \times 10^{-3})\ (210) = 0.82\ M^{-1}\ s^{-1}$ as the predicted specific rate of hydrolysis of the nine-membered cyclic vinyl ether oxacyclonon-2-ene, **4**, which is only a factor of three greater

4 **5**

than the observed specific rate of hydrolysis of the corresponding six-membered ring substrate, 2,3-dihydropyran, **5** (13).

This comparison shows that there is no significant ring-size effect on the rate of hydrolysis of a vinyl ether functional group when this group is incorporated into a six- or a nine-membered ring. The unusually great reactivity of the vinyl ether group in 9-methoxyoxacyclonon-2-ene, **1**, i.e. the factor of 500 by which the rate of hydrolysis of this substance exceeds that of its six-membered ring model, 2-methoxy-2,3-dihydropyran, **2**, must then be due to some other cause.

Acknowledgement

We are grateful to the Natural Sciences and Engineering Research Council of Canada for its financial support of this research.

1. (*a*) P. SALOMAA, A. KANKAANPERA, and M. LAJUNEN. Acta Chem. Scand. **20**, 1790 (1966); A. J. KRESGE and Y. CHIANG. J. Chem. Soc. B, 53 (1967); 57 (1967); (*b*) A. J. KRESGE, H. L. CHEN. Y. CHIANG, E. MURRILL, M. A. PAYNE, and D. S. SAGATYS. J. Am. Chem. Soc. **93**, 413 (1971); (*c*) A. J. KRESGE, D. S. SAGATYS, and H. L. CHEN. J. Am. Chem. Soc. **99**, 7228 (1977); (*d*) T. OKUYAMA, T. FUENO, H. NAKATSUJI, and J. FURUKAWA. J. Am. Chem. Soc. **89**, 5826 (1967); M. M. KREEVOY and R. ELIASON. J. Phys. Chem. **72**, 1313 (1968).
2. J. D. COOPER, V. P. VITULLO, and D. L. WHALEN. J. Am. Chem. Soc. **93**, 6294 (1971).
3. W. MAAS, M. J. JANSSEN, E. J. STAMHUIS, and H. WYNBERG. J. Org. Chem. **32**, 1111 (1967); J. K. COWARD and T. C. BRUICE. J. Am. Chem. Soc. **91**, 5329 (1969); P. Y. SOLLENBERGER and R. B. MARTIN. J. Am. Chem. Soc. **92**, 4261 (1970).
4. J. L. PIQUARD and L. HEVESI. Tetrahedron Lett. **21**, 1901 (1980); L. HEVESI, J. L. PIQUARD, and H. WAUTIER. J. Am. Chem. Soc. **103**, 870 (1981).
5. T. OKUYAMA and T. FUENO. J. Am. Chem. Soc. **102**, 6590 (1980); T. OKUYAMA, S. KAWAO, and T. FUENO. J. Am. Chem. Soc. **105**, 3220 (1983); T. OKUYAMA and T. FUENO. J. Am. Chem. Soc. **105**, 4390 (1983).
6. H. WAUTIER, S. DESAUVAGE, and L. HEVESI. J. Chem. Soc. Chem. Commun. 738 (1981).
7. (*a*) A. J. KRESGE and H. J. CHEN. J. Am. Chem. Soc. **94**, 2818 (1972); A. J. KRESGE and W. K. CHWANG. J. Am. Chem. Soc. **100**, 1249 (1978); Y. CHIANG, A. J. KRESGE, and C. I. YOUNG. Can. J. Chem. **56**, 461 (1978); Y. CHIANG, W. K. CHWANG, A. J. KRESGE, and S. SZILAGYI. Can. J. Chem. **58**, 124 (1980); (*b*) R. A. BURT, Y. CHIANG, and A. J. KRESGE. Can. J. Chem. **58**, 2199 (1980).
8. J. K. CRANDALL, D. B. BANKS, R. A. COLYER, R. J. WATKINS, and P. J. ARRINGTON. J. Org. Chem. **33**, 423 (1968).
9. J. K. CRANDALL and P. J. WATKINS. Tetrahedron Lett. 1717 (1967).
10. R. A. COX and K. YATES. Can. J. Chem. **59**, 2116 (1981).
11. A. J. KRESGE, H. J. CHEN, G. L. CAPEN, and M. F. POWELL. Can. J. Chem. **61**, 249 (1983).
12. A. SKRABAL and R. SKRABAL. Z. Phys. Chem. Abt. A, **181**, 449 (1938).
13. A. KANKAANPERA. Acta Chem. Scand. **23**, 1465 (1969).
14. Y. CHIANG, A. J. KRESGE, W. F. WHITE, and H. MARSHALL. J. Org. Chem. **48**, 2627 (1983).

Can. J. Chem. Downloaded from www.nrcresearchpress.com by 210.87.254.40 on 09/06/12
For personal use only.

Enzymes in organic synthesis. 30.[1] Reaction conditions – control of enantiomeric purities. Horse liver alcohol dehydrogenase-catalyzed reductions of 2-alkylcyclohexanones and their thiopyran analogs

J. BRYAN JONES AND TETSUO TAKEMURA[2]
Department of Chemistry, University of Toronto, Toronto, Ont., Canada M5S 1A1

Received May 6, 1983

J. BRYAN JONES and TETSUO TAKEMURA. Can. J. Chem. **62**, 77 (1984).

The effects of buffer, pH, reaction time, and [enzyme]/[substrate] ratio on the enantiomeric purities of the alcohol products of horse liver alcohol dehydrogenase-catalyzed reductions of (±)-α-alkylcyclohexanones and -tetrahydrothiopyranones have been studied. For poor substrates of this type, formation of enantiomerically pure products is assured when pH 8 and $<0.5 \times 10^{-4}$ [E]/[S] ratio conditions are used.

J. BRYAN JONES et TETSUO TAKEMURA. Can. J. Chem. **62**, 77 (1984).

On a étudié les effets de tampon, de pH, de temps de réaction et du rapport [enzyme]/[substrat] sur la pureté énantiomorphe des alcools obtenus par la réduction des (±)α-alkylcyclohexanones et des tétrahydrothiopyranones catalysées par la déshydrogénase de l'alcool du foie de cheval. Dans le cas des substrats pauvres de ce type, on s'assure de la formation de produits énantiomorphes purs lorsque le pH est de 8 et le rapport [E]/[S] $< 0,5 \times 10^{-4}$.

[Traduit par le journal]

Can. J. Chem. Downloaded from www.nrcresearchpress.com by 210.87.254.105 on 09/06/12
For personal use only.

In recent years the requirements of synthetic organic chemists for reagents capable of effecting asymmetric tranformations have increased dramatically. Nowadays, only reagents capable of yielding products that are enantiomerically pure, or almost of 100% ee, can be considered to be of practical asymmetric synthetic value. Enzymes present unique opportunities in this regard, with horse liver alcohol dehydrogenase (HLADH)[3] being one of the best documented enzymes of synthetic value. HLADH is a commercially available enzyme that catalyzes oxidoreductions of the type depicted in eq. [1].

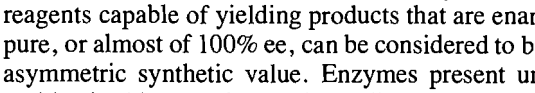

[1] $\text{>C=O} + \text{NADH} + \text{H}^+ \rightleftharpoons \text{>CHOH} + \text{NAD}$

Many HLADH-catalyzed reactions lead to enantiomerically pure products, particularly when the substrates are rapidly transformed (2, 3). However, for poor racemic substrates such as 2-alkylcyclohexanones (±)-**1** and 3-alkyltetrahydrothiopyranones (±)-**2**, for which both enantiomers can fit productively at the active site, products of <100% ee can result (4). We have now investigated the influence of reaction conditions on product ee. In this paper, limiting conditions are identified that guarantee enantiomerically pure products in HLADH-catalyzed reductions of poor substrates.

Results

2-Ethylcyclohexanone ((±)-**1***b*) and 3-ethyltetrahydrothiopyran-4-one ((±)-**3***b*) were selected as being representative of poor ketone substrates. Their HLADH-catalyzed reductions (Scheme 1) were studied under preparative-scale conditions on up to 2 g of the ketones, employing ethanol to effect coupled-substrate (3) recycling of the catalytic amount of nicotinamide coenzyme employed. The course of the reductions was monitored by glc and the *trans*-alcohol products **2***b* and **4***b* of primary interest were separated from the unchanged ketones by mplc.

Minor (<2%) amounts of the *cis*-alcohol isomers were isolated in a number of reactions (4). These by-products were discarded. The ees of the *trans*-alcohol products **2**,**4***b* were measured directly by ^{1}H nmr examination of the methoxyl peaks of their MTPA esters in the presence of Eu(fod)$_3$ (5). The ees of the recovered thiopyran ketones (−)-**3***b*, and of the cyclohexyl ketones (−)-**1***a*,*b* of Scheme 2 were established by ^{13}C nmr determinations on their (2*R*,3*R*)-2,3-butanediol ketals (6). The optical purities of the recovered 2-ethylcyclohexanones (−)-**1***b* of the Scheme 1 reactions were assigned from their optical rotations. The absolute configurations of the ketones (−)-**1**,**3***b* and alcohols (+)-**2**,**4***b* were verified by comparison with previously authenticated (4) samples.

The survey of reaction condition effects was begun by examining the influence of pH on the yield and rate of formation of the *trans*-alcohols **2***b* from (±)-**1***b*. The results are summarized in Table 1. The practical rates of reduction are slowest at the lowest pH's and reach a maximum at pH 8. Accordingly, the subsequent delineation of reaction conditions that maximize both yield and ee of the *trans*-alcohol products was largely performed at pH 8, using Tris-HCl buffer for convenience. The effects of varying the [E]/[S] ratio, the extent of reduction, and the reaction time are recorded in Table 2. The best yields and highest ees of both **2***b* and **4***b* are obtained with the shortest reaction times and employing the lowest [E]/[S] ratios.

HLADH-catalyzed oxidations of the racemic *trans*-alcohols **2***a*,*b* were carried out in order to confirm that the (1*S*,2*S*)-2-alkylcyclohexanol stereoisomers that formed preferentially in the Scheme 1 reductions were also the enantiomers most readily oxidized. This was found to be so, with the (1*R*,2*R*)-stereoisomers of **2***a*,*b* being recovered as shown in Scheme 2. FMN was used to effect recycling (7) of the NAD coenzyme in these experiments.

Discussion

All reactions were assayed under preparative-scale conditions since a practical, rather than kinetic, evaluation of the effects of reaction conditions on product ee was desired. The

[1]For Part 29, see ref. 1.

[2]On leave from the Department of Chemistry, Faculty of Science, Science University of Tokyo, Tokyo, Japan.

[3]Abbreviations used: HLADH, horse liver alcohol dehydrogenase; NAD/H, oxidized and reduced forms respectively of nicotinamide adenine dinucleotide; MTPA, (+)-2-methoxy-2-trifluoromethylphenylacetyl; Eu(fod)$_3$, tris(6.6.7.7.8.8.8-heptafluoro-2,2-dimethyl-3,5-octanedionato)europium(III); FMN, flavin mononucleotide.

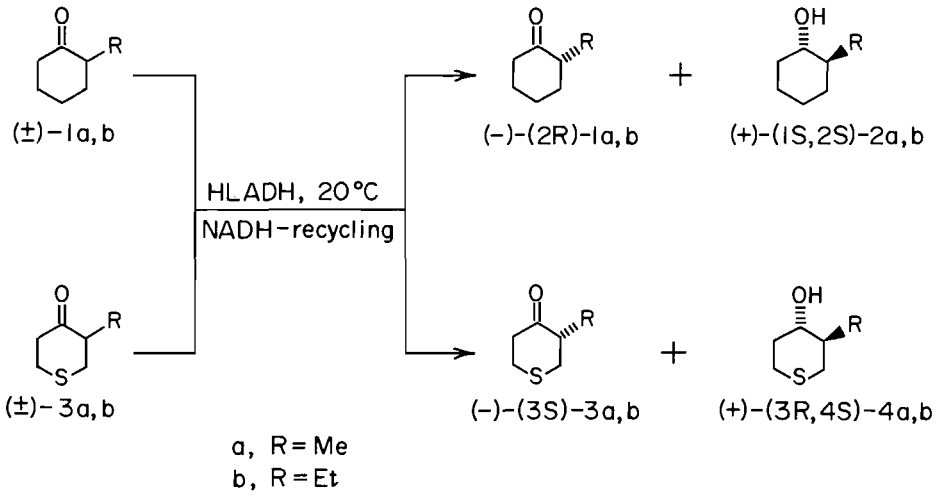

SCHEME 1.

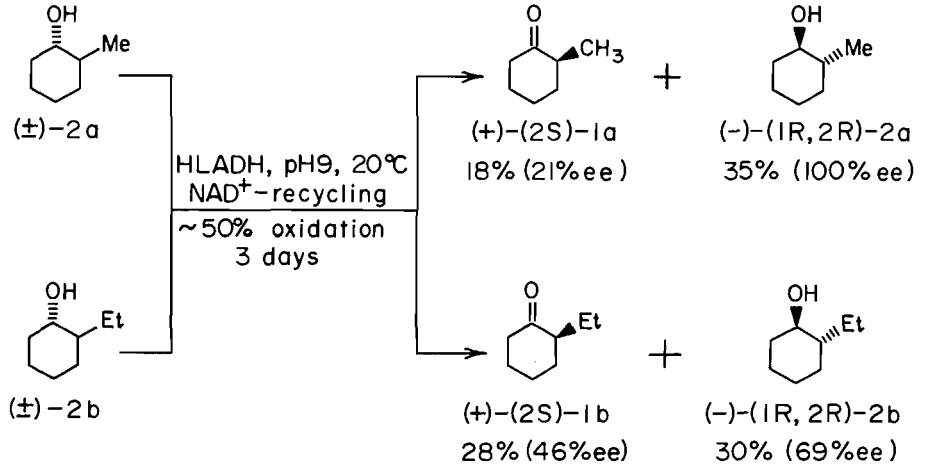

SCHEME 2.

TABLE 1. Influence of pH on the formation of **2***b* during HLADH-catalyzed reduction of (±)-**1***b*[a]

Buffer	pH	Reaction time (h)	% Yield **2***b*[b]
Phosphate	6	17	6.7
	6	63	13.2
	8	17	33.0
	8	65	53.8
Tris-HCl	7	26	18.6
	7	65	28.6
	8	17	43.0
	8	65	54.8
	9	17	43.0
	9	65	54.2

[a]Assays were performed on 0.4 *M* buffer solutions with [E]/[S] 3.1×10^{-4} at 20°C.
[b]By glc.

thiopyranone (±)-**3***b* was a better substrate than its cyclohexane analog (±)-**1***b* (Table 2), but the responses of both substrates to the reaction conditions were very similar in stereospecificity terms, as expected (4). In keeping with the asymmetric synthetic thrust of the investigation, the products were isolated prior to their characterization and analysis. The ees of the *trans*-alcohols (+)-**2**,**4***b* of primary interest were determined directly by nmr and are considered accurate to ±3%. The optical purities of the recovered ketones (−)-**1***a*,*b* and (−)-**3***b* of Schemes 1 and 2 were too far below asymmetric synthetically valuable levels to warrant the precision of direct ee determinations, and optical rotation values, previously correlated with nmr-based ees (4), were used to calculate all but a few of their optical purities.

Each of the Table 1 and 2 assays was terminated at ≤50% reduction since the substrates were racemates. However, the reductions will proceed beyond the 50% point if longer reaction times are employed (Table 1), due to slow reductions of the less reactive ketone enantiomers. The latter also epimerize slowly under the reaction conditions, thereby gradually regenerating the more rapidly reduced enantiomers of **1**,**3***b*.

Of the two buffers used, Tris-HCl was the more suitable. Reactions in phosphate proceeded somewhat more slowly. More significantly, the latter also gave *trans*-alcohol products of somewhat lower ee. At the buffer concentrations used in this study phosphate is known (8) to bind to the active site of HLADH. Although this could presumably affect the stereospecificity, many different buffers have been used successfully in HLADH-catalyzed oxidoreductions (2) and, with one or two exceptions (9), the nature of the buffer used is usually unimportant. Of much greater significance is the pH of the medium. The rate of reduction is greatly influenced by pH, with the rate

Can. J. Chem. Downloaded from www.nrcresearchpress.com by 210.87.254.105 on 09/06/12
For personal use only.

TABLE 2. Effect of reaction conditions on yields and optical purities of *trans*-alcohol products and recovered ketones from HLADH-catalyzed reductions of (±)-**1**,**3***b*[a]

Substrate	[E]/[S] ($\times 10^4$)	Reaction time	% Reduction[b]	Recovered ketone (%yield;[c] %ee)	Alcohol product (%yield;[c] %ee[d])
(±)-**1***b*	1.7[f]	10 days	49	(±)-**1***b* (19;7[d])	(±)-**2***b* (23;31)
(±)-**1***b*	1.2[f]	8 days	41	(±)-**1***b* (45;23[d])	(±)-**2***b* (24;44)
(±)-**1***b*	4.9	1 days	48	(±)-**1***b* (35;68[e])	(±)-**2***b* (31;70)
(±)-**1***b*	3.3	9 h	29	(±)-**1***b* (48;52[e])	(±)-**2***b* (26;100)
(±)-**1***b*	3.3	1 days	43	(±)-**1***b* (39;64[e])	(±)-**2***b* (37;80)
(±)-**1***b*	0.65	9 days	47	(±)-**1***b* (32;47[e])	(±)-**2***b* (26;83)
(±)-**1***b*	0.44	3 days	26	(±)-**1***b* (57;32[e])	(±)-**2***b* (18;100)
(±)-**1***b*	0.44	9 days	49	(±)-**1***b* (17;44[e])	(±)-**2***b* (22;100)
(±)-**3***b*	1.8	7 h	46	(±)-**3***b* (49;43[d])	(±)-**4***b* (35;79)
(±)-**3***b*	1.1	10 h	34	(±)-**3***b* (49;43[d])	(±)-**4***b* (35;79)
(±)-**3***b*	1.1	18 h	44	(±)-**3***b* (57;40[d])	(±)-**4***b* (41;83)
(±)-**3***b*	0.34	3 days	49	(±)-**3***b* (53;41[d])	(±)-**4***b* (43;90)

[a]In 0.4 *M* Tris-HCl buffer pH 8 at 20°C.
[b]By glc.
[c]Of isolated, purfied material.
[d]By nmr.
[e]From optical rotation.
[f]In phosphate buffer, pH 7.

reaching a maximum at pH ≥ 8 (Table 1).

The reduction rates are greatest at the highest enzyme concentrations, as expected from the Michaelis–Menten equation (10). However, the maximum ees are obtained when the [E]/[S] ratio is lowest, or when the reduction is <~30% complete. This is in accord with expectation for a kinetically controlled process involving preferential reduction of one enantiomer (2*a*, *b*). The lowerings in %ee of the (+)-*trans*-alcohol products as the reaction times increase are due to the slow accumulation of the opposite enantiomers via the unfavoured pathway for reduction of the much less reactive (−)-enantiomers of **1**,**3***b*.

A low [E]/[S] ratio is essential if *trans*-alcohol products of 100% ee are required. This conclusion is supported by the results of the Zurich (2*a*) and Antwerp (2*d*) groups for HLADH-mediated 2-alkylcyclohexanone reductions, in which enantiomerically pure alcohols were obtained using [E]/[S] ratios ~5–10-fold lower than the lowest values of Table 2. The practical lower limit of [E]/[S] will vary for different substrates. For poor substrates such as **1***a*,*b*, reductions become very slow at [E]/[S] ratios $<10^{-6}$.

Another factor contributing to lower ees of the *trans*-alcohol products (+)-**2**,**4***a*,*b* of long reductions at high [E] is that the reverse oxidation reaction can become significant. The more facile oxidation of (+)- than (−)-**2***a*,*b* was confirmed by the Scheme 2 reactions, during which the less reactive (1*R*,2*R*)-substrate enantiomers accumulated. The 2-methyl alcohol (−)-**2***a* isolated was of 100% ee while the lower optical purity of (−)-**2***b* indicates that manipulation of the [E]/[S] ratio could be beneficial in the oxidation mode also.

These results are believed to be generally valid for all HLADH-catalyzed reduction of poor substrates. In such cases the highest product ees will be attained at pH 8 by maximizing the rate of reduction with as high an enzyme concentration as feasible, while keeping the [E]/[S] ratio as low as possible and less than 0.5×10^{-4}.[4]

[4]A general formulation of the experimental conditions favouring formation of enantiomerically pure products from enzyme-catalyzed reactions has been published recently (11).

Experimental

The instrumentation and general purification and analytical procedures used were as described previously (4*b*). HLADH (EC 1.1.1.1) was 1× crystallized material from Sigma. The activity of each batch of enzyme was determined (12) prior to use; amounts of HLADH quoted refer to mg of active enzyme. NAD was obtained from Kyowa Hakko Kogyo, New York and FMN from Sigma. The physical and spectral properties of all racemic and optically active ketones **1**,**3***a*,*b* and alcohols **2**,**4***a*,*b*, and of their respective ketals with (−)-(2*R*,3*R*)-2,3-butanediol and MTPA esters, were identical with those reported previously for the fully characterized compounds (4).

*HLADH-catalyzed reductions of (±)-**1**,**3**b*

The following general procedure was employed. The ketone substrate and some ethanol were dissolved in buffer solution at 20°C. NAD was then added and the reduction was initiated by the addition of HLADH. The reaction mixture was kept at 20°C and the extent of reduction monitored by glc on Superpac 20 or 3% OV-101 on Chromasorb GHP columns. When sufficient (25–50%) reduction had occurred, the mixture was brought to pH 7 with 1 *N* HCl if buffer pH >7 was used, then saturated with NaCl and continuously extracted with chloroform for 2 days. The dried ($MgSO_4$) chloroform extract was analyzed by glc for the Table 1 runs, and, for the Table 2 experiments, evaporated and the residue purified by mplc on silica (ICN 0.032–0.063 mm) with ethyl acetate/hexane (1:8 for cyclohexane derivatives, 1:5 for thiopyrans). The individual compounds were then Kugelrohr-distilled.

*Effect of pH on reduction of (±)-**1**b*

2-Ethylcyclohexanone ((±)-**1***b*, 40 mg, 0.4 m*M*), EtOH (0.1 mL), NAD^+ (79 mg, 0.12 mmol), and HLADH (10 mg, 0.125×10^{-6} *M*) were reacted by the above procedure in 10 mL of 0.4 *M* potassium phosphate (pH 6, 8) or Tris-HCl (pH 6, 7, 8) buffer for 17–65 h. The results are summarized in Table 1.

*Influence of [E] and reaction time on reduction of (±)-**1**,**3**b*

The reductions were studied using the general procedure (4) on (±)-**1***b* (500 mg – 1.0 g, 3.96–7.92 mmol), EtOH (0.3–1.92 mL), NAD (150 mg – 1.48 g, 0.23–2.23 mmol), and HLADH (11–214 mg, 0.1382.68 × 10^{-6} mol) in 0.4 *M* Tris-HCl buffer (pH 8, 70–190 mL). For long reactions, the enzyme and NAD were added portion-wise every 2 days. The concentration ranges used were [S] 4.1–5.6 × 10^{-2} mol, [E] 1.94–20.8 × 10^{-6} *M*. The reactions were terminated after 26–49% reduction. The recovered ketones **1***b* (17–57% yields), typical bp 80°C (14 Torr) (lit. (4) bp 82–85°C

Can. J. Chem. Downloaded from www.nrcresearchpress.com by 210.87.254.105 on 09/06/12
For personal use only.

Can. J. Chem. Downloaded from www.nrcresearchpress.com by 210.87.254.105 on 09/06/12
For personal use only.

(22 Torr)), had rotations $[\alpha]_D^{25}$ −2.9 to −12.9° (*c* 1−2, EtOH) which were used to calculate the %ee (lit. (2*a*) (−)-(2*R*)-**1***b*, $[\alpha]_D$ −18° (*c* 1.8, EtOH)). The *trans*-alcohols **2***b* (18−37% yields), typical bp 70°C (13 Torr) (lit. (4) bp 80°C (18 Torr)), had rotations $[\alpha]_D^{25}$ +17.0 −63.0° (*c* 0.6−1, EtOH) (lit. (2*a*) (+)-(1*S*,2*S*)-**2***b*, $[\alpha]_D$ +59.2° (*c* 1.5, EtOH)). The ees of the (+)-**2***b* samples were measured by nmr examinations of the methoxyl protons of their MTPA esters (5), prepared and characterized as described previously (4). The thiopyranone reductions were carried out similarly on (±)-**3***b* (4) (590 mg − 2.0 g, 4.09−48.2 mmol), EtOH (1.1−3.6 mL), NAD (0.9−3.2 g, 1.36−4.82 mmol), and HLADH (35.6−203 mg, 0.45−2.54 × 10^{-6} mol) in 0.4 *M* Tris-HCl buffer (pH 8, 200−700 mL). The concentration ranges used were [S] 2.0 × 10^{-2} *M*, [E] 0.67−3.63 × 10^{-6} *M*. The reductions were terminated after 34−49% reaction. The recovered ketones **3***b* (49−57% yields), typical bp 100°C (8 Torr), (lit. (4) bp 92°C (7 Torr)) had rotations $[\alpha]_D^{25}$ −16.5 to 27.5° (*c* 1−2, $CHCl_3$) (lit. (4) (−)-(3*S*)-**3***b* (58% ee), $[\alpha]_D^{25}$ −36.0° (*c* 1, $CHCl_3$)). The *trans*-alcohols **4***b* (21−43% yields), typical bp 100°C (1.3 Torr) (lit. (4) bp 90°C (2.5 Torr)), had rotations $[\alpha]_D^{25}$ +47.0−51.4° (*c* 0.6−2, $CHCl_3$) (lit. (4) (+)-(3*R*,4*S*)-**4***b* (78% ee), $[\alpha]_D^{25}$ +39.5° (*c* 1.1, $CHCl_3$)). The ees of the ketones (−)-**3***b* were determined by ^{13}C nmr measurements on their ketals with (−)-(2*R*,3*R*)-2,3-butanediol (6), and of the alcohols (+)-**4***b* via ^1H nmr determinations of their MTPA esters as before (4). The results are summarized in Table 2.

*HLADH-catalyzed oxidations of (±)-2*a,b

Both substrates were oxidized under the same general conditions. The *trans*-alcohol (±)-**2***a* or *b* (5.05 mmol) was dissolved in 0.05 *M* glycine−NaOH buffer (pH 9, 500 mL) at 20°C. NAD (880 mg, 1.3 mmol) and FMN (9.65 g, 20.2 mmol) were added and the pH readjusted to 9 with 2 *N* aqueous NaOH. HLADH (56 mg) was then added and the mixture kept at 20°C. The reaction mixture turned black within 2 h and the progress of the oxidation was monitored by glc analysis (3% OV 101 columns) of small aliquots. This analysis is accurate to ±5−10%.

When the reaction was ~50% complete (3 days), the solution was saturated with NaCl and continuously extracted with chloroform for 2 days. The chloroform extract was filtered through a short column of Hyflo Super Cel (4 cm) containing Norite (1 cm) and then dried ($MgSO_4$), filtered, and evaporated. The components were separated by medium pressure liquid chromatography on silica gel (ICN 0.032−0.063 mm) with ethyl acetate/hexane (1:8) elution and the products Kugelrohr-distilled.[5] The ees of the recovered alcohols were determined by the MTPA ester method and of the product ketones using the ^{13}C nmr-ketal approach (4). The individual reactions gave the following results.

*Oxidation of (±)-2*a (578 mg) for 3 days (~46% oxidation) yielded (+)-(2*S*)-**1***a* (102 mg, 18% yield, 21% ee), bp 45°C (7 Torr) (lit. (13) bp 89−90°C (20 Torr)); $[\alpha]_D^{20}$ +9.8° (*c* 1.57, EtOH) (lit. (13) $[\alpha]_D$ +12.1° (neat), (2*a*) $[\alpha]_D$ +14.4° (*c* 1.03, EtOH)), and (−)-(1*R*,2*R*)-**2***a* (200 mg, 35%yield, 100% ee), bp 75°C (7 Torr) (lit. (14) bp 78°C (20 Torr)); $[\alpha]_D^{20}$ −41.4° (*c* 0.96, EtOH (lit. (14) (1*S*,2*S*), $[\alpha]_D^{20}$ +34.38° (neat), (2*a*) $[\alpha]_D$ +40.8° (*c* 0.7, EtOH).

*Oxidation of (±)-2*b (647 mg) for 3 days (~52% oxidation) afforded (+)-(2*S*)-**1***b* (182 mg, 28% yield, 46% ee), bp 55°C (7 Torr) (lit. (4) bp 82−85°C (22 Torr)); $[\alpha]_D^{20}$ +18.3° (*c* 2.8, EtOH) (lit. (2*a*) $[\alpha]_D$ +19° (*c* 0.26, EtOH)), and (−)-(1*R*,2*R*)-**2***b* (195 mg, 30% yield, 69% ee) bp 70−75°C (15 Torr) (lit. (4) bp 80°C (18 Torr)); $[\alpha]_D^{20}$ −45.9° (*c* 0.98, EtOH) (lit. (2*a*) (1*S*,2*S*), $[\alpha]_D$ +59.2° (*c* 1.45, EtOH)).

[5]The relatively low yields of the Scheme 2 reactions are due to mechanical losses during chromatographic and distillation purification of small amounts of liquid products. High yields will result on optimization of scale and conditions (2*a*).

Acknowledgements

We thank the Natural Sciences and Engineering Research Council and the Atkinson Charitable Foundation for generous financial support.

1. G. S. Y. NG, L-C. YUAN, I. J. JAKOVAC, and J. B. JONES. Tetrahedron. In press.
2. (*a*) V. PRELOG. Pure Appl. Chem. **9**, 119 (1964); R. E. HELMCHEN-ZEIER. Ph.D. thesis 4991, ETH, Zürich (1973); (*b*) J. B. JONES and J. F. BECK. Tech. Chem. N.Y. **10**, 107 (1976); J. A. HASLEGRAVE and J. B. JONES. J. Am. Chem. Soc. **104**, 4666 (1982); (*c*) M. NAKAZAKI, H. CHIKAMATSU, and M. TANIGUCHI. Chem. Lett. 1762 (1982); (*d*) T. A. VAN OSSELAER, G. L. LEMIERE, E. M. MERCKX, J. A. LEPOIVRE, and F. C. ALDERWEIRELDT. Bull. Soc. Chim. Belg. **87**, 799 (1978); (*e*) H. GERLACH and B. ZAGALAK. Chem. Commun. 274 (1973); (*f*) J. W. CORNFORTH, F. P. ROSS, and C. WAKSELMAN. J. Chem. Soc. Perkin Trans. 1, 429 (1975); (*g*) A. R. BATTERSBY, P. W. SHELDRAKE, J. STAUNTON, and D. C. WILLIAMS. J. Chem. Soc. Perkin Trans. 1, 1056 (1976).
3. B. ZAGALAK, P. A. FREY, G. L. KARABATSOS, and R. H. ABELES. J. Biol. Chem. **241**, 3028 (1966).
4. J. B. JONES and T. TAKEMURA. Can. J. Chem. **60**, 2950 (1982); J. Org. Chem. **48**, 791 (1983).
5. J. A. DALE, D. L. DULL, and H. S. MOSHER. J. Org. Chem. **34**, 2543 (1969).
6. H. HIEMSTRA and H. WYNBERG. Tetrahedron Lett. 2183 (1977).
7. J. B. JONES and K. E. TAYLOR. Can. J. Chem. **55**, 2969 (1976).
8. K. H. DAHL and J. S. MCKINLEY-MCKEE. Eur. J. Biochem. **103**, 47 (1980).
9. H. SUND and H. THEORELL. *In* The enzymes. Vol. 7. 2nd ed. *Edited by* P. D. Boyer, H. Lardy, and K. Myrback. Academic, New York. 1963. pp. 25−83.
10. M. DIXON and E. C. WEBB. Enzymes. 3rd ed. Academic, New York. 1979. Chapt. 4.
11. C-S. CHEN, Y. FUJIMOTO, G. GIRDAUKAS, and C. J. SIH. J. Am. Chem. Soc., **104**, 7294 (1982).
12. K. DALZIEL. Acta Chem. Scand. **11**, 397 (1957).
13. A. SKITA. Ber. **56**, 1016 (1923).
14. G. A. GOUGH, H. HUNTER, and J. KENYON. J. Chem. Soc. 2052 (1926).

Salting-out of triethylphosphate by inorganic electrolytes[1]

NORMAN H. SAGERT and DANNY W. P. LAU

Research Chemistry Branch, Atomic Energy of Canada Limited, Whiteshell Nuclear Research Establishment, Pinawa, Man., Canada R0E 1L0

Received May 24, 1983

NORMAN H. SAGERT and DANNY W. P. LAU. Can. J. Chem. **62**, 81 (1984).

The salting-out of triethylphosphate (TEP) from water was measured at 25°C for twelve inorganic electrolytes. If salting out is taken as an additive property of ions, then the effectiveness for salting TEP out of water is $I^- < Br^- < Cl^- < \frac{1}{2}SO_4^{2-} < \frac{1}{2}CO_3^{2-}$ for anions and $\frac{1}{3}La^{3+} < Na^+ \approx NH_4^+ < Cs^+ < \frac{1}{2}Ca^{2+} \approx \frac{1}{2}Mg^{2+} < K^+ < \frac{1}{2}Ba^{2+}$ for cations. The results were fitted to three theories. The distribution theory of Conway, Desnoyers, and Smith predicts the order of magnitude of the experimental results, but does not discriminate well between salts of the same valence type. The electrostriction theory of McDevit and Long discriminates well between ions but gives results three or five times larger than those observed. Scaled particle theory predicts the results reasonably well, but the predictions depend critically on the choice of ionic and molecular parameters. Thus, none of these theories is entirely satisfactory.

NORMAN H. SAGERT et DANNY W. P. LAU. Can. J. Chem. **62**, 81 (1984).

On a mesuré le relargage du phosphate de triéthyle (PTE) à partir de l'eau à 25°C pour 12 électrolytes inorganiques. Si on considère le relargage comme une propriété additive des ions, l'efficacité du relargage du PTE à partir de l'eau est alors: $I^- < Br^- < Cl^- < \frac{1}{2}SO_4^{2-} < \frac{1}{2}CO_3^{2-}$ pour les anions et de $\frac{1}{3}La^{3+} < Na^+ \approx NH_4^+ < Cs^+ < \frac{1}{2}Ca^{2+} \approx \frac{1}{2}Mg^{2+} < K^+ < \frac{1}{2}Ba^{2+}$ pour les cations. Les résultats sont analysés à l'aide de trois théories. La théorie de distribution de Conway, Desnoyers et Smith prédit l'ordre de grandeur des résultats expérimentaux mais elle ne fait pas de distinction nette entre les sels de même type de valence. La théorie d'électrostriction de McDevit et Long prédit la différence entre les ions mais donne des résultats 3 à 5 fois supérieurs à ceux observés. La théorie des sphères rigides prédit les résultats raisonnablement bien mais les prédictions dépendent d'une façon critique du choix des paramètres ionique et moléculaire. Ainsi aucune de ces théories n'est entièrement satisfaisante.

[Traduit par le journal]

Introduction

Neutral organic phosphates are the active extractants in many industrial processes, including those used for reprocessing nuclear fuel (1). We are studying interfacial properties relevant to these extraction systems (2, 3), and need to know distribution coefficients for organic phosphates between hydrocarbons and various aqueous media (4), including aqueous media with added salt. Measuring such distribution coefficients is equivalent to measuring the salting coefficients (5).

The salting-out of non-electrolytes from aqueous solutions has been of interest for many years (6, 7). Many non-electrolytes, both polar and non-polar, have been used, but few data are available for organic phosphates. Some results have been reported for tri-*n*-butylphosphate (TBP) (1, 8), but results for smaller phosphates do not appear to be available. These phosphates are of some interest as solutes since they have a higher dipole moment (9) than most polar non-electrolytes previously studied, but have a considerable hydrophobic character (10). Recently, Treiner and Fromon (11) measured the salting-out of acetonitrile, which also has a high dipole moment but little hydrophobic character. The availability of data on the salting-out of organic phosphates should help to test the limits of the currently available theories. Therefore, in the work reported here we have measured salting coefficients of triethylphosphate (TEP) using several salts and have compared our results to three conventional theories.

Experimental

Vials containing 5.0 cm^3 of dodecane, 5.0 cm^3 of aqueous salt solution and, appropriate amounts of TEP were prepared as previously described (4) and shaken for at least 40 h in a water bath, controlled by a thermostat to ±0.1 K. Samples were withdrawn for analysis while keeping the vials in the water bath. Analyses for TEP were done by gas chromatography, as previously described (4). Since most of the TEP goes into the water phase (4), it was possible to determine distribution coefficients by analyzing the organic phase before and after equilibration, and using a mass balance. Thus, the necessity of analyzing aqueous solutions with high salt concentrations was avoided. The salt solutions were prepared by volume and were converted to molalities using known densities (12).

The sources and purification of dodecane, water, and TEP have been described (2, 4). The inorganic salts were of ACS reagent-grade purity, or better, and were used without further purification. All salts were dried above 140°C for at least 40 h and were stored in a desiccator.

Results

Distribution ratios, D, defined as the concentration of TEP in the organic phase divided by that in the aqueous phase, are shown in Fig. 1 for 2.15 mol kg^{-1} KCl at 25°C, as a function of TEP concentration in the aqueous phase. Also shown in the figure are the distribution ratios in the absence of salt, D_0, obtained previously (4). From Fig. 1 it is apparent that the distribution ratios do not change materially with TEP concentration in the concentration range investigated here and that ratios obtained with about 0.1 mol dm^{-3} TEP in the aqueous phase are essentially equivalent to those determined at infinite dilution.

Following Friedman (13, 14), we define a salting coefficient, k_s, by eq. [1]:

$$[1] \quad k_s = -\left(\frac{\partial \ln m_{TEP}}{\partial m_E}\right)_{\mu_{TEP}}$$

where m denotes molality, μ is chemical potential, and E refers to the electrolyte. Since our distribution ratios do not vary with m_{TEP}, then, to a good approximation, eq. [2] holds:

$$[2] \quad k_s = \frac{\partial \ln (D/D_0)}{\partial m_E}$$

[1]Issued as AECL-8035.

Can. J. Chem. Downloaded from www.nrcresearchpress.com by 210.87.254.105 on 09/06/12
For personal use only.

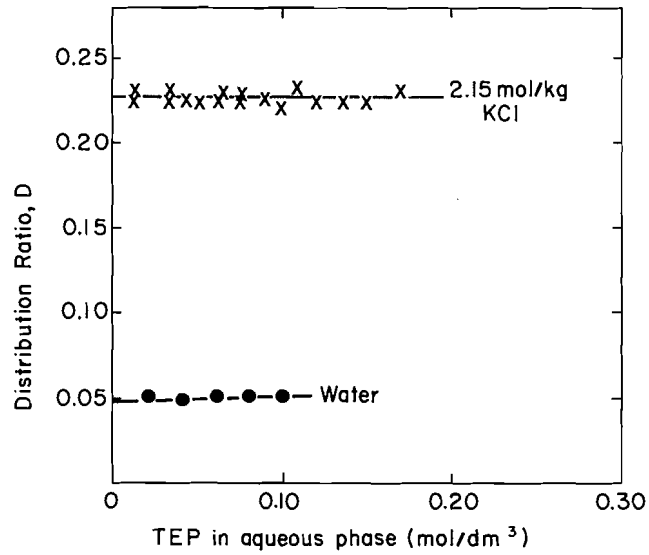

FIG. 1. Distribution ratios at 25°C as a function of TEP concentration, with 2.15 mol kg^{-1} KCl in the aqueous phase (×), and with pure water as the aqueous phase (●) (ref. 4).

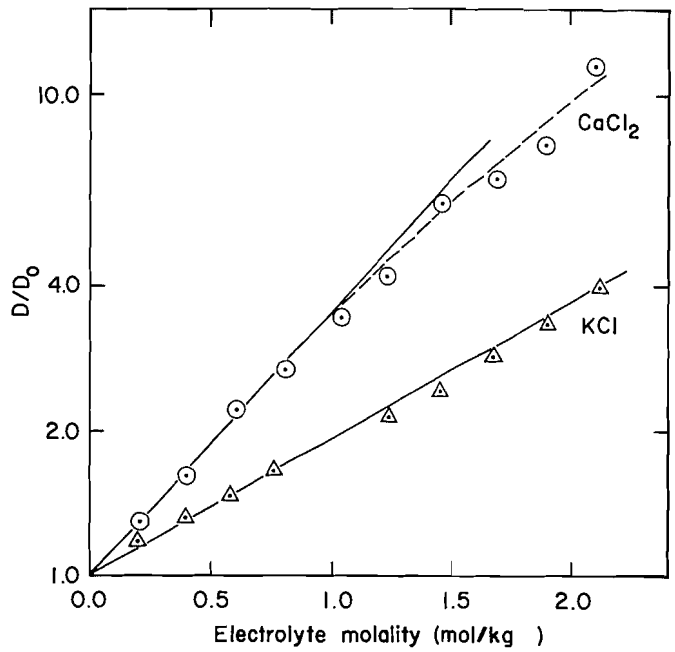

FIG. 2. The distribution ratio in the presence of salt divided by that in its absence, as a function of electrolyte molality at 25°C, for KCl (△) and $CaCl_2$ (○).

Figure 2 shows plots of the logarithm of (D/D_0) against electrolyte molality for both KCl and $CaCl_2$ solutions. The TEP concentration is close to 0.1 mol dm^{-3}. Reasonably good straight lines resulted, and from the slopes of these lines salting coefficients were obtained. Where some curvature was noted, the initial slopes were used. Table 1 lists experimental salting coefficients for the twelve electrolytes studied, along with theoretical values calculated by methods described below. Consideration of various sources of error led us previously (4) to ascribe an error of ±5% to the individual distribution ratios. Thus, the salting coefficients are likely reliable to within ±5%.

The definition of k_s in eq. [1] is such that, when multiplied by RT, k_s gives the standard Gibbs energy change accompanying the transfer of 1 mol of TEP at constant and low concentration from water to a 1-molal solution of salt (5). To obtain the standard Gibbs energy of transfer using the unit mole fraction standard states frequently (15), but not universally (16), employed, it is necessary to add to k_s the quantity $(0.0181\ \nu - \phi_0/1000)$, where ν is the number of moles of ions produced by the dissolution of 1 mol of electrolyte, and ϕ_0 is the apparent molal volume of the electrolyte (5). This quantity is quite small, usually within experimental error. For example, for KCl, the k_s for TEP transfer corresponds to a standard Gibbs energy of transfer of 1.593 kJ/mol for the concentration-based standard state and 1.616 kJ/mol for the mole fraction one.

Discussion

If salting-out results from additive contributions from the various ions in solution (6), then the effectiveness for salting-out of TEP is in the order

$$\tfrac{1}{3}La^{3+} < Na^+ \approx NH_4^+ < Cs^+ < \tfrac{1}{2}Ca^{2+} \approx \tfrac{1}{2}Mg^{2+} < K^+ < \tfrac{1}{2}Ba^{2+}$$

and

$$I^- < Br^- < Cl^- < \tfrac{1}{2}SO_4^{2-} < \tfrac{1}{2}CO_3^{2-}$$

For anions, the sequence is similar to that observed by others (5, 17) for salting-out of butanols. However, for cations, larger ones such as Cs^+ are somewhat more effective for salting-out TEP than for salting-out butanol. This is shown more clearly in Fig. 3, where k_s is plotted against cation ionic diameter for the alkali-metal chlorides and against anion ionic diameter for the potassium halides. The salting coefficient for KBr was calculated from those of KCl, NH_4Cl, and NH_4Br, assuming additivity. Also shown are results of Perron *et al.* (17) for *t*-butanol solutions at 25°C. For *t*-butanol, salting-out is less efficient for the larger cations, but for TEP, salting-out by these larger cations remains higher than for sodium ions. The salting coefficient for salting TEP from NaCl solution is close to that predicted by Treiner (18) for a polar solute, using a hard-sphere diameter for TEP calculated from the liquid density. Thus, it is the larger cations that give anomalously high results.

The TEP molecule is bifunctional. Its hydrocarbon chains are hydrophobic and should be strongly salted out. On the other hand, the phosphate group is highly polar and should be salted-in. Wilcox and Schrier (19) recognized that a similar, if less marked, situation would exist for alcohols. They studied the salting-out of a number of alcohols and devised an additivity scheme for the groups in the molecules. Using their numbers for CH_2 and CH_3, then, for NaCl, the hydrocarbon chains of TEP should be salted-out with a k_s of 1.02, and since the experimental value is 0.57, the phosphate is salted-in with a k_s of 0.45, or 1.12 kJ/mol. Thus the salting-out of TEP is clearly a balance between the strong salting-out tendency of the hydrocarbon chains and the weaker salting-in tendency of the phosphate group.

Three types of theories have frequently been used to account for salting coefficients (7). These are the distribution theories associated with many authors (7, 20), the electrostriction theory of McDevit and Long (21), and the scaled particle theory orginated by Reiss, Frisch, and Lebowitz (22). We will examine our data with these three theories and will not attempt to use the statistical-mechanical theory of Krishnan and Friedman (14). All three theories are deficient in that they do not take into account explicitly the bifunctional nature of the TEP molecule. However, since they have been applied to alcohols in the past, it is instructive to use them here to see how well they predict the behavior of TEP.

Can. J. Chem. Downloaded from www.nrcresearchpress.com by 210.87.254.105 on 09/06/12
For personal use only.

TABLE 1. Experimental and theoretical salting coefficients at 25°C

Salt	k_s (exp) (kg mol^{-1})	k_s (CDS) (kg mol^{-1})	k_s (McDL) (kg mol^{-1})	k_s (SPT) (kg mol^{-1})	k_s (SPTMS) (kg mol^{-1})
KCl	0.64	0.444	1.474[a]	0.438	0.609
KI	0.34	0.430	1.154	0.669	0.750
$LaCl_3$	1.53	1.194	7.508	1.596	2.394
CsCl	0.59	0.436	1.108[a]	0.140	0.462
$MgCl_2$	1.24	0.848	4.039	1.272	1.577
Na_2CO_3	2.25	0.859	7.370	2.371	2.172
$CaCl_2$	1.16	0.835	5.117	0.965	1.448
NH_4Cl	0.57	0.440	0.728	0.488	0.596
NH_4Br	0.42	0.436	1.168	0.642	0.800
NaCl	0.57	0.464	1.884[a]	0.767	0.825
Na_2SO_4	2.21	0.839	5.907[a]	3.724	2.939
$BaCl_2$	1.36	0.827	4.677	0.768	1.376

[a]Calculated from "effective pressures".

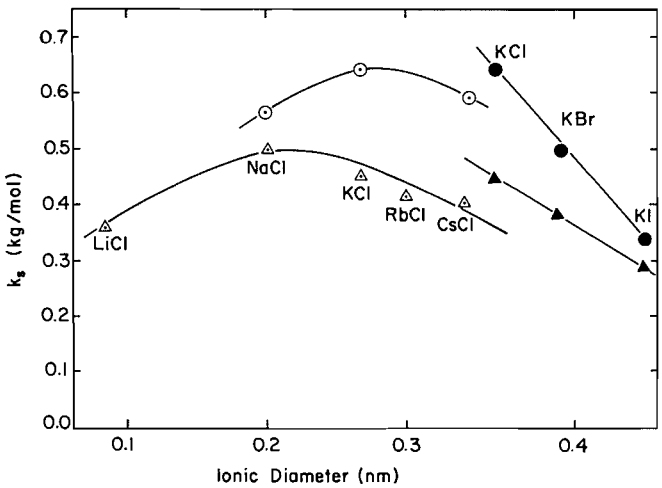

FIG. 3. Salting coefficients at 25°C as a function of ionic diameter. The open symbols refer to the cations of alkali-metal chlorides, the closed symbols the anions of potassium halides. Our results for TEP are shown as circles, and the results of Perron *et al.* (17) for *t*-butanol are shown as triangles.

Distribution theories

These theories treat salting-out by considering the behavior of polarizable solvent and solute molecules in the field of the ion. If, as is usually the case, the solvent, H_2O, is more polarizable than the solute, the ion − induced dipole interaction will preferentially attract solvent and result in a lower solubility for the solute. Such factors as proper handling of the potential function, dielectric saturation, and the use of realistic polarization functions have to be considered (7). A good approach is that of Conway *et al.* (20), who derived eq. [3]:

$$[3]\quad k_s = \frac{\pi N_A}{6000}(\sigma_h^3 - \sigma^3) + \frac{Z^2e^2}{2000\,kT\epsilon_0^2}\left(V_{TEP}\epsilon_0 - \frac{9}{2}P_{TEP}\right) \times \left[\frac{2}{\sigma_h} - \frac{1}{R}\right]$$

where N_A is the Avogadro's number, σ_h is the diameter of the hydrated ion, σ is the ionic diameter, Z is the charge on the ion, ϵ_0 is the dielectric constant, V_{TEP} is the molar volume of TEP, R is the co-sphere radius, and P_{TEP} is the total molar polarization of TEP. Equation [3] gives the salting coefficient for each ion, and it is necessary to sum the ionic contributions to get the salting coefficient for a given electrolyte. Calculated values (CDS) for each electrolyte are shown in Table 1. The hard-sphere ionic diameters used are those given in Table 2. The hydrated ionic diameters were taken from Nightingale (29). P_{TEP} was calculated from the refractive index and dipole moment of TEP (9). In general, this theory gives salting coefficients of the right order; however, it does not discriminate well between different salts of the same valence type.

Electrostriction theory

This theory is almost entirely due to McDevit and Long (21). The compression of solvent by the ions is used to derive an expression for the salting coefficient. This is done by considering the excess work that must be done to create a volume and noting that this work is proportional to the volume change on mixing the salt with water. The result is eq. [4]:

$$[4]\quad k_s = \frac{V_{TEP}(V_E - \phi_0)}{kT\beta}$$

where β is the compressibility of water and V_E is the hypothetical molar volume of the liquid salt at temperature T. Where "effective pressures" of the electrolyte in water are known, V_E can be calculated from them (21). Otherwise V_E can be taken as the molar volume of the crystalline state. Table 1 shows theoretical values (McDL) of k_s, the noted values being calculated from "effective pressures". The calculated values are several times larger than the experimental values, although they do discriminate well between different salts of the same valence type. This variation is not totally unexpected because the theory really takes into account differences between experimental densities. These density differences incorporate some of the specific interactions that other theories try to explain.

Scaled particle theory

Scaled particle theory purports to calculate the energy expended to form a cavity in the solvent large enough for a solute molecule, and then to calculate the energy regained by solute−solvent interaction when a solute molecule is placed in this cavity. It was originally developed for spherical non-polar molecules (22), but in recent years has been applied to systems involving polar molecules, with varying degrees of success (5, 11, 18). Masterton and Lee (30) developed equations specifically for calculating salting coefficients and, although these are given for 1:1 electrolytes, they are readily adapted for use with all electrolytes. The equations of Masterton and Lee (30) use the Mavroyannis−Stephen equation (31), eq. [5], to calculate

Can. J. Chem. Downloaded from www.nrcresearchpress.com by 210.87.254.105 on 09/06/12
For personal use only.

TABLE 2. Properties of salts used in scaled particle theory calculations

Salt	ϕ_0^a ($cm^3\ mol^{-1}$)	σ^+ (nm)	σ^- (nm)	α^+ ($10^{-3}\ nm^{-3}$)	α^- ($10^{-3}\ nm^{-3}$)
KCl	26.8	0.264[b]	0.364[b]	0.87[f]	3.02[f]
KI	45.4	0.264[b]	0.448[b]	0.87[f]	6.28[f]
$LaCl_3$	14.4	0.230[c]	0.364[b]	1.30[e]	3.02[f]
CsCl	39.2	0.344[b]	0.364[b]	2.79[f]	3.02[f]
$MgCl_2$	14.5	0.130[c]	0.364[b]	0.10[e]	3.02[f]
Na_2CO_3	−6.7	0.202[b]	0.370[d]	0.21[f]	1.63[h]
$CaCl_2$	17.8	0.198[c]	0.364[b]	0.60[e]	3.02[f]
NH_4Cl	35.7	0.307[b]	0.364[b]	1.84[g]	3.02[f]
NH_4Br	32.7	0.307[b]	0.390[b]	1.84[g]	4.17[f]
NaCl	16.6	0.202[b]	0.364[b]	0.21[f]	3.02[f]
Na_2SO_4	11.6	0.202[b]	0.460[d]	0.21[f]	1.55[h]
$BaCl_2$	23.2	0.270[c]	0.364[b]	0.17[e]	3.02[f]

[a]Reference 23.
[b]Reference 24.
[c]Pauling diameters as listed by Conway (ref. 7, p. 73).
[d]Thermochemical diameters as listed by Conway (ref. 7, p. 62).
[e]Reference 25.
[f]Reference 26.
[g]Reference 27.
[h]Reference 28.

the energy parameter ϵ/k for the ions:

$$[5]\quad \frac{\epsilon_i}{k} = 721\,\frac{\alpha_i^{3/2} Z_i^{1/2}}{\sigma_i^6}$$

where α_i is the polarizability of the ion in nm^3, σ_i is its molecular diameter in nm, and Z_i is the total number of electrons in the ion. Thus, for the salt, it is necessary to know the apparent molar volume, ϕ_0, at infinite dilution and the diameters and polarizabilities of the ions. For TEP, the molecular diameter, the energy parameter and the polarizability must be known. For water, ϵ/k is usually taken as 85.3 K and the diameter as 0.275 nm (30). The values of the parameters used here are given in Table 2.

For TEP, values of ϵ/k and σ are not readily available, although the polarizability can be calculated from the refractive index to be 16.24×10^{-3} nm^3. Two approaches were used to obtain the values of ϵ/k and σ. One approach, suggested by Aveyard and Heselden (5), was to use empirical equations produced by Stiel and Thodos (32) for organic molecules. These equations predict the values of ϵ/k and σ from the critical properties. Since the critical properties of TEP are also unavailable, they were estimated from vapor-pressure data at lower temperatures (ref. 12, p. C429), using the procedures of Curl and Pitzer (33). These gave a critical pressure of 2.11 MPa, a critical temperature of 684 K, and a critical volume of 0.696 dm^3. The correlation of Stiel and Thodos (32) then gave a value of 340.3 K for ϵ/k and 0.84 nm for σ. Another procedure for calculating ϵ/k and σ, which has been used with some success (30, 34), is to calculate ϵ/k using the Mavroyannis–Stephen equation, eq. [5]. In this case, ϵ/k was found to be 190.9 K and σ was taken as 0.69_5 nm, as obtained from a correlation suggested by Stiel and Thodos (35) for polar molecules, which is closer to the value of 0.66 nm derived from the liquid density.

Our calculated salting coefficients are shown in the last two columns of Table 1. The second last column (SPT) shows results obtained using ϵ/k = 340.3 K and σ = 0.84 nm, while the last column (SPTMS) uses ϵ/k = 190.9 K (from the Mavroyannis–Stephen equation) and $\sigma = 0.69_5$ nm. In general, reasonable fits are obtained in both cases, with exceptions. The calculated salting coefficients of KI and NH_4Br are too high, by about a factor of two. For some salts, such as KCl, CsCl, Na_2SO_4, and $BaCl_2$, the parameters obtained from the Mavroyannis–Stephen equation give a better fit, but for other salts, such as $LaCl_3$ and possibly $MgCl_2$, the parameters derived from the Stiel–Thodos equations give a better fit. Thus, scaled particle theory can give good fits, but the choice of parameters is critical.

If the polar solute correlation of Stiel and Thodos (35) is used with the critical constants determined previously, then ϵ/k is predicted to be 613.5 K and σ, as before, is 0.69_5 nm. These parameters give very low calculated salting coefficients, e.g., 0.038 for KCl and 0.297 for NaCl, as is frequently observed for polar solutes (11, 30). Treiner and Fromon (11) observed that, with many polar molecules, very low values are obtained, but the fit is improved immensely if the anion interaction term is deleted. When this was done, very large calculated salting coefficients were obtained, e.g., 1.264 for KCl and 1.523 for NaCl. Thus, it is clearly not appropriate, for TEP, to say that the anions are solvated entirely by water; some form of preferential solvation cannot be ruled out.

In summary, none of the three theories described gives a really satisfactory fit to our experimental results. Scaled particle theory can give good fits under certain circumstances, but the choice of parameters is critical and, when a key parameter is not well known, as is the case with the ϵ/k value for TEP, the validity of any fit is questionable. Furthermore, scaled particle theory is not really expected to work well for polar molecules with a high dipole moment in a complex solvent like water. New theoretical approaches, ones recognizing explicitly the bifunctional nature of these solutes, are clearly required.

Acknowledgements

We thank our colleagues at the Whiteshell Nuclear Research Establishment and especially R. J. Lemire, J. Paquette, and M. J. Quinn for their advice and encouragement.

Can. J. Chem. Downloaded from www.nrcresearchpress.com by 210.87.254.105 on 09/06/12
For personal use only.

1. Y. MARCUS and A. S. KERTES. Ion exchange and solvent extraction of metal complexes. John Wiley, New York. 1969. pp. 650–657.
2. N. H. SAGERT and W. LEE. Can. J. Chem. **58**, 2789 (1980).
3. N. H. SAGERT, W. LEE, and M. J. QUINN. Can. J. Chem. **60**, 1244 (1982).
4. N. H. SAGERT and W. LEE. Can. J. Chem. **58**, 1463 (1980).
5. R. AVEYARD and R. HESELDEN. J. Chem. Soc. Faraday I, **71**, 312 (1975).
6. F. A. LONG and W. F. MCDEVIT. Chem. Rev. **51**, 119 (1952).
7. B. E. CONWAY. Ionic hydration in chemistry and biophysics. Elsevier, Amsterdam. 1981. pp. 444–465.
8. C. E. HIGGINS, W. H. BALDWIN, and B. A. SOLDANO. J. Phys. Chem. **63**, 113 (1959).
9. D. M. PETKOVIĆ, B. A. KEZELE, and D. R. RAJIĆ. J. Phys. Chem. **77**, 922 (1973).
10. S. LINDENBAUM, D. STEVENSON, and J. H. RYTTING. J. Solution Chem. **4**, 893 (1975).
11. C. TREINER and M. FROMON. J. Chem. Soc. Faraday I, **76**, 1062 (1980).
12. R. C. WEAST (*Editor*). Handbook of chemistry and physics, 50th ed. Chemical Rubber Co., Cleveland. 1969. pp. D172–D210.
13. H. L. FRIEDMAN. J. Solution Chem. **1**, 387 (1972).
14. C. V. KRISHNAN and H. L. FRIEDMAN. J. Solution Chem. **3**, 727 (1974).
15. C. TANFORD. J. Phys. Chem. **83**, 1802 (1979).
16. A. BEN-NAIM. J. Phys. Chem. **83**, 1803 (1979).
17. G. PERRON, D. JOLY, J. E. DESNOYERS, L. AVEDIKIAN, and J.-P. MOREL. Can. J. Chem. **56**, 552 (1978).
18. C. TREINER. Can. J. Chem. **59**, 2518 (1981).
19. F. L. WILCOX and E. E. SCHRIER. J. Phys. Chem. **75**, 3757 (1971).
20. B. E. CONWAY, J. E. DESNOYERS, and A. C. SMITH. Phil. Trans. R. Soc. London, A**256**, 389 (1964).
21. W. F. MCDEVIT and F. A. LONG. J. Am. Chem. Soc. **74**, 1773 (1952).
22. H. REISS, H. L. FRISCH, and J. L. LEBOWITZ. J. Chem. Phys. **31**, 369 (1959).
23. F. J. MILLERO. Chem. Rev. **71**, 147 (1971).
24. T. C. WADDINGTON. Trans. Faraday Soc. **62**, 1482 (1966).
25. A. F. WELLS. Structural inorganic chemistry. Clarendon Press, Oxford. 1975. pp. 259–267.
26. B. E. CONWAY. Electrochemical data. Elsevier, London. 1952. p. 26.
27. E. A. MOELWYN-HUGHES. Physical chemistry. Pergamon Press, Oxford. 1964. pp. 381–400.
28. J. W. WEST. Electrodeposition and corrosion processes. Van Nostrand, London. 1970. p. 123.
29. E. R. NIGHTINGALE, JR. J. Phys. Chem. **63**, 1381 (1959).
30. W. L. MASTERTON and T. P. LEE. J. Phys. Chem. **74**, 1776 (1970).
31. C. MAVROYANNIS and M. J. STEPHEN. Mol. Phys. **5**, 629 (1962).
32. L. I. STIEL and G. THODOS. J. Chem. and Eng. Data **7**, 234 (1962).
33. R. F. CURL, JR. and K. S. PITZER. Ind. Eng. Chem. **50**, 265 (1958).
34. Y-L. T. CHANG, M. Y. SCHRIER, and E. E. SCHRIER. J. Phys. Chem. **78**, 165 (1974).
35. L. I. STIEL and G. THODOS. AIChE J. **10**, 266 (1964).

Can. J. Chem. Downloaded from www.nrcresearchpress.com by 210.87.254.105 on 09/06/12
For personal use only.

Kinetics of the reaction $H + C_2H_6 \rightarrow H_2 + C_2H_5$ in the temperature region of 1000 K

J.-R. CAO[1] AND M. H. BACK

The Ottawa–Carleton Institute for Research and Graduate Studies in Chemistry, University of Ottawa, Ottawa, Ont., Canada K1N 9B4

Received May 10, 1983

J.-R. CAO and M. H. BACK. Can. J. Chem. **62**, 86 (1984).

A system for the measurement of rate constants for elementary reactions of hydrogen atoms in the temperature region of 1000 K is described. The concentration of hydrogen atoms is controlled by the equilibrium constant for dissociation of hydrogen molecules. The kinetics of the rate of conversion of ethane to ethylene in this system has been studied over the temperature range 876–1016 K. The results show that the rate-controlling step is

$$H + C_2H_6 \rightarrow H_2 + C_2H_5$$

and the value obtained for the rate constant is

$$\log k \text{ (L mol}^{-1} \text{ s}^{-1}) = 11.72 \pm 0.05 - \frac{12\,800 \pm 200}{2.3RT}$$

(R = 1.987 cal mol^{-1} deg^{-1}). This value is compared with values obtained from other methods over the temperature range 300–1400 K. Combination with a recent measurement of the rate constant for the reverse reaction yields an experimental value for the equilibrium constant for the reaction.

J.-R. CAO et M. H. BACK. Can. J. Chem. **62**, 86 (1984).

On décrit un système qui permet de mesurer les constantes de vitesse des réactions élémentaires des atomes d'hydrogène aux environs de 1000 K. La constante d'équilibre de la dissociation des molécules d'hydrogène contrôle la concentration des atomes d'hydrogène. On a étudié la cinétique de la vitesse de transformation de l'éthane en éthylène dans ce système dans l'intervalle de température allant de 876 à 1016 K. Les résultats révèlent que l'étape déterminante est la réaction suivante:

$$H + C_2H_6 \rightarrow H_2 + C_2H_5$$

pour laquelle la constante de vitesse est de:

$$\log k \text{ (L mol}^{-1} \text{ s}^{-1}) = 11{,}72 \pm 0{,}05 - \frac{12\,800 \pm 200}{2{,}3RT}$$

(R = 1,987 cal mol^{-1} deg^{-1}). On a comparé cette valeur à celles obtenues par les autres méthodes dans l'intervalle de température de 300–1400 K. Lorsqu'on combine cette valeur avec les mesures récentes de la constante de vitesse de la réaction inverse, on obtient une valeur expérimentale de la constante d'équilibre de la réaction.

[Traduit par le journal]

Introduction

Measurements of rate constants for reactions of hydrogen atoms with hydrocarbons and other molecules have been attempted through a variety of techniques for many years. Published data have been recently summarized (1). Accurate values for such rate constants are essential for a proper understanding of the mechanisms of the wide variety of reactions in which hydrogen atoms play an important role. The main problem encountered in these measurements is the determination of the concentration of hydrogen atoms. A direct measure of the instantaneous concentration of atoms is undoubtedly the most desirable. During the past few years the technique of atomic resonance absorption has been successfully applied to measurements of the concentration of hydrogen atoms in several systems (2) and rate constants for reactions both producing (3) and consuming (4) hydrogen atoms have been obtained. Because of the high temperatures involved in these shock-heated reactants, however, rate constants involving only the most stable reactants have been reported. Measurements of rate constants for reaction of hydrogen atoms with ethane and higher hydrocarbons at lower temperatures have, except for studies using esr detection (5), relied on a relative measure of the hydrogen atom concentration.

In most systems the concentration of hydrogen atoms, unlike that of radicals, is not controlled by their rate of mutual combination, either homogeneously or heterogeneously, and other reactions consuming hydrogen atoms must be used as a reference. In the range of temperature 800–1100 K studies on the addition of hydrocarbons to reacting mixtures of hydrogen and oxygen (6) have used the reference reaction

$$H + O_2 \rightarrow OH + O$$

At slightly lower temperatures, 500–750 K, Marshall, Purnell, and co-workers have shown that in a flow system at low pressures with reactants ethylene (7) and ethane (8) the combination reaction

$$H + C_2H_5 \rightarrow 2CH_3$$

is the main competing process for removal of hydrogen atoms. At lower temperatures Yang (9) measured rate constants for abstraction reactions relative to $H + C_3H_6$, and other relative rate constants involving various abstraction and addition reactions have been reported. There is fairly good agreement among these various methods but there is no doubt that better accuracy is needed to give confidence to modelling studies and to assess the extent of curvature in the Arrhenius expression over the temperature range covered by the measurements.

A new method for the measurement of rates of hydrogen-atom reactions applicable in the temperature region of 1000 K

[1]Permanent address: Chemistry Department, Peking University, Peking, The People's Republic of China.

Can. J. Chem. Downloaded from www.nrcresearchpress.com by 210.87.254.40 on 09/06/12
For personal use only.

Can. J. Chem. Downloaded from www.nrcresearchpress.com by 210.87.254.40 on 09/06/12
For personal use only.

has been developed in this laboratory. The method is based on the fact that at moderate pressures of hydrogen in this temperature region the equilibrium concentration of hydrogen atoms provides a sufficient source for measurable reaction and on the assumption, which may be tested, that the dissociation equilibrium is rapidly attained in the system used. To this system is added a small quantity of reactant, a few ppm, and its rate of consumption measured. If the reaction is not too fast, the equilibrium concentration of hydrogen atoms should not be disturbed. The system was tested using the reactant ethylene (10) and from the results a value for the rate constant for reaction of ethyl radicals with hydrogen molecules was obtained. The present paper describes the results obtained with the reactant ethane and the values measured for the rate constant for the abstraction of hydrogen atoms from ethane.

$$H + C_2H_6 \rightarrow H_2 + C_2H_5$$

Experimental

The reaction was studied in a static system using a cylindrical quartz reaction vessel of 182 cm^3 volume. A second vessel packed with quartz tubes to give a S/V ratio of 7.5 cm^{-1} was used to test for the importance of surface reactions. Mixtures were prepared for introduction into the reaction vessel and tested for homogeneity. Research grade hydrocarbons were obtained from Matheson of Canada, Whitby, Ont. Hydrogen was purified by passage through a molecular seive 5A column at liquid nitrogen temperature with a residence time of about 2 s. The reactant and products were analyzed on a 1.2 m column of Durapak (Phenylisocyanate on Porasil) maintained at 30°C, using a Hewlett Packard Model 5750 Gas Chromatograph. Other details are described in earlier publications (10, 11).

Concentrations of ethane in hydrogen ranged from 16 to 56 ppm with total pressures from 50 to 125 Torr. Experiments covered the temperature range 876–1016 K. Reaction times ranged from 1 to 40 min.

Results and discussion

At temperatures below about 975 K ethylene was the principal product. Methane was a minor product, which became undetectable below about 900 K. Figure 1 shows a set of yield–time curves for formation of ethylene at various concentrations of ethane with a fixed total pressure. From such curves initial rates of formation of ethylene were obtained over the range of pressure and temperature indicated, and the data are summarized in Table 1.

The rate of formation of ethylene may be expressed as follows:

$$R_{C_2H_4} = k[H_2]^m[C_2H_6]^n$$

where k is an overall rate constant and m and n represent the order of the rate with respect to hydrogen and ethane, respectively. The measurements of the rate for a particular mixture of ethane and hydrogen at various total pressures provides data for the estimation of the total order, $m + n$. These results are shown in Fig. 2, as log of the initial rate of formation of ethylene as a function of log of the total pressure. From the slope of these plots, $m + n = 1.70 \pm 0.05$. To determine n the rate was measured at a constant total pressure for various mixtures of ethane in hydrogen (as illustrated in Fig. 1). Figure 3 shows some examples of these measurements, as a plot of log of the initial rate of formation of ethylene as a function of log of the concentration of ethane, giving a value of n of 1.25 ± 0.05. The value of m is therefore 0.45 ± 0.1. The order of the rate with respect to hydrogen may therefore be considered to be

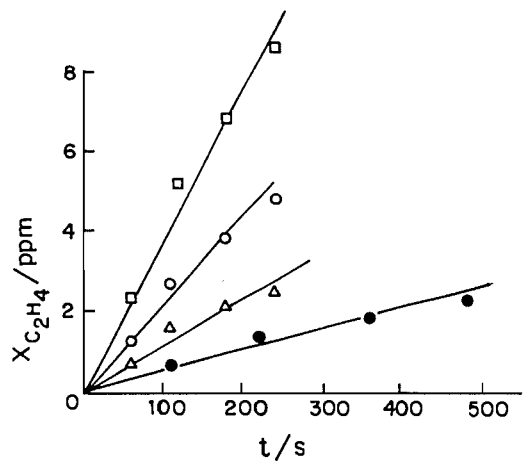

FIG. 1. Yield of ethylene, expressed as mole fraction, as a function of time at 922 K and total pressure of 113.5 Torr. $X_{C_2H_6}$ (ppm): ●, 16.4; △, 24.8; ○, 37.8; □, 56.

TABLE 1. Initial rate of formation of C_2H_4, 922 K, S/V = 1.0 cm^{-1}

Total pressure (Torr)	$X_{C_2H_6}$ (ppm)	$[C_2H_6] \times 10^7$ (mol L^{-1})	$R^0_{C_2H_4} \times 10^{11}$ (mol L^{-1} s^{-1})
175.0	16.4	1.71	15.4
	24.8	1.15	10.2
	37.8	0.755	4.87
	56	0.500	3.05
113.0	16.4	1.10	9.21
	24.8	0.744	4.15
	37.8	0.488	2.28
	56	0.328	1.08
82.5	16.4	0.804	4.48
	24.8	0.543	2.40
	37.8	0.356	1.38
	56	0.236	0.775
52.0	16.4	0.507	1.84
	24.8	0.342	0.869
	37.8	0.224	0.543
	56	0.148	0.296
36.5	16.4	0.356	0.830
	24.8	0.240	0.508
	37.8	0.158	0.270
	56	0.104	0.171

0.5 while the order with respect to ethane is somewhat greater than 1.

The rate of the reaction was measured in the packed vessel at four temperatures and for a range of pressures and concentration of ethane. The results are given in Table 2. At temperatures where the rate of formation of methane was measurable no change in its rate was observed in the packed vessel. The rate of formation of ethylene, however, was increased by a factor between two and three. Furthermore, the order of the rate of formation of ethylene with respect to the concentration of ethane was close to two, a stronger dependence than was observed in the unpacked vessel. In both vessels the order was essentially constant over the temperature range of the experiments. Using the values for the order observed in the packed vessel (S/V = 7 cm^{-1}) and the unpacked vessel (S/V = 1 cm^{-1}) a linear extrapolation to S/V = 0 gives an order of 1.1. It seems reasonable to conclude, therefore, that the homogeneous reaction producing ethylene is first order

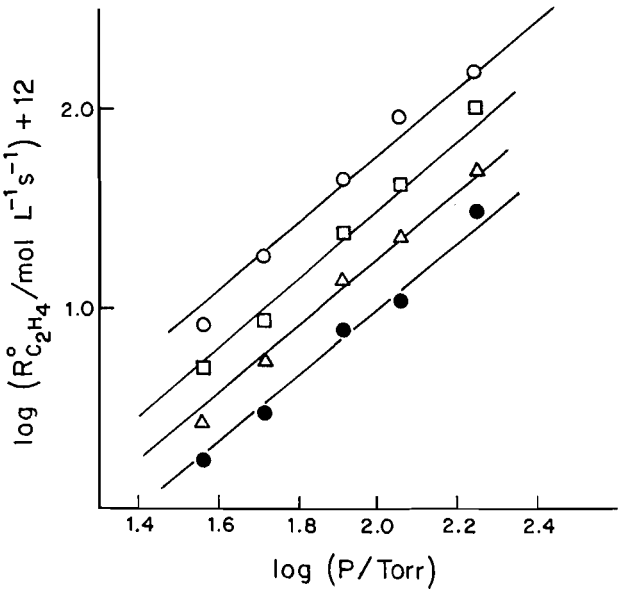

FIG. 2. log–log plot of the initial rate of formation of ethylene as a function of the total pressure at 922 K. $X_{C_2H_6}$ (ppm): ●, 16.4; △, 24.8; ○, 37.8; □, 56.

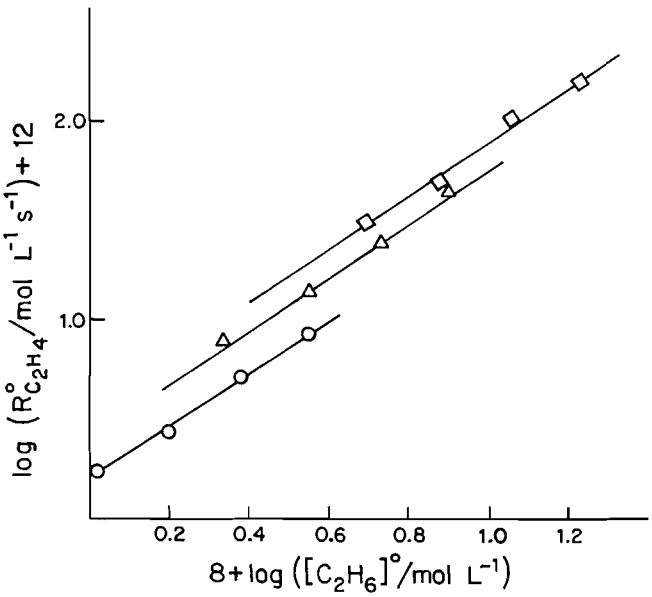

FIG. 3. log–log plot of the initial rate of formation of ethylene as a function of the concentration of ethane at 922 K. Total pressure (Torr): ○, 36.5; △, 82.5; ◇, 175.

with respect to the concentration of ethane and 0.5 order with respect to the concentration of hydrogen. The rate measured in the unpacked vessel has nevertheless a significant contribution from the heterogeneous reaction and a correction is required in order to obtain a rate constant relating to the homogeneous reaction [2]. The estimation of the correction as well as possible reasons for the strong dependence of the rate on the concentration of ethane in the packed vessel will be discussed later.

These results suggest that the formation of ethylene from reaction of ethane may occur through the following set of reactions:

[1] $H_2 \rightleftarrows 2H$

[2] $H + C_2H_6 \rightarrow C_2H_5 + H_2$

TABLE 2. Initial rate of formation of C_2H_4, S/V = 7.0 cm^{-1}

T (K)	P (Torr)	$X_{C_2H_6}$ (ppm)	[C_2H_6] × 10^7 (mol L^{-1})	$R^0_{C_2H_4}$ × 10^{11} (mol L^{-1} s^{-1})
894	185	7.96	0.264	0.896
		17.5	0.581	6.64
		35.7	1.190	16.6
956	120	9.70	0.195	5.23
		20.7	0.416	24.1
		39.8	0.800	64.3

[3] $C_2H_5 \rightarrow C_2H_4 + H$

In this simple mechanism the hydrogen atom concentration is controlled by the equilibrium with hydrogen molecules and every ethyl radical produced in reaction [2] yields ethylene by reaction [3]. Evidence was presented from the results obtained in a similar study (10) to show that an equilibrium concentration of hydrogen atoms was maintained under these conditions. Other reactions of the ethyl radical which may be important are,

[4] $H + C_2H_5 \rightarrow C_2H_6$

[−2] $C_2H_5 + H_2 \rightarrow C_2H_6 + H$

Taking into account reactions [1] to [4] the steady-state concentration of ethyl radicals may be expressed as follows:

$$[C_2H_5] = \frac{k_2(K_1[H_2])^{1/2}[C_2H_6]}{k_3 + k_{-2}[H_2] + k_4(K_1[H_2])^{1/2}}$$

and the rate of formation of ethylene is therefore

$$R_{C_2H_4} = k_3\left[\frac{k_2(K_1[H_2])^{1/2}[C_2H_6]}{k_3 + k_{-2}[H_2] + k_4(K_1[H_2])^{1/2}}\right]$$

The observed dependence of the rate on the concentration of hydrogen is a strong indication that neither reaction [−2] nor [4] is important. The rate definitely increased as the pressure of hydrogen increased whereas if reaction [−2] were important the rate should decrease as the pressure of hydrogen increased, or if reaction [4] were important, should remain independent of pressure of hydrogen. The relative magnitudes of the terms in the denominator may be estimated using a value for k_3 interpolated from the data of Lin and Back (12), whose measurements were made under similar conditions of temperature and pressure. Their data at 913 K indicate that at 120 Torr the ratio k_3/k_3^{∞} is about 0.3. Using their value for k_3, $10^{13.6-38\,000/RT}$, k_3 at 922 K and 120 Torr is about 1×10^4 s^{-1}. In the presence of hydrogen instead of ethane as a third body, this value may be further reduced by about a factor of four (13) to 0.25×10^4 s^{-1}. Taking an average value for k_{-2} of 5×10^5 L mol^{-1} s^{-1} (10) the product $k_{-2}[H_2]$ is about 1.1×10^3 s^{-1}, and therefore about half the value for k_3. At the lowest temperature, 876 K, the two rates become approximately the same. Although these estimates are only approximate, it might be expected that reaction [−2] could be important, particularly at the lower temperatures. Contribution from this reaction would reduce the rate of removal of ethylene and lead to too low a value for k_2. Although we believe from the measurements of the order of the rate with respect to hydrogen that this error is not serious, it might lead to a slight over-estimate of the activation energy for k_2. Using a collision rate constant for k_4 of 5×10^{10} L mol^{-1} s^{-1} the product $k_4(K_1[H_2])^{1/2}$ is about 10^4 times less than k_3 and this termination may be neglected.

Can. J. Chem. Downloaded from www.nrcresearchpress.com by 210.87.254.40 on 09/06/12
For personal use only.

TABLE 3. log k_2 (L mol^{-1} s^{-1})

T (K)	Packed vessel S/V = 7.0 cm^{-1}	Unpacked vessel S/V = 1.0 cm^{-1}	S/V = 0
956.0	9.194	8.822	8.759
915.5	9.094	8.696	8.656
894.0	9.005	8.625	8.569

Further evidence in support of this mechanism is provided by the value for the measured activation energy of the rate of formation of ethylene, E_r, of 70 kcal/mol. With the simple mechanism,

$$E_r = E_2 + \tfrac{1}{2}\Delta H_1$$

and E_r may be estimated as 64 kcal/mol, using the present value for E_2. If reaction [−2] is important in controlling the concentration of ethyl radicals then $E_r = E_3 + \Delta H_2 + \tfrac{1}{2}\Delta H_1$ and E_r would have a value of about 92 kcal/mol. If reaction [4] is important the value of E_r would be higher still. It appears, therefore, that the simple sequence of reactions [1] to [3] can account for the formation of ethylene in the initial stages of the reaction.

The rate of formation of ethylene may therefore be expressed as

$$[5] \quad R_{C_2H_4} = k_2 K_1^{1/2}[H_2]^{1/2}[C_2H_6]$$

Values for k_2 were calculated using eq. [5] and the rates obtained for concentrations of ethane in the neighbourhood of 20 ppm where the contribution from heterogeneous processes was a minimum. To estimate the correction for the heterogeneous reaction the rate constant k_2 was calculated in the same way for the measurements made in the packed vessel. Using both values for k_2 an extrapolation was made to S/V = 0. The values obtained were about 15% lower than the values obtained in the unpacked vessel. Examples are given in Table 3. The data for the determination of the temperature dependence of k_2 are given in Table 4, which includes the corrected values for k_2. The Arrhenius plot is shown in Fig. 4. The value of k_2 may be expressed as follows:

$$\log k_2 \text{ (L mol}^{-1}\text{ s}^{-1}\text{)} = 11.72 \pm 0.05 - \frac{12\,800 \pm 200}{2.3RT}$$

(R = 1.987 cal mol^{-1} deg^{-1}).

The values for the Arrhenius parameters of k_2 measured over the small temperature range of this study are not themselves as significant as the values obtained for the rate constant and their relation to other values measured with other techniques. This relation is shown in Fig. 5 where previous measurements covering the range 300−1400 K are shown. We have not included values of k_2 which, although quoted in the recent compilation (1), were not directly measured in the work described, for example, by Skinner and Ringrose (14), Bradley (15), and Clark, Izod, and Kistiakowsky (16). We have also omitted the early measurements by Darwent and Roberts (17) because it has been shown that the photolysis of H_2S, which was used as a source of hydrogen atoms, produced "hot" hydrogen atoms with consequent possibility for over-estimation of the rate of reaction (18).

Rate constants measured by addition of hydrocarbon to reacting mixtures of hydrogen and oxygen are determined relative to the branching reaction of hydrogen atoms with oxygen,

$$[6] \quad H + O_2 \rightarrow OH + O$$

Although there is essential agreement on the rate parameters for this reaction the actual values used by different laboratories may differ by as much as a factor of three. For comparison we have normalized the results of Tikhomirova and Voevodsky (19), Parsamyan *et al.* (20), and Gorban and Nalbandyan (21) to the value of k_6 used by Baldwin and Melvin (22).

$$\log k_6 \text{ (L mol}^{-1}\text{ s}^{-1}\text{)} = 11.33 - \frac{16\,500}{2.3RT}$$

This procedure has the effect of increasing the values of k_2 reported in these references and giving better consistency among values reported by this method.

The agreement between the results obtained by our method and those obtained from the H_2/O_2/hydrocarbon systems is useful confirmation for both techniques, particularly because all measurements reported above 750 K were obtained by the latter technique, except the unpublished data of Dove and Wagner, quoted in ref. 23, which are not included in Fig. 5.

The question of non-linearity in the Arrhenius relation has been much discussed for abstraction reactions of small radicals (23, 24) and has undoubtedly been observed in some cases. In Fig. 5 we have included as a dotted line the value of k_2 calculated by Clark and Dove (23). This calculation included such non-Arrhenius effects as temperature variation of quantum effects on vibrations and quantum mechanical tunnelling corrections. Camilleri *et al.* (8) concluded after an examination of the data that the variation of k_2 with temperature was best described by an Arrhenius relation over the range of temperature covered by the measurements shown in Fig. 5. This relation was expressed as follows:

$$[7] \quad \log k_2 \text{ (L mol}^{-1}\text{ s}^{-1}\text{)} = 11.0 \pm 0.1 - \frac{9600 \pm 200}{2.3RT}$$

R = 1.987 cal mol^{-1} deg^{-1}.

For our collection of data we did not make corrections to the results obtained below 770 K, but reasonable corrections based on stoichiometry discussed by Camilleri *et al.* (8) bring the data of Berlie and LeRoy (25) and Azatyan *et al.* (5) closer to an average value. It also appears that the value reported by Yang (9) measured relative to the addition of hydrogen atoms to propylene will be increased by using a more recent value for the reference reaction (1). Nevertheless, an examination of Fig. 5 shows that the correlation of the data with the calculated curve is almost as satisfactory as with a simple Arrhenius relation. The present measurements of k_2 are in agreement with either relation, but the measured value of the activation energy, 12.8 kcal mol^{-1}, is in good agreement with the value obtained from the calculated curve and suggests a small increase in activation energy with increasing temperature. Measurements of activation energies are, of course, subject to systematic errors and are less reliable than the rate constants themselves. The measured value of the frequency factor for k_2, $10^{11.7}$ L mol^{-1} s^{-1}, is between the values of $10^{11.1}$ and $10^{11.8}$ L mol^{-1} s^{-1} estimated by Benson (26) at 800 K for a transition state linear or non-linear, respectively. Taking our value for k_2 at 1000 K together with the lowest value calculated for the frequency factor, $10^{11.1}$ L mol^{-1} s^{-1}, a value for E_2 of 10.0 kcal mol^{-1} is obtained, which is reasonably close to the average value obtained from the Arrhenius relation. The present results, therefore, do not allow a clear choice between an Arrhenius or

Can. J. Chem. Downloaded from www.nrcresearchpress.com by 210.87.254.40 on 09/06/12
For personal use only.

TABLE 4. k_2 as a function of temperature

T (K)	P_{H_2} (Torr)	[H] (10^{-13} mol L^{-1})	[C_2H_6] (10^{-8} mol L^{-1})	$R^{\circ}_{C_2H_4}$ (10^{-11} mol L^{-1} s^{-1})	log k_2 (L mol^{-1} s^{-1})	log k_2* (L mol^{-1} s^{-1})
908	113.0	7.84	4.73	1.74	8.672	8.620
920	113.0	11.45	4.67	2.89	8.733	8.681
921.5	113.5	11.45	7.44	4.15	8.688	8.636
931	113.0	15.25	4.62	4.68	8.822	8.770
899	112.5	5.99	4.76	1.14	8.602	8.550
975.5	52.5	35.1	2.05	5.11	8.851	8.799
986	52.5	45.9	2.03	8.29	8.950	8.898
1005.5	37.5	59.8	1.42	8.08	8.978	8.926
1016	37.5	82.3	1.40	12.7	9.042	8.990
876	112.5	2.89	11.1	1.15	8.554	8.502
996	37.5	49.5	1.43	5.38	8.881	8.829
977	52.5	36.8	2.08	5.22	8.842	8.790

*Corrected for heterogeneous reaction.

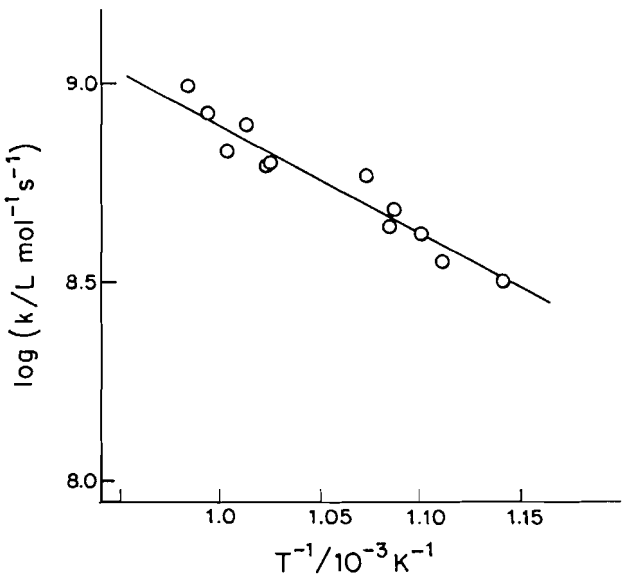

FIG. 4. Arrhenius plot of the corrected values of k_2.

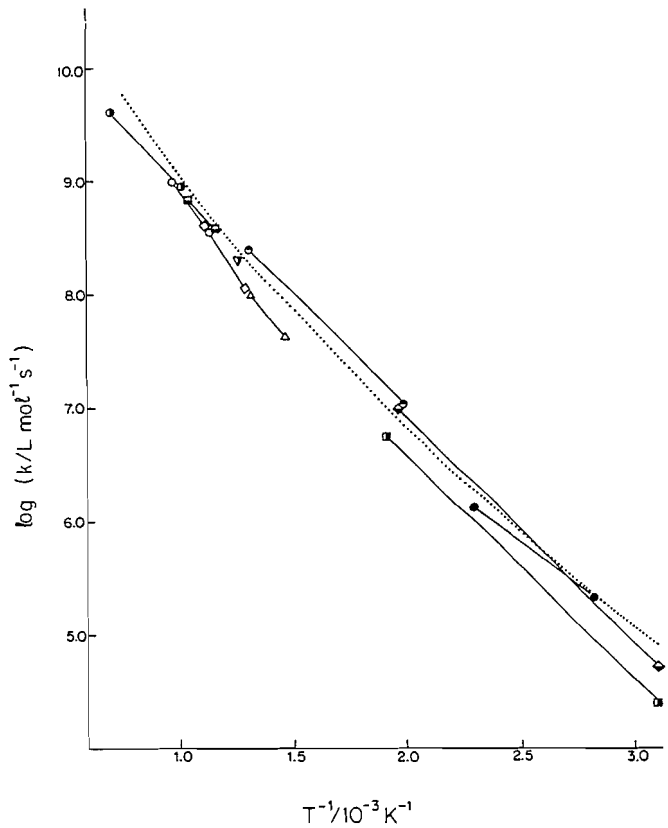

FIG. 5. Arrhenius plot of measurements of k_2 covering the temperature range 300–1400 K. ◑, ref. 28; ⬓, ref. 19; ◇, ref. 18; ▽, ref. 29; △, ref. 21; ◓, ref. 8; ⬙, ref. 5; ●, ref. 24; ◨, ref. 9; ○, present work. Dotted line: calculated curve, ref. 23.

non-Arrhenius relation for the dependence of k_2 on temperature. The equation suggested by Camilleri *et al.* (8) is probably the best average value of all the measurements.

The present values of k_2 may be compared to the values obtained for k_{-2} from the same method (10) through the equilibrium constant. This comparison, not only of our own results but of other published data on this system, provides evidence in support of a value for $\Delta H_f(C_2H_5)$ of 28 kcal mol^{-1} and will be presented and discussed in a forthcoming publication.

Finally we wish to comment on the results obtained in the packed reaction vessel. In the previous study of the kinetics of the hydrogenation of ethylene in a similar system the rates were not affected by a change in S/V ratio. It was concluded that the concentration of hydrogen atoms in the system was not altered in the packed vessel and that the equilibrium concentration was attained in both cases. This conclusion should also be valid in the present experiments and the heterogeneous reactions must involve the ethane molecule or its products. The rate of formation of methane, although only measurable at the highest temperature, was not altered in the packed vessel. Similar observations have been reported in studies of the thermal decomposition of ethane and it has been concluded that the dissociation reaction of ethane into two methyl radicals is a homogeneous process. In a recent study of heterogeneous processes in the pyrolysis of ethane, Pacey and Wimalasena (27) have concluded that the most important process occurring on the surface is a termination reaction of the ethyl radical. Such a reaction may occur in our system but would not affect the measured rate of formation of ethylene, since the rate-controlling step is reaction [2]. It seems more likely that a new decomposition process of the ethane molecule may be induced on the quartz surface, to give either an ethyl radical or ethylene directly. This type of reaction was not suggested in the pyrolysis of ethane itself because the ethylene formed by such a reaction would be negligible in comparison to the product

Can. J. Chem. Downloaded from www.nrcresearchpress.com by 210.87.254.40 on 09/06/12
For personal use only.

formed by the chain decomposition and would not, therefore, be observable. The actual rate of the surface process in the present system, where a chain decomposition does not occur, is only slightly larger than the homogenous initiation rate in the decomposition of ethane. Without more details of the surface process an empirical correction to the rate constant, such as that mentioned above, seems a reasonable method to obtain a rate constant which describes the homogeneous reaction.

In summary, the results presented here and previously demonstrate the validity of the technique for the utilisation of the equilibrium concentration of hydrogen atoms, obtained through the thermal dissociation of the hydrogen molecule for the measurement of rate constants for reactions of hydrogen atoms, and other small radicals. It should be noted that the principal assumption in the measurements is maintenance of an equilibrium concentration of hydrogen atoms and that under these circumstances absolute rather than relative values of the rate constants are obtained.

Acknowledgments

The authors wish to thank the Natural Sciences and Engineering Research Council of Canada for financial support of this work. J. R. Cao also thanks the government of the People's Republic of China for financial support during the course of this work.

1. J. A. KERR and S. J. MOSS (*Editors*). Handbook of bimolecular and termolecular gas reactions. CRC Press, Boca Raton, FL. 1981.
2. P. ROTH and T. H. JUST. NBS Special Publication No. 561. p. 1339 (1979).
3. P. ROTH, U. BARNER, and R. LÖHR. Ber. Bunsenges. Phys. Chem. **83**, 929 (1979).
4. J. V. MICHAEL, D. T. OSBORNE, and G. N. SUESS. J. Chem. Phys. **58**, 2800 (1973).
5. V. V. AZATYAN, S. B. FILIPPOV, A. B. NALBANDYAN, and L. B. RAMANOVICH. Arm. Khim. Zh. **22**, 193 (1969).
6. V. V. VOEVODSKY and V. N. KONDRATIEV. Prog. Reaction Kinet. **1**, 41 (1961).
7. M. P. HALSTEAD, D. A. LEATHARD, R. M. MARSHALL, and J. H. PURNELL. Proc. R. Soc. A**316**, 575 (1970).
8. P. CAMILLERI, R. M. MARSHALL, and J. H. PURNELL. J. Chem. Soc. Far. Trans. 1, **70**, 1434 (1974).
9. K. YANG. J. Phys. Chem. **67**, 562 (1963).
10. J.-R. CAO and M. H. BACK. Can. J. Chem. **60**, 3039 (1982).
11. J.-R. CAO and M. H. BACK. Carbon, **20**, 505 (1982).
12. M. C. LIN and M. H. BACK. Can. J. Chem. **44**, 2357 (1966).
13. S. C. CHAN, B. S. RABINOVITCH, J. T. BRYANT, L. D. SPICER, T. FUJIMOTO, Y. N. LIN, and S. P. PAVLOU. J. Phys. Chem. **74**, 3160 (1970).
14. G. B. SKINNER and G. H. RINGROSE. J. Chem. Phys. **43**, 4129 (1965).
15. J. N. BRADLEY. Proc. R. Soc. London, A**337**, 199 (1974).
16. T. C. CLARK, T. P. J. IZOD, and G. B. KISTIAKOWSKY. J. Chem. Phys. **54**, 1295 (1971).
17. B. DE B. DARWENT and R. ROBERTS. Discuss. Faraday Soc. **14**, 55 (1953).
18. B. DE B. DARWENT and M. J. ALLARD. J. Phys. Chem. **71**, 2346 (1967).
19. N. N. TIKHOMIROVA and V. V. VOEVODSKY. Chain oxidation of hydrocarbons in the gas phase (Russ). Moscow. 1955.
20. N. I. PARSAMYAN, E. A. ARAKELYAN, V. V. AZATYAN, and A. B. NALBANDYAN. Izv. Akad. Nauk SSSR, Ser. Khim. 496 (1968).
21. N. I. GORBAN and A. B. NALBANDYAN. Russ. J. Phys. Chem. **36**, 946 (1962).
22. R. R. BALDWIN and A. MELVIN. J. Chem. Soc. 1785 (1964).
23. T. C. CLARK and J. E. DOVE. Can. J. Chem. **51**, 2147 (1973).
24. W. C. GARDINER. Acc. Chem. Res. **10**, 326 (1977).
25. M. R. BERLIE and D. J. LEROY. Discuss. Faraday Soc. **14**, 50 (1953).
26. S. W. BENSON. Thermochemical kinetics. 2nd ed. John Wiley, New York. 1976. p. 154.
27. P. D. PACEY and J. H. WIMALASEMA. Can. J. Chem. In press.
28. C. P. FENIMORE and G. W. JONES. 9th Int. Symp. Comb. Academic Press, New York. 1963. p. 597.
29. R. R. BALDWIN, D. E. HOPKINS, and R.W. WALKER. Trans. Faraday Soc. **66**, 189 (1970).

Can. J. Chem. Downloaded from www.nrcresearchpress.com by 210.87.254.40 on 09/06/12
For personal use only.

Correlation of ^{13}C and ^{15}N nuclear magnetic resonance chemical shifts with polarographic reduction potentials of *para*-substituted benzenediazonium salts and their electronic structures[1]

R. M. ELOFSON, N. CYR, J. K. LAIDLER, K. F. SCHULZ, and F. F. GADALLAH
Alberta Research Council, Edmonton, Alta., Canada T6G 2C2

Received November 2, 1982[2]

R. M. ELOFSON, N. CYR, J. K. LAIDLER, K. F. SCHULZ, and F. F. GADALLAH. Can. J. Chem. **62**, 92 (1984).

Carbon-13 and nitrogen-15 nmr chemical shifts of benzenediazonium salt and its *para*-substituted derivatives have been measured in sulfolane solutions. The chemcial shifts of $^{13}C1$ correlate linearly with the polarographic half-wave potentials. This relation indicates the linear increase of electron densities at C1 with the increase of electron-donating power of the substituents. Non-linear relationships between ^{15}N shifts of both nitrogen nuclei and the half-wave potentials were partly attributed to the second-order paramagnetic contributions to the ^{15}N shifts. This contribution is approximately proportional to the inverse of the uv absorption frequencies. Overall results suggest that in the ground state resonance structures of the benzenediazonium salts, the rehybridization of the C1—N1 bond is very unlikely and this bond remains as a single bond.

R. M. ELOFSON, N. CYR, J. K. LAIDLER, K. F. SCHULTZ et F. F. GADALLAH. Can. J. Chem. **62**, 92 (1984).

Faisant appel à la rmn du ^{13}C et du ^{15}N, on a mesuré les déplacements chimiques des sels de benzènediazonium et de ses dérivés substitués en position *para* en solution dans le sulfolane. Il y a une corrélation linéaire entre les déplacements chimiques du $^{13}C1$ et les potentiels de demi-onde polarographique. Cette relation indique une augmentation linéaire de la densité électronique en C1 avec l'augmentation du pouvoir électronneur des substituants. On attribue partiellement les relations non linéaires entre les déplacements chimiques du ^{15}N des deux noyaux de nitrogène et les potentiels de demi-onde, à des contributions paramagnétiques de second ordre aux déplacements du ^{15}N. Cette contribution est approximativement proportionnelle à l'inverse des préférences d'absorptions en uv. Les résultats généraux suggèrent que dans l'état fondamental de la structure de résonance des sels de benzènediazonium, la rehybridation de la liaison C1—N1 est inhabituelle et cette liaison demeure une liaison simple.

[Traduit par le journal]

Can. J. Chem. Downloaded from www.nrcresearchpress.com by 210.87.254.105 on 09/06/12
For personal use only.

Introduction

Some time ago, Elofson and Gadallah obtained a good correlation of polarographic half-wave potentials of substituted benzenediazonium salts with Hammett substituent constants, $\sigma(1)$. We have had occasion to measure the ^{13}C nmr shifts of a number of substituted benzenediazonium salts in sulfolane, the solvent in which the polarographic correlation was obtained. We also obtained the natural abundance ^{15}N chemical shifts of some of the compounds.

Other workers (2–6) have noted various unusual aspects of the ^{13}C and ^{15}N chemical shifts, in particular, the very highfield shift of the C1 carbons and lowfield shift of diazo nitrogens in benzenediazonium salts, especially with electron-donating substituents. We have now extended the series and compared the nmr results with polarographic half-wave potentials which are a direct measure of the electrophilicity of these compounds. It was not surprising to find a good linear correlation between the polarographic half-wave potentials and $^{13}C1$ shifts. Nitrogen-15 nmr shieldings are found to be affected in opposite directions from those of $^{13}C1$ and they do not correlate linearly with the half-wave potential or the Hammet σ constants.

Sulfolane was chosen as a solvent for the nmr measurements in order to avoid the complications of specific solvation effects. Recently the effects of some other solvents on ^{15}N chemical shifts have been noted to be significant (7, 8). Also, the polarographic measurements in sulfolane have produced a good correlation and, with the most positive values for half-wave potentials, an indication of minimum solvation effects. It has been noted also in this laboratory that the chloride ion causes large displacement of $E_{1/2}$ to more negative potentials. This has been attributed to complex formation.[3] Therefore, chloride or other halide ions were carefully excluded from the diazotization procedures and tetrafluoroborate salts were used, except for sulfanilic acid diazonium zwitterion, in order to avoid specific interactions. Inclusion of chloride ions in diazotization procedures was largely responsible for the failure of early workers to obtain a correlation between $E_{1/2}$ and σ or σ^+.

Various resonance structures have been suggested for the ground state of aryldiazonium compounds (see Chart 1), including those with rehybridized C1—N1 and N1—N2 bonds (**3***a* and **3***b*). Significance of these resonance structures is discussed and, from the evidence of ^{13}C and ^{15}N chemical shifts, it is concluded that C1—N1 remains as a single bond.

Experimental

Carbon-13 and nitrogen-15 nmr spectra of benzenediazonium tetrafluoroborates were measured in approximately 15 mL of 1.5% sulfolane solutions on a Bruker WH-200 nmr spectrometer operating at 50.323 MHz for ^{13}C and 20.279 MHz for ^{15}N. Nitrogen chemical shifts were calculated from ammonia using the spectral reference numbers. Internal TMS was used as a carbon reference. Five percent of the solvent was perdeuterated sulfolane to provide a deuterium source for the field-frequency lock. All the measurements were made at 5°C and tetrabutylammonium fluoroborate (~0.1 *M*) was added to the solutions to prevent them from freezing.

Ultraviolet absorptions of the fluoroborate salts were measured in sulfolane/CH_3CN (9:1) in approximately 10^{-4} molar solutions using a Beckman Acta C-111 spectrophotometer.

Assignment ^{13}C signals

For *p*-CN benzenediazonium salt, the asssignments for C1, C4, and the cyano carbon were not straightforward. There are three peaks at 123.4, 119.3, and 116.1 ppm. First, a proton coupled ^{13}C spectrum showed that the signals at 123.4 ppm and 116.1 ppm were simple triplets and that at 119.3 ppm was a triplet of triplets. This indicates that the peak at 119.3 ppm was coupled to two sets of two equivalent protons. Therefore, this peak is not due to the cyano carbon, since there are only two protons which could couple to the carbon, and they

[1]Alberta Research Council Contribution Number 1233.
[2]Revision received March 17, 1983.
[3]R. M. Elofson and J. K. Laidler. Unpublished results.

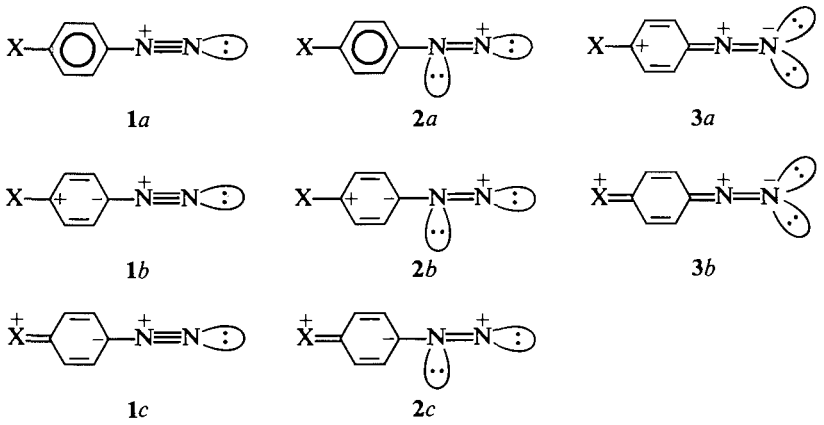

CHART 1. Possible resonance structures of *p*-substituted benzenediazonium salts.

TABLE 1. Chemical shifts, half-wave potentials, and Hammett constants of *para*-substituted benzenediazonium salts

	^{13}C shifts*				^{15}N shifts†			
Substituents	C(1)	C(2, 6)	C(3, 5)	C(4)	N(1)	N(2)	$E_{1/2}$	σ or σ^+
$N(CH_3)_2$	88.4	133.8	114.4	156.8	246.9	345.5	−0.095	−1.70
OCH_3	102.4	136.1	117.9	170.4	234.2	322.0	+0.140	−0.778
CH_3	111.0	132.5		155.7	232.4	316.5	+0.250	−0.311
		132.8						
Phenyl	112.3	Not assigned		—	—	—	+0.275	−0.179
H	115.1	131.9		141.9	231.4	314.2	+0.295	0
		132.8						
Cl	113.5	132.4		148.5	—	—	+0.350	+0.114
		134.4						
SO_3H	116.8	128.5		153.7	—	—	+0.297	+0.090
		133.1						
CN	119.8	133.2		123.5	229.1	314.7	+0.433	+0.660
		116.4						
		135.4 (CN)			269.2 (CN)			
NO_2	120.9	126.8		154.3	228.7	314.8	+0.450	+0.778
		134.8						

*From TMS in ppm.
†From NH_3 in ppm.

are separated from it by three bonds. Secondly, benzenediazonium fluoroborate wth the terminal nitrogen enriched with 95% ^{15}N was prepared, and its proton decoupled ^{13}C nmr spectrum, showed that the peak at 119.3 ppm was a doublet of ~5.5 Hz, indicating that this peak is due to the nearest carbon, C1. The other two peaks remained as singlets. From the above two experiments and the expected chemical shift of cyano carbons, the assignments were confirmed.

Results and discussion

The high stability of *p*-substituted benzenediazonium salts with electron-releasing substituents has been explained by Zollinger (9) as the result of strong contributions to the ground state structure from mesomeric forms **3***a* and **3***b* where the C1—N1 bond is a double bond. Although X-ray studies (10–15) have since shown the C1—N1 bond length in these compounds to be that of an ordinary single bond, and the N1—N2 distance to be the length of a normal triple bond, contributions to the structure from forms **3***a* and **3***b* have been invoked to explain the decrease in calculated bond order by Sukigara and Kikuchi (16), the lengthing of the N1—N2 bond in *p*-dimethylamino benzenediazonium salt by Polynova *et al.* (13), and the linear relationship between half-wave potentials and Hammett constants by this laboratory (1). Recently, studies of ^{13}C nmr chemical shifts of C4 (2, 6) and ^{15}N shifts of N1 and N2 (3, 7) again suggested significant contribution by structures **3***a* and **3***b* to the ground state of *p*-substituted benzenediazonium salts with electron-donating groups.

Carbon-13 and nitrogen-15 chemical shifts are listed in Table 1 together with the polarographic half-wave potential measured in the previous study (1). The equation for the linear correlation between ^{13}C1 shifts, δ, and half-wave potentials, $E_{1/2}$ in Fig. 1, is:

$$[1] \quad E_{1/2} = 0.016\,\delta - 1.51 \quad \text{corr. coeff.} = 0.979$$

where δ is in ppm from TMS. These results indicate a nearly linear increase in shielding of C1 as the electron-donating power of the substituents increases or the $E_{1/2}$ (electrophilicity) decreases. Since a linear relationship between the Hammett constants and $E_{1/2}$ has already been found (1), the ^{13}C chemical shifts also relate linearly with the Hammett constants according to the equation:

$$[2] \quad \delta = 13.216\,(\sigma \text{ or } \sigma^+) + 113.1 \quad \text{corr. coeff.} = 0.979$$

These results agree closely with those of Olah and Grant (2) and Ustynyk *et al.* (6).

The large upfield shifts of ^{13}C1 in various substituted benzenediazonium salts (refs. 2, 3, 5, 6 and footnote 2) indicate

Can. J. Chem. Downloaded from www.nrcresearchpress.com by 210.87.254.105 on 09/06/12
For personal use only.

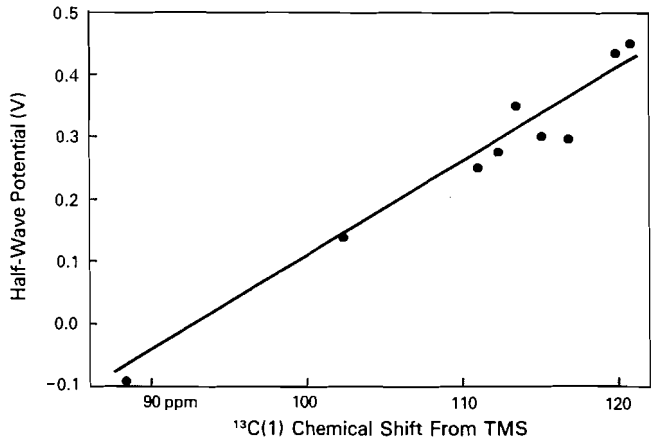

FIG. 1. Linear correlation between ^{13}C1 chemical shifts and polarographic half-wave potentials, $E_{1/2}$, of some aryl diazonium salts.

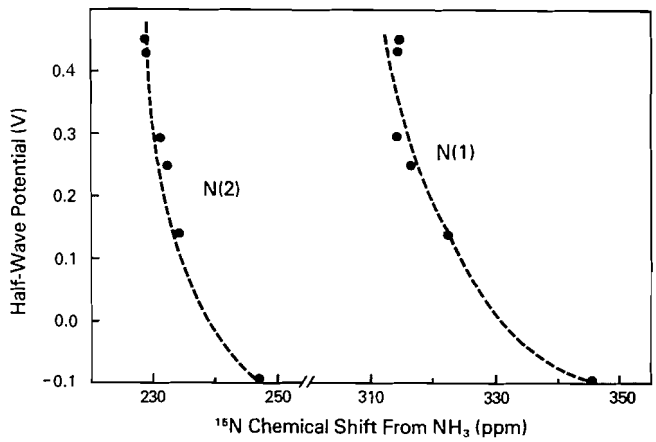

FIG. 2. Plots of ^{15}N chemical shifts with polarographic half-wave potentials, $E_{1/2}$, of some aryl diazonium salts.

the unusual effect of the diazonium group. These high shieldings are partly associated with the small second-order paramagnetic shift due to the N1≡N2 triple bond. The much higher shieldings of C1 found in phenylacetylene, 121.5 ppm (17), and in benzonitrile, 109.7 ppm(18), than found in styrene, 138.2 ppm (18), are analogous to the present observation.

The accumulation of electron charge on C1 is partly due to contributions from some of the accepted resonance structures of *para*-substituted benzenediazonium salts (Chart 1). Contributions from structures **1***b* and **1***c* reasonably explain the unusually high shielding of C1, and are particularly important when the substituent is capable of mesomeric donation of electrons to the ring.

In contrast to the ^{13}C chemical shifts, ^{15}N resonance absorptions shift downfield as the substituents become more electron donating. As shown in Fig. 2, the ^{15}N resonance shift generally to highfield as the half-wave potential, $E_{1/2}$, increases. The correlation is not linear.

The effect of rehybridization involving the phenyl ring and the *para* substituent (**1***b* and **1***c*) can be also seen from the ^{15}N chemical shifts. The large downfield shift in the amino ^{15}N resonance is the result of the loss of some electrons from this nitrogen to the ring. The ^{15}N chemical shift of the amino nitrogen of *p*-dimethylamino benzenediazonium salt is 128 ppm compared with a much more shielded value of 44.6 ppm dimethyl aniline (17), where such resonance structures as **1***b* and **1***c* make less contribution.

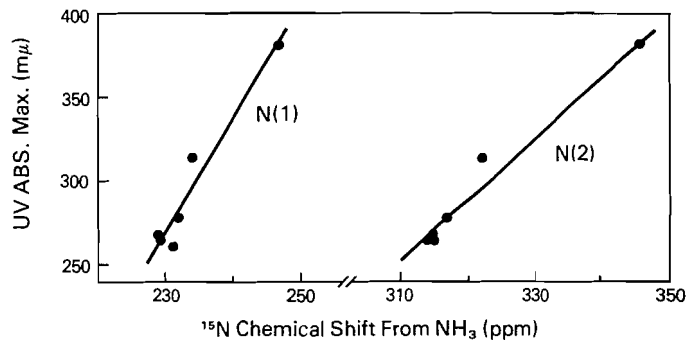

FIG. 3. Correlations between ^{15}N chemical shifts and the uv absorption maxima of some aryl diazonium salts.

The observed downfield shift of N1 and N2 with electron donating substituents may be further explained by including the resonance structues, **2***a*, **2***b*, or **2***c*. N1 shifts downfield by gaining a lone pair and N2 by gaining a positive charge (**1***a* → **2***a*, **2***b* or **2***c*). If we consider those resonance structures for compounds with electron-donating substituents, the correlation of ^{15}N chemical shifts, in the opposite direction from ^{13}C1 chemical shifts, with the half-wave potentials may be understood. The lack of a linear relationship between ^{15}N shifts and $E_{1/2}$ seems to indicate that differt mechanisms from those in the ^{13}C shifts dominate in ^{15}N chemical shifts.

The lengthening of the C1—N1 bond distance from 1.415 Å in benzenediazonium cations (11) to 1.48 Å in *o*-OCH_3 or *p*-$N(CH_3)_2$ derivatives (13, 14) predicts only about 5 ppm shift in ^{15}N resonance to the downfield if we consider only the decrease of diamagnetic contribution.[4] Second-order paramagnetic contributions due to the mixing of some excited states to the ground state may become important in this case. In Fig. 3, ultraviolet absorption maxima of the compounds studied here are plotted against ^{15}N chemical shifts. Figure 3 indicates that as the electron-donating property of the substituent increases, the absorption maxima shift toward the longer wavelength (lower excitation energy). The absorption of the dimethylamino compound is at a particularly long wavelength. If we assume that the mean excitation energy in the expression of the second-order paramagnetic shifts (19):

$$[3]\quad \sigma_p = -\frac{e^2h^2}{2m^2C^2\Delta E}\left\langle\frac{1}{r^3}\right\rangle_{2p}\left[Q_{NN} + \sum_{B\neq N} Q_{NB}\right]$$

can be approximated by the observed uv excitation energy (20), the non-linearity of the plot of the ^{15}N chemical shifts (see Fig. 2) with $E_{1/2}$ may be due mainly to the dominance of this term.

Resonance structures **2***a*, **2***b*, and **2***c* are also compatible with the slight lengthening of the N—N bond (14) and the calculated lower bond order (16) for the electron-donating dimethylamino derivative. These structures also agree with the single bond length found for C1—N1 bonds by X-ray studies (11–15). The downfield shift of ^{13}C4 (2) may also be due to the accumulation of positive charge on C4 (**1***b* and **2***b*). Moreover, the overall findings from the X-ray studies which eliminate structures **3***a* and **3***b* are fully supported here. Gadallah and Elofson (1) have shown that electrochemical reduction of aryldiazonium salts at controlled potentials in aprotic solvents produces phenyl radicals and N_2 gas as the only products, indicating an intact N≡N triple bond.

[4]N. Cyr. Unpublished results.

Can. J. Chem. Downloaded from www.nrcresearchpress.com by 210.87.254.105 on 09/06/12
For personal use only.

The increased shielding of C1 correlates well not only with $E_{1/2}$ as illustrated in Fig. 1 but also with coupling rates (21). The coupling rates of p-NO_2, unsubstituted, and p-OCH_3 benzenediazonium cations with 1-naphtholate are in the order of $NO_2 \gg H \gg OCH_3$. Again, no simple relationship exists between the $^{15}N1$ and $^{15}N2$ shifts and coupling rates. Perhaps the slightly decreased shielding of $^{15}N2$ observed by Casewit *et al.* (7) and in this study for p-NO_2, p-COOH, and p-CN compounds are significant. These shifts, although less than 1 ppm, are in the same direction (downfield) as the $^{13}C1$ resonances, compared to the unsubstituted compound. The maximum in the plot of $^{15}N2$ shifts against σ^+ (Fig. 2 in ref. 7) may be related to the well-known and still unexplained fact that both the p-NO_2 and p-OCH_3 derivatives decompose more slowly (22) in acid than the unsubstituted salt ($H > p$-$NO_2 \gg p$-OCH_3).

Acknowledgements

The authors thank Dr. T. Nakashima and Mr. G. Bigham for recording ^{13}C and ^{15}N nmr spectra and for their valuable discussions, and Mrs. L. Gadallah for editing the manuscript.

1. R. M. ELOFSON and F. F. GADALLAH. J. Org. Chem. **34**, 854 (1969).
2. G. A. OLAH and J. L. GRANT. J. Am. Chem. Soc. **97**, 1546 (1975).
3. R. O. DUTHALER, H. G. FORSTER, and J. D. ROBERTS. J. Am. Chem. Soc. **100**, 4974 (1978).
4. R. RADEGLIA and K. JACKOWSKI. Z. Chem. **15**, 311 (1975).
5. A. V. DUSHKIN, T. V. LESHINA, O. I. SHUVAEVA, R. Z. SAGDEEV, A. J. REZVUKHIN, M. V. KAZANKOV, N. M. MAKSHANOVA, and S. M. SHEIN. Zh. Org. Khim. **13**, 1132 (1977). English translation.
6. Y. A. USTYNYUK, O. A. SUBBOTIN, L. M. BUCHNEVA, V. N. GRUZDNEVA, and L. A. KAZITSYNA. Dokl. Akad. Nauk SSSR, **227**, 175 (1976). English translation.
7. C. J. CASEWIT. *In* Nitrogen-15 and carbon-13 nuclear magnetic resonance studies of aryl-diazonium compounds. Effect of substituent, solvent and 18-crown-6. Ph.D. Thesis. California Institue of Technology, 1981; C. Casewit, J. D. Roberts, and R. A. Bartsch. J. Org. Chem. **47**, 2875 (1982).
8. S. H. KORZENIOWSKI, A. LEOPOLD, J. R. BEADLE, M. F. AHERN, W. A. SHEPPARD, R. K. KHANNA, and G. W. GOKEL. J. Org. Chem. **46**, 2153 (1981).
9. H. ZOLLINGER. Azo and diazo chemistry. Interscience Publishers. Inc., New York. 1961. p. 42.
10. C. ROMMING. Acta Chem. Scand. **13**, 1260 (1959).
11. C. ROMMING. Acta Chem. Scand. **17**, 1444 (1963).
12. C. ROMMING. Acta Chem. Scand. **26**, 523 (1972).
13. T. N. POLYNOVA, N. G. BOKII, and M. A. PORAI-KOSHITS. Zh. Strukt. Khim. **6**, 877 (1965).
14. Y. M. NESTEROVA and M. A. PORAI-KOSHITS. Zh. Strukt. Khim. **12**, 108 (1971).
15. M. CYGLER, M. PRZYBYLSKA, and R. M. ELOFSON. Can. J. Chem. **60**, 2852 (1982).
16. M. SUKIGARA and I. KIKUCHI. Bull. Chem. Soc. Jpn. **40**, 461 (1967).
17. M. P. SIBI and R. L. LICHTER. J. Org. Chem. **42**, 2999 (1977).
18. J. B. STOTHERS. *In* Carbon-13 NMR spectroscopy. Academic Press, New York. 1972. p. 197.
19. M. KARPLUS and J. A. POPLE. J. Chem. Phys. **38**, 2803 (1963).
20. W. G. PROCTOR and F. C. YU. Phys. Rev. **81**, 20 (1951).
21. A. F. HEGARTY. *In* The chemistry of diazonium and diazo groups. *Edited by* S. Patai. John Wiley and Sons, New York. 1978. p. 548.
22. M. L. CROSSLEY, R. H. KIENLE, and C. H. BENBROOK. J. Am. Chem. Soc. **62**, 1400 (1940).

Can. J. Chem. Downloaded from www.nrcresearchpress.com by 210.87.254.105 on 09/06/12
For personal use only.

Diastereomers of the insect repellent 3-acetyl-2-(2′,6′-dimethyl-5′-heptenyl)oxazolidine. Isolation by high pressure liquid chromatography and characterization by ^{13}C nuclear magnetic resonance spectroscopy

WESLEY G. TAYLOR
Agriculture Canada Research Station, Lethbridge, Alta., Canada T1J 4B1

AND

TOM T. NAKASHIMA
Department of Chemistry, University of Alberta, Edmonton, Alta., Canada T6G 2G2

Received July 12, 1983

WESLEY G. TAYLOR and TOM T. NAKASHIMA. Can. J. Chem. **62**, 96 (1984).

Preparative-scale high pressure liquid chromatography on 3-acetyl-2-(2′,6′-dimethyl-5′-heptenyl)oxazolidine (**1**), a complex acetamide derivative of citronellal, resulted in isolation of the diastereomeric forms of this insect repellent. The two diastereomers were designated as **1***a* and **1***b* on the basis of their order of elution from silica gel and from a variety of capillary gas chromatography columns. Interpretation of the ^{13}C nuclear magnetic resonance spectra of **1***a* and **1***b* was accomplished by comparison with model compounds and by off-resonance proton-decoupling experiments. Absolute stereochemical assignments were not made. Because of the amide group, the diastereomers existed in solution at ambient temperature as *cis* and *trans* rotational isomers, which caused nonequivalence of most of the carbon atoms, including the olefinic carbons at C-5′ and C-6′. *trans* Isomer (**5**) was concluded to be the major contributor to the rotational equilibrium. The spectrum of 3-acetyl-2-(4′-methyl-3′-pentenyl)oxazolidine (**7**) was also recorded for comparison.

WESLEY G. TAYLOR et TOM T. NAKASHIMA. Can. J. Chem. **62**, 96 (1984).

La chromatographie liquide à haute pression à l'échelle préparative de l'acétyl-3 (diméthyl-2′,6′ heptène-5′ yl)-2 oxazolidine (**1**), un dérivé acétamide complexe du citronellal, a permis d'isoler deux formes diastéréoisomères de ce produit qui repousse les insectes. On désigne ces deux diastéréoisomères **1***a* et **1***b* en fonction de leur temps d'élution sur du gel de silice et en fonction d'analyses chromatographiques en phase gazeuse sur des colonnes capillaires. On a interprété les spectres de rmn du ^{13}C des composés **1***a* et **1***b* par comparaison avec des composés modèles et par des expériences de découplage hors résonance du proton. On n'a pas déterminé la stéréochimie absolue à cause du groupe amide; en solution les diastéréoisomères existent, à la température ambiante, sous forme d'isomères rotationnels *cis* et *trans*, ce qui provoque la non équivalence de ce plupart des atomes de carbone, y compris les carbones oléfiniques en C-5′ et C-6′. On conclut que l'isomère *trans* (**5**) est celui qui contribue d'avantage a l'équilibre rotationnel. On a également enregistré le spectre de l'acétyl-3 (méthyl-4′ pentène-3′-yl)-2 oxazolidine (**7**) en vue d'établir des comparaisons.

[Traduit par le journal]

Can. J. Chem. Downloaded from www.nrcresearchpress.com by 210.87.254.42 on 09/06/12
For personal use only.

Introduction

A number of 2-substituted N-acetyloxazolidines, for example (±)-3-acetyl-2-(2′,6′-dimethyl-5′-heptenyl)oxazolidine (**1**), have insect repellent properties (1, 2) and **1** has been registered in some countries as a biting fly repellent.[1] Despite these initial claims on the identity of **1**, which was synthesized from (±)-citronellal (**2**), its structure and stereochemistry have not been investigated in detail. This is due, in large part, to the presence of four optical isomers, arising from the asymmetric centers at C-2 and C-2′. To our knowledge, the diastereomers of **1** and their enantiomeric counterparts have never been isolated in quantity. Recently, however, one pair of diastereomers (**1***a* and **1***b*) were separated by high resolution capillary gas chromatography (capillary gc) with achiral liquid phases and their mass spectra were compared (3). The ratio of **1***a* to **1***b*, calculated from integrated capillary gc peak areas, was 45:55 in various samples of **1**. As part of continuing efforts to understand the complexities of this unusual insect repellent, we now describe the isolation of **1***a* and **1***b* by preparative high pressure liquid chromatography (hplc) and the confirmation of structure of these diastereomeric components by ^{13}C nuclear magnetic resonance spectroscopy (^{13}C nmr).

Results and discussion

Synthesis, chromatography, and purity assessments

Starting from **2** enriched in the (*R*) (+) enantiomer, **1** was obtained by the condensation of this aldehyde with ethanolamine followed by acetylation with acetic anhydride. Capillary gc with a variety of columns and conditions showed 45% of the first eluting diastereomer (**1***a*) and 55% of the second eluting diastereomer (**1***b*) as the two major products. As previously described (3), attempts were made to separate **1***a* and **1***b* by thin layer and column chromatography but without success.

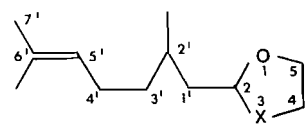

1 X = $NCOCH_3$

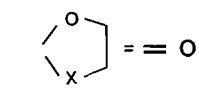

2

3 X = O

The separation of **1***a* and **1***b* was, however, accomplished by hplc with commercial silica gel cartridges. With a solvent mixture of ethyl acetate – methylene chloride and using the shave–recycle technique (4), **1***a* and **1***b* were partially separated after one recycling of the mixture. Compound **1***a* was collected by shaving the upslope of the first peak whereas **1***b*

[1]Citronyl, S. C. Johnson and Son.

TABLE 1. ^{13}C nuclear magnetic resonance chemical shifts of **2** and **3** in deuterochloroform solution[a]

Compound	2	4	5	1′	2′	2′-CH_3	3′	4′	5′	6′	6′-CH_3	7′	C=O
2	—	—	—	51.0[b] (?)[c]	27.9 (d)	19.9 (q)	37.0 (t)	25.5 (t)	124.1 (d)	131.7 (s)	17.6 (q)	25.7 (q)	202.7 (d)
3	103.9 (d)	64.7[d] (t)	64.6[d] (t)	41.0 (t)	29.1 (d)	19.8 (q)	37.5 (t)	25.4 (t)	124.7 (d)	131.1 (s)	17.6 (q)	25.7 (q)	—

[a]The temperature was 302–304 K.
[b]For ease of comparison to the remaining compounds, the carbons of **2** are labelled as primed numbers, with the carbon α to the aldehyde carbonyl being C-1′.
[c]The multiplicities (s, singlet; d, doublet; t, triplet; q, quartet) of signals from single-frequency off-resonance decouplings are given in brackets. The appearance of C-1′ under these conditions was more complex than the expected triplet.
[d]These signals may be interchanged.

TABLE 2. ^{13}C nuclear magnetic resonance chemical shifts of **1***a* and **1***b* in deuterochloroform solution[a]

Compound	Isomer[b]	2	4	5	1′	2′	2′-CH_3	3′	4′	5′	6′	6′-CH_3	7′	$NCOCH_3$	$NCOCH_3$
1*a*	**5**	88.6 (d)	45.6 (t)	65.2 (t)	39.8 (t)	29.2 (d)	20.3 (q)	36.6 (t)	25.3 (t)	124.8 (d)	131.0 (s)	17.6 (q)	25.7 (q)	167.9 (s)	23.2 (?)[c]
	6	88.2 (d)	43.3 (t)	64.6 (t)	41.6 (t)	29.2	20.3	36.3 (t)	25.3	124.3 (d)	131.3 (s)	17.6	25.7	167.0 (s)	22.4 (?)[c]
1*b*	**5**	88.2 (d)	45.6 (t)	65.2 (t)	39.4 (t)	29.0 (d)	19.1 (q)	37.7 (t)	25.4 (t)	124.8 (d)	131.0 (s)	17.6 (q)	25.7 (q)	167.8 (s)	23.2 (?)[c]
	6	87.7 (d)	43.3 (t)	64.6 (t)	41.3 (t)	28.8 (d)	19.1	37.7	25.4	124.4 (d)	131.4 (s)	17.6	25.7	167.2 (s)	22.3 (?)[c]

[a]The experimental conditions are given in Table 1.
[b]The peak height ratio of **5**:**6** was 72:28 ± 2%.
[c]The expected quartet was difficult to find in the off-resonance decoupled spectrum.

was isolated by shaving the backslope of the second peak. After redistillation of each sample, reasonable yields of **1***a* (20–25%) and **1***b* (40–60%) were isolated in at least 99% purity as shown by capillary gc with splitless injections. Each diastereomer also gave correct combustion analyses for its elements.

Samples of **1***a* and **1***b* (>98% diastereomeric purity by capillary gc) were checked for impurities by chemical ionization mass spectrometry using a direct insertion probe. Only the quasimolecular ion for **1***a* and **1***b* was detected, thus confirming the high purity of these samples.

The possibility existed that some chemical changes, such as rearrangement of the olefinic bond to give positional isomers, may have occurred during contact of the samples with silica gel, which would not have been detected by all of the above techniques. This did not occur because samples of **1** before hplc gave ^1H (3) and ^{13}C nmr spectra that were the same as the sum of the resonances in the purified diastereomers. Thirty resonances were detected in the ^{13}C nmr spectrum of **1**, which possessed 14 carbon atoms. Unfortunately, the ^1H nmr spectra (60 MHz) of **1***a* and **1***b* were virtually superimposable and the ^{13}C nmr spectra (22.6 MHz), although noticeably different, were still very complicated because two signals with unequal peak heights were observed for most of the carbon atoms, including the sp^2 carbons of the trisubstituted double bond. In attempts to characterize **1***a* and **1***b*, chemical shifts were first assigned, then reasons for the doubling of carbon signals in this system were investigated.

Assignments

Before commencing spectral analyses of **1***a* and **1***b*, the ^{13}C nmr spectra of **2** and citronellal ethylene acetal (**3**, ref. 5) were examined to aid in the interpretation. Chemical shift assignments (Table 1) were based on single-frequency off-resonance decoupling information and on available chemical shift data for related olefinic and isoprene compounds with analogous carbon structures (6–8). Couperus *et al.* (6) have reported the ^{13}C chemical shifts for a number of olefins and this work was of particular interest. The closest model for our system was 2,6-dimethyl-2-octene (**4**), shown below with the reported chemical shifts. From these values, the assignments for **2** and **3** followed directly.

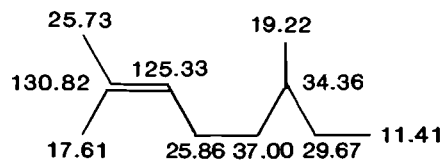

4

The spectra of **2** and **3** were very similar for C-3′ to C-7′ and for the methyl groups at C-2′ and C-6′. In **2**, C-1′ was deshielded by 10 ppm and C-2′ was shielded by 1.2 ppm compared to the same carbons in **3**. The dioxolane ring carbons were readily identified (Table 1) and the assignments agreed with reported values for related aliphatic acetals (9). C-4 and C-5 displayed a small difference in chemical shift (0.1 ppm).

The highly purified samples of **1***a* and **1***b* in deuterochloroform solution gave ^{13}C nmr chemical shifts as shown in Table 2. Where doubling of carbon signals occurred, the paired signal of larger intensity was considered first. Assignments of carbon shifts to the 5′-heptenyl side chain, with the exception of C-1′, were based on comparisons to **2**–**4** and the assignments were supported by off-resonance decoupling experiments. Chemical shift assignments for C-1′ at 39.8 ppm (**1***a*) and 39.4 ppm (**1***b*) were based on C-1′ being the only remaining methylene carbon that would be expected to resonate

Can. J. Chem. Downloaded from www.nrcresearchpress.com by 210.87.254.42 on 09/06/12
For personal use only.

near 40 ppm.

Assignment to C-2 of the oxazolidine ring (88.6 ppm for **1***a*; 88.2 ppm for **1***b*) was straightforward because of the expected large downfield shift from the other sp^3 hybridized tertiary carbon (C-2′). C-5 was deshielded relative to C-4, as noted in related N-nitrosooxazolidines (10). The only remaining carbons to assign were those of the N-acetyl group. As expected, the amide carbonyl carbon resonated near 168 ppm, whereas the main signal for the methyl group occurred at 23.2 ppm for both diastereomers. The latter carbon could be distinguished from C-2′ CH_3 by considering the similar chemical shifts for C-2′ CH_3 in **2** and **3** and by comparison to reported chemical shifts for related acetamides (11).

Compounds **1***a* and **1***b* gave very similar ^{13}C nmr spectra (Table 2). The largest differences in chemical shifts were found for C-2′ CH_3 (1.2 ppm), followed by C-3′ (1.1 ppm), C-2 (0.4 ppm) and C-1′ (0.4 ppm). These differences were not considered sufficiently large to attempt *R* or *S* stereochemical assignments at C-2.

cis–trans *Isomerism*

The ^{13}C nmr spectra of **1***a* and **1***b* showed that each diastereomer possessed nine nonequivalent carbons when recorded at ambient temperature in deuterochloroform solution. Four sites of nonequivalence were in the 5′-heptenyl side chain and the remainder were associated with the five carbon atoms of the N-acetyloxazolidine group (Table 2). With the exception of C-1′ and C-4, the chemical shifts of the paired signals differed by less than 1 ppm. The appearance of paired signals in **1***a* and **1***b* was different in one respect. In **1***a*, C-2′ gave one signal (29.2 ppm) and C-3′ gave two (36.6/36.3 ppm), whereas **1***b* gave two signals for C-2′ (29.0/28.8 ppm) and one for C-3′ (37.7 ppm).

Although N-acetyloxazolidines had not previously been examined by ^{13}C nmr, the carbon chemical shifts of N-acyl piperidines (12), N-acyl morpholines (13), N-acyl prolines (14), pyrrolidine-containing peptides (15), and other model amides (16) were influenced by the effects of restricted rotation about the amide bond, giving rise to sites of equivalence because of the existence of an equilibrium mixture of *cis* and *trans* rotational isomers. Thus, two well separated ^{13}C resonances have been observed at temperatures corresponding to a slow rate of amide bond rotation on the nmr time-scale. If **1***a* and **1***b* behaved similarly, the *trans* (**5**) and *cis* (**6**) isomers[2] must be present, and in unequal amounts, to account for the doubling of carbon signals when the spectra were recorded at ambient temperature.

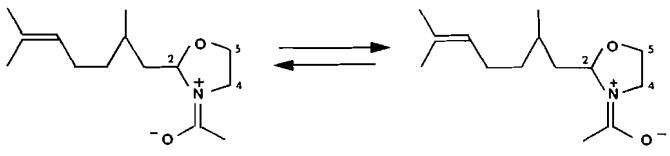

5 6

To demonstrate the involvement of **5** and **6**, a variable-temperature ^{13}C nmr experiment was performed on **1***b*, the diastereomer isolated in larger quantity. It was predicted that **5** and **6** would interconvert rapidly as the temperature rose and at a temperature corresponding to a fast rate of interconversion of these isomers on the nmr time-scale, nonequivalence would disappear, leading to a simplified ^{13}C nmr spectrum. The ^{13}C nmr spectra were recorded from 250–330 K at 20 K intervals. The spectra were virtually identical up to 310 K but at 330 K, the upper practical limit with deuterochloroform as solvent, the paired signals began to coalesce.

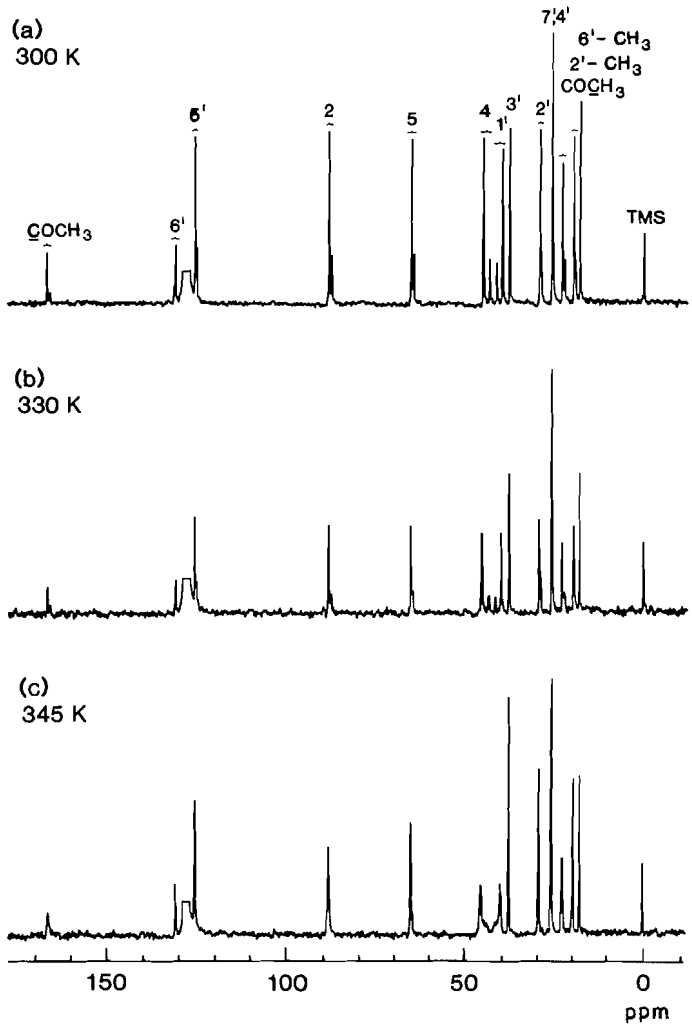

FIG. 1. The ^{13}C nmr spectra of 3-acetyl-2-(2′,6′-dimethyl-5′-heptenyl)oxazolidine (isomer **1***b*) at (a) 300 K, (b) 330 K, and (c) 345 K. The spectra were recorded with inverse gated decoupling with operating parameters as follows: decoupler delay, 2.2 s; decoupler switching delay 0.002 s; pulse width, 9 μs; acquisition time, 0.3 s; number of scans, 500. Peaks for the solvent (deuterobenzene) near 128 ppm have been truncated.

In order to extend the upper temperature limit the spectrum was recorded in deuterobenzene solution (Fig. 1). At 345 K, it can be seen that the paired signals had collapsed to singlets. This provided evidence for the existence of **5** and **6** and for the remarkable influence of these isomers on the doubling of signals for carbon atoms close to, and remote from, the amide group.

Comparison of the spectra run in deuterobenzene and in deuterochloroform solution at 300 K, representing the slow rate of interconversion on the nmr time-scale, was informative. The intensity of the nonequivalent carbon signals was unequal in both solvents but there was a higher population of one rotational isomer in deuterobenzene (~75:25 ratio) than in deuterochloroform (~70:30 ratio).

[2]This geometry (14, 15) designates orientation of the substituent at C-2 relative to the methyl group of the N-acetyl moiety.

Can. J. Chem. Downloaded from www.nrcresearchpress.com by 210.87.254.42 on 09/06/12
For personal use only.

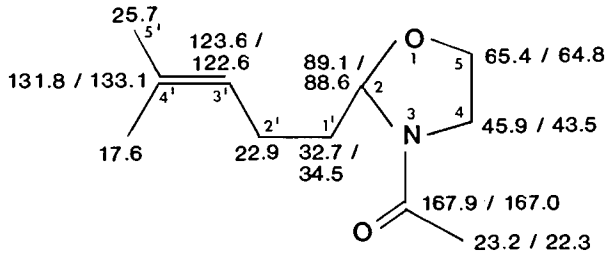

FIG. 2. Structure and ^{13}C nmr chemical shifts for 3-acetyl-2-(4′-methyl-3′-pentenyl)oxazolidine (**7**) in deuterochloroform at 303 K. Where doubling of carbon resonances occurred, the paired signal of larger intensity is given first.

Comparisons with other amides

With five- and six-membered N-acylated heterocycles, ^{13}C nmr studies have shown that a methylene carbon atom located *anti* to the carbonyl oxygen of the amide group is deshielded relative to the corresponding carbon in the *cis* isomer (12–15). This "α-to-nitrogen effect", when applied to C-4 of **1***a* and **1***b*, led to the conclusion that the major isomer in deuterobenzene and deuterochloroform had the *trans* geometry (**5**). In fact, under conditions of slow interconversion (Table 2), the main signal for C-4 in **1***a* and **1***b* occurred downfield by 2.3 ppm compared to the signal for C-4 in the minor isomer. This deshielding effect, although smaller, was also evident at the β-position (C-5).

The previous studies with amides also showed that an α-carbon *syn* to the carbonyl oxygen (in the *trans* isomer) was shielded relative to the same carbon atom in the *cis* isomer. This effect has been observed in aqueous solution with α-substituted pyrrolidines (15), the closest model we found to the oxazolidine system. With **1***a* and **1***b*, however, the main signal for C-2 resonated downfield by 0.4–0.5 ppm (Table 2). In fact, the main signals for C-1′ and C-6′ were the only paired signals that were shielded relative to the minor signal (Fig. 1). The evidence therefore suggested that 2-substituted N-acetyloxazolidines were exceptions to the "α-to-nitrogen effect" because not one but both of the α-carbons in the *trans* isomer (**5**) were deshielded compared to the α-carbons in the *cis* isomer (**6**). This anomaly is not entirely surprising because all of the factors influencing the carbon shifts of rotational isomers have not been elucidated. It was interesting to find that both the endocyclic (C-5) and exocyclic (C-1′) β-carbons behaved as the *syn–anti* argument had predicted.

3-Acetyl-2-(4′-methyl-3′-pentenyl)oxazolidine (**7**) was synthesized to compare its ^{13}C nmr spectrum with that of **1***a* and **1***b*. All carbons of the oxazolidine ring again gave two signals (~70:30 peak height ratio) and the main signal resonated downfield relative to the minor signal of the pair (Fig. 2). C-3′ of the 3′-pentenyl group behaved similarly. The other two nonequivalent carbons (C-1′ and C-4′) gave the main signal upfield relative to the minor signal as found with the comparable carbons in **1***a* and **1***b*. The presence of *cis* and *trans* isomers of **7** was again established by variable-temperature ^{13}C nmr, with slow, intermediate, and fast rates of interconversion in deuterobenzene solution corresponding to temperatures of 300, 330, and 345 K. As with **1***b*, the population of *trans* isomer was slightly higher in deuterobenzene than in deuterochloroform solution when the spectra were recorded at 300 K.

The techniques described here allow the exploration of **1** as an interesting stereochemical probe for investigating the metabolism (21) and mode of action of insect repellents. Differences in the repellent activity of both optical and *cis–trans* isomers may exist and further studies to examine these possibilities are in progress.

Experimental

High pressure liquid chromatography was performed with a Waters Prep LC/System 500 A instrument equipped with Prep PAK Silica cartridges (Waters Associates, Inc.) and a refractive index detector. Capillary gas chromatography was performed with a Hewlett–Packard 5838A chromatograph equipped with a flame ionization detector and a model 18835B capillary inlet system. The carrier gas was helium (30 cm/s flow velocity) and the makeup gas was nitrogen (30 mL/min). Injector and detector temperatures were 225°C and 250°C, respectively. Capillary columns, prepared by the method of Grob and Grob (17) or available commercially, were wall-coated with FFAP (fused silica, 25 m × 0.31 mm id, Quadrex Corporation, Woodbridge, CT), Carbowax 20M-TPA (Pyrex, 22 m × 0.33 mm), Carbowax 20M-TPA (Pyrex, 60 m × 0.29 mm), OV-105 (Pyrex, 30 m × 0.3 mm), SP2300 (Pyrex, 20 m × 0.29 mm), and OV-275 (Pyrex, 22 m × 0.33 mm). Samples were normally injected by the split technique. For mass spectrometry, a Hewlett–Packard 5985B instrument was used, with sample introduction by a capillary gc column of Carbowax 20M-TPA (15 m × 0.32 mm, splitless injections) or by a temperature-programmed direct insertion probe. Electron-impact mass spectra were recorded at 70 eV, whereas positive chemical ionization mass spectra were recorded using isobutane as the reagent gas at a source pressure of 0.5 Torr. Citronellal from commercial samples enriched in the (+)-enantiomer was obtained from Eastman Kodak Co., Rochester, NY or from Tridom/Fluka Chemical Corp., Hauppauge, NY. Mallinckrodt CC-7 silica gel was used for column chromatography. Elemental analyses were obtained from Dr. C. Daessle, Montreal, Quebec. Boiling points were recorded during vacuum distillations and are uncorrected. Evaporations were performed with a Buchi rotary evaporator at water aspirator vacuum below 50°C.

Fourier-transform ^{13}C nmr spectra (^{1}H broadband decoupled) were obtained at ambient temperature in deuterochloroform solution on a Bruker HFX-90 instrument at a frequency of 22.6 MHz. Single-frequency off-resonance ^{1}H decoupled spectra were also obtained with this spectrometer. Variable-temperature spectra were measured with a Bruker WM-250 instrument operating at 62.9 MHz and equipped with a BVT-1000 temperature control unit. Samples (0.75–1.5 mmol) were dissolved in 1.5 mL of solvent (10-mm nmr tubes) containing tetramethylsilane (TMS) as the internal standard. The ^{13}C chemical shifts are expressed downfield from TMS = 0.

*3-Acetyl-2-(2′,6′-dimethyl-5′-heptenyl)oxazolidine (**1**)*

A mixture of (+)-**2** (30.85 g, 0.2 mol), ethanolamine (26.9 g, 0.44 mol), and benzene (300 mL) was heated under reflux for 4 h (Dean–Stark trap) and acetic anhydride (45 g, 0.44 mol) was added at 5°C. After stirring at room temperature overnight, the product was isolated as described previously (method B in ref. 3) Distillation at 116–128°C (0.1 Torr) gave 39.27 g (82% yield) of a nearly colorless oil, which was a mixture of 44–46% **1***a* and 54–56% **1***b* by capillary gc with the columns indicated below. This sample was identical (capillary gc, ^{13}C nmr) to an analytical standard of **1** prepared from (±)–**2** (kindly supplied by S.C. Johnson and Son, Racine, WI); capillary gc retention times (in min), FFAP: 14.8 for **1***a*; 15.1 for **1***b*; 130–200°C at 3°C/min; 22 m Carbowax 20M-TPA: 18.8 for **1***a*; 19.5 for **1***b*; 180°C isothermally; 60 m Carbowax 20M-TPA: 36.9 for **1***a*; 38.0 for **1***b*; 180°C isothermally; OV-105: 8.9 for **1***a*; 9.0 for **1***b*; 160–220°C at 3°C/min; SP2300: 8.0 for **1***a*; 8.3 for **1***b*; 200°C isothermally; OV-275:9.7 for **1***a*; 9.9 for **1***b*; 200°C isothermally; ^{13}C nmr (WM-250, $CDCl_3$, 297 K) δ: 167.8, 167.0, 131.4, 131.0, 124.8, 124.3, 88.6, 88.1, 87.7, 65.2, 64.6, 45.6, 43.3, 41.5, 41.2, 39.8, 39.4, 37.7, 36.6, 36.3, 29.2, 28.9, 28.8, 25.7, 25.4, 23.2, 22.3, 20.3, 19.0, 17.6.

Can. J. Chem. Downloaded from www.nrcresearchpress.com by 210.87.254.42 on 09/06/12
For personal use only.

Can. J. Chem. Downloaded from www.nrcresearchpress.com by 210.87.254.42 on 09/06/12
For personal use only.

Isolation of **1**a *and* **1**b

The hplc was operated isocratically with a solvent system of ethyl acetate – methylene chloride (1:1 v/v, Caldeon ACS grade) and a flow rate of 250 or 300 mL/min. Samples of the mixture were diluted with the above solvent to give an injection volume of 5–7 mL. Before elution of the main peak, at 2.9–3.7 column volumes, the instrument was switched to the recycle mode. After one recycle, two partially resolved components were detected (~1:1 peak height ratio) and collections were initiated by shaving the leading and trailing peaks. Between collections, the mixture was recycled and collections were continued for 4–6 recycles.

In a typical experiment, 1 g of mixture (45% **1***a* and 55% **1***b* by capillary gc) was separated on a single silica cartridge and with 5 recycles (4 collections per isomer) over 60 min. The fractions were combined and concentrated by rotary evaporation of the solvents. Capillary gc (22 m Carbowax 20M-TPA) showed that the first fractions contained primarily **1***a* (7.7% of **1***b*), whereas the last fractions were enriched in **1***b* (5.7% of **1***a*). Samples of **1***a* from three runs were combined and one gram was repurified by hplc by recycling and collecting **1***a*. Fractions of **1***b* were discarded. This was repeated for combined (1 g) samples of **1***b*. Vacuum distillation gave 275 mg of **1***a* and 397 mg of **1***b*, with diastereomeric purities by capillary gc of 98–99%. The overall isolated yields, based on distilled samples and on the 45:55 mixture, were 25% for **1***a* and 36% for **1***b*. Capillary gc (FFAP, 20 m Carbowax 20M-TPA, SP2300, OV-275, 30-s splitless injection, 35°C for 1 min, 35–160°C at 25°C/min, 160–220°C at 1°C/min) indicated chemical purities of 99–99.5% for the samples of **1***a* and **1***b*.

Additional separations were performed with 2 g of the mixture and with two silica cartridges connected in series. The yields, based on the weight of products isolated after the two hplc separations and a final distillation, were 19–24% for **1***a* and 38–61% for **1***b*. The diastereomeric purities, determined by capillary gc with FFAP, Carbowax 20M-TPA, SP2300, or OV-275, ranged from 95–99%.

If traces of solvent impurities were suspected of being present, as evidenced by a slight coloration in the concentrated fractions from hplc, the samples were passed through a small column of silica gel (silicAR CC-7), by eluting first with hexane and then with mixtures of methylene chloride and hexane (both Caledon glass distilled grade). The fractions containing **1***a* or **1***b* were dried ($MgSO_4$), evaporated, and distilled *in vacuo*. No impurities were detected by tlc under conditions previously reported (3). *Anal.* calcd. for $C_{14}H_{25}NO_2$: C 70.25, H 10.53, N 5.85; found (**1***a*): C 70.21, H 10.68, N 5.98; found (**1***b*): C 69.90; H 10.15, H 5.77.

Purified samples of **1***a* and **1***b* were analyzed by chemical ionization mass spectrometry, using a direct insertion probe (temperature programmed from 30°C to 250°C at 15°C/min, then maintained at 250°C for 20 min) and with scanning from *m/z* 130–800. Under these conditions, one intense ion (at *m/z* 240) was found which corresponded to MH^+ for **1***a* and **1***b*.

Citronellal ethylene acetal (**3**)

This compound was prepared and purified as previously described (5).

3-Acetyl-2-(4'-methyl-3'-pentenyl)oxazolidine (**7**)

5-Methyl-4-hexenal was prepared from 2-methyl-3-buten-2-ol as described in the literature (18–20). This aldehyde (2.2 g, 0.02 mol) was reacted with ethanolamine (2.69 g, 0.044 mol) and acetic anhydride (4.5 g, 0.044 mol) as described for the preparation of **1**. A portion (1.4 g) of the crude product was purified by column chromatography with hexane and ether to give 0.86 g (45.2%) of **7** as a colorless oil: bp 91–114°C (0.05 Torr); ^{13}C nmr (see Fig. 2); ei–ms *m/z*: (% relative abundance): 197 ($M^{+\bullet}$, 1.5), 154 (23), 140 (17), 114 (18), 99 (11), 98 (22), 86 (14), 72 (100), 44 (13), 43 (18), 41 (11); ci–ms: 198 (MH^+, 100); ci–ms (direct insertion probe, as described for **1***a* and **1***b*) gave only one prominent ion, at *m/z* 198. Purified samples of **7** were homogeneous by capillary gc (FFAP) and tlc (3). *Anal.* calcd. for $C_{11}H_{19}NO_2$: C 66.97, H 9.71, N 7.21; found: C 66.86, H 9.98, N 7.21.

Acknowledgements

We thank Mr. A. Hewitt for skillfully operating the high pressure liquid chromatograph, Mr. G. Bitz (Defence Research Establishment Suffield, Ralston, Alberta) for drawing glass capillary tubing, and Dr. C. Preston and Mr. H. Lie (Chemistry and Biology Research Institute, Agriculture Canada, Ottawa, Ontario) for their cooperation in recording the variable-temperature spectra.

1. T. A. LAJINESS (to S. C. Johnson and Son). U.S. Patent No. 3,707,541 (December 26, 1972); Chem. Abstr. **78**, 72165r (1973).
2. T. A. LAJINESS (to S. C. Johnson and Son). U.S. Patent No. 3,825,555 (July 23, 1974); Chem. Abstr. **81**, 120605v (1974).
3. W. G. TAYLOR. J. Agric. Food Chem. **30**, 409 (1982).
4. R. P. W. SCOTT. *In* Contemporary liquid chromotography. Techniques of chemistry. Vol. XI. *Edited by* A. Weissberger. John Wiley and Sons, Inc., New York. 1976. p. 318.
5. W. G. TAYLOR. Can. J. Chem. **60**, 1847 (1982).
6. P. A. COUPERUS, A. D. H. CLAGUE, and J. P. C. M. VAN DONGEN. Org. Magn. Reson. **8**, 426 (1976).
7. S. L. ABIDI. Anal. Chem. **54**, 510 (1982).
8. L. CROMBIE, R. W. KING, and D. A. WHITING. J. Chem. Soc. Perkin Trans. 1, 913 (1975).
9. I. A. VASILENKO, V. N. KLYKOV, A. V. CHEBYSHEV, G. A. SEREBRENNIKOVA, and R. P. EVSTIGNEEVA. J. Org. Chem. U.S.S.R. **15**, 2220 (1979).
10. J. W. LOWN and S. M. S. CHAUHAN. J. Med. Chem. **24**, 270 (1981).
11. L. F. JOHNSON and W. C. JANKOWSKI. Carbon-13 nmr spectra. John Wiley and Sons, New York. 1972. p. 85.
12. J. A. HIRSCH, R. L. AUGUSTINE, G. KOLETAR, and H. G. WOLF. J. Org. Chem. **40**, 3547 (1975).
13. B. M. PINTO, D.M. VYAS, and W. A. SZAREK. Can. J. Chem. **55**, 937 (1977).
14. D. L. RABENSTEIN and A. A. ISAB. Anal. Chem. **54**, 526 (1982).
15. D. A. TORCHIA, J. R. LYERLA, and C. M. DEBER. J. Am. Chem. Soc. **96**, 5009 (1974).
16. G. C. LEVY, R. L. LICHTER, and G. L. NELSON. Carbon-13 nuclear magnetic resonance spectroscopy. 2nd ed. John Wiley and Sons, New York. 1980. p. 150.
17. K. GROB and G. GROB. J. Chromatogr. **125**, 471 (1976).
18. R. MARBET and G. SAUCY. Helv. Chim. Acta, **50**, 2095 (1967).
19. T. TAKIGAWA, K. MORI, and M. MATSUI. Agric. Biol. Chem. **39**, 249 (1975).
20. R. C. LAROCK, K. OERTLE, and G. F. POTTER. J. Am. Chem. Soc. **102**, 190 (1980).
21. W. G. TAYLOR. Drug Metab. Dispos. In press.

The structure of cubane mono and 1,4-dicarboxylic acids in lyotropic liquid crystalline solution

ALAN S. TRACEY
Department of Chemistry, Simon Fraser University, Burnaby, B.C., Canada V5A 1S6

Received July 26, 1983

ALAN S. TRACEY. Can. J. Chem. **62**, 101 (1984).

Proton nmr studies of cubane mono and 1,4-dicarboxylic acids in lyotropic liquid crystalline solution show that these molecules are distorted from the cubane structure. The protons of cubane dicarboxylate which are vicinal to their respective carboxylate group are displaced towards those groups along the C_3 axis resulting in an elongation relative to a cube. In cubane monocarboxylate there is also a displacement of vicinal protons toward the carboxyl group, but this is accompanied by a displacement of the protons one carbon further removed, away from the carboxyl groups. The shape of this latter compound is comparable to that of a section of a cone with the narrow end of the cone defining the proton positions adjacent to the carboxyl group while the wide end of the cone defines the positions of the adjacent set of protons. The remaining proton of course sits on the C_3 axis which determines the centre of symmetry of the cone.

ALAN S. TRACEY. Can. J. Chem. **62**, 101 (1984).

Les études en rmn du proton des acides mono et dicarboxyliques-1,4 du cubane dans un cristal liquide lyotrope révèlent que ces molécules sont déformées par rapport à la structure du cubane. Les protons du dicarboxylate de cubane qui sont vicinaux avec leur groupe carboxylate respectif se déplacent vers les groupes le long de l'axe C_3 provoquant une élongation par rapport au cubane. Dans le monocarboxylate de cubane, il y a également un déplacement des protons vicinaux vers le groupe carboxyle; mais ce déplacement des protons vicinaux s'accompagne aussi d'un déplacement des protons qui sont sur la position suivante par rapport aux groupes carboxyles. La forme de ce dernier composé est comparable à celle d'une section d'un cône avec l'extrémité étroite du cône définissant la position du proton adjacent au groupe carboxyle tandis que l'extrémité plus large du cône définit les positions des ensembles de protons adjacents. Le proton restant se situe naturellement sur l'axe C_3 qui détermine le centre de symétrie du cône.

[Traduit par le journal]

Can. J. Chem. Downloaded from www.nrcresearchpress.com by 210.87.254.42 on 09/06/12
For personal use only.

Introduction

The structures of pentacyclo[4.2.$0^{2,5}$.$0^{3,8}$.$0^{4,7}$]octane (cubane) derivatives are of considerable importance from a theoretical point of view since these are symmetric rigid molecules with a cagelike structure. Distortions from cubic symmetry are of interest. Although various theoretical studies of the cubane geometry have been reported (1–4), no structure determinations of cubane derivatives other than that of cubane itself (5) are available.

Lyotropic liquid crystalline materials are known to be good solvents for use in the structure determination of ionic solutes (6) and have been found to be free from the anomalous effects which are frequently encountered when thermotropic liquid crystals are employed (7–9).

In this study, the structures of the mono- and 1,4-dicarboxylates of cubane have been investigated by nuclear magnetic resonance (nmr) spectroscopy. The proton spectra give information about the relative proton positions via the interproton dipolar couplings (10, 11). These cubane derivatives have C_3 symmetry and consequently each requires one order parameter to describe its preferred alignment in the magnetic field of the nmr spectrometer.

The nmr spectrum of pentacyclo[4.2.$0^{2,5}$.$0^{3,8}$.$0^{4,7}$]octane-1,4-dicarboxylic acid (cubane dicarboxylate) is characterized by one chemical shift, three direct couplings, and three indirect coupling constants. The relative proton positions are determined by one ratio of internuclear distances and the alignment by one internuclear distance. Two dipolar couplings are therefore sufficient to determine both the proton positions and the molecular alignment. The structure is overdetermined by one coupling.

Pentacyclo[4.2.$0^{2,5}$.$0^{3,8}$.$0^{4,7}$]cubane-1-carboxylic acid (cubane monocarboxylate) provides an nmr spectrum characterized by six direct couplings, six indirect couplings, and three chemical shifts. Of the six direct couplings, four are required to specify internuclear distance ratios and the alignment. The structure of cubane monocarboxylate is therefore overdetermined by two couplings.

Experimental

The lyotropic mesophases used in this study were prepared according to standard procedures (6, 11) and had the following composition: decylammonium chloride, 385 mg; decanol, 8 mg; sodium chloride, 16 mg; deuteriated water, 607 mg. To separate preparations of this material, 10 mg of either cubane 1,4-dicarboxylic acid or cubane monocarboxylic acid was added. The preparation of these cubane derivatives is reported elsewhere and the compounds used here were received as a gift from those authors (12).

The nmr spectra were obtained from the lyotropic solution using a Bruker WM-400 nmr spectrometer operating at ambient temperature. The liquid crystalline solutions were allowed to equilibrate for 30 minutes in the spectrometer before nmr spectra were obtained.

Results and discussion

The nmr spectra of the two compounds investigated were well resolved and the spectra sufficiently overdetermined for good spectrum analysis. The six coupling constants (direct and indirect) and one chemical shift of cubane dicarboxylate were determined by 22 assigned transitions in the nmr spectrum. The three chemical shifts and 12 coupling constants of cubane monocarboxylate were determined from 90 assigned transitions. Table 1 gives the values obtained and their probable errors. The indirect couplings agree well with those previously reported (12). All spectra were analysed using the nmr program DIPUEA (13).

Figure 1 shows the coordinate system and position labelling adopted for this analysis. The structural and orientational parameters were obtained using the computer program SHAPE (14). For the structure analysis, the dipolar couplings were weighted according to the inverse of the probable error so that the best determined couplings had the most influence on struc-

Can. J. Chem. Downloaded from www.nrcresearchpress.com by 210.87.254.42 on 09/06/12
For personal use only.

TABLE 1. Direct dipolar D and indirect J couplings obtained from cubane mono and dicarboxylates in lyotropic liquid crystalline solution

Couplings (H-2)	Cubane monocarboxylate	Cubane dicarboxylate	Couplings (H-2)	Cubane monocarboxylate	Cubane dicarboxylate
$D_{12} = D_{13} = D_{26} = D_{34} = D_{45} = D_{56}$	4.76±0.04	6.05±0.03	$J_{12} = J_{13} = J_{26} = J_{34} = J_{45} = J_{56}$	5.18±0.03	5.32±0.04
$D_{14} = D_{16} = D_{46}$	−166.30±0.04	−108.77±0.04	$J_{14} = J_{16} = J_{46}$	2.51±0.04	2.15±0.34
$D_{23} = D_{25} = D_{35}$	−164.26±0.04		$J_{23} = J_{25} = J_{35}$	2.41±0.05	
$D_{15} = D_{24} = D_{36}$	−58.70±0.06	−38.37±0.04	$J_{15} = J_{24} = J_{36}$	−0.42±0.05	−0.60±0.11
$D_{17} = D_{47} = D_{67}$	165.94±0.04	—	$J_{17} = J_{47} = J_{67}$	2.24±0.04	—
$D_{27} = D_{37} = D_{57}$	−0.41±0.06	—	$J_{27} = J_{37} = J_{57}$	4.86±0.05	—
$W_1^* = W_4 = W_6$	−82.6	0.4			
$W_2^* = W_3 = W_5$	27.7	0.4			
W_7^*	−11.1	—			
RMS error	0.19	0.09			

*Chemical shifts provide only relative values.

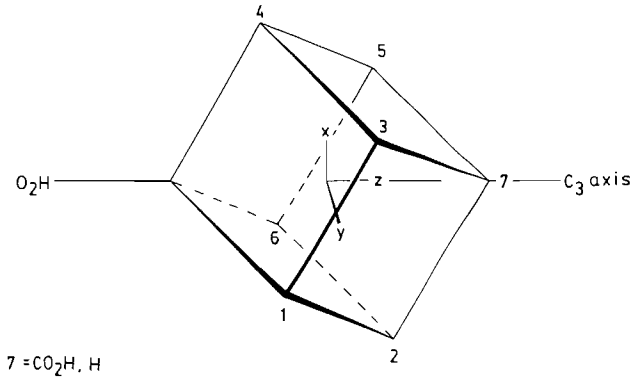

FIG. 1. The coordinate system and position labelling adopted for the structural analysis of cubane mono and 1,4-dicarboxylic acids.

tural parameters. A vicinal H—H distance of about 2.810 Å can be calculated from the X-ray structure for cubane. Using this value, the structural parameters of Tables 2, 3, and 4 were obtained. Any error in the reference distance will result in the appropriate scaling factor being applied to the tables. An important question raised by the analysis in Table 2 is why the RMS error of the fit is so large. The dipolar couplings are matched to an agreement generally no better than about 10 times their probable errors. The explanation in this case is quite straightforward. For an unperturbed cubane structure, the vicinal coupling constants D_{12} and D_{27} (see Table 1) are equal to zero since their corresponding internuclear vector lies at the zero transition (magic) angle and these dipolar couplings vanish. When bending motions occur, this vector deviates from the magic angle and a dipolar coupling arises. Even when the equilibrium angle is slightly removed from the magic angle, these bending contributions can be proportionately very important. An estimate of these contributions can easily be obtained by simply ignoring those couplings when performing the structure analysis. In this case, both structures are just determined. The results are shown in Table 3. It is clear that the contributions introduced to the dipolar couplings by the bending motions are of the same magnitude as the unperturbed coupling would be. On further consideration of Table 3, it can be seen that the major bending motion which contributes to the dipolar coupling is along the C_3 axis between geminal carbons. Thus H1, H4, and H6 preferentially bend toward position 7, while H2, H3, and H5 bend away from position 7. As a result of this bending, the contribution to D_{12} is negative, while that to D_{27} is positive, in agreement with Table 3. The remaining couplings are much less sensitive to the vibrational motions because the internuclear vectors do not lie near the magic angle. They consequently provide a much more accurate structure, though of course it is preferable to have an overdetermined structure.

A cube is defined by two distance ratios as 1:1.4142:1.7321. The values which correspond in the cubane dicarboxylate are 1:1.4035:1.7233, while two such sets of ratios can be obtained for the monocarboxylate. They are 1:1.4031:1.7254 and 1:1.4222:1.7417, where the second set of ratios is derived from distances to H7. These results show that there is an elongation of the cubane structure along the C_3 axis in the direction of the carboxyl groups. Considering for the moment the monocarboxylate, this result could mean that hydrogens 2, 4, and 6 are displaced towards the carboxyl group, leading to the r_{12} length of 2.837 Å compared to 2.810 Å for

TABLE 2. Approximate structure parameters of cubane mono and dicarboxylates obtained from the dipolar couplings when vibrational contributions to the dipolar couplings are ignored

Parameter	Cubane monocarboxylate	Cubane dicarboxylate
$r_{12} = r_{13} = r_{26} = r_{34} = r_{45} = r_{56}$	2.812	2.810*
$r_{14} = r_{16} = r_{46}$	3.957	3.953
$r_{23} = r_{25} = r_{35}$	3.975	3.953
$r_{15} = r_{24} = r_{36}$	4.862	4.850
$r_{17} = r_{47} = r_{67}$	3.975	—
$r_{27} = r_{37} = r_{57}$	2.810*	—
S_{C_3}	−0.0859	−0.0559
RMS error	0.258	0.212

*Reference distance in units of 10^{-10} m.

TABLE 3. Structural parameters obtained for the cubane mono and 1,4-dicarboxylic acids

Parameter	Cubane monocarboxylate*	D(calcd.)	D(expt.)	Cubane dicarboxylate*	D(calcd.)	D(expt.)
$r_{12} = r_{13} = r_{26} = r_{34} = r_{15} = r_{56}$	2.837	10.59	4.76	2.810†	9.11	6.05
$r_{14} = r_6 = r_{46}$	3.980			3.944		
$r_{23} = r_{25} = r_{35}$	3.996			3.944		
$r_{15} = r_{25} = r_{36}$	4.894			4.842		
$r_{17} = r_{47} = r_{67}$	3.989			—		
$r_{27} = r_{37} = r_{57}$	2.810†	−10.74	−0.41	—		
S_{C_3}	−0.0873			−0.0556		

*Probable errors in distances are less than 0.001 Å (see Table 4).
†Reference distance in units of 10^{-10} m.

TABLE 4. Nuclear coordinates obtained from the structural analysis of cubane monocarboxylate and the corresponding values for a cube

	X		Y		Z	
Nucleus*	Expt.	Cube	Expt.	Cube	Expt.	Cube
1	−1.1489	−1.1472	1.9900	1.9870	3.2603	3.2447
2	−2.3074	−2.2944	0.0	0.0	1.6038	1.6224
3	1.1537	1.1472	1.9982	1.9870	1.6038	1.6224
4	2.2979	2.2944	0.0	0.0	3.2603	3.2447
5	1.1537	1.1472	−1.9982	−1.9870	1.6038	1.6224
6	−1.1489	1.1472	−1.9900	−1.9870	3.2603	3.2447
7	0.0	0.0	0.0	0.0	0.0	0.0

*Note that $X_4 = -2X_1 = -2X_6, X_2 = -2X_3 = -2X_5, Y_1 = -Y_6 = -\sqrt{3}X_1$, and $Y_3 = -Y_5 = -\sqrt{3}X_3$. Error in X_1 and $X_3 = 0.0004$; in $Z_1 = Z_4 = Z_6 = 0.0010$; in $Z_2 = Z_3 = Z_5 = 0.0003$.

the r_{27} distance. Similarly the distance r_{14} is 0.009 Å shorter than the corresponding distance, r_{17}, of 3.989 Å. It is known from deuterium nmr studies that C—D bonds bend toward polar substituents in aromatic systems (15, 16) and the same could be occurring here.

Concurrent with the displacement of hydrogens 2, 4, and 6, there is a corresponding movement of nuclei 1, 3, and 5 in the opposite direction. In this case, the latter set of nuclei become relatively further apart as is shown by the two distances r_{14} = 3.980 Å compared to 3.996 Å for r_{23}. These conclusions are perhaps made clearer by Table 4 where the experimental nuclear coordinates are compared to those for an undistorted cube.

Conclusions

Pentacyclo[4.2.$0^{2,5}$.$0^{3,8}$.$0^{4,7}$]octane 1-mono and 1,4-dicarboxylic acids (cubane mono and dicarboxylates) have been studied in lyotropic liquid crystalline solution by proton nmr spectroscopy. The results showed that rather large distortions from the cubane structure occur. The distortion is apparent as an elongation of the proton skeleton of the molecule along the C_3 axis of symmetry. This distortion results from a displacement of hydrogen atoms toward the adjacent carboxyl groups. No information concerning carbon positions was obtained.

The structure of the monocarboxylate can best be related to a section of a cone with the C_3 axis defining the rotation axis of the cone. The protons adjacent to the carboxyl sit on the narrow end of the conic section while those protons one carbon removed are located on the wide end of the cone. The remaining proton is located on the symmetry axis.

It was found that large vibrational contributions to vicinal hydrogen dipolar coupling constants occurred. This resulted from the fact that the H—H internuclear vectors are close to the zero splitting (magic) angle which leads to the large con-

Can. J. Chem. Downloaded from www.nrcresearchpress.com by 210.87.254.42 on 09/06/12
For personal use only.

tributions. The major contribution to the vicinal dipolar couplings apparently arises from a bending of the C—H bond along the C_3 axis between the geminal carbon atoms.

Acknowledgements

Thanks are gratefully extended to Dr. P. G. Farrell of McGill University for his gift of the compounds used in this study. This work was supported by the Natural Sciences and Engineering Research Council of Canada by an operating grant, No. A1558.

1. J. ALMLÖF and T. JONVIK. Chem. Phys. Lett. **92**, 267 (1982).
2. K. KOVACEVIC and Z. B. MANIC. J. Org. Chem. **39**, 539 (1974).
3. W. SCHUBERT, M. YOSHIMINE, and J. PACANSKY. J. Phys. Chem. **85**, 1340 (1981).
4. P. BISCHOF, P. E. EATON, R. GLEITER, E. HEILBRONNER, T. B. JONES, H. MUSSO, A. SCHNELZER, and R. STOBER. Helv. Chim. Acta, **61**, 547 (1978).
5. E. B. FLEISCHER. J. Am. Chem. Soc. **86**, 3889 (1964).
6. L. W. REEVES, A. S. TRACEY, and M. M. TRACEY. J. Am. Chem. Soc. **95**, 3799 (1973).
7. P. DIEHL, S. SYKORA, W. NIEDERBERGER, and E. E. BURNELL. J. Magn. Reson. **14**, 260 (1974).
8. P. DIEHL, M. REINHOLD, A. S. TRACEY, and E. WULLSCHLEGER. Mol. Phys. **30**, 1781 (1975).
9. J. JOKISAARI, P. DIEHL, J. AMREI, and E. IJÄS. J. Magn. Reson. **52**, 193 (1983).
10. P. DIEHL and C. L. KHETRAPAL. NMR: Basic Princ. Prog. **1**, 7 (1969).
11. C. L. KHETRAPAL, A. C. KUNWAR, A. S. TRACEY, and P. DIEHL. NMR: Basic Princ. Prog. **9**, 13 (1975).
12. J. T. EDWARD, P. G. FARRELL, and G. E. LANGFORD. J. Am. Chem. Soc. **98**, 3075 (1976).
13. L. D. FIELD, S. STERNHELL, and A. S. TRACEY. J. Am. Chem. Soc. **99**, 5249 (1977).
14. P. DIEHL, P. M. HENRICKS, and W. NIEDERBERGER. Mol. Phys. **20**, 139 (1971).
15. P. DIEHL and A. S. TRACEY. Mol. Phys. **30**, 1917 (1975).
16. P. DIEHL and A. S. TRACEY. Can. J. Chem. **53**, 2735 (1975).

Can. J. Chem. Downloaded from www.nrcresearchpress.com by 210.87.254.42 on 09/06/12
For personal use only.

The photochemical addition of *N*-haloamides to olefins: a comparison of cyclic and acyclic *N*-halo-*N*-alkylamides and *N*-halo-*N*-acylamides (*N*-haloimides)[1,2]

JEAN LESSARD,[3] YVON COUTURE, MARTINE MONDON,[4] AND DANIEL TOUCHARD[5]
Département de chimie, Université de Sherbrooke, Sherbrooke (Qué.), Canada J1K 2R1

Received April 15, 1983

JEAN LESSARD, YVON COUTURE, MARTINE MONDON, and DANIEL TOUCHARD. Can. J. Chem. **62**, 105 (1984).

Upon photochemical decomposition in the presence of cyclohexene and 1-octene, an *N*-halo-*N*-acylamide (*N*-haloimide) leads to better yields of addition than its *N*-halo-*N*-alkyl analogue, and cyclic *N*-halo-*N*-alkyl- and *N*-halo-*N*-acylamides add more efficiently than their acyclic analogues. The yields of addition were higher with *N*-chlorosuccinimide which has been added also to 1-methylcyclohexene than with *N*-bromosuccinimide which did not add to 1-methylcyclohexene.

JEAN LESSARD, YVON COUTURE, MARTINE MONDON et DANIEL TOUCHARD. Can. J. Chem. **62**, 105 (1984).

L'addition-1,2, par voie photochimique, d'un *N*-halo-*N*-acylamide (*N*-haloimide) aux cyclohexène et 1-octène est plus efficace que celle d'un analogue *N*-alkyle et celle d'un *N*-halo-*N*-acyl- ou d'un *N*-halo-*N*-alkylamide cyclique, plus efficace que celle d'un analogue acyclique. Le *N*-chlorosuccinimide, qui a été additionné également au 1-méthylcyclohexène, donne de meilleurs rendements en addition que le *N*-bromosuccinimide qui ne s'additionne pas au méthyl-1 cyclohexène.

Can. J. Chem. Downloaded from www.nrcresearchpress.com by 210.87.254.6 on 09/06/12
For personal use only.

Introduction

Recently, we have identified a number of factors having an influence on the yield of 1,2-addition in the photochemical reactions of *N*-haloamides (ZCONRX) with olefins (1): replacing the *N*-hydrogen (R = H) by an *N*-methyl group (R = CH_3) does cause a dramatic decrease in the yield of 1,2-addition; the 1,2-addition is favored when replacing X = Br for X = Cl, when lowering the temperature, and when increasing the electron-withdrawing power of Z.

This paper delineates further the scope and limitations of the radical addition of *N*-haloamides to olefins for the synthesis of *N*-(2-haloalkyl) amides by identifying two other factors having an effect on the yield of 1,2-addition: (*i*) an *N*-halo-*N*-acylamide (R = acyl) leads to better yields of addition than its *N*-halo-*N*-alkyl (R = alkyl) analogue and (*ii*) cyclic *N*-halo-*N*-alkyl and *N*-halo-*N*-acylamides add more efficiently than their acyclic analogues.[6]

The photochemical addition of *N*-chlorosuccinimide (NCS) and *N*-bromosuccinimide (NBS) to olefins has been described in ref. 2. Since then, reports on the successful radical addition of NCS (3), NBS (3, 4),[7] and *N*-bromo-3,3-dimethylglutarimide (3) to olefins, initiated by light, have been published. We had reported earlier the radical addition of NCS to cyclohexene promoted by chromous chloride (5).[8]

Results and discussion

The results are recorded in Table 1 and Table 2 for the photochemical additions to cyclohexene and to 1-octene respectively and in Scheme 2 for the addition of NCS (**9**) to 1-methylcyclohexene. The reaction conditions were the same as those used in ref. 1 and are specified in footnote *a* of the tables. No dark reaction was observed in the case of the *N*-chloro derivatives even after three days. With NBS (**10**), there was essentially no dark reaction during the time required for the photochemical reaction to be completed. After three days in the dark at room temperature the following results were obtained: in the presence of cyclohexene, 95% of NBS was consumed (iodometric titration) and 7% of *trans* 1,2-adduct **20** was isolated;[9] in the presence of 1-octene, 20% of NBS was consumed and no addition product was detected.

The orientation of the photochemical additions to 1-octene (Table 2) and to 1-methylcyclohexene (Scheme 2) – the amide moiety being added on the least substituted carbon atom – and the failure of the dark reactions strongly suggest that 1,2-addition occurs through a radical chain mechanism (eqs. [1] to [3]) as previously shown for the photochemical addition to olefins of a variety of *N*-haloamides (1), of NCS (3), NBS (3, 4), and *N*-bromo-dimethylglutarimide (3, 7).

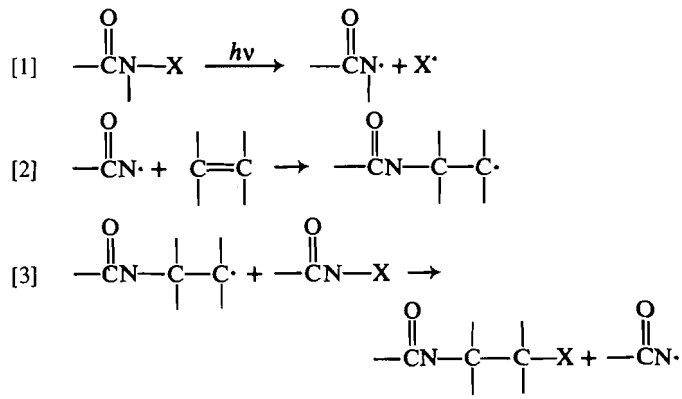

[1] —CN(O)—X —hν→ —CN(O)· + X·

[2] —CN(O)· + C=C → —CN(O)—C—C·

[3] —CN(O)—C—C· + —CN(O)—X → —CN(O)—C—C—X + —CN(O)·

[1]Part XII in the series "Radical Reactions of *N*-Haloamides with Olefins". For part XI, see ref. 1.

[2]Taken in part from the Ph.D. Thesis of D. Touchard, Université de Sherbrooke, Sherbrooke, Québec, 1974.

[3]Author to whom correspondence should be addressed.

[4]Arts Council of Canada Predoctorate Fellow, 1973–75. Present address: Laboratoire de Chimie XII, E.R.A. 556, 40 Ave du Recteur Pineau, 86022 Poitiers, France.

[5]France–Quebec Predoctorate Fellow, 1970–72. Present address: Institut Universitaire de Technologie, Université de Nantes, 44606 Saint-Nazaire, France.

[6]The influence of these factors on the halogenation of cyclohexene will be reported in a forthcoming paper.

[7]The few reports on the addition of NBS to olefins, some of them being ionic, have been reviewed in ref. 4. *N*-Bromophthalimide has also been added to olefins (6), many of the additions involving most probably an ionic mechanism.

[8]The chromous chloride promoted addition of NBS to cyclohexene was reported also in ref. 5. However, attempts to repeat this addition were unsuccessful. The sole products isolated were succinimide (35%, not fully recovered because of its high solubility in water), *trans*-2-bromo-methoxycyclohexane (32%), and *trans*-2-bromocyclohexanol (25%). Thus electrophilic bromination appears to be faster than radical 1,2-addition.

[9]When the reaction mixture was saturated with oxygen, 15% only of NBS was consumed after three days in the dark: no 1,2-adduct was detected.

TABLE 1. Photochemical additions of *N*-haloamides and *N*-haloimides to cyclohexene[a]

Entry	*N*-Haloamide	Lamps[b] (λ, nm)	Reaction time[c] (h)	1,2-Adduct(s) Structure	Yield[d] (*cis*/*trans*) (%)	Yield[d] of parent amide (%)	Material balance[e] (%)
1[f]	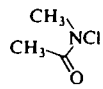 (**1**)	300	44		0	95–97	95–97
2	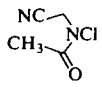 (**2**)	300	17		0	82	82
3	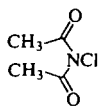 (**3**)	300	25	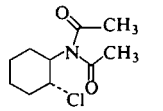 (**11**, *trans*)	24	57	81
4	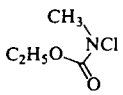 (**4**)	300		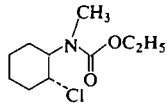 (**12**, *trans*)	<2[g]	23	56[h]
5	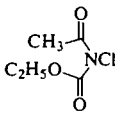 (**5**)	300		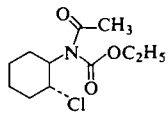 (**13**, *trans*)	62	42	104
6	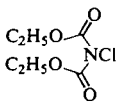 (**6**)	300		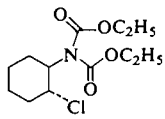 (**14**, *trans*)	55	39	94
7	(**7**)	254	16	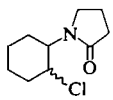 (**15**, *cis*) (**16**, *trans*)	9(0.3)	46	55
8	(**8**)	254	4.5	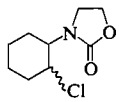 (**17**, *cis*) (**19**, *trans*)	34(0.8)	42(55)[i]	76(89)[i]
9	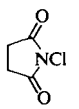 (**9**)	300	44	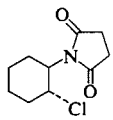 (**19**, *trans*)	54	38	92
10	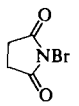 (**10**)	300	3	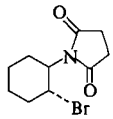 (**20**, *trans*)	22	72	94

[a]Reaction conditions: 15–20°C, CH_2Cl_2 (distilled over P_2O_5) as solvent, solutions 0.2 to 0.5 *M* in *N*-haloamide, 2 mol of cyclohexene per mol of *N*-haloamide, inert atmosphere (nitrogen or argon).

[b]Pyrex cell with the 300 nm lamps, Vycor cell with the 254 nm lamps.

[c]The reported reaction times represent a rough estimate. The reaction was normally stopped when the starch–iodide paper test was negative. However, if a *trace* amount of *N*-haloamide was still present, a faint coloration was appearing after 15 to 30 s. Depending on the experimentalist, the reaction was stopped either when the *N*-haloamide was entirely consumed or when a trace amount was still present, which could make a noticeable difference in the reaction time.

[d]Yield of chromatographically (preparative layer chromatography, plc) pure products based on the *N*-haloamide.

[e]Addition product(s), parent amide, plus any product containing the amide moiety or derived from the amide moiety.

[f]Taken from ref. 1.

[g]Many successive separations by plc led to a sample still contaminated with another product.

[h]Besides the parent amide, $C_2H_5OCON(CH_3)CH_2COOC_2H_5$ was isolated in a 31% yield (see ref. 1).

[i]By vpc.

One of the main features of Tables 1 and 2 is the increase in the yield of 1,2-addition when going from an *N*-chloro-*N*-alkylamide to its *N*-acyl analogue (*N*-chloroimide): compare entries 1 and 3, 4 and 5, 7 and 9 of Table 1; compare entries 1 and 2, 3 and 4, 6 and 8 of Table 2. This feature could be readily explained if both the rate of step [2] and that of step [3] of the addition chain are faster with an *N*-halo-*N*-acylamide than with its *N*-alkyl analogue, because the 1,2-addition process would then compete more effectively with the other chain processes such as halogenation (hydrogen abstraction processes). Indeed, an *N*-acylamidyl radical should react more rapidly with a carbon–carbon double bond than an *N*-

Can. J. Chem. Downloaded from www.nrcresearchpress.com by 210.87.254.6 on 09/06/12
For personal use only.

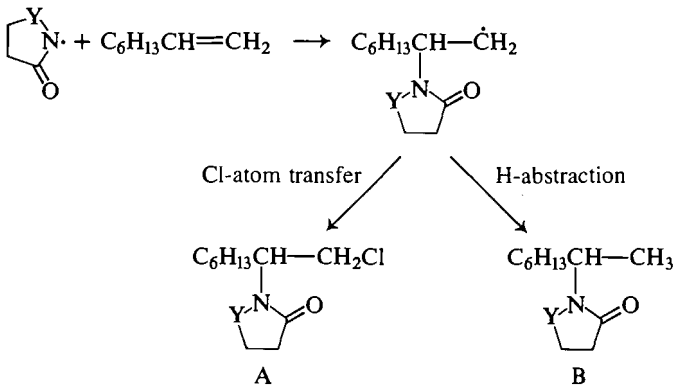

Y = C=O	**33**, 10%	**34**, ≤ 1% (not isolated)
Y = CH_2	**27**, ≤ 1% (not isolated)	**28**, 3%

SCHEME 1

alkylamidyl radical (step [2]) since the former, having two electron-withdrawing acyl groups linked to the nitrogen, should be more electrophilic (the SOMO should be lower in energy).[10] Furthermore, by analogy with the fact that the reactivity of ZCONHX as a halogen-atom transfer agent towards a carbon radical increases with the electron-withdrawing power of ZCO (10), an *N*-halo-*N*-acylamide should be a better halogen-atom donor (step [3]) than its *N*-halo-*N*-alkyl analogue.

Some evidence for the fact that an *N*-halo-*N*-acylamide is a better halogen-atom donor than its *N*-halo-*N*-alkyl analogue comes from a comparison of the addition of NCS (**9**) and of *N*-chlorobutyrolactam (**7**) to 1-octene (Table 2, entries 8 and 6 respectively). The adducts **33**, **34**, **27**, and **28** are derived from the addition of the amidyl radical on the most substituted carbon atom of the double bond (see Scheme 1). The 1,2-adducts **33** and **27** (see A) result from chlorine-atom transfer onto the intermediate radical adduct and the adducts **34** and **28** (see B) from hydrogen-atom abstraction. In the case of NCS (Y = C=O), A (**33**) (chlorine-atom transfer) was the major adduct, whereas in the case of *N*-chlorobutyrolactam (Y = CH_2), B (**28**) (hydrogen abstraction) was the major adduct. Therefore NCS (**9**) appears to be a better chlorine-atom donor than *N*-chlorobutyrolactam (**7**).

From entry 2 of Table 1, it can be seen that an *N*-cyanomethyl group is not electron-attracting enough to allow the observation of the 1,2-addition process with cyclohexene.

The other main feature of Tables 1 and 2 is the better yields of addition obtained with cyclic *N*-chloroamides as compared with their acyclic analogues: compare entries 1 and 7, 3 and 9, 4 and 8 of Table 1; and entries 1 and 6, 2 and 8, 3 and 7 of Table 2. To account for this second feature we propose that cyclic amidyls are more reactive in the addition step [2] than their acyclic analogues for steric and electronic reasons. In acyclic amidyls, Z and R (R = alkyl or acyl) must prefer the *trans* arrangement by analogy with carboxamides (11) and carboxylic esters (12), whereas in cyclic amidyls, Z and R are necessarily *cis* to each other:

acyclic amidyl (*trans*) cyclic amidyl (*cis*)

There are more steric interactions between the alkene and the attacking amidyl in the *trans* arrangement (acyclic amidyl) than in the *cis* arrangement (cyclic amidyl) according to the inspection of models. The activation entropy term ($-T\Delta S^{\ddagger}$) might also be larger in the case of acyclic amidyls. As for the electronic reasons, it is conceivable that the more reactive Σ_N electronic state could be more accessible in the case of cyclic amidyls than in the case of acyclic amidyls.[11]

As seen from Table 2, the additions of cyclic *N*-haloamides to 1-octene are less regioselective than those of their acyclic analogues. Indeed, cyclic *N*-haloamides gave addition products resulting from the attack of the amidyl radical on the most substituted atom of the double bond (entries 6 to 9) whereas in the case of acyclic *N*-haloamides, no such adducts were detected (entries 2 to 5).[12] Thus cyclic amidyls would be less regioselective. This lends support to the greater reactivity of cyclic amidyls in step [2].

The 1,2-adducts **33** and **36** (Table 2, entries 8 and 9) could have been formed via electrophilic halogenation of 1-octene but they most likely result from a radical process for the following reasons: (*i*) adduct **36** was not formed in the dark reaction of NBS with 1-octene; (*ii*) a similar ratio of regioisomer was obtained with NCS (**33**/**32** = 0.22) and NBS (**35**/**36** = 0.19) although NBS is a better electrophilic halogenating agent; (*iii*) the chromous chloride promoted addition of NCS to 1-octene gave also a mixture of regioisomers **32** and **33** in a 15% yield (**33**/**32** = 0.15) and electrophilic halogenation under these conditions leads to halohydrins and halomethoxy derivatives but not to 1,2-adducts (5).

In contrast to the addition to 1-octene, the radical addition of NCS (**9**) to 1-methylcyclohexene either photochemically initiated or promoted by chromous chloride (Scheme 2), appears to be regiospecific. This can be attributed to the larger steric hindrance of a trisubstituted carbon atom. Interestingly, the *cis* adduct **37** was formed whereas, with cyclohexene, only the *trans* adduct **19** (Table 1, entry 9) was isolated. This observation agrees with the general observation (1, 5) that, in radical 1,2-additions of *N*-haloamides, 1-methylcyclohexene gives a larger proportion of *cis* isomer than cyclohexene. NBS does not

[10]For an interpretation of the electrophilic character of radicals and their reactivity towards alkenes in terms of frontier orbital interactions, see ref. 8. An application to the reactivity of alkoxy radicals towards olefins has been reported in ref. 9.

[11]The electronic ground state of acyclic *N*-alkylcarboxamidyls (13–15) and of one cyclic carboxamidyl (14*b*) has been shown to be π_N. The ground state of succinimidyl is probably π_N also, according to MNDO (16) and INDO (17) calculations. However, Skell and co-workers (18*a*) have shown that two varieties of succinimidyl radicals, the π_N and the Σ_N states, can be produced from NBS and NCS according to the reaction conditions. In the radical addition to alkenes such as cyclohexene and tertiobutylethylene, the more energetic Σ_N state appears to be involved (18*b*) and this is supported by MNDO reaction path calculations for the attack of $CH_3^{\cdot}$ on NCS (17). By analogy, the Σ_N state of *N*-alkylcarboxamidyls could be involved in chemical reactions, as was suggested for some intramolecular additions to double bonds (19) and to an aromatic ring (20).

[12]Chow and co-workers (4) have studied the photochemical addition of NBS (**10**) to 1-hexene in acetonitrile and in the presence of ethylene oxide and reported that the addition is completely regiospecific, giving only the isomer with the succinimide moiety attached to the least substituted carbon atom.

Can. J. Chem. Downloaded from www.nrcresearchpress.com by 210.87.254.6 on 09/06/12
For personal use only.

Can. J. Chem. Downloaded from www.nrcresearchpress.com by 210.87.254.6 on 09/06/12
For personal use only.

TABLE 2. Photochemical additions of *N*-haloamides and *N*-haloimides to 1-octene[a]

Entry	*N*-Haloamide		Lamps[b] (λ, nm)	Reaction time[c] (h)	1,2-Adduct(s) Structure		Yield[d] (%)	Other adducts Structure	Yield[d] (%)	Yield[d] of parent amide (%)	Material balance[e] (%)
1[f]	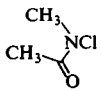	(**1**)	300	9			0			74	76[g]
2	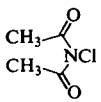	(**3**)	300	19	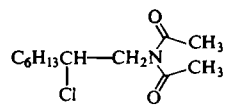	(**21**)	40			27	67
3[h]	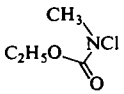	(**4**)	254	1.5	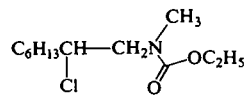	(**22**)	21			36	92[i]
4	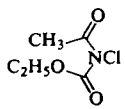	(**5**)	300	3.2	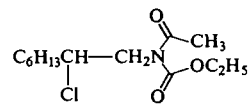	(**23**)	67			24	94
					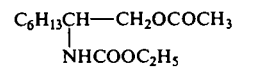	(**24**)	3				
5	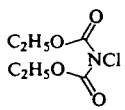	(**6**)	300	5		(**25**)	63			29	92
6		(**7**)	254	2	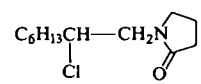	(**26**)	13				
					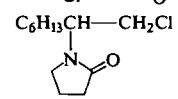	(**27**)	≤1[j]	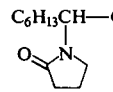	(**28**) 3	46	63

Can. J. Chem. Downloaded from www.nrcresearchpress.com by 210.87.254.6 on 09/06/12
For personal use only.

TABLE 2. (*Concluded*)

Entry	*N*-Haloamide	Lamps[b] (λ, nm)	Reaction time[c] (h)	1,2-Adduct(s) Structure		Yield[d] (%)	Other adducts Structure		Yield[d] (%)	Yield[d] of parent amide (%)	Material balance[e] (%)
7	(**8**)	254	1.2	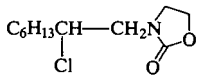	(**29**)	62					
				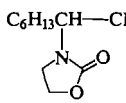	(**30**)	≤1[j]	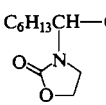	(**31**)	7	17	86
8	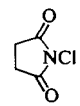 (**9**)	254	3	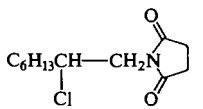	(**32**)	45(53)[k]					
				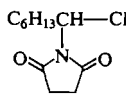	(**33**)	10(13)[k]	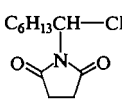	(**34**)	≤1[l]	39	95
9[m]	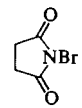 (**10**)	254	3	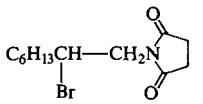	(**35**)	16(19)[k]					
				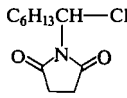	(**36**)	4(4)[k]				70	90

[a]Reaction conditions: 15−20°C, CH_2Cl_2 as solvent, solutions 0.2 to 0.5 *M* in *N*-haloamide, 2 mol of 1-octene per mol of *N*-haloamide, inert atmosphere (nitrogen or argon).
[b]Pyrex cell with the 300 and 350 nm lamps, Vycor cell with the 254 nm lamps.
[c]Rough estimate (see footnote *c* of Table 1).
[d]Yield of chromatographically pure (plc) product based on the *N*-haloamide.
[e]Addition product(s), parent amide, plus any product containing the amide moiety or derived from it.
[f]Reaction with 1-dodecene. Taken from ref. 1.
[g]Including about 2% of *N*-methyl-*N*,*N*′-bis-acetamide (see ref. 1).
[h]Taken from ref. 1.
[i]Including 35% of *N*-methyl-*N*,*N*′-bis-urethane (see ref. 1).
[j]Detected by ^{13}C nmr spectroscopy in chromatographic fractions (**27** + **28**, **30** + **31**) but not isolated.
[k]By vpc.
[l]Detected by ^1H nmr spectroscopy in chromatographic fractions (**34** + **33**) but not isolated.
[m]The addition was carried out at −78°C, in a 1:1 mixture of CH_2Cl_2 and CH_3CN. At 15−20°C and in CH_2Cl_2, using the 350 nm lamps, the yields were: **35**, 9%; **36**, 1.5%; succinimide, 82%.

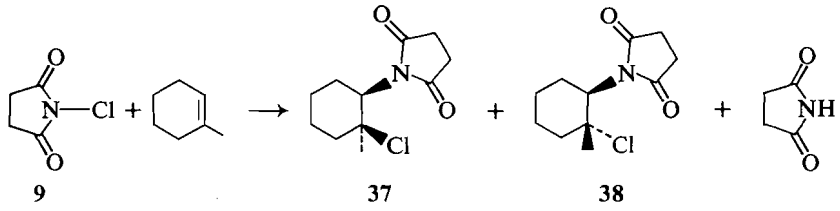

9	37	38
$h\nu$ (350 nm, 40 h)	41% (**38**/**37** = 5.9)	54%
$h\nu$ (254 nm, 4 h)	19% (**38**/**37** = 7.6)	63%
$CrCl_2$	15% (**38**/**37** = 4.0)	Not determined

SCHEME 2

add to 1-methylcyclohexene either photochemically or with chromous chloride.

Since we found that, with *N*-bromocarboxamides, lowering the temperature to −78°C caused a dramatic increase in the yield of 1,2-addition to cyclohexene (e.g. from 25% at 15−20°C to 95% in the case of *N*-bromoacetamide) (1, 21), the addition of NBS (**10**) was carried out at −78°C but without any improvement of the yield of 1,2-adduct **20**: 19% as compared to 22% at 15−20°C (Table 1, entry 10). However, NBS being practically insoluble in methylene chloride at −78°C, we used a 1:1 mixture of acetonitrile and methylene chloride as solvent and, in order to obtain a reasonable reaction time (7 h), the 254 nm lamps were used instead of the 300 nm lamps (see the Experimental). With 1-octene, the yield of addition was 20% at −78°C and 11% at 15−20°C (Table 2, entry 9).

Structure and stereochemistry of the addition products

All the addition products had ir and ^{1}H nmr spectra, an elemental analysis, and/or a mass spectrum consistent with their structure. For the 1,2-adducts derived from cyclohexene, the *cis* isomer was easily identified by ^{1}H nmr spectroscopy from the chemical shift of the equatorial proton at C-2 (carbon bearing the halogen), which is more deshielded than the axial proton of the *trans* isomer (1, 5).

The 1,2-adducts derived from 1-octene were compared (^{1}H nmr and, in a few cases, ^{13}C nmr spectrum) to adducts **35** and **36** whose structure was proven by hydrogenolysis of the C—Br bond.[13] The major adduct **35** gave *N*-(1-octyl)succinimide (**39**) whereas the minor adduct **36** gave *N*-(2-octyl)succinimide (**34**) (Scheme 3).

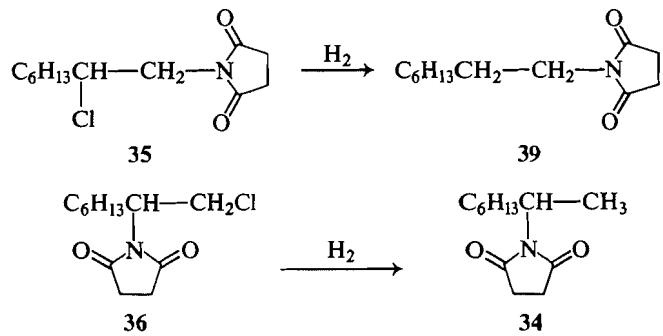

SCHEME 3

Hydrogenolysis of the 1,2-adducts **37**[14] and **38** obtained from 1-methylcyclohexene gave the stereoisomeric *N*-(2-methylcyclohexyl)succinimides **40** and **41** (Scheme 4), thus showing that the succinimido group was attached to the least substituted carbon atom and that the hydrogenolysis was not stereospecific. In the ^{1}H nmr spectrum of **40**, the axial proton at C-1 appears as a doublet of triplets (J = 13 and 4 Hz, ΣJ = 21 Hz) whereas in the case of **41**, it appears as a triplet of doublets (J = 11 and 4 Hz, ΣJ = 26 Hz). Therefore **40** must be the *cis* isomer (H2 equatorial) and **41**, the *trans* isomer (H2 axial). The *trans* stereochemistry was assigned to the major 1,2-adduct **38** on the basis that the addition of NCS (**9**) to cyclohexene gave exclusively the *trans* 1,2-adduct **19** (1, 5). We found that the proportion of *cis* addition is larger with 1-methylcyclohexene than with cyclohexene in all the radical additions of *N*-haloamides studied so far (1, 5).

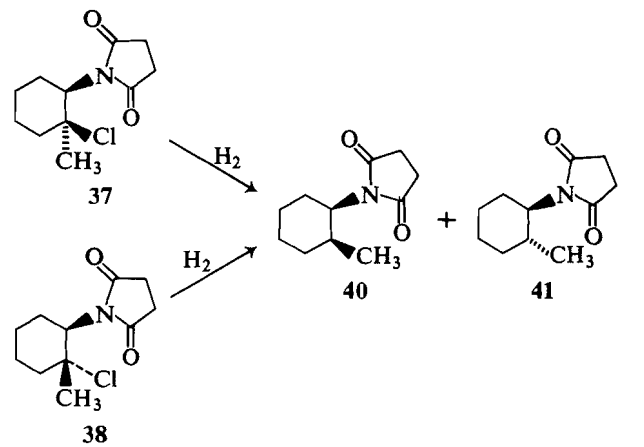

SCHEME 4

Experimental[15]

Most of the pertinent general information is the same as that given in refs. 1 and 5. The amides were obtained commercially.

N-Haloamides

NCS (**9**) and NBS (**10**) are commercially available and were recrystallized from water and methylene chloride (100% active halogen). The preparation of *N*-chloro-*N*-methylacetamide (**1**) and of ethyl *N*-chloro-*N*-methylcarbamate (**4**) has been reported (1). The following *N*-chloroamides were prepared by the chlorine method (1): *N*-chloro-

[13]The chloro analogue **33** was inert towards hydrogen under the same conditions.

[14]Since **37** could not be separated from **38**, the hydrogenolysis was carried out on a 40:60 mixture of **37** and **38**.

[15]For the new products not described in the experimental section, the microanalytical and/or mass spectral data, together with the ir and ^{1}H nmr characteristic absorptions, are available, at a nominal charge, from the Depository of Unpublished Data, CISTI, National Research Council of Canada, Ottawa, K1A 0R6.

Can. J. Chem. Downloaded from www.nrcresearchpress.com by 210.87.254.6 on 09/06/12
For personal use only.

Can. J. Chem. Downloaded from www.nrcresearchpress.com by 210.87.254.6 on 09/06/12
For personal use only.

N-cyanomethylacetamide (**2**) (55% yield, 83% active chlorine); ethyl *N*-chloro-*N*-acetylcarbamate (**5**) (60% yield, 90% active chlorine); diethyl *N*-chloro-imidomalonate (**6**) (65% yield, 80% active chlorine); *N*-chloro-2-pyrrolidone (**7**), mp 46–47°C (100% yield, 100% active chlorine); *N*-chloro-2-oxazolidone (**8**), mp 61–62°C (95% yield, 99.5% active chlorine). *N*-Chloro-*N*-acetylacetamide (**3**) was prepared by treating, in the dark, *N*-acetylacetamide with tertiobutylhypochlorite (1.1 equiv.) in carbon tetrachloride at room temperature: 60% yield, 75% active chlorine.

The ^{1}H nmr spectra of the crude *N*-chloroamides prepared by the chlorine method showed that they consisted of the pure *N*-chloroamide plus the extracting solvent (CH_2Cl_2). That explains why the active chlorine content was lower than 100%. Since the photochemical reactions were carried out in methylene chloride, no attempt was made to remove it completely. The ^{1}H nmr spectrum of crude **3** also showed that it consisted of pure **3** which then did contain some carbon tetrachloride.

Photochemical reactions

The general procedure was the same as that given in ref. 1. A typical procedure is described below.

Addition of N-*bromosuccinimide (**10**) to 1-octene at −78°C*

NBS (0.80 g, 4.49 mmol) in CH_2Cl_2 (40 mL) and CH_3CN (40 mL), both freshly distilled from P_2O_5, were placed in a Vycor cell. Nitrogen was bubbled through the solution for 10 min and the cell was cooled with acetone − Dry Ice (~−78°C)

1-Octene (1.0 g, ~9 mmol) was added. After degassing for a further 10 min and while maintaining a low stream of nitrogen, the solution was irradiated (254 nm lamps) until the starch−iodide paper test was negative (7 h). The reaction mixture was evaporated to dryness (rotating evaporator), then dissolved in methylene chloride (50 mL). The resulting solution was washed with water (3 × 10 mL), dried over Na_2SO_4, then evaporated to dryness (664 mg). The residue was separated by plc (ether−hexane 4:1) to give two main fractions. The less polar fraction consisted of N-*(1-chloro-2-octyl)succinimide* (**36**) (38 mg, 3%). Microdistillation at 90°C (0.005 Torr) afforded the analytical sample; ν_{max} ($CHCl_3$): 1780 (w) and 1710 (s) (C=O), 1390, 1370, 1135 cm^{-1}; δ ($CDCl_3$): 0.88 (CH_3), 2.73 (s, 4H), 3.4–4.6 ppm (complex pattern, 2H1 + H2); *m/e*: 289, 291 (1:1, M^+), 288, 290 (1:1, $M^+ - 1$), 210 ($M^+ - Br$), 100 (base peak, $C_4H_6NO_2^+$) (22). *Anal.* calcd. for $C_{12}H_{20}BrNO_2$: C 49.66, H 6.94; found: C 49.54, H 6.93.

The more polar fraction consisted of N-*(2-chloro-1-octyl)-succinimide* (**35**) (208 mg, 16%). Microdistillation at 100°C (0.004 Torr) gave the analytical sample; ν_{max} ($CHCl_3$): 1785 (w) and 1710 (s) (C=O), 1390, 1140 cm^{-1}; δ ($CDCl_3$): 0.89 (CH_3), 2.73 (s, 4H), 3.4–4.6 ppm (complex pattern, 2H1 + H2); *m/e*: 289, 291 (1:1, M^+), 288, 290 (1:1, $M^+ - 1$), 210 ($M^+ - Br$), 100 ($C_4H_6NO_2^+$) (22). *Anal.* calcd. for $C_{12}H_{20}BrNO_2$: C 49.66, H 6.94; found: C 49.54, H 6.79.

The aqueous phases were combined and continuously extracted with CH_2Cl_2 for 2 days to afford, after evaporating the solvent, succinimide, mp 116–119°C (31 mg, 70%).

Hydrogenolysis of 35

The procedure is based on that reported in ref. 23. Palladium (10%) on charcoal (15 mg) was prehydrogenated at room temperature in 95% ethanol (10 mL) at 40 lbs/in^2 for 30 min. The bromo derivative **35** (38 mg, 0.13 mmol) and potassium acetate (50 mg, 0.51 mmol) were added. After 42 h at room temperature under hydrogen (40 lbs/in^2), the catalyst was filtered, washed with 95% ethanol, and the filtrate evaporated to dryness. Water (15 mL) and ether (15 mL) were added. The mixture was shaken and the two phases were separated. The aqueous phase was extracted with ether. The organic phases were combined, dried over Na_2SO_4, and the solvent was evaporated to afford crude N-*(1-octyl)succinimide* (**39**) (15 mg, 55%). The analytical sample was prepared by microdistillation at 85°C (4 Torr); ν_{max} ($CHCl_3$): 1780 (w) and 1705 (s) (C=O), 1395, 1150, 1120 cm^{-1}; δ ($CDCl_3$): 0.85 (CH_3), 263 (s, 4H), and 3.45 ppm (t, J = 7 Hz, 2 H1); *m/e*: 211 (M^+), 100 (base peak, $C_4H_6NO_2^+$) (22). *Anal.* calcd. for $C_{12}H_{21}NO_2$: C 68.21, H 10.02; found: 68.06, H 9.99.

Hydrogenolysis of 36

It was carried out as above to afford N-*(2-octyl)succinimide* (**34**) (21 mg, 90%). The analytical sample was obtained by microdistillation at 90°C (4 Torr); ν_{max} ($CHCl_3$): 1780 (w) and 1705 (s) (C=O), 1390, 1370, 1360, 1160, 1110 cm^{-1}; δ ($CDCl_3$): 0.87 (CH_3), 1.36 (d, J = 7 Hz, CH_3), 2.65 (s, 4H), and 4.18 ppm (sextuplet, J = 7 Hz, H2); *m/e*: 211 (M^+), 100 (base peak, $C_4H_6NO_2^+$) (22). *Anal.* calcd. for $C_{12}H_{21}NO_2$: C 68.21, H 10.02; found: C 68.28, H 9.83.

Under the same conditions the chloro analogue **32** showed no sign of hydrogenolysis even after 9 days.

Hydrogenolysis of 38

It was carried out as above using 150 mg of Pd/C, 134 mg of **38** (0.45 mmol), 150 mg of potassium acetate (1.5 mmol), and a hydrogen pressure of 44 lbs/in^2. The hydrogenation was stopped after 6 days and the ^{1}H nmr spectrum of the crude product (139 mg) showed that it consisted of 41% (w/w) of starting material and 59% of a 64:36 mixture of *cis* and *trans* N-*(2-methylcyclohexyl)succinimides* (**40** and **41** respectively). Separation by plc on silica gel (ether−hexane 2:3) followed by microdistillation at 75°C (2 Torr) gave an analytical sample of a mixture of **40** and **41**; ν_{max} ($CHCl_3$): 1780 (w) and 1700 (s) (C=O), 1360, 1165, 1125 cm^{-1}; *m/e*: 196 ($M^+ + 1$), 195 (M^+), 100 ($C_4H_6NO_2^+$) (22). *Anal.* calcd. for $C_{11}H_{17}NO_2$: C 67.66, H 8.78; found: C 67.47, H 8.90. Homogeneous samples of **40** and **41** were obtained after several successive plc separations; **40**: δ ($CHCl_3$): 0.94 (d, J = 7 Hz, CH_3), 2.65 (s, 4H), and 4.08 ppm (d of t, J = 13 and 4 Hz); **41**: δ ($CHCl_3$): 0.73 (d, J = 7 Hz, CH_3), 2.64 (s, 4H), and 3.63 ppm (t of d, J = 11 and 4 Hz).

Hydrogenolysis of a mixture of 38 and 39

The conditions used above (50 mg of Pd/C, 40 mg of a 45:55 mixture of **38** and **39**, 50 mg of potassium acetate, 44 lbs/in^2 of hydrogen, 6 days) gave a mixture of starting material, **40**, and **41** in a 30:40:30 molar ratio.

Acknowledgements

We are grateful to the "Ministère de l'Education du Québec" and the Natural Sciences and Engineering Research Council of Canada for their financial support. We acknowledge the helpful assistance of C. Lebreux who carried out some of the reactions.

1. J. LESSARD, M. MONDON, and D. TOUCHARD. Can. J. Chem. **59**, 431 (1981).
2. D. TOUCHARD. Ph.D. Thesis, Université de Sherbrooke, Sherbrooke, Québec, 1974.
3. J. C. DAY, M. G. KATASAROS, W. D. KOCHER, A. E. SCOTT, and P. S. SKELL. J. Am. Chem. Soc. **100**, 1950 (1978).
4. F. L. LU, Y. M. A. NAGUIB, M. KITADANI, and Y. L. CHOW. Can. J. Chem. **57**, 1967 (1979).
5. H. DRIGUEZ, J. M. PATON, and J. LESSARD. Can. J. Chem. **55**, 700 (1977).
6. (*a*) K. ZIEGLER, A. SPATH, E. SCHAAF, W. SCHUMANN, and E. WINKELMANN. Ann. Chem. **551**, 80 (1942); (*b*) J. C. TRAYNARD. C. R. Acad. Sci. Paris, **239**, 63 (1954); (*c*) C. D. HURD, J. MOFFAT, and L. ROSNATI. J. Am. Chem. Soc. **77**, 2793 (1955); (*b*) A. GUILLEMONAT, G. PEIFFER, J. C. TRAYNARD, and A. LEGER. Bull. Soc. Chim. Fr. 1192 (1964); (*e*) G. PEIFFER, J. C. TRAYNARD, and A. GUILLEMONAT. Bull. Soc. Chim. Fr. 1910 (1966).
7. R. W. YIP, Y. L. CHOW, and C. BEDDARD. J. Chem. Soc. Chem. Commun. 955 (1981).
8. (*a*) J. FOSSEY. Thèse d'Etat, Université de Paris-Sud, 1974. pp. 69 ff; (*b*) I. FLEMING. Frontier orbitals and organic chemical reactions. John Wiley and Sons, Ltd., New York, NY. 1976. pp. 182–188.
9. M. P. BERTRAND and J. M. SURZUR. Tetrahedron Lett. 3451 (1976).

10. M. MONDON and J. LESSARD. Can. J. Chem. **56**, 2590 (1978).
11. M. B. ROBIN, F. A. BOVEY, and H. BASCH. *In* The chemistry of amides. *Edited by* J. Zabicky. John Wiley and Sons, Inc., New York, NY. 1970. pp. 19–22; W. E. STEWART and T. H. SIDDALL III. Chem. Rev. **70**, 517 (1970).
12. N. OKI and H. NAKANISHI. Bull. Chem. Soc. Jpn. **44**, 3419 (1970); G. I. JONES and N. L. OWENS. J. Mol. Struct. **18**, 1 (1973).
13. W. C. DANEN and R. W. GELLERT. J. Am. Chem. Soc. **94**, 6853 (1972).
14. (*a*) J. LESSARD, D. GRILLER, and K. U. INGOLD. J. Am. Chem. Soc. **102**, 3262 (1980); (*b*) R. SUTCLIFFE, D. GRILLER, J. LESSARD, and K. U. INGOLD. J. Am. Chem. Soc. **103**, 624 (1981).
15. C. BROWN and A. J. LAWSON. Tetrahedron Lett. 191 (1975).
16. T. CLARK. J. Am. Chem. Soc. **101**, 7746 (1979).
17. T. KOENIG and R. A. WIELESEK. Tetrahedron Lett. 2007 (1975).
18. (*a*) R. L. TLUMAK and P. S. SKELL. J. Am. Chem. Soc. **104**, 7267 (1982); R. L. TLUMAK, J. C. DAY, J. P. SLANGA, and P. S. SKELL. J. Am. Chem. Soc. **104**, 7257 (1982); (*b*) P. S. SKELL and J. C. DAY. Acc. Chem. Res. **11**, 381 (1978), and references therein.
19. P. MACKIEWICZ, R. FURSTOSS, B. WAEGELL, R. COTÉ, and J. LESSARD. J. Org. Chem. **43**, 3746 (1978).
20. S. A. GLOVER and A. GOOSEN. J. Chem. Soc. Perkin Trans. 1, 1348 (1977); Prog. Theor. Org. Chem. **2**, 297 (1977).
21. D. TOUCHARD and J. LESSARD. Tetrahedron Lett. 3827 (1973).
22. D. A. DENTON, F. J. MCQUILLIN, and P. L. SIMPSON. J. Chem. Soc. 5535 (1964).
23. H. BUDZIKIEWICZ, C. DJERASSI, and D. H. WILLIAMS. Mass spectrometry of organic compounds. Holden Day Inc., San Francisco. 1967. p. 363.

Can. J. Chem. Downloaded from www.nrcresearchpress.com by 210.87.254.6 on 09/06/12
For personal use only.

The intramolecular equilibrium in 2-*tert*-butylphenol and some derivatives. An anomalous $^5J_m^{H,OH}$ indicating steric distortion

TED SCHAEFER, RUDY SEBASTIAN, and SALMAN R. SALMAN[1]
Department of Chemistry, University of Manitoba, Winnipeg, Man., Canada R3T 2N2

Received June 28, 1983

TED SCHAEFER, RUDY SEBASTIAN, and SALMAN R. SALMAN. Can. J. Chem. **62**, 113 (1984).

The ^{1}H nmr spectral parameters in dilute carbon tetrachloride solution are reported for 2-*tert*-butylphenol, as obtained by decoupling of the sidechain protons. Long-range couplings between hydroxyl and ring protons are also reported for five derivatives of 2-*tert*-butylphenol. In the *cis* conformer of 2-*tert*-butylphenol an anomalous $^5J_m^{OH,H-5}$ occurs, most likely as a consequence of a significant distortion of the COH geometry. Such an anomaly, which leads to an incorrect estimate of the *cis*–*trans* equilibrium constant, does not occur in other alkyl phenols, for example, in 2-*tert*-butyl-6-methylphenol. The coupling constant data provide no evidence for out-of-plane conformational preferences of the hydroxyl group in these compounds.

TED SCHAEFER, RUDY SEBASTIAN et SALMAN R. SALMAN. Can. J. Chem. **62**, 113 (1984).

On rapporte les paramètres spectraux en rmn du ^{1}H obtenus en découplant les protons de la chaîne latérale du *tert*-butyl-2 phénol en solution dans le tétrachlorure de carbone. On rapporte également les couplages à longue distance entre le groupe hydroxyle et les protons du cycle de cinq dérivés du *tert*-butyl-2 phénol. Dans le conformère *cis* du *tert*-butyl-2 phénol, il se produit un $^5J_m^{OH,H-5}$ anomal qui serait une conséquence d'une déformation importante de la géométrie du groupe COH. Une telle anomalie, qui conduit à une évaluation incorrecte de la constante d'équilibre *cis*–*trans*, ne se produit pas dans les autres phénols alkylés: comme par exemple avec le *tert*-butyl-2 méthyl-6 phénol. Les données de constante de couplage n'apportent pas la preuve d'une préférence conformationnelle hors du plan du groupe hydroxyle de ces composés.

[Traduit par le journal]

Introduction

The first direct measurement (1) of the *cis*–*trans* equilibrium in solution for 2-methylphenol was based on the stereospecific spin–spin coupling between the hydroxyl proton and

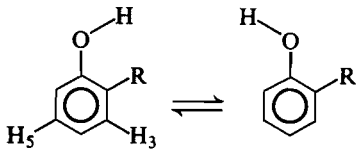

1*a* (*cis*) **1***b* (*trans*)

the ring protons in the *meta* position, $^5J_m^{H,OH}$. It was assumed, in line with data from a variety of phenol derivativs (2–6), that in **1***a* (R = CH_3) $^5J_m^{OH,H-3}$ is negligibly small as is $^5J_m^{OH,H-5}$ in **1***b*. Measurement of $^5J_m^{H,OH}$ then yields the free energy difference between **1***a* and **1***b* as $-RT \ln K = -RT \ln {}^5J_m^{OH,H-3}/{}^5J_m^{OH,H-5}$. In CCl_4 solution, this difference is -1590 ± 170 J/mol at 305 K (**1***b* more stable), in excellent agreement with an indirect measurement based on infrared band intensities in 2-*tert*-butylphenol and 2-*tert*-5,6-dimethylphenol (7).

As for 2-methylphenol, the hydroxyl stretching band in 2-isopropylphenol is also unresolvable into *cis* and *trans* components (7). It is shifted only 2 cm^{-1} from the phenol value. The $^5J_m^{H,OH}$ numbers give a free energy difference of -2510 ± 290 J/mol in CCl_4 solution at 305 K, **1***b* more stable for R = $CH(CH_3)_2$ (8). For 2-isopropyl-6-methylphenol the same procedure yields 1170 ± 330 J/mol as the free energy favoring the conformation in which the hydroxyl group lies *trans* to $CH(CH_3)_2$. Within experimental error this number agrees with the additive preference derived from the monosubstituted phenols.

Furthermore, the long-range couplings over five bonds involving the methine proton of the isopropyl group are also stereospecific and suggest the free energy difference between **1***a* and **1***b* in 2-isopropylphenol as -2340 ± 420 J/mol, to the advantage of **1***b*, in agreement with $^5J_m^{H,OH}$ as an indicator. This agreement implies that the methine C—H bond lies *cis* to the hydroxyl group in **1***b* and *trans* to it in **1***a*.

Now, in 2-*tert*-butylphenol the hydroxyl stretching band is resolvable into two components, one shifted to higher frequency by 32 cm^{-1} from the phenol band and the other, less intense, to lower frequency by 8 cm^{-1} (7). The free energy difference favoring **1***b* (R = *tert*-butyl) is 6570 J/mol and was derived from corrected band intensity ratios (7). A study of the temperature dependence of the band intensities in CCl_4 solution and in the vapour phase (9, 10) showed that the entropy difference between the two conformers was less than 1 J/mol K, indicating that the free energy differences are effectively enthalpy differences.

In this paper, $^5J_m^{H,OH}$ is reported for 2-*tert*-butylphenol and some of its derivatives. An apparently anomalous value of $^5J_m^{OH,H-5}$ is interpreted in terms of a pronounced distortion of the hydroxyl group geometry in **1***a*. The free energy difference derived from $^5J_m^{H,OH}$ in the 6-methyl derivative agrees with that based on infrared band intensities. Conclusions are also drawn about the possible presence of noncoplanar conformations of the hydroxyl group in these compounds.

Experimental

The 2-*tert*-butylphenol was a gift from Pitt–Consol Chemical Co., as were the 6-methyl- and the 6-*tert*-butyl derivatives from The Ethyl Corporation. The other compounds were acquired from Aldrich.

Solutions as dilute as 0.2 mol%, but never larger than 5 mol%, in CCl_4, containing ca. 4 vol.% of tetramethylsilane, were transferred to 5-mm od nmr sample tubes. The solutions were degassed by a number of freeze–pump–thaw cycles and were then flame-sealed under vacuum. Intermolecular proton exchange was retarded as described previously (5).

The ^{1}H nmr spectra were recorded in the frequency-sweep mode on a HA100 nmr spectrometer at a probe temperatur of 305 K. Careful calibrations of peak positions were made as described before in detail (11). Because the methyl protons of the *tert*-butyl groups caused

[1]Department of Chemistry, University of Baghdad, Baghdad, Iraq.

Can. J. Chem. Downloaded from www.nrcresearchpress.com by 210.87.254.42 on 09/06/12
For personal use only.

Can. J. Chem. Downloaded from www.nrcresearchpress.com by 210.87.254.42 on 09/06/12
For personal use only.

broadening of peaks from other protons, calibrations were usually combined with strong irradiation of the *tert*-butyl ^{1}H nmr peak or peaks. Because these δ values are relatively small, the decoupling fields were adjusted in amplitude so as not to perturb the TMS internal lock signal unduly.

The sign of $^4J_o^{H,OH}$ was determined by weak irradiation experiments (12) on 2-*tert*-butyl phenol, as was that of $^5J_m^{OH,H-5}$. The sign of $^5J_o^{OH,CH3}$ in the 6-methyl derivative was also determined.

Results and discussion

Spectral analyses

Full spectral analyses were carried out with the computer program LAME (13, 14). The ^{1}H nmr spectral parameters for 2-*tert*-butylphenol are given in Table 1. Figure 1 indicates the spectral quality and illustrates the necessity of decoupling the *tert*-butyl protons for a precise analysis. The signs of the coupling constants for the hydroxyl proton in Table 1 are relative to $^5J_m^{OH,H-3}$, which is positive (15).

The analysis of a 0.87 mol% solution of 2,6-di-*tert*-butylphenol in CCl_4 solution gave ν_{OH} as 497.292(6) Hz, $\nu_{3,5}$ as 702.403(7) Hz, and ν_4 as 666.477(7) Hz. $^3J^{H,H}$ is 7.852(8) Hz and decoupling of the hydroxyl proton narrowed line 3, the single transition between antisymmetric spin states in an AB_2 spin system, by ca. 0.03 Hz. Therefore $^6J_p^{H,OH} \leq 0.03$ Hz. $^5J_m^{H,OH}$ is 0.310(8) Hz, indicating $^5J_{trans}^{OH,H}$ as 0.62(2) Hz. Substitution by chlorine at the para position gave $^5J_m^{H,OH}$ as 0.314(6) Hz, suggesting $^5J_{trans}^{OH,H}$ as 0.63(2) Hz, for a 3 mol% solution in CCl_4, whereas the presence of a 4-methyl group gave $^5J_m^{H,OH}$ as 0.32(1) Hz. The average of the sum of the $^5J_m^{H,OH}$ values for the last four compounds in Table 2 is 0.62 Hz, whereas if there is only one *tert*-butyl substituent in the *ortho* position in these phenols, the sum is nearer 0.80 Hz.

The 1a ⇌ 1b *equilibrium in* 2-tert-*butylphenol*

$^5J_m^{OH,H-3}$ and $^5J_m^{OH,H-5}$ are 0.613(5) and 0.196(5) Hz, respectively. Writing $-RT \ln K = -RT \ln 0.613/0.196 = -RT \ln 3.13$, yields −2890 J/mol as the free energy difference favoring **1***b*. The infrared band intensities (7) yielded K as 13.3 and therefore a free energy difference of 6560 J/mol. The striking disagreement is unexpected in view of the discussion above. Agreement between the two equilibrium constants would demand a much smaller $^5J_m^{OH,H-5}$, roughly 0.05 instead of 0.196 Hz.

Furthermore, in 2-*tert*-butyl-6-methylphenol, the $^5J_m^{OH,H}$ numbers give a free energy difference of 4350 ± 570 J/mol to the advantage of the conformer in which the hydroxyl group lies *trans* to the larger alkyl substituent (the error is estimated on the basis of the errors in $^5J_m^{OH,H}$). The infrared band intensities gave 4400 J/mol for both the enthalpy and for the free energy differences (9, 10). Combined with the $^5J_m^{OH,H}$ data from previous work (1, 8, 16), in which a comparison of the free energy differences between *cis* and *trans* conformers of the 2-X-phenols allowed the prediction of those differences for the 2-X-6-Y phenols on an additive basis (X = CH_3, allyl, isopropyl, and the X−Y pairs being any two of these), this agreement, in conjunction with the apparently anomalous $^5J_m^{OH,H-5}$ in 2-*tert*-butylphenol, suggests a distortion of the hydroxyl group geometry in the *cis* conformer, **1***a*. Note also that the stretching band for this conformer is shifted to *high* frequency by a repulsive interaction.

INDO MO FPT (17) calculations of $^5J_m^{OH,H-5}$

If, as seems likely, the predominant distortion of the geometry of **1***a* involves bond angles, then it is of interest whether

TABLE 1. The ^{1}H nmr spectral parameters for a 2.0 mol% solution of 2-*tert*-butylphenol in CCl_4 at 305 K

Parameter	Value	Parameter	Value
ν_{CH_3}[a]	138.8	$^4J_{46}$	1.293(5)
ν_{OH}	440.395(3)[b,c]	$^5J_{36}$	0.310(5)
ν_3	716.297(3)	$^4J_o^{OH,H}$	−0.200(5)
ν_4	675.346(4)	$^5J_m^{OH,H-3}$	0.613(5)
ν_5	693.754(4)	$^5J_m^{OH,H-5}$	+0.196(5)
ν_6	649.232(3)	$^6J_p^{OH,H}$	−0.013(5)
$^3J_{34}$	7.814(5)	Calcd. transitions[d]	90
$^3J_{45}$	7.376(5)	Assigned transitions	77
$^3J_{56}$	7.858(5)	Peaks	58
$^4J_{35}$	1.631(5)	Deviation (r.m.s.)	0.012

[a]In Hz at 100.001$_2$ MHz (centerband) to low field of internal TMS.
[b]Numbers in parentheses are the standard deviations in the last significant figure.
[c]A 0.2 mol% solution has ν_{OH} equal to 436.99 Hz.
[d]Above a relative intensity of 0.05.

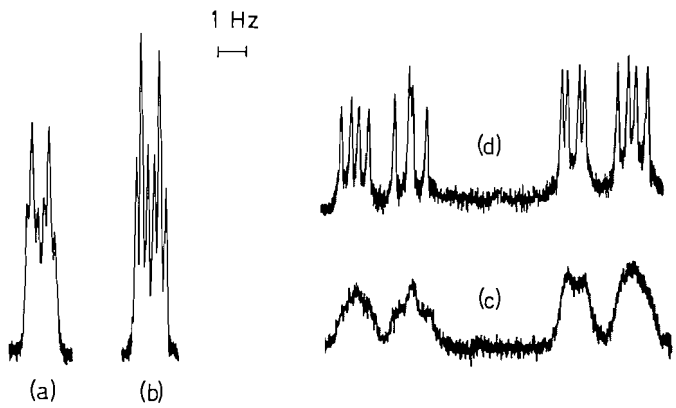

FIG. 1. In (a) is shown the ^{1}H nmr spectrum of the hydroxyl group of a 2.0 mol% solution of 2-*tert*-butylphenol at 100.001 MHz and 305 K. In (b) the hydroxyl proton peaks are displayed while the *tert*-butyl protons are being decoupled. The hydroxyl proton is coupled to H-3, H-5, and H-6. In (c) the ^{1}H nmr spectrum of H-3 is displayed and in (d) the same spectrum is shown while the *tert*-butyl protons are decoupled. Various weak irradiation experiments showed that the $^5J_m^{H,OH}$ numbers are positive, whereas $^4J_o^{H,OH}$ is negative.

INDO open shell calculations of $^5J_m^{OH,H}$ reflect such a distortion. It is known that INDO MO FPT computations give a *qualitatively* correct representation of a variety of five-bond coupling constants (18−20). The geometry of phenol is precisely known (21) and is given in **2** for the angles θ and ϕ. The INDO calculations assumed a standard geometry for the

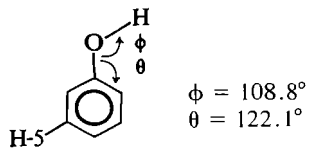

2

benzene ring, quite close to the actual geometry (21), and were done for a series of θ and ϕ values. It seemed likely that steric repulsion from a 2-*tert*-butyl group would increase both angles in **1***a*.

Angles θ and ϕ were varied between 120° and 126° and between 108.8° and 114°, respectively, yielding 20 combinations in all. In all cases, an increase in either angle increased

TABLE 2. Some relevant spectral parameters for 2-*tert*-butylphenol and some derivatives in CCl_4 solution at 305 K and 100.001 MHz

Compound[a]	$^5J_m^{OH,H-3}$	$^5J_m^{OH,H-5}$	ν_{OH} conc.
2-*tert*-Butyl (2)	0.613(5)	0.196(5)	440.395(3)[b]
2,4-Di-*tert*-butyl (3)	0.62(1)	0.17(2)[c]	433.2[f]
2,6-Di-*tert*-butyl (0.9)	0.310(8)	0.310(8)	497.292(6)
2-*tert*-Butyl-6-Me (2)	0.507(3)	0.09(1)	450.147(2)[e]
2,6-Di-*tert*-butyl-4-Cl (3)	0.314(6)	0.314(6)	496.835(5)
2,6-Di-*tert*-butyl-4-Me (2)	0.32(1)	0.32(1)[d]	477.2[f]

[a]Concentration in mol% is given in parentheses.
[b]436.99 Hz to low field of internal TMS for a 0.2 mol% solution.
[c]$^4J_o^{OH,H}$ is −0.21(1) Hz.
[d]The presence of this interaction was first noted by Freeman (ref. 34).
[e]$^5J_o^{OH,CH_3}$ is −0.22 ± 0.02 Hz.
[f]A full spectral analysis was not performed, leading to larger errors. The upfield shift of the hydroxyl proton peak is expected on the basis of electron release by the 4-methyl substituent (31).

$^5J_m^{OH,H-5}$ in **2**. For a given angle θ, increasing φ from 108.8° to 114° led to an increase of 0.12 to 0.13 Hz in this coupling. An increase of 2° in θ for a given φ increased the calculated ^5J by 0.04 Hz. In other words, the INDO MO FPT trends are in qualitative agreement with a model in which a repulsive interaction with a 2-*tert*-butyl substituent distorts the COH geometry in the *cis* form and entails an anomalously large $^5J_m^{H,OH}$ in that conformation. The present calculations did not allow for changes in C—O and O—H bond lengths and therefore for charge redistributions connected with such changes. Nevertheless, we suggest that the anomalous $^5J_m^{H,OH}$ data for 2-*tert*-butyl- and 2,4-di-*tert*-butylphenol can be accounted for in this manner.

CNDO MO FPT calculations gave results similar to the INDO trends, the calculated $^5J_m^{OH,H-5}$ values increasing by 0.16 Hz as θ and φ increased to 126° and 114°, respectively, that is, to 0.70 Hz. A precise X-ray or, better, a neutron diffraction study would be of interest.

It would follow that in the presence of another *ortho* substituent, the repulsive interaction is not large enough to cause significant angle changes of the COH moiety, as judged by the $^5J_m^{H,OH}$ values in Table 2. There is no evidence for significant out-of-plane conformations of the hydroxyl group in any of the compounds, as discussed further on in this paper.

Concerning the coplanarity of the hydroxyl group

The internal barrier to rotation about the C—O bond in phenol in the gas phase is 14.6 kJ/mol (22−24), apparently the same as when oriented in a nematic phase (25). For a 2,6-di-*tert*-butyl arrangement, dielectric relaxation (26), hydroxyl stretching frequencies (27), ultraviolet absorption (28), ^1H spin-lattice relaxation rates (27, 29), X-ray diffraction results (30, 31), and hyperfine splittings in a cation radical (32) are all consistent with a substantial coplanar preference of the hydroxyl group.

The present proton coupling data agree with such a preference, $^6J_p^{H,OH}$ and/or $^7J_p^{OH,CH_3}$ being ≤0.03 Hz for all the compounds in Table 2. These couplings should follow $\sin^2\theta$, where θ is the out-of-plane twist of the hydroxyl group, and might be as large as 1 Hz for θ = 90°(33). Accordingly, the discussion above in terms of **1***a* ⇌ **1***b* appears reasonable.

Conclusions

An anomalous $^5J_m^{OH,H-5}$ *in 2-tert*-butylphenol is very likely a consequence of a substantial distortion of the COH geometry in the *cis* conformer. The use of $^5J_m^{OH,H}$ values as indicators of *cis-trans* equilibria in phenol derivatives is reliable for other *ortho* alkyl phenols (methyl, isopropyl, allyl) and also for *ortho tert*-butylphenols which contain a second *ortho* alkyl group. All available evidence is compatible with an effectively coplanar conformation of the hydroxyl group, even in the presence of two *ortho tert*-butyl substituents.

Acknowledgments

We are grateful to Brenda Addison and to Rick Veregin for some preliminary measurements and calculations and thank the Natural Sciences and Engineering Research Council of Canada for financial assistance.

The referees offered some pungent criticism leading to a more sensible discussion.

1. T. SCHAEFER and K. CHUM. Can. J. Chem. **56**, 1788 (1978).
2. J. B. ROWBOTHAM and T. SCHAEFER. Can. J. Chem. **52**, 3037 (1974).
3. J. B. ROWBOTHAM, M. SMITH, and T. SCHAEFER. Can. J. Chem. **53**, 986 (1975).
4. T. SCHAEFER and J. B. ROWBOTHAM. Can. J. Chem. **54**, 2243 (1976).
5. T. SCHAEFER, J. B. ROWBOTHAM, and K. CHUM. Can. J. Chem. **54**, 3666 (1976).
6. R. FREEMAN, N. S. BHACCA, and C. A. REILLY. J. Chem. Phys. **38**, 293 (1963)
7. K. U. INGOLD and D. R. TAYLOR. Can. J. Chem. **39**, 471 (1961).
8. T. SCHAEFER, B. M. ADDISON, R. SEBASTIAN, and T. A. WILDMAN. Can. J. Chem. **59**, 1656 (1981).
9. K. U. INGOLD and D. R. TAYLOR. Can. J. Chem. **39**, 481 (1961).
10. K. U. INGOLD. Can. J. Chem. **40**, 111 (1962).
11. T. SCHAEFER and R. SEBASTIAN. J. Magn. Reson. **41**, 395 (1980).
12. R. FREEMAN and W. A. ANDERSON. J. Chem. Phys. **37**, 2053 (1962).
13. S. CASTELLANO and A. A. BOTHNER-BY. J. Chem. Phys. **41**, 3863 (1964).
14. C. W. HAIGH. Annu. Rep. NMR Spectrosc. **4**, 311 (1971).
15. S. FORSÉN and R. A. HOFFMAN. J. Mol. Spectrosc. **20**, 168 (1966).
16. T. SCHAEFER, R. SEBASTIAN, and T. A. WILDMAN. Can. J. Chem. **57**, 3005 (1979).
17. P. A. DOBOSH. Quantum Chemistry Program Exchange, **11**, 141 (1979).
18. J. KOWALEWSKI. Prog. Nucl. Magn. Reson. Spectrosc. **11**, 78 (1977).
19. R. WASYLISHEN and T. SCHAEFER. Can. J. Chem. **50**, 1852 (1972).
20. R. WASYLISHEN and T. SCHAEFER. Can. J. Chem. **49**, 3216 (1971).
21. N. W. LARSEN. J. Mol. Struct. **51**, 175 (1979).
22. E. MATHIER, D. WELTI, A. BAUDER, and HS. H. GÜNTHARD. J. Mol. Spectrosc. **37**, 63 (1971).
23. H. D. BIST, J. C. D. BRAND, and D. R. WILLIAMS, J. Mol. Spectrosc. **24**, 402 (1967).
24. N. W. LARSEN and F. M. NICOLAISEN. J. Mol. Struct. **22**, 29 (1974).
25. T. BJORHOLM and J. P. JACOBSEN. J. Mol. Struc. **96**, 315 (1983).
26. R. ISNARD, G. FROSSATI, J. GILCHRIST, and H. GODFRIN. Chem. Phys. **52**, 97 (1980).
27. M. ARONSON, P. BECKMANN, B. ROSS, and S. L. TAN. Chem. Phys. **63**, 349 (1981).
28. L. A. COHEN and W. M. JONES. J. Am. Chem. Soc. **85**, 3402 (1963).
29. P. BECKMANN. J. Magn. Reson. **36**, 199 (1979).

Can. J. Chem. Downloaded from www.nrcresearchpress.com by 210.87.254.42 on 09/06/12
For personal use only.

30. M. E. DRUYAN, A. H REIS, JR., E. GEBERT, S. W. PETERSON, G. W. MASON, and D. F. PEPPARD. J. Am. Chem. Soc. **98**, 4801 (1976).
31. M. ITOH, Y. TANIMOTO, and Y. IITAKA. J. Chem. Phys. **69**, 816 (1978).
32. F. NEMOTO, N. TSUZUKI, K. MUKAI, and K. ISHIZU. J. Phys. Chem. **85**, 2450 (1981).
33. T. SCHAEFER, T. A. WILDMAN, and S. R. SALMAN. J. Am. Chem. Soc. **102**, 107 (1980).
34. R. FREEMAN. Mol. Phys. **6**, 535 (1963).

Can. J. Chem. Downloaded from www.nrcresearchpress.com by 210.87.254.42 on 09/06/12
For personal use only.

An esr and CIDEP study of the photoreduction of chromone and chromanone and their organometallic radical adducts

BABATUNDE B. ADELEKE,[1] DOUGLAS WEIR, M. CATHERINE DEPEW, and JEFFREY K. S. WAN[2]
Department of Chemistry, Queen's University, Kingston, Ont., Canada K7L 3N6

Received February 28, 1983

BABATUNDE B. ADELEKE, DOUGLAS WEIR, M. CATHERINE DEPEW, and JEFFREY K. S. WAN. Can. J. Chem. **62**, 117 (1984).

The esr and CIDEP results show that the photoreduction of chromones and chromanones by phenol and by triethylamine proceeds via a spin polarized $T(n,\pi^*)$ triplet state which abstracts a hydrogen atom from the donor. Both chromone and chromanone are found to be reactive to the addition of organometallic radicals to form some radical adducts, including organotin, organosilicon, and organogermane.

BABATUNDE B. ADELEKE, DOUGLAS WEIR, M. CATHERINE DEPEW et JEFFREY K. S. WAN. Can. J. Chem. **62**, 117 (1984).

Les résultats de la rpe et du PEIDC montrent que la photoréduction des chromones et des chromanones par le phénol et la triéthylamine se produit par l'intermédiare d'un état triplet à spin polarisé $T(n, \pi^*)$ qui enlève un atome d'hydrogène du donneur. On a trouvé que la chromone et la chromanone réagissent lors de l'addition de radicaux organométalliques en donnant quelques adduits radicalaires comprenant l'organoétain, un organosilicium et un organogermane.

[Traduit par le journal]

Can. J. Chem. Downloaded from www.nrcresearchpress.com by 210.87.254.5 on 09/06/12
For personal use only.

Introduction

In nature benzopyran analogs are widespread and many of them have interesting biological and physical properties (1, 2). As a class of compounds, chromones and chromanones have been attracting much attention among chemists in different fields. In photochemistry, the early studies of substituted γ-pyrones have established a number of photochemical paths, including photodimerization (3), photorearrangement (4, 5), and photoaddition to olefins (6). In cycloalkane solvents, evidence of the primary photochemical processes involving the carbonyl chromophore has been documented (6). But the exact nature of the chemically active excited states of chromones and chromanones has remained controversial. Gallivan (7) and co-workers (8) have shown that chromones have two low-lying triplet states of $n\pi^*$ and $\pi\pi^*$ in character which are nearly isoenergetic and can thus be readily re-ordered by changing solvents. On the other hand, Wolfbeis and Knierzinger (9) have demonstrated the sensitivity of chromones towards acidic solvents, leading to protonation of the ground state molecule and consequent strong fluorescence. A more recent picosecond spectroscopic study by Hamanoue and co-workers (10) further concluded that in the primary photophysical processes involving chromone, chromanone, and flavone, the direct intersystem crossing from $S_1(n\pi^*)$ to the lowest triplet $T(\pi\pi^*)$ occurs efficiently in *polar* solvents while the corresponding transition to $T(n\pi^*)$ is observed in *non-polar* solvents. In general, it is recognized for carbonyl compounds triplet states of mixed orbital character such as the $T(\pi\pi^*)$ is much less chemically active than the $T(n\pi^*)$. However, for some biphenyl ketones the structure of their $T(\pi\pi^*)$ allows for substantial unpaired spin density on the carbonyl oxygen atom, thus making them fairly reactive (11). The carbonyl chromophore has been notoriously suited for initial electron polarization studies and many ketones and quinones have been used in our laboratory as model systems for CIDEP studies. We have, therefore, examined this interesting series of compounds the chromones and chromanones, by esr and CIDEP techniques. Our results will further shed some light on their triplet properties and their chemical behaviours towards photoreduction as well as in organometallic radical reactions.

Experimental

All of the benzopyran analogs used were supplied by Aldrich. Organic solvents and triethylamine were purified by the appropriate methods (12) before use. Sample solutions were all deoxygenated by bubbling with nitrogen gas immediately before photolysis. In cw experiments, samples were irradiated with a 200 W super pressure mercury lamp with Pyrex optics directly within the cavity of a X-band esr spectrometer with a 100 kHz field modulation. Magnetic fields were measured with a Bruker nmr oscillator and calibrated against DPPH. Microwave frequency was monitored by a Hewlett-Packard 5432 frequency counter. The transient spin-polarized radicals were generated by laser photolysis using a Molectron 1 MW nitrogen laser. The CIDEP apparatus and the method of estimating T_1 from the experimental data were described previously in detail (13).

Results and discussion

1. Chromone and chromone-2-carboxylic acid

The photolysis of chromone in either THF or ethanol at room temperature did not produce any significant esr observation. When a more reactive hydrogen donor, 2,6-di-*tert*-butylphenol, was added to the solution and irradiated, two radicals were clearly observed. The 2,6-di-*tert*-butylphenoxy radical was readily recognized and the other radical is assigned to the chromone ketyl radical (**I**) with the esr parameters listed in Table 1. The assignments of the two primary radicals formed in a primary photochemical act (see below) are further confirmed by the CIDEP observation of totally emissive polarization for both radicals. The photoreduction of chromone by phenol is therefore consistent with the following mechanism:

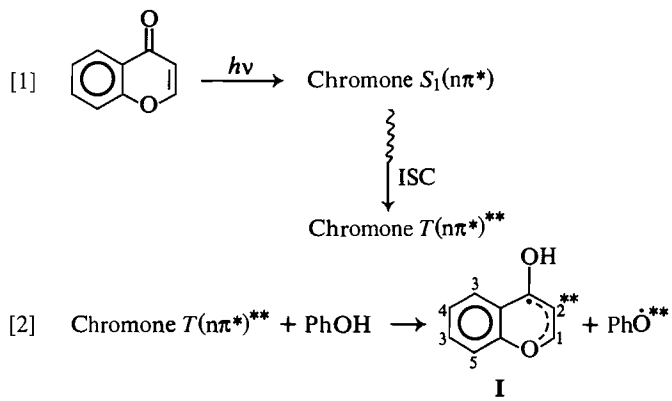

I

[1]CIDA–NSERC Summer Faculty Research Associate, 1979–1981; permanent address: Department of Chemistry, University of Ibadan, Ibadan, Nigeria.

[2]To whom all correspondence should be addressed.

TABLE 1. Electron spin resonance parameters of radicals produced by photoreduction of chromone, cromone-2-carboxylic acid, and thiachroman-4-one

Radical	Solvent	g	Proton hyperfine coupling constants* (G)
I	THF	2.0035±0.0002	$a_1 = 9.96$; $a_2 = a_3 = 2.92$ $a_4 = a_5 = 0.58$; $a_{OH} = 1.08$
I	THF	2.0034	$a_2 = a_3 = 2.15$ $a_{OH} = 0.3$
II	THF	—	$a_{1\alpha} = 30.4 \pm 0.4$

*Refer to diagrams in text for proton positions.

The symbol ** represents electron spin polarization. The initial polarization of the chromone triplet via the differential intersystem crossing processes to the T_{+1} sublevel is typical of many of the aromatic carbonyl compounds (14, 15). In order to preserve the spin polarization in the primary chemical processes [2], the reaction with phenol must proceed at a rate comparable to or greater than the relaxation process which can destroy the triplet spin polarization. Although phenol is a good hydrogen donor, the abstraction reaction [2] will only proceed efficiently if the triplet state is of $T(n\pi^*)$ character (11). Since very strong polarization of both radical **I** and the phenoxy radical is observed, we concluded that in THF or ethanol solution, the reactive triplet state of chromone in reaction [2] is indeed $T(n\pi^*)$. Gallivan and Brinen (8) have suggested that at low temperature the lowest triplet state of chromone is $T(\pi\pi^*)$ in ethanol and $T(n\pi^*)$ in 2-methyl tetrahydrofuran. They have also recognized that the two triplet states are almost isoenergetic. The present CIDEP experiments of chromone in ethanol and in THF confirmed the isoenergetic aspect of the two triplet states and at room temperature, regardless of the polarity of the solvent the chemically reactive triplet of chromone is $T(n\pi^*)$.

The photolysis of a THF solution containing chromone and triethylamine produced the same radical **I** which is also strongly polarized in the total emissive mode. This observation suggests that the primary photochemical reaction between the triplet chromone and the amine is not an electron transfer process but an abstraction of a hydrogen atom from the ethyl group of the amine. A similar reaction has been reported in the CIDEP study of benzophenone with triethylamine (16). Apparently, in THF solvent the chromone radical **I** does not undergo ionization to yield a radical anion.

Identical experiments were performed with a substituted chromone, the chromone-2-carboxylic acid. The corresponding chromone-2-carboxylic radical (**II**) was observed in all cases. The esr parameters of **II** is given in Table 1. The much

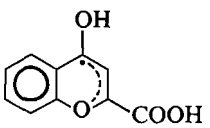

II

smaller hyperfine coupling constant of the hydroxylic proton in **II** as compared to **I** is typically due to the dynamic exchange between the hydroxylic proton and the carboxylic proton of the parent molecule and/or the radical. Similar CIDEP results were obtained also for the radical **II**.

T_1's of radicals **I** and **II** were measured at −15°C in THF solvent. The estimated values are 5.0 ± 0.3 and 6.3 ± 0.6 μs, respectively for radicals **I** and **II**. The larger T_1 of the radical **II**, the chromone-2-carboxylic acid radical, reflects the probable hydrogen-bonding character of the carboxylic proton. Both values, however, are comparable to the T_1 of the naphthosemiquinone (17) and consistent with the theoretical analysis of the T_1 data (18).

2. Chromanone and thiachroman-4-one

Many natural products, including vitamin E, contain the *chroman* ring as a common structural unit. The chroman unit can further be used to synthezise the corresponding chromones and chromenes. It is, therefore, most interesting to compare directly the photochemical properties of chromanones with chromones. Photolysis of 4-chromanone in toluene at room temperature did not produce any significant esr observation. The addition of triethylamine in room temperature photolysis of 4-chromanone did not improve the esr observation. When the temperature was lowered to −40°C, a poorly resolved esr spectrum became observable. There is no doubt that the esr spectrum is associated with the 4-chromanone radical but the poor intensity could be attributed to either the low reactivity of the triplet chromanone or the fast decay of the radicals themselves. In THF at −40°C, CIDEP showed that the chromanone radical is in emissive mode. The simple fact that CIDEP is observed in the photolysis of 4-chromanone with triethylamine indicates that the triplet reactivity is reasonable and therefore the $T(n\pi^*)$ of 4-chromanone is involved in the primary reaction. The low steady state concentration of the chromanone radical is due to the faster decay of the chromanone radical, as compared to radical **I**. This is reasonable, since in chromanone the ring is a smaller π-system:

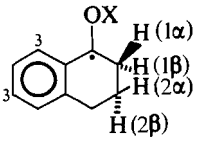

4-Chromanone radical

While it is disappointing that a good esr assignment of the above chromanone radical could not be made, very good esr results are obtained for the chromanone organometal radical adducts in which the hydroxylic proton is replaced by a variety of bulky organometallic group (see below). Thus, esr parameters for the basic chromanone ring still can be deduced and their interesting features will be discussed later.

Experiments with thiachroman-4-one and triethylamine in THF at −70°C produced a slightly better esr spectrum and a much better CIDEP observation of the emissive radical. The improved resolution allows us to report the largest proton hyperfine coupling in the 1α position (see the 4-chromanone radical formula above) of the thiachromanone radical in Table 1. A good estimate of the T_1 of the thiachromanone radical at −70°C gives a value of 9.5 μs. Thiachromanone also produces good concentrations of organometallic radical adducts for esr study which are given next.

3. Organometallic radical adducts of chromones, chromanone, and thiachromanones

Photolysis of a number of organometals in benzene in the presence of di-*t*-butyl peroxide usually generated the corresponding metal-centered radicals which can be trapped by carbonyl compounds such as quinones, aromatic ketones, and

Can. J. Chem. Downloaded from www.nrcresearchpress.com by 210.87.254.5 on 09/06/12
For personal use only.

TABLE 2. Electron spin resonance parameters of some organometallic radical adducts of chromone, chromanone, and thiachromanone in toluene solution

Organic moiety	Organometal	g	Proton coupling constants* (G)
	Ph_3Sn	2.0027±0.0002	$a_1 = 9.67$, $a_2 = 2.22$, $a_3 = 3.22$, $a_{4,5} = 0.57$
	Me_3Sn	2.0028	$a_1 = 9.99$, $a_2 = 2.20$, $a_3 = 3.35$, $a_{4,5} = 0.54$
	Ph_3Ge	2.0034	$a_1 = 9.93$, $a_2 = 2.24$, $a_3 = 3.31$, $a_{4,5} = 0.63$
	Ph_3Si	2.0031	$a_1 = 10.0$, $a_2 = 2.24$, $a_3 = 3.32$, $a_{4,5} = 0.54$
	Me_3Sn	2.0023	$a_{1\alpha} = 35.2$, $a_{1\beta} = 5.2$, $a_{2\alpha} = 5.9$, $a_3 = 1.4$
	Ph_3Ge	2.0029	$a_{1\alpha} = 37.4$, $a_{1\beta} = 5.1$, $a_{2\alpha} = 6.0$, $a_3 = 1.4$
	Ph_3Sn	2.0025	$a_{1\alpha} = 34.7$, $a_{1\beta} = 4.8$, $a_{2\alpha} = 5.82$, $a_3 = 1.6$
	Me_3Sn	2.0027	$a_{1\alpha} = 33.9$, $a_{1\beta} = 4.9$, $a_{2\alpha} = 5.82$, $a_3 = 1.6$
	Ph_3Ge	2.0037	$a_{1\alpha} = 36.2$, $a_{1\beta} = 4.7$, $a_{2\alpha} = 5.9$, $a_3 = 1.4$

*Refer to diagrams in text for proton positions.

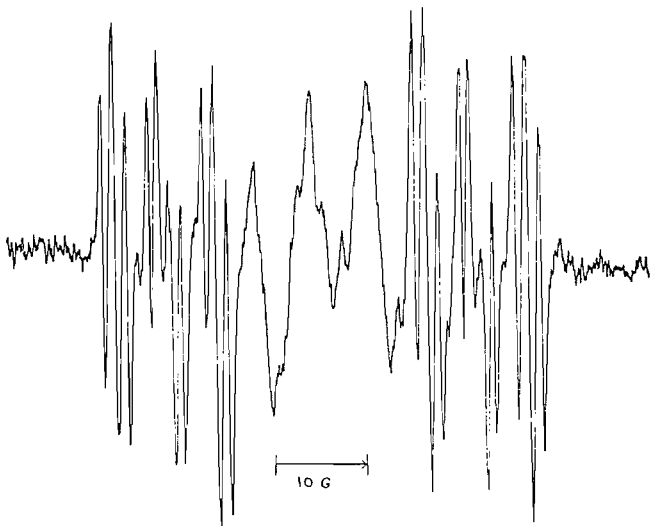

FIG. 1. The observed esr spectrum during the photolysis of thiachroman-4-one in THF at −60°C and in the presence of hexamethylditin.

thiobenzophenones (19). Thus, tin-, silicon-, and germanium-centered radicals are systematically added to chromones, chromanone, and thiachromanones and the resulting radical adducts are reported in Table 2. For the chromones, the addition of an organometallic group to the carbonyl oxygen does not alter significantly the spin densities of the chromone ring as compared to the radicals **I** and **II**. g-Factors of the organometallic adducts decrease from silyl to stannyl adducts which is consistent with other reports in literature (20). Similar observations and conclusions can be made for the chromanone and thiachromanone series of adducts. It is worth noting that in all the radical adducts reported in Table 2, hyperfine coupling constants due to the metallic nuclei had not been experimentally resolved, despite the fact that the radical adducts are rather persistent, giving excellent, intense spectra. For example, Fig. 1 shows the esr spectrum of the Me_3Sn−chromanone radical adduct and the chromanone radical is shown in the background for comparison. In the esr investigation of organometalloxy and organometalthio-pyryl radicals from the photolyses of heterocyclic pyrones and analogs, Alberti and co-workers (21) have found that the primary "ketyl" radicals of these compounds are too short-lived for esr observation, but the radical adducts can be readily detected. In their series, they observed a large Sn splitting order in the order of hundred gauss which they correctly assigned to a tin nuclei being non co-planar with the ring. A similar structure for the chromone and chromanone adducts would have produced also a large tin splitting. It is not immediately apparent to us why the chromone and chromanone radical adducts do not exhibit resolvable metal splittings and we intend to examine this fact further in an on-going CIDEP study of metal adducts to chromanones, as the T_1 values of these radical adducts should shed some light on the structure of the radicals. The results of the interaction of metals with chromones and chromanones should be of great interest to the biological properties of these compounds.

Acknowledgements

This research is supported by the Natural Sciences and Engineering Research Council of Canada. Douglas Weir wishes to acknowledge the award of an Ontario Graduate Scholarship.

1. H. J. KABBE and A. WIDDIG. Angew. Chem. Int. Ed. Engl. **21**, 247 (1982).
2. H. LUMBROSO, CH. LIEGEOIS, N. DEREU, L. CHRISTIAENS, and A. LUXEN. J. Mol. Struct. **67**, 251 (1980).
3. P. YATES and M. J. JORGENSON. J. Am. Chem. Soc. **85**, 2956 (1963).
4. A. PADWA and R. HARTMAN. J. Am. Chem. Soc. **88**, 1518 (1966).
5. M. SHIOZAKI and T. HIRAOKA. Tetrahedron Lett. **6**, 4655 (1972); N. ISHIBE, M. SUNAMI, and M. ODANI. J. Am. Chem. Soc. **95**, 463 (1973).
6. J. W. HANIFIN and E. COHEN. J. Am. Chem. Soc. **91**, 4494 (1969).
7. J. B. GALLIVAN. Can. J. Chem. **48**, 3928 (1970); **50**, 3601 (1972).
8. J. B. GALLIVAN and J. S. BRINEN. Chem. Phys. Lett. **10**, 455 (1971).
9. O. S. WOLFBEIS and A. KNIERZINGER. Z. Naturforsch. **34**a, 510 (1979).
10. K. HAMANOUE, T. NAKAYAMA, T. MIYAKE, and H. TERANISHI. Chem. Lett. 39 (1981).

Can. J. Chem. Downloaded from www.nrcresearchpress.com by 210.87.254.5 on 09/06/12
For personal use only.

11. H. M. VYAS and J. K. S. WAN. Can. J. Chem. **55**, 1175 (1977).
12. A. WEISSBERGER. Technique of organic chemistry. Vols. III and VII. Wiley Interscience, NY. 1955, 1956.
13. J. W. M. DEBOER, T. Y. C. CHUNG, and J. K. S. WAN. Can. J. Chem. **57**, 2971 (1979) and references therein.
14. J. K. S. WAN. Adv. Photochem. **12**, 283 (1980).
15. H. MURAI, T. IMAMURA, and K. OBI. Chem. Phys. Lett. **87**, 295 (1982).
16. A. J. DOBBS. Mol. Phys. **30**, 1073 (1975).
17. D. S. LENIART, H. D. CONNOR, and J. H. FREED. J. Chem. Phys. **63**, 165 (1975).
18. D. A. HUTCHINSON, J. RUSSELL, J. W. M. DEBOER, and J. K. S. WAN. Chem. Phys. **53**, 149 (1980).
19. K. A. CREBER, T. I. HO, M. C. DEPEW, D. WEIR, and J. K. S. WAN. Can. J. Chem. **60**, 1504 (1982) and references therein.
20. B. B. ADELEKE, K. S. CHEN, and J. K. S. WAN. J. Organomet. Chem. **208**, 317 (1981).
21. A. ALBERTI, F. P. COLONNA, and G. F. PEDULLI. Tetrahedron Lett. **36**, 3043 (1980).

Can. J. Chem. Downloaded from www.nrcresearchpress.com by 210.87.254.5 on 09/06/12
For personal use only.

The synthesis of trisubstituted cyclopentadienes and their reactivity in the intramolecular Diels–Alder reaction

SANDRA J. ALWARD AND ALEX G. FALLIS

Department of Chemistry, Memorial University of Newfoundland, St. John's, Nfld., Canada A1B 3X7

Received May 6, 1983

SANDRA J. ALWARD and ALEX G. FALLIS. Can. J. Chem. **62**, 121 (1984).

The intramolecular Diels–Alder reactivity of several trisubstituted cyclopentadienes is described and a general method for their preparation reported. In general, sidechain keto-ester functionality has an adverse effect on these internal cycloadditions.

SANDRA J. ALWARD et ALEX G. FALLIS. Can. J. Chem. **62**, 121 (1984).

On a examiné la réactivité de plusieurs cyclopentadiènes trisubstitués vis-à-vis des réactions de Diels–Alder intramoléculaires et on rapporte une méthode générale de synthèse de ces composés. En général, la fonction céto-ester de la chaîne latérale a un effet négatif sur ces cycloadditions internes.

[Traduit par le journal]

Introduction

The novel tricylic sesterterpene gascardic acid was isolated by Brochere and Polonsky in 1960 (1) from *Gascardia madagascariensis* and extensive work by Arigoni and Scartazzini (2)[1] led to the assignment of the tentative structure **1**. However, the complete structure was not determined until 1979 when Boeckman *et al.* (3) synthesized gascardic acid and established its structure as **2** by X-ray diffraction studies. These studies

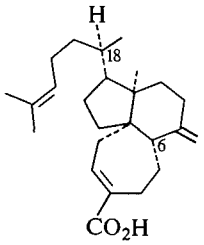

1

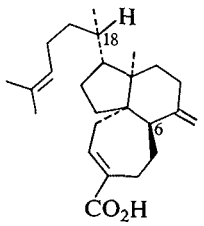

2

clarified the sidechain stereochemistry at C18 and necessitated a revision of the ring fusion at C6, which was previously felt to be *cis* (2) on the basis of chemical correlations.

In recent years the intramolecular Diels–Alder reaction has gained widespread popularity in synthetic studies (4). Although a great deal is known about this reaction, there is still much that remains a mystery, particularly the subtle effects of sidechain substituents (5). In order to use these cycloadditions synthetically one must be able to predict the feasibility of the cyclization with various substitution patterns in both the reacting units themselves and the connecting chain. In spite of these uncertainties, the synthesis of gascardic acid via an intramolecular Diels–Alder reaction was undertaken with the double aim of completing the synthesis and learning more about the Diels–Alder reaction.

The route under development is a general one for the construction of quarternary, spiro-fused tricyclic skeletons of varying ring size and relies on an intramolecular Diels–Alder/oxy-Cope rearrangement sequence, as outlined in Scheme 1. It provides stereochemical control and, depending upon the final target, gascardic acid, retigeranic acid, senoxydene, laurenene, etc., the length of the sidechain may be varied and the resulting cyclohexanone contracted or expanded as required.

[1]Also, R. Scartazzini, G. Wolf, and D. Arigoni, unpublished results.

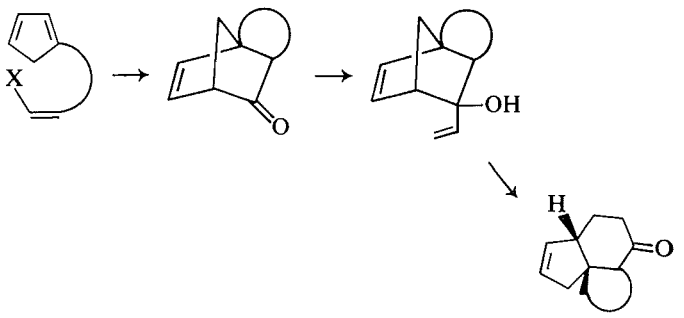

SCHEME 1

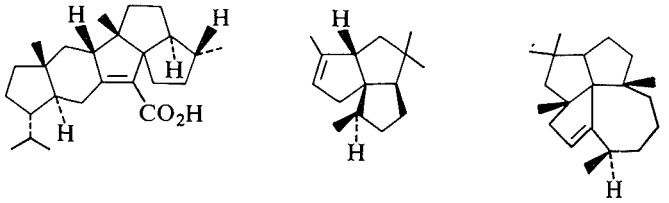

Retigeranic Acid Senoxydene Laurenene

Results and discussion

In order to prepare gascardic acid, the original plans called for intermediates such as keto-esters **3** and **4** which, after Diels–Alder cycloaddition, should afford **5** and **6** respectively. These tricyclic products possess the seven-membered ring required for gascardic acid **2** as well as a keto-ester moiety properly situated for development into the α,β-unsaturated car-

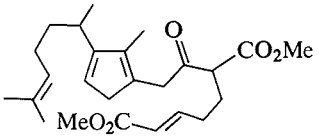

3

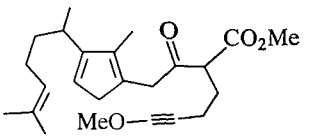

4

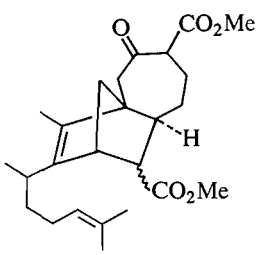

5

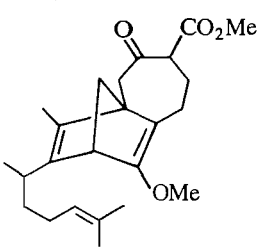

6

Can. J. Chem. Downloaded from www.nrcresearchpress.com by 210.87.254.5 on 09/06/12
For personal use only.

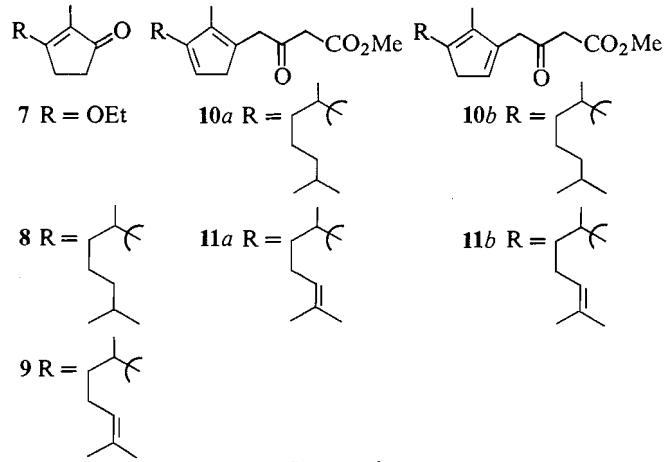

SCHEME 2

boxylic acid. Unfortunately, attempts to cyclize keto-esters **3** and **4** met with no success, yielding either starting materials or decomposition products. In light of these results it was decided to pursue some model studies to ascertain why the intramolecular Diels–Alder reaction was unsuccessful with compounds such as **3** and **4**.

Initially it appeared two factors might be contributing to the failure of the intramolecular Diels–Alder reaction. First it was possible that the entropy involved in forming a seven-membered ring might be too large to overcome, under the reaction conditions employed. There are no carbocyclic examples of substituted cyclopentadienes leading directly to cycloheptanes in the literature, although closely related heterocyclic cases have been reported (4). Secondly the keto-ester will likely be in equilibrium with its enol and, if it adopts the *E* geometry, then the dienophile is held in a position in which close approach to the cyclopentadiene is not feasible, thus inhibiting cyclization. In order to study these variables a number of suitable cyclopentadienes were synthesized.

The literature on trisubstituted cyclopentadienes is sparse but the route developed in Scheme 2 proved most versatile. Thus enone **7**, prepared in a manner analogous to 3-ethoxy-2-cyclohexen-1-one (6), was dissolved in ether and reacted with either 2-bromo-6-methylheptane or 2-bromo-6-methyl-5-heptene in the presence of lithium to yield the α,β-unsaturated ketones **8** and **9** respectively. Both products displayed evidence of the α,β-unsaturated ketone moiety in their ir spectra, which contained peaks at 1700 and 1640 cm^{-1}. Treatment of **8** or **9** with the dianion of methyl acetoacetate, generated by the method of Huckin and Weiler (7), gave a mixture of the cyclopentadienes **10***a* and **10***b* or **11***a* and **11***b* respectively. While five isomers of each of the cyclopentadienes are possible, the ^{1}Hmr spectra of the products show evidence of only the two isomers illustrated and there is no sign of the three possible C5-substituted isomers. Supporting this conclusion, the ^{1}Hmr spectrum of the mixture of **10***a* and **10***b* displayed a multiplet at δ 5.92 (1H, vinylic proton of cyclopentadiene) and a multiplet at δ 2.93 (2H, methylene of cyclopentadiene). A similar pattern was displayed in the ^{1}Hmr spectrum of **11***a* and **11***b*. These results were not unexpected since our studies on the trisubstituted cyclopentadiene **12**[2] showed evidence of isomers **12***a* and **12***b* only, in the ^{1}Hmr spectrum. Furthermore it was observed the ratio of these isomers of **12** showed no apparent change over the temperature range −50°C to 50°C.

[2]C. Mullaly, P. Moore, and S. J. Alward, unpublished results.

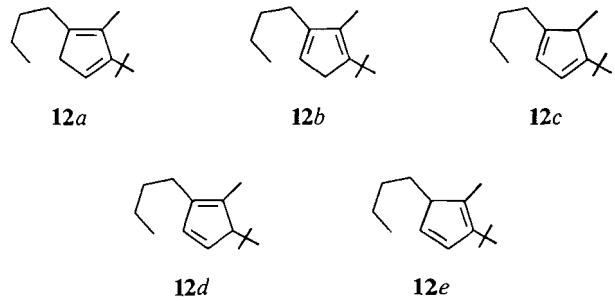

The incorporation of the dienophile into the molecule required reacting the keto-esters **10** and **11** with the appropriate alkylating agents. In view of the different acidic sites these keto-esters are prone to dialkylation but this could be controlled using potassium hydride to generate the keto-ester anion in dimethoxyethane followed by addition of the alkylating agent. The progress of the alkylations was followed by monitoring the disappearance of the characteristic methylene protons at approximately δ 3.3 (singlet, 2H, $COCH_2COOMe$) and the appearance of the methine proton at approximately δ 3.4 (triplet, J = 6.5 Hz, 1H, COCHRCOOMe) in their ^{1}Hmr spectra.

In this manner, cyclopentadienes **13** to **17** (see Table 1) were prepared from keto-esters **10** and **11**. (Only one of the cyclopentadiene isomers is depicted but both are present in all cases.) None of these compounds yielded intramolecular Diels–Alder products when heated in toluene at 180°C and under these reaction conditions only starting materials or extensive decomposition resulted. Since cyclization of **14**, **15**, and **17** would have led to six-membered ring products and since there are ample examples in the literature (4) of this type of reaction, it suggests that the failure to cyclize is a consequence of the sidechain functionality. Unfavourable entropy may inhibit the formation of a seven-membered ring (*vide infra*) but it should not retard cyclohexane generation.

The second complication involving the formation of an unfavourable geometry in the enol form of the keto-ester was automatically negated by the failure of the dialkylated compound **15** to undergo cyclization since no enol form is possible. Consequently there must be a third factor inhibiting cyclization.

In view of the influence sidechain substituents can have on the intramolecular Diels–Alder reaction (5), the ester functionality was removed to see if its absence would affect the reactivity. Thus the keto-ester **14** was heated in wet dimethyl sulfoxide with lithium chloride to give the ketone **18**. The absence of the methyl ester signal in the ^{1}Hmr and the evolution of gas during the reaction attested to the success of the decarboxylation. When ketone **18** was heated in toluene at 180°C for 3 days it gave the desired Diels–Alder product **22** in 77% yield. The ^{1}Hmr spectrum of **22** showed the absence of vinylic protons and the ir spectrum displayed a carbonyl peak at 1720 cm^{-1}, consistent with a ketone in a cyclohexanone. Clearly the β-ester functionality has a deleterious effect on the internal cycloaddition.

Encouraged by the results with ketone **18**, keto-ester **13** was decarboxylated to give ketone **19**. But when ketone **19** was heated in toluene at 180°C for 3 days no Diels–Alder product was formed and starting material was recovered with some sign of decomposition products. Thus it appears that the formation of a seven-membered ring in these systems is indeed disfavored. This result is in accord with the results of Bennett on bis-cyclopentadiene systems (4, 8).

Can. J. Chem. Downloaded from www.nrcresearchpress.com by 210.87.254.5 on 09/06/12
For personal use only.

TABLE 1. Trisubstituted cyclopentadienes

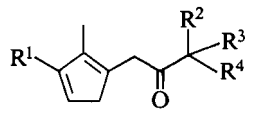

Compound	R^1	R^2	R^3	R^4
13	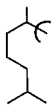	CO_2Me	H	$(CH_2)_2CH{=}CH_2$
14	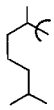	CO_2Me	H	$CH_2CH{=}CH_2$
15	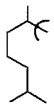	CO_2Me	$CH_2CH{=}CH_2$	$CH_2CH{=}CH_2$
16	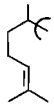	CO_2Me	H	$(CH_2)_2CH{=}CH_2$
17	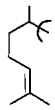	CO_2Me	H	$CH_2CH{=}CH_2$
18	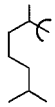	H	H	$CH_2CH{=}CH_2$
19	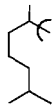	H	H	$(CH_2)_2CH{=}CH_2$
20	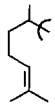	H	H	H
21	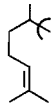	H	H	$CH_2CH{=}CH_2$

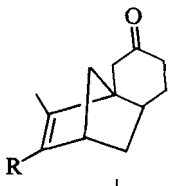

22 R = 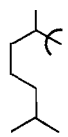

25 R = 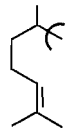

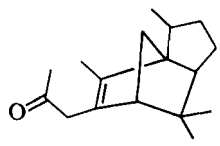

23

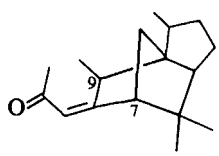

24

Cyclization to a cyclopentane was examined next. Keto-ester **11** was decarboxylated to give ketone **20** which on heating in toluene at 180°C for 7 days gave the cyclized product **24** in 53% yield. The reaction proceeds via ketone **23**, with the double bond then migrating into conjugation with the ketone to give **24**. The ir spectrum of **24** is consistent with the assigned structure, showing peaks at 1685 and 1620 cm^{-1} (α,β-unsaturated ketone), while the ^{1}Hmr spectrum shows no cyclopentadiene or vinylic methyl signals but does display signals at δ 0.87 and 1.05 (6H, s, tertiary methyls) and 6.00 (1H, m, vinylic proton).

Since these experimental results imply that the formation of a seven-membered ring intramolecular Diels–Alder product is improbable, a synthesis of gascardic acid will require a six-membered ring with subsequent ring expansion. In one contemplated route the two olefins may compete as dienophiles and a further model was examined to test the results of this competition. Hence, keto-ester **17** was decarboxylated in the usual manner to give ketone **21** which on heating in toluene at 180°C for 4 days gave the Diels–Alder product **25** in 76% yield. The structure of **25** was compatible with the ^{1}Hmr spectrum which lacked signals characteristic of the cyclopentadiene or $CH{=}CH_2$ systems, while a signal attributed to the side chain vinylic proton is present at δ 4.97 (1H, br t, $J \simeq 6.0$ Hz). The ir spectrum of **25** contains a peak at 1720 cm^{-1} consistent with a six-membered ring ketone. Thus, provided the dienophile is trisubstituted, cyclohexane ring formation takes precedence.

Can. J. Chem. Downloaded from www.nrcresearchpress.com by 210.87.254.5 on 09/06/12
For personal use only.

Can. J. Chem. Downloaded from www.nrcresearchpress.com by 210.87.254.5 on 09/06/12
For personal use only.

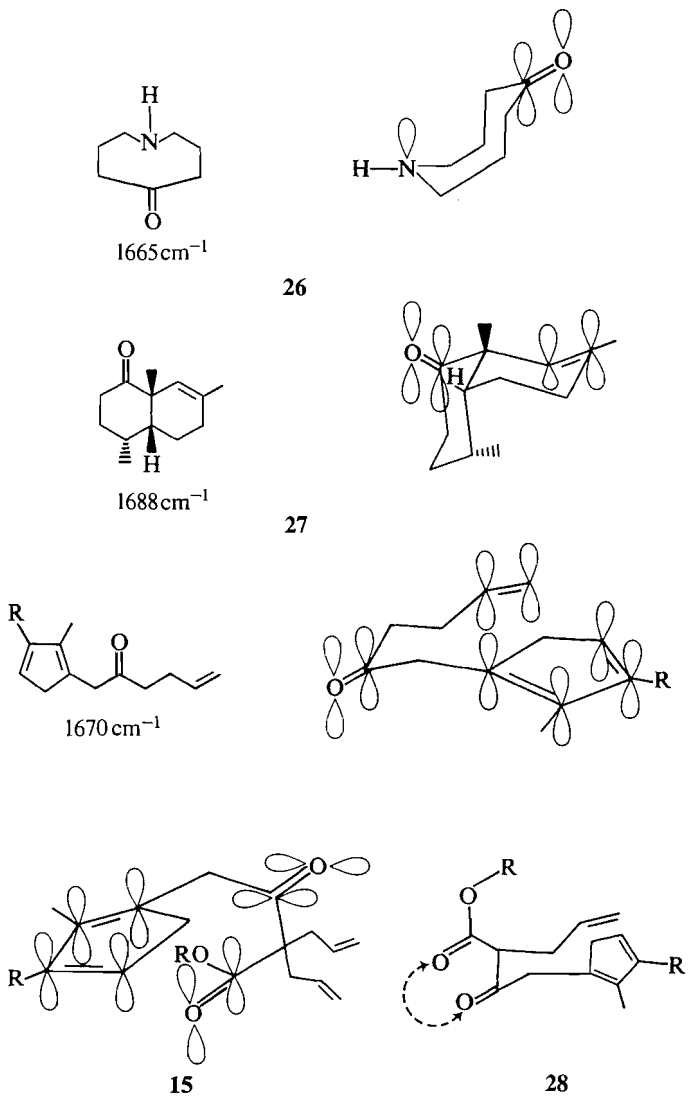

SCHEME 3

The ketones **18**–**21** display unusual infrared carbonyl absorptions and it seems likely that the success or failure of these intramolecular Diels–Alder reactions is largely a result of the stereochemical consequences induced by the alignment of the π systems which are responsible for these absorptions. The infrared spectra, of which **18** is typical, display a weak absorption at 1710, a strong signal at 1670, an intermediate peak at 1640, with the most intense band in the spectrum falling at 1575 cm^{-1}. The carbonyl band at 1670 cm^{-1} is certainly atypical for a non-conjugated ketone but is explicable for a pseudo conjugated carbonyl in which the π system of the diene has a direct influence. This band (1670 cm^{-1}) is not a double bond signal since the trisubstituted cyclopentadiene **12** displays only a very weak absorption at 1625 cm^{-1}. The ultraviolet spectrum of **12** contains a broad band at 250 nm (ϵ = 6 000) while the ketone **18** displays an intense absorption at 307 nm (ϵ = 27 000), unexpected for a saturated ketone but consistent with a through-space interaction between the π systems of the carbonyl and the cyclopentadiene, as illustrated in Scheme 3. This same influence is responsible for the 1670 cm^{-1} carbonyl absorption and finds analogy in the spectra of **26** (9) and **27** (10) in which the carbonyl bands are also shifted to lower frequency due to through-space overlap. The practical consequences of this overlap in the cyclopentadiene examples are that the dienophile can readily assume the orientation required for the Diels–Alder transition state. However, in the case of **19**, in spite of favourable spectral features, even this is insufficient to overcome the unfavourable entropy effect.

In contrast, when the ester is present it appears to interact preferentially with the cyclopentadiene, although this cannot be definitely ascertained from its infrared spectrum which is normal, placing the dienophile in a conformation remote from the diene as illustrated for **15**. If this analysis is correct, it should be possible to hold the keto-ester in the correct geometry for cycloaddition, either by coordination with a complexing agent or using an additional ring (cf. **28**). This is currently being explored.[3]

In other trienes the dominating influence of a carbonyl function on the course and stereochemistry of the adducts has been noted due to the desire of the carbonyl function to retain maximum overlap with the neighbouring π systems ("carbonyl coplanarity effect") (4, 11). These results add to our understanding of this phenomenon and will facilitate the application of these concepts in total synthesis.

Our work on the total synthesis of gascardic acid is continuing and, in view of the above, the route has been modified to proceed via a tricyclo[6.2.1.$0^{1,6}$]undecene which is suitably functionalized for subsequent ring expansion.

Experimental

General

The ir spectra were recorded as thin films with a Perkin–Elmer model 237B spectrophotometer. Proton magnetic resonance spectra were measured using a Varian Model EM-360 spectrometer in carbon tetrachloride solutions containing tetramethylsilane as an internal standard. Band positions are reported in parts per million downfield from tetramethylsilane (δ scale). High resolution mass spectrometric measurements were determined on a Kratos MS-50 spectrometer.

All reactions were carried out under a nitrogen atmosphere and, unless otherwise indicated, reaction products were isolated by the following procedure. The product was extracted into the specified solvent and the extract was washed two or three times with appropriate aqueous solutions as indicated. The original aqueous layer (if any) and the aqueous washings were extracted three times with the solvent and the combined extracts were dried over anhydrous magnesium sulfate, filtered, and evaporated on a Büchi rotary evaporator. Petroleum ether refers to the fraction with boiling range 30–60°C. Brine refers to a saturated aqueous solution of sodium chloride. Merck silica (230–400 mesh ASTM) was used for purification of products by flash chromatography (12).

3-Ethoxy-2-methyl-2-cyclopenten-1-one, 7

A solution of 2-methyl-1,3-cyclopentanedione (25 g, 0.22 mol, Aldrich) and *p*-toluenesulfonic acid (1.5 g, 7.9 mmol) in benzene (500 mL) and ethanol (300 mL) was refluxed through molecular sieves (4 Å) for 48 h. The solvent was evaporated and the residue was distilled to give enone **7** (28 g, 90%); bp 93–100°C (0.5 Torr); mp 36–38°C; ^{1}Hmr δ: 1.32 (3H, d, J = 6.5 Hz, OCH_2CH_3), 1.50 (3H, br s, $C{=}CRCH_3$) and 4.22 (2H, q, J = 6.5 Hz, OCH_2). The compound is air sensitive and gradually reverts to starting materials if not stored in a well-sealed container.

6-Methyl-2-heptanol

A mixture of 6-methyl-5-hepten-2-ol (25.0 g, 0.195 mol, Aldrich), 10% palladium on charcoal (2.0 g), and ethanol (150 mL) was hydrogenated (3 atm) for 7 h. The mixture was filtered to remove the

[3]Since submitting this manuscript, cyclization of a keto-ester has been accomplished with the lower homologue of **3** at 120°C in the presence of tetramethylethylenediamine as a complexing agent. This reaction failed in the absence of tetramethylethylenediamine.

Can. J. Chem. Downloaded from www.nrcresearchpress.com by 210.87.254.5 on 09/06/12
For personal use only.

catalyst and the catalyst was washed with ethanol. The solvent was evaporated and the residue distilled to give 6-methyl-2-heptanol (18.8 g, 74%); bp 78–80°C (12 Torr); ir: 3320 cm^{-1} (hydroxyl); ^{1}Hmr δ: 0.87 (6H, d, J = 6.5 Hz, $RCH(CH_3)_2$), 1.10 (3H, d, J = 6.5 Hz, $C(OH)CH_3$) and 3.63 (1H, m, H—COH). *Exact mass* calcd. for C_8H_{16} (mass − H_2O): 112.1252; found: 112.1258.

2-Bromo-6-methylheptane

To triphenylphosphine (32.52 g, 0.124 mol, Chemalog), suspended in cold (ice bath) dry acetonitrile (500 mL), a solution of bromine (19.8 g, 0.124 mol) in acetonitrile (100 mL) was added dropwise followed by pyridine (10.0 mL, 0.123 mol). The reaction mixture, after stirring for 0.25 h in the ice bath, was warmed to room temperature and a solution of 6-methyl-2-heptanol (see above) (16.5 g, 0.124 mol) was added dropwise. The resulting clear solution was left at 0°C overnight, the solvent was evaporated, and the residue was triturated with petroleum ether. The petroleum ether was evaporated and the crude product distilled to give 2-bromo-6-methylheptane (10.72 g, 45%); bp 75–76°C (12 Torr); ^{1}Hmr δ: 0.88 (6H, d, J = 6.5 Hz, $RCH(CH_3)_2$), 1.67 (3H, d, J = 6.5 Hz, $CBrCH_3$) and 4.00 (1H, sextet, J = 6.5 Hz, CHBr). *Exact Mass* calcd. for C_8H_{17} (mass − Br): 113.1330; found: 113.1324.

3-(1,5-Dimethylhexyl)-2-methyl-2-cyclopenten-1-one, 8

A mixture of enol ether **7** (10.0 g, 71.4 mmol) and 2% Na in Li alloy in ether (300 mL) was treated dropwise with 2-bromo-6-methylheptane (see above) (10.1 g, 52.3 mmol) while being irradiated in an ultrasonic bath (14) for 3.5 h. The mixture was then filtered to remove unreacted lithium and treated with 3 M aqueous hydrochloric acid (300 mL). The reaction mixture was worked up in the usual manner with ether and brine. The product was purified by flash chromatography (12) (30% ether/petroleum ether) to give enone **8** (4.86 g, 45%) as an oil; ir: 1700 and 1640 cm^{-1} (α,β-unsaturated ketone); ^{1}Hmr δ: 0.85 (6H, d, J = 6.5 Hz, $RCH(CH_3)_2$), 1.07 (3H, d, J = 6.5 Hz, R_2CHCH_3), 1.60 (3H, m, $C{=}CRCH_3$) and 2.83 (1H, sextet, J = 6.5 Hz, R_2CHMe). *Exact Mass* calcd. for $C_{14}H_{24}O$: 208.1827; found: 208.1829.

3-(1,5-Dimethyl-4-hexenyl)-2-methyl-2-cyclopenten-1-one, 9

The treatment of enol ether **7** (20.3 g, 0.145 mol) with 2-bromo-6-methyl-5-heptene (13) (27.6 g, 0.145 mol) in a manner analogous to the preparation of compound **8** gave the α,β-unsaturated ketone **9** (13.6 g, 46%) as an oil; ir: 1700 and 1640 cm^{-1} (α,β-unsaturated ketone); ^{1}Hmr δ: 1.15 (3H, d, J = 6.5 Hz, R_2CHCH_3), 1.60 (3H, br s, $C{=}CRCH_3$), 1.65 and 1.68 (6H, d, J = 2 Hz, $C{=}C(CH_3)_2$), 2.93 (1H, sextet, J = 6.5 Hz, R_2CHMe) and 5.07 (1H, br t, $J \simeq 6$ Hz, $CH{=}CMe_2$). *Exact Mass* calcd. for $C_{14}H_{22}O$: 206.1671; found: 206.1673.

Methyl 3-oxo-4-[2-methyl-3-(1,5-dimethylhexyl)cyclopentadienyl]-butyrate, 10

A mixture of sodium hydride, as a 60% oil dispersion (1.00 g, 25 mmol, Aldrich), in anhydrous tetrahydrofuran (70 mL) was cooled in an ice-water bath and treated dropwise with methyl acetoacetate (2.90 g, 25 mmol, Eastman). The solution was stirred for 10 min, then treated dropwise with a solution of 2.4 M butyllithium in hexane (10.5 mL, 25 mmol, Alfa) and stirred for another 10 min. The enone **8** (4.53 g, 22 mmol) was added in one portion and the resulting solution stirred for 20 min before adding to 3 M hydrochloric acid (100 mL). The mixture was stirred vigorously for 45 min and worked up in the usual manner with ether and brine. The product was flash chromatographed (30% ether/petroleum ether) to give cyclopentadiene **10** (4.53 g, 68%) as an oil; ir: 1745, 1670, 1635, 1605 and 1570 cm^{-1} (keto-ester and cyclopentadiene); ^{1}Hmr δ: 0.83 (6H, d, J = 6.5 Hz, $RCH(CH_3)_2$), 1.03 (3H, d, J = 6.5 Hz, R_2CHCH_3), 2.93 (2H, br m, $C{=}CCH_2C{=}C$), 3.32 (2H, s, $COCH_2COOR$), 3.63 (3H, s, OCH_3) and 5.92 (1H, br s, $C{=}CHCH_2C{=}C$). *Exact mass* calcd. for $C_{19}H_{30}O_3$: 306.2195; found: 306.2196.

Methyl 3-oxo-4-[2-methyl-3-(1,5-dimethyl-4-hexenyl)cyclopenta-dienyl]butyrate, 11

Following the method outlined for the preparation of compound **10**, enone **9** (3.99 g, 19 mmol) was converted to keto-ester **11** (5.08 g, 86%) after flash chromatography (30% ether/petroleum ether); ir: 1745, 1635, 1600 and 1570 cm^{-1} (keto-ester and cyclopentadiene); ^{1}Hmr δ: 1.07 (3H, d, J = 6.5 Hz, R_2CHCH_3), 1.53 to 1.73 (9H, $C{=}C(CH_3)_2$ and $C{=}CCH_3$), 2.95 (2H, br m, $C{=}CCH_2C{=}C$), 3.35 (2H, s, $COCH_2COOR$), 3.68 (3H, s, OCH_3), 5.03 (1H, br t, $J \simeq 6$ Hz, $HC{=}C(Me)_2$) and 6.00 (1H, t, $J \simeq 1$ Hz, $C{=}CHCH_2C{=}C$). *Exact Mass* calcd. for $C_{19}H_{28}O_3$: 304.2038; found: 304.2051.

Methyl 2-(3-butenyl)-3-oxo-4-[2-methyl-3-(1,5-dimethylhexyl)cyclo-pentadienyl]butyrate, 13

A mixture of potassim hydride, as a 35% oil dispersion (0.670 g, 5.86 mmol, Aldrich), in anhydrous dimethoxyethane (8 mL) was cooled in an ice-water bath and treated dropwise with a solution of keto-ester **10** (1.783 g, 5.83 mmol) in dimethoxyethane (10 mL). The ice bath was removed and 1-bromo-3-butene (2.8 g, 20.7 mmol, Aldrich) was added in one portion. The reaction mixture was stirred at 75°C for 2 h, then worked up in the usual manner with ether and brine. The residue was flash chromatographed (10% ether/petroleum ether) to give the alkylation product **13** (1.786 g, 85%) as an oil; ir: 1740, 1670, 1640 and 1560 cm^{-1} (keto-ester and cyclopentadiene); ^{1}Hmr δ: 0.87 (6H, d, J = 6.5 Hz, $RCH(CH_3)_2$), 1.07 (3H, d, J = 6.5 Hz, R_2CHCH_3), 0.97 (2H, br m, $C{=}CCH_2C{=}C$), 3.42 (1H, t, J = 6.5 Hz, COCHRCOOR), 3.67 (3H, s, OCH_3), 4.85 to 6.03 (3H, m, $CH{=}CH_2$) and 6.03 (1H, br s, $C{=}CHCH_2C{=}C$). *Exact Mass* calcd. for $C_{23}H_{36}O_3$: 360.2664; found: 360.2657.

Methyl 2-allyl-3-oxo-4-[2-methyl-3-(1,5-dimethylhexyl)cyclopenta-dienyl]butyrate, 14

A mixture of potassium hydride, as a 35% oil dispersion (0.414 g, 3.62 mmol, Aldrich), in anhydrous dimethoxyethane (3 mL) was cooled in an ice-water bath and treated dropwise with a solution of keto-ester **10** (1.05 g, 3.43 mmol) in dimethoxyethane (10 mL). The ice-bath was removed and allyl bromide (0.480 g, 3.97 mmol, Aldrich) was added in one portion. The reaction mixture was stirred at room temperature for 4.5 h, then worked up in the usual manner with ether and brine. The crude product was flash chromatographed (20% ether/petroleum ether) to give the desired product **14** (0.863 g, 73%) as an oil; ir: 1745, 1675, 1640 and 1570 cm^{-1} (keto-ester and cyclopentadiene); ^{1}Hmr δ: 0.85 (6H, d, J = 6.5 Hz, $RCH(CH_3)_2$), 1.05 (3H, d, J = 6.5 Hz, R_2CHCH_3), 2.97 (2H, br m, $C{=}CCH_2C{=}C$), 3.40 (1 H, t, J = 6.5 Hz, COCHRCOOR), 3.62 (3H, s, OCH_3), 4.77 to 5.93 (3H, m, $CH{=}CH_2$) and 5.93 (1H, br s, $C{=}CHCH_2C{=}C$). *Exact Mass* calcd. for $C_{22}H_{34}O_3$: 346.2508; found: 346.2506.

Methyl 2,2-diallyl-3-oxo-4-[2-methyl-3-(1,5-dimethylhexyl)cyclo-pentadienyl]butyrate, 15

A mixture of sodium hydride, as a 60% oil dispersion (0.220 g, 5.50 mmol, Aldrich), in anhydrous dimethoxyethane (3 mL) was cooled in an ice-water bath and treated dropwise with a solution of keto-ester **10** (1.53 g, 5.00 mmol) in dimethoxyethane (2 mL). The solution was warmed to room temperature for 10 min, then cooled in a Dry Ice/acetone bath and treated with allyl bromide (0.600 g, 5.04 mmol, Aldrich). The reaction mixture was stirred at room temperature for 1 h, then worked up in the usual manner with ether and brine. The crude reaction mixture was purified by flash chromatography (30% ether/petroleum ether) to give monoalkylated product **14** (0.727 g, 42%) as well as the desired dialkylation product **15** (0.617 g, 32%) as an oil; ir: 1730, 1665, 1640 and 1570 cm^{-1} (keto-ester and cyclopentadiene); ^{1}Hmr δ: 0.83 (6H, d, J = 6.5 Hz, $R_2CH(CH_3)_2$), 2.94 (2H, br m, $C{=}CCH_2C{=}C$), 3.59 (3H, s, OCH_3), 4.70 to 5.77 (6H, m, $CH{=}CH_2$) and 5.77 (1H, br s, $C{=}CHCH_2C{=}C$). *Exact Mass* calcd. for $C_{25}H_{38}O_3$: 386.2821; found: 386.2820.

Methyl 2-(3-butenyl)-3-oxo-4-[2-methyl-3-(1,5-dimethyl-4-hexenyl)-cyclopentadienyl]butyrate, 16

Alkylation of keto-ester **11** (1.256 g, 4.13 mmol) with 1-bromo-3-butene as outlined above in the preparation of **13** gave,

Can. J. Chem. Downloaded from www.nrcresearchpress.com by 210.87.254.5 on 09/06/12
For personal use only.

after flash chromatography (10% ether/petroleum ether), the desired product **16** (0.961 g, 65%) as an oil; ir: 1740, 1670, 1640 and 1570 cm^{-1} (keto-ester and cyclopentadiene); ^{1}Hmr δ: 1.07 (3H, d, J = 6.5 Hz, R_2CHCH_3), 1.54 to 1.75 (9H, m, $C{=}C(CH_3)_2$ and $C{=}CRCH_3$), 2.95 (2H, br m, $C{=}CCH_2C{=}C$), 3.40 (1H, br t, J = 6.5 Hz, COCHRCOOR), 3.67 (3H, s, OCH_3), 4.85 to 6.03 (4H, m, $CH{=}CH_2$ and $CH{=}C(Me)_2$) and 6.03 (1H, br s, $C{=}CHCH_2C{=}C$). *Exact Mass* calcd. for $C_{23}H_{34}O_3$: 358.2507; found: 358.2532.

Methyl 2-allyl-3-oxo-4-[2-methyl-3-(1,5-dimethyl-4-hexenyl)-cyclopentadienyl]butyrate, 17

Alkylation of keto-ester **11** (2.10 g, 6.91 mmol) with allyl bromide as outlined above in the preparation of **14** gave, along with some dialkylated compound, the desired keto-ester **17** (1.151 g, 48%) as an oil; ir: 1740, 1670, 1640 and 1575 cm^{-1} (keto-ester and cyclopentadiene); ^{1}Hmr δ: 1.05 (3H, d, J = 6.5 Hz, R_2CHCH_3), 1.55 to 1.73 (9H, m, $C{=}C(CH_3)_2$ and $C{=}CRCH_3$), 2.97 (2H, br m, $C{=}CCH_2C{=}C$), 3.42 (1H, t, J = 6.5 Hz, COCHRCOOR), 3.65 (3H, s, OCH_3), 4.83 to 5.97 (4H, m, $CH{=}CH_2$ and $CH{=}C(Me)_2$) and 5.97 (1H, t, $J \simeq 1$ Hz, $C{=}CHCH_2C{=}C$). *Exact Mass* calcd. for $C_{22}H_{32}O_3$: 344.2351; found: 344.2364.

2-Oxo-1-[2-methyl-3-(1,5-dimethylhexyl)cyclopentadienyl]-5-hexene, 18

A stock solution of wet dimethyl sulfoxide was prepared by adding water (0.31 mL) to anhydrous dimethyl sulfoxide (29 mL). A solution of keto-ester **14** (0.863 g, 2.49 mmol) in wet dimethyl sulfoxide (4.3 mL) was treated with lithium chloride (0.212 g, 5.00 mmol) and heated at 175°C for 0.5 h. The resulting mixture was worked up in the usual manner with ether and water and flash chromatographed (20% ether/petroleum ether) to give ketone **18** (0.478 g, 67%) as an oil; ir: 1710, 1670, 1640 and 1575 cm^{-1} (ketone and cyclopentadiene); uv (EtOH) λ_{max}: 307 nm (ε = 27 000); ^{1}Hmr δ: 0.83 (6H, d, J = 6.5 Hz, $RCH(CH_3)_2$), 1.02 (3H, d, J = 6.5 Hz, R_2CHCH_3), 1.68 (3H, $C{=}CRCH_3$), 2.93 (2H, br m, $C{=}CCH_2C{=}C$), 4.72 to 5.80 (3H, m, $CH{=}CH_2$) and 5.80 (1H, br s, $C{=}CHCH_2C{=}C$). *Exact Mass* calcd. for $C_{20}H_{32}O$: 288.2453; found: 288.2458.

2-Oxo-1-[2-methyl-3-(1,5-dimethylhexyl)cyclopentadienyl]-6-heptene, 19

Decarboxylation of keto-ester **13** (1.22 g, 3.39 mmol) as outlined above in the preparation of **18** yielded ketone **19** (0.720 g, 70%); ir: 1710, 1670, 1640 and 1575 cm^{-1} (ketone and cyclopentadiene); ^{1}Hmr δ: 0.85 (6H, d, J = 6.5 Hz, $RCH(CH_3)_2$), 1.05 (3H, d, J = 6.5 Hz, R_2CHCH_3), 1.70 (3H, br s, $C{=}CRCH_3$), 2.93 (2H, br m, $C{=}CCH_2C{=}C$), 4.80 to 5.90 (3H, m, $CH{=}CH_2$) and 5.90 (1H, t, J = 1 Hz, $C{=}CHCH_2C{=}C$). *Exact Mass* calcd. for $C_{21}H_{34}O$: 302.2609; found: 302.2563.

2-Oxo-1-[2-methyl-3-(1,5-dimethyl-4-hexenyl)cyclopentadienyl]-propane, 20

Decarboxylation of keto-ester **11** (3.288 g, 10.8 mmol) as outlined above in the preparation of **18** yielded ketone **20** (2.149 g, 81%); ir: 1700, 1670, 1645 and 1570 cm^{-1} (ketone and cyclopentadiene); ^{1}Hmr δ: 1.03 (3H, d, J = 6.5 Hz, R_2CHCH_3), 1.50 to 1.73 (9H, $C{=}C(CH_3)_2$ and $C{=}CRCH_3$), 2.08 (3H, s, $COCH_3$), 2.90 (2H, br m, $C{=}CCH_2C{=}C$), 4.97 (1H, br t, $J \simeq 6$ Hz, $CH{=}CMe_2$) and 5.83 (1H, br s, $C{=}CHCH_2C{=}C$). *Exact Mass* calcd. $C_{17}H_{26}O$: 246.1984; found: 246.1993.

2-Oxo-1-[2-methyl-3-(1,5-dimethyl-4-hexenyl)cyclopentadienyl]-5-hexene, 21

Decarboxylation of keto-ester **17** (1.165 g, 3.39 mmol) as outlined above in the preparation of **18** yielded ketone **21** (0.631 g, 65%) as an oil; ir: 1710, 1670, 1640 and 1575 cm^{-1} (ketone and cyclopentadiene); ^{1}Hmr δ: 1.03 (3H, d, J = 6.5 Hz, R_2CHCH_3), 1.55 to 1.75 (9H, $C{=}C(CH_3)_2$ and $C{=}CRCH_3$), 2.97 (2H, br m, $C{=}CCH_2C{=}C$), 4.80 to 6.17 (4H, m, $CH{=}CH_2$ and $CH{=}CMe_2$) and 5.90 (1H, br s, $C{=}CHCH_2C{=}C$). *Exact Mass* calcd. for $C_{20}H_{30}O$: 286.2297; found: 286.2297.

10-Methyl-9-(1,5-dimethylhexyl)tricyclo[6.2.1.0^{1,6}]-9-undecen-3-one, 22

A solution of ketone **18** (0.470 g, 1.63 mmol) in toluene (15 mL) was heated in a sealed tube at 180°C for 3 days. The solvent was evaporated and the residue was flash chromatographed (20% ether/petroleum ether) to give Diels–Alder adduct **22** (0.364 g, 77%) as an oil; ir: 1720 cm^{-1} (ketone); ^{1}Hmr δ: 0.80 to 1.10 (9H, m, $RCH(CH_3)_2$ and R_2CHCH_3), 1.61 (3H, br s, $C{=}CRCH_3$). *Exact Mass* calcd. for $C_{20}H_{32}O$: 288.2453; found: 288.2509.

2,6,6,9-Tetramethyl-8-(2-oxo-propylidenyl)tricyclo[5.2.1.0^{1,5}]-decane, 24

A solution of ketone **20** (1.00 g, 4.07 mmol) in toluene (15 mL) was heated in a sealed tube at 170°C for 7 days. The solvent was evaporated and the residue was flash chromatographed (20% ether/petroleum ether) to give ketone **24** (0.527 g, 53%) as an oil; ir: 1710, 1680 and 1620 cm^{-1} (α,β-unsaturated ketone); ^{1}Hmr δ: 0.87 and 1.05 (6H, s, *exo*- and *endo*-CH_3), 2.07 (3H, s, $COCH_3$), 3.00 to 3.53 (2H, overlapping m, C7 and C9 methines) and 6.00 (1H, br s, C=CH). *Exact Mass* calcd. for $C_{17}H_{26}O$: 246.1984; found: 246.2031.

10-Methyl-9-(1,5-dimethyl-4-hexenyl)tricyclo[6.2.1.0^{1,6}]-9-undecen-3-one, 25

A solution of ketone **21** (0.470 g, 1.64 mmol) in toluene (15 mL) was heated in a sealed tube at 180°C for 4 days. The solvent was evaporated and the residue flash chromatographed (20% ether/petroleum ether) to give cyclization product **25** (0.357 g, 76%) as an oil; ir: 1720 cm^{-1} (ketone); ^{1}Hmr δ: 0.93 and 1.02 (3H, d, J = 6.5 Hz, R_2CHCH_3), 1.55 and 1.64 (9H, $C{=}C(CH_3)_2$ and $C{=}CRCH_3$) and 4.97 (1H, br t, $J \simeq 6$ Hz, $CH{=}CMe_2$). *Exact Mass* calcd. for $C_{20}H_{30}O$: 286.2297; found: 286.2300.

Acknowledgements

The authors are grateful to Memorial University of Newfoundland and the Natural Sciences and Engineering Research Council of Canada for financial support; R. J. Anderson, T. Durst, and B. Gregory for high resolution mass spectra; and to the referee for constructive criticism.

1. G. Brochere and J. Polonsky. Bull. Soc. Chim. Fr. 993 (1960).
2. R. Scartazzini. Ph.D. Dissertation, ETH, Zurich (1966); D. Arigoni. Chem. Soc. of London Meeting, Nottingham (1965).
3. R. K. Boeckman Jr., D. M. Blum, and S. M. Arthur. J. Am. Chem. Soc. **101**, 5060 (1979); R. K. Boeckman Jr., D. M. Blum, E. V. Arnold, and J. Clardy. Tetrahedron Lett. **48**, 4609 (1979).
4. A. G. Fallis. Can. J. Chem. **62**, 183 (1984); E. Ciganek. Org. React. In press; G. Brieger and J. N. Bennett. Chem. Rev. **80**, 63 (1980); W. Oppolzer. Angew. Chem. Int. Ed. Engl. **16**, 19 (1977).
5. R. K. Boeckman, Jr. and S. S. Ko. J. Am. Chem. Soc. **104**, 1033 (1982); D. D. Sternbach and D. M. Rossana. Tetrahedron Lett. **23**, 303 (1982); W. R. Roush, H. R. Gillis, and A. I. Ko. J. Am. Chem. Soc. **104**, 2269 (1982); S. K. Attah-Poku, G. Gallacher, A. S. Ng, L. E. B. Taylor, S. J. Alward, and A. G. Fallis. Tetrahedron Lett. **24**, 677 (1983).
6. W. F. Gannon and H. O. House. Org. Synth. **40**, 41 (1960).
7. S. N. Huckin and L. Weiler. J. Am. Chem. Soc. **96**, 1082 (1974).
8. J. N. Bennett. M.S. Thesis, Oakland University (1978).
9. N. J. Leonard, R. C. Fox, M. Ōki, and S. Chiavarelli. J. Am. Chem. Soc. **76**, 630 (1954).
10. C. Schmidt and T. Breining. Can. J. Chem. In press.
11. R. K. Boeckman, Jr. and and D. M. Demko. J. Org. Chem. **47**,

1789 (1982); W. OPPOLZER and W. FRÖSTL. Helv. Chim. Acta, **58**, 590 (1975).
12. W. STILL, M. KAHN, and A. MITRA. J. Org. Chem. **43**, 2923 (1978).
13. E. BREITHOLLE and A. G. FALLIS. J. Org. Chem. **43**, 1964 (1978).
14. J. L. LUCHE and J. C. DAMIANO. J. Am. Chem. Soc. **102**, 7926 (1980).

Can. J. Chem. Downloaded from www.nrcresearchpress.com by 210.87.254.5 on 09/06/12
For personal use only.

Infrared and Raman spectra of alkali palmityl sulfates[1]

V. B. KARTHA,[2] L. C. LEITCH, AND H. H. MANTSCH
Division of Chemistry, National Research Council of Canada, Ottawa, Ont., Canada K1A 0R6

Received June 28, 1983

V. B. KARTHA, L. C. LEITCH, and H. H. MANTSCH. Can. J. Chem. **62**, 128 (1984).

Lithium, sodium, potassium, cesium, and ammonium palmityl sulfates were prepared by sulfonation of *n*-hexadecanol, followed by treatment with the corresponding alkali carbonates; selectively deuterated palmityl sulfates were also synthesized to aid the assignment of certain vibrational modes. The infrared and Raman spectra of the polycrystalline solids were interpreted and discussed in terms of acyl chain and head group vibrations. Spectral evidence is presented for the existence of different solid polymorphic forms.

V. B. KARTHA, L. C. LEITCH et H. H. MANTSCH. Can. J. Chem. **62**, 128 (1984).

On a préparé les sels de lithium, de sodium, de potassium, de césium et d'ammonium du sulfate de palmityle par une sulfonation du *n*-hexadécanol suivie de la réaction du sulfate acide avec les carbonates basiques correspondants. On a également synthétisé des sulfates de palmityle deutérés de façon sélective dans le but de faciliter l'identification de certains modes de vibration. On interprète les spectres infrarouge et Raman des solides polycristallins et on en discute en fonction des vibrations des chaines acylées et des groupes directeurs. On présente des preuves spectrales de l'existence de différentes formes de solides polymorphiques.

[Traduit par le journal]

Can. J. Chem. Downloaded from www.nrcresearchpress.com by 210.87.254.6 on 09/06/12
For personal use only.

Introduction

A considerable amount of work has been done on the amphiphilic properties and phase transitions of alkali salts of alkyl sulfates (for a review, see ref. 1), yet except for a few nmr studies (2, 3), mostly non-spectroscopic techniques were used. Recently, the technique of Fourier-transform infrared spectroscopy has been used by us extensively in the study of biological membranes and related amphiphilic systems to gain information about micellar aggregation (4–6) and thermotropic phase behavior (7–10). These studies have now been extended to alkali salts of alkyl sulfates which are common micelle forming surfactants and may be used as models for the thermotropic phase behavior of sulfolipids found in natural sources (11, 12).

In the present study we assign and discuss the vibrational bands of the alkali salts of palmityl sulfate in terms of crystal structure differences, and establish correlations between individual group frequencies and the nature of the counter-ions. We have chosen to study the palmityl rather than the better known dodecyl salts, as C_{16} is the most abundant chain length found in biological systems.

Experimental

Materials

As the alkali palmityl sulfates are not commercially available, the Li, NH_4, Na, K, Rb, and Cs palmityl sulfates were all prepared in our laboratory starting from *n*-hexadecanol. A solution of 13.5 g (0.05 mol) of *n*-hexadecanol (Chemical Sample Co., Columbus, OH) and 5 g (0.05 mol) of 98% sulfuric acid in 100 mL of petroleum ether (bp 30–60°C) was heated under reflux for 1/2 h. The pale reddish solution was subdivided into 10 mL aliquots for the preparation of individual alkali salts.

In a typical preparation the 10 mL aliquot of *n*-hexadecyl hydrogen sulfate was added to a mixture of 50 mL of *n*-butanol and 10 mL of water in a 100 mL round-bottomed flask and the reaction mixture was neutralized by adding small portions of the alkali carbonate or bicarbonate, with stirring until the pH was 7.5 on indicator paper. The solution was then evaporated to dryness under reduced pressure. The residue was extracted with 50 mL of hot chloroform–methanol (9:1 v/v) and filtered hot from a small excess of the carbonate. On cooling, the product crystallized in pearly white plates, which were filtered off with suction, washed with ether, and dried (yield 1.5 g). Elemental analyses were carried out for all the samples. A typical result for the cesium salt was: *Anal.* calcd. for $C_{16}H_{33}O_4SCs$: C 42.29, H 7.32, S 7.06; found: C 41.95, H 7.48, S 6.93.

The 1,1-d_2-palmityl sulfates were prepared starting with ethyl palmitate. A solution of 2.0 g of ethyl palmitate (Sigma Chemical Co., St. Louis, MO) in 50 mL ether was added to 0.5 g $LiAlD_4$ in 50 mL ether. The mixture was heated under reflux for 1 h and then decomposed by dropwise addition of dilute HCl. The ether layer was separated and dried over $MgSO_4$. Evaporation of the ether gave the 1,1-d_2-hexadecyl alcohol which crystallized at room temperature (yield ~2 g). From this alcohol, the 1,1-d_2-palmityl hydrogen sulfate and the corresponding alkali salts were obtained by the same procedure as described above for the preparation of the non-deuterated alkali palmityl sulfates.

Methods

Infrared spectra were obtained with KBr and CsI pellets. For the Li, Na, and K salts spectra were also recorded with Nujol and Fluorolube mulls; these spectra showed practically no differences from the pellet spectra. All infrared spectra were recorded on a BOMEM DA3-02 Fourier transform infrared spectrometer, equipped with a high-speed vector processor, and a PDP 11-03 computer for data processing. A germanium coated KBr beamsplitter and a high sensitivity, liquid nitrogen cooled mercury cadmium telluride detector were used for the 4000–500 cm^{-1} region, while a mylar beam splitter and a pyroelectric DTGS detector were used to cover the 700–200 cm^{-1} region. Typically, 250 scans were coadded at an apodized resolution of 1 cm^{-1}. Frequencies of absorption peaks were determined by computing centers of gravity of the bands by using programs developed in our laboratories (13). Shoulder peaks and very weak bands were measured visually on an expanded display by using the cursor position. For more accurate frequency measurements on overlapping bands the spectra were Fourier deconvoluted to produce sharper bands (14).

Raman spectra were recorded on a Spex 0.75 m double monochromator, equipped with a DATAMATE data collection system. Spectral slit-widths of 1.5–2 cm^{-1} were used. The DATAMATE was used in Burst Mode 1, where the spectrometer slews to the starting frequency, collects and integrates the photon counts for a specified integration time, then slews through an increment in frequency and repeats the collection and integration process. Frequency increments of 1 cm^{-1} with integration times of 3 s gave good spectra with 200–250 mW of laser power from the 514.5 nm line of a Coherent Radiation CRL Model 12 argon ion laser.

[1]NRCC No. 22545.

[2]Visiting Scientist from the Spectroscopy Division, Bhabha Atomic Research Centre, Trombay, Bombay, 400 085, India.

Can. J. Chem. Downloaded from www.nrcresearchpress.com by 210.87.254.6 on 09/06/12
For personal use only.

Results and discussion

Each of the alkali palmityl sulfates was purified by separate recrystallizations from *n*-butanol and from a chloroform–methanol mixture (9:1 v/v); for the sodium and potassium salts we found two different solid forms, whereas all other salts had identical infrared and Raman spectra regardless of whether they were obtained by recrystallization from *n*-butanol or from chloroform–methanol. The mid-infrared spectra of the lithium, ammonium, rubidium, and cesium salts of palmityl sulfate are shown in Fig. 1, along with the spectrum of the parent compound, *n*-hexadecanol; each of these solid salts was found to occur only in one polymorphic form. Figure 2 shows the infrared spectra of sodium palmityl sulfate and of the 1,1-d_2-palmityl salt, each obtained by recrystallization from *n*-butanol or chloroform–methanol (9:1 v/v); in this case two different polymorphs were obtained from both sodium salts. The Raman spectra of the alkali palmityl sulfates and that of *n*-hexadecanol are shown in Fig. 3 for the region of interest.

The vibrational spectra of these compounds are best discussed in terms of crystal structure differences, which are seen most clearly in the acyl chain modes, and in terms of the cation effect, which is most evident on the head group frequencies.

Acyl chain modes

As no crystal structure information is available on any of the alkali palmityl sulfates, one has to make use of correlations which have been established between certain infrared and Raman spectral features and known crystal structures of related compounds, such as *n*-alkanes or fatty acids. Thus, it can be seen that the infrared spectra of the lithium, ammonium, and rubidium salts in Fig. 1, like that of *n*-hexadecanol, show clear splitting of the CH_2 scissoring (1470 cm^{-1}) and the CH_2 rocking modes (720 cm^{-1}); these spectra resemble those of *n*-alkanes with a known orthorhombic subcell (15–18). The methylene scissoring and rocking modes are split in two components in the spectra of *n*-alkanes and polyethylene when the subcell is orthorhombic (19); this factor group or crystal field splitting arises from intermolecular interactions between the two chains in the orthorhombic subcell. Evidence for a two band system is also obtained from the corresponding Raman spectra. Thus, the two components of the CH_2 scissoring mode are clearly evident at 1420 and 1440 cm^{-1} in the Raman spectra of the lithium, ammonium, and rubidium salts as well as in that of *n*-hexadecanol (Fig. 3); the 1420 cm^{-1} component is absent in all the other salts. Furthermore, the Raman spectra of the CH_2 stretching modes, Fig. 4*A*, shows the 2848 cm^{-1} (symmetric CH_2 stretch) and 2880 cm^{-1} (antisymmetric CH_2 stretch) bands with intensities and widths observed in *n*-alkanes and fatty acids with the orthorhombic packing (17). These spectral features, which are compatible with an orthorhombic or monoclinic (which have a common orthorhombic subcell) packing pattern, we have designated as type I spectra.

As seen from Fig. 2 the spectrum of the sodium salt of palmityl sulfate depends on the method of crystallization. Samples crystallized from *n*-butanol show rather broad bands with practically no splitting, while samples crystallized from chloroform–methanol show very sharp bands. We designate these as type II and type III respectively since they possess spectral features similar to those observed in *n*-alkanes and fatty acids with known hexagonal and triclinic chain packing, respectively (15–18). The infrared spectrum of the cesium salt in Fig. 1 is quite different from that of the lithium, ammonium, and rubidium salts; like Na(III) it shows a larger number of

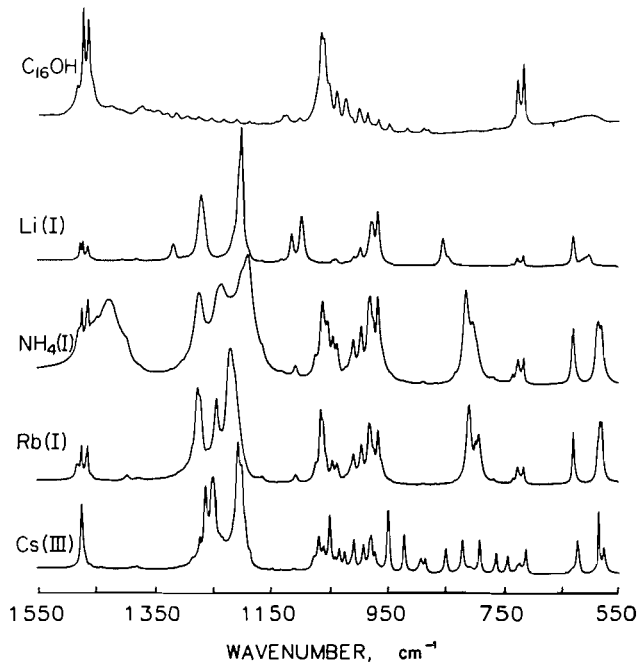

FIG. 1. FT-ir spectra of KBr pellets (1 mg sample/200 mg KBr) of polycrystalline *n*-hexadecanol and of lithium, ammonium, rubidium, and cesium palmityl sulfate in the 550–1550 cm^{-1} region.

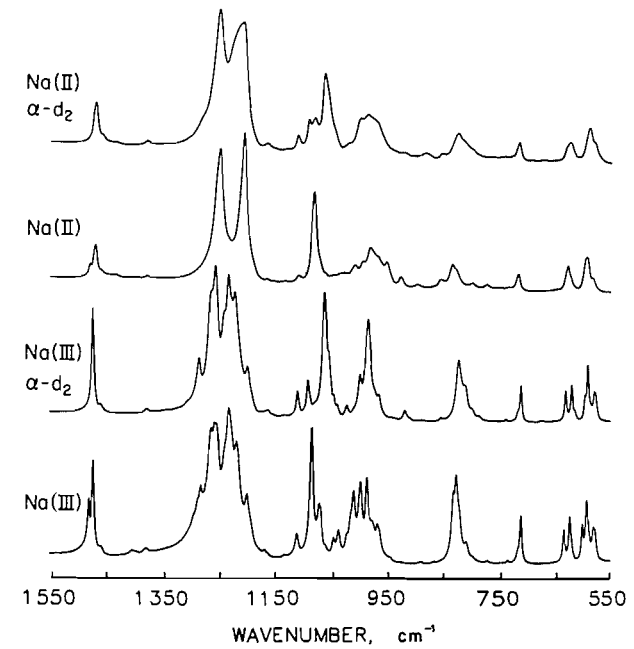

FIG. 2. Infrared spectra of type II and type III sodium palmityl and sodium 1,1-d_2-palmityl sulfate in the 550–1550 cm^{-1} region.

sharp bands. Neither type II nor type III spectra show splitting for the CH_2 rocking mode around 720 cm^{-1}; however, type III sodium palmitate shows an apparent splitting of the CH_2 scissoring mode with two bands at 1472 and 1479 cm^{-1} (Fig. 2). The absence of splitting of the CH_2 rocking mode makes it unlikely that the two bands in the CH_2 scissoring region belong to the same mode and deuteration of the α-CH_2 group in sodium and lithium palmitate have led to an unambigous assignment of the 1479 cm^{-1} band to the α-CH_2 scissoring mode. In fact, a band at 1479 ± 1 cm^{-1} is observed in practically all alkali

Can. J. Chem. Downloaded from www.nrcresearchpress.com by 210.87.254.6 on 09/06/12
For personal use only.

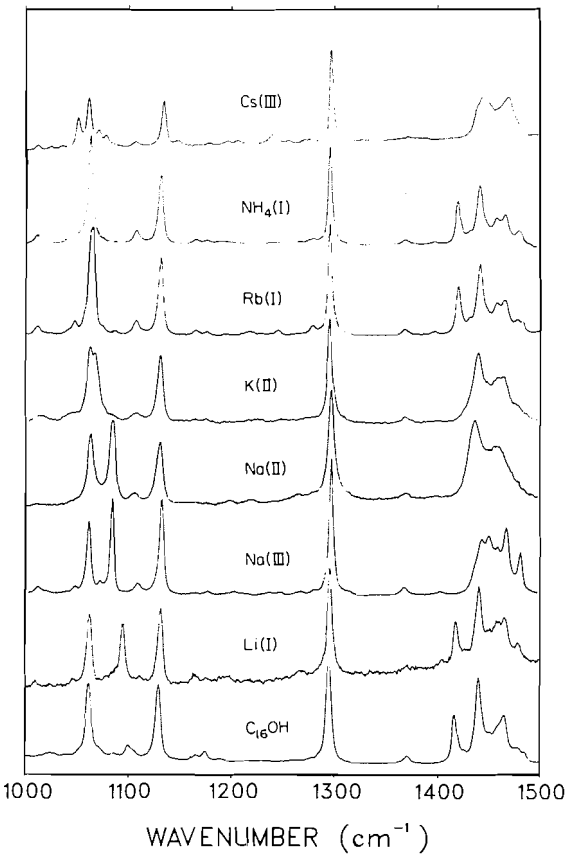

FIG. 3. Raman spectra of polycrystalline *n*-hexadecanol and of lithium, sodium (type II and type III), potassium, rubidium, ammonium, and cesium palmityl sulfate in the 1000–1500 cm^{-1} region.

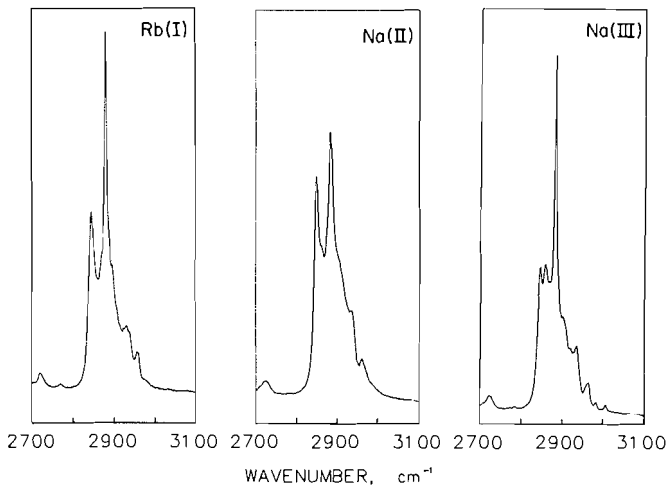

FIG. 4. Typical Raman spectra of type I, type II, and type III palmityl sulfates in the 2700–3100 cm^{-1} region.

palmityl sulfates, but as shown in the infrared spectra of 1,1-d_2-sodium palmityl sulfate in Fig. 2, this band disappears upon deuteration of the α-methylene group and is replaced by a new band at 1092 cm^{-1} which is also observed in the corresponding Raman spectra and can be assigned to the α-CD_2 scissoring vibration.

A detailed list of the infrared and Raman bands of all alkali palmityl sulfates, along with their assignment, is given in Table 1. The infrared frequencies of the CH_2 rocking modes are 721 cm^{-1} in type II and 716 cm^{-1} in type III samples. The values of the CH_2 scissoring and CH_2 rocking modes and the absence of any splitting, taken in conjunction with infrared spectra of *n*-alkanes and fatty acids of known crystal structure (15–18), strongly suggest a hexagonal packing for the acyl chains in type II and a triclinic packing in type III samples. Nevertheless, these conclusions eventually have to be confirmed by diffraction studies; therefore we prefer to use the nomenclature, type I, II, and III, instead of orthorhombic, hexagonal, and triclinic, respectively.

The assignments based on ir data are fully supported by the corresponding Raman data. As shown in Fig. 4, type II samples show the symmetric and antisymmetric CH_2 stretching modes with similar intensities (Fig. 4*B*), while type III samples possess two bands in the region of the symmetric CH_2 stretching mode (Fig. 4*C*, see also Table 1). These spectral features concur with those observed in the Raman spectra of crystalline hydrocarbons with hexagonal or triclinic packing, respectively (17). Furthermore, the 1420 cm^{-1} component of the CH_2 scissoring mode, characteristic of the orthorhombic subcell, is absent in both type II and type III spectra (Fig. 3).

Head group modes

Figures 1–3 show a number of strong infrared and Raman bands due to localized head group vibrations. It should be mentioned, however, that the concept of type I, type II, and type III packing applied to the acyl chain modes will not be applicable to the head groups modes. As has been shown by Sundell in the case of sodium dodecyl sulfate (20), the molecular arrangement in the system is too highly irregular to allow any formal subcell description for the whole molecule. The infrared and Raman spectra of the alkali hexadecyl sulfates reflect this aspect of the structure as shown by the complex splitting pattern observed for some of the head group bands.

The head group vibrations in these alkali palmityl sulfates involve four sulfur–oxygen stretching and five S—O angle bending modes of the SO_4 group; some of the vibrations could, in principle, be degenerate. The strongest bands in the infrared spectra of the alkali palmityl sulfates appear in the 1200–1300 cm^{-1} region and are due to the asymmetric SO_3 stretching modes (Figs. 1 and 2). These bands are absent or very weak in the corresponding Raman spectra (Fig. 3), where this region is dominated by an acyl chain mode, namely the strong CH_2 twisting band around 1300 cm^{-1}. The type II palmityl salts, as well as sodium dodecyl sulfate, show only two infrared bands around 1200 and 1270 cm^{-1}, while the type I and type III palmityl salts show at least three bands in the region of the asymmetric SO_3 stretching vibrations. In a planar arrangement, such as in a hexagonal subcell, all sulfate groups are equivalent and only two asymmetric SO_3 stretching modes are expected. This is indeed the case with type II salts. However, from the crystal structure of sodium dodecyl sulfate it is evident that the sulfate groups of adjacent molecules are alternately displaced by about 2 Å (20). The similarity of the infrared spectra of sodium dodecyl and sodium palmityl sulfate makes it not unrealistic to expect that this staggered structure also occurs in the palmityl sulfates; thus, different sulfate groups will have different environments, i.e. different sets of sites are occupied, producing an effect analogous to factor group splitting. In the more crystalline type I and type II palmityl salts, some of the sharp shoulder bands could also arise from the CH_2 wagging band progression (17). The spectra of the alkali palmityl salts in micellar solutions are identical with only two broad bands around 1210 and 1240 cm^{-1} (21).

Can. J. Chem. Downloaded from www.nrcresearchpress.com by 210.87.254.6 on 09/06/12
For personal use only.

TABLE 1. Infrared and Raman bands of alkali palmityl sulfates[a]

Lithium Type I		Ammonium Type I		Rubidium Type I		Potassium Type II		Sodium Type II		Sodium Type III		Cesium Type III		Tentative assignment
Infrared	Raman	Infrared	Raman	Infrared	Raman	Infrared	Raman	Infrared	Raman	Infrared	Raman	Infrared	Raman	
328 vw	328 m	331 w	330 m	330 vw	330 m	321 vw	331 m	332 vw	333 w	331 vw	330 m	336 vw	332 m	CCO bend
413 s	414 vw	412 w	411 w	412 vw	410 w	413 vw	414 vw	413 vw	415 vw	415 vw	411 w	415 vw	410 m	CCC bend
436 m	433 vw	431 w	427 m	430 w	426 m	431 w	429 m	431 w	425 m	436 w	435 vw	432 w	429 m	SO_3 o.o.p. rock
478 m	477 w	480 w	478 m	479 w	478 m	479 w	478 w	479 w	478 vw	481 w	479 w	488 w	487 m	SO_3 i.p. rock
517 m	520 sh	518 vw	520 vw	517 vw	517 vw	518 vw	515 w	517 vw	[b]	518 vw	[b]	525 w	521 w	SO_4 deformation
602 m	601 vw	585 s	587 s	583 s	586 s	583 s	583 m	594 s	593 m	594 s	593 m	585 s	584 m	SO_4 deformation
631 s	631 w	630 s	629 m	631 s	628 m	638 s	632 s	629 s	629 m	626 s	623 m	624 s	626 m	SO_4 deformation
720 m	—	720 m	—	720 m	—	720 m	—	721 m	—	716 m	—	716 m	—	$(CH_2)_n$ rock
730 m	—	730 m	—	730 m	—		—							
855 s	856 s	814 vs	814 vs	808 vs	810 s	808 s	810 m	834 m	838 m	827 vs	828 s	790 s	792 m	CO—S stretch
890 vw	890 m	887 vw	891 s	885 vw	891 m	889 w	889 m	897 w	893 m	888 w	892 m	885 m	884 m	CH_3 rock
945 sh	948 vw	948 sh	946 w	948 sh	947 vw	947 sh	949 vw	954 m	954 vw	945 m	947 vw	949 s	949 w	C—C stretch and C—O stretch
968 vs	969 vw	968 s	961 w	969 s	965 w	970 s	972 vw	970 s	969 vw	970 s	967 vw	973 m	972 w	
979 vs	981 vw	982 s	982 w	984 s	983 w	985 s	983 vw	983 s	982 vw	980 s	980 vw	979 s	978 w	
998 m	999 vw	997 s	997 vw	997 s	998 vw	999 s	998 vw	997 s	998 vw	1000 s	997 vw	993 m	994 w	
1009 m	1010 w	1011 m	1011 m	1011 m	1012 m	1013 s	1012 w	1011 m	1010 w	1013 s	1013 m	1009 s	1011 m	
1062 w	1062 vs	1062 s	1063 vs	1060 sh	1063 vs	1062 sh	1063 vs	1062 sh	1063 vs	1062 sh	1061 vs	1060 m	1061 vs	asym. C—C stretch
1096 vs	1095 vs	1062 s	1063 vs	1065 vs	1065 vs	1068 vs	1067 vs	1082 vs	1084 vs	1084 vs	1084 vs	1050 vs	1050 s	sym. SO_3 stretch
1112 vs	1111 vw	1106 m	1107 m	1106 w	1107 m	1107 m	1107 w	1107 m	1105 w	1108 m	1109 w	1108 vw	1106 w	C—C stretch
1131 w	1131 vs	1132 w	1131 vs	1130 vw	1130 vs	1130 vw	1130 vs	1130 vw	1130 vs	1130 vw	1131 vs	1131 vw	1133 vs	sym. C—C stretch
1202 vs	1196 w	1190 vs	1196 vw	1220 vs	1218 vw	1222 vs	1220 vw	1206 vs	1197 vw	1220 vs	1218 vw	1206 vs	1204 vw	asym. SO_3 stretch
1271 vs	1270 vw	1235 s	[b]	1244 s	1245 vw	1248 vs	1248 vw	1250 vs	1220 vw	1233 vs	1235 vw	1250 vs	1239 w	
1319 m	[b]	1273 s	1276 w	1276 s	1278 w	1273 s	1276 w	—	1261 vw	1256 vs	[b]	1263 vs	1254 vw	
—	—	—	—	—	—	—	—	—	—	1265 vs	1267 vw	1272 s	1276 vw	
1299 w	1296 vs	1298 sh	1295 vs	1295 sh	1295 vs	1296 sh	1295 vs	1297 sh	1296 vs	1298 sh	1296 vs	1295 sh	1297 vs	CH_2 twist
1380 w	1372 w	1380 sh	1370 m	1374 vw	1368 m	1379 w	1368 w	1379 w	1369 w	1379 w	1370 w	1378 w	1371 w	sym. CH_3 bend
1404 w	1406 w	1398 sh	1397 w	1396 w	1397 vw	1396 w	1397 vw	1397 w	1397 w	1402 w	1401 w	1390 sh	1386 sh	α-CH_2 wag
1463 m	1418 vs	1463 s	1420 vs	1463 s	1420 vs	1470 s	—	1468 vs	—	1472 vs	—	1473 vs	—	$(CH_2)_n$ scissoring
1473 m	1440 vs	1474 s	1442 vs	1474 s	1441 vs		1440 vs		1436 vs		1442 s		1444 vs	
—	1465 s	—	1465 s	—	1465 s	—	1463 vs	—	1461 sh	—	1466 vs	—	1468 vs	Fermi band
1479 m	1478 m	1478 sh	1479 m	1482 m	1478 m	1480 m	1478 sh	1478 m	1480 sh	1479 s	1480 s	[b]	[b]	α-CH_2 scissoring
2849 vs	2846 vs	2850 vs	2848 vs	2850 vs	2846 vs	2850 vs	2846 vs	2850 vs	2846 vs	2850 vs	2847 vs	2851 vs	2848 vs	sym. $(CH_2)_n$ stretch
2872 m	[b]	2870 m	[b]	2870 m	2870 sh	2872 m	[b]	2872 m	[b]	2868 m	[b]	2872 m	2871 m	sym. CH_3 stretch
2917 vs	2880 vs	2917 vs	2881 vs	2917 vs	2881 vs	2917 vs	2880 vs	2917 vs	2882 vs	2916 vs	2882 vs	2917 vs	2885 vs	asym. $(CH_2)_n$ stretch
2954 m	2959 w	2958 m	2959 m	2958 m	2957 w	2955 m	2955 w	2955 m	2959 w	2955 m	2861 m	2952 m	2952 w	asym. CH_3 stretch

[a]The frequencies (in cm^{-1}) are rounded off to the nearest integer.
[b]Too weak or masked by stronger bands.

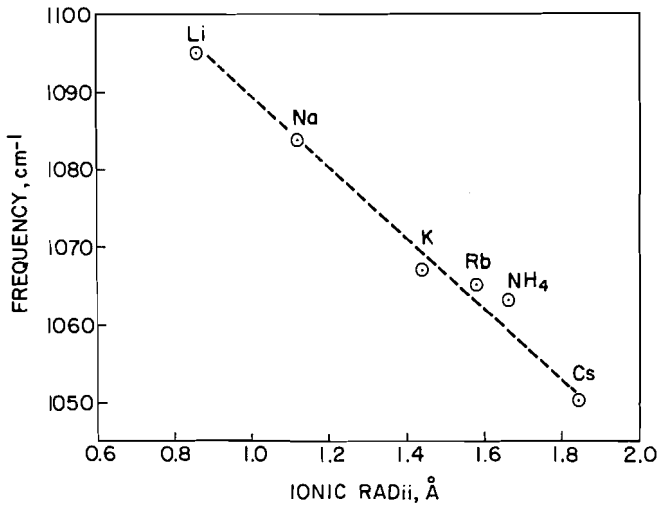

FIG. 5. Correlation between the position of the symmetric SO_3 stretching mode and the ionic radii of the alkali ions. The Ladd radii were used here (22), although the corresponding Pauling radii give a similar relationship with the same slope, but displaced by about 0.2 Å.

While we found no obvious correlation between the asymmetric SO_3 stretching bands and the nature of the alkali cations, the symmetric SO_3 stretching modes could be correlated with the ionic radius of the individual alkali cations. This umbrella-type vibration involves the concerted expansion and contraction of the three S—O bonds. The band is easily identified by its behavior on cation substitution, particularly in the Raman spectra. Figure 3 shows that the symmetric SO_3 stretching band occurs about midway between the two strong skeletal C—C bands at 1130 and 1062 cm^{-1} in the lithium salt, but with increasing cation size it moves towards the 1062 cm^{-1} band and even overtakes the latter in the cesium salt. As expected, the band is absent in the Raman spectrum of *n*-hexadecanol. Although the symmetric SO_3 stretching mode is quite strong in the infrared, it largely overlaps with the strong CCO stretching modes. The latter, however, show a considerable shift to lower frequencies upon deuteration of the α-methylene group, which allows a better assignment of the infrared modes in this region (Table 1).

As shown in Fig. 5 the frequency of the symmetric SO_3 stretching mode in the alkali palmityl sulfates decreases linearly with increasing ionic radius of the alkali ions (22). Furthermore, the symmetric S—O(C) stretching mode also shows a similar relationship between its frequency and the crystal radii of the alkali ions. This vibration yields a strong band at 855 cm^{-1} in the infrared and Raman spectra of the lithium salt which decreases also linearly with increasing cationic size; in the cesium salt this band was found at 796 cm^{-1} (Table 1).

The S—O angle bending modes of the SO_4 group can be identified in the 400–650 cm^{-1} region as a group of five medium strong bands around 430, 480, 520, 590, and 630 cm^{-1} (Table 1). Like in the case of the asymmetric SO_3 stretching mode no obvious correlation could be established between the frequency of these bands and the nature of the alkali cations.

In conclusion, the present study shows that while the vibrational modes of the palmityl moiety are invariant in the solid alkali palmityl sulfates, except for differences arising from packing of the methylene chains, some vibrational modes of the sulfate moiety show a linear relationship between their frequency and the crystal radii of the ions. The latter correlation becomes particularly important when studying the critical micellization temperature of these polycrystalline alkali palmityl sulfates (21).

Acknowledgements

We thank D. J. Moffatt for technical assistance and one of the reviewers for helpful comments.

1. B. LINDMAN and H. WENNERSTROM. Micelles. Amphiphilic aggregation in aqueous solution. Topics in current chemistry. Vol. 87. Springer-Verlag, Berlin. 1980. pp. 1–85.
2. E. J. STAPLES and G. J. T. TIDDY. J. Chem. Soc. Faraday Trans. I, **74**, 2530 (1978).
3. I. D. LEIGH, M. P. MCDONALD, R. M. WOOD, G. J. T. TIDDY, and M. A. TREVETHAN. J. Chem. Soc. Faraday Trans. 1, **77**, 2867 (1981).
4. J. UMEMURA, D. G. CAMERON, and H. H. MANTSCH. J. Phys. Chem. **84**, 2272 (1980).
5. J. UMEMURA, H. H. MANTSCH, and D. G. CAMERON. J. Colloid. Interface Sci. **83**, 558 (1981).
6. D. G. CAMERON, J. UMEMURA, P. T. WONG, and H. H. MANTSCH. Colloids Surfaces, **4**, 131 (1982).
7. H. H. MANTSCH, D. G. CAMERON, J. UMEMURA, and H. L. CASAL. J. Mol. Struct. **60**, 263 (1980).
8. D. G. CAMERON, H. L. CASAL, and H. H. MANTSCH. Biochemistry, **19**, 3665 (1980).
9. H. H. MANTSCH, A. MARTIN, and D. G. CAMERON. Biochemistry, **20**, 3138 (1981).
10. H. L. CASAL, D. G. CAMERON, H. C. JARRELL, I. C. P. SMITH, and H. H. MANTSCH. Chem. Phys. Lipids, **30**, 17 (1982).
11. G. L. MAYERS and T. HAINES. Biochemistry, **6**, 1665 (1967).
12. T. HAINES. Prog. Chem. Fats. Other Lipids, **11**, 297 (1971).
13. D. G. CAMERON, J. KAUPPINEN, D. J. MOFFATT, and H. H. MANTSCH. Appl. Spectrosc. **36**, 245 (1982).
14. J. K. KAUPPINEN, D. J. MOFFATT, H. H. MANTSCH, and D. G. CAMERON. Appl. Spectrosc. **35**, 271 (1981).
15. R. F. HOLLAND and J. R. NEILSEN. J. Mol. Spectrosc. **8**, 383 (1962); **9**, 436 (1962).
16. R. G. SNYDER. J. Chem. Phys. **71**, 4229 (1979).
17. R. G. SNYDER, S. L. HSU, and S. KRIMM. Spectrochim. Acta, **34A**, 395 (1978).
18. H. L. CASAL, H. H. MANTSCH, D. G. CAMERON, and R. G. SNYDER. J. Chem. Phys. **77**, 2825 (1982).
19. R. G. SNYDER. J. Mol. Spectrosc. **7**, 116 (1961).
20. S. SUNDELL. Acta Chem. Scand. A31, **10**, 799 (1977).
21. H. H. MANTSCH, V. B. KARTHA, and D. G. CAMERON. Proc. Symp. Surfactants in Solution. Vol. 1. *Edited by* K. I. Mittal. Plenum Pub. Corp., New York. 1984. pp. 673–690.
22. F. A. COTTON and G. WILKINSON. Adv. Inorg. Chem. 3rd ed. Interscience, New York. 1972. p. 198.

Can. J. Chem. Downloaded from www.nrcresearchpress.com by 210.87.254.6 on 09/06/12
For personal use only.

Résonance magnétique nucléaire ^{13}C des dérivés allyliques de la colonne IV-A,[1] de type $(C_6H_5)_3ECH_2CH{=}CH{-}CH_3$. Effets électroniques du substituant du noyau aromatique

E. MATARASSO-TCHIROUKHINE

Laboratoire de Recherches de Chimie Organique de l'E.N.S.C.P., 11, Rue Pierre et Marie Curie, 75231 Paris Cedex 05, France

Reçu le 24 janvier 1983[2]

E. MATARASSO-TCHIROUKHINE. Can. J. Chem. **62**, 133 (1984).

L'étude par rmn ^{13}C de la série $(C_6H_5)_3ECH_2CH{=}CH{-}CH_3$ **1***E* pour tous les éléments de la colonne IV-A a mis au jour les effets électroniques du substituant du noyau aromatique en fonction de l'élément E-IV-A; à savoir (a) un effet électro-accepteur par hyperconjugaison pour E = Si, Ge, Sn, (b) un effet inverse, électrodonneur par hyperconjugaison pour E = Pb, impliquant une électronégativité plus élevée pour cet élément et (c) un effet donneur par induction (I) pour E = C. L'énergie moyenne d'excitation de la molécule gouverne les déplacements chimiques des carbones *ipso* et *ortho*. Il semble qu'elle soit également déterminante quant au couplage $^1J(^{13}C{-}^{207}Pb)$.

E. MATARASSO-TCHIROUKHINE. Can. J. Chem. **62**, 133 (1984).

The ^{13}C nmr study of the series $(C_6H_5)_3ECH_2CH{=}CH{-}CH_3$ **1***E* shows, for the aromatic nucleus, a polarization consistent with a mesomeric electron withdrawing effect of the substituent in the case of E = Si, Ge, Sn; inversely, a mesomeric donating effect, in the case E = Pb, involving a higher electronegativity for Pb; and a donating π inductive effect, in the case E = C. The mean electronic excitation energy seems to dominate the chemical shifts of the aromatic carbons C_{ipso} and C_{ortho}, as well as the coupling $^1J(^{13}C{-}^{207}Pb)$.

Can. J. Chem. Downloaded from www.nrcresearchpress.com by 210.87.254.40 on 09/06/12
For personal use only.

L'étude comparative des déplacements chimiques et des couplages le long de la colonne IV-A pour une même série $R_3ECH_2CH{=}CH{-}CH_3$ **1***E*, *Z* ou $R_3ECH(CH_3)CH{=}CH_2$ **2** avait permis d'interpréter les résultats obtenus en termes d'hyperconjugaison $\sigma{-}\pi$ (1).

Dans le but d'apporter des renseignements quant aux comportement respectif des hétéroéléments Si, Ge, Sn et Pb vis à vis du noyau aromatique, il nous a paru souhaitable de compléter ces travaux par l'étude comparative du fragment aromatique de la série $(C_6H_5)_3ECH_2CH{=}CH{-}CH_3$, **1***E*.

En ce qui concerne *la partie expérimentale*, se rapporter à la *première partie* de ce travail (1).

Résultats et discussion

Paramètres $\delta^{13}C_{Ar}$

Les résultats numériques expérimentaux concernant les déplacements chimiques $\delta^{13}C_{Ar}$ se trouvent consignés dans le tableau 1.

Il convient de rappeler, d'une part, que l'introduction d'un substituant sur le noyau benzènique conduit à une polarisation des électrons π du noyau phényle. Cette polarisation est gouvernée à la fois par le facteur de polarité σ_I, et le facteur de résonance σ_R, du substituant; et, d'autre part, que (a) les déplacements chimiques $\delta^{13}C_p$ et $\delta^{13}C_m$ sont proportionnels à la charge totale, $q_t = q_\sigma + q_\pi$, portée respectivement par les carbones *para* et *meta*; ils sont liés aux paramètres d'induction σ_I et de résonance σ_R du substituant par une relation linéaire (2). Pour les carbones *ipso* C_i, et *ortho*, C_o, il faut ajouter l'effet stérique ainsi que toute contribution ayant pour origine l'effet d'anisotropie du substituant (3); et que (b) le paramètre $\Delta\delta^{13}C_p$ par rapport au benzène est fonction linéaire de $\Delta q_\pi{}^{C_p}$, lui-même proportionnel à $\Delta q_t{}^{C_p}$.

Il en résulte que le caractère donneur ou accepteur d'un substituant peut être déduit directement du déplacement chimique du carbone en *para*.

Il convient de distinguer $\Delta q_\pi{}^{C_p}$ et $\epsilon\Delta q_\pi$ (transfert de charge total) entre le substituant et le noyau aromatique, lequel dépend presque exclusivement de la constante σ_R, tandis que $\Delta q_\pi{}^{C_p}$ dépend de façon relativement importante de la polarité du substituant (2).

TABLEAU 1. Déplacements chimiques des carbones aromatiques, $\delta^{13}C_{Ar}$; composés **1***E*[a]

E	$\delta^{13}C_{Ar}$ ppm			
	C_i	C_o	C_m	C_p
Pb	151,19 [+22,69]	137,48 [+8,98]	129,16 [+0,66]	128,18 [−0,32]
Sn	138,64 [+10,14]	136,99 [+8,49]	128,37 [−0,13]	128,82 [+0,32]
Ge	136,66 [+8,16]	134,82 [+6,32]	127,88 [−0.62]	128,62 [+0,17]
Si	135,16 [+6,6]	135,92 [+7,42]	127,62 [−0,88]	129,26 [+0,76]
C	147,4 [+18,9]	129,42 [+0,92]	127,58 [−0,92]	125,79 [−2,71]

[a]Solutions saturées dans $CDCl_3$; référence interne TMS; précision: ±0,05 ppm. Entre parenthèses: déplacements chimiques rapportés au benzène, $\delta^{13}C_{C_6H_6}$ = 128,50 ppm. (12).

Effets électromères des substituants
—E(C₆C₅)₂(CH₂CH=CH—CH₃)

Les effets électromères observés sont faibles (Tableau 1).

(a) *E = C*

La polarisation du noyau benzènique ($\delta^{13}C_p < \delta^{13}C_m$) est congruente avec un *effet donneur pour le substituant*. Sur la base de résultats acquis antérieurement pour le méthylbenzène (4), admis pour le *tert*-butylbenzène (5) et sachant qu'une hyperconjugaison $\sigma{-}\pi$ nécessite des énergies comparables pour les orbitales σ et π, ce qui est réalisé dans le cas des composés organométalliques (6), tandis que dans le cas du composé **1***E* (E=C) cette hyperconjugaison se trouve très vraisemblablement minimisée du fait de la différence d'énergie entre les orbitales σ et π, nous concluons à une polarisation du noyau phényle par effets π inductifs du substituant.

[1]Voir réf. 1.

[2]Revision reçue le 20 juin 1983.

Can. J. Chem. Downloaded from www.nrcresearchpress.com by 210.87.254.40 on 09/06/12
For personal use only.

(b) *E = Si, Ge, Sn*

La polarisation du noyau benzènique ($\delta^{13}C_p > \delta^{13}C_m$) indique un effet *électroaccepteur pour le substituant*. Cet effet ne peut être attribué à des effets inductifs, car d'après l'échelle d'électronégativité établie pour les éléments E (1), un effet π inductif conduirait à un résultat inverse de celui observé. On peut conclure à un *effet électroaccepteur par résonance*.

(c) *E = Pb*

La polarisation du noyau phényle ($\delta^{13}C_p < \delta^{13}C_m$) est congruente avec un effet donneur pour le substituant. Pour des raisons exposées dans le cas précédent, on peut conclure à un *effet électrodonneur par résonance*. L'effet donneur par hyperconjugaison de la liaison C—E, favorisé par des énergies similaires pour les orbitales σ et π concernées, croît avec la densité électronique des orbitales *p* des atomes reliant les systèmes π et σ (6); il est favorisé par une électronégativité accrue de l'élément E (5). Le caractère électrodonneur par résonance distingue le dérivé du plomb des autres groupements $—E(C_6H_5)_2(CH_2CH{=}CH—CH_3)$ de la série E-IV-A; des résultats similaires ont été obtenus pour les groupements $E(C_6H_5)_3$ (E = Sn, Pb) (5, 10) rapprochant, de ce fait, les dérivés du plomb des dérivés arylmercuriques plûtot que des dérivés de l'étain (10).

La différence $\Delta = \delta^{13}C_p - \delta^{13}C_m$ est fonction linéaire du facteur de résonance σ_R^0 (9); les données de la littérature (9) ont été mises à profit pour déterminer des ordres de grandeur pour les effets de résonance σ_R^0 des substituants, étudiés en fonction de l'hétéroélément (Tableau 4).

La comparaison des paramètres $\delta^{13}C_{Ar}$ (Tableau 1) pour la série **1***E* avec les paramètres correspondants d'alkylbenzènes (7, 8) d'une part, et ceux des phényllithium et bromure de phénylmagnésium (11) de l'autre montre que: (a) le profil du spectre du dérivé ***1E*** du carbone (E = C) est similaire à ceux du toluène et du n-butylbenzène; (b) le profil des spectres des composés hétéroatomiques E = Si, Ge, Sn, Pb, présente une analogie (surtout marquée pour les dérivés du plomb) avec celui des spectres du phenyllithium et du bromure et de phenylmagnésium, à savoir, un déblindage des carbones *ipso* (C_i) (5−25 ppm/benzène) et *ortho* (C_o) (7 ppm/benzène).

Les déplacements chimiques paramagnétiques $\delta^{13}C_i$ et $\delta^{13}C_o$ pour le phényllithium et le bromure de phenylmagnesium avaient été interprétés (11) en suggérant que l'anisotropie de la liaison C_i—M était à l'origine des déplacements paramagnétiques $\delta^{13}C_i$ et $\delta^{13}C_o$ et que ceux-ci étaient gouvernés par l'énergie moyenne d'excitation de la molécule, ΔE ($\sigma_{C_i—M} \rightarrow \pi^*$); on sait que les déplacements chimiques du carbone sont essentiellement déterminés par le terme paramagnétique de la constante d'écran, δ_p^{AA}, qui peut être exprimé (2) en termes d'énergie moyenne d'excitation de la molécule, ΔE, à laquelle il est inversement proportionnel.

Pour les composés hétéroatomiques étudiés **1***E*, il paraît raisonnable d'interpréter les déplacements chimiques paramagnétiques des carbones C_i et C_o de la même manière; ΔE décroît de Si à Pb (6) ce qui est en accord avec le déplacement paramagnétique de C_i lorsque E varie de Si à Pb.

On remarque (Tableau 1) que pour le dérivé du silicium (à l'encontre des autres dérivés hétéroatomiques), le profil du spectre rmn ^{13}C correspond pour tous les carbones à une polarisation du noyau phényle induite par un substituant électroaccepteur. $\delta^{13}C_p > \delta^{13}C_m$ et $\delta^{13}C_{ortho} > \delta^{13}C_{ipso}$; le résultat s'accorde avec un effet électroaccepteur par résonance du groupement $(C_6H_5)_2(CH_3CH{=}CH—CH_2)E—$ qui serait relativement plus important pour le dérivé du silicium par rapport aux dérivés du germanium et de l'étain et qui serait déterminant; quant aux positions relatives des déplacements chimiques des carbones aromatiques. Ce résultat est en accord avec les travaux théoriques antérieurs (6).

TABLEAU 2. Couplages $^1J(^{13}C_{Ar}—E)$; composés **1***E*, *Z*; **2**

E		$J(^{13}C_{Ar}—E)$ (Hz) C_i	C_o	C_m	C_p
Sn	**1***E*	495,2; 472,8	34,8	48,3	11,1
	1*Z*		35,2	48,5	11,2
Pb	**1***E*	325,2	61,5	69,3	18,6
	1*Z*		62,7		
	2	277,6	58,7		

TABLEAU 3. Couplages $^1J(^{13}C_{Ar}—H)$; composé **1***E*

E	$^1J(^{13}C_{Ar}—H)$ (Hz) C_o	C_m	C_p
Si	166	157	162,3
Sn	159	156,7	159,6
Pb	161,2	159,7	159,2

TABLEAU 4. Paramètre de résonance, σ_R^0, pour le substituant, $—E(C_6H_5)(C_6H_5)(CH_2CH{=}CH—CH_3)$, au noyau aromatique; composé **1***E*

Paramètres	E Si	Ge	Sn	Pb
$\Delta = \delta C_p - \delta C_m$	+1,64	+0,79	+0,45	−0,98
σ_R^0	+0,085	+0,05	+0,035	−0,03

Couplages

Les résultats expérimentaux sont rassemblés dans les tableaux 2 et 3.

(a) *Couplage hétéroélément−carbone* $^1J(^{13}C—E)$

On remarque (Tableau 2), pour le dérivé de l'étain (E = Sn), un couplage $^1J(^{13}C—^{119,117}Sn)$ = 495,2; 472,8 Hz, donc très voisin d'un couplage "typique" d'une liaison étain tétrahédrique sp^3 − carbone sp^2 (13); en revanche pour le dérivé du plomb, E = Pb, on observe un couplage bien inférieur aux valeurs admises comme valeurs caractéristiques de la liaison plomb tetrahedrique sp^3 − carbone sp^2 (14), à savoir, pour $(C_6H_5)_4Pb$, $^1J(^{13}C—^{207}Pb)$ = 480,9 Hz et pour $(CH_2{=}CH)_4Pb$, $^1J(^{13}C—^{207}Pb)$ = 454,1 Hz. Il convient également de noter que pour $(C_6H_5)_3PbCH_3$, $^1J(^{13}C—^{207}Pb)$ = 439 Hz (15); comme il a été montré par de Vos, ^1J est fonction du nombre de phényles liés au plomb et décroît à 348 Hz, pour $(C_6H_5)Pb(CH_3)_3$; l'auteur interpréte ce phénomène en termes de charge effective portée par le plomb et du caractère *s* de la liaison C—Pb.

Rappelons que le terme de contact de Fermi gouverne le couplage $^1J(E—X)$ qui est (a) inversement proportionnel à l'énergie moyenne d'excitation de la molécule, ΔE, et (b) proportionnel à la charge effective du noyau et au caractère *s* de l'orbital hybride formant la liaison E—X.

Dans le cas du composé **1***E* (E = Pb) la faible valeur du couplage ^1J observée peut être rationalisée en termes

d'hyperconjugaison $\sigma-\pi$ de la liaison C—E et de la double liaison allylique; en effet, l'existence d'une hyperconjugaison conduit à un accroissement de la charge positive sur le plomb, ayant pour conséquence, un accroissement de ΔE, ce qui est congruent avec une diminution de $J(^{13}C—^{207}Pb)$.

(b) *Couplage carbone–proton* $J(^{13}C—H)$

Le tableau 3 montre pour les couplages $J(^{13}C—H)$ les résultats suivants: $^1J(^{13}C_m—H) < {}^1J(^{13}C_p—H)$ pour E = Si, Sn et $^1J(^{13}C_p—H) > {}^1J(^{13}C_m—H)$ pour E = Pb.

Ces résultats laissent entendre que ces couplages sont gouvernés par la charge effective des carbones C_m et C_p. Dans ce cas les inégalités observées correspondraient à une polarisation du noyau phényle induite par un substituant électro-accepteur, pour E = Si, Sn et par un substituant électrodonneur pour E = Pb; ce qui confirme les résultats déduits de l'étude des paramètres $\delta^{13}C_{Ar}$.

1. E. MATARASSO-TCHIROUKHINE et P. CADIOT. **61**, 2476 (1983).
2. W. J. HEHRE, R. W. TAFT, et R. D. TOPSOM. Prog. Phys. Org. Chem. **12**, 173 (1976), et références citées.
3. H. S. GUTOWSKY, D. W. MCCALL, B. R. MCGARVEY, et L. H. MEYER. J. Am. Chem. Soc. **74**, 4809 (1952).
4. L. LIBIT et R. HOFFMANN. J. Am. Chem. Soc. **96**, 1370 (1974).
5. M. L. BULLPITT, W. KITCHING, W. ADCOCK, et D. DODRELL. J. Organomet. Chem. **116**, 161 (1976).
6. C. G. PITT. J. Organomet Chem. **61**, 49 (1973).
7. W. R. WOOLFENDEN. Ph.D. Thesis, University of Utah, 1965.
8. J. B. STOTHERS. *Dans* Carbon-13 NMR spectroscopy. Academic Press, New York 1972. p. 97.
9. G. E. MACIEL et J. J. NATTERSTADT. J. Chem. Phys. **42**, 2427 (1965).
10. A. N. NESMEYANOV, D. N. KRAVTSOV, B. A. KVACOV, E. N. FEDIN et T. S. KHAZANOVA. Dokl. Akad. Nauk SSSR, **199**, 1078 (1971).
11. A. J. JONES, D. M. GRANT, J. G. RUSSEL et G. FRAENKEL. J. Phys. Chem. **73**, 1624 (1969).
12. G. L. NELSON, G. C. LEVY et J. D. CARGIOLI. J. Am. Chem. Soc. **94**, 3089 (1972).
13. H. G. KUIVILA, J. L. CONSIDINE, R. J. MYNOTT et R. H. SARMA. J. Organomet. Chem. **55**, C 11 (1973).
14. R. H. COX. J. Magn. Reson. **33**, 61 (1979).
15. D. DE VOS. J. Organomet. Chem. **104**, 193 (1976).

Can. J. Chem. Downloaded from www.nrcresearchpress.com by 210.87.254.40 on 09/06/12
For personal use only.

A kinetic study of the influence of alcohols on the nitrosation of morpholine in acid media. Equilibrium constants for the formation of alkyl nitrites

JULIO CASADO, FRANCISCO MANUEL LORENZO, MANUEL MOSQUERA, AND MARÍA FLOR RODRÍGUEZ PRIETO

Departamento de Química Física, Instituto de Investigaciones Químicas, C.S.I.C., Universidad de Santiago, E-Santiago de Compostela, Spain

Received April 20, 1983

JULIO CASADO, FRANCISCO MANUEL LORENZO, MANUEL MOSQUERA, and MARÍA FLOR RODRÍGUEZ PRIETO. Can. J. Chem. **62**, 136 (1984).

The effect of the aliphatic alcohols methanol, ethanol, propanol, isopropanol, 2-butanol, isobutanol, and *tert*-butanol on the rate of nitrosation of morpholine at pH 3 and 25°C has been studied. The inhibition observed is attributed to the formation of alkyl nitrites, which are poor nitrosating agents in acid media. The equilibrium constants for the formation of alkyl nitrites from nitrous acid and alcohols have been calculated both spectrophotometrically and from kinetic data for the inhibitory effect, and there is agreement between the two sets of results. The molar absorptivities at 265 nm of the alkyl nitrites have also been determined. When the concentration of alkyl nitrite is very low, a slight catalytic effect considered to be an effect of the medium has been observed.

JULIO CASADO, FRANCISCO MANUEL LORENZO, MANUEL MOSQUERA et MARÍA FLOR RODRÍGUEZ PRIETO. Can. J. Chem. **62**, 136 (1984).

Nous avons étudié l'effet des alcools aliphatiques: méthanol, éthanol, propanol, isopropanol, 2-butanol, isobutanol et *tert*-butanol sur la vitesse de nitrosation de la morpholine. On y trouve une inhibition attachée à la formation de nitrites d'alkyle qui sont faibles agents nitrosants dans milieu acide. On a utilisé l'étude cinétique de cet effet inhibiteur pour calculer les constants de formation des nitrites d'alkyle, dont les valeurs ont été aussi calculées par une méthode spectrophotométrique en obtenant par les deux voies résultats équivalents. On a mesuré aussi les absorptivités molaires des nitrites d'alkyle à 265 nm. Le faible effet catalytique observé a été interpreté comme un effet du milieu.

Can. J. Chem. Downloaded from www.nrcresearchpress.com by 210.87.254.105 on 09/06/12
For personal use only.

Introduction

Nitrosamines, which in weakly acid conditions are formed from nitrites and secondary or tertiary amines, constitute a risk to human health as carcinogenic substances present in the environment (1, 2). Their formation is affected by a number of chemical factors present in a normal everyday diet. The ions Cl^-, Br^-, I^-, and SCN^- all promote the formation of nitrosamines, whereas it is inhibited by ascorbic acid, hydroxylamine, sodium azide, and, under certain conditions, phenols.

In recent years a number of articles have been published reporting studies of the effect of alcohols on nitrosation reactions. Williams and Aldred (3) found the nitrosation of amines to be inhibited by alcohols, thiols, and carbohydrates in the presence of 0.08 *M* sulphuric acid or 0.04 *M* perchloric acid. However, Kurechi *et al.* (4) found inhibition at pH 3 but catalysis at pH 5. The present article reports a kinetic study which, given the importance of alcohols and other hydroxylated compounds such as carbohydrates and alkanolamines, has been undertaken with the intention of clarifying these findings. The effects of seven aliphatic alcohols upon the formation of *N*-nitrosomorpholine in acid media were studied.

Experimental

All reagents used were Merck p.a. except the Merck p.s. morpholine, whose perchlorate was used after recrystallization in ethanol.

For the measurements of reaction rate, a spectrophotometric technique has been used (5). The absorbance of *N*-nitrosomorpholine was determined at 265 nm, an isosbestic point for nitrite at which its molar absorptivity ($7.41 \pm 0.04\ M^{-1}\ cm^{-1}$) is much smaller than that of the nitrosamine ($1870 \pm 4\ M^{-1}\ cm^{-1}$). In the kinetic study, the initial rate method was used in view of the slowness of the reaction being studied and to avoid competition from the decomposition of nitrous acid. The percentage reaction followed never exceeded 2%. The initial reaction rates are given by the slope of the absorbance–time curves, which were all perfectly linear. All kinetic measurements were carried out at 25°C, pH 3, and an ionic strength of 0.5 *M* controlled using $NaClO_4$. No buffer was added to the medium because, for the short period of the reaction followed, the nitrite – nitrous acid system present sufficed for maintaining constant acidity.

The equilibrium constants of the reactions of formation of the alkyl nitrites were studied spectrophotometrically by measuring the absorbance of the reaction mixture at 265 nm. Equilibrium is rapidly established, and at 265 nm the difference between absorption by alkyl nitrites and nitrous acid is much greater than at longer wavelengths (6). These experiments were carried out at 25°C, an ionic strength of 0.5 *M*, and a concentration of perchloric acid of 0.1 *M*.

To measure absorbances a Perkin–Elmer–Coleman 55 spectrophotometer was used. Acidity was measured with a Radiometer PHM 82 pH-meter. The data were processed on a TI 59 programmable calculator.

Results and discussion

Mechanism and rate equation

Working conditions were chosen in which the only effective nitrosating agent in the absence of alcohol is N_2O_3. The mechanism in these conditions is (7):

1. $2HNO_2 \rightleftharpoons N_2O_3$ fast

2. $N_2O_3 + \text{O(CH}_2\text{)}_4\text{NH} \longrightarrow \text{O(CH}_2\text{)}_4\text{NNO} + HNO_2$ slow

so that the rate equation is:

$$[1] \quad v_0 = \frac{\alpha[\text{nit}]_0^2[\text{MOR}]_0}{[H^+](1 + K_a/[H^+])^2}$$

where $[\text{nit}]_0$ and $[\text{MOR}]_0$ are the initial stoichiometric concentrations of nitrite and morpholine, K_a is the acidity constant of the nitrous acid, and α the product of the equilibrium and rate constants. The order of the reaction with respect to nitrite and morpholine was found to remain unchanged when an alcohol (EtOH) was added to the medium.

The fact that no first order term in nitrite was observed shows that the alkyl nitrites, or more probably their protonated forms, are weak nitrosating agents, and agrees with the results ob-

Can. J. Chem. Downloaded from www.nrcresearchpress.com by 210.87.254.105 on 09/06/12
For personal use only.

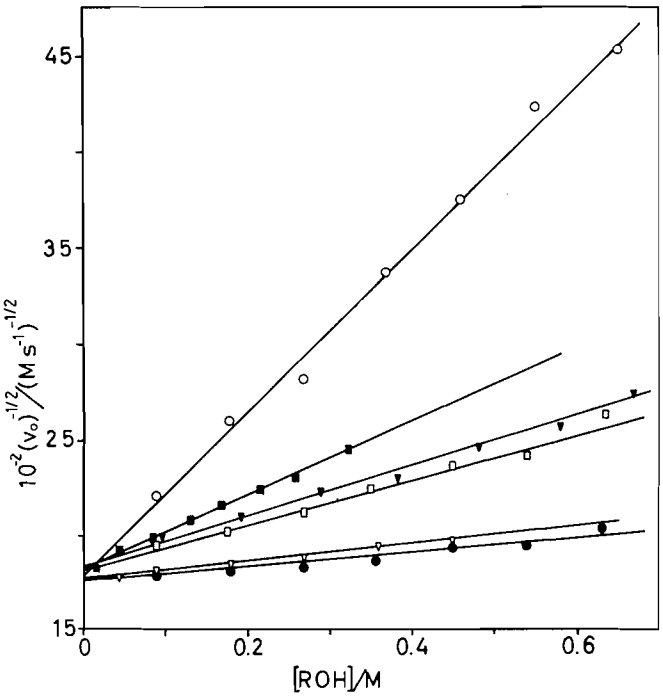

FIG. 1. Dependence of the initial rate of nitrosation of morpholine on the concentration of alcohol at 25°C, ionic strength 0.5 *M*, pH 3, $[nit]_0 = 1.09 \times 10^{-2}$ *M* and $[MOR]_0 = 7.2 \times 10^{-3}$ *M*. MeOH (○), isoBuOH (■), EtOH (▼), PrOH (□), 2-BuOH (▽), and isoPrOH (●).

tained by Aldred and Williams (8) in a kinetic study of nitrosation by propyl nitrite in 1-propanol.

The influence of the concentration of each alcohol on the reaction rate was determined in a series of experiments in which its concentration was varied. The reaction rate was in all cases found to decrease as the concentration of alcohol increased, in accordance with an equation of the form (Fig. 1):

$$[2] \quad (v_0)^{-1/2} = a + b[ROH]$$

The alcohols' inhibition of the formation of *N*-nitrosomorpholine may be explained (ref. 3) by supposing them to remove nitrous acid from the reaction medium to form alkyl nitrites, as a result of which the concentration of N_2O_3 falls. In the presence of alcohols, the mechanism for the nitrosation of morpholine shown above must therefore be supplemented by a third step, the fast equilibrium for the formation of alkyl nitrites:

$$3. \quad HNO_2 + ROH \overset{K}{\rightleftarrows} RONO + H_2O$$

If the concentration of alcohol is assumed to greatly exceed that of nitrite, the rate equation now becomes:

$$[3] \quad v_0 = \frac{\alpha[nit]_0^2[MOR]_0}{[H^+](1 + K_a/[H^+] + K[ROH])^2}$$

which in the working conditions of the present study may be expressed as:

$$[4] \quad (v_0)^{-1/2} = \frac{1 + K_a/[H^+]}{\beta} + \frac{K}{\beta}[ROH]$$

where β is a constant.

Equation [4] is of the same form as the experimental equation [2]. *K* may be calculated by simply dividing the slope of the experimental curves by the ordinate at the origin and multiplying by $(1 + K_a/[H^+])$. The value of pK_a used was 2.945, as found by Lumme and Tummavuori at 25°C and an ionic strength of 0.5 *M* (9). The resulting values of *K* are shown in Table 1, together with values obtained, likewise by kinetic methods, by Schmid and Riedl in a study of the influence of alcohols on the nitrosation of phenol (10) and by Aldred and Williams when studying the kinetics of the formation of alkyl nitrites from nitrous acid and alcohols (11).

The spectrophotometric determination of K

No direct spectrophotometric determination of *K* has so far been reported, and its purpose in the present study is not only to permit comparison of the results with the indirectly obtained values shown in Table 1, but also to confirm the proposed reaction mechanism. Since the measurements were carried out at constant ionic strength, an equilibrium constant for the formation of alkyl nitrites may be defined by:

$$[5] \quad K = \frac{[RONO]}{[HNO_2][ROH]}$$

In the conditions of acidity at which the experiments were carried out:

$$[6] \quad [nit] = [HNO_2] + [RONO]$$

so that:

$$[7] \quad A(1 + K[ROH]) = \epsilon_{HNO_2}[nit] + \epsilon_{RONO}[nit]K[ROH]$$

where *A* is the absorbance at 265 nm and ϵ_{HNO_2} and ϵ_{RONO} are the molar absorptivities of the nitrite and the alkyl nitrites at this wavelength.

To see whether the experimental results fit eq. [7], the parameter *K* was optimized using the unidimensional algorithm of Davies, Swann, and Campey implemented on a Texas TI 59 programmable calculator (12, 13). As can be seen in Fig. 2, there is a good fit between eq. [7] and the absorbance – concentration of alcohols curves, and the values of *K* and molar absorptivities of the alkyl nitrites calculated accordingly are shown in Table 1 beside the values of *K* obtained indirectly, which are in good agreement with the direct values.

The influence of the medium

Since Dix and Williams (14) found alcohols to cause an effect of the medium on their own nitrosation, we sought for a similar effect on the nitrosation of morpholine. Experiments were carried out under constant working conditions in tetrahydrofuran (THF), a solvent that does not react with nitrous acid. A catalysis of less than 30% was observed in 1 *M* THF, a higher concentration than that used in our kinetic experiments with alcohols. The same effect of the medium has been observed in the presence of acetic acid and other solvents such as DMSO and dioxane (15), and is comparable to that found by Schelly (16) in the diazotization of aniline in methanol–CCl_4 mixtures by NOCl which, like N_2O_3, is a neutral nitrosating agent. Schelly found that the reaction rate fell as the polarity of the medium increased. In the present case, since the effect of the medium is catalytic rather than inhibitory, it supports the assumption that the inhibition caused by alcohols at pH 3 is not due to such an effect.

When working with *tert*-butanol we have observed it to cause a slight catalytic effect. This we attribute to the effect of the medium in this case outweighing the inhibitory effect due to the reduction of the concentration of N_2O_3. In these conditions it has therefore been impossible to calculate *K*, though its value must clearly be small. That calculated by Schmid may perhaps have been influenced by an effect of the medium,

TABLE 1. Equilibrium constants of the formation of alkyl nitrites, and their molar absorptivities, $T = 25°C$

R	$K(M^{-1})$ This paper[a]	This paper[b]	Schmid[c]	Williams[d]	$\epsilon_{265}(M^{-1}\ cm^{-1})$[e]
Me	5.1±0.2	3.5±0.1	3.92	2.5	220±10
Et	1.39±0.04	1.20±0.06	1.81	0.88	315±20
Pr	1.42±0.04	1.3±0.1	1.61	0.66	380±30
isoPr	0.56±0.03	0.52±0.05	0.56	0.25	380±40
2-But	0.39±0.02	0.46±0.03	0.67	—	560±40
isoBut	1.90±0.02	1.53±0.05	1.88	—	425±20
tert-But	—	—	0.033	<0.05	—

[a]Kinetic results.
[b]Spectroscopic results.
[c]Cf. ref. 10.
[d]0°C, cf. ref. 11.
[e]This paper.

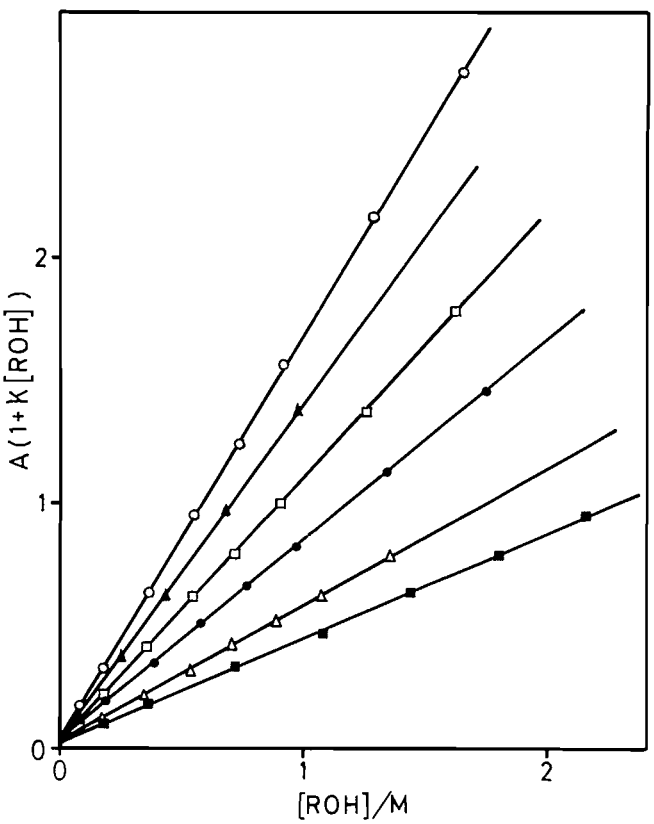

FIG. 2. Determination of the formation constants of the alkyl nitrites and their molar absorptivities. Verification of eq. [7] at 25°C, ionic strength 0.5 M, $[HClO_4] = 0.1\ M$ and $[nit] = 2.17 \times 10^{-3}\ M$. MeOH (○), isoBuOH (▲), PrOH (□), EtOH (●), 2-BuOH (△), and isoPrOH (■).

which is apparently inhibitory when, as in the nitrosation of phenols, the nitrosating agent is NO^+ (15, 17).

The effect of the medium may also explain the catalysis observed by Kurechi *et al.* (cf. ref. 4) in the nitrosation of dimethylamine and diethylamine at pH 5. At this pH the quantity of alkyl nitrites formed is very small and, since the concentrations of alcohol used were quite high (up to 42% by volume of ethanol), the effect of the medium may be expected to have prevailed over the inhibition caused by the formation of inefficient alkyl nitrites.

Acknowledgements

One of the authors (J.C.) wishes to thank the Spanish Comisión Asesora de Investigación Científica y Técnica for subsidizing the research reported in this article as part of an investigation into the mechanism of formation of carcinogenic nitroso compounds. F.M.L. likewise wishes to thank the Spanish Ministry of Education and Science for the grant (Formación de Personal Investigador) allowing him to take part in this research.

1. J. A. WOLF and A. E. WASSERMAN. Science, **177**, 15 (1972).
2. H. DRUCKREY, R. PREUSSMAN, S. IVAŃKOVIC, and D. SCHMAL. Z. Krebsforsch. **69**, 103 (1967).
3. D. L. H. WILLIAMS and S. E. ALDRED. Food Cosmet. Toxicol. **20**, 79 (1982).
4. T. KURECHI, K. KIKUGAWA, and T. KATO. Food Cosmet. Toxicol. **18**, 591 (1980).
5. J. M. CACHAZA, J. CASADO, A. CASTRO, and M. A. LÓPEZ QUINTELA. Z. Krebsforsch. **91**, 279 (1978).
6. R. N. HASZELDINE and B. J. H. MATTISON. J. Chem. Soc. 4172 (1955).
7. J. CASADO, A. CASTRO, M. A. LÓPEZ QUINTELA, M. MOSQUERA, and M. F. RODRÍGUEZ PRIETO. Monatsh. Chem. **114**, 647 (1983).
8. S. E. ALDRED and D. L. H. WILLIAMS. J. Chem. Soc. Perkin Trans. 2, 1021 (1981).
9. P. LUMME and J. TUMMAVUORI. Acta Chem. Scand. **19**, 617 (1965).
10. H. SCHMID and P. RIEDL. Monatsh. Chem. **98**, 1783 (1967).
11. S. E. ALDRED and D. L. H. WILLIAMS. J. Chem. Soc. Perkin Trans. 2, 777 (1982).
12. P. R. ADBY and M. A. H. DEMPSTER. Introduction to optimization methods. Chapman and Hall, London. 1974.
13. J. CASADO, M. MOSQUERA, A. RIVAS, M. F. RODRÍGUEZ PRIETO, and J. A. SANTABALLA. Comput. Chem. In press.
14. L. R. DIX and D. L. H. WILLIAMS. J. Chem. Res. (S), 190 (1982).
15. J. CASADO, J. R. LEIS, M. MOSQUERA, L. C. PAZ, and E. PEÑA. Monatsh. Chem. In press.
16. Z. A. SCHELLY. J. Phys. Chem. **74**, 4062 (1970).
17. H. SCHMID, G. MUHR, and P. RIEDL. Monatsh. Chem. **97**, 781 (1966).

Can. J. Chem. Downloaded from www.nrcresearchpress.com by 210.87.254.105 on 09/06/12
For personal use only.

Temperature dependence of the NH–proton hyperfine splitting in Bu^{t}NHO·[1]

ROBERTO HENRIQUEZ AND M. JOHN PERKINS[2]
Department of Chemistry, Chelsea College, Manresa Road, London, SW3 6LX England
AND
DAVID GRILLER
Division of Chemistry, National Research Council of Canada, Ottawa, Ont., Canada K1A 0R6

Received December 21, 1982[3]

ROBERTO HENRIQUEZ, M. JOHN PERKINS, and DAVID GRILLER. Can. J. Chem. **62**, 139 (1984).

Hyperfine splitting by the NH proton in Bu^{t}NHO· decreases markedly with increasing temperature, whilst the nitrogen hyperfine interaction shows a small increase. These observations are consistent with an increase in the out-of-plane bending as the temperature is raised.

ROBERTO HENRIQUEZ, M. JOHN PERKINS et DAVID GRILLER. Can. J. Chem. **62**, 139 (1984).

Le découplage hyperfin du proton du NH dans le Bu^{t}NHO· diminue fortement lorsque la température augmente tandis que l'interaction hyperfine de l'azote augmente légèrement. Ces observations sont en accord avec une augmentation de la déformation hors du plan lorsque la température augmente.

[Traduit par le journal]

Can. J. Chem. Downloaded from www.nrcresearchpress.com by 210.87.254.5 on 09/06/12
For personal use only.

The geometry of the nitroxide group has for years been a somewhat controversial subject (1). Molecular orbital calculations of varying degrees of sophistication have failed to agree in predicting whether the minimum energy geometry is planar (**1**) or pyramidal (**2**), although the majority favour a pyramidal structure in which the barrier for inversion is tiny (2). Indeed, for H_2NO·, all calculations agree in concluding that there is little energy difference between the planar structure and one pyramidalized as far as "sp^3" geometry. It seems reasonable, therefore, to expect an out-of-plane bending vibration, in unconjugated nitroxides, which has a large amplitude and low force constant, but no experimental probe has yet yielded unambigous evidence for this.

Recent infrared and Raman studies on bistrifluoromethyl nitroxide (3) led to the conclusion that this molecule probably has a planar energy minimum with a "soft" out-of-plane bending vibration,[4] and that simple dialkyl nitroxides would be expected to be more rigidly planar. Nevertheless, crystallographic studies have identified both bent (e.g. **3**), and planar (e.g. **4**) types among relatively strain-free di-*tert*-alkyl nitroxides (1), so that conformational and/or lattice forces are more than sufficient to overcome any inherent preference for a particular geometry at the nitrogen centre. The implied lack of well-defined intrinsic geometry for the nitroxide function has, in fact, been recognised for many years (1, 2*c*), but the obvious application of electron spin resonance to investigate changing vibration amplitude with variation in temperature has been relatively unproductive. For example, the tiny temperature dependence in a^N described recently for di-*tert*-butyl nitroxide (5) is within the range which might be expected solely on the basis of a *volume* change (6). In view of this, any attempt to interpret the observed reduction in $d(a^N)/dT$ as T increases in terms of an incipient turning point in the curve, as was suggested by Bullock and Howard (5), must remain open to question until the curvature has been established in a solvent which is not approaching its boiling point at the onset of curvature.

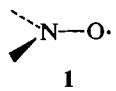

1

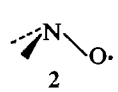

2

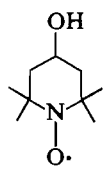

3

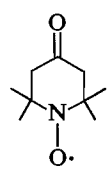

4

For simple dialkyl nitroxides, the insensitivity of a^N to out-of-plane vibrational amplitude may possibly be attributed to compensation of two effects. These are (*i*) the change in hybridization at nitrogen which causes a^N to increase as the molecule is bent, and (*ii*) change in spin distribution between oxygen and nitrogen which does the reverse (cf. ref. 2*c*). The two nitroxides **3** and **4**, which are respectively pyramidal and planar at nitrogen in the crystal, actually have almost identical isotropic a^N-values in solution (7).

Whilst the most sophisticated calculations of a^N for H_2NO· do suggest a change in value as the molecule is bent, the absolute values are markedly dependent on the level of refinement, and geometry optimization has not always been complete for bent structures. It is apparent, however, from published calculations, that *a larger dependence* of a^H upon nitroxide geometry might be expected (2*a*). We were unaware of any experimental test of this result, and have therefore examined the temperature dependence of a^H(NH) in the relatively accessible *tert*-butyl nitroxide, Bu^{t}NHO·.

Electron spin resonance spectra of Bu^{t}NHO· have been recorded on many occasions (7), but we found it difficult to adapt existing procedures in such a way as to obtain satisfactory spectra over a wide temperature range. However, we have observed that intense spectra of Bu^{t}NHO· may be obtained from solutions of *tert*-butylhydroxylamine and piperidine in toluene which have been shaken with PbO_2, filtered, and degassed. With these solutions, measurements were possible over the range −60° to +100°C. A regular dependence of a^H equal to ca. 8.4×10^{-3} gauss/degree (Fig. 1) was found over this range. The change in a^N, $d(a^N)/dT$, was much smaller (ca. 2.3

[1]Issued as NRCC No. 22646.
[2]Author to whom correspondence should be addressed.
[3]Revision received August 3, 1983.
[4]The uncertainty in this area is illustrated by an earlier assertion from the same laboratory (4) that "there can be no doubt that $(CF_3)_2NO$· is non-planar"!

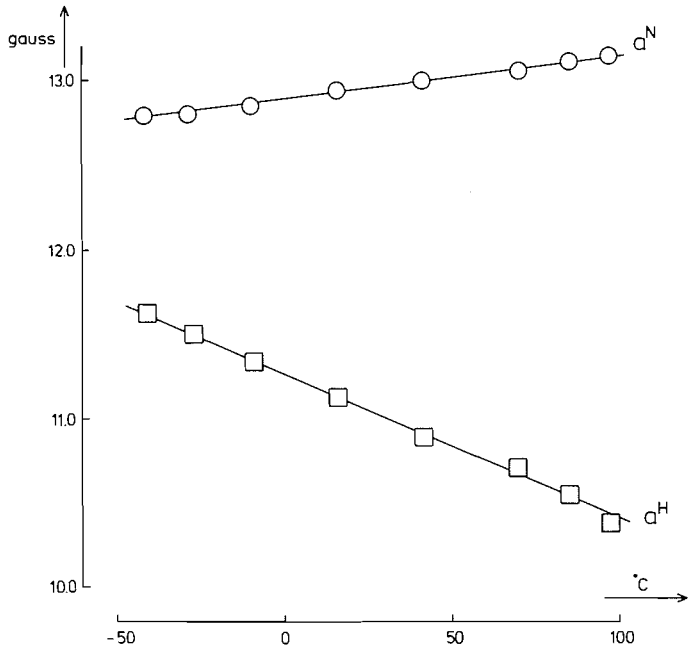

FIG. 1. Variation of a^N and a^H (NH) with temperature for Bu'NHO·.

$\times 10^{-3}$ gauss/degree), but, in contrast to the results with di-*tert*-butyl nitroxide (5, 6), was positive.

To eliminate the possibility that the piperidine exerted a significant solvent effect by complexing with the nitroxide, we repeated the experiments using ca. 0.01 *M* *tert*-butylhydroxylamine in toluene alone as solvent. Although the signals obtained were much weaker, the temperature dependencies of the hyperfine splittings were found to be the same, within experimental error. In addition, it should be noted that values of the hyperfine splittings measured in polar solvents (8) are substantially different to those reported herein which are typical of those measured in non-polar environments (8).

Salotto and Burnelle (2*a*) calculated splitting constants for planar and "best" bent structures of H_2NO·; the figures were 7.67 and 11.19 respectively for a^N, and −16.27 and −8.77 respectively for a^H (the out-of-plane angle for the bent structure being 26°). Clearly, the variations of a^N and a^H and their relative magnitudes now reported for Bu'NHO· are consistent with an interpretation in terms of increasing amplitude of the out-of-plane bending as the temperature is raised, although any attempt to give a quantitative analysis of the results in terms of an energy profile would be premature.

Experimental

Solutions of *tert*-butylhydroxylamine (10 mg) in a 1:1 mixture of toluene and piperidine (0.3 mL) were shaken with lead dioxide for 2 min, filtered, and thoroughly deoxygenated by passing purified nitrogen gas for a few minutes. Initial electron spin resonance spectra were recorded on a Varian E4 spectrometer, but measurements were made using a Varian E109 instrument equipped with field-frequency lock.

Acknowledgements

We thank the Ministry of Agriculture Fisheries and Food for a grant, and Professor A. G. Davies and Dr. B. P. Roberts, University College, London, for making available their E109 spectrometer.

1. J. LAJZEROWICZ-BONNETEAU. *In* Spin labelling. *Edited by* L. J. Berliner. Academic Press, New York. 1976. p. 239.
2. (*a*) A. W. SALOTTO and L. BURNELLE. J. Chem. Phys. **53**, 333 (1970); (*b*) L. EFSKIND. Acta Chem. Scand. **27**, 71, (1973); (*c*) Y. ELLINGER, R. SUBRA, A. RASSAT, J. DONADY, and G. BERTHIER. J. Am. Chem. Soc. **97**, 476 (1975); (*d*) T. D. DAVIS, R. E. CHRISTOFFERSEN, and G. M. MAGGIORA. J. Am. Chem. Soc. **97**, 1347 (1975).
3. D. A. C. COMPTON, C. CHATGILIALOGLU, H. H. MANTSCH, and K. U. INGOLD. J. Phys. Chem. **85**, 3093 (1981).
4. C. CHATGILIALOGHU and K. U. INGOLD. Can. J. Chem. **59**, 1745 (1981).
5. A. T. BULLOCK and C. B. HOWARD. J. Chem. Soc. Faraday Trans. 1, **76**, 1296 (1980).
6. D. GRILLER. J. Am. Chem. Soc. **100**, 5240 (1978).
7. A. R. FORRESTER. *In* Magnetic properties of free radicals. Vol. 9. Landolt-Bornstein, New Series, Group II, part C1, Springer Verlag, Berlin. 1979. pp. 192–1066.
8. TH. A. J. W. WAJER, A. MACKOR, and TH. J. DE BOER. Tetrahedron, **25**, 175 (1969).

Can. J. Chem. Downloaded from www.nrcresearchpress.com by 210.87.254.5 on 09/06/12
For personal use only.

Etude par spectroscopie infrarouge de l'action de $MgBr_2$ anhydre sur le *N*-méthylacétamide en solution dans CCl_4

SIMONE BLANCHARD ET ANNE-MARIE TISTCHENKO
DPC/SCM CEN/SACLAY, 91191 Gif-sur-Yvette Cedex, France

Reçu le 22 décembre 1982

SIMONE BLANCHARD et ANNE-MARIE TISTCHENKO. Can. J. Chem. **62**, 141 (1984).

La réaction du $MgBr_2$ anhydre sur le *N*-méthylacétamide en solution dans CCl_4 a été suivie par spectrométrie infrarouge mettant ainsi en évidence la formation progressive d'un composé d'addition NMA–$MgBr_2$.

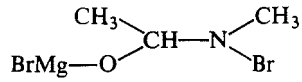

SIMONE BLANCHARD and ANNE-MARIE TISTCHENKO. Can. J. Chem. **62**, 141 (1984).

The reaction between anhydrous $MgBr_2$ and *N*-methylacetamide (NMA) in CCl_4 solution has been studied by infrared spectrometry. The temporal variation of the spectra has been followed and the final spectrum is attributed to a compound of structure

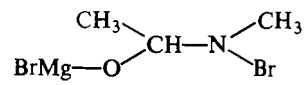

Can. J. Chem. Downloaded from www.nrcresearchpress.com by 210.87.254.6 on 09/06/12
For personal use only.

L'action des ions Mg^{2+} sur les protéines ou les peptides est un sujet de recherche de grande importance en biologie animale ou végétale. La spectrométrie infrarouge nous a permis de suivre dans le temps la transformation du *N*-méthylacétamide (NMA) en solution dans CCl_4 en présence de $MgBr_2$ anhydre. Nous avons pu à l'aide du spectre infarouge du composé final montrer la formation d'un organomagnésien de formule:

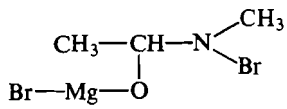

Conditions expérimentales

Le bromure de magnésium anhydre est préparé par action du magnésium sur le dibromoéthane en solution dans l'éther éthylique anhydre. Le NMA est un produit Merck, redistillé sous azote; le CCl_4 est un produit Merck, les dernières traces d'eau sont éliminées à l'aide de P_2O_5 pulvérulent; toutes les solutions sont faites en boite à gants à balayage d'azote. Les spectres infrarouge sont enregistrés sur un Perkin–Elmer 180.

Résultats

Le spectre infrarouge du NMA a été abondamment étudié et les attributions ont été faites par de nombreux auteurs; nous n'en citerons que deux (1) auxquelles nous nous référons. Le spectre infrarouge du produit final de l'action de $MgBr_2$ sur le NMA en solution dans CCl_4, subit une importante transformation (Fig. 1): (*i*) toutes les bandes caractéristiques du groupe peptidique, bande amide I, II et III, ont disparu; (*ii*) il n'existe plus de vibrateur NH (lié ou non) ni de vibrateur C=O (amidique, cétonique ou acide).

Discussion

La profonde modification au cours de la réaction des zônes spectrales, 3000 cm^{-1} – 2700 cm^{-1} et 1500 cm^{-1} – 1300 cm^{-1} des vibrations de valence et de déformation du CH_3, est représentée sur les figures 2 et 3. De nombreuses études, relatives aux fréquences de vibrations νCH et δCH des méthyles dans différents composés, ont mis en évidence l'influence de la nature de l'atome porteur et l'état d'hydridation du carbone porteur (2). Pour préciser et classer ces effets, nous avons entreprise l'étude méthodique des fréquences et des intensités des bandes d'absorption des CH_3, fixés sur le carbone, l'azote, l'oxygène ou le soufre, en solution dans CCl_4 (3). Les principales conclusions sont les suivantes.

Si l'atome porteur est un carbone d'hydbridation sp^2, la double liaison se faisant avec l'oxygène, le méthyle présente trois bandes νCH, d'intensité équivalente mais assez faible (coefficient d'extinction de l'ordre de 20 L mol^{-1} cm^{-1}) situées entre 3010 cm^{-1} et 2920 cm^{-1}. Par contre la vibration δ_s est très intense (coefficient de l'ordre de 50 L mol^{-1} cm^{-1}) et située vers 1360 cm^{-1}; les deux autres bandes δ_a et δ'_s faibles se trouvent entre 1440 et 1400 cm^{-1}.

Si le carbone porteur présente l'hybridation sp^3 et une substitution alcool, la vibration νCH se décompose en trois bandes d'intensité très inégale, dont l'une due à ν_{as} à 2972 cm^{-1} très intense (coefficient d'extinction égal à 45) et deux faibles à 2926 cm^{-1} et 2890 cm^{-1} comme le montre la figure 4 pour le propanol-2 dans CCl_4. Par contre la vibration δ_s est plus faible (coefficient d'extinction de l'ordre de 20) et toujours située à 1380 cm^{-1}; les deux autres δ_a et δ'_s faibles se trouvent au-dessus de 1450 cm^{-1}.

Si l'atome porteur est un azote d'hybridation sp^3, les bandes de vibration de valence sont très intenses et situées à des fréquences basses: entre 2900 et 2800 cm^{-1}, les bandes de vibration de déformation ont des intensités plus faibles et se trouvent toujours au-dessus de 1440 cm^{-1}. Dans le cas d'un azote d'hybridation sp^2, avec un groupe C=O en α comme dans le cas du groupe peptidique, les vibrations de valence des CH_3 sont très semblables, en intensité et position, à celles des CH_3 fixés sur un groupe C=O, la vibration de déformation δ_s est également très intense (coefficient d'extinction de l'ordre de 50) et la fréquence est voisine de 1400 cm^{-1}.

Quant aux vibrateurs OH et NH, leur coefficient d'extinction molaire est du même ordre de grandeur, soit environ 50, que celui des CH_3 fixé sur un carbone sp^3, s'ils existent ils sont donc aussi facilement détectables que les CH_3; le coefficient du vibrateur de la fonction alcool est environ une fois et demi celui de νCH_3 sur un carbone sp^3, quant au vibrateur C=O son intensité est au moins cinq fois celle d'un CH_3.

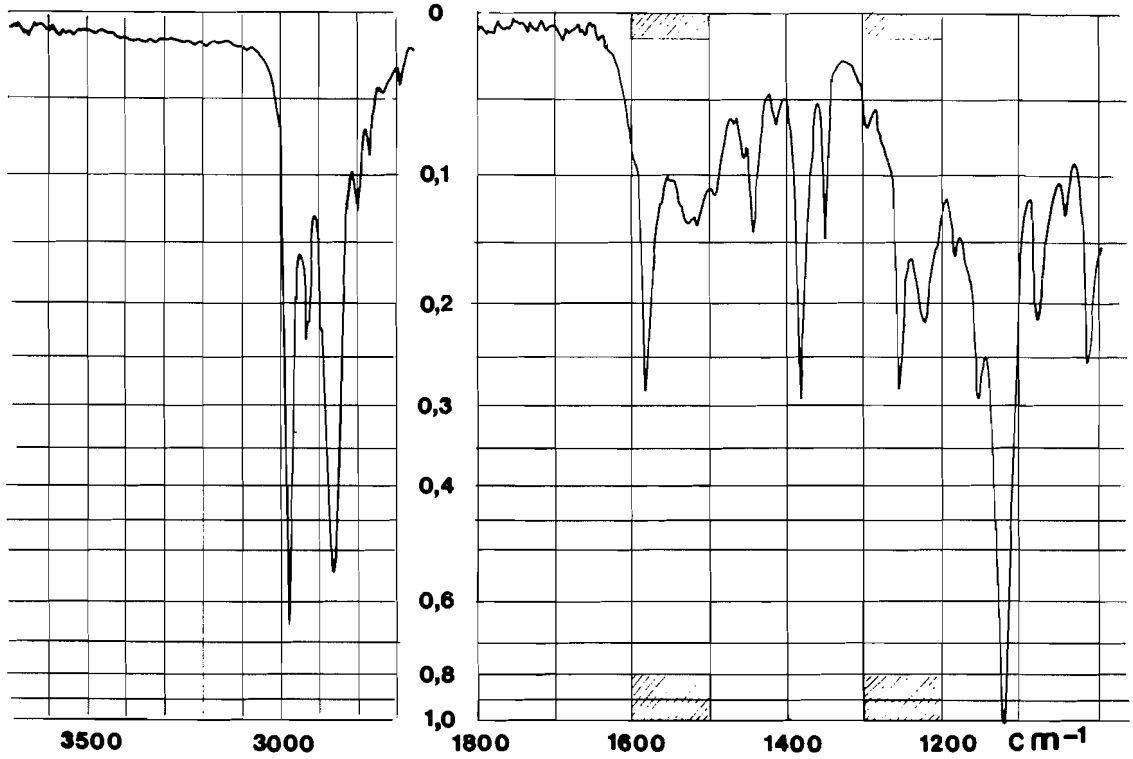

FIG. 1. Spectre infrarouge entre 4000 cm^{-1} et 1000 cm^{-1} de la solution de NMA laissée 24 h sur $MgBr_2$ anhydre. Les zônes hachurées correspondent aux zônes de forte absorption du CCl_4, les bandes y apparaissant ne sont donc pas significatives.

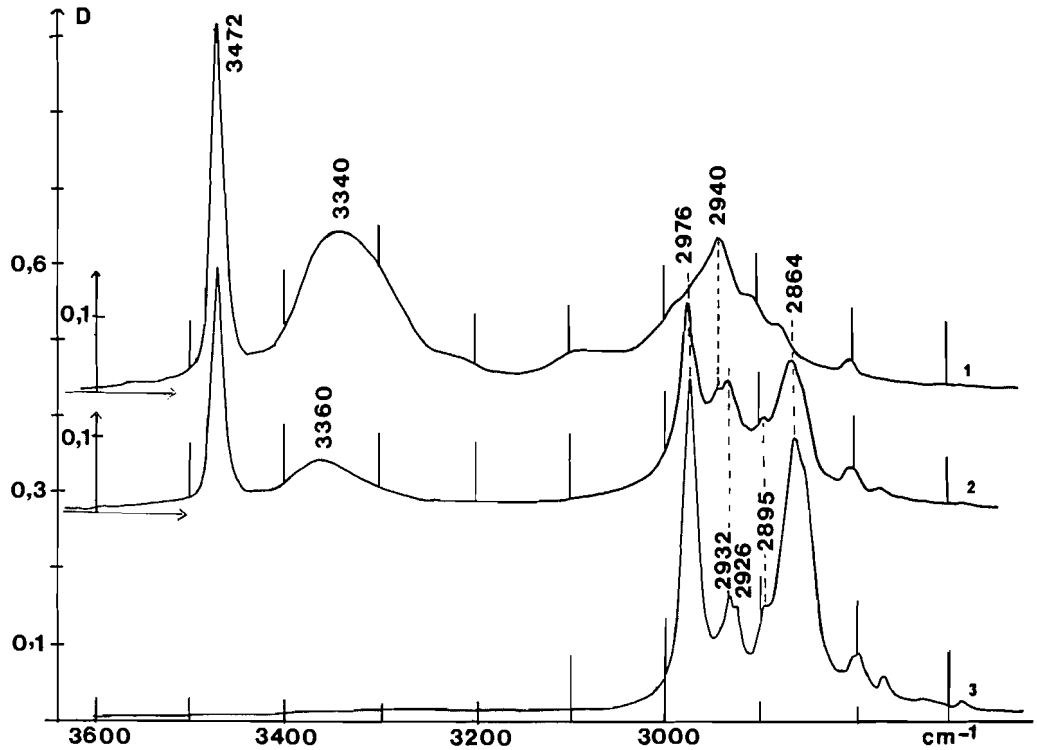

FIG. 2. Spectre infrarouge de la solution de NMA de 3600 à 2700 cm^{-1}; 1, solution NMA/CCl_4; c = 0,035 mol L^{-1}; 2, même solution laissée 4 h sur $MgBr_2$ anhydre; 3, même solution après après 24 h.

En conséquence le spectre infrarouge du produit final (Fig. 2 et 3) de la réaction $CH_3CONHCH_3$ + $MgBr_2$, montre qu'il n'y a plus qu'un CH_3 fixés sur un carbone sp^3, caractérisé par les bandes ν_a 2976 cm^{-1}, ν_s' 2926 cm^{-1} et ν_s 2895 cm^{-1}, la bande δ_s à 1380 cm^{-1} (provenant de la bande du NMA à 1365 cm^{-1} due à δ_s à C—CH_3, et environ deux fois et demi plus faible) et un CH_3 fixé sur un azote sp^3, caractérisé par la forte bande ν_s de 2864 cm^{-1} et une bande plus faible à 2932 cm^{-1}. La bande due à la vibration δ_s CH_3 du méthyl fixé sur l'azote du NMA à 1412 cm^{-1} disparaît progressivement également et est rempla-

Can. J. Chem. Downloaded from www.nrcresearchpress.com by 210.87.254.6 on 09/06/12
For personal use only.

Can. J. Chem. Downloaded from www.nrcresearchpress.com by 210.87.254.6 on 09/06/12
For personal use only.

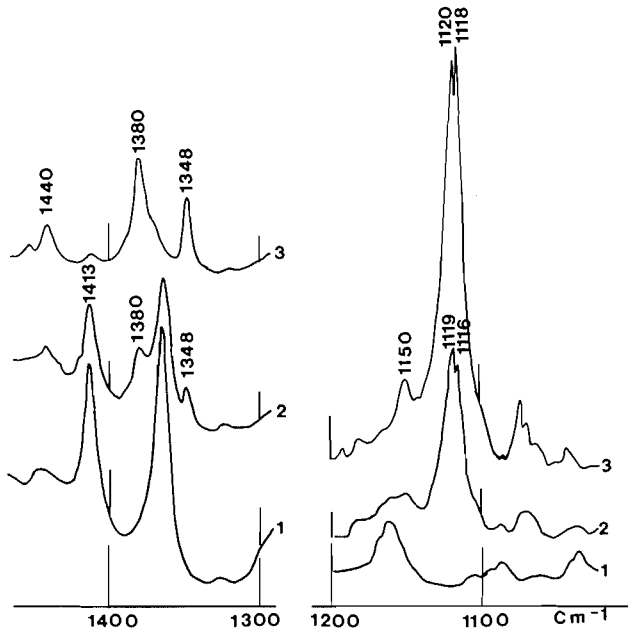

FIG. 3. Spectre infrarouge des mêmes solutions entre 1450 cm^{-1} et 1300 cm^{-1}.

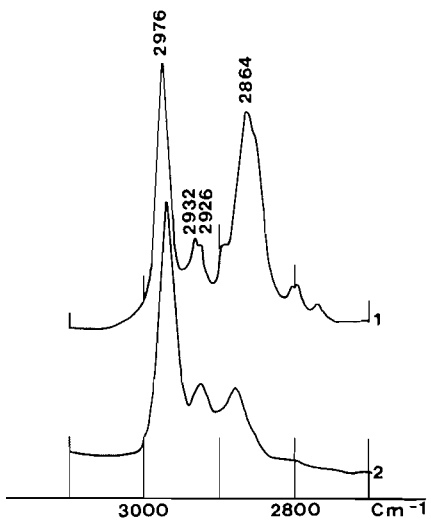

FIG. 4. Spectre infrarouge comparé de la solution 3 et de la solution propanol-2/CCl_4; c = 0,0228 mol L^{-1}.

cée par une bande faible à 1440 cm^{-1}, qui correspond bien à une vibration de déformation d'un méthyle fixé sur un azote sp^3. L'apparition d'une bande, intense, une fois et demie celle des δCH_3, à 1120 cm^{-1}, correspond bien à une bande de vibration de valence d'un C—O. Cette bande prend la forme d'un doublet, qui doit sans doute correspondre à la présence de deux isomères. La bande à 1348 cm^{-1} peut être attribuée à la vibration de déformation dans le plan du vibrateur CH qui s'est formé ou à la vibration de valence νC—N (4) des deux atomes C et N d'hybridation sp^3, ou aux deux à la fois. Pour confirmer ces deux hypothèses, il serait intéressant d'étudier la même réaction avec le NMA, N deutérié et substitué avec ^{15}N. De ces observations, il s'en suit que la formule du produit final peut s'écrire:

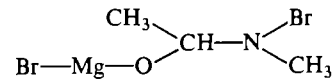

Il est possible d'intepréter la réaction de la façon suivante: en solution diluée le NMA est en équilibre sous trois formes I, II, III

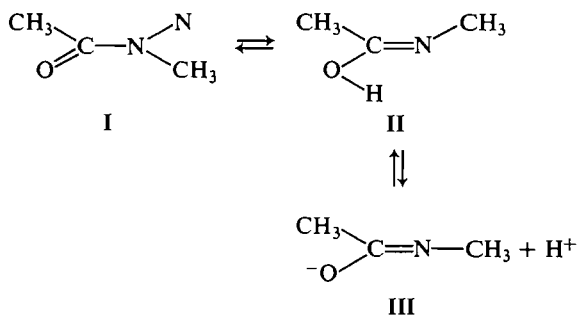

En présence de $MgBr_2$, l'équilibre est déplacé par disparition de la forme "énolique"

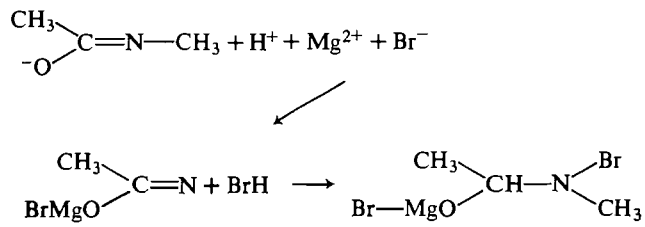

La forme II n'a jamais pu être mise en évidence, soit parce qu'elle est en infime proportion, soit parce qu'elle disparaît au fur et à mesure de sa formation.

Conclusion

Grâce à la spectrométrie infrarouge, nous avons pu mettre en évidence l'action des ions Mg^{2+} sur le NMA et la formation d'un organomagnésien, par addition du $MgBr_2$ sur le groupe peptidique CONH.

Cette réaction très importante doit sans doute représenter l'un des premiers maillons dans la chaîne de transmission de l'energie en biologie animale ou végétale.

1. T. MIYAZAWA, T. SHIMANOUCHI et S. I. MIZUSHIMA. J. Chem. Phys. **29**, 611 (1958); A. WARSHEL, M. LEVITT et S. LIFSON. J. Mol. Spectrosc. **33**, 84 (1970).
2. L. J. BELLAMY. Advances in infrared group frequencies. Methuen. 1968.
3. S. BLANCHARD et A. M. TISTCHENKO. Rapport CEA-R 5203 (1982).
4. R. N. JONES et C. SANDORFY. Chemical application of spectroscopy. Interscience, New York. 1956. p. 531.

Rate of lactamization of benzylstrychnine in acid solution

JOHN T. EDWARD AND SIN CHEONG WONG
Department of Chemistry, McGill University, 801 Sherbrooke St. W., Montreal, P. Q., Canada H3A 2K6

AND

ROBERT A. MCCLELLAND
Department of Chemistry, University of Toronto, 80 St.George St., Toronto, Ont., Canada M5S 1A1

Received June 21, 1983

JOHN T. EDWARD, SIN CHEONG WONG, and ROBERT A. MCCLELLAND. Can. J. Chem. **62**, 144 (1984).

The rate of lactamization of benzylstrychnine in aqueous solution at 25°C increases with acid concentration up to 5–10% sulfuric acid, and thereafter decreases. The maximum can be explained by taking account of the extent of protonation of the aromatic amino group with increasing acid concentration. This amino group is unusually weakly basic (pK_{BH^+} 0.3), perhaps because it is locked in an extremely rigid cage structure which opposes the rehybridization of N which must take place when it is protonated.

JOHN T. EDWARD, SIN CHEONG WONG et ROBERT A. MCCLELLAND. Can. J. Chem. **62**, 144 (1984).

La vitesse de lactamisation de la benzylstrychnine en solution aqueuse à 25°C augmente avec la concentration de l'acide sulfurique allant jusqu'à 5–10%, plus diminue. On peut expliquer le maximum en tenant compte du taux de protonation du groupe amino aromatique avec l'augmentation de la concentration de l'acide. Ce groupe amino est de façon inhabituelle faiblement basique (pK_{BH^+} 0,3) peut être à cause du fait qu'il est bloqué dans une structure en cage entièrement rigide qui s'oppose à la réhybridation de l'azote qui devrait se produire lorsqu'il est protoné.

[Traduit par le journal]

The lactam ring of benzylstrychninium ion (B in Scheme 1) is rapidly hydrolysed in warm sodium hydroxide, and the zwitterionic benzylstrychnine (A^-) crystallizes from the solution (1). In acid solution the amino acid HA recyclizes to the lactam (1). We wished to study the electrostatic effects of charged and dipolar substituents on the rates of lactamization of this and related amino acids, but first it was necessary to study the effects of acid concentration and temperature on the rate of lactamization of the parent compound, benzylstrychnine, in order to discover satisfactory conditions for kinetic studies. For convenience, it is desirable to have reasonably (but not excessively) rapid reactions; on the other hand, for interpreting the results in terms of electrostatic theory it is desirable that the ionic strength (acid concentration) be as low as possible; these two requirements are often in conflict.

The rate of the reaction at 25°C was studied in solutions ranging in aciditiy from very dilute acid (pH 3.5) to 71.6% sulfuric acid. The results[1] are shown in Fig. 1. The rate increases with acid strength to a flat maximum in 5–10% acid, and thereafter decreases.

In order to understand this result, it is necessary to know the protonation constants pK_1 and pK_2 of Scheme 1. The constant pK_1 for the equilibrium: $H_2A^+ \rightleftarrows H^+ + HA$ was determined by following the protonation of HA by the decrease in ultraviolet absorbance of the solution (cf. ref. 2). This occurred in the acid range pH 2 to $H_0 = -2$, exactly the region in which cyclization is occurring most rapidly. However, the ultraviolet absorbance could be obtained by stopped-flow methods before appreciable cyclization had occurred. Protonation followed H_0, and $pK_1 = 0.30$.

This is a pK without precedent in the literature of alkylated anilines. The pK of 5.43 for 8-methoxytetrahydrocarbazole is reduced to 2.66–2.70 for the aromatic amino centre of de-

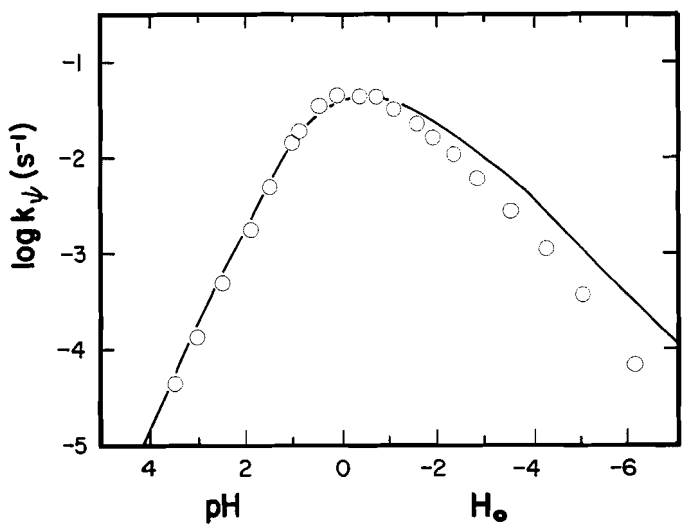

FIG. 1. Change in pseudo-first-order rate constant k_ψ for the lactamization of benzylstrychnine with change in acid concentration. Curve: theoretical, from eq. [1]. Points: experimental.

acetylaspidospermine (**1***a*) and its $N_{(b)}$-methyl derivative (**1***b*) (3), chiefly (it is to be presumed) because of the electrostatic

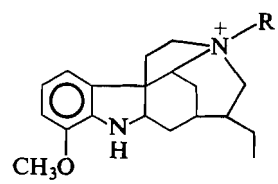

1*a* (R = H)
b (R = Me)

effect of the positive charge on $N_{(b)}$ transmitted across the low-dielectric molecular cavity. Another effect must be operating in the closely-similar HA to reduce the basicity by about another two pK units. We suggest this may be steric. The

[1]Rate constants k_ψ in different concentrations of acid and at different temperatures are available, at a nominal charge, from the Depository of Unpublished Data, CISTI, National Research Council of Canada, Ottawa, Ontario, Canada K1A 0R6.

Can. J. Chem. Downloaded from www.nrcresearchpress.com by 210.87.254.42 on 09/06/12
For personal use only.

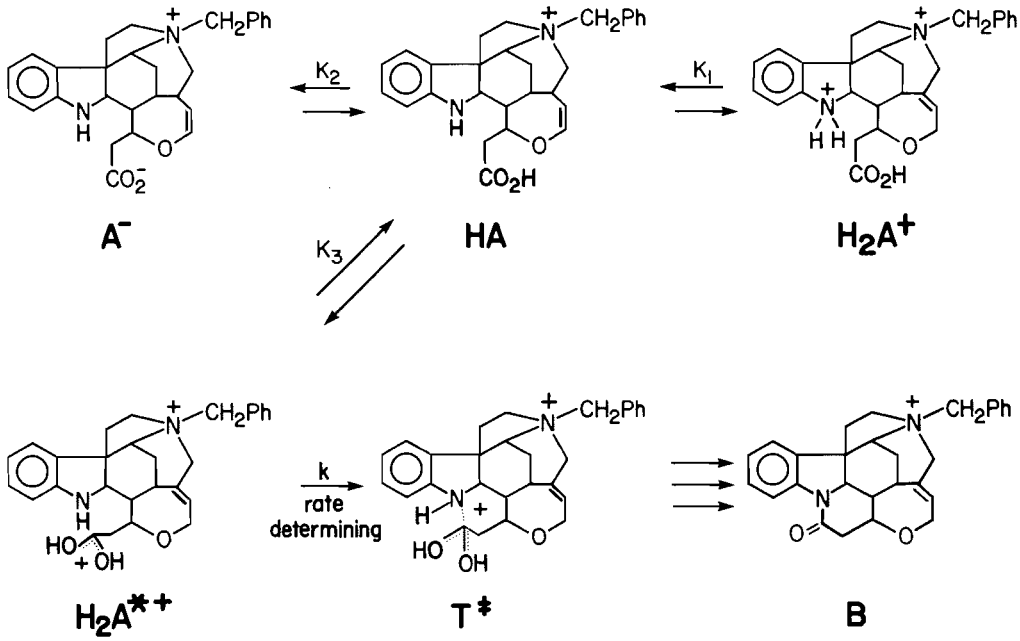

SCHEME 1

nitrogen of aniline is probably a flattened pyramid, whose angles are reduced towards tetrahedral values on protonation (4). CPK models show that the fusion of the benzo ring to the cage structure of HA is very strained with trigonal nitrogen, and even more strained with tetrahedral nitrogen.

The zwitterion A^- has extremely low solubility in water. Advantage was taken of this property to determine pK_2 by following the change in absorbance (due to a constant amount of A^- and increasing amounts of HA in solution) as the pH of the solution was lowered (5). The pK_2 of 4.20 ± 0.04 is about the value expected from the acid-strengthening effect of the distant quaternary nitrogen atom.

It is possible that formation of the lactam ring of B proceeds by way of the carboxyl-protonated intermediate H_2A^{*+} going through the transition state $T^{\ddagger}$.[2] The protonation of most carboxyl groups (7) is governed by the H_A acidity function (8). Accordingly, application of the Bronsted–Bjerrum treatment to the mechanism of Scheme 1 yields the following equation:

$$[1] \quad k_\psi = k[HA]h_A f_{H_2A^{*+}}/K_3([A^-] + [HA] + [H_2A^+])f_{T^{\ddagger}}$$

$$[1a] \quad = \frac{k}{K_3}\left(\frac{h_a}{1 + \frac{K_2}{[H^+]} + \frac{h_0}{K_1}}\right)\left(\frac{f_{H_2A^{*+}}}{f_{T^{\ddagger}}}\right)$$

where k_ψ is the pseudo-first-order rate constant for the lactamization of benzylstrychnine in the large excess of acid used, and the f's are activity coefficients. The curve shown in Fig. 1 was calculated using this equation, assuming log $k/K_3 = -0.69$ and log $(f_{H_2A^{*+}}/f_{T^{\ddagger}}) = 0$. The latter assumption is unlikely to be exactly true (9), particularly in the higher acid concentrations, and protonation of the carboxyl of HA may follow an acidity function differing slightly from H_A (8),[3] so the deviations of the experimental points from the theoretical curve at the higher acid concentrations are not serious.

We can now understand why the rate goes through a maximum with increasing concentration of acid. Going from low acidities to pH 1, A^- is being converted to HA, and thence to H_2A^{*+} (trace) and H_2A^+ (preponderance) in a ratio determined by K_3/K_1: hence the increase in rate. However, by the time the acidity has risen to $H_0 = -1.4$, protonation of HA to H_2A^+ is effectively complete, and $[A^-] \approx [HA] \approx 0$. Consequently, [1] can be simplified to

$$[2] \quad k_\psi = \frac{k\,K_1}{K_3}\left(\frac{h_A}{h_0}\right)\left(\frac{f_{H_2A^{*+}}}{f_{T^{\ddagger}}}\right)$$

With increasing acid concentration h_A increases much more slowly than h_0 (8), and hence k_ψ must decrease.

The position of the maximum is determined by pK_1, a value greater than 0.30 shifting the peak of the calculated curve to the left of the position shown in Fig. 1, and a smaller value shifting the peak to the right. Consequently, the curve offers support for the pK_1 of 0.3.

The activation parameters for the lactamization reaction[1] are

[2] The experimental results are equally compatible with a transition state involving acid-catalysed breakdown rather than formation of the neutral tetrahedral intermediate. A referee has pointed out that "the reaction is the reverse of acid-catalysed amide hydrolysis, and differs from that reaction only because the equilibrium position is over towards the amide in this case. A similar transition state to that supposed to obtain in acid-catalysed amide hydrolysis would therefore be expected . . . . . McClelland . . . . . has shown that very little oxygen exchange accompanies acid-catalysed amide hydrolysis (6), and this and other evidence has by several workers been taken to indicate a transition state which in the hydrolysis direction comes before the tetrahedral intermediate and involves attack of water on the O-protonated amide. In reverse, therefore, hydronium ion catalysed breakdown of a neutral tetrahedral intermediate (the immediate product of which is the O-protonated amide which then loses a proton) seems more likely and is equally consistent with all the other observations . . . . " We agree with this comment.

[3] A better fit in the higher acidities would almost certainly be obtained using an acidity function h_0^m with m as a variable. In light of the uncertainties in the activity coefficient and acidity function terms, the significance of this would, however, be questionable.

Can. J. Chem. Downloaded from www.nrcresearchpress.com by 210.87.254.42 on 09/06/12
For personal use only.

TABLE 1. Activation parameters for the acid-catalysed lactamization of benzylstrychnine

Acidity	ΔH (kcal/mol)	ΔS (eu)
0.003 *M* HCl	11	−36
0.01	11	−33
0.03	11	−33
0.1	10	−32
1.0% H_2SO_4	10	−33
2.1	10	−30
5.3	11	−26
9.7	11	−26
15.3	13	−20
20.7	14	−20
31.6	14	−18
43.6	15	−18
57.8	17	−14
71.6	19	−14

given in Table 1. Over the region 0.003 *M* − 0.1 *M* hydrochloric acid, benzylstrychnine exists essentially completely as HA, and the activation parameters for this region refer to the overall change: HA → $T^{\pm}$. On the other hand, in concentrations of sulfuric acid greater than 20.7% in Table 1, benzylstrychnine exists essentially completely as H_2A^+, and activation parameters refer to the overall change: $H_2A^+ \rightarrow T^{\ddagger}$. Since H_2A^+ will almost certainly be more hydrated (and more stabilized) than HA, one can understand the higher $\Delta H^{\pm}$ and the higher $\Delta S^{\pm}$ values required to reach the common $T^{\pm}$ state. Furthermore, the decreasing activity of water as the sulfuric acid concentration is increased to 71.6% will result in a progressive loss of stabilizing hydration from both H_2A^+ and $T^{\pm}$. In spite of its more diffuse charge, $T^{\pm}$ is likely to receive greater stabilization from hydration than H_2A^+, because oxonium ions are more hydrated than ammonium ions (9). Consequently, the progressive dehydration should lead to an increase in $\Delta H^{\ddagger}$ and in $\Delta S^{\ddagger}$ with increased acid concentration over the range 31.6−71.6%, as is observed.

Experimental

Determination of pK_1

A 10^{-4} molar solution of A^- in 0.002 *M* NaOH was placed in one syringe of a Durrum−Gibson stopped-flow apparatus, and mixed with acids ranging from pH 2.5 to $H_0 = -2$. The absorbance at 293 nm was recorded immediately after mixing (stopped-flow dead-time − 2 ms). The sigmoidal curve of absorbance vs. pH (H_0) so obtained was treated in the normal fashion to give pK_1.

Determination of pK_2

pK_2 was determined by noting the increase in absorbance at 293 nm of saturated solutions (containing fixed amounts of A^- and variable amounts of HA) obtained by shaking an excess of A^- with buffer solutions of decreasing pH. Theory and practical details are given in ref. 5.

Rate measurements

The lactamization of benzylstrychnine (λ_{max} 293 nm) is accompanied by a large increase in absorbance at 254 nm as the benzylstrychninium ion (λ_{max} 254 nm) is formed. Rate measurements were carried out by monitoring the increase in absorbance at 254 nm. For activation parameters, rates were obtained at three temperatures, chosen from 5°, 15°, 25°, 35° 45°, and 65°C, according to the concentration of acid.[1]

Acknowledgments

Financial support from the Natural Sciences and Engineering Research Council of Canada is gratefully acknowledged. In addition, two of us (J.T.E. and S.C.W.) are grateful to the Ministry of Education, Province of Quebec for a travel grant (Coopération Québec−Ontario) which made our cooperative efforts possible.

1. O. ACHMATOWICZ, G. R. CLEMO, W. H. PERKIN, and R. ROBINSON. J. Chem. Soc. 267 (1932).
2. L. P. HAMMETT. Physical organic chemistry. McGraw−Hill, New York. 1940. p. 60.
3. A. J. EVERETT, H. T. OPENSHAW, and G. F. SMITH. J. Chem. Soc. 1120 (1957).
4. B. M. WEPSTER. Recl. Trav. Chim. Pays-Bas, **72**, 661 (1953).
5. J. T. EDWARD, P. G. FARRELL, S. A. SAMAD, and S. C. WONG. J. Org. Chem. **42**, 225 (1977).
6. R. A. MCCLELLAND. J. Am. Chem. Soc. **97**, 5281 (1975).
7. J. T. EDWARD and S. C. WONG. J. Am. Chem. Soc. **99**, 4229 (1977).
8. K. YATES, J. B. STEVENS and A. R. KATRITZKY. Can. J. Chem. **42**, 1957 (1964); J. T. EDWARD and S. C. WONG. Can. J. Chem. **55**, 2492 (1977).
9. T. A. MODRO, K. YATES, and J. JANATA. J. Am. Chem. Soc. **97**, 1492 (1975); R. A. MCCLELLAND, T. A. MODRO, M. F. GOLDMAN, and K. YATES. J. Am. Chem. Soc. **97**, 5223 (1975); J. T. EDWARD and S. C. WONG. J. Am. Chem. Soc. **99**, 7224 (1977); J. T. EDWARD and S. C. WONG. J. Am. Chem. Soc. **100**, 7023 (1978).

Can. J. Chem. Downloaded from www.nrcresearchpress.com by 210.87.254.42 on 09/06/12
For personal use only.

The crystal and molecular structure of 5-(propyn-1-yl)-1-(β-D-arabinofuranosyl)uracil. A very short C≡C triple bond

MIROSLAW CYGLER[1] AND WAYNE F. ANDERSON

The MRC Group on Protein Structure and Function, Department of Biochemistry, University of Alberta, Edmonton, Alta., Canada T6G 2H7

AND

JERZY GIZIEWICZ[2] AND MORRIS J. ROBINS

Department of Chemistry, University of Alberta, Edmonton, Alta., Canada T6G 2G2

Received May 10, 1983

MIROSLAW CYGLER, WAYNE F. ANDERSON, JERZY GIZIEWICZ, and MORRIS J. ROBINS. Can. J. Chem. **62**, 147 (1984).

The crystal structure of 5-(propyn-1-yl)-1-(β-D-arabinofuranosyl)uracil, an analog of the active antiherpes nucleoside 1-(β-D-arabinofuranosyl)thymine, was determined by X-ray diffraction. The compound crystallizes in the space group $P2_12_12_1$ with $a = 4.925(1)$, $b = 14.326(2)$, $c = 17.454$ Å. Reflections were measured on a diffractometer and the structure was solved by direct methods. Least-squares refinement converged at $R = 0.032$ for 1159 observed reflections. The sugar ring exhibits an ^3E or a C(3′)*endo* conformation with a pseudorotation angle $P = 28.3°$ and puckering amplitude $\tau_m = 31.7°$. The orientation of the —CH_2OH side chain is g^+. The base is in an *anti* conformation with respect to the sugar ring, with a glycosidic torsion angle $\chi = 33.7°$. Changes in the C(5)—C(6) and C(6)—N(1) bond lengths suggest some interaction of the propynyl group with the pyrimidine ring. The C≡C bond length of 1.121 Å is very short. Its shortening could result from intermolecular interactions with the neighboring pyrimidine ring and nearby oxygen atoms.

MIROSLAW CYGLER, WAYNE F. ANDERSON, JERZY GIZIEWICZ et MORRIS J. ROBINS. Can. J. Chem. **62**, 147 (1984).

On a déterminé, par diffraction des rayons-X, la structure cristalline du (propyne-1 yl)-5 (β-D-arabinofurannosyl)-1 uracyle, un analogue du nucléoside actif contre l'herpes, la (β-D-arabinofurannosyl)-1 thymine. Le composé cristallise dans le groupe d'espace $P2_12_12_1$ avec $a = 4{,}925(1)$, $b = 14{,}326(2)$, $c = 17{,}454$ Å. On a mesuré les réflexions à l'aide d'un diffractomètre et on a résolu la structure par des méthodes directes et on l'a affinée par la méthode des moindres carrés jusqu'à une valeur de $R = 0{,}032$ pour 1159 réflexions observées. Le cycle du sucre a une conformation ^3E ou C(3′)*endo* avec un angle de pseudorotation $P = 28{,}3°$ et une amplitude de gauchissement $\tau_m = 31{,}7°$. L'orientation de la chaine latérale —CH_2OH est g^+. La base a une conformation "anti" par rapport au cycle du sucre avec un angle de torsion glycosidique de $\chi = 33{,}7°$. Les variations des longueurs de liaison C(5)—C(6) et C(6)—N(1) suggèrent l'existence d'une interaction entre le groupe propynyle et le cycle pyrimidine. La longueur de la liaison C≡C, 1,121 Å, est très courte. Son racourcissement peut être dû à des interactions intermoléculaires avec le cycle pyrimidine voisin et avec les atomes d'oxygène situés à proximité.

[Traduit par le journal]

Introduction

A number of 5-substituted pyrimidine 2′-deoxyribo- and arabino-nucleosides have been shown to exhibit selective biological activity (1). Beside the clinically effective 5-iodo (2), 5-trifluoromethyl (3), and 5-ethyl derivatives (4), several other 5-substituted 2′-deoxyuridines have been found to be potent antiviral agents (1). Among these analogues, (*E*)-5-(2-halovinyl)-2′-deoxyuridines (bromo and iodo derivatives) are the most potent and selective known inhibitors of Herpes simplex type I virus replication in cell cultures and experimental animals (5, 6). It has also been shown that some 5-alkyl and alkenyl derivatives of 1-(β-D-arabinofuranosyl)uracil (araU) effectively inhibit HSV replication without significant effect on host cell growth (7, 8). A number of derivatives of araU containing a two carbon unit at the 5-position, including the (*E*)-(2-halovinyl) group, have recently been synthesized and tested. Some have shown highly selective inhibition of HSV multiplication (9, 10).

The 5-(alkyn-1-yl)pyrimidine nucleosides represent a new group of analogues with antiviral and antitumor activities. Only 5-ethynyluracil and 5-ethynylcytosine and their nucleosides had been synthesized (11, 12) and biologically evaluated (5, 13, 14). A convenient and high-yield method for the preparation of 5-(alkyn-1-yl)uracil nucleosides has recently been developed (15, 16) and utilized for the synthesis and biological investigation of selected 2′-deoxy- and arabinofuranosides (17).

In comparison to ribo- and deoxyribonucleosides our understanding of solid state conformations of arabino-, xylo-, and lyxonucleosides is much more limited. There is only one structure of a β-D-lyxonucleoside (18) and one of a β-D-xylonucleoside (19) reported in the literature. Arabinonucleosides are better represented with 15 solid state structures reported.[3] Such a number allows some generalizations on their conformational trends to be drawn. One of the first observed conformations of the arabinofuranosyl ring was O(4′)*endo*—C(1′)*exo* (20), which is rarely observed in ribonucleosides. When more structures were determined it became clear that this conformation also is not common for arabinonucleosides. However, such a conformation might be of some importance in solution. Ekiel *et al.* (21) concluded from a compilation of nmr spectra of arabinonucleosides that the *S*-type state in solution may either be a mixture of C(2′)*endo*—C(3′)*exo* and O(4′)*endo*—C(1′)*exo* conformations or is shifted from C(2′)*endo*—C(3′)*exo* toward the C(2′)*endo*—C(1′)*exo* conformation.

[1] To whom all correspondence should be addressed. On leave from Department of Crystallography, Institute of Chemistry, University of Łódź, Poland.

[2] Present address: Faculty of Pharmacy and Pharmaceutical Sciences, University of Alberta, Edmonton, Alta., Canada T6G 2N8.

[3] Structures of 2′-anhydro-β-D-arabinofuranosylnucleosides are not included here as the conformations of their sugar rings are highly influenced by the additional ring fusion. For discussion see ref. 49.

We now report the molecular structure of 5-(propyn-1-yl)-1-(β-D-arabinofuranosyl)uracil (17) (araU-5-propyne). This compound is an acetylenic analog of the antiherpes active 1-(β-D-arabinofuranosyl)thymine (araT (22)) and also the biologically active 5-vinyl, 5-halovinyl, and other 5-alkenyl and 5-ethynyl-2′-deoxyuridines (13).

Experimental

Colorless, needle-shaped crystals of araU-5-propyne (17) were obtained from ethanol–water solution by slow cooling to 0°C. Systematic absences on precession photographs indicated the orthorhombic space group $P2_12_12_1$. The cell dimensions, determined on a Syntex $P2_1$ diffractometer using 15 high angle reflections, are: $a = 4.925(1)$, $b = 14.326(2)$, $c = 17.454(2)$ Å, $V = 1231.5$ Å^3, $Z = 4$. A crystal chosen for data collection had the dimensions $0.09 \times 0.10 \times 0.32$ mm (see Discussion). There were 1200 independent reflections measured up to 2θ of 126° with Ni-filtered CuKα radiation, of which 1159 had $I > 2.5\sigma(I)$. The $\theta/2\theta$ scan mode was used with the scan width $\Delta(2\theta) = 1.5° + \alpha_1 - \alpha_2$ splitting. The background was measured at each end of the scan for the total time equal to half that of the scan through the peak. Scan speed was in the range 1.4–15°/min (2θ motor). Every 400 reflections the orientation matrix of the crystal was redetermined. Three reflections were used as the intensity controls. Their intensities fluctuated by ±1.5% during data collection from their average values. They were used for appropriate scaling. The intensities of measured reflections were reduced to F values in the usual way. No absorption correction was applied.

The structure was solved by direct methods using SHELX 76 (23). All non-hydrogen atoms were located on the best E-map. After a few cycles of the full-matrix least-squares refinement, first with isotropic, and later with anisotropic temperature factors, a difference map was calculated and it revealed positions of all hydrogen atoms. Peaks corresponding to the H atoms of the methyl group, C(9), were relatively weak and these atoms, when included in the refinement, drifted away from C(9) (up to 1.3 Å). These atoms were refined with restraints put on their geometry. A weighting scheme $w^{-1} = \sigma^2(F_o) + 0.0033\,|F_o|$, where the $\sigma(F_o)$ are from counting statistics, was used at the end of the refinement. The largest shift/esd in the final cycle of the refinement was 0.05 for 237 refined parameters. There were no peaks above 0.15 e/Å^3 on the final difference map. Three low angle reflections probably affected by extinction were given zero weight in the refinement. At convergence the agreement indices were $R = 0.032$, $R_w = 0.038$ for 1155 observed reflections and $R = 0.034$, $R_w = 0.040$ for all measured reflections.

Final atomic parameters are given in Table 1.[4]

TABLE 1. 5-(Propyn-1-yl)-1-(β-D-arabinofuranosyl)uracil: final fractional coordinates with esd's in parentheses and isotropic temperature factors ($\times 10^4$, $\times 10^3$ for H atoms)

Atom	X	Y	Z	U_{eq}
N(1)	1.1578(4)	0.5853(1)	0.6368(1)	287(7)
C(2)	1.1421(4)	0.6543(1)	0.5822(1)	286(7)
O(2)	1.2875(4)	0.7242(1)	0.5843(1)	416(7)
N(3)	0.9544(4)	0.6399(1)	0.5260(1)	331(7)
C(4)	0.7853(4)	0.5634(1)	0.5174(1)	308(8)
O(4)	0.6332(4)	0.5579(1)	0.4624(1)	461(7)
C(5)	0.8074(4)	0.4948(1)	0.5783(1)	309(8)
C(6)	0.9911(4)	0.5100(1)	0.6349(1)	307(8)
C(7)	0.6279(4)	0.4125(1)	0.5778(1)	310(7)
C(8)	0.4807(5)	0.3529(2)	0.5779(1)	424(8)
C(9)	0.2865(6)	0.2754(2)	0.5782(2)	576(9)
C(1′)	1.3405(4)	0.6023(1)	0.7029(1)	291(7)
C(2′)	1.1940(4)	0.6542(1)	0.7688(1)	315(7)
O(2′)	0.9456(3)	0.6961(1)	0.7463(1)	416(7)
C(3′)	1.1413(4)	0.5771(1)	0.8268(1)	307(8)
O(3′)	1.1433(5)	0.6115(1)	0.9023(1)	550(8)
C(4′)	1.3683(4)	0.5080(1)	0.8121(1)	281(7)
O(4′)	1.4245(3)	0.5147(1)	0.7312(1)	329(6)
C(5′)	1.3100(5)	0.4069(1)	0.8321(1)	371(8)
O(5′)	1.0464(4)	0.3769(1)	0.8111(1)	449(7)
H(3)	0.927(1)	0.686(1)	0.490(1)	27(1)
H(6)	1.023(1)	0.464(1)	0.679(1)	23(1)
H(91)*	0.376(1)	0.214(1)	0.582(1)	78(1)
H(92)*	0.171(1)	0.282(1)	0.526(1)	139(1)
H(93)*	0.159(1)	0.271(1)	0.621(1)	184(1)
H(1′)	1.488(1)	0.637(1)	0.686(1)	25(1)
H(2′)	1.308(1)	0.699(1)	0.790(1)	17(1)
H(2″)	0.968(1)	0.760(1)	0.740(1)	127(1)
H(3′)	0.985(1)	0.553(1)	0.816(1)	26(1)
H(3″)	1.065(1)	0.569(1)	0.938(1)	91(1)
H(4′)	1.526(1)	0.534(1)	0.843(1)	40(1)
H(5′)	1.328(1)	0.398(1)	0.893(1)	46(1)
H(5″)	1.409(1)	0.375(1)	0.808(1)	63(1)
H(05′)	0.947(1)	0.379(1)	0.860(1)	87(1)

*Restraints were used to refine these atoms.

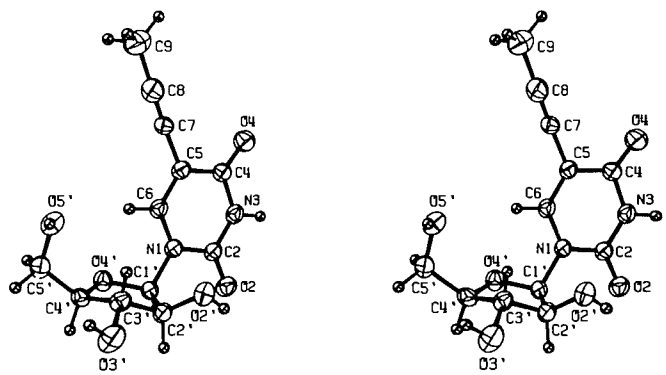

FIG. 1. Stereoscopic view of 5-(propyn-1-yl)-1-(β-D-arabinofuranosyl)uracil with the numbering scheme. Thermal ellipsoids correspond to a 50% probability level.

Discussion

The conformation of araU-5-propyne is shown in a stereoview in Fig. 1. Bond distances and valence angles are shown in Fig. 2 and selected torsion angles are given in Table 2.

The length of C(7)≡C(8) triple bond obtained in this study is unusually short. To check that this is not an artifact, we collected a new data set from a slightly larger crystal and used longer counting times and a more intense X-ray beam. Experimental details given in the previous section correspond to this more precise data set. Positional parameters of non-hydrogen atoms refined independently with both data sets do not differ by more than three standard deviations and 88% of them are within two esd's. Virtually identical values for the length of the C≡C bond were obtained from the two data sets. Atomic parameters (Table 1) and geometrical details given below are based on the second, more precise data set, which gave lower estimated standard deviations.

Arabinofuranose ring

The sugar ring exhibits an ^3E or a C(3′)*endo* conformation (N

[4] Tables of anisotropic temperature factors of the non-hydrogen atoms, observed and calculated structure amplitudes, and the table of C≡C bond lengths and compound codes obtained through a search of the Cambridge Database are available, at a nominal charge, from the Depository of Unpublished Data, CISTI, National Research Council of Canada, Ottawa, Ont., Canada K1A 0S2.

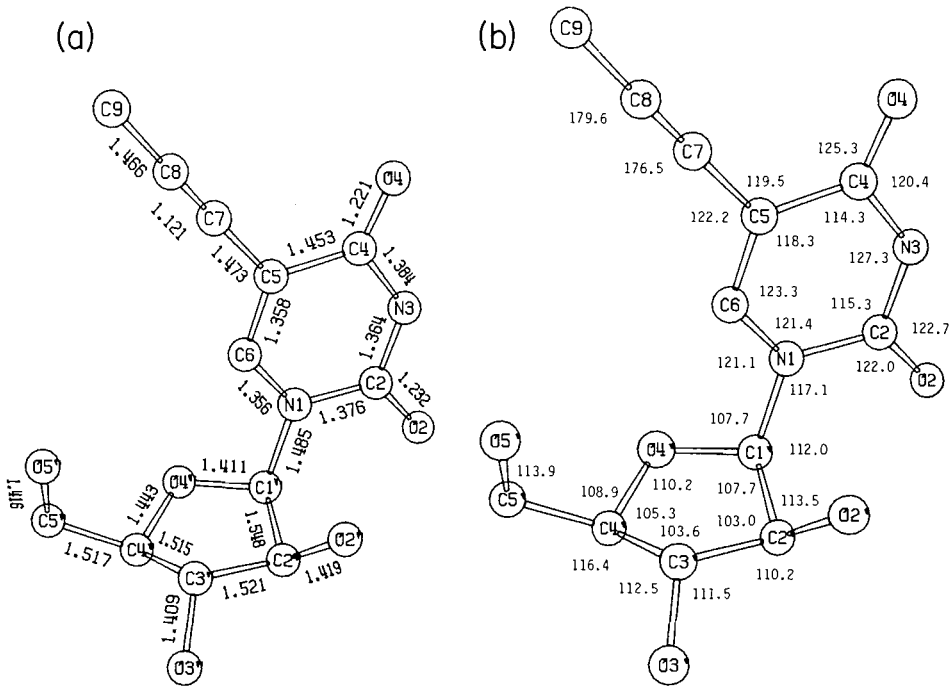

FIG. 2. (*a*) Bond distances (Å) and (*b*) valence angles (deg) in 5-(propyn-1-yl)-1-(β-D-arabinofuranosyl)uracil. Estimated standard deviations are in the range 0.003–0.004 Å for bonds and 0.01–0.03° for angles.

TABLE 2. Selected torsion angles for araU-5-propyne

Atoms	Angle* (deg)
O(4′)—C(1′)—C(2′)—C(3′)	−14.7
C(1′)—C(2′)—C(3′)—C(4′)	27.9
C(2′)—C(3′)—C(4′)—O(4′)	−32.0
C(3′)—C(4′)—O(4′)—C(1′)	23.6
C(4′)—O(4′)—C(1′)—C(2′)	−5.4
C(3′)—C(4′)—C(5′)—O(5′)	41.3
C(6)—N(1)—C(1′)—O(4′)	33.7

*Estimated standard deviations are in the range 0.3–0.5°.

type according to the nomenclature of Altona and Sundaralingam (24)). The pseudorotation parameter is $P = 28.3°$ and the puckering amplitude is $\tau_m = 31.7°$.

The amplitude of puckering is rather low, ~7° lower than the average pucker of a ribose ring, but is not unusual. Similar or even lower puckering was found in some 9-(β-D-furanosyl)purine 5′-phosphates (see Table 2 in ref. 25) and, for example, in N^6-(*N*-threonylcarbonyl)adenosine (26) and 8-bromo-9-(β-D-xylofuranosyl)adenine (19). Such a flattened conformation has not been observed in arabinonucleosides. The lowest pucker, with $\tau_m = 35.9°$, was found in arabinofuranosylcytosine hydrochloride (27).

Similar to other nucleosides the C(4′)—O(4′) bond is longer than O(4′)—C(1′) (by 0.03 Å). The C(1′)—C(2′) bond (1.548 Å) is long and C(2′)—C(3′) is short (1.521 Å). This pattern is typical for arabinonucleosides but opposite to that observed in ribonucleosides. It reflects different steric interactions of the 2′-hydroxyl group with neighboring atoms.

Endocyclic angles are typical for the C(3′)*endo* conformation of the sugar ring. From an analysis of sugar conformations observed in the solid state, Westhof and Sundaralingam (28) derived the relationship between τ_m and the average endocyclic angle $\langle\theta\rangle$:

$$\langle\theta\rangle = 108° - 0.00202\ \tau_m^2$$

The value of $\langle\theta\rangle$ calculated from this relationship for the present molecule (105.97°) is in excellent agreement with the experimental value of 105.96°.

The exocyclic angles show a usual pattern, with smaller values inside the O(2′)—C(2′)—C(3′)—O(3′) fragment and larger values outside, and with an opening of the C(3′)—C(4′)—C(5′) angle to 116.7°. The O(2′) atom, which is on the same side of the furanose ring as the pyrimidine base, is in close contact with the N(1) atom; the O(2′)...N(1) distance of 2.696(3) Å is shorter than the sum of the van der Waals radii of these two atoms.

The CH_2OH side chain is found in a g^+ conformation with a C(3′)—C(4′)—C(5′)—O(5′) torsion angle of 41.3°. There is no intramolecular hydrogen bond between O(2′) and O(5′) because of the unfavorable sugar ring conformation. Such a hydrogen bond is possible with a C(2′)*endo* conformation of the ring and a g^+ orientation of the side chain, and was observed in arabinofuranosylcytosine (29) and arabinofuranosyluracil (30, 31). In arabinofuranosylcytosine hydrochloride (27) the sugar ring also exhibits a C(2′)*endo* conformation but the CH_2OH side chain is in the *t* orientation and no intramolecular hydrogen bond is formed.

The distribution of pseudorotation angles, *P*, in arabinofuranose rings is shown in Fig. 3*a*.[3] For seven observed *N*-type states, *P* spans a very narrow range from 9.3 to 28.3°, clustering around 11° and 25°. More structures, however, have to be determined to evaluate the significance of this clustering. The *S*-type states fall into two categories: an O(4′)*endo*—C(1′)*exo* conformation with $P \cong 106°$ (two structures) and a C(2′)*endo* conformation with *P* in the range 156.3 to 171.3° (six structures).

Base moiety

The pyrimidine ring is planar. The average deviation of an

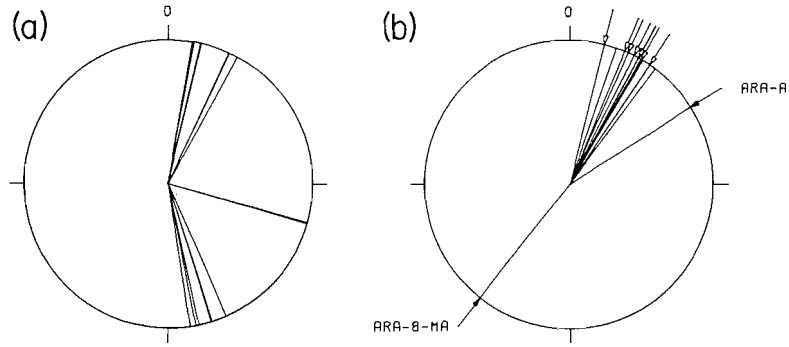

FIG. 3. Distribution of (*a*) pseudorotation angles ***P*** and (*b*) glycosidic torsion angles χ in arabinonucleosides (the torsion angle is measured positive if the far bond is rotated clockwise). The following structures are represented in the diagrams (***P***, χ in parentheses): 9-(β-D-arabinofuranosyl)adenine hydrochloride (43) (9.3°, 29.7°), 5-iodo-1-(2-deoxy-2-fluoro-β-D-arabinofuranosyl)cytosine (44) (10.0°, 19.0°), 1-(β-D-arabinofuranosyl)cytosine-5′-monophosphate (45) (12.6°, 30.7°), 4-thio-1-(β-D-arabinofuranosyl)uracil (37) (12.9°, 36.6°), 8-*N*-morpholino-1-(β-D-arabinofuranosyl)adenine (38) (ara-8-Ma; 24.5°, −142.1°), 9-(β-D-arabinofuranosyl)adenine (39) (araA; 24.8°, 57.8°), 5-(propyn-1-yl)-1-(β-D-arabinofuranosyl)uracil (this paper; 28.3°, 33.7°), 1-(β-D-arabinofuranosyl)thymine (33) (105.5°, 24.1°), 5-bromo-1-(β-D-arabinofuranosyl)uracil (20) (106°, 30°), 1-(β-D-arabinofuranosyl)uracil (30, 31) (156.3°, 34.0°), 1-(β-D-arabinofuranosyl)cytosine (29) (162.3°, 28.8°), 1-(β-D-arabinofuranosyl)-5-methylcytosine (46) (162.7°, 22.6°), 1-(3-methoxy-β-D-arabinofuranosyl)cytosine (47) (167.8°, 28.7°), 1-(β-D-arabinofuranosyl)cytosine hydrochloride (27) (169.0°, 26.7°), 1-(β-D-arabinofuranosyl)cytosine Pt(II) complex (48) (171.3°, 14.0°). Open arrows in (*b*) indicate *S*-type states.

TABLE 3. The geometry of hydrogen bonds

D—H . . . A	Symmetry of A	D . . . A (Å)	D—H (Å)	A . . . H (Å)	∠D—H—A (deg)
N(3)—H(3) . . . O(2)	$x - 1/2, 3/2 - y, 1 - z$	2.860	0.92	1.96	168
O(2′)—H(2″) . . . O(5′)	$2 - x, 1/2 + y, 3/2 - z$	2.778	0.93	1.89	157
O(3′)—H(3″) . . . O(4)	$3/2 - x, 1 - y, 1/2 + z$	2.974	0.95	2.11	151
O(5′)—H(O5′) . . . O(4)	$3/2 - x, 1 - y, 1/2 + z$	2.936	0.98	2.04	150
O(5′)—H(O5′) . . . O(2)	$2 - x, y - 1/2, 3/2 - z$	3.290	0.98	2.68	120

atom from the mean plane of the ring is 0.0115 Å with the largest being 0.0174 Å. The O(2) atom lies in the plane of the ring, while O(4) and C(1′) deviate slightly from it in opposite directions by 0.0525 and 0.0981 Å, respectively. The C(5)—C(6) and N(1)—C(6) bond lengths differ slightly from those in thymidine (32) and araU (30, 31).[5] The former bond in araU-5-propyne is ~0.015 Å longer and the latter is ~0.020 Å shorter than in the two reference structures, which might suggest some conjugation with the propyn-1-yl group. Comparably small changes were also observed in 5-ethynyl-2′-deoxyuridine (34) (dUrd-5-ethyne) and 5-acetyl-α-2′-deoxyuridine (35). Those authors suggested a degree of conjugation of the C(5)=C(6) double bond with the 5-substituent.

The C(2)—O(2) bond of 1.232(3) Å in araU-5-propyne is ~0.01 Å longer than in all of the above mentioned compounds, and this is accompanied by a shortening of the C(2)—N(3) bond also by ~0.01 Å. In the present compound the O(2) atom forms a strong intermolecular O . . . H—N hydrogen bond and makes another short contact with the 5′-hydroxyl group (Table 3). Similar lengthening of C(2)—O(2) and simultaneous shortening of the C(2)—N(3) bond was observed in thymine monohydrate crystals (36). In that compound the O(2) atom also forms two hydrogen bonds. In most of the other compounds mentioned above the O(2) atom is not involved in hydrogen bonding. In araU (30, 31) and arabinofuranosyl-4-thiouracil (37), O(2) forms a strong O . . . H—O bond. However, the C(2)—O(2) and C(2)—N(3) bonds are of normal length in the two latter structures.

The pyrimidine moiety of araU-5-propyne is in an *anti* orientation with respect to the sugar ring. The distances from the C(6) atom to O(4′) and O(2′) are 2.718(3) and 3.307(3) Å, respectively. The glycosidic torsion angle, C(6)—N(1)—C(1′)—O(4′) (χ), is 33.7°. It falls in the upper range of the values observed in arabinonucleosides.

The distribution of the glycosidic torsion angles observed in the solid state is shown in Fig. 3*b*. The *syn* conformation was observed only in 8-morpholino-1-(β-D-arabinofuranosyl)-adenine (38), in which a very bulky group was attached at C(8). This conformation was additionally stabilized by an intramolecular O(5′)—H . . . N(3) hydrogen bond. When *n*-butylamine was substituted at C(8) the usual *anti* conformation was found. The reported angles span a narrow range from 14 to 37° (except for arabinofuranosyladenine (39)), with very little dependence on the sugar conformation. The average value for five molecules with the *N*-type conformation is 30.0°, and for eight molecules with the *S*-type conformation is 25.5°. This χ angle distribution differs markedly from that for ribo- and deoxyribonucleosides in the *anti* conformation. The average values in the N type state are $\langle\chi\rangle$ = 19° for ribo- and 20° for deoxyribonucleosides (with very limited data for the 2′-deoxy series); for the *S*-type state $\langle\chi\rangle$ = 52° for ribo- and 39° for deoxyribonucleosides (25). Similar conclusions regarding the narrowing of the range of the χ angle in arabinonucleosides and

[5] The structure of arabinofuranosylthymine has also been determined (33); however, the somewhat lower precision of this study does not warrant a meaningful comparison for such small effects.

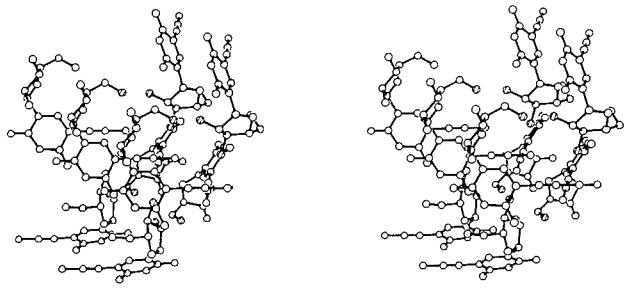

FIG. 4. Stereoscopic view of the environment of the propynyl group (shown in the center of the diagram). Surrounding oxygen atoms are dashed.

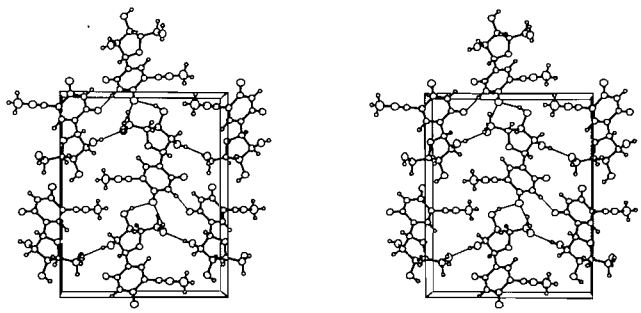

FIG. 5. Stereoscopic view of the unit cell with hydrogen bonds marked.

different dependence on the sugar conformation than found in ribonucleotides were put forward by Yathindra and Sundaralingam (40) on the basis of semi-empirical energy calculations.

Propynyl group

This group is nearly linear and is inclined by 3.7° to the pyrimidine ring plane. The C(7)≡C(8) triple bond, at 1.121(3) Å, is very short. The average C≡C bond in the propynyl group obtained from a search of the Cambridge Database (41) is 1.189 Å (for 34 compounds). In a related compound, dUrd-5-ethyne, the C≡C bond length of 1.182 Å is in the usual range. The pyrimidine C(5) to C≡C single bond is 0.03 Å shorter in dUrd-5-ethyne than in araU-5-propyne. The shortest reported triple bond in a propynyl group was observed in *N,N*-dimethyl-(*O*-ethyl)phenylpropiolamidium tetrafluoroborate (42) and was 1.149 Å. The authors suggested that this shortening could result from an intermolecular interaction of the C≡C bond with a neighboring aromatic six-membered ring. They also observed the shortening of a bond in the ring closest and parallel to the C≡C bond. The distance between the centers of these bonds was 3.47 Å. A similar arrangement is also present in araU-5-propyne. The environment of the propynyl group is shown in Fig. 4. The C(7)≡C(8) bond is parallel to the N(1)—C(6) bond and the corresponding distances are C(7)...N(1) = 3.542(3) Å and C(8)...C(6) = 3.445(3) Å. In addition, each C atom of the propynyl group is in close contact with an oxygen atom: C(7)...O(4′) = 3.212(3) Å, C(8)...O(3′) = 3.165(3) Å, and C(9)...O(3′) = 3.179(3) Å.

The atoms of the propynyl group vibrate with increasing amplitude the further they are from the center of the ring (see Fig. 1). The equivalent isotropic temperature factor, U_{iso}, increases by 0.011 from C(7) to C(8) and by 0.015 from C(8) to C(9). Due to the large vibrational movements of the terminal methyl group the positions of the C(9) H atoms are poorly determined.

Crystal packing and hydrogen bonding

As was mentioned above there are no intramolecular hydrogen bonds. Instead, all H-bonding groups take part in an extensive network of intermolecular interactions. A stereoview of the unit cell is shown in Fig. 5 and the hydrogen bond geometry is presented in Table 3. The O(4) atom accepts two hydrogen bonds from the O(3′) and O(5′) hydroxyl groups in the molecule related by the $^{-}2_1$ screw axis. These bonds join molecules into chains parallel to the *z*-axis. These chains are joined through O(2′)—H...O(5′) bonds into layers parallel to the *yz* plane, and these in turn are joined through O(2)...H—N(3) bonds into a three dimensional network. As a result the crystals exhibit a high melting point, mp = 242°C.

1. E. DE CLERCQ and P. F. TORRENCE. J. Carbohydr. Nucleosides Nucleotides, **5**, 187 (1978).
2. W. H. PRUSOFF, M. S. CHEN, P. H. FISHER, T.-S. LIN, G. T. SHIAN, and R. F. SCHINAZI. Adv. Ophthalmol. **38**, 3 (1979).
3. F. BIGAR. Adv. Ophthalmol. **38**, 105 (1979).
4. K.-L. ELZE. Adv. Ophthalmol. **38**, 134 (1979).
5. E. DE CLERCQ, J. DESCAMPS, P. DE SOMER, P. J. BARR, A. S. JONES, and R. T. WALKER. Proc. Natl. Acad. Sci. USA, **76**, 2947 (1979).
6. E. DE CLERCQ, J. DESCAMPS, G. VERHELST, R. T. WALKER, A. S. JONES, P. F. TORRENCE, and D. SHUGAR. J. Infect. Dis. **141**, 563 (1980).
7. H. MACHIDA, S. SAKATA, A. KUNINAKA, H. YOSHINO, C. NAKAYAMA, and M. SANEYOSHI. Antimicrob. Agents Chemother. **16**, 158 (1979).
8. H. MACHIDA, A. KUNINAKA, H. YOSHINO, K. IKEDA, and Y. MIZUNO. Antimicrob. Agents Chemother. **17**, 1030 (1980).
9. H. MACHIDA, S. SAKATA, S. SHIBUYA, K. IKEDA, C. NAKAYAMA, and M. SANEYOSHI. *In* Antiviral chemotherapy: design and inhibitors of viral functions. *Edited by* K.K. Gauri. Academic Press Inc., New York. 1981. pp. 207–217.
10. H. MACHIDA, S. SAKATA, A. KUNINAKA, and H. YOSHINO. Antimicrob. Agents Chemother. **20**, 47 (1981).
11. J. PERMAN, R. A. SHARMA, and M. BOBEK. Tetrahedron Lett. 2427 (1976).
12. P. J. BARR, A. S. JONES, P. SERAFINOWSKI, and R. T. WALKER. J. Chem. Soc. Perkin Trans. **I**, 1263 (1978).
13. E. DE CLERCQ. Meth. Find. Exptl. Clin. Pharmacol. **2**, 253 (1980).
14. E. DE CLERCQ, J. DESCAMPS, G.-F. HUANG, P. F. TORRENCE, D. E. BERGSTROM, A. S. JONES, P. SERAFINOWSKI, G. VERHELST, and R. T. WALKER. MOL. PHARMACOL. **21**, 217 (1982).
15. M. J. ROBINS and P. J. BARR. Tetrahedron Lett. 421 (1981).
16. M. J. ROBINS and P. J. BARR. J. Org. Chem. **48**, 1854 (1983).
17. E. DE CLERCQ, J. DESCAMPS, J. BALZARINI, J. GIZIEWICZ, P. J. BARR, and M. J. ROBINS. J. Med. Chem. **26**, 661 (1983).
18. I. EKIEL, E. DARZYNKIEWICZ, G. I. BIRNBAUM, and D. SHUGAR. J. Amer. Chem. Soc. **101**, 4724 (1979).
19. G. I. BIRNBAUM, M. CYGLER, I. EKIEL, and D. SHUGAR. J. Am. Chem. Soc. **104**, 3957 (1982).
20. P. TOUGARD. Biochem. Biophys. Res. Commun. **37**, 961 (1969).
21. I. EKIEL, M. REMIN, E. DARZYNKIEWICZ, and D. SHUGAR. Biochim. Biophys. Acta, **562**, 177 (1979).
22. G. A. GENTRY and J. F. ASWELL. Virology, **65**, 294 (1975).
23. G. M. SHELDRICK. SHELX76: Program for crystal structure determination. University of Cambridge, England. 1976.
24. C. ALTONA and M. SUNDARALINGAM. J. Am. Chem. Soc. **94**, 8205 (1972).
25. H. P. M. DE LEEUW, C. A. G. HAASNOOT, and C. ALTONA. Isr. J. Chem. **20**, 108 (1980).
26. R. PARTHASARATHY, J. M. OHRT, and G. B. CHHEDA. Biochem-

istry, **16**, 4999 (1977).
27. J. SHERFINSKI and R. E. MARSH. Acta Crystallogr. B**29**, 192 (1973).
28. E. WESTHOF and M. SUNDARALINGAM. J. Am. Chem. Soc. **102**, 1493 (1980).
29. P. TOUGARD and O. LEFEBVRE-SOUBEYRAN. Acta Crystallogr. B**30**, 86 (1974).
30. P. TOLLIN, H. R. WILSON, and D. W. YOUNG. Acta Crystallogr. B**29**, 1641 (1973).
31. J. SHERFINSKI and R. E. MARSH. Acta Crystallogr. B**30**, 873 (1974).
32. D. W. YOUNG, P. TOLLIN, and H. R. WILSON. Acta Crystallogr. B**25**, 1423 (1969).
33. P. TOUGARD. Acta Crystallogr. B**29**, 2227 (1973).
34. P. J. BARR, T. A. HAMOR, and R. T. WALKER. Acta Crystallogr. B**34**, 2799 (1978).
35. T. A. HAMOR, M. K. O'LEARY, and R. T. WALKER. Acta Crystallogr. B**33**, 1218 (1977).
36. R. GERDIL. Acta Crystallogr. **14**, 333 (1961).
37. W. SAENGER. J. Am. Chem. Soc. **94**, 621 (1972).
38. V. SWAMINATHAN, M. SUNDARALINGAM, J. B. CHATTOPADHYAYA, and C. B. REESE. Acta Crystallogr. B**36**, 828 (1980).
39. G. BUNICK and D. VOET. Acta Crystallogr. B**30**, 1651 (1974).
40. N. YATHINDRA and M. SUNDARALINGAM. Biochim. Biophys. Acta, **564**, 301 (1979).
41. F. H. ALLEN, S. BELLARD, M. D. BRICE, B. A. CARTWRIGHT, A. DOUBLEDAY, H. HIGGS, T. HUMMELINK, B. G. HUMMELINK-PETERS, O. KENNARD, W. D. S. MOTHERWELL, J. R. RODGERS, and D. G. WATSON. Acta Crystallogr. B**35**, 2331 (1979).
42. M. VAN MERSSCHE, G. GERMAIN, and J. P. DECLERCQ. Acta Crystallogr. B**33**, 1622 (1977).
43. A. K. CHWANG, M. SUNDARALINGAM, and S. HANESSIAN. Acta Crystallogr. B**30**, 2273 (1974).
44. G. I. BIRNBAUM, M. CYGLER, K. A. WATANABE, and J. J. FOX. J. Am. Chem. Soc. **104**, 7626 (1982).
45. J. S. SHERFINSKI, R. E. MARSH, A. K. CHWANG, and M. SUNDARALINGAM. Acta Crystallogr. B**35**, 2141 (1979).
46. G. I. BIRNBAUM. Private communication.
47. G. I. BIRNBAUM, E. DARZYNKIEWICZ, and D. SHUGAR. J. Am. Chem. Soc. **97**, 5904 (1975).
48. S. NEIDLE, G. L. TAYLOR, and A. B. ROBINS. Acta Crystallogr. B**34**, 1838 (1978).
49. J. L. SMITH, A. CHWANG, and M. SUNDARALINGAM. Acta Crystallogr. B**36**, 833 (1980); D. H. HARRISON, R. F. SCHINAZI, and B. H. RUBIN. J. Med. Chem. **25**, 1507 (1982), and references cited therein.

The hydration parameter and the excess acidity functions in $H_2SO_4-H_2O$ and $HClO_4-H_2O$ media

PIETRO GIUSEPPE TRAVERSO
Istituto di Chimica Industriale, Università, calle Larga S. Marta 2137, 30123 Venezia, Italy

Received June 20, 1983

PIETRO GIUSEPPE TRAVERSO. Can. J. Chem. **62**, 153 (1984).

Excess acidities, X, for aqueous H_2SO_4 and $HClO_4$ are derived under conditions of fixed pK_{BH^+} and m^* in both media, and of fixed m^* only, and compared among themselves and with newly derived and previous scales obtained without constraint, or with fixed pK_{BH^+} values. Analysis shows few or no real differences among these scales, which means that the equation $\log I + \log C_{H^+} = pK_{BH^+} + m^*X$ applies without the necessity of involving a "second-order" $m^{**}X^2$ term, at least for these media.

PIETRO GIUSEPPE TRAVERSO. Can. J. Chem. **62**, 153 (1984).

On a dérivé les acidités en excès, X, des milieux aqueux de H_2SO_4 et de $HClO_4$ pour des conditions où le pK_{BH^+} et le m^* sont fixés dans les deux milieux ainsi que lorsqu'uniquement m^* est fixé; on compare ces valeurs entre elles, avec les nouvelles échelles ainsi qu'avec les anciennes échelles obtenues sans contrainte ou avec des valeurs fixés de pK_{BH^+}. L'analyse ne révèle que peu ou pas de différence réelle parmi ces échelles, ce qui signifie que l'équation $\log I + \log C_{H^+} = pK_{BH^+} + m^*X$ s'applique sans la nécessité de faire intervenir un terme du "second degré" $m^{**}X^2$, au moins pour ces milieux.

[Traduit par le journal]

Introduction

In the last ten years the original Bunnett–Olsen (1) method of defining the basicity of organic bases has begun to be replaced by the excess acidity method, at least in aqueous H_2SO_4 and $HClO_4$. The latter method is a logical development of the first. Two parameters, pK_{BH^+} and the "solvation parameter", ϕ_e (1), n (2, 3), or m^* (4), are judged to be necessary (and sufficient) to describe the protonation equilibria of weak bases. Solvation parameters are becoming more important, mainly due to the results obtained by measuring the protonation of some representative compounds in the gas phase (5), for estimating the hydration behaviour of different classes of base (5, 6).

$$[1] \quad \log I - \log C_{H^+} = pK_{BH^+} + m^*X$$

The excess acidity functions X arise from a "first-order" approximation (7), defined by eq. [1] according to Cox and Yates' symbolism (4, 7).[1] The parameter m^* in eq. [1] is invariant with acid concentration.

$$[2] \quad \log I - \log C_{H^+} = pK_{BH^+} + m^*X + m^{**}X^2$$

A "second-order" approximation (7) has recently been proposed. Edward *et al.* (9) analyzed some data obtained in aqueous DMSO mixtures, and showed that the first-order approximation was insufficiently accurate in that case. Accordingly the new relation [2] was suggested (7, 9). It states that the m^* term in eq. [1] would *not* be invariant with acid concentration. The second-order approximation is undoubtedly superior to the first one, in principle. Hence one is forced to suspect that the results which have been obtained to date by the first-order approximation (e.g. equilibrium constants, hydration parameters, also the interpretations of them and of some reaction mechanisms), might suffer from error, possibly larger than that expected from experimental uncertainties only.

The aim of this paper is to show that this seems not to be the case, at present, in the most studied aqueous acid solutions, H_2SO_4 and $HClO_4$.

Experimental

All the computations used the mathematical procedure previously described (2, 3), partially modified to allow two parameters, m^* and pK_{BH^+}, to be fixed. In order to constrain both parameters, a slight change was adopted in step (*ii*) of the mathematical procedure in ref. 3. For each indicator, a 2×2 system was required, having the above parameters as unknowns. The same system had to be a 3×3 one in the case of pairs of corresponding indicators for the two acid media, since three unknowns were required for two connected indicators. When both parameters were fixed for the pair, as happens in the present case, a 2×2 system again results, now involving data for two indicators. Only a few experimental $\log I$ values were discarded, mainly those measured in the lowest acidity ranges (up to 0.2 M). This is because very small errors in C_{H^+} may cause large errors in the $\log I - \log C_{H^+}$ values.

The solutions obtained by the mathematical treatments are a mass of m^* and pK_{BH^+} values, and a generatrix (3) excess acidity function which is analytically expressed in polynomial form. The algorithm converges starting from the option *zero*,[2] that is by choosing the starting set $a_0 = a_1 = \ldots = a_i = 0$ (a_i are the polynomial coefficients).

The excess acidity functions which are compared in Fig. 1 are the generatrix functions obtained. The ones on the y axis of plots (e) and (f) in Fig. 1. were obtained as follows. The tabulated generatrix functions were multiplied by $m_f/m_{f'}$, where m_f is the hydration parameter of ferrocene, and $m_{f'}$ is the value related to the excess acidity function on the x axis. It is gratifying to observe that the slopes of plots (e) and (f) are very close to the expected value of unity.

Results and discussion

Three main arguments induce us to believe that the m^{**} term in eq. [2] is probably unnecessary, at least at present, in aqueous H_2SO_4 and $HClO_4$: (a) the discussions of Scorrano and co-workers (5, 6) showing how the parameter m^* in eq. [1] (in terms of ϕ_e) can be used to compare the solvation requirements of weak bases; (b) the latest results of Marziano *et al.* (3),

[1] Cox and Yates' symbolism is adopted in this paper because it has gained much more diffusion in the literature than the one previously proposed in ref. 2. The term m^*X represents the "excess acidity" of the weak base B, according to Perrin's definition (8). X itself represents the excess acidity of a defined hypothetical indicator.

[2] This option is chosen, as usual, in order to avoid misleading interpolations (14). A starting set of parameters must necessarily be chosen in order for the program to operate.

Can. J. Chem. Downloaded from www.nrcresearchpress.com by 210.87.254.105 on 09/06/12
For personal use only.

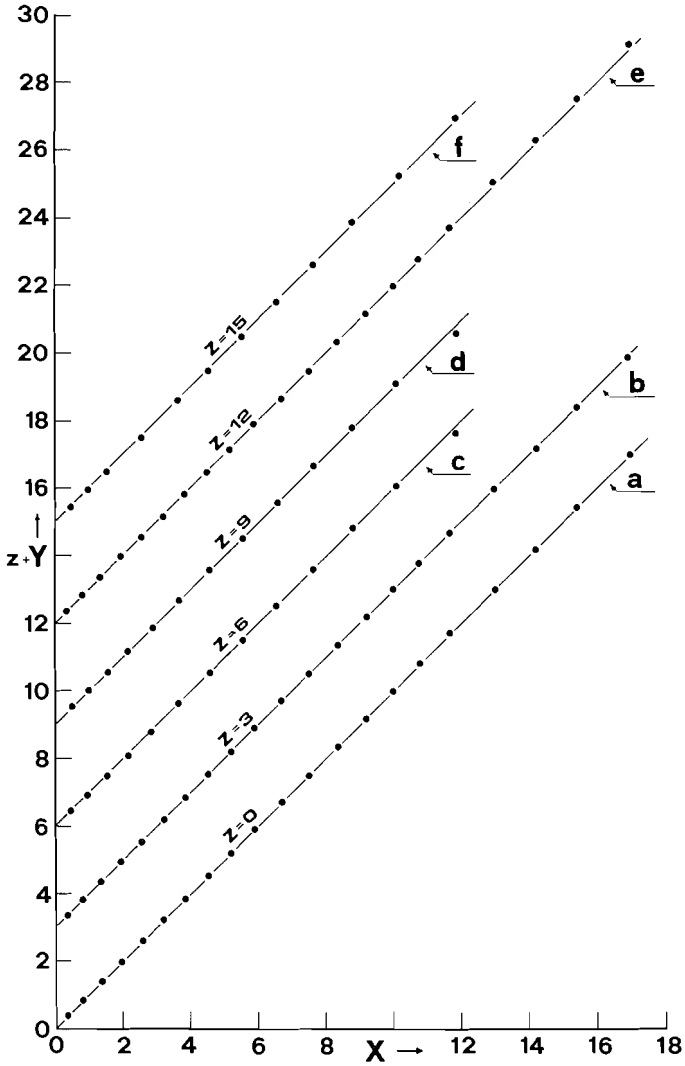

FIG. 1. Comparisons between the differently obtained excess acidity functions in this paper. x axis, excess acidities with: m^* and pK_{BH^+} fixed in $H_2SO_4-H_2O$ and in $HClO_4-H_2O$. y axis, excess acidities with: line a (H_2SO_4), m^* fixed; line b (H_2SO_4), pK_{BH^+} fixed; line c ($HClO_4$), m^* fixed; line d ($HClO_4$), pK_{BH^+} fixed; line e (H_2SO_4) and line f ($HClO_4$), no term fixed.

which have shown that the first-order approximation is compatible with the possibility of obtaining the same pK_{BH^+} values for the same indicators regardless of medium ($H_2SO_4-H_2O$ or $HClO_4-H_2O$); and (c) the observation that the ($-H_{GF}$ − log C_{H^+}) functions (10) are linearly related to the X (or M_C) functions (3, 5) and give equal m^* values in both acid media.[3]

If the first approximation can be accepted, and *if* the m^* terms are solvation parameters, one may expect the m^* values to be the same for the same bases regardless of the aqueous medium. They should be invariant because water is the common reference state. If the m^{**} terms were not very small in both aqueous solutions, the results in ref. 3 could hardly have been obtained.

We will examine this question (1) by calculating excess acidity functions for H_2SO_4 and $HClO_4$ simultaneously, forcing the weak bases to have the same m^* values regardless of medium; (2) by recalculating previous functions simultaneously, forcing the indicators to have the same pK_{BH^+} and m^* values regardless of medium; and (3) by comparing these results to each other and to the results which can be obtained without any constraint, or with the constraint in ref. 3.

TABLE 1. Multiple correlation coefficients (r), standard errors (S.E.), and slopes of the plots in Fig. 1

Line	r	S.E.	Slope
a	0.99999	1.03×10^{-3}	1.00±0.02
b	0.99999	0.81×10^{-3}	1.00±0.02
c	0.99986	5.1×10^{-3}	1.00±0.02
d	0.99981	5.9×10^{-3}	1.01±0.03
e	0.99995	2.04×10^{-3}	1.06±0.05
f	0.99990	4.2×10^{-3}	0.95±0.04

Lines a, b, c, d: 95% confidence interval from a simple regression analysis; lines e, f: the standard errors of estimate of each m^*_{lcc} values are also accounted for.

TABLE 2. Mean-square errors of the excess acidity functions obtained

Fixed term	Acid	σ^2
None	H_2SO_4	1.87×10^{-3}
None	$HClO_4$	1.49×10^{-3}
m^*	Both	1.92×10^{-3}
pK_{BH^+}	Both	1.93×10^{-3}
m^*, pK_{BH^+}	Both	2.78×10^{-3}

Some new carefully-measured log I values (11) were added to the set of data previously used in defining the M_C scale (2, 3). In addition ($-H_{GF}$ − log C_{H^+}) values derived from ref. 10 were processed. Inorganic anion values, and some kinetic data for benzene and halobenzenes used in (3), were discarded.[4] Seventy-one weak bases in $HClO_4-H_2O$ (782 experimental values), and 138 in $H_2SO_4-H_2O$ (1235 experimental values) were processed; results for 31 "key" indicators (3) were available in both media.

The plots in Fig. 1 show the comparisons among the excess acidity functions obtained in the acidity ranges 0−18.4 M H_2SO_4 and 0−13 M $HClO_4$. No essential difference among the derived functions can be deduced from the plots. The depicted points have excellent straight-line correlations; quantitative data are given in Table 1. The standard errors and r-values show that almost exactly the same excess acidity functions are obtained if pK_{BH^+}, or m^*, or m^* and pK_{BH^+}, are fixed, or when no term is fixed. This observation is reinforced by the analysis and comparison of the mean-square errors (σ^2 values) in Table 2. These are affected very little whether no, one, or two parameters are fixed; a variation of 0.95×10^{-3} units in σ^2 is too small to interpret, unless by accepting that it is due entirely to experimental uncertainty.

In Figs. 2 and 3 two very expressive comparisons are shown. The plots in Fig. 2. show the comparisons among the pK_{BH^+} values which have been obtained by processing the experimental data in $H_2SO_4-H_2O$ and $HClO_4-H_2O$ simultaneously, ensuring that indicators have the same pK_{BH^+} values, or the

[3]This fact can easily be observed by comparing the interpolated X and M_C functions, related to the same reference base, and the ($-H_{GF}$ − log C_{H^+}) functions (which are also excess acidity functions) in the cited media.

[4]Satisfactory straight lines for the discarded data were found by plotting the cited values against the M_C functions (2, 3), but the interpretations of such observations are still an open problem (12).

Can. J. Chem. Downloaded from www.nrcresearchpress.com by 210.87.254.105 on 09/06/12
For personal use only.

Can. J. Chem. Downloaded from www.nrcresearchpress.com by 210.87.254.105 on 09/06/12
For personal use only.

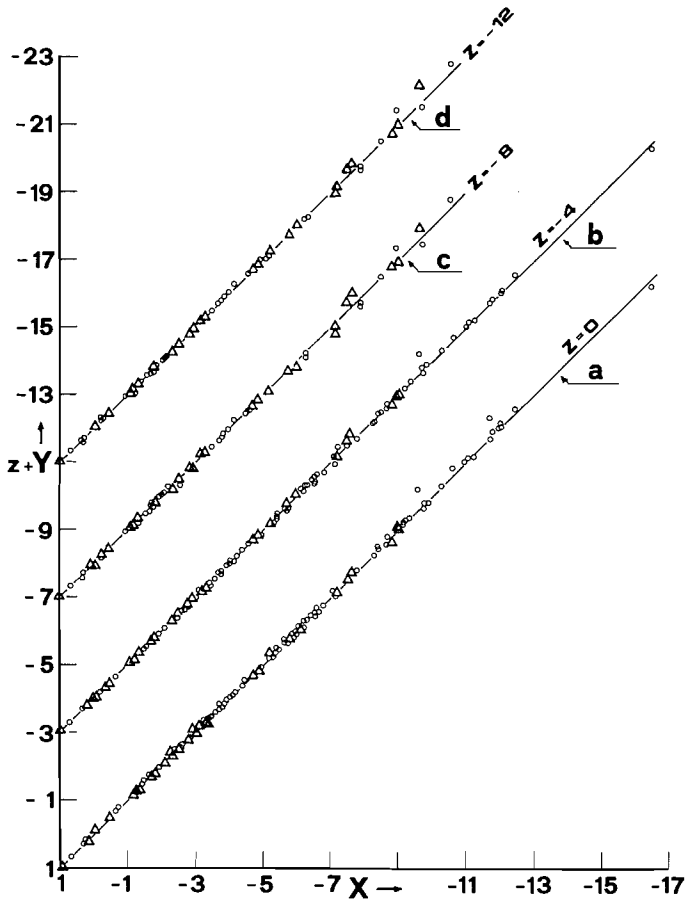

FIG. 2. Comparisons between the differently obtained pK_{BH^+} values in this paper. x axis: m^* and pK_{BH^+} are fixed in $H_2SO_4-H_2O$ and in $HClO_4-H_2O$. y axis: lines a and b (H_2SO_4), m^* or pK_{BH^+} fixed, respectively; lines c and d ($HClO_4$), m^* or pK_{BH^+} fixed, respectively. (△ = key compounds).

same m^* values, or the same pK_{BH^+} and m^* values, regardless of medium. The depicted points show that the imposed constraints do not essentially modify the pK_{BH^+} values.

The plots in Fig. 3 lead to the same conclusions one derives from Fig. 2, now referring to the hydration parameters m^*. Only four points are outside the expected ranges around the diagonals in Fig. 3. These are analyzed in Table 3. The σ values show that the experimental log I data are well correlated by all of the excess acidity functions. Hence these "exceptions" are only apparent ones, easily justified by the experimental uncertainties.

The data comparison in Figs. 2 and 3 is also shown in Table 4, where the results obtained by regression analysis are given. Only the data referring to the "key" indicators have been processed, because they have (and are expected to have) a wider spread around the diagonals. These results show no reason to deny the strong suggestion that the same indicators have the same pK_{BH^+} and m^* values regardless of medium.

Conclusions

All the results of the previous analysis are in accord with the opinion that the second-order approximation (7) is unnecessary in $H_2SO_4-H_2O$ and in $HClO_4-H_2O$, at least at present. The results must mean that the term m^{**} in eq. [2] is very small. Hence the chemical information which has been obtained to date by means of the excess acidity functions can still be reasonably accepted. Nothing has been found which suggests that the uncertainties are larger than the ranges suggested by the random experimental errors.

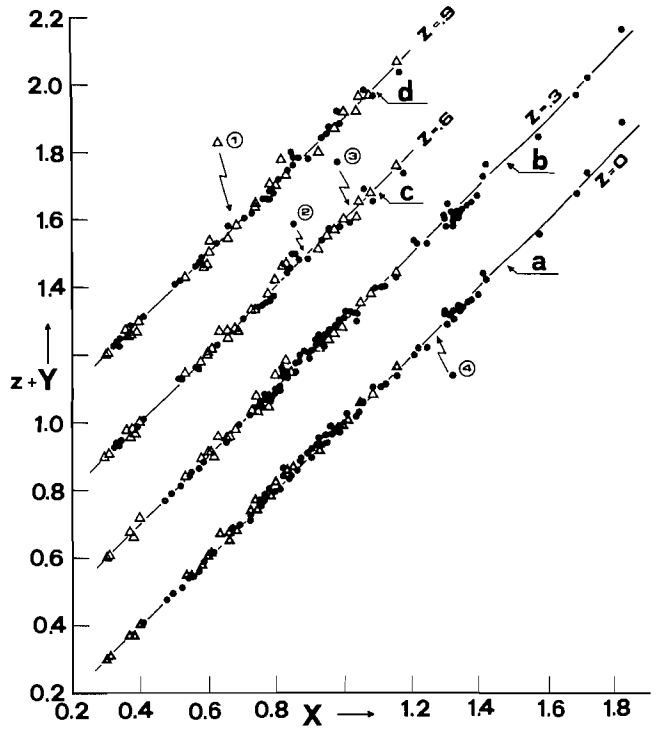

FIG. 3. Comparisons between the differently obtained hydration terms m^*. x axis: m^* and pK_{BH^+} are fixed. y axis: lines a and b (H_2SO_4), m^* or pK_{BH^+} fixed, respectively; lines c and d ($HClO_4$), m^* or pK_{BH^+} fixed, respectively. (△ = key compounds.) The x and y axes are expanded with respect to (4); the depicted m^* hydration term of ferrocene on the x axis is 1.156. (1): 4-Nitroaniline; (2): *N*,*N*-diethyl-2,4-dinitroaniline; (3): *N*,*N*-dimethyl-4-nitroaniline; (4): 2-methylindole.

TABLE 3. The quadratic means of errors (σ), obtained by comparing the excess acidity functions of indicators 1–4 (Fig. 3) with the experimental log I − log C_{H^+} values

	Fixed term				
No.	m^*	pK_{BH^+}	m^*, pK_{BH^+}	None, H_2SO_4	None, $HClO_4$
1	0.032	0.030	0.033	0.031	0.027
2	0.009	0.008	0.008	—	0.009
3	0.017	0.017	0.017	—	0.017
4	0.009	0.010	0.010	0.009	—

The differences between the excess acidity functions derived in this paper and previous ones (2–4) are small enough to dissuade us from suggesting new scales and from tabulating new pK_{BH^+} and m^* (or n) values.[5]

When the excess acidity scales of different authors have to be compared, a common "reference" must be found. This is still an open problem. Some interesting proposals have been advanced (13, 14), but some complications remain. During the work presented in this paper it was observed that the ($-H_{GF}$ − log C_{H^+}) functions show large m^* values (more than twice as

[5]The new acidity scales and/or m^* and pK_{BH^+} values, and the computer program used, can be obtained from the author on request.

TABLE 4. A comparison among slopes, intercepts, and some relevant statistical values, for the plots in Figs. 2 and 3[a]

Figure, line	r	Slope	Intercept	S.E.[b]	S.E.I.[c]
2, a	0.9998	1.00±0.01	-2.9×10^{-2}	4.0×10^{-3}	1.9×10^{-2}
2, c	0.9990	0.99±0.02	7.0×10^{-2}	8.4×10^{-3}	4.5×10^{-2}
2, b or d	0.9997	0.99±0.02	8.1×10^{-3}	4.5×10^{-3}	2.1×10^{-2}
3, a or c	0.9975	0.99±0.01	-2.7×10^{-3}	1.3×10^{-2}	1.0×10^{-2}
3, b	0.9952	1.00±0.04	-7.2×10^{-2}	1.9×10^{-2}	1.4×10^{-2}
3, d	0.9964	0.97±0.04	1.4×10^{-3}	1.6×10^{-2}	1.2×10^{-2}

[a]Only point 1 in plot d, Fig. 3, is discarded.
[b]S.E. = standard error of estimate.
[c]S.E.I. = standard error of intercept.

large as the nitroanilines). Moreover the experimental H_{GF} values are spread over wide acidity ranges. These facts might suggest a choice of the excess acidity function of ferrocene as the reference, notwithstanding some approximations (15). We have followed this suggestion in order to obtain plots (e) and (f) in Fig. 1. It is apparent that both slopes are strictly unity, as expected when a good reference is chosen.

As a corollary it can be underlined that the results in this paper suggest that Wojcik's theoretical objection (16) is not likely to be of serious consequence in $H_2SO_4-H_2O$ and in $HClO_4-H_2O$ media. Nevertheless we advise against the opinion that the second-order approximation might be unnecessary in general. Many acid solutions probably exist where the first-order approximation is not sufficient. This will form the thesis of a future paper.

Acknowledgements

Robin A. Cox and Keith Yates generously made their paper "Acidity functions: an update" available to us before publication. We also wish to thank Dr. Cox for some suggestions, and for help with the English version of this paper. We are deeply indebted to A. Tomasin and to E. Moretti for their support in the mathematical treatments.

1. J. F. BUNNETT and F. P. OLSEN. Can. J. Chem. **44**, 1899 (1966).
2. N. C. MARZIANO, P. G. TRAVERSO, A. TOMASIN, and R. C. PASSERINI. J. Chem. Soc. Perkin Trans. 2, 309 (1977).
3. N. C. MARZIANO, A. TOMASIN, and P. G. TRAVERSO. J. Chem. Soc. Perkin Trans. 2, 1070 (1981).
4. R. A. COX and K. YATES. J. Am. Chem. Soc. **100**, 3861 (1978).
5. E. M. ARNETT and G. SCORRANO. Adv. Phys. Org. Chem. **13**, 83 (1976).
6. P. BONVICINI, A. LEVI, V. LUCCHINI, C. MODENA, and G. SCORRANO. J. Am. Chem. Soc. **95**, 5960 (1973); A. LEVI, G. MODENA, and G. SCORRANO. J. Am. Chem. Soc. **96**, 6585 (1974); R. CURCI, F. DI FURIA, A. LEVI, V. LUCCHINI, and G. SCORRANO. J. Chem. Soc. Perkin Trans. 2, 341 (1975); V. LUCCHINI, G. MODENA, G. SCORRANO, and U. TONELLATO. J. Am. Chem. Soc. **99**, 3387 (1977); G. PERDONCIN and G. SCORRANO. J. Am. Chem. Soc. **99**, 6983 (1977).
7. R. A. COX and K. YATES. Can. J. Chem. **61**, 2225 (1983).
8. C. PERRIN. J. Am. Chem. Soc. **86**, 256 (1964).
9. J. T. EDWARD, M. SJÖSTRÖM, and S. WOLD. Can. J. Chem. **59**, 2350 (1981).
10. J. JANATA and G. JANSEN. J. Chem. Soc. Faraday Trans. 1, **68**, 1656 (1972).
11. J. T. EDWARD, G. D. DERDALL, and S. C. WONG. Can. J. Chem. **55**, 2331 (1977); J. T. EDWARD and S. C. WONG. Can. J. Chem. **57**, 1980 (1979).
12. P. G. TRAVERSO, N. C. MARZIANO, and R. C. PASSERINI. J. Chem. Soc. Perkin Trans. 2, 845 (1977); N. C. MARZIANO, P. G. TRAVERSO, and G. G. CIMINO. J. Chem. Soc. Perkin Trans. 2, 574 (1980); R. G. COOMBES, R. B. MOODIE, and K. SCHOFIELD. J. Chem. Soc. B, 800 (1968).
13. R. A. COX and K. YATES. Can. J. Chem. **59**, 2116 (1981).
14. V. LUCCHINI, G. MODENA, G. SCORRANO, R. A. COX, and K. YATES. J. Am. Chem. Soc. **104**, 1958 (1982).
15. Y. A. MODRO, K. YATES, and J. JANATA. J. Am. Chem. Soc. **97**, 1942 (1975).
16. J. F. WOJCIK. J. Phys. Chem. **86**, 145 (1982).

Can. J. Chem. Downloaded from www.nrcresearchpress.com by 210.87.254.105 on 09/06/12
For personal use only.

Fall-off shape and incubation times in weak-collision thermal unimolecular reactions

H. O. PRITCHARD

Centre for Research in Experimental Space Science, York University, Downsview, Ont., Canada M3J 1P3

Received March 30, 1983

H. O. PRITCHARD. Can. J. Chem. **62**, 157 (1984).

A new formula for the weak-collision unimolecular rate constant is readily interpretable in terms of bottleneck concepts. This formula is used to explore the correlation between variations in relaxation structure and fall-off shape in weak-collision thermal unimolecular reactions; some information is also presented relating to collision efficiency factors β_c, and to incubation times.

It is conjectured that randomisation failure is an important feature which causes near-Lindemann behaviour to occur in practical weak-collision thermal reactions.

H. O. PRITCHARD. Can. J. Chem. **62**, 157 (1984).

Une nouvelle formule pour la constante de vitesse unimoléculaire pour les collisions faibles peut être interprétée facilement en fonction de concepts "d'emboutaillage". On utilise cette formule pour étudier la corrélation existant entre les variations dans la structure de relaxation et la forme de chute des réactions thermiques unimoléculaires à faibles collisions. On présente également quelques informations relatives au facteur d'efficacité de collision β_c et aux temps d'incubation. Il est possible que le fait que la distribution au hasard ne s'établisse pas soit une caractéristique importante qui provoque un comportement pratiquement égal à celui prevu par Lindemann lors de réactions thermiques à faibles collisions.

[Traduit par le journal]

Can. J. Chem. Downloaded from www.nrcresearchpress.com by 210.87.254.6 on 09/06/12
For personal use only.

Introduction

It was shown recently that the placing of a bottleneck in the activation process for a thermal unimolecular reaction could lead to the occurrence of strict Lindemann behaviour in the fall-off (1); it has also been found that if the randomisation processes become rate-limiting, strict Lindemann behaviour likewise ensues (2). Since several weak-collision thermal systems exhibit fall-off behaviour which is very close indeed to strict Lindemann (3), it is important to decide whether such behaviour may result from a bottleneck in the activation ladder or from a bottleneck in the randomisation process (or, perhaps, a combination of both). Unfortunately, our original model of a bottleneck in the activation ladder (1) was an extremely artificial one, for which the same fall-off shape results no matter at what point below threshold the bottleneck is placed. In the present note, therefore, we investigate numerically an extremely simple stepladder model of a weak-collision thermal reaction, in order to find out what kinds of patterns of activation parameters might lead to the occurrence of strict Lindemann behaviour; also, since it may be possible to make a classification into weak- or strong-collision behaviour on the basis of the observed ratio of the incubation time (τ_{inc}) to the relaxation time (τ_{rel}) (4–6), a cursory inspection of these ratios is also undertaken.

The use of tridiagonal matrices to describe weak-collision unimolecular reactions

The rate constant for a thermal unimolecular reaction is calculated as the smallest eigenvalue γ_0 of a reaction matrix $[\mathbf{A} + \mathbf{D}]$ where $\mathbf{A}$ is (the negative of) the symmetrised form of the matrix $\mathbf{Q}$ describing relaxation processes among the states of the reactant molecule, and $\mathbf{D}$ is a diagonal matrix of decay rate constants for states above reaction threshold (6). Given the enormous number of states in any polyatomic molecule of practical interest, the individual elements of $\mathbf{Q}$ and $\mathbf{D}$ must represent suitably averaged rate constants which may be applied to groups of states (grains), in any feasible calculation.

Now, provided that the matrix $\mathbf{Q}$ does not have degenerate eigenvalues, it may be reduced by a similarity transformation to a tridiagonal matrix having non-zero entries on the codiagonal (7); the same is true of $\mathbf{A}$ or $[\mathbf{A} + \mathbf{D}]$. Also, in view of the complexity of the molecule, there can be no special relationships between the elements of $\mathbf{Q}$ so that, in general, it must be a non-degenerate matrix; in the unlikely event that a chance degeneracy could occur, it can always be removed by making an alternative choice for the graining. Thus, except for the strong-collision case, where the matrix $\mathbf{A}$ is totally degenerate (6, 8), any (weak-collision) unimolecular reaction process can be described by a tridiagonal reaction matrix, and the use of a tridiagonal matrix to represent the process does not imply a restriction to step-ladder or nearest-neighbour processes. As a consequence, those properties of a unimolecular reaction system which depend only upon the eigenvalues can be explored by the use of a tridiagonal matrix $[\mathbf{B} + \mathbf{D}]$. On the other hand, those unimolecular reaction properties which require the knowledge of the eigenvector(s) of $[\mathbf{A} + \mathbf{D}]$ will be defective unless the similarity transformation required to reduce the original, true, relaxation matrix $\mathbf{A}$ to the tridiagonal form $\mathbf{B}$ is known.

The rate constant for a tridiagonal reaction matrix

The rate constant for a tridiagonal reaction matrix was first derived in Theorem 4 of ref. 8, but the result was given in a rather forbidding recursive form which, although easy to compute, did not lend itself to intuitive analysis. More recently, Vatsya (9) has found a much more direct result, which may be written as

$$[1] \quad \gamma_0^{-1} = -\sum_{j=0}^{N-1} \frac{1}{J_{j+1}} \left[\sum_{i=0}^{j} \beta_i^{1/2} \prod_{l=1}^{j-1} \{B_{l,l+1}/J_{l+1}\} \right]^2$$

where N is the order of the matrix, β_i is the Boltzmann population in grain i, B_{ij} are the elements of the (symmetric) tridiagonal matrix, and

$$J_1 = -(B_{00} + D_{00})$$

$$J_{i+1} = -(B_{ii} + D_{ii} + B_{i-1,i}^2/J_i)$$

Equation [1] is valid provided only that γ_0 is small compared with the non-zero eigenvalues of $\mathbf{B}$, i.e. the relaxation rates; notice that unlike previous analytic solutions to the weak-collision problem, this solution is valid for all pressures, any pattern of transition probabilities, and any distribution of

Can. J. Chem. Downloaded from www.nrcresearchpress.com by 210.87.254.6 on 09/06/12
For personal use only.

energy levels. Furthermore, eq. [1] simplifies enormously at the low-pressure limit to a form which is amenable to intuitive analysis. Recalling our earlier discussion of bottleneck effects in diatomic dissociation (10), we may write an effective impedance associated with a transition between states j and $j + 1$ as

$$[2] \quad t_j = \left(\sum_{k=0}^{j} \beta_k\right)^2 / \beta_j q_{j,j+1}$$

which is obtained from eq. [17] of ref. 10 by neglecting some small quantities, and in which $q_{j,j+1}$ is the rate constant for the transition from state j to state $j + 1$, i.e. the codiagonal element of the unsymmetrised form of **B**. Let j_+ be the index of the first grain above the thermal threshold, and j_- be the index of the last grain below it. Then, providing that the total equilibrium population of the reactive states

$$\sum{}' \beta_j = \sum_{j=j_+}^{N-1} \beta_j$$

is negligible in comparison with the total population

$$\sum_{j=0}^{N-1} \beta_j = 1$$

the limiting low-pressure rate constant is given by

$$[3] \quad k_0 = \left[\sum_{j=0}^{j=j_-} t_j\right]^{-1}$$

Previous steady-state treatments of this problem have yielded [3], but with a slightly different form for the t_j (11–13); a proof of this result will be provided in a separate communication.

Thus, we have the potential for the occurrence of bottleneck effects in weak-collision unimolecular reactions similar to those which have been supposed to occur in diatomic dissociation (10) or inert-gas ionisation (14) processes; eq. [3] provides a straightforward vehicle for the examination of such effects.

A simple reaction model for exploring bottleneck properties

In order to make an initial exploration of possible bottleneck effects, it is useful to have a very simple reaction model, and the one used here is chosen to follow, in a rough and ready manner, the thermal dissociation of carbon dioxide. An energy span of 160 kcal mol^{-1} was divided into 40 equally spaced grains labelled 0 to 39: of these, 30 were below reaction threshold, and 10 above.

The tridiagonal relaxation matrix **Q** (unsymmetrised) was chosen in the form

$$[4a] \quad q_{i,i-1} = i^p q_{10}$$

where p is variable; the value q_{10}, the deactivation rate constant for the first excited grain, was taken to be fixed throughout the whole series of calculations, as 2.5×10^3 Torr^{-1} s^{-1}. The symmetrisation operation (6, 8, 10) requires a knowledge of the grain populations β_i, and two different models were explored, one labelled F where the state density was taken to be constant for all energies, and another labelled V in which the actual state densities for carbon dioxide were used; these two models give rise to markedly different population distribution functions β_i.

Likewise, the elements of the **D** matrix were chosen to have a very simple form, viz.

$$[4b] \quad d_i = \left(\frac{i - 29}{i}\right)^2 \times 10^{11} \text{ s}^{-1}$$

in other words, of RRK form with $s = 3$. The temperature was considered to be 4000 K throughout.

The major features examined in this series of numerical experiments were the fall-off shape, the apparent collision efficiency β_c, and the incubation time τ_{inc}, and their dependence, if any, on bottleneck features introduced into the system by variations in eqs. [4a] and [4b].

We introduce at this stage a very simple device for making comparison between the shapes of fall-off curves; the inappropriateness of the traditional measure, the Kassel s parameter, has been discussed extensively elsewhere (6, 8). Because the Lindemann form is a limiting shape (15, 16), we simply make a comparison between the observed shape and the strict Lindemann curve having the same high-pressure and low-pressure limits; this is most easily done by defining the area enclosed between the two curves, plotted in the usual log k vs. log p fashion, as a quantity Δ. We will consider two such quantities, Δ_S, the area between the strong-collision curve and Lindemann, and Δ_W, the area between the fall-off curve for the tridiagonal system and Lindemann.

The apparent collision efficiency β_c is defined in the usual way. The hard-sphere collision number for carbon dioxide at 4000 K is $\omega = 2.07 \times 10^6$ Torr^{-1} s^{-1}, given a collision diameter of 3.73 Å (17); thus, since the limiting low-pressure strong-collision rate constant is $k_{0,S} = \omega \Sigma' \beta_i$ (8), the apparent collision efficiency $\beta_c = k_0/k_{0,S} = k_0/\omega\Sigma'\beta_i$.

Calculation of the incubation time requires a knowledge of the eigenvector Ψ_0 of $[\mathbf{A} + \mathbf{D}]$ corresponding to γ_0, whence (4)

$$[5] \quad \tau_{inc} = \gamma_0^{-1} \ln [\mathbf{E}^{1/2}\boldsymbol{\beta}(0), \Psi_0)/(\Psi_0, \Psi_0)]$$

where $\mathbf{E}^{-1/2}$ is a matrix arising in the transformation symmetrising **Q** to **A** (6, 8, 10), and $\boldsymbol{\beta}(0)$ is the initial distribution, taken to be $\beta_0 = 1$, $\beta_i = 0$, $i \neq 0$. The notation (,) in [5] denotes the scalar product of two vectors, Ψ_0 is normalised so that $(S_0, \Psi_0) = 1$, and S_0 is the eigenvector of **A** corresponding to its zero eigenvalue. Unfortunately, the zeroth eigenvector ϕ_0 of $[\mathbf{B} + \mathbf{D}]$ is not equal to the zeroth eigenvector Ψ_0 of $[\mathbf{XBX}^T + \mathbf{D}]$, where $\mathbf{X}, \mathbf{X}^T$ denote the similarity transformation matrices required to reduce the original full symmetric relaxation matrix **A** to the tridiagonal form **B**; hence, the substitution of ϕ_0 for Ψ_0 in [5] restricts the conclusions concerning incubation times to a truly tridiagonal (i.e. step-ladder) model. However, it seems likely that the differences between step-ladder systems and general systems will only be in matters of detail, so that we can infer qualitative conclusions about incubation times from these calculations. It is usual to make a comparison of τ_{inc}/τ_{rel} and the relaxation time τ_{rel} is taken to be λ_1^{-1}, where λ_1 is the first non-zero eigenvalue of **B**. This is not strictly the relaxation time (4, 6), but the exact connection between τ_{rel} and λ_1^{-1} cannot be known unless the structure of the relaxation is known at a molecular level *within* grains; nevertheless, in practice, the disparity between τ_{rel} and λ_1^{-1} is not likely to be very severe when the uptake of vibrational energy is large (6), as it is in a reacting system.

Numerical results

Except for the high-pressure limit where the rate constant is $k_\infty = \Sigma \beta_i d_i$, and at the low-pressure limit where eq. [3] can be used, eq. [1] provides the most efficient method for calculating the rate constant as a function of pressure; standard matrix numerical methods are considerably slower.

Table 1 summarises two sets of calculations in which the value of p in eq. [4a] is varied, with designations F_p, V_p, for

TABLE 1. Variation of unimolecular reaction properties as a function of the parameter p in eq. [4a]

Case*	E_0 (kcal mol^{-1})	k_0 (Torr^{-1} s^{-1})	β_c	Δ_W	λ_1 (s^{-1})	τ_{inc}/τ_{rel}
F0	103.5	1.95×10^{-4}	3.1×10^{-4}	0.68	2.2×10^{2}	4.4
F1	102.8	5.52×10^{-3}	8.8×10^{-3}	0.64	1.6×10^{3}	3.2
F2	101.9	1.55×10^{-1}	2.5×10^{-1}	0.60	3.1×10^{3}	1.7
F3	100.6	4.31	6.8	0.56	3.7×10^{3}	1.2
Standard values: E_∞ = 129.2 kcal mol^{-1}; k_∞ = 2.47 × 10^2 s^{-1}; Δ_S = 0.29						
V0	75.1	1.56×10^{-1}	1.7×10^{-4}	0.66	1.0×10^{2}	3.2
V1	73.5	4.23	4.7×10^{-3}	0.61	1.0×10^{3}	3.1
V2	71.3	1.12×10^{2}	1.2×10^{-1}	0.55	2.2×10^{3}	1.8
V3	67.3	2.75×10^{3}	3.0	0.47	2.4×10^{3}	1.2
Standard values: E_∞ = 106.2 kcal mol^{-1}; k_∞ = 4.68 × 10^5 s^{-1}; Δ_S = 0.28						

*The case designation F means fixed state-density model, V means variable state-density model; the digit following is the (integer) value of p. Δ_S is the area contained between the strong-collision fall-off curve and the strict Lindemann form.

fixed, variable, state densities, respectively. Apart from some necessary differences, the two sets of calculations are remarkably similar: the rates are much higher in the variable density case because of the greater populations at higher energies, and the activation energies E_∞, E_0, are lower because the larger populations change more slowly with temperature.

In both sets, the low-pressure limiting rate constant increases strongly with increasing p in eq. [4a], despite the fact that q_{01}, q_{10}, remain unchanged throughout each set; along with this, β_c increases strongly too, and soon exceeds the value of unity! The increase in relaxation rate, λ_1 with p is much weaker.

In both sets too, the ratio of the incubation time to the relaxation time exceeds unity, as expected (4), by amounts typical of earlier numerical experiments (18, 19); notice that increasing p corresponds to an increasingly strong acceleration of the relaxation among the higher states of the molecule, causing τ_{inc} to decrease more quickly with p than does τ_{rel}. Also, although not detailed in Table 1, the ratio τ_{inc}/τ_{rel} appears to be rather insensitive to the degree of fall-off: for example, the values listed are for conditions close to the high-pressure limit, whereas at $p_{1/2}$, the ratio is 3.1 for case F1 and 3.0 for case V1.

The most startling feature of both calculations is that the computed fall-off curves are uniformly *much* broader than the strong-collision shape; the case F1 is shown in Fig. 1. This is in strong conflict with the experimental observation that many weak-collision thermal systems exhibit almost pure Lindemann behaviour (3) i.e. $\Delta_W \approx 0$, and conversely, that fall-off shapes broader than the strong-collision one are not seen. Thus, a major concern is how to choose a set of grained transition rates in such a way that we can achieve Lindemann behaviour, a problem which is examined in the next series of numerical experiments.

Certain conditions for the existence of strict Lindemann behaviour have been established recently as follows: (*i*) if there is only one (grained) reactive state above threshold, regardless of the form of the transition matrix **A** (8); (*ii*) if **A** is the strong-collision relaxation matrix, and all reactive grains have the same decay rate constant (8); (*iii*) if the relaxation above threshold is *very* much faster than that below threshold (1) — this was only proved for the case when both relaxations are of strong-collision form, but it may be true more generally; (*iv*) a fourth condition, proposed in ref. 3, has been shown to be unattainable (8).

Table 2 shows the results of a series of experiments to test

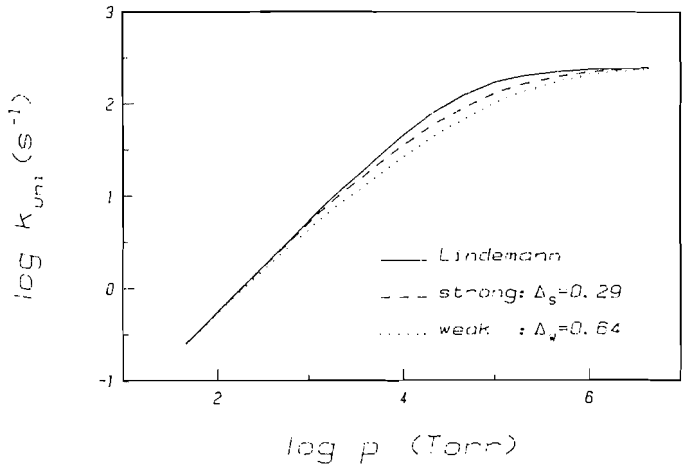

FIG. 1. Illustration of the method for characterising the shape of a unimolecular fall-off curve; the curves shown here are for the calculation labelled F1 in Table 1.

these points, with the results for cases F1 and V1 transcribed from Table 1 for comparison. Cases F1(1) and V1(1) are for p = 1 in eq. [4a], but with [4b] altered to read $d_i = 10^{11}$ s^{-1} for all $i \geq j_+$; these results are consistent with point (*ii*) above. Cases F1(0) and V1(0) are similar, but with $d_i = 10^{11}$ s^{-1} for $i = j_+$ only, and all other $d_i = 0$; this illustrates point (*i*). Point (*iii*) is partly illustrated in Table 1 because the larger the value of p in eq. [4a], the faster are the transitions between the reactive states. A further test of this point is made in cases V1(*a*), V1(*b*), and V1(*c*) in Table 2; notice that the differences between the F series and the V series of experiments are always small, and from here on, only the (more realistic) variable state-density results will be reported. These three cases all have the same relaxation matrix as case V1, except that the transition rates between grains *above threshold only* are all multiplied by a constant factor of 30, 100, or 1000 respectively; a significant progression towards strict Lindemann behaviour is found.

Since the transition probability distributions [4a] are smooth functions of the degree of excitation, none of the numerical experiments, except the last three, exhibits significant bottleneck effects in the sense described in ref. 10 and 14, i.e. that one of the t_j of eq. [2] is significantly *larger* than its neighbours — c.f. Fig. 1 of ref. 10. However, the arbitrary multiplication of all probabilities above threshold by these large factors auto-

Can. J. Chem. Downloaded from www.nrcresearchpress.com by 210.87.254.6 on 09/06/12
For personal use only.

TABLE 2. Results of some calculations yielding Lindemann behaviour*

Case	k_0 (Torr^{-1} s^{-1})	k_∞ (s^{-1})	Δ_S	Δ_W
F1	5.52×10^{-3}	2.47×10^{2}	0.29	0.64
F1(1)	5.52×10^{-3}	3.04×10^{5}	Zero	0.13
F1(0)	5.52×10^{-3}	1.20×10^{5}	Zero	Zero
V1	4.23	4.69×10^{5}	0.28	0.61
V1(1)	4.23	4.36×10^{7}	Zero	0.13
V1(0)	4.23	1.42×10^{7}	Zero	Zero
V1(*a*)	4.23	4.69×10^{5}	0.28	0.066
V1(*b*)	4.23	4.69×10^{5}	0.28	0.025
V1(*c*)	4.23	4.69×10^{5}	0.28	0.004

*Cases F1 and V1 are the standard cases transcribed for Table 1. The designation 1(1) means that *all* states above threshold have the same decay rate constant; the designation 1(0) means that *only one* state above threshold has a non-zero decay rate. The designations (*a*), (*b*), (*c*) mean that all transitions *above* threshold are artificially accelerated by constant factors of 30, 100, 1000, respectively. For all cases listed in this table τ_{inc}/τ_{rel} lies between 3.0 and 3.2 near the high pressure limit, or between 2.9 and 3.1 at $p_{1/2}$.

TABLE 3. Changes in shape of the fall-off curve as the result of single-transition perturbations

Case*	k_0 (Torr^{-1} s^{-1})	Δ_W
V1	4.23	0.61
V1(+1→+2)×30	4.23	0.52
V1(−→+1)×30	4.23	0.44
V1(−→+)×30	5.75	0.71
V1(−1→−)×30	5.22	0.67
V1(−6→−5)×30	4.46	0.63
V1(−→+)/30	0.47	0.16
V1(−6→−5)/30	1.65	0.36
V1(−11→−10)/30	3.10	0.52
V1(−11→−10)/100	1.88	0.39
V1(−11→−10)/1000	0.31	0.12

*The designation (+→+1) means that the transition rate for $j = j_+$ to $j = j_+ + 1$ was perturbed by the operator following the bracket; likewise (−6 → −5) refers to the transition between $j = j_- - 6$ and $j = j_- - 5$.

matically creates a bottleneck between grains j_- and j_+, and the stronger this bottleneck effect, the closer to Lindemann behaviour we find. This clearly establishes a link between Lindemann behaviour and activation bottlenecks.

The question now arises as to whether bottlenecks placed in other positions in the activation ladder can affect the shape of the fall-off curve, and the results of these experiments are summarised in Table 3. The first five entries show what happens when the rate of a specific transition (and its reverse), either just above or just below threshold, are multiplied by an arbitrary factor of 30; the unimolecular reaction properties of the system are insensitive to variations of this kind further away from the threshold level. Above threshold, k_0 is independent of the variations in q_{ij} as required by eq. [3], although the fall-off shape changes somewhat; otherwise, the rate is most sensitive to the rate of transport *across* the threshold, and the further below the threshold one arbitrarily lowers the impedance, the smaller is the effect on k_0 and Δ_W. Lowering the impedance anywhere above threshold narrows the fall-off curve — the same effect as in case V1(*a*) above, but not as marked — whereas lowering the impedance elsewhere broadens the fall-off, with the largest effect at the cross-threshold transition.

This multiplication of a specific rate by an arbitrary factor does not create a bottleneck in the accepted sense — it only creates an implied bottleneck at the preceding step. Consequently, the second set of five entries in Table 3 shows the effect of making arbitrary reductions in a specific transition rate, giving rise to a strong increase in impedance for that step. The first three experiments in this class show that as this extra impedance is moved down the activation ladder, we approach the normal behaviour of case V1; however, extra impedance for the transition *across* threshold does lead to a marked sharpening of the fall-off curve, $\Delta_W = 0.16$, which is actually a sharper curve than the strong-collision fall-off shape, $\Delta_S = 0.28$ for the variable state-density case. The same effect can be generated by placing the artificial bottleneck further below threshold, but the severity of the bottleneck has to be made much greater in order to achieve the same result, as is shown in the final three entries of this group.

Concluding remarks

The numerical experiments described in this paper have been used to explore three facets of the weak-collision unimolecular reaction problem, incubation times, collision efficiencies, and fall-off shapes; this development is based upon a new expression for the weak-collision rate, valid for all pressures.

The results obtained for the incubation times are the least satisfactory in that they do not throw a great deal of light on the cause of the inequality $\tau_{inc} > \tau_{rel}$ in weak-collision systems (4). Moreover, these results are strictly valid only for step-ladder probabilities because of the difference between ϕ_0 and Ψ_0, but it has often been found in the past that step-ladder calculations are of qualitative value. Only three points of substance stand out, a confirmation that $\tau_{inc} > \tau_{rel}$, that the ratio τ_{inc}/τ_{rel} is not very sensitive to the extent of the fall-off, but that τ_{inc} is sensitive to variations in the transition rates among some of the higher states.

The result that the apparent collision efficiency, β_c, can exceed unity may seem odd at first; it only means that the weak-collision rate is greater than the strong-collision rate at the low-pressure limit. It is quite easy to see how this can happen with the help of eq. [3]. At the low-pressure limit, the strong-collision rate is $k_{0,S} = \omega\Sigma'\beta_i$, where as we have noted, $\omega \simeq 2 \times 10^6$ Torr^{-1} s^{-1}, and $\Sigma'\beta_i$ is of the order of 3×10^{-7} (4×10^{-4}) for the F (V) series respectively; thus, the values of $k_{0,S}$ are 6×10^{-1} (8×10^2) Torr^{-1} s^{-1}. On the other hand, q_{10} is fixed at 2.5×10^3 Torr^{-1} s^{-1} in both cases, and since the temperature is 4000 K, q_{01} is of a similar magnitude too; the actual values of t_0 calculated by eq. [2] are 2.5×10^{-4} (1×10^{-6}) Torr s respectively. Now imagine an extremely artificial set of transition rates, such that all $t_j \approx 0$, $j \geq 1$: in other words, at the low-pressure limit, virtually any molecule which succeeds in being excited out of the bottom state will dissociate. Then $k_0 \approx t_0^{-1} \approx 4 \times 10^3$ (1×10^6) Torr^{-1} s^{-1}, whence $\beta_c \approx 10^4$ (10^3); this is what happens in the thermal ionisation of atoms (14). In the present case, the appearance of values of $\beta_c > 1$ is associated with values of $q_{j+1,j} > \omega$ near threshold; since there is no strong evidence that transition rates for high vibrational states grossly exceed those for lower states, β_c will not be expected to exceed unity in practice.

However, the major conclusion from this set of numerical experiments is that it is not easy to choose a set of transition rates which will lead to Lindemann or near-Lindemann behav-

Can. J. Chem. Downloaded from www.nrcresearchpress.com by 210.87.254.6 on 09/06/12
For personal use only.

iour, as appears to be the case for most so-called weak-collision thermal reactions (3). The only way, in fact, in which it can be done is to construct the transition rates in such a manner that the rate of relaxation among the reactive states *far exceeds* the rate constants for activation to those states. This was shown by the last three cases in Table 2 and, in fact, the last three entries in Table 3 are examples of the same effect, constructed in a slightly different manner. In the absence of this bottleneck effect, the fall-off curves are *much* too broad, broader in fact than the strong-collision shape.

It is not clear that the requirement of a collisional relaxation among the reactive states greatly exceeding (by a factor of at least an order of magnitude) the rate of collisional excitation across threshold, is a reasonable one, and yet, within the framework of the usual model of unimolecular reaction, it would have to be so if we are to account for the common observation of near-Lindemann behaviour in weak-collision systems. Rather than attempt to force agreement by postulating a new effect in collisional relaxation processes associated with only the reactive states, it is preferable to look for other possible causes for the common occurrence of this near-Lindemann behaviour; it is known already that a restriction in the randomisation rates among the reactive states can lead to strict Lindemann behaviour if it is sufficiently severe (2), and since the reactive states are relatively far apart in energy in these simple molecules (6), this seems to be the logical cause to pursue in this case, at least for the time being.

1. S. R. VATSYA and H. O. PRITCHARD. Chem. Phys. **63**, 383 (1981).
2. H. O. PRITCHARD AND S. R. VATSYA. Can .J. Chem. **59**, 2575 (1981).
3. A. W. YAU and H. O. PRITCHARD. Chem. Phys., Lett. **60**, 140 (1978).
4. H. O. PRITCHARD and S. R. VATSYA. Chem. Phys. **72**, 447 (1982).
5. H. O. PRITCHARD. J. Phys. Chem. **87**, 3179 (1983).
6. H. O. PRITCHARD. Quantum theory of unimolecular reactions. Cambridge University Press. 1984.
7. J. H. WILKINSON. The algebraic eigenvalue problem. Clarendon Press, Oxford. 1965.
8. S. R. VATSYA and H. O. PRITCHARD. Proc. R. Soc. London, A**375**, 409 (1981).
9. S. R. VATSYA. J. Phys. A**16**, 201 (1983).
10. A. W. YAU and H. O. PRITCHARD. J. Phys. Chem. **83**, 134 (1979).
11. E. E. NIKITIN and N. D. SOKOLOV. J. Chem. Phys. **31**, 1371 (1959).
12. E. V. STUPOCHENKO and A. I. OSIPOV. Russian J. Phys. Chem. **33**, 36 (1959).
13. J. KECK and G. CARRIER. J. Chem. Phys. **43**, 2284 (1965).
14. A. W. YAU and H. O. PRITCHARD. Proc. R. Soc. London, A**362**, 113 (1978).
15. N. S. SNIDER. J. Chem. Phys. **77**, 789 (1982).
16. S. R. VATSYA and H. O. PRITCHARD. J. Chem. Phys. **78**, 1624 (1983).
17. J. S. ROWLINSON. Q. Rev. **8**, 168 (1954).
18. A. W. YAU and H. O. PRITCHARD. Can. J. Chem. **57**, 1723 (1979).
19. W. FORST and A. P. PENNER. J. Chem. Phys. **72**, 1435 (1980).

Can. J. Chem. Downloaded from www.nrcresearchpress.com by 210.87.254.6 on 09/06/12
For personal use only.

Oxidation of sulfur compounds. I. The photolysis of CH_3SH and $(CH_3S)_2$ in the presence of NO[1]

R. JEFFREY BALLA AND JULIAN HEICKLEN

Department of Chemistry and Center for Air Environment Studies, The Pennsylvania State University, University Park, PA 16802, U.S.A.

Received May 10, 1983

This article is dedicated to Professor Harry E. Gunning on the occasion of his 65th birthday

R. JEFFREY BALLA and JULIAN HEICKLEN. Can. J. Chem. **62**, 162 (1984).

Both CH_3SH and $(CH_3S)_2$, as well as their mixtures, were photolyzed in the presence of NO at 23 ± 1°C. The photolyses were carried out in a 631 mL quartz vessel with a pinhole bleed to a quadrupole mass spectrometer for continual analysis of products. After the termination of exposure, further product analysis was made by gas chromatography.

The identified products of the reaction were CH_3SNO, $(CH_3S)_2$, H_2, and N_2. Hydrogen atoms, formed from the photolysis of CH_3SH, reacted with both NO and CH_3SH:

[4] $H + NO + M \rightarrow HNO + M$

[5] $H + CH_3SH \rightarrow H_2 + CH_3S$

with $k_5/k_4 = 626 \pm 42$ Torr for NO as a chaperone. The CH_3S radical adds to NO

[2*a*] $CH_3S + NO \rightleftarrows CH_3SNO\dagger$

[2*b*] $CH_3SNO\dagger + M \rightarrow CH_3SNO + M$

with $k_{-2a}/k_{2b} = 83 \pm 52$ Torr. As the CH_3SNO accumulates, CH_3S also reacts with CH_3SNO

[6] $CH_3S + CH_3SNO \rightarrow (CH_3S)_2 + NO$

with $k_6/k_{2a} \simeq 0.84 \pm 0.27$. At high NO pressures a chain process occurs which is attributed to:

[7] $H + NO \rightarrow \text{adduct} \xrightarrow{CH_3SH} H + \xi CH_3S$

where ξ is probably 4.0. Termination is most easily represented by

[8] $HNO \rightarrow$ termination

with $k_8/k_7 = 85.0 \pm 7.8$ Torr.

R. JEFFREY BALLA et JULIAN HEICKLEN. Can. J. Chem. **62**, 162 (1984).

On a photolysé le CH_3SH et le $(CH_3S)_2$ ainsi que leurs mélanges en présence du NO à 23 ± 1°C. On a réalisé les photolyses dans un récipient en quartz de 631 mL muni d'un très petit orifice relié à un spectromètre de masse quadrupolaire en vue d'une analyse continuelle des produits. A la fin de la photolyse, on analyse les produits par chromatographie en phase gazeuse.

On a identifié les produits suivants: CH_3SNO, $(CH_3S)_2$, H_2 et N_2. Les atomes d'hydrogène formés au cours de la photolyse du CH_3SH réagissent avec le NO et le CH_3SH.

[4] $H + NO + M \rightarrow HNO + M$

[5] $H + CH_3SH \rightarrow H_2 + CH_3S$

avec $k_5/k_4 = 626 \pm 42$ Torr pour le NO comme chaperon. Le radical CH_3S s'additionne au NO.

[2*a*] $CH_3S + NO \rightleftarrows CH_3SNO\dagger$

[2*b*] $CH_3SNO\dagger + M \rightarrow CH_3SNO + M$

avec $k_{-2a}/k_{2b} = 83 \pm 52$ Torr. Au fur et à mesure que le CH_3SNO s'accumule, le CH_3S réagit également avec lui

[6] $CH_3S + CH_3SNO \rightarrow (CH_3S)_2 + NO$

avec $k_6/k_{2a} \simeq 0{,}84 \pm 0{,}27$. Pour de fortes pressions de NO, il se produit une réaction en chaine que l'on attribue à

[7] $H + NO \rightarrow \text{adduit} \xrightarrow{CH_3SH} H + \xi CH_3S$

ou ξ est probablement égal à 4. On représente plus facilement la fin de la réaction par

[8] $HNO \rightarrow$ Fin de réaction

avec $k_8/k_7 = 85{,}0 \pm 7{,}8$ Torr.

[Traduit par le journal]

[1]CAES Report No. 679-83.

Can. J. Chem. Downloaded from www.nrcresearchpress.com by 210.87.254.5 on 09/06/12
For personal use only.

Can. J. Chem. Downloaded from www.nrcresearchpress.com by 210.87.254.5 on 09/06/12
For personal use only.

Introduction

The photolysis of CH_3SH in the presence of NO has been studied by Steer and Knight (1). They studied the reaction in steady-state photolysis and analyzed the products after termination of irradiation. They found that the H_2 formed in the absence of NO decreased in yield as the NO pressure was increased. The major product of the reaction was CH_3SNO. The sum of its yield plus twice the $(CH_3S)_2$ yield was constant for NO pressures <20 Torr, but at higher NO pressures, the yields of both compounds increased indicating a chain reaction. N_2 was also a major product at high NO pressures and it must also be formed in the chain process. They also found that both CH_3SNO and N_2 were produced in post-irradiation dark reactions, though the H_2 concentration was not affected. There was no dark reaction between NO and CH_3SH. The investigators were unable to provide a mechanism for their observations.

Recently the photolysis of CH_3SNO has been examined by Niki *et al.* (2) who also measured its uv and ir absorption cross sections. They found $(CH_3S)_2$ and NO to be produced in stoichiometric amounts. From this they concluded the mechanism to be

$$[1] \quad CH_3SNO + h\nu \rightarrow CH_3S + NO$$

$$[2] \quad CH_3S + NO \rightarrow CH_3SNO$$

$$[3] \quad 2CH_3S \rightarrow (CH_3S)_2$$

We have studied the reaction of CH_3S radicals with NO and report the results here. Most of our studies were done using the photolysis of CH_3SH as the source of CH_3S. However, we also have results using $(CH_3S)_2$ photolysis as the source of CH_3S.

Experimental

Photolysis was performed in a 631-mL spherical quartz cell equipped with Pyrex-quartz graded seals which contributed no more than 4% to the dead volume. Radiation was from one, two, or three unfiltered low-pressure Hanovia mercury lamps, No. Z1400-013, which emit essentially only 254 and 185 nm radiation (3). The 185 nm line is absorbed by air between the lamps and reaction vessel. All experiments were performed at 23 ± 1°C.

Gases were admitted to the reaction cell by using a conventional grease- and mercury-free vacuum line equipped with Teflon stopcocks. Gas pressures were measured by a Whittaker Model CD25 pressure transducer, oil manometer, or 0–800 Torr Wallace and Tiernan gauge. The transducer and manometer were calibrated with respect to a McLeod gauge which was kept carefully isolated from the vacuum system.

Continuous product analysis was performed by allowing the contents of the cell to bleed through a small pinhole into an Extranuclear type II quadrupole mass spectrometer. In the course of these experiments the total pressure in the cell ranged from 20 to 300 Torr pressure. In order to maintain the operating pressure of the mass spectrometer below 4×10^{-6} Torr, a series of three glass pinholes of different area were used. The glass pinholes were used over the following total pressure ranges: 20–60 Torr, 60–150 Torr, and 150–300 Torr. Under all experimental conditions, sample depletion never exceeded 5%. Mass spectrometric determinations were performed with 40 eV electrons by measuring the product ion current peaks relative to the $m/e = 40$ peak from a known amount of argon which was added to the mixture prior to irradiation. This reduces errors from instrumental and other periodic fluctuations. Methylthionitrite (CH_3SNO) and dimethyldisulfide $(CH_3S)_2$ were quantitatively determined by measuring their relative signals at $m/e = 77$ and $m/e = 94$, respectively, to that of argon at $m/e = 40$.

The H_2 produced was expanded into a sample loop after irradiation for analysis by gas chromatography. Separation was performed on a 12 ft.-long × 1/4 in.-diameter stainless steel column containing molecular sieve 5A maintained at room temperature. Nitrogen was used as the carrier gas with a flow rate of 40 mL/min. All gases which would not pass through the column were retained in the sample loop using an isopentane slush bath maintained at −160°C. Analysis for N_2 was performed using a 4 ft.-long × 1/4 in.-diameter stainless steel column packed with molecular sieve 5A at 23°C with a helium flow rate of 40 mL/min. An isopentane slush bath was used to retain the larger molecules, such as CH_3SH, in the sample loop in order to prevent column contamination. N_2O was analyzed with a 6 ft.-long × 1/4 in.-diameter stainless steel column packed with Porapak QS at 23°C with a helium flow rate of 55 mL/min.

TABLE 1. Mass spectrum of CH_3SNO[a]

m/e	Fragment	% relative height
14	CH_2	5.6
15	CH_3	14.6
30	NO	61.1
31	$^{15}NO/N^{17}O$	0.4
32	$N^{18}O$	0.1
44	CS	9.3
45	CHS	35.9
46	CH_2S	15.8
47	CH_3S	26.2
48	$^{13}CH_3S/CH_3{}^{33}S$	0.6
49	$CH_3{}^{34}S$	1.1
61	CH_3SN	2.3
64	?	6.9
77	CH_3SNO	100.0
78	CH_3SNO (^{13}C, ^{15}N, ^{33}S, ^{17}O)	2.3
79	$CH_3{}^{34}SNO$, $CH_3SN^{18}O$	4.5

[a]Taken on an Extranuclear Type II mass spectrometer at 40 eV electron energy.

Methylmercaptan, obtained from Matheson at 99.5% minimum purity, was distilled trap-to-trap from −94 to −160°C. Matheson C.P. grade nitric oxide was distilled from −186 to −196°C and thoroughly degassed prior to experimental use. Matheson prepurified argon was used without further purification. Gold label dimethyldisulfide, obtained from Aldrich, was distilled from 0 to −63°C prior to use. Methylthionitrite was prepared by photolyzing $(CH_3S)_2$ at 254 nm in the presence of a threefold excess of NO. Its mass spectrum is given in Table 1. Purification was accomplished by trap-to-trap distillation from −84 to −160°C. The purified material was stored in a darkened bulb at −196°C to prevent thermal as well as photolytic decomposition (4).

NO_2 (Matheson) was purified as follows. One hundred Torr of NO was mixed with 600 Torr O_2. This mixture was frozen at −196°C, then allowed to warm to room temperature. The freeze–thaw procedure was repeated until the blue color of N_2O_3 disappeared and the frozen mixture became pure white. The NO_2 was then distilled from −63 to −130°C. The pure NO_2 was kept in a dark storage bulb and degassed prior to each experiment.

Mass spectra of all gases were obtained and compared with the EPA-NIH mass spectral data base. In all cases, no extraneous peaks were obtained.

Actinometry was performed by photolysis of methylmercaptan at 254 nm. The products obtained, dimethyldisulfide and hydrogen, have quantum yields of 0.99 ± 0.1 (5) and 1.00 ± 0.05 (1), respectively. In all cases, the absorbed intensity, I_a, obtained from $(CH_3S)_2$ by mass spectrometry and from H_2 by gas chromatography, agreed within a few percent. For the photolysis of $(CH_3S)_2$ at 254 nm, CH_3SH was used as an actinometer at matched absorbances. We found the extinction coefficients to be 8.27×10^{-3} (to base 10) $Torr^{-1}\ cm^{-1}$ for $(CH_3S)_2$ and 2.36×10^{-3} (to base 10) $Torr^{-1}\ cm^{-1}$ for CH_3SH. Our extinction coefficient for CH_3SH agrees exactly with that of $2.4 \times 10^{-3}\ Torr^{-1}\ cm^{-1}$ reported by Bridges and White (5).

Some runs were done in which $(CH_3S)_2$ was photolyzed in the presence of CH_3SH. This could be done because $(CH_3S)_2$ absorbs light

slightly beyond 300 nm, while the extinction coefficient for CH_3SH is negligible above 275 nm. In these experiments three Hanovia medium-pressure Hg lamps were used with two Corning 0-53 filters to remove radiation <280 nm. To be certain that CH_3SH was not absorbing any radiation, an experiment was performed in which pure CH_3SH was irradiated, and no $(CH_3S)_2$ was found.

Results

When mixtures of CH_3SH and NO were photolyzed with 254 nm radiation, the products found were CH_3SNO, $(CH_3S)_2$, H_2, and N_2. Possibly NO_2 is also formed, but we were unable to analyze for it. The CH_3SNO and $(CH_3S)_2$ were monitored continuously throughout the run by mass spectrometry. The H_2, and in some cases N_2, was measured by gas chromatography after the termination of the irradiation. These results are in accord with the findings of Steer and Knight (1).

Curves of growth for CH_3SNO and $(CH_3S)_2$ are shown for two different runs in Figs. 1 and 2. In both cases, $[CH_3SNO]$ is proportional to irradiation time initially, but then rises less rapidly as the CH_3SH is consumed and $(CH_3S)_2$ is produced. The $(CH_3S)_2$ is formed with an induction period in both cases. The run at lower intensity shows a much more pronounced induction period. The major difference between the two runs is that there is no further growth of products after the termination of radiation for the run with 6.0 Torr NO (Fig. 1), whereas there is a post-irradiation dark reaction for the run with 50.0 Torr NO (Fig. 2).

To see if the post-irradiation dark reaction could be caused by the presence of CH_3SNO, mixtures of ≃200 Torr NO, ≃10 Torr CH_3SNO, ≃15 Torr of Ar, and either 0 or ≃16 Torr CH_3SH were allowed to stand for 775–1050 s in the dark. In none of these experiments did any reaction take place.

Figure 3 shows log–log plots of $[(CH_3S)_2]$ vs. reaction time for the irradiation of three different CH_3SH–NO mixtures. During most of the run, the plots can be fitted by lines of slope 2.0, indicating that $[(CH_3S)_2]$ is proportional to the square of the irradiation time.

The data for all of our runs in the CH_3SH–NO system are tabulated in Table 2, where the values listed for $\Phi\{CH_3SNO\}$ are initial values. The initial quantum yields of CH_3SNO formation rise from about 2 at low NO pressure to about 8 at 200 Torr NO, thus confirming the chain reaction demonstrated by Steer and Knight (1). In agreement with their findings $\Phi\{H_2\}$ decreases as the NO pressure is raised, reaching values as low as 0.21 with 200 Torr NO and 6 Torr CH_3SH. The quantity $[(CH_3S)_2]/t^2$ varies widely with changes in reaction conditions. In general it increases with I_a and decreases with increasing NO pressure.

The N_2 is produced in the dark reaction (1), so that measuring its quantum yield by gas chromatography is not very meaningful. We did confirm that N_2 is a product of the reaction, but report no quantum yields.

We had expected that N_2O might be a product, since it is formed from the interaction of two HNO molecules which are produced in the H + NO reaction. We looked for, but did not find, N_2O. For an experiment with 20.5 Torr NO, 21.5 Torr CH_3SH, 16.0 Torr Ar, and $I_a = 3.7 \times 10^{-4}$ Torr/s, $\Phi\{N_2O\} < 0.011$. Likewise for an experiment with 173 Torr NO, 21.0 Torr CH_3SH, 17.0 Torr Ar, and $I_a = 3.6 \times 10^{-4}$ Torr/s, $\Phi\{N_2O\} < 0.005$.

Another probable product of the reaction is NO_2. Possibly this molecule could be responsible for the post-irradiation dark reaction. We could not analyze for this molecule because the CH_3SH mass spectral cracking peaks interfered with m/e 46. However, we mixed NO_2 with CH_3SH and did find a dark reaction. A sample run is shown in Fig. 4, where the reaction was monitored continuously by mass spectrometry. The CH_3SH is rapidly removed by NO_2, and $(CH_3S)_2$ is formed as a stable product. CH_3SNO is also produced, as reported previously by Fierce *et al.* (6). However, its concentration rises to a maximum in <50 s, and then decreases as the CH_3SH is consumed.

We examined the photolysis of $(CH_3S)_2$ in the presence of NO. The sole reaction product is CH_3SNO, and it is formed linearly with time. There is no dark reaction either prior to or after irradiation. The quantum yields of CH_3SNO are given in Table 3. They are independent of pressure and have an average value of 2.04 ± 0.06.

Three experiments were also done in which $(CH_3S)_2$–NO mixtures were photolyzed at 280–300 nm in the presence of CH_3SH. The reaction conditions were $[CH_3SH] \simeq 8$ Torr, $[(CH_3S)_2] \simeq 10$ Torr, $[NO] \simeq 201$ Torr, $[Ar] \simeq 14$ Torr, and $I_a \simeq 0.49$ mTorr/s. One of these runs is shown in Fig. 5. There is no dark reaction, either prior to or following irradiation. During irradiation CH_3SNO is formed at a constant rate, its average quantum yield for the 3 experiments being 2.16 ± 0.14, based on the assumption that $\Phi\{CH_3SNO\} = 2.0$ in the absence of CH_3SH.

Discussion

The photolysis of CH_3SH at 254 nm is a clean source of CH_3S radicals. Inaba and Darwent (7) photolyzed CH_3SH with a medium pressure Hg arc and found the only important noncondensable gas to be H_2, with some CH_4 being formed in secondary processes. From this they concluded that the sole primary process was

$$CH_3SH + h\nu \rightarrow CH_3S + H \qquad \text{Rate} = I_a$$

Steer and Knight (1) came to the same conclusion. They found the quantum yield of H_2 with 254 nm radiation to be 1.00 ± 0.05 at low pressure and concluded that the above reaction proceeded with unit quantum yield. However, Bridges and White (5) obtained $\Phi\{H_2\} = 0.83 \pm 0.03$, $\Phi\{CH_4\} = 0.16 \pm 0.03$, and $\Phi\{(CH_3S)_2\} = 0.99 \pm 0.1$ with 254 nm radiation. From this they concluded that the quantum yield for the above reaction was only 0.93 and that CH_3 + SH was produced with a quantum yield of 0.07.

We have used the yield of $(CH_3S)_2$ as an actinometer, since a quantum yield of 1.0 for this compound is consistent with all three earlier studies. At low NO pressures, $\Phi\{H_2\}$ is close to 1.0, which supports the conclusion of Steer and Knight (1) and Inaba and Darwent (7) that the formation of CH_3S + H is the only primary process. However, if small amounts of CH_3 and SH are produced, our conclusions should not be affected significantly.

The H atoms produced can react with either NO or CH_3SH in well-known reactions:

[4] $\quad H + NO + M \rightarrow HNO + M$

[5] $\quad H + CH_3SH \rightarrow H_2 + CH_3S$

CH_3SNO is formed as a primary product. The indicated reaction is an addition of CH_3S to NO, which may be in the pressure fall-off region. Thus

[2*a*] $\quad CH_3S + NO \rightleftarrows CH_3SNO\dagger$

Can. J. Chem. Downloaded from www.nrcresearchpress.com by 210.87.254.5 on 09/06/12
For personal use only.

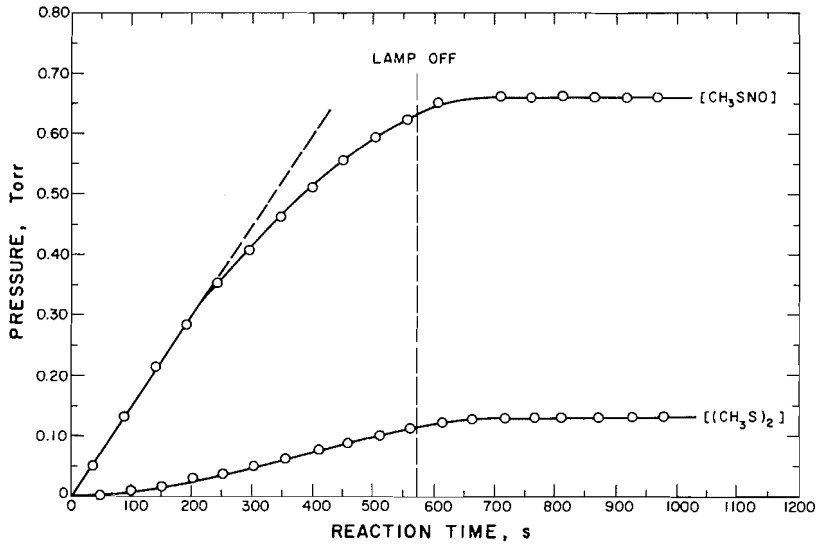

FIG. 1. Plot of product concentrations vs. reaction time for a mixture of 6.18 Torr CH_3SH, 6.00 Torr NO, and 15.4 Torr Ar at 23°C with I_a = 0.83 mTorr/s.

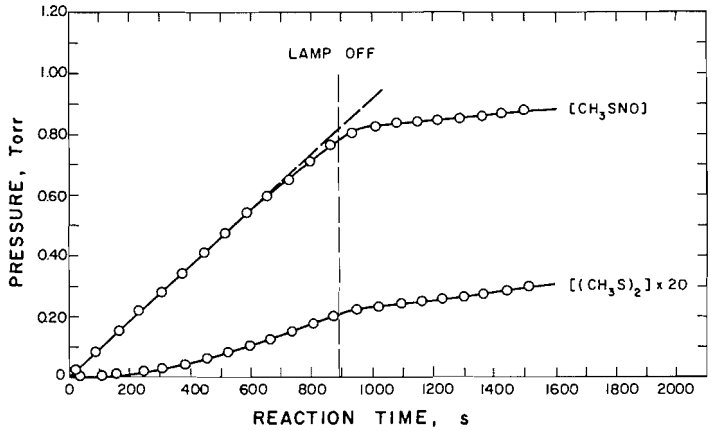

FIG. 2. Plot of product concentrations vs. reaction time for a mixture of 21.8 Torr CH_3SH, 50.0 Torr NO, and 16.3 Torr Ar at 23°C with I_a = 0.38 mTorr/s.

[2b] $CH_3SNO\dagger + M \rightarrow CH_3SNO + M$

The $(CH_3S)_2$ is formed with an induction period and thus is not a primary product. It cannot be formed by direct combination of two CH_3S radicals via reaction [3]. It must be formed by the reaction of CH_3S with a primary product. The indicated reaction is

[6] $CH_3S + CH_3SNO \rightarrow (CH_3S)_2 + NO$

The above reactions account for the formation of the measured products: CH_3SNO, H_2, and $(CH_3S)_2$. They do not account for the long chains or the post-radiation dark reaction observed under some conditions. Our results on the photolysis of $(CH_3S)_2$–NO mixtures in the absence or presence of CH_3SH show no chain or post-irradiation dark reaction. Thus these phenomena must be associated with the HNO species. In order to fit the data we need two reactions such as the following:

[7] $HNO + NO \rightarrow \text{adduct} \xrightarrow{CH_3SH} H + \xi CH_3S$

[8] $HNO \rightarrow \text{termination}$

where ξ is for the moment an unspecified stoichiometric factor. For the time being we shall leave reactions [7] and [8] in this form, and show that they lead to a mechanism that fits the data. These reactions will be discussed in more detail later. The reaction of two HNO species to give $H_2O + N_2O$ is omitted since we looked for, but could not find N_2O.

The mechanism leads to the following rate law for H_2 production:

$$[I] \qquad (\Phi\{H_2\}^{-1} - 1)^{-1} \frac{[NO][M]}{[CH_3SH]} = \frac{k_5}{k_4}\left(1 + \frac{k_7[NO]}{k_8}\right)$$

If [M] can be evaluated, then the left-hand side of eq. [I] can be computed and plotted vs. [NO]. We have evaluated [M] by using various efficiencies for NO, Ar, and CH_3SH as chaperone gases. The results are quite insensitive to the values chosen, and the expression

$$[M] \equiv [NO] + [Ar] + 3[CH_3SH]$$

fits the data as well as anything else. Figure 6 shows the appropriate plot for eq. [I]. The plot can be fitted by a straight line which gives least-square parameters for the intercept and slope of 626 ± 42 Torr and 7.64 ± 0.20 (uncertainties are one standard deviation). Thus k_5/k_4 = 626 ± 42 Torr and k_8/k_7 = 85.0 ± 7.8 Torr.

Equation [I] can be rearranged to:

Can. J. Chem. Downloaded from www.nrcresearchpress.com by 210.87.254.5 on 09/06/12
For personal use only.

TABLE 2. Product yields in CH_3SH–NO photolysis at 253.7 nm

[NO] (Torr)	I_a (mTorr/s)	$\Phi\{CH_3SNO\}$	$\Phi\{H_2\}$	$10^3[(CH_3S)_2]/t^2$ [a] (mTorr/s^2)
[CH_3SH] = 6.3 ± 0.3 Torr, [Ar] = 15.9 ± 0.8 Torr				
1.91	0.77	1.66	0.98	1.25
1.91	0.76	1.63	0.93	1.23
1.99	0.85	2.05	1.00	2.50
2.07	0.85	1.94	0.88	1.32
5.09	0.84	—	0.95	—
6.00	0.81	1.90	0.85	0.80
6.00	0.83	1.95	0.91	0.76
6.00	0.88	1.78	0.90	1.00
6.12	0.78	2.14	0.82	0.71
6.26	0.78	1.85	0.83	0.42[c]
6.82	0.22	1.81	—	0.060
19.46	0.20	2.49	0.88	0.0167
20.0	0.75	1.87	0.75	0.228
20.0	0.75	2.00	0.79	0.219
20.0	0.84	1.64	0.64	0.222
20.0	0.21	2.49	0.88	0.0167[c]
20.6	0.76	1.89	0.62	0.066
22.0	0.86	1.78	0.51	—
24.0	0.78	2.66	0.85	0.194
60.0	0.76	2.46[b]	0.60	—
60.0	0.74	2.46[b]	0.69	—
68.0	0.85	2.43[b]	—	—
119	0.94	5.73[b]	0.33	—
150	0.94	6.80[b]	0.27	—
180	0.96	8.92[b]	0.26	—
198	0.85	7.06[b]	—	—
200	0.75	5.36[b]	0.23	—
200	0.75	6.60[b]	0.22	—
200	0.82	6.73[b]	—	—
204	0.93	9.79[b]	0.22	—
[CH_3SH] = 21 ± 1 Torr, [Ar] = 16.1 ± 1.0 Torr				
0.98	0.36	1.87	0.99	—
2.00	0.52	—	1.00	—
10.0	0.35	2.46	0.99	0.0277[c]
19.5	1.28	1.82	—	0.275
20.0	0.50	—	0.94	—
20.0	0.37	2.08	0.89	0.0127[c]
20.0	0.76	2.11	—	0.090[c]
20.0	2.18	2.03	—	0.88
20.5	0.37	2.06	—	0.0260[c]
20.7	2.20	1.92	—	0.82
21.0	1.28	1.88	—	0.254[c]
50.0	0.38	2.16[b]	0.78	0.0139[b,c]
60	0.50	—	0.74	—
99	0.36	3.53[b]	0.62	—
100	0.28	4.48[b]	0.60	0.0107[b,c]
140	0.39	5.37[b]	0.55	0.0207[b,c]
147	0.30	6.28[b]	0.53	0.0134[b,c]
200	0.50	—	0.45	—
301	0.32	—	0.33	—
400	0.50	—	0.29	—
400	0.31	—	0.29	—
[CH_3SH] = 60 ± 1 Torr, [Ar] = 15.0 Torr				
2.10	2.40	1.77	1.00	4.22
2.10	2.40	1.99	1.04	5.33
6.07	2.40	2.37	1.00	1.92
6.29	2.40	2.50	1.11	2.28
20.6	2.40	2.17	1.06	0.91
21.0	2.40	2.74	1.10	0.81
60.0	2.40	2.89[b]	0.96	0.35[b,c]
60.0	2.40	3.64[b]	0.97	0.39[b]
200	2.40	4.44[b]	0.83	—
200	2.40	4.44[b]	0.87	—

[a] Initial slope.
[b] Exhibited growth in dark after irradiation terminated.
[c] Runs with ≤20% uncertainty. Other runs have much larger uncertainties.

Can. J. Chem. Downloaded from www.nrcresearchpress.com by 210.87.254.5 on 09/06/12
For personal use only.

$$[II] \quad \alpha(\Phi\{H_2\}^{-1} - 1)^{-1} = k_5[CH_3SH]/k_4[NO][M]$$

where

$$\alpha \equiv (1 + k_7[NO]/k_8)^{-1}$$

The left-hand side of eq. [II] can be computed using the value of k_8/k_7 obtained from eq. [I] and Fig. 6. This is plotted vs. $[CH_3SH]/[NO][M]$ on a log–log plot in Fig. 7. This plot extends the range of variables over that in Fig. 6. The data are force-fitted to a line of slope 1.0. The least-squares intercept of this plot gives log $(k_5/k_4) = 2.803 \pm 0.37$ or $k_5/k_4 = 636 \times/ 2.4$. While the uncertainty for k_5/k_4 is much greater from this plot than from Fig. 6, the value is essentially the same in the two plots. The reason for the larger uncertainty in Fig. 7 than in Fig. 6 is that, at large values of the ordinate, $\Phi\{H_2\} \simeq 1$, so that their difference has a large error.

Another way to estimate k_5/k_4 is to incorporate the data on CH_3SNO. In the initial phase of each run, all the CH_3S produced forms CH_3SNO. This fact leads to the rate law

$$[III] \quad \frac{(1-\alpha)\Phi\{H_2\}}{\Phi\{CH_3SNO\} - \Phi\{H_2\} - 1} = \frac{k_5[CH_3SH]}{\xi k_4[NO][M]}$$

The left-hand side of eq. [III] is computed using the value for k_8/k_7 obtained from eq. [I] and Fig. 6. It is plotted vs. $[CH_3SH]/[NO][M]$ in a log–log plot in Fig. 8. Again the data can be fitted by a line of slope 1.0. The intercept gives log $(k_5/\xi k_4) = 2.185 \pm 0.141$ or $k_5/\xi k_4 = 154 \times/ 1.38$ Torr. To make this value consistent with the value of $k_5/k_4 = 626 \pm 42$ Torr found from Fig. 1, ξ should be 4.1 ± 1.3 (1σ). A later discussion of the detailed mechanism for reaction [7] will suggest that ξ is likely to be 4.0. If so then Fig. 8 gives $k_5/k_4 = 616 \times/ 1.38$ Torr. The absolute value for k_4 with Ar as a chaperone has been reported to be 1.99×10^{-32} cm^6/s at 296 K (8). If we accept the value for k_5/k_4 to be 626 Torr, then $k_5 = 4.1 \times 10^{-13}$ cm^3/s.

Later in the reaction, $(CH_3S)_2$ is formed by reaction [6] giving rise to the rate law:

$$d[(CH_3S)_2]/dt = k_6[CH_3SNO][CH_3S]$$

Over most of the reaction, the rate of CH_3SNO formation is constant. Thus

$$[CH_3SNO] \simeq \Phi\{CH_3SNO\} I_a t$$

$$[CH_3S] = \Phi\{CH_3SNO\} I_a/\beta k_3[NO]$$

where $\beta \equiv (1 + k_{-2a}/k_{2b}[M])^{-1}$. Substitution of these expressions into the rate equation and integration gives

Can. J. Chem. Downloaded from www.nrcresearchpress.com by 210.87.254.5 on 09/06/12
For personal use only.

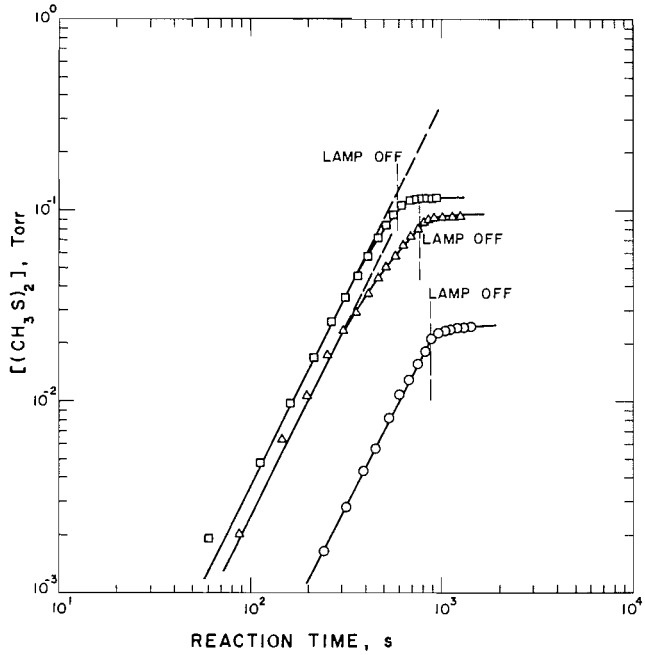

FIG. 3. log–log plot of the $(CH_3S)_2$ concentration as a function of reaction time: ○, $[CH_3SH]$ = 20.0 Torr, [NO] = 10.0 Torr, [Ar] = 16.9 Torr, I_a = 0.35 mTorr/s; △, $[CH_3SH]$ = 21.0 Torr, [NO] = 21.0 Torr, [Ar] = 15.7 Torr; I_a = 1.29 mTorr/s; □, $[CH_3SH]$ = 60.0 Torr, [NO] = 60.0 Torr, [Ar] = 15.0 Torr, I_a = 2.40 mTorr/s.

TABLE 3. Photolysis of $(CH_3S)_2$–NO mixtures at 253.7 nm

[NO] (Torr)	$[(CH_3S)_2]$ (Torr)	[Ar] (Torr)	I_a (mTorr/s)	$\Phi\{CH_3SNO\}$
5.4	9.62	14.2	1.72	2.02
11.9	9.22	16.5	1.65	2.08
30.0	2.46	14.9	0.44	2.06
30.0	5.30	14.2	0.95	1.96
30.1	9.08	15.0	1.62	2.14
49.6	10.05	20.3	0.62	2.14
50.0	9.76	15.4	1.74	2.03
100.0	14.0	19.5	0.85	1.93
198.2	9.00	14.8	1.61	2.01

$$[IV] \quad \frac{2[NO]\{[(CH_3S)_2]/t^2\}}{(\Phi\{CH_3SNO\}I_a)^2} = \frac{k_6}{k_{2a}}\left(1 + \frac{k_{-2a}}{k_{2b}[M]}\right)$$

If all the data are used to plot the left-hand side of eq. [IV] vs. $[M]^{-1}$, the data are very badly scattered. A somewhat better, but still badly scattered plot, is obtained if only the 12 data points involving the most accurate measurements of $[(CH_3S)_2]/t^2$, i.e. the runs giving the best straight line plots of $[(CH_3S)_2]$ vs. t^2, are used. This plot is shown in Fig. 9. The data are fitted by a least-squares line of intercept 0.84 ± 0.27 and slope = 0.069 ± 0.023 Torr. Thus k_6/k_{2a} = 0.84 ± 0.27 and k_{-2a}/k_{2b} = 83 ± 52 Torr.

Equation [IV] can be rearranged to

$$[V] \quad 2\beta\{[(CH_3S)_2]/t^2\} = k_6(\Phi\{CH_3SNO\}I_a)^2/k_{2a}[NO]$$

The left-hand side of this equation is plotted vs. $(\Phi\{CH_3SNO\}I_a)^2/[NO]$ for all of the data on a log–log plot in Fig. 10. This plot extends the range of variables over that in Fig. 9. The data are fitted to a line of slope 1.0 and the least-squares intercept gives log k_6/k_{2a} = −0.005 ± 0.30 or

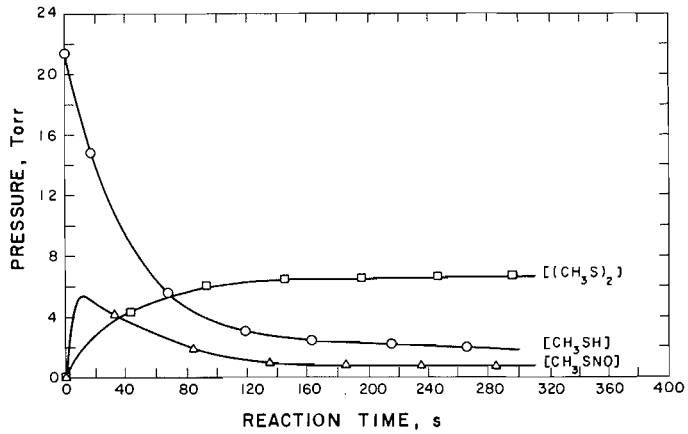

FIG. 4. Concentration profile vs. reaction time in the dark reaction of a mixture initially containing 21.4 Torr CH_3SH, 16.0 Torr NO_2, and 16.8 Torr Ar.

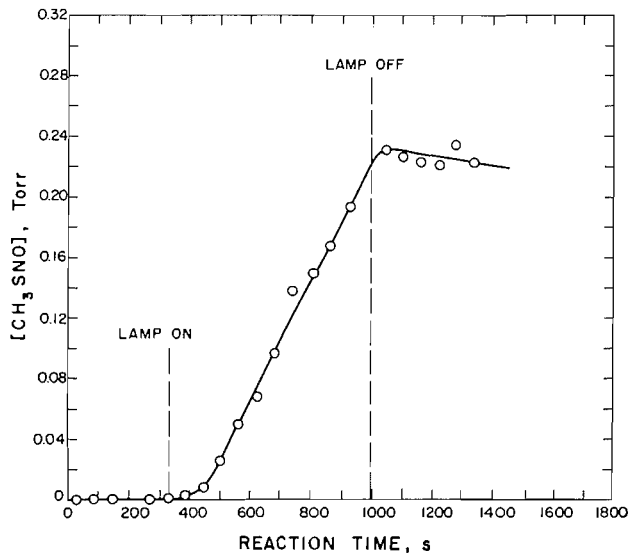

FIG. 5. Plot of $[CH_3SNO]$ vs. reaction time for the photolysis of 10.06 Torr $(CH_3S)_2$ at 280–300 nm in the presence of 7.54 Torr CH_3SH, 13.6 Torr Ar, and 200.8 Torr NO. I_a = 0.50 mTorr/s.

k_6/k_{2a} = 0.99 ×/ 2.0. This value is in good agreement with the value of 0.84 ± 0.27 obtained from Fig. 9. (If only the data from Fig. 9 are used in plotting Fig. 10, the intercept is −0.098 ± 0.148 or k_6/k_{2a} = 0.80 ×/ 1.4.)

A summary of the rate coefficient ratios obtained in our work is given in Table 4.

We now turn to a discussion of the reactions of HNO. In the presence of excess NO at room temperature, the known reactions are (9):

$$[9] \quad 2HNO \rightarrow N_2O + H_2O$$

$$[10a] \quad HNO + 2NO \rightarrow HNO_3 + N_2$$

$$[10b] \quad \rightarrow H + N_2 + NO_3 \xrightarrow{NO} 2NO_2$$

Reaction [9] is reported to be bimolecular with a rate coefficient ≃2.4 × 10^6 M^{-1} s^{-1} (10). However, we believe reaction [9] is too slow to be occurring in our system for two reasons: (*1*) our results are adequately fitted if the termination step is first-order in HNO, and (*2*) we looked for, but did not find N_2O as a product.

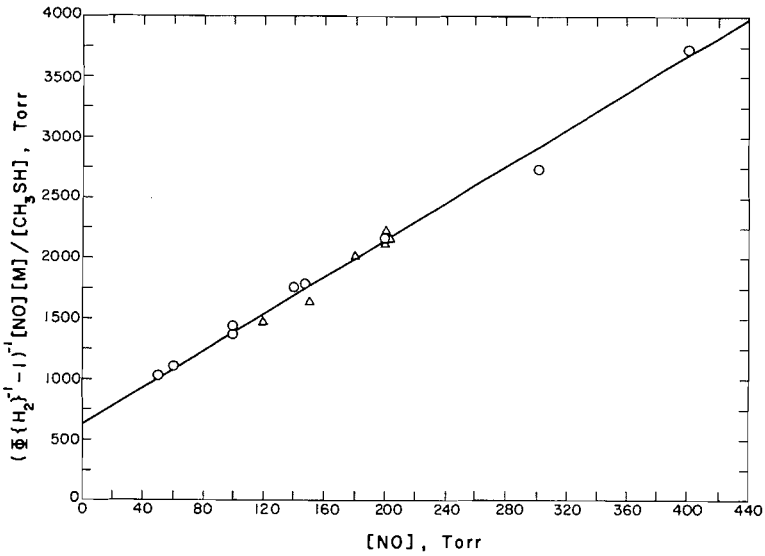

FIG. 6. Plot of $(\Phi\{H_2\}^{-1} - 1)^{-1}[NO][M]/[CH_3SH]$ vs. [NO]: △, 6.3 Torr CH_3SH; ○, 21 Torr CH_3SH.

Likewise we do not believe that reaction [10] is important in our system because the data are fitted by a termination step zero order in NO and not by one second order in NO. Reaction [10] proceeds in detail via:

[11] $HNO + NO \rightleftarrows H(NO)_2$

[12] $H(NO)_2 + NO \rightarrow HNO_3 + N_2$ or $H + N_2 + NO_3$

with reaction [12] being so slow that reaction [11] is always in equilibrium. We speculate that in the presence of CH_3SH, the $H(NO)_2$ intermediate is always intercepted by CH_3SH in a rapid reaction such as the following:

[13] $H(NO)_2 + 4CH_3SH \rightarrow$ 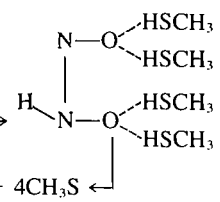

$H + N_2 + 2H_2O + 4CH_3S$

The pair of reactions [11] followed by [13] leads to a reaction which is first-order in both HNO and NO (i.e. reaction [7]) and has the overall stoichiometry

[14] $HNO + NO + 4CH_3SH \rightarrow H + N_2 + 2H_2O + 4CH_3S$

This reaction also provides the rational for $\xi = 4$ in reaction [7].

The bond dissociation energy for the S—H bond of CH_3SH would have to be $\leq$79.3 kcal/mol for reaction [14] to be thermal neutral or exothermic based on the enthalpies of formation listed in Table 5. This is very much smaller than the value of $\geq$87.0 ± 2 kcal/mol obtained from the most recent measurement of ΔH_{298} for CH_3S (11).

It is possible for reaction [13] to be rapid and yet be $\simeq$32 kcal/mol endothermic. Reaction [13] involves the scission of seven bonds. These could proceed by seven successive steps, each of which is $\simeq$5 kcal/mol endothermic, and this could proceed readily at room temperature. However, another possibility is that the bond dissociation enthalpy for the S—H bond of CH_3SH is much weaker than 87 kcal/mol, since this value is in part computed, and is not obtained entirely from experimental measurements.

Further evidence that the bond dissociation energy for the S—H bond of CH_3SH may be <87 kcal/mol comes from our work on the thermal reaction of NO_2 with CH_3SH. Presumably this reaction is initiated by either:

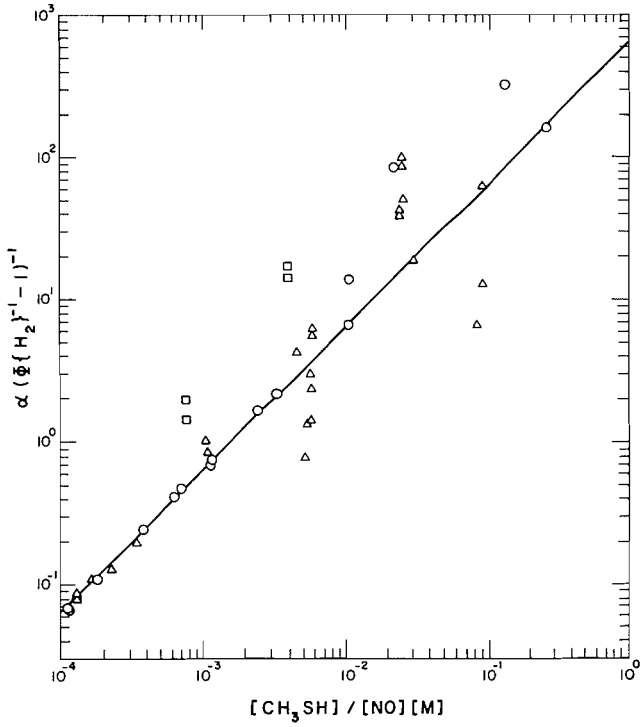

FIG. 7. log–log plot of $\alpha(\Phi\{H_2\}^{-1} - 1)^{-1}$ vs. $[CH_3SH]/[NO][M]$: △, 6.3 Torr CH_3SH; ○, 21 Torr CH_3SH; □, 60 Torr CH_3SH.

[15*a*] $CH_3SH + NO_2 \rightarrow CH_3S + HNO_2$

[15*b*] $\rightarrow CH_3SNO + HO$

Since the CH_3S—NO bond presumably is weaker than the HO—NO bond, reaction [15*b*] is energetically less favorable than reaction [15*a*]. For reaction [15*a*] to be thermal neutral or exothermic, the bond dissociation energy for S—H bond in CH_3SH would have to be $\leq$78.35 kcal/mol.

The details of the termination step, reaction [8], are not clear. One possibility is that HNO is removed by the wall in a

Can. J. Chem. Downloaded from www.nrcresearchpress.com by 210.87.254.5 on 09/06/12
For personal use only.

Can. J. Chem. Downloaded from www.nrcresearchpress.com by 210.87.254.5 on 09/06/12
For personal use only.

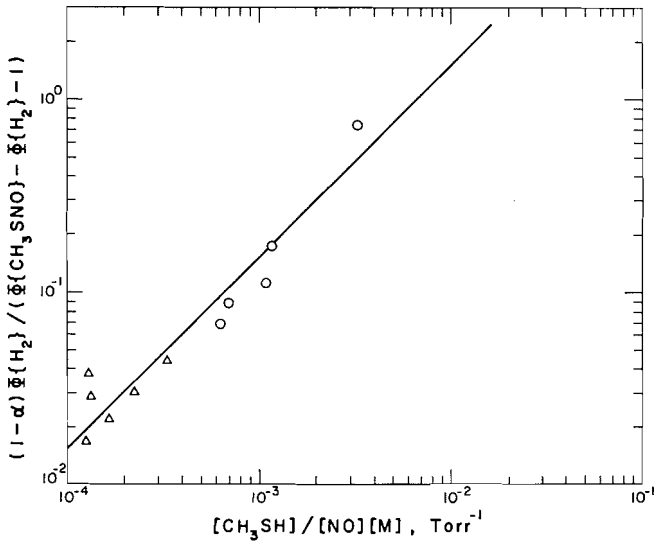

FIG. 8. log–log plot of $(1 - \alpha)\,\Phi\{H_2\}/(\Phi\{CH_3SNO\} - \Phi\{H_2\} - 1)$ vs. $[CH_3SH]/[NO][M]$: △, 6.3 Torr CH_3SH; ○, 21 Torr CH_3SH.

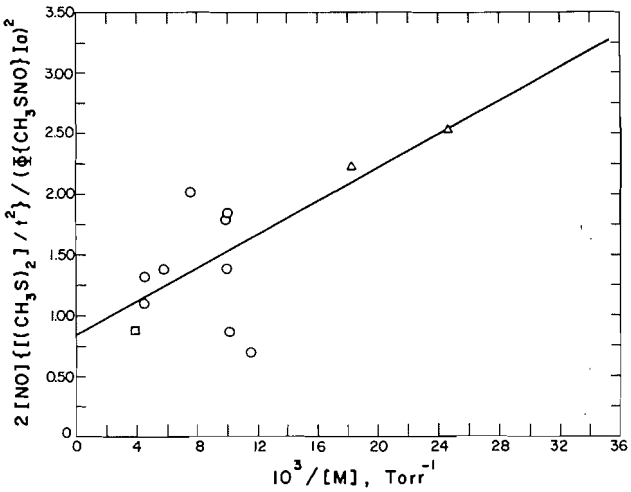

FIG. 9. Plot of $2[NO]\{[(CH_3S)_2]/t^2\}/(\Phi\{CH_3SNO\}I_a)^2$ vs. $[M]^{-1}$: △, 6.3 Torr CH_3SH; ○, 21 Torr CH_3SH; □, 60 Torr CH_3SH. Plot based on 12 most reliable data points for $[(CH_3S)_2]/t^2$.

TABLE 4. Summary of rate coefficient data

Ratio	Units	Value[a]	Source
k_5/k_4	Torr	626 ± 42	Eq. [I], Fig. 6
k_5/k_4	Torr	636 ×/ 2.4	Eq. [II], Fig. 7
k_5/k_4	Torr	616 ×/ 1.38[b]	Eq. [III], Fig. 8
k_8/k_7	Torr	85.0 ± 7.8	Eq. [I], Fig. 6
k_6/k_{2a}	None	0.84 ± 0.27	Eq. [IV], Fig. 9
k_6/k_{2a}	None	0.99 ×/ 2.0	Eq. [V], Fig. 10
k_{-2a}/k_{2b}	Torr	83 ± 52	Eq. [IV], Fig. 9

[a]All uncertainties are one standard deviation. ×/ sign denotes uncertainty by factor of.
[b]Based on $\xi = 4.0$.

first-order process and then reacts with NO on the wall according to reaction [10]. In any event the removal reaction is one that does not produce N_2O as a product.

The reason for the post-irradiation dark reaction with high NO pressures has not been explained yet. We suspect that it comes from reaction of CH_3SH with NO_2, the NO_2 being

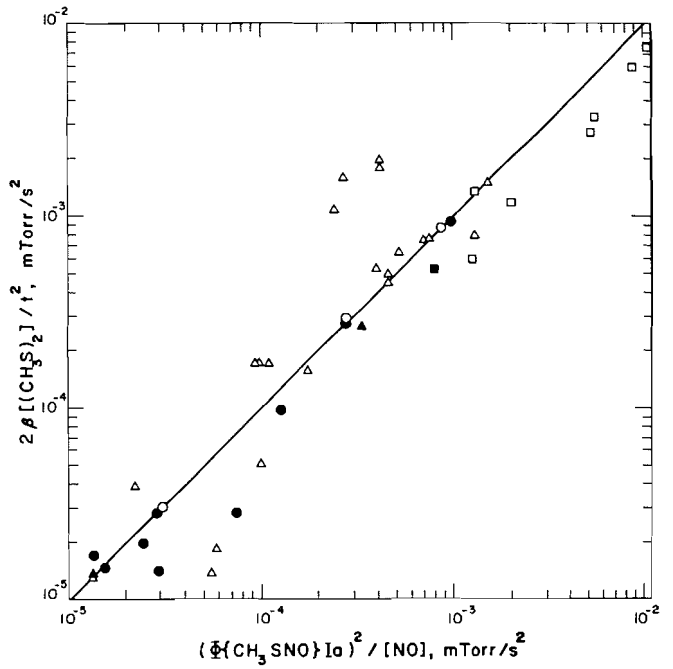

FIG. 10. log–log plot of $2\beta[(CH_3S)_2]/t^2$ vs. $(\Phi\{CH_3SNO\}I_a)^2/[NO]$. △, 6.3 Torr CH_3SH; ○, 21 Torr CH_3SH; □, 60 Torr CH_3SH. Filled symbols are for the 12 most reliable data points for $[(CH_3S)_2]/t^2$.

TABLE 5. Enthalpies of formation

Species	$\Delta H_f\{298\}$	Reference
H	52.103	12
HO	9.492	13
HNO	23.800	14
HNO_2	−18.340	14
H_2O	−57.798	14
NO	21.580	14
NO_2	7.910	14

formed as a product of the photochemical reaction. It is not clear how the NO_2 is produced, possibly from reactions [8] or [10*b*]. However, explanation of the post-irradiation dark reaction must await further work.

Acknowledgments

This work was supported in part by a grant from the Du Pont de Nemours and Co. to the Center for Air Environmental Studies at The Pennsylvania State University for which we are grateful.

1. R. P. STEER and A. R. KNIGHT. J. Phys. Chem. **72**, 2145 (1968).
2. H. NIKI, P. D. MAKER, C. M. SAVAGE, and L. P. BREITENBACH. J. Phys. Chem. **87**, 7 (1983).
3. S. L. MUROV. Handbook of photochemistry. Marcel Dekker, Inc., NY. 1973.
4. R. P. STEER, B. L. KALRA, and A. R. KNIGHT. J. Phys. Chem. **71**, 783 (1967).
5. L. BRIDGES and J. M. WHITE. J. Phys. Chem. **77**, 295 (1973).
6. W. L. FIERCE, R. L. WEICHMAN, and W. J. SANDNER. U. S. Patent 3,134,798 (1964).
7. T. INABA and B. DE B. DARWENT. J. Phys. Chem. **64**, 1431 (1960).
8. E. R. ALLEN and G. K. MOORTGAT. Third Intern. Symp. Gas Kinet. Abstract D1, Brussels (1973).

9. J. HEICKLEN and N. COHEN. Adv. Photochem. **5**, 157 (1968).
10. D. L. BAULCH, D. D. DRYSDALE, and D. G. HORNE. Evaluated kinetic data for high temperature reactions. Vol. 2. Homogeneous gas phase reactions of the $H_2-N_2-O_2$ systems. Butterworths, London. 1973.
11. L. G. S. SHUM and S. W. BENSON. Intern. J. Chem. Kinet. **15**, 433 (1983).
12. M. W. CHASE, J. L. CURNUTT, H. PROPHET, R. A. MCDONALD, and A. N. SYVERUD. J. Phys. Chem. Ref. Data, **4**, 1 (1975).
13. M. W. CHASE, J. L. CURNUTT, A. T. HU, H. PROPHET, A. N. SYVERUD, and L. C. WALKER. J. Phys. Chem. Ref. Data, **3**, 311 (1974).
14. D. R. STULL and H. PROPHET. National Bureau of Standards Report NBRDS–NBS 37 (1971) JANAF Thermochemical Tables 2nd ed.

Can. J. Chem. Downloaded from www.nrcresearchpress.com by 210.87.254.5 on 09/06/12
For personal use only.

The effect of pH and complexation on redox reactions between RS· radicals and flavins

RIZWAN AHMAD AND DAVID A. ARMSTRONG
Department of Chemistry, University of Calgary, Calgary, Alta., Canada T2N 1N4

Received April 14, 1983

RIZWAN AHMAD and DAVID A. ARMSTRONG. Can. J. Chem. **62**, 171 (1984).

Elementary considerations indicate that thiol radicals, RS·, should have a high redox potential ($E_2^0 \sim 1.0$ V):

[2] $RS\cdot + e^- = RS^-$

However, the equilibrium [4],

[4] $RS^- + RS\cdot = RS\dot{S}R^-$

which is established in the presence of excess RS^-, would convert RS· to $RS\dot{S}R^-$, which is a reducing species. Experimentally it was demonstrated that thiol radicals made by γ radiolysis of β-mercaptoethanol solutions effected two-electron oxidation of dihydroflavin FlH_2 at pH 6.3 and of FlH^- at pH 8. On the other hand, $RS\dot{S}R^-$ readily reduced Fl to FlH_2 or FlH^- as expected. At pH 9, photostationary states were established after a few minutes radiolysis and the ratios $[FlH^-]_{ss}/[Fl]_{ss}$ were a function of $[RS\dot{S}R^-]/[RS\cdot]$. The main reactions occurring were:

[19] $Fl + RS\dot{S}R^- \rightarrow \cdot Fl^- + RSSR$

[−23] $2\cdot Fl^- + H^+ \rightarrow FlH^- + Fl$

[22] $FlH^- + RS\cdot \rightarrow \cdot Fl^- + RSH$

The values of k_{19} and k_{22} were both large. The ratio k_{19}/k_{22} was ~0.8 for lumiflavin and ~0.3 for flavin adenine dinucleotide.

The cyclic disulphide anions of lipoamide and dithiothreitol ($L\dot{S}_2^-$ and $D\dot{S}_2^-$) also effected two-electron reductions of flavins. However, the protonated form of $L\dot{S}_2^-$ (i.e. $L\dot{S}_2H$) oxidized FlH_2, and the photostationary ratio $[FlH^-]_{ss}/[Fl]_{ss}$ was an approximate linear function of $[L\dot{S}_2^-]/[L\dot{S}_2H]$. The implications of the observed changes in redox properties of sulphur radicals on complexation with RS^- and protonation were briefly considered.

RIZWAN AHMAD et DAVID A. ARMSTRONG. Can. J. Chem. **62**, 171 (1984).

Des considérations élémentaires indiquent que les radicaux thiyles, RS·, doivent avoir un potentiel rédox élevé ($E_2^0 \sim 1{,}0$ V):

[2] $RS\cdot + e^- = RS^-$

Cependant, l'équilibre [4]

[4] $RS^- + RS\cdot = RS\dot{S}R^-$

qui s'établit en présence d'un excès de RS^-, transforme RS· en $RS\dot{S}R^-$ qui est une espèce réductrice. On démontre expérimentalement que les radicaux thiyles produits par radiolyse aux rayons γ de solutions de β-mercaptoéthanol provoquent une oxydation à deux électrons de la dihydroflavine (FlH_2) à un pH de 6,3 et de la FlH^- à un pH de 8. Par ailleurs, le composé $RS\dot{S}R^-$ réduit facilement la Fl en FlH_2 ou en FlH^- tel qu'attendu. A un pH de 9 il s'établit des états photostationnaires après quelques minutes de radiolyse et les rapports $[FlH^-]_{ss}/[Fl]_{ss}$ dépendent du rapport $[RS\dot{S}R^-]$ [RS·]. Les principales réactions qui se produisent sont les suivantes:

[19] $Fl + RS\dot{S}R^- \rightarrow \cdot Fl^- + RSSR$

[−23] $2\cdot Fl^- + H^+ \rightarrow FlH^- + Fl$

[22] $FlH^- + RS\cdot \rightarrow \cdot Fl^- + RSH$

Les valeurs de k_{19} et de k_{22} sont élevées. Le rapport k_{19}/k_{22} est de ~0,8 pour la lumiflavine et de ~0,3 pour le dinucléotide flavine adénine. Les anions disulfures cycliques du lipoamide et du dithiothréitol ($L\dot{S}_2^-$ et $D\dot{S}_2^-$) provoquent également des réductions à deux électrons des flavines. Cependant la forme protonée de $L\dot{S}_2^-$ ($L\dot{S}_2H$) oxyde la FlH_2 et le rapport photostationnaire $[FlH^-]_{ss}/[Fl]_{ss}$ est une fonction approximativement linéaire de $[L\dot{S}_2^-]/[L\dot{S}_2H]$. On considère brièvement les effets des changements observés dans les propriétés redox des radicaux sulfurés sur la complexation avec RS^- et sur la protonation.

[Traduit par le journal]

Introduction

Sulphur structures play important roles in the chemistry of redox proteins. In metal-containing enzymes, such as xanthine oxidase (1) and copper proteins (2), thiol groups frequently serve as binding ligands, while in other systems they may be involved as separate entities in the electron transport pathway. For example, in glutathione reductase, lipoamide dehydrogenase and thioredoxin reductase, for which the substrates themselves are sulphur-containing species, the electron transfer pathway in the direction of substrate oxidation is considered to be (3–5):

[1] $\text{Substrate} \xrightarrow{1} S{-}S \xrightarrow{2} Fl \xrightarrow{3} NAD^+$

Here the disulphide (S—S) is covalently bound to the protein, while the flavin (Fl) is strongly but non-covalently bound.

An understanding of the mechanisms of electron transport in such highly intricate systems clearly requires a knowledge of the relative redox potentials of the various sulphur species, and

Can. J. Chem. Downloaded from www.nrcresearchpress.com by 210.87.254.6 on 09/06/12
For personal use only.

Can. J. Chem. Downloaded from www.nrcresearchpress.com by 210.87.254.6 on 09/06/12
For personal use only.

of the effects on these of complexation and protonation. This publication is concerned with redox reactions of the thiol radical – thiolate ion couple:

[2] $RS\cdot + e^- = RS^-$

and the disulphide–disulphide anion:

[3] $RSSR + e^- = R\dot{S}SR^-$

The species RS· and $R\dot{S}SR^-$ are linked through the reversible reaction:

[4]/[−4] $RS\cdot + RS^- = R\dot{S}SR^-$

and, given time, equilibrium is readily established between them (6–8). As examples, values of K_4 are $1.8 \times 10^3\ M^{-1}$ for β-mercaptoethanol (6, 9) and $1.3 \times 10^3\ M^{-1}$ (8) for β-mercaptopropionic acid.

The standard reduction potential E^0 for reaction [5] with typical biological thiols

[5] $RSSR + 2H^+ + 2e^- = 2RSH$

like cysteine and glutathione is about 0.074 V (10). From this and the thiol pK, which is typically 8.3 (e.g. for cysteine (11)), it can be shown that $E^0_{5a} = -0.42$ V. If one takes D as the free energy of dissociation of the disulphide bond in reaction [6]

[5a] $RSSR + 2e^- = 2RS^-$

[6] $RSSR = 2RS\cdot$

in solution in J mol^{-1}, elementary thermodynamics then leads to $E^0_2 = -0.41 + d$, $E^0_3 = -0.24 - d$ and $E^0_7 = -0.19 + d$, where $d = D\ (2 \times 96487\ c\ mol^{-1})^{-1}$ and reaction [7] is:

[7] $R\dot{S}SR^- + e^- \rightarrow 2RS^-$

Unfortunately D is not a readily measurable quantity. However, as a first approximation one may neglect the entropy change in reaction [6] and set D equal to the S—S bond dissociation energy. That quantity has been reported (12) to be 280 ± 25 kJ mol^{-1}, and d is therefore about +1.5 V. Thus, despite the present approximation, it is evident that: E^0_2 (~+1.1 V) and E^0_7 (~+1.3 V) are positive, while E^0_3 (~−1.7 V) is strongly negative.

The large magnitudes of E^0_3 and E^0_7 would suggest that $R\dot{S}SR^-$ might serve as both a powerful oxidant and reductant. While this is true in a thermodynamic sense, $R\dot{S}SR^-$ is not expected to be capable of rapid reactions as an electron acceptor. This is because the additional electron must enter an antibonding orbital, and the energy of the —S—S— system would be prohibitively high until dissociation occurred. No such restriction applies to electron loss, and from a *dynamic point of view* $R\dot{S}SR^-$ should therefore be primarily a reductant. This is borne out in its reaction with oxygen and several other substances (11). On the other hand, the large positive value of E^0_2 indicates the role of a general oxidant. In this study we shall demonstrate the transition between these characteristics for RS· and $R\dot{S}SR^-$, using as references the flavin half reactions:

[8] $Fl + H^+ + e^- = \cdot FlH;\quad E^0_8 = 0.17$ (13)

and

[9] $\cdot FlH + H^+ + e^- = FlH_2;\quad E^0_9 = 0.22$ (13)

Two reports of one electron transfer from $R\dot{S}SR^-$ species to Fl have already been made (14, 15).

One other point deserves further attention here. While $R\dot{S}SR^-$ anions formed by reaction [4] are highly unstable with respect to reaction [−4] (8), those made by electron attachment to protein-bound S—S groups are stabilised by the tertiary protein structures and have been seen to have lifetimes extending into the 1 s range (16). This stabilisation can be simulated with small molecules, if the disulphide group is present in a ring having three or four aliphatic carbon atoms. In the case of lipoic acid or lipoamide:

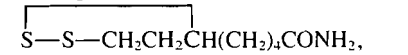

which we shall abbreviate to LS_2, both the anion $L\dot{S}_2^-$ and its conjugate acid $L\dot{S}_2H$ are believed to be cyclic in structure (8, 14, 17, 18). This is also true of the anion of dithiothreitol DS_2 (19). The pK's for protonation of both $L\dot{S}_2^-$ and $D\dot{S}_2^-$ are in the region of 5.4–5.6 (14, 17–19). Also either anion can be produced by H atom abstraction from the disulphydryls $L(SH)_2$ and $D(SH)_2$ (14, 18, 19), for example:

[10] $L(SH)_2 + \cdot OH(\text{or } H\cdot) \rightarrow L\dot{S}_2H + H_2O\ (\text{or } H_2)$

[11] $L\dot{S}_2H = H^+ + L\dot{S}_2^-$

In the present study the directions and stoichiometry of electron transfer between flavins and $D\dot{S}_2^-$, $L\dot{S}_2^-$, and $L\dot{S}_2H$ were also investigated. These and the other sulphur radicals RS· and $R\dot{S}SR^-$ were produced by ^{60}Co γ radiolysis through the sequence of reactions

[12] $4.2\ H_2O \xrightarrow{^{60}CO\,\gamma} 2.7\ e^-_{aq} + 0.5\ H\cdot + 2.8\ \dot{O}H + 2.7\ H^+_{aq} + 0.5\ H_2 + 0.7\ H_2O_2$

[13] $e^-_{aq} + N_2O + H_2O \rightarrow N_2 + OH^- + \cdot OH$

[14] $\cdot OH\ (\text{or } H\cdot) + RSH \rightarrow H_2O\ (\text{or } H_2) + RS\cdot$

[12]–[13]–[14] or [12]–[13]–[10]–[11]. As in earlier studies (14, 17–21) solute concentrations were adjusted so that ·OH, H·, and e^-_{aq} did not react directly with the flavin. The two flavins used were lumiflavin (LFl) and flavin adenine dinucleotide (FAD). A preliminary report of a small part of this work was presented in 1982 (15). The inspiration for it came partly from ref. 14.

Experimental

Materials

Lumiflavin, flavin adenine dinucleotide, lipoamide, β-mercaptoethanol, and β-mercaptopropionic acid were obtained from Sigma Chemical Company. Reduced dithiothreitol was from Kodak Chemical Company. Dihydrolipoamide was made by the method of Reed *et al.* (22). The water for preparing solutions was redistilled, first from alkaline permanganate and then from acid dichromate.

Apparatus and procedure

All experiments were conducted at room temperature (24 ± 1°C) with solutions containing 5 mM phosphate buffer. Irradiations were performed in an A.E.C.L. ^{60}Co γ cell with a steady dose rate of ~15 grays per min. This was checked periodically as described earlier (20). Oxidation and reduction of flavins was followed by recording the spectra of the solutions on a Cary 219 UV-Visible spectrophotometer. Extinction coefficients used were 12320 at 440 nm and 11300 at 450 nm for LF and FAD, respectively (21).

Precautions were taken to prevent air oxidation in the preparation of sulphydryl solutions. The buffer solution and other solutions were placed in the volumetric flask and then the RSH or $D(SH)_2$ was added. Immediately after that the solution was deaerated with N_2O, which had been passed through a "ridox" column supplied by the Fisher Scientific Company. In the case of $L(SH)_2$ the solution was deaerated

Can. J. Chem. Downloaded from www.nrcresearchpress.com by 210.87.254.6 on 09/06/12
For personal use only.

before adding the sulphydryl. Finally the pH was adjusted by adding NaOH or $HClO_4$.

Calculation of moles of sulphur radicals produced

As explained in ref. 15*b*, the number of mol per L of radicals produced, e, was calculated with the equation:

$$[15] \qquad e = 1.04 \times 10^{-7}\, Qt\,(g_r + aG^{M}_{H_2O_2})$$

Here Q was the dose rate in grays per min; t, the radiation time; g_r, the number of radicals formed per 100 eV of radiation energy; and $G^{M}_{H_2O_2}$, the yield of hydrogen peroxide in molecules per 100 eV. The inclusion of this term was necessary because H_2O_2 oxidised FlH_2 in a 1:1 stoichiometry (15*b*). The coefficient a has values of +2 and −2 for oxidising the reducing radicals, respectively, for pH ≤ 8. From data in ref. 23 it can be shown that above pH 8 reaction with RS^- would remove H_2O_2, and therefore a can be set equal to zero. The magnitudes of g_r and $G^{M}_{H_2O_2}$ were taken from the data of Draganić and Draganić (24) or from published yields of $G(LS_2)$ in lipoate (14) or lipoamide (18) solutions. Typical values were 6.0 and 0.6 for 2 m*M* formate and 6.3 and 0.6 for 2 m*M* lipoamide, respectively.

Results

Thermal reactions

A number of experiments were carried out to check the rate of the thermal reduction of the flavins by lipoamide and mercaptans. In agreement with the earlier data of Gascoigne and Radda (25) and others (26)[1] the rates were found to be negligible below the p*K* of RSH. Even at pH 10, where the thiol groups were ionised, with typical conditions of 2 m*M* $L(SH)_2$ and 20 μ*M* Fl the half life of reaction [16] was still several hours. Since our radiolysis experiments were complete in ~20

$$[16] \qquad L(SH)_2 + Fl \rightarrow LS_2 + FlH^- + H^+$$

min, the thermal reactions could be neglected. One may note that p*K* of FlH_2 is ~6.7 (13), so that at pH 7 it would be present mainly as FlH^-.

Reduction with $L\dot{S}_2^-$ and $D\dot{S}_2^-$ at pH 7

The changes in absorbance which occurred in the wavelength region 250 to 520 nm on treatment of 14.6 μ*M* lumiflavin with $L\dot{S}_2^-$ radicals are shown in Fig. 1*a*. As in our earlier study with $\cdot CO_2^-$, the initial flavin spectrum with peaks at ~365 and ~440 nm was bleached during each successive exposure to $L\dot{S}_2^-$ until finally the spectral changes ceased. This has been illustrated in Fig. 2*a*, where the decrease in absorbance, ΔA, at 440 nm has been plotted against the ratio of the number of equivalents of $L\dot{S}_2^-$ produced per L of solution to the initial molar concentration of flavin. A similar titration plot for a more concentrated LFl solution has also been presented.

As will be demonstrated below, the spectrum after irradiation (dashed line, Fig. 1*a*) was indicative of FlH^- formation. This was consistent with the fact that the initial spectrum of Fl was restored on admission of air (dotted line). The small increase in absorbance in the 290 to 370 nm region can be attributed to the LS_2 produced in the overall reaction:

$$[17] \qquad 2L\dot{S}_2^- + Fl + H^+ \rightarrow 2LS_2 + FlH^-$$

This compound has negligible absorption above 400 nm and a maximum at 330 nm with $\epsilon = 127\ M^{-1}\ cm^{-1}$ (Fig. 1*b*). Hence by taking into account excess absorbance at 330 nm after oxidation with air, one can calculate the LS_2 concentration and thence obtain a corrected spectrum of the reduced flavin product per se. This has been presented in Fig. 1*b*, where it has been

[1] Loechler and Hollocher cite other studies in ref. 26.

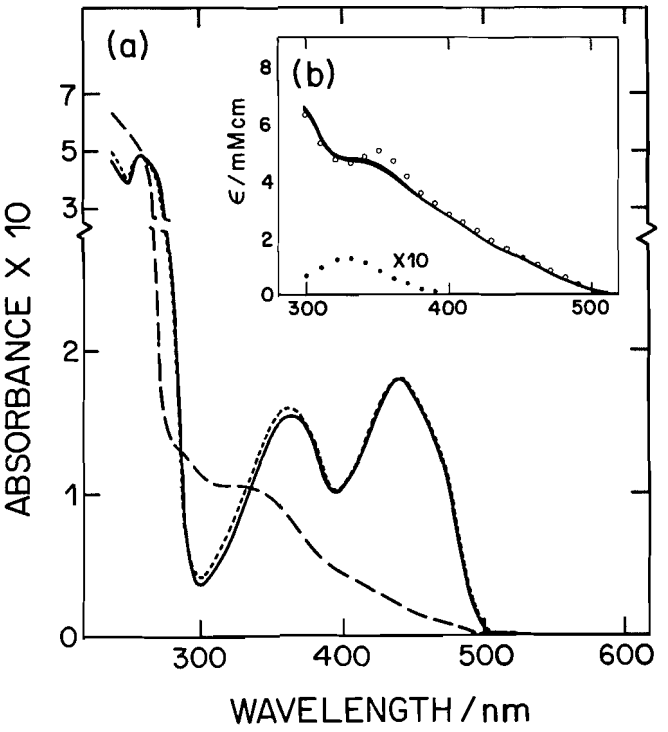

FIG. 1. (*a*) Spectra obtained from N_2O saturated solution of 14.61 μ*M* LF in 2 m*M* $L(SH)_2$ at pH 6.9 before irradiation (—), when the spectral changes ceased (– – –) and after addition of air to the irradiated solution (- - -). (*b*) Spectrum of fully reduced flavin ($LFlH^-$) obtained by: $\cdot CO_2^-$ reduction (thick line), $L\dot{S}_2^-$ reduction (open circles). The dots are the spectrum of LS_2.

compared with the spectrum of FlH^- prepared by $\cdot CO_2^-$ reduction under otherwise similar conditions. Both are the mean of replicate determinations, with extremes of the deviations for $\cdot CO_2^-$ shown by the thickness of the line.

Although it could be argued that the peak at 350 nm was due to insufficient correction for absorbance by LS_2 in some instances, it was observed repeatedly with $L\dot{S}_2^-$, being of the same magnitude over the pH range studied (see below). A similar peak was seen with FAD and $L\dot{S}_2^-$ and with both flavins and $D\dot{S}_2^-$ as reductant. This suggests that some addition compounds, e.g. H—Fl—SLSH, were formed, since thiol C-4a adducts of flavins have absorption maxima in that region with ϵ_{max} ~8000 M^{-1} cm^{-1} (27). The weakness of the present absorption peak demonstrates that the product was largely (≳85%) FlH^-. Also, unlike the addition products observed with aliphatic carbon radicals (15*b*), the flavin derivatives formed here were all readily converted to Fl by air oxidation.

Similar absorption changes were seen following reaction of LFl with $D\dot{S}_2^-$, and FAD with $L\dot{S}_2^-$ and $D\dot{S}_2^-$. Using the absorbance coefficients of the products at 440 nm from Fig. 1*b* and at 450 nm from an analogous plot for FAD and the known absorbance coefficients of the flavins, one can calculate the percentage of flavin reacted when spectral changes ceased. These percentages have been summarised in Table 1. For each case where there was 98+% conversion, η, the number of radicals reacting per flavin, was calculated from the break in the titration plot (see arrows, Fig. 2*a* and *c*). For lower conversions it was found from the initial slope of a plot of Δ[Fl] versus e (Cf. Fig. 2*b*). Values of η have also been listed in Table 1. For $L\dot{S}_2^-$ the percentage reduction and η were independent of LFl or $L(SH)_2$ concentration.

TABLE 1. Flavin reduction at pH 7

$[Fl]_0/\mu M$	Radical	Radical source (Conc./mM)	η, radicals reacted per Fl molecule	Percent Fl reacted at steady state
LFl				
15–20	$\cdot CO_2^-$	HCO_2^- (2.0)	2.1*	99+
15	$L\dot{S}_2^-$	$L(SH)_2$ (2.0)	1.8	99
28	$L\dot{S}_2^-$	$L(SH)_2$ (2.0)	1.9	98
21	$D\dot{S}_2^-$	$D(SH)_2$ (2.0)	4.2	~60
FAD				
4.8	$L\dot{S}_2^-$	$L(SH)_2$ (0.4)	2.1	99
4.5	$L\dot{S}_2^-$	$L(SH)_2$ (0.8)	2.1	98
5.2	$L\dot{S}_2^-$	$L(SH)_2$ (1.5)	1.9	98
19	$D\dot{S}_2^-$	$D(SH)_2$ (1.0)	2.8	~84

*From ref. 21.

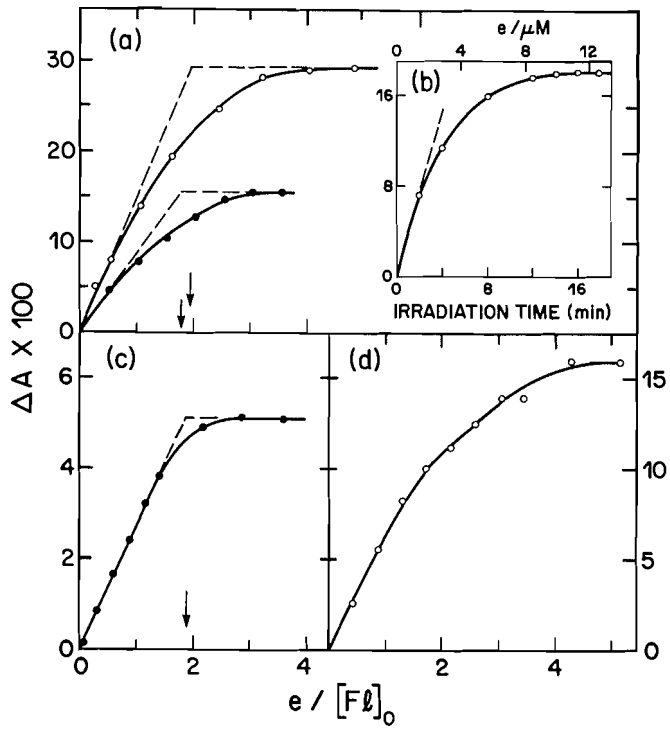

FIG. 2. Change in absorbance of flavin versus equivalents of reducing species produced by γ radiation in N_2O saturated solutions of 1–2 mM $L(SH)_2$ or $D(SH)_2$ and 13.5 mM RSH. (*a*) $L\dot{S}_2^-$ + LFl 27.5 μM (○) and 14.6 μM (●); (*b*) $RSSR^-$ + LFl 24.2 μM; (*c*) $L\dot{S}_2^-$ + FAD 5.2 μM; (*d*) $D\dot{S}_2^-$ + FAD 18.7 μM; pH = 9 in (*b*) and 7 for all others; dose rate = 1.4 gray min^{-1} in (*c*) and 12–16 gray min^{-1} otherwise.

Plots of absorbance changes for FAD titrated with $L\dot{S}_2^-$ and $D\dot{S}_2^-$ are presented in Fig. 2*c* and *d*.

The pH dependence of reactions with $R\dot{S}SR^-$ and RS·

Similar spectral changes and complete return to Fl on subsequent addition of air were also observed in RSH solutions at pH 9 and 10. However, as illustrated in Fig. 2*b* for 24.2 μM LFl in 13.5 mM β-mercaptoethanol at pH 9, the extent of reduction when steady state was reached at RSH concentrations in the range 2–15 mM was never complete.

The concentrations of flavin and reduction product at steady state were calculated from the changes in absorption as described above. The ratios $[FlH^-]/[Fl]$ at steady state have been plotted in Fig. 3 against the ratio $y = [R\dot{S}SR^-]/[RS\cdot]$. This was calculated from expression [18].

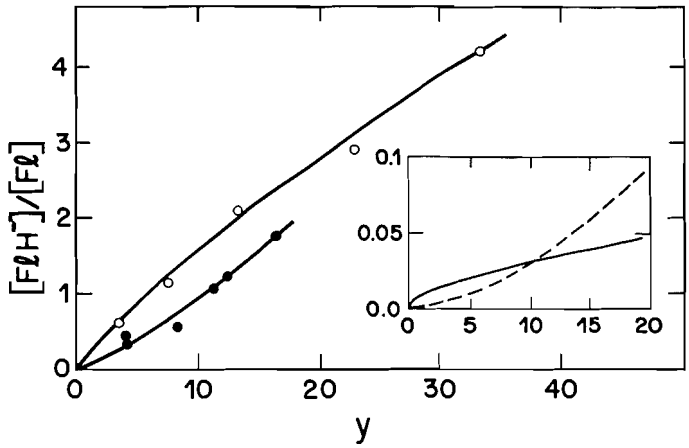

FIG. 3. The ratio of $[FlH^-]$ to [Fl] at stationary state obtained on γ radiolysis plotted as a function of y, the ratio of $[R\dot{S}SR^-]/[RS\cdot]$, for: 20 μM LFl (closed symbols; abscissa scale × 0.1) and FAD (open symbols). Inset: plots of $[\cdot Fl^-]_{ss}/[Fl]_{ss}$ (—) and $y[\cdot Fl^-]_{ss}/[Fl]_{ss}$ (– – –) versus y.

$$[18] \qquad [R\dot{S}SR^-]/[RS\cdot] = [\text{Total RSH}] \times K_4 \times \{1 + [H^+]/K_i\}^{-1}$$

The required assumption that reactions [4] and [−4] were sufficiently rapid to maintain equilibrium [4] can be justified from rate constants in refs. 6 and 8. The term K_i is the thiol ionisation constant. The results of similar experiments with 20 μM FAD at pH 9 have also been given. The steady-state ratios $[FlH^-]_{ss}/[Fl]_{ss}$ in all cases increased with y. The form of that increase will be discussed later. For all of the reductions reported in Fig. 3 the values of η from initial slopes of plots like that in Fig. 2*b* were 2.0–2.5.

In earlier work with β-mercaptoethanol and FAD at pH 7, where $[R\dot{S}SR^-]/[RS\cdot]$ is several hundredfold less than at pH 10 (K_i of β-mercaptoethanol $\simeq 10^{10}$ (6, 9)), we actually observed *oxidation* of FAD dihydroflavin by RS· (15*b*). Using the same procedure of reduction with $\cdot CO_2^-$ followed by addition of RSH, in the present series of experiments we demonstrated that the RS· radicals from a second thiol — β-mercaptopropionic acid — also oxidised the dihydroflavin of FAD. Oxidation with $\eta = 2.0–2.4$ was observed at pH 6.3, 6.9, and 8.1 in solutions containing 20 μM FlH_2 and 0.28 M RSH. However, at pH 9, where the ratio $[R\dot{S}SR^-]/[RS\cdot]$ would have become significant, oxidation did not occur.

Effect of pH on steady-state reduction with $L\dot{S}_2^-$ and $L\dot{S}_2H$ radicals

The pH dependence of the fraction of flavin reduced at steady state was examined in N_2O saturated solutions, which contained 16 to 24 μM LFl, 2 mM $L(SH)_2$, and 5 mM phosphate buffer. Concentrations of Fl and FlH_2 were calculated from absorbances at 440 nm as above. The values of η from initial slopes were in the region 1.8 to 2.2. The results have been shown as triangles in Fig. 4. The solid line is a pK curve with a pK value of 5.5.

Discussion

Reactions of RS· and $R\dot{S}SR^-$

The increase in the extent of reduction of flavin with the rise

Can. J. Chem. Downloaded from www.nrcresearchpress.com by 210.87.254.6 on 09/06/12
For personal use only.

Can. J. Chem. Downloaded from www.nrcresearchpress.com by 210.87.254.6 on 09/06/12
For personal use only.

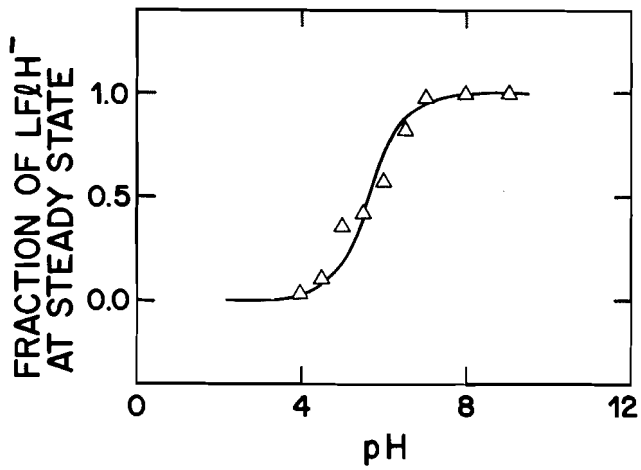

FIG. 4. Fraction of flavin present in reduced form, when stationary state was reached in the γ radiolysis of N_2O saturated 16–24 μ*M* LFl solutions containing 2 m*M* $L(SH)_2$ and 5 m*M* phosphate buffer, plotted as a function of pH.

in $[R\dot{S}SR^-]/[RS\cdot]$ in Fig. 3 demonstrates that $R\dot{S}SR^-$ reduces Fl. The first step in that process must be

[19] $\quad R\dot{S}SR^- + Fl \rightarrow RSSR + \cdot Fl^-$

(The $\cdot Fl^-$ form of the radical predominates at pH 9, because the p*K* is ~8.4 (13).) Independent evidence for reaction [19] has recently been obtained from a pulse radiolysis study at pH 9 and 10, which gave k_{19} values of 4×10^8 for FAD at pH 9 and 7×10^8 and $\sim 2 \times 10^8\ M^{-1}\ s^{-1}$ for LFl and FAD respectively at pH 10 (28). Thus the original observation of a reaction between lipoate $L\dot{S}_2^-$ and FAD by Chan, Chan, and Bielski (14) has now been extended to include $R\dot{S}SR^-$ ions and $D\dot{S}_2^-$ (15), and can be considered a general reaction of —S—$\dot{S}^-$-anions and flavins. Likewise the oxidation of FlH_2—FlH^-, which was reported earlier for $HOCH_2CH_2S\cdot$ radicals at pH 7 (15*b*) and confirmed here for $\cdot SCH_2CH_2CO_2^-$ radicals at pH 6.3, 7, and 8.0, now appears to be a general characteristic of thiyl radicals.

In addition to the primary reactions of $R\dot{S}SR^-$ with Fl and of $RS\cdot$ with FlH^-, one must examine the possibility that the overall two-electron reductions at pH 9 involve reactions between these sulphur radicals and flavin radicals. The reactions which must be considered are therefore [4], [19], and [20] to [23]:

[20] $\quad R\dot{S}SR^- + \cdot Fl^- + H^+ \rightarrow RSSR + FlH^-$

[21] $\quad RS\cdot + \cdot Fl^- \rightarrow RS^- + Fl$

[22] $\quad RS\cdot + FlH^- \rightarrow RS^- + \cdot Fl^- + H^+$

[23]/[−23] $\quad Fl + FlH^- = 2 \cdot Fl^- + H^+$

The fact that the initial values of η were never significantly less than 2 rules out the possibility of reaction [−22], which would have caused a chain reduction of Fl and low values of η. The absence of evidence for this process is consistent with the large

[−22] $\quad RS^- + \cdot Fl^- + H^+ \rightarrow RS\cdot + FlH^-$

positive value estimated for E_2^0 in the Introduction. Likewise there is no evidence for $RS\cdot$ addition to Fl or of $\cdot Fl^-$ + RSSR reactions.

A consideration of the kinetic equation for the above reactions when steady $[FlH^-]_{ss}$ and $[Fl]_{ss}$ have been reached, yields eq. [24]:

$$[24] \qquad \frac{[FlH^-]_{ss}}{[Fl]_{ss}} = \frac{k_{19}y}{k_{22}} + \frac{k_{20}}{k_{22}} \times y\frac{[\cdot Fl^-]_{ss}}{[Fl]_{ss}} - \frac{k_{21}}{k_{22}} \times \frac{[\cdot Fl^-]_{ss}}{[Fl]_{ss}}$$

The second and third terms on the right hand side are concerned with the radical + radical reactions, and for the following reasons are expected to be small relative to the first at any $[FlH^-]_{ss}/[Fl]_{ss}$ in Fig. 3. From the known magnitude of $k_{-23} = 3 \times 10^8\ M^{-1}\ s^{-1}$ (28) and the dose rate used one can show that the value of $[\cdot Fl^-]_{ss}$ would be 0.02 μ*M*, if reactions [23], [20], and [21] were neglected. The highest possible $[\cdot Fl^-]_{ss}$ would be realised if the equilibrium [23]/[−23] were maintained, giving

$$[\cdot Fl^-]_{ss} = \sqrt{K_{23}[Fl]_{ss}[FlH^-]_{ss}}$$

Taking $K_{23} = 10^{-3}$ at pH 9 (calculated from eq. [2] and the parameters for lumiflavin —3-CH_2COO^- in ref. 29) one can show that $[\cdot Fl^-]$ would not exceed 0.4 μ*M* when the total flavin concentration is 20 μ*M*. The calculated values of $y \times [\cdot Fl^-]_{ss}/[Fl]_{ss}$ and $[\cdot Fl^-]_{ss}/[Fl]_{ss}$ which apply to the reduction of LFl in Fig. 3 have been plotted as a function of *y* in the insert. The first of these is seen to rise more slowly, but eventually it crosses the second and increases very rapidly. Both are less than 0.03 over the range of *y* from zero to ten.

A detailed analysis of the plots in Fig. 3 is not possible, because specific values of K_{23} are lacking and too many rate constants are unknown. However, the curvature exhibited by the points for FAD suggests that the third term in eq. [24] is more important than the second (i.e. k_{21}/k_{22} is probably larger than k_{20}/k_{22}), while the opposite appears true for LFl. Approximate values of k_{19}/k_{22} obtained from the initial slopes of the experimental points in Fig. 3 where $[\cdot Fl^-]_{ss}/[Fl]_{ss}$ is small are 0.8 for LFl and 0.3 for FAD, respectively. From the magnitudes of k_{19} noted above it follows that k_{22} is in the region of 0.5 to $2 \times 10^9\ M^{-1}\ s^{-1}$ for these flavins. It is hoped that some of the other rate constants may be determined by independent techniques.

Reactions of $L\dot{S}_2^-$ and $L\dot{S}_2H$

The magnitudes of η in Table 1 and the spectral changes described in the second section of Results have demonstrated that, like $\cdot CO_2^-$, $L\dot{S}_2^-$ radicals effect a two-electron reduction of FAD and LFl in accord with reaction [17] at pH 7. The reactions responsible must be [19*l*], [23], and possibly also [20*l*].

[19*l*] $\quad L\dot{S}_2^- + Fl + H^+ \rightarrow LS_2 + \cdot FlH$

[20*l*] $\quad L\dot{S}_2^- + \cdot FlH \rightarrow LS_2 + FlH^-$

The role of [20*l*] cannot at present be assessed, since its rate constant has not been determined. However, the spectral evidence for a small amount of C4-a HSLS—FlH adduct (Fig. 1*b*) suggested that some radical + radical reactions had occurred as follows:

[20′*l*] $\quad L\dot{S}_2^- + \cdot FlH \rightarrow {}^-SLS—FlH$

Recent investigations (25, 26) of reaction [16] imply that such adducts decompose to $FlH^- + LS_2$, which would give the same stoichiometry as reaction [20*l*].

Although the rate constant for reaction of $D\dot{S}_2^-$ with FAD ($=9 \times 10^8\ M^{-1}\ s^{-1}$ (15)) is similar to k_{19l} ($=2.4 \times 10^8\ M^{-1}\ s^{-1}$ (14)), the percentage reduction observed at steady state was much less for the former (see Table 1). The same pattern was

Can. J. Chem. Downloaded from www.nrcresearchpress.com by 210.87.254.6 on 09/06/12
For personal use only.

observed with LFl. It is apparent therefore that reactions other than [19*l*], [20*l*], and [23] can occur, and that their relative importance varies from one disulphide anion to the next. This is also seen from a comparison of the titration plots in Fig. 2*a*, *c*, and *d*. From those the titration of FAD by $L\dot{S}_2^-$ (Fig. 2*c*) was most efficient, as judged by the linearity of the ΔA versus $e/[Fl]_0$ plot.

As shown in Fig. 4 the fraction of flavin reduced to FlH_2 at steady state falls with decreasing pH. We attribute this to the fall off in the fraction of lipoamide radicals present in the deprotonated $L\dot{S}_2^-$ form. Also reaction [22*l*] and possibly also [21*l*] must occur, otherwise the yield of FlH_2 would have

[22*l*] $\quad L\dot{S}_2H + FlH_2 \rightarrow L(SH)_2 + \cdot FlH$

[21*l*] $\quad L\dot{S}_2H + \cdot FlH \rightarrow L(SH)_2 + Fl$

been maintained through the sequence [11]–[19*l*]–[23].

It is apparent that reactions [19*l*] to [22*l*] are analogous to [19] to [22] and that an equation similar to [24] should also apply here. Neglecting [20*l*] and [21*l*] because of the low value of $[\cdot FlH]_{ss}/[Fl]_{ss}$ as justified above, one has in first approximation: $[FlH_2]_{ss}/[Fl]_{ss} = yk_{19l}/k_{22l}$. When k_{19l}/k_{22l} is unity, this equation is equivalent to:

(Fraction of flavin as $FlH_2)_{ss}$ = (Fraction of radicals as $L\dot{S}_2^-$)

The pK of lipoamide $L\dot{S}_2^-$ has recently been found by us (18) to be 5.5, in good agreement with the published values for lipoic acid $L\dot{S}_2^-$ (14, 17). The solid line in Fig. 4 shows the fraction of radicals present as $L\dot{S}_2^-$, calculated from that pK. The fit to the observed values of (fraction of flavin as $FlH_2)_{ss}$ is excellent, indicating that k_{19l}/k_{22l} must be near unity. Since k_{19l} is $= 2.4 \times 10^8\ M^{-1}\ s^{-1}$ (14) it follows that k_{22l} is of a similar magnitude.

From pK_5 = 5.5 one can show that $E^0_{3'l}$ is 0.33 V larger than

[3′*l*] $\quad LS_2 + H^+ + e^- = L\dot{S}_2H$

[3*l*] $\quad LS_2 + e^- = L\dot{S}_2^-$

E^0_{3l}. Thus the failure of $L\dot{S}_2H$ to act as a reductant of Fl can be rationalised. However, its ability to oxidise FlH_2 deserves further comment. Reaction [22*l*] may proceed as written, or as an electron transfer,

[22′*l*] $\quad L\dot{S}_2H + FlH_2 \rightarrow LSH.S^- + FlH_2^+$

followed by proton exchange. However, both [22*l*] and [22′*l*] assume simultaneous breakdown of the cyclic $L\dot{S}_2H$ (see comment on $R\dot{S}SR^-$ as an oxidant in Introduction). This inhibitory requirement does not apply to ·H and e^- transfers of the non-cyclic LSH.S· radical, and its reactions should therefore be faster. Thus we cannot eliminate the possibility that a small proportion of that species is always in equilibrium with $L\dot{S}_2H$ and is in fact the oxidant. In the related case of $D\dot{S}_2H$ the relatively small absorbance near 390 nm (19) suggests that the open radical structure DSH.S· may actually dominate over the cyclic radical. If the oxidation of FlH_2 by DSH.S· is fast (i.e. $k \gtrsim 10^9\ M^{-1}\ s^{-1}$) the residual proportion of DSH.S· at pH 7 may be sufficient to cause the large values of η and low percentages of reductant seen in Table 1.

Summary

This study has confirmed the strong oxidising nature of the RS· radical and its conversion to a reducing species on complexation with RS^- to form $R\dot{S}SR^-$. In the cyclic stable disulphides protonation is seen to increase E^0. These findings are clearly of importance in considering the role of sulphur species in electron transfer mechanisms and structures of redox proteins. For example, in the specific case of the flavoproteins mentioned in the Introduction flavin and sulphur radical pair species have been considered (30) as possibly existing in the doubly reduced form of lipoamide dehydrogenase. From this study the

S· ·FlH

structure is seen to be unstable. Actually radical pair structures have been discarded in favour of forms with either doubly reduced disulphide or flavin. Careful spectrophotometric studies demonstrate that charge transfer and base interactions play very important stabilising roles (4, 5). The enzymatic reactions require fast transfer of e^-/H^+ pairs between the sulphur and flavin entities in these stable structures. The rapidity of the reactions observed between the flavin and sulphur species studied here (all reactions were close to the diffusion control limit) implies that $S\dot{S}^-$ anions coupled with ·FlH or $\cdot Fl^-$ radicals could be transitory intermediates. However, before the feasibility of sequential one electron transfers involving such species can be properly assessed, one must also examine interactions between thiolate ions and ·FlH or $\cdot Fl^-$, since these could markedly effect E^0_8 and/or E^0_9 and the rates of electron transfer. One thiol group in lipoamide dehydrogenase and glutathione reductase is known to be in close proximity to the flavin, and a charge transfer interaction between its ionised form and the flavin has already been postulated (3–5).

Acknowledgements

Financial support from the Natural Sciences and Engineering Research Council of Canada under grant A3571 and from the University of Calgary is gratefully acknowledged.

1. P. HEMMERICH and H. LAUTERWEIN. Inorganic biochemistry. *Edited by* G. L. Eichhorn. Vols. 1 and 2. Elsevier. 1973. Chapt. 32.
2. E. I. SOLOMON, J. W. HAVE, D. M. DOOLEY, J. H. DAWSON, P. J. STEPHENS, and H. B. GRAY. J. Am. Chem. Soc. **102**, 168 (1980).
3. C. H. WILLIAMS, JR. Enzymes, **13**, 89 (1976).
4. K. D. WILKINSON and C. H. WILLIAMS, JR. J. Biol. Chem. **254**, 852 (1979).
5. L. D. ARSCOTT, C. THORPE, and C. H. WILLIAMS, JR. Biochemistry, **20**, 1514 (1981).
6. W. KARMANN, A. GANZOW, G. MEISSNER, and A. HENGLEIN. Int. J. Radiat. Phys. Chem. **1**, 395 (1969).
7. G. E. ADAMS and P. WARDMAN. Free radicals in biology. Vol. 3. *Edited by* W. A. Pryor. Academic Press. Chapt. 2.
8. M. Z. HOFFMAN and E. HAYON. J. Am. Chem. Soc. **94**, 7950 (1972); J. Phys. Chem. **77**, 990 (1973).
9. G. G. JAYSON, D. A. STIRLING, and A. J. SWALLOW. Int. J. Radiat. Biol. **19**, 143 (1971).
10. M. FRIEDMAN. The chemistry and biochemistry of the sulphydryl group in amino acids, peptides and proteins. Pergamon, New York. 1973.
11. J. E. PACKER. *In* The chemistry of the thiol group. Part 2. *Edited by* S. Patai. Wiley, London. 1974. p. 481.
12. S. SUNNER. Acta Chem. Scand. **9**, 837 (1955); H. MACKLE, Tetrahedron, **19**, 1159 (1963).
13. T. C. BRUICE. Progress in bioorganic chemistry. **4**, 1 (1979).
14. S. W. CHAN, P. C. CHAN, and B. H. J. BIELSKI. Biochim. Biophys. Acta, **338**, 213 (1974).

15. (*a*) A. J. ELLIOT, R. AHMAD, L. MCINTOSH, D. BURKE, K. J. STEVENSON, and D. A. ARMSTRONG. *In* Flavins and flavoproteins. *Edited by* V. Massey and C. H. Williams, Jr. Elsevier, New York. 1982. p. 533; (*b*) R. AHMAD and D. A. ARMSTRONG. Biochemistry, **21**, 5445 (1982), and to be published.
16. J. R. CLEMENT, W. S. LIN, D. A. ARMSTRONG, N. V. KLASSEN, and H. A. GILLIS. Int. J. Radiat. Biol. **26**, 571 (1974).
17. M. FARAGGI, J. L. REDPATH, and Y. TAL. Radiation Res. **64**, 452 (1975).
18. Z. WU, R. AHMAD and D. A. ARMSTRONG. Rad. Phys. Chem. In press.
19. J. L. REDPATH. Rad. Res. **54**, 364 (1973); P. C. CHAN and B. H. J. BIELSKI. J. Am. Chem. Soc. **95**, 5504 (1973); A. J. ELLIOT and F. C. SOPCHYSHYN. Radiat. Phys. Chem. **19**, 417 (1982).
20. I. G. DRAGANIĆ and Z. D. DRAGANIĆ. The radiation chemistry of water. Academic Press, New York. 1971.
21. L.-S. L. YEH and L. L. INGRAHAM. *In* Flavins and flavoproteins. *Edited by* T. P. Singer. Elsevier, New York. 1976; L. G. WHITBY. Biochemistry, **54**, 437 (1953).
22. L. J. REED, M. KOIKE, M. E. LEVITCH, and F. R. LEACH. J. Biol. Chem. **232**, 143 (1958).
23. J. P. BARTON, J. E. PACKER, and R. J. SIMS. J. Chem. Soc. Perkin II, 1547 (1973).
24. Z. D. DRAGANIĆ and I. G. DRAGANIĆ. J. Phys. Chem. **75**, 3950 (1971); **77**, 765 (1973).
25. M. GASCOIGNE and G. K. RADDA. Biochim. Biophys. Acta, **131**, 498 (1967).
26. E. L. LOECHLER and T. C. HOLLOCHER. J. Am. Chem. Soc. **97**, 3235 (1975).
27. W.-R. KNAPPE and P. HEMMERICH. Liebigs Ann. Chem. 2037 (1976).
28. R. AHMAD, P. S. SURDHAR, and D. A. ARMSTRONG. To be published.
29. A. EHRENBERG, F. MÜLLER, and P. HEMMERICH. Eur. J. Biochem. **2**, 286 (1967).
30. V. MASSEY, A. H. GIBSON, and C. VEEGAR. Biochem. J. **77**, 341 (1960).

Can. J. Chem. Downloaded from www.nrcresearchpress.com by 210.87.254.6 on 09/06/12
For personal use only.

Influence of temperature and concentration on the densities and viscosities of solutions of $CsNO_3$ in a low-melting nitrate melt

MAURICE ABRAHAM AND MARIE-CHRISTINE ABRAHAM

Département de Chimie, Université de Montréal, C.P. 6210, Succ. A, Montréal (Qué.), Canada H3C 3V1

Received May 12, 1983

MAURICE ABRAHAM and MARIE-CHRISTINE ABRAHAM. Can. J. Chem. **62**, 178 (1984).

The densities and viscosities of solutions of $CsNO_3$ in a low melting nitrate melt ($AgNO_3$ + $TlNO_3$) have been measured in the temperature range 371−403 K. The mole fraction X_{Cs} of $CsNO_3$ in the solution was varied between 0 and 0.1. The viscosities follow an Arrhenius relation:

$$\eta = A \exp (E^*/RT)$$

in which both ln A and E^* were found to be linear functions of X_{Cs}:

$$E^* \text{ (kJ mol}^{-1}) = 19.06X_{Cs} + 27.18$$

$$\ln A \text{ (cP)} = -4.273X_{Cs} - 5.687$$

These results are explained considering the preservation of ionic species in the mixtures when the mole fraction X_{Cs} is varied, and the assumption of the predominance of short range interactions.

MAURICE ABRAHAM et MARIE-CHRISTINE ABRAHAM. Can. J. Chem. **62**, 178 (1984).

On a mesuré les densités et les viscosités de solutions de $CsNO_3$ dans un mélange de nitrates à bas point de fusion ($AgNO_3$ + $TlNO_3$) dans l'intervalle de température 371−403 K. On a fait varier la fraction molaire X_{Cs} de $CsNO_3$ dans les solutions entre 0 et 0,1. Les viscosités obéissent à une relation d'Arrhénius:

$$\eta = A \exp (E^*/RT)$$

où ln A et E^* apparaissent tous deux comme des fonctions linéaires de X_{Cs}:

$$E^* \text{ (kJ mol}^{-1}) = 19{,}06X_{Cs} + 27{,}18$$

$$\ln A \text{ (cP)} = -4{,}273X_{Cs} - 5{,}687$$

Ces résultats s'expliquent par la conservation des espèces ioniques dans les mélanges quand on fait varier X_{Cs} et par la prédominance d'interactions à courte distance.

Can. J. Chem. Downloaded from www.nrcresearchpress.com by 210.87.254.42 on 09/06/12
For personal use only.

Introduction

Several studies have been recently performed on solutions where a molten ($AgNO_3$ + $TlNO_3$) eutectic mixture is the solvent (1, 2). The mole composition of this mixture is (3):

$AgNO_3$: 0.515, $TlNO_3$: 0.485

and its freezing point is 83°C.

Our understanding of the properties of molten salts mixtures is often restricted by a lack of precision in the measurements due to the high temperatures required to obtain the liquid states and associated technological difficulties. The above solvent gives solutions with other nitrates at low concentrations which lend themselves to investigations by experimental methods similar to those used at ordinary temperature.

In a study of solutions of $Cd(NO_3)_2$, simple empirical equations were found, giving the molar volume and viscosity as functions of the temperature and solute mole fraction (2).

The viscosity of a liquid is often expected to decrease with increasing temperature, following an Arrhenius type equation:

[1] $$\eta = A \exp (E^*/RT)$$

and this was again true with these solutions of $Cd(NO_3)_2$. But, for the first time, we believe, both the activation energy E^* and the logarithm of the preexponential factor A were found to be linear functions of the solute mole fraction X_{Cd}:

[2] $$E^* = \alpha X_{Cd} + \beta$$

[3] $$\ln A = \gamma X_{Cd} + \delta$$

in the solute mole fraction range $0 < X_{Cd} < 0.1$ and the temperature range $98 < \theta < 130$°C.

The sign of the parameters α, β, γ, and δ are equally noticeable:

$$\alpha, \beta > 0 \text{ and } \gamma, \delta < 0$$

When $Cd(NO_3)_2$ mole fraction increases, E increases whereas A decreases.

Before an answer can be brought to any question arising from these results, more experimental investigation is needed. In the present work, attention is focused on Cs^+ which is a cation with large ionic radius and polarizability (4). A study of the influence of temperature and solute mole fraction on the molar volume and viscosity of solutions containing this particular ion is made.

Experimental

The densities were measured by a picnometric method and the viscosities with an Ostwald−Ubbelhode viscometer. Most of the technological details, measurements procedures, origins of reagents, preparation and storage of solutions, purifications when necessary are given elsewhere (5). $CsNO_3$ from K and K Laboratories (99.9%) and from Aldrich Chemical Co. (99.99%) were used as received. Emphasis has been laid on improving the device to ensure perpendicularity of the capillary tube of the viscometer. The essential feature is the alignment of the capillary tube with respect to a metallic rod fixed up in a vertical position, with a plumb-line as a reference. For this reason the viscosities of the solvent itself have been measured again.

Can. J. Chem. Downloaded from www.nrcresearchpress.com by 210.87.254.42 on 09/06/12
For personal use only.

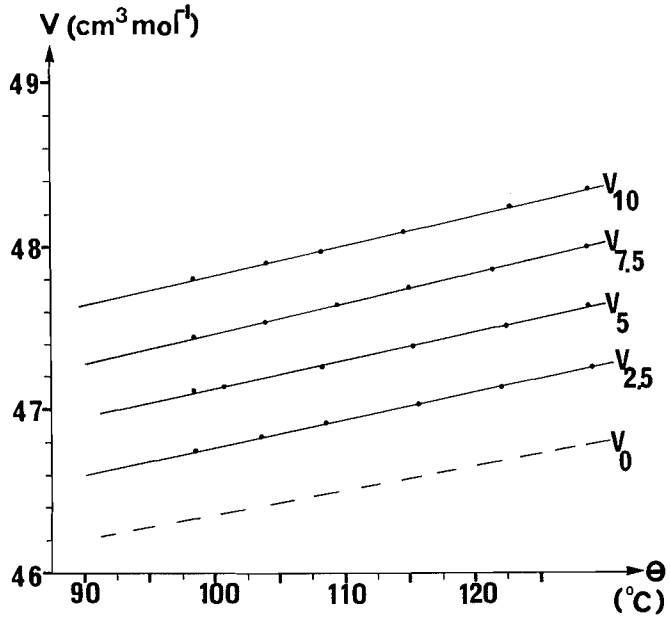

FIG. 1. The molar volume as a function of the temperature for various mole fractions X_{Cs}. V_{10}, $V_{7.5}$, ...: X_{Cs} = 0.100, 0.075, ...

TABLE 1. Parameters of eq. [5], $V = aT + b$, for solutions of $CsNO_3$, in the temperature range 95−130°C

X_{Cs}	$100a$ (cm³ mol⁻¹ K⁻¹)	b (cm³ mol⁻¹)
0	1.563*	40.50*
0.025	1.659	40.58
0.050	1.702	40.69
0.075	1.796	40.75
0.100	1.797	40.97

*Reference 2.

Results and discussion

Experimental values of the density ρ, molar volume V, and viscosity η are given elsewhere.[1]

The density and molar volume are related by

[4] $$V = (X_{Ag}M_{Ag} + X_{Tl}M_{Tl} + X_{Cs}M_{Cs})/\rho$$

Figure 1 shows that, at a given composition, the molar volume is a linear function of the temperature, in the range studied (100−130°C):

[5] $$V = aT + b$$

Values of the empirical parameters a and b are given for each composition in Table 1.

The viscosity conforms quite closely to eq. [1]. Figure 2 shows, for two compositions, an Arrhenius type plot of the viscosity:

[6] $$\ln \eta = f(1/T) = \ln A + E^*/RT$$

The preexponential factor A and activation energy E^* vary with the composition of the solution. Values of A and E^* are given for each composition in Table 2, together with those of the coefficient of correlation r for the fitting of ln η to eq. [6]. The effect of the solute mole fraction X_{Cs} on E^* and A, shown in Figs. 3 and 4, may be expressed by the equations:

[7] $$E^* \text{ (kJ mol}^{-1}) = 19.06X_{Cs} + 27.18$$

[8] $$\ln A \text{ (cP)} = -4.273X_{Cs} - 5.687$$

and the simultaneous effect of T and X_{Cs}, by the equation:

[9] $$\ln \eta \text{ (cP)} = -5.687 - 4.273\,X_{Cs} + 3269T^{-1} + 2292X_{Cs}T^{-1}$$

Cs^+ gives empirical linear relations as does Cd^{2+} previously studied (2). To explain this simple result, reference will be made to a closely related work (8). In the study of very concentrated aqueous solutions of nitrates simple additivity properties of the BET constants (6, 7) for the dissolution of water, were analysed (8). These properties were found to be compatible with several characteristics which are often met with in molten salts, and likely to appear when there is no chemical reaction or complex formation on mixing of the salts. It was put forward that the additivity properties of the BET constants may be the result of complete ionic dissociation in both single and mixed salts, the preservation of ionic species when the salts are mixed and the predominance of short range interactions in the phenomenon of adsorption of water. When water molecules come between a cation and its nearest neighbours, which are anions, the BET constants r_{BET} and E_{BET} depend particularly upon the nature of the cations and nearest anions neighbours. Surrounding cations which are further distant would influence r_{BET} and E_{BET} relatively little. Configurational characteristics reflected by r_{BET} and energetic characteristics reflected by E_{BET} would essentially be determined by the local environment. When one substitutes a cation M_1 for a cation M_0, one changes the local $r_{0,BET}$ to $r_{1,BET}$ and the local $E_{0,BET}$ to $E_{1,BET}$. The preservation of ionic species in mixtures means that the values of local $r_{0,BET}$, $r_{1,BET}$, $E_{0,BET}$, and $E_{1,BET}$ in mixtures are close to their values in single salt melts. Thus in a mixture one measures a mean of $r_{0,BET}$ and $r_{1,BET}$ and a mean of the products $(r_{0,BET}) \times (E_{0,BET})$ and $(r_{1,BET}) \times (E_{1,BET})$. Deviations from these additivity properties can be expected when the mixing takes place with chemical reactions.

In the above explanation one assumption should be underscored because it is likely to appear more and more important in the study of all kinds of highly ionic liquids, whether containing water or not: the predominance of short range interactions. Thus the same sort of explanation would hold good for some aspects of the present work on anhydrous molten nitrates. Although the electrostatic forces have long range effect, the net field action on an ion in a highly ionic liquid may be the result of the predominance of short range effects not purely ionic. The high density of packing ions and the lack of long range order in conjunction with the presence of holes (9−12) may produce compensation phenomena of long distance effects. We will consider that in a binary mixture of strongly ionic melts containing a common anion, the cations may be thought of as moving in a matrix of anions which continuously adjust their positions so that anions and cations move simultaneously to maintain electroneutrality. The Gibbs free energy of activation, ΔG^*, most of which is required to form the cationic holes for the particles to jump into, depends particularly upon the nature of the cations and nearest neighbours. Surrounding cations and anions which are further distant would influence ΔG^* relatively little, thus being essentially determined by the local

[1]A complete set of experimental data is available, at a nominal charge, from the Depository of Unpublished Data, CISTI, National Research Council of Canada, Ottawa, Ont., Canada K1A 0S2.

Can. J. Chem. Downloaded from www.nrcresearchpress.com by 210.87.254.42 on 09/06/12
For personal use only.

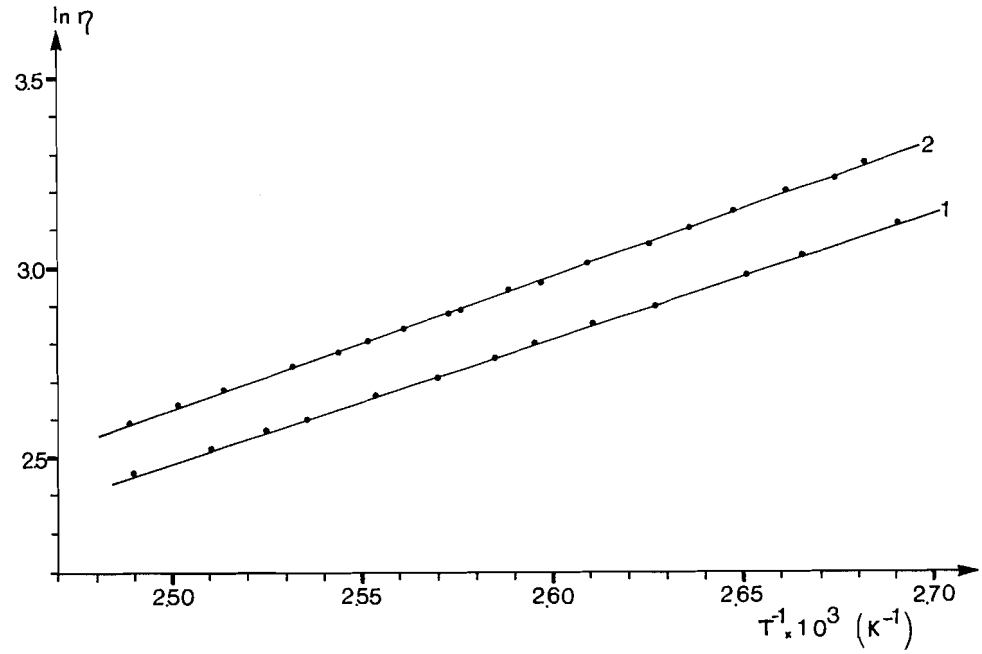

FIG. 2. Arrhenius type plot of viscosity: *1*, $X_{Cs} = 0$; *2*, $X_{Cs} = 0.100$.

TABLE 2. Parameters of eq. [1], $\eta = A \exp(E^*/RT)$, for solutions of $CsNO_3$, in the temperature range 95–130°C

X_{Cs}	1000 A (cP)	E^* (kJ mol^{-1})	r
0	3.38	27.188	0.9998
0.025	3.02	27.662	0.9997
0.050	2.76	28.128	0.9996
0.075	2.48	28.568	0.9997
0.100	2.19	29.117	0.9997

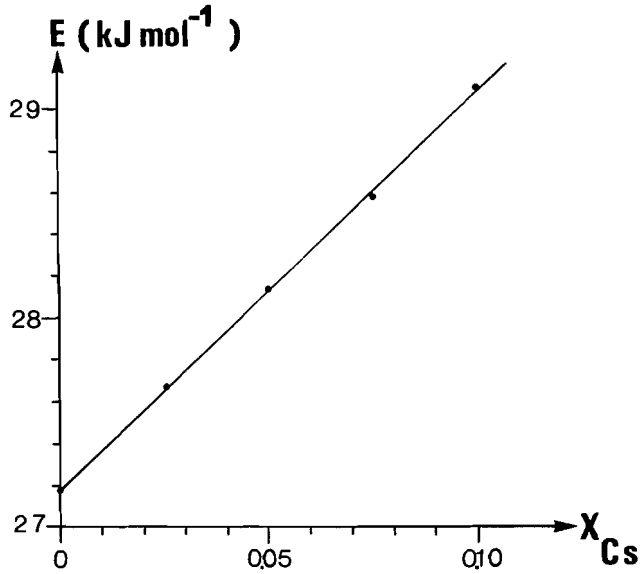

FIG. 3. The effect of the solute mole fraction on the activation energy.

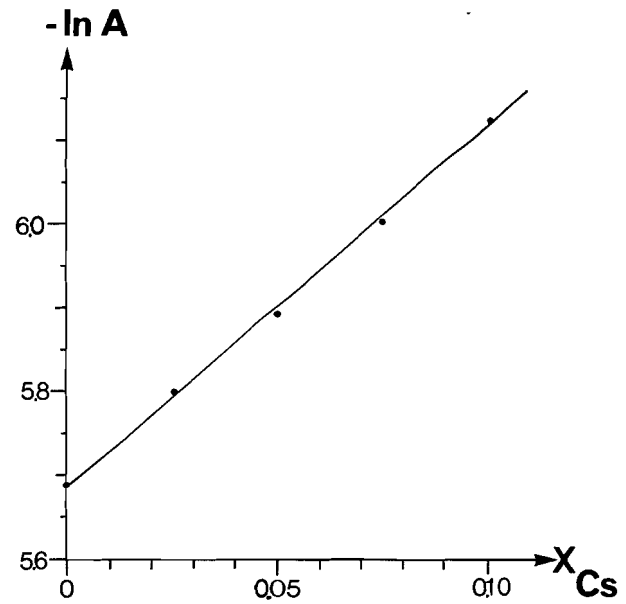

FIG. 4. The effect of the solute mole fraction on the preexponential factor.

environment. When one substitutes a cation M_1 for a cation M_0, one changes the local ΔG_0^* to ΔG_1^*. The preservation of ionic species in mixed melts, if there are no chemical reactions or complex formations, means that the local values of ΔG_0^* and ΔG_1^* in mixtures are close to their values in single salt melts. Thus, one measures a mean of ΔG_0^* and ΔG_1^*:

$$[10] \quad \Delta G^* = X_0 \Delta G_0^* + X_1 \Delta G_1^*$$

This equation can be interpreted in terms of entropy and enthalpy contributions, the latter being close to the energy ΔE^* in eq. [1]

$$[11] \quad \Delta G^* = X_0 \Delta E_0^* + X_1 \Delta E_1^* - T(X_0 \Delta S_0^* + X_1 \Delta S_1^*)$$

The complete and explicit expression of A in eq. [1] is unknown for the liquids under study in the present work. But it may be assumed that it is proportional to $\exp(-\Delta S^*/R)$ by analogy with classical theories (8), thus giving

$$[12] \quad \eta = \kappa \exp - \frac{X_0 \Delta S_0^* + X_1 \Delta S_1^*}{R} \exp \frac{X_0 \Delta E_0^* + X_1 \Delta E_1^*}{RT}$$

Provided κ is much less dependent on the composition of the solution than the exponential factors, the linear relation [7] and [8] are clear consequences of eq. [12] in the concentration and temperature ranges experimentally covered.

Moreover, the numerical coefficients in eq. [12] satisfactorily express the difference in behaviour between Cs^+ and Cd^{2+}. The extrapolated values of E^* and $-\ln A$ for the pure salts are much greater for Cd^{2+} than for Cs^+.

Acknowledgment

We thank the Natural Sciences and Engineering Research Council of Canada for financial aid.

1. J.-M. SANGSTER, M.-C. ABRAHAM, and M. ABRAHAM. Can. J. Chem. **56**, 348 (1978).
2. M.-C. ABRAHAM, M. ABRAHAM, and J.-M. SANGSTER. J. Chem. Eng. Data **27**, 200 (1982).
3. M. LEDUC. Mémoire de Maîtrise, Département de Chimie, Université de Montréal (Qué.) Canada. 1970.
4. J. LUMSDEN. Thermodynamics of molten salt mixtures. Academic Press. 1966.
5. M.-C. ABRAHAM, M. ABRAHAM, A. COMBEY, and J. SANGSTER. J. Chem. Eng. Data, **28**, 259 (1983).
6. S. BRUNAUER, P. M. EMMET, and E. TELLER. J. Am. Chem. Soc. **60**, 309 (1938).
7. R. H. STOKES and R. A. ROBINSON. J. Am. Chem. Soc. **70**, 1870 (1948).
8. M. ABRAHAM. Electrochim. Acta, **26**, 1397 (1981).
9. J. FRENKEL. Kinetic theory of liquids. Dover, New York. 1955.
10. S. GLASSTONE, K. LAIDLER, and E. EYRING. The theory of rate processes. McGraw-Hill, New York. 1941.
11. M. ABRAHAM and J. BRENET. C. R. Acad. Sci. **251**, 2921 (1960).
12. D. E. GOLDSACK and R. FRANCHETTO. Can. J. Chem. **55**, 1062 (1977).

Can. J. Chem. Downloaded from www.nrcresearchpress.com by 210.87.254.42 on 09/06/12
For personal use only.

REVIEW/SYNTHÈSE

The intramolecular Diels–Alder reaction: recent advances and synthetic applications

ALEX G. FALLIS

Department of Chemistry, Memorial University of Newfoundland, St. John's, Nfld., Canada A1B 3X7

Received March 7, 1983

ALEX G. FALLIS. Can. J. Chem. **62**, 183 (1984).

Recent advances and examples of the intramolecular Diels–Alder reaction are summarized and applications to the total synthesis of natural products, both completed and in progress, noted. A detailed discussion of trienes leading to bicyclo[4.3.0]nonene skeletons is followed by examples of bicyclo[4.4.0]decenes and adducts arising from *ortho*-quinodimethane precursors. Cycloadditions affording bicyclo[*n*.4.0] systems and bridged-ring adducts from cyclic dienes conclude this survey which is followed by a discussion of unreactive trienes and a brief analysis of synthetic strategy to complete the review.

ALEX G. FALLIS. Can. J. Chem. **62**, 183 (1984).

On résume les récents développements et des exemples de réaction de Diels–Alder intramoléculaire et on note leur utilisation dans la synthèse des produits naturels déjà effectués de même que dans celles qui sont en cours. Une discussion détaillée des triènes conduisant aux squelettes bicyclo[4.3.0]nonène est suivie d'exemples de bicyclo[4.4.0]décenes et d'adduits provenant de précurseurs *ortho*-quinodiméthane. Les cycloadditions conduisant aux systèmes bicyclo[*n*.4.0] et à des adduits cycliques pontés à partir de dièns servent de conclusion à cette étude qui est suivie d'une discussion sur les triènes non réactifs et d'une brève analyse de stratégie en vue de compléter cette étude.

[Traduit par le journal]

Introduction

In the arsenal of the synthetic organic chemist the Diels–Alder reaction occupies a position of particular prominence. A partial survey of carbon–carbon bond forming reactions reveals that this [4π + 2π] cycloaddition is one of the most widely used synthetic procedures, rivaling alkylation methods for ring formation (1). This utility is enhanced by the formation of two bonds "simultaneously" with the introduction of up to four new asymmetric centres and its widespread application is a consequence of its good yields, mild reaction conditions, high stereoselectivity, and predictability.

In the past decade, interest in the intramolecular Diels–Alder reaction, where the diene and dienophile are constrained in the same molecule, has increased exponentially. Obviously, when the reacting components are themselves cyclic and/or have ring substituents, complex multicyclic arrays, such as those contained in drugs and natural products, can be constructed in a single step (Scheme 1). Often the syntheses of molecules of this complexity are more difficult and lengthy by other routes. The additional intramolecular advantages gained due to entropy, reactivity, regio-, stereo-, and diastereoselectivity account for the explosive growth in the study and application of this internal cycloaddition for the synthesis of natural products.

Indicative of this worldwide activity is the frequency with which reviews of this rapidly expanding field have appeared during the recent past: 1974 (2), 1976 (3), 1977 (4), and 1980 (5). While this manuscript was in its infancy, I learned of three other accounts of the intramolecular Diels–Alder reaction that were in preparation: a chapter in Organic Reactions (6) which includes comprehensive tables, a monograph (7) which includes a chapter on triene preparations, and a section of a chapter on asymmetric cycloadditions for a book (8). This knowledge, plus space limitations, influences the orientation and scope of this review. Emphasis is placed on recent developments in our understanding of the intramolecular Diels–Alder reaction and its application to total synthesis. The literature since 1979 has been carefully scrutinized and the majority of these publications are summarized. In addition, a broad cross-section of earlier examples is included to represent the major structural types, particularly those cyclizations which have culminated in total syntheses. As organic chemists we read "by structures"; to facilitate comparison, a standard format for representing the trienes is adopted and adducts are listed in tabular form according to structural class. Of necessity this results in "unnatural" orientations and occasionally the opposite optical series for some molecules in order to emphasize the Diels–Alder component. Although prone to transcription error, this is frequently a useful exercise when contemplating a total synthesis. Synthetic targets are identified by name and if they have been totally synthesized by an internal [4 + 2] cycloaddition sequence the name is underlined. It is hoped that this account will stimulate further study of the Diels–Alder reaction itself, of improved procedures for triene preparation, etc., and that, as our knowledge increases, this reaction will be even more widely used in order to occupy a central place in synthetic design and methodology.

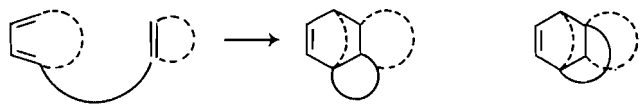

SCHEME 1

Background

The first example of an intramolecular Diels–Alder reaction appears to have been reported by Alder and Schumaker in 1953 (9), although it was not until the early sixties that isolated examples were published (10–13). Particularly relevant were the synthesis of γ-apopicropodophyllin (14), an attempted synthesis of longifolene (15), a systematic study of methyl

Can. J. Chem. Downloaded from www.nrcresearchpress.com by 210.87.254.6 on 09/06/12
For personal use only.

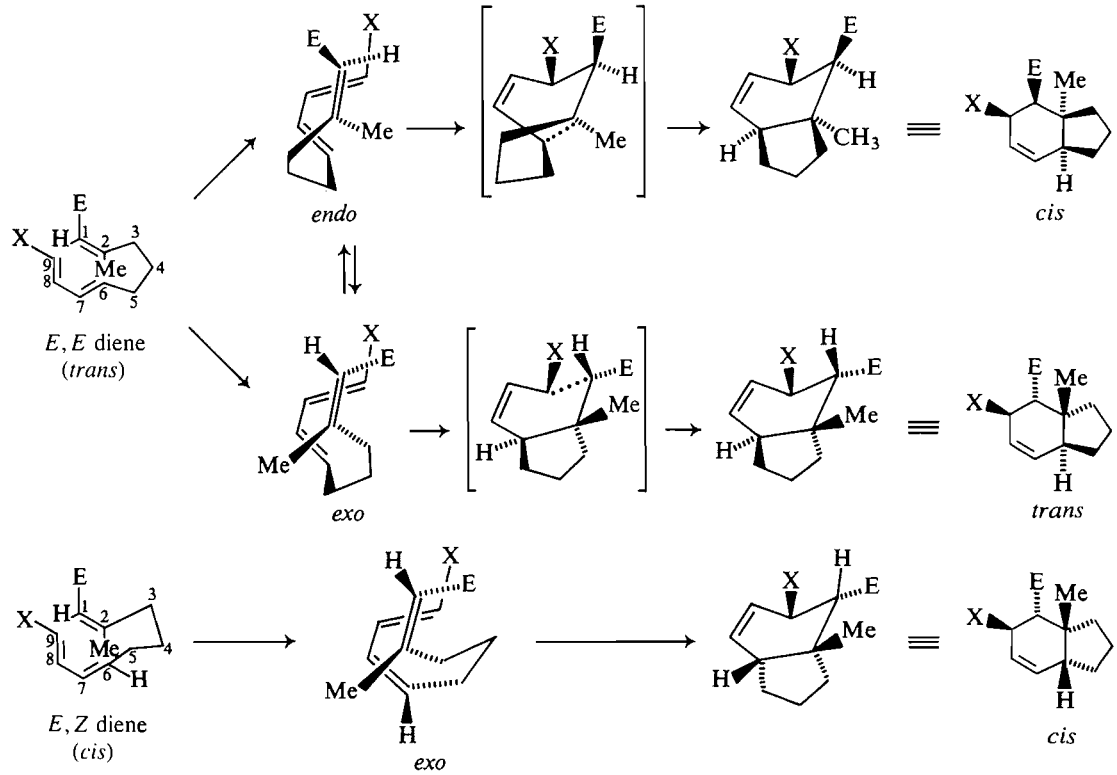

SCHEME 2

2,7,9-decatrienoates (16), an investigation of the intramolecular reactivity of diverse cyclohexadienes (17), the exploration of the *in situ* generation and internal cyclization of *ortho*-quinodimethanes (18), and the application of this strategy to the total synthesis of chelidonine (19). These studies set the stage for the more recent developments of the past decade.

Bicyclo[4.3.0]nonenes (tetrahydroindans, perhydroindenes, hydrindenes

The first detailed studies in this area are those of House and Cronin (16), who showed that the preparation of a bicyclo-[4.2.0]octene is not feasible by an intramolecular Diels–Alder reaction and thus the chain linking the diene and dienophile must contain three or more atoms for the reaction to succeed, although in certain specialized cyclic and bridged cases this generalization is not valid. The reactions are regiospecific and give annulated (fused) rather than bridged-ring products. The products result from a kinetically-controlled reaction and this regiochemical pattern, to fused adducts, is encountered in most cases as a consequence of geometric constraints present in competing orientations, irrespective of dienophile substitution. It is only with longer connecting chains (Table 5) and with cyclic dienes (Table 6(*a*)) that this influence can be overridden by other factors. Thus the resulting perhydroindenes are "*meta*-substituted" in contrast to the "*ortho*-substitution" pattern encountered in related intermolecular cases.

Several recent studies of related triene systems, carrying a variety of substituents, are summarized in Table 1(*a*). The tables follow a general sequence used throughout, listing carbocycles first, followed by heterocycles in which the heteroatom is in the connecting (side) chain, and then heterocycles with heteroatom dienophiles or dienes. Temperatures, times, and yields are included to provide a relative measure of reactivity and utility.[1]

In all cases, the stereochemistry of the cyclization is established by the spatial orientation of the dienophile as it approaches the diene, so that cyclization may proceed in a suprafacial–suprafacial manner. The ring fusion is determined by a complex interplay of conformational, steric, and electronic effects which may vary independently. Scheme 2 outlines the case for a model triene and illustrates the subtleties involved. The influence of sidechain substituents (at C3, C4, C5) should be noted. A C7 substituent experiences a nonbonded interaction with groups at C3, while C7 and C4 experience partial eclipsing in the *endo* transition state. These features are alleviated in the *exo* conformation and thus increased selectivity for *trans*-fused adducts should result, as has been found.

In general, steric effects are more important than electronic ones because the bicyclic products are predominantly *trans*-fused, yet this selectivity, especially in the case of terminally activated dienophiles, is independent of dienophile (*E* or *Z*) stereochemistry (20). Thus in these intramolecular reactions the Alder *endo* rule fails, emphasizing that secondary orbital interactions are not of prime importance in most instances. However, when Lewis acid catalysts are employed, the rates increase and selectivity improves in certain cases. This is a consequence of the increased dienophile polarization which results in a lowering of the LUMO energy at C2 for terminally activated systems and, in the case of *trans*-dienophiles, produces a marked increase in stereoselectivity so that *trans*-adducts are produced exclusively. In these cases (**3**–**6**) the

[1]E = CO_2CH_3 throughout unless otherwise indicated; ⌐ = compounds generated *in situ*. Many reactions are run in sealed tubes and are improved by additives, silanized glassware, etc.; however, except for Lewis acids, which are indicated, space precludes their inclusion. Reference numbers are in parentheses on the right-hand side.

Can. J. Chem. Downloaded from www.nrcresearchpress.com by 210.87.254.6 on 09/06/12
For personal use only.

TABLE 1(*a*). Bicyclo[4·3·0]nonenes

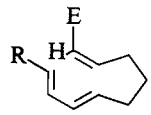

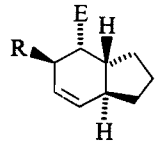

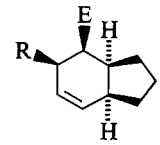

(20)

1 R = H		65	35
2 R = iPr	180°C, 5 h, 75%	67	33

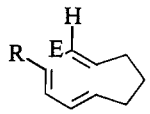

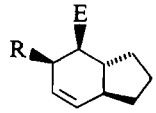

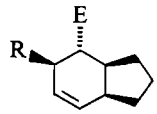

(20)

3 R = H		60	40
	MenthylOAlCl$_2$, 23°C, 60 h, 78%	100	0
4 R = iPr	150°C, 40 h, 72%	72	28
	MenthylOAlCl$_2$, 23°C, 48 h, 82%	100	0

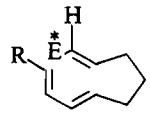

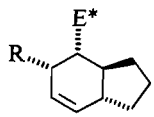

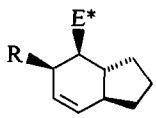

(20)
(21)

5 R = H	MenthylOAlCl$_2$, 23°C, 144 h, 40%	75	25(50%de)

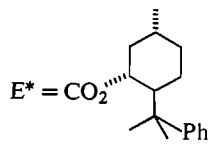

6 −-BornylOAlCl$_2$, 8°C, 144 h, 72%		86	14(72%de)
R = iPr TiCl$_4$, 23°C, 144 h, 8%		86	14(72%de)
MenthylOAlCl$_2$, 23°C, 84 h, 75%		68	32(36%de)

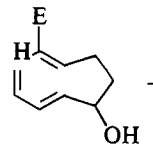

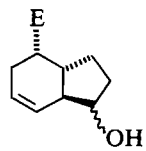

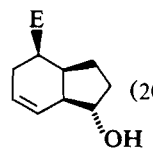

(20)

7 68 32

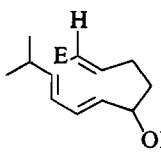

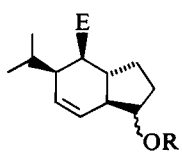

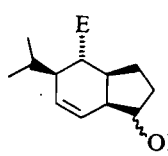

(22)
(23)

8 R = H, Bz, Ac, THP, SiMe$_3$ 76 ± 7 24 ± 7

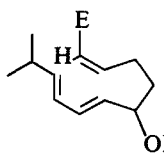

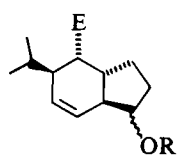

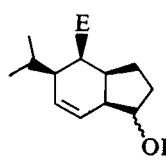

(22)

9 R = H, Bz, Ac, THP, SiMe$_3$ 72 ± 5 28 ± 5

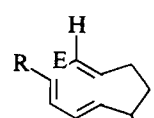

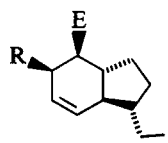

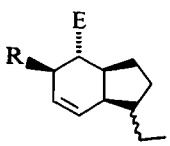

10 R = CH$_2$OSiPh$_2$*t*Bu		85	15 (24)
11 R = CH$_2$OMEM	110°C, 70 h, 100%	>90	(25)
E = CO_2Et			
12 R = CH=CH—E	Et$_2$AlCl, 0°C, 1.5 h, 71%	100	0 (26)

Can. J. Chem. Downloaded from www.nrcresearchpress.com by 210.87.254.6 on 09/06/12
For personal use only.

TABLE 1(*a*). (*Continued*)

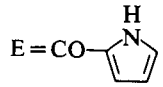

13 R = CH_2OH 110°C, 17 h, 67% >75 <25 (26)

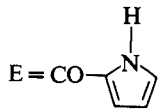

14 R = CH=CH—CH= 40°C, <39 h, 70% 72 28 (27)

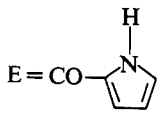

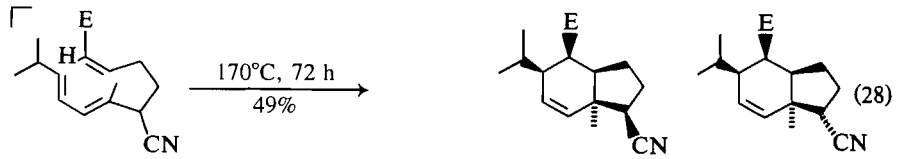

15 52 48

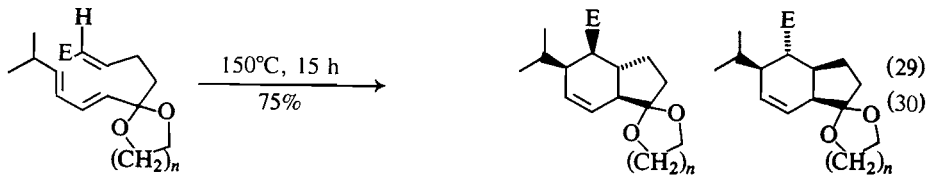

16 *n* = 1 83 17
n = 2 180°C, 0.5 h, 90%

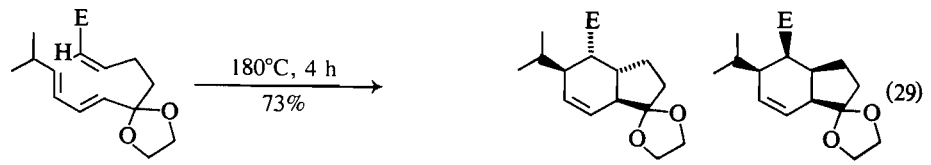

17 79 21

18 70 : 30

19 80 : 20

20 E = CH_2OH 50 : 50
21 200°C, 6 h, 100% 50 : 50

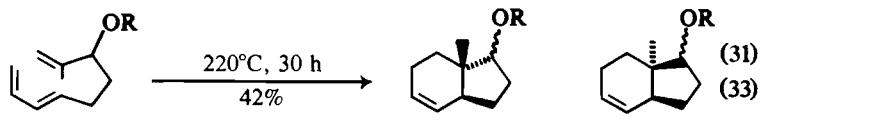

22 **50** : **50**

Can. J. Chem. Downloaded from www.nrcresearchpress.com by 210.87.254.6 on 09/06/12
For personal use only.

TABLE 1(*a*). (*Continued*)

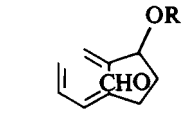

150°C, 16 h
87%

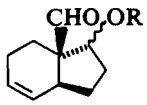

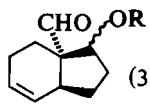

(31)

23 22 : 72

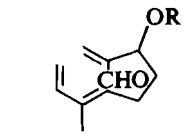

110°C, 18 h

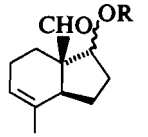

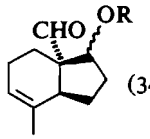

(34)

24 Minor Major

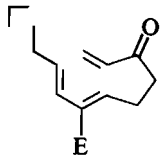

180°C, 3 h
92%

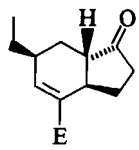

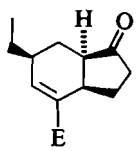

25 E = 100 0 (35)

26 E = CO_2Et 180°C, 4 h, 96% 40 60 (36)

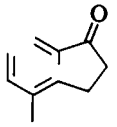

190°C, 18 h

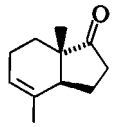

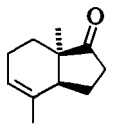

(34)

27 31 69

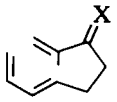

170°C, 24 h
100%

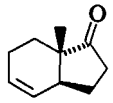

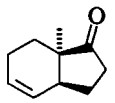

28 X = O 30 70 (37)

29 X = 170°C, 24 h, 98%(H^+) 72 28 (38)

30 X = 170°C, 24 h, 98%(H^+) 70 30

31 X = 200°C, 15 h, 85%(H^+) 75 25 (33)

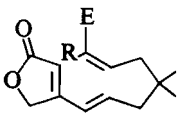

200°C, 0.5 h
92%

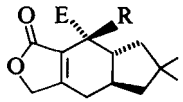

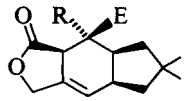

(39)

32 R = CH_2OAc Trace H^+ 50 50
75 25

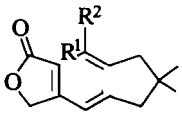

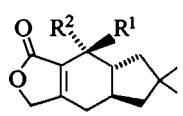

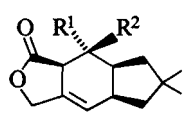

(40)

33 $R^1 = R^2 = CO_2Me$ 150°C, 0.25 h, 90% 100 0
34 $R^1 = CO_2Me$, $R^2 = CN$ 110°C, 4 h, 75% 100 0
35 $R^1 = R^2 = CN$ 110°C, 2.5 h, 80% 100 0

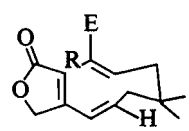

230°C, 32 h
80%

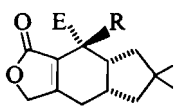

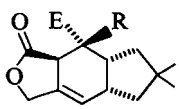

(41)

36 R = CH_2OAc

Can. J. Chem. Downloaded from www.nrcresearchpress.com by 210.87.254.6 on 09/06/12
For personal use only.

TABLE 1(*a*). (*Continued*)

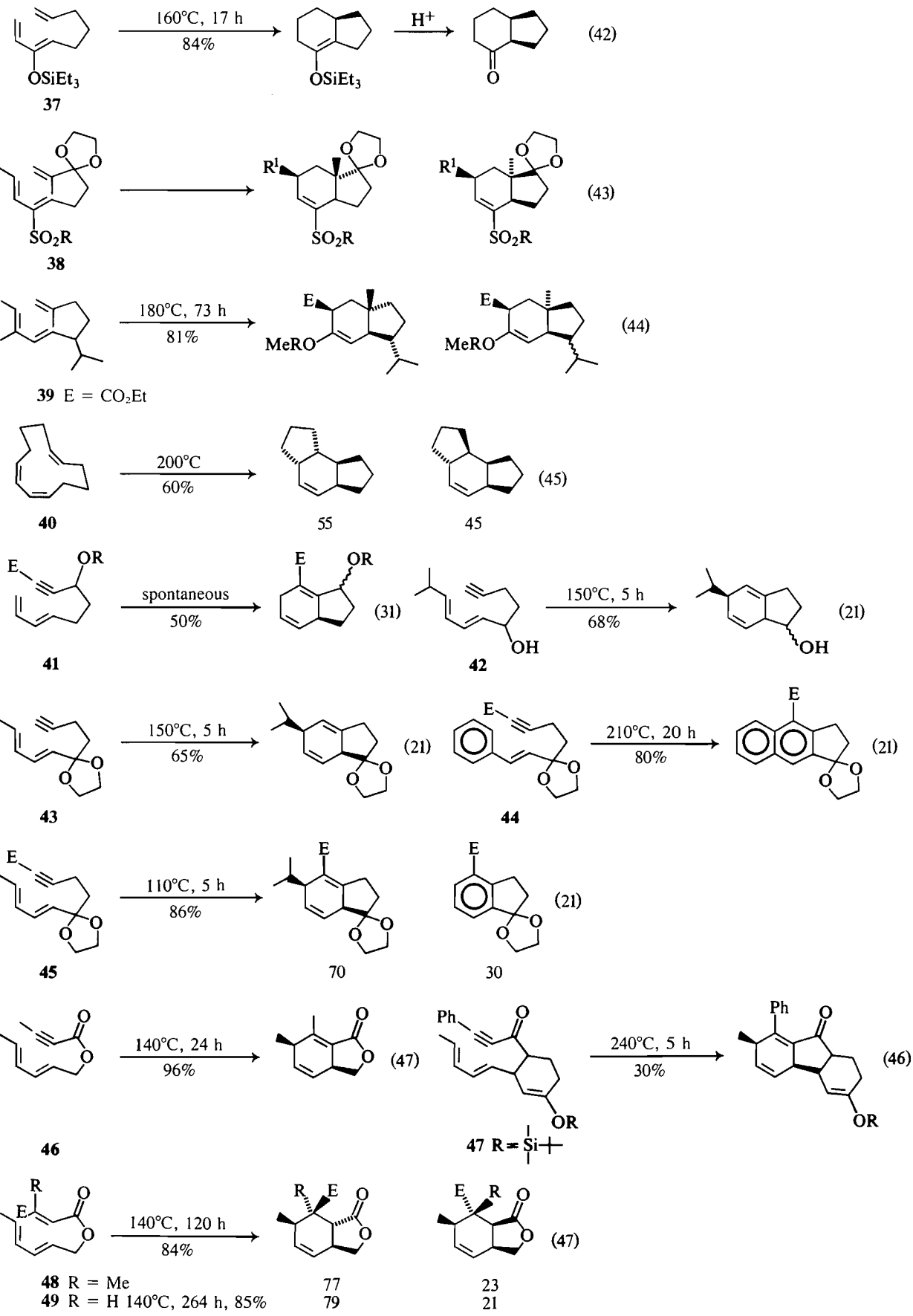

Can. J. Chem. Downloaded from www.nrcresearchpress.com by 210.87.254.6 on 09/06/12
For personal use only.

TABLE 1(*a*). (*Continued*)

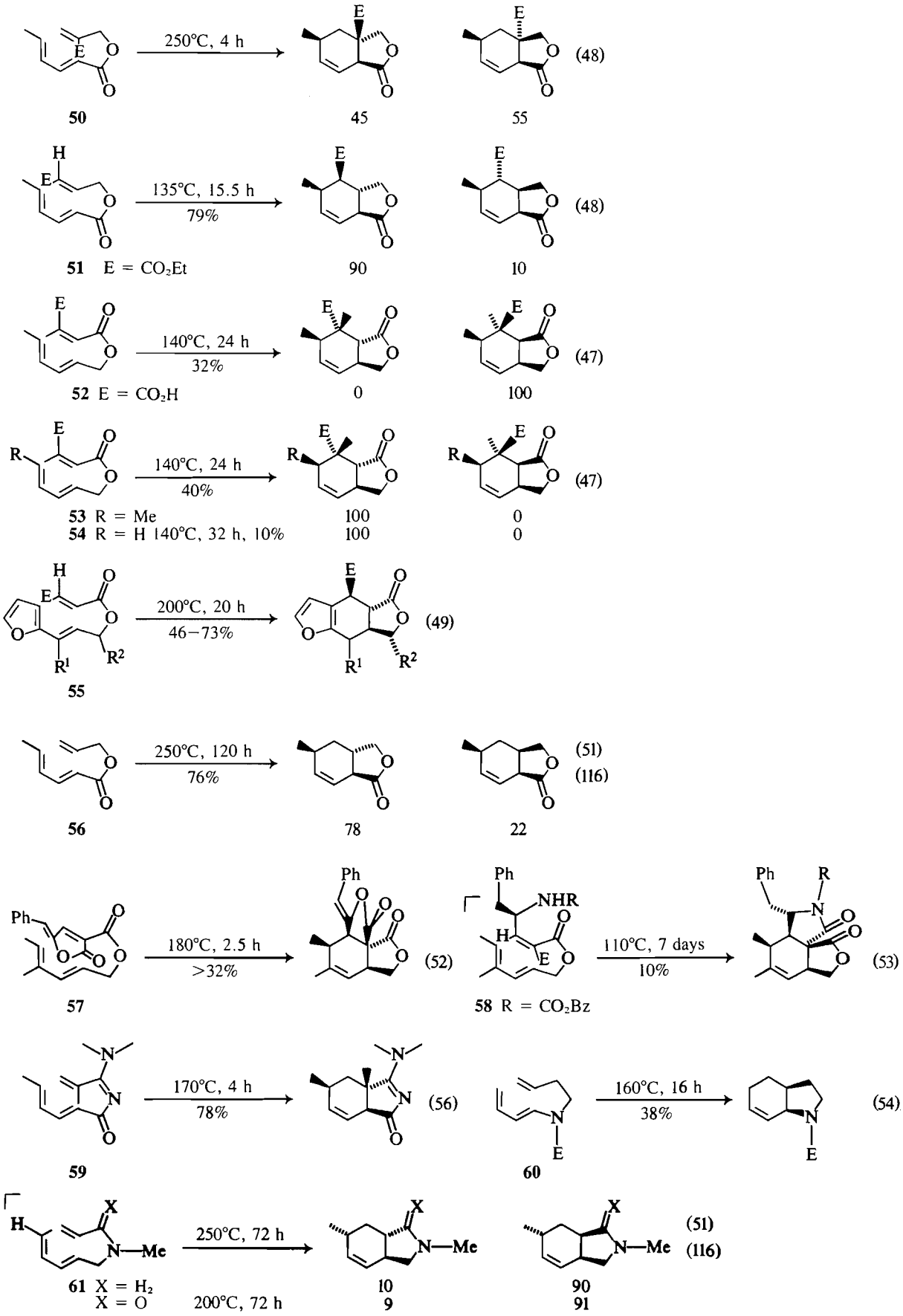

Can. J. Chem. Downloaded from www.nrcresearchpress.com by 210.87.254.6 on 09/06/12
For personal use only.

TABLE 1(*a*). (*Continued*)

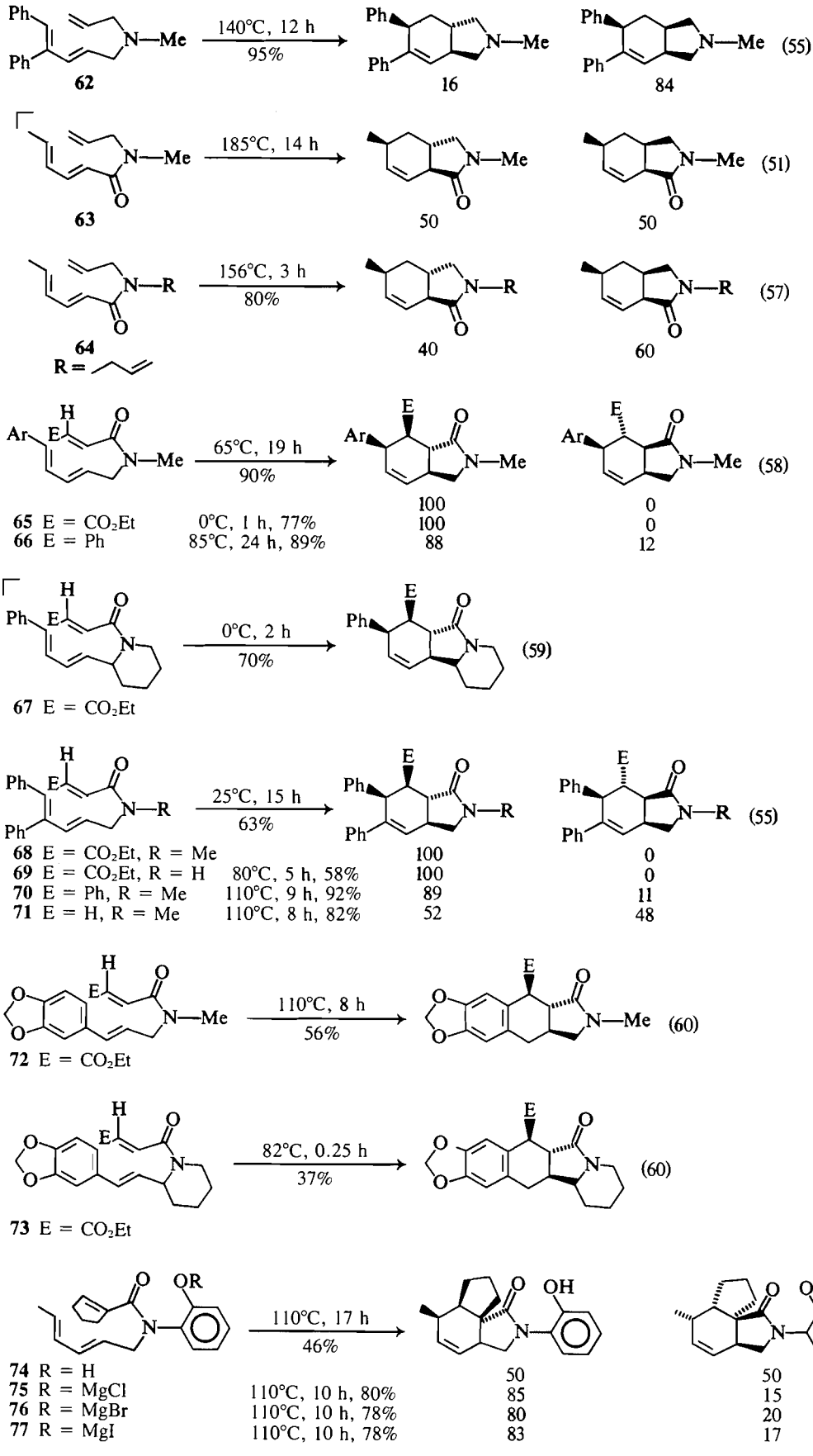

Can. J. Chem. Downloaded from www.nrcresearchpress.com by 210.87.254.6 on 09/06/12
For personal use only.

TABLE 1(*a*). (*Continued*)

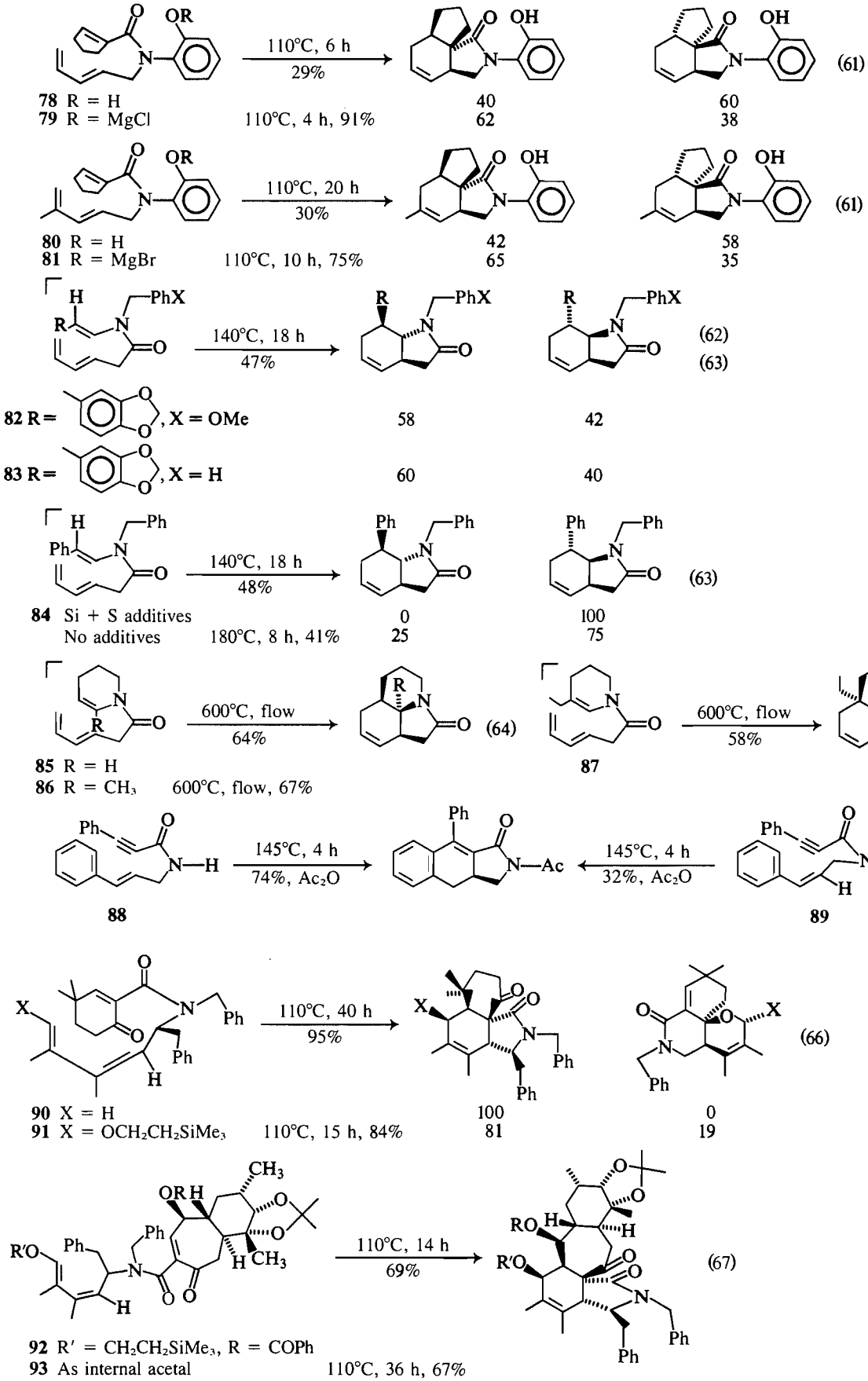

Can. J. Chem. Downloaded from www.nrcresearchpress.com by 210.87.254.6 on 09/06/12
For personal use only.

TABLE 1(*a*). (*Continued*)

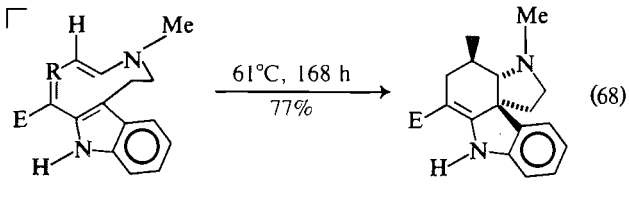

94 R = H
95 R = Me 60°C, 48 h, 84%
96 R = Et 61°C, 16 h, 94%

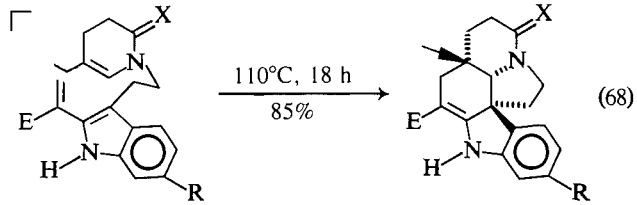

97 R = H, X = O
98 R = H, X = H_2 110°C, 100 h, 84%
99 R = Me, X = H_2 110°C, 72 h, 37%
100 R = OMe, X = H_2 110°C, 72 h, 92% (69)

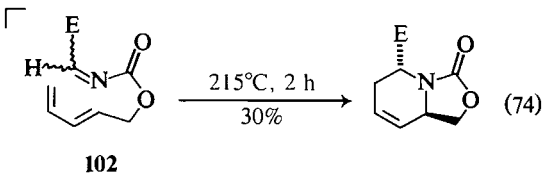

102

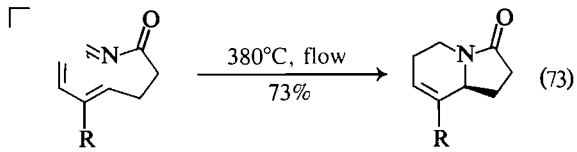

103 R = H
104 R = Me 800°C, flow, 20% (76)

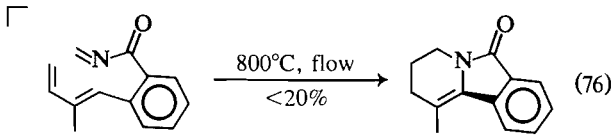

105

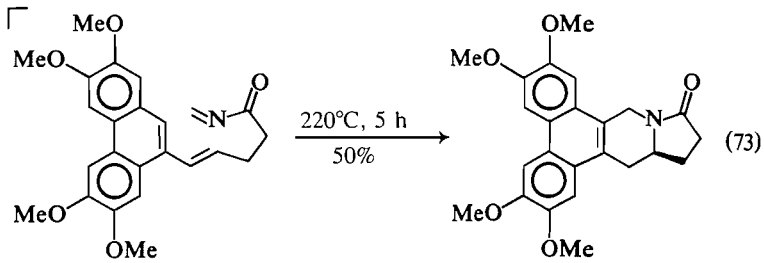

106

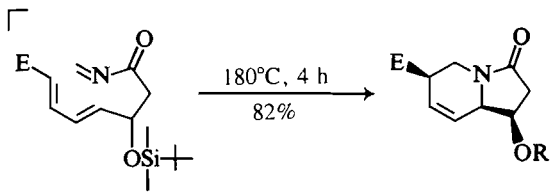

107 **36** **64** (75)

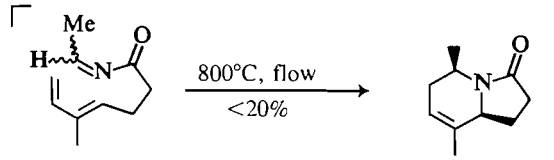

108 **33** **67**

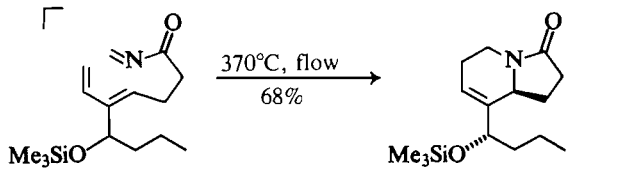

109 **55** **45**

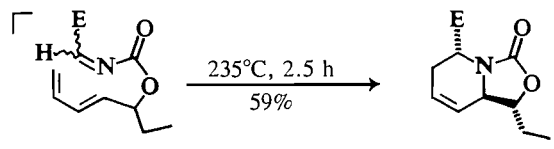

110 **45** **55**

Can. J. Chem. Downloaded from www.nrcresearchpress.com by 210.87.254.6 on 09/06/12
For personal use only.

TABLE 1(*a*). (*Concluded*)

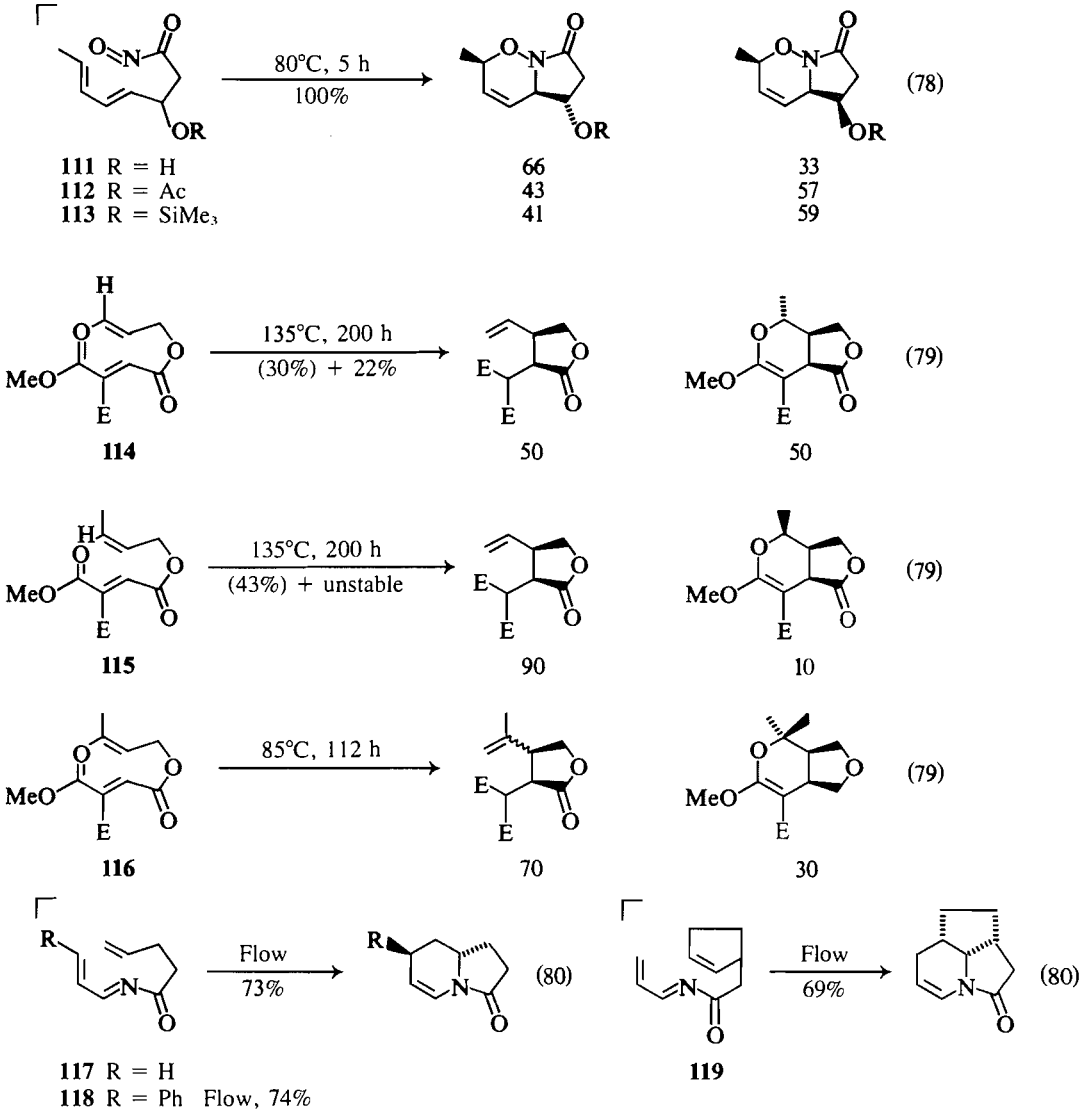

combined influence of the preferred transition state geometry (*endo*) and secondary orbital interactions are additive. In contrast, for *cis*-dienophiles, these factors are opposed and poor yields of mixtures are obtained. Catalysts also fail when ether oxygen substituents are present and chiral Lewis acids give negligible induction even for **3** and **4**. It is necessary to use the catalysts stoichiometrically, the best being ethylaluminum dichloride, diethylaluminum chloride, and methoxyaluminum dichloride. The combination of Lewis acid catalysts and a chiral dienophile affords diastereomeric excesses (de) of 30 to 75% (**5** and **6**).

In spite of the general failure of the *endo* rule, secondary orbital interactions do have an influence and several authors (31, 34, 40, 47) have pointed out that the rationalization of product distributions is facilitated if one postulates a nonsynchronous bond formation. The reaction is still concerted, in the sense that both bonds are initiated simultaneously, but an unsymmetric transition state is achieved by minimizing nonbonded interactions and bonding occurs preferentially between the termini with the largest LUMO coefficients. Thus with terminally activated dienophiles the C2 coefficient will be larger than C1 (as in Lewis acid cases above), facilitating formation of the C2—C6 bond so a "cyclopentane"-like species is formed early in the transition state leading preferentially to *trans*-adducts. In systems such as **20**–**22**, which lack dienophile activation, this influence is reduced and selectivity declines unless other steric demands are introduced as in **29**–**31**. In contrast, when the activating group is attached to C2 (e.g., carbonyl replaces methyl and E = H in Scheme 2), the LUMO coefficients are reversed and the outer termini (C1 and C9) may bond preferentially, leading to a *cis*-like transition state via a "cyclononene"-like species in which nonbonded interactions are minimized so that *cis*-fused adducts tend to dominate (cf., **23**, **24**, **26**, **50**). However, this influence may often be counteracted sterically by the choice of suitable substituents as in **25**, because entropy effects frequently override frontier orbital influences in intramolecular Diels–Alder reactions. If angularly methylated *trans*-perhydroindans are desired, maximum selectivity is achieved with terminally activated dienophiles such as **18** and **19**. In examples **33**–**35**, a four-fold rate increase is generated by the sidechain geminal methyl substituents at C4. An additional rate enhancement

Can. J. Chem. Downloaded from www.nrcresearchpress.com by 210.87.254.6 on 09/06/12
For personal use only.

Can. J. Chem. Downloaded from www.nrcresearchpress.com by 210.87.254.6 on 09/06/12
For personal use only.

is encountered with **35** as a consequence of the linearity (decreased bulk) of the nitrile functions and the lowering of the LUMO energy. Activated acetylenes are particularly useful dienophiles and generally cyclize under relatively mild conditions, as found for **41** and **45**.

The difference in transition state energies for the *endo* and *exo* conformations is not large, ~0.5−1 kcal/mol, but with careful choice of substituents and activating groups it is possible to significantly influence the product distribution. Thus, with the selective introduction of suitable nonbonded interactions, the *trans*-selectivity may be increased and is further enhanced by lower cyclization temperatures, consistent with kinetic products.

These studies have culminated in the total synthesis of several diverse natural products which incorporate a bicyclo[4.3.0]-nonane component (Table 1(*b*)). The *E,Z* triene corresponding to **15** (i.e., **492**) experiences severe steric congestion (cf. Scheme 2) in the conformation required for bonding and thermally isomerizes to **15** whose adduct was used for the total synthesis of 8-epi-dendrobine (28). More recently, the propylene glycol acetal corresponding to **16** ($n = 2$) has been employed in an improved synthesis of dendrobine by Roush and Gillis (29) which previously proceeded via **8** ($R = SiMe_3$) (23). Three groups, Nicolaou (24), Ley (25), and Roush (26) and their collaborators have approached the right-hand portion of antibiotic X-14547A using the trienes **10** to **14** and the total synthesis has been completed by Nicolaou *et al.* (50). Consistent with the suggestion that the natural product may be formed biosynthetically via an intramolecular Diels−Alder sequence is recent evidence (27) that **14** cyclizes spontaneously to give predominantly the *trans*-fused adduct. Two syntheses of coronafacic acid, derived from coronatine, have employed **25** (35) and **26** (36) respectively. The interesting terpene marasmic acid has been prepared by Boeckman and Ko (39) from **32** in which both adducts were utilized. They are also developing a related approach to the fused ring tricyclic system in ikarugamycin (81).

The furan system **55** is a key component in an approach to secofuranoeremephilane (49). Several different groups (32, 33, 38, 43) intend to use systems such as **21**, **30**, **31**, and **38** to generate the C-D rings of steroids such as vitamin D, 11-oxy-estrones, and cortisone, and **39** is destined for use in an approach to the total synthesis of retigeranic acid (44).

As the model system in Scheme 2 illustrates, *E,Z* dienes are restricted to a single transition state geometry which should afford the *cis*-fused adduct exclusively. Although, in principle, *Z* dienes can isomerize via a 1,5-sigmatropic rearrangement, as appears to happen for **15** (28), **61** (51, 116), and possibly **89** (65), sterically less demanding cases, even though highly substituted, do not present a practical difficulty and **36** selectively affords the *cis*-product. Not surprisingly, due to the congested transition state, the reaction is slower (~42×) than for the *E* diene **32** (41).

For unsymmetrically substituted chiral dienes, asymmetric induction should be feasible if the reaction occurs from a single diastereotopic face of the dienophile. This has been achieved by placing a chiral centre in the sidechain (at C5), which directs the cycloaddition so as to minimize nonbonded interactions and gives only one *cis*-fused adduct as illustrated in examples **90−93**. Fuchs and co-workers (66, 67) have developed this concept into a practical procedure for the introduction of five new asymmetric relationships simultaneously. The resulting adducts are being utilized in a total synthesis of cytochalasin C.

Kuehne *et al.* (68−70) have generated *in situ* several dehydrosecodines **94−100** which are *Z* dienes. These have been employed for a variety of biomimetic aspidospermine alkaloid syntheses which include tabersonine, vincadifformine, minovine, and ervinceine, etc. In these syntheses the natural products arise from a formal [4 + 2] cycloaddition as was postulated earlier (71), although in some cases an alternative stepwise ionic mechanism cannot be ruled out.

A number of heterocyclic systems have been prepared in which the heteroatom is in the sidechain. The lactone examples afford a product distribution similar to the carbocyclic cases in which the *trans*-adduct is dominant. Example **52**, which gives the thermodynamically favoured *cis*-fused lactone, is an exception, perhaps due to a reversible reaction (47). The esters **57** and **58** afford the tricyclic lactones with the correct stereochemistry for further elaboration into cytochalasin A and proxiphomine respectively (52, 53). These cases provide excellent examples of the stereo and regio control available in the intramolecular Diels−Alder reaction.

Sidechain hetero-atoms and/or carbonyl substituents influence the product distribution, but the trends are not clear. A carbonyl prefers to retain π overlap in the transition state (carbonyl coplanarity effect, *vide infra*); however, carbonyl−diene coplanarity results in a rather strained transition state for reactions leading to bicyclo[4.3.0]nonenes, so mixtures are generally encountered. It should be noted that the predominance of *trans*-adducts in the lactams **74** to **81** is governed by internal chelation with magnesium salts (61). In contrast, lactam products with the nitrogen adjacent to the dienophile are usually *cis* and advantage of this has been taken by Martin *et al.* to develop routes to the aspidospermine nucleus from **87** (64) and lycorine from **84** (63). Benz-[f]isoindoline derivatives are formed stereoselectively from various styrenes (120).

Imino dienophiles have been used by Weinreb *et al.* to prepare indolizidine alkaloids, including γ-coniceine, from **103** (73), elaeokanine A and B from **109** (72), slaframine from **107** (75), and tylophorine from **106** (77). Nitroso groups generated *in situ* will also function as dienophiles as exemplified by **111−113**, and related systems form the key construction for total syntheses of heliotridine and retronecine (78). A few cases of heteroatom dienes have been reported (**114−119**) and, although the ene reaction competes, in the case of **114** it is being employed in a synthesis of elenolic acid (79).

Bicyclo[4.4.0]decenes (decalins, octalins)

The addition of an extra methylene unit to the sidechain connecting the unsaturated centres in decatrienes permits the adoption of both *endo* and *exo* transition states with greater facility (cf. Scheme 2), leading to mixtures of *cis*- and *trans*-fused adducts, although in the absence of bulky substituents there is a slight preference for *cis*-products (Table 2(*a*)). This statement oversimplifies the situation, however, since substituents, sidechain heteratoms, adjacent rings, and carbonyl functions can markedly alter the ratio. The well established preference of six-membered rings to adopt a chair conformation and the tendency of substituents to adopt an equatorial rather than axial orientation frequently manifests itself in the highly ordered Diels−Alder transition state so that the dominant conformation is the one with the least bond-angle strain and fewest nonbonded interactions. This equatorial substituent effect is apparent in case **122** compared to **127**; however, the danger of oversimplification and the subtleties involved are illustrated by

TABLE 1(*b*). Synthetic targets

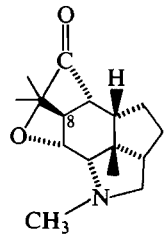

Dendrobine

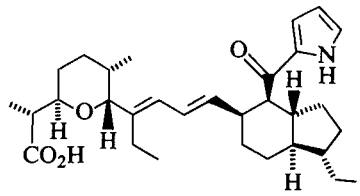

X—14547A

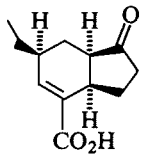

Coronafacic acid

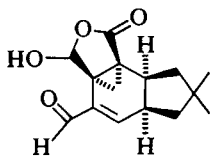

Marasmic acid

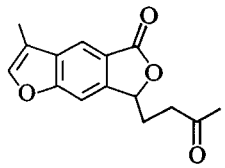

Secofuranoeremephilane

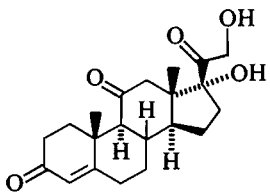

Cortisone

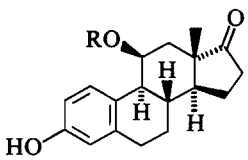

11-Oxy estrone

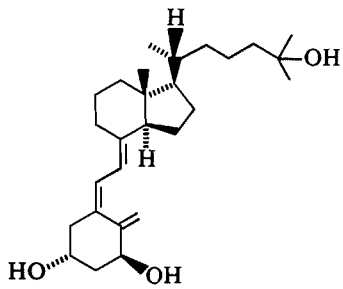

Vitamin D

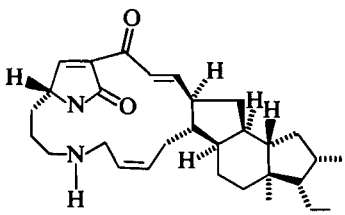

Ikarugamycin

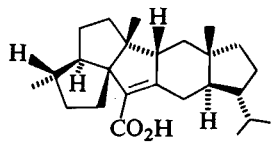

Retigeranic acid

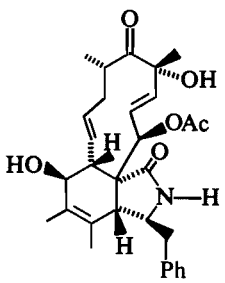

Cytochalasin C

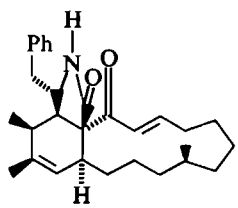

Proxiphomine

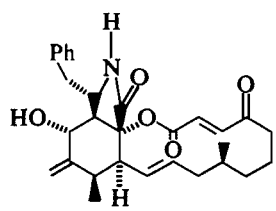

Cytochalasin A

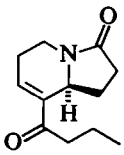

Elaeokanine A

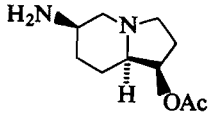

Slaframine

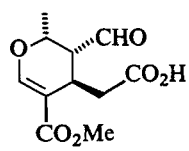

Elenolic acid

Can. J. Chem. Downloaded from www.nrcresearchpress.com by 210.87.254.6 on 09/06/12
For personal use only.

TABLE 1(*b*). (*Concluded*)

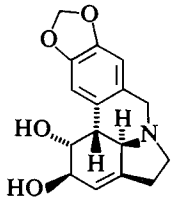

Lycorine

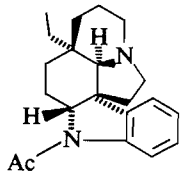

Aspidospermine

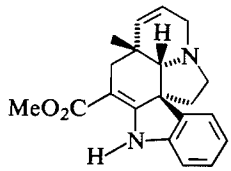

Tabersonine

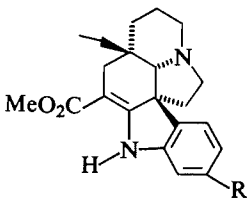

R = H, Vincadifformine
R = Me, Minovine
R = OMe, Ervinceine

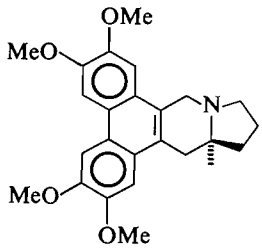

Tylophorine

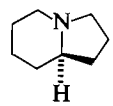

γ-Coniceine

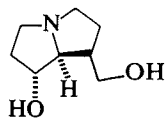

Heliotridine

the different product ratios from **127** and **128**. A γ-diene substituent promotes the formation of *trans*-fused products due to nonbonded interactions with sidechain functionality including hydrogen (cf. **120**, **121**, **125**, **126**, **132**). Although secondary orbital effects play a role, especially if sidechain ketones are present, these effects are generally of lesser importance. The stereochemical controlling influence of a carbonyl group, alluded to in the previous section, due to overlap between the adjacent π systems, was first noted by Oppolzer and Fröstl (54) with amides **173** and **175**. The major products result from adoption of the conformation in which overlap is most easily retained in the transition state. Thus judicious placement of a carbonyl group often permits the preparation of the desired adduct stereoselectively as a consequence of "carbonyl coplanarity control". In the carbocyclic series, *trans*-products often predominate when the sidechain carbonyl is in conjugation with the diene, as is evident by comparing **133** with **141**–**144** in which this coplanar effect is absent and the stereoselectivity is reversed. An additional contribution to *trans*-product domination can arise from facile enolization after cycloaddition. In similar fashion, replacing the sp^2 hybridized carbon by a cyclic acetal (**149**–**151**) affords mostly *cis*-fused products. These *cis*-adducts also usually dominate in cases where the sidechain carbonyl is adjacent to the dienophile (**156**–**164**), thus encouraging an *endo* transition state. This has been used to advantage in the cyclization of **170**, a key intermediate in the total synthesis of gibberellic acid by Corey *et al.* (85).

As in the perhydroindene series, secondary orbital interactions derived from C1 ester substituents are of minor importance and product selectivity is independent of dienophile stereochemistry. However, Lewis acid catalysis of simple esters can promote selective adduct formation (**146** and **148**) (21). Example **135**, in which internal coordination is assumed, provides a dramatic contrast with the closely related case **136**. Further studies with metal assisted systems (21) such as $MeTiCl_3$ and $MeNbCl_4$ hold promise to exercise stereocontrol but at present polymerization is a practical problem. An interesting construction of 11-keto steroids, developed by Stork *et al.*, employs **163** which gives mostly the desired *cis*-adduct upon catalysis with trifluoroacetic acid (86). This selectivity was further improved when **164** was cyclized in the presence of rhodium chloride (87).

In view of the widespread occurrence of decalin systems in nature, a number of natural products, in addition to those above, have been synthesized by internal Diels–Alder reactions (Table 2(*b*)). These include α-eudesmol, stereoselectively from **122** (88), epizonarene from **125** (89), selina-3,7(11)-diene from **132** (90), and eremoligenol and valerianol from **140** (91). Compound **162** cyclizes spontaneously to the required stereoisomer for the synthesis of torreyol (92) and **160** is utilized for γ-cadinene (93) by analogy with the route followed from **161** for khusitene (104). The alleged chiloscyphone has been synthesized from **158** (94) and cyclostachine B was prepared from **137** using a presumed biomimetic approach (95). The required *trans-anti-trans* perhydrophenanthrene skeleton is formed by cyclization of **123** for conversion to fichtelite (96). Compactin has recently been synthesized in enantioselective fashion from **156** (97). Two other approaches being developed to compactin employ the allene **153** (98) and the Lewis acid catalyzed cyclization of **155** (99). A route to chlorotricolide, based on the cyclization of the acetylenes **165** and **166**, is being developed (100).

A number of amide systems have been studied and many form the basis for total syntheses. Pumiliotoxin C has been prepared in both racemic and chiral form from **172** (114). Cyclization of **199** provides a building block for the yohimbane skeleton (116) while a different sequence is planned using **188** (51). Andranginine results from heating **171** via a presumed biomimetic cycloaddition (113). The lycorane skeleton of the amaryllidaceane alkaloids is generated stereospecifically from **182** (117) and a closely related cyclization of **183** is employed in the preparation of *cis*-dihydrolycoricidine (119). The same lycorane ring system has been synthesized by construction of a

Can. J. Chem. Downloaded from www.nrcresearchpress.com by 210.87.254.6 on 09/06/12
For personal use only.

TABLE 2(*a*). Bicyclo[4·4·0]decenes

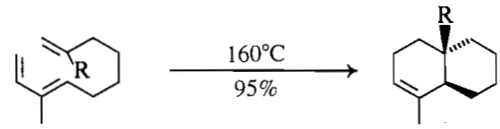

(90)

120 R = H
121 R = Me 190°C, 30%

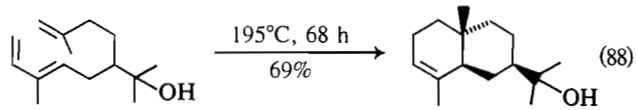

(88)

122

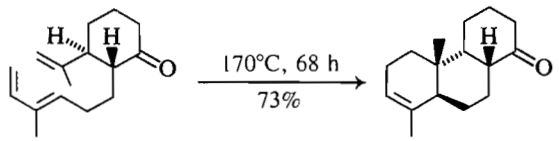

(96)

123

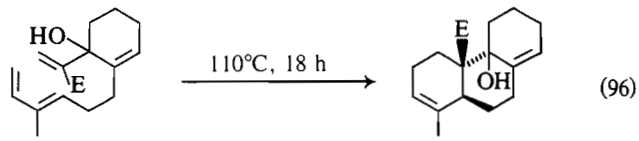

(96)

124 E = CO_2Et

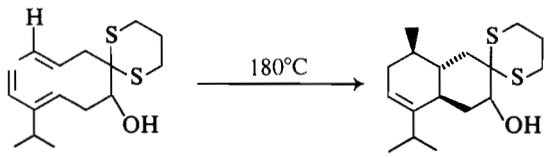

(89)

125

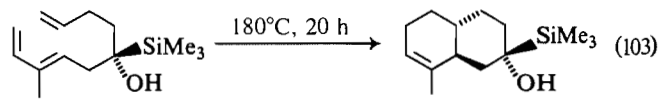

(103)

126

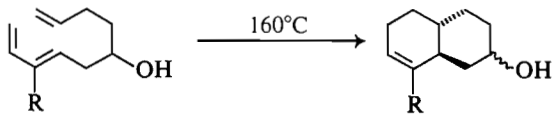

(101)

127 R = H 55 45
128 R = Me 160°C, 57% 94 6

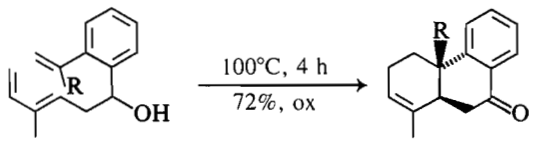

(102)

129 R = H 25 75
130 R = Me TMS ether, 33 67
180°C, 24 h, >43%

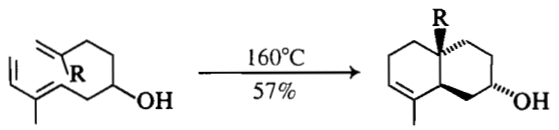

(90)

131 R = H 42 48
132 R = Me TMS ether, 37 58 *cis* 5
200°C, 100 h, 95%

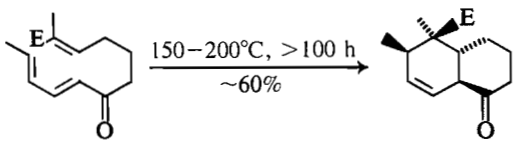

(106)

133 Major Minor

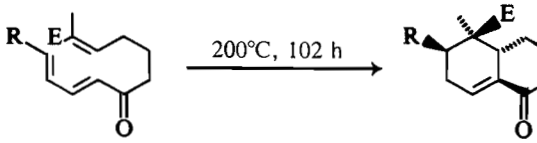

(106)

134 R = $\sim\!\!\sim CO_2Me$ 62 38

Can. J. Chem. Downloaded from www.nrcresearchpress.com by 210.87.254.6 on 09/06/12
For personal use only.

TABLE 2(*a*). (*Continued*)

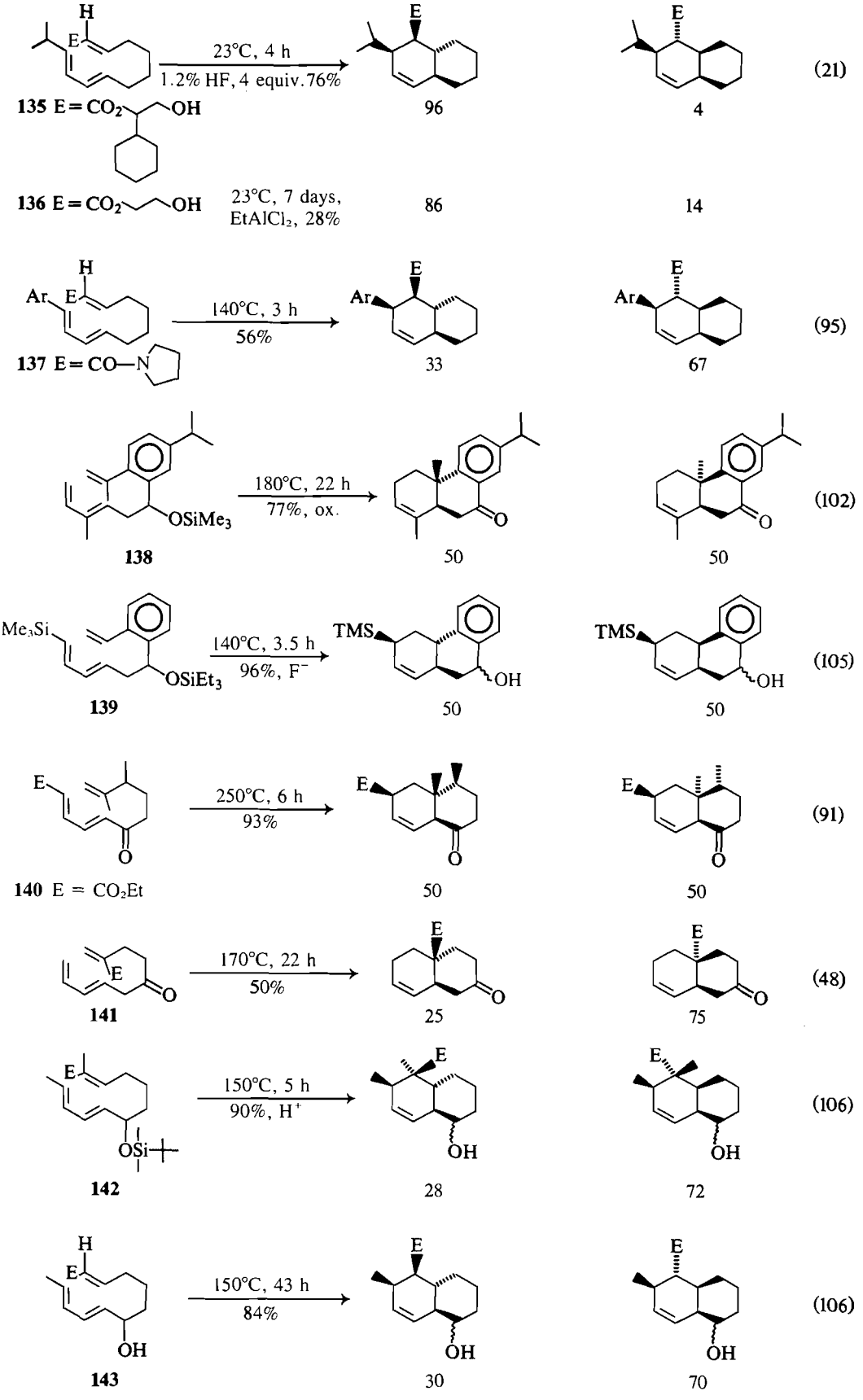

Can. J. Chem. Downloaded from www.nrcresearchpress.com by 210.87.254.6 on 09/06/12
For personal use only.

TABLE 2(*a*). (*Continued*)

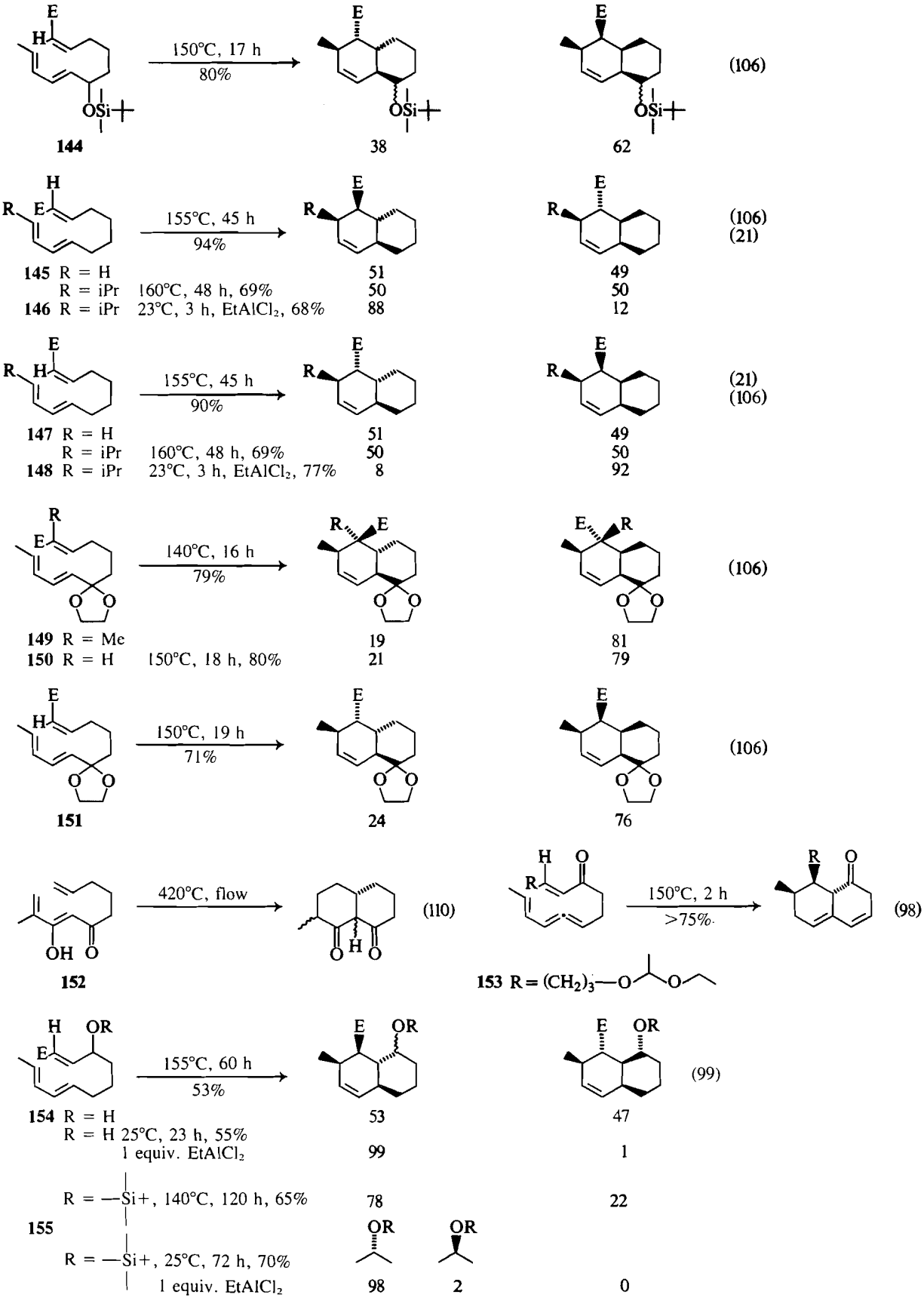

Can. J. Chem. Downloaded from www.nrcresearchpress.com by 210.87.254.6 on 09/06/12
For personal use only.

TABLE 2(*a*). (*Continued*)

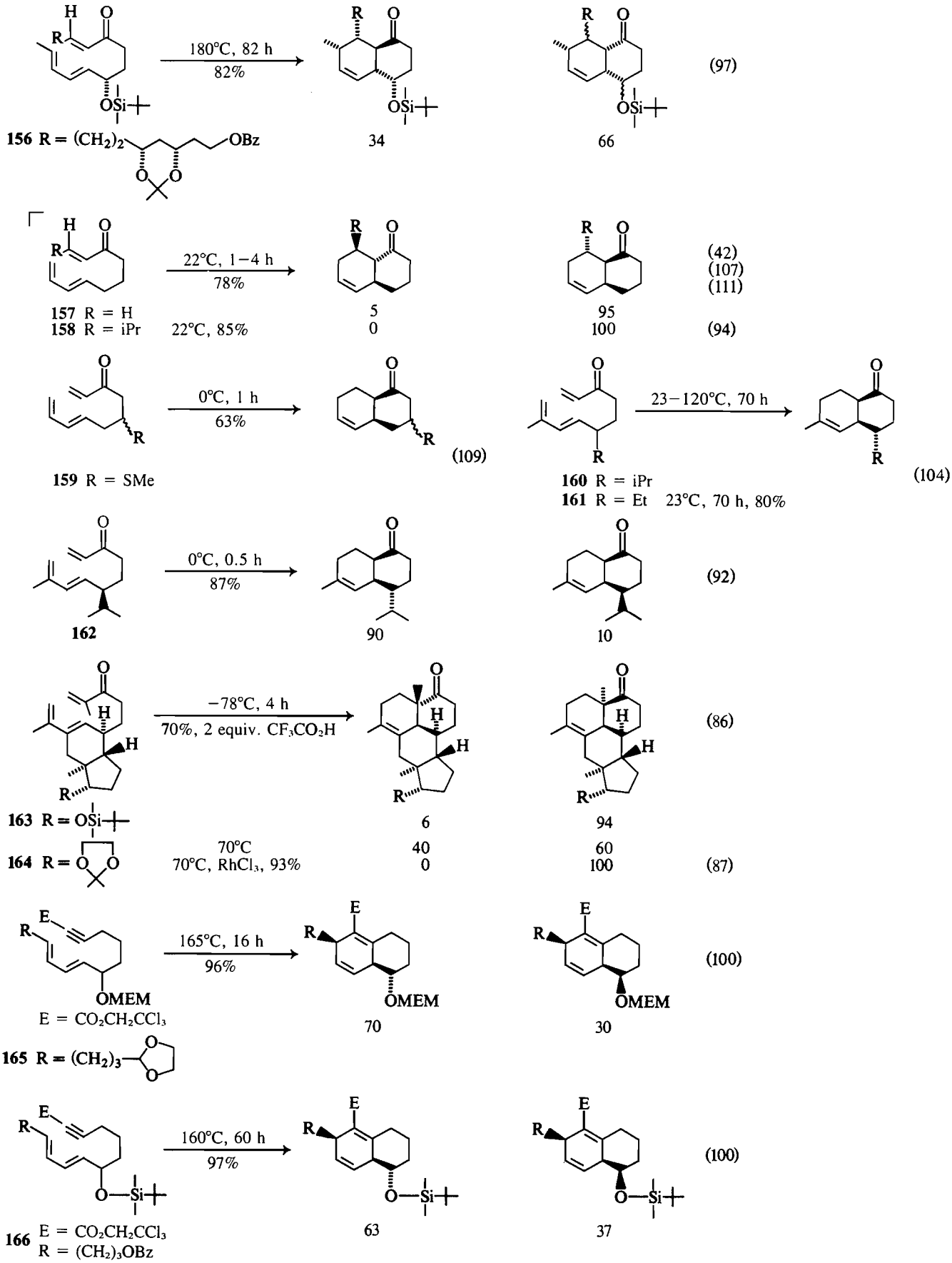

Can. J. Chem. Downloaded from www.nrcresearchpress.com by 210.87.254.6 on 09/06/12
For personal use only.

TABLE 2(*a*). (*Continued*)

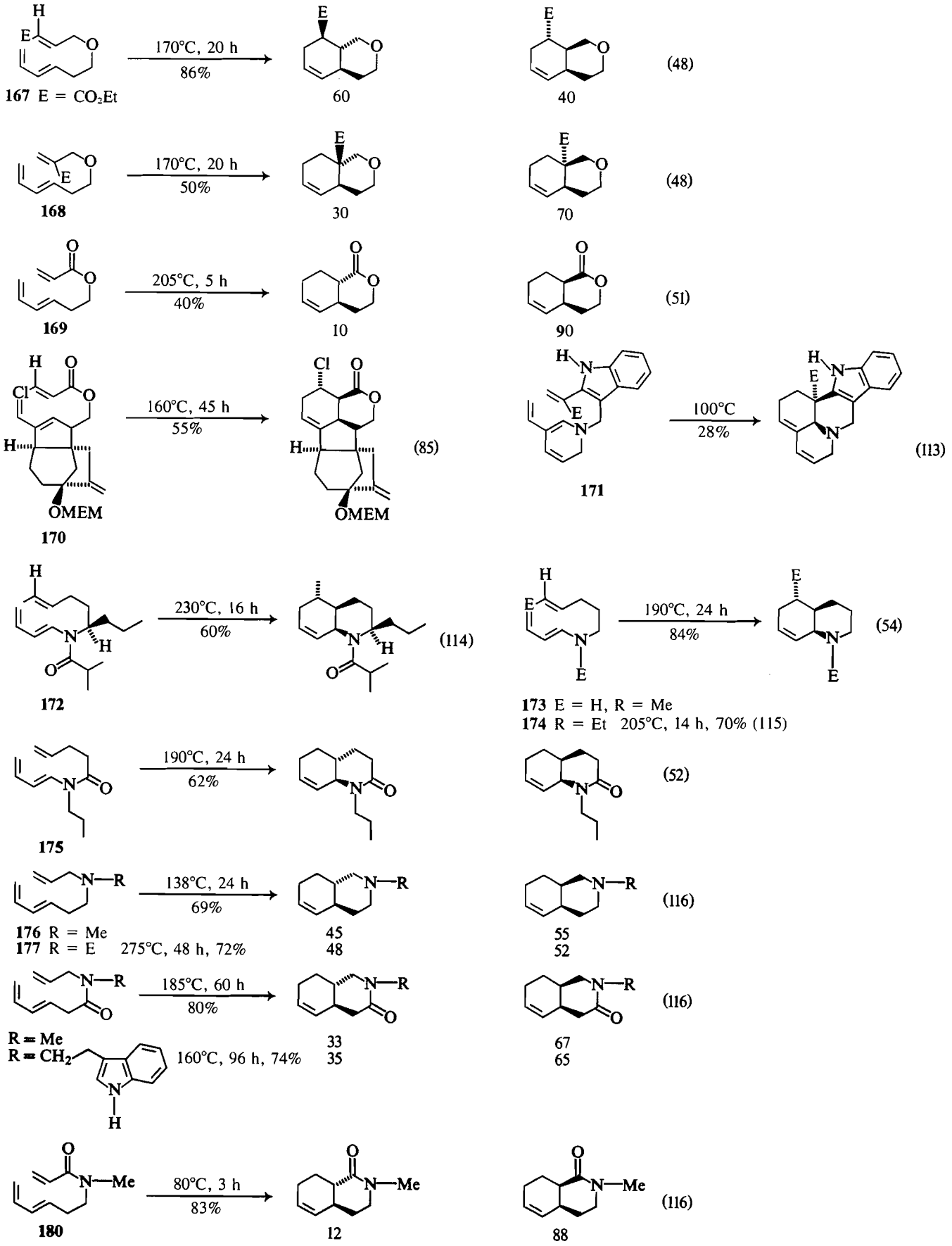

Can. J. Chem. Downloaded from www.nrcresearchpress.com by 210.87.254.6 on 09/06/12
For personal use only.

TABLE 2(*a*). (*Continued*)

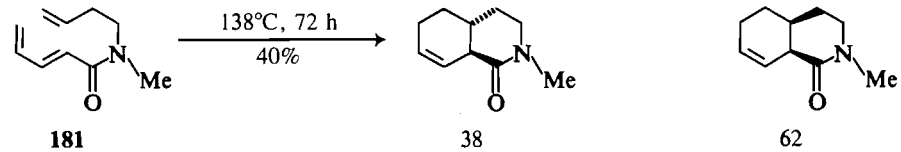

181 38 62

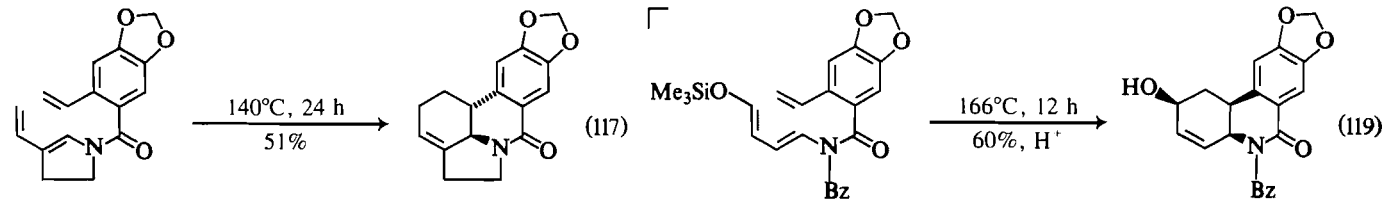

182 **183**

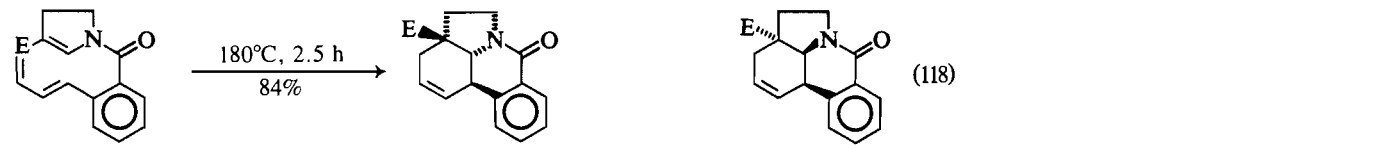

184 47 53

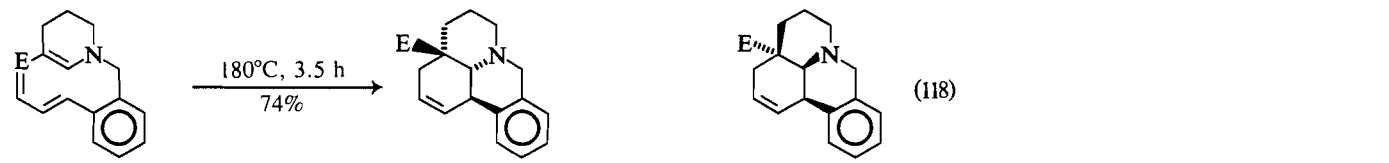

185 67 33

186 R = H 33 67
187 R = CH 600°C, flow, 43% 50 50

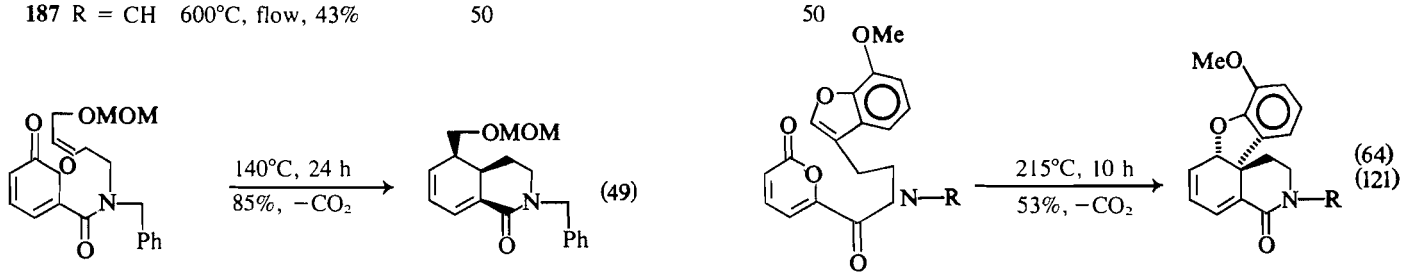

188 **189** R = Me
190 R = Bz 50%
191 R = CH_2—◁ 67%

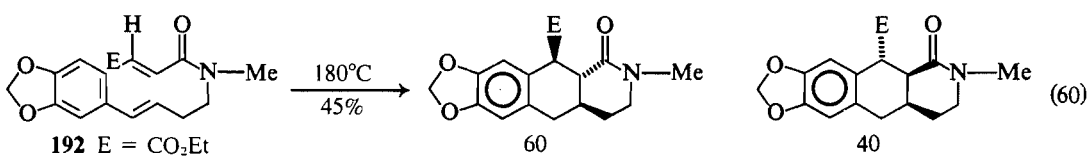

192 E = CO_2Et 60 40

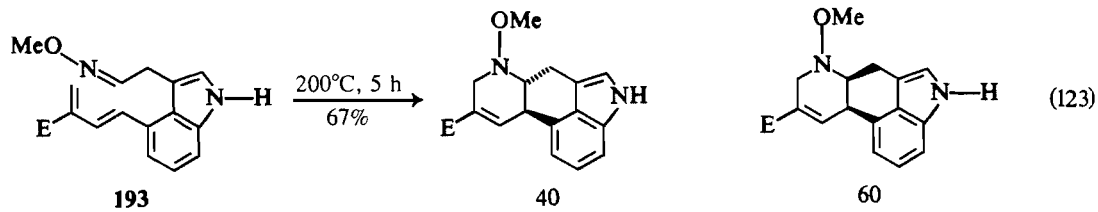

193 40 60

Can. J. Chem. Downloaded from www.nrcresearchpress.com by 210.87.254.6 on 09/06/12
For personal use only.

TABLE 2(*a*). (*Concluded*)

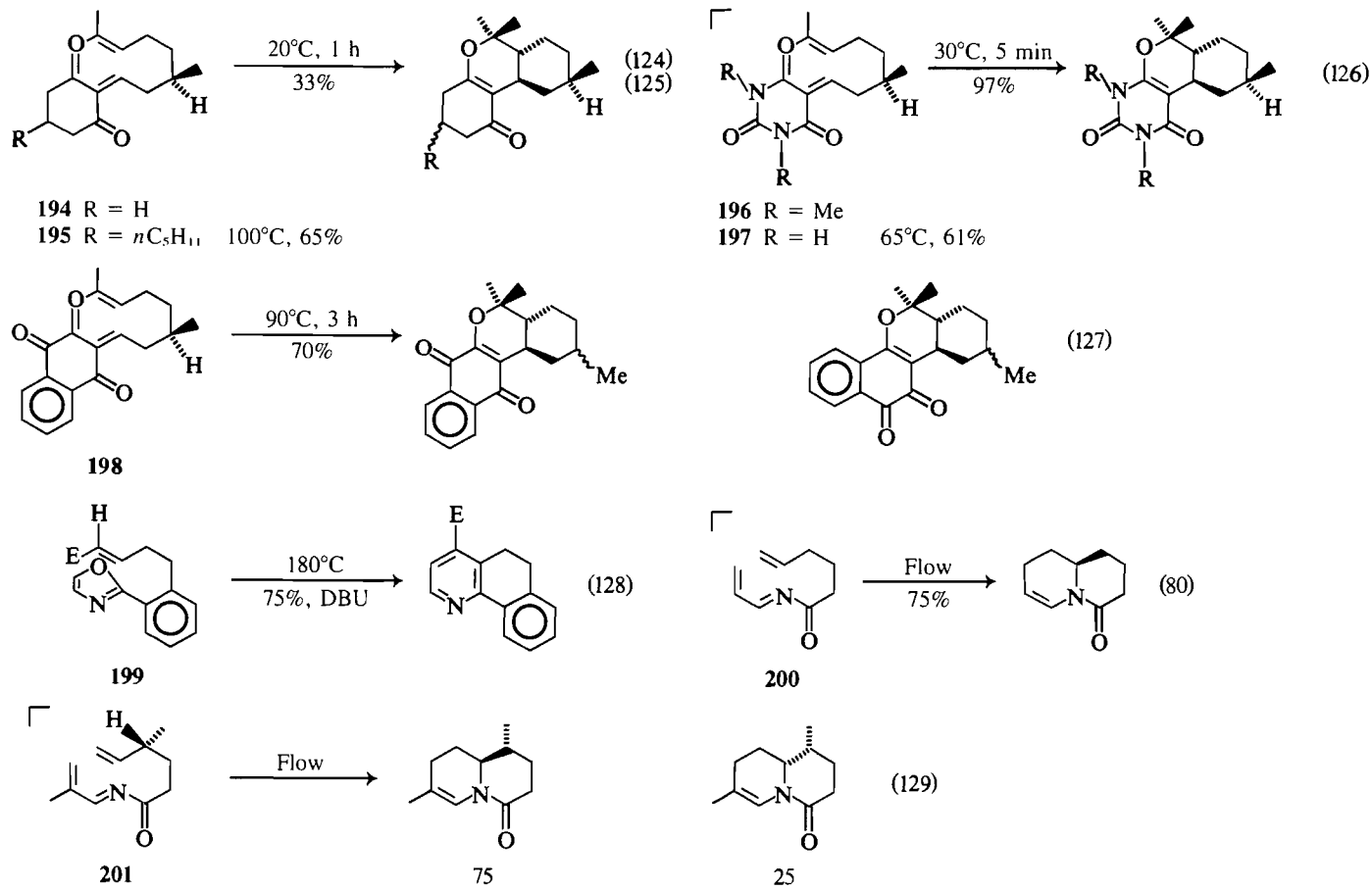

TABLE 2(*b*). Synthetic targets

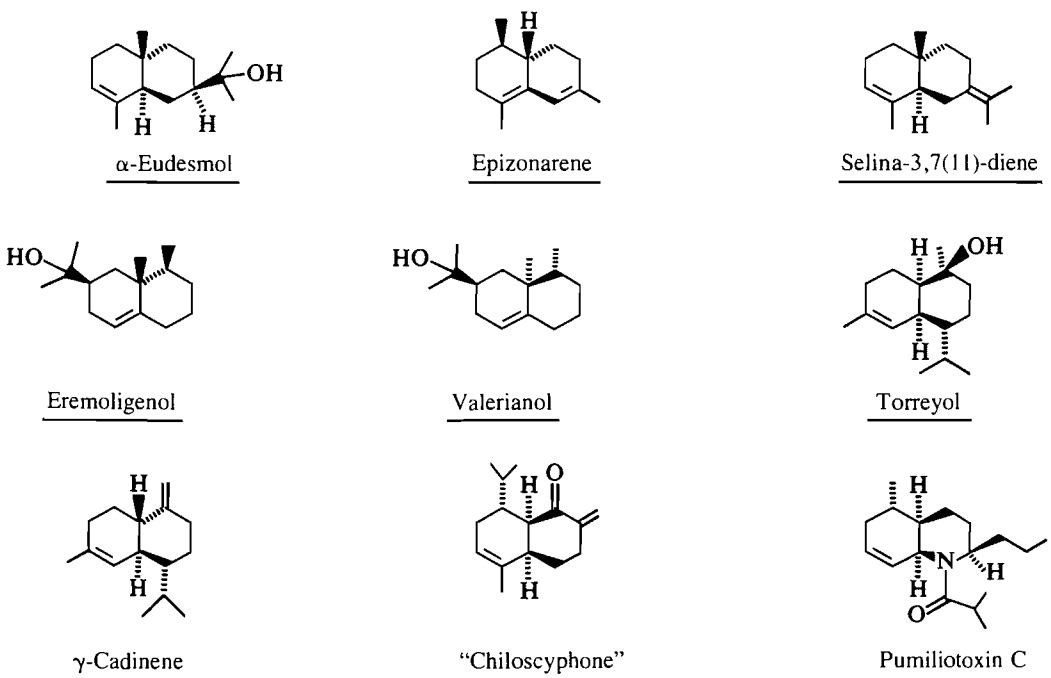

Can. J. Chem. Downloaded from www.nrcresearchpress.com by 210.87.254.6 on 09/06/12
For personal use only.

TABLE 2(*b*). (*Concluded*)

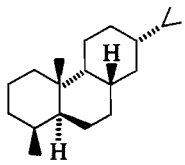

Fichtelite

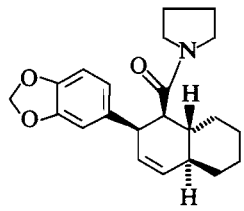

Cyclostachine B

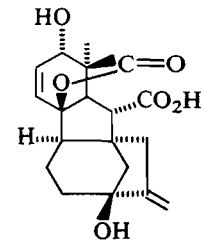

Gibberellic acid

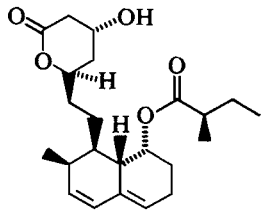

Compactin

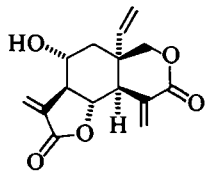

Vernolepin

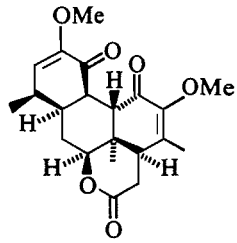

Quassin

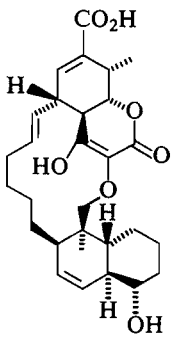

Chlorotricolide

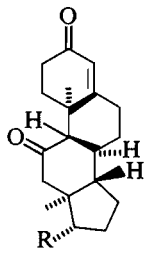

11-Oxygenated steroids

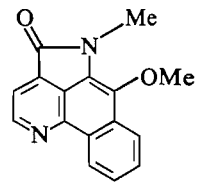

Lupolauramine

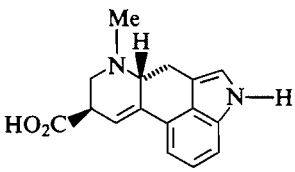

Lysergic acid

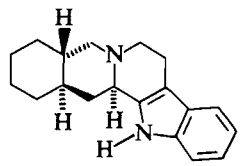

Yohimbane

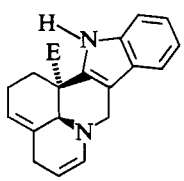

Andranginine

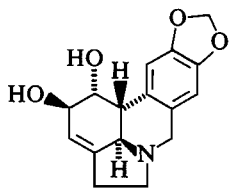

≡

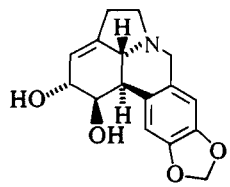

Lycorine

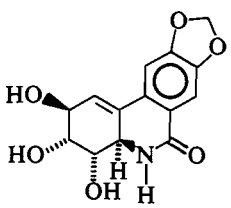

Lycoricidine

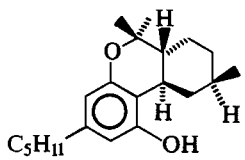

Hexahydrocannabinol

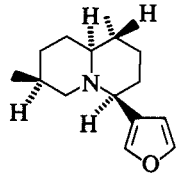

Deoxynuphanidine

Can. J. Chem. Downloaded from www.nrcresearchpress.com by 210.87.254.6 on 09/06/12
For personal use only.

Can. J. Chem. Downloaded from www.nrcresearchpress.com by 210.87.254.6 on 09/06/12
For personal use only.

different cyclohexane unit using **184** (118). The imino ether **193** is utilized in the synthesis of lysergic acid (123). Heteroatom dienes are used to prepare the hexahydrocannabinol skeleton enantioselectively from **195** (125), in which cyclization is directed by the chiral methyl centre. An intermediate for an approach to eupolauramine is generated from the oxazole **199** (128) and a recently completed total synthesis of deoxynuphanidine employs **201** (129).

ortho-Quinodimethane adducts

The *in situ* generation of *ortho*-quinodimethanes which are trapped intramolecularly by a dienophile to give fused ring systems was developed by Oppolzer and Keller (4, 18, 19) and has been studied extensively, particularly for the total synthesis of steroids. Several reviews have appeared (134–138) and thus recent applications to natural product synthesis are highlighted. The success of this methodology has stimulated the development of a number of procedures, in addition to benzocyclobutene fragmentation, for the preparation of the *ortho*-quinodimethane unit. One of the more versatile utilizes the thermal cheletropic elimination of sulphur dioxide (139, 140), while the mildest employs fluoride anion-induced silyl elimination (141–143) permitting diene generation and cycloaddition below 100°C. Generally *E*-quinodimethanes are formed preferentially and cyclize regioselectively to the fused ring product. They may be regarded as special examples of the preceding sections in which the selectivity (generally *trans* ring fusion) is enhanced due to the increased planarity of the reactive components. It is possible in many instances to direct the intramolecular cycloaddition towards the dominant formation of either the *endo*- or *exo*-adduct by modifications of the sidechain functionality and application of "carbonyl coplanarity control" as exemplified in examples such as **256–257** and **262–263** (145). In addition, several asymmetric syntheses have been conducted, particularly of steroids, by using a chiral ring D unit.

Steroid approaches have utilized a C,D ring construction as in **202–204** for the preparation of intermediates directed towards estradiol, cortisone, and progesterone (147, 148), while cyclization of **205** forms the basis for an approach to grayanotoxin-I (148).

Many groups have synthesized estradiol and its relatives based on a B,C ring assembly and typical examples **210–217** are tabulated (Table 3(*a*)). Kametani and co-workers are developing different Diels–Alder approaches to the quassinoid klaineanone; one route employs **223** (159), another the tetracyclic intermediate derived from **243** (160).

Chiral cyclohexane derivatives have proved useful for asymmetric synthesis of chenodeoxycholic acid from **227** (161) and as an entry to the pregnanes from **224** (162, 163). The ring fusion stereochemistry is changed to *cis* by the presence of a nitrile, as in **228** and **229**, providing intermediates from which the crustacean molting hormone 20-hydroxyecdysone was synthesized (164) (cf. **231** and **232**). Similar ring contraction of the adduct from **230** provides an alternative route to estrone (165).

Key intermediates for the total synthesis of the triterpenes alnusenol and friedelin have been prepared from **231** and **232**, respectively (166). The formal total synthesis of the diterpene alkaloids atisine, veatchine, garryine, and also gibberellin A_{15} was accomplished from **236**, in which the nitrile substituent again promotes the *cis*-product (167).

An alternative route to *o*-xylylenes has been developed by Funk and Vollhardt (137, 169), using cobalt-mediated co-oligomerization of bis(trimethylsilyl)acetylene and 1,5-hexadiyne so that the steroid nucleus can be generated in a single chemical operation. Cases **237–242** are representative and include the synthesis of estrone from **240** and **241** (169).

Kametani and co-workers have utilized exocyclic dienophiles to generate the tetracyclic nuclei of diverse terpenes. These studies have resulted in the total synthesis of hibaol from **246** (170) and approaches to isoatisirene and grayanotoxin I are being pursued from **244** and **245**, respectively (171, 172).

Magnus and co-workers have generated indole-2,3-quinodimethanes such as **254** which was employed in a synthesis of aspidosperimidine (177). Two syntheses of chelidonine have been completed by Oppolzer and Keller (19, 178), the most recent of which employs **259** in a highly stereoselective cycloaddition via an *exo* (with respect to nitro group) transition state.

The basic skeleon of aphidicolin has been constructed using the five-carbon sidechain contained in **271** (182), while the lignan carpanone was prepared by a biosynthetic-type cyclization of **270** (181) and, in related fashion, **273** afforded deoxybruceol (122).

Bicyclo[5.4.0]undecenes

Only two preparations of this ring system appear to have been reported (130, 131), each of which was used to synthesize himachalene (Table 4). As expected, the extra freedom in the sidechain and the carbonyl coplanar effect combine to give exclusively *cis*-fused products from **274** and **275**, although epimerization is possible in the latter case.

Bicyclo[*n*.4.0] skeletons

Only a few examples with sidechains containing more than five atoms have been studied (see Table 5). In general, with increased chain length both stereo- and regioselectivity diminish, as is evident for cases **276** and **277** (132) which resemble related intermolecular examples. However, the more sterically demanding dienophile in **278** cyclizes with greater regioselectivity and forms the basis for an approach to cytochalasin B (133). Part of the loss of selectivity in these examples is a consequence of entropy and free energy of activation changes, since the 5–7 kcal/mol reduction in activation barriers found for intramolecular cycloadditions (59) is largely forfeit with lengthy connecting chains.

Bridged ring adducts (cyclic dienes)

Cyclic dienes (Table 6(*a*)) have received a considerable amount of attention, initially as a consequence of the total synthesis of diverse bridged sesquiterpenes (Table 6(*b*)) by various Swiss chemists. The structural format used to this point has been altered to better reflect the actual transition states involved and to facilitate comparison with the synthetic targets.

5-Alkylcyclopentadienes undergo rapid 1,5-sigmatropic rearrangement to the C1 isomer from which intramolecular cyclization usually occurs. This has been used to advantage by Breitholle and Fallis in the cyclization of **283** for the total synthesis of cedrene and cedrol (186). Although this sigmatropic rearrangement leading to **280** foiled an early approach to longifolene (15), a similar ring system from **284** is currently being investigated as a route to the sesterterpene gascardic acid (187).

As a consequence of the strain inherent in the competing pathways, it was found that systems such as **291** afford a single

TABLE 3(*a*). *ortho*-Quinodimethane adducts

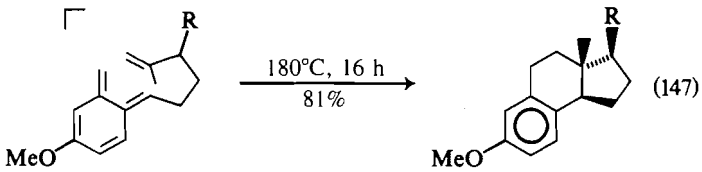

(147)

202 R = OH

203 R =

195°C, 7 h, 64% (148)

204 R =

180°C, 6 h, 86%

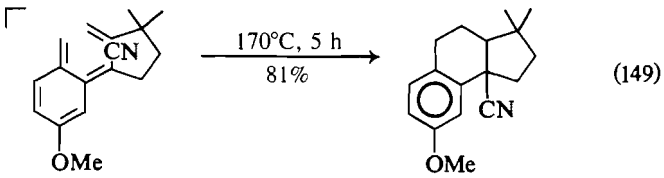

205 (149)

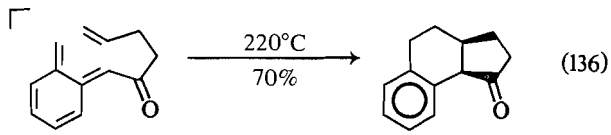

206 (136)

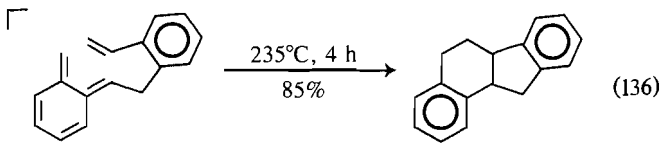

207 (136)

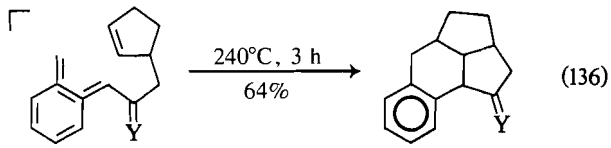

(136)

208 Y = H_2

209 Y = O 220°C, 4 h, 45%

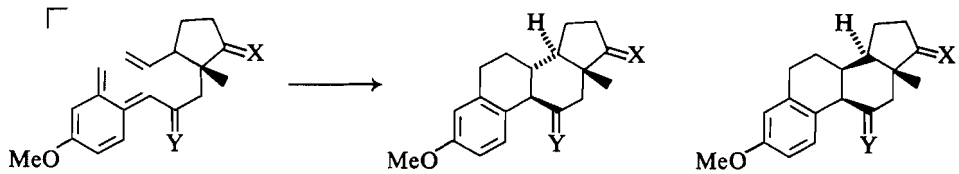

210 X = Y = O	150°C, 12 h, 56%	95	5 (150)
211 X = O, Y = H_2	82°C, 1.5 h, 86%	100	0 (142)
212 X = O, Y =	23°C, 20 h, 70%	100	0 (143)
213 MeO = H; X = O, Y = H_2	210°C, 8 h, 85%	94	6 (140)
214 MeO = CN; X = 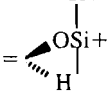 Y = H_2	213°C, 3 h, 80%	100	0 (151)
215 X = 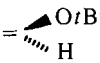 Y = H_2	180°C, 3 h, 84%	100	0 (152)
216 X = Y = H_2	200°C, 7.5 h, 78%	100	0 (153)

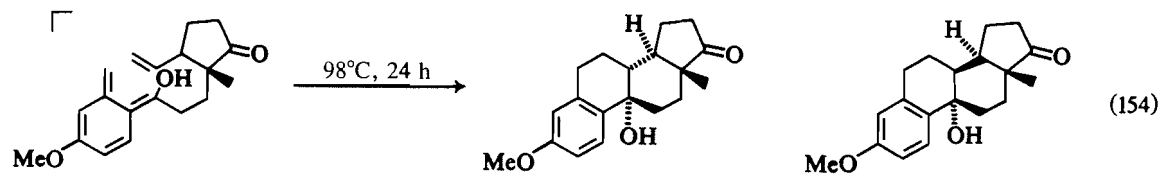

(154)

217 **95** **5**

Can. J. Chem. Downloaded from www.nrcresearchpress.com by 210.87.254.6 on 09/06/12
For personal use only.

TABLE 3(*a*). (*Continued*)

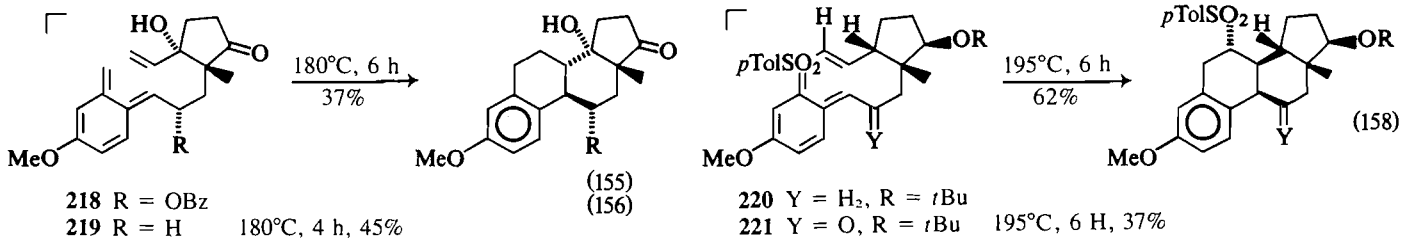

218 R = OBz
219 R = H 180°C, 4 h, 45%

(155)
(156)

220 Y = H_2, R = *t*Bu
221 Y = O, R = *t*Bu 195°C, 6 H, 37%

(158)

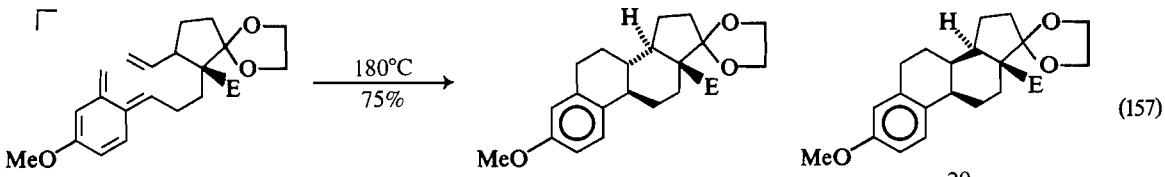

222 E = CH_2OH 180°C, 75%

80
100

20

(157)

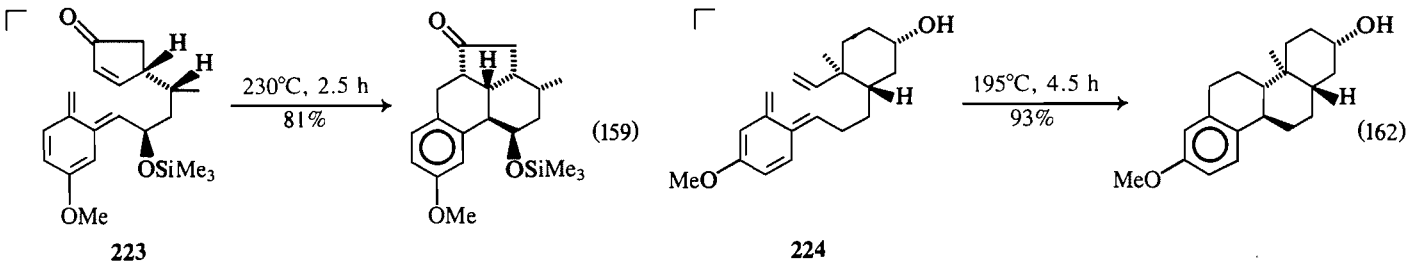

223

224

(159)

(162)

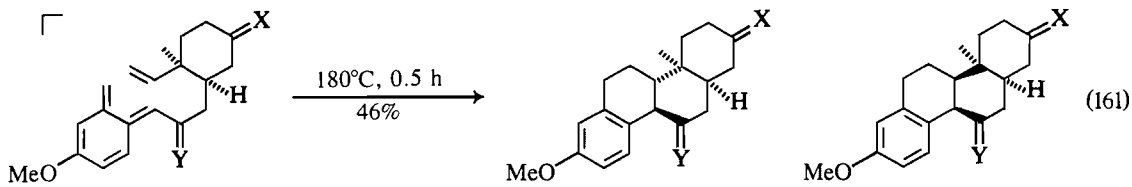

225 X = Y = O		57	43
226 X = 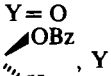 , Y =	180°C, 4 h, 65%	100	0
227 X = 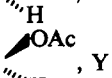 , Y = O	180°C, 0.75 h, 43%	100	0

(161)

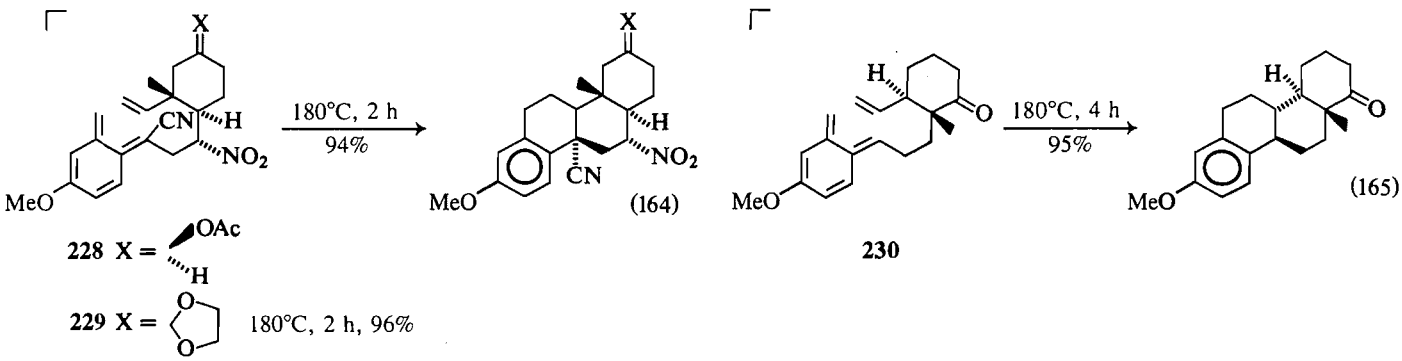

228 X =

229 X = 180°C, 2 h, 96%

230

(164)

(165)

Can. J. Chem. Downloaded from www.nrcresearchpress.com by 210.87.254.6 on 09/06/12
For personal use only.

TABLE 3(*a*). (*Continued*)

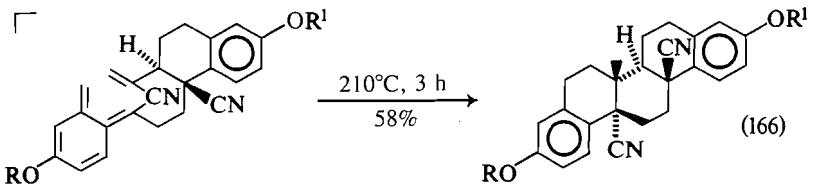

(166)

231 R = Et, R' = Me
232 R = Me, R' = Et 210°C, 3 h, 60%

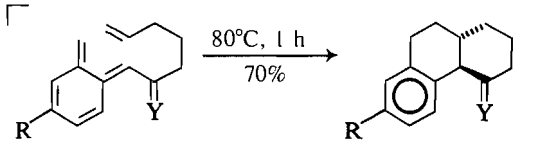

(141)
(136)

233 R = Y = H
234 R = OMe, Y = H_2 180°C, 90%
235 R = OMe, Y = O 220°C, 80%

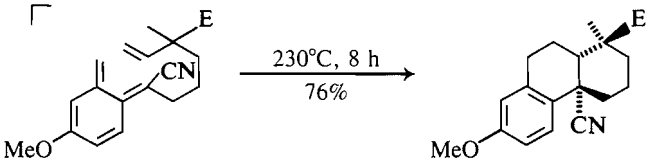

(167)

236 180–230°C, 3 h, 52%

16
0

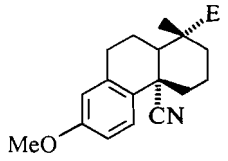

84
100

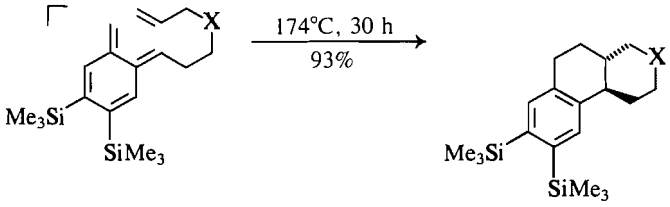

(168)

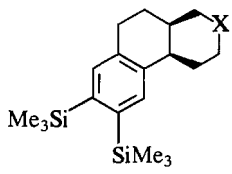

237 X = O
238 X = CH_2 174°C, 30 h, 97%

80
95

20
5

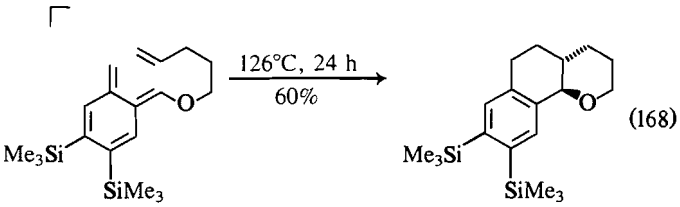

(168)

239

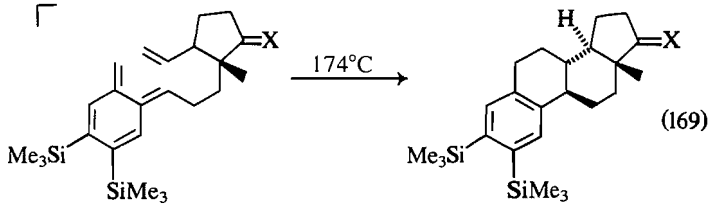

(169)

240 X = 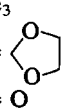
241 X = O 136°C, 35 h, 71%

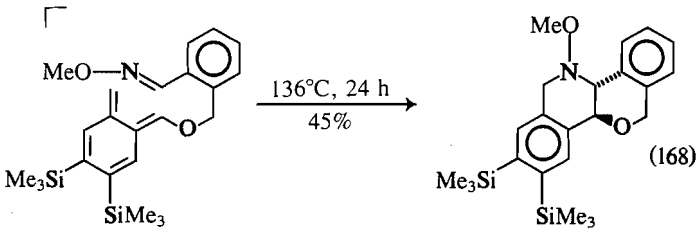

(168)

242

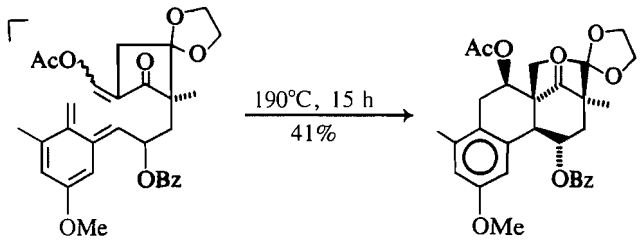

(160)

243

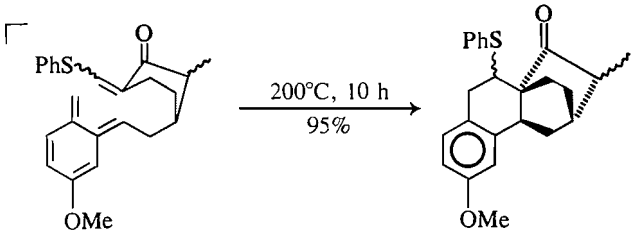

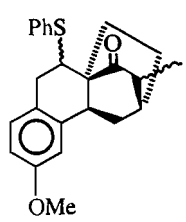

(171)

244

~30

~70

Can. J. Chem. Downloaded from www.nrcresearchpress.com by 210.87.254.6 on 09/06/12
For personal use only.

TABLE 3(*a*). (*Continued*)

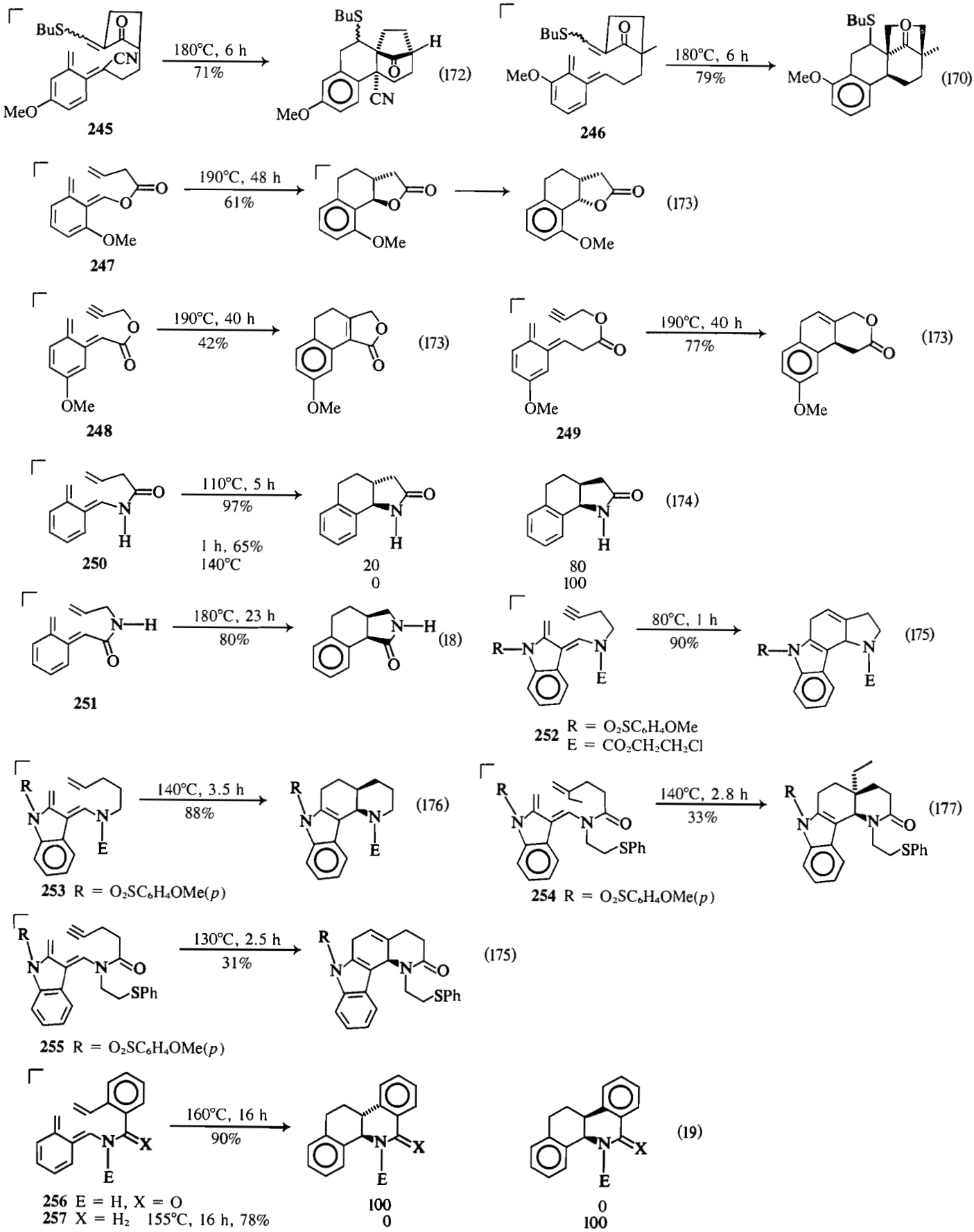

Can. J. Chem. Downloaded from www.nrcresearchpress.com by 210.87.254.6 on 09/06/12
For personal use only.

TABLE 3(*a*). (*Concluded*)

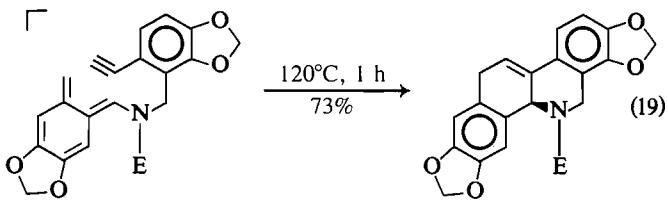

258 E = $CO_2C_7H_7$

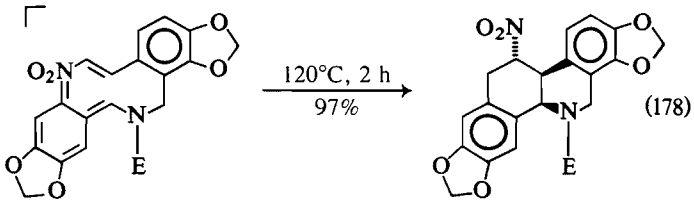

259 E = $CO_2C_7H_7$

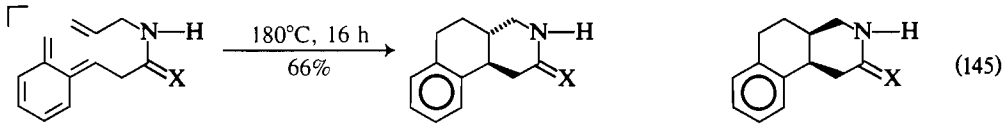

260 X = H_2 87 12
261 X = O 180°C, 16 h, 78% 20 79

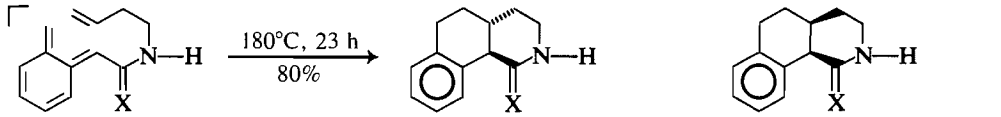

262 X = O 0 100
263 X = H 180°C, 16 h, 60% 72 27

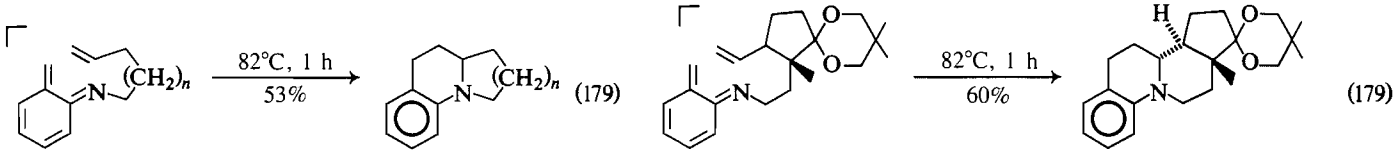

264 *n* = 1
265 *n* = 2 82°C, 1 h, 58%

266

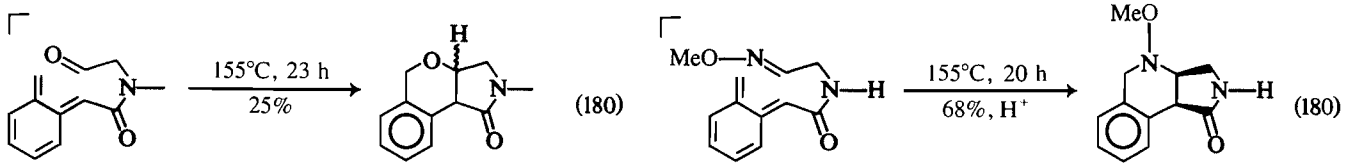

267 **268**

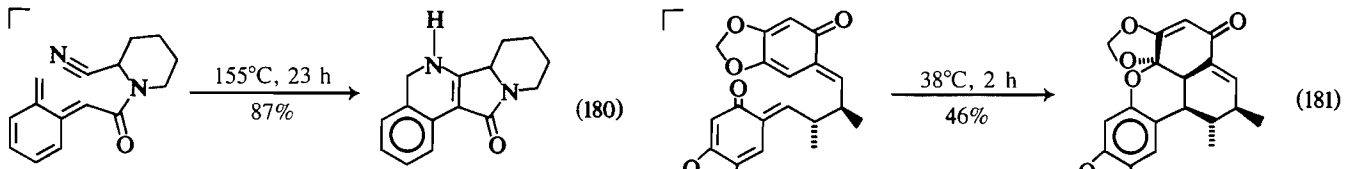

269 **270** 23°C, 15 h, 90%

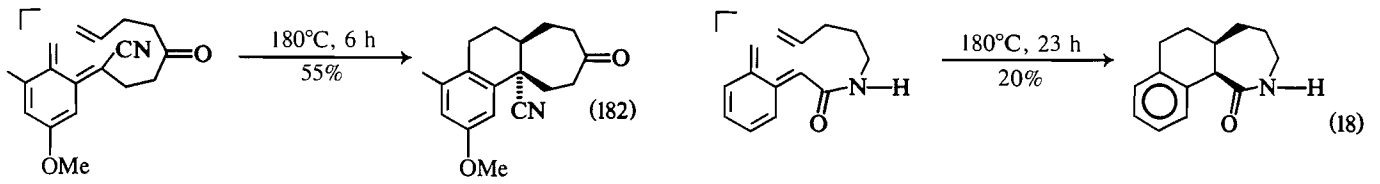

271 **272**

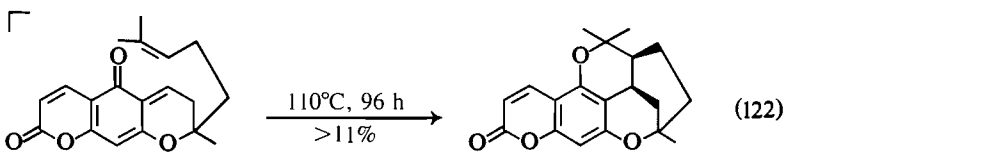

273

Can. J. Chem. Downloaded from www.nrcresearchpress.com by 210.87.254.6 on 09/06/12
For personal use only.

TABLE 3(*b*). Synthetic targets

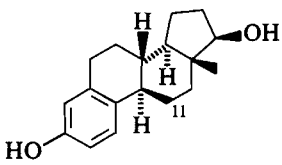

Estradiol
11-oxo, 11-hydroxy

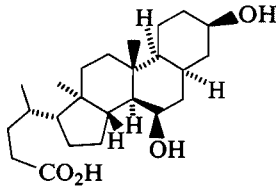

Chenodeoxycholic acid

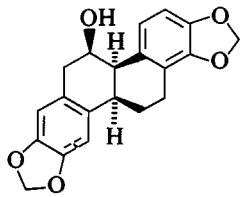

Chelidonine

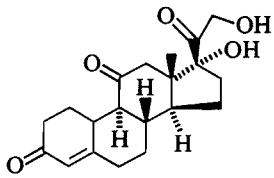

Cortisone

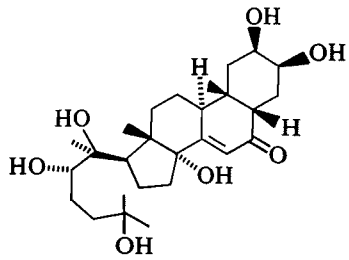

20-Hydroxyecdysone

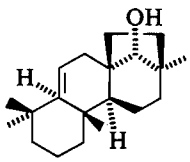

Hibaol

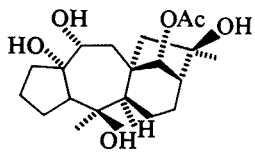

Grayanotoxin I

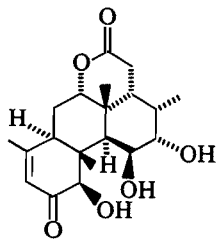

Klaineanone

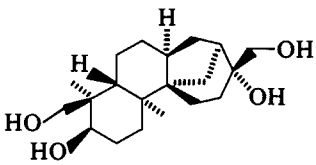

Aphidicolin

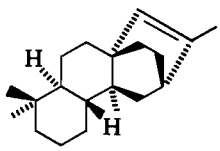

Isoatisirene

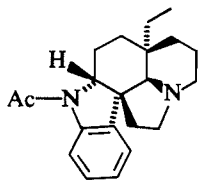

Aspidospermidine

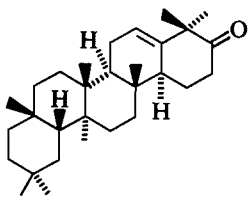

Alnusenol

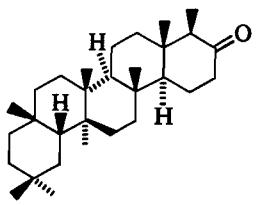

Friedelin

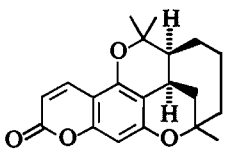

Deoxybruceol

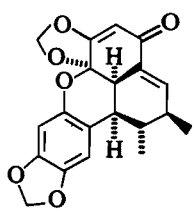

Carpanone

Can. J. Chem. Downloaded from www.nrcresearchpress.com by 210.87.254.6 on 09/06/12
For personal use only.

TABLE 4. Bicyclo[5.4.0]undecenes

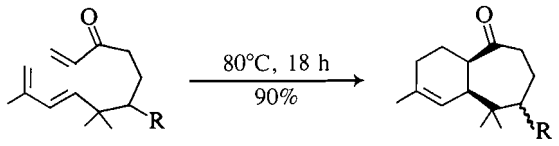

274 R = $OPO(OEt)_2$ (131)
275 R = H 110°C, $AlCl_3$, 70% (130)

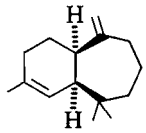

α and β-Himachalene

adduct from the C5 isomer. The regiochemistry varies with the cyclopentadiene and dienophile substituents. In the case of **293** it is regioselective, in accord with frontier molecular orbital correlations, and Snowden has utilized this in a total synthesis of sativene (190). A related cyclization is being studied in an approach to sinularene (191) from **295** and a fused cyclopentadiene **296** plays a key role in a route being developed to capnellene (195). An early stage of the recently completed total synthesis of dodecahedrane (193) depends upon the cyclization of **297** (192).

An alternative solution to the pestiferous cyclopentadiene rearrangement problem is to use a suitable blocking group, although chlorine was found to be unsatisfactory (198). This has been accomplished with a cyclopropane unit and **302** is employed in a recently completed total synthesis of the marine sesquiterpene sinularene (196). In similar fashion, an asymmetric total synthesis of longifolene is being developed from **303**, in which the chiral cyclopropane centre directs the cyclization (197).

Cyclohexadienes are more civilized in their behaviour and cyclization of **304** forms the basis for a total synthesis of khusimone by Büchi *et al.* (199), while the related higher homologue **306** provides an entry to a pleasant smelling, acid catalyzed rearrangement product of thujopsene (201). The aromatic triene system **307** is being developed into a synthesis of the diterpene alkaloid atisine (202). Of the five total syntheses of 9-isocyanopupukeanane or the ketone derived from it, four employ an intramolecular Diels–Alder cycloaddition as a key step from **308**, **318**, **319**, and **320** respectively (203–206). The regiochemistry of these cyclizations usually disfavours the "twistane" type product; however, the planarity of the sidechain, the presence of a carbonyl group, and nonbonded interactions can tip this balance, as in **309** and **310** compared to **308**. In these three examples the "twistane" (bridged) product is anticipated on the basis of molecular orbital considerations, although in the cases of **308** and **309** they may be converted (250°C, 5 min, for **308**) to the thermodynamically more stable isomers. The adducts from **310** and **312** have been utilized in a total synthesis of seychellene (208) and norseychellanone (209). A chiral synthesis of patchouli alcohol by Näf *et al.* (215) employs **314** in which the sidechain methyl function directs the reaction, since only one diastereomer cyclizes, and a related triene **317** is used for norpatchoulenol (216). Examples **280**, **283**, **304–307**, **370–375**, **382–383**, **413–420** illustrate the difficulty of predicting whether the new ring will be *exo* or *endo* in view of subtle substituent effects, but there is a preference for cyclopentanes (three connecting atoms) to be *exo*.

Obviously, when the sidechain contains rings (cf. Scheme 1), multicyclic systems can be constructed using cyclohexadienes, anthracenes, cycloheptadienes, etc., and representative examples are tabulated. Recently Nicolaou *et al.* have completed the total synthesis of endiandric acids A, B, and C from **335** and **336**, respectively (274, 275). (A and B actually possess a bicyclo[4.3.0]nonene nucleus but are included here for convenient comparison.) These studies lend support to the suggestions of Black and co-workers (270) that these compounds arise in nature, where they are found in racemic form, from a series of electrocyclizations culminating in an internal Diels–Alder reaction. *In situ* generation of the appropriate polyunsaturated, acyclic ester precursors **337** and **338** affords, after brief heating, the natural products A or B and C in which 4 new rings and 8 asymmetric centres are formed (276). They arise via a fascinating sequence involving an 8π electron conrotatory ring closure to a cyclooctatriene, rearrangement via 6π electron disrotatory cyclobutene formation (shown), followed by an intramolecular $\pi 4s + \pi 2s$ cycloaddition.

A large number of heterocyclic dienes have been studied but relatively few have been employed in total syntheses in spite of their potential for the introduction of diverse groups and selective functionalization of more than one position. Furans of type **381–383** are being utilized by De Clercq and co-workers in interesting approaches to gibberellic acid (232) and functionalized steroids (233). In the latter case formation of the kinetic product is facilitated by using water as a solvent (234). Cyclization of the furanobenzyne **374** provides an intermediate employed in the preparation of mansone E (231), and Keay and Rodrigo (273) have recently completed a total synthesis of resistomycin from the isobenzofuran **384**. Karahana ether has been synthesized by Mukaiyama *et al.* using the magnesium complexed triene **394** (237), which fails to cyclize as the free alcohol **393** possibly due to a diminished population of the required *s-cis* amide conformer and the absence of the Lewis acid contribution of the complex. They have utilized the same procedure for the asymmetric preparation of farnesiferol C from **414**, in which the chiral substituent on nitrogen directs the cyclization (239).

Facile bridge loss after cycloaddition is characteristic of many *bis*-heteroatom dienes and advantage is taken of this in a total synthesis of actinidine from **461** by Sammes and co-workers (254). Oxazoles also behave in this fashion (cf. **200**) and cyclization of **436** affords evodone (243) while the related systems **434** and **435** were used by Jacobi and Walker (244) to synthesize ligularone and petasalbine, respectively.

A different approach to bicyclic skeletons involves the use of butadienes with the connecting chain attached to the β position. Shea and his co-workers have studied a number of trienes which afford bridgehead olefins and intend to use this approach for taxane skeletons (144), such as taxusin.

Troublesome trienes

A risk involved in the application of the intramolecular Diels–Alder reaction to total synthesis is the failure of the carefully synthesized triene to cyclize! This can occur even when there are closely related literature precedents of successful cyclizations, as is evident by comparing these trienes with those in earlier sections. As a guide to future work several examples which failed to cyclize under the conditions examined are tabulated (Table 7). In cases designated with an

Can. J. Chem. Downloaded from www.nrcresearchpress.com by 210.87.254.6 on 09/06/12
For personal use only.

TABLE 5. Bicyclo[n.4.0] skeletons

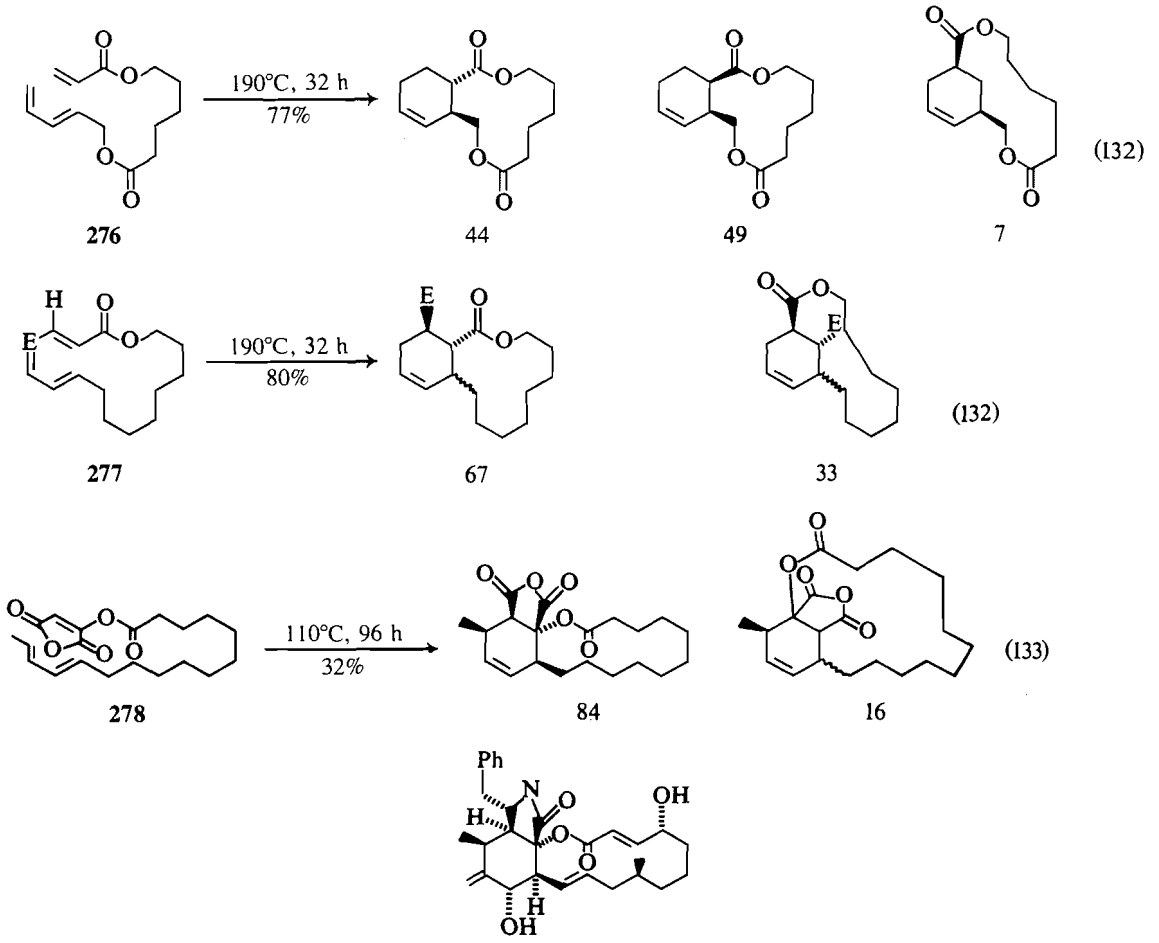

asterisk, other Diels–Alder adducts were formed as a result of isomerization of the original compound. Example **548** is a special case in which a [2 + 2] sequence, involving a vinylcyclobutane intermediate, takes precedence and the formal bridged [4 + 2] adduct **549** arises from further thermolysis via a diradical reaction (265).

The beneficial effects of a sidechain carbonyl group in altering product stereochemistry were discussed above; however, it can also be a liability due to its preference for coplanarity. This "carbonyl coplanarity effect" is often sufficient to inhibit cyclization. In cases **503** and **504**, part of an approach to vernolepin, no cyclization was observed below 220°C and at higher temperatures diene isomerization into conjugation precedes cycloaddition. In spite of the strain, overlap may be more readily maintained, in the transition state leading to the perhydroindene skeleton (cf. **50**, **51**) (46). It is likely, given the large number of compounds with connecting chain carbonyls in the table, that some of these suffer from a similar effect. In principle, it should be possible to circumvent this difficulty by alteration of the carbonyl functionality (reduction, protection, etc.) but even this may fail, as in **522** (233), and the examples in **519** only cyclize when a homoallylic oxygen substituent is present (196).

Deleterious steric effects are probably the prime culprit preventing cyclization in many instances and examples **488–490**, **492**, **493**, **508**, and **509** are representative. Although **508** and **509** could not be used in an approach to quassin (264), a different disconnection holds promise for realizing this goal (108). A related phenomenon is the restricted geometry imposed by the sidechain so that efficient diene–dienophile overlap cannot be achieved (**484**, **485**, **510**, etc.). At the other extreme, when the connecting chain is lengthened to 5 bridging atoms, the preferred conformations are not the folded ones required for cyclization, and the barrier to achieve them is increased. For example, **521** reacts preferentially with the trisubstituted olefin to form a five- rather than a seven-membered ring. This reluctance to form cycloheptanes is also exemplified by **538–540** and **547**. In intermolecular cases, the tendency of furan adducts to dissociate is well established and the large number of reluctant furan systems may reflect, in part, some situations where the equilibrium with the adduct is unfavourable, rather than the inability of the cyclization to actually occur. A recent study (266) of a furan intramolecular Diels–Alder cycloaddition confirmed the existence of a negative volume contribution from the approach of the reacting centres which, although smaller than intermolecular examples, suggests that high pressure should facilitate cyclization in difficult cases.

In view of the well defined geometric and electronic requirements of the Diels–Alder transition state, it is likely that detailed conformational analysis coupled with molecular orbital calculations might provide some insight into these sys-

Can. J. Chem. Downloaded from www.nrcresearchpress.com by 210.87.254.6 on 09/06/12
For personal use only.

TABLE 6(*a*). Bridged-ring adducts

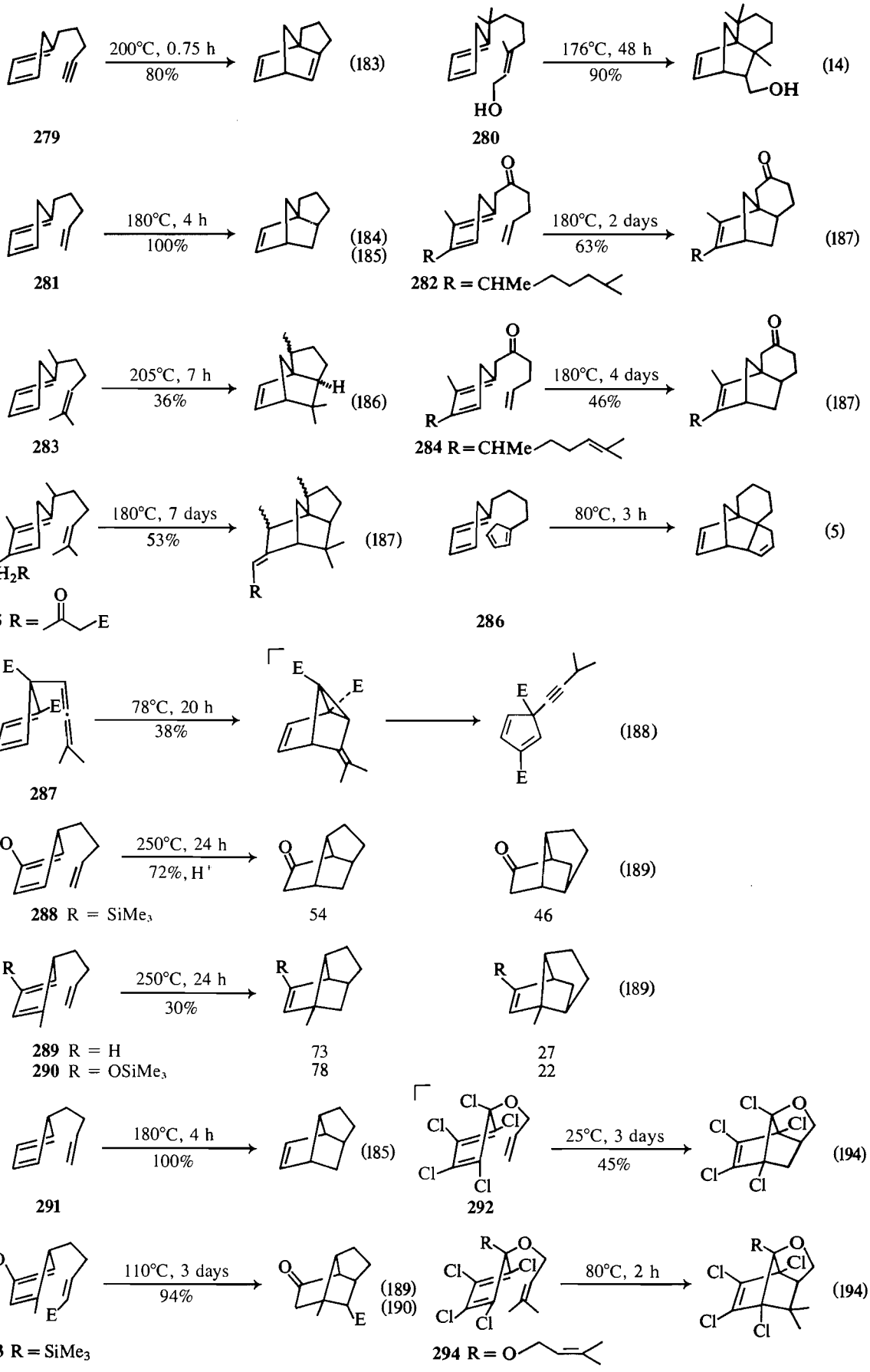

Can. J. Chem. Downloaded from www.nrcresearchpress.com by 210.87.254.6 on 09/06/12
For personal use only.

TABLE 6(*a*). (*Continued*)

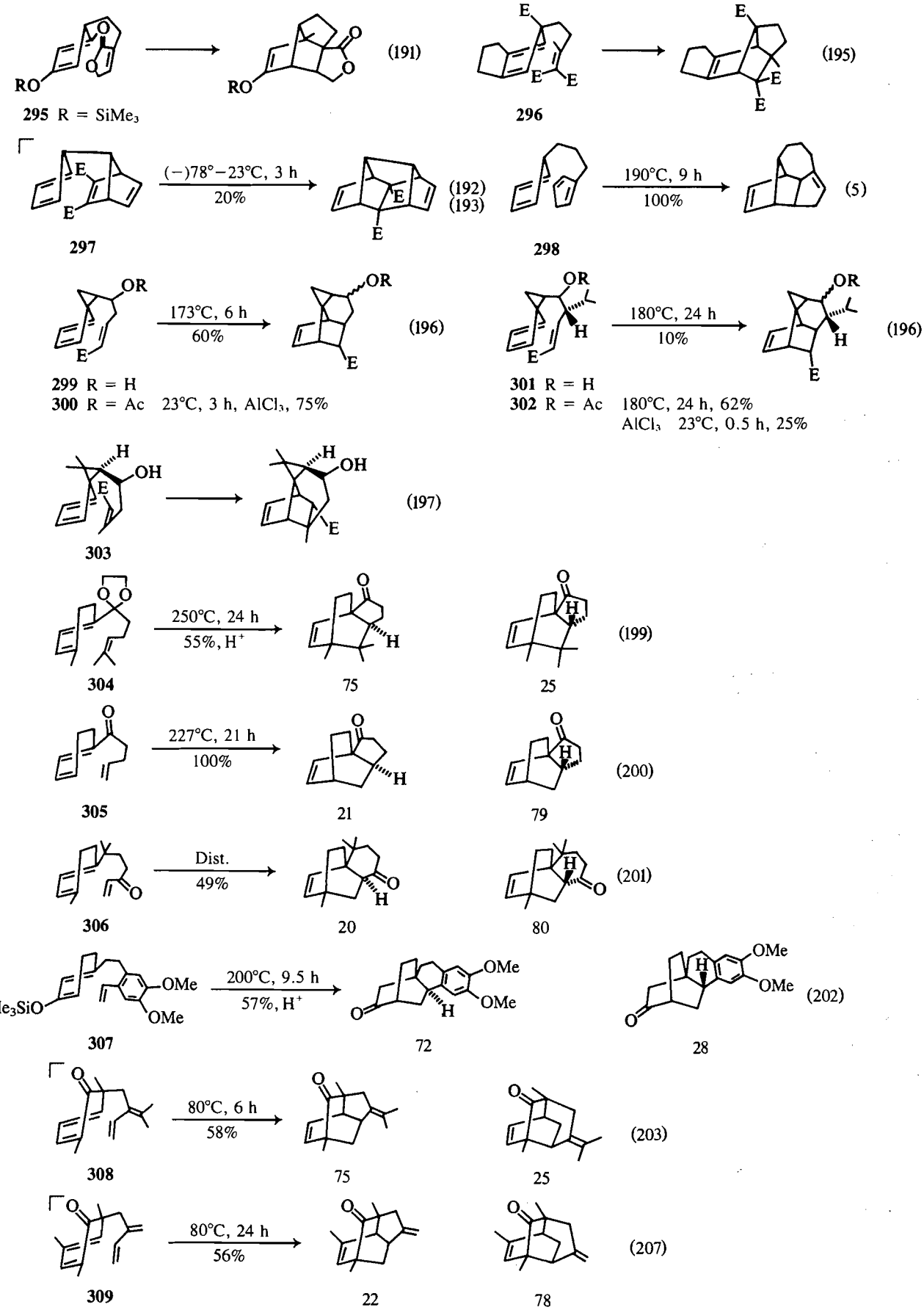

Can. J. Chem. Downloaded from www.nrcresearchpress.com by 210.87.254.6 on 09/06/12
For personal use only.

TABLE 6(*a*). (*Continued*)

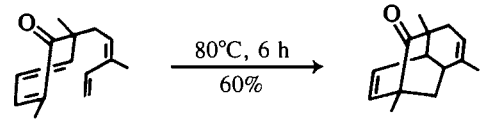

310 80°C, 6 h, 60% → 25

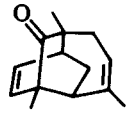

75 (208)

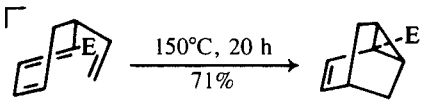

311 150°C, 20 h, 71% (210)

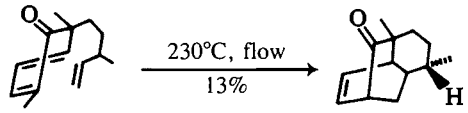

312 230°C, flow, 13% (209)

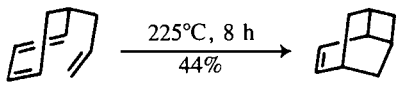

313 225°C, 8 h, 44% (211)

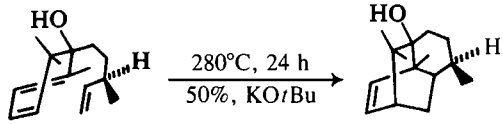

314 280°C, 24 h, 50%, KO*t*Bu (215)

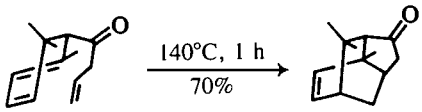

315 140°C, 1 h, 70% (212)

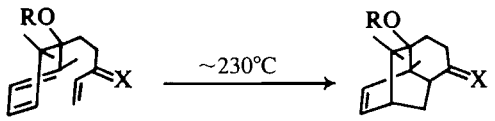

316 R = H, X = H_2
317 R = $SiMe_3$, X = O 230°C, 12 h, 76% (215)

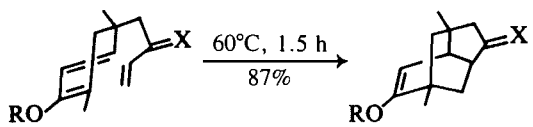

318 R = Me, X = O (204)

319 R = $SiMe_3$, X = 160°C, 0.5 h, 100% (205)

320 R = $P(OEt)_2$, X = 140°C, 4.5 h, 99% (206)

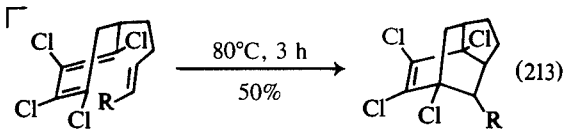

321 R = H
322 R = Me 80°C, 3 h, 48%

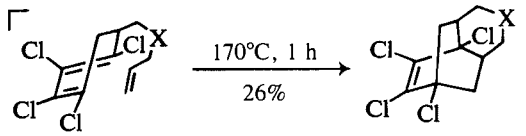

323 X = CH_2
324 X = O 170°C, 1 h, 65%
325 X = S 170°C, 3 h, 66%
326 X = NAc 170°C, 0.5 h, 59%
327 X = CH_2CN 170°C, 0.2 h, 75%

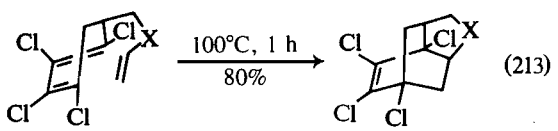

328 X = O
329 X = S 150°C, 0.2 h, 75%

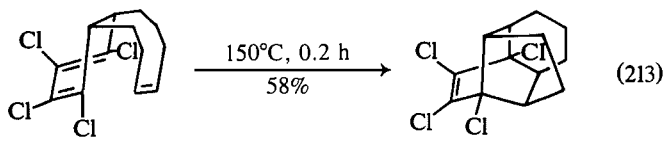

330

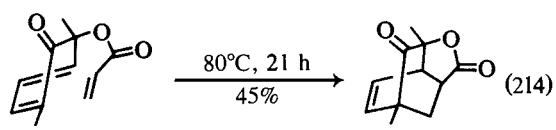

331

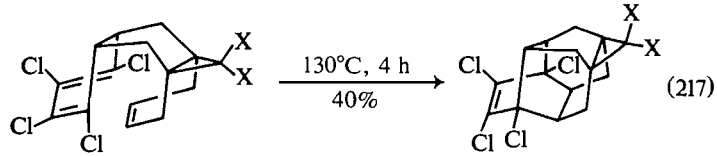

333 X = Cl
334 X = Br 130°C, 4 h, 50%

Can. J. Chem. Downloaded from www.nrcresearchpress.com by 210.87.254.6 on 09/06/12
For personal use only.

TABLE 6(*a*). (*Continued*)

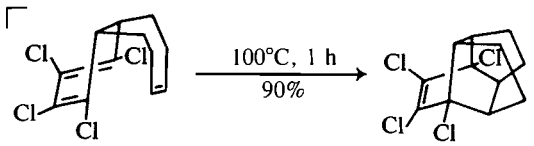

(213)

332

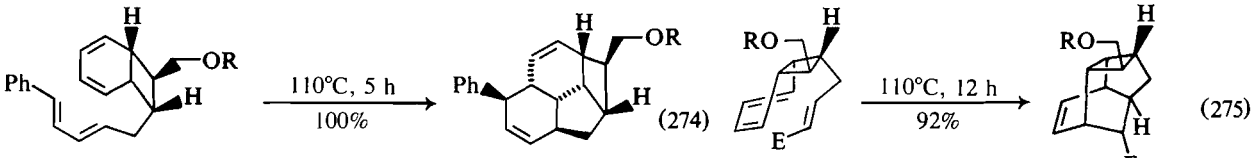

(274) (275)

335 R = Si*t*BuPh$_2$ **336** R = Si*t*BuPh$_2$

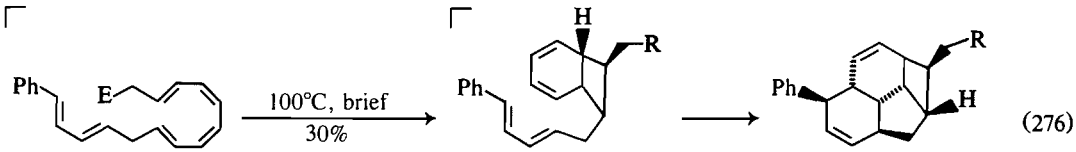

(276)

337 R = E; R = E **A** R = E; **B** R = E

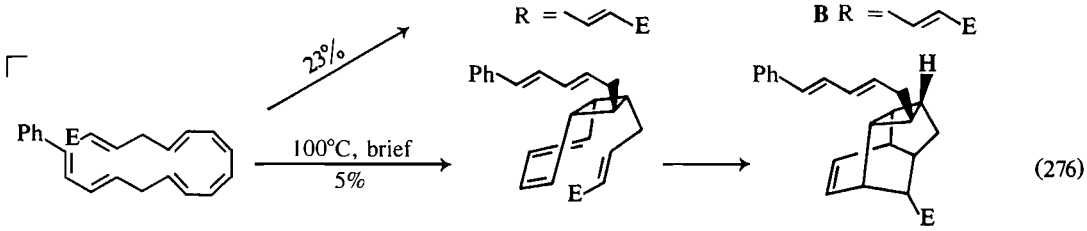

(276)

338 **C**

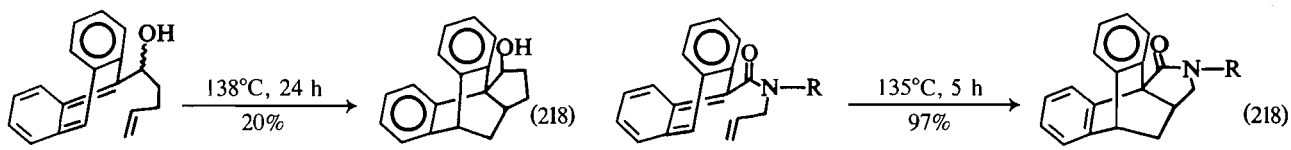

(218) (218)

339 **340** R = H; **341** R = Me 125°C, 1 h, 77%

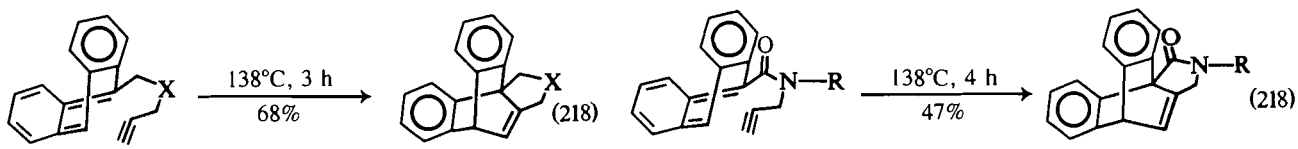

(218) (218)

342 X = O; **343** X = S 138°C, 3 h, 74% **344** R = H; **345** R = Me 111°C, 4 h, 70%

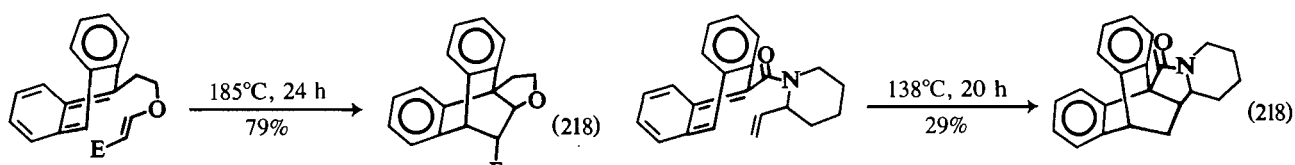

(218) (218)

346 **347**

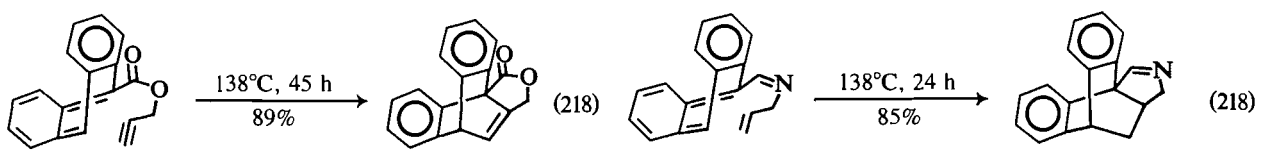

(218) (218)

348 **350**

Can. J. Chem. Downloaded from www.nrcresearchpress.com by 210.87.254.6 on 09/06/12
For personal use only.

TABLE 6(*a*). (*Continued*)

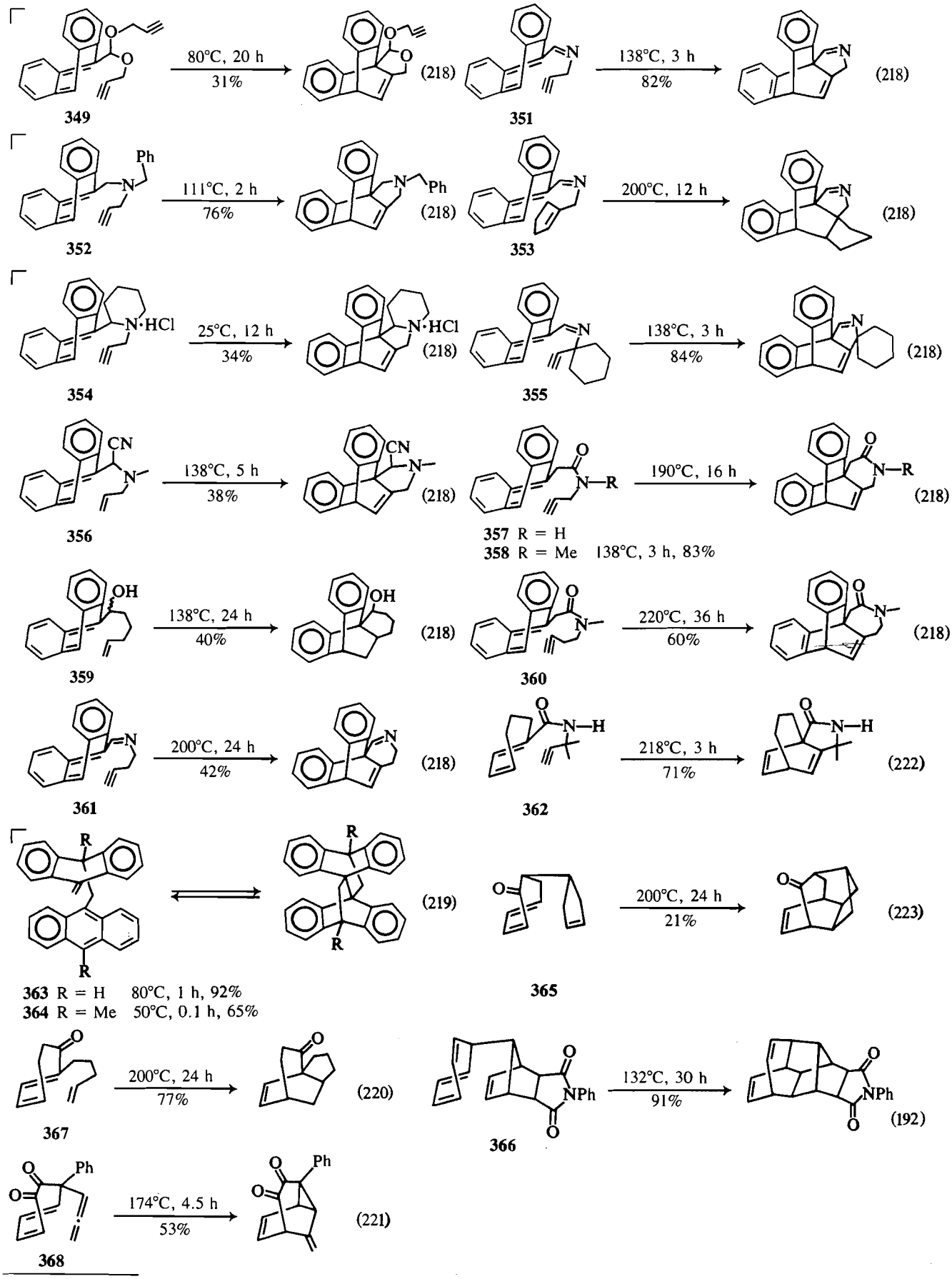

349 **351** **352** **353** **354** **355** **356**

357 R = H
358 R = Me 138°C, 3 h, 83%

359 **360** **361** **362**

363 R = H 80°C, 1 h, 92%
364 R = Me 50°C, 0.1 h, 65%

365 **366** **367** **368**

Can. J. Chem. Downloaded from www.nrcresearchpress.com by 210.87.254.6 on 09/06/12
For personal use only.

TABLE 6(*a*). (*Continued*)

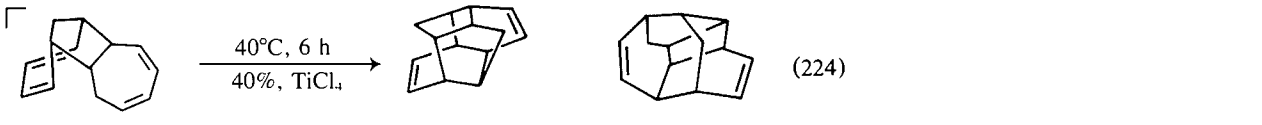

369 10 90 (224)

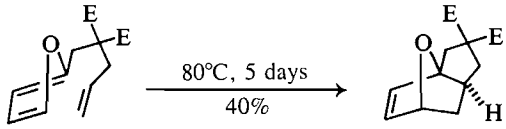

370 E = CO_2Et (225)

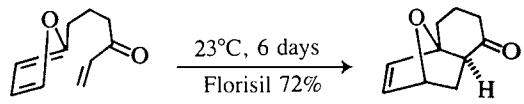

371 (230)

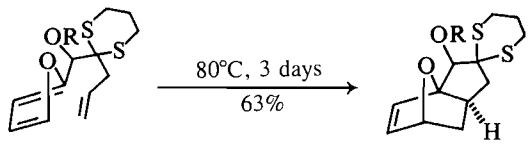

R = H
372 R = H 80°C, $EtOH/H_2O$ 5:2; 93%
R = H 89°C, 6 h, H_2O, β-cyclodextrin, 91% (227)
373 R = COPh 80°C, 14 days, 62%
(226)

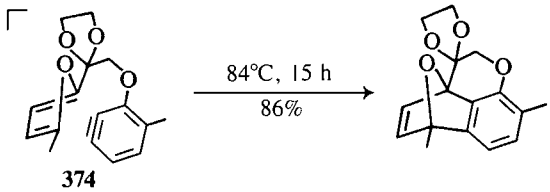

374 (231)

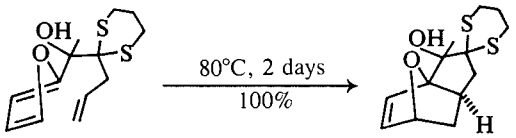

375 (226)

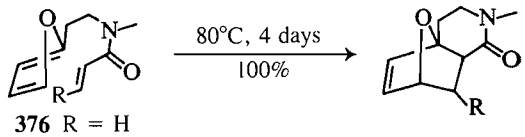

376 R = H
377 R = Me 80°C, 6 days, 12%
(225)

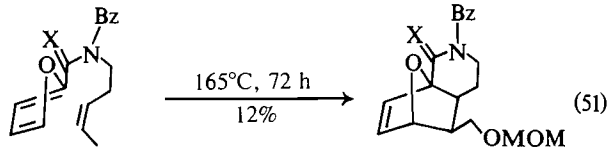

$MOMOCH_2$
379 X = O
380 X = H_2 135°C, 72 h, 10%
(51)

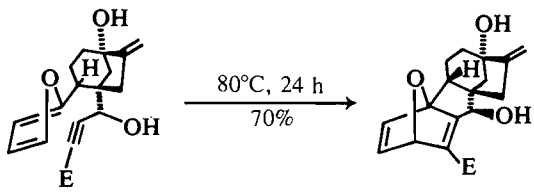

381 E = CO_2Et 80°C, 160 h, 70% 25 50

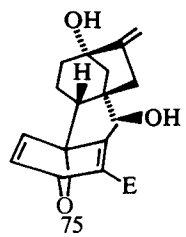

75 50 (232)

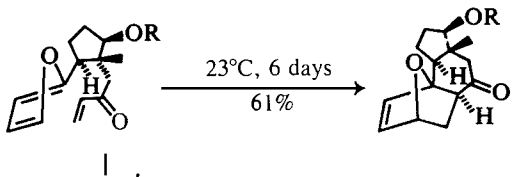

R = Si 12

382 R = Si 80°C, 6 days, 50% 90

383 R = H H_2O, 23°C, 0.5 h, >80% 0

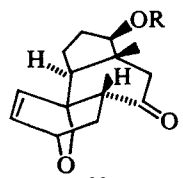

88 10 100 (233) (234)

Can. J. Chem. Downloaded from www.nrcresearchpress.com by 210.87.254.6 on 09/06/12
For personal use only.

TABLE 6(*a*). (*Continued*)

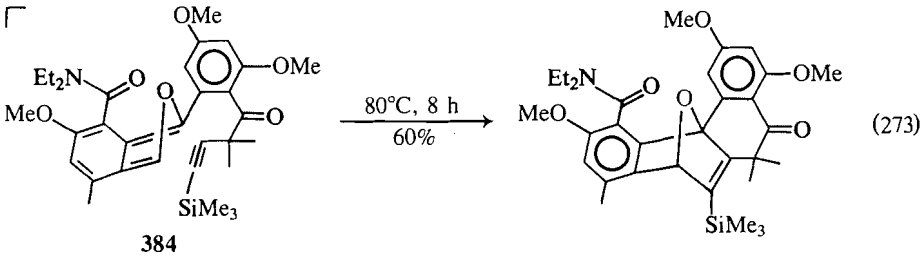

(273)

384

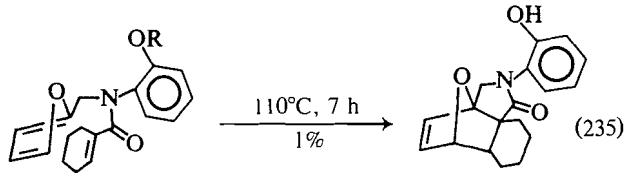

(235)

385 R = H
386 R = MgCl 110°C, 14 h, 41%

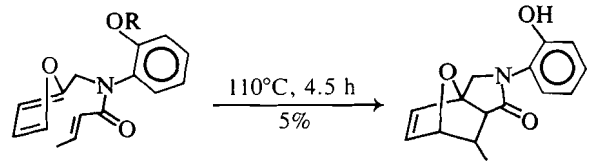

(236)

387 R = H
388 R = MgCl 110°C, 4.5 h, 63%
389 R = MgBr 110°C, 4.5 h, 53%
390 R = MgI 110°C, 4.5 h, 46%

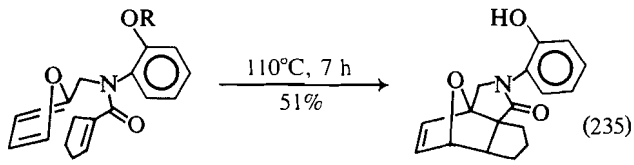

(235)

391 R = H
392 R = MgBr 110°C, 1 h, 85%

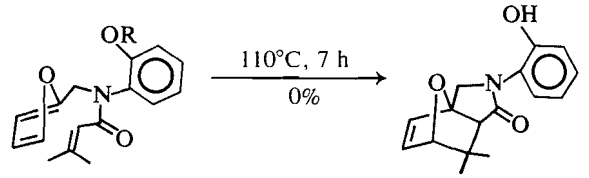

(237)

393 R = H
394 R = MgBr 110°C, 7 h, 76%

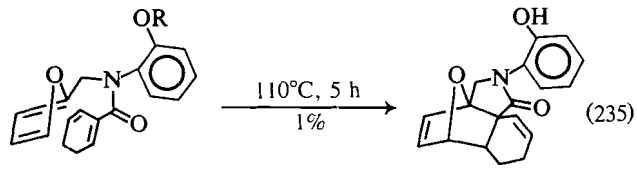

(235)

395 R = H
395 R = MgBr 110°C, 5 h, 75%

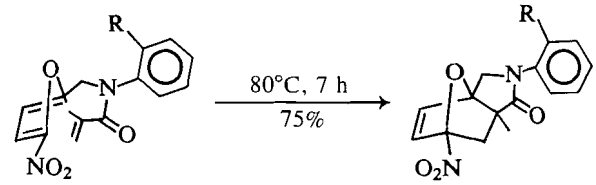

(238)

396 R = OH
397 R = OMgBr 80°C, 7 h, 57%
110°C, 7 h, 94%

398 R = H 80°C, 7 h, 30%
399 R = OMe 80°C, 7 h, 11%

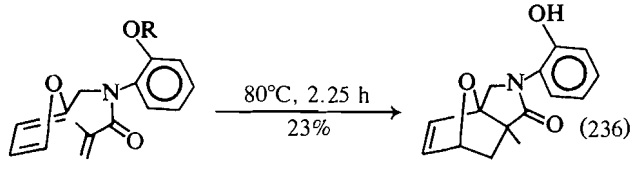

(236)

400 R = H
401 R = Li 80°C, 2.25 h, 45%
402 R = Na 80°C, 2.25 h, 29%
403 R = K 80°C, 2.25 h, 40%
404 R = MgCl 80°C, 2.25 h, 79%
405 R = MgBr 80°C, 2.25 h, 90%
406 R = MgI 80°C, 2.25 h, 95%
407 R = Mg 80°C, 2.25 h, 80%
408 R = Zn 80°C, 2.25 h, 55%

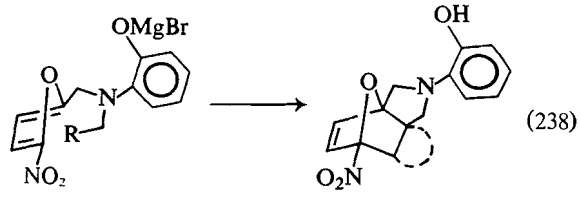

(238)

409 R = C=CH2 110°C, 9 h, 93%
410 R = C=C< 110°C, 9 h, 73%
411 R = 110°C, 7 h, 96%
412 R = 110°C, 9 h, 30%

Can. J. Chem. Downloaded from www.nrcresearchpress.com by 210.87.254.6 on 09/06/12
For personal use only.

TABLE 6(*a*). (*Continued*)

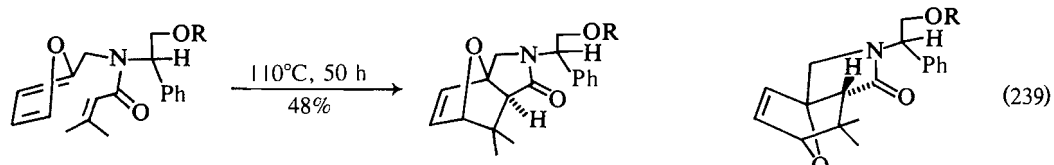

413 R = H		50	50
414 R = MgCl	110°C, 7 h, 86%	86	14
415 R = MgBr	110°C, 7 h, 77%	88	12
416 R = MgI	110°C, 7 h, 72%	81	19

(239)

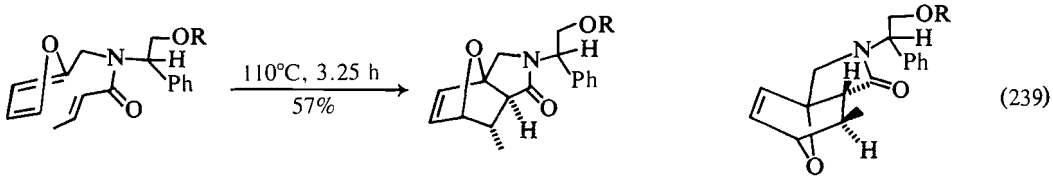

417 R = H		57	43
418 R = MgCl	110°C, 3.25 h, 82%	83	17

(239)

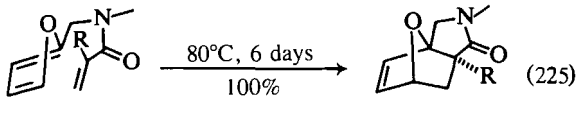

419 R = H
420 R = Me 80°C, 5 days, 100%

(225)

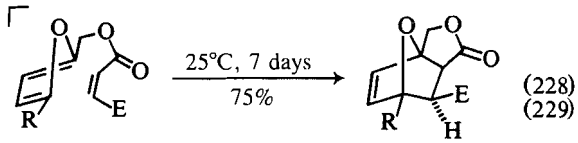

421 R = H, E = CO_2H
422 R = Me, E = CO_2H 25°C, 7 days, 70%

(228)
(229)

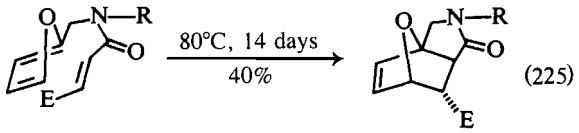

423 E = R = Me
424 R = Ph 23°C, 48 h, 100% (266)

(225)

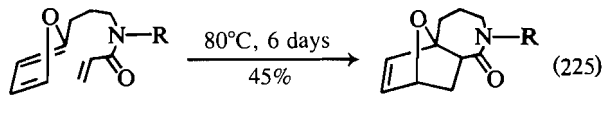

426 R = Me
427 R = Bz 80°C, 6 days, 75%

(225)

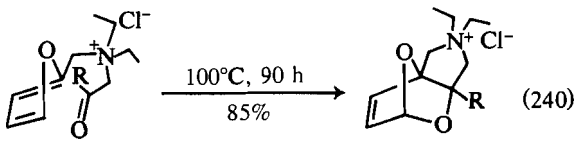

428 R = OMe

(240)

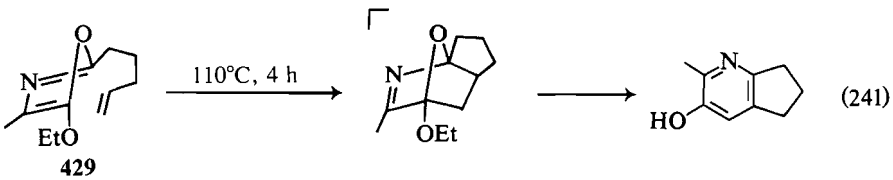

429

(241)

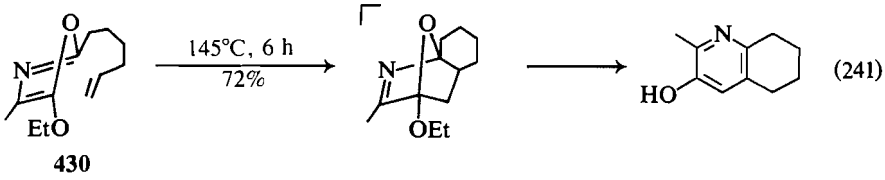

430

(241)

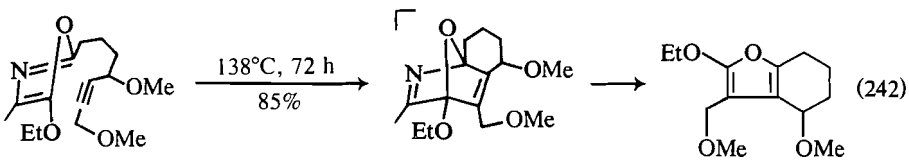

431

(242)

Can. J. Chem. Downloaded from www.nrcresearchpress.com by 210.87.254.6 on 09/06/12
For personal use only.

TABLE 6(*a*). (*Continued*)

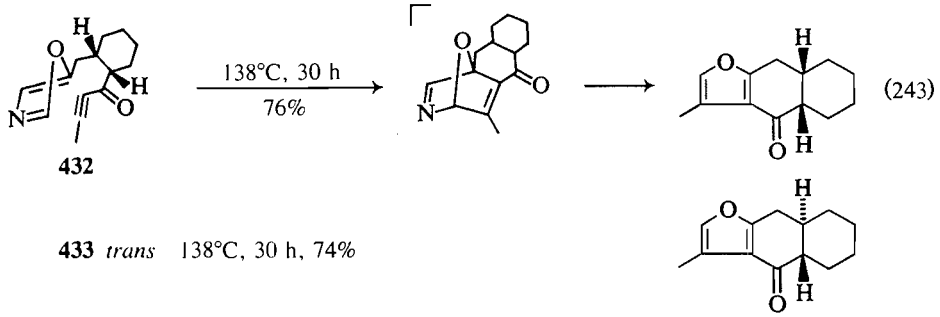

432

433 *trans* 138°C, 30 h, 74%

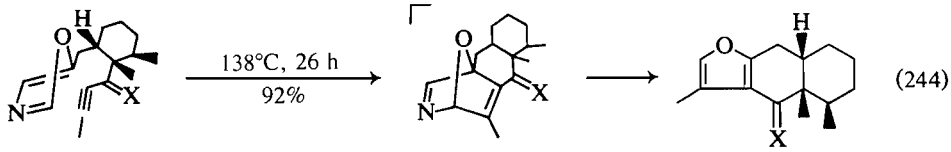

434 X = O

435 X = OH, H 138°C, 84%

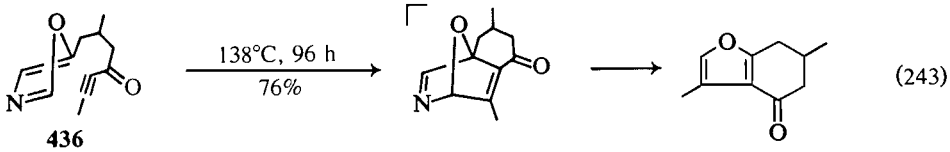

436

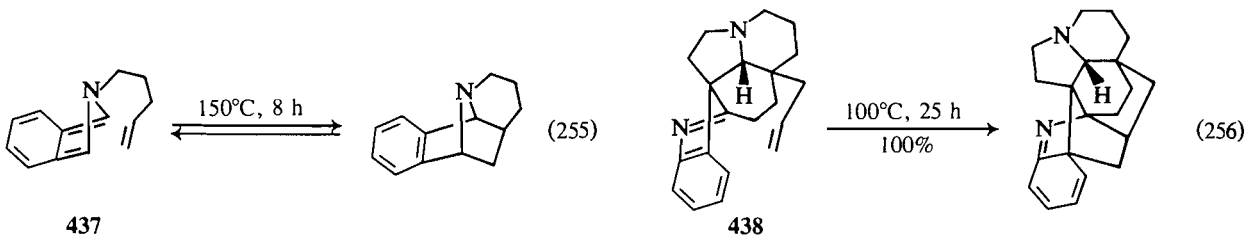

437 **438**

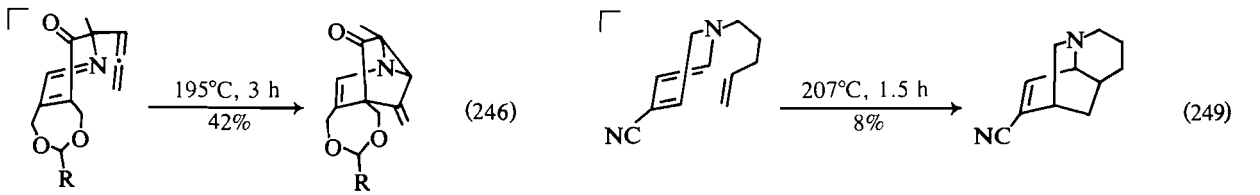

439 R = iPr

440 R = Me, Me 190°C, 10 h, 35%

441

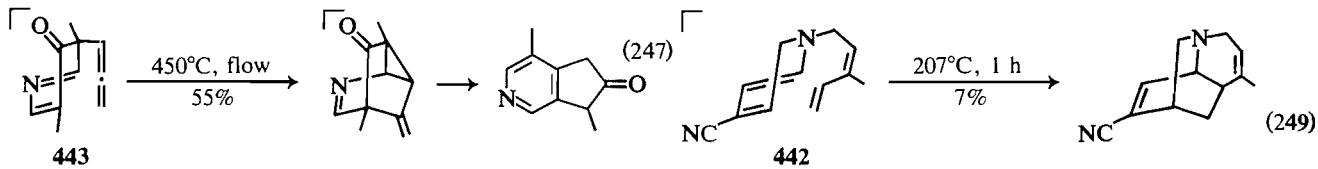

443 **442**

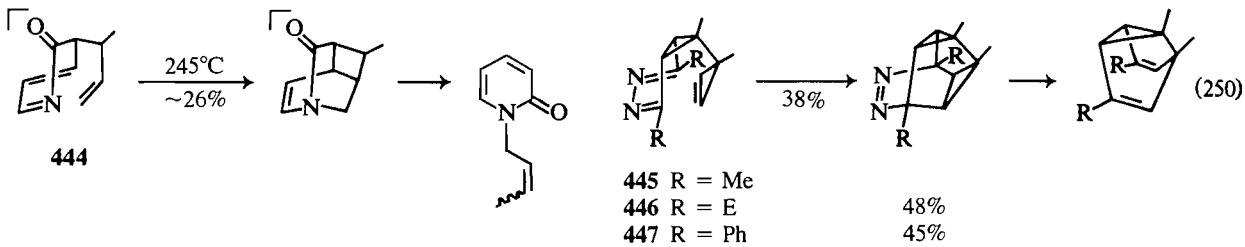

444

445 R = Me

446 R = E 48%

447 R = Ph 45%

Can. J. Chem. Downloaded from www.nrcresearchpress.com by 210.87.254.6 on 09/06/12
For personal use only.

TABLE 6(*a*). (*Continued*)

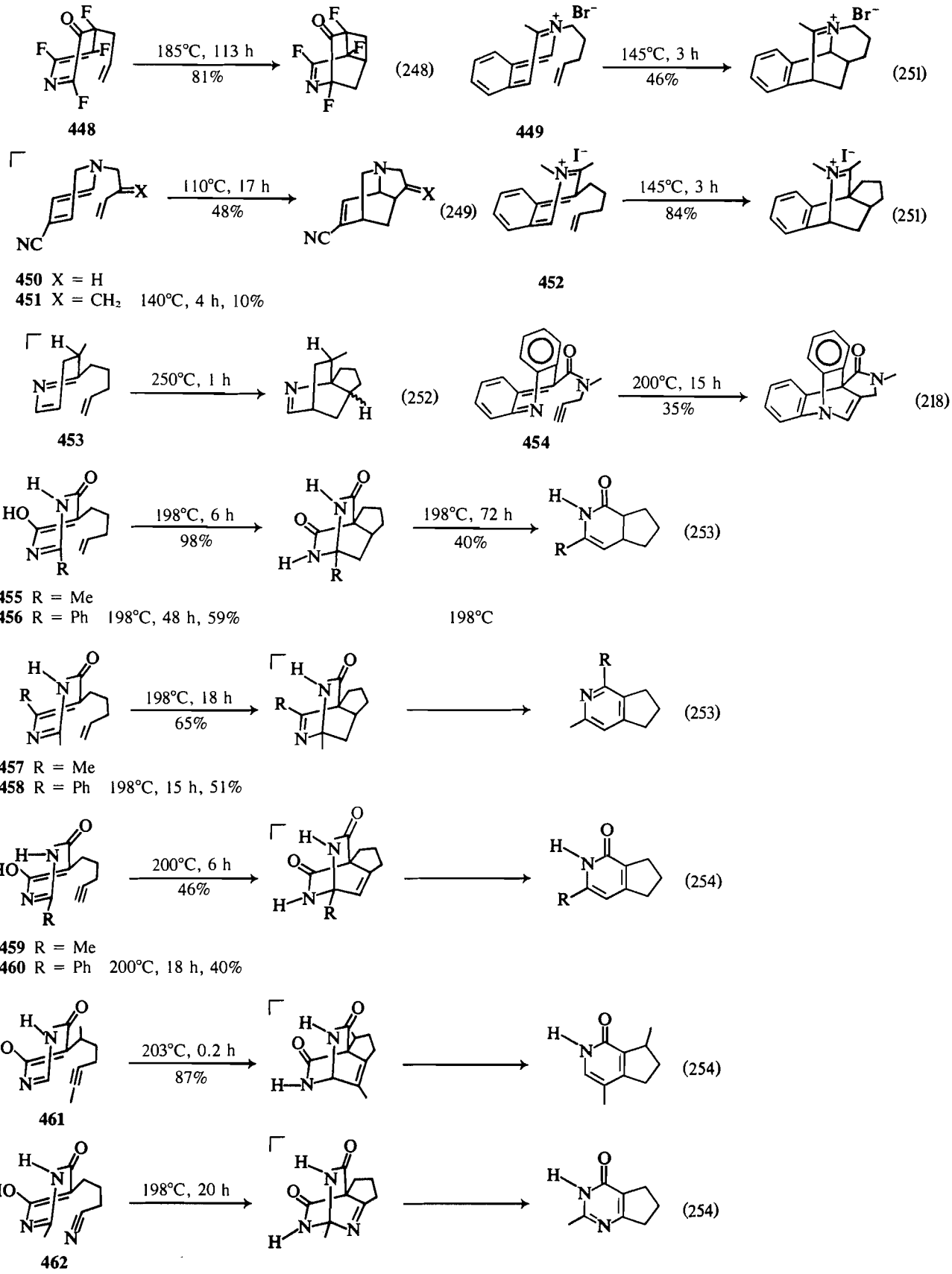

448

449

450 X = H
451 X = CH_2 140°C, 4 h, 10%

452

453

454

455 R = Me
456 R = Ph 198°C, 48 h, 59%

198°C

457 R = Me
458 R = Ph 198°C, 15 h, 51%

459 R = Me
460 R = Ph 200°C, 18 h, 40%

461

462

Can. J. Chem. Downloaded from www.nrcresearchpress.com by 210.87.254.6 on 09/06/12
For personal use only.

TABLE 6(*a*). (*Continued*)

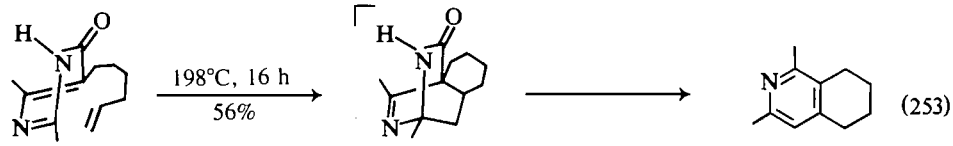

463

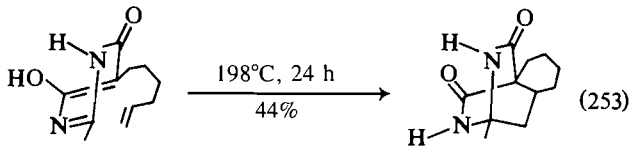

464

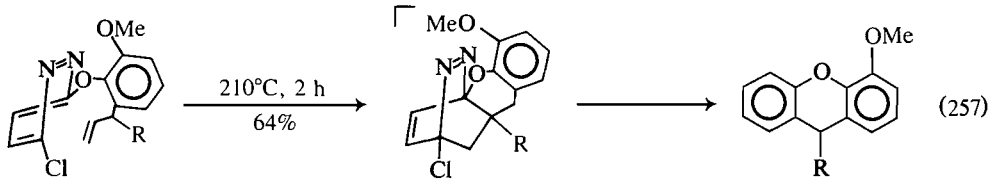

465 R = H
466 R = Me 210°C, 3.5 h, 100%

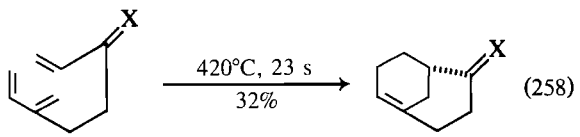

467 X = H_2
468 X = CH_2 400°C, 7 s, 10% (259)
469 X = O 395°C, 18 s, 72% (258)

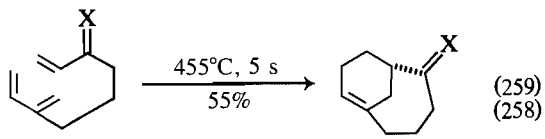

470 X = H_2
471 X = O 398°C, 8 s, 85%
201°C, 0.25 h, 57%

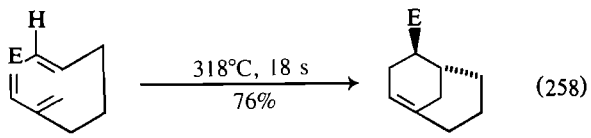

472

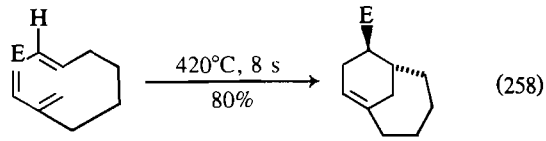

473 E = CO_2Et 206°C, 2 h, 91%

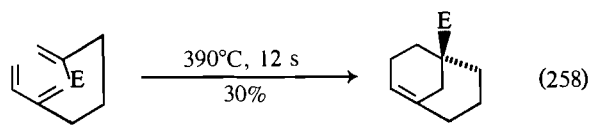

474 E = CO_2Et

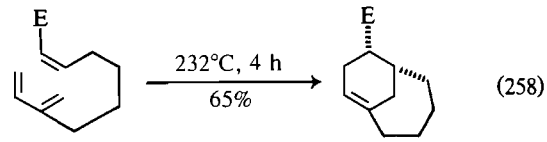

475 E = CO_2Et

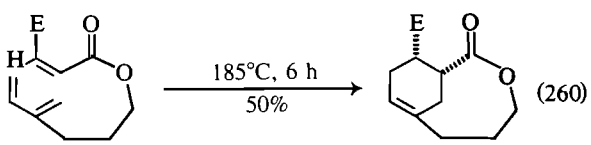

476

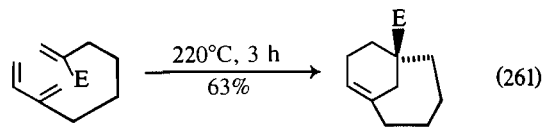

477 E = CO_2Et

Can. J. Chem. Downloaded from www.nrcresearchpress.com by 210.87.254.6 on 09/06/12
For personal use only.

TABLE 6(*a*). (*Concluded*)

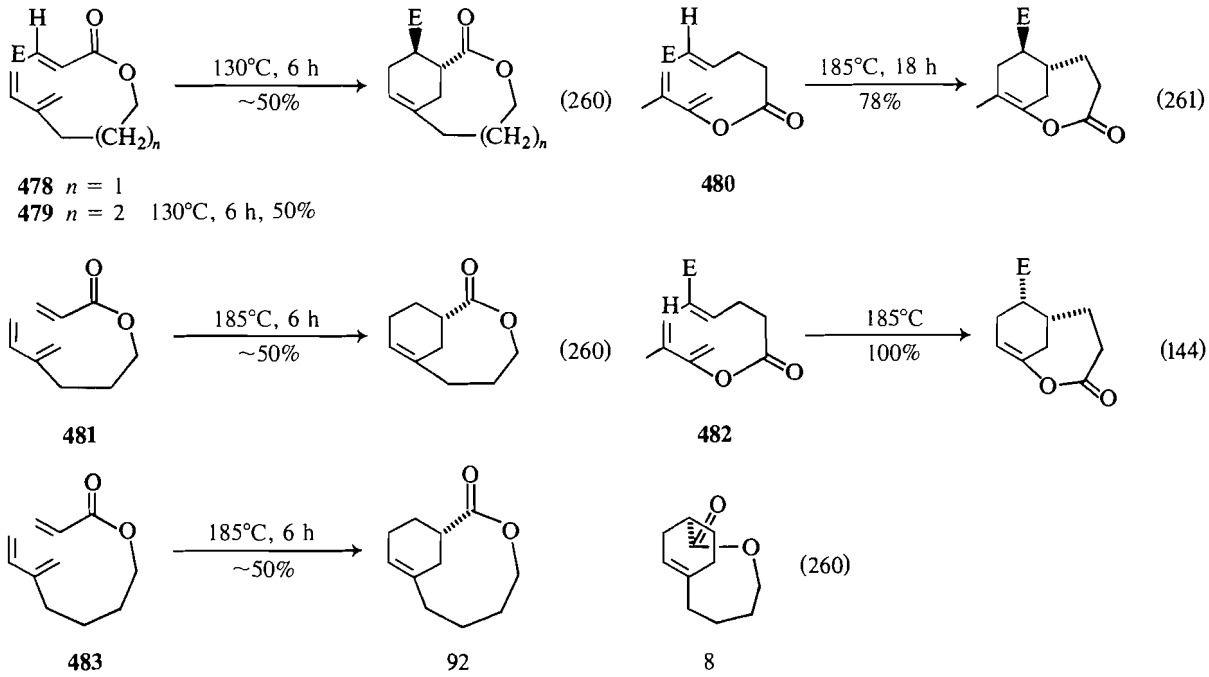

tems. If closely related successful and unsuccessful cases were calculated and compared, it might improve our understanding and provide a better predictive basis for future work. A partial step in this direction has been taken by Wilson and Huffman (101) using the data base available in the Cambridge Crystallographic Data File.

Synthetic strategy

To date, most applications of the intramolecular Diels–Alder reaction to total synthesis have involved construction of a bi- or tricyclic ring system which may be readily discerned by retro-synthetic inspection of the natural product. Many examples are apparent upon comparison of the tables and related synthetic targets depicted above. In some cases, as mentioned, these follow a possible biomimetic route, for although an internal cycloaddition has been suggested for the biosynthesis of a variety of natural products, in most cases rigorous proof is lacking. Nevertheless, increasing circumstantial evidence is provided by a number of laboratory cyclizations under mild conditions to give the natural ring systems. An example of the caution required is provided by a recent synthesis of a stabilized dehydrosecodine which failed to undergo the anticipated intramolecular cycloaddition(s) to the alkaloid skeleton(s) (267) even though other evidence suggests some Aspidosperma and Iboga skeletons may be formed in this way (68–70, 113, 269). Additional natural products for which an internal [4 + 2] cyclization has been implicated include ikarugamycin (82), X-14547A (26), iricinianin (268), cyclostachines, cyclopiperstachine (95), carpanone (181), lachananthocarpone (269), endiandric acid (270), morellin (271), gambogic acid (272), some other lignans (277), and possibly also the Aspergillus metabolite andibenin B (278).

In the hierarchy of synthesis, schemes which are short (efficient), chiral, stereocontrolled, and proceed under mild (neutral) conditions are particularly desirable. Frequently the intramolecular Diels–Alder approach fulfills these requirements for cyclohexenes, as noted, but its application need not be limited to six membered rings since ring expansion, contraction, and cleavage sequences facilitate the construction of many different skeletons. Indeed, the wide range of complex functionality that is compatible with this cycloaddition suggests that this strategy can often be used to best advantage when the adduct constructed is not part of the final target. Several examples illustrate these features. Rearrangement of suitable intermediates was used for seychellene (208) and khusimone (199), while ring expansion of the Diels–Alder adducts afforded the required skeletons for cedrene, cedrol (186), and sativene (190). Cleavage of the cyclized intermediate for subsequent elaboraion is important in the preparation of sinularene (196), mansone E (231), resistomycin (273), farnesiferol C (239), karahana ether (237), and in approaches to gibberellic acid (232), longifolene (197), and capnellene (195). Useful variations on this cyclization–cleavage approach are those schemes in which extra rings are attached to the modified (cleaved) adduct, frequently by annulation, base catalyzed condensation, addition, or rearrangement reactions. Total syntheses of gibberellic acid (85), oxygenated steroids (86, 87), dodecahedrane (193), and approaches to gascardic acid (187), klaineanone (160), and grayanotoxin I (172) fall in this general category. Given the current level of chemical ingenuity, the array of reagents available, and the range of complex targets that warrant attention, it is likely that many more sophisticated schemes whose net result is a synthetic simplification will continue to be reported. Indeed, if a molecule is worth synthesizing, an intramolecular Diels–Alder approach is worth considering.

NOTE: The following refer to intramolecular Diels–Alder papers which arrived after November 1, 1982. Allenecarboxanilides (279); see example **14** (280); see cases **145–148** (281); heterodienophiles review (282); intra-

Can. J. Chem. Downloaded from www.nrcresearchpress.com by 210.87.254.6 on 09/06/12
For personal use only.

TABLE 6(*b*). Synthetic targets

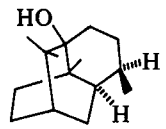

Patchouli alcohol

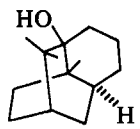

Norpatchoulenol

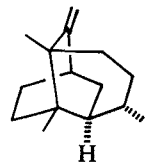

Seychellene

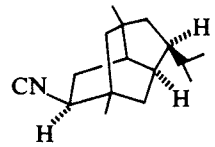

9-Isocyanopupukeanane

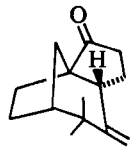

Khusimone

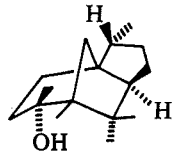

Cedrol

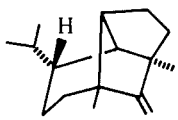

Sativene

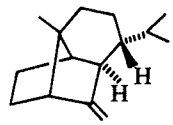

≡

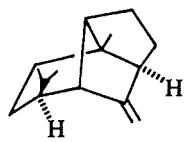

Sinularene

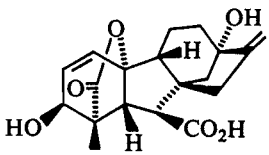

Gibberellic acid

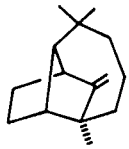

Longifolene

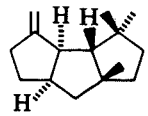

Capnellene

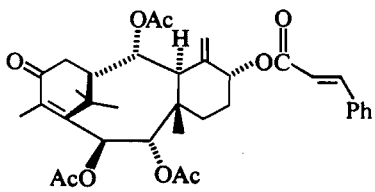

Taxusin

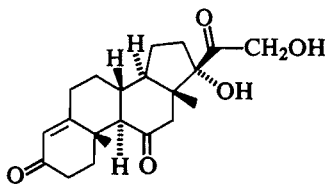

Cortisone

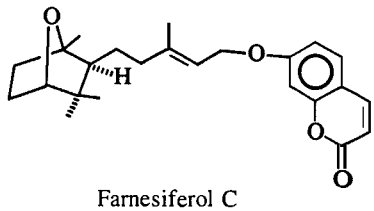

Farnesiferol C

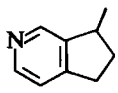

Actinidine

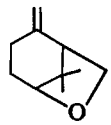

Karahana ether

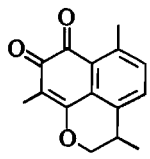

Mansone E

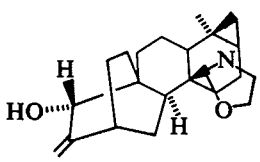

Atisine

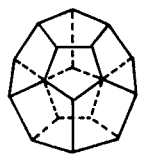

Dodecahedrane

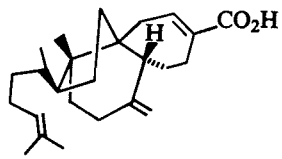

Gascardic acid

Can. J. Chem. Downloaded from www.nrcresearchpress.com by 210.87.254.6 on 09/06/12
For personal use only.

TABLE 6(*b*). (*Concluded*)

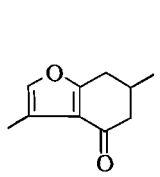

Evodone

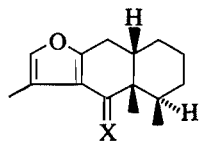

X = O Ligularone

Petasalbine

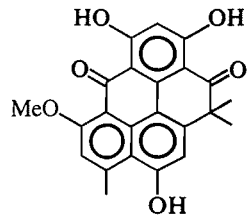

Resistomycin

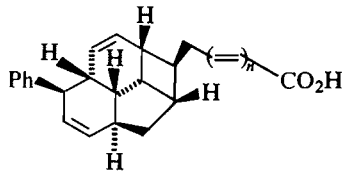

Endiandric acid A (*n* = 0)

Endiandric acid B (*n* = 1)

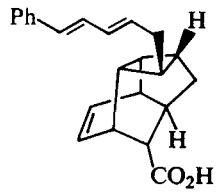

Endiandric acid C

TABLE 7. Troublesome trienes

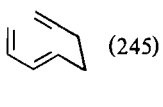

(245)

484

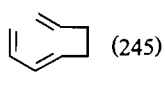

(245)

485

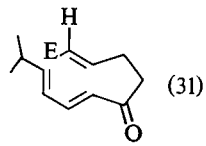

(31)

486

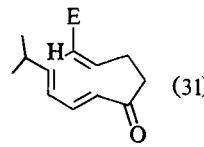

(31)

487

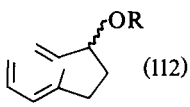

(112)

488

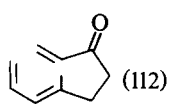

(112)

489

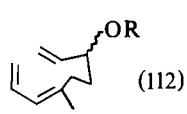

(112)

490

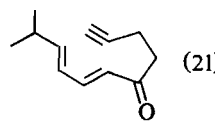

(21)

491

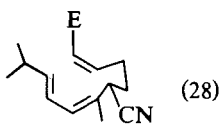

(28)

*__492__

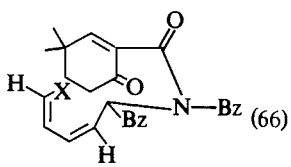

(66)

489

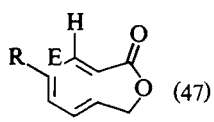

(47)

R = H, CH_3

494

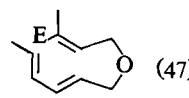

(47)

E = CO_2H

495

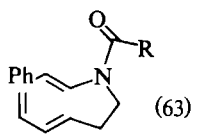

(63)

R = OMe, Me, CCl_3

496

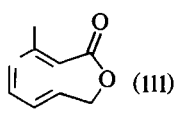

(111)

497

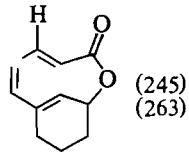

(245)
(263)

498

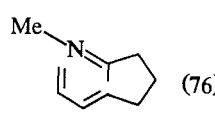

(76)

499

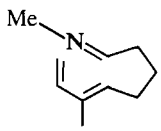

(76)

500

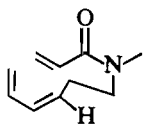

(51)
(116)

*__501__

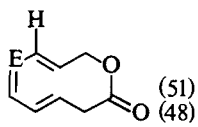

(51)
(48)

502 E = H
*__503__ E = CO_2Et

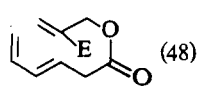

(48)

*__504__

Can. J. Chem. Downloaded from www.nrcresearchpress.com by 210.87.254.6 on 09/06/12
For personal use only.

TABLE 7. (*Continued*)

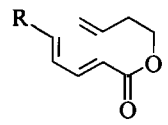
(51)
(262)

R = Me, $CO_2(CH_2)_2CH{=}CH_2$

505

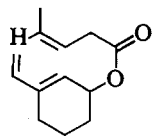
(263)

506

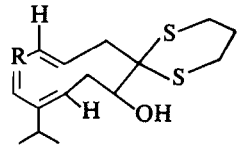
(89)

R = H, Me

507

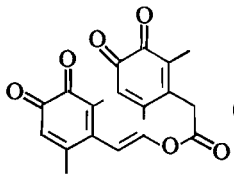
(264)

508

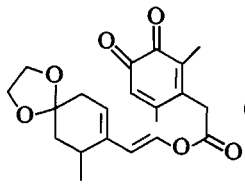
(146)

509

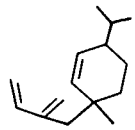
(245)

510

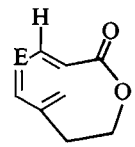
(144)

511

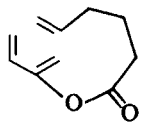
(110)

512

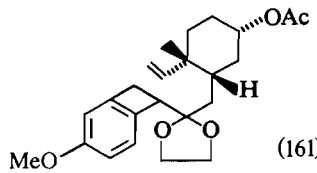
(161)

513

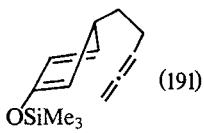
(191)

514

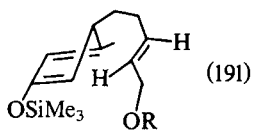
(191)

515

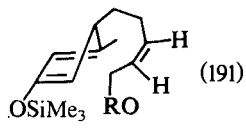
(191)

516

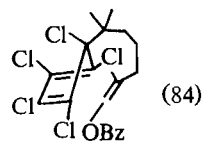
(84)

517

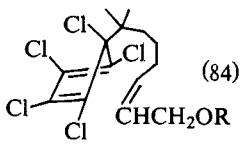
(84)

R = H, Me, Ac, Bz

518

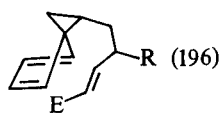
(196)

R = H, iPr

519

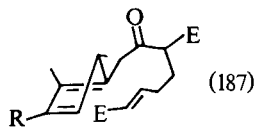
(187)

R = $CHMe(CH_2)_2CH{=}CMe_2$

520

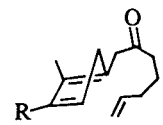
(187)

R = $CHMe(CH_2)_2CH{=}CMe_2$

*521

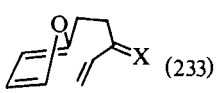
(233)

X = O, H, OH

522

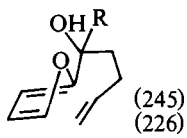
(245)
(226)

R = H, Me

523

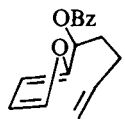
(226)

524

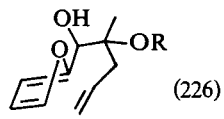
(226)

R = H, Bz

525

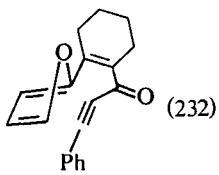
(232)

526

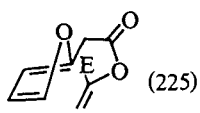
(225)

E = CO_2Et, H

527

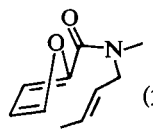
(225)

528

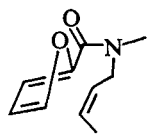
(225)

529

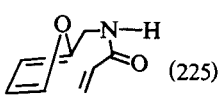
(225)

530

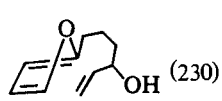
(230)

531

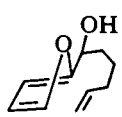
(245)

532

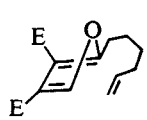
(241)

533

Can. J. Chem. Downloaded from www.nrcresearchpress.com by 210.87.254.6 on 09/06/12
For personal use only.

TABLE 7. (*Concluded*)

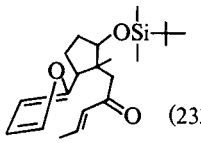
(233)

534

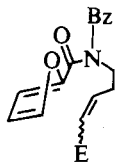
(51)

535

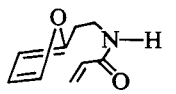
(225)

536

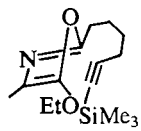
(241)

537

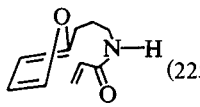
(225)

538

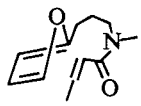
(225)

539

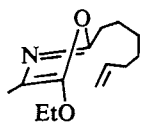
(241)

540

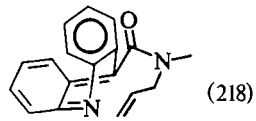
(218)

541

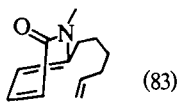
(83)

542

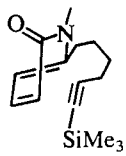
(83)

543

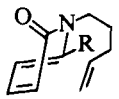
(83)

R = H, Me

544

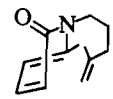
(241)

545

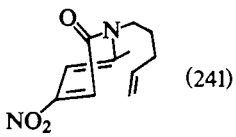
(241)

546

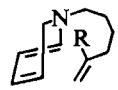
(252)

R = H, E

*547

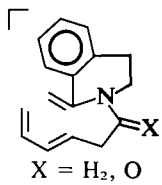

X = H_2, O

548

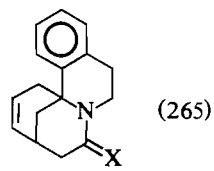
(265)

549

Can. J. Chem. Downloaded from www.nrcresearchpress.com by 210.87.254.6 on 09/06/12
For personal use only.

molecular [6 + 4] cycloadditions (283); 3-acetoxyisotwist-8-en-2-ones (284); epilupinine synthesis (285); C/D *trans*-hydrindan ring system (286); isoatisirene skeleton (287); androstan-2,17-dione synthesis (288); *o*-xylylenes (289, 290); intramolecular retro-Diels–Alder (291); *o*-quinodimethanes (292); inverse electron demand (293); bridgehead alkenes (294); ref. 295; 8-azobicyclo[4.3.0]non-4-en-7-ones (296); silicon-substituted dienes (297); quassinoid attempt (298); eupolauramine total synthesis, see **200** (299); *o*-quinodimethane cyclizations (300); kopsanone synthesis (301); cytochalasan approach (302); quadrone synthesis (303); 5-hydroxy-4-pyrone systems (304); sclerosporin synthesis (305); silyl dienes (306); phenylbenzo[*g*] indolinone (307); C-aromatic taxane (308); X-14547A synthesis (309); chelidonine synthesis (310); furan example (311); ref. 312; *N*-sulfinylimides, sphingosine synthesis (313); quassin approach (314); iceane derivatives (315); indole-2,3-quinodimethanes (316); 1-12b-didehydrolycorane synthesis (317); *cis*-decahydroquinolines (318); 11-keto-steroids (319); triptycenes (320); cytochalasin B synthesis (321); transition metal catalysts (322); mevinolin approach (323); cyclopentadienes (324); cedranediol synthesis (325); *trans*-decalins (326); bruceantin model (327); dihydropyridine cage system (328); cycloheptatriene–allene system (329); polycyclic systems (330); azadienes review (331).

Acknowledgements

I thank Mrs. K. Stewart and Ms. T. Barker for their typing and Mrs. C. Chen for transforming my hieroglyphics into lucid structures. I am particularly indebted to chemists around the world who generously supplied information on their Diels–Alder research, including their "troublesome trienes". Fruitful discussions with my colleagues and frequent collaborators Professors S. J. Alward and J. F. Kingston facilitated the preparation of this manuscript and we are grateful to Memorial University of Newfoundland and the Natural Sciences and Engineering Research Council of Canada for financial support of our research. It is also a pleasure to acknowledge the assistance of our co-workers W. L. Brown, R. R. Bukownik, J. Hellou, R. S. Smith, Drs. K. Antczak, and S. K. Attah-Poku whose skill and dedication are bringing our ideas to fruition.

1. N. ANAND, J. S. BINDRA, and S. RANGANATHAN. Art in organic synthesis. Holden-Day Inc., San Francisco. 1970. p. 377.
2. R. G. CARLSON. Ann. Rep. Med. Chem. **9**, 270 (1974).
3. G. MEHTA. J. Chem. Educ. **53**, 551 (1976).
4. W. OPPOLZER. Angew. Chem. Int. Ed. Engl. **16**, 10 (1977).
5. G. BRIEGER and J. N. BENNETT. Chem. Rev. **80**, 63 (1980).
6. E. CIGANEK. Org. React. In press.
7. D. F. TABER. Intramolecular Diels–Alder reactions and Alder ene reactions. Springer Verlag, New York. 1984. In press.
8. L. A. PAQUETTE. Asymmetric cycloaddition reactions. *In* Asymmetric synthesis. Vol. 3. *Edited by* J. E. Morrison. Academic Press, New York. In press.
9. K. ALDER and M. SCHUMAKER. Fortschr. Chem. Org. Naturst. **10**, 66 (1953).
10. D. J. CRAM and G. R. KNOX. J. Am. Chem. Soc. **83**, 2204 (1961); D. J. CRAM, C. S. MONTGOMERY, and G. R. KNOX. J. Am. Chem. Soc. **88**, 515 (1966).
11. E. T. MCBEE, J. O. STOFFER, and H. P. BRAENDIN. J. Am. Chem. Soc. **84**, 4540 (1962).
12. H. H. WASSERMAN and A. R. DOUXAUX, JR. J. Am. Chem. Soc. **84**, 4611 (1962); H. H. WASSERMAN, A. R. DOUXAUX,

Can. J. Chem. Downloaded from www.nrcresearchpress.com by 210.87.254.6 on 09/06/12
For personal use only.

JR., and R. E. DAVIS. J. Am. Chem. Soc. **88**, 4517 (1966).
13. D. BILOVIC, Z. STROJANAC, and V. HAHN. Tetrahedron Lett. 2071 (1964).
14. L. H. KLEMM and K. W. GOPINATH. Tetrahedron Lett. 1243 (1963); L. H. KLEMM, K. W. GOPINATH, D. HSU LEE, F. W. KELLY, E. TROD, and T. M. MCGUIRE. Tetrahedron, **22**, 1797 (1966).
15. G. BRIEGER. J. Am. Chem. Soc. **85**, 3783 (1963).
16. H. O. HOUSE and T. CRONIN. J. Org. Chem. **30**, 1061 (1965).
17. A. A. KRANTZ. Ph.D. Thesis, Yale University, 1967.
18. W. OPPOLZER. J. Am. Chem. Soc. **93**, 3833 (1971); **93**, 3834 (1971).
19. W. OPPOLZER and K. KELLER. J. Am. Chem. Soc. **93**, 3836 (1971).
20. W. R. ROUSH, H. R. GILLIS, and A. I. KO. J. Am. Chem. Soc. **104**, 2269 (1982).
21. H. R. GILLIS, JR. Ph.D. Thesis, Mass. Inst. of Technology, 1982.
22. W. R. ROUSH. J. Org. Chem. **44**, 4008 (1979).
23. W. R. ROUSH. J. Am. Chem. Soc. **102**, 1390 (1980).
24. K. C. NICOLAOU and R. L. MAGOLDA. J. Org. Chem. **46**, 1506 (1981).
25. M. P. EDWARDS, S. V. LEY, and S. G. LISTER. Tetrahedron Lett. **22**, 361 (1981).
26. W. R. ROUSH and A. G. MYERS. J. Org. Chem. **46**, 1509 (1981).
27. W. R. ROUSH. Personal communication.
28. R. F. BORCH, A. J. EVANS, and J. J. WADE. J. Am. Chem. Soc. **99**, 1612 (1977).
29. W. R. ROUSH and H. R. GILLIS. J. Org. Chem. **45**, 4238 (1980).
30. W. R. ROUSH, A. I. KO, and H. R. GILLIS. J. Org. Chem. **45**, 4264 (1980).
31. W. R. ROUSH and S. M. PESECKIS. J. Am. Chem. Soc. **103**, 6696 (1981).
32. K. A. PARKER and T. IQBAL. J. Org. Chem. **47**, 337 (1982).
33. S. A. BAL and P. HELQUIST. Tetrahedron Lett. **22**, 3933 (1981).
34. D. F. TABER, C. CAMPBELL, B. P. GUNN, and I. C. CHIU. Tetrahedron Lett. **22**, 5141 (1981).
35. A. ICHIHARA, R. KIMURA, S. YAMADA, and S. SAKAMURA. J. Am. Chem. Soc. **102**, 6353 (1980).
36. M. E. JUNG and K. M. HALWEG. Tetrahedron Lett. **22**, 2735 (1981).
37. J. J. S. BAJOREK and J. K. SUTHERLAND. J. Chem. Soc. Perkin Trans. 1, 1559 (1975).
38. M. E. JUNG and K. M. HALWEG. Tetrahedron Lett. **22**, 3929 (1981).
39. R. K. BOECKMAN, JR. and S. S. KO. J. Am. Chem. Soc. **102**, 7146 (1980).
40. R. K. BOECKMAN, JR. and S. S. KO. J. Am. Chem. Soc. **104**, 1033 (1982).
41. R. K. BOECKMAN, JR. and T. R. ALESSI. J. Am. Chem. Soc. **104**, 3216 (1982).
42. W. OPPOLZER, R. L. SNOWDEN, and D. P. SIMMONS. Helv. Chim. Acta, **64**, 2002 (1981).
43. P. HELQUIST. Personal communication.
44. S. K. ATTAH-POKU, F. CHAU, R. S. SMITH, S. J. ALWARD, and A. G. FALLIS. Unpublished work.
45. F. TURECEK, V. HANUS, P. SEDMERA, H. ANTROPIUSORA, and K. MACH. Tetrahedron, **35**, 1463 (1979).
46. G. A. KRAUS and M. J. TASCHNER. J. Am. Chem. Soc. **102**, 1974 (1980).
47. J. D. WHITE and B. G. SHELDON. J. Org. Chem. **46**, 2273 (1981).
48. R. K. BOECKMAN, JR. and D. M. DEMKO. J. Org. Chem. **47**, 1789 (1982).
49. H. KOTSUKI, A. KAWAMURA, and M. OCHI. Chem. Lett. 917 (1981).
50. K. C. NICOLAOU, D. A. CLAREMON, D. P. PAPAHATIJUS, and R. L. MAGOLDA. J. Am. Chem. Soc. **103**, 6969 (1981).
51. S. MARTIN. Personal communication.
52. J. AUERBACH and S. M. WEINREB. J. Org. Chem. **40**, 3311 (1975).
53. T. SCHMIDLIN, W. ZÜRCHER, and C. TAMM. Helv. Chim. Acta, **64**, 235 (1981); T. SCHMIDLIN and C. TAMM. Helv. Chim. Acta, **61**, 2096 (1978).
54. W. OPPOLZER and W. FRÖSTL. Helv. Chim. Acta, **58**, 590 (1975).
55. H. W. GSCHWEND, A. O. LEE, and H. P. MEIER. J. Org. Chem. **38**, 2169 (1973).
56. R. PREWO, J. H. BIERI, U. WIDMER, and H. HEIMGARTNER. Helv. Chim. Acta, **64**, 1515 (1981); U. WIDMER, H. HEIMGARTNER, and H. SCHMID. Helv. Chim. Acta, **61**, 815 (1978).
57. G. FRATER. Tetrahedron Lett. 4517 (1976).
58. H. W. GSCHWEND and H. P. MEIER. Angew. Chem. Int. Ed. Engl. **11**, 294 (1972).
59. H. W. GSCHWEND. Helv. Chim. Acta, **56**, 1763 (1973).
60. M. T. COX. Chem. Commun. 903 (1975).
61. T. TAKEBAYASHI, N. IWASAWA, and T. MUKAIYAMA. Chem. Lett. 579 (1982).
62. S. F. MARTIN and C. TU. J. Org. Chem. **46**, 3763 (1981).
63. S. F. MARTIN, C. TU, M. KIMURA, and S. H. SIMONSEN. J. Org. Chem. **47**, 3634 (1982).
64. S. F. MARTIN, S. R. DESAI, G. W. PHILLIPS, and A. C. MILLER. J. Am. Chem. Soc. **102**, 3294 (1980).
65. L. H. KLEMM, T. M. MCGUIRE, and K. W. GOPINATH. J. Org. Chem. **41**, 2571 (1976).
66. S. G. PYNE, M. J. HENSEL, and P. L. FUCHS. J. Am. Chem. Soc. **104**, 5719 (1982); S. G. PYNE, M. J. HENSEL, S. R. BYRN, A. T. MCKENZIE, and P. L. FUCHS. J. Am. Chem. Soc. **102**, 5960 (1980).
67. S. G. PYNE, D. C. SPELLMEYER, S. CHEN, and P. L. FUCHS. J. Am. Chem. Soc. **104**, 5728 (1982).
68. M. E. KUEHNE, T. H. MATSKO, J. C. BOHNERT, L. MOTYKA, and D. OLIVER-SMITH. J. Org. Chem. **46**, 2002 (1981).
69. M. E. KUEHNE, J. A. HUEBNER, and T. H. MATSKO. J. Org. Chem. **44**, 2477 (1979); M. E. KUEHNE, C. L. KIRKEMO, T. H. MATSKO, and J. C. BOHNERT. J. Org. Chem. **45**, 3259 (1980); M. E. KUEHNE, T. H. MATSKO, J. C. BOHNERT, and C. L. KIRKEMO. J. Org. Chem. **44**, 1063 (1979).
70. M. E. KUEHNE, J. F. OKUNIEWICZ, C. L. KIRKEMO, and J. C. BOHNERT. J. Org. Chem. **47**, 1335 (1982).
71. E. WENKERT. J. Am. Chem. Soc. **84**, 78 (1962); A. I. SCOTT. Acc. Chem. Res. **3**, 151 (1970); Bioorg. Chem. **3**, 398 (1974); E. LEETE and S. A. SLATTERY. J. Am. Chem. Soc. **98**, 6326 (1976).
72. H. F. SCHMITTHENER and S. M. WEINREB. J. Org. Chem. **45**, 3372 (1980).
73. S. M. WEINREB, N. A. KHATRI, and J. SHRINGARPURE. J. Am. Chem. Soc. **101**, 5073 (1979).
74. B. NADER, R. W. FRANCK, and S. M. WEINREB. J. Am. Chem. Soc. **102**, 1153 (1980).
75. R. A. GOBAO, M. L. BREMMER, and S. M. WEINREB. J. Am. Chem. Soc. **104**, 7065 (1982).
76. R. A. EARL and K. P. C. VOLLHARDT. Heterocycles, **19**, 265 (1982).
77. N. A. KHATRI, H. F. SCHMITTHENNER, J. SHRINGARPURE, and S. M. WEINREB. J. Am. Chem. Soc. **103**, 6387 (1981).
78. G. E. KECK. Tetrahedron Lett. 4767 (1978); G. E. KECK and D. G. NICKELL. J. Am. Chem. Soc. **102**, 3632 (1980).
79. B. B. SNIDER, D. M. ROUSH, and T. A. KILLINGER. J. Am. Chem. Soc. **101**, 6023 (1979).
80. Y-S. CHENG, F. W. FOWLER, and A. T. LUPO, JR. J. Am. Chem. Soc. **103**, 2090 (1981).
81. R. K. BOECKMAN, JR. Abstract No. OR1-2, 65th Canadian Chemical Conference of the Chemical Institute of Canada, Toronto, Ont., May 30 – June 2, 1982.
82. S. ITO and Y. HIRATA. Tetrahedron Lett. 2557 (1972).

Can. J. Chem. Downloaded from www.nrcresearchpress.com by 210.87.254.6 on 09/06/12
For personal use only.

83. G. P. GISBY, S. E. ROYALL, and P. G. SAMMES. J. Chem. Soc. Perkin Trans. 1. 169 (1982).
84. R. S. GLASS. Personal communication.
85. E. J. COREY, R. L. DANHEISER, S. CHANDRASEKARAN, G. E. KECK, B. GOPALAN, S. D. LARSEN, P. SIREL, and J. L. GRAS. J. Am. Chem. Soc. **100**, 8034 (1978); E. J. COREY and R. L. DANHEISER. Tetrahedron Lett. 4477 (1973).
86. G. STORK, G. CLARK, and C. S. SHINER. J. Am. Chem. Soc. **103**, 4948 (1981).
87. G. STORK and D. H. SHERMAN. J. Am. Chem. Soc. **104**, 3758 (1982).
88. D. F. TABER and S. A. SALEH. Tetrahedron Lett. **23**, 2361 (1982).
89. S. R. WILSON and R. N. MISRA. J. Org. Chem. **45**, 5079 (1980).
90. S. R. WILSON and D. T. MAO. J. Am. Chem. Soc. **100**, 6289 (1978).
91. F. NÄF, R. DECORZANT and W. THOMMEN. Helv. Chim. Acta, **62**, 114 (1979); Helv. Chim. Acta, **65**, 2212 (1982).
92. D. F. TABER and B. P. GUNN. J. Am. Chem. Soc. **101**, 3992 (1979).
93. O. P. VIG, I. R. TREHAN, N. MALIK, and R. KUMAR. Indian J. Chem. **16B**, 449 (1978).
94. J. L. GRAS. J. Org. Chem. **46**, 3738 (1981); J. D. CONNOLLY, L. J. HARRISON, and D. S. RYCROFT. Chem. Commun. 1236 (1982).
95. B. S. JOSHI, N. VISWANATHAN, D. H. GAWAND, V. BALAKRISHNAN, and W. V. PHILIPSBORN. Helv. Chim. Acta, **58**, 2295 (1975).
96. D. F. TABER and S. A. SALEH. J. Am. Chem. Soc. **102**, 5085 (1980).
97. M. HIRAMA and M. UEI. J. Am. Chem. Soc. **104**, 4251 (1982).
98. E. A. DEUTSCH and B. B. SNIDER. J. Org. Chem. **47**, 2682 (1982).
99. R. L. FUNK and W. E. ZELLER. J. Org. Chem. **47**, 180 (1982).
100. S. E. HALL and W. R. ROUSH. J. Org. Chem. **47**, 4611 (1982).
101. S. R. WILSON and J. C. HUFFMAN. J. Org. Chem. **45**, 560 (1980).
102. S. R. WILSON and D. T. MAYO. J. Org. Chem. **44**, 3093 (1979).
103. S. R. WILSON, M. S. HAGUE, and R. N. MISRA. J. Org. Chem. **47**, 747 (1982).
104. O. P. VIG, I. R. TREHAN, and R. KUMAR. Indian J. Chem. **15B**, 319 (1977).
105. W. OPPOLZER, S. C. BURFORD, and F. MARAZZA. Helv. Chim. Acta, **63**, 555 (1980).
106. W. R. ROUSH and S. E. HALL. J. Am. Chem. Soc. **103**, 5200 (1981).
107. J. L. Gras and M. BERTRAND. Tetrahedron Lett. 4549 (1979).
108. T. R. HOYE and A. S. MAGEE. Abstract Orgn. 35, 184th A.C.S. National Meeting, Kansas City, MO. Sept. 12–17, 1982.
109. W. OPPOLZER, R. L. SNOWDEN, and P. H. BRINER. Helv. Chim. Acta, **64**, 2022 (1981); W. OPPOLZER and R. L. SNOWDEN. Tetrahedron Lett. 4187 (1976).
110. K. J. SHEA and E. WADA. Tetrahedron Lett. **23**, 1523 (1982).
111. B. G. SHELDON. Ph.D. Thesis, Oregon State Univ. 1981.
112. P. MAGNUS. Personal communication.
113. C. KAN-FAN, G. MASSIOT, A. AHOND, B. C. DAS, H. P. HUSSON, P. POTIER, A. I. SCOTT, and C. C. WEI. Chem. Commun. 164 (1974).
114. W. OPPOLZER and E. FLASKAMP. Helv. Chim. Acta, **60**, 204 (1977); W. OPPOLZER, W. FRÖSTL, and H. P. WEBER. Helv. Chim. Acta, **58**, 593 (1975).
115. D. T. WITIAK, K. TOMITA, and R. J. PATCH. J. Med. Chem. **24**, 788 (1981).
116. S. F. MARTIN, S. A. WILLIAMSON, R. P. GIST, and K. M. SMITH. J. Org. Chem. In press.
117. G. STORK and D. J. MORGANS. J. Am. Chem. Soc. **101**, 7110 (1979).
118. D. J. MORGANS and G. STORK. Tetrahedron Lett. 1959 (1979).
119. G. E. KECK, E. BODEN, and U. SONNEWALD. Tetrahedron Lett. **22**, 2615 (1981).
120. W. OPPOLZER, R. ACHINI, E. PFENNINGER, and H. P. WEBER. Helv. Chim. Acta, **59**, 1186 (1976).
121. E. CIGANEK. J. Am. Chem. Soc. **103**, 6261 (1981).
122. M. J. BEGLEY, L. CROMBIE, D. A. SLACK, and D. A. WHITING. J. Chem. Soc. Perkin Trans. 1. 2402 (1977).
123. W. OPPOLZER, E. FRANCOTTE and K. BÄTTIG. Helv. Chim. Acta, **64**, 478 (1981).
124. L. F. TIETZE, G. V. KIEDROWSKI, K. HARMS, W. CLEGG, and G. SHELDRICK. Angew. Chem. Int. Ed. Engl. **19**, 134 (1980).
125. L. F. TIETZE, G. V. KIEDROWSKI, and B. BERGER. Angew. Chem. Int. Ed. Engl. **21**, 221 (1982).
126. L. F. TIETZE and G. V. KIEDROWSKI. Tetrahedron Lett. **22**, 219 (1981).
127. V. F. FERREIRA, L. C. COUTADA, M. C. F. R. PINTO, and A. V. PINTO. Synth. Commun. **12**, 195 (1982).
128. S. M. WEINREB. Personal communication.
129. F. W. FOWLER. Personal communication.
130. E. WENKERT and K. NAEMURA. Synth. Commun. 45 (1973).
131. W. OPPOLZER and R. L. SNOWDEN. Helv. Chim. Acta, **64**, 2592 (1981).
132. E. J. COREY and M. PETRZILKA. Tetrahedron Lett. 2537 (1975).
133. D. J. WILLIAMS, S. J. BAILEY, E. J. THOMAS, and J. A. J. JARVIS. Tetrahedron, **36**, 3571 (1980); S. J. BAILEY, E. J. THOMAS, W. B. TURNER, and J. A. J. JARVIS. Chem. Commun. 474 (1978).
134. W. OPPOLZER. Synthesis, 793 (1978).
135. T. KAMETANI and K. FUKUMOTO. Kagaku No Ryoiki, Zokan. 81 (1980).
136. W. OPPOLZER. Heterocycles, **14**, 1615 (1980).
137. R. L. FUNK and K. P. C. VOLLHARDT. Chem. Soc. Rev. **9**, 41 (1980).
138. T. KAMETANI and H. NEMOTO. Tetrahedron, **37**, 3 (1981).
139. W. OPPOLZER, D. A. ROBERTS, and T. G. C. BIRD. Helv. Chim. Acta, **62**, 2017 (1979).
140. K. C. NICOLAOU, W. E. BARNETTE, and P. MA. J. Org. Chem. **45**, 1463 (1980).
141. Y. ITO, M. NAKATSUKA, and T. SAEGUSA. J. Am. Chem. Soc. **102**, 863 (1980).
142. Y. ITO, M. NAKATSUKA, and T. SAEGUSA. J. Am. Chem. Soc. **103**, 476 (1981).
143. S. DJURIC, T. SARKAR, and P. MAGNUS. J. Am. Chem. Soc. **102**, 6885 (1980).
144. K. T. SHEA. Personal communication.
145. W. OPPOLZER. Tetrahedron Lett. 1001 (1974).
146. L. MANDEL. Personal communication.
147. T. KAMETANI, H. MATSUMOTO, T. HONDA, and F. FUKUMOTO. Tetrahedron Lett. **21**, 4847 (1980).
148. T. KAMETANI, H. MATSUMOTO, T. HONDA, M. NAGAI, and K. FUKUMOTO. Tetrahedron, **37**, 2555 (1981).
149. T. KAMETANI, M. TSUBUKI, H. NEMOTO, and K. FUKUMOTO. Chem. Pharm. Bull. **27**, 152 (1979).
150. W. OPPOLZER, K. BÄTTIG, and M. PETRZILKA. Helv. Chim. Acta, **61**, 1945 (1978).
151. W. OPPOLZER and D. A. ROBERTS. Helv. Chim. Acta, **63**, 1703 (1980).
152. T. KAMETANI, H. MATSUMOTO, H. NEMOTO, and K. FUKUMOTO. J. Am. Chem. Soc. **100**, 6218 (1978).
153. P. A. GRIECO, T. TAKIGAWA, and W. J. SCHILLINGER. J. Org. Chem. **45**, 2247 (1980).
154. G. QUINHERT, W.-D. WEBER, U. SCHWARTZ, and G. DÜRNER. Angew. Chem. Int. Ed. Engl. **19**, 1027 (1980); G. QUINKERT, U. SCHWARTZ, H. STARK, W.-D. WEBER, H. BAIER, F. ADAM, and G. DÜRNER. Angew. Chem. Int. Ed. Engl. **19**, 1029 (1980).
155. T. KAMETANI, M. AIZAWA, and H. NEMOTO. J. Chem. Soc. Perkin Trans. 1. 2793 (1980).
156. T. KAMETANI and H. NEMOTO. Tetrahedron Lett. 3309 (1979).
157. J. TSUJI, H. OKUMOTO, Y. KOBAYASHI, and T. TAKAHASHI.

Tetrahedron Lett. **22**, 1357 (1981).
158. T. KAMETANI, M. AIZAWA, and H. NEMOTO. Tetrahedron, **37**, 2547 (1981).
159. K. FUKUMOTO, M. CHIHIRO, Y. SHIRATORI, M. IHARA, T. KAMETANI, and T. HONDA. Tetrahedron Lett. **23**, 2973 (1982).
160. T. KAMETANI, M. CHIHIRO, T. HONDA, and K. FUKUMOTO. Chem. Pharm. Bull. **28**, 2468 (1980).
161. T. KAMETANI, K. SUZUKI, and H. NEMOTO. J. Org. Chem. **47**, 2331 (1982); T. KAMETANI, K. SUZUKI, and H. NEMOTO. J. Am. Chem. Soc. **103**, 2890 (1981).
162. T. KAMETANI, K. SUZUKI, and H. NEMOTO. J. Org. Chem. **45**, 2204 (1980).
163. T. KAMETANI, K. SUZUKI, and H. NEMOTO. J. Chem. Soc. Perkin Trans. 1, 2805 (1980).
164. T. KAMETANI, M. TSUBUKI, and H. NEMOTO. J. Org. Chem. **45**, 4391 (1980); T. KAMETANI, M. TSUBUKI, and H. NEMOTO. Tetrahedron Lett. **21**, 4855 (1980).
165. T. KAMETANI, H. NEMOTO, H. ISHIKAWA, K. SHIROYAMA, H. MATSUMOTO, and K. FUKUMOTO. J. Am. Chem. Soc. **99**, 3461 (1977).
166. T. KAMETANI, Y. HIRAI, Y. SHIRATORI, K. FUKUMOTO, and F. SATOH. J. Am. Chem. Soc. **100**, 554 (1978).
167. T. KAMETANI, Y. KATO, F. SATOH, and K. FUKUMOTO. J. Org. Chem. **42**, 1177 (1977); T. KAMETANI, Y. KATO, T. HONDA, and K. FUKUMOTO. J. Am. Chem. Soc. **98**, 8185 (1976).
168. R. L. FUNK and K. P. C. VOLLHARDT. J. Am. Chem. Soc. **102**, 5245 (1980).
169. R. L. FUNK and K. P. C. VOLLHARDT. J. Am. Chem. Soc. **99**, 5483 (1977); R. L. FUNK and K. P. C. VOLLHARDT. J. Am. Chem. Soc. **101**, 215 (1979).
170. T. KAMETANI, K. SUZUKI, H. NEMOTO, and K. FUKUMOTO. J. Org. Chem. **44**, 1036 (1979); T. KAMETANI, H. NEMOTO, and K. FUKUMOTO. Chem. Commun. 400 (1976).
171. H. NEMOTO, M. HASHIMOTO, K. FUKUMOTO, and T. KAMETANI. Chem. Commun. 699 (1982).
172. T. KAMETANI, H. MATSUMOTO, T. HONDA, and K. FUKUMOTO. Tetrahedron Lett. **22**, 2379 (1981).
173. T. KAMETANI, T. HONDA, H. MATSUMOTO, and K. FUKUMOTO. J. Chem. Soc. Perkin Trans. 1, 1383 (1981); T. KAMETANI, T. HONDA, and K. FUKUMOTO. Heterocycles, **14**, 419 (1980).
174. W. OPPOLZER. J. Am. Chem. Soc. **93**, 3834 (1971).
175. C. EXON, T. GALLAGHER, and P. MAGNUS. Chem. Commun. 613 (1982).
176. T. GALLAGHER and P. MAGNUS. Tetrahedron, **37**, 3889 (1981).
177. T. GALLAGHER, P. MAGNUS, and J. C. HUFFMAN. J. Am. Chem. Soc. **104**, 1140 (1982).
178. W. OPPOLZER. Pure Appl. Chem. **53**, 1181 (1981).
179. Y. ITO, S. MIYATA, M. NAKATSUKA, and T. SAEGUSA. J. Am. Chem. Soc. **103**, 5250 (1981).
180. W. OPPOLZER. Angew. Chem. Int. Ed. Engl. **11**, 1031 (1971).
181. O. L. CHAPMAN, M. R. ENGEL, J. P. SPRINGER, and J. C. CLARDY. J. Am. Chem. Soc. **93**, 6696 (1971); M. MATSUMOTO and K. KURODA. Tetrahedron Lett. **22**, 4437 (1981).
182. T. KAMETANI, T. HONDA, Y. SHIRATORI, H. MATSUMOTO, and K. FUKUMOTO. J. Chem. Soc. Perkin Trans. 1, 1386 (1981); T. KAMETANI, T. HONDA, Y. SHIRATORI, and K. FUKUMOTO. Tetrahedron Lett. **21**, 1665 (1980).
183. F. J. JÄGGI and C. GANTER. Helv. Chim. Acta, **63**, 866 (1980).
184. E. J. COREY and R. S. GLASS. J. Am. Chem. Soc. **89**, 2600 (1967).
185. G. BRIEGER and D. R. ANDERSON. J. Org. Chem. **36**, 243 (1971).
186. E. G. BREITHOLLE and A. G. FALLIS. Can. J. Chem. **54**, 1991 (1976); J. Org. Chem. **43**, 1964 (1978).
187. S. J. ALWARD and A. G. FALLIS. Can. J. Chem. **62**, 121 (1983).
188. S. F. NELSON, J. P. GILLESPIE, P. J. HINTZ, and E. D. SEPPANEN. J. Am. Chem. Soc. **95**, 8380 (1973).
189. R. L. SNOWDEN. Tetrahedron Lett. **22**, 97 (1981).
190. R. L. SNOWDEN. Tetrahedron Lett. **22**, 101 (1981).
191. R. L. SNOWDEN. Personal communication.
192. L. A. PAQUETTE, M. J. WYVRATT, H. C. BERK, and R. E. MOERCK. J. Am. Chem. Soc. **100**, 5845 (1978); L. A. PAQUETTE and M. J. WYVRATT. J. Am. Chem. Soc. **96**, 4671 (1974).
193. R. J. TERNANSKY, D. W. BALOGH, and L. A. PAQUETTE. J. Am. Chem. Soc. **104**, 4503 (1982).
194. M. E. JUNG and L. A. LIGHT. J. Org. Chem. **47**, 1084 (1982).
195. J. HELLOU, J. F. KINGSTON, and A. G. FALLIS. Unpublished work.
196. S. K. ATTAH-POKU, G. GALLACHER, A. S. NG, L. E. B. TAYLOR, S. J. ALWARD, and A. G. FALLIS. Tetrahedron Lett. **24**, 677 (1983), and unpublished work.
197. R. BUKOWNIK, J. F. KINGSTON, and A. G. FALLIS. Unpublished work.
198. R. S. GLASS, J. D. HERZOG, and R. L. SOBCZAK. J. Org. Chem. **43**, 3209 (1978).
199. G. BÜCHI, A. HAUSER, and J. LIMACHER. J. Org. Chem. **42**, 3323 (1977).
200. A. KRANTZ and C. Y. LIN. J. Am. Chem. Soc. **95**, 5662 (1973).
201. R. F. TRAVARES and E. KATTEN. Tetrahedron Lett. 1713 (1977).
202. T. KAMETANI, T. HONDA, K. FUKUMOTO, M. TOYOTA, and M. IHARA. Heterocycles, **16**, 1673 (1981).
203. G. FRATER and J. WENGER. Unpublished results.
204. G. A. SCHIEHSER and J. D. WHITE. J. Org. Chem. **45**, 1864 (1980).
205. H. YAMAMOTO and H. L. SHAM. J. Am. Chem. Soc. **101**, 1609 (1979).
206. E. PIERS and M. WINTER. Ann. 973 (1982).
207. H. GREUTER and H. SCHMID. Helv. Chim. Acta, **55**, 2382 (1972).
208. G. FRATER. Helv. Chim. Acta, **57**, 172 (1974).
209. N. FUKAMIYA, M. KATO, and A. YOSHIKOSHI. J. Chem. Soc. Perkin Trans. 1. 1843 (1973).
210. T. IMAGAWA, T. NAKAGAWA, M. KAWANISI, and K. SISIDO. Bull. Chem. Soc. Jpn. **52**, 1506 (1979).
211. A. KRANTZ. J. Am. Chem. Soc. **94**, 4020 (1972).
212. G. BÜCHI and H. WÜEST. Helv. Chim. Acta, **54**, 1767 (1971).
213. M. S. RAASCH. J. Org. Chem. **45**, 856 (1980).
214. P. YATES and H. AUKSI. Can. J. Chem. **57**, 2853 (1979).
215. F. NÄF, R. DECORZANT, W. GIERSCH, and G. OHLOFF. Helv. Chim. Acta, **64**, 1387 (1981); F. NÄF and G. OHLOFF. Helv. Chim. Acta, **57**, 1868 (1974).
216. W. OPPOLZER and R. L. SNOWDEN. Tetrahedron Lett. 3505 (1978).
217. D. P. G. HAMON and P. R. SPURR. Chem. Commun. 372 (1982).
218. E. CIGANEK. J. Org. Chem. **45**, 1497 (1980).
219. H. D. BECKER, K. SANDROS, and A. ARVIDSSON. J. Org. Chem. **44**, 1336 (1979); H. D. BECKER, K. ANDERSSON, and K. SANDROS. J. Org. Chem. **45**, 4549 (1980).
220. L. HODAKOWSKI and C. A. CUPAS. Tetrahedron Lett. 1009 (1973).
221. R. M. HARRISON, J. D. HOBSON, and A. W. MIDGLEY. J. Chem. Soc. Perkin Trans. 1. 2403 (1976).
222. G. FRATER. Tetrahedron Lett. 4517 (1976).
223. C. S. CUPAS and L. HODAKOWSKI. J. Am. Chem. Soc. **96**, 4668 (1974).
224. F. TURECEK, V. HANUS, P. SEDMERA, H. ANTROPIUSOVA, and K. MACH. Collect. Czech. Chem. Commun. **46**, 1474 (1981).
225. K. A. PARKER and M. R. ADAMCHUK. Tetrahedron Lett. 1689 (1978).
226. D. D. STERNBACH and D. M. ROSSANA. Tetrahedron Lett. **23**, 303 (1982).
227. D. D. STERNBACH and D. M. ROSSANA. J. Am. Chem. Soc. **104**, 5853 (1982).
228. R. IMAGAWA, T. NAKAGAWA, K. MATSUURA, T. AKIYAMA, and M. KAWANISI. Chem. Lett. 903 (1981).

Can. J. Chem. Downloaded from www.nrcresearchpress.com by 210.87.254.6 on 09/06/12
For personal use only.

Can. J. Chem. Downloaded from www.nrcresearchpress.com by 210.87.254.6 on 09/06/12
For personal use only.

229. A. PELTER and B. SINGARAM. Tetrahedron Lett. **23**, 245 (1982).
230. P. J. DE CLERCQ and L. A. VAN ROYEN. Synth. Commun. **9**, 771 (1979).
231. W. M. BEST and D. WEGE. Tetrahedron Lett. **22**, 4877 (1981).
232. W. M. GROOTAERT and P. J. DE CLERCQ. Tetrahedron Lett. **23**, 3291 (1982).
233. L. A. VAN ROYEN, R. MIJNGHEER, and P. J. DE CLERCQ. Tetrahedron Lett. **23**, 3283 (1982).
234. P. J. DE CLERCQ. Personal communication.
235. T. MUKAIYAMA. Personal communication.
236. T. MUKAIYAMA, T. TSUJI, and N. IWASAWA. Chem. Lett. 697 (1979).
237. T. MUKAIYAMA, N. IWASAWA, T. TSUJI, and K. NARASAKA. Chem. Lett. 1175 (1979).
238. T. MUKAIYAMA and T. TAKEBAYASHI. Chem. Lett. 1013 (1980).
239. T. MUKAIYAMA and N. IWASAWA. Chem. Lett. 29 (1981).
240. K. T. TAGMAZYAN, G. O. TOROSYAN, R. S. MKRTCHYAN, and A. T. BABAYAN. Arm. Khim. Zh. **29**, 352 (1976); Chem. Abstr. **86**, 42746 (1977).
241. P. G. SAMMES. Personal communication.
242. P. A. JACOBI and T. CRAIG. J. Am. Chem. Soc. **100**, 7748 (1978).
243. P. A. JACOBI, D. G. WALKER, and I. M. A. ODEH. J. Org. Chem. **46**, 2065 (1981).
244. P. A. JACOBI and D. G. WALKER. J. Am. Chem. Soc. **103**, 4611 (1981).
245. G. BRIEGER. Personal communication.
246. J. BRUHN, J. ZSINDELY, and H. SCHMID. Helv. Chim. Acta, **61**, 2542 (1978).
247. M. NITTA, A. SEKIGUCHI, and H. KOBA. Chem. Lett. 933 (1981).
248. G. M. BROOKE, R. S. MATTHEWS, and N. S. ROBSON. J. Chem. Soc. Perkin Trans. 1, 102 (1980); F. J. DINAN and H. TIECKELMANN. J. Org. Chem. **29**, 892 (1964).
249. H. GREUTER and H. SCHMID. Helv. Chim. Acta, **57**, 1204 (1974).
250. D. PASKE, R. RINGSHANDL, I. SELLNER, H. SICHERT, and J. SAUER. Angew. Chem. Int. Ed. Engl. **19**, 456 (1980).
251. G. P. GISBY, P. G. SAMMES, and R. A. WATT. J. Chem. Soc. Perkin Trans. 1, 249 (1982).
252. I. HASAN and F. W. FOWLER. J. Am. Chem. Soc. **100**, 6696 (1978).
253. L. B. DAVIES, O. A. LECI. P. G. SAMMES, and R. A. WATT. J. Chem. Soc. Perkin Trans. 1, 1293 (1978).
254. L. B. DAVIES, S. G. GREENBERG, and P. G. SAMMES. J. Chem. Soc. Perkin Trans. 1, 1909 (1981).
255. E. CIGANEK. J. Org. Chem. **45**, 1512 (1980).
256. J. HÁJICÉK and J. TROJÁNEK. Tetrahedron Lett. 1823 (1981).
257. T. JOJIMA, H. TAKESHIBA, and T. KINOTO. Chem. Pharm. Bull. **28**, 198 (1980); T. JOJIMA, H. TAKESHIBA, and T. KONOTSUNE. Chem. Pharm. Bull. **10**, 2191 (1972).
258. K. J. SHEA, S. WISE, L. D. BURKE, P. D. DAVIS, J. W. GILMAN, and A. C. GREELEY. J. Am. Chem. Soc. **104**, 5708 (1982).
259. K. J. SHEA and S. WISE. J. Am. Chem. Soc. **100**, 6519 (1978).
260. K. J. SHEA, P. S. BEAUCHAMP, and R. S. LIND. J. Am. Chem. Soc. **102**, 4544 (1980).
261. K. J. SHEA and E. WADA. J. Am. Chem. Soc. **104**, 5715 (1982).
262. F. NAF. Personal communication.
263. R. L. FUNK. Personal communication.
264. L. MANDELL, D. E. LEE, and L. F. COURTNEY. J. Org. Chem. **47**, 610 (1982).
265. S. F. MARTIN, C. TU, and T. CHOU. J. Am. Chem. Soc. **102**, 5274 (1980); S. F. MARTIN, T. CHOU, and C. TU. Tetrahedron Lett. 3823 (1979).
266. N. S. ISAACS and P. VAN DER BEEKE. Tetrahedron Lett. **23**, 2147 (1982).
267. R. M. WILSON, R. A. FARR, and D. J. BURLETT. J. Org. Chem. **46**, 3293 (1981).
268. W. HOFHEINZ and P. SCHÖNHOLZER. Helv. Chim. Acta, **60**, 1367 (1977).
269. A. C. BAZAN, J. M. EDWARDS, and U. WEISS. Tetrahedron, **34**, 3005 (1978).
270. W. M. BANDARANAYAKE, J. E. BANFIELD, and D. ST. C. BLACK. Chem. Commun. 902 (1980).
271. G. KARTHA, G. N. RAMACHANDRAN, H. B. BHAT, P. MADHAVAN NAIR, V. K. V. RAGHAVAN, and K. VENKATARAMAN. Tetrahedron Lett. 459 (1963).
272. P. YATES, S. D. KARMARKAR, D. ROSENTHAL, G. H. STOUT, and F. V. STOUT. Tetrahedron Lett. 1623 (1963); D. J. BICHAN and P. YATES. J. Am. Chem. Soc. **94**, 4773 (1972); Can. J. Chem. **53**, 2054 (1975).
273. B. A. KEAY and R. RODRIGO. J. Am. Chem. Soc. **104**, 4725 (1982).
274. K. C. NICOLAOU, N. A. PETASIS, R. E. ZIPKIN, and J. UENISH. J. Am. Chem. Soc. **104**, 5555 (1982).
275. K. C. NICOLAOU, N. A. PETASIS, J. UENISH, and R. E. ZIPKIN. J. Am. Chem. Soc. **104**, 5557 (1982).
276. K. C. NICOLAOU, N. A. PETASIS, and R. E. ZIPKIN. J. Am. Chem. Soc. **104**, 5560 (1982).
277. R. S. WARD. Chem. Soc. Rev. **11**, 75 (1982).
278. J. S. E. HOLKER and T. J. SIMPSON. Chem. Commun. 626 (1978).
279. G. HIMBERT and L. HENN. Angew. Chem. Int. Ed. Engl. **21**, 620 (1982).
280. W. R. ROUSH and S. M. PESECKIS. Tetrahedron Lett. **23**, 4879 (1982).
281. W. R. ROUSH and H. R. GILLIS. J. Org. Chem. **47**, 4825 (1982).
282. S. M. WEINREB and R. R. STAIB. Tetrahedron, **28**, 3087 (1982).
283. Y. N. GUPTA, M. J. DOA, and K. N. HOUK. J. Am. Chem. Soc. **104**, 7336 (1982).
284. T. S. MACAS and P. YATES. Tetrahedron Lett. **24**, 147 (1983).
285. M. L. BREMMER and S. M. WEINREB. Tetrahedron Lett. **24**, 261 (1983).
286. S. R. WILSON and M. S. HAGUE. J. Org. Chem. **47**, 5411 (1982).
287. H. NEMOTO, M. HASHIMOTO, and T. KAMETANI. Chem. Commun. 699 (1982).
288. T. KAMETANI, Y. SUZUKI, H. FURNYAMA, and T. HONDA. J. Org. Chem. **48**, 31 (1983).
289. T. TUSCHKA, K. NAITO, and B. RICKBORN. J. Org. Chem. **48**, 70 (1983).
290. J. M. HORNBACK and R. D. BARROWS. J. Org. Chem. **48**, 90 (1983).
291. R. S. BLY, R. K. BLY, and T. SHIBATA. J. Org. Chem. **48**, 101 (1983).
292. Y. ITO, M. NAKATSUKA, and T. SAEGUSA. J. Am. Chem. Soc. **104**, 7609 (1982).
293. L.-F. TIETZE, H. STEGELMEIER, K. HARMS, and T. BRUMBY. Angew. Chem. Int. Ed. Engl. **21**, 863 (1982).
294. K. J. SHEA and J. W. GILMAN. Tetrahedron Lett. **24**, 657 (1983).
295. M. E. GARST, J. D. FRAZIER, B. J. MCBRIDE, and J. R. DOUGLASS. 185th American Chemical Society National Meeting, Seattle, Wash. March 20–25, 1983. Abstract ORGN 114; P. A. WENDER and D. J. WOLANIN. Abstract ORGN 124; K. J. SHEA and P. D. DAVIS. Abstract ORGN 125; D. D. STERNBACH, J. HUGHES, D. BURDI, and R. FORSTOT. Abstract ORGN 174; M. K. EBERLE. Abstract ORGN 215.
296. R. BRETTLE and I. A. JAFRI. J. Chem. Soc. Perkin Trans. 1, 387 (1983).
297. S. D. BURKE, S. M. S. STRICKLAND, and T. H. POWNER. J. Org. Chem. **48**, 454 (1983).
298. M. VOYLE, K. S. KYLER, S. ARSENIYADIS, N. K. DUNLAP, and D. S. WATT. J. Org. Chem. **48**, 470 (1983).
299. J. I. LEVIN and S. M. WEINREB. J. Am. Chem. Soc. **105**, 1397 (1983).

300. Y. ITO, Y. AMINO, M. NAKATSUKA, and TAKEO SAEGUSA. J. Am. Chem. Soc. **105**, 1586 (1983).
301. T. GALLAGHER and P. MAGNUS. J. Am. Chem. Soc. **105**, 2086 (1983).
302. S. J. BAILEY, E. J. THOMAS, S. M. VATHER, and J. WALLIS. J. Chem. Soc. Perkin Trans. 1, 851 (1983).
303. R. H. SCHLESSINGER, J. L. WOOD, A. J. PRASS, R. A. NUGENT, and W. H. PARSONS. J. Org. Chem. **48**, 1146 (1983).
304. M. E. GARST, B. J. MCBRIDE, and J. G. DOUGLASS III. Tetrahedron Lett. **24**, 1675 (1983).
305. M. KATAYAMA and S. MARUMO. Tetrahedron Lett. **24**, 1703 (1983).
306. S. R. WILSON, A. SHEDRINSKY, and M. S. HAGUE. Tetrahedron, **39**, 895 (1983).
307. L. H. KLEMM, Y. M. HWANG, and J. N. LOURIS. J. Org. Chem. **48**, 1451 (1983).
308. K. J. SHEA and P. D. DAVIS. Angew. Chem. Int. Ed. Engl. **22**, 419 (1983).
309. M. P. EDWARDS, S. V. LEY, S. G. LISTER, and B. D. PLAMER. Chem. Commun. 630 (1983).
310. W. OPPOLZER and C. ROBBIANI. Helv. Chim. Acta, **66**, 1119 (1983).
311. D. A. SCHWARTZ and P. YATES. Can. J. Chem. **61**, 1126 (1983).
312. D. S. WATT and N. K. DUNLAP. 186th American Chemical Society National Meeting, Washington, D.C. Aug. 28 – Sept. 2, 1983. Abstract ORGN 4; R. L. FUNK and W. E. ZELLER. Abstract ORGN 7; B. B. SNIDER, B. W. BURBAUM, and E. A. DEUTSCH. Abstract ORGN 8; S. F. MARTIN, S. W. WILLIAMSON, R. P. GIST, K. M. SMITH, and S. W. GRZEJSZCZAK. Abstract ORGN 119; D. D. STERNBACH and J. W. HUGHES. Abstract ORGN 205; S. D. BURKE, D. R. MAGNIN, J. A. OPLINGER, J. P. BAKER, and A. ABDELMAGID. Abstract ORGN 208; S. R. WILSON and M. S. HAQUE. Abstract ORGN 234; D. D. STERNBACH, J. HUGHES, and D. BURDI. Abstract ORGN 295; D. D. STERNBACH and D. M. ROSSANA. Abstract ORGN 296.
313. R. S. GARIGIPATI and S. M. WEINREB. J. Am. Chem. Soc. **105**, 4499 (1983).
314. C. J. NORTHCOTT. Ph.D. Thesis, University of New Brunswick, 1983.
315. P. R. SPURR and D. P. G. HAMON. J. Am. Chem. Soc. **105**, 4734 (1983).
316. C. EXON, T. GALLAGHER, and P. MAGNUS. J. Am. Chem. Soc. **105**, 4739 (1983).
317. G. HWANG and P. MAGNUS. Chem. Commun. 693 (1983).
318. D. L. COMINS, A. H. ABDULLAH, and R. K. SMITH. Tetrahedron Lett. **24**, 2711 (1983).
319. L. A. VAN ROYEN, R. MIJNGHEER, and P. J. DE CLERCQ. Tetrahedron Lett. **24**, 3145 (1983).
320. H-D. BECKER and K. ANDERSSON. Tetrahedron Lett. **24**, 3273 (1983).
321. G. STORK and E. NAKAMURA. J. Am. Chem. Soc. **105**, 5510 (1983).
322. M. S. BAILEY, B. J. BRISDON, D. W. BROWN, and K. M. STARK. Tetrahedron Lett. **24**, 3037 (1983).
323. E. A. DEUTSCH and B. B. SNIDER. Tetrahedron Lett. **24**, 3701 (1983).
324. D. D. STERNBACH, J. W. HUGHES, D. F. BURDI, and R. M. FORSTOT. Tetrahedron Lett. **24**, 3295 (1983).
325. D. W. LANDRY. Tetrahedron, **39**, 2761 (1983).
326. S. D. BURKE, T. H. POWNER, and M. KAGEYAME. Tetrahedron Lett. **24**, 4529 (1983).
327. K. SHISHIDO, T. SAITOH, K. FUKUMOTO, and T. KAMETANI. Chem. Commun. 852 (1983).
328. O. TSUGE, S. KANEMAIA, and S. TAKENAKA. Chem. Lett. 519 (1983).
329. T. TODA, N. SHIMAZAKI, H. HOTTA, T. HATAKEYAMA, and T. MUKAI. Chem. Lett. 523 (1983).
330. H. SCHUSTER and J. SAUER. Tetrahedron Lett. **24**, 4087 (1983).
331. D. L. BOGER. Tetrahedron, **39**, 2869 (1983).

Can. J. Chem. Downloaded from www.nrcresearchpress.com by 210.87.254.6 on 09/06/12
For personal use only.

The importance of the $\sigma^*-\pi^*$ orbital mixing for the nucleophilic displacement on the unsaturated carbon

SHINICHI YAMABE,[1] TSUTOMU MINATO, AND YUMI KAWABATA
Department of Chemistry, Nara University of Education, Takabatake-cho, Nara 630, Japan

Received January 31, 1983

SHINICHI YAMABE, TSUTOMU MINATO, and YUMI KAWABATA. Can. J. Chem. **62**, 235 (1984).

The reactivity of carbonyl and aromatic compounds for the nucleophilic displacement is investigated theoretically. LUMO (lowest unoccupied MO) obtained by the mixing of the π^* MO with the σ^* MO is a uniform criterion of the relative reactivity of substrates. The presence or absence of the tetrahedral intermediate is found to depend on the energy difference between the π^* and σ^* MO's.

SHINICHI YAMABE, TSUTOMU MINATO et YUMI KAWABATA. Can. J. Chem. **62**, 235 (1984).

On a étudié sur une base théorique la réactivité des composés carbonylés et aromatiques lors d'un déplacement nucléophile. Le critère uniforme de la réactivité de ces substrats est le LUMO obtenu en mélangeant une OM π^* avec une OM σ^*. On a trouvé que la présence ou l'absence d'un intermédiaire tétraédrique dépend de la différence d'énergie entre les OM π^* et σ^*.
[Traduit par le journal]

I. Introduction

A nucleophilic substitution on the unsaturated carbon (e.g., the acyl carbon) is known to proceed via a tetrahedral intermediate.

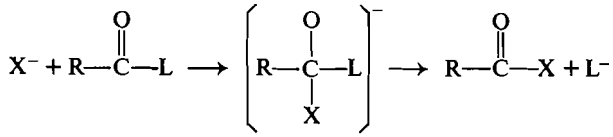

The mechanistic details of the reactions like ester hydrolysis have been extensively investigated, because of the relevance to the enzymatic catalysis in reactions of carboxylic acids (see, for example, ref. 1). Using the ion cyclotron resonance spectroscopy, Brauman and co-workers studied the kinetics of the gas-phase nucleophilic displacement (2). Such solvent-free data provide important information on the difference of the potential-energy surfaces between reactions in the gas phase and in the liquid phase. In our previous work (3), we sought the minimum-energy path of the gas-phase nucleophilic displacement on the acyl chloride. The reaction is initiated by the formation of the π $X^- \cdots CH_3CO—Cl$ complex and takes place in a concerted manner. No tetrahedral intermediate is found. The bent-out motion of the C—Cl bond from the *XZ* plane lowers the lowest unoccupied MO (LUMO) to enhance the charge-transfer (CT) interaction (LUMO−CT relation).

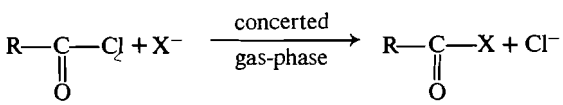

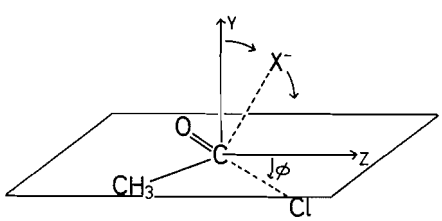

[1]To whom correspondence should be addressed.

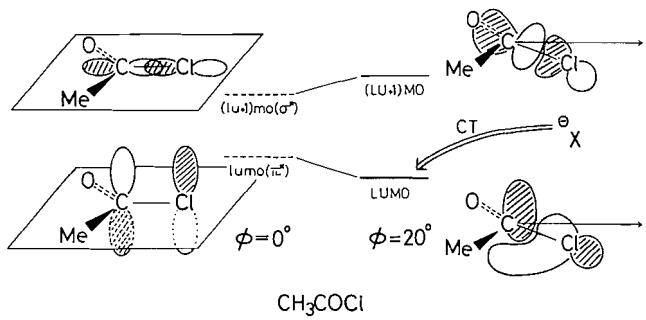

In this work, we would like to compare the reactivity of various carbonyl compounds theoretically, extending the concept of the LUMO−CT relation. An aromatic nucleophilic substitution is also studied to examine whether the tetrahedral intermediate is formed. Finally, the possibility of the intermediate is evaluated in terms of the extent of the $\pi^*-\sigma^*$ MO mixing. The solvent effect on the potential energy surface is discussed.

II. The reactivity of carbonyl compounds in the nucleophilic displacement

The order of the reactivity toward a nucleophile is established experimentally (see, for example, ref. 4).

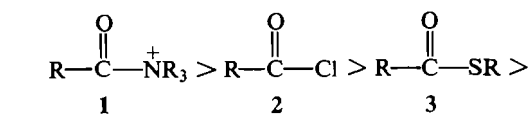

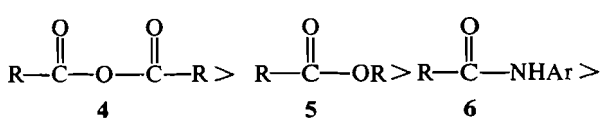

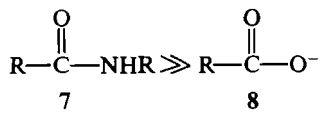

The order is explained in terms of both the activity of the leaving group (L) and the extent of the conjugation to the carbonyl group. More systematic and uniform comparison may

Can. J. Chem. Downloaded from www.nrcresearchpress.com by 210.87.254.6 on 09/06/12
For personal use only.

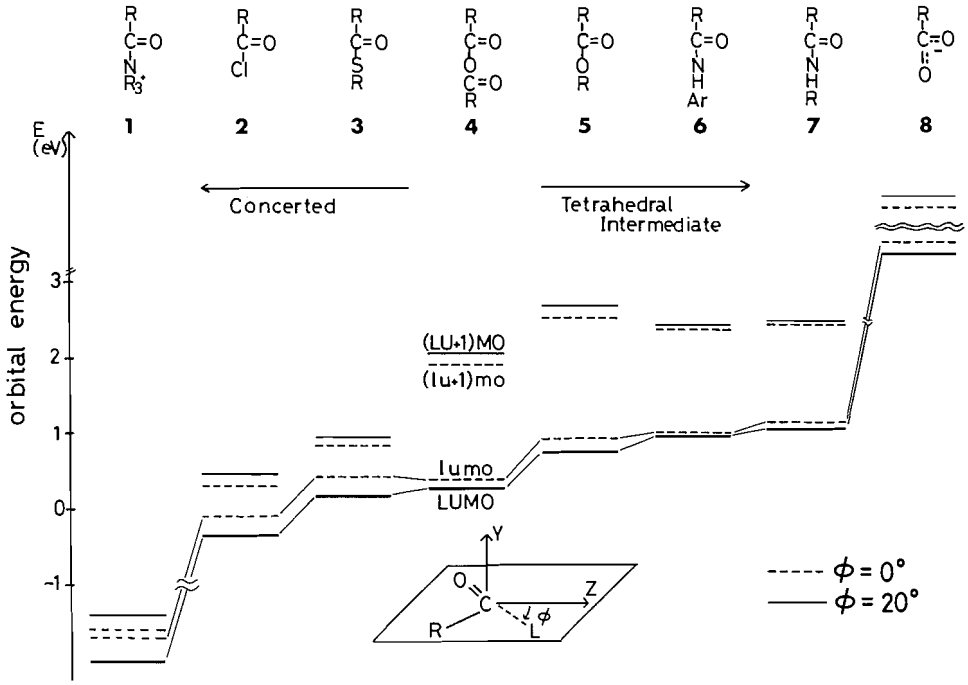

FIG. 1. The unoccupied-orbital energies of carbonyl compounds computed with the MNDO MO method. The broken levels, lumo and (lu + 1)mo, are for the equilibrium geometry. The full-line levels, LUMO and (LU + 1)MO, are for the bent-out geometry. lumo means the lowest unoccupied MO, and (lu + 1)mo the second lowest unoccupied MO. Substituent R is the methyl group and Ar is the phenyl ring in the MO calculation.

be made by applying the frontier orbital theory (5). In Fig. 1, lumo and (lu + 1)mo are displayed by broken lines. The lowest unoccupied MO, lumo, of the equilibrium geometry ($\theta = 0°$) is the π^* orbital, and (lu + 1)mo is σ^*_{C-L}. Although lumo's are almost in the correct order, we find a discrepancy between **3** and **4**. That is, lumo of **3** is higher than that of **4**, which is in disagreement with the experimental order. Here, we calculate LUMO and (LU + 1)MO which are obtained by bending the C—L bond ($\theta = 20°$). Since the angle θ may be taken arbitrarily as a non-zero value, 20° is used throughout this study. The deformation causes the destabilization of the substrates by 2.7 ~ 5.4 kcal/mol. This energy loss is, however, so small that the electronic stabilization is expected to overcome it readily. The distortion intermixes the π^* MO with the σ^* MO, resulting in the enlargement of the energy separation. These two energy levels denoted by full lines are also shown in the diagram below. When the levels of LUMO's (bold lines) are compared, they are found to be just in the right order. The discrepancy appearing in **3** and **4** is removed by the larger intermixing of π^* and σ^* in **3**.

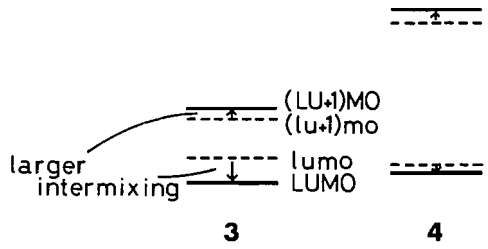

lumo(**3**) is higher than lumo(**4**)
but LUMO(**3**) is lower than LUMO(**4**)

This result indicates that the relative reactivity of the carbonyl compounds *should not* be evaluated by lumo alone. LUMO which is given by the small distortion along the reaction coordinate predicts the proper reactivity. The energy lowering by lumo → LUMO (i.e., $\phi = 0 \rightarrow 20°$) is larger, when the energy difference between lumo and (lu + 1)mo is smaller. π^* MO calls for the nucleophile X^-, and σ^* MO causes the C—L bond scission after the electronic charge of X^- is accepted. LUMO is a uniform criterion involving these two operations.

The σ^* level reflects the C—L bond strength. For **2** with the weak C—L bond, no tetrahedral intermediate is found (3). The intermediacy seems, however, to be a matter of degree of the σ^* level. To examine this, we seek the structure of $F^- \cdots HCOOCH_3$ (as **5**) and $H^- \cdots H_2C{=}O$ (as model) with the *ab initio* MO of the 4-31G basis set. Although the latter is not realistic,[2] its C—L (C—H) bond is the strongest and formaldehyde is a good model to check the intermediacy. As a result of calculation, those two are found to be intermediates. In Fig. 2, these geometries are exhibited together with that of the transition state of $Cl^- \cdots CH_3CO{-}Cl$ reported previously (3). By the MNDO calculation, the orbital energies of π^* and σ^*_{C-Cl} of **2** are −0.09 and 0.30 eV, respectively (shown in Fig. 1). Those of **5** are 1.20 and 2.75 eV, and those of the model are 0.93 and 3.86 eV. The $\pi^* - \sigma^*$ energy gap is in the order, **2** > **5** > model. Thus, the intermediacy depends on the energy difference between π^* and σ^* MO's. It is surprising in Fig. 2 that the C—O bond length in **2** is the same as that in the transition state (1.18 Å). This is in contrast to the result for the latter systems. This apparent maintenance arises from the back-donation of the $\bar{\pi}$ charge of the carbonyl oxygen to the carbon, schematically illustrated below. For $F^- \cdots HCOOCH_3$, such back-donation (although smaller) makes the C—O bond shorter (1.30 Å) than the standard value (~1.43 Å).

[2]The potential energy of the model reaction was computed in ref. 6.

Can. J. Chem. Downloaded from www.nrcresearchpress.com by 210.87.254.6 on 09/06/12
For personal use only.

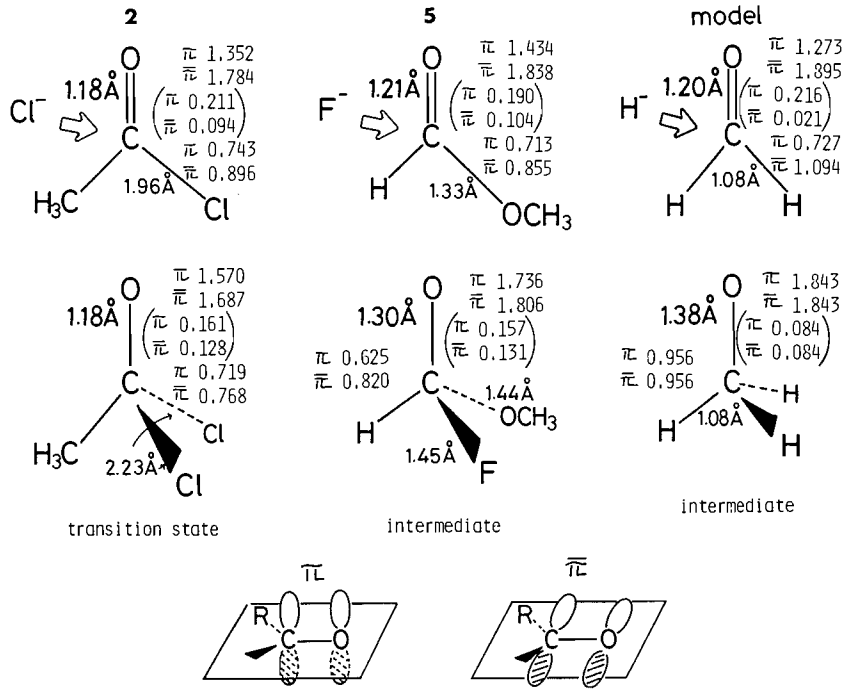

FIG. 2. The optimized structures of substrates, acyl chloride (as **2**), methyl formate (as **5**), and formaldehyde (as model). Those of the transition state and two intermediates are also shown. The numbers of π and $\bar{\pi}$ are orbital electron densities, and those in parentheses are π-type bonding electron densities between carbon and oxygen atoms. Densities are calculated with a fixed C—O bond length (of the substrate) for comparison. All calculations are made with the 4-31G basis set.

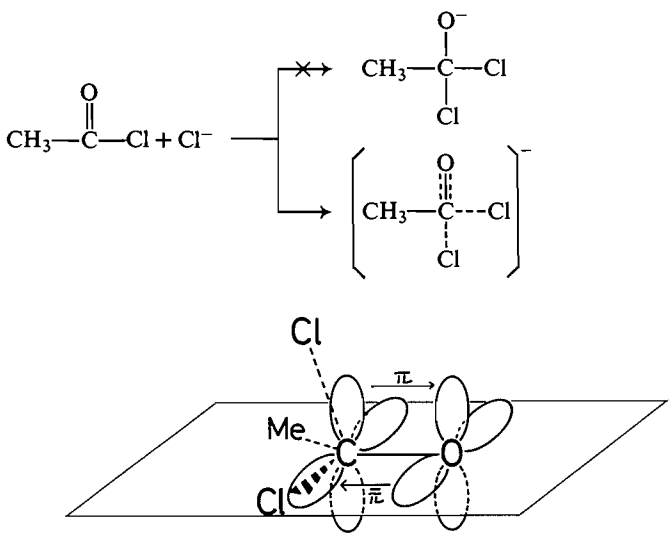

III. The aromatic nucleophilic displacement

In contrast to the S_N2 reaction of the alkyl halide, the aromatic nucleophilic substitution is thought to proceed via the benzenium-ion intermediate. This ion is stabilized by the nitro substituent on the phenyl ring (7).

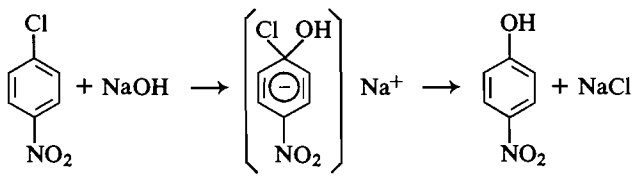

To examine the intermediacy, the minimum-energy path of the alkaline hydrolysis of *para*-nitrochlorobenzene is traced theoretically. In Fig. 3, the potential-energy profile is exhibited together with the optimized parameters. In Fig. 4, the snapshot of the minimum-energy path is given. The curve in Fig. 3 shows that there is no energy maximum corresponding to the transition state. Since this theoretical datum does not include the solvent effect at all, the energy variation is for the gas-phase reaction. In Fig. 5, the change of the orbital energies and spatial extensions along the bending is illustrated. There are three π^* MO's in the substrate of the planar structure. Through bending, lumo and (lu + 1)mo intermix with (lu + 3)mo, respectively, resulting in the larger energy splitting.

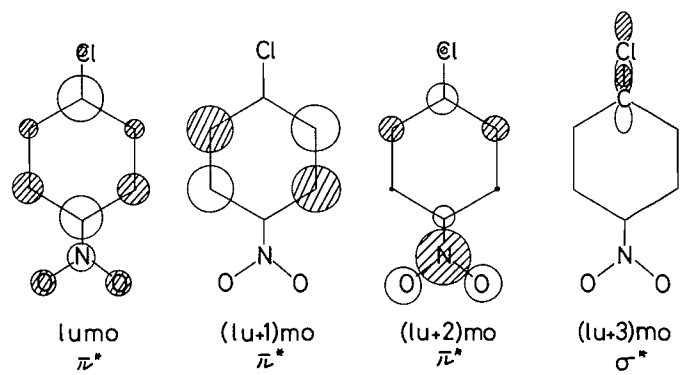

As a substrate, *para*-nitrochlorobenzene has the enough low σ^* level to mix effectively with π^* orbitals. This leads to the concerted nucleophilic displacement. In contrast to this type, the substrate with the high-lying σ^* orbital may generate the tetrahedral intermediate. 1-Methoxy-2,4,6-trinitrobenzene (A) is readily converted to 1-ethoxy-2,4,6-trinitrobenzene (C) via a stable intermediate (B) of the red crystal (8).

Can. J. Chem. Downloaded from www.nrcresearchpress.com by 210.87.254.6 on 09/06/12
For personal use only.

Can. J. Chem. Downloaded from www.nrcresearchpress.com by 210.87.254.6 on 09/06/12
For personal use only.

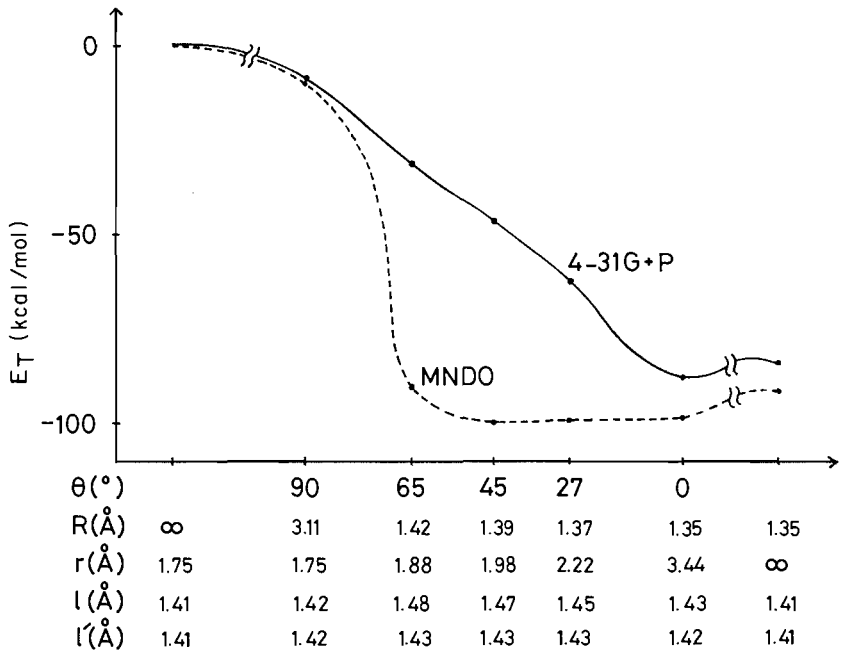

θ(°)		90	65	45	27	0	
R(Å)	∞	3.11	1.42	1.39	1.37	1.35	1.35
r(Å)	1.75	1.75	1.88	1.98	2.22	3.44	∞
l(Å)	1.41	1.42	1.48	1.47	1.45	1.43	1.41
l′(Å)	1.41	1.42	1.43	1.43	1.43	1.42	1.41

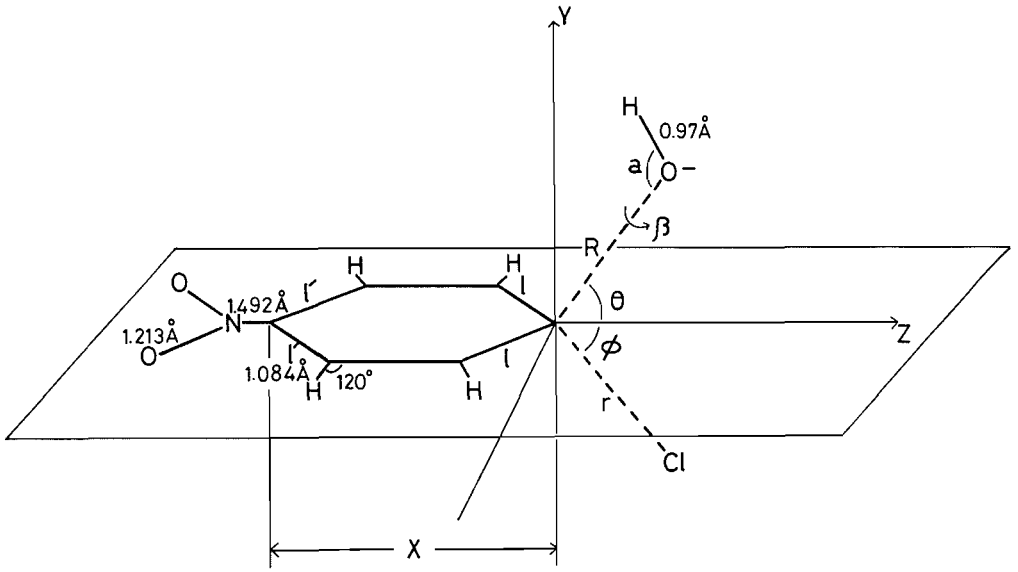

FIG. 3. The potential-energy profiles of the gas-phase reaction between *para*-nitrochlorobenzene and hydroxide ion. At a given angle θ, eight parameters, R, φ, r, l, l', X, α, and β, are optimized with the MNDO MO method. The total energy (E_T) given by the full line is calculated with the 4-31G + p (on Cl atom) + p' (on O atom) basis set. E_T is uniformed to zero at $R = \infty$. The C—N bond fixed here to 1.492 Å is found to be almost constant (at most 0.02 Å shortened) during the substitution.

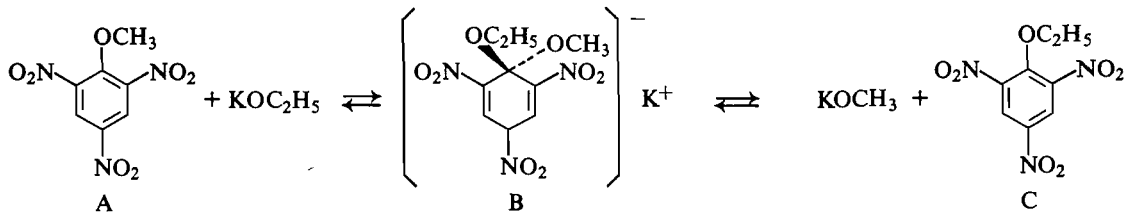

In Fig. 6, the MO energy levels of 4-nitromethoxybenzene (A′) and its intermediate (B′) are displayed. Omitting two *ortho* nitro groups, we adopt A′ for comparison with the reaction of *p*-nitrochlorobenzene in Fig. 3. The substantial difference of σ* levels as well as π lumo levels gives the different mechanism. Thus, similar to the nucleophilic displacement on the carbonyl carbon, the energy of the σ* level may be the criterion for the intermediacy.

Can. J. Chem. Downloaded from www.nrcresearchpress.com by 210.87.254.6 on 09/06/12
For personal use only.

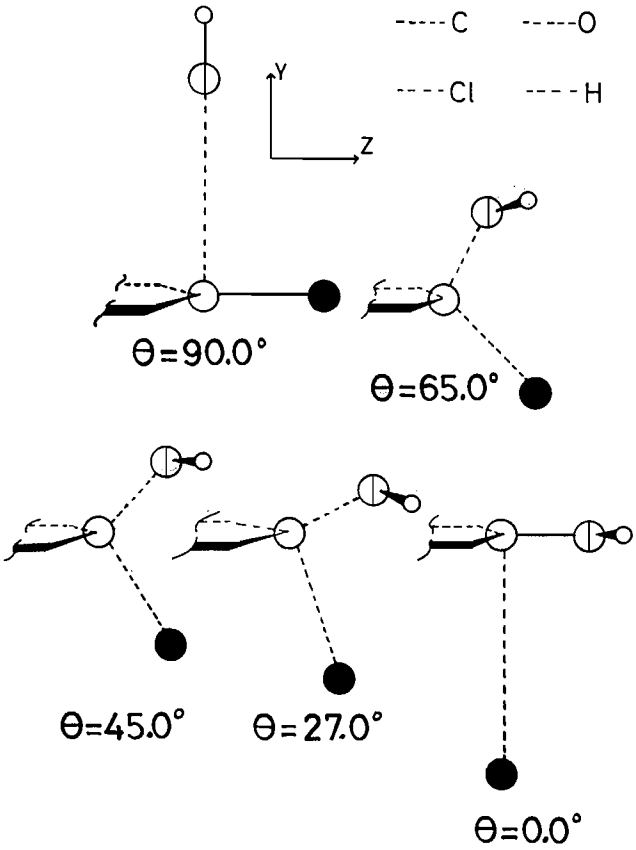

FIG. 4. The calculated path of the nucleophilic displacement on the phenyl α carbon.

IV. Concluding remarks

Different from the S_N2 reaction of the alkyl substrate, the nucleophilic displacement on the unsaturated carbon needs the $\pi^*-\sigma^*$ orbital mixing during the reaction.

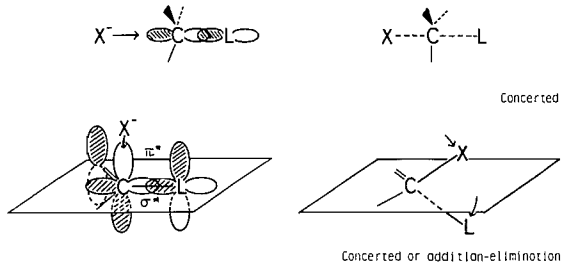

In the latter case, the σ^* level determines the mechanism (concerted or stepwise). In other words, if the C—L bond is weak, the concerted process is likely, and vice versa. The discussion made so far is based purely on the electronic structure of the substrate in the gas phase. To rationalize the application of the frontier-orbital theory to the liquid-phase reaction, comparison of the potential energies in the gas phase and in the liquid phase is necessary. Brauman *et al.* showed such comparison for the S_N2 reaction of the alkyl substrate (9). In Fig. 7, three types of the potential energies are suggested. Protic solvents such as water and alcohols are considered for the liquid phase. In Type I, the intermediate appears in both phases. The activation barrier is brought about by solvation or desolvation. The rate-determining step depends on the extent of the solvation ability. In the aromatic S_N2 reaction, however, the first energy barrier is known to control the kinetics (7). When X and L are first-row

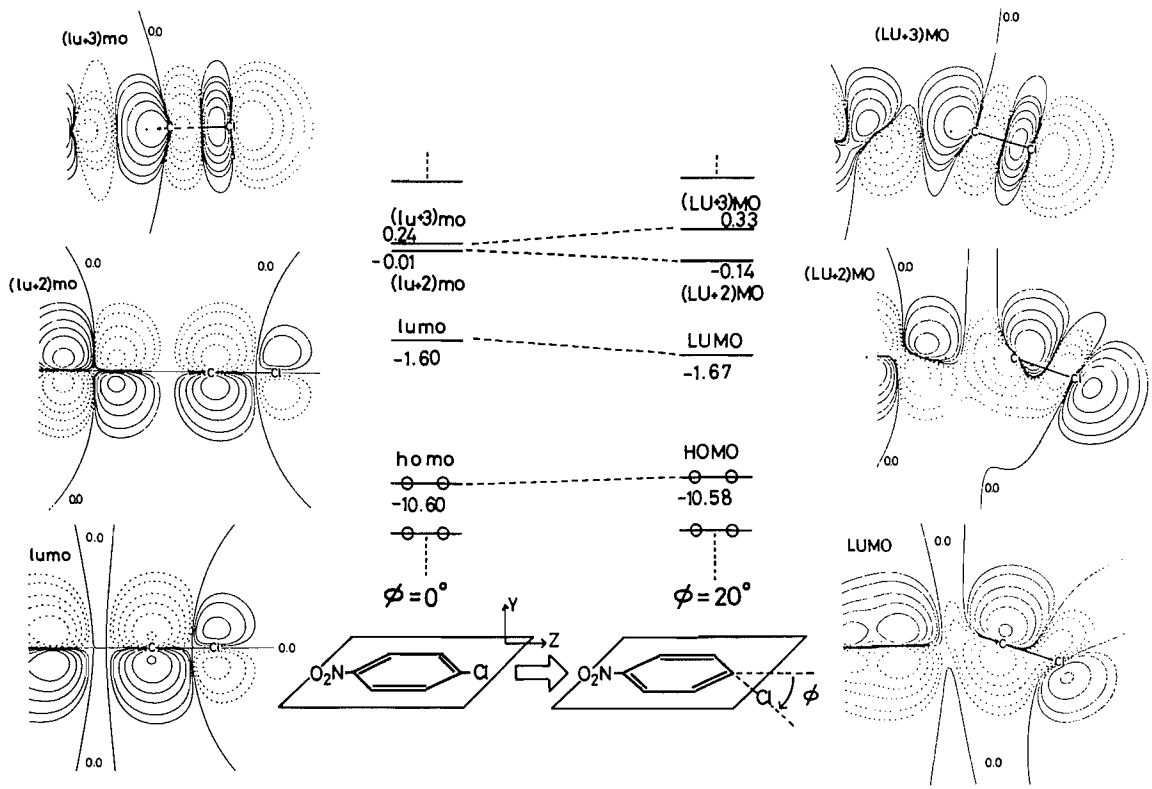

FIG. 5. The change of the orbital energies (in eV) and the shapes through bending the C—Cl bond out of the phenyl plane. The values attached to the contour lines in the *YZ* plane are ±0.5, ±0.2, ±0.1, ±0.05, ±0.02, ±0.01, and 0.0 $(e/Å^3)^{1/2}$ from inside to outer side.

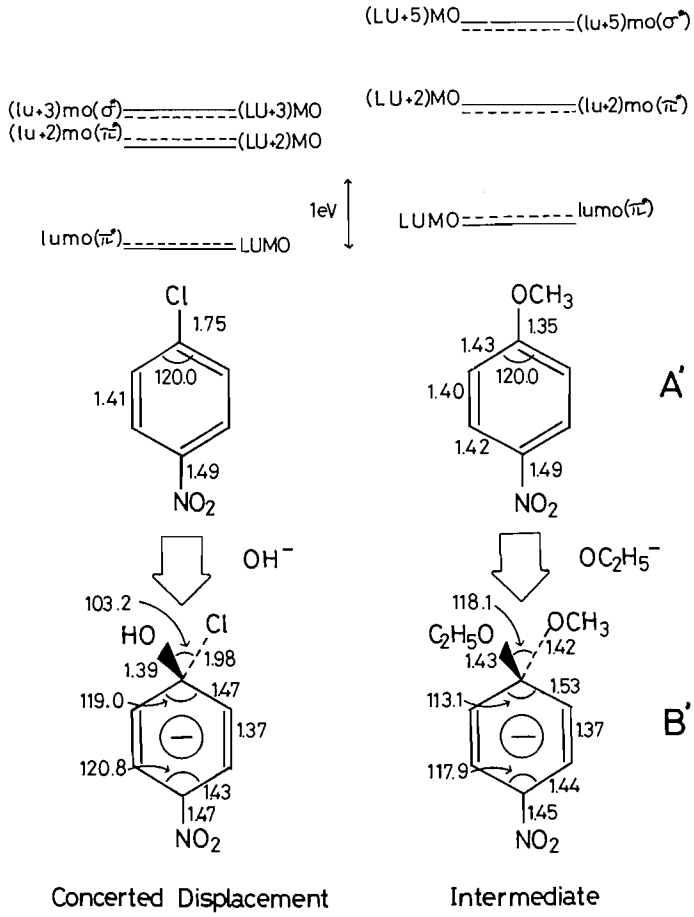

FIG. 6. The low-lying unoccupied levels (ϕ = 0 and 20°) of 4-nitrochlorobenzene and 4-nitromethoxybenzene (A'). For the former substrate, the geometry of the reacting system of θ = 45° (see Fig. 3) is shown. For the latter, the geometry of the intermediate (B') is exhibited. The optimization of geometries is carried out with the MNDO MO method. The bond length is in Å and angle in deg.

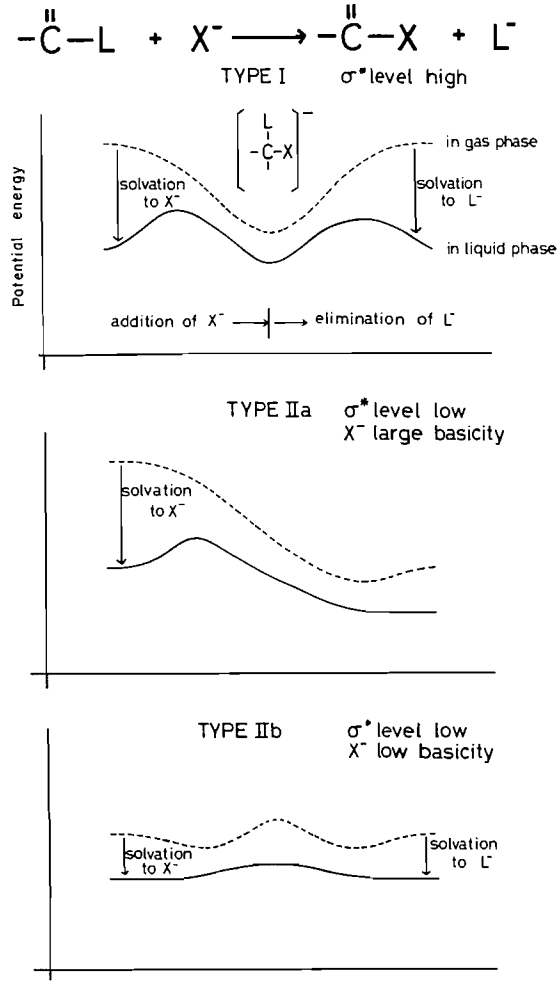

FIG. 7. Schematic sketch of three kinds of the potential energy diagram of the nucleophilic displacement on the unsaturated carbon. Full curves denote the liquid-phase reactions, and the broken curves the gas-phase reactions.

atoms or groups such as F and OCH_3, this type of the energy curves is likely. In Type IIa, the activation barrier is again due to the solvation to X^-. F^- + CH_3—CO—Cl and OH^- + O_2N—ϕ—Cl are the examples. In Type IIb, the energy barrier is given by bond interchange. Cl^- + CH_3—CO—Cl is the case. In Type II, no tetrahedral intermediate is formed. In all types, the rate-determining step is related to the energy change at the initial stage of the reaction. The energy lowering by the solvation is almost entirely for the nucleophile, X^-, and the energy of the substrate is hardly affected by solvation. Therefore, the frontier-orbital theory dealing with LUMO of the substrate may predict the proper relative reactivity, regardless of the type of the potential energy.

Acknowledgments

All *ab initio* calculations are performed with the GAUSSIAN 70 and its extended version GAUSSIAN 127 (10).[3] The authors thank the Institute for Molecular Science (IMS) for allotment of the CPU time of the HITAC M-200H computer. Permission to use the FACOM M-382 computer at the Data Processing Center, Kyoto University, is also acknowledged. They are grateful to Dr. Satoshi Inagaki for his valuable advice on the change of the C—O bond length in Fig. 2. The program of MNDO MO calculation is taken from the QCPE library (11).

[3]It is extended to GAUSSIAN 127 by K. Kitaura and K. Morokuma of the Institute for Molecular Science.

1. S. PATAI (*Editor*). The chemistry of the carbonyl group. Interscience, New York. 1966.
2. O. I. ASUBIOJO and J. I. BRAUMAN. J. Am. Chem. Soc. **101**, 3715 (1979).
3. S. YAMABE and T. MINATO. J. Org. Chem. **48**, 2972 (1983).
4. J. B. HENDRICKSON, D. J. CRAM, and G. S. HAMMOND. Organic chemistry. III ed. McGraw-Hill, New York. 1970. Chapt. 13.
5. K. FUKUI. Theory of orientation and stereoselection. Springer-Verlag, Heidelberg. 1970.
6. H. B. BÜRGI, J. M. LEHN, and G. WIPFF. J. Am. Chem. Soc. **96**, 1956 (1974).
7. L. M. STOCK. Aromatic substitution reactions. Foundations of Modern Organic Chemistry Series. *Edited by* Kenneth L. Rinehart, Jr. Prentice-Hall, Inc. New Jersey. 1968.
8. J. B. AINSCOUGH and E. F. CALDIN. J. Chem. Soc. 2528 (1956).
9. W. N. OLMSTEAD and J. I. BRAUMAN. J. Am. Chem. Soc. **99**, 4219 (1977).
10. W. J. HEHRE, W. A. LATHAN, R. DITCHFIELD, M. D. NEWTON, and J. A. POPLE. GAUSSIAN 70. Program No. 236, QCPE, Indiana University. 1973.
11. W. THIEL. MNDO. Program No. 353 (IBM Version), QCPE, Indiana University. 1981.

Can. J. Chem. Downloaded from www.nrcresearchpress.com by 210.87.254.6 on 09/06/12
For personal use only.

Synthesis of a purine acyclonucleoside series having pronounced antiviral activity. The glyceropurines[1]

KELVIN K. OGILVIE,[2] NGHE NGUYEN-BA, MICHAEL F. GILLEN, BRUNO K. RADATUS, UKKEN O. CHERIYAN, AND H. RIZK HANNA

Department of Chemistry, McGill University, Montreal, P.Q., Canada H3A 2K6

AND

KENDALL O. SMITH AND KAREN S. GALLOWAY

Department of Microbiology, The University of Texas, San Antonio, TX 78284, U.S.A.

Received May 19, 1983

KELVIN K. OGILVIE, NGHE NGUYEN-BA, MICHAEL F. GILLEN, BRUNO K. RADATUS, UKKEN O. CHERIYAN, H. RIZK HANNA, KENDALL O. SMITH, and KAREN S. GALLOWAY. Can. J. Chem. **62**, 241 (1984).

The synthesis of a series of purine analogues of the acyclonucleoside compound A* (A-Star, **1**) is described. Compounds in this series have been shown to have pronounced activity against herpesviruses. These compounds have been designated "the glycerosides". The glyceropurines are described in this report. Nucleotides have been constructed containing glyceroadenine (A*, compound **1**). These nucleotides are resistant to degradation by phosphodiesterases. The compound A* is both a poor substrate and a poor inhibitor of adenosine deaminase.

KELVIN K. OGILVIE, NGHE NGUYEN-BA, MICHAEL F. GILLEN, BRUNO K. RADATUS, UKKEN O. CHERIYAN, H. RIZK HANNA, KENDALL O. SMITH et KAREN S. GALLOWAY. Can. J. Chem. **62**, 241 (1984).

On décrit la synthèse d'une série de purines qui sont des analogues du composé acyclonucléoside A* (A étoilé-**1**). Les composés de cette série ont une activité assez marquée contre les virus de l'herpès. On les appelle "les glycérosides". Dans ce travail, on décrit les glycéropurines. On a construit des nucléotides contenant la glycéroadénine (A*, composé **1**). Ces nucléotides résistent à la dégradation par les phospodiestérases. Le composé A* est à la fois un substrat pauvre et un pauvre inhibiteur de la désaminase adénosine.

[Traduit par le journal]

Introduction

During our studies on cyclonucleosides we observed that 8,2′-thioanhydroadenosine was a good substrate for adenosine deaminase (1). This was surprising since 8-methylthioadenosine was a very poor substrate of adenosine deaminase. We reasoned (1) that 8-methylthioadenosine must prefer the "*syn*" conformation about the *N*−glycoside bond. Since 8,2′-thioanhydroadenosine is locked in the "*anti*" conformation, the implication drawn was that adenosine deaminase would recognize as substrates only those adenosine derivatives capable of existing in the "*anti*" conformation (1).

It was also known at the time that many adenosine derivatives are biologically active in vitro but are inactive in vivo because of deamination by adenosine deaminase to inactive inosine derivatives. We then made the assumption that a molecule (such as **1**) which has all of the chemical features of deoxyadenosine, but which lacks a rigid carbohydrate ring structure, would be a poor substrate of adenosine deaminase. We further reasoned that if compound **1** were also a poor inhibitor (i.e. had low binding to the enzyme) of adenosine deaminase, then it might serve as an excellent antiviral agent. This reasoning was purely intuitive and was based on the assumption that key viral enzymes would have a less rigorous structural requirement in their substrates than would the equivalent mammalian enzymes. Thus a molecule such as **1** might be exempt from degradation by adenosine deaminase and other mammalian enzymes but might be accepted as a substrate by replicative enzymes in viral systems.

We therefore began a program to synthesize a series of molecules based on the general structure **1**. One such molecule,

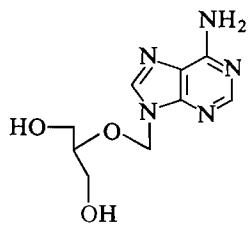

1

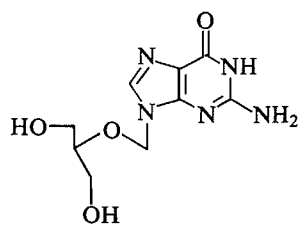

2

the guanine analogue **2** known as BIOLF-62, has shown remarkable activity against herpesviruses (2−5). The pyrimidine derivatives generally have lower activity toward the herpesviruses HSV-1 and HSV-2 (2*b*, 2*c*). In this report we wish to describe the synthesis of compound **1**, nucleotides derived from **1**, and a series of modified purine analogues of **1**. A preliminary account of some of these results has appeared (6).

Discussion and results

The general procedure for the synthesis of compound **1** and its analogues is outlined in Scheme 1. The chloromethyl ether **3** is prepared from 1,3-dichloro-2-hydroxypropane as shown. Compound **3** can be coupled directly to purines. For example, 6-chloropurine reacts with **3** in DMF to produce the 9-alkylated product **4** and the N-7 isomer **5**. Heating the mixture of products **4** and **5** results in the complete conversion of **5** into **4** resulting in a good overall yield of the desired product. Treatment of **4** or **5** with methanolic ammonia results in the adenine compounds **6** or **7**. The benzyl groups can easily be removed from **6** by catalytic hydrogenation to give **1**. Compound **1** is 9-[[2-hydroxy-1-(hydroxymethyl)ethoxy]methyl]adenine. For simplicity we have referred to this molecule as A* or A-Star.

An alternate route to compound **1** involved the direct (Scheme 2) condensation of adenine with **3**. In DMF with triethylamine only 17% of the desired product **6** was obtained.

[1]Part V in a series on antiviral and ring-open nucleoside analogues. Parts III and IV are refs. 2*b* and 2*c* respectively.

[2]Author to whom correspondence may be addressed.

Can. J. Chem. Downloaded from www.nrcresearchpress.com by 210.87.254.6 on 09/06/12
For personal use only.

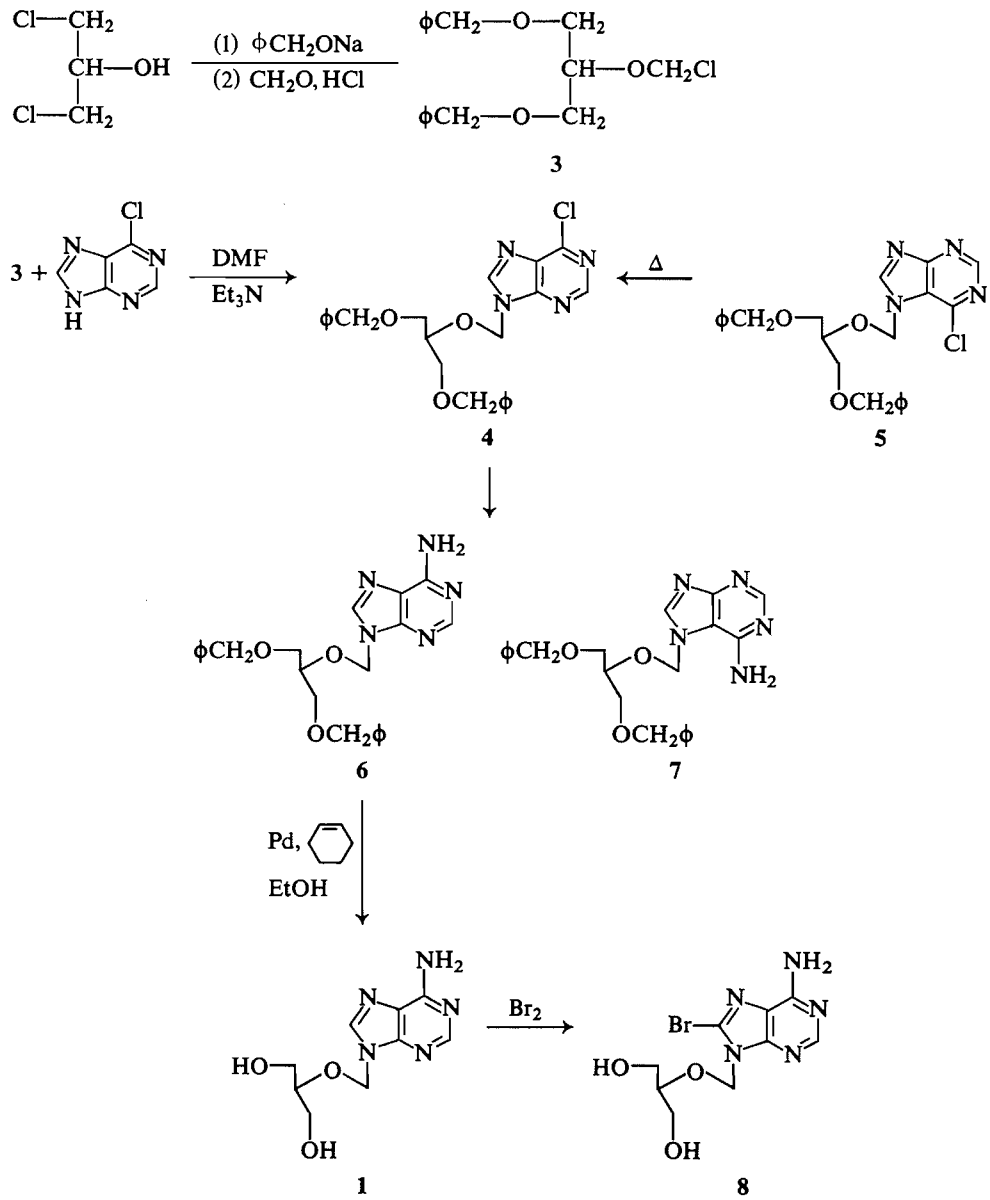

SCHEME 1

The major product (40%) was the N-7 isomer (**7**). The mercuric cyanide catalyzed coupling of adenine to **3** gave the desired product **6** in 30% yield.

Adenosine deaminase studies on 1

Initial velocities for the deamination of A* and adenosine in buffered solutions of varying substrate concentrations were determined and the data plotted according to the method of Lineweaver and Burk (7). The results are shown below.

Substrate	$K_m(M\times10^5)$	Rel. V_{max}
Adenosine	4.83	1.00
A*	187	2.55×10^{-2}

Clearly A* is weakly bound to the enzyme relative to adenosine. It appears that while A* had the structural features that should enable it to bind to the enzyme (8, 9), its conformational flexibility prevents efficient binding. In order to obtain an initial idea of the effect of base substituents on deaminase activity, 8-bromoA* (**8**) was prepared by standard procedures

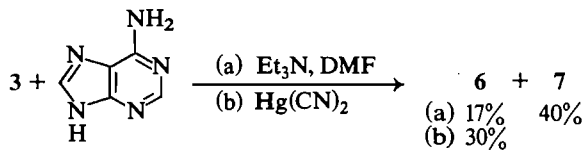

SCHEME 2

(10). A* and 8-bromoA* were treated with high concentrations of adenosine deaminase and 8-bromoA* was found to be 140 times less reactive than A*. A* is a weak competitive inhibitor of adenosine deaminase with a K_i value of 2.04×10^{-4} *M*.

*Dinucleotides from A**

It was of interest to synthesize dinucleoside monophosphate analogues from A*. This was readily accomplished (Scheme 3) by preparing the monomethoxytrityl derivative **9** (MMT-A*). The isomers of **9** were not resolved and the nucleotide **10** was prepared by coupling two equivalents of **9** with 1 equivalent of 2,2,2-trichloroethylphosphorodichloridite. The isolated yield of **10** was 56% and after complete deprotection the nucleotide analogue **11** was obtained.

Can. J. Chem. Downloaded from www.nrcresearchpress.com by 210.87.254.6 on 09/06/12
For personal use only.

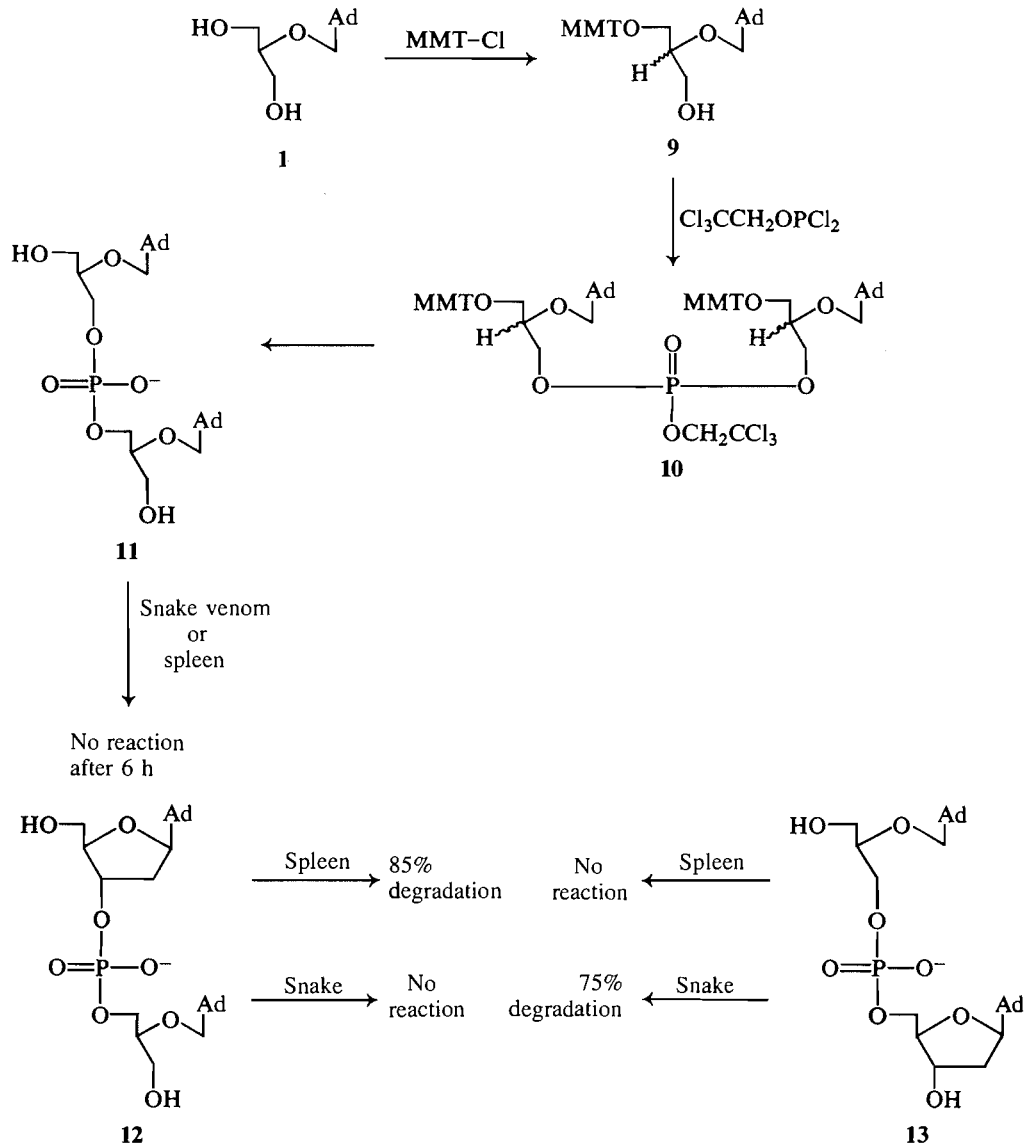

SCHEME 3

Compound **11** was completely resistant to both snake venom and spleen phosphodiesterases for 6 h under standard conditions. On the other hand, the mixed nucleotides **12** and **13**, each containing a unit of deoxyadenosine and A*, showed some degradation. For example, after 6 h, **12** was 85% degraded by spleen but was unaffected by snake venom. The reverse was true for **13**. These results indicate that the ring-open structure of A* is not recognized as a normal substrate by phosphodiesterases.

*Changes in the acyclic portion of A**

In order to determine the effect of replacement of the hydroxyl groups of A* with regard to biological activity, the azido and amino derivatives **18**, **22**, **23**, and **24** were prepared. The synthesis of these compounds is outlined in Scheme 4.

The mono and bis tosylated derivatives **16** and **20** were prepared by standard procedures. Sodium azide in DMF gave clean displacement of the tosyl groups in both cases and after deprotection the azido derivatives **18** and **22** were obtained. Compound **18** and **22** could be obtained directly from A* as an easily separable mixture using the procedure of Hata and co-workers (11). Direct reduction of the azido derivatives gave the monoamino derivative **23** and the diamino derivative **24**.

Changes in the purine base

Numerous purines have conferred biological activity to nucleoside structures. Among those of most interest, other than the guanine analogue, were purine, 2-aminopurine, 2,6-diaminopurine, 2-fluoro-6-aminopurine, isoguanine, 6-chloropurine, and 6-chloroguanine. 2,6-Diaminopurine nucleosides have shown activity against herpesviruses (12) while the purine, nebularine, is a nucleoside antibiotic (13). The 2-halopurine nucleosides have shown activity against malignant lymphoblasts (14) while isoguanine derivatives have shown a range of biological activities including uses as muscle relaxants and anti-inflammatory agents (15, 16).

Direct coupling of 2,6-diaminopurine to **3** was not successful under the usual conditions. However N^2,N^6-diacetyl-2,6-diaminopurine coupled to **3** to give **25** in 55% yield (Scheme 5). Removal of acetyl and benzyl groups produced the desired compound (**27**).

The 2-amino group in 2,6-diaminopurine derivatives can be

Can. J. Chem. Downloaded from www.nrcresearchpress.com by 210.87.254.6 on 09/06/12
For personal use only.

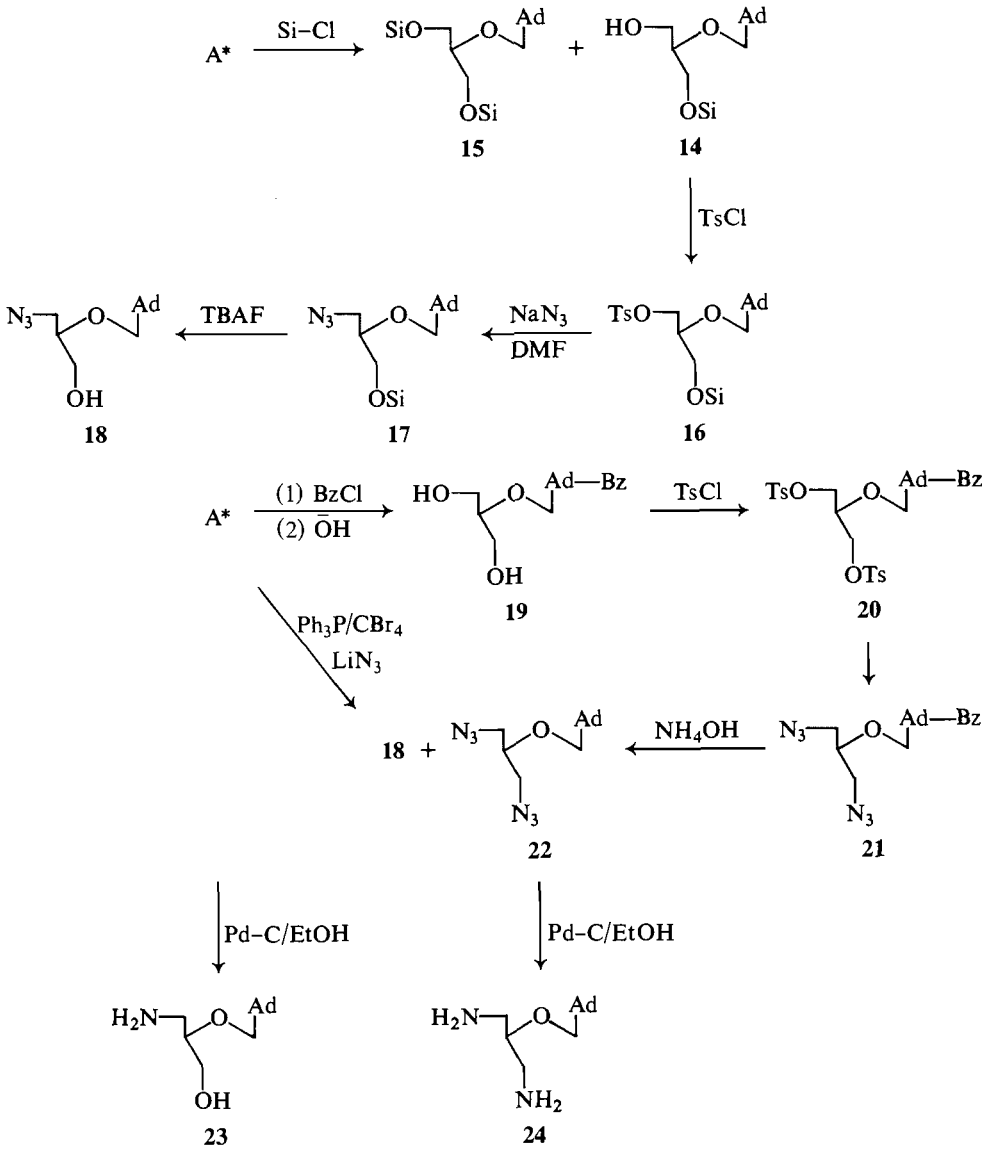

SCHEME 4

selectively replaced by halogens using procedures described by Robins and Uznanski (17). Treatment of **26** with *tert*-butylnitrite in 60% HF/pyridine gave the desired 2-fluoro derivative **28** in 35% yield. These reaction conditions also resulted in the partial loss of benzyl groups and compound **29** was obtained in 15% yield. Complete removal of benzyl groups from **28** produced **30** in 88% yield.

The 2-amino group in **26** could also be selectively diazatized to an oxygen function giving rise to the isoguanine structure **31** in 55% yield. Removal of the benzyl groups from **31** gave the isoguanine derivative **32** which is isomeric to BIOLF-62 (**2**).

While compounds A* (**1**) and **27** are not good substrates for adenosine deaminase they do undergo deamination when a large excess of enzyme is used. This process can be used on a preparative scale. In this work the 2,6-diaminopurine derivative **27** was treated with an excess of adenosine deaminase and was quantitatively converted into BIOLF-62 (**2**). Similar treatment of A* led to a 90% isolated yield of the inosine derivative **33**.

The chlorine atom in position 6 of the 6-chloropurine and 6-chloroguanine derivatives **4** and **34** could be hydrogenolyzed without any significant loss of benzyl protecting groups (18). The benzyl groups in **35** were quite resistant to hydrogenolysis under standard conditions. However, the boron trichloride method (19) worked well. In fact, this method led to cleavage of the benzyl groups from **4** and **34** without affecting the chlorine atom at position 6, producing the 6-chloropurine and 6-chloroguanine compounds **37***a* and **37***b* (Scheme 6).

Biological activity

The compounds described in this report were all tested for activity against HSV-1. The two most active compounds were the guanine derivative, **2**, and the 6-chloroguanine derivative, **37***b*. The ED-50 values vs. HSV-1 were 0.13 μg/mL and 6.6 μg/mL respectively. Neither compound showed any detectable toxicity towards cells at concentrations up to 1000 μg/mL. All other compounds had ED-50 values ≥ 100 μg/mL. Compounds **30** and **37***a* showed significant cellular toxicity at concentrations of 32 μg/mL.

Compound **2** is also active against HSV-2 with an ED-50 value of 0.25 μg/mL. It has previously and erroneously been reported (2, 3) that compound **2** is inactive against cytomegalovirus (CMV). In fact, compound **2** is very active against CMV with an ED-50 value of 20 μg/mL. Compounds **1**, **37***a*,

Can. J. Chem. Downloaded from www.nrcresearchpress.com by 210.87.254.6 on 09/06/12
For personal use only.

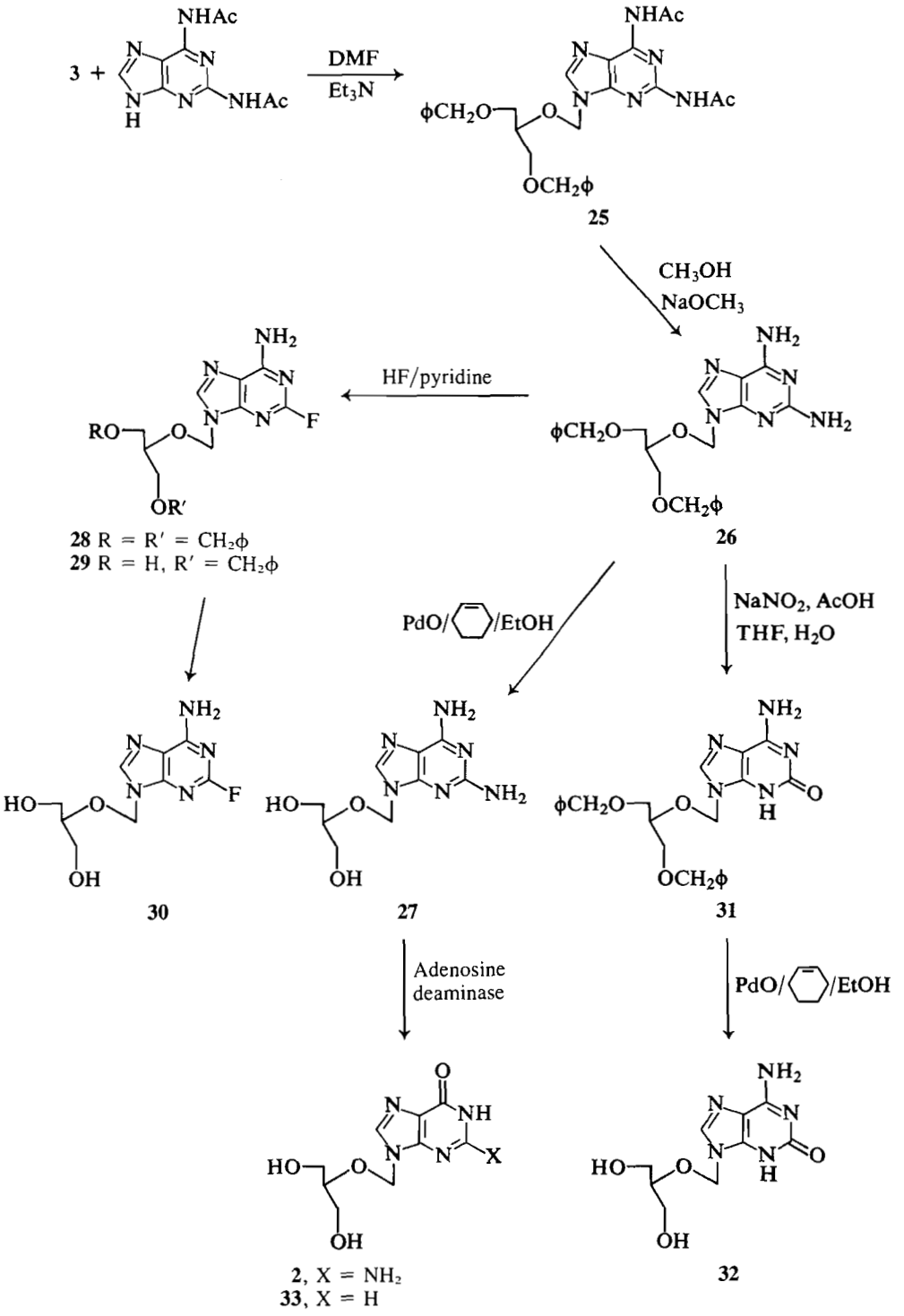

SCHEME 5

and **37***b* are also active against cytomegalovirus with viral ED-50 values of 20, 60, and 32 μg/mL repsectively. The results of complete biological testing will be reported elsewhere.

Experimental

General methods

Products from preparative scale reactions were isolated by column chromatography using Merck silica gel 60 (230–400 mesh) packed in glass columns (15 g of silica per gram of crude material). Thin-layer chromatographic data (R_f values) are recorded from Merck Kieselgel 60F254 analytical sheets. Purine bases were purchased from Sigma Chemical Co. Ultraviolet spectra were recorded on a Cary 17 spectrometer. Nuclear magnetic resonance spectra were recorded using a Bruker WH-90, a Varian XL-200, and a Varian T60A spectrometer.

Elemental analyses

C, H, and N analyses were performed by Canadian Microanalytical Service. Analyses of new compounds were ±0.4% of the calculated values.

1,3-Dibenzyloxy-2-propanol

Benzyl alcohol (500 mL) was placed in a three-neck round-bottom flask (2 L) through which dry nitrogen was passed continuously.

Can. J. Chem. Downloaded from www.nrcresearchpress.com by 210.87.254.6 on 09/06/12
For personal use only.

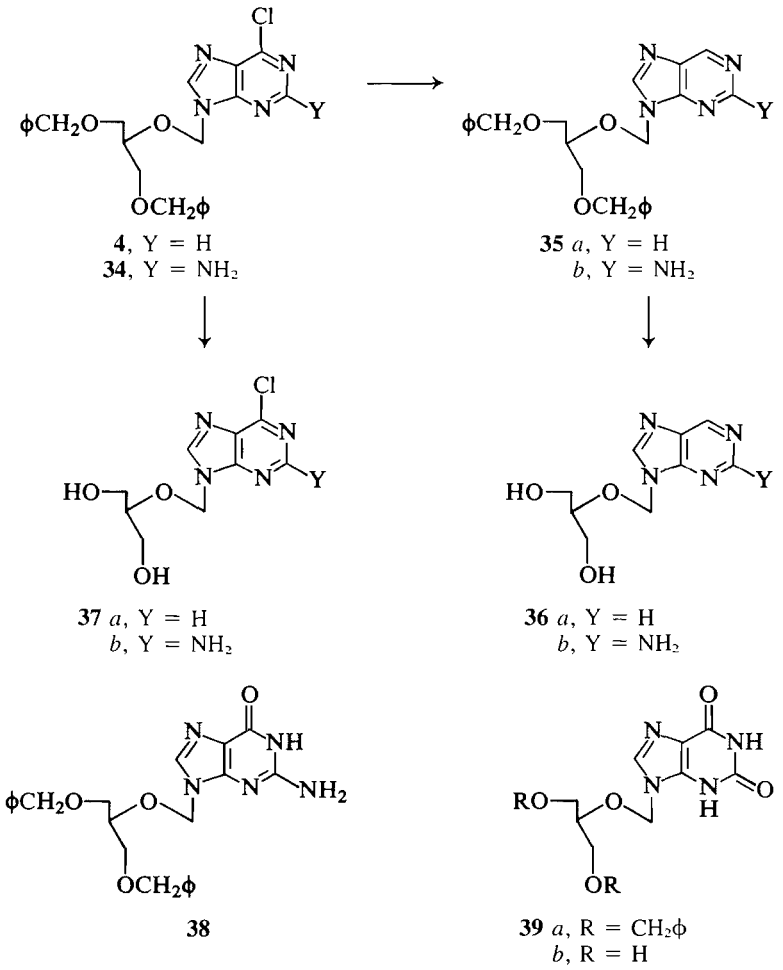

SCHEME 6

Sodium hydride (40 g of 50% NaH in oil, 0.834 mol of NaH) was washed with hexanes and added in portions to the benzyl alcohol with stirring. The addition required 15 min and stirring was continued for an additional hour. 1,3-Dichloropropan-2-ol was added and the system was heated at 100°C overnight. The reaction mixture was extracted with ether which was then washed sequentially with water, 20% aqueous HCl, and water (2×). The ether solution was dried over sodium sulfate and the ether was removed at reduced pressure. The excess benzyl alcohol was removed on a horizontal evaporator at reduced pressure. The remaining oil distilled under high vacuum to give 53 g (96%) of 1,3-dibenzyloxy-2-propanol (bp 195–210°C at 3 Torr). The product had R_f 0.35 in ether–hexane (1:1) and showed peaks in the ^{1}Hmr (60 MHz, $CDCl_3$) at δ: 2.92 (1H, OH), 3.58 (d, 4H, —$CH_2CHOHCH_2$—), 4.03 (m, 1H, —$CH_2CHOHCH_2$—), 4.58 (s, 4H, 2 × $PhCH_2$—), and 7.45 (m, 10H, 2 × Ph). The mass spectrum showed a molecular ion at *m/e* 272.

1,3-Dibenzyloxy-2-chloromethoxypropane (3)

1,3-Dibenzyloxy-2-propanol (50 g, 0.18 mol) was added to 1,2-dichloroethane (350 mL, distilled from P_2O_5) followed by paraformaldehyde (8 g). The reaction mixture was cooled in an ice bath and dry HCl gas was bubbled through the stirred solution for 6 h. Anhydrous calcium chloride was then added and after stirring for a few minutes the solution was collected by filtration. The filtrate was evaporated at reduced pressure to yield 53.5 g (91%) of compound **3** as a sirup. The product, which showed the following peaks in the ^{1}Hmr (60 MHz, $CDCl_3$), δ: 3.70 (d, 4H, —CH_2CHCH_2—), 4.13 (m, 1H, —CH_2CHCH_2—), 4.58 (s, 4H, 2 × $PhCH_2$—), 5.70 (s, 2H, OCH_2—Cl), and 7.38 (m, 10H, 2 × Ph), was used directly in coupling experiments.

9-[[2-Benzyloxy-1-(benzyloxymethyl)ethoxy]methyl]-6-chloropurine (4) and 7-[[2-benzyloxy-1-(benzyloxymethyl)ethoxy]methyl]-6-chloropurine (5)

6-Chloropurine (9 g, 58.5 mmol) was dissolved in DMF (50 mL) and triethylamine (7 g) was added. The solution was cooled in an ice–salt bath and compound **3** (58.5 mmol in 50 mL of DMF) was added. Triethylamine hydrochloride precipitated immediately. After 1 h the mixture was removed from the ice bath and was allowed to stand at room temperature for 12 h. The solution was collected by filtration and the solvents were removed at reduced pressure on a horizontal evaporator to yield 26.6 g of sirup. The residue was dissolved in a minimum of chloroform and applied to a silica gel column (24 × 6.3 cm) eluted with 1% methanol in chloroform. The yield of compound **4** was 14.8 g (60%) and that of compound **5** was 6.1 g (23%).

Compound **4** showed λ_{max}: 264 nm (pH 1), 264 nm (H_2O), and 264 nm (pH 13). The nmr spectrum in $CDCl_3$ showed signals at δ (ppm) of 3.53 (d, 4H, J = 5.5 Hz, —CH_2CHCH_2—), 4.03 (m, 1H, —CH—), 4.45 (s, 4H, 2 × $PhCH_2$—), 5.88 (s, 2H, —OCH_2N—), 7.33 (m, 10H, 2 × Ph—), 8.23 (s, 1H, H-2), and 8.78 (s, 1H, H-8).

Compound **5** had λ_{max} 268 nm at pH 1, 7, and 13. The nmr spectrum ($CDCl_3$) gave signals at δ (ppm) of 3.53 (d, 4H, J = 5.0 Hz, —CH_2CHCH_2—), 3.82 (m, 1H, —CH—), 4.47 (s, 4H, $PhCH_2$—), 5.98 (s, 2H, —OCH_2N—), 7.27 (m, 10H, 2 × Ph—), 8.33 (s, 1H, H-2), and 8.82 (s, 1H, H-8).

Compound 4. Direct route

6-Chloropurine (15.6 g) was dissolved in DMF (75 mL) and triethylamine (11.1 g) was added. The solution was cooled in an ice–salt bath and 32.3 g of **3** in DMF (50 mL) was added. After 2 h

Can. J. Chem. Downloaded from www.nrcresearchpress.com by 210.87.254.6 on 09/06/12
For personal use only.

TABLE 1. Physical properties of purine derivatives

Compound	Melting point (°C)	R_f*	λ_{max} (nm) pH 1 (ε)	pH 7 (ε)	pH 14 (ε)
1	193–195	0.37[a]	256(13 700)	259(13 750)	259(14 200)
18	200–204	0.27[b]	256(14 600)	259(18 975)	259(15 850)
19	188–190	0.46[c]	288(25 750)	279(20 600)	298(12 450)
22	168–170	0.49[b]	256(14 900)	259(13 900)	259(15 350)
23	135–136	0.45[^]	256(14 600)	259(14 850)	259(15 100)
24	106–109	0.40[^]	256(13 800)	259(13 550)	254(14 200)
27	183–185	0.68[^]	291(9 200)	278.5(9 840)	278.5(10 050)
			252(10 800)	255(9 200)	255(9 520)
30	232–233	0.65[^]	261.5(13 000)	261.5(14 700)	261.5(14 875)
32	dec.>200°C	0.45[^]	282(12 200)	291.5(10 100)	284(9 880)
			234(6 600)	247(8 130)	249(6 930)
33	193–195	0.58[^]	248(11 860)	248(14 260)	252(14 710)
36*a*	137–138	0.36[c]	262.5(6 300)	262.5(7 650)	262.5(8 400)
36*b*	156–157	0.33[a], 0.72[^]	313(3 840)	303(6 730)	303(7 000)
			246(5 380)	244(6 700)	244(7 250)
37*a*	126–128	0.52[c]	264(9 700)	264(8 720)	264(10 000)
37*b*	132 dec	0.35[c]	309(10 800)	309(11 300)	309(10 600)
			246(11 500)	247(12 000)	246(10 800)
39*b*	dec.>270°C	0.61[^]	261(8 930)	276(8 640)	276(9 500)
			233(8 000)	247(10 000)	247(10 960)

*Solvents for tlc: dichloromethane–methanol (a) 7:3; (b) 9:1; (c) 8:2. Solvent for paper chromatography: A (*i*PrOH–NH_4OH–H_2O; 7:1:2, v/v/v).

the mixture was removed from the ice bath and allowed to stand at room temperature for 18 h. The work-up was the same as in the above experiment except that the sirup obtained (48 g) was not applied directly to silica gel but was heated at 90°C for 24 h. Nuclear magnetic resonance showed that all of **5** had disappeared and the only product present was **4**. The product was further purified by chromatography on silica gel using $CHCl_3$–EtOAc (7:3) as eluant. Compound **4** was obtained as a sirup in 69% yield.

9[[2-Benzyloxy-1-(benzyloxymethyl)ethoxy)]methyl]adenine (6)

Compound **4** (22.3 g, 0.05 mol) was dissolved in methanol (15 mL) and 60 mL of saturated methanolic ammonia was added. The solution was sealed in a steel bomb which was then placed in an oil bath maintained at 110°C for 36 h. On cooling, the mixture was removed from the bomb, concentrated to about half its original volume, and then shaken with a mixture of water and chloroform. The organic phase was separated, washed with water, and dried over sodium sulfate. On evaporation of the solvent, 20 g of crude product was obtained. After recrystallization from ethanol, a total of 18.8 g (88%) of compound **6** was obtained as a white solid, mp 129–131°C. Compound **6** had a λ_{max} at 258 nm (pH 1), 260 nm (pH 7), and 260 nm (pH 13). The nmr spectrum ($CDCl_3$) showed signals at δ (ppm) of 3.55 (d, 4H, —CH_2—CH—CH_2—), 4.03 (m, 1H, —CH—), 4.47 (s, 4H, 2 × $PhCH_2$—), 5.77 (s, 2H, —OCH_2N—), 6.47 (bs, 2H, —NH_2), 7.28 (m, 10H, 2 × Ph—), 7.93 (s, 1H, H-2), and 8.38 (s, 1H, H-8).

7[[2-Benzyloxy-1-(benzyloxymethyl)ethoxy]methyl]adenine (7)

Compound **5** (2 g, 4.6 mmol) was treated as above for **4**. The product was purified from tlc using MeOH—$CHCl_3$ (5:95). The product crystallized from ethanol to give 1.03 g (54%) of **7** (mp 91–93°C). Compound **7** had a λ_{max} at 273 nm (pH 1) and 268 nm at pH 7 and 13. The nmr spectrum ($CDCl_3$) showed signals at δ (ppm) of 3.53 (d, 4H, —CH_2CHCH_2—), 3.93 (m, 1H, —CH—), 4.43 (s, 4H, 2 × $PhCH_2$—), 5.72 (s, 2H, —OCH_2N—), 7.82 (s, 1H, H-2), and 8.42 (s, 1H, H-8).

9-[[2-Benzyloxy-1-(benzyloxymethyl)ethoxy]methyl]adenine (6)

Adenine (500 mg) was suspended in HMDS (30 mL) and ammonium sulfate (200 mg) was added. The mixture was heated at reflux until a clear solution was obtained. The excess HMDS was removed at reduced pressure and the residue was dissolved in benzene (30 mL) to which mercuric cyanide (1.12 g) was added. After heating this mixture at reflux for 10 min, compound **3** (2.52 g dissolved in 10 mL of benzene) was added and refluxing was continued for 2 h. After cooling to room temperature, the solution was filtered from some insoluble material and was then extracted with methylene chloride (3 × 100 mL). The methylene chloride solution was washed successively with 30% aqueous potassium chloride (2 × 100 mL) and water (100 mL) and then dried over magnesium sulfate. The solvent was removed at reduced pressure to leave a residue that was dissolved in methanol (50 mL) and the resulting solution was heated at reflux for 1 h. The solution was concentrated to a small volume and subjected to silica gel chromatography using methylene chloride – methanol (9:1). Compound **6** was obtained in 30% yield (465 mg).

9-[[2-Hydroxy-1-(hydroxymethyl)ethoxy]methyl]adenine (1)

Compound **6** (20.5 g) was dissolved in hot ethanol (500 mL) and fresh palladium oxide (10 g) and cyclohexene (200 mL) were added. The reaction mixture was stirred overnight (18 h) at room temperature followed by heating at reflux for 2-1/2 h. The mixture was cooled and filtered. The residue was washed with 800 mL of hot ethanol. The filtrate and washings were combined and evaporated to yield 10.7 g of crude product. The crude product was treated with decolorizing carbon in hot water. Crystals were obtained by diluting a solution of the product in 10 mL of hot water with 400 mL of ethanol. A total of 9 g of compound **1** (77%, mp 193–195°C) was obtained. Signals in the nmr spectrum (DMSO-d_6) occurred at δ (ppm): 3.40 (m, 4H), 3.98 (m, 1H), 4.58 (t, 2H), 5.61 (s, 2H), 7.2 (s, 2H, —NH_2), 8.06 (s, 1H), and 8.13 (s, 1H). Other properties are collected in Tables 1 and 2.

8-BromoA (8)*

8-BromoA* was prepared according to a standard procedure (10). A* (72 mg, 0.3 mmol) was dissolved in 0.5 mL of 0.5 *M* Na^+OAc^- buffer (adjusted to pH 4.3 with AcOH). A saturated solution of bromine–water (0.25 mL) was then added and the reaction mixture was allowed to stir at 22°C for several hours. Thin-layer chromatography was used to monitor the reaction and after ~3 h most of A* had been converted to a faster moving material. A few milligrams of sodium bisulfite were then added to the reaction mixture until the red color had disappeared. The solution was then evaporated to dryness, dissolved in ~1 mL of 95% EtOH, and applied to two thick-layer silica gel plates. The plates were developed in $CHCl_3$–EtOH

Can. J. Chem. Downloaded from www.nrcresearchpress.com by 210.87.254.6 on 09/06/12
For personal use only.

TABLE 2. ^{13}C nuclear magnetic resonance data (δ, ppm) for purine acyclonucleosides*

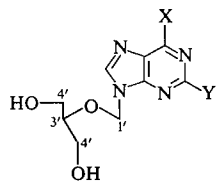

Compound	C-2	C-4	C-5	C-6	C-8	C-1′	C-3′	C-4′
1	152.95	149.71	118.69	156.08	141.35	71.82	80.50	60.97
18	152.89	149.71	118.58	156.02	141.13	71.38	78.45	60.70, 51.04
22	152.89	149.65	118.53	155.97	140.97	71.11	76.56	51.20
23	153.00	149.76	118.69	156.13	141.35	71.70	81.03	61.56, 42.52
24	153.16	149.82	118.74	156.24	141.45	71.54	81.84	42.89
27	158.56	151.76	112.54	154.73	139.03	71.65	80.23	60.97
30	159.04 (J_{CF} 205.07 Hz)	151.11 (J_{CF} 19.53 Hz)	117.10 (J_{CF} 3.66 Hz)	157.72 (J_{CF} 20.75 Hz)	141.78	72.03	80.66	60.91
32	154.08	152.62	109.36	150.25	139.89	72.19	80.39	60.91
33	148.52	146.20	123.98	156.94	140.65	72.19	80.66	60.91
36*a*	151.43	152.46	133.70	147.98	147.50	72.13	81.14	60.97
36*b*	160.82	153.22	126.78	149.22	143.13	71.32	80.39	60.86
37*a*	149.17	152.19	130.93	152.03	147.93	72.78	81.41	60.91
37*b*	154.24	149.44	123.28	160.02	143.35	71.92	80.66	60.92
39*b*	151.11	140.70	115.83	158.13	137.20	73.16	80.34	60.92

*Spectra were obtained in DMSO-d_6 on a Bruker WH90 spectrometer.

(8:2) and a band at R_f 0.24 was eluted with methanol. The methanol was then evaporated to leave 78 mg (82%) of 8-bromoA* as a white solid (mp 172–174°C); R_f: 0.24 ($CHCl_3$–EtOH (8:2)), 0.09 ($CHCl_3$–EtOH (6:1)); uv (95% EtOH), λ_{max}: 264 nm; λ_{min}: 233 nm; ^{1}Hmr (DMSO-d_6), δ: 8.17 (1H, s, C2—H), 7.37 (2H, s, NH_2), 5.6 (2H, s, O—CH_2—N), 4.67 (2H, t, OH), 4.0 (1H, m, H—C—O), 3.43 (4H, d, (HO—CH_2)$_2$—CHO).

Monomethoxytrityl A (9)*

Compound **1** (598 mg, 2.5 mmol) was dissolved with gentle heating in "dry" pyridine (40 mL) and the solution was cooled to room temperature. Monomethoxytrityl chloride (781 mg, 2.53 mmol) was then added and the reaction mixture was stirred at 22°C for 24 h. Pyridine was then removed under reduced pressure by co-distilling with toluene to leave a gummy foam which was dissolved in $CHCl_3$ (6 mL) and applied to 12 thick-layer silica gel plates. The plates were developed in $CHCl_3$–EtOH (8:2) and a uv absorbing band at R_f 0.63 was eluted with methanol. The methanol was then evaporated to leave a gum which was dissolved in $CHCl_3$ (5 mL). Addition of hexanes (25 mL) resulted in the precipitation of a fluffy white material which after drying under vacuum afforded 767 mg (60%) of the desired product (mp 94–97°C); R_f: 0.16 (EtOAc), 0.63 ($CHCl_3$–EtOH; 4:1), 0.35 (THF–EtOAc; 1:1); uv (95% EtOH) λ_{max}: 259, 231 nm; λ_{min}: 246, 227 nm; ^{1}Hmr ($CDCl_3$), δ: 8.3 (1H, s, C8—H), 7.83 (1H, s, C2—H), 6.7–7.43 (14H, m, trityl), 6.1 (2H, s, NH_2), 5.73 (2H, s, O—CH_2—N), 4.83 (1H, s, OH), 3.77 (4H, m, OCH_3, H—C—O), 3.25 (4H, d, (HO—CH_2)$_2$—CHO).

General procedure for the preparation of nucleotides

$$\overset{O}{\overset{\|}{}}$$

A. *Preparation of (MMT-A*)$_2$ $POCH_2CCl_3$ (10)*

Collidine (4.2 equiv.) was added to THF (0.5 mL) in a vial fitted with a rubber septum and a magnetic stirrer. The vial was then cooled to −78°C in a Dry Ice − acetone bath. 2,2,2-Trichloroethylphosphorodichloridite (0.55 equiv.) was then added. A solution containing MMT-A* (0.5 mmol) in THF (0.5 mL) was added dropwise over a 5-min period. The reaction mixture was vigorously stirred throughout the addition. Stirring was continued for an additional 30 min at −78°C followed by 30 min at 22°C.

Iodine (1.1 equiv.) and pyridine (2 drops) in THF–H_2O (2:1, v/v, 1.5 mL) was then added and the septum was removed. After 20 min the solvents were removed at reduced pressure. The residue was dissolved in chloroform which was washed successively with 5% $NaHSO_3$ (20 mL) solution and water (20 mL). The chloroform solution was concentrated to a small volume and applied to six thick-layer plates developed in $CHCl_3$–EtOH (6:1). The product band was eluted with ethyl acetate and the product was obtained by precipitation with hexane. The yield of **10** was 56% (mp 103–104°C). The product had an R_f of 0.42 in $CHCl_3$–EtOH (6:1) and showd λ_{max} at 258 nm (95% EtOH).

The product **10** was deprotected in the sequence (1) removal of methoxytrityl, (2) removal of the trichloroethyl group by Zn–Cu couple in DMF to give the nucleotide **11** (A*pA*). Compound **11** had λ_{max} at 258 nm (95% EtOH) and had $R_f^{\wedge}$ of 0.32 (paper chromatography) and E_m^{Tp} of 0.22 (pH 7.5).

B. *Mixed nucleotides d-ApA* (12) and A*pdA (13)*

This procedure was similar to that above except that 0.2 mmol of MMT-dA and 0.22 mmol of $TCEOPCl_2$ were used and stirring was continued for only 10 min at −78°C. At this point MMT-A* (0.18 mmol) in THF (0.5 mL) containing collidine (0.75 mmol) was added rapidly with stirring. The solution was stirred at −78°C for 20 min followed by 20 min at 22°C. Iodine was added as described in A above and the rest of the procedure is also as described in A. The yield of

$$\overset{O}{\overset{\|}{}}$$

MMT-dA P(OTCE) A*MMT was 65% (mp 112–116°C); R_f 0.62 ($CHCl_3$–EtOH; 6:1); λ_{max}: 258 (95% EtOH).

This material was deprotected as in A above to give dApA*, λ_{max} 258 nm (95% EtOH), $R_f^{\wedge}$ of 0.36, and E_m^{Tp} of 0.20.

The nucleotide of A*pdA (**13**) was prepared in a similar manner and had λ_{max} 258 nm (95% EtOH), $R_f^{\wedge}$ of 0.33, and E_m^{Tp} of 0.20.

Enzyme assays

A. *Adenosine deaminase*

(a) *Substrate studies*

A stock solution of adenosine was prepared by dissolving the nucleoside (10.22 μmol, 2.730 mg) in 100 mL of a stock solution of potassium phosphate (KH_2PO_4) buffer (pH 7.5, 0.055 *M*). Aliquots of the adenosine stock solution were then taken to prepare solutions with

Can. J. Chem. Downloaded from www.nrcresearchpress.com by 210.87.254.6 on 09/06/12
For personal use only.

Can. J. Chem. Downloaded from www.nrcresearchpress.com by 210.87.254.6 on 09/06/12
For personal use only.

adenosine concentrations of 81.72 μ*M*, 61.29 μ*M*, 51.08 μ*M*, 40.86 μ*M*, and 20.43 μ*M*. Each solution was prepared by placing the appropriate stock solution aliquot in a 10-mL volumetric flask and adjusting to volume with KH_2PO_4 buffer solution.

A stock solution of adenosine deaminase was prepared by weighing the enzyme (1 mg) into a 10-mL volumetric flask and adjusting to volume with the stock solution of KH_2PO_4 buffer solution.

The following procedure was then carried out to measure deaminase activity.

(*i*) An aliquot (2 mL) of each adenosine solution was placed in a 1 cm × 1 cm quartz cuvette (sample cell). KH_2PO_4 buffer solution (0.5 mL) was then added and the solution shaken to enhance mixing. KH_2PO_4 buffer solution (2.5 mL) was then placed in a second cuvette (reference cell) and the absorbance of each adenosine solution measured at 259 nm at 22°C on a Cary 17 spectrophotometer. The reading for each solution was recorded as absorbance at time of mixing, i.e. at $T = 0$.

(*ii*) Procedure (*i*) above was then repeated for each adenosine solution. However, instead of 0.5 mL of buffer being added to the sample cell, 0.5 mL of the adenosine deaminase stock solution was added. The reference cell contained 2 mL of KH_2PO_4 buffer and 0.5 mL of the adenosine deaminase stock solution. For each sample, when the deaminase solution was added, a timer was started and absorbance readings at 259 nm were taken every 10 s for 1.5 min. For all sample solutions, the absorbance was found to decrease linearly with time over the first 60 s.

(*iii*) The change in absorbance for each adenosine solution (for the first minute of reaction) was converted to change in concentration (for the conversion of adenosine to inosine at 259 nm, $\Delta A = 7400 \cdot b \cdot \Delta C$, (where b = cell path length)), the reaction velocity, V, in μmol/min/mg of enzyme was determined, and a plot of $1/S$ (S = substrate concentration) vs. $1/V$ made. Thus, by the method of Lineweaver and Burk, the Michaelis and maximum velocity constants, K_m and V_{max} respectively, were determined.

The above procedure was then repeated for the adenosine analogue A*. The initial stock solution of A* was 50 μ*M* (1.185 mg/100 mL of KH_2PO_4 buffer solution) and the enzyme stock solution contained 20 mg of enzyme/mL of buffer. Ultraviolet readings were taken over a period of 1.5 min. As with adenosine itself, K_m and V_{max} for A* were determined according to the methods of Lineweaver and Burk. The results are summarized in the discussion section.

(b) *Inhibition studies*

The general procedure described above for the determination of deaminase activity with adenosine as substrate was followed. However, substrate solutions in this assay contained A* in addition to the natural nucleoside.

Stock solutions of adenosine in KH_2PO_4 buffer (2.73 mg/50 mL buffer) and A* in KH_2PO_4 buffer (2.39 mg A*/50 mL buffer) were first prepared. A series of substrate solutions to be used in the assay were then prepared as follows. Aliquots (5 mL, 4 mL, 3 mL, 2.5 mL, 2 mL, and 1 mL) of the adenosine stock solution were placed in 10-mL volumetric flasks. To each flask, 5 mL of the A* stock solution was added. Each volumetric was then brought to volume with KH_2PO_4 buffer solution. Deaminase activity was then measured as described above. The apparent Michaelis constant, K_1, was determined according to the methods of Lineweaver and Burk.

B. *Snake venom phosphodiesterase (Russel's viper venom)*

Two hundred units of lyophilized enzyme obtained from Calbiochem were dissolved in 1 mL of tris-(hydroxymethyl)amino methane buffer (adjusted to pH 9.2 with 0.1 *N* HCl). The enzyme solution (0.1 mL) was then added to the nucleotide (0.2 to 0.5 mg) in a small vial and the reaction mixture was incubated at 37°C for 6 h. The solution was then applied to Whatman 3 MM paper as a 3-cm wide band. Papers were developed in solvent A or solvent F and nucleoside and nucleotide bands were cut out, eluted with water, and diluted to a known volume. The ultraviolet absorbance of each band was recorded against the absorbance of appropriate blanks. Blanks were prepared by cutting bands from the paper directly opposite the nucleotide bands and of the same size and shape as the nucleotide bands. The blanks were eluted with water and brought to the same volume as the corresponding nucleotide bands. Absorbances were measured for each solution in 1-cm path length quartz cells.

C. *Spleen phosphodiesterase (bovine, type 1)*

Ten to fifteen units of lyophiized enzyme obtained from Nutritional Biochemicals Corp. were dissolved in 1 mL of 0.01 *M* sodium pyrophosphate buffer (adjusted to pH 6.5 with phosphoric acid). The enzyme solution (0.1 mL) was added to the nucleotide (0.2–0.5 mg) previously dissolved in 0.2 mL of 0.05 *M* ammonium acetate buffer (adjusted to pH 6.5 with acetic acid). The mixture was then incubated at 37°C for 6 h. Degradation products were separated and ratios determined spectrophotometrically as described in B above.

Silylation of A (production of **14** and **15**)*

Compound **1** (1.0 g, 4.17 mmol) and imidazole (0.34 g, 1.2 equiv.) were suspended in DMF (30 mL). TBDMS-Cl (0.63 g) was added in portions over a 20-min period and the mixture was stirred for an additional 10 min. Solvents were removed at reduced pressure and the residue was chromatographed on silica gel (column) using methylene chloride – methanol (9:1) as eluant. The bis-silylated A* (**15**) was obtained in 25% yield (0.45 g, mp 160–161°C, R_f 0.59 (CH_2Cl_2–MeOH; 9:1). Compound **15** showed signals in the nmr (DMSO-d_6) at δ (ppm): 0.90 (s, 18H), 3.65 (m, 5H), 3.73 (s, 2H), 6.60 (bs, 2H, NH_2), 7.93 (s, 1H), and 8.33 (s, 1H).

In addition to compound **15**, starting material (360 mg, 36% recovery) and monosilyl derivative **14** (550 mg, 38%) were also recovered. Compound **14** had mp 153–155°C, R_f 0.29 (CH_2Cl_2–MeOH; 9:1) and showed signals in the nmr (DMSO-d_6) at δ: 0.00 (s, 6H, $(CH_3)_2Si$), 0.86 (s, 9H, $(CH_3)_3C$), 3.38–3.68 (m, 4H, —CH_2CH—CH_2—), 4.72 (t, 1H, —CH), 5.72 (s, 2H, —CH_2N), 7.18 (b, 2H, NH_2), 8.25 (s, 1H, H-2), and 8.3 (s, 1H, H-8).

*Tosylation of compound **14***

Compound **14** (725 mg) was dissolved in pyridine (15 mL) and the solution cooled to 0°C in an ice bath. *p*-Toluenesulfonyl chloride (470 mg, recrystallized) was added and the solution was stirred at 0°C for 2 h followed by 18 h at −10°C. Solvents were removed at reduced pressure and by coevaporation of benzene to remove the last traces of pyridine. The residue was purified by silica gel chromatography using CH_2Cl_2–MeOH (9:1). In addition to 100 mg of starting material, 810 mg (90%) of compound **16** was obtained, mp 115–118°C, R_f of 0.49 (CH_2Cl_2–MeOH; 9:1), and showing signals in the nmr ($CDCl_3$) at δ (ppm): 0.0 (s, 6H, $(CH_3)_2Si$), 0.8 (s, 9H, $(CH_3)_3C$), 2.45 (s, 3H, CH_3—), 3.5 (d, 2H, —CH_2—OSi), 3.8–4.2 (m, 3H, —CH—CH_2OTs), 5.65 (s, 2H, —CH_2—N), 6.24 (b, 2H, NH_2), 7.2–7.4, 7.63–7.78 (9H aromatic), 8.0 (s, 1H, H-2), and 8.4 (s, 1H, H-8).

Preparation of N*-benzoylA* (**19**)*

Compound **1** (2.7 g, 11.3 mmol) was suspended in pyridine (60 mL) and benzoyl chloride (12 equiv.) was slowly added. The mixture was stirred at room temperature for 20 h and then diluted with methanol (20 mL). Solvents were removed at reduced pressure to leave a sirup which was dissolved in methylene chloride. The solution was washed with water (2×), dried over sodium sulfate, and concentrated to a viscous residue at reduced pressure. The residue was washed with ethanol (5 mL) which was separated by filtration and discarded. The white solid remaining was dissolved in pyridine (80 mL) to which 2 *N* NaOH (100 mL) was added. After stirring for 1 h the solution was neutralized with Dowex 50 WX8 (H^+ form). The solvent was collected by filtration and concentrated to a small volume at reduced pressure. The product was isolated by silica gel column chromatography using methylene chloride – methanol (9:1, 500 mL) followed by the same solvents in a 7:3 ratio. The product **19** was obtained as a white solid, mp 188–190°C (52%). The nmr spectrum (DMSO-d_6) showed signals at δ (ppm): 3.67 (bm, 5H), 5.86 (s, 2H), 7.66 (m, 3H, aromatic), 8.12 (m, 2H, aromatic), 8.63 (s, 1H), and 8.80 (s, 1H). Other properties are collected in Tables 1 and 2.

Tosylation of N*-benzoylA**

Compound **19** (2.4 g) was dissolved in pyridine (50 mL) and the solution was cooled in an ice bath. *p*-Toluenesulfonyl chloride (6 g,

Can. J. Chem. Downloaded from www.nrcresearchpress.com by 210.87.254.6 on 09/06/12
For personal use only.

~5 equiv.) was added and, after stirring for 1 h, the solution was kept in a cold chest (−10°C) for two days. The solvent was removed at reduced pressure and the residue was dissolved in methylene chloride which was washed with water and dried over sodium sulfate. The solvent was removed at reduced pressure to leave a viscous gum. This material did not solidify after numerous attempts at crystallization. The material appeared homogeneous on tlc and nmr and was used directly in subsequent steps; R_f 0.5 (CH_2Cl_2−CH_3OH; 9:1); signals appeared in the nmr ($CDCl_3$) with δ (ppm) of 2.43 (s, 3H, CH_3—), 3.83−4.13 (m, 4H, —CH(CH_2O—)$_2$), 5.63 (s, 2H, —CH_2—N), 7.2−8.06 (m, 13H, aromatic), 8.1 (s, 1H, H-2), 8.76 (s, 1H, H-8), and 9.16 (b, 1H, —NHC(=O)—).

9[[2-Azido-1-(azidomethyl)ethoxy]methyl]-N-*benzoyladenine* (**21**)

Compound **20** (4 g) was dissolved in DMF (50 mL) and sodium azide (2 g) was added. The mixture was heated at 90−95°C for 3 h. The solvent was removed at reduced pressure and the residue was dissolved in methylene choride which was washed with water and dried over sodium sulfate. The solvent was removed at reduced pressure and the residue crystallized from ethanol to yield 1.86 g (77%) of compound **21** (mp 130−133°C). Compound **21** (R_f 0.65; CH_2Cl_2−CH_3OH (9:1)) had λ_{max} at 292 nm (pH 1), 282 nm (pH 7), and 302 nm (pH 14). The infrared spectrum (KBr) had a signal at 2100 cm^{-1} (—N_3). The nmr spectrum ($CDCl_3$) showed signals at δ (ppm) of 3.36 (d, 4H, —CH_2N_3, J = 6 Hz), 4.03 (t, 1H, —CH—), 5.83 (s, 2H, —OCH_2N—), 7.76 (m, 5H, Ph—), 8.20 (s, 1H, H-2), 8.80 (s, 1H, H-8), and 8.99 (b, 1H, —NHC(=O)—).

9-[[2-Azido-1-(azidomethyl)ethoxy]methyl]adenine (22)

Compound **21** (1.21 g) was dissolved in pyridine (15 mL) and 29% aqueous NH_4OH solution (60 mL) was added. The mixture was heated at 55°C for 3 h with stirring. The solvent was then removed at reduced pressure to leave a solid which crystallized from ethanol to give compound **22** (787 mg, 89%, mp 168−170°C). The nmr spectrum (DMSO-d_6) showed signals at δ (ppm): 3.20 (d, 4H), 4.10 (t, 1H), 5.70 (s, 2H), 7.23 (b, 2H, —NH_2), 8.13 (s, 1H), and 8.23 (s, 1H). Other properties are collected in Tables 1 and 2.

Direct conversion of A to 8 and 22*

Compound **1** (A*, 1 mmol), triphenylphosphine (2 mmol), and lithium azide (10 mmol) were dissolved in DMF (20 mL). Carbon tetrabromide (2 mmol) was added and the mixture was stirred at room temperature for 24 h. The solvents were removed at reduced pressure and the residue was dissolved in a minimum amount of pyridine and subjected to flash chromatography on silica gel using methylene chloride − methanol (9:1) as eluant. The minor product was compound **22** obtained in 14% yield. The major product was 9[[2-azido-1-(hydroxymethyl)ethoxy]methyl]adenine (**18**) obtained in 53% yield (mp 200−204°C, ir (KBr): 2080 cm^{-1} (—N_3)). The nmr spectrum (DMSO-d_6) showed signals at δ (ppm): 3.50 (d, 2H), 3.78 (d, 1H), 4.0 (m, 1H), 5.80 (s, 2H), 8.25 (s, 1H), and 8.35 (s, 1H). Other properties are collected in Tables 1 and 2.

Conversion of 17 into 18

Compound **17** (200 mg in THF (10 mL)) was treated with tetrabutylammonium fluoride (0.68 *M* in THF (3 mL)) for 2 h. After removal of solvents and chromatography of the residue on silica gel using methylene chloride − methanol (4:1), 110 mg of compound **18** was obtained (80% yield). The product was identical to the material obtained above.

9-[[2-Amino-1-(aminomethyl)ethoxy]methyl]adenine (24)

Compound **22** (300 mg) was dissolved in ethanol (50 mL) and subjected to hydrogenation at room temperature and one atmosphere of hydrogen over 5% palladium on charcoal (100 mg) for 18 h. The solvent was collected by filtration and the residue was washed with ethanol (200 mL). The combined filtrate and washings were concentrated at reduced pressure. The residue crystallized from ether to yield compound **24** (220 mg, 90%, mp 106−109°C). The nmr spectrum (DMSO-d_6) showed signals at δ (ppm): 2.56 (d, 4H), 3.43 (t, 1H), 5.63 (s, 2H), 8.16 (s, 1H), and 8.27 (s, 1H). Other properties are collected in Tables 1 and 2.

Conversion of 18 to 9-[[2-Amino-1-(hydroxymethyl)ethoxy]methyl]-adenine (23)

Compound **18** (400 mg) was dissolved in 70% aqueous ethanol and 5% Pd on charcoal (150 mg) was added. The mixture was subjected to room temperature hydrogenation under 30 psi of hydrogen for 2 h. The solution was collected by filtration and the residue washed with 95% ethanol (200 mL). The combined filtrate and washings were evaporated to dryness. The residue crystallized from ethanol−ether to give compound **23** (210 mg, 52%). The nmr spectrum (DMSO-d_6) showed signals at δ (ppm): 3.45 (bm, 5H), 5.73 (s, 2H), 8.28 (s, 1H), and 8.37 (s, 1H). Other properties are collected in Tables 1 and 2.

9-[[2-Hydroxy-1-(hydroxymethyl)ethoxy]methyl]-2,6-diamino-purine (27)

N^2,N^6-Diacetyl-2,6-diaminopurine (4.45 g) was suspended in DMF (350 mL). Triethylamine (2.3 g) and compound **3** (7.3 g in DMF (20 mL)) were added and the resulting solution was stirred for 60 h at room temperature, followed by heating at 40°C for 1 h. The clear solution was concentrated at reduced pressure and the residue was dissolved in chloroform (50 mL). The chloroform solution was washed with a saturated solution of sodium chloride, followed by water, and then dried over magnesium sulfate. The solvent was removed to give a viscous residue which crystallized from ethanol to give 5.4 g of white, crystalline **25** (mp 188−192°C); the nmr spectrum in $CDCl_3$ showed signals with δ (ppm) of 2.5 (s, 3H, CH_3CO—), 2.6 (s, 3H, CH_3CO—), 3.54 (d, 4H, 2 × —CH_2—O), 4.1 (q, 1H, —CH), 4.43 (s, 4H, 2 × —CH_2C), 5.75 (s, 2H, —CH_2—N),7.3 (s, 10H, 2 × —C_6H_5—), 8.3 (s, 1H, H-8), 9.7 (s, 1H, —NH—CO), 9.8 (s, 1H, —NH—CO).

Compound **25** (5.15 g) was dissolved in 400 mL of methanol containing 460 mg of sodium. The mixture was heated at reflux for 2 h and then stirred at room temperature for 12 h. The solution was neutralized with acetic acid and the solvent was removed at reduced pressure. The residue was dissolved in chloroform (500 mL) which was washed with water and then dried over magnesium sulfate. The solvent was removed at reduced pressure to leave a white solid (4.2 g) which crystallized from methylene chloride − ether to give compound **26** (3.7 g, 85%, mp 85−87°C). The nmr spectrum of **26** in $CDCl_3$ showed signals at δ (ppm) of 3.50 (d, 4H, 2 × CH_2O), 4.0 (q, 1H, —CH), 4.43 (s, 4H, 2 × —$CH_2\phi$), 5.18 (bs, 2H, —NH_2), 5.6 (s, 2H, —CH_2N—), 6.0 (bs, 2H, —NH_2), 7.15 (s, 10H, 2 × C_6H_5—), and 7.6 (s, 1H, H-8).

Compound **26** (800 mg) was dissolved in ethanol (100 mL) to which palladium oxide (400 mg) and cyclohexene (60 mL) were added. The mixture was heated at reflux for 3 h, cooled, filtered, and the residue washed with 70% aqueous ethanol (200 mL). The combined filtrates and washings were evaporated to dryness. The residue crystallized from ethanol to yield compound **27** (370 mg, 80%). The nmr spectrum (DMSO-d_6) showed signals at δ (ppm): 3.60 (bm, 5H), 5.53 (s, 2H), 6.93 (b, —NH_2), and 7.93 (s, 1H). Other properties are collected in Tables 1 and 2.

Enzymatic conversion of compound 27 to BIOLF-62

Compound **27** was subjected to adenosine deaminase (0.4 mg/mg **27**) at pH 7.5 (0.05 *m* phosphate buffer, 0.2 mL/mg **27**). The solution was allowed to stand at 25°C for 18 h. At this point tlc showed that compound **27** had been completely converted into BIOLF-62 (compound **2**). The yield of **33** was virtually quantitative and properties were identical to those previously reported (2).

Enzymatic conversion of A to 33*

The above procedure was repeated using 30 mg of adenosine deaminase and 500 mg of A* in 25 mL of buffer solution at 20°C for 24 h. The solvent was concentrated at reduced pressure to 2 mL and poured into hot ethanol (100 mL). The precipitate was removed by

Can. J. Chem. Downloaded from www.nrcresearchpress.com by 210.87.254.6 on 09/06/12
For personal use only.

filtration. The filtrate was concentrated to a dry residue which crystallized from water to yield 455 mg (90%) of compound **33**. The nmr spectrum (DMSO-d_6) showed signals at δ (ppm): 3.51 (m, 5H), 5.70 (s, 2H),6.73 (b, —NH), 8.10 (s, 1H), and 8.23 (s, 1H). Other properties are collected in Tables 1 and 2.

*9-[[2-Hydroxy-1-(hydroxymethyl)ethoxy]methyl]-2-fluoroadenine (**30**)*

Compound **26** (2 g) was dissolved in 60% HF in pyridine (16 mL) at −70°C (Dry Ice − acetone). The temperature of the mixture was allowed to rise to −40°C, at which point *tert*-butylnitrite (750 μL) was added. The mixture was stirred at −30 to −40°C for 15 min and then poured into ice-water (100 g). The aqueous mixture was extracted with chloroform (5 × 100 mL) and the combined chloroform extracts were washed successively with 5% sodium bicarbonate solution and water. After drying over magnesium sulfate, the solvent was removed at reduced pressure and the residue chromatographed on silica gel using methylene chloride − methanol (92:8) as eluant. In addition to recovery of starting material (300 mg), 200 mg of the monobenzyl product **29** and 200 mg of the dibenzyl product **28** were obtained. Compound **29** (mp 190−193°C) had signals in the nmr spectrum (DMSO-d_6) at δ (ppm) of 3.4 (bd, 4H, —CH_2O—), 3.8 (m, 1H, —CH), 4.4 (s, 2H, —$CH_2\phi$), 5.6 (s, 2H, —CH_2N—), 7.27 (s, 5H, C_6H_5), 7.77 (bs, 2H, —NH_2), and 8.2 (s, 1H, H-8). Compound **28** (mp 142−145°C) had signals in the nmr spectrum ($CDCl_3$) with δ (ppm) of 3.45 (d, 4H, 2 × —CH_2O—), 4.0 (g, 1H, —CH), 4.5 (s, 4H, 2 × —CH_2O), 5.70 (s, 2H, —CH_2N—), 6.37 (bs, 2H, —NH_2), 7.3 (s, 10H, 2 × C_6H_5—), and 7.90 (s, 2H, H-8).

Compound **28** (600 mg) was dissolved in ethanol (100 mL) to which was added palladium oxide (300 mg) and cyclohexene (60 mL). The mixture was heated at reflux for 3 h and worked up in the usual manner to yield, after crystallization from ethanol, compound **30** in 88% yield (313 mg). The nmr spectrum (DMSO-d_6) showed signals at δ (ppm): 3.6 (bm, 5H), 5.57 (s, 2H), 7.70 (bs, 2H, —NH_2), and 8.20 (s, 1H). Other properties are collected in Tables 1 and 2.

*9-[[2-Hydroxy-1-(hydroxymethyl)ethoxy]methyl]isoguanine (**32**)*

Compound **26** (660 mg) was dissolved in a mixed solvent containing tetrahydrofuran (15 mL) and water (10 mL). Sodium nitrite (600 mg) was added to the solution, followed by glacial acetic acid (8 mL). The solution was stirred at 50°C for 90 min, at which point additional sodium nitrite (600 mg), acetic acid (3 mL), and water (5 mL) were added and stirring at 50°C was continued for an additional 60 min. The mixture was cooled to room temperature, neutralized with 28% aqueous ammonium hydroxide, and extracted with methylene chloride (3 × 100 mL). The extracts were washed with water, dried over magnesium sulfate, and evaporated. The residue was chromatographed on silica gel using methylene chloride − methanol (4:1). Compound **31** was obtained in 55% yield and, on crystallization from methylene chloride − ether, had mp 183−185°C. In the nmr ($CDCl_3$), compound **26** showed signals at δ (ppm) of 3.50 (bd, 4H, 2 × —CH_2O—), 4.0 (m, 1H, —CH), 4.43 (s, 4H, 2 × —$CH_2\phi$), 5.53 (bs, 2H, —CH_2N—), 7.2 (s, 10H, 2 × C_6H_5—), and 7.50 (s, 1H, H-8).

Compound **31** (980 mg) was dissolved in ethanol (200 mL) and palladium oxide (500 mg) and cyclohexene (100 mL) were added. The mixture was heated at reflux for 12 h and filtered while hot. The residue was washed with hot 70% aqueous ethanol (300 mL). The combined filtrate and washings were evaporated and the residue was dissolved in hot water (20 mL). Ethanol (70 mL) was added and the solution was allowed to stand at room temperature. After 24 h the precipitate was collected by filtration to yield compound **32** (460 mg, 80%). The nmr spectrum (D_2O) showed signals at δ (ppm): 3.40 (bm, 5H), 5.33 (s, 2H), and 7.73 (s, 1H). Other properties are collected in Tables 1 and 2.

*9-[[2-Hydroxy-1-(hydroxymethyl)ethoxy]methyl]purine (**36**a)*

Compound **4** (1.7 g) was dissolved in absolute ethanol (100 mL) and 5% palladium on carbon (400 mg) and anhydrous sodium acetate (500 mg) were added. Hydrogenation was conducted at room temperature under 40 psi of hydrogen for 18 h. The residue was collected by filtration and washed with CH_2Cl_2−CH_3OH (1:1, 200 mL). The combined filtrate and washings were concentrated at reduced pressure to a dry residue. After chromatography on silica gel using CH_2Cl_2−CH_3OH (95:5), compound **35**a (1.37 g, 87%) was obtained as a viscous sirup; nmr, δ (ppm): 3.50 (d, 4H, —CH_2CHCH_2—), 4.0 (m, 1H, —CH—), 4.40 (s, 4H, 2 × $PhCH_2$—), 5.77 (s, 2H, —OCH_2N—), 7.20 (s, 10H, 2 × Ph—), 8.13 (s, 1H, H-2), 8.90 (s, 1H, H-8), and 9.90 (s, 1H, H-6).

Compound **35**a (767 mg) was dissolved in CH_2Cl_2 (50 mL) and the solution was cooled to −78°C. 1 *N* BCl_3 in CH_2Cl_2 (15 mL) was added to the solution under a nitrogen atmosphere. After 3 h at −78°C, the solution was diluted with CH_2Cl_2−CH_3OH (1:1, 100 mL) and allowed to stand at room temperature for 1 h. Upon addition of excess aqueous ammonia (28%), a precipitate formed. The solution was collected by filtration, concentrated to dryness, and the residue was extracted with methanol (50 mL). Silica gel (10 g) was added to the methanol solution and the excess solvent was removed at reduce pressure. The silica gel was added to a prepared silica gel column and the whole solumn was eluted with CH_2Cl_2−CH_3OH (8:2). Compound **36**a was obtained pure in 87% yield (370 mg). General properties of **36**a are collected in Tables 1 and 2. The nmr spectrum (DMSO-d_6) showed signals at δ (ppm): 3.40 (m, 5H), 4.60 (t, 2H), 5.80 (s, 2H), 8.70 (s, 1H), 8.96 (s, 1H), and 9.13 (s, 1H).

*9-[[2-Hydroxy-1-(hydroxymethyl)ethoxy]methyl]-2-aminopurine (**36***b*)*

Compound **34** (1.54 g) was treated as above for compound **4**. Compound **35***b* was obtained as a viscous sirup in 98% yield (R_f 0.42 (CH_2Cl_2−CH_3OH; 9:1); nmr, δ (ppm): 3.50 (d, 4H, —CH_2CH—CH_2—), 4.0 (m, 1H, —CH—), 4.37 (s, 4H, $PhCH_2$—), 5.60 (s, 2H, —OCH_2N—), 6.03 (b, 2H, —NH_2), 7.20 (s, 10H, 2 × Ph), 7.93 (s, 1H, H-8), and 8.56 (s, 1H, H-6). Compound **35***b* was treated with BCl_3 as described above for **35***a*. Compound **36***b* was obtained in 70% yield and general properties are collected in Tables 1 and 2. The nmr spectrum (D_2O) showed signals at δ (ppm): 3.33 (bm, 5H), 5.53 (s, 2H), 8.03 (s, 1H), and 8.37 (s, 1H).

*9-[[2-Hydroxy-1-(hydroxymethyl)ethoxy]methyl]-6-chloropurine (**37**a)*

Compound **4** (2.8 g) was treated with the 1N BCl_3 in CH_2Cl_2 solution as described above for compounds **35**. The product **37***a* was obtained pure from silica gel chromatography in 70% yield (1.16 g). General properties of **37***a* are collected in Tables 1 and 2. The nmr spectrum (DMSO-d_6) showed signals at δ (ppm): 3.56 (bm, 5H), 4.6 (t, 2H), 5.83 (s, 2H), and 8.82 (s, 2H).

*9-[[2-Hydroxy-1-(hydroxymethyl)ethoxy]methyl]-6-chloro-2-aminopurine (**37**b)*

Compound **34** (600 mg) was treated as above for compound **4**. The product, compound **37***b*, was obtained pure in 95% yield (345 mg). General properties are collected in Tables 1 and 2. The nmr spectrum (DMSO-d_6) showed signals at δ (ppm): 3.40 (bm, 5H), 5.52 (s, 2H), 6.35 (bs, 2H, —NH_2), and 8.15 (s, 1H).

*9-[[2-Hydroxy-1-(hydroxymethyl)ethoxy]methyl]xanthine (**39**b)*

Compound **38** (1 g) was dissolved in glacial acetic acid (100 mL) and water (50 mL). A solution containing 1 g of sodium nitrite in water (10 mL) was added dropwise over a period of 75 min at room temperature. The mixture was stirred for a further 3 h at room temperature. The solvents were removed at reduced pressure and the residue was extracted with dichloromethane. The extracts were washed with 5% aqueous sodium bicarbonate followed by saturated sodium chloride. The solution was dried over sodium sulfate and concentrated to a small volumne. The product **39***a* (mp 176−178°C, 60%) was obtained from silica gel chromatography using CH_2Cl_2−CH_3OH (92:8). The nmr spectrum in DMSO-d_6 showed signals at δ (ppm) of 3.50 (d, 4H, —CH_2CH—CH_2—), 4.0 (m, 1H, —CH—), 4.66 (s, 4H, 2 × $PhCH_2$—), 5.66 (s, 2H, —OCH_2N—), 7.30 (s, 10H, 2 × Ph), 7.80 (s, 1H, H-8), and 10.76 (b, 1H, NH).

Compound **39***a* was treated with BCl_3 as previously described. The

product, **39***b*, crystallized from ethanol–water and was obtained in 85% yield. The nmr spectrum (DMSO-d_6) showed signals at δ (ppm): 3.55 (bm, 5H), 5.53 (s, 2H), 7.20 (b, 1H, —NH), 7.80 (s, 1H), and 10.76 (b, —NH). Properties are collected in Tables 1 and 2.

Acknowledgements

We gratefully acknowledge financial assistance from Bio Logicals Inc. and the Natural Sciences and Engineering Research Council of Canada.

1. K. K. OGILVIE, L. SLOTIN, and P. RHEAULT. Biochem. Biophys. Res. Commun. **45**, 297 (1971).
2. (*a*) K. K. OGILVIE, U. O. CHERIYAN, B. K. RADATUS, K. O. SMITH, K. S. GALLOWAY, and W. L. KENNELL. Can. J. Chem. **60**, 3005 (1982); (*b*) K. K. OGILVIE, R. G. HAMILTON, M. F. GILLEN, B. K. RADATUS, K. O. SMITH, and K. S. GALLOWAY. Can. J. Chem. **62**, 16 (1984); (*c*) K. K. OGILVIE, D. M. DIXIT, B. K. RADATUS, and K. O. SMITH. Nucleosides Nucleotides. **2**, 147 (1983).
3. K. O. SMITH, K. S. GALLOWAY, W. L. KENNELL, K. K. OGILVIE, and B. K. RADATUS. Antimicrob. Agents Chemother. **22**, 55 (1982).
4. K. O. SMITH, K. S. GALLOWAY, K. K. OGILVIE, and U. O. CHERIYAN. Antimicrob. Agents Chemother. **22**, 1026 (1983).
5. K. O. SMITH, S. L. HODGES, K. S. GALLOWAY, K. K. OGILVIE, and U. O. CHERIYAN. J. Infect. Dis. In press.
6. K. K. OGILVIE and M. F. GILLEN. Tetrahedron Lett. **21**, 327 (1980).
7. M. F. GILLEN. PhD Thesis, McGill University, 1980.
8. A. BLOCH, M. J. ROBINS, and J. R. MCCARTHY. J. Med. Chem. **10**, 908 (1967).
9. J. L. YORK and G. A. LEPAGE. Can. J. Biochem. **44**, 331 1966).
10. H. ROKOS, A. MYLES, W. HUTZENLAUB, and W. PFLEIDERER. Chem. Ber. **108**, 2872 (1975).
11. I. YAMAMOTO, M. SEKINE, and T. HATA. J. Chem. Soc. Perkin Trans. 1, 306, (1980).
12. H-J. LEE and R. VINCE. J. Pharm. Sci. **69**, 1019 (1980).
13. H. IWAMURA and T. HASHIZUME. J. Org. Chem. **33**, 1796 (1968).
14. D. A. CARSON, D. B. WASSON, J. KAYE, B. ULLMAN, D. W. MARTIN, R. K. ROBINS, and J. A. MONTGOMERY. Proc. Natl. Acad. Sci. **77**, 6865 (1980).
15. Y. H. KIM, R. J. NACHMAN, L. PAVELKA, F. A. FUHRMAN, and G. J. FUHRMAN. J. Nat. Prod. **44**, 206 (1981).
16. A. F. COOK, R. T. BARTLETT, R. P. GREGSON, and R. J. QUINN. J. Org. Chem. **45**, 4020 (1980).
17. M. J. ROBINS and B. UZNANSKI. Can. J. Chem. **59**, 2608 (1981).
18. R. S. VICKERS, J. F. GERSTER, and R. K. ROBINS. Synthetic procedures in nucleic acid chemistry. Vol. I. Intersience, New York. 1968. p. 244.
19. F. SEELA and S. MENKHOFF. Justus Liebigs Ann. Chem. 813 (1982).

Can. J. Chem. Downloaded from www.nrcresearchpress.com by 210.87.254.6 on 09/06/12
For personal use only.

On the structure and energies of protonated cations of H_2CS, HFCS, and F_2CS

FRIEDRICH GREIN

Department of Chemistry, University of New Brunswick, Fredericton, N.B., Canada E3B 6E2

Received May 20, 1983

FRIEDRICH GREIN. Can. J. Chem. **62**, 253 (1984).

Using 4-31G basis sets, the geometries of H_2CS, HFCS, and F_2CS as well as their protonated cations were optimized. In each case, three protonation sites, S, C, and H (for H_2CS) or F (for HFCS and F_2CS) were considered. The H or F protonation leads to molecular complexes of the form $HX \ldots YCS^+$. For H_2CS and F_2CS, the S-protonation site is favored, whereas for HFCS the linear complex $HF \ldots HCS^+$ is the most stable protonated form. Predicted proton affinities are 177.4 for H_2CS (180.9 experimental), 172.0 for HFCS, and 149.1 kcal/mol for F_2CS.

FRIEDRICH GREIN. Can. J. Chem. **62**, 253 (1984).

Faisant appel aux ensembles de base 4-31G, on a optimisé les géométries du H_2CS, du HFCS et du F_2CS et de leurs cations protonés. On a considéré dans chaque cas trois sites de protonation, S, C et H pour (H_2CS) ou F (pour HFCS et F_2CS). La protonation de H ou de P conduit à des complexes moléculaires de la forme: $HX \ldots YCS^+$. Dans le cas de H_2CS et de F_2CS, le site de protonation S est favorisé tandis que pour HFCS le complexe linéaire $HF \ldots HCS^+$ est la forme protonée la plus stable. Les prédictions d'affinités pour le proton sont de: 177,4 pour H_2CS (valeur expérimentale 180,9), de 172,0 pour HFCS et de 149,1 kcal/mol pour F_2CS.

[Traduit par le journal]

Can. J. Chem. Downloaded from www.nrcresearchpress.com by 210.87.254.40 on 09/06/12
For personal use only.

Introduction

Experimental studies of reactions yielding the thiomethoxy cation H_3CS^+ and the thiolmethyl carbonium ion H_2CSH^+ have been reported in the literature (1–4). Experimental work is presently in progress to find and characterize protonated species of HFCS and F_2CS (5).

Theoretical investigations of cation structure and related proton affinities have been shown to be very useful. In the following, *ab initio* calculations at the 4-31G level will be reported for geometries and energies of cations resulting from the protonation of H_2CS, HFCS, and F_2CS. Besides the two obvious protonation sites — sulfur and carbon — molecular complexes of the form $HX \ldots YCS^+$, where X and Y are H or F, formally corresponding to protonation at the H or F site, were also considered, leading to some interesting and unexpected results.

Method

All geometry optimizations were performed using the 4-31G basis set (6), and the HONDO 5 (7), the GAUSSIAN 70 (8), and an IBM version (9*a*) of the GAUSSIAN 80 (9*b*) computer program. Unless stated otherwise, restricted Hartree–Fock (RHF) energies are given for singlet states. Several triplet states were calculated with the unrestricted Hartree–Fock (UHF) method. In general, gradient optimization techniques were employed. For each compound, three different protonation sites were investigated.

Results

H_2CS and protonated forms

The results for H_2CS, H_2CSH^+, H_3CS^+ (singlet), and $H_2 \ldots HCS^+$ are given in Table 1. Here, and in the following text, the various protonated isomers are distinguished by the placement of the additional H in the molecular formula. H_2CSH^+ refers to protonation at the sulfur site, H_3CS^+ to protonation at carbon, whereas $H_2 \ldots HCS^+$ indicates a molecular complex with weak interaction between the components H_2 and HCS^+. Thioformaldehyde, H_2CS, has been the topic of several *ab initio* studies (10–15). The 4-31G geometry and energy obtained by Bernardi *et al.* (12) agrees with ours. Experimental geometry parameters (16) are included in Table 1. The best geometry optimization was performed by Jaquet *et al.* (15), using a good double ζ plus polarization (DZP) basis set, and the CEPA-PNO method. Their CS and CH bond distances agree with the experimental values within 0.002 Å. The S-protonated structure H_2CSH^+, which is overall the most stable (singlet) isomer, was also studied by Bernardi *et al.* (12). Their optimized geometry parameters and energy are very similar to ours. These authors also investigated nonplanar conformations of H_2CSH^+ and a linear C—S—H^+ arrangement, but found them to be less stable. The optimized geometry obtained for H_2CSH^+ is very similar to that of protonated H_2CO, which for obvious reasons prefers oxygen as protonation site (17).

In C_{3v} symmetry, H_3CS^+ has the electron configuration $\ldots 2e^4 1a_1^2 3e^2$, which normally leads to a lowest-energy singlet state of A_1 symmetry. For this state, the single-determinant SCF method is unable to form the required linear combination, and the SCF wavefunction corresponds to a mixture of symmetry species. A two-determinant wavefunction of the form $e_x^2 + e_y^2$ would be required for the correct linear combination. On the other hand, an SCF geometry optimization in C_s symmetry overcomes the problem of the symmetry impurity, and the results are expected to be very close to the C_{3v} results for $^1A_1$. Therefore, a C_s SCF optimization was carried out. The results are given in Table 1. Dill and McLafferty (3) gave for the STO-3G optimized C_s geometry of H_3CS^+ (R_{CS} = 1.790 Å, R_{CH} = 1.103/1.091 Å) the 4-31G energy of −436.21806 hartree, only marginally higher than our energy. In each case, the CS distance increases by more than 0.2 Å relative to H_2CS.

Yamabe *et al.* (18) reported results for the triplet e^2 state of H_3CS^+, which according to Hund's rule is expected to be of lower energy than the singlet. Their UHF optimized geometry is R_{CS} = 1.94 Å, R_{CH} = 1.08 Å, and ∠HCS = 105.8°. The UHF energy is −436.30362 hartree, much lower than the RHF singlet energy. Since the UHF method is not subject to the symmetry restriction, a comparison of UHF with RHF energies is not meaningful. The triplet state resulting from the e^2 orbital occupation would have A_2 symmetry. Dill and McLafferty (3) obtained a similarly low energy for the triplet state of H_3CS^+ (−436.30145 hartree). By estimating the difference in correlation energies for triplet and singlet states, they came to the conclusion that the singlet C_{2v} structure (H_2CSH^+) is more

TABLE 1. 4-31G geometry optimization results for H_2CS and protonated singlet species; distances are in Å, angles in deg

Parameter	Value			
	H_2CS	H_2CSH^+	H_3CS^+	$H_2\cdots HCS^+$
CS	1.628(1.6109)[a]	1.654	1.859	1.488
CH	1.073(1.0925)[a]	1.073/1.074[b]	1.097/1.076[c]	1.069
$SH/H_2\cdots H/HH$		1.360		2.342/0.732[d]
∠HCS	122.2(121.56)[a]	101.6	102.7/109.6[c]	180.0
∠CSH		124.3/117.3[b]		
Symmetry	C_{2v}	C_s	C_s	C_{2v}
E (hartree)	−435.99188	−436.27456	−436.21925	−436.21001
PA[e] (kcal/mol)		177.4	142.7	136.9

[a]Experimental values in parentheses, ref. 16.
[b]H_1 is listed before H_2. See diagram.
[c]The first value refers to the hydrogen in the molecular symmetry plane. The dihedral angles of H_2 and H_3 for rotation about CS are ±116.2°.
[d]2.342 Å is the distance from the midpoint of H_2 to H of HCS^+. 0.732 Å is the H_2 distance.
[e]Calculated proton affinity.

stable than triplet C_{3v} by about 10 kcal/mol. This agrees qualitatively with their experimental findings. Roy and McMahon (4), in an experimental study designed to observe the different proton transfer reactions resulting from the two isomers H_3CS^+ and H_2CSH^+, failed to discover any evidence of H_3CS^+. From a theoretical point of view, configuration-interaction calculations on both triplet H_3CS^+ and singlet H_2CSH^+ are required, using in each case RHF molecular orbitals. Attempts to confirm the UHF-triplet H_3CS^+ results mentioned above (3, 18) failed. For the geometry reported by Yamabe *et al.*, a higher energy (−436.20176 hartree) was obtained. For other geometries, either a higher energy or convergence difficulties were encountered.

In the last column of Table 1, results are given for the $H_2\ldots HCS^+$ molecular complex, formally corresponding to protonation at one of the H-sites. The optimal geometry is of C_{2v} symmetry, corresponding to a weak bond between H_2 and HCS^+, with a stabilization energy relative to $H_2 + HCS^+$ of 0.70 kcal/mol. In the same basis (4-31G), the geometry of isolated HCS^+ is R_{CS} = 1.488 Å, R_{CH} = 1.068 Å, with an energy of −435.08206 hartree, and the H—H distance of isolated H_2 is 0.730 Å, with an energy of −1.12682 hartree. Only extremely small distortions are encountered in the formation of the complex. The distance of the center of mass (CM) of H_2 to H of HCS^+ was optimized to be 2.342 Å. However, due to the weak interaction between the two components, a complete distance optimization is beyond the accuracy of the employed methods. Yamabe *et al.* (18) reported the same stabilization energy of 0.7 kcal/mol, but an H_2 (CM)..H distance of 3.5 Å. For protonated H_2CO, a similar complex, $H_2\ldots HCO^+$, was proposed by Schleyer *et al.* (19).

Of the three isomers of protonated H_2CS studied here, the S-protonated H_2CSH^+ is the most stable, corresponding to a proton affinity of 177.4 kcal/mol. Lossing (1) obtained 181.6 kcal/mol, and Roy and McMahon reported a very similar experimental value of 180.9±1 kcal/mol. The agreement with the *ab initio* result is excellent.

HFCS and protonated forms

Thioformyl fluoride, HFCS, is not known. $HFCSH^+$ occurs in mixtures of H_2S and CHF_3 which are currently under experimental study (5). So far, there is no knowledge about the likely structure of the $HFCSH^+$ ion.

Results of the 4-31G geometry optimizations are given in Table 2. HFCS has CS and CH distances similar to H_2CS, and a normal CF single bond distance. The geometry of HFCS, as well as F_2CS, was optimized by Kapur *et al.* (13) using an STO-3G basis set.

Protonation of HFCS at the sulfur site gives a proton affinity of 162.5 kcal/mol. Note that the proton is *cis* with F. In the *trans* form, the energy is only insignificantly higher (1×10^{-5} hartree). Nonplanar configurations of $HFCSH^+$ were also considered, but were found to be less stable than the planar ones.

The C-protonated singlet isomer H_2FCS^+ is again characterized by a long CS distance, about 0.3 Å over the normal CS double bond distance. Due to the proximity of F, the CH distances also increase significantly. The proton affinity of this singlet isomer is quite small. Not given are the results of a UHF geometry optimization for triplet H_2FCS^+. The CS distance is 2.105 Å, CF 1.345 Å, CH 1.072 Å, the FCS angle is 103.1°, HCS 102.9°, and the dihedral angle of H with respect to the FCS plane, for rotation about CS, is 118.2°. The UHF energy, corresponding to this geometry, is −534.99760 hartree. This energy should not be compared with the RHF values for singlet states. But since it is higher than the RHF energy of $HFCSH^+$ one may conclude that triplet H_2FCS^+ is no competitor for the most stable protonated form of HFCS. The situation with respect to triplet states is quite different from the previous case of H_3CS^+. There, the C_{3v} symmetry allowed for degenerate orbitals, and the two highest-energy electrons resided in an *e*-orbital. For such cases, qualitative predictions place the triplet state lower than the singlet. The C_s symmetry of H_2FCS^+, on the other hand, does not lead to any symmetry-caused degeneracies, and only doubly occupied orbitals are expected. The same situation will apply to HF_2CS^+.

The geometry optimization of the F-protonated species was started with a proton attached sideways to the fluorine of HFCS. The gradient optimization eventually lead to the linear arrangement $HF\ldots HCS^+$, data of which are contained in Table 2. It is seen that the HCS^+ part of the complex has a

Can. J. Chem. Downloaded from www.nrcresearchpress.com by 210.87.254.40 on 09/06/12
For personal use only.

TABLE 2. 4-31G geometry optimization results for HFCS and protonated singlet species; distances are in Å, angles in deg

	Value			
Parameter	HFCS	$HFCSH^+$ 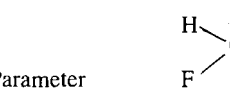	H_2FCS^+ 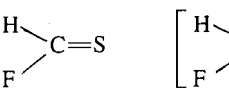	$HF\cdots HCS^+$ 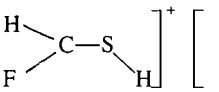
CS	1.611	1.672	1.910	1.492
CF/F···H	1.351	1.296	1.353	F··H:1.696
CH	1.069	1.072	1.215	1.083
θ_H/SH/HF	—	SH:1.363	θ_H:120.8[a]	HF:0.928
∠FCS	126.9	122.5	109.5	—
∠HCS/∠CSH	123.4	121.8/99.1	105.0	180
Symmetry	C_s	C_s	C_s	$C_{\infty v}$
E (hartree)	−534.722 62	−534.981 52	−534.914 40	−534.996 71
PA[b] (kcal/mol)	—	162.5	120.3	172.0

[a] θ_H is the dihedral angle of H with respect to the FCS plane, for rotation about C—S.
[b] Calculated proton affinity.

structure very similar to isolated HCS^+, and the HF bond length in the complex (0.928 Å) is similar to the optimized bond distance of 0.922 Å for HF (the 4-31G energy of HF is −99.88728 hartree). Relative to HF + HCS^+, the complex is stabilized by 17.2 kcal/mol. If one considers HF . . . HCS^+ as a proton-bound dimer of HF with CS, then the stabilization energy is 209.0 kcal/mol. (Isolated CS is calculated to have an optimal CS bond distance of 1.555 Å and an energy of −434.77617 hartree). For a proton-bound dimer, such as $H_2O \ldots H^+ \ldots OH_2$, or $H_2O \ldots H^+ \ldots OCH_2$, one expects the protons to be more evenly spaced between the two monomers (see refs. 20, 21), and not closely attached to one of them with a regular AH single bond distance.

The HF . . . HCS^+ molecular complex has a lower energy than $HFCSH^+$, and corresponds therefore to the most stable protonated form of HFCS. Experimental investigations on this ion would be of great interest. According to our results, the S-protonated $HFCSH^+$ is still more stable than isolated HF + HCS^+ (by about 8 kcal/mol), and should therefore not decompose.

F_2CS and protonated forms

Optimized geometries and energies of thiocarbonyl fluoride F_2CS and its various protonated forms are given in Table 3. The CS and CF bond distances of F_2CS are larger than the experimental values (22) by about 0.02 Å. With polarization functions on S, the CS bond shortens to 1.581 Å, while the CF bond length remains similar (14). The STO-3G optimized CS distance is 1.588 Å (13), slightly shorter than the experimental distance.

The sulfur protonated form, F_2CSH^+, shows regular bond distances and bond angles. The proton affinity of F_2CS relative to this isomer is 149.1 kcal/mol. The carbon protonated ion HF_2CS^+ shows an even longer CS bond than the corresponding ions of H_2CS and HFCS, but has regular CF and CH distances. The corresponding proton affinity is only 105.1 kcal/mol. UHF geometry optimizations on triplet HF_2CS^+ resulted in very weak CS bonds, with bond distances moving between 2.5 and 3 Å without much change in total energy. Due to this, the gradient optimization did not converge.

The optimized geometry of the HF . . . FCS^+ complex is shown in the diagram of Table 3. FCS^+ is almost linear, whereas HF is attached to one side, with a long CF distance of 2.373 Å. Geometry optimization of linear FCS^+ gave a CS distance of 1.499 Å, a CF distance of 1.239 Å, and an energy of −533.76976 hartree. The CF distance of the complex is exactly the same, and the CS distance differs by 0.001 Å only. The HF distance of the complex is identical to that of the HF . . . HCS^+ complex. So again, the complex is composed of FCS^+, very weakly interacting with HF. The stabilization with respect to HF + FCS^+ is 14.9 kcal/mol. A proton bound dimer explanation is not possible.

A linear complex with an HF . . . F atomic arrangement is not expected to be stable. Geometry optimizations on a linear complex with an FH . . . F arrangement were done, but the complex was found to dissociate. For F_2CS, the most stable protonated form is calculated to be F_2CSH^+, with a proton affinity of 149.1 kcal/mol. The HF . . . FCS^+ molecular complex is only 6 kcal/mol less stable, and formation in gas-phase ion experiments should be possible.

Discussion

In Table 4, the calculated proton affinities are summarized for the three possible protonation sites. The S-protonation energy decreases from H_2CS to F_2CS. Similarly, the C-protonation energy decreases quite regularly with increasing fluorine substitution, and the C-site proton affinities are always well below the S-site values. A very irregular behavior, however, is seen for the H or F protonation, which leads to molecular complexes. The HF . . . HCS^+ complex is exceptionally stable, about 30 kcal/mol more stable than HF . . . FCS^+, relative to the parent molecules.

The high stability of HF . . . HCS^+ causes an irregularity in the "best" proton affinity (last column of Table 4), which switches from the S-site for H_2CS to the F-site for HFCS and back to the S-site for F_2CS. The structure and stability of the complexes of H_2 or HF with HCS^+ or FCS^+ are of interest in their own right. In Table 5, shapes, distances, and stabilization energies are summarized. Again, HF . . . HCS^+ shows to be an exception in terms of stabilization energy and distortion. Whereas for $H_2 \ldots HCS^+$ and HF . . . FCS^+ distortions relative to the isolated species are in general only 0.002 Å or less (0.006 Å for the HF distance of HF . . . FCS^+), the HF distance

Can. J. Chem. Downloaded from www.nrcresearchpress.com by 210.87.254.40 on 09/06/12
For personal use only.

TABLE 3. 4-31G geometry optimization results for F_2CS and protonated singlet species; distances are in Å, angles in deg

Parameter	Value			
	F_2CS	F_2CSH^+	HF_2CS^+	$HF\cdots FCS^+$
	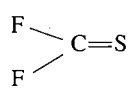	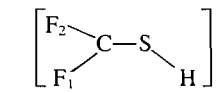	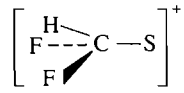	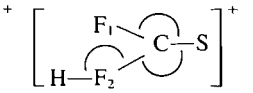
CS	1.611(1.589)[a]	1.702	2.149	1.500
CF_1/CF_2	1.328(1.315)[a]	1.282/1.277	1.317	1.239/2.373
SH/CH/HF	—	1.363	1.068	0.928
$\angle F_1CS/\angle F_2CS/\angle HSC$	126.3(126.45)[a]	124.3/121.2/96.4	105.0/101.7[b]	175.8/101.9/148.5[c]
Symmetry	C_{2v}	C_s	C_s	C_s
E (hartree)	−633.452 34	−633.689 96	−633.620 23	−633.680 81
PA[d] (kcal/mol)	—	149.1	105.4	143.4

[a]Experimental values in parentheses, ref. 16.
[b]The angles listed are ∠HCS/∠FCS. The dihedral angle of F with respect to the HCS plane, rotation about C—S, is 122.4°.
[c]The angles listed are $\angle F_1CS/\angle F_2CS/\angle HF_2C$; see diagram for definition of angles.
[d]Calculated proton affinity.

TABLE 4. Comparison of 4-31G proton affinities (in kcal/mol)

Molecule	S proton	C proton	H/F proton	Best site	Best PA
H_2CS	177.4	142.7	H:136.9	S	177.4
HFCS	162.5	120.3	F:172.0	F	172.0
F_2CS	149.1	105.4	F:143.4	S	149.1

TABLE 5. Shapes and stabilization energies of complexes (relative to H_2/HF plus HCS^+/FCS^+)[a]

Molecule	Shape	R	CS	CH/CF	HH/HF	ΔE
H_2CS	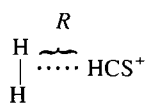	2.342	1.488 (1.488)	1.069 (1.068)	0.732 (0.730)	0.7
HFCS	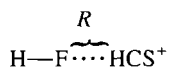	1.696	1.492 (1.488)	1.083 (1.068)	0.928 (0.922)	17.2
F_2CS	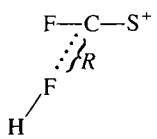	2.373	1.500 (1.499)	1.239 (1.239)	0.928 (0.922)	14.9

[a]Distances in Å, energies in kcal/mol. Values in parentheses were optimized for the isolated monomers H_2/HF and HCS^+/FCS^+.

of $HF\ldots HCS^+$ is elongated by (the same) 0.006 Å, but the CH distance by 0.015 Å. Such distortions are representative of the interactions taking place between the two components of the complex. One may say that $HF\ldots HCS^+$ shows a very small amount of proton-bound-dimer character, which becomes noticeable in its larger stabilization energy.

Summary

Proton affinities of H_2CS, HFCS, and F_2CS were calculated, considering in each case three different protonation sites. In general, protonation at sulfur leads to the greatest stabilization, and therefore to the most likely to be encountered protonated species. However, for HFCS the linear molecular complex of the form $HF\ldots HCS^+$ is calculated to be more stable than the S-protonated form $HFCSH^+$. The elongation of the CH distance relative to isolated HCS^+ shows that a small amount of charge transfer in the direction $F^{(-)}\ldots H^{(+)}$ takes place, which cannot be so easily accomplished for the other two complexes, $H_2\ldots HCS^+$ and $HF\ldots FCS^+$. In the case of $HF\ldots FCS^+$, HF is attached to C, the most electropositive element of FCS^+. Here, only a small energy difference of 6 kcal/mol between the S-protonated form and the molecular complex is predicted.

The question of a possible triplet H_3CS^+ ion, which, from qualitative arguments, should have lower energy than (singlet) H_2CSH^+, has not been addressed. A comparison of UHF energies for triplet H_3CS^+ with RHF energies of singlet H_2CSH^+ is not valid. RHF calculations on triplet H_3CS^+ can, in principle, be performed, and the calculated energies be compared with those of H_2CSH^+. However, due to symmetry problems and the different amounts of correlation energy expected for triplet and singlet states, it appears that the only acceptable method of treating this problem is by configuration interaction calculations on both triplet H_3CS^+ and singlet H_2CSH^+. Such work is being planned.

Inclusion of d-orbitals as well as diffuse functions in the basis set would undoubtedly lead to more accurate results. This, however, would require a much higher amount of computer time. Since the calculated proton affinity of H_2CS agrees well with the experimental one, and the inclusion of polarization and diffuse functions usually changes optimized geometries and energies very little, no compelling reason can be seen at this time for carrying out more expensive calculations with larger basis sets.

Acknowledgements

Dr. T. B. McMahon suggested this investigation. His continuous help and interest is gratefully acknowledged. Neilan Mehta, Chris Grein, and Uday Sishta performed many of the calculations. The financial support by NSERC and the generous allocation of computer time by the University of New Brunswick were essential to the success of this study.

1. F. P. LOSSING. Private communication.
2. R. E. KUTINA, A. K. EDWARDS, G. L. GOODMAN, and J. BERKOWITZ. J. Chem. Phys. **77**, 5508 (1982).

Can. J. Chem. Downloaded from www.nrcresearchpress.com by 210.87.254.40 on 09/06/12
For personal use only.

3. J. D. DILL and F. W. MCLAFFERTY. J. Am. Chem. Soc. **101**, 6526 (1979).
4. M. ROY and T. B. MCMAHON. Org. Mass. Spectrom. **17**, 392 (1982).
5. T. B. MCMAHON. Private communication.
6. R. DITCHFIELD, W. J. HEHRE, and J. A. POPLE. J. Chem. Phys. **54**, 724 (1971).
7. M. DUPUIS, J. RYS, and H. KING. QCPE, **11**, 338 (1977).
8. W. J. HEHRE, W. A. LATHAN, D. DITCHFIELD, M. D. NEWTON, and J. A. POPLE. QCPE, **10**, 236 (1973).
9. (*a*) P. N. VAN KAMPEN, F. A. A. M. DE LEEUW, G. F. SMITS, and C. ALTONA. QCPE, **14**, 437 (1982); (*b*) J. S. BINKLEY, R. A. WHITESIDE, R. KRISHNAN, R. SEEGER, D. J. DEFREES, H. B. SCHLEGEL, S. TOPIOL, L. R. KAHN, and J. A. POPLE. QCPE, **13**, 406 (1981).
10. N. C. BAIRD and J. R. SWENSON. J. Phys. Chem. **77**, 277 (1973).
11. (*a*) P. J. BRUNA, S. D. PEYERIMHOFF, R. J. BUENKER, and P. ROSMUS. Chem. Phys. **3**, 35 (1974); (*b*) P. G. BURTON, S. D. PEYERIMHOFF, and R. J. BUENKER. Chem. Phys. **73**, 83 (1982).
12. F. BERNARDI, I. G. CSIZMADIA, B. SCHLEGEL, and S. WOLFE. Can. J. Chem. **53**, 1144 (1975).
13. A. KAPUR, R. P. STEER, and P. G. MEZEY. J. Chem. Phys. **70**, 745 (1979).
14. H. OBERHAMMER and J. E. BOGGS. J. Mol. Struct. **55**, 283 (1979).
15. R. JAQUET, W. KUTZELNIGG, and V. STAEMMLER. Theoret. Chim. Acta, **54**, 205 (1980).
16. D. R. JOHNSON, F. X. POWELL, and W. H. KIRCHHOFF. J. Mol. Spectrosc. **39**, 136 (1971).
17. J. E. DEL BENE and A. VACCARO. J. Am. Chem. Soc. **98**, 7526 (1976).
18. T. YAMABE, K. YAMASHITA, F. FUKUI, and K. MOROKUMA. Chem. Phys. Lett. **63**, 433 (1979).
19. P. V. R. SCHLEYER, E. D. JEMMIS, and J. A. POPLE. Chem. Commun. 190 (1978).
20. P. J. DESMEULES and L. C. ALLEN. J. Chem. Phys **72**, 4731 (1980).
21. I. H. WILLIAMS, G. MAGGIORA, and R. L. SCHOWEN. J. Am. Chem. Soc. **102**, 7831 (1980).
22. A. J. CARELESS, H. W. KROTO, and B. M. LANDSBERG, Chem. Phys. **1**, 371 (1973).

Can. J. Chem. Downloaded from www.nrcresearchpress.com by 210.87.254.40 on 09/06/12
For personal use only.

The structure of a minor alkaloid from *Argemone grandiflora* Sweet subsp. *grandiflora*

R. E. MITCHELL, K. ANN KERR, and M. H. BENN[1]

Department of Chemistry, The University, Calgary, Alta., Canada T2N 1N4

Received July 22, 1983

R. E. MITCHELL, K. ANN KERR, and M. H. BENN. Can. J. Chem. **62**, 258 (1984).

Grandiflorine, a minor alkaloid of *Argemone grandiflora* Sweet subsp. *grandiflora*, is shown to be identical with ribasine (and most likely limogine) and have the carbinolamine ether-bridged indanobenzazepine structure **1**.

R. E. MITCHELL, K. ANN KERR et M. H. BENN. Can. J. Chem. **62**, 258 (1984).

On a déterminé que la grandiflorine, un alcaloïde mineur d'*Argemone grandiflora* Sweet (sous-espèce *grandiflora*), est identique à la ribasine (et fort probablement à la limogine) et possède la structure **1** d'un éther carbinolamine–indanobenzazepine ponté.

[Traduit par le journal]

Can. J. Chem. Downloaded from www.nrcresearchpress.com by 210.87.254.5 on 09/06/12
For personal use only.

Recent reports (1, 2) of the isolation of an alkaloid with the structure **1** prompt us to describe our own characterization of this compound.[2]

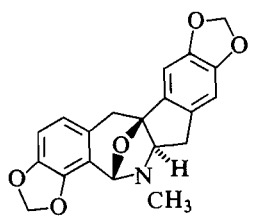

1

In 1969, during a study of the alkaloids of *Argemone grandiflora* Sweet subsp. *grandiflora*, we isolated small amounts of a base which we first designated alkaloid F, and subsequently called grandiflorine. High-resolution mass spectrometry indicated that grandiflorine had the molecular composition $C_{20}H_{17}NO_5$, and this was substantiated by X-ray crystallography of the hydrobromide salt (q.v.). Infrared spectroscopy revealed that grandiflorine did not contain hydroxyl or carbonyl groups, while ^{1}H nmr indicated the presence of two disubstituted methylenedioxybenzene units, a benzylic CH_2, an N—CH_3, and what appeared to be a carbinolamine ether (cf. Table 1). The uv spectrum showed that the two benzenoid chromophores were nonconjugated.

The genus *Argemone* is a rich source of tetrahydrobenzylisoquinoline derivatives (4), and indeed the major and all minor alkaloids which we isolated (5) from *A. grandiflora* subsp. *grandiflora* proved to belong to this group; so we anticipated that grandiflorine would, too. However, the spectroscopic data seemed to be accommodated by several structures and, as a paucity of material prevented extensive chemical investigations, we decided to solve the problem by X-ray crystallography of grandiflorine hydrobromide.

The crystals of this salt were orthorhombic, space-group $P_{2_1}P_{2_1}P_{2_1}$, $a = 11.10_4$, $b = 18.80_5$, $c = 9.21_0$ Å, with 4 molecules to the unit cell, $d_{obs} = 1.490$ (mol. wt. ≡ 431.4; calcd. for $C_{20}H_{18}BrNO_5$: 432.3). Intensity data were estimated visually from multiple-film Weissenberg photographs taken with CuK_α radiation, and the structure was solved by normal heavy atom methods. By present-day standards, these methods were primitive and the *R*-factor, for 1045 independent reflexions and 153 parameters, was large (17.5%). The standard deviation of an observation of unit weight was 0.787. No correction was made for absorption or anomalous dispersion. Nevertheless, the results revealed that grandiflorine had the *relative stereochemistry* shown in **1**, a structure in full accord with the other spectroscopic data.

Having exhausted our stock of grandiflorine and pending another, still unmade, collection of more plant material, we set aside the problem of determing the absolute stereochemistry of grandiflorine. There matters rested until Castedo and coworkers announced (1) that X-ray crystallography of an alkaloid which his group had isolated from *Sarcocapnos crassifolia*, and *Corydalis claviculata*, and named ribasine, had the structure *including absolute stereochemistry* shown in **1**. The physical constants reported for ribasine (1) left little doubt that it was the same as our alkaloid, and a comparison of the ir spectra of the two compounds clinched this identification.

Although limogine, isolated from *C. claviculata* by another group, was reported to be amorphous, the phsysical data given (2) leave no doubt that it is **1**; i.e. grandiflorine, ribasine, and limogine are identical.

Experimental

Instrumental methods were as described previously (6).

Grandiflorine was isolated from the minor bases of *A. grandiflora* subsp. *grandiflora* by preparative tlc on silica gel, using the solvent system MeOH–$CHCl_3$ 2:98 (v/v); or column chromatography on alumina using anhydrous Et_2O as eluant. It amounted to ca. 0.6% of the total alkaloid content, and had the following properties: mp 202.5–203.5°C; $[\alpha]_D$ +125° (*c* 1, $CHCl_3$); uv (EtOH) λ_{max} (log ε): 238 sh (3.79 and 297 nm (3.78), λ_{min} 260 nm; ir (KBr) ν_{max}: 3030 (w), 2960 (w), 2950 (m), 2890 (m), 2880 (m), 2860 (m), 2840 (m), 2770 (m), 1600 (w), 1480 (m), 1460 (s), 1435 (s), 1355 (m), 1310 (s), 1280 (w), 1265 (m), 1230 (br s), 1205 (m), 1185 (m), 1165 (m), 1150 (m), 1115 (m), 1090 (w), 1070 (m), 1055 (w), 1030 (br s), 1010 (s), 995 (s), 955 (s), 935 (s), 905 (m), 860 (m), 815 (m), 790 (m), 785 (m), 755 (w), 730 (w), 710 (w), 685 (w), 660 (w), 640 (w), 630 (w), 605 (w), 525 (w), 545 (w), 510 (w), 485 (w), 455 (m) cm^{-1}, superimposable upon that of ribasine; ^{1}H nmr, see Table 1; ms (70 eV EI) *m/z*: 351.1106 (87) (calcd. for $C_{20}H_{17}NO_5$: 351.1107), 350 (100), 322 (15), 287 (12), 189 (13), 188 (72), 165 (12), 147 (14), 135 (11), 89 (12), 77 (14), 63 (10), 51 (10) and 42 (22). Hydrobromide salt, mp 220–240°C (dec.) (lit. (1) mp for ribasine 194–195°C), $[\alpha]_D$ +126 (*c* 0.13, $CHCl_3$); uv (EtOH) λ_{max} (log ε): 213 (4.37), 240 sh (4.01), and 292 (4.07) nm.

[1]Author to whom correspondence should be addressed.

[2]Our findings, including structure **1** for grandiflorine, were first presented at the 54th annual meeting of the Chemical Institute of Canada, Halifax, N.S., June 1st, 1971.

TABLE 1. ^{1}H nuclear magnetic resonance data for grandiflorine

Signal position (δ) integrated intensity, multiplicity	Downfield shift (Δδ) upon addition of CF_3CO_2H (cf. ref. 3)	Assignment
2.33, 3H, s	0.57	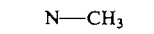
2.67 H, 1H, d, J = 16 Hz	0.22	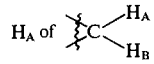
ca. 3.0, 3H, m	0.35, 0.45, ca. 0.6	—
3.60, 1H, d, J = 16 Hz	0.18	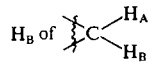
5.64, 1H, s	0.85	
ca. 5.95, 4H, s (some fine structure J < 2 Hz)	<0.1	2 × —OCH_2O—
6.60, 1H, d, J = 7.5 Hz	0.17	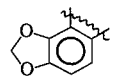
6.77, 1H, d, J = 7.5 Hz	0.20	
6.68, 1H, s	<0.1	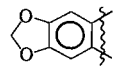
6.88, 1H, s	<0.1	

*In $CDCl_3$; $(CH_3)_4Si$ internal standard; 60 MHz.

Acknowledgements

Financial support for this work was provided by the National Research Council of Canada. We are indebted to Professor Luis Castedo for the generous gift of a reference specimen of ribasine.

1. J. M. BOENTE, L. CASTEDO, R. CUADROS, J. M. SAÁ, R. SUAU, A. PERALES, M. MARTINEZ-RIPOLL, and J. FAYOS. Tetrahedron Lett. 2029 (1983).
2. D. P. ALLAIS, H. GUINAUDEAU, A. J. FREYER, M. SHAMMA, N. C. GANGULI, B. TALAPATRA, and S. K. TALAPATRA. Tetrahedron Lett. 2445 (1983).
3. J. B. DAVIS. Chem. Ind. (London) 1094 (1968).
4. F. R. STERMITZ, D. E. NICODEM, C. C. WEI, and K. O MCMURTREY. Phytochemistry, **8**, 615 (1969).
5. M. H. BENN and R. E. MITCHELL. Phytochemistry, **11**, 461 (1972).
6. M. H. BENN and R. E. MITCHELL. Can. J. Chem. **47**, 3701 (1969).

Can. J. Chem. Downloaded from www.nrcresearchpress.com by 210.87.254.5 on 09/06/12
For personal use only.

Synthesis of selectively modified cellulose derivatives via reductive amination of 2-oxy- and 3-oxy-cellulose intermediates

MANSSUR YALPANI[1] and LAURANCE D. HALL
Department of Chemistry, University of British Columbia, Vancouver. B.C., Canada V6T 1W5

AND

JACQUES DEFAYE and ANDRÉE GADELLE
Centre de Recherches sur les Macromolécules Végétales, C.N.R.S., 53X, 38041, Grenoble, France

Received June 22, 1983

MANSSUR YALPANI, LAURANCE D. HALL, JACQUES DEFAYE, and ANDRÉE GADELLE. Can. J. Chem. **62**, 260 (1984).

Diamagnetic and paramagnetic amine derivatives of cellulose have been prepared from selectively oxidized cellulose precursors via the reductive amination method using sodium cyanoborohydride. 4-Amino-2,2,6,6-tetramethylpiperidine-1-oxyl was employed in the syntheses of nitroxide spin labelled cellulose derivatives **4** and **5** from 3-oxy-cellulose (**1**) and 6-*O*-triphenylmethyl-2-oxy-cellulose (**2**). Conversion of the linear polymer **1** into a highly branched, water soluble 3-deoxy-cellulose derivative **6** was accomplished by attachment of glucosamine side chains. 3-Amino-3-deoxy-cellulose **7** was obtained using ammonium acetate. A novel type of organometallic cellulose conjugate **8** was prepared by condensation of **2** and *p*-toluidine chromium tricarbonyl. Similarly, 1,10-diazo-18-crown-6 was added to **2** to form the crown ether derivative **9**. The synthetic strategies involving either 6-*O* protected or unprotected oxy-cellulose intermediates are compared in terms of reaction yields and product properties.

MANSSUR YALPANI, LAURANCE D. HALL, JACQUES DEFAYE et ANDRÉE GADELLE. Can. J. Chem. **62**, 260 (1984).

Faisant appel à la méthode d'amination réductrice utilisant le cyanoborohydrure de sodium, on a préparé des dérivés aminés diamagnétiques et paramagnétiques de la cellulose à partir de celluloses oxydées de façon sélective. L'amino-4 tétraméthyl-2,2,6,6 pipéridineoxyle-1 réagit avec de l'oxy-3 cellulose (**1**) et la *O*-triphénylméthyl-6- oxy-2- cellulose (**2**) pour conduire aux dérivés **4** et **5** de la cellulose contenant le nitroxyde comme marqueur de spin. On a transformé le polymère linéaire **1** en un dérivé de la déoxy-3 cellulose fortement ramifié et soluble dans l'eau en y attachant des chaines latérales de glucosamine. En utilisant l'acétate d'ammonium, on a obtenu l'amino-3 déoxy-3 cellulose **7**. On a préparé un nouveau type de conjugué organométallique de la cellulose **8** en condensant le composé **2** sur la *p*-toluidine chrome tricarbonyle. De la même façon, on a additionné le diazo-1,10 18-couronne-6 sur le composé **2** pour obtenir l'éther couronne **9**. Les méthodes de synthèse font intervenir soit des intermédiaires oxycellulose protégés ou non en position *O*-6 et on les compare du point de vue du rendement et des propriétés des produits.

[Traduit par le journal]

Introduction

Products derived from cellulose and other natural polysaccharides play prominent roles in various industrial and biomedical applications (1). The requirement for constant improvement of the properties of such products for specific, and often narrowly-defined end-uses, as well as the growing interest in the fundamental relationship between polysaccharide structure and properties (2), have prompted the development of new chemical approaches for the selective modification of the native biopolymers.

Substantial advances have recently been achieved in this regard for amylose and cellulose by the selective oxidation of secondary hydroxyl functions and their subsequent characterization (3). Using the mild acetic anhydride – dimethylsulfoxide reagent system, the 6-*O*-(triphenylmethyl) derivatives of amylose (4) and cellulose (5) or the corresponding 6-*O*-acetyl derivative of cellulose (3) can be selectively oxidized at the C-2 position, while for the C-6 unprotected polymers, the same oxidative reagent, in conjunction with the dimethylsulfoxide–paraformaldehyde solvent system leads to oxidation at C-3 (3). We report here on the utility of 2-oxy- and 3-oxy-cellulose derivatives, in combination with the reductive amination procedure.

[1]Present address: B.C. Research, Chemical Technology Division, 3650 Wesbrook Mall, Vancouver, British Columbia, Canada, V6S 2L2.

Results and discussion

The preparation and characterization of 3-oxy-cellulose, **1**, and the 6-*O*-triphenylmethylated 2-oxy analogue, **2**, have previously been reported (3,5). Both derivatives **1** and **2** had a carbonyl content (degree of oxidation) of about 0.8 and a degree of polymerization of approximately 150.

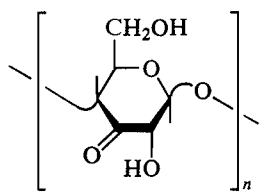

1

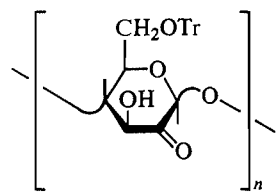

2

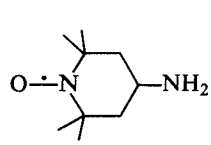

3

Derivatizations of the oxy-cellulose intermediates were performed using both the protected and unprotected species in order to evaluate the effects of the 6-*O*-triphenylmethyl substituent on parameters such as reaction yield and product solubility. Thus reductive amination of the oxy-celluloses **1** and **2**, using 4-amino-2,2,6,6-tetramethylpiperidine-1-oxyl, **3**, and

Can. J. Chem. Downloaded from www.nrcresearchpress.com by 210.87.254.42 on 09/06/12
For personal use only.

sodium cyanoborohydride in methanolic medium at ambient temperature afforded the corresponding spin-labelled derivatives **4** and **5** with degrees of substitution (d.s.) of 0.28 and 0.09, respectively. The relatively low d.s. value of derivative **5** appears to be principally attributable to steric hindrance by the bulky C6-trityl group.

The trityl group also contributes to the expected solubility differences observed for the two spin-labelled products. Derivative **4** is water soluble but insoluble in organic solvents, whereas derivative **5** is water insoluble but soluble in chloroform and other organic solvents. These solubility characteristics

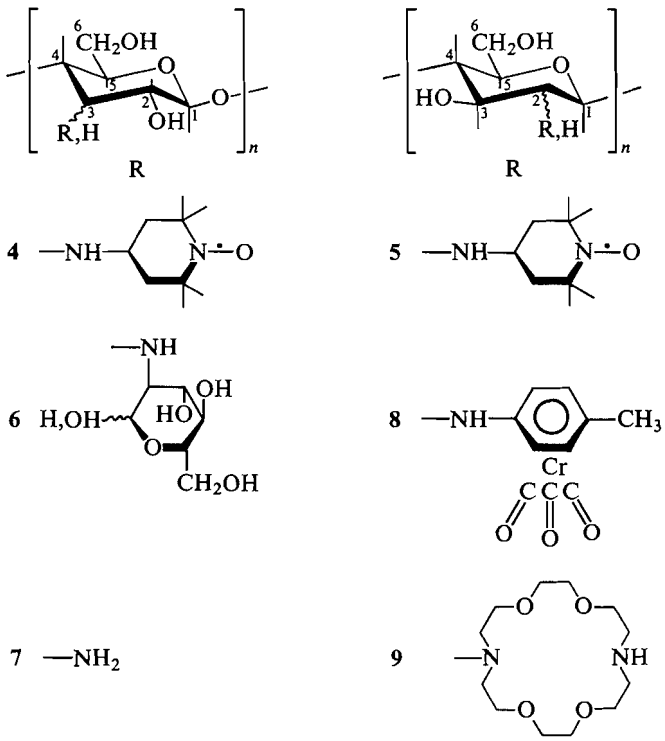

are also reflected in the esr spectra of the materials (Fig. 1): the ambient temperature spectrum of derivative **4** in water reveals typical triplet features of a nitroxide moiety tumbling in solution (Fig. 1a), whereas derivative **5** produces an immobilized, "polycrystalline" spectrum (Fig. 1b) in the same medium. Conversely, the latter derivative in chloroform solution produces a three-line spectrum indicative of a highly mobile nitroxide moiety (Fig. 1d), whereas derivative **4** exhibits a powder spectrum (Fig. 1c). Two further features of the esr spectra of these materials should be noted. First, the residual signals which are superimposd on the spectral envelope of the covalently-linked nitroxide moiety of derivative **5** (Fig. 1b) arise from trace quantities of unreacted amine spin label **3** that could not be removed despite exhaustive washing (6). Second, pronounced exchange narrowing is observed in Figs. 1c and e as a result of dipolar nitroxide interactions in the relatively highly substituted derivative **4**; these dipolar interactions are absent in the powder spectrum of the less substituted derivative **5** (Fig. 1f).

We subsequently prepared a series of diamagnetic cellulose derivatives employing the reductive amination procedure. Using, for example, the primary amine function of glucosamine, we converted the linear 3-oxy-cellulose derivative **1** into a highly-branched (d.s. 0.7), water soluble derivative **6**. Derivative **6** was prepared in analogy to a series of branched chitosan derivatives whose preparation (7) and rheological properties (8) we have described elsewhere.

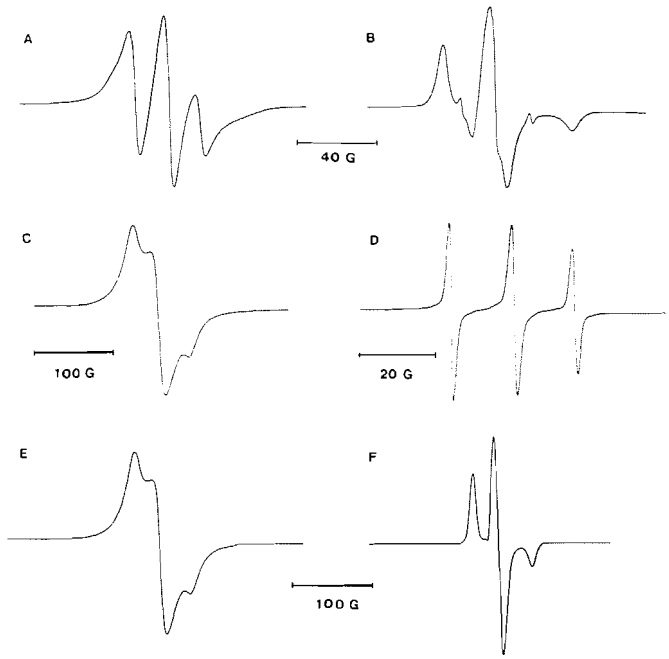

FIG. 1. Ambient temperature esr spectra of derivatives (a) **4** and (b) **5** in water, and derivatives (c) **4** and (d) **5** in chloroform. Powder spectra (at 77°K) of derivatives (e) **4** and (f) **5**.

The ketone derivatives **1** and **2** also constitute useful precursors for the synthesis of aminocellulose derivatives, as exemplified here by the reductive amination of derivative **2** using ammonium acetate, which afforded the 3-amino-3-deoxycellulose derivative **7** (d.s. 0.3). It may be noted that for the preparation of aminocellulose derivatives the reductive amination procedure is more facile than the procedure involving oximation and subsequent lithium aluminium hydride reduction as described by, for example, Teshirogi *et al.* (9). The method described here appears to offer the additional advantage of leading to substantially lower extents of polymer degradation (10).

The preparation of two other types of novel cellulose derivatives is illustrated here by the reductive amination of derivatives **1** and **2**, using *p*-toluidine chromium tricarbonyl and 1,10-diazo-18-crown-6, which afforded derivatives **8** (d.s. 0.25) and **9** (d.s. 0.06), respectively. The crown ether derivative **9** was soluble in organic solvents and is of potential interest as macromolecular complexing agent or phase transfer catalyst (11). The cellulose chromium derivative **8** constitutes, to our knowledge, the first covalent organometallic polysaccharide conjugate, and may find applications in catalysis.

Conclusions

We have demonstrated here the versatility of the combined selective oxidation–reductive amination method for obtaining a range of new cellulose products. It is worthwhile to briefly compare the relative merits of synthesizing selectively modified cellulose derivatives via either *O*-6-protected or unprotected oxy-intermediates. The major advantage of retaining the protective function on the primary hydroxyl groups of 2-oxy-cellulose intermediates derives from the fact that it assists in achieving homogeneous conditions in reactions involving hydrophobic reagents. The bulky size of the trityl group imposes, however, limitations on reaction yields. Conversely, removal of the triphenylmethyl group prior to deriva-

Can. J. Chem. Downloaded from www.nrcresearchpress.com by 210.87.254.42 on 09/06/12
For personal use only.

tization leads to improved yields and avoids exposure to hydrolytic conditions of any acid-labile amine moieties, such as nitroxide labels, attached to the cellulose matrix. One can, of course, alternatively use *O*-6 unsubstituted cellulose as substrate using the dimethylsulfoxide–paraformaldehyde route (3), which is more facile and avoids the polymer degradation (10) and side reactions (12) generally associated with tritylation reactions, but gives access only to 3-deoxy-cellulose products.

Experimental

General methods and materials

Sodium cyanoborohydride and 4-amino-2,2,6,6-tetramethylpiperidine-1-oxyl were purchased from Aldrich Chemical Co. Ammonium acetate was from Malinckrodt, glucosamine hydrochloride from Sigma Chemical Co., *p*-toluidine chromium tricarbonyl from Strem Chemicals, and 1,10-diazo-18-crown-6 from Chemical Dynamics Corp. 3-Oxy-cellulose and 6-*O*-triphenylmethyl-2-oxy-cellulose were prepared as described previously (3, 5). *Anal.* calcd. for **1**, d.s. 0.8, $[(C_6H_8O_5)_{0.8}(C_6H_{10}O_5)_{0.2}]\cdot 0.18\ H_2O$: C 44.00, H 5.39; found: C 43.78, H 5.20. *Anal.* calcd. for **2**, d.s. 0.85 $[(C_{25}H_{23}O_5)_{0.85}(C_6H_{10}O_5)_{0.15}]\cdot 0.2\ H_2O$: C 71.71, H 5.83; found: C 71.94, H 5.63.

Microanalyses were performed by the Microanalytical Laboratory, Department of Chemistry, University of B.C. and Canadian Microanalytical Services, Vancouver. The esr spectra were recorded at X-band using a Varian E-3 instrument and methods described elsewhere (6).

*Preparation of nitroxide-labelled cellulose derivatives **4** and **5***

A dispersion of 3-oxy-cellulose (378 mg, 2.36 mmol) in methanol (7 mL) was treated with amine spin label **3** (412 mg, 2.41 mmol) and sodium cyanoborohydride, $NaBH_3CN$ (400 mg, 6.4 mmol). A few drops of water were added and the mixture was shaken for 33 h at ambient temperature. The product was isolated by filtration, successive washing with water (100 mL), ethanol (150 mL), acetone (50 mL), and diethyl ether (50 mL), and subsequent drying *in vacuo* (50°C). Derivative **4** had a d.s. value of 0.28. *Anal.* calcd. for $[(C_{15}H_{27}N_2O_5)_{0.28}(C_6H_8O_5)_{0.52}(C_6H_{10}O_5)_{0.2}]\cdot 1.55\ H_2O$: C 44.11, H 7.31, N 3.38, (C/N 13.04); found: C 43.73, H 5.97, N 3.37 (C/N 12.98). 2-Oxy-6-*O*-trityl cellulose **2** was labelled under the same conditions yielding a product **5** with d.s. ~0.09. *Anal.* calcd. for $[(C_{34}H_{41}N_2O_5)_{0.086}(C_{25}H_{22}O_5)_{0.764}\ (C_6H_{10}O_5)_{0.15}]\cdot 0.31\ H_2O$: C 71.61, H 5.94, N 0.62; found: C 71.22, H 5.54, N 0.61.

*Preparation of 3-N-(2-amino-2-deoxy-D-glucose)-3-deoxycellulose derivative, **6***

An aqueous sodium bicarbonate solution (10 mL) of glucosamine hydrochloride (600 mg, 2.8 mmol) containing $NaBH_3CN$ (800 mg, 12 mmol) was added under stirring to a methanolic solution of derivative **1** (259 mg, 1.6 mmol, 20 mL). After stirring the reaction mixture for 30 h at ambient temperature, the product was precipitated with chloroform (200 mL), filtered, washed with 100 mL each of chloroform and methanol, and dried. The resulting white material had a d.s. of 0.7. *Anal.* calcd. for $[(C_{12}H_{21}NO_9)_{0.7}(C_6H_8O_5)_{0.15}(C_6H_{10}O_5)_{0.15}]\cdot 1.41\ H_2O$: C 40.81, H 6.80, N 3.27; found: C 40.48, H 6.24, N 3.11.

*Preparation of 3-amino-3-deoxycellulose **7***

A dispersion of derivative **1** (204 mg, 1.28 mmol) in aqueous methanol (15 mL) was treated with an aqueous solution of ammonium acetate (500 mg, 8 mmol) and $NaBH_3CN$ (800 mg, 12 mmol, 10 mL). After stirring the reaction mixture for 30 h, the product was filtered, exhaustively washed with water and chloroform, and dried, yielding derivative **7** with d.s. 0.3. *Anal.* calcd. for $[(C_6H_{11}NO_4)_{0.3}(C_6H_8O_5)_{0.5}(C_6H_{10}O_5)_{0.2}]\cdot 0.36\ H_2O$: C 43.07, H 6.04, N 2.51; found: C 42.85, H 6.31, N 2.27.

Preparation of p*-toluidine chromium tricarbonyl cellulose derivative **8***

A chloroform dispersion of derivative **1** (322 mg, 1.99 mmol, 20 mL) was purged with nitrogen and treated with a solution of *p*-toluidine chromium tricarbonyl (623 mg, 2.56 mmol) and $NaBH_3CN$ (800 mg, 12 mmol) in chloroform (10 mL) in the dark and under a nitrogen atmosphere for 30 h. The resulting green solution was precipitated by the addition of aqueous methanol (100 mL). The product was filtered, exhaustively washed and dried, yielding a fine turquoise powder (193 mg, 56%), d.s. 0.25. *Anal.* calcd. for $[(C_{16}H_{17}CrNO_7)_{0.25}(C_6H_8O_5)_{0.6}(C_6H_{10}O_5)_{0.15}]\cdot 0.1\ H_2O$: C 46.60, H 4.95, N 1.60, Cr 5.94; found: C 46.61, H 4.95. N 1.28, Cr 6.18.

*Preparation of 1,10-diazo-18-crown-6-cellulose derivative **9***

To a solution of derivative **2** (300 mg, 0.77 mmol) in methylene chloride (50 mL) was added 1,10-diazo-18-crown-6 (326 mg, 2.3 mmol) and $NaBH_3CN$ (400 mg, 6 mmol); the reaction mixture was stirred for 48 h at room temperature, then diluted with methanol to 100 mL, and the product precipitated with diethyl ether (1 L), yielding derivative **9**, d.s. 0.06, after filtration, washing (diethyl ether), and drying. *Anal.* calcd. for $[(C_{37}H_{48}N_2O_8)_{0.06}\ (C_{25}H_{23}O_5)_{0.79}(C_6H_{10}O_5)_{0.15}]\cdot 0.05\ H_2O$: C 71.73, H 5.97, N 0.44; found: C 71.25, H 5.57, N 0.36.

Acknowledgement

This work was supported by operating grants from the Natural Sciences and Engineering Research Council of Canada.

1. R. M. ROWELL and R. A. YOUNG (*Editors*). Modified cellulosics. Academic Press, New York. 1978; I. W. COTTRELL and K. S. KANG. Dev. Ind. Microbiol. **19**, 117 (1978).
2. E. M. MORRIS. *In* Techniques and applications of fast reactions in solution. *Edited by* W. J.Gettins and E. Qyn-Jones. Wiley, New York. 1979. p. 379; D. A. Rees. Polysaccharide shapes. Chapman and Hall, London. 1977.
3. C. BOSSO, J. DEFAYE, A GADELLE, C. C. WONG, and C. PEDERSEN. J. Chem. Soc. Perkin Trans. 1, 1579 (1982).
4. M. L. WOLFROM and P. Y. WANG. Carbohydr. Res. **12**, 109, 1970; D. HORTON and T. USUI. *In* Carbohydrate sulfates. *Edited by* G. Schweiger. ACS Symp. Ser. **77**, 95 (1978).
5. K. BREDERECK. Tetrahedron Lett. 695 (1967).
6. M. YALPANI and L. D. HALL. Can. J. Chem. **59**, 3105 (1981).
7. M. YALPANI and L. D. HALL. Submitted; L. D. Hall and M. Yalpani. J. Chem. Soc. Chem. Commun. 1153 (1980).
8. M. YALPANI, L. D. HALL, M. A. TUNG, and D. E. BROOKS. Nature, **302**, 812 (1983).
9. T. TESHIROGI, H. YAMAMOTIM, M. SAKAMOTO, and H. TONAMI. Sen'i Gakkaishi, **36**, T 501 (1980).
10. O. LARM, E. SCHOLANDER, and O. THEANDER. Abstract of Papers, 185th ACS National Meeting, Seattle, Washington, 1983. Carb. 17.
11. J. M. HARRIS, M. YALPANI, J. M. VAN ALSTINE, E. C. STRUCK, M. CHASE, M. S. PALEY, and D. E. BROOKS. J. Polym. Sci. Polym. Chem. Ed. In press.
12. J. W. GREEN. Methods Carbohydr. Chem. 3, 327 (1963).

Can. J. Chem. Downloaded from www.nrcresearchpress.com by 210.87.254.42 on 09/06/12
For personal use only.

An investigation of the effects of the medium and the type of fluoride on the hydrogen bond assisted alkylation of phenols

M. M. ALAUDDIN AND JACK M. MILLER[1]
Department of Chemistry, Brock University, St. Catharines, Ont., Canada L2S 3A1

AND

JAMES H. CLARK
Department of Chemistry, University of York, York, England Y01 5DD

Received January 25, 1983[2]

M. M. ALAUDDIN, JACK M. MILLER, and JAMES H. CLARK. Can. J. Chem. **62**, 263 (1984).

Several sources of the fluoride anion have been compared as electron donors in the hydrogen bond assisted alkylation of phenols.

M. M. ALAUDDIN, JACK M. MILLER et JAMES H. CLARK. Can. J. Chem. **62**, 263 (1984).

On compare plusieurs sources de l'anion fluorure en tant que donneur d'électrons dans l'alkylation des phénols assistée par la liaison hydrogène.

[Traduit par le journal]

Can. J. Chem. Downloaded from www.nrcresearchpress.com by 210.87.254.5 on 09/06/12
For personal use only.

Introduction

A large number of H-bond assisted reactions involving fluoride have now been reported, and a wide variety of types of fluorides and reaction solvents have been suggested for such reactions (1, 2). As part of our studies on the use of fluorides in organic synthesis (3, 4), we have carried out some investigations on the effects of varying the fluoride, and of varying the solvent, on the course and efficiency of the alkylation of phenols with benzyl halides.

Results and discussion

In the reaction of a phenol with a benzyl halide in the presence of a fluoride, the reaction may follow up to four pathways giving O-alkylated and C-alkylated phenols. Benzyl fluoride and benzyl alcohol are possible products, as shown below (Scheme 1). Further products may result from participation of the solvent in the reaction. We have compared the results from the reactions of phenols with benzyl bromide in a typical non-polar aprotic solvent (toluene) and in a typical polar aprotic solvent (DMF) using the most popular sources of fluoride, KF (oven dried) and tetra-n-butylammonium fluoride (as a solid hydrate). The results are summarized in Table 1.

It is interesting to note that only in one case is any C-alkylated phenol observed, and this occurs when the reaction may be considered to be totally heterogeneous (KF/toluene) as opposed to partially homogeneous (KF/DMF) or totally homogeneous (TBAF reactions). Presumably, in solution we are dealing with an H-bonded, F···HOAr complex where the negative charge is highly localized on the electron donor (fluoride) and electron acceptor (HO—) species. The concept of

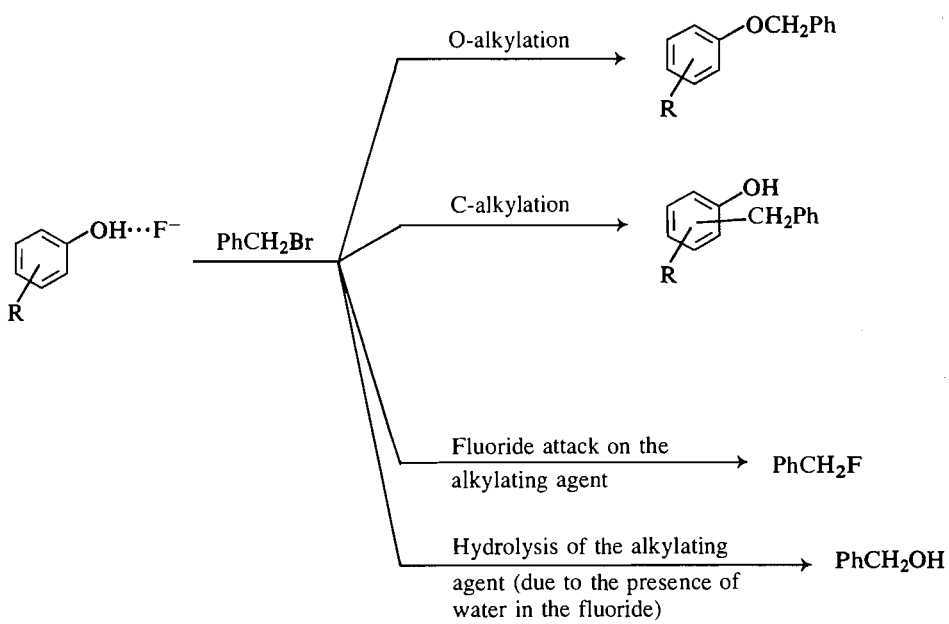

SCHEME 1

[1]Author to whom correspondence may be addressed.
[2]Revision received August 3, 1983.

TABLE 1. Products from the reactions of phenols with benzyl bromide in the presence of KF (oven dried) or TBAF (solid hydrate)[a]

Phenol	Fluoride	Solvent	Conditions (time(h)/temp(°C))	O-alkylated fluoride	Fluoride
Phenol	KF	Toluene	27/60	—	—[b]
Phenol	KF	DMF	24/60	67	10
Phenol	TBAF	Toluene	24/82	20[c]	76[c,d]
Phenol	TBAF	DMF	78/23	54[c]	40[c,e]
Phenol	TBAF	Benzene +10% DMF	24/70	15[c]	80[c,e]
p-Nitrophenol	KF	Toluene	72/80	—	—
p-Nitrophenol	KF	DMF	19/60	76	—
p-Nitrophenol	TBAF	DMF	24/23	76	—
p-Nitrophenol	TBAF	Benzene +25% DMF	1/23	75	—
2,6-Di-*t*-butyl-4-methylphenol[f]	TBAF	Toluene	24/82	—	80
2,6-Di-*t*-butyl-4-methylphenol	TBAF	DMF	24/23	—	48[g]

[a] Isolated yield unless stated otherwise.
[b] 20% C-alkylated phenol.
[c] Yield based on ^{1}H nmr.
[d] Along with 4% benzyl alcohol.
[e] Along with 5–6% benzyl formate.
[f] No reaction using KF in toluene or DMF.
[g] Along with 8% benzyl formate and 44% unidentified products.

H-bond charge localization is consistent with the current theory on hydrogen bonds involving fluoride based on the theoretical calculations (see, for example, ref. 5), on ion cyclotron resonance studies (6), and on other experimental observations (2). The reverse selectivity observed in the heterogeneous system is interesting and of potential importance to fluoride chemistry. Heterogeneous reactions showing unusual reaction selectivity is a subject of considerable current interest (see, for example, ref. 7).

In some of our reactions, we detected significant amounts of benzyl formate. DMF is known to be susceptible to hydrolysis, and under basic conditions should produce methanoic acid. The acid should compete for the fluoride and through the resulting H-bond activation be capable of attacking the alkylating agent as shown below.

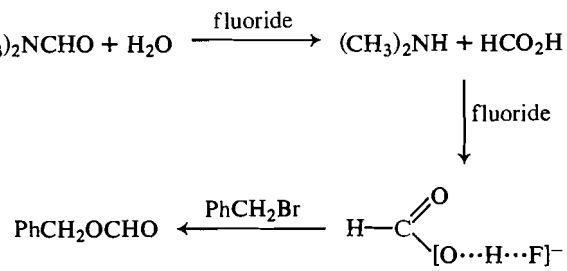

In reactions where KF was employed and the water content could be assumed to be very small, no hydrolysis products (benzyl formate or benzyl alcohol) could be detected. Introduction of water into KF–DMF reactions resulted in the production of benzyl formate as a side product.

Recently, it has been reported that the method of drying the KF may affect the course or efficiency of KF promoted reactions (8). We have compared oven dried KF and freeze dried KF in assisting the reaction of phenol with benzyl bromide in DMF. Whereas the oven dried KF produces both O-alkylated and fluorinated products (Table 1), freeze dried KF produced the O-alkylated product only (73% recovered yield after 24 h at 60°C). It is possible that freeze drying produces a material of higher surface area and hence either of higher solubility in DMF, or of greater reactivity if the reactions occur in part on the surface of the KF.

TABLE 2. The course of fluoride promoted alkylations of phenols using benzyl halides

Fluoride	Reaction
KF/toluene	Slow C-alkylation
KF(oven dried)/DMF	O-alkylation + fluoride (for unactivated phenols)
KF(freeze dried)/DMF	O-alkylation
KF/Bu^n_4NBr(catalytic)/DMF	O-alkylation (more rapid than KF alone)
TBAF/toluene	Mixture
TBAF/DMF	Mixture (unless phenol is activated)

Finally, we carried out some phenol alkylations under solid–liquid phase transfer conditions (KF/R_4NBr). When carried out under anhydrous conditions, these reactions gave good results using benzyl chloride or benzyl bromide as the alkylating agent. In all cases, only O-alkylation resulted, and isolated yields of 60% after 4–10 hours at 60°C were obtained easily. It is important to note that the role of the "onium" salt in these reactions is truly catalytic. The use of as little as 1 mol% (with respect to the KF) reduced the reaction time for complete conversion of the phenol to one-half of that required when KF was used alone. Furthermore, the phase transfer reactions gave only the one product. Tordeux and Wakselman (9) have recently reported simple fluorinations using similar KF/R_4NF systems to produce acylfluorides and fluoroformates.

In conclusion, it is apparent from our work that the nature of both the fluoride and the reaction medium can affect the course and rate of fluoride assisted reactions. Not surprisingly, TBAF reactions occur more rapidly than those employing KF, although this is at the cost of selectivity, halogen exchange with

Can. J. Chem. Downloaded from www.nrcresearchpress.com by 210.87.254.5 on 09/06/12
For personal use only.

the alkylating agent and solvent participation being the most common competing reactions where TBAF is used. O-alkylation is the major reaction at the phenol, especially when the phenol is activated or the solvent is polar aprotic. C-alkylation occurs only under totally heterogeneous conditions. Our results are summarized in Table 2.

Acknowledgements

We thank NSERC (Canada) for an operating grant (to J.M.M.) and NATO for a travel grant (for J.H.C. and J.M.M.).

1. J. EMSLEY. Chem. Soc. Rev. **9**, 91 (1980).
2. J. H. CLARK. Chem. Rev. **80**, 429 (1980).
3. J. H. CLARK, J. M. MILLER, S. R. CATER, and K.-H. SO. Can. J. Chem. **57**, 2629 (1979); J. H. CLARK, J. D. PYLE, J. M. MILLER, S. PAONE, and S. Y. TAN. Can. J. Chem. **60**, 1815 (1982).
4. A. L. JAZZAA, J. H. CLARK, and J. M. MILLER. Synthesis, 89 (1983).
5. J. EMSLEY, O. P. A. HOYTE, and R. E. OVERILL. J. Am. Chem. Soc. **100**, 3303 (1978).
6. J. W. LARSON and T. B. MCMAHON. J. Am. Chem. Soc. **105**, 2944 (1983).
7. D. G. LEE and N. A. NOURELDIN. J. Am. Chem. Soc. **105**, 3188 (1983).
8. J. YAMAWAKI, T. ANDO, and T. HANAFUSA. Chem. Lett. 1143 (1981); N. ISHIKAWA, T. KITAZUME, and M. KOKOBAYASHI. Chem. Lett. 1089 (1980); T. KITAZUME and N. ISHIKAWA. Chem. Lett. 1327 (1980); N. ISHIKAWA, T. KITAZUME, T. YAMAZAKI, Y. MOCHIDA, and T. TATSUNO. Chem. Lett. 761 (1980).
9. M. TORDEUX and C. WAKSELMAN. Synth. Commun. **12**, 513 (1982).

Can. J. Chem. Downloaded from www.nrcresearchpress.com by 210.87.254.5 on 09/06/12
For personal use only.

A Fourier transform infrared study of the electrophilic attack at the N_7-site of guanosine-5′-monophosphate

H. A. TAJMIR-RIAHI AND T. THEOPHANIDES
Département de Chimie, Université de Montréal, Montréal (Qué), Canada H3C 3V1

Received June 2, 1983

H. A. TAJMIR-RIAHI and T. THEOPHANIDES. Can. J. Chem. **62**, 266 (1984).

Fourier transform infrared spectra of several N_7-bound cations of guanosine-5′monophosphate disodium salt (5′-$GMPNa_2$), such as N_7-H^+GMP, N_7-MeGMP, and N_7-MGMP, where Me = CH_3^+ and M = divalent metal ions, Cd, Mn, Co, Ni, Cu, Pt, and Mg, have been recorded and a correlation between the spectral changes and the nature of the electrophile (H^+, CH_3^+, and M^{2+}) bound has been established. Spectroscopic evidence shows that methylation of the N_7-position of 5′-$GMPNa_2$ causes larger perturbation on the guanine ring system than protonation or metalation, in the order $Me^+ > H^+ > M^{2+}$. The effect of an N_7-electrophilic attack on the vibrational frequencies of the purine, the sugar, and the phosphate group is discussed.

H. A. TAJMIR-RIAHI et T. THEOPHANIDES. Can. J. Chem. **62**, 266 (1984).

On a enregistré les spectres infrarouges en transformation de Fourier de plusieurs cations du sel de sodium de la guanosine-5′ monophosphate, ($GMPNa_2$-5′) liés par l'azote en position 7, tels le N_7-H^+GMP, le N_7-MeGMP et le N_7-MGMP où Me = CH_3^+, et M = ions métalliques bivalents: Cd, Mn, Co, Ni, Cu, Pt et Mg et on a établi une corrélation entre les variations du spectre et la nature de l'électrophile de la liaison (H^+, CH_3^+ et M^{2+}). Les preuves spectroscopiques montrent que la méthylation de l'azote en position 7 du $GMPNa_2$-5′ provoque une plus grande perturbation sur le cycle de la guanine que la protonation ou la métallation, dans l'ordre suivant: $Me^+ > H^+ > M^{2+}$. On discute de l'effet d'une attaque électrophile en N_7 sur les fréquences de vibration de la purine, du sucre et du groupe phosphate.

[Traduit par le journal]

Introduction

The interaction of the electrophilic agents, H^+, R^+, and M^{2+} with the nucleic acids and their components has been the subject of recent studies (1–3). The interest in this area of research lies in the anti-tumor activity of the alkylating agents (1) (nitrogen mustards), the *cis*-platinum (*cis*-$Pt(NH_3)_2Cl_2$) and other related platinum compounds (4) which are assumed to interact with the DNA molecule *in vivo*. Raman and nmr spectroscopy has often been used (1, 2, 5–8) to characterize the nature of such electrophilic interaction with mono- and polynucleotides, whereas ir is the least used technique for this purpose, so far (9–11).

In the present work, we wish to describe and analyse the FT-IR spectra of a number of structurally known N_7-bonded metal–GMP complexes (12–16) and the corresponding protonated (17) and methylated analogs. Having at our disposal unambiguous structural information (12–17) on some N_7-bonded compounds, we have recorded and analyzed their FT-IR spectra in order to establish a correlation between the spectral changes and the nature of the N_7-electrophile bound (H^+, CH_3^+, and M^{2+}) on the guanine base. We have also studied the ribose–phosphate vibrational frequencies of these systems for a possible phosphate interaction. The structure and atomic numbering of 5′-$GMPNa_2$ is illustrated below.

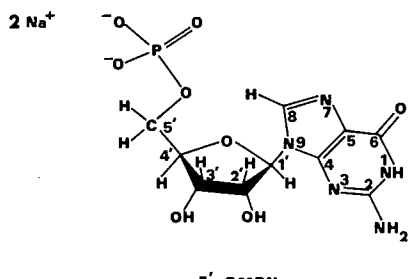

Experimental

The 5′-GMP acid, the N_7-MeGMP, and the Na salt of the mononucleotide were purchased from Sigma Chemical Company. The K_2PtCl_4 was purchased from Johnson Matthey Ltd., and was converted to *cis*- and *trans*-$Pt(NH_3)_2Cl_2$ by published methods (18, 19). All the other chemicals were BDH reagent grade and were used without further purification.

Preparation of the N_7-species

The metal–GMP complexes were synthesized and recrystallized following published methods (12–16). The preparation of Pt^{2+} and Mg^{2+} complexes was described earlier (20). The free 5′-GMP acid was used as N_7-protonated and was recrystallized by the reported method (17).

Elemental analysis

C, H, and N were analyzed by Schwarzkopf microanalysis (U.S.A.). The metal ions and the halide were determined as previously reported (20).

Physical measurements

The FT-IR spectra have been recorded on a DIGILAB FTS-15/C Fourier Transform Michelson Interferometer, equipped with a high-sensitivity HgCdTe detector and a KBr beam splitter with a spectral resolution of 2–4 cm^{-1}, and KBr pellets. The bands are accurate to ± 1 cm^{-1}.

Results and discussion

Structural data show (12–15) that [$(H_2O)_5M$(5′-GMP)].$3H_2O$, where M = Cd^{2+}, Mn^{2+}, Co^{2+}, and Ni^{2+}, contains a six-coordinated metal cation bonded to the N_7-site of guanine and five water molecules (three of the remaining water molecules are waters of crystallization). The Cu^{2+} ion is five coordinated, binding to the phosphate group and to the N_7 atom of guanine, as well as to three water molecules in Cu_3(5′-GMP)$_3$.$8H_2O$ (16). The free 5′-GMP acid exists in a zwitterionic form (17) with protonation at the N_7-position of the guanine and at an ionic phosphate oxygen. The N_7-$MeGMPNa_2$ is known (21) to contain a CH_3^+ group at the N_7-site of the purine ring (the crystal structure of this compound is not known). In this work the FT-IR spectra of these N_7-bonded species have been recorded in the region of 4000–400 cm^{-1} and a comparison with the spectrum of 5′-$GMPNa_2$ (which is free of N_7-bonding) has been made.

Can. J. Chem. Downloaded from www.nrcresearchpress.com by 210.87.254.105 on 09/06/12
For personal use only.

Can. J. Chem. Downloaded from www.nrcresearchpress.com by 210.87.254.105 on 09/06/12
For personal use only.

4000–2700 cm^{-1}

In this region, the asymmetric and symmetric stretching vibrations of the NH_2, NH, H_2O, OH, CH_2, and CH of the sugar moiety and the base residue of the free 5′-$GMPNa_2$ have been studied (22, 23) and show no considerable changes in the spectra of all these N_7-bonded species. The small shifts observed in this region of the spectra are due to a rearrangement of the hydrogen-bonding network of the free ligand upon N_7-complexation. Due to the presence of a strong hydrogen-bonding system in the free mononucleotides and their N_7-adducts, one cannot draw a conclusion on the nature of the electrophilic attack at the N_7-site of the ring system from this region.

1800–400 cm^{-1}

Drastic spectral changes occurred in this region upon formation of the N_7-electrophile compounds, these are dealt with separately.

N_7-protonation

Sundaralingam *et al.* (24) have demonstrated the zwitterionic character of the free acid form of the mononucleotide, 5′-$GMPNa_2$ in the solid state. The crystal structure of 5′-GMP acid protonated at N_7 exists in a zwitterionic form with an ionized phosphate group (17). The proton at the N_7-site is linked to the phosphate group via three hydrogen-bonded water molecules (A). The C_6=O group is shielded from hydrogen

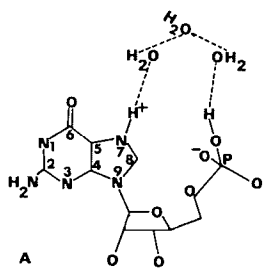

A

bonding, whereas the NH_2 group and the nitrogen atoms of the pyrimidinic ring as well as the sugar moiety are involved in a strong hydrogen-bonding network (17). The FT-IR spectra of this acid exhibits (Fig. 1*c*) a strong absorption band at 1705 cm^{-1} related to the free C_6=O stretching frequency (25), whereas in the 5′-$GMPNa_2$ salt the corresponding absorption band appears at 1692 cm^{-1} (Fig. 1*a* and Table 1). The small shift of the C_6=O stretching vibration to a lower frequency in the sodium salt is mainly due to the hydrogen bonding of the C_6=O group through the oxygen atom. The crystal structure of 5′-$GMPNa_2$ (26) shows an indirect Na–carbonyl interaction through a coordinated water molecule. The scissoring motion of the NH_2 group appeared (25) as a shoulder absorption band at 1600 cm^{-1} in the spectrum of the 5′-$GMPNa_2$ and shifted to a lower frequency at 1641 cm^{-1} in the spectrum of the free 5′-GMP acid. The shift of the scissoring vibration of the NH_2 group to a lower frequency and that of the NH_2 stretching vibration at 3400 cm^{-1} to a higher frequency is indicative of a rearrangement of the strong hydrogen-bonding system of the NH_2 group in 5′-$GMPNa_2$ upon N_7-protonation. The weaker hydrogen-bonding network of the NH_2 group causes an increase of the NH_2 stretching and a lowering of the NH_2 scissoring frequency. The N_7-protonation also produces small intensity changes and shifting of the absorption bands at 1600, 1580, and 1535 cm^{-1}, which are mainly assigned (25) to the C_4—N_3, C_5—C_4, and C_4—N_9 skeletal frequencies, respectively. Since protonation of the N_7-position of the guanine ring has been found (24) to have a considerable effect on the purine ring geometry, therefore, it should also perturb the electron distribution within the ring system and produce changes in the skeletal vibrational frequencies. An absorption band with a medium intensity at 1478 cm^{-1}, in the spectra of 5′-$GMPNa_2$ was assigned to a purine ring vibrational frequency (1). This frequency involves mainly stretching of C_8=N_7 and C_8—H bending motions and is shifted to a higher frequency (1480 cm^{-1}) in the N_7-protonated compound. The shift of the C_8=N_7 stretching to a higher frequency upon protonation is consistent

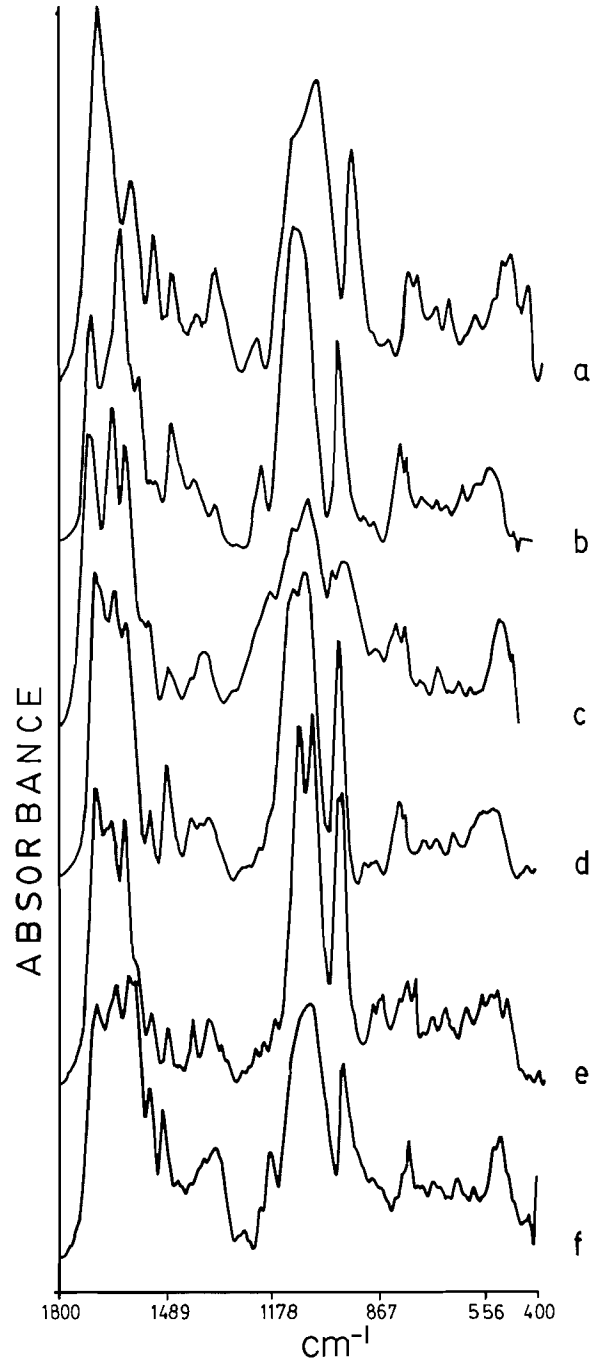

FIG. 1. FT-IR Spectra of 5′-$GMPNa_2$ and its N_7-bonded electrophile in the region of 1800–400 cm^{-1} for *a*, 5′-$GMPNa_2$; *b*, N_7-MeGMP; *c*, N_7-H^+GMP; *d*, Cd(5′-GMP).$8H_2O$; *e*, Cu_3(5′-GMP)$_3$.$8H_2O$; and *f*, *cis*-[$Pt(NH_3)_2$(5′-GMP)$_2$]Cl_2.$6H_2O$.

Can. J. Chem. Downloaded from www.nrcresearchpress.com by 210.87.254.105 on 09/06/12
For personal use only.

TABLE 1. Selected FT-IR bands (cm^{-1}) with possible

5′-GMPNa$_2$	N_7-H$^+$GMP. $3H_2O$	N_7-MeGMP	Mn(GMP). $8H_2O$	Co(GMP). $8H_2O$	Ni(GMP). $8H_2O$	$Cu_3(GMP)_3$. $8H_2O$	Cd(GMP). $8H_2O$
1692 bs	1705 vs	1703 s	1690 vs	1690 vs	1690 vs	1694 vs	1694 vs
			1655 sh	1656 sh	1656 sh	1663 sh	1656 s
1660 sh	1641 vs	1620 vs					
			1645 s	1640 s	1640 s	1648 s	1643 sh
1600 s	1603 s	1590 sh	1611 s	1611 s	1611 s	1611 s	1610 s
1580 sh	1557 sh	1566 m	1570 m	1570 m	1560 m	1551 sh	1550 sh
1535 m	1535 w	1533 w	1533 m	1535 m	1535 m	1539 m	1533 m
		1516 w	1476 m	1478 m	1479 m	1489 sh	1479 m
1478 m	1480 m	1467 s					
			1465 sh	1465 sh	1466 sh	1450 w	—
1415 m	1408 sh	1400 m	1425 w	1423 vw	1423 vw	1416 m	1420 sh
1410 sh	—	—	1410 vw	1412 vw	1412 vw	—	1412 m
1359 s	1369 s	1378 sh	1389 m	1391 w	1391 m	1374 m	1379 m
			1352 m	1352 m	1354 m	1350 sh	1358 m
1330 sh	—	1342 m					
			1290 vw	1300 w	1300 w	1300 w	1300 sh
			1280 w	1280 w	1290 w	1290 w	1290 w
1255 sh	1270 sh	1290 vw					
			1260 w	1260 w	1260 w	1260 vw	1265 m
1234 s	1250 sh	1225 sh	1236 m	1235 m	1236 m	1240 m	1236 m
			1216 sh	1215 sh	1216 sh	—	1216 sh
1204 m	1205 sh	1197 s					
			1205 s	1206 s	1208 s	1208 m	1204 m
			1177 m	1177 m	1175 m	1178 m	1175 m
1175 m	1170 m	—					
			1155 m	1153 m	1155 m	—	1150 m
1125 sh	1105 sh	1105 s	1109 sh	1107 sh	1109 sh	1111 vs	1112 sh
—			—	—	—	1040 sh	—
1075 bs	1065 s	110 sh	1084 vs	1080 vs	1080 vs	1076 vs	1080 bs
—	1035 sh		—	—	—	1001 sh	—
975 s	990 m	975 s	981 s	982 s	980 s	991 vs	979 vs
—	957 s		—	—	—	975 sh	—
800 s	798 m	789 s	802 s	802 s	802 s	815 s	802 s
—			—	—	—	790 w	—
682 m	680 m	681 w	688 m	686 m	688 m	700 m	688 m

*s, strong; m, medium; b, broad; sh, shoulder; w, weak; v, very; δ, bending; ν, stretching.

with the C=N$^+$ frequencies, which were experimentally found (27, 28) to be higher than the parent C=N groups. A strong absorption band at 1359 cm^{-1} in the spectrum of the free base related to a pyrimidinic ring vibration (29) lost intensity and shifted to a higher frequency (1369 cm^{-1}) upon protonation. The shift observed for that absorption frequency is most likely due to the different hydrogen binding system of the pyrimidinic ring upon N_7-protonation than to any inductive effects caused by N_7-binding, since the effect of electrophilic attack at the N_7-site hardly goes beyond the purine ring system (24). The other absorption bands at 1330 (sh), 1255 (m), 1234 (m), and 1175 cm^{-1} (m) in the spectra of 5′-GMPNa$_2$ are attributed mainly to C_8—N_9, C_5—N_7, C_8—N_7, stretchings and to the bending mode of C_8—H (25, 30). The bands showed considerable changes in the spectra upon N_7-protonation. The first absorption band disappeared and the rest shifted to lower frequencies (Table 1). These absorption bands are mainly related to the purine ring vibrational frequencies. Structural studies show (24) that protonation of N_7- in purines causes a large alteration on the bond distances of N_7—C_5, N_7—C_8, C_8—N_9, and the angles of N_7—C_8—N_9, C_5—N_7—C_8, C_4—C_5—N_7 distorting the molecular structure (Table 2). Therefore, it seems that an electrophilic attack at the N_7-position does perturb mainly the electron distribution of the imidazol ring system, where the vibrations are mostly localized and imposes a predominant distortion to the whole purine ring system. The band of medium intensity at 682 cm^{-1} in the spectrum of the 5′-GMPNa$_2$ related to the guanine ring breathing mode (25) shifted slightly to about 680 cm^{-1} in the spectrum of the N_7-protonated compound.

The effect of N_7-protonation on the phosphate and sugar vibrations

The ir spectra of the mononucleotide phosphate group has been reported earlier (20). The phosphate group of $ROPO_3^{2-}$ moiety in 5′-GMPNa$_2$ shows five vibrational frequencies in the region 1100−350 cm^{-1} (20, 23). The strong and broad absorption at 1075 cm^{-1} is assigned to the PO_3^{2-} degenerate stretching, the sharp band at 975 cm^{-1} is assigned to the PO_3^{2-} symmetric stretching, the absorption band with the medium intensity at about 800 cm^{-1} is assigned to the P—O stretching frequency, and the two other weaker absorption bands at about 450 and 400 cm^{-1} are assigned to the PO_3^{2-} symmetric and degenerate deformations, respectively (23). The three absorption bands at 1075, 975, and 800 cm^{-1} in the spectrum of 5′-GMPNa$_2$ show considerable changes upon direct or indirect phosphate−electrophile interaction. Deprotonation of the phosphate group and protonation of the N_7-position of the gua-

assignments for free 5′-GMPNa$_2$ and its N$_7$-bonded electrophile*

cis-[Pt(NH$_3$)$_2$(GMP)$_2$]Cl$_2$.6H$_2$O	Pt(GMP)$_2$Cl$_2$.6H$_2$O	Mg(GMP).10H$_2$O	Mg(GMP).6H$_2$O	Possible assignments
1694 vs	1693 s	1697 bs	1695 s	$\nu C_6{=}O > \nu C_6{=}C_5$ (25)
1653 sh	1655 sh	1660 sh	1655 sh	$\delta NH_2 > \nu C_2{-}N_2$ (25)
1643 s	1643 vs	1645 w	1638 w	
1599 s	1597 vs	1611 m	1616 sh	$\nu C_4{-}N_3 > \nu C_4{-}C_5 > \nu C_5{-}N_7$ (25)
1550 w	1543 sh	1550 sh	1560 sh	$\nu C_5{-}C_4 > \delta N_1{-}H > \nu C_6{-}N_1$ (25)
1543 m	1537 m	1536 m	1535 m	$\nu C_4{-}N_9 > \nu C_6{=}O > \nu C_2{-}N_1$ (25)
1503 m	1501 s	1483 m	1483 m	$\delta C_8{-}H > \nu C_8{-}N_7$ (1)
—	—	—	1466 sh	
1423 w	1422 vw	—	1420 w	$\delta CH + \delta CH_2$ (23, 33)
1412 vw	1410 vw	1414 w	1410 sh	
1383 m	1385 vw	1383 m	1375 w	ν(pyrimidine ring) (29)
1348 m	1350 m	1357 m	1367 m	$\nu C_8{-}N_9 > \nu C_8{-}N_7 > \delta N_1{-}H > \nu C_2{-}N_2$ (25, 30)
1300 sh	1310 sh	1330 sh	1330 sh	
1290 vw	1250 sh	—	—	
1270 vw	—	1254 m	1250 m	$\nu C_6{-}N_1 > \nu C_5{-}N_7$ (25)
—	—	—	—	
1218 w	1215 sh	1220 sh	—	$\delta C_8{-}H > \nu C_8{-}N_7$ (25)
1205 s	1205 m	1206 m	1208m	
1175 w	1177 w	1175 sh	1182 sh	$\nu C_8{-}N_7 > \nu N_9$—sugar $> \nu C_4{-}N_3$ (25)
—	—	—	—	
1109 vs	1110 sh	1107 bs	1102 bs	C—O of the sugar ring (23, 33)
—	—	—	—	
1084 s	1069 bs	1080 sh	1076 sh	νPO_3^{2-} deg. (20, 23)
—	—	—	1052 s	
974 s	976 s	993 s	976 s	νPO_3^{2-} sym. (20, 23)
—	—	—	940 s	
800 s	800 m	792 m	802 m	νP—O (20, 23)
—	—	—	—	
685 m	668 m	689 m	700 m	Guanine ring breathing mode (25)

nine ring, as well as indirect interaction of the proton-phosphate group through hydrogen bonded water molecules (A), brings considerable changes to the phosphate vibrational frequencies. Splitting of the bands at 1075 and 975 cm^{-1} in the spectrum of 5′-GMP acid upon N$_7$-protonation is indicative of the strong proton−phosphate interaction via the hydrogen-bonded water molecules. In the corresponding spectrum of the free ligand where the Na−OPO$_3$ interaction is largely electrostatic (26), such splitting and shifting of the phosphate absorption bands does not occur (Fig. 1*a* and Table 1). It is worth noting that the indirect interaction between the N$_7$-proton and the phosphate oxygens allows the phosphate group to approach the purine ring system (31) with a torsion angle ϕ (C5′—O5—P) of about −164° (17). These conformational changes around the phosphate−sugar bond (32) induce intensity changes and shifting of the ribose−phosphate vibrational frequencies centered at 900−700 cm^{-1} (33) in the spectrum of the N$_7$-protonated 5′-GMP molecule.

N$_7$-metalation

The polymeric copper complex, Cu$_3$(5′-GMP)$_3$.8H$_2$O, shows (16) that each Cu^{2+} ion is five-coordinated. The crystal structure analysis shows that binding takes place through the N$_7$-atom of the guanine ring and the oxygen atoms of the phosphate group, as well as through three water molecules, whereas the corresponding Cd, Mn, Co, and Ni complexes are only N$_7$-bonded and coordinated to five water molecules (12−15). Two of these water molecules are strongly hydrogen-bonded to a phosphate group, and the carbonyl group is also indirectly bound to the central metal cation via a coordinated water molecule (B).

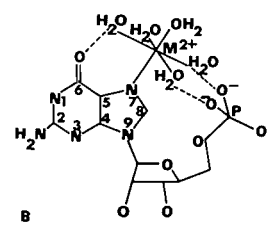

B

The FT-IR spectrum of the free 5′-GMPNa$_2$ shows a strong and broad absorption band at 1692 cm^{-1}, which is assigned to the C$_6$=O and the C$_6$—C$_5$ stretching frequencies (25). This absorption band lost intensity and appeared almost in the same position in the spectra of structurally known N$_7$-bonded metal complexes (Fig. 1*d* and Table 1). The small changes of the C$_6$=O stretching frequency are mainly due to the indirect metal−carbonyl interaction via a coordinated water molecule

Can. J. Chem. Downloaded from www.nrcresearchpress.com by 210.87.254.105 on 09/06/12
For personal use only.

TABLE 2. The effect of the N_7-electrophile bound on the bond lengths and the bond angles of the imidazol ring

Compounds	N_7—C_8 (Å)	N_7—C_5 (Å)	C_8—N_9 (Å)	$\angle N_7$—C_8—N_9 (deg)	$\angle C_5$—N_7—C_8 (deg)	$\angle C_4$—C_5—N_7 (deg)	Reference
5′-GMPNa$_2$.7H$_2$O	1.310	1.389	1.370	113.10	104.21	110.77	26
H$^+$—N$_7$-GMP.3H$_2$O	1.320	1.375	1.342	109.80	108.20	107.60	17
Cd(5′-GMP).8H$_2$O	1.340	1.330	1.340	111.00	105.00	111.00	12
Cu$_3$(5′-GMP)$_3$.8H$_2$O (A)	1.321	1.500	1.470	113.30	104.30	108.30	16
Cu$_3$(5′-GMP)$_3$.8H$_2$O (B)	1.290	1.390	1.350	119.00	100.00	111.00	16
Cu$_3$(5′-GMP)$_3$.8H$_2$O (C)	1.320	1.420	1.360	115.00	104.00	109.00	16

upon N_7-metalation. The bending mode of the NH_2 group of the free ligand absorbs (25) at 1660 cm^{-1}. This vibration appears as a strong absorption band at a slightly lower frequency in the spectra of the N_7-metalated complexes (Fig. 1 and Table 1). The shifting and splitting of the NH_2 bending motion to a lower frequency, together with the shift of the NH_2 stretching frequency at 3400 cm^{-1} to a higher frequency, is indicative of weaker hydrogen-bonding network of the NH_2 group in the N_7-metalated complexes. The absorption bands at about 1600, 1580, and 1535 cm^{-1}, in the spectra of the free base were mainly assigned to the skeletal vibrations (25) of the ring system and showed intensity changes and shifting in the spectra of the N_7-metalated compounds similar to those of the N_7-protonated compound (see N_7-protonated section). The absorption band at 1478 cm^{-1} in the spectrum of the free 5′-GMPNa$_2$ shifted to a higher frequency ($\Delta\nu$ = 10–20 cm^{-1}) in the spectra of the N_7-bonded platinum metal complexes (Fig. 1*f* and Table 1). Since this absorption band contains the C_8—N_7 stretching and the C_8—H bending vibrational frequencies (1), it seems to follow that metalation of the N_7-site induces an increase of the C_8—N_7 stretching frequency. Similar behaviour was observed (34) in the spectra of the structurally known metalated C=N group for some lanthanide Schiff base complexes. The pyrimidine ring vibration (29) at 1359 cm^{-1} in the spectra of the free ligand splits into two weak absorption bands at higher and lower frequencies in the spectra of the N_7-metal derivatives (Fig. 1 and Table 1). The changes observed for that absorption frequency are mainly due to the alteration of the hydrogen-bonding network of the pyrimidine ring system (base pairing) upon N_7-metalation (20). The absorption bands at 1330, 1255, 1234, and 1175 cm^{-1} with medium intensities in the spectrum of the free base show considerable changes (shifting and splitting), in the spectra of the N_7-metal complexes. These absorption bands have been primarily assigned (25, 30) to the purine ring vibrational frequencies, involving C_8—N_7, C_5—N_7 stretching and N_7—C_8—N_9 and C_8—H bending vibrations. It seems, therefore, that the distortion of the molecular geometry (12–16) of the ring system caused by N_7-metalation (Table 2) brings a large perturbation to the purine ring electronic distribution and alters the imidazol ring vibrational frequencies the most. The guanine ring breathing mode (25) of the free ligands at 682 cm^{-1} shifted towards higher frequencies (~700 cm^{-1}) in the spectra of the N_7-bonded metal cations and this is a characteristic feature of the N_7-metal bonding in DNA and its components (8, 20).

The effect of N_7-metalation on the phosphate and sugar vibrations

The phosphate absorption bands at 1075, 975, and 800 cm^{-1} in the spectrum of the free base show considerable changes upon direct or indirect metal–phosphate interaction. The effect of direct and indirect metal–phosphate binding on the vibrational frequencies of the $ROPO_3^{2-}$ of the mononucleotides has been described earlier (20). The ir spectra of the N_7-bonded copper complex Cu$_3$(5′-GMP)$_3$.8H$_2$O (20) shows splitting and shifting of the bands at 1075, 975, and 800 cm^{-1} (Fig. 1 and Table 1). These absorption bands have been assigned (20, 23) to the PO_3^{2-} degenerate and symmetric stretching vibrations, as well as to the P—O stretching frequency. The indirect metal–phosphate interaction through the hydrogen-bonded water molecules in the N_7-bonded metal complexes (Cd, Mn, Co, and Ni) caused shifting of the phosphate vibrational frequencies at 1075, 975, and 800 cm^{-1} (Table 1). The direct metal–phosphate interaction observed in the N_7-bonded Mg(5′-GMP).6H$_2$O synthesized in acidic solution (20) shows shifting and splitting of the phosphate vibrational frequencies (Table 1). The spectra of Mg^{2+} and Pt^{2+}—GMP complexes, on the other hand, obtained at neutral pH values with indirect metal–phosphate bonding and direct N_7-bonding (20) exhibit small shifting of the phosphate vibrational frequencies (Table 1). A shoulder absorption band at 1124 cm^{-1} in the spectrum of the free 5′-GMPNa$_2$ assigned to the C—O stretching of the sugar moiety (23) as well as the absorption bands near 900–700 cm^{-1} assigned mainly to the phosphate–ribose stretching vibrations (33) show intensity changes and shifting in the spectra of the N_7-bonded metal-complexes. The small changes occurred are mainly due to the conformational changes around the phosphate–ribose bond (32) and to the rearrangement of the hydrogen-bonding system of the sugar residue, upon direct or indirect metal–phosphate bonding. The torsional angle (ϕ) found (16) for Cu$_3$(5′-GMP)$_3$.8H$_2$O is about 122–151° (direct metal–phosphate bonding) and 153° for Cd(5′-GMP).8H$_2$O (indirect Cd–phosphate interaction) (12), which is indicative of the closer approach of the phosphate moiety towards the purine ring system upon direct metal OPO_3^{2-} interaction.

N_7-methylation

It has been suggested (1, 21) that the N_7-methylguanosine-monophosphate (N_7-MeGMP) molecule exists in equilibrium between a zwitterionic form (D) and a keto form (C), in aqueous solution. The crystal structure of this compound is not yet known. The CH_3^+ group is bound to the N_7-position of the ring system and shows the zwitterionic character (D) in basic solution (pH = 9), whereas in acidic media (pH = 4) the keto form

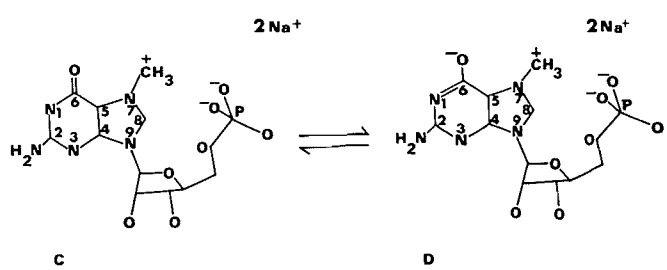

Can. J. Chem. Downloaded from www.nrcresearchpress.com by 210.87.254.105 on 09/06/12
For personal use only.

Can. J. Chem. Downloaded from www.nrcresearchpress.com by 210.87.254.105 on 09/06/12
For personal use only.

(C) is more predominant (1). The FT-IR spectrum of the N_7-MeGMP shows a strong absorption band at 1703 cm^{-1}, assignable to the C_6=O stretching frequency (25). The position of this band is similar to the corresponding band in the N_7-protonated species (Fig. 1*b*), which is also indicative of a free carbonyl group (shielded by the methyl group from hydrogen-bonding) in the N_7-MeGMP molecule. The bending motion of the NH_2 group appears as a strong absorption band at 1620 cm^{-1}, similar to the NH_2 bending mode in the N_7-protonated compound (Fig. 1*b*), which is consistent with the presence of the NH_2 group in a similar hydrogen-bonding network found (17) for the N_7-protonated species. It has been demonstrated (1) that the N_7-MeGMP shows a strong Raman line at 1620 cm^{-1} (pH = 9) with no carbonyl line at 1692 cm^{-1}, which indicates the presence of the N_7-MeGMP in the zwitterionic form (D) and therefore the line at 1620 cm^{-1} was tentatively assigned (1) to the C—O^- stretching frequency. Solution studies of the O_6-methylated inosine molecule (10) show that the absence of the band at 1690 cm^{-1} (C_6=O stretching) is accompanied by the appearance of a new absorption band at 1300 cm^{-1} in basic media which was related to the presence of the C—O^- stretching frequency. Therefore, the latter assignment of the C—O^- stretching vibration at 1300 cm^{-1} is more realistic, unless the double bond character of the C_6=O is still predominant in the former case (1). The presence of the strong absorption band at 1703 cm^{-1} and the absence of any new absorption band at 1300 cm^{-1} here indicates that the N_7-MeGMP molecule exists in a keto form (C). The other absorption bands at 1590, 1566 and 1533 cm^{-1}, in the spectra of the N_7-MeGMP show marked similarities with that of the corresponding N_7-protonated species. Since, these absorption bands have been mainly assigned to skeletal vibrations of the ring system (23), it seems that protonation and methylation of the N_7-position of the guanine ring perturbs in a similar fashion as the ring vibrational frequencies. The absorption band at 1478 cm^{-1} in the spectrum of the free 5′-$GMPNa_2$ has been shifted to a lower frequency at 1467 cm^{-1} in the spectrum of the N_7-methylated compound (Fig. 1*c*). The shift of this absorption band to a lower frequency on methylation is not consistent with that of protonation or metalation of the N_7-site in 5′-GMP, which on the contrary induces an increase to that absorption frequency. Since this absorption band has been mainly assigned (1) to the C_8—N_7 stretching and C_8—H bending frequencies, it appears that methylation of the N_7-site induces different electronic perturbation within the ring system, which could be explained by the more covalent character of the N_7—CH_3^+ bond compared to the corresponding protonated and metalated compounds. It has been shown (1) that the Raman line at 1480 cm^{-1} in the spectra of 5′-GMP disappears upon N_7-methylation (1, 35) and it shifts upon deuteration of H_8 (33), whereas heavy metalation, particularly platination (4, 35), affects that Raman line to a lesser extend. The pyrimidinic ring vibration (29) at 1359 cm^{-1} in the spectra of the free base loses intensity and disappears or remains as a weak band at 1378 cm^{-1} in the spectra of the N_7-methylated compound (Fig. 1*b*). The changes observed for this absorption frequency are mainly related to the rearrangement of the hydrogen-bonding network of the pyrimidinic ring nitrogen atoms. The absorption bands at 1330, 1255, 1234, and 1175 cm^{-1} in the spectrum of the free ligand, attributed mainly to the C_8—N_7, C_5—N_7, C_8—N_9 stretchings, and C_8—H bending frequency (25, 30) lose intensity and shift to higher frequencies in the spectra of the N_7-MeGMP compound (Table 1). Similar trends are observed in the spectra of the N_7-metalated species and since these absorption bands have been assigned to the purine ring vibrations, it seems that the addition of CH_3^+ to the N_7-position of the ring system produces large electronic perturbations within the purine ring and distorts the imidazol ring system. The absorption band at 682 cm^{-1} in the spectrum of free 5′-$GMPNa_2$ assigned to the guanine ring breathing mode (25) decreases in intensity and appears in the same position in the spectrum of the N_7-MeGMP compound (Table 1).

The effect of N_7-methylation on the phosphate and sugar vibrations

The phosphate vibrational frequencies of the free 5′-$GMPNa_2$ at 1075, 975, and 800 cm^{-1} (described in the protonation and metalation sections) shift moderately in the spectra of the N_7-MeGMP (shift of the above bands to 1100, 975, and 789 cm^{-1}, respectively). The changes occurred are mainly due to the hydrogen bonding of the phosphate via water molecules. Similar changes were also observed in the ir spectra of the structurally known N_7-bonded Cd^{2+}, Mn^{2+}, Co^{2+}, and Ni^{2+}—GMP complexes (20), that contain hydrogen-bonded phosphate groups through water molecules. The other absorption bands at 1125 cm^{-1} (assigned to the C—O stretching of the sugar moiety) and at 900−800 cm^{-1}, assigned to the phosphate−ribose stretching frequencies (23, 33), exhibit slight shifting and intensity decreases. The alteration of these absorption bands is mainly related to the hydrogen-bonding system of the sugar and the conformational changes around the phosphate−ribose bond upon N_7-methylation of the 5′-GMP molecule (32).

Conclusion

The vibrational modes of the guanine ring system are strongly coupled and it is difficult to observe characteristic vibrations localized between two atoms. The vibrations are spread over the entire molecule. The N_7-site coordination, however, may be a useful probe for studying and understanding the vibrational problem in these molecules. Comparing the FT-IR spectra of each type of N_7-electrophile bound with existing X-ray crystal structural data, systematic spectral changes have been observed depending on the strength of the N_7-electrophilic attack. The FT-IR results in this work support the following statements:

(*1*) Methylation and protonation at the N_7-site of the guanine ring shield the C_6=O group from hydrogen-bonding and shifts this band towards higher frequencies near 1703 cm^{-1}. The N_7-metalation, on the other hand, seems to involve indirectly the carbonyl group, via a coordinated hydrogen-bonded H_2O molecule. Intensity changes and/or slight shifting of the C_6=O stretching frequency ($\Delta\nu$ = ±5 cm^{-1}) have been observed.

(*2*) The scissoring motion of the NH_2 group at 1660 cm^{-1} (sh), in the spectrum of the free 5′-$GMPNa_2$, appears as a strong absorption band at 1650 cm^{-1} in the metal complexes, at 1641 cm^{-1} in the protonated species, and at 1620 cm^{-1} in the methylated species. The shift of the NH_2 bending mode to a lower frequency is indicative of a rearrangement and the weakening of the hydrogen-bonding network of the NH_2 group. The order of the perturbation is as follows: $CH_3^+ > H^+ > M^{2+}$.

(*3*) The effect of the N_7-bonding on the skeletal vibrations of the ring system at about 1600 cm^{-1}, 1580 and 1535 cm^{-1}, in the free ligand spectra is related to the nature of the N_7-electrophilic addition. The maximum perturbation has been observed for methylation and protonation rather than for metalation (CH_3^+

$> H^+ > M^{2+}$).

(*4*) The medium absorption band at 1478 cm^{-1} in the free base spectrum related to the C_8—N_7 and C_8—H of the purine ring vibrational frequencies is shifted to a higher frequency, upon metalation and protonation ($\Delta\nu$ = 2−20 cm^{-1}). The N_7-methylation, on the contrary, induced a decrease to this absorption frequency ($\Delta\nu$ = −10 cm^{-1}). The largest perturbation has been observed for N_7-methylation and metalation rather than for protonation ($CH_3^+ > M^{2+} > H^+$). The increase of this absorption band upon metalation or protonation may be due to the formation of the —C=N^+—, which has in general higher frequencies than the parent C=N group.

(*5*) The pyrimidinic ring vibration at 1359 cm^{-1} in the spectra of the free base was perturbed largely by metalation (splitting and shifting) rather than by protonation or methylation of the N_7-site of the guanine ring system ($M^{2+} > CH_3^+ > H^+$).

(*6*) The purine ring vibrational frequencies at about 1330, 1255, 1234, and 1175 cm^{-1} in the free base spectrum were strongly affected by the electrophilic attack at the N_7-site of the ring system. The larger perturbation has been observed for the N_7-metalation and protonation rather than for methylation. The structural studies of the N_7-metalated and protonated compounds show large alteration of the bond distances and the angles (Table 2). It seems that the distortion of the molecular dimensions of the purine ring system is accompanied by a perturbation of the electronic distribution of the ring system (due to the charge transfer from the ring nitrogen atom to the H^+, M^{2+}, and CH_3^+), which affects the vibrations associated with the local attack at N_7. Such perturbation of the electronic distribution of the purine ring system upon N_7-protonation was indicated from theoretical calculations on protonated DNA components in a recent study (36).

(*7*) A large perturbation of the phosphate vibrational frequencies at 1075, 975, and 800 cm^{-1} is observed for direct metal−phosphate interactions and to a lesser extent for an indirect metal or proton−phosphate interaction through hydrogen-bonded water molecules. Methylation at the N_7-site affects little the phosphate vibrational frequencies. The order of perturbation upon N_7-coordination on the phosphate vibrational frequencies is: direct metal−phosphate bonding > indirect metal−phosphate > proton−phosphate > CH_3^+.

(*8*) The sugar and sugar−phosphate vibrational frequencies at 1125 cm^{-1} and near 900−700 cm^{-1} are also mostly affected by the direct and indirect N_7−metal and proton−phosphate interaction, which induces conformational changes around the sugar−phosphate bond. The N_7-methylation shows little effect on these vibrational frequencies. This is most probably due to the absence of any strong hydrogen-bonding of the methyl group with the phosphate oxygen atoms.

(*9*) Finally, the guanine ring breathing mode at 682 cm^{-1} in the free 5′-GMPNa_2 is perturbed more by metalation at the N_7-site than by protonation or methylation, in the order $M^{2+} > H^+ > CH_3^+$.

Acknowledgements

We wish to thank the Natural Sciences and Engineering Research Council of Canada for financial support. The loan of platinum salts from Johnson Matthey Ltd. is also gratefully acknowledged.

1. S. MANSY and W. L. PETICOLAS. Biochemistry, **15**, 2650 (1975).
2. S. MANSY, W. L. PETICOLAS, and R. S. TOBIAS. Spectrochim. Acta, **35A**, 315 (1979).
3. T. G. SPIRO. Nucleic acid − metal ion interaction. Wiley, New York. 1980.
4. G. Y. H. CHU, S. MANSY, R. E. DUNCAN, and R. S. TOBIAS. J. Am. Chem. Soc. **100**, 593 (1978); **100**, 607 (1978).
5. G. M. CLORE and A. M. GRONENBORN. J. Am. Chem. Soc. **104**, 1369 (1982).
6. A. T. MARCELIS, C. G. VAN KRALINGEN, and J. REEDIJK. J. Inorg. Biochem. **13**, 213 (1980).
7. M. POLISSIOU, M. T. PHAN VIET, M. ST-JACQUES, and T. THEOPHANIDES. Can. J. Chem. **59**, 3297 (1981).
8. A. J. ALIX, L. BERNARD, M. MANFAIT, P. K. GANGULI, and T. THEOPHANIDES. Inorg. Chim. Acta, **55**, 147 (1981).
9. T. THEOPHANIDES. Appl. Spectrosc. **35**, 471 (1981).
10. A. PSODA and D. SHUGAR. Biochim. Biophys. Acta, **247**, 507 (1971).
11. A. PASINI and R. MENA. Inorg. Chim. Acta, **56**, L17−L19 (1981).
12. K. AOKI. Acta Crystallogr. B**32**, 1454 (1974).
13. P. DE MEESTER, D. M. L. GOODGAME, T. J. JONES, and A. C. SKAPSKI. Biochem. J. **139**, 791 (1974).
14. P. DIOE MEESTER, D. M. L. GOODGAME, T. J. JONES, and A. C. SKAPSKI. C.R. Acad. Sci. Paris, **22**, 667 (1974).
15. P. DE MEESTER, D. M. L. GOODGAME, A. C. SKAPSKI, and B. T. SMITH. Biochim. Biophys. Acta, **340**, 113 (1974).
16. K. AOKI, G. R. CLARK, and J. D. ORBELL. Acta Crystallogr. B**34**, 2119 (1978).
17. J. EMERSON and M. SUNDARALINGAM. Acta Crystallogr. B**36**, 1510 (1980).
18. S. C. DHARA. Indian J. Chem. **8**, 193 (1970).
19. G. B. KAUFFMAN and D. O. COWAN. Inorg. Synth. 239 (1963).
20. H. A. TAJMIR-RIAHI and T. THEOPHANIDES. Can. J. Chem. **61**, 1813 (1983).
21. P. D. LAWLEY and P. BROOKS. Nature (London), **192**, 1081 (1961).
22. R. C. LORD and G. J. THOMAS. Spectrochim. Acta, **23A**, 2551 (1967).
23. M. TSUBOI. Infrared and Raman spectroscopy in basic principles in nucleic acid chemistry. Vol. 1. Academic Press. 1974. p. 407; Adv. Chem. Phys. **7**, 435 (1964).
24. M. SUNDARALINGAM and P. PRUSINE. Nucleic Acids Res. **5**, 4375 (1978).
25. M. TSUBOI, S. TOKAHOSHI, and I. HORADA. Physicochemical properties of nucleic acid. Vol. 2. *Edited by* J. Dunhense. Academic Press, New York. 1973. p. 91.
26. S. K. KATTI, T. P. SESHADRI, and M. A. VISWAMITRA. Acta Crystallogr. B**37**, 1825 (1981).
27. C. SANDORFY. The chemistry of the carbon−nitrogen double bond. *Edited by* S. Patai. John Wiley, New York. 1970. p. 42.
28. J. I. BULLOCK, M. F. C. LADD, D. C. POVEY, and H. A. TAJMIR-RIAHI. Acta Crystallogr. B**35**, 2013 (1979).
29. A. LAUTI and A. NOVAK. J. Chem. Phys. **71**, 415 (1974).
30. L. CHINSKY, P. Y. TURPIN, and J. BRAHMS. Biopolymers, **17**, 1347 (1978).
31. M. SUNDARALINGAM. Biopolymers, **7**, 821 (1969).
32. P. PAPAGIANNAKOPOULOS, G. MAKRIGIANNIS, and T. THEOPHANIDES. Inorg. Chim. Acta, **46**, 263 (1980).
33. M. J. LANA and G. J. THOMAS JR. Biochemistry, **18**, 3839 (1979).
34. F. A. HART, M. UL-HUQUE, and C. N. CAUGHLAN. Chem. Commun. 1240 (1970); J. Inorg. Nucl. Chem. **31**, 145 (1969).
35. T. THEOPHANIDES. Interaction of metal ions with nucleic acids. *In* Infrared and Raman spectroscopy of biological molecules. *Edited by* T. Theophanides. R. Reidel Publishing Co., Dordrecht, Holland. 1979. p. 205.
36. J. E. DEL BENE. J. Phys. Chem. **87**, 367 (1983).

Can. J. Chem. Downloaded from www.nrcresearchpress.com by 210.87.254.105 on 09/06/12
For personal use only.

Substituent effects in the hydrogenation of $\Delta^{1,9}$-octalins

CIRILL SCHMIDT AND TIBOR BREINING[1]

Department of Chemistry, University of Prince Edward Island, Charlottetown, P.E.I., Canada C1A 4P3

Received May 30, 1983

CIRILL SCHMIDT and TIBOR BREINING. Can. J. Chem. **62**, 273 (1984).

The presence of the 4α-methyl group in olefin **4** or in conjugated ketone **10** prevents catalytic hydrogenation from the α side, leading exclusively to *cis*-fused decalins.

CIRILL SCHMIDT et TIBOR BREINING. Can. J. Chem. **62**, 273 (1984).

On rapporte que l'hydrogénation catalytique de l'oléfine **4** ou de la cétone conjuguée **10** conduit exclusivement a la *cis*-décaline correspondante étant donné la présence du groupement méthyle-4α qui empêche la réaction de s'effectuer du côté α de la molécule.

[Traduit par le journal]

Can. J. Chem. Downloaded from www.nrcresearchpress.com by 210.87.254.40 on 09/06/12
For personal use only.

We wish to report an example which might improve the predictability of ring junctures in decalins resulting from the catalytic hydrogenation of substituted $\Delta^{1,9}$-octalins **1**. The known cases are collected in Table 1. They show that any particular combination of methyl groups near the double bond profoundly influences the *cis*/*trans* isomer ratio of the decalins formed. However, these influences are not entirely understood.

Admittedly, the predominant and exclusive formation of *trans*-fused decalins from octalins **1***a* (1), **1***c* (3), and their derivatives (4) can readily be explained as the result of preferential adsorption of the less hindered side of the substrate on the surface of the catalyst. On the other hand, the predominance of the *cis* isomer in the hydrogenation of octalin **1***b*, containing an angular methyl group, is contrary to this explanation (2).

Octalin **1***d* should also be examined in this context, but to our knowledge this compound and its hydrogenation have not been reported. We have therefore prepared hydroxyketone **4** for this purpose.

The sterically hindered keto group in the recently reported dioxolane **2** (5) was reduced to the equatorial alcohol **3** with $LiAlH_4$ in refluxing THF as evidenced by a coupling constant of 11 Hz. After deketalization, hydroxyketone **4** was hydrogenated in acetic acid, in the presence of Adam's catalyst, to a single hydroxy ketone **5***a*, which will be shown to possess a *cis*-fused system.

We recently reported the preparation of the *trans*-fused ketone **11** from dimethylether **10** (5). The latter compound was hydrogenated to ketone **9** which, after elimination, led to ketone **8**, isomeric with the authentic *trans*-fused ketone **11**.[2]

Since the only possible stereochemical difference is due to the ring juncture, ketone **8** must be *cis*-fused. The same ketone was also obtained by elimination of mesylate **5***b* to olefin **6**, followed by reduction to alcohol **7***a* (8), methylation to **7***b* (9), and allylic oxidation to ketone **8** (10). It is to be mentioned that the only reagent which produced the pure equatorial alcohol **7***a* was Na in liquid ammonia (8). With complex hydrides, the undesired axial alcohol was also present.

The catalytic hydrogenations **4** → **5***a* and **10** → **9** led exclusively to *cis*-fused systems, even under the most *trans*-producing conditions (11). This indicated that the 4α-equatorial methyl group seriously inhibited the absorption of the substrate by the α side. This stereochemical result seems similar to that found in the selective reduction of diketone **12** to keto-alcohol **13** by $NaBH_4$, in which the hydride ion attacks from the β side (5), in spite of the usual α-attack encountered in the case of 6-ketosteroids (12). Clearly the 4α-methyl group seriously decreases the accessibility of the α side in both reactions.

It could be suggested that some secondary force of attraction may exist between the catalyst and the angular methyl group in octalin **1***b*, promoting the formation of a *cis*-fused system (55%), and, since hydrogenation leading to the *trans* product is prevented by the 4α-methyl group in compound **4**, the *cis*-decalin **5***a* is the only product formed. However, this attractive force between an angular methyl group and the catalyst in octalin **1***c* cannot operate, due to the presence of the second axial group.

Experimental

All melting points were taken on a Fisher–Johns melting point apparatus and are uncorrected. The elemental analyses were carried out by Pascher Mikroanalytical Laboratorium, Bonn, West Germany, and Schwarzkopf Mikroanalytical Laboratory, Woodside, N.Y. The ir spectra were recorded on a Perkin–Elmer Model 137B infracord spectrophotometer. The uv spectrograms were taken on a Coleman–Hitachi Model 124 double-beam grating spectrophotometer. The nmr spectra were recorded on a Varian Associates T60 spectrophotometer. The mass spectra were obtained with a Hitachi Perkin–Elmer Model RMS-4 spectrometer.

*8β-Hydroxy-4α,7α,8aβ-trimethyl-3,4,6,7,8,8a-hexahydronaphthalen-1(2*H*)-one ethylene ketal* **3**

A solution of 2α,5α,8aβ-trimethyl-3,6,7,8a-tetrahydronaphthalen-1,8 (2*H*,5*H*)-dione-8-ethylene ketal **2** (30.00 g, 0.119 mol) dissolved in dry THF (150 mL) was dropped into a magnetically stirred suspension of $LiAlH_4$ (4.55 g, 0.119 mol) in dry THF (150 mL). The reaction mixture was stirred while refluxing for 4 h, then the stirring was continued at room temperature for 14 h. Water (50 mL) was dropped carefully into the chilled suspension. The resulting suspension was filtered through Celite and the filter cake was washed with ether (100 mL). After separation of the ether layer, the aqueous phase was extracted with ether (4 × 50 mL). The combined organic phase was washed with water (50 mL), dried ($MgSO_4$), and concentrated *in vacuo* leading to crystalline, tlc (silica gel, benzene/ether 4:1) homogeneous product (28.4 g, 93.9%). An analytical sample was prepared by recrystallizing from pentane, mp 78–79°C; ir: 3460, 2850, 2820, 1450, 1095, 1050 cm^{-1}; nmr ($CDCl_3$, 60 MHz), δ: 1.02 (d, 6, J = 6 Hz, 4-CH_3 and 7-CH_3), 1.50 (s, 3, 8a-CH_3), 3.28 (dd, 1, J = 11 Hz, 4 Hz, 8-proton), 4.07 (m, 4, O—CH_2—CH_2—O), 4.33 (d, 1, J = 4 Hz, OH), 5.47 (m, 1, olefinic proton); mass spectrum (70 eV) m/e (relative intensity): 252 (9, M^+), 100 (32), 99

[1]On leave from Chinoin Pharmaceutical and Chemical Works Ltd., Budapest, Hungary.

[2]Ketone **11** was also prepared by P. Grieco *et al.* by an entirely different route (6, 7).

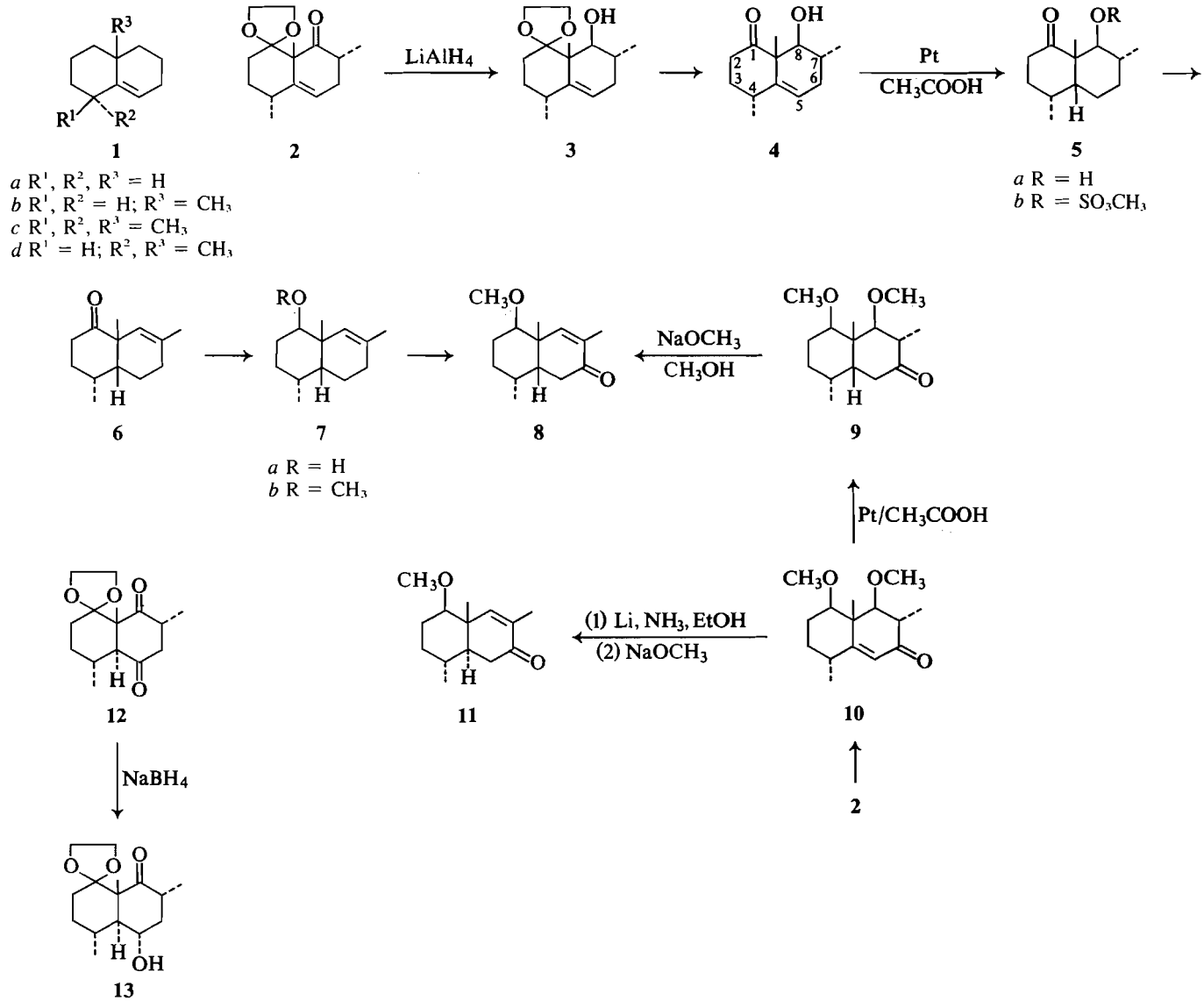

(100). *Anal.* calcd. for $C_{15}H_{24}O_3$: C 71.39, H 9.59; found: C 71.31, H 9.63.

8β-Hydroxy-4α,7α,8aβ-trimethyl-3,4,6,7,8,8a-hexahydronaphthalen-1(2H)-one **4**

A solution of 8β-hydroxy-4α,7α,8aβ-trimethyl-3,4,6,7,8,8a-hexahydronaphthalen-1(2*H*)-one-ethylene ketal **3** (15.00 g, 0.059 mol) dissolved in diethyl ether (150 mL) was magnetically stirred for 14 h at room temperature with a solution of *p*-toluenesulfonic acid (1.5 g) in water (75 mL). After separating the two phases, the water layer was extracted with ether (2 × 50 mL). The combined ether extracts were washed with 10% $NaHCO_3$ solution (20 mL), dried ($MgSO_4$), and concentrated *in vacuo* furnishing a tlc (silica gel, benzene/ether 4:1) homogeneous oil (12.0 g, 96%), which was converted to **5***a* without further purification; ir ($CHCl_3$): 3500, 2960, 2930, 2880, 1678, 1655, 1460, 1045 cm^{-1}; nmr ($CDCl_3$, 60 MHz), δ: 1.07 (d, 3, J = 5 Hz, CH_3), 1.08 (d, 3, J = 6 Hz, CH_3), 1.62 (s, 3, 8a-CH_3), 2.98 (after the addition of D_2O, d, 1, J = 11 Hz, 8-proton), 3.85 (d, 1, J = 11 Hz, OH), 5.50 (m, 1, olefinic proton); mass spectrum (70 eV) *m/e* (relative intensity): 208 (82, M^+), 151 (100), 138 (60), 135 (69), 123 (78).

8β-Hydroxy-4α,7α,8aβ-trimethyl-3,4,4aβ,5,6,7,8,8a-octahydronaphthalen-1(2H)-one **5**a

A solution of 8β-hydroxy-4α,7α,8aβ-trimethyl-3,4,6,7,8,8a-hexahydronaphthalen-1(2*H*)-one **4** (10.00 g, 0.048 mol) in acetic acid (100 mL) was hydrogenated at room temperature until the consumption of one equivalent hydrogen (1152 mL) at atmospheric pressure in the presence of prehydrogenated Pt (obtained from 50 mg of Adam's catalyst). After filtration, most of the acetic acid was distilled off at reduced pressure (5 Torr). Traces of CH_3COOH were removed by codistillation with ethyl acetate. The resulting colorless oil, homogeneous in tlc (silica gel, benzene/ether 4:1) was used without further purification for the preparation of mesylate **5***b*; ir ($CHCl_3$): 3510, 2995, 2950, 2930, 2870, 1680, 1450, 1050, 1036 cm^{-1}; nmr ($CDCl_3$, 60 MHz), δ: 1.00 (d, 3, J = 7 Hz, CH_3), 1.05 (d, 3, J = 6 Hz, CH_3), 1.57 (s, 3, 8a-CH_3), 2.62 (with D_2O, d, 1, J = 10 Hz, 8-proton), 3.37 (d, 1, J = 11 Hz, OH); mass spectrum (70 eV) *m/e* (relative intensity): 210 (67, M^+), 193 (55), 192 (90), 159 (100), 149 (98), 133 (73).

8β-Methanesulfonyloxy-4α,7α,8aβ-trimethyl-3,4,4aβ,5,6,7,8,8a-octahydronaphthalen-1(2H)-one **5**b

Methanesulfonyl chloride (5 mL) was dropped into a chilled solution of 8β-hydroxy-4α,7α,8aβ-trimethyl-3,4,4aβ,5,6,7,8,8a-octahydronaphthalen-1(2*H*)-one **5***a* (5.00 g, 0.024 mol) in dry pyridine (25 mL), over a 15-min period, while stirring magnetically. The reaction mixture was stirred at room temperature for 3 h, then it was poured into a mixture of crushed ice (25 g) and 10% H_2SO_4 (25 mL). After extraction with chloroform (4 × 20 mL), the combined extracts were washed in succession with 10% H_2SO_4 (2 × 30 mL), 10%

Can. J. Chem. Downloaded from www.nrcresearchpress.com by 210.87.254.40 on 09/06/12
For personal use only.

TABLE 1. The influence of substituents on the catalytic hydrogenation of $\Delta^{1,9}$-octalins

Substrate	Percentage of isomers *trans*	*cis*	Conditions	Reference
1*a*, R^1, R^2, R^3 = H	77	23	Pd/CH_3COOH	1
1*b*, R^1, R^2 = H; R^3 = CH_3	45	55	Pd/C_2H_5OH or CH_3COOH	2
1*c*, R^1, R^2, R^3 = CH_3	100	0	Pt/CH_3COOH	3,4
4, R^1 = H; R^2, R^3 = CH_3	0	100	Pt/CH_3COOH	This article
10, R^1 = H; R^2, R^3 = CH_3	0	100	Pt/CH_3COOH	This article

$NaHCO_3$ (20 mL), and water (20 mL). After drying ($MgSO_4$) and concentration *in vacuo*, diethyl ether (10 mL) was added to the residue. The product crystallized on scratching with a glass rod, after 15 min (5.35 g, 78%, mp 140–142°C). It was used without purification for the preparation of olefin **6**; ir ($CHCl_3$); 3010, 2960, 2930, 2865, 1695, 1320, 1158, 1145, 910, 890, 876 cm^{-1}; nmr ($CDCl_3$, 60 MHz), δ: 1.07 (d, 3, J = 7 Hz, CH_3), 1.05 (d, 3, J = 6 Hz, CH_3), 1.57 (s, 3, 8a-CH_3), 3.10 (s, 3, CH_3—SO_2), 4.08 (d, 1, J = 11 Hz, 8-proton).

4α,7,8aβ-Trimethyl-3,4,4aβ5,6,8a-hexahydronaphthalen-1(2H)-one **6**

Into a stirred suspension of Li_2CO_3 (1.50 g) and LiBr (1.50 g) in dry DMF (10 mL), a solution of 8β-methanesulfonyloxy-4α,7α,-8aβ-trimethyl-3,4,4aβ,5,6,7,8,8a-octahydronaphthalen-1(2*H*)-one **5***b* (3.00 g, 0.0104 mol) dissolved in DMF (30 mL) was dropped at 160°C under an atmosphere of dry nitrogen. The reaction mixture was then stirred at 170°C for 30 min. After cooling to room temperature, the solution was diluted with water (50 mL) and extracted with benzene (3 × 15 mL). The combined extracts were washed with water (2 × 30 mL), dried ($MgSO_4$), and concentrated *in vacuo* giving a yellow tlc (silica gel, benzene) homogeneous oil (1.97 g, 98.5%) which was used without purification for the preparation of unsaturated alcohol **7***a*; ir ($CHCl_3$); 2955, 2930, 2870, 1688, 1442, 1120 cm^{-1}; nmr ($CDCl_3$, 60 MHz), δ: 1.03 (d, 3, J = 7 Hz, 4-CH_3), 1.32 (s, 8a-CH_3), 1.72 (d, 3, J = 1 Hz, 7-CH_3), 5.38 (m, 1, olefinic proton); mass spectrum (70 eV) *m/e* (relative intensity): 192 (62, M^+), 159 (27), 149 (100), 135 (70).

4α,7,8aβ-Trimethyl-1,2,3,4,4aβ,5,6,8a-octahydronaphthalen-1β-ol **7**a

To a stirred solution of 4α,7,8aβ-trimethyl-3,4,4aβ,5,6,8a-hexahydronaphthalen-1(2*H*)-one **6** (3.00 g, 0.0156 mol) in ether (15 mL), ethanol (15 mL), and liquid ammonia (100 mL), freshly cut pieces of sodium (3 g) were added. The 500-mL three-neck flask was cooled with Dry Ice/acetone and was equipped with a Dry Ice condenser attached to a drying tube containing soda lime. The reduction was allowed to proceed for 30 min after the appearance of the blue color. After the evaporation of ammonia (1 h), water (30 mL) was added and the product was extracted with ether (4 × 10 mL). The combined extracts were washed with water (10 mL), dried ($MgSO_4$), and concentrated *in vacuo* giving a tlc (silica gel, benzene/ether 4:1) homogeneous oil (2.80 g, 92.4%) which was used without further purification for the preparation of methyl ether **7***b*; ir ($CHCl_3$): 3450, 2900, 1450, 1370, 1040, 1010 cm^{-1}; nmr ($CDCl_3$, 60 MHz), δ: 0.87 (d, 3, J = 6 Hz, 4-CH_3), 1.00 (s, 3, 8a-CH_3), 1.63 (d, 3, J = 1 Hz, 7-CH_3), 2.50 (broad s, 1, OH), 3.65 (dd, 1, J = 10 Hz, 6 Hz, 1-proton), 5.38 (m, 1, olefinic proton); mass spectrum (70 eV) *m/e* (relative intensity): 194 (94, M^+), 192 (68), 176 (94), 136 (86), 135 (100).

4α,7,8aβ-Trimethyl-1,2,3,4,4aβ,5,6,8a-octahydronaphthalen-1β-ol methyl ether **7**b

In a dry 100-mL three-neck flask equipped with reflux condenser, drying tube ($CaCl_2$), dropping funnel, and magnetic stirrer, sodium hydride (as 50% oil suspension, 2.00 g, 41.66 mmol, Alfa Inorganics) was placed under an atmosphere of dry nitrogen. After washing it by decantation with dry pentane (3 × 5 mL), the last traces of pentane were removed with a stream of dry nitrogen. Then tetrabutylammonium iodide (1 g) and dry THF (20 mL) were added.

A solution of 4α,7,8aβ-trimethyl-1,2,3,4,4aβ,5,6,8a-octahydronaphthalen-1β-ol **7***a* (2.00 g, 10.29 mmol) dissolved in dry THF (20 mL) was dropped into the stirred suspension. The suspension was stirred at room temperature, then methyl iodide (2.0 mL) was added over a 15-min period. The reaction mixture was stirred for 14 h at room temperature. After the addition of water (10 mL), most of the THF was removed by distillation at atmospheric pressure, using a short fractionating column. The residue was taken up in diethyl ether and the mixture of water and ether was filtered through Celite. After separation, the water phase was extracted with ether (2 × 10 mL). The combined ether extracts were washed with water (2 × 10 mL), dried ($MgSO_4$), and concentrated *in vacuo* giving a tlc (silica gel, benzene) homogeneous, slightly yellow oil (1.86 g, 86.8%) which was converted to the unsaturated ketone **8** without further purification; ir ($CHCl_3$): 2900, 1450, 1370, 1090 cm^{-1}; nmr ($CDCl_3$, 60 Hz), δ: 0.88 (d, 3, J = 7 Hz, 4-CH_3), 1.00 (s, 3, 8a-CH_3), 1.67 (d, 3, J = 1 Hz, 7-CH_3), 3.33 (s, 3, CH_3O), 5.47 (m,1 , olefinic proton); mass spectrum (70 eV) *m/e* (relative intensity): 208 (46, parent peak), 176 (31), 135 (100), 108 (59), 107 (96).

5β-Methoxy-3,4aβ,8α-trimethyl-4a,5,6,7,8,8aβ-hexahydronaphthalen-2(1H)-one **8**

(a). *By the allylic oxidation of methyl ether* **7**b

3,5-Dimethylpyrazole (1.66 g, 17.28 mmol) was added all at once to a magnetically stirred suspension of chromium trioxide (dried over P_2O_5 for 24 h, 1.73 g, 17.28 mmol) in dry methylene chloride (15 mL), at −20°C. The mixture was stirred for 15 min at −20°C, then a solution of 4α,7,8aβ-trimethyl-1,2,3,4,4aβ,5,6,8a-octahydronaphthalen-1β-ol methyl ether **7***b* (300 mg, 1.44 mmol) dissolved in dry CH_2Cl_2 (5 mL) was dripped in 5 min. The reaction mixture was stirred for 4 h at −10 to −20°C, then 5 *N* NaOH (10 mL) was added and the solution was stirred at 0°C for 1 h. After extracting with ether (3 × 30 mL), the combined organic extracts were washed in succession with 10% H_2SO_4 (2 × 10 mL) and 10% $NaHCO_3$ (10 mL). After drying ($MgSO_4$) and concentration (to 10 mL) the solution was passed through a short column of Fluorosil (10 g). The eluted colorless solution was concentrated to an oil (240 mg, 75%), whose spectroscopic properties were identical with those prepared from dimethoxy ketone **9** (see next paragraph).

(b). *By the base-catalyzed elimination of dimethoxy ketone* **9**

To a solution of 4β,5β-dimethoxy-3α,4aβ,8α-trimethyl-3,4,4a,-5,6,7,8aβ-octahydronaphthalen-2(1*H*)-one **9** (300 mg, 1.17 mmol) in methanol (5 mL), a solution of sodium methylate (20 mg) in methanol (2 mL) was added. The reaction mixture was allowed to stand at room temperature for 14 h, then it was diluted with water (15 mL) and extracted with ether (4 × 5 mL). The combined ether extracts were washed with water (2 × 5 mL), dried ($MgSO_4$), and concentrated *in vacuo* furnishing a slightly yellow oil (240 mg, 92%). The tlc (silica gel, benzene/ether 9:1) homogeneous oil was microdistilled, 115°C/0.1 Torr. Infrared ($CHCl_3$): 2950, 2930, 2870, 1660, 1455, 1362, 1092 cm^{-1}; $uv_{\lambda max}$: 238 nm (ε = 10 110); nmr ($CDCl_3$, 60 MHz), δ: 0.85 (d, 3, J = 6 Hz, 8-CH_3), 1.17 (s, 3, 4a-CH_3), 1.78 (d,

Can. J. Chem. Downloaded from www.nrcresearchpress.com by 210.87.254.40 on 09/06/12
For personal use only.

3, J = 1 Hz, olefinic 3-CH_3), 3.30 (s, 3, CH_3O), 6.73 (d, 1, J = 1 Hz, olefinic proton); mass spectrum (70 eV) *m/e* (relative intensity): 222 (30, parent peak), 190 (12), 175 (11), 140, (52), 123 (100), 122 (41). *Anal.* calcd. for $C_{14}H_{22}O_2$: C 75.63, H 9.97; found: C 75.70, H 10.01.

4β,5β-Dimethoxy-3α,4aβ,8α-trimethyl-3,4,4a,5,6,7,8,8aβ-octahydronaphthalen-2(1H)-one **9**

A solution of 4β-5β-dimethoxy-3α,4aβ,8α-trimethyl-4,4a,5,6,7,8-hexahydronaphthalen-2(3*H*)-one **10** (250 mg, 0.99 mmol) in acetic acid (2 mL) was hydrogenated at room temperature, while stirring magnetically, in the presence of prehydrogenated Pt (prepared from 50 mg of Adam's catalyst) until the consumption of one equivalent hydrogen (24 mL). After filtering the catalyst, the filtrate was dropped to a saturated solution of $NaHCO_3$ (30 mL), while stirring, and extracted with chloroform (4 × 10 mL). The combined organic extracts were washed with 10% $NaHCO_3$ (10 mL), dried ($MgSO_4$), and concentrated *in vacuo*, furnishing a colorless tlc (silica gel, benzene/ether 4:1) homogeneous oil (0.25 g, 99%) which was eliminated to the unsaturated ketone **8** without further purification. Infrared ($CHCl_3$): 2990, 2930, 1703, 1452, 1092 cm^{-1}; nmr ($CDCl_3$, 60 MHz), δ: 0.82 (d, 3, J = 7 Hz, CH_3), 1.18 (d, 3, J = 6 Hz, CH_3), 1.25 (s, 3, 4a-CH_3), 3.40 (s, 3, CH_3O), 3.50 (s, 3, CH_3O); mass spectrum (70 eV) *m/e* (relative intensity): 254 (8, parent peak), 222 (78), 190 (24), 175 (19), 149 (100), 139 (49), 125 (30), 123 (94).

Acknowledgements

The financial assistance of the Natural Sciences and Engineering Research Council of Canada and the Research Committee of the University of Prince Edward Island is gratefully acknowledged.

1. J. F. SAUVAGE, R. H. BAKER, and A. S. HUSSEY. J. Am. Chem. Soc. **83**, 3874 (1961).
2. F. SONDHEIMER and D. ROSENTHAL. J. Am. Chem. Soc. **80**, 3995 (1958).
3. G. DEFAYE. C. R. Acad. Sci. **260**, 2843 (1965).
4. B. GASPERT, T. G. HALSALL, and D. WILLIS. J. Chem. Soc. 624 (1958).
5. C. SCHMIDT and T. BREINING. Tetrahedron. In press.
6. P. A. GRIECO, T. OGURI, C. L. WANG, and E. WILLIAMS. J. Org. Chem. **42**, 4113 (1977).
7. P. A. GRIECO, G. VIDARI, and S. FERRINO. Tetrahedron Lett. **21**, 1619 (1980).
8. H. L. DRYDEN, JR. *In* Organic reactions in steroid chemistry. Vol. 1. *Edited by* J. Fried and J. A. Edwards. Van Nostrand Reinhold, Co., New York. 1972. p. 36.
9. C. A. BROWN and D. BARTON. Synthesis, 434 (1974).
10. W. G. SALMOND, M. A. BARTA, and J. L. HAVENS. J. Org. Chem. **43**, 2057 (1978).
11. R. L. AUGUSTINE. Catalytic hydrogenation. Marcel Dekker, Inc., New York. 1965.
12. D. M. S. WHEELER and M. M. WHEELER. *In* Organic reactions in steroid chemistry. Vol. 1. *Edited by* J. Fried and J. A. Edwards. Van Nostrand Reinhold, Co., New York. 1972. p. 61.

Can. J. Chem. Downloaded from www.nrcresearchpress.com by 210.87.254.40 on 09/06/12
For personal use only.

O—O stretching frequencies of cyclic peroxides. Stabilization of peroxides by alkoxy substituents[1]

KARL R. KOPECKY and RODRIGO RICO GOMEZ[2]
Department of Chemistry, University of Alberta, Edmonton, Alta., Canada T6G 2G2

Received June 9, 1983

KARL R. KOPECKY and RODRIGO RICO GOMEZ. Can. J. Chem. **62**, 277 (1984).

The O—O stretching frequencies of some alkyl substituted 1,2-dioxacyclohexanes are near 730 cm^{-1} and those of some alkyl substituted 1,2-dioxetanes are in the range 670 ± 20 cm^{-1}. Alkoxy substituents cause the frequency to increase; that for tetramethoxy-1,2-dioxetane is 752 cm^{-1}. Alkoxy substituents appear to stabilize peroxides.

KARL R. KOPECKY et RODRIGO RICO GOMEZ. Can. J. Chem. **62**, 277 (1984).

Les fréquences d'élongation de la liaison O—O de certains dioxa-1,2 cyclohexanes ayant un substituant alkyle sont à environ 730 cm^{-1} et celles des dioxétanes-1,2 ayant des substituants alkyles sont à 670 ± 20 cm^{-1}. Les substituants alkoxy provoquent une augmentation de la fréquence; cette fréquence est de 752 cm^{-1} pour le tétraméthoxy dioxétane-1,2. Les substituants alkoxy semblent stabiliser les peroxydes.

[Traduit par le journal]

Can. J. Chem. Downloaded from www.nrcresearchpress.com by 210.87.254.6 on 09/06/12
For personal use only.

Introduction

The luminescent thermolysis of 1,2-dioxetanes has been proposed (1) to proceed by a two-step process with initial cleavage of the O—O bond to a diradical intermediate as the rate determining step, eq. [1]. While values of the activation

[1] 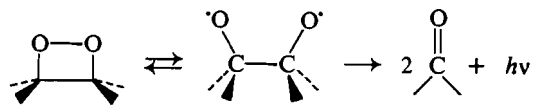

parameters for the thermolysis of a variety of alkyl and aryl substituted 1,2-dioxetanes, as estimated by thermochemical calculations (1) based on this mechanism, are in good agreement with the values determined experimentally, there are also 1,2-dioxetanes for which a significant difference has been found between calculated and observed parameters (2). Steric effects must be involved in alkyl substituted 1,2-dioxetanes and both steric and electronic effects may be present in 1,2-dioxetanes with other substituents. The factors which influence the stability of 1,2-dioxetanes are still being studied (1–3).

In the present report it is suggested that the inductive effect of alkoxy subsituents may strengthen the O—O bond of a 1,2-dioxetane and an attempt is made to detect the difference in the O—O bond strengths of alkyl and alkoxy substituted 1,2-dioxetanes by measuring the O—O stretching frequencies of these compounds.

Results and discussion

There is a marked effect of substituents on the O—O bond strengths and stretching frequencies of peroxides, Table 1. A molecular orbital explanation of this effect proposes (4)[3] that electronegative substituents bonded to oxygen donate little electron density into the antibonding orbitals of the peroxide and the O—O bond order is accordingly decreased by a small amount from that in the oxygen molecule. Substituents which can donate more electron density into the antibonding orbitals cause a greater reduction of the O—O bond order. According to this reasoning, alkoxy substituted 1,2-dioxetanes should have stronger O—O bonds and higher O—O stretching frequencies than the alkyl substituted analogues.

TABLE 1. Stretching frequencies and dissociation energies of some O—O bonds

Compound	ν_{O-O} (cm^{-1})	Ref.	D_{O-O} (kcal/mol)	Ref.
O_2	1556	6	118	7
FOOF	1306	8	62	9
CF_3OOCF_3	886	10	46	11
HOOH	877	12	50.3	13
CH_3OOCH_3	779	14	37.6	2*b*, 15
$(CH_3)_3COOC(CH_3)_3$	771	14	38.0	2*b*, 16

In an early report it was suggested that peroxides absorb in the range 890–830 cm^{-1} in the infrared (17). A number of 1,2-dioxetanes have been found to absorb in this region and this was taken as evidence for the 1,2-dioxetane ring system. However, it has been pointed out that the O—O stretch of peroxides should give rise to very weak infrared absorption and be Raman active, and this was shown to be so (14). The present study confirms these observations for a variety of cyclic peroxides (Table 2), and extends the structural diversity of peroxides for which O—O stretching frequencies have been determined.

The O—O stretching frequencies were identified in the following way. All the bands listed in Table 2 are either absent or very weak in the infrared spectra of these molecules. Only one intense band is present between 1400 and 500 cm^{-1} in the Raman spectra of several of these compounds. One additional strong band is present in this region in the spectra of the other molecules. The Raman spectra of the diperoxides of acetone and cyclohexanone each contain a second strong band at 895 and 860 cm^{-1}, respectively, but these are also infrared active. A strong band at 778 cm^{-1} is present in the Raman spectrum of the dioxetane of adamantylideneadamantane, but this appears to be associated with the adamantyl skeleton as the spectra of adamantane and 1-adamantanol exhibit strong bands at 762 and 778 cm^{-1}, respectively. A medium intensity band at 832 cm^{-1}

[1]This research was supported by a grant from the Natural Sciences and Engineering Research Council of Canada and was presented at the 65th Chemical Conference of the Chemical Institute of Canada, Toronto, Ontario, 30 May to 2 June, 1982, Abstract PH 7-2.

[2]Present address: Departamento de Química Orgánica, Facultad de Ciencias, Universidad de Málaga, Malaga, Spain.

[3]Some modifications of the original proposal have been suggested (5).

TABLE 2. O—O Stretching frequencies and energies of activation for thermolysis of some cyclic peroxides

Compound	ν_{O-O} (cm^{-1})	E_a (kcal/mol)	Ref.
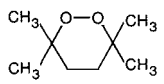	729	33	18
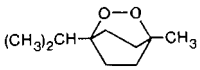	729	33[a]	19
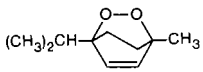	731	31.5	20
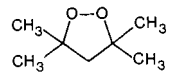	798	46	21
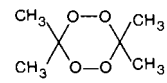	765	—	—
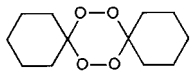	735	40	22
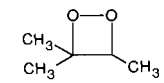	650	24	23
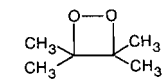	672	26	23
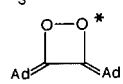	690	37	24
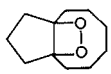	652	29	25
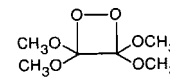	752	29	3

*Ad = Adamantylidene
[a]Value for 2,3-dioxabicyclo[2.2.2]octane.

in the Raman spectrum of tetramethoxy-1,2-dioxetane is infrared active. Thus, it seems fairly secure that the frequencies listed in Table 2 are associated with the O—O stretch.

The O—O stretching frequencies of the cyclic peroxides do depend upon structure and all those listed in Table 2, except that of the tetramethyldioxacyclopentane, are significantly lower than those of the acyclic dialkyl peroxides dimethyl and di-*tert*-butyl peroxide. With the limited data available here it appears as if each class of cyclic peroxide containing only alkyl substituents has a characteristic range of O—O stretching frequencies: near 730 cm^{-1} for the dioxacyclohexanes, whether mono- or bicyclic, and near 670 ± 20 cm^{-1} for dioxetanes. Oxygen substitution does result in an increased frequency of the O—O stretch and an increase in the energy of activation for thermolysis, and the former effect is especially marked for tetramethoxy-1,2-dioxetane. It is tempting to use this as evidence in support of the suggestion made above that alkoxy substituents stabilize dioxetanes by withdrawing electron density from the antibonding orbitals of the peroxy group relative to alkyl substituted dioxetanes. However, it should be pointed out that the O—O stretch of peroxides is strongly coupled with other vibrations in these molecules (26) and an unambiguous assessment of the various factors will be difficult. Nevertheless, it appears to be possible to determine whether a peroxy group is part of a four, five, or six membered ring on the basis of the O—O stretching frequency.

Experimental

Raman spectra were recorded on a Beckman Model 700 Laser Raman spectrometer using the 514.5 nm exciting line from a Coherent Radiation Model 52 argon laser. The spectra of the five and six membered cyclic peroxides and of the dioxetane of adamantylideneadamantane were obtained from the neat liquids or crystals in capillary tubes at ambient temperatures. Those of the other dioxetanes were obtained from solid films in a flat bottomed cylindrical rotating cell at −20 to −50°C with the incident light focused on the bottom edge of the cell. Infrared spectra were recorded on a Perkin–Elmer Model 457 spectrometer.

The dioxetane of adamantylideneadamantane was a gift from Prof. A. P. Schaap, acetone (27) and cyclohexanone (28) diperoxides were prepared as described, tetramethoxyethylene was oxygenated (3) to prepare the dioxetane, the other dioxetanes were available from previous studies (23, 25) and the other peroxides were prepared by Prof. R. S. Brown (29).

Acknowledgements

We thank Prof. R. S. Brown for stimulating discussions and Mr. R. N. Swindlehurst for determining the Raman spectra.

1. (*a*) H. E. O'NEAL and W. H. RICHARDSON. J. Am. Chem. Soc. **92**, 6553 (1970); (*b*) W. H. RICHARDSON, M. B. YELVINGTON, and H. E. O'NEAL. J. Am. Chem. Soc. **94**, 1619 (1972); (*c*) W. H. RICHARDSON, F. C. MONTGOMERY, M. B. YELVINGTON, and H. E. O'NEAL. J. Am. Chem. Soc. **96**, 7525 (1974); (*d*) W. H. RICHARDSON, F. C. MONTGOMERY, P. SLUSSER, and M. B. YELVINGTON. J. Am. Chem. Soc. **97**, 2819 (1975); (*e*) W. H. RICHARDSON, J. H. ANDEREGG, M. E. PRICE, W. A. TAPPEN, and H. E. O'NEAL. J. Org. Chem. **43**, 2236 (1978).
2. (*a*) E. J. H. BECHARA and T. WILSON. J. Org. Chem. **45**, 5261 (1980); (*b*) A. L. BAUMSTARK and C. E. WILSON. Tetrahedron Lett. 4363 (1981); (*c*) A. L. BAUMSTARK and T. DUNAMS. J. Org. Chem. **47**, 3754 (1982).
3. T. WILSON, D. E. GOLAN, M. S. HARRIS, and A. L. BAUMSTARK. J. Am. Chem. Soc. **98**, 1086 (1976).
4. R. D. SPRATLEY and G. C. PIMENTEL. J. Am. Chem. Soc. **88**, 2394 (1966).
5. (*a*) S. J. TURNER and R. D. HARCOURT. Chem. Commun. 4 (1967); (*b*) D. E. TEVAULT and R. R. SMARDZEWSKI. J. Am. Chem. Soc. **100**, 3955 (1978); (*c*) L. J. LAWLER, K. VASUDEVAN, and F. GREIN. J. Am. Chem. Soc. **100**, 8062 (1978).
6. G. HERTZBERG. Molecular spectra and molecular structure. I: Spectra of diatomic molecules. Van Nostrand Co., Princeton, NJ. 1950.
7. A. E. DOUGLAS. J. Phys. Chem. **59**, 109 (1955).
8. K. R. LOOS, D. T. GOETCHEL, and V. A. CAMPANILE. J. Chem. Soc. Chem. Commun. 1633 (1968).
9. A. D. KIRSCHENBAUM, A. V. GROSSE, and J. G. ASTON. J. Am. Chem. Soc. **81**, 6398 (1959).
10. J. R. DURIG and D. W. WERTZ. J. Mol. Spectrosc. **25**, 467 (1968).
11. B. DESCAMPS and W. FORST. Can. J. Chem. **53**, 1442 (1975).
12. E. HIROTA. J. Chem. Phys. **28**, 839 (1958).
13. P. GRAY. Trans. Faraday Soc. **55**, 408 (1959).
14. K. O. CHRISTIE. Spectrochim. Acta Part A, **27**, 463 (1971).
15. (*a*) Y. TAKEZAKI and C. TAKEUCHI. J. Chem. Phys. **22**, 1527 (1954); (*b*) J. R. BAKER, S. W. BENSON, and D. M. GOLDEN. Int. J. Chem. Kinet. **9**, 31 (1977).
16. L. BATT and S. W. BENSON. J. Chem. Phys. **36**, 895 (1962).
17. G. J. MINKOFF. Proc. R. Soc. London Ser. A, **224**, 176 (1954).
18. W. ADAM and J. SANABIA. J. Am. Chem. Soc. **99**, 2735 (1977).

Can. J. Chem. Downloaded from www.nrcresearchpress.com by 210.87.254.6 on 09/06/12
For personal use only.

19. D. J. COUGHLIN and R. G. SALOMON. J. Am. Chem. Soc. **101**, 2761 (1979).
20. J. BOCHE and O. RUNQUIST. J. Org. Chem. **33**, 4285 (1968).
21. W. H. RICHARDSON, R. MCGINNESS, and H. E. O'NEAL. J. Org. Chem. **46**, 1887 (1981).
22. J. R. SANDERSON and P. R. STORY. J. Org. Chem. **39**, 3463 (1974).
23. K. R. KOPECKY, J. E. FILBY, C. MUMFORD, P. A. LOCKWOOD, and J.-Y. DING. Can. J. Chem. **53**, 1103 (1975).
24. G. B. SCHUSTER, N. J. TURRO, H.-C. STEINMETZER, A. P. SCHAAP, G. FALER, W. ADAM, and J. C. LIU. J. Am. Chem. Soc. **97**, 7110 (1975).
25. K. R. KOPECKY, P. A. LOCKWOOD, R. RICO GOMEZ, and J.-Y. DING. Can. J. Chem. **59**, 851 (1981).
26. M. E. B. BELL and J. LAANE. Spectrochim. Acta, Part A, **28**, 2239 (1972).
27. A. BAEYER and V. VILLIGER. Chem. Ber. **32**, 3625 (1899).
28. G. LOHAUS. Justus Liebigs Ann. Chem. **583**, 6 (1953).
29. R. S. BROWN. Can. J. Chem. **53**, 3439 (1975).

Can. J. Chem. Downloaded from www.nrcresearchpress.com by 210.87.254.6 on 09/06/12
For personal use only.

Micellar properties of sodium alkyl sulfoacetates and sodium dialkyl sulfosuccinates in water

DAVID J. JOBE and VINCENT C. REINSBOROUGH
Chemistry Department, Mount Allison University, Sackville, N.B., Canada E0A 3C0

Received July 8, 1983

DAVID J. JOBE and VINCENT C. REINSBOROUGH. Can. J. Chem. **62**, 280 (1984).

Viscosity, conductivity, density, and fluorescence quenching studies were conducted in aqueous micellar solutions at 25.0°C of sodium alkyl sulfoacetates and sodium dialkyl sulfosuccinates in a comparison of one-tailed and two-tailed surfactant systems. The hexyl, octyl, and decyl members of the former group and the dihexyl and dioctyl members of the latter group were investigated. The results indicated that the sulfoacetates most likely form spherical micelles with aggregation numbers 20 for hexyl, 42 for octyl, and 70 for decyl with three methods for size determination giving concordant results. For the sulfosuccinates, the aggregation numbers from fluorescence quenching were 38 for the dihexyl and 56 for the dioctyl in agreement with the results from the conductance technique which means that spherical micelles are likely formed also. Volume changes on micellization were obtained for the sulfoacetates.

DAVID J. JOBE et VINCENT C. REINSBOROUGH. Can. J. Chem. **62**, 280 (1984).

On a étudié la viscosité, la conductivité, la densité et l'extinction de fluorescence de solutions micellaires aqueuses d'alkylsulfoacétates de sodium et de dialkylsulfosuccinates de sodium à 25°C en comparant les surfactants à une tête et à deux têtes. On a étudié les dérivés hexyle, octyle et décyle sulfoacétates et les dihexyl et dioctylsulfosuccinates. Les résultats indiquent que les sulfoacétates forment plus communément des micelles sphériques avec des nombres d'aggrégation de 20 pour l'hexyle, de 42 pour l'octyle et de 70 pour le décycle. Les trois méthodes de détermination de la grosseur utilisées donnent des résultats concordants. Pour les sulfosuccinates, les nombres d'aggrégation obtenus par extinction de fluorescence sont de 38 et de 56 pour le dihexyle et le dioctyle respectivement en accord avec les résultats obtenus à partir de la technique de conductance ce qui indique qu'il se forme également des micelles sphériques. On a obtenu des changements de volumes lors de la formation des micelles dans le cas des sulfoacétates.

[Traduit par le journal]

Can. J. Chem. Downloaded from www.nrcresearchpress.com by 210.87.254.105 on 09/06/12
For personal use only.

Introduction

Two-tailed surfactants are generally thought to form bilayer vesicles in water while single-tailed surfactants form micelles (1–3). If the carbon chains are long enough, for example with dioctadecyldimethylammonium chloride (DODAC) and dihexadecylphosphate (DHP), there seems to be little doubt that vesicles do form with two-tailed surfactants and these can be useful in membrane mimetic studies (4). The phospholipids of natural membranes may be two-tailed for this very reason. On the other hand, short-chained phospholipids can form micelles (5) and vesicles can be made in some instances from single-chain amphiphiles (6). Chain length appears critical in determining whether two-tailed surfactants will form vesicles or micelles.

This study examines the solution properties of two closely allied families of ionic surfactants of short to medium carbon chain length that differ essentially only by having either one tail or two tails of equal length. The aim was to provide insight into the size and shape of the surfactant aggregates in these solutions and to see whether the extra appendage changed the basic nature of this aggregate. The families selected for this study were the sodium alkyl sulfoacetates and the sodium dialkyl sulfosuccinates which, despite their different names, have the same sulfonate head group and differ essentially only in the number of their tails. In the former family, the hexyl (SHSA), octyl (SOSA), and decyl (SDSA) homologs were studied while in the latter, the dihexyl (SDHSS) and dioctyl (SDOSS) members received attention. Sodium didecyl sulfosuccinate was synthesized but its solubility range in water proved too limited. The hexyl homologs were chosen as the other extreme since amphiphiles seem to require at least a six carbon chain before micellization is possible below one molal in aqueous solution. It should be noted here that the well-known surfactant, Aerosol OT or AOT, is a sodium dialkyl sulfosuccinate where the alkyl group is 2-ethylhexyl. Athough well characterized in non-aqueous solvents as a bilayer vesicle (7, 8), its aqueous solution structure beyond the critical micelle concentration (cmc) is still a matter of conjecture, mainly because it has rarely been studied in water.

The results from a variety of experimental techniques are reported here because no one technique can unambiguously characterize micellar size and form. Measurements were made on the viscosities, conductivities, densities, and fluorescence quenching abilities of the five surfactant systems.

Experimental

Viscosities of the surfactant solutions were obtained with a Hoeppler precision viscometer (precision ±0.1%) which was wrapped in glass wool to avoid heat loss.

Conductivities were measured with a Beckman RC-18A conductivity bridge with the solutions in a Jones-Bollinger cell calibrated with KCl solutions of known concentration. Temperature control to ±0.1°C ensured a precision of ±0.1% in the conductivity data.

A Sodev OD2 digital flow densimeter was used to measure the solution densities in conjunction with a Fluke 1952A frequency meter. Temperature control to ±0.005°C enabled the densities to be measured with a relative error of 3 ppm (9).

Fluorescence quenching data were obtained by the single photon counting technique at the University of Kent at Canterbury (U.K.) with apparatus described by Bridge and Solomon (10). The fluorescent probe was acridinium (1.18×10^{-3} mol dm^{-3}) and the quencher was Co^{2+} (4.5×10^{-4} to 1.0×10^{-3} mol dm^{-3}). Decay profiles (log intensity against channel number) were recorded for the background and for the surfactant solutions with and without quencher. The surfactant concentrations were approximately twice the cmc for the sulfoacetates and SDHSS and twenty times the cmc for SDOSS.

The sulfoacetates were synthesized using a modified Hikota and Meguro approach (11). Equimolar quantities (usually 0.1 mol of each) of chloroacetyl chloride and the appropriate alcohol were mixed to

TABLE 1. Micellar parameters for sodium alkyl sulfoacetates and sodium dialkyl sulfosuccinates in water

Surfactant	cmc[a] (mol dm^{-3})	cmc[b] (mol dm^{-3})	η_0 (cP)	l^c (Å)	f	ΔV_m (cm^3 mol^{-1})	$\bar{n}^a$	$\bar{n}^b$	$\bar{n}^d$
SHSA	0.21	0.17	0.9595	15	0.48	2.0±.2	25	16	—
SOSA	0.070	0.066	0.9196	18	0.36	6.3±.5	34	37	42
SDSA	0.025	0.022	0.8995	21	0.29	13.6±1.0	40	69	71
SDHSS	0.014	0.0138	0.8786	—	0.38	16±5	—	30	36
SDOSS	—	6.8×10^{-4}	0.8130	—	0.36	—	—	59	56

[a]From viscosities.
[b]From conductances.
[c]Estimated monomeric length.
[d]From fluorescence quenching.

form the chlorester. Then, 100 cm^3 of 2 mol dm^{-3} aqueous sodium sulfite was added and the solution refluxed overnight. Vacuum drying at 50°C removed most of the water leaving a residue that was further dried in a dessicator overnight. This residue was extracted several times with hot ethanol. Crystallization of the surfactant occurred from the cooled extracts. Recrystallization was effected from hot ethanol also.

Caryl's procedure (12) formed the basis for obtaining the sodium dialkyl sulfosuccinates. To 0.1 mol of maleic anhydride was added 0.22 mol of the appropriate alcohol. After heating for 2 h, 100 cm^3 of 2 mol dm^{-3} aqueous sodium bisulfite was added and the mixture refluxed overnight. As with the alkyl sulfoacetates, several extractions with hot ethanol followed with the surfactants crystallizing in the cooled extracts. Recrystallization was carried out as outlined by Williams *et al.* (13) which ensured that the product was the monohydrate. The yields of both procedures were in the 60–65% range.

The structures of the surfactants were confirmed by nmr and their purities determined gravimetrically by precipitation as barium salts (purity >98%). All other reagents were the best obtainable commercially and were not further purified. All measurements were conducted at 25.0°C except for the SDOSS solutions which were done at 30.0°C because of solubility problems at the lower temperature (SDOSS appears to have a Krafft point around 27°C).

Results

The density, viscosity, and conductivity data for the five surfactant systems have been deposited.[1] In each system for each property usually about 15 determinations at different concentrations were required above and below the cmc. The cmc was determined by the break in the conductivity and viscosity curves and these values, which agreed with literature values where available, are listed in Table 1 (11, 14). For SDOSS, this break point was too uncertain from the viscosity and conductivity data (this is probably why such a wide range of cmc values is found in the literature for this compound (14)) so the cmc in this system was detected by the dye solubility method using pyridine-2-azo-*p*-dimethylaniline (PADA). The solubility of PADA is low in water (2.8×10^{-4} mol dm^{-3} at 30.0°C) and does not change until micelles are present when a several fold uptake of PADA occurs as the surfactant concentration is increased. This is a markedly sensitive method of detecting the cmc especially with long chained surfactants. The cmc for SDOSS at 30.0°C was thus determined to be 6.8×10^{-4} mol dm^{-3}.

The cmc values of the sulfoacetates correspond approximately to those for the sulfonates having two more carbon atoms in the chain reflecting the effective lengthening of the chain with the insertion of the acetyl group. The cmc values of the sulfosuccinates fall in line with the usual observation with double-tailed surfactants that they are intermediate between the cmc for the longest chain, single-tailed counterpart and the cmc for the single-tailed counterpart where the chains are laid end on end (15) (Fig. 1). Thus the cmc for SDHSS is roughly the cmc for SDSA.

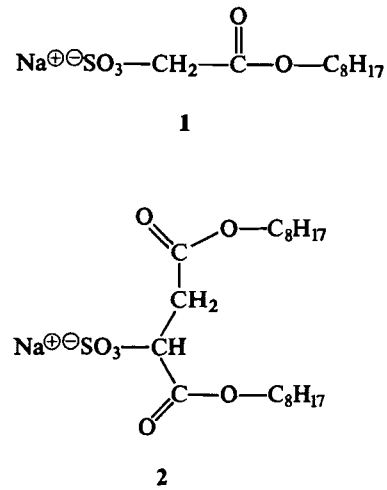

FIG. 1. Structural representations for sodium octyl sulfoacetate (*1*) and sodium dioctyl sulfosuccinate (*2*).

Aggregation numbers were calculated from the fluorescence quenching, viscosity, and conductivity data. Of these three methods, the first is probably the most reliable being less dependent on the model being assumed for micelle structure. The chief assumptions entail the rates of quenching and fluorescent decay, the distribution of probe and quencher, and the strength of the association of both to the micelle (16, 17). From the total intensities of the quenched (I) and unquenched (I_0) curves, the aggregation number can be determined from

$$I = I_0 \exp(-C_Q/C_{MIC})$$

where C_Q is the concentration of the quencher and C_{MIC} that of the micelles. C_{MIC} is given by $(C - \text{cmc})/\bar{n}$ where C is the total surfactant concentration and $\bar{n}$ is the mean aggregation number. A detailed analysis of the technique is given by Almgren and Löfroth (17).

Figure 2 depicts the unquenched and quenched decay profiles for 0.463 mol dm^{-3} SDSA. The aggregation number obtained from the slope of the computer linearizing of ln I against the inverse of the micellar concentration was 71 ± 2. With the smaller size of the SOSA micelle the difference between the

[1]Copies of the data are available upon request, at a nominal charge, to the Depository of Unpublished Data, CISTI, National Research Council of Canada, Ottawa, Ont., Canada K1A 0S2.

Can. J. Chem. Downloaded from www.nrcresearchpress.com by 210.87.254.105 on 09/06/12
For personal use only.

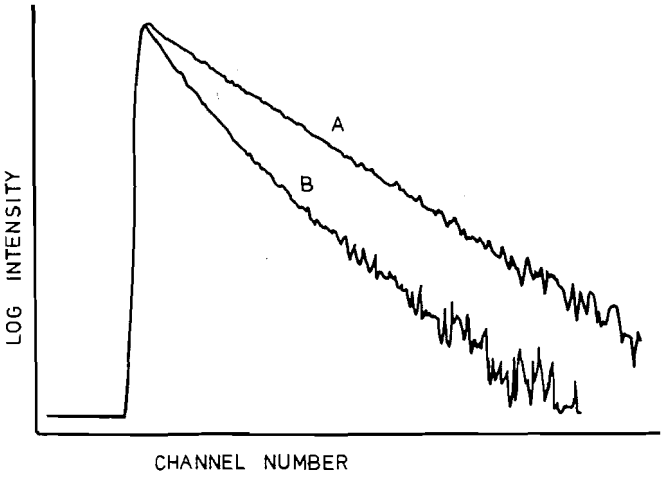

FIG. 2. Fluorescence decay profiles for 4.63×10^{-2} mol dm^{-3} sodium decyl sulfoacetate with no quencher (A) and with 9.45×10^{-4} mol dm^{-3} $CoSO_4$ as quencher (B).

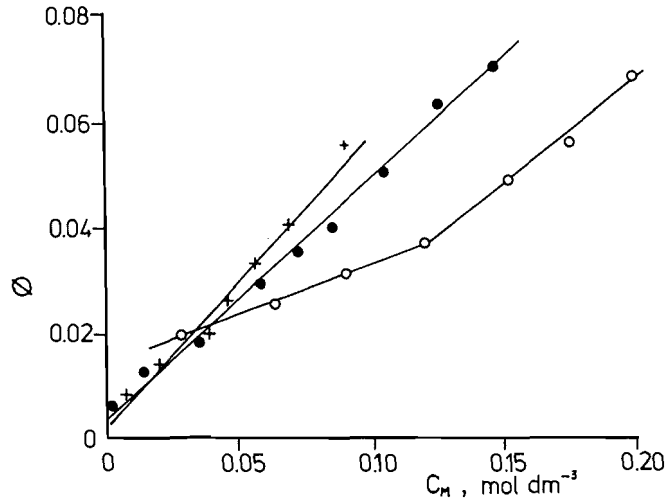

FIG. 3. Volume fraction (ϕ) dependence upon surfactant micellar concentration(C_M): ○, SHSA; ●, SOSA; +, SDSA.

two curves for the intensities was less pronounced with a value of $\bar{n} = 42 \pm 3$ being the result. For SHSA, the two curves differed so slightly at the quencher concentrations employed that meaningful estimates of the aggregation number were not possible. The decay profiles for the two-tailed SDHSS and SODSS surfactants were similar to the sulfoacetates with values of 38 ± 3 and 56 ± 2, respectively, being obtained for the mean aggregation numbers.

For short-chained (C_6—C_{10}) ionic surfactants, viscosity measurements provide micellar size parameters (18). The chief assumptions relate to the sphericity of the micelles and the neglecting of the electroviscous effect.

The volume fraction of the micelles (ϕ) is first calculated through the Guth and Simha equation (19, 20):

$$\eta = \eta_0(1 + 5\phi/2 + 109\phi^2/14)$$

where η is the solution shear viscosity and η_0 is its value at the cmc. With spherical micelles

$$\phi = 4\pi l^3 N_{ave} C_M/3000\bar{n}$$

where l is the radius of the hydrated micelle in cm and N_{ave}, Avogadro's number. C_M is the concentration of the surfactant in the micellar phase.

In Fig. 3 is shown the volume fraction dependence on micellar surfactant concentration for the three alkylsulfoacetate systems. From the best straight lines drawn through the points, the ratios of $l^3/\bar{n}$ were obtained. For SHSA, the curve consisted of two straight lines intersecting at roughly twice the cmc. The shortest chained sodium alkylsulfates showed a similar behaviour (18). This is interpreted as indicating that only beyond twice the cmc do SHSA micelles achieve a relatively constant size.

It was found previously that, by putting l equal to the "dry" extended length of the surfactant monomeric ion, statisfactory aggregation numbers were obtained for short-chained, ionic surfactants. This was attempted here also by estimating l as equal to the extended length of the hydrocarbon chain as reckoned by Tanford's formula (21) with 6 Å added to account for the $CO_2CH_2SO_3$ portion of the alkylsulfoacetate monomeric ion. The 6 Å extra extended length was estimated from crystallographic radii and geometry. These values of l were used to calculate $\bar{n}$ from the least error slopes. Both l and $\bar{n}$ values thus obtained are listed in Table 1.

This treatment was also extended to the viscosity data for the two-tailed surfactant SDHSS but two problems developed. First, the cmc was too low to neglect the electroviscous effect in all but concentrated micellar solutions. Second, estimates of the extended, "dry" length of the two-tailed monomeric ion are dependent upon the amount of spreading of the two tails. An unrealistic value of $\bar{n} = 10$ resulted for $l = 15$ Å, the estimated length of the SDHSS monomer with the two chains packed in closely side-by-side.

Evans (22) has developed a procedure by which conductivity data can yield micellar aggregation numbers.The equivalent conductance of the micellar solution is assumed to be the sum of the contributions of the conductances of the ionic species in solution, i.e. Λ_{Na}, Λ_S, and Λ_M, where the subscripts S and M refer to the surfactant monomer and the micelle:

$$1000\,K = \text{cmc}\,(\Lambda_{Na} + \Lambda_S) + C_M\Lambda_M/\bar{n} + C_M(n - g)\,\Lambda_{Na}/\bar{n}$$

where K is the specific conductance and g is the number of counter-ions associated with each micelle. From Stokes' theorem and noting that at the cmc $\Lambda_{Na} + \Lambda_S = 1000K_0/\text{cmc}$ (K_0 is the specific conductance at the cmc), this equation reduces to

$$1000S_1 = f^2\bar{n}^{2/3}(1000\,S_2 - \Lambda_{Na}) + f\Lambda_{Na}$$

where S_1 is the slope of the specific conductance plot below the cmc, S_2 is the corresponding slope above the cmc, and f is the fraction of free counter-ion, i.e. $(\bar{n} - g)/\bar{n}$. Values of $\bar{n}$ and f can be found by computer-fitting the observed slopes of the conductance curves to the above equation to give least error. These best-fit values of $\bar{n}$ and f are listed in Table 1.

The aggregation numbers obtained through conductances are in agreement with the fluorescence quenching $\bar{n}$ values for both the single-tailed and double-tailed surfactants. The viscometrically derived $\bar{n}$ values agree with those from the other two methods for the single-tailed surfactants. The apparent underestimate of $\bar{n}$ for SDSA was found also with sodium decylsulfate (18) and signifies that the electroviscous assumption of the viscometric technique is beginning to break down when the alkyl chain is ten carbons in length. The calculated fractions of unbound counter-ion in each system are in the expected range when compared to other surfactant systems and decrease

Can. J. Chem. Downloaded from www.nrcresearchpress.com by 210.87.254.105 on 09/06/12
For personal use only.

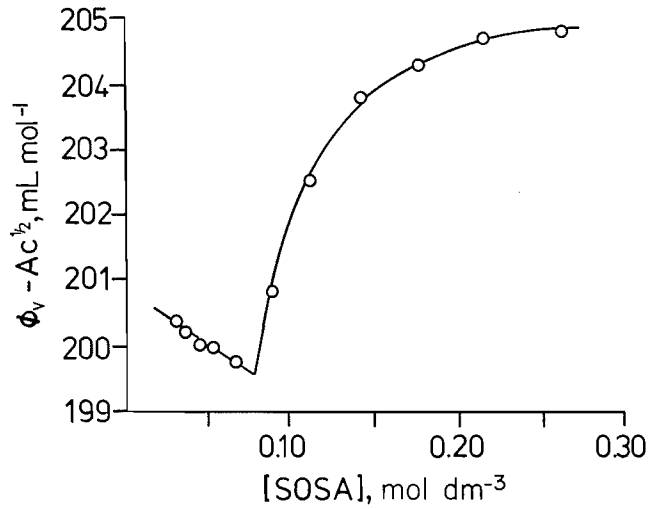

FIG. 4. Concentration dependence of apparent molal volume at 25.0°C for sodium octyl sulfoacetate solutions.

in the usual fashion with increasing aggregation in a particular series of surfactants.

Apparent molal volumes (ϕ_v) were calculated from the density data (9, 23) for each of the surfactant systems. Plots of $\phi_v - 1.868c^{1/2}$ against molarity for both the sulfoacetates and sulfosuccinates gave curves typical of micelle formers (Fig. 4). The curves consisted essentially of two plateaus with a sharp increase in $\phi_v - 1.868c^{1/2}$ in the cmc region. Volume changes upon micellization (ΔV_m) can be obtained from noting the height of the step in these plots (24, 25) or from partial molal volumes which entailes plotting $\Delta(m\phi_v)/\Delta m$ against the mean molarity (26). The latter method is more thermodynamically correct but leads to greater scatter in the experimental points.

Both methods were used to obtain ΔV_m and the mean value was listed for each surfactant in Table 1. The two determinations of ΔV_m agreed to within at least 1 mL mol^{-1} for the single-tailed surfactants. The low cmc values for both SDHSS and SDOSS prevented accurate estimates of ΔV_m for both these surfactants by this technique. The best estimate of ΔV_m for SDHSS was 16 ± 5 mL mol^{-1} which appears high in view of Lang's recent ultrasonic ΔV_m determinations for dialkylmethylammonium chloride micelles which were in the 8–10 mL mol^{-1} range (27).

The ΔV_m values for the sulfoacetates are reasonable when compared to literature values of one-tail surfactants of comparable chain length (23, 25). The positive value of ΔV_m for surfactants is generally observed and is attributed to the loss of hydrocarbon–water contact with the transfer of the surfactant molecule from bulk water to the micelle.

Discussion

The aggregation numbers of the single-tailed sulfoacetates are in accord among the three methods of determination which suggests that the basic premises of each method are correct. Even the short-fall of the $\bar{n}$ value determined by viscometry for SDSA is exactly what happens with sodium decylsulfate which forms spherical micelles. Thus, the sulfoacetates from the hexyl to the decyl member likely form spherical micelles beyond the cmc with micellar radii approximating the length of the extended monomeric hydrocarbon chain and with unbound counter-ion fractions in the 0.5 to 0.3 range. This probably means that there is considerable chain folding in the micelle but that hydration of the head group and counter-ion binding nullifies this loss in length in making the hydrated micellar radius roughly equivalent to the extended, "dry" monomeric length. The magnitudes of the volume changes upon micellization and the constant effective surface area per head group of about 100 Å^2 support this view since these are what are found with similar surfactants that form micelles.

The shorter the chain the less stable is the micelle (28), so that the SHSA micelles are relatively unstable. This is reflected in the small ΔV_m value of 2.0 mL mol^{-1} suggesting a loose association of monomers for SHSA micelles in which water has significant penetration. Otherwise, a value of ΔV_m larger than 7 mL mol^{-1} would be expected from assuming that half the ΔV_m value for SDSA would be the micellar volume contribution of an unwetted pentyl chain.

If all other factors were equal, the ΔV_m values for the sulfosuccinates should be roughly twice the values for the sulfoacetates with the hydrocarbon surface area being doubled. However, both SHSA and SOSA form relatively unstable micelles compared to SDHSS and SDOSS (micellar stability can be estimated from ultrasonic characteristic frequencies which vary generally as the cmc values (27, 28)) so that the ΔV_m values for the latter should exceed twice the ΔV_m values for the former. This appears to be the case with SDHSS with its ΔV_m of 16 reflecting a 10% in volume in the transition from bulk water to the micellar environment. The corresponding increase in ΔV_m for SOSA is 3% (see Fig. 4).

With the dialkyl sulfosuccinates SDHSS and SDOSS, agreement in aggregation numbers between the conductance and fluorescence quenching methods argues for near sphericity for these micelles. The fluorescence quenching technique is the more reliable because it is less model-dependent and, in particular, does not require that the micelles be spherical. This assumption is implicit in the conductance derivation since Stokesian flow of the aggregates and monomers is assumed. The apparent failure of the viscosity technique to obtain reasonable values of $\bar{n}$ for SDHSS may be due to several reasons as explained previously and non-sphericity in the micelles could be added to these. A referee has suggested that SDHSS micelles could be discs with thickness of 15 Å consisting of 30–36 monomers, i.e. about 70 chains, as obtained by the other two methods. This possibility cannot be ruled out but, in light of the agreement in $\bar{n}$ values obtained in fluorescence quenching and conductimetrically, spherical micelles are more likely present in these two micellar dialkyl sulfosuccinate systems.

Acknowledgements

Appreciation is expressed to Drs. Brian Robinson, Paul Fletcher, and James Bridge of the University of Kent at Canterbury for technical assistance and to the Natural Sciences and Engineering Research Council of Canada for financial support.

1. H. HOFFMAN. Ber. Bunsenges. Phys. Chem. **82**, 988 (1978).
2. E. I. FRANSES, Y. TALMON, L. E. SCRIVEN, H. T. DAVIS, and W. G. MILLER. J. Colloid Interface Sci. **86**, 449 (1982).
3. E. RUCKENSTEIN and R. NAGARAJAN. Micellization, solubilization and microemulsions. Vol. 1. *Edited by* K. L. Mittal. Plenum Press, New York. 1977. p. 133.
4. J. H. FENDLER. Acc. Chem. Res. **13**, 7 (1980).
5. R. J. M. TAUSK, J. VANESCH, J. KARMIGGELT, G. VOORDOUW, and J. T. G. OVERBEEK. Biophys. Chem. **1**, 184 (1974).

Can. J. Chem. Downloaded from www.nrcresearchpress.com by 210.87.254.105 on 09/06/12
For personal use only.

6. W. R. HARGREAVES and D. W. DEAMER. Biochemistry, **17**, 3759 (1978).
7. R. A. DAY, B. H. ROBINSON, J. H. R. CLARKE, and J. V. DOHERTY. J. Chem. Soc. Faraday Trans. I. **75**, 132 (1979).
8. J. R. LALANNE, B. POULIGNY, and E. SELN. J. Phys. Chem. **87**, 696 (1983).
9. P. PICKER, E. TREMBLAY, and C. JOLICOEUR. J. Solution Chem. **3**, 377 (1974).
10. N. J. BRIDGE and D. W. SOLOMON. J. Chem. Soc. Faraday Trans. II, **76**, 472 (1980).
11. T. HIKOTA and K. MEGURO. J. Am. Oil Chem. Soc. **46**, 579 (1969).
12. C. R. CARYL. Ind. Eng. Chem. **33**, 741 (1941).
13. E. F. WILLIAMS, N. T. WOODBERRY, and J. K. DIXON. J. Colloid Sci. **12**, 452 (1957).
14. P. MUKERJEE and K. J. MYSELS. Critical micelle concentrations of aqueous surfactant systems. National Bureau of Standards (U.S.) NSRDS-NBS 36, Washington. 1971 p. 135.
15. C. TANFORD. The hydrophobic effect. 2nd ed. John Wiley, New York. 1980. p. 69.
16. N. J. TURRO and A. YEKTA. J. Am. Chem. Soc. **100**, 5951 (1978).
17. M. ALMGREN and J.-E. LÖFROTH. J. Colloid Interface Sci. **81**, 486 (1981).
18. D. A. W. ADAIR, J. R. HICKS, D. J. JOBE, and V. C. REINSBOROUGH. Aust. J. Chem. **36**, 1021 (1983).
19. E. GUTH and R. SIMHA. Kolloid-Z. **74**, 266 (1936).
20. D. STIGTER. J. Colloid Interface Sci. **23**, 379 (1967).
21. C. TANFORD. op. cit. p. 52.
22. H. C. EVANS. J. Chem. Soc. 579 (1956).
23. G. M. MUSBALLY, G. PERRON, and J. E. DESNOYERS. J. Colloid Interface Sci. **48**, 494 (1974).
24. T. S. BRUN, H. HØILAND, and E. VIKINGSTAD. J. Colloid Interface Sci. **63**, 89 (1978).
25. K. M. KALE and R. ZANA. J. Colloid Interface Sci. **61**, 312 (1977).
26. J. E. DESNOYERS, F. DELISI, and G. PERRON. Pure Appl. Chem. **52**, 433 (1980).
27. J. LANG. J. Phys. Chem. **86**, 992 (1982).
28. D. A. W. ADAIR, V. C. REINSBOROUGH, N. PLAVAC, and J. P. VALLEAU. Can. J. Chem. **52**, 429 (1974).

Can. J. Chem. Downloaded from www.nrcresearchpress.com by 210.87.254.105 on 09/06/12
For personal use only.

The crystal and molecular structure of bis(2,3-butanedione dioximato)chloro-(hydroxodiphenylarsine)cobalt(III): assignment of the nature of the arsenic-based ligand

MONICA PIZZEY, LYNN MIHICHUK,[1] RICHARD J. BARTON, AND BEVERLY E. ROBERTSON
Faculty of Science, University of Regina, Regina, Sask., Canada S4S 0A2

Received July 21, 1983

MONICA PIZZEY, LYNN MIHICHUK, RICHARD J. BARTON, and BEVERLY E. ROBERTSON. Can. J. Chem. **62**, 285 (1984).

The Co(II) cobaloximes, (B)Co(dmgH)$_2$ (where B = phosphine or phosphite; dmgH = dimethylglyoximato monoanion) react with $(C_6H_5)_2AsCl$ to form ClCo(dmgH)$_2$B and a compound of formula $C_{20}H_{25}AsClCoN_4O_5$. A crystal structure analysis of the arsenic compound indicated it to be bis(2,3-butanedione dioximato)chloro(diphenylhydroxoarsine)cobalt(III), $[(C_6H_5)_2As(OH)Co(dmgH)_2Cl]$. The crystals are orthorhombic, space group $Pna2_1$, a = 15.334(2), b = 11.173(2), c = 13.745(4) Å at 19(2)°C with Z = 4. The structure has been refined by the least-squares method to a weighted residual of 0.071 using 2345 independent reflections. The Co atom is bonded equatorially to two dmgH ligands (average [Co—N] = 1.89(1) Å) with a Cl atom above this plane ([Co—Cl] = 2.252(2) Å) and the As atom of the $(C_6H_5)_2As(OH)$ group below it ([Co—As] = 2.322(1) Å). The [As—O] bond length is 1.781(7) Å, corresponding to a single bond and is consistent with the observed H atom on the oxygen atom.

MONICA PIZZEY, LYNN MIHICHUK, RICHARD J. BARTON et BEVERLY E. ROBERTSON. Can. J. Chem. **62**, 285 (1984).

Les cobaloximes de type Co(II), (B)Co(dmgH)$_2$ (où B = phosphine ou phosphite; dmgH = le monoanion diméthylglyoximato) réagissent avec le $(C_6H_5)_2AsCl$ pour donner le ClCo(dmgH)$_2$B et un composé de formule $C_{20}H_{25}AsClCoN_4O_5$. L'analyse de la structure cristalline du composé de l'arsenic indique qu'il s'agit du bis(butanedione-2,3 dioximato)chloro-(diphénylhydroxoarsine)cobalt(III) $[(C_6H_5)_2As(OH)Co(dmgH)_2Cl]$. Les cristaux sont orthorhombiques et appartiennent au groupe d'espace $Pna2_1$, a = 15,334(2), b = 11,173(2), c = 13,745(4) Å à 19(2)°C avec Z = 4. On a résolu la structure et on l'a affinée par la méthode des moindres carrés jusqu'à une valeur de R = 0,071 pour 2345 réflexions indépendantes. L'atome du Co est lié équatorialement aux deux ligands dmgH (moyenne [Co—N] = 1,89(1) Å) avec l'atome de Cl au dessus de ce plan ([Co—Cl] = 2,252(2) Å) et l'atome de As du groupe $(C_6H_5)_2As(OH)$ en dessous de ([Co—As] = 2,322(1) Å). La longueur de la liaison [As—O] = 1,781(7) Å correspond à une liaison simple et est en accord avec l'atome d'hydrogène observé sur l'atome d'oxygène.

[Traduit par le journal]

Introduction

Compounds containing arsenic σ-bonded to transition metals have not been well documented (1–3). The Co—$\ddot{A}sR_2$ moiety is of particular interest because very little information is available concerning this system. As well, it has been suggested that the cobaloxime compounds containing σ-bonded —$\ddot{A}sR_2$ may have some relevance to models for the biological methylation of arsenic (4). We have studied the structure of **A**, $(C_6H_5)_2As(OH)Co(dmgH)_2Cl$, which is closely related to **B**, $(CH_3)(C_6H_5)As(O)Co(dmgH)_2Cl.H_2O$, recently reported by Mihichuk *et al.* (5). In the structure of the latter compound the authors concluded, based on their refinement in an ordered non-centrosymmetric space group and a disordered centrosymmetric space group, that the disordered model was to be preferred. Hence, they were unable to determine the order of the [As—O] bond.

The molecule in this investigation has two equivalent groups on the arsenic atom. If it adopts the same molecular packing as **B**, the molecule may be able to utilize the mirror plane in the space group *Pnam* and thereby avoid the disorder problem.

Experimental

$C_{20}H_{25}AsClCoN_4O_5$ mw = 569.74
Orthorhombic, space group $Pna2_1$, a = 15.334(3), b = 11.173(2), c = 13.745(4) Å, T = 19(2)°C, V = 2354.94 Å^3, Z = 4, D_x = 1.607 g cm^{-3}, D_m = 1.61 g cm^{-3}, μ(MoKα) = 22.69 cm^{-1}.

The compound **A** was prepared according to the method previously reported by Mihichuk *et al.* (5). Crystals of **A** were obtained by slow evaporation of a dichloromethane/hexane solution at 20°C.

Anal. calcd. for **A**: C 42.12, H 4.43, N 9.84; found: C 42.39, H 4.62, N 9.32.

A crystal in the form of an amber-coloured plate of dimensions 0.55 × 0.35 × 0.10 mm was chosen for study. Laue symmetry and systematic absences ($k + l = 2n + 1$ for $h = 0$, $h = 2n + 1$ for $k = 0$) indicated the orthorhombic space groups *Pnam* (standard notation, *Pnma*) or $Pna2_1$. The density was determined by flotation in a chloroform/bromoform mixture.

Intensity data were measured on a modified Picker diffractometer with graphite-monochromated MoKα radiation (λ = 0.71069 Å), using the NRCC diffractometer control system (6). Accurate cell dimensions were calculated from the centred settings of 65 reflections with 11° < 2θ < 60°. Diffraction intensities in the range 3° ≤ 2θ ≤ 60° were measured using a scan speed of 2 deg min^{-1} and a scan width of (1.6 + 0.692 tan θ) degs. Three standard reflections which were measured after every 47 reflections showed no systematic changes. The intensities of 3558 reflections were measured, of which 2345 were considered as observed with $I > 2.0\sigma(I)$. ($\sigma(I)$ is the standard deviation of the intensity derived both from the counting statistics of the individual reflection, and the extent to which the scatter in the intensities of the standard reflections exceeded that predicted from the counting statistics.) Absorption corrections were applied using μ = 22.69 cm^{-1} in the XRAY76 set of programs (7). Scattering factors for all atoms were taken from the XRAY76 system (7). Dispersion corrections which were taken from International tables for X-ray crystallography (8) were applied to the scattering factors of the Co, As, and Cl atoms.

The structure was solved by the heavy-atom method.The values of $\langle|E|\rangle$ and $\langle E^2 - 1\rangle$ were 0.802 and 0.949, respectively, which are intermediate between those expected for a centrosymmetric and a non-centrosymmetric space group but close to those expected for the centrosymmetric space group *Pnam*. We might expect that a centrosymmetric space group containing structural elements with local centers of symmetry, such as contained in **A**, would give parameters further removed from the theoretical non-centrosymmetric values.

[1]To whom all correspondence should be addressed.

Can. J. Chem. Downloaded from www.nrcresearchpress.com by 210.87.254.42 on 09/06/12
For personal use only.

TABLE 1. Atomic and thermal parameters ($\times 10^3$)[a]

Atom	x	y	z	U(iso)/ U (equiv)
C(11)	0.7205(8)	0.7730(11)	0.1984(9)	47(6)
C(12)	0.7094(7)	0.7597(11)	0.3053(8)	41(5)
C(13)	0.6668(10)	0.8612(13)	0.1389(11)	70(7)
C(14)	0.6474(8)	0.8327(12)	0.3682(12)	69(7)
N(11)	0.7726(6)	0.6933(9)	0.1652(7)	44(4)
N(12)	0.7593(6)	0.6803(8)	0.3440(6)	36(4)
O(11)	0.7878(6)	0.6840(9)	0.0708(6)	65(5)
O(12)	0.7534(5)	0.6537(7)	0.4396(5)	47(3)
H(11)[b]	0.825(6)	0.622(8)	0.062(7)	27(24)
C(21)	0.9558(7)	0.4308(9)	0.2053(10)	42(5)
C(22)	0.9492(9)	0.4278(14)	0.3122(11)	62(7)
C(23)	1.0178(11)	0.3571(14)	0.1451(14)	81(9)
C(24)	1.0054(10)	0.3413(14)	0.3765(14)	81(8)
N(21)	0.9009(7)	0.5047(10)	0.1682(7)	42(5)
N(22)	0.8908(5)	0.5003(10)	0.3482(7)	38(4)
O(21)	0.8938(6)	0.5158(10)	0.0756(6)	65(5)
O(22)	0.8794(6)	0.5070(10)	0.4465(6)	56(5)
H(22)[b]	0.840(5)	0.538(6)	0.456(6)	30(18)
C(31)	0.6379(5)	0.4625(7)	0.1520(7)	38(4)
C(32)	0.5740(6)	0.5482(9)	0.1602(8)	52(5)
H(32)	0.5707	0.5988	0.2201	20
C(33)	0.5160(6)	0.5695(10)	0.0844(10)	59(6)
H(33)	0.4719	0.6354	0.0882	20
C(34)	0.5171(7)	0.4946(16)	0.0029(10)	63(7)
H(34)	0.4740	0.5056	−0.0510	20
C(35)	0.5776(8)	0.4052(11)	−0.0036(9)	60(6)
H(35)	0.5315	0.4373	−0.0480	20
C(36)	0.6377(6)	0.3888(8)	0.0691(7)	44(4)
H(36)	0.6820	0.3236	0.0625	20
C(41)	0.7644(4)	0.2872(6)	0.2584(9)	38(4)
C(42)	0.8070(7)	0.2361(10)	0.1770(7)	46(5)
H(42)	0.8128	0.2802	0.1141	20
C(43)	0.8388(9)	0.1196(13)	0.1883(10)	71(7)
H(43)	0.8695	0.0817	0.1320	20
C(44)	0.8331(8)	0.0589(10)	0.2673(16)	90(8)
H(44)	0.8540	−0.0258	0.2707	20
C(45)	0.7949(9)	0.1141(11)	0.3530(10)	66(7)
H(45)	0.7952	0.0714	0.4170	20
C(46)	0.7602(7)	0.2251(10)	0.3454(8)	50(5)
H(46)	0.7304	0.2614	0.4030	20
Cl	0.93548(13)	0.73531(18)	0.26747(23)	50(2)
Co	0.83062(6)	0.59474(8)	0.25714(11)	28.1(5)
As	0.72281(4)	0.44905(6)	0.25000	29.8(4)
O(51)	0.6580(4)	0.4576(7)	0.3573(5)	52(3)
H(51)	0.6869	0.4597	0.3929	20

[a]Thermal parameters are of the form $\exp[-2\pi^2(U_{11}h^2a^{*2} + U_{22}k^2b^{*2} + U_{33}l^2c^{*2} + 2U_{12}hka^*b^* + 2U_{13}hla^*c^* + 2U_{23}klb^*c^*)]$ and U(equiv) = $(1/3)\sum_{i=1}^{3}\sum_{j=1}^{3}[U_{ij}a_i^*a_j^*(\mathbf{a}_i\cdot\mathbf{a}_j)]$.

[b]All H atoms except H(11) and H(22) were constrained during refinement.

Nevertheless, a structure solution was first attempted in the centrosymmetric space group.

The coordinates of the three heavy atoms, Co, Cl, and As were determined from a Patterson map, and the remaining non-hydrogen atoms were located in successive electron-density difference maps. The solution showed the molecule located on the mirror plane, but it was either disordered in the centrosymmetric space group or it was ordered in the non-centrosymmetric space group $Pna2_1$ and the apparent disorder was an artifact of an incorrect choice of space group. A disordered model for the structure would lead to severe steric problems involving overlap of phenyl rings of neighbouring molecules. This

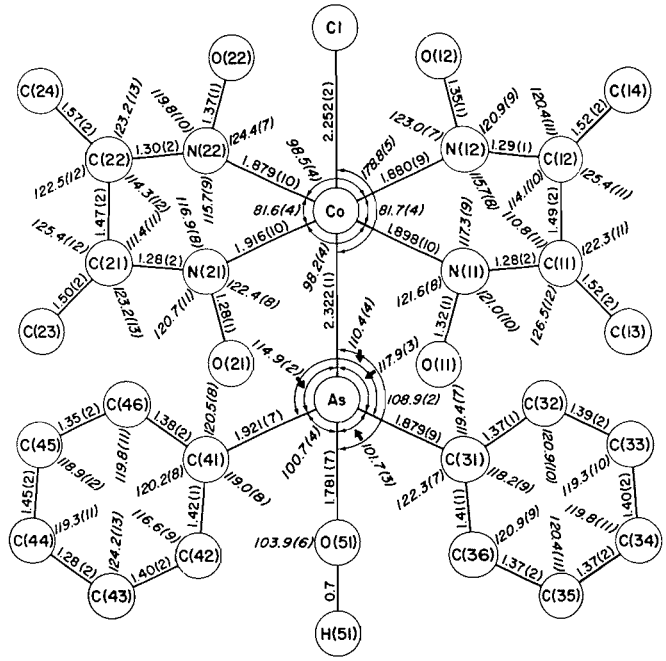

FIG. 1. Schematic diagram showing atom labelling, bond lengths, and angles for **A** with estimated standard deviations.

observation and the indefinite statistical results of the analysis of normalized structure factors suggested that the correct space group was $Pna2_1$.

Refinement was continued based on an ordered model in the non-centrosymmetric space group. The temperature factors of the non-hydrogen atoms were refined initially using isotropic temperature factors and then anisotropically. The positions of the hydrogen atoms on the phenyl rings were calculated and constrained to their corresponding carbon atoms during refinement. The three other H atoms bound to oxygen atoms in the structure were found from an electron density difference map. These three peaks in the difference map corresponded very nearly to an electron density of 1 electron $Å^{-3}$. The two hydrogen atoms on the equatorial oxime rings were refined with isotropic temperature factors. H(51), the hydrogen atom bonded to the oxygen atom O(51) was fixed at the position of maximum electron density as determined from the difference Fourier map. Least-squares refinement gave a position too close to the atom O(51). Because of computer core limitations it was necessary to refine the structure in five blocks of atoms. The blocks were chosen so as to retain any expected significant correlations between least-squares parameters. The agreement factors converged to:

$$R = \Sigma(|F_o| - |F_c|)/\Sigma|F_o| = 0.056$$

$$R_w = [\Sigma w(|F_o| - |F_c|)^2/\Sigma w|F_o|^2]^{1/2} = 0.071$$

The weighting scheme, which was chosen to remove bias with respect to $|F_o|$ from the distribution of $w(|F_o| - |F_c|)^2$, was $w = 1.0/(\sigma(|F_o|)^2 + 3 \times 10^{-5}(|F_o|)^3)$. The average shift/error and the maximum shift/error for a structural parameter were 0.022 and 0.14, respectively, at the termination of refinement.

The enantiomorphically alternative structure was refined to convergence and gave values of R and R_w which were 0.057 and 0.073, respectively, greater than for the molecular arrangement reported here. Using Hamilton's significance test (9) and assuming no systematic errors, the choice of enantiomer is correct with a significant level better than (1/2)%.

The atomic coordinates and equivalent isotropic thermal parameters for all atoms are listed in Table 1. Figure 1 shows the atomic labelling, the configuration of the molecule, and important bond lengths and angles. A stereoscopic view of the molecule drawn using ORTEP (10) is shown in Fig. 2. Orientation of the arsine moiety with respect to the

Can. J. Chem. Downloaded from www.nrcresearchpress.com by 210.87.254.42 on 09/06/12
For personal use only.

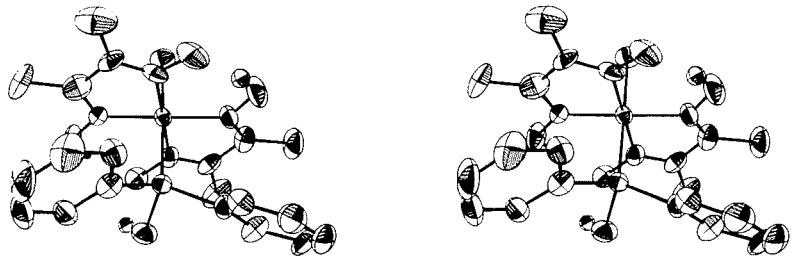

FIG. 2. Stereoscopic view of the molecule.

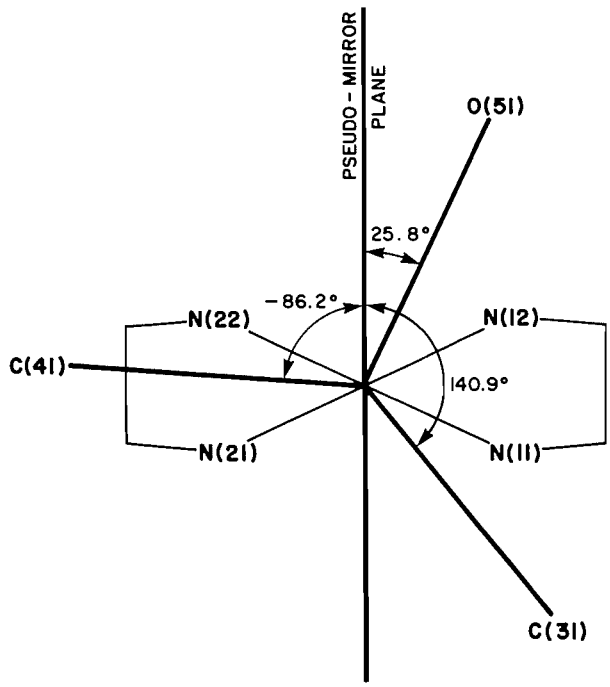

FIG. 3. Schematic view along the [As—Co] bond showing degree of rotation of the arsine moiety about the [As—Co] bond from the pseudo-mirror relating the two equatorial oxime ligands.

two equatorial oxime ligands is shown in a schematic diagram of the molecule in Fig. 3.[2]

Discussion

The coordination about the cobalt atom, is octahedral. The Co atom is coordinated to two bidentate dmgH ligands, related to each other by a pseudo-mirror plane passing through the cobalt atom. This plane is located equidistant between the two equatorial oxime ligands, and contains the Co—Cl vector. The dihedral angle formed by the planes of the two ligands is 4.2°. The cobalt atom is also coordinated to the Cl atom and the As atom of a $(C_6H_5)_2As(OH)$ group on opposite sides of the plane of the oxime ligands. The slight fold of the oxime ligands is away from the arsenic atom. The average [Co—N] distance is 1.90(2) Å and the [Co—Cl] and [Co—As] distances are 2.252(2) Å and 2.322(1) Å, respectively. The [N—Co—N] *bite* angles are approximately 81.6(4)°. These values are similar to those found for other $Co^{III}(dmgH)_2XY$ compounds (11). Bond lengths and bond angles within the dmgH ligands are in agreement with those for previously reported dmgH complexes.

The arsenic atom is bonded to the oxygen atom O(51), to the two phenyl rings, and to the cobalt atom. The average [C—C] distance in the phenyl rings is 1.38(2) Å. The observed molecular geometry associated with the carbon atom, C(44), is not reasonable. Furthermore, this atom is strongly influenced by the apparent libration of the phenyl ring and has unusually large temperature factors. The estimated standard deviations in its positional parameters are probably unrealistically low. There are no unusually short intermolecular contacts.

The arsenic-based ligand is strongly indicated to be $(C_6H_5)_2As^{III}$—OH and not $[(C_6H_5)_2As^{V}{=}O]^+$. The [As—O] bond length of 1.781(7) Å is longer than previously reported first-order [As—O] bonds; $(C_6H_5)_3As(OH)X$ (X = Cl, Br) (1.70(1) Å) (12) and $[(C_6H_5)_3As$—OH . . . Cl . . . HO—As-$(C_6H_5)_3]^+(ICl_2)^-$ (1.72 Å) (13). Also the hydrogen atoms located from electron-density difference maps show that each oxime ligand is mono-protonated. The atoms O(11) and O(22) are hydrogen-bond donors to O(21) and O(12), respectively, ([O(11)—H(11)] = 0.9(1) Å and [O(22)—H(22)] = 0.7(1) Å), making a pseudo two-fold axis along the [Cl—Co] vector relating the oxime ligands. The other hydrogen atom, H(51), is formally bonded to O(51), necessitating an [As—O(51)] single bond.

The oxime [O . . . O] intramolecular distances are slightly asymmetric ([O(12)—O(22)] = 2.54(1) Å and [O(21)—O(11)] = 2.49(1) Å). The greater value for [O(12)—O(22)] is consistent with the observation that the hydrogen atom of the OH group on the arsenic atom is hydrogen-bonded to O(12). ([O(51) . . . O(12)] = 2.871 Å, [O(51)—H(51)] = 0.7 Å, [Co—As—O(51) . . . O(12)] = 0.3°, [O(12) . . . H(51)—O(51)] = 116°, and [H(51) . . . O(12) = 2.5 Å).

The rotation angles between the pseudo-mirror plane of the cobaloxime moiety and the two [As—C] bonds and the [As—O] bond (Fig. 3) show that this plane does not apply to the arsine moiety. Looking along the Co—As vector, the angles define the degree of rotation from the pseudo-mirror relating the two equatorial oxime ligands. The angle with respect to O(51) is 25.8°, to C(31) is 140.9°, and to C(41) is 273.8°. These angles are set primarily by the hydrogen bond to O(12) from O(51). Therefore, the rotation angles between the atom O(51) and the atoms C(31) and C(41) of the phenyl rings are 115.1° and 112.0°, respectively. The rotation angle between the phenyl rings is 132.9°.

The orientation of the phenyl rings is further defined by the torsional angles about the As—C bonds which are 73.3° for [C(36)—C(31)—As—Co] and 77.6° for [C(46)—C(41)—As—Co]. The [As—C] distances are also significantly different at 1.879(9) and 1.922(9) Å but the reason for this is not readily apparent. The two phenyl rings are bent at the bridge-

[2]The structure amplitude table, a table of general anisotropic temperature factors, and a table of mean plane data are avaiable, at a nominal charge, from the Depository of Unpublished Data, CISTI, National Research Council of Canada, Ottawa, Ont., Canada K1A 0S2.

Can. J. Chem. Downloaded from www.nrcresearchpress.com by 210.87.254.42 on 09/06/12
For personal use only.

head carbon atoms so that the As atom is 0.142 and 0.071 Å out of their respective average planes. These parameters and the afore-mentioned upward tilt of the oxime ligands are related to the steric interactions between the oxime ligands and the arsenic ligands. Short contacts to the plane of the oxime ligand [N(11), C(11), C(12), N(12)] are: C(31), 3.30 Å; O(51), 2.79Å. The shortest contact to the plane of the ligand [N(21), C(21), C(22), N(22)] is: C(41), 3.14 Å.

Acknowledgements

We are grateful to the Natural Sciences and Engineering Research Council of Canada for financial support of this work in the form of operating grants to R.J.B., L.M., and B.E.R. Technical assistance in data collection from K.Wolbaum, University of Regina, Regina, Sask., is gratefully acknowledged.

1. W. MALISCH, H. ROSSNER, K. KELLER, and R. JANTA. J. Organomet. Chem. **133**, C21 (1977).
2. P. PANSTER and W. MALISCH. Chem. Ber. **109**, 3842 (1976).
3. W. MALISCH and M. KUHN. Angew. Chem. Int. Ed. Engl. **13**, 84 (1974).
4. G. N. SCHRAUZER, J. A. SECK, R. J. HOLLAND, T. M. BECKMAN, E. M. RUBIN, and J. W. SIBERT. Bioinorg. Chem. **2**, 93 (1972).
5. L. M. MIHICHUK, M. J. MOMBOURQUETTE, F. W. B. EINSTEIN, and A. C. WILLIS. Inorg. Chim. Acta, **63**, 189 (1982).
6. A. C. LARSON and E. J. GABE. Computing in crystallography. *Edited by* H. Shenk, R. Olthof-Hazekamp, H. van Koningsveld, and G. C Bassi. Delft University Press. 1978. pp. 81–89.
7. J. M. STEWART (*Editor*). The X-ray system of crystallographic programs – XRAY 76. Tech. Rep. TR-446. Computer Science Centre, University of Maryland, College Park, MD. March, 1976.
8. International Tables for X-ray Crystallography. Vol. 4. Kynoch Press, New York. 1974. pp. 99, 149.
9. W. C. HAMILTON. Acta Crystallogr. **18**, 502 (1965).
10. C. K. JOHNSON. ORTEP Report ORNL-3794. Oak Ridge National Laboratory, TN. 1965.
11. W. R. CULLEN, D. DOLPHIN, F. W. B. EINSTEIN, L. M. MIHICHUK, and A. C. WILLIS. J. Am. Chem. Soc. **101**, 6898 (1979).
12. G. FERGUSON and E. W. MACAULAY. Chem. Commun. 1288 (1968).
13. F. C. MARCH and G. FERGUSON. J. Chem. Soc. Dalton, 1381 (1975).

Can. J. Chem. Downloaded from www.nrcresearchpress.com by 210.87.254.42 on 09/06/12
For personal use only.

Novel gas phase ions. II. $[CH_2{=}CHOH/CH_3OH]^{+\cdot}$ and $[CH_2{=}CHOH/H_2O]^{+\cdot}$

JOHAN K. TERLOUW, WIGGER HEERMA, AND PETER C. BURGERS
Analytical Chemistry Laboratory, University of Utrecht, Croesestraat 77A, Utrecht, 3522 AD., The Netherlands

AND

JOHN L. HOLMES
Chemistry Department, University of Ottawa, Ottawa, Ont., Canada K1N 9B4

JOHAN K. TERLOUW, WIGGER HEERMA, PETER C. BURGERS, and JOHN L. HOLMES. Can. J. Chem. **62**, 289 (1984).

The title ions are generated by the loss of C_2H_4 from ionised 4-methoxybutan-1-ol and butan-1,4-diol, respectively, and are best described as complexes between $[CH_2{=}CHOH]^{+\cdot}$ and CH_3OH (dissociation energy 21 kcal mol^{-1}) and between ionised vinyl alcohol and H_2O (dissociation energy $\geq$ 13 kcal mol^{-1}). ΔH_f^0 of the ions $[CH_2{=}CHOH/H_2O]^{+\cdot}$ and $[CH_2{=}CHOH/CH_3OH]^{+\cdot}$ were measured as $\leq$110 and 112 kcal mol^{-1}, respectively.

JOHAN K. TERLOUW, WIGGER HEERMA, PETER C. BURGERS et JOHN L. HOLMES. Can. J. Chem. **62**, 289 (1984).

On obtient les ions mentionnés dans le titre respectivement à partir du méthoxy-4 butanol-1 et du butanediol-1,4 ionisés qui perdent du C_2H_4. On peut décrire très bien ces ions comme étant des complexes entre le $[CH_2{=}CHOH]^{+\cdot}$ et le CH_3OH (énergie de dissociation 21 kcal mol^{-1}) et entre l'alcool vinylique ionisé et le H_2O (énergie de dissociation $\geq$ 13 kcal mol^{-1}). On a mesuré le ΔH_f^0 des ions $[CH_2{=}CHOH/H_2O]^{+\cdot}$ et $[CH_2{=}CHOH/CH_3OH]^{+\cdot}$ et on a trouvé que les ΔH_f^0 sont de $\leq$110 et 112 kcal mol^{-1}, respectivement.

[Traduit par le journal]

Introduction

Examination of collisionally induced unimolecular fragmentations of ions in the gas phase has proved to be an important method for investigating the structures of ions having internal energies below their first dissociation threshold. This technique has been particularly valuable for distinguishing between isomeric ions which are able to interconvert below the threshold for their common unimolecular fragmentation of lowest energy requirement, because such ions cannot be distinguished by means of their metastable peak characteristics.

Recently, collisional activation (CA) mass spectra have successfully been used unequivocally to identify both odd and even electron ions having unusual structures. Examples include the series of methylene-onium ions $[CH_2XH]^{+\cdot}$, where X = OH, SH, NH_2, F, Cl, Br, I (1) and the oxycarbenes $[C(OH)_2]^{+\cdot}$, $[HCOH]^{+\cdot}$ (2), and $[COH]^+$ (3, 4). The $[CH_2XH]^{+\cdot}$ ions are the lowest members of a potential homologous series of ions $[C_nH_{2n}XH]^{+\cdot}$, some higher members of which have been reported for n = 2, X = OH (5), OCH_3 (1*a*), NH_2 (1*b*). These species have been referred to as radical – ion dipole complexes by virtue of their major dissociations leading to $[C_2H_4]^{+\cdot}$ + XH, behaviour quite unlike that of their isomers of conventional structure. In general, these new ions have heats of formation close to, or in some cases below, those of their conventional isomers.

In this short paper we present evidence for the existence of complexes between ionised vinyl alcohol and the polar methanol and water molecules.

Results and discussion

Structure assignment and heat of formation of $[CH_2{=}CHOH/CH_3OH]^{+\cdot}$

Ionised 4-methoxy-butan-1-ol generates an ion at m/z 76, $[C_3H_8O_2]^{+\cdot}$, of abundance ca. 10% of base peak (m/z 45).

The collisional activation (CA) mass spectrum of this ion displays only two peaks of significant abundance, m/z 44, $[C_2H_4O]^{+\cdot}$ (80%), and m/z 33, $[CH_3\dot{O}H_2]$ (20%). Both daughter ions are also prominently observed in the metastable ion mass spectrum of m/z 76. The m/z 44 daughter ions, generated in the ion source and in the m/z 76 → m/z 44 metastable

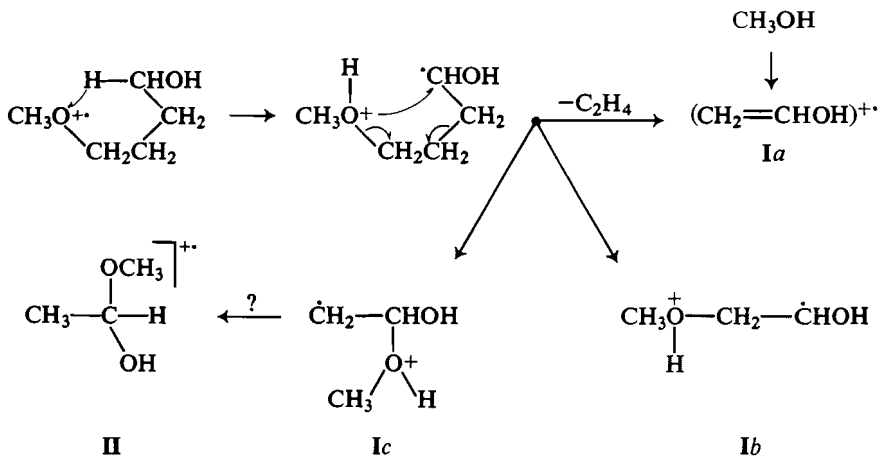

SCHEME 1

Can. J. Chem. Downloaded from www.nrcresearchpress.com by 210.87.254.6 on 09/06/12
For personal use only.

Can. J. Chem. Downloaded from www.nrcresearchpress.com by 210.87.254.6 on 09/06/12
For personal use only.

fragmentation, were shown by their CA mass spectrum (6) to consist solely of ionised vinyl alcohol, $[CH_2{=}CHOH]^{+\cdot}$. Furthermore, the appearance energy (AE) of the very narrow ($T_{0.5}$ = 3.9 meV) metastable peak (7) m/z 76 → 44, 10.7 ± 0.1 eV is close to that calculated for $[CH_2{=}CHOH]^{+\cdot}$, 10.6 eV. ($\Delta H_f^0[CH_3OCH_2CH_2CH_2CH_2OH]$ = −98.0 kcal mol^{-1} (by additivity (8), $\Delta H_f^0[C_2H_4]$ = 12.5 kcal mol^{-1} (9), $\Delta H_f^0[CH_3OH]$ = −48.1 kcal mol^{-1} (9), $\Delta H_f^0[CH_2{=}CHOH]^{+\cdot}$ = 181 kcal mol^{-1} (10).) Such a major loss of CH_3OH is not observed in either the normal or CA mass spectra of the $C_3H_8O_2$ isomers $HOCH_2CH_2CH_2OH$, $HOCH_2CH(OH)CH_3$, $CH_3OCH_2CH_2OH$, and $(CH_3O)_2CH_2$, all of which are dominated by m/z 45 or m/z 31.

Isomers of $[C_3H_8O_2]^{+\cdot}$, which could be expected prominently to lose CH_3OH, are the unconventional ions related to an ionised vinyl alcohol–methanol complex **I***a*, *b*, and *c* or possibly the ionised hemi-acetal $CH_3OCH(OH)CH_3$, **II** which are shown in Scheme 1, together with a possible mechanism for their formation. Ions **I***a*, *b*, and *c*, although formally structurally distinct symmetrical complex or σ-bonded ions, are unlikely to be distinguishable via their fragmentation characteristics. (Compare the similar systems $[C_2H_4 \cdot H_2O]^{+\cdot}$ (5) and $[CH_2CO \cdot H_2O]^{+\cdot}$ (11).) In the absence of further information concerning the relative stabilities of these ions (such as high-level *ab initio* calculations (12)), we will simply represent them by the formula $[CH_2{=}CHOH/CH_3OH]^{+\cdot}$.

This assignment is in keeping with observations on labelled compounds. $^{13}CH_3OCH_2CH_2CH_2CH_2OH$ cleanly produced m/z 77 which in turn only yielded m/z 44 and m/z 34 $[^{13}CH_3OH_2]^+$, i.e., no label retention in the $[CH_2{=}CHOH]^{+\cdot}$ ion; similarly, the CD_3 analogue produced only m/z 36 $[CD_3OH_2]^+$, m/z 44 with some (ca. 13%) m/z 45. The latter probably arises from exchange between the CH_3OH moiety and the vinyl alcohol hydroxyl group: m/z 77 from the OD precursor molecule again shows a clean displacement to m/z 34 $[CH_3ODH]^+$ whereas m/z 44 and m/z 45 are now of comparable abundance.

Ion **II** could also be generated via a more complex route than that shown in Scheme 1. Although they may play a role among reacting configurations (see below) ions of structure **II** cannot be the *stable* $[C_3H_8O_2]^{+\cdot}$ ions derived from 4-methoxybutan-1-ol.

First, ion **II** has as its *direct* bond cleavage of lowest energy requirement the reaction

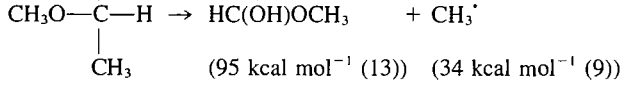

ΔH_f^0 products = 129 kcal mol^{-1}, an energy 4 kcal mol^{-1} *lower* than that for the rearrangement leading to ionised vinyl alcohol, ΔH_f^0 = 181 kcal mol^{-1}, plus methanol, ΔH_f^0 = −48 kcal mol^{-1}. Thus the CA mass spectrum of **II** would be dominated by m/z 61 rather than m/z 44. For ions **I**, the production of ionised vinyl alcohol plus CH_3OH is *their* direct bond cleavage of lowest energy requirement.

Secondly, the heat of formation, ΔH_f^0, of the $[C_3H_8O_2]^{+\cdot}$ ion was measured to be 112 ± 1 kcal mol^{-1} (AE m/z 76 = 9.64 ± 0.05 eV, energy selected electrons (14); AE metastable peak (7) = 9.7 ± 0.1 eV (Gaussian type peak, $T_{0.5}$ = 20 meV). The ΔH_f^0 for $[CH_3OCH(OH)CH_3]^{+\cdot}$ is unknown but can be estimated as follows: ΔH_f^0 for the neutral molecule = −98.4 kcal mol^{-1} (by additivity (8)) and its ionisation energy will be similar to that for $CH_3CH(OCH_3)_2$, 9.5 eV (15), leading to ΔH_f^0 for ionised **II** of ~ 121 kcal mol^{-1}. Alternatively, ΔH_f^0[**II**] may be estimated by considering OH substitution in $[CH_3CH_2OCH_3]^{+\cdot}$ or OCH_3 substitution in $[CH_3CH_2OH]^{+\cdot}$ and the enthalpy-structure correlations described elsewhere (16); these yield 118 and 117 kcal mol^{-1}, respectively. All three estimated values lie significantly above the observed ΔH_f^0 and are deemed unlikely to be in error by so large an amount.

We therefore conclude that the new m/z 76 ion is best described as $[CH_2{=}CHOH/CH_3OH]^{+\cdot}$.

From the above thermochemical results it is clear than an appreciable binding energy (21 ± 2 kcal mol^{-1}) exists between ionised vinyl alcohol and methanol, i.e. the ion–molecule reaction

$$[CH_2{=}CHOH]^{+\cdot} + CH_3OH \rightarrow \mathbf{I}$$

is exothermic by this amount.

Dissociation characteristics of $[CH_2{=}CHOH/CH_3OH]^{+\cdot}$

As described above the CA mass spectrum of the new ion contains only two intense peaks, m/z 44 and m/z 33; in marked contrast, the metastable $[C_3H_8O_2]^{+\cdot}$ ions undergo five competing fragmentations:

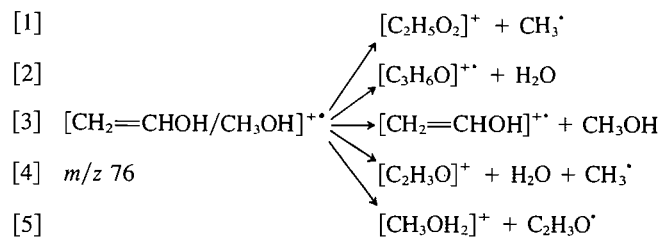

Only reaction [3] would be a direct bond cleavage for our proposed ion structure. This reaction becomes increasingly important among metastable ions of higher internal energy content, i.e. shorter lifetime. This can be seen from comparison of metastable peak abundances measured in the first field free region of a Kratos-AEI MS902S mass spectrometer (average ion lifetime ca. 1.8 μs (17)) 14:12:*100*:11:24, respectively, with those observed in the second field-free region of a VG Micromass ZAB-2F instrument (average ion lifetime ca. 13 μs (17)), relative abundances 100:75:*100*:54:44, respectively. These observations show that reaction [3] has a more steeply rising rate constant vs. internal energy curve than reactions [1], [2], [4], and [5]. The latter four would all require some rearrangement before fragmentation. The identifications of the daughter ions and mechanisms for reactions [1], [2], [4], and [5], which will provide insight as to the isomerisation of the complex ion, are being pursued.

Structure assignment and heat of formation of $[CH_2{=}CHOH/H_2O]^{+\cdot}$

Ionised butan-1,4-diol also loses C_2H_4 to produce an ion at m/z 62, $[C_2H_6O_2]^{+\cdot}$, of abundance ca. 3% of base peak (m/z 31). We propose that the ion m/z 62 has the structure $[CH_2{=}CHOH/H_2O]^{+\cdot}$, an analogue of the m/z 76 ion described above both in regard to its structure and mechanism of formation:

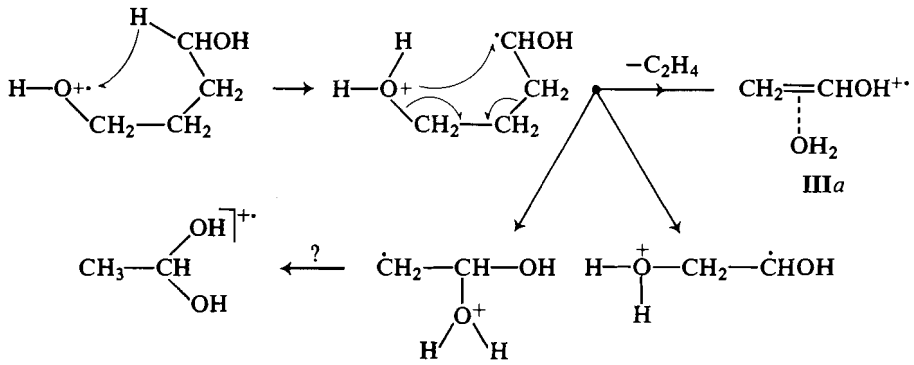

IV III*c* III*b*

Both MI and CA mass spectra are dominated by one peak, m/z 44, similarly shown to be ionised vinyl alcohol. Again the AE of the very narrow Gaussian type metastable peak, 10.5 ± 0.2 eV, showed that $[CH_2{=}CHOH]^{+\cdot}$ is generated ($\Delta H_f^0[HOCH_2CH_2CH_2CH_2OH] = -102.7$ kcal mol^{-1} (by additivity (8)), $\Delta H_f^0[H_2O] = -57.8$ kcal mol^{-1} (9) calculated AE for $[CH_2{=}CHOH]^{+\cdot} = 10.3$ eV). In addition the m/z 64 ion derived from the $(OD)_2$ derivative specifically loses HDO in the metastable dissociation and predominantly (82%) in the CA mass spectrum.

The ΔH_f^0 value for m/z 62 was measured as $\leq 110 \pm 1$ kcal mol^{-1} from AE = 9.78 ± 0.05 eV. Note that the apparent binding energy between $[CH_2{=}CHOH$ and $H_2O]^{+\cdot}$ in this ion is ca. 13 kcal mol^{-1}, less than that for the CH_3OH complex. However, it should be noted that the AE for m/z 62 is within experimental error, the same as the IE for butan-1,4-diol, 9.75 eV. Thus, the heat of formation of the ion may well represent an upper limit. The only isomeric $[C_2H_6O_2]^{+\cdot}$ ion which might be expected to yield $[CH_2{=}CHOH]^{+\cdot} + H_2O$ without major rearrangement is ion **IV**. (Note that $[HOCH_2CH_2OH]^{+\cdot}$ and $[CH_3OOCH_3]^{+\cdot}$ have no m/z 44 ion in their mass spectra.) However, an estimate of the heat of formation of **IV**, 132 ± 5 kcal mol^{-1} (by consideration of the effect of OH substitution on $[CH_3CH_2OH]^{+\cdot}$ (16)), indicates that such an ion would be "hot" with respect to fragmentation to $[CH_2{=}CHOH]^{+\cdot}$ and in any case lies well above the observed ΔH_f^0, 110 kcal mol^{-1}.

Finally, it must be re-emphasised that the experiments described above do not permit clear distinctions to be drawn between the proposed structures of these novel ions. Moreover, as cogently pointed out by a referee, another type of structure, to wit a proton-bound radical–molecule pair e.g.

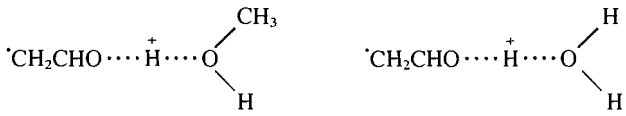

I*d* III*d*

may also be stable, by analogy with closed shell systems (18–20). Indeed the major fragmentations in the CA mass spectra of **I** and **III** can be rationalised by considering the relative proton affinities of the radical and molecules involved in **I***d* and **III***d*. High level *ab initio* quantum mechanical calculations are required to solve this dilemma.

Experimental

Collisional activation mass spectra and metastable peak shapes were measured with the VG ZAB-2F mass spectrometer as described elsewhere (21). Metastable peak abundances and appearance energies were measured using an AEI-Kratos MS902S mass spectrometer (7) and daughter ion AE values were obtained with an apparatus comprising an electrostatic electron monochromator with a quadrupole mass analyser and minicomputer data system (14).

Butan-1,4-diol was obtained from Aldrich Co. and 4-methoxybutan-1-ol was prepared by reacting the former with CH_3I (22); the labelled analogues required CD_3I and $^{13}CH_3I$, obtained from Merck, Sharp and Dohme.

Acknowledgements

We thank Dr. F. P. Lossing for appearance energy measurements and stimulating discussions and Prof. G. Dijkstra for his continuing enthusiastic support. J.H. thanks the Natural Sciences and Engineering Research Council of Canada and J.K.T. the Netherlands Organisation for the Advancement of Pure Research (Z.W.O.) for continuing financial support. J.K.T., P.C.B., and J.H. also thank the NATO Scientific Affairs Division for collaborative research award 0329.

1. (*a*) J. L. Holmes, F. P. Lossing, J. K. Terlouw, and P. C. Burgers. J. Am. Chem. Soc. **104**, 2931 (1982); (*b*) J. L. Holmes, F. P. Lossing, J. K. Terlouw, and P. C. Burgers. Can. J. Chem. **61**, 2305 (1983).
2. P. C. Burgers, A. A. Mommers, and J. L. Holmes. J. Am. Chem. Soc. **105**, 5976 (1983).
3. A. J. Illies, M. F. Jarrold, and M. T. Bowers. J. Chem. Phys. **77**, 5847 (1982).
4. P. C. Burgers and J. L. Holmes. Chem. Phys. Lett. **97**, 236 (1983).
5. J. K. Terlouw, W. Heerma, and G. Dijkstra. Org. Mass Spectrom. **16**, 326 (1981).
6. C. C. van der Sande and F. W. McLafferty. J. Am. Chem. Soc. **97**, 4613 (1975).
7. P. C. Burgers and J. L. Holmes. Org. Mass Spectrom. **17**, 123 (1982).
8. S. W. Benson, F. R. Cruickshank, D. M. Golden, G. R. Haugen, H. E. O'Neil, A. S. Rodgers, R. Shaw, and R. Walsh. Chem. Rev. **69**, 279 (1969).
9. H. M. Rosenstock, K. Draxl, B. W. Steiner, and J. T. Herron. J. Phys. Chem. Ref. Data Suppl. 6, No. 1 (1977).
10. J. L. Holmes, J. K. Terlouw, and F. P. Lossing. J. Phys. Chem. **80**, 2860 (1976).
11. J. K. Terlouw, C. G. Dekoster, W. Heerma, J. L. Holmes, and P. C. Burgers. Org. Mass Spectrom. **18**, 223 (1983).
12. W. J. Bouma, J. K. MacLeod, R. H. Nobes, and L. Radom. Int. J. Mass Spectrom. Ion Phys. **46**, 235 (1983), and references cited therein.
13. R. Yamdagni and P. Kebarle. J. Am. Chem. Soc. **98**, 1320 (1976).
14. F. P. Lossing and J. C. Traeger. Int. J. Mass Spectrom. Ion Phys. **19**, 9 (1976).

Can. J. Chem. Downloaded from www.nrcresearchpress.com by 210.87.254.6 on 09/06/12
For personal use only.

15. F. P. LOSSING. Private communication.
16. J. L. HOLMES and F. P. LOSSING. Can. J. Chem. **60**, 2365 (1982).
17. P. C. BURGERS and J. L. HOLMES. Int. J. Mass Spectrom. Ion Phys. In press.
18. I. H. WILLIAMS, G. M. MAGGIORA, and R. L. SCHOWEN. J. Am. Chem. Soc. **102**, 7831 (1980).
19. S. A. MCLUCKEY, D. CAMERON, and R. G. COOKS. J. Am. Chem. Soc. **103**, 1313 (1981).
20. J. W. LARSON and T. B. MCMAHON. J. Am. Chem. Soc. **104**, 6255 (1982).
21. J. K. TERLOUW, P. C. BURGERS, and H. HOMMES. Org. Mass Spectrom. **14**, 307 (1979).
22. L. PICHAT, C. BARET, and M. AUDINOT. Bull. Soc. Chim. Fr. 151 (1956).

Can. J. Chem. Downloaded from www.nrcresearchpress.com by 210.87.254.6 on 09/06/12
For personal use only.

Relative rates of radical–radical processes in the pyrolysis of ethane

PHILIP D. PACEY AND JAYANTHA H. WIMALASENA[1]
Department of Chemistry, Dalhousie University, Halifax, N.S., Canada B3H 4J3

Received May 6, 1983

PHILIP D. PACEY and JAYANTHA H. WIMALASENA. Can. J. Chem. **62**, 293 (1984).

Ethane has been pyrolysed in a flow system at 900 to 963 K, at residence times from 0.5 to 50 s and with $[C_2H_6]$ from 1×10^{-4} to 4×10^{-3} mol L^{-1}. From measurements of yields of minor products at 902 K, it is concluded that the combination reaction, [5*a*], and disproportionation reaction, [5*b*], of C_2H_5 radicals have the rate constant ratio, $k_{5b}/k_{5a} = 0.44 \pm 0.07$. It is suggested that this ratio has a curved Arrhenius plot, which is interpreted in terms of activated complex theory. The cross-combination of CH_3 and C_2H_5 radicals becomes significant at low pressures, reaching 1.5% of the sum of the rates of [5*a*] and [5*b*] when $[C_2H_6] = 10^{-3}$ mol L^{-1} at 902 K. With $[C_2H_6] = 10^{-4}$ mol L^{-1} at 963 K, the yield of CH_4 was greater in the presence of an SiO_2 surface than in the presence of a PbO surface, consistent with the occurrence of the atom-cracking reaction,

[7*a*] $H + C_2H_5 \rightarrow 2CH_3$

at 15% of the combined rates of [5*a*] and [5*b*]. Rate parameters are also reported for the C—C scission in C_2H_6, for the abstraction of H from C_2H_6 by CH_3, for the decomposition of C_2H_5, and for the reaction of C_2H_5 at PbO surfaces.

PHILIP D. PACEY et JAYANTHA H. WIMALASENA. Can. J. Chem. **62**, 293 (1984).

On a étudié la pyrolyse de l'éthane à faible avancement en réacteur dynamique entre 900 et 963 K avec $[C_2H_6]$ entre 1×10^{-4} et 4×10^{-3} mol L^{-1}. Le rapport $[C_3H_8]/[CH_4]$ avait une valeur moins de 0.8% et était en accord avec un mécanisme de formation de C_3H_8 par la combinaison de radicaux CH_3 et C_2H_5. En présence des parois de PbO, il y avait une légère diminution de la vitesse de formation de CH_4, expliquée par l'extinction de la réaction,

[7*a*] $H + C_2H_5 \rightarrow 2CH_3$

qui arrive 15% aussi souvent que les terminaisons des chaines à 963 K, avec $[C_2H_6]$ égale à 1×10^{-4} mol L^{-1}. Extrapolé à l'avancement nul et aux hautes pressions, le rapport $[CH_4]/[C_4H_{10}]$ correspond à la valeur de 0.44 ± 0.07 pour le rapport des constantes de vitesse de dismutation et de combinaison de radicaux C_2H_5. Pour la réaction de dismutation, avec l'aide de la théorie du complexe activé, on suggère que les paramètres d'Arrhénius varient avec la température. On trouve également des constantes de vitesse pour l'amorçage, pour l'arrachement de H de C_2H_6 par CH_3 et pour la disparition unimoléculaire homogène et hétérogène de C_2H_5.

Introduction

According to the simple mechanism for the pyrolysis of ethane, the ratio of the yield of CH_4 to that of n-C_4H_{10} is predicted to be close to two. Instead, it is found experimentally (1–3) that the ratio is often three or more. It has been suggested that minor heterogeneous and homogeneous processes are responsible for this difference. The heterogeneous processes have been examined recently in this laboratory (4). The purpose of this article will be to examine the minor, homogeneous, radical–radical processes.

The simple mechanism is as follows:

[1] $C_2H_6 \rightarrow 2CH_3$

[2] $CH_3 + C_2H_6 \rightarrow CH_4 + C_2H_5$

[3] $C_2H_5 \rightarrow C_2H_4 + H$

[4] $H + C_2H_6 \rightarrow H_2 + C_2H_5$

[5*a*] $2C_2H_5 \rightarrow C_4H_{10}$

[5*b*] $2C_2H_5 \rightarrow C_2H_6 + C_2H_4$

Making the steady-state assumption for this mechanism, it is found that $[CH_4]/[C_4H_{10}]$ is equal to $2k_5/k_{5a}$, where k_5 is the sum of the rate constants for reactions [5*a*] and [5*b*]. If k_{5b}/k_{5a} is assumed to have the value of 0.13 ± 0.02, as at room temperature (5), then $[CH_4]/[C_4H_{10}]$ should be 2.26 ± 0.04.

Additional reactions which could affect this ratio are as follows (2–4, 6):

[6] $C_2H_5 \xrightarrow{w}$ products

[7*a*] $H + C_2H_5 \rightarrow 2CH_3$

[7*b*] $H + C_2H_5 \rightarrow C_2H_6$

[7*c*] $H + C_2H_5 \rightarrow H_2 + C_2H_4$

[8*a*] $CH_3 + C_2H_5 \rightarrow C_3H_8$

[8*b*] $CH_3 + C_2H_5 \rightarrow CH_4 + C_2H_4$

Making the steady-state approximation and the long chain approximation, neglecting reactions of products and eliminating sums in the denominator or within square roots using the binomial expansion, retaining leading terms only, expressions for relative rates of product formation have been obtained.[2]

When termination is strongly dominated by reaction set [5], initial yield ratios are predicted to be as follows:

$$[9] \quad \left(\frac{[CH_4]}{[C_4H_{10}]}\right)_0 = \frac{2k_5}{k_{5a}}\left(1 + \frac{k_6}{2(k_1k_5[C_2H_6])^{1/2}} + \frac{k_3k_7}{k_4k_5[C_2H_6]} + \frac{k_1^{1/2}(k_{8a} + 2k_{8b})}{k_2k_5^{1/2}[C_2H_6]^{1/2}} - \cdots\right)$$

[1] Present address: Department of Chemistry, University of Sri Jayewardenepura, Nugegoda, Sri Lanka.

[2] An appendix, outlining this derivation, and a complete set of data are available at a nominal charge, upon request, from the Depository of Unpublished Data, CISTI, National Research Council of Canada, Ottawa, Ont., Canada K1A 0R6.

Can. J. Chem. Downloaded from www.nrcresearchpress.com by 210.87.254.42 on 09/06/12
For personal use only.

$$[10]\quad \left(\frac{[C_3H_8]}{[CH_4]}\right)_0 = \frac{k_1^{1/2}k_{8a}}{k_2k_5^{1/2}[C_2H_6]^{1/2}}\left(1 - \frac{k_6}{4(k_1k_5[C_2H_6])^{1/2}} - \frac{k_3(k_{7b} + k_{7c})}{2k_4k_5[C_2H_6]} - \frac{k_1^{1/2}(k_{8a} + 2k_{8b})}{k_2k_5^{1/2}[C_2H_6]^{1/2}} + \ldots\right)$$

These series converge; all terms but the first are less than unity.

Comparing rates of formation of CH_4 when reaction set [5] dominates termination, $R_{CH_4,5}$, and when reaction [6] dominates, $R_{CH_4,6}$, but when temperature and $[C_2H_6]$ are the same, one obtains

$$[11]\quad \frac{R_{CH_4,5}}{R_{CH_4,6}} = 1 + \frac{k_3k_{7a}}{k_4k_5[C_2H_6]}\left(1 - \frac{4k_1k_5[C_2H_6]}{k_6^2} - \ldots\right) - \frac{k_1^{1/2}k_{8a}}{k_2k_5^{1/2}[C_2H_6]^{1/2}}\left(1 - \frac{(4k_1k_5[C_2H_6])^{1/2}}{k_6}\ldots\right) - \ldots\ldots$$

In eq. [11], k_6 has its value when reaction [6] dominates termination, and the series converge.

Examining eq. [9], it is seen that $[CH_4]/[C_4H_{10}]$ should be greater than $2k_5/k_{5a}$ when the terms in k_6, k_7, and $(k_{8a} + 2k_{8b})$ are not zero. It should be possible to obtain information about the terms in k_7 and $(k_{8a} + 2k_{8b})$ by experimental studies applying eqs. [11] and [10], respectively, in which similar quotients appear. Based on the orders of k_1 and k_3 at 894 K (1), the orders of the terms in eq. [9] in k_6, k_7, and $(k_{8a} + 2k_{8b})$ are predicted to be -0.56 ± 0.01, -0.46 ± 0.04, and -0.44 ± 0.01, respectively. These are all close to -0.5, so a plot of $([CH_4]/[C_4H_{10}])_0$ as a function of $[C_2H_6]^{-1/2}$ should give a straight line of intercept $2k_5/k_{5a}$.

Experimental

Most of the apparatus and experimental techniques have been described in refs. 4 and 8. An additional, dual reactor system was constructed with two 3 mm inside diameter cylindrical quartz tubes placed side by side in an 11 mm inside diameter quartz tube, which was surrounded by an 18 mm outside diameter brass tube and an electrically heated furnace. Both inner tubes were washed with concentrated HNO_3 and distilled water. One was rinsed with a 1 *M* solution of $Pb(NO_3)_2$ and heated slowly to obtain a PbO deposit. Reagent flow was directed alternatively to these two reactor chambers.

Products were analyzed by gas chromatography (4).

Results

Propane formation

Experiments[2] to determine the yields of C_3H_8 have been performed in 8 and 17 mm inside diameter quartz reactors at temperatures from 900 to 905 K, at six C_2H_6 concentrations from 1.07×10^{-3} to 4.4×10^{-3} mol L^{-1} and at residence times from 1.4 to 50 s.

Values of the ratio $[C_3H_8]/[CH_4]$ have been extrapolated to initial time to eliminate interference by reactions of the products. The initial values, approximately equal to $k_1^{1/2}k_{8a}/(k_2k_5^{1/2}[C_2H_6]^{1/2})$ by eq. [10], had an order with respect to $[C_2H_6]$ of -0.33 ± 0.20, in agreement within experimental uncertainty with the value -0.44 ± 0.01, predicted by eq. [10]. (Here and elsewhere quoted uncertainties are standard deviations.) The largest value (at the lowest $[C_2H_6]$) was 7.7×10^{-3}, indicating that this is a very minor termination process.

The concentrations of products and reactant were also used to calculate $k_2/k_{-1,\infty}^{1/2}$, as in ref. 3. (The factor of $(1.15)^{1/2}$, included in ref. 3, was omitted. See footnote 2.) The order of the quotient, $k_2/k_{-1,\infty}^{1/2}$, was found to be 0.08 ± 0.12, or zero within experimental uncertainty. The average of the six values was 26 ± 4 $L^{1/2}$ $mol^{-1/2}$ $s^{-1/2}$. Taking $k_{-1,\infty}$ from ref. 8, it is found that $k_2 = 3.9 \times 10^6$ L mol^{-1} s^{-1}.

From CH_4 yields k_1 is calculated (1–3) to have values from 1.1×10^{-5} to 1.8×10^{-5} s^{-1}.

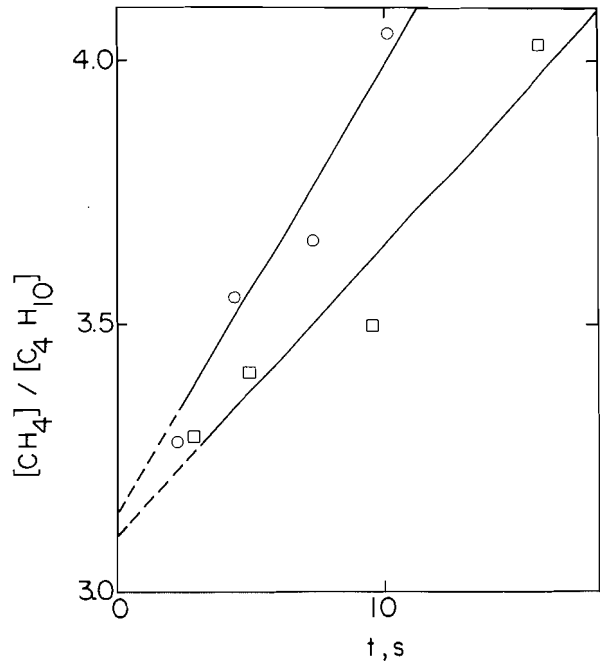

FIG. 1. Dependence of $[CH_4]/[n\text{-}C_4H_{10}]$ on residence time in the 8 mm diameter reactor at 902 K; □, 3.5×10^{-3} mol C_2H_6 L^{-1}; ○, 1.7×10^{-3} mol C_2H_6 L^{-1}; —, least-squares straight lines.

Dual reactor experiments

Pure C_2H_6 at a concentration of 1.05×10^{-4} mol L^{-1} was pyrolyzed in the dual reactor system at 963 K. Rates of formation of CH_4 and C_2H_4 in the presence of the SiO_2 and PbO surfaces are summarized[2] in Table 1. It can be seen that the PbO surface reduced the rate of formation of C_2H_4 by an order of magnitude and reduced the rate of formation of CH_4 by 10%. The difference in the CH_4 rates was small but by the test of analysis of variance it was significant at the 99% confidence level (9).

CH_4-to-C_4H_{10} ratio

The ratio of CH_4 to C_4H_{10} yields has been measured in experiments[2] at 900 to 902 K in clean quartz reactors of 8 mm diameter at $[C_2H_6]$ from 2.5×10^{-4} to 3.5×10^{-3} mol L^{-1}.

The dependence of this ratio on reactor residence time is shown in Fig. 1 for experiments at 3.5×10^{-3} and 1.7×10^{-3} mol L^{-1} at 902 K. It can be seen that the ratio increases sharply with increasing residence time, mainly because of secondary processes which reduce the later yields of C_4H_{10}. The data in Fig. 1 may be reliably extrapolated to determine the initial ratio, $([CH_4]/[C_4H_{10}])_0$. However, it was necessary that the shortest residence times be less than about 4 s in order to confidently predict this intercept.

Initial values of the ratios are shown in Fig. 2, plotted as a function of $[C_2H_6]^{-1/2}$, as suggested by eq. [9]. The solid, straight line is a least-squares fit. The intercept, which by eq. [9] should be equal to $2k_5/k_{5a}$, was found to be 2.88 ± 0.13. The disproportionation to combination ratio, k_{5b}/k_{5a}, is then calculated to be 0.44 ± 0.07. The ratio of slope to intercept,

Can. J. Chem. Downloaded from www.nrcresearchpress.com by 210.87.254.42 on 09/06/12
For personal use only.

Can. J. Chem. Downloaded from www.nrcresearchpress.com by 210.87.254.42 on 09/06/12
For personal use only.

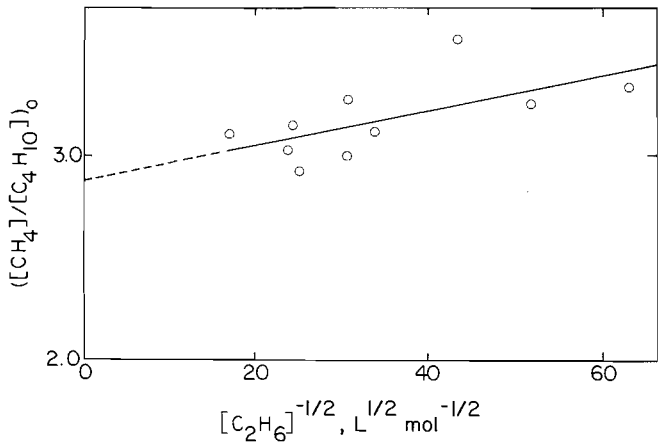

FIG. 2. Dependence of initial values of $[CH_4]/[n\text{-}C_4H_{10}]$ on $[C_2H_6]^{-1/2}$ at 900–902 K in the 8 mm diameter reactor; ○, intercepts of analogues of Fig. 1; —, least-squares straight line.

which is related to the terms in k_6, k_7, and $(k_{8a} + 2k_{8b})$ in eq. [9], is 3.0 (±1.3) × 10^{-3} $mol^{1/2}$ $L^{-1/2}$.

Discussion

Reactions [2] and [8a]

Possible sources of systematic error in the determination of $k_2/k_{-1,\infty}^{1/2}$ were thoroughly discussed in ref. 3. The value determined in this work, 26 ± 4 $L^{1/2}$ $mol^{-1/2}$ $s^{-1/2}$ may be compared with values calculated from Arrhenius parameters determined in the following temperature ranges: 21 $L^{1/2}$ $mol^{-1/2}$ $s^{-1/2}$, 931–1038 K (3); 24 $L^{1/2}$ $mol^{-1/2}$ $s^{-1/2}$, 880–1068 K (10); 5.9 $L^{1/2}$ $mol^{-1/2}$ $s^{-1/2}$, 303–797 K (11). The value from the present work is four times larger than that extrapolated from measurements at lower temperatures (11). There is growing evidence that the Arrhenius plot for reaction [−1] is straight (8, 12). The value of $k_2/k_{-1,\infty}^{1/2}$ determined in this work agrees well with the other data obtained at high temperatures and further confirms the suggested Arrhenius plot curvature (3, 10) for reaction [2].

It was seen in the Results section that $k_1^{1/2}k_{8a}/(k_2k_5^{1/2} \times [C_2H_6]^{1/2})$ is small under these conditions. It must make only a minor contribution in eqs. [9] and [11]. Applying the literature value of k_{8b}/k_{8a} (13), reactions [8*a*] and [8*b*] explain only 10% of the ratio of slope to intercept in Fig. 2.

Reactions [5a] and [5b]

Values of the disproportionation to combination ratio, k_{5b}/k_{5a}, calculated from the intercepts of graphs like Fig. 2, are shown as the solid points in Fig. 3. The results are based on the data of refs. 1, 2, and 3 as well as the present work. Results of experiments of ref. 1 at 873 and 894 K are not shown, as conversions were much greater than those in Fig. 1. The average of the values from C_2H_6 pyrolysis in Fig. 3 is 0.44 ± 0.12. These values could be fitted to an Arrhenius expression as follows

$$\log_{10}(k_{5b}/k_{5a}) = 0.5 \pm 0.4 - (15 \pm 6)\ \text{kJ mol}^{-1}/(2.3\ RT)$$

If one assumed a dependence on $[C_2H_6]^{-1}$ or an independence of $[C_2H_6]$ in Fig. 2, one would obtain k_{5b}/k_{5a} equals 0.52 ± 0.04 or 0.59 ± 0.10, respectively. Thus the conclusion, that k_{5b}/k_{5a} is about 0.5, does not depend on the interpretation of the small pressure dependence of $[CH_4]/[C_4H_{10}]$ in Fig. 2. For the conditions of the earliest points in Fig. 1, yields of C_3H_6 were only 2% of the yields of CH_4; the reaction,

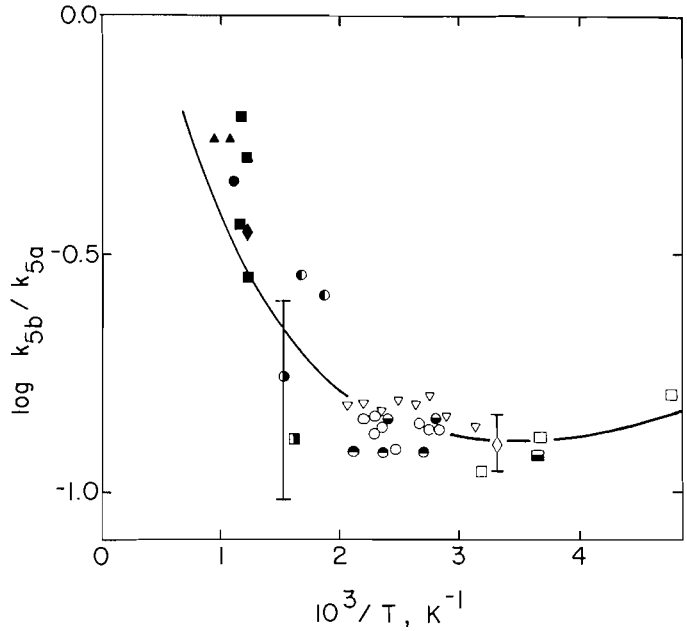

FIG. 3. Arrhenius plot for k_{5b}/k_{5a}: ■, extrapolated from the data of ref. 1; ◆, from ref. 2; ▲, from ref. 3; ◇, room temperature data from ref. 5; ◒, ref. 7; ◨, ref. 14; ◓, ref. 15; □, ref. 16; ▽, ref. 17; ○, ref. 18; ⬓, ref. 19; ◐, ref. 20; ◑, ref. 21; ●, this work; —, activated complex theory results.

$$C_2H_5 + C_2H_4 \rightarrow CH_3 + C_3H_6$$

is not a significant initial source of CH_4.

In the low pressure pyrolysis of azoethane at 860 K (22) the value of k_{5b}/k_{5a} was found to be 1.5, which would be reduced to about 0.7 when k_{5a} is adjusted to its limiting high pressure value. This value is similar to those from C_2H_6 pyrolysis.

The present authors consider that the most reasonable interpretation of the data is that the Arrhenius plot for reaction [5*b*] is a curve. In this way, it would join several other atom transfer reactions, for example, reaction [2], and the disproportionation of OH radicals (23). For these reactions, activation energies increase by 20 to 40 kJ mol^{-1} at high temperatures and pre-exponential factors approach collision numbers.

Also shown in Fig. 3 is a curved line calculated by activated complex theory. In this calculation, k_{5b} was favoured by a statistical factor of 6. Four free internal rotational degrees of freedom of ethyl radicals in the complex for combination were replaced by four vibrational modes (ω = 85 cm^{-1}) in the complex for disproportionation. The zero point energy for the disproportionation complex was 3 kJ mol^{-1} less than that for combination. Other parameters were identical for k_{5a} and k_{5b}. Replacement of the rotational modes by vibrational modes leads to the upward curvature at high temperatures. The small difference in zero point energies leads to the slight increase in the ratio at low temperatures. This increase is not clearly established experimentally (24). The illustrated model is not intended to be exact, but to indicate that most of the data were compatible with a single, reasonable explanation.

Reaction [7a]

The most straightforward interpretation of the reduction in the CH_4 yields observed in Table 1 is to suppose, following eq. [11], that this reduction is a measure of the reduction in the rate of formation of CH_3 by reaction [7*a*]. However, there are at least two other possible interpretations.

Can. J. Chem. Downloaded from www.nrcresearchpress.com by 210.87.254.42 on 09/06/12
For personal use only.

TABLE 1. Summary of experiments in dual 3 mm diameter reactors at 963 K with $[C_2H_6] = 1.05 \times 10^{-4}$ mol L^{-1}

Surface	$10^8 \times [CH_4]/t$ (mol L^{-1} s^{-1})	$10^6 \times [C_2H_4]/t$ (mol L^{-1} s^{-1})
SiO_2	2.75 ± 0.12	1.30 ± 0.08
PbO	2.48 ± 0.13	0.135 ± 0.007

One possibility is that CH_3 was removed at the PbO surface, without forming CH_4. This reaction could not be reaction [−1], as this reaction is not favoured by thermodynamics. However, such a reaction could have formed C_2H_4 and H_2, for example.

It is also possible that the greater rate of formation of CH_4 in the clean reactor was the result of the reaction,

$$[12] \quad H + C_2H_6 \rightarrow CH_4 + CH_3$$

In hot atom experiments (25) this reaction was found to be much slower than the process in which hydrogen atoms are simply exchanged. Even the latter process has a much higher threshold energy than reaction [4] and is unable to compete in thermal systems.

Neither of these possibilities can be completely eliminated, so Table 1 does not constitute a proof that reaction [7*a*] occurs in C_2H_6 pyrolysis. Nevertheless, we shall interpret Table 1 assuming that the change in CH_4 yields is a measure of the influence of reaction [7*a*] in order to compare our conclusions with those in the literature.

In eq. [11], the left hand side was calculated assuming that reaction set [5] dominates termination in the clean reactor and that reaction [6] dominates in the PbO reactor. From the relative C_2H_4 yields, by the methods of ref. 4, the quotient $(4k_1k_5[C_2H_6])^{1/2}/k_6$ (PbO) is found to be 0.10. Finding k_1 from CH_4 yields (1–3), adjusting our earlier value of $k_2/k_{-1,\infty}^{1/2}$ for temperature (3) and taking the cross-combination ratio (7), the quotient $k_1^{1/2}k_{8a}/(k_2k_5^{1/2}[C_2H_6]^{1/2})$ is calculated to be 0.039. The quotient, $k_3k_{7a}/(k_4k_5[C_2H_6])$, is then found from eq. [11] to be 0.15. Taking k_5 from ref. 26 and finding k_3 from C_2H_4 yields (4), $k_{7a}/(k_4k_5^{1/2})$ becomes 1.3 (±0.8) × 10^{-3} $mol^{1/2}$ $s^{1/2}$ $L^{-1/2}$. The latter quotient is important in flow discharge systems containing H atoms and C_2H_6 or C_2H_4. Taking the Arrhenius parameters of ref. 6 for k_4 and those of refs. 6, 27, or 28 for k_{7a} and k_5, the value of $k_{7a}/(k_4k_5^{1/2})$ at 963 K is calculated to be 1.6×10^{-3}, 0.9×10^{-3} or 0.4×10^{-3} $mol^{1/2}$ $s^{1/2}$ $L^{-1/2}$, respectively. Considering the extrapolation of 200 K or more, this is satisfactory agreement, supporting the present interpretation of the data in Table 1.

From the data of Table 1 the following kinetic parameters may also be calculated (1–4, 26): $k_1 = 1.2 \times 10^{-4}$ s^{-1}, $k_3 = 1300$ s^{-1}, k_6 (PbO) = 240 s^{-1}, $k_7/k_4 = 110$, γ (probability of termination per collision of C_2H_5 with PbO) = 8×10^{-4}. Residence times were an order of magnitude greater than those needed for the use of the steady-state assumption (26).

Reaction [7*a*] does not play a major role in C_2H_6 pyrolysis. This role becomes smaller at lower temperatures and higher pressures, where it would be hard to detect (2). The reaction would become more important at lower pressures or higher temperatures, but would be difficult to study because of reduced analytical sensitivity or increased competition from secondary reactions, respectively. Camilleri *et al.* (6) reported that the rate of reaction [7*c*] is about 5% of that of reaction [7*a*], independent of temperature. The ratio of dissociation, [7*a*], to stabilization, [7*b*], has been calculated using the method of ref. 29 and RRKM model of ref. 30. The integration was performed with energies of the complex starting at 410 kJ mol^{-1}. At 901 K, the ratio, k_{7b}/k_{7a}, was calculated to have values from 0.08 at 1.8×10^{-4} mol L^{-1} to 1.1 at 4.4×10^{-3} mol C_2H_6/L.

Taking $k_{7a}/(k_4k_5^{1/2})$ as above, increasing by 13% to allow for reactions [7*b*] and [7*c*], adjusting for the temperature dependence of k_4 (6), and taking k_3 and k_5 from ref. 26, it is predicted that the quantity, $k_3k_7/(k_4k_5[C_2H_6]^{1/2})$ would have the value 1.5×10^{-3} $mol^{1/2}$ $L^{-1/2}$ at 902 K. This is half the ratio of slope to intercept in Fig. 2.

Reaction [6]

According to the preceeding sections, 10% of the slope in Fig. 2 can be attributed to reaction set [8] and about 50% to reaction set [7]. The remainder could be attributed to reaction [6]. From eq. [9], then, $k_6(SiO_2)/(2k_1^{1/2}k_5^{1/2}) = 1.2$ (±1.6) × 10^{-3} $mol^{1/2}$ $L^{-1/2}$, small enough to ensure that reaction set [5] dominates termination in clean quartz reactors. This value may be shown (4) to correspond to a probability, $\gamma(SiO_2)$, of reaction per wall collision of 5 (±7) × 10^{-6}. The following values of γ have been calculated by the same method from the data of ref. 1: 823 K, unpacked, 40 (±30) × 10^{-6}, packed, 20 (±5) × 10^{-6}; 844 K, 11 (±16) × 10^{-6}; 858 K, 70 (±20) × 10^{-6}.

The above values of γ are imprecise. This reflects the uncertainty in the slopes and perhaps also a difference in the history of the surfaces. We have previously reported (4) a value of γ = 11 (±3) × 10^{-6} at 823 K based on the data of ref. 1 but calculated from the changes in C_4H_{10} yields on changing surface-to-volume ratio. The previous method is more direct and more reliable, as it avoids the need to measure small slopes and avoids assumptions regarding k_7 and k_8. The above values of γ are quoted only to show that their orders of magnitude are similar and that the present interpretation of the variation of CH_4 to C_4H_{10} ratios is reasonable.

It has been assumed by other workers (2, 31) that the heterogeneous reaction in pyrolysis is

$$[13] \quad H \xrightarrow{w} (1/2)H_2$$

It has been shown (4) that reaction [6] is more consistent with the data for C_2H_6 pyrolysis. However, if reaction [6] is replaced by reaction [13], the term in k_6 in eq. [9] would be replaced by $k_3k_{13}/(2k_4(k_1k_5)^{1/2}[C_2H_6]^{3/2})$, which has an order of −1.02 ± 0.04. The rate constants calculated herein for heterogeneous processes would lose their meaning, but those for homogeneous processes would not change significantly.

In summary the rate of reaction [8*a*] has been measured directly. Less direct and less reliable estimates have been obtained for the rates of reactions [6] and [7*a*]. The disproportionation to combination ratio, k_{5b}/k_{5a}, has been calculated from high pressure ratios of $[CH_4]/[C_4H_{10}]$. Arrhenius plot curvature has been confirmed for reaction [2] and is suggested for reaction [5*b*]. At high pressures reactions [5*a*] and [5*b*] are the dominant radical–radical processes, accounting for 70 and 30%, respectively, of the total. At lower pressures, especially at high temperatures, reactions [7*a*] and [8*a*] also contribute. Further studies of disproportionation reactions at high temperatures are recommended.

Acknowledgements

The authors wish to thank the Natural Sciences and Engineering Research Council of Canada for a grant in support of this work, and Dr. G. Scacchi for pointing out some of the

merits of studying the pyrolysis of ethane in contact with PbO. J.H.W. thanks the Dorothy J. Killam Trust for the award of a scholarship.

1. M. C. LIN and M. H. BACK. Can. J. Chem. **44**, 505 (1966).
2. G. SCACCHI, R. MARTIN, and M. NICLAUSE. Bull. Soc. Chim. Fr. 731 (1971).
3. P. D. PACEY and J. H. PURNELL. J. Chem. Soc. Faraday Trans. I, **68**, 1462 (1972).
4. P. D. PACEY and J. H. WIMALASENA. Can. J. Chem. **61**, 1086 (1983).
5. J. A. KERR and S. J. MOSS. Handbook of bimolecular and termolecular gas reactions. Vol. II. CRC Press, Boca Raton. 1981. p. 80.
6. P. CAMILLERI, R. M. MARSHALL, and J. H. PURNELL. J. Chem. Soc. Faraday Trans. I, **70**, 1434 (1974).
7. J. C. J. THYNNE. Trans. Faraday Soc. **58**, 676 (1962).
8. P. D. PACEY and J. H. WIMALASENA. J. Phys. Chem. **84**, 2221 (1980).
9. C. A. BENNETT and N. L. FRANKLIN. Statistical analysis in chemistry and the chemical industry. Wiley, New York. 1954.
10. C. J. CHEN, M. H. BACK, and R. A. BACK. Can. J. Chem. **54**, 3175 (1976).
11. J. A. KERR and M. J. PARSONAGE. Evaluated kinetic data on gas phase hydrogen transfer reactions of methyl radicals. Butterworths, London. 1976.
12. M. T. MACPHERSON, M. J. PILLING, and M. J. C. SMITH. Chem. Phys. Lett. **94**, 430 (1983).
13. M. J. GIBIAN and R. C. CORLEY. Chem. Rev. **73**, 441 (1973).
14. H. V. CARTER, E. I. CHAPPELL, and E. WARHURST. J. Chem. Soc. 106 (1956).
15. R. K. BRINTON and E. W. R. STEACIE. Can. J. Chem. **33**, 1840 (1955).
16. P. S. DIXON, A. P. STEFANI, and M. SZWARC. J. Am. Chem. Soc. **85**, 2551 (1963).
17. J. A. KERR and A. F. TROTMAN-DICKENSON. J. Chem. Soc. 1611 (1960).
18. D. G. L. JAMES and G. E. TROUGHTON. Trans. Faraday Soc. **62**, 120 (1966); **62**, 145 (1966).
19. J. GROTEWOLD and E. A. LISSI. J. Chem. Soc. B, 264 (1968).
20. L. E. REID and D. J. LEROY. Can. J. Chem. **46**, 3275 (1968).
21. A. C. LALONDE and S. J. W. PRICE. Can. J. Chem. **49**, 3367 (1971).
22. D. M. GOLDEN, K. Y. CHOO, M. J. PERONA, and L. W. PISZKIEWICZ. Int. J. Chem. Kinet. **8**, 381 (1976).
23. W. T. RAWLINS and W. C. GARDINER, JR. J. Chem. Phys. **60**, 4676 (1974).
24. D. G. HOOPER, M. SIMON, and M. H. BACK. Can. J. Chem. **53**, 1237 (1975).
25. D. URCH and R. WOLFGANG. J. Am. Chem. Soc. **83**, 2982 (1981).
26. P. D. PACEY and J. H. WIMALASENA. Chem. Phys. Lett. **76**, 433 (1980).
27. L. TENG and W. E. JONES. J. Chem. Soc. Faraday Trans. I, **68**, 1267 (1972).
28. G. PRATT and I. VELTMAN. J. Chem. Soc. Faraday Trans. I, **72**, 1733 (1976).
29. B. S. RABINOVITCH and D. W. SETSER. Adv. Photochem. **3**, I (1964).
30. J. A. CLARK and C. P. QUINN. J. Chem. Soc. Faraday Trans. I, **72**, 706 (1976).
31. K. KANAN, H. PURNELL, and A. SEPHERAD. Int. J. Chem. Kinet. **15**, 845 (1983).

Can. J. Chem. Downloaded from www.nrcresearchpress.com by 210.87.254.42 on 09/06/12
For personal use only.

Spirolucidine, a new *Lycopodium* alkaloid

WILLIAM A. AYER, LESLIE F. BALL, LOIS M. BROWNE, AND MOTOO TORI
Department of Chemistry, University of Alberta, Edmonton, Alta., Canada T6G 2G2

AND

LOUIS T. J. DELBAERE AND ALEXIS SILVERBERG
Department of Biochemistry, University of Saskatchewan, Saskatoon, Sask., Canada S7N 0W0

Received May 12, 1983

WILLIAM A. AYER, LESLIE F. BALL, LOIS M. BROWNE, MOTOO TORI, LOUIS T. J. DELBAERE, and ALEXIS SILVERBERG. Can. J. Chem. **62**, 298 (1984).

The structure of spirolucidine, a new type of *Lycopodium* alkaloid related to the lucidines, has been determined. Chemical and spectroscopic data, together with biogenetic considerations, led to the correct constitution of spirolucidine. An X-ray crystallographic study of tetrahydrodeoxyspirolucidine, the lithium aluminum hydride reduction product of spirolucidine, confirmed the constitution and established the relative stereochemistry of the alkaloid.

WILLIAM A. AYER, LESLIE F. BALL, LOIS M. BROWNE, MOTOO TORI, LOUIS T. J. DELBAERE et ALEXIS SILVERBERG. Can. J. Chem. **62**, 298 (1984).

On a déterminé la structure de la spirolucidine, un nouvel alcaloïde du type *Lycopodium*. Les données chimiques et spectroscopiques ainsi que des considérations portant sur la biogénèse conduisent à la structure exacte de la spirolucidine. Une étude par cristallographie aux rayons-X de la tétrahydrodéoxyspirolucidine, le produit de réduction de la spirolucidine par l'alanate de lithium, confirme la structure et établit la stéréochimie relative de l'alcaloïde.

[Traduit par le journal]

Can. J. Chem. Downloaded from www.nrcresearchpress.com by 210.87.254.105 on 09/06/12
For personal use only.

We have recently reported the structure of three $C_{30}N_3$ alkaloids isolated from *Lycopodium lucidulum* (1). These alkaloids represent a new structural type among the Lycopodium alkaloids, represented here by lucidine B (**1**).[1] We now wish to report the structure of a related weakly basic alkaloid, which we have named spirolucidine, isolated from the same source. Spirolucidine is shown to possess structure **2**, and is a possible biogenetic precursor of the lucidines. The conformational drawing of spirolucidine (**2***a*) shows the close relationship between the top portion of the molecule and the tricyclic alkaloid luciduline (**3**) (2).

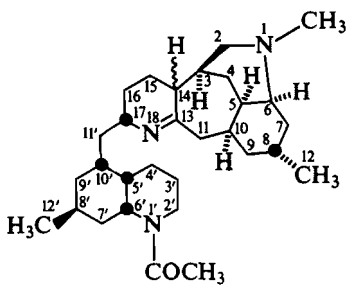

1

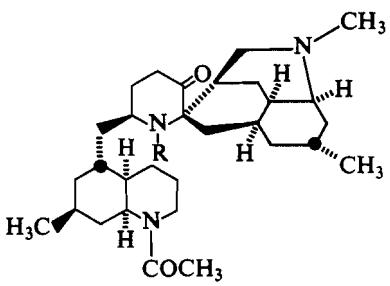

2 R = H
4 R = CHO

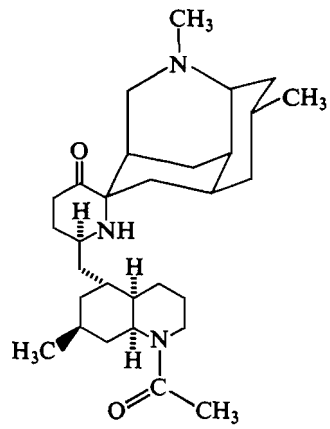

2*a*

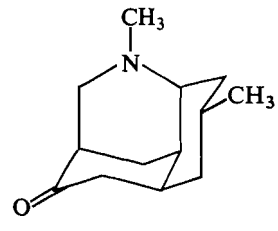

3

The weak bases of *L. lucidulum* were separated by 100-funnel countercurrent distribution as previously described (2). The weakest base fraction (tubes 1–12) was further separated by chromatography over neutral alumina to give luciduline (**3**) (least polar), dihydrolycolucine (1), and then spirolucidine (**2**) (most polar), obtained as a viscous gum which showed a single spot on tlc using several solvent systems.[2] High resolution mass spectrometry reveals that spirolucidine has the molecular formula $C_{30}H_{49}N_3O_2$. The infrared spectrum shows ketonic absorption at 1710 cm^{-1} and amide absorption at 1630 cm^{-1}. The ^1H nmr spectrum shows the presence of two secondary *C*-methyl groups (doublets at δ 0.82 and 0.89), an *N*-methyl group (s, δ 2.03), and an *N*-acetyl methyl (δ 2.08 and 2.09 (rotamers)).

The base peak in the mass spectrum of spirolucidine appears

[1]In ref. 1 the stereochemistry of lucidine B (**1**) and related compounds, at C-17, is incorrectly shown. The hydrogen should be above the plane, and the substituent below the plane, in accord with the X-ray structure shown as Fig. 1 in ref. 1.

[2]Full details of the separation may be found in ref. 3. In ref. 3 spirolucidine is referred to as "the 483-ketone".

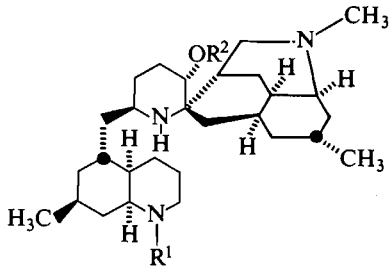

5 R' = $COCH_3$, R^2 = H
6 R' = R^2 = $COCH_3$
7 R' = CH_2CH_3, R^2 = H

at *m/z* 455, corresponding (hrms) to the loss of CO from the molecular ion, and was the first indication that we were dealing with an α-aminoketone (4). The infrared spectrum of spirolucidine does not show a clear N—H stretching vibration and attempted acetylation (Ac_2O-py) gave only starting material. However, treatment of spirolucidine with acetic formic anhydride gave *N*-formylspirolucidine (**4**) (δ 8.68, s, N—C*H*O; ν_{max}: 1710, 1650, 1630 cm^{-1}), confirming the presence of the secondary amino function and yet indicating its hindered nature.

Sodium borohydride reduction afforded dihydrospirolucidine (**5**) (ν_{max}: 3400, 1620 cm^{-1}) which on acetylation gave the *O*-acetyl derivative **6**. Reduction of spirolucidine (**2**) with lithium aluminum hydride provided tetrahydrodeoxyspirolucidine (**7**). Oxidation of **7** with Jones' reagent gave dihydrodeoxyspirolucidine (**8**) (ν_{max}: 1700 cm^{-1}). Treatment of **8** with sodium deuteroxide in D_2O—CH_3OD led to the incorporation of two C-bound deuterium atoms (mass spectrometry).

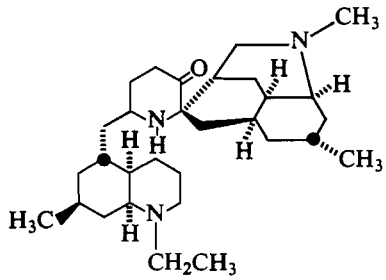

8

This finding, along with the fact that spirolucidine shows a *singlet* in the ^{13}C nmr at δ 65.9, in the region for carbons bonded to nitrogen, demonstrates that *spirolucidine does not have the same skeleton* as the lucidines (skeleton 1).

As has been pointed out (1, 5), the lucidine skeleton **1** may be biogenetically derived by the fusion of two $C_{11}N$ units such as that found in luciduline (**3**), with a piperidine ring as illustrated in **9**. The phlegmarines (skeleton 10) are a group of Lycopodium alkaloids in which one $C_{11}N$ unit is joined to a piperidine ring (6). The unusual biogenetic feature of the lucidine structure is that the C-3 to C-14 bond represents the fusion of a β (to nitrogen) carbon (C-3) of one ring system with the β (to nitrogen) carbon (C-14) of the piperidine ring. Normally this type of bond is from the β-carbon of one ring system (enamine) to the α-carbon of the other (immonium ion). It was this consideration, along with the finding that one carbon α to nitrogen was fully substituted, which led us to consider the spiro structure **11** for the new alkaloid. Location of the ketonic carbon at C-14 follows from the finding that there are two hydrogens α to the carbonyl. Location of the carbonyl oxygen at C-11′ is ruled out since this structure would not explain the facile loss of carbon monoxide from the molecular ion in the mass spectrum of spirolucidine (**2**).

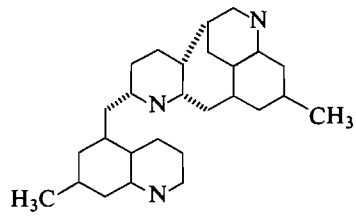

9

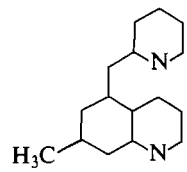

10

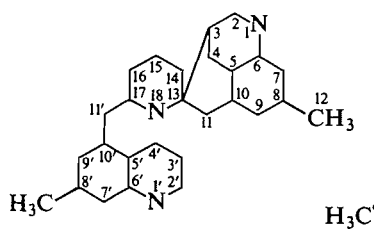

11

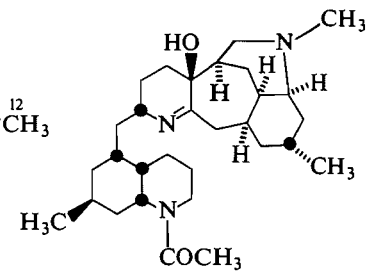

12

Attempts to bring about acid-catalyzed rearrangement of oxolucidine B (**12**) to the spiro ring system of spirolucidine were unsuccessful. The conditions investigated included treatment with aqueous sulfuric acid, aqueous hydrochloric acid, trifluoroacetic acid in tetrahydrofuran, and *p*-toluenesulfonic acid in refluxing benzene. Similarly, attempts to rearrange the spiro system of dihydrospirolucidine (**5**) by treatment with phosphorous oxychloride or by mesylation and solvolysis, led to the formation of many products, none of which appeared to have the lucidine skeleton.

Although spirolucidine and many of its derivatives could not be induced to crystallize, tetrahydrodesoxyspirolucidine (**7**), obtained by lithium aluminum hydride reduction, crystallizes nicely from ether–pentane to give colorless rhombic crystals, mp 149–152°C. In order to verify the structural hypothesis and to determine the stereochemistry of the alkaloid, an X-ray crystallographic study was carried out on tetrahydrodesoxyspirolucidine (**7**). A perspective drawing of the molecule is shown in Fig. 1. All of the six-membered rings are in a chair conformation. The major intermolecular contact (2.89 Å) is a hydrogen bond between the hydroxyl group of the molecule and the N-1′ of an adjacent molecule. The crystal packing of the molecule is illustrated in Fig. 2 which is a projection of the molecule down the $-a$-axis of the unit cell.

An unusual feature revealed by the X-ray crystal structure is the stereochemistry of the decahydroquinoline portion of the molecule. In lucidine B (**1**) and those compounds correlated with it (1), the *cis*-ring junction hydrogens (at C-5′ and C-6′) are *syn* to the methyl group located at C-8′, whereas in spirolucidine they are *anti* to the methyl. Another unexpected result is that the configuration at C-17 of spirolucidine is opposite to that in lucidine B.

Experimental

High resolution mass spectra were recorded on an A.E.I. MS-50 mass spectrometer coupled to a DS 50 computer. Unless diagnostically significant, only peaks greater than 20% of the base peak are

Can. J. Chem. Downloaded from www.nrcresearchpress.com by 210.87.254.105 on 09/06/12
For personal use only.

Can. J. Chem. Downloaded from www.nrcresearchpress.com by 210.87.254.105 on 09/06/12
For personal use only.

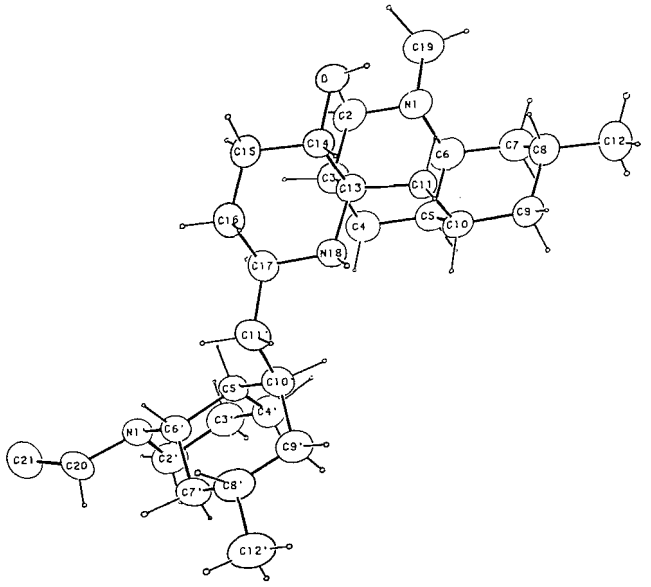

FIG. 1. Perspective drawing of tetrahydrodeoxyspirolucidine (11). For clarity, only one of the three partially-occupied positions of C-21 is illustrated.

reported. Infrared spectra were recorded on a Unicam SP 1000 or a Nicolet 7199 FT spectrometer. The nmr spectra were determined on a Varian HA-100 spectrometer (^{1}H nmr) interfaced to a Digilab FTS/NMR-3 data system and on a Bruker HFX-90 spectrometer (^{13}C nmr), with TMS as internal standard. Thin layer chromatography (tlc) was carried out on aluminum oxide GF_{254} (Type 60-E, E. Merck), aluminum oxide G (Type 60-E), or Woelm basic alumina for tlc, and the compounds were visualized using Dragendorff's reagent. Woelm neutral aluminum oxide (grade IV) or Woelm basic alumina (B-Super I, activity III) was used for column chromatography. Skellysolve B refers to Skelly Oil Company light petroleum, bp 62–70°C.

Isolation of spirolucidine

The "weak bases" of *L. lucidulum* (5.1 g) (2) were subjected to one-hundred funnel countercurrent distribution using chloroform (40 mL per tube) as the stationary phase and a saturated solution of potassium hydrogen tartrate (pH 3, 40 mL per tube) as the moving phase. Tubes 1–12 contained mainly three components (by tlc) and were combined (1.5 g). These very weak bases were chromatographed over alumina (150 g, activity IV). Elution with benzene gave luciduline (**3**, 0.06 g), benzene–ether (9:1) gave dihydrolycolucine (3.1 mg after further purification by preparative tlc), and benzene–ether (7:1) gave crude spirolucidine (0.28 g). This was further purified by column chromatography over basic alumina (activity I) and then preparative tlc to provide 88 mg of spirolucidine (**2**) as a viscous oil. Infrared ($CHCl_3$): 2790 (N—CH_3), 1710 (ketone), 1630 (amide) cm^{-1}; ^{1}H nmr ($CDCl_3$) δ: 0.82 (3H, d, J = 7 Hz), 0.89 (3H, d, J = 7 Hz), 2.03 (3H, s), 2.08 and 2.09 (3H, *N*-acetyl CH_3, two rotamers); ms *m/z*: 483 (M^+, 11%), 455 (100), 205 (99), 192 (69). *Mol. Wt.* calcd. for $C_{30}H_{49}N_3O_2$: 483.3825; found (hrms): 483.3828.

N-*Formylspirolucidine (4)*

Spirolucidine (**2**, 5.3 mg) was treated with acetic formic anhydride (1 mL) in CH_2Cl_2 (2 mL) at 0°C for 15 min, then at room temperature overnight. Methanol was added to decompose excess acetic formic anhydride and the reaction mixture was concentrated. The residue was dissolved in $CHCl_3$. The $CHCl_3$ extract was washed successively with 10% Na_2CO_3 solution, H_2O, and brine, then dried over anhydrous Na_2SO_4. The $CHCl_3$ extract was filtered and concentrated to give *N*-formylspirolucidine (**4**) (5.4 mg); ir ($CHCl_3$ cast): 2770, 1720, 1650 cm^{-1}; ^{1}H nmr ($CDCl_3$) δ: 0.82 (d, CH_3), 0.94 (d, CH_3), 2.03, 2.06 (s, NCH_3 and $NCOCH_3$), 8.68 (s, 1, N—CHO); ms *m/z*: 511 (M^+, 34), 483 (37), 192 (100).

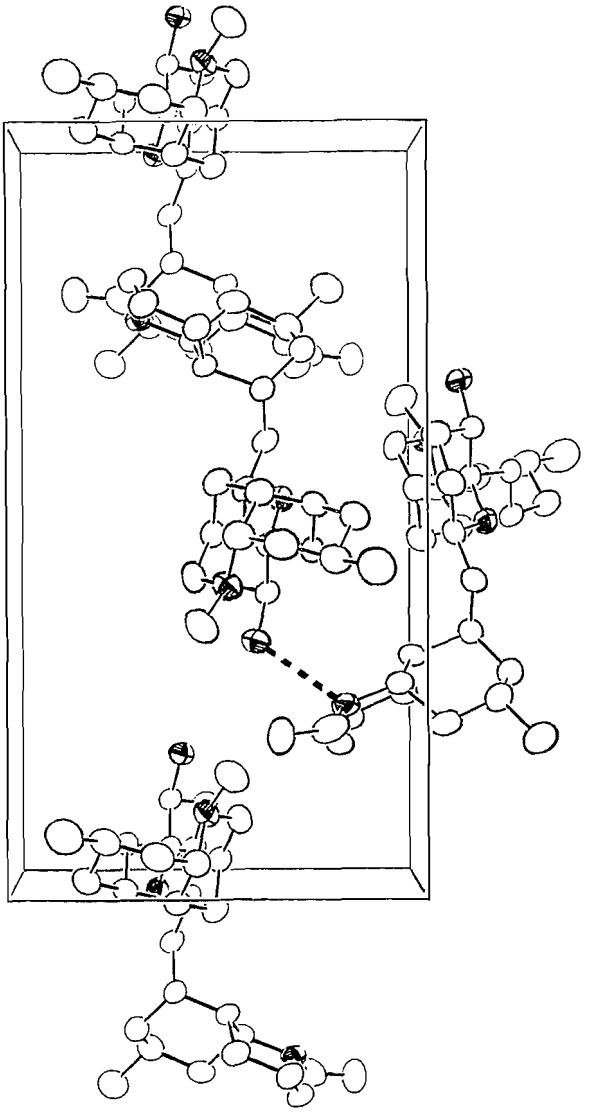

FIG. 2. Crystal packing diagram for tetrahydrodeoxyspirolucidine projected down the $-a$-axis of the unit cell. For clarity, only one of the three partially-occupied positions of C-21 is illustrated.

Dihydrospirolucidine (5)

Sodium borohydride (38 mg) was added to a stirred solution of spirolucidine (**2**, 28 mg) in methanol. The mixture was allowed to stir under a N_2 atmosphere overnight. The mixture was diluted with water and extracted with $CHCl_3$. The $CHCl_3$ extract was dried (anhydrous Na_2SO_4), filtered, and concentrated to give dihydrospirolucidine (**5**, 26 mg); ir ($CHCl_3$ cast): 3400 (br), 2780, 1620 cm^{-1}; ^{1}H nmr ($CDCl_3$) δ: 0.81 (d, J = 6 Hz, CH_3), 0.86 (d, J = 6 Hz, CH_3), 2.06, 2.08, 2.12 (s, N—CH_3 and N—$COCH_3$ rotamers); ms *m/z*: 485 (M^+, 23), 467 (6), 207 (100), 205 (47).

O-*Acetyldihydrospirolucidine (6)*

Dihydrospirolucidine (**5**, 3.3 mg) was treated with acetic anhydride (0.5 mL) in pyridine (1 mL) under a N_2 atmosphere at room temperature overnight. The reaction mixture was concentrated *in vacuo* by azeotropic distillation with toluene to give *O*-acetyldihydrospirolucidine (**6**, 3.5 mg); ir ($CHCl_3$ cast): 1720, 1620, 1250 cm^{-1}; ^{1}H nmr ($CDCl_3$) δ: 0.81 (d, J = 6 Hz, CH_3), 0.86 (d, J = 6 Hz, CH_3). 2.03, 2.04, 2.06, 2.07 (s, $OCOCH_3$, N—CH_3 and $NCOCH_3$ rotamers); ms *m/z*: 527 (M^+, 76), 467 (97), 333 (18), 319 (38), 273 (67), 259 (70), 205 (100).

Tetrahydrodeoxyspirolucidine (7)

Spirolucidine (**2**, 4.8 mg) in dry tetrahydrofuran was added to a

Can. J. Chem. Downloaded from www.nrcresearchpress.com by 210.87.254.105 on 09/06/12
For personal use only.

stirred solution of lithium aluminum hydride (48 mg) in dry tetrahydrofuran (8 mL) under a N_2 atmosphere. The reaction mixture was heated under reflux for 3 hours, cooled, and excess lithium aluminum hydride destroyed by cautious addition of dry ethyl acetate, then water. The reaction mixture was filtered and extracted with $CHCl_3$. The $CHCl_3$ extract was dried (anhydrous Na_2SO_4) and concentrated to give tetrahydrodeoxyspirolucidine (**7**, 4.6 mg) which was crystallized from ether–pentane, mp 149–152°C; ir ($CHCl_3$ cast): 3370 cm^{-1}; ^1H nmr ($CDCl_3$) δ: 0.85 (d, J = 6 Hz, CH_3), 0.89 (d, J = 6 Hz, CH_3), 1.10 (t, J = 7 Hz, NCH_2CH_3), 2.08 (s, NCH_3); ms m/z: 513 (M^+, 36), 453 (23), 178 (100).

Dihydrodeoxyspirolucidine (8)

Tetrahydrodeoxyspirolucidine (**7**, 3.2 mg) in acetone (3 mL) was treated with Jones' reagent (0.5 mL) under a N_2 atmosphere at room temperature for 30 min. Isopropyl alcohol was added to decompose unreacted oxidizer. The reaction mixture was filtered and concentrated. Purification by preparative tlc over alumina (ether–methanol, 98:2) gave dihydrodeoxyspirolucidine (**8**, 3.1 mg); ir ($CHCl_3$ cast): 1700 cm^{-1}; ^1H nmr ($CDCl_3$) δ: 0.82 (d, J = 6 Hz, CH_3), 0.91 (d, J = 6 Hz, CH_3), 1.14 (t, J = 7 Hz, NCH_2CH_3), 2.03 (s, NCH_3); ^{13}C nmr ($CDCl_3$) δ: 213.6 (s, C=O); ms m/z: 469 (M^+, 18), 441 (77), 205 (86), 192 (86), 180 (55), 178 (100).

Deuterium exchange on 8

To a stirred solution of sodium deuteriomethoxide (prepared from Na (80 mg) and CH_3OD (0.5 mL)) was added a solution of dihydrodeoxyspirolucidine (**8**, 6.5 mg) in CH_3OD (0.5 mL) at room temperature under a N_2 atmosphere. D_2O (0.25 mL) was added and the reaction mixture was allowed to stir for 2 h. Further D_2O was added and the reaction mixture was extracted with $CDCl_3$ (total 15 mL). The organic extract was washed with D_2O (5 mL), H_2O (5 mL), dried (anhydrous Na_2SO_4), and concentrated to give a residue which was analyzed (ms) directly without further purification.

Single crystal X-ray diffraction analysis of tetrahydrodeoxyspirolucidine

Tetrahydrodeoxyspirolucidine crystallized as {110} rhombic prisms and the crystal data were the following.

$C_{30}H_{53}N_3O$ mw = 471.8

$P2_12_12_1$, a = 14.482(1) Å, b = 19.434(1) Å, c = 10.507(1) Å, V = 2957.1 Å^3, Z = 4, ρ_c = 1.06 gm cm^{-3}, $F(000)$ = 1048e, radiation Ni-filtered Cu K_α λ = 1.5418 Å, $2\theta_{max}$ = 140°, crystal dimensions (mm) 0.24 × 0.40 × 0.38, max. decay correction 1.05, temp. = 14°C.

A single crystal was mounted about the c-axis on an Enraf–Nonius CAD4F diffractometer and data were collected with an $\omega/2\theta$ scan. A total of 2177 reflections (of 3075 total) had net $I > 3\sigma(I)$ and these reflections were used in the analysis. The data were corrected for Lorentz and polarization effects. Observational weights (7) for the reflections were derived from the formula:

$$W = (2I)^2/|F_o|^2(T + (0.02I)^2 + r^2B)$$

where I is the net intensity, F_o is the observed structure amplitude, T is the total peak count, B is the sum of the background counts, and r is the ratio of the peak-scan time to the total background-counting time (r = 2 for these data).

An initial model of the structure was chosen from the E map of the MULTAN 80 (8) trial solution which had the lowest R_{Karle} (9) value, 0.182, but this model resisted least-squares refinement. Subsequently, the trial solution which had the second lowest R_{Karle} value, 0.195, was shown to be correct. The E map of this latter solution contained a fused tricyclic fragment of fourteen atoms which refined by least-squares methods. Subsequent difference maps and least-squares refinement led to the location of all of the nonhydrogen atoms of the molecule. The terminal carbon atom (C-21) of the ethyl group bonded to N-1′ is disordered in the crystal structure, and three statistically occupied positions were assigned to this atom with occupancies of 0.4, 0.4, and 0.2 based on peak heights from difference maps. All of the hydrogen atoms of the molecule were found except for those on C-21 and also for one hydrogen on C-20. Block diagonal least-squares refinement of the atomic parameters (anisotropic temperature factors for the nonhydrogens and isotropic for the hydrogens) converged to a final R index ($R = (\sum_{hkl} |F_o| - |F_c|)/\sum_{hkl} |F_o|$) of 0.047 and R_w = 0.049 ($R_w = (\Sigma W\Delta^2/\Sigma W|F_o|^2)^{1/2}$). Crystallographic computations were carried out using the XRAY 76 System (10) on the DEC 2060 computer at the University of Saskatchewan. The nonhydrogen atom coordinates are given in Table 1.[3]

TABLE 1. Tetrahydrodeoxyspirolucidine nonhydrogen atom coordinates

Atom	x/a	y/b	z/c	U_{eq} (Å^2)
N(1)	0.5455(2)	0.4037(1)	−0.0259(3)	0.065
C(2)	0.4640(3)	0.4147(2)	0.0548(3)	0.069
C(3)	0.3984(2)	0.4705(2)	0.0072(3)	0.061
C(4)	0.4532(3)	0.5371(2)	−0.0045(4)	0.068
C(5)	0.5296(3)	0.5236(2)	−0.1005(4)	0.066
C(6)	0.5952(3)	0.4682(2)	−0.0515(4)	0.071
C(7)	0.6727(3)	0.4570(2)	−0.1485(4)	0.083
C(8)	0.6352(3)	0.4379(2)	−0.2789(4)	0.075
C(9)	0.5672(3)	0.4921(2)	−0.3259(3)	0.071
C(10)	0.4899(3)	0.5075(2)	−0.2313(3)	0.058
C(11)	0.4189(2)	0.4489(2)	−0.2271(3)	0.052
C(12)	0.7141(3)	0.4284(2)	−0.3746(5)	0.110
C(13)	0.3478(2)	0.4560(2)	−0.1205(3)	0.053
C(14)	0.2835(3)	0.3928(2)	−0.1199(3)	0.058
C(15)	0.2019(3)	0.4014(2)	−0.0300(3)	0.065
C(16)	0.1477(2)	0.4654(2)	−0.0628(3)	0.067
C(17)	0.2095(2)	0.5289(2)	−0.0707(3)	0.057
N(18)	0.2886(2)	0.5156(1)	−0.1536(2)	0.057
C(19)	0.6045(3)	0.3529(2)	0.0365(4)	0.096
O	0.3287(2)	0.3297(1)	−0.0911(2)	0.066
N(1′)	0.1251(2)	0.7532(1)	0.1898(3)	0.064
C(2′)	0.1987(3)	0.8036(2)	0.2047(3)	0.078
C(3′)	0.2924(2)	0.7703(2)	0.1768(4)	0.078
C(4′)	0.2951(2)	0.7393(2)	0.0448(3)	0.066
C(5′)	0.2127(2)	0.6904(1)	0.0260(3)	0.051
C(6′)	0.1196(2)	0.7251(2)	0.0582(3)	0.058
C(7′)	0.0893(2)	0.7764(2)	−0.0441(4)	0.068
C(8′)	0.0848(3)	0.7437(2)	−0.1749(4)	0.076
C(9′)	0.1791(3)	0.7125(2)	−0.2088(3)	0.072
C(10′)	0.2124(3)	0.6598(2)	−0.1103(3)	0.060
C(11′)	0.1582(2)	0.5921(2)	−0.1175(3)	0.062
C(12′)	0.0533(3)	0.7956(2)	−0.2741(5)	0.103
C(20)	0.0342(4)	0.7817(3)	0.2304(6)	0.112
C(21)*	0.003(2)	0.792(3)	0.349(4)	0.100
C(22)*	−0.033(1)	0.743(1)	0.254(1)	0.074
C(23)*	0.032(3)	0.792(5)	0.372(8)	0.082

$U_{eq} = (U_{11} + U_{22} + U_{33})/3$

*These represent the three disordered positions of C(21) with populations of 0.4, 0.4, and 0.2, respectively.

Acknowledgements

We thank the Natural Sciences and Engineering Research Council of Canada for the financial support, Prof. D. B. MacLean for a generous gift of crude weak bases of *L. lucidulum*, and Mr. R. St. Pierre for growing the large crystal of tetrahydrodeoxyspirolucidine.

[3]Tables of atomic parameters, bond lengths and angles, and structure factors are available, at a nominal charge, from the Depository of Unpublished Data, CISTI, National Research Council of Canada, Ottawa, Ont., Canada K1A 0S2.

1. W. A. AYER, L. M. BROWNE, Y. NAKAHARA, M. TORI, and L. T. J. DELBAERE. Can. J. Chem. **57**, 1105 (1979).
2. W. A. AYER, N. MASAKI, and D. S. NKUNIKA. Can. J. Chem. **46**, 3631 (1968).
3. L. F. BALL. Ph.D. Thesis, University of Alberta, Edmonton, Alberta. 1971.
4. Y. INUBUSHI, T. IBUKA, T. HARAYAMA, and H. ISHII. Tetrahedron, **24**, 3541 (1968).
5. A. LENIEWSKI, J. SZYCHOWSKI, and D. B. MACLEAN. Can. J. Chem. **59**, 2479 (1981).
6. L. NYEMBO, A. GOFFIN, C. HOOTELÉ, and J.-C. BRAEKMAN. Can. J. Chem. **56**, 851 (1978).
7. F. R. AHMED, S. R. HALL, M. E. PIPPY, and C. P. HUBER. N.R.C. Crystallographic Programs for the IBM/360 System. Accession Nos. 133–147 in J. Appl. Crystallogr. **6**, 309 (1973).
8. P. MAIN, S. J. FISKE, S. E. HULL, L. LESSINGER, G. GERMAIN, J.-P. DECLERCQ, and M. M. WOOLFSON. MULTAN 80. A system of computer programs for the automatic solution of crystal structures from X-ray diffraction data. University of York, England. 1980.
9. J. KARLE and I. L. KARLE. Acta Crystallogr. **21**, 849 (1966).
10. J. M. STEWART. The X-ray system of crystallographic computer programs. Computer Science Center, University of Maryland, College Park, MD. 1976.
11. C. K. JOHNSON. ORTEP-II. Report ORNL-5138. Oak Ridge National Laboratory, Oak Ridge, TN, U.S.A. 1976.

Can. J. Chem. Downloaded from www.nrcresearchpress.com by 210.87.254.105 on 09/06/12
For personal use only.

Transference numbers and solvation studies in *n*-butanol

J. S. BANAIT, K. S. SIDHU, and J. S. WALIA
Department of Chemistry, Punjabi University, Patiala-147002, India

Received March 11, 1983

J. S. BANAIT, K. S. SIDHU, and J. S. WALIA. Can. J. Chem. **62**, 303 (1984).

Transference numbers of tetrabutylammonium bromide have been measured in *n*-butanol at 25°C in the concentration range 5.79−12.86 × 10^{-2} mol dm^{-3}. The variation of transference number with concentration is negligible. The limiting transference number of tetrabutylammonium ion has been determined by the Longsworth method. Combining the limiting transference number and limiting equivalent conductance of this salt, limiting ionic conductances of tetrabutylammonium and bromide ions have been found to be 8.05 and 8.02 ohm^{-1} cm^2 mol^{-1}, respectively. From these values limiting ionic conductances of other univalent ions, effective ionic radii and solvation numbers have been computed. The solvation numbers of anions have been found to be more than those of cations which shows the protic nature of this solvent.

J. S. BANAIT, K. S. SIDHU et J. S. WALIA. Can. J. Chem. **62**, 303 (1984).

On a mesuré les facteurs de transport de bromure de tétrabutylammonium dans le *n*-butanol à 25°C dans l'intervalle de concentration allant de 5,79 à 12,86 × 10^{-2} mol dm^{-3}. La variation du facteur de transfert en fonction de la concentration est négligeable. On a déterminé le facteur de transfert limite de l'ion tétrabutylammonium selon la méthode de Longsworth. En combinant le facteur de transfert limite et la conductivité équivalente limite de ce sel, on a trouvé que les conductances limites des ions tétrabutylammonium et bromures sont respectivement de 8,05 et de 8,02 ohm^{-1} cm^2 mol^{-1}. On a calculé, a partir de ces valeurs les conductances ioniques limites des autres ions univalents, les rayons ioniques effectifs et les facteurs de solvation. On a trouvé que le facteur de solvation des anions est plus élevé que ceux des cations; ceci montre la nature protique de ce solvant.

[Traduit par le journal]

Can. J. Chem. Downloaded from www.nrcresearchpress.com by 210.87.254.42 on 09/06/12
For personal use only.

Introduction

Conductances of some alkyl substituted ammonium and alkali metal salts (1−3) in *n*-butanol have been reported. Due to the lack of transference number data, approximate limiting equivalent ionic conductances of various ions in this solvent have been computed on the basis of the Walden product of large ions and Kohlrausch's law of independent ion migration. However, this approximation has not been found satisfactory in many solvents (4−6). In order to evaluate limiting equivalent ionic conductances accurately, transference numbers of tetrabutylammonium bromide have been measured in *n*-butanol at 25°C using a modified Hittorf method. Effective ionic radii in solution and solvation numbers of ions have been calculated to throw light on ion−solvent interactions in this solvent.

Experimental

n-Butanol (BDH, Analar) was purified as described by Evans and Gardam (1). Freshly distilled solvent was used for each experiment and the physical constants (density, 0.80576 g mL^{-1}; viscosity, 2.589 cP; and specific conductance, $<2 \times 10^{-7}$ ohm^{-1} cm^{-1}) were checked before use.

Tetrabutylammonium bromide (Riedal pure) was crystallized from conductivity water and dried at 100°C in vacuum.

Transference numbers have been determined by Hittorf method. The apparatus and procedure were essentially the same as those reported by Paul *et al.* (7). The instruments have been calibrated and the precision of the results has been checked by determining the transference number of potassium chloride in water. A current of 0.5 to 2.0 mA was employed in various experiments. Transference numbers of anion have been determined by direct measurements and those of cation were put equal to $1 - t_-$.

In order to determine the concentration of the solutions after electrolysis, the solutions were analysed for bromide ions using Volhard's method (8).

Results and discussion

In view of the high resistance offered by the cell and the analytical difficulties, the measurements of transference numbers in *n*-butanol at 25°C have been carried out in a moderately high concentration range (5.79 −12.86 × 10^{-2} mol dm^{-3}). The results are given in Table 1. The cation transference numbers increase with an increase in concentration. However, the variation is very small. Variation of transference numbers with concentration can be written as (9):

TABLE 1. Transference numbers of tetrabutylammonium bromide in *n*-butanol at 25°C

Concentration (mol dm^{-3})	t_+	t_-
0.0000	0.5010	0.4990
0.0579	0.5015	0.4985
0.0866	0.5016	0.4984
0.1188	0.5018	0.4982
0.1286	0.5022	0.4978

$$[1] \quad \left(\frac{dt_\pm}{d\sqrt{C}}\right)_{C\to 0} = \frac{(t_\pm^0 - 0.5)\beta}{\Lambda_0}$$

where β is the electrophoretic parameter and all other symbols have their usual meanings.

It is clear from eq. [1] that the transference numbers of the ions increase with increasing concentration if they are more than 0.5 and decrease with increasing concentration if they are less than 0.5. It further shows that the closer the transference number of the ions are to 0.5, the less will be their variations with concentration. These conclusions have been verified by transference number measurements in various solvents (10−12). In the present study, the transference numbers of the ions are quite close to 0.5 and the variations with concentration are also negligible.

The limiting transference number ($t_\pm^0$) of tetrabutylammonium ion has been determined by using the Longsworth equation (13).

$$[2] \quad t_+^{0\prime} = \frac{t_+\Lambda' + (1/2)\beta C^{1/2}}{\Lambda' + \beta C^{1/2}} = t_+^0 + \beta' C$$

All the symbols have their usual meanings (13). While calcu-

Can. J. Chem. Downloaded from www.nrcresearchpress.com by 210.87.254.42 on 09/06/12
For personal use only.

lating Λ' and $t_+^{0\prime}$ at different concentrations, C has been replaced by αC (α being the degree of dissociation) because of ion-association of tetrabutylammonium bromide. The value of α has been computed with the help of association constant of this salt ($K_A = 860$) in *n*-butanol. The plot of $t_+^{0\prime}$ versus C is linear and its extrapolation given a value of 0.5007.

Limiting ionic conductances ($\lambda_\pm^0$) of tetrabutylammonium and bromide ions have been determined by combining (14) the limiting transference numbers ($t_\pm^0$) of these ions with the limiting equivalent conductance (Λ_0) of tetrabutylammonium bromide (1). The limiting ionic conductances of tetrabutylammonium and bromide ions have been found to be 8.05 and 8.02 ohm^{-1} cm^2 mol^{-1} respectively. Evans and Gardam (1) have reported conductance studies of various uni-univalent electrolytes in *n*-butanol at 25°C. They have computed the limiting ionic conductances on the basis of the Walden product of tetraalkylammonium salts. The present values of limiting ionic conductances differ by 0.21 ohm^{-1} cm^2 mol^{-1} from those reported by Evans and Gardam. Limiting ionic conductances obtained by transference number methods and the approximate methods such as Walden product method, equal division of the limiting equivalent conductances of the reference electrolyte etc., have been found to differ by up to 0.5 ohm^{-1} cm^2 mol^{-1} in other solvents also (4, 5, 15). However, the values obtained by transference number method are considered more accurate. This is because the molecules of different solvents have different modes of interactions with the ions. Thus a single approximation cannot be generalised for all the solvents.

The limiting ionic conductance of various ions has been computed from the conductance data (1–3, 16) and the limiting ionic conductance of tetrabutylammonium and bromide ions (present work) using Kohlrausch's law of independent ion migration. A few ions are arranged in the order of decreasing ionic conductances in *n*-butanol.

$$Et_4N^+ > Me_4N^+ > Pr_4N^+ > Li^+ > Bu_4N^+ > (i\text{-}Am)_3BuN^+\ ClO_4^- > I^- > Br^- > Cl^-$$

The limiting ionic conductances of tetraalkylammonium ions (except that of tetramethylammonium ion) decrease with the increase in the size of the ions. This is in accordance with the findings in other solvents. These ions remain unsolvated because of their large size. However, tetramethylammonium ion, being smallest in the series, seems to be slightly solvated as its conductance does not fit into the pattern. In some other solvents also, this ion has been found to be solvated (4, 17).

Solvated radii, corrected solvated radii in solution, and the solvation numbers of various ions have been determined by the method reported by Paul *et al.* (18). All the relevant data are given in Table 2.

Perusal of Table 2 reveals that the solvation number of anions decreases with an increasing anion size, this is in accord with the findings in various solvents (4, 14, 18, 19). Chloride and bromide ions are more solvated in this solvent than lithium ion though the crystallographic radii of these ions are more than three times that of lithium ion, which shows that the anions are heavily solvated in this solvent. This is due to the superimposition of hydrogen bonding on anion–dipole interactions whereas cations are solvated due to the cation–dipole interaction only.

According to Parker's (20) classification of solvents, protic solvents solvate the anions more whereas in aprotic solvents, solvation of anions is very small. Comparison of solvation numbers of anions in *n*-butanol with those in other protic solvents shows that except in lower alcohols, the solvation numbers of anions in *n*-butanol are higher than those in most of the solvents (21).

TABLE 2. Limiting ionic conductance ($\lambda_\pm^0$), crystallographic (r_c)*, solvated (r_s), and corrected (r_{corr}) radii, and solvation numbers (N) of various univalent ions in *n*-butanol at 25°C

Ion	$\lambda_\pm^0$ (ohm^{-1} cm^2 mol^{-1})	r_c (Å)*	r_s (Å)	r_{corr} (Å)	N
Li^+	8.38	0.60	4.60	4.80	3.08
NH_4^+	6.96	1.44	5.54	5.52	4.53
Me_4N^+	10.00	3.47	3.86	4.20	0.89
Et_4N^+	10.60	4.00	3.62	—	—
Pr_4N^+	9.03	4.52	4.27	—	—
Bu_4N^+	8.05	4.94	4.79	—	—
$(i\text{-}Am)_3BuN^+$	7.98	—	4.83	—	—
$Hept_4N^+$	6.66	5.88	5.88	—	—
Cl^-	7.41	1.81	5.22	5.27	3.85
Br^-	8.02	1.95	4.82	4.97	3.11
T^-	9.01	2.16	4.29	4.55	2.28
ClO_4^-	10.90	2.40	3.52	3.95	1.31

*Reference 22.

Higher solvation numbers of anions in alcohols than in other protic solvents like formamide, *N*-methylformamide, and *N*-methylacetamide can be explained on the basis of the structure of these solvent molecules:

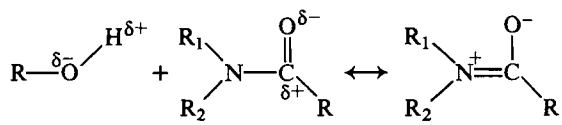

The approach of the anions to the positive end of the solvent molecules is easier in alcohols and seems to be sterically hindered in other solvents.

Solvation numbers of alkali metal, ammonium, and silver ions decrease with the increase in the size of these ions in most of the solvents. However, in *n*-butanol lithium ions are less solvated than ammonium ions (Table 2). In tetramethyl urea (4) and *N*,*N*-dimethyl acetamide (15), sodium ions have been found to be less solvated than potassium ions. Barker and Caruse (17) have attributed this to the fact that smaller ions are comparatively less solvated in these solvents because of the large size of the solvent molecules. In *n*-butanol less solvation of lithium ions can also be explained on the basis of similar steric factors.

1. D. F. EVANS and P. GARDAM. J. Phys. Chem. **73**, 158 (1969).
2. H. V. VENKATASETTY and G. M. BROWN. J. Phys. Chem. **66**, 2075 (1962).
3. H. V. VENKATASETTY and G. M. BROWN. J. Phys. Chem. **67**, 954 (1963).
4. R. C. PAUL, S. P. JOHR, J. S. BANAIT, and S. P. NARULA. J. Phys. Chem. **80**, 351 (1976).
5. M. DELLA MONICA, D. MASCIOPINTO, and G. TERSARD. Trans. Faraday Soc. **66**, 2872 (1970).
6. R. GOPAL and J. S. JHA. J. Phys. Chem. **78**, 2405 (1974).
7. R. C. PAUL, J. P. SINGLA, and S. P. NARULA. J. Phys. Chem. **73**, 741 (1969).
8. A. I. VOGAL. A textbook of quantitative inorganic analysis including elementary instrumental analysis. 3rd ed. Longmans, London. 1961. p. 267.

9. M. SPIRO. Physical chemistry of organic solvent systems. *Edited by* A. K. Covington and T. Dickinson. Plenum Press, London, New York 1973. p. 621.
10. J. A. DAVIES, R. L. KAY and A. R. GORDON. J. Chem. Phys. **19**, 749 (1957).
11. L. W. SHEMILT, J. A. DAVIES, and A. R. GORDON. J. Chem. Phys. **16**, 340 (1948).
12. M. CARMO SANTOS and M. SPIRO. J. Phys. Chem. **76**, 712 (1972).
13. L. G. LONGSWORTH. J. Am. Chem. Soc. **54**, 2741 (1972).
14. R. A. ROBINSON and R. H. STOKES. Electrolyte solutions. Butterworths Scientific Publishing Co. Ltd. 1959.
15. R. C. PAUL, J. S. BANAIT, and S. P. NARULA. Aust. J. Chem. **28**, 321 (1975).
16. T. SHEDLOWSKY. J. Am. Chem. Soc. **54**, 1405 (1932).
17. B. J. BARKER and J. A. CARUSE. J. Am. Chem. Soc. **93**, 1341 (1971).
18. R. C. PAUL, J. S. BANAIT, and S. P. NARULA. Z. Phys. Chem. Frankfurt am Main, **94**, 199 (1975).
19. R. L. KAY and J. L. DYE. Proc. Natl. Acad. Sci. U.S. **49**, 5 (1963).
20. A. J. PARKER. Q. Rev. **16**, 183 (1962).
21. R. GOPAL and M. M. HUSSAIN. J. Ind. Chem. Soc. **40**, 981 (1963).
22. L. PAULING. The nature of the chemical bond. 2nd ed. Cornell University Press, Ithaca, 1940. pp. 346, 350; J. F. COETZE and G. P. CUNNINGHAM. J. Am. Chem. Soc. **27**, 2569 (1965).

Can. J. Chem. Downloaded from www.nrcresearchpress.com by 210.87.254.42 on 09/06/12
For personal use only.

Synthesis of phthalideisoquinolines by direct coupling of phthalide anions with 3,4-dihydroisoquinolinium salts

RICHARD MARSDEN and DAVID B. MACLEAN[1]

Department of Chemistry, McMaster University, Hamilton, Ont., Canada L8S 4M1

Received July 19, 1983

RICHARD MARSDEN and DAVID B. MACLEAN. Can. J. Chem. **62**, 306 (1984).

The condensation of phthalide anions, derived from phthalide itself and from its 6,7- and 5,6-dimethoxy derivatives, with 6,7-dimethoxy-2-methyl-3,4-dihydroisoquinoline is described. The reaction products obtained in ca. 40% yield are easily separable mixtures of substituted (±)-*erythro* and (±)-*threo*-phthalidetetrahydroisoquinolines. The reaction is potentially useful for synthesis of naturally occurring akaloids of this family.

RICHARD MARSDEN et DAVID B. MACLEAN. Can. J. Chem. **62**, 306 (1984).

On décrit la condensation des anions phtalides, provenant du phtalide lui-même et de ses dérivés diméthoxy-6,7 et diméthoxy-5,6 sur la diméthoxy-6,7 méthyl-2 dihydro-3,4 isoquinoléine. Les produits de la réaction obtenus avec un rendement d'environ de 40% sont des mélanges facilement séparables de (±) *érythro* et de (±) *thréo* phtalidetétrahydroisoquinoléines substituées. La réaction est potentiellement utile pour la synthèse des alcaloïdes naturels de cette famille.

[Traduit par le journal]

Perkin and Robinson (1) reported in 1911 the first successful synthesis of a phthalideisoquinoline alkaloid, although in low yield, by treating cotarnine with meconin in boiling alcohol. Many synthetic approaches to these alkaloids have appeared in the intervening years, which are summarized in several reviews (2–6) and in a recent paper (7). Several reports describing new and efficient syntheses of these alkaloids based on the Perkin–Robinson approach have recently appeared. In 1979 a preliminary account appeared of the reaction between 3-halophthalides and 2-methyl-3,4-dihydroisoquinolinium salts in the presence of Zn metal or Zn–Cu couple (8) and a full account of this reaction was published in 1981 (7). The validity of this approach to phthalideisoquinoline alkaloid synthesis has recently been confirmed by Shono *et al.* (9) who carried out the same reaction in a different solvent system. The electrochemical coupling of bromophthalides and 3,4-dihydroisoquinolinium salts has also been reported (10). In another approach Prager *et al.* (11) have shown that 2-methylisoquinolinium salts condense with phthalides in the presence of sodium methoxide yielding adducts that may be reduced catalytically with hydrogen or with sodium cyanoborohydride to the 2-methylphthalidetetrahydroisoquinoline system present in the naturally occurring alkaloids. Prager *et al.* (11) noted that they were unable to carry out a similar addition to 3,4-dihydroisoquinolinium salts. In this laboratory we had encountered similar difficulties in the past. Now, however, by preparation of the phthalide anions at low temperature using LDA, we are able to report the direct coupling of phthalide anions with 3,4-dihydroisoquinolinium salts.

Phthalide anions have been prepared and used successfully by Broom and Sammes (12) as Michael donors. Sammes' group has also shown that they add to acyclic imines forming isoquinolones (13) and we have shown that they add to 3,4-dihydroisoquinolines (cyclic imines), forming in one step the berberine ring system (14). Their addition to iminium salts, derived from 3,4-dihydroisoquinolines, is described here.

The overall reaction is outlined in Scheme 1. The anion, prepared by treatment of the phthalide with LDA, was added to a slurry of the iminium salt in THF, both operations being conducted at low temperature. The reaction mixture was al-

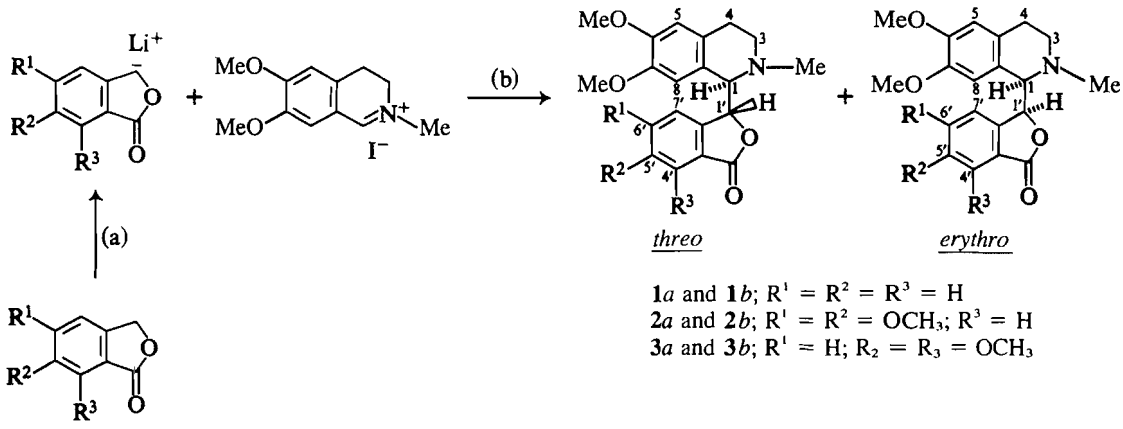

(a) LDA, THF, −70°C
(b) THF, −70°C, then at room temperature

SCHEME 1

[1]Author to whom correspondence may be addressed.

Can. J. Chem. Downloaded from www.nrcresearchpress.com by 210.87.254.5 on 09/06/12
For personal use only.

Can. J. Chem. Downloaded from www.nrcresearchpress.com by 210.87.254.5 on 09/06/12
For personal use only.

lowed to warm to room temperature and was worked up in the conventional manner, yielding the expected mixture of racemates in approximately equal amount and in an overall yield of approximately 40%. Attempts to improve the yield by variation of the reaction conditions were unsuccessful. Exchange of Li for Zn by treating the solution of Li phthalide with anhydrous $ZnCl_2$ before addition to the iminium salt did not improve the yield. Apparently deprotonation of the iminium salt competes with addition across the carbon–nitrogen double bond.

The racemic compounds prepared in this study have all been reported previously. Compounds **1***a* and **1***b* have recently been described by de Silva *et al.* (15), while the isocordrastines **2***a* and **2***b* (7, 16) and the cordrastines **3***a* (cordrastine I) and **3***b* (cordrastine II) (17–19) have been synthesized and examined by several groups. The structures of compounds **1**–**3** have been established by comparison of their properties with published data in the case of **1***a* and **1***b* or by direct comparison with samples previously prepared in this laboratory in the case of **2***a*, **2***b*, **3***a*, and **3***b*.

Through appropriate choice of substituted phthalide (now readily prepared by recently developed aromatic lithiation reactions (20–22)) and substituted 3,4-dihydroisoquinoline, this method should be applicable to the preparation of many of the naturally occurring alkaloids of this group (23).

Experimental

Apparatus, materials, and methods

The continuous wave ^{1}H nmr spectra were run on a Varian EM 390 spectrometer. Unless otherwise specified, the samples were dissolved in $CDCl_3$ using tetramethylsilane (TMS) as the internal standard. Chemical shifts, quoted as δ values, were measured in relation to TMS. The symbols s, singlet, d, doublet, q, quartet, and m, multiplet are used in reporting spectra.

Infrared spectra were recorded on a Perkin–Elmer 283 spectrometer in chloroform solution. Melting points were determined using a Gallenkamp apparatus and are uncorrected.

Thin layer chromatography (tlc) was performed using Polygram Sil G/UV_{254} plates. Preparative layer chromatography (plc) was performed using Silica Gel PF-254. Flash column chromatography was employed as described in the literature (24).

Diisopropylamine was refluxed over calcium hydride and distilled onto molecular sieves (4 Å). THF was dried by distillation from Na/benzophenone under a nitrogen atmosphere just prior to use. All the reactions described were carried out under a blanket of argon, using syringes and septa for transfer of reagents.

The following compounds were prepared by standard methods and gave satisfactory physical data: meconin (22), *m*-meconin (25), 6,7-dimethoxy-2-methyl-3,4-dihydroisoquinolinium iodide (26).

*6,7-Dimethoxy-2-methyl-1-phthalidyl-1,2,3,4-tetrahydroisoquinolines, 1*a *and 1*b

To a stirred solution of diisopropylamine (0.42 mL, 3 mmol) in dry THF (5 mL) at −10°C was added n-BuLi (2 mL of a 1.65 *M* solution in hexane, 3.3 mmol). After 5 min the LDA solution was cooled to −70°C (Dry Ice/acetone bath) and treated dropwise with a solution of phthalide (0.402 g, 3 mmol) in dry THF, producing initially an orange solution. Towards the end of the addition a suspension was observed; homogeneity was restored by adjusting the temperature to −35°C. After stirring at −35°C for 20 min the solution was added to a suspension of 6,7-dimethoxy-2-methyl-3,4-dihydroisoquinolinium iodide (1 g, 3 mmol) in dry THF at −35°C. Treatment and work up as for **2***a* and **2***b* below yielded a yellow oil which was subjected to flash chromatography (silica gel, applying the oil to the column in EtOAc/CH_2Cl_2, 1:1, then eluting with EtOAc) to give the following two components.

(a) *threo* Isomer **1***a*, 195 mg (19.2%), R_f 0.73 (silica gel, EtOAc), mp 165–167°C (from EtOH) (lit. (9) mp 163–164°C, (15) mp 168–170°C); ir ($CHCl_3$) ν_{max}: 1760 cm^{-1} (γ-lactone); ^{1}H nmr δ: 2.1–3.4 (4H, m, C-3 and C-4 H's), 2.66 (3H, s, —NCH_3), 3.69 (3H, s, —OCH_3), 3.78 (3H, s, —OCH_3), 4.14 (1H, d, J = 4 Hz, C-1 H), 5.72 (1H, d, J = 4 Hz, C-1′ H), 6.33 (1H, s, C-8H), 6.69 (1H, s, C-5H), 7.2–7.9 (4H, m, C-4′, 5′, 6′ and 7′ H's).

(b) *erythro* Isomer **1***b*, 215 mg (21.1%), R_f 0.34 (silica gel, EtOAc), oil; ir ($CHCl_3$) ν_{max}: 1760 cm^{-1} (γ-lactone); ^{1}H nmr δ: 2.2–2.3 (4H, m, C-3 and C-4 H's), 2.58 (3H, s, —NCH_3), 3.60 (3H, s, —OCH_3), 3.85 (3H, s, —OCH_3), 4.11 (1H, d, J = 4 Hz, C-1 H), 5.72 (1H, d, J = 4 Hz, C-1′ H), 6.25 (1H, s, C-8 H), 6.62 (1H, s, C-5 H), 6.95–7.1 and 7.4–7.9 (4H, m, C-4′, 5′, 6 and 7′ H's). The picrate of **1***b* was obtained as a yellow crystalline powder, mp 209–211°C (from MeOH) (lit. (9, 15) mp 208–210°C).

Isocordrastines **2**a *and* **2**b

An LDA (3 mmol) solution, prepared as described above, was treated dropwise with a solution of *m*-meconin (0.582 g, 3 mmol) in dry THF. The resulting clear orange solution was stirred for 20 min at −70°C and added dropwise to a suspension of 6,7-dimethoxy-2-methyl-3,4-dihydroisoquinolinium iodide (1 g, 3 mmol) in dry THF at −70°C. The mixture was kept at this temperature for 20 min, then allowed to warm to room temperature and stirred overnight. The THF was evaporated, 10% HCl (40 mL) added, and the aqueous phase extracted with CH_2Cl_2. The organic extracts were discarded and the acidic aqueous layer neutralized (to pH 7–9) with aqueous NaOH. Extraction with CH_2Cl_2, drying (Na_2SO_4), and evaporation of the solvent gave a yellow oil which was subjected to flash chromatography (silica gel, initial eluant EtOAc to obtain the faster running isomer, then EtOAc + 10% MeOH to recover the slower running isomer), yielding the following two components.

(a) *threo*-Isocordrastine **2***a*, 290 mg (24.2%), R_f 0.4 (silica gel, EtOAc), mp 146–148°C (from EtOH) (lit. (16, 27), mp 115–117°C, (7) mp 144–146°C; ir ($CHCl_3$) ν_{max}: 1755 cm^{-1} (γ-lactone); ^{1}H nmr δ: 2.3–3.3 (4H, m, C-3 and C-4 H's) 2.70 (3H, s, —NCH_3), 3.72 (3H, s, —OCH_3), 3.79 (3H, s, —OCH_3), 3.83 (3H, s, —OCH_3), 3.94 (3H, s, —OCH_3), 4.11 (1H, d, J = 4 Hz, C-1 H), 5.62 (1H, d, J = 4 Hz, C-1′H), 6.33 (1H, s, C-5 H), 6.69 (1H, s, C-8 H), 7.03 (1H, s, C-4′ H), 7.15 (1H, s, C-7′ H).

(b) *erythro*-Isocordrastine **2***b*, 240 mg (20.1%), R_f 0.08 (silica gel, EtOAc), mp 170–171°C (from EtOH) (lit (7, 9) mp 169–171°C); ir ($CHCl_3$) ν_{max}: 1750 cm^{-1} (γ-lactone); ^{1}H nmr δ: 2.1–3.2 (4H, m, C-3 and C-4 H's), 2.58 (3H, s, —NCH_3), 3.70 (3H, s, —OCH_3), 3.80 (3H, s, —OCH_3), 3.85 (3H, s, —OCH_3), 3.92 (3H, s, —OCH_3), 4.12 (1H, d, J = 4 Hz, C-1 H), 5.58 (1H, d, J = 4 Hz, C-1′ H), 6.29 (1H, s, C-7′ H), 6.38 (1H, s, C-8 H), 6.63 (1H, s, C-5 H), 7.26 (1H, s, C-4′ H).

Cordrastines **3**a *and* **3**b

An LDA solution (3 mmol), prepared as described above, was treated dropwise with a solution of meconin (0.582 g, 3 mmol) in dry THF. Treatment of the clear orange solution as in the preparation of the isocordrastines gave, after work-up, an orange oil. Flash chromatography (silica gel, initial eluant $CHCl_3$ + 1.5% MeOH to obtain the faster running isomer, then $CHCl_3$ + 2% MeOH to recover the slower running isomer) gave the following two components.

(a) *threo*-Cordrastine **3***a*, 270 mg (26.2%), R_f 0.41 (silica gel, EtOAc), mp 158–159°C (from EtOH) (lit. (17), mp 156–157°C); ir ($CHCl_3$) ν_{max}: 1760 cm^{-1} (γ-lactone); ^{1}H nmr δ: 2.3–3.2 (4H, m, C-3 and C-4 H's) 2.65 (3H, s, —NCH_3), 3.74 (3H, s, —OCH_3), 3.81 (6H, s, 2 × —OCH_3), 3.90 (3H, s, —OCH_3), 4.06 (1H, d, J = 4 Hz, C-1 H), 5.69 (1H, d, J = 4 Hz, C-1′H), 6.36 (1H, s, C-5 H), 6.71 (1H, s, C-8 H), 7.02 and 7.33 (2H, ABq, J = 8.5 Hz, C-6′ and C-7′ H's, respectively).

(b) *erythro*-Cordrastine (cordrastine II), **3b**, 225 mg (18.8%), R_f 0.09 (silica gel, EtOAc), oil; ir ($CHCl_3$) ν_{max}: 1765 cm^{-1} (λ-lactone); ^{1}H nmr δ: 2.3–3.2 (4H, m, C-3 and C-4 H's), 2.60 (3H, s, —NCH_3), 3.67 (3H, s, —OCH_3), 3.87 (3H, s, —OCH_3), 3.91 (3H, s, —OCH_3), 4.03 (3H, s, —OCH_3), 5.57 (1H, d, J = 4 Hz, C-1′ H), 6.29 (1H, s, C-8 H), 6.63 (1H, s, C-5 H), 6.59 and 7.14 (2H, ABq,

J = 8.5 Hz, C-7′ and C-6′ H's, respectively). The doublet at ca. 4.05 ppm is partially obscured by the singlet appearing at 4.03 ppm.

The picrate of **3***b* was obtained as a yellow crystalline powder, mp 204–205°C (lit. (9) mp 205°C, (17) mp 208°C).

When an ethanol/ether solution of the oil was seeded with an authentic sample of cordrastine II, crystals were deposited, mp 119–120°C (lit. (17, 18) mp 117–119°C.

Acknowledgement

We thank the Natural Sciences and Engineering Research Council for financial support of this work.

1. W. H. PERKIN, JR. and R. ROBINSON. J. Chem. Soc. **99**, 775 (1911).
2. M. SHAMMA. The isoquinoline alkaloids. Academic Press, New York. 1972, p. 360.
3. M. SHAMMA and J. L. MONIOT. Isoquinoline alkaloid research 1972–77. Plenum Press, New York. 1978. p. 307.
4. F. SÂNTAVY. *In* The alakaloids. Vol. XII. *Edited by* R. H. F. Manske. Academic Press, New York. p. 397.
5. F. SÂNTAVÝ. *In* The alkaloids. Vol. XVII. *Edited by* R. H. F. Manske and R. Rodrigo. Academic Press, New York. p. 467.
6. M. SHAMMA. *In* Chemistry of the alkaloids. *Edited by* S. W. Pelletier. Van Nostrand Reinhold Co., New York. 1970. p. 65.
7. C. E. SLEMON, L. C. HELLWIG, J.-P. RUDER, E. W. HOSKINS, and D. B. MACLEAN. Can. J. Chem. **59**, 3055 (1981).
8. D. B. MACLEAN. 11th Int. Symp. Chem. Nat. Prod. Golden Sands, Bulgaria. Symp. Papers 4(2), 204 (1979).
9. T. SHONO, H. HAMAGUCHI, M. SASAKI, S. FUJITA, and K. NAGAMI. J. Org. Chem. **48**, 1621 (1983).
10. T. SHONO, Y. USUI, and H. HAMAGUCHI. Tetrahedron Lett. 1351 (1980).
11. R. H. PRAGER, J. M. TIPPETT, and A. D. WARD. Aust. J. Chem. **34**, 1085 (1981).
12. N. J. P. BROOM and P. G. SAMMES. J. Chem. Soc. Perkin Trans. 1, 465 (1981).
13. D. J. DODSWORTH, M.-P. CALIAGNO, U. E. EHRMANN, and P. G. SAMMES. Tetrahedron Lett. 5075 (1980).
14. R. MARSDEN and D. B. MACLEAN. Tetrahedron Lett. 2063 (1983).
15. S. O. DE SILVA, I. AHMAD, and V. SNIECKUS. Can. J. Chem. **57**, 1598 (1979).
16. M. SHAMMA and V. ST. GEORGIEV. Tetrahedron, **32**, 211 (1976).
17. V. SMULA, N. E. CUNDASAWMY, H. L. HOLLAND, and D. B. MACLEAN. Can. J. Chem. **51**, 3287 (1973).
18. P. KEREKES, G. GAÁL, R. BOGNÁR, T. TÖRÓ, and B. COSTISELLA. Acta Chim. Acad. Sci. Hung. **105**, 283 (1980).
19. T. KAMETANI, T. HONDA, H. INOUE, and K. FUKUMOTO. J. Chem. Soc. Perkin Trans. 1, 1221 (1976).
20. F. E. ZIEGLER and K. W. FOWLER. J. Org. Chem. **41**, 1564 (1976).
21. V. SNIECKUS. Heterocycles, **14**, 1649 (1980), and references cited therein.
22. T. V. HUNG, B. A. MOONEY, R. H. PRAGER, and J. M. TIPPETT. Aust. J. Chem. **34**, 383 (1981).
23. G. BLASKÓ, D. J. GULA, and M. SHAMMA. J. Nat. Prod. **45**, 105 (1982).
24. W. C. STILL, M. KAHN, and A. MITRA. J. Org. Chem. **43**, 2923 (1978).
25. G. A. EDWARDS, W. H. PERKIN, JR., and F. W. STOYLE. J. Chem. Soc. **127**, 195 (1925).
26. W. M. WHALEY and M. MEADOW. J. Chem. Soc. 1067 (1953).
27. T. KAMETANI, T. OHSAWA, S. HIRATA, M. S. PREMILA, M. IHARA, and K. FUKUMOTO. Chem. Pharm. Bull. **25**, 321 (1977).

Can. J. Chem. Downloaded from www.nrcresearchpress.com by 210.87.254.5 on 09/06/12
For personal use only.

Synthetic cardenolides and related products. IV.[1] *D*-homo derivatives

J. M. FERLAND and Y. LEFEBVRE

Ayerst Research Laboratories, Montréal, P.Q., Canada H3C 3J1

Received June 1, 1983

J. M. FERLAND and Y. LEFEBVRE. Can. J. Chem. **62**, 309 (1984).

The synthesis of novel structures related to naturally occurring cardiotonic agents such as resibufogenin is described. These products retain the essential features of aglycones needed for biological activity. They are, however, thermodynamically stable and easily available from smilagenin. The methods of preparation, together with the proof of structures and configuration, are reported.

J. M. FERLAND et Y. LEFEBVRE. Can. J. Chem. **62**, 309 (1984).

On a synthétisé de nouveaux agents isomères de cardénolides naturels tels la résibufogénine. Ces produits retiennent les caractéristiques essentielles à l'activité biologique des aglycones. Ils sont cependant thermodynamiquement stables et ont été préparés à partir de la smilagénine, un produit naturel abondant. Les méthodes de synthèses ainsi que les preuves de structure et de configuration sont décrites.

Can. J. Chem. Downloaded from www.nrcresearchpress.com by 210.87.254.6 on 09/06/12
For personal use only.

Naturally occurring cardenolides exist in a thermodynamically unfavoured configuration (2): 17β-side chain, 14β-orientation, A/B and C/D *cis*-fused rings, and 3β-oriented substituents.

The preparation of such compounds is relatively difficult as emphasized by Sondheimer (2) in his review on "Synthesis in the Cardiac Active Steroid Field". However, these stereochemical features are important and often slight modifications will result in a net loss of biological activity (3, 4). It is also known that the synthetic cardenolides (1*a*), with a lactone isomeric to the natural one, retain biological activity (5).

It appeared interesting to synthesize compounds of types **A** and **B** which would retain the essential features of natural and synthetic aglycones, but would be thermodynamically more stable and easily available from the abundant smilagenin.

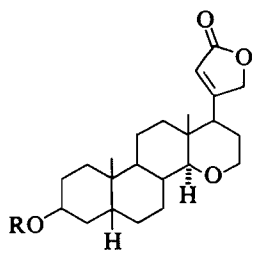

A

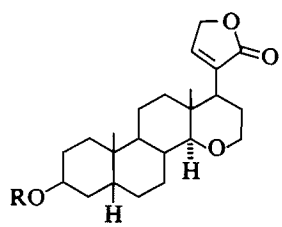

B

These products are analogous to the naturally occurring 14β,15β-oxido-steroids, such as resibufogenin **C**, or to 14β,15β-oxido-anhydrodigitoxigenin **D**, which are known to exhibit cardiotonic activity (6) insofar as the 15-oxygen of the *D*-homo-15-oxa ring of compounds **A** and **B** has the same configuration as the oxygen of the epoxide functions of compounds **C** and **D**.

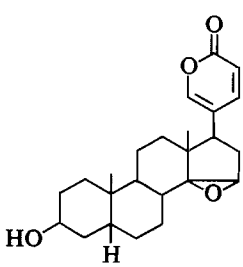

C

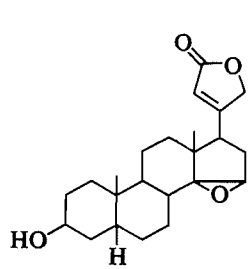

D

[1]For parts I–III, see ref. 1.

The key intermediate for such a synthesis was the 5β-androstan-15-one derivative **7**. This product was obtained from smilagenin which was degraded to the 17-ketone **1**. The latter was then transformed into ketone **7** by a route described by Kelly and Sykes (8). In order to differentiate between the 3- and the 17-hydroxyls in **7**, appropriate protecting groups had to be selected. These reactions are summarized in Scheme 1.

The stereochemistry of ketone **7** was confirmed by circular dichroism and optical rotary dispersion curves which showed a positive Cotton effect (9).

As shown in Scheme 2, the Baeyer–Villiger oxidation of ketone **7** to lactone **8** gave the expected rearrangement (10) with retention of configuration in C14 (11). Indeed, the coupling constant of the 14α-proton with the 8β-hydrogen (dihedral angle of 180°) is equal to $J = 10$ Hz. This is in agreement with reported values (12*b*) for lactones in ring A of steroids.

The lactone **8** was then hydrogenolysed to the cyclic ether **9** (13). The removal of the 3-chloroacetate (**9** → **10**) was not as selective as expected, and the amount of sodium bicarbonate used had to be carefully controlled in view of the ease of hydrolysis of the 17-acetate. This facile hydrolysis is most probably due to an anchimeric assistance from the 14β-oxygen, which is only possible with the proposed stereochemistry. The diol **11**, always present in the hydrolysis reaction, was oxidized to the dione **14**. Protection of the 3-OH in **10** as the THP ether, followed by hydrolysis of the 17-acetate and subsequent oxidation with the $Et_3N—SO_3$ complex afforded the 17-ketone **13**. Those reactions are described in Scheme 2.

The ketone **13** was then treated with 3-furyllithium to give two isomeric furyl derivatives **15** and **16** in a proportion of 2:1. These products were isolated and identified as the 3-acetyl derivatives **15***b* and **16***b*.

As expected (14), the 17α-furyl derivative **15** was the major isomer isolated. The nmr data (Table 1) are indicative of the proposed stereochemistry for products described in Scheme 3. The 18-CH_3 of products **15***b* and **17** with a 17α-furyl substituent is strongly deshielded in comparison with the 18-CH_3 of products **16***b* and **18** where the furyl moiety has the 17β-configuration. In the furyl derivatives **16**, it is interesting to note the deshielding of the 14α-proton *cis* to the 17β-hydroxyl group. This phenomenon is analogous to the one observed (15) with 17β-H, 14β-OH that exists in some naturally occurring cardenolides.

The unsaturated furyl derivative **17** was obtained on treat-

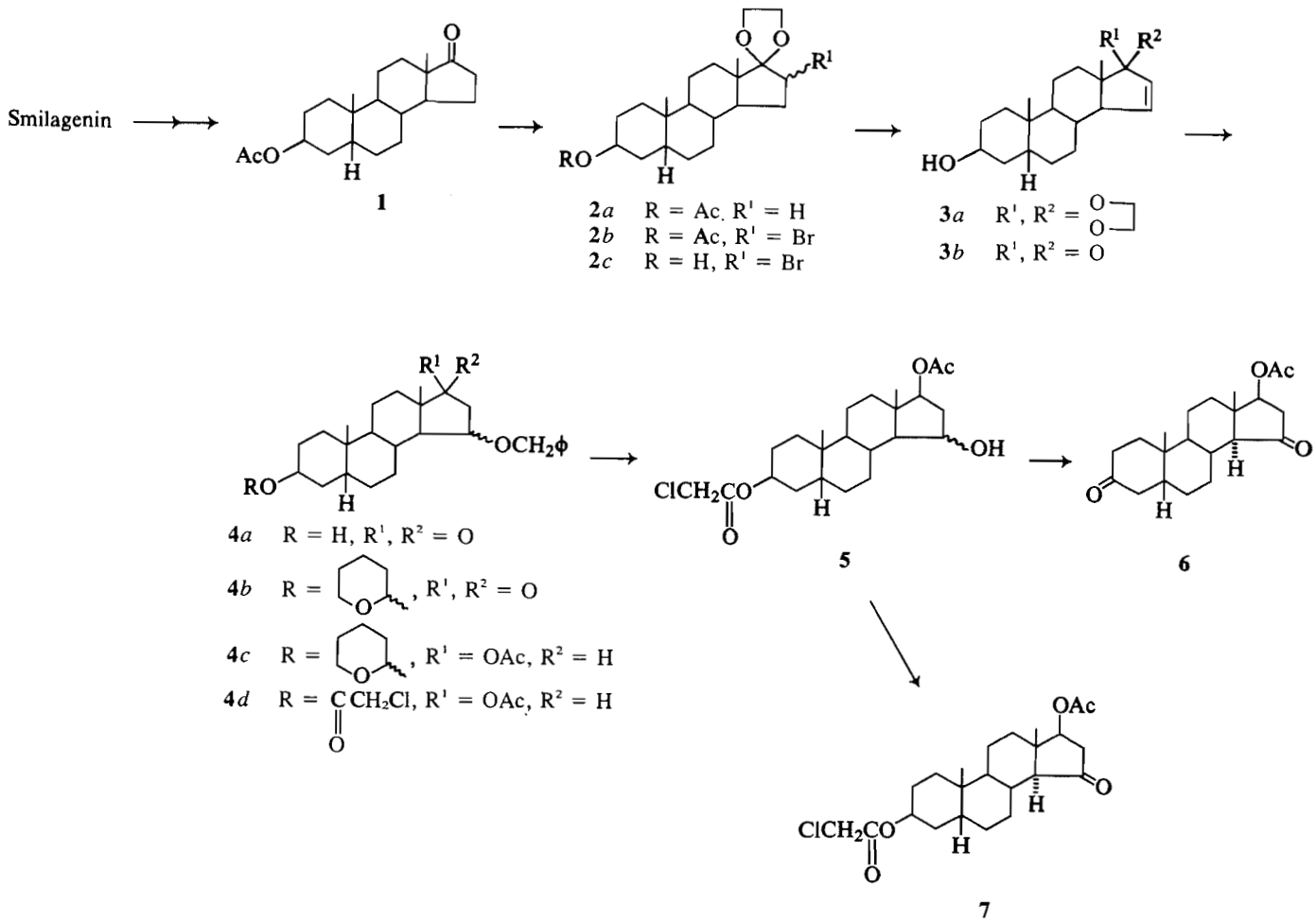

SCHEME 1

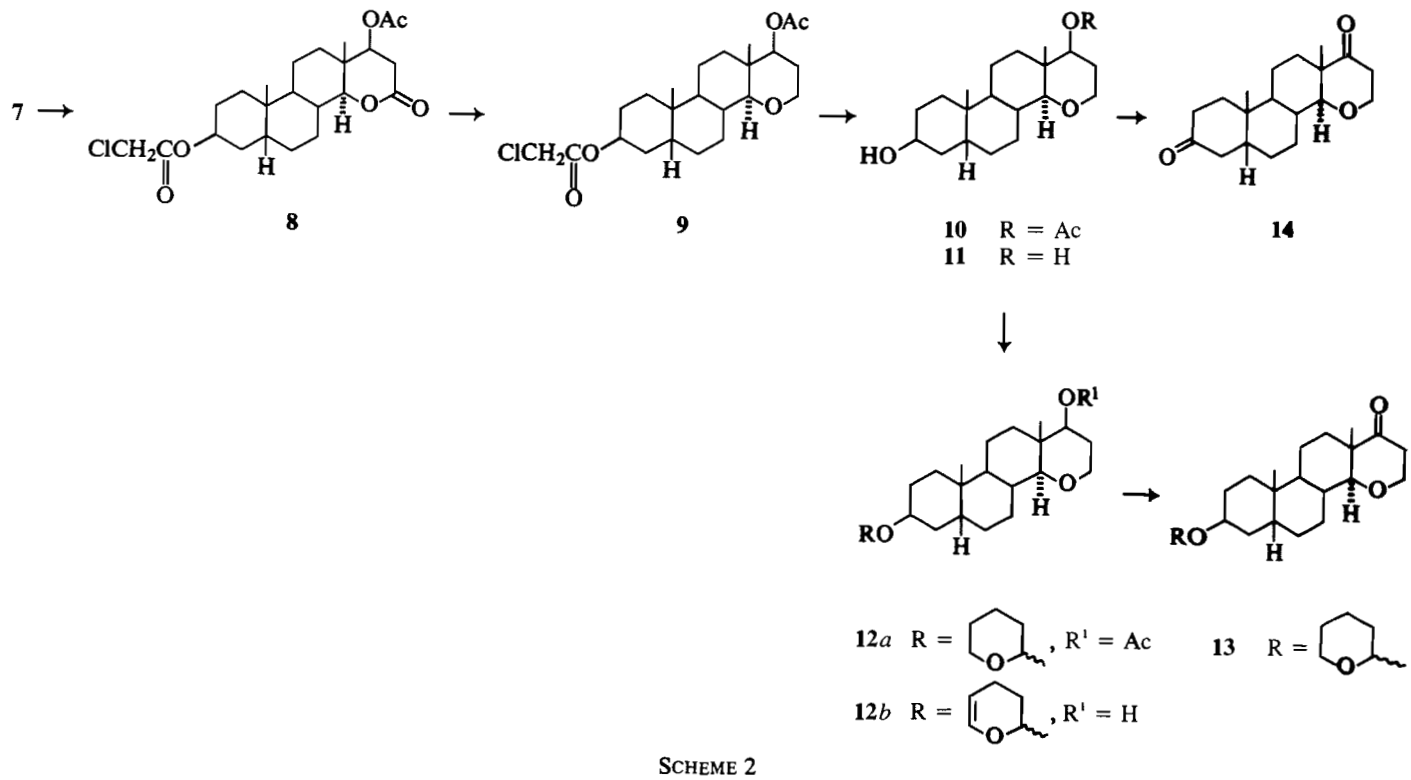

SCHEME 2

Can. J. Chem. Downloaded from www.nrcresearchpress.com by 210.87.254.6 on 09/06/12
For personal use only.

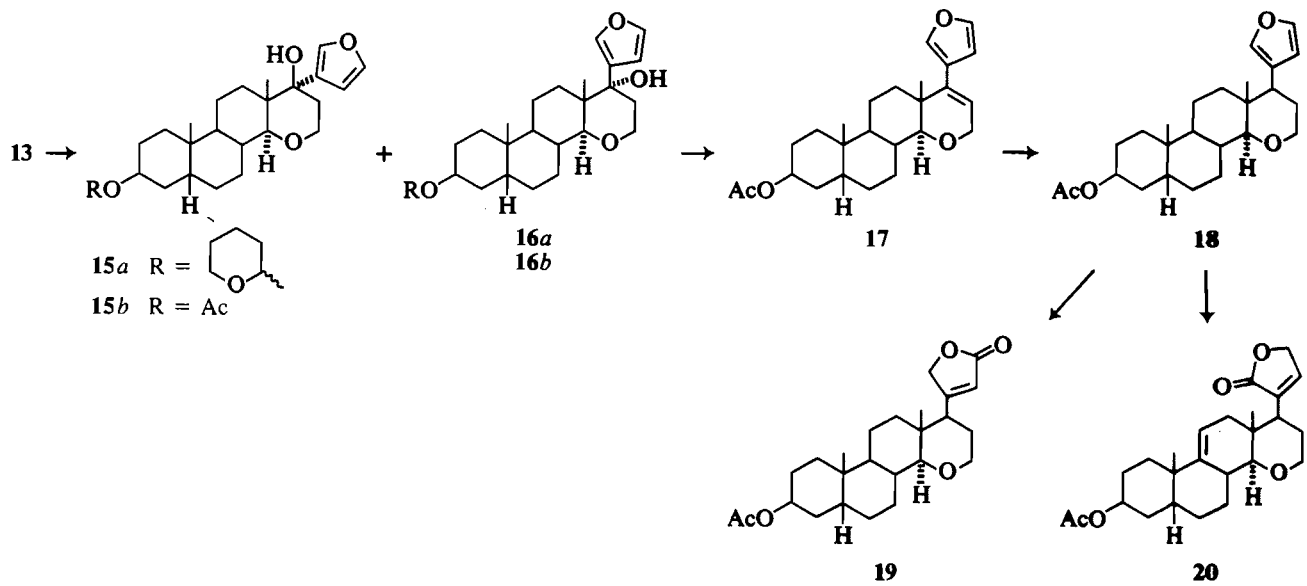

SCHEME 3

TABLE 1. Characteristic nuclear magnetic resonance of 17-substituted ethers (δ)

Products	14-H	18-CH_3	19-CH_3
15 (R = Ac)	2.86 (d, J = 8.5 Hz)	1.16	0.97
16 (R = Ac)	3.48 (d, J = 8.0 Hz)	0.86	0.95
17 (R = Ac)	3.05 (d, J = 9.0 Hz)	1.16	1.00
18 (R = Ac)	2.80 (d, J = 8.0 Hz)	0.84	0.96

ment of the 17-alcohols **15***b* and **16** with phosphorus oxychloride or from **15***b* when stirred in presence of 4 *N* HCl. Under the latter conditions the *trans*-diaxial alcohol **16***b* remained unchanged. These results can only be explained by a steric decompression resulting from the removal of the furyl moiety from the concave face of the molecule.

Hydrogenation of the unsaturated furyl derivative **17** yielded product **18**. The lactones **19** and **20** were obtained by oxidation (1*a*, 1*c*) of the furyl derivative **18** with *N*-bromosuccinimide for **20** and with peracetic acid followed by sodium borohydride reduction for **19**.

These lactones were found to be devoid of cardiotonic activity.

Experimental

Melting points are uncorrected. The ir spectra were taken on a Perkin–Elmer 225 ir spectrophotometer and nmr were recorded on a Varian A-60A spectrometer operating at 60 MHz; TMS was used as internal standard. Merck silica gel 60 (60–230 mesh) was used. The $[\alpha]_D$ were taken at 20–23°C in 1% chloroform solutions. Otherwise, the solvent is mentioned.

3β-Hydroxy-15-benzyloxy-5β-androstan-17-one (**4**a)

This product was prepared from **1** (**7**) following the methods described by Kelly and Sykes (8) in the androst 5-ene series. It was purified by chromatography (silica gel; EtOAc/hexane, 1:1), yield 62% as an oil; nmr ($CDCl_3$): 1.03 (C18—CH_3), 1.17 (C19—CH_3), 4.11 (C3 and C15—H), 4.33, 4.50, and 4.60 (unresolved peaks for —$OCH_2\phi$) and 7.30 (5 aromatic H) ppm.

In Table 2 are found some analytical data of the intermediates leading to product **4***a*.

15-Benzyloxy-3β-tetrahydropyranyloxy-5β-androstran-17-one (**4**b)

To a solution of the 3-OH derivative **4***a* (125 g) in $CHCl_3$ (5 L) and dihydropyran (600 mL) was added a solution of phosphorous oxychloride (2 drops) in EtOAc (10 mL). The reaction mixture was stirred at 50°C for 4 hours. The mixture was washed with water, 5% $NaHCO_3$, water, dried, and evaporated. The crude product was chromatographed on silica gel (hexane/EtOAC, 17:3) to give the title product (125 g) as an oil, yield 83%; nmr ($CDCl_3$): 1.01 (C19—CH_3), 1.17 (C18—CH_3), 3.67 (CH_2O—THP), 4.0 (C3 and C15—H), 4.33 and 4.57 (ϕCH_2O—), 4.65 (OCHO—THP), and 7.33 (5 aromatic H) ppm.

17β-Acetyloxy-15-benzyloxy-3β-tetrahydropyranyloxy-5β-androstane (**4**c)

To a solution at 0°C of the 17-ketone **4***b* (125 g) in methanol (6.25 L) was slowly added sodium borohydride (125 g) in water (1.25 L). The mixture was then stirred at room temperature for one hour and poured into ice-cold water. The solid obtained was filter dried and acetylated (pyridine/acetic anhydride). The product obtained was chromatographed on silica gel (hexane/EtOAc, 3:1) to give the title product (105 g) as an oil, yield 77%, nmr ($CDCl_3$): 0.80 (C18—CH_3), 0.97 (C19—CH_3), 2.03 (OAc), 3.55 (CH_2O—THP), 3.9 and 4.38 (ϕCH_2O—), 4.62 (OCHO—THP), and 7.28 (5 aromatic H) ppm.

17β-Acetyloxy-3β-chloroacetyloxy-15-benzyloxy-5β-androstane (**4**d)

A solution of the THP–ether (**4***c*) (105 g) in ethanol (2.6 L) and 0.1 *N* HCl (1.1 L) was stirred at 45°C for 4 hours. The ethanol was evaporated to half of its initial volume and the remaining solution poured into ice cold water. The crude alcohol obtained was filtered and dried (85 g). A sample was crystallized from CH_2Cl_2/hexane, yield 65%, mp 177–179°C; ir ($CHCl_3$): 3620, 3480, 1728, 1250, and 1027 cm^{-1}; nmr ($CDCl_3$): 1.0 (C18–CH_3), 1.05 (C19—CH_3), 1.72 (OH), 2.03 (OAc), 4.1 (C3 and C15—H), and 4.52 (C17—H, J = 8.5 Hz) ppm. *Anal.* calcd. for $C_{21}H_{34}O_4$: C 71.96, H 9.78; found: C 71.48, H 9.44. To this alcohol in dioxane (680 mL) and pyridine (170 mL) at 10°C was added, over a period of 15 minutes, a solution of chloroacetylchloride (51 mL) in dioxane (150 mL). The reaction mixture was stirred at 10°C for 10 min. It was then diluted with ether. The organic solution was washed once with water, then with brine, dried, and evaporated. The crude product obtained was chromatographed on silica gel (hexane/EtOAc, 3:1) to give **4***d* (83 g).

A solution of this derivative (65 g) in glacial acetic acid was hydrogenated at room temperature and atmospheric pressure over 10% Pd/C (16 g). The catalyst was removed by filtration and the acetic acid evaporated under reduced pressure. The residue was dissolved in EtOAc and the organic solution washed with $NaHCO_3$, brine, dried,

Can. J. Chem. Downloaded from www.nrcresearchpress.com by 210.87.254.6 on 09/06/12
For personal use only.

TABLE 2. Analytical data for derivatives **2** and **3**

Compound	Crystallization	Melting point (°C)	Yield (%)	Nuclear magnetic resonance (δ) C18	Nuclear magnetic resonance (δ) C19	Infrared (ν_{max} cm^{-1})
2*a*	MeOH/H_2O	109–111	90	0.83	0.97	1725, 1258, and 1020
2*b*	MeOH/H_2O	143–145	86	0.88	0.97	1725 and 1018
2*c*	MeOH/H_2O	210–212	95			
3*a*[a,b]	Ether/hexane	150–152	78	0.91	1.00	3620, 3480, 1665, and 1030
3*b*[b]	Acetone/H_2O	160–165	95			

[a]This product analyzed for $C_{21}H_{32}O_3$; C 75.86, H 9.70; found: C 75.51, H 9.73.
[b]The 3-phenylmethyloxy-(**16***a*, *b*) or the *tert*-butylsilyloxy-derivative (**16***c*) of these products has already been described.

and evaporated. The crude 17β-acetyloxy-3β-chloracetyloxy-15-hydroxy-5β-androstane (**5**) obtained (51 g) was used as such for the following reaction. The nmr ($CDCl_3$): 1.02 (C18—CH_3), 1.05 (C19—CH_3), 2.03 (OAc), 4.05 ($ClCH_2CO$), 4.53 (C17—H), and 5.20 (C3—H) ppm.

*17β-Acetyloxy-5β-androstane-3,16-dione (**6**)*

A mixture of 3-chloroacetyloxy-15-hydroxy derivative (**5**) (4.6 g) and $KHCO_3$ (1.3 g) in methanol (330 mL) and water (70 mL) was heated at reflux for 3 hours. Most of the methanol was evaporated under reduced pressure and the residue was taken into EtOAc. The organic solution was washed with brine, dried, and evaporated. The crude product obtained (4.8 g) was chromatographed on silica gel (toluene/EtOAc, 1:1).

The 3,15-diol obtained (3.3 g) was dissolved in acetone (150 mL) and oxidized at 0°C with 8 *N* Jones' reagent (4 mL). After 10 min the excess reagent was destroyed and the mixture concentrated under reduced pressure. It was then taken into EtOAc and the organic solution washed with brine, dried, and evaporated. The crude product obtained (2.3 g) was crystallized 3 times from acetone/hexane to give the pure title product (1.6 g), mp 170–172°C, $[\alpha]_D$ +60.2°; ir ($CHCl_3$): 1732 and 1704 cm^{-1}; nmr ($CDCl_3$): 0.90 (C18—CH_3), 1.05 (C19—C_3), 2.09 (OAc), and 5.00 (C17—H, t, J = 8.5 Hz) ppm. *Anal.* calcd. for $C_{21}H_{30}O_4$: C 72.80, H 8.73, found: C 72.86, H 8.82.

*17β-Acetoxy-3β-chloroacetoxy-5β-androstane-15-one (**7**)*

Jones' reagent was added dropwise (40 mL) to a stirred solution in acetone, at 0°C of the 15-OH derivative **5** (51 g) (obtained from the 17-ketone **1**). The mixture was stirred for 10 more minutes after the addition and the excess reagent destroyed with isopropanol. Most of the acetone was evaporated under reduced pressure and the residue was partitioned between ethyl acetate and water. The organic layer was washed with salt-saturated water, dried, and evaporated. The product obtained was chromatographed on silica gel (hexane/EtOAc, 3:1) to give the title compound (37 g). An analytical sample was crystallized twice from EtOAc/hexane, yield 62%, mp 148–150°C, $[\alpha]_D$ +35.4°; ord (*c* 8.5 mg/mL; dioxan) 20°C $[\phi]_{350}$ +2100°; $[\phi]_{322}$ +7000°; $[\phi]_{298}$ 0°; cd mμ (ΔE): 320 (+0.501), 301 (+2.90), 274 (+0.50); ir ($CHCl_3$): 1735 cm^{-1}; nmr ($CDCl_3$): 0.87 (C18—CH_3), 1.00 (C19—CH_3), 2.07 (OAc), 2.05 and 2.80 (H16 and H16′, 2d, $J_{16,16'}$ = 18 Hz, $J_{16,17}$ = $J_{16',17}$ = 8.5 Hz), 4.06 (CH_2Cl), 4.97 (H17, m), and 5.20 (H3, m) ppm. *Anal.* calcd. for $C_{23}H_{33}ClO_5$: C 65.01, H 7.84, Cl 8.35; found: C, 64.92, H 7.90, Cl 8.13.

*17β-Acetoxy-3β-chloroacetoxy-5β-D-homo-15-oxaandrostan-15-one (**8**)*

To a solution in CH_2Cl (720 mL) at 0°C of the 15-ketone **7** (36 g) was added bicarbonate (27 g) and *m*-chloroperbenzoic acid (36 g). The mixture was stirred at room temperature for 16 h, then heated under reflux for 2 h. The organic solution was washed in succession with ice-cold water, sodium sulfite, sodium bicarbonate, water, dried, and evaporated. The crude product obtained was chromatographed on silica gel (hexane/EtOAc, 2:1) to give the title compound (31 g).

The analytical sample was crystallized twice from acetone, yield 85% mp 220–222°C, $[\alpha]_D$ −34.8°; ir ($CHCl_3$): 1735 cm^{-1}; nmr ($CDCl_3$): 1.00 (C18 and C19—CH_3), 2.08 (17–OAc), 2.46, 3.18 (H16,16′, 2d for each proton, $J_{16,16'}$ = 18.5 Hz, $J_{16,17}$ = 9 Hz, $J_{16',17}$ = 8.5 Hz), 4.06 (CH_2Cl), and 3.68 (C14—H, d, J = 10 Hz) ppm. *Anal.* calcd. for $C_{23}H_{33}O_6Cl$: C 62.66, H 7.49; found: C 62.50, H 7.60.

*17-aβ-Acetoxy-3β-hydroxy-5β-D-homo-15-oxaandrostane (**10**)*

A solution of lactone **8** (31 g) in glacial acetic acid (750 mL) was hydrogenated over platinum oxide 85% (10.0 g) at atmospheric pressure and room temperature until no more hydrogen was absorbed (72 h). The catalyst was removed by filtration and the filtrate evaporated under reduced pressure to one-third of its initial volume. It was then diluted with ethyl acetate and the organic solution washed carefully with bicarbonate solution, salt-saturated water, dried, and evaporated. The crude product obtained was chromatographed on silica gel (pet. ether 60–80°C/ether, 2:1) to give the 17β-acetoxy-3β-chloroacetoxy-5β-D-homo-15-oxaandrostane (**9**) (25 g).

To a solution of this product (25 g) in methanol (2.4 L) was added a solution of potassium bicarbonate (6.0 g) in water (600 mL) over a period of 5 minutes. The mixture was heated under reflux for 2 hours. It was then poured into ice-cold water and the solid obtained filtered. It was chromatographed on silica gel (benzene/EtOAc, 3:1). The faster moving compound was the title product **10** (15 g).

The analytical sample was crystallized twice from methanol–water, yield 87%, mp 186–188°C, $[\alpha]_D$ −26.9°; ir ($CHCl_3$): 3620, 3480, 1715, 1240, 1110, and 1025 cm^{-1}; nmr ($CDCl_3$): 0.97 (C18 and C19—CH_3), 1.62 (OH), 2.03 (OAc), 2.69 (C14—H, d, J = 8 Hz), and 3.50 – 4.00 (C15—CH_2O,m) ppm. *Anal.* calcd. for $C_{21}H_{34}O_4$: C 71,96, H 9.78; found: C 71.99, H 9.92.

The slower moving compound (2.5 g) was assumed to be the 3,17-diol **11** and was oxidized with Jones' reagent as in **7**. The crude product obtained (1.6 g) was crystallized twice from acetone–hexane to give the pure 5β-D-*homo-15-oxaandrostane-3-17a-dione* (**14**), mp 158.160°, $[\alpha]_D$ −52.5°; ir ($CHCl_3$): 1700 and 1104 cm^{-1}; nmr ($CDCl_3$): 1.04 (C18—CH_3), 1.20 (C19—CH_3), 2.91 (C14—H, d, J = 9.0 Hz), and 3.33, 4.53 (C15—H, m) ppm. *Anal.* calcd. for $C_{19}H_{28}O_3$: C 74.96, H 9.27; found: C 74.79, H 9.34.

*3β-Acetoxy-17aβ-hydroxy-17α-[3-furyl]-5β-D-homo-androstane (**15**b) and 3β-acetoxy-17aα-hydroxy-17β-[3-furyl]-5β-D-homo-androstane (**16**b)*

A solution of phosphorous oxychloride (4 drops) in ethyl acetate (10 mL) was added to a solution at 50°C of the 3-OH, 17-aβ-acetate (**10**) (11.5 g) in chloroform (480 mL) and dihydropyran (50 mL). The mixture was stirred at this temperature for 1-1/2 hours, cooled, and washed carefully with 10% sodium bicarbonate solution and water. The organic layer was then dried, evaporated, and chromatographed on silica gel (hexane/ether, 1:1) to give the 3-tetrahydropyranyl ether derivative (*12a*) (15.5 g) as an oil which was used as such for the subsequent reaction.

To a solution of the 17-acetate (**12***a*) (15.5 g) in methanol (800 mL) was added a solution of potassium bicarbonate (5.0 g) in water (200 mL). The mixture was then heated under reflux for 1 hour. Most of the methanol was evaporated and the remaining oil was extracted with ethyl acetate. The organic solution was washed with water, dried,

Can. J. Chem. Downloaded from www.nrcresearchpress.com by 210.87.254.6 on 09/06/12
For personal use only.

Can. J. Chem. Downloaded from www.nrcresearchpress.com by 210.87.254.6 on 09/06/12
For personal use only.

and evaporated to give the *17-alcohol* (**12***b*) (14.5 g) which was used as such for the following reaction.

To a solution at room temperature of **12***b* (14.5 g) in DMSO (40 mL) and triethyl amine (42 mL) was added dropwise, over a period of 10 min, a solution of NEt_3—SO_3 complex (17.3 g) in DMSO (70 mL). The mixture was stirred for 1 hour, poured into water, and the solution neutralized to pH 3–4 with 1 *N* HCl. The solid obtained was filtered, washed with water, and dried. The crude 17-ketone (**13**) (14 g) was used as such for the following reaction.

A solution of this ketone (3.2 g) in anhydrous ether (100 mL) was added slowly to a solution of 3-furyl lithium (prepared at −70°C from 3-bromofuran (1.54 g) in anhydrous ether (60 mL) and 20% butyl lithium (2.94 mL)) maintained at −70°C. The mixture was then stirred at room temperature for 1 hour. Salt-saturated water was carefully added to the mixture. The organic layer was then washed with brine, dried, and evaporated. The crude product obtained was chromatographed on silica gel (Et_2O/pet. ether 60–110°C) to get a mixture of **15***a* and **16***a* (1.72 g); ir ($CHCl_3$): 3600, 3450, 1495, 1100, 1018, and 870 cm^{-1}; nmr ($CDCl_3$): 0.87 and 0.95 (C18—CH_3), 1.17 (C19—CH_3), 2.91 (C14—H, d, J = 9 Hz), 4.70 (OCHO, THP), 6.67 (C4′—H), 7.50 (C3′—H, m), and 7.64 (C2′—H, m) ppm.

A solution of these ethers (1.6 g) in ethanol (40 mL) and 0.1 *N* sulfuric acid (15 mL) was heated at 40°C for 4 hours. The crude alcohols isolated (1.3 g) were acetylated (pyridine/acetic anhydride) and the crude 3-acetate derivatives isolated were chromatographed on silica gel (ether/pet. ether 30–60°C, 3:1). The faster moving product (0.95 g) was crystallized twice from methanol–ether to give the pure *3β-acetoxy-17aβ-hydroxy-17α-[3-furyl], 5β-D-homo-15-oxaandrostane (15*b) mp 205–208°C $[\alpha]_D$ −7.1°; ir ($CHCl_3$): 3410, 1720, 1495, 1230, 1018, and 865 cm^{-1}; nmr ($CDCl_3$): 0.97 (C19—CH_3), 1.16 (C18—CH_3), 1.83 (17–OH), 2.03 (3-$OCOCH_3$), 2.86 (C14—H, d, J = 8.5 Hz), 6.56 (C4′—H,m), 7.40 (C5′—H, t, J = 1,5 Hz), and 7.53 (C2′—H, m) ppm. *Anal.* calcd. for $C_{25}H_{36}O_5$: C 72.08, H 8.71; found: C 72.21, H 8.81.

The fractions containing only the slower moving product were evaporated and the product obtained (0.090 g) was crystallized twice from CH_2Cl_2/EtOH/hexane to give *the pure 17β-[3-furyl]-derivative* (**16**b), mp 251–253°C, $[\alpha]_D$ −10.5°; ir ($CHCl_3$): 3600, 3460, 1720, 1577, 1495, and 868 cm^{-1}; nmr ($CDCl_3$): 0.86 (C18—CH_3), 0.95 (C19—CH_3), 1.74 (C17—OH), 2.05 (3-$OCOCH_3$), 3.48 (C14—H, d, J = 10 Hz, and 7.40 (C2′and C5′—H, m) ppm. *Anal.* calcd. for $C_{25}H_{36}O_5$: C 72.08, H 8.71; found: C 71.76, H 8.63.

*3β-Acetoxy-17a-[3-furyl]-5β-*D*-homo-15-oxaandrost-16-ene (**17**)*

Method A

A solution of the mixture of 17α- and 17β-[3-furyl]-3-THP ethers (**15***a* and **16***a*) (1.73 g) in ether (200 mL) and CH_2Cl_2 (70 mL) was stirred at room temperature for 1 hour in presence of 4 *N* HCl in water. After dilution with more ether, the organic phase was washed with brine until neutral, dried, and evaporated. The crude product obtained (1.25 g) was acetylated (pyridine/acetic anhydride). The crude 3-acetates obtained (1.3 g) were chromatographed on silica gel (ether/pet. ether 30–60°C, 2:1). The faster moving product (0.570 g) was crystallized from ether–methanol to give the pure title product **17** (0.475 g), mp 147–149°C, $[\alpha]_D$ +63.7; ir ($CHCl_3$): 1720, 1650, 1560, 1490, and 870 cm^{-1}; uv (MeOH): λ_{max} 224, ϵ 5500; nmr ($CDCl_3$): 1.00 (C18—CH_3), 1.16 (C19—CH_3), 2.05 (3-$OCOCH_3$), 3.05 (C14—H, d, J = 9 Hz), 4.34 (C15—H, d, J = 3 Hz), 5.64 (C16—H, t, J = 3 Hz), 6.40 (C4′—H, m), and 7.38 (C2′—H and C5′—H, m) ppm. *Anal.* calcd. for $C_{25}H_{34}O_4$: C 75.34, H 8.60; found: C 75.25, H 8.38.

The slower moving product (0.320 g) was isolated and proved to be identical (mp, ir and nmr spectroscopy, and $[\alpha]_D$) with the 17β-derivative **16***b* described above (0.19 g after crystallization).

Method B

A solution of the 17β-[3-furyl]-3 acetate derivative **16***b* (0.2 g) in pyridine (5 mL) and phosphorous oxychloride (0.62 mL) was heated at 100°C for 16 h. The cold solution was then poured onto ice-cold water and the solid obtained filtered and taken into ethyl acetate. The organic solution was washed with water, 10% sulfuric acid solution, brine, dried, and evaporated. The crude product obtained was chromatographed on silica gel (pet. ether 30–60°C/ether, 4:1). The product obtained was crystallized (0.120 g) and proved to be identical (mp, ir and nmr spectroscopy, and $[\alpha]_D$) with the unsaturated product **17**.

Under similar conditions **15***b* also yielded **17**.

*3β-Acetoxy-17aβ-[3-furyl]-*D*-homo-5β-androstane (**18**)*

A solution of the unsaturated furyl derivative **17** (8.1 g) in EtOAc (400 mL) was hydrogenated over 5% $Pd/CaCO_3$ (8.1 g) at room temperature and atmospheric pressure. The reaction was stopped after one equivalent of hydrogen was absorbed. The catalyst was filtered and the filtrate evaporated. The product obtained was chromatographed on silica gel (pet. ether 30–60°C/ether, 4:1) to give the title product (5.6 g) which was crystallized twice from methanol–hexane (5.0 g), mp 137–138°C, $[\alpha]_D$ 0°; nmr ($CDCl_3$): 0.84 (C18—CH_3), 0.96 (C19—CH_3), 2.06 ($OCCH_3$), 2.80 (C14—H, d, J = 8 Hz), 3.90 (C15—H, m), 6.34 (C4′—H, m), 7.28 (C5′—H, m), and 7.44 (C2′—H, m) ppm. *Anal.* calcd. for $C_{25}H_{36}O_4$: C 74.96, H 9.06; found: C 75.05, H 9.11.

*3β-Acetoxy-23-hydroxy-*D*-homo-24-nor-15-oxa-5β, 14α, 17a-chol-20(22)-en-21-oic acid γ lactone (21 → 23) (**20**)*

To a well-stirred solution of the 17β-furyl derivative (**18**) (2.5 g) in dioxane (125 mL) and water (10 mL) was added NBS (2.3 g) over a period of 10 min. The mixture was then diluted with salt-saturated and extracted with EtOAc. The organic solution was washed with 10% $NaHCO_3$, brine, dried, and evaporated. The product obtained was treated with zinc (25 g) in acetic acid (100 mL) for 1/2 hour. The zinc was filtered and the filtrate evaporated (bath temperature <40°C). The remaining oil was taken into chloroform and the organic solution washed with water, dried, and evaporated. The crude product was chromatographed on silica gel (pet. ether 30–60°C/ether, 2:1) to give the title product **20** (2.27 g). It was crystallized twice from methanol–hexane (1.33 g), mp 220–222°C $[\alpha]_D$ −9.1°; ir ($CHCl_3$): 1748, 1720, 1255, and 1100 cm^{-1}; nmr ($CDCl_3$): 0.88 (C_{18}—CH_3), O ‖ 0.95 (C19—CH_3), 2.05 ($OCCH_3$), 2.86 (C14—H, d, J = 8 Hz), 3.90 (C15—H), 4.86 (CH_2-lactone), and 7.25 (C=CH-lactone ring) ppm. *Anal.* calcd. for $C_{35}H_{36}O_5$: C 72.08, H 8.71; found: C 72.13, H 8.92.

*3β-Acetoxy-*D*-homo-15-oxa-5β,14α,17a-card-20(22)-enolide (**19**)*

A mixture of the 17-furyl derivative (**18**) (2.5 g), 40% peracetic acid (2.6 mL), and sodium acetate (2.6 g) in chloroform (75 mL) was stirred at room temperature for 3 hours. It was then diluted with more chloroform and the organic solution washed with water, 10% $NaHCO_3$, water, dried, and evaporated. The crude product obtained (2.8 g), in methanol (125 mL), was treated with sodium borohydride (2.34 g) in water (25 mL). The solution was poured onto a 5% ice-cold sulfuric acid solution. The solid obtained was filtered, taken into EtOAc, and the organic solution washed with brine, dried, and evaporated. The crude product obtained was chromatographed on silica gel (pet. ether 30–60°C/EtOAc, 2:1) to give the title product (2.214 g). This was crystallized twice from ethyl acetate (1.7 g), mp 212–215°C, $[\alpha]_D$ +13.6°; ir ($CHCl_3$): 1782 (weak), 1745, 1724, 1625 and 1250 cm^{-1}; nmr ($CDCl_3$): 0.94 and 0.96 (C18 and C19—CH_3), 2.06 ($OCCH_3$), 2.76 (C14—H, d, J = 8 Hz), 3.60 and 4.50 (C15—H, m), 4.83 (CH_2-lactone), and 5.92 (=CH, lactone) ppm. *Anal.* calcd. for $C_{25}H_{36}O_5$: C 72.08, H 8.71; found: C 72.16, H 8.81.

Acknowledgements

The authors wish to thank Dr. G. Schilling and his associates for the analytical data and Dr. K. Wiesner for stimulating discussions.

1. (*a*) J. M. FERLAND. Can. J. Chem. **52**, 1652 (1974); (*b*) J. M. FERLAND, Y. LEFEBVRE, R. DINOÏ, and R. DEGHENGHI. Can. J.

Chem. **49**, 2671 (1971); (*c*) J. M. FERLAND, Y. LEFEBVRE, R. DEGHENGHI, and K. WIESNER. Tetrahedron Lett. 3617 (1966).
2. F. SONDHEIMER. Chem. Br. **1**, 454 (1965).
3. CH. TAM. 1st International Pharmacological Meeting. Vol. 3. Permagon Press, New York. 1963. p. 11.
4. (*a*) R. THOMAS, J. BOUTAGY, and A. GELBART. J. Pharm. Sci. **63**, 1649 (1974); (*b*) S. F. CAMPBELL and J. C. DANILERWICZ. Annu. Rep. Med. Chem. **13**, 92 (1978).
5. G. PASTELIN and R. MANDEZ. Eur. J. Pharmacol. **19**, 291 (1972); (*b*) J. R. CUMMINGS and G. BEAULIEU. Arch. Int. Pharmacodyn. Ther. **228**, 92 (1977).
6. (*a*) M. OKADA and Y. SAITO. Chem. Pharm. Bull. **16**, 2223 (1968); (*b*) T. SHIGEI and M. MINESHITA. Experientia, **24**, 466 (1968); (*c*) T. SAWLERWICZ, H. H. A. LINDE, and K. MEYER. Helv. Chim. Acta, **51**, 1353 (1968).
7. (*a*) R. R. MARKER, R. B. WAGNER, and E. L. WITTBECKER. J. Am. Chem. Soc. **64**, 2093 (1942); (*b*) G. ROSENKRANZ, O. MANCERA, F. SONDHEIMER, and C. DJERASSI. J. Org. Chem. **21**, 520 P1956).
8. R. W. KELLY and P. J. SYKES. J. Chem. Soc. 416 (1968).
9. (*a*) G. R. PETTIT and T. H. BROWN. J. Chem. Soc. 2024 (1967); (*b*) R. TSCHESCHE and H. MÜLLER-ALBRECHT. Chem. Ber. **103**, 350 (1970).
10. (*a*) W. E. DOERING and L. SPEERS. J. Am. Chem. Soc. **72**, 5515 (1950); (*b*) S. L. FRIESS and N. FARNHAM. J. Am. Chem. Soc. **72**, 5518 (1950).
11. (*a*) R. B. TURNER. J. Am. Chem. Soc. **72**, 579 (1950); (*b*) J. T. EDWARD and P. F. MORAND. Can. J. Chem. **38**, 1325 (1960); (*c*) A. WINDAUS. Chem. Ber. **39**, 2008 (1906).
12. (*a*) M. KARPLUS. J. Chem. Phys. **30**, 11 (1959); (*b*) J. T. EDWARD and J. M. FERLAND. Can. J. Chem. **44**, 1311 (1966).
13. (*a*) J. T. EDWARD and J. M. FERLAND. Can. J. Chem. **44**, 1299 (1966); (*b*) J. T. EDWARD and J. M. FERLAND. Chem. Ind. London, 975 (1964).
14. (*a*) C. REVESZ and Y. LEFEBRE. J. Med. Chem. **18**, 217 (1975); (*b*) Y. LEFEBVRE, D. J. MARSHALL, and C. REVESZ. J. Med. Chem. **18**, 220 (1975).
15. K. TORI and K. AONO. Annual Report of Shionogi Research Laboratory, No. 15, 1965 p. 130.
16. (*a*) T. Y. R. TSAI, A. MINTA, and K. WIESNER. Heterocycles, **12**, 1397 (1979); (*b*) R. MARINI-BETTOLO, P. FLECKER, T. Y. R. TSAI, and K. WIESNER. Can. J. Chem. **59**, 1403 (1981); (*c*) V. BALOGH, J. C. BELOEIL, and M. FÉTIZON. Tetrahedron, **33**, 1321 (1977).

Can. J. Chem. Downloaded from www.nrcresearchpress.com by 210.87.254.6 on 09/06/12
For personal use only.

15-Oxa-*D*-homosteroids

J. M. FERLAND and Y. LEFEBVRE
Ayerst Research Laboratories, Montreal, P.Q., Canada H3C 3J1

Received June 1, 1983

J. M. FERLAND and Y. LEFEBVRE. Can. J. Chem. **62**, 315 (1984).
Novel 15-oxa-*D*-homosteroids related to pregnane and estrane derivatives have been prepared.

J. M. FERLAND et Y. LEFEBVRE. Can. J. Chem. **62**, 315 (1984).
On a préparé des stéroides 15-oxa-*D*-homo dont les structures sont reliées à celles des pregnanes et des estranes.

Can. J. Chem. Downloaded from www.nrcresearchpress.com by 210.87.254.40 on 09/06/12
For personal use only.

In a previous paper (1) we described the preparation of novel 15-oxa-*D*-homocardenolides which retain some of the essential stereochemical features of natural cardiotonic agents. It appeared interesting to prepare similar types of products related to pregnane and estrane derivatives.

The key intermediates to achieve the preparation of such products were the 15-oxa-14α-steroids of type **A** and **B**.

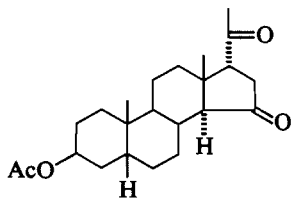

A

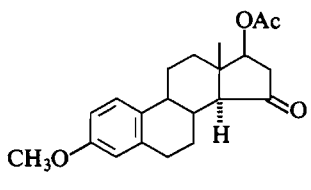

B

An attractive route to the preparation of such compounds has been described by Tschesche and Müller-Albrecht (2) in their partial synthesis of dehydrodiginigenon. However, the treatment with BF_3 of the epoxide **3** obtained from the known derivatives **1** and **2** (3) yielded the 14β-unsaturated ketone **5** which, on hydrogenation or treatment with zinc in acetic acid, gave the diketone **6**. This latter product was again obtained when the oxido derivative (**3**) was oxidized (CrO_3/AcOH) to the hydroxyketone **4** which was transformed to diketone **6** on treatment with zinc in acetic acid. In the 5α-series (4, 5), the more stable 14β,17α-pregnane-15,20-dione was obtained when the epoxide was treated under similar conditions. This discrepancy between Tschesche's results and ours is most certainly due to the lack of the proper substitution in ring C of our derivatives.

The 14β-configuration of the 15-ketones **4**, **5**, and **6** was further confirmed in the transformation of the last derivative **6** to the lactone **7** through a Baeyer–Villiger oxidation. This reaction is known to proceed with retention of configuration. The nmr spectrum of lactone **7** shows a band at 3.9 ppm with a $W/2$ equal to 3.5 Hz, a value in agreement with a dihedral angle of 0° to 10° and indicative (7) of a 14β-stereochemistry. The results are presented in Scheme 1 and Table 1.

In order to overcome this difficulty, the oxido derivative (**3**) was reduced with sodium borohydride. The 17α-derivative **8** obtained was then transformed into the esters **8***a* or **8***b*. On treatment with BF_3, the epoxide **8***a* rearranged to the 14α,15-oxo derivative **9***a* as evidenced by positive ord and cd curves (2, 6, 8). The epimeric ketone **10** (ord and cd curves are negative (2, 6, 8)) was obtained when **9***a* was treated under basic conditions followed by reacetylation. The nmr signal of the $18CH_3$ of **10** is strongly deshielded in comparison with the $18\text{-}CH_3$ of **9***a* (Table 1), thus further confirming the proposed

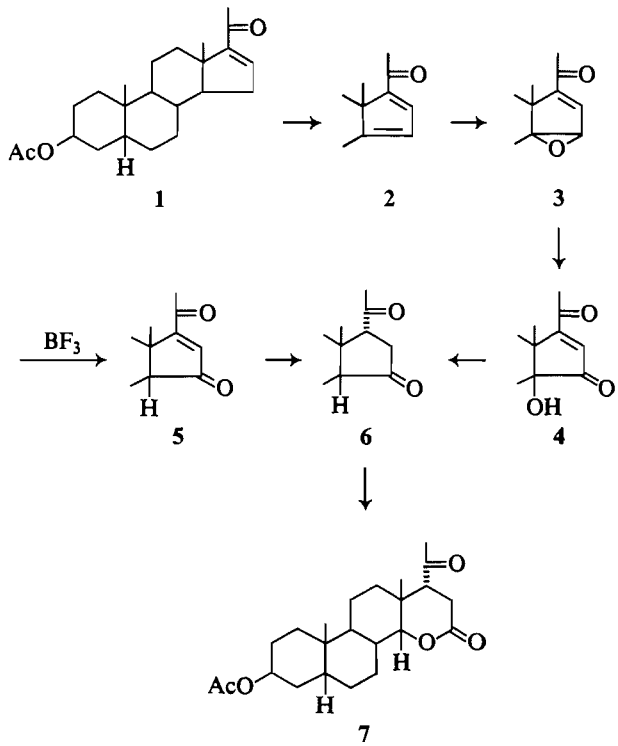

SCHEME 1

TABLE 1. Nuclear magnetic resonance data of some ketones, lactones, and ethers

Products	$18CH_3$ (δ)	14-H (δ)
6	1.32	
9*a*	0.98 (0.97 for **9***b*)	
10	1.25	
15	0.91	
7	1.17	3.90 ($W/2$ = 3.5 Hz)
11	1.09	3.77 (d, J = 8.5 Hz)
16	1.03	3.78 (d, J = 10 Hz)
13	1.12	3.40 (m)
14	1.01	
18	1.03	
21	0.96	
22	0.94	

stereochemistry.

When treated with BF_3, the epoxide **8***b* rearranged to the 14α,15-oxo derivative **9***b* which yielded the lactone **11** through a Baeyer–Villiger oxidation. This latter reaction proceeds with retention of configuration in the 14-position as evidenced by the coupling constant of the doublet for the 14-proton coupled

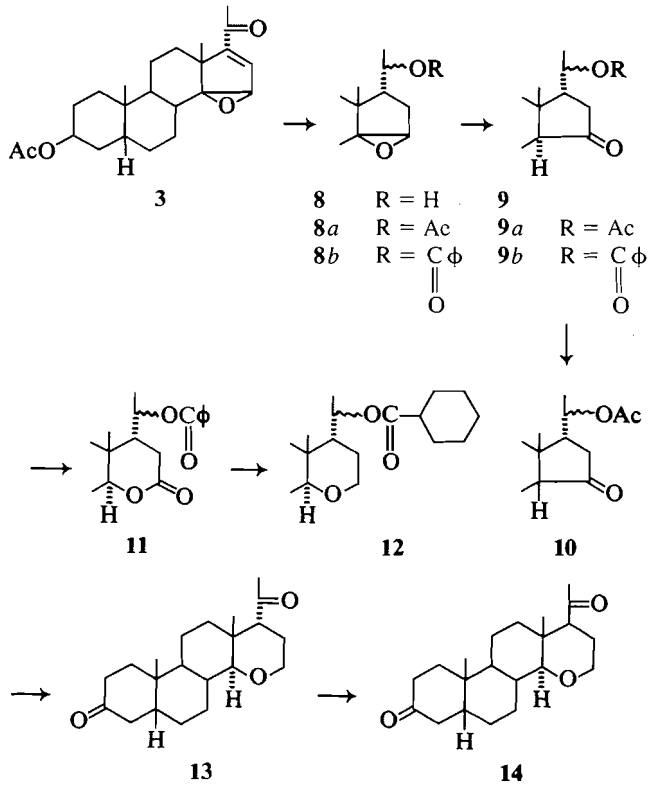

SCHEME 2

with the 8β-hydrogen which is equal to 8.5 Hz. This value is consistent with an angle of 180° (7), characteristic of a C/D ring junction.

Hydrogenolysis (9) of lactone **11** yielded the ether **12** which was then transformed by hydrolysis and oxidation (Jones' reagent) into diketone **13**. The latter yielded a novel diketone **14** when treated with KOH in MeOH. As demonstrated in Table 1, the position of the 18-CH_3 in **14** as compared with the one of **13** is indicative of the epimerization of the 17α-side chain. This is only possible with the proposed 14α-stereochemistry and constitutes an unequivocal proof. These results are shown in Scheme 2.

In a similar fashion, but starting this time from 15-oxo-estradiol (**15**) (8), the *D*-homo-oxaestradiol **19** and the 19-nor-*D*-homo-oxatestosterone derivatives **20**, **21**, and **22** were prepared. It is worthwhile to note that the ether **19** could not be obtained easily through the usual hydrogenolysis procedure. The aromatic ring of estrone was partially reduced in the presence of platinum. However, this difficulty was circumvented when the lactone **16** was reduced to lactol **17***a* using diisobutyl aluminum hydride. It was then acetylated (**17***b*) and hydrogenolysed to ether **18** using Pd/C. The methyl ether derivative **19** was then prepared (K_2CO_3; $(CH_3)_2SO_4$; KOH) and transformed into the derivatives **20**, **21**, and **22** using the classical Birch reduction method. These reactions are described in Scheme 3.

It is worthwhile to note in Table 1 that the 14β-H of the *cis*-lactone **7** is found at a lower field than the 14α-proton of lactones **11** and **16**. This deshielding effect is due to the anisotropy of the carbon–carbon bond and agrees (7*b*) with values described for ring A *cis* or *trans* lactones.

Experimental

Melting points are uncorrected. The ir spectra were taken on a Perkin–Elmer 225 ir spectrophotometer and nmr were recorded on a Varian A-60A spectrometer operating at 60 MHz; TMS was used as internal standard. Merck silica gel 60 (60–230 mesh) was used. The $[\alpha]_D$ were taken at 20–23°C in 1% chloroform solutions. Otherwise, the solvent is mentioned.

3β-Acetoxy-14,15β-epoxy-5β-pregn-16-en-20-one (3)

This product was prepared from 3β-acetoxy-5β-pregna-14,16-diene-20-one (**2**) (3) (520 g) using 85% *m*-chloroperbenzoic acid (200 g) according to the methods described by Nambara *et al.* (4) or by Tschesche and Müller-Albrecht (2).

The crude product obtained (520 g) was chromatographed on silica gel (ether–hexane, 1:1) to give the title product (220 g). The analytical sample was obtained after two crystallizations from methanol, mp 105–108°C $[\alpha]_D$ +60.2°; ir ($CHCl_3$): 3630, 3480, 1720, 1663, 1590, and 1250 cm^{-1}; nmr ($CDCl_3$): 1.00 (C19—CH_3), 1.32 (C18—CH_3), 2.05 (OAc), 2.26 (C21—CH_3), 3.84 (C15—H), 5.20 (C3—H), and 6.94 (C16—H) ppm. *Anal.* calcd. for $C_{23}H_{32}O_4$: C 74.16, H, 8.66; found: C 74.00, H 8.68

3β-Acetoxy-5β,14β,17α-pregnane-15,20-dione (6). Tschesche's method (2)

Method A

A freshly distilled solution of BF_3–ether complex (2.5 mL) in anhydrous ether (25 mL) was added, dropwise, to a stirred solution of the epoxide **3** (5.0 g) in dry benzene (1.25 L). The mixture was then stirred at room temperature for 64 h. It was washed with water, dried, and evaporated.The crude product obtained was chromatographed on silica gel (hexane–ether, 1:1) to give **5** (3.5 g).

A solution of the crude 16-ene derivative **5** (3.0 g) in absolute ethanol (75 mL) was hydrogenated at room temperature and atmospheric pressure over 10% Pd on barium sulfate (1.5 g) until no more hydrogen was absorbed (0.5 hour). The catalyst was removed by filtration and the filtrate evaporated. The crude product obtained was chromatographed on silica gel (ether–hexane, 1:1). The fractions containing the pure title product were mixed together and evaporated (1.3 g). The analytical sample was crystallized from CH_2Cl_2–ether, mp 188–190°C, $[\alpha]_D$ −40.1°; ir ($CHCl_3$): 1725, 1718, 1698, 1252, and 1018 cm^{-1}; nmr ($CDCl_3$): 0.92 (C19—CH_3), 1.43 (C18—CH_3), 2.04 (OAc), and 2.25 (C21—CH_3) ppm. *Anal.* calcd. for $C_{23}H_{34}O_4$: C 73.76, H 9.15; found: C 73.84, H 9.21.

Method B

On a treatment of the 16-ene derivative **5** (3.0 g) with zinc powder (12 g) in glacial acetic acid, the pure title product was again obtained after one crystallization from CH_2Cl_2–ether, yield 50%, mp 188–190°C.

Method C

3β-Acetoxy-14β-hydroxy-5β-pregn-16-ene-15,20-dione (4) (Method described by Mitsuhashi and Fukuoka (5))

A mixture of the epoxide (**3**) (44 g) in AcOH (1320 mL) was treated with CrO_3 (15.4 g) in AcOH (660 mL) and stirred at room temperature for 24 h. The acetic acid was removed under reduced pressure and the solid obtained taken into CH_2Cl_2. The organic layer was washed with 5% $NaHCO_3$, water dried, and evaporated. The residue was chromatographed on silica gel (benzene–EtOAc, 4:1) and the title product obtained crystallized from CH_2Cl_2–hexane to give the analytical sample, 19 g, mp 163–165°C, $[\alpha]_D$ +19.1°; nmr ($CDCl_3$): 0.93 (C19—CH_3), 1.26 (C18—CH_3), 2.46 (C21—CH_3), and 6.64 (=CH) ppm. *Anal.* calcd. for $C_{23}H_{32}O_5$: C 71.10, H 8.30; found: C 71.01, H 8.44.

3β-Acetoxy-5β,17α-pregnane-3,20-dione (6)

Zinc granules (70 g) were added to a solution of the dione (**4**) (7.0 g) and the mixture was heated under reflux for 1.5 hours. The solvent was removed under reduced pressure and the residue obtained was chromatographed on silica gel (benzene–EtOAc, 4:1). The title product obtained (5.6 g) was crystallized twice from CH_2Cl_2–ether (3.0 g), mp 186–189°C $[\alpha]_D$ −37.1°; nmr ($CDCl_3$): 0.92 (C19—CH_3), 1.43 (C18—CH_3), and 2.25 (C21—CH_3) ppm. *Anal.* calcd. for $C_{23}H_{34}O_4$: C 73.76, H 9.15; found: C 73.78, H 9.16.

Can. J. Chem. Downloaded from www.nrcresearchpress.com by 210.87.254.40 on 09/06/12
For personal use only.

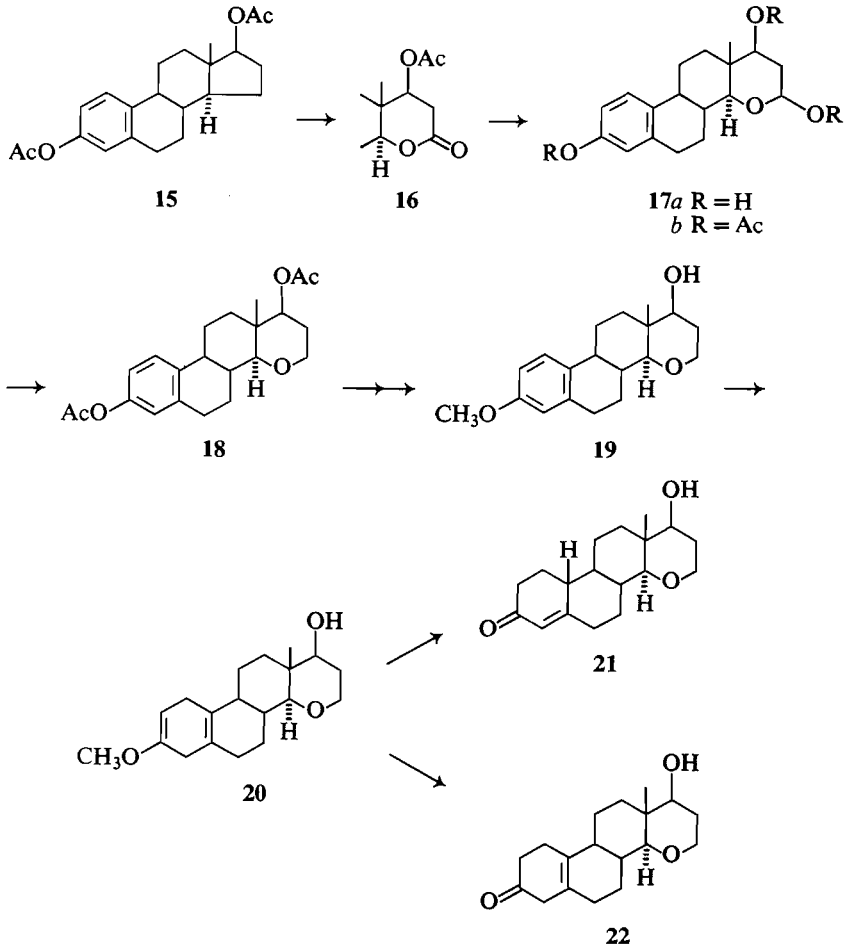

SCHEME 3

3β-Acetoxy-hydroxy-15-oxa-pregnan-16,20-dione (7)

A mixture of the dione (**6**) (1.0 g), $NaHCO_3$ (1.5 g), and *m*-chloroperbenzoic acid (2.0 g) was stirred in CH_2Cl_2 for 20 h. It was then heated under reflux for 3 hours. The mixture was diluted with more chloroform and washed in succession with $NaHCO_3$, water, 5% $Na_2S_2O_3$, water, dried, and evaporated. The crude product obtained was chromatographed on silica gel (benzene–EtOAc, 7:3) to give the title product (0.56 g). It was crystallized twice from ethane–hexane, mp 138–140°C, $[\alpha]_D$ +30.5°; ir ($CHCl_3$): broad C=O at 1715 cm^{-1}; nmr ($CDCl_3$): 0.96 (C19—CH_3), 1.17 (C18—CH_3), and 3.90 (C14—H, $W/2$ = 3.5 Hz) ppm. *Anal.* calcd. for $C_{23}H_{34}O_5$: C 70.74, H 8.78; found: C 70.91, H 8.81.

*3β-Acetoxy-20-benzoyloxy-14,15β-epoxy-5β,17α-pregnane (8*b)

A solution of $NaBH_4$ (50 g) in water (300 mL) was added to a solution at 0°C of the unsaturated ketone **3** (50 g) in methanol (3 L). The mixture was stirred at room for 2 hours and poured into water. The solid obtained was filtered, washed with water, dried, and crystallized from CH_2Cl_2–hexane to give the 20-alcohols (**8**) (25 g).

To a solution at 0°C of these alcohols (10 g) in pyridine (60 mL) was added benzoyl chloride (6 mL). The solution was let at room temperature overnight. It was then poured into water and the solid obtained filtered and dried. It was crystallized twice from EtOAc–hexane to give the pure title product (8.5 g), mp 204–206°C $[\alpha]_D$ +89.4°; ir ($CHCl_3$): 0.95 (C18—CH_3), 1.19 (C19—CH_3), 1.28 (C21—CH_3, d, J = 7 Hz), and 7.5 and 8.0 (5 aromatic H) ppm. *Anal.* calcd. for $C_{30}H_{40}O_5$: C 74.97, H 8.39; found: C 75.15, H 8.45.

*3β,20-Diacetoxy-14,15β-epoxy-5β,17α-pregnane (8*a)

The 20-alcohols **8** (1.0 g) were acetylated in the usual fashion and the product isolated used as such.

*3β,20-Diacetoxy-5β,14α-17α-pregnan-15-one (9*a)

A freshly distilled solution of ethereal BF_3 (0.55 mL) in dry ether (15 mL) was added dropwise over a period of 10 min to a solution of the diacetate **8***a* (1.0 g) in dry benzene (100 mL). The mixture was stirred overnight, washed with water, dried, and evaporated.

The crude product obtained (1.0 g) was chromatographed on silica gel (EtOAc/C_6H_6, 5:1) and the product obtained crystallized twice from ether–hexane to give the pure title product (315 mg), mp 136–138°C; ir: ($CHCl_3$): 1718, 1245, and 1014 cm^{-1}; ord (*C* 10.4 mg/mL; CH_3OH) 20°C: $[\phi]_{350}$ + 960°; $[\phi]_{316}$ + 3460°; $[\phi]_{298}$ O°; $[\phi]_{274}$ −5600; $[\phi]_{249}$ −3900; $[\phi]_{227}$ −5100; cd Mμ (ΔE); 320 (+0.4), 296 (+1.6), 267 (+0.4); nmr ($CDCl_3$): 0.88 (C19—CH_3), 0.98 (C18—CH_3), 1.25 (C21—CH_3, d, J = 6 Hz), and 2.04 (OAc) ppm. *Anal.* calcd. for $C_{25}H_{38}O_5$: C 71.74, H 9.15; found: C 71.71, H 9.13.

*3β-Acetoxy-20-benzoyloxy-5β,17α-pregnan-15-one (9*b)

This compound was prepared as for **9***a*, starting from **8***b* (8.6 g). The crude product isolated was chromatographed on silica gel to give the title product (6.2 g) which was used as such for the following reaction. The nmr spectrum ($CDCl_3$): 0.92 (C19—CH_3), 0.97 (C18—CH_3), 1.78 (C21—CH_3, d, J = 7 Hz), and 2.04 (OAc) and 7.56 and 8.0 (5 ar H) ppm.

3β,20-Diacetoxy-5β,14α,17α-pregnan-15-one (10)

A solution of the diacetate **9***a* (200 mg) in methanol (40 mL) containing KOH (2.0 g) was stirred at 60°C for 2 hours. Most of the methanol was evaporated under reduced pressure, water was added, and the solid obtained filtered. It was taken into CH_2Cl_2, the organic solution was washed with water, dried, and evaporated.

The crude product obtained (0.165 g) was acetylated (pyridine–Ac_2O) and the product isolated chromatographed on silica gel

Can. J. Chem. Downloaded from www.nrcresearchpress.com by 210.87.254.40 on 09/06/12
For personal use only.

Can. J. Chem. Downloaded from www.nrcresearchpress.com by 210.87.254.40 on 09/06/12
For personal use only.

(EtOAc–hexane, 1:5). The material obtained was crystallized twice from ether–hexane to give the pure title product (127 mg), yield 63%, mp 170–172°C; ir ($CHCl_3$): 1720, 1240, and 1017 cm^{-1}; ord (c 10.8 mg/mL; CH_3OH), 20°C: $[\phi]_{350}$ −670°; $[\phi]_{326}$ −2350°, $[\phi]_{308}$ 0°; $[\phi]_{285}$ +3400; $[\phi]_{233}$ +1800°; cd Mμ (ΔE) = 320 (−0.8), 305 (−1.48), 287 (−0.8); nmr ($CDCl_3$): 0.91 (C19—CH_3), 1.18 (C21—CH_3, d, J = 6 Hz), 1.25 (C18—CH_3), and 2.04 (OAc) ppm. *Anal.* calcd. for $C_{25}H_{38}O_5$: C 71.74, H 9.15; found: C 71.60, H 9.15.

*3β-Acetoxy-20-benzoyloxy-*D*-homo-15-oxa-17a-pregnan-16-one (**11**)*

An ice-cold solution made of trifluoroacetic anhydride (18.6 mL) and 90% hydrogen peroxide (3.7 mL) in CH_2Cl_2 (125 mL) was added dropwise to a stirred suspension of the 15-ketone **9***b* (6.2 g) and disodium hydrogen phosphate (12.4 g) in CH_2Cl_2 (150 mL). The mixture was then stirred at room temperature for 48 h, diluted with more CH_2Cl_2, washed with saturated solutions of $NaHCO_3$, NaI, $Na_2S_2O_3$, water, dried, and evaporated.

The product was chromatographed on silica gel (EtOAc–benzene, 1:1) to give the title product (3.8 g) as an oil. It was used as such for the following reaction. The nmr ($CDCl_3$): 0.96 (C19—CH_3), 1.09 (C18—CH_3), 1.38 (C21—CH_3, d, J = 5 Hz), 3.77 (C14—H, d, J = 8.5 Hz), and 7.54 and 8.03 (5 aromatic H) ppm.

*3β-Acetoxy-20-cyclohexylcarbonyloxy-*D*-homo-15-oxa-5β,17α-pregnane (**12**)*

A solution of lactone (**11**) (3.8 g) in acetic acid (50 mL) was added to a mixture of prehydrogenated 83% PtO_2 (1.8 g) in acetic acid (20 mL) containing perchloric acid (0.18 mL). The whole was stirred at room temperature and atmospheric pressure until no more hydrogen was absorbed.

The catalyst was removed by filtration and the filtrate diluted with CH_2Cl_2. The organic solution was washed with water, dried, and evaporated. The crude product obtained (3.5 g) was chromatographed on silica gel (ether/hexane, 1:1) to give the title product (1.2 g).

The analytical sample was crystallized three times from cold petroleum ether (30–60°C), mp 133–134°C, $[\alpha]_D$ −3.4°; nmr ($CDCl_3$): 0.96 (C19—CH_3), 1.10 (C18—CH_3), 1.25 (C21—CH_3, d, J = 7 Hz), and 5.25 (C20—H, quartet, J = 6.5 Hz) ppm. *Anal.* calcd. for $C_{30}H_{48}O_5$: C 73.73, H 9.90; found: C 73.67, H 10.00.

*D-Homo-15-oxa-5β,17aα-pregnan-3,20-dione (**13**)*

A solution of the diester (**12**) (1.0 g) in ethanol (50 mL) and water (10 mL) was heated under reflux in presence of KOH (1.0 g). Most of the ethanol was evaporated under reduced pressure, water was added, and the solid obtained filtered and dried.

A solution of the crude diol isolated (0.8 g) in acetone (30 mL) was oxidized with Jones' reagent in the usual fashion. The product obtained was chromatographed on silica gel (EtOAc/benzene, 1:3) to give the title product (0.5 g). The analytical sample was crystallized twice from acetone–hexane, mp 159–161°C, $[\alpha]_D$ −61.9°; ir ($CHCl_3$): 1698 and 1080 cm^{-1}; nmr ($CDCl_3$): 1.01 (C19—CH_3), 1.12 (C18—CH_3), 2.20 (C21—CH_3), and 3.40 (C14—H) ppm. *Anal.* calcd. for $C_{21}H_{32}O_3$: C 75.85, H 9.70 found: C 75.50, H 9.69.

*D-Homo-15-oxa,5β,17aβ-pregnane-3,2-dione (**14**)*

A solution of the dione (**13**) (6.0 g) in 5% KOH in methanol (1.2 L) was heated at 60°C for 2 hours. Most of the methanol was evaporated and the remaining diluted with water and extracted with EtOAc. The organic solution was washed until neutral, dried, and evaporated. The crude product isolated was chromatographed on silica gel (ether–hexane, 2:1) to give the title product (4.2 g). The analytical sample was crystallized twice from acetone–hexane (3.2 g), mp 133–135°C, $[\alpha]_D$ +42.1°; ir ($CHCl_3$): 1698 and 1100 cm^{-1}; nmr ($CDCl_3$): 1.01 (C19—CH_3 and C18—CH_3) and 2.16 (C21—CH_3) ppm. *Anal.* calcd. for $C_{21}H_{32}O_3$: C 75.86, H 9.70; found: 76.00, H 9.85.

*3β,17β-Diacetoxy-estra-1,3,5 (10)-trien-15-one (**15**)*

This compound was prepared from estrone as described by Pettit and Brown (8); mp 174–176°C, $[\alpha]_D$ 71.3°; (lit. mp 173–174°C, $[\alpha]_{589}$ + 90°, $[\alpha]_{350}$ +54°); nmr ($CDCl_3$): 0.91 (C18—CH_3) and 5.03 (C17—H, t, J = 8.5 Hz) ppm. *Anal.* calcd. for $C_{22}H_{26}O_5$: C 71.33, H 7.07; found: C 71.14, H 6.91.

*3,17aβ-Dihydroxy-*D*-homo-15-oxaestra-1,3,5(10)-trien-16-one (**16**)*

m-Chloroperbenzoic acid (13 g) was added to a cooled suspension of the 15-ketone (20 g) and sodium bicarbonate (10 g) in CH_2Cl_2 (400 mL). The mixture was stirred at room temperature for 24 h. More peracid (13 g) and bicarbonate (10 g) were added and stirring continued for two more hours. The material in suspension was removed by filtration and the filtrate washed with a 5% solution of sodium bisulfite, water, dried, and evaporated. The crude product obtained was chromatographed on silica gel (C_6H_6/EtOAc, 9:1). Some starting ketone (4.7 g) was recuperated, followed by the title product (16 g).

The latter was crystallized from CH_2Cl_2/ether, mp 156–158°C, $[\alpha]_D$ +12.9°; ir ($CHCl_3$): 1740, 1610, 1580, and 1495 cm^{-1}; uv (EtOH): λ_{max} 267, 274; ε, 695 and 665; nmr ($CDCl_3$): 1.03 (C18—CH_3), 3.78 (C14—H, d, J = 10.7 Hz), and 6.65 and 7.50 (3 ar H) ppm. *Anal.* calcd. for $C_{22}H_{20}O_6$: C 68.38, H 6.78; found: C 68.64, H 6.78.

*3,16,17aα-Triacetoxy-*D*-homo-15-oxaestra-1,3,5,(10)-triene (**17**b)*

A solution of 3.2 equiv. of diisobutyl aluminum hydride in hexane was added dropwise to a solution at −20°C of lactone **16** (2.0 g) in dry THF (60 mL). The mixture was stirred at −20°C for 30 min and the reaction quenched with a saturated solution of sodium potassium tartrate. The organic layer was separated and diluted with EtOAc. It was washed with water, dried, and evaporated. The crude product obtained was filtered on silca gel (acetone/benzene, 1:2) to give the triol **17***a* (1.3 g) which was acetylated in the usual fashion. The crude triacetate isolated was crystallized twice from i-propyl ether to give the pure title product, mp 184–185°C, $[\alpha]_D$ +43.9°; ir ($CHCl_3$): 1747, 1725 inflexion, and 1060 cm^{-1}; nmr ($CDCl_3$): 1.05 (C18—CH_3), and 6.67 and 7.50 (3 ar H) ppm. *Anal.* calcd. for $C_{24}H_{30}O_7$: C 66.96, H 7.06; found: C 66.77, H 7.05.

*3,17aα-Diacetate-*D*-homo-15-oxaestra-1,3,5(10)-triene (**18**)*

A solution of the triacetate **17***b* (6.0 g) in acetic acid (250 mL) was hydrogenated at room temperature and atmospheric pressure over 10% Pd/C (3.0 g) until no more hydrogen was absorbed (~48 h). The catalyst was removed by filtration and the filtrate evaporated. The crude product obtained was chromatographed on silica gel (hexane/EtOAc, 5:1) to give the title product (3.6 g). It was crystallized from hexane, mp 148–150°C, $[\alpha]_D$ +10.6°; ir ($CHCl_3$): 1748, 1723, 1608, 1580, and 1493 cm^{-1}; nmr ($CDCl_3$): 1.03 (C18—CH_3), and 6.67 and 7.50 (3 ar H) ppm. *Anal.* calcd. for $C_{22}H_{28}O_5$: C 70.94, H 7.58; found: C 70.94, H 7.39.

*The 15-oxa-*D*-homoestren-3-one derivatives **21** and **22***

A mixture of the diacetate **18** (3.2 g) and sodium carbonate (2.4 g) in methanol (380 mL) containing water (120 mL) was heated under reflux for 4 hours. Most of the methanol was evaporated and the remaining mixture extracted with CH_2Cl_2. The organic solution was dried and evaporated. The crude oil obtained (2.3 g) was treated with dimethylsulfate (18.5 mL) and 50% KOH (18.5 mL) in the usual manner to give the *3,17aβ-dihydroxy-*D*-homo-15-oxaestra-1,3,5(10)-triene-3-methylether (2.2 g) (**19**)*; uv (MeOH): λ_{max} 286, 275; ε = 2056, 2142. This product was used as such for the following reaction.

Lithium wire (2.25 g) was added in portions over a period of 10 min to a stirred solution at reflux of the 3-methyl ether **19** (2.1 g) in dry ether (120 mL) and distilled ammonia (~200 mL). Absolute ethanol (45 mL) was then added dropwise over a period of 1 hour. Ammonia was evaporated and the mixture diluted with water. The ether layer was recuperated and the water layer extracted once more with ether. The ethereal solution was washed with a solution made of KOH (35 g) in water (25 mL) and MeOH (100 mL) then with water, dried, and evaporated. The crude crystalline *17aβ-hydroxy-3-methoxy-15-oxa-*D*-homo-ester,2,5(10)-diene (**20**) isolated* (2.1 g) was used for the following reactions without further purification. Infrared ($CHCl_3$): 1695 and 1665 cm^{-1}.

A suspension of the methoxy-diene (**20**) (1.05 g) in methanol (20 mL) containing concentrated HCl (2.1 mL) was stirred at room temperature for 1 hour. It was then diluted with water and most of

the methanol evaporated under reduced pressure. The mixture was extracted with CH_2Cl_2. The organic solution was washed with water, dried, and evaporated. The crude product obtained was chromatographed on silica gel (EtOA/C_6H_6, 1:5) and the *17aβ-hydroxy-15-oxa*-D-*homoestr-4-en-3-one* obtained was crystallized from CH_2Cl_2/hexane to give the analytical sample, mp 162–164°C, $[\alpha]_D$ +13.7°; ir ($CHCl_3$): 3600, 3460, 1658, 1610, and 1095 cm^{-1}; nmr ($CDCl_3$): 0.96 (C18—CH_3), 2.03 (OH), 3.45 (C15—H, m), 4.04 (C17—H, m), and 5.86 (C4—H, s) ppm. *Anal.* calcd. for $C_{18}H_{26}O_3$: C 74.45, H 9.02; found: C 74.28, H 9.06.

A suspension of the methoxydiene (**20**) (1.05 g), methanol (21 mL), and acetic acid (2.1 mL) was heated under reflux for 15 min. It was cooled and poured into ice-cold water. The solid obtained was filtered, washed, and dried.

The crude product obtained was crystallized from CH_2Cl_2–hexane to give the *17αβ-hydroxy-15-oxa*-D-*homoestr-5(10-ene-3-one (22)* (0.5 g), yield 50%, mp 178–180°C; ir ($CHCl_3$): 3600, 3470, 1704, and 1090 cm^{-1}; nmr ($CDCl_3$): 0.94 (C18—CH_3), 1.85 (OH), 2.44 (C18—2H, m), 2.75 (C4–2H, m), 3.45 (C15—H, m) and 4.05 (C17—H, m) ppm. *Anal.* calcd. for $C_{18}H_{20}O_3$: C 74.45, H 9.02; found: 74.01, H 9.17.

Acknowledgements

The authors wish to thank Dr. G. Schilling and his associates for the analytical data and Dr. K. Wiesner for stimulating discussions.

1. J. M. FERLAND and Y. LEFEBVRE. Can. J. Chem. **62**, 309 (1984).
2. R. TSCHESCHE and H. MÜLLER-ALBRECHT. Chem. Ber. **103**, 350 (1970).
3. G. BACH, J. CAPITAINE, and CH. R. ENGEL. Can. J. Chem. **46**, 733 (1968).
4. T. NAMBARA, S. GOYA, J. GOTA, and K. SHIMADA. Chem. Pharm. Bull. **16**, 2228 (1968).
5. H. MITSUHASHI and M. FUKUOKA. Chem. Pharm. Bull. **14**, 809 (1966).
6. G. SNATZKE, H. PIEPER, and R. TSCHESCHE. Tetrahedron **20**, 107 (1964).
7. (*a*) M. KARPLUS. J. Chem. Phys. **30**, 11 (1959); (*b*) J. T. EDWARD and J. M. FERLAND. Can. J. Chem. **44**, 1311 (1966).
8. G. R. PETTIT and T. H. BROWN. J. Chem. Soc. 2024 (1967).
9. J. T. EDWARD and J. M. FERLAND. Can. J. Chem. **44**, 1299 (1966).

Can. J. Chem. Downloaded from www.nrcresearchpress.com by 210.87.254.40 on 09/06/12
For personal use only.

Studies in the usnic acid series. IX.[1] The biodegradation of (+)-usnic acid by *Mucor globosus*

JAMES P. KUTNEY, JEFFREY D. LEMAN, PHILLIP J. SALISBURY, AND TREVOR YEE
Department of Chemistry, University of British Columbia, 2036 Main Mall, University Campus, Vancouver, B.C., Canada V6T 1Y6

AND

IGNACIO H. SÁNCHEZ
Instituto de Química, Universidad Nacional Autónoma de México, Circuito Exterior, Ciudad Universitaria, Coyoacán 04510, México, D. F., México

Received July 8, 1983

JAMES P. KUTNEY, JEFFREY D. LEMAN, PHILLIP J. SALISBURY, TREVOR YEE, and IGNACIO H. SÁNCHEZ. Can. J. Chem. **62**, 320 (1984).

The microbial degradation of the lichen antibiotic (+)-usnic acid (**1**) by means of the fungal isolate *Mucor globosus* has been studied. It is shown that this organism provides the metabolite (+)-2-desacetylusnic acid (**2**) as a major component via a novel deacylation reaction.

JAMES P. KUTNEY, JEFFREY D. LEMAN, PHILLIP J. SALISBURY, TREVOR YEE et IGNACIO H. SÁNCHEZ. Can. J. Chem. **62**, 320 (1984).

On a étudié la dégradation microbienne de l'acide (+) usnique (**1**) un antibiotique de lichen, par le *Mucor globosus*, un produit isolé de champignons. On montre que le métabolite principal fournit par cet organisme est l'acide (+) désacétyl-2 usnique (**2**) formé par l'intermédiaire d'une nouvelle réaction de désacylation.

[Traduit par le journal]

Can. J. Chem. Downloaded from www.nrcresearchpress.com by 210.87.254.6 on 09/06/12
For personal use only.

As a continuation of our studies (1, 2) on the microbial degradation of the lichen antibiotic (+)-usnic acid (**1**) (3, 4), the fungal isolate *Mucor globosus* (Fischer, 1892) (5), isolated from surface soil samples collected in the Whistler Mountain area of British Columbia, was chosen as a promising candidate for further investigation. This organism is rather unique in the sense that it is capable of converting **1** quite efficiently via a novel and selective deacylation reaction predominantly to the metabolite (+)-2-desacetylusnic acid (**2**). In comparison, our preliminary studies of the biodegradation of **1** by the fungus *Mortierella isabellina* (1, 2) had yielded complex mixtures of metabolites. The new metabolite (**2**) was isolated from the fermentation broth of *Mucor globosus* essentially as a single major component. We wish to record our detailed investigations concerning the structure elucidation of **2** and its chemical reactions which are of general interest within the usnic acid area.

By following fermentation conditions similar to those developed during our other biodegradation studies (1, 2) (see Experimental), a *Mucor globosus* isolate, strain MU-1, was shown to degrade samples of (+)-usnic acid (**1**) to a single component, isolated in up to 32% yield as yellow crystals, mp 221–222°C, in addition to some recovered substrate (11%).

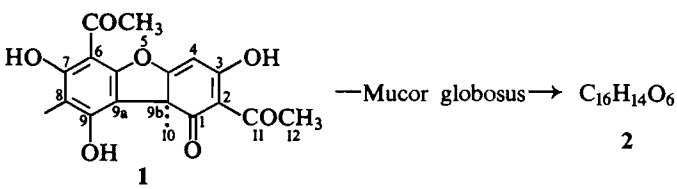

1 **2**

This material had the molecular formula $C_{16}H_{14}O_6$ as shown by high resolution mass spectrometry and elemental analysis, and was optically active, $[\alpha]_D^{27}$ +635° (CH_3CN). Its ultraviolet spectrum (λ_{max} (MeOH): 330, 287, 218 nm) resembled quite closely that of the starting material (6) and suggested that the aromatic chromophore was unaltered. However, important structural differences were indicated by its infrared spectrum, which lacked the band characteristic of the chelated non-aromatic ring C acetyl grouping, usually occurring in the 1560–1540 cm^{-1} region,[2] suggesting that a novel deacylation of the alicyclic β-triketone system had taken place.

The same conclusion was obtained upon analysis of its ^1H nmr spectrum, which showed the two three-proton singlets corresponding to the angular and aromatic methyl groups (δ: 1.70 and 2.05 ppm, respectively). Whereas in usnic acid (**1**) the absorption characteristics of the C2- and C6-acetyl groupings coalesce into a six-proton singlet at δ: 2.70, compound **2** shows only one singlet (3H) at δ: 2.65 assigned to the ring A acetyl since the corresponding chelated phenolic hydroxyl at the C-7 position appears at its normal position (δ: 13.31). Furthermore, the C-4 olefinic proton is now observed as a doublet (J = 2 Hz) centred at δ: 5.85 showing long range coupling (8) with a new one-proton doublet at δ: 5.38 that can now be attributed to the C-2 hydrogen atom.

As expected, its mass spectral fragmentation pattern (Scheme 1) completely agreed with the proposed structure **2**. Specifically, the retro Diels–Alder fragmentation pathway, arising from cleavage of the C-ring, produces a fragment with 42 mass units less than that resulting from the equivalent process in usnic acid (**1**) itself (9) and further pinpoints the place where the fungal deacylation had taken place.

Further evidence for structure **2** was obtained through the appropriate chemical degradation reactions or preparation of derivatives. On the one hand, acetylation and subsequent ozonolysis furnished the known (10) α-coumaranone diacetate **3**, whereas treatment with 75% aqueous potassium hydroxide afforded usnetic acid (**4**), identical to that obtained directly from **1** (11).

[1] For Part VIII, see ref. 1.

[2] For a discussion of the infrared spectrum of (+)-usnic acid (**1**), see ref. 7.

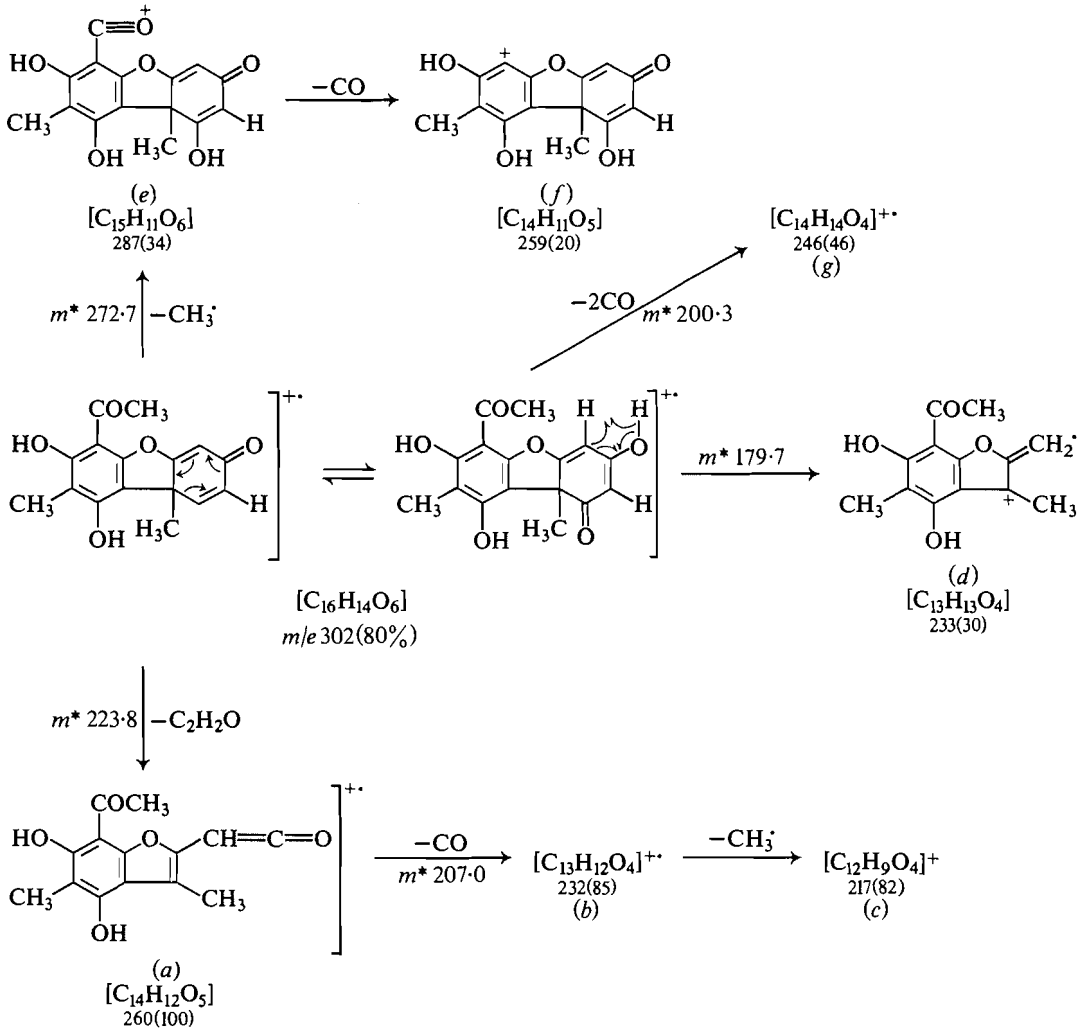

SCHEME 1. Postulated fragmentation pattern for (+)-2-desacetylusnic acid (**2**)

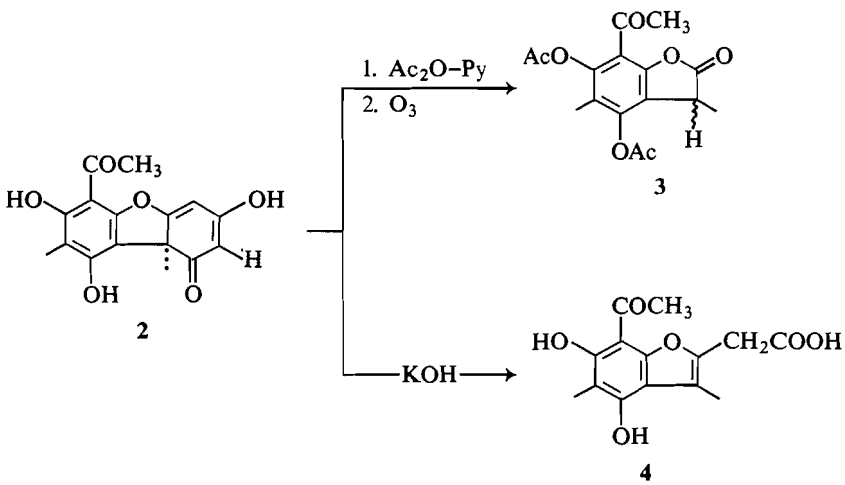

On the other hand, **2** was converted into ethyl acetusnetate (**5**) by conditions (4) (ethyl alcohol in a sealed tube at 150°C) under which usnic acid (1) gives rise to the C-acetyl analog, usnic acid ethoxide (**6**). However, under more vigorous treatment (12) (e.g., heating at 190°C in a sealed tube) cleavage of the C-ring in **1** occurs with concomitant deacylation to furnish again the β-ketoester **5**.

Further proof of the ring C enolic β-diketone system was obtained through the formation of its methyl enol ether **7** and the corresponding enol acetate **8** derivatives by treatment with excess ethereal diazomethane in methanolic solution,[3] or by a mild aluminium trichloride-catalyzed enol acetylation, respectively.

[3] For the formation of ether derivatives of (+)-usnic acid (**1**), see ref. 13.

Can. J. Chem. Downloaded from www.nrcresearchpress.com by 210.87.254.6 on 09/06/12
For personal use only.

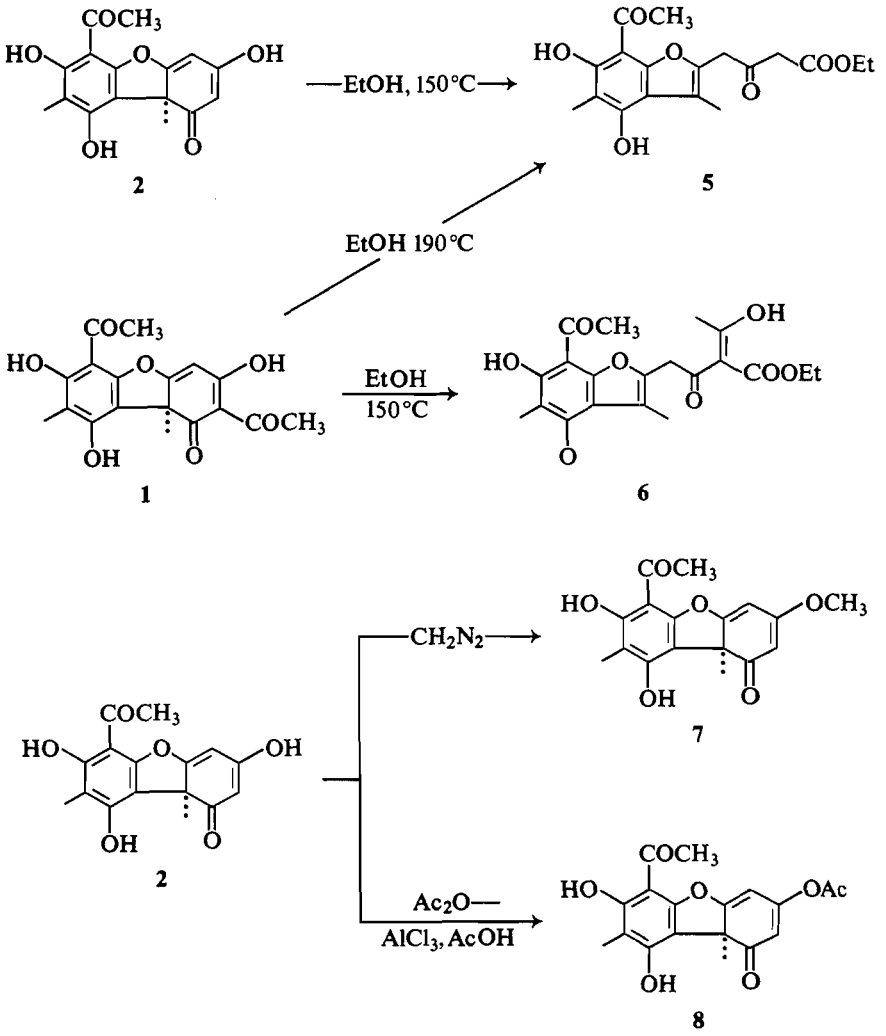

Finally, since the direct C-acylation of **2** was not possible, a direct chemical correlation with **1** was attempted by means of its laboratory preparation. The key step of our degradative scheme consisted of the generation of a C-ring α-acetoxy-β-diketone derivative by a chemoselective process whereby reaction would occur preferentially with an (alicyclic) enolic α-acetyl-β-diketone system rather than with a chelated aromatic methyl ketone. The type of transformation required here (i.e., a Baeyer–Villiger oxidation), has been successfully carried out in other alicyclic β-triketone systems using either alkaline peroxide (14) or peracids (15), although no information regarding the aromatic vs. alicyclic chemoselectivity was available. To our delight, when (+)-usnic acid (**1**) was reacted with 30% hydrogen peroxide in dry pyridine at room temperature, an 83% yield of the desired oily α-acetoxy derivative **9** was realized. This compound proved identical as well to another of the metabolites characterized during our studies with the fungal isolate *Mortierella isabellina* (1). Moreover, during this work we were also able to show that chromium(II) chloride reaction[4] of (natural or synthetic) **9** afforded a 72% yield of (+)-2-desacetyl usnic acid (**2**), identical in all respects to the isolated metabolite.

Finally, it should be noted that prior to the development and completion of the above chemistry, it was possible to obtain an X-ray analysis of **2**[5] and the latter eliminated any doubt about the structure as proposed herein. Also the isolation of **2** as a

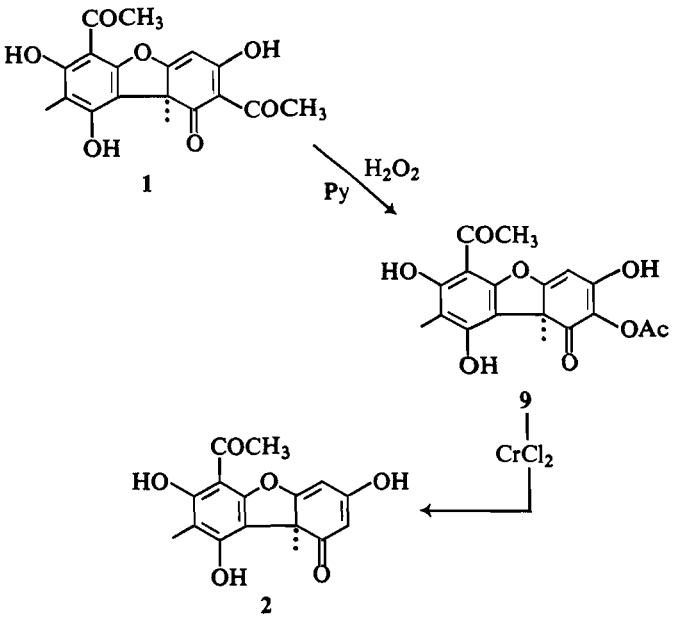

[4] For a recent review of the reduction of various functional groups with chromium(II) salts, see ref. 16.

[5] An X-ray diffraction study of (+)-2-desacetylusnic acid (**2**) has already been performed; see ref. 17.

Can. J. Chem. Downloaded from www.nrcresearchpress.com by 210.87.254.6 on 09/06/12
For personal use only.

Can. J. Chem. Downloaded from www.nrcresearchpress.com by 210.87.254.6 on 09/06/12
For personal use only.

minor component from our studies with *Mortierella isabellina* has been achieved (1).

Experimental

Melting points were determined on a Kofler block and are uncorrected. Ultraviolet (uv) spectra were recorded on a Cary 15 spectrophotometer in methanol solution (unless otherwise noted). The wavelength of the absorption maxima are reported in nanometres (nm). Infrared (ir) spectra were measured routinely on a Perkin–Elmer model 710 spectrophotometer. Analytical or comparison spectra were recorded on a Perkin–Elmer model 457 spectrophotometer using matched cells with a cell path of 0.2 mm in chloroform solution. Calibration was achieved using the 1601 cm^{-1} absorption band of polystyrene. The absorption maxima are quoted in wave numbers (cm^{-1}). Proton magnetic resonance (^{1}Hmr) spectra were measured at 60 or 100 MHz in deuterochloroform ($CDCl_3$) solution (unless otherwise indicated) at room temperature. Line positions are given in the δ (ppm) scale using tetramethylsilane (TMS) as internal standard. The integrated peak areas, multiplicity, and proton assignments are indicated in parentheses. Low resolution mass (ms) spectra were determined on either an AEI-902 or an Atlas CH-4B mass spectrometer, with high resolution mass spectra being recorded exclusively on an AEI-MS-902 mass spectrometer. Optical rotations ($[\alpha]_D$) were measured on a Perkin–Elmer model 141 polarimeter at the sodium D line in chloroform solution (unless otherwise noted) using cells with a 0.1-dm path. Circular dichroism (cd) spectra were obtained on a Jasco model J-20 spectropolarimeter in methanol solution. Microanalyses were performed by Mr. P. Borda of the Microanalytical Laboratory, University of British Columbia. Merck silica gel G (acc. to Stahl) impregnated with oxalic acid (2%) and with 2% fluorescent indicator added, was used as adsorbent for thin layer chromatography (tlc), unless otherwise noted. The tlc plates were activated in an oven at 90°C for 4 h before use. For qualitative chromatography, layers of 0.3-mm thickness were used and the spots were visualized by viewing under ultraviolet (uv) light or spraying with a 1% ethanolic ferric chloride solution. For preparative (plc) chromatography, large (20 × 20 and 20 × 60 cm) plates with a thicker layer (0.7 mm) were used. The developing systems were A, petroleum ether (30–60°C) – acetone (4:1), and B, chloroform – ethyl acetate (3:2), unless otherwise indicated. Column chromatography was performed on either Mackerey–Nagel (0.2–0.5 mm grain size) or Merck 60 (0.063–0.2 mm grain size) silica gel. (+)-Usnic acid was obtained from Koch-Light Laboratories, England.

Maintenance and growth conditions

A sample of the isolated used, identified as *Mucor globosus*, strain MU-1, was maintained on modified malt agar plates (2) by transfer every two weeks from a two-week old agar plate growth into a fresh sterile plate.

A "stock culture" of the purified fungal isolate was stored on modified malt agar in culture tubes placed in the refrigerator.

Aseptic techniques were used throughout in handling the cultures. To ensure proper aeration, the volume of the nutrient solution (2) should never exceed about two-fifths of the total volume of the flask.

Media and stock solutions have been fully described (2).

Fermentation conditions and extraction procedures

Surface soil samples obtained by Dr. J. D. Leman in the Whistler Mountain area produced, by serial dilution of soil and plating on modified malt agar, a fungal isolate able to degrade (+)-usnic acid (**1**). The culture has since been purified and was characterized as *Mucor globosus* by Dr. John J. Ellis of the United States Department of Agriculture, Agricultural Research Service, Northern Utilization Research and Development Division, Fermentation Laboratory, Peoria, Illinois 61604, U.S.A.

Inoculation of shake culture flasks was carried out by transferring a small segment (about 1/4-in. square) of active growth (not older than 2 weeks) and agar to a sterile Erlenmeyer flask containing an appropriate volume of nutrient medium.

The biodegradation of (+)-usnic acid (1). Isolation of (+)-2-desacetyl-usnic acid (2) (6-acetyl-1,9b-dihydro-8,9bα-dimethyl-3,7,9-trihydroxy-1-oxodibenzofuran)

The (+)-usnic acid (**1**) (190 mg, 0.552 mmol) was added as an acetone solution to a 3–4 days old liquid culture of *Mucor globosus* (strain MU-1, 300 mL) and the flask agitated on a rotary shaker at room temperature for 14 days. The cells were then filtered off, suspended in benzene (50 mL), and stirred at room temperature for one hour. The organic extract was dried over anhydrous sodium sulfate and evaporated under reduced pressure to produce (+)-usnic acid (**1**) (22.1 mg, 0.0642 mmol; 11.6%), yellow crystals from chloroform – ethyl alcohol, mp 201–202°C; mixture mp with authentic (+)-usnic acid, 201–203°C.

The clear filtrate (300 mL, pH 8) was extracted with ethyl acetate (2 × 100 mL), and the combined extracts washed with water, dried over anhydrous sodium sulfate, and evaporated under reduced pressure. The residue (46.2 mg) was shown by thin layer chromatography (silica gel – oxalic acid plates, solvent A, run twice) to consist mainly of dark brown polar and base line materials and was not investigated further.

The yellow mother liquors were then acidified with tartaric acid to pH 4 and extracted with ethyl acetate (2 × 100 mL). The combined extracts were washed with water, dried over anhydrous sodium sulfate, and evaporated under reduced pressure to afford a yellow residue (68.3 mg). Purification by preparative layer chromatography (silica gel – oxalic acid plates, solvent A) produced (+)-2-desacetylusnic acid (**2**) (54.2 mg, 0.179 mmol; 32.4%), bright yellow prisms from ethyl acetate – petroleum ether, mp 221–222°C; $[\alpha]_D^{26}$ (CH_3CN) +635° (*c*, 0.063); uv λ_{max} (log ε): 330 (3.49), 287 (4.03), 218 (4.28); ir (Nujol) ν_{max}: 3300–2500 (OH, chelated), 1670 (C=O, dienone system), 1625 (C=O, chelated aromatic acetyl), 1620, 1600 (C=C); ^{1}Hmr (100 MHz, $CDCl_3$ – DMSO-d_6) δ: 1.70 (3H, singlet, C9b—CH_3), 2.05 (3H, singlet, C8—CH_3), 2.65 (3H, singlet, C6—COCH_3), 5.38 (1H, doublet, *J* = 2 Hz, C2—*H*), 5.85 (1H, doublet, *J* = 2 Hz, C4—*H*), 11.85 (1H, broad, C9—O*H*), 13.31 (1H, singlet, C7—O*H*) ppm; ms (70 eV) *m/e*: 302 (M^+), 287 (*M* − 15), 260 (base peak), 246, 233, 232, 217. *Anal.* calcd. for $C_{16}H_{14}O_6$: C 63.57, H 4.67%; found: C 63.47, H 4.66%. High resolution molecular weight determination calcd.: 302.0789; found: 302.0749; cd λ_{max} (Δε): 375 (+0.94), 333 (+6.08), 298 (−4.32), 273 (+5.27), 238 (−5.67).

Ozonolysis of (+)-2-desacetylusnic acid (2). Isolation of (±)-7-acetyl-3,5-dimethyl-4,6-dihydroxy-coumaran-2-one diacetate (3)

A solution of (+)-2-desacetylusnic acid (**2**) (100 mg, 0.231 mmol) in a 1:1 mixture of acetic anhydride – pyridine (6 mL) was allowed to stand at room temperature overnight. The reaction mixture was then poured onto ice (20 g), extracted with ethyl acetate (3 × 10 mL), and the combined extracts washed with water, dried over anhydrous sodium sulfate, and evaporated under reduced pressure. The crude residue (135 mg) was dissolved in dry carbon tetrachloride (10 mL) and cooled to 0°C in an ice bath. Ozonized oxygen (26 mg O_3/minute) was then bubbled through until the yellow color was discharged and the crystalline ozonide began to precipitate. The resulting suspension was then diluted with distilled water (10 mL) and heated to reflux in a steam bath for 15 min. The organic fraction was then evaporated, washed with 2% sodium bicarbonate solution, water, dried over anhydrous sodium sulfate, and evaporated under reduced pressure to produce (+)-7-acetyl-3,5-dimethyl-4,6-dihydroxycoumaran-2-one diacetate (**3**) (32.1 mg, 0.100 mmol; 30%), colorless crystals from ethyl alcohol, mp 131–132°C (lit. (4) mp 130–132°C); $[\alpha]_D$ (CH_3CN) 0° (*c*, 0.17075); uv λ_{max} (log ε): 297 (3.19), 245 (3.65), 213 (4.14); ir ν_{max}: 1815 (C=O, lactone), 1765 (C=O, acetates), 1690 (C=O, aromatic acetyl), 1605 (C=C); ^{1}Hmr (100 MHz) δ: 1.50 (3H, doublet, *J* = 7.5 Hz, C3—CH_3), 1.98 (3H, singlet, C5—CH_3), 2.33 (3H, singlet, C4—OCOCH_3), 2.39 (3H, singlet, C6—OCOCH_3), 2.61 (3H, singlet, C7—COCH_3), 3.73 (1H, quartet, *J* = 7.5 Hz, C3—*H*) ppm; ms (70 eV) *m/e*: 320 (M^+), 278, 236 (base peak), 211, 208.

Can. J. Chem. Downloaded from www.nrcresearchpress.com by 210.87.254.6 on 09/06/12
For personal use only.

Anal. calcd. for $C_{16}H_{16}O_7 \cdot \frac{1}{4}H_2O$: C 59.16, H 5.12%; found: C 59.52, H 5.08%. High resolution molecular weight determination calcd. for $C_{16}H_{16}O_7$: 320.0895; found: 320.0877.

Base cleavage of (+)-2-desacetylusnic acid (2). Isolation of usnetic acid (4)

(+)-2-Desacetylusnic acid (**2**) (48 mg, 0.1589 mmol) in 75% potassium hydroxide (2 mL) was heated at 90–95°C (oil bath temperature) under nitrogen atmosphere for 25 min. The reaction mixture was cooled to 0°C (ice bath) and carefully acidified with 1 *N* hydrochloric acid. The resultant brown precipitate was filtered, washed with water, dried, and recrystallized from methanol to produce usnetic acid (27 mg, 0.0971 mmol; 61%), mp 208–210°C (lit. (4) mp 209–210°C); mixture mp with authentic usnetic acid, 209–210°C. Both samples displayed identical chromatographic and spectroscopic properties.

Conversion of (+)-2-desacetylusnic acid (2) to ethyl acetusnetate (5)

A suspension of (+)-2-desacetylusnic acid (**2**) (40 mg, 0.132 mmol) in absolute ethyl alcohol (8 mL) was heated in a sealed tube at 150°C for 5 hours. The tube was then cooled, opened, and stored at 0°C overnight. The pale yellow precipitate was filtered and recrystallized from ethyl alcohol to produce ethyl acetusnetate (5) (30 mg, 0.0862 mmol; 65%), pale yellow needles, mp 147–149°C (lit. (4) mp 150°C); mixture mp with authentic ethyl acetusnetate, 147–149°C; $[\alpha]_D$ (CH_3CN) 0° (*c*, 0.1775); uv λ_{max} (log ϵ): 346 (3.40), 301 (3.86), 243 (3.98); ir (Nujol) ν_{max}: 3600–3100, 2800–2400 (OH, chelated), 1725 (C=O, ester grouping of the β-ketoester side chain), 1700 (C=O, ketone of the β-ketoester side chain), 1620 (C=O, chelated aromatic acetyl; C=C), 1600 (C=C); ^{1}Hmr (100 MHz) δ: 1.22 (3H, triplet, J = 7 Hz, O—CH_2—CH_3), 2.10 (3H, singlet, C5—CH_3), 2.30 (3H, singlet, C3—CH_3), 2.70 (3H, singlet, C7—$COCH_3$), 3.49 (2H, singlet, CO—CH_2—CO), 4.16 (2H, quartet, J = 7 Hz, O—CH_2—CH_3), 4.18 (2H, singlet, C2—CH_2—CO), 5.86 (1H, singlet, C4—OH), 13.71 (1H, singlet, C6—OH) ppm; ms (70 eV) *m/e*: 348 (M^+), 260, 234, 223 (base peak), 219, 215, 69. *Anal.* calcd. for $C_{18}H_{20}O_7$: C 62.06, H, 5.78%; found: C 61.97, H 5.82%. High resolution molecular weight determination calcd: 348.1208; found: 348.1229.

Preparation of usnic acid ethoxide (6)

A suspension of (+)-usnic acid (**1**) (1 g, 2.9069 mmol) in absolute ethyl alcohol (25 mL) was heated in a sealed tube at 150°C for 4.5 hours. The tube was then cooled, opened, and stored at 0°C overnight. The pale yellow precipitate was filtered, dried, and recrystallized from ethyl alcohol to give usnic acid ethoxide (**6**) (680 mg, 1.743 mmol; 60%), yellow crystals, mp 103–105°C; $[\alpha]_D$ (CH_3CN) 0° (*c*, 0.0435); uv λ_{max} (log ϵ): 347 (3.41), 296 (3.91), 241 (4.01); ir ν_{max}: 3600–3100, 2800–2400 (OH, chelated), 1705, 1665 (C=O, β-ketoester side chain), 1620 (C=O, chelated aromatic acetyl; C=C), 1600 (C=C); ^{1}Hmr (100 MHz) δ: 1.33 (3H, triplet, J = 6 Hz, O—CH_2—CH_3), 2.05 (3H, singlet, C5—CH_3), 2.28 (3H, singlet, C3—CH_3), 2.38 (3H, singlet, C=C (OH) CH_3), 2.70 (3H, singlet, C2—$COCH_3$), 4.18 (2H, singlet, C2—CH_2—CO), 4.30 (2H, quartet, J = 6 Hz, O—CH_2—CH_3), 6.56 (1H, singlet, C4—OH), 13.66 (1H, singlet, C6—OH), 17.50 (1H, broad singlet, C=C (CH_3) OH) ppm; ms (70 eV) *m/e*: 390 (M^+), 344, 260, 234, 233 (base peak), 219, 217, 215, 191, 76. *Anal.* calcd. for $C_{20}H_{22}O_8$: C 61.54, H 5.64%; found: C 61.47, H 5.67%. High resolution molecular weight determination calcd.: 390.1314; found: 390.1322.

Treatment of (+)-2-desacetylusnic acid (2) with diazomethane. Isolation of (+)-2-desacetyl-3-methoxyusnic acid (7) (6-acetyl-1,9b-dihydro-7,9-dihydroxy-8,9bα-dimethyl-3-methoxy-1-oxodibenzofuran)

A solution of (+)-2-desacetylusnic acid (**2**) (50 mg, 0.165 mmol) in dry methanol (10 mL) was treated at 0°C with excess ethereal diazomethane and the reaction mixture allowed to stand in an ice bath for 30 min. The solvent was then evaporated under reduced pressure and the residue (55 mg) purified by preparative layer chromatography (silica gel – oxalic acid plates, solvent A) to produce (+)-2-desacetyl-3-methoxyusnic acid (**7**) (20 mg, 0.06329 mmol; 38%), yellow prisms from chloroform – petroleum ether, mp 163–165°C; $[\alpha]_D^{26}$ (CH_3CN) +622° (*c*, 0.07075); uv λ_{max} (log ϵ): 370 (2.60), 330 (3.25), 282 (4.00), 218 (4.23); ir ν_{max}: 3400–3200 (OH, chelated), 1692 (C=O, enone system), 1634 (C=O, chelated aromatic acetyl; C=C); ^{1}Hmr (100 MHz) δ: 1.71 (3H, singlet, C9b—CH_3), 2.04 (3H, singlet, C8—CH_3), 2.60 (3H, singlet, C6—$COCH_3$), 3.85 (3H, singlet, C3—OCH_3), 5.30 (1H, doublet, J = 1.8 Hz, C2—*H*), 5.74 (1H, doublet, J = 1.8 Hz, C4—*H*), 11.19 (1H, singlet, C9—O*H*), 13.26 (1H, singlet, C7—O*H*) ppm; ms (70 eV) *m/e*: 316 (M^+, base peak), 301, 273, 260, 232, 217, 69, 43. *Anal.* calcd. for $C_{17}H_{16}O_6$: C 64.55, H 5.10%; found: C 64.63, H 5.30%. High resolution molecular weight determination calcd.: 316.0946; found: 316.0971; cd λ_{max} ($\Delta\epsilon$): 375 (+4.62), 338 (+7.96), 300 (−7.49), 270 (−4.94), 253 (+0.95), 245 (−1.91), 231 (+9.88).

Preparation of (+)-2-desacetylusnic acid enol acetate (8) (3-acetoxy-6-acetyl-1,9b-dihydro-7,9-dihydroxy-8,9bα-dimethyl-1-oxodibenzofuran)

A suspension of (+)-2-desacetylusnic acid (**2**) (56 mg, 0.185 mmol) in acetic anhydride (5.6 mL) and glacial acetic acid (0.4 mL) was treated with anhydrous aluminum trichloride (25 mg, 0.1879 mmol), heated at 40°C (oil bath temperature) under nitrogen atmosphere for one hour and then stirred at room temperature overnight. The resulting bright yellow solution was poured onto crushed ice (15 g), extracted with ethyl acetate (3 × 5 mL), and the combined extracts washed with water, dried over anhydrous sodium sulfate, and evaporated under reduced pressure. The residue (62 mg) was recrystallized from methanol to produce (+)-2-desacetylusnic acid enol acetate (**8**) (54 mg, 0.156 mmol; 84%), yellow prisms, mp 159–160°C; $[\alpha]_D^{26}$ (CH_3CN) +564° (*c*, 0.078); uv λ_{max} (log ϵ): 386 (3.23), 338 (3.58), 282 (4.26), 214 (4.41); ir ν_{max}: 3600–3200 (OH, chelated), 1769 (C=O, enol acetate), 1681 (C=O, enone system), 1623 (C=O, chelated aromatic acetyl; C=C), 1215 (C—O, enol acetate); ^{1}Hmr (100 MHz) δ: 1.75 (3H, singlet, C9b—CH_3), 2.09 (3H, singlet, C8—CH_3), 2.31 (3H, singlet, C3—$OCOCH_3$), 2.65 (3H, singlet, C6—$COCH_3$), 5.89 (2H, singlet, C2—*H* and C4—*H*), 10.59 (1H, singlet, C9—O*H*), 13.29 (1H, singlet, C7—O*H*) ppm; ms (70 eV) *m/e*: 344 (M^+), 302, 287, 260 (base peak), 232, 217, 43. *Anal.* calcd. for $C_{18}H_{16}O_7$: C 62.78, H 4.69%; found: C 62.70, H 4.74%. High resolution molecular weight determination calcd.: 344.0895; found: 344.0881.

Preparation of (+)-2-acetoxyusnic acid (9) (2-acetoxy-6-acetyl-1,9b-dihydro-8,9bα-dimethyl-3,7,9-trihydroxy-1-oxodibenzofuran)

(+)-Usnic acid (**1**) (150 mg, 0.436 mmol) was dissolved in warm pyridine (2.5 mL), treated at room temperature with 30% hydrogen peroxide (0.1 mL, 0.885 mmol), and the reaction allowed to proceed with stirring for one hour. The resulting orange solution was cooled to 0°C (ice bath), acidified with 1 *N* hydrochloric acid, and extracted with ethyl acetate (3 × 5 mL). The combined extracts were washed with water, dried over anhydrous sodium sulfate, and evaporated under reduced pressure to produce a bright yellow foam (159 mg). Purification by preparative layer chromatography (silica gel – oxalic acid plates, solvent A), produced (+)-2-acetoxyusnic acid (**9**) (130 mg, 0.361 mmol; 83%), unstable bright yellow glassy material that could not be induced to crystallize; $[\alpha]_D^{26}$ (CH_3OH) +389° (*c*, 0.05525); uv λ_{max} (log ϵ): 334 (3.39), 289 (3.93), 223 (4.17); ir ν_{max}: 3400–2600 (OH, chelated), 1768 (C=O, acetate), 1715, 1695 (C=O, β-diketone), 1625 (C=O, chelated aromatic acetyl; C=C); ^{1}Hmr (100 MHz, $CDCl_3$ – DMSO-d_6) δ: 1.77 (3H, singlet, C9b—CH_3), 2.20 (3H, singlet, C8—CH_3), 2.24 (3H, singlet, C2—$OCOCH_3$), 2.61 (3H, singlet, C6—$COCH_3$), 5.86 (1H, singlet, C4—H), 9.30 (2H, broad, C3—O*H*, and C9—O*H*), 13.28 (1H, singlet, C7—O*H*) ppm; ms (70 eV) *m/e*: 360 (M^+), 318, 302, 300, 272, 262, 260, 232, 217, 202, 199, 97 (base peak), 84, 83. High resolution molecular weight determination calcd. for $C_{18}H_{16}O_8$: 360.0844; found: 360.0801.

Preparation of synthetic (+)-2-desacetylusnic acid (2)

(+)-2-Acetoxyusnic acid (**9**) (85 mg, 0.236 mmol) was dissolved in

dry acetone (10 mL) and at 0°C (ice bath) saturated with carbon dioxide (CO_2). Under a stream of carbon dioxide a freshly prepared solution of chromium(II) chloride (10 mL, 10.130 mmol $Cr^{II}Cl_2$) was added, the flask stoppered, sealed with Parafilm, and allowed to stand at room temperature in the dark for 3 days. The resulting green solution was concentrated under reduced pressure to one-third its original volume, diluted with cold distilled water (10 mL), and extracted with ethyl acetate (3 × 10 mL). The combined extracts were washed with water, dried over anhydrous sodium sulfate, and evaporated under reduced pressure. Purification by preparative layer chromatography (silica gel – oxalic acid plates, petroleum ether – acetone (3:2)) and recrystallization from ethyl acetate produced (+)-2-desacetylusnic acid (**2**) (51 mg, 0.168 mmol; 72%), bright yellow plates, mp 220–221°C; mixture mp with authentic (+)-2-desacetylusnic acid, 220–222°C; $[\alpha]_D^{26}$ (CH_3CN) +625° (*c*, 0.08); uv λ_{max} (log ϵ): 328 (3.52), 289 (4.04), 216 (4.32); ir (Nujol) ν_{max}: 3300–2300 (OH, chelated), 1670 (C=O, enone system), 1630, chelated aromatic acetyl; C=C), 1600 (C=C); ^{1}Hmr (100 MHz, $CDCl_3$ – DMSO-d_6) δ: 1.73 (3H, singlet, C9b—CH_3), 2.06 (3H, singlet, C8—CH_3), 2.65 (3H, singlet, C6—COCH_3), 5.41 (1H, doublet, J = 2 Hz, C2—H), 5.85 (1H, doublet, J = 2 Hz, C4—H), 11.96 (1H, broad, C9—OH), 13.43 (1H, singlet, C7—OH) ppm; ms (70 eV) *m/e*: 302 (M^+), 287, 260 (base peak), 233, 232, 217. *Anal.* calcd. for $C_{16}H_{14}O_6$: C 63.57, H 4.67%; found: C 63.42, H 4.62%. High resolution molecular weight determination calcd.: 302.0789; found: 302.0784; cd λ_{max} ($\Delta\epsilon$): 374 (+0.95), 333 (+6.10), 298 (−4.29), 272 (+5.23), 238 (−5.63).

Acknowledgement

Financial aid from the Natural Sciences and Engineering Research Council of Canada is gratefully acknowledged.

1. J. P. KUTNEY, W. A. BAARSCHERS, O. CHIN, Y. EBIZUKA, L. HURLEY, J. D. LEMAN, P. J. SALISBURY, I. H. SÁNCHEZ, T. YEE, and R. J. BANDONI. Can. J. Chem. **55**, 2930 (1977).
2. J. P. KUTNEY, J. D. LEMAN, P. J. SALISBURY, I. H. SÁNCHEZ, T. YEE, and R. J. BANDONI. Can. J. Chem. **55**, 2336 (1977).
3. C. F. CULBERSON. Chemical and botanical guide to lichen products. The University of North Carolina Press, Chapel Hill, NC. 1969. p. 171; Bryologist, **73**, 201 (1970).
4. A. ASAHINA and S. SHIBATA. Chemistry of lichen substances. Japan Society for the Promotion of Science, Tokyo. 1954. p. 171.
5. (*a*) N. A. NAUMOV. Clés des Mucorinées (Mucorales). *In* Encyclopédie Mycologique. Vol. IX. *Edited by* P. Lechevalier. Paris. 1939. pp. 1–137; (*b*) H. ZYCHA. Mucorinae. *In* Kryptogamenflora der Mark Brandenburg. Pilze II. Verlag von Gebrüder Borntraeger, Leipzig. 1935. pp. 42–57; (*c*) C. W. HASSELTINE. Mycologia, **47**, 344 (1953).
6. S. MACKENZIE. J. Am. Chem. Soc. **74**, 4067 (1952).
7. S. FORSÉN, M. NILSSON, and C. A. WACHTMEISTER. Acta Chem. Scand. **16**, 583 (1962).
8. R. M. SILVERSTEIN and G. C. BASSLER. Spectrometric identification of organic compounds. J. Wiley and Sons, Inc., New York. 1967. Chapt. 4.
9. J. P. KUTNEY, I. H. SÁNCHEZ, and T. YEE. Org. Mass Spectrom. **8**, 129 (1974).
10. H. TAGUCHI and S. SHIBATA. Chem. Pharm. Bull. **18**, 374 (1970); F. M. DEAN and A. ROBERTSON. J. Chem. Soc. 2166 (1955).
11. A. ROBERTSON and F. H. CURD. J. Chem. Soc. 1173 (1933).
12. Y. ASAHINA, M. YANAGITA, and S. MAYEDA. Ber. **70**, 1500 (1937).
13. J. P. KUTNEY and I. H. SÁNCHEZ. Can. J. Chem. **55**, 1085 (1977), and references cited therein.
14. (*a*) C. H. HASSALL. J. Chem. Soc. 50 (1948); (*b*) H. DAVIES, H. ERDTMAN, and M. NILSSON. Tetrahedron Lett. 2491 (1966).
15. A. A. AKHREM, A. M. MOISSENKOV, and V. A. KRIVORUCHKO. Bull. Acad. Sci. U.S.S.R. Chem. Sci. 1268 (1968).
16. J. R. HANSON. Synthesis, 1 (1974).
17. A. L. MACDONALD, S. J. RETTIG, and J. TROTTER. Can. J. Chem. **52**, 723 (1974).

Can. J. Chem. Downloaded from www.nrcresearchpress.com by 210.87.254.6 on 09/06/12
For personal use only.

Spin–spin coupling between hydroxyl and aldehydic protons in some salicylaldehyde derivatives. Correlation with the hydroxyl proton chemical shift

TED SCHAEFER, RUDY SEBASTIAN, REINO LAATIKAINEN,[1] AND SALMAN R. SALMAN[2]
Department of Chemistry, University of Manitoba, Winnipeg, Man., Canada R3T 2N2

Received June 27, 1983

TED SCHAEFER, RUDY SEBASTIAN, REINO LAATIKAINEN, and SALMAN R. SALMAN. Can. J. Chem. **62**, 326 (1984).

^{1}H nmr spectral parameters are reported for salicylaldehyde and 15 of its derivatives in dilute CCl_4 solutions. In those compounds in which sufficiently large substituents are placed *ortho* to either of the functional groups or in which substituents enhance the charge density in the carbonyl group, a positive spin–spin coupling is observed between the two sidechain protons. This coupling, formally over five bonds, correlates with the chemical shift of the hydroxyl proton. The coupling mechanism is discussed from various viewpoints. STO 3G MO calculations give an optimized planar structure for salicylaldehyde. Nonplanar structures are less stable than the planar form. The energy of the hydrogen bond in salicylaldehyde lies near 30 kJ/mol and increases to 36 kJ/mol in the 4,6-dimethoxy derivative. Other small long-range spin–spin coupling constants in these compounds are also discussed.

TED SCHAEFER, RUDY SEBASTIAN, REINO LAATIKAINEN et SALMAN R. SALMAN. Can. J. Chem. **62**, 326 (1984).

On rapporte les paramètres spectraux du salicylaldéhyde et de 15 de ses dérivés en solution diluée dans le CCl_4. On observe un couplage spin–spin positif entre les protons des chaînes latérales des composés dans lesquels des substituants assez volumineux sont en position *ortho* par rapport aux groupes fonctionnels ou dans lesquels les substituants augmentent la densité de charge du groupe carbonyle. Ce couplage, formellement établi à travers plus de 5 liaisons, est en accord avec les déplacements chimiques du proton hydroxylique. On discute du mécanisme du couplage à partir de diverses considérations. Les calculs STO 3G OM donnent une structure plane optimisée pour le salicylaldéhyde. Les structures non planes sont moins stables que la forme plane. L'énergie de la liaison hydrogène du salicylaldéhyde est d'environ 30 kJ/mol et augmente jusqu'à 36 kJ/mol dans le dérivé diméthoxy-4,6. On discute également d'autres faibles constantes de couplage spin–spin à longue distance observés dans ces composés.

[Traduit par le journal]

Introduction

At 308 K the chemical shift of the hydroxyl proton in phenol, δ_{OH}/(ppm), at infinite dilution in CCl_4 is 4.26 (1). In salicylaldehyde δ_{OH} is near 11 (2), reflecting the presence of a normal[3] intramolecular hydrogen bond in **1**, whose energy has been variously estimated as lying between 3.3 and 35.2 kJ/mol (3–8).

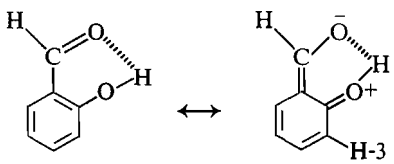

1 **1*a***

It is likely that the quinoid resonance structure (canonical form), **1*a***, is important. Indeed, it has been recommended that all phenols with strong hydrogen bonds be regarded as quinoids (9). This attitude is certainly valid for the keto–enol tautomerization observed in the Schiff bases derived from salicylaldehyde (9). However, it is unlikely that tautomerization or an (asymmetric) double minimum potential with a low barrier exists in **1** (10). Substitution of the hydroxyl proton by deuterium and tritium nuclei, together with the measurement of their chemical shifts (primary isotope effects), demonstrates this situation for **1**. As the proton moves nearer towards a point midway between the heavy atoms it becomes less shielded (11, 12) and a low-barrier double minimum potential is not indicated for δ_{OH} less than 12.7 ppm (10).

Nevertheless, it is of interest whether δ_{OH} in salicylaldehyde derivatives is sensitive to electronic and/or steric perturbations by the ring substituents. It turns out that, for a number of such compounds, there is a good correlation between δ_{OH} and $^5J_o^{OH,CHO}$, the spin–spin coupling constant over five formal bonds between the hydroxyl and the aldehydic protons. As far as we know, this coupling has not been previously observed.

Experimental

Of commercial origin, salicylaldehyde derivatives were prepared as dilute (<5 mol%) solutions in CCl_4, tetramethylsilane was added as an internal reference, transfer to 5-mm od nmr sample tubes was followed by degassing via freeze–pump–thaw cycles, and the tubes were flame-sealed after the last pump cycle. Calibration of the ^{1}H nmr spectra on an HA100 nmr spectrometer at a probe temperature of 305 K involved the procedure described in detail recently (13). STO 3G MO (14) and INDO MO FPT (15) calculations were performed on an Amdahl 470/V7 system.

Results and discussion

Spectral analyses

The computer program LAME (16, 17) was employed in spectral analytical procedures. Table 1 gives the spectral parameters obtained for salicylaldehyde as a 4.0 mol% solution in CCl_4. Although the linewidths at half-height were typically $\leq$0.1 Hz, no coupling between hydroxyl and aldehydic protons was evident in single or double resonance spectra. The presence of certain ring substituents gives rise to such a coupling. Thus, in 3,5-diiodosalicylaldehyde, this coupling is +0.125(3) Hz. Its sign was determined in a series of nine double resonance experiments, under conditions of weak irradiation (18), which showed that $^5J_m^{OH,H\text{-}4}/^5J_m^{OH,H\text{-}6} > 0$, $^5J_m^{OH,H\text{-}6}/^5J_o^{OH,CHO} > 0$, and $^5J_m^{OH,H\text{-}6}/^4J_o^{CHO,H\text{-}6} < 0$. Because $^5J_m^{OH,H\text{-}4}$ is certainly positive (19), $^5J_o^{OH,CHO}$ follows as positive. The signs of the ratios above

[1] Present address, Department of Chemistry, University of Kupio, Kupio 10, Finland.

[2] Present address, Department of Chemistry, University of Bhagdad, Bhagdad, Iraq.

[3] Emsley (8*b*) defines a weak or normal hydrogen bond as one whose strength is less than 50 kJ/mol.

Can. J. Chem. Downloaded from www.nrcresearchpress.com by 210.87.254.42 on 09/06/12
For personal use only.

Can. J. Chem. Downloaded from www.nrcresearchpress.com by 210.87.254.42 on 09/06/12
For personal use only.

TABLE 1. The ^{1}H nmr spectral parameters for a 4.0 mol% solution of salicylaldehyde in CCl_4 at 305 K and 100.001 MHz

Parameter	Value	Parameter	Value
ν_{CHO}[a]	985.102(2)[b]	$^4J_o^{H,HO}$	−0.011(3)[c]
ν_{OH}	1089.635(2)	$^5J_m^{CHO,H-3}$	0.623(4)
ν_3	691.793(2)	$^5J_m^{CHO,H-5}$	−0.015(3)[c]
ν_4	744.615(2)	$^5J_m^{OH,H-4}$	0.480(3)
ν_5	693.986(2)	$^5J_m^{OH,H-6}$	0.043(3)
ν_6	747.039(2)	$^5J_o^{OH,CHO}$	<0.02[d]
$^3J_{34}$	8.435(4)	$^6J_p^{OH,H}$	−0.001(3)
$^3J_{45}$	7.258(3)	$^6J_p^{CHO,H}$	0.003(3)
$^3J_{56}$	7.709(3)	Transitions calcd.	224[e]
$^4J_{35}$	1.040(3)	Transitions assigned	170
$^4J_{46}$	1.747(3)	Peaks observed	70
$^5J_{36}$	0.461(4)	Largest difference	0.022
$^4J_o^{H,CHO}$	−0.111(3)	Deviation r.m.s.	0.010

[a] In Hz to low field of internal TMS; ν_3 corresponds to the proton *ortho* to the hydroxyl group.
[b] Numbers in parentheses are the standard deviations in the last significant figure.
[c] No evidence for a finite value.
[d] From decoupling.
[e] Above 0.05 intensity.

are in agreement with previous sign determinations of $^5J_m^{OH,H-6}$ in 3-methoxysalicylaldehyde (19) and of $^4J_o^{OH,H-6}$ in 4-*N*,*N*-dimethylaminobenzaldehyde (20).

Figure 1 displays various multiplets, indicating the spectral quality obtainable with many of these molecules. Table 2 presents the spectral parameters of immediate interest for 15 compounds.

The correlation between δ_{OH} and $^5J_o^{OH,CHO}$

$^5J_o^{OH,CHO}$ is not observed for those compounds having only a fluorine or methoxy substituent *ortho* to the hydroxyl groups.[4] A larger substituent at this position *or* at the position *ortho* to the aldehyde function induces an observable $^5J_o^{OH,CHO}$; for example, 3-*tert*-butyl, 3-Br, or 6-Cl. Furthermore, a 4-methoxy group entails a $^5J_o^{OH,CHO}$ whose magnitude is enhanced by the further addition of a 6-methoxy substituent. By way of contrast, a 3- or a 5-methoxy group is associated with no observable $^5J_o^{OH,CHO}$. These observations (see Table 2) suggest, first, that large substituents placed *ortho* to the functional groups in salicylaldehyde exert steric or compressive forces which enhance the transfer of nuclear spin state information within the hydrogen bonded moieties; second, that a π-electron donor *para* to the aldehydic group provides, via resonance structures like **2**, additional electron density in the hydrogen bond region, again to the advantage of the coupling mechanism.

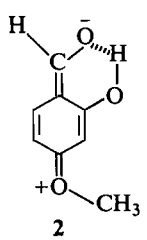

2

[4] In 3-methoxysalicylaldehyde, $^5J_o^{H,CH_3}$ is (−)0.27(1) Hz, see also ref. 21, showing that the methoxy group is oriented towards H-4, and therefore presenting only the oxygen atom to the hydroxyl group (22).

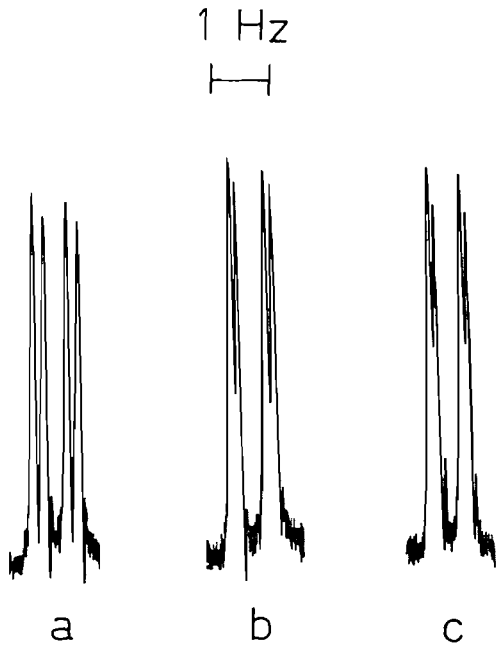

FIG. 1. In (a) the aldehydic proton resonance is displayed for a 2.0 mol% solution of 4,6-dichlorosalicylaldehyde in CCl_4 at 100 MHz and a probe temperature of 305 K. The smaller splitting of 0.195(3) Hz arises from coupling to the hydroxyl proton. In (b) the aldehydic proton peaks are shown for a 2.0 mol% solution of 4-methoxysalicylaldehyde in CCl_4 under conditions in which the hydroxyl proton is decoupled. The smaller splitting of 0.093(3) Hz represents the coupling to H-6. In (c) the hydroxyl proton peaks are given for a 2.0 mol% solution of 3,5-diiodosalicylaldehyde in CCl_4 while the aldehydic proton is being irradiated strongly. The smallest splitting of 0.098(6) Hz involves an interaction with H-6.

The latter structure might well increase the strength of the intramolecular hydrogen, increasing δ_{OH} (6), and because electron density is increased in the aldehydic region, the aldehydic proton resonance should shift to high field. Both phenomena are observed (Table 2). Steric compression usually causes deshielding, as noted for the aldehyde proton in these compounds in Table 2 with 6-substituents.

In Fig. 2, $^5J_o^{OH,CHO}$ is plotted versus the shift in Hz to low field of the hydroxyl proton relative to salicylaldehyde for the nine derivatives in which the coupling is observed. Equation [1] describes a linear relationship between the two quantities (r = 0.991), in which ν_S is the shift in salicylaldehyde. This

$$[1]\quad {}^5J_o^{OH,CHO}(\text{Hz}) = -0.002 + 1.807 \times 10^{-3}(\nu_{OH} - \nu_S)/(\text{Hz})$$

equation predicts a negligible coupling in salicylaldehyde itself. Note that the equation is not meant to hold for $\nu_{OH} < \nu_S$ and no coupling is actually observed for 5-methoxysalicylaldehyde in which $\nu_{OH} - \nu_S$ is −41 Hz; this number would imply $^5J_m^{OH,CHO}$ as -0.07_5, easily detectable. Very probably, structure **3** is a contributor, placing negative charge near the hydroxyl group, reducing its electron donation to the ring,

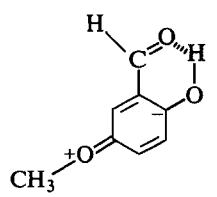

3

TABLE 2. Some ^{1}H nmr spectral parameters for some salicylaldehyde derivatives in CCl_4 solution at 100.001 MHz and 305 K

Compound	ν_{OH}	ν_{CHO}	$^5J_o^{OH,CHO}$	$^5J_m^{OH,H\text{-}6}$	$^5J_m^{OH,H\text{-}4}$	$^4J_o^{H,CHO}$
H(4.0)[a]	1089.635(2)	985.102(2)	<0.02	0.043(3)	0.480(3)	−0.111(3)
3-F(5.0)	1085.114(4)	989.137(4)	<0.02	<0.05	0.726(6)	−0.086(6)
3-OCH_3(3.0)	1081.690(4)	986.906(3)	<0.02	0.093(5)	0.674(5)	−0.122(4)
3-Allyl(5.0)	1123.687(4)	982.166(5)	0.046(7)	0.076(11)	0.617(10)	−0.059(9)
4-OCH_3(2.0)	1135.812(3)	967.003(2)	0.089(4)	<0.02	—	<0.02
5-OCH_3(2.0)	1048.519(10)	980.669(9)	<0.02	0.084(14)	0.620(17)	−0.098(14)
3-NO_2(<1.5)	1130.192(2)	1045.299(2)	<0.02	0.508(3)	<0.02	<0.02
5-Br(2.0)	1083.400(3)	982.320(3)	<0.02	0.065(6)	0.482(6)	−0.045(5)
3,4-DiOCH_3(2.0)	1102.740(1)	968.078(1)	<0.05	<0.02	—	−0.104(2)
3,5-DiBr(2.0)	1137.606(8)	979.804(7)	0.077(6)	0.090(5)	0.571(6)	−0.165(9)
3,5-Di-*t*-bu(2.0)	1165.802(10)	982.242(5	0.135(9)	≤0.05	0.648(9)	−0.155(8)
3,5-DiI(2.0)	1161.913(4)	969.769(4)	0.125(3)	0.098(6)	0.529(5)	−0.072(6)
3-Br-5-Cl(2.0)	1135.637(8)	980.275(7)	0.099(9)	0.099(9)	0.562(4)	−0.080(6)
3-Br-5-NO_2(1)	1211.574(3)	997.248(3)	0.139(4)	0.114(4)	0.626(4)	<0.02
4,6-DiCl(2.0)	1200.610(2)	1032.649(2)	0.195(3)	—	—	—
4,6-diOCH_3(2.0)	1237.173(2)	1001.785(2)	0.266(2)	—	—	—

[a]Concentrations in mol%.

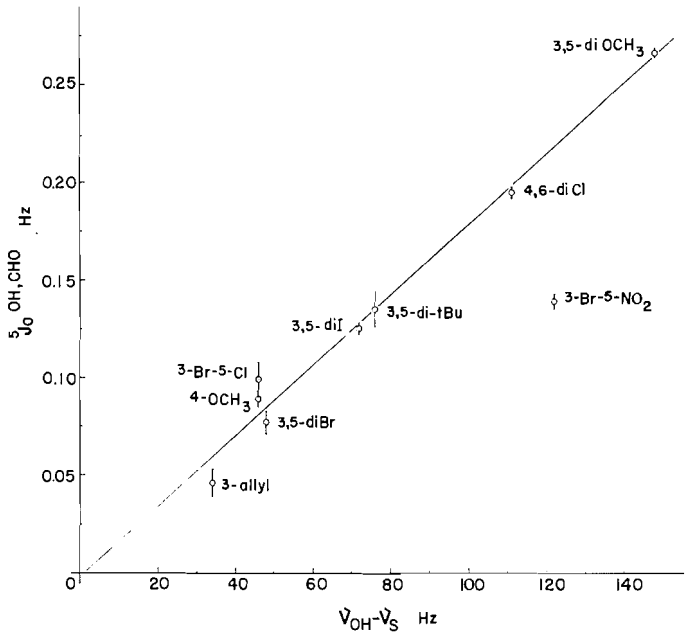

FIG. 2. $^5J_o^{OH,CHO}$ in Hz is plotted versus $\nu_{OH} - \nu_S$ in Hz at 100 MHz for a number of salicylaldehyde derivatives. ν_S is the shift of the hydroxyl proton in salicylaldehyde. The data are found in Table 2. Excluding the point for 3-bromo-5-nitrosalicylaldehyde yields the equation $^5J = -0.002 + 1.807 \times 10^{-3}(\nu_{OH} - \nu_S)$ with a correlation coefficient of 0.991 for 8 points. See text for further discussion.

and therefore leading to a somewhat weakened hydrogen bond and an increased shielding of the hydroxyl proton.

Further, note that 3-bromo-5-nitrosalicylaldehyde is excluded from the correlation in eq. [1]. Comparison with δ_{OH} and $^5J_o^{OH,CHO}$ in the 5-bromo (no coupling) and the 3,5-dibromo derivatives suggests that resonance structure **4** contributes to the excess low-field shift of the hydroxyl proton. Relative to the 3,5-dibromo compound, the low-field shift is 74 Hz and, allowing for the upfield shift of 6 Hz in the 5-bromo derivative relative to the parent compound, one arrives at 68 Hz for the deshielding by the 5-nitro group. In 4-nitro-2,6-di-*tert*-butylphenol, in which no intermolecular hydrogen bonding apparently occurs, the 4-nitro substituent causes a low-field

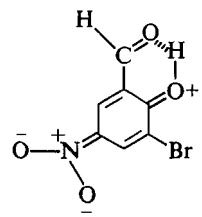

4

shift of 88 Hz in CCl_4 solution (23). Of course, a certain attenuation of the shift due a *para* nitro group would be expected in the salicylaldehyde, the hydroxyl proton region have already lost a significant amount of electron density (24). Although the 5-nitro substituent does lead to an increase in $^5J_o^{OH,CHO}$, its magnitude is less than that expected on the basis of δ_{OH} (see Fig. 2). One may argue as follows.

Examination of the substituent effects on $^5J_o^{OH,CHO}$ (Fig. 2 displays them most clearly) reinforces the suggestions at the beginning of this section. Steric compression (3-allyl; 3,5-diBr; 3-Br-5-Cl; 3,5-diI; 3,5-di-*t*-butyl; 4,6-diCl) by sufficiently large substituents placed *ortho* to either of the functional groups forces the hydroxyl proton closer to the carbonyl group. The hydrogen bond strengthens, leading to a larger δ_{OH}, and spin state information is transferred more efficiently via the $=\overset{+}{O}—H\cdots\bar{O}—C—H$ pathway. Via structure **2**, a 4-OCH_3 substituent strengthens the hydrogen bond by placing more negative charge density on the carbonyl oxygen and again enhances $^5J_o^{OH,CHO}$ by the pathway above. In the 4,6-dimethoxy derivative both steric compression and charge redistribution are active, leading to the largest observed $^5J_o^{OH,CHO}$. On this basis, the $^5J_o^{OH,CHO}$ in the 3-bromo-5-nitro compound falls off the correlation line in Fig. 2 because structure **4** interferes with **1***a*, as does a 5-methoxy substituent because of structure **3**.

Evidence for structures **1**a, **2**, **3**, *and* **4**

Some evidence for the contributions from resonance structures **1***a* to **4** can be adduced from $^3J^{H,H}$ values in these compounds. It is known that $^3J^{H,H}$ in di- and trisubstituted benzene derivatives depends in an additive way on the presence of substituents (25–28). For 14 trisubstituted benzenes in which no strong resonance interaction is expected between the substituents (27), the mean deviation between observed and calcu-

Can. J. Chem. Downloaded from www.nrcresearchpress.com by 210.87.254.42 on 09/06/12
For personal use only.

Can. J. Chem. Downloaded from www.nrcresearchpress.com by 210.87.254.42 on 09/06/12
For personal use only.

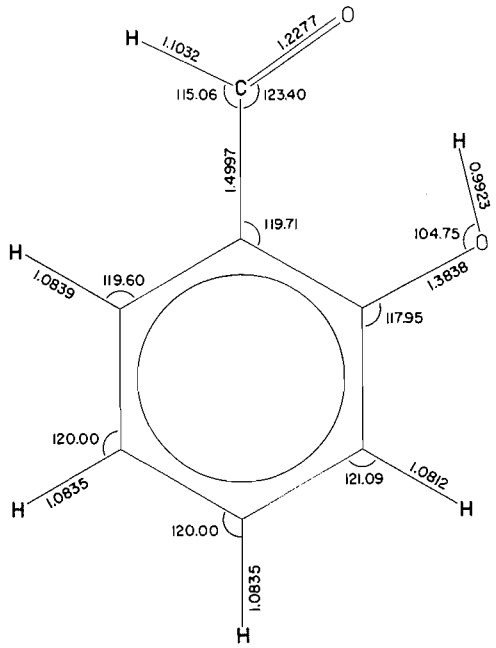

FIG. 3. The STO-3G geometry for salicylaldehyde in which the sidechain chain geometries have been optimized. The total energy is −412.96918 au. The dipole moment is 2.34 D, μ_x is 1.51 D, and μ_z is 1.79 D; the z axis lies along the C1—C2 bond. The geometry of the sidechains is remarkably similar to those found in phenol and benzaldehyde. See text for a discussion of nonplanar geometries.

lated values is ca. 0.05 Hz and for only two of these is the observed value significantly larger (0.05 and 0.13 Hz) than the one based on additivity. It was suggested very early (25) that appreciable deviations from additivity would indicate substituent interactions. This suggestion was later substantiated (29).[5] With reference to structure **1***a*, these studies imply that $^3J_{34}$ and $^3J_{56}$ should be larger than those predicted on an additivity basis and that $^3J_{45}$ should be smaller, reflecting partial double bond fixation (30). Indeed, they are +0.33, +0.11, and −0.07 Hz larger, respectively, than predicted on an additive basis (Table 1 and ref. 25). Furthermore, in 3-methoxysalicylaldehyde, $^3J^{H,H}$ is 0.29 Hz larger, in line with **2**, and is 0.27 Hz larger in the 5-methoxy compound, as expected if **3** is an important resonance structure.

Evidence from $^4J_o^{H,CHO}$

In *para* substituted benzaldehydes $^4J_o^{H,CHO}$ is an average of the *cis* and *trans* arrangements of the aldehydic and ring C—H bonds. This negative coupling increases in magnitude if the *para* substituent is a π electron donor and decreases if it is a π electron acceptor (20). It has been argued that this increase is a consequence of a shorter C—C bond for the aldehydic group (31); see structure **2**. Structure **4** should therefore have a smaller magnitude for $^4J_o^{H,CHO}$ than **1***a*. In salicylaldehyde, this coupling is −0.11 Hz and could not be detected in the 3-bromo-5-nitro derivative (careful decoupling experiments). However, in the 3-methoxy and 5-methoxy compounds $^4J_o^{H,CHO}$ is not significantly different from its value in salicylaldehyde. Therefore the evidence from this source for the importance of **1***a* to **4** is mixed.

STO 3G MO calculations of geometry and energy

The STO 3G optimization of the sidechain geometries gave the structure in Fig. 3. The exocyclic geometries are remarkably similar to the optimized geometries reported for phenol and benzaldehyde with the same minimal basis set (32). The only significant differences are that the COH angle has decreased by 0.7° and the C1—C7 (HO) bond length has decreased by 0.02 Å in salicylaldehyde. At this level of theory there is no evidence for an O—H bond as long as 1.15 Å, apparently found in the 3-methoxy derivative (33, 34) or as long as 1.16 Å, suggested for salicylaldehyde itself (35, 36). In a correlation of O—H and O···O bond lengths (37), an O···O distance of 2.63 Å as in Fig. 3 corresponds to an O—H distance of ca. 0.99 Å.

In a paper on quadrupole coupling constants (38) the O···O distance is quoted as 2.68 Å, whereas a microwave study suggests 2.62 Å (39). The latter also quotes an O—H bond length of 1.04 and an O—H···O separation of 1.76 ± 0.01 Å. According to a relationship (39*b*) between the deuterium quadrupole coupling constant and the H···O distance, together with the known value of 196 kHz in salicylaldehyde (39*c*), this distance is 1.70 Å. The STO 3G structure in Fig. 3 gives 1.72 Å.

In any event, it seems unlikely that the O—H bond length in salicylaldehyde is significantly longer than 1.00 Å. An interesting correlation (40) exists between δ_{OH} in solids and the O···O distance and is roughly compatible with the δ_{OH} for salicylaldehyde in Table 1 and a theoretical calculation (11).

A correlation of δ_{OH} and the energy of the intramolecular hydrogen bond in phenol derivatives (6) gives the energy of that bond in salicylaldehyde as 29.7 kJ/mol. Because an STO 3G calculation can give hydrogen bond energies in rough agreement with experiment,[6] the energies of **5**, **6**, and **7** were computed. These are, respectively, 23.6, 32.2, and 41.8 kJ/mol less stable than **1**. In another STO 3G MO computation

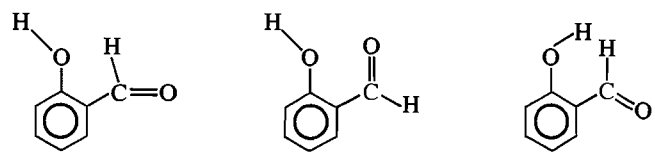

5 **6** **7**

(8), the energy difference between **1** and **6** was 31.1 kJ/mol and was taken as the hydrogen bond strength. In our opinion, **5** is the stable form of salicylaldehyde in the absence of a hydrogen bond (as found for 2-fluorobenzaldehyde, for example (41)). In any case, it appears that the energy of the hydrogen bond in **1** lies at the high end of the available estimates.

Parenthetically, the calculated dipole moment of 2.34 D for **1** is 0.52 D less than the observed 2.86 D (42). The STO 3G MO dipole moment of phenol agrees with experiment to within 0.01 D (32), but is too low by 1.4 D for benzaldehyde (43). The INDO MO value for **1** is 3.77 D, suggesting too large a charge separation.

INDO MO FPT calculations of $^5J_o^{OH,CHO}$

The INDO MO FPT value of $^5J^{OH,CHO}$ for the STO 3G geometry is −0.51 Hz[7] and the CNDO MO FPT number is −0.11 Hz. An STO 3G optimization of the enol structure yielded an energy 122 kJ/mol higher in energy than **1**. $^5J_o^{OH,CHO}$ now becomes $^3J^{HOCH}$ and is calculated as −2.49 Hz by INDO and as −1.03 Hz by CNDO!

[5] Also R. E. Wasylishen, private communication to T. Schaefer.

[6] See ref. 24, p. 115.

[7] The INDO values are exponentially dependent on the O—H bond length, $-7.8057 \times 10^{-6} \exp(11.17r)$ (r = 0.9994).

Can. J. Chem. Downloaded from www.nrcresearchpress.com by 210.87.254.42 on 09/06/12
For personal use only.

In an attempt at tracing the coupling path in **1**, Barfield's method (44), involving the deletion of certain off-diagonal elements in the Fock matrix, was employed. This approach prevents the development of spin polarization via the overlap of selected orbitals and can give useful information about coupling pathways. For $^5J_o^{OH,CHO}$ this technique gave somewhat ambiguous results. For example, if all elements involving the hydroxyl hydrogen 1*s* orbital and the 2*s* and 2*p* orbitals of C-2 are set to zero, the coupling becomes 0.11 Hz. This might be taken as an indication that elimination of a pathway via the ring orbitals gives rise to reasonable agreement with experiment. However, deletion of all elements containing the hydroxyl hydrogen orbital and the valence orbitals of C-1 and the aldehydic carbon and oxygen atoms, yields $^5J_o^{OH,CHO}$ as 0.05 Hz, whereas doing the same for the 1*s* orbitals of the two sidechain hydrogen atoms gave 0.19 Hz. Elimination of the carbonyl oxygen atom valence orbital elements gave 0.62 Hz. In other words, support for the pathway indicated by the experiments above could not be established.

The simplest explanation consistent with observation is that increased charge on the carbonyl oxygen atom, together with steric forces favouring a close approach of this atom to the hydroxyl proton, enhances $^5J_o^{OH,CHO}$.

Concerning a possible nonplanarity of salicylaldehyde

The microwave spectra of salicylaldehyde and two if its isotopomers yield a planar molecule (39), a COH angle of 109° (the INDO results above did not change appreciably for an angle of 108° as contrasted to the STO 3G angle), and allowed out-of-plane torsions of the sidechains. In a nematic phase, the observed dipolar couplings (45) were consistent with a nonplanar structure as well as with an average of nonplanar structures with energies greater than a planar minimum. The present STO 3G computations gave the following results, where θ_1 is

θ_1 (deg)	Energy (kJ)	θ_2 (deg)	Energy (kJ)
5	1.9	5	0.7
10	7.0	10	2.7
15	13.8	15	5.9
20	20.7	20	10.1

the angle by which both groups twist out of the ring plane so that the protons remain on the same side of the plane; θ_2 is the twist angle if the protons of the sidechains move to opposite sides of that plane. The second alternative is favoured and a twist of 10° is equal to *kT* at 305 K, in disagreement with the nmr results for a nematic solution, which favor the protons on the same side of the ring (45).

For none of the appropriate compounds in Table 2 were there observable $^6J_p^{H,CHO}$ or $^6J_p^{OH,H}$ numbers. Substantial nonplanarity, say 20° of torsion, should lead to easily observable couplings. For example, in 2,6-dichlorobenzaldehyde $^6J_p^{H,CHO}$ is −0.15 Hz (46) and is not observable in benzaldehyde (47). Our observations are consistent with a planar minimum for the energy of salicylaldehyde and the other compounds in Table 2. Apparently, steric compression is relieved by formation of a stronger hydrogen bond, stronger by as much as 6 kJ/mol on the basis of δ_{OH} and the empirical relationship mentioned above. Out-of-plane movement of the aldehyde group, for example in the 4,6-dichloro derivative, would furthermore lead to a high-field shift (ring anisotropy), but a low-field shift is observed.

Concerning $^5J_m^{OH,H-6}$

Spin–spin coupling over five bonds between sidechain protons and *meta* ring protons is stereospecific. For example, for benzaldehyde derivatives there is no evidence that $^5J_m^{CHO,H-5}$ in **8** is nonzero. In none of the compounds in Table 2 was there an observable $^5J_m^{CHO,H-5}$ (not tabulated), except of course for 3-nitrobenzaldehyde in which the internal hydrogen bond involves the nitro group. Again, $^5J_m^{H,SH}$ in thiophenol derivatives can be written as $^5J = A \sin^2\theta + B \sin^2(\theta/2)$, where θ is the angle by which the S—H bond twists out of the ring plane (48). *B* is the value of the coupling for θ = 180° (see **8**). A similar equation has been derived for toluene derivatives (49).

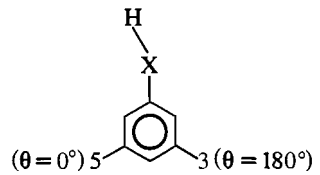

8

In a variety of phenol derivatives, no evidence for a $^5J^{OH,H}$ with θ = 0° exists (50–52), *except* for salicylaldehyde and its derivatives. A previous value of +0.13 ± 0.05 Hz in 3-methoxysalicylaldehyde (19) is substantiated in Table 2, where it is given as 0.093(5) Hz. The nitro group forms a stronger hydrogen bond to the hydroxyl group than does the carbonyl bond (see the 3-nitro derivative in Table 2). Yet the coupling analogous to that observed in salicylaldehyde is not present, nor does it appear in 2-fluoro-6-nitro- or 3-fluoro-6-nitrophenol (50). Its largest value is 0.11 Hz in 3-bromo-5-nitrosalicylaldehyde, in which the largest $^5J_o^{OH,CHO}$ and δ_{OH} also occur for those compounds where $^5J_o^{OH,CHO}$ is observable in Table 2. One possible explanation therefore involves a coupling pathway through the carbonyl group orbitals, an alternate five-bond interaction if the hydrogen bond is counted as a bond. However, no $^5J_m^{OH,H-6}$ is observed in the 4-methoxy or 3,4-dimethoxy derivatives, so that this coupling pathway must be considered tentative at best.

Conclusions

Salicylaldehyde and many of its derivatives most likely prefer a planar conformation. The intramolecular hydrogen bond has an energy near 30 kJ/mol and increases by as much as 6 kJ/mol in the presence of substituents which cause steric compression, increase the electron density in the carbonyl group, or decrease the electron density near the hydroxyl proton. As the hydrogen bond energy increases, a coupling between the hydroxyl and aldehydic protons appears, apparently transmitted via the hydrogen bond.

Acknowledgments

We are grateful to the Natural Sciences and Engineering Research Council of Canada and to the Research Council for the Natural Sciences of the Academy of Finland for financial support. We thank a referee for pointing out a real blunder in the original manuscript.

1. T. GRAMSTAD and E. D. BECKER. J. Mol. Struct. **5**, 253 (1970).
2. A. L. PORTE, H. S. GUTOWSKY, and I. M. HUNSBERGER. J. Am. Chem. Soc. **82**, 5057 (1960).
3. M. REMKO and J. POLCIN. Z. Phys. Chem. Leipzig, **258**, 219 (1977).
4. E. RAJAGOPAL, K. V. SIVAKUMAR, S. V. SUBRAHMANYAM, and K. C. REDDY. J. Chem. Soc. Faraday Trans. 1, **77**, 2149 (1981).
5. M. HIROTA, T. SUZUKI, and K. ABE. Bull. Chem. Soc. Jpn. **50**,

1129 (1977).
6. T. SCHAEFER. J. Phys. Chem. **79**, 1888 (1975).
7. P. SCHUSTER. Chem. Phys. Lett. **3**, 433 (1969).
8. (*a*) S. W. DIETRICH, E. C. JORGENSEN, P. A. KOLLMAN, and S. ROTHENBERG. J. Am. Chem. Soc. **98**, 8310 (1976); (*b*) J. EMSLEY. J. Chem. Soc. Rev. **9**, 91 (1980).
9. G. O. DUDEK and E. P. DUDEK. J. Chem. Soc. Chem. Commun. 464 (1965).
10. L. J. ALTMAN, D. LAUNGANI, G. GUNNARSON, H. WENNERSTROM, and S. FORSÉN. J. Am. Chem. Soc. **100**, 8264 (1978).
11. R. DITCHFIELD. J. Chem. Phys. **65**, 3123 (1976).
12. K. F. LAU and R. W. VAUGHAN. Chem. Phys. Lett. **33**, 550 (1975).
13. T. SCHAEFER and R. SEBASTIAN. J. Magn. Reson. **41**, 395 (1980).
14. W. J. HEHRE, W. A. LATHAN, R. DITCHFIELD, M. D. NEWTON, and J. A. POPLE. Quantum Chemistry Program Exchange, **11**, 236 (1979).
15. P. A. DOBOSH. Quantum Chemistry Program Exchange, **11**, 141 (1979).
16. S. CASTELLANO and A. A. BOTHNER-BY. J. Chem. Phys. **41**, 3863 (1964).
17. C. W. HAIGH. Annu. Rep. NMR Spectrosc. **4**, 311 (1971).
18. R. FREEMAN and W. A. ANDERSON. J. Chem. Phys. **37**, 2053 (1962).
19. S. FORSÉN and R. A. HOFFMAN. J. Mol. Spectrosc. **20**, 168 (1966).
20. S. S. DANYLUK, C. L. BELL, and T. SCHAEFER. Can. J. Chem. **47**, 4005 (1969).
21. S. FORSÉN, B. AKERMARK, and T. ALM. Acta Chem. Scand. **18**, 2313 (1964).
22. T. SCHAEFER and R. LAATIKAINEN. Can. J. Chem. **61**, 224 (1983).
23. L. A. COHEN and W. M. JONES. J. Am. Chem. Soc. **85**, 3402 (1963).
24. P. SCHUSTER. *In* The hydrogen bond. *Edited by* P. Schuster, G. Zundel, and C. Sandorfy. North-Holland Publishing Co., New York. 1976. pp. 73, 77.
25. S. CASTELLANO and R. KOSTELNIK. Tetrahedron Lett. 5211 (1967).
26. J. M. READ, JR., R. W. CRECELY, R. S. BUTLER, J. E. LOEMKER, and J. H. GOLDSTEIN. Tetrahedron Lett. 1215 (1968).
27. T. SCHAEFER, G. KOTOWYCZ, H. M. HUTTON, and J. W. LEE. Can. J. Chem. **46**, 2531 (1968).
28. V. A. CHERTKOV and N. M. SERGEYEV. J. Magn. Reson. **52**, 400 (1983).
29. W. B. SMITH, A. M. IHRIG, and J. W. ROARK. J. Phys. Chem. **74**, 812 (1970).
30. D. CREMER and H. GÜNTHER. Justus Liebigs Ann. Chem. **763**, 87 (1972).
31. W. F. REYNOLDS, I. R. PEAT, and G. K. HAMER. Can. J. Chem. **52**, 3415 (1974).
32. T. SCHAEFER, T. A. WILDMAN, and R. SEBASTIAN. J. Mol. Struct. Theochem. **89**, 93 (1982).
33. F. IWASAKI, I. TANAKA, and A. AIHARA. Acta Crystallogr. Sect. B, **32**, 1264 (1976).
34. N. G. FURMANOVA. Russ. Chem. Rev. **50**, 775 (1981); Usp. Khim. (English translation) **50**, 1491 (1981).
35. L. PAULING. The nature of the chemical bond. Cornell Univ. Press, Ithaca, NY. 1960.
36. M. BARFIELD, H. P. W. GOTTLIEB, and D. M. DODDRELL. J. Chem. Phys. **69**, 4504 (1978).
37. I. OLOVSSON and P.-G. JONSSON. *In* The hydrogen bond. *Edited by* P. Schuster, G. Zundel and C. Sandorfy. North-Holland Publishing Co., New York. 1976. p. 393.
38. L. G. BUTLER and T. L. BROWN. J. Am. Chem. Soc. **103**, 6541 (1981).
39. (*a*) H. JONES and R. F. CURL, JR. J. Mol. Spectrosc. **42**, 65 (1972); (*b*) M. J. HUNT and A. L. MACKAY. J. Magn. Reson. **15**, 402 (1974); (*c*) L. M. JACKMAN, J. C. TREWELLA, and R. C. HADDON. J. Am. Chem. Soc. **102**, 2519 (1980).
40. B. BERGLUND and R. W. VAUGHAN. J. Chem. Phys. **73**, 2037 (1980).
41. R. WASYLISHEN and T. SCHAEFER. Can. J. Chem. **49**, 3216 (1971).
42. H. LUMBROSO and P. RUMPF. Bull. Soc. Chim. Fr. 371 (1950).
43. Y. KAWASHIMA and K. KOZIMA. Bull. Chem. Soc. Jpn. **47**, 2879 (1974).
44. M. BARFIELD. J. Am. Chem. Soc. **102**, 1 (1980).
45. P. DIEHL and P. M. HENRICHS. J. Magn. Reson. **5**, 134 (1971).
46. C. L. BELL, S. S. DANYLUK, and T. SCHAEFER. Can. J. Chem. **47**, 3529 (1969).
47. R. J. KOSTELNIK, M. P. WILLIAMSON, D. E. WISNOSKY, and S. M. CASTELLANO. Can. J. Chem. **47**, 3313 (1969).
48. T. SCHAEFER, T. A. WILDMAN, and R. SEBASTIAN. Can. J. Chem. **60**, 1924 (1982).
49. T. SCHAEFER and R. LAATIKAINEN. Can. J. Chem. **61**, 2785 (1983).
50. J. B. ROWBOTHAM, M. SMITH, and T. SCHAEFER. Can. J. Chem. **53**, 986 (1975).
51. T. SCHAEFER, R. SEBASTIAN, and T. A. WILDMAN. Can. J. Chem. **57**, 3005 (1979).
52. T. SCHAEFER and K. CHUM. Can. J. Chem. **56**, 1788 (1978).

Can. J. Chem. Downloaded from www.nrcresearchpress.com by 210.87.254.42 on 09/06/12
For personal use only.

Complexes with macrocyclic ligands. II. The crystal structures of $HgCl_2 \cdot$ 18-crown-6 and $CdCl_2 \cdot$ 18-crown-6, and the FAB mass spectrum of $HgCl_2 \cdot$ 18-crown-6

CHRISTOPHER ROBIN PAIGE AND MARY FRANCES RICHARDSON
Department of Chemistry, Brock University, St. Catharines, Ont., Canada L2S 3A1

Received January 19, 1983[1]

CHRISTOPHER ROBIN PAIGE and MARY FRANCES RICHARDSON. Can. J. Chem. **62**, 332 (1984).

$HgCl_2$ and $CdCl_2$ form 1:1 complexes with 1,4,7,10,13,16-hexaoxacyclooctadecane (18-crown-6). The complexes are isostructural. The metal coordination is hexagonal bipyramidal, with chlorine atoms strongly coordinated in the axial positions and the 18-crown-6 in the equatorial place. The symmetry of the complex is crystallographically required to be $\bar{3}$ (C_{3i}), but is very nearly $\bar{3}m$ (D_{3d}). The Hg—Cl, Hg—O, Cd—Cl, and Cd—O distances are 2.314(1), 2.825(4), 2.3645(5), and 2.752(1) Å, respectively. Crystals of $HgCl_2 \cdot$ 18-crown-6 are rhombohedral, space group $R\bar{3}$, a = 7.746(2) Å, α = 95.26(3)°, Z = 1 unit of $HgCl_2C_{12}H_{24}O_6$, R = 0.026 for 543 independent reflections with $\theta < 25°$, $I > 3\sigma(I)$. Crystals of $CdCl_2 \cdot$ 18-crown-6 are also rhombohedral, space group $R\bar{3}$, a = 7.712(3) Å, α = 95.57(2)°, Z = 1 unit of $CdCl_2C_{12}H_{24}O_6$, R = 0.022 for 534 independent reflections with $\theta < 25°$, $I > 3\sigma(I)$.

CHRISTOPHER ROBIN PAIGE et MARY FRANCES RICHARDSON. Can. J. Chem. **62**, 332 (1984).

Les sels $HgCl_2$ et $CdCl_2$ forment des complexes 1:1 avec l'hexaoxa-1,4,7,10,13,16 cyclooctadécane (18-couronne-6). Les complexes sont isostructuraux. Le métal a une coordination hexagonale bipyramidale avec les atomes de chlore fortement coordonnés en position axiale et le 18-couronne-6 en position équatoriale. Du point de vue cristallographique le complexe devrait avoir une symétrie $\bar{3}$ (C_{3i}) mais elle est très proche de $\bar{3}m$ (D_{3d}). Les distances Hg—Cl, Hg—O, Cd—Cl et Cd—O sont respectivement de 2,314(1), 2,825(4), 2,3645(5) et 2,752(1) Å. Les cristaux du $HgCl_2 \cdot$ 18-couronne-6 sont rhomboédriques et appartiennent au groupe d'espace $R\bar{3}$ avec a = 7,746(2) Å, α = 95,26(3)°, Z = 1 unité de $HgCl_2C_{12}H_{24}O_6$, R = 0,026 pour 543 réflexions indépendantes avec $\theta < 25°$, $I > 3\sigma(I)$. Les cristaux de $CdCl_2 \cdot$ 18-couronne-6 sont également rhomboédriques et appartiennent au groupe d'espace $R\bar{3}$ avec a = 7,712(3) Å, α = 95,57(2)°, Z = 1 unité de $CdCl_2C_{12}H_{24}O_6$, R = 0,022 pour 534 réflexions indépendantes avec $\theta < 25°$, $I > 3\sigma(I)$.

[Traduit par le journal]

Can. J. Chem. Downloaded from www.nrcresearchpress.com by 210.87.254.42 on 09/06/12
For personal use only.

Introduction

Macrocyclic ligands are of great interest both because they are able to impose unusual coordination numbers and geometries on metal ions (1) and because they serve as models for metal ion transport across membranes (2). We have been investigating cadmium and mercury complexes of macrocyclic ligands (3). Mercury(II) has a strong tendency to linear two-coordination (4, 5), but this is not a special feature of cadmium(II) stereochemistry (4). In complexes of 18-crown-6, the ligand frequently adopts a true "crown" configuration with six oxygen donor atoms in a nearly planar arrangement about the enclosed metal ion (6). However, folded conformations are known to occur both in metal complexes and in uncomplexed 18-crown-6 (7–10). We thus decided that the complexes of $HgCl_2$ and $CdCl_2$ with 18-crown-6 provided a fascinating opportunity to observe unusual metal coordination or unusual crown configurations, and their structures are reported in this paper.

Experimental

Syntheses

$HgCl_2 \cdot$ 18-crown-6 was prepared as follows. Solutions containing 0.27 g $HgCl_2$ (1.0 mmol) in 20 mL 1-BuOH and 0.26 g 18-crown-6 (1.0 mmol) in 20 mL 1-BuOH were heated almost to boiling, and then mixed. Slow cooling yielded small transparent crystals. $CdCl_2 \cdot$ 18-crown-6 was synthesized in a similar manner, except $CdCl_2$ was dissolved in water. Crystals of the complex grew at the water–BuOH interface. Analyses of both compounds were satisfactory.

Structure determination and refinement for $HgCl_2 \cdot$ 18-crown-6

A crystal 0.05 × 0.16 × 0.70 mm was mounted with epoxy glue on a thin glass fiber. Preliminary oscillation and Weissenberg photographs initially suggested monoclinic symmetry. However, there were small differences between reflections which should have been equivalent in monoclinic symmetry. The crystal system was thus taken as triclinic (pseudomonoclinic) with the long axis of the crystal parallel to the pseudomonoclinic c-direction.

The crystal was transferred to a CAD-4 diffractometer, and cell dimensions were determined from 25 reflections having $9.5° < \theta < 22°$ (graphite-monochromatized MoKα radiation, λ = 0.7107 Å). The cell found by the INDEX routine of the CAD-4 had rhombohedral dimensions, but we chose to retain the triclinic (pseudomonoclinic) cell for data collection. For a C-centered triclinic cell having Z = 2, a = 10.444(2), b = 11.458(1), c = 7.745(1) Å, α = 90.04(1), β = 82.21(2), γ = 90.01(1)°. The full sphere of data was collected by the ω–2θ scan technique. The ω scan angle was 0.70 + 0.35 tan θ, the maximum ω scan speed was 2° min^{-1}, and the maximum scan time was 300 s. The orientation was checked every 100 reflections, and a standard was measured every hour. The standard decreased to about 85% of the starting value by the end of the data collection. Backgrounds were counted for one-quarter of the scan time at each end of the scan. A total of 4370 reflections was measured with $2° < \theta < 25°$. The reflections were corrected for variations in the standard intensity and for Lorentz and polarization effects. No absorption correction was applied. All reflections were observed.

The structure was solved in space group $C\bar{1}$ by the heavy-atom method. The Hg atoms were placed on centers of symmetry. Non-hydrogen atoms were given anisotropic thermal parameters; hydrogen atom positions were calculated, and hydrogen atoms assigned an isotropic U of 0.070 Å^2. Refinement was carried out by full-matrix least-squares on $\Sigma w(F_o - F_c)^2$ to R = 0.045. Scattering factors were from the International tables for X-ray crystallography (11). At this point the $\bar{3}$ symmetry of the complex strongly indicated that the rhombohedral cell was correct. Refinement was completed in $R\bar{3}$, with the mercury atom in the (1a) position ($\bar{3}$ symmetry required). Reflections equivalent in $R\bar{3}$ were averaged, yielding R = 0.058. Two cycles of least-squares refinement resulted in convergence at R = 0.026, R_w = 0.024, for 543 independent reflections. The weights used were $w = (\sigma^2(F) + 0.006F^2)^{-1}$. The final difference map had no features greater than 0.6 e Å^{-3} high.

$C_{12}H_{24}Cl_2HgO_6$ fw = 535.5
Rhombohedral, $R\bar{3}$, a = 7.746(2) Å, α = 95.26(3)°, V = 458.5 Å^3,

[1] Revision received September 6, 1983.

Can. J. Chem. Downloaded from www.nrcresearchpress.com by 210.87.254.42 on 09/06/12
For personal use only.

TABLE 1. Fractional coordinates and isotropic thermal parameters for $HgCl_2 \cdot$ 18-crown-6, with estimated standard deviations in parentheses, hydrogen atom positions were calculated

Atom	x/a	y/b	z/c	U_{eq}/U_{iso}[a]
Hg	0.0	0.0	0.0	0.039
Cl	−0.1908(2)	−0.1908(2)	−0.1908(2)	0.054
O	−0.2103(5)	−0.0158(5)	0.2785(5)	0.052
C(1)	−0.0638(8)	−0.2518(7)	0.3665(7)	0.057
C(2)	−0.2371(8)	−0.1874(8)	0.3264(7)	0.058
H(1)	−0.0806	−0.3733	0.4243	0.070
H(2)	0.0175	−0.1567	0.4565	0.070
H(3)	−0.3081	−0.1874	0.4401	0.070
H(4)	−0.3103	−0.2709	0.2203	0.070

[a] $U_{eq} = (1/3)\ \Sigma_i\Sigma_j U_{ij} a_i^* a_j^* \boldsymbol{a}_i \cdot \boldsymbol{a}_j$.

$\rho_o = 1.87$, $Z = 1$, $\rho_c = 1.93\ cm^{-3}$ (room temperature), $F(000) = 258$, $\mu(MoK\alpha) = 85.6\ cm^{-1}$.

Structure determination and refinement for $CdCl_2 \cdot$ 18-crown-6

A crystal 0.04 × 0.28 × 0.8 mm was used for the data collection. The determination of cell dimensions, collection of a full sphere of data, and data reduction were the same as described for $HgCl_2 \cdot$ 18-crown-6. There was no decrease in the standard during data collection.

$C_{12}H_{24}CdCl_2O_6$ fw = 447.3

Rhombohedral, $R\bar{3}$, $a = 7.712(3)$ Å, $\alpha = 95.57(2)°$, $V = 451.7$ Å^3, $\rho_o = 1.61$, $Z = 1$, $\rho_c = 1.64\ g\ cm^{-3}$ (room temperature), $F(000) = 226$, $\mu(MoK\alpha) = 14.6\ cm^{-1}$.

The structure was solved with the coordinates for $HgCl_2 \cdot$ 18-crown-6 as a starting point. Hydrogen atom positions were refined, together with an isotropic thermal parameter for the four hydrogen atoms. The final R and R_w were 0.022 and 0.027 for the 534 observed reflections, obtained by averaging the six equivalent *hkl* reflections for rhombohedral symmetry. The weights taken were $w = (\sigma^2(F) + 0.003F^2)^{-1}$. The final difference map had no features higher than 0.2 e Å^{-3}.

Computer programs used included SHELX (12) and ORTEP (13). The Cambridge Crystallographic Data Base (14), implemented as CRYSTOR by the Canadian Institute for Scientific and Technical Information, was searched for complexes of cadmium and mercury. The master file was used, complete with updates through September 1982 (34 246 entries).

Mass spectra

Conventional mass spectra were obtained with an AEI MS-30 double beam mass spectrometer operating at 4 kV acceleration potential and 70 eV ionization potential. The samples were vaporized by heating the probe. FAB (fast atom bombardment) mass spectra were obtained on the same instrument operating at a 2 kV acceleration potential. The samples were vaporized from a di-*t*-amylphenol matrix by xenon atom bombardment at 6 kV.

Results and discussion

Tables 1 and 2 present the fractional atomic coordinates of $HgCl_2 \cdot$ 18-crown-6 and $CdCl_2 \cdot$ 18-crown-6, and Table 3 lists important bond distances and angles. Table 4 reports deviations from least-squares planes. The numbering scheme and thermal ellipsoids of the mercury complex are shown in Fig. 1; numbering for the cadmium compound is analogous. Tables of the anisotropic thermal parameters and structure factors have been deposited.[2]

[2] This material is available, at a nominal charge, from the Depository of Unpublished Data, CISTI, National Research Council of Canada, Ottawa, Ont., Canada K1A 0S2.

TABLE 2. Fractional coordinates and isotropic thermal parameters for $CdCl_2 \cdot$ 18-crown-6, with estimated standard deviations in parentheses

Atom	x/a	y/b	z/c	U_{eq}/U_{iso}[a]
Cd	0.0	0.0	0.0	0.043
Cl	−0.19719(7)	−0.19719(7)	−0.19719(7)	0.047
O	−0.2098(2)	−0.0205(2)	0.2679(2)	0.047
C(1)	−0.0639(3)	−0.2527(3)	0.3657(3)	0.053
C(2)	−0.2380(3)	−0.1886(3)	0.3224(3)	0.053
H(2)	0.000(4)	−0.182(4)	0.440(4)	0.052(3)
H(1)	−0.086(3)	−0.375(4)	0.409(3)	0.052(3)
H(4)	−0.312(3)	−0.264(4)	0.239(4)	0.052(3)
H(3)	−0.293(4)	−0.181(4)	0.429(4)	0.052(3)

[a] $U_{eq} = (1/3)\ \Sigma_i\Sigma_j U_{ij} a_i^* a_j^* a_i \cdot a_j$.

TABLE 3. Bond distances and angles for $MCl_2 \cdot$ 18-crown-6, with estimated standard deviations in parentheses, symmetry superscripts are listed in Fig. 1

	Length, Å	
Bond	$HgCl_2 \cdot$ 18-crown-6	$CdCl_2 \cdot$ 18-crown-6
M—Cl	2.314(1)	2.3645(5)
M—O	2.825(4)	2.752(1)
O—C(2)	1.415(7)	1.404(3)
C(1)—C(2)	1.490(9)	1.495(3)
C(1)—O^{ii}	1.414(7)	1.422(3)
	Angle, deg	
Bond	$HgCl_2 \cdot$ 18-crown-6	$CdCl_2 \cdot$ 18-crown-6
Cl—M—O	94.3(1)	93.13(4)
O—M—O^{ii}	60.6(1)	60.30(4)
M—O—C(2)	111.5(3)	114.4(1)
M—O—C(1)^{iii}	113.8(3)	117.0(1)
C(1)^{iii}—O—C(2)	113.2(5)	112.5(1)
O—C(2)—C(1)	108.5(5)	108.4(2)
C(2)—C(1)—O^{ii}	109.1(5)	108.1(2)

The metal coordination

$HgCl_2 \cdot$ 18-crown-6 and $CdCl_2 \cdot$ 18-crown-6 are isostructural. The metal ions lie on crystallographic $\bar{3}$ axes. Each has a linear Cl—M—Cl^i group surrounded by the 18-crown-6 ligand (Fig. 1). The Hg—Cl and Hg—O distances are 2.314(1) and 2.825(4) Å, respectively. Corresponding distances for the cadmium complex are 2.3645(5) and 2.752(1) Å, respectively.

The problem arises of assigning a coordination number to the metal ions. They can either be regarded as two-coordinate or as eight-coordinate; the latter is rare for both cadmium and mercury (Table 5), and the former is not frequent for cadmium. The pattern of two short contacts and six long ones is a feature of the present complexes, $Ca(NCS)_2 \cdot$ 18-crown-6 (15), $[(CH_3)_2Tl \cdot$ dicyclohexano-18-crown-6$]^+$ (16), $[(CH_3)_2Tl \cdot$ dibenzo-18-crown-6$]^+$ (17), the CdI_2 and HgI_2 complexes of 7,16-diaza-18-crown-6 (18), and others, including UO_2^{2+} complexes (4). Most of these compounds have been taken as examples of the relatively rare hexagonal bipyramidal geometry, but $(CH_3)_2Tl^+$ was regarded as being "threaded" through the dibenzo-18-crown-6 cavity (17).

A van der Waals radius of 1.73 Å for mercury(II) has been recommended (19). This, coupled with the normal van der Waals radius for oxygen of 1.40 Å, suggests that the Hg—O distance of 2.825 Å in the 18-crown-6 complex should be treated as a bonding interaction, albeit a weak one. This gives

TABLE 4. Least-squares planes and deviations (in Å), asterisks designate atoms used in calculating the plane, symmetry superscripts are listed in Fig. 1

Plane equation, HgO_6: $-0.57198X - 0.52174Y - 0.63294Z = 0.00000$[a]			
O*	0.212	O^{iv*}	0.212
O^{i*}	−0.212	O^{v*}	0.212
O^{ii*}	−0.212	Hg	0.000
O^{iii*}	−0.212		
Plane equation, CdO_6: $-0.57129X - 0.51829Y - 0.63639Z = 0.00000$[a]			
O*	0.150	O^{iv*}	0.150
O^{i*}	−0.150	O^{v*}	0.150
O^{ii*}	−0.150	Cd	0.000
O^{iii*}	−0.150		

[a] X, Y, and Z are orthogonal coordinates in Å.

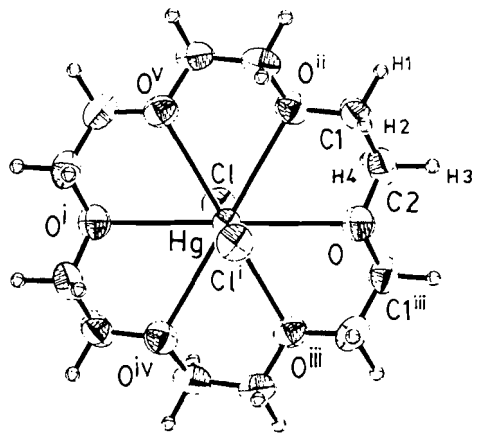

FIG. 1. A molecule of $HgCl_2 \cdot$ 18-crown-6, showing the numbering scheme and thermal ellipsoids. Symmetry superscripts: *i* $(-x, -y, -z)$; *ii* $(-y, -z, -x)$; *iii* $(-z, -x, -y)$; *iv* (y, z, x): *v* (z, x, y).

mercury a coordination number of eight and a hexagonal bipyramidal geometry. The Hg—Cl distance of 2.314(1) Å is somewhat longer than the value of 2.25 Å observed for $HgCl_2$ itself (5). This again supports the idea of bonding between $HgCl_2$ and 18-crown-6, as there is a steady lengthening of the Hg—Cl bonds as other ligands become progressively more strongly coordinated (5).

Also to be noted are the HgX_2 complexes of open-chain polyethers such as tetraethyleneglycol dimethyl ether (20) and 1,15-bis(2-bromophenyl)-2,5,8,11,14-pentaoxapentadecane (21). In both of these complexes, the Hg(II) atom organizes the five oxygen donor atoms around itself in a pentagonal arrangement, with the halides completing a pentagonal bipyramidal coordination. The Hg—O bond distances are 2.78–2.96 Å in the former complex and 2.718–3.059 Å in the latter.

The $CdCl_2$ complex of tetraethyleneglycol dimethyl ether (22) is quite different from the corresponding $HgCl_2$ complex. The two independent cadmium ions in this structure are both six-coordinate, with Cd—Cl and Cd—O distances of 2.425–2.682 and 2.409–2.735 Å, respectively. The upper limits of these values are not greatly different from the Cd—Cl and Cd—O bond distances in $CdCl_2 \cdot$ 18-crown-6. Thus cadmium, too, exhibits hexagonal bipyramidal coordination in its 18-crown-6 complex.

The shorter Cd—O and longer Cd—Cl distances, by comparison to these quantities for the mercury complex (Table 3), are in line with simple hard–soft acid–base predictions.

TABLE 5. Results of searching the Cambridge Crystallographic Data Base for complexes of cadmium and mercury (does not include purely inorganic compounds)

	No. of complexes with coordination number							
Metal	2	3	4	5	6	7	8	9+
Cd	16	7	51	22	94	20	6	0
Hg	185	59	145	23	20	3	2	0

The ligand structure

The 18-crown-6 ligand has nearly perfect D_{3d} symmetry, as shown in Fig. 1. The oxygen atoms lie alternately above and below the plane defined by the six oxygens (Table 4), which is typical for 18-crown-6 in this conformation (6). The chelate rings are all *gauche*. The bond distances and angles in the ligand are typical (6, 10).

Molecular packing

Figure 2 shows a view of the packing projected down the pseudomonoclinic *c*-axis, and Fig. 3 shows a projection down the rhombohedral $\bar{3}$ axis. The $HgCl_2$ and $CdCl_2$ units do indeed define a monoclinic unit cell with $C2/m$ symmetry, which accounts for the fact that the Weissenberg photographs initially looked as though they came from a monoclinic crystal. The monoclinic symmetry is destroyed by the crown ligands. The pseudomonoclinic to rhombohedral transformation is given by:

$$\begin{pmatrix} a \\ b \\ c \end{pmatrix}_{\text{rhombohedral}} = \begin{pmatrix} 0 & 0 & -1 \\ 0.5 & 0.5 & 0 \\ 0.5 & -0.5 & 0 \end{pmatrix} \begin{pmatrix} a \\ b \\ c \end{pmatrix}_{\text{pseudomonoclinic}}$$

There are no intermolecular contacts significantly shorter than the van der Waals distances.

Mass spectra

The normal mass spectrum of $HgCl_2 \cdot$ 18-crown-6 contained peaks due to Hg^+ and fragments from the 18-crown-6 ligand; with the exception of peaks due to the Hg^+ cluster, it was essentially identical to the mass spectrum of 18-crown-6 alone (23). However, the FAB-source mass spectrum clearly showed a cluster of peaks centered at m/z 501, attributable to the $[HgCl(18\text{-crown-6})]^+$ ion ($^{202}Hg^{35}Cl^{12}C_{12}{}^{1}H_{24}{}^{16}O_6$ has a mass of

Can. J. Chem. Downloaded from www.nrcresearchpress.com by 210.87.254.42 on 09/06/12
For personal use only.

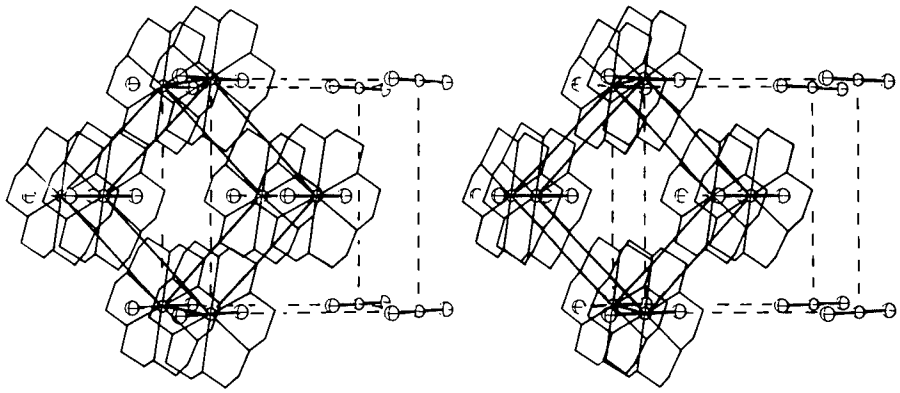

FIG. 2. Packing of $HgCl_2 \cdot$ 18-crown-6 as viewed down the pseudomonoclinic c-axis. The pseudomonoclinic a and b axes are horizontal and vertical, respectively. Dotted lines show the pseudomonoclinic cell; solid lines outline the true rhombohedral cell.

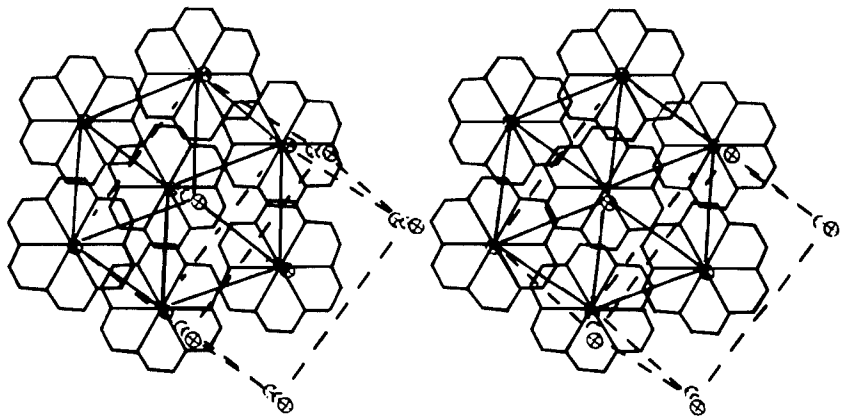

FIG. 3. Packing of $HgCl_2 \cdot$ 18-crown-6 as viewed down the rhombohedral $\bar{3}$ axis.

501 au). The appearance of this ion as the highest-mass peak is normal for chlorinated compounds, which usually exhibit much stronger $[M—Cl]^+$ peaks than $[M]^+$ peaks. The significance of the FAB-source spectrum is that it shows that the mercury ion remains associated with the 18-crown-6 ligand, in spite of the long, presumably weak, mercury–oxygen bonds. Thus, FAB mass spectroscopy may prove to be a useful tool in characterizing metal complexes, especially when they pyrolyze or dissociate upon heating in a conventional mass spectrometer probe.

Acknowledgements

We thank the Natural Sciences and Engineering Research Council of Canada for financial support, and are especially grateful to the Atkinson Charitable Foundation and the J. P. Bickell Foundation for grants towards the purchase of the CAD-4 diffractometer. We also thank Mr. Tim Jones for obtaining the mass spectra.

1. G. A. MELSON (*Editor*). Coordination chemistry of macrocyclic compounds. Plenum Press, New York. 1979.
2. J. H. FENDLER. Membrane mimetic chemistry. John Wiley and Sons, New York. 1982.
3. M. R. BURKE and M. F. RICHARDSON. Inorg. Chim. Acta, **69**, 29 (1983).
4. F. A. COTTON and G. WILKINSON. Advanced inorganic chemistry, 4th ed. John Wiley and Sons, New York. 1980.
5. P. A. W. DEAN. Prog. Inorg. Chem. **24**, 109 (1978).
6. M. DOBLER. Ionophores and their structures. John Wiley and Sons, New York. 1981.
7. G. BOMBIERI, G. DE PAOLI, and A. IMMIRZI. J. Inorg. Nucl. Chem. **40**, 1889 (1978).
8. G. BOMBIERI, G. DE PAOLI, and A. IMMIRZI. J. Inorg. Nucl. Chem. 799 (1978).
9. M. DOBLER, J. D. DUNITZ, and P. SEILER. Acta Crystallogr. B**30**, 2741 (1974).
10. E. MAVERICK, P. SEILER, W. B. SCHWEIZER, and J. D. DUNITZ. Acta Crystallogr. B**36**, 615 (1980).
11. International tables for X-ray crystallography. Vol. IV. The Kynoch Press, Birmingham. 1974.
12. G. M. SHELDRICK. SHELX-76 program for crystal structure determination. University of Cambridge, England. 1976.
13. C. JOHNSON. ORTEP-II. A thermal ellipsoid plot program for crystal structure illustrations. Oak Ridge National Laboratory, Oak Ridge, TN. 1976.
14. F. H. ALLEN, O. KENNARD, W. D. S. MOTHERWELL, and D. G. WATSON. J. Chem. Docum. **13**, 119 (1977).
15. J. D. DUNITZ and P. SEILER. Acta Crystallogr. B**30**, 2750 (1974).
16. D. L. HUGHES and M. R. TRUTER. J. Chem. Soc. Chem. Commun. 727 (1982).
17. K. HENRICK, R. W. MATTHEWS, B. L. PODEJMA, and P. A. TASKER. J. Chem. Soc. Chem. Commun. 118 (1982).
18. L. A. MALMSTEN. Acta Crystallogr. B**35**, 1702 (1979).
19. A. J. CANTY and G. B. DEACON. Inorg. Chim. Acta, **45**, L225 (1980).
20. R. IWAMOTO. Bull. Chem. Soc. Jpn. **46**, 1114 (1973).
21. G. WEBER. Acta Crystallogr. B**36**, 2779 (1980).
22. R. IWAMOTO and H. WAKANO. J. Am. Chem. Soc. **98**, 3764 (1976).
23. Y. C. LEE, A. I. POPOV, and J. ALLISON. Intl. J. Mass Spectry. Ion Phys. **51**, 267 (1983).

Can. J. Chem. Downloaded from www.nrcresearchpress.com by 210.87.254.42 on 09/06/12
For personal use only.

Reagents and synthetic methods. 31. Silylations with *N*-trimethylsilyl-2-oxazolidinone (TMSO)

JESÚS M. AIZPURUA AND CLAUDIO PALOMO[1]
Kimika Organikako Departamendua, Kimika Fakultatea, Donostia, Spain
AND
ANTONIO L. PALOMO
Departamento de Investigación Gema S.A., Beethoven 15, Barcelona-21, Spain

Received July 11, 1983

JESÚS M. AIZPURUA, CLAUDIO PALOMO, and ANTONIO L. PALOMO. Can. J. Chem. **62**, 336 (1984).

Silylation of ketones, alcohols, mercaptans, and carboxylic acids with *N*-trimethylsilyl-2-oxazolidinone (TMSO) and triflic acid as catalyst has been described from synthetic and mechanistic points of view.

JESÚS M. AIZPURUA, CLAUDIO PALOMO et ANTONIO L. PALOMO. Can. J. Chem. **62**, 336 (1984).

On décrit l'emploi de la *N*-triméthylsilyl-oxazolidinone-2 (TMSO) avec l'acide triflique comme catalyseur pour la silylation de cétones, d'alcools, de mercaptans et d'acides carboxyliques d'un point de vue mécanistique et de son application en synthèse.

[Traduit par le journal]

The utility of the silylation reaction in organic synthesis is well recognized (1, 2), and the introduction of new reagents and the modification of existing ones is a continuous challenge. Although there are numerous reports on different silylation methods, most of them require energetic conditions. Recently, silylations with trimethylsilyl triflate generated *in situ* from allyltrimethylsilane and triflic acid have been reported (3). However, in this method, the silylation of mercaptans needs high temperatures and long reaction times. In connection with our first reports (4, 5) on silylation of organic compounds by means of *N*-trimethylsilyl-2-oxazolidinone (TMSO), recent publications from our laboratory have revealed that this reagent is a powerful silylating agent for (a) carboxylic acids (6), (b) 1,3-dicarbonyl compounds (7), (c) alcohols (8), and (d) amino acids (4, 9).

We now wish to report that TMSO, together with triflic acid as catalyst, may be efficiently used for the silylation of carboxylic acids, alcohols, mercaptans, and carbonyl compounds.

Although we have recently described the use of this reagent for the synthesis of trimethylsilyl carboxylates and trimethylsilyl ethers under basic, neutral, or acidic catalysis, we have now found that trimethylsilylation of carboxylic acids and alcohols takes place almost instantaneously when 2–3 drops of triflic acid are added to a mixture of the substrate and *N*-trimethylsilyl-2-oxazolidone **1**, with the immediate precipitation of 2-oxazolidinone **4**. In order to provide fundamental

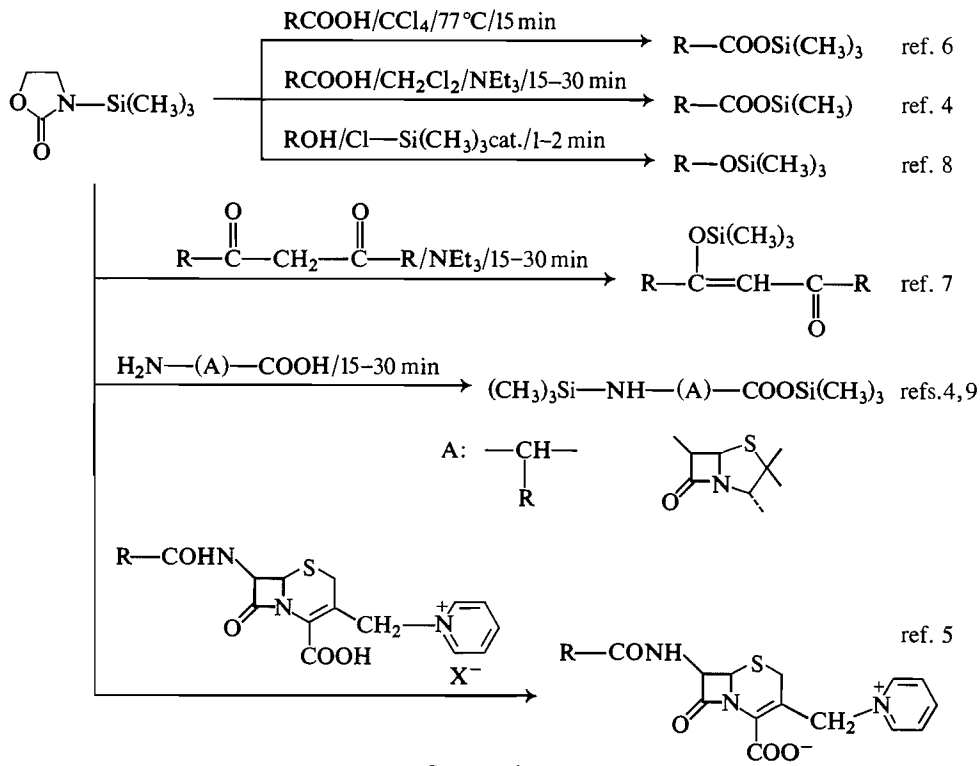

SCHEME 1

[1]Author to whom correspondence may be addressed.

Can. J. Chem. Downloaded from www.nrcresearchpress.com by 210.87.254.105 on 09/06/12
For personal use only.

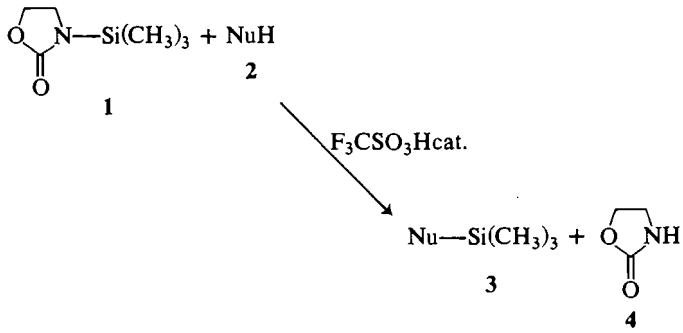

2*a*: RCOOH, 2*b*: ROH, 2*c*: R—SH

SCHEME 2

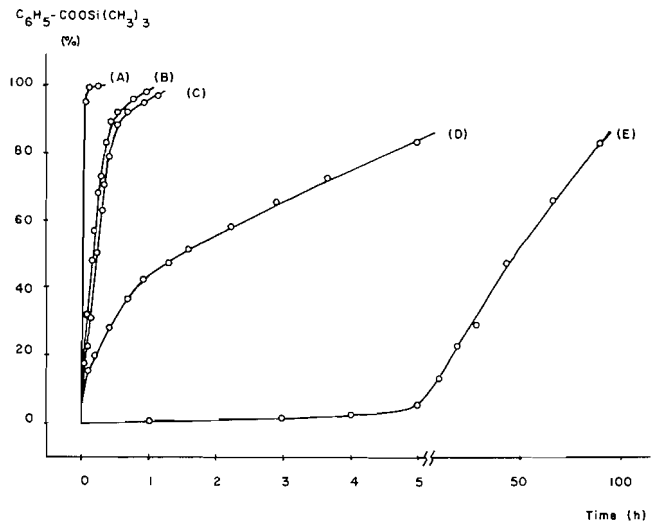

FIG. 1. Silylation of benzoic acid with TMSO at 25°C. Solvent: CH_2Cl_2. Reagent concentration: 0.5 *M*. Catalyst concentration: 2 mol%. Catalysts: (A) F_3CSO_3H, (B) DBU, (C) $N(C_2H_5)_3$, (D), $ClSi(CH_3)_3$, (E) none.

information regarding these factors, we have studied the effect of some catalysts on the outcome of the silylation of benzoic acid by means of this reagent **1**. Thus, an equimolecular mixture of *N*-trimethylsilyl-2-oxazolidinone **1** and the substrate in dichloromethane was treated at 25°C with different catalysts in an nmr sample tube, and the reaction was monitored mainly by observing the change of the relative intensities of the trimethylsilyl groups; the trimethylsilyl group of TMSO appeared consistently at a slightly higher field than that of the product. Measurements were done in the presence of a catalytic amount of triethylamine, 1,8-diazabicyclo[5.4.0]undec-7-ene, trimethylchlorosilane, triflic acid, and in their absence, and the results are shown in Fig. 1. While, in the absence of any catalyst, the transformation proceeds very smoothly, the catalytic assistance of triflic acid increases the silylation rate. Moreover, the reaction proceeds much faster than with basic catalysis.

The generalization of these results is shown in Table 1. The utility of this method can be observed in the silylation of phenylmalonic acid, which easily undergoes decarboxylation under basic or thermal conditions.[2]

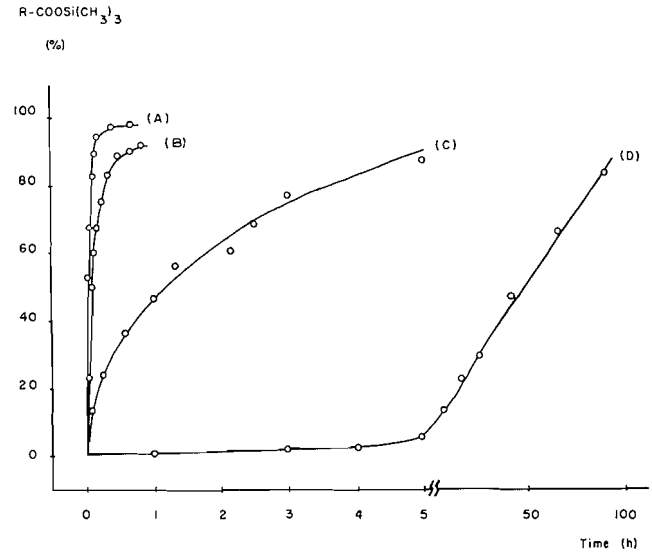

FIG. 2. Silylation of carboxylic acids with TMSO in the absence of catalyst at 25°C. Reagent concentration: 0.5 *M*. Solvent: CH_2Cl_2. Carboxylic acids: (A) Cl_3C—COOH (pK_a = 0.70), (B) Cl_2CH—COOH (pK_a = 1.48), (C) $NCCH_2$—COOH (a mixture of CH_2Cl_2/CH_3CN (9:1) was used as solvent) (pK_a = 2.45), (D) C_6H_5—COOH (pK_a = 4.19).

This aroused our interest in examining, in the same way, the silylation of some carboxylic acids with different pK_a values (Fig. 2). The rapid conversion of strong carboxylic acids into the corresponding silyl esters seems to indicate that the autocatalytic acid effect is important in the silylation rate. When triflic acid is present in the reaction mixture the transformation takes place almost instantaneously.

From a preparative point of view, the reaction of carboxylic acids or alcohols with the trimethylsilyl triflate generated *in situ* from *N*-trimethylsilyl-2-oxazolidinone **1** is carried out at room temperature and the by-product, 2-oxazolidinone **4**, can be separated by filtration or the silylated product **3** can be distilled directly from the reaction mixture.

The silylation of thiols under similar catalytic reaction conditions is shown in Table 2. In this case the acid catalysis is also more efficient than the basic catalysis and the trimethylsilyl thio derivatives were obtained in high yields and in a short time.[3]

This fast transformation may be rationalized by assuming that the equilibrium **1** + **2** $\rightleftharpoons$ **3** + **4** is shifted to the side of **3** by the precipitation of 2-oxazolidinone **4**.

It should be noted that the separation of the side product **4** from the reaction mixture is necessary, because the direct distillation of the mixture gives the starting products, as we have observed in the case of n-propylmercaptan.

Furthermore, the utility and general superiority of the present silylating system have been demonstrated by the silylation of carbonyl compounds. In these cases an equimolecular amount of triflic acid was needed to perform the silylation reaction. In this way we have found that trimethylsilyl triflate can be obtained from reagent **1** and not from other commercial silylating agents such as monotrimethylsilylacetamide (MSA), bistrimethylsilylacetamide (BSA), or

[2] Under neutral conditions the yield of the isolated product is also high, but the reaction proceeds more smoothly than in the method described here (6).

[3] In comparison, in the allyltrimethylsilane – triflic acid method, the trimethylsilyl thio derivatives are obtained upon reflux in carbon tetrachloride for 8–10 h (3).

Can. J. Chem. Downloaded from www.nrcresearchpress.com by 210.87.254.105 on 09/06/12
For personal use only.

TABLE 1. Silylation of alcohols and carboxylic acids by means of reagent **1** under triflic acid catalysis

Compound	Time[a]	Yield[b] (%)	Boiling point (°C/Torr) Found	Lit. (ref.)
Cl_3CCOOH	2 min	87	68–69/10	69/10(6)
C_6H_5COOH	5 min	95	220–222	221/760(1)
CH_3CH_2COOH	2 min	93	120–122	122/760(1)
HCOOH	2 min	95	83	86.5/760(1)
$C_6H_5—CH=CH—COOH$	3 min	91	142–143/10	102/1(1)
$CH_3—CH=CH—COOH$	2 min	97	52–54/16	47/9(1)
$(CH_3)_3C—COOH$	2 min	97	28/16	
$C_6H_5CHCOOH$ | COOH	15 min[c]	74	92–94/0.3	94–95/0.3–0.4(6)
$(CH_3)_3C—OH$	15 s	91	102–104/760	105/760(1)
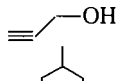	15 s	92	106–108/760	110/757(1)
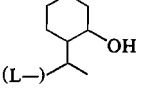	30 s	95	180–182/760	87–88/8(1)

[a] Reaction temperature 15°C, without solvent.
[b] Yield of isolated pure product.
[c] Tetrachloromethane was used as solvent.
[d] All compounds were identified by physical properties (bp, ir and ^1H nmr spectral characteristics).

TABLE 2. Trimethylsilyl thio derivatives prepared[a]

Compound	Catalyzer (2%)	Time (min)	Yield (%)	Boiling point (°C/Torr) Found	Lit. (ref.)
$CH_3CH_2—SH$	DBU[b]	30	82	128–130/760	130/760(1)
$CH_3CH_2—SH$	F_3CSO_3H	10	86		
$CH_3CH_2CH_2—SH$	DBU	30	78	152/760	151/760(1)
$CH_3CH_2CH_2—SH$	F_3CSO_3H	10	83		
$C_6H_5—SH$	DBU	60	89	40–42/0.3	72/8(12)
$C_6H_5—SH$	F_3CSO_3H	10	93		
$HOOCCH_2CH_2—SH$[c]	F_3CSO_3H	10	92	70–72/17[d]	

[a] All reactions were carried out at room temperature, without solvent.
[b] DBU: 1,8-diazabicyclo[5.4.0]undec-7-ene.
[c] From two equivalents of TMSO, the product obtained is $Me_3SiS—CH_2CH_2COOSiMe_3$, (see Experimental).
[d] O-silylated.

trimethylsilyl imidazole (TMSI), as is shown in Table 3. Thus, equimolecular amounts of TMSO **1** and triflic acid are mixed at room temperature and the trimethylsilyl triflate is directly distilled under vacuum from the mixture into a solution of the appropriate ketone and 1,8-diazabicyclo[5.4.0]undec-7-ene (DBU). The reaction takes place rapidly, 15–30 min, at room temperature and the desired silyl enol ethers are obtained in high yield.

It should be noted that the thermodynamic-to-kinetic isomer ratio for methylcyclohexanone, 89:11, was different from the ratio 78:22, reported by House *et al.*, with triethylamine in refluxing dimethylformamide (10). This seems to be due to the difference in reaction conditions.

The above-mentioned results clearly demonstrate that *N*-trimethylsilyl-2-oxazolidinone (TMSO) is indeed a highly effective reagent for the transformations studied, and may prove to be a useful alternative to other reagents in silylation reactions.

Experimental

General procedure for silylation of carboxylic acids **2**a *and alcohols* 2b

A mixture of *N*-trimethylsilyl-2-oxazolidinone **1** (3.1 mL, 20 mmol), triflic acid (0.05 mL, cat.), and the corresponding carboxylic acid **2***a* (20 mmol) or alcohol **2***b* (20 mmol) was stirred at 0°C for 3 min. Distillation of the reaction mixture afford the trimethylsilyl carboxylates **3***a* or trimethylsilyl ethers **3***b*, respectively.

General procedure for the preparation of trimethylsilyl thio ethers

A mixture of *N*-trimethylsilyl-2-oxazolidinone **1** (3.1 mL, 20 mmol), triflic acid (0.05 mL, cat.), and the corresponding thiol **2***c* (20 mmol) was stirred at room temperature for 10 min. n-Hexane (10 mL) was added and the reaction mixture stirred for 2 min again, after which 2-oxazolidinone **4** was filtered off. Evaporation of the solvent gave the crude trimethylsilyl thioether **3***c* which was purified by distillation.

S,O-*bis(trimethylsilyl)thio propionate: typical procedure*

A mixture of TMSO **1** (6.4 mL, 40 mmol), 3-mercaptopropionic acid (1.74 mL, 20 mmol), and triflic acid (0.05 mL, cat.) was stirred

Can. J. Chem. Downloaded from www.nrcresearchpress.com by 210.87.254.105 on 09/06/12
For personal use only.

TABLE 3. Preparation of trimethylsilyl triflate

Reagent	Time (min)	Yield[a] (%)
$CH_3-C(OSi(CH_3)_3)=N-Si(CH_3)_3$ (BSA)	5	43
$CH_3C(=O)-NH-Si(CH_3)_3$ (MSA)	5	35
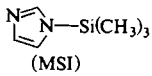 (MSI)	30	—[b]
$Cl_3C-C(=O)-OSi(CH_3)_3$	5	40
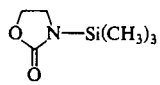 (TMSO)	2	80

[a] Yield of isolated pure product; bp 40°C/18 Torr (lit. (11) bp 36°C/12 Torr).
[b] A white solid mp 72–75°C was obtained: 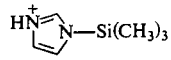 (see Experimental).

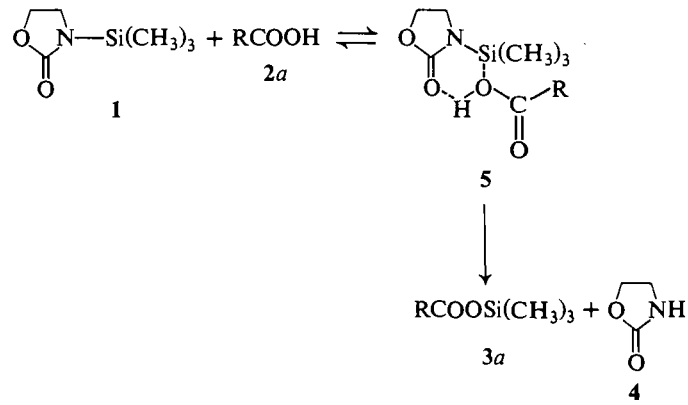

SCHEME 3

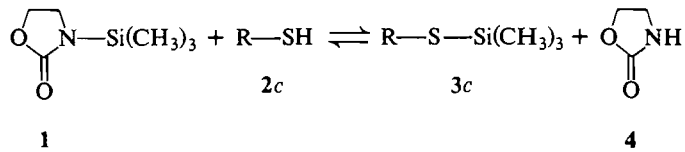

SCHEME 4

TABLE 4. Preparation of enol silyl ethers from ketones

Substrate	T (°C)	Time (min)	Products	Yield[a] (%)	Boiling point/Torr Found	Boiling point/Torr Lit. (3)
	15	15	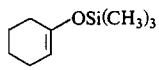	84	60–62/8	70–72/18–19
	0	20	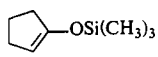	96	140–142/760	48–49/15
	0	30	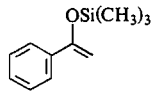	86	90–92/17	89–92/12–13
	15	10	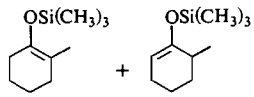 89:11	85[b]	102–106/30	79–85/20

[a] Yield of isolated product; purity of the product as determined by ^1H nmr is ≤95%.
[b] Isomer ratio calculated from ^1H nmr in CCl_4.

at room temperature for 10 min, after which n-hexane (25 mL) was added and the mixture stirred for 5 min again. The 2-oxazolidinone was filtered off and the solvent evaporated at reduced pressure to give crude *S,O*-bis(trimethylsilyl)thio propionate which was purified by distillation (2.30 g, 92%), bp 114–118°C/17 Torr (lit. (1) bp 120–121°C/16 Torr); ^1H nmr (CCl_4–TMS), 0.19 (s, 9H, CH_3), 0.21 (s, 9H, CH_3), 2.51 (m, 4H, CH_2), δ ppm.

Trimethylsilyl triflate

Triflic acid (1.76 mL, 20 mmol) was slowly added to TMSO **1** (3.2 mL, 20 mmol) and the resulting solution was stirred for 2 min and distilled at reduced pressure, affording trimethylsilyl triflate (3.55 g, 80%), bp: 40°C/18 Torr (lit. (11) bp 36°C/12 Torr); ^1H nmr (CCl_4–TMS), 0.50 (s, 9H, CH_3), δ ppm.

General procedure for the preparation of trimethylsilyl enol ethers

Triflic acid (1.32 mL, 15 mmol) was slowly added to cooled (0°C) and stirred *N*-trimethylsilyl-2-oxazolidinone **1** (2.40 mL, 15 mmol). The reaction mixture was then heated to reflux under reduced pressure (15–20 Torr) and simultaneously distilled into a solution of the corresponding carbonyl compound (10 mmol) and DBU (3.0 mL, 20 mmol). The resulting mixture was stirred at 0°C for 30 min and then distilled at reduced pressure to afford the corresponding enol silyl ether.

N-trimethylsilylimidazolium triflate

Triflic acid (0.44 mL, 5 mmol) was slowly added to cooled (0°C) and stirred trimethylsilylimidazole (MSI) (0.74 mL, 5 mmol). The resulting white solid was dried under reduced pressure (0.1 Torr) to give *N*-trimethylsilylimidazolium triflate (1.30 g, 96%), mp 72–75°C; ^1H nmr ($CDCl_3$–TMS), 0.53 (s, 9H, CH_3), 7.24 (bs, 2H, CH), 8.48 (s, 1H, N=CH), 13.35 (s, 1H, NH), δ ppm.

Acknowledgements

This work was supported by the Hezkuntza Saila of Eusko Jaurlaritza (Basque Government), and by Wacker-Chemie

Can. J. Chem. Downloaded from www.nrcresearchpress.com by 210.87.254.105 on 09/06/12
For personal use only.

GMBH (München, Germany) with gifts of BSU, MSI, and MSA reagents.

1. A. E. PIERCE. Silylation of organic compounds. Pierce Chemical Co., Rockford, Illinois. 1968.
2. E. COLVIN. Silicon in organic synthesis. Butherworths, London. 1981.
3. G. A. OLAH, A. HUSAIN, B. G. B. GUPTA, G. F. SALEM, and S. C. NARANG. J. Org. Chem. **46**, 5212 (1981), and references cited therein.
4. A. L. PALOMO. An. Quim. **77**(c), 35 (1981).
5. A. L. PALOMO and C. PALOMO. An. Quim. **77**(c), 87 (1981).
6. C. PALOMO. Synthesis, 809 (1981).
7. J. M. AIZPURUA and C. PALOMO. Synthesis, 280 (1982).
8. J. M. AIZPURUA and C. PALOMO. Bull. Soc. Chim. Fr. II, 265 (1982).
9. A. ARRIETA and C. PALOMO. Synthesis, 1050 (1982).
10. H. O. HOUSE, L. J. CZUBA, M. GALL, and H. D. OLMSTEAD. J. Org. Chem. **34**, 2324 (1969).
11. M. SCHMEIBER, P. SARTORI, and B. LIPPSMEIER. Chem. Ber. **103**, 868 (1970).
12. K. A. HOOTON and A. L. ALLRED. Inorg. Chem. **4**, 671 (1965).

Can. J. Chem. Downloaded from www.nrcresearchpress.com by 210.87.254.105 on 09/06/12
For personal use only.

MNDO calculations for some allotropes, hydrides, and oxides of phosphorus

N. COLIN BAIRD
Department of Chemistry, University of Western Ontario, London, Ont., Canada N6A 5B7

Received May 18, 1983

N. COLIN BAIRD. Can. J. Chem. **62**, 341 (1984).

Molecular orbital calculations by the MNDO method are reported for some allotropes, hydrides, and oxides of phosphorus. The aim of the study is to test further the ability of MNDO to reproduce the energetics of PP, PH, and PO bonds, and to apply MNDO to interesting problems in the chemistry of such systems. Different isomers of P_4, P_6, and P_8 are considered, as well as ions of P_3, P_5, and P_7. The method is found to overestimate strain energy in three-membered rings, and to underestimate the strength of three-electron PP bonds. The strength of PO π bonds apparently also is overestimated. Possible isomers of P_2O_2 and P_2O_3 are discussed.

N. COLIN BAIRD. Can. J. Chem. **62**, 341 (1984).

On rapporte des calculs d'orbitale moléculaire, selon la méthode MNDO, relatifs à quelques formes allotropes d'hydrures et d'oxyde de phosphore. Le but de l'étude est de vérifier d'avantage la capacité du MNDO à reproduire les liaisons énergétiques du PP, PH et PO et d'appliquer le MNDO à des problèmes intéressants dans la chimie de tels systèmes. On a considéré les différents isomères de P_4, de P_6 et de P_8 aussi bien que les ions de P_3, de P_5 et de P_7. On trouve que la méthode surestime l'énergie de contrainte des cycles à trois chainons et sous estime la force des liaisons PP à trois électrons. La force des liaisons π PO est apparamment surestimée également. On discute des isomères possibles de P_2O_2 et de P_2O_3.
[Traduit par le journal]

Can. J. Chem. Downloaded from www.nrcresearchpress.com by 210.87.254.40 on 09/06/12
For personal use only.

Introduction

Although sophisticated *ab initio* molecular orbital calculations are becoming feasible for larger and larger systems, semiempirical MO computations still are useful in many contexts — including reaction mechanisms and the study of molecules which contain many electrons. Two methods which are claimed to be sufficiently accurate and general for most purposes are the MINDO and MNDO schemes developed by Dewar and co-workers (1). Recently we have initiated a study of the use of the MNDO method in the field of covalent inorganic chemistry and have reported on applications to the various forms of elemental sulfur (2). In the present report we extend our analysis to the catenation behavior of phosphorus, and to some phosphorus oxides.

Method of calculation

All calculations reported herein were obtained by the MNDO method without CI unless otherwise indicated. Thiel's program (3) was used on the CDC cyber 170–835 computer at the University of Western Ontario.

Results and discussion

Phosphorus allotropes and hydrides

In analogy with nitrogen, phosphorus atoms could conceivably form triple, double, and single PP bonds in the various allotropes P_n and in the phosphorus hydrides P_nH_m. The simplest molecule, P_2, contains a P≡P bond. Since its predicted heat of formation (ΔH_f) in Table 1 exactly equals the experimental value, presumably this species was included in the MNDO parameterization procedure for this element.

To determine whether MNDO accounts quantitatively for the strength of unstrained phosphorus–phosphorus single bonds, a calculation for the infinitely polymeric "black" phosphorus would be desirable. Since this computation is not feasible with the current MNDO program, an indirect approach based upon the group additivity value for —P<, derived from predicted ΔH_f's for P_nH_m chains, has been used instead. From the MNDO ΔH_f's for the unbranched chains PH_3, P_2H_4, P_3H_6, and *n*-P_4H_8 listed in Table 2, we can derive a group value of −6.9 kcal for >PH (from the limiting $\Delta\Delta H_f$ along this series), −1.8 kcal for —PH_2 and +3.9 kcal for PH_3. Extrapolation of these values yields a group value for >P— of about −11 or −12 kcal. A more direct evaluation is obtained from an MNDO calculation for $P(PH_2)_3$; from its ΔH_f and the group value for PH_2, we obtain −14.4 kcal for —P<. Thus we conclude that the MNDO value for —P<, and thus the predicted ΔH_f per atom in black phosphorus, is about −14 kcal mol^{-1}. Since experimentally the heat of formation for the black allotrope is −9.4 kcal (4), we conclude that MNDO slightly overestimates, by about 3 kcal (i.e. 2/3 of the ΔH_f error for >P—) the energy of each unstrained PP single σ bond. A similar group value analysis for alkane chains does lead to the correct value for diamond if experimental ΔH_f's are used, but not if MNDO predictions are employed, because MNDO substantially underestimates the stability of highly-branched hydrocarbon chains. Our conclusion regarding P—P bond energy is also supported by the calculated ΔE for the reaction

$$2PH_2 \rightarrow P_2H_4$$

for which MNDO predicts −65.7 kcal compared to −61 ± 4 experimental (5). Thus the strength of the P—P single bond in P_2H_4 seems to be overestimated by 5 ± 4 kcal, which is not inconsistent with the value of 2 ± 3 obtained above.

Given that the total energy for the one σ and two π bonds in P_2 is correctly predicted, we can conclude that MNDO must underestimate the energy of each phosphorus–phosphorus π bond by about 1.5 kcal.

Since the MNDO ΔH_f's for P_nH_m chains are accurately duplicated using the group values derived above, strain energies in various conceivable cyclic structures formed by phosphorus atoms can be derived from their MNDO-predicted heats of formation (listed in Tables 1 and 2). Before proceeding with such an analysis, however, it is useful to note that a strong preference is evident in all MNDO calculations for PP single-bonded molecules for an *anti* conformation of the lone pair positions on adjacent phosphorus atoms. According to MNDO, it requires an input of 4.2 kcal to eclipse the lone pairs (and hydrogens) in P_2H_4, and 2.6 kcal to achieve *gauche* lone pairs relative to the *anti* conformations. The optimum conformations for all the P_nH_{n+2} chains studied is *anti* for adjacent lone pairs.

TABLE 1. MNDO calculations for P_n molecules and ions

System	ΔH_f (kcal mol^{-1})	Bond lengths (Å)	Bond angles (deg)	Dihedral angles (deg)
P_2	+40.7	1.693		
P_4				
A	+61.6	1.858(*1*—*2*) 2.063(*2*—*3*)	90.0(all)	0.0(*1234*)
B	+36.2	2.053(all)	60.0	
P_6				
A	+30.9	1.888(all)	120.0(all)	0.0(all)
B 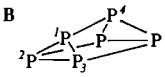	+25.9	2.066(*1*—*2*) 2.074(*1*—*4*)	60.0(*123*) 90.0(*214*)	
C 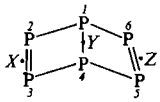	+35.6	2.020(*1*—*2*) 1.859(*2*—*3*) 2.086(*1*—*4*)	93.2(*123*) [120.0](*XYZ*)	−0.9(*1234*) 20.5(*1YZ6*) 150.9(*1YZ5*)
P_8 cubic	+4.1	2.075(all)		
P_3^+	+268.2	1.952(all)	60.0(all)	
P_5^+ 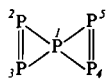	+264.6	2.007(*1*—*2*) 1.892(*2*—*3*)	61.9(*123*)	
P_5^- 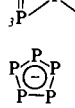	−77.4	1.894(all)	108.0(all)	0.0(all)
P_7^+ 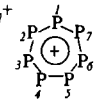	+288.7	1.897(*1*—*2*) 1.903(*2*—*3*) 1.897(*3*—*4*) 1.904(*4*—*5*) 1.897(*5*—*6*) 1.904(*6*—*7*)	128.3(*123*) 128.5(*234*) 128.4(*345*) 128.6(*456*) 128.7(*567*)	−2.5(*1234*) −1.7(*2345*) −1.2(*3456*) 9.0(*4567*)

TABLE 2. MNDO calculations for P_nH_m systems

System	ΔH_f (kcal mol^{-1})	Bond lengths (Å)	Bond angles (deg)	Dihedral angles (deg)
$PH_2(^2\pi)$	+31.4	1.334	96.2	
PH_3	+3.9	1.340	96.1	
P_2H_2 *trans*	+27.4	1.833(PP) 1.338(PH)	100.6	180.0
cis	+29.5	1.829(PP) 1.338(PH)	107.2	0.0
P_2H_3 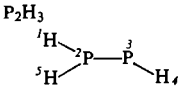	+23.2	1.340(*1*—*2*) 1.985(*2*—*3*) 1.336(*3*—*4*) 1.342(*2*—*5*)	98.2(*123*) 99.2(*234*) 100.9(*325*)	189.2(*1234*) −71.4(*4325*)
P_2H_4	−2.9	2.023(PP) 1.340(PH)	98.4	180.0($HPPH_1$) −81.5($HPPH_2$) +81.5($HPPH_3$)
P_3H 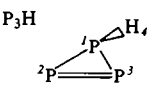	+38.0	2.039(*1*—*2*) 1.843(*2*—*3*) 1.340(*1*—*4*)	105.9(PPH)	
P_4H_2 (*cis* planar) 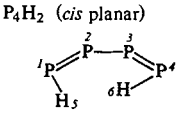	+47.3	1.827(*1*—*2*) 1.974(*2*—*3*) 1.340(*1*—*5*)	108.7(*512*) 123.2(*123*)	[0.0](*5123*) [0.0](*1234*)

Can. J. Chem. Downloaded from www.nrcresearchpress.com by 210.87.254.40 on 09/06/12
For personal use only.

TABLE 2 (*Concluded*)

System	ΔH_f (kcal mol^{-1})	Bond lengths (Å)	Bond angles (deg)	Dihedral angles (deg)
P_4H_4 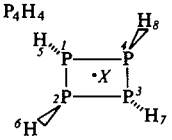	−19.1	2.034(PP) 1.340(PH)	86.1(*123*) 86.1(*234*) 126.4(*X15*) 106.3(*X26*) 126.4(*X37*) 107.4(*X48*)	−29.2(*1234*) 292.5(*2X15*) 270.2(*1X26*) 67.7(*2X37*) 88.4(*3X48*)
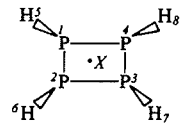	−2.8	2.049(PP) 1.340(*15,37*) 1.342(*26,48*)	87.3(*123*) 90.6(*234*) 110.2(*X15*) 97.3(*X26*) 110.3(*X37*) 97.2(*X48*)	15.1(*1234*) 90.7(*2X15*) 100.9(*3X26*) 89.2(*4X37*) 101.0(*1X48*)
P_4H_6 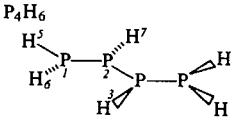	−17.4	2.024(*1—2*) 2.014(*2—3*) 1.341(*1—5*) 1.341(*1—6*) 1.342(*2—7*)	101.5(*123*) 98.0(*215*) 97.1(*216*) 98.9(*127*)	85.8(*5123*) 180.0(*1234*) 183.6(*3216*) 186.8(*5127*)
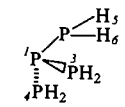	−19.8	2.011(*1—2*) 1.341(PH)	104.5(*213*) 97.1(PPH)	72.5(*5213*) 182.0(*5214*) 169.6(*4126*)
P_3H_3 singlets				
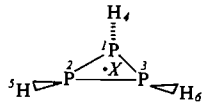	+4.2	2.034(*1—2*) 2.033(*2—3*) 1.400(*1—4*) (*2—5*)	104.6(*X14*) 103.8(*X25*)	90.0(*2X14*) 80.8(*1X25*)
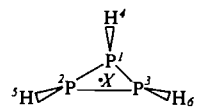	+10.2	2.040(PP) 1.340(PH)	106.5(*XPH*)	−94.1(*2X14*) 94.1(*3X25*) 90.0(*1X36*)
P_3H_3 triplet				
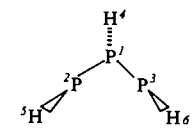	+39.3	1.961(PP) 1.340(*1—4*) 1.335(*2—5*)	112.9(*213*) 99.0(*125*)	64.7(*5213*) 185.6(*6314*)
P_3H_5 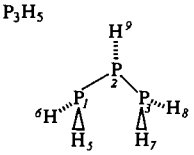	−10.5	2.018(*1—2*) 1.341(*1—5*) 1.341(*1—6*) 1.341(*2—9*)	102.6(*123*) 97.6(*512*) 97.6(*612*) 99.9(*129*)	187.2(*6123*) 289.4(*6129*) 189.4(*3215*) 179.1(*1237*) 276.8(1238)
P_6H_6 chair 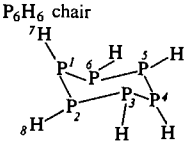	−43.4	2.019(PP) 1.343(PH)	101.7(PPP) 98.2(PPH)	74.9(*1234*) −74.9(*2345*) 74.9(*3456*) 175.6(*5617*) −175.6(*6128*)
P_7H_5 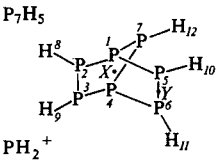	−46.6	2.019(*1—2*) 2.015(*1—7*) 1.342(*2—8*) 1.338(*7—12*)	104.1(*123*) 112.5(*4X7*) 99.5(*128*) 109.7(*X—9—12*)	−1.4(*1234*) 112.3(*34X7*) 108.8(*X128*) −20.1(*Y—X—7—12*)
PH_2^+	+260.3	1.329	95.3	
$P_2H_3^+$ 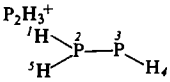	+228.0	1.359(*1—2*) 1.846(*2—3*) 1.336(*3—4*) 1.351(*2—5*)	120.3(*123*) 100.4(*234*) 128.6(*325*)	180.0(*1234*) 0.0(*4325*)

Can. J. Chem. Downloaded from www.nrcresearchpress.com by 210.87.254.40 on 09/06/12
For personal use only.

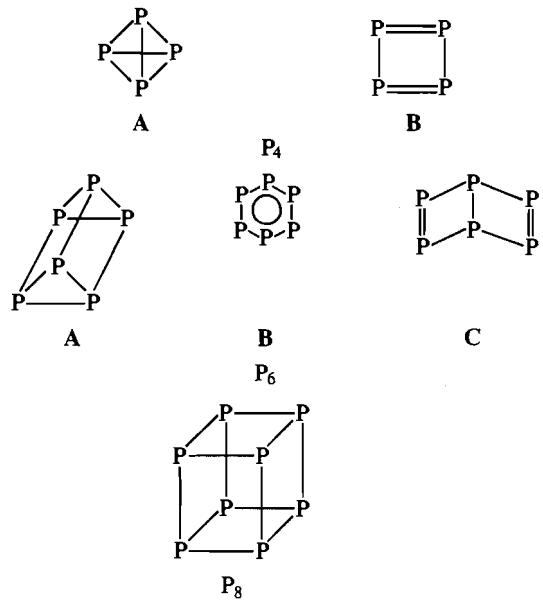

FIG. 1. Lewis structures for P_4, P_6, and P_8 molecules.

In all cases, disproportionation of the chains to elemental hydrogen and phosphorus (black) is predicted to be energy-releasing, which may account for the fact that such species have never been prepared:

$$P_nH_{n+2} \rightarrow nP + \left(\frac{n}{2} + 1\right)H_2 \qquad \Delta E < 0$$

MNDO predicts rather different stabilities for the two isomers of the three-membered $(PH)_3$ ring system; that with one hydrogen located on the side of the P_3 plane opposite to the other two is favoured by 6.0 kcal, presumably because it involves two less eclipsing lone pair − lone pair (and H−H) interactions, compared to the isomer with all three hydrogens on the same side of the P_3 plane. The strain energy of 24.9 kcal calculated for the stabler isomer of $(PH)_3$ presumably includes a contribution of 3 or 4 kcal from the one eclipsing lone pair − lone pair interaction and 21−22 kcal from bending to 60° the PPP angles from their preferred 101°−102° (predicted for unbranched chains) or 104.5° (predicted for $P(PH_2)_3$). These strainless angles are slightly larger than the values of 96.3° and 102.1° found experimentally in black phosphorus (6).

From the heat of formation calculated for gaseous white phosphorus, P_4 (isomer *A* in Fig. 1) which contains a tetrahedron of P atoms and therefore has four P_3 faces, an MNDO strain value of about 92 kcal is derived, i.e. the strain per PPP face is almost identical to that for $(PH)_3$. Experimentally, the ΔH_f for $P_4(g)$ is +14.1 kcal (4) which, when combined with the presumably strain-free value for —P< of −9.4 kcal yields a total strain energy of 51.7 kcal, i.e. 13 kcal per face. Thus MNDO apparently overestimates strain energy in three-membered rings of phosphorus, as it also does for hydrocarbons and rings of sulfur atoms (1*e*, 2).

For the four-membered ring $(PH)_4$, MNDO predicts that the isomer with hydrogen atoms alternating positions relative to the local P_3 planes is more stable by 16.3 kcal than that with all hydrogens on the same side; thus each of the four eclipsing lone pair − lone pair (or H−H) interactions in the latter destabilizes the molecule by 4.1 kcal. A strain energy of 8.5 kcal is derived from the calculated ΔH_f of the isomer which is free of lone pair − lone pair eclipsing interactions. This rather small value is not unexpected given that the average PPP angle in the ring of ~86° is not very different from the strain-free value (see above). The cross-ring[1,3] destabilizing interactions which contribute substantially to the net strain energy in other four-membered rings also operate here since the planar form of the ring (where such interactions are magnified) lies 5.3 kcal above the equilibrium geometry — in which the PPPP dihedral angle is 29°. Thus the total strain for a planar four-membered ring is 14 kcal.

We have performed MNDO calculations for the "cubane"-like isomer of P_8, i.e. with a geometry in which each phosphorus atom lies at the corner of a cube. The predicted ΔH_f of +4.1 kcal corresponds to 0.5 kcal per mol of P atoms, the lowest value we obtained for any of the finite P_n systems (n = 2, 4, 6, 8) studied herein. Nevertheless the total strain energy 116 kcal is large, and corresponds to 19 kcal per face, i.e. slightly more than that found for the planar $(PH)_4$ ring.

The strain energy computed for the stablest P_6 isomer we found, i.e. the phosphorus equivalent of prismane (P_6-**A**), is 110 kcal, i.e. 22 kcal per each of the five faces (two of which are three-membered rings and three four-membered rings). Since MNDO overestimates the strain energy of three-membered phosphorus rings, the prismane strain probably also is an upper limit. Unfortunately, there is no experimental data for any four-membered phosphorus ring from which we can decide the sign or magnitude of the MNDO error for such systems. If the MNDO results for sulfur rings are a guide here, the overestimate of strain in P_4 is approximately transferrable as a percentage, i.e. 60%, to four-membered rings.

For P_4 and P_6, we have performed calculations for isomers which contain phosphorus−phosphorus double bonds. For HP=PH itself, MNDO predicts the existence of two stable isomers, both planar, with the *trans* geometry more stable than the *cis* by 2.1 kcal. The PPH angle of 107.2° in the *cis* is larger than the 100.2° for the *trans*, due presumably to steric effects. The double bond in HP=PH is predicted to be less stable than the average of PP triple and single bonds, since for the disproportionation reaction

$$2\ P_2H_2 \rightarrow P_2 + P_2H_4$$

the ΔE predicted by MNDO is +17.0 kcal.

Since PP σ bonds are substantially more stable than the π bonds, it is not surprising that P_4 and P_6 isomers containing P=P are predicted to be less stable than isomers with P—P bonds only, notwithstanding the (overestimated) strain in the small rings found for the exclusively singly-bonded structures. Thus the P_4 analog of cyclobutadiene, (P_4-**B**), is calculated to be 25.4 kcal less stable than predicted for **A**, the analog of tetrahedrane (P_4-**A**).

In contrast to the cyclobutadiene analog (P_4-**B**) which is predicted to have bond lengths which alternate strongly (see Table 1), the phosphorus analog of benzene, P_6-**B**, is stabilized by resonance since even when the MNDO calculation is initiated with PP distances appropriate to an alternating Kekule-like structure, a planar structure with all bond lengths equal is obtained. The resonance effect in these molecules can be estimated by comparing their calculated ΔH_f to that expected from the group value for *cis* —P= of +8.9 kcal which was derived by combining the heats of formation of *cis* HP=PH and HP=P—P=PH (planar, all-*cis* conformation) listed in Table 2. (A comparable analysis of experimental values for hydrocarbons leads to 21.6 kcal for the resonance energy in benzene, i.e. the "Dewar Resonance Energy" value (7).) By this mea-

Can. J. Chem. Downloaded from www.nrcresearchpress.com by 210.87.254.40 on 09/06/12
For personal use only.

Can. J. Chem. Downloaded from www.nrcresearchpress.com by 210.87.254.40 on 09/06/12
For personal use only.

sure, the benzene analog is stabilized by 22.5 kcal, and the cyclobutadiene analog is destabilized by 26.0 kcal — due presumably to a combination of antiaromaticity and angle strain effects. (The destabilizations due to eclipsing lone pairs are automatically included by using group values appropriate to *cis* units.)

The prismane analog of P_6 is predicted to be 5 kcal more stable than the benzene analog (although the stability of the former probably is underestimated), and about 10 kcal more stable than the analog of Dewar benzene, i.e. P_6-**C** in Fig. 1. MNDO calculations for the $(PH)_6$ ring confirm that this molecule is strainless, at least in the chair conformation, since it adopts bond angles (averaging 101.7°) which are virtually identical to those in free chains and since its calculated ΔH_f actually is 2 kcal more negative than that expected from the group values.

It is somewhat disconcerting that MNDO calculations for various P_6 and P_8 systems predict heats of formation for P atoms which are comparable to that observed for P_4, and yet only the tetramer apparently is observed in the vapour phase of the element. The possibility of splitting P_6 rings from black phosphorus as it decomposes seems most feasible, given that the atoms occur in fused six-membered rings in this infinite polymer.

An MNDO calculation was performed for the P_7H_5 structure shown below. The P_7 framework here is of interest since red–violet phosphorus is known to contain such units, with each of the hydrogen atoms in P_7H_5 replaced by bonding to other P_7 units. The calculation we have done has all hydrogen atoms, except that of the bridgehead, pointing up toward the bridge, since this is the conformation in red–violet phosphorus (8). The calculated strain energy of 15.9 kcal amounts to 2.3 kcal per mol of phosphorus atoms. The actual strain energy in red–violet phosphorus should be larger than this, since the bond joining the bridgehead atoms is abnormally long (and therefore weak) and since additional strain may be associated with fusion of the rings.

Ions and radicals

In our calculations for elemental sulfur and the sulfur hydrides, it was established that whereas MNDO deals fairly successfully with the homonuclear π bonds in S_2, the strength of three-electron π bonding between nonequivalent sulfurs in free radicals is underestimated substantially (2). We suspect that an even more serious underestimation occurs for phosphorus molecules. In particular, MNDO calculations for the energy of hydrogen abstraction predict that the process for P_2H_4, whose resultant radical P_2H_3 can be stabilized by three-electron π bonding between the two P atoms, requires only 1.3 kcal less than that (27.5 kcal) for PH_3. Unfortunately no experimental information appears to be available regarding this process. In P_2H_3, the calculated PP distance of 1.985 Å is much closer to the values computed for single bonds (2.01–2.08 Å) than for double (1.83–1.86 Å). In addition, the geometry at the tricoordinate atom is distinctly pyramidal (see Table 2), and the unpaired electron is almost completely localized on the dicoordinate phosphorus.

Similarly, in the triplet state of the open-chain P_3H_3 the optimum geometry is so nonplanar at all three P atoms as to eliminate the possibility of any substantial three-electron π bonds. The calculated energy to remove two hydrogens from the P_3H_5 chain, one from each terminal atom, is only 5.2 kcal less than twice the energy to remove an H from PH_3.

π-Bonding is, however, predicted by MNDO calculations to be an important factor in stabilizing closed-shell cations of phosphorus rings and hydrides. The PH_2PH^+ system is predicted planar, with a PP distance of 1.846 Å and a stabilization energy of 25.5 kcal (as judged by the difference between the energies required to abstract a hydride ion from PH_3 and from P_2H_4) much of which can be attributed to π bonding:

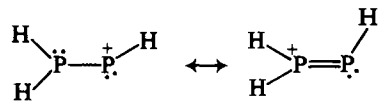

Encouraged by this result, we decided to investigate P_3^+ and P_7^+, the phosphorus analogs of the hydrocarbon analogs $C_3H_3^+$ and $C_7H_7^+$ both of which are known to be aromatic since they contain two and six π electrons respectively.

The optimum geometry for P_3^+ has equal bond lengths of 1.952 Å and an electron configuration corresponding to two π electrons. Its energy of formation via hydride abstraction from P_3H is virtually identical to that of PH_2PH^+ from P_2H_4.

The optimum geometry for P_7^+ has one phosphorus slightly out of the plane of the other six and some slight variation of bond lengths around the ring, but has an average PP distance (1.90 Å) almost as short as that (1.89 Å) predicted for the benzene-like analog of P_6.

The anion P_5^- in the geometry of a monocyclic ring is analogous to cyclopentadienyl anion and has six π electrons if planar. Although we began the MNDO calculations with a half-envelope geometry, in the geometry optimization the anion became planar with all bond lengths equal at 1.894 Å. Thus there appears to be some aromatic character associated with this system.

Calculations for planar, monocyclic P_5^+ were not performed due to the need for configuration interaction on this network. However, we did consider an interesting isomer (shown below) which is the analog of spiropentadiene. The length for the "double" bond here is 0.05 Å longer than for PH=PH (though shorter than for the P_3^+ system), whereas the "single" bonds are 0.03 Å shorter. These bond length variations are not

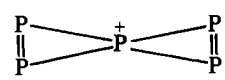

unexpected given that the filled π MO of one P=P pair is of the correct symmetry to donate electron density into the empty π^* MO of the other unit and vice-versa. As a result of such interactions, the bond orders for the formal double bonds are reduced but some bonding between the two P=P pairs is created, thus reducing the lengths of the "single" bonds (see also the analysis for spiro systems by Goldstein and Hoffmann (9)).

Phosphorus–oxygen molecules

The heats of formation and structures calculated by MNDO for several P_nO_m molecules of interest are summarized in Table 3. Since MNDO cannot handle quantitatively phosphorus in the pentavalent state, most of the interesting oxides and oxyacids were not considered.

TABLE 3. MNDO calculations for phosphorus oxides

System	ΔH_f (kcal mol^{-1})	Bond lengths (Å)	Bond angles (deg)	Dihedral angles (deg)
P═O	−21.1	1.424		
OPO	−47.2	1.460	117.4	
PPO	+33.6	1.459(PO) 1.726(PP)	164.2	
P_2O_2				
A	−7.1	1.919(PP) 1.640(PO) 1.284(OO)	78.8(OPP) 101.2(POO)	0.0(POOP)
B 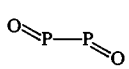	−60.8	1.444(PO) 2.118(PP)	106.2	182.3
C 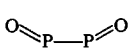	−62.9	1.444(PO) 2.097(PP)	110.0	85.0
D	−77.2	1.644(PO) 2.039(PP)	76.6(POP)	75.9(PO*X*O)
E	−112.3	1.592	80.9(OPO)	0.0(POPO)
P_2O_3	−181.9	1.650	84.9(POP)	
F				
G 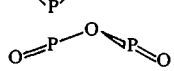	−172.8	1.563(P—O) 1.444(P═O)	158.0(POP) 103.8(OPO)	−41.4(O═POP) −33.7(POP═O)
P_2O_4 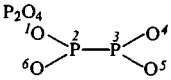	−75.5	1.463(PO) 2.157(PP)	119.0(OPP)	0.0(*1234*) 180.0(*1235*) 180.0(*5326*)

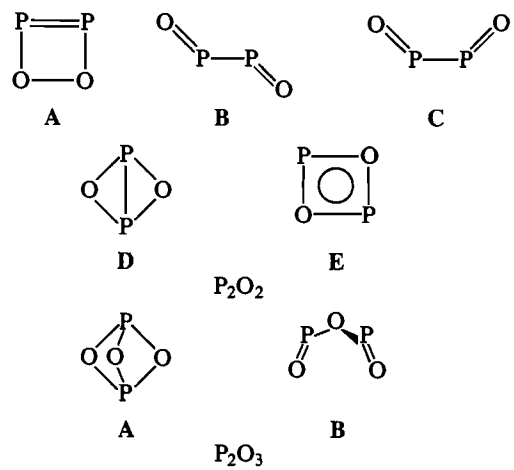

FIG. 2. Lewis structures for oxides of phosphorus.

Since MNDO overestimates, by 14.3 kcal, the stability of the ·P═O free radical in its π state (experimental ΔH_f = −6.8 kcal (4)), we suspect that this trend may appear as well in all structures containing the —P═O unit.

For ·PO_2, MNDO predicts that the unpaired electron occupies a σ orbital (as is found in the analogous ·NO_2 system) which is rather evenly delocalized over all three atoms. The phosphorus−nitrogen analogy breaks down somewhat for P_2O since although we obtained a PPO rather than a POP structure (no convergence obtained when the calculation was initiated with a POP geometry), the PPO angle is only 164° rather than 180°.

Five isomers, covering a range of stability of 105 kcal, were obtained in MNDO calculations for P_2O_2; see Fig. 2 for their Lewis structures. Least stable is **A** which contains P═P and O—O linkages. The chains **B** and **C** are next in stability, being each about 20 kcal more favourable than two separated ·P═O units. Although the (initially) *trans* isomer is almost planar, the (initially) *cis* geometry reverted to a twisted molecule similar to hydrogen peroxide. Although conjugation of the π bonds with each other is destroyed by twisting to this conformation, the geometry does allow donation of electron density from the lone pair of one phosphorus into the π* MO at the other end of the molecule. By this mechanism the PP bond is strengthened, as is manifested by its contraction of 0.021 Å relative to that in the *trans* and by the energetic preference for the twisted form of 2.2 kcal.

Even with the exaggerated stability for π bonds in MNDO and the strain associated with small rings, the inherent superiority of phosphorus−oxygen σ bonds to π bonds leads to the greater stability of the P_2O_2 isomers **D** and **E** compared to **B** and **C**. The "bicyclobutane" analog, **D**, possesses PO and PP σ bonds of usual length; the angle between the two POP planes is 76°. The "cyclobutadiene" analog **E** is much the stabler of the pair since it contains only a four-membered ring and since the π network contains six electrons and therefore is "aromatic" to some degree:

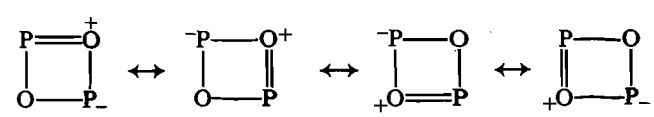

Can. J. Chem. Downloaded from www.nrcresearchpress.com by 210.87.254.40 on 09/06/12
For personal use only.

Can. J. Chem. Downloaded from www.nrcresearchpress.com by 210.87.254.40 on 09/06/12
For personal use only.

The PO bond lengths are all equal at 1.592 Å, which is the single bond length minus one quarter of the contraction associated with a double bond.

Given the experience above, the only isomers we considered for P_2O_3 are those having only phosphorus–oxygen bonds. Structure **A** contains only σ bonds whereas **B** has both σ, and π, the latter potentially conjugated via the central oxygen.

Energetically **A** is preferred to **B** by 9.1 kcal according to MNDO; this value probably is a lower limit given the method's underestimation of the preference for σ over π bonds in PO links. The phosphorus–oxygen bond lengths predicted for **A** are identical with those for other single bonds between these atoms; as a result the phosphorus–phosphorus distance is only 2.22 Å, i.e. only 10% greater than the P—P value. In **B**, the terminal bond lengths are those expected for P=O whereas the middle pair show significant contraction from the usual P—O length. Starting from both the all-*cis* and the all-*trans* planar forms for **B**, the same nonplanar structure is obtained (see Table 3 for details). The helix shape adopted by **B**, with a wide POP angle, allows for substantial overlap of the lone pairs on the central oxygen each with one of the π networks on the terminal atom pairs. The electron density associated with the p_π orbitals in each P=O is 2.11 electrons, indicating substantial donation from the central oxygen into each $\pi^*_{P=O}$ molecular orbital.

To our knowledge, none of the above-mentioned P_2O_2 or P_2O_3 molecules have been observed. Experimentally, the burning of phosphorus in (limited) oxygen produces P_4O_6, which contains only P—O bonds in a geometry which is rather strain-free, namely a tetrahedron on phosphorus atoms with one oxygen atom associated with (but pushed away from) each of the six edges of the P_4 tetrahedron. We performed an MNDO calculation for P_4O_6, starting with this symmetrical structure but allowing all bond lengths and angles to vary independently. After many iterations, a structure of rather low symmetry was obtained. The P—O bond lengths vary from 1.54 to 1.71 Å, compared to 1.64 Å experimentally (10), and the PP (nonbonded) distances vary from 2.75 to 3.02 Å. The POP angles, 126.4 ± 0.7° experimentally, vary in our structure from 119° to 137°, and the OPO angles vary from 70° to 80° compared to 99.8 experimentally (10). The calculated ΔH_f of −466.4 kcal is much more stable than that computed for $2P_2O_3$ units (by 102.6 kcal) and than that of −381.9 kcal obtained experimentally (5*b*). Frenking *et al.* report an MNDO calculation for P_4O_{10} with a calculated ΔH_f of −521.2 kcal, and a single PO length (11). The experimental ΔH_f they quote is −529.2 kcal, based presumably on the older determination (12).

Finally, we performed a calculation for P_2O_4, starting with a structure similar to that known for N_2O_4:

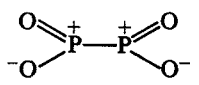

Although a nonplanar geometry was initially assumed, the MNDO calculations converged to an exactly planar structure, with PO lengths virtually identical to those in PO_2 and with a ΔH_f which is 19.9 kcal *less* stable than that for two PO_2 molecules. Analogous calculations for N_2O_4 yield a molecule which is 39.1 kcal less stable than $2NO_2$ and which is 90° twisted about the NN bond.

Conclusions

MNDO does quite well in predicting the strengths of both σ and π two-electron bonds between phosphorus atoms. The strain energy in three-membered rings, however, is overestimated, and the strength of three-electron π bonds apparently is underestimated. These trends are very similar to those obtained with sulfur, although there MNDO overestimated strain in other small rings as well, whereas this may not be true for phosphorus. The MNDO predictions for P_6 and P_8, and for the ions P_3^+, P_5^-, and P_7^+ indicate that these systems are relatively stable energetically, and should be capable of detection under appropriate experimental conditions. However, on the basis of *ab initio* and bond energy calculations Trinquier and co-workers predict that cubic P_8 will be substantially less stable than two tetrahedral P_4 due mainly to unfavourable bond–bond interactions in the former (13).

The experience with MNDO calculations for the oxides of trivalent phosphorus indicate that the method handles PO σ bonds very well but overestimates the strength of π bonds.

1. (*a*) M. J. S. DEWAR and G. KLOPMAN. J. Am. Chem. Soc. **89**, 3089 (1967); (*b*) N. C. BAIRD and M. J. S. DEWAR. J. Chem. Phys. **50**, 1262 (1969); (*c*) M. J. S. DEWAR and E. HASELBACH. J. Am. Chem. Soc. **92**, 590 (1970); (*d*) R. C. BINGHAM, M. J. S. DEWAR, and D. H. LO. J. Am. Chem. Soc. **97**, 1285 (1975); (*e*) M. J. S. DEWAR and W. J. THIEL. J. Am. Chem. Soc. **99**, 4899, (1977); **99**, 4907 (1977).
2. N. C. BAIRD. J. Comput. Chem. Submitted.
3. W. THIEL. Quantum Chemistry Program Exchange Program 438 (1982).
4. CRC handbook of chemistry and physics. 63rd ed. (1982–1983), CRC Press, Inc. FL. USA (*a*) D-81; (*b*) p. F-205.
5. A. J. HEAD. (*Editor*) Computer analysis of thermochemical data. National Physical Laboratory, Teddington, England. 1972.
6. A. BROWN and S. RUNDQUIST. Acta Crystallogr. **19**, 684 (1965).
7. N. C. BAIRD. J. Chem. Ed. **48**, 509 (1971).
8. H. THURN and H. KREBS Angew. Chem. Intl. Ed. **5**, 1047 (1966).
9. M. J. GOLDSTEIN and R. HOFFMANN. J. Am. Chem. Soc. **93**, 6193 (1971).
10. B. BEAGLEY, D. W. J. CRUICKSHANK, T. G. HEWITT, and K. H. JOST. Trans. Faraday Soc. **65**, 1219 (1969).
11. G. FRENKING, F. MARSCHNER, and H. GOETZ. Phosphorus Sulfur, **8**, 343 (1980).
12. S. B. HARTLEY and J. C. MCCOUBREY. Nature, **198**, 476 (1963).
13. G. TRINQUIER, J-P. MALRIEU, and J-P. DAUDEY Chem. Phys. Lett. **80**, 552 (1981).

Studies on double malonates. I. Sodium lanthanide malonates, $Na_5Ln(C_3H_2O_4)_4.7.5H_2O$ (Ln = Gd–Ho or Y)

MAHADEO A. NABAR AND BHARAT N. JUKAR

Department of Chemistry, University of Bombay, Vidyanagari, Bombay - 400 098, India

Received March 10, 1983

MAHADEO A. NABAR and BHARAT N. JUKAR. Can. J. Chem. **62**, 348 (1984).

A new series of double malonates of some of the lanthanides and yttrium with sodium having the formula $Na_5Ln(C_3H_2O_4)_4.7.5\ H_2O$ was synthesised. The compounds were characterised using X-ray powder diffractometry and infrared absorption spectroscopy.

MAHADEO A. NABAR et BHARAT N. JUKAR. Can. J. Chem. **62**, 348 (1984).

On a synthétisé une nouvelle série de malonates doubles de quelques lanthanides et de l'yttrium avec le sodium de formule: $Na_5Ln(C_3H_4O_4)_4.7.5H_2O$. On a caractérisé les composés en faisant appel à la diffraction des poudres par rayons-X et à la spectroscopie d'absorption dans l'infrarouge.

[Traduit par le journal]

Can. J. Chem. Downloaded from www.nrcresearchpress.com by 210.87.254.40 on 09/06/12
For personal use only.

Introduction

Davitashvili *et al.* have studied the reaction of different rare earth nitrates with alkali metal oxalates and ammonium oxalate in water (1–5). Formation of double oxalates, $M^ILn(C_2O_4)_2.xH_2O$ (M^I = alkali metal or ammonium, Ln = lanthanide) was observed in most cases. In a few cases, however, these compounds started dissolving at higher $C_2O_4^{2-}:Ln^{3+}$ ratio, with the formation of more stable soluble complexes, which did not precipitate even after a long duration. However, no further attempts were made to isolate them.

Research is in progress in this laboratory on the double salts of malonic acid, the next higher homologue of oxalic acid, to examine the systematics of these systems. The lighter lanthanide ions, in the presence of concentrated aqueous alkali metal (Na, K) malonates, precipitated the double salts of the type $M^ILn(C_3H_2O_4)_2{\cdot}xH_2O$. However, here again the soluble complexes at higher ionic ratios of $C_3H_2O_4^{2-}:Ln^{3+}$ could not be isolated. On the other hand, for heavier rare earth elements (Gd, Tb, Dy, Ho) and yttrium, the soluble complexes formed could be obtained in solid form by crystallization.

The present article describes the synthesis and study of some of the physicochemical properties of the isolated rare earth double malonates, $Na_5Ln(C_3H_2O_4)_4.7.5H_2O$, where Ln = Gd–Ho, or Y.

Experimental

Synthesis

An aqueous solution of sodium malonate (324 mg of $(C_3H_2O_4)^{2-}$ cm^{-3}) was mixed with the rare earth malonate in the ionic ratio $Ln^{3+}:C_3H_2O_4^{2-}$ as 1:4. The mixture was warmed on the water bath to get a clear solution, which on evaporation at ambient temperature gave the desired double malonate. The crystallised compound, after transferring to a filter, was washed with 50 cm^3 of 90% methanol and dried over silica gel under vacuum.

TABLE 1. Results of chemical analysis of $Na_5Ln(C_3H_2O_4)_4.7.5H_2O$

	Na(%)		Ln(%)		$C_3H_2O_4$(%)		H_2O(%)	
Ln	Calcd.	Obsd.	Calcd.	Obsd.	Calcd.	Obsd.	Calcd.	Obds.
Gd	14.10	13.87	19.28	19.20	50.00	49.56	16.40	15.90
Tb	14.08	14.28	19.45	19.30	49.94	49.45	16.53	16.20
Dy	14.01	13.90	19.81	19.60	49.73	49.90	16.45	*
Ho	13.97	13.98	20.04	20.00	49.51	49.00	16.40	16.06
Y	15.40	14.92	11.90	11.86	54.62	54.65	18.07	17.50

*Not analysed.

TABLE 2. Crystal data for $Na_5Ln(C_3H_2O_4)_4.7.5H_2O$

Ln	Mol. wt.	*a* (pm)	*b* (pm)	*c* (pm)	β (deg)	*V* (pm^3) × 10^6	$\rho_{calcd.}$ Mg m^{-3}	$\rho_{obsd.}$ Mg m^{-3}
Gd	815.26	1833 ±1	895 ±1	1609 ±1	92.44 ±0.08	2638	2.05	2.03
Tb	816.92	1830 ±2	894 ±1	1606 ±2	92.46 ±0.10	2624	2.07	2.08
Dy	820.51	1824 ±1	891 ±1	1602 ±1	92.42 ±0.06	2601	2.10	2.07
Ho	822.94	1823 ±1	890 ±1	1600 ±1	92.44 ±0.06	2595	2.11	2.11
Y	746.92	1825 ±1	890 ±1	1600 ±1	92.49 ±0.07	2598	1.91	1.91

TABLE 3. X-ray powder diffraction data for $Na_5Dy(C_3H_2O_4)_4.7.5H_2O$

$h\ k\ l$	$d_{calcd.}$	$d_{obsd.}$	I/I_0	$h\ k\ l$	$d_{calcd.}$	$d_{obsd.}$	I/I_0
2 0 0	912	909	100	5 2 $\bar{4}$	234	233	3
1 1 0	801	799	15	5 3 0	230		
0 0 $\underline{2}$	800			7 0 $\underline{3}$	230	230	4
1 1 $\bar{1}$	722	722	25	7 1 $\bar{3}$	230		
1 0 2	721			7 2 1	224	224	16
0 1 2	595	597	58	4 3 3	224		
1 1 2	561	561	20	8 1 $\underline{0}$	221	220	14
3 0 $\underline{1}$	560			1 1 $\underline{7}$	221		
3 0 $\underline{2}$	494	495	11	5 1 $\bar{6}$	213		
3 1 $\bar{1}$	484	482	10	2 1 7	213	213	5
0 2 $\underline{0}$	446	444	5	1 4 2	213		
4 0 $\underline{1}$	443			5 0 $\underline{6}$	211	211	5
1 0 $\bar{4}$	394	394	6	3 4 $\underline{1}$	208	208	4
1 2 2	379	379	19	4 0 $\bar{7}$	208		
4 1 2	357	357	5	0 4 3	206	206	4
5 1 $\underline{0}$	337	336	23	0 2 $\bar{7}$	203		
3 2 $\bar{2}$	331	332	23	3 4 $\bar{2}$	203	203	5
5 1 1	328	328	8	8 2 $\underline{0}$	203		
3 0 4	328			4 3 $\underline{5}$	198.7	198.8	11
1 3 0	293			9 0 $\bar{2}$	198.4		
4 2 2	293	292	9	7 0 5	197.9	197.5	6
1 2 $\underline{4}$	292			9 1 0	197.5		
6 1 $\underline{1}$	285	284	16	2 0 8	193.6		
2 3 $\bar{1}$	279	279	4	7 1 $\underline{5}$	193.2	193.3	3
3 0 5	278			5 1 $\bar{7}$	192.7		
0 0 6	267	266	14	3 4 $\underline{4}$	184.3		
7 0 0	260	261	9	9 2 $\bar{1}$	184.0	184.2	6
6 2 $\underline{0}$	251	252	7	5 4 2	184.1		
4 3 $\bar{2}$	239	239	3				
3 1 6	239						

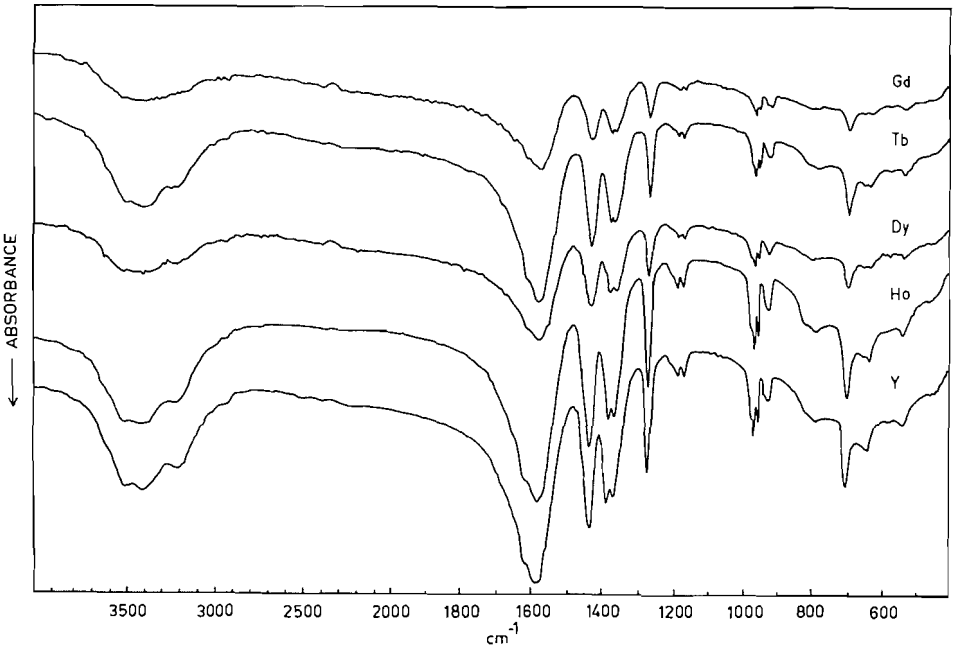

FIG. 1. Infrared spectra of $Na_5Ln(C_3H_2O_4)_4.7.5H_2O$.

Analyses

The sodium and rare earth contents in the double malonates were determined flame photometrically and complexometrically, respectively. Malonate ion percentage was estimated using ion exchange method. The water of crystallization was determined by isothermal dehydration at suitable temperature. Analytical results are given in Table 1.

Ni filtered CuK_α radiation was used for the X-ray powder diffraction study. The densities of the compounds were determined by the flotation method, using bromoform – *n*-hexane mixture as a working medium. Infrared absorption spectra of the double malonates were scanned in the frequency range 4000–400 cm^{-1} with a Perkin-Elmer Model 377 by CsBr disc method.

Can. J. Chem. Downloaded from www.nrcresearchpress.com by 210.87.254.40 on 09/06/12
For personal use only.

TABLE 4. Infrared spectral data in cm^{-1} for $Na_5Ln(C_3H_2O_4)_4.7.5H_2O$*

Gd	Tb	Dy	Ho	Y	Assignments
	3500 s	3500 s	3500 s	3510 s	
3400 s, b	3400 s, b	3400 s, b	3400 s, b	3400 s	ν(OH)
	3200 s, b	3200 s, b	3200 s, b	3200 s	
	3000 vw		3000 vw	3000 vw	$\nu(CH_2)$
	2920 vw	2920 vw	2920 vw	2920 vw	
1620 s	1620 s, sh	1625 s, sh	1618 s, sh	1625 s, sh	$\nu(OCO)_{asym.}$
1580 vs	1590 vs	1590 vs	1590 vs	1590 vs	
1430 s	1438 s	1435 s	1440 s	1440 s	$\delta(CH_2)$
1380 s	1380 s	1382 s	1378 s	1380 s	$\nu(OCO)_{sym.}$
1370 s	1370 s	1368 s	1370 s	1370 s	
1270 s	1275 s	1272 s	1280 s	1280 s	(CH_2)wag
			1215 sh		
1190 vw	1195 w	1192 w	1198 w	1198 w	$\nu(C—C)_{asym.}$
1175 vw	1178 w	1175 w	1180 w	1180 w	
982 sh	982 sh	985 sh	985 sh	988 sh	
972 m	972 m	972 m	977 m	978 m	$\nu(C—C)_{sym.}$
960 m	962 m	962 m	966 m	968 m	
932 m, b	932 m, b	932 m, b	938 m, b	940 m, b	(CH_2)rock
			825 sh		(OCO) Scissors?
	800 w, b	800 w, b	800 w, b	800 w, b	
710 s	710 s	710 s	715 s	712 s	(OCO)wag
			670 w		
	650 m	650 m	650 m	650 m	$\delta(CCO)_{asym.}$
550 w	550 w	550 w	550 w	550 w	$\delta(CCO)_{sym.}$

*s = strong, m = medium, w = weak, v = very, b = broad, sh = shoulder.

Results and discussion

X-ray diffraction

The double malonates are isomorphous and are indexed on a monoclinic cell using Ito's (6) method. The unit cell comprised four formula units and the probable space group assigned is $P2_1/m$, (systematic extinctions: $0k0:k = 2n + 1$). There is a linear decrease in lattice dimensions a, b, and c and hence in the volume (Table 2) from gadolinium to holmium, in accordance with the lanthanide contraction.

The indexed powder data of dysprosium double malonate are reported in Table 3, as a representative example.

Infrared absorption spectroscopy

The infrared spectra of the double malonates are similar to each other (Fig. 1). The spectral data of the compounds are reported in Table 4. The attributions of various vibrations are done by comparison with the published data (7–9). In particular, it may be pointed out that the $\nu(OCO)_{asym}$ (~1590 cm^{-1}) and $\nu(OCO)_{sym}$ (~1380 and 1370 cm^{-1}) frequencies for the double malonates appear at higher and lower frequencies, respectively, than the corresponding frequencies in potassium malonate (7), indicative of an increase in the covalent nature of Ln—O bond.

Acknowledgements

The authors are indebted to Mr. P. V. Adarkar for extending the spectral facility and to the Director, Tata Institute of Fundamental Research, Bombay, for the X-ray facility. One of the authors (B.N.J.) is grateful to the University of Bombay for the research fellowship.

1. E. G. DAVITASHVILI and M. E. MODEBADZE. Soobshch. Akad. Nauk Gruz. SSR, **39**, 305 (1965).
2. E. G. DAVITASHVILI, M. E. MODEBADZE, and N. G. SHELIYA. Soobshch. Akad. Nauk Gruz. SSR, **40**, 325 (1965).
3. E. G. DAVITASHVILI, N. G. SHELIYA, and M. E. MODEBADZE. Zh. Neorg. Khim. **14**, 917 (1969).
4. E. G. DAVITASHVILI, M. E. MODEBADZE, and N. G. SHELIYA. Zh. Neorg. Khim. **16**, 655 (1971).
5. ZH. SH. KUBLASHVILI and E. G. DAVITASHVILI. Zh. Neorg. Khim. **16**, 1526 (1971).
6. T. ITO. X-ray studies on polymorphism. Maruzen Co. Ltd., Tokyo. 1950. p. 187.
7. M. J. SCHMELZ, I. NAKAGAWA, S. MIZUSHIMA, and J. V. QUAGLIANO. J. Am. Chem. Soc. **81**, 287 (1959).
8. B. S. AZIKOV, S. E. KHARZEEVA, Z. A. GRANKINA, and V. V. SEREBRENNIKOV. Zh. Neorg. Khim. **13**, 1831 (1968).
9. J. MACH. Monatsh. Chem. **100**, 1839 (1969).

Can. J. Chem. Downloaded from www.nrcresearchpress.com by 210.87.254.40 on 09/06/12
For personal use only.

Pseudobase formation from 9-substituted 10-methylacridinium cations in aqueous solution

JOHN W. BUNTING, VIVIAN S. F. CHEW, SUDHIR B. ABHYANKAR, AND YUKIKO GODA
Department of Chemistry, University of Toronto, Toronto, Ont., Canada M5S 1A1

Received July 18, 1983

JOHN W. BUNTING, VIVIAN S. F. CHEW, SUDHIR B. ABHYANKAR, and YUKIKO GODA. Can. J. Chem. **62**, 351 (1984).

Rates of cation–pseudobase equilibration have been measured for a series of C-9 substituted (CH_3, CH_3CH_2, $C_6H_5CH_2$, $(CH_3)_2CH$, C_6H_5, 4-$(CH_3)_2NC_6H_4$) 10-methylacridinium cations in aqueous solution at 25°C over the pH range of approximately 9–13. Separation of the rate constants for formation (k_{OH}) and decomposition (k_2) of each of these pseudobases allowed the calculation of the pK_{R^+} value for each cation. The presence of a C-9 isopropyl substituent enhances the stability of the pseudobase relative to the cation, whereas all other C-9 substituted cations have pK_{R^+} values greater than the 10-methylacridinium cation. There is no simple quantitative relationship between pK_{R^+} and the size of the C-9 substituent. Rate constants (k_{OH}) for hydroxide ion attack on these C-9 substituted cations are in the order: H > primary alkyl > secondary alkyl > aryl, while rate constants (k_2) for pseudobase decomposition are less predictable but generally follow the order: H > primary alkyl > aryl > secondary alkyl. These phenomena are shown to be consistent with a competition between destabilization of the cation by *peri* interactions between the C-9 substituent and H(1) and H(8) and reduced pseudobase solvation for large C-9 substituents. Resonance interactions of 9-aryl substituents with the acridine moiety of these cations are shown to be quite small. 9-Aryl-10-methylacridinium cations are approximately 30-fold more reactive towards hydroxide ion attack than are their triphenylmethyl carbocation analogues.

JOHN W. BUNTING, VIVIAN S. F. CHEW, SUDHIR B. ABHYANKAR et YUKIKO GODA. Can. J. Chem. **62**, 351 (1984).

On a déterminé les vitesses d'équilibre de la pseudobase cationique d'une série de cations méthyl-10 acridinium ayant un substituant en position 9 (CH_3, CH_3CH_2, $C_6H_5CH_2$, $(CH_3)_2CH$, C_6H_5, $CH_3)_2NC_6H_4$-4), en solution aqueuse à 25°C, dans un intervalle de pH allant de 9 à 13. La séparation des constantes de vitesse de formation (k_{OH}) et de la décomposition (k_2) de chacune de ces pseudobases permet de calculer la valeur du pK_{R^+} de chaque cation. La présence d'un substituant isopropyle en C-9 augmente la stabilité de la pseudobase par rapport au cation tandis que tous les autres cations substitués en C-9 ont des valeurs de pK_{R^+} plus élevées que celle du cation méthylacridinium-10 lui-même. Il n'y a pas de relation quantitative simple entre le pK_{R^+} et la taille du substituant en C-9. Les constantes de vitesse (k_{OH}) de l'attaque de l'ion hydroxyde sur ces cations substitués sont dans l'ordre suivant: H > alkyle primaire > alkyle secondaire > aryle, tandis que les constantes de vitesse (k_2) de décomposition de la pseudobase sont plus difficiles à prédire mais suivent en général l'ordre: H > alkyle primaire > aryle > alkyle secondaire. On montre que ces phénomènes sont en accord avec une compétition entre la déstabilisation du cation par des interactions *péri* entre le substituant à C-9 et les hydrogènes H(1) et H(8) et la solvatation réduite de la pseudobase pour des substituants grands en C-9. On montre que les interactions de résonance, des substituants aryles avec l'unité acridine de ces cations, sont très faibles. Les cations aryl-9 méthyl-10 acridinium réagissent environ 30 fois plus rapidement avec les ions hydroxydes que les carbocations triphénylméthyles analogues.

[Traduit par le journal]

Previous attempts (1) to measure the pK_{R^+} values for pseudobase formation from 9-alkyl-10-methylacridinium cations (**1**) were hampered by the limited solubilities of these pseudobases (**2**) in strictly aqueous media. A further complication arises for those 9-alkyl substituents having hydrogen atoms on the carbon atom that is directly bonded to C-9 of the acridine moiety. In such cases, the formation of an anhydrobase (**3**) in a deprotonation reaction competes with the hydroxide ion addition reaction to form **2**. Based upon a limited number of observations (1), it seems that the pseudobase (**2**) is the kinetically-controlled product from **1** in basic solutions, whereas the anhydrobase (**3**) is the thermodynamically more stable product. Thus, attempts to measure equilibrium constants for pseudobase formation from the electronic absorption spectra of equilibrated basic aqueous solutions of **1** are frustrated by both limited solubility and a competing reaction.

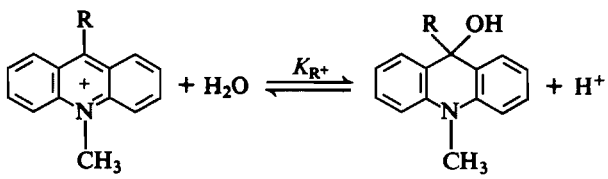

1 **2**

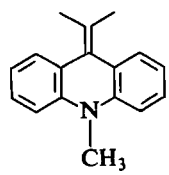

3

We have now overcome these complications by measuring pseudo-first-order rate constants for the approach to the cation–pseudobase equilibrium over the first few half-times of the reaction. Separation of the rate constants for the forward and reverse reactions then allows the calculation of pK_{R^+}.

Experimental

9-Alkylacridines and 9-phenylacridine were synthesized by the high temperature reaction of diphenylamine with the appropriate carboxylic acid (2). These bases were then methylated with dimethyl sulfate and the crude 9-alkyl-10-methylacridinium methylsulfates were converted to the corresponding chloride salts by Albert's general method (ref. 2, p. 343). These chloride salts were recrystallized several times from ethanol and characterized by ^{1}Hmr spectroscopy in trifluoroacetic acid solution.

9-(4-Dimethylaminophenyl)-10-methylacridinium chloride was prepared by refluxing 10-methylacridinium chloride with *N*,*N*-dimethylaniline in ethanol as described by Ballard *et al.* (3).

Rates of cation–pseudobase equilibration were followed spec-

Can. J. Chem. Downloaded from www.nrcresearchpress.com by 210.87.254.40 on 09/06/12
For personal use only.

Can. J. Chem. Downloaded from www.nrcresearchpress.com by 210.87.254.40 on 09/06/12
For personal use only.

trophotometrically in aqueous solution (ionic strength 0.1 (KCl + buffer)) at 25°C, by mixing a solution of the acridinium cation (within the range 0.01–0.02 m*M*) in water with appropriate buffer solutions on either a Varian Cary 210 spectrophotometer or a Durrum–Gibson stopped-flow spectrophotometer. Each cation was studied in 10–15 solutions of different pH over a range of at least 3 pH units spanning the pK_{R^+} value.

All reactions proved to be kinetically first-order in total acridine concentration for at least three half-lives, although deviations from strictly first-order behaviour were observable at longer reaction times, especially in the slower reactions. These deviations were readily attributable to either precipitation or anhydrobase formation. In general, rate constants were obtained by digitizing absorbance vs. time curves at approximately 40 points over the first three reaction half-times, and then fitting the data by the Guggenheim technique.

Results

Acridinium cations (**1**) display an intense electronic absorption maximum in the vicinity of 360 nm and a series of less intense maxima in the region 390–420 nm. The corresponding pseudobases (**2**) show an intense maximum only in the vicinity of 280 nm (where **1** only weakly absorbs), and are essentially transparent at all wavelengths longer than about 320 nm. Thus the rate of equilibration of **1** with **2** can be readily measured either from the increase in absorbance with time at 280 nm, or alternatively from the decrease in absorbance with time at essentially any wavelength between 320 and 450 nm. All rate constants reported in this work were independent of the wavelength of observation. Decreases in absorption in the region of 400 nm are consistent only with pseudobase formation since the anhydrobases show absorption maxima in the vicinity of 400 nm. The most basic solutions of **1**: R = CH_3, C_2H_5, and $C_6H_5CH_2$, the rates of cation–pseudobase equilibration were sufficiently rapid that stopped-flow spectrophotometry was required. In less basic solutions of the above cations, and also for **1**: R = $(CH_3)_2CH$ and 4-$(CH_3)_2NC_6H_4$ over the entire pH region, rates of equilibration were readily accessible on a recording spectrophotometer after manual mixing of solutions.

The pH dependences of the experimentally determined pseudo-first-order rate constants for cation–pseudobase equilibration are displayed in Fig. 1 for **1**: R = CH_3, CH_3CH_2 $(CH_3)_2CH$, $C_6H_5CH_2$, and 4-$(CH_3)_2NC_6H_4$. In each case k_{obs} is linear in $[HO^-]$ in the more basic solutions, but approaches pH independence in the less basic solutions. The data of Fig. 1 were fitted to eq. [1] by regression analysis, and the parameters k_{OH} and k_2 that were evaluated in this way are listed in Table 1.

$$[1] \quad k_{obs} = k_{OH}[HO^-] + k_2$$

In an earlier detailed kinetic study (4) of cation–pseudobase equilibration for **1**: R = H and C_6H_5, the rates of equilibration in the region pH > 9 (as used in the current work) were shown to be controlled by a kinetically second-order reaction between HO^- and **1** for pseudobase formation, and a pH-independent decomposition of pseudobase to cation by expulsion of hydroxide ion from **2**. Thus the empirically derived parameters of eq. [1] can be associated with the kinetic processes of eq. [2].

$$[2] \quad \mathbf{1} + HO^- \underset{k_2}{\overset{k_{OH}}{\rightleftharpoons}} \mathbf{2}$$

Thus pK_{R^+} for the equilibration of **1** and **2** can be calculated from

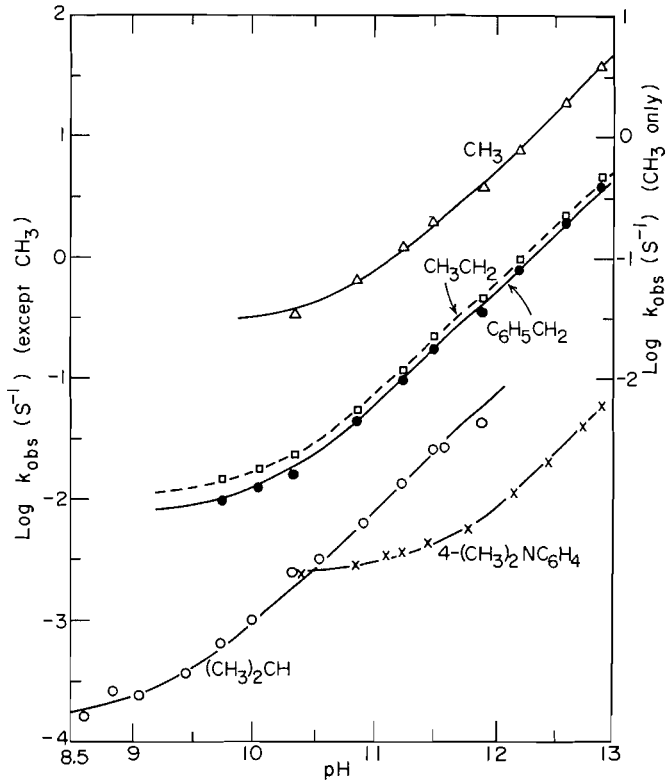

FIG. 1. pH dependence of k_{obs} for equilibration of **1** and **2** for various C-9 substituents as indicated. Curves are calculated from eq. [1] using the parameters in Table 1.

TABLE 1. Rate and equilibrium constants for equilibration of **1** and **2**[a]

R	pK_{R^+}	k_{OH} (M^{-1} s^{-1})	k_2 (s^{-1})
H[b]	10.01	550	0.058
CH_3	10.8	49±2	0.033±0.008
CH_3CH_2	10.3	59±3	0.011±0.001
$C_6H_5CH_2$	10.2	50±2	0.008±0.002
$(CH_3)_2CH$	9.3	7.7±0.5	1.6 (±0.6) × 10^{-4}
C_6H_5[b]	11.03	1.3	0.0014
4-$(CH_3)_2NC_6H_4$	11.54[c]	0.69±0.05	0.0024±0.0002

[a]In aqueous solution, ionic strength 0.1, 25°C.
[b]Data from ref. 4.
[c]pK_{R^+} = 11.51 from absorbance vs. pH of equilibrated basic solutions.

$$K_{R^+} = \frac{[H^+][\mathbf{2}]}{[\mathbf{1}]} = \frac{K_w \cdot [\mathbf{2}]}{[\mathbf{1}][HO^-]} = K_w \cdot k_{OH}/k_2$$

Values of pK_{R^+} evaluated in this way are included in Table 1. For **1**: R = 4-$(CH_3)_2NC_6H_4$, pK_{R^+} was also accessible from the pH dependence of the electronic absorption spectrum of the equilibrated mixture of cation and pseudobase. The pK_{R^+} value evaluated in this way is 11.51 and is in excellent agreement with the value obtained from the kinetic data.

Discussion

The pK_{R^+} values in Table 1 indicate that, whereas a C-9 methyl, ethyl, or benzyl group slightly stabilizes the 10-methylacridinium cation towards pseudobase formation, the presence of the more sterically hindered isopropyl substituent at C-9 actually somewhat enhances the thermodynamic stability of the pseudobase relative to the cation. This relative enhancement of pseudobase stability in the 9-isopropyl deriva-

Can. J. Chem. Downloaded from www.nrcresearchpress.com by 210.87.254.40 on 09/06/12
For personal use only.

tive is not reflected, however, in the rate of hydroxide ion attack to form the pseudobase. Thus, whereas the equilibrium constant for pseudobase formation is 5-fold larger for **1**: R = $(CH_3)_2CH$ than for **1**: R = H, the second-order rate constant for hydroxide ion attack at C-9 is 70-fold larger in the latter case. Although the 9-isopropyl pseudobase is the most thermodynamically stable of all the cases in Table 1, its rate of formation is slower than for all other 9-alkyl derivatives.

In general, the values of k_{OH} in Table 1 decrease with increasing size of the C-9 substituent (H > primary alkyl > secondary alkyl > aryl), and are presumably a simple reflection of steric hindrance to the rate of hydroxide ion attack at C-9. Values of k_2 show much less order than do those of k_{OH}, and it seems clear that it is the k_2 values that are primarily responsible for the unpredictable variation that is found for the dependence of pK_{R^+} upon the C-9 substituent.

Variation of the C-9 substituent will most directly influence the stability of **1** via increasingly unfavourable *peri* interactions between R and the C-1 and C-8 hydrogen atoms as R increases in size. Such steric interactions are relieved in the pseudobases relative to the cation, and also somewhat relieved in the transition state for cation–pseudobase interconversion. This phenomenon is quite obvious in the case of the 9-isopropyl derivative, both in the enhanced stability of the pseudobase relative to the cation (lowest pK_{R^+}), and also in the dramatic reduction in k_2 which reflects the enhanced steric congestion in the transition state relative to the pseudobase.

For the primary alkyl C-9 substituents (CH_3, CH_3CH_2, $C_6H_5CH_2$), the *peri* interactions are apparently not sufficiently great to produce a net increase in pseudobase stability relative to the cation when compared with the C-9 unsubstituted species. This suggests that there may be another factor which offsets to some extent the influence of the *peri* interactions in these species. We suggest that such a factor is probably to be found in the solvation requirements of the C-9 hydroxyl group in the pseudobases. The presence of a C-9 alkyl substituent will disrupt the solvation pattern of the hydroxyl group relative to the C-9 unsubstituted pseudobase species, and in so doing will result in a reduced pseudobase stability. Thus the 9-isopropyl derivative is the only case in Table 1 in which the unfavourable *peri* interactions in the cation are sufficiently great to completely offset this solvation effect, and therefore produce a net increase in pseudobase stability.

Within the series of methyl, ethyl, and benzyl C-9 substituents, the variations in pK_{R^+} and k_2 are probably mainly attributable to differences in the *peri* interactions of these substituents with H(1) and H(8). The essentially constant value for k_{OH} for these primary alkyl groups is presumably a reflection of the fact that hydroxide ion attack can occur from either face of the acridine ring system. The sp^3 hybridization of the α-methylene group of a primary alkyl group (RCH_2) will require the R group to lie on one side of the plane of the acridine ring system. Hydroxide attack from the other face of the acridine plane would then encounter a common steric interaction with the methylene group irrespective of the nature of R. The 9-isopropyl substituent can take up a conformation in which both methyl groups are on the same side of the acridine plane. The relatively small reduction in k_{OH} for the 9-isopropyl substituent relative to these primary alkyl groups can then be readily accounted for by hydroxide ion attack on the side away from these methyl groups. The smallest values for k_{OH} are observed for the 9-aryl substituents. These substituents are expected (5) to take up a conformation at a significant angle to the acridine plane, and therefore to inhibit attack at C-9 from both faces of the tricyclic system.

The 9-phenyl and 9-(4-dimethylaminophenyl) substituents both lead to enhanced cation stability towards pseudobase formation relative to the 9-unsubstituted cation. In these cases, possible contributions from resonance interactions for the stabilization of the cations must also be considered, in addition to the steric interactions and solvation effects considered above for 9-alkyl substituents. Resonance effects are most readily discussed by reference to the canonical structure **4**.

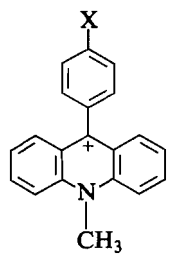

4

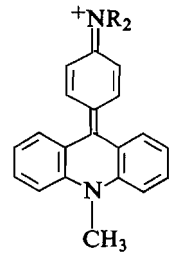

5

In view of the *peri* interactions of the 9-aryl substituents with the hydrogen atoms on C-1 and C-8, it is clear that the 9-phenyl ring cannot achieve coplanarity with the tricyclic acridine ring system. The dipole moment of 9-phenylacridine has been interpreted (5) as requiring an angle of greater than 40° between the planes of the phenyl and acridine rings. Such an angle should allow little overlap between the π-orbitals of the phenyl and acridine systems, and would suggest that there will be little resonance stabilization from the 9-phenyl substituent in **4**. On the other hand, the electronic absorption spectra of 9-(4-aminophenyl)acridinium cations show pronounced bathochromic shifts relative to 9-phenylacridinium cations, and these shifts have been interpreted in terms of resonance stabilization via **5** (ref. 2, p. 186).

The pK_{R^+} values for **4**: X = H and $(CH_3)_2N$ in Table 1 allow a quantitative evaluation of the importance of resonance stabilization in these systems. The 4-dimethylamino substituent does show an enhanced stability of the cation relative to the 9-phenyl substituent. However, based upon the observed $\Delta pK_{R^+} = 0.5$, this stabilization is only 0.7 kcal/mol. This is clearly much smaller than the stabilization of 3.3 kcal/mol ($\Delta pK_{R^+} = 2.45$) which is found upon comparison of the relative susceptibilities of the malachite green (**6**: X = H) and crystal violet (**6**: X = $(CH_3)_2N$) cations to carbinol formation (6). These comparisons, which should be free of solvation and steric influences, indicate that resonance interactions of the 9-aryl groups with the acridine π-system must be quite small. In fact, ΔpK_{R^+} for **4**: X = H and $(CH_3)_2N$ is even smaller than the electronic effect of a *para*-dimethylamino substituent upon the pK_a of benzoic acid ($\Delta pK_a = 0.83$ (7)).

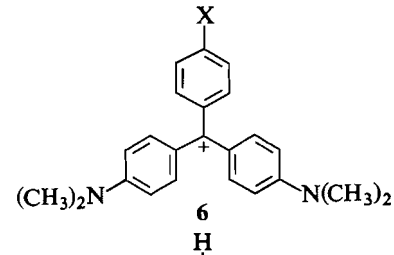

6

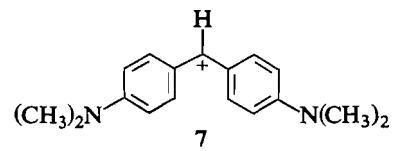

7

TABLE 2. Rate and equilibrium constants for hydroxide ion addition to **4** and **6**

Cation	X	pK_{R^+}	k_{OH} (M^{-1} s^{-1})	k_2 (s^{-1})
4	H	11.0	1.3	1.4×10^{-3}
4	$(CH_3)_2N$	11.54	0.69	2.4×10^{-3}
6	H[a]	6.94	2.18	1.5×10^{-7}
6	$(CH_3)_2N$[a]	9.39	0.205	4.7×10^{-6}
6	X[b]	11.0	0.04	4.0×10^{-5}

[a]Data from ref. 6.
[b]Rate constants calculated as described in text for a hypothetical cation **6** having $pK_{R^+} = 11.0$.

It is of interest that $\Delta pK_{R^+} = 1.0$ for **1**: R = C_6H_5 and H is of similar magnitude to $\Delta pK_{R^+} = 1.33$ for **6**: X = H and **7** (9). While this comparison might be used to argue for similar resonance interactions of the phenyl substituents with the electron-deficient benzylic carbon atom in these two cases, we feel that steric and solvation effects are unlikely to be negligible in such a comparison, and the similarity in pK_{R^+} values in this case is probably fortuitous.

It is of particular interest to compare rate and equilibrium effects upon pseudobase formation from **4**: X = H and $(CH_3)_2N$ with analogous data for the well studied carbinol formation from the malachite green and crystal violet cations. Rate and equilibrium data for these two series of cations are collected in Table 2.

Despite their unfavourable *peri* interactions which destabilize the cations relative to the pseudobases, the 9-aryl-10-methylacridinium cations are considerably less susceptible towards pseudobase formation than their triphenylmethyl carbocation analogs. This enhanced cation stability in the acridinium system can be attributed to the resonance stabilization that is available in the tricyclic acridine ring system. Consideration of the rate constants for cation–pseudobase equilibrium indicates that, whereas k_{OH} is similar for the 9-arylacridinium and triphenylmethyl cations, k_2 for loss of hydroxide ion from the pseudobase is quite different in these two systems. This comparison can also be extended to the activation parameters for the k_{OH} and k_2 reactions. Thus whereas the entropies and enthalpies of activation are similar for hydroxide attack on the 9-phenyl-10-methylacridinium ($\Delta H^{\ddagger} = 13.8$ kcal/mol, $\Delta S^{\ddagger} = -12$ eu (4)) and the crystal violet cation ($\Delta H^{\ddagger} = 15.3$ kcal/mol, $\Delta S^{\ddagger} = -10$ eu (6)), these parameters are quite different for the k_2 step in these two cases ($\Delta H^{\ddagger} = 14$ kcal/mol and $\Delta S^{\ddagger} = -24$ eu for **2**: R = C_6H_5 (4); $\Delta H^{\ddagger} = 21.9$ kcal/mol and $\Delta S^{\ddagger} = -10$ eu for the carbinol of **6**: X = 4-$(CH_3)_2N$ (6)).

The most direct comparison of rate constants for acridinium and triphenylmethyl cations would employ cations of similar pK_{R^+} values in the two series (8). Ritchie *et al.* (6) have reported rate and equilibrium data for carbinol formation from a variety of substituted triphenylmethyl cations. Their data can be analyzed to give the rate–equilibrium correlation of eq. [3]. The relatively low correlation coefficient is indicative of some scatter in the data; however, the greatest variation of any experimental k_{OH} value from this correlation equation is by less than a factor of 3.

$$[3] \quad \log k_{OH} = -0.40(\pm 0.05)\ pK_{R^+} + 3.0(\pm 0.3) \qquad (r = 0.965)$$

Equation [3] may be used to estimate that a triphenylmethyl cation of $pK_{R^+} = 11$ would have $k_{OH} = 0.04\ M^{-1}\ s^{-1}$. Comparison of this value with $k_{OH} = 1.3\ M^{-1}\ s^{-1}$ for **1**: R = C_6H_5 indicates that 9-arylacridinium cations are 30-fold more reactive towards attack by hydroxide ion than are triphenylmethyl carbocations. The simplest interpretation of this result is probably an indication that, whereas resonance delocalization of charge occurs over all three rings of the triphenylmethyl cations, geometric considerations allow delocalization only within the tricyclic acridine ring system and not to any significant extent into the pendant phenyl ring of the 9-arylacridinium cations.

Acknowledgement

We appreciate the continued support of this work by the Natural Sciences and Engineering Research Council of Canada through the award of an Operating Grant to J.W.B.

1. J. W. BUNTING and W. G. MEATHREL. Can. J. Chem. **52**, 981 (1974).
2. A. ALBERT. The acridines. 2nd ed. Edward Arnold Ltd., London. 1966. p. 100.
3. R. E. BALLARD, J. JONES, and E. SUTHERLAND. Tetrahedron Lett. **23**, 3677 (1982).
4. J. W. BUNTING and W. G. MEATHREL. Can. J. Chem. **51**, 1965 (1973).
5. C. W. N. CUMPER, R. F. A. GINMAN, and A. I. VOGEL. J. Chem. Soc. 4518 (1962).
6. C. D. RITCHIE, D. J. WRIGHT, D. S. HUANG, and A. A. KAMEGO. J. Am. Chem. Soc. **97**, 1163 (1975).
7. D. H. MCDANIEL and H. C. BROWN. J. Org. Chem. **23**, 420 (1958).
8. C. F. BERNASCONI. Pure Appl. Chem. **54**, 2335 (1982).
9. R. J. GOLDACRE and J. N. PHILLIPS. J. Chem. Soc. 1724 (1949).

Can. J. Chem. Downloaded from www.nrcresearchpress.com by 210.87.254.40 on 09/06/12
For personal use only.

Mechanistic aspects of the methoxide-catalyzed transformation of 4-acyloxy-1,3,4-oxadiazines to N-amino-oxazolidonylhydrazones

DONALD MACKAY AND DEANE DOUGLAS MCINTYRE

The Guelph–Waterloo Center for Graduate Work in Chemistry, University of Waterloo, Waterloo, Ont., Canada N2L 3G1

Received January 3, 1983[1]

DONALD MACKAY and DEANE DOUGLAS MCINTYRE. Can. J. Chem. **62**, 355 (1984).

When the 1,3,4-oxadiazine **2**, one of three known isomers formed by cycloaddition of 2,5-dimethyl-3,4-diphenylcyclopentadienone and dimethyl azodicarboxylate, is isomerized by MeO^-–MeOH to the hydrazone **4**, the MeO of the ester group of **2** is lost and MeO is incorporated into **4** from the solvent. In acid, e.g. trifluoroacetic acid, demethylation of **2** gives **14** in which the ester Me is lost. The hydrazone **4** also gives **14** with acid, but by a different pathway.

These results were established using the structurally isomeric oxadiazines **10** and **11** as mechanistic probes; an X-ray analysis of **10** established the individual identities of these.

DONALD MACKAY et DEANE DOUGLAS MCINTYRE. Can. J. Chem. **62**, 355 (1984).

La oxadiazine-1,3,4 (**2**), l'un des trois isomères obtenus dans la cycloaddition de la diméthyl-2,5 diphényl-3,4 cyclopentadiénone et de l'azodicarboxylate de diméthyle, s'isomérise en présence de MeO^-–MeOH en hydrazone **4**; le composé **2** perd un groupe MeO^- et ce dernier s'incorpore dans le composé **4** à partir du solvant. En milieu acide, par exemple l'acide trifluoroacétique, le composé **2** subit une déméthylation et conduit au composé **14** dans lequel de groupe Me de l'ester est perdu. L'hydrazone **4** conduit également au composé **14** en présence d'un acide mais selon un mécanisme différent.

On a établi ces résultats en utilisant les isomères de structure des oxadiazines **10** et **11** comme références; l'analyse par rayons-X du composé **10** permet d'identifier individuellement les isomères.

[Traduit par le journal]

Introduction

We have previously shown that heating of 2,5-dimethyl-3,4-diphenylcyclopentadienone with dimethyl azodicarboxylate rapidly gave the bridged adduct **1** which isomerized reversibly to the oxadiazine **2**, and more slowly, but irreversibly, to the diazetidine **3** (1). Recently we have described the conversion of **2** into another isomer, the dimethyl carbonate hydrazone **4** (2). The four isomers thus show a wide variety of bicyclic structural arrangments: [2.2.1], [3.4.0], [3.2.0], and [3.3.0].

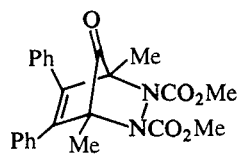

1

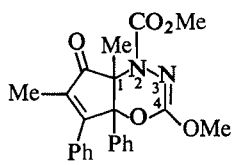

2

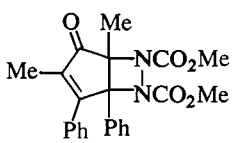

3

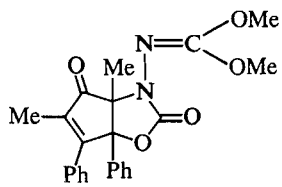

4

The formation of **4** required the use of a dilute solution of KOH or NaOMe in MeOH; KOH in EtOH or H_2O completely degraded **2**. This suggested that external MeOH was incorporated into **4**, confirmation of which came from the conversion of the oxadiazine **5** by KOH in MeOH into a mixture of the diastereomeric hydrazones **6** and **7**. Though **4** is an isomer of **1**–**3**, it is not an isomerization product.

We briefly describe here experiments which help to clarify the nature of the transformation of **2** into **4**. We also wish to comment further on the acid-catalyzed demethylation of the isomers **1**–**4**.

[1]Revision received July 28, 1983.

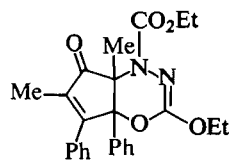

5

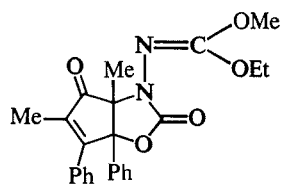

6

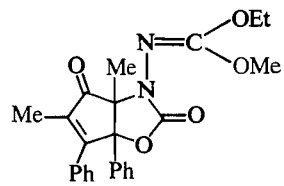

7

Base-catalyzed formation of the carbonate hydrazones

Reactions **2** → **4** and **5** → **6** + **7** leave us with the following questions. (*i*) Which MeO group in **2** is lost? One MeO (and only one) is lost since **5** gives **6** and **7**, but gives neither **4** nor the analogous di-ethoxy compound. (*ii*) Why does **5** gives *both* diastereomeric hydrazones? Restated for the transformation **2** → **4**, why are the MeO groups in **4** scrambled with respect to their origin from **2** and the solvent? (*iii*) Which N in **2** becomes the exocyclic N in **4**? (*iv*) Why is MeOH apparently so specific? The analogous transformation is not observed in other alcohols, e.g. ethanol.

(i) and (ii)

Further evidence for the inclusion of external MeOH came from repetition of the reaction of **2** with 0.1 *M* KOD in methanol-d_4 at 65°C. Disappearance of the MeO peaks of **2**, coincident at 3.67 (δ values in CD_3OD), was accompanied by the growth of new MeO peaks at 3.30 (**4** and MeOH) and 3.70 (**4**). Their ratios throughout indicated that the two peaks for **4** were growing at about the same rate. After work-up these MeO peaks were of equal intensity and each was half that of the C-Me peaks.

This result is consistent either with the intermediacy of a

Can. J. Chem. Downloaded from www.nrcresearchpress.com by 210.87.254.6 on 09/06/12
For personal use only.

Can. J. Chem. Downloaded from www.nrcresearchpress.com by 210.87.254.6 on 09/06/12
For personal use only.

symmetric precursor to **4**, containing one CH_3O and one CD_3O group, or, more likely, with the formation of a single diastereomeric hydrazone, which is rapidly *E,Z* equilibrated. This equilibration is certainly not catalyzed by addition of MeO^- to the imino carbon (thus allowing C—N rotation), since the CH_3O^- is not all lost in the labelled experiment. Thermal *E,Z* inerconversion is most likely. Though the MeO peaks of **4** in CD_3SOCD_3 ($\Delta\nu$ = 16.2 Hz at 80 MHz[2]) did not coalesce at 150°C (2), the lower limit associated with this barrier ($\Delta G^{\ddagger}$ = ca. 22 kcal/mol; the associated rotation frequency is 36 s^{-1}) does not allow us to rule out thermal rotation on the time scale of the experiment.[3]

An answer to the question of which MeO group in **2** is lost requires a distinction between these groups to be created, either isotopically or though the replacement of one of them by a constitutionally different variation. Perforce we chose the latter. Conditions necessary for removal of the ester group (acid or base) in **2**, and thence replacing it with an isotopically different methoxycarbonyl group, lead to rapid transformation of the heterocyclic ring.

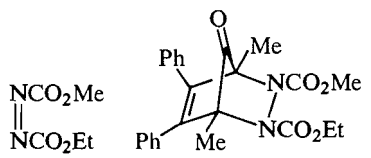

8

9

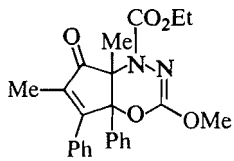

10

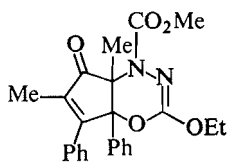

11

Our starting point was the unsymmetrical azo compound **8**. Its synthesis and that of its cyclone adduct **9** were unexceptional. Refluxing of **9** in MeCN for 40 h gave the equilibrium mixture of oxadiazines (cf. ref. 1), as well as traces of the diazetidines (cf. **3**). Separation of the individual oxadiazines from this five-component mixture was tedious, requiring column chromatography and repeated crystallizations. Small amounts were obtained pure with melting points 124.5−125.5°C and 133−135°C. The former was subjected to X-ray analysis and found to be the carboethoxy-containing isomer. Its crystal structure is shown in Fig. 1, which also confirms the *cis* ring junction stereochemistry which we have hitherto assumed (5). The two isomers were characterized for diagnostic purposes in subsequent experiments by their OMe

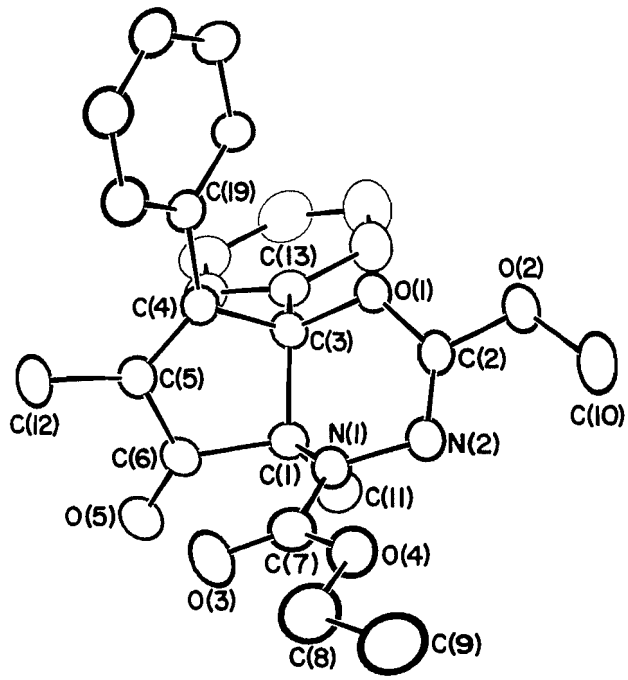

FIG. 1. ORTEP plot for compound **10**.

and OCH_2 ^1H nmr absorptions (δ, $CDCl_3$) at 3.80 and 4.22 for **10** and 3.77 and 4.16 for **11**.

A sample of **10** subjected to the conditions used for the conversion of **2** → **4** gave **4** as *the sole product*. By contrast, similar treatment of **11** gave the *same mixture* of **6** and **7** obtained from **5**. The alkoxy group of the ester is thus exclusively solvolyzed.

(iii)

The exocyclic N in **4** must surely be N_3 in **2**: for numbering see formula **2**. Given the demonstrated loss of the exocyclic MeO group in **2**, and the inclusion of one from the solvent, it is clear that the transformation which makes N_3 exocyclic requires at a minimum only the formal migration of O_5 from C_4 to C(=O). By contrast, to make N_2 exocyclic requires at a minimum the migration of C_1 from N_2 to N_3 and of OMe from C_4 to C(=O), as well as the loss of the exocyclic carbonyl O and the gain of an external O.[4]

(iv)

An appealing enough mechanism can be visualized for the transformation of **2** (Scheme 1), which accounts for the proven origin of the MeO groups in **4**, one from C4 and one from the solvent, and for the presumed migration of N_3 out of the ring.[5] If such a mechanism is valid it follows that k_{-1} is small compared with k_2 since otherwise more than one equivalent of CD_3O would have been incorporated into **4** in the labelled experiment, and in the reactions of **5** and **11** with MeO^- (from OH^-) a bias towards hydrazones with more MeO than EtO would have been observed.

Scheme 1 does not, however, explain why EtO^-−EtOH

[2]Diastereotopic shifts, though much smaller ones, were also observed by us in the MeO peaks in acyclic dimethyl carbonate hydrazones (2), and in the methyl (but not the methylene)absorptions of some acyclic diethyl carbonate hydrazones reported in the literature (3).

[3]The result at 150°C can be extrapolated to 65°C (the temperature of the deuteration experiment) by treating $\Delta G^{\ddagger}$ as temperature independent, a reasonable assumption since in most conformational rotation processes $\Delta S^{\ddagger}$ is usually very small (4). The rotation frequency drops from an upper limit of 36 s^{-1} to one of about 3 min^{-1}, still very fast on the experimental time scale.

[4]We are of course applying Occam's Razor here. We have no *proof* whatsoever of the origin of any of the atoms or groups in the oxazolidone ring of **4** or its side chain, except that one of its MeO groups was originally that on C_4 in **2**.

[5]Anions like **12** or **13** may not of course be involved, since two or more of the steps shown may be concerted.

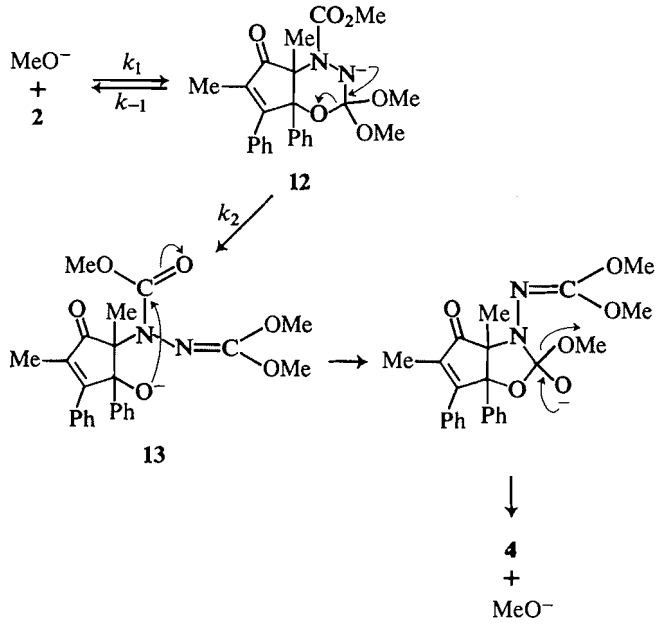

SCHEME 1

decomposes **2**,[6] as it also does **5** (2). Whether conversion of these first into hydrazones does occur cannot be determined, since in a control experiment the hydrazone **4** was rapidly and completely degraded by this reagent.

The decreasing efficiency in MOH of CN^- and CO_3^{2-} (as compared with MeO^- or OH^-) (2) is presumably related to their decreasing basicities. The equilibrium concentration of MeO^- generated by these anions would be extremely low.

A final comment about the hydrazone formation is in order. An alkoxy 1,3,4-oxadiazine like **2** is itself a cyclic hydrazone of an unsymmetrical carbonate, derived in this case from MeOH and a benzylic alcohol. Thus the reaction **2** → **4** represents the conversion of a cyclic hydrazone and an exocyclic urethane into an exocyclic hydrazone and a cyclic urethane.

Acid-catalyzed demethylation reactions

The acid hydrolysis product formed from each of **1**–**4** has been shown by X-ray analysis to be the oxazolidone **14** (footnote 5, ref. 2), the crystal structure of which is given in Fig. 2. We had concluded in earlier work on the hydrolysis of **1**–**3** that it had the structure **16** (5). The reaction of these three isomers in the presence of trifluoroacetic acid (TFA), as followed by nmr spectroscopy, was complex in dilute TFA in $CDCl_3$, isomerization between **1**, **2**, and **3** preceding solvolysis. In concentrated TFA (8% or greater) only solvolysis was observed, through a rapidly formed common intermediate which decayed to product with first-order kinetics. The rate constant of the solvolysis decreased with TFA concentration (e.g. 8% TFA, $t_{1/2}$ = 1.2 min; 100% TFA, $t_{1/2}$ = 30 min). We speculated that the intermediate, which had one very low-field MeO absorption (at δ 4.7 in neat TFA), was a mono- or multiprotonated form of **2**, but this view was biased by our belief that the final demethylation product had the 6-membered heterocyclic ring.

[6]A referee has pointed out that this experiment, done at reflux, represents more severe reaction conditions than those used in the transformation of **2** → **4** in refluxing MeOH. We have repeated the EtO^- (0.5 *M*) catalyzed reaction in scrupulously dried EtOH in a refluxing MeOH bath. Again, complete degradation of **2** was observed.

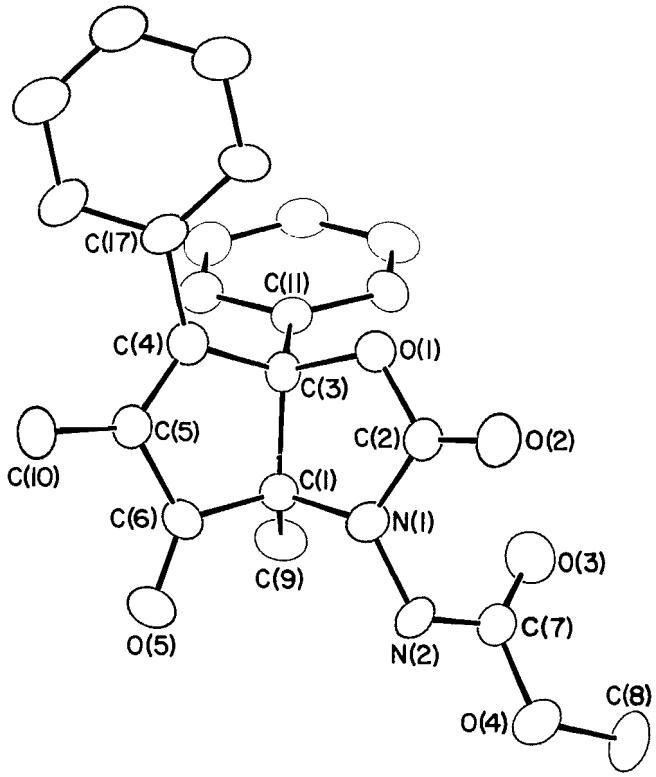

FIG. 2. ORTEP plot for compound **14**.

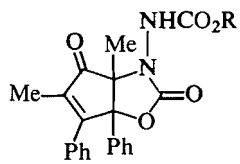

14, R = Me
15, R = Et

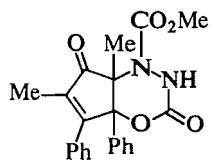

16

We are no clearer about the structure of the immediate precursor to **14**, but we have now shown that in the solvolysis of the oxadiazines it is the exocyclic (ester) site which is dealkylated, just as it is the exocyclic alkoxy group which is lost in the base-catalyzed hydrazone formation. This was determined using a 1:5 mixture of the oxadiazines **10**/**11**. In TFA the mixture of complexes obtained had the MeO peak at δ 4.7 as the major low-field alkoxy absorption. Work-up at the end of the reaction gave a 1:5 mixture of **14**/**15**. Protonation thus occurs on or near the ester group and it is its alkyl group that is solvolyzed.

The solvolysis of **4** → **14** in TFA goes through a different intermediate, characterized by *two* low-field MeO absorptions at δ 4.4 and 4.7. These decay together to **14**, faster ($t_{1/2}$ = 8 min) than the intermediate from **1**–**3** decays to **14**. This solvolysis thus goes by a different mechanism than the one common to the solvolysis of **1**, **2**, and **3**.

Experimental

The following spectrometers were used: infrared, Beckman IR-10; nuclear magnetic resonance, Perkin–Elmer R12-B or Bruker WP-80. Melting points are uncorrected. MeOH was dried by distillation from magnesium methoxide and ethanol by distillation from sodium ethoxide.

Can. J. Chem. Downloaded from www.nrcresearchpress.com by 210.87.254.6 on 09/06/12
For personal use only.

Can. J. Chem. Downloaded from www.nrcresearchpress.com by 210.87.254.6 on 09/06/12
For personal use only.

TABLE 1. Bond lengths and angles for compound **10**, $C_{24}H_{24}N_2O_5$

Bond	Length (Å)	Bond	Length (Å)
C(1)—N(1)	1.469(7)	C(1)—C(3)	1.561(7)
C(1)—C(6)	1.539(8)	C(1)—C(11)	1.539(8)
C(2)—O(1)	1.325(6)	C(2)—O(2)	1.334(7)
C(2)—N(2)	1.269(7)	C(3)—O(1)	1.461(6)
C(3)—C(4)	1.553(8)	C(3)—C(13)	1.530(7)
C(4)—C(5)	1.354(7)	C(4)—C(19)	1.471(7)
C(5)—C(6)	1.473(8)	C(5)—C(12)	1.507(8)
C(6)—O(5)	1.207(7)	C(7)—O(3)	1.209(7)
C(7)—O(4)	1.344(7)	C(7)—N(1)	1.353(7)
C(8)—O(4)	1.467(8)	C(8)—C(9)	1.529(10)
C(10)—O(2)	1.465(8)	N(1)—N(2)	1.421(6)
C(13)—C(14)	1.392(9)	C(14)—C(15)	1.419(10)
C(15)—C(16)	1.398(11)	C(16)—C(17)	1.389(11)
C(17)—C(18)	1.398(9)	C(18)—C(13)	1.398(8)
C(19)—C(20)	1.401(7)	C(20)—C(21)	1.408(8)
C(21)—C(22)	1.410(9)	C(22)—C(23)	1.390(9)
C(23)—C(24)	1.398(9)	C(24)—C(19)	1.411(8)

Bond	Angle (°)	Bond	Angle (°)
N(1)—C(1)—C(3)	104.7(2)	N(1)—C(1)—C(6)	111.1(2)
N(1)—C(1)—C(11)	110.8(2)	C(3)—C(1)—C(6)	98.9(2)
C(3)—C(1)—C(11)	117.7(2)	C(6)—C(1)—C(11)	112.9(2)
O(1)—C(2)—O(2)	108.7(2)	O(1)—C(2)—N(2)	129.0(2)
O(2)—C(2)—N(2)	122.3(2)	O(1)—C(3)—C(1)	111.4(2)
O(1)—C(3)—C(4)	110.3(2)	O(1)—C(3)—C(13)	106.6(2)
C(1)—C(3)—C(4)	103.3(2)	C(1)—C(3)—C(13)	112.8(2)
C(4)—C(3)—C(13)	112.5(2)	C(3)—C(4)—C(5)	110.1(2)
C(3)—C(4)—C(19)	122.1(2)	C(5)—C(4)—C(19)	127.5(3)
C(4)—C(5)—C(6)	108.8(3)	C(4)—C(5)—C(12)	131.1(3)
C(6)—C(5)—C(12)	119.6(3)	O(5)—C(6)—C(1)	124.5(2)
O(5)—C(6)—C(5)	127.2(2)	C(1)—C(6)—C(5)	107.7(2)
O(3)—C(7)—O(4)	124.3(2)	O(3)—C(7)—N(1)	123.2(2)
O(4)—C(7)—N(1)	112.5(2)	O(4)—C(8)—C(9)	105.3(3)
C(2)—O(1)—C(3)	119.0(3)	C(2)—C(2)—C(10)	115.8(3)
C(7)—O(4)—C(8)	114.0(3)	N(2)—N(1)—C(1)	115.8(2)
N(2)—N(1)—C(7)	118.3(3)	C(1)—N(1)—C(7)	124.7(3)
N(1)—N(2)—C(2)	110.1(2)	C(3)—C(13)—C(14)	120.4(3)
C(3)—C(13)—C(18)	118.9(3)	C(18)—C(13)—C(14)	120.8(3)
C(13)—C(14)—C(15)	118.2(3)	C(14)—C(15)—C(16)	121.0(4)
C(15)—C(16)—C(17)	119.6(4)	C(16)—C(17)—C(18)	120.0(3)
C(17)—C(18)—C(13)	120.3(3)	C(4)—C(19)—C(20)	121.3(2)
C(4)—C(19)—C(24)	119.3(3)	C(24)—C(19)—C(20)	119.4(3)
C(19)—C(20)—C(21)	119.8(3)	C(20)—C(21)—C(22)	120.5(3)
C(21)—C(22)—C(23)	119.3(3)	C(22)—C(23)—C(24)	120.7(3)
C(23)—C(24)—C(19)	120.3(3)		

*X-Ray analyses of compounds **10** and **14***[7]

Compound **10**: $C_{24}H_{24}N_2O_5$ Mol. wt. 420.47
Triclinic; a = 8.736(2), b = 8.816(3), c = 15.093(3) Å; α = 96.80(2), β = 94.81(2), λ = 107.92(2)°, V = 1089.5(5) Å^3, space group $P\bar{1}$, Z = 2, ρ_c = 1.282 g cm^{-3}, $F(000)$ = 444, λ = 0.71069 Å, μ(MoKα) = 0.98 cm^{-1}.

From a total of 3061 diffractometer measured reflections ($2\theta \leq 46°$), 2467 were considered observed ($I \geq 3\sigma(I)$). The structure was solved by direct methods (MULTAN 80) and refined with anisotropic thermal parameters to an R of 0.077.

Compound **14**: $C_{22}N_{20}N_2O_5$ Mol. Wt. 392.42
Orthorhombic; a = 14.263(3), b = 16.229(4), c = 16.585(4) Å, V = 3839(1) Å^3, space group $Pbca$, Z = 8, ρ_c = 1.358 g cm^{-3}, $F(000)$ = 1648, λ = 0.71069 Å, μ(MoKα) = 1.05 cm^{-1}.

From a total of 2529 independent diffractometer measured reflections ($2\theta \leq 45°$), 1527 were considered observed $I \geq 3\sigma(I)$). The structure was solved by direct methods (MULTAN 80) and refined with anisotropic thermal parameters to an R of 0.076 (cf. refinement of solution in footnote 5, ref. 2). Tables 1 and 4 give bond lengths and angles for compounds **10** and **14**.

Reaction of oxadiazine 2 with KOD − methanol-d_4

To a 0.1 *M* solution of KOD (made by repeated exchange of KOH in D_2O) in CD_3OD (0.5 mL) was added the oxadiazine (50 mg, 0.12 mmol) and the solution was heated in an nmr tube in refluxing MeOH (65°C). The ^{1}H nmr spectrum was monitored at intervals. The coincident MeO peaks of **2** at δ 3.67 decreased and new peaks for **4** at 3.30 and 3.37 grew, the latter being coincident with that of the MeOH displaced from **2**. The peaks for **4** were judged to be of equal intensity at all times. Work-up of the solution in the usual way (2) gave the deuterated hydrazone whose ^{1}H nmr spectrum in $CDCl_3$ showed the

[7]For both compounds the following are available at a nominal charge from the Depository of Unpublished Data, CISTI, National Research Council of Canada, Ottawa, Ont., Canada K1A 0S2; (*i*) atomic coordinates, (*ii*) anisotropic thermal parameters, and (*iii*) observed and calculated structure factor amplitudes (Tables 2, 3, 5, 6).

TABLE 4. Bond lengths and angles for compound **14**, $C_{22}H_{19}N_2O_5$

Bond	Length)Å)	Bond	Length (Å)
C(1)—N(1)	1.471(9)	C(1)—C(3)	1.569(9)
C(1)—C(6)	1.515(10)	C(1)—C(9)	1.530(10)
C(2)—O(1)	1.363(9)	C(2)—O(2)	1.183(9)
C(2)—N(1)	1.379(9)	C(3)—O(1)	1.466(8)
C(3)—C(4)	1.527(10)	C(3)—C(11)	1.507(10)
C(4)—C(5)	1.354(10)	C(4)—C(17)	1.487(10)
C(5)—C(6)	1.466(10)	C(5)—C(10)	1.511(10)
C(6)—O(5)	1.218(8)	C(7)—O(3)	1.201(11)
C(7)—O(4)	1.349(9)	C(7)—N(2)	1.379(11)
C(8)—O(4)	1.463(13)	N(1)—N(2)	1.384(8)
C(11)—C(12)	1.382(10)	C(12)—C(13)	1.403(11)
C(13)—C(14)	1.402(12)	C(14)—C(15)	1.399(12)
C(15)—C(16)	1.396(11)	C(16)—C(11)	1.409(10)
C(17)—C(18)	1.402(10)	C(18)—C(19)	1.423(10)
C(19)—C(20)	1.389(13)	C(20)—C(21)	1.398(13)
C(21)—C(22)	1.400(13)	C(22)—C(17)	1.398(11)

Bond	Angle (°)	Bond	Angle (°)
N(1)—C(1)—C(3)	101.1(3)	N(1)—C(1)—C(6)	107.2(3)
N(1)—C(1)—C(9)	113.9(3)	C(3)—C(1)—C(6)	103.3(3)
C(3)—C(1)—C(9)	117.8(3)	C(6)—C(1)—C(9)	112.2(3)
O(1)—C(2)—O(2)	123.2(3)	O(1)—C(2)—N(1)	108.4(3)
O(2)—C(2)—N(1)	128.4(3)	O(1)—C(3)—C(1)	104.6(3)
O(1)—C(3)—C(4)	108.7(3)	O(1)—C(3)—C(11)	109.0(3)
C(1)—C(3)—C(4)	104.7(3)	C(1)—C(3)—C(11)	115.3(3)
C(4)—C(3)—C(11)	114.0(3)	C(3)—C(4)—C(5)	112.1(3)
C(3)—C(4)—C(17)	119.8(3)	C(5)—C(4)—C(17)	128.0(4)
C(4)—C(5)—C(6)	109.5(4)	C(4)—C(5)—C(10)	129.3(4)
C(6)—C(5)—C(11)	121.1(4)	O(5)—C(6)—C(1)	124.0(3)
O(5)—C(6)—C(5)	125.7(3)	C(1)—C(6)—C(5)	110.4(3)
O(3)—C(7)—O(4)	125.9(3)	O(3)—C(7)—N(2)	126.6(3)
O(4)—C(7)—N(2)	107.5(3)	C(2)—C(1)—C(3)	112.0(4)
C(7)—O(4)—C(8)	114.9(5)	N(2)—N(1)—C(1)	122.7(3)
N(2)—N(1)—C(2)	119.1(4)	C(1)—N(1)—C(2)	113.7(4)
N(1)—N(2)—C(7)	116.1(4)	C(3)—C(11)—C(12)	121.4(4)
C(3)—C(11)—C(16)	118.1(3)	C(16)—C(11)—C(12)	120.5(4)
C(11)—C(12)—C(13)	119.9(4)	C(12)—C(13)—C(14)	120.6(4)
C(13)—C(14)—C(15)	118.7(4)	C(14)—C(15)—C(16)	121.2(4)
C(15)—C(16)—C(11)	119.1(4)	C(4)—C(17)—C(18)	120.6(4)
C(4)—C(17)—C(22)	118.7(4)	C(22)—C(17)—C(18)	120.6(4)
C(17)—C(18)—C(19)	119.5(4)	C(18)—C(19)—C(20)	119.6(4)
C(19)—C(20)—C(21)	120.1(5)	C(20)—C(21)—C(22)	120.9(5)
C(21)—C(22)—C(17)	119.1(5)		

MeO peaks to be equal in intensity and half the intensity of the C-Me peaks.

Methyl ethyl azodicarboxylate

This compound has been described in the patent literature (6).

A solution of ethyl carbazate (52 g, 0.50 mol) in methylene chloride (600 mL) was kept chilled in CO_2–acetone as necessary while methyl chloroformate (57 g, 0.60 mol) was carefully added, followed by sodium carbonate (56 g, 0.50 mol). The whole was stirred for 24 h (a check showed about 70% reaction in 5 h), evaporated to dryness, and extracted with hot ethyl acetate (600 mL, refluxed 1h). The hot solution was filtered and evaporated to give the crude methyl ethyl hydrazinedicarboxylate (98%). It could be recrystallized from ethyl acetate – isooctane in an overall yield of 75%; mp 84.5–86°C; δ ($CDCl_3$): 7.15 (broad, NHNH), 4.19 (q, J = 7.0 Hz, OCH_2), 3.75 s, OMe), 1.27 (t, Me).

The hydrazine (7 g, 74 mmol) was added all at once to a solution of *N*-bromosuccinimide (12 g, 67 mmol) and pyridine (5.3 mL, 67 mmol) in methylene chloride (250 mL) in a separatory funnel. There was an immediate orange coloration. After 30 min, during which the funnel was occasionally shaken to ensure dissolution of all the hydrazine, the whole was extracted with 4 × 250 mL water, dried, and evaporated. The residual orange oil (8.0 g, 66%) had δ($CDCl_3$): 4.45 (q, J = 7.0 Hz, OCH_2), 4.00 (s, OMe), 1.41 (t, Me).

*2-Ethoxycarbonyl-3-methoxycarbonyl-1,4-dimethyl-5,6-diphenyl-7-oxo-2,3-diazabicyclo[2.2.1]hept-5-ene (**9**)*

A solution of the azo ester (5.0 g, 31.2 mmol) and 2,5-dimethyl-3,4-diphenylcyclopentadienone (8.0 g, 30.8 mmol) in benzene (100 mL) was refluxed for 2 h. Evaporation and trituration of the residue with ether–hexane gave a colorless crystalline product (11 g, 85%). Recrystallization from ether–hexane gave prisms, mp 109–111°C; ν (Nujol): 1800 (bridging CO), 1748 (ester CO) cm^{-1}; δ ($CDCl_3$): 7.4–6.8 (m, 10H, Ph), 3.96 (A of ABX_3, J_{AB} = 9.3, J_{AX} = 7.1 Hz, 1H, OCH_2), 4.12 (B of ABX_3, J_{BX} = 7.1 Hz, 1H, OCH_2), 3.65 (s, OMe), 1.84 (s, Me), 1.80 (s, Me), 1.01 (t, Me). *Anal.* calcd. for $C_{24}H_{24}N_2O_5$: C 68.56, H 5.75, N 6.66; found: C 68.66, H 5.69, N 6.69.

*Isomerization of **9** to **10** and **11***

A sample of **9** (10 g) was refluxed in acetonitrile (250 mL) for 40 h. Evaporation gave a sticky residue whose ^1H nmr spectrum showed

Can. J. Chem. Downloaded from www.nrcresearchpress.com by 210.87.254.6 on 09/06/12
For personal use only.

unreacted **9** and the two expected oxadiazines, as well as small amounts of the isomeric diazetidines (cf. ref. 1). Chromatography was carried out on silica gel from 1:2 ether–hexane. Both diazetidines and the first runnings of the oxadiazines appeared in the first few fractions. The central fractions consisted only of the oxadiazines, with a bias towards **10** (as was later demonstrated by the X-ray analysis result) in the early, and towards **11** in the late, fractions. The last fractions contained **9**, **10**, and **11**.

The fractions richest in **10**, but also contaminated by the diazetidines, were crystallized from acetone–isooctane, and after removal of a first crop the filtrate slowly deposited crystals of pure oxadiazines in the ratio **10**/**11** = 5:1. This was recrystallized from ethyl acetate – isooctane and finally from MeOH to give pure **10**, mp 124.5–125.5°C; ν (Nujol): 1736 (ester CO), 1700 (ketone CO), 1662 (C=N) cm^{-1}; δ ($CDCl_3$): 7.6–7.0 (m, 10H, Ph), 4.22 (q, J = 7.1 Hz, OCH_2), 3.80 (s, OMe), 2.21 (s, vinylic Me), 1.31 (t, ester Me), 1.04 (s, *tert*-Me).

The fractions richest in **11** were crystallized, first from acetone–isooctane and then thrice from MeOH to give **11**, mp 133–135°C; ν (Nujol): 1735 (ester CO), 1701 (ketone CO), 1652 (C=N) cm^{-1}; δ ($CDCl_3$): 7.6–7.0 (m, 10H, Ph), 4.16 (q, J = 7.0 Hz, OCH_2), 3.77 (s, OMe), 2.21 (s, vinylic Me), 1.24 (t, alkoxy Me), 1.05 (s, *tert*-Me).

A representative sample of a mixture of pure **10** and **11** was analyzed. *Anal.* calcd. for $C_{24}H_{24}N_2O_5$: C 68.56, H 5.75, N 6.66; found: C 68.52, H 5.63, N 6.63.

A single crystal of **10** was subjected to X-ray analysis and found to have the assigned structure.

*Base-catalyzed conversion of **10** into **4***

A solution of **10** (35 mg, 0.083 mmol) in 0.2 *M* KOH–MeOH (5 mL) was refluxed for 3 h and worked up exactly as described for the isomerization of **2** to **4**. The glassy residue (33 mg, 98%) had a ^1H nmr spectrum ($CDCl_3$) identical with that of **4**, alone or in admixture with authentic **4**.

*Base-catalyzed conversion of **11** into **6** and **7***

A solution of **11** (contaminated with a trace of **10**) (44 mg, 0.10 mmol) was similarly solvolyzed. Work-up as before gave a glassy residue (41 mg, 94%) whose ^1H nmr spectrum was identical with that of the similarly prepared solvolysis product of **5**, viz. compounds **6** and **7**. Mixing of the two solutions in $CDCl_3$ gave a spectrum in which no new peaks could be observed. Peak separations and peak positions could be determined with great precision using the Bruker WP-80 spectrometer.

*Reaction of **4** with $EtO^- - EtOH$*

A solution of the hydrazone **4** (100 mg, 0.25 mmol) in 0.2 *M* NaOEt in EtOH (50 mL) became red-brown when refluxed for 30 min. It was worked up in the usual manner (2) and gave a residue with an extremely complex ^1H nmr spectrum.

*Solvolysis of the oxadiazines **10** and **11** with TFA*

A 1:5 mixture of **10**/**11** (50 mg) was dissolved in TFA (0.50 mL) in an nmr tube and the spectrum run repeatedly until reaction was complete (about 3 h). The most strongly downfield-shifted major peak, at a maximum when the spectrum was first run, was the MeO peak, at δ 4.7. The final mixture of **14** and **15** was worked up by blowing off the acid in a stream of N_2, and treating the residue with methylene chloride and aqueous sodium hydrogen carbonate. The dried organic layer was evaporated. Its ^1H nmr spectrum was that of a 1:5 mixture of **14**/**15**. Crystallization from ethyl acetate – isooctane gave **15**, identified by comparative ^1H nmr spectroscopy and mixture mp (5).

*Solvolysis of **4** with TFA*

A solution of **4** (50 mg, 0.12 mmol) in TFA (0.5 mL) was similarly kept and periodically monitored in an nmr tube. Both MeO peaks derived from **4** were observed at low field, δ 4.7 and 4.4, in the immediately formed protonated intermediate. The decay of the latter was much more rapid ($t_{1/2}$ = 8 min) than that of the corresponding intermediate from **2** ($t_{1/2}$ = 30 min (5)). Work-up as described earlier (2) gave compound **14**.

Acknowledgment

We thank the Natural Sciences and Engineering Research Council of Canada for support of this work.

1. D. MACKAY, C. W. PILGER, and L. W. WONG. J. Org. Chem. **38**, 1043 (1973).
2. D. MACKAY, D. D. MCINTYRE, N. J. TAYLOR, and L. L. WONG. Can. J. Chem. **61**, 1213 (1983).
3. D. J. BROWN and R. K. LYNN. Austl. J. Chem. **26**, 1689 (1973).
4. W. E. STEWART and T. H. SIDDAL III. Chem. Rev. **70**, 517 (1970).
5. D. MACKAY and C. W. PILGER. Can. J. Chem. **52**, 1114 (1974).
6. C. S. STEPHEN and L. W. KORCZYKOWSKI. Ger. Pat. 1 818 020 (1977); Chem. Abstr. **87**, 38848s (1977).

Can. J. Chem. Downloaded from www.nrcresearchpress.com by 210.87.254.6 on 09/06/12
For personal use only.

Propriétés physiques et basicité de l'oxydipropionitrile

JEAN-CLAUDE BOLLINGER,[1] GERMAINE YVERNAULT ET THÉOPHILE YVERNAULT
Laboratoire de Chimie Générale et Analytique, Faculté des Sciences, 123 Avenue Albert-Thomas, 87060 Limoges Cédex, France

ET

RAYMOND HOURIET
Institut de Chimie-Physique, Ecole Polytechnique Fédérale, Ecublens, 1015 Lausanne, Suisse

Reçu le 8 juillet 1983

JEAN-CLAUDE BOLLINGER, GERMAINE YVERNAULT, THÉOPHILE YVERNAULT et RAYMOND HOURIET. Can. J. Chem. **62**, 361 (1984).

On a déterminé les constantes physiques du 3,3′-oxydipropionitrile (ODPN) à 25°C (densité, indice de réfraction, viscosité, constante diélectrique, moment dipolaire, paramètre de solubilité), ainsi que certains critères de basicité (nombre donneur, déplacement chimique du proton de $CHCl_3$, basicité en phase gazeuse). Ces résultats sont comparés à ceux de quelques autres solvants usuels; ils permettent d'expliquer les propriétés de l'ODPN comme solvant pour des dosages acide–base, ainsi que l'existence de l'homoliaison-hydrogène dans ce milieu.

JEAN-CLAUDE BOLLINGER, GERMAINE YVERNAULT, THÉOPHILE YVERNAULT, and RAYMOND HOURIET.. Can. J. Chem. **62**, 361 (1984).

Physical constants (density, refractive index, viscosity, dielectric constant, dipole moment, solubility parameter) and some basicity parameters (donor number, proton chemical shift variation for $CHCl_3$, gas phase basicity) have been determined for 3,3′-oxydipropionitrile (ODPN) at 25°C. These results are compared with those for other usual solvents; they permit an explanation of its properties as a solvent for acid–base titrations, and the appearance of homohydrogen bonding in this medium.

Can. J. Chem. Downloaded from www.nrcresearchpress.com by 210.87.254.105 on 09/06/12
For personal use only.

Introduction

Plusieurs travaux récents ont montré l'intérêt du 3,3′-oxydipropionitrile $O(CH_2CH_2CN)_2$ ou ODPN, en tant que solvant pour des études électrochimiques (1–5) et d'extraction liquide–liquide (6, 7). Toutefois, on ne dispose pas actuellement d'un ensemble de valeurs précises de ses constantes physiques, mis à part certains résultats préliminaires indiqués dans la réf. 7; d'autre part, son emploi comme solvant pour des dosages acide–base, pur (5) ou en mélange avec l'eau (8), rend intéressantes les mesures que nous avons effectuées pour certains critères de basicité concernant ce produit.

Partie expérimentale

L'ODPN Fluka "purum" est déshydraté et conservé sur tamis 3 Å. Contrairement au solvant synthétisé par Persin et Gal (5), nos échantillons ne contenaient pas d'impuretés acido-basiques; leur teneur en eau, mesurée par le Karl–Fischer coulométrique, était de 50 à 80 mg L^{-1}.

Les indices de réfraction sont mesurés pour la raie D du sodium avec un réfractomètre d'Abbe, thermostaté à 25 ± 0,05°C et étalonné avec un verre d'indice n_D = 1,5166. Les mesures diélectriques sont réalisées, à la fréquence de 1 MHz, à l'aide d'un pont de capacité automatique Hewlett–Packard 4270 A, équipé d'une cellule type CS 601 Férisol thermostatée à 25 ± 0,05°C; la cellule est étalonnée à la même température avec des liquides organiques (9). Le moment dipolaire de l'ODPN, à dilution infinie dans le benzène Merck "pour spectroscopie", a été calculé selon la méthode de Guggenheim et Smith (10), à partir des résultats rassemblés dans le Tableau 1.

Pour les autres constantes physiques, on a utilisé: un densimètre SODEV 02D (11), couplé à un compteur/timer Hewlett–Packard 5308 A et à un système de mesures Hewlett–Packard 5300 B, thermostaté à 25 ± 0,01°C et étalonné par de l'azote et de l'eau; ainsi qu'un viscosimètre à capillaire (k = 15,05 × 10^{-9} m^2 s^{-2}) thermostaté à 25 ± 0,05°C.

La mesure du déplacement chimique du proton de $CHCl_3$ (spectromètre Varian EM 360) est réalisée à 60 MHz, sur une solution de 10 μL de chloroforme Merck "pour spectroscopie" dans 0,4 mL d'ODPN. Le nombre donneur selon Gutmann a été déterminé avec un ensemble microcalorimétrique LKB 8700, dans les conditions décrites par ailleurs (12); on obtient les valeurs suivantes: enthalpie de dissolution ΔH_d = (0,45 ± 0,06) × 10^3 J mol^{-1} et enthalpie de réaction ΔH_r = −(80,2 ± 0,2) × 10^3 J mol^{-1}, d'où DN = 79,75 kJ mol^{-1} ou 19,0 kcal mol^{-1}.

TABLEAU 1. Détermination du moment dipolaire de l'ODPN, à dilution infinie dans le benzène (T = 25°C)

Fraction en poids ODPN w_2	n_D	ϵ
0,00000	1,4978	2,274
0,01694	1,4971	$2,59_7$
0,03175	1,4968	$2,88_9$
0,07226	1,4948	$3,78_4$

$d\epsilon/dw_2 = 21,01_5$; $dn_D^2/dw_2 = -0,127_2$.

La basicité en phase gazeuse (GB) de l'ODPN a été déterminée par résonance cyclotronique des ions, à l'aide d'un dispositif expérimental dont les caractéristiques sont indiquées par ailleurs (13); afin de favoriser la formation d'ions ODPN.H^+, du méthane a été ajouté comme gaz réactant. Une série de mesures avec diverses bases B a été réalisée, dans les conditions suivantes: P_{CH_4} = 5 × 10^{-6} Torr, P_{ODPN} = 4 × 10^{-6} Torr, P_B = 4 × 10^{-6} Torr (env.), temps de piégeage = 100 ms. On aboutit à la séquence ci-dessous, pour laquelle on a fait réagir les divers partenaires B cités avec l'ODPN:

$$GB(Me_2O) < GB(Me_2CO) < \underline{GB(ODPN)} < GB(MeCOOMe) < GB(THF) < GB(Et_2O)$$

ce qui donne comme résultat final GB(ODPN) = 797 ± 2 kJ mol^{-1} (référence $GB(NH_3)$ = 821,7₄ kJ mol^{-1} (14)).

Le paramètre de solubilité de l'ODPN a été calculé à l'aide de son enthalpie de vaporisation, ΔH_v = 67,3 kJ mol^{-1}, calculée par nous à partir des valeurs rapportées dans la réf. 15, en utilisant la relation de Van't Hoff.

Résultats et discussion

Le Tableau 2 rassemble les résultats de nos mesures sur l'ODPN. On constate aisément que l'ODPN entre bien dans la

[1]Auteur à qui la correspondance doit être adressée.

TABLEAU 2. Propriétés physiques et basicités de l'ODPN à 25°C

Paramètre	Valeur	Paramètre	Valeur
Indice de réfraction	1,4390	Paramètre de solubilité ($MPa^{1/2}$)	23,4
Masse volumique ($g\ mL^{-1}$)	$1,04471_9$	Nombre donneur ($kJ\ mol^{-1}$)	79,75
Viscosité (10^{-3} Pa s)	$9,35_0$	Déplacement chimique du proton de $CHCl_3$ (ppm)	0,25
Constante diélectrique	66,66	Basicité en phase gazeuse ($kJ\ mol^{-1}$)	797
Moment dipolaire (D; dans C_6H_6)	4,91		

catégorie des solvants dipolaires à forte constante diélectrique; toutefois, on sait (5) que dans ce solvant les phénomènes d'association par homoliaison-hydrogène entre acide et base conjugués sont fréquents:

$$AH + A^- \rightleftarrows AHA^-; \qquad BH^+ + B \rightleftarrows BHB^+$$

ce qui le rapproche de l'acétonitrile (AN), du sulfolane (S) et du carbonate de propylène (CP) de constante diélectrique voisine; ce ne sont donc pas les seuls paramètres diélectriques qui interviennent dans cette propriété (16). Sa densité est voisine de l'unité, cependant sa viscosité élevée peut limiter son emploi.

L'enthalpie de vaporisation de l'ODPN peut être estimée à l'aide des paramètres empiriques de groupes ou de liaisons établis par Ducros et coll. (17), soit $\Delta H_v \simeq 74,9\ kJ\ mol^{-1}$ ou à partir des paramètres de Guthrie et Taylor (18), soit $72,0 \pm 1,7\ kJ\ mol^{-1}$ ou $74,9 \pm 1,7\ kJ\ mol^{-1}$. L'écart avec la valeur calculée par nous, $\Delta H_v = 67,3\ kJ\ mol^{-1}$, à partir de données de la littérature (15), est important, mais ceci peut être expliqué par la forte polarité de l'ODPN. Le paramètre de solubilité obtenu, $\delta = 23,4\ MPa^{1/2}$, est tout à fait comparable à ceux de l'acétonitrile, $\delta = 24,3\ MPa^{1/2}$, ou du propionitrile, $\delta = 22,1\ MPa^{1/2}$ (19).

Afin de caractériser ses propriétés basiques, nous avons déterminé ici trois paramètres différents: (a) le nombre donneur DN selon Gutmann (20), qui correspond à l'enthalpie de complexation avec $SbCl_5$, en solution infiniment diluée dans le dichloro-1,2 éthane:

$$ODPN_{soln} + SbCl_{5\,soln} \rightarrow ODPN.SbCl_{5\,soln} \qquad DN = -\Delta H$$

(b) la variation de déplacement chimique du proton du chloroforme, $\Delta\delta$, entre l'état libre et l'état lié par liaison-hydrogène (21):

$$ODPN + HCCl_3 \rightarrow ODPN \ldots . HCCl_3$$

$$\Delta\delta\ (ppm) = \delta_{CHCl_3\,libre} - \delta_{CHCl_3\,lié}$$

(c) la basicité en phase gazeuse GB, qui est la variation d'enthalpie libre pour la réaction de déprotonation en phase gazeuse (14):

$$ODPN.H^+_g \rightarrow ODPN_g + H^+_g \qquad GB = \Delta G°$$

Ces trois critères de basicité correspondent à des phénomènes fort différents, puisqu'ils caractérisent respectivement: (a) la molécule isolée, dispersée dans un solvant inerte; (b) le solvant en masse; (c) la molécule isolée en phase gazeuse. Ils donnent toutefois la même indication, à savoir que l'ODPN est un solvant très faiblement basique, comparable à l'éther diéthylique Et_2O; ceci permet de penser que le site basique de l'ODPN est probablement l'atome d'oxygène.

D'autre part, on observe les classements suivants, pour des solvants courants, avec les trois critères considérés ici:

$$AN < S \simeq CP < ODPN \simeq Et_2O < H_2O < HMPT \quad \text{pour DN}$$

$$ODPN < AN < Et_2O = S < HMPT \quad \text{pour } \Delta\delta$$

$$H_2O < AN < ODPN < Et_2O < HMPT \quad \text{pour GB}$$

De plus, l'ODPN se comporte également comme une base de Bronsted extrêmement faible, puisque nous n'avons pas pu le doser par $HClO_4$ dans le mélange sulfolane/benzène 98/2 p/p, qui permet pourtant des dosages de bases très faibles (22), y compris l'eau. On comprend ainsi mieux les propriétés de l'ODPN, qui permet lui-même des dosages acide/base non réalisables dans d'autres solvants, comme de différencier les acides qui sont forts dans l'eau, ou de doser des bases très faibles (urée, DMSO, HMPT) (5).

Remerciements

Les auteurs tiennent à remercier pour son amicale collaboration Mr. Michel Ducros, du Groupe de Calorimétrie et Thermochimie de l'E.N.S.T.A. (Palaiseau), chez qui JCB a effectué la détermination calorimétrique du DN, ainsi que le Professeur Jean-Yves Gal (Université de Montpellier) pour les nombreuses discussions qu'ils ont eues avec lui sur le sujet.

1. J. Y. GAL et M. PERSIN. C. R. Acad. Sci. (Paris) Sér. C, **280**, 1259 (1975).
2. J. Y. GAL et M. PERSIN. C. R. Acad. Sci. (Paris) Sér. C, **280**, 1305 (1975).
3. J. Y. GAL et M. PERSIN. C. R. Acad. Sci. (Paris) Sér. C, **283**, 37 (1976).
4. J. Y. GAL et M. PERSIN. J. Electroanal. Chem. **77**, 361 (1977).
5. M. PERSIN et J. Y. GAL. Can. J. Chem. **59**, 2491 (1981).
6. J. Y. GAL et M. PERSIN. C. R. Acad. Sci. (Paris) Sér. C, **284**, 987 (1977).
7. D. DE BARROS, J. Y. GAL, M. PERSIN et F. PERSIN. J. Electroanal. Chem. **99**, 347 (1979).
8. J. Y. GAL, M. PERSIN et B. CASTELAS. Can. J. Chem. **61**, 1189 (1983).
9. H. KIENITZ et K. N. MARSH. Pure Appl. Chem. **53**, 1847 (1981).
10. E. A. GUGGENHEIM. Trans. Faraday Soc. **45**, 714 (1949); J. W. SMITH. Trans. Faraday Soc. **46**, 394 (1950).
11. P. PICKER, E. TREMBLAY et C. JOLICOEUR. J. Solution Chem. **3**, 377 (1974).
12. J. C. BOLLINGER, G. YVERNAULT et T. YVERNAULT. Thermochim. Acta, **60**, 137 (1983).
13. R. HOURIET, H. RÜFENACHT, P. A. CARRUPT, P. VOGEL et M. TICHY. J. Am. Chem. Soc. **105**, 3417 (1983).
14. D. H. AUE et M. T. BOWERS. *Dans* Gas phase ion chemistry. Vol. 2. *Edité par* M. T. Bowers. Academic Press, New York. 1979. Chapt. 9.
15. G. CARRIERE. Chem. Techn. (Dortmund) **7**, 145 (1952).
16. I. M. KOLTHOFF. Anal. Chem. **46**, 1992 (1974).
17. M. DUCROS, J. F. GRUSON et H. SANNIER. Thermochim. Acta, **36**, 39 (1980); M. DUCROS, J. F. GRUSON, H. SANNIER et J. VELASCO. Thermochim. Acta, **44**, 131 (1981).
18. J. P. GUTHRIE et K. F. TAYLOR. Can. J. Chem. **61**, 602 (1983).
19. A. F. M. BARTON. Chem. Rev. **75**, 731 (1975).
20. V. GUTMANN. Electrochim. Acta, **21**, 661 (1976).
21. M. L. MARTIN. Ann. Phys. **7**, 35 (1962).
22. J. C. BOLLINGER, R. FAURE et T. YVERNAULT. Analusis, **10**, 270 (1982).

Can. J. Chem. Downloaded from www.nrcresearchpress.com by 210.87.254.105 on 09/06/12
For personal use only.

Additivity methods for estimating heat capacities of vaporization for organic compounds

J. PETER GUTHRIE[1] AND KATHLEEN F. TAYLOR
Department of Chemistry, University of Western Ontario, London., Ont., Canada N6A 5B7

Received July 14, 1983

J. PETER GUTHRIE and KATHLEEN F. TAYLOR. Can. J. Chem. **62**, 363 (1984).

Additivity methods permitting the estimation of heat capacities of vaporization for organic liquids have been developed, using atom, bond, and group additivity parameters. Previously it had been common to use an average value for all organic liquids, which can lead to considerable errors. For the atom level scheme, 193 compounds could be fitted using 20 parameters, with a standard deviation of 1.50 cal/deg/mol, and only 29 deviations greater than 2 cal/deg/mol. For the bond level scheme, 197 compounds could be fitted using 23 parameters, with a standard deviation of 1.47 cal/deg/mol, and only 37 deviations greater than 2 cal/deg/mol. For the group level scheme, 177 compounds could be fitted using 39 parameters, with a standard deviation of 1.05 cal/deg/mol, and only 13 deviations greater than 2 cal/deg/mol. The significant terms in the correlation matrix are given for each set of parameters.

J. PETER GUTHRIE et KATHLEEN F. TAYLOR. Can. J. Chem. **62**, 363 (1984).

On a développé des méthodes d'additivité permettant d'évaluer les capacités calorifiques de vaporisation de liquides organiques qui font appel à des paramètres d'additivité d'atomes, de liaisons et de groupes. Antérieurement, il était courant d'utiliser une valeur moyenne pour tous les liquides organiques et ceci pouvait entraîner des erreurs considérables. A l'aide du schéma au niveau des atomes, il est possible d'établir une corrélation pour 193 composés en utilisant 20 paramètres; la déviation standard est de 1,50 cal/deg/mol et il n'y avait que 29 déviations qui soient plus grandes que 2 cal/deg/mol. Au niveau des liaisons, il est possible d'établir une corrélation pour 197 composés en utilisant 23 paramètres; la déviation standard est de 1,47 cal/deg/mol et il n'y a que 37 déviations qui soient plus grandes que 2 cal/deg/mol. Au niveau des groupes, il est possible d'établir une corrélation pour 177 composés en utilisant 39 paramètres; la déviation standard est de 1,05 cal/deg/mol et il n'y a que 13 déviations qui soient plus grandes que 2 cal/deg/mol. On donne les termes importants de la matrice de corrélation pour chaque ensemble de paramètres.

[Traduit par le journal]

Can. J. Chem. Downloaded from www.nrcresearchpress.com by 210.87.254.42 on 09/06/12
For personal use only.

Introduction

In investigations of organic reaction mechanisms we have made use of free energies of formation calculated from heats of formation and various thermodynamic parameters obtained from the literature or estimated following accepted procedures. As part of this process it is frequently necessary to estimate the vapor pressure of an organic liquid at 25°C from meager vapor pressure data. In such estimations it is often not permissible to assume a constant heat of vaporization, because the heat of vaporization is well known to be a function of temperature (1). The next level of approximation is to assume a temperature independent heat capacity of vaporization. It has been suggested that the heat capacity of vaporization for any organic liquid may be taken as -12 ± 4 cal/deg/mol (2, 3). In the course of gathering data for a recent paper on estimation methods for heats of vaporization (4) we became aware that there were enough data for heat capacities of vaporization in the literature to allow an examination of this assumption. In fact it is clear that the heat capacity of vaporization does depend on structure, and can be estimated with useful precision by additivity methods at the atom, bond, or group (5) level of approximation.

It must be borne in mind that any such estimation procedure is only an interpolation technique and will decline rapidly in reliability as it is extrapolated to types of compound not used in the parameterization. This is particularly the case for polyfunctional compounds where there may well be interactions which need to be explicitly allowed for, and for which there are no parameters in the present set. Due caution is urged on anyone using the estimation procedures reported here. Despite these caveats, we feel that having estimation procedures will be of practical use in the application of thermodynamic calculations to real problems in organic chemistry. Since it is unlikely that measurements of thermodynamic properties will ever catch up to synthesis of new organic compounds, there will always be a need for estimation procedures.

[1]Author to whom correspondence may be addressed.

Results and discussion

Table 1 gives the compounds which we used, the experimental heat capacities of vaporization, and the values calculated at the atom, bond, and group levels of approximation. Data were gathered from the literature, from sources cited in Table 1, frequently in the form of heats of vaporization as a function of temperature. Such heats of vaporization were fitted by least squares (6, 7) to a straight line dependence on temperature, and the slope was taken as the heat capacity of vaporization. For a few compounds we used data for the heat capacity of the liquid, and calculated the heat capacity of vaporization by difference from the heat capacity of the gas. For the set of data in Table 1 used for the least squares fitting of parameters, the average value of ΔC_{vap} was -12.9 ± 5.7. Parameters were fitted by least squares (6, 7) using a computer program written for the purpose (8); in general, only parameters based on more than two independent compounds were determined by least squares. A number of additional parameters were calculated on the basis of 1 or 2 compounds. These values must be regarded as provisional only. In the least squares fitting, weights were calculated on the assumption of 20% errors in ΔC_{vap}, i.e. assuming constant relative error. This will be overly conservative for some data, but it is in many cases difficult or impossible to make a better estimate of the uncertainty, and the scatter in values from different laboratories is such as to inspire a certain caution.

In one case, that of ethyl bromide, the value of ΔC_{vap} calcu-

TABLE 1. Experimental and calculated heat capacities of vaporization[a]

Compound	Experimental		Calculated					
	$-\Delta C_{vap}$	Ref.	$-\Delta C_{vap}$ atom	δ	$-\Delta C_{vap}$ bond	δ	$-\Delta C_{vap}$ group	δ
(a) Aliphatic hydrocarbons								
Pentane	13.6	14	10.8	2.8	10.4	3.1	11.4	2.1
2-Methylbutane	10.9	3	10.8	0.2	10.4	0.5	10.7	0.2
Neopentane	13.7	14	10.8	3.0	10.4	3.3	8.9	4.8
n-Hexane	12.4	3	12.4	0.0	12.1	0.3	13.1	−0.7
n-Hexane	14.7	15	12.4	2.3	12.1	2.6	13.1	1.6
2-Methylpentane	11.7	3	12.4	−0.7	12.1	−0.4	12.3	−0.6
3-Methylpentane	11.4	3	12.4	−1.0	12.1	−0.7	12.3	−0.9
3-Methylpentane	14.2	15	12.4	1.8	12.1	2.1	12.3	1.9
2,3-Dimethylbutane	11.4	3	12.4	−1.0	12.1	−0.7	11.6	−0.2
2,2-Dimethylbutane	11.1	3	12.4	−1.3	12.1	−1.0	10.5	0.6
n-Heptane	14.0	3	14.1	−0.1	13.8	0.2	14.7	−0.7
n-Heptane	15.3	15	14.1	1.3	13.8	1.5	14.7	0.6
2-Methylhexane	15.5	15	14.1	1.5	13.8	1.7	14.0	1.5
3-Methylhexane	14.7	15	14.1	0.7	13.8	0.9	14.0	0.7
2,3-Dimethylpentane	13.9	15	14.1	−0.2	13.8	0.1	13.2	0.7
3,3-Dimethylpentane	13.9	14	14.1	−0.2	13.8	0.1	12.1	1.7
2,2,3-Trimethylbutane	10.7	3	14.1	−3.4	13.8	−3.1	13.8	−3.1
n-Octane	15.6	3	15.7	−0.1	15.4	0.2	16.3	−0.7
n-Octane	17.4	14	15.7	1.7	15.4	2.0	16.3	1.1
n-Octane	16.0	15	15.7	0.3	15.4	0.6	15.6	0.4
2-Methylheptane	16.0	15	15.7	0.3	15.4	0.6	15.6	0.4
4-Methylheptane	16.0	15	15.7	0.3	15.4	0.6	15.6	0.4
2,2,4-Trimethylpentane	13.9	15	15.7	−1.8	15.4	−1.5	13.0	0.9
2,3,4-Trimethylpentane	15.0	14	15.7	−0.7	15.4	−0.4	14.1	0.9
2,2,3,3-Tetramethylbutane	9.9	3	15.7	−5.8	15.4	−5.5	11.2	−1.3
n-Nonane	17.4	3	17.3	0.1	17.1	0.3	17.9	−0.5
n-Decane	19.1	3	19.0	0.1	18.7	0.4	19.5	−0.4
n-Undecane	21.0	3	20.6	0.4	20.4	0.6	21.1	−0.2
n-Dodecane	22.7	3	22.3	0.4	22.0	0.7	22.8	−0.1
n-Tridecane	24.7	3	23.9	0.8	23.7	1.0	24.4	0.3
n-Tetradecane	26.9	3	25.6	1.3	25.3	1.6	26.0	0.9
n-Pentadecane	28.8	3	27.2	1.6	27.0	1.8	27.6	1.2
n-Hexadecane	31.0	3	28.9	2.1	28.6	2.4	29.3	1.7
(b) Alicyclic hydrocarbons								
Cyclopentane	10.6	3	8.2	2.4	8.3	2.3	10.8	−0.2
Methylcyclopentane	11.8	3	9.9	1.9	9.9	1.9	11.7	0.1
Cyclohexane	11.0	3	9.9	1.1	10.2	0.9	10.9	0.1
Cyclohexane	12.7	15	9.9	2.8	10.2	2.6	10.9	1.8
Ethylcyclopentane	13.0	3	11.5	1.5	12.9	0.1	13.3	−0.3
Ethylcyclopentane	13.6	16	14.4	−0.8	12.9	0.7	13.3	0.3
1,1-Dimethylcyclopentane	12.7	3	11.5	1.2	12.9	−0.2	15.0	−2.3
cis-1,2-Dimethylcyclopentane	13.0	3	11.5	1.5	12.9	0.1	12.6	0.4
trans-1,2-Dimethylcyclopentane	13.0	3	11.5	1.5	12.9	0.1	12.6	0.4
trans-1,3-Dimethylcyclopentane	13.0	3	11.5	1.5	12.9	0.1	12.6	0.4
Methylcyclohexane	11.9	3	11.5	0.4	11.8	0.1	11.8	0.1
Methylcyclohexane	12.7	15	11.5	1.2	11.8	0.9	11.8	0.9
1-Methyl-1-ethylcyclopentane	14.6	14	16.0	−1.4	14.6	0.0	13.1	1.5
Ethylcyclohexane	12.0	3	13.2	−1.2	13.5	−1.5	13.4	−1.4
Ethylcyclohexane	14.9	16	13.2	1.8	13.5	1.4	13.4	1.5
1,2-Dimethylcyclohexane	13.0	3	13.2	−0.2	13.5	−0.5	11.0	2.0
cis-1,3-Dimethylcyclohexane	12.4	3	13.2	−0.8	13.5	−1.1	14.3	−1.9
trans-1,3-Dimethylcyclohexane	13.2	3	13.2	−0.0	13.5	−0.3	14.3	−1.1
cis-1,4-Dimethylcyclohexane	12.9	3	13.2	−0.3	13.5	−0.6	14.3	−1.4
trans-1,4-Dimethylcyclohexane	12.6	3	13.2	−0.6	13.5	−0.9	14.3	−1.7
Butylcyclopentane	17.4	16	17.6	−0.2	16.2	1.2	16.6	0.8
t-Butylcyclohexane	15.8	16	16.4	−0.6	16.8	−1.0	14.1	1.7
Propyl cyclopentane	14.7	29	16.0[f]	−1.3	14.6	0.1	15.0	−0.3
Butyl cyclopentane	16.3	29	17.7[f]	−1.4	16.2	0.1	16.6	−0.3
Decyl cyclopentane	26.7	29	27.6[f]	−0.9	26.1	0.6	26.3	0.4
Decyl cyclohexane	25.8	29	26.4[f]	−0.6	26.7	−0.9	26.4	−0.6

Can. J. Chem. Downloaded from www.nrcresearchpress.com by 210.87.254.42 on 09/06/12
For personal use only.

TABLE 1 (*Continued*)

Compound	Experimental		Calculated					
	$-\Delta C_{vap}$	Ref.	$-\Delta C_{vap}$ atom	δ	$-\Delta C_{vap}$ bond	δ	$-\Delta C_{vap}$ group	δ
(c) Unsaturated hydrocarbons								
Ethylene	4.0	[b]					4.0	−0.0
2-Methyl-1-butene	10.8	3	10.9	−0.1	10.6	0.2	10.2	0.6
3-Methyl-1-butene	8.9	3	10.9	−2.0	10.4	−1.5		
3-Methyl-2-butene	11.3	3	10.9	0.4	10.7	0.6	10.6	0.7
1-Pentene	10.9	3	10.9	0.0	10.6	0.3	10.7	0.2
cis-2-Pentene	12.0	3	10.9	1.1	8.7	3.4	11.7	0.3
trans-2-Pentene	11.7	3	10.9	0.8	8.7	3.1	11.7	−0.0
1-Hexene	12.2	3	12.6	−0.4	12.1	0.1	12.3	−0.1
2,3-Dimethyl-2-butene	11.2	3	12.6	−1.4	12.5	−1.3	11.8	−0.6
1-Heptene	13.4	3	14.2	−0.8	13.7	−0.3	13.9	−0.5
1-Octene	15.1	3	15.9	−0.8	15.4	−0.3	15.5	−0.4
1-Decene	18.3	3	19.1	−0.8	18.7	−0.4	18.7	−0.4
1-Undecene	19.9	3	20.8	−0.9	20.3	−0.4	20.4	−0.5
1-Dodecene	21.8	3	22.4	−0.6	22.0	−0.2	22.0	−0.2
1-Hexadecene	29.6	3	29.0	0.6	28.6	1.0	28.5	1.1
1,3-Butadiene	10.5	3	9.4	1.1	10.2	0.3		
1,4-Pentadiene	9.7	3	11.1	−1.4	10.4	−0.7		
2-Methyl-1,3-butadiene	11.7	3	11.1	0.6	12.0	−0.3		
2-Butyne	10.8	3	10.8	0.0				
(d) Aromatic hydrocarbons								
Benzene	12.9	3	10.3	2.6	10.7	2.2	12.2	0.7
Toluene	12.5	3	12.0	0.5	12.6	−0.1	12.9	−0.4
Ethylbenzene	13.8	3	13.6	0.2	14.0	−0.2	14.5	−0.7
p-Xylene	13.3	3	13.6	−0.3	14.5	−1.2	13.7	−0.4
p-Xylene	14.6	17	13.6	1.0	14.5	0.0	13.7	0.9
Ethylbenzene	14.7	17	13.6	1.0	10.5	4.2	14.5	0.2
1,2,3-Trimethylbenzene	14.9	3	15.3	−0.4	16.5	−1.6	14.5	0.4
1,2,4-Trimethylbenzene	14.5	3	14.5	−0.8	16.5	−2.0	14.5	0.0
1,3,5-Trimethylbenzene	14.2	3	15.3	−1.1	16.5	−2.3	14.5	−0.3
Indane	14.9	17	13.3	1.6	15.4	−0.5	14.6	0.3
Butyl benzene	15.5	29	16.9[f]	−1.4	17.6	−2.1	16.2	−0.7
(e) Oxygen compounds								
Methyl n-propyl ether	14.4	18	13.8	0.6	14.1	0.3	14.2	0.2
Methyl i-propyl ether	15.0	18	13.8	1.2	14.1	0.9	14.5	0.5
Diethyl ether	15.5	18	13.8	1.7	14.1	1.4	13.9	1.6
Diethyl ether	15.3	3	13.8	1.5	14.1	1.2	13.9	1.4
Methyl n-butyl ether	15.4	18	15.5	−0.1	15.7	−0.3	15.8	−0.4
Methyl *t*-butyl ether	15.1	18	15.5	−0.4	15.7	−0.6		
Ethyl n-propyl ether	15.9	18	15.5	0.5	15.7	0.2	15.5	0.4
Ethyl i-propyl ether	15.7	18	15.5	0.3	15.7	−0.0	15.8	−0.1
Ethyl n-butyl ether	16.5	18	17.1	−0.6	17.4	−0.9	17.2	−0.7
Di-n-propyl ether	15.9	18	17.1	−1.2	17.4	−0.3	17.8	−0.7
Di-i-propyl ether	17.1	18	17.1	0.0	17.4	−1.5	17.2	−1.3
Di-n-butyl ether	16.9	18	20.4	−3.5	20.7	−3.8	20.4	−3.5
Tetrahydrofuran	12.7	19	14.1	−1.4	15.8	−3.1	13.3	−0.6
Methanol	9.0	3	9.5	−0.5	9.2	−0.2	10.0	−1.0
Ethanol	11.3	3	11.1	0.2	10.8	0.5	11.3	−0.0
n-Propanol	13.4	3	12.8	0.7	12.5	0.9	13.0	0.4
i-Propanol	15.8	3	12.8	3.1	12.5	3.3	13.3	2.5
Acetaldehyde	7.9	[c]	9.6[f]	−1.7	9.5	−1.5	7.9	0.0
Acetone	12.2	3	11.3	1.0	11.7	0.5	12.7	−0.5
Methyl ethyl ketone	15.3	20	12.9	2.4	13.4	1.9	14.5	0.8
Diethyl ketone	16.0	28	14.6[f]	1.4	15.0	1.0	16.3	−0.3
Methyl i-propyl ketone	15.8	28	14.6[f]	1.2	15.0	0.8	15.6	0.2
Ethyl propyl ketone	17.2	28	16.2[f]	1.0	16.7	0.5	18.0	−0.8
Methyl isobutyl ketone	18.2	20	16.2	2.0	16.7	1.5	17.0	1.2
Methyl *s*-butyl ketone	17.0	20	16.2	0.8	16.7	0.3	17.2	−0.2
Methyl *t*-butyl ketone	16.3	20	16.2	0.1	16.7	−0.4		

Can. J. Chem. Downloaded from www.nrcresearchpress.com by 210.87.254.42 on 09/06/12
For personal use only.

TABLE 1 (*Continued*)

Compound	Experimental		Calculated					
	$-\Delta C_{vap}$	Ref.	$-\Delta C_{vap}$ atom	δ	$-\Delta C_{vap}$ bond	δ	$-\Delta C_{vap}$ group	δ
Formic acid	12.8	3	13.2	−0.4	12.0	0.8	13.1	−0.3
Acetic acid	13.4	3	14.9	−1.5	14.2	−0.8	13.1	0.3
Methyl formate	15.6	21	14.3	1.3	13.5	2.1	15.1	0.5
Ethyl formate	17.5	21	15.9	1.6	15.2	2.3	16.5	1.0
Methyl acetate	17.6	22	15.9	1.7	15.7	1.9	15.1	2.5
n-Propyl formate	18.1	21	17.6	0.5	16.8	1.3	18.1	0.0
Ethyl acetate	17.5	22	17.6	−0.1	17.4	0.1	16.4	1.1
Methyl propanoate	16.9	22	17.6	−0.7	17.4	−0.5	16.9	−0.0
n-Butyl formate	18.5	21	19.2	−0.7	18.5	0.0	19.7	−1.2
n-Propyl acetate	18.2	22	19.2	−1.0	19.1	−0.9	18.0	0.2
n-Propyl acetate	16.1	20	19.3	−3.1	19.1	−3.0	18.0	−1.9
i-Propyl acetate	16.4	20	19.2	−2.8	19.1	−2.7	18.3	−1.9
Ethyl propanoate	18.5	22	19.2	−0.7	19.1	−0.6	18.3	0.2
(f) Nitrogen compounds								
Methylamine	12.8	[d]	13.6[f]	−0.8	13.5	−0.6	13.5	−0.7
Dimethylamine	16.1	[d]	11.6[f]	4.5	12.0	4.1	17.2	−1.2
Trimethylamine	10.5	[d]	9.5[f]	1.0	10.5	−0.0	10.1	0.4
n-Propyl amine	18.6	23	16.9	1.7	16.8	1.8	18.2	0.4
i-Propyl amine	18.6	23	18.5	0.9	16.8	1.8	16.4	2.2
Methyl i-propyl amine	19.0	24	14.9	4.2	14.3	4.7	14.8	4.2
Diethyl amine	17.8	23	14.9	2.9	15.3	2.5	14.9	2.9
n-Butyl amine	19.4	23	18.5	0.9	18.4	1.0	18.2	1.2
i-Butyl amine	17.9	23	18.5	−0.6	18.4	−0.5	17.5	0.4
s-Butyl amine	17.7	23	18.5	−0.8	18.4	−0.7	18.0	−0.3
Ethyl i-propyl amine	17.0	24	16.5	0.5	17.0	0.0	16.3	0.7
Triethyl amine	13.9	23	14.5	2.9	15.5	−1.6	14.6	−0.7
n-Propyl i-propyl amine	16.7	24	18.1	−1.4	18.6	−1.9	17.9	−1.2
Di-i-propyl amine	17.4	24	18.1	−0.7	18.6	−1.2	17.7	−0.3
Ethyl n-butyl amine	17.5	24	18.1	−0.6	18.0	−0.5	18.1	−0.6
c-Hexyl amine	16.2	23	19.3	−3.1	19.6	−3.4	17.9	−1.7
n-Butyl i-propyl amine	17.7	24	19.8	−2.1	20.3	−2.6	19.6	−1.9
Aniline	20.1	3	19.8	0.3				
4-Methylpyridine	14.6	19	14.6[g]	0.0				
Acrylonitrile	11.6	3	11.6[g]	0.0				
Nitromethane	11.6	3	11.6[g]	0.0				
(g) Sulfur compounds								
Dimethyl sulfide	10.5	3	9.2	1.3	9.8	0.7	10.6	−0.1
Methyl ethyl sulfide	11.8	3	10.9	0.9	11.4	0.4	11.9	−0.1
Methyl propyl sulfide	12.8	3	12.5	0.3	13.1	−0.3	13.5	−0.7
Methyl i-propyl sulfide	12.4	3	12.5	−0.1	13.1	−0.7	12.5	−0.1
Diethyl sulfide	12.8	3	12.5	0.3	13.1	−0.3	13.2	−0.4
Methyl *t*-butyl sulfide	13.4	29	14.2[f]	−0.8	14.7	−1.3	13.1	0.3
Methyl butyl sulfide	14.2	3	14.2	0.0	14.7	−0.5	15.1	−0.9
Ethyl propyl sulfide	14.0	3	14.2	−0.2	14.7	−0.7	13.5	0.5
Dipropyl sulfide	15.3	3	15.8	−0.5	16.4	−1.1	15.1	0.2
Dibutyl sulfide	18.3	3	16.6	1.7	19.7	−1.4	16.3	2.0
Thiacyclopentane	12.6	3	12.8	−0.2	12.3	0.3	12.5	0.1
Thiacyclohexane	13.0	3	14.2	−1.2	12.8	0.2	12.6	0.4
Dimethyl disulfide	12.3	3	12.6	−0.3	12.0	0.3	12.3	0.0
Diethyl disulfide	14.8	3	15.9	−1.1	15.3	−0.5	14.8	−0.0
Methanethiol	9.6	29	7.8[f]	1.8	8.1	1.5	8.9	0.7
Ethanethiol	10.8	3	9.5	1.3	9.7	1.1	10.2	0.6
2-Propanethiol	11.6	3	11.1	0.5	11.4	0.2	10.8	0.8
Butanethiol	12.5	29	12.8[f]	−0.3	13.0	−0.5	13.4	−0.9
Butanethiol	12.9	3	12.8	0.1	13.0	−0.1	13.4	−0.5
2-Butanethiol	11.3	3	12.8	−1.5	13.0	−1.7	12.4	−1.1
2-Butanethiol	13.7	29	12.8[f]	0.9	12.8	−0.9	13.0	−0.7
Isobutanethiol	12.7	3	12.8	−0.1	13.0	−0.3	12.7	−0.0
t-Butanethiol	12.8	3	12.8	0.0	13.0	−0.2		
Pentanethiol	14.3	3	14.4	−0.1	14.7	−0.4	15.0	−0.7

Can. J. Chem. Downloaded from www.nrcresearchpress.com by 210.87.254.42 on 09/06/12
For personal use only.

TABLE 1 (*Concluded*)

Compound	Experimental $-\Delta C_{vap}$	Ref.	Calculated $-\Delta C_{vap}$ atom	δ	$-\Delta C_{vap}$ bond	δ	$-\Delta C_{vap}$ group	δ
2-Methyl-1-butanethiol	14.7	19	14.4	0.3	14.7	0.0	14.3	0.4
Cyclopentanethiol	13.6	3	14.7	−1.1	12.5	1.1	13.4	0.2
Cyclohexanethiol	13.9	19	13.5	0.4	14.4	−0.5	13.5	0.4
Thiophenol	13.9	3	14.0	−0.1				
(h) Halogen compounds								
Dichloromethane	12.4	25	8.6	3.8	8.9	3.5		
Chloroform	12.7	25	10.8	1.9	11.5	1.2		
Chloroform	11.9	3	10.8	1.1	11.5	0.4		
Carbon tetrachloride	11.4	3	13.1	−1.7	14.0	−2.6		
Carbon tetrachloride	12.1	25	13.1	−1.0	14.0	−1.9		
1,2-Dichloroethane	13.1	25	10.3	2.8	10.6	2.5	13.2	−0.1
1,1,1-Trichloroethane	13.2	25	12.5	0.7	13.1	0.1		
1,1,1-Trichloroethane	12.0	3	12.5	−0.5	13.1	−1.1		
1,1,2-Trichloroethane	14.4	25	12.5	1.9	13.1	1.3	14.2	0.2
1,1,2,2-Tetrachloroethane	15.0	25	14.7	0.3	15.6	−0.6	15.1	−0.1
Butyl chloride	14.1	26	10.1[f]	4.0	11.3	2.8	12.5	1.6
s-Butyl chloride	13.2	26	10.1[f]	3.1	11.3	1.9	14.1	−0.9
Pentyl chloride	14.7	26	13.0[f]	1.7	13.0	1.7	14.7	−0.0
2-Pentyl chloride	14.7	26	13.0[f]	1.7	13.0	1.7	15.8	−1.1
i-Pentyl chloride	13.6	26	13.0[f]	0.6	13.0	0.6	13.4	0.2
Hexyl chloride	15.9	26	14.6[f]	1.3	14.6	1.3	15.7	0.2
1,2-Dibromoethane	14.0	3	13.5	0.5	13.8	0.2	13.7	0.3
1,1-Dichloroethylene	10.5	3	10.4	0.1				
1,1,2-Trichloroethylene	12.0	25	12.6	−0.6	11.1	0.9		
Tetrachloroethylene	12.3	25	14.9	−2.6	13.0	−0.7		
Ethyl bromide	8.8	[e]	9.7[f]	0.9	9.6	−0.8	10.2	−1.3
Propyl bromide	14.6	9	11.3	3.3	11.3	3.3	11.8	2.8
Isopropyl bromide	13.6	9	11.3	2.3	11.3	2.3		
Butyl bromide	14.6	9	12.9	1.7	12.9	1.7	13.4	1.2
i-Butyl bromide	12.0	9	12.9	−0.9	12.9	−0.9	12.7	−0.7
Allyl bromide	13.8	9	11.4	2.4	11.2	2.6		
1,2-Dibromotetrafluoroethane	14.7	27	15.4	−0.7	14.9	−0.2		
1-Bromo-2-chloro-1,1,2-trifluoroethane	14.6	27	13.3	1.3	13.0	1.6		
1-Chloro-1,2-dibromo-1,1,2-trifluoroethane	13.5	27	17.1	−3.6	17.2	−3.7		
Fluorobenzene	12.4	3	10.8	1.6				
Chlorobenzene	11.3	3	12.6	−1.3				
Bromobenzene	12.9	3	14.2	−1.3				
Hexafluorobenzene	18.0	19	13.1[f]	4.9				
(i) Miscellaneous compounds								
Tetramethylsilane	16.3	3	16.3[g]	0.0				
Oxetane	12.4	19	12.4[f,g]	0.0				
Thiophene	11.3	29	11.2[f]	0.1				
2-Methylthiophene	12.1	29	12.8[f]	−0.7				
3-Methylthiophene	13.3	29	12.8[f]	0.5				
Anisole	16.0	28	16.7[f]	−0.7				

[a] C_{vap} is evaluated at 25°C; with adequately precise data we expect that C_{vap} will itself be a function of temperature.

[b] A synthetic value for ethylene had to be used to obtain convergence; the value used was taken as twice the value for $[C_dH_2]$ generated by the least squares program in a run which showed severe problems attributed to covariance among the parameters involving olefinic carbon. The synthetic value was assigned a large error to ensure it had low statistical weight.

[c] This value was obtained by using a heat capacity of the liquid calculated from data in ref. 31 and $C_p(g)$ from ref. 11.

[d] These values were obtained using heat capacity data for the liquids at various temperatures (30) fitted to linear equations by least squares to allow extrapolation to 25°C, and $C_p(g)$ from ref. 11.

[e] This value was obtained using a heat capacity for the liquid from ref. 10 and $C_p(g)$ from ref. 11.

[f] Not included in the least squares fit.

[g] Unique parameter.

lated from the temperature dependence of ΔH_{vap} (9) was seriously out of line with the trend for similar compounds; the value obtained for ethyl bromide was −18.1 cal/deg/mol (data from ref. 9) while the value for n-propyl bromide was −14.6 cal/deg/mol (data from ref. 9). A value based on $C_p(l)$ (10) and $C_p(g)$ (11) was in better agreement with expectation; this value was −8.8 cal/deg/mol.

The atom level parameters were the first to be determined; this was done using batch mode computations, where a deck of data cards was submitted for each run. This procedure was

Can. J. Chem. Downloaded from www.nrcresearchpress.com by 210.87.254.42 on 09/06/12
For personal use only.

TABLE 2. Atom level parameters for estimating heat capacities of vaporization

No.	Atom	Parameter	Error	Correlation matrix elements
Parameters determined by least squares[a]				
[1]	C_{te}	0.87	0.23	[2], −0.99; [3], 0.9
[2]	H_C	−1.26	0.11	[3], −0.9
[3]	C_{tr}	−0.46	0.12	
[4]	C_{di}	−2.49	0.47	
[5]	O	−4.69	0.38	[7], −0.6
[6]	CO	−5.44	0.50	
[7]	H_O	−1.86	0.43	
[8]	N_{te}	−0.80	1.16	[9], −0.9
[9]	H_N	−4.94	0.77	
[10]	N_{tr}	−4.37	0.43	
[11]	N_{di}	−4.40	0.47	
[12]	NO_2	−8.69	0.47	
[13]	S	−3.41	0.30	[14], −0.5
[14]	H_S	−1.51	0.42	
[15]	F	−1.73	0.30	[17], −0.5
[16]	Cl	−3.48	0.13	
[17]	Br	−5.09	0.39	
[18]	Si	−4.68	0.41	
[19]	5-Ring[b]	−2.81	0.48	
[20]	6-Ring[b]	0.03	0.50	
Parameters determined by few compounds				
[21]	4-Ring[b]	−2.8		
[22]	S_{tr}	−4.3		

[a]C means tetrahedral carbon; C_{tr} is trigonal carbon in an alkene or aromatic ring; C_{di} is acetyleneic (digonal) carbon; CO is treated as a divalent atom; N is amine nitrogen; N_{tr} is planar trigonal nitrogen in an aromatic ring; N_{di} is nitrogen of a nitrile, bonded to a C_{di}; the nitro group is treated as a monovalent atom; S is sulfur of a thiol, sulfide, or disulfide; S_{tr} is sulfur of an aromatic heterocycle; H_C is hydrogen attached to carbon; H_O, H_N, and H_S are hydrogens attached to the indicated heteroatom, and include any hydrogen bonding contribution.

[b]Correction for a flexible ring.

TABLE 3. Bond level parameters for estimating heat capacities of vaporization

No.	Bond	Parameter	Error	Correlation matrix
Parameters determined by least squares[a]				
[1]	C—C	0.26	0.24	[2], −0.99; [3], 0.8; [7], 0.5; [8], 0.6; [10], 0.6; [13], 0.7; [15], 0.7; [22], −0.6; [23], −0.7
[2]	C—H	−0.96	0.10	[3], −0.8; [7], −0.5; [8], −0.6; [10], −0.6; [13], −0.7; [15], −0.7; [22], 0.5; [23], 0.6
[3]	C—C_d	−0.26	0.39	[4], −0.7; [8], 0.5; [10], 0.5; [13], 0.5; [15], 0.5; [23], −0.5
[4]	C_d—H	−1.32	0.18	[5], −0.7
[5]	C_d—C_d	−2.29	1.34	
[6]	C_B—H	−1.78	0.16	
[7]	C_B—C	−0.84	0.32	
[8]	C—O	−2.50	0.34	[15], 0.5
[9]	O—H	−3.80	0.56	
[10]	C—CO	−2.97	0.40	[15], 0.5
[11]	O—CO	−4.52	0.69	
[12]	H—CO	−3.63	0.74	
[13]	C—N	−0.63	0.40	[14], −0.5; [15], 0.5
[14]	N—H	−4.98	0.43	
[15]	C—S	−2.01	0.33	[16], −0.5
[16]	S—H	−3.17	0.52	
[17]	S—S	−2.19	1.27	
[18]	C—F	−1.24	0.37	
[19]	C—Cl	−3.50	0.15	
[20]	C_d—Cl	−3.26	0.30	
[21]	C—Br	−5.10	0.49	
[22]	5-Ring[b]	−1.35	0.64	[23], 0.5
[23]	6-Ring[b]	−0.23	0.62	
Parameters determined by one or two compounds				
[24]	C—C_t	−2.5		
[25]	C_B—O	−1.7		
[26]	C_d—CN	−7.6		
[27]	C_B—N	3.7		
[28]	C—NO_2	−8.7		
[29]	C_B—S	−1.8		
[30]	C_B—F	−3.1		
[31]	C_B—Cl	−2.4		
[32]	C_B—Br	−4.0		
[33]	C—Si	−1.2		
[34]	4-Ring[b]	−1.6		

[a]C means tetrahedral carbon; C_d means doubly bonded (olefinic) carbon; C_B means aromatic carbon; C_t means triply bonded (acetylenic) carbon; CO is treated as a divalent atom; CN and NO_2 are treated as univalent atoms.

[b]Correction for flexible ring.

tedious, and altering the data set was a time consuming operation. For the bond and group schemes we entered the data using the SIR database management system on the Cyber 170/835 at the University of Western Ontario Computing Center, and used this system to handle corrections to the database and in preparation of a data file for the least squares program. Actual data entry was done using a Xitan microcomputer, and the data file was then transmitted to the Cyber for processing. The last few compounds for which values were found were not included in the atomic parameter calculations because it seemed unlikely that any significant change would result; manual calculation showed that the deviations were in the usual range.

Table 2 gives the atom level parameters which were evaluated by least squares fitting; Table 3 gives the bond level parameters and Table 4 gives the group level parameters. For the bond and group parameters we have followed Hine's notation (12) rather than Benson's (13). In all three tables we have included the significant (absolute value greater than 0.5) elements of the correlation matrix (4). This matrix is diagonal, so that only half the terms need be listed, and is sparse, with most terms being negligibly small.

For the compounds used in the atom parameterization we were able to fit 193 compounds using 20 parameters with a standard deviation of 1.50. Only 29 compounds gave deviations of more than 2 cal/deg/mol, and only 12 gave deviations of more than 3 cal/deg/mol. With the bond parameterization, we were able to fit 197 compounds using 23 parameters with a standard deviation of 1.47. Only 37 compounds gave deviations of more than 2 cal/deg/mol, and only 17 gave deviations of more than 3 cal/deg/mol. In this case the bond level scheme uses only slightly more parameters than the atom level scheme and is, if anything, poorer at representing the data. With a richer data set we would expect to see more bond level parameters required, and an improvement in estimation power relative to the atom level scheme. With the group parameterization scheme, we were able to fit 177 compounds using 39 parameters and a standard deviation of 1.05. Only 13 compounds gave deviations of more than 2 cal/deg/mol, and only 4 gave deviations of more than 3 cal/deg/mol. As is usually

Can. J. Chem. Downloaded from www.nrcresearchpress.com by 210.87.254.42 on 09/06/12
For personal use only.

TABLE 4. Group level parameters for estimating the heat capacity of vaporization

No.	Group	Parameter	Error	Correlation matrix
Parameters determined by least squares[a]				
[1]	$CH_3(X)$	−3.30	0.17	[2], −0.7; [3], −0.9; [4], −0.9; [8], −0.7; [10], −0.5; [27], −0.5; [28], −0.5; [38], 0.6; [39], 0.7
[2]	$CH_2(C)_2$	−1.62	0.06	[3], 0.5; [4], 0.6; [8], 0.5; [38], −0.7; [39], −0.7
[3]	$CH(C)_3$	0.78	0.34	[4], 0.8; [8], 0.6; [10], 0.5; [38], −0.7; [39], −0.7
[4]	$C(C)_4$	4.28	0.63	[8], 0.6; [10], 0.5; [38], −0.6; [39], 0.6
[5]	$CH_2(C)(C_d)$	−2.31	0.85	[6], −0.8; [7], −0.6
[6]	$C_dH(C)$	−1.43	0.61	
[7]	C_dH_2	−2.01	0.42	
[8]	$C_d(C)_2$	0.69	0.54	
[9]	C_BH	−2.03	0.13	[10], −0.6
[10]	$C_B(C)$	0.50	0.33	
[11]	$CH_2(C)(C_B)$	−1.56	0.62	
[12]	$O(C)_2$	−4.60	1.09	[13], 0.5; [14], −0.9; [15], −0.6
[13]	OH(C)	−6.68	0.63	
[14]	$CH_2(C)(O)$	−1.36	0.57	[15], 0.6; [26], −0.5
[15]	$CH(C)_2(O)$	0.01	0.78	
[16]	$CO(C)_2$	−6.07	0.93	[17], −0.7
[17]	$CH_2(C)(CO)$	−1.84	0.64	[22], 0.5
[18]	O(C)(CO)	−7.18	1.06	[19], −0.8; [20], −0.6; [21], 0.6
[19]	CO(O)(C)	−1.29	1.14	[20], 0.7; [21], −0.7
[20]	HCO(X)	−4.63	0.72	[21], −0.6
[21]	OH(CO)	−8.48	1.16	
[22]	$CH(C)_2(CO)$	0.34	1.35	
[23]	$CH(C)_2(N)$	0.39	0.62	
[24]	$NH(C)_2$	−5.32	0.64	
[25]	$CH_2(C)(N)$	−1.50	0.37	
[26]	$NH_2(C)$	−10.20	0.63	
[27]	$N(C)_3$	−0.23	0.96	
[28]	$S(C)_2$	−4.04	0.67	[29], −0.7; [30], 0.6
[29]	$CH_2(S)(C)$	−1.26	0.41	[30], −0.6; [31], 0.5
[30]	SH(C)	−5.63	0.52	[31], −0.6
[31]	$CH(C)_2(S)$	1.42	0.71	
[32]	S(C)(S)	−2.85	0.49	
[33]	$C(C)_3(S)$	4.15	0.99	
[34]	$CH_2Cl(C)$	−6.59	0.49	
[35]	$CHCl_2(C)$	−7.57	0.59	
[36]	$CHCl(C)_2$	−5.93	0.58	
[37]	$CH_2Br(C)$	−6.87	0.40	
[38]	5-Ring[b]	−2.74	0.50	[39], 0.7
[39]	6-Ring[b]	−1.18	0.57	[8], −0.5
Parameters determined by one or two compounds				
[40]	$C_dH(C_d)$	−3.2		
[41]	$CH_2(C_d)_2$	−2.8		
[42]	$C_d(C)(C_d)$	−1.1		
[43]	$C_t(C)$	−2.1		
[44]	$C(C)_3(O)$	2.7		
[45]	$C(C)_3(CO)$	3.0		
[46]	$C_B(O)$ + $O(C)(C_B)$	−2.6		
[47]	$C_B(N)$[c]	0.3		
[48]	$N_B(C_B)_2$	−3.7		
[49]	C_dHCN	−9.6		
[50]	$C(C)_3(S)$	2.7		
[51]	$C_B(S)$[d]	1.9		
[52]	$S_B(C_B)_2$	−3.6	0.7	
[53]	C_BF	−2.9	0.3	
[54]	$CCl_3(C)$	−9.9		
[55]	C_dCl_2	−6.9	1.4	

Can. J. Chem. Downloaded from www.nrcresearchpress.com by 210.87.254.42 on 09/06/12
For personal use only.

TABLE 4 (*Concluded*)

No.	Group	Parameter	Error	Correlation matrix
[56]	C_dHCl	−5.1		
[57]	C_BCl	−1.2		
[58]	C_BBr	−2.8		
[59]	$CHBr(C)_2$	−7.0		
[60]	$CH_2Br(C_d)$	−10.4		
[61]	CF_2Br	−7.4		
[62]	CHFCl	−7.3		
[63]	CFClBr	−6.2		
[64]	$Si(C)_4$	−3.1		
[65]	4-Ring[b]	−4.8		

[a]C means tetrahedral carbon; C_d means doubly bonded (olefinic) carbon; C_B means aromatic carbon; C_t means triply bonded (acetylenic) carbon; CO is treated as a divalent atom; CN and NO_2 are treated as univalent atoms; N_B means aromatic nitrogen of a heterocycle; S_B means aromatic sulfur of a heterocycle.
[b]Correction for flexible ring.
[c]Calculated assuming $[NH_2(C_B)] = [NH_2(C)]$.
[d]Calculated assuming $[SH(C_B)] = [SH(C)]$.

found (5), the group level scheme gives much better estimates at the price of a much larger parameter set.

A possibly fairer comparison of the three schemes is to take 177 compounds which can be handled by all three, and calculate the rms error for estimation by each scheme. The results were: atom, 1.42; bond, 1.45; group, 1.05. The numbers of serious deviations were: atom, 25 greater than 2, 12 greater than 3; bond, 28 greater than 2, 13 greater than 3; group, 13 greater than 2, 4 greater than 3.

In the atomic parameterization scheme we used C_{tr} and N_{tr} to represent both simple doubly bonded atoms and members of aromatic rings; it was not necessary to make any further correction for the rigid aromatic ring, although corrections were necessary for the presence of flexible rings. In the bond parameterization scheme, we were not able to include pyridines and thiophenes because this would require redefining the scheme to include C⋯C, C⋯N, and C⋯S bonds explicitly. The scheme which we used incorporated the aromatic C⋯C bonds in the C_B atoms so that one endocyclic bond was implicitly included in each explicitly defined exocyclic bond. Our experience with the parameterization of ΔH_{vap} (4) led to the expectation that there would be severe covariance problems if one used the more elaborate scheme, and there seemed little hope of including a realistic value for naphthalene, which was the key to obtaining convergence in the case of ΔH_{vap} (4). In the group parameterization scheme, we were able to include parameters for $N_B(C_B)_2$ and $S_B(C_B)_2$, representing the aromatic N and S atoms bonded to two aromatic C atoms, with these parameters incorporating all of the effects of the heteroatoms, so that the remaining C atoms in the rings were all represented by $C_B(X)$ with no distinction being made as to what atoms of the ring a C in the ring was bonded to. This is clearly not the proper way to set up the parameters, but the data set is too small at present to allow anything more realistic.

The clear conclusion is that at present there is no advantage to using a bond level scheme, and the group level scheme is better but not dramatically so. In a practical sense this is very convenient, because it means that a useful estimate of ΔC_{vap} can be made using a small set of atomic level parameters.

We also feel that the evidence is now conclusive that ΔC_{vap} is *not* a constant for all organic liquids, but should be measured or estimated for the particular compound of interest.

That ΔC_{vap} can be estimated from structural parameters has been implicit in the literature for some years. By definition, $\Delta C_{vap} = C_p(g) - C_p(l)$. Benson has shown (5, 13) that $C_p(g)$ can be estimated at various temperatures by his additivity procedures. Shaw (3) reported a scheme for $C_p(l)$ of organic liquids at 25°C and Benson and Luria (32) have reported an

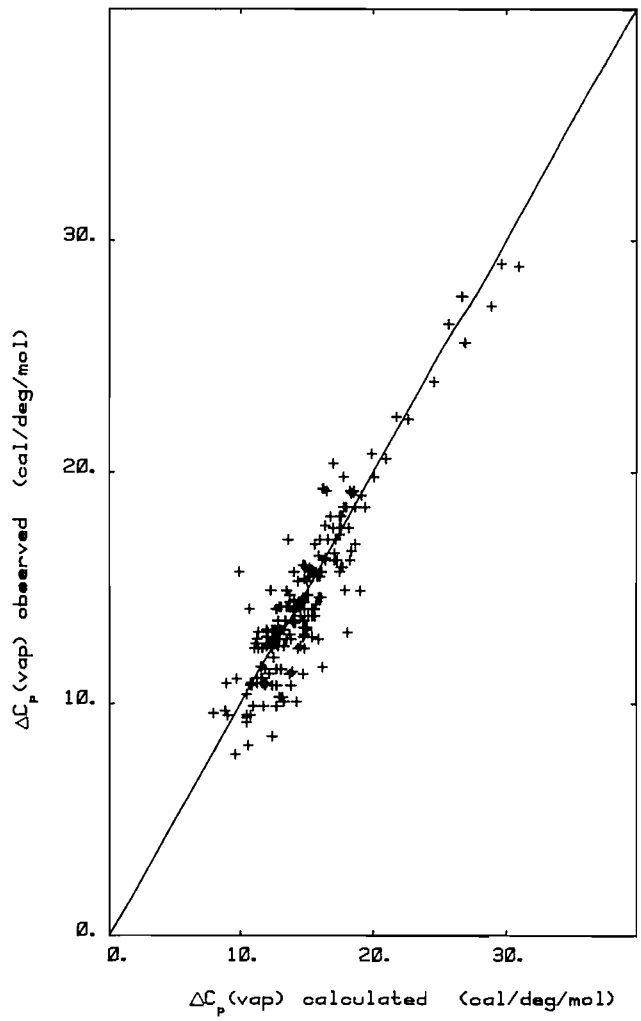

FIG. 1. Calculated vs. experimental values for the heat capacity of vaporization using atomic level parameters; data from Table 1.

Can. J. Chem. Downloaded from www.nrcresearchpress.com by 210.87.254.42 on 09/06/12
For personal use only.

Can. J. Chem. Downloaded from www.nrcresearchpress.com by 210.87.254.42 on 09/06/12
For personal use only.

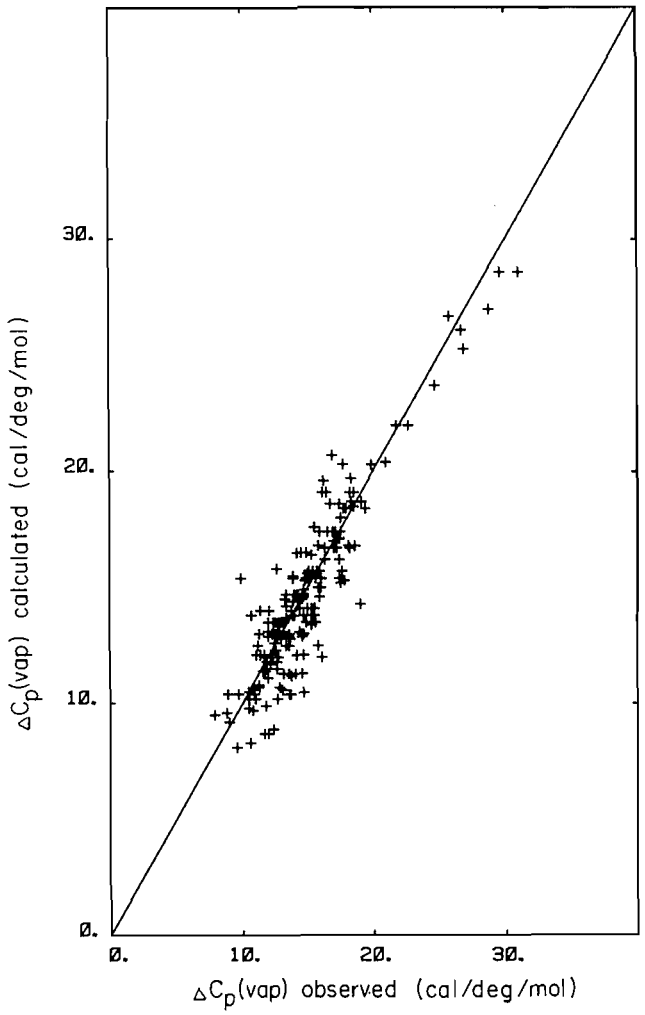

FIG. 2. Calculated vs. experimental values for the heat capacity of vaporization using bond level parameters; data from Table 1.

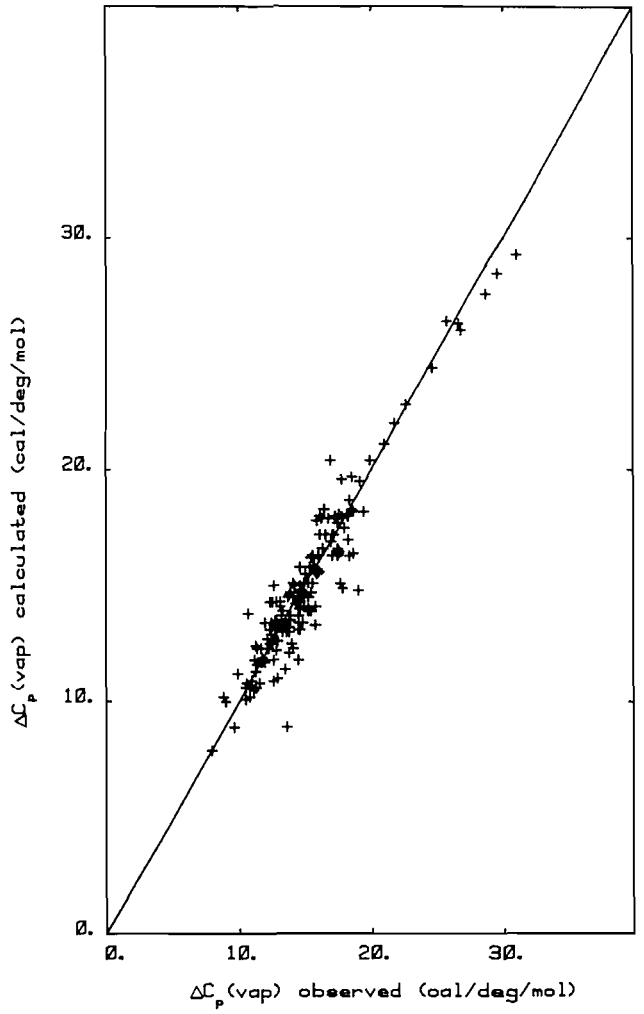

FIG. 3. Calculated vs. experimental values for the heat capacity of vaporization using group level parameters; data from Table 1.

additivity scheme for liquid hydrocarbons permitting the calculation of $C_p(l)$ as a function of temperature. Obviously ΔC_{vap} should also be a function of temperature, but at present the data permitting such a parameterization for a wide range of organic compounds simply do not exist.

The quality of the overall fit and the range of the available data are shown by Figs. 1, 2, and 3. Although it is clear that the data for heat capacity of vaporization values do not span as wide a range as would be desired for testing an estimation procedure, it is also clear that we can do much better by such procedures than by assuming a structure independent average value.

Acknowledgments

We thank the Natural Sciences and Engineering Research Council of Canada for financial support of this work.

1. K. DENBIGH. The principles of chemical equilibrium. 2nd ed. Cambridge University Press, Cambridge. 1966. p. 200.
2. S. W. BENSON and G. D. MENDENHALL. J. Am. Chem. Soc. **98**, 2046 (1976).
3. R. SHAW. J. Chem. Eng. Data. **14**, 461 (1969).
4. J. P. GUTHRIE and K. F. TAYLOR. Can. J. Chem. **61**, 602 (1983).
5. S. W. BENSON and J. H. BUSS. J. Chem. Phys. **29**, 546 (1958).
6. W. E. DEMING. Statistical adjustment of data. Dover, New York. 1964.
7. P. R. BEVINGTON. Data reduction and error analysis for the physical sciences. McGraw–Hill, New York. 1969.
8. J. P. GUTHRIE. Can. J. Chem. **55**, 3700 (1977).
9. V. SVOBODA, V. MAJER, F. VESELY, and J. PICK. Collect. Czech. Chem. Commun. **42**, 1755 (1977).
10. V. YA. KURBATOV. Zh. Obshch. Khim. **18**, 372 (1948); Chem. Abstr. **43**, 30a (1949).
11. D. F. STULL, E. F. WESTRUM, JR., and G. C. SINKE. The chemical thermodynamics of organic compounds. Wiley, New York. 1967.
12. J. HINE and P. K. MOOKERJEE. J. Org. Chem. **40**, 292 (1975).
13. S. W. BENSON. Thermochemical kinetics. 2nd ed. Wiley, New York. 1976.
14. I. A. HOSSENLOPP and D. W. SCOTT. J. Chem. Thermodyn. **13**, 415 (1981).
15. V. MAJER, V. SVOBODA, S. HALA, and J. PICK. Collect. Czech. Chem. Commun. **44**, 637 (1979).
16. V. SVOBODA, V. CHARVATOVA, V. MAJER, and J. PICK. Collect. Czech. Chem. Commun. **46**, 2983 (1981).
17. I. A. HOSSENLOPP and D. W. SCOTT. J. Chem. Thermodyn. **13**, 423 (1981).
18. V. MAJER, Z. WAGNER, V. SVOBODA, and V. CADEK. J. Chem. Thermodyn. **12**, 387 (1980).
19. I. A. HOSSENLOPP and D. W. SCOTT. J. Chem. Thermodyn. **13**, 405 (1981).
20. G. GEISELER, K. QUITZSCH, H. P. HOFMANN, and R. PFESTORF. Z. Phys. Chem. **252**, 170 (1972).
21. J. CIHLAR, V. HYNEK, V. SVOBODA, and R. HOLUB. Collect.

Czech. Chem. Commun. 41, 1 (1976).
22. V. SVOBODA, F. VESELY, R. HOLUB, and J. PICK. Collect. Czech. Chem. Commun. **42**, 943 (1977).
23. V. MAJER, V. SVOBODA, J. KOUBEK, and J. PICK. Collect. Czech. Chem. Commun. **44**, 3521 (1979).
24. L. PETROS, V. MAJER, J. KOUBEK, V. SVOBODA, and J. PICK. Collect. Czech. Chem. Commun. **44**, 3533 (1979).
25. V. MAJER, L. SVAB, and V. SVOBODA. J. Chem. Thermodyn. **12**, 843 (1980).
26. V. TEKAC, V. MAJER, V. SVOBODA, and V. HYNEK. J. Chem. Thermodyn. **13**, 659 (1981).
27. V. MAJER, V. SVOBODA, A. POSTA, and J. PICK. Collect. Czech. Chem. Commun. **46**, 817 (1981).
28. J. L. HALES, E. B. LEES, and D. J. RUXTON. Trans. Faraday Soc. **63**, 1876 (1967).
29. American Petroleum Institute Research Project 44. Selected values of properties of hydrocarbons and related compounds. Texas A and M University, College Station, TX 1973.
30. J. TIMMERMANS. Physico-chemical constants of pure organic compounds. Elsevier, New York. 1950.
31. D. LEB. COOPER. Proc. N.S. Inst. Sci. **17**, 82 (1927).
32. M. LURIA and S. W. BENSON. J. Chem. Eng. Data. **22**, 90 (1977).

Can. J. Chem. Downloaded from www.nrcresearchpress.com by 210.87.254.42 on 09/06/12
For personal use only.

Dipole oscillator strength distributions and properties for methanol, ethanol, and *n*-propanol

B. L. JHANWAR[1] AND WILLIAM J. MEATH[2]

Department of Chemistry, University of Western Ontario, London, Ont., Canada N6A 3K7

Received March 1, 1983[3]

B. L. JHANWAR and WILLIAM J. MEATH. Can. J. Chem. **62**, 373 (1984).

Dipole oscillator strength distributions (DOSDs) have been constructed for ground state methanol, ethanol, and *n*-propanol and used to evaluate integrated ("band") oscillator strengths and the dipole oscillator strength sums S_k and L_k (for a variety of k values) for these molecules. Each DOSD is constructed by using available experimental and theoretical photoabsorption cross sections and by constraining the resulting dipole oscillator strength data to satisfy the Thomas–Reiche–Kuhn sum rule and molar refractivity constraints. The discussion includes an analysis of the reliability of the results.

B. L. JHANWAR et WILLIAM J. MEATH. Can. J. Chem. **62**, 373 (1984).

On a évalué les distributions de force d'un oscillateur dipolaire (DFOD) pour l'état fondamental du méthanol, de l'éthanol et du *n*-propanol et on les a utilisées pour évaluer les forces d'un oscillateur intégré ("bande") et les sommes S_k et L_k, des forces d'un oscillateur dipolaire S_k et L_k (pour diverses valeurs k), de ces molécules. On a construit chaque DFOD en utilisant les sections droites de photoabsorption expérimentales et théoriques disponibles et en restreignant les données relatives à la force de l'oscillateur dipolaire de façon à satisfaire à la règle d'additivité de Thomas–Reiche–Kuhn et les contraintes de réfractivité molaire. La discussion comporte une analyse de la fiabilité des résultats.

[Traduit par le journal]

1. Introduction

The purpose of this paper is to present reliable results for many of the dipole properties of the methanol, ethanol, and *n*-propanol molecules. The results are obtained through the construction of globally reliable dipole oscillator strength distributions (DOSDs) for the molecules. The properties considered explicitly are the dipole oscillator strength sums S_k, $k = -10(1)2$, the logarithmic oscillator strength sums L_k, $k = -2(1)2$, and the molar refractivities R_λ for wavelengths λ associated with the visible and ultraviolet region of the spectrum.

The approach (Section 2) used to evaluate the properties is based on the relationship (1–11) between the dipole properties and the DOSDs and upon the construction of the DOSDs by using a quantum mechanical constraint procedure (9) and a given dipole oscillator strength (DOS) input data base. The initial DOSDs, and properties, obtained from the original experimental and theoretical DOS input are unreliable due to errors inherent in the original DOS data. In order to provide reliable results, the initial DOSDs are modified to satisfy the Thomas–Reiche–Kuhn sum rule (1, 12) and two other constraints provided by values of the molar refractivity of the relevant dilute gas. A variety of refractivity and experimental and/or mixture rule DOS sources are used for the evaluation of the dipole properties of the alcohols and results are also presented for various integrated ("band") oscillator strengths evaluated from the constructed DOSDs (Section 3). Experimental refractive index data are used to provide constraints for methanol whereas, because of a lack of experimental data, those for ethanol and *n*-propanol are generated by additivity relations. The discussion (Sections 3 and 4) contains an assessment of the reliability of the results for the dipole properties, with particular emphasis on errors arising from the lack of accurate experimental refractivity constraints, and a summary of the relevance of the results and the method by which they are obtained.

[1]On leave from the Department of Physics, Meerut University, Meerut, India.

[2]Associated with the Centre for Interdisciplinary Studies in Chemical Physics, University of Western Ontario, London, Ontario.

[3]Revision received September 6, 1983.

2. Construction of the dipole oscillator strength distributions (DOSDs)

Many important dipole properties (1–5) of molecules can be determined from DOSDs by evaluating dipole oscillator strength sums S_k and L_k defined by

$$[1] \quad S_k = \int_{E_0}^{\infty} \left(\frac{E}{2R}\right)^k \left(\frac{df}{dE}\right) dE$$

and

$$[2] \quad L_k = \int_{E_0}^{\infty} \left(\frac{E}{2R}\right)^k \left(\frac{df}{dE}\right) \ln E \, dE$$

where E_0 is taken to be the electronic absorption threshold for the molecule, R is the Rydberg constant of energy, and (df/dE) is the differential dipole oscillator strength of the molecule at excitation energy E. Related properties include the number of electrons N in the molecule, $S_0 = N$, the static dipole polarizability $\alpha_d = S_{-2}$, mean excitation energies (for various processes) $I_k = 2R \exp[L_k/S_k]$, and the molar refractivity of the dilute molecular gas, R_λ, which is related to the refractive index, $n(\lambda)$, of the gas at wavelength λ;

$$[3] \quad R_\lambda = \rho^{-1}[n^2(\lambda) - 1]/(n^2(\lambda) + 2]$$

$$= \frac{4\pi}{3} N_A (2R)^2 a_0^3 \int_{E_0}^{\infty} \frac{(df/dE)}{E^2 - (hc/\lambda)^2} dE$$

where ρ is the molar density of the gas, N_A is Avogadro's number, a_0 is the Bohr radius, h is Planck's constant, and c is the speed of light.

The choice of E_0 as the electronic (uv) absorption threshold is in a sense arbitrary, although this is the usual choice. For example, it is not difficult to include the effects of the ir part of the spectrum although for many (but not all) properties and/or molecules this has little effect on the calculated properties (6–8).

The evaluation of the molecular properties via results like eqs. [1]–[3] is straightforward if accurate values of molecular dipole oscillator strengths are available over a wide range of

Can. J. Chem. Downloaded from www.nrcresearchpress.com by 210.87.254.105 on 09/06/12
For personal use only.

Can. J. Chem. Downloaded from www.nrcresearchpress.com by 210.87.254.105 on 09/06/12
For personal use only.

excitation energies E. Generally, however, the direct use of such data is not a trivial matter since there are often large errors (typically 2−20%, e.g. ref. 9 and some of the references therein) associated with even good oscillator strength data and there is often a severe lack of molecular data over wide energy regions.

In order to obtain a recommended DOSD, from an initial data base of (df/dE) versus E values, we follow Zeiss *et al.* (9) (see also refs. 7, 8, 10) and divide the excitation energies for a given molecule into N regions from E_0 to very large values of E. The original differential oscillator strength data for the jth region is then modified according to

$$[4] \quad (df/dE)^j_{\text{mod}} = (1 + a_j)(df/dE)^j_{\text{initial}}, \quad j = 1, 2, \ldots, N$$

so that the total modified DOSD satisfies constraints through the choice of the parameters a_j. Particularly good constraints (4, 5, 7−11) are provided by the Thomas−Reiche−Kuhn sum rule (1, 12), $S_0 = N$, and values of R_λ for two well separated values of λ and these are used in the work reported in Section 3. The lack of reliable experimental values for R_λ is a limiting factor in this procedure (see refs. 10, 13 and the sequel).

The constraints S_0 and the R_λ are written as the sum of N integrals, one each for every value of j in [4]. If N_i sources of oscillator strength data are used for the ith spectral region, the total number of initial DOSDs is given by $\prod_{i=1}^{N} N_i$. The parameters a_j are determined for each initial DOSD by using the constrained least-squares procedure outlined in ref. 9 where the initial DOSD data are allowed to vary within their expected uncertainty while satisfying the imposed constraints. The final "recommended" DOSD for each molecule is that which requires the least overall adjustment in the original input DOSD data. Often DOSDs that differ considerably locally (e.g. pointwise as a function of E) agree well globally in the sense of yielding very similar results for a variety of dipole properties, see refs. 8, 14 and what follows. Thus while the constraint procedure can often be used to discriminate between various sources of DOSD input data, considerable care should be used in this application of the method.

Each DOSD is represented by a set of data points, E_l and $(df/dE)_l$, for $l = 1, 2, \ldots, N_p \gg N$, and a set of $(N_p - 1)$ interpolating functions. For very high energies $\gtrsim 10^9$ eV, (df/dE) is represented by the Born dipole formula (12) $AE^{-3.5}$. The "recommended" DOSDs for the molecules treated in this paper have been placed in the Depository for Unpublished Data.[4] The dipole properties [1]−[3] can be readily evaluated (9) using this representation of the DOSDs.

3. DOSDs and related properties for methanol, ethanol, and *n*-propanol

The following experimental photoabsorption cross sections σ were used in constructing the DOSDs for the primary alcohols: *Methanol (CH_3OH)*: 6.2−7.4 eV (Harrison *et al.* (15)); 6.2−10.0 eV (Salahub and Sandorfy (16)); 7.4−16 eV (Heubner and Cellota (17)); 7.4−21 eV and 10.0−11.8 eV (Person and Nicole, refs. 18 and 19, respectively); 30−100 eV (de Reilhac and Damany (20)). *Ethanol (C_2H_5OH)*: 6.1−7.4 eV (15); 6.1−10.3 eV (16); 7.4−16 eV (17); 7.4−21 eV (18); 10.3−11.8 eV (19); 27−100 eV (20). *N-Propanol (C_3H_7OH)*: 6.1−10 eV (16); 9.3−24 eV (Ogawa and Cook (21)); 25−100 eV (20). The data of Ogawa and Cook (21) are widely spaced in energy and are used explicitly to construct the DOSD for *n*-propanol only. The cross sections due to Heubner and Cellota (17) are obtained from electron energy loss spectra.

Apparently experimental refractive index data for the gaseous normal alcohols are available only for methanol (22).

Due to the limited direct experimental DOS and refractive index data available for these molecules, it is augmented by photoabsorption cross sections and molar refractivities generated by additivity rules. Many possible additivity rules can be developed using available literature DOSD data and those used here for σ and R_λ are meant to be representative examples. In general, additivity rules based on elementary substances that most closely reflect the environment of the atoms making up the molecule of interest yield the most reliable results. Additivity rules for the various molecular dipole properties, including the molar refractivity, the closely related static dipole polarizability, and the DOSD itself, have been discussed in detail in previous papers (10, 23, 24) and some of the references therein. These papers contain dicussions of how the usefulness of the additivity rules depends both on the index k occurring in [1] or [2] and on the choice of elemental substances used in the rules.

Very often when molecules are used as elemental substances in applications of the mixture or additivity rule for DOSDs, and in particular for the lower members of a homologous series of molecules, there is little to choose between various additivity schemes in that the differences between the DOS data produced are less than the expected experimental error in reliable DOS data. In general, the mixture rule is not useful if the photon energy E is too low. For example, in what follows the mixture rules involving O_2 and H_2O are considered only for $E > 20$ eV since the DOSDs for these substances have structure for lower photon energies. Mixture rules employing atomic DOS data become reasonable only for larger photon energies where the effects of intramolecular forces, which are responsible for the breakdown of atomic additivity, become less important.

In general, the additivity rules for molecular properties are less reliable as the index k decreases below zero. For this reason the molar refractivity additivity rules for ethanol and *n*-propanol used here are group additivity rules based on experimental methanol and CH_2 group refractivity data, the latter being generated by normal alkane results.

3.A. Methanol

No direct experimental cross section data are available between 21 and 30 eV. In the first instance cross sections for this region were obtained, following de Reilhac and Damany (20), by using a plot of ln σ versus ln E to extrapolate their data for $E < 30$ eV; the extrapolated data merge satisfactorily with those of Ogawa and Cook (21) for $E > 20$ eV.

The experimental data for methanol are augmented by using the following mixture rules:

$$[5] \quad (M.1)\ \sigma(CH_3OH) = \sigma(C) + 2\sigma(H_2) + \tfrac{1}{2}\sigma(O_2)$$

$$[6] \quad (M.2)\ \sigma(CH_3OH) = \sigma(CH_4) + \sigma(H_2O) - \sigma(H_2)$$

$$[7] \quad (M.3)\ \sigma(CH_3OH) = \sigma(CH_4) + \tfrac{1}{2}\sigma(O_2)$$

$$[8] \quad (M.4)\ \sigma(CH_3OH) = \tfrac{1}{2}\sigma(C_2H_6) + \sigma(H_2O) - \tfrac{1}{2}\sigma(H_2)$$

$$[9] \quad (M.5)\ \sigma(CH_3OH) = \tfrac{1}{2}[\sigma(C_2H_6) + \sigma(O_2) + \sigma(H_2)]$$

[4]The appendix is available, at a nominal charge, from the Depository of Unpublished Data, CISTI, National Research Council of Canada, Ottawa, Ont., Canada K1A 0S2.

Can. J. Chem. Downloaded from www.nrcresearchpress.com by 210.87.254.105 on 09/06/12
For personal use only.

The input for these mixture rules are our recommended (9, 10, 7) DOSDs for H_2, O_2, H_2O, CH_4, and C_2H_6 while the $\sigma(C)$ data are those used in our treatment (10) of the normal alkanes.

The molar refractivity constraints, at $\lambda = 6400$ and 4359 Å, are obtained from the refractive index data of Ramaswamy (22).

The energy spectrum for methanol is divided into thirty energy regions as indicated in Table 1 which includes our "recommended" integrated dipole oscillator strengths together with the original experimental and/or mixture rule values for each region. Four "recommended" DOSDs have been constructed.

First we considered the available experimental data for $E \leq 50$ eV, together with all the mixture rule data considered individually from 50−100 eV and (M.1) data used for $E > 100$ eV. DOSD-I is obtained by subjecting these data to the constraint procedures reviewed in Section 2. DOSD-II is constructed by using the experimental data only for $E \leq 21$ eV, mixture rules (M.2) to (M.5) considered individually for 21−100 eV, and (M.1) for $E > 100$ eV. DOSD-III is obtained analogously to DOSD-II except that only mixture rule (M.3) is used in the 21−100 eV energy range. DOSD-I was constructed under the assumption that de Reilhac and Damany's data are too low for $E > 50$ eV; see also refs. 8, 9. To help verify this DOSD-IV was constructed, analogously to DOSD-I, except that de Reilhac and Damany's data were included in the constraint procedure for $50 \leq E \leq 100$ eV.

It is clear from Table 1 that the mixture rule data are in good agreement with each other and with the recommended, and most of the available experimental, values for $E \gtrsim 20$ eV. All the DOSDs are very similar for all energy regions except between 21 and 24 eV where DOSD-III and/or DOSD-IV can be as much as 20% lower than DOSD-I or DOSD-II. It seems clear that the original DOS data from (20) are too small for $E > 50$ eV, and in particular for $50 \leq E \leq 70$ eV.

Table 2 compares our calculated values of R_λ with Ramaswamy's (22) experimental results as a function of λ and Table 3 contains our calculated values for S_k, $-10 \leq k \leq 2$, and L_k, $-2 \leq k \leq 2$, for the four DOSDs. The DOSD results for R_λ are in excellent agreement with the available experimental values and each other. The differences between the values of the dipole properties evaluated from the four DOSDs, see Table 3, are much less, for all k, than the expected errors inherent in the DOSD constraint method (9, 5), namely ~2−3% for $k = 1$ and 2 and ~1% for $-6 \leq k \leq 0$ assuming the refractivity constraints are accurate to within a few tenths of a percent. These results also strongly suggest that reliable values for the dipole properties of the molecule can be obtained by using mixture rule DOSD data for $E \gtrsim 21$ eV. Our result for $S_{-2} = 21.94$ is in reasonable agreement with the results 21.69 and 21.74 obtained by Kubo (25) and Cartright (26).

3.B. Ethanol

As in the case of methanol, de Reilhac and Damany's data are extrapolated to fill the gap in the cross section data between 21 and 27 eV and the following mixture rules are employed:

[10] (M.1) $\sigma(C_2H_5OH) = 2\sigma(C) + 3\sigma(H_2) + \frac{1}{2}\sigma(O_2)$

[11] (M.2) $\sigma(C_2H_5OH) = 2\sigma(CH_4) + \sigma(H_2O) - 2\sigma(H_2)$

[12] (M.4) $\sigma(C_2H_5OH) = \sigma(C_2H_6) + \sigma(H_2O) - \sigma(H_2)$

[13] (M.6) $\sigma(C_2H_5OH) = \frac{1}{2}\sigma(C_4H_{10}) + \sigma(H_2O) - \frac{1}{2}\sigma(H_2)$

[14] (M.7) $\sigma(C_2H_5OH) = \sigma(CH_3OH) + \sigma(CH_4) - \sigma(H_2)$

[15] (M.8) $\sigma(C_2H_5OH) = \sigma(CH_3OH) + \sigma(C_2H_6) - \sigma(CH_4)$

[16] (M.9) $\sigma(C_2H_5OH) = \sigma(CH_3OH) + \frac{1}{2}[\sigma(C_4H_{10}) - \sigma(C_2H_6)]$

The additional input for these mixture rules relative to those for methanol are the butane recommended DOSD of ref. 10 and DOSD-I for methanol. The group mixture rules (M.8) and (M.9) are used for $E \gtrsim 15$ eV while the other mixture rules are used explicitly to construct the ethanol DOSD only for $E \gtrsim 21$ eV.

Apparently there are no experimental refractive index data for gaseous C_2H_5OH. The initial molar refractivity contraints, at $\lambda = 6440$ and 2302 Å, are generated by the additivity rule

[17] $R_\lambda(C_2H_5OH) = R_\lambda(CH_3OH) + R_\lambda(C_2H_6) - R_\lambda(CH_4)$

and, as input, the experimental data of Watson and Ramaswamy (27) and Friberg (28, 29), as normalyzed to (27) at $\lambda = 5462$ Å, for C_2H_6 and CH_4 at $\lambda = 6440$ and 2302 Å respectively, the experimental data of Ramaswamy (22) for CH_3OH at $\lambda = 6440$ Å, and the result obtained from DOSD-I for CH_3OH at $\lambda = 2302$ Å (see Table 2). The constraints are $R(\lambda = 6440) = 13.0546$ and $R(\lambda = 2302) = 15.2096$ cm^3 mol^{-1}.

The molar refractivity constraints and the various dipole oscillator strength data are used to construct three ethanol DOSDs. DOSD-I and DOSD-II are obtained analogously to the corresponding DOSDs for methanol by using the mixture rules [10]−[16] for $E \gtrsim 50$ eV and $E \gtrsim 21$ eV, respectively. DOSD-III is constructed by constraining all the experimental data for $E \leq 15$ eV, the mixture rule (M.8) and (M.9) data for $15 \leq E \leq 100$ eV, and (M.1) data for $E \gtrsim 100$ eV. Table 4 contains the "recommended" integrated oscillator strengths, together with the initial experimental and/or mixture rule results used in the construction of the "recommended" DOSDs, for various spectral regions.

It is evident from Table 4 that the mixture rule data are in satisfactory agreement with one another and with the recommended DOSDs for $E \gtrsim 15$ eV. Mixture rule (M.9) data require the least overall adjustment of all the mixture rules for $15 \leq E \leq 100$ eV. As for methanol the DOS data from ref. 20 are considerably too small for larger energy values, in particular for $50 \leq E \leq 70$ eV.

The results for the dipole properties S_k and L_k for the three DOSDs are all very similar (the spread in the results are analogous to those for CH_3OH, see Table 3) and only those corresponding to DOSD-I are given in Table 5. Since experimental data for the refractivity results are not available, the reliability of our values for these dipole properties is open to question. To investigate this we generated other values for R_λ at 6440 and 2302 Å by using the additivity rules

[18] $R_\lambda(C_2H_5OH) = R_\lambda(CH_3OH) + R_\lambda(C_3H_8) - R_\lambda(C_2H_6)$

and

[19] $R_\lambda(C_2H_5OH) = R_\lambda(CH_3OH) + \frac{1}{2}[R_\lambda(C_4H_{10}) - R_\lambda(C_2H_6)]$

The additional input for [18] and [19], relative to [17], is the experimental data for C_3H_8 due to Watson and Ramaswamy (27) and Friberg (28), as normalyzed to ref. 27 at 5462 Å, the experimental data of ref. 27 at 6440 Å for *n*-butane, and the result obtained from our recommended C_4H_{10} DOSD (10) at 2302 Å. The resulting molar refractivity constraints are $R(\lambda = 6440) = 13.1134$, 13.0175 and $R(\lambda = 2302) = 15.3399$,

Can. J. Chem. Downloaded from www.nrcresearchpress.com by 210.87.254.105 on 09/06/12
For personal use only.

TABLE 1. Integrated dipole oscillator strengths for methanol*

Energy range (eV)	Recommended values I		II		III		IV		Original experimental and/or mixture rule values†
6.2–7.4	0.582 (−2)	(16)	0.576 (−2)	(16)	0.571 (−2)	(16)	0.591 (−2)	(16)	0.423 (−2) (15); 0.509 (−2) (16)
7.4–8.0	0.285 (−1)	(16)	0.283 (−1)	(16)	0.281 (−2)	(16)	0.288 (−1)	(16)	0.258 (−1) (16); 0.258 (−1) (18); 0.218 (−1) (17)
8.0–8.5	0.369 (−1)	(16)	0.367 (−1)	(16)	0.365 (−1)	(16)	0.373 (−1)	(16)	0.336 (−1) (16); 0.324 (−1) (18); 0.290 (−1) (17)
8.5–9.0	0.251 (−1)	(16)	0.250 (−1)	(16)	0.249 (−1)	(16)	0.252 (−1)	(16)	0.239 (−1) (16); 0.221 (−1) (18); 0.208 (−1) (17)
9.0–10.0	0.109	(18)	0.109	(18)	0.108	(18)	0.110	(18)	0.923 (−1) (16); 0.983 (−1) (18); 0.934 (−1) (17)
10.0–11.8	0.386	(18)	0.385	(18)	0.382	(18)	0.387	(18)	0.345 (18); 0.334 (17); 0.338 (19)
11.8–13.0	0.427	(18)	0.429	(18)	0.430	(18)	0.423	(18)	0.424 (18); 0.405 (17)
13–14	0.461	(18)	0.466	(18)	0.470	(18)	0.455	(18)	0.486 (18); 0.487 (17)
14–15	0.484	(18)	0.490	(18)	0.497	(18)	0.478	(18)	0.529 (18); 0.540 (17)
15–16	0.456	(18)	0.462	(18)	0.469	(18)	0.451	(18)	0.503 (18); 0.541 (17)
16–17	0.467	(18)	0.472	(18)	0.481	(18)	0.463	(18)	0.520 (18)
17–18	0.516	(18)	0.522	(18)	0.534	(18)	0.513	(18)	0.583 (18)
18–19	0.452	(18)	0.456	(18)	0.464	(18)	0.450	(18)	0.499 (18)
19–20	0.448	(18)	0.452	(18)	0.460	(18)	0.448	(18)	0.492 (18)
20–21	0.441	(18)	0.444	(18)	0.452	(18)	0.442	(18)	0.480 (18)
21–22	0.429	(20)	0.371	(M.4)	0.357	(M.3)	0.431	(20)	0.463 (20); 0.378 (M.5); 0.394 (M.4); 0.373 (M.3); 0.390 (M.2)
22–23	0.397	(20)	0.362	(M.4)	0.339	(M.3)	0.399	(20)	0.423 (20); 0.369 (M.5); 0.383 (M.4); 0.352 (M.3); 0.366 (M.2)
23–24	0.367	(20)	0.346	(M.4)	0.314	(M.3)	0.370	(20)	0.387 (20); 0.340 (M.5); 0.362 (M.4); 0.323 (M.3); 0.346 (M.2)
24–27	0.878	(20)	0.866	(M.4)	0.798	(M.3)	0.901	(20)	0.989 (20); 0.889 (M.5); 0.969 (M.4); 0.854 (M.3); 0.934 (M.2)
27–30	0.737	(20)	0.762	(M.4)	0.731	(M.3)	0.757	(20)	0.791 (20); 0.737 (M.5); 0.819 (M.4); 0.761 (M.3); 0.844 (M.2)
30–35	0.957	(20)	1.005	(M.4)	1.073	(M.3)	0.997	(20)	1.015 (20); 1.036 (M.5); 1.075 (M.4); 1.108 (M.3); 1.147 (M.2)
35–40	0.743	(20)	0.738	(M.4)	0.816	(M.3)	0.770	(20)	0.760 (20); 0.781 (M.5); 0.759 (M.4); 0.820 (M.3); 0.799 (M.2); 0.692 (M.1)
40–50	1.058	(20)	1.155	(M.4)	1.163	(M.3)	1.117	(20)	1.062 (20); 1.143 (M.5); 1.174 (M.4); 1.143 (M.3); 1.174 (M.2); 1.104 (M.1)
50–70	1.547	(M.4)	1.515	(M.4)	1.422	(M.3)	1.332	(20)	1.211 (20); 1.353 (M.5); 1.492 (M.4); 1.352 (M.3); 1.492 (M.2); 1.316 (M.1)
70–100	1.039	(M.4)	1.022	(M.4)	1.028	(M.3)	0.993	(20)	0.905 (20); 0.977 (M.5); 0.995 (M.4); 0.976 (M.3); 0.994 (M.2); 0.958 (M.1)
100–300	1.422	(M.1)	1.404	(M.1)	1.430	(M.1)	1.484	(M.1)	1.367 (M.1)
300–500	1.083	(M.1)	1.077	(M.1)	1.086	(M.1)	1.106	(M.1)	1.061 (M.1)
500–700	1.021	(M.1)	1.015	(M.1)	1.023	(M.1)	1.042	(M.1)	1.002 (M.1)
700–1000	0.740	(M.1)	0.739	(M.1)	0.740	(M.1)	0.743	(M.1)	0.736 (M.1)
1000–∞	0.839	(M.1)	0.839	(M.1)	0.839	(M.1)	0.839	(M.1)	0.839 (M.1)

*The table contains the recommended oscillator strengths, obtained by applying the constraint procedures discussed in the text, and the oscillator strengths obtained by using the unmodified experimental or mixture rule dipole oscillator strength data considered in constructing the recommended DOSDs. The reference given with each recommended value indicates the source of the original DOS data for each specified spectral region.

†Between 21 and 30 eV extrapolated results based on ref. 20 are employed.

Can. J. Chem. Downloaded from www.nrcresearchpress.com by 210.87.254.105 on 09/06/12
For personal use only.

TABLE 2. Comparison of the values of R_λ(DOSD) for methanol with the experimental values of the molar refractivity obtained from Ramaswamy (22)*

λ (Å)	R_λ(DOSD)	Experimental values
6440	8.3516	8.3516†
5462	8.4133	8.4120
5087	8.4476	8.4443
4801	8.4797	8.4808
4359	8.5434	8.5434†

*The values obtained from all four DOSDs of Table 1 are identical at the experimental λ values. For λ = 2302 Å, R_λ = 9.7363, 9.7355, 9.7344, and 9.7376 for DOSD-I through DOSD-IV respectively; all results for R_λ are in units of $cm^3\ mol^{-1}$.

†Used as constraints in the construction of the methanol DOSDs.

TABLE 3. Some dipole properties S_k and L_k for methanol corresponding to DOSDs I–IV of Table 1

	Value			
Property*	DOSD-I	DOSD-II	DOSD-III	DOSD-IV
S_2	13.97(3)	13.96(3)	13.97(3)	13.99(3)
S_1	14.70(1)	14.67(1)	14.71(1)	14.80(1)
S_0	18.00	18.00	18.00	18.00
S_{-1}	15.18	15.19	15.17	15.18
S_{-2}	21.94	21.94	21.94	21.94
S_{-3}	38.87	38.88	38.90	38.85
S_{-4}	78.91	78.92	78.94	78.88
S_{-6}	44.03(1)	43.97(1)	43.87(1)	44.14(1)
S_{-8}	33.40(2)	33.27(2)	33.11(2)	33.60(2)
S_{-10}	31.59(3)	31.41(3)	31.21(3)	31.86(3)
L_2	88.10(3)	80.08(3)	88.10(3)	88.16(3)
L_1	49.39(1)	49.29(1)	49.42(1)	49.68(1)
L_0	14.81	14.76	14.83	14.90
L_{-1}	−3.20	−3.19	−3.20	−3.22
L_{-2}	−10.71	−10.71	−10.73	−10.70

*The dipole properties evaluated from the four DOSDs are essentially identical. By the method of construction DOSD-I is marginally recommended. The results for S_{-5}, S_{-7}, and S_{-9} for this DOSD are 17.82(1), 11.74(2), and 10.04(3), respectively. Estimated errors for the properties are discussed in the main text.

15.2409 $cm^3\ mol^{-1}$, respectively, corresponding to [18] and [19]. These values were used to construct DOSD-I′ and I″ which are analogous to DOSD-I but with the molar refractivity constraints generated by [17] replaced by those obtained from [18] and [19], respectively. The corresponding values of the dipole properties S_k and L_k are included in Table 5.

There is little to choose between the results for the dipole properties evaluated using the three DOSDs until reliable experimental data for the molar refractivity of ethanol are available. On chemical grounds the molar refractivity rule [18] appears preferable to [19], and particularly [17], and we nominally choose our recommended values of the dipole properties to be those evaluated using DOSD-I′. An estimate of the error in these results is given by the magnitude of the maximum discrepancies between the values of the dipole properties evaluated using the three DOSDs. It appears the errors in the S_k and L_k, for $-2 \leq k < -4$, obtained from DOSD-I′ are of about the same size as those inherent in the DOSD method itself. Our result for S_{-2} = 34.29 is in good agreement with, and probably more reliable than, the literature values (30, 31) of 33.20 and 35.61. The errors in our calculated results for the dipole properties for $k \leq -4$ probably become progressively worse as k decreases; this is in agreement with the point that the S_k, increasingly so for increasing negative values of k, emphasize the low energy part of the photoabsorption spectra which is largely constrained by the values of R_λ (10, 23). Values of R_λ evaluated using DOSD-I′, for λ = 5462, 5087, 4801, and 4359 Å, are R_λ = 13.1513, 13.2049, 13.2552, and 13.3549 $cm^3\ mol^{-1}$, respectively.

It is clear from the above discussion that mixture rules based on group additivity schemes can be used with confidence for $E > 15$ eV for the purposes of calculating reliable dipole properties for the higher alcohols.

3.C. n-Propanol

The following mixture rules are used to augment the experimental photoabsorption cross section data for this molecule:

[20] (M.1) $\sigma(C_3H_7OH) = 3\sigma(C) + 4\sigma(H_2) + \frac{1}{2}\sigma(O_2)$

[21] (M.10) $\sigma(C_3H_7OH) = \sigma(C_3H_8) + \sigma(H_2O) - \sigma(H_2)$

[22] (M.7) $\sigma(C_3H_7OH) = \sigma(CH_3OH) + 2[\sigma(CH_4) - \sigma(H_2)]$

[23] (M.8) $\sigma(C_3H_7OH) = \sigma(CH_3OH) + 2[\sigma(C_2H_6) - \sigma(CH_4)]$

[24] (M.9) $\sigma(C_3H_7OH) = \sigma(CH_3OH) + \sigma(C_4H_{10}) - \sigma(C_2H_6)$

[25] (M.11) $\sigma(C_3H_7OH) = \sigma(C_2H_5OH) + \frac{1}{2}[\sigma(C_4H_{10}) - \sigma(C_2H_6)]$

[26] (M.12) $\sigma(C_3H_7OH) = 2\sigma(C_2H_5OH) - \sigma(CH_3OH)$

The additional input for these mixture rules relative to those for ethanol is the recommended DOSD of ref. 10 for propane and DOSD-I for ethanol. Mixture rules (M.7)–(M.11) are used explicitly to construct the propanol DOSD only for $E \geq 15$ eV while (M.12) is used for $E \geq 10$ eV; the mixture rules, in particular (M.12), provide an alternative to the widely spaced DOS data of Ogawa and Cook (21) between 9.3 and 24 eV.

The initial molar refractivity constraints for propanol are obtained from the group additivity rule

[27] $R_\lambda(C_3H_7OH) = R_\lambda(CH_3OH) + R_\lambda(C_3H_8) - R_\lambda(CH_4)$

The input data have been discussed previously in the context of additivity rules [17] and [18] and the constraints correspond to the R_λ values for λ = 6440 and 2302 Å (see Table 6).

In the constraint procedure the experimental data of Salahub and Sandorfy (16) was used for $E \leq 10$ eV, the mixture rule (M.12) was employed for $10 \leq E \leq 15$ eV, all the mixture rules were used individually between 15 and 100 eV, and (M.1) was used for $E > 100$ eV. The corresponding integrated oscillator strengths for the twenty-one spectral regions considered in constructing the DOSD for *n*-propanol are given in Table 7. For comparative purposes the integrated oscillator strengths for 10–23 eV, obtained from the relatively widely spaced DOS data of Ogawa and Cook (21), are also listed in this table; the agreement with the mixture rule data is generally satisfactory. As typical examples, DOSD-I and DOSD-II integrated oscillator strengths, which correspond to using (M.12) and (M.9) in the constraint procedure between 15 and 100 eV, are given in Table 7. It is evident from this table that mixture rules (M.7)–(M.12) are in satisfactory agreement with each other

Can. J. Chem. Downloaded from www.nrcresearchpress.com by 210.87.254.105 on 09/06/12
For personal use only.

TABLE 4. Integrated dipole oscillator strengths for ethanol*

Energy range (eV)	Recommended values			Original experimental and/or mixture rule values†
	I	II	III	
6.1–7.4	0.95 (−2) (16)	0.96 (−2) (16)	0.95 (−2) (16)	0.95 (−2) (16); 0.86 (−2) (15)
7.4–10.3	0.359 (16)	0.365 (16)	0.360 (16)	0.373 (16); 0.399 (18); 0.379 (17)
10.3–11.8	0.548 (18)	0.548 (18)	0.557 (18)	0.563 (18); 0.563 (17); 0.555 (19)
11.8–13.0	0.671 (18)	0.669 (18)	0.676 (18)	0.678 (18); 0.669 (17)
13–15	1.486 (18)	1.467 (18)	1.503 (18)	1.502 (18); 1.570 (17)
15–17	1.626 (18)	1.597 (18)	1.554 (M.9)	1.628 (18); 1.545 (M.9); 1.516 (M.8); 1.568 (M.7); 1.413 (M.6); 1.528 (M.4); 1.581 (M.2)
17–19	1.632 (18)	1.599 (18)	1.583 (M.9)	1.624 (18); 1.572 (M.9); 1.563 (M.8); 1.541 (M.7); 1.446 (M.6); 1.516 (M.4); 1.493 (M.2)
19–21	1.554 (18)	1.489 (18)	1.408 (M.9)	1.525 (18); 1.400 (M.9); 1.405 (M.8); 1.381 (M.7); 1.304 (M.6); 1.366 (M.4); 1.343 (M.2)
21–24	1.649 (20)	1.717 (M.9)	1.765 (M.9)	1.605 (20); 1.755 (M.9); 1.844 (M.8); 1.768 (M.7); 1.615 (M.6); 1.741 (M.4); 1.665 (M.2)
24–27	1.273 (20)	1.305 (M.9)	1.326 (M.9)	1.240 (20); 1.322 (M.9); 1.394 (M.8); 1.325 (M.7); 1.339 (M.6); 1.432 (M.4); 1.363 (M.2)
27–30	1.010 (20)	1.100 (M.9)	1.111 (M.9)	0.987 (20); 1.109 (M.9); 1.085 (M.8); 1.134 (M.7); 1.143 (M.6); 1.184 (M.4); 1.234 (M.2)
30–35	1.302 (20)	1.385 (M.9)	1.398 (M.9)	1.262 (20); 1.396 (M.9); 1.346 (M.8); 1.490 (M.7); 1.459 (M.6); 1.528 (M.4); 1.672 (M.2)
35–40	0.964 (20)	1.021 (M.9)	1.026 (M.9)	0.938 (20); 1.026 (M.9); 0.994 (M.8); 1.072 (M.7); 1.011 (M.6); 1.048 (M.4); 1.127 (M.2); 0.903 (M.1)
40–50	1.354 (20)	1.466 (M.9)	1.471 (M.9)	1.302 (20); 1.473 (M.9); 1.413 (M.8); 1.413 (M.7); 1.558 (M.6); 1.532 (M.4); 1.531 (M.2); 1.423 (M.1)
50–70	2.025 (M.9)	1.900 (M.9)	1.901 (M.9)	1.468 (20); 1.907 (M.9); 1.895 (M.8); 1.893 (M.7); 1.852 (M.6); 1.865 (M.4); 1.863 (M.2); 1.653 (M.1)
70–100	1.330 (M.9)	1.273 (M.9)	1.271 (M.9)	1.082 (20); 1.275 (M.9); 1.274 (M.8); 1.272 (M.7); 1.230 (M.6); 1.241 (M.4); 1.239 (M.2); 1.185 (M.1)
100–300	1.839 (M.1)	1.783 (M.1)	1.780 (M.1)	1.784 (M.1)
300–500	2.036 (M.1)	1.994 (M.1)	1.900 (M.1)	1.994 (M.1)
500–700	1.349 (M.1)	1.331 (M.1)	1.329 (M.1)	1.331 (M.1)
700–1000	0.939 (M.1)	0.936 (M.1)	0.936 (M.1)	0.936 (M.1)
1000–∞	1.045 (M.1)	1.045 (M.1)	1.045 (M.1)	1.045 (M.1)

*Details of the construction of the three DOSDs considered are given in the main text (see also the caption for Table 1).
†Between 21 and 27 eV extrapolated results based on ref. 20 are employed.

Can. J. Chem. Downloaded from www.nrcresearchpress.com by 210.87.254.105 on 09/06/12
For personal use only.

TABLE 5. Some dipole properties S_k and L_k for ethanol calculated using DOSD-I of Table 4, and DOSD-I′ and DOSD-I″ which are analogous to DOSD-I except that the molar refractivity constraints are generated by [18] and [19], respectively, rather than [17]

	Value		
Property*	DOSD-I	DOSD-I′	DOSD-I″
S_2	17.25(3)	17.26(3)	17.27(3)
S_1	19.74(1)	19.80(1)	19.86(1)
S_0	26.00	26.00	26.00
S_{-1}	23.09	23.06	22.92
S_{-2}	34.29	34.43	34.17
S_{-3}	61.26	62.09	61.70
S_{-4}	12.39(1)	12.71(1)	12.66(1)
S_{-6}	67.68(1)	71.01(1)	71.20(1)
S_{-8}	50.03(2)	53.38(2)	53.82(2)
S_{-10}	46.35(3)	49.79(3)	50.35(3)
L_2	10.75(4)	10.76(4)	10.76(4)
L_1	64.63(1)	64.79(1)	64.94(1)
L_0	19.79	19.93	20.14
L_{-1}	−5.79	−5.84	−5.73
L_{-2}	−17.30	−17.64	−17.51

*The properties evaluated using DOSD-I′ are nominally recommended. The results for S_{-5}, S_{-7}, and S_{-9} for this DOSD are 28.77(1), 18.87(2), and 15.94(3), respectively. Estimated errors for the properties are discussed in the main text.

TABLE 6. Comparison of the values of R_λ evaluated using the *n*-propanol DOSDs-I, I′, I″, I‴ as a function of λ for 2302 ≤ λ ≤ 6440 Å

	R_λ			
λ (Å)	DOSD-I	DOSD-I′	DOSD-I″	DOSD-I‴
6440*	17.8164	17.7575	17.8751	17.6832
5462	17.9517	17.8901	18.0130	17.8205
5087	18.0266	17.9636	18.0895	17.8966
4801	18.0969	18.0324	18.1612	17.9680
4359	18.2363	18.1690	18.3035	18.1097
2302*	20.8130	20.6828	20.9434	20.7453

*These values are used as constraints for the construction of the relevant DOSDs and are evaluated by using the molar refractivity additivity rules [27] through [30] respectively.

and with the recommended DOSDs for $15 < E < 100$ eV and that (M.1) merges nicely from below (9, 10) with the other mixture rules for $70 \leq E \leq 100$ eV. The results of de Reilhac and Damany (20) appear to be consistently too low.

The dipole properties for *n*-propanol, including R_λ for $6440 \geq \lambda \geq 2302$ Å, have been evaluated using the various DOSDs constructed from the input data discussed above. The results are all very similar (the differences being analogous to those for methanol, see Tables 2 and 3) and only those corresponding to DOSD-I are given in Tables 6 and 8.

To investigate possible errors in the calculated values of the properties arising from the use of [27], three other refractivity additivity rules were employed to generate R_λ constraint values at 6440 Å and 2302 Å;

$$[28]\quad R_\lambda(C_3H_7OH) = R_\lambda(CH_3OH) + 2[R_\lambda(C_2H_6) - R_\lambda(CH_4)]$$

$$[29]\quad R_\lambda(C_3H_7OH) = R_\lambda(CH_3OH) + 2[R_\lambda(C_3H_8) - R_\lambda(C_2H_6)]$$

$$[30]\quad R_\lambda(C_3H_7OH) = R_\lambda(CH_3OH) + R_\lambda(C_4H_{10}) - R_\lambda(C_2H_6)$$

The input used to generate the three sets of refractivity constraints corresponding to [28]−[30], see Table 6, is discussed in the context of [17]−[19]. These results are used to construct DOSD-I′ through DOSD-I‴, which are analogous to DOSD-I but with the molar refractivity constraints obtained from [27] replaced with those generated by [28]−[30], respectively. The dipole properties R_λ, S_k, and L_k evaluated using these DOSDs are included in Tables 6 and 8 and the integrated oscillator strengths for the first two DOSDs are given in Table 7 as illustrative examples.

Keeping the input DOS data the same and varying the refractivity constraints affects the final DOSDs only for relatively low values of the photon energy E; compare the integrated oscillator strengths of Table 7 corresponding to DOSDs-I, I′, and I″. This is in agreement with the fact that the molar refractivity constraints, like S_{-2}, are dominated by the low energy ($E \lesssim 30$ eV) portion of the DOSD (10, 23). Thus, as is clear from Table 8, the dipole properties determined from DOSD-I through DOSD-I‴ vary substantially only for $k < -2$ since the constraints do not vary drastically; for example, the discrepancies in Table 8 for S_{-2}, S_{-3}, and S_{-4} are 1.1, 2.1, and 3.8% respectively and the discrepancy for S_{-2} is, of course, essentially the same as that in Table 6 for the higher wavelength values of R_λ ($R_\infty \sim S_{-2}$). For recommended values of the dipole properties we nominally choose those corresponding to DOSD-I″ which are very similar to those obtained from DOSD-I‴ for all k. Our result for $S_{-2} = 46.9$ is probably more reliable than the literature value (30) of 45.5. It appears that the uncertainty in our results for S_k and L_k, $-2 \leq k \leq 0$, is ~1% while that for $k = 1$ and 2, which is related to the uncertainties in the high energy portion of the DOSD, is probably ~2% (9). The limiting factor in our treatment of *n*-propanol is the lack of accurate experimental refractivity data and because this molecule is further removed from methanol than is ethanol, it is probably prudent to increase the estimated errors for $-2 \leq k \leq 0$ to ~2%.

4. Discussion

For fixed R_λ constraints different DOS input data can yield DOSDs that differ from one another locally (for given photon energies E) while agreeing globally in the sense that they yield essentially identical results for a variety of dipole properties. Examples are furnished in Section 3 for the three molecules studied here and earlier work (14) using 1-butene as a model, see also ref. 9, indicates that DOSDs with considerably more local disagreement than those of Section 3 yield markedly similar results for the dipole properties.

A limiting factor in the constraint procedure for determining the dipole properties is the lack of reliable experimental values for the molar refractivity constraints for a variety of molecules. The effect on the calculated properties S_k and L_k of varying the R_λ constraints for fixed DOSD input data is also illustrated by some of the calculations of the properties of ethanol and *n*-propanol. As expected (10, 23) from the structure of the integrals [1] and [2] defining the properties, the effect is largest for $k \leq -2$, increases as k decreases from −2, and is the same as the discrepancy in the higher wave length R_λ constraint for S_{-2}. For the typical variations in the constraints investigated in Section 3 the changes induced in the calculated properties are small ($\lesssim$1%) for $k \geq -3$.

The results obtained for the properties of methanol have the errors normally associated with the constraint procedure assuming the molar refractivity constraints are reliable (~1−2%

TABLE 7. Integrated dipole oscillator strengths for *n*-propyl alcohol*

Energy values (eV)	Recommended values				Original experimental and/or mixture rule values
	I	II	I′	I″	
6.1−8.0	0.521 (−1) (16)	0.518 (−1) (16)	0.503 (−1) (16)	0.539 (−1) (16)	0.052 (16)
8−10	0.473 (16)	0.473 (16)	0.436 (16)	0.510 (16)	0.480 (16)
10−11	0.404 (M.12)	0.407 (M.12)	0.395 (M.12)	0.414 (M.12)	0.557 (21); 0.410 (M.12)
11−13	1.313 (M.12)	1.341 (M.12)	1.285 (M.12)	1.340 (M.12)	1.536 (21); 1.358 (M.12)
13−15	1.958 (M.12)	2.008 (M.12)	1.973 (M.12)	1.943 (M.12)	2.293 (21); 2.031 (M.12)
15−17	2.254 (M.12)	2.139 (M.9)	2.300 (M.12)	2.208 (M.12)	2.689 (21); 2.317 (M.12); 2.236 (M.11); 2.155 (M.9) 2.097 (M.8); 2.201 (M.7); 2.190 (M.10)
17−19	2.244 (M.12)	2.152 (M.9)	2.291 (M.12)	2.197 (M.12)	2.668 (21); 2.280 (M.12); 2.222 (M.11); 2.163 (M.9); 2.145 (M.8); 2.099 (M.7); 2.159 (M.10)
19−21	2.188 (M.12)	1.893 (M.9)	2.227 (M.12)	2.149 (M.12)	2.336 (21); 2.205 (M.12); 2.052 (M.11); 1.899 (M.9); 1.908 (M.8); 1.862 (M.7); 1.859 (M.10)
21−23	1.470 (M.12)	1.620 (M.9)	1.485 (M.12)	1.456 (M.12)	2.006 (21); 1.472 (M.12); 1.547 ((M.11); 1.623 (M.9); 1.710 (M.8); 1.624 (M.7); 1.520 (M.10)
23−25	1.228 (M.12)	1.286 (M.9)	1.236 (M.12)	1.220 (M.12)	1.226 (M.12); 1.256 (M.11); 1.287 (M.9); 1.465 (M.8); 1.340 (M.7); 1.196 (M.10)
25−30	2.353 (M.12)	2.616 (M.9)	2.369 (M.12)	2.337 (M.12)	2.088 (20); 2.331 (M.12); 2.475 (M.11); 2.619 (M.9); 2.627 (M.8); 2.645 (M.7); 2.479 (M.10)
30−35	1.658 (M.12)	1.827 (M.9)	1.659 (M.12)	1.657 (M.12)	1.475 (20); 1.640 (M.12); 1.734 (M.11); 1.827 (M.9); 1.728 (M.8); 2.015 (M.7); 2.206 (M.10)
35−40	1.195 (M.12)	1.307 (M.9)	1.193 (M.12)	1.197 (M.12)	1.095 (20); 1.183 (M.12); 1.245 (M.11); 1.308 (M.9); 1.243 (M.8); 1.400 (M.7); 1.471 (M.10)
40−50	1.678 (M.12)	1.890 (M.9)	1.670 (M.12)	1.686 (M.12)	1.516 (20); 1.651 (M.12); 1.770 (M.11); 1.890 (M.9); 1.771 (M.8); 1.770 (M.7); 1.907 (M.10); 1.741 (M.1)
50−70	2.587 (M.12)	2.293 (M.9)	2.557 (M.12)	2.617 (M.12)	1.701 (20); 2.514 (M.12); 2.403 (M.11); 2.292 (M.9); 2.267 (M.8); 2.264 (M.7); 2.252 (M.10); 1.988 (M.1)
70−100	1.666 (M.12)	1.522 (M.9)	1.650 (M.12)	1.683 (M.12)	1.246 (20); 1.633 (M.12); 1.577 (M.11); 1.522 (M.9); 1.521 (M.8); 1.517 (M.7); 1.486 (M.10); 1.413 (M.1)
100−300	2.233 (M.1)	2.201 (M.1)	2.216 (M.1)	2.250 (M.1)	2.201 (M.1)
300−500	2.984 (M.1)	2.927 (M.1)	2.953 (M.1)	3.016 (M.1)	2.926 (M.1)
500−700	1.671 (M.1)	1.660 (M.1)	1.665 (M.1)	1.677 (M.1)	1.660 (M.1)
700−1000	1.137 (M.1)	1.136 (M.1)	1.136 (M.1)	1.138 (M.1)	1.135 (M.1)
1000−∞	1.251 (M.1)	1.251 (M.1)	1.251 (M.1)	1.251 (M.1)	1.251 (M.1)

for $2 \geq k \geq -6$). For the other alcohols this estimate of the reliability of the properties applies only for $k \geq -3$. The properties of most interest for a variety of applications correspond to these latter values of k.

The accurate *ab initio* or non-empirical quantum mechanical evaluation of the dipole properties of even relatively simple molecules is a difficult problem. Similarly the accurate *direct* experimental determination of many of these properties is often very difficult (for example see ref. 4). The quantum mechanical constraint procedure used here for determining the dipole properties of the alcohols offers a method for the reliable determination of many molecular properties if suitable input data are available or can be constructed using additivity relations. The usefulness of results of this type for testing the *ab initio* and non-empirical approaches is clear (32). An important application of reliable results for the dipole properties lies in the construction of group or bond properties which can be used in additivity formalisms to evaluate the properties of large species from those of smaller molecules and/or atoms (23, 24). A preliminary report on some of the group properties associated with the alcohols studied here can be found in ref. 24 and a full study will be published in due course. One of the drawbacks of the approach used in this paper is that it is, at present, only generally applicable to the evaluation of the rotationally averaged (isotropic) dipole properties of molecules primarily because of the lack of symmetry adapted dipole oscillator strength data.

In this paper, we have taken the lower limit for the integrals over photon energy defining the dipole properties, see [1] and [2], to be the electronic (uv) absorption threshold, see Section 2. The effect of including the ir part of the spectrum on the values of S_{-2} has been considered for H_2O, CH_4, and CO_2 in refs. 7, 8, and 33 and for these and many other molecules in ref. 34. The influence of the ir oscillator strengths on the values

Can. J. Chem. Downloaded from www.nrcresearchpress.com by 210.87.254.105 on 09/06/12
For personal use only.

TABLE 8. Some dipole properties S_k and L_k for *n*-propanol calculated using DOSDs-I, I′, I″, and I‴

	Value			
Property*	DOSD-I	DOSD-I′	DOSD-I″	DOSD-I‴
S_2	20.54(3)	20.52(3)	20.54(3)	20.57(3)
S_1	24.77(1)	24.69(1)	24.85(1)	24.98(1)
S_0	34.00	34.00	34.00	34.00
S_{-1}	30.95	30.99	30.91	30.63
S_{-2}	46.77	46.63	46.91	46.40
S_{-3}	84.68	83.82	85.56	84.77
S_{-4}	17.31(1)	16.98(1)	17.63(1)	17.53(1)
S_{-6}	95.06(1)	91.77(1)	98.37(1)	98.76(1)
S_{-8}	68.77(2)	65.65(2)	71.91(2)	72.76(2)
S_{-10}	60.66(3)	57.62(3)	63.72(3)	64.78(3)
L_2	12.69(4)	12.69(4)	12.70(4)	12.70(4)
L_1	79.82(1)	79.62(1)	80.03(1)	80.36(1)
L_0	24.85	24.68	25.03	25.45
L_{-1}	−8.39	−8.34	−8.45	−8.23
L_{-2}	−24.30	−23.94	−24.66	−24.40

*The properties evaluated using DOSD-I″ are nominally recommended. The results for S_{-5}, S_{-7}, and S_{-9} for this DOSD are 40.01(1), 25.86(2), and 20.97(3) respectively. Estimated errors for the properties are discussed in the main text.

of the S_k, as a function of k, has been discussed in ref. 8 for CO_2 and in general the ir contribution can increase markedly as k decreases.

We have considered here only dipole properties involving one integral over the DOSD for the molecule of interest. Many other important properties, for example, the dipole−dipole and the triple-dipole interaction dispersion energies between molecules, depend on two or more such integrals. These properties are much more readily evaluated by constructing pseudo-DOSDs (35) and these and the dispersion energies involving the alcohols considered in this paper will be presented elsewhere.

Acknowledgement

This research was supported by a grant from the Natural Sciences and Engineering Research Council of Canada.

1. J. O. HIRSCHFELDER, W. BYERS BROWN, and S. T. EPSTEIN. Adv. Quantum Chem. **1**, 255 (1964).
2. A. DALGARNO and A. E. KINGSTON. Proc. Phys. Soc. London, **72**, 1053 (1958); **73**, 455 (1959); **78**, 607 (1961).
3. U. FANO and J. W. COOPER. Rev. Mod. Phys. **40**, 441 (1968); **41**, 724 (1969).
4. G. D. ZEISS, W. J. MEATH, J. C. F. MACDONALD, and D. J. DAWSON. Radiat. Res. **70**, 284 (1977); **63**, 64 (1975).
5. G. D. ZEISS and W. J. MEATH. Mol. Phys. **33**, 1155 (1976), and the discussion and references therein.
6. R. T. PACK. J. Chem. Phys. **61**, 2091 (1974).
7. G. F. THOMAS and W. J. MEATH. Mol. Phys. **34**, 113 (1977).
8. B. L. JHANWAR and W. J. MEATH. Chem. Phys. **67**, 185 (1982) and the discussion, and some of the references therein.
9. G. D. ZEISS, W. J. MEATH, J. C. F. MACDONALD, and D. J. DAWSON. Can. J. Phys. **55**, 2080 (1977).
10. B. L. JHANWAR, W. J. MEATH, and J. C. F. MACDONALD. Can. J. Phys. **59**, 185 (1981).
11. A. DALGARNO, I. H. MORRISON, and R. M. PENGELLY. Int. J. Quant. Chem. **1**, 161 (1967).
12. H. A. BETHE and E. E. SALPETER. Quantum mechanics of one- and two-electron atoms. Academic Press, New York. 1957.
13. B. L. JHANWAR and W. J. MEATH. Mol. Phys. **41**, 1061 (1980).
14. B. L. JHANWAR, W. J. MEATH, and J. C. F. MACDONALD. Can. J. Phys. **61**, 1027 (1983).
15. A. J. HARRISON, B. J. CEDERHOLM, and M. A. TERWILLIGER. J. Chem. Phys. **30**, 355 (1959).
16. D. R. SALAHUB and C. SANDORFY. Chem. Phys. Lett. **8**, 71 (1971).
17. R. H. HEUBNER and R. J. CELLOTA. Argonne Natl. Lab. Radiolog. Environ. Res. Div. Ann. Rep. 1971-72. ANL-7960, Part I.
18. J. C. PERSON and P. P. NICOLE. Argonne Natl. Lab. Radiolog. Environ. Res. Div. Ann. Rep. 1973-74. ANL-75-3, Part I.
19. J. C. PERSON and P. P. NICOLE. J. Chem. Phys. **55**, 3990 (1971).
20. L. DE REILHAC and N. DAMANY. J. Phys. (Paris) Colloq. **32**, C4-32 (1971).
21. M. OGAWA and G. R. COOK. J. Chem. Phys. **28**, 747 (1958).
22. K. L. RAMASWAMY. Proc. Indian Acad. Sci. A**4**, 675 (1936).
23. G. D. ZEISS, W. J. MEATH, J. C. F. MACDONALD, and D. J. DAWSON. Mol. Phys. **39**, 1055 (1980).
24. W. J. MEATH, D. J. MARGOLIASH, B. L. JHANWAR, A. KOIDE, and G. D. ZEISS. *In* Intermolecular forces. *Edited by* B. Pullman. Reidel, Dordrecht. 1981. pp. 101−115.
25. M. KUBO. Sci. Pap. Inst. Phys. Chem. Res. Jpn. **26**, 242 (1935).
26. U. J. E. CARTRIGHT. Proc. R. Soc. London **154**, 138 (1936).
27. H. E. WATSON and R. L. RAMASWAMY. Proc. R. Soc. London, **156**, 144 (1936).
28. S. FRIBERG. Z. Phys. **73**, 216 (1931).
29. S. FRIBERG. Z. Phys. **41**, 378 (1927).
30. M. KUBO. Sci. Pap. Inst. Phys. Chem. Res. Jpn. **39**, 122 (1936).
31. L. G. GROVES and U. S. SUGDEN. J. Chem. Soc. Part 2, 1094 (1934).
32. F. MULDER, G. F. THOMAS, and W. J. MEATH. Mol. Phys. **41**, 249 (1980); G. F. THOMAS, F. MULDER, and W. J. MEATH. Chem. Phys. **54**, 45 (1980); F. MULDER and W. J. MEATH. Mol. Phys. **42**, 629 (1981).
33. G. D. ZEISS and W. J. MEATH. Mol. Phys. **30**, 161 (1975).
34. D. M. BISHOP and L. M. CHEUNG. J. Phys. Chem. Ref. Data, **11**, 119 (1982).
35. D. J. MARGOLIASH and W. J. MEATH. J. Chem. Phys. **68**, 1426 (1978); D. J. MARGOLIASH, T. R. PROCTOR, and W. J. MEATH. Mol. Phys. **35**, 747 (1978).

Can. J. Chem. Downloaded from www.nrcresearchpress.com by 210.87.254.105 on 09/06/12
For personal use only.

Synthetic and Raman spectroscopic study of the fluorosulfates of zinc, cadmium, and mercury

S. P. MALLELA AND F. AUBKE

Department of Chemistry, The University of British Columbia, Vancouver, B.C., Canada V6T 1Y6

Received April 5, 1983

S. P. MALLELA and F. AUBKE. Can. J. Chem. **62**, 382 (1984).

The group IIB metal fluorosulfates of the type $M(SO_3F)_2$, with M = Zn, Cd, or Hg, are conveniently obtained in a simple one-step procedure: the metal oxidation in a mixture of bis(fluorosulfuryl)peroxide and fluorosulfuric acid. The resulting white polymeric solids are all excellent Raman scatterers and provide the first consistent set of Raman data for this structural type. Above 400 cm^{-1} six sharp Raman lines indicate retention of C_{3v} symmetry for the tridentate fluorosulfate groups, with coordination through oxygen evidenced by frequency shifts, in particular in the stretching range and the rigid polymeric structure causing a different band intensity pattern than the one found for ionic fluorosulfates. Bands below 300 cm^{-1} are observed as well and some are tentatively assigned to skeletal metal–oxygen vibrations.

S. P. MALLELA et F. AUBKE. Can. J. Chem. **62**, 382 (1984).

Utilisant un procédé simple en une étape, ou a pu obtenir facilement des fluorosulfates des métaux du groupe IIb du type $M(SO_3F)_2$, où M = Zn, Cd ou Hg: le procédé implique une oxydation du métal dans un mélange de peroxyde de bis-(fluorosulfuryl) et d'acide fluorosulfurique. Les solides polymériques blancs qui en résultent diffractent bien le Raman et permettent d'obtenir pour la première fois des données cohérentes en Raman pour ce type de structure. Au-dessus de 400 cm^{-1}, la présence de six lignes Raman bien définies indique que la symétrie C_{3v} est retenue pour les groupes fluorosulfates tridentates, avec une coordination par le biais de l'oxygène démontrée par des déplacements de fréquences, en particulier dans la région de l'élongation, et la structure polymérique rigide provoquant un changement dans l'arrangement des intensités des bandes par rapport à celui trouvé pour les fluorosulfates ioniques. On observe aussi la présence de bandes en-dessous de 300 cm^{-1} et on en attribue quelques-unes à des vibrations du squelette métal–oxygène.

[Traduit par le journal]

Introduction

The fluorosulfates of the metals zinc, cadmium, and mercury of the type $M(SO_3F)_2$ have been known for some time. Zinc fluorosulfate was first obtained by Goubeau and Milne (1) in the reaction of anhydrous $ZnCl_2$ with fluorosulfuric acid in the presence of potassium fluorosulfate. The same authors have reported the infrared spectrum down to ~100 cm^{-1}. Both $Cd(SO_3F)_2$ and $Zn(SO_3F)_2$ are also prepared by the solvolysis of the corresponding metal benzoates in an excess of HSO_3F (2), while $Hg(SO_3F)_2$ was obtained by the oxidation of mercury with an excess of bis(fluorosulfuryl)peroxide, $S_2O_6F_2$, in a rather slow reaction (3).

Structural proposals for all three and a number of other fluorosulfates of divalent metals (2) have involved a 3-dimensional polymer with the tridentate fluorosulfate group retaining C_{3v} symmetry and the metal achieving regular octahedral coordination (Fig. 1). Since all attempts so far have failed to obtain single crystals suitable for an X-ray diffraction study, and since the compounds are all high melting, do not sublime, and are completely insoluble in HSO_3F and other inert solvents, evidence has come from infrared spectra (2), and in case of some transition metal fluorosulfates like $Pd(SO_3F)_2$ (4), from their magnetic properties and the electronic spectra. Again a regular octahedral environment for Pd(II) is indicated (4).

Our interest in these compounds centered around three points. (*i*) Metal oxidation in a mixture of HSO_3F and $S_2O_6F_2$ had proven a very simple and efficient method to prepare metal fluorosulfates. This method should be extendable to the group IIB fluorosulfates as well. (*ii*) Controlled metal oxidation may even provide evidence for low valency, metal–metal bonded species, in particular in case of mercury. (*iii*) All compounds are colorless and should be excellent Raman scatterers. We hoped to settle some of the discrepancies found in the published infrared data (2, 3) and provide for the first time a detailed and consistent set of Raman data for compounds with a tridentate bridging fluorosulfate group. In addition, we hoped to find some spectral features in the low frequency region, characteristic of the suggested polymeric structure. Only for $Zn(SO_3F)_2$ are vibrational modes below 400 cm^{-1} reported (1). This region should be more easily accessible by Raman spectroscopy but so far no Raman data on these compounds have been reported.

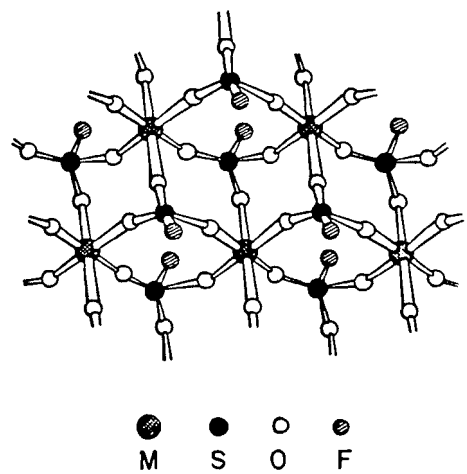

FIG. 1. Proposed structure of $M(SO_3F)_2$.

Experimental

Both zinc and cadmium were of analytical grade; mercury was doubly distilled. Bis(fluorosulfuryl)peroxide was prepared by catalytic (AgF_2) direct fluorination of sulfur trioxide according to Cady and Shreeve (5). Technical grade fluorosulfuric acid (Allied Chemical Corp.) was doubly distilled at atmospheric pressure in a counter stream of dry nitrogen.

Raman spectra were obtained with a Spex Ramalog 5, equipped with a Spectra Physics 164 argon ion laser. The line at 514.5 nm was

Can. J. Chem. Downloaded from www.nrcresearchpress.com by 210.87.254.105 on 09/06/12
For personal use only.

Can. J. Chem. Downloaded from www.nrcresearchpress.com by 210.87.254.105 on 09/06/12
For personal use only.

used for excitation and solid samples were contained in melting point tubes. A Perkin-Elmer 457 grating infrared spectrophotometer was used with samples pressed between AgCl windows.

All reactions were performed in Pyrex reaction vials of about 40 mL capacity, filled with Kontes Teflon stem valves. Volatile materials were manipulated using standard vacuum line techniques. Solids were handled in a Vacuum Atmosphere Corporation "Dri Lab", model No. HE-43-2 filled with purified dry nitrogen and equipped with a "Dri Train" model HE-93-2. All reactions were followed by weight.

Synthetic reactions

A mixture of fluorosulfuric acid and bis(fluorosulfuryl)peroxide ~1:1 by volume was used. About 200−300 mg of metal were allowed to react with approximately 5 to 8 mL of the mixture of HSO_3F and $S_2O_6F_2$. The reaction with mercury proceeded vigorously, and went to immediate completion with the reaction mixture initially at room temperature. The reactions of zinc and cadmium took 3−4 weeks with the temperature gradually raised to 90°C. Completion was judged by the disappearance of the grey colour due to unreacted metal. In all instances white powders precipitated out of solution. After completion of the reaction all volatiles were removed *in vacuo*.

Attempts to obtain lower valent compounds involving primarily mercury were performed in a similar way using small proportions of oxidizer.

Results and discussion

Metal oxidation by bis(fluorosulfuryl)peroxide is a simple, one-step route, resulting in the preparation of the group IIB metal fluorosulfates. The role of HSO_3F is crucial in all three instances. The preparation of $Hg(SO_3F)_2$ is speeded up and is essentially complete within minutes. The other two metals are both unreactive towards $S_2O_6F_2$ alone, but in the presence of fluorosulfuric acid quantitative conversion is achieved even though rather long reaction times are required. The advantage over solvolysis reactions of either anydrous chlorides or benzoates is threefold: (*a*) the starting materials are available at a very high degree of purity, (*b*) no preparation or drying of starting materials is needed, and (*c*) isolation of the final products by removal of all volatiles *in vacuo* is, in case of moisture-sensitive material, more advantageous than filtration and results in theoretical yields. While this procedure can be used for a wide range of metals, there are limitations to its use. Attempts by us to extend this study to the preparation of fluorosulfates of aluminum, boron, or indium were totally unsuccessful. Even at temperatures up to 110°C no reaction occurred.

In the case of the IIB metals the observed reactivity of mercury is somewhat surprising, since it is generally attested to be the least reactive of the three with the highest first and second ionization energies. We feel that the lack of reactivity for Zn and Cd may be caused by the initial formation of an unreactive coating on the metal surface preventing further reaction. The bis(fluorosulfates) of all three metals are indeed completely insoluble in HSO_3F, not inconsistent with their polymeric structure. Similar arguments apply to the observed lack of reactivity for the IIIA metals. Also unsuccessful were attempts to obtain lower valent fluorosulfates. Our attempts had centered primarily on mercury, because Hg_2^{2+} is by far the most stable of the three M_2^{2+} ions, and other chainlike ions such as Hg_3^{2+} and Hg_4^{2+} are known (6). In all instances where small amounts of $S_2O_6F_2$ are used, only $Hg(SO_3F)_2$ forms and unreacted mercury is noted as well.

All solid metal bis(fluorosulfates) are indeed excellent Raman scatterers and high quality spectra with a very good signal-to-noise ratio, reasonably straight baselines, and sharp Raman lines down to below 100 cm^{-1} are obtained. The spectrum of $Hg(SO_3F)_2$ is shown in Fig. 2. The Raman shifts observed are listed in Table 1 together with measured relative intensities in the region of the internal vibration of the SO_3F group. The noted base line shift in the region below 250 cm^{-1} allows only a rough estimation of intensities. Also listed are the corresponding infrared data. Our own infrared data agree reasonably well with the published data (1; 2); however, there are some minor exceptions. Two weak bands reported for $Hg(SO_3F)_2$ (2) at 581 and 574 cm^{-1} are not observed, nor is a weak band at 1067 cm^{-1} for $Zn(SO_3F)_2$ (1). None of these bands have Raman counterparts and may be due to combination bands or solid state effects. There is also, particularly in the SO— and SF stretching region, a discrepancy in the reported band position, up to about 20−25 cm^{-1} in some cases. This discrepancy is in our view caused by the rather broad bands found in the infrared spectra for these compounds in the stretching region. It should also be kept in mind that all materials are polymers with different synthetic routes at different reaction conditions, possibly resulting in a different degree of polymerisation. In addition, the reported infrared spectra were obtained on mulls with Nujol, hexachlorobutadiene, and fluorocarbon oils used as mulling agents (1,2), while our ir spectra were obtained on solid samples pressed between AgCl plates. In the deformation region the ir bands sharpen up and agreement is very good. The Raman spectrum of KSO_3F (7) is listed for reference purposes. Also listed are reported infrared data for $Pd(SO_3F)_2$ (4), where the electronic spectrum and the magnetic behavior indicate an undistorted environment and provide convincing evidence for the proposed structural type, so frequently encountered for metal bisfluorosulfates (1, 2, 4). Here the SO_3F^- ion has C_{3v} symmetry as well. Discussion of the spectra will first focus on the internal SO_3F vibrations.

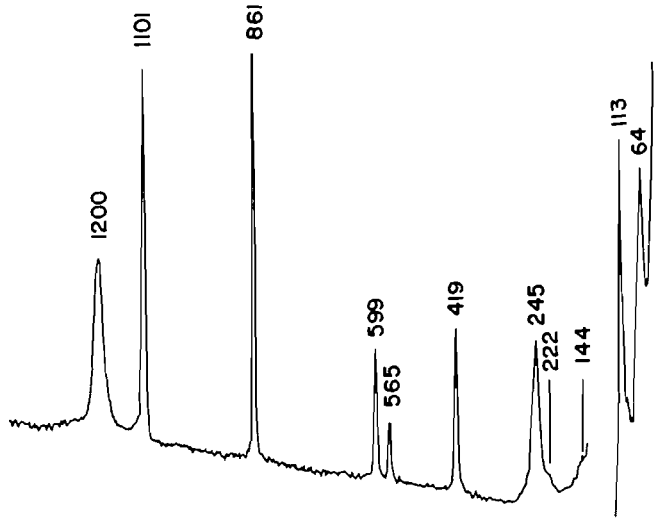

FIG. 2. Raman spectrum of $Hg(SO_3F)_2$.

Agreement with ir data in this region is generally good. The reported value of 832 cm^{-1} for νSF in $Zn(SO_3F)_2$ (1) may be abnormally low. Both in ref. 2 and in our own study, values of 854 and 859 cm^{-1} respectively are suggested in better agreement with the Raman shift of 871 cm^{-1}. Other discrepancies in the stretching region may be due to the various factors discussed above.

The proposed (2) retention of C_{3v} symmetry for the tridentate bridging fluorosulfate group is well confirmed by the Raman spectra for all three compounds. Only six fundamentals are

TABLE 1. Vibrational data for the fluorosulfates of Zn, Cd, and Hg[e]

KSO_3F[a] Raman $\Delta\nu$ (int) (cm^{-1})	$Pd(SO_3F)_2$ Infrared[d] ν (int) (cm^{-1})	$Zn(SO_3F)_2$ Raman $\Delta\nu$ (int) (cm^{-1})	$Zn(SO_3F)_2$ Infrared ν (int) (cm^{-1})	$Cd(SO_3F)_2$ Raman $\Delta\nu$ (int) (cm^{-1})	$Cd(SO_3F)_2$ Infrared ν (int) (cm^{-1})	$Hg(SO_3F)_2$ Raman $\Delta\nu$ (int) (cm^{-1})	$Hg(SO_3F)_2$ Infrared ν (int) (cm^{-1})	Assignment
1285(6)	1240 s, b	1240(24)	1245 vs	1237(31)	1230 vs	1200(52)	1200 vs	$\nu_4(E)$, asym SO_3 stretch
1079(100)	1090 m, s	1130(76)	1110 s	1119(100)	1100 s	1101(90)	1085 s	$\nu_1(A_1)$, sym SO_3 str.
745(10)	860 s	871(100)	854 s	862(83)	859 s	861(100)	850 s	$\nu_2(A_1)$, SF stretch
570(20)	610 s	606(48)	610 s	601(37)	600 vs	599(29)	598 vs	$\nu_3(A_1)$, sym SO_3 def.
594(18)	565 m	572(23)	568 m	569(15)	569 s	565(13)	561 m	$\nu_5(E)$, asym SO_3 def.
586(21)								
407(41)	421 m	430(27)	411 m	421(30)	411 m	419(37)	406 m	$\nu_6(E)$, SO_3F rock
		250 mw[c]	261 w[b]	230 mw		245 ms		sym. MO_6 str. A_{1g}
		218 w	205 s,b[b]	208 w		222 w, sh		MO_6 stretch E_{2g}
		148 m	159 w[b]			144 w, sh		
		108 s	114 w[b]	107 s		113 s		MO_6 deformation?
				90 s		64 s		

[a]Reference 7.
[b]Reference 1.
[c]Tentatively assigned as asymmetric MO_6 stretch.
[d]Reference 4.
[e]vs = very strong, s = strong, m = medium, w = weak, vw = very weak, b = broad, sh = shoulder, Raman = Raman shifts, infrared = infrared frequencies, int = intensities.

observed and in no instance is there any band splitting or shoulder noted, which might imply a removal of degeneracy for any of the three E modes. The intensities of the fundamentals show a rather interesting departure from the pattern usually observed for ionic fluorosulfate groups (1, 7). In two instances, the spectra for $Zn(SO_3F)_2$ and $Hg(SO_3F)_2$, the S—F stretching frequency is even more intense than ν_1, the symmetric SO_3 stretch, while for $Cd(SO_3F)_2$ ν_1 is only slightly more intense than νSF. In ionic fluorosulfates, ν_2 is commonly broad and of rather low intensity. This intensity reversal and the shift in band position discussed below becomes a diagnostic feature for the tridentate fluorosulfate group.

A reversal of intensities is noted for the two SO_3 bending modes ν_3 and ν_5 in all three spectra. The higher frequency band had been assigned as ν_5, in ionic compounds the asymmetric SO_3 bend (1, 7), and this assignment had been aided by an observable but small band splitting (7) and the relative intensities. For the group IIB metal fluorosulfates a rather intense band at ~600 cm^{-1} is followed in the Raman spectra by a weaker band at ~570 cm^{-1}.

It seems reasonable to reverse the assignment in this case with $\nu_3(A')$ now at ~600 cm^{-1} and $\nu_5(E)$ at 570 cm^{-1} for the tridentate bridging group.

The basic difference between ionic SO_3F^- and the tridentate bridging form encountered here is due to the rather rigid polymeric frame work, which eliminates disorder problems as they are encountered in KSO_3F (8) and produces a more even intensity pattern with sharp Raman lines.

The shift in band position can now also be seen more clearly and affects predominantly the stretching modes ν_1, ν_2, and ν_4. The band separation between ν_4 and ν_1, the SO_3 stretches, has decreased to about 110 ± 10 cm^{-1} from 206 cm^{-1} in KSO_3F (7) while ν_2, the SF stretch, has moved up by about 115 cm^{-1} compared to its position in KSO_3F. This reflects a change in $p_\pi - d_\pi$ back bonding on coordination through the three oxygen as has been noted before (2). The weighted average of the SO_3 stretching bands in $M(SO_3F)_2$ decreases from 1203 for Zn over 1198 to 1167 cm^{-1} for Hg and may reflect the increase in the mass of the metal tightly held in the polymeric structure.

The deformation modes show only rather small shifts and are obviously not as useful in recognizing the bonding mode of the SO_3F group.

Both intensity pattern and band positions in the range of internal vibrations of the fluorosulfate group are very indicative of a common structural type. The stated complete retention of C_{3v} symmetry suggests a regular octahedral environment for the MO_6— skeleton and indeed a common pattern emerges in the low frequency range as well with two minor exceptions. A strong increase in intensity at ~120 cm^{-1} has made it impossible to locate a weak Raman band, expected at ~150 cm^{-1} in the spectrum of $Cd(SO_3F)_2$, and a rather intense band at 245 cm^{-1} for $Hg(SO_3F)_2$ has weaker counterparts in the spectra of both $Zn(SO_3F)_2$ and $Cd(SO_3F)_2$. Agreement with infrared bands observed by Goubeau and Milne (1) is fair and assignment of bands at ~250 and 220 cm^{-1} as MO stretching modes is based on their original proposal for the related system. This assignment must remain tentative. Previous work on IIB metal compounds with coordinated oxyanions has rarely been extended down below 400 cm^{-1}. Infrared bands for $Zn(NO_3)_2$ at 317 and 287 cm^{-1} and for $Cd(NO_3)_2$ at 199 cm^{-1} have been attributed to M—O skeletal vibrations (9) and frequency trends for these and similar metal nitrates and carbonates have been rationalized with trends in the polarizing power of the various M^{2+} ions. In CH_3HgNO_3 a band at 292 cm^{-1} has been assigned to νHg—O (10), but in all these cases the coordination geometry around the metal is different from the octahedral environment suggested for the fluorosulfates.

Any further assignment would be hazardous in the absence of a detailed structure, but it is fair to say that the Raman spectra provide an additional recognition pattern for the polymeric structure in these metal fluorosulfates. The group IIB fluorosulfates have proven very useful indeed since neither interference from color nor from a distortion of the MO_6 skeleton causes problems.

Acknowledgement

Financial support by the National Sciences and Engineering Research Council of Canada is gratefully acknowledged.

Can. J. Chem. Downloaded from www.nrcresearchpress.com by 210.87.254.105 on 09/06/12
For personal use only.

1. J. GOUBEAU and J. B. MILNE. Can. J. Chem. **45**, 2322 (1967).
2. C. S. ALLEYNE, K. O'SULLIVAN-MAILER, and R. C. THOMPSON. Can. J. Chem. **52**, 336 (1974).
3. J. E. ROBERTS and G. H. CADY. J. Am. Chem. Soc. **82**, 353 (1960).
4. K. C. LEE and F. AUBKE. Can. J. Chem. **55**, 2473 (1977).
5. G. H. CADY and J. M. SHREEVE. Inorg. Synth. **7**, 124 (1963).
6. R. J. GILLESPIE and J. PASSMORE. Adv. Inorg. Chem. Radiochem. **17**, 49 (1975).
7. A. M. QURESHI, H. A. CARTER, and F. AUBKE. Can. J. Chem. **49**, 35 (1971).
8. K. O'SULLIVAN, R. C. THOMPSON, and J. TROTTER. J. Chem. Soc. A, 2024 (1967).
9. J. R. FERRARO and A. WALKER. J. Chem. Phys. **42**, 1273 (1965).
10. P. L. GOGGIN and L. A. WOODWARD. Trans. Faraday Soc. **58**, 1495 (1962).

Can. J. Chem. Downloaded from www.nrcresearchpress.com by 210.87.254.105 on 09/06/12
For personal use only.

Photochemistry of alkyl esters of benzoylformic acid[1]

M. V. ENCINAS AND E. A. LISSI
Departamento de Química, Facultad de Ciencias, Universidad de Santiago, Santiago, Chile
A. ZANOCCO
Departamento de Ciencias Formativas, Facultad de Ciencias Básicas Farmacéuticas, Universidad de Chile, Santiago, Chile
AND
L. C. STEWART AND J. C. SCAIANO
Division of Chemistry, National Research Council of Canada, Ottawa, Ont., Canada K1A 0R6

Received July 18, 1983

M. V. ENCINAS, E. A. LISSI, A. ZANOCCO, L. C. STEWART, and J. C. SCAIANO. Can. J. Chem. **62**, 386 (1984).

The photodecomposition of several alkyl benzoylformates has been examined using quantum yield and laser flash photolysis techniques. The Norrish Type II reaction is a major triplet deactivation path in all substrates having γ-hydrogen atoms. Representative triplet lifetimes are 670, 500, and 310 ns, for the methyl, ethyl, and isopropyl esters, respectively, in 1:4 chlorobenzene:*n*-heptane at 298 K. Product studies suggest that several competing reactions are involved in the decay of the 1,4-biradical; some of these lead to highly absorbing (and presumably quenching) products, that make it essential to extrapolate quantum yields to "zero conversion" conditions.

M. V. ENCINAS, E. A. LISSI, A. ZANOCCO, L. C. STEWART et J. C. SCAIANO. Can. J. Chem. **62**, 386 (1984).

On a étudié la photodécomposition de plusieurs benzoformates alkylées en utilisant les techniques du rendement quantique et de la photolyse flash au laser. La réaction de type Norrish II consiste principalement en une désactivation du triplet de tous les substrats ayant des atomes d'hydrogène en position γ. Les principaux temps de vie du triplet sont respectivement de 670, 500 et 310 ns pour les esters méthylique, éthylique et isopropylique à 298 K dans un mélange 1:4 de chlorobenzène–*n*-heptane. L'étude des produits suggère que plusieurs réactions compétitives sont impliquées dans la désintégration du biradical 1,4; certaines d'entres-elles conduisent à des produits qui absorbent fortement (et qui probablement s'inhibent) ce qui oblige d'extrapoler les rendements quantiques aux conditions "où il n'y a pas eu de transformation".

[Traduit par le journal]

The photochemistry of α-keto esters has been the subject of a limited number of studies (1–3). In particular, there are few reported data on the rate of photoprocesses taking place from excited aromatic keto esters. The only reported rate constant has been given by Zanocco *et al.* in a communication on the photolysis of methyl benzoylformate (4). The product distribution and product quantum yield in the photolysis of aliphatic esters of benzoylformic acid are extremely dependent both upon the solvent (1) and temperature (5). In solvents bearing labile hydrogen atoms the main products have been rationalized by a mechanism involving keto ester photoreduction (1). In the photolysis of ethyl benzoylformate in benzene, Leermakers *et al.* found carbon monoxide, benzaldehyde, and acetaldehyde as main products. These were explained in terms of a Type II intramolecular abstraction (6). Due to the large conversions involved, these products could alternatively arise from secondary photolysis of unstable primary photoproducts. Further, the reactive state has not been characterized and its lifetime has not been measured.

In this paper we report the results obtained in a study of the photochemistry of several esters of benzoylformic acid, **I–VIII**.

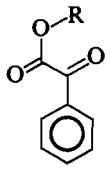

I, R = CH_3
II, R = C_2H_5
III, R = *n*-C_3H_7
IV, R = *n*-C_4H_9
V, R = *i*-C_4H_9
VI, R = *i*-C_3H_7
VII, R = *t*-C_4H_9
VIII, R = *i*-C_5H_{11}

[1]NRCC No. 22752.

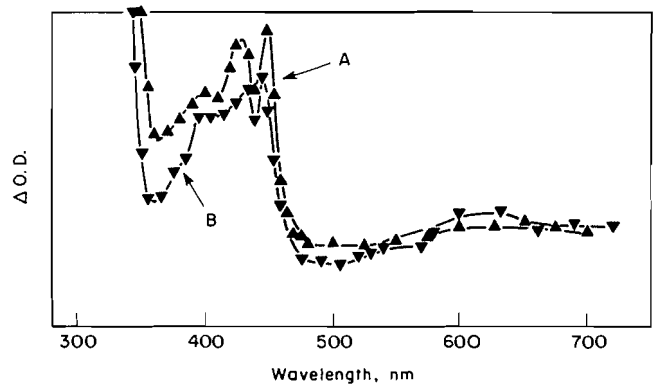

FIG. 1. Absorption spectra of the transients produced in the photolysis of **IV** (*A*) and **I** (*B*) in benzene at 298 K.

This study comprises both direct measurements of transient lifetimes and product analysis under a variety of experimental conditions.

Results

The absorption spectra of the transients produced in the photolysis of **I** and **IV** in benzene are shown in Fig. 1. The shape of the spectra was nearly independent of the delay following laser excitation and was similar for all compounds considered. In particular, it is relevant to the following discussion that the transient spectrum obtained employing compound **VII** was essentially the same as those obtained for the other compounds. These spectra can then be attributed to T–T transitions (4). The decay of the absorption followed first order kinetics and was independent of the monitoring wavelength. The lifetimes were measured at 440 nm; at this wavelength a small residual absorption was observed in some solvents (e.g. hexane

Can. J. Chem. Downloaded from www.nrcresearchpress.com by 210.87.254.105 on 09/06/12
For personal use only.

TABLE 1. Dependence of the triplet lifetimes on the R group at 298 K

Substrate	γH[a]	τ_T (ns) Decay[b]	τ_T (ns) Quenching[c]
I	Primary	645(1000)	~670[d]
II	Secondary		500
III	Secondary		450
IV	Secondary	480(500)	540
V	Secondary	(500)	
VI	Tertiary	420(415)	310
VII	None	2500(5600)	

[a] Type of hydrogen in γ-position to the carbonyl group.
[b] Data in *n*-heptane containing 20% chlorobenzene. Values in parentheses were obtained in benzene.
[c] Data in *n*-heptane containing 20% chlorobenzene.
[d] Measurement based only on benzaldehyde quenching.

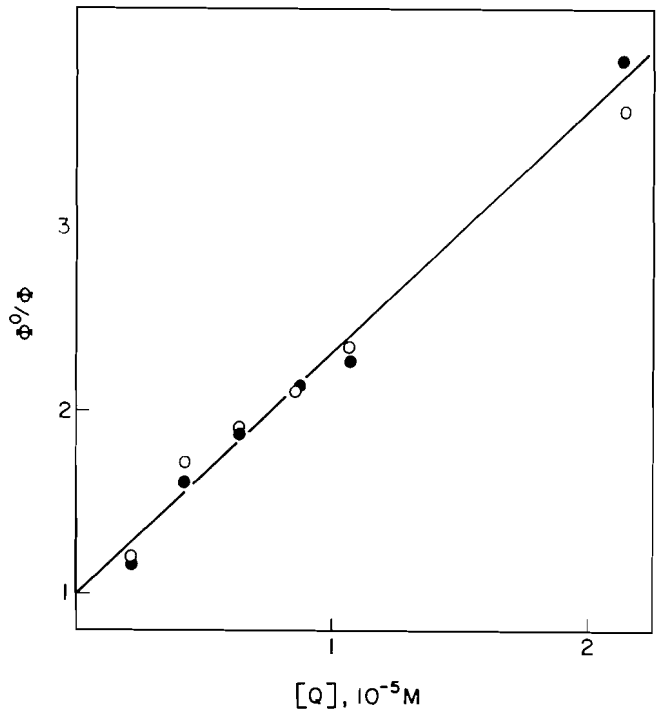

FIG. 2. Effect of the diene concentration upon benzaldehyde (○) and aliphatic carbonyl (●) yields in the photolysis of **VI**. Solvent: *n*-heptane containing 20% chlorobenzene.

or benzene). The lifetimes obtained were independent of the light intensity and of the ester concentration but decreased in the presence of triplet quenchers (e.g. amines and dienes). Quenching rates by 2,5-dimethyl-2,4-hexadiene were determined directly by following the change in triplet lifetimes as a function of added diene. The values obtained in *n*-heptane, benzene, and heptane containing 20% chlorobenzene were (4 ± 1) × 10^9 M^{-1} s^{-1} at 300 K, and, within the error limits given, were independent of the solvent used.

The τ_T values in benzene and *n*-heptane containing 20% chlorobenzene are given in Table 1. This table gives τ_T values measured directly by monitoring the triplet decay and values obtained from product quenching experiments. The latter were obtained from Stern–Volmer plots assuming a quenching rate constant of ~4 × 10^9 M^{-1} s^{-1} for 2,5-dimethyl-2,4-hexadiene.

Stern–Volmer plots were linear and similar results were obtained by measuring the effect of the diene upon benz-

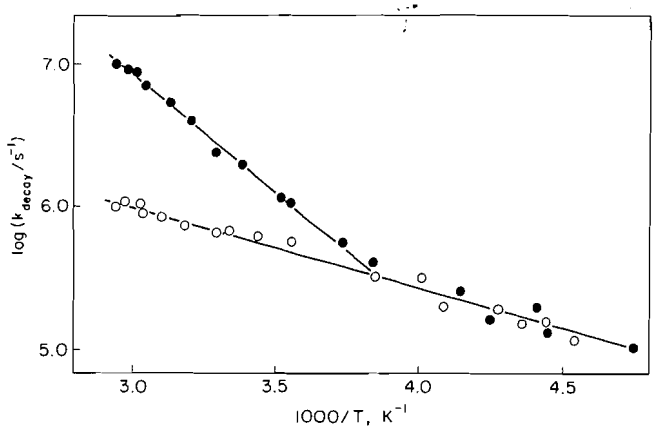

FIG. 3. Decay rate as a temperature function for **VI** (●) and **VII** (○). Solvent: *n*-heptane containing 20% chlorobenzene.

aldehyde or the aliphatic carbonyl compound (see Fig. 2 for a typical set of results).

Triplet lifetimes as a function of temperature were measured for **I**, **IV**, **VI**, and **VII**. The data obtained for **VI** and **VII** are given in Fig. 3. The data of **VI** show two distinct slopes, with a more pronounced temperature dependence at the higher temperatures. The same behaviour was observed for **IV** and **I**.

No measurable photoproducts ($\Phi < 0.01$) were observed in the photolysis of **VII**. In the photolysis of the other compounds (general formula PhCOC(O)OCHR'R), the only products detected by gas chromatography were benzaldehyde and the corresponding aliphatic carbonyl [RC(O)R']. Benzene, the alcohol RR'CHOH, the saturated hydrocarbon RR'CH_2, the olefins R(—H)CHR' and R'(—H)CHR were below our detection limit ($\Phi < 0.01$).

The product quantum yields were very dependent on the solvent and photolysis time. In several solvents (e.g. benzene, ethyl acetate, carbon tetrachloride, or dichloromethane) the reaction mixture develops, upon irradiation, a strong absorption at $\lambda \leq 430$ nm that makes the measurements of quantum yields relatively unreliable. The strongest absorption was observed in ethyl acetate. The change in uv spectra during the irradiation is shown in Fig. 4. When 1% of water was added to the solvent prior to the photolysis, the formation of the coloured compound was markedly diminished. Furthermore, this absorption is bleached when air is admitted to the reaction tube after photolysis.

The ir spectra of samples of methyl benzoylformate photolyzed in carbon tetrachloride show bands at 3390 and 2130 cm^{-1} that increase with irradiation time. The band at 2130 cm^{-1} disappears when the photolyzed sample is exposed to air. The bands at 2130 cm^{-1} and 3390 cm^{-1} could be attributed to the presence of >C=C=O and —OH linkages, respectively (7).

In hydrocarbon solvents (e.g. dodecane) a white precipitate was observed after prolonged photolysis. In methanol as solvent, the photolysis of methyl benzoylformate at long irradiation times gives a white crystalline solid (mp 156–158°C), nmr ($CDCl_3$, TMS): 3.85 (s, 3H), 4.9 (s, 1H), 7.15 (s, 5H). This spectrum agrees with that expected for dimethyl-2,3-dihydroxy-2,3-diphenyl succinate.

The product quantum yields were determined for all the compounds in *n*-heptane–chlorobenzene (4:1). This mixture was selected since no precipitate was observed and the absorption developed in the visible – near uv region is weak enough that it can be neglected at short irradiation times. The product

Can. J. Chem. Downloaded from www.nrcresearchpress.com by 210.87.254.105 on 09/06/12
For personal use only.

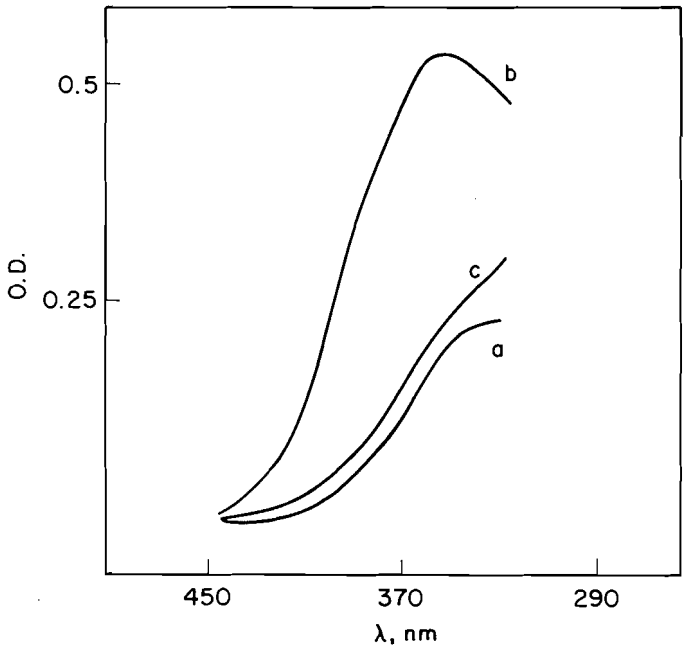

FIG. 4. Ultraviolet spectral change during the irradiation of *n*-propyl benzoylformate in ethyl acetate: (*a*) fresh solution, (*b*) after 15 min photolysis, (*c*) as (*b*), after 5 min exposure to air.

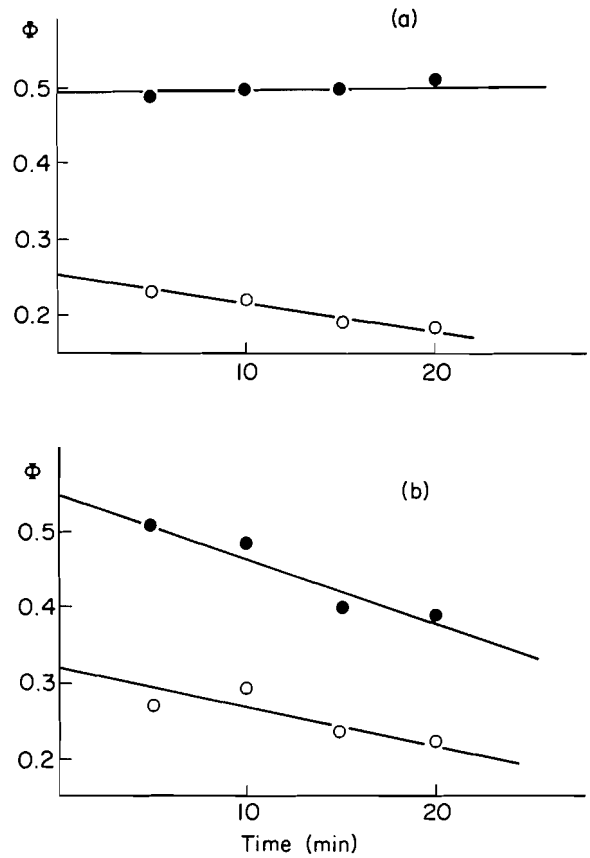

FIG. 5. Dependence of product yields as a function of irradiation time for (*a*) *n*-propyl benzoylformate isopropyl benzoylformate, (*b*) based on aliphatic carbonyl quantum yield (●) and benzaldehyde quantum yield (○).

yields were dependent upon the irradiation time. Those measured in the photolysis of **III** and **VI** are given in Fig. 5. A similar dependence was observed for the other compounds investigated. The yields obtained by extrapolation at zero irradiation time are given in Table 2.

TABLE 2. Product yields in *n*-heptane – chlorobenzene (4:1) extrapolated to zero irradiation time

Substrate	Carbonyl	$\Phi_{carbonyl}$	$\Phi_{benzaldehyde}$
I	CH_2O	[a]	0.09
II	CH_3CHO	0.4	0.25
III	CH_3CH_2CHO	0.50	0.25
IV	$CH_3CH_2CH_2CHO$	0.70	0.22
V	$CH_3CH(CH_3)CHO$	0.73	0.24
VI	CH_3COCH_3	0.55	0.32
VIII	$CH_3CH_2CH(CH_3)CHO$	0.70	—

[a] Formaldehyde was detected but not measured quantitatively.

TABLE 3. Arrhenius parameters and quantum yields for intramolecular hydrogen abstraction

Substrate	k_5[a] (10^6 s^{-1})	E_5[b]	log (A/s^{-1})	Φ_5[a]
I	0.60 ± 0.1	9.1 ± 1	12.4	0.4 ± 0.08
IV	1.3	9.1 ± 0.5	12.7	0.70 ± 0.10
VI	1.4	9.0 ± 0.5	12.7	0.66 ± 0.10
VII[c]	—	2.5	7.6	—

[a] Temperature 298 K.
[b] In kcal/mol.
[c] Arrhenius parameters for reaction [4].

Discussion

The data in Table 1 show that lifetimes measured by direct transient detection or by product quenching with a typical triplet quencher (e.g. 2,5-dimethyl-2,4-hexadiene) show a similar pattern. The differences observed between both sets of results are within the experimental error. This fact, together with the linearity of the Stern–Volmer plots, would indicate that all observed products originate from a single excited triplet. This conclusion is similar to that reached for other aromatic carbonyls (8). Furthermore, the fact that the triplet lifetime is related to the type of hydrogen in the γ-position to the carbonyl group and to the type of products obtained are compatible with a significant contribution of an intramolecular hydrogen abstraction to the triplet lifetime. The photochemistry of compounds **I** to **VIII** can be interpreted then in terms of the following reaction scheme

[1] $K \xrightarrow{h\nu} {}^1K$

[2] ${}^1K \rightarrow K$

[3] ${}^1K \rightarrow {}^3K$

[4] ${}^3K \rightarrow K$

[5] ${}^3K \rightarrow$ products

In this scheme, reaction [4] involves all processes that deactivate the triplet, other than intramolecular hydrogen abstraction. The most important process is likely to involve impurity quenching. This is supported by the triplet lifetime dependence on solvent for **VII** (see Table 1), and the Arrhenius parameters obtained for its triplet lifetime in *n*-heptane – chlorobenzene (see Fig. 3 and Table 3).

The product distribution, the dependence of the lifetime upon the type of γ-hydrogen and the lack of photoproducts in the

Can. J. Chem. Downloaded from www.nrcresearchpress.com by 210.87.254.105 on 09/06/12
For personal use only.

Can. J. Chem. Downloaded from www.nrcresearchpress.com by 210.87.254.105 on 09/06/12
For personal use only.

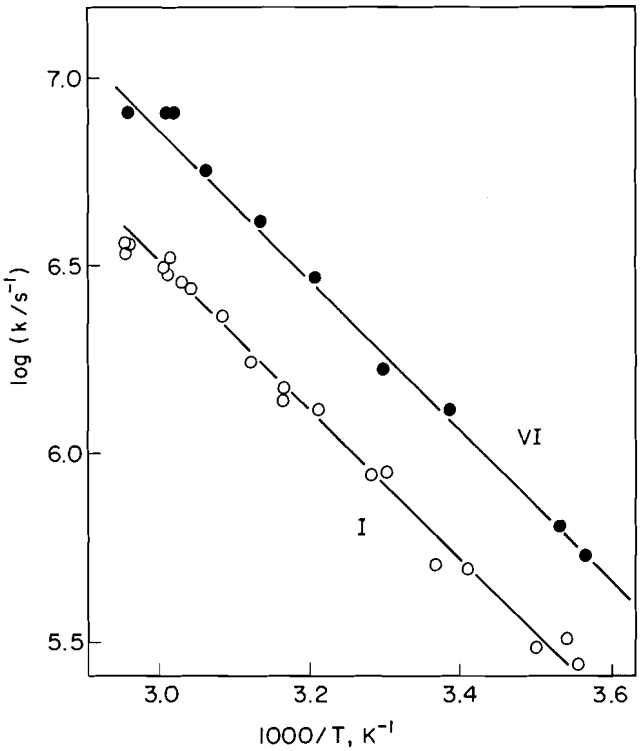

FIG. 6. Arrhenius plot for the intramolecular hydrogen abstraction for **I** (○) and **VI** (●).

irradiation of **VII** imply that Type I cleavage and intramolecular β-hydrogen abstraction are negligible. From the known behaviour of other $n\pi^*$ carbonyl compounds (9), the most likely pathway of reaction [5] is the Norrish Type II process, i.e.

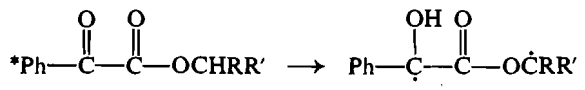

followed by reactions of the 1,4-biradicals.

The values of k_5 and their Arrhenius parameters can be obtained by subtracting from the high temperature lifetimes the values obtained by extrapolation of the low temperature data using the method described in an earlier report (10). The values of k_5 so obtained, plotted according to the Arrhenius equation, are shown in Fig. 6 for **I** and **VI**. The Arrhenius parameters obtained are collected in Table 3. This table also includes values of $(k_5\tau_T)$ estimated at 298 K. These values measure, according to the above reaction scheme, the 1,4-biradical quantum yield.

The *A*-factors obtained for the intramolecular hydrogen abstraction are, for three compounds considered, $\sim 5 \times 10^{12}$ s^{-1}. These values are nearly an order of magnitude higher than those reported for other Type II photoprocesses involving γ-hydrogen abstraction (10–12) and explained in terms of an adiabatic reaction. Nevertheless, this difference could be partly related to the restricted character of the internal rotation along the carbon bond between both carbonyl groups.

The activation energies given in Table 3 are higher than those measured for monocarbonyl ketones (10–12). This fact can be related to the lower triplet energy of the α-keto esters which implies a smaller exothermicity for the hydrogen abstraction process. In fact, for the carbonyl compounds in-

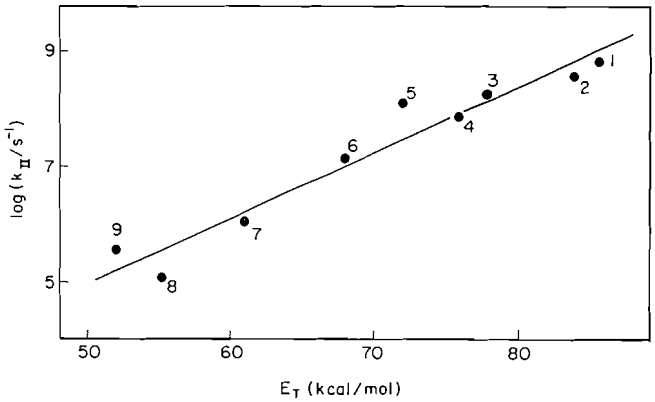

FIG. 7. Relationship between intramolecular secondary γ-hydrogen abstraction and excitation energy of the carbonyl group: (*1*) 2-heptanone singlet (ref. 21); (*2*) *n*-pentanal singlet (ref. 22); (*3*) 2-heptanone triplet (ref. 12); (*4*) *n*-pentanal triplet (ref. 22); (*5*) valerophenone triplet (ref. 20); (*6*) ethylpyruvate triplet (ref. 15); (*7*) *n*-butyl benzoylformate triplet (this work); (*8*) 2,3-heptanedione triplet (ref. 13); (*9*) 1-phenyl-1,2-pentanedione triplet (ref. 14).

vestigated to date there is a fair correlation between excited state energy and intramolecular hydrogen abstraction rate (Fig. 7).

The values of k_5 given in Table 3 show that the relative values of primary, secondary, and tertiary sites are 1:3.2:7.5, respectively, per reactive hydrogen. This small selectivity (manifested also in the similarity of the activation energies) contrasts with those observed in Type II processes of other carbonyl (10, 12) and α-dicarbonyl (13, 14) compounds, and appears to be a peculiarity of α-keto esters (2, 15). This indicates that in these systems there is no direct relationship between reactivity and selectivity. Wagner *et al.* (14) have suggested that a zwitterionic structure like

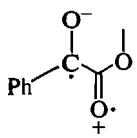

could contribute significantly to the electronic configuration in the excited triplet. In this case, the reactive oxygen should be highly nucleophilic. Substitution at the γ-carbon, while decreasing the strength of the C—H bond, will increase the charge density. The effect of substitution upon the rate of hydrogen abstraction could then be less than that expected from the C—H bond weakening. Another factor to be taken into account is the rather peculiar effect of oxygen atoms bound to the γ-carbon in the photolysis of aromatic ketones (16). Wagner and Kemppainen found that in the photolysis of ketones of general formula Ph—CO—CH_2—CH_2—CHR_1R_2, when $R_1 = CH_3$, the ketone with $R_2 = CH_3$ reacts four times faster than that with R_2 = H. However, when $R_1 = OCH_3$, the ketone with $R_2 = CH_3$ reacts 1.3 times slower than that with R_2 = H.

The product distribution depends strongly both upon the solvent and conversion. Nevertheless, the yields obtained at very low conversion in "inert" solvents (e.g. benzene, chlorobenzene, butyronitrile, *n*-heptane) are very similar to those given in Table 3.

Comparison of $\Phi_{carbonyl}$ (Table 2) with Φ_5 (Table 3) shows that for compounds **IV** and **VI**, both values are similar. This

Can. J. Chem. Downloaded from www.nrcresearchpress.com by 210.87.254.105 on 09/06/12
For personal use only.

indicates that the biradical cleaves almost quantitatively to produce carbonyl compound even in non-polar solvents. This behaviour contrasts with that observed in other 1,4-biradicals (9). Further, these results support the simplified reaction Scheme assumed, that disregards singlet photoprocesses other than intersystem crossing.

The data in Table 2 show that, for all compounds, the yield of aliphatic carbonyls extrapolated to zero time is larger than the benzaldehyde yield. This result can be explained in terms of the following competing 1,4-biradical reactions:

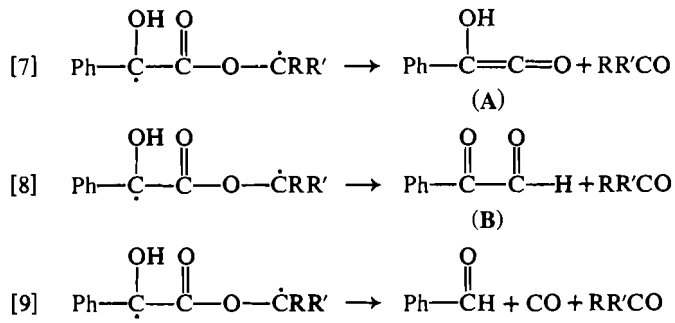

While the three processes give RR'CO, only reaction [9] gives benzaldehyde. The formation of **B** and **A** could explain the yellow colour developed during the photolysis in non-polar solvents. Nevertheless, the characteristics of the developed spectra are different from those shown by a solution of phenylglioxal in the same media. The lack of phenylglioxal formation (or accumulation) is also in agreement with previous results (1). On the other hand, the production of an hydroxy ketene as intermediate has been proposed both in the photolysis of alkyl benzoylformates (5), alkyl pyruvates, and oxoamides (17). The results obtained in the present work would support this suggestion. In particular, the response of the yellow absorption to the sample treatment and the ir spectra observed in carbon-tetrachloride would point to the formation of the ketene. The lack of yellow absorption in protic solvents and the product obtained in methanol can be also explained in terms of the fast solvolysis of the ketene. In methanol, the sequence could explain the production of **C**, although **C** may also result from photoreduction by the solvent followed by self-reaction of the ketyl radicals.

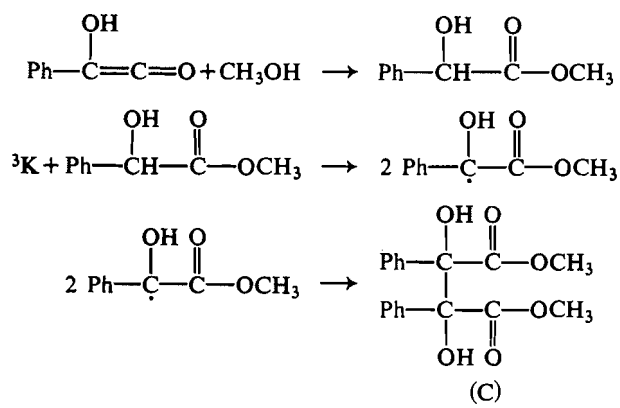

Experimental

Benzoylformic (phenylglyoxylic) acid (Fluka) was employed without further purification. The acid chloride was prepared as previously described (18). All benzoyl formic esters were prepared by reaction of the chloride of the benzoylformic acid with the aliphatic alcohol in basic media. A representative procedure is described below for **VI**.

Isopropyl benzoylformate (VI)

A solution of isopropanol (1.47 g) and pyridine (2.42 g) in 90 mL of dry benzene, cooled to 0°C, was added dropwise over 20 min to benzoylformic chloride (4.4 g) dissolved in 40 mL of dry benzene. The final mixture was stirred for 30 min. The white solid formed was filtered and to the filtrate were added 100 mL of ethyl ether. The organic phase was washed with 10% sodium bicarbonate, distilled water, and dried over Na_2SO_4. After solvent evaporation, the residue was distilled under reduced pressure yielding 4.6 g (92% yield) of the final product, bp 94–95°C, (1 Torr); nmr (CCl_4, TMS): 1.37 (d, 6H); 5.28 (m, 1H); 7.57 (m, 3H), 7.95 (m, 2H) ppm.

Methyl benzoylformate

Yield 94%, bp 75–76°C (1 Torr); nmr (CCl_4, TMS): 3.90 (s, 3H); 7.54 (m, 3H); 7.95 (m, 2H) ppm.

Ethyl benzoylformate

Yield 88%, bp 83–84°C (1 Torr); nmr (CCl_4, TMS): 1.40 (t, 3H); 4.43 (q, 2H), 7.54 (m, 3H); 7.98 (m, 2H) ppm.

n-*Propyl benzoylformate*

Yield 92%, bp 84–85°C (0.8 Torr); nmr (CCl_4, TMS): 0.97 (t, 3H); 1.73 (m, 2H); 4.33 (t, 2H); 7.54 (m, 3H); 7.95 (m, 2H) ppm.

n-*Butyl benzoylformate*

Yield 90%, bp 103–104°C (0.9 Torr); nmr (CCl_4, TMS): 0.94 (t, 3H); 1.55 (m, 4H); 4.37 (t, 2H); 7.54 (m, 3H); 7.95 (m, 2H) ppm.

Isobutyl benzoylformate

Yield 91%, bp 91–92°C (0.7 Torr); nmr (CCl_4, TMS): 0.95 (d, 6H); 1.80 (m, 1H); 4.12 (d, 2H); 7.54 (m, 3H); 7.95 (m, 2H) ppm.

t-*Butyl benzoylformate*

Yield 69%, bp 90–91°C (0.9 Torr); nmr (CCl_4, TMS): 1.62 (s, 9H); 7.54 (m, 3H), 7.95 (m, 2H) ppm.

Isoamyl benzoylformate

Yield 90%, bp 107–109°C (0.8 Torr); nmr (CCl_4, TMS): 0.95 (d, 6H); 1.67 (m, 3H); 4.37 (t, 2H); 7.54 (m, 3H); 7.97 (m, 2H) ppm.

Triplet spectra and triplet lifetimes were determined in nitrogen purged samples using for excitation the pulses from a Molectron UV-24 nitrogen laser (337.1 nm, ~8 ns, up to 10 mJ). The detection system makes use of a RCA-4840 photomultiplier tube whose signals were processed through an R-7912 Tektronix transient digitizer and analyzed using a PDP 11/23 computer. Further details can be found elsewhere (19).

Steady state photolyses at 20°C were carried out on deaerated samples. The light source was a medium pressure mercury lamp with a 366 nm glass filter. The reaction products were analyzed by gas chromatography using flame ionization detectors. The photofragmentation of valerophenone in *n*-hexane ($\phi_{acetophenone} = 0.33$ (20)) was used as an actinometer.

1. B. M. MONROE. Adv. Photochem. **8**, 77 (1971).
2. R. S. DAVIDSON and D. GOODWIN. J. Chem. Soc. Perkin Trans. II, 993 (1982).
3. R. S. DAVIDSON, D. GOODWIN, and P. F. DE VIOLET. Tetrahedron Lett. **22**, 2485 (1981).
4. A. ZANOCCO, F. CASTAÑEDA, J. C. SCAIANO, M. V. ENCINAS, and E. A. LISSI. Acta Sudam. Quim. **2**, 5 (1982).
5. E. S. HUYSER and D. C. NECKERS. J. Org. Chem. **29**, 276 (1964).
6. P. A. LEERMAKERS, P. C. WARREN, and G. F. VEREY. J. Am. Chem. Soc. **86**, 1768 (1964).
7. J. R. DYER. Applications of absorption spectroscopy of organic compounds. Prentice-Hall Inc. N.Y. 1965. pp. 34–36.
8. P. J. WAGNER. Acc. Chem. Res. **4**, 168 (1971).
9. J. C. SCAIANO, E. A. LISSI, and M. V. ENCINAS. Rev. Chem. Intermed. **2**, 139 (1978).
10. M. V. ENCINAS, E. A. LISSI, E. LEMP, A. ZANOCCO, and J. C. SCAIANO. J. Am. Chem. Soc. **105**, 1856 (1983).
11. J. GROTEWOLD, D. SORIA, C. M. PREVITALI, and J. C. SCAIANO.

J. Photochem. **1**, 471 (1972/73).
12. M. V. ENCINAS and E. A. LISSI. J. Photochem. **6**, 173 (1976/77).
13. N. J. TURRO and T. J. LEE. J. Am. Chem. Soc. **91**, 5651 (1969).
14. P. J. WAGNER, R. G. ZEPP, K. C. LIU, M. THOMAS, T. Y. LEE, and N. J. TURRO. J. Am. Chem. Soc. **98**, 8125 (1976).
15. M. V. ENCINAS and J. C. SCAIANO. Unpublished results.
16. P. J. WAGNER and A. E. KEMPPAINEN. J. Am. Chem. Soc. **94**, 7495 (1972).
17. N. C. YANG and A. MORDUCHOWITZ. J. Org. Chem. **29**, 1654 (1964); H. AOYAMA, T. HASEGAWA, and Y. OMOTE. J. Am. Chem. Soc. **101**, 5343 (1979).
18. H. C. J. OTTENHEIJM and J. H. M. DE MANS. Synthesis, 163 (1975).
19. J. C. SCAIANO. J. Am. Chem. Soc. **102**, 7747 (1980).
20. F. D. LEWIS and T. A. HILLIARD. J. Am. Chem. Soc. **94**, 3852 (1972).
21. M. V. ENCINAS and E. A. LISSI. J. Photochem. **4**, 321 (1975).
22. M. V. ENCINAS, E. A. LISSI, and F. A. OLEA. J. Photochem. **14**, 233 (1980).

Can. J. Chem. Downloaded from www.nrcresearchpress.com by 210.87.254.105 on 09/06/12
For personal use only.

COMMUNICATION

Olefin hydrogenation catalysed by chrysotile asbestos fibres and supported titanocene

DANIEL COZAK[1] AND CHRISTIAN DEBLOIS
Chemistry Department, Laval University, Quebec, P.Q., Canada G1K 7P4

Received September 22, 1983

DANIEL COZAK and CHRISTIAN DEBLOIS. Can. J. Chem. **62**, 392 (1984).

The double bond hydrogenation at NTP catalysed by both natural short fibre chrysotile asbestos and $(\eta^5\text{-}C_5H_5)_2TiCl$ treated fibres is reported for some linear and cyclic olefins.

DANIEL COZAK et CHRISTIAN DEBLOIS. Can. J. Chem. **62**, 392 (1984).

Nous avons étudié les propriétés hydrogénantes à TPN de la fibre d'amiante chrysotile et de la fibre traitée au $(\eta^5\text{-}C_5H_5)_2TiCl$. Nous rapportons ici les propriétés catalytiques des fibres naturelles et traitées, pour l'hydrogénation de quelques oléfines linéaires et cycliques.

Can. J. Chem. Downloaded from www.nrcresearchpress.com by 210.87.254.105 on 09/06/12
For personal use only.

Chrysotile is a naturally occurring magnesia–silicate mineral best described by the ideal formula $[3MgO \cdot 2SiO_2 \cdot 2H_2O] \cdot nH_2O$, where n is the number of loose water molecules. Furthermore, the natural fibre contains varying amounts (total < ca. 4 wt.%) of transition metals such as iron, manganese, chromium, and nickel. Moreover, chrysotile has a unique and highly organized structure made up typically of 16–18 rolled up coaxial brucite–silicate bilayers. This gives chrysotile fibres an hollow-tube-like morphology (1). Also, several bis(cyclopentadienyl)titanium complexes are known to be catalytically active for both the homogeneous phase (2) and for the mineral oxide supported heterogeneous phase hydrogenation of olefins (3–5). Bearing this in mind, we have prepared a titanocene, $(\eta^5\text{-}C_5H_5)_2TiCl$, treated fibre and studied its hydrogenating properties. We have, in the course of this work, observed a remarkably high activity and selectivity, reported here, for the untreated natural chrysotile asbestos comparable to the treated chrysotile catalyst. Hence we wish to report in this communication the hydrogenation curves and initial hydrogenation rates observed in the alkene-to-alkane conversion reaction of some olefins using both the untreated chrysotile and chrysotile–titanocene treated fibres as catalyst.

The chrysotile asbestos used in our study was of the short fibre variety, obtained by sedimentation and flocculation of commercial 4T30 chrysotile asbestos (6). The scanning electron microscope (SEM) revealed that the fibres were mainly 1–10 μm in length, 200–400 Å in diameter and monofibrils.

The titanocene treated chrysotile was obtained by reacting $(\eta^5\text{-}C_5H_5)_2TiCl$ with short fibres in refluxing toluene under a positive argon pressure for 12 h. The air-sensitive green solid product was then rinsed and thoroughly washed in a soxhlet extractor with benzene for 24 h. Also, we observed that it is possible to introduce up to 3.2 wt.% titanium on the fibre, depending on the initial complex concentration and reaction times, without destroying its morphology. The following equation is proposed for the reaction, based on both spectroscopic data and the reactivity of titanium chlorides with chrysotile (6, 7),

$$\text{chrysotile} + (\eta^5\text{-}C_5H_5)_2TiCl \xrightarrow{\text{toluene}} \text{chrysotile-Ti}(\eta^5\text{-}C_5H_5)_2 + HCl$$

Hydrogenation of the olefins was carried out in the following manner for all the experiments. The fibres (ca. 1.0 g) were placed in a glass reactor containing toluene (10 mL, temperature controlled 27 ± 0.1°C) and equipped with a mercury gas burette to monitor the hydrogen uptake. The fibres were then reduced with *n*-butyllithium (1.80 mmol) and the argon atmosphere replaced by pure hydrogen at atmospheric pressure (755 Torr). Gas uptake was measured immediately after adding the olefin from a dropping funnel to the stirred fibre suspension.

When natural chrysotile asbestos short fibres were used as catalyst in the reactor, hydrogen consumption was observed for cyclohexene, cyclooctene, 1-hexene, 1-heptene, 1-octene, 1-decene, and 1,4-hexadiene, with concomitant conversion of the olefin to the corresponding saturated alkane. The hydrogenation products and conversion yields were measured by gc (12 foot Carbowax column, 70°C) and by gc – mass spectroscopy. Table 1 summarizes the reaction conditions used and hydrogenation data for the studied olefins. All reactions were carried out at normal temperature and pressure (27°C, 755 Torr) and the alkene–alkane conversion yields were all quantitative when the gas consumption ceased.

Figure 1 shows the hydrogen uptake curves as a function of time for some monoolefins studied, measured during hydrogenation using chrysotile asbestos fibres. The curves show that the initial hydrogen uptake varies almost linearly. Hence, the slope or the hydrogenation rate is estimated to be constant for this portion of the reaction. The initial hydrogen uptake rates given in Table 1 were calculated from such curves. We have also noticed that this rate is of zero order in olefin concentration. Another feature observed in the hydrogenation reactions is the bending of the curve, leading to a plateau towards the end of the reaction, when most of the olefin is consumed. The hydrogenation curve for 1-hexene (curve *3*) illustrates well this phenomenon. Hence, for this curve the initial hydrogen consumption is 0.58 mL H_2 min^{-1} g^{-1} of chrysotile till approximately 75% of the heptene is converted to heptane. After this concentration there is a sharp bend in the curve and the slope slowly tapers off till the remaining olefin is hydrogenated. Another visible feature in several reactions is a sharp absorption step from 0 to 6 mL (0.27 mmol) when the olefin is added to the fibre suspension. For example, this is visible in curves *2* and *4* and is not believed to be directly related to the catalytic hydrogenation absorption by the olefins.

In one experiment, the catalytic behavior of the chrysotile fibres was checked by performing two successive hydro-

[1]To whom all correspondence should be addressed.

TABLE 1. Experimental data and initial hydrogen gas consumption rates for the hydrogenation of some alkenes by asbestos chrysotile short fibres at 27°C and 755 Torr[a]

Olefine to be hydrogenated	Olefine (mmol)	Chrysotile fibres (g) Untreated	Chrysotile fibres (g) Treated[b]	Initial rate of H_2 uptake during hydrogenation (mL of H_2 min^{-1} g^{-1} of chrysotile)[c]
Cyclohexene (*1*)[d]	1.97	1.51		0.37
	1.97		1.05	0.00
Cyclooctene (*2*)	1.69	1.05		0.026 (±0.005)
	1.69		1.02	0.061 (±0.005)
1-Hexene (*3*)	1.60	1.08		0.58
	1.60		1.26	0.84
1-Heptene (*4*)	1.42	0.93		0.65
	1.42		1.46	0.86
1-Octene	1.27	1.03		1.29
	1.27		1.02	0.24
1-Decene (*5*)	1.06	1.03		0.67[e]
	1.06		1.01	0.13
1,4-Hexadiene	0.85	1.01		0.85
	0.85		1.09	0.068 (±0.006)

[a]The hydrogenation cell was temperature-controlled to within ±0.1°C and pressure variations did not exceed ±5 Torr during the reaction. The values reported in this table have been corrected for atmospheric variations between readings on the gas burette.
[b]Asbestos chrysotile short fibres treated with $(\eta^5\text{-}C_5H_5)_2TiCl$. The fibres used here are all from the same reaction (50 g batch) and contained 0.99 wt.% Ti.
[c]Unless otherwise indicated, error = ±0.03.
[d]The numbering corresponds to the curves given in Fig. 1.
[e]A second addition of 1.27 mmol olefine to the same reaction mixture gave the same initial hydrogen uptake rate, see text.

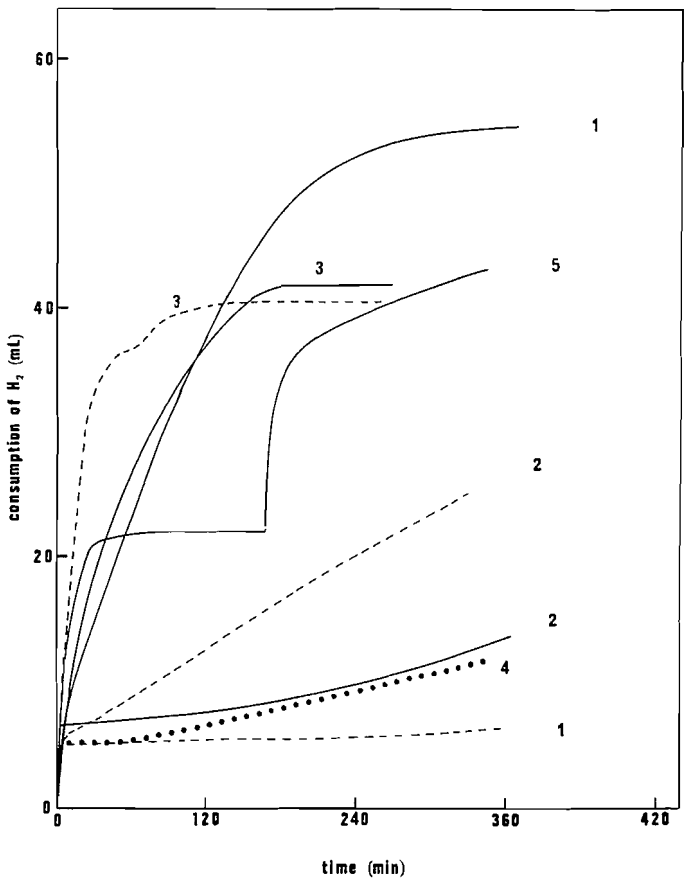

FIG. 1. Hydrogen consumption versus time curves for the hydrogenation of some monoolefins by chrysotile asbestos short fibres (—), chrysotile–titanocene short fibres (---), and commercial 4T30 Quebec chrysotile asbestos (···). The numbering corresponds to the alkenes in Table 1.

genation reactions using the same fibre. Curve *5* shows the hydrogen uptake for this experiment. The first part of the curve, segment A–B, corresponds to the gas uptake for the first 1.06 mmol 1-decene added to the reaction. Segment B–C shows the gas uptake after the second addition, 1.27 mmol 1-decene, to the same reaction mixture. These two segments are almost identical and the initial olefin reaction rates for both additions are the same (cf. Table 1).

In another experiment the hydrogenation of 1-heptene was carried out using commercial 4T30 chrysotile asbestos as received, curve *4* in Fig. 1. The hydrogenation rate of the commercial asbestos, 0.021 (±0.005) mL H_2 min^{-1} g^{-1} of chrysotile, is an order of magnitude slower than the rate for selected short fibres. We believe that this is due to the presence of amorphous mineral impurities usually associated with natural asbestos (8). Also chrysotile fibres containing non-bonded water were found to be less active for the hydrogenation of olefins.

Catalytic hydrogenation of the studied olefins was also observed for $(\eta^5\text{-}C_5H_5)_2TiCl$-treated fibres. The hydrogenation reaction conditions were identical to those used for the untreated chrysotile discussed above, and the experimental hydrogenation rates are given in Table 1. Figure 1 also shows the hydrogen consumption curves of some monoolefins for the chrysotile–titanocene catalyst. The fibres used in these experiments contained 0.99 wt.% titanium. The outstanding difference in the hydrogenation properties of untreated and titanocene treated fibres is the observed high selectivity of the latter for linear olefins over cyclohexene, as evidenced by the null hydrogenation rate observed for this olefin (cf. Table 1 and Fig. 1). Moreover, several hydrogenation experiments were carried out with different titanocene treated fibres[2] using equi-

[2]Both $(\eta^5\text{-}C_5H_5)_2TiCl$ and $(\eta^5\text{-}C_5H_5)_2TiCl_2$ reacted short fibre chrysotile containing up to 3.2 wt.% Ti were used in these experiments.

Can. J. Chem. Downloaded from www.nrcresearchpress.com by 210.87.254.105 on 09/06/12
For personal use only.

molar mixtures of 1-octene and cyclohexene. The only hydrogenation product detected in these experiments was octane. Furthermore, in all cases the cyclohexene was totally recovered, even after 3 days of reaction. This is, to the best of our knowledge, the first time such a selectivity for a titanocene catalyst is reported.

In order to verify if the observed hydrogenation was due to a homogeneous catalytic reaction arising from dissolved titanocenes, a new olefin addition was made to the decanted filtrate taken from a previous hydrogenation run. Under these conditions no hydrogen consumption was observed when 1-octene was added to the filtrate. Moreover, the amount of titanium measured in the filtrate of several runs never exceeded 8 ppm and is believed to be due mainly to small suspended fibres in the filtrate.

The fibrous structure and chemical composition of the catalysts were checked both before and after hydrogenation by elemental microanalysis,[3] SEM micrography, ir, and SEM-ED X-ray[4] spectroscopy. These results indicate that initial composition of the fibres is not significantly affected by the hydrogenation process and the fibre morphology is preserved. From microanalysis, high carbon and hydrogen values were found for both the titanocene-treated fibres and the fibres recovered after hydrogenation. Furthermore, SEM micrographs (20 000×) of the brown–black solid after catalysis show that the fibres retained their fibrous morphology. Also the SEM-ED X-ray spectra of the fibres after catalysis remained unchanged as evidenced from the Si/Mg and Ti/Mg intensity ratios. Similarly, the ir spectra (KBr pellet) of reacted fibres in all cases showed the characteristic brucite vibrations at 3685 and 3640 cm^{-1} and silicate vibrations at 1075, 1015, and 950 cm^{-1}. However, the intensity of the water bands at ca. 3400 and 1625 cm^{-1} increased in the spectra of the titanium-treated fibres and after hydrogenation reactions. Moreover, two new bands of weak intensity at 1260 and 795 cm^{-1} and slight changes for the silicate intensities at 1015 and 950 cm^{-1} are indicative of some chemical or structural modification in the fibres (9).

We are presently investigating the chemical origin of the observed catalytic property of natural chrysotile asbestos. The reaction rates measured so far seem to indicate that the active species in the natural chrysotile asbestos and the chemically modified chrysotile–titanocene fibres are not the same.

[3]Elemental microanalyses. *Anal.* calcd. for $Mg_3Si_2O_9H_4$: Si 20.27, Mg 26.31, H 1.44; found for the untreated chrysotile before catalysis (after catalysis): Si 18.89 (19.31), Mg 24.71 (24.59), Ti <0.05, C 0.25 (2.09), H 1.67 (1.38); found for the titanocene treated chrysotile before catalysis (after catalysis): Si 18.44 (19.18), Mg 24.80 (23.65), Ti 0.99 (0.93), C 1.67 (2.14), H 1.68 (1.29) %.

[4]The intensities were calculated by averaging the X-ray counts (300 s) from three spectra of the same sample. Found for chrysotile before catalysis (after catalysis): Si/Mg = 1.2 (1.2); found for the titanocene treated chrysotile before catalysis (after catalysis): Si/Mg = 1.2 (1.3) ± 0.1 and Ti/Mg = 0.03 (0.02) ± 0.002. Literature value Si/Mg = 1.3, from ref. 10.

Acknowledgments

The authors are grateful to the Natural Sciences and Engineering Research Council of Canada, the "Programme de formation de chercheurs et d'action concertée," and the "Institut de recherche et de développement sur l'amiante" for the financial support of this work. We also wish to thank the "Institut de recherche en santé et sécurité du travail du Québec" for a summer stipend awarded to C.D.

1. K. YADA. Acta Crystallogr. **23**, 704 (1967).
2. B. M. BULICHEV, E. V. EVDOKIMOVA, A. I. SIZOV, and G. L. SOLOVEICHIK. J. Organomet. Chem. **239**, 313 (1982).
3. W. SKUPINSKI, I. CIESLOWSKA, and S. MALINOWSKI. J. Organomet. Chem. **182**, C33 (1979).
4. R. JACKSON, J. RUDDLESDEN, D. J. THOMPSON, and R. WHELAN. J. Organomet. Chem. **125**, 57 (1977).
5. J. C. W. CHIEN and J. T. T. HSIEH. Coordination polymerization. *Edited by* J. C. W. Chien. Academic Press, NY. 1975. p. 305.
6. D. COZAK, C. BARBEAU, F. GAUVIN, J.-P. BARRY, C. DEBLOIS, R. DEWOLF, and F. KIMMERLE. Can. J. Chem. **61**, 2753 (1983).
7. R. DECHENNE and P. DECROLY. Ger. Pat. No. 2 130 677 (1971); Chem. Abstr. **76**, 114 154c (1972).
8. M. S. BADOLLET and J. P. MCGOURTY. Asbestos. A symposium of articles. *Edited by* M. S. Badollet. The Canadian Institute of Mining and Metallurgy. 1961. p. 44.
9. Z. JOHAN, J. GONI, C. SARCIA, G. BONNAUD, and J. BIGNON. Advances in organic geochemistry 1973. Proceedings of the 6th International Meeting on Organic Geochemistry. *Edited by* B. Tissot and F. Bienner. Editions Technip, Paris, France. 1973. p. 883.
10. E. S. CRAWFORD, D. A. JEFFERSON, J. M. THOMAS, and A. C. BISHOP. J. Chem. Soc. Chem. Commun. 986 (1979).

Can. J. Chem. Downloaded from www.nrcresearchpress.com by 210.87.254.105 on 09/06/12
For personal use only.

Stability and solubility relationships between some solids in the system $PbO-CO_2-H_2O$[1]

PETER TAYLOR AND VINCENT J. LOPATA

Research Chemistry Branch, Atomic Energy of Canada Limited, Whiteshell Nuclear Research Establishment, Pinawa, Man., Canada R0E 1L0

Received May 9, 1983

PETER TAYLOR and VINCENT J. LOPATA. Can. J. Chem. **62**, 395 (1984).

We have determined equilibrium conditions for each reaction in the solid interconversion sequence $PbO \rightleftharpoons Pb_{10}O(OH)_6(CO_3)_6$ (plumbonacrite) $\rightleftharpoons Pb_3(OH)_2(CO_3)_2$ (hydrocerussite) $\rightleftharpoons PbCO_3$ (cerussite), in aqueous carbonate solutions near 25°C. Our data yield the following Gibbs energies of formation from the elements, $\Delta_f G°$(298.15 K): plumbonacrite, -5310 ± 31 kJ mol^{-1}; hydrocerussite, -1705 ± 11 kJ mol^{-1}; cerussite, -628.0 ± 3.9 kJ mol^{-1}. Corresponding estimated values of $\Delta_f G°$(373 K) are -5120 ± 50, -1643 ± 18, and -612 ± 9 kJ mol^{-1}, respectively. We have demonstrated the existence of a narrow stability field for plumbonacrite, and convenient small-scale preparations of hydrocerussite and plumbonacrite are described. Gibbs energy data for the solids have been combined with selected data for aqueous lead species in a detailed computation of solubility behaviour for this system at 25°C.

PETER TAYLOR et VINCENT J. LOPATA. Can. J. Chem. **62**, 395 (1984).

Nous avons déterminé les conditions d'équilibre de chaque réaction dans les interconversions suivantes à l'état solide: $PbO \rightleftharpoons Pb_{10}O(OH)_6(CO_3)_6$ (plumbonacrite) $\rightleftharpoons Pb_3(OH)_2(CO_3)_2$ (hydrocérussite) $\rightleftharpoons PbCO_3$ (cérussite), dans des solutions aqueuses de carbonate à environ 25°C. Nos données fournissent les énergies de Gibbs suivantes pour la formation à partir des éléments $\Delta_f G°$(298,15 K): plumbonacrite, -5310 ± 31 kJ mol^{-1}; hydrocérussite -1705 ± 11 kJ mol^{-1}; cérussite $-628,0 \pm 3,9$ kJ mol^{-1}. Les $\Delta_f G°$(373 K) sont respectivement évalués comme étant suivantes; -5120 ± 50, -1643 ± 18 et -612 ± 9 kJ mol^{-1}. Nous avons démontré l'existence d'un champ étroit de stabilité pour le plumbonacrite et nous décrivons une préparation convenable à faible échelle de l'hydrocérussite et du plumbonacrite. On a combiné les données d'énergie de Gibbs des solides avec des données choisies pour des composés du plomb en solution aqueuse dans un calcul détaillé du comportement de ce système en ce qui a trait à la solubilité à 25°C.

[Traduit par le journal]

Introduction

Many solids exist in the system $PbO-CO_2-H_2O$. Of these, two polymorphs of PbO (litharge and massicot) and three carbonates (cerussite, $PbCO_3$; hydrocerussite, $Pb_3(OH)_2(CO_3)_2$; plumbonacrite, $Pb_{10}O(OH)_6(CO_3)_6$) occur in aqueous systems near ambient temperature and pressure (1, 2). Garrels and Christ (3) have discussed the stability fields of PbO, cerussite, and hydrocerussite in the system $Pb-O_2-CO_2-H_2O$ at 25°C. Recently, plumbonacrite was reported (4) to be metastable with respect to decomposition according to reaction [1]:

[1] $$Pb_{10}O(OH)_6(CO_3)_6 \rightarrow PbO + 3Pb_3(OH)_2(CO_3)_2$$

Several phases of the type $aPbCO_3 \cdot bPbO$ occur during thermal decomposition of the named carbonates, but do not normally occur in aqueous systems (5–7). Grisafe and White (7) determined the stability fields of these phases in the system $PbO-CO_2$ at elevated temperatures and pressures. A hydrated lead(II) oxide, $3PbO \cdot H_2O$ or $Pb_6O_4(OH)_4$, is also known (8–11), and early solubility measurements indicate that it may be marginally stable with respect to reaction [2] at ambient temperature (11):

[2] $$6PbO(s) + 2H_2O(l) \rightarrow Pb_6O_4(OH)_4(s)$$

Our interest arose from the possible use of lead compounds to precipitate $^{14}CO_3$ species, which are radioactive contaminants produced in the heavy-water moderator systems of Canadian nuclear reactors (12). The formation of lead carbonates may also be important in high-level radioactive waste disposal, since lead has been proposed as an investment material for used nuclear fuel in a deep underground disposal vault (13). Lead carbonates are also of some importance in the environmental and mineralogical behaviour of lead (14–18). We have studied interconversions among the five named solids to determine equilibrium constants and hence to compute solubility and stability relationships.

Experimental

Starting materials were reagent-grade PbO, KOH, K_2CO_3 (Fisher), and CO_2 (Matheson). Carbonate-free KOH solutions (J. T. Baker) were used in key determinations. Potassium salts were used in preference to sodium salts to avoid precipitation of $NaOH \cdot 2PbCO_3$, which is less soluble than $KOH \cdot 2PbCO_3$ (19). The PbO reagent was a mixture of litharge and massicot; this was adequate for most purposes, since their Gibbs energies of formation differ by only about 1 kJ mol^{-1} (20, 21). Samples of litharge and massicot were collected whenever they were obtained as pure reaction products. Recrystallized litharge, prepared in an earlier study (22), was also used in a few experiments.

(a) Preparation of cerussite

Pure cerussite was readily made by bubbling CO_2 through a suspension of PbO (20 g) in dilute acetic acid (10^{-3} mol dm^{-3}, 200 cm^3) at room temperature for 6 h. Unlike Olby (2), we did not obtain plumbonacrite or hydrocerussite as pure intermediates, although they did occur sequentially as major phases. Our preparation was on a smaller scale than Olby's, with a more dilute suspension of PbO.

(b) Preparation of hydrocerussite

Pure hydrocerussite was prepared by shaking a suspension of cerussite (5 g) in a solution of K_2CO_3 (8 g in 200 cm^3) for 48 h at room temperature. Alternatively, cerussite (5 g) was added to aqueous KOH (10^{-3} mol dm^{-3}, 200 cm^3), and the pH of the stirred suspension was maintained at 11 for 24 h, using an automatic titrator charged with KOH solution (0.1 mol dm^{-3}).

(c) Preparation of plumbonacrite

Hydrocerussite (5 g) was suspended in a solution (200 cm^3) of K_2CO_3 (13 g) and KOH (2 g), which was then stirred for 48 h at 100°C. The filtered product comprised plumbonacrite (>80%) and

[1] Issued as AECL-7974.

Can. J. Chem. Downloaded from www.nrcresearchpress.com by 210.87.254.42 on 09/06/12
For personal use only.

TABLE 1. Solution data for final series of hydrocerussite/cerussite equilibration runs (*a*) 5 days, (*b*) 13 days

Run*	Initial HCO_3^- (%)†	Final $[C_t] \times 10^3$ (mol dm^{-3}) (*a*)	(*b*)	pH(meter) (*a*)	(*b*)	pH(calcd)‡ (*a*)	(*b*)	Final HCO_3^- (%)†§ (*a*)	(*b*)	$p(CO_2)$‖ (Pa)
1	100	3.4	3.1	9.14	9.12	9.22	9.20	91.4	91.8	13.4
2	80	3.5	3.4	9.14	9.17	9.18	9.18	91.9	92.0	14.1
3	60	4.3	4.0	9.28	9.29	9.29	9.27	89.8	90.3	12.8
4	40	4.3	4.5	9.27	9.26	9.29	9.30	90.1	89.5	13.5
5	20	4.7	4.9	9.32	9.35	9.29	9.31	89.6	89.1	13.3
6	0	—	5.3	9.40	9.36	—	9.35	—	89.1	12.8

* Initial $[C_t] = 3 \times 10^{-3}$ mol dm^{-3}.
† Percentage of total carbonate concentration.
‡ Calculated from titration data.
§ Calculated from average of meter and calculated pH values.
‖ Calculated from average of all pH measurements and calculations.

hydrocerussite. This was crushed using a pestle and mortar, and returned to the solution for a further 24 h at 100°C. Care was needed to maintain the pH near 13, to remain within the narrow stability field of plumbonacrite (see below). This procedure was repeated until hydrocerussite was reduced to <5% (usually two or three cycles); it was difficult to eliminate completely.

(d) Interconversion reactions

Over 200 experiments were run, in which the various solids were exposed to solutions of different pH and total carbonate concentration, $[C_t]$.[2] Most experiments were run in screw-topped plastic bottles; long equilibration runs were performed in flame-sealed Pyrex glass vials. Solid products were identified and their purity estimated by X-ray powder diffractometry (XRD), using CuK_α radiation and a Philips PW-1150 diffractometer equipped with a diffracted-beam monochromator. When necessary, solutions were analyzed for lead by atomic absorption spectrophotometry, and for carbonate by titration or using a CO_2-sensing electrode (Orion model 95-02). Measurements of pH were made with a glass electrode. When precise pH measurements were needed (see Table 1), the electrode was calibrated with a fresh sodium borate buffer solution having pH = 9.00 or 9.18.

Results and discussion

(a) Theoretical considerations

The solid interconversion reactions are conveniently expressed by reactions [3] to [5] below. In reaction [3], distinction should be drawn between reactions involving litharge and massicot.

$$[3] \quad \tfrac{5}{3}PbO(s) + CO_2(g) + \tfrac{1}{2}H_2O(l) \overset{p_1}{\rightleftharpoons} \tfrac{1}{6}Pb_{10}O(OH)_6(CO_3)_6(s)$$

$$[4] \quad \tfrac{3}{2}Pb_{10}O(OH)_6(CO_3)_6(s) + CO_2(g) + \tfrac{1}{2}H_2O(l) \overset{p_2}{\rightleftharpoons} 5Pb_3(OH)_2(CO_3)_2(s)$$

$$[5] \quad Pb_3(OH)_2(CO_3)_2(s) + CO_2(g) \overset{p_3}{\rightleftharpoons} 3PbCO_3(s) + H_2O(l)$$

Although these reactions involve many aqueous species, the equilibrium constant for each reaction can be expressed simply as the reciprocal of a carbon dioxide partial pressure,[3] $p(CO_2)$ (3, 23). The anionic activity quotient, $\{OH^-\}^2/\{CO_3^{2-}\}$, obtained from equilibria such as [6], is sometimes more convenient.

$$[6] \quad Pb_3(OH)_2(CO_3)_2(s) + CO_3^{2-}(aq) \rightleftharpoons 3PbCO_3(s) + 2OH^-(aq)$$

The $p(CO_2)$ value associated with a solution is conveniently manipulated between 10^{-6} and 10^2 Pa by adjusting pH and $[C_t]$. Total carbonate activity $\{C_t\}$, proton activity $\{H^+\}$, and $p(CO_2)$ are interrelated at 25°C by expression [7], which is derived from equations given by Stumm and Morgan (ref. 23, chapt. 4) and accepted Gibbs energy data for water and carbonate species (e.g. 21, 24):

$$[7] \quad \frac{\{C_t\}}{p(CO_2)} = \left[1 + \frac{4.34 \times 10^{-7}}{\{H^+\}} + \frac{2.04 \times 10^{-17}}{\{H^+\}^2}\right] \times 3.4 \times 10^{-7} \text{ mol } kg^{-1} \text{ Pa}^{-1} (\approx \text{mol } dm^{-3} \text{ Pa}^{-1})$$

We have not distinguished between molal and molar concentration units, since the resulting errors are much less than the experimental uncertainties. We have used expression [8] as proposed by Davies (ref. 23, pp. 134–136; ref. 25) to estimate the mean ionic activity coefficient, $f_\pm$, and hence bicarbonate and carbonate activities, from the ionic charge, z, and the ionic strength, I.

$$[8] \quad -\log f_\pm = 0.5z^2\left[\frac{I^{1/2}}{1 + I^{1/2}} - 0.3I\right]$$

Where necessary, I was calculated from measured pH and $[C_t]$ values by an iterative procedure.

(b) Reactions of cerussite with KOH

Reactions between cerussite (0.25 g) and KOH solutions (40 cm^3; various concentrations up to 5 mol dm^{-3}) were investigated at room temperature (22 ± 2°C). Cerussite alone was recovered from reactions with final pH below about 9.5. Hydrocerussite was the major product in the pH range 9.5–12. Plumbonacrite and hydrocerussite occurred together at pH ≈ 12–13.5. Lead(II) oxide was formed at pH ≈ 13.5–14; both litharge and massicot occurred, often one or the other as a pure phase, but with no obvious pattern of occurrence. Above pH ≈ 14, clear undersaturated lead solutions were formed. These observations are consistent with McIntyre's stability calculations reported by Garrels and Christ (3), except for the occurrence of plumbonacrite. Further experiments were designed to define the stability fields more exactly, with special attention to plumbonacrite.

[2] In this account, $[C_t]$ and $\{C_t\}$ represent the sums of the concentrations and activities, respectively, of non-complexed carbonate species, i.e. "H_2CO_3", HCO_3^-, and CO_3^{2-}, and do not include complexes such as $PbCO_3^0$ and $Pb(CO_3)_2^{2-}$.

[3] Strictly speaking, this term should be fugacity, rather than partial pressure, but the two are indistinguishable at the pressures of concern here.

Can. J. Chem. Downloaded from www.nrcresearchpress.com by 210.87.254.42 on 09/06/12
For personal use only.

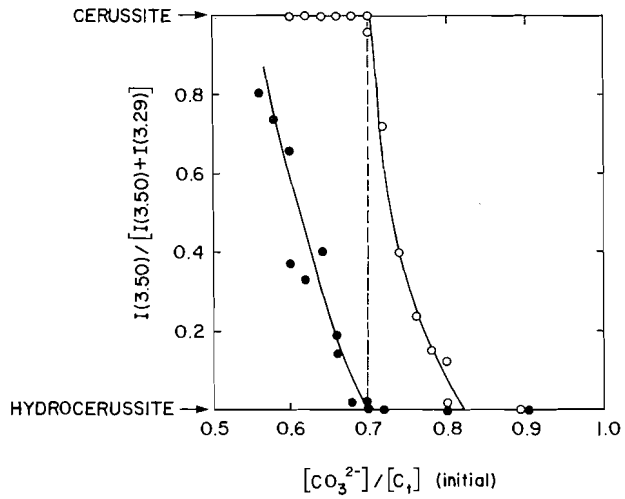

FIG. 1. Summary of X-ray diffraction data for products of reactions between cerussite (○) or hydrocerussite(o) with solutions having $[C_t] = [HCO_3^-] + [CO_3^{2-}] = 0.125$ mol dm^{-3}, for 48 h at 22°C. $I(3.50)$ and $I(3.29)$ are the peak heights of the most intense features in the cerussite and hydrocerussite diffraction patterns (3.50 Å and 3.29 Å, respectively). The ordinate function is thus an approximate measure of the extent of conversion.

(c) Cerussite–hydrocerussite interconversion

Experiments in which either cerussite or hydrocerussite was exposed to carbonate/bicarbonate solutions clearly showed that this interconversion is readily reversible at room temperature. XRD data, summarized in Fig. 1, indicated that hydrocerussite and cerussite were in equilibrium at $[CO_3^{2-}]/[C_t] = 0.70 \pm 0.02$ and $[C_t] = 0.125$ mol dm^{-3}. At lower $[CO_3^{2-}]/[C_t]$ ratios, hydrocerussite was converted to cerussite, and the reverse reaction occurred at higher ratios. Although equilibrium conditions are thus narrowly defined, ionic activities could not be estimated sufficiently well to calculate p_3 as precisely as we wished. Further experiments were therefore run at lower $[C_t]$, down to 10^{-3} mol dm^{-3}. At these lower concentrations, the quantity of hydrocerussite or cerussite consumed or formed in the reactions was too small to determine equilibrium conditions by XRD. We therefore deduced the direction of reaction, and judged whether equilibrium had been achieved, by careful measurement of pH and $[C_t]$.

Twenty-five experiments with $[C_t]$ between 10^{-3} and 10^{-2} mol dm^{-3} yielded values for p_3 between 8 and 16 Pa. In the final determination, duplicated experiments were run in sealed Pyrex glass vials, starting with a mixture of cerussite and hydrocerussite (0.5 g each) in solutions with various $[HCO_3^-]/[C_t]$ ratios and $[C_t] = 3 \times 10^{-3}$ mol dm^{-3}. This concentration provides the best compromise between the respective limitations of the carbonate analyses and the estimation of activity coefficients. One series of experiments ((*a*) in Table 1) was run for 5 days, and the second ((*b*) in Table 1) for 13 days. The pH was measured immediately after opening each vial. The solutions were then filtered and analyzed for carbonate and bicarbonate by titration; a pH value was then calculated from the titration data. Most measured and calculated pH values agreed within 0.04 units, the largest discrepancy being 0.08 units. We conclude that solution analyses were not substantially affected by exchange of CO_2 with the atmosphere. The results are summarized in Table 1. The values of p_3 at 25°C, determined from these runs, range from 12.8 to 14.1 Pa, with an average of 13.3 Pa. No correction was made for the actual experimental temperature of 22 ± 2°C, since the equilibrium quotient, $[CO_3^{2-}]/[C_t]$, changes only slightly between 22 and 100°C (see below).

Our determination of p_3 is in fair agreement with the value of 27 Pa obtained from the Gibbs energy data recommended by Sadiq and Lindsay (21). The discrepancy corresponds to a disagreement of about 1.8 kJ mol^{-1} in the Gibbs energy of reaction for reaction [5]. Our result is also consistent with Garrels' estimate of $p_3 \simeq 10$ Pa, which was based on deductions from the natural occurrence of cerussite and hydrocerussite (17).

(d) Interconversions involving plumbonacrite

Preliminary experiments indicated a narrow stability field for plumbonacrite, so subsequent work concentrated on confirming this observation and defining the boundaries of the field.

Plumbonacrite persisted unchanged for seven days in solutions with $[C_t] = 0.125$ mol dm^{-3} and [KOH] between 0.02 and 0.4 mol dm^{-3}. It was converted to massicot at [KOH] ≥ 0.6 mol dm^{-3}, with partial conversion occurring at 0.5 mol dm^{-3}. In similar experiments starting with PbO, plumbonacrite was formed at [KOH] = 0.1, but not at 0.5 mol dm^{-3}. Slow, partial conversion of plumbonacrite to hydrocerussite occurred at [KOH] ≤ 0.01 mol dm^{-3}, and the reverse reaction was observed in some runs with KOH concentrations between 0.05 and 0.08 mol dm^{-3}. The latter reaction, accelerated by heating to 100°C, provided the basis for our synthesis of plumbonacrite, described above. In triplicated experiments starting with mixtures of plumbonacrite and hydrocerussite at [KOH] = 0.01 and 0.1 mol dm^{-3}, the relative amount of plumbonacrite in the product was consistently higher at the higher KOH concentration. Although these interconversions are less clear-cut than the hydrocerussite–cerussite reaction, we could nevertheless observe reversible reactions in the sequence PbO ⇌ plumbonacrite ⇌ hydrocerussite, thus confirming that plumbonacrite has a narrow stability field. This narrowness can account for the scarcity of plumbonacrite in nature (4).

Further experiments in sealed glass vials were run for 7–14 days with mixtures of PbO and plumbonacrite (0.3 g each) in 20 cm^3 aliquots of solutions with various KOH concentrations at $[K_2CO_3] = 10^{-1}$, 10^{-2}, and 10^{-3} mol dm^{-3}. Most runs did not reach equilibrium, but the direction of reaction [9] (equivalent to reaction [3]) could be determined from solution analyses for carbonate and/or hydroxide.

$$[9] \quad \frac{5}{3}\,PbO + CO_3^{2-} + \frac{3}{2}\,H_2O \rightleftharpoons \frac{1}{6}\,Pb_{10}O(OH)_6(CO_3)_6 + 2OH^-$$

The results are presented in Fig. 2. From these we estimate the equilibrium constant $\{OH^-\}^2/\{CO_3^{2-}\} = 10^{0.1 \pm 0.6}$ mol dm^{-3}, which corresponds to $p_1 = 10^{-4.9 \pm 0.6}$ Pa. We did not discern reproducible differences between reactions involving PbO reagent and our synthetic litharge, except that the latter material reacted more lethargically. Based on the free energies of formation of massicot and litharge, p_1 values for the two forms of PbO should differ by a factor of about 1.5, whereas we estimate an error of a factor of four in p_1.

Interconversion between hydrocerussite and plumbonacrite was too slow at $[C_t] \leq 10^{-2}$ mol dm^{-3} to pin-point the equilibrium at low ionic strength. The close crystallographic similarity between these phases may promote epitaxial crystallization with consequent passivation of one phase by the other. Furthermore, their solubility behaviour is very similar (see Fig. 5), so the driving force for interconversion is slight.

Can. J. Chem. Downloaded from www.nrcresearchpress.com by 210.87.254.42 on 09/06/12
For personal use only.

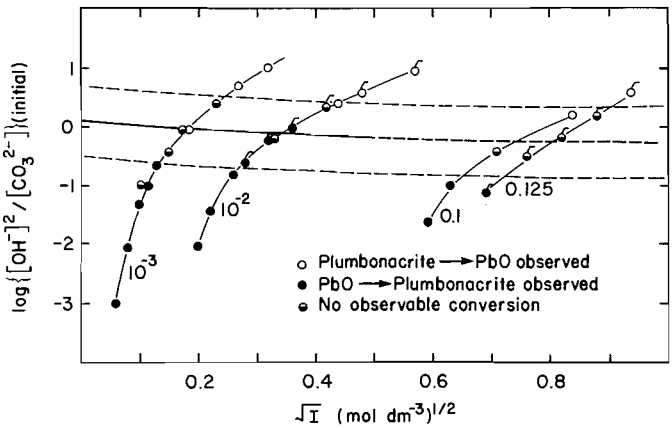

FIG. 2. Summary of conditions under which interconversion of PbO and plumbonacrite was observed. The numbering on the figure indicates carbonate concentration (mol dm^{-3}). The bold lines correspond to log $K = 0.1 \pm 0.6$ for eq. [9], using eq. [8] to estimate deviation from ideality. Flagged data points correspond to determinations by visual observation ($[CO_3^{2-}] = 0.01$ mol dm^{-3}) or X-ray diffraction ($[CO_3^{2-}] = 0.125$ mol dm^{-3}). The remaining observations are based on solution analyses.

Based on the results obtained at $[C_t] = 0.125$ mol dm^{-3} we estimate that p_2 exceeds p_1 by one to three orders of magnitude, so we assign the value $p_2 = 10^{-2.9 \pm 1.6}$ Pa. Since plumbonacrite and hydrocerussite differ only slightly in composition, calculated Gibbs energies and solubilities are much less sensitive to errors in p_2 than in p_1 or p_3, so precise measurement of p_2 is relatively unimportant in the overall description of the system, except in determining the plumbonacrite–hydrocerussite stability boundary (see expressions [12] and [13] below).

(e) Gibbs energies of formation of the carbonates

When expression [10] is applied successively to reactions [3] to [5], using Gibbs energy data from ref. 21, we obtain relationships [11] to [13]. These permit us to calculate the Gibbs energies of formation, $\Delta_f G°(298.15\ K)$, of the three lead carbonates from the $p(CO_2)$ data.[4]

[10] $\Delta_f G°(\text{products}) = \Delta_f G°(\text{reactants}) + RT \ln p(CO_2, \text{equilibrium, atmospheres})$

[11] $\Delta_f G°(\text{plumbonacrite, s, } 298.15\ K) = -(4970.8 - 34.25 \log p_1') = -5310 \pm 31\ \text{kJ mol}^{-1}$

[12] $\Delta_f G°(\text{hydrocerussite, s, } 298.15\ K) = -(1593.8 - 10.28 \log p_1' - 1.14 \log p_2') = -1705 \pm 11\ \text{kJ mol}^{-1}$

[13] $\Delta_f G°(\text{cerussite, s, } 298.15\ K) = -(583.7 - 3.43 \log p_1' - 0.38 \log p_2' - 1.90 \log p_3') = -628.0 \pm 3.9\ \text{kJ mol}^{-1}$

(Estimated errors include our own experimental uncertainties, plus those in Gibbs energies of formation of the parent oxides, as indicated in ref. 24, since the latter uncertainties are not stated in ref. 21. Data from ref. 21 were used for consistency with the solubility computations, shown below.)

[4] The data of ref. 21 refer to a standard state pressure of one atmosphere (1.013×10^5 Pa). In eqs. [11] to [13], p_1', p_2', p_3' are partial pressures in atm.

TABLE 2. Gibbs energy data used to determine equilibrium relationships

Species*	$\Delta G°_{f,298}$ (kJ mol^{-1})	Reference
$PbCO_3$(s)	−628.0	This work
$Pb_3(OH)_2(CO_3)_2$(s)	−1705	This work
$Pb_{10}O(OH)_6(CO_3)_6$(s)	−5310	This work
PbO(s) (litharge)	−189.3	21
CO_2(g)	−394.38	21
H_2O(l)	−237.18	21
"H_2CO_3(aq)"	−623.21	21
HCO_3^-(aq)	−586.89	21
CO_3^{2-}(aq)	−527.94	21
Pb^{2+}(aq)	−24.69	21
$PbOH^+$(aq)	−217.94	21
$Pb(OH)_2^0$(aq)	−397.73	21
$Pb(OH)_3^-$(aq)	−575.89	21
Pb_2OH^{3+}(aq)	−250.04	21
$Pb_3(OH)_4^{2+}$(aq)	−886.42	21
$Pb_4(OH)_4^{4+}$(aq)	−928.22	21
$Pb_6O(OH)_6^{4+}$(aq)	−1559.59	21, 38, 29, see text
$PbCO_3^0$(aq)	−593.37	44, 45
$Pb(CO_3)_2^{2-}$(aq)	−1141.17	44, 45

* Our grounds for omission of the following species are presented in the text: PbO(s) (massicot), $Pb(OH)_2$(s), $Pb_6O_4(OH)_4$(s), $Pb_3(OH)_3^{3+}$(aq), $Pb_3(OH)_5^+$(aq), $Pb_6(OH)_8^{4+}$(aq).

Our experimental Gibbs energy for cerussite, -628.0 ± 3.9 kJ mol^{-1}, lies within the range of reported values cited by Sadiq and Lindsay (21), −625.5 to − 629.0 kJ mol^{-1}, and is not significantly different from their recommended, recalculated value of −629.7 kJ mol^{-1}, originating from the calorimetric work of Adami and Conway (26). Our value of -1705 ± 11 kJ mol^{-1} for hydrocerussite agrees with their calculation of −1711.6 kJ mol^{-1}, derived from the pioneering solubility study by Randall and Spencer, the only source they cite (11, 21). Our estimate of -5310 ± 31 kJ mol^{-1} for plumbonacrite is much more negative than the value of −5121 kJ mol^{-1} reported by Haacke and Williams (4). The source of so large a discrepancy is not readily apparent, since few details are given in ref. 4. We emphasize that our value is consistent with extensive observations of interconversion reactions involving plumbonacrite.

(f) Calculation of solubility–stability relationships

Solubility calculations were performed using the computer program DIST, which was developed at these laboratories by Robert J. Lemire and Nava C. Garisto.[5] This program calculates species distributions, at given pH and ligand activities, from Gibbs energies of formation of the solid and solution species concerned. The results are expressed as activities, in molal units. We have used molar units throughout the discussion, since the resulting errors are negligible at the level of precision of our data. Our selected Gibbs energy data are shown in Table 2.

[5] Strictly speaking, this program calculates the activities of species in saturated solutions. It is reasonable to equate the total lead activity, $\{Pb_t\} = \Sigma x\{Pb_xL_y^{z+}\}$, to solubility at ionic strengths below about 0.01 mol dm^{-3}.

Can. J. Chem. Downloaded from www.nrcresearchpress.com by 210.87.254.42 on 09/06/12
For personal use only.

Can. J. Chem. Downloaded from www.nrcresearchpress.com by 210.87.254.42 on 09/06/12
For personal use only.

Although hydroxo- and carbonato-lead(II) complexes have received much experimental attention, some uncertainties about them persist. The most recent detailed assessment of thermochemical data for hydroxo-lead(II) complexes appears to be that reported by Sadiq and Lindsay (21), and most of our data are from this source. These data originate mainly from the work of Olin and Carell (27–30), as previously compiled by Baes and Mesmer (31) and by Smith and Martell (32). Sadiq and Lindsay have adjusted the Gibbs energy data tabulated by Smith and Martell for internal consistency with their recalculated values for PbO(s) and Pb^{2+}(aq).

We have omitted two species which were included in Sadiq and Lindsay's compilation: $Pb(OH)_4^{2-}$(aq) and $Pb(OH)_2$(s). The former had been included on the basis of a single report by Aksel'rud (33), cited by Karapet'yants and Karapet'yants (34). We found that its inclusion led to unrealistically high computed lead concentrations at high pH, exceeding 1 mol dm^{-3} above about pH = 13.5. The data selected by Sadiq and Lindsay imply that $Pb(OH)_2$(s) is stable relative to litharge and water by 26.0 kJ mol^{-1} at 25°C. This is based on two earlier thermochemical compilations, but the original source is obscure. However, there is considerable doubt about the very existence of solid $Pb(OH)_2$, many earlier reports being referable to basic lead nitrates (35–37). We noted above that the hydrated lead(II) oxide, $Pb_6O_4(OH)_4$, may be marginally stable with respect to PbO(s) and H_2O(l) (11). However, we have not observed it, except in some electrochemical experiments under conditions of high supersaturation.[6] We omitted massicot, since the consensus is that it is metastable with respect to litharge at 25°C (21, 24).

Two further species, $Pb_3(OH)_5^+$ and $Pb_3(OH)_3^{3+}$, have recently been reported (38–40). When we included $Pb_3(OH)_5^+$ in our data set, it led to unrealistically high computed solubilities for PbO around pH = 9 to 11, with a minimum solubility of about 5×10^{-4} mol dm^{-3}. The computed minimum solubility when $Pb_3(OH)_5^+$ was omitted was about 2.5×10^{-5} mol dm^{-3}, in better agreement with the experimental minimum solubility of litharge, 6.7×10^{-5} mol dm^{-3} (41). The species $Pb_3(OH)_5^+$ may thus be present, but its reported stability constant appears to be too high. We therefore omitted it from our final computations. We also omitted $Pb_3(OH)_3^{3+}$, since its formation constant has only been determined at high ionic strength (3.0 mol dm^{-3} $LiClO_4$) (39, 40). The quality of agreement between Olin's speciation model and experimental data indicates that the inclusion of further species will only have minor effects on computed solubility behaviour (27–30, 38–40). Ohtaki and co-workers (39, 40) present evidence that the species formerly identified as $Pb_6(OH)_8^{4+}$ is in fact $Pb_6O(OH)_6^{4+}$, which has also been observed in the solid state (10, 42, 43). We have incorporated this suggestion by subtracting the Gibbs energy of formation of H_2O(l) from that recommended for $Pb_6(OH)_8^{4+}$ in ref. 21, the two species being related by reaction [14]:

$$[14] \quad Pb_6(OH)_8^{4+} \rightleftharpoons Pb_6O(OH)_6^{4+} + H_2O$$

Several workers have measured formation constants, β, for the two lead carbonate complexes $PbCO_3^0$ and $Pb(CO_3)_2^{2-}$. Clever and Johnston (44) tentatively recommended the respective values $\beta = 2 \times 10^6$ and 6×10^9 at $I = 0.1$ mol dm^{-3}, as reported by Bilinski *et al.* (45). We have used these data, corrected to zero ionic strength using eq. [8]. We note that Bilinski and Schindler (14) recently reported somewhat lower formation constants (log β = 5.40 and 8.86, respectively, at $I = 0.3$ mol dm^{-3}).

It is convenient to discuss the solubility calculations in terms of pC_t and pPb_t, the negative logarithms of $\{C_t\}$ and $\{Pb_t\}$, respectively (cf. pH). We computed species distributions at pH intervals of 0.5 and pC_t intervals of 1.0. A finer grid was used to elucidate details of complex behaviour in some portions of the pH–pC_t matrix. Results are summarized in Figs. 3 to 5. Figure 3 is a composite solubility diagram, showing pPb_t and the stability fields of litharge and the three carbonates as functions of pH and pC_t. Figure 4 shows the computed fields of preponderance of the various aqueous lead species in saturated solutions, superimposed on solubility contours corresponding to Figure 3. Figure 5 shows the computed solubilities of the four solids, including conditions of their metastable occurrence, as a function of pH at $pC_t = 4$. Table 3 lists computed equilibrium pPb_t and pC_t values, as a function of pH, for the three stable solid assemblages (litharge + plumbonacrite; plumbonacrite + hydrocerussite; hydrocerussite + cerussite).

(g) Description of solubility–stability relationships

Figure 3 illustrates the development of the lead carbonate stability fields as total carbonate activity increases. At $pC_t > 9.5$ and $pPb_t > 0$, litharge is the sole stable solid, with a minimum computed solubility of $pPb_t \simeq 4.6$ at pH ≃ 10.3. (See top of Fig. 3; note that a portion of the PbO solubility curve at $pC_t = 10$ is obscured in this view of the solubility surface.) Most of the litharge solubility surface at pH < 9 is probably not accessible in practice without precipitation of basic lead salts. As pC_t decreases (i.e. total carbonate activity increases), solid lead carbonates progressively suppress lead solubility, and their stability fields encroach into that of litharge. Plumbonacrite initially appears at $pC_t \simeq 9.5$, hydrocerussite at $pC_t \simeq 9.0$, and cerussite at $pC_t \simeq 5.5$. The stability field boundaries (dashed lines in Fig. 3) progress to higher pH as pC_t decreases. Encroachment by the stability fields of the complex salts $MOH \cdot 2PbCO_3$ (not shown in Fig. 3) occurs at pH ≃ 10 and $pC_t < 1$ (M = Na) or $pC_t < 0$ (M = K), when Na and K are the counterions in the added carbonate salts.

The preponderance diagram (Fig. 4) shows that polymeric hydroxo-lead complexes are important only at about $pC_t > 8$ and pH < 10 for realistic lead concentrations. At lower pC_t values, polymerization is suppressed by precipitation of the solid carbonates. Lead solubility reaches a minimum, $pPb_t \simeq 6.6$, in slightly alkaline solution near $pC_t = 4$; at still lower pC_t values solubility is enhanced by carbonato-lead(II) complex formation. This behaviour is consistent with the solubility data of Bilinski and co-workers (14, 46). The field of predominance of $Pb(CO_3)_2^{2-}$ (Fig. 4) indicates that the best area for further experimental evaluation of the formation constant of this species would be near $pC_t = 1–2$ and pH = 9–11. The low and relatively constant computed lead solubility within the field of predominance of $PbCO_3^0$ indicates that solubility measurements are unlikely to shed further light on this complex.

There is some interest in whether cerussite or hydrocerussite is the stable form of lead carbonate in natural surface waters (14, 15). Our data indicate that cerussite should be the stable phase at the usual atmospheric $p(CO_2)$ of ≃ 30 Pa, but that only slight depletion of CO_2 would be necessary to enter the hydrocerussite stability field. However, Fig. 5 shows that the solubilities are similar, especially near neutral pH. This similarity also explains the substantial uncertainty in p_1, as determined

[6] Unpublished work, in collaboration with D. W. Shoesmith and M. G. Bailey.

Can. J. Chem. Downloaded from www.nrcresearchpress.com by 210.87.254.42 on 09/06/12
For personal use only.

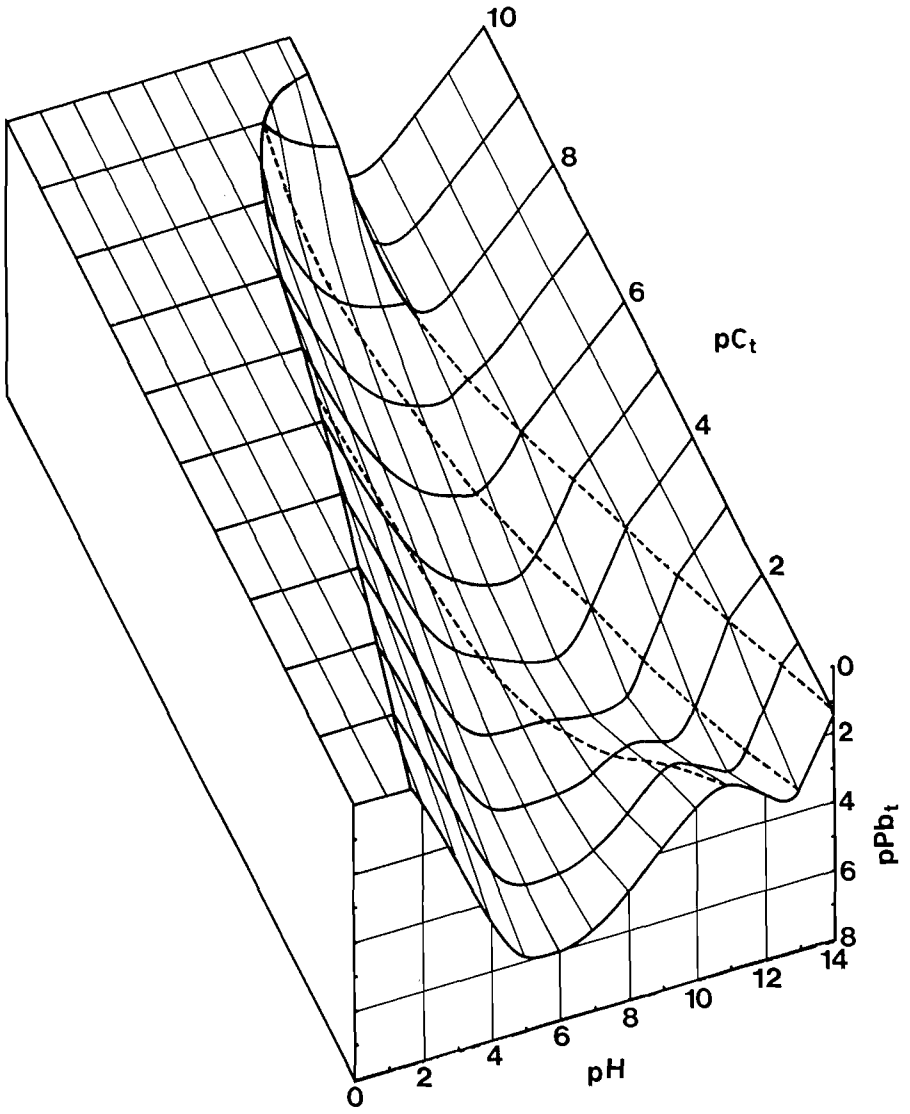

FIG. 3. Computed solid/solution equilibrium surface in the lead carbonate system at 25°C, expressed as negative logarithms of proton, total lead and total carbonate activities (pH, pPb_t, and pC_t, respectively). Dashed lines represent stability boundaries between solid phases in the sequence (left to right) cerussite, hydrocerussite, plumbonacrite, litharge.

from solubility measurements (14), compared with direct observation of phase transformations. Interestingly, the minimum computed lead solubility varies only within the narrow limits, $5.8 < pPb_t < 6.6$, as $p(CO_2)$ varies between 10^{-3} and 10^5 Pa, although the position of the minimum progresses from pH $\simeq$ 10 to 6.5.

Most of our lead solubility measurements were in the range pH > 10 and $pC_t < 3$, and thus lay within the predominance fields of $Pb(CO_3)_2^{2-}$ and $Pb(OH)_3^-$. These measurements were not sufficiently precise to permit any further critique of the computed solubilities, but the general trends paralleled the behaviour described in the appropriate portions of Figs. 3 and 4.

(h) Phase equilibria above 25°C

We briefly investigated the solid phase interconversions at 50, 75, and 100°C, in solutions with $[C_t]$ near 0.1 mol dm^{-3}. We found only a slight temperature dependence for all three equilibria, when expressed as concentrations of carbonate and bicarbonate or hydroxide. However, applying Helgeson's data for the dissociation equilibria of water and carbonic acid at

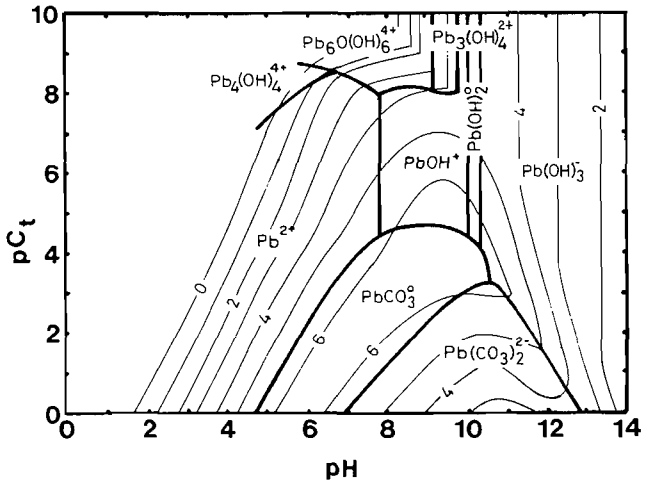

FIG. 4. Computed fields of preponderance of the various dissolved lead species (bold outlines) in saturated solutions corresponding to the equilibrium surface in Fig. 3. Numbered contours represent total lead activity, expressed as pPb_t.

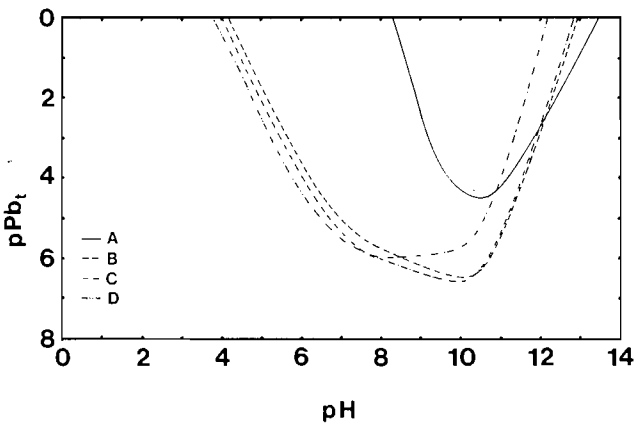

FIG. 5. Computed equilibrium dissolved lead activities for the four solids litharge (*A*), plumbonacrite (*B*), hydrocerussite (*C*), and cerussite (*D*) at $pC_t = 4$, as a function of pH.

TABLE 3. Computed ionic activities of saturated solutions in equilibrium with lead oxide/carbonate phase assemblages

Litharge + plumbonacrite			Plumbonacrite + hydrocerussite		Hydrocerussite + cerussite	
pH	pC_t	pPb_t	pC_t	pPb_t	pC_t	pPb_t
4.0		*		*	5.34	−0.86
4.5		*		*	5.34	0.16
5.0		*		*	5.33	1.17
5.5		*		*	5.29	2.17
6.0		*		*	5.19	3.16
6.5		*	8.99	−0.40	4.97	4.14
7.0		*	8.64	1.53	4.62	5.05
7.5		*	8.20	3.04	4.18	5.71
8.0		*	7.71	3.94	3.70	5.97
8.5	9.22	0.52	7.22	4.58	3.20	6.03
9.0	8.71	2.44	6.71	5.11	2.69	5.96
9.5	8.17	3.90	6.17	5.55	2.15	5.49
10.0	7.56	4.53	5.56	5.81	1.54	4.61
10.5	6.83	4.58	4.83	5.78	0.82	3.63
11.0	5.97	4.28	3.97	5.48	−0.05	2.63
11.5	5.02	3.85	3.03	5.04	−0.99	1.63
12.0	4.05	3.37	2.05	4.55	*	
12.5	3.05	2.87	1.05	4.02	*	
13.0	2.06	2.38	0.06	3.43	*	
13.5	1.06	1.88	−0.94	2.72	*	
14.0	0.06	1.38	*		*	

* Indicates impossibly high total lead or carbonate activity.

elevated temperatures (47) to the estimated equilibrium solution concentrations, we obtain substantial increases in all three equilibrium partial pressures, as expected. We estimate the following values at 100°C:

$$p_1 = 10^{-1.1 \pm 1.0}\ \text{Pa}$$

$$p_2 = 10^{+0.9 \pm 2.0}\ \text{Pa}$$

$$p_3 = 10^{+1.9 \pm 1.0}\ \text{Pa}$$

Combining these estimates with high-temperature Gibbs energy data for PbO, CO_2, and H_2O from ref. 23, we obtain the following estimates of Gibbs energies of formation:

$$\Delta_f G°(\text{plumbonacrite, s, 373 K}) = -5120 \pm 50\ \text{kJ mol}^{-1}$$

$$\Delta_f G°(\text{hydrocerussite, s, 373 K}) = -1643 \pm 18\ \text{kJ mol}^{-1}$$

$$\Delta_f G°(\text{cerussite, s, 373 K}) = -612 \pm 9\ \text{kJ mol}^{-1}$$

By analogy with the computed high-temperature Gibbs energy data reported (24) for aragonite, strontianite, and witherite, which are all isostructural with cerussite, and display similar $\Delta_f G°-T$ relationships, we would anticipate $\Delta_f G°$ (cerussite, s, 373 K) $\simeq -608$ kJ mol^{-1}, in reasonable agreement with our experimental estimate. The temperature dependence of p_3 appears to differ substantially from that of p_1 and p_2. Whereas p_3 increases by only about an order of magnitude between 25 and 100°C, p_1 and p_2 both increase by about four orders of magnitude. This is probably because H_2O is a reactant in the forward reaction of equilibria [3] and [4], but a product in reaction [5]. These $p(CO_2)-T$ relationships indicate that the stability field of cerussite encroaches on that of hydrocerussite with increasing temperature. The stability fields of hydrocerussite and plumbonacrite in the presence of H_2O(l) are likely to disappear at about 150 and 200°C, respectively. However, the phase diagram will probably be further complicated in this region by the emergence of stability fields for the anhydrous basic carbonates, $a\text{PbCO}_3 \cdot b\text{PbO}$ (8).

Acknowledgements

Part of this work was jointly funded by AECL and Ontario Hydro under the CANDEV agreement. We are grateful to A. M. Duclos for performing many of the XRD measurements, and to R. J. Lemire and J. Paquette for many helpful discussions.

1. E. W. ABEL. *In* Comprehensive inorganic chemistry. Vol. 2. *Edited by* J. C. Bailar, H. J. Emeléus, R. Nyholm, and A. F. Trotman-Dickinson. Pergamon Press. 1973. pp. 119–123.
2. J. K. OLBY. J. Inorg. Nucl. Chem. **28**, 2507 (1966).
3. R. M. GARRELS and C. L. CHRIST. *In* Solutions, minerals and equilibria. Harper and Row, New York. 1965. pp. 233–238.
4. D. F. HAACKE and P. A. WILLIAMS. J. Inorg. Nucl. Chem. **43**, 406 (1981).
5. J. YAMAGUCHI, Y. SAWADA, O. SAKURAI, K. UEMATSU, N. MIZUTANI, and M. KATO. Thermochim. Acta, **35**, 307 (1980).
6. J. YAMAGUCHI, Y. SAWADA, O. SAKURAI, K. UEMATSU, N. MIZUTANI, and M. KATO. Thermochim. Acta, **37**, 79 (1980).
7. D. A. GRISAFE and W. B. WHITE. Am. Miner. **49**, 1184 (1964).
8. G. TODD and E. PARRY. Nature, **202**, 386 (1964).
9. R. A. HOWIE and W. MOSER. Nature, **219**, 372 (1968).
10. A. OLIN and R. SODERQUIST. K. Tekn. Högsk. Handl. No. 289, 517 (1972).
11. M. RANDALL and H. M. SPENCER. J. Am. Chem. Soc. **50**, 1572 (1928).
12. R. R. STASKO and G. A. VIVIAN. An overview of the Ontario Hydro Carbon-14 Control Program. *In* Proceedings of International Conference on Radioactive Waste Management, Winnipeg, September 1982. Canadian Nuclear Society, Toronto. pp. 547–553.
13. J. BOULTON (*Editor*). Management of radioactive fuel wastes: the Canadian disposal program. Atomic Energy of Canada Ltd. Report AECL-6314. 1978.
14. H. BILINSKI and P. SCHINDLER. Geochim. Cosmochim. Acta, **46**, 921 (1982).
15. J. D. HEM and W. H. DURUM. J. Am. Water Works Assoc. **65**, 562 (1973).
16. R. M. HARRISON and D. P. H. LAXEN. Chem. Brit. **16**, 316 (1980).
17. R. M. GARRELS. Am. Miner. **42**, 780 (1957).
18. A. W. MANN and R. L. DEUTSCHER. Chem. Geol. **29**, 293 (1980).
19. M. H. BROOKER, S. SUNDER, P. TAYLOR, and V. J. LOPATA.

Can. J. Chem. Downloaded from www.nrcresearchpress.com by 210.87.254.42 on 09/06/12
For personal use only.

Can. J. Chem. **61**, 494 (1983).
20. M. W. CHASE, J. L. CORNUTT, A. T. HU, H. PROPHET, A. N. SYVERUD, and L. C. WALKER. J. Phys. Chem. Ref. Data, **3**, 311 (1974).
21. M. SADIQ and W. L. LINDSAY. Selection of standard free energies of formation for use in soil chemistry. Tech. Bull. 134, Colorado State Univ. Expt. Stn., 1979.
22. G. W. BIRD and V. J. LOPATA. *In* Scientific basis for nuclear waste management. Vol. 2. *Edited by* C. J. M. Northrup, Jr. Plenum, New York. 1980. pp. 419–426.
23. W. STUMM and J. J. MORGAN. Aquatic chemistry. 2nd ed. Wiley, New York. 1981.
24. R. A. ROBIE, B. S. HEMINGWAY, and J. R. FISHER. U.S. Geol. Surv. Bull. 1452 (reprinted with corrections, 1979).
25. C. W. DAVIES. *In* Ion association. Butterworths, London. 1962. Chapt. 3.
26. L. H. ADAMI and K. C. CONWAY. U.S. Bureau of Mines Report Inv. 6822, 7 pp (1966).
27. A. OLIN. Acta Chem. Scand. **14**, 126 (1960).
28. A. OLIN. Acta Chem. Scand. **14**, 814 (1960).
29. B. CARELL and A. OLIN. Acta Chem. Scand. **14**, 1999 (1960).
30. B. CARELL and A. OLIN. Acta Chem. Scand. **16**, 2350 (1962).
31. C. F. BAES, JR. and R. E. MESMER. *In* The hydrolysis of cations. Wiley-Interscience, New York. 1976. pp. 358–365.
32. R. M. SMITH and A. E. MARTELL. Critical stability constants. Vol. 4. Critical complexes. Plenum, New York. 1976.
33. N. V. AKSEL'RUD. Dokl. Akad. Nauk SSSR, **132**, 1967 (1960).
34. M. KH. KARAPET'YANTS and M. L. KARAPET'YANTS. Thermodynamic constants of inorganic and organic compounds. Ann Arbor-Humphrey, Ann Arbor. 1970.
35. A. E. NEWKIRK and V. B. HUGHES. Inorg. Chem. **9**, 401 (1970).
36. W. KWESTROO, C. LANGEREIS, and H. A. M. VAN HAL. J. Inorg. Nucl. Chem. **29**, 33 (1967).
37. J. ROBIN and A. THÉOLIER. Bull. Soc. Chim. Fr. 680 (1956).
38. R. N. SYLVA and P. L. BROWN. J. Chem. Soc. Dalton, 1577 (1980).
39. T. KAWAI, S. ISHIGURO, and H. OHTAKI. Bull. Chem. Soc. Jpn. **53**, 2221 (1980).
40. S. ISHIGURO and H. OHTAKI. Bull. Chem. Soc. Jpn. **54**, 335 (1981).
41. A. B. GARRETT, S. VELLENGA, and C. M. FONTANA. J. Am. Chem. Soc. **61**, 367 (1939).
42. T. G. SPIRO, D. H. TEMPLETON, and A. ZALKIN. Inorg. Chem. **8**, 856 (1969).
43. A. OLIN and R. SODERQUIST. Acta Chem. Scand. **26**, 3505 (1972).
44. H. L. CLEVER and F. J. JOHNSTON. J. Phys. Chem. Ref. Data, **9**, 751 (1980).
45. H. BILINSKI, R. HUSTON, and W. STUMM. Anal. Chim. Acta, **84**, 157 (1976).
46. H. BILINSKI and M. MARKOVIC. Croat. Chem. Acta, **50**, 125 (1977).
47. H. C. HELGESON. J. Phys. Chem. **71**, 3121 (1967).

Can. J. Chem. Downloaded from www.nrcresearchpress.com by 210.87.254.42 on 09/06/12
For personal use only.

Surface photochemistry: generation of benzyl radical pairs on dry silica gel[1]

BRADLEY FREDERICK, LINDA J. JOHNSTON, PAUL DE MAYO, AND S. KING WONG
Photochemistry Unit, Department of Chemistry, University of Western Ontario, London, Ont., Canada N6A 5B7

Received July 6, 1983

BRADLEY FREDERICK, LINDA J. JOHNSTON, PAUL DE MAYO, and S. KING WONG. Can. J. Chem. **62**, 403 (1984).

Singlet and triplet benzyl radical pairs have been generated on silica gel by photolysis of a benzyl phenylacetate, a dibenzyl ketone, and a dibenzyl sulfone. The extent of geminate radical recombination has been measured and requires that translational motion of radicals occur on the silica gel surface. This motion was affected by the radical pair multiplicity and the photolysis temperature, but was relatively insensitive to the state of hydration of the silica gel and the presence of coadsorbates. The presence of certain rearranged starting materials, which are not formed in solution, amongst the products from photolysis of both dibenzyl ketone and dibenzyl sulfone on silica gel indicates the restrictions on radical movement on the surface on the shorter timescale of the benzyl–phenylacetyl and benzyl – benzyl sulfonyl radical pairs.

BRADLEY FREDERICK, LINDA J. JOHNSTON, PAUL DE MAYO et S. KING WONG. Can. J. Chem. **62**, 403 (1984).

On a généré des paires de radicaux benzyles singulet et triplet sur du gel de silice par photolyse d'un acétate de phényle, d'une dibenzylcétone et d'une dibenzylsulfone. On a mesuré la quantité de recombinaison radicalaire geminée et on a observé que cette valeur requière que le mouvement translationnel des radicaux se produise à la surface du gel de silice. Ce mouvement est influencé par la multiplicité de la paire de radicaux et par la température de photolyse; il n'est toutefois pas sensible à l'état d'hydratation du gel de silice et à la présence de substances coadsorbées. Certains produits de départ transposés, qui ne se forment pas en solution, se retrouvent parmi les produits de photolyse de la dibenzylcétone ainsi que de la dibenzylsulfone sur le gel de silice; leur présence indique qu'il existe des restrictions au mouvement des radicaux sur la surface à l'échelle de temps plus courte pour les paires de radicaux benzyle–phénylacétyle et benzyle–benzylsulfonyle.

[Traduit par le journal]

Can. J. Chem. Downloaded from www.nrcresearchpress.com by 210.87.254.40 on 09/06/12
For personal use only.

Although radical pairs have been widely studied in solution (1) their behaviour, when adsorbed on solid surfaces, has not been extensively examined.[2] Modification of the normal solution behaviour is, however, to be expected for such adsorbed radicals. In a solution solvent-cage a spin correlated geminate radical pair, either singlet or triplet, may undergo a number of processes: (*A*) it may recombine to regenerate starting materials; (*B*) it may either recombine in a different manner, or it may disproportionate, to form new products; (*C*) it may be transformed into a new radical pair; or (*D*) it may diffuse apart to form free radicals. The rates of both processes (*A*) and (*B*) depend on the radical pair multiplicity since they can occur only with singlet radical pairs. Because intersystem crossing must precede reaction of a triplet radical pair, spin independent processes (*C*) and (*D*) compete more effectively with geminate recombination for triplet than for singlet pairs. Changing either the rate of intersystem crossing of the radical pair or its rate of diffusional separation will affect the relative contributions of processes (*A*–*D*) to the decay of a particular radical pair. For example, increasing the viscosity of the medium or generating the radical pair in an environment in which its movement is restricted, as, for example, in a micelle (9) or on a solid surface (3, 4, 7), will both affect the diffusional behaviour of the radical pair. Such effects may be readily evaluated by measuring the changes in the amount of geminate radical recombination under various conditions.

Until recently, few studies have examined the possibilities of movement of radicals adsorbed on inorganic solids such as silica gel, alumina, and porous Vycor (2–10). The examination of mobility of adsorbed closed-shell molecules has also been neglected although both the surface–adsorbate interaction and the nature of the surface have been investigated in detail (11).

On silica gel surfaces there are two functional groups: the silanols and siloxanes; physisorbed water molecules are also important (11). The presence of ~5 silanols/nm^2 for water-equilibrated surfaces appears to be generally accepted. The recent application of ^{29}Si nmr to the study of silica surfaces (12, 13) will probably resolve the controversy concerning the relative contributions from isolated, vicinal and geminal silanols. London dispersion forces, electrostatic interactions, and hydrogen bonding provide the major adsorption interactions for organic molecules on silica and the type of surface–adsorbate binding, as well as its strength, depends on the adsorbate polarity and the activation treatment of the silica. The surface silanols are thought to be the principal adsorption sites, but siloxanes and hydrogen-bonded water molecules may also be involved.

One of the earlier investigations of adsorbed radical mobility involved the generation of cyanopropyl radical pairs in a silica gel slurry (2). It was claimed therein, from product analysis, that the adsorbed radicals were not free to rotate on the surface. However, a later reinvestigation of this system indicated that both rotational and, to a lesser extent, translational motion occur for cyanopropyl radicals adsorbed on silica gel, both dry and in a slurry (3). Rotational and translational radical movement has also been suggested on the basis of esr studies of adsorbed free, persistent, radicals, but the conclusions may be oversimplified since the effects of surface heterogeneity were not considered (10). More recently, limited translational motion on a silica gel surface has been shown to precede recombination of a singlet radical pair generated in the photo-Fries rearrangement (4). Similarly, substantial surface mobility has been observed for radical pairs generated by photolysis of azocumene (5) and diacyl peroxides (6) on silica gel, although decomposition of the latter is reportedly complicated by the intervention of ionic processes. Evidence for restriction of the mobility of adsorbed radicals has been provided by the observation, on silica gel, of previously undetected reaction pathways in the photolysis of benzoin methyl ether (7).

Dibenzyl ketones (14–16), benzyl phenylacetates (17–20), and dibenzyl sulfones (17, 21, 22) have all been shown to

[1] Publication No. 307 from the Photochemistry Unit, Department of Chemistry, University of Western Ontario.

[2] Most of the previous work is contained or cited in refs. 3–9.

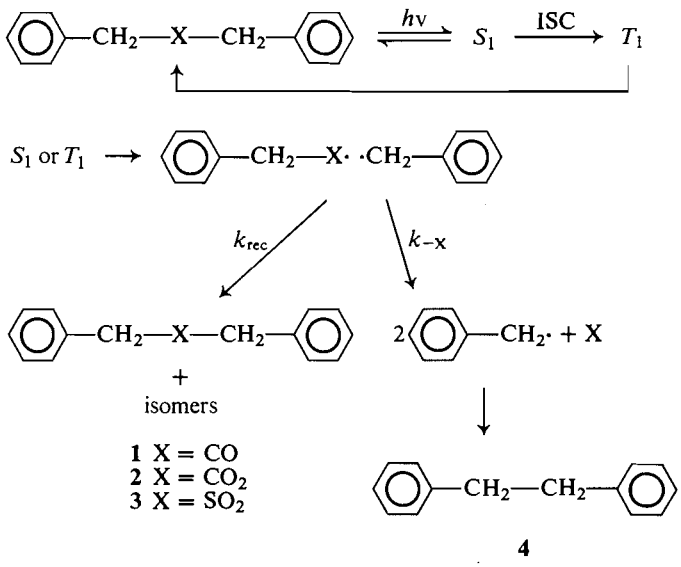

SCHEME 1

undergo photoextrusion reactions in solution to produce benzyl radical pairs (Scheme 1). Studies of the Type I photolysis of dibenzyl ketone, **1**, have shown that excitation is followed by rapid intersystem crossing to a short-lived triplet which undergoes α cleavage to generate a phenylacetyl–benzyl radical pair (15). Both the photodecarbonylation quantum yields of less than unity ($\phi = 0.7 \pm 0.1$ in benzene (15)) and the observation of CIDNP emission for the methylene protons of **1** during its photolysis (16) indicated that geminate recombination of the original radical pair to regenerate **1** occurs. However, in solution, diffusional separation provides the main decay pathway for the initial radical pair. The free phenylacetyl radicals then lose carbon monoxide ($k_{-CO} = 5-9 \times 10^6\ s^{-1}$ (23), depending on the solvent) to give benzyl radicals which combine to give quantitative yields of dibenzyl. The statistical dibenzyl product ratios obtained upon photolysis of unsymmetrical dibenzyl ketones (15) and CIDNP studies (16) showed that cage recombination of benzyl radicals does not occur.

The efficiency of photodecarboxylation of benzyl phenylacetates (18–20) varies considerably with substituents and solvent, but is always lower than that for the decarbonylation of dibenzyl ketones; for example, ϕ_{-CO_2} for benzyl phenylacetate, **2**, is 0.31 in dioxane (19*a*) and 0.19 in methanol (18). Although it has been concluded that the photolysis proceeds by a radical pathway, the multiplicity of the excited state involved and the nature of the decarboxylation step are less certain. Early claims that the photolysis of several phenylacetates involved triplet precursors have been disproved for naphthylmethyl phenylacetates (19). It is likely that the photolysis of **2** and its derivatives also follows a singlet pathway (21). The decarboxylation is thought to proceed by initial cleavage of the carbon – ether oxygen bond followed by rapid loss of carbon dioxide (19*c*). Recombination of the initial benzyl–phenylacetoxy radical pair has not been demonstrated. In contrast to results obtained for dibenzyl ketones, unsymmetrically substituted benzyl phenylacetates show substantial cage effects, particularly in relatively viscous solvents (19*a*, 20).

The photoextrusion of sulfur dioxide from several arylmethyl sulfones has been previously examined (17, 21, 22). Dibenzyl sulfone, **3**, shows both singlet and triplet reactivity and its photodecomposition and that of similar sulfones proceeds by cleavage of one bond to produce a benzylsulfonyl–benzyl radical pair. This either recombines to produce racemized starting material (as shown by the loss of optical activity in *S*-α-methyldibenzylsulfone recovered after partial photolysis), or loses sulfur dioxide to produce a benzyl radical pair (21*b*). The dibenzyl products are derived from both geminate and random free radical combination; decreased amounts of geminate recombination are observed for triplet sensitized photolysis (21).

We report here an account of the generation, on a silica gel surface, of benzyl radical pairs by photolysis of a dibenzyl ketone (**5**), a benzyl phenylacetate (**6**), and a dibenzyl sulfone (**7**). A preliminary account of part of this work has been published (24).

Results and discussion

The same three dibenzyl products, **8**, **9**, and **10** were formed from each of the three precursors (**5**, **6**, and **7**). Since the symmetrical dibenzyls, **8** and **10**, could arise only by nongeminate combination, i.e., by union of radicals which had escaped from their original partners, the product ratios provided a useful probe for translational radical movement on the surface.

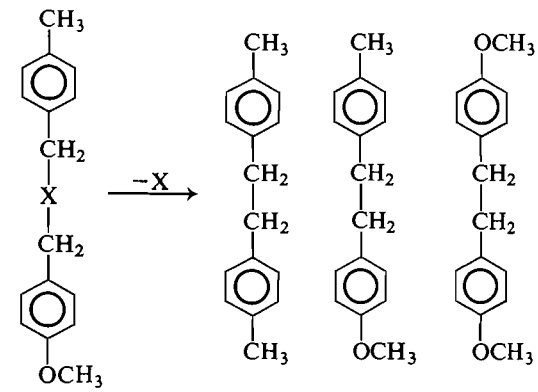

5 X = CO
6 X = CO_2
7 X = SO_2

8 **9** **10**

The solution photolysis of ester **6** had been previously examined by Givens (19*a*); the product dibenzyl distribution ranged from 1:2.5:1 in dioxane ($\eta = 1.087 \times 10^{-3}\ N\ s\ m^{-2}$) to 1:5.07:1 in 2-propanol ($\eta = 1.765 \times 10^{-3}\ N\ s\ m^{-2}$), a marked cage effect being noted in the more viscous solvents. In contrast, photolysis of ketone **5** in 2-propanol gave a statistical (1:2:1) product distribution; even at −78°C the product ratio of 1.0:2.2:1.0 indicated that most of the radicals escaped from the solvent cage before recombining. Photolysis of sulfone **7** yielded product distributions of 1.1:2.7:1.0 in dioxane and acetone and 1.1:2.9:1.0 in 2-propanol. These product ratios, since they were intermediate between those obtained for **5** (triplet) and **6** (singlet), suggested that both singlet and triplet excited states were involved in the photolysis of **7**.

Photolysis of 5, 6, and 7 on silica gel

Samples of **5**, **6**, and **7** were adsorbed on silica gel at various coverages; monolayer coverages were obtained either from Langmuir adsorption isotherms (Fig. 1) or by calculations based on the silica gel surface area and the molecular areas determined from space filling models. The agreement between the coverages obtained from isotherms or by calculation was acceptable given the errors involved in each method.

As in solution, dibenzyls **8**, **9**, and **10** were formed in good

Can. J. Chem. Downloaded from www.nrcresearchpress.com by 210.87.254.40 on 09/06/12
For personal use only.

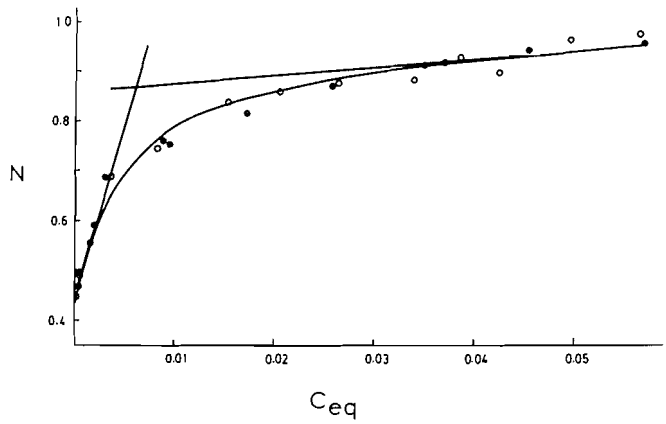

FIG. 1. Adsorption isotherms for ketone **5** (○) and ester **6** (●) on silica gel; N (mmol/g versus C_{eq} (M).

yield (75–100%) when **5**, **6**, and **7** were photolyzed on dry silica gel.

The dibenzyl product distribution (Table 1) was not far removed from statistical when ketone **5** was photolyzed on silica gel at room temperature. However, there was clear indication that some recombination of benzyl radicals with their original partners had occurred. Thus, for example, at 10% coverage the dibenzyl ratio indicated that 23% of the radicals recombined in the original geminate pair. The remaining radicals must have become "free" and found a radical from another pair with which to react. These results require that translational movement of the benzyl radicals occur even if the ketone molecules be unevenly distributed on the surface (e.g., small pools of ketone molecules and large areas of "bare" silica gel). The amount of movement, but not the necessity for its occurrence, will depend upon the adsorbate distribution. The probability of the generation of a second radical pair from a nearby substrate molecule is $\ll 1$, even if the radical pair has a lifetime of milliseconds (i.e., the chance of two photons being absorbed within the space occupied by 2 substrate molecules on this time-scale is negligibly low).

The fraction of geminate recombination did not increase at 50% coverage. Lowering the photolysis temperature to −55°C did, however, yield a larger amount of the unsymmetrical dibenzyl **9**, although the product distribution (1 : ~6 : 1, Table 1) still required some radical movement. Further lowering of the temperature to −165°C gave >95% of **9**. At this temperature on the time-scale of the experiment the ketone is presumably translationally immobile; the benzyl radicals may also be so, but on warming become mobile between this temperature and −55°C where the product ratios require movement. These results reflect the increased restrictions placed upon radical movement on the surface at low temperatures, and demonstrate that there is an activation energy for this radical motion.

Photolysis of ester **6** on dry silica gel at 10% coverage gave a dibenzyl distribution similar to that obtained in 2-propanol solution. As with ketone **5**, the product ratios did not change appreciably from 1 to 50% coverage. However, more geminate recombination to produce the unsymmetrical dibenzyl, **9**, was always observed for the ester than for the ketone under the same conditions. These differences were more pronounced at low temperature: at −50°C >96% of the unsymmetrical dibenzyl was obtained from **6** whereas much lower temperatures were required before similar results were obtained from **5**. It is apparent that less translational movement occurs before

TABLE 1. Photolysis of ketone **5**, ester **6**, and sulfone **7** on dry silica gel

Ketone	Coverage (%)[a]	Temperature (°C)	Dibenzyl ratio[b] 8	9	10
6	1	20	1.0	6.1	1.0
	10	20	1.4	5.5	1.0
	50	20	1.0	4.1	1.1
	10	−55		>96%	
5	1	20	1.2	3.7	1.0
	10	20	1.0	3.2	1.0
	50	20	1.0	3.1	1.0
	2	−55	1.2	9.0	1.0
	10	−55	1.0	6.3	1.0
	50	−55	1.0	6.2	1.0
	10	−165		>95%	
7	2	20	1.2	8.3	1.0
	10	20	1.0	6.2	1.0
	50	20	1.2	6.4	1.0
	−10	−55	1.0	30	1.2

[a]Coverages are based on monolayer coverages determined from adsorption isotherms.
[b]All product ratios are the average of two or more experiments.

recombination for radicals generated from **6** than for those from **5**.

The dibenzyl distribution (Table 1) obtained when sulfone **7** was photolyzed on silica gel at room temperature showed slightly more geminate recombination than did the ester. These results lead to the conclusion that translational motion on the surface of silica gel competes more effectively with radical recombination for **5** than for **6** or **7**. The benzyl radicals formed from all three are the same; only the distances between the radical centres and their multiplicities differ. The radical pair from **6** is formed with the greatest separation and should, therefore, be the most likely to diffuse apart and exhibit more nongeminate recombination. The opposite is observed so an explanation based on the multiplicity of the radical pair is favoured. The decomposition of **5** occurs from a triplet (15), whereas **6** is thought to decompose by a singlet pathway (19, 21). The singlet radical pair generated from **6** should recombine faster than the triplet pair from **5** and, thus, should show more geminate recombination, as the results indicate. Similarly, the increase in unsymmetrical dibenzyl formation for the ester as compared to the ketone in 2-propanol may also reflect this difference in spin multiplicity of the benzyl radical pair; additionally, it may also reflect the difference in the rate of formation of the benzyl radical pairs by decarboxylation as compared to decarbonylation.

The situation with sulfone **7** is less clear. The surface results, since they are similar to those obtained with the ester, suggest a singlet precursor. However, dibenzyl ratios for **7** in solution are intermediate between those of the ester and ketone and provide evidence for a mixture of singlet and triplet pathways. If a primarily singlet decomposition is occurring for the sulfone on the surface, the increase in geminate recombination for **7** as compared to **6** may reflect the slightly greater separation for the radical pair generated from the former.

The results for the adsorbed versus the solution phase sulfone could be interpreted as a reflection of changes in the relative amounts of singlet and triplet excited states. For example, changes in the rates of either intersystem crossing or radi-

Can. J. Chem. Downloaded from www.nrcresearchpress.com by 210.87.254.40 on 09/06/12
For personal use only.

TABLE 2. Photolysis of ketone **5** and ester **6** on modified silica gel

Coverage	Silica gel	Temperature (°C)	Dibenzyl ratio **8** : **9** : **10**
5, 0.09 mmol/g	Dehydrated	20	1.1 : 2.7 : 1.0
5, 0.45 mmol/g	Dehydrated	20	1.1 : 2.7 : 1.0
6, 0.45 mmol/g	Dehydrated	20	1.2 : 4.4 : 1.0
5, 2%	**10**, 0.45 mmol/g	−55	1.0 : 11 : 1.0
5, 2%	**10**, 0.093 mmol/g	−55	1.1 : 8.8 : 1.6
5, 2%	**10**, 0.020 mmol/g	−55	1.0 : 8.0 : 1.2

ationless deactivation processes could decrease the amount of triplet reaction occurring for the adsorbed sulfone. Previously observed variations in excited state energy levels (25) and in excited state lifetimes (8), because of changes in radiationless deactivation rates, have been well documented for adsorbed molecules and provide support for the above hypothesis. More information concerning the multiplicity of excited state sulfones is obviously needed before any conclusions can be reached.

The results obtained for adsorbed **5**, **6**, and **7** thus demonstrate that translational motion occurs for benzyl radicals adsorbed on the silica gel surface and that this movement has a significant activation energy. This will vary for movement from different adsorption sites. Thus, when interaction of a molecule with two (or more) silanols is possible, translational motion need not require the simultaneous disruption of all bonding, as would motion which occurred by vaporization. Furthermore, if the molecule moves toward a silanol group, bonding to it may occur as the original silanol bonding is disrupted. According to this model, the most rapid translational motion is to be expected for surfaces with large numbers of silanols or for ones with very few silanols. An energy profile may then be as first suggested by Dacey (26). The deepest wells correspond to the preferred sites and the height of the barrier will vary with the amount of bonding retained in the transition state. The preferred sites must represent some favorable arrangement of surface and silanols, and, hence, will depend, in part, on the specific molecules, especially if large.

Although translational motion was shown to depend on the radical pair multiplicity (and, hence, on its lifetime), movement of the radicals was unaffected by increased coverages of starting material. An increased amount of adsorbate might be expected either to interfere with, or to increase, radical movement. The latter could, presumably, occur because the probability of a specific molecule being adsorbed at a stronger binding site would be lower at higher coverages. Neither effect was, however, observed for benzyl radicals over the 1–50% coverage range.

An estimate of the effective surface "viscosity" of the silica gel at room temperature may be obtained for singlet derived benzyl radicals for which the surface product ratios have been shown to resemble those in 2-propanol. It should be noted that this apparent "viscosity" changes when either the radical pair multiplicity or the photolysis temperature is varied. Consequently, a surface viscosity can only be expressed with reference to a particular adsorbate and specified conditions.

The absence of evidence for preferential adsorption sites, that is, the insensitivity of the amount of geminate recombination to changes in surface coverage, in light of recent results,[3] could have been caused by the presence of sufficient water to fill the active surface sites. Although the present experiments were carried out under "dry" conditions (silica gel dried at 200°C), some water would have been added in even the dry solvent. Typically, the methylene chloride after drying contained 10 ppm water; the use of 4 mL/g silica would, thus, result in the addition of 0.5 mg water/g. Recently, the addition of similar amounts of water to dry silica gel has been shown to produce dramatic changes in the emission spectra for pyrene adsorbed at low coverage on dry silica gel.[3] These results suggest that either the preferred sites are already modified or occupied, or, more probably, that the occupancy of a preferred site for ketone, ester, or sulfone does not require that the subsequently formed benzyl radical also find itself in a preferred site.

Turro and Weed (9) have recently reported results for the photolysis of the unsymmetrical ketone, 1,3-diphenylbutan-2-one, adsorbed on porous glass and on silica gel tlc plates. The observed product ratios indicated "cage" effects of 38% and 9%, respectively. The authors attributed their results to the constraints imposed upon the diffusional separation of geminate radical pairs by the "super-cage" environment. It should be noted that this usage of the word "cage" referring to a surface is somewhat misleading; since, on the surface, a radical pair is not surrounded by a solvent "wall" (or anything else) as it is in solution. If a functional analogy be required — which is dubious — then, rather than invoke the misleading "super-cage" concept, recourse may be had to the relationship of flies to flypaper as more adequately representing the relationship of an adsorbed molecule to the adsorbent surface . . . .

The behaviour of adsorbed benzyl radical pairs may also be compared to that in micelles. Extensive geminate recombination has been recorded for benzyl radical pairs generated in micellar environments from **6** (24) and from **5** (24) and from several other dibenzyl ketones (9, 27). For example, the dibenzyl product mixture was ≥88% **9** when ester **6** was photolyzed in 0.08 *M* potassium dodecanoate. The micellar environment is apparently more effective in preventing diffusional separation of benzyl radicals than is the silica gel surface at room temperature.

Photolysis of ***5*** *and* ***6*** *on modified surfaces*

Several experiments aimed at determining the effects of modification of the silica gel surface were undertaken. Firstly, the silica gel was heated at 750°C, at which temperature most of the surface silanols are thought to be removed (11). Because the major adsorption interaction is with the silanols, an extensively dehydrated silica might be expected to provide less restriction to movement of adsorbed radicals or molecules. Photolysis of ketone **5** on dehydrated silica gel at two coverages at room temperature gave dibenzyl products in the ratios shown in Table 2. The small decrease in the unsymmetrical product yield from that on the normal hydrated surface is consistent with an

[3] R. K. Bauer. Private communication.

Can. J. Chem. Downloaded from www.nrcresearchpress.com by 210.87.254.40 on 09/06/12
For personal use only.

Can. J. Chem. Downloaded from www.nrcresearchpress.com by 210.87.254.40 on 09/06/12
For personal use only.

increased radical mobility on the dehydrated silica but is unimpressive.

Irradiation of ester **6** on this silica gel also showed only a small variation in the dibenzyl distribution and it would appear that large changes in mobility are not to be expected on partial dehydration. This may not have been carried far enough, since, assuming that approximately one isolated silanol/nm^2 remains on the silica surface (11) and using the calculated area of ~0.98 nm^2 for ester **6**, each substrate molecule should still be able to interact with one or two silanols. The results for the partially dehydrated silica are, therefore, not surprising.

Secondly, the effect of coadsorbates on the translational mobility of benzyl radicals on the silica gel was examined. Coadsorbates might be predicted to influence radical mobility in several ways: they could interfere with and, thus, decrease translational motion; they could adsorb preferentially on stronger adsorption sites leaving the substrate the weaker sites from which the radicals could more easily escape; or they could change the substrate distribution on the surface.

Ketone **5** was photolyzed on silica in the presence of coadsorbed cyclohexane diol, **10**, at −55°C: only small variation from the product distribution obtained on silica gel was observed in the presence of the highest concentration of coadsorbed diol (Table 2). The increase in the amount of unsymmetrical product for the higher diol coverage (~20%) was consistent with some interference by the diol with movement of the benzyl radicals.

Photolysis of dibenzyl ketone

Photolysis of dibenzyl ketone, **1**, in micellar solution has been shown by Turro and co-workers (28) to produce small amounts of a rearranged ketone, 1-phenyl-4′-methylacetophenone, **11**. This product presumably arises via recombination of the original acylbenzyl radical pair with subsequent rearomatization. Although 5–10% yields of **11** have been reported for photolysis of **1** in hexadecyltrimethylammonium micelles, the isomer has not been observed in homogeneous solution photolyses (28).

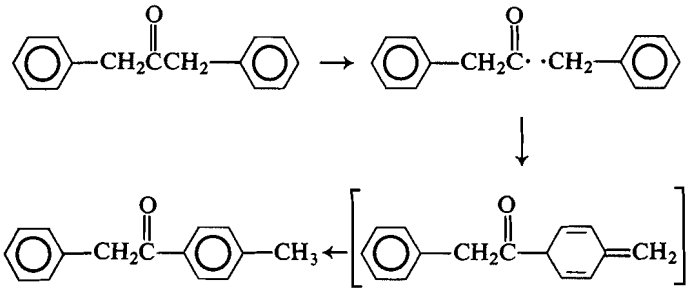

11

Irradiation of **1** on silica gel at 20°C yielded small amounts of **11** along with the major product, dibenzyl. The isomer was isolated and its identity confirmed by comparison with an authentic sample. Typical yields were from 1–2% for irradiation of **1** on silica (irrespective of the manner of drying) at 20°C; photolysis at −55°C resulted in higher yields of 3–4%. At both temperatures the percentage of **11** decreased considerably at higher conversions (e.g., 0.1–0.4% for >97% reaction), presumably owing to its photodecomposition.

There appeared to be no obvious reason for the formation of **11** but not that of the analogous *ortho* compound, 1-phenyl-2′-methylacetophenone, **12**; however, its formation has not previously been reported (28).

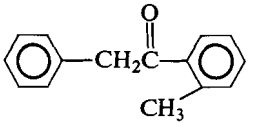

12

The gc retention times of **1** and **12** were identical on the SE 30 column normally used for analysis of reaction products, but the two were separable from each other, and from **11**, on a carbowax column. Analysis of the reaction products obtained in micelle solution showed the presence of isomer **12** (~2–4% yields) as well as **11**. Lesser amounts (<0.5%, estimated) of **12** were also detected in silica gel reaction mixtures at 20 and −55°C. The observation of both *ortho* and *para* rearranged starting material is consistent with the earlier observation of both *ortho* and *para* products in the photo-Fries rearrangement on dry silica gel (5) and with the suggestion that both *ortho* and *para* LATs are formed in the photoreduction of benzophenone (29).

Photolysis of dibenzyl sulfone

Solution photolyses of dibenzyl sulfone, **3** (in benzene (21, 22) and in ethanol (22)), have been reported to produce dibenzyl as the only isolated product, although in less than quantitative yields. No evidence for sulfur to oxygen migration has been found (21*a*). However, photolysis of **3** on silica gel at 20°C yielded small amounts of a rearranged starting material in addition to dibenzyl: the isomer was shown to be sulfinate **13** by comparison with an authentic sample. This ester is presumably formed by recombination of the benzyl — benzyl sulfonyl radical pair before its destruction either by desulfonylation or by diffusional separation. Sulfinates have been detected among the thermolysis and photolysis products from other sulfones (30).

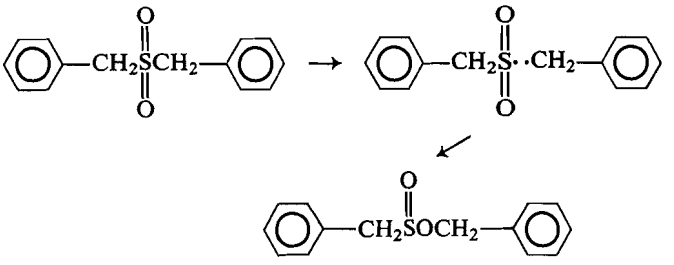

13

Following photolysis of **3** on silica gel at 20°C dibenzyl **4** and sulfinate **13** accounted for ~40% and ≤5%, respectively, of the decomposed sulfone. Decreasing the photolysis temperature to −55°C gave an increased yield of the sulfinate (10%). In contrast, photolysis of **3** in methanol at either 20 or −77°C gave much lower yields of **13** (~0.5%). The low overall recoveries may result from formation of toluene-α-sulfinic acid or toluene-α-sulfonic acid (22). The isolation of acidic products was not attempted.

The decreased yield of sulfinate at higher conversions on silica gel suggested that **13** was not stable on the silica gel surface. To test for this possibility two samples of **13** adsorbed on silica gel were prepared; one sample was kept in the dark for 24 h and the other was irradiated using the same conditions as those used for sulfone photolyses. The "dark" sample showed ~80% sulfinate recovery. From the irradiated sample there was obtained 63% unreacted **13** in addition to dibenzyl and dibenzyl sulfone, **3** (13% and 8%, respectively, based on sulfinate con-

TABLE 3. Photolysis of dibenzyl sulfone, **3**

Conditions	Temperature (°C)	Conversion (%)	Products (mol%)[a] **4**	**13**
Silica gel[b]	25	45	38	5.0
Silica gel	25	59	45	3.0
Silica gel	25	69	36	2.7
Silica gel	−55	30	24	10
Methanol, 0.011 *M*	20	52	35	0.4
Methanol, 0.0034 *M*	−77	52	64	0.6

[a] Based on amount of sulfone recovered.
[b] 0.250 mmol **10**/g silica gel.

Can. J. Chem. Downloaded from www.nrcresearchpress.com by 210.87.254.40 on 09/06/12
For personal use only.

sumed). The presence of a number of other unidentified compounds was also evident. An irradiated methanol solution of **13** similarly indicated the presence of dibenzyl, dibenzyl sulfone, and a number of unidentified compounds.

The above results indicate that recombination of the initial radical pair formed by photolysis of dibenzyl sulfone does occur with benzyl migration from sulfur to oxygen when the sulfone is adsorbed on silica gel. The reported yields of sulfinate represent lower limits because of the instability of **13** on silica gel and its photolability. Recombination of the radical pair can compete more effectively with its diffusional separation on the silica gel surface than in solution.

Conclusions

Translational motion of benzyl radicals adsorbed on silica gel has been demonstrated. The radical mobility has been shown to depend on both the radical pair multiplicity and the photolysis temperature, but was not particularly sensitive to the dehydration of the silica or to the presence of coadsorbed cyclohexanediol. The formation of rearranged starting materials amongst the products from the photolysis of adsorbed dibenzyl ketone and dibenzyl sulfone provided additional evidence for restrictions to radical movement on the surface.

Experimental

Apparatus

Ultraviolet spectra were recorded on a Varian Cary 219 spectrophotometer. Proton nmr spectra were recorded on either a Varian T-60 (60 MHz) or an XL-100 (100 MHz) spectrometer using tetramethylsilane as the internal standard. Mass spectra were measured on a Varian MAT 311A mass spectrometer. Melting points were measured on a Reichert hot stage and are uncorrected. Gas chromatography was done on a Varian 2400 instrument equipped with a flame ionization detector, a temperature programmer, and a 5′ × 1/4″ glass column packed with 10% SE 30 on Chromosorb W (except for the identification of **12** for which a Carbowax column was used). The carrier gas was helium, flow rate 40 mL/min. Operating conditions for the analysis of products from the photolysis of various substrates were as follows: **1**, **5**, **6**, **7**: injector, 225°C; column, 170°C (**1**), 185°C (**5**, **6**), and 185°C for 15 min followed by 200°C for 25 min (**7**); detector, 250°C; **3**, **13**: injector, 190°C; column, 170°C for 20 min followed by 176°C for 25 min; detector, 250°C. Irradiations were carried out with a 150 W or 1000 W XBO high pressure xenon lamp in a Photochemical Research Associates lamp housing (with an infrared water filter) or in a Rayonet reactor equipped with either 254.7 or 300 nm lamps.

Materials

Silica gel (35–70 mesh, Merck) was used as received or dried as outlined below. Dehydrated silica gel was prepared by heating the above silica slowly over a 6 h period to 750°C and leaving it at that temperature for 48 h at atmospheric pressure in an open container. The sample was then evacuated for 2 h at ~0.1 Torr, cooled slowly to 20°C while still under vacuum and stored over P_2O_5 until used. All solvents for solution photolyses or for preparation of silica gel samples were Fisher spectrograde. Methylene chloride was refluxed over P_2O_5 and distilled directly before use for adsorption of compounds onto dry silica gel. Cyclohexane, acetone, and dioxane were dried over molecular sieves. 2-Propanol was dried by refluxing over magnesium/iodine and was then distilled. Anhydrous ether (Fisher) was used as received or distilled from $LiAlCl_4$ when particularly dry ether was required. All other solvents were reagent grade and were used as received.

Dibenzyl ketone (ICN Pharmaceutical) was recrystallized from ether (at −78°C) or petroleum ether (40–60°C) (mp 30.5–32°C) and was stored at 0°C in the dark in a desiccator. Cyclohexanediol (Aldrich, *cis* and *trans*) was recrystallized twice from acetone. Dibenzyl sulfone (Fairfield Chemical Company) as received contained ~50% dibenzyl sulfoxide. The mixture was oxidized with 3-chloroperbenzoic acid and the sulfone obtained recrystallized three times from 95% ethanol (mp 153–155°C). The literature procedure (19*b*) for the preparation of 4-methylbenzyl-4-methoxyphenyl acetate was used (mp 31.5–32°C). 1-Phenyl-4′-methylacetophenone (31) was prepared by Friedel Crafts acylation of toluene (mp 108–109°C). 1-Phenyl-2′-methylacetophenone (32) was prepared by the literature procedure (33) for the preparation of substituted dibenzyl ketones. Benzyl-α-toluenesulfinate (34) was prepared by condensation of α-toluenesulfinyl chloride and benzyl alcohol (mp 49.5–50°C).

1-(4-Methylphenyl)-3-(4-methoxyphenyl)-2-propanone, 6

A general literature procedure (33) for the synthesis of other unsymmetrically substituted dibenzyl ketones was employed. The product was obtained as a yellow oil which contained ~30% dibenzyl and was purified by crystallization from ether at −77°C to give white crystals: mp 48–49°C; ^{1}H nmr (δ, $CDCl_3$) 7.1–6.8 (m, 8H), 3.79 (s, 3H), 3.65 (s, 2H), 3.64 (s, 2H), 2.33 (s, 3H); uv (cyclohexane) λ_{max} 275 nm (ε 1580 M^{-1} cm^{-1}).

4,4′-Methoxymethyldibenzyl sulfone, 7

The sulfone was prepared by condensation of 4-methylbenzyl chloride and 4-methoxybenzyl thiol, followed by hydrogen peroxide oxidation. The product was recrystallized from ethanol to give white plates: mp 141–142°C; ^{1}H nmr (δ, $CDCl_3$) 7.33–6.86 (m, 8H), 4.07 (s, 2H), 4.05 (s, 2H), 3.81 (s, 3H), 2.36 (s, 3H); uv (ethanol) λ_{max} 274 nm (ε 1520 M^{-1} cm^{-1}); mass spectrum (70 eV) *m/e* (relative intensity) 290 (0.4), 226 (6), 121 (100).

Monolayer coverages

Adsorption isotherms (35) were measured for **5** and **6** on silica gel using cyclohexane as solvent and uv analysis. Values obtained for 100% coverage were the same within experimental error for both substrates: 0.9 mmol/g from plots of N versus C_{eq} (Fig. 1) and 1.0 mmol/g from plots of C_{eq}/N versus C_{eq}. Monolayer coverages were also calculated from the surface area of the silica gel (560 m^2/g) and the molecular area determined from space filling molecular models (**5**, 0.94 nm^2; **6**, 0.98 nm^2; **10**, 0.37 nm^2).

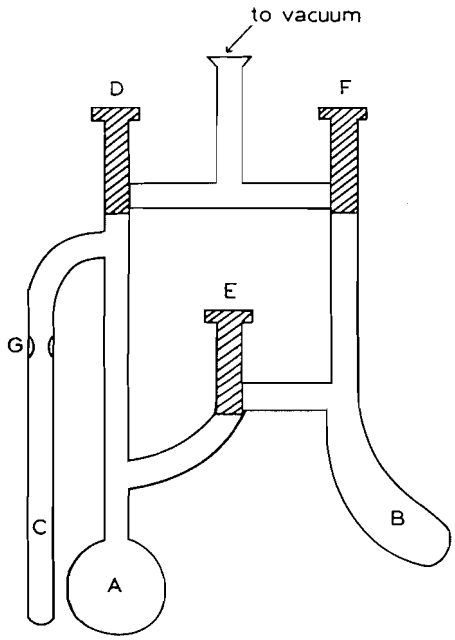

FIG. 2. Cell for preparation of dry silica gel samples.

Photolysis of 5, 6, and 7 on silica gel

Poor material balances and irreproducible product ratios resulted when **5** and **6** were photolyzed on silica gel which had not been dried in the following manner. A preweighed silica sample was heated at 200°C at ≤1 Torr for ≥5 h in compartment A of the cell shown in Fig. 2. The sample was cooled under vacuum and stopcocks D and E were closed. The substrate was then adsorbed without reexposing the silica gel to the atmosphere. A methylene chloride solution of the substrate was added through F to compartment B of the cell. After brief degassing of the solution, F was closed, E was opened, and the solution was poured onto the silica gel. Compartment B was rinsed with fresh solvent by closing E, adding ~2 mL solvent, degassing the solvent and adding it to the slurry in compartment A. The solvent was removed (E and F open, D closed) to give a free-flowing sample. All stopcocks were then closed and the cell was attached to a vacuum line and degassed to $\sim 10^{-5}$ Torr by three or more freeze–thaw cycles at liquid nitrogen temperatures. After degassing, the sample was transferred to irradiation tube C which was sealed at point G. For samples to be irradiated at low temperature, dry, deoxygenated nitrogen was added to the tube before it was sealed; this was necessary to ensure adequate sample cooling.

The rotated sample tubes were irradiated with the 150 W xenon lamp (**4**) or the Rayonet reactor (**5** and **6**) at room temperature with cold running water and air cooling, respectively. All low temperature irradiations were performed with the 1000 W xenon lamp. The light was focused on the end of a 16 mm quartz light pipe and the sample tube was rotated under the other end. Both the tube and the end of the light pipe were immersed in a cooling bath (methanol/dry ice or liquid nitrogen). All photolysis temperatures refer to internal sample temperatures.

The adsorbed products were removed from the silica gel by extraction with 100 mL of diethyl ether (**5** and **6**) or methylene chloride (**7**). The filtrate was concentrated and analyzed by gc after the addition of a known amount of tetracosane as internal standard. Calibration curves were constructed for all compounds analyzed quantitatively; the average of three or more injections was used for each determination.

Dibenzyls **8**, **9**, and **10** were isolated from preparative scale photolyses of each of **5**, **6**, and **7** on silica gel. They were separated by chromatography and recrystallized from methanol; the identity of each was established by comparison of its mp and spectra with those in the literature (19*b*).

Photolysis of 5 and 6 on modified silica

Samples of **5** and **6** on dehydrated silica gel were prepared, degassed, irradiated, and analyzed as outlined above. For silica samples containing coadsorbed cyclohexanediol, the diol was adsorbed first and then the ketone; all procedures were as outlined above.

Photolysis of 1, 3, and 13 on silica gel

Samples of **1**, **3**, and **13** were adsorbed on silica gel which had not been predried. A methylene chloride solution of the adsorbate was added to a preweighed silica sample in a round bottom flask. After solvent removal by evacuation, the sample was transferred to an irradiation cell. The sample was then evacuated at ~0.5 Torr for 15 min before being degassed. Dry, deoxygenated nitrogen was added before the tube was sealed. Samples of **1** were rotated and water cooled during irradiation with the 1000 W xenon lamp plus light pipe assembly. They were extracted with 100 mL ether and analyzed by gc with eicosane as the internal standard. Rotated samples of **3** and **13** were air cooled, irradiated in the Rayonet (254.7 nm), extracted with 100 mL methylene chloride, and analyzed by gc with docosane as the internal standard.

The isomeric ketones, **11** and **12** were isolated from a preparative scale photolysis of **1** on silica gel. Each was separated by chromatography and identified by comparison with an authentic sample. Sulfinate **13** was isolated from a preparative scale photolysis of **3** and also identified by comparison with an authentic sample. Products from the photolysis of **13** were identified tentatively by comparison of gc retention times but were not separated.

Solution photolyses

All solutions to be irradiated were deaerated by purging with nitrogen for 30 min. Ketone **5** was irradiated with the 150 W xenon lamp; all others were irradiated at 254 nm in the Rayonet with air cooling. Products were analyzed by gc, as already described.

Acknowledgement

We thank the Natural Sciences and Engineering Research Council of Canada for financial support.

1. (*a*) N. J. TURRO and B. KRAEUTLER. *In* Diradicals. *Edited by* W. T. Borden. John Wiley and Sons, Inc., New York. 1982. Chapt. 6; (*b*) H. SCHUH and H. FISCHER. Helv. Chim. Acta, **61**, 2130 (1978); (*c*) H. D. ROTH and M. L. SCHILLING. J. Am. Chem. Soc. **103**, 7210 (1981); (*d*) D. D. TANNER and P. M. RAHIMI. J. Am. Chem. Soc. **104**, 225 (1982).
2. (*a*) P. A. LEERMAKERS, L. D. WEIS, and H. T. THOMAS. J. Am. Chem. Soc. **87**, 4403 (1965); (*b*) P. A. LEERMAKERS, H. T. THOMAS, L. D. WEIS, and F. C. JAMES. J. Am. Chem. Soc. **88**, 5075 (1966).
3. L. J. JOHNSTON, P. DE MAYO, and S. K. WONG. J. Chem. Soc., Chem. Commun. 1106 (1982).
4. D. AVNIR, P. DE MAYO, and I. ONO. J. Chem. Soc. Chem. Commun. 1109 (1978).
5. J. E. LEFFLER and J. J. ZUPANCIC. J. Am. Chem. Soc. **102**, 259 (1980).
6. J. E. LEFFLER and J. T. BARBAS. J. Am. Chem. Soc. **103**, 7768 (1981).
7. P. DE MAYO, A. NAKAMURA, P. W. K. TSANG, and S. K. WONG. J. Am. Chem. Soc. **104**, 6824 (1982).
8. M. ANPO, T. WADA, and Y. KUBOKAWA. Bull. Chem. Soc. Jpn. **50**, 31 (1977).
9. N. J. TURRO and G. C. WEED. J. Am. Chem. Soc. **105**, 1861 (1983).
10. (*a*) C. MALLER and B. M. HOFFMANN. J. Phys. Chem. **80**, 842 (1976); (*b*) A. K. SELIVANOVSKII, V. B. GOLUBEV, E. V. LUNINA, and B. V. STRAKHOV. Russ. J. Phys. Chem. **50**, 990 (1975); (*c*) G. B. GARBUTT and H. D. GESSER. Can. J. Chem. **48**, 2685 (1970).
11. (*a*) R. K. ILER. *In* The chemistry of silica. John Wiley and Sons, Inc., New York. 1979. Chapt. 6; (*b*) A. V. KISELEV and V. I.

Can. J. Chem. Downloaded from www.nrcresearchpress.com by 210.87.254.40 on 09/06/12
For personal use only.

LYGIN. *In* Infrared spectra of surface compounds. Keterpress Enterprises, Jerusalem. 1975; (*c*) K. K. UNGER. *In* Porous silica. J. Chromatography Library. Vol. 16. Elsevier Scientific Publishing Company, Amsterdam. 1979.
12. (*a*) D. W. SINDORF and G. E. MACIEL. J. Am. Chem. Soc. **105**, 1487 (1983); (*b*) G. E. MACIEL and D. W. SINDORF. J. Am. Chem. Soc. **102**, 7606 (1980).
13. J. M. THOMAS, C. A. FYFE, S. RAMDAS, J. KLINOWSKI, and G. C. GOBBI. J. Phys. Chem. **86**, 3061 (1982).
14. P. S. ENGEL. J. Am. Chem. Soc. **92**, 6074 (1970).
15. W. K. ROBBINS and R. H. EASTMAN. J. Am. Chem. Soc. **92**, 6076 (1970); **92**, 6077 (1970).
16. (*a*) B. BLANK, P. G. MENNITT, and H. FISCHER. Spec. Lect. 23rd Congr. Pure Appl. Chem. **4**, 1 (1971); (*b*) H. LANGHALS and H. FISCHER. Chem. Ber. **111**, 543 (1978); (*c*) M. LEHNI, H. SCHUH, and H. FISCHER. Int. J. Chem. Kinet. **11**, 705 (1979).
17. R. S. GIVENS. *In* Organic photochemistry. Vol. 5. *Edited by* A. Padwa. Marcel Dekker, Inc., New York. 1981. p. 227.
18. T. O. MEIGGS, L. I. GROSSWEINER, and S. I. MILLER. J. Am. Chem. Soc. **94**, 7986 (1972).
19. (*a*) R. S. GIVENS and W. F. OETTLE. J. Org. Chem. **37**, 4325 (1972); (*b*) B. MATUSZEWSKI, R. S. GIVENS, and C. NEYWICK. J. Am. Chem. Soc. **95**, 595 (1973); (*c*) R. S. GIVENS, B. MATUSZEWSKI, N. LEVI, and D. LEUNG. J. Am. Chem. Soc. **99**, 1896 (1977).
20. A. A. M. ROOF, H. F. VAN WOERDEN, and H. CERFONTAIN. J. Chem. Soc. Perkin Trans. II, 841 (1980).
21. (*a*) R. S. GIVENS and B. MATUSZEWSKI. Tetrahedron Lett. 861 (1978); (*b*) J. H.-S. LIU. Ph.D. Dissertation, University of Kansas. 1980.
22. G. E. ROBINSON and J. M. VERNON. J. Chem. Soc. Perkin Trans. I, 1682 (1977).
23. (*a*) L. LUNAZZI, K. U. INGOLD, and J. C. SCAIANO. J. Phys. Chem. **87**, 529 (1983); (*b*) N. J. TURRO, I. R. GOULD, and B. H. BARETZ. J. Phys. Chem. **87**, 531 (1983).
24. D. AVNIR, L. J. JOHNSTON, P. DE MAYO, and S. K. WONG. J. Chem. Soc. Chem. Commun. 958 (1981).
25. (*a*) J. GRIFFITHS and H. HART. J. Am. Chem. Soc. **90**, 5296 (1968); (*b*) R. L. CARGILL, W. A. BUNDY, D. M. POND, A. B. SEARS, J. SALTIEL, and J. WINTERLE. Mol. Photochem. **3**, 123 (1971).
26. J. R. DACEY. Ind. Eng. Chem. **57**, 27 (1965).
27. N. J. TURRO and W. R. CHERRY. J. Am. Chem. Soc. **100**, 7431 (1978).
28. (*a*) N. J. TURRO, D. R. ANDERSON, and B. KRAEUTLER. Tetrahedron Lett. **21**, 3 (1980); (*b*) N. J. TURRO, M. F. CHOW, C. J. CHUNG, and B. KRAEUTLER. J. Am. Chem. Soc. **103**, 3886 (1981).
29. J. CHILTON, L. GIERING, and C. STEEL. J. Am. Chem. Soc. **98**, 1865 (1976).
30. (*a*) C. R. HALL and D. J. H. SMITH. Tetrahedron Lett. 3633 (1974); (*b*) J. SALTIEL and L. METTS. J. Am. Chem. Soc. **89**, 2232 (1967).
31. O. BEHAGEL and H. RATZ. Chem. Ber. **72**, 1257 (1939).
32. R. R. OTTER and R. L. SHRINER. J. Am. Chem. Soc. **73**, 887 (1951).
33. R. C. ELDERFIELD and K. L. BURGESS. J. Am. Chem. Soc. **82**, 1975 (1960).
34. Q. E. THOMPSON. J. Org. Chem. **30**, 2703 (1965).
35. R. L. HOFFMANN, D. G. MCCONNELL, G. R. LIST, and C. D. EVANS. Science, **157**, 550 (1967).

Can. J. Chem. Downloaded from www.nrcresearchpress.com by 210.87.254.40 on 09/06/12
For personal use only.

On catalyzed additions of *trans*-piperylene to 2-cyclohexenones. A short route to potential precursors of eremophilane sesquiterpenoids

JAGABANDHU DAS, MASATOSHI KAKUSHIMA, AND ZDENEK VALENTA[1]
Department of Chemistry, University of New Brunswick, Fredericton, N.B., Canada E3B 6E2

AND

KRZYSZTOF JANKOWSKI AND RHÉAL LUCE
Departement de Chimie, Université de Moncton, Moncton, N.B., Canada E1A 3E9

Received August 9, 1983

JAGABANDHU DAS, MASATOSHI KAKUSHIMA, ZDENEK VALENTA, KRZYSZTOF JANKOWSKI, and RHÉAL LUCE. Can. J. Chem. **62**, 411 (1984).

A chemical correlation is described by which the two adducts resulting from a catalyzed addition of *trans*-piperylene to 2-methyl-2-cyclohexenone, **7** and **8**, are proven to be stereoisomers. Various reaction conditions for the addition of *trans*-piperylene to 2-cyclohexenone are also summarized.

JAGABANDHU DAS, MASATOSHI KAKUSHIMA, ZDENEK VALENTA, KRZYSZTOF JANKOWSKI et RHÉAL LUCE. Can. J. Chem. **62**, 411 (1984).

On décrit une corrélation chimique qui permet de prouver que les deux adduits (**7** et **8**) provenant de l'addition catalysée du pipérylène-*trans* sur la méthyl-2 cyclohexénone-2 sont des stéréoisomères. On résume également différentes conditions de réaction pour l'addition du pipérylène-*trans* sur la cyclohexénone-2.

[Traduit par le journal]

Can. J. Chem. Downloaded from www.nrcresearchpress.com by 210.87.254.40 on 09/06/12
For personal use only.

It was assumed until recently that 2-cyclohexenone and its alkyl derivatives (as well as other 2-cycloalkenones) are not suitable for synthetically useful Diels–Alder reactions. Several reports during the last few years have shown, however, that catalyzed diene additions (1, 2) work efficiently, if somewhat slowly, to give good yields of the desired *cis*-octalones **1** or **2** (3–11) in which R^1 and R^2 can be an H-atom or an alkyl group and R^3 is an alkyl group. Concerning substitution of the dienophile olefinic bond, it is thus clear now that the 2-position can be unsubstituted (R^2 = H) or alkyl substituted (R^2 = alkyl). Also, the saturated C-atoms of the 2-cyclohexenone may bear alkyl groups.

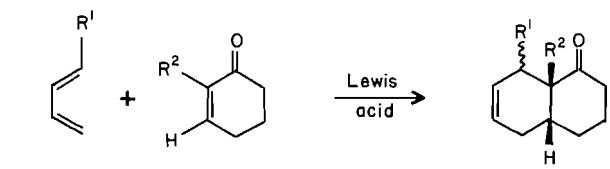

1

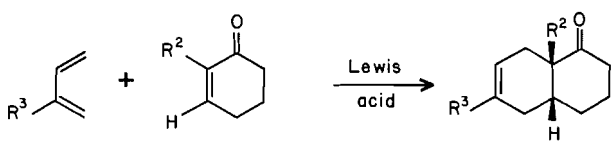

2

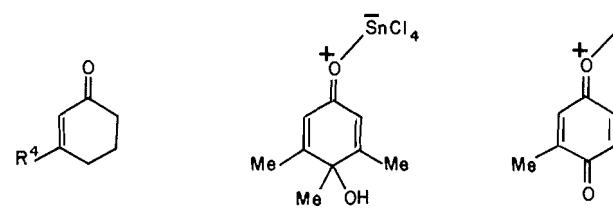

3 **4** **5**

[1]Author to whom correspondence may be addressed.

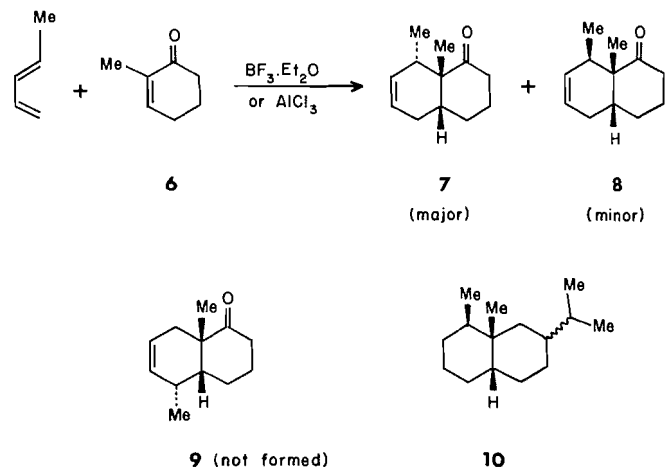

6 **7** (major) **8** (minor)

9 (not formed) **10**

SCHEME 1

In contrast, no additions (thermal or catalyzed) have been reported to simple 2-cyclohexenones of type **3** in which the 3-position is alkyl substituted. As suggested by Liotta *et al.* (12), this lack of reactivity is likely due to a combination of electronic and steric factors. Exceptions to this "rule of unreactivity" are instructive. Complexes **4** (12) and **5** (13, 14) have been reported to add to dienes with facility and this is presumably due to a lower lying LUMO (15) as well as a sterically less hindered approach of the diene in these cases.

In an important contribution, Wenkert and co-workers (11) have recently reported their extensive work on the $AlCl_3$-catalyzed addition of 1,3-butadiene, isoprene, and *trans*-piperylene to 2-cyclopentenones, 2-cyclohexenones, and 2-cycloheptenones, and their analysis of product structures, done mainly by ^{13}Cmr spectroscopy, has shown that the *ortho*- and *para*-rules of addition (16) are followed in all cases.

We wish to report in more detail on one of the additions described by them, that of *trans*-piperylene to 2-methyl-2-cyclohexenone **6** (Scheme 1). Our study was undertaken in order to establish rigorously whether the *ortho*-rule of addition

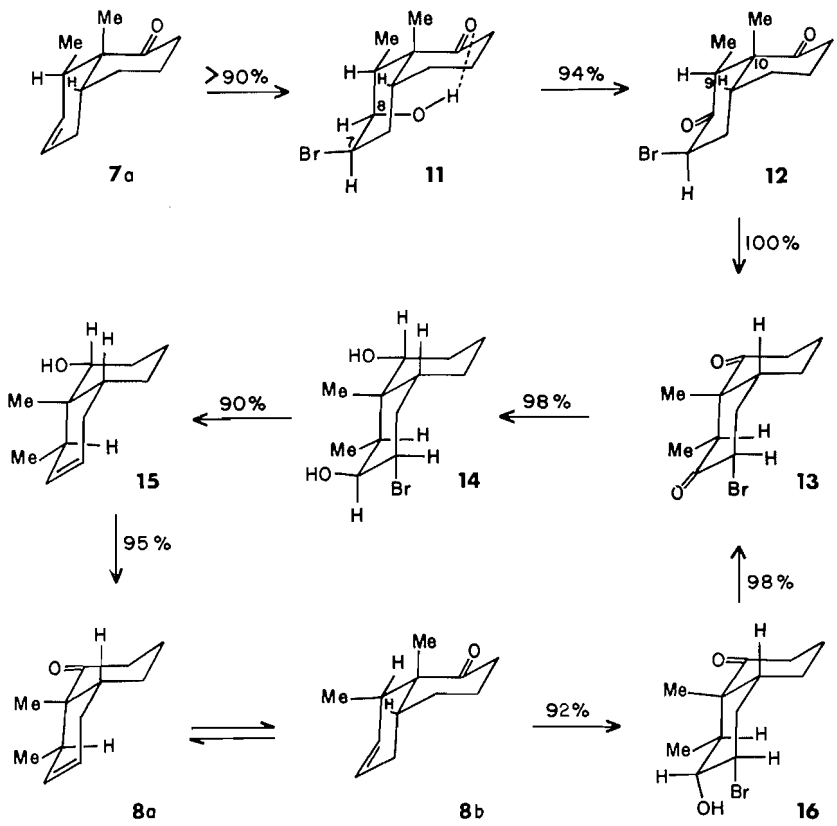

SCHEME 2

TABLE 1. Condensation of *trans*-piperylene with 2-methyl-2-cyclohexenone **6**

Catalyst	Solvent	*t* (h)	*T* (°C)	Total yield[a] (%)	Products (% of total) 7	8
$BF_3 \cdot Et_2O$	C_6H_6	48	20	75	67	33
$AlCl_3$	C_6H_6	72	20	80	78	22

[a]Yield based on the dienophile; diene was used in large excess. Total yield is the sum of isolated pure adducts.

is followed quantitatively in this case; a previous report (5) indicated the formation of a substantial amount of the *meta*-adduct **9** and we deemed it essential to find out whether this addition constitutes an important exception to the *ortho*-rule (16). Two adducts are formed and we have been able to convert the major (*endo-ortho*) adduct **7** into the minor (*exo-ortho*) adduct **8** in a 6-step sequence and an overall yield of 70% (17). This proves rigorously that the two products are stereoisomers (i.e., that the *meta*-adduct **9** is absent) and thus strengthens the structural assignments based on spectroscopy (11). From the synthetic standpoint, it furthermore makes *cis*-octalones of type **8** available in good yield. Eremophilane sesquiterpenoids (skeleton **10**) (18) provide one example for which the geometry present in **8** is required.

In order to establish best experimental conditions and analytical procedures, we have also studied catalyzed additions of *trans*-piperylene to 2-cyclohexenone (10, 11) in detail.

Catalyzed additions of trans*-piperylene to 2-methyl-2-cyclohexenone*

As summarized in Table 1, good yields (based on dienophile) of the two adducts were obtained in reactions of *trans*-piperylene with **6** in the presence of BF_3-etherate or $AlCl_3$.[2] The reactions were found to be relatively slow and the diene was used in excess since it was found to polymerize slowly under the reaction conditions. The mixture of the two adducts was first separated from polymers by distillation and the pure adducts were then obtained by chromatography on a silver nitrate impregnated silica gel column. Gas chromatography of the distilled mixture showed the presence of only two products in both reactions.

The following findings prove rigorously that the major adduct has the expected structure **7** and the minor one structure **8**. Treatment of **7** with bromine and sodium hydroxide in methylene chloride at −20°C gave an excellent yield of crystalline bromohydrin **11**. A broad peak at 3380 cm^{-1} (—OH) and a peak at 1690 cm^{-1} (C=O) in the ir spectrum of **11** indicated that the two functions are H-bonded. The ^{1}Hmr spectrum of **11**, after exchange of the hydroxyl H-atom with D_2O, showed two deshielded equatorial protons (Table 2), one at δ 3.8 and one at δ 4.4. The position and multiplicity of these signals, together with the ir data, are only compatible with structure and conformation **11**. Clearly, the only bromohydrin formed is the one expected after an attack of the double bond in **7***a* from the less hindered convex side followed by a *trans* diaxial opening of the intermediate bromonium ion.

Oxidation of **11** with Jones' reagent gave bromoketone **12** in a 94% yield after chromatography. The appearance of a sharp quadruplet in the ^{1}Hmr spectrum of **12** (H_A, Table 2) establishes that the secondary methyl group is located at C-9.[3]

[2]Wenkert and co-workers (11) have reported a yield of 92% (based on chromatographic analysis) and a product ratio **7**/**8** = 2.2:1 in a reaction catalyzed by $AlCl_3$ in toluene.

[3]See formula **17** for carbon numbering and proton notation.

Can. J. Chem. Downloaded from www.nrcresearchpress.com by 210.87.254.40 on 09/06/12
For personal use only.

TABLE 2. Proton magnetic resonance data for selected protons in compounds **7** to **16** (δ, ppm)[a]

Compound	Angular CH_3	CH—CH_3 (J, Hz)	H_A (J, Hz)	H_B (J, Hz)	H_C (J, Hz)	C_1(OH)(H)
7	1.3 (s)	1.1 (d, 7)		5.4 (s)	5.4 (s)	
8	0.9 (s)	0.8 (d, 7)		5.4 (m)	5.4 (m)	
11[b]	1.5 (s)	1.2 (d, 7)		3.8 (t, 3.5)	4.4 (q, 3)	
12	1.6 (s)	1.15 (d, 6.5)	2.95 (q, 6.5)		4.4 (t, 3.5)	
13	1.0 (s)	0.9 (d, 6.5)	3.3 (q, 6.5)		5.0 (t, 10)	
14	1.3 (s)	1.2 (d, 6.5)		3.8 (t, 3)	4.6 (o, 13, 5, 3)	3.2 ($W/2$ = 22)
15	1.05 (s)	1.1 (d, 7)		5.4 (m)	5.4 (m)	3.6 (m)
16[b]	1.15 (s)	0.9 (d, 7)			3.6 (t, 10)	4.35 (o, 11.5, 10, 7)

[a]Spectra taken on a Varian T-60 instrument in $CDCl_3$; see formula **17** for proton notation; s = singlet, d = doublet, t = triplet, q = quadruplet, o = octet, m = multiplet.
[b]D_2O added.

Irradiation of H_A changed the methyl doublet at δ 1.15 to a singlet as expected. A one-proton triplet (H_C) at δ 4.4 (J = 3.5 Hz) shows that the proton adjacent to the bromine atom is coupled to two protons and that the bromine is axially oriented.

On standing for three days at ambient temperature, either in crystalline state (!) or in chloroform solution, **12** was converted quantitatively into an isomer. The ^{1}Hmr signal corresponding to the proton adjacent to the bromine atom (δ 5.0; t, J = 10 Hz) in the spectrum of the new isomer showed that the compound contains an equatorial bromine. Clearly, there are two ways in which **12** can isomerize to give a product of greater stability. Epimerization at C-7 would lead to bromoketone **18**. Alternatively, a conformational flip and an epimerization at C-9 would give compound **13**. Both **13** and **18** contain the two epimerizable groups, bromine and secondary methyl, in an equatorial position. The quaternary methyl group at C-10 cannot be expected to have a decisive influence since it is axial to one ring and equatorial to the other ring in all the possible *cis*-decaline dione systems.

Structure **13** for the isomerization product was proven in the following simple way. Reduction of **13** with sodium borohydride gave diol **14** as the only product. Its ^{1}Hmr spectrum (Table 2) shows clearly that the hydroxyl group vicinal to bromine is axial (H_B; δ 3.8; t, J = 3 Hz), whereas the other OH-group is equatorial (C_1—H; δ 3.2; m, $W/2$ = 22 Hz). Interestingly, the screening of the bromoketone ring by the axial methyl group thus completely prevented the more commonly observed axial attack by the hydride ion.

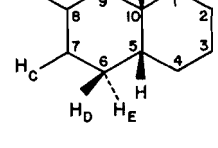

17

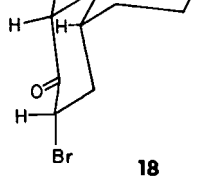

18

Reduction of **14** with zinc in acetic acid gave a 90% yield of olefin **15**. On Jones' oxidation, **15** was converted to a ketone which was found to be identical in all respects with minor Diels–Alder adduct **8**.

This correlation completely clarifies the whole series. Obviously, both Diels–Alder adducts have a methyl group at C-9 and must thus be epimeric at that position.[4] Furthermore, the isomerization of bromoketone **12** discussed above must involve a change of configuration at C-9, since otherwise the subsequent three steps (**13** → **14** → **15** → **8**) would have converted the isomerized product back to **7**, rather than **8**. Finally, the spectroscopic data for all compounds in this series make sense only if the major adduct is assigned structure **7** (*endo*-adduct) and the minor adduct structure **8** (*exo*-adduct).

The fact that diketone **13** has a configuration at C-9 identical to that of minor adduct **8** was further confirmed by a treatment of **8** with bromine and aqueous sodium hydroxide at ambient temperature for 2 h to form bromohydrin **16** in a high yield. The configuration and conformation of **16** follows clearly from its ^{1}Hmr spectrum (Table 2). Finally, Jones' oxidation of **16** gave diketone **13** in high yield.

The above results can be summarized in the following way. (1) *trans*-Piperylene adds to 2-methyl-2-cyclohexenone **6** in the presence of BF_3-etherate or $AlCl_3$ to give exclusively the *ortho*-adducts **7** and **8**. (2) The *endo*-adduct **7** can be isolated in a yield of 62% from the $AlCl_3$-catalyzed addition. (3) The *exo*-adduct **8** can be obtained in a maximum yield of 60–62% by a combination of direct isolation (Table 1) and of conversion of **7** (Scheme 2) from additions catalyzed by either BF_3-etherate or $AlCl_3$. (4) Diketone **13** can presumably be obtained from a mixture of **7** and **8** without the necessity of chromatographic separation (Scheme 2). (5) Adduct **7** reacts in conformation **7***a* in agreement with the conformation proposed for **7** on the basis of a ^{13}Cmr study (11). Not surprisingly, the addition of the elements of HOBr to adduct **8** is much slower than that to **7** since both faces of the double bond are screened in either conformation of **8** (Scheme 2). Nevertheless, one bromohydrin is formed exclusively (**16**) and it clearly arises from a diaxial opening of a bromonium ion corresponding to conformer **8***b*, followed by a conformational inversion.

Based on available evidence, it can be predicted that the exclusive *ortho*-addition will take place in catalyzed reactions of similar dienes and dienophiles in which the methyl groups (Scheme 1) have been replaced by other alkyl groups. A similar prediction concerning the *endo* (**7**)/*exo* (**8**) ratio would, however, be unwise. The amount of the *exo*-adduct **8** formed (Table 1) (11) is unusually large. Wenkert and co-workers have, furthermore, shown that this *exo*-addition is specific to 2-methyl-2-cyclohexenone; catalyzed additions of *trans*-piperylene to 2-methyl substituted 2-cyclopentenones and 2-cycloheptenones gave only the expected *endo*-adducts (11). A subtle nonbonded interaction is probably involved (11) and this could well be affected drastically by replacing the methyl groups in *trans*-piperylene and in **6** by larger alkyl groups.

[4]An ^{1}Hmr induced shift study using $Eu(fod)_3$ (see Experimental) is in full agreement with this conclusion.

Can. J. Chem. Downloaded from www.nrcresearchpress.com by 210.87.254.40 on 09/06/12
For personal use only.

TABLE 3. Condensation of *trans*-piperylene with 2-cyclohexenone

Catalyst (1 mol equivalent)	Solvent	*t* (h)	*T* (°C)	Total yield (%)	Products (% of total)					
							Isomers **21** or **22**			
					cis-**20**	*trans*-**20**	*cis*	*trans*	Unidentified	Method[a]
None	None	48	220	50	30	50	5	10	5	(a)
$AlCl_3$	C_6H_6	5	Reflux	85	62	30	3	Traces	—	(a)
	C_6H_6	10	20	70	65	35	Traces	—		(a)
	C_6H_6	48	20	62	84	16	—	—	—	(b)
$AlCl_3$·dioxane	C_6H_6	5	20	56	60	40	—	—	—	(a)
$AlCl_3$·THF	C_6H_6	5	20	50	60	40	—	—	—	(a)
BF_3·Et_2O	C_6H_6	20	20	97	84	16	—	—	—	(b)
BF_3·Et_2O	CH_2Cl_2	2	20	40	60	35	Traces	—		(a)
	CH_2Cl_2	10	20	45	60	30	Traces	—		(a)
$SnCl_4$	CH_2Cl_2	2	0–5	27	55	35	—	—	10	(a)
	CH_2Cl_2	2	20	22	50	50	—	—	20	(a)

[a]Method (a): product ratios obtained by gas chromatographic analysis (for retention times, see Table 4); Method (b): product ratios obtained by column chromatography and ^{1}Hmr integration.

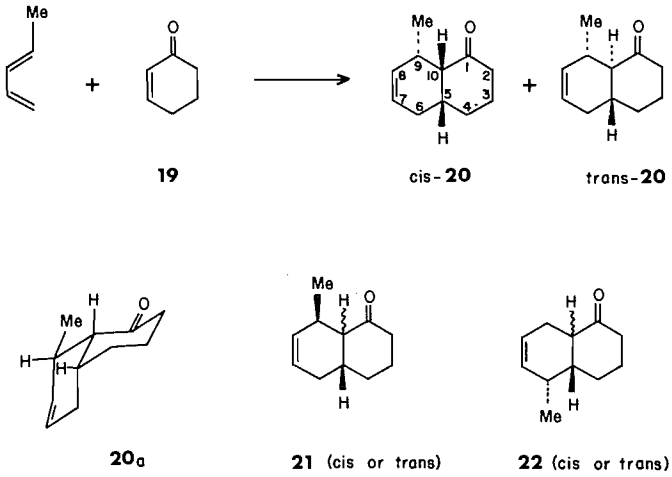

SCHEME 3

Catalyzed additions of trans*-piperylene to 2-cyclohexenone*

The results of all additions of *trans*-piperylene to **19** (Scheme 3) are summarized in Table 3. It should be noted that particularly good yields of the partially equilibrated *cis*–*trans* mixture of the expected *endo-ortho* adduct **20** are obtained using BF_3-etherate in benzene, while useful yields also result using $AlCl_3$ in benzene.[5] Tin tetrachloride proved to be an inferior catalyst in this case.

A high temperature thermal addition was performed (see Table 3) in order to acquire a comparison with the catalyzed additions and to obtain gas chromatographic data for the greatest possible number of adducts. Table 4 lists gc retention times and major ms peaks for the four products obtained in the thermal addition. Equilibrations with alumina clearly established that the two major products showing retention times of 9.5 and 10.8 min, respectively (see Table 4), are interconvertible *cis*-*trans* isomers and that the two minor products (retention times of 11.9 and 12.1 min, respectively) are similarly related.

Since the two minor products were formed in negligible quantities in the catalyzed additions (3% or less, Table 3), their structure elucidation was not pursued. This *cis*-*trans* pair must clearly result either from the *exo-ortho* adduct **21** or the *endo-meta* adduct 22.

Mixture of the two major products obtained in all additions gave up to 96% of *trans*-**20** on treatment with neutral alumina. The ^{1}Hmr data for the two compounds together with an induced shift study using $Eu(fod)_3$ (Table 5) clearly show that the CH_3 group is in the vicinity of the carbonyl group and that *cis*-**20** is thus the expected *ortho*-adduct. Furthermore, simulation of the ^{1}Hmr shift reagent experiments using the JULIE program (19)

[5]A yield of 81% was reported (11) for the addition using $AlCl_3$ in toluene.

TABLE 4. Gas chromatographic — mass spectral data of condensation of *trans*-piperylene with 2-cyclohexenone

Compound	Retention times[a] (min)	Mass spectra – *m*/*z* (*I*%) of selected ions				
		M^+	164	131	118	93
trans-**20**	9.5	100	78	85	82	
cis-**20**	10.8	100	65	70	68	
trans-**21** or **22**	11.9	100	63	55	60	
cis-**21** or **22**	12.1	100	52	60	70	

[a]For column details see Experimental.

TABLE 5. Proton magnetic resonance data for compounds *cis*-**20** and *trans*-**20** (δ, ppm)

	cis-**20**		*trans*-**20**	
	δ_0	$\Delta\delta_{rel}$[a]	δ_0	$\Delta\delta_{rel}$[b]
CH_3	1.25	1.00	0.93	1.00
Ring allylic protons (H-6)	2.20	0.54	2.30	0.58
CH—CH_3	2.70	1.06	2.70	1.00
H-10	2.40	1.78	2.40	1.10
H-2 eq	2.70	3.42	2.30	3.44
H-2 ax	2.30	2.40	2.60	2.26
H-7, H-8	5.5	0.71	5.46 5.57	0.42

[a]$\delta\Delta_{rel}$: relative induced shift; the true shift of 0.60 ppm (1.25 to 1.85) for CH_3 at 0.1 *M* $Eu(fod)_3$ has been normalized to unity.

[b]The true shift of 0.72 ppm (0.93 to 1.65) for CH_3 at 0.1 *M* $Eu(fod)_3$-d_{27} has been normalized to unity.

Can. J. Chem. Downloaded from www.nrcresearchpress.com by 210.87.254.40 on 09/06/12
For personal use only.

confirms the predominance of conformation **20***a* for the *cis*-isomer.

In contrast to the thermal addition which requires high temperature and gives a 50% total yield of a mixture of at least four products, a catalyzed addition of *trans*-piperylene to 2-cyclohexenone can thus be accomplished at 20°C to give a very high yield of the *ortho-endo* adduct **20**.[6]

Experimental

General

The ^{1}Hmr spectra were determined on a Varian T-60 or HR-220 MHz spectrometer in $CDCl_3$ (≃10%, TMS). The ir spectra were recorded on Perkin–Elmer 457 or 700-A spectrometers. The gc–ms analyses were perfomed using a PE-990 chromatograph coupled to a Hitachi RM-50 mass spectrometer. The column OV-101 (15% on WHP 80/100, 6 ft × 6 mm) was used in the programmed temperature mode. The mass spectra were recorded at 70 eV (EI); source temperature was kept at 200°C. High resolution mass spectra were determined by Dr. A. M. Hogg, University of Alberta. Elemental analyses were performed by Dr. F. Pascher, Bonn, West Germany. Melting points were determined on a Kofler hot stage and are uncorrected. Thin-layer chromatography was performed on 0.25-mm silica gel G plates containing a fluorescent indicator; preparative tlc was done on 0.75-mm silica gel G plates (20 × 20 cm). Solutions were dried over anhydrous magnesium sulfate.

Catalyzed addition of trans*-piperylene to 2-methyl-2-cyclohexenone*

1. 2-Methyl-2-cyclohexenone **6** (1.10 g, 10 mmol) prepared according to Warnhoff *et al.* (20) and *trans*-piperylene (6.80 g, 100 mmol) were dissolved in dry benzene (30 mL); BF_3-etherate (1.42 g, 10 mmol) was added in one lot at 5°C and the reaction mixture was maintained at 20°C for 48 h. It was then diluted with ether (50 mL), washed twice with a saturated $NaHCO_3$ solution, twice with water and twice with brine, and dried. Removal of solvent under reduced pressure gave a viscous oil which was distilled (75°C/0.04 Torr) to give a mixture of adducts **7** and **8** (1.28 g, 80%). Gas chromatographic study revealed the presence of only two compounds. Elution with 5% ether in hexane on chromatography on a silver nitrate-impregnated silica gel column (10% silver nitrate by weight) gave (1). minor adduct **8** (0.40 g, 25% yield) as colorless oil; ir (film): 1700 (C=O) cm^{-1}; ms m^+ 178; ^{1}Hmr: see Table 2; relative shifts on addition of [Eu(fod)$_3$]: C-10 methyl 3.7 ppm; C-9 methyl 1.9 ppm; (2). major adduct **7** (0.80 g, 50% yield) as colorless oil; ir (film): 1700 (C=O) cm^{-1}; ms m^+ 178; ^{1}Hmr: see Table 2; relative shifts on addition of [Eu(fod)$_3$]: C-10 methyl 2.5 ppm, C-9 methyl 2.0 ppm.

2. In a similar way, ketone **6** (2.20 g, 20 mmol) and *trans*-piperylene (3.40 g, 50 mmol) were reacted in benzene (25 mL) in the presence of aluminum chloride (0.66 g, 5 mmol; freshly sublimed in a stream of HCl) at 20°C for 72 h. Work-up identical to the one above gave adduct **8** (0.64 g, 18% yield) and adduct **7** (2.20 g, 62% yield) as colorless oils, homogeneous by tlc, gc, and ^{1}Hmr.

Conversion of adduct 7 into bromohydrin 11

A solution of adduct **7** (524 mg, 2.95 mmol) in methylene chloride (25 mL) was treated at −20°C with 50% aqueous sodium hydroxide (5 mL) followed by bromine (1 mL, 15 mmol). The mixture was stirred at −20°C for 5 min and then poured into water. The organic layer was separated and the aqueous layer was extracted with three 20-mL portions of methylene chloride. The combined organic layer was washed twice with water, twice with brine, and dried. Evaporation of solvent under reduced pressure gave an oily residue which crystallized from ether, mp 76–80°C (770 mg, 95% yield); ir ($CHCl_3$): 3380 (OH) and 1690 (C=O) cm^{-1}; ^{1}Hmr: see Table 2; ms M^+ calcd. for $C_{12}H_{19}O_2{}^{79}Br$: 274.05684; found: 274.05683.

[6]We do not ascribe much significance to the exact ratio of *cis* and *trans* isomers of **20** as listed for all the additions in Table 3. It can be assumed that the equilibration can partially take place both during the additions and in the process of analysis.

Oxidation to bromoketone 12

A 0.07 molar Jones' oxidation reagent (CrO_3–H_2SO_4–H_2O) (21) was added dropwise at 20°C to a stirred solution of bromohydrin **11** (214 mg, 0.78 mmol) in acetone (20 mL). The addition was continued until the color of the reagent persisted. The reaction mixture was stirred at 20°C for an additional 30 min and the excess of Jones' reagent was then destroyed by the addition of a saturated sodium bisulfite solution. The reaction mixture was then extracted three times with ether and the ethereal extract was washed twice with saturated sodium bicarbonate solution, twice with water, and twice with saturated brine. Drying and evaporation of solvent gave an oily residue which was chromatographed on silica gel plates. Elution with 30% ether in hexane gave ketone **12** (202 mg, 94% yield) as colorless crystals, mp 96–100°C; ir ($CHCl_3$): 1725 and 1710 cm^{-1} (shoulder) (carbonyls); ^{1}Hmr: see Table 2; ms m^+ 272 and 274. *Anal.* calcd. for $C_{12}H_{17}O_2Br$: C 52.40, H 6.23, O 11.63; found: C 52.66, H 6.32, O 11.62.

Isomerization to ketone 13

Crystalline bromoketone **12** (150 mg) was allowed to stand in the air at 20°C for 72 h to give pure **13**. The same transformation was observed in chloroform solution, monitored by ^{1}Hmr spectroscopy. Ketone **13** was crystallized from ether, mp 135–137°C; ir ($CHCl_3$): 1730 and 1710 cm^{-1} (carbonyls); ^{1}Hmr: see Table 2; ms m^+ 272 and 274. *Anal.* calcd. for $C_{12}H_{17}O_2Br$: C 52.40, H 6.23, O 11.63; found: C 52.18, H 6.25, O 11.13.

Reduction to diol 14

Ketone **13** (550 mg, 2 mmol) was reacted with sodium borohydride (228 mg, 6 mmol) in absolute ethanol at 20°C for 30 min. The reaction mixture was then poured into ice-water and extracted three times with ether. The combined ether extracts were washed twice with brine and dried. Evaporation of solvent gave **14** as a colorless oil (545 mg, 98% yield) homogeneous on tlc; ir ($CHCl_3$): 3600 and 3460 (OH) cm^{-1}; ^{1}Hmr: see Table 2; ms m^+ 276 and 278; M^+ calcd. for $C_{12}H_{19}O_2{}^{79}Br - H_2O$: 258.01619; found: 258.0636.

Formation of olefin alcohol 15

Diol **14** (414 mg, 1.5 mmol) was heated under reflux with reagent grade zinc dust (250 mg. 3.75 mmol) in glacial acetic acid (15 mL) for 1 h). The cooled reaction mixture was diluted with ether, residual zinc was filtered and washed with ether. The combined organic layer was evaporated to near dryness, the residue dissolved in ether (30 mL) and washed three times with saturated $NaHCO_3$ solution and twice with brine. Drying and evaporation of solvent gave an oily residue which was chromatographed on silica gel plates. Development with hexane–ether (1:2) gave oily olefin **15** (240 mg, 90% yield); ir ($CHCl_3$): 3605 and 3460 (OH) cm^{-1}; ^{1}Hmr: see Table 2; ms M^+ calcd. for $C_{12}H_{20}O$: 180.1514; found: 180.1519.

Oxidation of olefin alcohol 15 to diketone 8

Alcohol **14** (180 mg, 1 mmol) was oxidized in acetone (20 mL) with Jones' reagent (21) under conditions comparable to those described above for the formation of bromoketone **12**. A similar work-up gave an oil which was chromatographed on silica gel plates. Development with hexane–ether (2:1) gave an oil (170 mg, 95% yield) which was found to be identical with minor adduct **8** in ir, ^{1}Hmr, ms, tlc, and gc.

Conversion of adduct 8 into bromohydrin 16

A solution of adduct **8** (336 mg, 1.9 mmol) in methylene chloride (20 mL) was treated with 50% aqueous sodium hydroxide (5 mL) followed by bromine (1 mL, 15 mmol). The reaction mixture was stirred at 20°C for 2 h, when tlc showed that **8** had been consumed. Water was then added, the methylene chloride layer separated, and the aqueous layer extracted with two 20-mL portions of methylene chloride. The combined organic layer was washed three times with water, three times with brine, and dried. Evaporation of solvent gave an oily residue which on crystallization from ether gave colorless crystals of **16** (478 mg, 92% yield), mp 128–141°C; ir ($CHCl_3$): 3590 (OH) and 1705 (C=O) cm^{-1}; ^{1}Hmr: see Table 2; ms m^+ 274 and 276; M^+ calcd. for $C_{12}H_{19}O_2{}^{79}Br$: 274.05684; found: 274.05683.

Can. J. Chem. Downloaded from www.nrcresearchpress.com by 210.87.254.40 on 09/06/12
For personal use only.

*Oxidation of bromohydrin **16** to ketone **13***

Bromohydrin **16** (413 mg, 1.5 mmol) was oxidized in acetone (15 mL) under conditions comparable to those described above for the formation of ketone **12**. A similar work-up gave an oil (415 mg) which was chromatographed on silica gel plates. Development with 30% ether in hexane gave crystalline ketone **13** (400 mg, 98% yield), mp 135–137°C, identical in all respects with the product of isomerization of ketone **12**.

Condensation of trans*-piperylene with 2-cyclohexenone*

The two starting materials were obtained from the Aldrich Chemical Company.

(a) *Thermal*

Equimolar quantities of the two compounds were heated in a sealed tube at 220°C for 48 h in the presence of a few milligrams of hydroquinone. Extraction with $CHCl_3$ was followed by washing with 5% aqueous $NaHCO_3$ and saturated brine. The solution was dried and subjected to distillation. The fraction boiling at 93–105°C/0.2 Torr was analyzed by gc as shown in Table 4.

(b) *Catalytic*

For those experiments listed in Table 3 in which analysis was done by gc, equimolar quantities of cyclohexenone complex and diene were stirred in dry solvent according to details in Table 3. Isolation of the mixture of adducts was performed as above and this was followed by gc analysis.

For preparative purposes, two experiments were done in which separation was achieved by column chromotography.

1. Solution of 2-cyclohexenone (0.96 g, 10 mmol), *trans*-piperylene (2.04 g, 30 mmol), and BF_3-etherate (1.42 g, 10 mmol) in dry benzene (20 mL) was stirred for 20 h at 20°C. Work-up with ice-cold aqueous $NaHCO_3$ (5%), followed by washing with saturated brine, drying, and evaporation of solvent gave a yellow oil which was subjected to chromatography on a silica gel column. Elution with 10% ether in hexane gave two combined fractions: (*i*) a colorless oil (0.58 g, 35% yield) which proved to be a mixture of *cis*-**20** and *trans*-**20** in a 15:11 ratio (^{1}Hmr integration of the CH_3 signal); (*ii*) pure oily *cis*-**20** (1.02 g, 62% yield).

The compound (*cis*-**20**) proved homogeneous by tlc, gc, and ^{1}Hmr; ms M^+ calcd. for $C_{11}H_{16}O$: 164.1202; found: 164.1204. For gc and ms data, see Table 4; for ^{1}Hmr data, see Table 5.

2. An experiment similar to the above was performed in which $AlCl_3$ (1.33 g, 10 mmol), freshly sublimed in a stream of dry HCl gas, was used as a catalyst and the reaction was allowed to proceed for 48 h at 20°C. A work-up identical to the above gave, on silica gel chromatography: (*i*) a mixture of *cis*-**20** and *trans*-**20** (0.35 g, 24% yield) in a 15:11 ratio; (*ii*) pure *cis*-**20** (0.56 g, 38% yield); (*iii*) unreacted 2-cyclohexenone (60 mg).

Equilibrations of cis–trans *isomers*

The mixture of *cis*-**20** and *trans*-**20** obtained above (0.5 g) was stirred with neutral alumina (grade I, 2 g) in dry chloroform (25 mL) at 20°C for periods of 1–48 h. The alumina was then filtered, washed repeatedly with methanol, and the combined organic extracts were evaporated *in vacuo*. The residue was subjected to gc analysis. After 24 h, the composition was 92% *trans*-**20**, 8% *cis*-**20**; after 48 h, the composition was 96% *trans*-**20** and 4% *cis*-**20**.

For gc and ms data on compound *trans*-**20**, see Table 4; for ^{1}Hmr data, see Table 5.

Acknowledgements

We are grateful to the Natural Sciences and Engineering Research Council of Canada for financial support.

1. P. YATES and P. EATON. J. Am. Chem. Soc. **82**, 4436 (1960).
2. R. ROBINSON and G. I. FRAY. J. Am. Chem. Soc. **83**, 249 (1961).
3. T. HARAYAMA, H. CHO, M. OHTANI, and Y. INUBUSHI. Chem. Pharm. Bull. Jpn. **22**, 2784 (1974).
4. T. HARAYAMA, H. CHO, and Y. INUBUSHI. Tetrahedron Lett. 2693 (1975).
5. I. NAGAKURA, H. OGATA, M. UENO, and Y. KITAHARA. Bull. Chem. Soc. Jpn. **48**, 2995 (1975).
6. W. OPPOLZER and M. PETRZILKA. J. Am. Chem. Soc. **98**, 6722 (1976); Helv. Chim. Acta, **61**, 2755 (1978).
7. C. F. FRINGUELLI, F. PIZZO, A. TATICCHI, and E. WENKERT. Synth. Commun. **9**, 391 (1979).
8. H. J. LIU and E. N. C. BROWNE. Can. J. Chem. **57**, 377 (1979).
9. P. A. GRIECO, S. FERRINO, and G. VIDARI. J. Am. Chem. Soc. **102**, 7586 (1980).
10. W. G. DAUBEN and D. M. MICHNO. J. Am. Chem. Soc. **103**, 2284 (1981).
11. F. FRINGUELLI, F. PIZZO, A. TATICCHI, T. D. J. HALLS, and E. WENKERT. J. Org. Chem. **47**, 5056 (1982).
12. D. LIOTTA, M. SAINDANE, and C. BARNUM. J. Am. Chem. Soc. **103**, 3224 (1981).
13. R. A. DICKINSON, R. KUBELA, G. A. MACALPINE, Z. STOJANAC, and Z. VALENTA. Can. J. Chem. **50**, 2377 (1972).
14. N. STOJANAC, A. SOOD, Z. STOJANAC, and Z. VALENTA. Can. J. Chem. **53**, 619 (1975).
15. K. N. HOUK. Acc. Chem. Res. **8**, 361 (1975).
16. A. S. ONISHCHENKO. Diene synthesis. Israel Program of Scientific Translations, Jerusalem, 1964; J. SAUER. Angew. Chem. Int. Ed. Engl. **6**, 16 (1967).
17. J. DAS. Ph.D. Dissertation, University of New Brunswick, Fredericton, 1977.
18. T. K. DEVON and A. I. SCOTT. Handbook of naturally occurring compounds, Vol. 2. Academic Press, New York. 1972, pp. 129–134
19. H. TOMISAWA, H. HONGO, J. B. CHIASSON, and K. JANKOWSKI. Heterocycles, **19**, 1257 (1982).
20. E. W. WARNHOFF, D. G. MARTIN, and W. S. JOHNSON. Org. Synth. Coll. Vol. IV, 162 (1963).
21. A. BOWERS, T. G. HALSALL, E. R. H. JONES, and A. J. LEMIN. J. Chem. Soc. 2555 (1953).

Can. J. Chem. Downloaded from www.nrcresearchpress.com by 210.87.254.40 on 09/06/12
For personal use only.

Chemiluminescence from the reactions of ozone with sulphur compounds

P. K. ARORA AND J. P. S. CHATHA
Air Monitoring Section, Bhabha Atomic Research Centre, Bombay-400 085, India

Received April 18, 1983

P. K. ARORA and J. P. S. CHATHA. Can. J. Chem. **62**, 417 (1984).

Emissions from excited SO_2 in its singlet state ($^1B_1$ and/or $^1A_2$) and triplet state ($^3B_1$) have been observed in gas-phase chemiluminescent reactions of ozone with a number of sulphur compounds. The compounds studied are carbon disulphide, thiophene, diallyl sulphide, diallyl disulphide, dimethyl sulphide, dimethyl disulphide, and thiophenol. The reaction pathways responsible for the formation of excited molecules are discussed. The remarkable similarity between the emission spectra of the reactions and the chemiluminescence from the SO + O_3 reaction confirms that SO is a precursor for the observed chemiluminescence. Disulphides are found to be more chemiluminescent than monosulphides. The absence of chemiluminescence from HCHO* in the reactions of ozone with allyl sulphide and disulphide indicates that the attack of ozone molecule is on the C—S bond in organic sulphides.

P. K. ARORA et J. P. S. CHATHA. Can. J. Chem. **62**, 417 (1984).

On a observé des émissions à partir du SO_2 excité à l'état singulet ($^1B_1$ et/ou $^1A_2$) et à l'état triplet ($^3B_1$) au cours de réactions chimiluminescentes, en phase gazeuse, de l'ozone avec un certain nombre de composés soufrés. On a étudié les composés suivants: le disulfure de carbone, le thiophène, le sulfure de diallyle, le disulfure de diallyle, le sulfure de diméthyle, le disulfure de diméthyle et le thiophénol. On discute des chemins réactionnels responsables de la formation des molécules excitées. La similitude frappante existant entre les spectres d'émission des réactions et la chimiluminescence à partir de la réaction SO + O_3 confirme que le SO est un précurseur de la chimiluminescence observée. On a trouvé que les disulfures sont plus chimiluminescents que les monosulfures. L'absence de chimiluminescence à partir de HCHO* dans la réaction de l'ozone avec le sulfure et le disulfure d'allyle indique que l'attaque de la molécule d'ozone à lieu sur la liaison C—S des sulfures organiques.
[Traduit par le journal]

Can. J. Chem. Downloaded from www.nrcresearchpress.com by 210.87.254.40 on 09/06/12
For personal use only.

Introduction

Chemiluminescence spectra from the reactions of ozone with H_2S, CH_3SH, and CH_3SCH_3 were first studied by Akimoto *et al.* (1). The emitting species was identified as $SO_2(^1B_1)$. They suggested that SO is a radical intermediate in these reactions and SO_2^* is formed by the reaction

[1] $$SO + O_3 \rightarrow SO_2^* + O_2$$

$$\Delta H = -106 \text{ kcal/mol}$$

Toby *et al.* (2) also observed emissions due to $SO_2(^1B_1)$ in the chemiluminescent reactions of ozone with CS_2 and thiophene. However, no bands due to triplet $SO_2(^3B_1)$ were observed in these reactions as reported by Halstead and Thrush (3) in the chemiluminescent emission from reaction [1]. Recently, Glinski *et al.* (4, 5) have reexamined the reactions of O_3 with CH_3SH and H_2S under beam-gas conditions and shown that the vibrationally resolved phosphorescent spectra are due to first triplet excited state of SO_2.

In this work we report detailed studies on the reactions of ozone with different types of sulphur compounds which provide definite evidence that SO is a common radical intermediate in all these chemiluminescent reactions. All the emission spectra are identical and there is a marked similarity with the spectrum observed by Halstead and Thrush (3) in the reaction of SO with O_3. The effects of reactant concentration on the spectra and on total signal have also been studied in some cases. The possible reaction pathways for formation of SO radicals are discussed.

Experimental

The experimental system used for studying the chemiluminescence spectra has been described in detail elsewhere (6). The reaction cell of 200 cm^3 volume had a 50 mm diameter window and was made of quartz. Ozone in O_2 was produced by a calibrated ozone generator based on the silent electric discharge technique (7). Known concentrations of sulphur compounds were introduced by controlling the flow of a helium stream saturated with the reactant at 0°C. The flows of gases were measured by Matheson rotameters. The pressure in the reaction cell was measured with a MKS Baratron pressure sensor system (Type 310 BHS-1000).

The light emissions from reaction cell were analyzed with a scanning monochromator (Jarrel-Ash 0.25 meter) having two gratings blazed at 300 and 500 nm. Photomultiplier tube EMI 9635 QA was used for uv and visible region and a thermoelectrically cooled EMI 9659 A for the region up to 900 nm. Signal from photomultiplier tube was fed either to a dc amplifier or a photon counter.

CS_2 (E. Merck, Proanalyst), dimethyl sulphide (Fluka AG Purum), and dimethyl disulphide (BDH England) from fresh bottles were used as received. Thiophene and thiophenol were distilled before use. Diallyl disulphide was prepared by the method of Carson and Wong (8). It was purified by vacuum distillation and was found to be more than 98% pure (9). Diallyl sulphide was prepared by the action of allyl chloride (2 mol) on sodium sulphide (1 mol). It was then vacuum distilled and purity was better than 99%.

Results

Chemiluminescence in the region of 200–900 nm was studied from the reaction of ozone with CS_2, C_4H_4S, $(CH_3)_2S$, $(CH_3)_2S_2$, $(CH_2{=}CHCH_2)_2S$, $(CH_2{=}CHCH_2)_2S_2$, and C_6H_5SH. No chemiluminescence was observed from the reaction of ozone with dimethyl sulphoxide. Detailed observations on individual compounds are given below.

Carbon disulphide

The chemiluminescence spectrum from the reaction of ozone with CS_2 is shown in Fig. 1. It consists of a broad continuum from 270 to 470 nm and a number of peaks starting from 380 nm superimposed on the continuum. The broad structureless continuum is due to the fluorescence from excited singlet SO_2 while the bands from 380 nm onwards are due to $SO_2(^3B_1)$.

The effect of CS_2 concentration on the emission bands of $SO_2(^3B_1)$ is shown in Fig. 2. The spectra were recorded at different partial pressures of CS_2 as indicated in the figure. The ozone concentration and the total pressure were kept constant. As the CS_2 concentration was increased the emission from

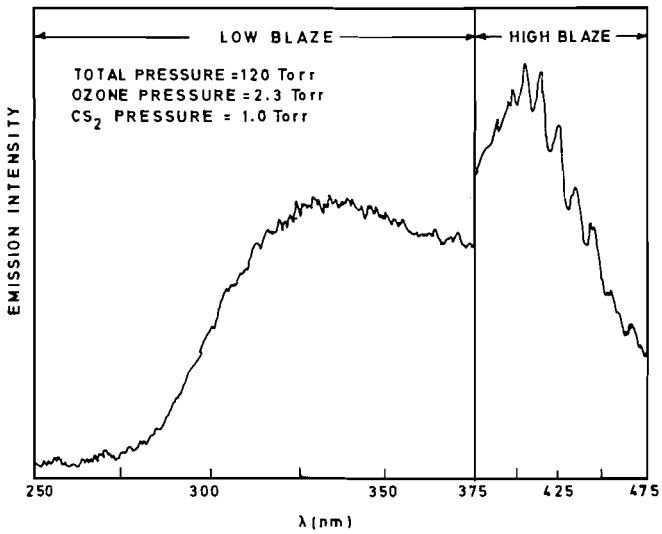

FIG. 1. Chemiluminescence spectrum from the reaction of ozone with carbon disulphide: spectral slitwidth, 0.8 nm; range, 5 nA.

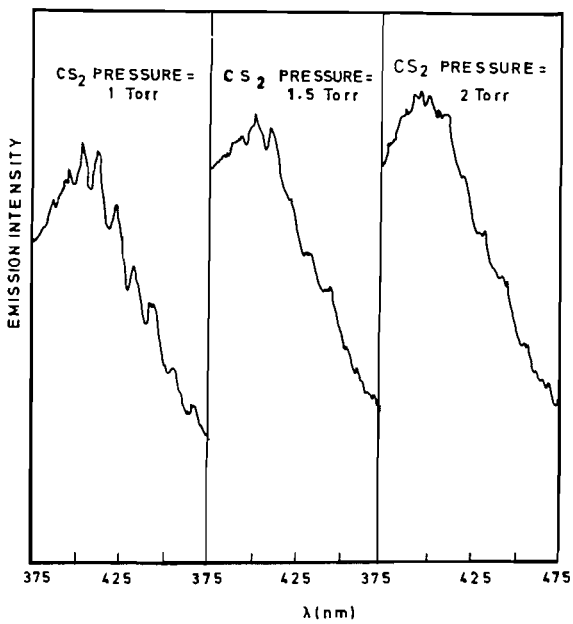

FIG. 2. Effect of CS_2 pressure on triplet SO_2 emission: total pressure, 120 Torr; ozone pressure, 2.3 Torr.

triplet SO_2 became weaker and the structure less well defined.

Figure 3 shows the effect of ozone concentration on the total signal. Ozone concentration from the ozone generator was varied in such a way that O_3/O_2 flow entering the reaction cell did not vary. It is seen that the total signal increases linearly with the square of the ozone concentration.

Thiophene

The chemiluminescence spectrum arising from the reaction of ozone with thiophene is shown in Fig. 4. The emissions are due to the transitions from excited SO_2 in its singlet and triplet state. The intensity of bands due to triplet SO_2 is much stronger than in the case of CS_2. Emissions in the region of 500 to 800 nm were also recorded and number of bands, similar to those reported by Toby *et al.* (2), was observed. These are due to the electronically excited HSO radical ($^2A'$) (10). A brown-coloured coating was formed in the reaction cell and a charred smell was noticed after the experiments.

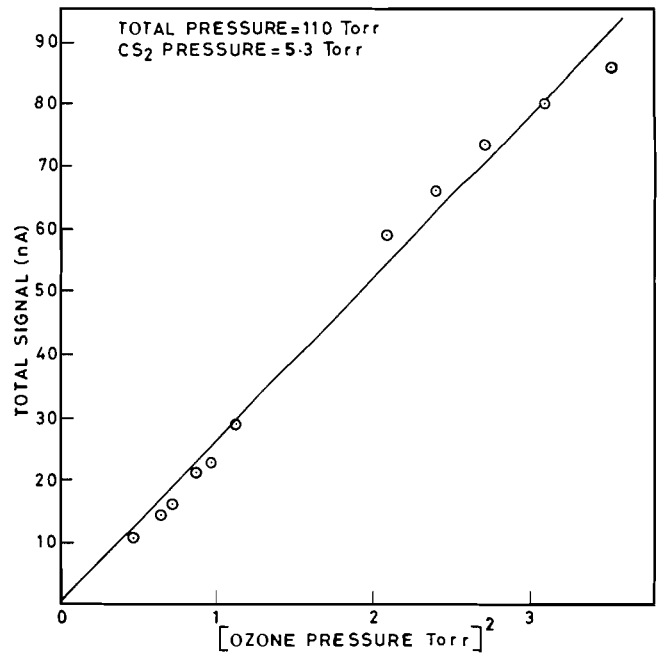

FIG. 3. Effect of ozone concentration on total signal.

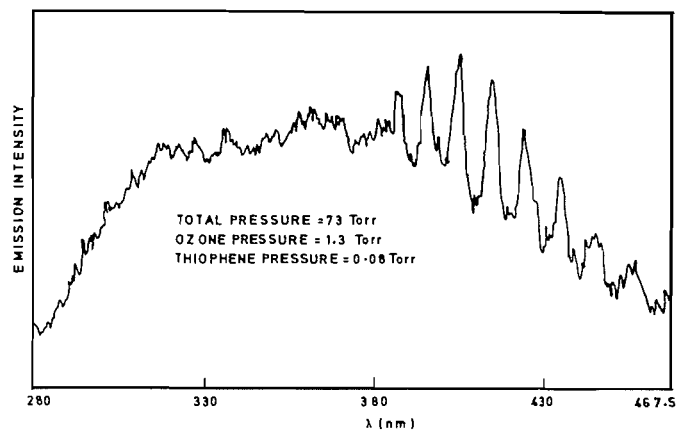

FIG. 4. Chemiluminescence emission from the reaction of ozone with thiophene: spectral slitwidth, 1.65 nm; range, 2 nA.

Dimethyl sulphide and dimethyl disulphide

The chemiluminescence spectra from the reaction of ozone with dimethyl sulphide and dimethyl disulphide are shown in Fig. 5. The partial pressures of dimethyl sulphide and disulphide in these reactions are indicated in the figure. The emissions due to triplet SO_2, superimposed on the continuum, are not as strong as those observed with other sulphur compounds. Keeping other parameters constant when the concentration of DMS was increased to 95 mTorr, the peaks due to triplet SO_2 completely vanished even though the emission intensity increased by a factor of two. In the case of dimethyl disulphide, the emission intensity was very high and the spectrum was taken with a spectral slitwidth of 0.4 nm. No vibrational structure of emission due to singlet SO_2 is observed even at this resolution.

Well-resolved emissions from vibrationally excited OH were also observed in these reactions. These are shown in Fig. 6 for dimethyl disulphide. The peaks are identical to the Meinel bands, thus indicating that the formation of H atoms takes place in these reactions.

Can. J. Chem. Downloaded from www.nrcresearchpress.com by 210.87.254.40 on 09/06/12
For personal use only.

Can. J. Chem. Downloaded from www.nrcresearchpress.com by 210.87.254.40 on 09/06/12
For personal use only.

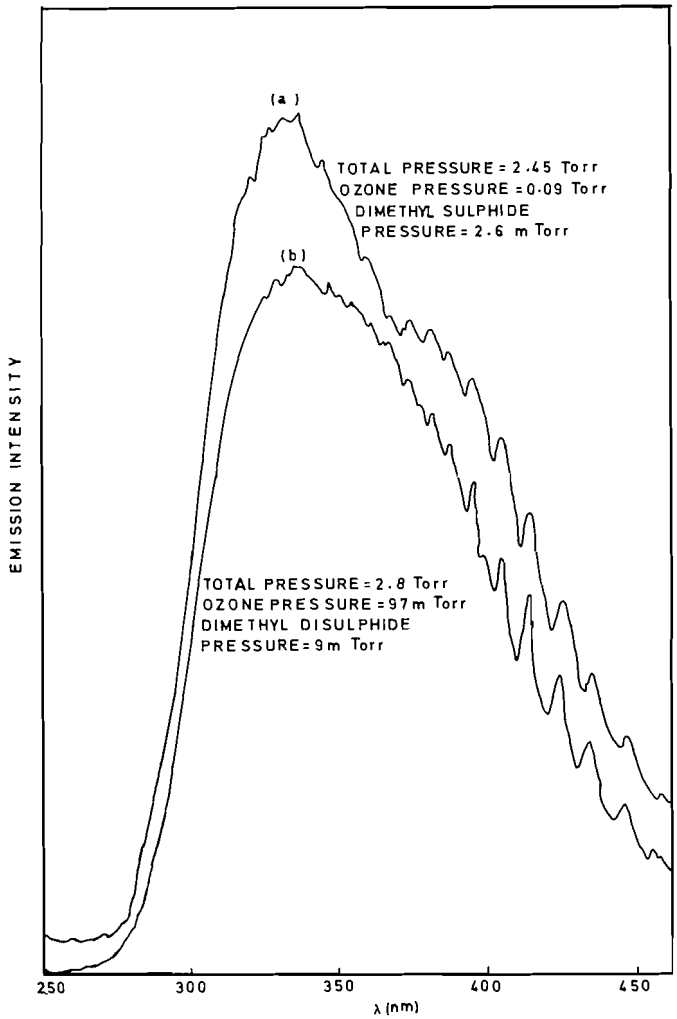

FIG. 5. Chemiluminescence spectra from the reaction of ozone with (*a*) dimethyl sulphide: spectral slitwidth, 1.65 nm; range, 1000 cps; (*b*) dimethyl disulphide: spectral slitwidth, 0.4 nm; range, 2000 cps.

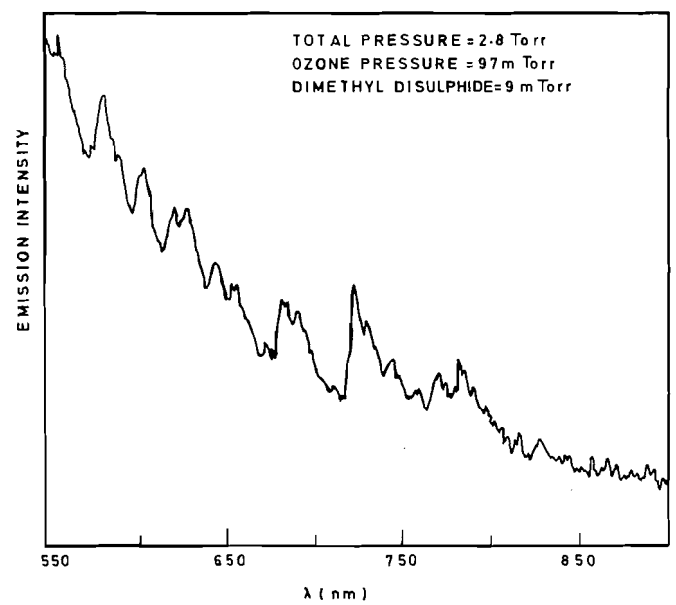

FIG. 6. Chemiluminescence emission from the reaction of ozone with dimethyl disulphide: spectral slitwidth, 3.3 nm; range, 100 pA.

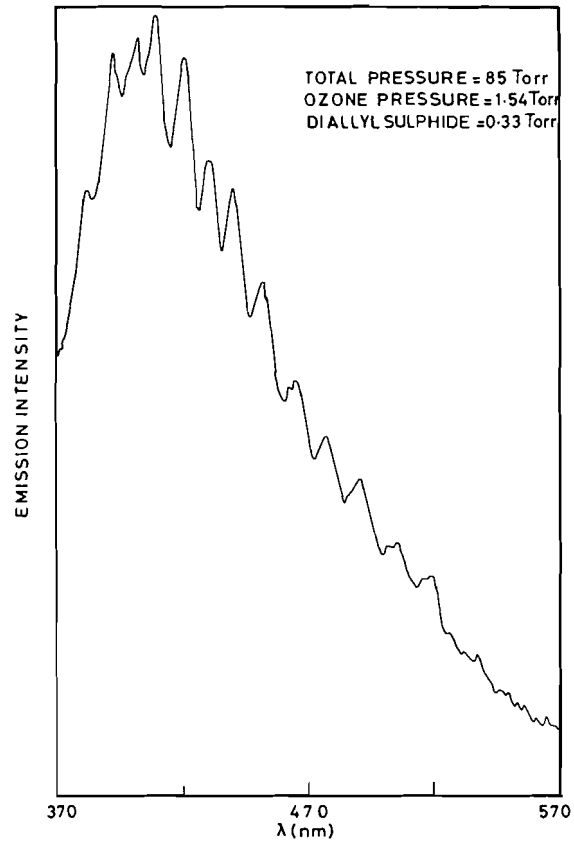

FIG. 7. Emission spectrum from the reaction of ozone with diallyl sulphide; spectral slitwidth, 3.3 nm; range, 5 nA.

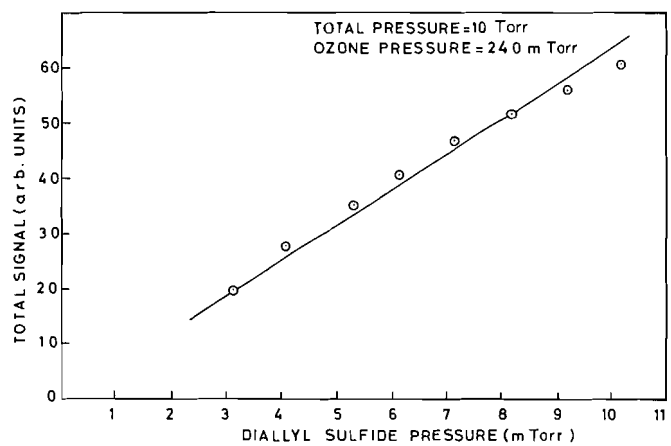

FIG. 8. Effect of diallyl sulphide concentration on total signal.

Diallyl sulphide and diallyl disulphide

The reaction of ozone with diallyl sulphide gave emission similar to that observed in the reactions with other sulphur compounds. However, the emission from triplet SO_2 is quite strong and extremely well defined as is shown in Fig. 7. The effect of diallyl sulphide concentration on the total signal was also studied and is shown in Fig. 8. It is observed that the total signal increases linearly with concentration.

Figure 9(*a*) shows the emission observed in the reaction of ozone with diallyl disulphide. The intensity of peaks due to $SO_2(^3B_1)$ is quite high. No other emission due to either excited HCHO or OH was observed in these reactions in spite of the presence of double bond in the allyl compounds.

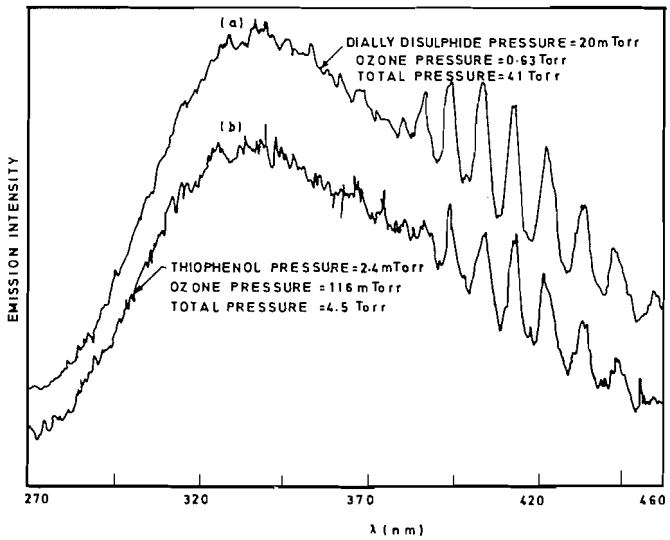

FIG. 9. Chemiluminescence spectra from the reaction of (*a*) ozone with diallyl disulphide: range, 5 nA; (*b*) ozone with thiophenol: range, 2 nA; spectral slitwidth, 1.65 nm.

Thiophenol

The spectrum from this reaction is shown in Fig. 9(*b*). The emissions are identical to those observed with other organic compounds, thus confirming that SO_2^* is the emitting species.

Discussion

Spectroscopic studies of SO_2 yield the following low-lying electronic states (and their origin in cm^{-1}): $X\,^1A_1$ (0,0), $a\,^3B_1$ (25766), $b\,^3A_2$ (26000), $A\,^1A_2$ (27930), and $B\,^1B_1$ (31950) (11). The transition of SO_2 which appears over the region of 260–340 nm was initially believed to be $^1A_1 \rightarrow {}^1B_1$. However, the recent rotational analysis of high resolution absorption spectra (12, 13) shows that the upper state is electronically $^1A_2$ and vibronically $^1B_1$ with the $\nu_3(b_2)$ antisymmetric stretching vibration. Magnetic rotations and Zeeman broadenings are found in the region of 295–325 nm (14), which evidence the additional coupling with triplet and/or ground electronic state. Fluorescence spectra originating from a variety of single vibronic bands have recently been analyzed by Shaw *et al.* (15) in terms of the levels of the zero-order $^1B_1$ electronic state which are vibronically coupled with many $^1A_2$ levels.

The weak absorption in the region of 3400–3900 Å is attributed to the spin-forbidden $a\,^3B_1 \leftarrow X\,^1A_1$ transition (16). The rotational analysis of several absorption bands of this $a \leftarrow X$ system have shown that the bands at higher energy have irregular contours and are strongly perturbed due to vibronic interaction with the nearby $^3A_2$ state.

Brus and McDonald (17) and Su *et al.* (18) measured the fluorescence decay of excited SO_2 and reported that it decays biexponentially with two independent lifetimes: 10–80 μs and 100–600 μs. It was proposed that the short-lived component was due to $^1A_2$ and the long-lived one to $^1B_1$ which was immersed in a large number of ground vibronic levels through the Renner–Teller coupling. Recently, Holtermann *et al.* (19) excited the single rotational level of the *E* band and found that the emission decayed single exponentially with a lifetime of 13 μs. They claimed this to be the lifetime of the pure $^1A_2$ state. Very recently, Watanabe *et al.* (20) have measured the lifetime of rotationally cooled $SO_2(^1A_2)$ and reported biexponential decay with a short lifetime of 3–5 μs and a long one of 15–30 μs. Compared to this the lifetime of triplet $SO_2(^3B_1)$ has been measured to be ~8 ms (21).

We have studied the reaction of ozone with seven different sulphur compounds and find that a common feature of all these chemiluminescent reactions is the nearly identical emission in the region of 270–470 nm. The spectra show a series of sharp bands, starting from 388 nm superimposed on the featureless broad band. These spectra have a strong similarity to the luminescent spectra reported by Strickler (22) and to the chemiluminescence spectra reported by Halstead and Thrush (3) from reaction [1]. Following the work of Gaydon (23) and Halstead and Thrush (3), these bands can easily be assigned to transitions from the first excited triplet state of SO_2 to the ground state. We have observed only those transitions which originate from $V' = (0,0,0)$ of the $^3B_1$ state to various $V'' = (n,m,0)$ of the $^1A_1$ ground state. This corresponds to a fully relaxed vibrational distribution at ambient temperature. This is due to the fact that at the higher pressures used in the present studies the molecules will undergo multiple collisions before they can radiate since the phosphorescence lifetime is so long. However, Glinski *et al.* (4) have recently observed emission from higher vibrational levels of SO_2 excited triplet in the low pressure chemiluminescent reaction of ozone with methyl mercaptan.

The spectrum which appears as a continuous emission from 270 nm to 470 nm with a maximum at 340 nm can be attributed to transitions from $^1B_1$ and/or $^1A_2$ state to ground state. No band structure due to any of these states could be observed even in the reaction of ozone with dimethyl disulphide where the spectral slitwidth was 0.4 nm. The short wavelength limit of 270 nm in the observed chemiluminescence is set by the energetics of the reaction [1] which is 106.5 kcal/mol exothermic.

The formation of triplet $SO_2(^3B_1)$ takes place from singlet $SO_2(^1B_1$ and/or $^1A_2)$ by collisionally-induced intersystem crossing. The spin and thermodynamically allowed process

$$[2]\quad SO(^3\Sigma) + O_3(^1A) \rightarrow {}^3SO_2 + O_2(^1\Delta_g) \qquad \Delta H = -10 \text{ kcal/mol}$$

does not seem to operate since Halstead and Thrush failed to discover $O_2(^1\Delta_g)$ or $O_2(^1\Sigma_g{}^+)$ in their original work. Recently, Glinski *et al.* (4) have observed emission from $SO_2(^3B_1)$ and attributed it to the collisions of He atoms with excited singlet state of SO_2 inducing a transfer to this triplet state. They have also studied the effect of ozone pressure on the fluorescence and phosphorescence intensity of SO_2. From the correlation of the onset of phosphorescence with the loss of fluorescence they have suggested that $^1A_2$ state is the precursor state to much of observed phosphorescence. The persistence of fluorescent intensity at higher pressure has been attributed to emission from $^1B_1$ state. In the present studies it is difficult to suggest whether the emission is from $^1B_1$ state or $^1A_2$ state. However, taking into account the lifetime of $^1A_2$ state and the high pressures used it is probably the $^1B_1$ state which is responsible for the broad featureless band observed in the present studies. The following reaction steps can be written for the formation of excited singlet and triplet states of SO_2.

$$[3]\quad SO + O_3 \rightarrow {}^1SO_2(^1B_1 \text{ and/or } {}^1A_2) + O_2$$

$$[4]\quad SO + O_3 \rightarrow SO_2(^1A_1) + O_2$$

$$[5]\quad {}^1SO_2 \rightarrow SO_2(^1A_1) + h\nu_f$$

$$[6]\quad {}^1SO_2 \rightarrow SO_2(^1A_1)$$

Can. J. Chem. Downloaded from www.nrcresearchpress.com by 210.87.254.40 on 09/06/12
For personal use only.

Can. J. Chem. Downloaded from www.nrcresearchpress.com by 210.87.254.40 on 09/06/12
For personal use only.

[7] $^1SO_2 \rightarrow SO_2(^3B_1)$

[8] $^1SO_2 + M \rightarrow SO_2(^1A_1) + M$

[9] $^1SO_2 + M \rightarrow SO_2(^3B_1) + M$

[10] $SO_2(^3B_1) \rightarrow SO_2(^1A_1) + h\nu_p$

[11] $SO_2(^3B_1) \rightarrow SO_2(^1A_1)$

[12] $SO_2(^3B_1) + M \rightarrow SO_2(^1A_1) + M$

where M represents some quencher molecule including SO_2.

The efficiency with which $SO_2(^3B_1)$ molecules are formed in the spin inverting reaction is of primary importance and has been measured by Wampler *et al.* (24) for O_2 and other atmospheric gases. They reported the values of bimolecular intersystem crossing ratio $k_9/(k_8 + k_9)$ to be 0.03, 0.034, 0.025, 0.052, and 0.045 for O_2, N_2, Ar, CO_2, and CO respectively. This explains why emission from $SO_2(^3B_1)$ is very weak compared to the total integrated emission observed from $SO_2(^1B_1)$.

The quenching rate constants of $SO_2(^3B_1)$ with a variety of chemically reactive and unreactive molecules have been determined by Wampler *et al.* (25). Becker *et al.* (10) have measured the rate constants for the quenching of triplet SO_2 by various sulphur compounds. They report values of 3×10^{10}, 5×10^{10}, 9×10^{10}, and 14×10^{10} L/mol s for H_2S, CS_2, CH_3SH, and $(CH_3)_2S$, respectively.

The quenching rate constants of $SO_2(^1B_1)$ have been measured for SO_2, O_2, and CO_2 and their values are 1.5×10^{10}, 4.7×10^9, and 1.1×10^{10} L/mol s, respectively (26).

Carbon disulphide

The reaction of ozone with CS_2 probably takes place via

[13] $CS_2 + O_3 \rightarrow CS + SO + O_2$

$\Delta H = -5.5$ kcal/mol

$SO + O_3 \rightarrow SO_2^* + O_2$

Olszyna and Heicklen (27) have studied the reaction of ozone with CS_2 and postulated that the SO radicals arise from reaction of oxygen atoms, produced by ozone decomposition, with CS_2.

[14] $CS_2 + O \rightarrow CS + SO$

However, thermochemical calculations show that even reaction of ozone with CS_2 can produce SO radicals directly (reaction [13]). The intensity of SO_2^* will then be proportional to the square of the ozone concentration. This agrees with the experimental observation where emission from SO_2^* was found to be second order in ozone (Fig. 3).

The effect of increasing the CS_2 concentration was found to be the reduction of the emission from triplet SO_2. This is due to the very high quenching rate constant of CS_2 with $SO_2(^3B_1)$. This rate constant ($k = 5 \times 10^{10}$ L/mol s) (10) is even higher than the highest reported rate constant of $SO_2(^1B_1)$ with ground state SO_2 ($k = 1.5 \times 10^{10}$ L/mol s) (26).

Thiophene

The reaction between ozone and thiophene has been studied by Kaduk and Toby (28) at low pressure; they found the most abundant product to be O_2 with smaller amounts of CO_2 and SO_2. The mass balance for O_2 and sulphur was found to be 100% while that for carbon was found to be 25%. Since they did not observe any H-containing product, it was suggested that the missing product is a hydrocarbon which may be a polymer. The following mechanism was proposed.

[15] 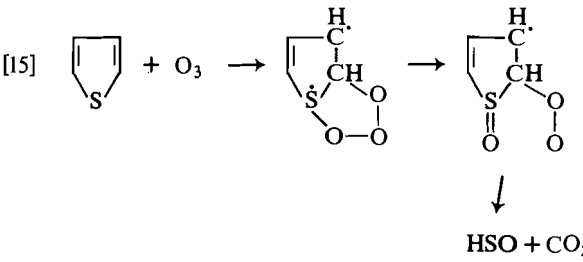

The HSO radical may undergo the following reactions leading to the formation of excited HSO and SO_2.

[16] $HSO + O_3 \rightarrow HS + 2O_2$

$\Delta H = -13$ kcal/mol

[17] $HSO + O_3 \rightarrow HO + SO + O_2$

$\Delta H = -36$ kcal/mol

[18] $HS + O_3 \rightarrow HSO + O_2$

$\Delta H = -56$ kcal/mol

[1] $SO + O_3 \rightarrow SO_2^* + O_2$

The enthalpy of the reactions has been calculated on the basis of $\Delta H_f^0(HSO) = 13$ kcal/mol (10). Reaction [18] is sufficiently exothermic to produce HSO in an electronically excited state. The short wavelength limit of 517 nm agrees well with the enthalpy of the reaction. Formation of excited SO_2 takes place via reaction [1]. The emission due to $SO_2(^3B_1)$ is quite strong. This is because of the reduced quenching rate due to the small concentration of thiophene in the reaction chamber.

Dimethyl sulphide

The gas phase reaction of ozone with dimethyl sulphide (DMS) has been studied at low pressure by Martinez and Herron (29). The major products of this reaction were found to be H_2CO, H_2O, CO, and SO_2. This shows that C—S bond scission takes place in the gas phase reaction contrary to the general trend in solutions where ozonolysis of organic sulphides leads to the formation of sulphoxides and sulphones. The initial product yield was found to be

$$1.0\ DMS \xrightarrow{O_3/O_2} 0.93H_2CO + 0.32SO_2 + 0.43H_2O + 0.34CO + 0.07CO_2$$

It was proposed that the initial attack of ozone on DMS gives rise to radicals which act as chain carrier.

[19] $DMS + O_3 \rightarrow CH_3O + CH_3SO_2$

$\Delta H = -82$ kcal/mol

[20] $\rightarrow CH_2O + H + CH_3SO_2$

$\Delta H = -61$ kcal/mol

[21] $\rightarrow CH_3O_2 + CH_3SO$

$\Delta H = -6.6$ kcal/mol

[22] $\rightarrow (CH_3)_2SO + O_2$

$\Delta H = -60$ kcal/mol

We propose that the formation of SO takes place by reaction of ozone with CH_3SO

[23] $CH_3SO + O_3 \rightarrow CH_3O + SO + O_2$

$\Delta H = -41$ kcal/mol

[24] $\rightarrow CH_3OO + SO_2$

$\Delta H = -110$ kcal/mol

[25] $\rightarrow CH_3S + 2O_2$

$\Delta H = -13.5$ kcal/mol

Reaction of CH_3S with ozone can also lead to the formation of SO.

[26] $CH_3S + O_3 \rightarrow CH_3OO + SO$

$\Delta H = -58$ kcal/mol

The reaction of SO with ozone will lead to the formation of excited SO_2 by reaction [1]. It is seen that reaction [24] can directly lead to the formation of excited SO_2. This may be responsible for the high intensity of SO_2 emission observed in the DMS + O_3 reaction.

The triplet SO_2 emission is not very strong and vanishes on increasing the concentration of DMS. This is due to very high quenching rate of $SO_2(^3B_1)$ with DMS ($k = 1.4 \times 10^{11}$ L/mol s) (10).

Dimethyl disulphide

The reaction of ozone with dimethyl disulphide gives rise to very intense emission due to SO_2^*. It is also noted that the short wavelength limit in this chemiluminescence is less than 260 nm which corresponds to 110 kcal/mol. The following mechanism is proposed to explain these features.

[27] $(CH_3)_2S_2 + O_3 \rightarrow CH_3SO + CH_3SO_2$

$\Delta H = -78$ kcal/mol

[28] $\rightarrow CH_3 + SO + CH_3SO_2$

$\Delta H = -53$ kcal/mol

[29] $\rightarrow CH_3S + CH_3SO + O_2$

$\Delta H = -16$ kcal/mol

The SO and CH_3SO thus formed may react again with ozone giving rise to excited SO_2.

[30] $CH_3SO + O_3 \rightarrow CH_3OO + SO_2$

$\Delta H = -110$ kcal/mol

The formation of SO_2^* via reaction [30] explains the high intensity of chemiluminescence observed in this reaction since SO_2^* is formed in two steps only. This also explains why more emission is observed in disulphide than in DMS since each of the two reaction pathways [27] and [28] may lead to the formation of excited SO_2. The short wavelength limit of less than 260 nm observed in this reaction is due to the exothermicity of reaction [30]. Intense Meinel bands were observed in this reaction. This is due to the very efficient formation of H atoms in the system which are formed by

[31] $CH_3 + O_3 \rightarrow HCHO + O_2 + H$

$\Delta H = -39$ kcal/mol

This reaction is similar to the reaction of an O atom with a CH_3 radical which leads to the formation of H atoms and HCHO. The reaction of H atoms with O_3 leads to the formation of the Meinel bands

[32] $H + O_3 \rightarrow OH^\dagger + O_2$

$\Delta H = -77$ kcal/mol

Diallyl sulphide and diallyl disulphide

The reactions of ozone with diallyl sulphide and diallyl disulphide give emissions due to singlet and triplet SO_2. No emission due to excited HCHO was observed in these reactions as was observed in the reaction of ozone with allyl chloride and allyl alcohol (30). This indicates that the attack of ozone takes place on the S atom instead of —C=C— bond as in olefins. This leads to the scission of the —C—S bond in organic sulphides. The mechanism of formation of SO should follow pathways which are similar to those in the reactions of ozone with dimethyl sulphide and dimethyl disulphide. The intensity of SO_2^* was found to be comparable in the two reactions even though the concentration of diallyl disulphide was about 15 times less than that of diallyl sulphide. This also agrees with the earlier observation that disulphides give rise to more emission than sulphide. However, no $OH^\dagger$ emission was observed in the reaction. This is due to the absence of methyl group in the reacting molecule.

Thiophenol

The reaction of ozone with thiophenol gives rise to emission from excited SO_2. The following mechanism is proposed.

[33] $C_6H_5SH + O_3 \rightarrow C_6H_5SO_2 + OH$

[34] $\rightarrow C_6H_5O + SO + OH$

[35] $\rightarrow C_6H_5SO + HO_2$

Reaction of C_6H_5SO with ozone may also lead to the formation of excited SO_2 via reactions which are similar to those postulated for the reactions with CH_3SO. However, the short wavelength limit of 275 nm suggests that excited SO_2 is formed by the reaction of SO radicals with ozone.

1. H. AKIMOTO, B. J. FINLAYSON, and J. N. PITTS JR. Chem. Phys. Lett. **12**, 199 (1971).
2. S. TOBY, F. S. TOBY, and B. A. KADUK. J. Photochem. **6**, 296 (1976/77).
3. C. J. HALSTEAD and B. A. THRUSH. Proc. R. Soc. A **295**, 380 (1966).
4. R. J. GLINSKI, J. A. SEDARSKI, and D. A. DIXON. J. Phys. Chem. **85**, 2440 (1981).
5. R. J. GLINSKI, J. A. SEDARSKI, and D. A. DIXON. J. Am. Chem. Soc. **104**, 1126 (1982).
6. P. K. ARORA and K. G. VOHRA. Chem. Phys. Lett. **96**, 161 (1983).
7. J. P. S. CHATHA, P. K. ARORA, NALINI RAJA, and P. B. KULKARNI. Ind. J. Technol. **19**, 300 (1981).
8. J. F. CARSON and F. F. WONG. J. Org. Chem. **24**, 175 (1959).
9. S. V. AMONKAR and A. BANERJI. Science, **174**, 1343 (1971).
10. K. H. BECKER, M. A. INOCENCIO, and U. SCHURATH. Int. J. Chem. Kinet. Symp. **1**, 205 (1975).
11. E. K. C. LEE and G. L. LOPPER. *In* Radiationless transitions. *Edited by* S. H. Lin. Academic Press, New York. 1980. Chapt. 1.
12. Y. HAMADA and A. J. MERER. Can. J. Phys. **52**, 1443 (1974).
13. Y. HAMADA and A. J. MERER. Can. J. Phys. **53**, 2555 (1975).
14. J. C. D. BRAND, J. L. HARDWICK, D. R. HUMPHREY, Y. HAMADA, and A. J. MERER. Can. J. Phys. **54**, 186 (1976).
15. R. J. SHAW, J. E. KENT, and M. F. O'DWYER. Chem. Phys. **8**, 155 (1976); **8**, 165 (1976).
16. J. C. D. BRAND, V. T. JONES, and C. DILAURO. J. Mol. Spectrosc. **45**, 404 (1973).
17. L. E. BRUS and J. R. MCDONALD. Chem. Phys. Lett. **61**, 97 (1974).
18. F. SU, J. W. BOTTENHEIM, H. W. SIDEBOTTOM, J. G. CALVERT, and E. K. DAMON. Int. J. Chem. Kinet. **10**, 125 (1978).

Can. J. Chem. Downloaded from www.nrcresearchpress.com by 210.87.254.40 on 09/06/12
For personal use only.

19. D. L. HOLTERMANN, E. K. C. LEE, and R. NANES. Chem. Phys. Lett. **75**, 91 (1980).
20. H. WATANABE, S. TSUCHLYA, and S. KODA. J. Phys. Chem. **87**, 906 (1983).
21. F. SU, J. W. BOTTENTHEIM, D. L. THORASELL, J. G. CALVERT, and E. K. DAMON. Chem. Phys. Lett. **49**, 305 (1977).
22. S. STRICKLER and D. HOWELL. J. Chem. Phys. **49**, 1947 (1968).
23. A. G. GAYDON. Proc. R. Soc. **146**, 901 (1934).
24. F. B. WAMPLER, J. G. CALVERT, and E. K. DAMON. Int. J. Chem. Kinet. **5**, 107 (1973).
25. F. B. WAMPLER, K. OTSUKA, J. G. CALVERT, and E. K. DAMON. Int. J. Chem. Kinet. **5**, 669 (1973).
26. T. N. RAO and J. G. CALVERT. J. Chem. Phys. **74**, 681 (1970).
27. K. J. OLSZYNA AND J. HEICKLEN. J. Chem. Phys. **74**, 4188 (1970).
28. B. KADUK and S. TOBY. Int. J. Chem. Kinet. **9**, 829 (1977).
29. R. I. MARTINEZ and J. T. HERRON. Int. J. Chem. Kinet. **10**, 433 (1978).
30. P. K. ARORA. Ph.D. Thesis, University of Bombay, Bombay 400 001, 1982.

Can. J. Chem. Downloaded from www.nrcresearchpress.com by 210.87.254.40 on 09/06/12
For personal use only.

Photoinduced electron transfer C—C bond cleavage reactions; oxidations and isomerizations[1]

L. W. REICHEL, G. W. GRIFFIN, AND A. J. MULLER
University of New Orleans, Department of Chemistry, New Orleans, LA 70148, U.S.A.

P. K. DAS
Radiation Laboratory, University of Notre Dame, Notre Dame, IN 46556, U.S.A.

AND

SEYHAN N. EGE
University of Michigan, Department of Chemistry, Ann Arbor, MI 48109, U.S.A.

Received June 2, 1983

This paper is dedicated to Professor Harry E. Gunning on the occasion of his 65th birthday

L. W. REICHEL, G. W. GRIFFIN, A. J. MULLER, P. K. DAS, and SEYHAN N. EGE. Can. J. Chem. **62**, 424 (1984).

We have shown that radical cations generated by photoinduced electron transfer (ET) in 1,2-diarylethanes, aryl pinacols, and their derivatives undergo fragmentation reactions. In the presence of oxygen oxidative products are obtained. Time-resolved laser flash photolysis and other ancillary techniques have permitted us to define the mechanisms of certain oxidative processes observed.

L. W. REICHEL, G. W. GRIFFIN, A. J. MULLER, P. K. DAS et SEYHAN N. EGE. Can. J. Chem. **62**, 424 (1984).

Nous avons montré que les cations radicalaires générés par transfert d'électron (TE) dans les diaryl-1,2 éthanes, les pinacols aryliques et leurs dérivés subissent des réactions de fragmentation. En présence d'oxygène, on obtient des produits d'oxydation. La photolyse flash ou laser résolue en fonction du temps, et d'autres techniques ancillaires nous permettent de définir le mécanisme de certaines réactions d'oxydation observées.

[Traduit par le journal]

Can. J. Chem. Downloaded from www.nrcresearchpress.com by 210.87.254.6 on 09/06/12
For personal use only.

Introduction

The classic work by Weller and co-workers (2*a*–*c*) on charge-transfer processes, exciplexes, and the dissociation of the latter has captured the attention of photochemists and has stimulated extensive research in the field of photoinduced electron transfer (ET) reactions (1–15). The primary focus in this field has revolved around ET reactions induced by excitation of specific compounds (so called "sensitizers") to the singlet state possessing augmented electron donor (D) or electron acceptor (A) properties (i.e., enhanced oxidation or reduction potentials). In most cases studied to date, and in those described in this communication, the electron acceptor species is designated as the "sensitizer". The excited singlet state of this "sensitizer" or acceptor (A) has a greater tendency to be reduced than the ground state and may accept an electron from a suitable ground state donor substrate with concomitant formation of a radical cation ($D^{\ddagger}$) and an acceptor radical anion ($A^{\bar{\cdot}}$) (Scheme 1) in their ground states. Such processes proceed directly through an encounter complex in polar solvents where potential exciplex formation may be circumvented. In contrast, donor–acceptor exciplexes, which may be characterized by emission spectroscopy, are observed in nonpolar solvents where dissociation is unfavorable.

Fragmentation of donor radical cations in polar solvents to a cation and radical is a reaction of primary significance. Among other reactions observed for radical cations generated by photoinduced ET are the following: (a) coupling with the radical anion followed by cyclization and/or rearrangement to give a neutral adduct (3), (b) addition to alkenes (4), cyclodimerization (5), and cross-cycloaddtion (5*f*, 6), (c) reduction of radical cations derived from arenes with metal hydrides (7), (d) reaction with nucleophiles, alcohols, and cyanide ion, to give saturated products (i.e., ethers and nitriles, respectively (4*a*, 5*a*, 8)), (e) rearrangement of cyclopropanes and cyclopropenes (9), (f) coupling with triplet ground state oxygen (10), singlet oxygen and/or superoxide (3*d*, 11) and (g) isomerization of alkenes (11*g*), oxiranes, (1*b*, 12) and cyclopropanes (13).

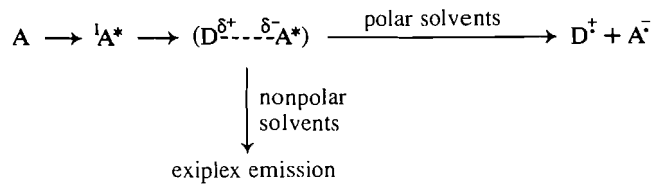

SCHEME 1

The radical anions derived by ET in turn may serve to reduce the fragment cation and/or radical formed by fragmentation of the initial radical cation to a radical and/or anion, respectively, a process loosely designated as "back electron donation". Competitive reactions include (a) interaction with the donor radical cation as noted above (3), (b) reduction of triplet oxygen to superoxide anion which is capable of oxidizing radical cations of alkenes and alkynes (11*a*–*c*, *e*–*j*), polyaryl oxiranes as well as cyclopropanes (11*k*), and sulfur compounds (11*b*, *d*), (c) reductive cleavage of protecting groups (14), and (d) reduction of arenes (15).

Our interest in the area of fragmentation reactions which proceed through photoinduced ET mechanisms had its inception in continuing studies on the photocycloelimination and isomerization reactions of small-ring systems, such as vicinal diaryl substituted oxiranes and cyclopropanes, to give reactive transients (carbenes (16), carbonyl ylides (17), and diradicals (18)). The isomerization of stilbene oxides by electron transfer "sensitization" reported by Albini and Arnold (12) impinged upon current photochemical studies being conducted in our laboratory (1*a*) and we were encouraged by Arnold to expand our efforts in this area.

Arnold's work (19) on the photoinduced ET-sensitized

[1]For preliminary reports of our work in this area, see ref. 1.

Can. J. Chem. Downloaded from www.nrcresearchpress.com by 210.87.254.6 on 09/06/12
For personal use only.

cleavage of 2,2-diphenylethyl 2-propyl ether in acetonitrile–methanol, using 1,4-dicyanobenzene (DCB) as sensitizer, established that the radical cation of the ether undergoes C—C bond cleavage to give the benzhydryl radical and an α-alkoxycarbocation.[2] Reduction of the benzhydryl radical to the benzhydryl anion by "back electron transfer" from the radical anion of 1,4-dicyanobenzene and subsequent protonation is advanced to explain diphenylmethane formation. Solvolysis of the carbocation with methanol would explain the formation of the other product, namely the 2-propyl methyl acetal of formaldehyde.

Arnold recognized that stilbene oxides also incorporate a key structural element in common with the diphenylethyl 2-propyl ether, namely an Ar—C— C—O bond sequence, and found that irradiation of either *cis*- or *trans*-stilbene oxide in CH_3CN solution containing 1,4-dicyanonaphthalene (DCN) resulted in a common mixture (1:5, respectively) of both isomers (12).[3] "Equilibration" of the stilbene oxides is attributed to cleavage of the oxirane C—C bond of an initially-formed cyclic radical cation to give open planar isomeric 1,3-radical cations which may recyclize or undergo reduction by "back electron transfer" in the formal sense to the radical site to give the carbonyl ylide.[4] The intermediate carbonyl ylide(s) in the interconversion of stilbene oxides may be intercepted with electron-poor dipolarophiles, affording tetrahydrofuran (THF) adducts. Carbonyl ylides of 2,3-dimethylstilbene oxides formed through photoinduced ET conditions have also been trapped with dipolarophiles (1*a*).

Concurrent isomerization of the open radical cation cannot be excluded despite the fact that carbonyl ylides are intercepted. A case has been reported where the open radical cation of *trans*-stilbene oxide may be intercepted with an electron-rich dipolarophile, 2,5-dimethoxy-2,5-dihydrofuran, in an electron transfer reaction induced by singlet excited DCB (20). Evidence for recyclization of the open radical cation of this stilbene oxide followed by "back electron transfer" has been obtained from laser flash spectroscopy. Clearly the timing of the radical cation reduction, orbital topology, and the species responsible for recyclization (carbonyl ylide, zwitterions, or diradical) (21) remain to be clarified and may be a function of the system.

Substituents exert a marked influence on the ET photoinduced *cis–trans* isomerization of vicinal diaryl oxiranes bearing electron-withdrawing carbomethoxy and cyano groups at the 2 and 3 positions of the oxirane ring (1*c*, 22). The parent 2,3-dicarbomethoxy-2,3-diphenyl oxiranes fail to undergo ET photoinduced interconversion with DCN, unlike stilbene oxides (12) and 2,3-dimethylstilbene oxides (1*a*); however, the oxiranes that embody electron-donating 4-methyl and 4-methoxy substituents on the aromatic nuclei do isomerize upon ET sensitization with DCN. Clearly the presence of the electron-donating substituents on the *para* position of the phenyl rings alters the oxidation potential of these systems to a more favorable level for ET, as evidenced by fluorescence quenching rate studies conducted with DCN (22). Oxiranes bearing the better donor 4-methoxy substituents on the aromatic nuclei quench DCN flourescence 200 times as fast as the parent oxirane, *trans*-2,3-dicarbomethoxystilbene oxide, while only a 2.5 increase in the DCN quenching efficiency is observed with the 4-methyl substituted oxiranes. The cyano substituted oxiranes still proved unreactive even when substituted by methyl groups on the aryl rings; however, unexpectedly, *trans*-2,3-dicyano-2,3-bis(4-methoxyphenyl)-oxirane proved labile and decomposed to 4-methoxy benzoyl cyanide (22).

Despite the magnitude of the difference in quenching rates measured for the methoxy and methyl substituted oxiranes, isomerization still proceeds in both cases and we can only speculate on why isomerization of the parent oxirane becomes unfavorable. Perhaps, in the absence of the donor substituents, we reach a point where destabilization of the open radical cation by the α-carbomethoxy groups is sufficient to preclude C—C bond cleavage despite electron transfer to give a radical cation of the parent oxirane i.e., the relative oxidative potentials do not appear to be the controlling factor.

Aryl substituted cyclopropanes which undergo isomerization upon direct irradiation through a diradical-like intermediate also undergo photoinduced ET interconversions in the presence of 1-cyanonaphthalene (MCN) (13). Hixson *et al.* confirmed that an ET mechanism is implicated by observing the fluorescence quenching of MCN. Photo-CIDNP studies confirm that radical ions and 1,3-diradical species are produced in the ET process (23). As with the oxiranes, steric strain should provide additional driving force for the requisite C—C bond cleavage.

The DCN photoinduced ET isomerizations and opening of selected stilbene oxides (1, 12, 20, 22), as well as of vicinal diaryl substituted cyclopropanes (13), stimulated our interest in the potential cleavage of C—C bonds flanked by aryl substituents in other less complex systems such as substituted bibenzyls. The detailed results of our studies of substituted bibenzyls, as well as of several other systems incorporating similar structural elements, are described below.

Results and discussion

The selection of the activated bibenzyls, 1,2-bis(4-methoxyphenyl)ethane (**1***a*) and 1,2-bis(4-methylphenyl)ethane (**1***b*) as potential reactive candidates in ET reactions was predicated on our experience with diaryl oxiranes (1*a*) and the premise that a favorable decrease in oxidation potential of bibenzyl (**1***c*) should accompany the introduction of electron donor aryl substituents, i.e., CH_3O and CH_3 groups (Scheme 2). This expectation was validated by comparison of DCN singlet fluorescence quenching rates of **1***a* and **1***b* as determined by Stern–Volmer methods ($k_q = 1.7 \times 10^{10}\ M^{-1}\ s^{-1}$ and $1.3 \times 10^{10}\ M^{-1}\ s^{-1}$, respectively).[5,6] These values approach the dif-

[2]Cleavage in the gas phase, as in a mass spectrometer, gives the more highly delocalized diphenylmethyl carbonium ion; however, in solution, the more localized α-alkoxycarbocation is stabilized by solvation.

[3]The oxidation potentials of 2,2-diphenylethyl ethers are considerably lower than those of aliphatic ethers; however, they are essentially identical with that of 1,1-diphenylethane suggesting that the aromatic nuclei serve as the electron donor sites rather than the oxygen atom in the electron transfer process.

[4]It remains to be established if orbital topology plays a role in dictating the course of electrocyclic opening of such odd electron systems. In the absence of data to the contrary we are prejudiced (1*a*, 1*b*, 21*d*) in favor of the thermally more stable *exo–exo* isomer for the ring-opened stilbene oxides.

[5]Steady state fluorescence measurements were carried out using a photon counting spectrofluorimeter from SLM. The description of the apparatus is given in ref. 24.

[6]The measured fluorescence lifetime (τ_F) for DCN is 9.5 ns which is in agreement with the previously reported value 10.06 (19).

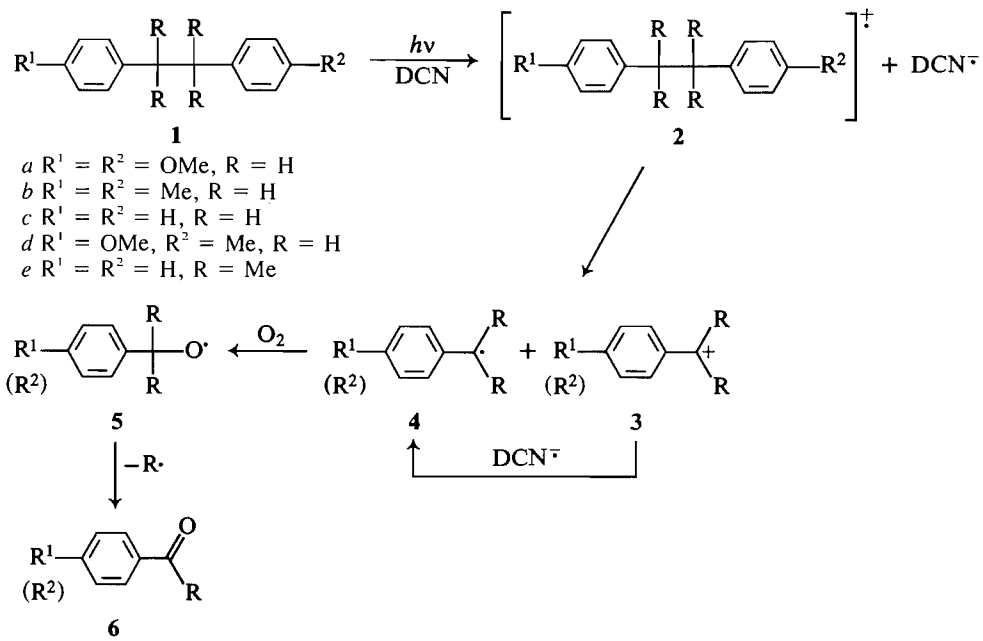

1

a $R^1 = R^2$ = OMe, R = H
b $R^1 = R^2$ = Me, R = H
c $R^1 = R^2$ = H, R = H
d R^1 = OMe, R^2 = Me, R = H
e $R^1 = R^2$ = H, R = Me

2 5 4 3 6

SCHEME 2

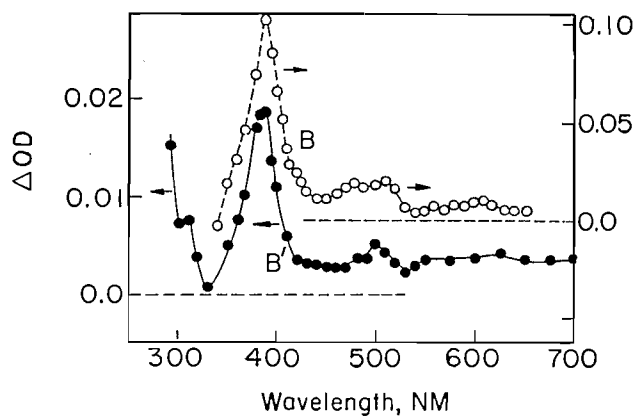

FIG. 1. B-$DCN^{\cdot-}$ observed by pulse radiolysis of DCN in 2-propanol. B'-$DCN^{\cdot-}$ observed by electron transfer from triethylamine to ^{1}DCN.

fusion controlled rate constant of 1.8×10^{10} M^{-1} s^{-1} for CH_3CN solutions at 20°C (19).

Time-resolved laser flash studies (the description of the flash photolysis set-up is given in ref. 25) were performed in CH_3CN (deoxygenated) to confirm that electron transfer mechanisms are responsible for DCN fluorescence quenching by **1***a* and **1***b* and to characterize, through spectral absorption techniques, those transients produced. The absorption spectrum of the transient radical anion ($DCN^{\cdot-}$) is characterized by a sharp intense spectral peak at 390 nm, observed upon near total quenching of excited singlet DCN in deoxygenated acetonitrile by ET from triethylamine and 1,2,4-trimethoxybenzene. Furthermore, pulse radiolysis (26) of DCN in 2-propanol gives rise to a transient having similar spectral features (Fig. 1).

Upon laser excitation of DCN in CH_3CN (deoxygenated), transient spectral phenomena are observed which consist of a strong band at 275 nm and a less intense broad absorption at 400–500 nm (maximum at 455 nm) attributed to DCN triplet–triplet transitions. A spectrum with a maximum at 455 nm is also observed upon DCN quenching of triplet benzophenone in CH_3CN.

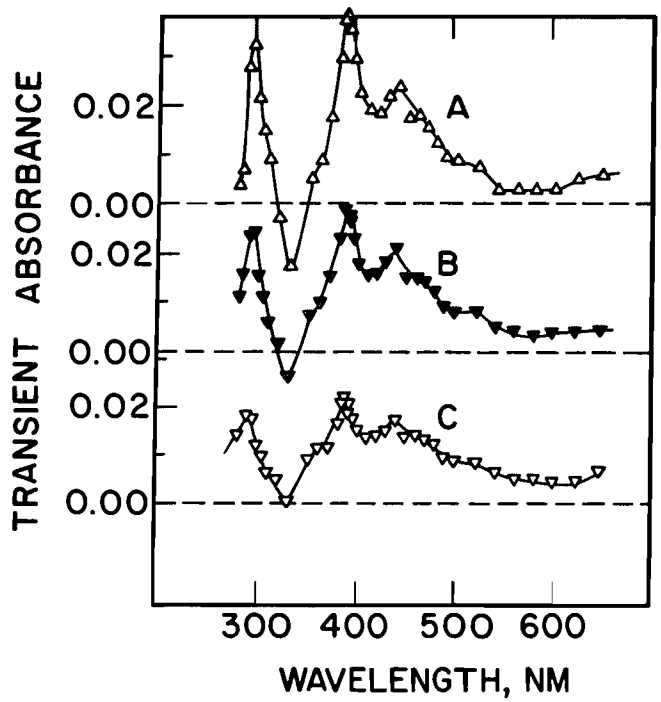

FIG. 2. Transient absorption spectra observed upon 337.1 nm laser flash photolysis of a deoxygenated acetonitrile solution of the bibenzyl **1***a* (12.4 m*M*) and DCN (0.25 m*M*) at approximately 0.4 (A), 1.4 (B), and 3.4 (C) μs following the laser flash.

The transient spectra obtained upon laser flash photolysis of bibenzyls **1***a* and **1***b* (and indeed of all the other substrates discussed later in this paper) in CH_3CN (deoxygenated) containing DCN display the well-defined band for $DCN^{\cdot-}$ (390 nm) in addition to bands at 295 nm and 400–500 nm assignable to ^{3}DCN and radical cations from **1***a* and **1***b* (Fig. 2), constituting clear evidence that ET occurs from **1***a* and **1***b* to excited DCN. Despite our efforts to increase the concentraton of the electron donor substrate to ensure that ET from ^{1}DCN competes effectively with intersystem crossing to its triplet, the $DCN^{\cdot-}$ spectrum is always accompanied by the broad absorption char-

Can. J. Chem. Downloaded from www.nrcresearchpress.com by 210.87.254.6 on 09/06/12
For personal use only.

Can. J. Chem. Downloaded from www.nrcresearchpress.com by 210.87.254.6 on 09/06/12
For personal use only.

acteristic of ^{3}DCN, which may obscure spectral bands for other transients. Within our detection limits, no spectral characteristics of the benzylic radical **4***a*, anticipated as a fragmentation product of the radical cation **2***a*, are observed in the laser flash spectrum of **1***a*. This species, which absorbs at 310 nm, was generated independently by flash photolysis of di-*tert*-butyl peroxide in the presence of 4-methylanisole.

Crossover experiments were conducted in an attempt to discern if the radical cations **2** do in fact fragment to solvent-separated cations **3** and radicals **4** which, for reasons unknown at this time, escape spectroscopic detection. No crossover product, namely 4-methyl-4′-methoxy-1,2-diphenylethane (**1***d*), was detected by glc when an equimolar mixture of **1***a* and **1***b* in CH_3CN (deoxygenated) containing DCN was irradiated. Conversely, the bibenzyls **1***a* and **1***b* were not detected as products upon irradiation of an authentic sample of **1***d* under similar conditions, though the unsymmetrically substituted bibenzyl **1***d* quenches the fluorescence of DCN by electron transfer at near diffusion-controlled rates in acetonitrile (19) (k_q = $1.3 \times 10^{10}\ M^{-1}\ s^{-1}$) (24).

Products identified as aldehydes were formed in trace amounts upon steady state irradiation of CH_3CN solutions of **1***a–c* when samples were not deoxygenated carefully. In order to evaluate the potential significance of this observation, solutions of **1***a* and **1***b*, as well as **1***d*, respectively, in CH_3CN (oxygenated) containing DCN were irradiated for prolonged periods. Under these conditions, 4-anisaldehyde (**6***a*) (83%) and 4-tolualdehyde (**6***b*) (58%) are obtained (Scheme 2). In contrast, only a trace of benzaldehyde (**6***c*) is produced from bibenzyl (**1***c*) under similar conditions. This affirms the significance of the relative efficiency of the initial ET step to form the radical cations **2** derived from **1***a*, **1***b*, and **1***d*, respectively, as well as of enhanced stabilization of the transition state leading to fragment cations **3** and radicals **4** for the compounds with electron-donating substituents on the aryl rings.

Oxygen may play a dual role in the oxidative conversions of **1***a*, **1***b*, and **1***d* to the corresponding aldehydes **6***a*, **6***b*. It is known that 9,10-dicyanoanthracene (DCA) radical anion is capable of reducing ground state oxygen to superoxide anion ($O_2^{\cdot-}$) in a reaction which is exothermic (−6.9 kcal/mol), while the corresponding reaction for $DCN^{\cdot-}$ is more exothermic (−17.6 kcal/mol).[7] Ground state oxygen may act as an electron sink by accepting an electron from $DCN^{\cdot-}$, thus suppressing "back electron transfer" to the initial radical cation, which then enjoys an extended lifetime and enhanced opportunity for cleavage. Our experiments show a decrease in lifetime for $DCN^{\cdot-}$ upon flash photolysis of **1***a*, **1***b*, and **1***d* in CH_3CN (air saturated) relative to that observed under deoxygenated conditions. Oxygen in its ground or excited singlet state and/or superoxide also may be responsible for intercepting the fragments produced; however, a discussion of the oxidation process at this time would be premature and speculative.

Our studies were then expanded to include 2,3-dimethyl-2,3-diphenylbutane (**1***e*) in an effort to ensure that the oxidation products generated from **1***a*, **1***b*, and **1***d* do not arise in whole or in part by oxidation of stilbenes (11*b*, *h*) produced initially from the bibenzyls **1**. Continuous irradiation of **1***e* CH_3CN (oxygenated) containing DCN affords acetophenone (**6***e*) (60%) (Scheme 2). Despite the moderate conversion level observed and incomplete product identification, the results confirm that photooxidative cleavage of 1,2-diphenylethanes may occur even in the absence of benzylic hydrogens; this precludes an oxidation mechanism involving initial formation and subsequent cleavage of isomeric stilbenes by $O_2^{\cdot-}$.

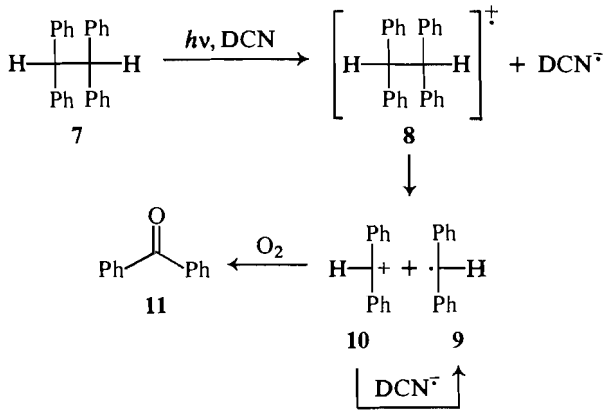

SCHEME 3

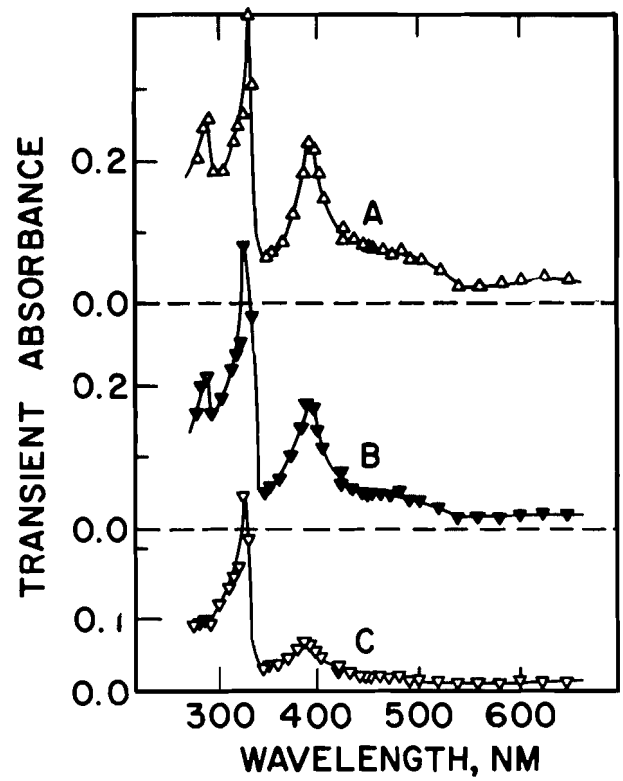

FIG. 3. Transient absorption spectra observed upon 337.1 nm laser flash photolysis of a deoxygenated acetonitrile solution of **7** (22.9 m*M*) and DCN (0.25 m*M*). A: end-of-pulse; B: 0.4 μs; and C: 3.4 μs (following laser flash).

The transient phenomena induced upon laser flash photolysis (25) of 1,1,2,2,-tetraphenylethane (**7**) (Scheme 3) proved more informative than those observed for the bibenzyl systems **1**. Singlet quenching of DCN by **7** occurs with a rate constant of $k_q = 1.0 \times 10^{10}\ M^{-1}\ s^{-1}$. In addition to the transient absorption bands for ^{3}DCN and $DCN^{\cdot-}$; an intense band at 330 nm, which is attributed to benzhydryl radical **9**, is observed in the laser flash spectrum of **7** obtained in CH_3CN (deoxygenated) containing DCN (Fig. 3). Laser flash studies of diphenylmethane

[7]The reversible reduction potential for DCA in acetonitrile vs. SCE is −0.87 V (ref. 27). The reduction potential of DCN is −1.67 V (19) in CH_3CN vs. Ag/0.1 *M* $AgNO_3$. Reduction potential for oxygen $E^0_{1/2}$ = −0.57 V vs. SCE in water (11*b*).

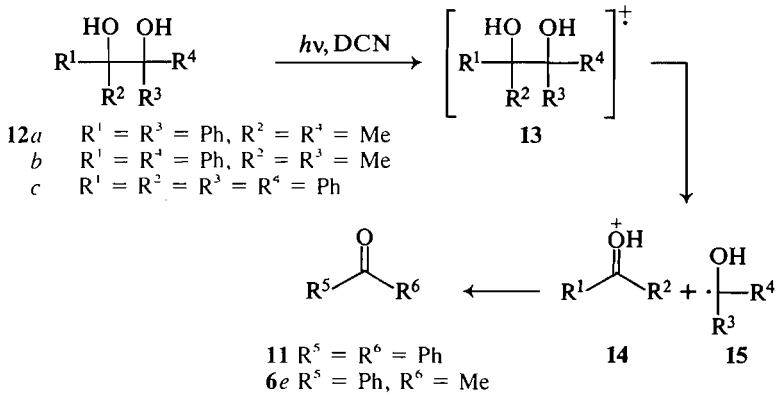

SCHEME 4

in benzene containing di-*tert*-butylperoxide affords benzhydryl radical **9**, the absorption spectrum of which corresponds to that of the transient generated from **7**. Our success in observing the benzhydryl radical **9** derived from **7** by laser flash spectroscopy, when we failed to detect the benzylic radicals **4** under similar conditions, may be ascribed to enhanced stabilization of the incipient benzhydryl cation **10** and radical **9** centers in the transition state leading to fragmentation of the radical cation **8**. It remains to be established if the benzhydryl cation **10** and/or the radical **9** derived from **7** contributes to absorption in the region of 400–500 nm. Experiments are in progress to determine if efficient electron transfer from $DCN^{\cdot-}$ to cation **10** to form the radical **9** may account for our inability to observe an absorption band for the cation **10** in the absence of oxygen and for possible augmentation of the spectral band assigned to **9** (330 nm) (Fig. 3).

The steady-state irradiation of **7** in CH_3CN (oxygenated) containing DCN gives benzophenones (**11**) (41%) (Scheme 3). While many mechanisms may be envisioned for the conversion of benzhydryl radical **9** and cumyl radical **4***e* and/or their respective cations to benzophenone (**11**) and acetophenone (**6***e*) respectively, with active oxygen ($^3O_2$, $^1O_2$, $O_2^{\cdot-}$), no attempt has yet been made to determine which species is or are implicated in this oxidations. Obviously, elimination of two methyl groups must accompany oxidation leading to **6***e*, and the absence of detectable cumyl hydroperoxide or dicumyl peroxide as products suggests that ET-induced decomposition may be implicated in the homolysis of hydroperoxy and/or peroxy intermediates to oxy radicals such as **5***e*, i.e., the conversion of hydroperoxy or peroxy intermediates to products must be efficient (28).

Pinacols and pinacol ethers derived from aryl ketones constitute another class of readily available compounds which incorporate the Ar—C—C—Ar bond sequence. Steady-state irradiation of samples of the racemic and *meso* pinacols **12***a* and **12***b*, respectively, in CH_3CN (deoxygenated) containing DCN gives acetophenone (**6***e*) (Scheme 4) in moderate yields (65%) which increase to 81% when the CH_3CN is saturated with oxygen. The conversion proceeds through initial formation of the radical cation **13**, followed by fragmentation to give the cation **14** and ketyl radical **15**, observed upon laser flash photolysis by its characteristic absorption band at 275 nm. Acetophenone (**6***e*) could be derived from either **14** (by deprotonation) or **15** (by loss of a hydrogen atom) (29).

When benzopinacol (**12***c*) is irradiated under conditions identical to those employed with the pinacols **12***a* and **12***b* in deoxygenated and oxygenated CH_3CN, benzophenone (**11**) is produced in high yields (72% and 100%, respectively) (Scheme 4). All of the pinacols are converted more efficiently to ketone when oxygen is present, conceivably because ET from $DCN^{\cdot-}$ to oxygen occurs to give superoxide anion, a less efficient donor to the radical cation **13**, prolonging its lifetime while increasing the opportunity to fragment. Not surprisingly, no silver chloride precipitate was observed under these conditions. Finally, fragmentation does not occur upon irradiation of CH_3CN solutions of **12***c* for prolonged periods in the absence of DCN.

In an attempt to define the mechanism of this pinacol cleavage we investigated a series of *O*-methyl substituted derivatives to assess the effect of such groups on the fragmentation process. Racemic acetophenone pinacol dimethyl ether **16** undergoes cleavage to acetophenone (**6***e*) (53%) and epimerization to the *meso* isomer **17** (16%) upon irradiation in CH_3CN (deoxygenated) containing DCN (Scheme 5). Control experiments confirm that **16** is photostable upon irradiation in the absence of the electron acceptor DCN under otherwise identical conditions. It is reasonable to assume that the epimerization of the pinacol dimethyl ether **16** occurs through initial fragmentation of the radical cation **18** to cation **19** and radical **20** which recombine Re, Si (or Si, Re) (30) prior (Path a) or subsequent (Path b) to reduction. Acetophenone (**6***e*) formation competes effectively with recombination and may arise by loss of methyl radicals from **20** if electron transfer precedes β-scission of a methyl cation, a process not without precedent for α-methoxy radicals of type **20** (31). Conversely, fragmentation may intercede and **19** may give methyl cation and acetophenone (**6***e*) directly. In order to discern whether an energy transfer mechanism from triplet acetophenone (**6***e*) initiates cleavage and epimerization in these systems, samples of **16** were irradiated in CH_3CN (deoxygenated) containing acetophenone (**6***e*), and, in the absence of DCN, no cleavage or epimerization is observed. Thus a triplet excited state mechanism may be discounted for the conversions observed with **16** and **17**.

Acetophenone (**6***e*) (80%) is the sole product formed when the *meso* isomer **17** is irradiated under conditions similar to those employed with **16** (Scheme 5). In contrast to **16**, however, solubility problems in CH_3CN were encountered with **17** and it was necessary to stir the mixture throughout the course of the irradiation and to extend the time period ten-fold in order to achieve conversion of **17** to **6***e* at levels commensurate with that observed with **16**.

We attribute the absence of racemization upon photoinduced fragmentation of **17** to the greater steric encumbrance of the

Can. J. Chem. Downloaded from www.nrcresearchpress.com by 210.87.254.6 on 09/06/12
For personal use only.

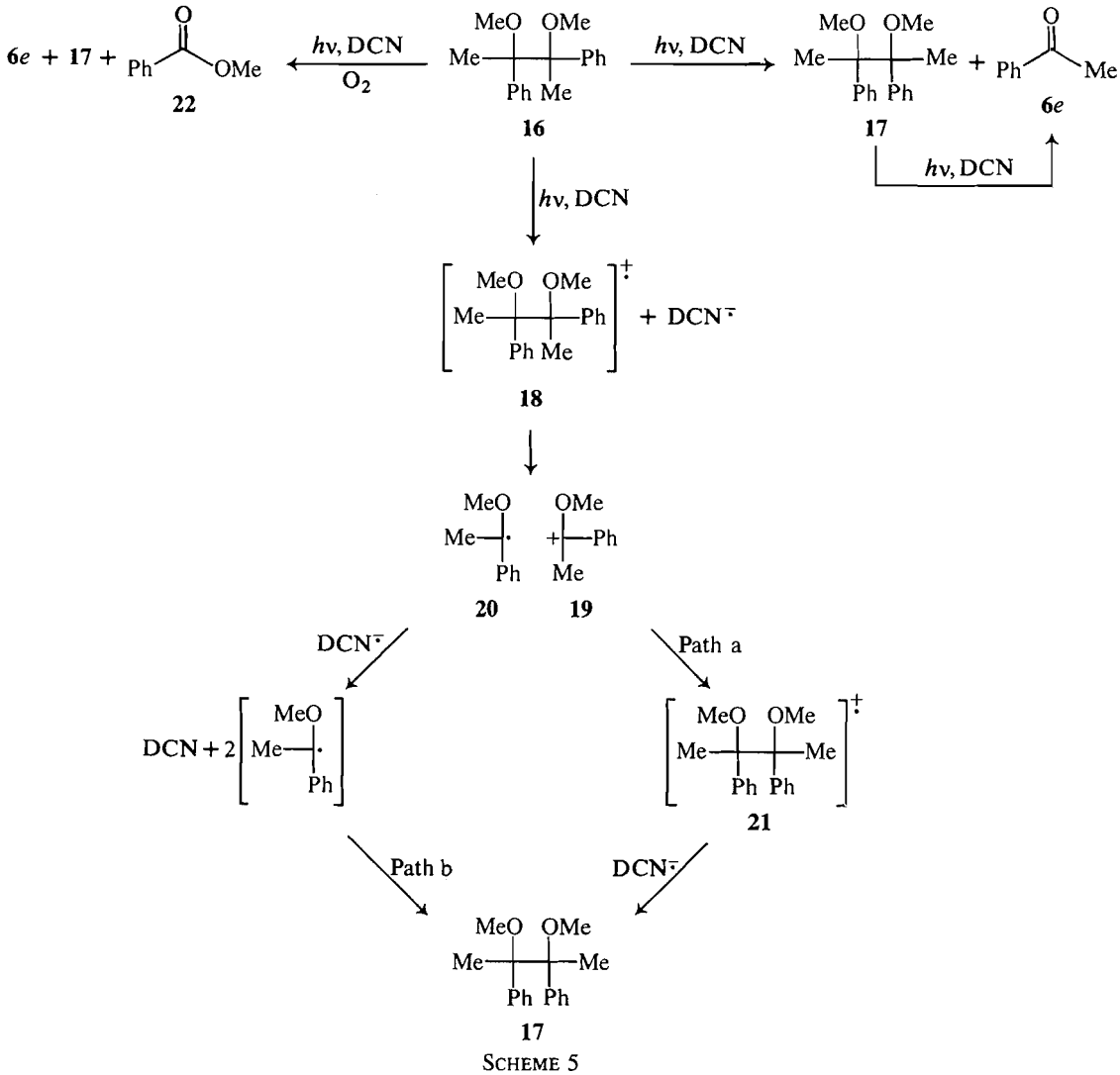

SCHEME 5

transition state for the requisite recombination, to give racemic pinacol dimethyl ether **16** regardless of the specific mechanism of inversion (Path a and/or Path b), than that leading to *meso* pinacol dimethyl ether **17**. *meso* Acetophenone pinacol **12***b* is formed preferentially upon peroxide-induced thermal pinacolization of acetophenone (**6***e*) (32), which validates this conclusion. Furthermore, the *meso* pinacol dimethyl ether **17** is formed to the exclusion of the racemic modification **16** upon free radical induced coupling of methyl α-phenethyl ether (33).

Oxidative cleavage to methyl benzoate (**22**) competes with fragmentation to acetophenone (**6***e*) in the case of the racemic and *meso* diastereomeric acetophenone pinacol dimethyl ethers **16** and **17**, respectively, when irradiated in CH_3CN (oxygenated) containing DCN (Scheme 5). The conversion to acetophenone (**6***e*) and methyl benzoate (**22**) appears more efficient with **16** (95% total conversion) than with the *meso* counterpart **17** (78% total conversion). Control experiments with oxygen and DCN in CH_3CN were performed in order to ensure that methyl benzoate (**22**) is not a secondary oxidation product formed from acetophenone (**6***e*) and $O_2^{\cdot-}$. That an ET mechanism is operate in these conversions was demonstrated in control experiments by irradiating CH_3CN solutions (oxygenated) of both **16** and **17** in the absence of DCN. No detectable epimerization or oxidative cleavage is observed under these control conditions.

4-Tolualdehyde (**6***b*) is formed under photoinduced ET conditions in the absence of oxygen in CH_3CN containing DCN and *meso*-1,2-bis(4-methylphenyl)-1,2-dimethoxyethane (**23**) (Scheme 6). A second product, namely methyl 4-toluate (**24**) (55%) is formed in addition to 4-tolualdehyde (**6***b*, 35%) when **22** is irradiated in the presence of oxygen. We presume that the ester **24** is formed through interception of the α-methoxy benzyl cation **25** and radical **26** (Scheme 6) by triplet ground state oxygen or perhaps an activated state ($^1O_2$ or $O_2^{\cdot-}$).

The behavior observed for the benzopinacol dimethyl ether **27** when subjected to photoinduced ET cleavage under deoxygenated conditions parallels that observed for benzopinacol (**12***c*) and *meso* acetophenone pinacol dimethyl ether (**17**) and the sole product isolated is benzophenone (**11**) (34%) (Scheme 7). Extensive quantities of intractable product(s) were formed and the amount of starting material **27** recovered was high (33%). It is interesting that no ester is detected when **27** is irradiated under oxygenated conditions, though more benzophenone (**11**) is formed (54%). This reaction also gives intractable product(s), less starting material is recovered, and the material balance is low. When **27** is thermolyzed (34) in the presence of oxygen, methyl benzoate (**22**) is formed by way of α-methoxybenzhydryl radicals **28**, characterized by esr spectroscopy. No methyl benzoate (**22**) is formed from **27** under ET conditions. We infer from these data that β-scission competes

Can. J. Chem. Downloaded from www.nrcresearchpress.com by 210.87.254.6 on 09/06/12
For personal use only.

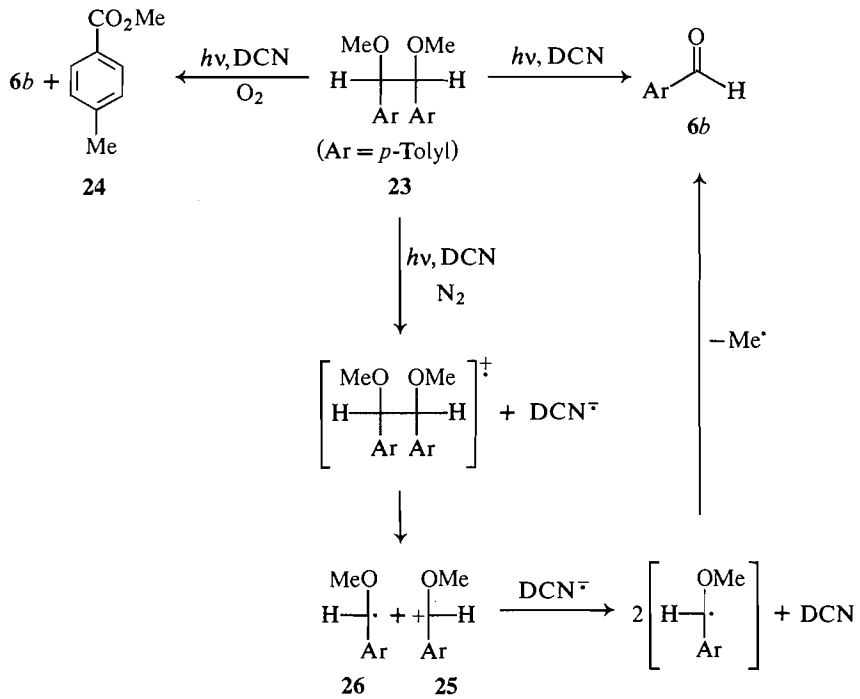

SCHEME 6

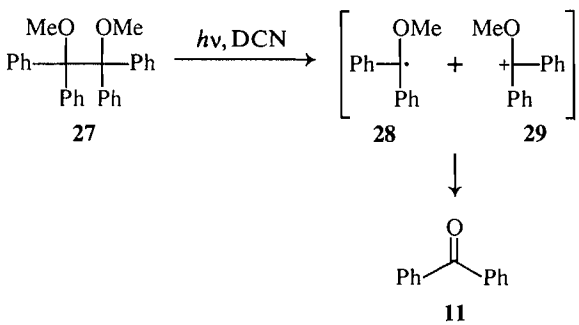

SCHEME 7

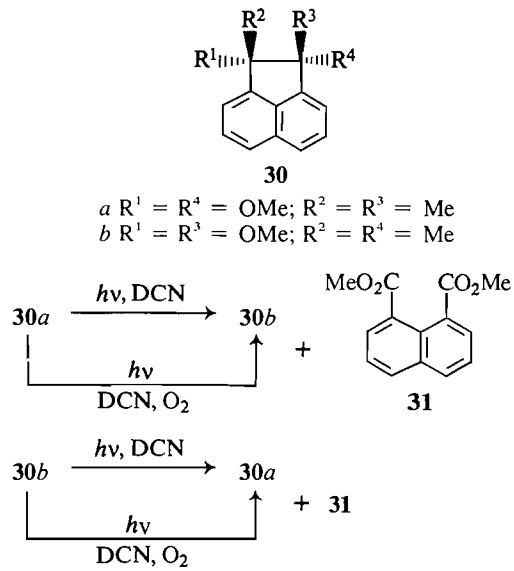

SCHEME 8

favorably with oxidation of the α-methoxy benzhydryl radical **28**. No products are found in control experiments when a deoxygenated CH_3CN solution of **27** is irradiated in the absence of DCN; however, benzophenone (**11**) is formed in CH_3CN (oxygen saturated). Perhaps the conversion of **27** in an oxygen atmosphere occurs through an electron transfer mechanism in which radical cations of **27** are generated through photoexcitation of a charge transfer (CT) complex between oxygen and the pinacol dimethyl ether **27**. Tokumaru and co-workers (35) have reported that the photooxidation of hexamethylbenzene and the dimerization of 4-methoxystyrene to cyclobutane dimers proceeds through a radical cation mechanism in which oxygen behaves as the electron acceptor in a polar solvent.

The presence of the *meso* isomer **17** among the ET-induced oxidation products of racemic acetophenone pinacol dimethyl ether **16** indicates that cation and radical or radical recombination competes with oxidation. How effectively remains to be determined. This observation led us to study the cyclic acenaphthene pinacol dimethyl ethers **30***a* and **30***b* (Scheme 8) which are constrained in such a manner as to enhance recombination of the cation and radical and/or radical centers with the objective of decreasing the efficiency of β-scission, loss of methyl cation, and addition of oxygen, while enhancing epimerization. Irradiation of *meso*-1,2-dimethyl-1,2-dimethoxyacenaphthene (**30***a*) in CH_3CN (deoxygenated) containing DCN affords the racemic modification **30***b* (23%). It is significant that no diketone is produced and the material balance is high (91%). Less dramatic results are obtained with the corresponding racemic pinacol dimethyl ether **30***b* where recyclization via an open radical cation or diradical mechanism to form the *meso* isomer **30***a* (7.4%) is sterically less favorable than recyclization to the enantiomeric pair **30***b*. The *meso* isomer **30***a* is photostable upon irradiation in the absence of DCN; however, the racemic substrate **30***b* undergoes limited epimerization to **30***a* (2.5%). This is undoubtably due to direct absorption of radiation by **30***b* which incorporates an acenapthene moiety (36).

Dramatically different results are observed when the di-

Can. J. Chem. Downloaded from www.nrcresearchpress.com by 210.87.254.6 on 09/06/12
For personal use only.

Can. J. Chem. Downloaded from www.nrcresearchpress.com by 210.87.254.6 on 09/06/12
For personal use only.

methyl acenaphthene pinacol dimethyl ethers **30***a* and **30***b* are irradiated in the presence of DCN in CH_3CN (oxygen saturated) (Scheme 8). Under these conditions substantial amounts of dimethyl 1,8-naphthalate (**31**) are obtained (30% and 16%, respectively). The presence of this oxidation product **31** attests to the fact that interception of the open radical cation by ground state oxygen or an activated form ($^1O_2$ or $O_2^{\cdot-}$) competes with β-scission, recyclization, and, conceivably, reduction of the radical cation by "back electron transfer". An open diradical cannot be excluded as a viable mechanistic alternative responsible for the observed results if "back electron transfer" is competitive with recyclization.

The conversion levels of **30***a* and **30***b* (37% and 62%, respectively) to the alternate isomer and diester **31** in each case are higher with the more sterically strained *meso* isomer **30***a*. These results are comparable to those obtained with the open chain acetophenone pinacol dimethyl ethers **16** and **17** (Scheme 5) where the racemic form constitutes the sterically less favorable substrate in this case.

It is noteworthy that oxygen should exert such a marked influence on the ET-sensitized isomerization and oxidation of the *meso* isomer **30***a*. The course of this reaction was monitored by thin-layer chromatography and the isomerization to **30***b* (46%) maximized, i.e., the extent of epimerization is enhanced by a factor of two when the CH_3CN is saturated with oxygen rather than nitrogen. Furthermore, no such enhancement is observed upon irradiation of the enantiomeric pair **30***b* under similar conditions, even when the irradiation period is extended. The mechanism by which oxygen enhances epimerization of *meso* diether **30***a* to **30***b* is of great interest. Conceivably, superoxide anion, a less efficient electron donor, is formed when oxygen is present, which intercepts the electron transferred from $DCN^{\cdot-}$, delaying its return to the radical cation, and thus exerts a favorable influence on the extent of the isomerization process by extending the radical cation lifetime (11*j*).

A control experiment was run with the *meso* isomer **30***a* in CH_3CN (oxygen saturated) in the absence of DCN, and limited epimerization (9%) was observed upon irradiation. In the case of the racemic modification, however, the extent of isomerization is equivalent to that observed with DCN present, and some diester **31** (6.7%) is also formed. Presumably cleavage, isomerization, and oxidation here are due to direct absorption and reaction through the singlet and/or triplet state. It is noteworthy, however, that irradiation of the *meso* pinacol dimethyl ether **30***a* in deoxygenated acetonitrile in the absence of DCN with added benzophenone (**11**) (in polar solvents E_T = 69.2 kcal/mol) (37, 38) induced only 8.2% isomerization to the racemic modification **30***b*. Thus a triplet mechanism cannot explain the more extensive isomerization observed with DCN, although the irradiation time was longer in the latter case. Certainly, triplet sensitization of the isomerization of **30***a* to **30***b* by DCN may be excluded on the basis of relative triplet energies, i.e., the DCN triplet energy (E_T = 55.5 kcal/mol) (19) is lower than that estimated for **30***a* (59.2 kcal/mol) (38, 39), based on the parent hydrocarbon acenaphthene. Intersystem crossing then provides the only mechanism for populating the triplet manifold of **30***a* and, while this is a relatively efficient process (Φ_{ISC} = 0.45−0.58 for acenapthene) (37, 40, 41), the triplet state cannot be implicated in the isomerization of **30***a* to **30***b*, based on the negative results obtained with benzophenone as a sensitizer.

rac-9,10-Dimethoxy-9,10-dimethyl-9,10-dihydrophenanthrene (**32**), another cyclic pinacol dimethyl ether, was irradiated in acetonitrile containing DCN under conditions analogous to those employed with the acenaphthene counterparts **30***a* and **30***b*. In a nitrogen atmosphere, **32** is converted in low yield (9%) to the *meso* epimer **33** and 84% of the precursor **32** was recovered (eq. [1]). We attribute the low conversion levels achieved, once again, to unfavorable thermodynamic factors, i.e., recyclization of the open radical cation (or diradical) to the *meso* radical ion corresponding to **33** is sterically less favorable than recyclization of the original enantiomeric radical cations of **32**. In CH_3CN (oxygenated) the conversion of **32** to **33** is enhanced to 24% upon irradiation in the presence of DCN and over half the substrate **32** (56%) is recovered. The effect of oxygen is thus general in all of the examples presented. It remains to be established whether the postulate of electron relay from DCN radical anion to oxygen, forming superoxide anion to explain the extended lifetime of the radical cation, is correct. Oxidation products, in particular the diester, are conspicuously absent in this case, a result which may be due to more rapid recyclization. Experimental difficulties were encountered with the preparation of the *meso* isomer **33** which precluded studies in this case. Control experiments with **32** under deoxygenated conditions revealed no isomerization; however, in oxygenated acetonitrile in the absence of DCN, 21% of **33** was observed, which is nearly equivalent to that achieved with DCN present, probably as a result of absorption by the 9,10-dihydrophenanthrene chromophore (42). The diether **32** was irradiated in the presence of benzophenone (**11**) in acetonitrile under similar deoxygenated conditions and detectable isomerization was observed. It is unlikely, however, that ^{3}DCN can transfer energy to **32** in view of the magnitude of its triplet energy (E_T = 55.5 kcal/mol) (19).

[1] 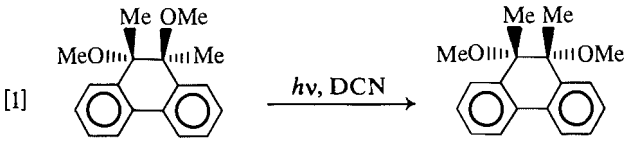

32 **33**

On the basis of the foregoing data it should be possible to design unsymmetrical reactive substrates which, like the substituted bibenzyl systems described above, would undergo facile fragmentation of the corresponding radical cations generated by photoinduced electron transfer reactions to give cations and free radicals.

Our initial endeavors in this area were devoted to a study of substrates incorporating the pyrazolinone nuclei in which a radical center at C-4 displays marked stability as a consequence of merostabilization (also known as captodative and push−pull stabilization) (43). The pyrazolinone nucleus should impart fragmentation lability to radical cations embodying this moiety coupled to a substituent capable of manifesting independent existence as a cationic species.

1-Phenyl-3-methyl-4-benzhydryl-2-pyrazolin-5-one (**34**) was selected as the initial member of these series to be evaluated. Upon irradiation of **34** in CH_3CN (oxygen saturated) containing DCN, 1-phenyl-3-methyl-2-pyrazolin-4,5-dione (**35**) (27%)

[2] 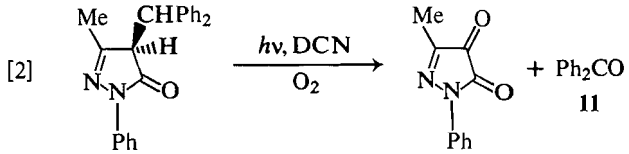

34 **35**

(44) and benzophenone (**11**) (41%) are produced (eq. [2]). The oxidative cleavage of **34** to the dione **35** and benzophenone (**11**) under electron transfer conditions is consistent with the results obtained with 1,1,2,2-tetraphenylethane (**7**) in which benzhydryl radical **9**, identified by laser flash spectroscopy, and benzhydryl cation **10**, are presumably oxidized to benzophenone (**11**) under similar conditions. On the basis of this experiment it is clear that a host of other substituted pyrazolinone and related heterocyclic systems will also cleave in a similar fashion when converted to their respective radical cations by electron transfer process.

Experimental

The 60 MHz proton magnetic resonance spectra were obtained on a Varian A-60, Hitachi Perkin–Elmer R-20B, or a Varian EM-360A spectrometer with 1% tetramethylsilane as an internal standard. Mass spectra were recorded on a Hitachi Perkin–Elmer RMU-6E spectrometer. Infrared spectra were determined using either a Perkin–Elmer 257 or 735B instrument. All melting point determinations were performed using a Thomas–Hoover capillary melting point apparatus and are uncorrected.

Silica Gel G (PF 254; Brinkman Co.) coated on glass plates was used for all preparative thick-layer chromatographic separations. Eastman Chromagram sheets (silica gel) were employed in analytical thin-layer applications. Visualization of resolved bands was achieved utilizing short-wavelength ultraviolet lamps (Black–Ray UVL-21). Preparative gas chromatographic separations were accomplished using a Varian Aerograph Model 90P gas chromatograph equipped with a 10 ft × 0.25 in. SE-30 (30% on Chromosorb P) column. All elemental combustion analyses were performed by Galbraith Laboratories, Inc., (Knoxville, TN) and were found to be within acceptable limits.

Acetonitrile (Bardick and Jackson Spectro Grade), the solvent of choice for all electron transfer sensitization experiments conducted, was dried over activated silica gel, then distilled from P_2O_5 in an atmosphere of dry nitrogen. Other anhydrous solvents, when required, were purified and dried just prior to use by standard procedures (45). 1,4-Dicyanonaphthalene was prepared by heating 1,4-dibromonaphthalene (Eastman) with cuprous cyanide and pyridine according to a modification of the procedure described for the conversion of 1-bromonaphthalene to the corresponding α-naphthonitrile and purified by column chromatography on neutral alumina followed by recrystallization from toluene (46). The results of the photoinduced electron transfer cleavage reactions are described in Table 1.

*Preparation of 1,2-bis(4-methoxyphenyl)ethane (**1**a)*

The substituted bibenzyl **1***a* was prepared from 4-methoxybenzyl bromide (47) (from 4-methylanisole and *N*-bromosuccinimide) by the general method of Trahanovsky and Brixius (48) or by a reduction of 4,4′-dimethoxy stilbene (Aldrich); mp 122–123°C (ethanol, lit (48) mp 125–126°C).

*Preparation of 1,2-bis(4-methylphenyl)ethane (**1**b)*

The Grignard coupling method described above for the preparation of **1***a* was used to convert 0.64 g (2.7 mmol) of 4-methylbenzyl bromide (Aldrich) to the hydrocarbon **1***b*, 1.2 g (21%); mp 81–82°C (ethanol, lit. (48) mp 83–84°C).

*Preparation of 1-(4-methylphenyl)-2-(4-methoxyphenyl)ethane (**1**d)*

trans-4-Methyl-4′-methoxy stilbene (49) (prepared from the Wittig reaction of 4-methylbenzyltriphenylphosphonium bromide (50) with 4-anisaldehyde in the presence of lithium ethoxide) was hydrogenated (H_2, 45 psi, 10% Pd/C) in ethanol. After removal of the volatile solvents under reduced pressure, the residual solid was recrystallized from ethanol to afford 0.38 g (63%) of the desired 1,2-diphenylethane **1***d*: mp 63–64°C ir (Nujol): 1610 (s), 1510 (s), 1380 (s), 1300 (s), 1250 (s), 1178 (s), 1038 (m), 830 (m), 820 (s) cm^{-1}; nmr ($CDCl_3$) δ: 2.28 (s, 3H, CH_3), 2.81 (s, 4H), 3.77 (s, 3H, OCH_3), 7.05 (m, ArH). *Anal.* calcd. for $C_{16}H_{18}O$: C 84.91, H 8.02; found: C 85.09, H 8.14.

*Preparation of 2,3-dimethyl-2,3-diphenylbutane (**1**e)*

To a mixture of 6.8 g of sodium hydroxide, 100 mL of bleach, and 5 drops of the phase transfer agent Aliquot 336 in 100 mL of hexane was added 2.0 g (6.00 mmol) of *N*,*N*′-bis(1-methyl-1-phenylethyl)sulfamide (51). The mixture was allowed to stir at room temperature for a period of 72 h. The resulting hexane solution was washed in turn with water, 5% hydrochloric acid, 5% sodium bicarbonate, and finally water, and then dried over magnesium sulfate. The solvent was removed under reduced presure at room temperature and the remaining solid was added to 50 mL of toluene and subsequently heated at the reflux temperatue for 24 h. Toluene was removed under reduced pressure and the residue was recrystallized from 95% ethanol to provide 1.3 g (46%) of **1***e*: mp 120–121°C (lit. (52) mp 115°C).

Preparation of rac- *and* meso-*2,3-dimethoxy-2,3-diphenylbutane (**16** and **17**, respectively)*

The methylation procedure of Gillis (53) was used for the conversion of the corresponding pinacols *rac*- and *meso*-2,3-butanediols, **12***a* and **12***b*, to the diethers **16** and **17**, respectively. The corresponding racemic or *meso* pinacol (54) (500 mg, 2.1 mmol) was added to a finely powdered suspension of sodium hydroxide (0.67 g, 18 mmol) in 15 mL of DMSO. Methyl iodide (1.2 g, 8.2 mmol) was then introduced and the resulting mixture was stirred at room temperature for 30 min and then quenched with 10 mL of water. The desired product was extracted using three 10-mL portions of chloroform and the combined organic extracts were washed twice with water and then dried over magnesium sulfate. Removal of the solvent under reduced pressure and recystallization of the residue from methanol afforded white crystals of the desired diol dimethyl ether **16** or **17**. Racemic diol dimethyl ether **16**: mp 111.0–111.5°C (0.46 g, 80%); ir (KBr): 3050 (m), 3010 (m), 2970 (s), 2930 (m), 2830 (s), 1440 (w), 1360 (m), 1140 (s), 1090 (s), 1150 (s), 880 (s), 800 (s), 760 (s), 710 (s) cm^{-1}; nmr ($CDCl_3$) δ: 1.65 (s, 6H, CH_3), 3.10 (s, 6H, OCH_3), 6.73–7.28 (m, 10H, ArH); mass spectrum, *m/e*: 135 ($M^+ - C_9H_{11}O$), 105 ($M^+ - C_9H_{11}O - CH_2O$), 77, 43, 51. *Anal.* calcd. for $C_{18}H_{22}O_2$: C 79.96, H 8.20; found: C 79.95, H 8.03. *meso* Diol dimethyl ether **17**: mp 164–166°C (377 mg, 67%) (lit. (55) mp 171–173°C); nmr ($CDCl_3$) δ: 1.43 (s, 6H, CH_3), 3.01 (s, 6H, OCH_3), 7.25 (s, 10H, ArH).

Preparation of meso-*1,2-bis(4-dimethylphenyl)-1,2-dimethoxyethane (**23**)*

The procedure for methylation devised by Gillis (53) was used to convert 1,2-bis(4-methylphenyl)-1,2-dihydroxyethane (56) to the diether **23**. To a finely powered suspension of sodium hydroxide (0.32 g, 8.0 mmol) in 15 mL of dimethyl sulfoxide was added the pinacol (0.24 g, 1.0 mmol), followed by methyl iodide (0.57 g, 4.0 mmol). The resulting reaction mixture was allowed to stir for 30 min and then 10 mL of water were added. The combined chloroform extracts were washed twice with water and dried over magnesium sulfate. Removal of the solvent under reduced pressure and recystallization of the residue from ligroin afforded 0.23 g (85%) of the diether **23** in the form of white crystals: mp 126–128°C; ir ($CHCl_3$): 2990 (m), 2940 (m), 2830 (s), 1515 (s), 1455 (m), 1100 (w), 830 (m) cm^{-1}; nmr ($CDCl_3$) δ: 7.09 (s, 8H, ArH), 4.23 (s, 2H), 3.12 (s, 6H, OCH_3), 2.32 (s, 6H, CH_3). *Anal.* calcd. for $C_{18}H_{22}O_2$: C 79.96, H 8.20; found: C 80.17, H 8.29.

*Preparation of 1,2-dimethoxy-1,1,2,2-tetraphenylethane (**27**)*

This pinacol dimethyl ether was prepared in an indirect manner by free radical induced coupling of diphenylmethyl methyl ether according to the procedure described by Hartzell and Huyser (33). In our hands, this conversion gave an overall yield of 5.2% based on benzhydrol: mp 155–158°C (lit. (57) mp 157–159°C).

Preparation of meso- *and* rac-*1,2-dimethoxy-1,2-dimethylacenaphthene (**30**a and **30**b, respectively)*

The method of Gillis (53) was employed for the methylation of the isomeric 1,2-dimethylacenaphthane-1,2-diols (58). To a fine suspension of sodium hydroxide (0.74 g, 19 mmol) in 15 mL of dimethyl sulfoxide was added the diol (0.56 g, 2.3 mmol) and then methyl iodide (1.3 g, 9.2 mmol). The mixture was then stirred for 30 min and

Can. J. Chem. Downloaded from www.nrcresearchpress.com by 210.87.254.6 on 09/06/12
For personal use only.

TABLE 1. Photoinduced electron transfer cleavage reactions

Compound	Amount	DCN (amount)	O_2 present?	Time of irradiation	Products (yield)	Methods of isolation and identification
1*a*	200 mg	20 mg	Yes	4 days	**6***a* (83%)	tlc (benzene), nmr
1*b*	200 mg	17 mg	Yes	4 days	**6***b* (58%)	nmr
1*d*	20 mg	3 mg	Yes	4 days	**6***a*+**6***b* (4:3, 54%)	nmr
1*e*	200 mg	24 mg	Yes	63 h	**6***e* (61%);	
					1*e* (17%)	tlc (benzene–hexane, 1:1)
7	130 mg	12 mg	Yes	88 h	**11** (41%);	
					7 (14%)	tlc ($CHCl_3$)
12*a* or **12***b*	200 mg	20 mg	No	4 days	**6***e* (66%)	tlc (ether–hexane, 1:1)
12*a* or **12***b*	250 mg	25 mg	Yes	98 h	**6***e* (81%)	tlc (hexane–chloroform, 4:1) nmr
12*c*	250 mg	29 mg	No	90 h	**11** (72%)	tlc ($CHCl_3$)
12*c*	250 mg	26 mg	Yes	90 h	**11** (100%)	tlc (hexane–chloroform, 4:1) nmr
16	150 mg	17 mg	No	24 h	**6***e* (53%);	tlc (benzene–hexane, 2:1)
					17* (16%)	nmr
16	150 mg	15 mg	Yes	26 h	**6***e* (39%);	
					22 (56%);	
					17* (3%);	tlc (benzene–hexane, 2:1) nmr
17	260 mg	27 mg	No	260 h	**6***e* (80%);	
					17 (9%)	tlc (benzene–hexane, 3:1)
17	260 mg	27 mg	Yes	159 h	**6***e* (57%);	
					22 (21%);	
					17 (14%)	tlc (benzene–hexane, 2:1)
23	200 mg	20 mg	No	4 days	**6***a* (75%)	tlc (benzene)
23	200 mg	20 mg	Yes	4 days	**6***a* (35%);	
					24 (55%)	tlc (benzene)
27	240 mg	26 mg	No	99 h	**11** (33);	
					27 (34%)	tlc (chloroform)
27	220 mg	23 mg	Yes	88 h	**11** (54%);	
					27 (9%)	tlc (chloroform)
30*a*	250 mg	24 mg	No	98 h	**30***b* (23%);	
					30*a* (68%)	tlc (hexane–chloroform, 1:1)
30*a*	230 mg	26 mg	Yes	60 h	**30***b* (46%);	
					31 (16%);	
					30*a* (41%)	tlc (chloroform) synthesis of **31**†
30*b*	280 mg	28 mg	No	131 h	**30***a* (7.4%);	
					30*b* (86%)	tlc (chloroform)
30*b*	260 mg	26 mg	Yes	113 h	**30***a* (7.3%);	
					31 (30%);	
					30*b* (41%)	tlc (chloroform)
32	210 mg	19 mg	No	120 h	**33** (9%);	
					32 (84%)	tlc (chloroform) ir, nmr, ms for **33**‡
32	150 mg	12 mg	Yes	98 h	**33** (24%);	
					32 56%)	tlc (chloroform)
34	200 mg	22 mg	Yes	25 h	**11** (41%)	
					35 (27%)	tlc (chloroform)

*Difficulty was encountered in separating the racemic and *meso* diethers **16** and **17** and analyses of mixtures of these substrates were achieved by integration of the resolvable methyl protons of the mixture of the isomeric pair.

†Reference 60.

‡Compound **33** was characterized by the following spectral data: ir ($CHCl_3$(; 2980 (m), 2930 (m), 2810 (m), 2730 (m), 1450 (m), 1360 (m), 1220 (m), 1200 (m), 1110 (s), 1060 (s), 1040 (s), 850 (s), 800 (s), 760 (s), 750 (s) cm^{-1}; nmr ($CDCl_3$) δ: 1.40 (s, 6H, CH_3), 3.15 (s, 6H, OCH_3), 7.18–7.33, 7.63–7.80 (m, 8H, ArH); mass spectrum, *m/e*: 268 (M^+), 253 ($M^+ - CH_3$), 209, 197.

quenched with 10 mL of water. The desired products in each case were extracted using three 10-mL portions of chloroform. The combined organic extracts were washed with water, dried over magnesium sulfate, and concentrated by removal of the solvent under reduced pressure. The *meso* diol dimethyl ether **30***a* was separated on a silica gel column using 1:1 hexane–chloroform as the eluent to give a very light yellow oil (0.36 g, 64%) which was not induced to crystallize. The racemic diol dimethyl ether **30***b* was recrystallized from hexane to give 0.27 g (48%) of white crystals; mp 107–108°C (102–103°C, MeOH). *meso* Diol dimethyl ether **30***a*: ir (neat): 2950 (m), 2800 (s), 1430 (s), 1360 (m), 1260 (m), 1200 (m), 1100 (m), 880 (s), 830 (s), 780 (s), 760 (s) cm^{-1}; nmr ($CDCl_3$) δ: 1.63 (s, 6H, CH_3), 3.3 (s, 6H, OCH_3), 7.20–7.75 (m, 6H, ArH); mass spectrum, *m/e*: 242 (M^+), 227 ($M^+ - CH_3$), 195 ($M^+ - CH_3 - CH_2O$), 165, 162. Racemic dimethyl ether **30***b*: ir (KBr): 2930 (m), 2830 (s), 2730 (m), 1450 (w), 1360 (m), 1250 (w), 1200 (m), 1110 (w), 1040 (m), 860 (s), 840 (s),

Can. J. Chem. Downloaded from www.nrcresearchpress.com by 210.87.254.6 on 09/06/12
For personal use only.

800 (s) cm^{-1}; nmr ($CDCl_3$) δ: 1.70 (s, 6H, CH_3), 2.90 (s, 6H, OCH_3), 7.35−7.80 (m, 6H, ArH); mass spectrum, as for **30***a*. *Anal.* calcd. for $C_{16}H_{18}O_2$: C 79.31, H 7.49; found: C 79.12, H 7.36.

Preparation of rac-*9,10-dimethoxy-9,10-dimethyl-9,10-dihydrophenanthrene (32)*

rac-9,10-Dihydroxy-9,10-dimethyl-9,10-dihydrophenanthrene (59) (1.0 g, 4.2 mmol) was added to a suspension of finely divided sodium hydroxide (1.3 g, 33 mmol) in a 15 mL of dimethyl sulfoxide and then methyl iodide (2.3 g, 16.2 mmol) was introduced (53). The resulting mixture was stirred at room temperature for 30 min and quenched with 10 mL of water. The resulting slurry was extracted using three 10-mL portions of chloroform and the combined organic extracts were washed twice with water and dried over magnesium sulfate. Removal of the solvent under reduced pressure and recrystallization of the residue from hexane afforded 0.44 g (40%) of **32**: mp 110−114°C; ir (KBr): 2980 (m), 2930 (s), 2810 (m), 2730 (m), 1450 (m), 1360 (m), 1200 (w), 1110 (s), 1060 (m), 1040 (m), 850 (s), 750 (s) cm^{-1}; nmr ($CDCl_3$) δ: 1.58 (s, 6H, CH_3), 3.03 (s, 6H, OCH_3), 7.10−7.80 (m, 8H, ArH); mass spectrum, *m/e*: 268 (M^+), 253 ($M^+ - CH_3$), 209, 179. *Anal.* calcd. for $C_{18}H_{20}O_2$: C 80.56, H 7.51; found: C 80.67, H 7.62.

Preparation of 1-phenyl-3-methyl-4-benzhydryl-2-pyrazolin-5-one (34)

3-Methyl-1-phenyl-2-pyrazolin-5-one (Aldrich, 1.70 g, 10 mmol) was heated for 2.5 h with benzhydrol (1.84 g, 10 mmol) in glacial acetic acid (35 mL) with 4 drops of concentrated hydrochloric acid. Dilution of the solution with water gave 1.40 g (41%) crystals, mp 221−221.5°C dec. (ethanol, lit. (61) mp 220°C).

Conventional method for sample preparation and irradiation in the photoinduced electron transfer reactions

Samples to be irradiated and DCN were placed in 15 × 1.2 cm (id) Pyrex test tubes and 20 mL of acetonitrile were added. The vessel was then sealed with a serum cap which was wired in place. The solution was deoxygenated or oxygenated by inserting hypodermic needles to introduce either nitrogen or oxygen (15 to 30 min), respectively, and to provide an exit port. Irradiations were conducted in an air-cooled Rayonet RPR-100 Chamber Reactor (The Southern New England Ultraviolet Co., Middletown, Conn.) equipped with sixteen F8T5/BLB broad emission (280−420 nm) 8-W low pressure mercury lamps (General Electric Company) operating at a temperature of approximately 40°C. Utilization of the F8T5/BLB lamps (emission max. 350 nm,) coupled with a Pyrex filter (opaque below 290 nm) effectively precludes excitation of the substrate and ensures that the electron transfer sensitizer is excited preferentially. Control experiments were conducted under similar conditions in the absence of the electron transfer sensitizer. In order to ensure uniform exposure of individual samples during multiple irradiations and kinetic experiments, the same reactor was fitted with a continuously rotating MGR-100 Merry-Go-Round adapter (Southern New England Ultraviolet Co.). The residue obtained after removal of solvent under reduced pressure was analyzed by tlc and/or nmr. The results of these experiments are summarized in Table 1.

*Attempted triplet−triplet energy sensitized isomerizations of **16**, **30**a, and **32***

A procedure similar to that used for the foregoing electron transfer sensitized reactions was employed, with the exception that acetophenone (**6***e*) (10 mg, 0.08 mmol) was used as a sensitizer in the case of **16** (0.1 g, 0.4 mmo), and benzophenone (**11**) (10 mg, 0.05 mmol) for **30***a* (0.1 g, 0.4 mmol) and **32** (0.1 g, 0.4 mmol) in the place of the electron transfer agent DCN. Solutions of the various substrates in 20 mL of acetonitrile contained in a Pyrex test tube were deoxygenated with nitrogen in the specified manner. The resulting solutions **16**, **30***a*, and **32** were irradiated for 71 h, 56 h, and 48 h, respectively, and the volatile solvent was then removed. The nmr analysis of the resulting residues revealed that no isomerization had occurred with **16** and **32**; however, 8.2% of the racemic compound was found in the case of **30***a*.

Acknowledgements

This investigation at the University of New Orleans (G.W.G.) was supported in part by the National Science Foundation (Grant CHE 78-00615). Those phases of the project conducted in the Radiation Laboratory at the University of Notre Dame were financed by funds from the Office of Basic Energy Science of the United States Department of Energy (P.K.D.). This is document No. NDRL 2373 from the Radiation Laboratories. Appreciation is also expressed to Ms. Tekla Teleshak, Karen Deogracias, and Frances Caldwell for their assistance in the preparation of the manuscript and Dr. Eleanor Elder for technical library assistance. Drawings were done by Dr. David Lankin and we are indebted to Dr. Pesi Umrigar for technical assistance.

1. (*a*) J. P. K. WONG, A. A. FAHMI, G. W. GRIFFIN, and N. S. BHACCA. Tetrahedron, **37**, 3345 (1981); (*b*) G. W. GRIFFIN, J. P. K. WONG, and A. A. FAHMI. J. Photochem. **17**, 104 (1981); (*c*) G. W. GRIFFIN, J. P. K. WONG, A. A. FAHMI, P. P. UMRIGAR, A. J. MULLER, and S. N. EGE. J. Photochem. **17**, 327 (1982); (*d*) G. W. GRIFFIN, J. P. K. WONG, A. A. FAHMI, P. P. UMRIGAR, A. J. MULLER, and S. N. EGE. Xth International Conference on Photochemistry, Iraklion, Crete, Greece. September 6−12, 1981; (*e*) G. W. GRIFFIN, A. J. MULLER, L. W. REICHEL, A. P. TAMVAKIS, and J. D. TIMPA. 183rd ACS National Meeting, Las Vegas, Nevada. March 28 − April 2, 1982; (*f*) G. W. GRIFFIN, A. J. MULLER, L. W. REICHEL, A. P. TAMVAKIS, and J. D. TIMPA. Symposium on Pure and Applied Photochemistry in honor of Harry E. Gunning, Chemical Institute of Canada 65th Annual Conference, Toronto, Ontario. May 30 − June 2, 1982; (*g*) G. W. GRIFFIN, A. J. MULLER, L. W. REICHEL, A. P. TAMVAKIS, J. D. TIMPA, and P. K. DAS. IX Symposium IUPAC de Photochemie, Pau, France. July 25−30, 1982; (*h*) G. W. GRIFFIN, A. J. MULLER, L. W. REICHEL, A. P. TAMVAKIS, J. D. TIMPA, and P. K. DAS. ACS 34th Annual Southeastern Regional Meeting, Birmingham, Alabama. Nov. 3−5, 1982; (*i*) G. W. GRIFFIN, A. J. MULLER, L. W. REICHEL, A. P. TAMVAKIS, J. D. TIMPA, and P. K. DAS. ACS 38th Southwest and 6th Rocky Mountain Combined Regional Meeting, El Paso, Texas. Dec. 1−3, 1982.
2. (*a*) H. LEONHARD and A. WELLER. Ber. Bunsenges. Phys. Chem. **67**, 791 (1963); (*b*) D. REHM and A. WELLER. Ber. Bunsenges. Phys. Chem. **73**, 834 (1969); (*c*) D. REHM and A. WELLER. Isr. J. Chem. **8**, 259 (1970), and references therein.
3. (*a*) C. PAC and H. SAKURAI. Tetrahedron Lett. 3829 (1969); (*b*) J. J. MCCULLOUGH and W. S. WU. J. Chem. Soc. Chem. Commun. 1136 (1972); (*c*) J. J. MCCULLOUGH, R. C. MILLER, and W. S. WU. Can. J. Chem. **55**, 2909 (1977); (*d*) K. A. BROWN-WENSLEY, S. L. MATTES, and S. FARID. J. Am. Chem. Soc. **100**, 4162 (1978); (*e*) D. R. ARNOLD, P. C. WONG, A. J. MAROULIS, and T. S. CAMERON. Pure Appl. Chem. **52**, 2609 (1980); (*f*) M. YASUDA, C. PAC, and H. SAKURAI. Bull. Chem. Soc. Jpn. **53**, 502 (1980); (*g*) R. M. BORG and D. R. ARNOLD. Gunning Symposium on Photochemistry, Toronto, Canada. May 30 − June 2, 1982.
4. (*a*) K. MIZUNO, R. KAJI, H. OKADA, and Y. OTSUJI. J. Chem. Soc. Chem. Commun. 594 (1978); (*b*) K. MIZUNO, M. ISHII, and Y. OTSUJI. J. Am. Chem. Soc. **103**, 5570 (1981).
5. (*a*) R. A. NEUNTEUFEL and D. R. ARNOLD. J. Am. Chem. Soc. **95**, 4080 (1973); (*b*) S. KUWATA, Y. SHIGEMITSU, and Y. ODAIRA. J. org. Chem. **38**, 3803 (1973); (*c*) M. YAMAMOTO, T. ASANUMA, and Y. NISHIJIMA. J. Chem. Soc. Chem. Commun. 53 (1975); (*d*) T. ASANUMA, M. YAMAMOTO, and Y. NISHIJIMA. J. Chem. Soc. Chem. Commun. 608 (1975); (*e*) T. GOTOH, M. YAMAMOTO, and Y. NISHIJIMA. J. Polym. Sci. Polym. Lett. Ed. **17**, 143 (1979); (*f*) D. R. ARNOLD, R. M. BORG, and A. ALBINI. J. Chem. Soc. Chem. Commun. 138 (1981).

Can. J. Chem. Downloaded from www.nrcresearchpress.com by 210.87.254.6 on 09/06/12
For personal use only.

Can. J. Chem. Downloaded from www.nrcresearchpress.com by 210.87.254.6 on 09/06/12
For personal use only.

6. (*a*) K. MIZUNO, H. OKAMOTO, C. PAC, and H. SAKURAI. J. Chem. Soc. Chem. Commun. 839 (1975); (*b*) A. J. MAROULIS and D. R. ARNOLD. J. Chem. Soc. Chem. Commun. 351 (1979).
7. (*a*) K. MIZUNO, R. KAJI, and Y. OTSUJI. Chem. Lett. 1027 (1977); (*b*) M. YASUDO, C. PAC, and H. SAKURAI. J. Org. Chem. **46**, 788 (1981).
8. (*a*) Y. SHIGEMITSU and D. R. ARNOLD. J. Chem. Soc. Chem. Commun. 407 (1975); (*b*) K. MIZUNO, C. PAC, and H. SAKURAI. J. Chem. Soc. Chem. Commun. 553 (1975); (*c*) A. J. MAROULIS, Y. SHIGEMITSU, and D. R. ARNOLD. J. Am. Chem. Soc. **100**, 535 (1978); (*d*) A. J. MAROULIS and D. R. ARNOLD. Synthesis, 819 (1979); (*e*) D. R. ARNOLD and A. J. MAROULIS. J. Am. Chem. Soc. **99**, 7355 (1977); (*f*) S. L. MATTES and S. FARID. J. Am. Chem. Soc. **104**, 1454 (1982); (*g*) V. R. RAO and S. S. HIXSON. J. Am. Chem. Soc. **101**, 6458 (1979).
9. (*a*) D. R. ARNOLD and R. W. R. HUMPHREYS. J. Am. Chem. Soc. **101**, 2743 (1979); (*b*) A. PADWA, C. S. CHOU, and W. F. RIEKER. J. Org. Chem. **45**, 4555 (1980).
10. I. SAITO, K. TAMOTO, and T. MATSUURA. Tetrahedron Lett. 2889 (1979).
11. (*a*) G. RIO and J. BERTHELOT. Bull. Soc. Chem. Fr. 3609 (1969); (*b*) J. ERIKSEN, C. S. FOOTE, and T. L. PARKER. J. Am. Chem. Soc. **99**, 6455 (1977); (*c*) N. BERENJIAN, P. DE MAYO, F. H. PHOENIX, and A. C. WEEDON. Tetrahedron Lett. 4179 (1979); (*d*) W. ANDO, T. NAGASHIMA, K. SAITO, and S. KOHMOTO. J. Chem. Soc. Chem. Commun. 154 (1979); (*e*) L. E. MANRING, J. ERIKSEN, and C. S. FOOTE. J. Am. Chem. Soc. **102**, 4275 (1980); (*f*) L. T. SPADA and C. S. FOOTE. J. Am. Chem. Soc. **102**, 391 (1980); (*g*) A. P. SCHAAP, K. A. ZAKLIKA, B. KASKAR, and L. W. M. FUNG. J. Am. Chem. Soc. **102**, 389 (1980); (*h*) J. ERIKSEN and C. S. FOOTE. J. Am. Chem. Soc. **102**, 6083 (1980); (*i*) S. L. MATTES and S. FARID. J. Chem. Soc. Chem. Commun. 457 (1980); (*j*) J. E. MANRING, M. K. KRAMER, and C. S. FOOTE. J. Am. Chem. Soc. In press; (*k*) A. P. SCHAAP, L. LOPEZ, and S. D. GAGNON. J. Am. Chem. Soc. **105**, 663 (1983); (*l*) S. FUTAMURA, S. KUSUNOSE, H. OHTA, and Y. KAMIYA. J. Chem. Soc. Chem. Commun. 1223 (1982).
12. A. ALBINI and D. R. ARNOLD. Can. J. Chem. **56**, 2985 (1978).
13. S. S. HIXSON, J. BOYER, and C. GALLUCCI. J. Chem. Soc. Chem. Commun. 540 (1974).
14. T. HAMADA, A. NISHIDA, Y. MATSUMOTO, and O. YONEMITSU. J. Am. Chem. Soc. **102**, 3978 (1980).
15. (*a*) J. A. BARLTROP and R. J. OWERS. J. Chem. Soc. Commun. 1462 (1970); (*b*) J. A. BARLTROP. Pure Appl. Chem. **33**, 179 (1973).
16. (*a*) N. R. BERTONIERE and G. W. GRIFFIN. *In* Carbenes. Vol. I. *Edited by* M. Jones, Jr. and R. A. Moss. Wiley, New York. 1973. Chapt. 3. pp. 305–349; (*b*) G. W. GRIFFIN. Angew. Chem. **83**, 604 (1971); Angew. Chem. Int. Ed. Engl. **10**, 537 (1971); (*c*) H. KRISTINSSON and G. W. GRIFFIN. Angew. Chem. **77**, 859 (1965); Angew. Chem. Int. Ed. Engl. **4**, 868 (1965); (*d*) H. KRISTINSSON and G. W. GRIFFIN. J. Am. Chem. Soc. **88**, 1579 (1966); (*e*) P. C. PETRELLIS, H. DIETRICH, E. MEYER, and G. W. GRIFFIN. J. Am. Chem. Soc. **89**, 1967 (1967); (*f*) P. C. PETRELLIS and G. W. GRIFFIN. J. Chem. Soc. Chem. Commun. 691 (1967); (*g*) P. C. PETRELLIS and G. W. GRIFFIN. J. Chem. Soc. Chem. Commun. 1099 (1968); (*h*) A. M. TROZZOLO, W. A. YAGER, G. W. GRIFFIN, H. KRISTINSSON, and I. SARKAR. J. Am. Chem. Soc. **89**, 3357 (1967); (*i*) H. DIETRICH, G. W. GRIFFIN, and R. C. PETTERSON. Tetrahedron Lett. 153 (1968); (*j*) R. M. G. NAIR, E. MEYER, and G. W. GRIFFIN. Angew. Chem. **80**, 442 (1968); Angew. Chem. Int. Ed. Engl. **7**, 462 (1968); (*k*) R. S. BECKER, J. KOLC, R. O. BOST, H. DIETRICH, P. PETRELLIS, and G. W. GRIFFIN. J. Am. Chem. Soc. **90**, 3292 (1968); (*l*) R. S. BECKER, R. O. BOST, J. KOLC, N. R. BERTONIERE, R. SMITH, and G. W. GRIFFIN. J. Am. Chem. Soc. **92**, 1302 (1970); (*m*) T. DOMINH, A. M. TROZZOLO, and G. W. GRIFFIN. J. Am. Chem. Soc. **92**, 1402 (1970); (*n*) P. C. PETRELLIS, G. W. GRIFFIN, M. E. HENDRICK, and M. JONES, JR. J. Chem. Soc. Chem. Commun. 1002 (1972); (*o*) G. W. GRIFFIN, N. BRIGHTWELL, K. ISHIKAWA, I. LEV, and S. SATRA. VIII Int. Conf. Photochem., Edmonton, Alberta, Canada. August 7–13, 1975. Abstr. I–1; (*p*) J. P. WASACZ, M. M. JOULLIE, U. MENDE, I. FUSS, and G. W. GRIFFIN. J. Org. Chem. **41**, 572 (1976); (*q*) G. W. GRIFFIN, K. NISHIYAMA, H. TERASAWA, M. YAMAUCHI, J. WONG, A. J. MULLER, and L. KOLACZKOWSKI. Preprints, **24**, Division of Petroleum Chemistry, Inc., American Chemical Society; Washington, D.C. 1979. pp. 56–78.
17. (*a*) G. W. GRIFFIN, I. LEV, and K. ISHIKAWA. Vth IUPAC Symp. on Photochem., Enschede, the Netherlands. July 22–26, 1974. Contr. Paper No. 20, p. 62; (*b*) G. W. GRIFFIN and A. PADWA. *In* Photochemistry of Heterocyclic Compounds. *Edited by* O. Buchardt. Wiley, New York. 1976. Chapt. 2. pp. 41–122; (*c*) I. J. LEV, K. ISHIKAWA, N. S. BHACCA, and G. W. GRIFFIN. J. Chem. Soc. **98**, 5697 (1976); (*e*) K. ISHIKAWA, G. W. GRIFFIN, and I. J. LEV. J. Org. Chem. **41**, 3747 (1976); (*f*) G. W. GRIFFIN, K. NISHIYAMA, and K. ISHIKAWA. J. Org. Chem. **42**, 180 (1977); (*g*) K. NISHIYAMA, K. ISHIKAWA, I. SARKER, D. C. LANKIN, and G. W. GRIFFIN. Heterocycles, **6**, 1337 (1977); (*h*) C. E. GRIFFIN, E. KRAAS, H. TERASAWA, G. W. GRIFFIN, and D. C. LANKIN. J. Heterocycl. Chem. **15**, 523 (1978).
18. R. S. BECKER, L. EDWARDS, R. BOST, M. ELAM, and G. W. GRIFFIN. J. Am. Chem. Soc. **94**, 6584 (1972).
19. D. R. ARNOLD and A. J. MAROULIS. J. Am. Chem. Soc. **98**, 5931 (1976).
20. T. M. LESLIE. Ph.D. Dissertation, University of Notre Dame, Notre Dame, IN. 1980.
21. (*a*) K. YAMAGUCHI and T. FUENO. Chem. Phys. Lett. **22**, 471 (1973); (*b*) K. YAMAGUSHI. Chem. Phys. Lett. **33**, 330 (1975); (*c*) K. YAMAGUCHI, T. FUENO, A. NISHIO, and S. YABUSHITA. Chem. Lett. 1479 (1977); (*d*) K. N. HOUK, N. G. RONDAN, C. SANTIAGO, C. J. GALLO, R. W. GANDOUR, and G. W. GRIFFIN. J. Am. Chem. Soc. **102**, 1504 (1980); (*e*) Y. JEAN and F. VOLATRON. Chem. Phys. Lett. **83**, 91 (1981); (*f*) P. C. HIBERTY and C. LEFORSTIER. J. Am. Chem. Soc. **100**, 2012 (1978).
22. A. J. MULLER. Ph.D. Dissertation, University of New Orleans, New Orleans, LA. 1982.
23. (*a*) H. D. ROTH and M. L. M. SCHILLING. J. Am. Chem. Soc. **102**, 7956 (1980); (*b*) P. C. WONG and D. R. ARNOLD. Tetrahedron Lett. 2101 (1979).
24. S. K. CHATTOPADHYAY, P. K. DAS, and G. L. HUG. J. Am. Chem. Soc. **104**, 4507 (1982).
25. (*a*) R. D. SMALL, JR. and J. C. SCAIANO. J. Phys. Chem. **82**, 2662 (1978); (*b*) J. Phys. Chem. **81**, 828 (1977); **81**, 2126 (1977).
26. (*a*) N. V. RAGHAVAN, P. K. DAS, and K. BOBROWSKI. J. Am. Chem. Soc. **103**, 4569 (1981); (*b*) L. M. DORFMAN. Acc. Chem. Res. **3**, 224 (1970); (*c*) H. LEVANON, P. NETA, and A. M. TROZZOLO. Chem. Phys. Lett. **54**, 181 (1978).
27. S. FARID and K. A. BROWN. J. Chem. Soc. Chem. Commun. 564 (1976).
28. M. S. KHARASCH, A. FONO, and W. NUDENBERG. J. Org. Chem. **16**, 105 (1951).
29. (*a*) G. W. GRIFFIN, E. J. O'CONNELL, and H. A. HAMMOND. J. Am. Chem. Soc. **85**, 1001 (1963); (*b*) G. W. GRIFFIN and E. J. O'CONNEL. J. Am. Chem. Soc. **84**, 4148 (1962); (*c*) H. E. ZIMMERMAN and V. J. HULL. J. Am. Chem. Soc. **92**, 6515 (1970).
30. V. PRELOG and G. HELMCHEN. Angew. Chem. Int. Ed. Engl. **21**, 567 (1982).
31. J. W. TIMBERLAKE and M. L. HODGES. Tetrahedron Lett. 4147 (1970).
32. J. H. STOCKER and D. H. KERN. J. Org. Chem. **35**, 1708 (1970).
33. G. E. HARTZELL and E. S. HUSYER. J. Org. Chem. **29**, 3341 (1964).
34. G. E. HARTZELL, C. J. BREDEWEG, and B. LOY. J. Org. Chem. **30**, 3119 (1965).
35. (*a*) K. ONODERA, H. SAKURAGI, and K. TOKUMARU. Tetrahedron

Lett. **21**, 2831 (1980); (*b*) M. KOJIMA, H. SAKURAGI, and K. TOKUMARU. Tetrahedron Lett. **22**, 2889 (1981).
36. UV atlas of organic compounds. Vol. III. Plenum Press, New York. 1967. p. E1/16.
37. S. L. MUROV. Handbook of photochemistry. Marcel Dekker, Inc., New York. 1973.
38. S. L. MUROV. Ph.D. Thesis, University of Chicago, Chicago, IL. 1966.
39. A. P. MARCHETTI and D. R. KEARNS. J. Am. Chem. Soc. **89**, 768 (1967).
40. (*a*) A. R. HORROCKS and F. WILKINSON. Proc. R. Soc. London, Ser. A, **306**, 257 (1968); (*b*) T. MEDINGER and F. WILKINSON. Trans. Faraday Soc. **61**, 620 (1965).
41. C. A. PARKER and T. A. JOYCE. Chem. Commun. 108 (1966); C. A. PARKER and T. A. JOYCE. Trans. Faraday Soc. **62**, 2785 (1966).
42. (*a*) K. MISLOW, S. HYDEN, and H. SCHAEFER. J. Am. Chem. Soc. **84**, 1449 (1962); (*b*) R. N. JONES. J. Am. Chem. Soc. **67**, 2127 (1945); (*c*) J. Am. Chem. Soc. **63**, 1658 (1941).
43. (*a*) L. STELLA, Z. JANOUSEK, R. MERENYI, and H. G. VIEHE. Angew. Chem. Int. Ed. Engl. **17**, 691 (1978); (*b*) R. W. BALDCOCK, P. HUDSON, A. R. KATRIZKY, and F. SOTI. J. Chem. Soc. Perkin Trans. 1, 1422 (1974); (*c*) A. T. BALABAN. Rev. Roum. Chim. **16**, 725 (1971); (*d*) A. T. BALABAN *et al.* Tetrahedron, **33**, 2249 (1977).
44. F. SACHS and H. BARSCHALL. Chem. Ber. **35**, 1437 (1902); W. HAENSEL. Justus Liebigs Ann. Chem. 1380 (1976).
45. D. D. PERRIN and W. L. ARMAREGO. Purification of laboratory chemicals. Pergamon Press; London. 1966.
46. (*a*) E. C. HORNING. Org. Synth. Coll. Vol. 3. John Wiley and Sons, Inc., New York. 1965. p. 631; (*b*) D. R. ARNOLD and A. J. MAROULIS. J. Am. Chem. Soc. **98**, 5931 (1976); (*c*) W. S. TSANG, G. W. GRIFFIN, M. G. HORNING, and W. G. STILLWELL. J. Org. Chem. **47**, 5339 (1982).
47. A. LAPWORTH and J. B. SHOESMITH. J. Chem. Soc. 1391 (1922).
48. W. S. TRAHANOVSKY and D. W. BRIXIUS. J. Am. Chem. Soc. **95**, 6778 (1973).
49. N. ONO, S. KAWAI, K. TANAKA, and A. KAJI. Tetrahedron Lett. 1733 (1979).
50. R. N. MCDONALD and T. W. CAMPBELL. J.Org. Chem. **24**, 1969 (1959).
51. J. W. TIMBERLAKE, J. ALENDER, A. W. GARNER, M. L. HODGES, C. OZMERAL, S. SZILAGYI, and J. O. JACOBUS. J. Org. Chem. **46**, 2082 (1981).
52. M. S. KHARASCH, H. C. MCBAY, and W. H. URRY. J. Org. Chem. **10**, 401 (1945).
53. R. G. GILLIS. Tetrahedron Lett. 1413 (1968).
54. (*a*) W. A. MOSHER and N. D. HEINDEL. J. Org. Chem. **28**, 2154 (1963); (*b*) J. H. STOCKER, P. SIDISUNTHORN, B. M. BENJAMIN, and C. J. COLLINS. J. Am. Chem. Soc. **82**, 3913 (1960).
55. D. J. CRAM and K. P. KOPECKY. J. Am. Chem. Soc. **81**, 2748 (1959).
56. J. GRIMSHAW and J. S. RAMSEY. J. Chem. Soc. C, 653 (1966).
57. E. BERGMAN and S. FUJISE. Ann. **483**, 65 (1930).
58. D. F. TAVARES and J. P. BORGER. Can. J. Chem. **44**, 1323 (1966).
59. D. M. HALL, J. E. LADBURY, M. S. LESSLIE, and E. E. TURNER. J. Chem. Soc. 3475 (1956).
60. (*a*) T. A. GEISSMAN and L. MORRIS. J. Am. Chem. Soc. **66**, 716 (1944); (*b*) H. O. HOUSE, R. C. STRICKLAND, and E. J. ZAIKO. J. Org. Chem. **41**, 240 (1976).
61. A. MUSTAFA, W. ASKER, A. H. HARHASH, and N. A. L. KASSAB. Tetrahedron, **19**, 1577 (1963).

Can. J. Chem. Downloaded from www.nrcresearchpress.com by 210.87.254.6 on 09/06/12
For personal use only.

A new glucosinolate synthesis

THOMAS H. KELLER, LOIS J. YELLAND, AND M. H. BENN
Chemistry Department, The University, Calgary, Alta., Canada T2N 1N4

Received July 25, 1983

THOMAS H. KELLER, LOIS J. YELLAND, and M. H. BENN. Can. J. Chem. **62**, 437 (1984).

The *tert*-butyldimethylsilyl nitronate derived from 1-nitropropane was condensed with 2,3,4,6-tetra-*O*-acetyl-β-D-glucopyranosylthiol to yield two geometrically isomeric thiohydroximates; the Z-isomeric form was then converted by conventional procedures into potassium ethylglucosinolate ("glucolepidiin").

THOMAS H. KELLER, LOIS J. YELLAND et M. H. BENN. Can. J. Chem. **62**, 437 (1984).

La condensation du nitronate de *tert*-butyldiméthylsilyle, provenant du nitro-1 propane, sur le tétra-*O*-acétyl-2,3,4,6 β-D-glucopyrannosylthiol conduit à deux isomères géométriques thiohydroximates; on a transformé l'isomère Z à l'aide de méthodes conventionnelles, en éthylglucosinolate de potassium ("glucolépidiin").

Some years ago Copenhaver (1) recorded the preparation of some thiohydroximates (**1**) by means of a base-induced condensation of primary nitroalkanes with thiols (eq. [1]).

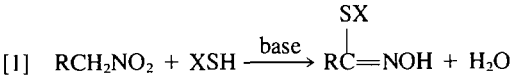

[1] $RCH_2NO_2 + XSH \xrightarrow{base} \underset{\displaystyle SX}{\underset{|}{RC}}{=}NOH + H_2O$

1

We thought of using this reaction to make glucosinolates, a compact group of naturally occurring thiohydroximate derivatives characterized by the structure **2** (2).

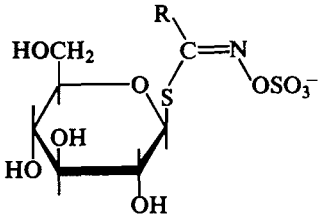

2

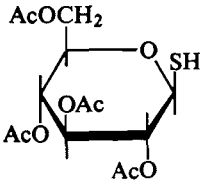

3

Our idea was to condense a primary nitroalkane with 2,3,4,6-tetra-*O*-acetyl-β-D-glucopyranosylthiol (**3**) to provide the corresponding thiohydroximate (**1**, X = tetraacetyl-β-D-glucopyranosyl) which could then be converted to **2** by established procedures involving sulphonation and subsequent deacetylation (3). However, in its original form, the Copenhaver reaction did not seem well suited to our purpose since the drastic conditions employed (refluxing tributylamine, or hot aqueous solutions containing alkali metal hydroxide) were unlikely to be compatible with **3**. This supposition was borne out by experiments: the reaction of 1-nitropropane with tetraacetyl-β-D-glucosylthiol under "typical" Copenhaver conditions yielded only small amounts of the desired thiohydroximate (detected by tlc), and much tarry material. Milder conditions were also unpromising.

As shown in Scheme 1, a plausible mechanism for the Copenhaver reaction involves the intermediacy of an *aci*-nitroalkane, or nitronate anion (4).

With this in mind, we decided to try modifying the Copenhaver reaction by replacing the nitroalkane with a nitronate. For this purpose we selected the trialkylsilyl derivatives (**4**), which are relatively readily available (5). What follows is

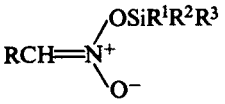

4

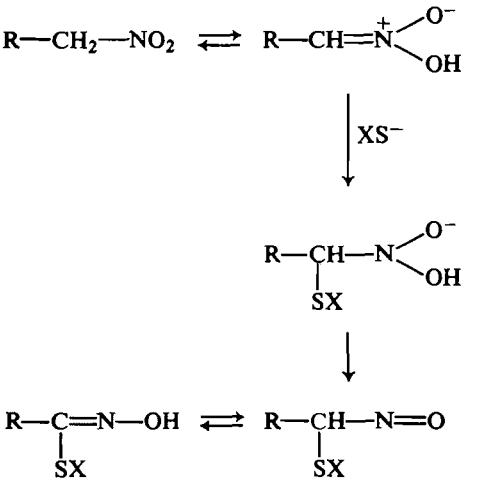

SCHEME 1. A possible mechanism for the Copenhaver reaction.

an account of our experiences with the use of the *tert*-butyldimethylsilyl nitronate **5** (**4**, R = Et, $R^1 = R^2 = Me$, R^3 = *t*-Bu) derived from 1-nitropropane for the synthesis of potassium ethylglucosinolate ("glucolepidiin"), the putative parent of ethyl isothiocyanate formed by *Lepidium menziesii* DC (6).

As outlined in Scheme 2, the slow addition of the trialkylsilyl nitronate **5** to a solution of equimolar amounts of tetraacetyl-β-D-glucopyranosylthiol and triethylamine in tetrahydrofuran, at room temperature, afforded two thiohydroximates. These were separated by flash chromatography, and obtained as homogeneous crystalline solids **6***a* (28%) and **6***b* (56%). Complete characterization of these isomers by spectroscopic methods and combustion analyses established their relationship as a pair of geometric isomers. The reaction of nitrile oxides (generated *in situ* from hydroxamoyl halides and triethylamine) with thiols affords *Z*-thiohydroximates (7), and authentic **6***b* was thus prepared from **3** and **7**. (It may be noted that this observation excludes the intermediacy of a nitrile oxide intermediate in the formation of the thiohydroximates from the silyl nitronates; i.e., if the mechanism of that reaction involved eliminative loss of silanol to generate a nitrile oxide which then reacted with thiolate to give the thiohydroximate, **6***b* would be the product formed.)

The *E*-isomer **6***a* was indefinitely stable in the crystalline form in the dark at 0°C, but underwent slow thermal or photochemical isomerization to **6***b* in solution.

It is known that there is rapid O → O migration of the silyl group in trialkylsilyl nitronates (5), and this may be invoked to

Can. J. Chem. Downloaded from www.nrcresearchpress.com by 210.87.254.6 on 09/06/12
For personal use only.

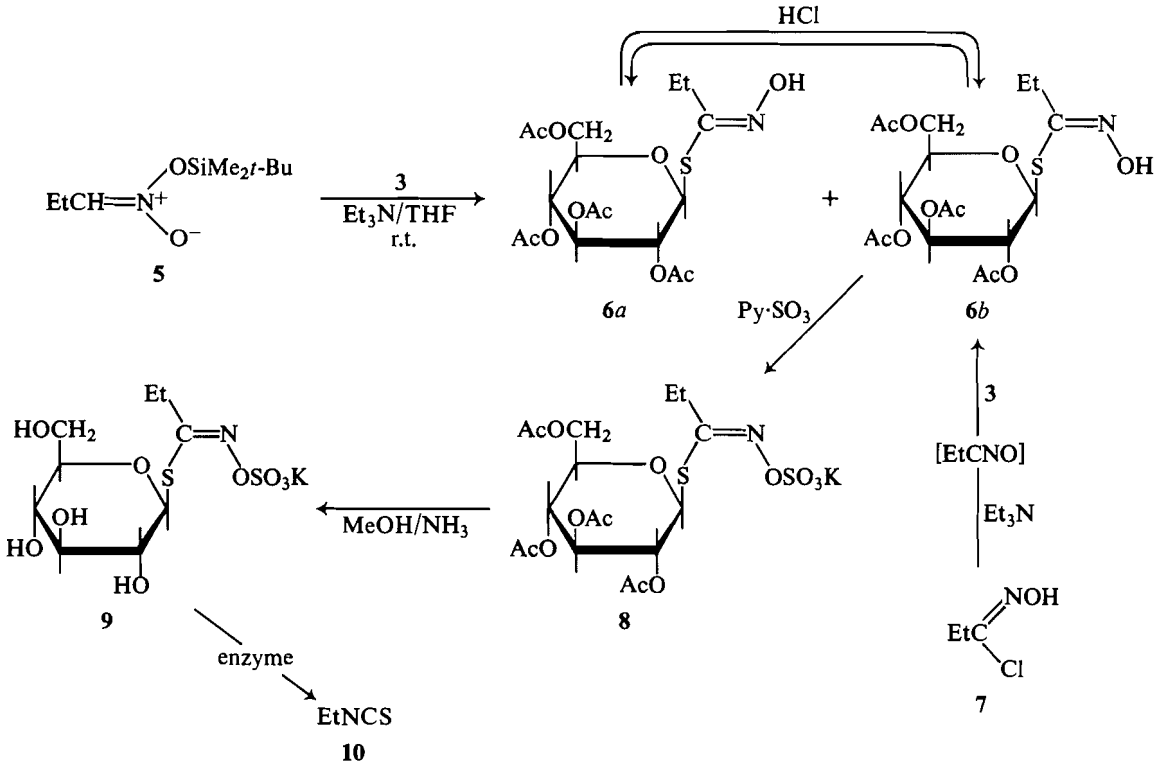

SCHEME 2. The silylnitronate route to ethylglucosinolate.

provide a rationalization for the formation from **3** and **5** of **6***a* and **6***b* in comparable amounts (Scheme 3).

The success of our modification of the Copenhaver reaction was pleasing: we had had some worries that although the thiolate nucleophile was soft, and the Si—S bond weak (8), it might attack at silicon rather than carbon, leading to desilylation and regeneration of the nitroalkane.

The formation of both geometrical isomers of the thiohydroximate, although at first sight inconvenient since only one of these (**6***b*) has the requisite stereochemistry for conversion to the natural (*Z*)-glucosinolates, was not unwelcome. Apart from the fact that the *E*-isomer can be isomerized to the *Z*-form, and then utilized for glucosinolate synthesis, there has been considerable speculation on the catabolic consequences of changing the configuration of glucosinolates from *Z* to *E* (9, 10), but no direct experimental tests of these hypotheses. Although geometrically isomeric pairs of *S*-alkyl thiohydroximates have been made before, usually via photoequilibration of the *Z*-isomer (11), no *E*-glucosinolates have been prepared. (Photolysis of an indolylglucosinolate has been reported to lead to extensive decomposition (12), and our own, unpublished, attempts to achieve the photoisomerization of *E*-**1** (R = $PhCH_2$, X = tetraacetyl-β-D-glucopyranosyl) were unsuccessful.[1]) Thus it appears likely that our modified Copenhaver reaction will make the "unnatural" *E*-glucosinolates accessible, for the first time.

Sulphonation of **6***b* with pyridine – sulphur trioxide and subsequent treatment with potassium hydrogen carbonate gave the nicely crystalline potassium tetraacetylethylglucosinolate (**8**), which was then deacetylated with methanolic ammonia to afford potassium ethylglucosinolate **9** as an amorphous, but homogeneous, solid whose spectroscopic and analytical properties were in accord with expectation. When an aqueous solution of **9** was stirred with white mustard seed flour, ethyl isothiocyanate **10** was released, demonstrating that ethylglucosinolate can indeed function as a source of that mustard oil.

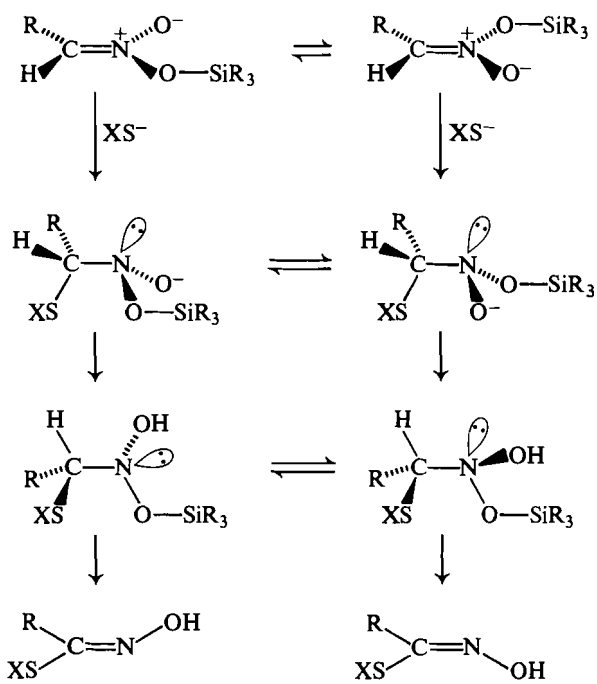

SCHEME 3. *E*- and *Z*-thiohydroximates from silylnitronates.

Experimental

The instruments and operating conditions were as previously described (13). In the ^{13}C nmr spectrum of **8**, methanol (δ = 49.0) was used as an internal reference.

[1]P. K. Oommen and M. H. Benn, unpublished results.

Can. J. Chem. Downloaded from www.nrcresearchpress.com by 210.87.254.6 on 09/06/12
For personal use only.

Can. J. Chem. Downloaded from www.nrcresearchpress.com by 210.87.254.6 on 09/06/12
For personal use only.

The tert-*butyldimethylsilyl ester of* aci-*1-nitropropane (5)*

To a stirred solution of diisopropylamine (3.03 g, 30 mmol) in dry THF (70 mL), at −78°C, under an atmosphere of dry nitrogen, was added a solution of butyllithium in hexane (1.0 *M*, 30 mL, 30 mmol). After the addition was complete, the cooling bath was removed and the mixture stirred for 30 min. The reaction mixture was then again cooled to −78°C, and 1-nitropropane (2.5 g, 28 mmol) was added. This yielded a gel which was kept at −78°C for a further 30 min. To this, at the same temperature, was then added a solution of *tert*-butyldimethylsilyl chloride (4.82 g, 32 mmol) in dry THF (10 mL) and the mixture was stirred for 30 min.

The cooling bath was removed and the mixture was allowed to warm to room temperature and stirred overnight. The stirrer-bar was then removed and the reaction mixture concentrated at room temperature (rotatory evaporator) under reduced pressure (oil pump, ca. 15 Torr) to a semi-solid residue. This material was suspended in dry pentane (100 mL) and filtered through a Celite pad. The reaction flask and filter were washed with dry pentane (4 × 20 mL). Removal of solvent from the combined filtrate and washings (room temperature, ca. 0.1 Torr) left a residual orange liquid which was purified by bulb-to-bulb distillation (48°C, 0.03 Torr) to yield **5** as a colourless oil (4.0 g, 70%); ν_{max} (film): 3100 (w), 1615 (s), 1250 (s), 1110 (s), 835 (vs), and 790 (s) cm^{-1}; ^1H nmr ($CDCl_3$) δ: 0.25 (6H, s), 0.89 (9H, s), 1.05 (3H, t, J = 7 Hz), 2.21 (2H, q, J = 7 Hz), and 5.95 (1H, t, J = 7 Hz).

The preparation of S-*(2',3,4',6'-tetra-*O*-acetyl-*β*-D-glucopyranosyl)-propiothioydroximates, **6**a and **6**b*

(a) *From preformed* tert-*butyldimethylsilyl nitronate **5***

A solution of the *tert*-butyldimethylsilyl nitronate **5** (1.02 g, 5 mmol) in dry THF (10 mL) was added dropwise, under an atmosphere of dry nitrogen, over 12 h and at room temperature, to a solution of 2,3,4,6-tetra-*O*-acetyl-β-D-glucopyranosylthiol (1.82 g, 5 mmol) and triethylamine (0.5 g, 5 mmol) in dry THF (30 mL). The reaction mixture was concentrated (<40°C; aspirator, ca. 15 Torr) to a semi-solid residue which was then kept under high vacuum (ca. 0.1 Torr) for 1 h to remove *tert*-butyldimethylsilanol, after which it was subjected to flash chromatography (Merck silica gel 60, with hexane − ethyl acetate 1:1 v/v as eluant). This afforded **6***a* and **6***b* as colourless crystalline solids. After recrystallization from hexane − ethyl acetate, **6***a* had mp 134−135°C; $[\alpha]_D$ +8.4° (*c* 1.0, $CHCl_3$); ^1H nmr ($CDCl_3$) δ: 1.15 (3H, t, J = 7 Hz), 2.01, 2.02, 2.05, and 2.07 (4 × 3H, s), 2.48 (1H, dq, J = 7 and 16 Hz), 2.61 (1H, dq, J = 7 and 16 Hz), 3.77 (1H, ddd, J = 9, 4, and 2 Hz), 4.15 (1H, dd, J = 12.5 and 2 Hz), 4.32 (1H, dd, J = 12.5 and 4 Hz), 5.2 (4H, m), and 8.22 (1H, s); ^{13}C nmr ($CDCl_3$) δ: 10.4 (q), 20.6 (q, $4CH_3$), 24.1 (t), 61.8 (t), 68.0 (d), 69.5 (d), 73.9 (d), 75.9 (d), 81.1 (d), 158.3 (s), 169.4 (s, 2C=O), 170.2 (s), and 170.7 (s). *Anal.* calcd. for $C_{17}H_{25}NO_{10}S$: C 46.89, H 5.79, N 3.22; found: C 47.21, H 5.82, N 3.29%. The yield of **6***a* was 28% (0.61 g). Similarly, **6***b* had mp 155−156°C; $[\alpha]_D$ −16.4° (*c* 1.0, $CHCl_3$); ^1H nmr ($CDCl_3$) δ: 1.22 (3H, t, J = 7 Hz), 2.02, 2.04, 2.05, and 2.07 (4 × 3H, s), 2.54 (1H, dq, J = 7 and 16 Hz), 2.67 (1H, dq, J = 7 and 16 Hz), 3.75 (1H, ddd, J = 9, 5, and 3 Hz), 4.15 (2H, m), 5.0−5.4 (4H, m), and 8.18 (1H, bs); ^{13}C nmr ($CDCl_3$) δ: 11.7 (q), 20.6 (q, $4CH_3$), 26.1 (t), 62.3 (t), 68.2 (d), 70.2 (d), 73.8 (d), 76.0 (d), 79.9 (d), 154.4 (s), 169.2 (s), 169.4 (s), 170.2 (s), and 170.5 (s). *Anal.* calcd. for $C_{17}H_{25}NO_{10}S$: C 46.89, H 5.79, N 3.22; found: C 46.65, H 5.83, N 3.10%. The yield of **6***b* was 56% (1.23 g).

(b) *From propanaldoxime*

A slow stream of chlorine gas was passed into a solution of propanaldoxime (6.2 g, 50 mmol) in dry Et_2O (250 mL), cooled in an ice−salt bath, for 1 h. Excess chlorine and some Et_2O were then removed under aspirator vacuum until the solution changed colour from green to blue. To this was then added a solution of tetraacetyl-β-D-glucopyranosylthiol (5 g, 14 mmol) in EtOH (10 mL) and Et_2O (200 mL) followed, with swirling, by a solution of triethylamine (15 mL, 100 mmol) in Et_2O (15 mL). The reaction mixture was kept at room temperature for 30 min, then poured into 1.5 *M* aqueous H_2SO_4 (300 mL) and ice. After shaking this mixture, the Et_2O phase was separated, washed with more 1.5 *M* aqueous H_2SO_4 (100 mL), then H_2O (100 mL), dried ($MgSO_4$), and evaporated to a crystalline residue. This material was recrystallized from ethanol−hexane to provide **6***b*, mp 156°C (2.0 g, 34%), identical in all respects with **6***b* prepared as in (a).

*Interconversion of **6**a and **6**b*

When a solution of **6***a* in $CHCl_3$ was kept in a 5-mm ^1H-nmr tube, in sunlight, slow isomerization occurred to produce **6***b*. Attempts to accelerate this process by uv irradiation resulted in extensive decomposition. If a trace of HCl was added to a $CHCl_3$ solution of **6***a* or **6***b*, an equilibrium mixture of the two isomers was attained within 1 h, at room temperature, 3:7 **6***a*/**6***b* as revealed by ^1H and ^{13}C nmr and tlc.

Potassium tetraacetylethylglucosinolate (8)

Freshly prepared pyridine−SO_3 complex (0.9 g, 5.6 mmol) was added to a solution of **6***b* (1.8 g, 4 mmol) in dry pyridine (ca. 35 mL). This mixture was stirred at room temperature for 48 h, then poured in H_2O (250 mL) containing $KHCO_3$ (1.7 g, 7 mmol). The mixture was filtered and then extracted with Et_2O (2 × 200 mL). The aqueous phase was then freeze-dried. The residue so obtained was then extracted with boiling 95% (v/v) aqueous EtOH and filtered hot. The filtrate was chilled to 0°C and the crystalline precipitate which separated was collected and recrystallized from 95% EtOH to yield a product, mp 205−207°C (dec.) (1.9 g, 98%); $[\alpha]_D$ −18.6° (*c* 1.0, H_2O); ^1H nmr (DMSO-d_6) δ: 1.14 (3H, t, J = 7 Hz), 1.96, 2.00, 2.01, and 2.02 (4 × 3H, s), 2.65 (2H, q, J = 7 Hz), 4.1 (3H, m), 4.92 (1H, dd, J = 9 Hz), 5.5 (1H, dd, J = 9 Hz), 5.8 (1H, d, J = 9 Hz); ^{13}C nmr (D_2O) δ: 11.4 (q), 20.0 (4 × CH_3, q), 26.2 (t), 62.1 (t), 68.1 (d), 70.1 (d), 74.0 (d), 75.2 (d), 79.4 (d), 163.8 (s), 172.3 (s), 172.6 (s), 173.0 (s), and 173.6 (s). *Anal.* calcd. for $C_{17}H_{24}NO_{13}S_2K$: C 36.88, H 4.37, N 2.53; found: C 36.91, H 4.42, N 2.43%.

Potassium ethylglucosinolate (9)

Potassium tetraacetylethylglucosinolate (200 mg, 0.6 mmol) was dissolved in dry MeOH (15 mL) saturated with NH_3. The solution was stirred overnight at room temprature, then evaporated to dryness (aspirator vacuum, <40°C) and the residue extracted with $CHCl_3$ (30 mL). The residue was dissolved in methanol, the solution so obtained was evaporated to dryness as before, and the residue again extracted with $CHCl_3$ (30 mL). This process was repeated once more and the glassy $CHCl_3$-insoluble residue thus obtained was then dissolved in water (ca. 3 mL), and the solution freeze-dried to yield **9** as an amorphous white powder (120 mg, 86%); $[\alpha]_D$ −20.5° (*c* 0.6, H_2O); ^1H nmr (D_2O) δ: 1.25 (3H, t, J = 7.4 Hz), 2.74 (2H, q, J = 7.4 Hz), 3.40−4.0 (6H, m), and 5.01 (1H, d, J = 9.4 Hz); ^{13}C nmr (D_2O) δ: 11.5 (q), 26.1 (t), 60.7 (t), 69.2 (d), 72.0 (d), 77.2 (d), 80.0 (d), 81.7 (d) and 165.0 (s). *Anal.* calcd. for $C_9H_{18}NO_9SK$: C 28.04, H 4.18, N 3.63; found: C 27.85, H 4.39, N 3.41%. This material was homogeneous by tlc (on Merck silica gel 60-F254, using n-PrOH − EtOAc−H_2O (7:1:2 v/v) as the solvent system) (ref. 14); R_f 0.53; under these conditions potassium allylglucosinolate had R_f 0.61.

Enzymatic cleavage of ethylglucosinolate

To a solution of **9** (50 mg, 0.13 mmol) in phosphate buffer (3 mL, pH 6.7) was added white mustard seed flour (20 mg, prepared by pulverizing the seeds, and then regrinding the flour in hexane to remove fats, after which it was air-dried at room temperature). This mixture was cooled in an ice bath, and stirred for 1 h, after which Et_2O (3 mL) was added. Gas chromatographic and gc−ms analyses (on 3% OV-17 at 65°C) of the Et_2O phase revealed the presence of ethyl isothiocyanate (identical R_t and fragmentation pattern as an authentic reference specimen). The Et_2O layer was separated, dried ($MgSO_4$), and aniline (5 drops) added. After 48 h the Et_2O solution was washed with 1 *M* aqueous HCl (1 mL), dried ($MgSO_4$), and evaporated. The residue recrystallized from EtOH−hexane yielded crystals (5 mg), mp 105−107°C, with an ir spectrum superimposable upon that of an authentic specimen of *N*-ethyl-*N'*-phenylthiourea, mp 105−107°C, prepared from ethyl isothiocyanate and aniline.

Acknowledgements

Financial support of this work was provided by grants-in-aid from the National Research Council and the Natural Sciences and Engineering Research Council of Canada. One of us (T.K.) is indebted to the Alberta Heritage Foundation for Medical Research for a scholarship.

1. J. W. COPENHAVER. U.S. Patent 2,786,965 (1954); Chem. Abstr. **51**, 13920 (1957); J. B. BUCHANAN. Fr. Patent 1,573,102 (1969). Chem. Abstr. **72**, 100,080 (1970).
2. E. W. UNDERHILL. *In* Secondary plant products. *Edited by* E. A. Bell and B. V. Charlwood. Springer Verlag, Berlin. 1980. p. 493, and references therein.
3. (*a*) M. G. ETTLINGER and A. J. LUNDEEN. J. Am. Chem. Soc. **79**, 1764 (1957); (*b*) M. H. BENN. Can. J. Chem. **42**, 163 (1964).
4. M. G. ETTLINGER and A. KJAER. *In* Advances in phytochemistry. Vol. 1. *Edited by* T. J. Mabry, R. E. Alston, and V. C. Runeckles. Appleton–Century–Crofts, New York. 1968. p. 60.
5. E. W. COLVIN, A. K. BECK, B. BASTANI, D. SEEBACH, Y. KAI, and J. D. DUNITZ. Helv. Chim. Acta, **63**, 697 (1980).
6. A. KJAER and I. LARSEN. Acta Chem. Scand. **8**, 699 (1954).
7. M. H. BENN. Can. J. Chem. **42**, 2393 (1964).
8. E. COLVIN. Silicon in organic synthesis. Butterworths, London. 1981. p. 4.
9. M. H. BENN. Pure Appl. Chem. **49**, 197 (1977).
10. X. HASAPIS and A. J. MACLEOD. Phytochemistry, **21**, 1009 (1982).
11. J. H. DAVIES, R. H. DAVIS, and P. KIRBY. J. Chem. Soc. (C), 431 (1968).
12. N. MICHAJLOVSKIJ. Experientia, **24**, 223 (1968).
13. H. RÜEGER and M. H. BENN. Can. J. Chem. **60**, 2918 (1982).
14. M. MATSUO. J. Chromatogr. **49**, 323 (1970).

Can. J. Chem. Downloaded from www.nrcresearchpress.com by 210.87.254.6 on 09/06/12
For personal use only.

Quantitative IR-ATR spectrometry of asbestos fibers on membrane filters

F. M. KIMMERLE,[1] LUC NOËL, AND JALEH KHORAMI

Programme de Recherche sur l'Amiante, Université de Sherbrooke, Sherbrooke, (Qué.), Canada J1K 2R1

Received April 11, 1983

F. M. KIMMERLE, L. NOËL, and J. KHORAMI. Can. J. Chem. **62**, 441 (1984).

We have developed a new IR-ATR spectroscopic technique for the identification and quantification of fibers collected on PVC filters. This nondestructive method has a detection limit of about 10 μg, involves no sample preparation, and is relatively insensitive to nonserpentine dusts normally associated with the asbestos mining and milling industries.

An analysis of the ATR phenomena for a fiber matt indicates that the logarithmic ratio of the reflectivity varies with the surface concentration C as:

$$\log \frac{R_0}{R} = A\alpha \frac{C_S}{2r} \lambda \left[1 - \exp\left(-\frac{7.2rC}{\lambda}\right)\right]$$

where C_S is the concentration for a monolayer of fiber, r the mean fiber diameter. Thus, the absorption should reach a plateau when a sufficient thickness is obtained, and this nonlinear region should be attained at lower wavelength, and at lower concentrations for long fibers having a high aspect ratio. We further predict that the relative absorption $A(\lambda_1)/A(\lambda_2)$ where $\lambda_1 < \lambda_2$, should decrease with fiber dimension.

The ATR signal at 303 cm^{-1}, corresponding to a lattice vibration, varies linearly with fiber concentration up to 100 $\mu g/cm^2$, whereas the intensity of this band relative to the OH stretching band at 3690 cm^{-1} is a monotonic function, representing the fiber morphology. Dust levels and fiber morphology established from the IR-ATR spectroscopy are consistent with measurements by light and electron microscopy.

F. M. KIMMERLE, L. NOËL et J. KHORAMI. Can. J. Chem. **62**, 441 (1984).

Nous avons développé une nouvelle technique par spectroscopie IR-ATR pour l'identification et la quantification des fibres collectées sur des membranes de PVC. Cette méthode est non destructive, la limite de détection se situe vers les 10 μg et les échantillons ne requièrent aucun traitement. De plus, la présence de poussière autre que celle du groupe de la serpentine associée à l'amiante ne semble pas être un obstacle pour les mines et les industries.

Une analyse du phénomène ATR pour un certain recouvrement de fibres indique que le rapport logarithmique de la réflectivité varie avec la concentration à la surface C tel que:

$$\log \frac{R_0}{R} = A\alpha \frac{C_S}{2r} \lambda \left[1 - \exp\left(-\frac{7.2rC}{\lambda}\right)\right]$$

où C_S est la concentration pour une monocouche de fibre et r le diamètre moyen de la fibre. Pour une concentration de surface suffisante, un plateau sera obtenu plus rapidement pour les courtes longueurs d'ondes et pour les fibres ayant un rapport longueur/diamètre élevé. Nous pouvons prédire que l'absorption relative $A(\lambda_1)/A(\lambda_2)$, où $\lambda_1 < \lambda_2$, doit diminuer en fonction de la dimension des fibres.

Le signal ATR à 303 cm^{-1}, caractéristique de la vibration de la maille cristalline, varie linéairement avec une concentration de 100 $\mu g/cm^2$ de fibres tandis que les rapports des bandes d'absorption de 303 cm^{-1}/3690 cm^{-1} (3690 cm^{-1} = vibration OH) nous donnent plutôt une fonction monotone représentative de la morphologie des fibres.

Les niveaux d'empoussiérage et la morphologie moyenne des fibres peuvent être établis par ATR, et les résultats sont compatibles avec ceux de la microscopie optique et de la microscopie électronique.

Introduction

The accepted analytical technique for asbestos fiber control in the workplace or the environment has traditionally involved fiber counting by phase contrast light microscopy and, more recently, by electron microscopy (TEM and SEM) (1). X-ray diffraction of air samples collected on membrane filters has been variously proposed (2–4), but IR analysis has not found very wide acceptance. It has been shown to be sufficiently sensitive (detection limit 10–20 μg) to monitor present legal dust levels (5, 6), but suffers from three apparent drawbacks. The possible interference due to other airborne pollutants is not well established, the IR signal will respond to fibrous and nonfibrous serpentine materials, and the sample preparation has been relatively tedious since it was felt necessary to incorporate the fibers collected on a membrane filter in a KBr disk prior to IR analysis.

The IR spectra of chrysotile asbestos and related materials are well known (7) although accurate wavelength tabulations are relatively scarce (8), particularly those below $\bar{\nu}$ = 500 cm^{-1}.

Coates (9) recently examined the IR spectra of various asbestos varieties and proposed a classification scheme which would allow the identification of amphibole and serpentine materials. The sharp peak of the hydroxyl doublet at 3690 cm^{-1} has been used traditionally (6, 10–12) for quantitative analysis of chrysotile asbestos, although it was not always adequately resolved from the asymmetric OH vibration at 3646 cm^{-1}. The silicate triplet (ν_{as}(Si—O—Si) at 1080 cm^{-1}, ν_{Si-O} at 1020 cm^{-1}, and ν_{Si-O} at 945 cm^{-1}) constitutes by far the most prominent feature of the IR spectra (13), but overlaps the major, broad bands of all silicate materials, including quartz, to such an extent that it becomes practically useless. Flick (14) suggested that several peaks should be examined to minimize interferences. Luce (15) confirmed Brindley and Zussmanns' (10) observation that the fibrous chrysotile could be distinguished from the host rock, antigorite, which lacks the central silicate bond.

Typically, chrysotile fibers were collected as for microscopy examination (11), on a 47 mm diameter Millipore membrane,

[1] Present address: Laboratoire de Recherche appliquée et Centre de génie expérimental, Alcan International, Jonquière, Québec.

Can. J. Chem. Downloaded from www.nrcresearchpress.com by 210.87.254.5 on 09/06/12
For personal use only.

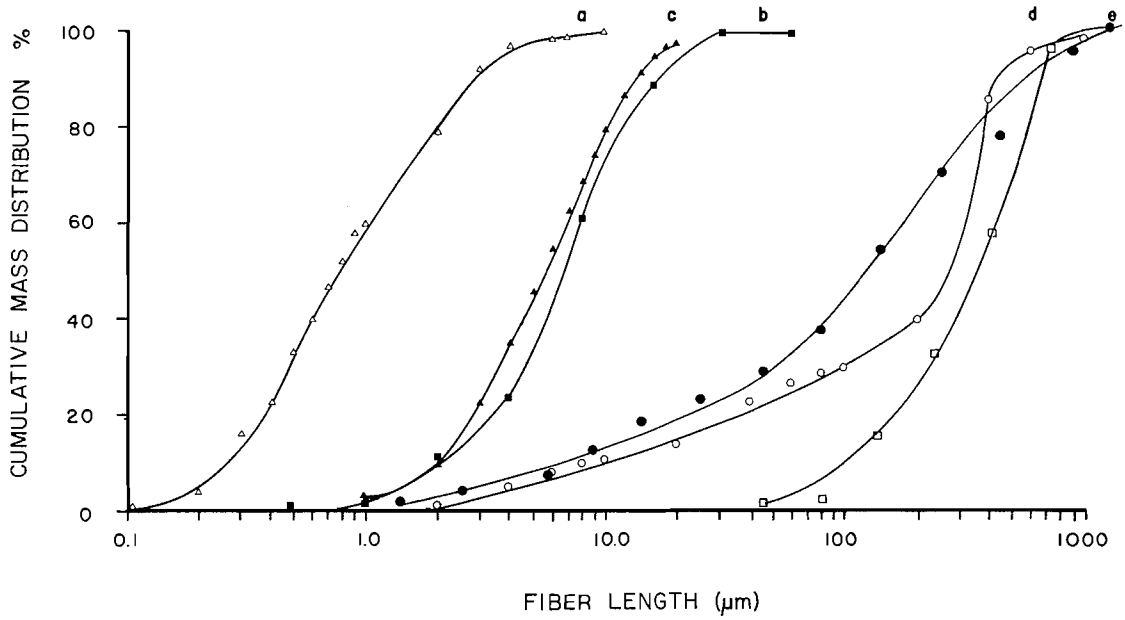

FIG. 1. Distribution of fibers length by optical microscopy, transmission electronic microscopy, and scanning electronic microscopy (OM, SEM, TEM): (*a*) very short fiber (19) △ = TEM; (*b*) UICC-B chrysotile (18) ■ = OM; (*c*) Calidria COF-25 (16) ▲ = SEM; (*d*) Plastibest #20 (16) ● = SEM and (22) ○ = OM; (*e*) Paperbestos #3 (20, 22) □ = OM.

TABLE 1. Morphology of reference fibers

Parameter	Value				
	Very short chrysotile	UICC-B Chrysotile	Calidria COF-25	Plastibest #20	−35 + 200 Paperbestos #3
Specific surface ($m^2\ g^{-1}$)	37.7	24.3	55.4	14.2	12.9
Average fiber diameter (nm)	41.8	72.2	28.4	111	122
Mean fiber length (μm)	0.8	11.6	8.0	100	370
Aspect ratio	19	160	280	910	3025
C_S^a ($\mu g\ cm^{-2}$)	8.4	14.4	5.6	22.2	24.4
C_S^r ($\mu g\ cm^{-2}$)	0.56	0.115	0.026	0.031	0.010
C_S ($\mu g\ cm^{-2}$)	2.16	1.28	0.38	0.831	0.501
C^* ($g\ cm^{-3}$)	0.52	0.177	0.134	0.075	0.041

the filter was calcinated and the residue incorporated in a KBr disk. Heidermanns' technique (16) used in the Staubforschungsinstitut at Bonn probably constitutes the most successful version of this approach. Similar techniques (12), where separation of the asbestos fibers was attempted through a centrifugation step in a high density liquid, suffer from a reduced detection limit.

Results

Chrysotile reference materials

Some of the reference materials related to the chrysotile fibers used in this study have been described in the literature (16–19) and others have been isolated in our laboratory (20). Although the Calidria chrysotile contains more trace metals and less brucite than the Quebec chrysotiles, no major differences in composition are evident. The rather high brucite content of the UICC-B chrysotile might be attributed to fibers from the Carey mine incorporated in the original sample; the other three chrysotile samples have been isolated from fibers of the Jeffrey mine.

The fiber length distribution for the shortest and the longest fraction were calculated from the transmission micrographies and optical microscopy measurements respectively. Results for the other materials are taken from the literature and are presented as % cumulative volume fractions in Fig. 1. The fiber diameter distributions are less reliably established, except for the electron microscopy results. The mean diameter of the Quebec monofibril has been given as 350 Å, that of the Calidria fibril as 280 Å (21), but we preferred to calculate an "average" diameter for all five materials from indirect measurements (22).

If the fibers and fiber bundles can be approximated as cylinders of length l and radius r, their specific surface area S is given as:

$$[1] \quad S = \frac{\pi r l + 2\pi r^2}{\rho \pi r^2 l}\ (m^2\ g^{-1})$$

where ρ, the density of chrysotile asbestos $\simeq 2.54 \times 10^6\ g\ m^{-3}$. Except for extremely short fibers with a very low aspect ratio, $l/2r$, the average diameter is inversely proportional to the surface area and can be estimated immediately. The surface area measured from nitrogen adsorption isotherms, the calculated average diameter, and the mean length estimated from optical and electron micrographies (50% volume shorter or longer than $\langle l \rangle$ for the reference fibers) are given in Table 1.

Can. J. Chem. Downloaded from www.nrcresearchpress.com by 210.87.254.5 on 09/06/12
For personal use only.

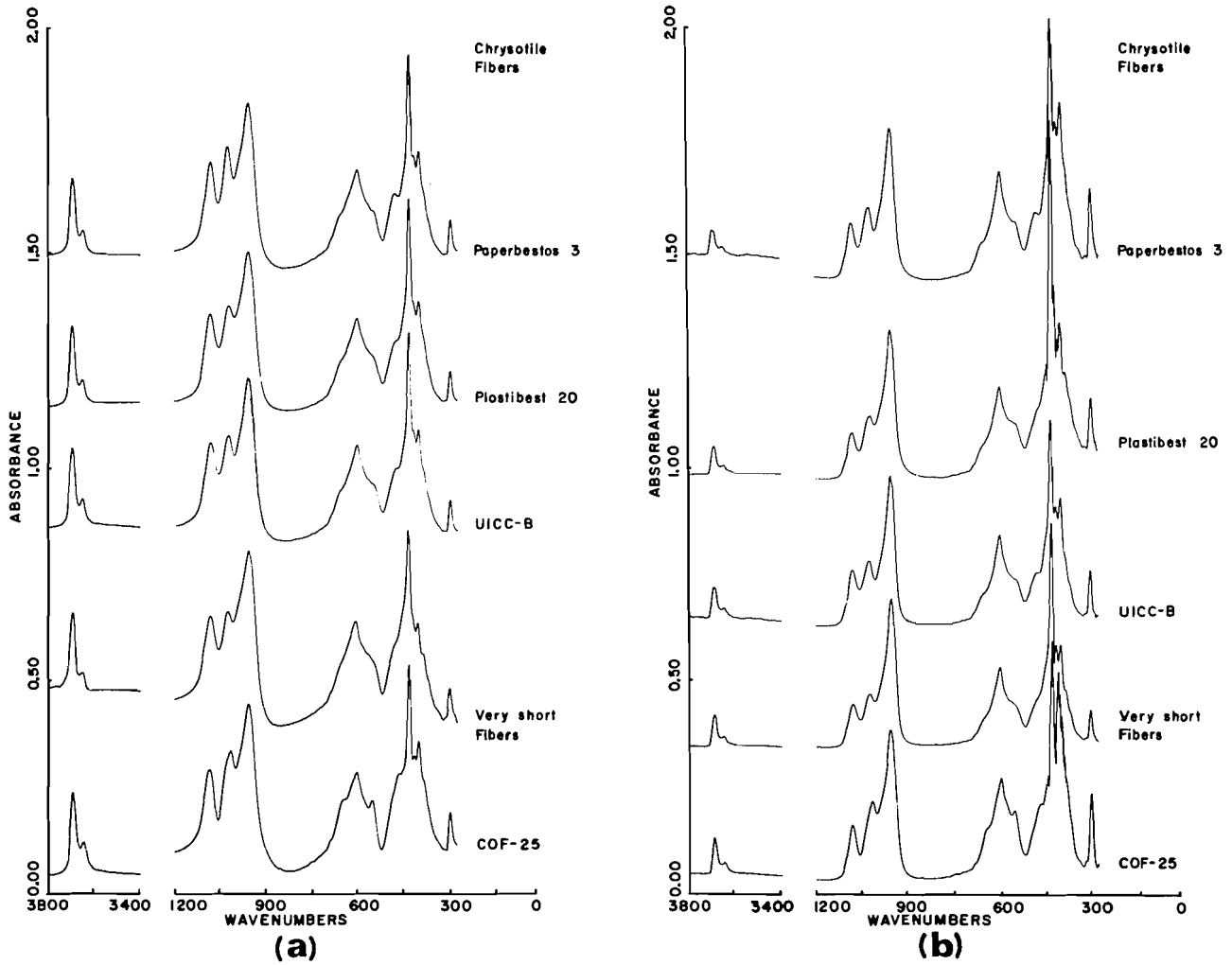

FIG. 2. Infrared spectra of different chrysotile fibers; (*a*) transmission spectra obtained from a KBr disk; (*b*) multiple internal reflection obtained with a IRE KRS-5.

IR spectra — transmission versus reflectance

Compared to the transmission spectra, Fig. 2*a*, obtained from a KBr disk, the IR spectra in the reflectance mode, Fig. 2*b*, shows relatively sharper peaks at lower wave numbers and relatively lower peaks at higher wave numbers. The increased noise level above $\bar{\nu} = 3000\ cm^{-1}$, due to the absorption characteristics of the Internal Reflection Element (IRE) and the beam splitter of the Nicolet MX-1 Fourier Transform Spectrophotometer, is practically without consequence except for the lowest chrysotile concentrations.

Variations of the IR transmission spectra with fiber type may reflect differences in impurity levels and crystal structure. Increased geometric size will eventually cause peak broadening and degradation of the signal, due to light dispersion and reflection, as was elegantly shown for calcite particles by Duyckaerts (23). Since aspect ratios $l/2r \simeq 200$ are not common, fibers almost 1 mm long may be encountered. Their thickness, $\ll$ 5 μm, would otherwise pose few optical problems, but their length makes them most difficult to incorporate in a transparent KBr disk. Extensive grinding would defiberize the material and eventually shorten the length of the fiber bundles, defeating the purpose of this study (24).

The IR spectra of all five materials are very similar and a detailed examination is necessary to identify their distinguishing features. The Calidria COF-25 chrysotile shows significant differences in the far-infrared region (Fig. 2, note that the peak at 303 cm^{-1} is considerably higher than for other chrysotiles). Since its chemical and mineralogical composition varies little from the other reference materials, these differences would be consistent with minor alteration in the crystal structure. Whereas the others occur as crossfibers in ultrabasic rocks, the Calidria chrysotile consists of extremely short fibers dispersed in a carbonate deposit. The differences in crystal structure could be attributed to an average fibril diameter some 100 Å smaller than that of Quebec chrysotile monofibers, and manifested by slightly different lattice vibrations.

Because of the characteristics of the ATR (attenuated total reflectance) technique (25), the morphology of the fibers has a much greater intrinsic effect. The signal will vary with the depth of penetration into sample, which can be expected to vary with fiber size and wavelength. We have undertaken this study in order to evaluate whether the reflectance mode can be used to quantitatively measure chrysotile fibers of respirable dimension (aerodynamic diameter < 7 μm). Before examining the experimental results, it is perhaps useful to analyse the predictions of a simplified model of the ATR phenomena.

IR spectra ATR mode comparison of reference fibers

For a uniform film of sufficient thickness, d, deposited on the surface of an appropriate internal reflectance element, it has

Can. J. Chem. Downloaded from www.nrcresearchpress.com by 210.87.254.5 on 09/06/12
For personal use only.

Can. J. Chem. Downloaded from www.nrcresearchpress.com by 210.87.254.5 on 09/06/12
For personal use only.

been established (25) that the depth of penetration of the photon into the sample, d_p, varies with the wavelength (measured in vacuum), refractive index, n, and the angle of incidence, θ, as:

$$[2] \quad d_p = \frac{\lambda}{2\pi (\sin^2 \theta - n_{21}^2)^{1/2}}$$

For $\theta = 45°$, n_1(KRS-5) = 2.4, $n_{2\,(\text{chrysotile})} = 1.55$, we can estimate:

$$[3] \quad n_{21} = \frac{n^2}{n_1} \text{ and } d_p \simeq 0.55\lambda$$

The amplitude of the electromagnetic radiation extending out of the internal reflection element into the sample should decrease exponentially with distance x according to:

$$[4] \quad E = E_0 \exp\left(-\frac{x}{d_p}\right)$$

Thus parts of the sample with an intimate contact at the surface will absorb a far greater fraction of the energy, E, than parts of sample lying at $x > d_p$.

A comprehensive treatment of the ATR has been given recently on the basis of the Lorentz–Lorentz's law and Fresnel equations for thick sample films (26), i.e., absorbing molecules dispersed in a nonabsorbing medium. Another recent evaluation of the measured absorbance values as a function of various sample parameters, including the surface morphology of a sample film, using a 45° KRS-5 internal reflection element, approaches our problem (27). However, for discrete particles in general, and fibrous materials in particular, no such complete analysis is available. We are dealing with fiber diameters of the order of 0.03 to 0.15 μm (where the thin layer approximation would normally hold for a continuous film), which are discrete particles where the "concentration" takes on a new meaning.

Following Harrick's approach in relating the reflectivity R logarithmically to the concentration C^*

$$[5] \quad R = R_0 \exp(-N\epsilon C^* d_{\text{eff}})$$

where ϵ is the extinction coefficient, N, the number of reflections in the IRE, and d_{eff}, the effective layer thickness which has been calculated by considering the interaction of the electromagnetic field of the incident light wave and sample media. For limited adsorption

$$[6] \quad d_{\text{eff}} = \frac{n_{21}}{\cos\theta} \int_0^d E^2\, dx = \frac{n_{21}}{\cos\theta} \int_0^d E_0^2 \exp\left[\frac{-2x}{d_p}\right] dx$$

where we suppose that the medium has a finite thickness d.

For $d \ll \lambda$ or $d \gg \lambda$, the thin and thick layer approximations are well known. For materials where the sample thickness is of the same order as the penetrating depth d_p, we estimate:

$$[7] \quad d_{\text{eff}} \simeq \frac{n_{21}}{4\pi \cos\theta} E_0^2 \frac{\lambda}{(\sin^2\theta - n_{21}^2)^{1/2}} \left(1 - \exp\left[-\frac{2d}{d_p}\right]\right)$$

where E_0, the relative electric field amplitude, is greater for $\parallel$ polarization than for $\perp$ polarization. For $n_1 = 2.4$, $n_2 = 1.55$, $n_3 = 1$, $E_\perp$ will vary from 1.55 to 1.8 and $E_\parallel$ from 1.59 to 2.6 for thin and thick films respectively. Taking 1.8 as an approximate value for E_0, we calculate for unpolarized radiation:

$$[8] \quad d_{\text{eff}} \simeq 0.52\lambda\left(1 - \exp\left[-\frac{3.6d}{\lambda}\right]\right)$$

This expression, plotted in Fig. 3, indicates an initial linear variation between effective thickness and sample thickness and an eventual limiting value $d_{\text{eff}} \simeq 0.52\lambda$. It also indicates that the thin layer approximation may be valid at low wavelengths, e.g., $\lambda_1 = 2.5$ μm ($\bar{\nu} = 4000$ cm^{-1}) and hold for longer wavelengths, e.g., $\lambda_2 = 25$ μm ($\bar{\nu} = 400$ cm^{-1}).

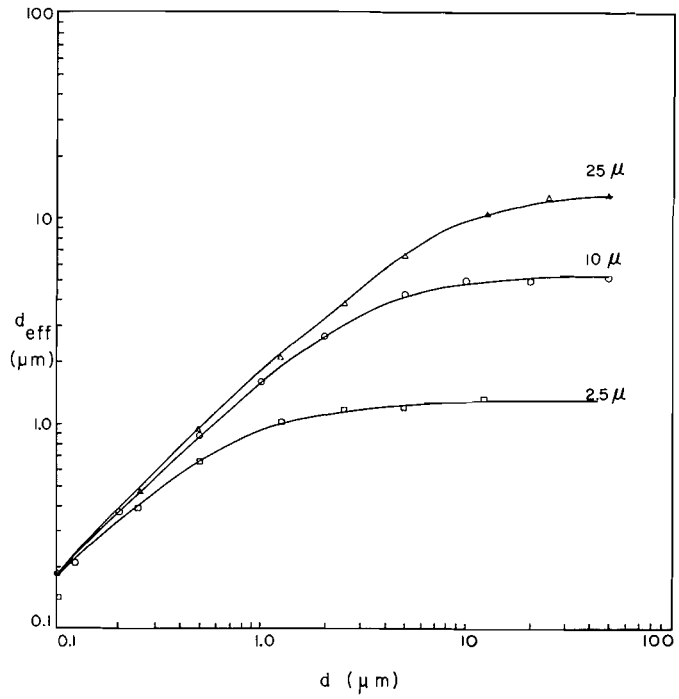

FIG. 3. Variation of effective thickness with sample thickness.

As indicated schematically in Fig. 4*a*, if the sample thickness $d \gg d_p$, then the reflectivity will not vary with a further increase in sample thickness. If $d_p(\lambda_1) \ll d$ and $d_p(\lambda_2) \gg d$, then the absorbance will continue to increase for sample thickness at λ_2 only. For a fixed number of discrete sample particles, Fig. 4*b*, it is expected that the amount of energy absorbed will be proportional to their surface concentration. Thin samples should absorb less than thicker samples, subject to the constraint $d_p > d$.

Surface concentration of chrysotile fibers

For a monolayer coverage, $\theta = 1$, illustrated in Fig. 4*c*, by perfectly aligned cylindrical fibers of uniform length and diameter, we would estimate a surface concentration

$$[9] \quad C_S^a \simeq \frac{\pi r^2 l}{2rl}\rho = \frac{\pi r}{2}\rho$$

or 200 μg/cm^2 for a fiber 1 μ thick.

If full rotational freedom (Fig. 4*d*) were allowed during fiber settling on the membrane surface, some overlapping of fibers would occur beyond a surface concentration

$$[10] \quad C_S^r = \frac{\pi r^2 l\rho}{\pi l^2/4} = \frac{4r^2\rho}{l}$$

or 2.54 μg/cm^2 for fibers 1 μ thick having an aspect ratio $l/2r = 100$. A better estimate of the mean surface concentration is probably given by

$$[11] \quad C_S = \sqrt{C_S^r \cdot C_S^a} = \left(\frac{2\pi r}{l}\right)^{1/2} r\rho \text{ (g cm}^{-2}\text{)}$$

and the "bulk" concentration as employed in eq. [5] is given by $C^* = C_S/2r$ (g cm^{-3}).

Can. J. Chem. Downloaded from www.nrcresearchpress.com by 210.87.254.5 on 09/06/12
For personal use only.

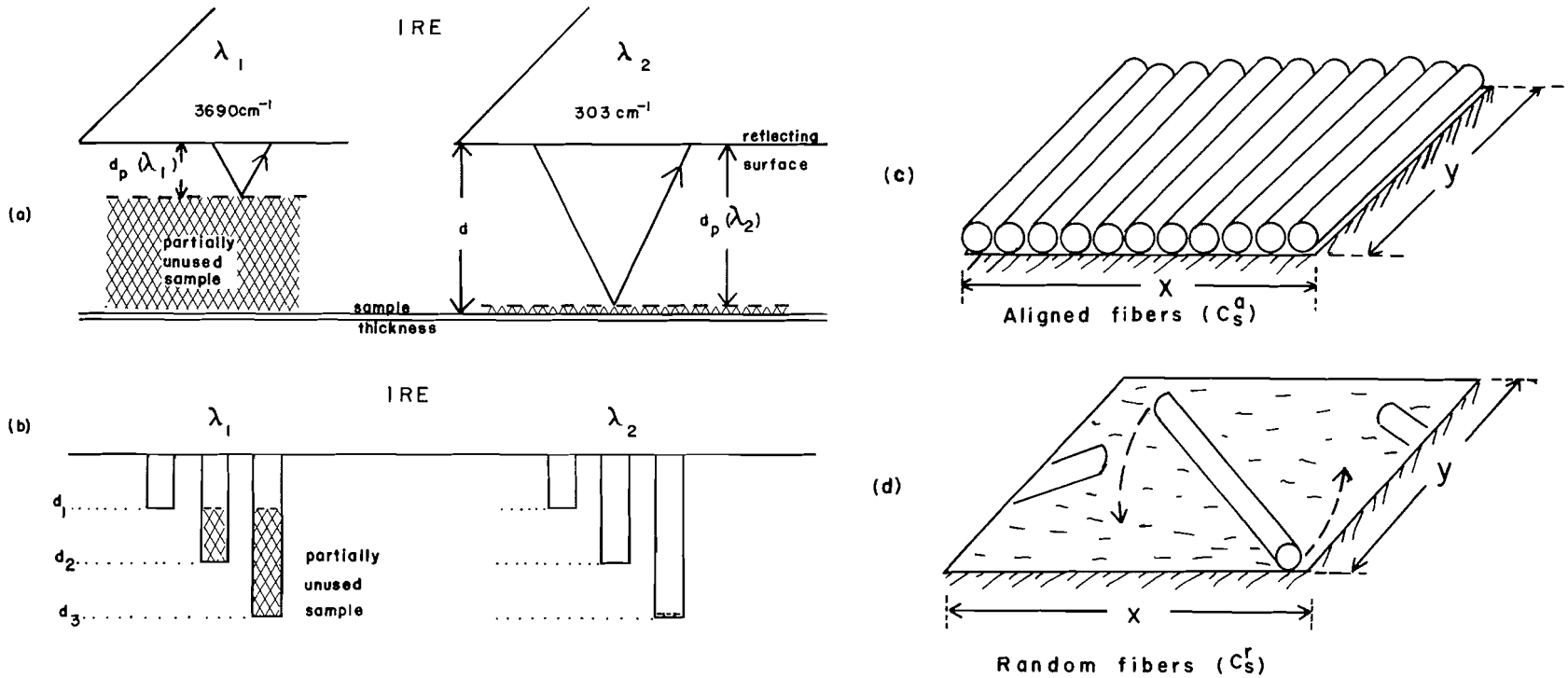

FIG. 4. (*a*) Scheme of sample thickness for $d \gg dp$; (*b*) the energy absorbed is proportional to the surface concentration for a fixed number; (*c*) concentration for aligned fibers (C_s^a) at the surface membrane (eq. [9]); (*d*) concentration for a random fibers (C_s^r) at the surface membrane (eq. [10]).

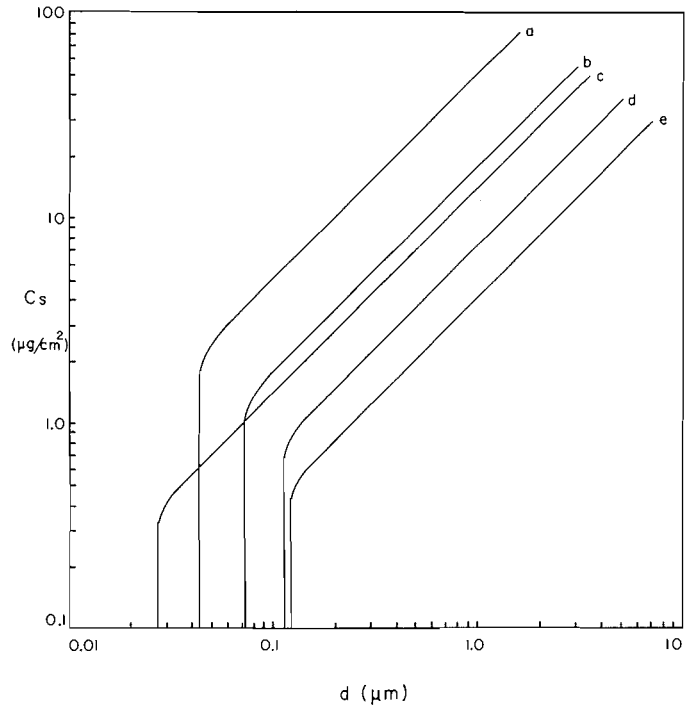

FIG. 5. Correlation between sample concentration, C_S, and thickness of the fiber matt for the five reference fibers; (*a*) very short chrysotile; (*b*) UICC-B chrysotile; (*c*) Calidria COF-25; (*d*) Plastibest #20; (*e*) Paperbestos #3.

For $\theta > 1$, closepacked, aligned fibers, the surface concentration would increase linearly with thickness of the fiber matt and independently of fiber length. For randomly aligned fibers the surface concentration would increase linearly but the slope would depend on the square root aspect ratio. For the five reference fibers, Table 1, both the mean diameter and the mean length vary. Thus, below $\theta < 1$, the thickness of the fiber matt will be determined by the diameter of the fibers, and the surface concentration can be given as θC_S. Beyond monolayer coverage the thickness can be approximated as $2r\theta$, where θ will vary according to eq. [11] with fiber type. The correlation between sample weight and thickness of the fiber matt is illustrated in Fig. 5 for the five reference fibers.

Thus, for a fiber deposit 10 μg/cm² of the longest reference fiber, the matt would be some 2.5 μm thick. At this thickness, according to Fig. 3, we are approaching the limiting value for d_{eff} at $\lambda = 2.5$ μm, but the entire sample will still absorb photons at $\lambda = 25$ μm. Similarly, for the shortest fibers we would estimate a thickness from Fig. 5, of 0.2 μm for the fiber matt for a deposit of 10 μg/cm², according to Fig. 3, and the entire sample would absorb radiation over the entire IR range.

The variation of absorbance with sample weight can be predicted by combining eqs. [5], [8], and [11]. Thus

$$[12] \quad A = \ln \frac{R_0}{R} = N\epsilon C^* d_{eff}$$

$$= 0.52\, N\epsilon \frac{C_S}{2r} \lambda \left(1 - \exp\left[-\frac{3.6d}{\lambda}\right]\right)$$

where C^* is the concentration on the membrane (specific to the density of the fiber, see Table 1) and C is the weight of fiber deposited on the membrane surface. In fact d represents the thickness of the fiber at the film surface, where

$$d = \frac{C}{C^*} = \frac{2rC}{C_S} = \frac{2}{\rho} \frac{C}{\sqrt{2\pi r/l}}$$

Equation [12] will be examined below.

Undoubtedly, these predictions are grossly oversimplified; the diffraction and reflection at the air/sample and air/reflectance element interfaces have been neglected, fibers and fiber bundles have been treated as a continuous film, the surface concentration for monolayer coverage has only been estimated, etc. Nevertheless, this simple model indicates that: (*i*) the absorption curve should plateau out when sufficient sample thickness is attained; (*ii*) this nonlinear region should be attained at much lower concentrations at $\lambda_1 < \lambda_2$, and at lower concentrations for long fibers of high aspect ratio than for short fibers having a low aspect ratio; and (*iii*) the relative absorption $A(\lambda_1)/A(\lambda_2)$, where $\lambda_1 < \lambda_2$ should decrease with fiber dimension.

If such be the case, it should be possible to use the ATR technique not only to measure fiber concentrations, but also to estimate mean fiber dimensions.

Variation of reflectivity with concentration

The calibration curves for three of the reference fibers, illustrated in Fig. 6, show a linear relationship between the measured absorbance $A = \log R_0/R$ and the sample weight at low concentrations for all three wavelengths investigated (3690, 960, and 303 cm⁻¹). At 303 cm⁻¹ the sensitivity (absorbance/(μg/cm²)) is relatively independent of fiber type and linear over the range investigated <1.2 mg/filter (or ~150 μg/cm²). At the longer wavelengths the sensitivity becomes increasingly dependent on fiber type. At 3690 cm⁻¹, for a given sample weight, the shortest fibers yield a signal twice as high as that observed for the longest fibers investigated. Moreover, the deviation from linearity occurs at lower surface concentrations, as predicted for the longer fibers.

The agreement of this rather complicated behavior with semiquantitative calculations is surprisingly good. The absorbance values predicted by eq. [12] are plotted in Fig. 7 on a log–log scale. This treatment emphasizes the difference in behavior at different wavelengths and attributes the differences between fiber types to differing aspect ratios. Since natural fibers consist of bundles having varying lengths and diameters, the concentration corresponding to monolayer coverage may differ somewhat from that calculated from eq. [11], which would shift the concentration where the deviation from linearity occurs (to somewhat higher or lower values).

The comparison between the experimental results and the model predictions is well illustrated in Fig. 8 for $\bar{\nu} = 3690$ cm⁻¹. Deviation from linearity occurs at higher concentrations than predicted. This observation is consistent with the fact that thin fibers can be readily accommodated within the thicker bundles without substantially increasing the thickness of the fiber matt. At $\bar{\nu} = 303$ cm⁻¹ our predictions indicate a linear correlation between absorbance and concentration up to about 100 μg/cm², with a higher sensitivity for the very short fibers.

Thus at $\bar{\nu} = 303$ cm⁻¹ the absorbance varies linearly with concentration, whereas at higher wavenumbers the reflectivity depends not only on concentration but also on fiber type. Let us examine in somewhat more detail this dependence on fiber morphology at sufficiently low concentrations, $C_S < 10$ μg/cm², where a linear concentration dependence still holds.

Variation of relative reflectivity with fiber type and incident wavelength

The intensity of the peaks in the ATR mode vary with the degree of contact, and thus the applied pressure, the angle of incidence, and the number of reflections; hence it is difficult to

Can. J. Chem. Downloaded from www.nrcresearchpress.com by 210.87.254.5 on 09/06/12
For personal use only.

Can. J. Chem. Downloaded from www.nrcresearchpress.com by 210.87.254.5 on 09/06/12
For personal use only.

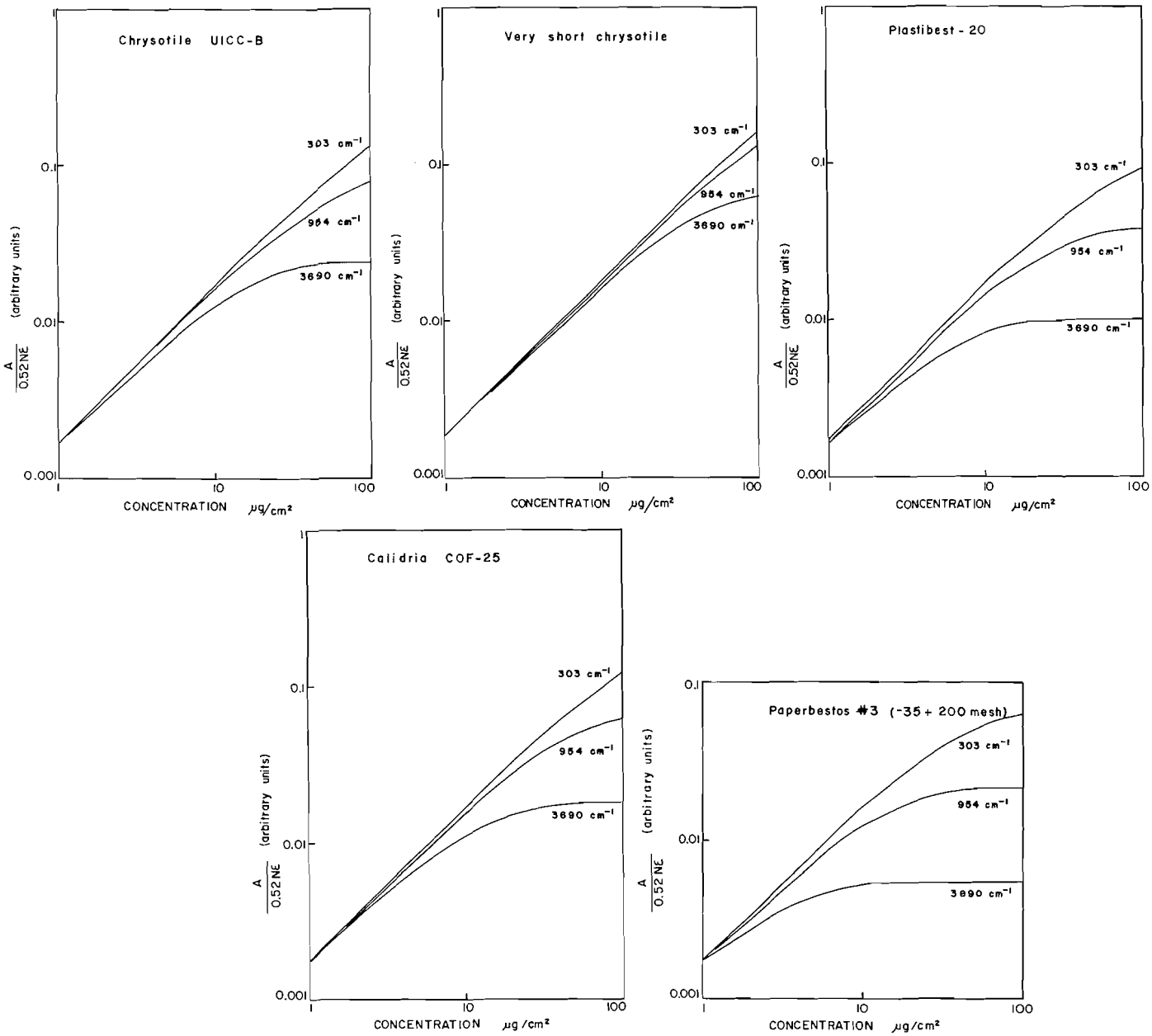

FIG. 6. Variation of the multiple internal reflection with concentration for the five reference fibers.

compare absolute values of the extinction coefficients, except as they pertain to a particular experimental ATR system (S_{ATR}). In order to eliminate the possibility of spectral interference, we preferred to deposit the fibers directly on the IRE without a backing plate. We therefore normalized the absorbance values with respect to one major peak ($\bar{\nu}$ = 954 cm^{-1}) and minimized effects of minor variations in fiber concentration.

These absorbance ratios are given in Table 2 for the major absorption peaks. By definition, both the normalized signal

$$[13] \quad S_{ATR} = \log \frac{R_0(\bar{\nu})}{R(\bar{\nu})} \Big/ \log \frac{R_0(954\ \text{cm}^{-1})}{R(954\ \text{cm}^{-1})}$$

and for the transmission system (S_T or KBr disk),

$$[14] \quad S_T = A(\bar{\nu})/A(954\ \text{cm}^{-1})$$

both are equal to 1.00 at $\bar{\nu}$ = 954 cm^{-1}. The absorbance ratios in the transmission mode are consistent, except for the Calidria chrysotile. A trend seems to exist between fiber length and peak height at 303 cm^{-1}. The ratio of the peak heights at 3690 cm^{-1} and 3645 cm^{-1} increases from a value of 3 : 1 for the long fiber bundles to 4 : 1 for the shortest fibers. This would be consistent with the assignment of the peak at 3645 cm^{-1} to the interstitial hydroxyl stretching bond, since the relative number of surface OH bonds increases for highly defiberized material.

The ratio of the absorbance values in the ATR mode vary in a monotone fashion for the remaining four fiber types. When classified in order of absorbance ratios $A(\bar{\nu})/A(954\ \text{cm}^{-1})$, the shortest fibers have the largest ratios at the shortest wavelengths (e.g. $\bar{\nu}$ = 3690 cm^{-1}) and the longest fibers have the largest ratios at the longest wavelengths (e.g. $\bar{\nu}$ = 303 cm^{-1}).

It is possible to normalize the ATR results by dividing them by peak height in the transmission mode. The normalized data should reflect primarily the effect of morphology since, for nonpolarised radiation, it may be presumed that the extinction coefficient for the evanescent wave is similar to that found for the same IR band for transmitted radiation. These normalized

Can. J. Chem. Downloaded from www.nrcresearchpress.com by 210.87.254.5 on 09/06/12
For personal use only.

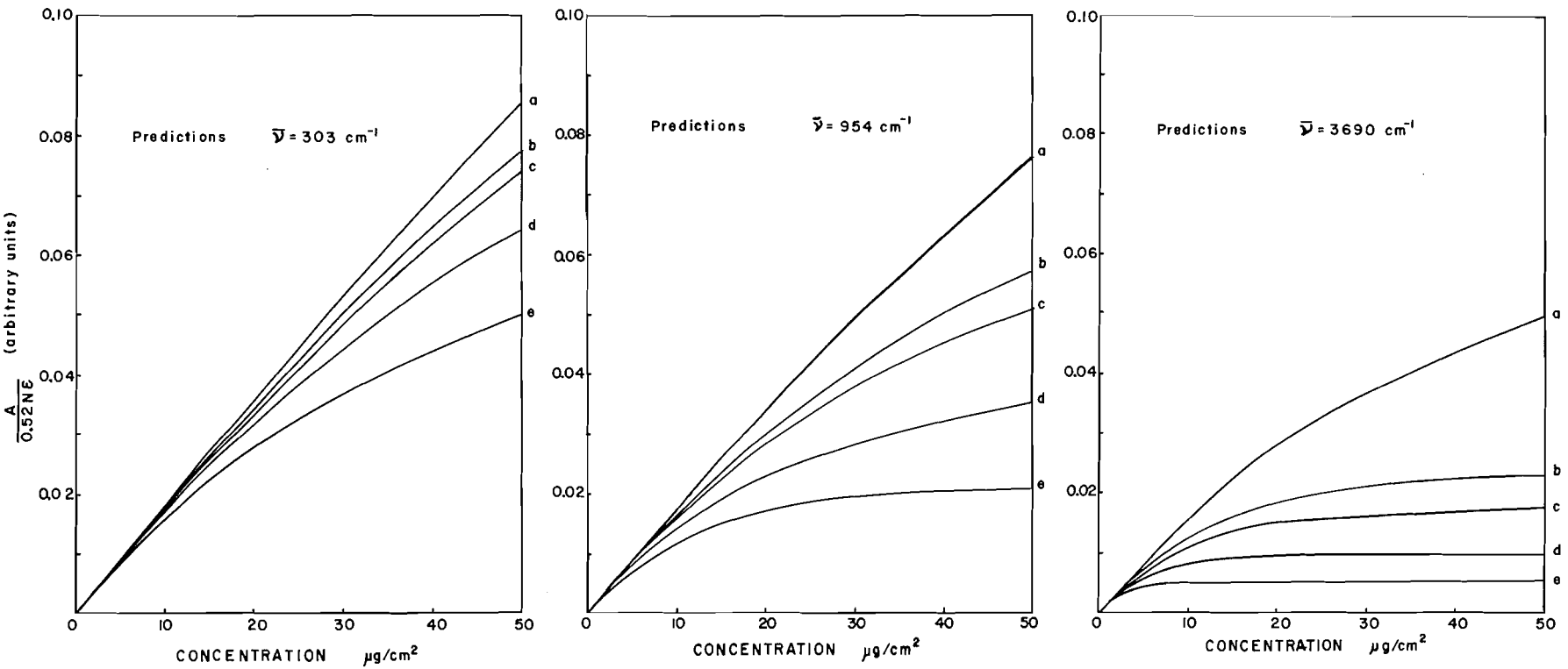

FIG. 7. Multiple internal reflection (theoretical value) predicted by eq. [12] for the five reference fibers: (*a*) very short chrysotile; (*b*) UICC-B chrysotile; (*c*) Calidria COF-25; (*d*) Plastibest #20; (*e*) Paperbestos #3.

Can. J. Chem. Downloaded from www.nrcresearchpress.com by 210.87.254.5 on 09/06/12
For personal use only.

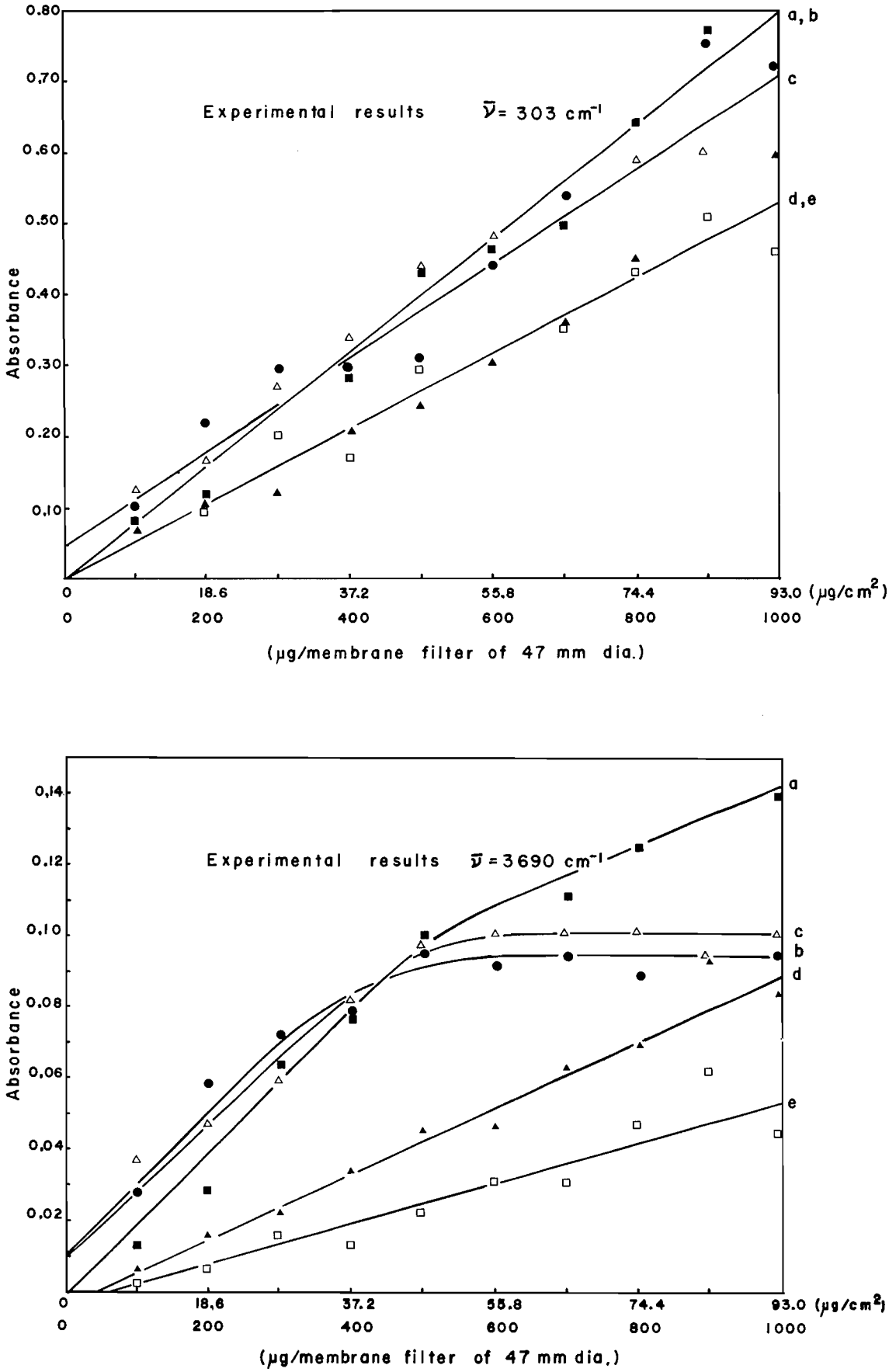

FIG. 8. Multiple internal reflection (experimental value) obtained for the five reference fibers: (*a*) very short chrysotile; (*b*) UICC-B chrysotile; (*c*) Calidria COF-25; (*d*) Plastibest #20; (*e*) Paperbestos #3.

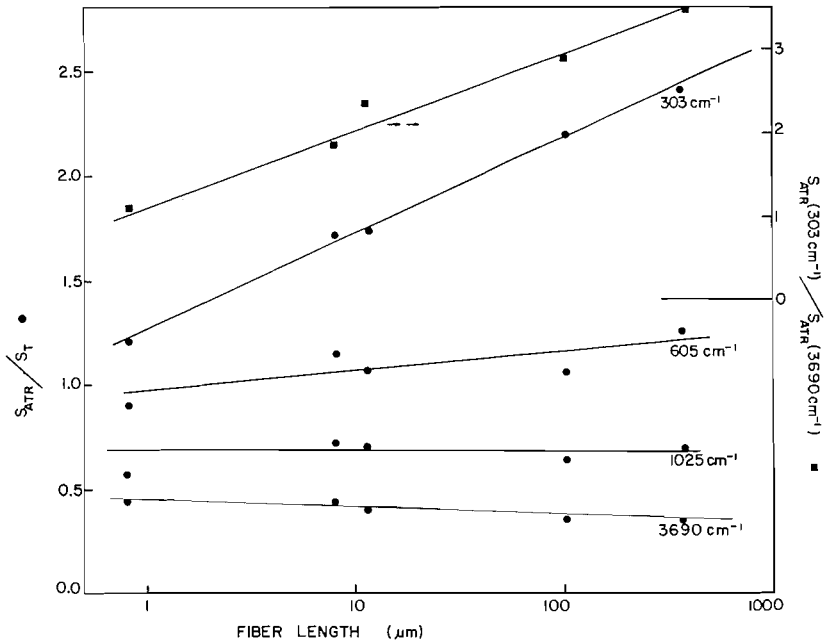

FIG. 9. Ratio of S_{ATR}/S_T versus the fiber length (●); ratio of S_{ATR} (303 cm^{-1})/S_{ATR} (3690 cm^{-1}) versus the fiber length (□).

TABLE 2. Absorbance ratio ($A(\bar{\nu})/A(954\ cm^{-1})$) classified for the major absorption peaks of chrysotile fiber

	Very short fiber (*a*)			UICC-B (*b*)		
$\bar{\nu}$ (cm^{-1})	S_{ATR}	S_T	S_{ATR}/S_T	S_{ATR}	S_T	S_{ATR}/S_T
3690	0.21	0.48	0.44	0.20	0.52	0.40
3646	0.07	0.12	0.57	0.08	0.20	0.38
1080	0.29	0.60	0.48	0.38	0.58	0.66
1025	0.36	0.63	0.57	0.44	0.63	0.70
605	0.54	0.60	0.90	0.61	0.57	1.07
303	0.24	0.20	1.20	0.38	0.22	1.73
	Calidria COF-25 (*c*)			Plastibest #20 (*d*)		
3690	0.24	0.54	0.44	0.19	0.53	0.36
3646	0.08	0.13	0.57	0.06	0.18	0.36
1080	0.37	0.60	0.62	0.31	0.61	0.51
1025	0.52	0.73	0.72	0.42	0.67	0.63
605	0.68	0.59	1.15	0.62	0.59	1.05
303	0.58	0.34	1.71	0.55	0.25	2.20
	Paperbestos #3 (*e*)					
3690	0.17	0.50	0.34			
3646	0.06	0.17	0.37			
1080	0.36	0.61	0.59			
1025	0.47	0.69	0.68			
605	0.70	0.57	1.22			
303	0.60	0.25	2.40			

values are plotted in Fig. 9 as a function of the fiber length. The trends noted above in Table 2 become evident and reflect the effective depth of penetration with respect to the major silicate band at $\bar{\nu} = 954\ cm^{-1}$. Even the Calidria COF-25 data fall in the line with the remaining points when plotted in terms of average fiber length, as in Fig. 9, or as a function of the aspect ratio.

The ratio S_{ATR} (303 cm^{-1})/S_{ATR} (3690 cm^{-1}) varies linearly with log (fiber length) as in Fig. 9 RHS ordinate scale. This result provides a very simple means to characterize the asbestos samples collected on the air filter. The absorbance at 303 cm^{-1} could be used to establish the concentration ($\mu g/cm^2$) independent of fiber dimension. The absorbance ratio with respect to the peak at 3690 cm^{-1} would allow an estimate of the mean length (Fig. 9) and hence eventually the number of fibers collected (Fig. 8).

Acknowledgements

The authors wish to thank the Institut de Recherche et de Développement de l'Amiante (IRDA) and the Le Conseil de Recherche en Science Naturelle et en Génie (CRSNG) for their financial support.

1. E. J. CHATFIELD. Measurement of asbestos fibers in the workplace and in the general environment. *In* Mineralogical techniques of asbestos determination. *Edited by* R. L. Ledoux. Mineral. Ass. of Canada, 1979.
2. A. RICHARDS. Anal. Chem. **44**, 1872 (1972).
3. B. A. LANGE and J. C. HAARTZ. Anal. Chem. **51**, 4 (1979); **51**, 520 (1979).
4. N. KOHYAMA. Ind. Health, **18**, 69 (1980).
5. S. T. BECKETT, A. P. MIDDLETON, and J. DODGSON. Ann. Occup. Hyg. **18**, 313 (1975).
6. G. HEIDERMANNS. BIA Report 3-78, (1978); Staub-Reinhalt. Luft. **33**, 3 (1973); **33**, 66 (1973).
7. R. J. P. LYON. Infrared spectroscopy of silicates and related compounds. *Edited by* J. Zussmann. Academic Press. 1971. pp. 371–403.
8. L. J. MONKMAN. Asbestos — recent developments. *In* Applied fiber science 3. *Edited by* F. Happey. London, Academic Press. 1979. pp. 163–196.
9. J. P. COATES. The infrared analysis of quartz and asbestos. Perkin-Elmer Ltd., Maxwell Road, Beaconsfield, Bucks, England. 1979.
10. G. W. BRINDLEY and J. ZUSSMAN. Am. Mineral **44**, 185 (1959).
11. J. A. GADSEN, J. PARKER, and W. L. SMITH. Atmos. Environ. **4**, 667 (1970).
12. R. P. BAGIONI. Environ. Sci. Technol. **9**, 262 (1975).
13. R. E. HEFFELFINGER. Atmos. Environ. **5**, 565 (1971).
14. K. FLICK. Arbeitsschutz. Z. 161 (1969).
15. R. W. LUCE. U.S. Geol. Survey. Prof. Paper 750-13, pp. B-199–201 (1970).

Can. J. Chem. Downloaded from www.nrcresearchpress.com by 210.87.254.5 on 09/06/12
For personal use only.

16. W. J. CAMPBELL, C. W. HUGGINS, and A. G. WYLIE. Chemical and physical characterization of amosite, chrysotile, crocidolite and non fibrous tremolite for oral ingestion studies by the NIEHS. RI report 8452 (1980).
17. R. E. G. RENDALL. Pneumoconiosis Proceed. 3rd Int. Conf., Johannesburg, 1969.
18. V. TIMBRELL. Characteristics of the international union against cancer standard reference samples of asbestos. Pneumoconiosis. Proceedings of the International Conference. Johannesburg. *Edited by* Shapiro. II. R., Oxford University Press, Capetown. 1969. pp. 28–36.
19. C. JOLICOEUR, P. ROBERGE, and J. L. FORTIER. Can. J. Chem. **59**, 1140 (1981).
20. F. M. KIMMERLE and R. STEELE. Preparation of a purified grades asbestos fraction. Société Nationale de l'Amiante à Sherbrooke, Québec, Rapport 8, 109:99 (1980). Unpublished.
21. S. SPEIL and J. P. LEINWEBER. Environ. Res. **2**, 166 (1969).
22. L. NOËL. Mesure pondérale de l'amiante chrysotile par spectroscopie infrarouge à réflexion interne. Mémoire de maîtrise. Université de Sherbrooke, Sherbrooke, Qué., Sept. 1982.
23. G. DUYCKAERTS. Ann. Chem. **84**, 201 (1959).
24. A. M. LANGER, M. S. WOLFF, A. N. ROHL, and I. J. SELIKOFF. J. Toxicol. Environ. Health. **4**, 173 (1978).
25. N. J. HARRICK. Internal reflectance spectroscopy. Interscience, New York, NY. 1967.
26. G. GIDALY and R. KELLNER. Fresenius Z. Anal. Chem. **302**, 4 (1980); **302**, 257 (1980).
27. G. MUELLER, K. ABRAHAM, and M. SCHALDACH. Appl. Opt. **20**, 7 (1981); **20**, 1182 (1981).

Can. J. Chem. Downloaded from www.nrcresearchpress.com by 210.87.254.5 on 09/06/12
For personal use only.

Across-space double bond interactions: the crystal and molecular structures of two chlorinated *endo-endo*-dienes and comparisons with a third homolog

DAO CONG DONG,[1] WINNIE WONG-NG,[2] STANLEY C. NYBURG, AND PIK YUEN SIEW
Department of Chemistry, University of Toronto, Toronto, Ont., Canada M5S 1A1

AND

J. T. EDWARD
Chemistry Department, McGill University, Montreal, P.Q., Canada H3A 2K6

Received August 5, 1982[3]

DAO CONG DONG, WINNIE WONG-NG, STANLEY C. NYBURG, PIK YUEN SIEW, and J. T. EDWARD. Can. J. Chem. **62**, 452 (1984).

The crystal structures of two *endo-endo*-dienes, 5,6,7,8,9,9-hexachloro-1,4,4*a*,5,8,8*a*-hexahydro-*endo-endo*-1,4-ethano (and propano)-5,8-dimethanonaphthalene, **I***b* and **I***c* have been determined. These, together with the methano-homolog **I***a* (of known structure), are shown to exhibit decreasing across-space double-bond/double-bond repulsion which correlates with the observed decrease in the ease of cyclization in solution.

DAO CONG DONG, WINNIE WONG-NG, STANLEY C. NYBURG, PIK YUEN SIEW et J. T. EDWARD. Can. J. Chem. **62**, 452 (1984).

On a déterminé les structures cristallines de deux dienes *endo-endo*, les hexachloro-5,6,7,8,9,9 hexahydro-1,4,4*a*,5,8,8*a* éthano-1,4 (et propano)-*endo-endo* diméthano-5,8 naphtalène (**I***b* et **I***c*). On démontre que ces composés, ainsi que l'homologue méthano **I***a* (de structure connue) présentent des répulsions double liaison/double liaison à travers l'espace qui vont en décroissant: ceci est en accord avec les facilités relatives de cyclisation en solution qui ont été observées.

[Traduit par le journal]

Introduction

This paper reports the crystal and molecular structures of two hexachlorinated *endo-endo*-dienes, **I***b*, **I***c* which, together with **I***a* of known structure (1), form a homologous series. Interest

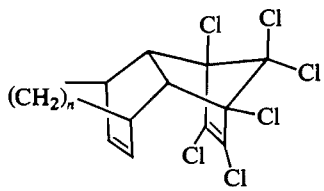

I*a,b,c*, ($n = 1,2,3$)

in these compounds lies in the marked differences in their ease of cyclization in which the opposing double bonds are opened to form a four-membered ring. Dong and Edward (2) have shown that when bromine is added to carbon tetrachloride solutions of the dienes which are then irradiated with uv light, the speed of cyclization is in the order **I***a* > **I***b* > **I***c*. These authors attribute this sequence to decreasing molecular strain with increasing n, an interpretation supported by the results reported here.

Experimental

Both crystal specimens were prepared as described by Dong and Edward (2). The crystals were, in both cases, colorless and well formed. Unit cell dimensions were determined from diffractometer setting angles of seven or more centered reflections using Zr-filtered MoKα radiation. Intensity data were collected on a Picker four-circle diffractometer in θ−2θ scan mode at 2° min^{-1} in the range θ < 25°. In both cases the initially colorless crystals became cloudy and there was loss in reflection intensity. Corrections linear in time were applied to compensate for these intensity losses. Reflections were considered to be of significant intensity on the criterion $F_o > 2\sigma(F_o)$ where $\sigma(F)$ was taken as $\{[\sigma(I)\cdot Lp]^2 + 0.02F_o^4\}^{1/2}/2F_o$, Lp being the Lorentz-polarization factor.

TABLE 1. Molecule **1***b*: fractional atomic co-ordinates, ×10^4 for non-hydrogen atoms, ×10^3 for hydrogen atoms

Atom	*x*	*y*	*z*
Cl(1)	3171(2)	4548(2)	2473(1)
Cl(2)	3533(1)	2951(2)	4232(2)
Cl(3)	2252(2)	4686(2)	5146(1)
Cl(4)	719(2)	5440(2)	3614(1)
Cl(5)	1022(2)	4168(2)	1759(1)
Cl(6)	2792(1)	2509(2)	2040(1)
C(1)	2472(4)	3504(5)	2759(4)
C(2)	2496(4)	3236(5)	3773(4)
C(3)	2061(4)	4193(5)	4116(4)
C(4)	1463(5)	4488(5)	3535(4)
C(5)	1478(4)	3745(5)	2766(4)
C(6)	1106(4)	2710(5)	3075(4)
C(7)	1807(4)	2362(5)	3782(4)
C(8)	1325(4)	2077(5)	4662(4)
C(9)	712(5)	2902(5)	4966(5)
C(10)	110(5)	3195(5)	4373(5)
C(11)	159(4)	2654(5)	3496(5)
C(12)	709(5)	1189(6)	4401(5)
C(13)	25(5)	1535(6)	3708(5)
H(6)	102	225	249
H(7)	217	167	366
H(8)	181	193	518
H(9)	75	322	563
H(10)	−37	378	451
H(11)	−32	299	305
H(121)	37	91	499
H(122)	111	59	412
H(131)	10	110	310
H(132)	−64	142	398

[1]Present address: Uniroyal Research Laboratories, Guelph, Ont., Canada N1H 6N3.

[2]Present address: JCPDS-International Center for Diffraction Data, 1601 Park Lane, Swarthmore, PA 19806, U.S.A.

[3]Revision received September 16, 1983.

Can. J. Chem. Downloaded from www.nrcresearchpress.com by 210.87.254.105 on 09/06/12
For personal use only.

TABLE 2. Compound **1***c*: (molecule **A**, unprimed, **B**, primed). Fractional atomic co-ordinates $\times 10^4$ for non-hydrogen atoms, $\times 10^3$ for hydrogen atoms

Atom	*x*	*y*	*z*	Atom	*x*	*y*	*z*
Cl(1)	4074(1)	3016(1)	2272(0)	Cl(1)′	9263(2)	3741(1)	1859(1)
Cl(2)	2832(2)	1251(1)	3115(1)	Cl(2)′	10393(1)	1041(1)	1915(1)
Cl(3)	3500(2)	2331(1)	4203(1)	Cl(3)′	8992(2)	−221(1)	915(1)
Cl(4)	5173(2)	4758(1)	4116(1)	Cl(4)′	6931(2)	1581(1)	205(1)
Cl(5)	5551(1)	5208(1)	2968(1)	Cl(5)′	7100(2)	3975(1)	748(1)
Cl(6)	2256(1)	4006(1)	2895(1)	Cl(6)′	7038(1)	2162(1)	1692(1)
C(1)	3903(4)	3305(4)	2888(2)	C(1)′	8590(5)	2669(4)	1468(2)
C(2)	4090(5)	2301(4)	3227(2)	C(2)′	9709(5)	1786(4)	1390(2)
C(3)	4095(5)	2890(4)	3706(2)	C(3)′	8831(5)	1130(4)	997(2)
C(4)	4756(5)	3818(4)	3669(2)	C(4)′	8039(5)	1834(4)	724(2)
C(5)	5195(4)	3896(3)	3168(2)	C(5)′	8385(4)	2959(4)	923(2)
C(6)	6413(4)	3066(3)	3114(2)	C(6)′	9924(4)	3267(4)	840(2)
C(7)	5663(4)	1953(4)	3159(2)	C(7)′	10863(4)	2461(4)	1174(2)
C(8)	6451(5)	1215(4)	3562(2)	C(8)′	11950(5)	1837(4)	906(2)
C(9)	6958(6)	1859(5)	4012(2)	C(9)′	11299(6)	1442(4)	424(2)
C(10)	7592(5)	2786(5)	3970(2)	C(10)′	10490(6)	2115(5)	138(2)
C(11)	7793(5)	3194(4)	3474(2)	C(11)′	10266(5)	3240(4)	305(2)
C(12)	7760(6)	684(4)	3356(2)	C(12)′	13241(6)	2592(6)	846(2)
C(13)	8602(7)	1439(5)	3072(3)	C(13)′	12906(16)	3616(13)	697(6)
C(14)	9025(5)	2555(4)	3279(2)	C(13)″	13003(18)	3482(16)	442(5)
				C(14)′	11635(7)	3915(5)	272(2)
H(6)	685	318	278	H(6)′	1013	411	93
H(7)	566	143	285	H(7)′	1160	284	145
H(8)	572	60	366	H(8)′	1229	113	112
H(9)	679	155	436	H(9)′	1149	62	31
H(10)	798	325	429	H(10)′	1000	185	−21
H(11)	805	405	350	H(11)′	936	358	8
H(121)	737	2	312	H(121)′	1386	224	60
H(122)	848	37	366	H(122)′	1390	266	120
H(131)	797	157	273	H(121)″	1413	210	77
H(132)	958	102	302	H(122)″	1354	301	120
H(141)	987	245	357	H(131)′	1385	397	59
H(142)	942	303	300	H(132)′	1262	405	102
				H(131)″	1344	319	14
				H(132)″	1364	420	59
				H(141)′	1200	378	−8
				H(142)′	1137	479	29
				H(141)″	1165	412	−11
				H(142)″	1150	469	46

The structures were solved by direct methods using the SHELX (3) package. Anisotropic least-squares refinement was by SHELX using the atomic scattering factors and anomalous dispersion corrections (for chlorine) provided by the program.

5,6,7,8,9,9-Hexachloro-1,4,4a,5,8,8a-hexahydro-endo-endo-*1,4-ethano-5,8-dimethanonaphthalene*, ***I***b

A fragment ca. 0.04 × 0.46 × 0.21 mm was cut for X-ray structure analysis. Crystal data are as follows:

$C_{13}H_8Cl_6$ $M_r = 376.95$

Orthorhombic, *Pbca*, $a = 15.01(4)$, $b = 13.27(3)$, $c = 15.00(4)$ Å, $U = 2988$ Å^3, $Z = 8$ molecules per cell, $D_c = 1.68$, D_m (not det.) Mg m^{-3}, μ(MoKα) = 10.4 cm^{-1}.

Out of 2488 reflections 1528 were deemed significant. Structure solution was based on the most probable set of phases derived from the 286 *E* values greater than 1.6. In the penultimate refinement cycle, hydrogen atoms were added in theoretical positions using d(C—H) = 1.08 Å. Their temperature factors were refined overall to $U = 0.068$ Å^2. Final atomic co-ordinates are given in Table 1. (Anisotropic temperature factors and the F_o, F_c table have been deposited.)[4] The final unweighted and weighted *R* values were 0.057 and 0.063, respectively. The molecule of **1***b* is illustrated in Fig. 1.[5,6]

5,6,7,8,9,9-Hexachloro-1,4,4a,5,8,8a-hexahydro-endo-endo-*1,4-propano-5,8-dimethanonaphthalene*, ***I***c

A fragment ca. 0.87 × 0.54 × 0.17 mm was cut for X-ray structure analysis. Crystal data are as follows:

$C_{14}H_{12}Cl_6$ $M_r = 392.97$

Monoclinic, $P2_1/c$, $a = 9.42(2)$, $b = 12.30(4)$, $c = 27.84(10)$ Å, $\beta = 97.27(6)°$, $U = 3200$ Å^3, $Z = 8$ molecules per cell, $D_c = 1.63$, D_m (not det.) Mg m^{-3}, μ(MoKα) = 10.61 cm^{-1}.

Out of 5557 reflections, 3945 were considered of significant intensity. There was a 15% loss in reflection intensity during data collection. Structure solution was from the most probable set of phases obtained from the 286 *E* values greater than 1.7.

There are two molecules **A**, **B** in the asymmetric unit whose atomic designations are unprimed and primed, respectively. The former molecule presented no refinement problems but molecule **B** had initially a virtually coplanar propanobridge system and large anisotropic temperature factors for atom C(13)′. This was attributed to disorder and it was possible to resolve and separately refine the two positions for this atom. The positions are named C(13)′ and C(13)″. Refinement of occupancy gave 0.46(5) and 0.54(5); these were then

[4]Complete set of data is available at a nominal charge, upon request, from the Depository of Unpublished Data, CISTI, National Research Council of Canada, Ottawa, Ont., Canada K1A 0S2.

[5]Molecule **I***a* is illustrated in ref. 1.

[6]Atomic numbering used here differs from the systematic.

Can. J. Chem. Downloaded from www.nrcresearchpress.com by 210.87.254.105 on 09/06/12
For personal use only.

TABLE 3.
(*a*) Central bonds

Type	Bond	Length Ia*	Ib	IcA	IcB
	C(1)—Cl(1)	1.75(2)	1.790(7)	1.776(5)	1.775(5)
	C(1)—Cl(6)	1.86(2)	1.771(7)	1.777(5)	1.774(5)
a	C(3)—C(4)	1.34(2)	1.311(9)	1.311(6)	1.320(6)
d	C(6)—C(7)	1.53(2)	1.564(8)	1.552(6)	1.556(6)
a'	C(9)—C(10)	1.30(2)	1.33(1)	1.299(8)	1.321(8)
	C(12)—C(13)	—	1.53(1)	—	—

(*b*) Pseudo-*m* related bonds

Type	Bonds	Length Ia*	Ib	IcA	IcB
	C(2)—Cl(2), C(5)—Cl(5)	1.74(2) 1.74(2)	1.744(7) 1.750(6)	1.755(5) 1.754(4)	1.775(4) 1.764(5)
	C(3)—Cl(3), C(4)—Cl(4)	1.70(2) 1.69(2)	1.701(6) 1.691(7)	1.700(5) 1.708(4)	1.686(5) 1.699(5)
	C(1)—C(2), C(1)—C(5)	1.48(2) 1.51(2)	1.563(9) 1.526(9)	1.551(6) 1.542(6)	1.548(6) 1.548(7)
b'	C(2)—C(3), C(4)—C(5)	1.43(2) 1.46(2)	1.518(9) 1.518(9)	1.518(6) 1.506(6)	1.517(6) 1.511(7)
c'	C(2)—C(7), C(5)—C(6)	1.57(2) 1.58(2)	1.554(9) 1.553(9)	1.577(6) 1.557(6)	1.549(6) 1.543(6)
c	C(7)—C(8), C(6)—C(11)	1.59(2) 1.64(2)	1.552(9) 1.557(9)	1.558(7) 1.544(6)	1.546(7) 1.564(7)
b	C(8)—C(9), C(10)—C(11)	1.45(2) 1.50(2)	1.50(1) 1.50(1)	1.506(7) 1.504(7)	1.484(8) 1.483(8)
	C(8)—C(12), C(11)—C(12)	1.44(2) 1.44(2)	—	—	—
	C(8)—C(12), C(11)—C(13)	—	1.55(1) 1.53(1)	—	—
	C(8)—C(12), C(11)—C(14)	—	—	1.569(8) 1.555(7)	1.555(8) 1.546(8)
	C(12)—C(13), C(13)—C(14)	—	—	1.507(8) 1.522(8)	1.35(2)‡ 1.61(2)‡
	C(12)—C(13)†, C(13)†—C(14)	—	—	—	1.56(2)‡ 1.42(2)‡

*Calculated from ref. 1.
†Second of two disordered positions.
‡Clearly the disordered positions of C(13) given by least-squares refinement are very inaccurate.

both set to 0.5 and kept fixed. Separate, resolvable positions could not be found for C(12)′ or for C(14)′.

All hydrogen atoms of molecule **A** and all those of **B** (apart from those attached to C(12)′, C(13)′, C(13)″, and C(14)′) were found on the ΔF map with density 0.3–0.7 e Å^{-3}. Their positions were fixed theoretically and their individual isotropic temperature factors, U, refined. Temperature factors for the remaining hydrogen atoms of molecule **B** were refined overall to a U value of 0.11 (1) Å^2. Final atomic co-ordinates are listed in Table 2. (Anisotropic temperature factors and the F_o, F_c table have been deposited.)[4] The final unweighted and weighted R values were 0.052 and 0.061, respectively. Molecule **A** is illustrated in Fig. 2 (molecule **B** is not illustrated).

No unusually short intermolecular contacts were reported for the crystal structure of **I***a* and none were found in the crystal structures of **1***b* or **I**c.

Discussion

All four molecules **I***a*, **I***b*, **I***c***A**, and **I***c***B** show nearly exact (non-crystallographic) *m* (C_s) symmetry. This can be shown by using the best molecular fitting program BMFIT (4), which gives the following small sums of the squared atomic displacements from *m* symmetry: **I***a*, 0.065, **I***b*, 0.011, **I***c***A**, 0.02 Å^2. Accordingly, in the lower part of Table 3, pseudo-*m* related bond lengths are paired off, some being designated by lower case letters to facilitate discussion. It will be seen that, for molecules **I***b*, **I***c***A**, and **I***c***B**, all bond lengths agree well (except for the disordered atom in positions C(13)′ and C(13)″). The bond lengths of **I***a* match less well, especially those of types *b* and *c*. In fact, there seems to be a number of bond lengths of **I***a* which are not in good accord with those of **I***b* or

Can. J. Chem. Downloaded from www.nrcresearchpress.com by 210.87.254.105 on 09/06/12
For personal use only.

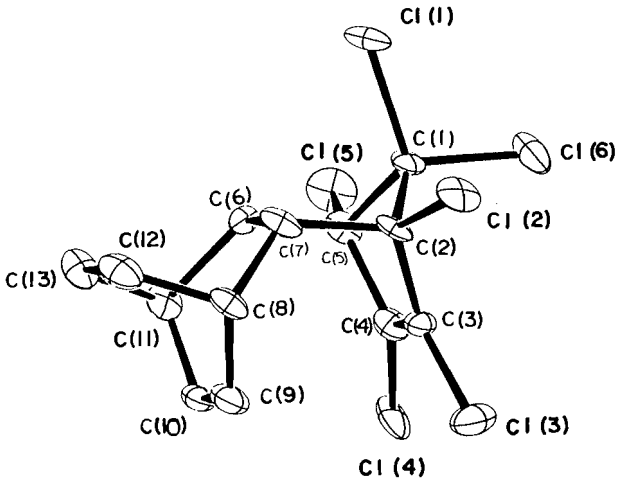

FIG. 1. ORTEP plot (10) of molecule **1***b* showing atomic numbering and 50% probability ellipsoids.

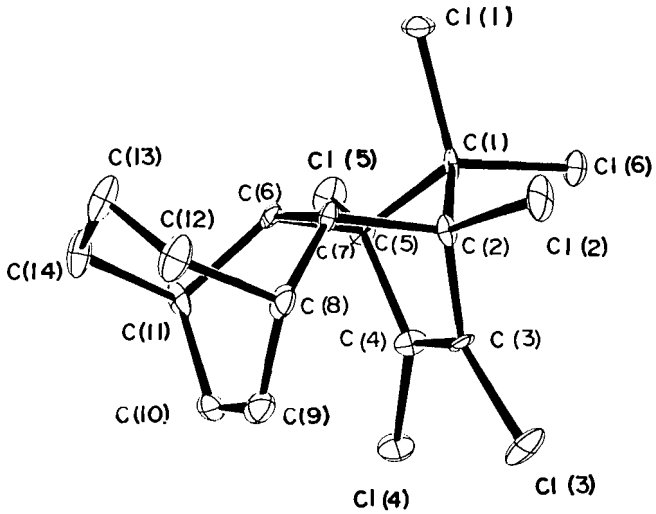

FIG. 2. ORTEP plot of molecule **1***cA*.

I*c*. Accordingly, we carried out a structure analysis on a specimen of **I***a*, but the rapid deterioration of the crystal in X-rays prevented a good data set from being collected. Indeed, we found the same general differences in bond lengths with molecules **I***b* and **I***c* as were found by Kennard *et al.*(1), in particular, that bonds of types *c* and *c'* are, on average, longer than in molecules **I***b* and **I***c*. This effect appears to be directly related to the decreasing repulsion between bonds *a* and *a'* which appears to bring in its train a second effect, a change in the state of hybridization of atoms C(2) and C(5) involved in the *c'*-type bonds. There is a steady increase in the dihedral between planes I and II (see Figure in Table 4): 112°, 119°, and 120°. This, in turn, causes Cl(6) to be brought into repulsive conflict with Cl(2) and Cl(5) causing C(1)—Cl(6) to stretch. It is because of this stretching (which decreases through the series, see Table 3) that the mean distance between Cl(6) and the conflicting chlorine atoms Cl(2) and Cl(5) remains approximately constant: 3.36, 3.40, and 3.45 Å. In the absence of this stretching these distances would have been unacceptably short.

Our main preoccupation is with the nature of the interaction between the double bonds *a*, *a'*. For molecules **I***a* and **I***b* it is possible, using known geometries of suitable molecular fragments, to infer what the geometries of these molecules would have been in the absence of any interaction between bonds *a* and *a'*. Table 4 shows the sources from which the required bond lengths and angles have been taken. Each molecule can be considered to be made up of two parts at bond *d* (i.e. C(6)—C(7)), one part being the same in all three molecules, the other varying with *n*, the number of bridging methylene groups. In the case of molecule **I***c* we could find no precedent for this second half so we have used the geometry of the molecule itself and connected it to the idealised constant part. We find that this molecule shows the least double-bond/double-bond interaction of the three so that, probably, the hypothetical molecule (completely free from this interaction) would have similar bond lengths and angles to those found experimentally.

TABLE 4. Bond lengths and angles assumed to calculate geometry of hypothetical molecules in absence of double-bond/double-bond interaction

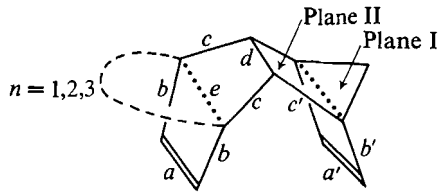

	Length		
Bond	*n* = 1	*n* = 2	*n* = 3¶
a	1.32*	1.32‡§	1.31
b	1.509*	1.505‡§	1.49
c	1.550*	1.538‡§	1.55
d	1.520*	1.54‡	1.54
e	2.235*	2.566‡	2.745
	Angle		
Bonds	*n* = 1	*n* = 2	*n* = 3
b ^ *c*	105°*	108.9°‡	112.4°
c ^ *c'*	112°*†	112°‖	112°

*Bicyclo[2.2.1]hept-2-ene (5).
†Bicyclo[2.2.1]heptane (6).
‡Bicyclo[2.2.1]octene (7).
§Tricyclo[4.4.2.0^{25}]decadiene (8).
‖Dodecahydrotriptycene (9).
¶This paper.

From the dimensions assumed in Table 4 it is possible to calculate exactly what the distances between the mid-points of bonds *a* and *a'* would have been in the absence of any double-bond/double-bond interaction across space. The results are 2.03, 2.37, and 2.67 Å for **I***a*, **I***b*, and **I***c*, respectively. The experimental distances are: **I***a*, 2.87 (calculated from ref. 1), **I***b*, 2.94, **I***c***A**, 2.99 and **I***c***B**, 3.01 Å. These results imply that there is a repulsive interaction between the double bonds in these molecules which decreases through the homologous series, the differences between observed and hypothetical distances decreasing: 0.84, 0.57, and 0.33 (mean) Å. (It is possible that changes in the state of hybridization of atoms C(9) and C(10) also play some part in this trend. The mean bond angle *a* ^ *b* increases significantly through the series: 108.0°, 114.9°, 119.1°.)

In conclusion, since the double-bond/double-bond interaction across space decreases in the order **I***a* > **I***b* > **I***c*, the strain within the molecules must decrease in the same order. Dong and Edward (2) came to the same conclusion using

Can. J. Chem. Downloaded from www.nrcresearchpress.com by 210.87.254.105 on 09/06/12
For personal use only.

Dreiding molecular models and, as noted earlier, attributed this decreasing strain to the decreasing speed of cyclization in uv-irradiated solutions.

Acknowledgement

Financial assistance from the Natural Sciences and Engineering Research Council of Canada is gratefully acknowledged.

1. C. H. L. KENNARD, G. SMITH, and S. HOVMÖLLER. Acta Crystallogr. B**35**, 493 (1979).
2. D. C. DONG, and J. T. EDWARD. J. Org. Chem. **45**, 2395 (1980).
3. G. SHELDRICK. X-Ray System Report. University of Cambridge. 1976.
4. P.-S. YUEN, and S. C. NYBURG. J. Appl. Crystallogr. **12**, 258 (1979).
5. G. EVRARD, R. THOMAS, B. R. DAVIS, and I. BERNAL. J. Organomet. Chem. **124**, 59 (1977).
6. G. CHAPUIS, A. ZALKIN, and D. H. TEMPLETON. Acta Crystallogr. B**33**, 560, (1977).
7. S. G. DYKES, and R. E. DAVIS. Acta Crystallogr. B**33**, 3243 (1977).
8. J. T. LEMLEY, J. J. STEZOWSKI, and R. E. HUGHES. Acta Crystallogr. B**32**, 1212 (1976).
9. A. ALBINATI, S. BRÜCKNER, and G. ALLEGRA. Acta Crystallogr. B**33**, 229 (1977).
10. C. K. JOHNSON. ORTEP. Report ORNL-3974. Oak Ridge National Laboratory, TN.

Can. J. Chem. Downloaded from www.nrcresearchpress.com by 210.87.254.105 on 09/06/12
For personal use only.

Calculation of phase diagrams and thermodynamic properties of 14 additive and reciprocal ternary systems containing Li_2CO_3, Na_2CO_3, K_2CO_3, Li_2SO_4, Na_2SO_4, K_2SO_4, LiOH, NaOH, and KOH[1]

A. D. PELTON, C. W. BALE, AND P. L. LIN
Ecole Polytechnique, C. P. 6079, Succ. "A", Montréal (Qué.), Canada H3C 3A7

Received November 25, 1982[2]

A. D. PELTON, C. W. BALE, and P. L. LIN. Can. J. Chem. **62**, 457 (1984).

Phase diagrams and thermodynamic properties of five additive molten salt ternary systems and nine reciprocal molten salt ternary systems containing the ions Li^+, Na^+, K^+/CO_3^{2-}, SO_4^{2-}, OH^- are calculated from the thermodynamic properties of their binary subsystems which were obtained previously by a critical assessment of the thermodynamic data and the phase diagrams in these binary systems. Thermodynamic properties of ternary liquid phases are estimated from the binary properties by means of the Conformal Ionic Solution Theory. The ternary phase diagrams are then calculated from these thermodynamic properties by means of computer programs designed for the purpose. It is found that a ternary phase diagram can generally be calculated in this way with a maximum error about twice that of the maximum error in the binary phase diagrams upon which the calculations are based. If, in addition, some reliable ternary phase diagram measurements are available, these can be used to obtain small ternary correction terms. In this way, ternary phase diagram measurements can be smoothed and the isotherms drawn in a thermodynamically correct way. The thermodynamic approach permits experimental data to be critically assessed in the light of thermodynamic principles and accepted solution models. A critical assessment of error limits on all the calculated ternary diagrams is made, and suggestions as to which composition regions merit further experimental study are given.

A. D. PELTON, C. W. BALE et P. L. LIN. Can. J. Chem. **62**, 457 (1984).

On a calculé les diagrammes de phase et les propriétés thermodynamiques de 5 systèmes ternaires additifs de sels fondus et de 9 systèmes ternaires réciproques de sels fondus contenant des ions Li^+, Na^+, K^+/CO_3^{2-}, SO_4^{2-}, OH^-; ces calculs ont été effectués à partir des propriétés thermodynamiques de leurs sous-systèmes binaires que l'on a obtenues antérieurement par un évaluation critique des données thermodynamiques et des diagrammes de phase de ces systèmes binaires. On a évalué les propriétés thermodynamiques des phases liquides ternaires en faisant appel à la théorie des solutions ioniques conformales. On calcule alors les diagrammes de phases ternaires à partir de ces propriétés thermodynamiques au moyen de programmes d'ordinateurs réalisés dans ce but. On a trouvé qu'un diagramme de phase ternaire peut généralement être calculé de cette façon avec une erreur maximale qui n'est que le double de l'erreur maximale obtenue avec les diagrammes de phases binaires sur lesquels reposent ces calculs. De plus, si on dispose de mesures fiables pour les diagrammes de phases ternaires, on peut alors utiliser ces mesures pour déduire des petits termes de correction ternaires. De cette façon, on peut raffiner les mesures de diagrammes de phases ternaires et tracer les isothermes d'une manière qui est thermodynamiquement correcte. L'approche thermodynamique permet d'évaluer les données expérimentales d'une façon critique à la lumière de principes thermodynamiques et de modèles acceptables pour les solutions. On a fait une évaluation critique des limites d'erreur sur tous les diagrammes ternaires calculés et on fait des suggestions relatives aux zones de composition qui méritent des études expérimentales plus approfondies.

[Traduit par le journal]

Introduction

In the molten carbonate fuel cell being developed by the U.S. Department of Energy, the electrolyte consists nominally of a mixture of liquid lithium and potassium carbonates. It has been proposed that sodium carbonate might also be added. The gas phase contains a mixture of hydrocarbons, H_2, CO, CO_2, O_2, N_2, etc. Significant quantities of sulfur may also be present as impurity in the gas phase as SO_2, SO_3, S_2, H_2S, etc. Since the gas is recirculated between electrode compartments, the sulfur can accumulate in the electrolyte.

Reaction between the gas and liquid phases can result in changes in electrolyte composition through the appearance of OH^- and SO_4^{2-} ions dissolved in the molten carbonate and through volatilization of hydroxides. Under certain conditions, S^{2-} ions may also be present, but the principal ions expected in solution will be Li^+, K^+, Na^+, CO_3^{2-}, OH^-, and SO_4^{2-}. The composition of the electrolyte is important to the operating characteristics of the cell. In particular, too large a shift from the nominal $Li_2CO_3-K_2CO_3$ composition could result in the precipitation of solid phases. In addition, volatilization of the electrolyte can occur through the formation of hydroxide vapour species such as LiOH and $Li_2(OH)_2$.

The composition of the electrolyte depends upon the composition of the gas phase with which it is in contact. The entire system cannot be at equilibrium since the gases in the anode and cathode compartments are different. Hence, composition gradients will be observed in the electrolyte. At the high operating temperature (650°C) of the cell, however, it is likely that local gas–liquid equilibrium is attained.

It would be desirable to have a complete thermodynamic analysis of the system such that, for a given temperature and total pressure, a given overall gas composition, and a given Li/K ratio in the electrolyte one could find, at equilibrium, (*i*) the partial pressures of all the species in the gas phase and the extent of electrolyte volatilization, and (*ii*) the composition of the electrolyte. It would also be desirable to have the phase diagram of the Li, Na, K/CO_3, OH, SO_4 system, especially near the nominal alkali composition of the operating cell, to know whether the precipitation of any solid phases is expected. The results should be important for fully defining the chemistry of cell operation and for understanding how different variables (e.g. changes in fuel composition) influence the chemistry of the cell and volatilization.

[1]This work was sponsored by the U.S. Department of Energy under Contract DE-AC02-79ET15416. The views, opinions, and/or findings in this article are those of the authors and should not be construed as an official U.S. Government or Department of Energy position, policy, or decision.

[2]Revision received September 6, 1983.

Can. J. Chem. Downloaded from www.nrcresearchpress.com by 210.87.254.6 on 09/06/12
For personal use only.

TABLE 1. Thermodynamic properties of pure salts

Compound	Phase transformation I → II	Temperature of transformation T^0_{Tr} (°C)	Enthalpy of transformation T^0_{Tr} (kcal/mol)	Change in molar heat capacity $\Delta C_p = C_p^{II} - C_p^{I} = a + bT + c/T^2$ (cal/mol K)		
				a	$b \times 10^3$	$c \times 10^{-5}$
Li_2CO_3	α → l	720	10.7	40.887	−43.2	
	β → α	410	0.535	0		
Na_2CO_3	α → l	850	7.09	33.33	−30.85	
K_2CO_3	α → l	901	6.6	26.595	−22.008	2.368
Li_2SO_4	α → l	859	3.3	13.3	−13.5	
	β → α	586	6.5	14.6	−18.8	
Na_2SO_4	α → l	884	5.5	12.512	−13.049	
	β → α	249	2.584	14.992	−23.844	
K_2SO_4	α → l	1069	8.8	14.2	−13.4	
	β → α	583	2.14	4.83	−10.4	4.26
LiOH	α → l	471	5.01	8.75	−8.24	2.27
NaOH	α → l	320	1.52	0.83	−1.4	
	β → α	293	1.52	16.946	−29.2	
KOH	α → l	400	2.24	1.06		
	β → α	249	1.515	8.604	−18.395	

Such a complete thermodynamic analysis has recently been performed by the authors (1) using the facilities of the F*A*C*T computerized thermodynamic data bank and data treatment center (2). The results of the first stage of this project, the optimizational analysis of the phase diagrams and thermodynamic properties of the 18 binary systems containing the ions Li^+, Na^+, K^+/SO_4^{2-}, CO_3^{2-}, OH^-, was reported in a previous publication (3). In the present article are reported the results of the second stage, the calculation of the thermodynamic properties and phase diagrams of 14 ternary additive and reciprocal fused salt systems containing these ions.

The calculation of phase diagrams of ternary fused salt systems — general methodology

The calculation of the ternary phase diagrams was carried out in the following manner. First, all available thermodynamic data and measured phase diagrams of the binary subsystems of each ternary system were critically assessed and an optimization analysis (4) was carried out in order to obtain mathematical expressions for the Gibbs energies of all phases as functions of temperature and composition which "best" reproduce the experimental thermodynamic properties and phase diagrams. Second, interpolation procedures were used to estimate the Gibbs energies of the ternary liquid phases from the Gibbs energies of the binary liquid phases. Finally, the ternary phase diagrams were calculated from these estimated ternary thermodynamic properties.

This type of calculation has been carried out for a large number of ternary salt systems by the present authors (5−10) and by others (11−14). This experience has shown that, in general, the maximum uncertainty in an estimated ternary phase diagram is about twice that of the binary phase diagrams upon which the calculations are based. If the binary phase diagrams have been measured to ±5°C, then the ternary diagram estimated therefrom is probably accurate to ±10°C.

If, in addition, some ternary phase diagram measurements have been made, a small adjustable ternary term can be added to the expression for the Gibbs energy in order to increase the precision. Even when ternary phase diagram data are available, this type of approach serves to smooth the data and to yield ternary isotherms whose interpolated shape is consistent with basic thermodynamic principles.The data can be checked for internal consistency, discrepancies can be identified and frequently resolved, and areas in which further experimentation is required can be identified.

Thermodynamic properties of the pure components

Thermodynamic properties of the nine pure salts are listed in Table 1. Data are taken mainly from ref. 15. Details of the sources and accuracy of these data are given in refs. 1 and 3.

Temkin ideal mixing terms

The Gibbs energy of a molten salt solution can be written as the sum of ideal and excess terms. For the ideal terms, experience has shown that the Temkin model in which cations and anions mix randomly on their respective sublattices, regardless of charge, invariably gives the best results and is consistent with observations in the limiting dilute concentration regions. In the Temkin model, the ideal entropy of mixing referred to the pure neutral salts is given by:

$$[1] \quad \Delta S = -R\Sigma n_k \ln X_k$$

where n_k is the number of moles of ions k in solution, and X_k is either the cationic or anionic molar fraction of ion k defined as:

$$[2] \quad X_k = n_k / \sum_{\text{cations}} n_i$$

in the case of a cation, or

$$[3] \quad X_k = n_k \Big/ \sum_{\text{anions}} n_j$$

in the case of an anion.

It is also necessary for the following discussion to define the equivalent ionic fraction, Y_k, of ion k as:

$$[4] \quad Y_k = q_k n_k / \Sigma q_i n_i$$

where q_k is the absolute value of the charge on ions k, and the summation in eq. [4] is over all cations if k is a cation or over all anions if k is an anion.

Thermodynamic/phase diagram analysis of binary systems

There are nine binary common anion systems (e.g.

Can. J. Chem. Downloaded from www.nrcresearchpress.com by 210.87.254.6 on 09/06/12
For personal use only.

$Li_2CO_3-K_2CO_3$) and nine binary common cation systems (e.g. $LiOH-Li_2CO_3$) formed among the ions Li^+, Na^+, K^+/CO_3^{2-}, SO_4^{2-}, OH^-. Expressions were obtained (3) for the thermodynamic properties of all phases in these systems as functions of temperature and composition.

In the liquid binary phases and in any binary solid solutions, the enthalpy of mixing, Δh^{mix}, and the excess entropy of mixing, s^E, per equivalent of solution, are expressed as power series in the equivalent ionic fractions as follows:

$$[5] \quad \Delta h^{mix} = \sum_{i,j} h_{ij} Y_A^i Y_B^j$$

$$[6] \quad s^E = \sum_{i,j} s_{ij}^E Y_A^i Y_B^j$$

and so the equivalent excess Gibbs energy is given as:

$$[7] \quad g^E = \sum_{i,j} \phi_{ij} Y_A^i Y_B^j = \sum_{i,j} (h_{ij} - T s_{ij}^E) Y_A^i Y_B^j$$

where Y_A, Y_B are the equivalent ionic fractions of the anions in the case of a common-cation binary system, or the equivalent ionic fractions of the cations in the case of a common-anion system.

h_{ij} and s_{ij}^E are empirical coefficients found by a least-squares optimization procedure to be discussed shortly. The number of coefficients required to give a satisfactory representation varies from system to system. Experience has shown that the use of equivalent ionic fractions rather than molar ionic fractions in the polynomial expansions frequently reduces the number of coefficients required to yield a satisfactory fit. In the present study, no more than three terms were ever required.

Δh^{mix}, s^E, and g^E in eqs. [5], [6], [7] are expressed per equivalent of solution. One equivalent of solution contains one equivalent of anions and one equivalent of cations. Hence, this method of representation is unambiguous, whereas normalization in terms of a "mole of solution" would be ambiguous since, with ions of different absolute charges, the number of moles of cations and the number of moles of anions in solution are not necessarily equal.

Dilute binary solid solutions are treated as Henrian solutions. The Henrian activity coefficient γ^0 is expressed as:

$$[8] \quad RT \ln \gamma^0 = A + BT$$

where A and B are adjustable parameters. Often, B can be set equal to zero. Values of A and B are generally calculated so as to reproduce the measured solubilities in the binary solid phases.

Finally, it is necessary to obtain expressions for the Gibbs energies of fusion of all known binary intermediate solid compounds, $(M_mX)_x(N_nY)_{(1-x)}$, as follows:

$$[9] \quad \Delta g^0_{fusion} = a + bT$$

For many of the 18 binary systems, Δh^{mix} has been measured calorimetrically for the liquid phases. For all but one of the systems, experimental phase diagrams are available. For a few intermediate compounds, Δg^0_{fusion} has been measured. A critical optimization analysis of all these data was performed (3) in order to find the "best" set of coefficient h_{ij}, s_{ij}^E, A, B, a, b of eqs. [5]–[9] for each system. For those intermediate compounds for which Δg^0_{fusion} has not been measured, the coefficients a, b of eq. [9] were found from phase diagram analysis after all the other coefficients had been determined. The choice of which coefficients are "best" is based upon the authors' judgment of the reliability of the various sets of data, of whether certain values of thermodynamic properties are plausible or not based upon experience with similar systems, and so on. The choice is made partially subjectively and partially objectively. A computer program called "FITBIN" (2) has been written to assist in this critical analysis. The different sets of data (thermodynamic data and parameters, liquidus compositions, etc.) are read directly into the computer interactively along with appropriate weighting factors. The computer program linearizes the data and performs a least-squares optimization procedure. The operator can interact with the program until the "best" analysis is obtained. This interaction can involve changing the weighting factors for certain data points or data sets, varying the numbers of coefficients used in the polynomial expansions and so on. The choice of the "best" coefficients must always be made with a large measure of subjectivity based upon an assessment of the reliability of the various data sets, upon a knowledge of the behaviour of similar systems, and upon experience. However, the computer-assisted analysis assures thermodynamic consistency and plausibility, permits the thermodynamic data and the phase diagram data to be treated simultaneously, and ensures that the rules of solution theory such as adherence to Raoult's Law in concentrated solutions are obeyed. The interactive nature of the computer programs takes the tedium out of the calculations and permits the operator to concentrate on the analysis itself rather than on the mechanical details.

Complete details of the analysis for all 18 binary systems are given in ref. 3. A summary of the optimized parameters is given in Table 2. Binary phase diagrams calculated from these parameters are given in ref. 3 and are also shown as the edges of the ternary diagrams in Figs. 3–16 of the present article. The optimization analysis also aids in the assessment of the accuracy of the calculated diagrams. These accuracies are listed in Table 2 as "probable maximum deviations". This is the estimated probable maximum difference between the true diagrams and the calculated diagrams which can be regarded as the best present estimates of the true diagrams.

Procedures used for the calculation of ternary phase diagrams

Once all the binary systems have been analysed, the thermodynamic properties of the ternary systems may be estimated by means of interpolation procedures.

Additive ternaries

The additive ternary systems in the present study are those composed of three salts with a common cation such as $Li_2CO_3-Li_2SO_4-LiOH$, or three salts with a common anion such as $Li_2CO_3-Na_2CO_3-K_2CO_3$. Compositions are expressed on the standard "Gibbs triangle".

The interpolation formulae for estimating ternary Gibbs energies from binary Gibbs energies which have proved successful in the case of additive fused salt systems are the Conformal Ionic Solution (CIS) equation (16) and a group of "geometrical" formulae, most notably the Kohler (17) and Toop (18) equations.

CIS equation

The CIS equation, which is based upon statistical mechanical perturbation theory, for the excess Gibbs energy of an additive ternary molten salt system with components 1–2–3 is derived (16) as:

Can. J. Chem. Downloaded from www.nrcresearchpress.com by 210.87.254.6 on 09/06/12
For personal use only.

Can. J. Chem. Downloaded from www.nrcresearchpress.com by 210.87.254.6 on 09/06/12
For personal use only.

TABLE 2. Thermodynamic properties of the binary systems (all units in cal per mol, T in K)

Binary system		Solution phase coefficients h_{ij}, s^{E}_{ij} (eqs. [5], [6])				Henrian solid phases $RT \ln \gamma_i^0 = A + BT$			Solid phase A_xB_{1-x} $\Delta g^0_{fusion} = a + bT$			Probable maximum deviation of calculated diagram from true diagram
A	B	i,j =	1,1	1,2	1,3	i	A	B	x	a	b	
$Na(CO_3)_{1/2}$	$Li(CO_3)_{1/2}$	h(liq)	−1183	−309.5		$Li(CO_3)_{1/2}$	3200					±5°C Li_2CO_3 side
		s(liq)	−1.0352									±10°C Na_2CO_3 side
$K(CO_3)_{1/2}$	$Li(CO_3)_{1/2}$	h(liq)	−3293.5	−1314.5		$Li(CO_3)_{1/2}$	2900		0.5	4350	−5.6	±5°C central portion
		s(liq)	−2.1923									±10°C elsewhere
$K(CO_3)_{1/2}$	$Na(CO_3)_{1/2}$	h(liq)	−601	−151.75								
		s(liq)	0									±5°C
		h(s)	766	774								
$Li(SO_4)_{1/2}$	$Na(SO_4)_{1/2}$	h(liq)	−1025	−265		$Li(SO_4)_{1/2}$	757		0.5	2343.7	−2.660	±20°C liquidus
		s(liq)	0			$Na(SO_4)_{1/2}$	747		0.333	2888.7	−3.121	±35°C solidus
$Li(SO_4)_{1/2}$	$K(SO_4)_{1/2}$	h(liq)	−2560	−930		$Li(SO_4)_{1/2}$	2500		0.5	2990.6	−2.977	±10°C $X(K_2SO_4)>0.3$
		s(liq)	0						0.667	4186.3	−4.990	±25°C elsewhere
$K(SO_4)_{1/2}$	$Na(SO_4)_{1/2}$	h(liq)	−525									
		s(liq)	0									±10°C
		h(s)	1282.6	−2581.6	3160.5							
NaOH	LiOH	h(liq)	−1625.2	−71.7		LiOH	8480	14	0.5	3178.3	−6.018	±10°C
		s(liq)	−0.0849	−1.5534	0.86651							
KOH	LiOH	h(liq)	−2731.8	−3016.3	1037.3				0.333	4456.9	−7.551	±5°C
		s(liq)	0.609	−3.797	1.735							
KOH	NaOH	h(liq)	−616.63	117.1		NaOH	3100	−4.17				±10°C
		s(liq)	−1.9879	−2.3115								
Li_2CO_3	Li_2SO_4	h(liq)	−1251			Li_2CO_3	4600					±20°C near eutectic
		s(liq)	0									±15°C elsewhere
Li_2CO_3	LiOH	h(liq)	−752.9			LiOH	10150	−8.5				±10°C
		s(liq)	0									
LiOH	Li_2SO_4	h(liq)	−900									±30°C
		s(liq)	0									
Na_2CO_3	Na_2SO_4	h(liq)	0									±5°C liquidus
		h(s)	820									±10°C solidus
Na_2CO_3	NaOH	h(liq)	3.596	−134.5								±5°C near eutectic
		s(liq)	0									±15°C above 725 K
NaOH	Na_2SO_4	h(liq)	−903.1						0.5	5035	−6.706	±15°C
		s(liq)	0									
K_2CO_3	K_2SO_4	h(liq)	0									±15°C
		h(s)	1300									
K_2CO_3	KOH	h(liq)	361.93	174.36								±15°C
		s(liq)	0									
KOH	K_2SO_4	h(liq)	−915.3									±5°C below 975 K
		s(liq)	0									±10°C above 975 K

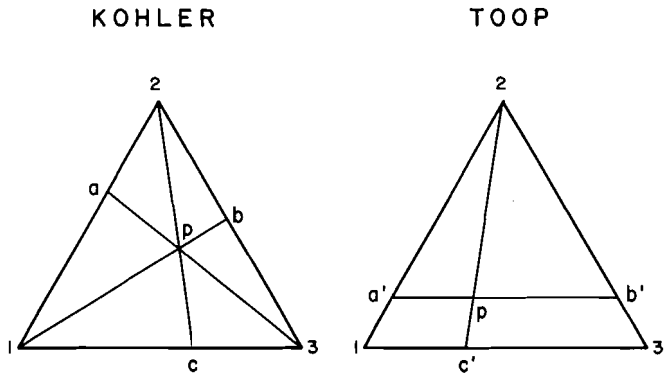

FIG. 1. Composition triangle illustrating the geometrical basis of the Kohler and Toop equations [11], [12].

$$[10]\quad g^E = \sum_m \sum_{n<m} \phi_{11(mn)} Y_m Y_n + \sum_{m \neq n} \phi_{21(mn)} Y_m^2 Y_n + \sum_{m<n} \phi_{22(mn)} Y_m^2 Y_n^2 - (\phi_{21(12)}^{1/3} + \phi_{21(13)}^{1/3})(\phi_{21(23)}^{1/3} + \phi_{21(21)}^{1/3}) \times (\phi_{21(31)}^{1/3} + \phi_{21(32)}^{1/3}) Y_1 Y_2 Y_3 + \sum_{m \neq n < k} 2(\phi_{22(mn)} \phi_{22(mk)})^{1/2} Y_m^2 Y_n Y_k$$

where g^E is expressed per equivalent of solution and where Y_1, Y_2, Y_3 are the equivalent ionic fractions of the non-common ions. Hence, g^E in the ternary can be calculated from a knowledge of the coefficients $\phi_{11(mn)}$, $\phi_{21(mn)} = -\phi_{21(nm)}$, and $\phi_{22(mn)} = \phi_{22(nm)}$ of the three binary subsystems.

Kohler and Toop equations

The Kohler equation (17) for the ternary excess Gibbs energy is

$$[11]\quad g^E_{(P)} = (1 - X_3)^2 g^E_{(a)} + (1 - X_1)^2 g^E_{(b)} + (1 - X_2)^2 g^E_{(c)}$$

The Toop equation (18) is as follows:

$$[12]\quad g^E_{(P)} = \frac{X_1}{X_1 + X_3} g^E_{(a')} + \frac{X_3}{X_1 + X_3} g^E_{(b')} + (1 - X_2)^2 g^E_{(c')}$$

where, in the 1–2–3 ternary system of Fig. 1, $g^E_{(P)}$ is the excess Gibbs energy at point p in the ternary system and $g^E_{(a)}$, $g^E_{(a')}$, ... are the excess Gibbs energies in the binary systems at the points indicated. X_1, X_2, X_3 are the molar ionic fractions of the non-common ions, and g^E in eqs. [11], [12] is expressed per mol of non-common ions in the solution.

Equations [11], [12] are based on regular solution theory, and both equations are exact if the binary and ternary solutions are regular. The Kohler equation has the advantage over the Toop equation of being symmetrical with respect to the three components. Therefore, the Kohler equation is preferred over the Toop equation for charge symmetrical additive ternary systems. For ternary charge asymmetrical fused salt systems such as $MOH-M_2SO_4-M_2CO_3$, the Toop equation is preferred over the Kohler equation, with the asymmetrical component (MOH) as component 2 in Fig. 1. In this case, the first two terms on the right hand side in eq. [12] represent a linear interpolation between the two asymmetrical binary systems 2–1 and 2–3 at the same mole fraction X_2, while the third term, which is the same as the third term in eq. [11], represents the contribution from the charge-symmetrical 1–3 system.

The CIS equation [10] applies equally to charge symmetrical and charge-asymmetrical systems and is, in general, to be preferred over both the Kohler and Toop equations for fused salt solutions since it is based on firmer theoretical ground and has been developed specifically for liquid salt solutions, whereas the Kohler and Toop equations are more general and are semi-empirical. However, for solid solutions, the more general equations are preferable, since the theoretical basis for the CIS equations no longer holds. In the present study for dilute ternary solid solutions which extend a short distance into the ternary system from one side of the composition triangle, the Toop equation, asymmetric in the third component, is preferable on grounds of symmetry.

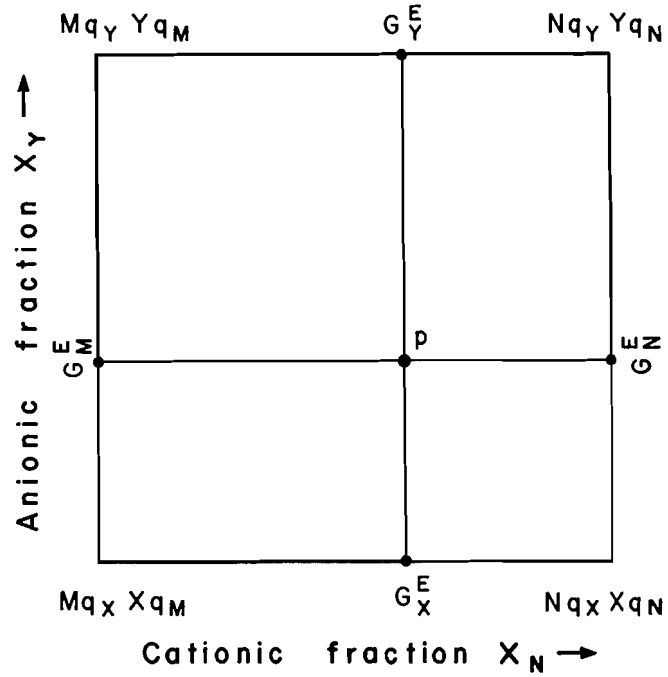

FIG. 2. Composition square of a reciprocal ternary system illustrating the geometrical basis of the CIS equation [13].

Equations [10], [11], [12] have been shown (4–14) to give good approximations for a large number of ternary salt systems.

If a measured ternary phase diagram is available, and if the calculated and measured diagrams do not agree within the experimental error limits of the latter, then ternary terms of the form $\phi_{ijk} Y_1^i Y_2^j Y_3^k$ with adjustable parameters ϕ_{ijk} ($i, j, k \geq 1$) can be added to eqs. [10], [11], [12], although this was not required in the present study.

Reciprocal ternaries

A reciprocal ternary system is defined as one containing two cations, M, N and two anions, X, Y. Although such a system contains four ions, the condition of charge neutrality removes one degree of freedom. Concentrations in a reciprocal ternary system are most conveniently plotted on a composition square as shown in Fig. 2 in which the horizontal and vertical axes are the cationic and anionic mole fractions, X_N and X_Y. The corners of this square represent compositions corresponding to the pure neutral salts $M_{q_X} X_{q_M}$, etc. (where q_M, q_N, q_X, q_Y are the absolute charges on the ions), and the edges of the square represent compositions in the binary subsystems.

The extended CIS theory (19, 20) for reciprocal ternary systems has been applied with success (6, 9, 21–23) to calculate the thermodynamic properties of a large number of ternary reciprocal systems from the properties of the binary subsystems. The excess Gibbs energy per equivalent of solution at a point P (see Fig. 2) within the ternary system relative to the

Can. J. Chem. Downloaded from www.nrcresearchpress.com by 210.87.254.6 on 09/06/12
For personal use only.

TABLE 3. The Gibbs energy of the exchange reactions and the Λ term

Reaction	ΔG^{EX} (cal)	Λ (cal)
$\frac{1}{2}K_2CO_{3(l)} + \frac{1}{2}Li_2SO_{4(l)} = \frac{1}{2}K_2SO_{4(l)} + \frac{1}{2}Li_2CO_{3(l)}$	$-2030 - 20.00T + 2.34T \ln T$	$-2170 + 0.721T$
$\frac{1}{2}K_2CO_{3(s)} + \frac{1}{2}Li_2SO_{4(s)} = \frac{1}{2}K_2SO_{4(s)} + \frac{1}{2}Li_2CO_{3(s)}$	$-11731 + 5.63T$	$-6501 + 4.845T$
$\frac{1}{2}Na_2CO_{3(l)} + \frac{1}{2}Li_2SO_{4(l)} = \frac{1}{2}Na_2SO_{4(l)} + \frac{1}{2}Li_2CO_{3(l)}$	$-2825 - 2.26T + 0.3T \ln T$	$-917 + 0.541T$
$\frac{1}{2}K_2CO_{3(l)} + \frac{1}{2}Na_2SO_{4(l)} = \frac{1}{2}K_2SO_{4(l)} + \frac{1}{2}Na_2CO_{3(l)}$	$+795 - 17.75T + 2.04T \ln T$	$-313 - 0.029T$
$\frac{1}{2}K_2CO_{3(l)} + LiOH_{(l)} = \frac{1}{2}Li_2CO_{3(l)} + KOH_{(l)}$	$11900 - 34.235T + 3.72T \ln T$	$-4502 + 3.802T$
$\frac{1}{2}Li_2CO_{3(l)} + NaOH_{(l)} = \frac{1}{2}Na_2CO_{3(l)} + LiOH_{(l)}$	$-4375 + 1.065T + 0.15T \ln T$	$-1469 + 1.19T$
$NaOH_{(l)} + \frac{1}{2}K_2CO_{3(l)} = KOH_{(l)} + \frac{1}{2}Na_2CO_{3(l)}$	$7525 - 33.17T + 3.87T \ln T$	$-910 + 0.802T$
$\frac{1}{2}K_2SO_{4(l)} + NaOH_{(l)} = \frac{1}{2}Na_2SO_{4(l)} + KOH_{(l)}$	$6730 - 15.42T + 1.83T \ln T$	$-2452 + 1.781T$
$\frac{1}{2}Li_2SO_{4(l)} + KOH_{(l)} = \frac{1}{2}K_2SO_{4(l)} + LiOH_{(l)}$	$-13930 + 14.23T - 1.38T \ln T$	$-12928 + 8.237T$
$\frac{1}{2}Li_2SO_{4(l)} + NaOH_{(l)} = \frac{1}{2}Na_2SO_{4(l)} + LiOH_{(l)}$	$-7200 - 1.19T + 0.45T \ln T$	$-4722 + 3.412T$

pure components $M_{q_X}X_{q_M}$, $N_{q_X}X_{q_N}$ and $N_{q_Y}Y_{q_N}$, is given by the CIS theory as:

$$[13] \quad g^E = Y_M Y_Y \Delta G^{EX} + (Y_M g_M^E + Y_N g_N^E + Y_X g_X^E + Y_Y g_Y^E) + Y_M Y_N Y_X Y_Y \Lambda$$

where g_M^E, g_N^E, g_X^E, g_Y^E are the excess equivalent Gibbs energies in the four binary subsystems at the ends of horizontal and vertical lines passing through point P in Fig. 2, and where ΔG^{EX} is the Gibbs energy of the "exchange reaction" among one equivalent of each of the pure salts according to:

$$[14] \quad (q_M q_X)^{-1} M_{q_X} X_{q_M} + (q_N q_Y)^{-1} N_{q_Y} Y_{q_N} = (q_M q_Y)^{-1} M_{q_Y} Y_{q_M} + (q_N q_X)^{-1} N_{q_X} X_{q_N}$$

The factor Λ in eq. [13] is composition-independent. It has been shown (19, 20) that, for liquid salts, to a first approximation Λ is given by:

$$[15] \quad \Lambda = -(\Delta G^{EX})^2 / 2ZRT$$

where the parameter Z is commonly taken as $Z = 6$.

For solid reciprocal ionic phases, larger deviations from the CIS equation are to be expected since the theoretical assumptions on which the CIS model are based are not as good for solids. In particular, there is probably little justification to the use of eq. [15] for solid phases. If a measured ternary diagram of sufficient accuracy is available, and if the measured and calculated diagrams do not agree within the experimental error limits, then Λ can be taken as an adjustable ternary parameter. Although for a liquid phase the value of Λ should not deviate too far from that given by eq. [15] and should in theory always be negative, in the case of a solid reciprocal salt phase much larger deviations are to be expected.

Values of ΔG^{EX} taken from ref. 15 for the exchange reactions (expressed in terms of one equivalent of each reactant and product) for the nine reciprocal systems in the present study are listed in Table 3. Values of Λ from eq. [15], linearized with respect to temperature over the temperature range of interest, are also listed in Table 3.

It is to be noted that the most important term in eq. [13] as regards its influence upon g^E and hence upon the calculated phase diagram is the term containing ΔG^{EX}. The "binary terms" are of lesser importance, and the term containing Λ is generally of least significance.

Detailed calculations for ternary systems

The techniques discussed above cannot, of course, predict the existence of ternary compounds. If a ternary compond is known to exist, then it can be included in the calculations. In general, for systems treated here, the existence of unknown ternary compounds with large negative Gibbs energies of formation from neighouring compounds which could significantly affect the liquidus surface is unlikely.

Details of the calculations of the 14 ternary additive and reciprocal phase diagrams considered in the present study will now be given. Calculated polythermal projections of the liquidus surfaces are presented along with the values of any ternary parameters. Reproductions of measured ternary diagrams are also given for each system when available. The calculated diagrams were prepared with the computer programs TERNFIG and RECIPFIG which are available as part of the F*A*C*T (2) interactive computer system.

The accuracy of the calculated phase diagrams depends strongly upon the composition region in question. In general, near any binary subsystem the error in the ternary diagram is about the same as that given in Table 2 for the binary system. Accuracies quoted in the following discussions of individual ternary systems are given as estimated "probable maximum deviations" between the calculated diagrams and the true diagrams ("true" diagram means the real correct diagram, not the experimental diagram). However, in most composition regions, the probable deviation will generally be less than the quoted "maximum" value.

In the calculated polythermal projections, temperatures are in °C. The symbols e, p, and m refer to binary eutectics, peritectics, and minima, and the symbols E and P refer to ternary eutectics and peritectics. The maximum extent of solid solubility in the binary subsystems is indicated by hatching along the axes of the diagrams. In Figs. 11, 12, 13, 16, for certain systems containing OH^-, the components are indicated as $(LiOH)_2$, $(NaOH)_2$, and $(KOH)_2$. In these cases the anionic fraction axes are not the anionic molar fractions, X_{OH} but rather the anionic equivalent fractions, Y_{OH}. This was done in order to facilitate comparison with the measured diagrams which are drawn in this way.

$Li/CO_3,SO_4,OH$ (Fig. 3)
$Na/CO_3,SO_4,OH$ (Fig. 4)
$K/CO_3,SO_4,OH$ (Fig. 5)

No measured phase diagrams were found. The phase diagrams were calculated via the CIS equation [10]. When the calculations were repeated with the Toop equation [12] with the hydroxide as the "asymmetric component" the results agreed with those of the CIS theory within 2°C.

Can. J. Chem. Downloaded from www.nrcresearchpress.com by 210.87.254.6 on 09/06/12
For personal use only.

Can. J. Chem. Downloaded from www.nrcresearchpress.com by 210.87.254.6 on 09/06/12
For personal use only.

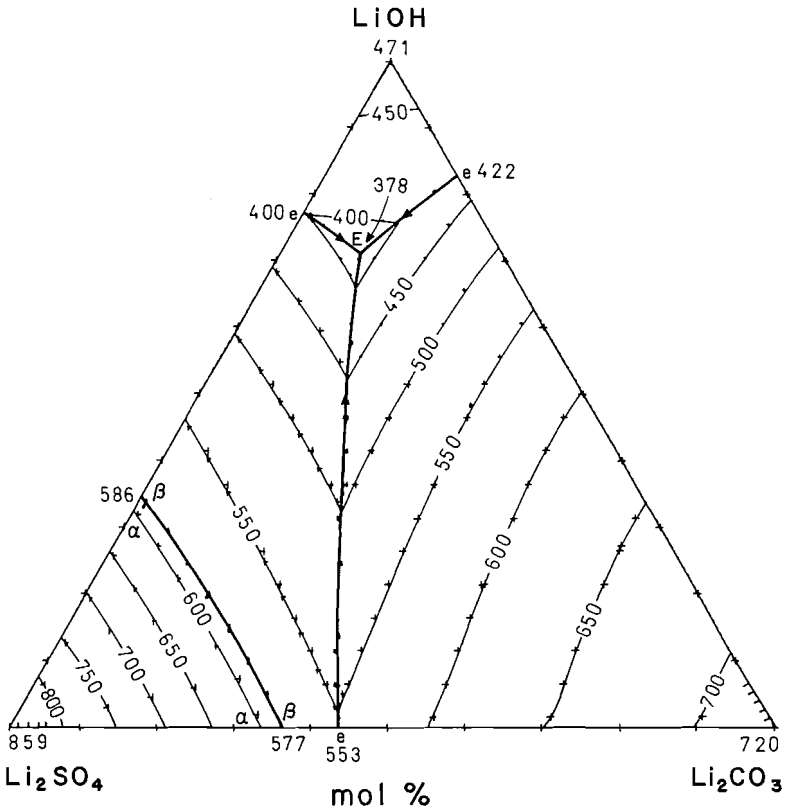

FIG. 3. $Li_2CO_3-Li_2SO_4-LiOH$ phase diagram calculated via the CIS equation (°C).

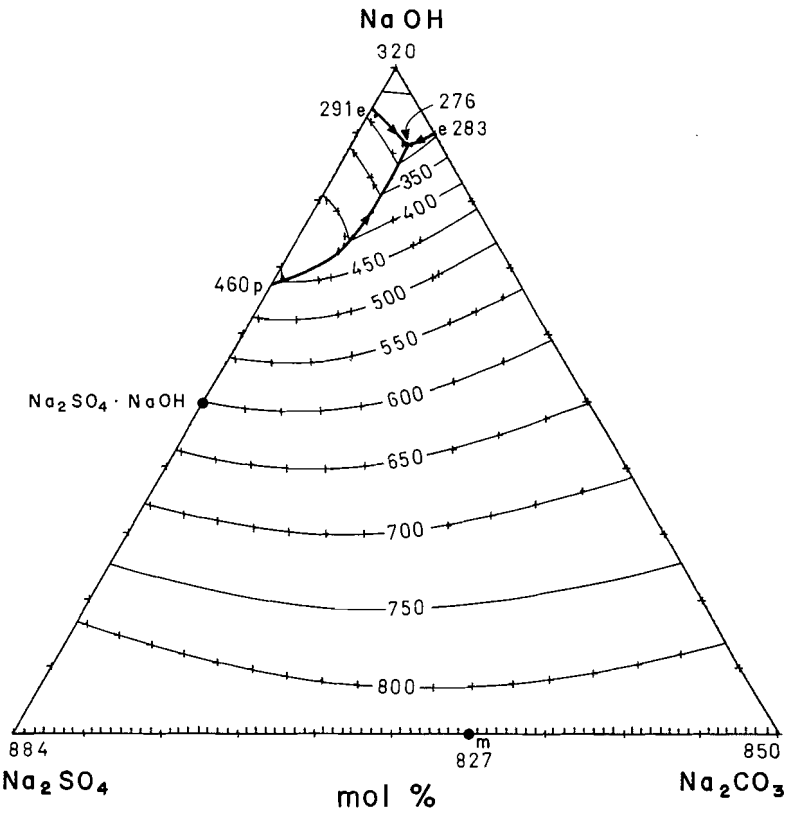

FIG. 4. $Na_2CO_3-Na_2SO_4-NaOH$ phase diagram calculated via the CIS equation (°C).

Probable maximum deviations: for all three diagrams near a binary side, the accuracy is about the same as that given in Table 2 for that binary system. Maximum deviations in the calculated ternary eutectics are estimated as follows:

$Li/CO_3,SO_4,OH$: ±35°C, ±5 mol%

$Na/CO_3,SO_4,OH$: ±20°C, ±2 mol%

$K/CO_3,SO_4,OH$: ±20°C, ±2 mol%

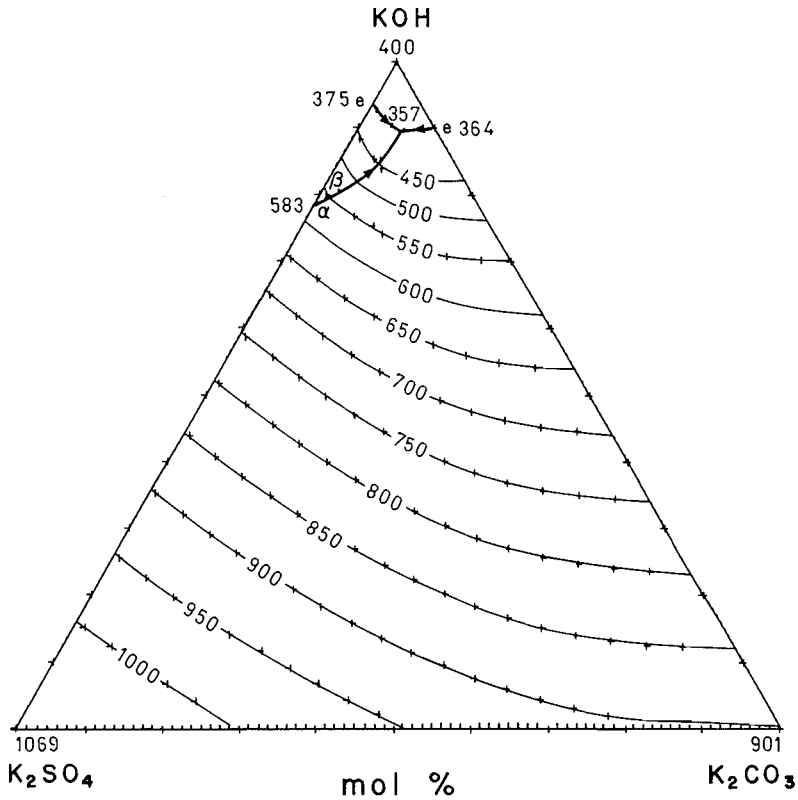

FIG. 5. $K_2CO_3-K_2SO_4-KOH$ phase diagram calculated via the CIS equation (°C).

Li,Na,K/CO₃ (Fig. 6)

Three measured diagrams (25–27) are available which agree with each other within ±10°C. That of Janz and Lorenz (25) is probably the most accurate. For the solid solution which extends into the ternary from the $K_2CO_3-Na_2CO_3$ binary, the Toop equation [12] was used. For the ternary liquid phase, two equations were used: the Kohler equation [11] and the CIS equation [10] without ternary terms. Both equations gave ternary diagrams which were virtually indistinguishable from each other except right at the ternary eutectic where the Kohler equation gave 401°C and the CIS gave 406°C. The measured (25) eutectic temperature is 397°C. Both calculated ternary eutectic compositions and the measured agree within 1 mol%. The measured ternary eutectic temperature of 397°C has been marked on the calculated diagram.

Probable maximum deviation: ±5 to 10°C

Ternary eutectic: ±5°C, ±2 mol%

Li,Na,K/SO₄ (Fig. 7)

A ternary phase diagram has been measured by Akopov and Bergman (28) who report the existence of eight ternary phase fields, but who do not identify the composition of the ternary compounds associated with each. Only one of these compounds, that labelled "VII" by the authors (28), appears to affect the liquidus surface significantly, since for all other reported ternary phase fields the liquidus isotherms bend only very slightly as they cross the univariant lines between these fields. Indeed, in the analysis of this system by Janz *et al.* (29), all the compounds "I to VI" are simply grouped together into one "ternary" field which has little influence on the liquidus isotherms, and compound "VIII" is not reported at all. Only compound VII is significant.

Since the compositions of the ternary compound(s) are unknown, they were not included in the present calculations. Hence, the central portion of the calculated diagram is not reported. More experimental work must be done on this system in this region.

In the calculations, the CIS equation [10] was used for the liquid phase, and the Toop equation [12] was used for the solid phase which extends into the ternary from the $K_2SO_4-Na_2SO_4$ binary. The calculated diagram agrees within 10 to 15°C with that of Akopov and Bergman (except, of course, for the central portion). However, it should be noted that the $Na_2SO_4-Li_2SO_4$ and $Na_2SO_4-K_2SO_4$ binaries reported on their measured ternary diagram already disagree by over 10°C with the calculated binaries from the present study.

Probable maximum deviation: ±30° near Li_2SO_4 corner; ±20°C elsewhere (except in central region)

Li,Na/CO₃,SO₄ (Fig. 8)

The liquidus has been measured (30). However, the reported diagram is thermodynamically incorrect. If one follows the diagonal from Li_2CO_3 to Na_2SO_4, the liquidus descends to 500°C and then rises again to 517°C within the phase field of stoichiometric Li_2CO_3.Hence, the measured diagram is probably not very reliable. There is a ternary solid phase extending into the ternary system from the $Na_2SO_4-Na_2CO_3$ binary as well as a small ternary solid phase near the Li_2SO_4 corner. When the CIS equation [13] was applied to both the liquid and the solid phases with Λ calculated via eq. [15] for both solid and liquid, the calculated diagram at its central point was 20°C higher than the measured. This agreement is within the error limits of the measurements. However, as discussed previously, when dealing with a solid solution phase there is little justification for calculating Λ via eq. [15]. Hence, it was decided in the present case to treat Λ for the solid phases as an adjustable

Can. J. Chem. Downloaded from www.nrcresearchpress.com by 210.87.254.6 on 09/06/12
For personal use only.

Can. J. Chem. Downloaded from www.nrcresearchpress.com by 210.87.254.6 on 09/06/12
For personal use only.

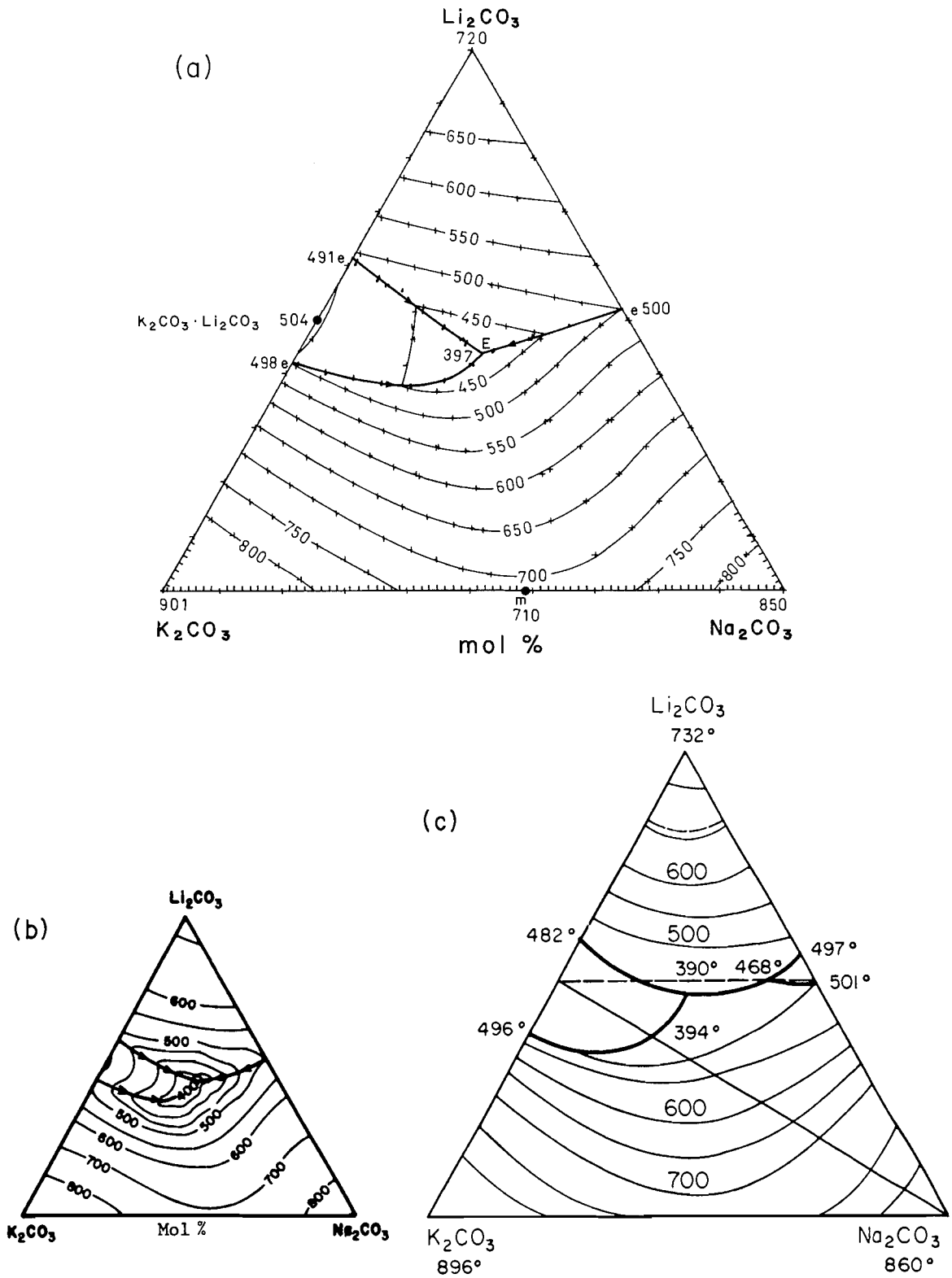

FIG. 6. $Li_2CO_3-Na_2CO_3-K_2CO_3$ phase diagram (°C): (*a*), calculated; (*b*), ref. 25; (*c*), ref. 26, taken from ref. 24.

parameter in order to reproduce the measured diagram more closely in the central region. However, Λ for the liquid was calculated via eq. [15]. With Λ^{solid} set equal to +3200 cal for both solid phases, the calculated and measured diagrams agree within ±5°C except in the Li_2SO_4 corner. The maximum deviation occurs at the ternary eutectic where the calculated diagram is 39°C higher than the measured although the position of the ternary eutectic agreed within 2 mol%. However, this eutectic is near the Li_2SO_4 corner of the system and, as discussed in ref. 3, there were large inaccuracies observed in all binary systems at high concentrations of Li_2SO_4. The calculated $Li_2SO_4-Li_2CO_3$ binary and that reported on the measured (30) ternary diagram are already in disagreement by 14°C.

In shape of the isotherms and in position of the invariants,

Can. J. Chem. Downloaded from www.nrcresearchpress.com by 210.87.254.6 on 09/06/12
For personal use only.

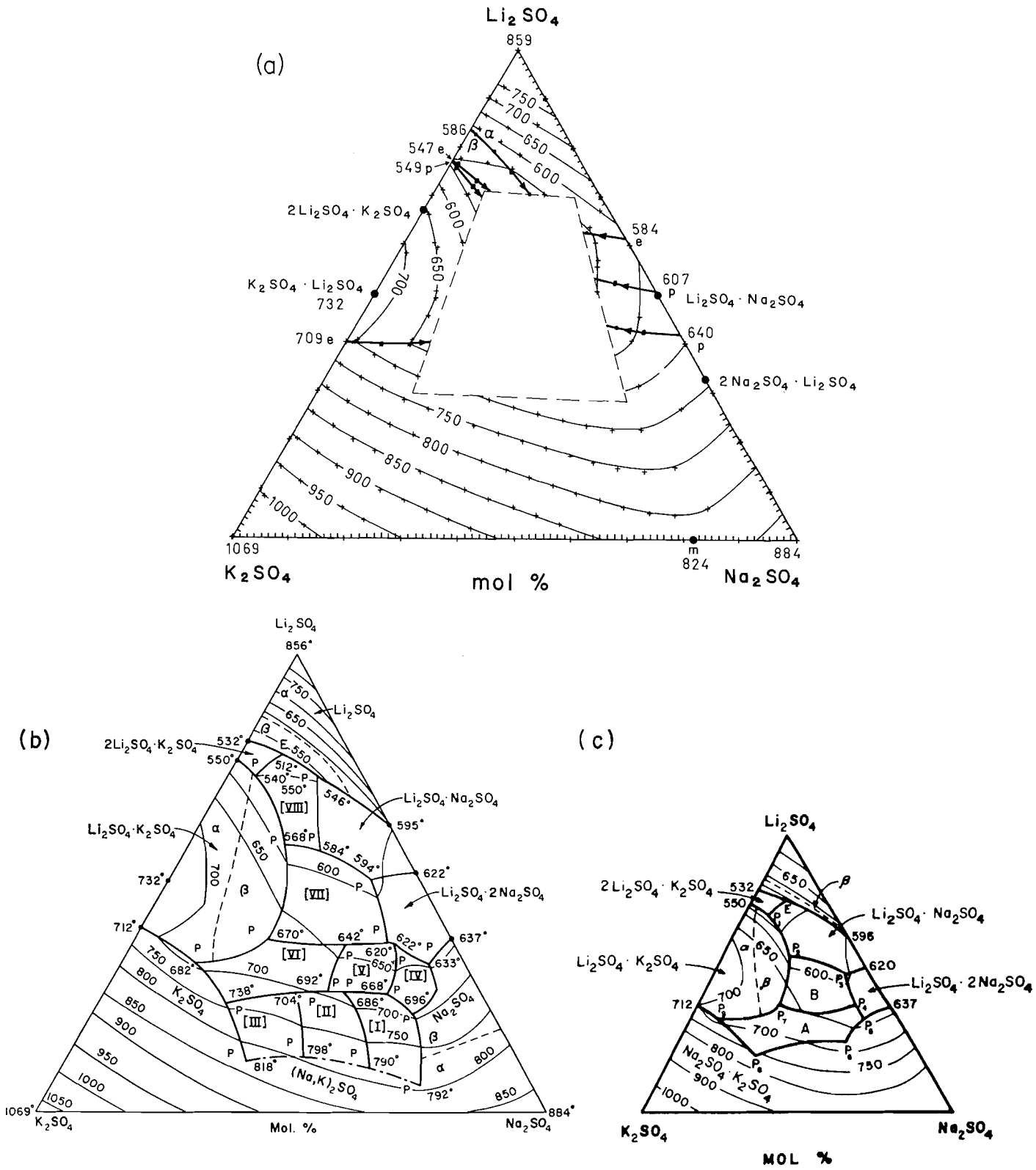

FIG. 7. $Li_2SO_4-Na_2SO_4-K_2SO_4$ phase diagram (°C): (*a*), calculated; (*b*), ref. 28, taken from ref. 24; (*c*), ref. 29.

the calculated and measured diagrams agree very well.

Ternary data

Λ^{solid} = +3200 cal for both solid phases

Probable maximum deviation: ±20°C
except at ternary eutectic: ±40°C, ±3 mol%

$Li,K/CO_3,SO_4$ (Fig. 9)

No measured diagram was found for this system. There exists one solid ternary phase extending slightly into the ternary system from the $K_2CO_3-K_2SO_4$ binary. The CIS equation [13] with Λ calculated via eq. [15] was applied to both solid and liquid phases. The two intermediate solid binary compounds $K_2SO_4 \cdot Li_2SO_4$ and $K_2CO_3 \cdot Li_2CO_3$ were assumed to be immis-

Can. J. Chem. Downloaded from www.nrcresearchpress.com by 210.87.254.6 on 09/06/12
For personal use only.

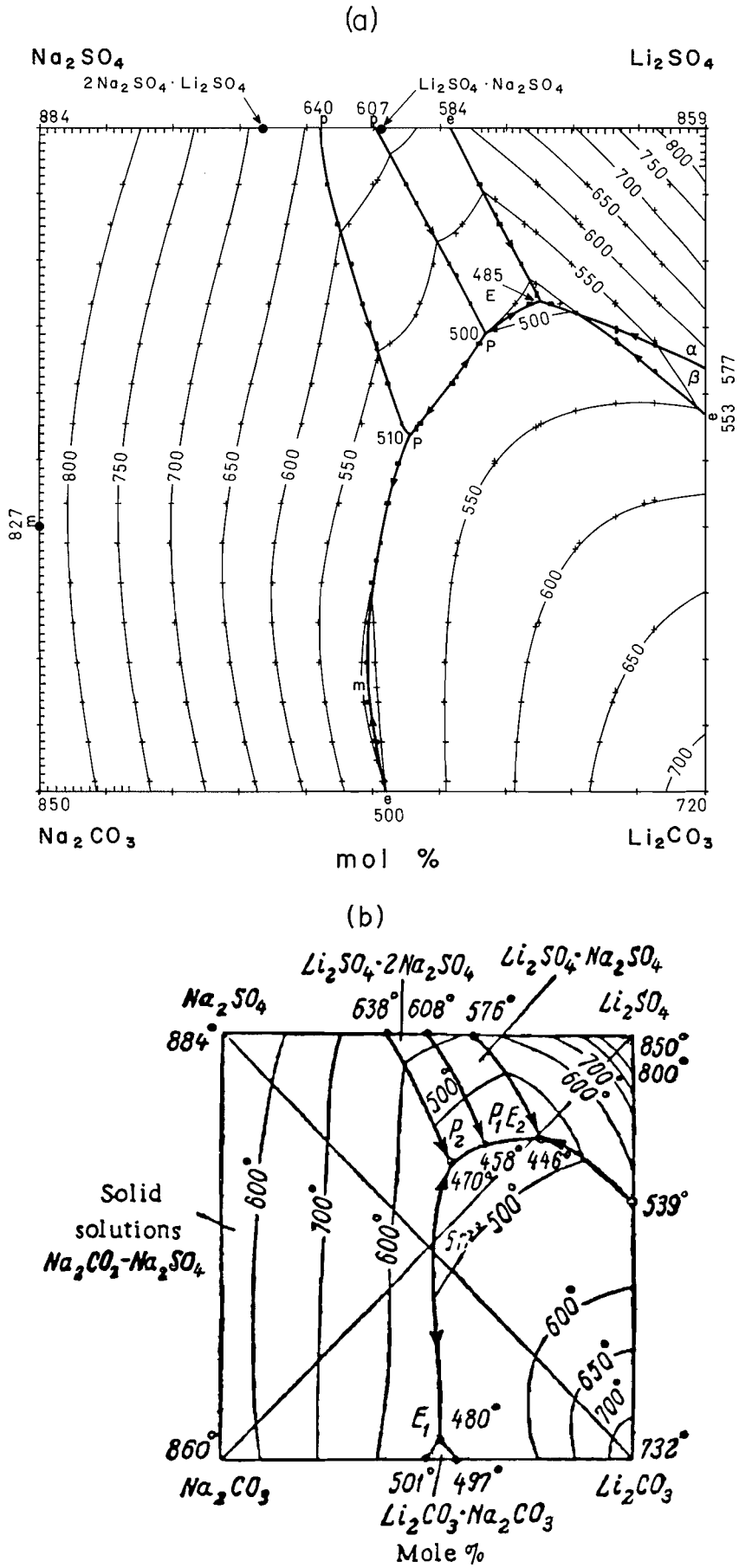

FIG. 8. Li,Na/CO_3,SO_4 phase diagram (°C); (*a*), calculated; (*b*), ref. 30, taken from ref. 24.

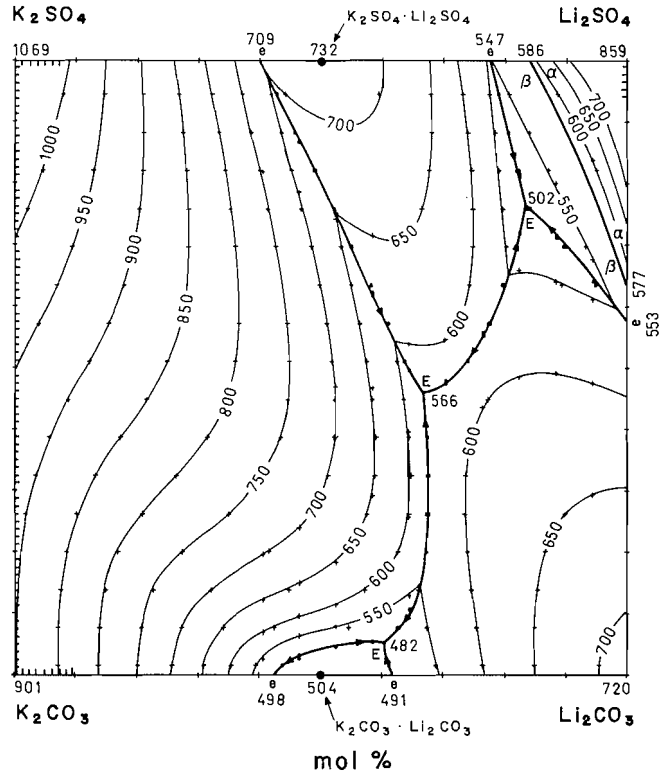

FIG. 9. Li,K/CO_3,SO_4 phase diagram calculated from the CIS equation (°C).

cible. However, in view of the complete solid solubility observed between K_2CO_3 and K_2SO_4, and in view of the similar stoichiometry of these two intermediate 1:1 compounds, the existence of quasi-binary solid solution between them is possible. (In this connection it should be noted, however, that Li_2SO_4 and Li_2CO_3 are immiscible in the solid state.) Hence, the ternary diagram was re-calculated under the assumption of complete solid solubility between the two compounds with $\Delta h^{mix(s)}$ and $s^{E(s)}$ taken to be the same as for the K_2CO_3–K_2SO_4 binary. This probably represents the other extreme possibility. The diagram so calculated agreed with the diagram calculated for no solubility within 6°C everywhere. The greatest difference (6°C) occurred at one ternary eutectic which was changed from 482 to 488°C. The correct value is most likely closer to 482°C.

From the results of the calculations on the other two reciprocal systems containing CO_3^{2-} and SO_4^{2-} (Na,Li/CO_3,SO_4 and Na,K/CO_3,SO_4) for which measured diagrams are available, the calculated liquidus in the present system may be somewhat high, but the general shape of the isotherms and the position of the invariant points are probably quite accurate.

Probable maximum deviation: ±20°C
(±30°C near Li_2SO_4 corner)

Na,K/CO_3,SO_4 (Fig. 10)

This system exhibits complete miscibility in the solid state. One experimental determination of the liquidus (31) is available which, on the basis of experience with measurements on similar systems by these authors, is probably correct to within ±10 to 20°C.

The CIS equation [13] with Λ for the solid and liquid phases calculated via eq. [15] was applied to both the solid and liquid phases. The calculated diagram agreed very well in shape of the

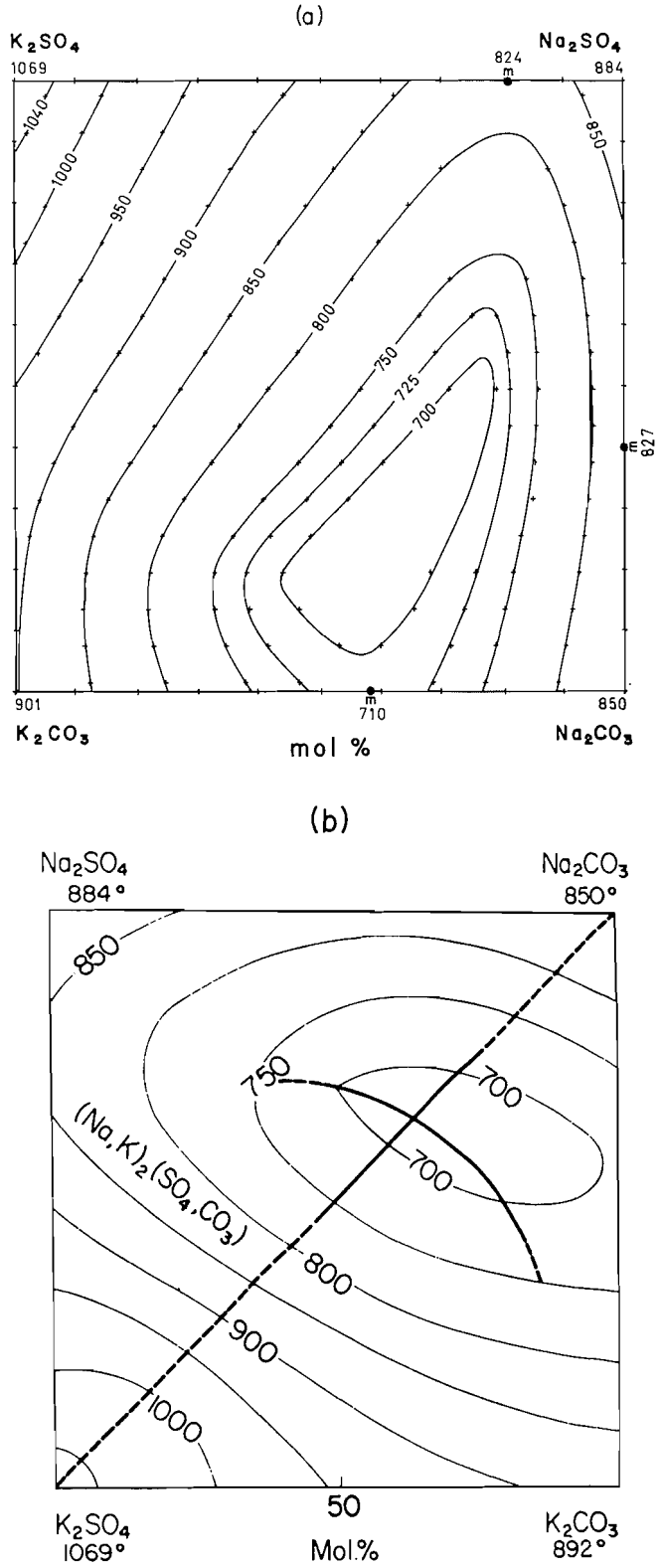

FIG. 10. Na,K/CO_3,SO_4 phase diagram (°C): (*a*), calculated; (*b*), ref. 31, taken from ref. 24.

isotherms with the measured, but near the centre of the ternary system the calculated was up to 40°C higher than the measured. Since, as discussed above, there is reason to believe that the measurements are more accurate than this and since, for a solid phase, deviation from the CIS equations are expected, Λ for the solid phase was taken as an adjustable parameter. (For the

Can. J. Chem. Downloaded from www.nrcresearchpress.com by 210.87.254.6 on 09/06/12
For personal use only.

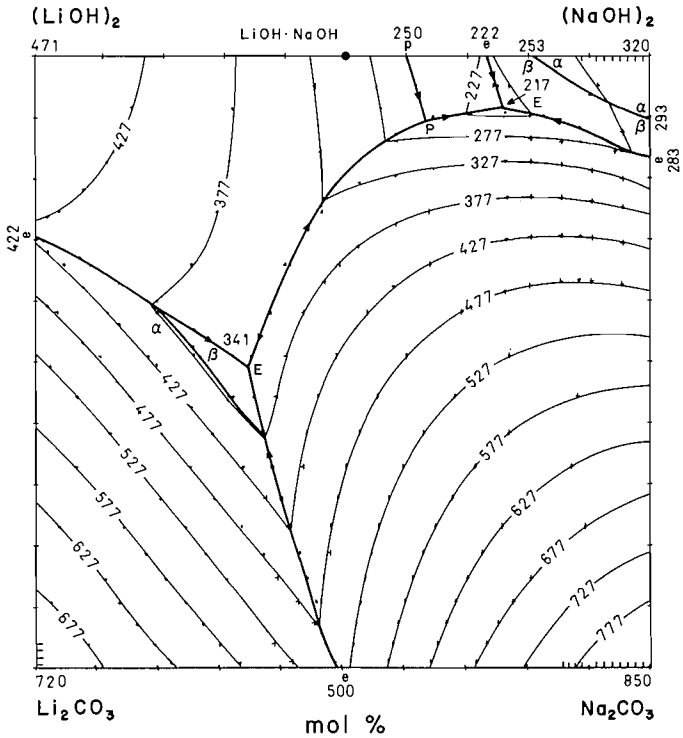

FIG. 11. Li,Na/CO_3,OH phase diagram calculated from the CIS equation (°C).

liquid phase, however, Λ was calculated by eq. [15].) With Λ^{solid} set equal to +3000 cal, the measured and calculated diagrams agreed within ±5°C everywhere.

Ternary data

Λ^{solid} = 3000 cal

Probable maximum deviation: ±20°C

Li,Na/CO_3,OH (Fig. 11)

No measured diagram was found for this system. The diagram was calculated from the CIS equation [13] for the liquid with Λ given by eq. [15]. The dilute solid solutions were assumed to be strictly binary.

Probable maximum deviation at ternary eutectic:

±25°C and ±5 mol%

Li,K/CO_3,OH (Fig. 12)

One measured phase diagram (32) exists for this system. The binary K_2CO_3–Li_2CO_3 data reported on the ternary diagram differ by 30°C from the most recent binary data used in the present study, and the LiOH–Li_2CO_3 binary data reported on the ternary diagram would seem to be equally inaccurate as discussed in ref. 3. Hence, the measured ternary diagram is probably not very accurate. One ternary compound, $Li_2CO_3 \cdot K_2CO_3 \cdot 8LiOH$, has been reported (32) with a congruent melting point of 425°C. The enthalpy of fusion of this compound was chosen so as to fit the measured ternary diagram as well as possible. The calculated and measured diagrams agree very well in the shape of the isotherms, and along the LiOH–K_2CO_3 diagonal the maximum deviation is 20°C.

Ternary data

$\Delta g^0_{fusion} = 2792 - 4.00T$ cal/mol for $K_{0.2}Li_{1.0}(OH)_{0.8}(CO_3)_{0.2}$

Probable maximum deviation: ±25°C

Na,K/CO_3,OH (Fig. 13)

One measured phase diagram (33) exists for this system, but three of the binary subsystems on the reported diagram differ by 10 to 30°C from the most recent binary diagrams chosen in the present study. Hence, the accuracy of the measured ternary diagram is no better than this. The calculated and measured diagrams do agree well in shape of the isotherms, however, and across the KOH–Na_2CO_3 diagonal, the maximum deviation is 20°C.

Probable maximum deviation: ±25°C

Li,Na/SO_4,OH (Fig. 14)

Since LiOH and Li_2SO_4 are immiscible and since NaOH and Na_2SO_4 are immiscible in the solid state, it may be assumed that the two solid 1:1 compounds LiOH·NaOH and $LiNaSO_4$ are also immiscible. No measured diagram was found. The diagram was calculated from the CIS equation [13] for the liquid with Λ given by eq. [15].

Probable maximum deviation: ±40°C with the largest uncertainty near the Li_2SO_4 corner

Li,K/SO_4,OH (Fig. 15)

No measured diagram was found. The diagram was calculated from the CIS equation [13] for the liquid with Λ given by eq. [15]. The dilute solid solution was assumed to be strictly binary.

Probable maximum deviation: ±40°C with the largest uncertainty near the Li_2SO_4 corner

Na,K/SO_4,OH (Fig. 16)

One measured phase diagram (34) exists for this system, but the work appears to be imprecise. A phase field of the compound $3K_2SO_4 \cdot Na_2SO_4$ is reported as being stable below 750°C. However, the reference for the K_2SO_4–Na_2SO_4 binary system (35) indicates that no intermediate phases exist in this system above 500°C. Since the ternary phase field for this compound below 500°C is very small, it has been ignored in the calculations. The calculated and measured diagrams agree quite well in general shape of the isotherms. The maximum deviation is about 20°C, but this is probably within the experimental error limits.

Probable maximum deviation: ±30°C

Calculation of iso-activity curves in reciprocal ternary systems at 650°C

From the CIS equation [13], the Gibbs energies of the liquid phases in the reciprocal ternary systems were calculated, and from these Gibbs energy expressions the reciprocal ternary phase diagrams were calculated as has been discussed. The same Gibbs energy expressions can also be used to calculate the activities of the components in the reciprocal ternary liquid phases.

Iso-activity curves for all four components at 650°C, which is the temperature of operation of the molten carbonate fuel cell, were presented in ref. 1. These plots are very useful in the computation of fuel gas–liquid electrolyte equilibria as was discussed in ref. 1.

The iso-activity curves at 650°C in the Li,K/CO_3, SO_4 and Li,K/CO_3,OH systems, which are the two most important systems from a practical standpoint, are shown in Figs. 17, 18.

Can. J. Chem. Downloaded from www.nrcresearchpress.com by 210.87.254.6 on 09/06/12
For personal use only.

Can. J. Chem. Downloaded from www.nrcresearchpress.com by 210.87.254.6 on 09/06/12
For personal use only.

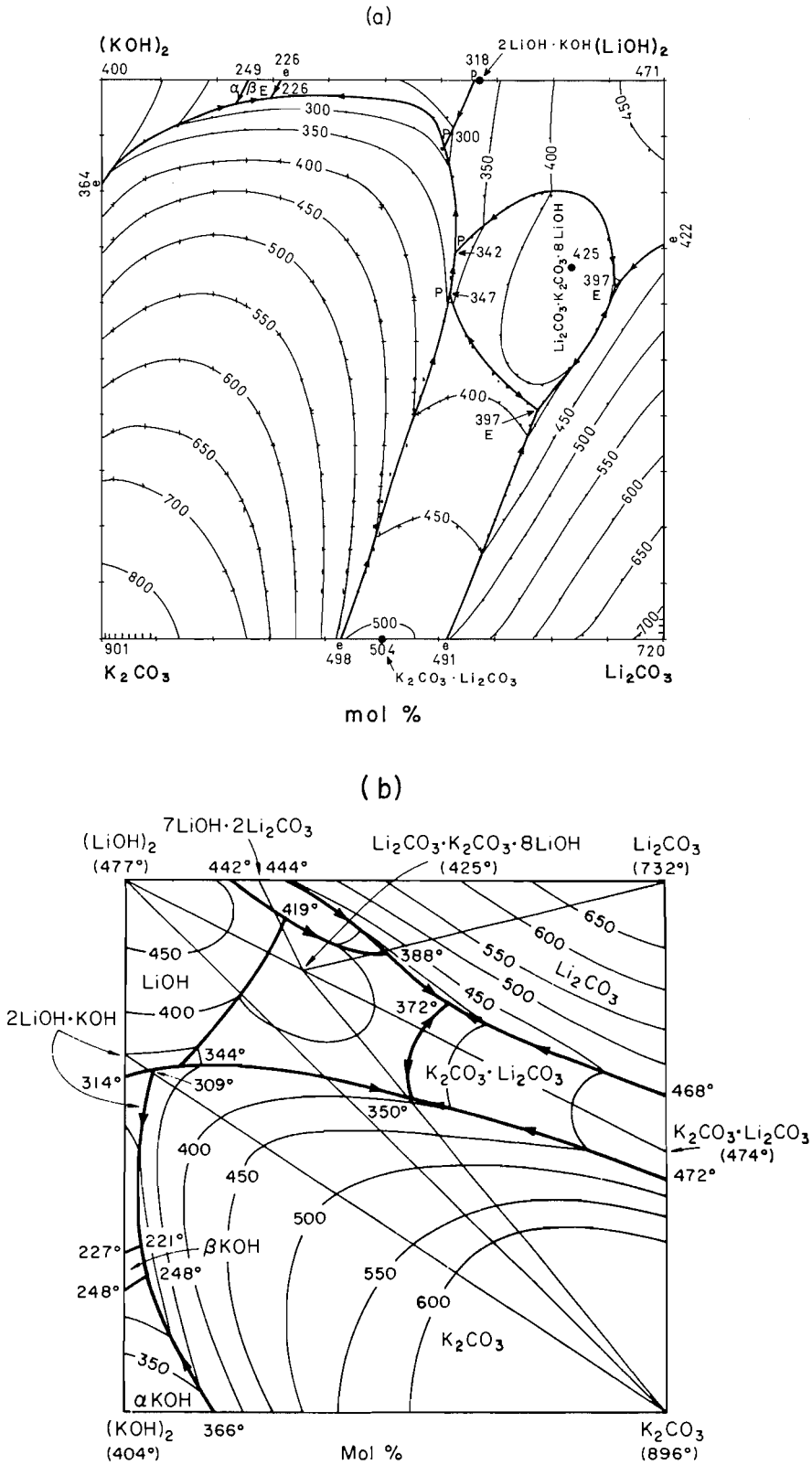

FIG. 12. Li,K/CO_3,OH phase diagram (°C): (*a*), calculated; (*b*), ref. 32, taken from ref. 24.

Conclusions and identification of areas where further measurements are desirable

Once its binary subsystems have been analysed by a coupled thermodynamic/phase diagram analysis, the phase diagram of a ternary system can usually be calculated with a maximum error no greater than about twice that of the maximum error in any of the binary phase diagrams. Hence, in order to minimize the experimental effort, one should concentrate on re-measuring regions of the binary diagrams where required. The ternaries and quaternaries can then be re-calculated.

Can. J. Chem. Downloaded from www.nrcresearchpress.com by 210.87.254.6 on 09/06/12
For personal use only.

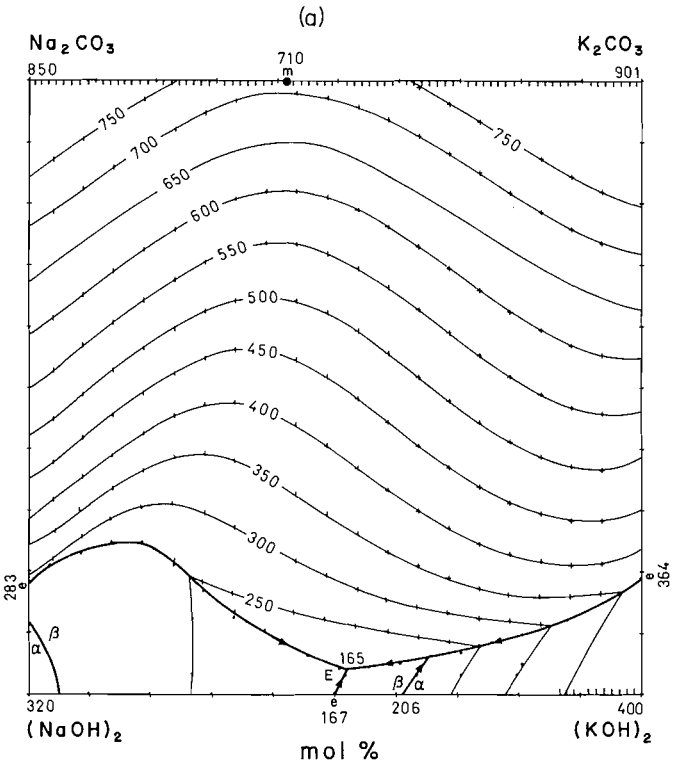

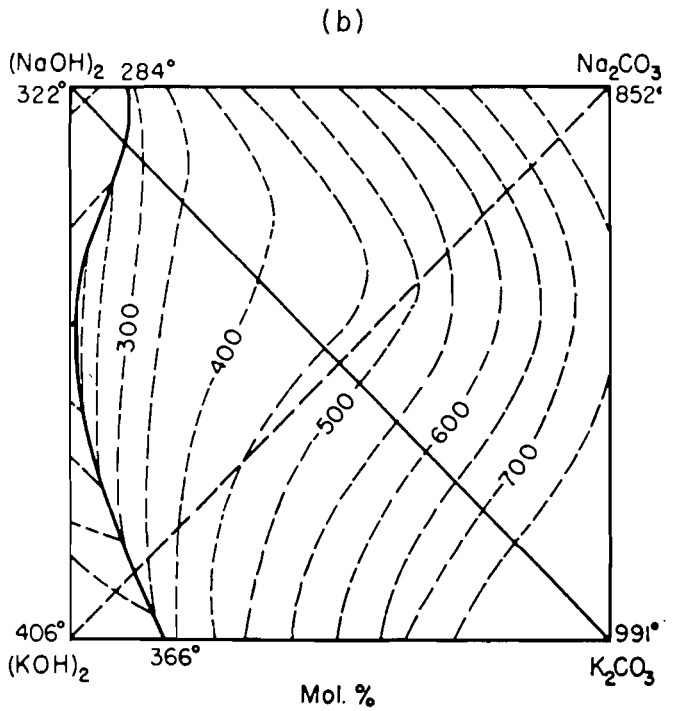

FIG. 13. $Na,K/CO_3,OH$ phase diagram (°C): (*a*), calculated; (*b*), ref. 33, taken from ref. 24.

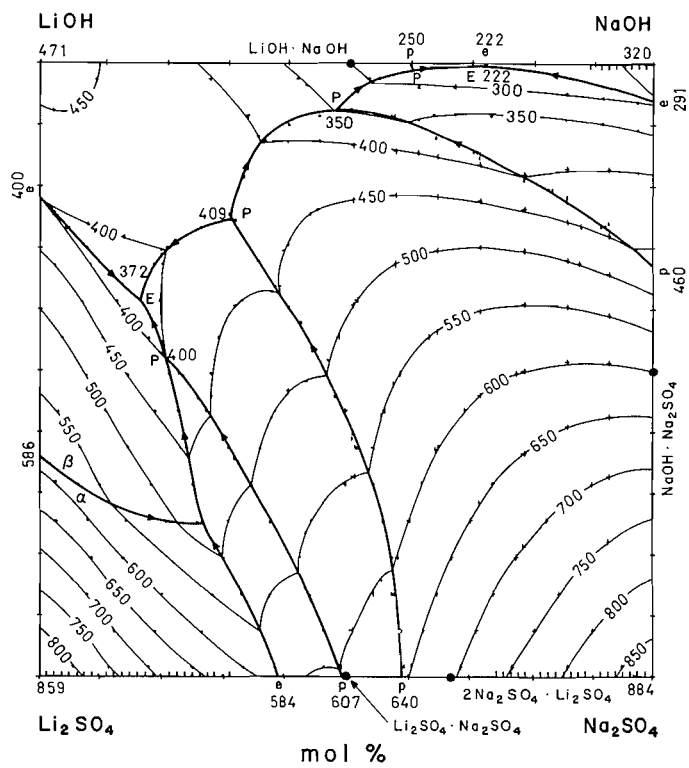

FIG. 14. $Li,Na/SO_4,OH$ phase diagram calculated from the CIS equation(°C).

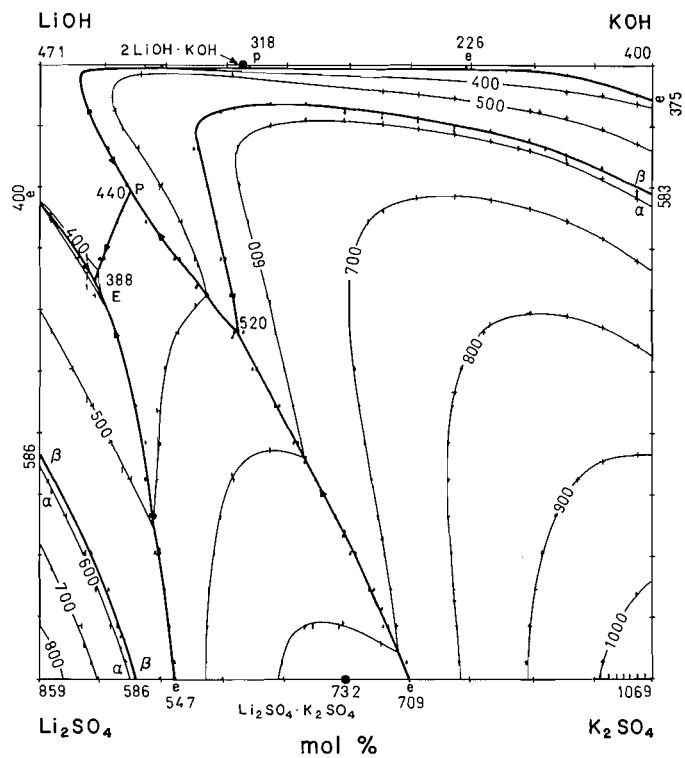

FIG. 15. $Li,K/SO_4,OH$ phase diagram calculated from the CIS equation (°C).

Furthermore, the general shape of the isotherms of the calculated ternary diagrams and the compositions of the calculated ternary invariant points are quite insensitive to relatively large changes in the thermodynamic parameters. Calculated and measured diagrams nearly always agree well in this regard. Hence, the experimental measurement of one or two ternary phase diagram temperatures (often just a ternary eutectic temperature) is sufficient to permit an adjustable ternary term to be determined so as to result in a very good calculated ternary diagram. Usually, only one such ternary term is required.

With these points in mind it is proposed that the following

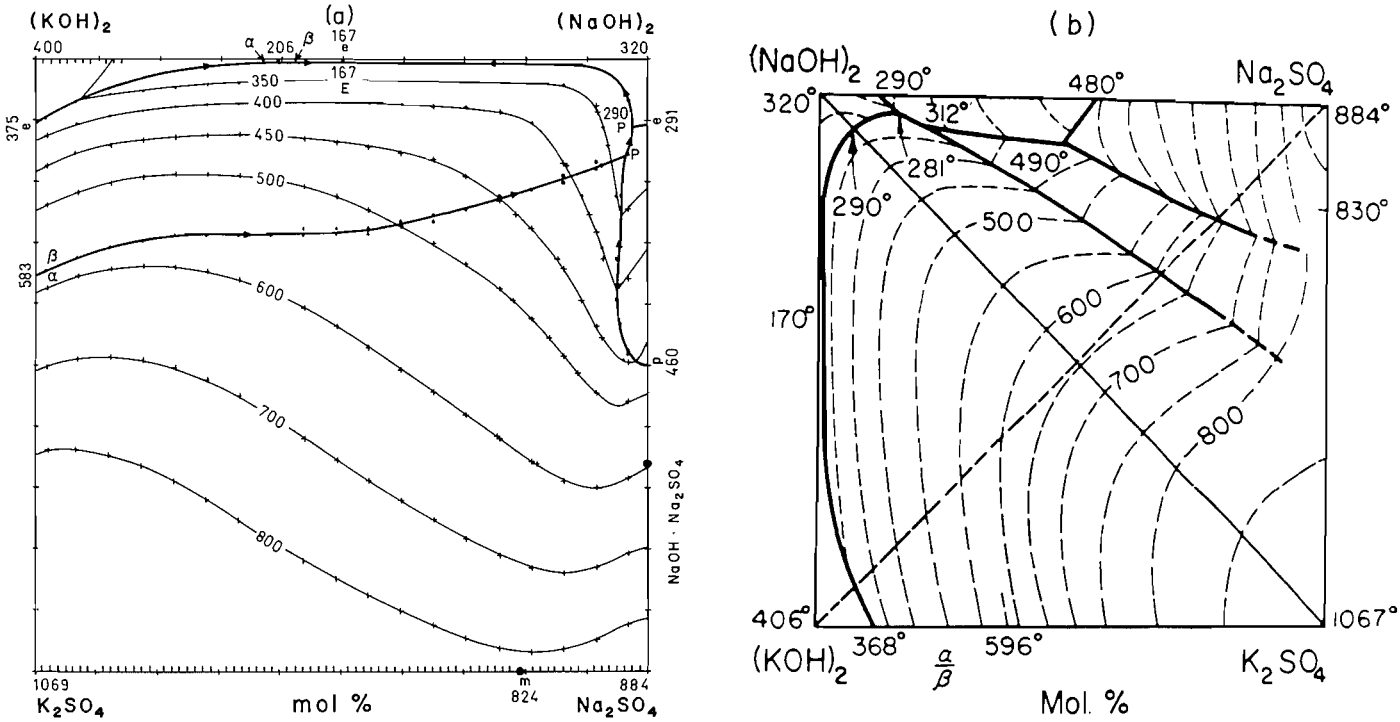

FIG. 16. Na,K/SO_4,OH phase diagram (°C): (*a*), calculated; (*b*), ref. 34, taken from ref. 24.

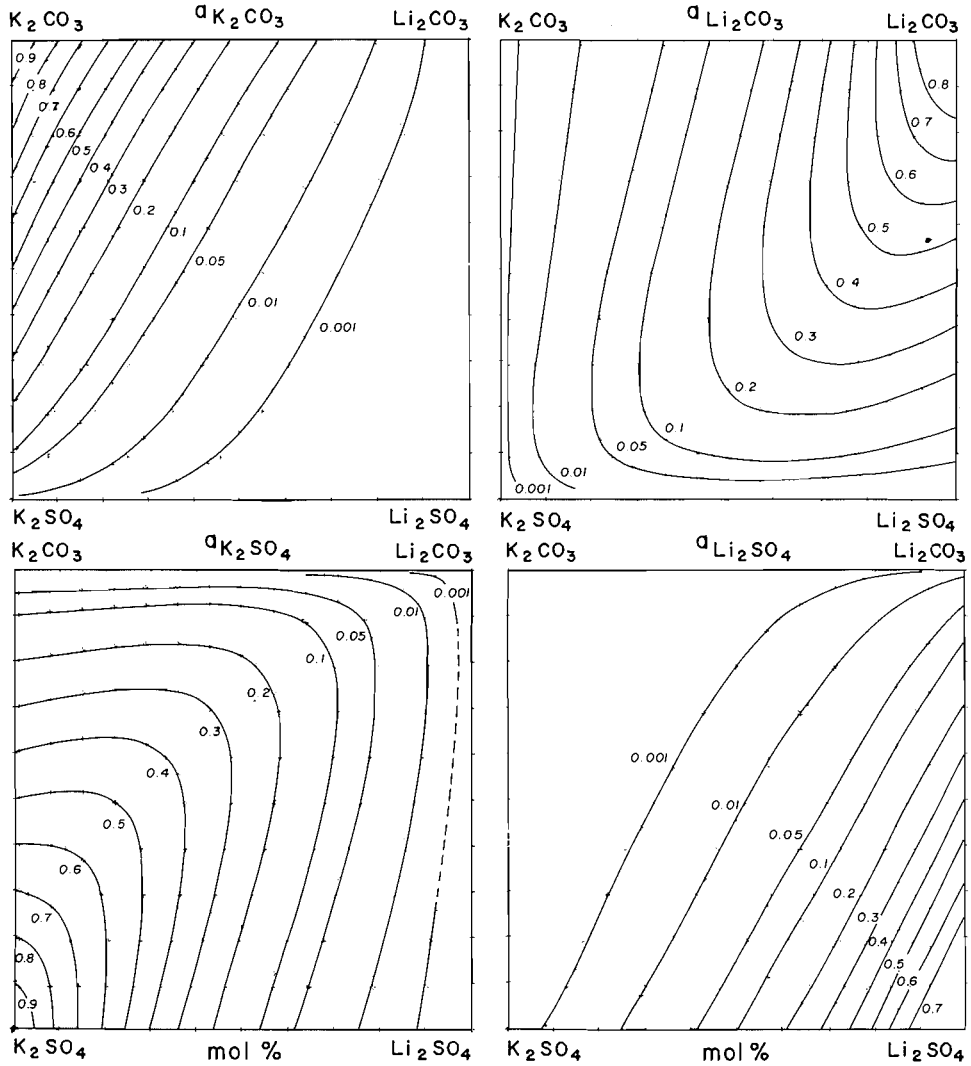

FIG. 17. Iso-activity curves at 650°C in the Li,K/CO_3,SO_4 system calculated via the CIS equation.

Can. J. Chem. Downloaded from www.nrcresearchpress.com by 210.87.254.6 on 09/06/12
For personal use only.

Can. J. Chem. Downloaded from www.nrcresearchpress.com by 210.87.254.6 on 09/06/12
For personal use only.

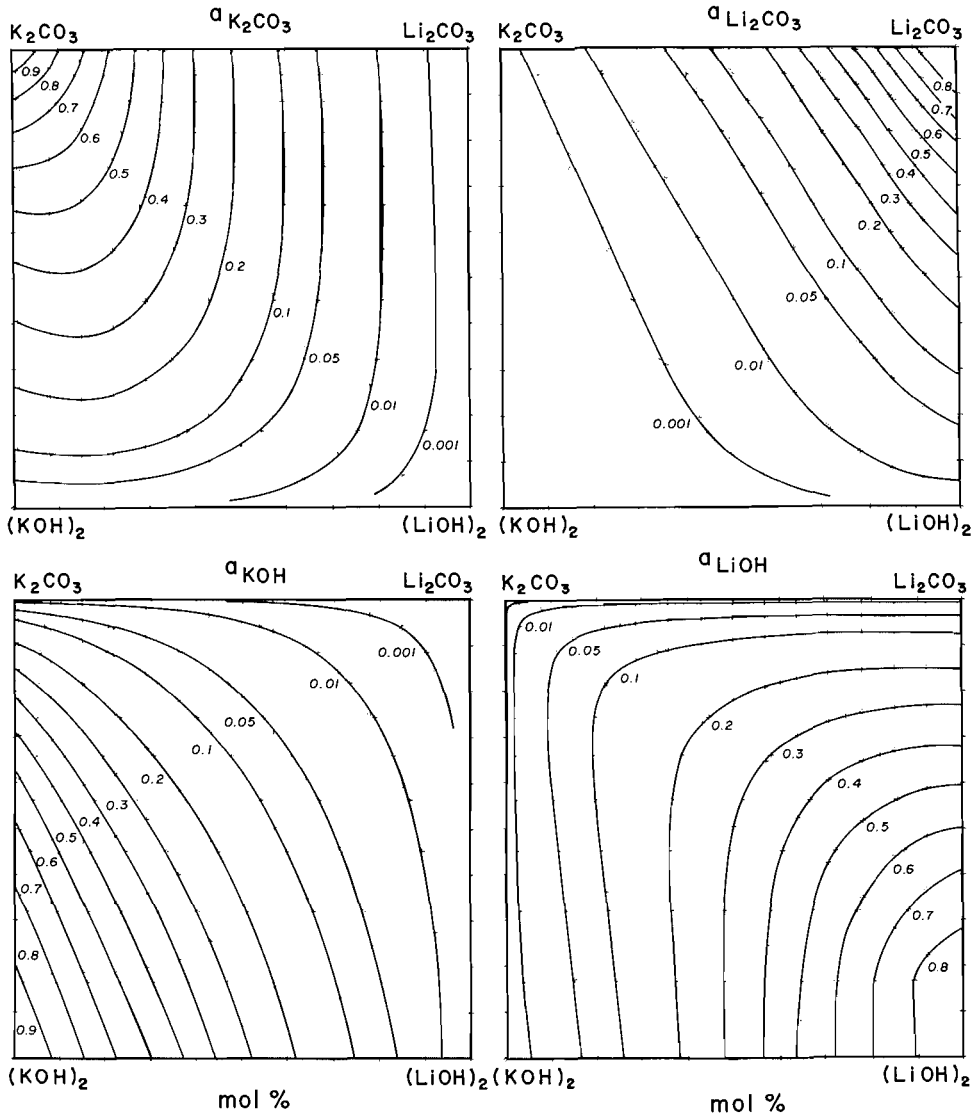

FIG. 18. Iso-activity curves at 650°C in the Li,K/CO_3,OH system calculated via the CIS equation.

regions of the binary and ternary phase diagrams could profitably be re-measured. The greatest uncertainties in all the binary and ternary diagrams center around the component Li_2SO_4. Diagrams for the same system measured by different authors are usually in large disagreement for compositions rich in Li_2SO_4. Furthermore, some of the measured diagrams are thermodynamically inconsistent with the enthalpy of the $\alpha-\beta$ transformation of Li_2SO_4. Possibly, the metastable solidification of β in regions where α is thermodynamically stable is responsible for some of the discrepancies. The $Li_2CO_3-Li_2SO_4$ and $Li_2SO_4-K_2SO_4$ binary liquidus should thus be re-examined in the Li_2SO_4-rich regions and particularly around the eutectics, care being taken to identify the $\alpha-\beta$ phase transition. The $LiOH-Li_2SO_4$ system has never been measured. The $Li_2SO_4-Na_2SO_4$ system should be completely re-examined particularly in the central regions. The solidus of this system should also be re-measured. The ternary eutectic temperature of the Li,Na/CO_3,SO_4 system should be re-measured in order to resolve a seemingly too large discrepancy in this system. The entire central region of the Li,Na,K/SO_4 system should be re-examined, and the compositions of the ternary compound(s) identified. For *any* of the ternary phase diagrams, one simple experimental determination of the ternary eutectic temperature would permit a large increase in the accuracy of the calculated diagram to be made. In view of the importance of the Li,K/CO_3,SO_4 system to the DOE carbonate fuel cell project, it is suggested that the ternary eutectic temperature (for the ternary eutectic near the $Li_2CO_3-K_2CO_3$ binary) be carefully re-measured.

Acknowledgements

This project was supported by the U.S. Department of Energy, contract number DE-AC02-79ET15416. The authors wish to thank the project director, Dr. John Ackerman, for guidance. We are also indebted to Dr. M.-L. Saboungi and Dr. M. Blander for their assistance at all stages of this work.

1. (*a*) A. D. PELTON, C. W. BALE, and P. L. LIN. Vol. 1. Binary, ternary and quaternary phase diagrams containing Li^+, Na^+, K^+, $CO_3^=$, $SO_4^=$, and OH^-; C. W. BALE, A. D. PELTON, and J. MELANÇON. Vol. II. Equilibria between the carbonate electrolyte and the C—H—O—S gas phase; vapour pressures and volatilization of the alkali species. *In* Calculation of thermodynamic equilibria in the carbonate fuel cell. U.S. Dept. of Energy, Contract No. DE-AC02-79ET15416 May 1981; (*b*) C. W. BALE and A. D. PELTON. Proc. Symp. Molten Carbonate Fuel Cell Technology, Electrochem. Soc., Montreal. 1982.

2. C. W. BALE, A. D. PELTON, and W. T. THOMPSON. F*A*C*T — Facility for the Analysis of Chemical Thermodynamics. User's Guide. Edition 1, McGill University/Ecole Polytechnique. 1979.
3. C. W. BALE and A. D. PELTON. CALPHAD J. **6**, 255 (1982).
4. C. W. BALE and A. D. PELTON. Met. Trans. **14B**, 77 (1983).
5. P. L. LIN, A. D. PELTON, and C. W. BALE. J. Am. Ceram. Soc. **62**, 414 (1979).
6. A. D. PELTON, C. W. BALE, and W. T. THOMPSON. Calculation of liquidus surfaces, vapour pressures, and decomposition potentials in certain ternary and quaternary fused salt systems. CANMET Report, Can. Dept. of Energy, Mines and Resources, Contract No. SQ23440-8-9076 (1979).
7. J. M. SKEAFF, C. W. BALE, A. D. PELTON, and W. T. THOMPSON. CANMET Report No. 79-23, Minister of Supply and Services Canada (1980).
8. P. L. LIN, A. D. PELTON, and M. L. SABOUNGI. Met. Trans. **13B**, 61 (1982).
9. P. L. LIN, C. W. BALE, and A. D. PELTON. Proceedings of TMS-AIME Symposium on Calculation of Phase Diagrams. *Edited by* Y. A. Chang and J. F. Smith. Milwaukee, 1979. pp. 26–44.
10. W. W. LIANG, P. L. LIN, and A. D. PELTON. High Temp. Sci. **12**, 41 (1980); **12**, 71 (1980).
11. M. BLANDER and M. L. SABOUNGI. Fundamental aspects of ternary molten salt solutions and their application in technology. *In* Molten salts. Electrochem. Soc. Inc. 1976. pp. 93–107.
12. T. FOOSNAES, T. ØSTVOLD, and H. A. ØYE. Acta Chem. Scand. **A32**, 973 (1978).
13. M. L. SABOUNGI and P. CERISIER. J. Electochem. Soc. **121**, 1258 (1974).
14. M. L. SABOUNGI and M. BLANDER. J. Am. Ceram. Soc. **58**, 1 (1975).
15. I. BARIN, O. KNACKE, and O. KUBASCHEWSKI. Thermochemical properties of inorganic substances; and supplement. Springer-Verlag, Dusseldorf. 1973.
16. M. L. SABOUNGI and M. BLANDER. J. Chem. Phys. **63**, 212 (1975).
17. F. KOHLER. Mh. Chem. **91**, 738 (1960).
18. G. W. TOOP. TMS-AIME, **233**, 850 (1965).
19. M. BLANDER and S. J. YOSIM. J. Chem. Phys. **39**, 2610 (1963).
20. M. L. SABOUNGI and M. BLANDER. J. Am. Ceram. Soc. **58**, 1 (1975).
21. G. HATEM, M. GAUNE-ESCARD, and A. D. PELTON. J. Phys. Chem. **86**, 3039 (1982).
22. M. L. SABOUNGI, P. L. LIN, P. CERISIER, and A. D. PELTON. Met. Trans. **11B**, 493 (1980).
23. A. D. PELTON, J. M. SKEAFF, C.W. BALE, and P. L. LIN. Can. J. Chem. **60**, 1664 (1982).
24. E. M. LEVIN, C. R. ROBBINS, and H. F. MCMURDIE. Phase diagrams for ceramists. Nat. Bur. Stand. *Edited and Published by* Am. Ceram. Soc., Inc. 1964; supplement 1969; supplement 1975.
25. G. J. JANZ and M. R. LORENZ. J. Chem. Eng. Data, **6**, 321 (1961).
26. L. F. VOLKOVA. Izvest. Sibirsk. Otdel. Akad. Nauk SSSR, No. 7, 34 (1958).
27. M. ROLIN and J. M. RECAPET. Bull. Soc. Chim. Fr. 2504 (1964).
28. E. K. AKOPOV and A. G. BERGMAN. Zhur. Neorg. Khim. **4**, 1151 (1959).
29. G. J. JANZ (*Editor*). Physical properties data compilations relevant to energy storage, II. Molten salts. National Bureau of Standards, Washington, 1979.
30. N. N. VOLKOV and L. F. VOLKOVA. Izv. Fiz. Khim. Nauchno. Issled. Inst. Irkutsk. Gos. Univ. **2**, 65 (1963).
31. A. K. SEMENTSOVA, K. A. EVDOKIMOVA, and A. G. BERGMAN. Zhur. Neorg. Khim. **4**, 146 (1958).
32. N. A. RESHETNIKOV and O. G. PERFIL'EVA. Zh. Neorg. Khim. **13**, 1662 (1968); Russ. J. Inorg. Chem. **13**, 870 (1968).
33. V. A. KHITROV. Izv. Sekt. Fiz. Khim. Anal. Inst. Obshch. Neorg. Khim. Akad. Nauk SSSR, **25**, 243 (1954).
34. A. G. BERGMAN and V. A. KHITROV. Izv. Sekt. Fiz. Khim. Anal. Inst. Obshch. Neorg. Khim. Akad. Nauk SSSR, **21**, 207 (1952).
35. C. PERRIER and A. BELLANCA. Period. Mineral. Rome, **11**, 169 (1940).

Can. J. Chem. Downloaded from www.nrcresearchpress.com by 210.87.254.6 on 09/06/12
For personal use only.

Optical and magnetic resonance studies of the interaction of metallo tetraphenylporphyrins with nitrobenzofuroxan

T. K. CHANDRASHEKAR AND V. KRISHNAN[1]

Department of Inorganic and Physical Chemistry, Indian Institute of Science, Bangalore-560012, India

Received January 20, 1983[2]

T. K. CHANDRASHEKAR and V. KRISHNAN. Can. J. Chem. **62**, 475 (1984).

Metallo tetraphenylporphyrins form 1:1 molecular complexes with 4,6-dinitrobenzofuroxan. The molecular association is described in terms of $\pi-\pi$ interaction with porphyrins functioning as donors. The association constants and thermodynamic parameters have been evaluated using optical absorption and ^1H nmr spectral methods. Based on the binding constants, the donor ability of various metalloporphyrins can be arranged in the following order: Pd(II) > Co(II) > Cu(II) > Ni(II) ~ VO(IV) ~ 2H > Zn(II). Electron paramagnetic resonance studies of the complexes reveal that the π-complexation results in changes in the electronic structure of the central metal ions which are reflected in the changes in the M–N σ bonding. The dipolar contribution to the acceptor proton chemical shifts in the CoTPP complex has been partitioned from ring current contributions using the shifts observed in the ZnTPP complex. The shifts, along with the line broadening ratios observed for the CoTPP complex, are used to arrive at the possible solution structures of the complexes.

T. K. CHANDRASHEKAR et V. KRISHNAN. Can. J. Chem. **62**, 475 (1984).

Les métallotétraphénylporphyrines forment des complexes moléculaires 1:1 avec le dinitro-4,6 benzofuroxane. On décrit l'association moléculaire en fonction des interactions $\pi-\pi$ avec les porphyrines agissant comme donneurs. On a évalué les constantes d'association et les paramètres thermodynamiques en faisant appel à l'absorption optique et à la rmn du ^1H. En se basant sur les constantes de liaison, on peut établir la capacité des diverses métalloporphyrines en tant que donneur dans l'ordre suivant: Pd(II) > Co(II) > Cu(II) > Ni(II) ~ VO(IV) ~ 2H > Zn(II). Les études de rpe des complexes révèlent que la complexation π est due à des changements dans la structure électronique de l'ion métallique central qui se réflète dans les variations de la liaison σ M–N. On a partagé la contribution dipolaire aux déplacements chimiques de l'accepteur de proton dans le complexe CoTPP, à partir du courant de cycle, en utilisant les déplacements observés dans le complexe ZnTPP. On a utilisé les déplacements chimiques ainsi que le taux d'élargissement des raies observé dans le complexe CoTPP pour arriver à déterminer les structures possibles des complexes.

[Traduit par le journal]

Introduction

The molecular interactions of porphyrins with neutral organic molecules is either donor–acceptor type or coordinative, depending on the functional groups present in the organic molecules. Nitroaromatics essentially function as π-acceptors and form donor–acceptor complexes with porphyrins (1). Among the nitroaromatics, the most widely used acceptor is sym. trinitrobenzene (TNB). Earlier we employed TNB as an acceptor and investigated the donor properties of tetraphenylporphyrin, phthalocyanin, pheophytin, and their metallo derivatives (2). 4,6-Dinitrobenzofuroxan is another member of the nitroaromatics and an examination of its structure reveals two canonical forms indicating planar structure of the compound. (Fig. 1). This bears a close resemblance to the structure of TNB. It is known that nitrobenzofuroxans form highly coloured complexes with aromatic donors exhibiting charge transfer bands in the visible region (3). The π-acceptor behaviour of benzofuroxans towards Co(II) derivatives of *meso*-porphyrin IX dimethyl ester and etioporphyrin has earlier been reported (4). In our continuing interest in the study of donor ability of porphyrins and their metallo derivatives with various acceptors, we chose to investigate the acceptor behaviour of 4,6-dinitrobenzofuroxan (BFO) in the expectation that near coplanarity of BFO may promote plane–plane overlap with the donor, thereby contributing significantly to the stability of the complexes. Moreover, such a study would make a comparative study with the TNB complexes more meaningful and help to delineate any specific site interaction that may prevail in the complexes.

The various donor porphyrins employed in the study are

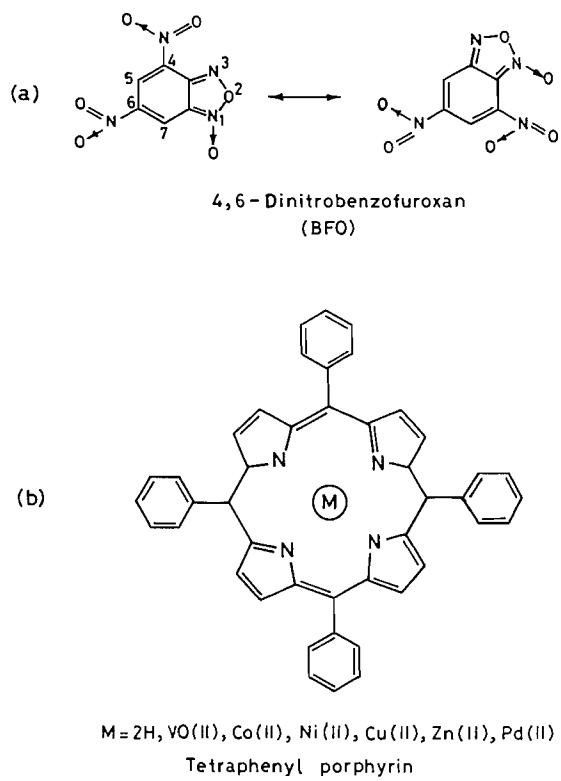

FIG. 1. (a) Different canonical forms of 4,6-dinitrobenzofuroxan. (b) chemical structure of metallo porphyrin.

5,10,15,20-tetraphenylporphyrin (TPP) and its metallo VO(II), Co(II), Ni(II), Cu(II), Zn(II), and Pd(II) derivatives. Besides employing the optical absorption method for the evaluation of

[1]Author to whom correspondence should be addressed.

[2]Revision received August 3, 1983.

Can. J. Chem. Downloaded from www.nrcresearchpress.com by 210.87.254.5 on 09/06/12
For personal use only.

Can. J. Chem. Downloaded from www.nrcresearchpress.com by 210.87.254.5 on 09/06/12
For personal use only.

association constants and thermodynamic parameters, the use of the ^1H nmr method is exploited for the determination of binding constants of BFO with ZnTPP and CoTPP's. The choice of ZnTPP as a donor is to apportion the ring current contributions to the proton chemical shifts of BFO in the CoTPP complex to evaluate the dipolar shifts. The esr measurements, coupled with the magnitude of the dipolar shifts and line broadening effects in the paramagnetic TPP's, are useful in arriving at the possible solution structures of the molecular complexes. The paramagnetic resonance parameters of the complexes provide information regarding the manner in which the $\pi-\pi$ interaction is transmitted through the metal–porphyrin bonding framework.

Experimental

The donor porphyrin (TPP) was procured from Aldrich, USA. The metal derivatives of TPP have been prepared according to the published procedures (5). 4,6-Dinitrobenzofuroxan was prepared from the nitration reaction of nitrosobenzene (6). It was crystallized twice from acetic acid, mp 172°C. All the solvents employed in the study were distilled before use. The preparation of solutions and all manipulations were carried out in dim light under a blanket of nitrogen. The spectra of the solutions were recorded immediately after mixing.

The optical absorption method employed for the evaluation of association constants involves the measurements of absorbance of the Q bands of porphyrin and its derivatives in the solvent CH_2Cl_2 on increasing addition of BFO. The concentration of the donor porphyrins is held constant ($\sim 10^{-5}$ *M*) and the range of concentration of BFO employed is 1.0×10^{-4} to 2.0×10^{-2} *M*. The spectrometer used was the same as described previously (2).

The ^1H nmr spectra were recorded on a WH-Bruker 270 MHz FT instrument using $CDCl_3$ as a solvent and TMS as an internal standard. The nmr titration experiment was performed as follows. To a constant volume of $CDCl_3$ solution of BFO (1×10^{-2} *M* varying amounts of ZnTPP/CoTPP in $CDCl_3$ were added, and the ^1H nmr spectra recorded, the temperature of measurement being 27°C. The shifts are with respect to TMS and the accuracy of the shifts lies in the range ± 0.005 δ. In both the optical and ^1H nmr experiments, the spectra of several sets of solutions were recorded to check reproducibility of the data obtained.

Electron spin resonance measurements of the solutions containing the donors and acceptors were recorded on a Varian E 109 esr spectrometer using toluene as the solvent. The spectra reported are at a temperature of 100 K. The field strength was calibrated using an nmr probe.

Results

BFO in CH_2Cl_2 exhibits well-defined intense absorption bands at 422 mm ($\log \epsilon = 2.87$), 333 nm ($\log \epsilon = 2.77$), 276 nm ($\log \epsilon = 3.14$), 261 nm ($\log \epsilon = 3.11$), and 233 nm ($\log \epsilon = 2.96$). Addition of increasing amounts of BFO to the donor porphyrins in CH_2Cl_2 causes a progressive decrease in the absorbance of Q bands in the region 500 to 600 nm (Fig. 2). Association constants were evaluated using the method of Nash (7). A typical plot of C_A^{-1} versus $d^0 (d^0 - d)^{-1}$ where C_A, d^0, and d denote the concentration of BFO, the absorbance value of the pure donor, and the absorbance value of the donor in presence of acceptor respectively, is shown in Fig. 3. The linearity of the plots suggests that the complexes formed are of 1:1 stoichiometry. The absorbance measurements taken at different temperatures permit the evaluation of thermodynamic parameters. The values of *K* and related parameters obtained in the present study are given in Table 1. The reliability of the *K* values is tested using Deranleau's saturation factor criterion (8). This is defined as the ratio of the concentration of the

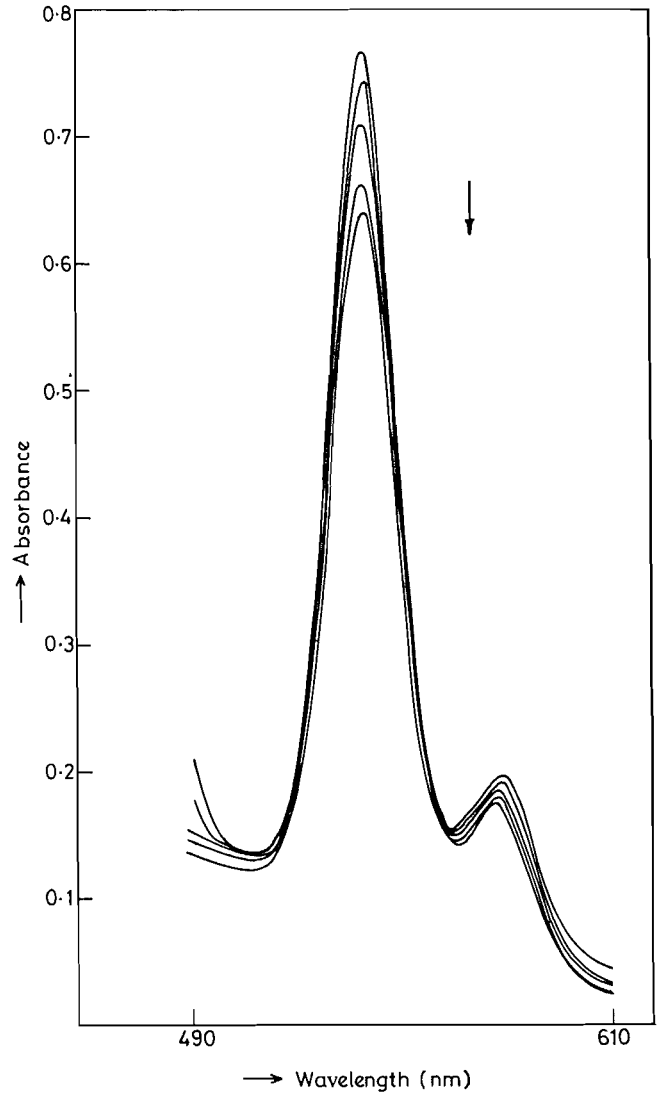

FIG. 2. Visible spectrum of (a) ZnTPP (5.6×10^{-5} *M*) containing increasing amounts of BFO in CH_2Cl_2 (3.9×10^{-4} to 5.5×10^{-2} *M*).

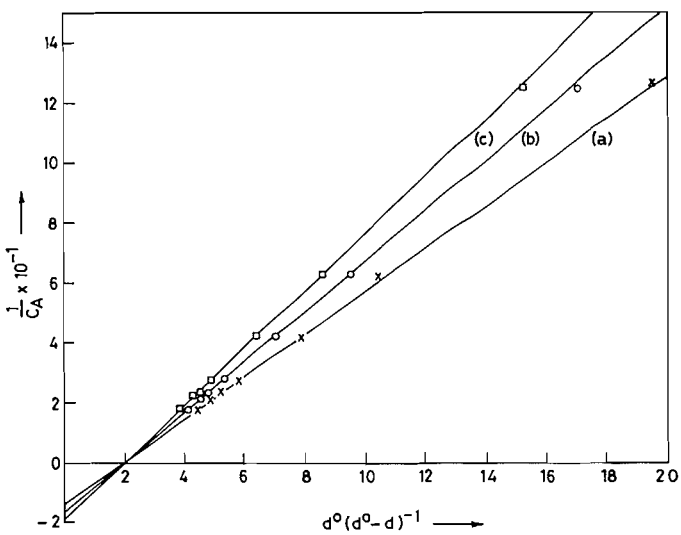

FIG. 3. Plots of $d^0 (d^0 - d)^{-1}$ versus 1/C for the interaction of ZnTPP with BFO at (a) 25°C; (b) 16°C; and (c) 9°C.

TABLE 1. Association constants and thermodynamic parameters for MTPP–BFO interaction in CH_2Cl_2

Complex	Temperature °C	K $dm^3\ mol^{-1}$	$-\Delta H$ kJ mol^{-1}	ΔS J $mol^{-1}\ deg^{-1}$
VOTPP–BFO	25.0	53±7.0		
	17.0	67±11.0	16.20±2.5	−21.20±2.5
	8.0	79±12.0		
PdTPP–BFO	25.0	132±22.0		
	17.0	161±28.0	12.90±3.6	−2.92±9.5
	9.0	178±31.0		
CuTPP–BFO	25.0	77±10.0		
	17.0	101±12.0	18.90±2.5	−27.15±4.0
	9.0	119±13.0		
NiTPP–BFO	25.0	55±6.0		
	18.0	65±9.0	13.80±3.0	−13.20±5.0
	10.0	74±7.0		
H_2TPP–BFO	25.0	56±7.0		
	16.0	71±11.0	16.80±3.0	−22.90±40
	10.0	80±9.0		
CoTPP–BFO	25.0	105±12.0		
	16.0	114±15.0	8.70±2.0	9.20±3.0
	10.0	127±14.0		
ZnTPP–BFO	25.0	14.2±3.0		
	16.0	16.8±2.5	14.0±2.0	−25.10±4.5
	9.0	19.6±3.0		

complex to that of the acceptor and in the present study this is within the range of 0.2–0.8 for well-defined K values.

The ^{1}H nmr spectrum of BFO in $CDCl_3$ consists of resonances centered at δ 9.150 and δ 8.847, corresponding to H_7 and H_5 protons respectively. On increasing addition of MTPP, the acceptor resonances are shifted to higher fields (Fig. 4). The multiplet structure of H_7 and H_5 proton resonances remains unaffected on addition of ZnTPP. On the other hand, these resonances are broadened and shifted to higher fields (relative to the ZnTPP complex) on addition of CoTPP (Table 2). The appearance of only one set of resonances in the ^{1}H nmr spectra of the complexes reveals that the rate of exchange between the free and complexed BFO is fast in the time scale. It can be shown that the observed proton resonance shifts (Δ) of the acceptor on increasing addition of donor porphyrins are related to the association constant, K, through the expression

$$[1]\quad \frac{1}{\Delta} = \frac{1}{D\Delta_c} A\left(1 - \frac{\Delta}{\Delta_c}\right) + \frac{1}{\Delta_c} + \frac{1}{KD\Delta_c}$$

where D and A represent the concentration of donor porphyrins and acceptor respectively and Δ_c is the shift in the fully formed complex. To obtain the best values of K and Δ_c we adopted a procedure similar to that described in the literature (1). This involves an initial neglect of the first term in eq. [1] to obtain

$$[2]\quad \frac{1}{\Delta} = \frac{1}{\Delta_c} + \frac{1}{KD\Delta_c}$$

Plots of $1/\Delta$ vs. $1/D$ for both H_5 and H_7 protons of BFO in the ZnTPP and CoTPP addition versus the concentration of donor porphyrin yield straight lines, with a slope of $1/K\Delta_c$ and an intercept of $1/\Delta_c$. The least-squares fit of these values thus obtained is fitted into expression [1] in a manner to get the best fit. A regression analysis programme was employed to arrive at the best values of K and Δ_c satisfying expression [1]. The values of K and Δ_c obtained for H_5 and H_7 protons are listed in Table 3.

The values of K obtained for H_5 and H_7 protons are similar in magnitude, indicating that the π-complexation effect is felt by the protons equally. The magnitudes of K obtained using the nmr method are at variance with those obtained by the visible spectral method. We attribute the variance in K values to the different concentration ranges employed in the respective methods.

The values of Δ_c are composed of ring current and dipolar effects. Thus

$$[3]\quad \Delta_c = \Delta_{(ring)} + \Delta_{(dipolar)}$$

where $\Delta_{(ring)}$ are the shifts due to the ring current of the porphyrin and $\Delta_{(dipolar)}$ are the additional shifts due to the single unpaired electron in CoTPP. A reasonable assumption, that the shift due to the ring current in CoTPP is identical to that of ZnTPP owing to their structural similarity except for the metal ion, permits the calculation of the contribution from the dipolar term to the shifts. The pseudo contact shifts obtained for H_5 and H_7 protons are represented below. It is seen that both H_5 and H_7 protons of BFO experience shifts of similar magnitude unlike

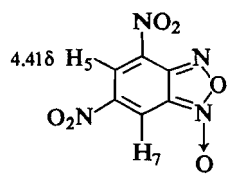

those reported for other acceptor systems (1).

The esr spectra of the BFO complexes of Cu and VOTPP's are highly characteristic, permitting an evaluation of esr parameters (Table 4). Addition of BFO shifts the signals to higher fields, thereby decreasing the values of $g_\parallel$ and $g_\perp$ (Fig. 5). The small changes observed in metal hyperfine coupling constants and a decrease in $A_\parallel^M$ relative to the MTPP's signify molecular complexation. In the case of the CuTPP complex, a simultaneous increase in $A_\parallel^N$ and $A_\perp^N$ values is observed. The esr spectrum of the CoTPP–BFO complex is often plagued with the

Can. J. Chem. Downloaded from www.nrcresearchpress.com by 210.87.254.5 on 09/06/12
For personal use only.

Can. J. Chem. Downloaded from www.nrcresearchpress.com by 210.87.254.5 on 09/06/12
For personal use only.

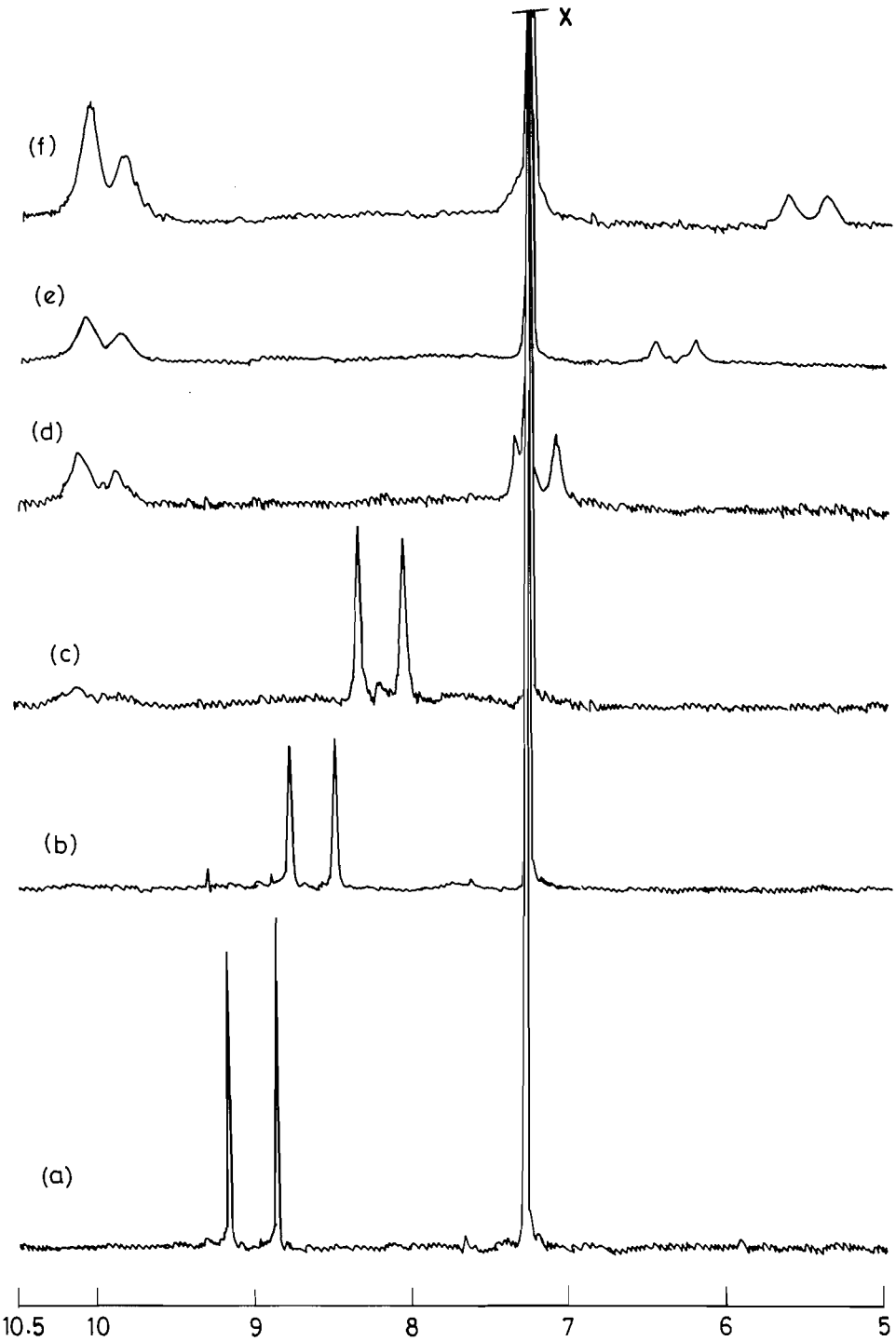

FIG. 4. Chemical shifts of BFO (1.09×10^{-2} *M*) proton resonances with increasing addition of CoTPP; (a) nil; (b) 7.5×10^{-4} *M*; (c) 2.55×10^{-4} *M*; (d) 4.51×10^{-3} *M*; (e) 6.01×10^{-3} *M*; and (f) 7.51×10^{-3} *M*. Mark (X) denotes solvent peak.

signals arising from its molecular oxygen adduct. The spectrum obtained exhibits a strong signal at $g \simeq 2.08$, typical of an oxygen adduct (9), and weak signals in the low-field region, resembling closely that of the CoTPP–TNB complex (2) and indicating the existence of a mixture of pure CoTPP–BFO complex and its oxygen adduct. In view of this, the esr parameters of the oxygen-free CoTPP–BFO complex could not be calculated unambiguously. The π-complexation by metal TPP's causes a change in the electron distribution over the porphyrin core, affecting the electronic energy levels of the central metal ions. Though a manifestation of this effect is seen only in the changes of $A_{\parallel}^{M}$ values to VOTPP, it has been possible to quantitatively assess this in the CuTPP complexes. The perturbance of electronic levels of Cu is seen in the slight decrease in the value of the covalency factor α^2. It is calculated using the procedure described by Kievelson and Neiman (10); the change in the α^2 value relative to CuTPP is found to be -0.01391, signifying that the σ bonding is slightly more covalent in the molecular complex. Such changes are interpreted in terms of a small increase in the π-electron density of N or in

TABLE 2. Concentrations of MTPP and the observed shifts (δ) of BFO protons[a,b]

Concentration of MTPP $\times 10^{-3}$ mol/dm^3	H_7	Shift	H_5	Shift
ZNTPP				
BFO	9.151	—	8.848	—
1.12	9.065	0.086	8.755	0.093
2.24	8.986	0.165	8.669	0.179
4.48	8.383	0.313	8.510	0.338
6.72	8.708	0.443	8.369	0.479
8.40	8.635	0.516	8.289	0.559
CoTPP				
BFO	9.150 (4)	—	8.847 (4)	—
0.75	8.791 (8)	0.359	8.500 (6)	0.347
2.25	8.339 (12)	0.811	8.059 (14)	0.788
4.51	7.318 (18)	1.832	7.064 (19)	1.783
6.01	6.473 (23)	2.677	6.198 (24)	2.649
7.51	5.635 (30)	3.515	5.392 (31)	3.455

[a]Concentration of BFO employed is 1.09×10^{-2} *M*.
[b]The values in parenthesis represent the linewidths in Hertz.

TABLE 3. The ^{1}H nuclear magnetic resonance data evaluated for Zn and CoTPP–BFO complexes

Proton	Δ_c (δ)	*K* dm^3 mol^{-1}
ZnTPP–BFO		
H_5	2.514±0.210	58.3±10
H_7	2.733±0.210	56.0±10
CoTPP–BFO		
H_5	7.010±0.315	70.7±12
H_7	7.140±0.315	69.9±12

TABLE 4. Electron spin resonance parameters of MTPP complexes with BFO in toluene at 100 K

Complex	$g_\parallel$	$g_\perp$	$10^4 A_\perp^M$ cm^{-1}	$10^4 A_\parallel^M$ cm^{-1}	$10^4 A_\perp^N$ cm^{-1}	$10^4 A_\parallel^N$ cm^{-1}
CuTPP	2.185	2.047	31.50	208.10	15.70	14.70
CuTPP–BFO	2.179	2.038	32.82	206.66	16.81	15.72
VOTPP	1.968	1.997	57.60	164.30	—	—
VOTPP–BFO	1.961	1.989	59.10	160.71	—	—
CoTPP	1.971	2.80	210.00	141.00	—	—
CoTPPP–BFO[a]	2.007	2.120	—	—	—	—

[a]Corresponds to CoTPP–BFO:O_2.

the increase in electronic charge on copper in the molecular complex relative to CuTPP (2).

Discussion

An examination of Table 1 reveals that the association constants for the BFO interaction with MTPP's follow the order $Pd^{2+} > Co^{2+} > Cu^{2+} > Ni^{2+} \sim VO^{2+} \sim 2H > Zn^{2+}$, similar to that observed for the corresponding complexes of TNB. However, the magnitudes of *K* are higher than those observed for the TNB complexes. This can be interpreted in terms of the planar disposition of the NO_2 groups in BFO. Shinomiya (11) has pointed out that a maximum stability in the complexes can

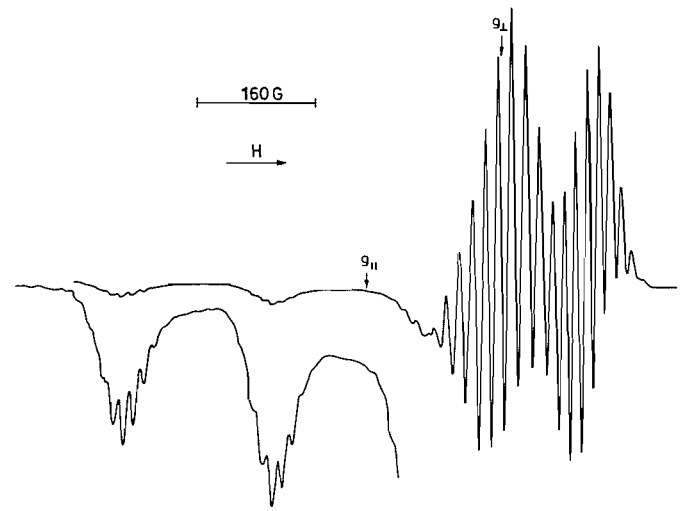

FIG. 5. The esr spectrum of the CuTPP–BFO complex in toluene at 110 K.

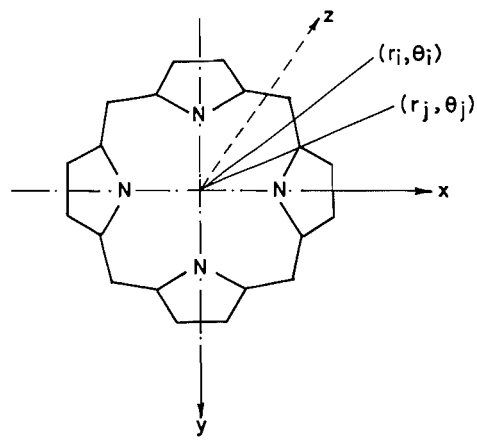

FIG. 6. Coordinate system for metal and acceptor protons.

be accomplished if the nitro groups are allowed to be coplanar with the benzene ring to which they are attached. It is worthwhile to point out that the magnitudes of *K* are lower than those observed for polynitro fluorenone complexes (12). We attribute this to the relatively smaller size of BFO. The thermodynamic parameters of the MTPP–BFO interaction are not significantly different on variation of the metal. It is worthy to mention here that the decreases in ΔH values observed in the present study are higher than those observed for TNB complexes. In molecular complexing systems, the values of ΔH signify the efficiency of packing of donor and acceptor in the complex. This can be enhanced if the molecules involved in the complex formation are planar, such that plane-to-plane overlap leads to a better packing of the donor and acceptor. We believe such effects are operative in the present study. Attempts to obtain single crystals of these complexes have so far been unsuccessful.

In order to demonstrate that the interaction of BFO with MTPP is not of the coordinative type, we studied the ir spectra of the complexes. The strong band, ~1550 cm^{-1}, in BFO has been assigned to the N→O stretching frequency (13). The —C=$\overset{+}{N}$— stretching vibration in BFO occurs as a weak band at 1625 cm^{-1}, while the asymmetric and symmetric stretching vibrations of the NO_2 groups appear at 1530 and 1320 cm^{-1}, respectively. In the complexes, these vibrations remain virtu-

Can. J. Chem. Downloaded from www.nrcresearchpress.com by 210.87.254.5 on 09/06/12
For personal use only.

ally unaffected. Further, the donor porphyrin vibrations are only marginally affected. These observations indicate the absence of any specific site interaction of BFO with MTPP's. Moreover, the esr spectral changes, i.e. decrease in g values and increase in A values, are in contrast to those observed in the interaction of MTPP's with axially coordinating ligands (14).

An attempt has been made here to probe into possible solution structures of the molecular complexes using ^{1}H nmr and esr data of the complexes. The dipolar shifts and broadening of the acceptor proton signals in the CoTPP–BFO complex are used to locate the protons of BFO with respect to the Co(II) centre in the complex. The linewidths of the BFO proton resonances on addition of CoTPP are given in Table 2. The broadening ratios are obtained using the expression of Sternlicht (15). The estimates of broadening ratios were obtained at 270 MHz by subtracting the diamagnetic line widths of BFO multiplets from those in the presence of CoTPP. This indicated that both H_5 and H_7 proton resonances were about seven times as broad as in free BFO. The absence of any preferential broadening of acceptor protons underscores the plane–plane overlap of the acceptor with donor in these complexes. The dipolar shifts experienced by the acceptor protons in the CoTPP–BFO complex are all to higher fields, justifying that there exists no direct spin-transfer. Calculation of such shifts is based on the evaluation of the geometric factors, $(3\cos^2\theta - 1)\,r^{-3}$, where θ is the angle the acceptor proton subtends with Co(II) and the said proton (Fig. 6). The X-ray structure of CoTPP (14) was taken to define the stereochemistry, and the bond angles and bond lengths of BFO are approximated to that of TNB. The molecular framework of the complex is then defined by placing BFO parallel to CoTPP at a distance R, such that the centre of the aryl ring passes through the Co(II) ion. Moreoever, for a fixed distance R, tilt angles are varied from 0 to 30°. The distances r_0 and r_j from Co(II) to H_5 and H_7 protons of the acceptor and the angles subtended are computed for various values of R (3.5–4.0 Å) and tilt angles. The dipolar shifts are calculated using the geometric factors according to ref. 16.

$$[4]\quad \left(\frac{\Delta H}{H}\right)_i \Big/ \left(\frac{\Delta H}{H}\right)_j = (3\cos^2\theta_i - 1)\,r_i^{-3}/(3\cos^2\theta_j - 1)\,r_j^{-3}$$

Most of the structures scanned in this fashion do not fit well into the experimentally observed ratio of dipolar shifts, probably because of the random orientations of the molecules in the solvent. The determination of structure must, however, await a detailed X-ray examination. The present study points out that the interaction of BFO with porphyrins occurs only in the periphery.

Acknowledgements

One of the authors (TKC) is grateful to the University Grants Commission for the Fellowship.

1. (*a*) G. P. FULTON and G. N. LAMAR. J. Am. Chem. Soc. **98**, 2119 (1976); **98**, 2124 (1976); (*b*) C. D. BARRY, H. A. O. HILL, B. E. MANN, P. J. SADLER, and R. J. P. WILLIAMS. J. Am. Chem. Soc. **95**, 4545 (1973); (*c*) H. A. O. HILL, P. J. SADLER, and R. J. P. WILLIAMS. J. Chem. Soc. 1663, 1973.
2. T. K. CHANDRASHEKAR and V. KRISHNAN. Inorg. Chem. **20**, 2782 (1981).
3. (*a*) A. S. BAILEY and J. R. CASE. Proc. Chem. Soc. 176 (1956); (*b*) Tetrahedron, **3**, 113 (1958).
4. H. A. O. HILL, A. J. MACFARLANE, and R. J. P. WILLIAMS. J. Chem. Soc. 1704 (1969).
5. (*a*) P. ROTHEMUND and A. R. MENNOTTI. J. Am. Chem. Soc. **70**, 1808 (1948); (*b*) G. D. DOROUGH, J. R. MILLER, and F. M. HUENNEKENS. J. Am. Chem. Soc. **73**, 4315 (1951).
6. A. G. GREEN and R. M. ROW. J. Chem. Soc. **103**, 2023 (1913).
7. C. J. NASH. J. Phys. Chem. **64**, 950 (1960).
8. D. A. DERANLEAU. J. Am. Chem. Soc. **91**, 4044 (1969).
9. F. A. WALKER. J. Magn. Reson. **15**, 201 (1974).
10. D. KIEVELSON and R. NIEMAN. J. Chem. Phys. **35**, 149 (1961).
11. T. SHINOMIYA. Bull. Chem. Soc. Jpn. **92**, 137 (1940).
12. T. K. CHANDRASHEKAR and V. KRISHNAN. Inorg. Chem. Acta, **62**, 259 (1982).
13. C. N. R. Rao. *In* The chemistry of nitro and nitroso groups. Part I. *Edited by* Henry Fever. Interscience, New York (1969).
14. (*a*) F. A. WALKER. J. Am. Chem. Soc. **92**, 4235 (1970); (*b*) H. YOKI and M. IWAIZUMI. Bull. Chem. Soc. Jpn. **53**, 1489 (1980).
15. H. STERNLICHT. J. Chem. Phys. **42**, 2250 (1965).
16. G. N. LAMAR. *In* NMR of paramagnetic molecules: principles and applications. *Edited by* W. Horrocks. Academic Press, New York. 1973.

Can. J. Chem. Downloaded from www.nrcresearchpress.com by 210.87.254.5 on 09/06/12
For personal use only.

On the structure of the adduct from the aluminium chloride catalyzed Diels–Alder reaction of 2-methyl-2-cyclohexenone with isoprene

JAGABANDHU DAS and ZDENEK VALENTA[1]
Department of Chemistry, University of New Brunswick, Bag Service #45222, Fredericton, N.B., Canada E3B 6E2

AND

HSING-JANG LIU[1] and TENG KO NGOOI
Department of Chemistry, University of Alberta, Edmonton, Alta., Canada T6G 2G2

Received July 19, 1983

JAGABANDHU DAS, ZDENEK VALENTA, HSING-JANG LIU, and TENG KO NGOOI. Can. J. Chem. **62**, 481 (1984).

An unequivocal correlation of keto ester **3** and the adduct obtained from the aluminium chloride catalyzed Diels–Alder reaction of 2-methyl-2-cyclohexenone with isoprene confirms the structure of the adduct to be **2**.

JAGABANDHU DAS, ZDENEK VALENTA, HSING-JANG LIU et TENG KO NGOOI. Can. J. Chem. **62**, 481 (1984).

On a déterminé que le produit d'addition obtenu de la réaction de Diels–Alder catalysée par le chlorure d'aluminium entre la méthyl-2-cyclohexèn-2-one et l'isoprène possède la structure **2**, en se basant sur une corrélation non-équivoque du céto-ester **3** et du produit d'addition.

[Traduit par le journal]

Can. J. Chem. Downloaded from www.nrcresearchpress.com by 210.87.254.5 on 09/06/12
For personal use only.

In 1975, the aluminium chloride catalyzed Diels–Alder reaction of 2-methyl-2-cyclohexenone with isoprene was described (1). The reaction produced in high yield an adduct to which structure **1** was assigned. This structural assignment has been suspected to be in error in light of its violation of the "*para*" rule (2) for Diels–Alder addition. The incorrectness of the assignment has been pointed out in a recent report (3) which provided spectral evidence in support of structure **2** for the adduct resulting from the normal mode of "*para*" addition. Concurrently, we have reached the same conclusion on the basis of the following chemical correlation which confirms unambiguously this structural assignment.

In the presence of stannic chloride, the reaction of 2-carbomethoxy-2-cyclohexenone with isoprene gave a 61% yield of a single adduct **3** (4) showing thirteen lines in the ^{13}Cmr spectrum. Its regiochemistry was unambiguously determined as follows. Keto ester **3** was subjected to decarbomethoxylation with lithium iodide dihydrate in refluxing 2,4,6-collidine (5, 6) to give a mixture of two epimeric ketones **4** in 40% yield. Oxidation of this mixture with *N*-bromosuccinimide in refluxing carbon tetrachloride in the presence of a small amount of benzoyl peroxide (7, 8) gave aryl ketone **5** in 64% yield. The ^{1}Hmr spectrum of this compound displayed a signal due to a *peri*-proton (C-8 H) (6, 8, 9) as a doublet (J = 8 Hz) at δ 7.92. Such a coupling is in agreement only with structure **5**.

Ketalization of keto ester **3** under standard conditions afforded a 92% yield of ketal ester **6** which was reduced with lithium aluminium hydride to the corresponding alcohol **7** (96% yield). Conversion of alcohol **7** to its phosphorodiamidate derivative **8** using *n*-butyllithium, *N*,*N*-dimethylphosphoramidic dichloride, and dimethylamine (10), followed by lithium–ethylamine reduction (11) of **8** gave ketal **9** in an overall yield of 40%. Upon treatment with *p*-toluenesulfonic acid in acetone, ketal **9** was transformed quantitatively to the corresponding ketone **2** which was shown to be identical in all respects with the adduct prepared from 2-methyl-2-cyclohexenone and isoprene according to the described procedure (1).

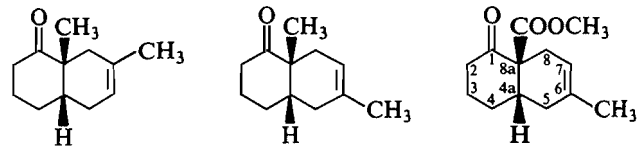

1 **2** **3**

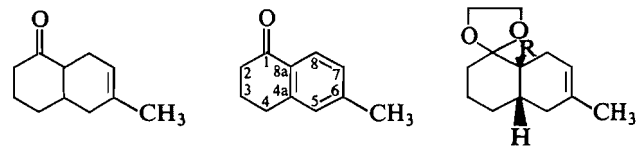

4 **5**

6 R = $COOCH_3$
7 R = CH_2OH
8 R = $CH_2OPO[N(CH_3)_2]_2$
9 R = CH_3

Experimental

General

Elemental analyses were performed by the microanalytical laboratory of the Department of Chemistry, University of Alberta. Infrared spectra were recorded on a Nicolet 7-199 FT-IR spectrophotometer. The ^{1}Hmr spectra were recorded on a Varian HA-100, Bruker WH-200, or WH-400 spectrometer and, except where otherwise stated, were obtained on solutions in deuteriochloroform with tetramethylsilane as internal reference. The ^{13}Cmr spectra were recorded on a Bruker WP-60/Nicolet BNC-12 system or a Bruker WH-400 spectrometer and were obtained on solutions in deuteriochloroform using tetramethylsilane as internal reference. Mass spectra (ms) were recorded using A.E.I. model MS12 or MS50 mass spectrometers. Anhydrous magnesium sulfate was used for drying organic solutions.

Preparation of keto ester 3

At 0°C, anhydrous stannic chloride (1.16 g, 4.45 mmol) was added to a solution of 2-carbomethoxy-2-cyclohexenone (12) (1.37 g, 8.9 mmol) and isoprene (6.10 g, 89 mmol) in ether (20 mL). After stirring under an argon atmosphere for 6 h, the reaction mixture was poured into ice-cold water and extracted with ether. The organic solution was dried, filtered, and concentrated. Flash chromatography (13) of the residue on silica gel, eluting with 7% ethyl acetate in petroleum ether, gave keto ester **3** (1.2 g; 61% yield); ir (film): 1743 (ester) and 1715 (ketone) cm^{-1}; ^{1}Hmr δ: 1.63 (s, 3H, —CH_3), 3.73 (s, 3H, —OCH_3), and 5.32 (m, 1H, =CH—); ^{13}Cmr δ: 208.3 (C-1), 172.8 (—COO—), 131.5 (C-6), 116.8 (C-7), 60.6 (C-8a), 52.3

[1]Authors to whom correspondence should be addressed.

Can. J. Chem. Downloaded from www.nrcresearchpress.com by 210.87.254.5 on 09/06/12
For personal use only.

(—OCH_3), 37.5 (C-4a), 23.6 (—CH_3), 38.1, 32.2, 27.8, 27.0, and 24.1 (C-2, C-3, C-4, C-5, and C-8); ms M^+: 222.1256 (calcd. for $C_{13}H_{18}O_3$: 222.1256). *Anal.* calcd. for $C_{13}H_{18}O_3$: C 70.23, H 8.17; found: C 70.20, H 8.20.

Decarbomethoxylation of keto ester 3

Finely divided anhydrous lithium iodide (750 mg, 5.6 mmol) was suspended in 2,4,6-collidine (5 mL) wth vigorous stirring. Water (202 μL, 11.2 mmol) was added and the suspension rapidly dissolved. Keto ester **3** (580 mg, 2.6 mmol) was dissolved in this solution under an atmosphere of argon. The mixture was heated at reflux for 16 h. The mixture was cooled to room temperature, poured into ice-cold aqueous 1 *N* hydrochloric acid, and extracted with ether. The extracts were washed with water, dried, filtered, and concentrated. Flash chromatography of the residue on silica gel, eluting with 5% ethyl acetate in petroleum ether, gave a mixture of epimeric ketones **4** (170 mg; 40% yield); ir (film): 1714 (C=O) cm^{-1}; ^{1}Hmr (CCl_4) δ: 1.60 (br s, 3H, —CH_3) and 5.37 (m, 1H, =CH—); ms M^+: 164.1197 (calcd. for $C_{11}H_{16}O$: 164.1197).

Dehydrogenation of ketones 4

The mixture of epimeric ketones **4** (140 mg, 0.85 mmol) was dissolved in carbon tetrachloride (10 mL). Benzoyl peroxide (5 mg, 0.02 mmol) and *N*-bromosuccinimide (310 mg, 1.74 mmol) were added.The reaction mixture was heated at reflux for 16 h under an atmosphere of argon. Filtration and concentration gave an oily residue which was subjected to flash chromatography on silica gel. Elution with 5% ethyl acetate in petroleum ether afforded aryl ketone **5** (87 mg, 64% yield); ir (film): 1682 (C=O) and 1608 (aromatic C=C) cm^{-1}; ^{1}Hmr δ: 2.11 (m, 2H, —$CH_2CH_2CH_2$—), 2.37 (s, 3H, —CH_3), 2.61 (dd, 2H, J = 8, J' = 6 Hz, =C—CH_2—), 2.90 (t, 2H, J = 6 Hz, —CH_2CO—), 7.04 (s, 1H, C-5 H), 7.10 (d, 1H, J = 8 Hz, C-7 H) and 7.92 (d, 1H, J = 8 Hz, C-8 H); ^{13}Cmr δ: 197.9 (C-1), 144.5 (C-4a), 144.1 (C-8a), 130.6 (C-6), 129.2, 127.6, 127.4 (C-5, C-7, and C-8), 39.2 (C-2), 29.9 (C-4), 23.5 (C-3), and 21.6 (—CH_3); ms M^+: 160.0879 (calcd. for $C_{11}H_{12}O$: 160.0887).

Ketalization of keto ester 3

A solution of keto ester **3** (750 mg, 3.38 mmol), ethylene glycol (2.09 g, 33.7 mmol), and *p*-toluenesulfonic acid (10 mg, 0.05 mmol) in benzene (50 mL) was refluxed with a Dean–Stark water separator under an argon atmosphere for 55 h. After cooling to room temperature, the resulting mixture was made basic with 10 mL of saturated aqueous sodium bicarbonate. The organic layer was separated and washed with water. Drying, filtration, and concentration gave an oil which was purified by flash chromatography on silica gel. Elution with 5% ethyl acetate in petroleum ether gave 101 mg of the starting material **3**. Further elution with the same solvent system afforded ketal ester **6** (713 mg; 92% yield based on consumed starting material); ir (film): 1728 (C=O) cm^{-1}; ^{1}Hmr δ: 1.60 (s, 3H, —CH_3), 3.70 (s, 3H, —OCH_3), 3.86 (m, 4H, —OCH_2CH_2O—), and 5.28 (m, 1H, =CH—); ms M^+: 266.1517 (calcd. for $C_{15}H_{22}O_4$: 266.1512). *Anal.* calcd. for $C_{15}H_{22}O_4$: C 67.63, H 8.33; found: C 67.25, H 8.27.

Reduction of ketal ester 6

At 0°C, lithium aluminium hydride (236 mg, 6.21 mmol) was added to a solution of ketal ester **6** (550 mg, 2.07 mmol) in ether (10 mL). After stirring at room temperature under an argon atmosphere for 10 h, the reaction mixture was cooled to 0°C and water was slowly added. The resulting mixture was extracted with methylene chloride. The extracts were dried, filtered, and concentrated. Flash chromatography of the residue on silica gel, eluting with 15% ethyl acetate in petroleum ether, gave alcohol **7** (474 mg; 96% yield); ir (film): 3550 (OH) cm^{-1}; ^{1}Hmr δ: 1.66 (s, 3H, —CH_3), 3.41, 3.75 (both d, 1H each, J = 12 Hz each, —CH_2OH), 3.76 (s, 1H, —OH), 4.02 (m, 4H, —OCH_2CH_2O—), and 5.21 (m,. 1H, =CH—); ms M^+: 238.1565 (calcd. for $C_{14}H_{22}O_3$: 238.1563). *Anal.* calcd. for $C_{14}H_{22}O_3$: C 70.54, H 9.30; found: C 70.55, H 9.35.

Preparation of phosphorodiamidate 8

At 0°C, to a solution of ketal alcohol **7** (220 mg, 0.93 mmol) in *N*,*N*,*N'*,*N'*-tetramethylethylenediamine and 1,2-dimethoxyethane (1:4; 10 mL), was added a 2.35 *M* solution of *n*-butyllithium in hexane (1 mL, 2.35 mmol) under an argon atmosphere. After stirring for 15 min, *N*,*N*-dimethylphosphoramidic dichloride (2.5 g, 15.7 mmol) was added. The reaction mixture was stirred at room temperature for 24 h and an excess of dimethylamine (3 mL) was added at 0°C. After 30 min, the resulting mixture was poured into water and extracted with ether. The extracts were washed with water, dried, filtered, and concentrated. Column chromatography of the residue on silica gel, eluting with ether, afforded 30 mg of starting alcohol **7**. Further elution with 5% methanol in ether gave phosphorodiamidate **8** (290 mg; 98% yield based on consumed starting material); ir (film): major absorption bands at 2926, 1458, 1300, 1227, 1180, 1090, 1047, 995, and 751 cm^{-1}; ^{1}Hmr δ: 1.68 (s, 3H, —CH_3), 2.69 (d, 12H, J = 10 Hz, 2 × —$N(CH_3)_2$), 3.75 (dd, 1H, J = 11, J' = 3 Hz, —OC*H*H—), 3.90–4.12 (m, 5H, —OCH_2CH_2O— and —OC*H*H—), and 5.23 (m, 1H, =CH—); ms M^+: 372.2181 (calcd. for $C_{18}H_{33}N_2O_4P$: 372.2170).

Reduction of phosphorodiamidate 8

Lithium ribbon (349 mg; 55 g-at.) was added in small pieces over a 10-min period to 5 mL of ethylamine (freshly distilled from calcium hydride) at 0°C under an atmosphere of argon. After 30 min, a solution of phosphorodiamidate **8** (188 mg, 0.51 mmol) and *tert*-butyl alcohol (75 mg, 1.01 mmol) in tetrahydrofuran (3 mL) was added dropwise over 5 min and stirring was continued for 30 min. Water was slowly added and the resulting mixture extracted with ether. After washing with water, the organic solution was dried, filtered, and concentrated. Flash chromatography of the residue on silica gel, eluting with 3% ethyl acetate in petroleum ether, afforded ketal **9** (46 mg; 41% yield); ir (film): major absorption bands at 2924, 2853, 1464, 1171, 1095, 1063, 955, and 896 cm^{-1}; ^{1}Hmr δ: 0.80 (s, 3H, —CH_3), 1.81 (br s, 3H, =C—CH_3), 3.85 (s, 4H, —OCH_2CH_2O—) and 5.17 (m, 1H, =CH—); ms M^+: 222.1617 (calcd. for $C_{14}H_{22}O_2$: 222.1614). *Anal.* calcd. for $C_{14}H_{22}O_2$: C 75.62, H 9.98; found: C 75.59, H 10.06.

Deketalization of ketal 9

Ketal **9** (30 mg, 0.14 mmol) was dissolved in acetone (2 mL) and *p*-toluenesulfonic acid (13 mg, 0.07 mmol) was added. After stirring at room temperature under an argon atmosphere for 2 h, the reaction mixture was made basic with saturated aqueous sodium bicarbonate and extracted with methylene chloride. The extracts were washed with water, dried, and filtered. Concentration gave the crude product which was purified by column chromatography on silica gel. Elution with 20% ethyl acetate in petroleum ether gave ketone **2** (24 mg; quantitative yield); ir (film): 1705 (C=O) cm^{-1}; ^{1}Hmr δ: 1.12 (s, 3H, —CH_3), 1.68 (s, 3H, =C—CH_3), and 5.32 (m, 1H, =CH—); ms M^+: 178.1356 (calcd. for $C_{12}H_{18}O$: 178.1353). Ketone **2** was shown to be identical with the adduct prepared from 2-methyl-2-cyclohexenone and isoprene according to the reported procedure (1), by direct comparison of their chromatographic and spectral properties.

Acknowledgments

We are grateful to the Natural Sciences and Engineering Research Council of Canada for financial support and to the Alberta Heritage Foundation for Medical Research for a Studentship to T.K.N.

1. I. NAGAKURA, H. OGATA, M. UENO, and Y. KITAHARA. Bull. Chem. Soc. Jpn. **48**, 2995 (1975).
2. A. S. ONISHCHENKO. Diene synthesis. Israel Program of Scientific Translations, Jerusalem. 1964.
3. F. FRINGUELLI, F. PIZZO, A. TATICCHI, T. D. J. HALLS, and E. WENKERT. J. Org. Chem. **47**, 5056 (1982).
4. H. J. LIU and T. K. NGOOI. Synth. Commun. **12**, 715 (1982).

5. F. ELZINGER. Org. Synth. **45**, 7 (1965).
6. H. J. LIU and E. N. C. BROWNE. Can. J. Chem. **59**, 601 (1981).
7. R. A. BARNES. J. Am. Chem. Soc. **70**, 145 (1948).
8. H. J. LIU and E. N. C. BROWNE. Can. J. Chem. **57**, 377 (1979).
9. L. M. JACKMAN and S. STERNHELL. Applications of nuclear magnetic resonance spectroscopy in organic chemistry. 2nd ed. Pergamon Press, Oxford. 1969.
10. H. J. LIU, S. P. LEE, and W. H. CHAN. Can. J. Chem. **55**, 3797 (1977).
11. R. E. IRELAND, D. C. MUCHMORE, and U. HENGARTNER. J. Am. Chem. Soc. **94**, 5908 (1972).
12. H. J. REICH, J. M. RENGA, and L. T. REICH. J. Am. Chem. Soc. **97**, 5434 (1975).
13. W. C. STILL, M. KAHN, and A. MITRA. J. Org. Chem. **43**, 2923 (1978).

Can. J. Chem. Downloaded from www.nrcresearchpress.com by 210.87.254.5 on 09/06/12
For personal use only.

Thermodynamics of solution of gypsum and anhydrite in water over a wide temperature range

HORACIO R. CORTI AND ROBERTO FERNANDEZ-PRINI[1]

Departamento Química de Reactores, Comisión Nacional de Energía Atómica, Av. Libertador 8250, CP-1429, Capital Federal, Argentina

Received June 29, 1983

HORACIO R. CORTI and ROBERTO FERNANDEZ-PRINI. Can. J. Chem. **62**, 484 (1984).

The solubility of calcium sulphate in water at different temperatures is important for the description of chemical processes occurring in heat exchangers as well as in geothermal processes. Great discrepancies have been reported between experimental and predicted solubilities at high temperature and the transition temperature for the phase transition process (gypsum → anhydrite) is ill-defined.

We have analyzed the available data for the solubility of calcium sulphate in water with no added electrolyte. Ion-pairing has been taken into account to calculate the standard thermodynamic properties of the solution process.

It is found that the solubility data for gypsum and anhydrite are thermodynamically very consistent. It is possible to obtain the thermodynamic properties of the phase transition from solution data and, at 298.15 K and 101.325 kPa, they are in very good agreement with reported values from measurements with the pure phases. The transition temperature is calculated to be 315.7 ± 0.4 K.

It is also shown that the experimental data agree with values predicted for high temperature by employing well-established methods of calculation of solution thermodynamic properties (e.g., principles of correspondence and of constant charge).

HORACIO R. CORTI et ROBERTO FERNANDEZ-PRINI. Can. J. Chem. **62**, 484 (1984).

La solubilité du sulfate de calcium dans l'eau à diverses températures est importante pour la description de processus chimiques se produisant dans des échangeurs de chaleur de même que dans des processus géothermiques. De grandes disparités ont été rapportées entre les solubilités prédites et expérimentales à haute température et la température de transition pour le processus de transition de phase (gypse → anhydrite) est mal défini.

Nous avons analysé les données disponibles pour la solubilité du sulfate de calcium dans de l'eau où il n'y a pas d'électrolytes ajoutés. On a tenu compte des paires d'ions pour calculer les propriétés thermodynamiques standards des processus en solution.

On a trouvé que les données de solubilité pour la gypse et l'anhydrite sont thermodynamiquement très consistantes. Il est possible d'obtenir les propriétés thermodynamiques de la phase de transition à partir des données en solution; pour 298.15 K et 101,325 kPa, ces propriétés sont en très bon accord avec les valeurs rapportées pour ces quantités lorsqu'elles ont été mesurées avec les phases pures. On a calculé que la température de transition est 315,7 ± 0,4 K.

On a aussi montré que les données expérimentales sont en accord avec les valeurs que l'on peut prédire pour les hautes températures en employant des méthodes bien établies pour le calcul de propriétés thermodynamiques en solution (par exemple, les principes de correspondance et de charge constante).

[Traduit par le journal]

Can. J. Chem. Downloaded from www.nrcresearchpress.com by 210.87.254.42 on 09/06/12
For personal use only.

Introduction

Knowledge of the thermodynamics of aqueous solutions of calcium sulphate is of great practical importance because of its influence in scale formation on surfaces exposed to heat exchange. Moreover, it is also of interest in geothermal and hydrothermal processes.

The solubilities of anhydrite ($CaSO_4$) and gypsum ($CaSO_4 \cdot 2H_2O$) are known over a wide temperature range. They have been determined by several authors studying either the pure binary systems (1–6) or their mixtures with other strong electrolytes (6, 7). However, when these data were compared to those calculated by well-established methods for prediction of thermodynamic properties at high temperatures, no agreement was found (e.g., at 573 K they differ by a factor greater than 10^3) (8). Consequently, doubts have been expressed regarding the reliability of experimental solubility data for calcium sulphate aqueous solutions; this in turn makes uncertain the choice of the values for the solubility of anhydrite at high temperature which must be employed to model the chemistry in heat exchangers (9). Even the phase transition process between both crystalline calcium sulphates is not yet well established, as witnessed (10) by an uncertainty of about 22 K in the transition temperature at 101.325 kPa.

The purpose of the present work was to reassess the available experimental information about the solubility of anhydrite and gypsum in pure water up to 573 K. From this analysis we conclude that there is very good thermodynamic consistency among the solubility data available in the literature, those calculated with methods which predict the solubility at high temperatures on the basis of thermodynamic properties for room temperature, and the values established for the standard thermodynamic properties of the phase transition process at 298.15 K.

Since one of the methods used to predict thermodynamic properties makes use of the solubility data of barite ($BaSO_4$), the thermodynamic properties of solution of $BaSO_4$ also had to be considered in this work. It was found to be consistent with the rest of the thermodynamic information.

Calculation of standard thermodynamic properties of solution

The dissolution of calcium sulphate may be described by the following two processes:

$$[I] \quad CaSO_4 \cdot nH_2O(s) \rightleftharpoons Ca^{2+}(aq) + SO_4^{2-}(aq) + nH_2O(l)$$

$$[II] \quad Ca^{2+}(aq) + SO_4^{2-}(aq) \rightleftharpoons CaSO_4(aq)$$

The second process describes the association of oppositely charged ions to form ion pairs.

In order to calculate the standard Gibbs free energies of solution, $\Delta_{sol}G^0$, from solubility data, it is necessary to correct

[1]Author to whom correspondence should be addressed.

Can. J. Chem. Downloaded from www.nrcresearchpress.com by 210.87.254.42 on 09/06/12
For personal use only.

the experimental solubilities for the effect of ion association. If K_I and K_A represent the equilibrium constants characterizing reactions [I] and [II], respectively, the solubility s may be expressed by

$$[1] \quad s = K_I K_A + \frac{K_I^{1/2}}{\gamma_\pm}$$

The association constant was calculated with Bjerrum's expression for ion-pair formation (11–13):

$$[2] \quad K_A = 4\pi N_A \int_a^d r^2 \exp\left\{\frac{(ze)^2}{\epsilon kT}\right\} dr$$

where d, the distance of closest approach of free ions, was fixed at the value $(ze)^2/2\epsilon kT$. If the contact distance of ion pair, a, is assumed to be temperature independent, it is only necessary to know K_A at one temperature to establish ionic association over all the temperature range from eq. [2]. Using K_A = 209 mol kg^{-1} at 298.15 K, which was obtained from conductivity (14) and emf (15) measurements for calcium sulphate aqueous solutions, the value 4.45 Å was calculated for a from eq. [2]. This result, when compared to the sum of crystal radii (3.72 Å), shows that solvent-separated pairs predominate in solution, a conclusion which agrees with evidence from relaxation spectrometry (16).

The mean activity coefficients, $\gamma_\pm$, in eq. [1] were calculated by means of the extended Debye–Hückel equation

$$[3] \quad \ln \gamma_\pm = -\frac{AI^{1/2}}{1 + dBI^{1/2}}$$

where I is the ionic strength of the saturated solution, and A and B have the usual meaning (12). To ensure consistency (13), the distance parameter in eq. [3] must be the same as that in eq. [2]. The dielectric constant of water, ϵ, at different temperatures was obtained from ref. 17.

A strong support for the method used here to calculate K_A is the fact that the values determined for pK_A in all the temperature range differed less than 0.3 units from those reported by Yeatts and Marshall (7), whose results were obtained from solubility measurements in aqueous solutions of calcium sulphate in Na_2SO_4–$NaNO_3$ mixtures having ionic strengths between 0.25 to 6 molal in the temperature range 273 to 623 K. These experimental conditions enabled the authors to obtain K_I and K_A by means of an extrapolation procedure, which entails more uncertainty than the method employed in this work to deal with the pure binary system.

Gardner and Glueckauf (18, 19) have used previously a similar method to treat the solubility of calcium sulphate in water up to 473 K. They have employed a more complicated equation for $\gamma_\pm$ and have required the additional assumption that triplet and quadruplet ions exist in solution. In spite of using more adjustable parameters, their agreement with experimental data was not too satisfactory at high temperatures (7, 19).

Figures 1 and 2 show the temperature dependence of the solubility of the binary systems containing either gypsum or anhydrite in pure water. The transition temperature for the reaction

$$[III] \quad CaSO_4 \cdot 2H_2O(s) \rightleftharpoons CaSO_4(s) + 2H_2O(l)$$

is in the vicinity of 313 K (*vide infra*). Nevertheless, there are a number of solubility data corresponding to both solid phases above and below the transition temperature. These solids can

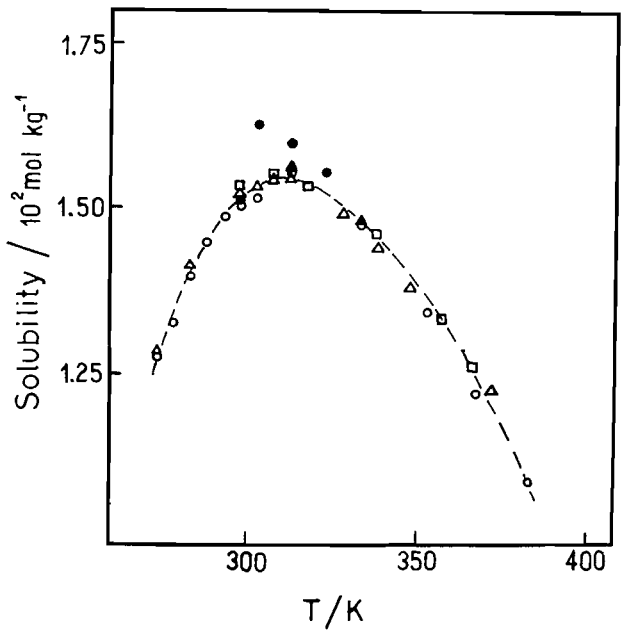

FIG. 1. Solubility of gypsum in water versus temperature. Sources of data: ▲, ref. 1; ○, ref. 2; □, ref. 3; △, ref. 4; ●, ref. 5.

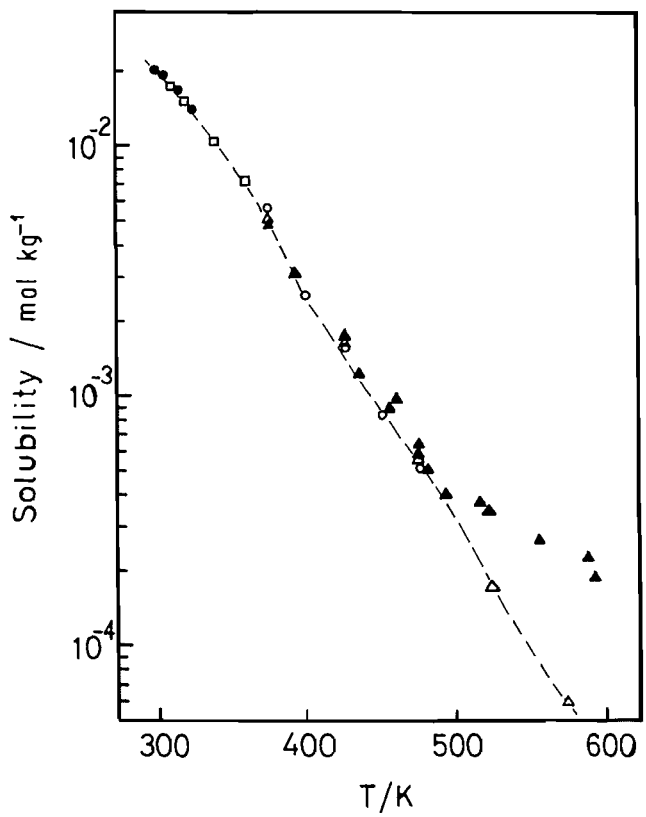

FIG. 2. Solubility of anhydrite in water versus temperature. Sources of data: ○, ref. 1; □, ref. 3; ▲, ref. 4; ●, ref. 5; △, ref. 6.

exist under metastable conditions; thus it is possible to cover a temperature range which extends outside the stability region for each solid. The solubility data for gypsum between 273 and 383 K (Fig. 1) show good agreement among the different sources of data, except for those reported by Bock (5) which differ markedly from all the rest and were not included in the present analysis. For anhydrite, the agreement among different

TABLE 1. Coefficients of eq. [4] for gypsum and anhydrite

	b_0	b_1	b_2	b_3	σ
$CaSO_4 \cdot 2H_2O$ (273–383 K)	−20.680	0.48011	−59.188	−43.188	0.058
$CaSO_4$ (298–373 K)	−19.913	−12.520	−97.157	158.330	0.052
$CaSO_4$ (298–573 K)	−19.756	−17.543	−37.809	−71.640	0.272

TABLE 2

(*a*) Thermodynamic properties for the solution of calcium sulphate in water at 298.15 K

	$CaSO_4 \cdot 2H_2O$	$CaSO_4$
$\Delta_{sol}G^0$ (kJ mol^{-1})	25.795 ± 0.021	24.84 ± 0.05
$\Delta_{sol}H^0$ (kJ mol^{-1})	0.58 ± 0.29	−15.6 ± 2.4
$\Delta_{sol}S^0$ (J (mol K)$^{-1}$)	84.5 ± 0.8	−135.5 ± 7.9

(*b*) Standard thermodynamic properties of phase transition at 298.15 K

	Circ. 500 NBS (21)	This work
$\Delta_{trs}G^0$ (kJ mol^{-1})	−0.807	−0.958 ± 0.075
$\Delta_{trs}H^0$ (kJ mol^{-1})	−16.52	−16.2 ± 2.6
$\Delta_{trs}S^0$ (J (mol K)$^{-1}$)	−52.7	−51.0 ± 8.8

authors is reasonably good up to 493 K. Above this temperature we have only considered the solubility data of Blount and Dickson (6) after a careful analysis of the experimental procedures convinced us that the precautions of these authors to ensure the attainment of equilibrium give great reliability to their solubility data at high temperatures.

In order to calculate the standard thermodynamic quantities describing process [I] over the temperature range, the values of ln (K_I) for gypsum and for anhydrite were fitted to a polynomial in the reduced temperature according to Clarke and Glew (20).

For gypsum it was found that the whole set of data could be well represented by the four-parameter equation

$$[4] \quad \ln K_I(T) = b_0 + b_1u_1 + b_2u_2 + b_3u_3$$

where

$$u_1 = \frac{x}{1 - x}$$

$$u_2 = x^2 \sum_{n=1}^{\infty} \frac{n}{n+1}(-x)^{n-1}$$

$$u_3 = x^3 \sum_{n=1}^{\infty} \frac{n}{n+2}(-x)^{n-1}$$

and the reduced temperature $x = (T/\theta - 1)$, θ being the reference temperature here, taken as 298.15 K. Coefficients b_0, b_1, b_2, and b_3 are simply related to $\Delta_{sol}G^0(\theta)$, $\Delta_{sol}H^0(\theta)$, $\Delta_{sol}S^0(\theta)$, and $\Delta_{sol}C_p^0(\theta)$, respectively (20).

For anhydrite dissolution, eq. [4] was found to describe adequately the two sets of data corresponding to the lower temperature range (298 to 373 K) (3, 5). The deviation from eq. [4] increased when all the data were considered together, as a result of increased experimental uncertainty in the data at higher temperatures. In order to calculate the standard thermodynamic properties at 298.15 K for anhydrite, only those data up to 373 K, which are believed to be the most accurate ones, were considered. Table 1 reports the coefficients of eq. [4] for gypsum and two sets of coefficients for anhydrite, one corresponding to the low temperature range and the other obtained from the whole set of data with a somewhat reduced precision.

TABLE 3. Standard thermodynamic properties for the solution of gypsum in water in the range of 273 to 383 K

T (K)	$\Delta_{sol}G^0$ (kJ mol^{-1})	$\Delta_{sol}H^0$ (kJ mol^{-1})	$\Delta_{sol}S^0$ (J (mol K)$^{-1}$)
273.15	23.94 ± 0.04	6.40 ± 1.05	−64.2 ± 3.7
298.15	25.80 ± 0.02	0.59 ± 0.29	−84.5 ± 1.0
323.15	28.17 ± 0.03	−5.98 ± 0.38	−105.6 ± 1.2
348.15	31.08 ± 0.03	−13.30 ± 0.33	−127.5 ± 1.0
373.15	34.55 ± 0.04	−21.4 ± 1.2	−149.9 ± 3.2
383.15	36.09 ± 0.07	−24.8 ± 1.8	−159.0 ± 4.7

Table 2 gives the values found for the standard thermodynamic properties of solution at 298.15 K. A comparison between the values of the thermodynamic properties of the phase transition process [III] given in the literature (21) with those calculated here from solubility data is shown in Table 2. The good agreement observed lends strong support to the consistency of the thermodynamic properties calculated for gypsum and anhydrite from solubility data because the values reported for this phase transition process in Circular 500 of NBS come from experimental data obtained for the pure solid phases and for water. From eq. [4] for gypsum and anhydrite, it was possible to calculate the transition temperature of [III] to be 315.7 ± 0.4 K at atmospheric pressure; this value is close to that reported by Marshall and Slusher (2).

Tables 3 and 4 list the thermodynamic properties for the dissolution of gypsum and anhydrite in water at different temperatures calculated from eq. [4] for ln (K_I). It is of interest to mention the good agreement between the values of the thermodynamic properties calculated for anhydrite and those reported by Yeatts and Marshall (7) on the basis of measurements of calcium sulphate solubility at constant ionic strength, because there have been previous reports (8) of a lack of agreement.

Prediction of ln K_I for anhydrite at high temperatures

It is important to compare ln K_I calculated from the $\Delta_{sol}G^0$ ($CaSO_4$(s)) values at different temperatures in Table 4, with those calculated by well-established predictive methods. This is because previous calculations have yielded doubtful results (8) and also because good predictive procedures are of practical importance to obtain reliable values of the solubility outside the experimental temperature range.

Both the correspondence principle introduced by Criss and Cobble (22) and the principle of constant charge (8) have been employed in this work.

(a) Correspondence principle

The modification proposed by Lewis (23) of the correspondence principle has been followed. It relates the standard molar heat capacity of ion i in solution to its standard entropy at a reference temperature, i.e.,

$$[5] \quad C_{p,i}^0 = (k + lS_i^0(\theta))T$$

Can. J. Chem. Downloaded from www.nrcresearchpress.com by 210.87.254.42 on 09/06/12
For personal use only.

TABLE 4. Standard thermodynamic properties for the solution of anhydrite in water in the range of 298 to 573 K[a]

T (K)	$\Delta_{sol}G^0$ (kJ mol^{-1})		$\Delta_{sol}H^0$ (kJ mol^{-1})		$\Delta_{sol}S^0$ (J (mol K)$^{-1}$)	
298.15	24.85 ± 0.04[b]	(24.3)	−15.6 ± 2.4[b]	(−24.3)	−135.5 ± 7.9[b]	(−163.1)
323.15	28.74 ± 0.13	(28.6)	−26.5 ± 1.6	(−28.6)	−170.7 ± 6.7	(−176.9)
373.15	38.15 ± 0.17	(38.3)	−39.4 ± 0.8	(−41.1)	−207.9 ± 4.6	(−212.5)
423.15	49.61 ± 0.13	(50.2)	−57.4 ± 1.5	(−58.6)	−252.7 ± 5.4	(−256.4)
473.15	63.55 ± 0.16	(64.0)	−80.4 ± 1.6	(−80.7)	−304.1 ± 5.4	(−306.2)
523.15	80.11 ± 0.25	(80.7)	−108.3 ± 3.2	(−108.3)	−360.2 ± 3.8	(−361.5)
573.15	99.65 ± 0.59	(100.4)	−141.4 ± 9.1	(−140.6)	−420 ± 15	(−422)

[a] Values given in parentheses are from Yeatts and Marshall (7).
[b] This value is obtained with the low temperature polynomial reported in Table 1.

TABLE 5. Predicted and experimental values of pK_I for anhydrite between 298 and 623 K

T (K)	pK_I			
		Correspondence principle		
	Experimental	(*a*)	(*b*)	(*c*)
298.15	4.35	4.35	4.35	4.35
323.15	4.65	4.65	4.63	4.61
373.15	5.34	5.39	5.33	5.29
423.15	6.13	6.25	6.16	6.10
473.15	7.02	7.19	7.07	6.99
523.15	8.00	8.18	8.03	7.94
573.15	9.08	9.21	9.03	8.93
623.15	10.24[d]	10.27	10.06	9.95

[a] With $\Delta_{sol}S^0$ (298.15 K) = −144.7 J (mol K)$^{-1}$ and $\Delta_{sol}C_p^0$ = −70.20 − 0.7806 T J (mol K)$^{-1}$ (21).
[b] With $\Delta_{sol}S^0$ (298.15 K) = −139.7 J (mol K)$^{-1}$ and $\Delta_{sol}C_p^0$ = −70.20 − 0.7639 T J (mol K)$^{-1}$ (24).
[c] With $\Delta_{sol}S^0$ and $\Delta_{sol}C_p^0$ calculated in this work (cf. Table 4 and text).
[d] Extrapolated with eq. [4].

where k and l are the correspondence principle constants (22) for that ionic class. The change of heat capacities of process [I] may be expressed by

$$[6]\quad \Delta_{sol}C^0_{p,I} = \alpha + \beta T + \gamma T^{-2}$$

This leads to the following expression for ln K_I:

$$[7]\quad \ln K_I(T) = \frac{\theta}{T}\ln K_I(\theta) + \frac{1}{R}\left\{\frac{x}{x+1}\Delta_{sol}S^0(\theta)\right\} - \alpha\left\{\frac{x}{x+1} - \ln(x+1)\right\} - \frac{\beta}{2}\left\{\frac{\theta x^2}{x+1}\right\} - \frac{\gamma}{2}\left\{\frac{x(x+2)}{\theta^2(x+1)^2}\right\}$$

with θ = 298.15 K. The value of ln $K_I(\theta)$ = −10.022 was obtained from the value for $\Delta_{sol}G^0(\theta)$ reported in Table 2. For $\Delta_{sol}S^0(\theta)$ we have used the value obtained in this work (cf. Table 2) as well as those calculated from the ionic entropies reported by Cobble *et al.* (21, 22) and those given by Wagman *et al.* (24) which have been recently used by Cobble and coworkers (8).

Table 5 compares the values of ln K_I calculated with the correspondence principle to the experimental ones. It may be noted that the correspondence principle with any of the $\Delta_{sol}S^0(\theta)$ values used in this work predicts a temperature dependence for ln K_I which is very close to that experimentally observed even at temperatures above 573 K. Furthermore, the pK_I value reported by Yeatts and Marshall (7) for 623.15 K is 10.30, in good agreement with the value 10.24 extrapolated with eq. [4] as reported in Table 5.

Table 5 appears to contradict the observation of Cobble and Murray (8) because it shows that the thermodynamic pattern emerging from the analysis of solubility measurements is quite consistent and in agreement with the behaviour predicted at high temperature.

(b) Constant charge principle

When an equilibrium involving ionic species is written in such a way that the process does not imply change in the number of charges, the assumptions on the values of ΔC_p^0 are greatly simplified (25). Cobble and Murray (8) have used this method for $CaSO_4$ solution by combining reaction [I] with that describing the dissolution of barite. Hence, the process they studied was

$$[IV]\quad BaSO_4(s) + Ca^{2+}(aq) \rightleftharpoons Ba^{2+}(aq) + CaSO_4(s)$$

The values of K_I for $CaSO_4$ which they obtained differ by more than three orders of magnitude from the experimental values.

We have calculated the equilibrium constant K_{IV} of process [IV] with the correspondence principle (23) and with the constant charge principle (8) with various choices for the change of heat capacity. Table 6 reports these values and compares them to experimental ones obtained from the solubility measurements of Blount (26).[2] Table 6 confirms the very good agreement between the solubility measurements and the predicted pK_{IV}, the only exception being the principle of constant charge with $\Delta C_p^0 = 0$, which is a rather extreme assumption.

Conclusions

A great consistency is observed in the thermodynamic data evaluated in the present work. The standard thermodynamic properties for the solution of gypsum and anhydrite in water at 298.15 K obtained from the solubility data are in good agreement with those reported in the literature. It was possible to establish the phase transition temperature within 0.4 K.

The principles of correspondence and of constant charge used with appropriate values for the heat capacities are good enough for predicting the solubilities of anhydrite and barite up to 573 K. The values of the thermodynamic properties of solution of anhydrite in water above 573 K, which may be obtained by extrapolation with eq. [4], should be considered as highly reliable. In fact, the value for pK_I quoted for 623 K in Table 5

[2] For $BaSO_4$ solutions it is not necessary to correct solubilities for ion pair formation because the saturated solutions are very dilute.

Can. J. Chem. Downloaded from www.nrcresearchpress.com by 210.87.254.42 on 09/06/12
For personal use only.

TABLE 6. Predicted and experimental equilibrium constants (pK_{IV}) for the process $BaSO_4(s) + Ca^{2+}(aq) \rightleftharpoons Ba^{2+}(aq) + CaSO_4(s)$

Temperature (K)	Experimental	Correspondence principle		Constant charge principle		
		(*a*)	(*b*)	(*c*)	(*d*)	(*e*)
298.15	5.61	5.61	5.61	5.61	5.61	5.61
323.15	5.06	5.01	5.03	5.01	5.03	5.03
373.15	4.25	4.09	4.14	4.09	4.13	4.09
423.15	3.60	3.43	3.50	3.41	3.47	3.38
473.15	3.20	2.95	3.02	2.89	2.97	2.82
523.15	2.50	2.59	2.67	2.50	2.58	2.36
573.15	2.36	2.32	2.40	2.19	2.28	1.99

[a] With $\Delta_{sol}S^0$ (298.15 K) = 42.2 J (mol K)$^{-1}$ and $\Delta_{sol}C_p^0 = -71.20 - 0.0142T + 35.27 \times 10^5 T^{-2}$ J (mol K)$^{-1}$ (21).
[b] With $\Delta_{sol}S^0$ (298.15 K) = 37.2 J (mol K)$^{-1}$ and $\Delta_{sol}C_p^0 = -71.20 - 0.00167T + 35.27 \times 10^5 T^{-2}$ J (mol K)$^{-1}$ (24).
[c] With $\Delta_{sol}C_p^0 = -35.77$ J (mol K)$^{-1}$ (21).
[d] With $\Delta_{sol}C_p^0 = -32.00$ J (mol K)$^{-1}$ (24).
[e] With $\Delta_{sol}C_p^0 = 0$ J (mol K)$^{-1}$.

is close to that reported by Yeatts and Marshall (7) from the study of mixed electrolyte solutions.

It is recommended that the values of the thermodynamic properties of solution for high temperature, which are reported here, be used in the calculations involved in the modelling of chemical processes that take place on heat exchanging surfaces or in hydrothermal processes.

Acknowledgement

The authors are grateful to SUBCYT (Argentina) for partial financial support in this project.

1. W. L. MARSHALL, R. SLUSHER, and E. V. JONES. J. Chem. Eng. Data, **9**, 187 (1964).
2. W. L. MARSHALL and R. SLUSHER. J. Phys. Chem. **70**, 4015 (1966).
3. W. H. POWER, B. M. FABUSS, and C. N. SATTERFIELD. J. Chem. Eng. Data, **11**, 149 (1966).
4. A. SEIDELL. Solubility of inorganic compounds. Vol. 1. Am. Chem. Soc. 1958. p. 660.
5. E. BOCK. Can. J. Chem. **39**, 1746 (1961).
6. C. W. BLOUNT and F. W. DICKSON. Geochim. Cosmochim. Acta, **33**, 227 (1969).
7. L. B. YEATTS and W. L. MARSHALL. J. Phys. Chem. **73**, 81 (1969).
8. R. C. MURRAY and J. W. COBBLE. 41st Int. Water Conf. Pittsburgh. 1980. J. W. COBBLE, R. C. MURRAY, P. J. TURNER, and K. CHEN. EPRI NP-2400, Project 1167-1, Final Report. 1982.
9. R. J. BAWDEN. Centr. Electr. Res. Lab. Lab. Note RD/L/2108 N81. 1981.
10. L. A. HARDIE. Am. Mineral. **52**, 171 (1967).
11. N. BJERRUM. K: Danske Vidensk. Selsk. Mat-fys. **7**, No. 9 (1926).
12. R. A. ROBINSON and R. H. STOKES. Electrolyte solutions. Butterworths. 1968.
13. R. FERNÁNDEZ-PRINI. *In* The physical chemistry of organic solvents. *Edited by* A. K. Covington and T. Dickinson. Plenum. 1973.
14. A. D. PETHYBRIDGE and S. S. TABA. J. Chem. Soc. Faraday Trans. I, **78**, 1331 (1982).
15. R. G. AINSWORTH. J. Chem. Soc. Faraday Trans. I, **69**, 1028 (1973).
16. M. EIGEN and L. DE MAEYER. *In* Tech. Org. Chem. *Edited by* S. L. Friess, E. S. Lewis, and A. Weissberger. Vol. 8. Part II. Interscience. 1963. p. 895; G. ATKINSON and S. PETRUCCI. J. Phys. Chem. **70**, 3122 (1966); G. ATKINSON and S. K. KOR. J. Phys. Chem. **71**, 673 (1967).
17. M. UEMATSU and E. U. FRANCK. J. Phys. Chem. Ref. Data, **9**, 1291 (1980).
18. A. W. GARDNER and E. GLUECKAUF. Proc. R. Soc. A**313**, 131 (1969).
19. A. W. GARDNER and E. GLUECKAUF. Trans. Faraday Soc. **66**, 1081 (1970).
20. E. C. W. CLARKE and D. N. GLEW. Trans. Faraday Soc. **62**, 539 (1966).
21. F. D. ROSSINI, D. D. WAGMAN, W. H. EVANS, S. LEVINE, and I. JAFFE. Natl. Bur. Stand. Circular 500. 1952.
22. C. M. CRISS and J. W. COBBLE. J. Am. Chem. Soc. **86**, 5385 (1964).
23. D. LEWIS. Arkiv Kemi, **32**, 384 (1971).
24. D. D. WAGMAN, W. H. EVANS, V. B. PARKER, I. HALOW, S. M. BAILEY, and R. H. SCHUMM. N.B.S. Tech. Notes 270-3. 1968. Tech. Notes 270-6. 1975.
25. W. T. LINDSAY. 41st Int. Water Conf. Pittsburgh. 1980.
26. C. W. BLOUNT. Am. Mineral. **62**, 942 (1977).

Can. J. Chem. Downloaded from www.nrcresearchpress.com by 210.87.254.42 on 09/06/12
For personal use only.

Synthesis and electron paramagnetic resonance studies of chiral spin-labeled crown ethers

H. DUGAS AND P. KEROACK

Department of Chemistry, Université de Montréal, C. P. 6210, Succ. A, Montréal (Qué), Canada H3C 3V1

AND

M. PTAK

Centre de Biophysique Moléculaire, C.N.R.S. et Université d'Orléans, 45045 Orléans Cédex, France

Received January 10, 1983[1]

H. DUGAS, P. KEROACK, and M. PTAK. Can. J. Chem. **62**, 489 (1984).

The synthesis of *syn* and *anti* chiral dinitroxide [18]-crown-6 ethers and of a tetranitroxide crown ether is described. The existence of a spin–spin interaction for the *syn* isomer makes this spin-labeled crown ether probe particularly useful to follow by epr the effects of K^+ ion binding, pH, solvent, and temperature. These observations are discussed in terms of a global dynamical fluctuation of the substituted crown ether.

H. DUGAS, P. KEROACK et M. PTAK. Can. J. Chem. **62**, 489 (1984).

Cet article décrit la synthèse de dinitroxydes couronne-[18]-éthers-6 chirales, *syn* et *anti* et un éther couronne tétranitroxyde. La présence d'interactions spin–spin pour l'isomère *syn* rend cet éther couronne marqueur de spin particulièrement utile pour suivre par rpe les effets de fixation d'ions K^+, de pH, de solvant et de température. Ces observations sont discutées en terme d'une fluctuation dynamique et globale de l'éther couronne substitué.

Introduction

Precise conformational data on free and complexed crown ethers are obtainable mainly from X-ray structure determinations. Studies in solution using spectroscopic methods are often rather limited because of the reduced number of parameters which change significantly with various conformations and interactions. These features are inherent in the $—CH_2—O—CH_2—CH_2—O—CH_2—$ sequence and in the symmetry properties of the corresponding crown ether. We have recently developed methods of labeling crown ethers with nitroxide radicals with the following in mind: (a) synthesis of doubly labled crown ethers to prepare subtituted macrocyclic molecules with different complexing abilities, and (b) to take advantage of the spin–spin exchange interaction to investigate conformations and motions of these molecules.

We have reported in a communication (1) the first synthesis of two stereochemically distinct chiral dinitroxide crown ethers, the *syn* isomer **2** and the *anti* isomer **3**. In the present paper we would like to expand this work to the corresponding tetranitroxide molecule **4** which is symmetric relative to the crown ether ring. It should be particularly interesting to compare this compound with the di-SL-*syn* isomer **2** (SL for spin label) in which there is a dissymmetry in the molecule that can be referred to as "face discriminated" relative to the crown ether plane (2). That is, one face of the molecule can be selectively modified (ionized for instance) while the paramagnetic

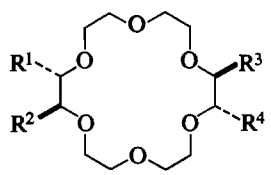

1 $R^1 = R^2 = R^3 = R^4 =$ COOH, tetraacid
2 $R^1 = R^4 =$ COOH, $R^2 = R^3 =$ CONH-SL, di-SL-*syn*
3 $R^1 = R^3 =$ COOH, $R^2 = R^4 =$ CONH-SL, di-SL-*anti*
4 $R^1 = R^2 = R^3 = R^4 =$ CONH-SL, tetra-SL
5 $R^1 = R^4 = COOCH_3$, $R^2 = R^3 =$ CONH-SL, di-SL-*syn* dimethyl ester

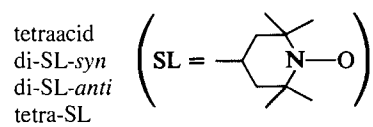

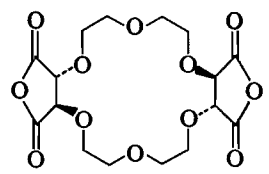

6

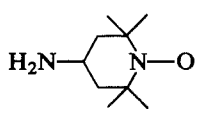

7

[1]Revision received September 15, 1983.

Can. J. Chem. Downloaded from www.nrcresearchpress.com by 210.87.254.5 on 09/06/12
For personal use only.

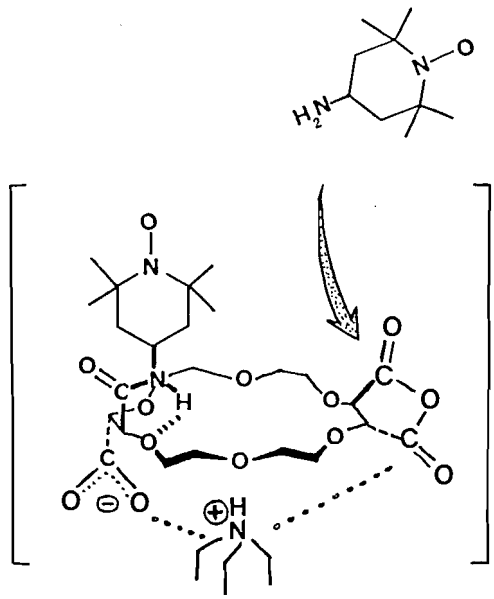

SCHEME 1

probes on the other face could act as reporters to monitor structural and dynamical perturbations. Such an architecture of the molecule should also confer toposelectivity in complexation processes with chiral organic cations (3).

In a first step we report here how the epr spectra of these molecules are affected by solute–solvent interactions, temperature, K^+ binding, and the state of ionization of the carboxyl groups (for the dinitroxide derivative).

This study should serve as a basis for further detailed investigations of complexation processes.

Results and discussion

Chemistry

The tetraacid-bis-tartro-[18]-crown-6 **1** was readily obtained from (+)-*R*,*R*-tartaric acid by well-established procedures (4, 5). The corresponding anhydride **6** was used to prepared the dinitroxides **2** and **3** by reaction with tempamine **7** following the methodology developed by Lehn's group (2). Mixtures were separated by column chromatography and, when the reaction with **6** was performed in the presence of triethylamine, only one isomer (*syn* **2**) was formed (1). The reason for this probably lies in the fact that, in the transition state of the reaction (Scheme 1), the base is involved in electrostatic interactions with the carboxylate group newly formed on one side of the macrocyclic ring, and thus tempamine **7** can approach and react with the second anhydride function only from the opposite (top side) face of the crown ether ring. Esterification of **2** with diazomethane gave **5** in almost quantitative yield.

The tetranitroxide **4** was obtained by reaction of tempamine **7** with the tetraacid chloride (via PCl_5) of **1** in dichloromethane (3). The neutral product was purified by chromatography.

Generalities

The global conformation of the spin-labeled [18]-crown-6 ethers depends on three sets of parameters: (a) 18 intracyclic rotations around $(O—CH_2—CH_2—O)_4$ and $(O—\overset{*}{C}HX—\overset{*}{C}HY—O)_2$ bonds describing the conformation of the crown ring (X, Y = side chains); (b) 6 side-chain rotations around $(\overset{*}{C}H—COOH)_2$, $(\overset{*}{C}H—CONH\dot{R})_2$, $(CONH—\dot{R})_2$ bonds where $\dot{R}$ = 2,2,6,6-tetramethylpiperidine-1-oxyl; and

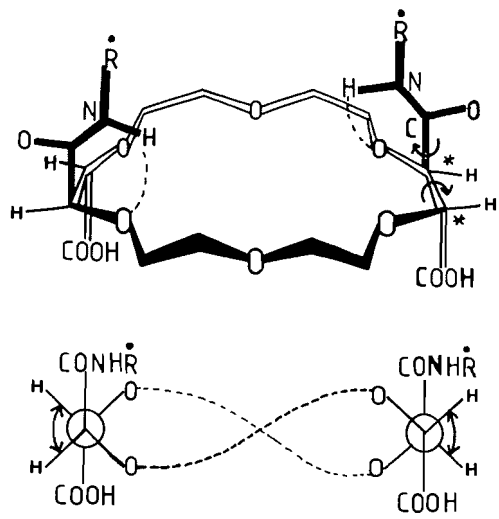

SCHEME 2

(c) 6 internal rotations of the $\dot{R}$ piperidine ring. Scheme 2 shows a three-dimensional presentation and a Newman projection of the di-SL-*syn* isomer **2**.

A priori, one could assume that the global conformation of the free and complexed compounds remains of C_2 symmetry. The shape of the epr signal of biradicals and tetraradicals will depend strongly on the exchange integral $\bar{J}$ and on the modulation of this integral by internal motions. It is particularly important to recall that for a biradical, the linewidth of $M_I = \pm 1$ lines and of two components of the central line depends on the ratio: $j(\bar{J})/(\bar{J})^2$ (6). Unfortunately, the exact dependence of $\bar{J}$ on the conformation and on the nature of motions determining the spectral density $j(\bar{J})$ is not available. Therefore, the positions of the epr signals and the linewidths will depend simultaneously on parameters such as temperature, pH, and solvent, all having an effect on the internal motions and the average conformation of the molecule.

Spectra of the different spin-labeled crown ethers

Figure 1 represents the epr spectra of dinitroxides, *syn* **2** and *anti* **3**, and of the tetranitroxide **4**, in water at ambient temperature. Because of the orientation of the nitroxide groups on opposite faces of the crown ether ring, the spectrum of the *anti* isomer **3** does not reveal any spin–spin interaction. On the other hand, such an interaction is clearly detected for the *syn* isomer **2** by the appearance of small intermediate lines between the three main lines where the intensity, the position, and the shape depend on $\bar{J}$ and $j(\bar{J})$. Such spectra have been described before for different families of linear flexible biradicals (7, 13). The spectrum of the tetranitroxide **4** is more complex since thirteen lines are readily distinguished. Assuming a nearly axial position (8) for the spin-labeled side chains with respect to the plane of the crown ether ring, one should consider this tetraradical as two independent biradicals since all *trans* spin–spin interactions (opposite side) should be negligible compared with the *cis* ones (same side) (*trans* nitroxide–nitroxide distances $\geqslant$ 12 Å). The position of satellite and intermediate small lines is very similar to the spectrum of a biradical with a weak exchange interaction with $J \approx 2a$ (a = isotropic hyperfine splitting) (7). Their intensities, however, seem to be too small, as compared to the three main lines, to correspond to a unique species which would be a rigid biradical with a fixed nitroxide–nitroxide distance.

Can. J. Chem. Downloaded from www.nrcresearchpress.com by 210.87.254.5 on 09/06/12
For personal use only.

Can. J. Chem. Downloaded from www.nrcresearchpress.com by 210.87.254.5 on 09/06/12
For personal use only.

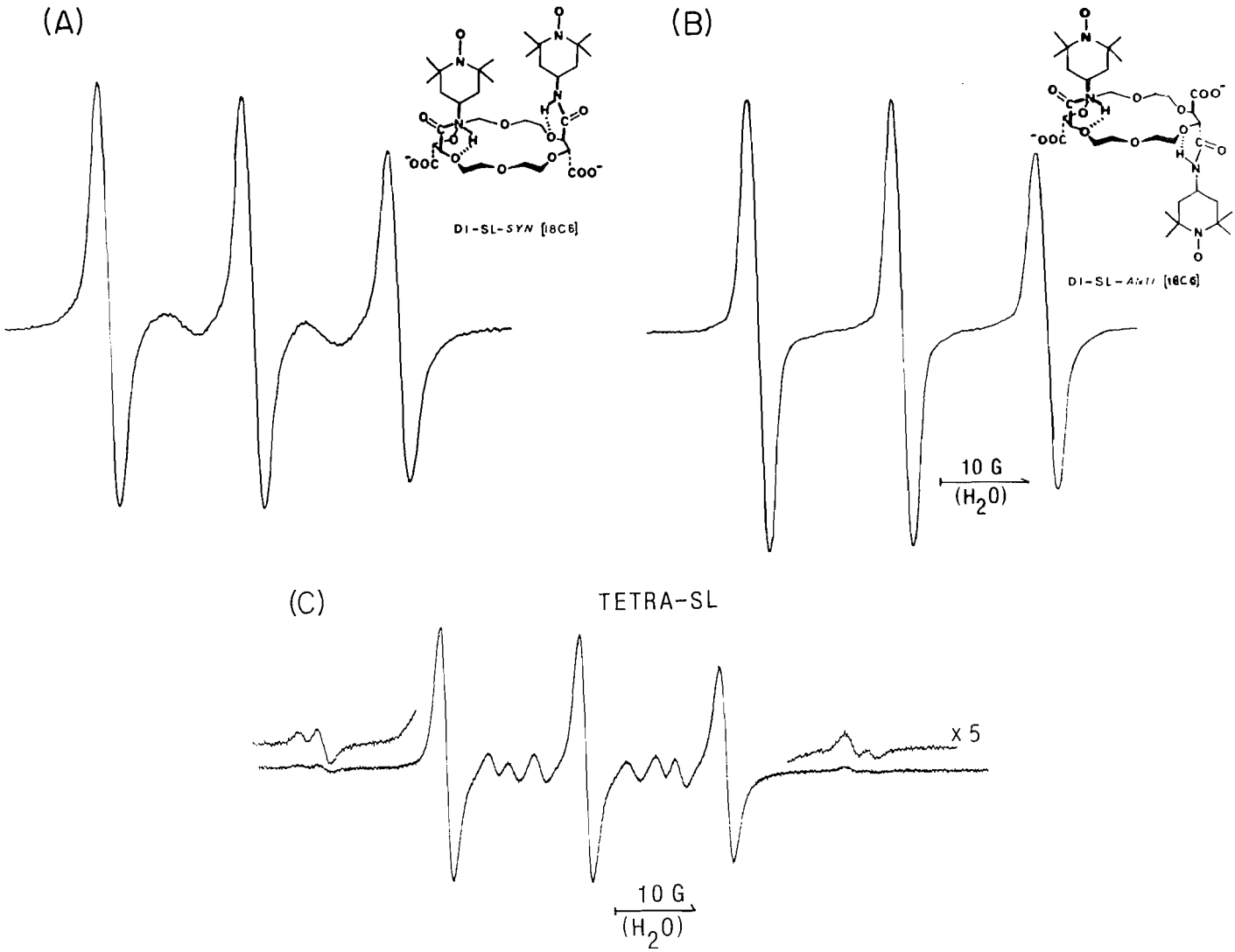

FIG. 1. Electron paramagnetic resonance spectra in water at room temperature of di-SL-*syn* **2** (A), di-SL-*anti* **3** (B), and tetra-SL **4** (C).

More likely one has to consider the existence of a slow equilibrium ($\tau \leq 10^{-7}$ s) between a so-called "closed" conformation where two *syn* nitroxides are interacting and an "open" one where they are more distant. The presence of four bulky substitutents and the absence of a strong effect upon K^+ complexation suggest a limited flexibility of the crown ether ring. Therefore, the spin–spin interactions seem to depend more on the motions and the conformations of the side chains which are also sensitive to solute–solvent interactions since in ethanol only six small broad intermediate lines are observed.

The temperature has only small effects on the spectra. This could be explained by the symmetry of the internal motions; that is, an increase in the interaction between the nitroxide group on one face of the crown ether ring is compensated by an opposite effect on the other side. The internal molecular motions should be significantly different for the dinitroxide-*syn* **2** because of the dissymmetry of the molecule. Furthermore, the flexibility of the crown ether is expected to be greater and the presence of two carboxylic groups should make the molecule particularly sensitive to ionization and to interaction with the solvents and ions (see below).

Solute–solvent interactions

At room temperature, the positions and the shape of the small intermediate lines in the epr spectrum of di-SL-*syn* isomer **2** change when going from $CHCl_3$ or DMSO to ethanol and water, as seen in Fig. 2. Clearly the solvation has an effect on the exchange integral $\bar{J}$ as well as on the spectral density $j(\bar{J})$, i.e., on the nature and the frequency of the intramolecular motions and on the related averaged conformations. Traces of water in $CHCl_3$ have significant effects on the spectrum, certainly because of a preferential solvation of the two carboxyl groups. Furthermore, if traces of acid are present one should also consider the possibility of complexation of the H_3O^+ oxonium cation by the crown ether (9).[2]

In bulk water, both carboxyl groups are ionized and their repulsion affects the interactions of the nitroxide groups on the other face of the macrocylic ring. Therefore, in addition to global effects of the solvent similar to those just described for the tetranitroxide, there are specific effects on the two acidic groups located on one side of the molecule. A comparison with the nmr of non-paramagnetic di-anilide *syn* analogue (2) brings supplementary information. In $CDCl_3$ and DMSO-d_6, the two $\dot{C}HX$—$\dot{C}HY$ protons appear as well-separated doublets in 250 MHz ^1H nmr spectra, with different values for the coupling

[2]Also, J. M. Lehn, personal communication.

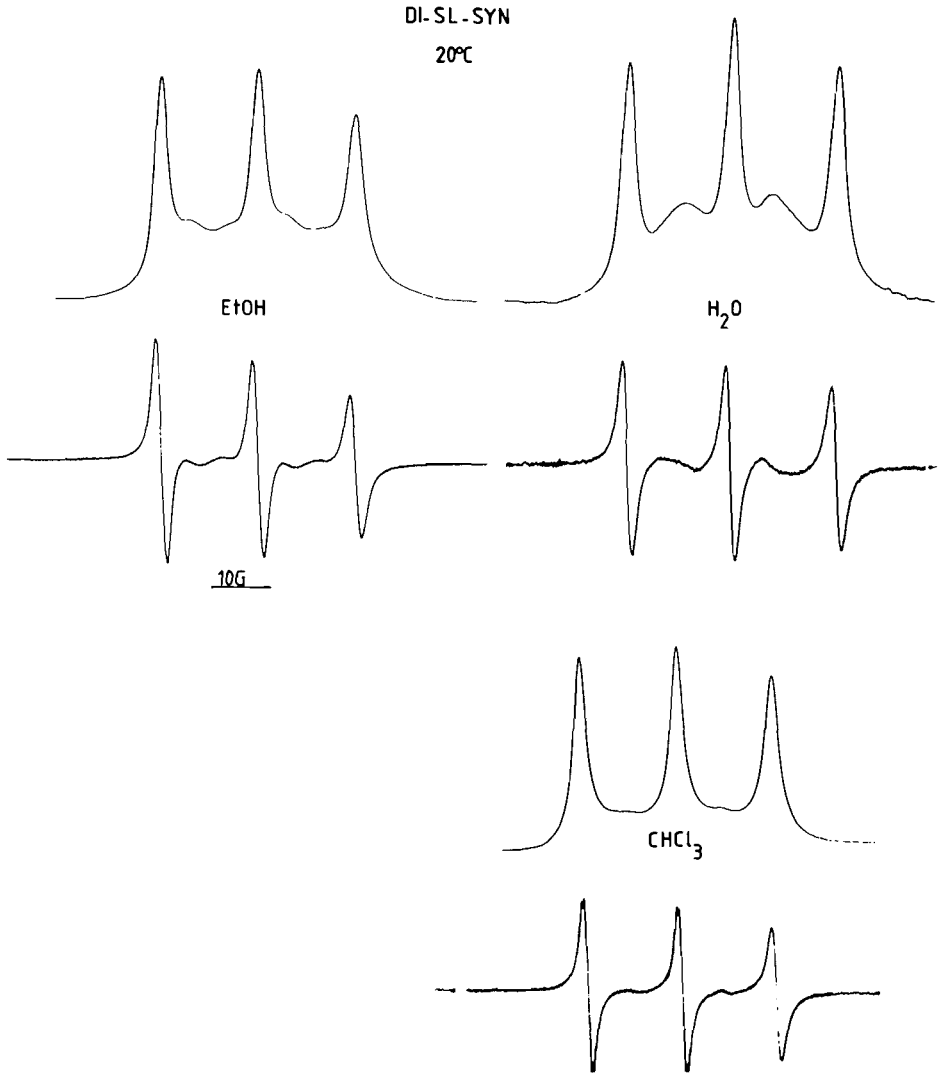

FIG. 2. Electron paramagnetic resonance spectra (first derivative and absorption) of di-SL-*syn* **2** in three different solvents (degassed) at room temperature (20°C).

constant: ^3J = 2.0 Hz ($CDCl_3$), ^3J = 4.7 Hz (DMSO). In D_2O, these doublets coalesce into a singlet. These coupling constants are sensitive to traces of water which, as noted previously, have an effect on spin–spin interactions. Such observations further corroborate how critically the conformation of the crown ether can be influenced by the nature of the solvent.

Assuming a nearly *trans*-diaxial orientation of the CONHR and COOH side chains (Scheme 2), one relates an increase in the coupling constant ^3J to a decrease of the corresponding dihedral angle, according to the classical Karplus relationship (10). Such a change in the conformation of the crown ether backbone does not influence appreciably the nitroxide–nitroxide distance in the spin-labeled compound since the epr spectra of di-*syn* **2** in $CHCl_3$ and DMSO are very similar and correspond to a smaller interaction than in more polar solvents. The most important solute–solvent interactions certainly involve the two *syn* acidic chains, while in $CHCl_3$ and also in DMSO these groups are probably implicated in a strong intramolecular hydrogen bond, COOH····OCOH, which stiffens the conformation of the whole molecule and does not favor nitroxide–nitroxide interactions on the opposite side of the crown ether. On the other hand, more polar solvents (ethanol and water) weaken the interaction between the carboxyl groups, producing a global conformational change and resulting in the closeness of the spin-labeled side chains.

Temperature effects

Figure 3 shows that the positions and the shape of the intermediate lines in the epr spectra of di-SL-*syn* **2** in organic solvents, as well as in water, depend on the temperature. Similar effects have been previously observed for flexible biradicals for which there was extensive line broadening (11). For the more rigid spin-labeled crown ether, the spectral change indicates that the exchange integral J increases with temperature. One can assume that an increase of temperature very likely induces a conformational change of the whole molecule and not only a modification of the intramolecular motions, i.e., on $j(\bar{J})$ and linewidth.

As for the solvent effects, an ^1H nmr study of the di-anilide *syn* again provided some useful information on the conformational behaviour of the spin-labeled analogue. In $CDCl_3$ and in DMSO-d_6 the $\overset{*}{C}HX—\overset{*}{C}HY$ coupling constants remain independent of temperature between 20° and 50°C. This shows that this chiral barrier fragment is thus relatively rigid and consequently the fluctuations observed in the epr spectra should be related to a more flexible portion of the molecule, mainly the

Can. J. Chem. Downloaded from www.nrcresearchpress.com by 210.87.254.5 on 09/06/12
For personal use only.

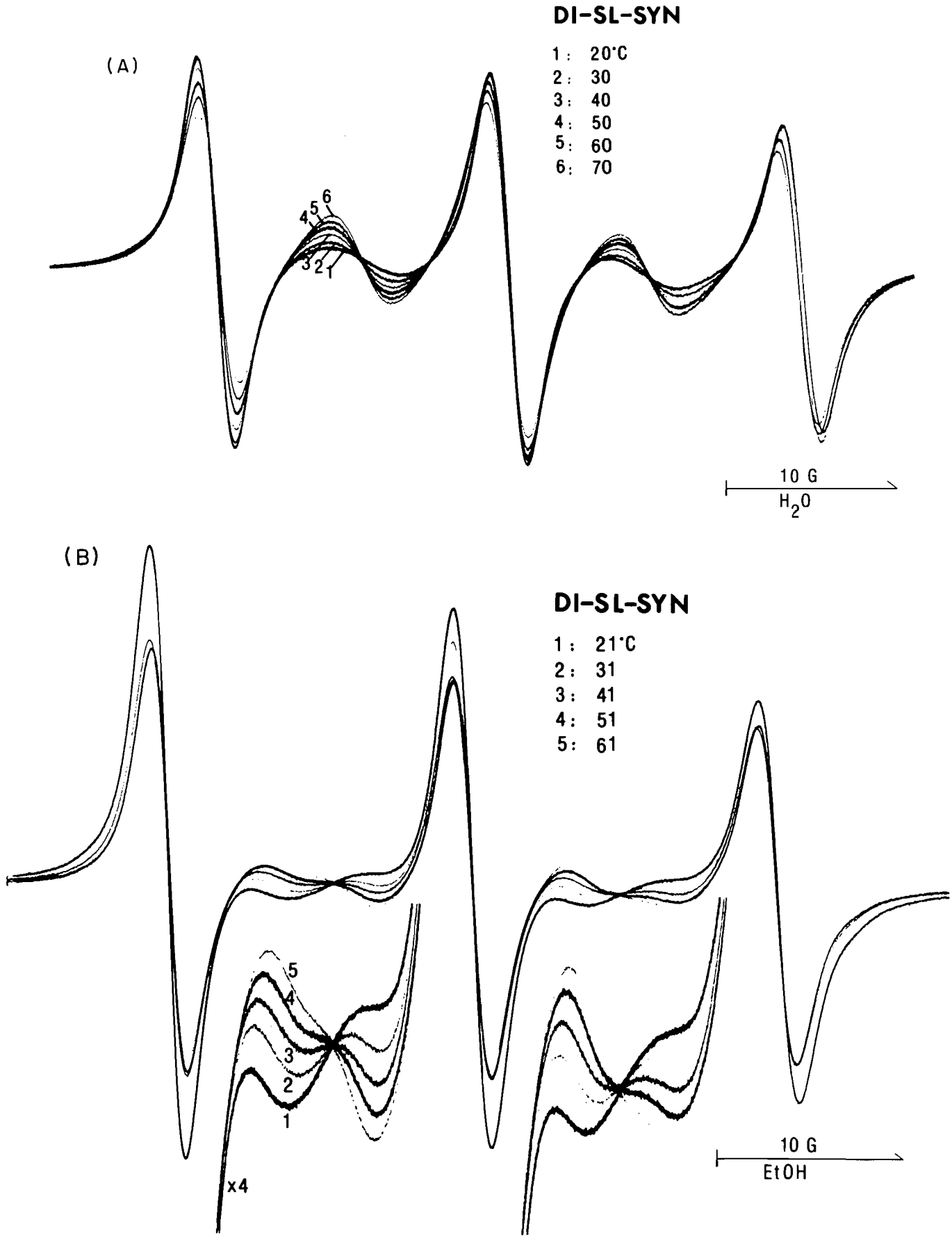

FIG. 3. Electron paramagnetic resonance spectra of di-SL-*syn* **2** in water (A) and ethanol (B) as a function of temperature.

Can. J. Chem. Downloaded from www.nrcresearchpress.com by 210.87.254.5 on 09/06/12
For personal use only.

macrocylic ring itself. Such molecular perturbations induced by temperature can be schematized in the following way:

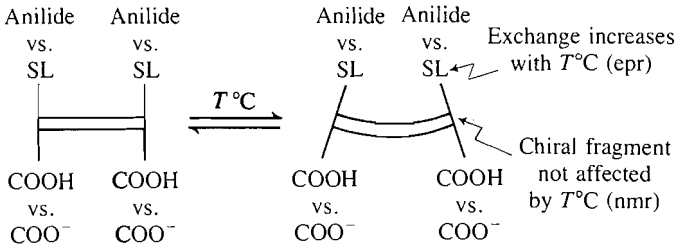

Another spectroscopic observation worth mentioning is that the chemical shift of the amide N*H* decreases as the temperature increases. Therefore, the temperature-dependent N*H* shielding ($\Delta\delta_{NH}/\Delta T$) was used to evaluate the accessibility of the amide proton by the solvent. In DMSO-d_6, this temperature coefficient has a value of 2.3×10^{-3} ppm/degree, a value currently found for groups screened from the solvent or engaged in internal hydrogen bonds. On the other hand, in $CDCl_3$, $\Delta\delta_{NH}/\Delta T$ is about 9.5×10^{-3} ppm/degree. Such a high value is usually found when both the internal motion of the solute and the thermal motion of the solvent dictate simultaneously the accessibility of the N*H* protons. The accessibility of the spin-labeled face seems to depend on the nature (structure and size) of the solvent, this effect being combined with a more selective solvation of the acidic groups on the opposite face of the crown ether ring.

Since the temperature acts simultaneously on several conformational parameters and spectral parameters (isotropic splitting, linewidth) it is especially difficult to quantify the corresponding epr spectral changes. One of the major difficulties is to maintain the instrumental sensitivity strictly constant and to avoid small changes of the linewidth in successive experiments. Very small variations of the linewidth of the three main lines due, for instance, to remaining traces of oxygen have similar consequences. Independent of such experimental conditions, two isoclinic points (12) were always found between the three main epr lines (Fig. 3). We have verified that the maxima of the three main lines in the corresponding absorption curve remain at constant values of the magnetic field while the shape of the absorption spectrum for the intermediate isoclinic points is significantly modified in these regions. In ethanol, changes occur progressively from two small intermediate lines to a unique higher line when the temperature is raised. In water, principally a progressive decrease of the linewidth of the intermediate lines is seen while the total spectrum gradually takes on the appearance of a five-line spectrum corresponding to a biradical with strong exchange. The two intermediate lines remain small due to symmetric linewidth variation and because of conformational equilibria.

A more quantitative interpretation of such spectra would require simulation in which one would introduce symmetric linewidth variations and conformational changes.

pH Effects

To confirm that the degree of ionization of the carboxyl groups could have an effect on the epr signal, the spectra were recorded at different pH values; three of them are presented in Fig. 4. Ionization of the carboxyl groups in water significantly increases the intensity of the intermediate lines of the di-SL-*syn* **2**. A similarity with the effect of temperature was at the origin of a controversy on the interpretation of spectral changes induced by temperature and pH for linear flexible biradicals (11, 13). For the spin-labeled crown ether **2**, the ionization of the carboxyl groups results in a strong electrostatic charge–charge repulsion on one face of the molecule, which induces a conformational change and then a modification of the exchange integral $\bar{J}$. Notice also the presence of isoclinic points, which could be considered as characteristic of an equilibrium between a neutral and an ionic form. As expected, such nitroxide–nitroxide interactions depend on the ionic strength since addition of an excess of TMA (tetramethylammonium), which is not complexed by the crown ether, causes a decrease of the intermediate lines.

The pK_a and pK_s values for the complexed (with K^+) and non-complexed forms of di-SL-*syn* **2** and di-SL-*anti* **3** have been measured (5) by Fyles and a more complete study on the effect of pH will be reported separately. Suffice to say that this preliminary result indicates that compounds such as **2** could be used as pH-sensitive spin probes. Only a few mono-spin-label compounds display this property (14, 15).

K^+ complexation

As stressed in a previous paper (1), the complexation of K^+ ion by the di-SL-*syn* **2** significantly modifies the spin–spin interaction. The nitroxide–nitroxide distance is reduced and the symmetric broadening is diminished. Two types of interaction are taking place in such a complexation process: (a) binding of K^+ within the cavity of the crown ether (internal position); and (b) a simultaneous interaction of another K^+ ion with some crown oxygen atoms and the two lateral carboxyl groups, corresponding to an external position of the cation. The existence of these two positions was recently established by Lehn and co-workers (16) on the crystal structure of the tetradimethyl amide of the **1**-K^+ complex. For the dimethyl ester derivative **5**, the cavity effect corresponding to the first type of interaction should be predominant. As shown in Fig. 5, the presence of the K^+ ion does not drastically modify the epr spectrum since the intermediate lines are undetectable. The esterification of the carboxyl groups seems to modify appreciably the spectral density $j(\bar{J})$, leading to extreme symmetric broadening even in the presence of K^+, as compared to free acidic side chains (compound **2**) (1).

The K^+ complexation also has an effect on the conformation of the crown ether since in the ^1H nmr spectrum (2), the dianilide-*syn* shows a decrease of the $\dot{C}HX—\dot{C}HY$ coupling constant; i.e. an increase in the dihedral angle. Moreover, in DMSO-d_6, the addition of K^+ ion produces an increase of the $\Delta\delta_{NH}/\Delta T$ coefficient for the N*H* protons (4.6×10^{-3} ppm/degree); i.e. an increase of their accessibility to the solvent. Clearly, the binding of K^+ in the crown ether weakens the interaction by hydrogen bonds of the N*H* protons with the proximal ether oxygen atoms.

These observations reinforce several features previously described, namely that any modification in the environment of the carboxyl groups located on one face of the crown ether ring profoundly affects the distance between the two nitroxide groups on the other side.

Conclusion

It is certainly premature to try to give a complete view of the conformational properties of the spin-labeled crown ethers from the present study. Nevertheless, several fundamental features do emerge. First of all, the interactions between the acidic side chains of di-SL-*syn* **2** on one face of the crown ether ring

Can. J. Chem. Downloaded from www.nrcresearchpress.com by 210.87.254.5 on 09/06/12
For personal use only.

Can. J. Chem. Downloaded from www.nrcresearchpress.com by 210.87.254.5 on 09/06/12
For personal use only.

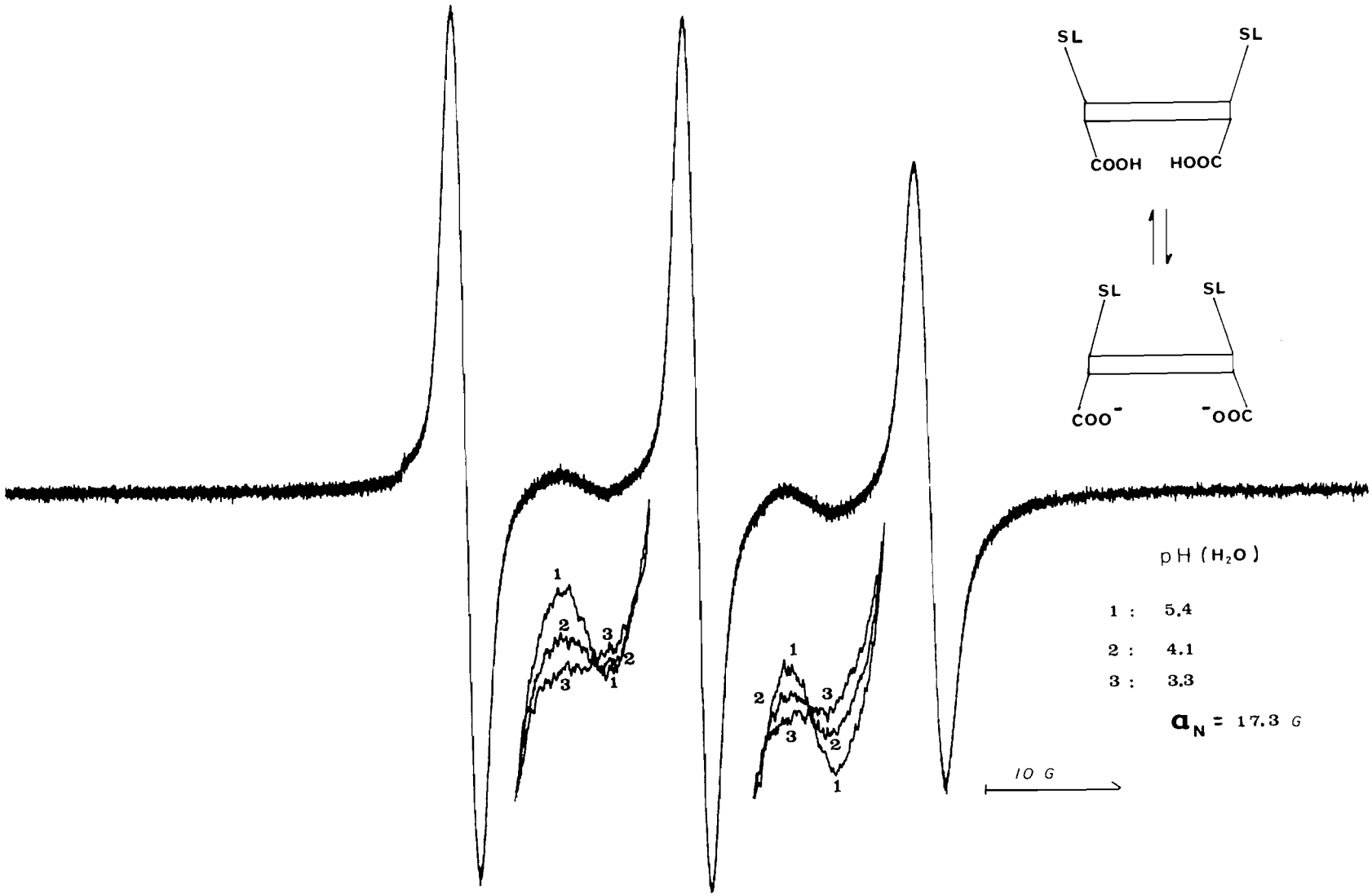

FIG. 4. Electron paramagnetic resonance spectra of di-SL-*syn* **2** in water at pH 5.9, 20°C, and at three different pH values (expanded scale by a factor of 5). The diagram is a schematic representation of the relative position of the nitroxide group (SL for spin label) before and after ionization of the carboxyl group.

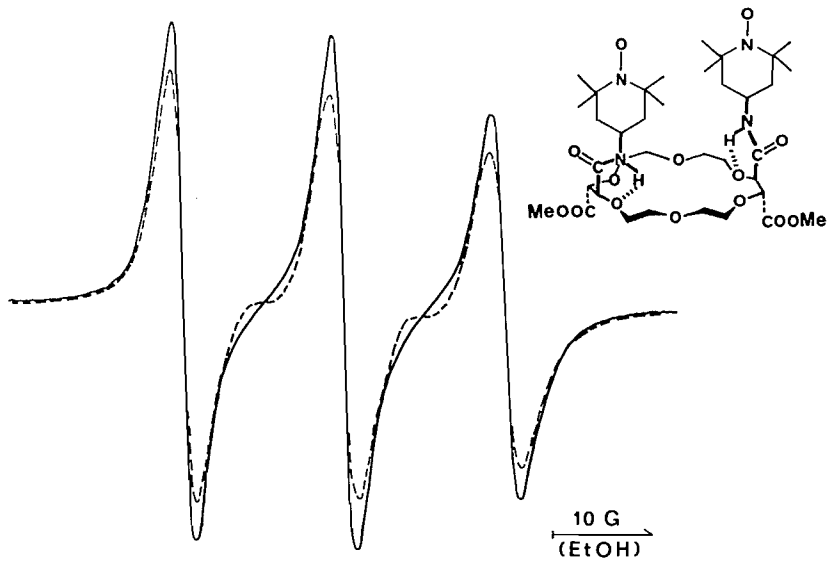

FIG. 5. Electron paramagnetic resonance spectra of the di-SL-*syn* dimethyl ester **5** in ethanol at room temperature in the presence of KSCN (dotted lines); complex 1:1.

play a major role on the global conformation of the whole molecule. Any modifications induced by either the solvent, the complexation with K^+, or by the degree of ionization have a profound effect on the nitroxide–nitroxide distance on the other face. Secondly, the crown ether backbone is rather flexible and changes of its conformation are readily detected by measuring the CHX—CHY coupling constant in ^1H nmr. Interestingly, it is to be noted that temperature does not modify the conformation of this chiral fragment, contrary to solvation, pH, or K^+ complexation.

Thirdly, the nitroxide–nitroxide interactions depend in a complex manner on all the parameters describing the conformation. In fact, one of the most striking features is the presence of a so-called "conformational reflex effect" (3) in which perturbation of the interactions between the carboxyl groups on one side of the crown results in a modification of the spin–spin interaction on the other side. The dinitroxide **2** is a very flexible molecule and the population of spin–spin interacting states increases with the temperature without reaching a point equivalent to a biradical with a strong interaction with a five-line spectrum (6). Nevertheless, the way is now open for a more complete analysis of interactions with different substitutents on spin-labeled crown ether receptors in order to see how the dissymmetry of the molecules influences the binding process.

Experimental

General details

Melting points were taken using a Reichart hotstage microscope and are uncorrected. The ir spectra were recorded using a Perkin–Elmer 710A spectrometer in $CHCl_3$ as solvent unless otherwise stated. The proton nmr spectra were recorded using a Varian 360 (60 MHz), a Bruker-WH90 (90 MHz), and a Cameca (250 MHz) spectrometer, using $CDCl_3$ or DMSO-d_6 as solvent, and containing tetramethylsilane (TMS) as internal standard. Specific rotations were calculated from optical rotation values obtained using a Perkin–Elmer 241 polarimeter and a 1-dm cell. Microanalyses were performed by H. Seguin of the National Research Council of Canada, Ottawa. For tlc, commercial plates of silica gel (Eastman or Macherey–Nagel) were used. Nitroxide groups give white spots on a blue background with molybdenum blue (Zinzadze) reagent.

The epr spectra were taken on a Bruker 414S or ER-200D spectrometer, equipped with a temperature control unit.

Procedure for the preparation of syn- *and* anti-*dinitroxide [18]-crown-6 diacid (2 and 3)*

A solution of dry tempamine **7** (1.2 g, 8 mmol) in 9 mL of dichloromethane was added dropwise over a 10-min period to a stirred solution of the dianhydride **6** (1.85 g, 4 mmol) in 15 mL of dry dichloromethane. After 2 hours at room temperature in the dark, the mixture was evaporated to dryness to yield 3.9 g of a crude orange foamy mixture of dinitroxide diacids. Chromatography on Kieselgel 60 Merck (5 × 15 cm) and elution with 30:8:5 $CHCl_3/CH_3OH/NH_4OH$ allowed the *anti* isomer **3** (0.35 g) to be eluted first, followed by elution with 70:30:7:1 $CHCl_3/CH_3OH/H_2O/NH_4OH$ to elute a mixture of *anti* and *syn* isomers (0.84 g) (that can be rechromatographed) and finally the *syn* isomer **2** (0.42 g), all as ammonium salts. Passage over Dowex 50-X8 (H^+ form) resin in 8:2 CH_3OH/H_2O yielded, after crystallization from C_2H_5OH/H_2O mixture, 127 mg of *anti* isomer **3** as orange needles (mp 235–240°C) and 269 mg of the *syn* isomer **2** as a pink crystalline material (mp 157–159°C); ir: 3500–3000 (OH), 1720 (COOH), 1660 (CONH) cm^{-1} for both compounds. The purity of both compounds was verified by hplc (Perkin–Elmer Series 3B) with a HS-SC18 column using 70:30:4 $CH_3OH/H_2O/NH_4Cl$ as eluant; $[\alpha]_D^{24}$ +58.9° (*c* 1.0, CH_2Cl_2) for **3** and +45.3° (*c* 1.5, C_2H_5OH) for **2**. *Anal.* calcd. for $C_{34}H_{58}N_4O_{14}\cdot 3H_2O$ for **3**: C 51.32, H 7.30, N 7.04; found: C 50.74, H 7.66, N 7.70 and for $C_{34}H_{58}N_4O_{14}\cdot 4H_2O$ for **2**: C 50.18, H 7.13, N 6.88; found: C 49.62, H 7.95, N 6.89.

Procedure for the preparation of only the syn *isomer (2): 2R,3R,11R,12R–(+)-N,N'-di-4'(2',2',6',6'-tetramethylpiperidine-1'-oxyl)-2-11-dicarboxamido-3,12-dicarboxyl-1,4,7,10,-13,16-hexaoxacyclooctadecane*

A solution of the dianhydride **6** (200 mg, 0.49 mmol) in 2 mL of dry dichloromethane was added dropwise to a solution of tempamine **7** (70 mg, 0.4 mmol) and triethylamine (20 drops) in 1 mL of dichloromethane. After stirring in the dark for 30 min the reaction mixture was evaporated to dryness to give a crude pink foam which was passed on a Kieselgel 60 Merck (1 × 10 cm) column. The excess tempamine was eluted first with CH_2Cl_2 and the *syn* isomer **2** (150 mg) with 30:8 CH_2Cl_2/CH_3OH. The material was shaken for a few minutes with a small amount of Dowex 50-X8 (H^+ form) resin to remove traces of remaining tempamine and to convert the *syn* isomer **2** (99 mg) in the carboxylic acid form as a glassy orange oil that can be crystallized from wet methanol (mp 160°C); epr: a_N = 16.3 G (C_2H_5OH), 17.2 G (H_2O). *Anal.* calcd. for $C_{34}H_{58}N_4O_{14}\cdot 2CH_3OH\cdot H_2O$: C 52.14, H 8.30, N 6.76; found: C 52.17, H 7.92, N 6.26.

Can. J. Chem. Downloaded from www.nrcresearchpress.com by 210.87.254.5 on 09/06/12
For personal use only.

Dimethyl ester (5)

A small amount of **2** was esterified in methanol with diazomethane in the usual way to give a semi-solid yellow compound **5**: ir: 1650 (CONH), 1745 ($COOCH_3$) cm^{-1}; $[\alpha]_D^{20}$ +36.0° (*c* 1.0, C_2H_5OH). *Anal.* calcd. for $C_{36}H_{62}N_4O_{14}$: C 55.870, H 8.07, N 7.23; found: C 55.96, H 8.49, N 7.02.

Tetranitroxide [18]-crown-6 (4): 2R,3R,11R,12R-(+)-N,N',N'',N'''-2,3,11,12-tetrakis-4'-(2',2',6',6'-tetramethylpiperidine-1'-oxyl)-2,3,11,12-tetracarboxyamido-1,4,7,10,13,16-hexaoxacyclooctadecane

To the tetraacid **1** (85 mg, 0.2 mmol) in 2 mL of dry dichloromethane was added freshly sublimed PCl_5 (100 mg) and the solution was stirred at room temperature overnight so as to dissolve most of the PCl_5. This clear solution was added to the tempamine **7** (120 mg, 0.8 mmol) and triethylamine (200 mg, 2 mmol) in 2 mL of dichloromethane. After 1 hour, 1 g of alumina and 2 mL of methanol were added and the mixture evaporated *in vacuo*. Purification by passage over an alumina column (2 × 5 cm) using $CHCl_3$, followed by 10:1 $CHCl_3/CH_3OH$ as eluant, afforded 85 mg of a reddish oil. After elution on a Bio-Rad AG 50W-X8 (H^+ form) resin with CH_3OH, 70 mg of **4** as a clean orange oil was obtained. The oil solidified upon scratching the wall of the flask (mp 106–109°C); $[\alpha]_D^{24}$ +42.7° (*c* 1.0, C_2H_5OH). *Anal.* calcd. for $C_{52}H_{92}N_8O_{14}$: C 59.29, H 8.80, N 10.64; found: C 59.52, H 9.10, N 9.85.

Acknowledgments

Financial support from the Natural Sciences and Engineering Research Council of Canada, the Ministère de l'Éducation du Québec (H.D. and P.K.), and from CNRS and the Université d'Orléans, France (M.P.) is acknowledged. The di-anilide *syn* crown ether was a gift of Dr. J. P. Behr (Stasbourg).

1. H. DUGAS and M. PTAK. J. Chem. Soc. Chem. Commun. 710 (1982).
2. J. P. BEHR, J. M. LEHN, D. MORAS, and J. C. THIERRY. J. Am. Chem. Soc. **103**, 701 (1981).
3. J. J. DALY, P. SCHÖNHOLZER, J. P. BEHR, and J. M. LEHN. Helv. Chim. Acta, **64**, 1444 (1981).
4. J. P. BEHR, J. M. GIRODEAU, R. C. HAYWARD, J. M. LEHN, and J. P. SAUVAGE. Helv. Chim. Acta, **63**, 2096 (1980).
5. L. A. FREDERICK, T. M. FYLES, N. P. GURPRASAD, and D. M. WHITFIELD. Can. J. Chem. **59**, 1724 (1981).
6. G. R. LUCKHURST. *In* Spin labeling, theory and applications. Vol. 1. *Edited by* L. J. Berliner. Academic Press, New York, NY. 1976. p. 133.
7. H. LEMAIRE. J. Chim. Phys. **64**, 559 (1967).
8. J. P. BEHR, J. M. LEHN, and P. VIERLING. Helv. Chim. Acta, **65**, 1853 (1982).
9. R. M. IZATT, B. L. HAYMORE, and J. J. CHRISTENSEN. J. Chem. Soc. Chem. Commun. 1308 (1972).
10. A. A. BOTHNER-BY. *In* Advances in magnetic resonance. Vol. 7. *Edited by* J. J. Waugh. Academic Press, New York, NY. 1965. p. 195.
11. G. F. LUCKHURST and G. F. PEDULLI. J. Am. Chem. Soc. **92**, 4738 (1970).
12. T. B. MARRIOTT and O. H. GRIFFITH. J. Magn. Reson. **13**, 45 (1974).
13. P. FERRUTI, D. GILL, M. P. KLEIN, and M. CALVIN. J. Am. Chem. Soc. **91**, 7765 (1969).
14. C. R. NAKAIE, G. GOISSIS, S. SCHREIER, and A. C. M. PAIVA. Braz. J. Med. Biol. Res. **14**, 173 (1981).
15. J. F. W. KEANA, M. J. ACARREGUI, and S. L. M. BOYLE. J. Am. Chem. Soc. **104**, 827 (1982).
16. J. P. BEHR, J. M. LEHN, A. C. DOCK, and D. MORAS. Nature, **295**, 526 (1982).

Can. J. Chem. Downloaded from www.nrcresearchpress.com by 210.87.254.5 on 09/06/12
For personal use only.

Membrane transport systems. V. Coupled countertransport of alkaline earth cations and protons

LYNN M. DULYEA, THOMAS M. FYLES, AND DENNIS M. WHITFIELD
Department of Chemistry, University of Victoria, P.O. Box 1700, Victoria, B.C., Canada V8W 2Y2

Received June 30, 1983

LYNN M. DULYEA, THOMAS M. FYLES, and DENNIS M. WHITFIELD. Can. J. Chem. **62**, 498 (1984).

The extraction and transport of alkaline earth cations from a basic to an acidic solution across an artificial membrane by crown ether carboxylic acids are reported. Monocarboxylate carriers achieve the transport via 2:1 complexes or by ternary complexes in the presence of readily extractible anions, while dicarboxylate carriers transport cations as 1:1 complexes. Both types of carrier exhibit two regimes of kinetic behaviour depending on the relative concentrations of the carrier and the metal ion: a zero order regime in which the rate depends only on the carrier concentration, and a reversible consecutive first order regime in which the rate depends only on the metal ion concentration. In the former, the rate of adsorption of the carrier on the interface is presumed to be rate limiting while in the latter, the diffusion of metal ion to the interface is rate limiting. Carrier structure exerts a general influence over both the rate and selectivity of transport but this influence varies with the kinetic regime considered.

LYNN M. DULYEA, THOMAS M. FYLES et DENNIS M. WHITFIELD. Can. J. Chem. **62**, 498 (1984).

On rapporte des extractions et des transports de cations d'alcalino-terreux de solutions basiques vers des solutions acides à travers une membrane artificielle effectués par des éthers couronnes d'acides carboxyliques. Les transporteurs monocarboxylés permettent d'effectuer les transferts via des complexes 2:1 ou par le biais de complexes ternaires en présence d'anions qui peuvent être extraits facilement; par ailleurs, les transporteurs dicarboxylés effectuent le transport des cations sous forme de complexes 1:1. Les deux types de transporteurs présentent deux régimes de comportement cinétique différents suivant les concentrations relatives de transporteur et d'ion métallique: un régime d'ordre zéro dans lequel la vitesse dépend uniquement de la concentration de transporteur et un régime du premier ordre consécutif et réversible dans lequel la vitesse dépend uniquement de la concentration de l'ion métallique. Dans le premier régime, on suppose que la vitesse d'adsorption du transporteur à l'interface est l'étape déterminante alors que dans le dernier régime, la diffusion de l'ion métallique à l'interface serait l'étape déterminante. La structure du transporteur exerce une influence générale à la fois sur la vitesse et sur la sélectivité du transport mais cette influence varie avec le régime cinétique considéré.

[Traduit par le journal]

Can. J. Chem. Downloaded from www.nrcresearchpress.com by 210.87.254.6 on 09/06/12
For personal use only.

The extraction and transport of ionic species across membranes is central to the functioning of biological systems and is of increasing importance for the recovery and upgrading of resources using artificial membranes (1–6). One approach to the development of practical separation schemes seeks inspiration from the processes which occur in natural systems and, in particular, the behaviour of certain carboxylate antibiotics (7). These ionophores are capable of transporting a cation against its concentration gradient using a coupled counterflow of protons to drive the process. Numerous studies of these antibiotics *in vivo* and *in vitro* have confirmed a carrier mechanism in which proton loss and cation uptake occur to give a complex which diffuses across the membrane (8). Artifical systems incorporating the more readily available of these antibiotics have been examined in detail (9–11).

Extending this concept to a completely artificial system could follow one of several routes. Carriers might be designed to mimic structural features of the antibiotic ionophores (12–14) or, alternatively, the essential features of the transport might be adapted to other ionophoretic materials such as crown ethers or cryptands. From the point of view of synthesis, the latter approach based on crown ethers represents an important compromise. Candidate structures are of sufficient complexity to achieve the necessary control of ion bindings and physical properties, yet are sufficiently simple so that structural modifications throughout a series can be investigated without a massive investment of synthetic effort for each carrier. This approach has been investigated for the countertransport of alkali metal cations and protons (15–19). A schematic mechanism of the process is given in Fig. 1, A. At the basic interface the carrier is deprotonated and cation complexation occurs to give a neutral complex which can diffuse across the membrane. At

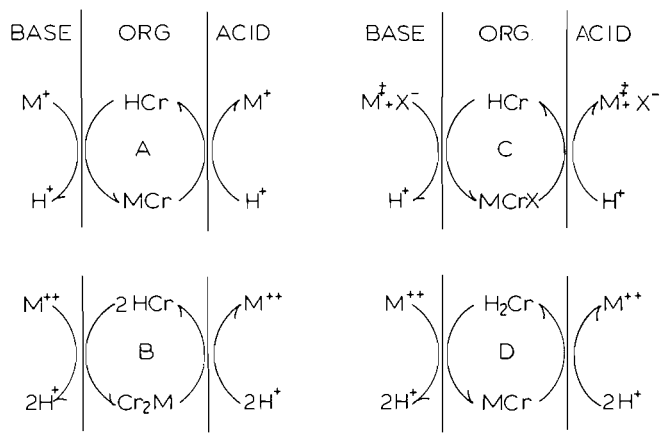

FIG. 1. Schematic mechanisms of cation–proton coupled countertransport. A: Monocarboxylate carrier/alkali metal cation. B: Monocarboxylate carrier/alkaline earth cation, 2:1 complexes. C: Monocarboxylate carrier/alkaline earth cation/extracted anion, ternary complex. D: Dicarboxylate carrier/alkaline earth cation.

the acidic interface the reverse process occurs; protonation and metal ion loss regenerates the carrier and completes the cycle. In the systems studied to date, ion extraction is rate limiting under most circumstances (16, 17) and two different kinetic regimes can be recognized. One type is a "zero order" regime in which the transport rate depends only on the carrier concentration in the membrane phase while the other type is a "consecutive first order regime" in which the rate depends on the interfacial concentration of a carrier/metal ion complex (17). A mechanism consistent with these observations involves rate limiting adsorption of carrier or desorption of complex

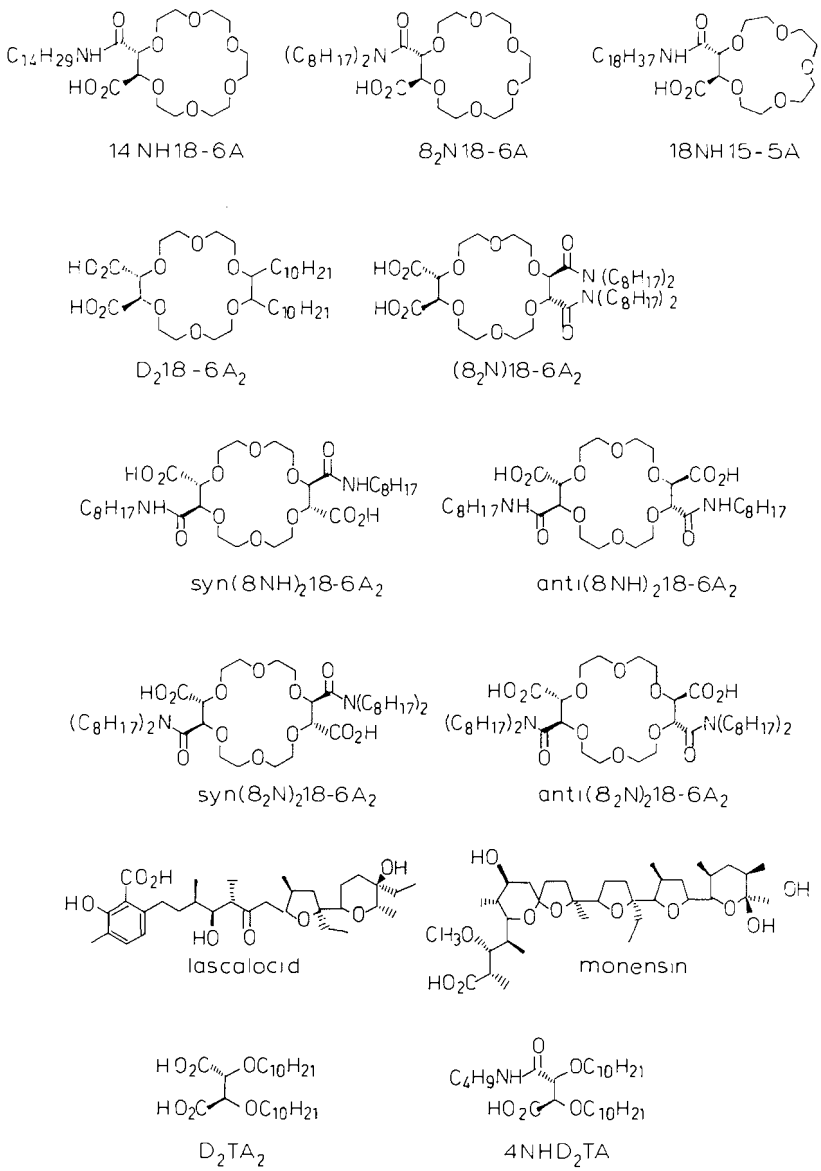

from the interface (17).

Recently we have prepared a number of dicarboxylic acid carriers (20) which we anticipated would be capable of the extraction and transport of alkaline earth cations in exchange for two protons countertransported. For purposes of comparison we have also examined divalent ion transport by the monocarboxylic acid carriers previously prepared. This report outlines the transport behaviour of these two types of carriers and further probes the details of the interfacial exchange of cations and protons. Formulae of the carriers considered are shown, together with line notations indicating general structural features. Thus 14NH18-6A is a tetradecyl 1° amide (14NH) on an 18-crown-6 periphery (18-6) and a monocarboxylic acid (A), while *syn* (8NH)$_2$18-6A$_2$ is an 18-crown-6 diacid (18-6A$_2$) bearing two octyl 1° amides (8NH)$_2$. Positional isomerism is generally ignored (2,3 vs. 2,11 diacids) except for the important differences noted by the prefixes *syn* or *anti*.

Results and discussion

The transport of alkaline earth cations was examined using a U-tube cell (16, 17). The membrane phase was a chloroform solution of the carrier in the base of the U separating aqueous phases floating on the chloroform in the arms of the U. Transport of cations was followed by analysis of aliquots withdrawn from the aqueous phases. Initially, the two aqueous phases were at equal concentration but during the countertransport the concentration on the acidic side increased at the expense of a decrease of concentration on the basic side. Typical curves are shown in Figs. 2 and 3. As previously, two distinctly different kinetic regimes were noted. An excess of metal ion produces the zero order behaviour noted in Fig. 2 while approximately equal concentrations of metal ion and carrier produce nonlinear behaviour (Fig. 3). The two kinetic regimes are controlled by selection of the initial conditions but the concentration ranges accessible within each regime are limited by the tendency for most carriers to emulsify the cell contents at concentrations greater than 5×10^{-3} *M* and by the limits of the sampling and analysis protocols used (experimental section).

Zero order kinetic regime

In order to preserve electroneutrality the transport of divalent ions by monocarboxylate carriers requires either 2:1 carrier/metal ion complexes (Fig. 1, B) or anion dependent transport via ternary complexes (Fig. 1, C). Despite the

Can. J. Chem. Downloaded from www.nrcresearchpress.com by 210.87.254.6 on 09/06/12
For personal use only.

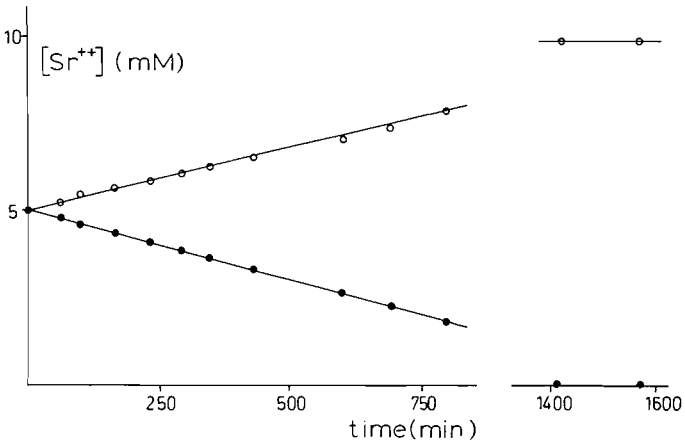

FIG. 2. Transport of strontium by the dicarboxylate carrier $D_2$18-6A_2 (Table 3, entry 35). Lower line, solid circles = basic phase; upper line, open circles = acidic phase. This experiment is typical of the zero order kinetic behaviour.

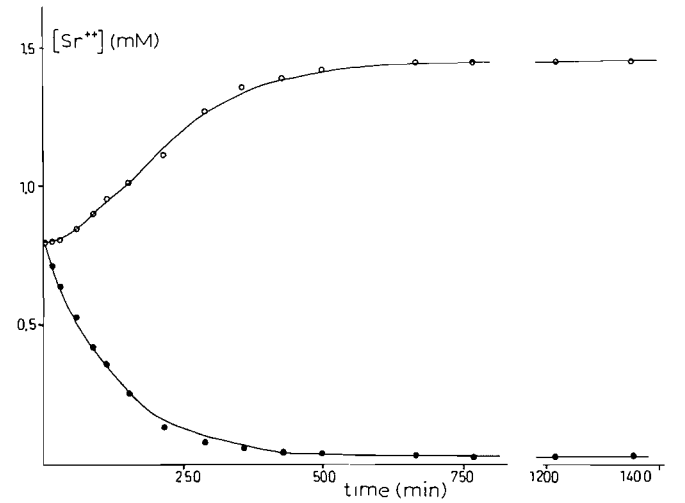

FIG. 3. Transport of strontium by the dicarboxylate carrier *anti* $(8NH)_2$18-6A_2 (Table 4, entry 9). Lower line, filled circles = basic phase; upper line, open circles = acidic phase. This experiment is typical of reversible consecutive first order kinetic behaviour.

demands of the structural organization required, transport of divalent ions occurs readily at rates comparable to the rates of monovalent ions (Table 3, 1–33). Typically, 10^{-3} *M* carrier and 10^{-2} *M* cation solutions produce transport behaviour which can be described as zero order in transported cation for all cases. Zero order behaviour at these concentrations is directly comparable to the alkali metal cation transport examined previously utilizing the same carriers (16, 17). In order to further explore the similarities, we considered the effect of pH on transport rate (Table 3, 8–13, no significant variation) as well as the effect of carrier concentration. As previously (17), the extraction in the zero order regime is presumed to follow the rate law:

[1] $\text{rate} = k[\text{HCr(org)}]^c$

where c is the order in carrier, which yields at time = 0.

[2] $\log(\text{rate})_0 = c \log([\text{HCr(org)}]_0) + \text{const.}$

where the subscripts denote initial values. The cell consisted of fixed concentrations of Ca^{2+} and buffers with variable initial

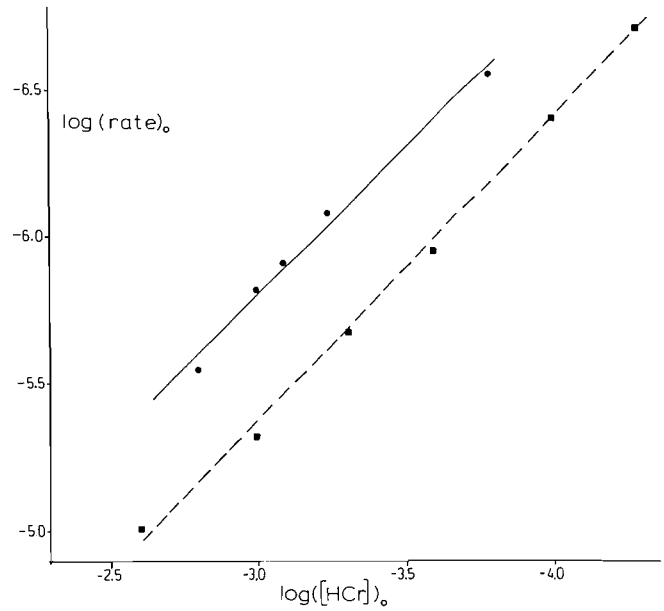

FIG. 4. A plot of log $(\text{rate})_0$ as a function of log $([\text{HCr}]_{org})$ for the zero order transport of Ca^{2+} by 14NH18-6A (upper curve, –●–, Table 3; 1, 5, 6, 7, 16) and of Sr^{2+} by *anti* $(8NH)_2$18-6A_2 (lower curve, –■–, Table 3; 47, 49, 51–54).

concentrations of 14NH18-6A. A graph of initial transport rate according to [2] is given in Fig. 4 (solid line) which shows a line of slope 0.98 (r^2 = 0.991) clearly indicating that calcium transport is first order in carrier. The very close similarities between these experiments and the transport of K^+ by 14NH18-6A suggests that the transport rate in this case is similarly rate limited by the adsorption of the carrier at the interface (17).

Although this result clarifies the extraction kinetics, it sheds no light on the nature or stoichiometry of the complexes which traverse the membrane. The two principal possibilities are sketched in Fig. 1 (B and C). The two choices are distinguished by different cation–proton stoichiometries ($2H^+ = M^{2+}$ vs. $H^+ = M^{2+}X^-$) and by their anion dependencies. The cycle described in Fig. 1, C would be expected to depend on the nature of the extracted anion as observed in other systems (21); more liposoluble anions (picrate, I^-) would be expected to enhance the rate while more hydrophilic anions (F^-, SO_4^{2-}) would retard the rate. Various buffers were prepared in which the normally available anion (Cl^-) was replaced by NO_3^-, ClO_4^-, or SO_4^{2-} but these substitutions did not significantly alter the rate (Table 3; 16–19). Moreover, addition of an extremely liposoluble anion such as picrate or 1-naphthylacetate did result in rate increases (typically 2 to 2.5-fold enhancement, Table 3; 14, 15, 30, 31). These results suggest that under normal conditions the major mode of transport is via 2:1 complexes (Fig. 1, B) while the anion dependent cycle may be induced with readily extracted anions (Fig. 1, C). The accompanying paper (32) examines this point in more detail and we propose a structure based on nmr studies for the 2:1 complex in which the metal ion occupies one macrocycle while the other macrocycle provides a coordinating carboxylate. Thus the second carrier is simply a liposoluble anion which presumably could be replaced by ion exchange with picrate or 1-naphthylacetate when present.

Unlike the monocarboxylate carriers, the dicarboxylate carriers could provide electrically neutral transport via 1:1 com-

Can. J. Chem. Downloaded from www.nrcresearchpress.com by 210.87.254.6 on 09/06/12
For personal use only.

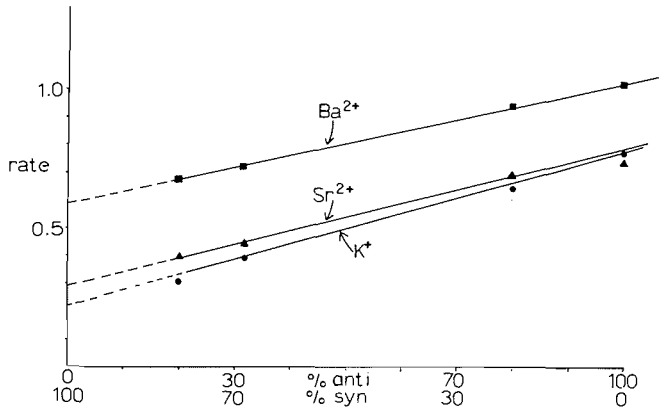

FIG. 5. Transport rates, normalized to 5×10^{-4} *M*, for mixtures of *syn* and *anti* $(8_2N_2)18\text{-}6A_2$. Data from Table 3; 57–72, (Ca^{2+} omitted for clarity of presentation).

plexes which require two protons per metal ion transferred (Fig. 1, D). At a divalent ion concentration of 10^{-2} *M* and a carrier concentration of 10^{-3} *M*, transport occurred readily with the concentration vs. time curves similar to the one shown in Fig. 2. The transport in this case is zero order in divalent ion and independent of pH. The kinetic order in carrier may be assessed by the same methods outlined above and the results are present in Fig. 4 (dashed line). The line in this case has a slope of 1.04 ($r^2 = 0.998$) and indicates the transport is first order in carrier. By analogy with the other cases examined, the adsorption of carrier is presumably rate limiting in this case as well.

In the majority of cases the carriers were available in reasonable quantity and high purity. Unfortunately the separation of *syn* and *anti* $(8_2N)_218\text{-}6A_2$ gave only the *anti* isomer isomerically pure. The *syn* isomer was available only in mixtures although these mixtures were chemically pure. The isomer composition of each mixture was obtained from the ^1H nmr spectrum by integration and the overall transport rate for the mixture was obtained in the normal fashion. The observed rates, normalized to a common carrier concentration, were plotted as a function of mixture composition to give the transport rate for pure *syn* $(8_2N)_218\text{-}6A_2$ by extrapolation as shown in Fig. 5. In most cases the experimental points lie directly on the least-squares line, hence the values obtained for *syn* $(8_2N)_218\text{-}6A_2$ are presumed to be about as reliable as those directly determined (±15%).

Transport selectivities

The issue of transport selectivity can be examined utilizing the normalized data of Tables 1 and 2. Selectivity among ions is easily indicated as a ratio relative to some reference, e.g. Ca^{2+} in Tables 1 and 2. By this criterion the selectivities observed are modest at best, while for some carriers, notably *anti* $(8NH)_218\text{-}6A_2$, the transport is essentially nonselective. In most cases 18-crown-6 derivatives exhibit some preference for Sr^{2+} over the other alkaline earth cations. This is in agreement with stability constant data for these carriers (accompanying paper) and crown ethers in general, which show optimal binding of the cation whose radius matches that of the macrocycle (22). As noted previously (16), binding selectivity does not directly result in transport selectivity of the same magnitude, although overall complex stability and selectivity both play a role in the transport process (23). In this system, the rate is controlled by the ability of the ligand to adsorb to the interface but, once in position, equilibrium considerations will govern the fraction of the surface crown ether which will be occupied by metal ion, hence will control the amount of metal ion extracted. The selectivity, or lack of it, among the alkaline earth cations is comparable to other crown ether based systems (24).

Comparisons between carriers reveal more substantial differences. One of the most important comparisons is between the acyclic carriers $4NHD_2TA$ and D_2TA_2 and the other cyclic carriers for Ca^{2+} transport. The acyclic carriers have only two possible donor atoms for cation complexation, yet transport at a significant fraction of the rate of much more elaborate carriers (Table 1). This must indicate that the important interaction for cation transport is primarily electrostatic and that a relatively simple complex is sufficient to permit the extraction to occur. This is also consistent with the lack of selectivity noted above, since electrostatic effects will note only the charge and only indirectly the size of the ion.

In general, the effect of carrier concentration on selectivity is relatively minor (Tables 1 and 2), especially for 14NH18-6A which is essentially the same at the two concentrations. Larger differences can be noted for other carriers and carriers with similar structures such as $D_218\text{-}6A_2$ and $(8_2N)_218\text{-}6A_2$. The major changes in selectivity are for *syn/anti* pairs and K^+ transport. The more lipophilic carriers *syn/anti* $(8_2N)_218\text{-}6A_2$ transport K^+ more readily and are more Ba^{2+} selective than the comparable $(8NH)_218\text{-}6A_2$ homologs. This may be a result of steric factors rather than differences in lipophilicity similar to the difference between $8_2N18\text{-}6A$ and 14NH18-6A. The steric effect might take the form of direct blocking of the binding site or might simply be due to blocking of positions normally occupied by coordinated water.

The naturally occurring ionophore antibiotics lascalocid (X537A) and monensin are included for comparison with the synthetic ionophores. Monensin is a sodium specific ionophore which is incapable of transporting Ca^{2+} (Table 3; 80). Lascalocid is a calcium selective ionophore which is presumed to transport using 2:1 complexes in both artificial and natural systems (7, 10, 11). Our initial attempts to achieve Ca^{2+} transport using X537A were uniformly unsuccessful, and we recovered only lascalocid as the free acid at the end of the transport experiments (judged by nmr (25)). The problem was traced to the use of Tris[1] as a buffer component. Lascalocid is known to complex and transport primary amines (8) and in this case must form a complex at the interface which blocks Ca^{2+} transport. With Tricine[1] as buffer component the rate of transport is comparable to the rate reported in a similar but smaller U-tube cell (10) (1.44 μmol/h our cell; 1.35 μmol/h calculated from (10) normalized to 10^{-3} *M* and corrected for interfacial area). The difference might have been expected to be greater as the two experimental protocols are different; our system examines transport against a gradient in total Ca^{2+} while previous workers examined transport down the concentration in Ca^{2+} (ref. 10, also refs. 8, 11).

On closer examination this distinction is not as marked, due to the composition of our buffer system. On the acidic side, the major buffer components all form complexes with Ca^{2+} and Sr^{2+} and will diminish the concentration of "free" metal on the acidic side. The analytical concentrations of the acidic buffer

[1] Tris = tris(hydroxymethyl)aminomethane; Tris H^+ = protonated Tris; Tricine = *N*-tris(hydroxymethyl)methylglycine; MES = 2-(*N*-morpholino)ethane sulfonic acid; TEA = triethanolamine; $TEAH^+$ = protonated TEA.

Can. J. Chem. Downloaded from www.nrcresearchpress.com by 210.87.254.6 on 09/06/12
For personal use only.

TABLE 1. Zero order transport rates for various carriers at 10^{-3} M^a

Carrier	Metal ion (Rate, μmol/h (selectivity relative to Ca^{2+}))			
	Ca^{2+}	Sr^{2+}	Ba^{2+}	K^+
18NH15-5A	0.77 (1.0)	1.59 (2.06)	1.25 (1.62)	
14NH18-6A	1.50 (1.0)	2.61 (1.74)	1.99 (1.32)	3.91 (2.60)
$D_2$18-6A_2	3.02 (1.0)	2.57 (0.85)	2.22 (0.74)	0.31 (0.10)
anti $(8NH)_2$18-6A_2	4.29 (1.0)	5.15 (1.20)	4.55 (1.06)	<0.1 (<0.02)
syn $(8NH)_2$18-6A_2	2.68 (1.0)	3.82 (1.42)	3.70 (1.38)	<0.1 (<0.03)
Lascalocid	1.44			
D_2TA_2	0.79			
4NHD_2TA	0.62			

[a] Rates normalized to 10^{-3} M in carrier assuming first order dependence for carrier concentration.

TABLE 2. Zero order transport rates for various carriers at 5×10^{-4} M^a

Carrier	Metal ion (Rate, μmol/h (selectivity relative to Ca^{2+}))			
	Ca^{2+}	Sr^{2+}	Ba^{2+}	K^+
14NH18-6A	0.37 (1.0)	0.66 (1.78)	0.49 (1.32)	0.96 (2.60)
8_2N18-6A	0.50 (1.0)	0.93 (1.86)	0.68 (1.38)	1.44 (2.90)
$(8_2N)_2$18-6A_2	0.61 (1.0)	1.07 (1.75)	0.27 (0.64)	0.21 (0.35)
syn $(8_2N)_2$18-6A_2	0.30 (1.0)	0.27 (0.90)	0.57 (1.90)	0.22 (0.73)
anti $(8_2N)_2$18-6A_2	0.70 (1.0)	0.75 (1.07)	1.04 (1.48)	0.77 (1.10)

[a] Rates normalized to 5×10^{-4} M in carrier assuming first order dependence for carrier concentration.

components (Ca^{2+} or Sr^{2+}, phosphate, TEA, pH) and the stability constants of the species formed in solution[2] (26–28) allow the concentration of free Ca^{2+} or Sr^{2+} to be calculated (29). The major Ca^{2+} or Sr^{2+} species at pH 2.3 was $M^{2+}HPO_4^{2-}$ and the free metal ion concentration was typically 3×10^{-4} M for the total concentrations of metal ion typical of those encountered in the course of an experiment (1 to 2×10^{-2} M). On the basic side of the cell the free metal ion concentration is not substantially altered by complex formation with buffer components, although a weak complex with Tris (28) diminishes the concentration to about 60% of the analytical values at all points during a typical transport run (10^{-2} to 10^{-4} M). Thus, at least in the initial stages, the transport of M^{2+} occurs *up a concentration gradient in TOTAL* M^{2+} but *down a concentration in FREE* M^{2+}. Despite this potential problem there is no evidence to suggest any additional complications. Transport rates in the zero order regime are insensitive to pH, to buffer type and concentration, and to stirring rate. In this respect, the zero order transport regime is very well defined and quite selective for metal ions in the presence of large excesses of buffer components.

Consecutive first order kinetic regime

With the zero order behaviour closely similar to previously examined cases, we anticipated that it would be possible to alter the initial concentrations to enter a kinetic regime of consecutive first order reactions (16, 17). In fact, at metal ion and carrier concentrations about 10^{-3} M, nonlinear curves of concentration as a function of time were observed as shown in Fig. 3. However, the curves did not fit with the irreversible cases examined previously, notably late in the transport where the basic phase was not entirely depleted in metal ion and the mass balance indicated that substantial amounts of metal ion were still held in the membrane. Considering only the early portions of the curves, the irreversible consecutive first order kinetic analysis used previously gave an adequate fit to the data. The final concentrations attained did not vary over a considerable time, which suggests that the overall behaviour could be an example of reversible consecutive first order reactions. This would give a kinetic scheme as in [3].

$$[3]\quad [M^{2+}]_{basic} \underset{k_{21}}{\overset{k_{12}}{\rightleftharpoons}} [M^{2+}]_{org} \underset{k_{32}}{\overset{k_{23}}{\rightleftharpoons}} [M^{2+}]_{acidic}$$

The general case of two reversible consecutive first order reactions has been discussed in detail and methods for the calculation of species concentrations for a given set of rate constants have been outlined (30). Utilizing these procedures, a nonlinear optimization program for the calculation of rate constants from concentration vs. time data was written. The experimental value for $[M^{2+}]_{org}$ was calculated from the mass balance equation, utilizing the analytical concentrations in both aqueous phases and the total concentration initially. The experimental values were compared with calculated concentrations and the set of rate constants was varied to minimize the differences between the experimental and calculated values. The solid line drawn in Fig. 3 is the calculated curve derived for the experimental data shown. Since the experimental value for $[M^{2+}]_{org}$ is obtained indirectly, the uncertainty in this concentration is greater than for directly determined concentrations. Consequently the degree of uncertainty in the rate constants derived, especially k_{21} and k_{23}, is greater than was

[2] Species considered: H_3PO_4, $H_2PO_4^-$, HPO_4^{2-}, PO_4^{3-}, TEA, $TEAH^+$, $M^{2+}PO_4^{3-}$, $M^{2+}HPO_4^{2-}$, $M^{2+}H_2PO_4^-$, M^{2+}TEA.

Can. J. Chem. Downloaded from www.nrcresearchpress.com by 210.87.254.6 on 09/06/12
For personal use only.

TABLE 3. Zero order transport experiments

Entry	Carrier	Initial				Rate, μmol h^{-1}
		Conc, m*M*	Ion	Conc, m*M*	Buffers[a]	
1	14NH18-6A	1.0	Ca^{2+}	10	A 8.3/2.3	1.50
2	14NH18-6A	1.0	K^+	10	A 8.3/2.3	3.91
3	14NH18-6A	0.96	Sr^{2+}	10	A 8.3/2.3	2.61
4	14NH18-6A	0.96	Ba^{2+}	10	A 8.3/2.3	1.99
5	14NH18-6A	1.6	Ca^{2+}	10	A 8.3/2.3	2.87
6	14NH18-6A	0.81	Ca^{2+}	10	A 8.3/2.3	1.25
7	14NH18-6A	0.16	Ca^{2+}	10	A 8.3/2.3	0.28
8	14NH18-6A	0.99	Ca^{2+}	10	A 7.9/2.3	1.35
9	14NH18-6A	0.99	Ca^{2+}	10	A 8.3/2.3	1.65
10	14NH18-6A	0.99	Ca^{2+}	10	A 9.0/2.3	1.88
11	14NH18-6A	0.90	Ca^{2+}	10	A 8.3/1.3	1.52
12	14NH18-6A	0.90	Ca^{2+}	10	A 8.3/2.3	1.31
13	14NH18-6A	0.90	Ca^{2+}	10	A 8.3/3.0	1.25
14	14NH18-6A	1.0	Ca^{2+}	10	B 8.3/2.3	3.92
15	14NH18-6A	1.0	Ca^{2+}	10	C 8.3/2.3	3.88
16	14NH18-6A	0.58	Ca^{2+}	10	A 8.3/2.3	0.8
17	14NH18-6A	0.58	Ca^{2+}	10	D 8.3/2.3	1.03
18	14NH18-6A	1.0	Ca^{2+}	10	E 8.3/2.3	1.70
19	14NH18-6A	1.0	Ca^{2+}	10	F 8.3/2.3	1.83
20	14NH18-6A	0.48	K^+	1	A 8.3/2.3	0.93
21	14NH18-6A	0.48	Ca^{2+}	1	A 8.3/2.3	0.36
22	14NH18-6A	0.48	Sr^{2+}	1	A 8.3/2.3	0.64
23	14NH18-6A	0.48	Ba^{2+}	1	A 8.3/2.3	0.47
24	14NH18-6A	0.96	Ca^{2+}	10	G 8.1/2.3	1.20
25	8_2N18-6A	0.51	K^+	1	A 8.3/2.3	1.42
26	8_2N18-6A	0.51	Ca^{2+}	1	A 8.3/2.3	0.51
27	8_2N18-6A	0.51	Sr^{2+}	1	A 8.3/2.3	0.95
28	8_2N18-6A	0.51	Ba^{2+}	1	A 8.3/2.3	0.70
29	18NH15-5A	1.0	Ca^{2+}	10	A 8.3/2.3	0.77
30	18NH15-5A	1.0	Ca^{2+}	10	B 8.3/2.3	1.55
31	18NH15-5A	1.0	K^+	1	A 8.3/2.3	0.06
32	18NH15-5A	1.0	Sr^{2+}	10	A 8.3/2.3	1.59
33	18NH15-5A	1.0	Ba^{2+}	10	A 8.3/2.3	1.25
34	$D_2$18-6A_2	0.96	Ca^{2+}	5	A 8.3/2.3	2.90
35	$D_2$18-6A_2	0.96	Sr^{2+}	5	A 8.3/2.3	2.47
36	$D_2$18-6A_2	0.96	Ba^{2+}	5	A 8.3/2.3	2.13
37	$D_2$18-6A_2	0.45	K^+	10	A 8.3/2.3	0.14
38	$D_2$18-6A_2	0.85	Ca^{2+}	6.7	A 8.3/2.3	2.21
39	$D_2$18-6A_2	0.57	Ca^{2+}	6.7	A 8.3/2.3	1.42
40	$D_2$18-6A_2	0.31	Ca^{2+}	3.3	A 8.3/2.3	0.61
41	*syn* $(8NH)_2$18-6A_2	0.91	Ca^{2+}	10	A 8.3/2.3	2.42
42	*syn* $(8NH)_2$18-6A_2	0.89	Sr^{2+}	10	A 8.3/2.3	3.60
43	*syn* $(8NH)_2$18-6A_2	0.91	Ba^{2+}	10	A 8.3/2.3	3.46
44	*syn* $(8NH)_2$18-6A_2	0.89	K^+	10	A 8.3/2.3	<0.1
45	*anti* $(8NH)_2$18-6A_2	0.96	Ca^{2+}	10	A 8.3/2.3	4.13
46	*anti* $(8NH)_2$18-6A_2	1.63	K^+	10	A 8.3/2.3	0.1
47	*anti* $(8NH)_2$18-6A_2	0.94	Sr^{2+}	10	A 8.3/2.3	4.86
48	*anti* $(8NH)_2$18-6A_2	0.94	Ba^{2+}	10	A 8.3/2.3	4.29
49	*anti* $(8NH)_2$18-6A_2	2.5	Sr^{2+}	25	A 8.3/2.3	10.8
50	*anti* $(8NH)_2$18-6A_2	5.0	Sr^{2+}	50	A 8.3/2.3	15.5
51	*anti* $(8NH)_2$18-6A_2	0.5	Sr^{2+}	5	A 8.3/2.3	2.07
52	*anti* $(8NH)_2$18-6A_2	0.25	Sr^{2+}	2.5	A 8.3/2.3	1.10
53	*anti* $(8NH)_2$18-6A_2	0.099	Sr^{2+}	0.5	A 8.3/2.3	0.39
54	*anti* $(8NH)_2$18-6A_2	0.050	Sr^{2+}	0.25	A 8.3/2.3	0.19
55	*anti* $(8NH)_2$18-6A_2	0.53	Ca^{2+}	10	G 8.3/2.3	1.64
56	*anti* $(8NH)_2$18-6A_2	0.70	Sr^{2+}	10	B 8.3/2.3	3.68
57	*anti* $(8_2N)_2$18-6A_2	0.50	K^+	1	A 8.3/2.3	0.78
58	*anti* $(8_2N)_2$18-6A_2	0.50	Ca^{2+}	1	A 8.3/2.3	0.71
59	*anti* $(8_2N)_2$18-6A_2	0.50	Sr^{2+}	1	A 8.3/2.3	0.76
60	*anti* $(8_2N)_2$18-6A_2	0.50	Ba^{2+}	1	A 8.3/2.3	1.05
61	[b]	0.43	K^+	1	A 8.3/2.3	0.48
62	[b]	0.43	Ca^{2+}	1	A 8.3/2.3	0.59
63	[b]	0.43	Sr^{2+}	1	A 8.3/2.3	0.60

Can. J. Chem. Downloaded from www.nrcresearchpress.com by 210.87.254.6 on 09/06/12
For personal use only.

TABLE 3. (*Continued*)

Entry	Carrier	Initial Conc, m*M*	Ion	Conc, m*M*	Buffers[a]	Rate, μmol h^{-1}
64	[b]	0.43	Ba^{2+}	1	A 8.3/2.3	0.82
65	[c]	0.48	K^+	1	A 8.3/2.3	0.39
66	[c]	0.48	Ca^{2+}	1	A 8.3/2.3	0.40
67	[c]	0.48	Sr^{2+}	1	A 8.3/2.3	0.42
68	[c]	0.48	Ba^{2+}	1	A 8.3/2.3	0.71
69	[d]	0.52	K^+	1	A 8.3/2.3	0.33
70	[d]	0.52	Ca^{2+}	1	A 8.3/2.3	0.39
71	[d]	0.52	Sr^{2+}	1	A 8.3/2.3	0.42
72	[d]	0.52	Ba^{2+}	1	A 8.3/2.3	0.70
73	$(8_2N)_2$18-6A_2	0.54	Ca^{2+}	1	A 8.3/2.3	0.66
74	$(8_2N)_2$18-6A_2	0.54	Sr^{2+}	1	A 8.3/2.3	1.15
75	$(8_2N)_2$18-6A_2	0.36	K^+	1	A 8.3/2.3	0.15
76	$(8_2N)_2$18-6A_2	0.36	Ba^{2+}	1	A 8.3/2.3	0.19
77	X537A	1.2	Ca^{2+}	10	A 8.3/2.3	<0.1
78	X537A	1.0	Ca^{2+}	10	G 8.3/2.3	1.44
79	X537A	1.2	Ca^{2+}	10	B 8.3/2.3	0.47
80	Monensin	1.0	Ca^{2+}	10	A 8.3/2.3	≪0.1
81	D_2TA_2	1.0	Ca^{2+}	10	A 8.3/2.3	0.79
82	4NHD_2TA	1.1	Ca^{2+}	10	A 8.3/2.3	0.62

[a]A–G refer to buffer type, 8.3/2.3 indicates initial pH values on basic/acidic sides of the cell. A = basic side: 0.125 *M* Tris to pH with HCl; acidic side: 0.125 *M* H_3PO_4 to pH with TEA. B = A plus 10^{-2} *M* naphthylacetic acid added to the basic side. C = A plus 2×10^{-2} *M* picric acid added to basic side. D = A with H_2SO_4 used in place of HCl. E = A with HNO_3 used in place of HCl. F = A with $HClO_4$ used in placed of HCl. G = basic side: 0.125 Tricine to pH with HCl.

[b]20:80 Mixture of *syn/anti* $(8_2N)_2$18-6A_2.

[b]67:33 Mixture of *syn/anti* $(8_2N)_2$18-6A_2.

[d]81:19 Mixture of *syn/anti* $(8_2N)_2$18-6A_2.

TABLE 4. Reversible consecutive first order transport experiments

Entry	Carrier	Conc, m*M*	Ion	Conc, m*M*	Cond[a]	$-\log k_{12}$[b]	$-\log k_{21}$[b]	$-\log k_{23}$[b]	$-\log k_{32}$[b]
1	*anti* $(8NH)_2$18-6A_2	0.96	Ca^{2+}	1.0	A 8.3/2.3	3.91	4.32	3.73	5.19
2	*anti* $(8NH)_2$18-6A_2	0.91	Sr^{2+}	0.8	A 7.0/2.3	3.81	4.18	3.71	4.74
3	*anti* $(8NH)_2$18-6A_2	0.91	Sr^{2+}	0.8	A 8.1/2.3	3.94	4.05	3.65	4.67
4	*anti* $(8NH)_2$18-6A_2	0.91	Sr^{2+}	0.8	B 6.6/2.3	3.88	4.54	3.70	4.62
5	*anti* $(8NH)_2$18-6A_2	0.91	Sr^{2+}	0.8	B 7.1/2.3	3.85	4.40	3.95	5.06
6	*anti* $(8NH)_2$18-6A_2	1.0	Sr^{2+}	0.8	C 8.3/0.33	3.98	5.04	3.85	5.09
7	*anti* $(8NH)_2$18-6A_2	1.0	Sr^{2+}	0.8	C 8.3/0.59	3.93	4.71	3.86	5.06
8	*anti* $(8NH)_2$18-6A_2	1.0	Sr^{2+}	0.8	C 8.3/1.25	3.94	4.64	3.85	5.12
9	*anti* $(8NH)_2$18-6A_2	0.49	Sr^{2+}	0.8	D 6.1/2.3	3.90	5.11	3.78	4.83
10	*anti* $(8NH)_2$18-6A_2	2.0	Sr^{2+}	0.8	D 6.1/2.3	3.86	[d]	[d]	[d]
11	$D_2$18-6A_2	1.0	Sr^{2+}	0.8	A 8.3/2.3	3.40	4.72	4.03	4.85
12	$D_2$18-6A_2	0.84	Sr^{2+}	0.8	C 8.3/0.33	3.45	4.48	4.10	5.06
13	14NH18-6A	0.96	Sr^{2+}	0.8	D 6.1/2.3	4.66	4.54	4.24	5.32
14	14NH18-6A	1.0	Ca^{2+}	1.0	C 7.5/2.3	4.48	[c]	3.78	[c]
15	14NH18-6A	1.0	Ca^{2+}	1.0	C 8.0/2.3	4.26	[c]	3.79	[c]
16	14NH18-6A	1.0	Ca^{2+}	1.0	C 8.5/2.3	4.25	[c]	3.60	[c]
17	14NH18-6A	1.0	Ca^{2+}	1.0	C 9.5/2.3	4.33	[c]	3.66	[c]
18	*syn*$(8NH)_2$18-6A_2	0.85	Sr^{2+}	0.8	A 8.3/2.3	3.90	4.22	3.94	5.13
19	*anti*$(8NH)_2$18-6A_2	0.49	Sr^{2+}	0.8	E 6.1/2.3	3.71	[c]	3.70	[c]
20	*anti*$(8NH)_2$18-6A_2	0.49	Sr^{2+}	0.8	F 6.1/2.3	4.07	4.70	3.23	5.17

[a]A–D refer to buffer type, 8.3/2.3 indicates initial pH values on basic/acidic sides of the cell. A = basic side: 0.125 *M* Tris to pH with HCl; acidic side: 0.125 *M* H_3PO_4 to pH with TEA. B = 0.125 *M* H_3PO_4 to pH with TEA both sides. C = basic side: 0.125 *M* Tris to pH with HCl; acidic side: HCl to pH. D = basic side: 0.01 *M* MES to pH with $(CH_3)_4NOH$; acidic side: 0.125 *M* H_3PO_4 to pH with TEA. E, buffer D, stirring at 800 rpm. F, buffer D, stirring at 200 rpm.

[b]Rate constants calculated as described in text. Uncertainties: log k_{12} ±0.1, log k_{23} ±0.15, log k_{21}, log k_{32} ±0.3.

[c]Irreversible consecutive first order kinetic model fit the data well.

[d]Initial intake rate only calculated from log (conc.) vs. time.

previously the case with irreversible consecutive first order cases (17). Nonetheless, the values given in Table 4 are reproducible between duplicates, within the errors noted.

The collapse to a consecutive first order behaviour is different than was noted previously (17). In the present case the uptake rate and overall cell behaviour is independent of pH

Can. J. Chem. Downloaded from www.nrcresearchpress.com by 210.87.254.6 on 09/06/12
For personal use only.

Can. J. Chem. Downloaded from www.nrcresearchpress.com by 210.87.254.6 on 09/06/12
For personal use only.

(from 6.0–9.0, Table 4; 1–10, 13–17) and is also independent of carrier concentration. Thus the kinetic scheme [3] completely describes the transport kinetics with no additional concentration terms for protons or carrier concentration. In this regime the rate limiting step must be remote from the interface and adsorbed carrier, hence must lie in the water layer on the basic side of the cell. One possibility is that the rate is limited by diffusion of the metal ion across the unstirred boundary layer near the interface. If this deduction is correct, the rate should depend on stirring conditions, which was found to be the case (Table 4; 9, 19, 20); increased stirring enhanced the rate while decreased stirring retarded the rate. The U-tube cells utilized in this work are suitable for achieving a relatively reproducible set of stirring conditions but are incapable of permitting detailed control of hydrodynamic conditions at the interface. Further studies of this aspect of transport are in progress, utilizing a different cell with more closely controlled hydrodynamic parameters.

Nonetheless, some transport results have been obtained for a limited selection of carriers and ions (Table 4). Complex stability again plays a role in the transport process as the various carriers transport at differing rates. The diffusion rate will depend on the concentration gradient in the diffusing ion. If the complex formed at the interface is stable, the free ion concentration will be low and the gradient established will provide a higher flux of ions. By this argument the apparent complex stabilities follow the sequence $D_2$18-6A_2 > *anti*~*syn* $(8NH)_2$18-6A_2. A similar sequence is noted in the stability constants for complexation in homogeneous solution (accompanying paper).

To summarize the results of the transport, it is important to note that the simple mechanisms outlined in Fig. 1 adequately present the overall stoichiometry of the countertransport, but the extraction steps involve considerably more complexity when examined in detail. At least three distinct types of behaviour have been noted for a given carrier and two different, but closely related, ions (e.g. 14NH18-6A/K^+ or Sr^{2+}). For each of these, the structures of the carriers play a role with respect to both overall shape and ion binding, but the essential structural components remain relatively poorly defined. The carrier must be able to complex ions, but it is not essential that the complex be structurally well defined (e.g. D_2TA/Ca^{2+}). The carrier must have some surfactant activity, but even poorly arranged carriers (*anti* $(8NH)_2$18-6A_2) are active. Ultimately, the structural requirements will depend on the source phase concentrations and the separation required, as this will in part dictate where the rate limiting step of the transport will appear.

Experimental

Transport experiments were performed in a U-shaped apparatus constructed of 15-mm id Pyrex tubing bent to a 20-mm radius bend. The U-tube had a total volume of 35 mL and was jacketted and thermostatted at 25 ± 0.1°C. The membrane phase was 12 mL of $CHCl_3$ in the base of the U and aqueous phases of 10 mL each were placed in the arms of the U. All three phases were stirred at 400 ± 1 rpm. The interfaces were 1.54 cm^2 and remained quiescent throughout the experiments. The general methods for purification of carriers and kinetic analyses were as previously described (15, 16, 17, 20, 31). The syntheses of the carriers D_2TA_2 and $4NHD_2TA$ are described below. Details of experiments (concentrations, buffers) and the transport rates are in Tables 3 and 4. Kinetic data reported were determined in duplicate. Experiments for the determination of kinetic order were conducted in a preliminary fashion to determine optimal sampling times and analytical procedures but these results are not included in the final values. Care is required in setting up the cell so that the interfaces always lie in the same position in the U and the stirring is regular. Under typical, controlled conditions, reproducibility between duplicates from the same stock solution of carrier was better than ±4% for the values reported in Table 3. Due to the sensitivity of the consecutive reversible first order regime to stirring conditions, the reproducibility between duplicates was ±10% for the values reported in Table 4. Longer term reproducibility, working from different preparations of carriers, different stock solutions, and different dates was somewhat poorer (±6% Table 3; ±15% Table 4). High purity carriers must be used; minor impurities, particularly ammonium salts from the synthesis, decrease the transport rate. The reported behavior should be regarded as system dependent; other sizes or shapes of U tube with different relative phase volumes will influence the conditions necessary to provoke a particular kinetic regime. The synthesis of the two carriers prepared for this work followed general procedures previously described.

R,R-*Di*-O-*decyltartaric acid (D_2TA_2)*

To a solution of 4.5 g of *R,R-N,N,N',N'*-tetramethyltartaramide in 60 mL of DMF under an argon atmosphere at ambient temperature was added 3.7 mL of thallous ethoxide followed by 11.8 g of n-decyl iodide. The mixture was stirred and heated at 50–55°C for 14 h, cooled, diluted with 100 mL of water, and filtered to removed Tll. The filtrate was evaporated, passed down a short alumina column with 600 mL of CH_2Cl_2, evaporated, and pumped to remove traces of DMF. The product was purified by column chromatography on alumina using a toluene–$CHCl_3$ gradient to give 5.3 g (50% yield) of a waxy solid, mp 48–49°C; ir (cm^{-1}): 1640, 1100; $[\alpha]_D$ +53.8 (*c* 0.08, $CHCl_3$); ^{1}H nmr: 0.89 (6H, bt), 1.25, −1.55 (32H, bs), 2.84 (6H, s), 3.14 (6H, s), 3.52 (4H, bt), 4.68 (8H, s); ^{13}C nmr: 13.9, 22.5, 26.0, 29.3(m), 29.9, 35.6, 37.1, 64.7, 77.3, 169.7; ms (*m/e*): 485 (M + 1,100), 440 (19), 412 (3). *Anal.* calcd. for $C_{28}H_{56}N_2O_4$: C 69.38, H 11.54, N 5.78; found: C 69.42, H 12.10, N 5.73.

The tetramethyldiamide was hydrolysed in 25% aqueous HCl at reflux for 36 h, the mixture was cooled, and the diacid was isolated by solvent extraction (100 mL CH_2Cl_2) and purified by chromatography on alumina using 10% CH_3OH in $CHCl_3$ as eluent to give the diacid D_2TA_2 as a solid, mp 56–58°C; ir (cm^{-1}): 3600–2400, 1725, 1110; $[\alpha]_D$ +21.8 (*c* 0.106, $CHCl_3$); ^{1}H nmr: 0.87 (6H, bt), 1.24 (32H, bs), 3.49 (2H, dt, *J* = 9, 7), 3.68 (2H, dt, *J* = 9, 7), 4.37 (2H, s); ^{13}C nmr: 14.0, 22.6, 25.7, 29.5 (m), 31.8, 73.1, 79.4, 174.0; ms (*m/e*): 431 (M + 1, 1), 141(100). *Anal.* calcd. for $C_{24}H_{46}O_6$: C 66.94, H 10.77, found: C 66.90, H 10.78.

R,R-N-*Butyl-di*-O-*decyltartaric acid ($4NHD_2TA$)*

The monoamide of D_2TA_2 was prepared from the diacid in a manner identical to previously published procedures for crown ether monoacid – monoamides (15, 31) to give $4NHD_2TA$ as a viscous oil. Infrared (cm^{-1}): 3600–2400, 1725, 1670, 1530, 1090; $[\alpha]_D$ +25.2 (*c* 0.52, $CHCl_3$); ^{1}H nmr: 0.86 (9H, m), 1.23 (36H, bs), 3.30 (2H, bq), 3.49–3.63 (4H, m), 4.20 (1m, bs), 4.39 (1H, bs), 6.70 (1H, bt); ^{13}C nmr: 13.6, 20.0, 31.6, 39.8 (butyl), 14.0, 22.6, 26.0, 29.5 (m), 31.9, 73.3, 73.4, 80.4, 81.2, 169.3, 172.1; ms (*m/e*): 486 (M + 1, 100). *Anal.* calcd. for $C_{28}H_{58}NO_5$: C 69.23, H 11.41, N 2.90; found: C 69.36, H 11.24, N 2.88.

Acknowledgements

This work was supported by the Natural Sciences and Engineering Research Council and by Dow Chemical Canada Inc. through the University Fellowship Program. We are grateful to both these organizations for their assistance.

1. E. L. CUSSLER. AIChE J. **17**, 1300 (1971).
2. R. W. BAKER, M. E. TUTTLE, D. J. KELLY, and H. K. LONSDALE. J. Membr. Sci. **2**, 213 (1977).
3. K. H. LEE, D. F. EVANS, and E. L. CUSSLER. AIChE J. **24**, 860 (1978).
4. J. STRZELBICKI and W. CHAREWICZ. J. Inorg. Nucl. Chem. **40**,

1415 (1978).
5. M. SUGIURA. J. Colloid Interface Sci. **81**, 385 (1981).
6. W. C. BABCOCK, R. W. BAKER, E. D. LACHAPELLE, and K. L. SMITH. J. Membr. Sci. **7**, 71 (1980).
7. J. W. WESTLEY. Adv. Appl. Microbiol. **22**, 177 (1977).
8. B. C. PRESSMAN and N. T. DEGUZMAN. Ann. N.Y. Acad. Sci. **256**, 373 (1976).
9. E. M. CHOY, D. F. EVANS, and E. L. CUSSLER. J. Am. Chem. Soc. **96**, 7085 (1974).
10. J. BOLTE, C. DEMUYNCK, G. JEMINET, J. JUILLARD, and C. TISSIER. Can. J. Chem. **60**, 981 (1982).
11. W. J. MAILAISSE, I. VALVERDE, G. DEVIS, G. SOMERS, and E. COUTURIER. Biochemie, **61**, 1185 (1979); E. COUTURIER and W. J. MAILAISSE. Biochemie, **62**, 177 (1980).
12. J. O. GARDNER and C. C. BEARD. J. Med. Chem. **21**, 357 (1972).
13. M. J. UMEN and A. SCARPA. J. Med. Chem. **21**, 505 (1978).
14. W. WIERENGA, B. R. EVANS, and J. H. WOLTERSOM. J. Am. Chem. Soc. **101**, 1334 (1979).
15. L. A. FREDERICK, T. M. FYLES, N. P. GURPRASAD, and D. M. WHITFIELD. Can. J. Chem. **59**, 1724 (1981).
16. T. M. FYLES, V. A. MALIK-DIEMER, and D. M. WHITFIELD. Can. J. Chem. **59**, 1734 (1981).
17. T. M. FYLES, V. A. MALIK-DIEMER, C. A. MCGAVIN, and D. M. WHITFIELD. Can. J. Chem. **60**, 2259 (1982).
18. S. SHINKAI, M. KINDA, T. SONE, and O. MANABE. J. Chem. Soc. Chem. Commun. 125 (1982).
19. S. SHINKAI, H. KINDA, Y. ARARAGI, and O. MANABE. Bull. Chem. Soc. Jpn. **56**, 559 (1983).
20. T. M. FYLES, C. A. MCGAVIN, and D. M. WHITFIELD. In press.
21. J. D. LAMB, J. J. CHRISTENSEN, S. R. IZATT, K. BEDKE, M. S. ASTIN, and R. M. IZATT. J. Am. Chem. Soc. **102**, 3399 (1980).
22. R. M. IZATT, R. E. TERRY, B. L. HAYMORE, L. D. HANSEN, N. K. DALLEY, A. G. AVONDET, and J. J. CHRISTENSEN. J. Am. Chem. Soc. **98**, 7620 (1976).
23. J. D. LAMB, J. J. CHRISTENSEN, J. L. OSCARSON, B. L. NIELSEN, B. W. ASAY, and R. M. IZATT. J. Am. Chem. Soc. **102**, 6820 (1980).
24. J. D. LAMB, R. M. IZATT, D. G. GARRICK, J. S. BRADSHAW, and J. J. CHRISTENSEN. J. Membr. Sci. **9**, 83 (1981).
25. M. J. O. ANTEUNIS. Bioorg. Chem. **5**, 327 (1976).
26. L. G. SILLEN and A. E. MARTELL (*Editors*). Stability constants of metal-ion complexes. Special Publication No. 17, Chemical Society, London. 1964.
27. H. GNEPF, O. GUBELI, and G. SCHWARZENBACH. Helv. Chim. Acta, **45**, 1171 (1962).
28. K. H. SCHELLER, T. H. J. ABEL, D. E. POLANYI, P. K. WENK, B. E. FISCHER, and H. SIGEL. Evr. J. Biochem. **107**, 455 (1980).
29. B. GINZBERG. Talanta, **23**, 149 (1976).
30. A. A. FROST and R. G. PEARSON. Kinetics and mechanism. Wiley, New York. 1961.
31. T. M. FYLES and C. A. MCGAVIN. Anal. Chem. **54**, 2103 (1982).
32. T. M. FYLES and D. M. WHITFIELD. Can. J. Chem. **62**, 507 (1984).

Can. J. Chem. Downloaded from www.nrcresearchpress.com by 210.87.254.6 on 09/06/12
For personal use only.

Membrane transport systems. VI. Complexation of cations by lipophilic crown ether carboxylic acids

THOMAS M. FYLES AND DENNIS M. WHITFIELD
Department of Chemistry, University of Victoria, P.O. Box 1700, Victoria, B.C., Canada V8W 2Y2

Received June 30, 1983

THOMAS M. FYLES and DENNIS M. WHITFIELD. Can. J. Chem. **62**, 507 (1984).

The complexation of alkali metal and alkaline earth cations by crown ether carboxylic acids has been studied by potentiometric titration and by infrared and nuclear magnetic resonance spectroscopy. Complexation in methanol–water solution is governed by the electrostatic interactions between the cation and the carboxylate, hence discrimination among cations on the basis of ionic radius is poor. The isomers *syn* and *anti* $(8NH)_2$18-6A_2 exhibit differing complexation behaviour towards cations with the *anti* isomer giving the stronger complexes. Interaction between the carboxylates across the face of the macrocycle of *syn* $(8NH)_2$18-6A_2 can be inferred from the potentiometric data. Combined infrared and nuclear magnetic resonance studies of the complexes in chloroform solution show that the cation is held as an asymmetric tight ion pair with the carboxylate. The dimeric salt $(4NH18\text{-}6)_2Ca$ exhibits both a tight and a symmetric or loose ion pair between the cation and the two carboxylates. The substituents on the macrocycle are pseudoaxially disposed and in some cases *gauche* ethylenedioxy units can be recognized from the spectra. The complexes are monomeric in solution and in most cases the conformations are unaffected by small amounts of water in the chloroform solution. The structural results correlate with observations from transport experiments.

THOMAS M. FYLES et DENNIS M. WHITFIELD. Can. J. Chem. **62**, 507 (1984).

On a étudié la complexation de cations de métaux alcalins et alcalino-terreux par des acides carboxyliques d'éthers couronnes en faisant appel à des titrages potentiométriques et à la spectroscopie infrarouge et rmn. La complexation dans une solution eau–méthanol dépend des interactions électrostatiques entre le cation et le carboxylate; il en résulte que la discrimination entre les cations sur la base du rayon ionique est faible. Les isomères *syn* et *anti* du $(8NH)_2$18-6A_2 présentent des comportements de complexation différents vis-à-vis les cations; l'isomère *anti* donne les complexes les plus forts. L'interaction entre les carboxylates *syn* à la surface du macrocycle $(8NH)_2$18-6A_2 peut être déduite des données potentiométriques. La combinaison des études infrarouges et rmn des complexes en solution dans le chloroforme montre que le cation est maintenu dans une paire intime d'ions avec le carboxylate. Le sel dimère $(4NH18\text{-}6)_2$ Ca présente à la fois une paire d'ion intime et symétrique ainsi qu'une paire d'ion plus lâche entre le cation et les deux carboxylates. Les substituants du macrocycle sont disposés de façon pseudoaxiale et dans certains cas on peut reconnaître, dans le spectre, des unités d'éthylènedioxy *gauche*. Les complexes sont monomères en solution et, dans la plupart des cas, les conformations ne sont pas affectées par de faibles quantités d'eau dans le chloroforme. Les résultats structuraux sont en accord avec les expériences de transport.

[Traduit par le journal]

Can. J. Chem. Downloaded from www.nrcresearchpress.com by 210.87.254.40 on 09/06/12
For personal use only.

The discovery of the complexing properties of synthetic macrocyclic polyethers (crown ethers) has sparked a wide range of activity in fields ranging from synthesis of related compounds to analytical applications (1–3). An important property of crown ethers is their ability to dissolve ionic solids in nonpolar media leading to solutions of "naked anions" for synthetic applications (1, 2) to phase transfer catalysis (4) and to cation extraction and membrane transport across artificial membranes (5). The structures of the ligands and their complexes in the solid state and in solutions have been the subject of numerous studies (1, 2). In a "typical" complex the metal ion occupies a site in the center of the macrocycle with ligating donor atoms from the ring providing a full or partial inner coordination sphere for the ion. The exterior of the complex is lipophilic to provide for dissolution in the nonpolar solvent.

Our interest in crown ethers centers on a series of lipophilic crown ether carboxylic acids (6–10) which are capable of mediating cation–proton coupled countertransport (11). Representative structures of the carriers examined to date are shown below together with a line notation (10) indicating structural features. A simple schematic mechanism for the net countertransport of monocations and protons is given in Fig. 1. At the basic interface, the carrier gives up a proton in exchange for a cation from the aqueous phase. The resultant complex is neutral and readily traverses the membrane phase to the acidic interface, whereupon the reverse ion exchange process occurs. The net result is the exchange of a cation for a proton across the membrane barrier. As long as the proton gradient exceeds the cation gradient the system will "pump" cations against their concentration gradient. This strategy has potential application for the recovery of metal ions from dilute solution and related systems have been developed for copper and uranium recovery using acyclic complexing agents (12–14).

Our continuing studies are directed toward the synthesis and characterization of carriers for multivalent ions and as a first step we have prepared carriers for alkaline earth cations. Transport kinetics studies of the extraction step for alkali metal (8) and alkaline earth (10) cations generally support the schematic mechanism described above. However, such studies have provided relatively little information on the nature of the complexes which traverse the membrane beyond the apparent stoichiometry of the complex. Structural information is more readily available from common spectroscopic methods such as infrared and nuclear magnetic resonance spectroscopy and from potentiometric titrations. Our goal in this report is to build up an overview of the structures of the carriers and their complexes in the bulk membrane phase. The key questions concern the nature of the ion binding site, the overall conformations of the carrier, the role of water in the complexation, and the degree of aggregation of the carriers.

Results and discussion

Complex formation in methanol/water solution

Although the membrane phase of the transport experiments is typically chloroform (7, 10), equilibrium complexation studies require a more polar solvent to produce observable

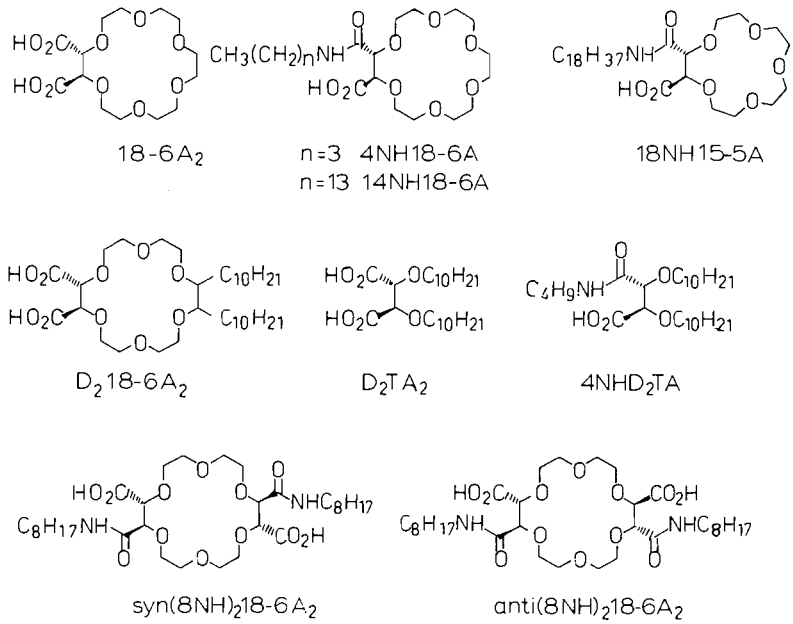

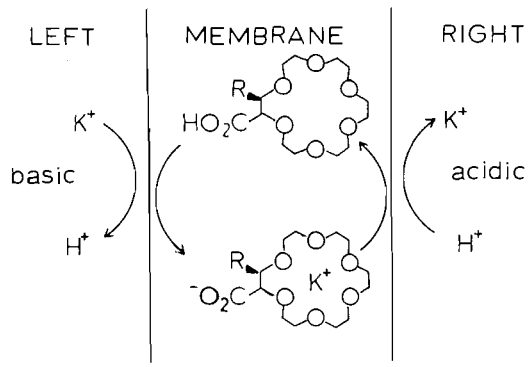

FIG. 1. A schematic mechanism for cation–proton coupled countertransport.

concentrations of free ligand. Accordingly the complexation behaviour was examined in 90:10 methanol–water (v/v). As previously (6), the complexation is examined using a generalized cumulative association constant β_{lmh} defined as $\beta_{lmh} = [L_lM_mH_h]/[L]^l[M]^m[H]^h$ (charges omitted) where the integers *l*, *m*, and *h* refer to the number of ligands, metal ions, and protons bound in a given complex. Note that this association constant is defined in terms of concentrations rather than activities. The ligand is defined as the most deprotonated form of the carrier, thus β_{110} refers to a complex of the monoanion of a monocarboxylate carrier or the dianion of a dicarboxylate carrier with a single metal ion in each case. The overall charge on the complex will thus depend on the specific case being considered. The experiment involves two stages: acid/base titration of the ligand alone to determine its acidity constant(s), followed by an acid/base titration of the ligand in the presence of the metal ion. Computer analysis of the titration curves (6) gave a set of β_{lmh} values for each of the systems examined. The results are presented in Table 1. For the dicarboxylate carriers, stepwise association constants for defined equilibria are more informative than the cumulative constant calculated. In particular, the apparent stability of complexes of the monoprotonated ligand may be calculated from the β_{lmh} values by subtraction of the first pK_a from log β_{lmh} (6, 15); thus for $LH^- + M^{2+} \rightleftharpoons LHM^+$, $\log K = \log \beta_{111} - \log \beta_{101}$ (pK_1). These results appear in parentheses where appropriate in Table 1. The complexes of ammonium are proton ambiguous in a fashion similar to polyammonium and polyguanidinium/anion complexes (15); the overall stoichiometry of the complex is known but it is not known if the proton is associated with the ligand or the ammonia. For the dicarboxylate carriers it is productive to assume that the complex whose β_{111} is calculated refers to $NH_4^+ + L^{2-}$ rather than $NH_3 + LH^-$. Thus the appropriate stepwise association constants may be calculated from log β_{111} by subtraction of the pK_a of NH_4^+, determined by titration to be 9.38 in 90:10 methanol–water. These values are given in Table 1 as well.

The difference between pK_1 and pK_2 has been used to characterize the structures of the isomers *syn* and *anti* $(8NH)_2$18-6A_2 (9), and this difference can be further utilized to infer solution structures for these two carriers. Acidity constants for dicarboxylic acids reflect a mixture of statistical and electrostatic factors (16, 17); in general, as the distance and local dielectric between the two carboxylates decreases, the difference in their two pK_a's (ratio of K_a's) increases due to electrostatic destabilization of the dianion. The principles are well-developed for simple diacids in water and may be presumed to extend at least qualitatively to 90:10 methanol–water and more complex diacids. Considering the 2,3-dicarboxylic acids 18-6A_2 and $D_2$18-6A_2, the pK_a differences are similar (2.16 and 2.02) and comparable to the values for fumaric acid (15) (pK_1 7.44, pK_2 5.23, difference 2.21). Structural studies of tetra-carboxy crown ethers have amassed considerable evidence for pseudo axial dispositions of substituents (18–21). The pK_a differences noted here are consistent with such a diaxial arrangement of carboxylates but not with a diequatorial interaction between the carboxylates. The fragment derived from tartaric acid thus retains the same conformation as the parent acid in aqueous solution (22).

An examination of CPK models of *syn* and *anti* $(8NH)_2$18-6A_2 in a variety of plausible conformations suggests that the separation of the carboxylates is about 6.5–7.5 Å for both isomers. A fully extended (all *anti*) conformation of adipic acid provides a model for 6.5 Å separation of carboxylates and the pK_a's were found to be pK_1 7.88, pK_2 6.82 (difference 1.06) in 90:10 methanol–water. The difference observed for adipic acid is greater than that observed for the *anti* isomer

Can. J. Chem. Downloaded from www.nrcresearchpress.com by 210.87.254.40 on 09/06/12
For personal use only.

TABLE 1. Logarithm of cumulative stability constants for complexation[a]

Metal	β_{lmh}	4NH18-6A	18NH15-5A	$D_2$18-6A_2	18-6A_2	*syn* $(8NH)_2$18-6A_2	*anti* $(8NH)_2$18-6A_2
H^+	101	6.23	6.24	7.77	7.77	7.38	7.04
	102	*	*	13.38 (5.61)	13.52 (5.75)	12.70 (5.32)	13.30 (6.26)
K^+	110	5.8[b]	2.9[b]	6.3	6.1	5.4	6.4
	111	10.7[b] (4.5)	8.3[b] (2.1)	12.1[c] (4.3)	12.0 (4.2)	11.0[d] (3.6)	11.8 (4.8)
Ca^{2+}	110	5.8	3.5	9.4	9.1	8.9	10.1
	210	9.9	7.1	<	<	<	<
	111	<	<	13.8 (6.0)	13.3 (5.5)	12.7 (5.3)	<
Sr^{2+}	110	5.5	4.1	10.1	9.3	8.9	10.0
	210	11.4	8.5	<	<	<	<
	111	<	<	14.4 (6.6)	13.4 (5.6)	12.8 (5.4)	<
Ba^{2+}	110	5.5	4.4	9.8	9.2	8.0	9.5
	210	11.4	8.2	<	<	<	<
	111	<	<	14.1 (6.3)	13.4 (5.6)	12.1 (4.3)	<
NH_4^+[e]	111	13.0 (3.6)	—	—	—	14.6 (5.2)	14.7 (5.3)
	112	18.5[g] (3.1)	—	—	—	19.5[f] (2.7)	20.1 (3.3)

[a] In 90:10 methanol/water (v/v), total ionic strength = 0.05 *M* (Me_4NCl) at 25 ± 0.1°C. Values in parentheses are stepwise formation constants. The symbol * indicates the complex stoichiometry is not applicable; the symbol < indicates a complex of the given stoichiometry is not required to model the experimental curve, thus is too weak to be detected. Values precise to log β_{lmh} ± 0.2.

[b] Determined at I = 0.10 *M* (6).

[c] $K^+/D_2$18-6A_2 β_{120} = 9.5.

[d] K^+/*syn* $(8NH)_2$18-6A_2 β_{120} = 8.1.

[e] pK_a (NH_4^+) = 9.38. Complexes are proton ambiguous (ref. 15, text) but assume NH_4^+ is the complexed species.

[f] NH_4^+/*syn* $(8NH)_2$18-6A_2 β_{122} = 26.8 (8.1 for L^{2-} + $2NH_4^+$).

[g] NH_4^+/4NH18-6A β_{122} = 24.7 (6.0 for L^- + $2NH_4^+$).

(0.78), thus it is likely that *anti* $(8NH)_2$18-6A_2 represents a case where there is no direct interaction between carboxylates other than the general effect of a second charge about 7 Å away.

The case of *syn* $(8NH)_2$18-6A_2 is clearly an anomaly; pK_1 is in the expected range for carboxylate on a crown ether periphery, but pK_2 is too low for an electrostatic effect alone. The monoanion is thus stabilized relative to the diacid, presumably by some interaction across the face of the macrocycle. A direct hydrogen bond ($CO_2H\cdots\bar{O}_2C$) can be accommodated with CPK models but a water-bridged structure ($CO_2H\cdots O(H)\cdots\bar{O}_2C$) involves minimal distortion of the crown ether periphery. This may also be viewed as a weak complex of H_3O^+ by the dianion. In any event, the interaction will destabilize metal ion complexes of the monoanion if the complexation disrupts whatever structural organization is present.

The notable feature of the rest of the stability constant data is the lack of selectivity exhibited by the carriers. This is most marked in the case of the 18-6 diacid with alkaline earth cations; the ligand is incapable of distinguishing among Ca^{2+}, Sr^{2+}, and Ba^{2+} even though the neutral parent, 18-crown-6, shows a range of stability constant in water of over three orders of magnitude along the same series (23). It is clear that the complexation is governed to a large extent by electrostatic attraction of the carboxylates for the metal ion, while the size selectivity of the ligand plays a minor role. The ion binding might not even involve the ring donor sites and be simply an ion-pairing interaction. Transport data for simple carriers such as D_2TA_2 show that the ring structure is not essential for transport (10) although the range of transport rates observed suggests that the ring does provide additional stabilization for the extracted ion. A metal binding structure which emerges is primarily an ion-pairing arrangement with the carboxylate plus additional ligation by the oxygen donors of the macrocycle.

Not only is a given ligand relatively unselective, among the dicarboxylate carriers there are only relatively minor differences in the complexation of a given cation. The additional decyl groups of $D_2$18-6A_2 clearly do not perturb the parent 18-6A_2 structure since the complexation constants of these two ligands are so closely similar. The largest differences occur between the isomers *syn* and *anti* $(8NH)_2$18-6A_2 with the complexes of the *syn* isomer uniformly less stable by an order of

Can. J. Chem. Downloaded from www.nrcresearchpress.com by 210.87.254.40 on 09/06/12
For personal use only.

Can. J. Chem. Downloaded from www.nrcresearchpress.com by 210.87.254.40 on 09/06/12
For personal use only.

magnitude than the complexes of the *anti* isomer. These results are in direct contradiction to the assertion that "*syn* isomers . . . complex cations much more strongly than the corresponding *anti* isomers" (19), which refers to the complexation of NH_4^+ in water by *syn* and *anti* dianilide dicarboxylate crown ethers. Significantly, the stability constants of the ammonium complexes of *syn* and *anti* $(8NH)_2$18-6A_2 are more closely similar than for any of the other cations examined. The *syn*/K^+ data more closely parallel the *syn*/NH_4^+ data than occurs with the *anti*/K^+ or NH_4^+ data. Both *anti* $(8NH)_2$18-6A_2 and 4NH18-6A complex K^+ more readily than NH_4^+; thus it appears that the *syn* isomer has a higher relative affinity for NH_4^+ than would be predicted from an examination of the complexation data for spherical metal ions alone. The ammonium complexes of *syn* $(8NH)_2$18-6A_2 must thus possess additional stabilization. Along with the pK_a anomaly noted above, a likely candidate structure for the ammonium complex is a bridging structure

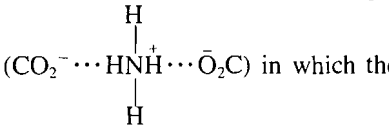

bridging H_2O or H_3O^+. The close similarity between K^+ and NH_4^+ binding by *syn* $(8NH)_2$18-6A_2 further suggests that the bridging site is the "normal" binding site for K^+ as well. In any event, the binding of NH_4^+ does not correctly reflect the binding of all other metal cations. Together with the differences in ligand, solvent, conditions, and method, these results are reconciled with previous observations.

To place the potentiometric results in the context of bulk membrane transport experiments (7, 10) it is essential to note that, even in relatively polar media (methanol–water), electrostatic effects dominate metal ion complexation. In the less polar membrane solvent chloroform, the electrostatic effects will be even more pronounced; hence a very close association between cations and the carrier carboxylate is highly likely.

Site of cation binding

The lack of size selectivity for ion complexation in homogeneous solution and the observation that relatively simple carriers could extract and transport alkaline earth cations suggest that the primary interaction is electrostatic. There are a variety of ways this might be accomplished both between different ligands and within a given complex. The two limiting structures to consider are one in which the metal ion lies near the center of the macrocycle as in a "typical" crown ether complex and the other in which the metal ion lies out of the macrocycle but closely ion-paired with the carboxylate. Between these extremes are asymmetric structures with variable ligation of the metal ion by the crown ether donor sites and/or additional water molecules. The environment of the carboxylate can be probed using infrared spectroscopy. A free carboxylate ion exhibits two bands: a strong asymmetric stretching band (ν_{AS}) near 1650–1550 cm^{-1} and a weaker symmetric stretching band (ν_S) near 1400 cm^{-1} (24). Interaction of a metal ion with carboxylate can occur with a variety of geometries and radii of interactions. The two main types are shown below:

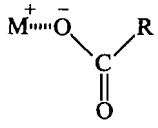

A

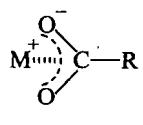

B

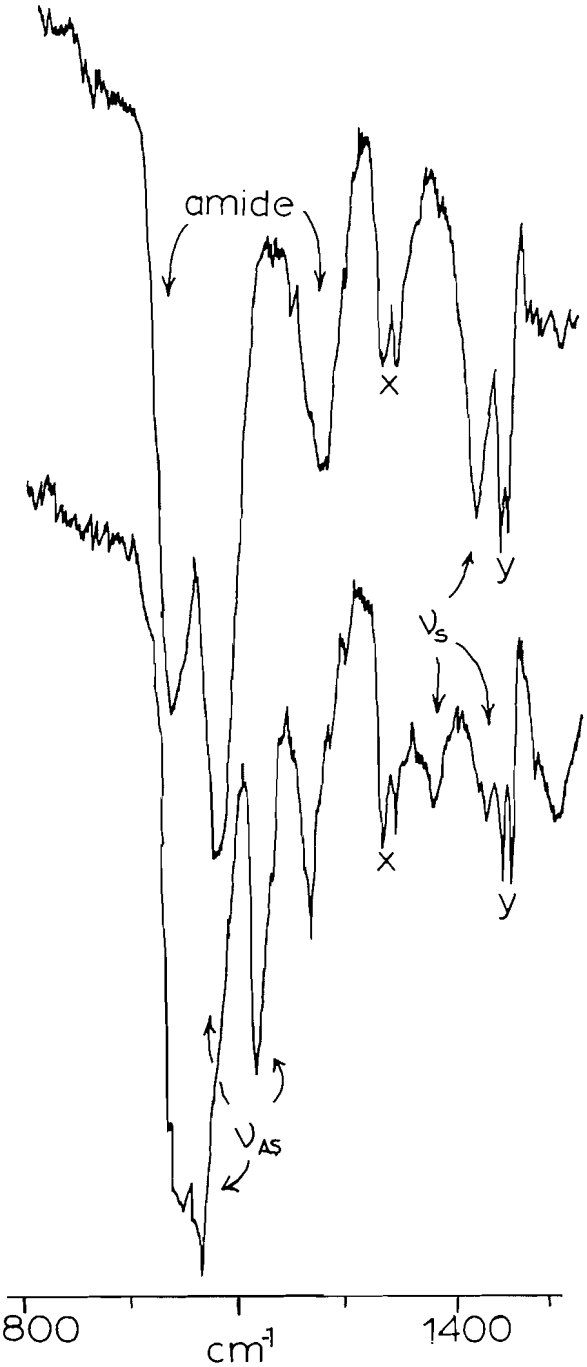

FIG. 2. Infrared spectra of carriers and complexes in chloroform solution (5×10^{-2} *M*). Upper Curve, 4NH18-6 Na; lower curve, $(4NH18\text{-}6)_2Ca$.

The type A interaction will increase ν_{AS} toward the frequency of a C=O group while the ν_S will fall towards the frequency of a C—O group (25). As a consequence $\Delta\nu = \nu_{AS} - \nu_S$ will measure the asymmetry of the interaction; $\Delta\nu$ larger than 225 cm^{-1} is characteristic of a tight ion pair of type A geometry (25) while values of $\Delta\nu$ lower than 225 cm^{-1} indicate a looser ionic interaction, either of the type B geometry or a solvent-separated ion pair (25).

The key bands are shown in Fig. 2. The free acid 4NH18-6A shows bands at 1755 (CO_2H), 1670, and 1530 cm^{-1} (amide I and II) and a pair of bands marked x and y due to —CH_2— groups in the molecule. Formation of the sodium salt

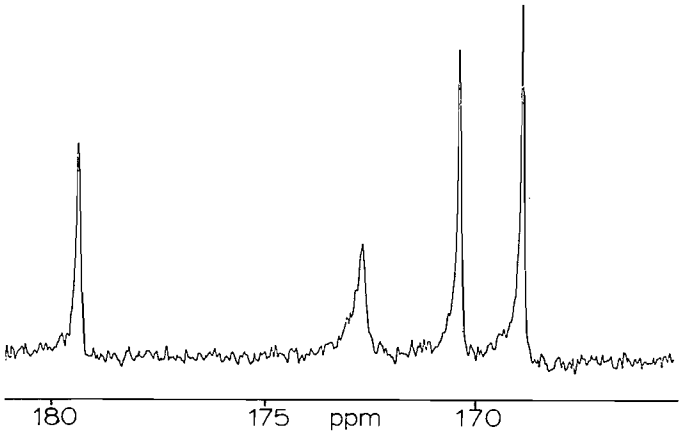

FIG. 3. Carbonyl region of the ^{13}C nmr spectrum of $(4NH18\text{-}6)_2Ca$.

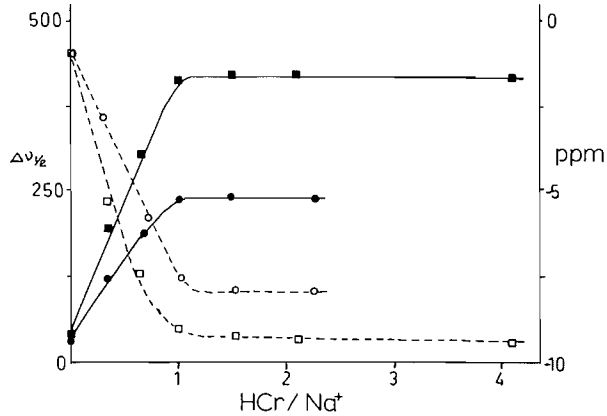

FIG. 4. ^{23}Na chemical shift (dashed lines) and linewidth ($\Delta\nu_{1/2}$) (solid lines) as a function of added 4NH18-6A. $[Na^+] = 5 \times 10^{-2}$ *M* in CD_3OD/H_2O (90:10 v/v); circles, pH* = 2.0 (HCl); squares pH* = 8.0 (Tris).

4NH18-6A Na results in a shift of the principal carboxylate band to 1625 cm^{-1} in the range typical of ν_{AS}. The two amide bands, and x and y, are unaffected and leave only a weak band at 1385 cm^{-1} assigned as ν_S. The value of $\Delta\nu$ = 240 cm^{-1} suggests an asymmetric, type A ion pair. More importantly, the calcium salt $(4NH18\text{-}6A)_2Ca$ shows two sets of carboxylate bands: ν_{AS} at 1635 and 1585 cm^{-1} and ν_S at 1430 and 1380 cm^{-1}. The pair of bands which resemble the sodium salt have $\Delta\nu$ = 255 cm^{-1} while the remaining pair give $\Delta\nu$ = 1585 − 1430 = 155 cm^{-1}. The two distinct sets of carboxylate bands suggest two different metal–carboxylate interactions; one, like the sodium salt of the asymmetric tight ion-pair type and the other, a looser or symmetrical ion pair (type B).

Both the ^1H and ^{13}C nmr spectra of $(4NH18\text{-}6A)_2Ca$ show two sets of resonances for two distinctly different types of ligand within the complex. As an example, Fig. 3 shows the carbonyl region of the ^{13}C nmr spectrum of $(4NH18\text{-}6A)_2Ca$ showing four carbonyl resonances (two amide and two carboxylate). In a wide range of ligands and complexes the amide resonances occur at 170 ± 1 ppm and for simple salts the carboxylate resonances occur at 172 ± 3 ppm. The carboxylate resonance is typically broadened, possibly due to interaction with the metal ion nuclear quadrupole. In Fig. 3 the sharp resonance at 179.5 ppm is anomalous for the range of complexes examined and is presumed to be the type B or loosely bound carboxylate.

Taken together, these results suggest that $(4NH18\text{-}6)_2Ca$ exists as a dimer with the metal ion occupying one of the two crown ether rings and bound in a tight ion pair with the carboxylate of that ring. The second carboxylate is more loosely coordinated and the macrocycle of that carboxylate is empty. From the transport studies conducted, the normal transport of calcium by 4NH18-6A may be disrupted in the presence of extractible anions such as picrate or 1-naphthylacetate. As judged by infrared and nmr, 14NH18-6 and its calcium salt are strongly similar to the 4NH18-6A case discussed above. However, extraction of calcium into $CDCl_3$ from solutions containing picrate gave a different type of complex containing 1:1 picrate–14NH18-6 by integration. The ligand present was of the asymmetrical ion-pair type characterized by high ν_{AS} and a broadened carbonyl resonance in the ^{13}C nmr. The loosely bound macrocycle has evidently been exchanged for the picrate anion as an additional counterion in the ternary complex.

Cation binding in the remaining complexes can be compared with one or the other of the two modes identified with $(4NH18\text{-}6)_2Ca$: asymmetric, tight ion pair ν_{AS} ~ 1630 cm^{-1} and broad carbonyl resonance ~ 172 ppm; or symmetric, loose ion pair ν_{AS} ~ 1580 cm^{-1} and sharp carbonyl resonance ~ 180 ppm. By these criteria the majority of the salts prepared (listed in Experimental) and are tightly ion-paired in chloroform solution. Exceptions are $D_2$18-6 Ca and 18-6 Ca, which presumably cannot allow close contact of both carboxylates simultaneously. Consequently, at least one carboxylate is only loosely bound to the metal ion.

The symmetry of ion binding with respect to the metal ion may be assessed by direct nmr observation of a complexed ion; of the group I and II cations the most convenient is sodium (^{23}Na, I = 3/2, 100% abundance). Sodium nmr has been used to probe solvation and complexation of sodium by synthetic and naturally occurring ionophores (26–29). The relaxation of the ^{23}Na nucleus, hence the linewidth of the resonance, is dominated by the interaction of the nuclear quadrupole moment with the electric field gradient at the nucleus. In a symmetric environment, the quadrupole coupling constant will be low and the linewidth will be narrow; as the asymmetry of the environment increases, the linewidth will increase proportionately. The sodium chemical shift is also sensitive to complexation and the upfield shift of the sodium resonance line on addition of complexing agents can be used to determine complex stability constants (29).

Figure 4 shows the evolution of ^{23}Na chemical shift and peak width at half maximum for the addition of 4NH18-6A to sodium chloride in $CD_3OD–H_2O$ (90:10) containing excess acid or base. Considering the chemical shift data, the complex is virtually completely formed after the addition of one equivalent of 4NH18-6 in either acidic or basic solution. The complexation shifts are comparable and indicate roughly the same shielding electron density, hence roughly the same coordination at the sodium nucleus in both acidic and basic solution. The linewidth parameter, however, shows a larger difference between acidic and basic complexation; the limiting $\Delta\nu_{1/2}$ values are 425 Hz for the basic case and 230 Hz for the acidic case. It is clear that the deprotonation increases the asymmetry of the environment about the sodium ion. The values of $\Delta\nu_{1/2}$ for other crown ether complexes in methanol are in the range 200–250 Hz (28, 29) which presumably is typical of a complex with the sodium ion near the center of the macrocycle and axially ion-paired with a counter ion (28). Since the value observed for acidic 4NH18-6A is in this range, it is likely that the carrier is simply behaving as other crown ethers. The basic complex is more

Can. J. Chem. Downloaded from www.nrcresearchpress.com by 210.87.254.40 on 09/06/12
For personal use only.

Can. J. Chem. Downloaded from www.nrcresearchpress.com by 210.87.254.40 on 09/06/12
For personal use only.

closely similar to the antibiotics nigericin and monensin which have carboxylates as donor sites for sodium complexation ($\Delta\nu_{1/2} > 300$ Hz) (ref. 28). A shift of position of the metal ion within the macrocycle towards the carboxylate on deprotonation is a plausible explanation for the differences noted in the ^{23}Na nmr experiments and is completely consistent with the infrared experiments described above.

Conformations of identifiable structural fragments

In principle, ^{1}H nmr provides a powerful method for the determination of the conformations of the carriers and their complexes but, in practice, the spectra obtained are highly overlapped in the regions of interest and provide relatively little information. Nonetheless, certain structural fragments may be identified which permit a general picture to be built up from results at a variety of temperatures and concentrations and by careful comparisons between the carriers and their salts. The experimental section outlines the range of cases examined.

The most readily observable unit is the —CHX—CHY— unit derived from tartaric acid in various carriers where X and Y are the amide and carboxylate groups. Vicinal coupling constants for all carriers are typically 2–3 Hz. Binding of metal ions results in some slight broadening of the resonances and a clear shift to smaller vicinal coupling constant (<1 Hz); many salts exhibit only singlets for the methine resonances. The small coupling constant is consistent with a diaxial conformation of the amide and carboxyl groups as noted in X-ray crystal structures (19, 20) and by nmr (18, 19) of related derivatives. The shift to smaller coupling constant on ion complexation could represent a shift of equilibrium from a minor diequatorial conformer (18) or a decrease in the O—CHX—CHY—O dihedral angle to produce a HCCH dihedral angle near to 90°. In view of the requirement that the carboxylate be ion-paired with the metal ion, which probably will involve distortion, the latter possibility is appealing.

Variation of the temperature results in general changes in the ^{1}H nmr spectra of carriers and complexes but few of the changes are well-defined. The ring protons in particular broaden and shift somewhat in chemical shift as the temperature is lowered but no clearly defined limit is attained. The most clearly defined changes are noted with the 1° amide groups. At high temperatures (>35°C), the methylenes adjacent to the amide appear as a broad quartet. On cooling, this collapses to a multiplet which separates further on cooling to a pair of multiplets. This is attributed to the onset of slow exchange between *cis* and *trans* conformations of the amide. Infrared spectra show the amide N—H to be hydrogen bonded over a range of concentration. An intermolecular hydrogen bond would be expected to show a concentration or temperature dependence of the NH chemical shift in the ^{1}H nmr spectrum. Over a wide range of solvents, concentrations, and conditions the NH singal is virtually invariant suggesting that the hydrogen bond is intramolecular. Hydrogen bonding of the amide hydrogen to the adjacent ether oxygen (bent 5-membered ring) has been inferred from the crystal structures of *syn* and *anti* dianilide crown ethers (19) and it is reasonable to propose that this structure is retained in solution as a general feature throughout the series examined.

The conformational possibilities for the ethylenedioxy fragments have been described for simple crown ethers as deduced from crystal structures, nmr, and force-field calculations (30–32). In general, these units adopt conformations with a *gauche* relationship between the oxygens although distortions are common. As a closely related example, the *syn* dianilide crown ether adopts an all-*gauche* arrangement in the solid state but the *anti* isomer contains two eclipsed fragments (19). A recurring feature of many variable temperature spectra is the appearance of a broad triplet downfield of the main CH_2O multiplets. This is shown in Fig. 5 for the case of *anti* $(8NH)_2$18-6Ca. Decoupling experiments establish that the downfield feature is coupled to a multiplet on the upfield edge of the CH_2O multiplet; the downfield signal consists of two large couplings (10 and 12 Hz) plus smaller couplings (~2 Hz) while the upfield signal contains the 12 Hz coupling plus smaller couplings (2 × 2 Hz). With reference to the *gauche* ethylenedioxy fragment pictured in Fig. 5, the coupling pattern observed is the one expected for the geminal pair H_a, H_b. Pseudoaxial H_a shows two large couplings ($J_{ab} \sim 12$ Hz, $J_{ad} \sim 10$ Hz) with a smaller coupling J_{ac}, while the equatorial proton H_b shows one large coupling (J_{ab}) with two smaller coupling ($J_{bc} \sim J_{bd} \sim 2$ Hz). Integration shows the downfield signal to be only one of the sixteen ring protons. This is tentatively identified as one axial proton in the shielding region of the acid carbonyl; the bent hydrogen bonding of the NH rigidifies the amide CH—OCH unit and brings one of the ring protons into the shielding zone of the carbonyl. If this is the case, the overall conformation of the macrocycle must be restricted to one major conformer only at one "end" of the macrocycle; the other end is unconstrained. The features discussed with particular reference to *anti* $(8NH)_2$18-6Ca may be identified in most of the other spectra but are usually less well defined. The conclusion which may be drawn is that essentially all the cases examined exhibit the same overall conformation.

The samples examined typically contained small amounts of water, usually less than one molar equivalent. Completely anhydrous samples were prepared in some cases which exhibited the same behaviour as did slightly more hydrated samples. The only exception found was *anti* $(8NH)_2$18-6A_2 and its salts, shown in Fig. 5 for a partly hydrated sample. Samples with excess water failed to show the downfield multiplet described above and had a markedly different overall lineshape for the CH_2O multiplets. It may therefore be suggested that the conclusions drawn above refer to a conformation which requires some small amount of additional water for stabilization. A further discussion of the role of hydration by bulk water is given below.

Degree of aggregration

The carriers and their salts are amphiphilic molecules and might be expected to form aggregrated species in solution. As the acid, dimerization might occur but is somewhat improbable due to unfavourable steric factors. Infrared spectra of various carriers at concentrations up to 10^{-1} *M* failed to indicate any dimerization (2650 cm^{-1}, 920 cm^{-1} dimer bands) (24, 25). This result is consistent with kinetic studies (8, 10) where the rate is a first order process in carrier; higher nonintegral orders would be expected for aggregrated species.

Aggregration of the complexes might occur to form reversed micelles within the chloroform phase during the transport. The general phenomenon of aggregation may be followed by observation of a discontinuity in some parameter as a function of concentration (33). A convenient probe for ionophores is the dependence of proton spin-lattice relaxation times (T_1) on concentration. This technique has been used to probe dimerization of acids (34), micellization of phospholipids (35), and aggregation of calcium ionophores (36). On a qualitative level, a

TABLE 2. Selected spin-lattice relaxation times for carboxylate crown ethers[a]

Carrier	Ring methine	Ring methylene	Amide N—CH_2	Chain methylene	Chain methyl
4NH18-6A	1.1	0.5	0.75	1.1	1.4
$(4NH18\text{-}6)_2Ca$	0.15	0.25	0.30	0.6	0.9
14NH18-6A	0.30	0.18	0.30	0.85	2.0
$D_218\text{-}6A_2$	0.40	0.23	—	0.8	1.9
$D_218\text{-}6Ca$	0.35	0.21	—	0.6	1.6
syn $(8NH)_218\text{-}6A_2$	0.36	0.19	0.30	0.9	1.7
anti $(8NH)_218\text{-}6A_2$	0.40	0.23	0.35	0.8	1.9
anti $(8NH)_218\text{-}6Ca$	0.40	0.17	0.23	0.75	1.7

[a]In s^{-1} determined in $CDCl_3$ at 25°C, values reported are averages obtained at different concentrations and for different portions of the multiplet when more than one proton is involved. Ranges: methines ± 0.05, ring methylenes ± 0.04, chain methylenes ± 0.1.

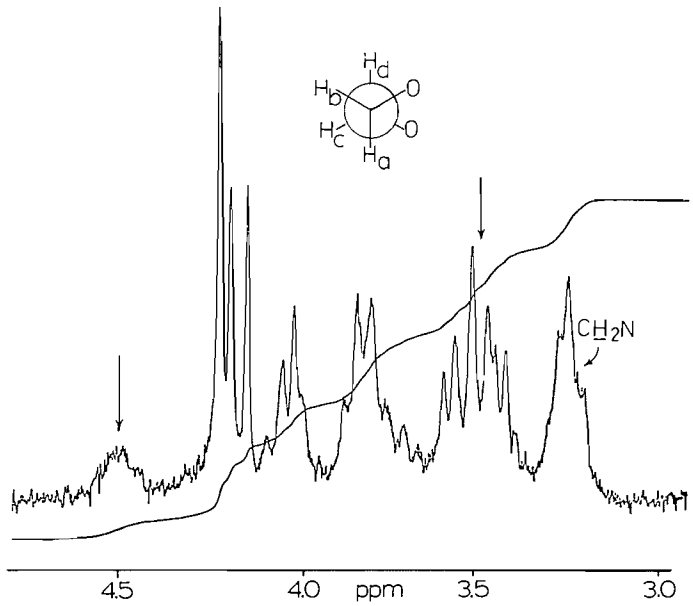

FIG. 5. Ring proton region of the ^1H nmr spectrum of *anti* $(8NH)_218\text{-}6A_2$ in $CDCl_3$ at 25°C. Arrows indicate mutually coupled upfield and downfield multiplets.

freely diffusing, rotating molecule in solution will be characterized by a set of T_1's which would be expected to dramatically diminish as association occurs to provide a larger aggregate with a longer correlation time. Typical values for the carriers are given in Table 2 and, in general, confirm that the carriers behave as surfactants. The head group and closely held protons have short T_1's which gradually lengthen along the hydrocarbon tail (35).

The data reported apply over a range of concentration from 10^{-3} to 10^{-4} *M*; throughout this range the values vary slightly but there are no discontinuities. Minor effects are noted in changing an acid to its salt, which probably reflect changes in overall conformation. The general conclusion is that aggregation is unimportant for these complexes under the transport conditions. The one case where dimerization is clearly evident from other data, namely $(4NH18\text{-}6)_2Ca$, is the one case where the T_1's differ substantially from the free acid to the complex. The change is very marked, indicating that this technique would be sufficient to detect any aggregation had it occurred.

Effect of hydration

Water is soluble in chloroform to the extent of about 5×10^{-3} *M* at equilibrium, hence under the transport conditions there is an excess of water available in the membrane phase. Salts of the carriers are readily prepared by extraction of the cation from basic aqueous solutions (9). The amount of extracted water may be determined by integration of the proton nmr spectrum of these extraction solutions. The metal salts of the carriers apparently enhance the solubility of water in the chloroform; typically a solution of carrier salt (1×10^{-3} *M*) contains a tenfold excess of water (1×10^{-2} *M* H_2O). It is likely that this additional water is associated with the crown ether and the metal ion and provides additional ligation. With one exception, these water saturated solutions are identical with samples prepared with minimal amounts of water (above), thus the additional water does not perturb the conformational preferences deduced. The principal exception is *anti* $(8NH)_218\text{-}6A_2$ and its salts, which give variable spectra which depend on the amount of water present. The solid state structure shows both carboxylates closely coordinated to the central cation (19) which results in ring distortions. As the amount of water increases, the necessity for ion-pairing is relaxed, water molecules can take up the role of metal ligation and carboxylate stabilization, and the macrocycle can relax to the more stable all-*gauche* arrangement of ethylenedioxy units.

Summary of solution structures

Taken together, the experiments described above lead to a relatively simple picture of the solution structures of the carriers and their complexes. The solution species are monomeric but will have some associated water under the conditions of the membrane experiment. The crown ether portion adopts a single predominant conformation incorporating at least four sets of *gauche* OCCO fragments, axially disposed groups at the tartrate derived positions, and, when amides are present, an intramolecular N—H hydrogen bond possibly within a 5-membered ring. When required by stoichiometry, dimeric complexes form in which the metal ion occupies one macrocycle while the other carrier provides a liposoluble counterion which may be exchanged for another counterion such as picrate. In all the complexes the carboxylate forms an asymmetric contact ion pair with the metal ion in the macrocycle. It is encouraging to note that this simple picture is essentially the one considered at the design stage of the project (6) based on simple extrapolations from previous data on crown ether complexes, stability constants, and X-ray crystal structures.

Experimental

The syntheses, purification, and characterization of carriers were previously described (6, 9). All samples were purified just prior to use and were pumped at high vacuum to remove volatile impurities. An-

Can. J. Chem. Downloaded from www.nrcresearchpress.com by 210.87.254.40 on 09/06/12
For personal use only.

hydrous samples were prepared by drying the material at 80°C and 0.1 Torr over P_2O_5 for 16 h.

Stability constant determinations

The general procedures outlined previously for the determination of association constants from pH metric titration (6) were used in this study, but the apparatus consisted of a fully automatic titration system programmed for equilibrium aliquot titrations. The buret (Metrohm 655) and pH/mV meter (Metrohm 632) were linked to an HP85 microcomputer which controlled all functions of the buret. In one cycle of program control, the pH/mV data are examined until equilibrium is established in the cell, the buret volume and current cell potential are recorded, and the buret adds a further aliquot of titrant (typically 5 or 10 μL). The data file may be plotted, stored, printed, edited, and endpoints may be determined. The pH electrode (Metrohm EA 109) was conditioned for use in 90:10 v/v methanol–water. The reference electrode (Fisher calomel electrode) was linked to the cell via a porous plug salt bridge containing 0.1 *M* Me_4NCl. Standardization of pH*, procedures, and calculations utilizing the modified version of SCOGS (37) followed previously outlined procedures (6).

Infrared experiments

All infrared spectra were recorded using a Perkin–Elmer 283 infrared spectrometer and the spectral calibration was checked with polystyrene. Solution spectra in $CHCl_3$ were recorded using matched KBr cells with 0.1 or 0.5-mm path lengths. The discussion in the text summarizes the following set of carriers and counterions: 4NH18-6A, Li, Na, K, Ca, Ba; 14NH18-6A, K, Ca; 18-6A_2, Ca; $D_2$18-6A_2, Ca; *syn* and *anti* $(8NH)_2$18-6A_2, Ca, Sr, Ba.

Nuclear magnetic resonance experiments

All spectra were recorded on a Bruker WM 250 spectrometer at 250 MHz for ^1H, 62.84 MHz for ^{13}C, and 66.16 MHz for ^{23}Na. Spectral data are relative to TMS (^1H, ^{13}C) or external 3 *M* NaCl in water (^{23}Na). The temperature controller was calibrated using a methanol–water standard. All samples involving consideration of linewidths, for relaxation measurement, and for ^{23}Na experiments were degassed immediately prior to recording the spectra. Spin-lattice relaxation times were determined by inversion recovery and calculated using an integral program of the WM 250. The conclusions drawn in the text summarize the following set of experiments.

^1H in $CDCl_3$: 18NH15-5A, K, Ca; 4NH18-6A (VT, T_1), Na (VT), K (VT, T_1), Ca (VT, T_1), Ba (VT, T_1), 1/2 equiv. KPF_6 (VT), excess KPF_6 (VT); 14NH18-6A (T_1), Na, K, Ca; 18-6A_2 (T_1, VT), Ca (T_1, VT); $D_2$18-6A_2 (T_1, VT), Ca (T_1, VT); *syn* $(8NH)_2$18-6A_2 (T_1, VT), Ca + 10% CD_3OD; *anti* $(8NH)_2$18-6A_2 (T_1, VT), Ca (VT, T_1) Sr, Ba; D_2TA$_2$, Ca (VT).

^{13}C in $CDCl_3$: 4NH18-6A, Na, K, Ca, Ba; ^{14}NH18-6A, K, Ca; $D_2$18-6A_2, Ca; *syn* $(8NH)_2$18-6A_2, Ca, Ba; *anti* $(8NH)_2$18-6A_2, Ca, Sr, Ba.

^{23}Na in CD_3OD: H_2O (90:10 v/v): 4NH18-6A + NaCl.

Extraction from basic aqueous buffers ^1H and ^{13}C: no carrier, 14NH18-6A, Na, Ca, Ca + picrate, Sr, Ba; 18NH15-5A, K, Ca, Ca + 1-naphthylacetate; $D_2$18-6A_2, Ca; *syn* $(8NH)_2$18-6A_2, K, Ca; *anti* $(8NH)_2$18-6A_2, K, Ca, Sr.

Concentration dependence 10^{-1} to 10^{-5} *M* (^1H) and 10^{-1} to 10^{-3} *M* (^{13}C): 4NH18-6A, K, Ca; 14NH18-6A, K, Ca; *anti* $(8NH)_2$18-6A_2, Ca.

Acknowledgements

We wish to thank the Natural Sciences and Engineering Research Council of Canada for continued support of membrane transport studies.

1. R. M. IZATT and J. J. CHRISTENSEN (*Editors*). Progress in macrocyclic chemistry. Vol. 1. Wiley–Interscience, New York. 1979.
2. F. VOGTLE. Top. Curr. Chem. **98** and **101** (1981).
3. G. W. GOKEL and S. H. KORZENIOWSKI. Macrocyclic polyether synthesis. Springer-Verlag, New York. 1982.
4. E. V. DEHMLOW and S. S. DEHMLOW. Phase transfer catalysis, Verlag-Chemie, Weinheim. 1980.
5. C. F. REUSCH and E. L. CUSSLER. AIChE J. **19**, 736 (1973).
6. L. A. FREDERICK, T. M. FYLES, N. P. GURPRASAD, and D. M. WHITFIELD. Can. J. Chem. **59**, 1724 (1981).
7. T. M. FYLES, V. A. MALIK-DIEMER, and D. M. WHITFIELD. Can. J. Chem. **59**, 1734 (1981).
8. T. M. FYLES, V. A. MALIK-DIEMER, C. A. MCGAVIN, and D. M. WHITFIELD. Can. J. Chem. **60**, 2259 (1982).
9. T. M. FYLES, C. A. MCGAVIN, and D. M. WHITFIELD. In press.
10. L. M. DULYEA, T. M. FYLES, and D. M. WHITFIELD. Can. J. Chem. **62**, 000 (1984).
11. E. L. CUSSLER. AIChE J. **17**, 1300 (1971).
12. W. C. BABCOCK, R. W. BAKER, E. D. LACHAPELLE, and K. L. SMITH. J. Membr. Sci. **7**, 71 (1980).
13. J. STRZELBICKI and W. CHAREWICZ. J. Inorg. Nucl. Chem. **40**, 1415 (1978).
14. T. KATAOKA, T. NISHIKI, and K. UEYAMA. Bull. Chem. Soc. Jpn. **55**, 1306 (1982).
15. B. DIETRICH, D. L. FYLES, T. M. FYLES, and J. M. LEHN. Helv. Chim. Acta, **62**, 2763 (1979).
16. J. GREENSPAN. Chem. Rev. **12**, 339 (1933).
17. J. G. KIRKWOOD and F. H. WESTHEIMER. J. Chem. Phys. **6**, 506 (1938).
18. J. P. BEHR, J. M. GIRODEAU, R. C. HAYWARD, J. M. LEHN, and J. P. SAUVAGE. Helv. Chim. Acta, **63**, 2096 (1980).
19. J. P. BEHR, J. M. LEHN, D. MORAS, and J. C. THIERRY. J. Am. Chem. Soc. **103**, 701 (1981).
20. J. J. DALY, P. SCHONHOLZER, J. P. BEHR, and J. M. LEHN. Helv. Chim. Acta, **64**, 1444 (1981).
21. H. DUGAS and M. PTAK. J. Chem. Soc. Chem. Commun. 710 (1982).
22. J. ASCENSO and V. M. S. GIL. Can. J. Chem. **58**, 1376 (1980).
23. R. M. IZATT, R. E. TERRY, B. L. HAYMORE, L. D. HANSEN, N. K. DALLEY, A. G. AVONDET, and J. J. CHRISTENSEN. J. Am. Chem. Soc. **98**, 7620 (1976).
24. R. M. SILVERSTEIN, G. C. BASSLER, and T. C. MORELL. Spectrometric identification of organic compounds. 3rd ed. J. Wiley and Sons, New York. 1974. pp. 99–102.
25. D. T. SAWYER and P. J. PAULSEN. J. Am. Chem. Soc. **81**, 819 (1959).
26. L. LEVY, M. MUZZI, and H. D. HURWITZ. J. Chem. Soc. Faraday Trans. 1, **78**, 1011 (1982).
27. J. BOUQUANT, A. DEVILLE, J. GRANDJEAU, and P. LASZLO. J. Am. Chem. Soc. **104**, 686 (1982).
28. D. C. HAYNES, B. C. PRESSMAN, and A. KOWALSKY. Biochemistry, **10**, 852 (1971).
29. A. KAIFER, H. D. DURST, L. ECHEGOYEN, D. M. DISHONG, R. A. SCHULTZ, and G. W. GOKEL. J. Org. Chem. **47**, 3195 (1982).
30. M. DOBLER. Ionophores and their structures. Wiley–Interscience, New York. 1981.
31. J. DALE. Isr. J. Chem. **20**, 3 (1980).
32. G. WIPFF, P. WEINER, and P. KOLLMAN. J. Am. Chem. Soc. **104**, 3249 (1982).
33. J. H. FENDLER. Membrane mimetic chemistry. Wiley–Interscience, New York. 1982.
34. G. C. LEVY and D. TERPSTRA. Org. Magn. Reson. **8**, 658 (1976).
35. N. M. J. BIRDSALL, A. G. LEE, Y. K. LEVINE, and J. C. METCALFE. J. Chem. Soc. Chem. Commun. 1171 (1971).
36. C. M. DUBBER and D. R. PFEIFFER. Biochemistry, **15**, 132 (1976).
37. I. G. SAYCE. Talanta, **15**, 1397 (1968); **18**, 653 (1971).

Can. J. Chem. Downloaded from www.nrcresearchpress.com by 210.87.254.40 on 09/06/12
For personal use only.

Structural studies of organoboron compounds. XIX.[1] 1,7-Dimethyl-3,5-diphenyl-2,4,6-trioxa-7-aza-1-azonia-3-bora-5-boratabicyclo[3.3.0]octane

WOLFGANG KLIEGEL

Institut für Pharmazeutische Chemie, der Technischen Universität Braunschweig, 3300 Braunschweig, Beethovenstraße 55, Bundesrepublik Deutschland

AND

STEVEN J. RETTIG AND JAMES TROTTER

Department of Chemistry, University of British Columbia, 2036 Main Mall, Vancouver, B.C. V6T 1Y6

Received July 25, 1983

WOLFGANG KLIEGEL, STEVEN J. RETTIG, and JAMES TROTTER. Can. J. Chem. **62**, 515 (1984).

Crystals of 1,7-dimethyl-3,5-diphenyl-2,4,6-trioxa-7-aza-1-azonia-3-bora-5-boratabicyclo[3.3.0]octane are triclinic, a = 10.559(2), b = 15.156(3), c = 10.338(2) Å, α = 99.14(1), β = 89.90(1), γ = 96.73(1)°, Z = 4, space group $P\bar{1}$. The structure was solved by direct methods and was refined by full-matrix least-squares procedures to R = 0.032 and R_w = 0.038 for 2396 reflections with $I \geq 3\sigma(I)$. The structure consists of two crystallographically independent, but virtually identical, molecules containing sterically lengthened N—B coordinative bonds (mean 1.740(3) Å). The structurally inequivalent (in the solid state) pairs of N-methyl and B-phenyl groups are observed by variable temperature ^{1}H nmr to be magnetically equivalent in solution, implying a rapid interconversion of "valence tautomers" at temperatures down to −60°C.

WOLFGANG KLIEGEL, STEVEN J. RETTIG et JAMES TROTTER. Can. J. Chem. **62**, 515 (1984).

Les cristaux de diméthyl-1,7 diphényl-3,5 trioxa-2,4,6-aza-7 azonia-1 bora-3 borata-5 bicyclo[3.3.0] octane sont tricliniques, a = 10,559(2), b = 15,156(3), c = 10,338(2) Å, α = 99,14(1), β = 89,90(1), γ = 96,73(1)°, Z = 4, groupe d'espace $P\bar{1}$. On a résolu la structure par des méthodes directes et on l'a affinée par la méthode des moindres carrés (matrice complète) jusqu'à des valeurs de R = 0,032 et R_w = 0.038 pour 2396 réflexions avec $I \geq 3\sigma(I)$. La structure comprend deux molécules qui sont cristallographiquement indépendantes mais qui sont pratiquement identiques; elles comportent des liaisons coordinantes N—B qui sont stériquement allongées (valeur moyenne de 1,740(3) Å). Par rmn du proton à température variable, on peut observer que les paires de groupes *N*-méthyle et B-phényle, qui structuralement ne sont pas équivalents, sont équivalents en solution; ce résultat implique une interconversion rapide des "tautomères de valence" à des températures allant jusqu'à −60°C.

[Traduit par le journal]

Can. J. Chem. Downloaded from www.nrcresearchpress.com by 210.87.254.40 on 09/06/12
For personal use only.

Introduction

The condensation of phenylboronic acid, *N*-methylhydroxylamine, and formaldehyde leads to the isolation of a stable crystalline compound. Both the elemental analysis and spectroscopic data for this material indicate an eight-membered ring system, the structure of which could not be unambiguously determined (1). "Magnetic equivalence" of the identical functional groups in the molecule would correspond to the simple cyclocondensate **1**, to the strained tricyclooctane system **2** (containing a pair of transannular N—B coordinative bonds), or to the less strained dimer of **1** with the pentacyclohexadecane structure **3**.

In addition, the transannular mono-coordinated structure **4** had to be considered, at least in the solid state, by analogy to the very stable compounds possessing a bicyclo[3.3.0]octane structure such as **5** (2) and **6** (3, 4) or similar compounds such as **7** (5) and **8** (6). ^{1}H nmr spectra of $CDCl_3$ solutions of **4**, however, showed only one methyl and one phenyl signal, even at temperatures as low as −60°C.[2] The ^{11}B nmr spectrum as well indicated only one type of boron atom, which could not be clearly assigned to trigonal sp^2 or to tetrahedral sp^3 boron (1). This situation could arise from a temperature-dependent equilibrium between two virtually identical valence tautomers ("coordination topomers") **4** which would cause coalescence of the nmr signals (1). In order to determine unambiguously the solid state structure of this compound an X-ray crystallographic analysis was performed.

Experimental

*1,7-Dimethyl-3,5-diphenyl-2,4,6-trioxa-7-aza-1-azonia-3-bora-5-boratabicyclo[3.3.0]octane, **4***

The compound was prepared by reported (1) methods. Suitable crystals were obtained by recrystallization from benzene/petroleum ether, mp 179–181°C. ^{1}H nmr (400 MHz, $CDCl_3$/TMS) δ (ppm) at 0, −10, −20, −30, and −40°C without change: 2.70 (s, $2CH_3$), 3.77 (s, N—CH_2—N), 7.37 (m, 6 phenyl-H, *meta* and *para*), 7.79 (d, 2 phenyl-H, *ortho*); at −60°C: 2.70 (s, $2CH_3$), 3.88 (s, N—CH_2—N), 7.37 (m, 6 phenyl-H, *meta* and *para*), 7.79 (d, 2 phenyl-H, *ortho*).

X-ray crystallographic analysis

A crystal bounded by the six faces (followed by their distances in mm from a common origin): ±(0 1 0), 0.05, ±(0 1 −1), 0.13, ±(3 0 1), 0.18 was mounted in a general orientation. Unit-cell parameters were refined by least-squares on 2 sin θ/λ values for 25 reflections (2θ = 25–36°) measured on a diffractometer with Mo-Kα_1 radiation (λ = 0.70903 Å). Crystal data at 22°C are:

$C_{15}H_{18}B_2N_2O_3$ fw = 295.94

Triclinic, a = 10.559(2), b = 15.156(3), c = 10.338(2) Å, α = 99.14(1), β = 89.90(1), γ = 96.73(1)°, V = 1621.9(5) Å^3, Z = 4, ρ_c = 1.212 g cm^{-3}, $F(000)$ = 624, μ(Mo-Kα) = 0.77 cm^{-1}. Absent reflections: none, space group $P\bar{1}$ (C_i^1, No. 2, reduced cell) from structure analysis.

Intensities were measured with graphite-monochromated Mo-Kα radiation (λ = 0.71073 Å) on an Enraf-Nonius CAD4-F diffractometer. An ω–2θ scan at 0.57–6.71° min^{-1} over a range of (0.55 + 0.35 tan θ) deg in ω (extended by 25% on both sides for background measurement) was employed. Data were measured to 2θ = 55°. The

[1] Part XVIII: ref. 14.

[2] See Experimental section for low temperature ^{1}H nmr data, further information in ref. 1.

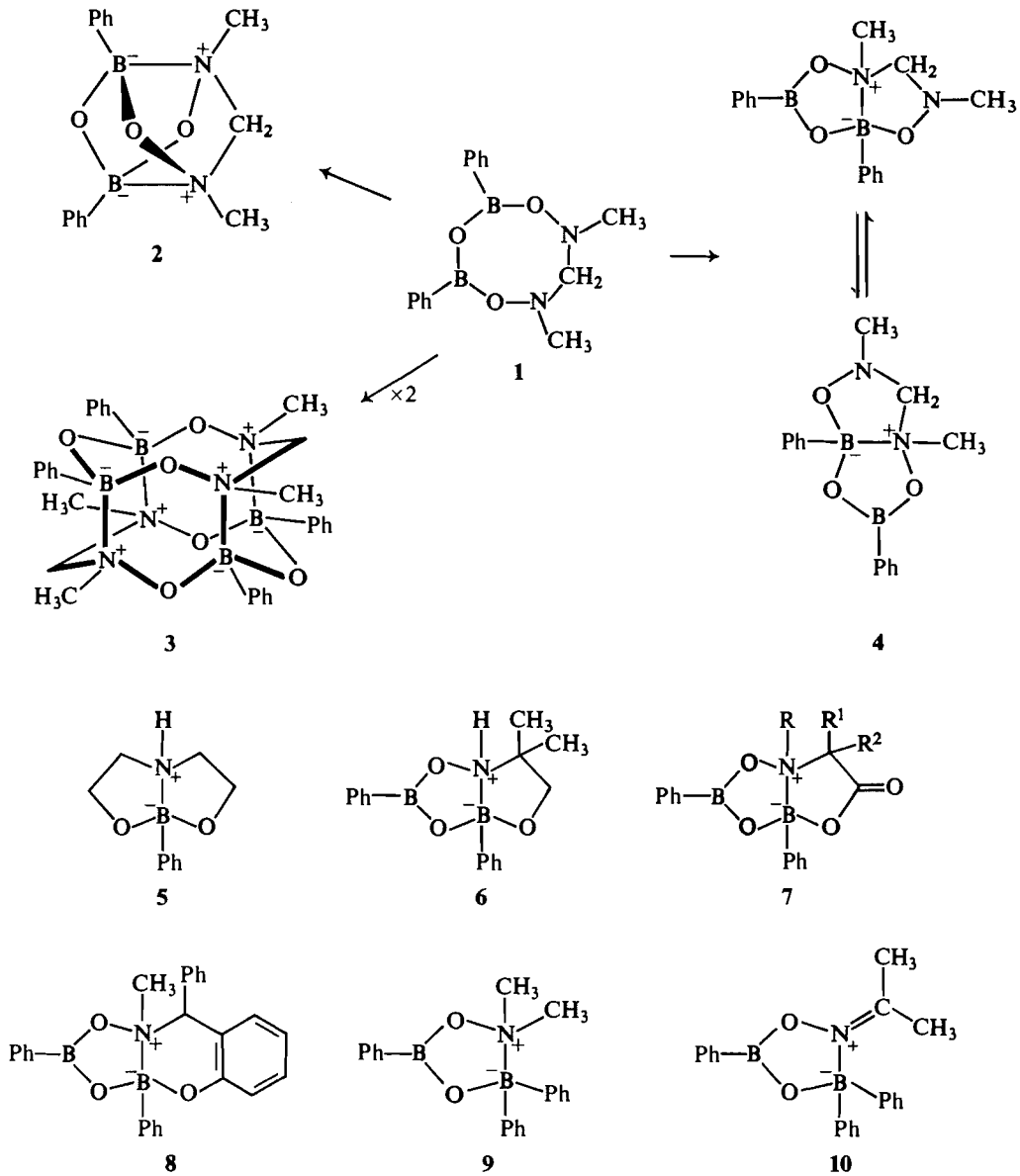

intensities of three check reflections, measured every 3600 s throughout the data collection, remained constant to within ±3.5%. Of the 7417 independent reflections measured and processed,[3] 2396 (32.3%) had intensities greater than $3\sigma(I)$ above background where $\sigma^2(I) = S + 2B + (0.04(S - B))^2$ with S = scan count and B = normalized background count.

The structure was solved by direct methods in the centrosymmetric space group $P\bar{1}$ which was strongly indicated by the E-statistics, the coordinates of all non-hydrogen atoms being determined from an E-map. Full-matrix least-squares refinement of the non-hydrogen atoms with anisotropic thermal parameters reduced R to 0.103, at which point a difference map clearly revealed the positions of all hydrogen atoms. Due to the relatively small number of observed reflections, hydrogen atoms were included as fixed atoms in idealized positions (C(sp^2)—H = 0.97, C(sp^3)—H = 0.98 Å) in subsequent cycles of refinement. These positions and thermal parameters were readjusted after each least-squares cycle. The scattering factors of ref. 7 were used for non-hydrogen atoms and those of ref. 8 for hydrogen atoms. The weighting scheme, $w = 1/\sigma^2(F)$ where $\sigma^2(F)$ is derived from the previously defined $\sigma^2(I)$, gave uniform average values of $w(|F_o| - |F_c|)^2$ over ranges of both $|F_o|$ and $\sin\theta/\lambda$ and was employed in the final stages of refinement. Convergence was reached at $R = 0.032$ and $R_w = 0.038$ for 2396 reflections with $I \geq 3\sigma(I)$. For all 7417 reflections $R = 0.182$. The function minimized was $\Sigma w(|F_o| - |F_c|)^2$, $R = \Sigma||F_o| - |F_c||/\Sigma|F_o|$ and $R_w = (\Sigma w(|F_o| - |F_c|)^2/\Sigma w|F_o|^2)^{1/2}$.

On the final cycle of refinement the mean and maximum parameter shifts corresponded to 0.04 and 0.23σ, respectively. The mean error in an observation of unit weight was 1.678. A final difference map showed maximum fluctuations of ±0.12 e Å^{-3}. The final positional and thermal parameters appear in Tables 1 and 5,[4] respectively. Measured and calculated structure factors have been placed in the Depos-

[3] The computer programs used include locally written programs for data processing and locally modified versions of the following: MULTAN 80, multisolution program by P. Main, S. J. Fiske, S. E. Hull, L. Lessinger, G. Germain, J. P. Declercq, and M. M. Woolfson; ORFLS, full-matrix least-squares, and ORFFE, function and errors, by W. R. Busing, K. O. Martin and H. A. Levy; FORDAP, Patterson and Fourier syntheses, by A. Zalkin; ORTEP II, illustrations, by C. K. Johnson.

[4] The structure factor table, Table 5 (anisotropic thermal parameters) and other material mentioned in the text are available, at a nominal charge, from the Depository of Unpublished Data, CISTI, National Research Council of Canada, Ottawa, Canada K1A 0S2.

Can. J. Chem. Downloaded from www.nrcresearchpress.com by 210.87.254.40 on 09/06/12
For personal use only.

TABLE 1. Final positional (fractional × 10^4) and isotropic thermal parameters ($U \times 10^3$ Å^2) with estimated standard deviations in parentheses

Atom	x	y	z	U_{eq}*	Atom	x	y	z	U_{eq}*
O(1)	8173(2)	3183(1)	8304(2)	58	O(1′)	6940(2)	−2449(1)	1876(2)	62
O(2)	9179(2)	1280(1)	8905(2)	62	O(2′)	5394(2)	−2793(1)	4555(2)	67
O(3)	7249(1)	1858(1)	9215(1)	51	O(3′)	7545(2)	−2469(1)	4154(2)	56
N(1)	8792(2)	2614(1)	7283(2)	62	N(1′)	5927(2)	−3196(2)	1846(2)	70
N(2)	9529(2)	2242(1)	9171(2)	55	N(2′)	5419(2)	−2190(1)	3596(2)	61
C(1)	9974(3)	2532(2)	7934(3)	66	C(1′)	4880(3)	−2716(2)	2356(3)	76
C(2)	9018(3)	3123(2)	6204(3)	92	C(2′)	5713(4)	−3576(2)	465(3)	108
C(3)	10508(3)	2420(2)	10221(3)	74	C(3′)	4697(3)	−1445(2)	4145(3)	90
C(4)	7962(2)	3324(2)	10761(2)	52	C(4′)	7550(2)	−957(2)	3313(3)	54
C(5)	7539(3)	2955(2)	11849(3)	69	C(5′)	7983(3)	−449(2)	4489(3)	81
C(6)	7389(3)	3469(2)	13041(3)	88	C(6′)	8466(4)	454(2)	4589(3)	98
C(7)	7636(3)	4376(3)	13189(3)	97	C(7′)	8540(3)	853(2)	3487(4)	91
C(8)	8035(3)	4778(2)	12144(4)	97	C(8′)	8128(3)	365(2)	2322(3)	84
C(9)	8213(3)	4251(2)	10942(3)	77	C(9′)	7624(3)	−521(2)	2220(3)	66
C(10)	7204(3)	146(2)	8531(2)	53	C(10′)	6896(3)	−3606(2)	5713(2)	51
C(11)	7908(3)	−575(2)	8202(3)	73	C(11′)	5903(3)	−4145(2)	6178(3)	66
C(12)	7296(4)	−1449(2)	7888(3)	83	C(12′)	6113(4)	−4751(2)	6993(3)	85
C(13)	6003(4)	−1608(2)	7907(3)	87	C(13′)	7339(4)	−4826(2)	7366(3)	87
C(14)	5295(3)	−908(2)	8226(3)	95	C(14′)	8350(3)	−4299(2)	6935(3)	79
C(15)	5888(3)	−45(2)	8533(3)	72	C(15′)	8124(3)	−3692(2)	6109(2)	63
B(1)	8101(3)	2704(2)	9404(3)	50	B(1′)	7008(3)	−1987(2)	3203(3)	55
B(2)	7844(3)	1124(2)	8884(3)	51	B(2′)	6659(3)	−2935(2)	4780(3)	55

*U_{eq} = (1/3) trace U_{diag}.

TABLE 2. Bond lengths (Å) with estimated standard deviations in parentheses

	Length (Å)			Length (Å)	
Bond	Uncorr.	Corr.	Bond	Uncorr.	Corr.
O(1)—N(1)	1.458(2)	1.462	O(1′)—N(1′)	1.460(3)	1.464
O(1)—B(1)	1.440(3)	1.445	O(1′)—B(1′)	1.436(3)	1.442
O(2)—N(2)	1.444(2)	1.447	O(2′)—N(2′)	1.450(2)	1.451
O(2)—B(2)	1.402(3)	1.406	O(2′)—B(2′)	1.403(3)	1.409
O(3)—B(1)	1.464(3)	1.466	O(3′)—B(1′)	1.466(3)	1.469
O(3)—B(2)	1.339(3)	1.343	O(3′)—B(2′)	1.335(3)	1.338
N(1)—C(1)	1.447(3)	1.452	N(1′)—C(1′)	1.447(4)	1.453
N(1)—C(2)	1.459(3)	1.462	N(1′)—C(2′)	1.460(4)	1.462
N(2)—C(1)	1.475(3)	1.479	N(2′)—C(1′)	1.475(4)	1.481
N(2)—C(3)	1.472(3)	1.476	N(2′)—C(3′)	1.474(3)	1.478
N(2)—B(1)	1.736(3)	1.742	N(2′)—B(1′)	1.729(3)	1.737
C(4)—C(5)	1.385(3)	1.400	C(4′)—C(5′)	1.379(4)	1.392
C(4)—C(9)	1.382(3)	1.396	C(4′)—C(9′)	1.394(3)	1.407
C(4)—B(1)	1.577(4)	1.582	C(4′)—B(1′)	1.584(4)	1.589
C(5)—C(6)	1.369(4)	1.375	C(5′)—C(6′)	1.391(4)	1.397
C(6)—C(7)	1.353(4)	1.367	C(6′)—C(7′)	1.370(4)	1.384
C(7)—C(8)	1.365(4)	1.379	C(7′)—C(8′)	1.353(4)	1.366
C(8)—C(9)	1.391(4)	1.397	C(8′)—C(9′)	1.374(4)	1.379
C(10)—C(11)	1.390(3)	1.399	C(10′)—C(11′)	1.386(3)	1.399
C(10)—C(15)	1.386(4)	1.404	C(10′)—C(15′)	1.387(3)	1.396
C(10)—B(2)	1.543(4)	1.548	C(10′)—B(2′)	1.548(4)	1.554
C(11)—C(12)	1.394(4)	1.399	C(11′)—C(12′)	1.378(4)	1.384
C(12)—C(13)	1.359(4)	1.377	C(12′)—C(13′)	1.374(4)	1.383
C(13)—C(14)	1.367(4)	1.375	C(13′)—C(14′)	1.373(4)	1.386
C(14)—C(15)	1.371(4)	1.375	C(14′)—C(15′)	1.391(3)	1.398

itory of Unpublished Data.[4]

The ellipsoids of thermal motion for the non-hydrogen atoms are shown in Fig. 1. The thermal motion has been analysed in terms of the rigid-body modes of translation, libration, and screw motion (9). The rms standard error in the temperature factors σU_{ij} (derived from the least-squares analysis) is 0.0018 Å^2. For each of the two independent molecules analysis of the entire molecule indicated significant independent motion of the phenyl rings. The 7-atom BPh group and 12-atom group consisting of the bicyclo[3.3.0]octane backbone plus all atoms directly bonded to it were separately analysed (rms ΔU = 0.0024–0.0048 Å^2). The appropriate bond distances have been corrected for libration (9, 10), using shape parameters q^2 of 0.08 for all atoms involved. Corrected bond lengths appear in Table 2 along with the uncorrected values; corrected bond angles do not differ by more than 1σ from the uncorrected values given in Table 3. Intra-annular torsion angles defining the conformations of five-membered rings are

Can. J. Chem. Downloaded from www.nrcresearchpress.com by 210.87.254.40 on 09/06/12
For personal use only.

Can. J. Chem. Downloaded from www.nrcresearchpress.com by 210.87.254.40 on 09/06/12
For personal use only.

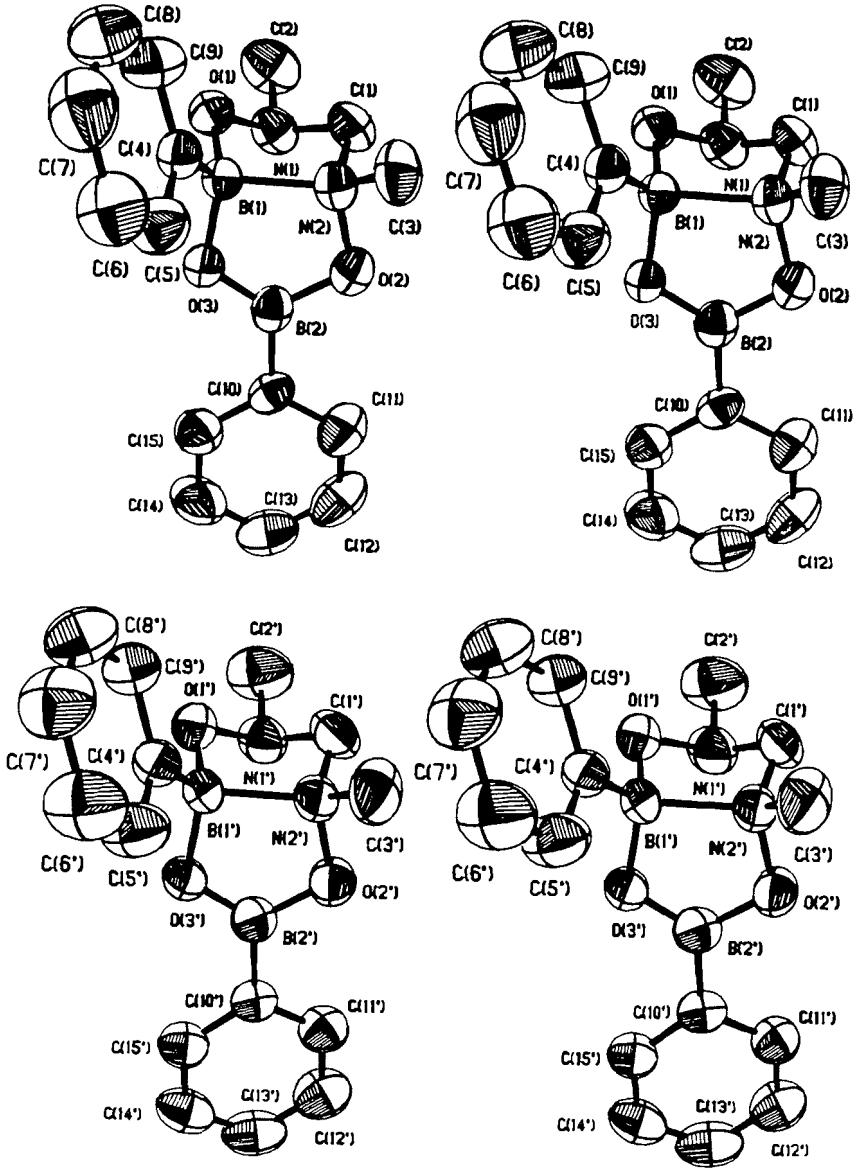

FIG. 1. Stereoscopic views of two independent 1,7-dimethyl-3,5-diphenyl-2,4,6-trioxa-7-aza-1-azonia-3-bora-5-boratabicyclo[3.3.0]octane molecules. 50% probability thermal ellipsoids are shown for the non-hydrogen atoms. The (1*S*,5*R*,7*S*) isomers are shown; for molecule B (primed labels) this is the mirror image of the molecule whose coordinates are presented in Table 1.

listed in Table 4. Calculated hydrogen coordinates and thermal parameters and a complete listing of torsion angles (Tables 6, 7) are included as supplementary material.

Results and discussion

The X-ray crystallographic analysis confirms the bicyclo[3.3.0]octane structure **4** in the solid state. In solution the compound must exist either as the cyclocondensate **1** or must undergo rapid interconversion between the two valence tautomers **4** in order to be consistent with the observed variable temperature ^{1}H nmr data. Based on the known structures and stabilities of the related molecules **5**–**8** (2–6), the latter situation seems most likely.

The centrosymmetric crystal structure of **4** contains equal numbers of (1*S*,5*R*,7*S*)- and (1*R*,5*S*,7*R*)-1,7-dimethyl-3,5-diphenyl-2,4,6-trioxa-7-aza-1-azonia-3-bora-5-boratabicyclo-[3.3.0]octane molecules, the former depicted in Fig. 1. The two crystallographically independent molecules which comprise the asymmetric unit are essentially equivalent, differing only slightly from one another in both the orientation of the B(2)-phenyl group and in the conformation of the BOBON ring. These small, but statistically significant, differences between molecules **A** and **B** (the latter denoted by primed atom labels) may safely be ascribed to differences between the packing environments. Intermolecular distances generally correspond to normal van der Waals interactions, the only nonbonded intermolecular contacts of any possible significance being a pair of C—H···O contacts (C(1′)—H(1′a)···O(3) ($1-x, -y, 1-z$), C···O = 3.279(3), H···O = 2.46 Å, C—H···O = 141°; C(1′)—H(1′b)···O(1) ($1-x, -y, -z$), C···O = 3.267(3), H···O = 2.57 Å, C—H···O = 128°).

The markedly folded bicyclo[3.3.0]octane molecular backbone consists of the pair of *cis*-fused five-membered rings, structurally very similar to those observed in **5** (2) and **6** (3). In

TABLE 3. Bond angles (deg) with estimated standard deviations in parentheses

Bonds	Angle (deg)	Bonds	Angle (deg)
N(1)—O(1)—B(1)	104.9(2)	N(1′)—O(1′)—B(1′)	105.7(2)
N(2)—O(2)—B(2)	107.4(2)	N(2′)—O(2′)—B(2′)	107.3(2)
B(1)—O(3)—B(2)	114.1(2)	B(1′)—O(3′)—B(2′)	113.3(2)
O(1)—N(1)—C(1)	101.4(2)	O(1′)—N(1′)—C(1′)	100.5(2)
O(1)—N(1)—C(2)	106.6(2)	O(1′)—N(1′)—C(2′)	105.8(2)
C(1)—N(1)—C(2)	111.3(2)	C(1′)—N(1′)—C(2′)	111.2(3)
O(2)—N(2)—C(1)	107.5(2)	O(2′)—N(2′)—C(1′)	107.8(2)
O(2)—N(2)—C(3)	107.0(2)	O(2′)—N(2′)—C(3′)	107.0(2)
O(2)—N(2)—B(1)	105.5(2)	O(2′)—N(2′)—B(1′)	105.1(2)
C(1)—N(2)—C(3)	113.8(2)	C(1′)—N(2′)—C(3′)	114.0(2)
C(1)—N(2)—B(1)	102.2(2)	C(1′)—N(2′)—B(1′)	101.2(2)
C(3)—N(2)—B(1)	120.0(2)	C(3′)—N(2′)—B(1′)	120.9(2)
N(1)—C(1)—N(2)	102.4(2)	N(1′)—C(1′)—N(2′)	102.6(2)
C(5)—C(4)—C(9)	116.0(2)	C(5′)—C(4′)—C(9′)	116.6(2)
C(5)—C(4)—B(1)	120.6(2)	C(5′)—C(4′)—B(1′)	121.8(2)
C(9)—C(4)—B(1)	123.4(2)	C(9′)—C(4′)—B(1′)	121.5(2)
C(4)—C(5)—C(6)	122.6(3)	C(4′)—C(5′)—C(6′)	122.1(3)
C(5)—C(6)—C(7)	120.2(3)	C(5′)—C(6′)—C(7′)	119.4(3)
C(6)—C(7)—C(8)	119.7(3)	C(6′)—C(7′)—C(8′)	119.5(3)
C(7)—C(8)—C(9)	119.8(3)	C(7′)—C(8′)—C(9′)	121.4(3)
C(4)—C(9)—C(8)	121.7(3)	C(4′)—C(9′)—C(8′)	121.0(3)
C(11)—C(10)—C(15)	117.4(2)	C(11′)—C(10′)—C(15′)	117.4(2)
C(11)—C(10)—B(2)	122.1(3)	C(11′)—C(10′)—B(2′)	121.8(3)
C(15)—C(10)—B(2)	120.5(2)	C(15′)—C(10′)—B(2′)	120.8(2)
C(10)—C(11)—C(12)	120.4(3)	C(10′)—C(11′)—C(12′)	121.9(3)
C(11)—C(12)—C(13)	120.4(3)	C(11′)—C(12′)—C(13′)	119.5(3)
C(12)—C(13)—C(14)	120.0(3)	C(12′)—C(13′)—C(14′)	120.4(3)
C(13)—C(14)—C(15)	120.1(3)	C(13′)—C(14′)—C(15′)	119.4(3)
C(10)—C(15)—C(14)	121.7(3)	C(10′)—C(15′)—C(14′)	121.3(3)
O(1)—B(1)—O(3)	115.2(2)	O(1′)—B(1′)—O(3′)	115.0(2)
O(1)—B(1)—N(2)	97.9(2)	O(1′)—B(1′)—N(2′)	98.8(2)
O(1)—B(1)—C(4)	113.6(2)	O(1′)—B(1′)—C(4′)	112.7(2)
O(3)—B(1)—N(2)	97.5(2)	O(3′)—B(1′)—N(2′)	98.1(2)
O(3)—B(1)—C(4)	114.5(2)	O(3′)—B(1′)—C(4′)	115.2(2)
N(2)—B(1)—C(4)	116.0(2)	N(2′)—B(1′)—C(4′)	115.1(2)
O(2)—B(2)—O(3)	115.2(2)	O(2′)—B(2′)—O(3′)	115.6(2)
O(2)—B(2)—C(10)	118.4(2)	O(2′)—B(2′)—C(10′)	117.9(2)
O(3)—B(2)—C(10)	126.4(3)	O(3′)—B(2′)—C(10′)	126.5(3)

TABLE 4. Intra-annular torsion angles (deg) standard deviations in parentheses

Atoms	Torsion angle (deg)
B(1)—O(1)—N(1)—C(1)	−57.0(2)
O(1)—N(1)—C(1)—N(2)	51.6(2)
B(1)—N(2)—C(1)—N(1)	−28.0(2)
C(1)—N(2)—B(1)—O(1)	−4.2(2)
N(1)—O(1)—B(1)—N(2)	35.0(2)
B(1′)—O(1′)—N(1′)—C(1′)	55.2(2)
O(1′)—N(1′)—C(1′)—N(2′)	−53.5(2)
B(1′)—N(2′)—C(1′)—N(1′)	32.1(2)
C(1′)—N(2′)—B(1′)—O(1′)	0.4(2)
N(1′)—O(1′)—B(1′)—N(2′)	−31.6(2)
B(2)—O(2)—N(2)—B(1)	2.7(2)
O(2)—N(2)—B(1)—O(3)	0.4(2)
B(2)—O(3)—B(1)—N(2)	−3.7(2)
B(1)—O(3)—B(2)—O(2)	6.2(3)
N(2)—O(2)—B(2)—O(3)	−5.5(3)
B(2′)—O(2′)—N(2′)—B(1′)	1.5(3)
O(2′)—N(2′)—B(1′)—O(3′)	−5.3(2)
B(2′)—O(3′)—B(1′)—N(2′)	7.7(3)
B(1′)—O(3′)—B(2′)—O(2′)	−8.1(3)
N(2′)—O(2′)—B(2′)—O(3′)	3.6(3)

both molecules **A** and **B** the BONCN rings have slightly distorted N(1)-envelope conformations (see Table 4). The now well-characterized five-membered BOBON rings are significantly non-planar although not greatly so (mean and maximum deviations from the mean planes being 0.024 and 0.047(2) Å), the rings having flattened B(2)- and O(3′)- envelope conformations in molecules **A** and **B** respectively. The corresponding rings in **6** (3) and **10** (12) are planar, that in **8** (6) slightly less planar than in **4**, while that in **9** (11) is markedly non-planar. Steric factors responsible for distortions of the BOBON rings from planarity have been discussed at length for **8** (6), analogous arguments pertaining to the present structure.

The long mean[5] transannular N—B bond of 1.740(3) Å in **4** lies between the values of 1.728(3) Å in **9** and 1.754(3) Å in **8**, both of which are lengthened by NMe–BPh steric interactions as is that in **4**. These values may be compared with those of 1.666(3), 1.692(2), and 1.676(4) Å in **5**, **6**, and **10** wherein this particular interaction is absent. Bond distances involving the trigonal planar boron atom are essentially equal in all five structures containing the BOBON ring; the very short

[5] Here and elsewhere in this report mean values refer to weighted means with rms deviations from the mean in parentheses.

Can. J. Chem. Downloaded from www.nrcresearchpress.com by 210.87.254.40 on 09/06/12
For personal use only.

anhydridic B—O(B) distance of 1.341(3) Å and the shortened B—O(N) and B—C distances of 1.408(2) and 1.551(3) Å may be compared with the corresponding mean values of 1.337(3), 1.412(9), and 1.553(4) Å for the closely related structures **6**, **8**, **9**, and **10**. The B(sp^3)—O bond lengths do not differ significantly from those observed in **5**, **6**, and **8** (in which the boron atom is similarly coordinated). It is noteworthy that the N—O bonds involving the trivalent N atoms are significantly longer than those involving the tetrahedral N atoms (mean values of 1.463(1) and 1.449(2) Å, respectively).

The trigonally coordinated B(2) and B(2′) atoms are displaced 0.013(3) and 0.001(3) Å from the planes of their substituents. The B(2) phenyl groups (both of which are planar to within experimental error) are twisted out of the respective B(2/2′) coordination planes by 1.1(1) and 8.6(1)°, these values being normal for derivatives of phenylboronic acid (refs. 3, 6, 11, 12, and references therein). The two B(1) phenyl rings are slightly, but significantly, non-planar (χ^2 = 21.9 and 23.7, maximum deviation from the mean plane 0.010(4) Å). The B—C distances and the substituent induced geometrical distortions of the phenyl rings are normal (13).

Acknowledgments

We thank the Natural Sciences and Engineering Research Council of Canada for financial support and the University of British Columbia Computing Centre for assistance. We are indebted to Dr. V. Wray, Gesellschaft für Biotechnologische Forschung mbH, Braunschweig-Stöckheim, for running the low temperature ^{1}H nmr spectra.

1. W. KLIEGEL. J. Organomet. Chem. To be published.
2. S. J. RETTIG and J. TROTTER. Can. J. Chem. **53**, 1393 (1975).
3. S. J. RETTIG, J. TROTTER, W. KLIEGEL, and H. BECKER. Can. J. Chem. **54**, 3142 (1976).
4. W. KLIEGEL and H. BECKER. Chem. Ber. **110**, 2090 (1977); W. KLIEGEL, B. ENDERS, and H. BECKER. Liebigs Ann. Chem. 1712 (1982).
5. W. KLIEGEL and J. GRAUMANN. Chemiker-Zeitg. **106**, 378 (1982).
6. W. KLIEGEL, D. NANNINGA, S. J. RETTIG, and J. TROTTER. Can. J. Chem. Part XVII. To be published.
7. D. T. CROMER and J. B. MANN. Acta Crystallogr. Sect. A, **24**, 321 (1968).
8. R. F. STEWART, E. R. DAVIDSON, and W. T. SIMPSON. J. Chem. Phys. **42**, 3175 (1965).
9. V. SCHOMAKER and K. N. TRUEBLOOD. Acta Crystallogr. Sect. B, **24**, 63 (1968).
10. D. W. J. CRUICKSHANK. Acta Crystallogr. **9**, 747 (1956); **9**, 754 (1956); **14**, 896 (1961).
11. W. KLIEGEL, H.-W. MOTZKUS, S. J. RETTIG, and J. TROTTER. Can. J. Chem. To be published.
12. W. KLIEGEL, D. NANNINGA, S. J. RETTIG, and J. TROTTER. Can. J. Chem. **61**, 2329 (1983).
13. A. DOMENICANO, A. VACIAGO, and C. A. COULSON. Acta Crystallogr. Sect. B, **31**, 221 (1975); **31**, 1630 (1975).
14. W. KLIEGEL, D. NANNINGA, S. RETTIG, and J. TROTTER. Can. J. Chem. **61**, 2493 (1983).

Can. J. Chem. Downloaded from www.nrcresearchpress.com by 210.87.254.40 on 09/06/12
For personal use only.

"Through-space" spin–spin coupling between thallium and hydrogen in *o*-alkylphenylthallium compounds

BRUCE VICTOR CHEESMAN[1] AND RAYMOND FREDERICK MARTIN WHITE

Department of Chemistry, Sir John Cass School of Science and Technology, City of London Polytechnic, Jewry Street, London, England EC3N 2EY

Received October 25, 1982[2]

BRUCE VICTOR CHEESMAN and RAYMOND FREDERICK MARTIN WHITE. Can. J. Chem. **62**, 521 (1984).

In this study a comparison was made of the Tl···H sidechain coupling constants for mono- and di-arylthallium derivatives in which a series of alkyl groups (CH_3, C_2H_5, i-C_3H_7, *t*-C_4H_9) are *o*- and *p*- to the thallium atom. The results provide evidence of "through-space" coupling between thallium and hydrogen in some of the *o*-alkylphenylthallium compounds, with the "through-space" contribution to $^5J(Tl\cdots C(CH_3)_3)$ in the *o-tert*-butylphenylthallium derivatives being considerable.

BRUCE VICTOR CHEESMAN et RAYMOND FREDERICK MARTIN WHITE. Can. J. Chem. **62**, 521 (1984).

Dans ce travail, on compare les constantes de couplage Tl···H des chaînes latérales des dérivés mono- et di-arylthallium dans lesquels une série de groupes alkyles (CH_3, C_2H_5, i-C_3H_7, *t*-C_4H_9) sont en positions *ortho* et *para* par rapport à l'atome de thallium. Les résultats révèlent un couplage à "travers l'espace" entre le thallium et l'hydrogène dans certains composés *o*-alkylphénylthallium avec une contribution considérable à "travers l'espace" au $^5J(Tl\cdots C(CH_3)_3)$ dans les dérivés *o-tert*-butylphénylthallium.

[Traduit par le journal]

Introduction

"Through-space" coupling can occur if the internuclear distance between a pair of coupled nuclei is abnormally small (1, 2). Observation of a coupling constant which is larger than might otherwise be expected is taken to be indicative of a "through-space" mechanism (3–6). Unambiguous examples of "through-space" coupling involving nuclei other than hydrogen and fluorine are few. Petrakis and Sederholm (1) suggested "through-space" coupling involves lone pair orbitals, but this has led in most cases to the existence of lone pair orbitals, on one or both of the atoms involved in coupling, being taken as indicative that the important mechanism in such couplings is "through-space". McFarlane (7) suggested this type of coupling is likely between fluorine and the magnetic nuclei of elements larger than helium, in their *o*-trifluoromethyl derivatives, because of van der Waals penetration which depends upon the extent to which other substituents allow close approach of the trifluoromethyl group. Mercury and phosphorus(III) are favourable in this respect and evidence for "through-space" coupling in *o*-trifluoromethyl derivatives of these nuclei has been reported by McFarlane (7) and Grim *et al.* (8) respectively.

Values of J_{Tl-H} for arylthallium compounds were first reported by Maher and Evans (9), who proposed that the coupling involves essentially the same mechanism as that involved in hydrogen–hydrogen coupling, that is, via Fermi contact, by using the 6*s*-orbital of the thallium atom. They also observed (9, 10) an increase in the magnitude of J_{Tl-H} in the series Ar_3Tl, Ar_2Tl^+, and $ArTl^{2+}$ (where Ar is aryl), which was qualitatively interpreted on the basis of the Fermi contact term as due to the increase in both the effective nuclear charge (Z_{eff}) of the thallium atom and the *s*-character of the outer electrons of the thallium atom, an interpretation supported by other workers (11, 12). McKillop *et al.* (13) have measured the magnitude of $J_{Tl\cdots H}$ and $J_{Tl\cdots CH_3}$ for a range of arylthallium trifluoroacetates prepared by the direct thallation technique, and the results of their studies were in complete agreement with those of Maher and Evans (9, 10). The very large differences in the coupling constants for Tl—*o*H, Tl—*m*H, and Tl—*p*H make possible the unambiguous determination of the orientation of the carbon–thallium bond in both mono- and di-arylthallium compounds, and distinguish between the two types of organothallium compounds. Ernst (14) has measured ^{13}C chemical shifts, $^nJ(^{13}C, ^{205}Tl)$, where $n = 2-6$, for some alkyl-substituted arylthallium trifluoroacetates, and $^6J_{Tl\cdots pH}$ for *p*-Me, *p*-Et, and *p*-i-Pr-phenylthallium bis(trifluoroacetates). He discussed substituent effects on chemical shifts and coupling constants for the ^{13}C data and found $^6J_{Tl\cdots pC}$ was dependent upon the conformation of the *p*-alkyl side-chains.

The aim of the present work was to investigate the possibility of "through-space" coupling in suitable *o*-alkylphenylthallium compounds. To detect the effects of "through-space" coupling it is necessary to compare coupling constants in structurally similar compounds which differ only in the proximities of possible interacting groups. In this study, mono- and diarylthallium compounds in which the groups of interest are *o*- and *p*- to the thallium atom, are compared. "Through-space" coupling might be expected for the *o*-substituted derivatives, as the alkyl groups would be close to the thallium atom, whereas in the *p*-substituted compounds there is no possibility of a "through-space" contribution to the coupling because of the distance separating the coupled nuclei. Thus the *p*-substituted compounds act as a control for investigating "through-space" effects in the *o*-derivatives. Compounds in which the alkyl control groups are *p*-, rather than *m*-, to thallium were used for two reasons. Firstly, $J_{(Tl-H(p\text{-}R))}$ is larger than $J_{(Tl-H(m\text{-}R))}$, where R is an alkyl group, so any "through-space" effects would be more difficult to evaluate if $J_{(Tl-H(o\text{-}R))}$ was being compared with $J_{(Tl-H(m\text{-}R))}$. Secondly, the preparation of *p*-alkylphenylthallium bis(trifluoroacetates) is more convenient since *p*-thallation is easier than at the *m*-position, *p*-substitution occurring at room temperature rather than at elevated temperatures. In general, *p*-alkylphenylthallium compounds are more readily obtained than the *m*-substituted ones, even via other preparative routes. Evidence is presented of "through-space" coupling between thallium and hydrogen in some of the *o*-alkylphenylthallium compounds, with the "through-space" contribution to

[1]Present address: Department of Chemistry, University of Alberta, Edmonton, Alta., Canada T6G 2G2.

[2]Revision received July 5, 1983.

Can. J. Chem. Downloaded from www.nrcresearchpress.com by 210.87.254.42 on 09/06/12
For personal use only.

$^5J(Tl\cdots C(CH_3)_3)$ in the *o-tert*-butylphenylthallium derivatives being considerable.

Results

All spectra were assigned on a first-order basis. In the alkyl sidechains, $^3J_{H\cdots H}$ was in the order of 7 Hz. The results for the Tl···H sidechain coupling constants in the *o*-alkylphenylthallium **1** and *p*-alkylphenylthallium compounds are presented

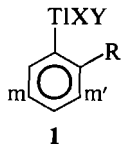

1

X = Cl, Y = Cl for a monoarylthallium compound
X = *o*-alkylphenyl (same as existing one),
Y = Cl, for a diarylthallium compound
R = alkyl group

in Table 1. Only in three bis(*p*-alkylphenyl)thallium compounds, containing ethyl and isopropyl groups, the methylene/methine peaks are broad and fine structure was not resolved. Line broadening in these large molecules could be due to $^{203}Tl/^{205}Tl$ isotopes ($^{205}\gamma/^{203}\gamma = 1.0098$) (11) and some self association process, or the ^1H T_1 values may be short enough to give broad peaks. Estimation of $^6J_{Tl\cdots pH}$ from these broad peaks is highly uncertain and values obtained are not presented here since their inclusion is unnecessary for confirmation of "through-space" coupling in the *o*-alkylphenylthallium compounds.

Computer programmes were used to calculate thallium···hydrogen internuclear distances (on the assumption of free rotation of the alkyl groups) in the *o*-alkylphenylthallium derivatives discussed. The range of carbon–thallium bond lengths employed in these calculations would cover both mono- and di-compounds. It was assumed that carbon–hydrogen bond lengths, carbon–carbon bond lengths (for C_2 and above), and HCH bond angles were constant in the alkyl sidechains. The thallium···hydrogen internuclear distances ($R_{Tl\cdots H}$) for hydrogens on the carbon atom at position 4 (Fig. 1) in *o*-methyl, *o*-ethyl-, and *o*-isopropylphenylthallium compounds were calculated using a five-atom chain for thallium···hydrogen dihedral angles at intervals of rotation of 60° (about the C3—C4 bond (Fig. 1)) in the range 0–300°. A six-atom chain was used in the calculation of $R_{Tl\cdots H}$ for hydrogens (on the carbon atom at position 5 (Fig. 1)) of methyl groups in *o*-ethyl, *o*-isopropyl-, and *o-tert*-butylphenylthallium compounds, which involved consideration of both thallium···carbon and thallium···hydrogen dihedral angles. The same range, 0–300° (represented by the subscript 0–5), and interval, 60°, were used for both dihedral angles, so the five-atom chain produced six values of $R_{Tl\cdots H}$, J_0–J_5. Thirty six values of $R_{Tl\cdots H}$, I_{00}–I_{55}, obtained from the different combinations of thallium···carbon and thallium···hydrogen dihedral angles, were produced by the six-atom chain. The two subscripts indicate thallium···carbon and thallium···hydrogen dihedral angle, in units of 60°, respectively. The use of these thallium···hydrogen internuclear distances for the *o*-methyl- and *o*-isopropylphenylthallium derivatives is illustrated (Fig. 2). The values of $R_{Tl\cdots H}$ produced for both the five- and six-atom chain calculations were then averaged and are presented, together with $R_{Tl\cdots H_{min}}$ and $R_{Tl\cdots H_{max}}$ (Table 2), for three carbon–thallium bond lengths.

TABLE 1. Tl···H sidechain coupling constants for solutions of mono- and di-arylthallium compounds at 23°C

Compound	$^4J_{Tl\cdots oH}$ (Hz)	$^5J_{Tl\cdots oH}$ (Hz)
o-$CH_3C_6H_4TlCl_2$	95 (P)[a]	—
o-$CH_3CH_2C_6H_4TlCl_2$	84 (P)	2 (P)
o-$(CH_3)_2CHC_6H_4TlCl_2$	81 (P)	3 (P)
o-$(CH_3)_3CC_6H_4TlCl_2$	—	22 (P)
$(o\text{-}CH_3C_6H_4)_2TlCl$	47 (P)	—
$(o\text{-}CH_3CH_2C_6H_4)_2TlCl$	58 (P)	4 (P)
$(o\text{-}(CH_3)_2CHC_6H_4)_2TlCl$	93 (P)	5 (P)
$(o\text{-}(CH_3)_3CC_6H_4)_2TlCl$	—	19 (P)
	$^6J_{Tl\cdots pH}$	
p-$CH_3C_6H_4Tl(OCOCF_3)_2$	64 (P)	
p-$CH_3CH_2C_6H_4Tl(OCOCF_3)_2$	51 (P)	
p-$(CH_3)_2CHC_6H_4Tl(OCOCF_3)_2$	27 (P)	
$(p\text{-}CH_3C_6H_4)_2TlOCOCF_3$	24 (D)[a]	
$(p\text{-}CH_3CH_2C_6H_4)_2TlOCOCF_3$	[b] (P)	
$(p\text{-}CH_3CH_2C_6H_4)_2TlCl$	[b] (D)	
$(p\text{-}(CH_3)_2CHC_6H_4)_2TlOCOCF_3$	[b] (P)	

[a]Solvent: P = C_5D_5N, D = $(CD_3)_2SO$.
[b]Methylene/methine peaks were broad and fine structure not resolved. Estimation of $^6J_{Tl\cdots pH}$ highly uncertain (see Results).

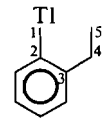

FIG. 1. Schematic diagram of the five-atom chain used for thallium···hydrogen internuclear distance calculations.

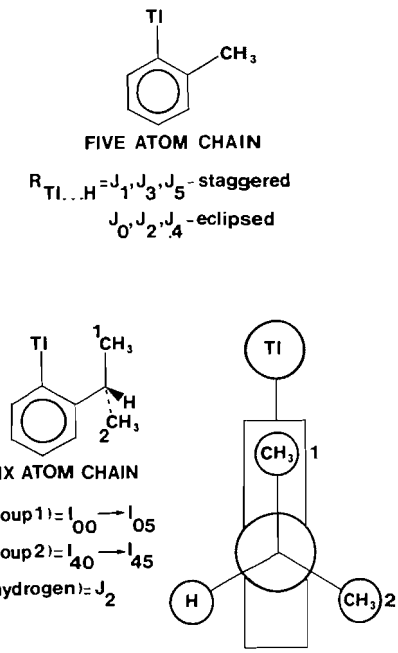

FIG. 2. The use of $R_{Tl\cdots H}$ for the *o*-methyl- and *o*-isopropylphenylthallium derivatives. A view obtained by looking down the C4 → C3 bond is illustrated for the *o*-isopropylphenylthallium derivative; for methyl groups 1 and 2 the Tl···C dihedral angles are 0° and 240° respectively, whilst the Tl···H dihedral angle is varied in the range 0–300°, at intervals of 60°. The methine hydrogen has a Tl···H dihedal angle of 120°.

Can. J. Chem. Downloaded from www.nrcresearchpress.com by 210.87.254.42 on 09/06/12
For personal use only.

TABLE 2. Values of $R_{Tl\cdots H}$ (five- and six-atom chains)

C—Tl (nm)	0.208	0.218	0.228
5 Atom $R_{Tl\cdots H_{min}}$ (nm)	0.252	0.256	0.260
5 Atom $R_{Tl\cdots H_{max}}$ (nm)	0.432	0.439	0.445
6 Atom $R_{Tl\cdots H_{min}}$ (nm)	0.122	0.125	0.129
6 Atom $R_{Tl\cdots H_{max}}$ (nm)	0.526	0.531	0.537
5 Atom $R_{Tl\cdots H_{ave}}$ (nm)	0.348	0.354	0.359
6 Atom $R_{Tl\cdots H_{ave}}$ (nm)	0.391	0.395	0.399

Discussion

The thallium···proton coupling constants (Table 1) for the *p*-alkylphenylthallium bis(trifluoroacetates) indicate that $^6J_{Tl\cdots pH}$ decreases as the methyl hydrogens in *p*-tolylthallium bis(trifluoroacetate) are replaced by methyl groups. An analogous situation exists for dialkylthallium halides,[3] where further alkyl substitution effects a reduction of $^2J_{Tl\cdots H}$. For the mono- and bis- *p*-Et, *p*-i-Pr, and *p*-*t*-Bu-phenylthallium derivatives, $^7J_{Tl\cdots pH}$ could not be observed and must be smaller than 1 Hz, as concluded previously (14) for *p*-*tert*-butylphenylthallium bis(trifluoroacetate). Comparing the results for the *o*-alkylphenylthallium compounds with those of the *p*-compounds, it is found that the change in $^4J_{Tl\cdots oH}$ for *o*-alkylphenylthallium dichlorides, as *ortho*-hydrogens are replaced by methyl groups, is much less than the change in $^6J_{Tl\cdots pH}$ for *p*-alkylphenylthallium bis(trifluoroacetates). Considering $^5J_{Tl\cdots oH}$, the replacement of the methine hydrogen in *o*-isopropylphenylthallium dichloride by a methyl group, as in *o*-*tert*-butylphenylthallium dichloride, results in an increase in $^5J_{Tl\cdots oH}$ from 3 to 22 Hz. In the bis(*o*-alkylphenyl)thallium chlorides $^4J_{Tl\cdots oH}$ *increases* when methyl groups are substituted for hydrogen atoms and for the *o*-isopropylphenylthallium compounds both $^4J_{Tl\cdots oH}$ and $^5J_{Tl\cdots oH}$ are larger in the diarylthallium derivatives than in the monoarylthallium derivatives. Replacement of the methine hydrogen in bis(*o*-isopropylphenyl)thallium chloride by a methyl group, as in bis(*o*-*tert*-butylphenyl)thallium chloride, leads to an increase in $^5J_{Tl\cdots oH}$ from 5 to 19 Hz. Additionally, $^5J_{Tl\cdots oH}$ in *o*-$(CH_3)_3CC_6H_4TlX_2$ is practically insensitive to the nature of X. These unusual results suggest the possibility of a substantial "through-space" contribution involving coupling between thallium and hydrogen in some of the *o*-alkylphenylthallium derivatives. For the *o*-*tert*-butylphenylthallium derivatives the indications are that the "through-space" component to $^5J_{Tl\cdots oH}$ is considerable. In the *o*-isopropylphenylthallium compounds there must be a slight preference for a conformation such as **2** rather than **3**, but there can be no preferred conformation in the *o*-*tert*-butylphenylthallium derivatives, where thallium is adjacent to three methyl groups **4**. There is no experimental evidence of non-equivalence of the hydrogen nuclei in the methyl groups of these arylthallium derivatives, so their overall rate of rotation must be rapid on the nmr time scale. Changes with temperature, not detailed here (15), are not large enough to be significant; this suggests that conformational preferences are small.

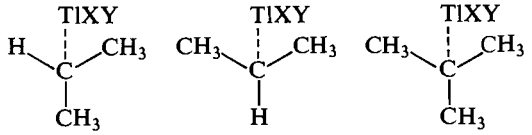

2 **3** **4**

X = Cl, Y = Cl for a monoarylthallium derivative
X = *o*-alkylphenyl (same as existing one),
Y = Cl, for a diarylthallium derivative

The calculation of internuclear distances and penetration of van der Waals radii of nuclei have frequently been used to support cases of "through-space" coupling (16). A reliable covalent radius for Tl(III) is not available; for the halides, TlX_3, a value of 0.133 nm is obtained, whilst a value ranging from 0.145 to 0.155 nm is evaluated from complexes possessing six halogen neighbours. The radius of Tl(III) is calculated as 0.141 nm (17) for diethyl(salicylaldehydato)thallium(III), by subtraction of the single bond radius of carbon from the average thallium–carbon bond length. This value lies within the range determined for the six-coordinate halide complexes.

It is impossible to calculate accurate internuclear distances for $ArTl^{2+}$ or Ar_2Tl^+ (Ar is aryl), firstly because there have been relatively few measurements of thallium–carbon bond energies or bond lengths. Nevertheless carbon–thallium bond lengths, for the compounds measured so far, lie within the range 0.207–0.227 nm. Secondly, van der Waals radii of Tl^+ and Tl^{2+} are not known accurately. Hence, measurements and deductions of internuclear distances involving thallium are tentative. The smallest ($R_{Tl\cdots H_{min}}$) and average ($R_{Tl\cdots H_{ave}}$) thallium···hydrogen internuclear distances for the *o*-alkylphenylthallium derivatives are presented (Table 3) for three carbon–thallium bond lengths.

In the *o*-alkylphenylthallium compounds and for a carbon–thallium bond length of 0.218 nm, the average $Tl\cdots CH_3$ internuclear distances are ca. 0.350 nm (*o*-methylphenylthallium derivatives) and ca. 0.400 nm for the others, while the shortest instantaneous thallium···hydrogen separations are only ca. 0.260 nm (*o*-methylphenylthallium derivatives) and ca. 0.130 nm (others); these are probably the more significant figures since McFarlane (7) suggests it is likely "through-space" coupling depends upon $\langle r^{-n} \rangle$ where r is the internuclear distance between a pair of coupled nuclei exhibiting "through-space" coupling, and n is fairly large. Furthermore, $R_{Tl\cdots H_{ave}}$ has been calculated assuming no conformational preference, so the shortest instantaneous thallium···hydrogen separations are probably more important.

Van der Waals radii of Tl^+ and Tl^{2+} (the ionic radius of which was taken as half-way between Tl^+ and Tl^{3+}) have been approximately deduced (at 0.08 nm greater than the ionic radii) as 0.229 nm and 0.201 nm respectively. Since the van der Waals radius of the hydrogen atom is 0.12 nm, the sums of the van der Waals radii are 0.349 nm (for Ar_2Tl^+) and 0.321 nm (for $ArTl^{2+}$). This indicates the possibility of steric overcrowding both for an *o*-methyl group and terminal methyl groups in *o*-ethyl-, *o*-isopropyl-, and *o*-*tert*-butylphenylthallium compounds. The effect is more pronounced in Ar_2Tl^+ than in $ArTl^{2+}$, where penetrations of van der Waals radii (for *o*-alkylphenylthallium derivatives having a carbon–thallium bond length of 0.218 nm) are, Ar_2Tl^+: *o*-methyl 0.093 nm, terminal methyl 0.224 nm; $ArTl^{2+}$: *o*-methyl 0.065 nm, terminal methyl 0.196 nm. It might reasonably be expected that all these derivatives would show "through-space" coupling. The "through-space" interaction between thallium and hydrogen occurring in *o*-alkylphenylthallium derivatives is more significant in bis(*o*-alkylphenyl)thallium chlorides because of a larger van der Waals radius and hence greater overlap of orbitals than in *o*-alkylphenylthallium dichlorides.

[3]Manuscript in preparation.

Can. J. Chem. Downloaded from www.nrcresearchpress.com by 210.87.254.42 on 09/06/12
For personal use only.

TABLE 3. Tl···H internuclear distances for methyl groups in *o*-alkylphenylthallium derivatives

	o-Me			*o*-Et			*o*-i-Pr			*o*-*t*-Bu		
C—Tl (nm)	0.208	0.218	0.228	0.208	0.218	0.228	0.208	0.218	0.228	0.208	0.218	0.228
$R_{Tl\cdots H_{min}}$	0.252	0.256	0.260	0.122	0.125	0.129	0.122	0.125	0.129	0.122	0.125	0.129
$R_{Tl\cdots H_{ave}}$	0.348	0.354	0.359	0.391	0.395	0.399	0.391	0.395	0.399	0.391	0.395	0.399

The main points of this discussion of thallium − sidechain hydrogen coupling constants are summarized below.

(a) Calculations, using a range of carbon−thallium bond lengths that would cover both mono- and di-arylthallium derivatives, indicate that sidechain hydrogen atoms five or six atom distances from the thallium atom can approach within the sum of the thallium and hydrogen van der Waals radii.

(b) When an ethyl or isopropyl group is *ortho* to thallium, the conformational preference is for the hydrogen rather than the methyl group to be *gauche* (or closer) to thallium.

(c) The pattern of $J_{Tl\cdots H}$ suggests a "through-space" effect is occurring. For an *ortho* ethyl or isopropyl group, the conformational preference results in CH_2 or CH showing the effect, while in the case of *o*-*tert*-butylphenylthallium derivatives, all conformations are equally probable and thus the methyl groups show the effect.

(d) The "through-space" effect is less pronounced for *o*-alkylphenylthallium dichlorides than for bis(*o*-alkylphenyl)-thallium chlorides.

Experimental

Instrumentation

The ^1H nmr spectra (measured in dimethyl sulphoxide-d_6 or pyridine-d_5 solution) were obtained on a JEOL C-60-H spectrometer operating at 60 MHz, using 5-mm spinning samples. Spectra were recorded in the field-sweep mode with the field-frequency stabilization circuitry activated by the signal from an external water sample. The coupling constants were virtually independent of concentration for the moderately (0.08−1 *M*) concentrated solutions used.

Sample preparation

The dependence of $J_{Tl\cdots H}$ and ^1H chemical shifts for arylthallium compounds on concentration, temperature, the addition of a common ion, and water in the solvent was investigated (15) during the primary study of "through-space" coupling. It was evident that the coupling constants and chemical shifts for pyridine or dimethyl sulphoxide solutions are not strongly dependent on the concentration of arylthallium compound present, although the low solubility of some of the compounds restricted this study. The main factors affecting coupling constants were found to be water (or deuterium oxide) concentration, concentration of thallic chloride, and soluble chloride anion concentration. Thorough washing and drying (under vacuum) of organothallium compounds before recording spectra eliminates the last two factors. Both pyridine-d_5 and dimethyl sulphoxide-d_6 as supplied contained water/deuterium oxide. In the case of pyridine this could have been removed by refluxing over sodium hydroxide pellets followed by distillation under nitrogen, and dimethyl sulphoxide may be dried over calcium hydride followed by distillation under reduced pressure. A more practical and more economical approach adopted in the present work is to use the solvents as supplied and monitor the water peak as a guide. It should be noted that in the interpretation of the results, variations in coupling constants of about 2% (15) may arise from differences in the water content of the solvent. The low solubilities of some of the arylthallium compounds prepared for the "through-space" study restricted the number of solutions that could be examined.

Chemicals

Where a number of compounds were prepared by a particular procedure, full details are given for one compound and, if necessary, comments are given on cognate preparations. Analyses are reported for new compounds only. A starting material for the preparation of *o*-isopropylphenylboronic acid, *o*-bromoisopropylbenzene, was synthesized from *o*-isopropylaniline by the method of Kiersznicki *et al.* (18). The synthesis of *o*-bromo-*tert*-butylbenzene, used in the preparation of *o*-*tert*-butylphenylboronic acid, involved four preparative stages; nitration of *tert*-butylbenzene (Nelson and Brown (19)), bromination of *p*-nitro-*tert*-butylbenzene (Derbyshire and Walters (20)), reduction of 2-bromo-4-nitro-*tert*-butylbenzene (using granulated tin and concentrated hydrochloric acid), and deamination of 2-bromo-4-amino-*tert*-butylbenzene (Crawford and Stewart (21)).

All arylboronic acids were prepared by the method of Bean and Johnson (22) which involves reaction of an aryl Grignard reagent with tri-n-butyl borate at −60°C and subsequent hydrolysis to give the arylboronic acid, $ArB(OH)_2$. These acids were prepared for Ar = p-$CH_3C_6H_4$, o-$C_2H_5C_6H_4$, o-i-$C_3H_7C_6H_4$, and o-t-$C_4H_9C_6H_4$; experimental data are summarized in Table 4 for *o*-isopropylphenyl- and *o*-*tert*-butylphenylboronic acid.

Syntheses of organothallium compounds

Monoarylthallium compounds were prepared by the following methods: (a) direct thallation of substituted benzenes by thallic trifluoroacetate; (b) reaction of an arylboronic acid with thallic chloride.

Diarylthallium compounds were synthesized as follows: (a) reaction of a monoarylthallium derivative with trimethyl phosphite; (b) reaction of thallic chloride with excess arylboronic acid; syntheses of arylthallium compounds are detailed below.

Monoarylthallium bis(trifluoroacetates)

These were prepared by the method of McKillop *et al.* (23). Arylthallium bis(trifluoroacetates) can be recrystallized from 1,2-dichloroethane, but most were analytically pure as isolated. In a number of cases of thallation the development of intense colours was noted. This is most probably due[4] to a small amount of oxidation of the aromatic substrate by thallic trifluoroacetate. Arylthallium bis(trifluoroacetates), $ArTl(OCOCF_3)_2$, were prepared for Ar = p-$CH_3C_6H_4$, p-$C_2H_5C_6H_4$, and p-i-$C_3H_7C_6H_4$.

Diarylthallium trifluoroacetates

These were prepared by the method of McKillop *et al.* (13) which involves addition of the solid arylthallium bis(trifluoroacetate) to trimethyl phosphite. Diarylthallium trifluoroacetates, $Ar_2TlOCOCF_3$, were prepared for Ar = p-$CH_3C_6H_4$, p-$C_2H_5C_6H_4$, and p-i-$C_3H_7C_6H_4$.

Arylthallium chlorides

(a) *Using arylboronic acids*

These syntheses are based on the method developed by Challenger and Parker (24), which is suitable for the preparation of both monoaryl and diarylthallium chlorides. The product obtained depends on the relative quantities of the reactants. Details of typical preparations, for phenylthallium chlorides, are given below.

Diphenylthallium chloride

Thallic chloride (0.0048 mol) in 6 mL of water was refluxed with 0.0098 mol of phenylboronic acid, giving a white solid after one minute. Diphenylthallium chloride so obtained was filtered off, washed with cold water, recrystallized from pyridine, and dried. This method was satisfactory for the preparation of all diarylthallium chlorides, with the exceptions of bis(*o*-isopropylphenyl)thallium chloride

[4]A. McKillop, personal communication.

Can. J. Chem. Downloaded from www.nrcresearchpress.com by 210.87.254.42 on 09/06/12
For personal use only.

TABLE 4. Experimental data for compounds

Compound	Analysis	Comments
(1) o-i-$C_3H_7C_6H_4B(OH)_2$	Calcd. C 65.91, H 7.99, B 6.59 Found C 65.89, H 7.87, B 6.45	
(2) o-t-$C_4H_9C_6H_4B(OH)_2$	Calcd. C 67.46, H 8.49, B 6.07 Found C 67.31, H 8.37, B 5.90	
(3) $(o\text{-}C_2H_5C_6H_4)_2TlCl$[a]	Calcd. C 42.69, H 4.03, Cl 7.88, Tl 45.40 Found C 42.47, H 3.89, Cl 7.73, Tl[b]	From arylboronic acid
(4) o-i-$C_3H_7C_6H_4TlCl_2$	Calcd. C 27.40, H 2.81, Cl 17.98, Tl 51.81 Found C 27.42, H 2.75, Cl 17.87, Tl 52.06	From arylboronic acid (1)
(5) $(o\text{-i-}C_3H_7C_6H_4)_2TlCl$	Calcd. C 45.21, H 4.64, Cl 7.41, Tl 42.74 Found C 45.04, H 4.52, Cl 7.20, Tl 42.51	From (4) by reaction with trimethyl phosphite
(6) o-t-$C_4H_9C_6H_4TlCl_2$	Calcd. C 29.40, H 3.21, Cl 17.36, Tl 50.03 Found C 29.63, H 3.21, Cl 17.24, Tl 49.75	From arylboronic acid (2)
(7) $(o\text{-}t\text{-}C_4H_9C_6H_4)_2TlCl$	Calcd. C 47.45, H 5.18, Cl 7.00, Tl 40.37 Found C 47.68, H 5.19, Cl 6.79, Tl 40.27	From (6) by reaction with trimethyl phosphite
(8) $(p\text{-}t\text{-}C_4H_9C_6H_4)_2TlOCOCF_3$	Calcd. C 45.26, H 4.49, F 9.76, Tl 35.01 Found C 44.69, H 4.34, F 9.16, Tl 35.15	

[a] o-$C_2H_5C_6H_4TlCl_2$ reported (without analysis) in ref. 25, which states that satisfactory analysis was obtained for o-$C_2H_5C_6H_4B(OH)_2$; see also ref. 26.
[b] Insufficient sample for determination of thallium.

and bis(*o-tert*-butylphenyl)thallium chloride. In these cases, reaction of the appropriate arylboronic acid with thallic chloride produced a mixture of monoarylthallium chloride and unreacted arylboronic acid, so the compounds were synthesized from the monoarylthallium dichloride and trimethyl phosphite, the method for diarylthallium trifluoroacetates.

Phenylthallium dichloride

Thallic chloride (0.0145 mol) in 6 mL of water was refluxed with 0.00492 mol of phenylboronic acid for one minute, giving a precipitate of phenylthallium dichloride. The product was filtered off, washed with a small quantity of cold water, recrystallized from methanol, and dried.

Arylthallium chlorides, $ArTlCl_2$ and $(Ar)_2TlCl$, were prepared by reaction of arylboronic acid with thallic chloride for Ar = p-$CH_3C_6H_4$, o-$C_2H_5C_6H_4$, o-i-$C_3H_7C_6H_4$ (only $ArTlCl_2$), and o-t-$C_4H_9C_6H_4$ (only $ArTlCl_2$); experimental data are summarized in Table 4 for Ar = o-$C_2H_5C_6H_4$, o-i-$C_3H_7C_6H_4$, and o-t-$C_4H_9C_6H_4$.

(b) *Using arylthallium dichlorides and trimethyl phosphite*

Bis(*o*-isopropylphenyl)thallium chloride and bis(*o-tert*-butylphenyl)thallium chloride were prepared from the arylthallium dichlorides and trimethyl phosphite using the method (13) for preparation of diarylthallium trifluoroacetates. A larger volume of trimethyl phosphite was found necessary for reaction than for arylthallium bis(trifluoroacetates), reaction times were longer, and the diarylthallium chlorides produced required washing with large quantities of water to remove traces of trimethyl phosphite/phosphate. Experimental data for these diarylthallium chlorides, Ar_2TlCl, Ar = o-i-$C_3H_7C_6H_4$ and o-*tert*-$C_4H_9C_6H_4$, are summarized in Table 4.

Acknowledgements

One of us (BVC) thanks the Inner London Education Authority for the award of a Research Assistantship during the period, 1975–1978, when the present study was done. This work formed part of a Ph.D. thesis (Council for National Academic Awards, 1980) for BVC.

Microanalyses were provided by the Analytical Service Laboratory of this department.

1. L. PETRAKIS and C. H. SEDERHOLM. J. Chem. Phys. **35**, 1243 (1961).
2. S. NG and C. H. SEDERHOLM. J. Chem. Phys. **40**, 2090 (1964).
3. H. S. GUTOWSKY and V. D. MOCHEL. J. Chem. Phys. **39**, 1195 (1963).
4. J. JONAS, L. BOROWSKI, and H. S. GUTOWSKY. J. Chem. Phys. **47**, 2441 (1967).
5. F. J. WEIGERT and J. D. ROBERTS. J. Am. Chem. Soc. **90**, 3577 (1968).
6. K. L. SERVIS and K. N. FANG. J. Am. Chem. Soc. **90**, 6712 (1968).
7. W. MCFARLANE. J. Chem. Soc. Chem. Commun. 609 (1971).
8. S. O. GRIM, G. R. MILLER, and A. W. YANKOWSKY. J. Chem. Phys. **51**, 3185 (1969).
9. J. P. MAHER and D. F. EVANS. J. Chem. Soc. 637 (1965).
10. J. P. MAHER and D. F. EVANS. Proc. Chem. Soc. London, 176 (1963).
11. J. V. HATTON. J. Chem. Phys. **40**, 933 (1964).
12. K. HILDENBRAND and H. DREESKAMP. Z. Phys. Chem. (Frankfurt/Main) **69**, 171 (1970).
13. A. MCKILLOP, J. D. HUNT, and E. C. TAYLOR. J. Organomet. Chem. **24**, 77 (1970).
14. L. ERNST. J. Organomet. Chem. **82**, 319 (1974).
15. B. V. CHEESMAN. Ph.D. Thesis (CNAA), City of London Polytechnic, 1980.
16. J. HILTON and L. H. SUTCLIFFE. Prog. Nucl. Magn. Reson. Spectrosc. **10**, 27 (1975).
17. G. H. W. MILBURN and M. R. TRUTER. J. Chem. Soc. A, 648 (1967).
18. T. KIERSZNICKI, Z. KULICKI, and C. TROSZKIEWICZ. Zesz. Nauk. Politech. Slask. Chem. **40**, 113 (1967).
19. K. L. NELSON and H. C. BROWN. J. Am. Chem. Soc. **73**, 5605 (1951).
20. D. H. DERBYSHIRE and W. A. WATERS. J. Chem. Soc. 573 (1950).
21. M. CRAWFORD and F. H. C. STEWART. J. Chem. Soc. 4443 (1952).
22. F. R. BEAN and J. R. JOHNSON. J. Am. Chem. Soc. **54**, 4415 (1932).
23. A. MCKILLOP, J. S. FOWLER, M. J. ZELESKO, J. D. HUNT, E. C. TAYLOR, and G. MCGILLIVRAY. Tetrahedron Lett. **29**, 2427 (1969).
24. F. CHALLENGER and B. PARKER. J. Chem. Soc. 1462 (1931).
25. J. P. MAHER, M. EVANS, and M. HARRISON. J. Chem Soc. Dalton Trans. 188 (1972).
26. W. J. DALE and J. E. RUSH. J. Org. Chem. **27**, 2598 (1962).

Can. J. Chem. Downloaded from www.nrcresearchpress.com by 210.87.254.42 on 09/06/12
For personal use only.

Hétérocycles à fonction quinone. V. Réaction anormale de la butanedione avec la diamino-1,2 anthraquinone; structure cristalline de la naphto[2,3-*f*]quinoxalinedione-7,12 obtenue[1]

MICHEL BARON, SYLVIANE GIORGI-RENAULT, JEAN RENAULT[2] ET PATRICK MAILLIET

Département de chimie organique, Faculté des Sciences pharmaceutiques et biologiques (Université René Descartes), 4 avenue de l'Observatoire, 75270 Paris Cédex 06, France

ET

DANIEL CARRÉ ET JEAN ETIENNE

Département de physique, Faculté des Sciences pharmaceutiques et biologiques (Université René Descartes), 4 avenue de l'Observatoire, 75270 Paris Cédex 06, France

Reçu le 11 juillet 1983

MICHEL BARON, SYLVIANE GIORGI-RENAULT, JEAN RENAULT, PATRICK MAILLIET, DANIEL CARRÉ et JEAN ETIENNE. Can. J. Chem. **62**, 526 (1984).

La butanedione réagit à chaud avec la diamino-1,2 anthraquinone pour donner, non pas la diméthyl-2,3 naphto[2,3-*f*]quinoxalinedione-7,12 **3** attendue, mais l'(hydroxy-2 méthyl-2 oxo-3 butyl)-2 méthyl-3 naphto[2,3-*f*]quinoxalinedione-7,12 **4***a* dont la structure est établie par diffraction de rayons-X. Elle cristallise dans le groupe d'espace triclinique $P\bar{1}$ avec les dimensions de maille a = 9,091 (1), b = 16,966 (4), c = 12,375 (3) Å, α = 100,75 (2), β = 101,83 (2), γ = 100,29 (2)°, V = 1789 Å^3, Z = 4. La structure a été résolue par des méthodes directes et affinée jusqu'à une valeur de R = 0,039 pour 3027 réflexions indépendantes. La conformation générale de la molécule est sensiblement plane. La caractéristique principale est la présence de deux cycles potentiels dûs à une liaison hydrogène bifurquée intramoléculaire. La diméthyl-2,3 naphto[2,3-*f*]quinoxalinedione-7,12 est l'intermédiaire de la réaction.

MICHEL BARON, SYLVIANE GIORGI-RENAULT, JEAN RENAULT, PATRICK MAILLIET, DANIEL CARRÉ, and JEAN ETIENNE. Can. J. Chem. **62**, 526 (1984).

Butanedione reacts on heating with 1,2-diaminoanthraquinone to give, not the expected 2,3-dimethylnaphtho[2,3-*f*]quinoxaline-7,12-dione **3**, but 2-(2-hydroxy-2-methyl-3-oxobutyl)-3-methylnaphtho[2,3-*f*]quinoxaline-7,12-dione **4***a* whose structure was established by X-ray diffraction. This compound crystallizes in the triclinic $P\bar{1}$ space group with unit cell dimensions of a = 9.091 (1), b = 16.966 (4), c = 12.375 (3) Å; α = 100.75 (2), β = 101.83 (2), γ = 100.29 (2)°, V = 1789 Å^3, Z = 4. The structure was resolved by the direct method and refined to R = 0.039 for 3027 independent reflections. The overall conformation of the molecule is essentially planar. The principal characteristic is the presence of two cyclic arrangements caused by intramolecular hydrogen bonding. 2,3-Dimethylnaphtho[2,3-*f*]quinoxaline-7,12-dione is the intermediate in this reaction.

[Journal translation]

Introduction

Dans un travail précédent (2), il a été constaté que les quinoxalinediones-5,8 sont peu cytotoxiques. Leur manque d'activité a été attribué à la trop faible surface de la molécule par rapport à celle des acridinediones-1,4 (3). Nous avons donc préparé des benzo[*g*]quinoxalinediones-5,10, dont certaines se montrent très actives (à paraître). Pour augmenter encore la surface de la molécule, nous avons tenté la synthèse de la diméthyl-2,3 naphto[2,3-*f*]quinoxalinedione-7,12 **3** par condensation classique de la diamino-1,2 anthraquinone **1** avec la butanedione **2** selon le schéma 1. Or quelles que soient les conditions opératoires (réaction de l'amine **1** avec la dicétone **2** en quantités équimolaires en présence d'acide acétique à 80°C ou mieux chauffage de l'amine **1** dans la butanedione à l'ébullition), on n'obtient pas le dérivé diméthylé **3** mais un seul produit qui, d'après les résultats de la microanalyse et les données spectrales (ir et rmn) répond à la formule d'un des racémiques **4***a* ou **4***b*. La diffraction de rayons-X permet de lui attribuer la structure **4***a*. Cette molécule essayée selon la technique décrite dans la réf. 3 ne possède aucune cytotoxicité sur la cellule leucémique L1210.

[1] Précedente publication: voir la réf. 1.

[2] Auteur à qui toute correspondance doit être adressée.

Résultats et discussion

A. *Structure*

Le spectre ir montre la présence d'une liaison hydrogène intramoléculaire forte (bande intense fine à 3400 cm^{-1}). La rmn corrobore ce fait: le proton alcoolique est déblindé à 7,41 ppm. On constate également que les deux protons du CH_2 sont inéquivalents ($\Delta\delta \simeq 0{,}7$ ppm) et fortement couplés (J = 20 Hz) par la présence du carbone chiral en α qui les rend diastéréotopiques. Ces données sont compatibles avec les structures **4***a* ou **4***b*.

La structure **4***a* a été établie sans ambiguité par diffraction de rayons-X. Les coordonnées atomiques relatives et les facteurs d'agitation thermique isotropes équivalents obtenus sont rassemblés dans le tableau 1. L'unité asymétrique comprend deux molécules indépendantes, chacune correspondant à un énantiomère. La lettre A identifie les atomes correspondant à une molécule et la lettre B à l'autre molécule. Les distances interatomiques et les angles sont représentés sur les Figs. 1(*a*) et (*b*).

La structure **4***a*, dont la vue stéréoscopique de l'unité asymétrique est indiquée sur la Fig. 2, montre la présence d'une liaison hydrogène intramoléculaire bifurquée entre l'hydroxyle de la chaîne latérale et les atomes O(2) et N(1). En effet, H(O3) se trouve à une distance similaire des atomes O(2) et N(1) bien inférieure aux distances de Van der Waals. Les différentes grandeurs intéressant cette liaison hydrogène sont précisées sur

Can. J. Chem. Downloaded from www.nrcresearchpress.com by 210.87.254.5 on 09/06/12
For personal use only.

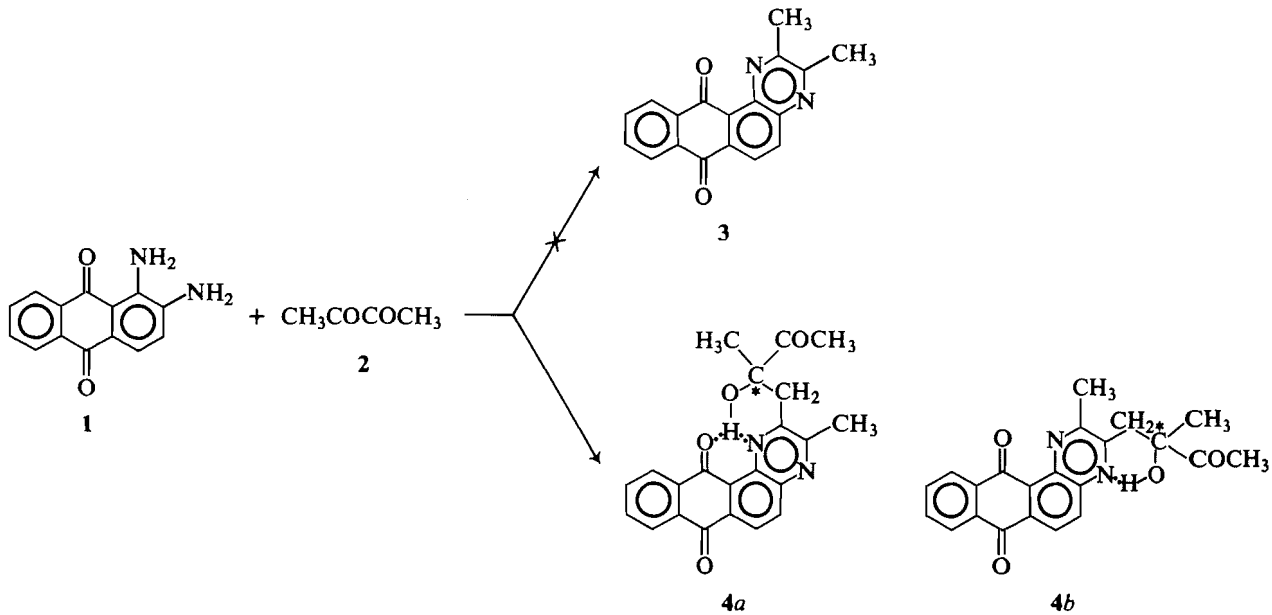

SCHÉMA 1

les Figs. 1(*a*) et (*b*).

L'intérêt de cette liaison hydrogène bifurquée est d'engendrer la formation de deux cycles potentiels de six atomes H(O3), N(1), C(2), C(13), C(14), O(3) et H(O3), N(1), C(12b), C(12a), C(12), O(2). Ce type de liaison a été décrit par la réf. 4 et les angles et distances relatives à cette liaison ont été rapportés aux calculs *ab initio* de Newton *et al.* (5). Dans le cas présent, les distances et les angles observés sont en accord avec ceux indiqués par ces auteurs.

Les molécules A et B présentent la même conformation qui est globalement plane. Une étude de planéité des différents cycles ou groupes d'atomes a été réalisée. Elle consiste à calculer par la méthode des moindres carrés le plan moyen déduit d'un ensemble d'atomes. Pour chaque plan moyen calculé, le tableau 2 indique l'équation de ce plan, la valeur du χ^2 et la distance de l'atome qui s'en écarte le plus, ce qui permet d'évaluer les éventuelles distorsions dans les cycles.[3]

Des angles dièdres entre plans moyens complètent la description: cycle IV et le plan formé par les atomes C(13)—C(2)—N(1)—H(O3)—O(3): A 7,55°; B 12,86°. Cycles IV et VI: A 11,87°; B 11,31°. Cycles VI et le plan formé par les atomes C(13)—C(2)—N(1)—H(O3)—O(3): A 4,35°; B 3,38°.

Ces différents résultats montrent que les molécules A et B présentent de légères dissemblances au plan typologique, les distorsions des cycles par rapport à la planéité attendue étant légèrement plus grandes pour la molécule B. Cette constatation se retrouve aussi au niveau des oxygènes O(1) et O(2) qui s'écartent très significativement du plan moyen du cycle II mais de manière plus importante pour la molécule B (O(1)B: 0,19 Å; O(2)B: 0,27 Å) que pour la molécule A (O(1)A: 0,06 Å; O(2)A: 0,14 Å).

La seule liaison hydrogène possible étant intramoléculaire, les deux molécules A et B indépendantes dans la maille cristalline sont reliées par des liaisons de van der Waals.

[3]On peut obtenir le tableau 2 et ces données à un prix nominal en s'adressant au Dépôt de données non publiées, ICIST, Conseil national de recherches du Canada, Ottawa (Ont.), Canada K1A 0S2.

B. *Origine de* **4**a

Le dérivé **4***a* provient de la condensation de deux moles de butanedione avec une mole de diamine **1**. Deux hypothèses peuvent rendre compte de la formation de **4***a*.

La première admet la dimérisation préalable de la dicétone **2** suivie de la condensation avec la diamine **1**. Diels *et al.* (6) ont montré que la butanedione se dimérise en présence de base forte (KOH) pour donner un composé qui, selon Birch et Moyle (7), est l'acétyl-5 diméthyl-2,5 hydroxy-2 oxo-3 tétrahydrofuranne, susceptible de réagir comme l'hydroxy-5 méthyl-5 heptatrione-2,3,6. Si cette dimérisation de la butanedione a lieu avec une base faible comme la diamine **1**, elle devrait également se produire avec la diamino-2,3 anthraquinone. Or, Gorelik (8) a montré que les pK_a de ces deux amines sont voisins (pK_a respectifs: 5,68 et 5,8) et que la diamine en −2,3 réagit normalement avec la butanedione.

Dans la deuxième hypothèse, le dérivé diméthylé **3** se forme et réagit ensuite sur une deuxième mole de dicétone **2**. Cette origine peut être retenue puisqu'en opérant la condensation à froid dans le tétrahydrofuranne, il est possible d'isoler une faible quantité de composé **3** dont la structure a été établie par rmn. Dans la butanedione à reflux, il se transforme rapidement en dérivé **4***a*.

L'un de nous (9) a proposé un mécanisme de cette réaction anormale.

Partie expérimentale

Etude chimique

Les spectres ^{1}H rmn sont enregistrés dans $CDCl_3$ sur appareil Brucker 270 MHz, les déplacements chimiques sont exprimés en ppm par rapport au HMDS pris comme référence interne; s = singulet, d = doublet, m = multiplet. Le spectre ir est réalisé sur spectromètre Perkin–Elmer 157G (KBr). Les résultats d'analyses (C,H,N) correspondent aux valeurs théoriques ± 0,4%.

(Hydroxy-2 méthyl-2 oxo-3 butyl)-2 méthyl-3 naphto[2,3-f]quinoxalinedione-7,12 **4**a

On chauffe à reflux sous azote pendant deux heures une solution de 11,9 g (0,05 mol) de diamino-1,2 anthraquinone dans 220 mL de butanedione. Après élimination de la cétone sous vide, on lave le solide à l'eau. On le chromatographie sur colonne de silice Merck

Can. J. Chem. Downloaded from www.nrcresearchpress.com by 210.87.254.5 on 09/06/12
For personal use only.

Can. J. Chem. Downloaded from www.nrcresearchpress.com by 210.87.254.5 on 09/06/12
For personal use only.

TABLEAU 1. Coordonnées relatives avec écarts-types et facteurs de température isotropes équivalents

Atome	x	y	z	B_{eq} (Å^2)
N(1)A	0,5013 (3)	0,4818 (2)	0,1853 (2)	3,4 (3)
C(2)A	0,3609 (4)	0,4818 (2)	0,1300 (3)	3,5 (3)
C(3)A	0,2333 (4)	0,4143 (2)	0,1167 (3)	3,7 (4)
N(4)A	0,2497 (3)	0,3547 (2)	0,1687 (2)	3,9 (4)
C(4a)A	0,3942 (4)	0,3551 (2)	0,2290 (3)	3,6 (4)
C(5)A	0,4118 (5)	0,2924 (2)	0,2865 (4)	4,6 (5)
C(6)A	0,5540 (5)	0,2886 (2)	0,3423 (4)	4,5 (4)
C(6a)A	0,6845 (4)	0,3461 (2)	0,3414 (3)	3,8 (4)
C(7)A	0,8376 (4)	0,3375 (2)	0,4052 (3)	4,0 (4)
C(7a)A	0,9776 (4)	0,3947 (2)	0,4022 (3)	3,8 (4)
C(8)A	0,1220 (5)	0,3872 (3)	0,4598 (3)	4,6 (5)
C(9)A	0,2534 (5)	0,4419 (3)	0,4606 (3)	5,0 (5)
C(10)A	0,2449 (5)	0,5047 (3)	0,4035 (3)	4,7 (5)
C(11)A	0,1020 (4)	0,5127 (2)	0,3450 (3)	3,9 (4)
C(11a)A	0,9680 (4)	0,4572 (2)	0,3437 (3)	3,4 (3)
C(12)A	0,8161 (4)	0,4661 (2)	0,2793 (3)	3,5 (3)
C(12a)A	0,6735 (4)	0,4100 (2)	0,2859 (3)	3,2 (3)
C(12b)A	0,5232 (4)	0,4163 (2)	0,2319 (3)	3,2 (3)
C(13)A	0,3386 (5)	0,5541 (2)	0,0800 (4)	4,3 (4)
C(14)A	0,4677 (4)	0,6318 (2)	0,1309 (3)	3,9 (4)
C(15)A	0,4827 (5)	0,6613 (2)	0,2578 (3)	4,1 (4)
C(16)A	0,6393 (6)	0,7024 (3)	0,3353 (4)	5,6 (6)
C(17)A	0,4296 (6)	0,7014 (3)	0,0745 (4)	5,1 (5)
C(18)A	0,0776 (5)	0,4091 (3)	0,0442 (4)	5,3 (5)
O(1)A	0,8417 (3)	0,2846 (2)	0,4601 (2)	5,6 (5)
O(2)A	0,8149 (3)	0,5167 (2)	0,2210 (2)	5,5 (5)
O(3)A	0,6120 (3)	0,6191 (2)	0,1100 (2)	4,5 (4)
O(4)A	0,3691 (3)	0,6531 (2)	0,2951 (3)	6,3 (6)
N(1)B	0,8499 (3)	0,0363 (2)	0,6362 (2)	3,1 (3)
C(2)B	0,8452 (4)	0,0151 (2)	0,7322 (3)	3,0 (3)
C(3)B	0,7297 (4)	−0,0521 (2)	0,7381 (3)	3,4 (3)
N(4)B	0,6224 (3)	−0,0951 (2)	0,6473 (2)	3,7 (4)
C(4a)B	0,6276 (4)	−0,0736 (2)	0,5462 (3)	3,2 (3)
C(5)B	0,5114 (4)	−0,1176 (2)	0,4483 (3)	3,6 (4)
C(6)B	0,5121 (4)	−0,0971 (2)	0,3467 (3)	3,6 (4)
C(6a)B	0,6276 (4)	−0,0328 (2)	0,3388 (3)	3,2 (3)
C(7)B	0,6174 (4)	−0,0122 (2)	0,2259 (3)	3,8 (4)
C(7a)B	0,7270 (4)	0,0599 (2)	0,2173 (3)	3,4 (3)
C(8)B	0,7087 (5)	0,0881 (3)	0,1173 (3)	4,4 (4)
C(9)B	0,8139 (5)	0,1543 (3)	0,1083 (3)	5,0 (5)
C(10)B	0,9430 (5)	0,1918 (3)	0,1976 (3)	4,7 (5)
C(11)B	0,9623 (4)	0,1636 (2)	0,2966 (3)	3,9 (4)
C(11a)B	0,8539 (4)	0,0991 (2)	0,3081 (3)	3,2 (3)
C(12)B	0,8750 (4)	0,0731 (2)	0,4181 (3)	3,1 (3)
C(12a)B	0,7467 (4)	0,0109 (2)	0,4326 (3)	2,8 (3)
C(12b)B	0,7428 (4)	−0,0086 (2)	0,5396 (3)	2,9 (3)
C(13)B	0,9676 (4)	0,0643 (2)	0,8366 (3)	3,4 (3)
C(14)B	1,0541 (4)	0,1462 (2)	0,8228 (3)	3,2 (3)
C(15)B	0,9407 (4)	0,2017 (2)	0,8000 (3)	3,5 (3)
C(16)B	0,9645 (6)	0,2581 (3)	0,7230 (4)	5,2 (5)
C(17)B	1,1732 (5)	0,1916 (3)	0,9346 (3)	4,1 (4)
C(18)B	0,7260 (6)	−0,0758 (3)	0,8491 (4)	4,6 (5)
O(1)B	0,5167 (3)	−0,0539 (2)	0,1432 (2)	5,7 (5)
O(2)B	0,9955 (3)	0,1023 (2)	0,4908 (2)	4,0 (4)
O(3)B	1,1389 (3)	0,1349 (2)	0,7389 (2)	3,7 (3)
O(4)B	0,8366 (3)	0,1999 (2)	0,8465 (2)	5,2 (4)
H(5)A	0,3165 (48)	0,2502 (25)	0,2869 (34)	
H(6)A	0,5648 (47)	0,2464 (25)	0,3804 (35)	
H(8)A	0,8750 (48)	0,6619 (26)	0,4993 (36)	
H(9)A	0,6452 (50)	0,5636 (26)	0,5028 (36)	
H(10)A	0,3426 (51)	0,5447 (27)	0,4018 (35)	
H(11)A	0,0968 (47)	0,5565 (25)	0,2998 (34)	
H(131)A	0,6781 (48)	0,4644 (25)	0,0026 (37)	
H(132)A	0,2391 (49)	0,5697 (24)	0,0939 (35)	
H(161)A	0,6939 (54)	0,6573 (29)	0,3211 (38)	
H(162)A	0,6198 (52)	0,7177 (27)	0,4192 (41)	
H(163)A	0,6845 (52)	0,7463 (29)	0,3019 (39)	
H(171)A	0,3264 (53)	0,7129 (27)	0,0856 (36)	
H(172)A	0,5714 (50)	0,3183 (27)	0,0088 (39)	
H(173)A	0,5083 (52)	0,7543 (28)	0,1097 (37)	
H(181)A	0,0354 (55)	0,4504 (30)	0,0696 (39)	
H(182)A	0,9142 (52)	0,5770 (28)	0,0289 (41)	
H(183)A	0,0034 (55)	0,3598 (30)	0,0430 (38)	
H(O3)A	0,6289 (48)	0,5758 (26)	0,1464 (35)	
H(5)B	0,4331 (44)	0,8374 (23)	0,4564 (31)	
H(6)B	0,4306 (46)	0,8758 (24)	0,2785 (33)	
H(8)B	0,6079 (48)	0,0594 (25)	0,0519 (36)	
H(9)B	0,7957 (49)	0,1737 (26)	0,0381 (37)	
H(10)B	0,0146 (49)	0,2375 (26)	0,1870 (35)	
H(11)B	0,0472 (46)	0,1912 (24)	0,3601 (34)	
H(131)B	0,0746 (43)	0,9280 (23)	0,0942 (33)	
H(132)B	0,9604 (44)	0,9701 (23)	0,1441 (32)	
H(161)B	0,9267 (52)	0,7025 (26)	0,2458 (36)	
H(162)B	0,1107 (51)	0,7054 (27)	0,2723 (35)	
H(163)B	0,0240 (51)	0,7674 (27)	0,3455 (38)	
H(171)B	0,8812 (49)	0,8003 (25)	0,0012 (37)	
H(172)B	0,7442 (50)	0,8415 (26)	0,0511 (35)	
H(173)B	0,7732 (49)	0,7561 (28)	0,0741 (35)	
H(181)B	0,3631 (53)	0,1201 (28)	0,1592 (37)	
H(182)B	0,2826 (51)	0,0311 (28)	0,0940 (39)	
H(183)B	0,1791 (54)	0,0862 (27)	0,1178 (38)	
H(O3)B	0,9268 (45)	0,8882 (24)	0,3307 (34)	

(0,2–0,5 mm) (solvant: chloroforme); (8 g) 43%; F = 213°C (chlorure de méthylène – éther de pétrole); ir: 1670 et 1705 (C=O), 3400 (O—H lié) cm^{-1}; ^{1}H rmn, δ: 1,47 (s, 3, CH_3—C(=O)—O), 2,37 (s, 3, CH_3—C(=O)—), 2,73 (s, 3, CH_3 en 3), 3,08 (d, 1, 1H du CH_2, J(H—C—H) = 20 Hz), 3,79 (d, 1, 1H du CH_2), 7,41 (s, 1, OH, éch D_2O), 7,77 (m, 2, H-9, -10), 8,27 (m, 3, H aromatiques), 8,55 (d, 1, H-5 ou -6, J(H-5/H-6) = 8,5 Hz).

Diméthyl-2,3 naphto[2,3-f]quinoxalinedione-7,12 3

On agite à la température ambiante sous azote pendant 21 jours une suspension de 0,5 g (0,0021 mol) de diamino-1,2 anthraquinone dans un mélange de 0,18 g de butanedione (0,0021 mol) et de 200 mL de tétrahydrofuranne (THF). Après évaporation du THF, on lave le solide à l'eau puis l'extrait au CH_2Cl_2 que l'on évapore sous pression réduite. Le produit obtenu (0,13 g) est chromatographié sur colonne d'alumine Merck (0,063–0,200 mm) (solvant: éther de pétrole/CH_2Cl_2 65:35). On obtient 3 mg (0,5%) d'un dérivé beige clair monotache en chromatographie sur couche mince d'alumine GF 254 Merck (solvant: benzène/$CHCl_3$ 35:65); F = 180°C (décomposition); ^{1}H rmn, δ: 2,73 (s, 3, CH_3 en 3), 2,85 (s, 3, CH_3 en 2), 7,77 (m, 2, H-9, -10), 8,27 (m, 3, H aromatiques), 8,55 (d, 1, H-5 ou -6, J(H-5/H-6) = 8,5 Hz).

Etude cristallographique

$C_{22}H_{18}N_2O_4$ M = 374,3

Triclinique, a = 9,091 (1), b = 16,966 (4), c = 12,375 (3) Å, α = 100,75 (2), β = 101,83 (2), γ = 100,29° (2), V = 1789 Å^3, Z = 4, d_c = 1,39, d_o = 1,40 (2) g cm^{-3}, 20°C, MoK$_\alpha$ λ = 0,707 Å, μ = 1,03 cm^{-1}.

Les cristaux sont obtenus par évaporation lente, à l'abri de la lumière, d'une solution de **4*a*** dans un mélange de chloroforme et de propanol.

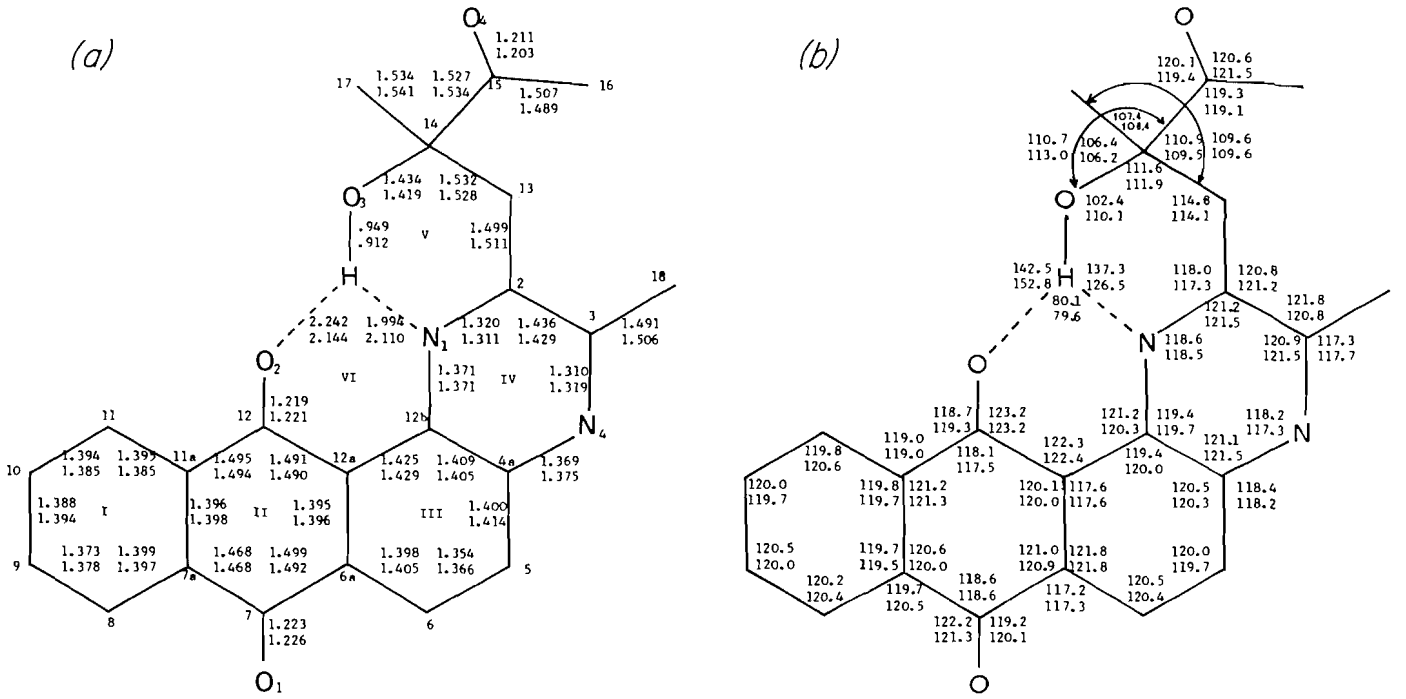

FIG. 1. (*a*) Distance (Å) entre les différents atomes lourds. La valeur supérieure correspond à la molécule A et la valeur inférieure à la molécule B. Les écart-types sont de 0,005 Å. (*b*) Angles (°) entre les différents atomes lourds. La valeur supérieure correspond à la molécule A et la valeur inférieure à la molécule B. Les écart-types sont de 0,3°.

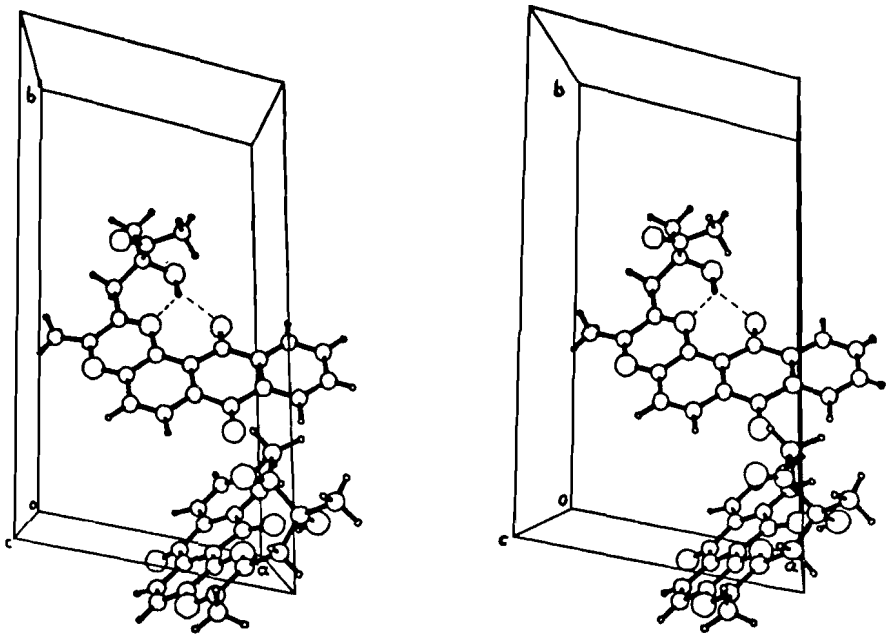

FIG. 2. Vue stéréoscopique de l'unité asymétrique. La liaison hydrogène bifurquée est en pointillé.

L'étude de la structure est effectuée sur un monocristal ayant la forme d'une aiguille allongée parallèlement à C, de dimensions 150 × 200 × 500 μm. L'absence de symétrie observée sur les clichés de Weissenberg correspond aux deux seuls groupes $P1$ et $P\bar{1}$. 5000 réflexions indépendantes telles que $2\theta \leq 50°$ sont mesurées sur un diffractomètre automatique à quatre cercles Syntex en utilisant le rayonnement K_α du molybdène (monochromateur de graphite). Seules sont conservées les 3027 réflexions indépendantes dont les intensités I sont telles que $I > 3\sigma(I)$, $\sigma(I)$ étant l'écart-type sur la mesure de l'intensité I. Ces intensités sont corrigées des facteurs de Lorentz polarisation et mises en échelle absolue par la méthode statistique de Wilson. Les facteurs de structure normalisés E sont calculés pour toutes les réflexions en prenant comme facteur d'agitation thermique celui obtenu par la méthode statistique de Wilson, soit $B = 4{,}3$ Å^2. La distribution statistique de ces facteurs de structure normalisés permet de prévoir la présence d'un centre de symétrie, ce qui nous conduit à choisir le groupe d'espace $P\bar{1}$. La structure est déterminée par utilisation des méthodes directes (programme MULTAN (10)). Le calcul de la densité électronique correspondant à la meilleure figure de mérite permet de déterminer la position de 48 atomes lourds sur 56. Les 8 atomes lourds restant ainsi que tous les atomes d'hydrogène sont positionnés par examen de différences de Fourier. Les facteurs de

Can. J. Chem. Downloaded from www.nrcresearchpress.com by 210.87.254.5 on 09/06/12
For personal use only.

diffusion sont ceux donnés par la réf. 11. L'affinement de la structure est effectué avec le programme à matrice complète ORFLS (12) en faisant varier indépendamment et successivement d'une part les coordonnées atomiques de tous les atomes, y compris les atomes d'hydrogène, et d'autre part les facteurs de température anisotropes des seuls atomes lourds. Nous donnons aux atomes d'hydrogène les facteurs de température isotropes équivalents de l'atome lourd correspondant. Après correction de l'extinction secondaire, on obtient pour l'ensemble des 3027 réflexions un facteur $R = \Sigma||F_o| - |F_c||/\Sigma|F_o|$ de 0,039 et un facteur $R_w = (\Sigma w(|F_o| - |F_c|)^2/\Sigma w|F_o|^2)^{1/2}$ de 0,40.

Remerciements

Les auteurs remercient l'INSERM de l'aide matérielle qui leur a été apportée (contrat de recherche libre 78.1160-3) et S. Cros pour la détermination de la cytotoxicité.

1. J. RENAULT, S. GIORGI-RENAULT, M. BARON, P. MAILLIET, C. PAOLETTI, S. CROS et E. VOISIN. J. Med. Chem. Sous presse.
2. J. RENAULT, M. BARON, P. MAILLIET, S. GIORGI-RENAULT, C. PAOLETTI et S. CROS. Eur. J. Med. Chem. **16**, 545 (1981).
3. J. RENAULT, S. GIORGI-RENAULT, P. MAILLIET, M. BARON, C. PAOLETTI et S. CROS. Eur. J. Med. Chem. **16**, 24 (1981).
4. L. DUPONT, O. DIDEBERG, J. DELARGE, G. DIVE et L. THUNUS. Acta Crystallogr. Sect. B, **38**, 1495 (1982).
5. M. D. NEWTON, G. A. JEFFREY et S. TAKAGI. J. Am. Chem. Soc. **101**, 1997 (1979).
6. O. DIELS, W. M. BLANCHARD et H. V. D. HEYDEN. Ber. 2355 (1914).
7. A. J. BIRCH et C. J. MOYLE. J. Chem. Soc. 412 (1957).
8. M. V. GORELIK, H. IV. KWONG, N. P. VINOGRADOVA et B. A. KOROLEV. J. Org. Chem. (USSR) **12**, 2503 (1976).
9. M. BARON. Etude de quinones dérivées d'hétérocycles azotés à activité antitumorale potentielle. Thèse Doct. ès Sciences pharmaceutiques, Université R. Descartes, Paris. 1982.
10. G. GERMAIN, P. MAIN et M. M. WOOLFSON. Acta Crystallogr. Sect. A, **27**, 208 (1971).
11. International tables for X-ray crystallography. Tome IV. Kynoch Press, Birmingham. 1974.
12. W. R. BUSING, K. O. MARTIN et H. A. LEVY. ORFLS. Report ORNL-TM-305. Oak Ridge National Laboratory, Tennessee. 1962.

Can. J. Chem. Downloaded from www.nrcresearchpress.com by 210.87.254.5 on 09/06/12
For personal use only.

Studies on the biosynthesis of the sterpurenes[1]

WILLIAM A. AYER, THOMAS T. NAKASHIMA, AND M. HOSSEIN SAEEDI-GHOMI
Department of Chemistry, University of Alberta, Edmonton, Alta., Canada T6G 2G2

Received August 29, 1983

WILLIAM A. AYER, THOMAS T. NAKASHIMA, and M. HOSSEIN SAEEDI-GHOMI. Can. J. Chem. **62**, 531 (1984).

The sterpurenes are a unique group of sesquiterpenes produced by the fungus *Stereum purpureum*. Biosynthetic studies utilizing [1-^{13}C] and [2-^{13}C] acetate indicate that sterpuric acid (**2**) and sterpurene-3,12,14-triol (**3**) are formed from acetate via humulene (**5**) and the protoilludane cation (**6**) by one of the paths shown in Scheme 2.

WILLIAM A. AYER, THOMAS T. NAKASHIMA et M. HOSSEIN SAEEDI-GHOMI. Can. J. Chem. **62**, 531 (1984).

Les sterpurènes sont un groupe unique de sesquiterpènes qui sont produits par le *Stereum purpureum*. Des études de biosynthèse utilisant des acétates [1-^{13}C] et [2-^{13}C] indiquent que l'acide sterpurique (**2**) et que le sterpurènetriol-3,12,14 (**3**) se forment à partir de l'acétate via l'humulène (**5**) et que le cation protoilludane (**6**) se forme par une des voies représentées dans le schéma 2.

[Traduit par le journal]

The sterpurenes are a unique type of sesquiterpene possessing the carbon skeleton **1** (1, 2). They are produced by the fungus *Stereum purpureum* (class Basidiomycetes), the causative agent of the so-called silver leaf disease of many fruit and ornamental trees (3). The hydrocarbon **1** has been isolated from the mycelium of *S. purpureum* (2), while sterpuric acid (**2**) and sterpurene-3,12,14-triol (**3**) are the major components of the broth extract (1, 2). The latter two compounds have been utilized in the biosynthetic studies described below.

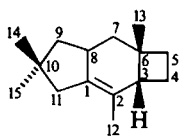

1

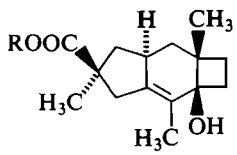

2 R = H
2*a* R = CH_3

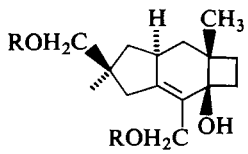

3 R = H
3*a* R = $COCH_3$

The sterpurene skeleton may be derived from farnesyl pyrophosphate via humulene without rearrangement as shown in Scheme 1. In fact, this "biogenetic" consideration was useful in the determination of the structure of sterpuric acid (**2**) (1). Farnesyl pyrophosphate is derived in nature from acetate via mevalonic acid[2] and "active isoprene". To determine whether a pathway such as is shown in Scheme 1 is followed, we have undertaken a study of the incorporation of ^{13}C-labelled acetate by *S. purpureum* into sterpuric acid (**2**) and sterpurenetriol (**3**).

In order to follow the labelling pattern of ^{13}C enriched metabolites, it was first necessary to assign the chemical shifts of the carbons of methyl sterpurate (**2***a*, the ester is much more soluble in $CDCl_3$ than sterpuric acid itself) and the 12,14-*O*,*O*-diacetyl derivative (**3***a*) of sterpurenetriol (**3**) (again chosen for solubility reasons). The chemical shift assignments are shown in Table 1. These assignments are based largely on off-

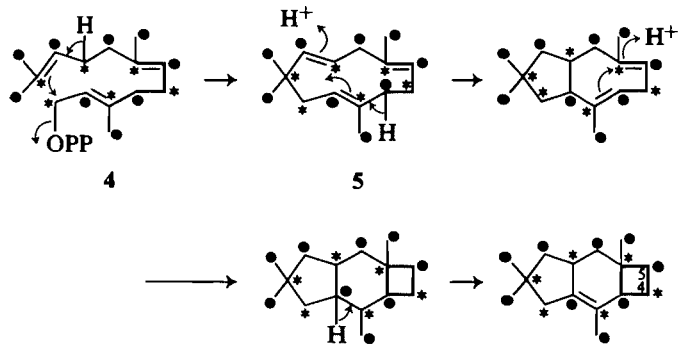

SCHEME 1

resonance and single frequency decoupling (selective proton decoupling) experiments (5). The assignments of sp^2 carbons and the quaternary carbons are based on comparison of the chemical shifts of these centers with reference compounds reported in the literature (6).

Incorporation of ^{13}C-labelled acetate by cyclization of farnesyl pyrophosphate (**4**) to humulene (**5**) and subsequent cyclization as depicted in Scheme 1 would give rise to labelling as shown, where the asterisked carbons arise from the carboxyl group of acetate, and the dotted carbons originate from the methyl group. *S. purpureum* was grown in liquid culture in the presence of [1-^{13}C] acetate and, separately, in the presence of [2-^{13}C] acetate. Examination of the proton noise decoupled ^{13}C nmr spectrum of methyl sterpurate (**2***a*) isolated from the culture containing [1-^{13}C] acetate showed that carbons 2, 5, 6, 8, 10, and 11 were enriched (about 5% incorporation) relative to the natural abundance spectrum. This is consistent with the pathway shown in Scheme 1 *except that this route predicts enrichment at C-4 rather than C-5*. The spectrum also exhibits induced couplings between C-5 and C-6, indicating that rearrangement has occurred at some point during the formation of sterpuric acid. To our disappointment, when *S. purpureum* was grown in the presence of [2-^{13}C] acetate, we were unable to isolate sufficient sterpuric acid to obtain a ^{13}C nmr spectrum. Fortunately, however, it was possible to isolate sufficient quantities of enriched sterpurene-3,12,14-triol (**3**) from both the [1-^{13}C] and the [2-^{13}C] acetate experiments. The ^{13}C nmr spectra of the diacetyl triol **3***a* derived from [1-^{13}C] acetate showed the same labelling pattern as that of methyl sterpurate (**2***a*); again C-2, C-5 (and not C-4), C-6, C-8, C-10, and C-11 were

[1] Presented in part at the 28th IUPAC Congress, Vancouver, B.C., Aug. 1981. Abstract OR4.

[2] For a review of terpenoid biosynthesis, see ref. 4.

Can. J. Chem. Downloaded from www.nrcresearchpress.com by 210.87.254.105 on 09/06/12
For personal use only.

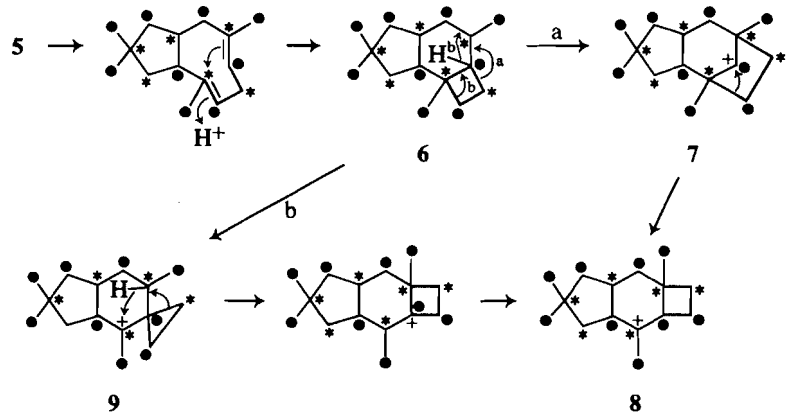

SCHEME 2

TABLE 1. Carbon-13 chemical shifts of methyl sterpurate (**2***a*) and 12,14-*O*,*O*-diacetylsterpurene-3,12,14-triol (**3***a*)

Carbon	**2***a* δ (multiplicity)	**3***a* δ (multiplicity)
1	138.3 (s)	147.6 (s)
2	127.8 (s)	127.2 (s)
3	73.4 (s)	72.9 (s)
4	34.4 (t)	35.3 (t)
5	22.1 (t)	22.1 (t)
6	43.9 (s)	44.2 (s)
7	34.9 (dd)	35.2 (dd)
8	36.8 (d)	37.1 (d)
9	44.3 (t)	42.9 (dd)
10	47.1 (s)	40.6 (s)
11	41.3 (dd)	40.0 (t)
12	12.8 (q)	62.1 (t)
13	23.4 (q)	23.9 (q)
14	178.6 (s)	72.4 (t)
15	25.4 (q)	24.9 (q)
2 × —O—C(=O)—CH$_3$		171.2 (s)
—O—C(=O)—CH$_3$		21.0 (q)
—O—C(=O)—CH$_3$		20.9 (q)
—C(=O)—O—CH$_3$	51.9 (q)	

enriched. This spectrum also exhibits induced coupling between C-5 and C-6 (J = 29.1 Hz) and C-10 and C-11 (J = 34.3 Hz). The ^{13}C nmr spectrum of **3***a* obtained from the [2-^{13}C] acetate labelling experiment shows enrichment at C-1, C-3, C-4, C-7, C-9, and at the C-methyl and hydroxymethyl carbons. Again this is as expected for the pathway illustrated in Scheme 1, *except that C-4 is enriched rather than C-5*. Induced coupling between C-3 and C-4 (J = 31.4 Hz) is observed in this case. These findings indicate that a molecular rearrangement is occurring at some point in the transformation of farnesyl pyrophosphate to the sterpurenes.

Many sesquiterpenoid metabolites of fungi of the class Basidiomycetes arise via humulene (**5**) and the so-called protoilludane cation (**6**, Scheme 2) (7). Rearrangement of cation **6** to the bicyclo[3.2.1]octane cation **7**, followed by another 1,2-shift as indicated in Scheme 2 leads to the sterpurane cation **8** in which the labelling pattern is that observed in the labelling studies. Alternatively, the protoilludane cation **6** may undergo rearrangement to the illudane cation **9** which on ring expansion as shown in Scheme 2 also leads to the sterpurane skeleton. Provided that the latter rearrangement is stereoselective, this would also account for the observed labelling pattern. We thus feel that the sterpurenes arise via humulene (**5**) and the protoilludane cation (**6**) by one of the pathways illustrated in Scheme 2.

Finally, it is worthwhile to point out that we have previously suggested that the sterpurane cation **8** may be the precursor of the so-called isolactarane sesquiterpenoids (8).

Experimental

Instrumentation

The ^{13}C nmr spectra were determined in chloroform-d_1 (1% tetramethylsilane as standard) at a concentration of 3.6% w/v for methyl sterpurate (**2***a*) and 5.6% w/v for samples of 12,14-*O*,*O*-diacetylsterpuren-3,12,14-triol (**3***a*) in 5-mm sample tubes using a Bruker WH-400 spectrometer operating in the Fourier transform mode.

Materials

Sodium [1-^{13}C] acetate and sodium [2-^{13}C] acetate (90% enriched) were purchased from Merck, Sharp and Dohme Canada Ltd. Column chromatography was carried out using Macherey Nagel Kieselgel (0.08 mm, 100 g/g substrate). Flash chromatography was carried out using Merck silica gel 60 (0.040–0.063 mm). All compounds for which spectral data are reported showed single spots on tlc using at least two different solvent systems.

*Incorporation of ^{13}C-labelled acetate into sterpuric acid (**2**) and sterpurene-3,12,14-triol (**3**)*

Stereum purpureum (strain C-663, Canadian Forestry Service) was grown in liquid still culture at room temperature in a medium of malt extract (25 g/L), dextrose (13 g/L), and peptone (0.7 g/L) in 2.8-L Fernbach flasks (1 liter of medium per flask). After ten days of growth, sodium [1-^{13}C] acetate (0.082 g, 1 mmol) dissolved in sterile water (5 mL) was injected into each flask. After a further 7, and then 14, days another 1.0 mmol of labelled acetate was injected into each flask. After a total of 30 days of growth the mycelium was removed by filtration and the broth was extracted three times with an equal volume of ethyl acetate. The ^{13}C-enriched samples of sterpuric acid and sterpurenetriol were isolated as previously described (1, 2). Methyl sterpurate (**2***a*) (1) and 12,14-*O*,*O*-diacetylsterpurene-3,12,14-triol (**3***a*) (2) were prepared as previously described.

The experiments with sodium [2-^{13}C] acetate were carried out in the same way as described above for [1-^{13}C] acetate.

Acknowledgements

We thank the Natural Sciences and Engineering Research

Can. J. Chem. Downloaded from www.nrcresearchpress.com by 210.87.254.105 on 09/06/12
For personal use only.

Council of Canada for financial support, and Dr. Y. Hiratsuka, Northern Forest Research Centre, Edmonton, for slant tube cultures of *S. purpureum*.

1. W. A. AYER, M. H. SAEEDI-GHOMI, D. VAN ENGEN, B. TAGLE, and J. CLARDY. Tetrahedron, **37**, Suppl. No. 1, 379 (1981).
2. W. A. AYER and M. H. SAEEDI-GHOMI. Can. J. Chem. **59**, 2536 (1981).
3. C. WESTCOTT. Plant disease handbook. 3rd ed. Van Nostrand Reinhold, Toronto. 1971. pp. 354–355.
4. D. V. BANTHORPE and B. V. CHARLWOOD. *In* Chemistry of the terpenes and terpenoids. *Edited by* A. A. Newman. Academic Press, New York, NY. 1972. pp. 337–411.
5. A. A. MCINNES, J. A. WALTER, J. L. C. WRIGHT, and L. C. VINING. *In* Topics in carbon-13 nmr spectroscopy. Vol. 2. *Edited by* J. C. Levy. John Wiley and Sons, New York, NY. 1976. p. 125.
6. J. B. STOTHERS. Carbon-13 nmr spectroscopy. Academic Press, New York, NY. 1972. pp. 150, 168, 188, 296, 430, 435, 436.
7. W. A. AYER and L. M. BROWNE. Tetrahedron Report No. 110, Tetrahedron, **37**, 2199 (1981).
8. W. A. AYER and M. H. SAEEDI-GHOMI. Tetrahedron Lett. **22**, 2071 (1981).

Can. J. Chem. Downloaded from www.nrcresearchpress.com by 210.87.254.105 on 09/06/12
For personal use only.

Ambident nucleophilic reactivity in σ-complex formation. Part 5.[1] Reaction of 1-phenyl-2,4,6-trinitrobenzene with methoxide and phenoxide ions

ERWIN BUNCEL, SURESH KUMAR MURARKA, AND ALBERT RICHARD NORRIS
Department of Chemistry, Queen's University, Kingston, Ont., Canada K7L 3N6

Received June 13, 1983

ERWIN BUNCEL, SURESH KUMAR MURARKA, and ALBERT RICHARD NORRIS. Can. J. Chem. **62**, 534 (1984).

The reactions of 1-phenyl-2,4,6-trinitrobenzene (**4**) with methoxide and phenoxide ions in DMSO and DMSO–methanol solutions have been investigated. MeO^- gives rise to a 1,3 adduct through kinetic control and a 1,1 adduct through thermodynamic control. These processes persist also in the reaction of **4** with potassium phenoxide in DMSO–methanol. However, reaction of **4** with potassium phenoxide in DMSO gives rise to a 1,3 adduct as the only observed species in which phenoxide is bonded to the nitroaromatic moiety via the *para* phenoxy carbon, in accord with previous observations on the ambident reactivity of phenoxide ion. The results are considered in terms of various steric and electronic effects and it is concluded that *F*-strain, relief of steric compression, and delocalizability considerations play dominant roles in accounting for the observed reaction course.

ERWIN BUNCEL, SURESH KUMAR MURARKA et ALBERT RICHARD NORRIS. Can. J. Chem. **62**, 534 (1984).

On a étudié les réactions du phényl-1 trinitro-2,4,6 benzène (**4**) avec les ions méthanolates et phénolates en solution dans le DMSO et dans le mélange DMSO–méthanol. L'ion MeO^- donne des adduits 1,3 qui sont des produits de contrôle cinétique et des adduits 1,1 résultant du contrôle thermodynamique. Ce processus se manifeste également dans la réaction du composé **4** avec le phénolate de potassium dans le mélange DMSO–méthanol. Cependant, cette même réaction effectuée dans le DMSO conduit à un adduit 1,3; c'est la seule espèce observée dans laquelle l'ion phénolate est lié à la portion nitroaromatique par l'intermédiaire du carbone en position *para* du groupe phénoxy en accord avec les observations antérieures relatives à l'ion phénolate qui possède deux positions de réaction. On considère ces résultats en fonction des effets stériques et électroniques et on conclut que l'encombrement *F*, la décompression stérique et la possibilité de délocalisation jouent un rôle majeur dans l'évolution de la réaction.

[Traduit par le journal]

Can. J. Chem. Downloaded from www.nrcresearchpress.com by 210.87.254.6 on 09/06/12
For personal use only.

As part of a continuing study on the interactions of nitroaromatic compounds with bases (1–3), in this paper we present results pertaining to the formation of 1,1 and 1,3 σ-complexes and the ambident reactivity of phenoxide ion (4).

Among the various structure–reactivity relationships in σ-complex formation processes (5–11), one which has received considerable attention is the generally observed kinetic preference for 1,3, and thermodynamic preference for 1,1 adduct formation, in the reactions of bases with 1-X-2,4,6-trinitrobenzenes and related substrates. The first instance of this type of result was the discovery by Servis in 1965 (12) through ^1H nmr spectroscopy that 2,4,6-trinitroanisole (TNA, **1**), on reaction with methoxide ion in dimethyl sulfoxide (DMSO) – methanol solution (90:10 v/v), yielded initially the 1,3 adduct (**2**), which then decayed and was replaced by the more stable 1,1 adduct (**3**), Scheme 1.

While in the majority of subsequent studies this trend in kinetic versus thermodynamic control was confirmed, several exceptions have been observed (13–15). Hence it appeared that a unique theory for this phenomenon could not apply and several proposals evolved to account for its origin (*vide infra*). It occurred to us that structural modification could produce useful information and, while use of alkyl substituted nitroaromatics could be considered, study of 2,4,6-trinitrotoluene has shown that alkoxide ion can partake in proton abstraction to give a nitrobenzylic anion in addition to σ-complex formation (16–19). On the other hand, use of 1-phenyl-2,4,6-trinitrobenzene (**4**) would preclude proton abstraction from occurring, while providing a model to test the importance of steric and delocalization effects. In addition to choosing methoxide as the standard nucleophile, we selected phenoxide ion in the expectation that this could act either as an oxygen nucleophile

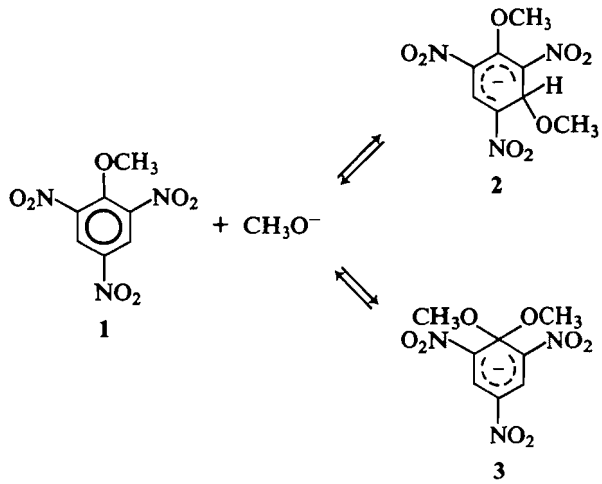

SCHEME 1

to yield **5** and/or **6**, or as a carbon nucleophile to give **7** and/or **8**. The ability of phenoxide to act as an ambident nucleophile towards 1,3,5-trinitrobenzene (TNB) has been reported previously (20–23). Similar observations have been made with naphthoxide (24) and indolide (25) anions.

Previous work on anionic σ-complexes (5–7) has shown that structural characterization of these species can generally be accomplished through ^1H nmr spectroscopy. However, uv–visible absorption spectroscopy can provide valuable supporting evidence, especially in differentiating between bonding via oxygen or via carbon in the case of a potential ambident nucleophile such as phenoxide ion. As will be shown in the following, the results of these studies have in fact allowed complete structural characterization of the σ-complexes formed in the reaction of **4** with methoxide and phenoxide ions as nucleophiles. The significance of the findings is considered.

[1] Parts 3 and 4: see refs. 39 and 40.

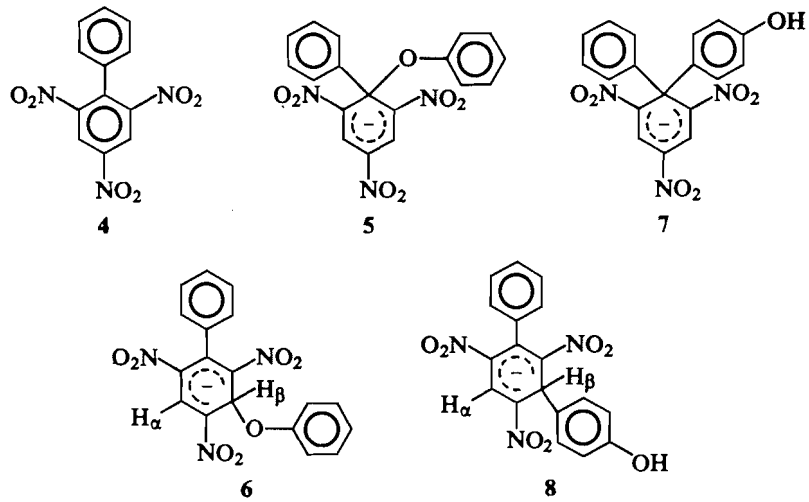

Results

σ-Complex formation between 4 and methoxide

An orange-red colored solution resulted on addition of equimolar methanolic sodium methoxide to **4** in $(CD_3)_2SO$ (final solvent composition, 90:10 v/v $(CD_3)_2SO$/MeOH; reactant concentrations, 0.46 *M*). An nmr spectrum recorded 3 min after mixing showed the absence of a signal at δ 9.10 due to H-3(5) of **4**, and the appearance of new peaks at δ 8.68 (d, J = 1.5 Hz) and δ 6.25 (d, J = 1.5 Hz), integral ratio 1.1:1. An unresolved multiplet centered around δ 7.3 (5H) also present could be ascribed to the phenyl ring protons of the resulting complex. The region below δ 4.5 was blanked out by the solvent. On further monitoring of the spectra with time, the doublets at δ 6.25 and δ 8.68 were found to decrease while a singlet at δ 8.72 increased in intensity; after 8 h only the δ 8.72 singlet was present and had an integral value twice that of the doublets at δ 8.68 and δ 6.25 seen initially.

The above spectral changes can be interpreted as follows. The appearance of two doublets at δ 8.68 and 6.25 is ascribed to the H_α and H_β protons of **9**, while the singlet at δ 8.72 is assigned to $H_{\alpha'}$ of **10**. The chemical shift values observed correspond closely to literature data obtained for these types of protons (5–7). As well, the rapid formation of **9** followed by its slow transformation into **10** is in accord with previous observations on the kinetic preference for formation of 1,3 adducts, and their transformation into the thermodynamically more stable 1,1 complexes.

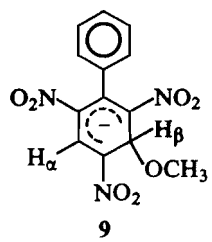

9

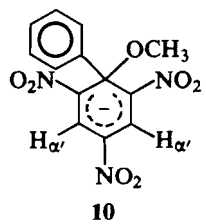

10

Complementary evidence was obtained by following the reaction course through uv–visible spectroscopy. In Fig. 1 are shown the visible absorption spectra, as a function of time, of solutions in DMSO–MeOH (90:10 v/v) obtained by ca. 1000-fold dilution of a reaction mixture having the same composition as in the nmr experiment. It is seen that initially the spectra exhibit absorption maxima at 428 and 506 nm but in time these maxima shift to 436 and 520 nm with a concurrent

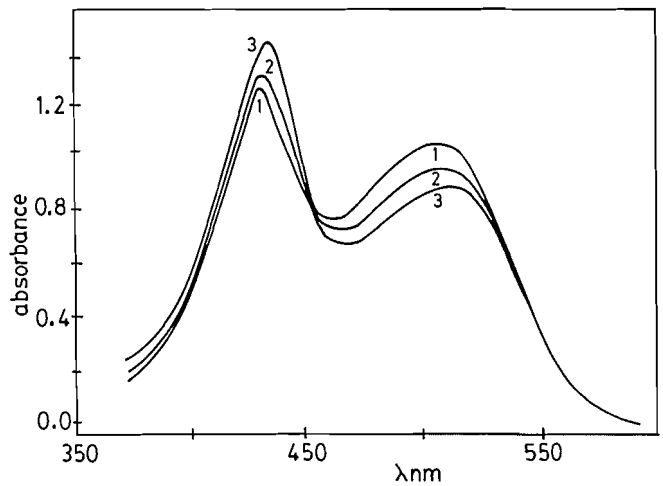

FIG. 1. Ultraviolet–visible absorption spectra as function of time in reaction of 1-phenyl-2,4,6-trinitrobenzene with methoxide ion in DMSO–methanol indicating transformation of 1,3 and 1,1 σ-complexes: (1) 1.5 min; (2) 3.5 h; (3) 24 h.

change in intensities. Addition of acid caused the absorptions to disappear. The acid lability and the general characteristics of these spectra, i.e. two absorptions with the one at lower wavelength the more intense, are typical of methoxide adducts of trinitrobenzene derivatives. Though these spectra do not differentiate between 1,3 and 1,1 adducts, they are, however, in complete agreement with our assignment. It is also of interest that, in the majority of systems studied in the past, the 1,3 adduct was formed as a transient intermediate whose visible spectrum could only be reconstructed through repeated stopped-flow experiments performed as a function of wavelength. Thus the present system appears to be one of the few where the spectrum of the metastable species, as well as its transformation, were readily measurable by standard spectrophotometric techniques.

Another estimate of the relative stabilities of the complexes **9** and **10** was obtained as follows. The diluted solutions whose spectra are given in Fig. 1 were kept in the dark for 24 h, following which the spectra were again recorded. The resulting spectra correspond exactly, in the positions of the absorption maxima and their relative intensities, to the final spectrum shown in Fig. 1. Thus the 1,3 adduct **9** decomposed on standing, while the 1,1 adduct **10** was completely stable for the extended period of time.

Can. J. Chem. Downloaded from www.nrcresearchpress.com by 210.87.254.6 on 09/06/12
For personal use only.

Can. J. Chem. Downloaded from www.nrcresearchpress.com by 210.87.254.6 on 09/06/12
For personal use only.

σ-Complex formation by phenoxide ion

Due to the ambident nature of phenoxide ion, its reaction with **4** can potentially lead to the formation of both oxygen-bound and carbon-bound σ-complexes. The use of nmr and electronic absorption spectroscopy, when coupled with other properties such as stability (or lack of) to acidification, enables one to differentiate among the various possibilities.

The nmr spectrum of a solution of **4** and potassium phenoxide in $(CD_3)_2SO$ (final concentrations 0.49 *M* and 0.57 *M*, respectively), when recorded immediately on mixing and then monitored with time, was found to exhibit no further changes during the next 24 h. A typical spectrum showed two somewhat poorly resolved doublets at δ 8.60 and δ 5.65 with integral ratios of 1.1:1.0. A complex multiplet between δ 6.2 and δ 7.8 was also present, arising from the phenyl protons in the complex as well as any excess phenoxide ion that was present.

The appearance of the doublets at δ 8.60 and 5.65 is indicative of the formation of a 1,3 complex but not of a 1,1 complex. The two possibilities consistent with these features are the O-bound complex **6** and the C-bound complex **8**. The following considerations serve to differentiate between these possibilities. The shielding of the H_β protons in **6** and **8** will depend on the electronegativity of the atom bonded to C-3. On the basis of literature data (5–7), one would expect δ values close to 6.2 for **6**, and 5.7 for **8**. The observed value, δ 5.65 for the resonance assigned to H_β, is thus in accord with complex **8**. Furthermore, literature data indicate that the difference in the H_α and H_β shieldings for O-bound complexes lies between 2.2 and 2.6 ppm, whereas for C-bound complexes this value is ~3.0 ppm. The observed value in the present case is 2.95 ppm, which again favors structure **8**.

Further evidence concerning the nature of the complexes was obtained from their uv–visible spectral characteristics. When the reaction between **4** and PhOK in DMSO was monitored by uv–visible spectroscopy, a characteristic spectrum was obtained immediately on mixing and then underwent no further changes for the duration of the experiment (24 h), as had previously been found in the nmr experiment. The resulting spectrum exhibited maxima at 465 and 556 nm, the former being the more intense. From literature data (5–7) one would predict that for an O-bound complex the two absorption maxima should lie in the region of 430 and 495 nm, which is not in accord with the present result. In the case of the C-bound phenoxide adduct of TNB (20), the corresponding absorption maxima occurred at 468 and 570 nm (broad). Thus the uv–visible spectra are strongly indicative of the formation of a carbon-bound complex, **8**, rather than an oxygen-bound complex, **6**. Assuming that the molar extinction coefficient of **8** is of the same order of magnitude as that of the phenoxide adduct of TNB, one estimates that **8** was formed in ~25% yield.

Acidification of the solutions from the reaction of **4** with phenoxide caused no change in the spectrum of the resulting solution. This result rules out the possibility of formation of an O-bound complex since such species are known to be destroyed by acid. Thus the evidence from nmr and uv–visible spectroscopy fully supports structure **8** for the phenoxide complex of **4**.

A contrasting result from the TNB–phenoxide system was found when the reaction of **4** with potassium phenoxide was conducted in DMSO–methanol (80:20 v/v). In the TNB system it was found (20) that reaction gave rise immediately to the TNB–methoxide σ-complex, through solvolysis, which was then slowly transformed to the TNB–phenoxide adduct. When the reaction was performed with **4** and followed by both nmr and uv–vis spectroscopy, as above, it was found that the methoxide complex **9** was immediately obtained and was replaced over 1 h by **10**, which then remained stable over an extended period (24 h). Thus formation of the C-bounded phenoxide adduct was not detected in this system. The significance of this result will be considered further in the following discussion.

Discussion

Steric and electronic effects in σ-complex formation

A number of theories have been proposed to explain the origin of the generally observed kinetic preference for 1,3 adduct formation and the thermodynamic preference for 1,1 adduct formation (26–29). The nitroaromatic substrate under investigation in this study differs structurally from compounds previously investigated in σ-complex formation, which enables us to critically assess the various proposals, as discussed under the five headings below.

1. *Resonance stabilization involving alkoxy and nitro groups*

Resonance structures involving conjugation between the methoxy and nitro functionalities could potentially contribute towards stabilization of the reactants as well as products in nitroaromatic–base interactions. Thus contribution by structures **1***a* and **2***a* would serve to stabilize the ground state of TNA (**1**) and the 1,3 adduct (**2**), respectively, but this interaction would no longer be possible in the 1,1 adduct (**3**). The transition state leading up to **2** could similarly benefit from this stabilization, but not that for formation of **3**. Therefore the transition state for 1,3 adduct formation would be effectively lowered in energy relative to that for 1,1 adduct formation.

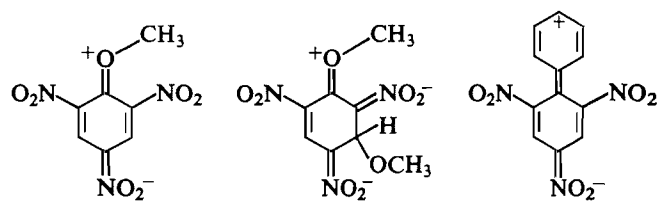

1*a* **2***a* **4***a*

In the present system, for ground state stabilization to be effective, one would have to invoke structure **4***a* as a contributing form. However, it could be expected that the phenyl group in **4** would be disposed substantially out-of-plane relative to the TNB ring, noting that one *ortho* nitro group in biphenyl derivatives results in an angle of rotation between the two rings of the order of 50–60° (30–32). On this basis, the extent of contribution by **4***a* would be minimal. One can hence effectively eliminate this possibility as a source of the kinetic preference for 1,3 adduct formation in this system.

2. *Geminal alkoxy substitution as a stabilizing effect*

Multiple substitution by electronegative groups at an sp^3 carbon center is recognized as a stabilizing electronic influence through a negative type of hyperconjugation (33, 34), and this has been considered to contribute to the greater stability of 1,1 relative to 1,3 dimethoxy complexes. However, although the phenyl group can be considered as an electron-withdrawing substituent, it appears unlikely that this could assume a role similar to OMe, F, etc. since resonance structures involving a phenyl anion would be prohibitively high in energy. It is also noted that in the case of attack by CN^- on TNA, the 1,1 adduct was found to be of lower stability than the 1,3 adduct (13),

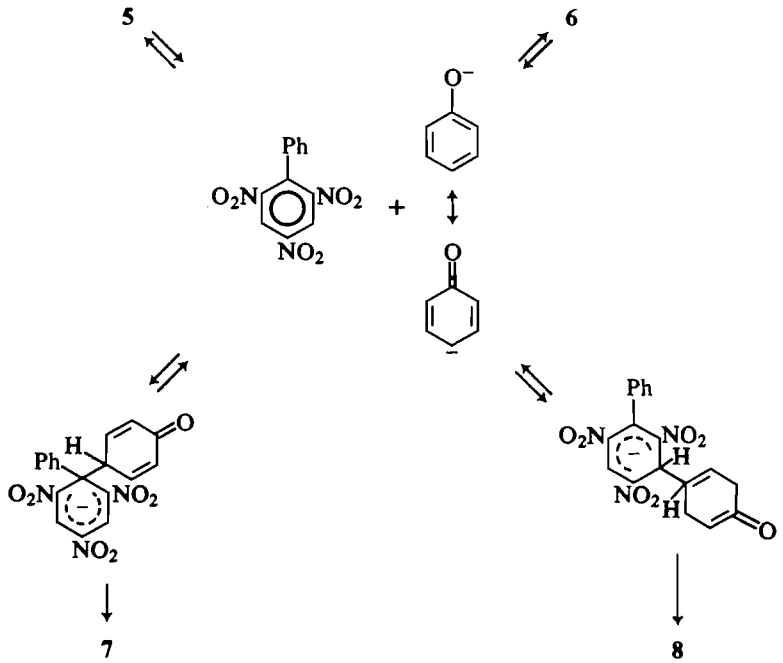

SCHEME 2

which could indicate that two unlike electron-withdrawing substituents are not effective in stabilizing σ-complexes by this type of mechanism.

3. *Structural effects on delocalizing ability*

A variety of evidence points to the fact that, in σ-complex formation by 1-X-2,4,6-trinitrobenzene, negative charge is predominantly delocalized onto the nitro group which is *para* with respect to the formed sp^3 carbon center. In 1,1 adduct formation, this *para* nitro group bearing negative charge can achieve maximum coplanarity with respect to the overall π electron system. However, in a 1,3 complex, the NO_2 situated *para* to the sp^3 carbon is also *ortho* to the substituent X, which will result in deviation from coplanarity depending on the degree of steric interaction between X and NO_2. In the present system, steric inhibition of resonance should be of considerable importance due to the large steric requirement of the C-1 phenyl, thus leading to stabilization of the 1,1 adduct **10** relative to the 1,3 adduct **9**.

4. *Relief of steric strain*

A substituent X in 1-X,2,4,6-trinitrobenzene will tend to cause the *ortho* nitro groups to deviate from coplanarity with the ring as a result of steric compression. For example, in 1-ethoxy-2,4,6-trinitrobenzene, the 2- and 6-nitro groups are rotated from the ring plane by 32° and 61° respectively (35). Formation of the σ-complex results in relief of this steric interaction as the C-1 centre becomes tetrahedral. In the present system, the phenyl ring in **4** could be expected to be substantially out-of-plane relative to the TNB ring and there can only be slight relief of this type of steric strain on formation of the 1,1 adduct. However, there will nevertheless be an appreciable increase in librational motion compared to the reactant where rotation about the C-1 bond should be severely restricted. This effect will serve to stabilize the 1,1 adduct relative to the 1,3 adduct since in the latter case this relief of steric strain would not arise.

5. F *strain*

Formation of a 1,1 adduct will in general be subject to greater steric hindrance (*F* strain) in the approach of the nucleophile compared to formation of a 1,3 adduct. Since the nucleophile will approach from a direction perpendicular to the TNB ring plane, this effect will be particularly important in the present system owing to interaction between the approaching nucleophilic reagent and the phenyl group at C-1. On the other hand, attack at C-3 will be relatively unhindered, thus favoring 1,3 adduct formation. We conclude that *F*-strain is probably a dominant factor leading to kinetic preference for 1,3 adduct formation in this system.

The ambident reactivity of phenoxide ion

The results obtained in the reaction of **4** with phenoxide can be discussed in relation to Scheme 2 which considers both oxygen-bound and carbon-bound σ-complexes. Of the various possibilities shown in this scheme, the pathway leading to formation of **8** is the only one which was detected in the PhOK/DMSO system. The finding of the C-bonded adduct is in agreement with the results obtained by us previously for the TNB/PhOK/DMSO system (20), but contrasts with the report of Shein *et al.* (22, 23) that reaction of TNB gives rise initially to the O-bonded phenoxide adduct observable by standard nmr techniques. On the other hand, 2,4,6-trimethylphenoxide ion was found by us to react with TNB to give the O-bonded σ-complex (21).

When the present reaction was performed in DMSO–MeOH (80:20 v/v) we observed the formation, through solvolysis, of the methoxy complexes **9** and **10** as the intial and final products of reaction, respectively. A phenoxy complex was not obtained in this system, contrasting with the course of reaction observed with TNB under corresponding conditions (20).

It has been shown by Bernasconi and Muller (15), using fast reaction techniques (stopped flow and T-jump), that the reaction of TNA with phenoxide ion in DMSO–water media gives rise in a rapid process to the O-bonded 1,1 phenoxide adduct as a transient species which is then converted to the 1,3 hydroxide adduct of TNA. Comparison with the results for reaction of MeO^- with TNA showed that PhO^- attack (H_2O) is faster than MeO^- attack (MeOH) by a factor of 2.9, but PhO^- expulsion is faster by 4.5×10^6, with the result that the equilibrium

Can. J. Chem. Downloaded from www.nrcresearchpress.com by 210.87.254.6 on 09/06/12
For personal use only.

constant for 1,1 phenoxide adduct formation is smaller than for 1,1 methoxide adduct formation by 1.5×10^6.

Our own observation, that in the PhOK/DMSO–MeOH system MeO^- attack on **4** is preferred over PhO^- attack, contrasts with Bernasconi's report (15) that $k_{PhO^-} > k_{MeO^-}$ for reaction with TNA, although the different time scales of the two studies could affect the overall result. It could thus be possible that, at extremely short reaction times, attack by PhO^- to form an O-bonded complex might be detected in our system as well, and that the observed result is the outcome of a secondary rather than a primary process. However, our observation in the PhOK/DMSO–MeOH system of the initial 1,3 and subsequent 1,1 MeO^- adduct formation, with the latter *not* replaced by a C-bonded phenoxide adduct, is remarkable in view of the contrasting result observed in the TNB/PhOK/DMSO–MeOH system (20), and may reflect widely different stabilities of the MeO^- adducts in the two cases.

Perhaps the most significant difference between the present work and the results obtained by Bernasconi (15) is that attack by PhO^- on TNA occurs preferentially at C-1 whereas PhO^- attacks **4** at C-3. Presumably attack by phenoxy oxygen at C-1 of **4** to give **5** would be subject to steric interactions fairly comparable to those for attack by MeO^-, although attack at C-1 of **4** through carbon of phenoxide to give **7** would be sterically much less favorable. This result further demonstrates the importance of *F*-strain in the present system. It appears that this factor overrides the delocalizability criterion which normally results in 1,1 adducts being thermodynamically more stable than 1,3 adducts.

Conclusions

The study has shown that the title compound **4** reacts with phenoxide ion in DMSO to form a carbon-bonded σ-complex **8** through an irreversible process, whereas oxygen attack by phenoxide would occur reversibly (Scheme 2). This is in accord with our previous observations with TNB (20). In contrast to the observations with TNB, reaction of **4** with potassium phenoxide in DMSO–methanol gives rise, through solvolysis, only to the 1,3 and 1,1 methoxy adducts **9** and **10**, formed sequentially. Under the same conditions, TNB gave rise first to the methoxy adduct and then, in a slower process, to the phenoxy adduct. The ease of formation of the 1,1 methoxy adduct of **4** indicates that **4** reacts in a conformation in which the C-1 phenyl and the C-2,6 nitro groups are oriented in a propeller-like configuration, thus minimizing steric hindrance to approach of the nucleophile. The σ-complex formation reaction is expected to occur through an early transition state, as should be the case also for S_NAr processes (36, 37) in highly activated nitroaromatics such as 1-X-2,4,6-trinitrobenzene derivatives where X is a bulky substituent ($C_5H_5N^+$, SO_2Ph, etc.).

While reaction of **4** with methoxide ion gives rise to the 1,3 adduct **9** and the 1,1 adduct **10** through kinetic and thermodynamic control, as in the case of TNA, the two sets of observations differ in origin. Dominant factors in the present system are believed to be the delocalizing ability of *para* nitro substituents in absorbing of negative charge, *F*-strain with respect to approach of nucleophile, and the relief of steric compressions in the ground state in passing to the transition state for σ-complex formation.

Experimental

Materials and methods

Dimethyl sulfoxide was distilled from calcium hydride under nitrogen at reduced pressure. Methanol was distilled from magnesium metal. Potassium phenoxide was prepared according to Kornblum and Lurie (4). Sodium methoxide solutions were prepared from freshly cut sodium metal and methanol, or methanol-O-*d*, and standardized before use. DMSO-d_6 was dried before use over molecular sieves.

1-Phenyl-2,4,6-trinitrobenzene (**4**) was prepared by the Ullmann synthesis from picryl chloride, iodobenzene, and copper bronze using the method described by Gull and Turner (38). The product, recrystallized from ethanol, was obtained as pale yellow needles, mp 129° (lit. (38) mp 130°C); nmr $(CD_3)_2SO$, δ: 9.12 (s, 2H), 7.22–7.56 (m, 5H).

The nmr spectra were recorded on a Varian EM360 or HA100 spectrometer. Chemical shifts are given in ppm downfield from tetramethylsilane (TMS) used as an internal standard. Ultraviolet–visible spectra were recorded on a Unicam SP800B spectrophotometer.

*Reaction of **4** with methoxide ion in DMSO–MeOH*

For the nmr experiments, reaction solutions were prepared by addition of NaOMe/MeOH to **4** in $(CD_3)_2SO$, giving a solution 0.46 *M* in **4** and in NaOMe, and a solvent composition 90:10 (v/v) DMSO–MeOH. Visible spectra were taken following 7×10^3 dilution with DMSO of reaction solutions with concentrations of **4** and NaOMe of same order as in the nmr experiments. The uv–vis spectra were recorded immediately on dilution and again after standing for 1 day.

*Reaction of **4** with potassium phenoxide in DMSO*

The $(CD_3)_2SO$ solution in the nmr experiment was 0.49 *M* in **4** and 0.57 *M* in PhOK. Ultraviolet–vis spectra were obtained following 3×10^3 dilution. To test the reversibility of complex formation, 3 mL of the diluted solution was acidified with 50 μL 1 *N* HCl and the uv–visible spectrum recorded.

*Reaction of **4** with potassium phenoxide in DMSO–MeOH*

The experiments were performed as above but the solution in the nmr experiment was prepared using $(CD_3)_2SO$ and methanol-O-*d* (80:20 v/v). The concentration of PhOK was varied between 0.51 and 0.98 *M* while keeping **4** constant at 0.46 *M*.

Acknowledgements

Continuing financial support of this research by the Natural Sciences and Engineering Research Council of Canada is gratefully acknowledged, as are discussions with Drs. S. Hoz and R. Y. Moir.

1. E. BUNCEL. The chemistry of amino, nitro and nitroso compounds. Supplement F. *Edited by* S. Patai. Wiley, London. 1982.
2. E. BUNCEL and A. W. ZABEL. Can. J. Chem. **59**, 3168 (1981); **59**, 3177 (1981).
3. E. BUNCEL, J. A. ELVIDGE, J. R. JONES, and K. T. WALKIN. J. Chem. Res. (S) 272 (1980).
4. N. KORNBLUM and A. P. LURIE. J. Am. Chem. Soc. **81**, 2705 (1959).
5. M. R. CRAMPTON. Adv. Phys. Org. Chem. **7**, 211 (1969).
6. M. J. STRAUSS. Chem. Rev. **70**, 667 (1970).
7. C. A. FYFE. The chemistry of the hydroxyl group. Part 1. *Edited by* S. Patai. Wiley, London. 1971.
8. J. H. FENDLER, W. L. HINZE, and L. J. LIU. J. Chem. Soc. Perkin Trans. 2, 1768 (1975).
9. C. F. BERNASCONI. Chimia, **34**, 1 (1980).
10. F. TERRIER. Chem. Rev. **82**, 77 (1982).
11. G. A. ARTAMKINA, M. P. EGOROV, and I. P. BELETSKAYA. Chem. Rev. **82**, 427 (1982).
12. K. L. SERVIS. J. Am. Chem. Soc. **87**, 5495 (1965).
13. A. R. NORRIS. Can. J. Chem. **47**, 2895 (1969).
14. G. BIGGI and F. PIETRA. J. Chem. Soc. Perkin Trans. 1, 1980 (1973).
15. C. F. BERNASCONI and M. C. MULLER. J. Am. Chem. Soc. **100**, 5530 (1978).

Can. J. Chem. Downloaded from www.nrcresearchpress.com by 210.87.254.6 on 09/06/12
For personal use only.

16. C. F. BERNASCONI. J. Org. Chem. **36**, 1671 (1971).
17. E. BUNCEL, A. R. NORRIS, K. E. RUSSELL, P. J. SHERIDAN, and H. WILSON. Can. J. Chem. **52**, 1750 (1974).
18. C. A. FYFE, C. D. MALKIEVICH, S. W. H. DAMJI, and A. R. NORRIS. J. Am. Chem. Soc. **98**, 6983 (1976).
19. A. JARCZEWSKI, P. PRUSZYNSKI, and K. T. LEFFEK. Can. J. Chem. **57**, 669 (1979).
20. (*a*) E. BUNCEL and J. G. K. WEBB. J. Am. Chem. Soc. **95**, 8470 (1973); (*b*) E. BUNCEL, A. JONCZYK, and J. G. K. WEBB. Can. J. Chem. **53**, 3761 (1975).
21. E. BUNCEL, R. Y. MOIR, A. R. NORRIS, and A.-P. CHATROUSSE. Can. J. Chem. **59**, 2470 (1981).
22. S. M. SHEIN and O. G. BYVAL'KEVICH. Zh. Org. Khim. **8**, 328 (1972).
23. S. M. SHEIN, O. G. BYVAL'KEVICH, and A. D. KHMELINSKAYA. Zh. Org. Khim. **12**, 134 (1976).
24. V. MAHACEK, V. STERBA, and A. STERBOVA. Collect. Czech. Chem. Commun. **41**, 2556 (1976).
25. J. C. HALLE, M. J. POUET, M. P. SIMONNIN, F. DEBLEDS, and F. TERRIER. Can. J. Chem. **60**, 1988 (1982).
26. J. H. FENDLER, E. J. FENDLER, and C. E. GRIFFIN. J. Org. Chem. **34**, 689 (1969).
27. C. F. BERNASCONI. J. Am. Chem. Soc. **92**, 4682 (1970).
28. G. BALDINI, G. DODDI, G. ILLUMINATI, and F. STEGEL. J. Org. Chem. **41**, 2153 (1976).
29. M. R. CRAMPTON. J. Chem. Soc. Perkin Trans. 2, 1442 (1977).
30. L. FALLON and H. L. AMMON. J. Cryst. Mol. Struct. **4**, 63 (1974).
31. H. H. SUTHERLAND and J. H. C. HOGG. Acta. Crystallogr. Sect. B, **30**, 1562 (1974).
32. N. I. SADOVA and L. V. VILKOV. Russ. Chem. Rev. **51**, 87 (1982).
33. J. HINE. J. Am. Chem. Soc. **85**, 3239 (1963).
34. J. HINE, L. G. MAHONE, and C. L. LIOTTA. J. Am. Chem. Soc. **89**, 5911 (1967).
35. C. M. GRAMACCIOLI, R. DESTRO, and M. SIMONETTA. Acta. Crystallogr. Sect. B, **24**, 129 (1968).
36. J. MILLER. Nucleophilic aromatic substitution. Elsevier, Amsterdam. 1968.
37. J. F. BUNNETT, S. SEKIGUCHI, and L. A. SMITH. J. Am. Chem. Soc. **103**, 4865 (1981).
38. H. C. GULL and E. E. TURNER. J. Chem. Soc. 498 (1929).
39. M. J. STRAUSS, R. A. RENFROW, and E. BUNCEL. J. Am. Chem. Soc. **105**, 2473 (1983).
40. E. BUNCEL, R. A. RENFROW, and M. J. STRAUSS. Can. J. Chem. **61**, 1690 (1983).

Can. J. Chem. Downloaded from www.nrcresearchpress.com by 210.87.254.6 on 09/06/12
For personal use only.

Aminosulfonic acids. Part 1. Crystal structures of *N*-methylaminomethanesulfonic acid, $MeNHCH_2SO_3H$, and disodium *N*-methyliminobis(methanesulfonate) dihydrate, $MeN(CH_2SO_3Na)_2 \cdot 2H_2O$

T. STANLEY CAMERON, WALTER J. CHUTE, AND OSVALD KNOP[1]

Department of Chemistry, Dalhousie University, Halifax, N.S., Canada B3H 4J3

Received May 30, 1983

T. STANLEY CAMERON, WALTER J. CHUTE, and OSVALD KNOP. Can. J. Chem. **62**, 540 (1984).

The crystal structure of *N*-methylaminomethanesulfonic acid ($P2_12_12_1$, a = 5.455(1) Å, b = 7.791(1) Å, c = 11.925(2) Å, Z = 4) consists of $^+MeNH_2CH_2SO_3^-$ zwitterions hydrogen-bonded to form infinite chains about screw axes parallel to a. In the structure of $MeN(CH_2SO_3Na)_2 \cdot 2H_2O$ (*Pbcn*, a = 10.469(1) Å, b = 6.039(3) Å, c = 17.549(3) Å, Z = 4), layers of $MeN(CH_2SO_3^-)_2$ anions alternate with layers of Na^+ ions parallel to (001). The anions are linked by O—H···O bonds between the water molecules and the O(2) atoms of the sulfonate groups. Because of the twofold orientational disorder of the N—CH_3 groups the space group *Pbcn* is only statistical.

The S—C, C—N, and S—O bond lengths in solid aminosulfonic acids and their salts are discussed with a view to detecting the existence of effects due to deprotonation of the amino group and to hydrogen bonding.

T. STANLEY CAMERON, WALTER J. CHUTE et OSVALD KNOP. Can. J. Chem. **62**, 540 (1984).

La structure cristalline de l'acide *N*-méthylaminométhanesulfonique ($P2_12_12_1$, a = 5,455(1) Å, b = 7,791(1) Å, c = 11,925(2) Å; Z = 4) consiste en des zwitterions $^+MeNH_2CH_2SO_3^-$ liés par des liaisons hydrogène; ces liaisons forment des chaînes infinies autour des axes hélicoïdaux parallèles à a. Dans la structure du $MeN(CH_2SO_3Na)_2 \cdot 2H_2O$ (*Pbcn*, a = 10,469(1) Å, b = 6,039(3) Å, c = 17,549(3) Å; Z = 4), les couches d'anions $MeN(CH_2SO_3^-)_2$ alternent avec des couches d'ions Na^+ parallèles à (001). Les anions sont liés par des liaisons O—H···O entre les molécules d'eau et des atomes d'oxygène O(2) des groupes sulfonates. La symétrie *Pbcn* n'est que statistique du fait que deux orientations alternatives équivalentes sont disponibles à chaque groupe N—CH_3.

On discute des longueurs des liaisons S—C, C—N et S—O des acides aminosulfoniques solides et de leurs sels dans le but de déceler l'existence d'effets dûs à le déprotonation du groupe amino et à la liaison hydrogène.

Can. J. Chem. Downloaded from www.nrcresearchpress.com by 210.87.254.42 on 09/06/12
For personal use only.

The main aim of this series of investigations is to study, by X-ray and nmr methods, some of the changes which free aminosulfonic acids undergo on deprotonation of the amino group, i.e., on conversion of the zwitterion to the corresponding sulfonate anion.

The effect of the deprotonation on bond lengths is a natural object of attention. In principle, it can be followed in a straightforward manner by determining and comparing pairs of structures, the structure of the free acid with that of one of the corresponding normal (i.e., non-chelated, preferably alkali) salts. However, for reasons to be discussed in more detail in a subsequent paper of this series, the alkali salts of aliphatic amino acids in general are notoriously difficult to obtain in the solid state.[2] In the specific case of the aminoalkanesulfonic acids, the simplest member of that class, sulfamic acid, presents little problem in this regard as its salts can be readily obtained, but this is not so with its homologues. Condensation of $^-O_3S(CH_2)_nNRH_2^+$ (R = H or alkyl) to $NR[(CH_2)_nSO_3^-]_2$ tends to take place in aqueous solution at high pH, with the result that the alkali salt obtained on crystallization is that of the dibasic anion instead of the desired $RNH(CH_2)_nSO_3^-M^+$. The existence of this process seriously hinders the prospect of determining the effect of deprotonation by direct comparison of zwitterion/anion pairs, since it renders the required "monomer" salt inaccessible. However, the effects of deprotonation associated with the formation of the $NR[(CH_2)_nSO_3^-]_2$ anions are equally little known, and as no structure containing these sulfo analogues of the iminodicarboxylate anions appears to have been reported, it seemed worthwhile to compare the molecular structures and dimensions of at least one such zwitterion/iminodisulfonate anion pair.

In the following, $^+MeNH_2CH_2SO_3^-$ is compared with the $MeN[CH_2SO_3^-]_2$ anion as present in the dihydrate of the disodium salt, and the structure features of these two species are further compared with those of the aminosulfonic acids and their salts that have been investigated to date.

Experimental

The preparation of all the compounds used in this series of investigations (including the two title compounds) will be described in Part 2.

A CAD-4 diffractometer was used in the determination of the unit-cell dimensions and to collect intensities (θ = 2–25°). The intensities were reduced by routine procedures (2). Lorentz and polarization factors were applied but not absorption or extinction corrections. The scattering factors for neutral atoms were taken from ref. 3. The structures were solved by the heavy atom method using the SHELX system (4). Full-matrix least-squares ($w\Delta F^2$ = minimum) refinements were carried out with isotropic temperature factors on heavy atoms until R was reduced to a suitably low value. After appropriate intervention (see below) the refinements were continued with anisotropic temperature factors on the non-hydrogen atoms and isotropic factors on the hydrogens until the final R values (Table 1). Least-squares weights were calculated from expressions of the type $w^{-1} = \sigma|F_o| + kF_o^2$, where σ is the weight for an individual reflection derived from the diffractometer counting statistics and k is a refined variable. The anisotropic temperature factor is defined as $T = \exp[-2\pi^2(U_{11}h^2a^{*2} + U_{22}k^2b^{*2} + U_{33}l^2c^{*2} + 2U_{23}klb^*c^* + 2U_{13}hla^*c^* + 2U_{12}hka^*b^*)]$.

The crystal data and particulars of the refinements are listed in Table 1.

$MeNHCH_2SO_3H$

The crystal used in the determination was 0.3 × 0.3 × 0.4 mm^3 in size. In the late stages of the refinement the bond lengths and angles

[1] To whom all correspondence should be addressed.

[2] For the difficulty in preparing pure alkali salts of aminocarboxylic acids, see ref. 1.

Can. J. Chem. Downloaded from www.nrcresearchpress.com by 210.87.254.42 on 09/06/12
For personal use only.

TABLE 1. Crystal data of $MeNH.CH_2SO_3H$ and $MeN(CH_2SO_3Na)_2 \cdot 2H_2O$[a]

Parameter	Value	
	$C_2H_7NO_3S$	$C_3H_{11}NNa_2O_8S_2$
fw	125.15	299.22
μ_{Mo}, cm^{-1}	4.7	15.4
a, Å	5.455(1)	10.469(1)
b, Å	7.791(1)	6.039(3)
c, Å	11.925(2)	17.549(3)
V, $Å^3$	506.8(3)	1109.5(9)
Z	4	4
ρ_c, g/cm^3	1.640(2)	1.791(3)
$F(000)$	264	616
Space group	$P2_12_12_1$ (No. 19)	$Pbcn$ (No. 60)
Reflections		
Total measured	658	924
Unique measured[b]	612	824
Used in refinement	609	824
$100R$; $100R_w$	2.92; 2.89	5.36; 5.36

[a] Mo $K\alpha_1$, λ = 0.70926 Å (graphite monochromator).
[b] $I > 1\sigma(I)$.

involving H atoms were constrained (4) to be chemically reasonable: C—H at 1.08(2) Å, N—H at 1.02(2) Å, and the bond angles at the appropriate near tetrahedral values. The CH_2 and CH_3 groups were refined as rigid bodies. No other geometric restrictions were placed on the molecule.

The positional and thermal parameters are listed in Table 2, structure factors in Table 3,[3] and interatomic distances and bond angles in Table 4.

$MeN(CH_2SO_3Na)_2 \cdot 2H_2O$

The size of the crystal used was 0.4 × 0.3 × 0.8 mm^3. As in the case of $MeNHCH_2SO_3H$, the C—H bond lengths and bond angles were constrained in the later stages of the refinement. However, the twofold orientational disorder of the N—C_{Me} groups (see below) imposed these additional constraints: C_{CH_2}—N at 1.47(1) Å (in analogy with $MeNHCH_2SO_3H$), N—C_{CH_3} at 1.50(1) Å, and the C—N—C angles at 110(2)°.

The positional and thermal parameters are listed in Table 5, structure factors in Table 6,[3] and interatomic distances and bond angles in Table 7.

Description of the structures

$MeNHCH_2SO_3H$

As would be expected, the structure consists entirely of the zwitterions $^+MeNH_2CH_2SO_3^-$. These are arranged in chiral symmetry ($P2_12_12_1$) and are joined by hydrogen bonds involving the O(1) and O(2) oxygens and both N-hydrogens to form infinite chains about screw axes parallel to the a-axis. One of the hydrogen bonds (N(C)—H(2C)···O(1A″) in Fig. 1) is nearly straight, with an H···O separation of only 1.76 Å (Table 4). The bond involving H(1) is nominally trifurcated, but two of the H···O distances are much longer than the third (2.47 and 2.51 as against 1.97 Å) and the NHO angle corresponding to the largest of these H···O distances is only 102°. This angle would correspond to an intramolecular hydrogen bond between H(1) and O(1), but in view of its smallness and of the considerable H···O distance the H(1)···O(1) interaction must be very weak.

The only hydrogen-bond interaction between the infinite zwitterion chains is through one of the components of the trifurcated N—H(1)···3O bond, involving the H(1) atoms of one chain and O(3) atoms of the adjacent chains. The interchain H···O distance is only 2.47 Å and the NHO angle, 117°. The trifurcated bond might thus be more correctly viewed as a

TABLE 2. $^+MeNH_2CH_2SO_3^-$: positional and thermal parameters (×10^4)

Atom	x y z	U_{11} U_{22} U_{33}	U_{12} U_{13} U_{23}
S	1631(2) 1125(1) 8497(1)	230(3) 227(3) 285(3)	−17(3) −38(3) −28(3)
O(1)	−0987(4) 1416(3) 8684(2)	239(10) 388(11) 335(9)	−23(8) 28(8) −25(9)
O(2)	2811(5) 0413(3) 9479(2)	486(16) 344(12) 574(14)	−101(11) −260(13) 149(11)
O(3)	2125(5) 0245(3) 7455(2)	367(13) 428(13) 503(13)	−60(11) 84(11) −219(11)
N	2046(5) 4376(3) 9205(2)	247(12) 219(10) 301(10)	−16(9) 28(9) −25(9)
H(1)[a]	0121(20) 4414(61) 9262(37)	557(127)[b]	
H(2)[a]	2731(95) 3965(70) 9988(23)	744(155)[b]	
C(1) CH_2	2913(5) 3224(4) 8310(2)	297(15) 231(11) 266(12)	−28(11) 29(11) −19(9)
H(11)	2231(5) 3664(4) 7510(2)	555(128)[b,c]	
H(12)	4886(5) 3120(4) 8275(2)	476(115)[b,c]	
C(2) CH_3	2893(6) 6191(4) 9076(2)	395(17) 195(12) 397(14)	−39(12) −29(13) −15(12)
H(21)	2181(6) 6738(4) 8310(2)	918(193)[b,c]	
H(22)	4868(6) 6290(4) 9079(2)	771(171)[b,c]	
H(23)	2156(6) 6879(4) 9786(2)	622(146)[b,c]	

[a] N—H distances constrained in refinement (see text); esd's unreliable.
[b] U_{iso}.
[c] Rigid-body refinement.

[3] This table has been deposited. Complete set of data is available, at a nominal charge, from the Depository of Unpublished Data, CISTI, National Research Council of Canada, Ottawa, Ont., Canada K1A 0S2.

TABLE 4. $^{+}MeNH_2CH_2SO_3^{-}$: interatomic distances (Å) and bond angles (deg) (see Fig. 1)[a]

Atoms	Distance	Atoms	Angle
S—O(1)	1.463(2)	O(1)—S—O(2)	111.8(2)
S—O(2)	1.447(3)	O(1)—S—O(3)	112.7(2)
S—O(3)	1.445(3)	O(2)—S—O(3)	115.5(2)
S—C(1)	1.793(3)	O(1)—S—C(1)	104.9(3)
N—C(1)	1.473(4)	O(2)—S—C(1)	106.1(1)
N—C(2)	1.496(4)	O(3)—S—C(1)	104.6(1)
N—H(1)	1.05(1)	S—C(1)—N	109.8(2)
N—H(2)	1.05(1)	C(1)—N—C(2)	113.7(2)
N(C)···O(2A′)	2.798(4)		
N(C)···O(1A″)	2.805(3)		
N(C)···O(1C)	2.905(3)		
N(C)···O(3B)	3.091(4)		
N(C)···O(2A″)	3.518(3)		
N—H···O up to H···O = 2.8 Å:			
H(1C)···O(2A′)	1.97(3)	N(C)—H(1C)···O(2A′)	133(3)
H(1C)···O(3B)	2.47(3)	N(C)—H(1C)···O(3B)	117(2)
H(1C)···O(1C)	2.51(3)	N(C)—H(1C)···O(1C)	102(2)
H(2C)···O(1A″)	1.76(5)	N(C)—H(2C)—O(1A″)	172(4)
H(2C)···O(2A′)	2.80(5)		
C—H···O up to H···O = 2.8 Å:		Symmetry code:	
O(1C)···H(21B′)	2.48(1)	A x y z	
O(1C)···H(11B′)	2.66(1)	B $\frac{1}{2}-x$ $\bar{y}$ $z-\frac{1}{2}$	
O(1C)···H(12C′)	2.66(1)	C $\frac{1}{2}+x$ $\frac{1}{2}-y$ $1-z$	
O(2A″)···H(22C)	2.70(1)	D $\bar{x}$ $\frac{1}{2}+y$ $\frac{3}{2}-z$	
O(2C)···H(12C)	2.79(1)	A′ = A + (00$\bar{1}$)	
O(2C)···H(23C″)	2.80(1)	A″ = A + (10$\bar{1}$)	
O(3B)···H(12C′)	2.48(1)	B′ = B + (010)	
O(3B)···H(22C′)	2.59(1)	C′ = C + ($\bar{1}$00)	
O(3C)···H(11C)	2.67(1)	C″ = C + ($\bar{1}$10)	
O(3C)···H(11B′)	2.68(1)		
O(3C)···H(21B)	2.78(1)		

[a] Librational corrections for distances involving two non-hydrogen atoms do not exceed 0.002 Å and are thus entirely within the stated esd's.

highly-bent (NHO = 133°) rather than a trifurcated hydrogen bond.[4]

Some of the $H_C\cdots O$ distances are quite short, the shortest being 2.48 Å (Table 4). The organization of the structure resembles in its main features that reported for ^{+}i-$PrNH_2CH_2SO_3^{-}$ (7).

$MeN(CH_2SO_3Na)_2\cdot 2H_2O$

The structure consists of layers of $MeN(CH_2SO_3^{-})_2$ anions alternating with layers of Na^{+} ions parallel to (001) (Fig. 2). The anions are linked by the water molecules through $O_w—H\cdots O_S$ hydrogen bonds to the O(2) atoms. Each H_2O is four-coordinated, more or less tetrahedrally, by two O(2) atoms and two Na^{+} ions (Fig. 3). The Na^{+} ion is surrounded by two O_w and four O_S atoms to form an irregular $NaO_4(H_2O)_2$ octahedron; the two H_2O oxygens are *cis*, as are the two O(1) and the two O(3) atoms (Na(D), O(1D), O(1F), O(3B), O(3F′), O(4D), and O(4H) in Fig. 2).

The space group symmetry requires the anion to have the symmetry C_2. However, the N atom of an individual anion is not on a twofold axis, consequently the $N—C_{Me}$ bonds in the crystal are orientationally disordered (Fig. 2). The existence of the disorder is consistent with the expected sp^3 geometry at the N atom. The CH_3 group and the two O(1) oxygens of an anion are *cis* to the N atom; the O(2) and O(3) pairs are coplanar ‖ (010) on the opposite side of N.

Since the anion was refined in its average, pseudo-C_2 conformation, only the average bond lengths and angles can be calculated. Specifically, the effect of the CH_3 group on O(1) will not be the same as that of the lone pair on the N atom. The shortest (average) $H_{Me}\cdots O(1)$ distances (Fig. 2) are quite different, H(22)···O(1A) ~ 2.7 Å, H(21)···O(1B) ~ 3.2 Å, which makes the significance of the value of the S—C(1)—N angle, 126° (Table 7), uncertain. Similarly, the N—C(1) and N—C(2) bond lengths and the C(1)—N—C(1) angle must be interpreted with caution, especially when attempting comparison between the dimensions of the zwitterion and the anion.

Nevertheless, it is found that the C(1)—N—C(1) angle of ~115° is, perhaps not surprisingly, in the range of C—N—C angles reported for iminodiacetic acid and its salts, 109–116° (refs. 8 and 9 and further references therein). Furthermore, the S—C bond length, 1.797(5) Å, coincides with the mean of the S—C bond lengths in the aminosulfonic acids and their salts listed in Table 8, 1.791(29) Å, and there is no indication from these data that a class difference in d(S—C) exists between the zwitterions and the anions. The S—C(1)—N angle of 126°, which is significantly larger than the corresponding angles in $^{+}MeNH_2CH_2SO_3^{-}$, ^{+}i-$PrNH_2CH_2SO_3^{-}$ and the two Na salts **15**

[4] This situation is reminiscent of taurine, $^{+}H_3N(CH_2)_2SO_3^{-}$, where H(7) is involved in a bifurcated bond, $H(7)\cdots O(3)_{intra}$ ~ 2.3 Å (NHO ~ 133°), $H(7)\cdots O(3)_{inter}$ ~ 2.4 Å (NHO ~ 132°) (5). The stretching frequency of the N—H(7) bond exhibits a temperature dependence characteristic of strongly bent hydrogen bonds (6).

Can. J. Chem. Downloaded from www.nrcresearchpress.com by 210.87.254.42 on 09/06/12
For personal use only.

Can. J. Chem. Downloaded from www.nrcresearchpress.com by 210.87.254.42 on 09/06/12
For personal use only.

TABLE 5. $MeN(CH_2SO_3Na)_2 \cdot 2H_2O$: positional and thermal parameters ($\times 10^4$)

Atom	x y z	U_{11} U_{22} U_{33}	U_{12} U_{13} U_{23}
S	−0526(1)	214(6)	−6(6)
	3809(2)	125(6)	−10(6)
	1174(1)	260(7)	−4(6)
O(1)	−0292(4)	303(22)	1(18)
	1845(6)	183(19)	−4(19)
	0707(2)	352(22)	−96(18)
O(2)	0629(4)	260(21)	−107(19)
	5140(7)	243(20)	44(19)
	1292(2)	436(24)	−32(19)
O(3)	−1604(4)	306(22)	77(19)
	5143(7)	239(21)	−83(19)
	0908(2)	429(24)	57(20)
O(4) H_2O	2834(4)	311(23)	10(18)
	3394(6)	155(19)	12(19)
	0626(2)	427(23)	39(18)
H(41)	3431(77)	2145(212)[a]	
	2297(141)		
	0805(53)		
H(42)	2447(100)	1995(211)[a]	
	3973(154)		
	1081(38)		
C(1) CH_2	−0966(5)	278(30)	−47(26)
	2886(7)	255(29)	9(26)
	2111(3)	264(29)	53(25)
H(11)	−1267(20)	301(132)[a]	
	4465(20)		
	2346(6)		
H(12)	−1810(12)	382(142)[a]	
	1942(32)		
	1963(8)		
C(2)[b] CH_3	0109(16)	817(100)	173(109)
	−0589(11)	92(44)	−205(95)
	2418(12)	1062(119)	−136(108)
H(21)[b]	0636(106)	2859(221)[a]	
	−1391(65)		
	2868(35)		
H(22)[b]	0661(103)	1239(216)[a]	
	−0593(46)		
	1900(41)		
H(23)[b]	−0785(25)	2655(221)[a]	
	−1437(61)		
	2327(71)		
N[b]	−0154(0)	381(55)	−19(42)
	1703(4)	106(33)	31(45)
	2640(0)	1(55)	17(30)
Na	1525(2)	300(12)	−19(10)
	1239(4)	155(10)	−4(10)
	−0214(1)	364(12)	8(10)

[a] U_{iso}.
[b] Half occupancy.

and **16** of Table 8, 110–114°, and even than the S—C—S angle in $CH_2(SO_3^-)_2$, 116–120° (10, 11), may be the consequence of the *cis*-O(1), CH_3 conformation of the anion (see above). It may be noted that the P—O—C angle in **23** is also quite large, 119° (12).

Discussion of bond lengths

S—C bond lengths

The S—C bond lengths in the two title compounds are indistinguishable. Furthermore, there is no indication from the available evidence (only two salts, cf. Table 8) that a class difference exists between the free-acid zwitterions and the sulfonate anions. A more definite statement on this point can only be made when direct comparisons are available for matching $^+H_3N\cdots SO_3^-/H_2N\cdots SO_3^-$ pairs. At present it would seem that any zwitterion/anion difference that may exist will be absorbed in the d(S—C) variation due to the *chemical* differences between zwitterions and to the bond-length uncertainties of the individual structure determinations.

S—O bond lengths[5]

By itself, comparison of d(S—O) in the two title compounds is not illuminating, although the S—O bond length involving the non-hydrogen-bonded oxygen O(3) in $^+MeNH_2CH_2SO_3^-$ appears to be slightly shorter than the corresponding S—O(1) and S—O(3) bond lengths in the Na disulfonate. On the other hand, the shorter hydrogen-bonded S—O(2) bond in the zwitterion is shorter than the hydrogen-bonded S—O(2) bond in the disulfonate anion, but then the particulars of the two hydrogen bonds are different.

To obtain a clearer idea of the effect of hydrogen bonding on d(S—O) it is necessary to extend the comparison to other aminosulfonic acids. Table 9 lists the d(S—O) values (uncorrected for thermal motion)[6] in all the ω-aminosulfonic and related acids and their salts we have found in the literature. In some of the structures one (or even two) of the oxygens can be clearly identified as non-hydrogen-bonded, while in others all three oxygens engage in hydrogen bonding. The unbiased means of the S—O bond lengths are as follows (with the number of values in brackets):

All values [72]	1.450(14) Å
Oxygen clearly identified as non-hydrogen-bonded [10]	1.451(8) Å
Oxygen clearly identified as hydrogen-bonded [26][7]	1.455(11) Å

From these means we cannot conclude that hydrogen bonding produces a lengthening of the S—O bond. However, if the comparison is restricted to those structures in which both hydrogen-bonded and non-bonded oxygens are known to be simultaneously present (nine determinations in all), then the following result is obtained:

Oxygen non-hydrogen-bonded [10]	1.451(8) Å
Oxygen hydrogen-bonded [17]	1.460(7) Å

Analysis of variance as well as a paired t test show that the hypothesis that these two sample means come from the same population can be rejected at the 0.5% significance level. Thus for the self-consistent sets of d(S—O) determinations the available evidence strongly suggests that there is a class effect, i.e., hydrogen bonding causes the S—O bonds in the aminosulfonic acids and their salts to be lengthened.

[5] In the following, *sample* standard deviations of the unweighted means are quoted in parentheses.

[6] Librational corrections for the three S—O bonds in $^+MeNH_2CH_2SO_3^-$ amount to 0.001 Å (cf. Table 4). This order of magnitude may be taken as representative of the corrections for the S—O bonds listed in Table 9.

[7] When determinations by photographic methods are not included, the mean is 1.457(10) Å.

Can. J. Chem. Downloaded from www.nrcresearchpress.com by 210.87.254.42 on 09/06/12
For personal use only.

TABLE 7. $MeN(CH_2SO_3Na)_2 \cdot 2H_2O$: interatomic distances (Å) and bond angles (deg) (see Fig. 2)

Atoms	Distance	Atoms	Angle
S—O(1)	1.462(4)	O(1)—S—O(2)	112.7(2)
S—O(2)	1.467(4)	O(1)—S—O(3)	113.4(2)
S—O(3)	1.462(4)	O(2)—S—O(3)	112.3(2)
S—C(1)	1.797(5)	O(1)—S—C(1)	107.7(2)
N—C(1)	1.447(5)	O(2)—S—C(1)	104.5(2)
N—C(2)	1.464(15)	O(3)—S—C(1)	105.4(2)
Na(D)···O(4H)	2.361(5)	S—C(1)—N	126.2(3)
Na(D)···O(4D)	2.397(5)	C(1A)—N(A)—C(1B)	114.8(8)
Na(D)···O(1F)	2.426(4)	C(1)—N—C(2)	113.8(8)
Na(D)···O(3B)	2.453(5)	O(4D)—Na(D)—O(3F′)	78.8(1)
Na(D)···O(3F′)	2.503(5)	O(1F)—Na(D)—O(4H)	79.3(1)
Na(D)···O(1D)	2.523(4)	O(3B)—Na(D)—O(4H)	80.5(2)
O(4D)···O(2H)	2.794(6)	O(4D)—Na(D)—O(4H)	81.3(2)
O(4D)···O(2D)	2.796(6)	O(1D)—Na(D)—O(4H)	85.4(1)
H(41D)···O(2H)	1.84(9)	O(1D)—Na(D)—O(1F)	86.5(1)
H(42D)···O(2D)	2.06(12)	O(1D)—Na(D)—O(4D)	88.1(2)
		O(3B)—Na(D)—O(1F)	89.2(1)
		O(3B)—Na(D)—O(3F′)	91.7(2)
Symmetry code:		O(3B)—Na(D)—O(4D)	91.9(2)
A x y z		O(1D)—Na(D)—O(3F′)	102.1(2)
B $\bar{x}$ y $\frac{1}{2}-z$		O(1F)—Na(D)—O(3F′)	120.9(2)
C $\frac{1}{2}+x$ $\frac{1}{2}-y$ $\bar{z}$		O(3F′)—Na(D)—O(4H)	158.4(2)
D $\frac{1}{2}-x$ $\frac{1}{2}-y$ $\frac{1}{2}+z$		O(1F)—Na(D)—O(4D)	160.2(2)
E $\frac{1}{2}-x$ $\frac{1}{2}+y$ z		O(1D)—Na(D)—O(1F)	166.0(2)
F $\frac{1}{2}+x$ $\frac{1}{2}+y$ $\frac{1}{2}-z$		Na(D)—O(4D)—Na(H′)	100.0(2)
G $\bar{x}$ $\bar{y}$ $\bar{z}$		H(41)—O(4)—H(42)	104(8)
H x $1-y$ $\frac{1}{2}+z$		O(4D)—H(41D)—O(2H)	157(20)
X′ = X + (0$\bar{1}$0)		O(4D)—H(42D)—O(2D)	142(20)

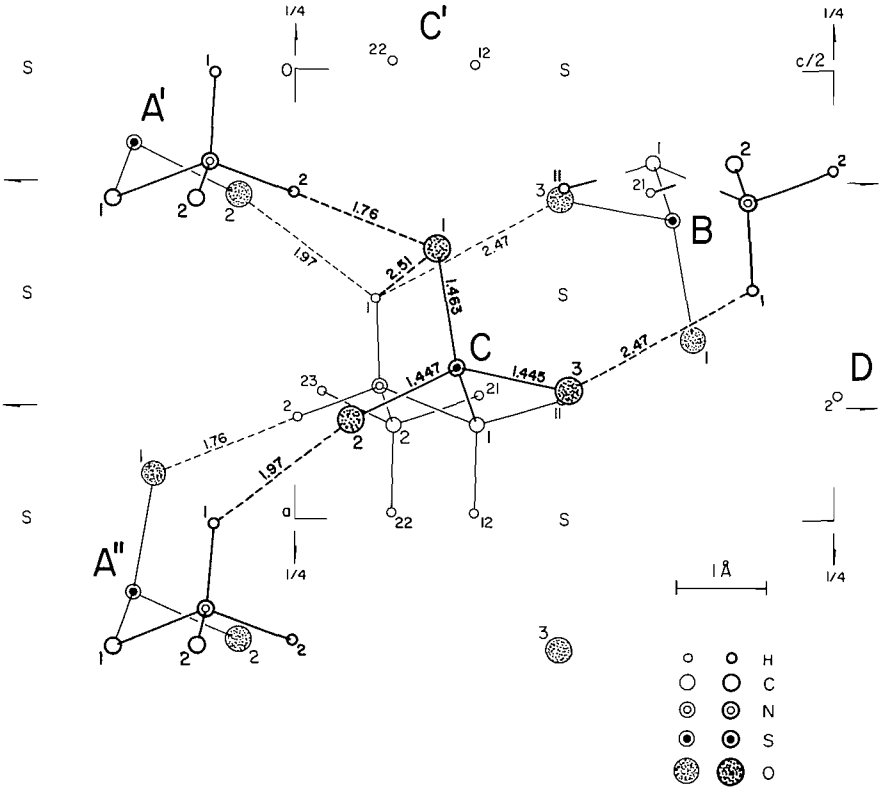

FIG. 1. Hydrogen bonding in $^+MeNH_2CH_2SO_3^-$ (projection of a portion of the crystal structure on (010)). Positions of the screw axes are indicated by S. For symmetry code and additional interatomic distances and bond angles see Table 4.

TABLE 8. Uncorrected bond lengths (Å) in ω-aminosulfonic, ω-aminophosphonic and related acids and their salts

No.	Compound	S—C P—C S—N	C—N	N—C_N
	Zwitterions			
1	$^{+}MeNH_2CH_2SO_3^{-}$ (this work)	1.793(3)	1.473(3)	1.496(4)
2	^{+}i-$PrNH_2CH_2SO_3^{-}$ (7)	1.793(3)	1.487(3)	1.521(3)
3	$^{+}H_3N(CH_2)_2SO_3^{-}$ (5)	1.780(2)	1.484(2)	—
4	α-$^{+}H_3N(CH_2)_3SO_3^{-}$ (13)	1.761(4)	1.486(6)	—
5	$HO(CH_2)_2NH_2^{+}(CH_2)_2SO_3^{-}$ (14)	1.782(3)	1.490(3)	1.492(3)
6	$^{+}MeNH_2CH_2CH[3,4\text{-}C_6H_3(OH)_2]SO_3^{-}\cdot\frac{1}{2}H_2O$ (15)	1.817(6)	1.499(7)	1.494(8)
6	$^{+}MeNH_2CH_2CH[3,4\text{-}C_6H_3(OH)_2]SO_3^{-}\cdot\frac{1}{2}H_2O$ (16)	1.809(5)	1.488(7)	1.500(8)
7	$PhNH.CH(\beta\text{-}pyH^{+})SO_3^{-}\cdot MeOH$ (17)	1.845(4)	1.424(5)	1.421(5)
8	$^{+}H_3N.CH_2CONH(CH_2)_2SO_3^{-}$ (18)	1.781(4)	1.469(5) 1.478(5)	—
9	$^{+}H_3N.CH(COOH)CH_2SO_3^{-}\cdot H_2O$ (19)	1.785	1.497	—
10	$^{+}H_3N.CH(COOH)(CH_2)_2SO_3^{-}$ (20)	1.767(10)	1.470(10)	—
11	$^{+}H_3N(CH_2)_2SSO_3^{-}$ (21)	1.76(1) 1.88(1)	1.51(1) 1.50(1)	—
12	^{+}o-$H_3NC_6H_4SO_3^{-}$ (22)	1.773	1.466	—
13	^{+}m-$H_3NC_6H_4SO_3^{-}$ (23)	1.80(1)	1.44(2)	—
14	^{+}p-$H_3NC_6H_4SO_3^{-}\cdot H_2O$ (24)	1.77(2)	1.49(3)	—
	Salts			
15	$PhNHCH_2SO_3Na\cdot H_2O$ (25)	1.795(3)	1.426(4)	1.400(3)
16	$p\text{-}BrC_6H_4NHCH_2SO_3Na\cdot\frac{3}{2}H_2O$ (26)	1.769(10)	1.419(13)	1.417(12)
17	8-CH_3S-quinoline-5-$SO_3Na\cdot\frac{1}{2}H_2O$ (27)	1.78(1) 1.76(2)	—	—
18	8-HS-quinoline-5-SO_3K (28)	1.80	—	—
19	$MeN(CH_2SO_3Na)_2\cdot 2H_2O$ (this work)	1.797(5)	1.447(5)	1.464(9)
	Zwitterions			
20	β-$^{+}H_3NCH_2PO_3H^{-}$ (29)	1.817(3)	1.485(4)	—
21	β-$^{+}H_3N(CH_2)_2PO_3H^{-}$ (30)	1.807(4)	1.488(5)	—
22	$^{+}H_3N(CH_2)_3PO_3H^{-}$ (31)	1.808(12)	1.524(21)	—
23	$^{+}H_3N(CH_2)_2OPO_3H^{-}$ (12, 32)	—	1.491(7)	—
24	$^{+}H_3NCH_2P(CH_3)O_2^{-}$ (33)	1.825(6) 1.807(6)[a]	1.486(6)	—
	Zwitterion			
25	$^{+}H_3N.SO_3^{-}$ (34)	1.772(1)	—	—
25	$^{+}H_3N.SO_3^{-}$, 78 K (35)	1.772(1)	—	—
	Salts			
26	$H_2N.SO_3K$ (36)	1.666(6)	—	—
27	$H_2N.SO_3NH_4$ (37)	1.63(1)	—	—
27	$H_2N.SO_3NH_4$ (38)	1.640(10)	—	—
28	$HN(SO_3K)_2$ (39)	1.655(7)	—	—
28	$HN(SO_3K)_2$ (11)	1.662(5)	—	—
29	$N(SO_3K)_3\cdot 2H_2O$ (40)	1.70(2) 1.71(2) 1.72(2)	—	—

[a] P—C_{Me}.

Can. J. Chem. Downloaded from www.nrcresearchpress.com by 210.87.254.42 on 09/06/12
For personal use only.

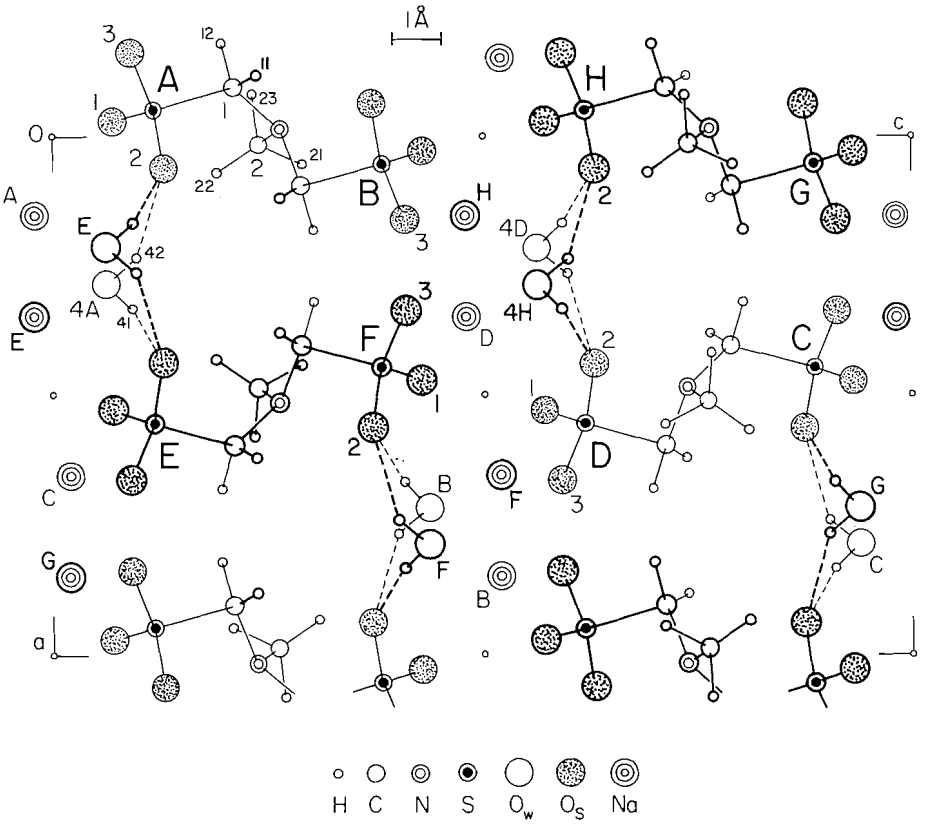

FIG. 2. Projection of the $MeN(CH_2SO_3Na)_2 \cdot 2H_2O$ structure on (010). Note the twofold orientational disorder of the N—CH_3 groups with respect to the twofold axes (parallel to *b*, midway between the C(1) atoms). O_w—H···O_S hydrogen bonds are indicated by dashed lines, centres of symmetry by the smallest circles. For symmetry code, interatomic distances and bond angles see Table 7.

The data of Table 9 are insufficient in number and quality for an investigation of the possible existence of a class difference between the zwitterions and the anions. Nevertheless, a weak indication that such a difference *may* exist is obtained when the above set of ten S—O bond lengths involving non-hydrogen-bonded oxygens is split into a subset of six (zwitterions) and one of four (sulfonate anions). The respective sample means are 1.446(4) and 1.459(6) Å. These are different at the 0.5% significance level, suggesting the order of magnitude to be expected if the class difference proves to be real.

C—N bond lengths in the S···N chains

The *d*(C—N) value in $^+MeNH_2CH_2SO_3^-$, 1.473(3)Å, is within 1σ of the unbiased mean for the zwitterions of Table 8 (excluding **7**), 1.483(17) Å. The corresponding value in $MeN(CH_2SO_3^-)_2$, 1.447(5) Å, is lower, but the difference must be viewed with caution because of the uncertainties in the positional parameters resulting from having to refine a structure containing orientational disorder.

The only two salts in Table 8 that can be contrasted with the zwitterions, **15** and **16**, have a *d*(C—N) mean, 1.423(5) Å, indisputably lower than the mean for the zwitterions. However, the comparison is not informative on the effect of deprotonation. The bond shortening is undoubtedly due to the aromatic substitution at the nitrogen, similar to that in the zwitterion **7**, and is consistent with the observed C—N—C_{Ph} angles in **15** and **16**, ~122° and ~126° respectively, which are larger than the corresponding C—N—C_{alkyl} angles in the other compounds, ~113–~116°, and with the N—C_{Ph} bonds in **15** and **16**, which are significantly shorter than the corresponding N—C_{alkyl} bonds.

The question of whether the C—N bond length in the zwitterionic acids undergoes observable change on deprotonation of the amino group thus remains unanswered.

Comparison of aminoalkanesulfonic and aminoalkanephosphonic acids

Only the zwitterion forms (Table 8) can be compared, as no phosphonate structures appear to have been determined.

The means of the uncorrected S—C and P—C distances are statistically indistinguishable, 1.799(34) Å as against 1.813(8) Å. Similarly, the means of the C—N bond lengths in the two classes of acids are statistically not different, 1.491(11) Å compared with 1.495(16) Å. However, comparing only $^+H_3N(CH_2)_nSO_3^-$ and $^+H_3N(CH_2)_nPO_3H^-$, $n = 1-3$, and using $^+MeNH_2CH_2SO_3^-$ instead of $^+H_3NCH_2SO_3^-$ (the structure of which has not been reported), the means are 1.778(16) Å for S—C and 1.811(6) Å for P—C, and these are significantly different at the 5% level. Clearly, both a more extensive and more accurate set of bond lengths would be required to estimate the actual difference between the mean values of *d*(S—C) and *d*(P—C) in the two groups of acids.

The means of the C—N bond lengths in the two classes of zwitterions, 1.483(17) Å and 1.495(16) Å, are statistically indistinguishable. The P—O distances have not been scrutinized.

Concluding remarks

Analysis of the currently available bond lengths leads to

Can. J. Chem. Downloaded from www.nrcresearchpress.com by 210.87.254.42 on 09/06/12
For personal use only.

TABLE 9. Dimensions of the SO_3 group in ω-aminosulfonic and related acids and their salts (uncorrected distances, in Å)[a]

No.	S—O	X	O···X	O···H	OHX°
1	1.445(3)	—			
	1.447(3)	N	2.798(4)	1.97(3)	133(3)
	1.463(2)	N	2.805(3)	1.76(5)	172(4)
		N	2.905(3)	2.51(3)	102(2)
2	1.441(2)	—			
	1.463(2)	N	2.844(3)	1.93(5)	171
	1.463(2)	N	2.842(3)	2.05(5)	168
3	1.448(2)	—			
	1.461(2)	N	2.793	1.92	166
	1.465(2)	N	2.893	2.12	162
		N	2.926(2)	2.29	133
		N	3.016	2.38	132
4	1.445(4)	N	2.892		
	1.469(3)	N (2×)	2.837		
5	1.453(3)	N	2.855(2)	2.10(3)	149(3)
	1.459(3)	N	2.812(2)	2.02(3)	158(2)
	1.466(3)	O(OH)	2.731(2)	2.00(4)	160(4)
6 (15)	1.447(4)	—			
	1.459(4)	O(OH)	2.84	1.78	170
		N	2.84	1.93	151
		N	2.90	2.01	148
	1.465(4)	O(OH)	2.67	1.50	170
		O(w)	2.86	1.68	166
6 (16)	1.442(4)	—			
	1.454(4)	O(OH)	2.84	2.01	176
		N	2.89	2.01	147
	1.460(4)	O(OH)	2.67	1.89	170
		O(w)	2.86	1.79	169
7	1.450(3)	—			
	1.453(3)	O(MeOH)	2.834(5)	2.27(6)	170(4)
	1.461(3)	N	2.731(4)	2.17(6)	134(3)
8	1.451(3)	N	2.860	1.86	163
	1.456(4)	N	2.888	1.86	175
	1.460(4)	N	2.872	1.86	164
9	1.437	O(w)	2.780(8)	1.82(2)	165
	1.453	O(w)	2.814(7)	1.89(2)	174
	1.461	N	2.943(8)	1.99(3)	157
		N	2.967(8)	1.99(2)	172
10	1.435(7)	N	2.78(2)	2.02(12)	151(10)
		N	2.96(2)	2.36(14)	132(10)
	1.457(9)	N	2.77(2)	1.80(11)	153(11)
	1.461(6)	O	2.66(2)	1.75(11)	149(8)
11	1.41(1)	N	2.83	2.08	145
	1.48(1)	N	2.89	1.88	149
		N	2.78	2.18(8)	107
	1.48(1)	N	2.85	2.14	113
		N	3.00	2.20	128
	1.39(1)	N	2.96	1.85	162
	1.47(1)	N	2.98	2.41(10)	110
		N	2.84	2.42	111
		N	2.86	2.46	105
	1.48(1)	N	2.87	2.34	118
		N	3.15	2.40	132
12	1.427	N	2.823	1.92	145
	1.435	N	2.774	1.80	161
	1.438	N	2.753	1.80	163
13	1.44(1)	N	2.84		
	1.44(1)	N	2.84		
	1.44(1)	N	2.85		
14	1.42(2)	N	2.91		
	1.44(2)	O(w)	2.83		
		N	2.86		
	1.46(2)	O(w)	2.73		
15	1.450(2)	N	3.079(3)	2.30(6)	172(6)
	1.455(2)	O(w)	2.978(3)	2.67(6)	108(5)
	1.469(2)	O(w)	2.968(3)	2.17(6)	163(6)
16	1.450(5)	—			
	1.459(6)	O(w)	2.947(8)	2.16(9)	149(9)
	1.478(5)	O(w)	2.842(8)	2.29(9)	118(8)
		O(w)	2.892(6)	2.10(8)	170(11)
17	1.44(1)				
	1.45(1)	(2×)			
	1.46(1)	(3×)			
18	1.45				
	1.48				
	1.50				
19	1.463(4)	—			
	1.463(4)	—			
	1.467(4)	O(w)	2.794(6)	1.84(9)	157(20)
		O(w)	1.797(5)	2.06(12)	142(20)
25 (34)	1.435(1)	N	2.931		
		N	3.004		
	1.436(1)	N	2.986		
	1.438(1)	N	2.929		
		N	2.963		
25 (35)	1.439(1)	N			
		N			
	1.444(1)	N			
	1.444(1)	N			
		N			
26	1.459(7)	—			
	1.454(4)	N (2×)			
27 (37)	1.45(1)				
	1.46(1)				
	1.49(1)				
27 (38)	1.432(8)				
	1.442(8)				
	1.450(8)				
28 (39)	1.438(10)				
	1.448(8)				
	1.454(9)				
29	1.42(2)	(3×)			
	1.44(2)	(2×)			
	1.47(2)				

[a] The esd's of the original papers are given in parentheses. For numbering of compounds and references see Table 8.

disappointing results, in that the volume of data and the assortment of compounds are not adequate to permit definite conclusions about the effect of deprotonation of the amino group. This is in striking contrast with the effect of deprotonation and condensation on the S—N bond length and on bond angles in sulfamic acid (Table 8), where the reasons for the large variation have been discussed, in terms of the presence or the absence of a d_π–p_π overlap, by Cruickshank (11).

Can. J. Chem. Downloaded from www.nrcresearchpress.com by 210.87.254.42 on 09/06/12
For personal use only.

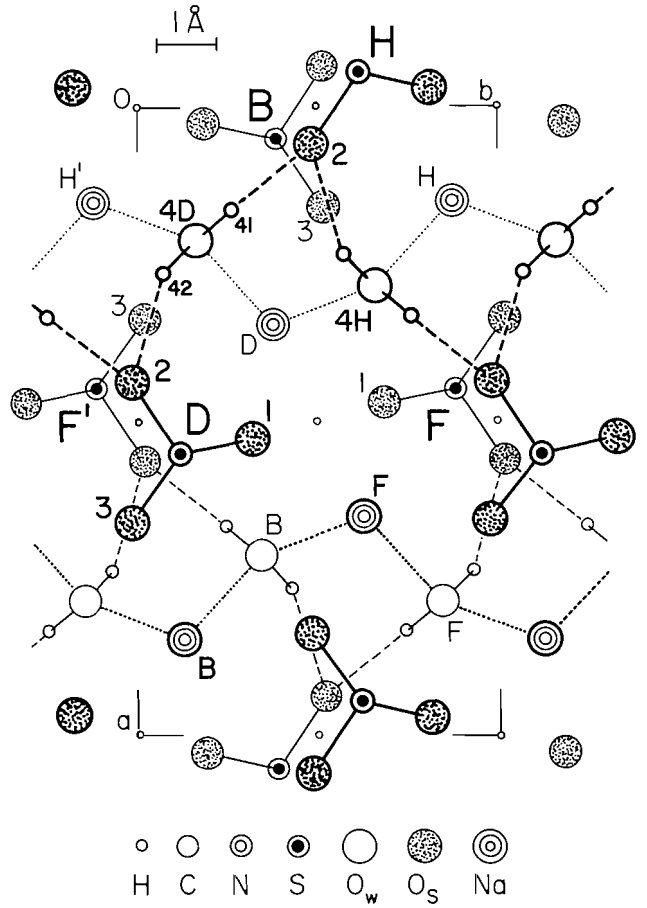

FIG. 3. Hydrogen bonding in $MeN(CH_2SO_3Na)_2 \cdot 2H_2O$ (projection of a portion of the unit-cell contents on (001)). Each water molecule is coordinated approximately tetrahedrally by two O(2) atoms (dashed lines, O_w—H···O_S hydrogen bonds) and two Na^+ ions (dotted lines). For symmetry code, interatomic distances and bond angles see Table 7.

Acknowledgment

This investigation was supported by research grants from the Natural Sciences and Engineering Research Council of Canada to T.S.C. and O.K.

1. W. VOSS and R. GUTTMANN. Ber. Deutsch. Chem. Ges. **63**, 1726 (1930).
2. T. S. CAMERON and R. E. CORDES. Acta Crystallogr. B, **35**, 748 (1979).
3. International tables for X-ray crystallography. Vol. IV. The Kynoch Press, Birmingham, England. 1974.
4. G. SHELDRICK. X-Ray system report. University Chemical Laboratories, Lensfield Road, Cambridge, England. 1976.
5. Y. OKAYA. Acta Crystallogr. **21**, 726 (1966).
6. O. KNOP, W. J. WESTERHAUS, and M. FALK. Can. J. Chem. **58**, 867 (1980).
7. J. R. LECHAT. Acta Crystallogr. B, **36**, 3148 (1980).
8. H. HERBERTSSON. Acta Crystallogr. B, **33**, 830 (1977).
9. J. BERNSTEIN. Acta Crystallogr. B, **35**, 360 (1979).
10. F. CHARBONNIER, R. FAURE, and H. LOISELEUR. Acta Crystallogr. B, **35**, 1773 (1979).
11. D. W. J. CRUICKSHANK. J. Chem. Soc. 5486 (1961).
12. J. KRAUT. Acta Crystallogr. **14**, 1146 (1961).
13. S. UEOKA, T. FUJIWARA, and K. TOMITA. Bull. Chem. Soc. Jpn. **45**, 3634 (1972).
14. N. GALEŠIĆ, M. HERCEG, and B. MATKOVIĆ. Acta Crystallogr. B, **37**, 265 (1981).
15. A. R. GARAFALO, E. MILANO, D. A. WILLIAMS, and T. F. BRENNAN. Cryst. Struct. Commun. **8**, 823 (1979).
16. J. G. HENKEL, J. B. ANDERSON, M. RAPPOSCH, and G. HITE. Acta Crystallogr. B, **36**, 953 (1980).
17. K. STADNICKA, J. MIREK, and A. BUDA. Pol. J. Chem. **54**, 811 (1980).
18. C. GARRIGOU-LAGRANGE, H. JENSEN, and M. COTRAIT. J. Mol. Struct. **36**, 275 (1977).
19. M. RAMANADHAM, S. K. SIKKA, and R. CHIDAMBARAM. Acta Crystallogr. B, **29**, 1167 (1973).
20. G. R. CLARKE and E. G. STEWARD. J. Cryst. Mol. Struct. **7**, 41 (1977).
21. W. E. KEEFE and J. M. STEWART. Acta Crystallogr. B, **28**, 2469 (1972).
22. S. R. HALL and E. N. MASLEN. Acta Crystallogr. **22**, 216 (1967).
23. S. R. HALL and E. N. MASLEN. Acta Crystallogr. **18**, 301 (1965).
24. A. 1. M. RAE and E. N. MASLEN. Acta Crystallogr. **15**, 1285 (1962).
25. J. R. LECHAT. Acta Crystallogr. B, **35**, 183 (1979).
26. J. R. LECHAT. Cryst. Struct. Commun. **10**, 553 (1981).
27. A. D. OZOLA, YA. K. OZOLS, A. A. KEMME, YA. YA. BLEIDELIS, and YA. V. ASHAKS. Zh. Strukt. Khim. **23** [6], 98 (1982).
28. A. D. OZOLA, YA. K. OZOLS, and YA. V. ASHAKS. Zh. Strukt. Khim. **21** [6], 119 (1980).
29. M. DARRIET, J. DARRIET, A. CASSAIGNE, and E. NEUZIL. Acta Crystallogr. B, **31**, 469 (1975).
30. Y. OKAYA. Acta Crystallogr. **20**, 712 (1966).
31. T. GŁOWIAK and W. SAWKA-DOBROWOLSKA. Acta Crystallogr. B, **36**, 961 (1980).
32. W. G. FERRIER, A. R. LINDSAY, and D. W. YOUNG. Acta Crystallogr. **15**, 616 (1962).
33. T. GŁOWIAK and W. SAWKA-DOBROWOLSKA. Acta Crystallogr. B, **33**, 1522 (1977).
34. A. F. CAMERON and F. D. DUNCANSON. Acta Crystallogr. B, **32**, 1563 (1976).
35. J. W. BATS, P. COPPENS, and T. F. KOETZLE. Acta Crystallogr. B, **33**, 37 (1977).
36. G. W. COX, T. M. SABINE, V. M. PADMANABHAN, NGUYEN TU BAN, M. K. CHUNG, and A. J. SURJADI. Acta Crystallogr. **23**, 578 (1967).
37. V. K. WADHAWAN and V. M. PADMANABHAN. Acta Crystallogr. B, **28**, 1903 (1972).
38. E. B. CAIN and F. A. KANDA. Z. Kristallogr. **135**, 253 (1972).
39. G. A. JEFFREY and D. W. JONES. Acta Crystallogr. **9**, 283 (1956).
40. J. V. TILLACK and C. H. L. KENNARD. J. Chem. Soc. A, 1637 (1970).

Can. J. Chem. Downloaded from www.nrcresearchpress.com by 210.87.254.42 on 09/06/12
For personal use only.

Alternaric acid. Proof of biosynthesis via condensation of two polyketide chains. Complete assignment of the ^1H and ^{13}C magnetic resonance spectra by 2D techniques[1,2]

ALBERT STOESSL AND J. B. STOTHERS

London Research Centre, Agriculture Canada and the Department of Chemistry, University of Western Ontario, London, Ont., Canada N6A 5B7

Received August 12, 1983

ALBERT STOESSL and J. B. STOTHERS. Can. J. Chem. **62**, 549 (1984).

Incorporation studies utilizing [1,2-$^{13}C_2$]acetate have established that the fungal phytotoxin alternaric acid is biosynthesized by an uncommon condensation of two polyketide chains rather than from a single chain undergoing an a priori possible, albeit improbable, rearrangement. Unequivocal assignments for the ^{13}Cmr spectra followed from the results of three 2D experiments, namely, homonuclear (^{1}H) and heteronuclear (^{1}H, ^{13}C) correlation spectra and double quantum coherence (^{13}C). Attempts to distinguish between the two possible loci of the chain junction were unsuccessful, suggesting that the synthesis may proceed on a single enzyme complex, without intervention of discrete intermediates.

ALBERT STOESSL et J. B. STOTHERS. Can. J. Chem. **62**, 549 (1984).

Des études d'incorporation d'acétates [$^{13}C_2$-1,2] ont permis d'établir que la biosynthèse de l'acide alternarique de la phytotoxine fongique se produit par le biais d'une condensation peu commune de deux chaînes de polycétides plutôt qu'à partir d'une chaîne unique subissant une transposition qui est a priori possible mais qui est peu probable. On a fait des attributions non-ambigues des spectres rmn du ^{13}C en faisant appel à trois expériences en 2D, soit des spectres de corrélation homonucléaire (^{1}H) et hétéronucléaire (^{1}H, ^{13}C) et une cohérence quantique double (^{13}C). On a essayé en vain de localiser les deux points éventuels de jonction des chaînes; ceci suggère que la synthèse peut se produire sur un complexe enzymatique unique sans l'intervention d'intermédiaires discrets.

[Traduit par le journal]

Can. J. Chem. Downloaded from www.nrcresearchpress.com by 210.87.254.5 on 09/06/12
For personal use only.

Alternaric acid (**1***a*) (1–3) is a phytotoxic metabolite of the fungus *Alternaria solani* (4–6). Its biosynthesis has been investigated by Turner (7) who showed, in an elegant application

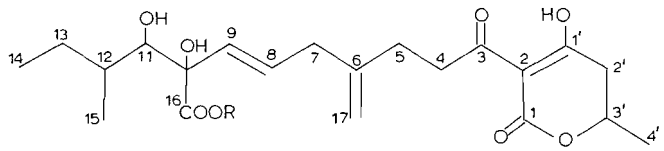

1 a R = H
b R = Me

of radiotracer techniques, that the odd-numbered carbon atoms, 1,3,5 . . . . 13, 1′, and 3′, are derived from C-1 and the even-numbered carbons, 2,4,6 . . . . 14, 2′, and 4′, from C-2 of acetate, while C-15, -16, and -17 originate from the C_1 pool. Mevalonate was not incorporated into **1***a* in significant amount. Alternaric acid is, therefore, a polyketide but it remained unknown whether it was the product of an uncommon condensation of two chains as in either Scheme 1 or 2 (8) or by rearrangement of a single nonaketide as in Scheme 3. In seeking an answer to this question, we have examined **1**, isolated from incorporation experiments with [1,2-$^{13}C_2$]acetate and some likely competitors, using nmr spectroscopic methods.

A prerequisite for these studies was the complete assignment of the signals in the ^{13}Cmr spectra of **1***a* or its more soluble methyl ester **1***b*. This problem was facilitated by heteronuclear correlation with the ^{1}Hmr spectrum which itself was readily assigned as follows. For **1***b*, the four olefinic absorptions consisted of two broadened singlets, δ 4.77 and 4.81, attributable to the C-17 protons, and a pair of doublets of triplets at δ 6.02 (J = 7.3, 15.5 Hz) and 5.58 (J = 2.5, 15.5 Hz), assignable to H-8 and -9, respectively, with each multiplet exhibiting long range coupling. A broadened doublet of doublets (δ 2.81 (2H), J = 2.5, 7.3 Hz) was easily ascribed to the protons on C-7. Methyl absorptions at δ 0.86 (d, J = 6.8 Hz), 0.865 (t, J = 7.3 Hz), and 1.45 (d, J = 6.3 Hz) could be directly assigned to the 15-, 14-, and 4′-methyl protons, respectively. A sharp doublet, J = 1.8 Hz, at δ 3.92 arose from the carbinyl proton on C-11,

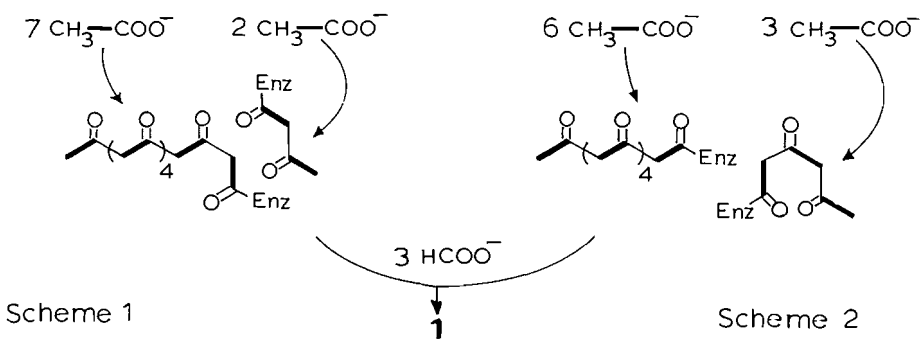

SCHEMES 1 AND 2

[1] Part X of the Series "Metabolites of *Alternaria solani*"; for Part IX see ref. 21; for Part VIII see ref. 22; for Part VII see ref. 23.
[2] Part 108 in the series "^{13}Cmr studies"; for Part 107 see ref. 24; for Part 106 see ref. 25; for Part 105 see ref. 26.

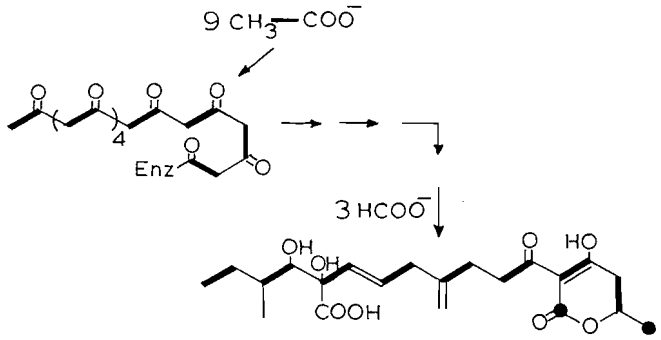

SCHEME 3

close to a methoxyl singlet at δ 3.82. A one-proton multiplet at δ 4.53 could be attributed to H-3′ which was coupled to a 2-proton multiplet near 2.6 ppm. These two absorption patterns were duplicated by spin simulation calculations to show that the C-2′ protons absorb at 2.60 and 2.63 with $J = -12.0$ Hz and are coupled at H-3′ with $J = 4.3$ and 11.0 Hz, respectively. The remaining one-proton multiplet at δ 1.65 ($J = 1.8$, 6.8, 7.2 Hz) must arise from H-12 while 2-proton multiplets at δ 3.2, 2.35, and 1.27 were assignable to the 4-, 5-, and 13-methylene protons, respectively. All of these assignments were confirmed through a homonuclear correlation experiment (9) using the HOMCOR pulse sequence of the XL-200 software.

The ^{13}Cmr spectrum of **1***b* in $CDCl_3$ contained 22 sharp signals indicating either rapid equilibration between various tautomeric forms or its existence as a single tautomer; in CD_3CN solution, six of these signals are significantly broadened.[3] For **1***a*, all 21 signals are sharp in $CDCl_3$ while six are markedly broadened[3] in CD_3OD solution. Of the 22 signals for **1***b*, eight were readily assigned after the APT spectrum (10) was recorded; these included the $COOCH_3$ group at 175.3 and 53.2 ppm, the $C{=}CH_2$ group at 145.9 and 111.0 ppm, C-2, -4′, -10, and -12 at 103.0, 20.5, 81.3, and 35.2 ppm, respectively. Definitive assignments for the other sp^3 carbons, all of which are protonated, were obtained by a $^{13}C-^1H$ chemical shift correlation experiment (11) using the HETCOR pulse sequence of the XL-200 software. Thus the carbinyl methine signals at 70.2 and 76.0 ppm were found to arise from C-3′ and C-11, respectively, while the methyl signals at 11.7 and 12.8 ppm were readily assigned to C-14 and -15, respectively. The five methylene signals at 28.2, 30.5, 36.8, 38.8, and 38.9 ppm were found to be correlated with the methylene proton multiplets centred at δ 1.27, 2.34, 3.17, 2.6, and 2.81, respectively, thereby leading to the ^{13}C assignments at C-13, -5, -4, -2′, and -7, respectively, since the proton assignments had been established as described above. Unequivocal assignments for the five remaining signals for **1***b* were obtained by the double quantum coherence technique (12) with **1***b*-$^{13}C_x$ isolated from the incorporation experiments utilizing [1,2-$^{13}C_2$]acetate. The key feature of the ^{13}Cmr spectrum of this material was the fact that each of the absorptions for the carbons in the main skeleton contained ^{13}C satellites confirming the polyketide origin of the skeleton and establishing the incorporation of nine intact doubly labelled acetate units. In principle, one can identify the individual acetate units by pairing the coupling constants given by the satellite separations provided the J values are significantly different. For **1***b*, this is not the case since the methylene carbons at 30.5, 36.8, 38.8, and 38.9 ppm each exhibited satellites separated by 42–43 Hz. In a two-dimensional INADEQUATE experiment, however, coupled spins are identified by the double quantum coherence which is equal to the sum of the chemical shifts of the two carbon sites measured with respect to the transmitter frequency. This technique with natural abundance material can establish the connectivity of the carbons in a molecular skeleton, as was first illustrated for 5α-androstane (13), but relatively large samples are required because of the low probability of occurrence, ca. $(0.01)^2$, of contiguous ^{13}C nuclei. In an enriched compound obtained from experiments utilizing doubly labelled acetate, however, the double quantum coherence of the pairs of carbons arising by incorporation of intact acetate units is much more readily determined even at low incorporation levels and, thus, smaller samples are required to identify these coupled pairs. With this technique it was found that the four methylene signals at 30.5, 36.8, 38.8, and 38.9 ppm are directly bonded to the carbons absorbing at 145.9, 203.5, 128.9, and 194.5 ppm, respectively, and that the 129.0 ppm olefinic carbon is bonded to C-10 (81.3 ppm). This information completed the ^{13}C assignments as set out in **2** for which the individual coupling constants for the bonds labelled by intact acetate units are given in parentheses.

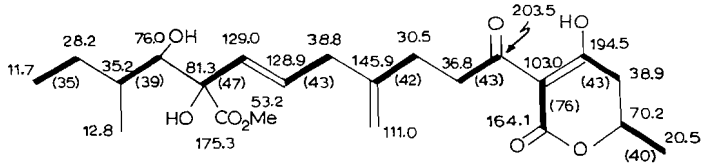

2

It may be noted that the observed shieldings for C-1′, -1, -2, and -3 in **1***b* are very similar to those found for the corresponding centres in podoblastin A (**3**) (14) and in 5,6-dihydrodehydroacetic acid (**4**).[4] The assignments shown in **4** were

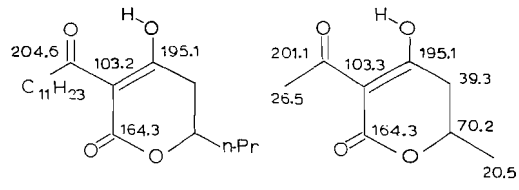

3 **4**

obtained by a 2D INADEQUATE experiment which provided the required double quantum frequencies. Similar shieldings have also been reported for 2-acetyldimedone (15) for which the endo- and exo-cyclic "carbonyl" carbons were found to absorb at δ 196.3 and 201.6, respectively. Although drawn as a 3-acyl-4-hydroxy-6-methylpyrone in **2**, **1***b* can exist in a variety of tautomeric forms (see **5**). The absence of a protonated carbon signal for C-2 shows that **5***a* is a very minor contributor but a clear distinction between **5***b* and *c* is not possible from the available data.

[3] The broadening (for the C-1, -2, -3, -4, -1′, and -2′ signals, see below) is presumably due to a change in tautomeric equilibration rate with solvent.

[4] A generous sample of **4** was kindly provided by D. Figueroa, University of Alberta, for the spectroscopic studies.

Can. J. Chem. Downloaded from www.nrcresearchpress.com by 210.87.254.5 on 09/06/12
For personal use only.

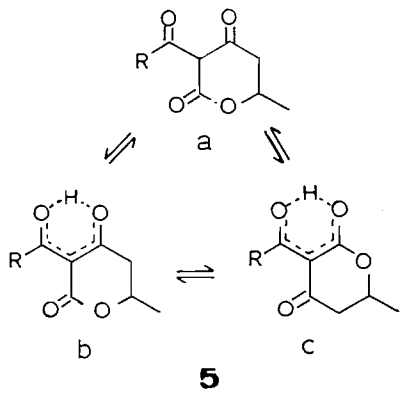

5

The ^{13}Cmr spectra of samples of **1**-$^{13}C_x$, isolated from still cultures of *A. solani* that had been amended with sodium [1,2-$^{13}C_2$]acetate at the time of maximal alternaric acid synthesis, showed that the labelled precursor had been incorporated in the pattern shown in **2** where the heavy bars indicate nine intact acetate units. For each of the labelled carbons the relative intensities of the satellites and the central signal corresponding to the absorption of natural abundance material provided a measure of the ^{13}C enrichment (16). For carbons 1–12 as well as 1′ and 2′, the incorporation level was found to be 0.5 ± 0.1% while C-13, -14, -3′, and -4′ were more highly labelled, ca. 0.8%. The latter values constitute distinct starter effects establishing that **1** must arise by condensation of two polyketide chains. In addition, the rearrangement required for the genesis of **1** from a single nonaketide chain (Scheme 3) would lead to enhanced singlet signals lacking pronounced satellites for C-1 and -4′, and common couplings for C-1′ and -2 as well as for C-2′ and -3′. The absence of all of these features proves that **1** does not arise from a single chain precursor.

In principle, a distinction between the alternatives shown in Schemes 1 and 2 is possible if the acetate incorporation levels differ for the two polyketide chains. Unfortunately, several incorporation experiments with [1,2-$^{13}C_2$]acetate failed to provide **1**-$^{13}C_x$ with significantly different degrees of labelling of the pertinent carbon atoms. In other words, these experiments did not reveal whether the C-1, -2 unit was a terminal unit for either the C-3 to -14 or the C-1′ to -4′ chains. An exactly analogous failure has been reported (17) from a study of [1,2-$^{13}C_2$]acetate incorporation into radicinin (**6**) which, like **1**, is one of very few compounds whose origin from two polyketide chains is indicated.[5]

In further attempts to obtain differential incorporation into

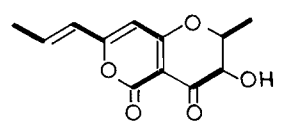

6

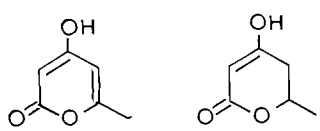

7 8

[5]Other recent cases are those of citreothiolactone and citreopyrone from *Penicillium viride* (18) and the podoblastins from the higher plant *Podophyllum peltatum* (14).

the two moieties of **1**, labelled acetate was administered to fungal cultures together with unlabelled compounds which had some promise as possible competitors. Thus, in separate experiments, [1,2-$^{13}C_2$]acetate was administered together with triacetic acid lactone (**7**) and its dihydro derivative (**8**) as well as with sodium acetoacetate and 3-hydroxybutyrate as possible specific precursors for a C_6 or C_4 chain, respectively. In all four cases, the alternaric acid which was isolated exhibited essentially equal labelling in both moieties, as in the earlier experiments. Alternaric acid isolated from fungal cultures amended only with either dideuteriotriacetic acid lactone or 3-deuterio--3-hydroxybutyrate was unlabelled according to ^{2}Hmr spectroscopy.

The consistent absence of differential labelling by acetate, other than that arising from starter effects, both in these experiments and in those described by Seto and Urano (17) suggests that both molecules may be biosynthesized rapidly on one multiple enzyme complex, with the intervention of intermediates in a manner analogous to that presumably operative in fungal fatty acid synthesis (19).

Experimental

Melting points were determined on the Kofler hot stage. Organic solvents were reagent grade and redistilled before use. Ethanol was the 96% product. Thin layer chromatography was done on precoated plates of silica gel (Macherey–Nagel Polygram SIL N-HR/UV$_{254}$; 0.2 mm) with MeOH/$CHCl_3$ (3:7) or concentrated ammonia solution/EtOH (1:9) as irrigants and detection by uv light, I_2 vapour, or vanillin (1%) in 50% phosphoric acid at 120°C.

Sodium [1,2-$^{13}C_2$]acetate (90% ^{13}C), sodium borodeuteride, and deuterated solvents were obtained from Merck, Sharp, and Dohme Canada Ltd., Pointe Claire-Dorval. Triacetic acid lactone (4-hydroxy-6-methyl-2-pyrone (**7**)) was used as received from Aldrich Chem. Co., Milwaukee, U.S.A. Its 5,6-dihydro derivative **8** was prepared by hydrogenation in EtOAc over Pd/C as described in the literature (20); it had mp 128°C (lit. (20) mp 120–121°C; 124°C) and contained a little unreduced pyrone even after recrystallization from EtOH (^{1}Hmr spectrum). Material enriched in 5,6-dideuterio-4-hydroxy-6-methyl-2-pyrone, mp 123–124°C, was prepared analogously with $^2H_2$ (99.6%; Canada Liquid Air Ltd., Montreal), analysis of its ^{1}Hmr spectrum indicating that it consisted mainly of the expected 5,6-dideuterio compound (ca. 33%) and, for unclarified reasons, the 5,6-dihydro compound (ca. 66%). Sodium acetoacetate was prepared by hydrolysis of redistilled ethyl acetoacetate with the calculated volume of aqueous 0.93% NaOH at 4°C during 3 days, the crude product being diluted with EtOH (2.2 vol.) before use. Sodium (±)-3-deuterio-3-hydroxybutyrate was prepared by reduction of ethyl acetoacetate (1.3 g) with an excess of sodium borodeuteride (126 mg) in ice-cold MeOH (10 mL), hydrolysis of the resulting ester (^{13}Cmr, δ_C: 13.9, 22.2, 42.8, 60.4, 63.7 (J_{CD} = 22 Hz), 172.5) with the calculated volume of 1 *M* NaOH (room temperature; 2 days), and recrystallization from absolute EtOH; mp 162–165°C; ^{13}Cmr, δ_c: 25.4, 50.2, 69.1 (J_{CD} = 22 Hz), 184.3.

Alternaria solani (Ell. & Mart.) Sorauer, strain ATCC 11078, was obtained from the American Type Culture Collection, Rockville, Maryland, and maintained on V8 juice agar slants (23). Inocula were prepared by culturing mycelium scraped from one or more slants on Brian's medium T (23) (25 mL) in 100-mL Delong flasks for 10 days, collecting the mycelial mats, washing with several rinses of sterile distilled water, and homogenizing in a Waring blender in sterile distilled water. The homogenates were used without delay, at the rate of 2 mL/bottle, to inoculate fresh medium T contained in 1-L Roux bottles (100 mL/bottle). Cultures were maintained at room temperature (ca. 24°C) in diffuse artificial light, alternaric acid production being monitored by tlc of the $CHCl_3$ extracts of filtrates, obtained from 2 cultures at a time, at intervals. Concentrations were estimated by relating the product [spot area × intensity (determined photo-

Can. J. Chem. Downloaded from www.nrcresearchpress.com by 210.87.254.5 on 09/06/12
For personal use only.

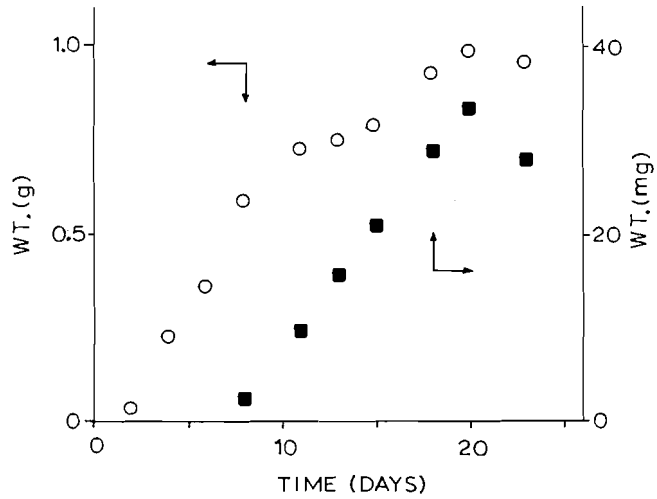

FIG. 1. Mycelial growth rate and alternaric acid production by *Alternaria solani*. ○ dry weight of mycelium (g/Roux bottle); ■ alternaric acid (mg/Roux bottle).

densitometrically)] to a calibration curve constructed likewise with reference samples of known concentration. The results (Fig. 1) indicated that production of **1***a* occurred at a maximal rate about 15 to 20 days after inoculation. Essentially identical observations were made consistently in other experiments which, however, were limited to visual inspection of the tlc's.

*Isolation of alternaric acid (**1**a) and methyl alternarate (**1**b)*

Culture filtrates were acidified (few drops HCl), extracted with $CHCl_3$ (3 × 1 vol.), the extracts reextracted in turn with 5% $NaHCO_3$ (2 × 0.2 vol.), the combined alkaline extracts acidified and extracted with $CHCl_3$ (3 × 0.5 vol.). The washed acidic $CHCl_3$ extracts were evaporated (15 Torr), the residue being crystallized from EtOAc or C_6H_6 and recrystallized (when necessary) from aqueous MeOH. Pure samples had mp 135–136°C but material with mp > 130°C is sufficiently pure for spectroscopy. The methyl ester, mp 103–105°C, was prepared as in the literature (1).

Incorporation experiments

(a) A sterile solution of sodium [1,2-$^{13}C_2$]acetate (669 mg; ca. 8 mmol) in H_2O (162 mL) was added in equal portions to four sets of four Roux bottle cultures 16 days after inoculation. Three of the sets were further supplemented immediately with either (*i*) triacetic acid lactone, (*ii*) its 5,6-dihydro derivative, or (*iii*) its 5,6-dideuterated derivative as 0.084 *M* solutions in EtOH (1 mL/bottle). The cultures were extracted after another 6 days and the purified alternaric acid which was obtained (110 ± 10 mg from each set of 4 bottles) was converted into the methyl ester **1***b* for spectroscopic study.

(b) In a similar series, three sets of three cultures each were supplemented 15 days after inoculation with sodium [1,2-$^{13}C_2$]acetate (0.05 *M* in H_2O, 10 mL/bottle) together with (*i*) 70% EtOH (1 mL/bottle), (*ii*) (±)-3-hydroxybutyrate (0.14 *M* in 70% EtOH, 1 mL/bottle), or (*iii*) sodium acetoacetate (0.78 *M* in 70% EtOH, 1 mL/bottle). Alternaric acid, isolated after 3 days' further incubation, was obtained only in greatly reduced yields (2–4 mg/bottle) and was used for spectroscopy without conversion to the ester. Similarly low yields were obtained also from unamended cultures, nor were they improved by the use of newly obtained cultures of the strain.

(c) Six cultures were amended with sodium (±)-3-deuterio-3-hydroxybutyrate (0.068 *M* in 4% EtOH, 2 mL/bottle) 14 days and, again, 15.5 days after inoculation. The alternaric acid (6.4 mg) isolated after another 2 days did not contain detectable amounts of deuterium (^{2}Hmr spectrum).

Nuclear magnetic resonance spectra

A Varian XL-200 spectrometer was used to record the ^{1}H and ^{13}C spectra at 200 and 50.3 MHz, respectively. Although initially some selective decoupling experiments were done to aid the analysis of the ^{1}H spectra, all of the coupling interactions were identified by homonuclear correlation using the HOMCOR pulse sequence resident in the XL-200 software. The correlated spectrum was obtained using a 512 × 1024 data point matrix transforming 1024 points in both domains with a spectral width of 1200 Hz in both domains. The ^{13}Cmr spectra of **1***a* and *b* in $CDCl_3$ solution contained 21 and 22 signals, respectively, and the degree of protonation of each was determined by recording the APT spectrum for each. Specific assignments of the protonated carbon signals shown in **2** were obtained by heteronuclear correlation with the proton spectrum using the HETCOR pulse sequence of the XL software. The ^{13}C–^{1}H chemical shift correlation utilized a 2048 × 256 data matrix with a 3600 Hz spectral width for ^{13}C and a 1 KHz width for ^{1}H, tranforming 2048 and 512 points, respectively. The results of this experiment unequivocally identified the five individual methylene signals. To complete the ^{13}C assignments, a clear distinction between C-1′ and C-3 was required. As noted in the text, **1**-$^{13}C_x$ isolated from the [1,2-$^{13}C_2$]acetate incorporation experiments gave rise to ^{13}Cmr spectra in which nine pairs of carbons exhibited AX patterns of satellites characteristic of bonded labelled carbons. However, the similar J_{AX} values for four of the methylene carbons precluded positive identification of their labelled partners and a third 2D experiment was required in which the double quantum coherence of the pairs of labelled carbons was determined. With the CCC2D pulse sequence of the XL software a 2K × 128 data point matrix transforming 2048 and 256 points, respectively, with 10 000 Hz sweep widths in both domains, was employed to obtain the double quantum frequencies for the labelled carbons. Through this 2D INADEQUATE spectrum, the labelled pairs of carbon atoms arising from incorporation of intact doubly labelled acetate units were unequivocally identified as shown in **2**. It may be noted that the J_{AX} values were most readily determined with a one-dimensional INADEQUATE spectrum using the C13SAT sequence of the XL software. The spin simulation program used to analyse the proton pattern for the 2′, 3′, and 4′ protons is supplied with the XL software. The 2D INADEQUATE experiment for **4** utilized 2048 × 128 data matrix, 10 KHz in both dimensions, transforming 2K and 512 points, respectively.

Acknowledgements

We are grateful for the financial support provided by the Natural Sciences and Engineering Research Council of Canada and the technical assistance of G. L. Rock.

1. J. F. GROVE. J. Chem. Soc. 4056 (1952).
2. J. R. BARTELS-KEITH. J. Chem. Soc. 860 (1960).
3. J. R. BARTELS-KEITH. J. Chem. Soc. 1662 (1960).
4. P. W. BRIAN, P. J. CURTIS, H. G. HEMMING, C. H. UNWIN, and J. M. WRIGHT. Nature (London), **164**, 534 (1949).
5. P. W. BRIAN, P. J. CURTIS, H. G. HEMMING, E. G. JEFFERYS, C. H. UNWIN, and J. M. WRIGHT. J. Gen. Microbiol. **5**, 619 (1951).
6. P. W. BRIAN, G. W. ELSON, H. G. HEMMING, and J. M. WRIGHT. Ann. Appl. Biol. **39**, 308 (1952).
7. W. B. TURNER. J. Chem. Soc. 522 (1961).
8. W. B. TURNER. Fungal metabolites. Academic Press, London and New York. 1971. p. 136.
9. A. BAX, R. FREEMAN, and G. A. MORRIS. J. Magn. Reson. **42**, 169 (1981).
10. S. L. PATT and J. N. SHOOLERY. J. Magn. Reson. **46**, 535 (1982).
11. G. A. MORRIS and L. D. HALL. J. Am. Chem. Soc. **103**, 4703 (1981).
12. A. BAX, R. FREEMAN, T. A. FRENKIEL, and M. H. LEVITT. J. Magn. Reson. **43**, 478 (1981).
13. A. BAX, R. FREEMAN, and T. A. FRENKIEL. J. Am. Chem. Soc. **103**, 2102 (1981).
14. M. MIYAKADO, S. INOUE, Y. TANABE, K. WATANABE, N. OHNO, H. YOSHIOKA, and T. MABRY. Chem. Lett. 1539 (1982).

Can. J. Chem. Downloaded from www.nrcresearchpress.com by 210.87.254.5 on 09/06/12
For personal use only.

15. D. T. W. CHU, S. N. HUCKIN, E. BERNSTEIN, D. L. GARMAISE, R. S. EGAN, and R. S. STANASZEK. Can. J. Chem. **59**, 763 (1981).
16. R. E. LONDON, V. H. KOLLMAN, and N. A. MATWIYOFF. J. Am. Chem. Soc. **97**, 3565 (1975).
17. H. SETO and S. URANO. Agric. Biol. Chem. **39**, 915 (1975).
18. Y. SHIZURI, M. NIWA, H. FURUKAWA, and S. YAMAMURA. Tetrahedron Lett. **24**, 1053 (1983).
19. P. WALKER and M. WOODBINE. The biosynthesis of fatty acids. *In* The filamentous fungi. Vol. 2. Biosynthesis and metabolism. *Edited by* J. E. Smith and D. R. Berry. John Wiley and Sons, New York. 1976. p. 137.
20. A. I. SCOTT, H. GUILFORD, and D. SKINGLE. Tetrahedron, **27**, 3039 (1971).
21. J. E. HOLENSTEIN and A. STOESSL. Phytopathol Z. In press.
22. A. STOESSL and J. B. STOTHERS. Can. J. Chem. **61**, 378 (1983).
23. A. STOESSL, C. H. UNWIN, and J. B. STOTHERS. Can. J. Chem. **61**, 372 (1983).
24. J. F. KING, S. SKONIECZNY, K. C. KHEMANI, and J. B. STOTHERS. J. Am. Chem. Soc. **105**, 6514 (1983).
25. J. E. HOLENSTEIN, H. KERN, A. STOESSL, and J. B. STOTHERS. Tetrahedron Lett. **24**, 4059 (1983).
26. A. J. RAGAUSKAS and J. B. STOTHERS. Can. J. Chem. **61**, 2254 (1983).

Can. J. Chem. Downloaded from www.nrcresearchpress.com by 210.87.254.5 on 09/06/12
For personal use only.

Metal salt catalyzed carbenoids. XVIII.[1] The electron impact mass spectral behavior of diazocarbonyl compounds. I.

D. S. WULFMAN,[2] JAMES ROBERTS,[3] DENNIS K. HENDERSON,[3] J. C. ROMINE,[3] R. S. MCDANIEL, JR., L. CARVER, AND D. W. BEISTEL

Department of Chemistry, University of Missouri-Rolla, Rolla, MO 65401, U.S.A.

Received March 29, 1983[4]

D. S. WULFMAN, JAMES ROBERTS, DENNIS K. HENDERSON, J. C. ROMINE, R. S. MCDANIEL, JR., L. CARVER, and D. W. BEISTEL. Can. J. Chem. **62**, 554 (1984).

Electron impact (EI) mass spectral studies of methyl diazoacetate, ethyl diazoacetate (**1**), methyl diazoacetoacetate (**2**), and dimethyl diazomalonate (**3**) indicate that loss of N_2 is exceedingly difficult from the parent ion and was observed only with **3**. Diazoacetylacetone exhibits an appreciable $(M - 28)^+$. *Exact Mass* and metastable transitions indicate fragmentation occurs in part via 1,2,3-oxadiazolium ion-radicals (**6**) or α-lactones (**7**) to furnish N_2O and hyponitrite esters. $(M - 28)^+$ from **1** results from loss of ethylene.

D. S. WULFMAN, JAMES ROBERTS, DENNIS K. HENDERSON, J. C. ROMINE, R. S. MCDANIEL, JR., L. CARVER et D. W. BEISTEL. Can. J. Chem. **62**, 554 (1984).

Des études de spectrométrie de masse par impact électronique du diazoacétate de méthyle, du diazoacétate d'éthyle (**1**), du diazoacétoacétate de méthyle (**2**) et du diazomalonate de diméthyle (**3**) indiquent que la perte d'azote moléculaire est difficile à partir des ions moléculaires; on ne l'observe qu'avec **3**. Avec la diazoacétylacétone, il y a un pic important à $(M - 28)^+$. Les masses exactes et les transitions métastables indiquent que la fragmentation se produit en partie par le biais des ions radicaux oxadiazolium-1,2,3 (**6**) ou des lactones-α (**7**) qui fournissent du N_2O et des esters hyponitreux. L'ion à $M - 28^+$, obtenu à partir de **1**, provient d'une perte d'éthylène.

[Traduit par le journal]

Can. J. Chem. Downloaded from www.nrcresearchpress.com by 210.87.254.42 on 09/06/12
For personal use only.

There are surprisingly few studies of the mass spectra of diazo compounds (2–12). Frequently the generation of the ion $[RCN_2]^+$ occurs (presumably the diaza analog of the cyclopropenium ion) (2, 3, 5, 6, 11, 12). The reported spectrum of diazomethane (2) exhibited this as a peak of 8.4% intensity and interestingly, possesses an M^+ of 96.5%. Paulett and Ettinger (2) also found a value for $D(CH_2 - H_2)$ of 1.9 eV and for $D(CH_2 - N_2)^+$, 3.3 eV.

Our observation (10) that dimethyl diazomalonate failed to lose N_2 to form a $(M - 28)^+$ ion is somewhat unique since the M^+ ion might be expected to readily lose N_2 to furnish a carbene-cation-radical stabilized by its substituents. This would have mimicked the reported photochemical behavior (13), a common occurrence in photochemistry and mass spectroscopy (14). The lack of mimicry here is especially surprising since the π system is fully conjugated. Ions possessing the necessary lifetime to pass through a mass spectrometer might be expected to have sufficient time to undergo electronic decay to the most stable cation radicals regardless of which electron had been ejected by electron bombardment. (Luinenberg *et al.* (12) failed to observe any $(M - N_2)^+$ with four diazomethylsulphones.)

We have now completed a study of the series of structurally related diazo carbonyl compounds, ethyl diazoacetate (**1**), methyl diazoacetoacetate (**2**), dimethyl diazomalonate (**3**), and 3-diazopentane-2,4-dione (**4**). Their low and medium-high resolution EI mass spectra are tabulated in Tables 1–5. Spectra were obtained at ~75, ~30, and ~13 eV. The experiments were performed using a JEOL-D100 double focussing mass spectrometer equipped with a JEOL data system and a JEOL ion defocussing attachment capable of scanning accelerating voltage and thus observing metastable transitions (15). The D-100 can be operated in either a low resolution mode or a medium-high resolution mode (up to ~10 000 resolution). For the mass ranges and compositions encountered here, it was possible to distinguish between the various elemental compositions for the ions of interest. The inlet system is all glass up to the gap before the ionizing source. Thus, this study was free from the plague of metal catalyzed processes to be expected of diazo compounds and observed in some of the earlier studies in this area (3). Table 6 reveals some of the common fragmentations observed. Table 7 is a listing of all of the nitrogen-containing fragments found in the ms of methyl diazoacetoacetate.

Schemes 1–3 reveal the fragmentation sequences obtained by ion defocussing.

All of the esters exhibit the typical fragmentation patterns associated with esters, e.g., loss of alkoxyl and, with **1**, elimination of olefin from the ester alkyl group (21). In some cases it was not possible to observe metastable transitions. This does not preclude a possible pathway. Such transitions are shown by – – – lines. With the metastable ion determination of the source of $m/z = 59$ in the mass spectrum of **3** some difficulty was encountered. However, we were able to find low intensity metastable ions showing that some (and perhaps all) $m/z = 59$ derived from ions having $m/z = 102$ and 74.

The decomposition of **3** via the pathways 158–130–102–74–59; 102–59; 74–43, and presumably 102–43 is of particular note in that it requires the stepwise loss of three molecules of CO from a material possessing only two initial carbonyl groups, migration of CH_3O to N and CH_3 to N′. Although we were unable to obtain an acceptable *Exact Mass* at $m/z = 102$ from **3**, it must contain N_2 since one of the two paths from it to $m/z = 59$ furnishes CH_3ON_2. Similarly, $m/z = 43$ (CH_3N_2) had its origin in $m/z = 74$ which arose from $m/z = 102$. Since the daughter ions possessed N_2, the parent did as well. The loss of ethylene is not possible in this case and the loss of 28 amu must therefore be attributed to loss of CO. We presume that an oxygen migration has occurred via an

[1] For paper XVII, see ref. 1.

[2] Author to whom correspondence may be addressed.

[3] Undergraduate research participant.

[4] Revision received October 14, 1983.

TABLE 1. Ethyldiazoacetate

m/z	Intensity @75.4 eV	Intensity @25.3 eV	Intensity @13.0 eV	*Exact Mass* (found) @75.4 eV	Assignments	*Exact Mass* (calcd.)	Comments
34	16						
39	24	8		39.0141	C_2HN	39.01089	
40	335	299		40.0029	CN_2	40.00614	
41	480	307		41.0017	C_2HO	41.00273	$I_{rel} = 15$
41	33			41.0173	CHN_2	41.01396	$I_{rel} = 1$, diazacyclopropenium ion
42	231	262	76	42.0073	C_2H_2O	42.01055	Ketene
42				42.0270	CH_2N_2	42.02178	
43	186	213	7	43.0162	C_2H_3O	43.01837	
43				43.0252	CH_3N_2	43.02960	
44	120	65	2	43.9913	CO_2	43.98982	
44				43.9984	N_2O	44.00105	
44				44.0189	C_2H_4O	44.02619	
45	118	151	31	45.0288	C_2H_5O	45.03401	$CH_3CH_2—O^+$
45				45.0481	CH_5N_2	45.04524	
54	2						
57	74	131	100	57.0238	C_2H_3NO	57.02144	?
57				57.0367	$C_2H_5N_2$	57.04524	
58	91	118	107	57.9963	$C_2H_2O_2$	58.00546	$(CHCO_2H)^+$
69	1000	1000	93		C_2HN_2O	69.00887	$(M - OC_2H_5)^+$ interference from CF_3
70	26						
86	28	32	62	86.01414*	$C_2H_2N_2O_2$	86.01160	$(N_2CHCO_2H)^+$
99	3			99.01878*	$C_3H_3N_2O_2$	99.01942	$(N_2CHCO_2CH_2)^+$
114	643	823	1000	114.04220*	$C_4H_6N_2O_2$	114.04288	M^+
115	37	49	78	115.0465	$C^{13}C_3H_6N_2O_2$	115.04624	$(M + 1)^+$

*Average of 27 determinations all within ±0.005 amu of theory.

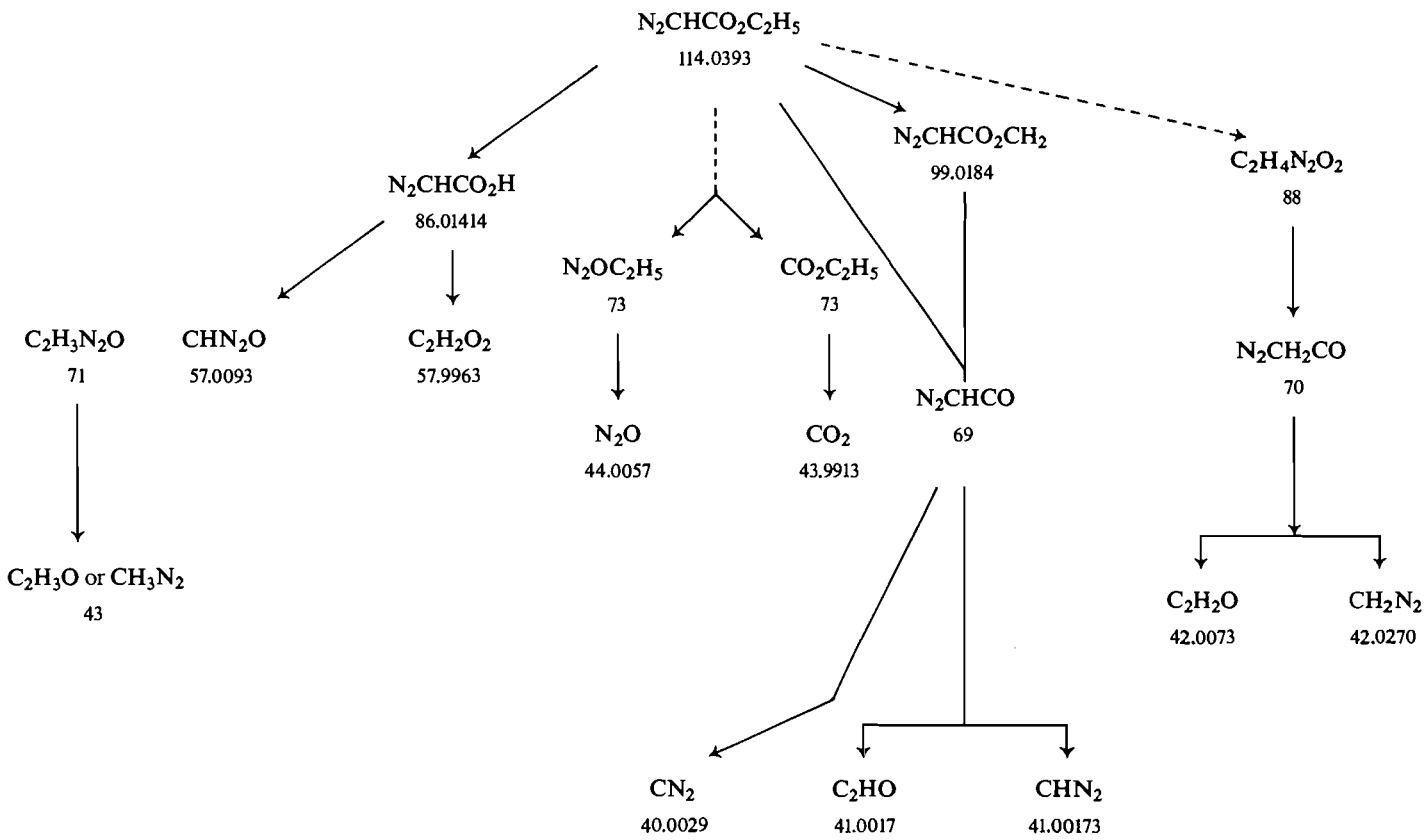

SCHEME 1. Observed metastable transitions with ethyl diazoacetate.

Can. J. Chem. Downloaded from www.nrcresearchpress.com by 210.87.254.42 on 09/06/12
For personal use only.

TABLE 2. Methyldiazoacetoacetate

m/z	Intensity @75.4 eV	Intensity @25.3 eV	Intensity @13.0 eV	*Exact Mass* (found) @75.4 eV	Assignments	*Exact Mass* (calcd.)	Comments
34	73				NH_4O		
37	77				C_3H		
39	89	4			C_2HN		
40	1000	123			CN_2	40.00614	
41	142			41.0161	CHN_2	41.01396	Diazacyclopropenium ion
42	398	25		42.0245	CH_2N_2	42.02178	
42				42.0070	C_2H_2O	42.01055	
43	4158	1000	1000	43.0315	CH_3N_2	43.02960	
43				43.0153	C_2H_3O	43.01837	
44	398	47		44.0351	CH_4N_2	44.03742	
44				44.0214	C_2H_4O	44.02619	
44				43.9865	CO_2	43.98982	
45	93			45.0411	CH_5N_2	45.04524	
53	130			53.0024	C_3HO	53.00273	
53				53.0141	C_2HN_2	53.01396	
54	146	26		54.0168	$C_2H_2N_2$	54.02178	
54				54.0141	C_3H_2O	54.01055	
55	365	66	82	55.0247	$C_2H_3N_2$	55.02960	
				55.0185	C_3H_3O	55.01837	
58	36			58.0425	C_3H_6O	58.04183	
59	495	70		59.0137	$C_2H_3O_2$	59.01328	CO_2CH_3
				59.0246	CH_3N_2O	59.02451	
68	113			67.9905	C_2N_2O	68.00105	?
69	252	42	89	—	C_2HN_2O	69.00887	PFK interference at 68.99520
72	101	25	146	72.0248	$C_3H_4O_2$	72.02110	
74	77			74.0340	$C_3H_6O_2$	74.03674	
83	296	57		83.0246	$C_3H_3N_2O$	83.02451	$(M - CO_2CH_3)$
84	52		63	84.0314	$C_3H_4N_2O$	84.03233	?
84				84.0224	$C_4H_4O_2$	84.02110	
85	109	33			$C_3H_5N_2O$	85.04015	Absent
85				85.0276	$C_4H_5O_2$	85.02892	
86	48		57	86.0380	$C_4H_6O_2$	86.03674	
86				—	$C_3H_6N_2O$	86.04797	Absent
99	69			99.0164	$C_3H_3N_2O_2$	99.01942	$(M - COCH_3)^+$
101	56			101.0237	$C_4H_5O_3$	101.02383	
111	150	26		111.0186	$C_4H_3N_2O_2$	111.01942	$(M - OCH_3)^+$
142	769	140	726	142.0399	$C_5H_6N_2O_3$	142.03779	M^+
143	44		39	—	$C^{13}C_4H_6N_2O_3$	—	$(M + 1)^+$

α-lactone intermediate (**7**) which then successively loses two CO to furnish an azo-carbamate (**8**) which can collapse via CO loss to the species $CH_3N_2OCH_3$ or loss of N_2OCH_3 to CO_2CH_3.

It is clear from the fragmentation pathways of both **1** and **3** that initial retention of N_2 is highly favored. Thus we see that, in all cases where N_2 is present, either *Exact Mass* measurements were possible or, when such measurements were not possible due to closeness in mass with the PFK standards, subsequent daughters were found containing N_2.[5] Similar behavior was observed for **3**.

The generation of oxadiazolium ion radicals (**6**) will account for the generation of the ions $(N_2O)^+$ and $(N_2OR)^+$ (Scheme 4). The relatively low intensities of these ions is consistent with this not being an important pathway. Historically, the structure of α-diazo ketones had been questioned and the 1,2,3-oxadiazole structure proposed (16, 17). However, currently no 1,2,3-oxadiazoles are known and the alternate structure has been discarded (18). The related radical cation clearly offers an adequate representation of ionized diazo esters.

In the case of ethyl diazoacetate, an $(M - 28)^+$ ion was observed. At 72 eV *Exact Mass* measurements indicated that this ion resulted solely from loss of ethylene. Due to sensitivity problems, we were not able to ascertain if this was also the case at the lower ionizing voltages. At 30 eV, one would expect less fragmentation and the $(M - 28/M)$ ratio decreased. Unfortunately, at 13 eV it increased. Thus, the possibility existed that loss of N_2 might occur at the lowest ionizing voltage for **1**. (The $M - 28$ ion from **3** arises via a rearrangement process. Such processes have small frequency factors and low activation energies and consequently will become more important at lower energies.) Although the authors consider it unlikely, the argument can be made that failure to lose N_2 by cleavage of what is traditionally viewed as a weak C—N bond is a consequence of the excess energy leading to cyclization to oxadiazolium ion radicals (**6**). The failure to lose N_2 from **2** or **3** at low voltages might seem to argue against such an interpretation. The counter argument that ethyl diazoacetate behaves differently than **2** and **3** could be made. The related ester,

[5] The nature of the JEOL computer program for high resolution studies precludes the use of other *Exact Mass* standards. The program is written in machine language and a listing is not available.

Can. J. Chem. Downloaded from www.nrcresearchpress.com by 210.87.254.42 on 09/06/12
For personal use only.

TABLE 3. Dimethyldiazomalonate

m/z	Intensity @75.2 eV	Intensity @25.3 eV	Intensity @13.1 eV	*Exact Mass* (found) @75.2 eV	Assignments	*Exact Mass* (calcd.)	Comments
31	45			31.0257	CH_3O	31.01837	
33	4						
34	45						
40	650	404		40.0097	CN_2	40.00614	
41	55			41.0174	CHN_2	41.01396	Diazacyclopropenium ion
42	36				CH_2N_2		
43	113	108		43.0281	CH_3N_2	43.02960	
44	239	82		44.0057	N_2O	44.00105	
44				44.0412	CH_4N_2	44.03742	
45	36			45.0433	CH_5N_2	45.04524	
55	93						
58	46						
59	1000	1000	1000	59.0247	CH_3N_2O	59.02451	$I_{rel} = 29$ $(N_2OCH_3)^+$
59				59.0124	$C_2H_3O_2$	59.01328	$I_{rel} = 71$ $(CO_2CH_3)^+$
60	27	5					
68	107			67.9898	C_3O_2	67.98982	
69	137	150					
70	16			70.0014	$C_3H_2O_2$	70.00546	
74	38						
77	22						
91	15						
99	73			99.01972	$C_3H_3N_2O_2$	99.01942	$(M - CO_2CH_3)^+$
100	5			100.0272	$C_3H_4N_2O_2$	100.02724	$(M - C_2H_2O_2)^+$
101	39						
102	34						
114	7			114.0399	$C_4H_6N_2O_2$	114.0428	$(M - CO_2)^+$
127	102	51		127.0143	$C_4H_3N_2O_3$	127.01433	$(M - OCH_3)^+$
128	5			128.0221	$C^{13}C_3H_3N_2O_3$	128.01769	$(M + 1 - OCH_3)^-$
130	6			130.0264	$C_5H_6O_4$	130.02656	$(M - N_2)^+$
				130.0374	$C_4H_6N_2O_3$	130.0379	$(M - CO)^+$
158	173	170	582	158.0317	$C_5H_6N_2O_4$	158.03270	M^+
159	12			159.0328	$C^{13}C_4H_6N_2O_4$	159.03606	$(M + 1)^+$

TABLE 4. 3-Diazopentane-2-4-dione

m/z	Intensity @74 eV	Tentative assignments
15	39	CH_3
18	59	H_2O
19	287	
26	39	CN
27	95	HCN
39	30	C_3H_3
42	66	CH_2CO
43	1000	CH_3CO
44	59	C_2H_4O and/or N_2O
45	57	C_3HO
55	78	C_3H_3O
56	53	C_3H_4O
60	43	CH_4N_2O
67	30	C_4H_3O
70	33	$C_3H_2O_2$ and/or $C_2H_2N_2O$
83	51	$(M - CH_3 - N_2)^+$ and/or $(M - CH_3CO)^+$
98	107	$(M - N_2)^+$
126	55	M^+

methyl diazoacetate (**5**) was prepared. The data at 72, 30, and 13 eV are given in Table 5. No loss of N_2 to furnish $(M - 28)^+$ is observed.

The failure to lose N_2 from the diazoesters is consistent with the thermal chemistry of these same compounds (for discussions of this point, see ref. 19). Both **1** and **3** can withstand prolonged heating in refluxing toluene solutions. One might suspect that much of the instability of pure diazo compounds results from chain reactions. In solution these chains are interrupted by solvent molecules. The retention of N_2 when bombarded with electrons of 300, 960, and 1656 kcal/g-at. should cast considerable doubt as to the ability of photons in the energy range 80–115 kcal/g-at. to generate nitrogen-free species such as carbenes. Indeed, the observation by Voigt and Meier (20) that photolysis of diazo isatin furnished a diazirine points in the same direction as the observation of a temperature dependence of the photolysis of **3** by Wulfman *et al.* (10), the observation by Tomioka *et al.* (22) of a non-carbenic path C—H inseration product in the course of the photolysis of the diethylamide of diazoacetic acid, and the observation of a diazoacetylonium ion intermediate in the photolysis of **1** in isopropyl alcohol (23). As noted previously (1), the carbene pathway rationale is extremely attractive but is a house-of-cards. No one has demonstrated where along the reaction coordinate N_2 is lost and addition to substrate occurs. There most probably exists a broad range of reactivities amongst diazo compounds in which carbenes represent only an extreme case. The various substitution patterns available would be expected to modify the ease with which N_2 is lost. What is clear, is that diazo esters and diazo ketones behave differently from each other under thermal, photochemical, and mass spectral conditions. In the case of diazoacetoacetic esters, the ester functionality is controlling.

Can. J. Chem. Downloaded from www.nrcresearchpress.com by 210.87.254.42 on 09/06/12
For personal use only.

TABLE 5. Methyldiazoacetate

	Intensity				
m/z	@75.2 eV	@29.3 eV	@13.0 eV	@14.0 eV	Assignments
30	52				CH_2O
31	69	15			CH_3O
40	32				CN_2
41	581	375			CHN_2
42	124	101			CH_2N_2 and/or $CH_2{=}C{=}O$
43	261	226	218	276	CH_3N_2 and/or C_2H_3O
44	21				N_2O and/or CO_2
59	61				CH_3ON_2
69	849	648		62	M − OCH_3
70	19				M + 1 − OCH_3
100	1000	1000	1000	1000	M
101	47				M + 1

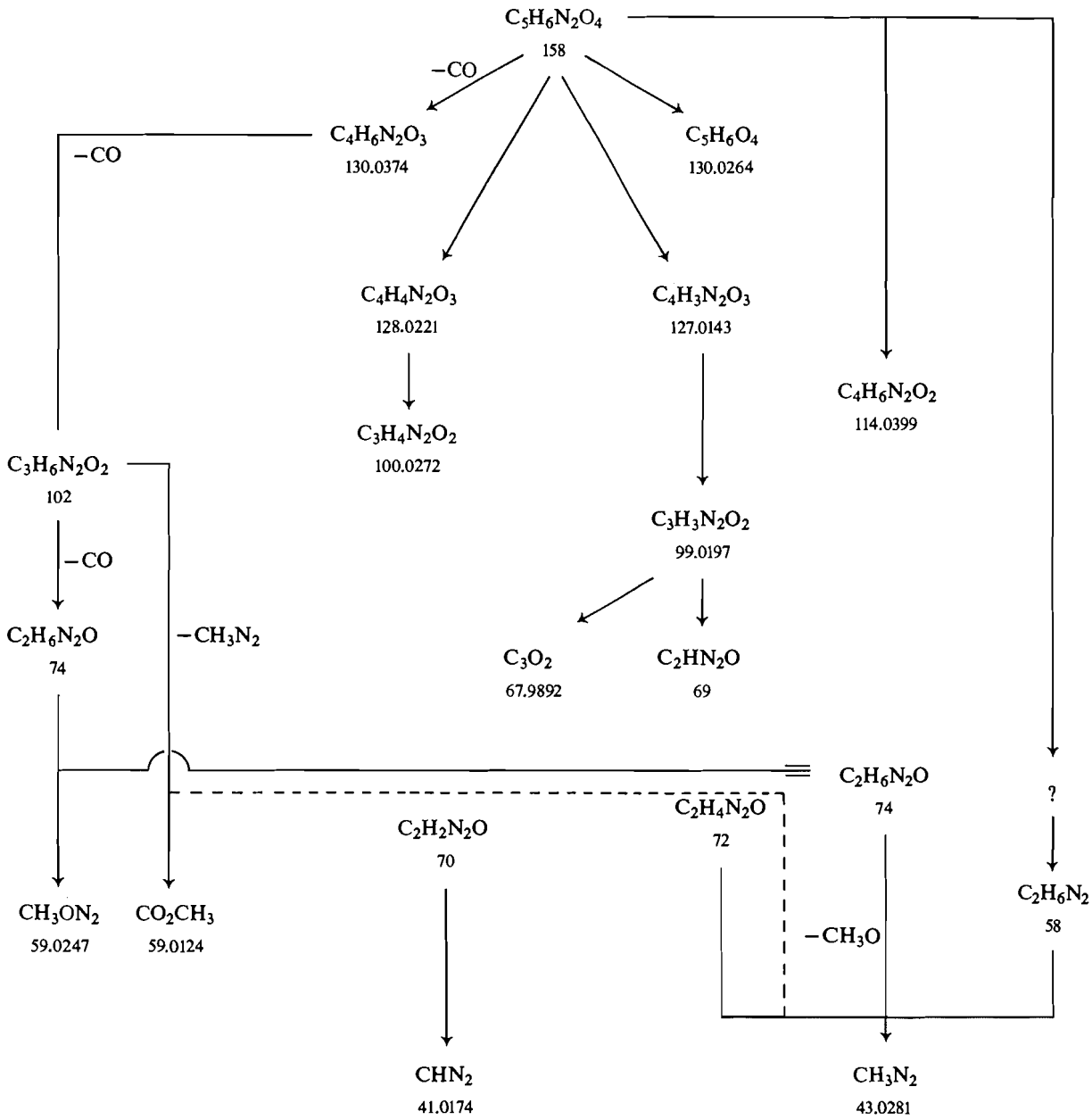

SCHEME 2. Observed metastable transitions of dimethyldiazomalonate.

Can. J. Chem. Downloaded from www.nrcresearchpress.com by 210.87.254.42 on 09/06/12
For personal use only.

TABLE 6. Fragmentations of diazo esters and ketone

Compound	Fragment lost (−) and found (+)								
	P − N_2	±OR	±CH_3CO	±CO_2R	HCN	−CH_3	+N_2OR	+N_2O	+RN_2
$N_2CHCO_2CH_3$	No	Yes	N/A	Yes	Yes	No	Yes	Yes	Yes
$N_2CHCO_2CH_2CH_3$	No	Yes	N/A	Yes	Yes	Yes	No	Yes	Yes
$CH_3COCN_2CO_2CH_3$	No	Yes	Yes	Yes	Yes	Yes	Yes	Yes	Yes
$CH_3O_2CCN_2CO_2CH_3$	No*	Yes	N/A	Yes	Yes	Yes	Yes	Yes	Yes
$CH_3COCN_2COCH_3$	Yes	N/A	Yes	N/A	Yes	Yes	N/A	?	No

*Function of instrument conditions; 0.6% of 100% peak in Table 3.

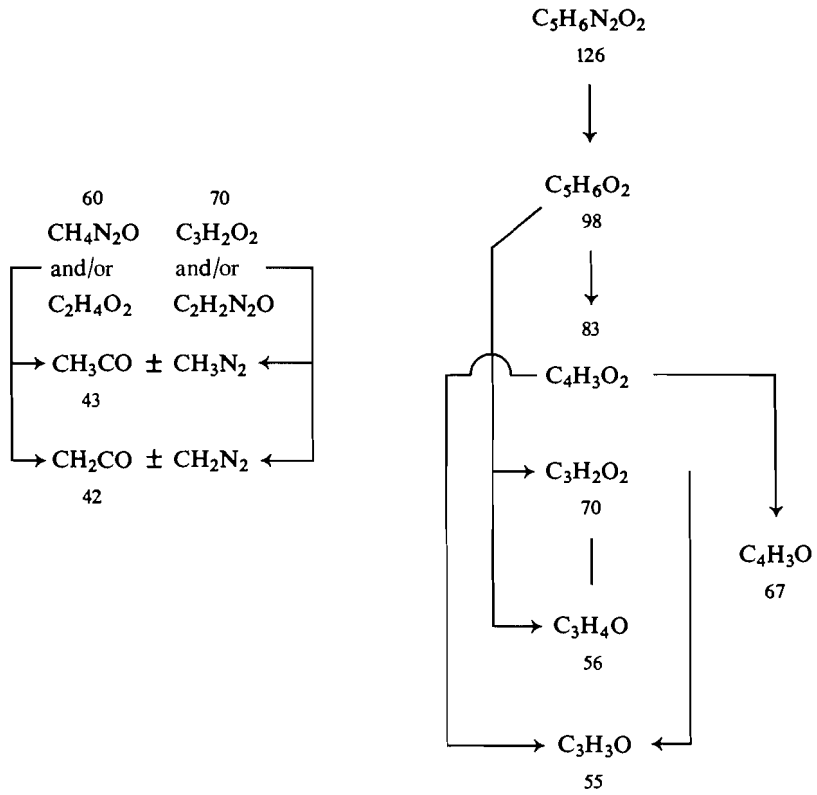

SCHEME 3. Metastable transitions observed with 3-diazopentane-2,4-dione.

TABLE 7. Nitrogen containing fragments from methyl diazoacetoacetate at 10 000 resolution

CHN_2	CH_2N_2	CH_3N_2	CH_3N_2H	CH_3N
	CH_3NH_2	CH_5N_2	HCN	N_2OCH_3
	C_2HN_2	$C_2H_2N_2$		$C_2H_3N_2$
	CH_3COCN_2	$CN_2CO_2CH_3$		CH_3COCN_2CO
		CH_3COCN_2CO		
		N_2O		

Clearly, strong parallels do exist, and in the case of the mass spectral behavior, N_2 is not readily lost from diazo esters. Thus, the cautionary statement of Wolfgang Kirmse (24) – "The long-lasting fascination of the carbene concept for organic chemists appears to have emotional rather than empirical grounds" – appears to have been prescient.

The mass spectrum of dimethyl diazomalonate has been reported previously (*6b*). However, we were unable to observe the reported ions having m/z of 39, 86, and 92. In most instances, we also failed to observe m/z = 130 $(M - N_2)^+$ and found its appearance was more frequent as the temperature of the glass inlet was raised and as the age of the instrument increased. (In 1974 typically the M^+ ion at 75 eV would reach intensities of 50+ percent and there would be no $(M - N_2)^+$.) The differences between the present low resolution work on **3** and that of Zeller *et al.* (6) are minor and most probably reflect instrumental factors.

The mass spectra of *p*-substituted phenyl triazines derived from glycine ethyl ester (**9**) exhibit of an ion $C_4H_6N_2O_2$ which appears to be isomeric with that derived from the diazo ester.

p-X—C_6H_4N=N—$NHCH_2CO_2C_2H_5$

9

This phenomenon is currently under investigation along with the fragmentation behavior of a variety of 1,2,3-triazenes, triazolones, diazoacetamides and anilides, and aliphatic diazoketones.

Can. J. Chem. Downloaded from www.nrcresearchpress.com by 210.87.254.42 on 09/06/12
For personal use only.

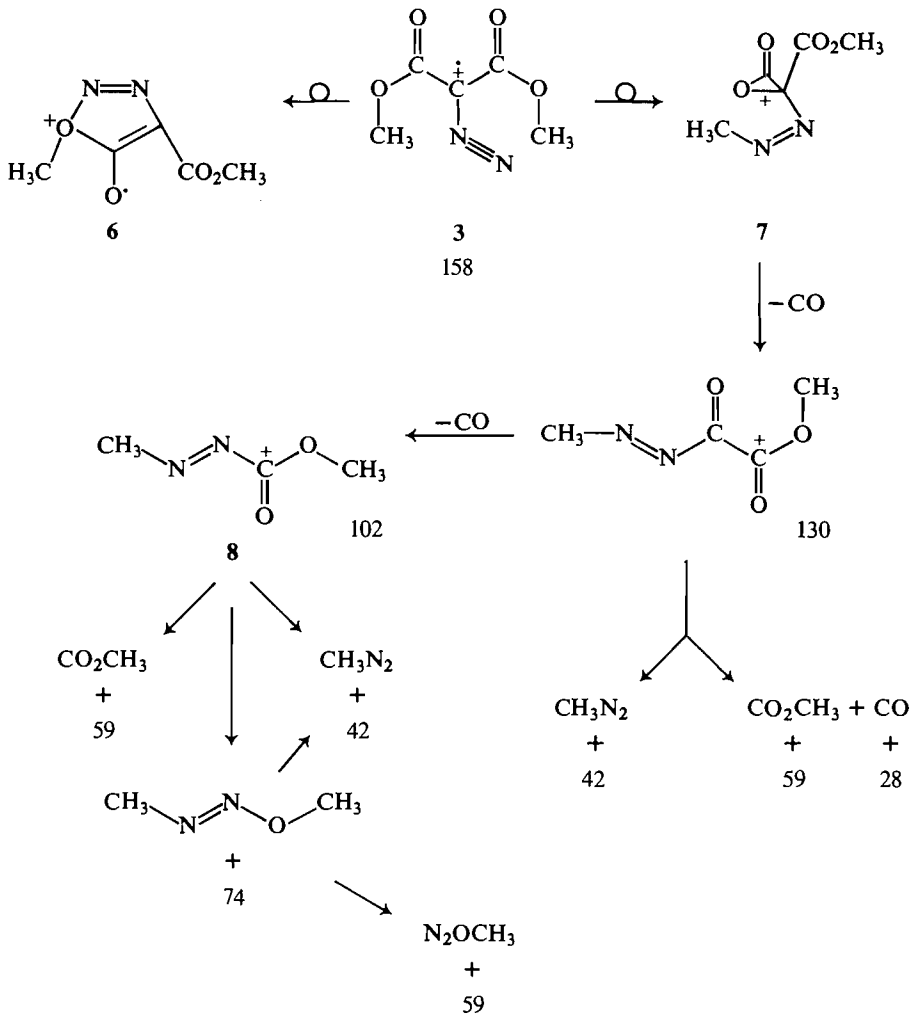

SCHEME 4

1. D. S. WULFMAN and B. POLING. *In* Reactive intermediates. *Edited by* R. A. Abramovitch. Plenum, New York. 1980. pp. 321–512.
2. G. S. PAULETT and R. ETTINGER. J. Chem. Phys. **39**, 825 (1963); **39**, 3534 (1963).
3. A. FOFFANI, S. PIGNATARO, B. CANTONE, and F. GRASSO. Nuovo Cimento, **29**, 918 (1960).
4. K.-P. ZELLER. Org. Mass Spectrom. **10**, 317 (1975).
5. K.-P. ZELLER, H. MEIER, and E. MÜLLER. Ann. **749**, 178 (1971).
6. (*a*) K.-P. ZELLER, H. MEIER, and E. MÜLLER. Org. Mass Spectrom. **5**, 373 (1971); (*b*) Tetrahedron, **28**, 5831 (1972).
7. D. C. DEJONGH, R. Y. VAN FOSSEN, L. R. DUSOLD, and M. P. CAVA. Org. Mass Spectrom. **3**, 31 (1970).
8. P. KINSON and B. TROST. Tetrahedron Lett. 1075 (1968).
9. O. THORSTAD and K. UNDHEIM. Chem. Scr. **6**, 222 (1974).
10. D. S. WULFMAN, B. POLING, and R. S. MCDANIEL, JR. Tetrahedron Lett. 4519 (1975).
11. C. W. THOMAS and L. L. LEVESON. Org. Mass Spectrom. **13**, 39 (1978).
12. O. LUINENBURG, J. B. F. N. ENGBERTS, and W. D. WERINGA. Org. Mass Spectrom. **9**, 837 (1974).
13. R. C. DOUGHERTY. Top. Curr. Chem. **45**, 93 (1974).
14. M. JONES, JR., W. ANDO, M. E. HENDRICK, A. KULCZYCKI, JR., P. M. HOWLEG, K. F. HUMMEL, and D. S. MALAMENT. J. Am. Chem. Soc. **94**, 7469 (1972).
15. S. SASAKI, E. YAMAUCHI, Y. ITASAKI, M. NAITO, and E. WATANABE. Qual. Anal. (Tokyo), **15**, 179 (1965); Anal. Chem. **40**, 1000 (1968).
16. L. WOLFF. Ann. **312**, 119 (1900).
17. L. WOLFF and A. A. HALL. Ber. **36**, 3612 (1903).
18. M. REGITZ. Diazoalkane, Eigenschaften und Synthesen. George Thieme Verlag, Stuttgart. 1977. p. 3.
19. D. W. WULFMAN, G. LINSTRUMELLE, and C. F. COOPER. *In* The chemistry of the diazonium and diazo groups. *Edited by* S. Patai. Wiley–Interscience, Chichester. 1978. pp. 823 and 833.
20. E. VOIGT and H. MEIER. Angew. Chem. **87**, 109 (1975); Chem. Ber. **110**, 2242 (1977).
21. H. BUDZIKIEWICZ, C. DJERASSI, and D. H. WILLIAMS. Mass spectrometry of organic compounds. Holden-Day, San Francisco. 1967.
22. H. TOMIOKA, H. KITAGAWA, and Y. IZAWA. J. Org. Chem. **44**, 3072 (1979).
23. T. DOMINH, O. P. STRAUSZ, and H. E. GUNNING. J. Am. Chem. Soc. **91**, 1261 (1969).
24. W. KIRMSE. Carbene chemistry. 2nd ed. Academic Press, New York. 1971, p. 3.

Can. J. Chem. Downloaded from www.nrcresearchpress.com by 210.87.254.42 on 09/06/12
For personal use only.

Structure determination of the hexosulose dimers

PEDRO ANTONIO GARCÍA RUIZ,[1] INMACULADA CARTAGENA TRAVESEDO, AND ANTONIO SOLER MARTÍNEZ
Department of Organic Chemistry, Faculty of Science, University of Murcia, Murcia, Spain

Received October 21, 1982[2]

PEDRO ANTONIO GARCÍA RUIZ, INMACULADA CARTAGENA TRAVESEDO, and ANTONIO SOLER MARTÍNEZ. Can. J. Chem. **62**, 561 (1984).

The structure determination of the dimers of three hexosuloses has been achieved by mass spectrometry of their acetates and trimethylsilyl derivatives. The analysis of the mass spectra and the chemical evidence for the claim that the dimers are 1,2′:2,1′-di-hexosulofuranose dianhydrides have been reported.

PEDRO ANTONIO GARCÍA RUIZ, INMACULADA CARTAGENA TRAVESEDO et ANTONIO SOLER MARTÍNEZ. Can. J. Chem. **62**, 561 (1984).

On a determiné la structure des dimères de trois hexosuloses en faisant appel à la spectrométrie de masse de leurs acétates et de leurs derivés triméthylsilylés. On rapporte l'analyse de leurs spectres de masse et les preuves chimiques qui confirment que les dimères sont des dianhydrides de di-hexosulofurannoses-1,2′:2,1′.

[Traduit par le journal]

Can. J. Chem. Downloaded from www.nrcresearchpress.com by 210.87.254.6 on 09/06/12
For personal use only.

Introduction

It is very well known that upon concentration of hexosulose solutions, or upon dehydration of the osone by heating at 56°C, under vacuum (1), a dimerization process occurs, but there are no studies of the structure of the osulose dimers.

Also, it is known that mass spectrometry is now a conventional method for the structural analysis of monosaccharides (2–4), disaccharides, and dialdose dianhydrides (5–7).

In the present paper, the dimers of three hexosuloses previously isolated as their monomers by gas–liquid and paper chromatography, are studied. The structural elucidation of the osulose dimers is carried out on the basis of the mass spectral data obtained from their acetate and trimethylsilyl derivatives. In addition, some chemical evidence for the proposed structures is reported.

Results and discussion

The structures of the D-*arabino*, D-*lyxo*, and L-*xylo* hexosulose dimers were identified as the 1,2′:2,1′-dianhydrides of the 2,5-hexosulofuranoses (Fig. 1), by means of the interpretation of their mass spectrometric behaviour.

Some of the more abundant peaks, upon which the identification of D-*arabino* hexosulose dimer as the peracetate or pertrimethylsilyl derivative was based, are given in Table 1 (see Fig. 1). These peaks occur also in the spectrum of the corresponding derivatives of D-*lyxo* and L-*xylo* hexosulose dimers. The relative intensities of the peaks have not been corrected for the isotopic contribution of peaks of lower masses.

The assignment of structure was made on the basis of the presence or absence of characteristic fragments. Moreover, the mass spectra of the structurally analogous compounds have been used to confirm the proposed fragmentations.

The assignment of structure will be discussed in the following sections.

A. *The molecular weight determination*

In accordance with the bibliographic criteria, when no molecular ion peak is present, the molecular weight can be deduced for trimethylsilyl derivatives (8) and acetates (2, 3, 9) from the fragment ions in the region near the molecular weight.

Table 1 shows fragments at $M^{+\cdot} - OR$, $M^{+\cdot} - Me - OR$, $M^{+\cdot} - R - OR$, $M^{+\cdot} - 2OR$, and $M^{+\cdot} - 3OR$, which are indicative of a molecular weight of 932 for the trimethylsilyl derivatives (R = $SiMe_3$), and fragments at $M^{+\cdot} - R$, $M^{+\cdot} - OR$, $M^{+\cdot} - R - OR$, and $M^{+\cdot} - 2OR - R$, which are indicative of a molecular weight of 692 for the acetates (R = $CO—CH_3$).

Also, the molecular weight is confirmed by other characteristic fragments obtained from the molecular ion peak, such as those described in the following sections ($M^{+\cdot} - a$, (see Fig. 1), $M^{+\cdot} - a - R$, $M^{+\cdot} - a - OR$, $M^{+\cdot} - c - OR$, etc.).

B. *The CH_2OR group determination*

The loss of the substituents alpha (α) to the ring oxygen gave rise to the most significant fragment series. As is typical of this group (2, 3, 6, 8–10), the fragments at $M^{+\cdot} - CH_2OR$ ($M^{+\cdot} - a$), $M^{+\cdot} - CH_2OR - Me$ ($M^{+\cdot} - a - Me$), $M^{+\cdot} - a - R$, $M^{+\cdot} - a - OR$, $M^{+\cdot} - a - R - OR$, $M^{+\cdot} - b - R$, a, b + H, and b − Me reported in Table 1 (see Fig. 1) confirm its presence. Moreover, the fragments at $M^{+\cdot} - 2a - 2OR$, $M^{+\cdot} - c - b - OR$, $M^{+\cdot} - h - a$, $h - a - R$, and $g - a - OR - CHO$ are indicative of the presence of two CH_2OR groups. Although some of these fragments (e.g. $h - a - R$) can be considered as derived from some other isomeric structures having only one CH_2OR group, the simultaneous detection of all of them and their complementary fragments (e.g. $M^{+\cdot} - h$) is only possible when the molecule contains two CH_2OR groups.

C. *The furanose ring determination*

In accordance with the results obtained for other mono and oligosaccharide derivatives (11–15), the fragments $M^{+\cdot} - c - OR$ and $M^{+\cdot} - d - OR$ and their corresponding series (see Table 1) are characteristic of the fragmentation of the furanose rings, as well as the abundances of the peaks of the lowest ratio *m/e*: protonated furan, protonated furaldehyde, b − Me, and the abundance ratio for the fragments at *m/e* 217 and *m/e* 204, in the case of TMS derivatives.

Furthermore, as can be seen in Fig. 1 (Table 1), all of them present the fragments $M^{+\cdot} - h$, $M^{+\cdot} - h - OR$, and $h - R$, corresponding to the loss of the lactonic moiety of a pentonic acid which may lose one CH_2OR group (fragments $h - a - R$ and $M^{+\cdot} - h - a$). Also, the symmetric fragmentation g gave rise to two moieties of six carbon atoms (fragments $g - OR$, $g - OR - OR$) which may lose the CH_2OR and CHO groups

[1]Author to whom correspondence may be addressed.
[2]Revision received October 31, 1983.

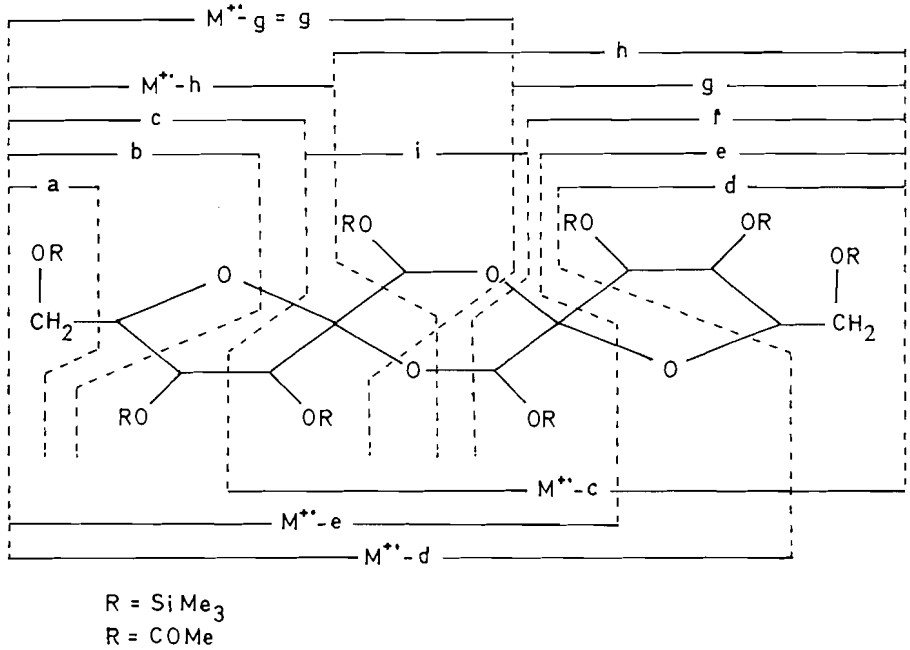

FIG. 1. Hexosulose dimers, mass spectral fragment ions (refer to Table 1 for mass values).

TABLE 1. Mass spectra (70 eV) of the acetates and TMS derivatives of the D-*arabino* hexosulose dimer and their assignment

TMS		Acetate		
m/e	I^a	*m/e*	I^a	Assignment[b]
932	0	692	0	$M^{+\cdot}$
—	—	649	1.9	$M^{+\cdot}$ − R
843*	2.6	633	1.6	$M^{+\cdot}$ − OR
829	0.8	619	0.1	$M^{+\cdot}$ − a
828*	1.2	—	—	$M^{+\cdot}$ − Me − OR
814	1.7	—	—	$M^{+\cdot}$ − a − Me
770	2.3	590	0.1	$M^{+\cdot}$ − R − OR
756	3.0	—	—	$M^{+\cdot}$ − a − R
754*	3.2	—	—	$M^{+\cdot}$ − 2OR
740	1.4	560	0.5	$M^{+\cdot}$ − a − OR
727	1.0	547	0.7	$M^{+\cdot}$ − b − R
—	—	531	0.8	$M^{+\cdot}$ − 2OR − R
667	0.8	517	0.3	$M^{+\cdot}$ − a − R − OR
665*	2.7	—	—	$M^{+\cdot}$ − 3OR
636*	1.4	488	0.5	$M^{+\cdot}$ − 3OR − CHO
609	1.2	459	1.8	$M^{+\cdot}$ − c − OR
599	1.6	—	—	$M^{+\cdot}$ − $C_4H_3O(OR)_3$
596	0.7	446	1.6	$M^{+\cdot}$ − e
548	0.4	—	—	$M^{+\cdot}$ − 2a − 2OR
536	5.8	416	0.4	$M^{+\cdot}$ − c − OR − R
523	2.6	403	1.4	$M^{+\cdot}$ − d − OR
495	0.7	375	1.1	h − R
476	0.3	357	3.9	$M^{+\cdot}$ − c − b − OR
464	0.4	344	2.1	$M^{+\cdot}$ − 2c
540	7.1	330	0.3	f
447	19.1	357	3.9	$M^{+\cdot}$ − c − OR − R − OR
434	24.9	344	2.1	$M^{+\cdot}$ − d − OR − OR
405	0.8	315	2.2	$M^{+\cdot}$ − d − OR − OR − CHO
392	1.7	302	2.4	h − a − R
377	4.6	287	18.0	f − OR
375	1.1	—	—	$M^{+\cdot}$ − 2C − OR
364	1.3	274	6.5	$M^{+\cdot}$ − h
361	2.3	271	4.3	f − OR
333	2.8	—	—	$C_4H_2O(OR)_3$
319	1.7	—	—	d − H
305	3.0	—	—	ROCH=COR—CHOR
288	25.0	228	2.1	g − OR − OR
—	—	215	3.7	$M^{+\cdot}$ − h − OR
273	1.0	213	3.2	$M^{+\cdot}$ − 2C − $CH(OR)_2$
261	1.9	201	2.0	$M^{+\cdot}$ − h − a
259	8.6	—	—	g − OR − OR − CHO
258	7.0	198	3.3	g − OR − ROH − CHO
245	2.6	185	21.0	g − a − OR − CHO
243	4.8	—	—	$C_4HO(OR)_2$
233	1.9	173	5.1	C − H
232	4.6	172	7.8	$\frac{M^{+\cdot} - 2C}{2}$
217	35.1	157	1.1	CHORCHCHOR
204	6.7	—	—	CHORCHOR
—	—	145	0.8	R_3O
191	8.6	131	0.7	$CH(OR)_2$
189	4.6	—	—	$CHORCHOSiMe_2$
159	3.1	129	10.0	i − R
—	—	125	25.1	CHOR—C=C—CHO
147	9.2	—	—	$ROSiMe_2$
133*	16.5	103	10.1	b + h
130	12.8	100	6.0	CHORCO
117	5.6	—	—	b − Me
103*	6.2	73	18.0	CH_2OR = a
97	16.3	97	22	Protonated furaldehyde
—	—	85	16.1	ROCHCH
89*	2.4	59	17.2	OR
73*	100	43	100	R
69*	30.4	69	46.0	Protonated furan

[a] I represents relative intensity.
[b] Structure of the fragments and losses from M^+ (see Fig. 1).
*Analogous fragments (see section F).

Can. J. Chem. Downloaded from www.nrcresearchpress.com by 210.87.254.6 on 09/06/12
For personal use only.

Can. J. Chem. Downloaded from www.nrcresearchpress.com by 210.87.254.6 on 09/06/12
For personal use only.

(fragments g − OR − OR − CHO, g − OR − ROH − CHO, g − OR − a − CHO), in accordance with the presence of two 2,5-furanose rings.

D. *Fragmentation data and elimination of alternative structures*

In the preceding sections A–C were determined unambiguously the molecular weight and the presence of the unsubstituted 2,5-furanose rings exclusively. The assigned structure is the only one which explains all the facts observed, because other glycosidic links (such as 1,2′:2,3′) should give different molecular weights, should present other groups (such as —$CH(OR)_2$) which give strong peaks when present in the structures, or should present the peaks corresponding to substituted furans which are absent in the spectra.

For similar reasons other alternative structures should be excluded.

E. *The 1,2′:2,1′-glycosidic links*

The intensities of the peaks that appeared in the high-mass region were relatively low and the aA_i fragments (g − OR and their fragment series) had high intensities as occur in the spectra of the peracetates (5, 15) and trimethylsilyl derivatives (14, 16, 17) of 1→2-linked disaccharides.

The furanose ring fragmentations (2, 13) at $M^{+\cdot}$ − d − OR, $M^{+\cdot}$ − c − OR, f, f − OR, and i − R are those expected because the fragmentation of oligosaccharides generally takes place in such a way that the constituent sugar residues are degraded independently (3, 4, 18, 19).

Other fragmentations, such as the one assigned to the permethylated dialdose 1,2′:2,1′-dianhydrides (6), are the fragments $M^{+\cdot}$ − 2c, f, f − OR, and i − R, which are indicative of the two 1,2-glycosidic links.

On the other hand, the absence of the fragments from the free monomer of the aldehydic aldosulose excludes the presence of only one 1→2-glycosidic link, and the absence of the fragments from the alternative dioxane rings confirms the structure.

F. *Mass spectra analogies with the pertrimethylsilyl 1,2′:2,1′-di-D-fructofuranose dianhydride*

In the trimethylsilyl derivatives, the fragments that contain the intact dianhydride ring require a shift of 176 mass units more (changing two —CH_2— groups for two —CHOR— groups) for the osulose dimers in relation to D-fructofuranose dianhydride. When the fragements contain only one —CH_2— group, the required shift (to —CHOR—) is 88 mass units more.

On the basis of the preceding shifts, the fragments at $M^{+\cdot}$ − OR, $M^{+\cdot}$ − Me − OR, $M^{+\cdot}$ − 2OR, $M^{+\cdot}$ − OR − a, $M^{+\cdot}$ − R − b, $M^{+\cdot}$ − 3OR, $M^{+\cdot}$ − 3OR − CHO, and those others marked with an asterisk in Table 1, are analogous in both cases.

However, it was concluded that other types of linkage are not formed (as occur in the fructose anhydrides) because only a single peak in glc and a single spot in paper chromatography are detected, while the di-D-fructose anhydrides show one peak and one spot for each isomer.

G. *Structure of the osulose monomers*

Structure of the osulose monomers (1) and their derivatives (20–23), and the facile formation of formyl acetals (24–26), are in agreement with the assigned structures for the osulose dimers.

H. *Chemical evidence*

The following evidence is in accordance with the presence of two glycosidic linkages of the nonreducing sugar type.

(*i*) Paper chromatography, using solvents containing water and some acid, causes partial hydrolysis of the dimers (as readily as some nonreducing disaccharides).

(*ii*) Color reactions for paper chromatography (see experimental analytical methods) show nonreducing character under the normal conditions used for paper chromatographic determination of reducing sugars.

(*iii*) In the Raney nickel reduction, the hexoses are effectively hydrogenated while the osulose dimers (like the disaccharides (27)) are more difficult to convert into their polyols.

(*iv*) Aldoses and ketoses are not detected as reduction, nor as reduction and hydrolysis, products of the inulobiose (reduction is not possible without hydrogenolysis) and osulose dimers (as occur for their monomers), while D-glucose is detected in the maltose reduction and hydrolysis. This is in accordance with the nature of the linkages between the two molecules of the osulose.

Experimental

Starting products

The mono and oligosaccharides were obtained commercially: D-glucose anhydrous, Fluka A.G. Puriss p.a. Ref. 49140; D-galactose, Fluka A.G. Puriss p.a. Ref. 48260; L-sorbose, Fluka A.G. Puriss p.a. Ref. 85542; D-maltose monohydrate, Fluka A.G. Puriss p.a. Ref. 63419.

The 1,2′:2,1′-di-D-fructose anhydrides were prepared according to the literature methods (28, 29) using commercial D-fructose (Fluka A.G. Puriss p.a. Ref. 47740).

Inulobiose was isolated from the hydrolysis of inulin, by paper chromatography. Inulin Merck, Ref. 4733.

The hexosuloses were prepared by the benzaldehyde method (30, 31) from the phenylosazones of D-glucose, D-galactose, and L-sorbose. D-*arabino* hexosulose, mp 103.3°C (dec.); uv λ_{max}: 245 nm and 279 nm. *Anal.* calcd. for $C_6H_{12}O_7$: C 36.73, H 6.12; found: C 37.38, H 6.14. D-*lyxo* hexosulose, mp 89.9°C (dec.); uv λ_{max}: 220 nm and 275 nm. *Anal.* found: C 36.01, H 5.92. L-*xylo* hexosulose, mp 92.1°C (dec.); uv λ_{max}: 218 nm and 282 nm. *Anal.* found: C 36.41, H 5.84.

Preparation of the volatile derivatives

For the preparation of the TMS derivatives (32), the solvent (pyridine) was replaced by *N,N*-dimethylformamide (1, 33).

The acetates (34) were prepared by the acetic anhydride – sodium acetate method.

Analytical methods

Paper chromatography was accomplished by the descending method in a 20°C thermostated chamber by the use of Whatman no. 1 paper irrigated with acetone – *n*-butanol – water (7:2:1). The detection reagents were (35): aniline hydrogen phthalate, orcinol–HCl, orcinol–CCl_3COOH, anthrone, and ammoniacal $AgNO_3$ and triphenyltetrazolium chloride for reducing sugars.

Gas–liquid chromatography was performed on a Perkin–Elmer F-30 gas chromatograph equipped with a flame-ionization detector and stainless steel columns (6 ft × 1/8 in.) packed with 3% SE-30 or SE-52 on a support such as Chromosorb W HP 80–100. The carrier gas was nitrogen at a flow rate of 30 mL/min.

For the glc–ms analyses, a Hewlett–Packard 5980-A gas chromatograph was employed in combination with a Hewlett–Packard 5710-A mass spectrometer, operating at 70 eV under the conditions described above for glc; the carrier gas was helium.

Isolation of hexosulose dimers

The isolation of the dimers was effected by paper chromatography on Whatman no. 1 paper strips, according to the method of Flood *et al.* (36) from each osulose sirup obtained by the following procedures. I. Osulose (2.5 g) was dissolved in 25 mL of water and concentrated

at 60°C under reduced pressure. II. Osulose (2.5 g) was refluxed 20 h with 20 mL of HCl (0.1 *M* in water), passed through IR-45 Amberlite resin (20–50 mesh, OH form), and concentrated at 60°C under reduced pressure.

The dimers isolated by both methods were identical, although a greater amount was obtained by the second method.

Raney nickel reduction

The reduction was performed for maltose, inulobiose, and the three osulose dimers studied, by reflux (3 and 7 hours) under atmospheric pressure (37). The resulting products obtained by reduction, and reduction followed by hydrolysis, are identified (by comparison of pure standards using glc and mass spectrometry) as the corresponding isomeric hexitols (in all cases), D-glucose (only of reduction and hydrolysis of maltose), and the starting products (in the 3-hour reaction).

1. S. BAYNE and J. A. FEWSTER. Adv. Carbohydr. Chem. **11**, 43 (1956).
2. R. BARKER and D. L. MACDONALD. J. Am. Chem. Soc. **82**, 2301 (1960).
3. K. M. HODORSEN. Carbohydr. Res. **63**, 61 (1978).
4. K. K. SEN GUPTA, S. SEN GUPTA, and S. N. BASU. Carbohydr. Res. **71**, 75 (1979).
5. T. FUJIWARA and K. ARAI. Carbohydr. Res. **86**, 17 (1980).
6. T. FUJIWARA and K. ARAI. Carbohydr. Res. **87**, 201 (1980).
7. R. U. LEMIEUX and R. NAGARAJAN. Can. J. Chem. **42**, 1270 (1964).
8. D. C. DEJONGH *et al.* J. Am. Chem. Soc. **91**, 1728 (1969).
9. F. JASSON and B. LINDBERG. Carbohydr. Res. **86**, 287 (1980).
10. A. ROSSENTHAL. Carbohydr. Res. **8**, 61 (1968).
11. D. C. DEJONGH and K. BIEDMANN. J. Am. Chem. Soc. **86**, 64 (1964).
12. N. K. KOCHETKOV, O. S. CHIZHOV, and N. V. MOLODTSOV. Tetrahedron, **24**, 5587 (1968).
13. J. F. KENNEDY and S. M. ROBERSTON. Carbohydr. Res. **58**, 1 (1978).
14. J. P. KAMERLING and J. F. G. VLIEGENTHART. Tetrahedron, **28**, 4375 (1972).
15. T. FUJIWARA and K. ARAI. Carbohydr. Res. **87**, 11 (1980).
16. K. BIEDMANN. Angew. Chem. **74**, 102 (1962).
17. N. K. KOCHETKOV and O. S. CHIZHOV. Methods in carbohydrate chemistry. Vol. VI. *Edited by* R. L. Whistler and J. BeMiller. Academic Press Inc., New York. 1972. pp. 540–552.
18. K. K. SEN GUPTA and S. N. BASU. Carbohydr. Res. **72**, 139 (1979).
19. K. K. SEN GUPTA and S. N. BASU. Carbohydr. Res. **80**, 223 (1980).
20. G. M. CREE, D. M. MACKIE, and A. S. PERLIN. Can. J. Chem. **47**, 511 (1969).
21. D. M. MACKIE and A. S. PERLIN. Carbohydr. Res. **24**, 67 (1972).
22. G. H. R. CHITTENDEN. Carbohydr. Res. **11**, 424 (1969).
23. R. W. BINKLEY. J. Org. Chem. **42**, 1216 (1977).
24. S. BAYNE, G. A. COLLIS, and J. A. FEWSTER. J. Chem. Soc. 2766 (1962).
25. A. HASEGAWA and M. KISO. Carbohydr. Res. **79**, 265 (1980).
26. A. ASSARSSON and O. THEANDER. Acta Chem. Scand. **17**, 47 (1963).
27. J. V. KARABINOS and A. T. BALLUM. J. Am. Chem. Soc. **75**, 4501 (1953).
28. H. W. HILTON. *In* Methods in carbohydrate chemistry. Vol. II. *Edited by* R. L. Whistler and M. L. Wolfrom. Academic Press Inc., New York. 1963. pp. 199–203.
29. M. L. WOLFROM, H. W. HILTON, and W. W. BINKLEY. J. Am. Chem. Soc. **74**, 2867 (1952).
30. S. BAYNE. *In* Methods in carbohydrate chemistry. Vol. II. *Edited by* R. L. Whistler and M. L. Wolfrom. Academic Press Inc., New York. 1963. pp. 421–423.
31. E. C. TAYLOR and P. A. JACOBI. J. Am. Chem. Soc. **98**, 2305 (1976).
32. C. C. SWEELEY, R. BENTLEY, M. MAKITA, and W. W. WELLS. J. Am. Chem. Soc. **85**, 2497 (1963).
33. W. C. ELLIS. J. Chromatogr. **41**, 325 (1969).
34. M. L. WOLFROM and A. THOMPSON. *In* Methods in carbohydrate Chemistry. Vol. II. *Edited by* R. L. Whistler and M. L. Wolfrom. Academic Press Inc., New York. 1963. p. 212.
35. A. SOLER, P. A. GARCÍA RUIZ, and M. C. MARTINEZ SÁNCHEZ. An. Quim. **72**, 957 (1976).
36. A. W. FLOOD, E. L. HIRST, and J. N. K. JONES. J. Chem. Soc. 1679 (1948).
37. J. V. KARABINOS. *In* Methods in carbonhydrate chemistry. Vol. II. *Edited by* R. L. Whistler and M. L. Wolfrom. Academic Press Inc., New York. 1963. p. 78.

Can. J. Chem. Downloaded from www.nrcresearchpress.com by 210.87.254.6 on 09/06/12
For personal use only.

Electrochemical oxidation of 4-substituted *N*,*N*-dimethylaniline in the presence of silyl enol ether. Effect of the substituent on the formation of Mannich bases. II.[1]

ROGER N. RENAUD,[2] CAMPBELL J. STEPHENS, AND GAÉTAN BROCHU
Division of Chemistry, National Research Council, Ottawa, Ont., Canada K1A 0R6

Received June 27, 1983

ROGER N. RENAUD, CAMPBELL J. STEPHENS, and GAÉTAN BROCHU. Can. J. Chem. **62**, 565 (1984).

The formation of Mannich bases from the electrochemical oxidation of 4-substituted *N*,*N*-dimethylaniline in the presence of silyl enol ether was studied. The yield of bases obtained depended on the relative oxidation potentials of the starting amine compound and the base formed. An electron-donating substituent on the amine showed a large difference in the oxidation potentials and gave the highest yield of product. On the other hand, the oxidation potentials were very close with an electron-withdrawing substituent and the yield in base was relatively much lower. Furthermore, the main product in the case of an electron-withdrawing group in the presence of 1-trimethylsilyloxy-1-cyclohexene was 4-substituted 2-(2-oxocyclohexyl)-*N*,*N*-dimethylaniline. Some side products were also isolated and were identified as *N*,*N*-diketonic compounds.

ROGER N. RENAUD, CAMPBELL J. STEPHENS et GAÉTAN BROCHU. Can. J. Chem. **62**, 565 (1984).

On a étudié la formation des bases de Mannich par oxydation électrochimique de *N*,*N*-diméthylanilines substituées en position 4 en présence d'éthers énoliques silylés. Les rendements en bases dépendent des potentiels relatifs d'oxydation des amines de départ et des bases formées. Un substituant électrodonneur sur l'amine provoque une grande différence dans les potentiels d'oxydation et conduit à un rendement plus élevé en produit. D'un autre coté, avec des substituants électro-affinitaires, les potentiels d'oxydation sont très voisins et les rendements en base sont relativement beaucoup plus faibles. De plus, le produit majoritaire obtenu dans le cas d'un réactif portant un groupe électroaffinitaire réaggisant en présence du triméthylsilyloxy-1 cyclohexène-1 est une(oxo-2 cyclohexyl)-2 *N*,*N*-diméthylaniline substituée en position 4. On a également isolé quelques produits secondaires et on les a identifiés comme étant des composés *N*,*N*-dicétoniques.

[Traduit par le journal]

Can. J. Chem. Downloaded from www.nrcresearchpress.com by 210.87.254.40 on 09/06/12
For personal use only.

The first paper of this series (1) described the synthesis of Mannich bases from the electrochemical oxidation of *N*,*N*-dimethylmesidine in the presence of silyl enol ethers. It was noticed that the reaction depended upon the relative electrochemical oxidation potentials of the silyl enol ether, the amine, and the product. In this paper, a selection of 4-substituted *N*,*N*-dimethylanilines was chosen in order to examine the effect of the substituent on the formation of the Mannich base:

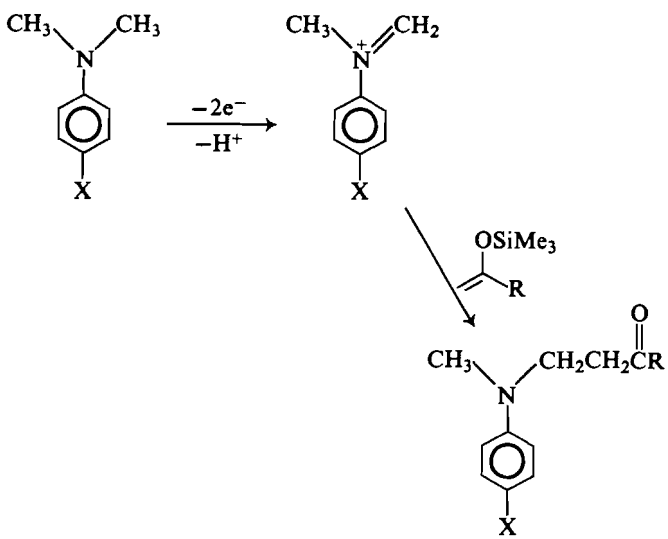

1*a* X = CH_3
b X = OCH_3
c X = $COOCH_3$
d X = $COCH_3$
e X = H

Results and discussion

In order to compare the effect of the substituent on the yield of Mannich base formed, the experimental conditions for all the runs were kept constant. The only variable was the reaction oxidation potential (E). This potential was controlled at such a voltage that a current of 100 mA was attained at the beginning of the electrolysis (Fig. 1, arrows). Then, the current dropped slowly to about 50 mA or less after the passage of 2 F/mol.

The silyl enol ethers chosen for this study, 1-trimethylsilyloxy-1-cyclohexene **3** and 1-phenyl-1-trimethylsilyloxyethylene **4**, are known from the previous study to give good yield of Mannich bases in the presence of the iminium salt of *N*,*N*-dimethylmesidine. The halfwave potentials ($E_{1/2}$'s) of the two silyl enol ethers are 1.25 V and 1.30 V vs. $Ag/AgNO_3$ respectively. The $E_{1/2}$'s of the amino compounds **1** are shown in Table 1 and they are all much less anodic than those of the silyl enol ethers **3** and **4**. On the other hand, the halfwave potentials of the amines **1** are, as expected, relatively more anodic for an electron-withdrawing substituent than for an electron-donating substituent. The yield of products **5** and **8** was markedly higher with an electron-donating group (Tables 1 and 2).

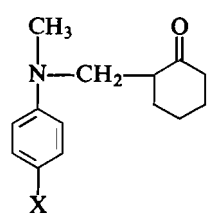

5

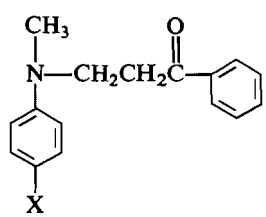

8

The oxidation potentials of at least three compounds must also be considered: the silyl enol ether, the amine **1**, and the Mannich base formed. As for the silyl enol ethers **3** and **4**, their E's are somewhat much too anodic to affect the result of the

[1]NRCC No. 22856.
[2]Author to whom correspondence should be addressed.

Can. J. Chem. Downloaded from www.nrcresearchpress.com by 210.87.254.40 on 09/06/12
For personal use only.

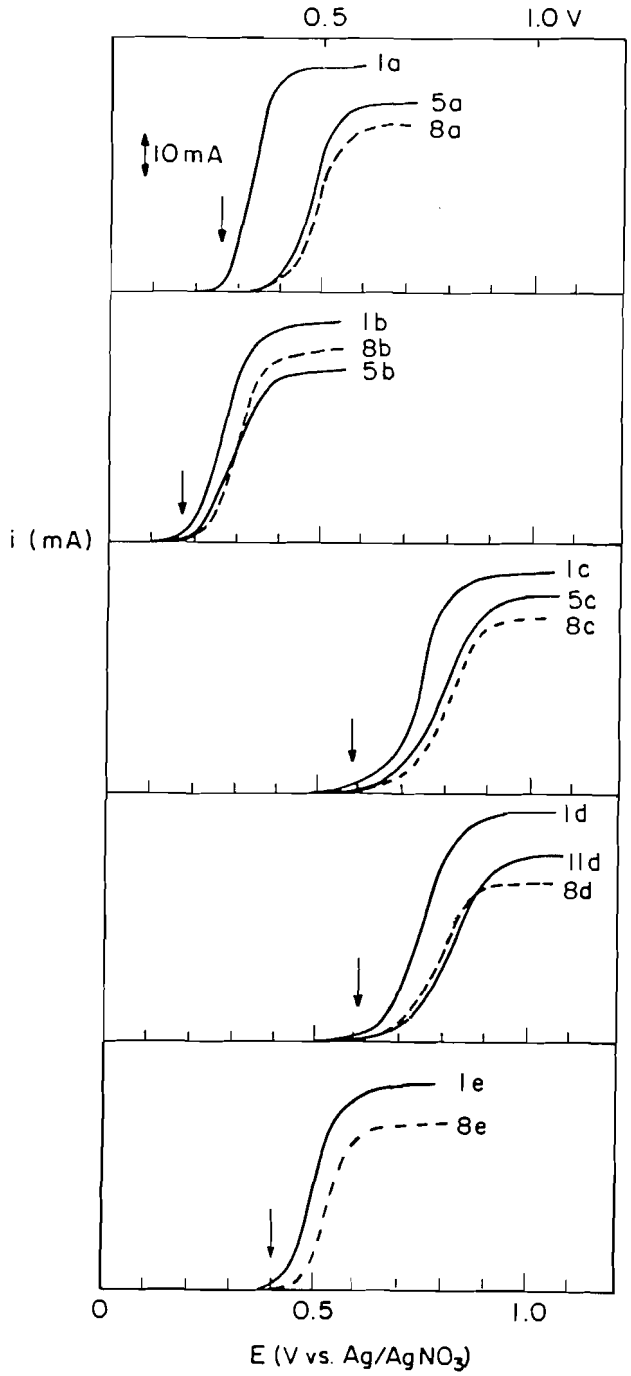

FIG. 1. Current–potential curves of 4-substituted *N*,*N*-dimethylanilines and the corresponding Mannich bases. The arrows indicate the reaction oxidation potentials *E*. Concentration: $\approx 10^{-3}$; scan rate: 2 mV/s.

reaction. Therefore, the relative *E*'s of the amine **1** and the products **5** and **8** are most important. The current–potential curves for the amine **1** and the products **5** and **8** are shown in Fig. 1. The *E*'s of the amines having an electron-donating substituent (**1***a* and **1***b*) are more cathodic than the *E*'s of the corresponding products **5** and **8** (Fig. 1, arrows) and the Mannich bases were obtained in good yield. However, the difference between the *E*'s of the amine **1***c* and the product **5***c* was very small and the yield in Mannich base was low. The main compound obtained from this reaction was methyl 3-(2-oxocyclohexyl)-4-*N*,*N*-dimethylaminobenzoate **11***c*. The structure of **11***c* was determined by nuclear magnetic resonance spectroscopy. Two structures are plausible:

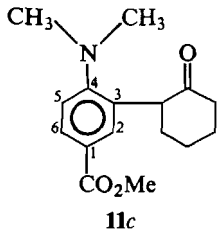

11*c*

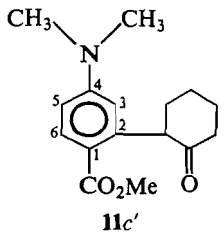

11*c*′

The broad singlet for the proton at the position 2 is at the low field side of the AB system of the two protons at positions 5 and 6. Therefore, it corresponds to a proton *ortho* to the carbonyl group (structure **11***c*). A proton at position 3 (structure **11***c*′) would show the singlet at the high-field side of the AB system. No product corresponding to **5***d* was observed from **1***d*. The main compounds isolated, in this case, were the amine **1***d*, the product **11***d*, and polymers. The mechanism for the formation of **11** is still not clear but it is most likely the attack of a radical intermediate **a** on the silyl enol ether to give a stabilized ether radical **b** (2, 3).

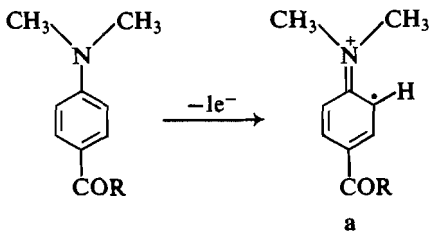

a

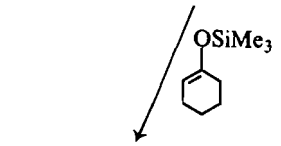

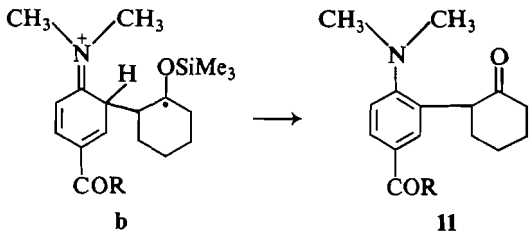

b **11**

The electrochemical oxidation of **1***c*–**1***e* in the presence of the silyl enol ether **4** gave low yields of **8***c*–**8***e* as the main products. No compound corresponding to **11** was observed.

Besides the major products **5** and **8**, some side products **6**, **7**, **9**, and **10** were also obtained in low yield. They are formed as a result of further oxidation of **5** and **8** to give a new iminium salt, which reacts either with another molecule of silyl enol ether to give **6** and **9** respectively or with residual water in the medium to give **7** and **10** respectively. Compounds **7** and **10** may also be formed from the hydrolysis of the iminium salt formed from **1**, followed by the electrolysis of the resulting *N*-methylaniline derivative[3] to give another iminium salt which

[3]The infrared spectrum showed that the starting compound **1***b* was free of monomethylanisidine.

TABLE 1. Controlled potential electrolysis of *p*-substituted *N*,*N*-dimethylanilines in the presence of 1-trimethylsilyloxy-1-cyclohexane **3**

Amine **1**				Product **5**				Product **6**, **7**, or **11**			
	X	$E_{1/2}$	E^a (V vs. Ag/$AgNO_3$)		Melting point (°C)	Yield	$E_{1/2}$		Melting point (°C)	Yield	$E_{1/2}$
1*a*	CH_3	0.34	0.26	**5***a*	27–28	50.5	0.48	**6***a*	96–97	13.8	0.47
1*b*	OCH_3	0.28	0.16	**5***b*	Oil	34.6	0.30	**7***b*	61–62	13.1	0.31
1*c*	$COOCH_3$	0.72	0.57	**5***c*	82–83	6.4	0.79	**11***c*	Oil	16.7	0.81
1*d*	$COCH_3$	0.81	0.60	**5***d*	—	—	—	**11***d*	93–94	20.0	0.83
1*e*	H	0.49	0.34	Polymers							

[a]The reaction potential.

TABLE 2. Controlled potential of *p*-substituted *N*,*N*-dimethylamilines in the presence of 1-phenyl-1-trimethylsilyolxyethylene **4**

Amine **1**				Product **8**				Product **9** or **10**			
	X	$E_{1/2}$	E^a (V vs. Ag/$AgNO_3$)		Melting point (°C)	Yield	$E_{1/2}$		Melting point (°C)	Yield	$E_{1/2}$
1*a*	CH_3	0.34	0.29	**8***a*	56–57	45.2	0.47	**9***a*	91–92	9.1	0.50
1*b*	OCH_3	0.28	0.18	**8***b*	57–58	31.9	0.30	**9***b*+**10***b*	99–100	≈5.0	—
1*c*	$COOCH_3$	0.72	0.64	**8***c*	78–79	19.5	0.81	**9***c*	150–151	3.1	0.84
1*d*	$COCH_3$	0.81	0.62	**8***d*	93–94	6.0	—	—	—	—	—
1*e*	H	0.49	0.39	**8***e*	58–59	13.4[b]	0.52	—	—	—	—

[a]The reaction potential.
[b]The same yield was obtained using collidine instead of sodium carbonate.

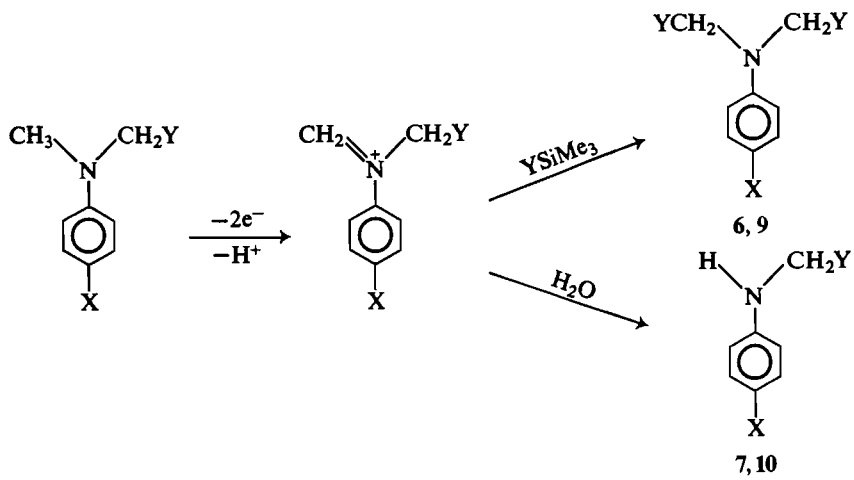

Y = ketonic substituent

can react with the silyl enol ether. The yields of compounds **6***c*, **6***d*, and **9***d* were very low and these compounds could not be obtained pure enough for identification. However, **6***a*, **9***a*, and **9***c* were isolated pure, and identified. With X = OCH_3 (**1***b*), demethylated product **7***b* and a mixture of **9***b* and **10***b* in a 1:1 ratio were obtained.

Experimental

The *para*-substituted *N*,*N*-dimethylanilines were obtained from Aldrich or prepared by the methylation of *para*-substitued anilines (4). The silyl enol ethers were prepared according to methods described in the literature (5). The acetonitrile was purified as reported in the literature (6). Flash chromatography was performed using silica gel 230–400 mesh (7). All melting points reported are uncorrected. Infrared spectra were recorded on a Perkin–Elmer Model 267 spectrophotometer. Proton magnetic resonance spectra were taken in deuteriochloroform on a Varian Associates spectrometer model E.M. 360 or a Bucker WP-80 apparatus and are reported in the δ scale. The mass spectra were obtained from a Hewlett–Packard model 5585 gc–ms spectrometer or from a VG 7070 type mass spectrometer. The molecular weight determinations were done on a Mechrolab vapor pressure osmometer model 301A. The electrochemical instrumentation is described in the previous publication (1) with two modifications. The source of energy for the preparative scale synthesis was obtained from a 100-V 10-A Kepco power supply and the potential of the working electrode was controlled by an esc potentiostatic controller model 410.

General procedure

The anodic solution was a well-stirred mixture of $LiClO_4$ (1.34 g), Na_2CO_3 (2.12 g), silyl enol ether (3 mL), and *para*-substituted

Can. J. Chem. Downloaded from www.nrcresearchpress.com by 210.87.254.40 on 09/06/12
For personal use only.

Can. J. Chem. Downloaded from www.nrcresearchpress.com by 210.87.254.40 on 09/06/12
For personal use only.

N,N-dimethylaniline (0.005 mol) in acetonitrile (125 mL). The cathodic solution was $LiClO_4$ (0.1 *M*) in acetonitrile. The potential was controlled at such a voltage that 100 mA was obtained. That potential was kept constant until 2 F/mol has been passed. At the end of the electrolysis the current dropped to about 50 mA. The anodic solution was filtered and concentrated on a high vacuum system. The solvent was collected in a cold trap. The oily residue was extracted with two 100-mL portions of boiling n-pentane or until the pentane solution was negative to tlc. Sometimes an extraction with ether was necessary, but less pure product was isolated. The organic solvent was removed on the vacuum system and the residue pumped under a pressure of 10^{-2} Torr for 3–5 h at room temperature in order to remove the excess of silyl enol ether. The combined low vapor pressure oil or solid was fractionated by flash chromatography (7) using a column of 2-cm diameter by 40 cm long. The residue of the different fractions was purified further either by a bulb-to-bulb distillation at 10^{-2} Torr or by recrystallization from ethanol in a Craig tube.

Physical properties of the products

(A) *Electrolysis of the amine* **1** *in the presence of 1-trimethylsilyloxy-1-cyclohexene* **3**

From **1***a*: the crude mixture, obtained after the evaporation of the high vapor pressure fraction, showed one major and three minor spots on the tlc plate. The separation of the products by flash chromatography using hexane – ethyl acetate (8:1) gave four fractions. First fraction: a very small quantity of starting amine **1***a*. Second fraction: an oil corresponding to **5***a*. It was further purified by a bulb-to-bulb distillation at 80°C under a pressure of 10^{-2} Torr to give 0.54 g (50.5%) of a white solid melting at 27–28°C; ir ($CHCl_3$): 1710 (C=O) cm^{-1}; ^1H nmr δ: 1.70 (broad m including the aromatic CH_3 group, 12H), 2.90 (s, 3H), 3.42 (AB q, 2H), 6.86 (AB q, 4H); ms *m/e*: 231 (M^+, 29), 134 ($M^+ - C_6H_9O$, 100). *Anal.* calcd. for $C_{15}H_{21}NO$: C 77.92, H 9.09, N 6.06; found: C 77.88, H 9.26, N 6.17. Third fraction: a white solid (0.21 g; 13.8%) melting at 96–97°C which corresponded to **6***a*; ir ($CHCl_3$): 1705 (C=O) cm^{-1}; ^1H nmr δ: 1.20–3.90 (broad m including the aromatic CH_3 group, 25H), 7.02 (q, AB, 4H); ms *m/e*: 327 (M^+, 10), 2.30 ($M^+ - C_6H_9O$, 100). *Anal.* calcd. for $C_{21}H_{29}NO_2$: C 77.06, H 8.87, N 4.28; found: C 76.96, H 8.88, N 4.37. Fourth fraction: impure oil (**7***a*) (10 mg); ir (neat): 3400 (NH), 1705 (C=O) cm^{-1}; ms *m/e*: 217 (M^+, 5) 129 ($M^+ - C_6H_{10}O$, 100).

From **1***b*: the oily residue (1.07 g) obtained after the removal of the high vapor pressure fraction showed one major and one minor spots on the tlc plate. Two fractions were obtained by flash chromatography. First fraction: an oil corresponding to **5***b*. It was purified further by a bulb-to-bulb distillation at 60°C under a pressure of 10^{-2} Torr to give a yellow oil (0.43 g; 34.6%); ir (film): 1703 (C=O) cm^{-1}; ^1H nmr δ: 1.20–2.45 (m, 9H), 2.83 (s, 3H), 3.15 and 3.86 (2d, AB, 2H), 3.70 (s, 3H), 6.71 (m, 4H); ms *m/e*: 247 (M^+, 19) 150 ($M^+ - C_6H_9O$, 100). *Anal.* calcd. for $C_{15}H_{21}NO_2$: C 72.87, H 8.50, N 5.67; found: C 73.41, H 8.56, N 5.51. Second fraction: a white solid melting at 61–62°C after a bulb-to-bulb distillation at 100°C (10^{-2} Torr). The compound analyzed as **7***b* (154 mg; 13.1%); ir ($CHCl_3$): 3395 (NH), 1702 (C=O) cm^{-1}; ^1H nmr δ: 1.20–2.52 (m, 9H), 3.02 (m, 3H), 3.51 (broad s, 1H), 3.73 (s, 3H), 6.66 (m, 4H); ms *m/e*: 233 (M^+, 51), 136 ($M^+ - C_6H_9O$, 100). *Anal.* calcd. for $C_{14}H_{19}NO_2$: C 72.10, H 8.15, N 6.01; found: C 71.86, H 8.23, N 6.11.

From **1***c*: the crude product showed three major spots on the tlc plate. They were separated by flash chromatography. First fraction: a white solid melting at 99–101°C corresponding to **1***c* (170 mg). Second fraction: a white solid (**5***c*) melting at 82–83°C (88 mg; 6.4%); ir ($CHCl_3$): 1700 (C=O) cm^{-1}; ^1H nmr δ: 1.2–2.7 (broad m, 9H), 3.08 (s, 3H), 3.59 (q, AB, 2H), 3.85 (s, 3H), 7.18 (q, 4H); ms *m/e*: 275 (M^+, 18), 178 ($M^+ - C_6H_9O$, 100). *Anal.* calcd. for $C_{16}H_{21}NO_3$: C 69.82, H 7.64, N 5.09; found: C 69.85, H 7.71, N 5.05. Third fraction: an oil (**11***c*) (0.23 g; 16.7%); ir (neat): 1720 (C=O), 1705 (C=O) cm^{-1}; ^1H nmr δ: 1.05–2.40 (m, 8H), 2.61 (s, 6H), 3.00 (m, 1H), 3.80 (s, 3H), 7.05 (d, 1H), 7.80 (d and s, 2H); molecular weight determination: 273: ms *m/e*: 275 (M^+, 100), 260 ($M^+ - CH_3$, 6). *Anal.* calcd. for $C_{16}H_{21}NO_3$: C 69.82, H 7.64, N 5.09; found: 69.90, H 7.75, N 5.15.

From **1***d*: the tlc of the crude material showed two major spots which were separated by flash chromatography. First fraction: recovered amine **1***d* (0.21 g). Second fraction: a white solid corresponding to **11***d* (0.26 g; 20.0%) which melted at 93–94°C after recrystallization from ethanol; ir ($CHCl_3$): 1705 (C=O) 1670 (C=O) cm^{-1}; ^1H nmr δ: 1.50–24.0 (m, 7H), 2.58 (s, 3H), 2.69 (broad s, 7H), 7.28 (m, 2H), 7.90 (m, 2H); ms *m/e*: 259 (M^+, 100), 244 ($M^+ - CH_3$, 31), 216 ($M^+ - CH_3CO$, 40). *Anal.* calcd. for $C_{16}H_{21}NO_2$: C 74.13, H 8.11, N 5.41; found: C 73.94, H 8.13, N 5.29.

From **1***e*: practically only polymeric compounds were obtained. A very small quantity of soluble material in ether was isolated and no compound could be obtained pure enough for proper identification.

(B) *Electrolysis of the amine* **1** *in the presence of 1-phenyl-1-trimethylsilyloxy-ethylene* **4**

From **1***a*: the crude product showed two major and two minor spots on the tlc plate, which were separated by flash chromatography. First fraction: a white solid melting at 56–57°C and corresponding to **8***a* (0.57 g; 45.2%); ir ($CHCl_3$): 1680 (C=O) cm^{-1}; ^1H nmr δ: 2.21 (s, 3H), 2.90 (s, 3H), 3.14 (t, 2H), 3.78 (t, 2H), 6.40–7.92 (m, 9H); ms *m/e*: 253 (M^+, 57), 134 ($M^+ - C_8H_7O$, 100). *Anal.* calcd. for $C_{17}H_{19}NO$: C 80.63, H 7.51, N 5.53; found: C 80.46, H 7.45, N 5.60. Second fraction: a white solid melting at 91–92°C. It analyzed as **9***a* (0.17 g; 9.1%); ir ($CHCl_3$): 1680 (C=O) cm^{-1}; ^1H nmr δ: 2.21 (s, 3H), 3.16 (t, 4H), 3.86 (t, 4H), 6.40–7.90 (m, 14H); ms *m/e*: 371(M^+, 14), 252 ($M^+ - C_8H_7O$, 100). *Anal.* calcd. for $C_{25}H_{25}NO_2$: C 80.86, H 6.74, N 3.77; found: C 80.56, H 6.62, N 3.92. The two minor products could not be obtained pure enough for identification.

From **1***b*: the crude product was obtained from an ether extraction after addition of water to the reaction mixture. One major and two minor spots showed on the tlc plate. The compounds were separated by flash chromatography. First fraction: a white solid (**8***b*) melting at 57–58°C (0.43 g; 31.9%); ir ($CHCl_3$): 1680 (C=O) cm^{-1}; ^1H nmr δ: 2.50–4.10 (m, including the two CH_3 groups, 10H), 6.41–7.95 (m, 9H); ms *m/e*: 269 (M^+, 38), 150 ($M^+ - C_8H_7O$, 100). *Anal.* calcd. for $C_{17}H_{19}NO_2$: C 75.84, H 7.06, N 5.20; found: C 75.98, H 7.04, N 5.28. Second fraction: a white solid (87 mg) which melted at 99–100°C after recrystallization from ethanol. The analysis of this solid indicated a mixture of **9***b* and **10***b* by mass spectrometry. The analysis was done by direct injection and the temperature was programmed from 60–270°C.

From **1***c*: water (50 mL) was added to the reaction mixture which was then extracted with ether. The crude product (two important spots on tlc) was purified by a bulb-to-bulb distillation at 10^{-2} Torr. First fraction (60°C): 50 mg of starting amine **1***c*. Second fraction (140°C): an oil corresponding to **8***c*, which crystallized on standing. It was purified further by recrystallization from ethanol in a Craig tube. A white solid melting at 78–79°C (0.29 g; 19%) was obtained; ir ($CHCl_3$): 1700 (C=O), 1690 (C=O) cm^{-1}; ^1H nmr δ: 3.03 (s, 3H), 3.31 (m, 2H), 4.09 (m, including the single of N—CH_3), 6.89 (d, 2H), 7.60 (m, 3H), 8.10 (m, 4H); ms *m/e*: 297 (M^+, 21), 178 ($M^+ - C_8H_7O$, 100). *Anal.* calcd. for $C_{18}H_{19}NO_3$: C 71.58, H 6.67, N 4.91; found: C 71.65, H 6.56, N 4.79. A small amount of solid, not very soluble in ether, was also obtained. This compound (**9***c*) melted at 150–151°C after recrystallization from ethanol (78 mg; 3.1%). *Anal.* calcd. for $C_{26}H_{25}NO_4$: C 75.18, H 6.02, N 3.37; found: C 75.06, H 6.24, N 3.41.

From **1***d*: the crude product showed two spots on the tlc plate. First fraction from flash chromatrography: the amine **1***d* (66 mg; 8%). Second fraction: a white solid (**8***d*) melting at 93–94°C (85 mg; 6%); ir ($CHCl_3$): 1680 (C=O), 1660 (C=O) cm^{-1}; ^1H nmr δ: 2.47 (s, 3H), 3.03 (s, 3H), 3.25 (t, 2H), 3.89 (t, 2H), 6.72 (d, 2H), 7.39 (m, 3H), 7.82 (m, 4H); ms *m/e*: 281 (M^+, 53), 162 ($M^+ - C_8H_7O$, 100). *Anal.* calcd. for $C_{18}H_{19}NO_2$: C 76.87, H 6.76, N 4.98; found: C 76.67, H 6.67, N 5.02.

From **1***e*: to the gummy residue, obtained after the evaporation of the high vapor pressure fraction, was added water (50 mL), and the resulting mixture was extracted with two portions of 50 mL of ether. The crude product gave one major and many minor spots on the tlc plate. The major compound was isolated by flash chromatography. A white solid melting at 58−59°C was obtained after recrystallization from ethanol. This compound corresponded to **8***e* (0.16 g; 13.4%); ir ($CHCl_3$): 1678 (C=O) cm^{-1}, ^1H nmr δ: 2.98 (s, 3H), 3.20 (t, 2H), 3.85 (5, 2H), 6.52−8.00 (m, 10H); ms *m/e*: 239 (M^+, 19), 120 ($M^+ - C_8H_7O$, 100). *Anal.* calcd. for $C_{16}H_{17}NO$: C 80.33, H 7.11, N 5.86; found: C 80.15, H 7.22, N 5.68.

Acknowledgements

We wish to thank Mr. H. Séguin for the elemental analyses and the molecular weight determination, and Dr. J. L. Holmes of the University of Ottawa for the mass spectral determinations.

1. R. N. RENAUD, D. BÉRUBÉ, and C. J. STEPHENS. Can. J. Chem. **61**, 1379 (1983).
2. (*a*) D. M. MOHILNER, R. N. ADAMS, and W. J. ARGERSINGER, JR. J. Am. Chem. Soc. **84**, 3618 (1962); (*b*) Z. GALUS and R. N. ADAMS. J. Am. Chem. Soc. **84**, 1061 (1962); (*c*) Z. GALUS, R. N. WHITE, F. S. ROWLAND, and R. N. ADAMS. J. Am. Chem. Soc. **84**, 2065 (1962).
3. H. G. VIEHE, R. MERENYI, L. STELLA, and Z. JANOUSEK. Angew. Chem. Int. Ed. Engl. **18**, 917 (1979).
4. (*a*) F. P. BOGERT and F. P. NABENHAUER. J. Chem. Soc. 1702 (1924); (*b*) A. I. VOGEL. A textbook of practical organic chemistry. Longmans, Green and Co., New York. 1956. p. 572; (*c*) H. RIVIER and C. SCHNEIDER. Helv. Chem. Acta, 718 (1919).
5. (*a*) R. WEST. J. Org. Chem. **23**, 1552 (1958); (*b*) C. AINSWORTH, F. CHEN, and Y-N. KUO. J. Organometal Chem. **46**, 59 (1972); (*c*) H. O. HOUSE, L. J. CZUBA, M. GALL, and H. D. OLMSTEAD. J. Org. Chem. **34**, 2324 (1969).
6. G. CAUQUIS, H. F. FAHMY, G. PIERRE, and M. H. ELNAGDI. Electrochim. Acta, **24**, 391 (1979).
7. W. C. STILL, M. KAHN, and A. MITRA. J. Org. Chem. **43**, 2923 (1978).

Can. J. Chem. Downloaded from www.nrcresearchpress.com by 210.87.254.40 on 09/06/12
For personal use only.

Structural studies on the dichlorocarbene adducts with (−)-*R*-carvone. I. The crystal structures of [1*R*, 4*R*, 6*R*, 9*R*]-7,7-dichloro-1-methyl-4-[2′,2′-dichloro-1′-methylcyclopropyl]-bicyclo[4.1.0]-heptan-2-one and [1*R*, 4*R*, 6*R*, 9*S*]-7,7-dichloro-1-methyl-4-[2′,2′-dichloro-1′-methylcyclopropyl]-bicyclo[4.1.0]-heptan-2-one

J. Zukerman-Schpector, E. E. Castellano, and G. Oliva

Instituto de Física e Química de São Carlos, Universidade de São Paulo, Caixa Postal 369, 13.560-São Carlos-SP, Brazil

AND

Timothy John Brocksom and Elisabete Terezinha Canevarolo

Departamento de Química, Universidade Federal de São Carlos, Caixa Postal 676, 13.560-São Carlos-SP, Brazil

Received May 25, 1983

J. Zukerman-Schpector, E. E. Castellano, G. Oliva, Timothy John Brocksom, and Elisabete Terezinha Canevarolo. Can. J. Chem. **62**, 570 (1984).

The crystal structures of the title compounds have been determined from diffractometric X-ray data and refined by full-matrix least-squares to final *R* factors of 0.047 and 0.060 from 830 and 620 independent reflections above background, respectively. The space group and the number of molecules per unit cell are the same in both cases: $P2_12_12_1$ and $Z = 4$. Cell dimensions are: $a = 7.982(2)$, $b = 9.538(3)$, $c = 18.785(3)$ Å for the *S* form and $a = 10.339(3)$, $b = 11.510(3)$, and $c = 11.886(6)$ Å for the *R* form. The molecules, produced simultaneously in the same chemical reaction, have essentially identical configuration except for the location of the chlorine atoms at C-11 (in the *S* case) and at C-10 (in the *R* case). This difference gives rise to a completely different molecular packing of the structures. In each compound the two cyclopropane rings present a *cis* relationship to one another, with an identical dihedral angle of 77.0°.

J. Zukerman-Schpector, E. E. Castellano, G. Oliva, Timothy John Brocksom et Elisabete Terezinha Canevarolo. Can. J. Chem. **62**, 570 (1984).

Faisant appel à la diffraction de rayons-X, on a déterminé les structures cristallines des composés mentionnés dans le titre et on les a affinées par la méthode des moindres carrés (matrice entière) jusqu'à des valeurs conventionnelles de $R = 0{,}047$ et de 0,060 pour 830 et 620 réflexions indépendantes observées au-dessus de l'état fondamental. Le groupe d'espace et le nombre de molécules par maille sont les mêmes dans les deux cas soit: $P2_12_12_1$ et $Z = 4$. Les dimensions de la maille sont: $a = 7{,}982(2)$, $b = 9{,}538(3)$, $c = 18{,}785(3)$ Å pour la forme *S* et $a = 10{,}339(3)$, $b = 11{,}510(3)$ et $c = 11{,}886(6)$ Å pour la forme *R*. Les molécules, qui sont produites simultanément par la même réaction chimique, ont essentiellement la même configuration sauf en ce qui a trait à la position des atomes de chlore en C-11 (dans le cas de la forme *S*) et à celle du groupe C-10 (dans le cas de la forme *R*). Cette différence conduit à un entassement moléculaire des structures complètement différent. Dans chaque composé, les deux cycles cyclopropanes sont en position *cis* avec un angle dièdre identique de 77,0°.

[Traduit par le journal]

Introduction

In connection with recent studies on the synthesis of biologically active sesquiterpenes using simple monoterpenes as starting materials (1), we have investigated the stereochemistry of the addition of carbenes to *p*-menth-1-ene monoterpenes (**I**). Apart from helping to elucidate the reaction mechanism, the structure of the adducts is important in the prediction of the structures of products in subsequent reactions. We have prepared a series of adducts from the reaction of dichlorocarbene and dibromocarbene with simple monoterpenes such as limonene, α-terpineol, and carvone. However, the only product which presents crystals in an adequate form for three-dimensional structure determination is the bis-adduct of dichlorocarbene with (−)-*R*-carvone (**II**), which forms the subject matter of the present article.

A literature search on these carbene−monoterpene adducts (2−6), demonstrates clearly the lack of concrete information about their stereochemistry. Occasional comments (6) suggest a preferential *trans* relationship between the bulky isopropenyl group and the incoming carbene unit, by analogy with the well defined stereochemistry of epoxidation of carvone (7). In this regioselective and stereoselective reaction, epoxidation occurs exclusively at the conjugated double bond with the formation of the epoxi-carvone (**III**) indicated. The reaction of dichlorocarbene with carvone, in our hands, is not regioselective as the

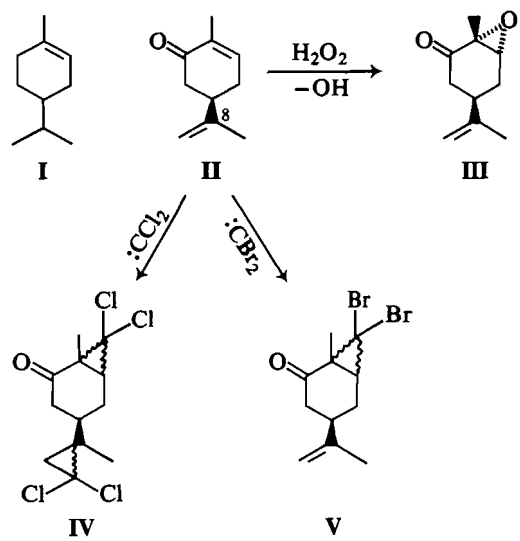

attack of the carbene occurs at both double bonds (**IV**), whereas the dibromocarbene adduct (**V**) is formed regioselectively (5).

Stereochemical analysis of the bisdichlorocarbene adduct (**IV**) suggests nonstereoselective formation of dichlorocyclopropanes at the nonconjugated double bond (Δ-8 of carvone (**II**)). Thus, by analogy with the completely stereo-

Can. J. Chem. Downloaded from www.nrcresearchpress.com by 210.87.254.105 on 09/06/12
For personal use only.

TABLE 1. Summary of data collection and processing parameters

Parameter	Value (9*S*)	Value (9*R*)
Space group	$P2_12_12_1$	$P2_12_12_1$
Cell constants	a = 7.982(2)	10.339(3) Å
	b = 9.538(3)	11.510(3)
	c = 18.785(3)	11.886(6)
	V = 1430(1)	1415(2) Å^3
Crystal size (approx.)	0.18×0.4×0.5	0.12×0.18×0.20 mm
Molecular formula	$C_{12}H_{14}OCl_4$	$C_{12}H_{14}OCl_4$
Molecular weight	316.06	316.06
Molecules per cell	Z = 4	4
Density (calcd.)	ρ = 1.47	1.48 g·cm^{-3}
Absorption coefficient	μ = 7.4	7.5 cm^{-1}
Collection range	$0° < \theta < 23°$	$0° < \theta < 23°$
Scan width	0.8 + 0.35 tan θ	1.0 + 0.35 tan θ
Scan rate	6.6 to 20	5.0 to 30 deg min^{-1}
Total data collected	1179	1150
Data with $I > 3\sigma(I)$	832	
Data with $I > 2\sigma(I)$		620
$R = \Sigma\|\|F_o\| - \|F_c\|\|/\Sigma\|F_o\|$	0.047	0.060
$R_w = [\Sigma w(\|F_o\| - \|F_c\|)^2/\Sigma w\|F_o\|^2]^{1/2}$	0.052	0.054
Weights	$w = [\sigma^2(F_o) + 0.00584F_o^2]^{-1}$	$[\sigma^2(F_o) + 0.00062F_o^2]^{-1}$

TABLE 2. (9*S*) Atomic coordinates and calculated isotropic temperature factors with esd's in parentheses; the standard deviation of B_{iso} was calculated as $\sigma(B_{iso}) = \sum_{ij} T_{ij}\sigma(B_{ij})$

Atom	*X*/*A*	*Y*/*B*	*Z*/*C*	B_{iso} (Å^2)
Cl-1	−0.4905(3)	−0.1155(2)	−0.7616(1)	5.98(8)
Cl-2	−0.7337(3)	−0.2554(2)	−0.6737(1)	5.23(6)
Cl-3	−1.1975(4)	−0.2245(2)	−0.5242(1)	7.9(1)
Cl-4	−1.3812(4)	0.0099(3)	−0.4694(2)	8.9(1)
O-1	−1.0575(7)	−0.1457(6)	−0.7835(3)	5.1(2)
C-1	−0.8186(9)	−0.0152(8)	−0.7523(4)	3.3(2)
C-2	−0.995(1)	−0.0665(9)	−0.7417(4)	3.7(2)
C-3	−1.0880(8)	−0.0042(8)	−0.6798(4)	3.8(2)
C-4	−0.989(1)	−0.0110(7)	−0.6103(3)	3.4(2)
C-5	−0.8191(9)	0.0639(8)	−0.6181(4)	4.0(3)
C-6	−0.7297(9)	0.0395(7)	−0.6873(4)	3.7(2)
C-7	−0.6849(9)	−0.1006(8)	−0.7174(4)	3.9(3)
C-8	−0.793(1)	0.0541(8)	−0.8247(4)	4.8(3)
C-9	−1.088(1)	0.0513(8)	−0.5495(4)	3.9(2)
C-10	−1.036(2)	0.010(1)	−0.4749(4)	6.6(4)
C-11	−1.191(1)	−0.0456(9)	−0.5055(4)	5.2(3)
C-12	−1.158(1)	0.1967(8)	−0.5612(4)	5.2(3)

TABLE 3. (9*R*) Atomic coordinates and calculated isotropic temperature factors with esd's in parentheses; the standard deviation of B_{iso} was calculated as $\sigma(B_{iso}) = \sum_{ij} T_{ij}\sigma(B_{ij})$

Atom	*X*/*A*	*Y*/*B*	*Z*/*C*	B_{iso} (Å^2)
Cl-1	−0.8885(3)	0.2693(3)	−0.6380(3)	4.9(1)
Cl-2	−1.1438(3)	0.1758(3)	−0.6031(3)	6.1(1)
Cl-3	−0.3928(3)	−0.0923(3)	−0.7092(4)	6.2(1)
Cl-4	−0.5207(3)	0.1019(3)	−0.6057(3)	5.1(1)
O-1	−0.9365(9)	0.2815(9)	−0.9276(8)	6.6(2)
C-1	−1.013(1)	0.136(1)	−0.804(1)	4.3(2)
C-2	−0.911(1)	0.188(1)	−0.881(1)	4.6(2)
C-3	−0.791(1)	0.126(1)	−0.902(1)	4.4(2)
C-4	−0.731(1)	0.080(1)	−0.792(1)	2.9(2)
C-5	−0.825(1)	0.001(1)	−0.724(1)	3.7(2)
C-6	−0.961(1)	0.046(1)	−0.722(1)	2.5(2)
C-7	−1.003(1)	0.164(1)	−0.685(1)	3.6(2)
C-8	−1.143(1)	0.117(1)	−0.857(1)	5.9(2)
C-9	−0.603(1)	0.019(1)	−0.819(1)	4.0(2)
C-10	−0.495(1)	0.026(1)	−0.733(1)	3.8(2)
C-11	−0.485(1)	0.091(1)	−0.838(1)	4.0(2)
C-12	−0.615(1)	−0.092(1)	−0.882(1)	5.2(2)

selective epoxidation of carvone, one expects to obtain two diastereomers in approximately equal amounts (diastereomeric at C-9).[1] On the other hand, partially stereoselective attack of the carbene at the conjugated double bond should lead to two pairs of the four possible diastereomers formed in unequal amounts. Careful gas chromatographic analysis of the product obtained indicated the presence of one component only (one peak). As no conventional spectroscopic method or chemical correlation would really define the full stereochemical structure, we chose to perform a three-dimensional crystal structure analysis.

[1]We have used standard *p*-menthane numbering for carvone (**II**), whereas the products obtained in the reaction were given conventional IUPAC numbering as in Figs. 1 and 2.

Experimental

The compounds were prepared as described elsewhere (1). Crystals were grown from ether solution by slow evaporation at 8°C. Visual inspection of the crystalline material showed the presence of two shades of yellow samples which turned out to correspond to the *S* and *R* forms of the compound. Crystal data are given in Table 1. Intensities were measured on an Enraf-Nonius CAD-4 diffractometer by the ω-2θ scan technique, with scan rates determined from fast prescans on each reflection, using graphite monochromated MoKα (λ = 0.71069 Å) radiation. The intensities of two standard reflections were essentially constant over the duration of both experiments. Data were corrected for Lorentz and polarization effects but not for absorption or extinction.

Structures solution and refinements

Both structures were solved using MULTAN-80 (8) and refined by full-matrix least-squares with the SHELX-76 (9) system of programs.

Can. J. Chem. Downloaded from www.nrcresearchpress.com by 210.87.254.105 on 09/06/12
For personal use only.

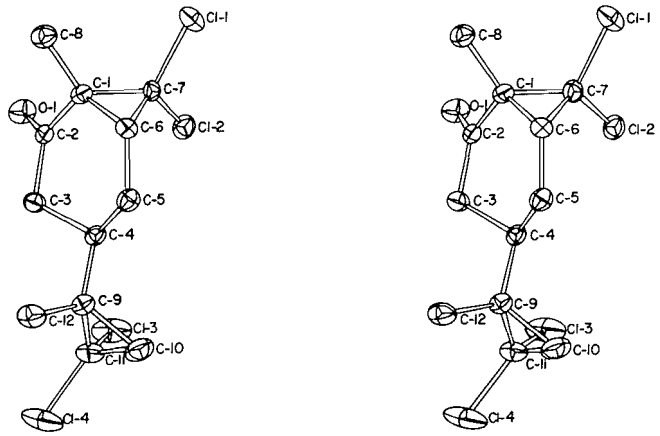

FIG. 1. Stereoscopic view and atom-labeling scheme for (9*S*).The thermal ellipsoids are 45% equiprobability envelopes.

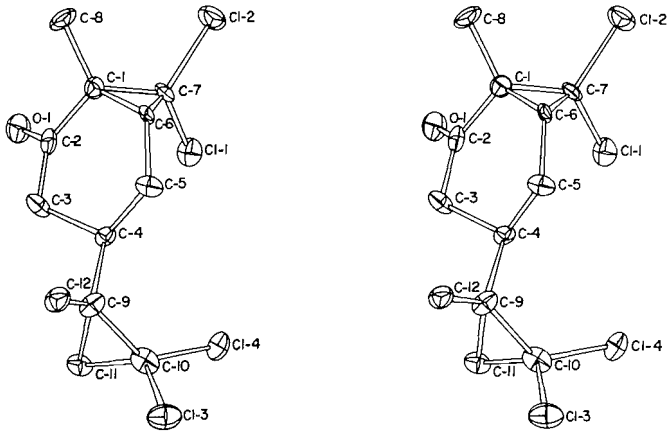

FIG. 2. Stereoscopic view and atom-labeling scheme for (9*R*). The thermal ellipsoids are 45% equiprobability envelopes.

TABLE 4. Intramolecular bond distances (Å) with esd's in parentheses

Bond	Distance (9*S*)	(9*R*)
Cl-1—C-7	1.769(8)	1.78(1)
Cl-2—C-7	1.727(8)	1.76(1)
Cl-3—C-11	1.731(9)	—
Cl-4—C-11	1.75(1)	—
Cl-3—C-10	—	1.75(1)
Cl-4—C-10	—	1.77(1)
C-1—C-2	1.50(1)	1.52(2)
C-1—C-6	1.51(1)	1.52(2)
C-1—C-7	1.49(1)	1.46(2)
C-1—C-8	1.53(1)	1.50(2)
C-2—C-3	1.51(1)	1.45(2)
C-2—O-1	1.20(1)	1.24(2)
C-3—C-4	1.54(1)	1.54(2)
C-4—C-5	1.54(1)	1.56(2)
C-4—C-9	1.52(1)	1.53(2)
C-5—C-6	1.51(1)	1.50(2)
C-6—C-7	1.49(1)	1.49(2)
C-9—C-10	1.52(1)	1.52(2)
C-9—C-11	1.49(1)	1.49(2)
C-9—C-12	1.50(1)	1.49(2)
C-10—C-11	1.46(2)	1.46(2)

The usual sequence of isotropic and anisotropic refinement, using unit weights, was followed. All hydrogen atoms were then located from a difference Fourier synthesis. Further anisotropic refinement proceeded with all hydrogen atom positions fixed and their isotropic temperature factors set to the common value of 4.0 Å^2. The final weighting schemes used are described in Table 1. In both cases refinement was considered complete when the shifts/esd ratios were less than 0.01. Bonded H-atom scattering factors (10) and complex neutral scattering factors (11, 12) for the remaining atoms were employed. No unusually high correlations were noted in either refinement. A final difference Fourier map showed no features of chemical significance. Measured and calculated structure factors, anisotropic thermal parameters for non-hydrogen atoms, and H-atoms parameters have been deposited. Atomic coordinates together with calculated isotropic temperature factors are given in Tables 2 and 3, where the expression for B_{iso} is of the form:

$$B_{iso} = \frac{4}{3}\sum_{ij} T_{ij}B_{ij}$$

where T_{ij} are the elements of the metric tensor and B_{ij} are the elements of the thermal tensor usually obtained by least-squares refinement (13).

Discussion

The main result of the present paper is the unambiguous determination of the existence of the two forms (*S* and *R*) of the reaction product mentioned in the Introduction, which are diastereomeric at C-9, according to **VI**, where **VI***a* and **VI***b* correspond to the *S* and *R* forms, respectively. It should be pointed out that the fact that the two compounds produced crystals of different colours is really a fortunate situation, since no standard organic chemistry method would have distinguished and allowed separation between the two forms. Indeed, careful gas chromatographic analysis does not separate these diastereomers.

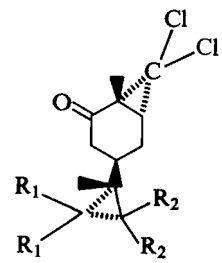

VI*a* R_1 = Cl, R_2 = H
VI*b* R_1 = H, R_2 = Cl

Figures 1 and 2 are stereoscopic projections (14) of the two molecules, showing the numbering scheme, displayed in similar orientations to facilitate comparison. Since the absolute configuration was not determined (the Hamilton test was insensitive to enantiomorph reversal) we choose for both molecules the same configuration as that of natural (−)-*R*-carvone (**II**). Interatomic distances and bond angles are given in Tables 4 and 5. The two molecules have essentially the same configuration except for the location of the chlorine atoms at C-11 in the *S* case and C-10 in the *R* case. This difference, however, gives rise to a completely different molecular packing of the structures. Superposition of the two molecules (excluding hydrogens and chlorines Cl-3 and Cl-4) using the best least-squares orthogonal transformation as defined by Kabsch (15), gave a root-mean-square distance between equivalent atoms of 0.26 Å. The cyclopropane rings are in a *cis* relationship to one another with the same dihedral angle of 77.0° in both

Can. J. Chem. Downloaded from www.nrcresearchpress.com by 210.87.254.105 on 09/06/12
For personal use only.

TABLE 5. Intramolecular bond angles (deg) with esd's in parentheses

Bond	Angle (9*S*)	Angle (9*R*)
C-2—C-1—C-6	116.3(6)	114(1)
C-2—C-1—C-7	115.9(6)	117(1)
C-2—C-1—C-8	112.5(6)	115(1)
C-6—C-1—C-7	59.3(5)	60.2(9)
C-6—C-1—C-8	121.2(6)	119(1)
C-7—C-1—C-8	122.1(6)	120(1)
C-1—C-2—C-3	116.1(6)	120(1)
C-1—C-2—O-1	120.3(7)	118(1)
C-3—C-2—O-1	123.5(7)	122(1)
C-2—C-3—C-4	113.2(6)	112(1)
C-3—C-4—C-5	110.7(5)	113(1)
C-3—C-4—C-9	111.4(6)	109(1)
C-5—C-4—C-9	110.7(6)	112.3(9)
C-4—C-5—C-6	115.5(6)	113(1)
C-1—C-6—C-5	122.4(6)	124(1)
C-1—C-6—C-7	59.7(5)	57.7(8)
C-5—C-6—C-7	125.6(6)	126(1)
C-1—C-7—Cl-1	117.5(5)	120.1(9)
C-1—C-7—Cl-2	120.6(5)	119.8(9)
C-1—C-7—C-6	60.9(5)	62.1(9)
C-6—C-7—Cl-1	117.6(5)	121.2(8)
C-6—C-7—Cl-2	121.3(5)	118.4(9)
Cl-1—C-7—Cl-2	110.9(4)	108.9(7)
C-4—C-9—C-10	118.3(6)	118(1)
C-4—C-9—C-11	117.5(7)	119(1)
C-4—C-9—C-12	116.1(6)	115(1)
C-10—C-9—C-11	58.2(6)	58.0(9)
C-10—C-9—C-12	118.3(7)	117(1)
C-11—C-9—C-12	116.2(7)	118(1)
C-9—C-10—C-11	59.7(6)	—
C-9—C-11—C-10	62.1(6)	—
C-9—C-11—Cl-3	120.4(6)	—
C-9—C-11—Cl-4	121.0(6)	—
C-10—C-11—Cl-3	117.2(7)	—
C-10—C-11—Cl-4	118.2(7)	—
Cl-3—C-11—Cl-4	110.4(5)	—
C-9—C-10—Cl-1	—	60.2(9)
C-9—C-10—Cl-3	—	120.9(9)
C-9—C-10—Cl-4	—	119.5(9)
C-11—C-10—Cl-3	—	120.0(1)
C-11—C-10—Cl-4	—	119.3(9)
Cl-3—C-10—Cl-4	—	109.7(8)
C-9—C-11—C-10	—	61.8(9)

structures.

The rather poor quality of the crystals, especially that of the *R*-form, prevented us from obtaining a good number of reflections per parameter ratio. As a result, the standard deviations for bond distances and angles are rather large, as expected after Cruickshank (16).

Acknowledgements

We thank Dragoco, São Paulo, for a very generous gift of natural (−)-*R*-carvone.

This work has received the support of CAPES, FAPESP, FINEP, and the CNPq-NAS (Washington) bilateral program in chemistry; these organizations are hereby gratefully acknowledged.

1. T. J. BROCKSOM and E. T. CANEVAROLO. To be published.
2. G. C. JOSHI, N. SINGH, and L. M. PANDE. Tetrahedron Lett. 1461 (1972).
3. T. HIYAMA, H. SAWADA, M. TSUKANAKA, and H. NOZAKI. Tetrahedron Lett. 3013 (1975).
4. Y. KIMURA, K. ISAGAWA, and Y. OTSUJI. Chem. Lett. 951 (1977).
5. L. SYDNES and L. SKATTEBØL. Tetrahedron Lett. 4603 (1975).
6. R. J. GIGUERE, G. VON ILSEMANN, and H. M. R. HOFFMANN. J. Org. Chem. **47**, 4948 (1982).
7. E. KLEIN and G. OHLOFF. Tetrahedron, **19**, 1091 (1963).
8. P. MAIN, M. M. WOOLFSON, G. GERMAIN, and J. P. DECLERCQ. MULTAN-80. A System of Computer Programs for the Automatic Solution of Crystal Structures. University of York, England, and University of Louvain la Neuve, Belgium.
9. G. M. SHELDRICK. SHELX program for crystal structure determination. University of Cambridge, England. 1976.
10. R. F. STEWART, E. R. DAVIDSON, and W. T. SIMPSON. J. Chem. Phys. **42**, 3175 (1965).
11. D. T. CROMER and D. LIBERMAN. J. Chem. Phys. **53**, 1891 (1970).
12. D. T. CROMER and J. B. MANN. Acta Crystallogr. A**24**, 321 (1968).
13. W. C. HAMILTON. Acta Crystallogr. **12**, 609 (1959).
14. C. K. JOHNSON. ORTEP, Report no. ORNL-3794, Oak Ridge National Laboratory, Oak Ridge, TN. 1965.
15. W. KABSCH. Acta Crystallogr. A**32**, 922 (1976).
16. D. W. J. CRUICKSHANK. Acta Crystallogr. **13**, 774 (1960).

Can. J. Chem. Downloaded from www.nrcresearchpress.com by 210.87.254.105 on 09/06/12
For personal use only.

Synthesis and spreading behaviour of some reactive derivatives of long-chain alcohols and carboxylic acids

DAVID A. HOLDEN
Department of Chemistry, University of Waterloo, Waterloo, Ont., Canada N2L 3G1

Received September 12, 1983

DAVID A. HOLDEN. Can. J. Chem. **62**, 574 (1984).

Procedures are described for the synthesis of several azides, diimides, and azodiformates from long-chain alcohols and fatty acids. These reactive compounds have potential applications as thermal and photochemical curing agents, and as surface-modifying agents for the preparation of filled plastics and chromatographic packings. The surface activity of the compounds was characterized by investigations of their spreading behaviour in monolayers on water. Unlike the single-chain azides and azo compounds, which give well-defined monolayers at all temperatures, monolayers of diacyl diimides and dialkyl azodiformates with two long-chain substituents are unstable with respect to collapse to the bulk solid. The photoreaction of monolayers of octadecanoyl azide to give a mixture of products derived from an intermediate isocyanate was demonstrated by ir and mass spectrometry.

DAVID A. HOLDEN. Can. J. Chem. **62**, 574 (1984).

On décrit des méthodes de synthèse de plusieurs azotures, diimides et azodiformates à partir d'acides gras et d'alcools à longues chaînes. Ces composés réactifs peuvent éventuellement être utilisés comme agents de durcissement thermique ou photochimique ou comme agents modifiant la surface lors de la préparation de garnissages chromatographiques ou de plastiques remplis. On a caractérisé l'activité de surface des composés en étudiant leur comportement lorsqu'ils se répandent sous forme de monocouches sur l'eau. Contrairement aux composés azotures et azo ne comportant qu'une seule chaîne, qui donnent des monocouches bien définies à toutes les températures, les monocouches des diimides de diacyles et des azodiformates de dialkyles portant comme substituants deux longues chaînes carbonées ne sont pas stables. On a démontré par ir et par spectrométrie de masse que la photoréaction de monocouches de l'azoture d'octadécanoyle conduit à un mélange de produits qui proviennent d'un intermédiaire isocyanate.

[Traduit par le journal]

Can. J. Chem. Downloaded from www.nrcresearchpress.com by 210.87.254.5 on 09/06/12
For personal use only.

Introduction

There is considerable scientific and technical interest in the reactions of compounds incorporated into thin layers at interfaces. Recent activity in this field is concentrated in several areas: in efforts to duplicate or imitate biological processes in synthetic bilayer membranes (1–3), in photochemically cured coatings designed to avoid the use of toxic solvents (4), and in potential applications of monomolecular films in the optical and electronics industries (5).

In a number of applications involving amphiphilic molecules it is necessary to introduce a complex functional group into a surface-active molecule without destroying the surface activity. This surface activity causes the molecules to organize spontaneously into structures such as monolayers at interfaces or bilayer vesicles resembling simple cell membranes, while the functional group remains intact and available for subsequent reaction. In particular it may be desirable to have long-chain compounds with the same potential for surface reactions as octadecyltrichlorosilane, for example, but with higher surface activity and greater resistance to hydrolysis.

The present publication describes the synthesis from fatty acids and alcohols of a number of surface-active derivatives containing reactive functional groups. These include the azo compounds **1** and **2** having two long hydrocarbon chains and the related compounds **3** to **5** having only a single long hydrocarbon chain. Such compounds are potential thermal and photochemical sources of free radicals for curing and polymerization reactions in thin films. Several long-chain azides **6**–**8**, with potential applications as surface-modifying agents, were also synthesized. The spreading behaviour of these new compounds in monolayers is reported, as well as the results of an investigation of the photochemistry of octadecanoyl azide in monolayers.

Scheme 1 shows the sequence of reactions by which the

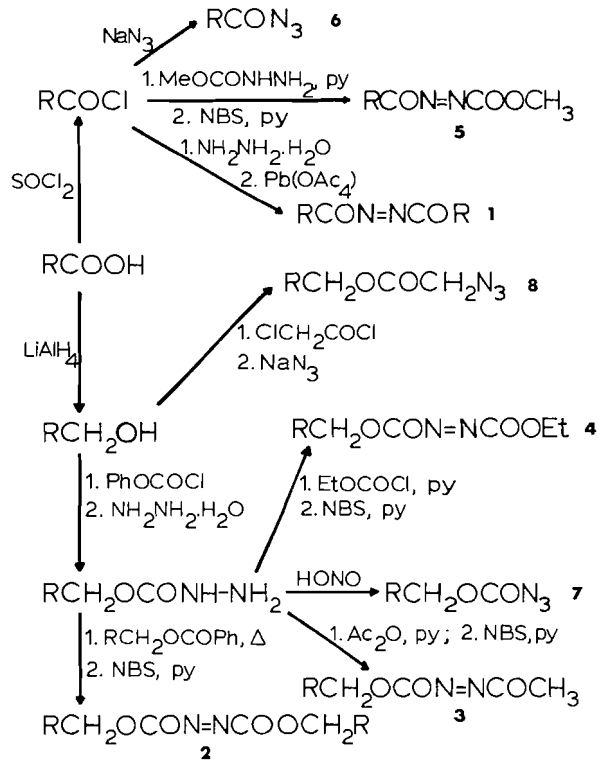

SCHEME I

compounds were prepared. While procedures exist for the synthesis of short-chain analogues of these compounds, it was necessary to modify these procedures substantially in several cases. The lower solubility of fatty acids and alcohols in organic solvents required more vigorous reaction conditions. New solvent systems were necessary in several cases because

the long-chain starting materials had negligible solubility in water. Distillation of the unstable products was not practical and washing of organic solutions of the products often gave intractable emulsions. Instead, suitable solvent systems for purification of the products by low-temperature recrystallization were found. It is hoped that such procedures may be more easily scaled up than purification steps requiring liquid chromatography.

Experimental

Melting points of compounds were recorded in capillaries using a Büchi oil immersion apparatus and are uncorrected. The ^{1}H nmr spectra were recorded on JEOL or Perkin–Elmer R-12B 60 MHz instruments using $CDCl_3$ as solvent and Me_4Si as internal reference. Infrared spectra were recorded on Perkin–Elmer 457 and Beckman Acculab 10 instruments, either as melts or in paraffin oil mulls.

Materials

Stearic acid (99%) was obtained from Sigma Chemicals. Myristic and lauric acids (Merck) were used as received. Palmitic acid (Fisher reagent grade) was recrystallized twice from acetone between 50°C and 0°C. Acid chlorides were obtained by overnight stirring of the corresponding acid with 1.1 equivalents of $SOCl_2$ catalysed by the addition of one drop of *N*,*N*-dimethylformamide. The excess $SOCl_2$ was removed on a water aspirator and the acid chloride was fractionally distilled under high vacuum. 1-Hexadecanol was obtained by $LiAlH_4$ reduction of palmitic acid in refluxing THF. All of the following compounds were stored in the dark at −20°C.

1,2-Dihexadecanoyl hydrazine

Symmetric hydrazides were prepared by a modification of the Sonntag method (6). A solution of 0.56 NaOH and 0.337 g 85% hydrazine hydrate in 25 mL H_2O was stirred at 0°C while 3.13 g palmitoyl chloride in 5 mL CH_2Cl_2 was added dropwise over 30 min. The reaction mixture was stirred overnight at room temperature and the precipitate was filtered by suction. The dried product was recrystallized several times from toluene between its boiling point and room temperature to give 2.7 g (92%) of crystals melting at 144.5–145°C; ir (Nujol): 3260, 1610 cm^{-1}.

Dihexadecanoyl diimide (7)

Lead tetraacetate (Merck) was washed free of excess acetic acid with dry hexanes, dried by suction, and used immediately. Benzene was purified by distillation from P_2O_5 under nitrogen. A suspension of 2.0 g 1,2-dihexadecanoyl hydrazine in 250 mL purified benzene was heated to the boiling point of the solvent and stirred vigorously while 1.8 g lead tetraacetate was added all at once. After 15 s the hot solution was filtered by suction through a medium porosity sintered glass funnel and the benzene was evaporated off at 20°C under reduced pressure. The product was recrystallized twice from 50 mL 2:1 CH_2Cl_2–hexane solution between 30°C and −20°C. The yield of yellow crystals was 1.0 g (51%), mp 69–71°C with decomposition; ir (Nujol): C=O at 1750 cm^{-1}; no NH or amide C=O bands remaining; ^{1}H nmr δ: 0.86 (t, 6H, $2CH_3$), 1.27 (m, 52H, $26CH_2$), 2.55 (t, 4H, $2CH_2CO$); uv (1:1 hexane–dichloromethane, Cary 118) λ_{max}: 454 nm (ε 23.0 M^{-1} cm^{-1}). Other long-chain diacyl diimides were obtained from the corresponding hydrazides by the same procedure. High purity of the starting materials was necessary, otherwise the diimides decomposed rapidly at room temperature.

Ditetradecanoyl diimide

Melting point 70–71°C with gas evolution (oil bath preheated to 65°C); ir (Nujol): 1755 cm^{-1}; nmr δ: 0.88 (t, 6H) 1.22 (m, 44H), 2.52 (t, 4H); uv (distilled THF) λ_{max}: 452 nm (ε 24.4 M^{-1} cm^{-1}). The extinction coefficient at 254 nm is 342 M^{-1} cm^{-1}. *Anal.* calcd. for $C_{28}H_{54}N_2O_2$: C 74.61, H 12.08, N 6.21%; found: C 74.25, H 12.33, N 6.20%.

Didodecanoyl diimide

Melting point 62–63°C with gas evolution (oil bath preheated to 55°C); ir (Nujol): 1755 cm^{-1}; nmr δ: 0.85 (t, 6H), 1.22 (m, 36H), 2.56 (t, 4H); uv (purified THF) λ_{max}: 452 nm (ε 24.3 M^{-1} cm^{-1}). The extinction coefficient at 254 nm is 322 M^{-1} cm^{-1}. *Anal.* calcd. for $C_{24}H_{46}N_2O_2$: C 73.04, H 11.75, N 7.10%; found: C 72.99, H 12.09, N 7.13%.

Dioctadecanoyl diimide

Melting point 79.5–80.5°C with decomposition (oil bath preheated to 75°C); ir (Nujol): 1760 cm^{-1}; nmr δ: 0.90 (t, 6H), 1.27 (m, 60H), 2.55 (t, 4H); uv (cyclohexane) λ_{max}: 450 nm (ε 22.9 M^{-1} cm^{-1}). The extinction coefficient at 254 nm is 350 M^{-1} cm^{-1}. *Anal.* calcd. for $C_{36}H_{70}N_2O_2$: C 76.81, H 12.53, N 4.98%; found: C 76.93, H 12.88, N 4.91%.

Phenyl hexadecyl carbonate (8)

To a stirred solution of 8.0 g 1-hexadecanol and 5.0 g *N*,*N*-dimethylaniline in 50 mL CH_2Cl_2 at room temperature, 5.2 g phenyl chloroformate (Eastman) was added over 2 hours. After overnight stirring the solution was extracted twice with 50 mL water, three times with 1 *M* HCl, twice with 5% Na_2CO_3 solution, and once with water, and was dried over Na_2SO_4. Removal of the solvent left a crystalline product, mp 33–34°C, following recrystallization from ethanol; ir (melt): 1760 cm^{-1}.

Hexadecyl carbazate (8)

A mixture of 11.0 g phenyl hexadecyl carbonate and 2.8 g 85% hydrazine hydrate was stirred at 80°C for 16 h. The product was dissolved in 150 mL CH_2Cl_2 and the organic layer was extracted four times with 50-mL lots of 2.5 *M* NaOH and twice with water. The solution of the product was dried over Na_2SO_4 and the solvent was removed on a rotary evaporator. The product was recrystallized from methanol between its boiling point and 0°C, filtering the hot solution. The yield of colourless crystals having mp 79–80°C was 7.1 g (74%); ir (Nujol): 3320, 1690, 1610 cm^{-1}.

Hexadecyl azidoformate (9)

A solution of 3.0 g hexadecyl carbazate in 150 mL glacial acetic acid was cooled in ice until the acid began to freeze, at which point a solution of 0.76 g $NaNO_2$ in 3 mL H_2O was added dropwise with stirring. The mixture was allowed to warm up to room temperature overnight. The solution was diluted to 600 mL with water and was extracted three times with 50-mL lots of CH_2Cl_2. The combined organic extracts were washed with three 50-mL volumes of 3% $NaHCO_3$ and once with water, and were dried over Na_2SO_4. Evaporation of the solvent left a white solid which was dissolved in 8 mL CH_2Cl_2, diluted to 50 mL with hexanes, and cooled to 0°C. A small amount of a solid, mainly unreacted starting material, was filtered off and discarded. Cooling the filtrate to −78°C gave pure white crystals, which were filtered by suction and dried *in vacuo*. The yield of product, mp 33°C, was 2.2 g; ir (melt): 2180, 2130, 1725 cm^{-1}; nmr δ: 0.95 (t, 3H) 1.30 (m, 28H), 4.24 (t, 2H); uv (abs. ethanol): shoulder at 255 nm (ε 175 M^{-1} cm^{-1}), shoulder at 218 nm (ε 3180 M^{-1} cm^{-1}).

1,2-Bis(hexadecyloxyformyl) hydrazine

A mixture of 1.50 g phenyl hexadecyl carbonate and 1.24 g hexadecyl carbazate was melted in an oil bath and maintained at 80–100°C for 4 days. The cooled product was dissolved in 50 mL hot $CHCl_3$, and the solution was treated with Norite and filtered. Chilling the solution in Dry Ice initiated crystallization. The filtered product was recrystallized a second time from 30 mL hot ethanol to give 1.1 g of colourless crystals, mp 67–68°C; ir (Nujol): 3280 cm^{-1}, split carbonyl band with maxima at 1740, 1720, 1710 cm^{-1}.

Dihexadecyl azodiformate (10)

A suspension of 0.5532 g 1,2-bis(hexadecyloxyformyl) hydrazine and 0.0805 g dry pyridine in 25 mL dry CH_2Cl_2 was stirred at room temperature and 0.165 g *N*-bromosuccinimide was added all at once. After 5 minutes the solution was filtered to remove a small amount of precipitate. The clear filtrate was evaporated to dryness at reduced pressure and the solids were transferred to a filter funnel and washed many times with water. Recrystallization of the insoluble product from 50 mL 95% ethanol between 50°C and 0°C, filtering the warm

Can. J. Chem. Downloaded from www.nrcresearchpress.com by 210.87.254.5 on 09/06/12
For personal use only.

Can. J. Chem. Downloaded from www.nrcresearchpress.com by 210.87.254.5 on 09/06/12
For personal use only.

solution, gave 0.37 g (67%), mp 37.5–38°C; nmr δ: 0.87 (t, 6H), 1.24 (m, 56H), 4.38 (t, 4H); uv (hexanes) λ_{max}: 401 nm (ε 35.6 M^{-1} cm^{-1}). The extinction coefficient at 250 nm is 480 M^{-1} cm^{-1}.

1-Hexadecyloxyformyl 2-acetyl azene **3**

A solution of 6.2 g hexadecyl carbazate in 75 mL pyridine at 40°C was stirred while 5 mL (5.5 g) of acetic anhydride in 20 mL pyridine was added all at once. After 1 hour of stirring the solution was diluted to 300 mL with ice water and the product was filtered by suction and washed with water. The hydrazide was recrystallized from 200 mL 95% ethanol to give 6.0 g of product, mp 82.5–83°C; ir (Nujol): 3200, 1720, 1670, 1610 cm^{-1}.

A suspension of 2.00 g of the above hydrazide in 75 mL CH_2Cl_2 containing 0.475 mL dry pyridine was stirred while 1.045 g *N*-bromosuccinimide was added all at once. After 5 minutes further stirring the solvent was removed on the rotary evaporator. The product was taken up in hexanes and filtered by suction from insoluble by-products and residual starting material. Evaporation of the solvent at reduced pressure left 1.55 g (78%) of an orange oil, n_D^{24} = 1.4507; ir (neat): 1765 cm^{-1}; nmr δ: 0.89 (t, 3H), 1.29 (m, 28H), 2.38 (s, 3H), 4.45 (t, 2H); uv (cyclohexane) λ_{max}: 430 nm (ε 29.2 M^{-1} cm^{-1}). Attempts to recrystallize this compound at low temperature gave material of much lower purity.

Ethyl hexadecyl azodiformate **4**

A solution of 1.30 g hexadecyl carbazate and 0.45 mL pyridine in 75 mL dichloromethane was stirred at room temperature while 0.50 g ethyl chloroformate was added dropwise over 5 minutes. After overnight stirring the solution was washed with 1 *M* HCl, 5% $NaHCO_3$ solution and water, and was dried over Na_2SO_4. Following evaporation of the solvent the hydrazide was recrystallized from 75 mL absolute ethanol between 75°C and 0°C to give 1.1 g white crystals, mp 71.5–73°C; ir (Nujol): 3220, 1740, 1680 cm^{-1}.

To a stirred suspension of 1.0 g of the above product in 75 mL CH_2Cl_2 containing 1.1 equivalents of dry pyridine, 0.48 g *N*-bromosuccinimide was added all at once. After all of the starting material had dissolved, the clear orange solution was washed with 0.5 *M* HCl and water and was dried over Na_2SO_4. The yield of pure ethyl hexadecyl azodiformate after two low-temperature recrystallizations was 0.20 g (20%), mp 29.5–30°C; ir (Nujol): 1770 cm^{-1}; nmr δ: 0.85 (t, 3H), 1.1–1.9 (m, 31H, $14CH_2$ and $1CH_3$), 4.2–4.7 (m, 4H, 2 overlapping —CH_2—O—); uv (cyclohexane) λ_{max}: 404 nm (ε 35.3 M^{-1} cm^{-1}).

1-Octadecanoyl 2-methoxyformyl azene **5**

A solution of 10 g stearoyl chloride in 50 mL benzene was added to a stirred solution of 3.0 g methyl carbazate in 20 mL dry pyridine. After 1 hour further stirring the reaction mixture was poured into 750 mL water and the product was filtered by suction and washed with water. The yield of product following recrystallization from 200 mL 95% ethanol was 8.7 g, mp 103–103.5°C; ir (Nujol): 3200, 1730, 1700, 1670, 1645, 1600 cm^{-1}.

This hydrazide was converted to the azo-compound **5** following the procedure for compound **4**. The product was recrystallized twice from 60 mL 1:2 CH_2Cl_2–hexanes between room temperature and −78°C to give 2.65 g (87%) orange crystals, mp 39–40°C; ir (Nujol): 1765 cm^{-1}; nmr δ: 0.88 (t, 3H), 1.26 (m, 30H), 2.63 (t, 2H), 4.05 (s, 3H); uv (cyclohexane) λ_{max}: 429 nm (ε 32.0 M^{-1} cm^{-1}).

Octadecanoyl azide (11)

A solution of 5.0 g distilled stearoyl chloride in 30 mL acetone was added dropwise with stirring to a solution of 3.1 g sodium azide in 75 mL H_2O cooled to 5–10°C. After three hours stirring at 10°C the reaction mixture was diluted with 100 mL H_2O and the white solid was filtered by suction and washed several times with water. The product was dissolved in 150 mL 1:1 ether–ethanol at 30°C, filtered through a filter cone filled with Na_2SO_4, and cooled to −20°C. The filtered crystals were dried for one hour over P_2O_5 under high vacuum to give 4.3 g of a white crystalline solid which decomposes with nitrogen evolution at 42–43°C; ir (Nujol): 2145, 1710 cm^{-1}. The 2275 cm^{-1} band of 1-heptadecyl isocyanate is virtually absent; nmr δ: 0.090 (t, 3H), 1.23 (m, 30H), 2.35 (t, 2H); uv (cyclohexane): no absorption maxima above 220 nm. The extinction coefficient at 254 nm is 162 M^{-1} cm^{-1}. The half-life of the solid azide at 20°C is approximately 72 h. Following prolonged storage the compound was repurified by recrystallization from acetone between 30°C and −20°C.

Hexadecyl 2-chloroacetate (12)

A solution of 15.0 g 1-hexadecanol and 7.5 g *N*,*N*-dimethylformamide in 75 mL dry CH_2Cl_2 was stirred at 0°C while 7.1 g chloroacetyl chloride (Merck) was added dropwise over 15 min. After one hour the solution was washed three times with 10% HCl, twice with 5% $NaHCO_3$, and once with water. After overnight drying over Na_2SO_4 the solvent was removed at reduced pressure, leaving 18.5 g (94%) of a solid, mp 28.5–29°C; ir (neat): 1745 cm^{-1}. The crude product was used directly in the following reaction.

Hexadecyl 2-azidoacetate (13)

A solution of 10.0 g crude hexadecyl 2-chloroacetate in 60 mL acetone was added at room temperature to a stirred solution of 5.0 g sodium azide in 40 mL H_2O. The two-phase system was refluxed gently for 18 h, after which the bath temperature was raised to 70°C and 50 mL acetone was distilled off. The residual liquids were diluted to 100 mL with water and the product was separated. The aqueous layer was extracted three times with ether and the combined organic layers were washed twice with water and once with saturated NaCl and were dried over Na_2SO_4. Removal of the solvent left a solid, which was recrystallized twice from 75 mL hexanes between 25°C and −20°C. A total of 7.1 g (70%) colourless crystals, mp 35.5–36.5°C, was obtained; ir (melt): 2100, 1740 cm^{-1}; nmr ($CDCl_3$) δ: 0.90 (t, 3H), 1.24 (m, 28H), 3.88 (s, 2H), 4.22 (t, 2H). *Anal.* calcd. for $C_{18}H_{35}N_3O_2$: C 66.42, H 10.84, N 12.91%; found: C 68.2, H 11.4, N 12.2%. It is probable that slight decomposition of the product occurred in the several days which elapsed between removal of the sample from the freezer and performing the elemental analysis.

Methods

Measurements of surface spreading behaviour

Two commercial Langmuir troughs, one a rectangular trough (MGW Lauda) and the other a Fromherz circular trough (14), were used in studies of monolayers. Temperature control of the subphase was provided by a Lauda Model K4R constant temperature bath and circulating pump. Compounds were spread as dilute (1 mg/mL) solutions in chloroform or hexane on the surface of pure unbuffered water. After five minutes to allow the spreading solvent to evaporate completely, the surface pressure – area curves were recorded continuously at a compression rate of 0.05 nm^2 $molecule^{-1}$ min^{-1}. All measurements were performed at least twice. The reproducibilities of the surface pressure and surface area values for consecutive measurements were typically 0.5 mN m^{-1} and 0.005 nm^2 $molecule^{-1}$ respectively.

Irradiation of monolayers of octadecanoyl azide on water

For photochemical studies the cover of the Lauda trough was modified to hold a 250-mA low-pressure mercury lamp (Gräntzel, Karlsruhe), which was driven at a constant current of 120 mA. Octadecanoyl azide was spread from a fresh cold (0°C) solution in chloroform on the subphase. The solvent was allowed to evaporate for two minutes and the monolayer was irradiated at 254 nm at a constant surface area of 0.65 nm^2/molecule for 20 min. The lamp was switched off and the surface pressure – area curve of the irradiated monolayers recorded at a compression rate of 0.05 nm^2 $molecule^{-1}$ min^{-1}.

Analysis of photoproducts from irradiation of monolayers of octadecanoyl azide

The entire water surface below the low-pressure lamp of the Lauda trough was used as a reaction surface. Monolayers were irradiated at a constant area of 0.25 nm^2/molecule for 30 min. They were then compressed to a 0.5-cm strip, removed from the surface with a clean metal spatula, and dried *in vacuo* over P_2O_5. A total of 8 monolayers was collected to yield about 1 mg of a white solid, mp 69–74°C. The infrared spectrum of the product was recorded in carefully dried KBr against a KBr reference pellet; ir (Perkin–Elmer 457): 3300, 2900, 2840, 1760, 1710, 1635, 1540, 1464, 1373, 1235, 1090, 1035, 718

cm^{-1}; ms (electron impact, 200°C sample holder, main peaks only) *m/z:* 565 (relative intensity 2), 564 (5), 537 (4), 536 (10), 522 (10), 521 (28), 520 (7), 394 (2), 380 (3), 366 (6), 353 (6), 352 (5), 338 (5), 324 (7), 312 (3), 310 (22), 298 (19), 297 (75), 284 (24), 283 (7), 282 (23), 268 (5), 267 (6), 256 (14), 255 (8), 254 (17), 241 (5), 240 (5), 226 (4), 212 (4), 198 (5), 185 (6), 184 (5), 170 (5), 156 (6), 142 (7), 129 (14), 128 (10), 114 (20), 113 (19), 112 (27), 99 (59), 98 (19), 97 (21), 57 (93), 43 (100).

Thermal stability of diacyl diimides

Dilute solutions of dihexadecanoyl diimide in xylenes (J. T. Baker) were maintained at constant temperature in an air-free microcell in the thermostatted sample compartment of a Cary 118 uv–visible spectrometer. The decrease of the sample absorbance at 450 nm was recorded continuously.

Results and discussion

Surface spreading behaviour

Figure 1 shows the surface pressure – area diagrams of hexadecyl azidoformate, hexadecyl azidoacetate, and octadecanoyl azide on pure water. All three compounds form stable monolayers, but show individual behaviour reflecting the interplay between the length of the hydrocarbon chain and the polarity of the head group. Both hexadecyl azidoformate and hexadecyl azidoacetate show expanded phases over part of the accessible temperature range. Above 15°C the azidoformate forms liquid-analog monolayers similar to those of oleic acid. Monolayers of hexadecyl azidoacetate undergo a transition from a solid-analog to an expanded state at 8.5°C. At all temperatures a steep increase in the surface pressure at 0.24 nm^2 $molecule^{-1}$ corresponds to transition from an expanded phase to a closest-packed solid-analog phase. This behaviour is reminiscent of that of fatty acids of intermediate chain length, such as pentadecanoic acid, and was shared by 1-diazo-2-pentadecanone, as described in a previous publication (15). Monolayers of octadecanoyl azide exhibit quite different behaviour, showing only solid-analog phases up to 30°C, which was considered to be the maximum temperature at which spreading behaviour could be investigated without contamination by thermal decomposition products. Here the longer hydrocarbon chain resists the formation of liquid-analog phases, so that curves similar to those of stearic acid are observed.

None of the new compounds having two hydrocarbon chains form stable monolayers by themselves. Monolayers of dihexadecyl azodiformate have borderline stability, so that at high compression rates $\pi-\sigma$ diagrams with collapse areas close to 0.40 nm^2 $molecule^{-1}$ are observed. At normal compression rates collapse of the monolayer under pressure is able to keep pace with the change in surface area until much lower surface areas are reached, as shown in Fig. 2. Monolayers of the four diacyl diimides are unstable at all experimentally accessible rates of compression. This instability may be attributed to the high symmetry and insufficient polarity of the head-group.

Figure 3 shows the surface pressure – area curves of the azo-compounds **4** and **5**. The spreading behaviour of the unsymmetrical azodiformate **4** is similar to that of hexadecyl azidoformate, except that there does not appear to be a transition to a more compact monolayer at low temperatures in the case of compound **4**. Compound **5** gives solid-analog monolayers at all experimentally accessible temperatures, reflecting the greater length of the hydrocarbon chain in this derivative. The curves of Fig. 3 show that it is possible to build the aliphatic azo chromophore into a molecule having only a single long hydrocarbon chain and still retain high surface activity.

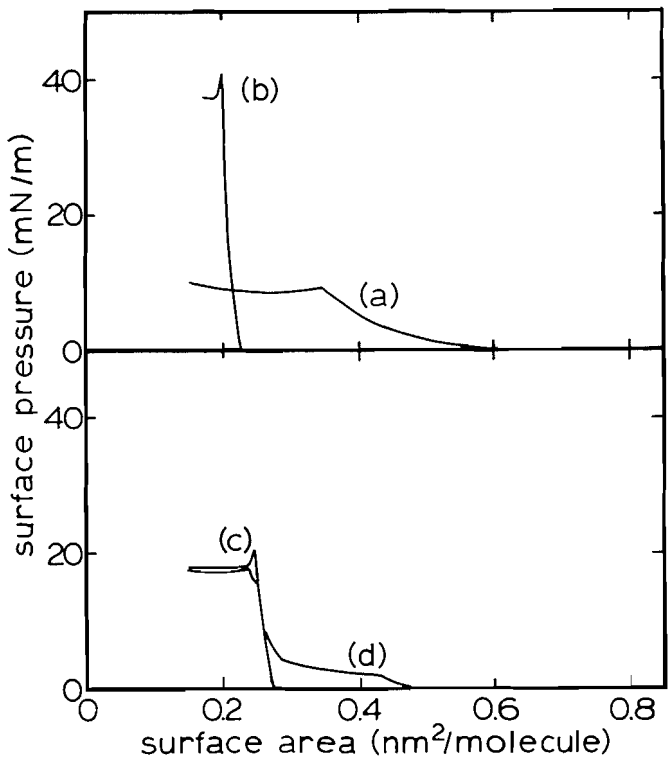

FIG. 1. Surface pressure – area diagrams of monolayers on pure water. (a) Hexadecyl azidoformate, 24.0°C; (b) octadecanoyl azide, 12.9°C; (c) hexadecyl azidoacetate, 4.1°C; (d) hexadecyl azidoacetate, 10.1°C.

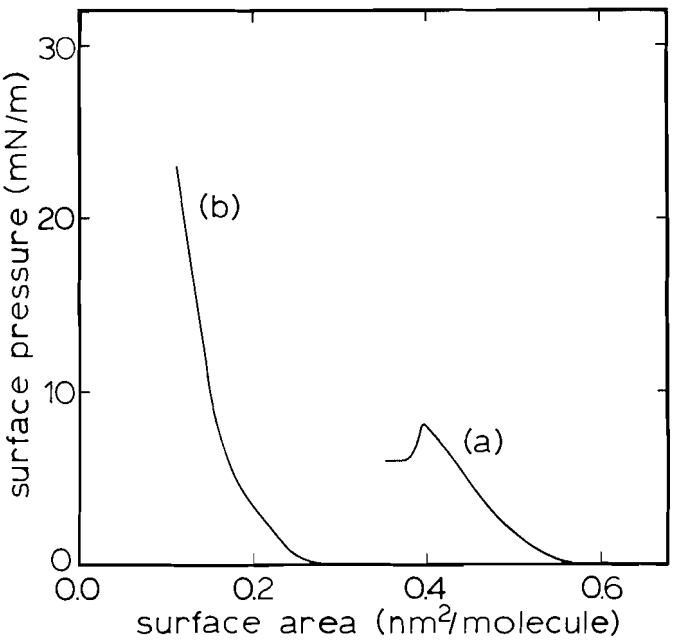

FIG. 2. Surface pressure – area diagrams of dihexadecyl azodiformate on pure water at 24.0°C. (a) Compression rate 0.52 nm^2 $molecule^{-1}$ min^{-1}; (b) compression rate 0.025 nm^2 $molecule^{-1}$ min^{-1}.

Thermal stability of diacyl diimides

A Japanese patent which described the synthesis of aliphatic diacyl diimides suggested that these compounds were useful polymerization initiators (7). Initial attempts to prepare diacyl diimides from fatty acid hydrazides by the same route gave impure products which were indeed very unstable, often de-

Can. J. Chem. Downloaded from www.nrcresearchpress.com by 210.87.254.5 on 09/06/12
For personal use only.

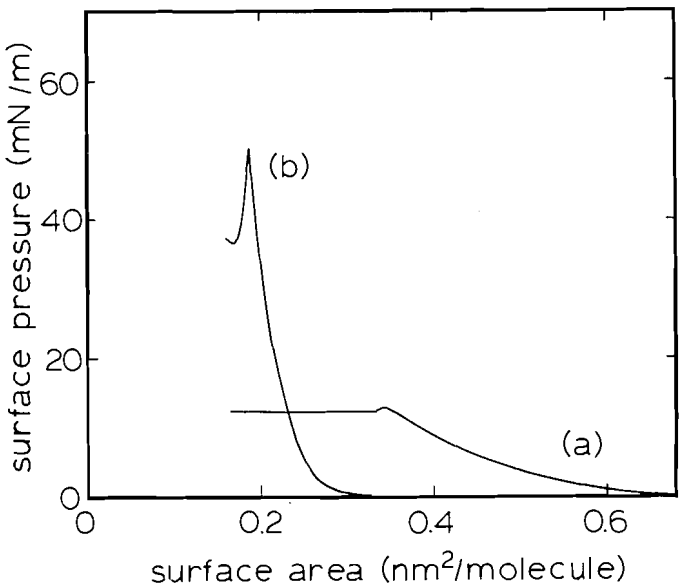

FIG. 3. Surface pressure – area diagrams of monolayers of single-chain azo-compounds on water. (a) Compound **4**, 10.1°C; (b) compound **5**, 10.1°C.

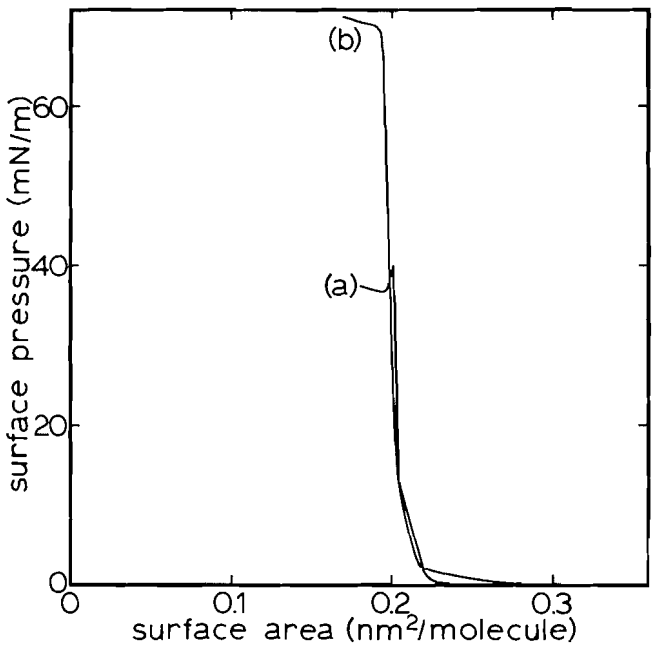

FIG. 4. Surface pressure – area diagrams of monolayers of octadecanoyl azide on pure water at 20.1°C. (a) Before irradiation; (b) after 20 minutes of 254 nm irradiation in air at 0.65 nm^2 $molecule^{-1}$ min^{-1}.

composing unpredictably in solution with the evolution of nitrogen. It was found that if the newly-formed diimide is removed as quickly as possible from the solution in which it is prepared and freed from acetic acid and lead compounds by several low-temperature recrystallizations, it is quite stable. Dihexadecanoyl diimide, for example, has a half-life of 40 h at 73°C in xylene solution. Such decomposition temperatures are too high for these compounds to function as thermal initiators of polymerization in mixed monolayers on water, but they may be used to initiate radical reactions at solid surfaces.

Photochemistry of octadecanoyl azide in monolayers

Figure 4 shows the changes in the surface spreading behaviour of octadecanoyl azide which occur on 20-min 254-nm irradiation of monolayers at a constant surface area of 0.65 nm^2 $molecule^{-1}$. Unlike the long-chain diazoketones investigated previously (15), long irradiation times are necessary to achieve complete decomposition of the azide. This is merely a consequence of the low absorbance of a monolayer of the azide at 254 nm and has little to do with differences in quantum yield of photoreaction between the two classes of compounds. As Fig. 4 shows, the photoreaction of the azide leads to a pronounced increase in the collapse pressure of the monolayer, but without the appearance or disappearance of an expanded phase.

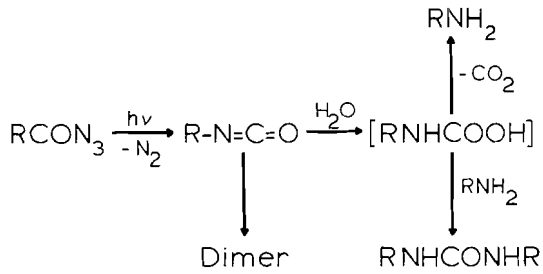

SCHEME 2

An infrared spectrum of the photoproduct mixture indicates that complete decomposition of the azide has occurred, as shown by the absence of the $—N_3$ band at 1710 cm^{-1}. The photoproduct possesses new carbonyl bands at 1760, 1710, and 1635 cm^{-1} and a weak NH band at 3300 cm^{-1}. Notably absent is the 2275 cm^{-1} band of the aliphatic isocyanate.

Further insight into the photochemistry of octadecanoyl azide is obtained from the mass spectrum of the product mixture. A peak at m/z 536 corresponds to sym-diheptadecyl urea. This compound arises by the photochemical conversion of the azide to an isocyanate (16), followed by reaction with water and addition of the resulting amine to a second mole of isocyanate. At higher mass ratios a second molecular ion peak at m/z 564 corresponds to the unexpected isocyanate dimer. In this respect the photoreactions of monolayers of aliphatic acyl azides and α-diazoketones are similar. One of the products of the irradiation of monolayers of 1-diazo-2-nonadecanone, for example, was the β-lactone formed by dimerization of the primary photoproduct, a long-chain ketene (15). Thus even though the ketene or isocyanate functional groups are in contact with pure water, their concentration and mobility within the surface layer are sufficiently high for dimerization to compete successfully with hydrolysis. At lower mass ratios the characteristic breakup pattern of a long hydrocarbon chain, with peaks separated by 14 mass units, is evident. A moderately strong peak at m/z 255 corresponds to heptadecylamine, formed by hydrolysis of the long-chain isocyanate, while at still lower mass ratios is the pattern of peaks corresponding to disintegration of the second alkyl chain.

Scheme 2 summarizes the photochemistry of octadecanoyl azide monolayers on water. With the exception of the dimer, the products are similar to those reported for an aromatic acyl azide in a previous communication (15). In that case, however, the high susceptibility of the aromatic amine to further photodegradation and photooxidation gave a much more complex product mixture.

The risk of explosion normally prevents the isolation of primary aliphatic acyl azides, which are converted directly to isocyanates by controlled heating of solutions. Nevertheless the present work shows that azides containing a long hydrocarbon

Can. J. Chem. Downloaded from www.nrcresearchpress.com by 210.87.254.5 on 09/06/12
For personal use only.

chain are sufficiently stable to be isolated and purified by low-temperature recrystallization, and their physical and chemical properties may be investigated safely up to room temperature.

Summary

The goal of this research was to create compounds with reactive functional groups which retained the high surface activity of their fatty-acid and long-chain alcohol precursors. It was important for the range of proposed applications that these derivatives retain their reactivity in contact with water. Three long-chain azides were synthesized which fulfilled these requirements, ranging from the highly reactive octadecanoyl azide to the much more stable hexadecyl azidoacetate. The compound hexadecyl azidoformate, which has intermediate reactivity as a grafting agent, is a surface-active analog of *tert*-butyl azidoformate, a blocking agent used extensively in peptide synthesis. One promising application of this compound is therefore as a grafting agent for attaching bilayer membranes to supports, and proteins to these synthetic membranes.

The need for long-chain radical initiators having higher purity and greater resistance to hydrolysis than commercial diacyl peroxides has led to the successful synthesis of several new diacyldiimides and azodiformates. While not all of these compounds gave stable monolayers on water, they may still have applications as polymerization initiators in thin films on solid supports.

Acknowledgements

This research was begun at the University of Mainz, West Germany, with the support of an Alexander von Humboldt Research Fellowship (1981–1982). The author thanks Professor Helmut Ringsdorf of the Institute of Organic Chemistry for his constant support and encouragement. The financial assistance of the Natural Sciences and Engineering Research Council is gratefully acknowledged. Thanks are extended to Mrs. Margret Deptolla for her technical assistance, and to Dr. M. Breton and Dr. P. S. Vincett of the Thin Film Science and Memory Group, Xerox Research Centre of Canada, for assistance with the investigations of surface spreading behaviour.

1. J. H. FENDLER. Acc. Chem. Res. **13**, 7 (1980).
2. T. KUNITAKE. J. Macromol. Sci. Chem. **13**, 587 (1979).
3. H. GERISCHER and J. KATZ (*Editors*). Light-induced charge separation in biology and chemistry. Dahlem Konferenzen, West Berlin. 1979.
4. G. A. DELZENNE. Adv. Photochem. **11**, 1 (1979).
5. M. BRETON. J. Macromol. Sci. Rev. Macromol. Chem. **21**, 61 (1981).
6. N. O. V. SONNTAG. J. Am. Oil Chem. Soc. **45**, 571 (1968).
7. Y. TAKADA, K. OYA, and R. WAKASA. Japanese Patent No. 73 19, 501 (1973).
8. L. A. CARPINO, B. A. CARPINO, C. A. GIZA, R. W. MURRAY, A. A. SANTILLI, and P. H. TERRY. Org. Synth. **44**, 22 (1964).
9. L. A. CARPINO, B. A. CARPINO, P. J. CROWLEY, C. A. GIZA, and P. H. TERRY. Org. Synth. **44**, 15 (1964).
10. L. A. CARPINO and P. J. CROWLEY. Org. Synth. **44**, 18 (1964).
11. C. F. H. Allen and A. BELL. Org. Synth. Coll. Vol. **3**, 846 (1955).
12. R. H. BAKER. Org. Synth. Coll. Vol **3**, 144 (1955).
13. A. T. MOORE and H. N. RYDON. Org. Synth. Coll. Vol. **5**, 586 (1973).
14. P. FROMHERZ. Rev. Sci. Instrum. **46**, 1380 (1975).
15. D. A. HOLDEN, H. RINGSDORF, and M. HAUBS. J. Am. Chem. Soc. Submitted.
16. W. LWOWSKI. Nitrenes. Interscience, New York. 1970.

Can. J. Chem. Downloaded from www.nrcresearchpress.com by 210.87.254.5 on 09/06/12
For personal use only.

Formation and spectra of flavin radicals in the presence of β-mercaptoethanol at pH 9 and 10

PARMINDER S. SURDHAR, RIZWAN AHMAD, AND DAVID A. ARMSTRONG
Department of Chemistry, University of Calgary, Calgary, Alta., Canada T2N 1N4

Received July 25, 1983

PARMINDER S. SURDHAR, RIZWAN AHMAD, and DAVID A. ARMSTRONG. Can. J. Chem. **62**, 580 (1984).

Spectral changes and rates of reaction of flavins and several radical species have been investigated at pH 7, 9, and 10 in the presence and absence of β-mercaptoethanol. The radicals $\cdot CO_2^-$, e_{aq}^-, and $LS_2^{\cdot -}$ reacted with FAD at pH 10 to give a spectrum of FAD $\cdot Fl^-$ with rate constants of $7 \pm 1 \times 10^8$ and $4 \pm 1 \times 10^8\ M^{-1} s^{-1}$ for $\cdot CO_2^-$ and $LS_2^{\cdot -}$ respectively. At pH 7 only $\cdot FlH$ was observed and at pH 9 a mixture of $\cdot FlH$ and $\cdot Fl^-$.

Interactions between flavin radicals and sulphydryl at $10^{-4}\ M$ concentration did not cause perturbations in the uv–visible spectra until either the radical and/or the sulphydryl were ionized. With FAD at pH 9 or 10 and LFl at pH 10 the 370 nm peak of $\cdot Fl^-$ was enhanced by about 15% and a second larger growth occurred near 450 nm in the presence of 10^{-4} to $10^{-2}\ M$ sulphydryl. We attribute this to the formation of labile intermediate $RSHFl\cdot^-$, which must also be involved in the reduction of Fl by $RS\dot{S}R^-$ at pH 9 or 10.

The second order rate constant k_{13} for reaction of $RS\dot{S}R^-$ with FAD at pH 9 and 10 was found to be $4.2 \pm 0.5 \times 10^8\ M^{-1} s^{-1}$ and $2.0 \pm 0.4 \times 10^8\ M^{-1}\ s^{-1}$ respectively. The rate constant for the reaction between $RS\dot{S}R^-$ and LFl at pH 10 was slightly faster, $7 \pm 1 \times 10^8\ M^{-1}\ s^{-1}$, probably reflecting the fact that LFl lacks the bulky negatively charged adenine dinucleotide group of FAD.

PARMINDER S. SURDHAR, RIZWAN AHMAD et DAVID A. ARMSTRONG. Can. J. Chem. **62**, 580 (1984).

Opérant à des pH de 7, 9 et 10 et en présence ou en l'absence de β-mercaptoéthanol, on a étudié les changements spectraux et les vitesses de réaction de flavines et de plusieurs espèces radicalaires. Les radicaux $\cdot CO_2^-$, e_{aq}^- et $LS_2^{\cdot -}$ réagissent avec FAD à un pH de 10 pour donner un spectre de FAD $\cdot Fl^-$ avec des constantes respectives de vitesses de $7 \pm 1 \times 10^8$ et $4 \pm 1 \times 10^8\ M^{-1}\ s^{-1}$ pour $\cdot CO_2^-$ et $LS_2^{\cdot -}$. A un pH de 7, on n'observe que $\cdot FlH$ alors qu'à un pH de 9, il y a formation d'un mélange de $\cdot FlH$ et $\cdot Fl^-$.

Les interactions entre les radicaux flavines et sulfhydryles à des concentrations de $10^{-4}\ M$ ne provoquent pas de perturbations dans les spectres uv–visible tant que le radical et/ou le sulfhydryle n'est pas ionisé. Avec le FAD à un pH de 9 ou 10 et avec le LFl à un pH de 10, il y a une augmentation d'environ 15% du pic à 370 nm dû au $\cdot Fl^-$ et une deuxième augmentation plus importante se produit près de 450 nm en présence de sulfhydryle à des concentrations allant de 10^{-4} à $10^{-2}\ M$. On attribue ces résultats à la formation de l'intermédiaire labile $RSFl\cdot^-$ qui doit aussi être impliqué dans la réduction de Fl par $RS\dot{S}R^-$ à des pH de 9 ou 10.

On a trouvé que les constantes de vitesse du deuxième ordre, k_{13}, pour la réaction de $RS\dot{S}R^-$ avec FAD à des pH de 9 et 10 sont respectivement de $4{,}2 \pm 0{,}5 \times 10^8\ M^{-1}\ s^{-1}$ et $2{,}0 \pm 0{,}4 \times 10^8\ M^{-1}\ s^{-1}$. La constante de vitesse pour la réaction entre RSSR et LFl à un pH de 10 est légèrement supérieure, $7 \pm 1 \times 10^8\ M^{-1}\ s^{-1}$; ceci est probablement dû au fait que LFl ne porte pas le volumineux groupe chargé négativement qu'est l'adénine dinucléotide du FAD.

[Traduit par le journal]

Introduction

The chemistry of disulphide anions has been investigated in several laboratories (1–7). Anions for cyclic disulphides and protein disulphides are relatively stable (3, 4, 6, 7), and can be formed by reactions with solvated electrons (e_{aq}^-) or formate radical anions ($\cdot CO_2^-$). Typical examples of cyclic disulphides are dithiothreitol and lipoamide, viz. $\overline{S—S—CH_2-CHOHCHOHCH_2}$ and $\overline{S—S—CH_2CH_2CH(CH_2)_4CONH_2}$, which are represented below by the abbreviated formulae DS_2 and LS_2 respectively. Formation of the anions occurs, for example, in reaction [1]:

[1] $$\cdot CO_2^- + LS_2 \rightarrow CO_2 + LS\dot{S}^-$$

Non-cyclic disulphides (RSSR) also form anions. However, here reactions [2] and [−2] are both rapid, and $RS\dot{S}R^-$ is only observed in the presence of appreciable concentrations of

[2]/[−2] $$RS\cdot + RS^- \rightleftharpoons RS\dot{S}R^-$$

thiolate (RS^-) ion, which drives equilibrium [2] to the right. Examples of K_2 are $1.8 \times 10^3\ M^{-1}$ for β-mercaptoethanol (1,5) and $(1.3 \times 10^3\ M^{-1}$ (3) for β-mercaptopropionic acid.

Apart from their intrinsic interest to the field of sulphur chemistry, it has been recognised that disulphide anions may be involved in electron transport (4, 8). Flavin molecules are important prosthetic groups for a large variety of redox enzymes (9, 10) and in the specific cases of glutathione reductase, lipoamide dehydrogenase, and thioredoxin reductase protein-bound disulphides are involved in the *two-electron-transfer* pathways, which in the direction of substrate oxidation can be represented as (11–13):

[3] $$\text{Substrate} \xrightarrow{1} S—S \xrightarrow{2} Fl \xrightarrow{3} NAD^+$$

Here Fl represents a strongly bound flavin molecule and NAD^+ is the oxidized nicotinamide cofactor. From biochemical studies it is apparent that step 1 leaves the enzyme disulphide doubly reduced (11–13), while step 2 transfers the electrons to the flavin. The structures existing before and after step 2 are thus taken to be:

[4] $$\begin{array}{ccc} SH & S^- \cdots Fl & \xrightarrow{2} \\ \llcorner\!\!\lrcorner & \llcorner\!\!\lrcorner & \end{array} \quad \begin{array}{cc} S—S & FlH^- \\ \llcorner\!\!\lrcorner & \llcorner\!\!\lrcorner \end{array}$$

Chan *et al.* (4) and more recently Ahmad and Armstrong (14) have pointed out that disulphide anion – flavin one-electron transfers are rapid and relatively clean. Hence, as in the mechanisms proposed for monoamine (15, 16) and alcohol (9), oxidations by flavin cofactors in enzymes, one should consider the possibility that step 2 occurs through a sequence of two one-

Can. J. Chem. Downloaded from www.nrcresearchpress.com by 210.87.254.40 on 09/06/12
For personal use only.

Can. J. Chem. Downloaded from www.nrcresearchpress.com by 210.87.254.40 on 09/06/12
For personal use only.

electron transfers with a radical pair, such as I, as a short-lived intermediate:

$$[4a] \quad SH \quad S^- \cdots Fl \rightleftharpoons \underset{I}{S^{\cdot} \cdots S^- \cdots FlH} \rightleftharpoons S{-}S \quad FlH^-$$

The preceding discussion has made it apparent that adjacent thiolate ions would stabilize a protein RS· ($\Delta G_2 = -18.2 \pm 0.4$ kJ mol^{-1} for the examples cited). Thiolate ion or RSH might also interact with flavin radicals and this could have an important effect on the stability of I and the rate of step 2. As a means of determing whether such interactions occur, the spectra of flavin radicals $\cdot Fl^-$ and $\cdot FlH$ have been investigated in the presence and absence of a sulphydryl solute at several pH's. The experiments were performed by the technique of pulse radiolysis (17). The flavin radicals were produced via the following reactions (17, 18):

$$[5] \quad 4.2H_2O \rightsquigarrow 2.7e_{aq}^- + 0.6\cdot H + 2.8\cdot OH + 2.7H^+ + 0.5H_2 + 0.7H_2O_2$$

$$[6] \quad e_{aq}^- + N_2O + H_2O \rightarrow N_2 + OH^- + \cdot OH$$

$$[7] \quad \cdot OH(or \cdot H) + HCO_2^- \rightarrow H_2O(or\ H_2) + \cdot CO_2^-$$

$$[8] \quad \cdot CO_2^- + Fl \rightarrow CO_2 + \cdot Fl^-$$

$$[9] \quad e_{aq}^- + Fl \rightarrow \cdot Fl^-$$

$$[10]/[-10] \quad \cdot FlH \rightleftharpoons \cdot Fl^- + H^+$$

In addition, the rate of the reaction between $\dot{L}S_2^-$ and $RS\dot{S}R^-$ and Fl was also investigated and the species produced by electron transfer from these anions to flavins were shown to be similar to those formed by $\cdot CO_2^-$. The flavins used were flavin adenine dinucleotide (FAD) and lumiflavin (LFl). The sulphydryl compound was β-mercaptoethanol, which has a low vapour pressure, is water soluble, and has been studied extensively in previous radiation chemical investigations (1, 5). It possess a pK of 10.0 ± 0.2 (1.5).

Experimental

The pulse radiolysis experiments were performed by utilizing 2-μs pulses of electrons with a dose of 0.2 to 0.4 gray from the 1.5-meV Van de Graaff generator described earlier (19). A 1.0-cm path-length optical cell was used with a fresh solution for each pulse. Dosimetry was based on absorbance changes in N_2O-saturated 7×10^{-3} M potassium ferrocyanide solutions with ($G \times \epsilon_{420}$) taken as 6.4×10^3 molecules (100 eV)$^{-1}$ M^{-1} cm^{-1} (20). Here G is the yield of the product (ferricyanide) in molecules per 100 eV of radiation energy and ϵ_{420} the difference in molar absorbance coefficients of ferri- and ferrocyanide at 420 nm.

Flavin adenine dinucleotide (FAD) and lumiflavin (LFl) were used as supplied by the Sigma Chemical Co. All other chemicals were the purest available commercial products.

All solutions were prepared from triply distilled water and purged with N_2O or argon as indicated. These gases were first passed through a column of Ridox (Fisher Scientific Co.) to remove traces of oxygen. All solutions were buffered with 10 mM phosphate, and protected from light as much as possible before pulsing.

Solutions requiring RSH were prebubbled before addition of the RSH. This was done to minimize air oxidation of the sulphydryl. The solutions were then adjusted to the required pH and purged again with the required gas before irradiation.

Absorption spectra of FAD and LFl in deaerated solutions at pH 9 and 10 were taken on a Cary 219 spectrophotometer. They were found to be stable over the time of our experiments in the absence and presence of ten millimolar concentrations of RSH. Values of ΔA, the change in absorbance per unit dose observed at any given time after the radiation pulse, were converted to [ε(Fl radical) − ε(Fl)] at each wavelength by dividing ΔA by the concentration of radicals produced per kilogray. Values of ε(Fl radical) were obtained by adding ε(Fl). Radical yields used were 6.6×10^{-4} M and 7.0×10^{-4} M for 20 mM and 0.2 M formate solutions respectively and 7.0×10^{-4} M for 10^{-2} M RSH. These were estimated from solute–radical reactivities (21), and are concentrations per kilogray of absorbed radiation energy.

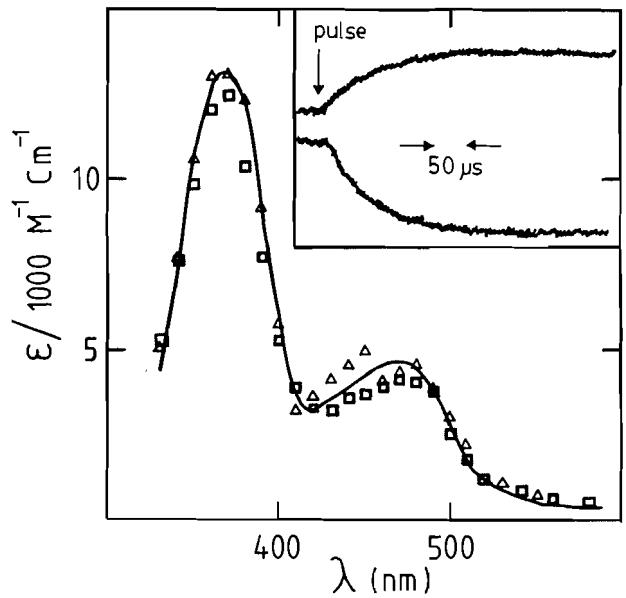

FIG. 1. Absorption spectra following pulse radiolysis of FAD at pH 10, in phosphate buffer. Reacting radicals: (—) CO_2^- in formate solutions (20×10^{-3} M and 0.2 M), N_2O-saturated; (Δ) e_{aq}^- + $\cdot CO_2^-$ in formate solution, argon-saturated; (□) $LS_2^{\cdot -}$ in 0.2 M formate solution containing 2 mM LS_2, argon-saturated. Inserted are oscilloscope traces of transmission changes at 370 nm (top) and 440 nm (bottom). Spectra were independent of [FAD] over the range used, 10–40 μM.

Results and discussion

Initial experiments were performed at pH 7, where both the flavin radical (p$K_{10} \simeq 8.4$ (22)) and β-mercaptoethanol are protonated. Both the FAD and LFl the spectra of the $\cdot FlH$ radicals formed via reactions [8] and [−10] were the same in the presence and absence of RSH at a concentration of 10^{-4} M. It is conceivable that interactions causing spectral changes might occur at higher concentrations. However, since $\cdot CO_2^-$ reacts with RSH with a rate constant of about 1×10^8 M^{-1} s^{-1} (22) and k_8 is 1 to 4×10^9 M^{-1} s^{-1} at pH 7 (ref. 23 and references therein, and ref. 24), the use of larger [RSH] would have caused complications and was not pursued.

Attention is now focused on experiments performed at pH 10, where the flavin radicals should be fully ionized and the sulphydryl about 50 percent ionized, and pH 9, where the former is still largely ionized and the latter about 10 percent ionized. The series of experiments carried out with FAD at both pH's and with LFl at pH 10 were very similar and are not all described in detail.

FAD at pH 10

Reaction with $\cdot CO_2^-$, e_{aq}^-, and $LS_2^{\cdot -}$

The solid line in Fig. 1 is the absorption spectrum of the FAD radical produced in reactions [5]–[8] in N_2O-saturated solutions. This spectrum, which is the mean of five determinations,

Can. J. Chem. Downloaded from www.nrcresearchpress.com by 210.87.254.40 on 09/06/12
For personal use only.

was independent of formate and FAD concentrations over the ranges 0.02 to 0.2 M and 10 to 40 μM respectively. The triangular data points demonstrate that a similar spectrum, was obtained in argon-saturated solutions, where e_{aq}^- and $\cdot CO_2^-$ would have reacted with FAD in approximately equimolar amounts.

It should be noted that the peak at 370 nm was reproducible to within about 5 percent between experiments, but absorbances in the wavelength range 410 to 480 nm tended to scatter more, both in N_2O- and argon-saturated solutions. That feature has been illustrated by the data points shown.

The major characteristics of the spectrum, a strong peak at 370 nm and a second weaker broad peak in the region of 470 nm, resemble those reported for the negative $\cdot Fl^-$ ion of lumiflavin-3-$CH_2COOC_2H_5$ by Ehrenberg *et al.* (ref. 25, Fig. 3). As reported by Land and Swallow (24) the riboflavin radical anion also has a strong peak near 370 nm and a weaker one at 480 nm. The riboflavin radical $\cdot FlH$ has a pK of 8.3 (24), and one would assume a similar pK for FAD $\cdot FlH$. Therefore it seems clear that the spectrum in Fig. 1 is that of FAD $\cdot Fl^-$ formed in reaction [8] or [9].

The insert in Fig. 1 illustrates changes in absorbance with time for a 20 μM FAD solution on reaction with $\cdot CO_2^-$. These changes were found to be first order in time, and a second order rate constant was obtained from a plot of the pseudo first order rate constant versus FAD concentration in the range 10 to 40 μM. The value at ionic strength 0.06 was $7 \pm 1 \times 10^8\ M^{-1}\ s^{-1}$.

Although the transients in the inset of Fig. 1 exhibited no evidence of decay on the time scale shown at the above given ionic strength, significant decay was seen when it was increased to 0.24. That observation is consistent with bimolecular decay of a species bearing a negative charge. The buildup was faster as well. This was not pursued in detail here, but would be expected as $\cdot CO_2^-$ and FAD are both negatively charged at pH 10.

The squares in Fig. 1 exhibit the spectrum of the species produced on completion of the reaction between $LS_2\cdot^-$ and FAD. It is the mean of results at two FAD concentrations and is, within experimental error, the same as that formed by $\cdot CO_2^-$ and $\cdot CO_2^- + e_{aq}^-$. The initial spectrum was that of $LS_2\cdot^-$, and the spectral changes during reaction were very similar to those described below for $RS\dot{S}R^-$ (Figure 3a). From analysis of these at different FAD concentrations, the rate constant for reaction [11] was found to be

$$[11] \qquad LS_2^{\cdot -} + Fl \rightarrow LS_2 + Fl\cdot^-$$

$$k_{11} = 4 \pm 1 \times 10^8\ M^{-1}\ s^{-1}$$

Reaction with $\cdot CO_2^-$ in the presence of 10^{-4} M β-mercaptoethanol[1]

At pH 10 in these solutions one has $[RS^-] = [RSH] = 5 \times 10^{-5}\ M$. As shown by a comparison of the data points and dashed line in Fig. 2a, when $\cdot Fl^-$ was formed by reaction [8] in 0.02 M formate containing the above sulphydryl–thiolate ion mixture, the spectrum exhibited an enhancement of the 370 nm peak and the absorption in the 400 to 480 nm region was almost doubled. However, the rate of growth of the transient species, as given by traces like those in the inset of Fig. 1, remained the same as in the absence of RSH and RS^-. These results suggest that $\cdot Fl^-$ was still formed in reaction [8], but subsequently underwent a rapid secondary reaction with either RS^- or RSH to form the species responsible for the new spectrum. For practical purposes this is subsequently referred to as $RSHFl\cdot^-$.

Reaction with $RS\dot{S}R^-$ in 10^{-2} M β-mercaptoethanol

When these N_2O-saturated solutions containing flavin were pulsed, the initial absorbance was that of $RS\dot{S}R^-$, which would have been formed in reactions [5]–[7], [12], and [2] (1).

$$[12] \qquad \cdot OH(\text{or } \cdot H) + RSH \rightarrow H_2O(\text{or } H_2) + RS\cdot$$

This has been illustrated in Fig. 3a, where the circles represent the initial absorbances for $10^{-2}\ M$ RSH solutions containing 10 μM FAD and the line through them is the absorption spectrum of $RS\dot{S}R^-$ obtained under the same conditions with no flavin present. The spectrum agrees with that in ref. 1.

The absorbance changed with time, exhibiting a small growth between 340 and 380 nm and a strong decrease between 400 and 500 nm. The signals were constant from 140 μs to at least 400 μs. The triangles in Fig. 3a display the absorbances at 400 μs. An abolute spectrum calculated from these and the absorption spectrum of the unirradiated flavin solution is shown by the solid line in Fig 2a.

Comparison of the solid line and circles in Fig. 2a shows that at 400 μs the 370 nm peak of the products of the $RS\dot{S}R^-$ and $\cdot CO_2^-$ reactions with FAD in the presence of $10^{-4}\ M$ total sulphydryl were the same. The 420–480 nm absorptions were slightly different from each other, but both exhibited strong enhancement over the peak height seen in the absence of sulphydryl. Therefore the species formed by $RS\dot{S}R^-$ in $10^{-2}\ M$ β-mercaptoethanol is probably structurally similar to $RSHFl\cdot^-$. Furthermore, since one-electron reductions of flavins by $LS_2^{\cdot -}$ above and other cyclic disulphides (23) have been observed to produce flavin radicals in the absence of RS^- or RSH, it is reasonable to propose that reaction [13] occurred and was followed by a process similar to that which produced $RSHFl\cdot^-$ in

$$[13] \qquad RS\dot{S}R^- + Fl \rightarrow RSSR + \cdot Fl^-$$

the $10^{-4}\ M$ β-mercaptoethanol solutions.

The rate of reaction between $RS\dot{S}R^-$ and Fl was calculated in the following way from oscilloscope traces at 420 to 460 nm. The difference, a, between the absorbance at time t and at 400 μs (i.e. $t = \infty$) was divided by the same difference for $t = 0$ (i.e. a_∞) to give (a/a_∞). As demonstrated in Fig. 3b, plots of $\ln(a/a_\infty)$ versus time were linear, indicating that the reaction was pseudo first order. For a given FAD concentration the plots were independent of RSH concentration in the range 10^{-2} to $2 \times 10^{-2}\ M$ (see squares and circles in Fig. 3b). The second order rate constant k_{13} for reaction of $RS\dot{S}R^-$ with FAD was found from a plot of the pseudo first order rate constants against [FAD] to be $2.0 \pm 0.4 \times 10^8\ M^{-1}\ s^{-1}$.

FAD at pH 9

Reaction with $\cdot CO_2^-$

As shown in Fig. 2b, the spectrum produced on reaction of $\cdot CO_2^-$ with FAD in the absence of mercaptan at this pH exhibits a much smaller peak at 370 nm and stronger absorbance in the 500 to 600 nm region. Neutral flavin radicals possess

[1] If the rate constant of the reaction $\cdot CO_2^- + RSH \rightarrow HCO_2^- + RS\cdot$ is similar to that for abstraction of H from dithiothreitol, which is 1×10^8 (22), then at pH 10 in $10^{-4}\ M$ RSH with $[Fl] \geq 4 \times 10^{-5}\ M$, 15% or less of the $\cdot CO_2^-$ would react with RSH and the remainder with Fl. The spectral intensities of $\cdot Fl^-$ observed here suggest that the proportion of $\cdot CO_2^-$ undergoing reaction with RSH is actually much less.

Can. J. Chem. Downloaded from www.nrcresearchpress.com by 210.87.254.40 on 09/06/12
For personal use only.

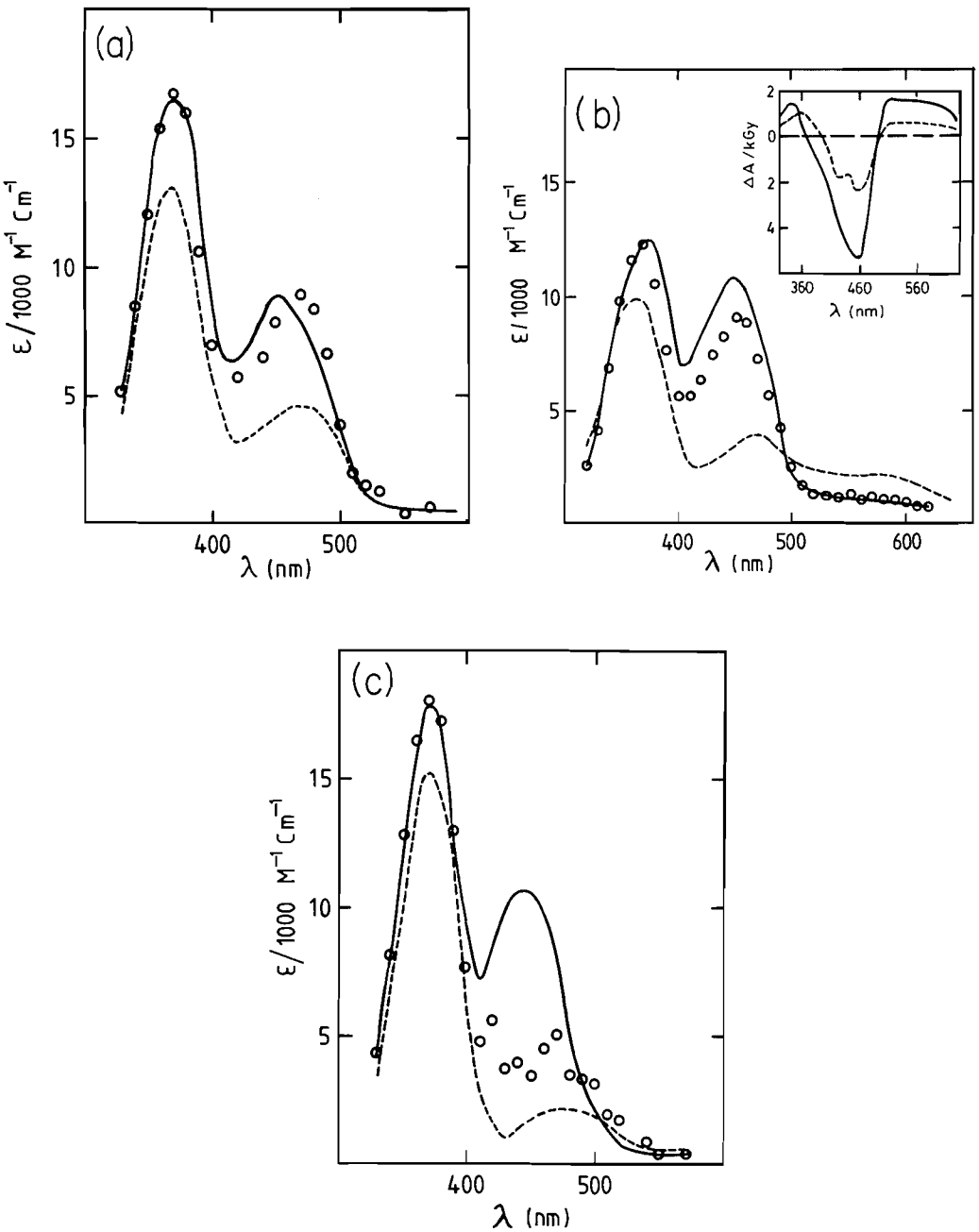

FIG. 2. Spectra of flavin solutions following pulse radiolysis of N_2O-saturated solutions. Reacting radicals: (----) $\cdot CO_2^-$ in formate solutions, (○) $\cdot CO_2^-$ in formate solution with 1×10^{-4} *M* RSH and (—) $RSS\dot{R}^-$ in 10^{-2} *M* RSH solution. (a) FAD at pH 10; (b) FAD at pH 9; (c) LFl at pH 10. The inset in (b) shows difference spectra following pulse radiolysis of FAD (36×10^{-6} *M*) in 20×10^{-3} *M* sodium formate measured 20 μs after pulse (----) and 400 μs after pulse (—).

stronger absorbtions ($\epsilon \sim 4000\ M^{-1}\ cm^{-1}$) in the 500–600 nm region and lower absorptions from 330 to 400 nm ($\epsilon_{max} \sim 8000\ M^{-1}\ cm^{-1}$ at 340 nm) than $\cdot Fl^-$ (24, 25). Thus both of the above features are consistent with the presence of a significant proportion of $\cdot FlH$ at pH 9. A second feature worth noting was that the spectrum did not grow homogeneously. This has been illustrated in the inset of Fig. 2b by the absorbance changes measured at 20 and 400 μs. The 20 μs difference spectrum exhibited much smaller changes in intensity at 460 and 560 relative to that at 360 nm and would correspond more closely to the absolute spectrum of $\cdot Fl^-$ in Fig. 2a. It would appear, therefore, that $\cdot Fl^-$ was formed first in reaction [8], and then the equilibrium [10] was established.

Reaction with $\cdot CO_2^-$ and $RSS\dot{R}^-$ in the presence of 10^{-4} M and 10^{-2} M β-mercaptoethanol respectively

As was the case at pH 10, the absorption of the flavin radical over the 350 to 480 nm region was enhanced in the presence of 10^{-4} *M* mercaptan. A further but much smaller enhancement was seen from 380 to 470 nm when $RSS\dot{R}^-$ was the reducing species in 10^{-2} *M* mercaptan solutions. The rate constant for the reaction of FAD with $RSS\dot{R}^-$ was now larger, viz. $k = 4.2 \pm 0.5 \times 10^8\ M^{-1}\ s^{-1}$, when calculated by the same method as used at pH 10.

LFl at pH 10

The results obtained with LFl are in principle similar to

Can. J. Chem. Downloaded from www.nrcresearchpress.com by 210.87.254.40 on 09/06/12
For personal use only.

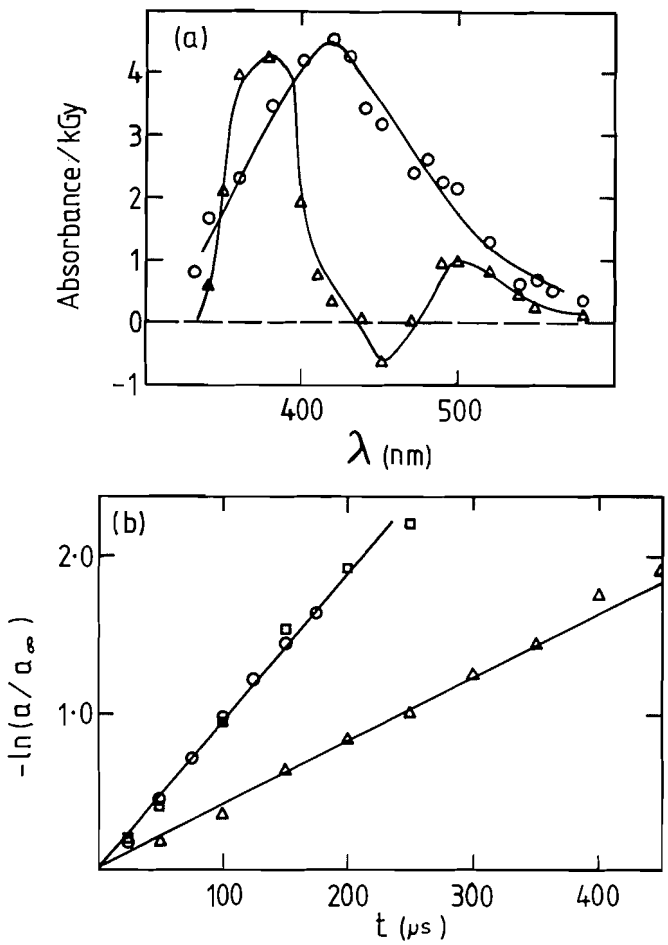

FIG. 3.(a) Difference spectra following the pulse radiolysis of FAD (10×10^{-6} *M*) at pH 10 in N_2O-saturated phosphate buffer containing 1×10^{-2} *M* RSH. The spectra were measured (○) 20 μs after pulse and (Δ) 400 μs after pulse. The line through the circles is the spectrum of $RSS\dot{R}^-$ in N_2O-saturated phosphate buffer containing 1×10^{-2} *M* RSH at pH 10 and no flavin. (b) Plot of ln (a/a_∞) vs. time for the formation of transient species produced following the pulse radiolysis of 10×10^{-6} *M* FAD containing 1×10^{-2} RSH (Δ); 40×10^{-6} *M* FAD containing 2×10^{-2} *M* RSH (○); and 1×10^{-2} *M* RSH (□). All the solutions were in N_2O-saturated phosphate buffer.

those observed with FAD and need only a cursory discussion. As shown by the dashed line in Fig. 2c, the spectrum of $Fl\cdot^-$ for this flavin has a stronger absorption at 370 nm and the extinction coefficient more closely matches that of Ehrenberg *et al.* for lumiflavin-3-$CH_2COOC_2H_5$ $Fl\cdot^-$ (ϵ = 17 500 M^{-1} m^{-1} (25)). At the same time, the 480 nm peak was weaker than that of FAD $\cdot Fl^-$.

As in the case of FAD, the peak heights were enhanced in the presence of β-mercaptoethanol. Also the enhancement was fully saturated in 10^{-4} *M* solutions for the wavelength region 330 to 380 nm. However, this did not apply in the 400 to 500 nm region. Furthermore, the data there exhibited considerable scatter for 10^{-4} *M* solutions.

The rate constant for the reaction between $RSS\dot{R}^-$ and LFl in 10^{-2} *M* β-mercaptoethanol solutions was $7 \pm 1 \times 10^8$ M^{-1} s^{-1}, as calculated from absorption changes over the 420 to 460 nm range. That it was larger than for FAD probably reflects the fact that LFl lacks the bulky negatively charged adenine dinucleotide group of FAD.

Summary and conclusions

The complexation of flavin radicals by various amino acids has been reported before and flavins are known to bind up to two ligands per molecule (26). However, we are unaware of publications dealing with sulphydryl species interacting with $\cdot Fl^-$ or $\cdot FlH$.

The present study has demonstrated that interactions between flavin radicals and β-mercaptoethanol at the 10^{-4} *M* level do not cause measurable perturbations in the uv–visible spectra until either the radical and/or the sulphydryl are appreciably ionized. At pH 9 and 10 with FAD and at pH 10 with LFl 330 to 370 nm absorption was enhanced in the presence of β-mercaptoethanol, and the effect in all three cases was saturated at 10^{-4} *M* mercaptan. In addition, the sulphydryl compound caused the growth of a strong peak with a maximum near 450 nm, and at pH 9 there was a factor of two reduction in the absorbance above 500 nm. These observations imply that the perturbations in the spectral regions are probably due to sulphydryl–FlH or $\cdot Fl^-$ interactions which form a species $RSHFl^{\cdot-}$. However, it may be that more than one mercaptan is bound to the flavin radical in the 10^{-2} *M* solutions, and the present results do not resolve that point.

In addition, one cannot state whether the formation of $RSHFl\cdot^-$ is a reversible process or not. However, it is evident that this species would have to be an intermediate in the two-electron reduction of Fl by $RSS\dot{R}^-$ in the presence of RSH at pH 9 or 10, and the only significant product of that reaction was FlH^- (14). Therefore it is evident that $RSHFl\cdot^-$ is a fairly labile species, possible reacting with RS· as follows.

[14] $\quad RS\cdot + RSHFl\cdot^- \rightarrow RSSR + FlH^-$

That process would be the equivalent of the second half of step 2 (reaction [4*a*] of Introduction).

Extensive speculation concerning the structure of $RSHFl\cdot^-$ is not warranted here, but it should be pointed out that one type of interaction may involve a three-electron bond between N-5 and the thiolate ion, viz.

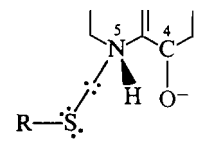

The structure would be rendered more stable with N-5 protonated as shown, and could be formed by reaction of RS^- and $\cdot FlH$ or RSH and $Fl\cdot^-$. Hiller and Amus (27) have postulated a transitory S—N three-electron bond to explain aspects of methionine chemistry and Musker *et al.* (28) have observed such bonds in cyclic amino-thio ethers.

As a final point, in our view the tendency for scatter in the 410- to 480-nm range may be an indication that other substances, also capable of causing spectral perturbations, bind to Fl radicals. Fluctuations in the concentrations of trace reaction products or impurities may cause the pulse-to-pulse variations. Studies of spectral perturbations by species other than mercaptans will be undertaken.

Acknowledgements

This research was supported by NSERC grant A3571. We are grateful to S. Przepiora for technical assistance.

1. W. KARMANN, A. GANZOW, G. MEISSNER, and A. HENGLEIN. Int. J. Radiat. Phys. Chem. **1**, 395 (1969).

2. G. E. ADAMS and P. WARDMAN. Free radicals in biology. Vol. 3. *Edited by* W. A. Pryor. Academic Press, New York. 1977. Chapt. 2.
3. M. Z. HOFFMAN and E. HAYON. J. Am. Chem. Soc. **94**, 7950 (1972); J. Phys. Chem. **77**, 990 (1973).
4. S. W. CHAN, P. C. CHAN, and B. H. J. BIELSKI. Biochim. Biophys. Acta, **338**, 213 (1974).
5. G. G. JAYSON, D. A. STIRLING, and A. J. SWALLOW. Int. J. Radiat. Biol. **19**, 143 (1971).
6. M. FARAGGI,, J. L. REDPATH, and Y. TAL. Radiat. Res. **64**, 452 (1975).
7. Z. WU, R. AHMAD, and D. A. ARMSTRONG. Radiat. Phys. Chem. In press.
8. M. H. KLAPPER and M. FARAGGI. Q. Rev. Biophys. **12**, 465 (1979).
9. T. C. BRUICE. Prog. Bioorg. Chem. **4**, 2 (1976).
10. P. HEMMERICH and H. LAUTERWEIN. Inorganic biochemistry. Vols. 1 and 2. *Edited by* G. L. Eichhorn. Elsevier, London. 1973 Chapt. 32.
11. C. H. WILLIAM, JR. Enzyme, **13**, 89 (1976).
12. K. D. WILKINSON and C. H. WILLIAMS, JR. J. Biol. Chem. **254**, 852 (1979).
13. L. D. ARSCOTT, C. THORPE, and C. H. WILLIAMS, JR. Biochemistry, **20**, 1514 (1981).
14. R. AHMAD and D. A. ARMSTRONG. Can. J. Chem. **62**, 000 (1984).
15. R. B. SILVERMAN, S. J. HOFFMAN, and W. B. CATUS III. *In* Flavins and flavoproteins. *Edited by* V. Massey and C. H. Williams, Jr. Elsevier, New York. 1982. p. 213.
16. T. P. SINGER and M. HUSAIN. *In* Flavins and flavoproteins. *Edited by* V. Massey and C. H. Williams, Jr. Elsevier, New York. 1982. p. 389.
17. B. H. J. BIELSKI and J. M. GEBICKI. Free radicals in biology. Vol. 3. *Edited by* M. Pryor. Academic Press, New York. 1977. p. 2.
18. I. G. DRAGANIĆ and Z. D. DRAGANIĆ. The radiation chemistry of water. Academic Press, New York. 1971.
19. A. J. ELLIOT, F. WILKINSON, and D. A. ARMSTRONG. Int. J. Radiat. Biol. **38**, 1 (1980).
20. R. H. SCHULER, L. K. PATTERSON, and E. JANATA. J. Phys. Chem. **84**, 2089 1980.
21. Z. D. DRAGANIĆ and I. G. DRAGANIĆ. J. Phys. Chem. **75**, 3950 (1971); **77**, 765 (1973).
22. A. J. ELLIOT, A. S. SIMSONS, and F. C. SOPCHYSHYN. To be published.
23. A. J. ELLIOT, R. AHMAD, L. MCINTOSH, D. BURKE, K. J. STEVENSON, and D. A. ARMSTRONG. *In* Flavins and flavoproteins. *Edited by* V. Massey and C. H. Williams, Jr. Elsevier, New York. 1982. p. 533.
24. E. J. LAND and A. J. SWALLOW. Biochemistry, **8**, 2117 (1969).
25. A. EHRENBERG, F. MÜLLER, and P. HEMMERICH. Eur. J. Biochem **2**, 286 (1967).
26. L.-S.L. YEH and L. L. INGRAM. *In* Flavins and flavoproteins. *Edited by* T. P. Singer. Elsevier, Amsterdam. 1976. p. 765.
27. K.-O. HILLER and K.-D. ASMUS. Int. J. Radiat. Biol. **40**, 583 (1981).
28. W. K. MUSKER, A. S. HIRSCHON, and J. T. DOI. J. Am. Chem. Soc. **100**, 7754 (1978).

Can. J. Chem. Downloaded from www.nrcresearchpress.com by 210.87.254.40 on 09/06/12
For personal use only.

Chemical behavior of an α-azidosulfide, and the related sulfoxide and sulfone, in the tetrahydrothiophene series[1,2]

IAN W. J. STILL,[3] WILLIAM L. BROWN,[4] ROBIN J. COLVILLE,[4] AND GERALD W. KUTNEY

J. Tuzo Wilson Research Laboratories and Department of Chemistry, University of Toronto, Mississauga, Ont., Canada L5L 1C6

Received July 15, 1983

IAN W. J. STILL, WILLIAM L. BROWN, ROBIN J. COLVILLE, and GERALD W. KUTNEY. Can. J. Chem. **62**, 586 (1984).

The thermal, photochemical, base-catalyzed, and Lewis acid-catalyzed reactivity of 2-azidotetrahydrothiophene (**1***a*) and the related α-azidosulfoxide and sulfone have been found to lead to a number of interesting rearrangement products. The ^{13}C nmr data for these compounds are also reported and discussed and the results of attempted deoxygenation of the α-azidosulfoxide **1***b* with a variety of reagents are compared.

IAN W. J. STILL, WILLIAM L. BROWN, ROBIN J. COLVILLE et GERALD W. KUTNEY. Can. J. Chem. **62**, 586 (1984).

On a trouvé que les réactions thermique et photochimique de l'azido-2 tétrahydrothiophène (**1***a*) et des α-azido-sulfoxyde et sulfone correspondants ainsi que leurs réactions catalysées par les bases ou par les acides de Lewis conduisent à un certain nombre de produits de transposition intéressants. On rapporte aussi des données de la rmn du ^{13}C relatives à ces composés et on les discute; on compare les résultats obtenus lors de divers essais effectués en vue de désoxygéner l'α-azido-sulfoxyde **1***b* à l'aide de divers réactifs.

[Traduit par le journal]

Can. J. Chem. Downloaded from www.nrcresearchpress.com by 210.87.254.40 on 09/06/12
For personal use only.

Introduction

The stimulus for the work described below arose from our own earlier work with organic azides (1, 2). In addition, successful attempts to trap nitrene intermediates using divalent sulfur compounds (3, 4) and the first reports of the preparation of the α-azidosulfide class of compounds by Böhme *et al.* (5, 6) combined to induce us to embark upon a detailed study of the thermal, photochemical, and acid- and base-catalyzed reactions of 2-azidotetrahydrothiophene (**1***a*) and its related sulfoxide (**1***b*) and sulfone (**1***c*), the results of which are described below. Since this study was initiated interesting reports on some aspects of this relatively new type of bifunctional organosulfur compound have appeared from two sets of authors. Trost *et al.* have studied the effects of Lewis acids upon α-azidosulfides (7) and, more recently, the potential synthetic utility of phenylthiomethyl azide as a synthon for NH_2^+ (8). Jarvis *et al.* have reported on the thermal (9) and base-catalyzed (10) decomposition reactions of α-azidosulfides, sulfoxides, and sulfones.

Results and discussion

The syntheses of 2-azidotetrahydrothiophene (**1***a*) and its 1-oxide (**1***b*) and 1,1-dioxide (**1***c*) analogs were generally unremarkable and were carried out as outlined in Scheme 1. The replacement of chloride by azide ion is considerably facilitated by the use of a quaternary ammonium salt as a phase-transfer catalyst. In order to produce **1***b* or **1***c* in reasonable yields, oxidation must be carried out *subsequent* to the introduction of the azide group. The ^1H nmr and ^{13}C nmr data for each compound are listed in Table 1, along with the corresponding data for the related 2-azido-4-thiochromanone 1-oxide (**2***b*) and 2-azido-4-thiochromanone 1,1-dioxide (**2***c*)[5] prepared by us earlier (1, 2), for comparison. From the data in Table 1, while

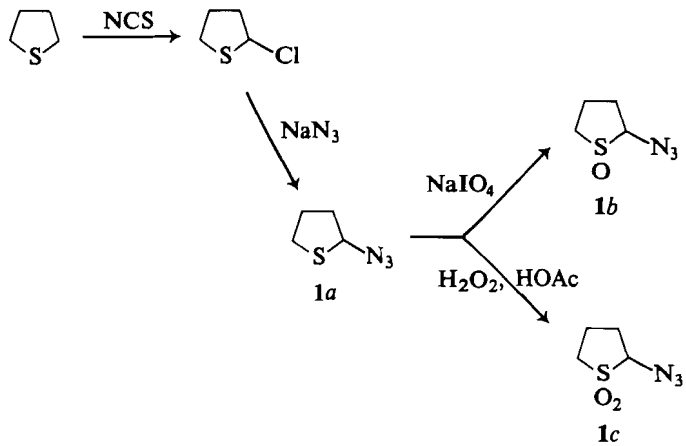

SCHEME 1

it appears that the substituent chemical shift (S.C.S.) effects for the N_3 group are somewhat conformation dependent, the α-effect produces deshielding ranging between 23–39 ppm, with the high value of +39 being observed only for one α-azidosulfide (**1***a*), most values falling in the range 23–29 ppm. The β-effect of the N_3 group is also deshielding, but this time typically in a relatively narrow range from ~5–8 ppm. The γ-effect observed for N_3, in contrast, is small and shielding in nature, ranging from −2.3 to −4.0 ppm. This pattern of S.C.S. effects is reminiscent of that noted by us for the phenyl group in an earlier study (11), at least in so far as the α- and β-deshielding effects are concerned, although the α-effect is not as great for phenyl (~14–18 ppm). Further data are clearly needed before more detailed conclusions can be drawn, but Table 1 provides useful qualitative insight into the S.C.S. effects of the previously little studied azide group.

Attempts were also made to synthesize 2-cyanotetrahydrothiophene **3** as another suitable model for the ^{13}C nmr study. Reaction of 2-chlorotetrahydrothiophene with cyanide ion, however, under conditions similar to those used for the preparation of the azide, always seemed to give **3** contaminated by 2,3-dihydro-4-(2-thiolanyl)thiophene **4**. Presumably this known compound (12) arises as a result of partial dehydrochlorination of the chloro compound in the presence of the

[1] Presented in part at the 65th Annual Conference of the C.I.C., Toronto, Ontario, May 30 – June 2, 1982.

[2] Taken in part from the M.Sc. Thesis of G.W.K., University of Toronto, 1978.

[3] Author to whom all correspondence should be addressed.

[4] Undergraduate research participant.

[5] 2-Azido-4-thiochromanone (**2***a*) appears to be unstable (2).

TABLE 1. ^{13}C nuclear magnetic resonance chemical shift data for **1***a–c*, **2***b*, *c*, and related model compounds[a]

Compound	C-2	C-3	C-4	C-5
1*a*	70.4	38.9	28.4	32.6
1*b*	83.8	30.6	24.3	52.0
1*c*	74.4	28.0	18.8	48.8
	31.4	31.2	31.2	31.4[b]
	51.5	22.8	22.8	51.5[b]
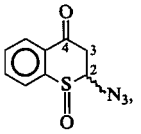 **2***b*	(*trans*) 76.3 (*cis*) 72.7	37.7 38.1	189.2 189.6	[c] —
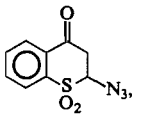 **2***c*	73.8	42.4	187.4	—
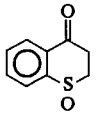	47.1	30.7	191.9[d]	—
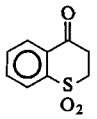	49.3	36.8	190.1[d]	—

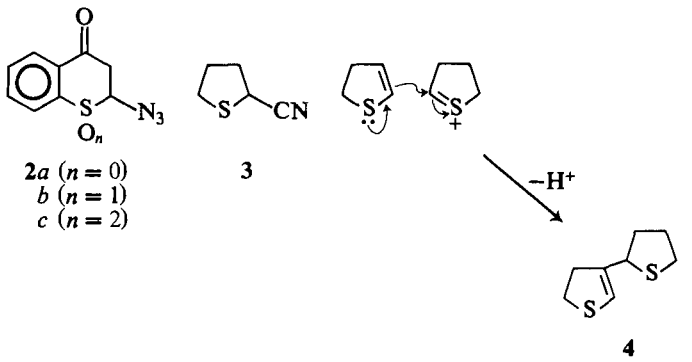

2*a* (*n* = 0)
b (*n* = 1)
c (*n* = 2)

3 **4**

SCHEME 2

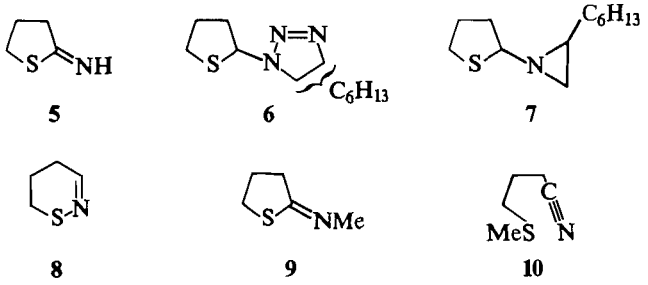

5 **6** **7**

8 **9** **10**

SCHEME 3

more basic cyanide ion, followed by dimerization, as shown in Scheme 2.

Turning to the reactivity of the azido derivatives **1***a–c*, it has been found that the thermal decomposition of 2-azidotetrahydrothiophene **1***a* at 130°C, in the absence of solvent, afforded a product with a strong ir band at 1610 cm^{-1}, characterized as tetrahydrothiophen-2-imine **5**, in 4% yield, accompanied by material of higher molecular weight. Better yields of the imine (21–25%) were obtained when the thermal reaction was carried out in refluxing toluene and slightly higher yields (25–30%) when one equivalent of bromobenzene was present.[6] The reaction presumably involves a [1,2] sigmatropic rearrangement of the initially formed singlet nitrene (13). In a series of attempts to trap the intermediate nitrene, tetrahydrothiophene, 1-butanol, dimethyl acetylenedicarboxylate, and 1-octene were all tried, but only the 1-octene was successful in leading to an identifiable product, presumably the 1-(2-thiolanyl)-2-hexylaziridine **7**, in 22% yield. It is not certain that the formation of **7** requires the intermediacy of a nitrene, since one of the two possible regioisomeric triazolines **6** might first be formed (Scheme 3). Similar thermal decomposition reactions of the somewhat more stable α-azidosulfoxide and sulfone (**1***b, c*) led mainly to recovered starting materials or, at higher temperatures, to uncharacterizable products of higher molecular weight. While these results are somewhat disappointing, it must be borne in mind that the mechanism proposed by Jarvis *et al.* (9) for the decomposition of an α-azidosulfide is probably not available in our system (**1***a*) because of steric constraints. It is also quite likely that the product (**8**) which one would expect from this mechanism would be much less stable than the diaryl-substituted sulfenamide obtained by the earlier

[6] This increase in yield on adding bromobenzene is probably insufficient to conclude that diversion of the mechanistic pathway from a singlet to a triplet manifold is occurring here, via the heavy-atom effect.

Can. J. Chem. Downloaded from www.nrcresearchpress.com by 210.87.254.40 on 09/06/12
For personal use only.

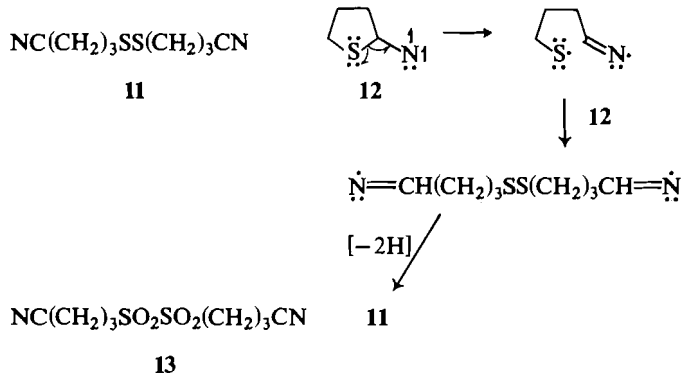

SCHEME 4

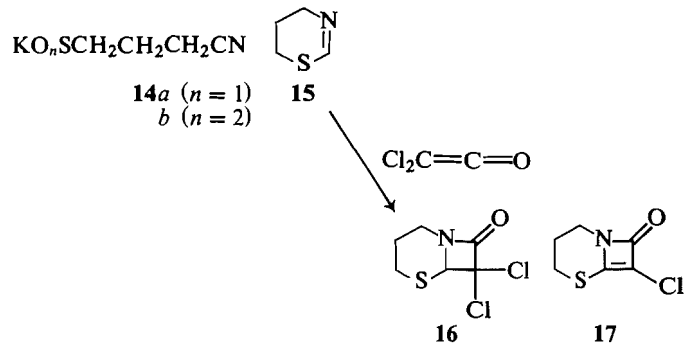

SCHEME 5

workers. Similar comments may apply to the decomposition of **1***b, c*.

Extensive attempts to carry out the base-catalyzed methylation of tetrahydrothiophen-2-imine under a wide variety of conditions have met with little success and neither the expected product of N-methylation **9** nor of S-methylation **10** has been characterized. Some (^{1}H nmr) spectral evidence for C-methylation of **5** was noted under very strongly basic conditions, but as the yields were very low no further work was attempted.

The photochemical decomposition of **1***a* was next carried out. Irradiation in various solvents (including cyclohexane, methanol, and acetonitrile) afforded a liquid product with a strong C≡N band in the ir at 2250 cm^{-1}, eventually characterized by further spectral and elemental analyses, as the previously known 4,4′-dithiodibutanenitrile **11** (14), in yields ranging from 12–26%. Some starting material was usually recovered, even after irradiation for 20 hours. Attempted sensitization of the reaction by the addition of triplet sensitizers such as acetophenone or benzophenone led only to lesser amounts of **11** being formed. At first sight it appears surprising that none of the imine **5** formed in the thermal reaction, nor its open-chain γ-mercaptonitrile tautomer, was observed. To explain this dichotomy we propose that a pathway via the triplet nitrene **12** may be involved (Scheme 4). Again, as was the case for the corresponding thermolyses, the azidosulfoxide and azidosulfone analogs **1***b* and **1***c* were much more stable towards irradiation (in acetonitrile), but mass spectral evidence indicated the formation of the α-disulfone analog **13** in very low (<2%) yield, accompanying large amounts of recovered **1***c*.

The recent work of Jarvis and Nicholas (10) on the base-catalyzed conversion of α-azidosulfides, sulfoxides, and sulfones to nitriles, prompted us to examine the effects of base upon **1***a–c*. Jarvis has noted that the utility of this procedure is limited by the fact that many nitriles may not be stable under the basic conditions used. Exposure of **1***a* to potassium *tert*-butoxide led only to high molecular weight materials, but comparable treatment of **1***b* and **1***c* with *tert*-butoxide for short periods of time at 0°C led to the isolation of uncrystallizable solid materials, tentatively identified by analogy with the work above as the expected **14***a, b*, in yields of 60 and 68%, respectively. As expected, since the acidity of the methine proton in even **1***c* is significantly less than the corresponding (benzylic) protons in some of Jarvis' compounds, milder bases such as triethylamine were without effect.

Somewhat more interesting results were obtained from attempts to rearrange the azidosulfide **1***a* in the presence of acids. Trost *et al.* (7) have recently shown that cyclic α-azidosulfides, prepared by the novel reaction of a thioketal with iodine azide, can be converted to the corresponding ring-expanded lactams on treatment with trifluoroacetic acid or the corresponding cyclic imino-sulfides with a Lewis acid such as $SnCl_4$. Treatment of **1***a* with trifluoroacetic acid was unfruitful, but with $SnCl_4$ or $TiCl_4$, **1***a* could be converted smoothly to 5,6-dihydro-4*H*-1,3-thiazine **15** in 85–90% yields. Somewhat lower yields were obtained with other Lewis acids such as $AlCl_3$ or BF_3 etherate. The characteristic C-2 proton of **15** is visible at δ 9.85 and other ^{1}H and ^{13}C nmr, as well as mass spectral, data support this assignment. The reaction of **15** with dichloroketene, generated from trichloroacetyl chloride by the improved procedure of Krepski and Hassner (15), was next attempted as a route to the interesting β-lactam system **16**. The initial product, however, appears to undergo unusually facile dehydrochlorination. Attempts to extend this approach to 2-substituted analogs of **15** have so far not met with success.

Another reaction which we were interested in trying was the reduction of 2-azidotetrahydrothiophene 1-oxide **1***b*, given our previous interest in sulfoxide reduction (16–18) and since the effect of the various literature methods available on the azide group has never been explored. Interestingly contrasting results were obtained with the procedures employed. The use of phosphorus pentasulfide (16) proved to be the most effective method for the conversion of **1***b* to **1***a*, in 81% yield, although iodotrimethylsilane (19) also afforded **1***a*, in 60% yield. In sharp contrast, the use of thiophosphoryl bromide (17) or the triphenylphosphine–iodine – sodium iodide procedure of Olah *et al.* (20) led to the rapid destruction of **1***b*. Treatment of **1***b* with the $TiCl_4$–Zn reagent described by Drabowicz and Mikolajczyk (21), even for brief periods, led only to the isolation of 5,6-dihydro-4*H*-1,3-thiazine **15** in 30% yield, presumably by Lewis acid-catalyzed rearrangement of the initially formed α-azidosulfide. A small amount (10%) of **15** also accompanied the deoxygenation of **1***b* to **1***a* (34%) using the trifluoroacetic anhydride – sodium iodide procedure of Drabowicz and Oae (22), and **15** was detectable in very small amount (3%) in the more successful reduction of **1***b* to **1***a* using phosphorus pentasulfide already discussed above. Somewhat surprisingly, no reaction was observed between **1***b* and diazomethane. Perhaps less surprisingly, the attempted reduction of the α-azidosulfone **1***c* on a small scale, using our two-step diazonium salt – sodium borohydride procedure (23), produced a violent decomposition and is not recommended.

In summary, we have shown in our study of the, presumably typical, cyclic α-azidosulfur derivatives **1***a–c* that these interesting bifunctional compounds reveal unusual aspects of chemical reactivity but also maintain in certain reactions the patterns of reactivity expected from simple organosulfur compounds or organic azides.

Can. J. Chem. Downloaded from www.nrcresearchpress.com by 210.87.254.40 on 09/06/12
For personal use only.

Can. J. Chem. Downloaded from www.nrcresearchpress.com by 210.87.254.40 on 09/06/12
For personal use only.

Experimental

Infrared spectra were recorded in chloroform on a Perkin–Elmer 298 grating spectrophotometer and the uv spectra in acetonitrile on a Unicam SP-8000 spectrophotometer. The ^{1}H nmr spectra were obtained on a Varian T-60 or EM-360 spectrometer in $CHCl_3$-*d* solution unless otherwise indicated and the natural abundance ^{13}C nmr spectra on either the Varian XL-200 or CFT-20 instruments, at 32 ± 3°C. Routine (low-resolution) mass spectra were obtained with a Bell and Howell 21-490 spectrometer and the high-resolution data on the AEI-MS 3074 instrument. Column chromatography and tlc (analytical and preparative) were carried out on silica gel supplied by E. Merck (Darmstadt). Elemental analyses were performed by the Scandinavian Microanalytical Laboratory, Box 25 DK2730, Herlev, Denmark. Melting points are uncorrected.

Synthesis of 2-azidotetrahydrothiophene, **1**a

To 2.00 g (22.73 mmol) of tetrahydrothiophene in 30 mL of benzene was added 3.03 g (22.69 mmol) of *N*-chlorosuccinimide, over a 15 min period. The mixture was stirred for a further 30 min, filtered, and the solvent removed *in vacuo*. The resulting 2-chlorotetrahydrothiophene was quickly added to 6.94 g (106.75 mmol) of sodium azide in 30 mL of distilled water containing a few drops of Adogen® 464 (Aldrich, phase transfer reagent). After 21 h of vigorous stirring at 25°C, the aqueous solution was extracted three times with 25 mL of dichloromethane. The organic layers were combined and dried. Column chromatography and elution with carbon tetrachloride – dichloromethane (9:1) yielded 2-azidotetrahydrothiophene (45%) as a yellow liquid, bp 50–52°C/6 Torr; ir ν: 2110(N_3) cm^{-1}; uv λ_{max}: 222 (log ϵ, 2.95) nm; ^{1}H nmr δ: 2.05 (m, 4H), 2.90 (m, 2H), 5.10 (t, 1H, J = 2 Hz) ppm; ms m/z: 101 ($M^+ - N_2$). *Anal.* calcd. for $C_4H_7N_3S$: C 37.19, H 5.46, N 32.53, S 24.82; found: C 37.16, H 5.40, N 32.58, S 24.77.

2-Azidotetrahydrothiophene 1-oxide, **1**b

2-Azidotetrahydrothiophene (1.29 g, 10 mmol) was added to a solution of $NaIO_4$ (2.25 g,10.50 mmol) in 210 mL of water, at 0°C. After stirring for 20 h, the aqueous solution was filtered and extracted thoroughly with chloroform to give a yellow oil which could be crystallized from petroleum ether – dichloromethane as white crystals (1.01 g, 72%), mp 31–31.5°C; ir ν: 2120 (N_3), 1055 (SO) cm^{-1}; uv λ_{max}: 223 (log ϵ, 2.98), 286 (1.80) nm; ^{1}H nmr δ: 2.15 (m, 4H), 2.89 (m, 2H), 4.88 (t, 1H, J = 4 Hz) ppm; ms m/z: 117 ($M^+ - N_2$). *Anal.* calcd. for $C_4H_7N_3OS$: C 33.07, H 4.87, N 28.95, S 22.09; found: C 32.73, H 4.95, N 28.47, S 21.55.

2-Azidotetrahydrothiophene 1,1-dioxide, **1**c

To a solution of **1***a* (2.58 g, 20 mmol) in glacial acetic acid (50 mL) was added a solution of 30% hydrogen peroxide (7.20 g, 60 mmol) in acetic acid (50 mL), dropwise over a period of 45 min. After stirring for 48 h, the reaction mixture was diluted with water and extracted with dichloromethane. Washing of the organic extract (10%Na_2SO_3, $NaHCO_3$, H_2O), drying, and evaporation gave a colorless oil, which could be crystallized from petroleum ether – benzene as a white solid (2.46 g, 85%), mp 36–37°C; ir ν: 2120 (N_3), 1335 and 1115 (SO_2) cm^{-1}; uv λ_{max}: 229 (log ϵ 3.69), 253 (3.48), 283 (3.38) nm; ^{1}H nmr δ: 2.10 (m, 4H), 2.95 (m, 2H), 4.33 (t, 1H, J = 5 Hz) ppm; ms m/z: 133 ($M^+ - N_2$). *Anal.* calcd. for $C_4H_7N_3O_2S$: C 29.81, H 4.38, N 26.07, S 19.89; found: C 29.86, H 4.71, N 25.63, S 20.02.

2-Azidothiochroman-4-one 1-oxide, **2**b

Thiochromone 1-oxide (24) (0.4 g, 2.2 mmol) was dissolved in chloroform (30 mL) and a solution of HN_3 (9 mmol) in chloroform, prepared from sodium azide by the method of Fieser (25), was added slowly with stirring. After stirring 4 h at 25°C, removal of the solvent left a dark residue which was redissolved in chloroform and treated with charcoal to remove the colored impurities. Evaporation of the solvent and recrystallization of the solid residue from hexane – carbon tetrachloride gave **2***b* as yellow crystals (50%), mp 116–118°C. The ir and ms data were similar to those reported previously (2), but the ^{1}H nmr indicated a mixture of *trans* and *cis* isomers in a 60:40 ratio, as estimated from the ratio of the methine protons; δ: 3.1–3.4 (m), 3.5–3.9 (m), 5.18 (dd, J = 3, 6 Hz, *cis*), 5.38 (dd, J = 2, 4 Hz, *trans*), 7.3–8.2 (m) ppm.

2-Azidothiochroman-4-one 1,1-dioxide, **2**c

The preparation and characterization of this compound have been described previously (2).

Thermolysis of **1**a

(a) 2-Azidotetrahydrothiophene (1.50 g, 11.7 mmol) was refluxed for 20 h in degassed toluene under nitrogen, in the presence of bromobenzene (1.83 g, 11.7 mmol). Preparative tlc (hexane–acetone 2:1) afforded tetrahydrothiophene-2-imine **5** (0.72 g, 62%) as a yellow oil; ir ν: 1610 (C=N) cm^{-1}; ^{1}H nmr δ: 2.2 (m, 4H), 3.1 (t, 2H, J = 4 Hz), 7.85 (br s, 1H) ppm; ^{13}C nmr δ: 16.5 (C-4), 26.1 (C-5), 29.4 (C-3), 157.2 (C=NH) ppm; ms m/z: 101 (M^+). *Exact Mass* calcd. for C_4H_7NS: 101.0299; found (high resolution ms): 101.0299.

Attempts to carry out the methylation of **5** using methyl iodide or dimethyl sulfate in the presence of various bases, including potassium carbonate, DBU, sodium hydride, and even LDA, in anhydrous acetone or THF, were unsuccessful.

(b) 2-Azidotetrahydrothiophene (0.50 g, 3.88 mmol) in 100 mL of degassed 1-octene was refluxed under nitrogen for 20 h. Column chromatography yielded the aziridine **7** (0.12 g, 22%); ms m/z: 213 (M^+). *Exact Mass* calcd. for $C_{12}H_{23}NS$: 213.1553; found (high resolution ms): 213.1551.

Photolysis of **1**a *(typical procedure)*

2-Azidotetrahydrothiophene (0.50 g, 3.88 mmol) in 100 mL of degassed acetonitrile was irradiated with a 400-W medium pressure lamp for 20 h. Thick layer chromatography yielded 4,4′-dithiodibutanenitrile **11** (14), (0.10 g, 26%); ir ν: 2250 (CN) cm^{-1}; ^{1}H nmr δ: 1.9–3.75 (m, 12H) ppm. *Exact Mass* calcd. for $C_8H_{12}N_2S_2$: 200.0445; found (high resolution ms): 200.0442. *Anal.* calcd. for $C_8H_{12}N_2S_2$: C 47.97, H 6.04, N 13.98, S 31.95; found: C 47.80, H 6.74, N 13.81, S 31.73.

Similar irradiation of **1***c* produced mainly recovered starting material, along with a small amount (2%) of a compound which appeared from the mass spectrum (m/z = 264) to be **13**.

Base-catalyzed reactions of **1**b *and* **1**c

To a solution of 2-azidotetrahydrothiophene 1-oxide (0.50 g, 3.5 mmol) in 40 mL of dry tetrahydrofuran at 0°C, potassium *tert*-butoxide (0.56 g, 5.0 mmol) was added. After stirring for 30 min under N_2, water (20 mL) was added to quench the reaction. After evaporation to dryness, the product was dissolved in a small amount of water which was re-extracted with dichloromethane. Evaporation of the organic layer gave only starting material (0.20 g, 40%). Evaporation of the aqueous phase afforded a pale brown solid (0.19 g, 60%), which could not be recrystallized; ir (KBr) ν: 2270 (CN) cm^{-1}; ^{1}H nmr (D_2O) δ: 1.85 (m, 2H), 2.35 (m, 4H) ppm.

Reaction of **1***c* under identical conditions afforded a similar, water-soluble, non-crystalline solid (68%), suspected to be **14***b*; ir (KBr) ν: 2280 (CN), 1040, 970 cm^{-1}; ^{1}H nmr (D_2O) δ: 2.0 (m, 2H), 2.5 (m, 4H) ppm.

Lewis acid-catalyzed rearrangement of **1**a*: 5,6-dihydro-4H-1,3-thiazine,* **15**

To a solution of α-azidosulfide **1***a* (0.69 g, 5 mmol) in dry acetonitrile (25 mL), anhydrous stannic chloride (1.42 g, 5.50 mmol) was added slowly under N_2. After stirring 1.5 h a yellow solid appeared, mp 90–95°C (dec.), believed to be the $SnCl_4$ complex of **15**. Upon dissolution in water (200 mL), addition of a few drops of concentrated hydrochloric acid, and stirring for 0.5 h, extraction with dichloromethane, drying, and evaporation afforded a yellow oil (0.46 g, 85%). (Similar results were obtained with $TiCl_4$ as the catalyst.) Spectral data were ^{1}H nmr δ: 2.0 (m, 2H), 2.7 (m, 4H), 9.85 (t, 1H, J = 1 Hz) ppm; ^{13}C nmr (CH_3NO_2-d_3) δ: 15.0 (C-5), 24.4 (C-6), 36.3 (C-4), 118.3 (C-2) ppm; ms m/z: 101 (M^+).

Reaction of **15** *with dichloroketene*

The preparation of trichloroacetyl chloride from the acid and the

activation of the zinc were carried out according to the procedure of Krepski and Hassner (15). To a mixture of compound **15** (0.54 g, 5.4 mmol) and activated zinc (0.69 g, 10.5 mmol) in anhydrous diethyl ether (25 mL), was slowly added a mixture of trichloroacetyl chloride (1.83 g, 10.0 mmol) and phosphorus oxychloride (1.53 g, 10.0 mmol) dissolved in anhydrous ether (10 mL). After refluxing 1 h, work-up according to the literature procedure led to the isolation of a yellow oil (possibly the dehydrochlorination product **17**) in low yield; ^{1}H nmr δ: 2.10 (m, 2H), 2.75 (m, 4H) ppm.

*Reduction of 2-azidotetrahydrothiophene 1-oxide, 1*b

These reactions, the results of which are summarized in the text, were carried out according to the respective literature procedures (16–22).

Acknowledgements

This work has been supported generously by the Natural Sciences and Engineering Research Council of Canada and the J. P. Bickell Foundation. The authors are grateful to Dr. V. A. Sayeed for assistance with the methylation of tetrahydrothiophene-2-imine.

1. I. W. J. Still, M. T. Thomas, and A. M. Clish. Can. J. Chem. **53**, 276 (1975).
2. I. W. J. Still and T. S. Leong. Can. J. Chem. **58**, 369 (1980).
3. W. Ando. Acc. Chem. Res. **10**, 179 (1977).
4. S. E. Carroll, B. Nay, E. F. V. Scriven, H. Suschitzsky, and D. R. Thomas. Tetrahedron Lett. 3175 (1977).
5. H. Böhme and D. Morf. Chem. Ber. **90**, 446 (1957).
6. H. Böhme and F. Ziegler. Justus Liebigs Ann. Chem. 734 (1974).
7. B. M. Trost, M. Vaultier, and M. L. Santiago. J. Am. Chem. Soc. **102**, 7929 (1980).
8. B. M. Trost and W. H. Pearson. J. Am. Chem. Soc. **103**, 2483 (1981).
9. B. B. Jarvis, P. E. Nicholas, and J. O. Midiwo. J. Am. Chem. Soc. **103**, 3878 (1981).
10. B. B. Jarvis and P. E. Nicholas. J. Org. Chem. **45**, 2265 (1980).
11. M. S. Chauhan and I. W. J. Still. Can. J. Chem. **53**, 2880 (1975).
12. J. M. Cox and L. N. Owen. J. Chem. Soc. (C), 1130 (1967).
13. N. J. Turro. Modern molecular photochemistry. Benjamin–Cummings, Menlo Park, CA. 1978. pp. 550 et seq.
14. G. G. Stoner and G. Dougherty. J. Am. Chem. Soc. **63**, 987 (1941).
15. L. R. Krepski and A. Hassner. J. Org. Chem. **43**, 2879 (1978).
16. I. W. J. Still, S. K. Hasan, and K. Turnbull. Can. J. Chem. **56**, 1423 (1978).
17. I. W. J. Still, J. N. Reed, and K. Turnbull. Tetrahedron Lett. 1481 (1979).
18. J. A. M. Kuipers, B. H. M. Lammerink, I. W. J. Still, and B. Zwanenburg. Synthesis, 295 (1981).
19. G. A. Olah, B. G. B. Gupta, and S. C. Narang. Synthesis, 583 (1977).
20. G. A. Olah, B. G. B. Gupta, and S. C. Narang. Synthesis, 137 (1978).
21. J. Drabowicz and M. Mikolajczyk. Synthesis, 138 (1978).
22. J. Drabowicz and S. Oae. Synthesis, 404 (1977).
23. I. W. J. Still and S. Szilagyi. Synth. Commun. **9**, 923 (1979).
24. I. W. J. Still, P. C. Arora, and S. N. Sokolowsky. Org. Prep. Proced. Int. **7**, 159 (1975).
25. L. F. Fieser. Reagents for organic synthesis. Vol. 1. Wiley, New York, NY. 1967. p. 446.
26. L. F. Johnson and W. C. Jankowski. Carbon-13 nmr spectra. Wiley–Interscience, New York, NY. 1972. pp. 77–78.

Can. J. Chem. Downloaded from www.nrcresearchpress.com by 210.87.254.40 on 09/06/12
For personal use only.

A ^{19}F, ^{119}Sn nuclear magnetic resonance and ^{119}Sn Mössbauer study of the SnF_2-MF-H_2O system

THOMAS BIRCHALL[1] AND GEORGES DÉNÈS
Department of Chemistry, McMaster University, Hamilton, Ont., Canada L8S 4M1

Received October 20, 1983

THOMAS BIRCHALL and GEORGES DÉNÈS. Can. J. Chem. **62**, 591 (1984).

^{19}F and ^{119}Sn nmr spectroscopy has been used to study the SnF_2-MF-H_2O (M = Li^+, Na^+, K^+, Rb^+, Cs^+, and $[NH_4]^+$) system. The nmr data have been supplemented by frozen solution ^{119}Sn Mössbauer measurements. The evidence suggests that the dominant species in the SnF_2-H_2O system is a hydrated stannous fluoride, probably $SnF_2 \cdot H_2O$ having Mössbauer parameters of δ = 3.46 mm s^{-1} and Δ = 1.70 mm s^{-1}. When F^- is added to these solutions rapid F^- exchange occurs with the hydrated SnF_2 and the dominant species becomes $[SnF_3]^-$. The ^{119}Sn nmr chemical shift of $[SnF_3]^-$ is ~ -700 ppm from $(CH_3)_4Sn$. The ^{119}Sn Mössbauer parameters for frozen solutions of $[SnF_3]^-$ are $\delta = \sim 3.1$ mm s^{-1}, Δ = 1.9 mm s^{-1}. These spectroscopic data are cation dependent. We could find no strong evidence for high concentrations of $[Sn_2F_5]^-$ in any of these solutions.

THOMAS BIRCHALL et GEORGES DÉNÈS. Can. J. Chem. **62**, 591 (1984).

L'étude du système SnF_2-MF-H_2O (M = Li^+, Na^+, K^+, Rb^+, Cs^+ et $[NH_4]^+$) a été entreprise à l'aide de la rmn ^{19}F et ^{119}Sn ainsi que par spectroscopie Mössbauer ^{119}Sn sur des solutions gelées. Il est suggéré que l'espèce prédominante dans le système SnF_2-H_2O est un hydrate du fluorure stanneux, probablement $SnF_2 \cdot H_2O$ ayant les paramètres Mössbauer suivants: δ = 3,46 mm^{-1} et Δ = 1,70 mm s^{-1}. L'addition d'ions F^- à ces solutions entraîne un échange rapide du fluor entre ions F^- et SnF_2 hydraté, l'espèce prédominante en solution étant maintenant $[SnF_3]^-$. Le déplacement chimique de $[SnF_3]^-$ en rmn ^{119}Sn est ~ -700 ppm par rapport à $(CH_3)_4Sn$. Les paramètres Mössbauer ^{119}Sn pour les solutions gelées de $[SnF_3]^-$ sont $\delta = \sim 3,1$ mm s^{-1} et Δ = 1,9 mm s^{-1}. Les résultats spectroscopiques montrent une certaine variation avec la nature du cation. Il n'a pas éte observé d'évidence pour l'existence de fortes concentrations en $[Sn_2F_5]^-$ dans aucune de ces solutions.

Introduction

The structure of α-stannous fluoride is now well established (1, 2) and consists of cyclic tetramers of SnF_2. In this structure there are two different tin environments which may be represented as SnF_3E and SnF_5E, where E represents a non-bonding electron pair and only one F, on each tin, is of the terminal type, the others being bridging fluorines. The ^{119}Sn Mössbauer spectrum of α-SnF_2, the monoclinic form, has been reported by several researchers (3–5) with some variation in the parameters reported by the various groups. Stannous fluoride forms salts of the general type, $M[Sn_2F_5]$ and $M[SnF_3]$ with alkali metal fluorides, (6, 7) but $Na_4[Sn_3F_{10}]$ has also been characterized (8). The X-ray crystal structure of $Na[Sn_2F_5]$ has been reported (9) and consists of $[Sn_2F_5]^-$ units in which each tin has three close fluorines, one of them bridging the two tin atoms to give a distorted tetrahedral environment to the Sn(II) and the non-bonding 5*s* electron pair occupying the fourth coordination site. Weaker fluorine bridges link the $[Sn_2F_5]^-$ units into a polymeric chain. For the $M[SnF_3]$ composition the X-ray crystal structures of $[NH_4][SnF_3]$ (10, 11) and $K[SnF_3] \cdot 0.5H_2O$ (12) have been reported. In $[NH_4][SnF_3]$ there are isolated $[SnF_3]^-$ ions while $K[SnF_3] \cdot 0.5H_2O$ consists of infinite chains of $[SnF_4]^{2-}$ pyramids connected at corners. In both cases the non-bonding electron pair is stereochemically active and occupies the vacant site of each polyhedron. ^{119}Sn Mössbauer spectra for both series of solids, $M[Sn_2F_5]$ and $M[SnF_3]$, have been reported (13) and interpreted in terms of the geometries discussed above. The Mössbauer parameters for the two series are not very different but the trends in each series appear to be cation dependent.

The salts of $[Sn_2F_5]^-$ and $[SnF_3]^-$ were prepared from aqueous solution and while evidence for the existence of these anions in solution has been presented (14, 15) only one frozen solution Mössbauer study has been reported for Sn^{2+} in $HF-H_2O$ (16). Since the nmr and Mössbauer methods can provide unique information about the degree of Sn–ligand interaction we decided to examine the $MF-SnF_2-H_2O$ system using ^{19}F and ^{119}Sn nmr and ^{119}Sn Mössbauer spectroscopy in the hope that we could further quantify the evidence for the $[Sn_2F_5]^-$ and $[SnF_3]^-$ ions in aqueous solution, and to see what evidence, if any, there was for species such as $SnF_2 \cdot H_2O$. The results presented below appear to confirm the earlier results for the existence of $[SnF_3]^-$ but that of $[Sn_2F_5]^-$ appears more doubtful. There is clearly rapid exchange of F^- occurring in these solution and equilibria of the type [1] and [2] undoubtedly exist. Rapid exchange of F^-

$$[1] \quad [SnF_3]^- + H_2O \rightleftarrows SnF_2 \cdot H_2O + F^-$$

$$[2] \quad [Sn_2F_5]^- + H_2O \rightleftarrows [SnF_3]^- + SnF_2 \cdot H_2O$$

with $[SnF_3]^-$ and $[GeF_3]^-$ in aqueous solution has already been reported by Meutterties using ^{19}F nmr techniques (17). Similar results have recently been published for SnF_2 in donor solvents such as DMSO and HMPA (18). The concentration of $[Sn_2F_5]^-$ present at any one time could be quite low and the isolation of $M[Sn_2F_5]$ salts from aqueous solution could occur only because it is the least soluble.

Experimental

The α-SnF_2, monoclinic form, was used as supplied by O.S.I.; ^{119}Sn Mössbauer spectra show that this contains a small amount of Sn(IV) impurity. The alkali metal fluorides were supplied by Ventron Corpn. Mössbauer spectra were recorded with a Promeda multichannel analyzer and ancilliary equipment which has already been described (19). The Mössbauer source, $Ca^{119m}SnO_3$ supplied by Spire Corporation, was maintained at room temperature for all measurements while the samples were quenched in liquid nitrogen and then transferred to an Air Products Heli-Trans system precooled to 80 K. Periodic checks were made on the frozen samples to ensure that no crystallization of the tin fluoride salts had occurred. Spectra were fitted using the computer program of Ruebenbauer and Birchall (20). The spectra were referenced against a standard $CaSnO_3$ absorber and

[1] To whom all correspondence should be addressed.

Can. J. Chem. Downloaded from www.nrcresearchpress.com by 210.87.254.5 on 09/06/12
For personal use only.

TABLE 1. ^{119}Sn Mössbauer data of frozen aqueous solutions of the SnF_2–MF system

Composition*	Concentration	δ (mm s^{-1})	Δ (mm s^{-1})	Γ (mm s^{-1})		χ^2/d.f.†
SnF_2	Solid (α-phase)	3.461(4)	1.546(4)	0.98(2)	0.91(1)	0.862
	1 M	3.464(6)	1.688(6)	1.24(3)	1.05(3)	0.903
	0.5 *M*‡	3.517(7)	1.703(6)	1.34(3)	1.18(3)	1.053
	0.5 *M*§	3.544(6)	1.705(6)	1.40(3)	1.14(2)	1.060
$NH_4Sn_2F_5$	0.50 *M*	3.251(5)	1.934(5)	1.34(3)	1.25(4)	1.485
	1.00 *M*	3.23(1)	1.91(1)	1.11(7)	1.29(10)	0.698
NH_4SnF_3	0.20 *M*	3.42(2)	1.83(2)	1.67(12)	1.57(16)	0.878
	1.00 *M*	3.267(5)	1.893(5)	1.12(3)	1.11(3)	0.763
$LiSn_4F_9$	1.00 *M*	3.464(6)	1.763(2)	1.28(4)	1.53(3)	0.939
$LiSn_2F_5$	1.00 *M*	3.445(7)	1.760(10)	1.30(4)	1.18(4)	1.196
$LiSnF_3$	1.00 *M*	3.410(6)	1.766(10)	1.17(4)	1.05(4)	0.921
$NaSn_4F_9$	1.00 *M*	3.437(4)	1.820(6)	1.52(5)	1.22(2)	0.963
$NaSn_2F_5$	0.82 *M*	3.343(3)	1.869(5)	1.28(2)	1.22(2)	1.263
$NaSnF_3$	1.50 *M*	3.183(3)	1.941(3)	1.22(1)	1.14(2)	1.206
$Na_4Sn_3F_{10}$	1.23 *M*	3.149(6)	1.994(8)	1.52(3)	1.52(4)	1.014
Na_2SnF_4	1.00 *M*	3.027(4)	1.955(6)	1.26(2)	1.23(3)	1.071
Na_6SnF_8	0.56 *M*	3.065(6)	1.936(9)	1.15(4)	1.14(4)	0.963
KSn_4F_9	0.10 *M*	3.40(1)	1.74(2)	1.48(3)	1.02(8)	0.928
KSn_2F_5	0.10 *M*	3.274(6)	2.005(2)	1.11(4)	1.08(4)	1.058
$KSnF_3$	0.10 *M*	3.163(6)	1.928(9)	1.08(3)	1.14(4)	0.993
$K_{3.64}SnF_{5.64}$	0.10 *M*	3.062(6)	1.767(8)	1.04(3)	1.06(4)	0.885
$K_{7.29}SnF_{9.29}$	0.10 *M*	3.067(5)	1.838(7)	1.01(3)	1.08(3)	0.986
$RbSn_4F_9$	1.00 *M*	3.338(8)	1.89(1)	1.34(5)	1.13(4)	0.892
$RbSn_2F_5$	1.00 *M*	3.275(8)	1.996(8)	1.16(3)	1.04(4)	0.884
$RbSnF_3$	1.00 *M*	3.182(9)	1.951(9)	1.29(4)	1.19(4)	0.971
Rb_6SnF_8	0.50 *M*	3.02(3)	1.79(3)	0.99(10)	1.03(11)	1.079
$CsSn_4F_9$	1.00 *M*	3.34(1)	1.835(10)	1.65(4)	1.35(4)	1.058
$CsSn_2F_5$	1.00 *M*	3.149(6)	1.962(8)	1.56(4)	1.39(4)	1.060
$CsSnF_3$	1.00 *M*	3.118(5)	1.97(2)	1.27(6)	1.23(6)	2.87
Cs_6SnF_8	0.50 *M*	3.09(2)	1.94(2)	0.88(6)	0.97(7)	1.043

* Composition refers to the atomic ratios of the alkali metal, tin, and fluorine and is not meant to imply that these compounds exist in solution.

† χ^2/d.f. = chi-squared/number of degrees of freedom.

‡ Contains 2% Sn(IV) impurity.

§ Contains 14% Sn(IV) impurity after standing 48 h.

Can. J. Chem. Downloaded from www.nrcresearchpress.com by 210.87.254.5 on 09/06/12
For personal use only.

calibrated using a ^{57}Co source and a standard iron foil absorber. The concentration of the solutions used for Mössbauer spectroscopy was usually ~1 *M* in Sn except for the potassium salts where a concentration of ~0.1 *M* in Sn was used because of their low solubility. ^{19}F and ^{119}Sn nmr spectra were recorded on a Bruker W.H.90 at 84.669 MHz and 33.545 MHz, respectively. The ^{19}F spectra were referenced against CCl_3F and the ^{119}Sn spectra against $(CH_3)_4Sn$ as zero chemical shift, negative shifts being to higher magnetic field strength.

Results and discussion

The ^{119}Sn Mössbauer data for α-SnF_2 solid and for the frozen aqueous solutions of SnF_2 and MF are given in Table 1. We have shown that a small Sn(IV) impurity is present in the α-SnF_2 used in these studies. A freshly prepared solution of commercial α-SnF_2 in water which has been frozen to 80 K, within ~30 min of dissolution, and its Mössbauer spectrum recorded, shows no growth in intensity of this Sn(IV) component. After this solution had stood for 48 h in air at room temperature and the frozen solution spectrum recorded again the spectrum showed that some augmentation of the Sn(IV) component had occurred (Table 1), indicating that oxidation of Sn(II) to Sn(IV) had taken place. It is clear that this process is not fast as has been claimed (21), and our findings corroborate those of Muetterties (17) who also found this process to be slow.

On dissolution in water there is a small increase in the isomer shift and a significant increase in the quadrupole splitting, indicating a small increase in *s* electron density at tin while at the same time a more asymmetric tin environment is produced. This suggests that the cyclic tetrameric α-SnF_2 structure has been disrupted perhaps to give $SnF_2 \cdot H_2O$ with the oxygen coordinated to the tin to maintain the pyramidal geometry. Addition of MF ($M = NH_4^+, Li^+, Na^+, K^+, Rb^+, Cs^+$) to these solutions results in a decrease in isomer shift and an increase in

Can. J. Chem. Downloaded from www.nrcresearchpress.com by 210.87.254.5 on 09/06/12
For personal use only.

quadrupole splitting. These changes indicate a greater involvement of the Sn(II) 5*s* electrons in the bonding between the tin and the ligands surrounding it. If the species in solution prior to the addition of MF was indeed $SnF_2 \cdot H_2O$, we assume that the water molecule is displaced by the F^- added. These changes are progressive as the amount of MF is increased but appear to reach more or less constant values for each alkali metal or ammonium ion at $MF:SnF_2$ ratio $> 1:1$, i.e., when there is an excess of F^- over the composition of $MSnF_3$. The Mössbauer parameters at this stage are very similar to the data reported for the corresponding solid $M[SnF_3]$ species (13) after allowance is made for the different isomer shift references that have been used. This supports the idea that the $[SnF_3]^-$ anion is the dominant tin species present in these frozen solutions. The solid state data appeared to show a smooth variation in the values of the Mössbauer parameters as the size of the cation was increased and this was interpreted as reflecting the decreasing polarizing power of the cation: in the case of the $[NH_4]^+$ cation the differences were attributed to hydrogen bonding to the $[SnF_3]^-$ anions (13). In the frozen aqueous solutions of composition $M[SnF_3]$ the Mössbauer parameters follow the solid state trends but are of smaller magnitude. For example, from $[NH_4]^+$ to Cs^+ the isomer shift of the $M[SnF_3]$ species decreases by 0.25 mm s^{-1} while the quadrupole splitting decreases by 0.12 mm s^{-1}: the corresponding changes in the frozen aqueous solutions are 0.15 mm s^{-1} and 0.08 mm s^{-1}. These latter changes are barely outside the 3σ standard deviation of errors involved in the measurement. This suggests that the degree of cation–anion interaction in these frozen systems is small. In the $LiF-SnF_2-H_2O$ system the Mössbauer parameters obtained for all compositions are very close to those obtained for frozen solutions of SnF_2 in water (Table 1). This suggests that the tin species present is $SnF_2 \cdot H_2O$ and not $[SnF_3]^-$ or $[Sn_2F_5]^-$. The lithium ion, being strongly polarizing, must form a strong ion pair with the fluoride ion and so prevent the coordination of F^- to SnF_2 to produce the fluorostannate(II) ions. This could be the reason why no solid lithium fluorostannate salts have been obtained from aqueous solutions.

For the composition corresponding to $M[Sn_2F_5]$, similar trends in Mössbauer parameters are also noted with changing cation, that is, the isomer shifts decrease as the cation size increases. Isomer shifts vary by ~0.2 mm s^{-1} while quadrupole splittings change by ~0.1 mm s^{-1}. In view of the fact that all frozen solutions did not have the same concentration of tin, due to solubility problems for some salts, it is difficult to compare these results absolutely. The isomer shifts for the $M[Sn_2F_5]$ composition appear to be slightly more positive that those for the $M[SnF_3]$ composition, particularly for the smaller cations such as $[NH_4]^+$, Na^+, K^+, but the quadrupole splittings for these two compositions are virtually the same. On the basis of Mössbauer spectroscopy it is unlikely that $[SnF_3]^-$ and $[Sn_2F_5]^-$ can be distinguished in these frozen aqueous solutions. This is disappointing, but perhaps not surprising, since the measurements on the pure solid compounds only show isomer shift differences of 0.2 mm s^{-1}. At higher ratios of SnF_2 to MF the Mössbauer parameters approach those for the SnF_2-H_2O frozen solutions, the isomer shift being the most sensitive in this regard. In addition there is a noticeable broadening of the low velocity component of the quadrupole doublet in these cases, indicating the presence of overlapping, unresolvable peaks (Fig. 1). The species present probably are due to $[SnF_3]^-$ and $SnF_2 \cdot H_2O$ with the possibility that $[Sn_2F_5]^-$ is also present, although nmr data presented below seem to eliminate the latter possibility. We attempted to fit these spectra to two overlapping doublets without success.

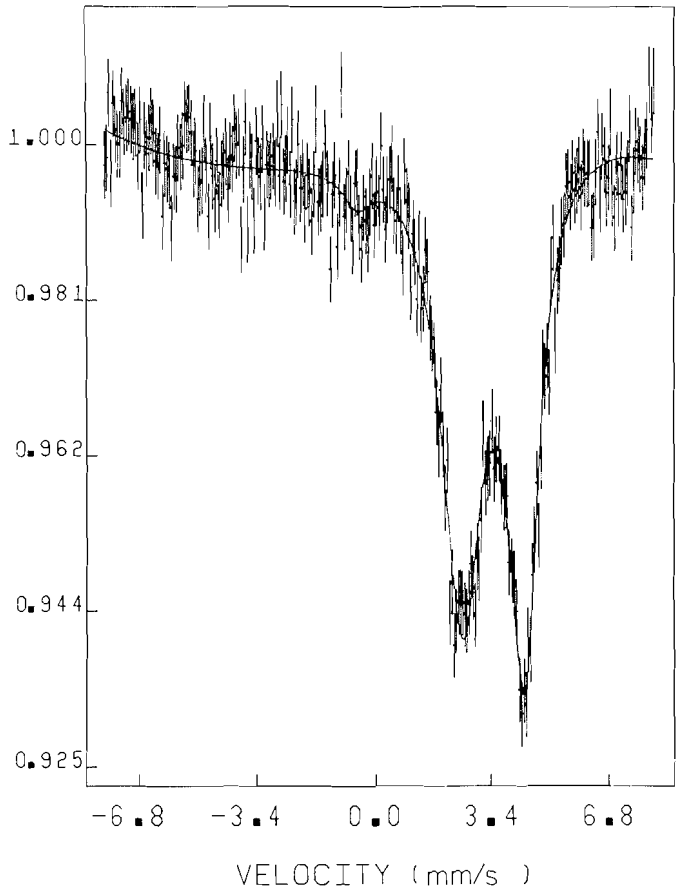

FIG. 1. ^{119}Sn Mössbauer spectrum of a frozen aqueous solution of $K[Sn_4F_9]$ composition at 80 K.

Nuclear magnetic resonance data

In an attempt to obtain further information on the species present in solution, ^{19}F and ^{119}Sn nmr measurements were carried out at ambient temperature. The ^{19}F nmr spectra of solutions of stannous fluoride in water consisted of one major, fairly broad peak (~30 Hz wide) at −80 to −90 ppm from $CFCl_3$, with minor peaks (<5%) at ~−128, −141, −148, and −154 ppm. The nature of these minor components is not clear but they probably arise from the small amount of the Sn(IV) impurity detected by Mössbauer spectroscopy in the SnF_2 used. The main fluorine signal is broad, suggesting that a slow exchange process is taking place. Some of these solutions were cooled to ~−10°C in an attempt to slow down the exchange process but the ~40°C reduction in temperature produced no visible effect on the spectra.

Figure 2 shows a plot of ^{19}F chemical shifts vs. concentration of SnF_2 in water, which is linear from 4 *M* to ~0.5 *M*. At lower concentrations the plot deviates from linearity and extrapolates to a chemical shift of ~−93 ppm at infinite dilution. This value represents the chemical shift of the $SnF_2 \cdot (x + 1)H_2O$ species where at least one of the water molecules is strongly bound to the tin.

Addition of MF to these solutions results in a narrowing of the ^{19}F resonance, which would be expected since an easy mechanism for fluorine exchange is now possible via [3].

[3] $SnF_2 \cdot (x + 1)H_2O + F^- \rightleftarrows [SnF_2F]^- \cdot (x)H_2O + H_2O$

Can. J. Chem. Downloaded from www.nrcresearchpress.com by 210.87.254.5 on 09/06/12
For personal use only.

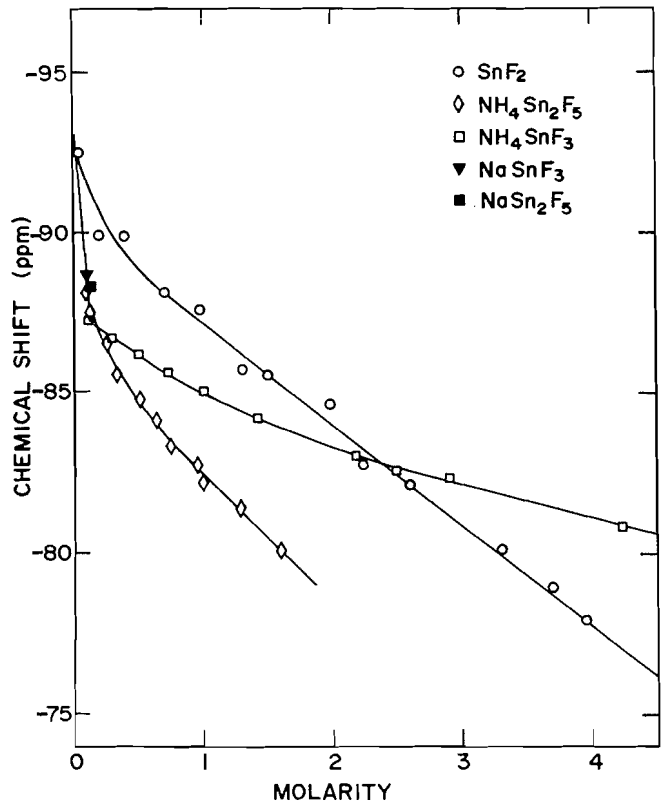

FIG. 2. ^{19}F nmr chemical shift of solutions of SnF_2, $[NH_4][SnF_3]$, $[NH_4][Sn_2F_5]$ vs. concentration.

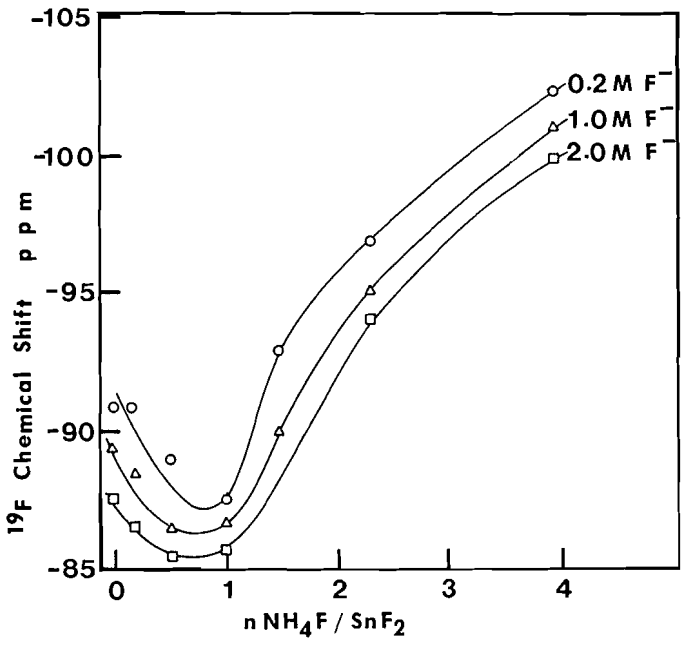

FIG. 3. ^{19}F nmr chemical shift of solutions of SnF_2 vs. amount of $[NH_4]F$, for three constant concentrations in fluoride ion.

No coupling of fluorine to tin is observed, confirming rapid exchange. Plots of ^{19}F chemical shift vs. concentration for solutions of composition $[NH_4][SnF_3]$ and $[NH_4][Sn_2F_5]$ in water are also shown in Fig. 2. These plots are not linear and since ^{19}F exchange is rapid, represent the time-averaged chemical shift of the $[SnF_3]^-$, SnF_2, F^-, and $[Sn_2F_5]^-$, $[SnF_3]^-$, SnF_2,

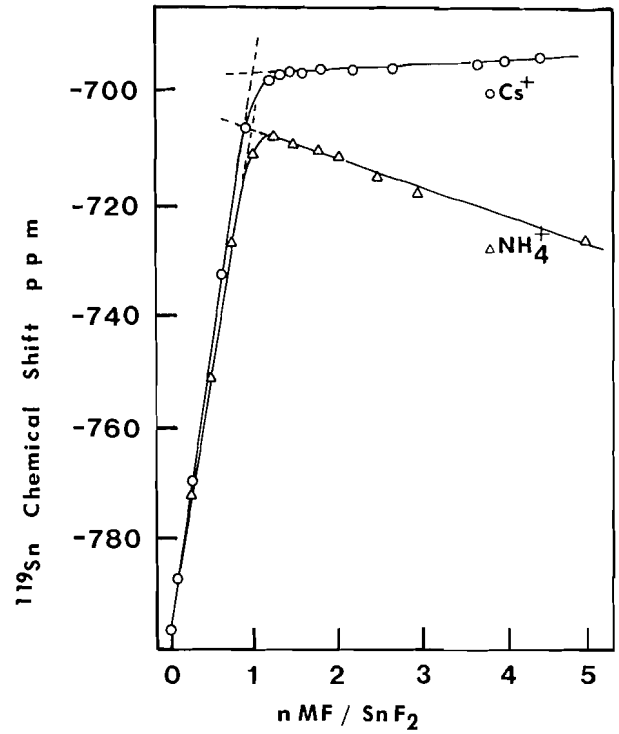

FIG. 4. ^{119}Sn nmr chemical shift of solutions of SnF_2 vs. amount of CsF and $[NH_4]F$, for a constant concentration (2 *M*) in tin.

and F^- for the $[NH_4][SnF_3]$ and $[NH_4][Sn_2F_5]$ solutions as in [3] and [4], respectively,

[4] $[Sn_2F_5]^- \rightleftarrows [SnF_3]^- + SnF_2$

with all Sn—F species presumably also interacting and exchanging with the solvent water molecules. At concentrations less than 0.2 *M* the curves for $[SnF_3]^-$ and $[Sn_2F_5]^-$ appear to merge with the extrapolated value at infinite dilution being ~ -97 ppm. This would suggest complete dissociation of both $[SnF_3]^-$ and $[Sn_2F_5]^-$ into SnF_2 and F^- whose chemical shifts at low concentration are ~93 ppm and ~ -118 ppm, respectively. Increasing the pH of both SnF_2 and $[SnF_3]^-$ solutions above pH = 6 causes the ^{19}F chemical shift to become more negative until at pH 10.7 the resonance has almost reached that of free F^-. Under those conditions hydrated $Sn(OH)_2$ and/or $[Sn(OH)_3]^-$ are probably the dominant tin species with all fluoride ions having been displaced.

Figure 3 shows the effect of added $[NH_4]F$ to solutions containing three different concentrations of SnF_2. As $[NH_4]F$ is increased from zero the ^{19}F chemical shift first decreases and after a 1:1 molar ratio of F^-:SnF_2 is reached there is a steady increase in ^{19}F shifts. For all three SnF_2 concentrations the minimum in the curve occurs close to a 1:1 ratio, this minimum being sharper for the less concentrated solution. These data indicate that $[SnF_3]^-$ is the dominant species at the 1:1 ratio. The more concentrated solution results in a broader, less well-defined minimum, and probably reflects the presence of larger amounts of $[Sn_2F_5]^-$ and an increasing contribution from equilibrium [4].

Equilibria such as [3] and [4], since they affect the ^{19}F chemical shifts, should certainly have an influence on the ^{119}Sn resonance. Dean (22) has noted the large range of ^{119}Sn chemical shifts for compounds of tin(II) and we were therefore hopeful of obtaining evidence for the hydrated SnF_2, $[SnF_3]^-$,

and $[Sn_2F_5]^-$ species. Solutions of SnF_2 (2 *M*) have a linewidth of ~20 Hz and as with the ^{19}F spectra, no $J_{^{119}Sn-^{19}F}$ coupling is observed. Addition of F^- causes a broadening which reaches a maximum of about ~30 Hz, again at a 1:1 mole ratio of $MF:SnF_2$, but excess F^- causes this to decrease as exchange according to [3] becomes more prevalent. The ^{119}Sn chemical shift of a 2 *M* solution of SnF_2 in water is ~−800 ppm from $(CH_3)_4Sn$. As F^- ion is added the resonance shifts to lower field strength, as was observed for the ^{19}F shifts, and reaches a minimum value of ~−700 ppm at the composition $M[SnF_3]$, Fig. 4. The ^{119}Sn chemical shift of the $CsF-SnF_2$ system remains fairly constant once the $Cs[SnF_3]$ composition has been reached, but the shift observed for the $[NH_4]F-SnF_2$ system reaches a lower minimum value and begins to increase again as the amount of $[NH_4]F$ is increased. This may be attributed to a stronger cation–anion interaction in the ammonium ion case via H—F hydrogen bonds. Figure 4 shows an essentially linear relationship between $\delta^{119}Sn$ and MF concentration up to the $M[SnF_3]$ composition with no noticeable break at the $M[Sn_2F_5]$ composition, perhaps indicating that the concentration of $[Sn_2F_5]^-$ is never very significant. This contrasts with the earlier evidence presented by Donaldson and co-workers (14) who suggested that the concentration of $[Sn_2F_5]^-$ anion was appreciable in aqueous solutions of this composition.

Acknowledgements

G.D. thanks the Laboratoire de Chimie Minérale D, LA No. 254, Université de Rennes, France, and the C.N.R.S. for a leave of absence and the C.N.R.S. and the N.R.C. Canada for a research exchange grant. The efficient technical assistance and stimulating nmr discussions of B. G. Sayer is gratefully acknowledged. NSERC is thanked for financial support.

1. R. C. McDonald, H. H.-K. Hau, and K. Eriks. Inorg. Chem. **15**, 762 (1976).
2. G. Dénès, J. Pannetier, J. Lucas, and J. Y. Le Marouille. J. Solid State Chem. **30**, 335 (1979).
3. M. Cordey-Hayes. *In* Chemical applications of Mössbauer spectroscopy. *Edited by* V. I. Goldanskii and R. H. Herber. Academic Press, New York. 1968. p. 317.
4. J. D. Donaldson, R. Oteng, and B. J. Senior. Chem. Commun. 618 (1965).
5. T. Birchall, G. Dénès, K. Ruebenbauer, and J. Pannetier. J. Chem. Soc. Dalton, 1831 (1981).
6. L. L. Abbas, G. Jourdan, C. Avinens, and L. Cot. C. R. Acad. Sci. Paris, **279**C, 307 (1974).
7. A. L. Lavassini, L. Cot, C. Geneys, and C. Avinens. C. R. Acad. Sci. Paris, **280**C, 1211 (1975).
8. G. Bergerhoff and L. Goost. Acta Crystallogr. B**26**, 19 (1970).
9. R. R. McDonald, A. C. Larson, and D. T. Cromer. Acta Crystallogr. **17**, 1104 (1964).
10. G. Bergerhoff and L. Goost. Acta Crystallogr. B**29**, 632 (1973).
11. G. Bergerhoff and N. Namgung. Acta Crystallogr. B**34**, 699 (1978).
12. G. Bergerhoff, L. Goost, and E. Schultze-Rhonhof. Acta Crystallogr. B**24**, 803 (1968).
13. J. D. Donaldson and B. J. Senior. J. Chem. Soc. A, 1798 (1966).
14. J. D. Donaldson and J. D. O'Donoghue. J. Chem. Soc. 271 (1964).
15. J. D. Donaldson, J. D. O'Donoghue, and R. Oteng. J. Chem. Soc. 3876 (1965).
16. H. S. Cheng, C. M. Hsu, Y. C. Chang, and H. W. Wei. Radiochem. Radioanal. Lett. **49**, 167 (1981).
17. E. L. Muetterties. Inorg. Chem. **1**, 342 (1962).
18. H. M. M. Yeh and R. A. Geanangel. Inorg. Chim. Acta, **52**, 113 (1981).
19. T. Birchall and J. P. Johnson. Can. J. Chem. **57**, 160 (1979).
20. K. Ruebenbauer and T. Birchall. Hyperfine Int. **1**, 125 (1979).
21. W. Pugh. J. Chem. Soc. 1934 (1953).
22. P. A. W. Dean. Can. J. Chem. **60**, 2921 (1982).

Can. J. Chem. Downloaded from www.nrcresearchpress.com by 210.87.254.5 on 09/06/12
For personal use only.

The cathodic reduction of PbO in the passive layer on lead in aqueous sulphuric acid

R. G. BARRADAS AND D. S. NADEZHDIN

The Ottawa–Carleton Institute for Graduate Studies and Research in Chemistry, Department of Chemistry, Carleton University, Ottawa, Ont., Canada K1S 5B6

Received August 2, 1983

R. G. BARRADAS and D. S. NADEZHDIN. Can. J. Chem. **62**, 596 (1984).

The cathodic reduction of the lead monoxide layer formed on lead in 30% aqueous H_2SO_4 under anodic oxidation at 0.6 V (vs. $Hg/HgSO_4$ reference electrode) was investigated by linear sweep voltammetry, potential step and admittance measurements. The experimental data were analyzed respectively in terms of thin-layer electrochemistry, electrocrystallisation, and changes of resistance of the PbO layer under reduction. The results seem to be best interpreted from the theory of three-dimensional electrocrystallisation as PbO is reduced to Pb. At sub-zero temperatures the PbO peak observed on our voltammograms and potentiostatic current time transients reveals the splitting of the curves into two peaks, which may be a result of reduction of the same material but of different phases, namely, orthorhombic and tetragonal PbO.

R. G. BARRADAS et D. S. NADEZHDIN. Can. J. Chem. **62**, 596 (1984).

Faisant appel à la voltamétrie à balayage lineaire, au palier de potentiel et aux mesures d'admission, on a étudié la réduction cathodique de la couche de monoxyde de plomb qui se forme sur le plomb en solution aqueuse de H_2SO_4 à 30% sous oxydation anodique à 0,6 V (par rapport à une électrode de référence de $Hg/HgSO_4$). On a analysé les données expérimentales en fonction respectivement de l'électrochimie de la couche mince, de l'électrocristallisation et des variations de la résistance de la couche de PbO lors de la réduction. Les résultats semblent mieux s'interpréter à partir de la théorie de l'électrocristallisation en 3 dimensions lorsque le PbO est réduit en Pb. A des températures sous zéro, le pic de PbO observé sur nos voltamogrammes et le temps provisoire de courant potentiostatique révèlent le dédoublement des courbes en deux pics qui peuvent résulter de la réduction du même produit mais dans des phases différentes soit les PbO orthorhombique et tétragonal.

[Traduit par le journal]

Introduction

It is well established that the passive layer on lead formed under anodic oxidation in a certain potential region between the equilibrium potentials of $Pb/PbSO_4$ and $PbO_2/PbSO_4$ systems consists of an outer porous layer of $PbSO_4$ and an inner layer of lead monoxide (PbO). According to Ruetschi (1), the inner part of the solution in the pores is separated from the bulk of the solution with a semipermeable $PbSO_4$ membrane.

Ruetschi and Angstadt (2) showed that the process of the cathodic reduction of the PbO under galvanostatic conditions is highly irreversible. A number of publications have shown a cathodic peak for PbO on cyclic voltammograms (3–7).

In this paper we wish to report some new experimental data on the cathodic reduction of the PbO layer.

Experimental

The experiments consisted of the anodic passivation of pure lead (99.997% Pb, Cominco of Canada Ltd.) in a 30% solution of H_2SO_4 (Aristar) in triply distilled water at the constant potential of 0.6 V (all potential vs. Hg/Hg_2SO_4, 30% H_2SO_4 reference electrode) followed by cathodic reduction under potential linear sweep at different sweep rates or under potential step conditions. Duration of the passivation and temperature of the solution were varied. The apparent electrode area was 0.040 cm^2. The experimental technique has been described in a previous communication (8).

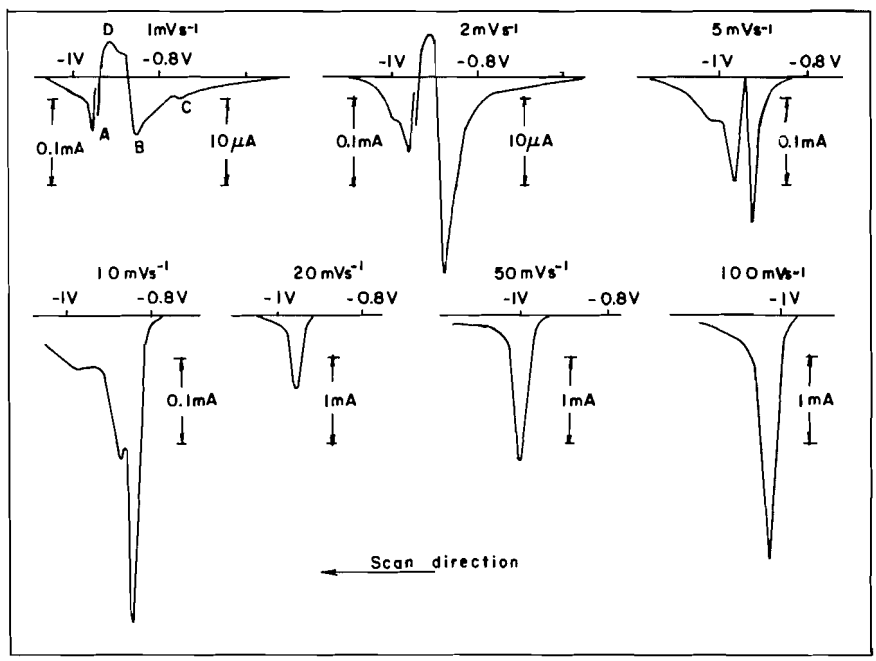

FIG. 1. Cathodic linear sweep voltammogram (LSV) at different scan rates after passivation for 20 min at 0.6 V and 22°C.

Can. J. Chem. Downloaded from www.nrcresearchpress.com by 210.87.254.6 on 09/06/12
For personal use only.

Can. J. Chem. Downloaded from www.nrcresearchpress.com by 210.87.254.6 on 09/06/12
For personal use only.

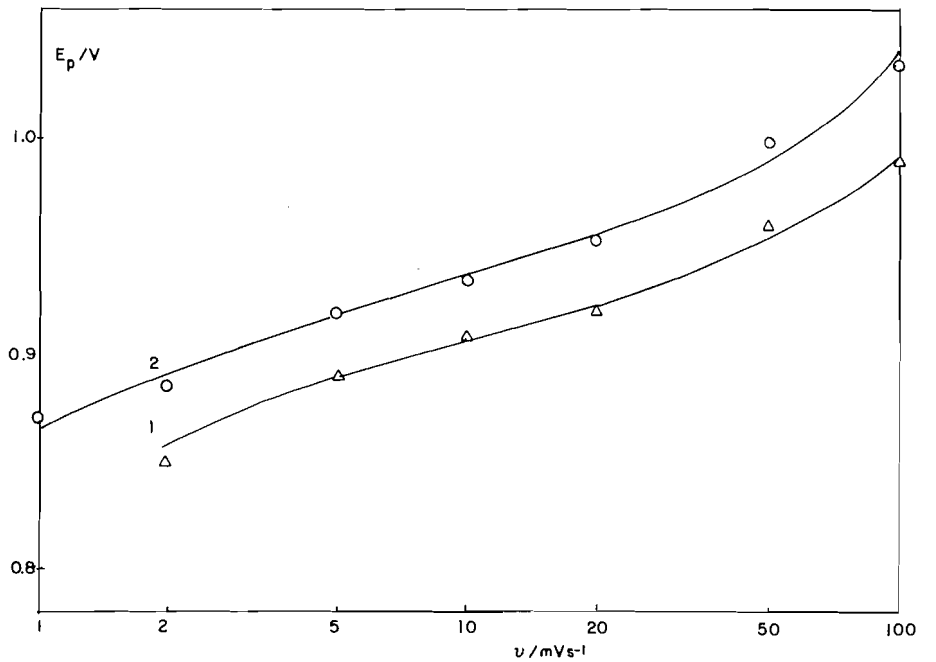

FIG. 2. Dependence of the PbO peak potential on scan rate for the LSV after passivation for 10 (*1*) and 20 (*2*) min.

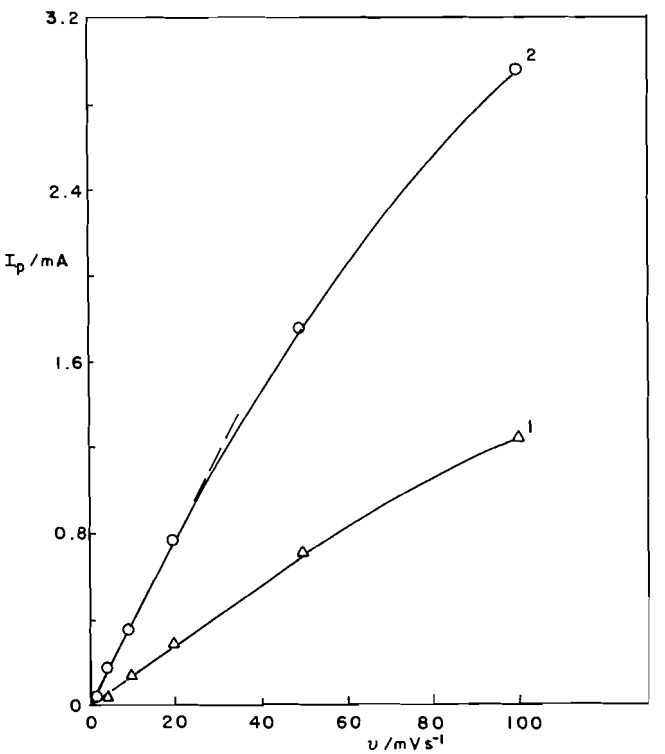

FIG. 3. Dependence of the PbO peak current on scan rate for the LSV after passivation for 10 (*1*) and 20 (*2*) min.

Admittance measurements were carried out at a frequency of 1 kHz and a peak-to-peak amplitude of 11 mV using an EG&G PARC Lock-in-Amplifier, Model 128A, a Hewlett-Packard 3310B Function Generator, and a Hewlett-Packard 7123A Chart Recorder.

Results and discussion

(a) Linear sweep voltammograms

Figure 1 shows cathodic linear sweep voltammograms (LSV) obtained at different sweep rates (from 1 to 100 mV s^{-1}) after passivation for 20 min at 22°C. The LSV at scan rates 1, 2, 5, and 10 mV s^{-1} show two cathodic peaks A and B, which can be related to the reduction of $PbSO_4$ and PbO, respectively (3–7). With increasing scan rate the peak potential (E_p) for peak A has not changed; however, the E_p for peak B has shifted significantly towards more negative potentials. The peak current (I_p) for both peaks A and B has increased, but the increase for peak B is much larger. This peak, whose height is relatively small at a scan rate of 1 mV s^{-1}, has become equal to and significantly larger than peak A at a scan rate of 5 and 10 mV s^{-1}, respectively. At a scan rate of 20 mV s^{-1} peak B has overlapped peak A and a resulting peak has shifted towards negative potentials and its height increased with scan rate from 50 to 100 mV s^{-1}. A small cathodic peak C on the LSV for 1 mV s^{-1} at a potential around −0.75 V will be considered later in context of our experiments at low temperatures. A small anodic excursion D between peaks A and B appears to be similar to that reported by Valeriote and co-workers (4) and is believed to represent re-oxidation of metallic lead formed by reduction of PbO at peak B, volume contraction due to reduction creating pores and thereby exposing such lead to the electrolyte.

Figures 2 and 3 present dependencies of the E_p and I_p for the PbO peak on scan rate (v) for LSV after passivations for 10 and 20 min. Both dependencies have a linear part in the middle region of v, which can be expressed, respectively, as

$$[1] \quad E_p = a - b \cdot \log v$$

and

$$[2] \quad I_p = cv$$

where a, b, and c are constants. The electrochemical reduction of thin oxide films may be described in terms of an analogous mathematical treatment of the theory of thin layer electrochemistry (9), which is consistent with eqs. [1] and [2]. However, detailed calculations based on such a treatment gave

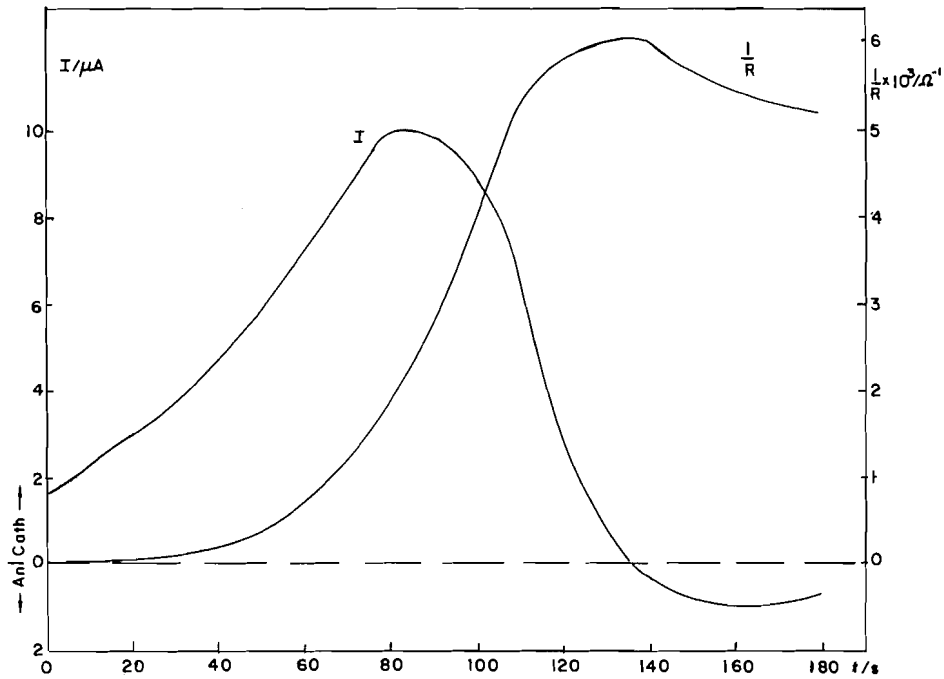

FIG. 4. Current (I) and admittance ($1/R$) transients for the potential step to −0.85 V after passivation at 0.6 V and 22°C for 20 min.

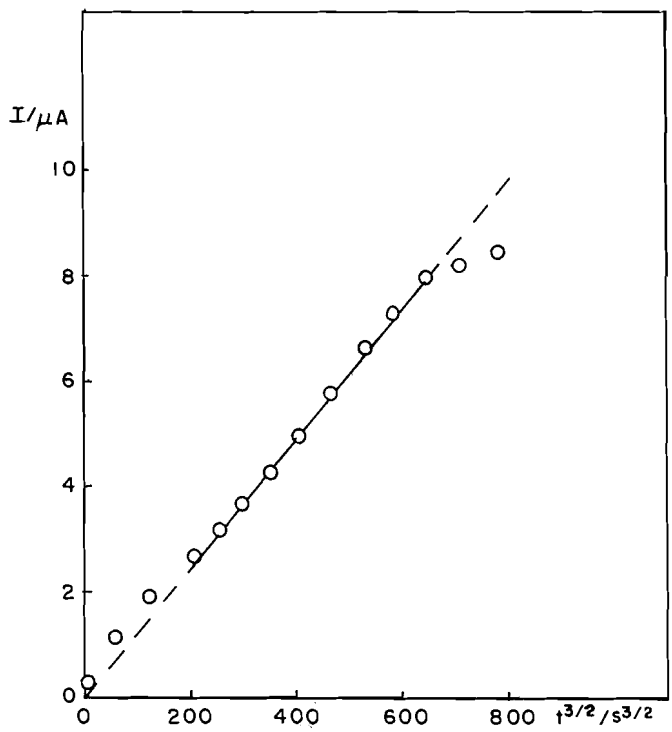

FIG. 5. Plot of the net current vs. $t^{3/2}$ for the ascending branch of the current transient on Fig. 4.

I_p values considerably smaller than the ones obtained experimentally.

(b) Potential step transient

Figure 4 (curve I vs. t) presents a current transient for a potential step from the potential of passivation, 0.6 V (passivation for 20 min at 22°C) to the potential of reduction, −0.85 V. The rising form of the transient permits one to consider the reduction process on the basis of the nucleation and growth model of electrocrystallisation (10). In our case it represents the three-dimensional crystallisation and consequent deposition of metallic lead as the reduction of PbO proceeds to completion.

Figure 5 shows that the dependence of the net current on time for the ascending branch of the transient is

$$[3] \quad I = kt^{3/2}$$

where k is a constant. This is characteristic of the model of progressive nucleation and three-dimensional growth with slow diffusion (10). It is interesting to note that a similar type of transient was reported by Valeriote and Gallop (11) for oxidation of PbO to α-PbO_2 in a passive layer on lead in sulphuric acid. A possible explanation for the positive deviation of the current in the initial portion of the transient could be that the proper diffusion conditions are established with some time lag. At the end of the transient the current becomes anodic (Fig. 4). It corresponds with the aforementioned anodic excursion D on the LSV (Fig. 1).

Figures 6 and 7 present plots of the I_p and E_p vs. $v^{1/2}$ for the PbO peak. The shapes of the curves are similar to those for the I_p and E_p vs. $v^{1/2}$ dependence obtained by a computer simulation of the voltammogram describing the nucleation and growth of a three-dimensional deposit by electrocrystallisation (12).

(c) Admittance measurements

Another reason for the rising potentiostatic transient lies in a decrease of the PbO layer resistance resulting from conversion of the highly resistive PbO into less resistive metallic Pb.

Figure 4 presents direct current and the in-phase component of the electrode admittance transients obtained simultaneously at the potential step to −0.85 V after passivation at 0.6 V. The value of the in-phase component ($1/R$) at the end of passivation lies around $5 \times 10^{-5}\ \Omega^{-1}$. Taking into account the charge passed for layer reduction (Q = ca. 800 μC) and assuming that the PbO layer is uniformly distributed on the electrode area, the value of conductivity of the PbO layer (σ) calculated from

Can. J. Chem. Downloaded from www.nrcresearchpress.com by 210.87.254.6 on 09/06/12
For personal use only.

Can. J. Chem. Downloaded from www.nrcresearchpress.com by 210.87.254.6 on 09/06/12
For personal use only.

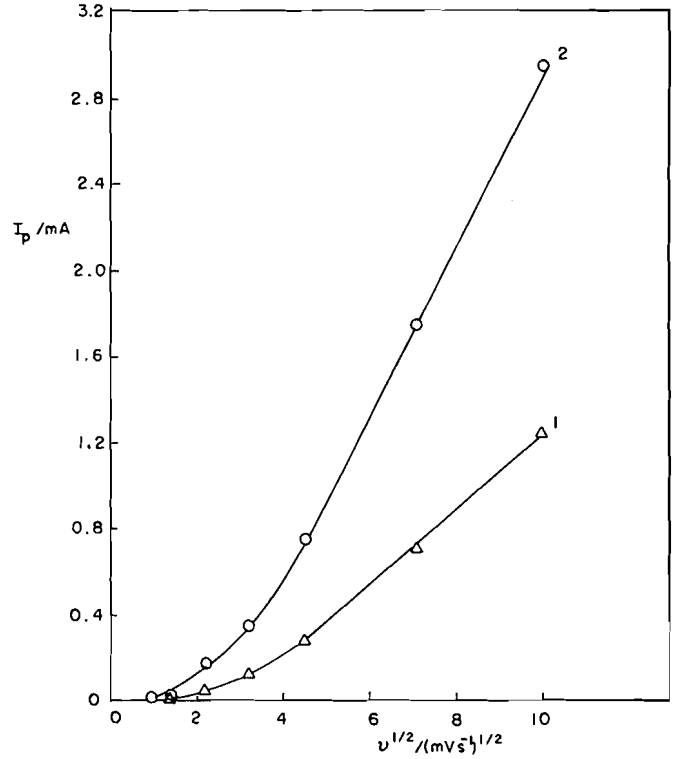

FIG. 6. Plot of the PbO peak current vs. $v^{1/2}$ after passivation for 10 (*1*) and 20 (*2*) min.

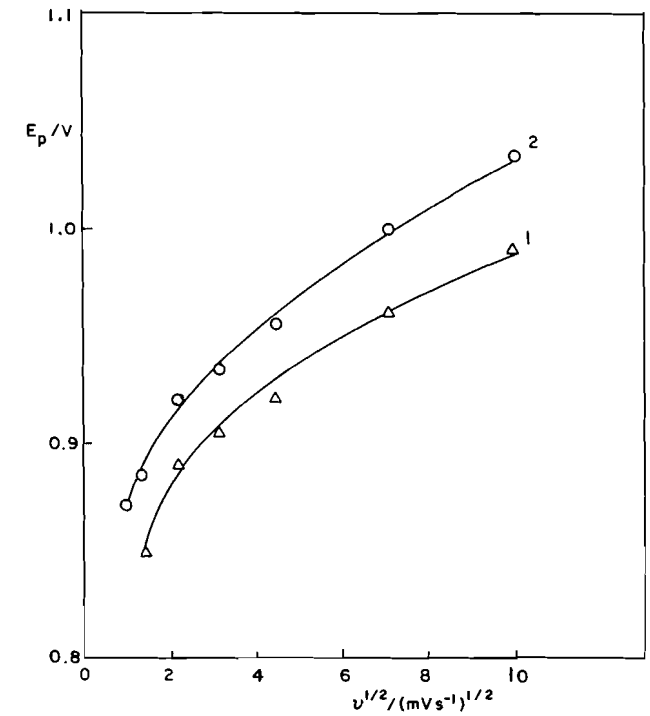

FIG. 7. Plot of the PbO peak potential vs. $v^{1/2}$ after passivation for 10 (*1*) and 20 (*2*) min.

$$[4] \quad \sigma = \frac{M_{PbO}Q}{2Fd_{PbO}A^2}\frac{1}{R}$$

(M_{PbO} = 223; F = 96 500; d_{PbO} = 9.5 g cm^{-3} (13); A = 0.04 cm^2) is equal to 0.3 × 10^{-8} Ω^{-1} cm^{-1}.

Recently, Peter's admittance measurements have estimated

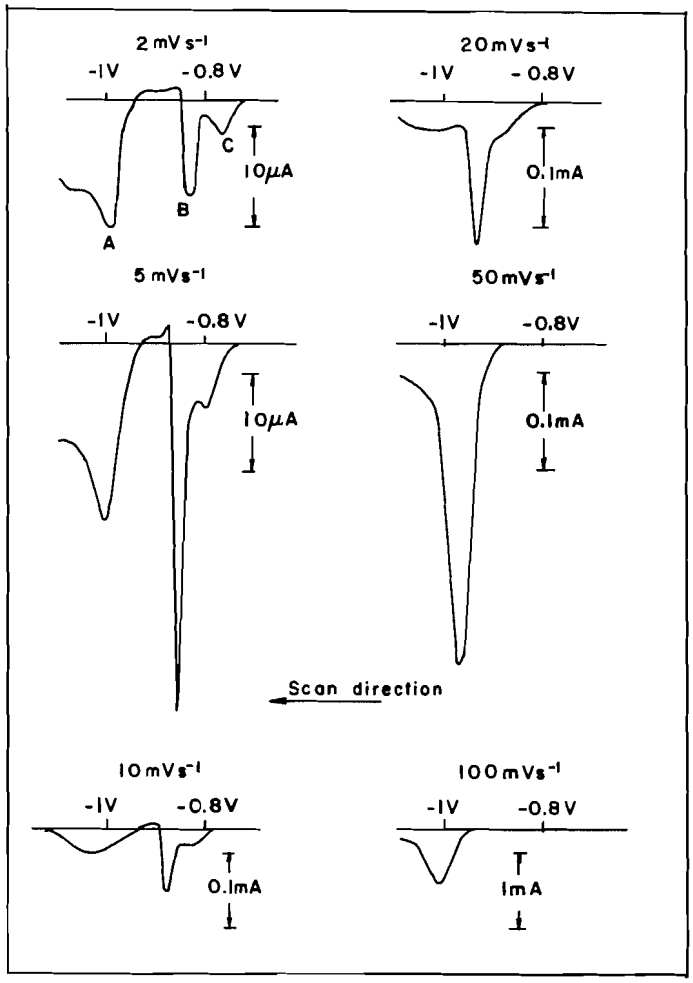

FIG. 8. Cathodic LSV at different scan rates after passivation for 20 min at 0.6 V and −20°C.

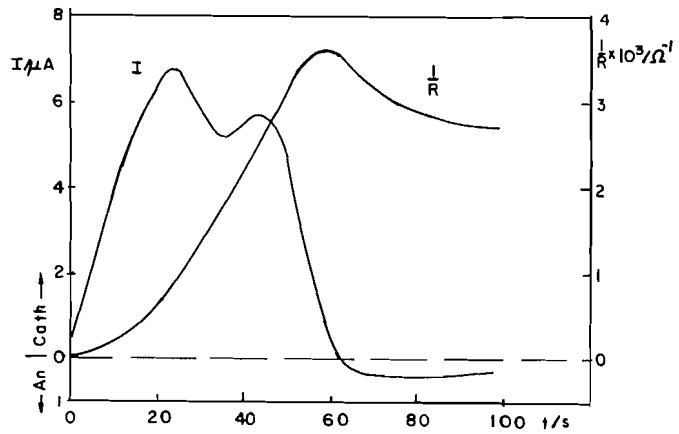

FIG. 9. Current (*I*) and admittance ($1/R$) transients for the potential step to −0.85 V after passivation at 0.6 V and −20°C for 20 min.

the conductivity of a reduced α-PbO_2 film, formed and reduced in aqueous sodium tetraborate, to be lower than 10^{-7} Ω^{-1} cm^{-1} (14).

Using direct current measurements, Laws (15) obtained the value of resistance of ca. 60 kΩ at 20°C for a PbO layer of area 3.1 cm^2 and of thickness 9.6 μm formed by anodic oxidation of lead in H_2SO_4, then removed from the solution and dried. Calculations from Laws' data give the value of conductivity σ

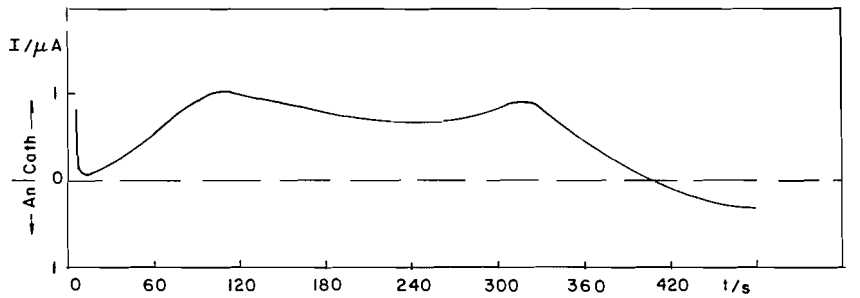

FIG. 10. Current transient for the potential step to −0.75 V after passivation at 0.6 V and −11°C.

of ca. $0.5 \times 10^{-8}\ \Omega^{-1}\ cm^{-1}$, which is close to the σ value found in the present investigation. It suggests that the ohmic resistance of the PbO layer is the major component of the impedance measured.

The conductance transient (Fig. 4, curve $1/R$ vs. t) shows a maximum, which corresponds with the region on the current transient where current changes from cathodic to anodic. This is probably associated with the anodic excursion designated as point D on the LSV (Fig. 1) which represents an oxidation of Pb to $PbSO_4$. The passive layer conductance decreases accordingly to this process. The ascending branches of both I and $1/R$ transients have similar character (although they are not parallel).

In the process of reduction the conductance has increased ca. 120 times, while the current has increased only ca. 7 times, thus one can infer that the conductance is a function of the current, but not vice versa. The current is determined by a process other than changes in the layer resistance and most likely by the process of electrocrystallisation of metallic lead as described in section (*b*).

(d) Low temperature effects

Figure 8 shows cathodic LSV produced at different scan rates after passivation for 20 min at −20°C. The LSV are in general similar to those after passivation at 22°C. However, the cathodic peak C at −0.75 V which at 22°C was observed as a very small one only at a scan rate of 1 mV s^{-1}, has become quite distinctive at −20°C and is observed at scan rates up to 5 mV s^{-1}, as a peak and up to 20 mV s^{-1} as a shoulder.

A similar observation was detected in experiments at −11°C.

The dependences I_p and E_p vs. $\nu^{1/2}$ for the PbO peak are comparable to the ones for 22°C (Figs. 6 and 7).

Figure 9 presents direct current and in-phase component of the electrode admittance transients for the potential step from 0.6 to −0.85 V, i.e. to the potential corresponding to the peak B on the LSV (Fig. 8). The current transient reveals two peaks, which corresponds with two cathodic peaks on the LSV. The shape of the conductance transient does not show the appearance of the second peak.

A splitting of the PbO peak, especially at low temperatures, was obtained on cyclic voltammograms by Chang *et al.* (4). These authors found the splitting to be more pronounced with an increase of the potential shift in a positive direction into the PbO_2 region. A probable explanation for the split peak may be a reduction of two different basic divalent lead formed beneath $PbSO_4$ due to an alkalinity gradient within the film.

The two forms may be related to PbO and some form of basic lead sulphate or to orthorhombic and tetragonal polymorphs of PbO. Bullock *et al.* (16) have recently shown, using microprobe laser Raman spectroscopy, that both orthorhombic and tetragonal form of PbO may be simultaneously present in the passive layer on lead. Figure 10 presents a current transient for the potential step from 0.6 V to −0.75 V, i.e. to the potential corresponding to the peak C on the LSV (Fig. 8). The transient shows two peaks in this case also. It ean conceivably be that both peaks may be related to the same material.

Acknowledgements

This work has been supported by a Strategic Grant from the Natural Sciences and Engineering Council of Canada. The authors are grateful to T. VanderNoot for very useful discussions. Pure lead for the preparation of electrodes has been generously donated as a gift by Cominco of Canada Ltd.

1. P. RUETSCHI. J. Electrochem. Soc. **120**, 331 (1973).
2. P. RUETSCHI and R. T. ANGSTADT. J. Electrochem. Soc. **111**, 1323 (1964).
3. M. VISSCHER. J. Power Sources **1**, 257 (1976/1977).
4. T. G. CHANG, M. M. WRIGHT, and E. M. L. VALERIOTE. *In* Power sources. Vol. 6. *Edited by* D. H. Collins. Academic Press, NY. 69 (1977).
5. B. K. MAHATO. J. Electrochem. Soc. **126**, 365 (1979).
6. S. FLETCHER and D. B. MATTHEWS. J. Electroanal. Chem. **126**, 131 (1981).
7. R. G. BARRADAS, D. S. NADEZHDIN, and N. SHAH. J. Electroanal. Chem. **147**, 193 (1983).
8. R. G. BARRADAS and D. S. NADEZHDIN. J. Electroanal. Chem. **158**, 165 (1983).
9. A. J. BARD and L. R. FAULKNER. Electrochemical methods. Wiley and Sons, NY. 1980. pp. 413, 525.
10. H. R. THIRSK and J. A. HARRISON. A guide to the study of electrode kinetics. Academic Press, London. 1972. p. 115.
11. E. M. L. VALERIOTE and L. D. GALLOP. J. Electrochem. Soc. **124**, 370 (1977).
12. R. G. BARRADAS, F. C. BENSON, and S. FLETCHER. J. Electroanal. Chem. **80**, 305 (1977).
13. H. BODE. Lead acid batteries. Wiley and Sons, NY. 1977.
14. L. M. PETER. J. Electroanal. Chem. **144**, 315 (1983).
15. K. L. LAWS. J. Chem. Phys. **39** 1924 (1963).
16. K. R. BULLOCK, G. M. TRISCHAN, and R. G. BURROW. J. Electrochem. Soc. **130**, 1283 (1983).

Can. J. Chem. Downloaded from www.nrcresearchpress.com by 210.87.254.6 on 09/06/12
For personal use only.

The crystal and molecular structure of the bis(*N*,*N*,*N*′,*N*′-tetramethylethanediamine) adduct of I(Br)InInBr$_2$, In$_2$Br$_3$I.2C$_6$H$_{16}$N$_2$, an indium–indium bonded molecule

MASOOD A. KHAN, CLOVIS PEPPE, AND DENNIS G. TUCK[1]

Department of Chemistry, University of Windsor, Windsor, Ont., Canada N9B 3P4

Received September 19, 1983

MASOOD A. KHAN, CLOVIS PEPPE, and DENNIS G. TUCK. Can. J. Chem. **62**, 601 (1984).

The crystal structure of the title compound has been determined by the heavy atom method. The crystals are orthorhombic, space group *Pbca*, with unit cell dimensions a = 22.795(3) Å, b = 17.518(2) Å, c = 12.396(3) Å, Z = 8; R = 0.0409 for 1527 unique "observed" reflections. The structure is disordered, with each halogen site (X) occupied by 75% Br, 25% I. The molecule consists of two X_2(tmen)In units (tmen = *N*,*N*,*N*′,*N*′-tetramethylethanediamine) with distorted trigonal bipyramidal geometry, joined by an In—In bond 2.775(2) Å in length.

MASOOD A. KHAN, CLOVIS PEPPE et DENNIS G. TUCK. Can. J. Chem. **62**, 601 (1984).

On a déterminé la structure cristalline du composé mentionné dans le titre grâce à la méthode des atomes lourds. Les cristaux sont orthorhombiques, groupe d'espace *Pbca*, avec des dimensions a = 22,795(3), b = 17,518(2), c = 12,396(3) Å, Z = 8; R = 0,0409 pour 1527 réflexions observées. La structure est désordonnée alors que chaque site d'halogène (X) est occupé à 75% par Br et 25% par I. La molécule comporte deux unités X_2(tmen)In (tmen = *N*,*N*,*N*′,*N*′-tétraméthyléthanediamine), avec une géométrie trigonale-bipyramidale déformée, unies par une liaison In—In de 2,775(2) Å de longueur.

[Traduit par le journal]

Can. J. Chem. Downloaded from www.nrcresearchpress.com by 210.87.254.5 on 09/06/12
For personal use only.

Introduction

The chemistry of indium in the +II oxidation state has been the subject of a number of recent studies. The dihalides are now known to be mixed oxidation state ionic dimers (1), but both the anionic complexes $In_2X_6^{2-}$ (X = Cl, Br, I) (2) and the adducts of In_2X_4 (3, 4) have been formulated as genuine compounds of indium(II), all involving indium–indium bonds. The general trend here is very similar to that of gallium(II), for which X-ray studies have demonstrated the presence of Ga—Ga bonding in $Ga_2X_6^{2-}$ anions (5, 6), and in the 1,4-dioxane and pyridine adducts of Ga_2Br_4 (7, 8).

We now report the crystal structure of the compound $In_2Br_3I.2tmen$ (tmen = *N*,*N*,*N*′,*N*′-tetramethylethanediamine) prepared by the low temperature reaction of InI and $InBr_3$ in toluene/tmen mixtures (9). The structural determination confirms the presence of the postulated indium–indium bond. In addition to the parameters of the I(Br)InInBr$_2$ moiety, there are some features of interest in the structure of the ligand, and these are compared with previous results in the literature.

Experimental section

A small prismatic yellow crystal of $In_2Br_3I.2tmen$ (see Table 1 for dimensions and other relevant data) was sealed in a capillary and mounted on a Syntex P2$_1$ diffractometer for X-ray data collection. The crystals decompose slowly on exposure to the atmosphere. Details of the data collection procedures have been given previously (10, 11). During the data collection, the intensity of three monitor reflections decreased by approximately 3.5%, and an appropriate scaling factor was used to correct for this. We observed a rapid decrease in intensities beyond 2θ = 30°, ascribed to disorder (see below) and to the high thermal motion of the carbon atoms. Most of the reflections beyond 2θ = 30° were rejected on the basis of peak profile test during data reduction, and were accordingly not used in subsequent calculations, resulting in only 44% of the measured reflections being given "observed" status (see Table 1). The data were further corrected for Lorentz and polarization effects, and analytical absorption corrections were applied. The systematic absences ($0kl$, $k = 2n + 1$; $h0l$, $l = 2n + 1$, and $hk0$, $h = 2n + 1$) indicated the space group *Pbca*.

The positions of the indium atoms were obtained from a sharpened Patterson synthesis, which showed evidence of I/Br disorder, since the In—I and I—I vectors did not have the expected height. In addition, the magnitude of the In—X vectors was approximately equal, suggesting disorder at all four halogen sites. A similar situation was observed earlier (12) in the structures of the $InBrCl_3^-$ and $InBr_3Cl^-$ anions, and there, as here, the model on which the refinement was based assumed that each halide ligand could be treated as 75% Br + 25% I. Subsequent refinement of the data justified this assumption.

The positions of the remaining non-hydrogen atoms were obtained from subsequent difference Fourier synthesis based on the coordinates of the two indium atoms. The structure was then refined by full-matrix least-squares methods, with all the non-hydrogen atoms being treated anisotropically. This refinement converged at R = 0.0467 and R_w = 0.0523, at which stage some peaks appeared in the difference map at plausible hydrogen atom locations. All hydrogen atoms were subsequently included in idealized positions (C—H = 0.95 Å), with the thermal parameters being assigned the same values as those of the appropriate bonded carbon atoms. After six more cycles of refinement, convergence was achieved with the final R = 0.0409 and the final R_w = 0.0433 for 1527 unique "observed" ($I > 2\sigma(I)$) reflections. The final difference map showed no features of any chemical significance, with the largest peak being 0.8 e Å^{-3}, and close to the halide species X (2). In the final cycle of refinement, the largest shift:error ratio was 0.1. The computer programmes and scattering factor tables used were those given previously (11).

Positional and thermal parameters are given in Table 2 and interatomic distances and bond angles in Table 3. Figure 1 shows the molecule, with the atomic numbering scheme, and Fig. 2 gives the cell packing; hydrogen atoms are excluded from these figures for the sake of clarity.

Tables of structure factors, anisotropic thermal parameters, and hydrogen atom coordinates are available as supplementary data.[2]

Results and discussion

The results show that the structure of $In_2Br_3I.2tmen$ consists of discrete molecules, with no significant intermolecular interactions. Each indium atom is coordinated by two halogen atoms and a bidentate tmen ligand.

Perhaps the most interesting feature of the molecule is the indium–indium bond, of length 2.775(2) Å. There have been

[1] To whom all correspondence should be addressed.

[2] Complete set of data is available upon request, at a nominal charge, from the Depository of Unpublished Data, CISTI, National Research Council of Canada, Ottawa, Ont., Canada K1S 0A2.

Can. J. Chem. Downloaded from www.nrcresearchpress.com by 210.87.254.5 on 09/06/12
For personal use only.

TABLE 1. Summary of crystal data, intensity collection, and structural refinement for $In_2Br_3I.2tmen$

Cell constants	a = 22.795(3) Å, b = 17.518(2) Å c = 12.396(3) Å
Cell volume	4950(1) Å^3
Space group	*Pbca* (No. 61)
Z	8
M_r	828.36
ρ(calc)	2.224 g cm^{-3}
Absorption coefficient	64.02 cm^{-1}
Min/max absorption correction	6.335/8.933
Crystal dimensions	0.36 × 0.30 × 0.32 mm
Radiation	MoK$_\alpha$ (λ = 0.71069 Å)
T (°C)	22
2θ angle	4–45°
Scan type	Coupled θ(crystal)/2θ(counter)
Scan width	$K_{\alpha 1}$ − 1° to $K_{\alpha 2}$ + 1°
Scan speed	2.0–5.0° min^{-1}
Background time/scan time	0.5
Total reflections measured	3487 (h,k,l)
Unique data used	1527 $(I > 2\sigma(I))$
No. of parameters	199
$R = (\|\|F_o\| - \|F_c\|\|/\Sigma\|F_o\|)$	0.0409
$R_w = [\Sigma w(\|F_o\| - \|F_c\|)^2/\Sigma\|F_o\|^2]^{1/2}$	0.0433

TABLE 2. Atomic coordinates for non-hydrogen atoms in $In_2Br_3I.2tmen$

Atom	x	y	z	$\bar{U}_{eq}$(Å^2 × 10^3)[a]
In(1)	0.0966(1)	0.4254(1)	0.2174(1)	52.9
In(2)	0.1408(1)	0.5650(1)	0.2856(1)	48.6
X(1)[b]	0.0575(1)	0.3887(1)	0.0257(2)	93
X(2)[b]	0.2108(1)	0.3672(1)	0.1794(2)	97
X(3)[b]	0.0825(1)	0.6851(1)	0.3470(2)	91
X(4)[b]	0.1543(1)	0.5164(1)	0.4956(2)	88
N(1)	0.0785(9)	0.3194(9)	0.3258(15)	78
N(2)	−0.0058(7)	0.4429(8)	0.2842(12)	54
N(3)	0.2367(7)	0.6081(10)	0.2889(13)	67
N(4)	0.1574(8)	0.6255(9)	0.1093(13)	63
C(1)	0.0161(10)	0.3222(13)	0.3696(21)	109
C(2)	−0.0112(12)	0.3927(19)	0.3724(26)	166
C(3)	0.2540(11)	0.6395(14)	0.1798(15)	92
C(4)	0.2048(12)	0.6724(18)	0.1228(18)	153
C(11)	0.1236(10)	0.3144(12)	0.4154(18)	87
C(12)	0.0809(10)	0.2508(11)	0.2549(20)	99
C(21)	−0.0124(10)	0.5114(15)	0.3339(22)	143
C(22)	−0.0543(10)	0.4321(17)	0.2119(18)	137
C(31)	0.2364(10)	0.6709(14)	0.3732(18)	118
C(32)	0.2788(10)	0.5467(16)	0.3202(18)	120
C(41)	0.1647(12)	0.5724(13)	0.0316(17)	108
C(42)	0.1093(13)	0.6761(18)	0.0727(22)	162

[a] $\bar{U}_{eq}$ is calculated from the refined anisotropic thermal parameters (supplementary material) ($U_{eq} = (1/3)\Sigma_{i=1}^{3}(\text{rmsd})_i^2$, with rmsd values taken from ORTEP output).
[b] X = 75% Br, 25% I.

no previous structural results on this bond, but relevant values are available for the solids In_6S_7 and In_6Se_7, in which short In—In distances of 2.741(2) Å and 2.760(5) Å have been found (13, 14), suggesting the presence of In_2^{4+} cations. Further evidence of indium–indium bonding was found in the solids In_4Se_3 and In_4Te_3 (15), whose structures show the presence of the catenated species [In—In—In]$^{5+}$, with In—In distances averaging 2.78 Å. These values agree well with the In—In distance reported in the present work. In the complex lattice of the mixed oxide $In_6La_{10}O_6S_{17}$, pairs of indium atoms are found to be 2.863(4) Å apart (16), implying a somewhat weaker bond than in the previous cases. Comparison with the Sn—Sn distance of 2.770(4) Å found from the X-ray study of hexaphenyldistannane (17) demonstrates the similarities in the M—M bonding properties of indium and tin. Finally we note that the distance of 2.775 Å yields a covalent radius of 1.39 Å for the indium atom. The values reported previously (12, 18) for r(In—Cl), r(In—Br), and r(In—I), when combined with standard values for the covalent radii of the halogen atoms, give r(In) = 1.36(2) Å, in reasonable agreement with the above result, although it should be emphasised that In—X bonds are not in practice purely covalent (19).

TABLE 3. Interatomic distances (Å) and angles (deg), with e.s.d.'s in parentheses, for $In_2Br_3I.2tmen$

(*a*) Bonding distances

Bond	Distance	Bond	Distance
In(1)—In(2)	2.775(2)		
In(1)—X(1)[a]	2.618(2)	In(2)—X(3)	2.602(2)
In(1)—X(2)	2.834(2)	In(2)—X(4)	2.756(2)
In(1)—N(1)	2.33(2)	In(2)—N(3)	2.32(2)
In(1)—N(2)	2.50(2)	In(2)—N(4)	2.46(2)
N(1)—C(1)	1.52(2)	N(3)—C(3)	1.51(2)
N(1)—C(11)	1.52(3)	N(3)—C(31)	1.52(3)
N(1)—C(12)	1.49(2)	N(3)—C(32)	1.49(3)
N(2)—C(2)	1.41(3)	N(4)—C(4)	1.37(3)
N(2)—C(21)	1.36(2)	N(4)—C(41)	1.35(3)
N(2)—C(22)	1.44(2)	N(4)—C(42)	1.48(3)
C(1)—C(2)	1.38(3)	C(3)—C(4)	1.45(3)

(*b*) Angles

Bonds	Angle	Bonds	Angle
In(2)—In(1)—X(1)	128.0(1)	In(1)—In(2)—X(3)	128.1(1)
In(2)—In(1)—X(2)	92.0(1)	In(1)—In(2)—X(4)	93.2(1)
In(2)—In(1)—N(1)	126.2(5)	In(1)—In(2)—N(3)	129.4(4)
In(2)—In(1)—N(2)	97.4(3)	In(1)—In(2)—N(4)	99.5(4)
X(1)—In(1)—X(2)	94.2(1)	X(3)—In(2)—X(4)	91.7(1)
X(1)—In(1)—N(1)	105.5(5)	X(3)—In(2)—N(3)	102.3(4)
X(1)—In(1)—N(2)	90.7(4)	X(3)—In(2)—N(4)	89.4(4)
X(2)—In(1)—N(1)	88.4(5)	X(4)—In(2)—N(3)	88.8(4)
X(2)—In(1)—N(2)	163.4(3)	X(4)—In(2)—N(4)	162.9(4)
N(1)—In(1)—N(2)	75.0(6)	N(3)—In(2)—N(4)	74.3(6)
In(1)—N(1)—C(1)	110(1)	In(2)—N(3)—C(3)	110(1)
In(1)—N(1)—C(11)	110(1)	In(2)—N(3)—C(31)	104(1)
In(1)—N(1)—C(12)	107(1)	In(2)—N(3)—C(32)	112(1)
C(1)—N(1)—C(11)	112(2)	C(3)—N(3)—C(31)	111(2)
C(1)—N(1)—C(12)	106(2)	C(3)—N(3)—C(32)	109(2)
C(11)—N(1)—C(12)	111(2)	C(31)—N(3)—C(32)	110(2)
In(1)—N(2)—C(2)	105(1)	In(2)—N(4)—C(4)	106(1)
In(1)—N(2)—C(21)	111(1)	In(2)—N(4)—C(41)	111(1)
In(1)—N(2)—C(22)	120(1)	In(2)—N(4)—C(42)	115(2)
C(2)—N(2)—C(21)	101(2)	C(4)—N(4)—C(41)	114(2)
C(2)—N(2)—C(22)	110(2)	C(4)—N(4)—C(42)	105(2)
C(21)—N(2)—C(22)	108(2)	C(41)—N(4)—C(42)	107(2)
N(1)—C(1)—C(2)	117(2)	N(3)—C(3)—C(4)	112(2)
N(2)—C(2)—C(1)	120(3)	N(4)—C(4)—C(3)	116(2)

[a]Here, and throughout, X = 75% Br, 25% I.

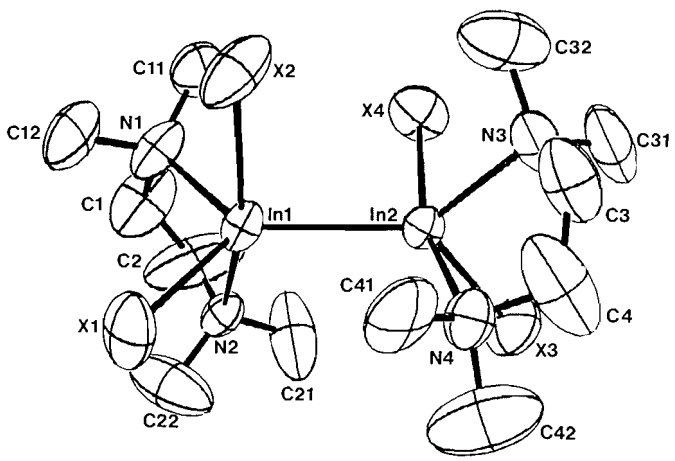

FIG. 1. The molecular structure of $In_2Br_3I.2tmen$ (X = 75% Br, 25% I).

It is unfortunate that the disorder problem (see Experimental section) prevented the measurement of the individual In—Br and In—I bond distances, so that we cannot compare the lengths of these bonds as they appear in In(III) and In(II) complexes. One significant feature is the difference between the equatorial and axial indium–halogen bonds, with the axial bonds 0.185 Å longer than those in the equatorial plane (see below for a discussion of the indium stereochemistry). A similar effect is found in the In—N bonds, with the (average) In—N distances 2.48(2) and 2.33(2) Å in the axial and equatorial positions, respectively. Previously reported values for In—N are 2.276(4) and 2.299(4) Å in $InCl_2$(acac)(bpy) (acac = 2,3-pentanedionate, bpy = 2,2′-bipyridine) (20); 2.238(3), 2.268(3), and 2.228(3) Å in $InCl_3$.terpy (terpy = 2,2′,2″-terpyridine (21); 2.442(3) and 2.482(2) Å in bis{2-[(dimethylamino)methyl]phenyl}chloroindium(III) (10); 2.250(5) and 2.300(6) Å in dichloro(benzoato)bispyridineindium(III) (11); 2.32(3), 2.31(2), and 2.28(3) Å in $InBr_3$.3py (py = pyridine)

Can. J. Chem. Downloaded from www.nrcresearchpress.com by 210.87.254.5 on 09/06/12
For personal use only.

TABLE 4. Least-squares planes as $Ax + By + Cz + D = 0$, and atomic deviations (Å) therefrom, for $In_2Br_3I.2tmen$

Plane[a]	Atomic deviations				*A*	*B*	*C*	*D*
1	In(1) (0.0537)	In(2) (−0.0188)	X(1) (−0.0166)	N(1) (−0.0183)	0.9170	−0.3288	−0.2258	1.0919
2	In(2) (0.0463)	In(1) (−0.0165)	X(3) (−0.0139)	N(3) (−0.0159)	0.0668	−0.3274	0.9425	−0.2641

[a]Dihedral angles between planes *1* and *2* = 92.5°.

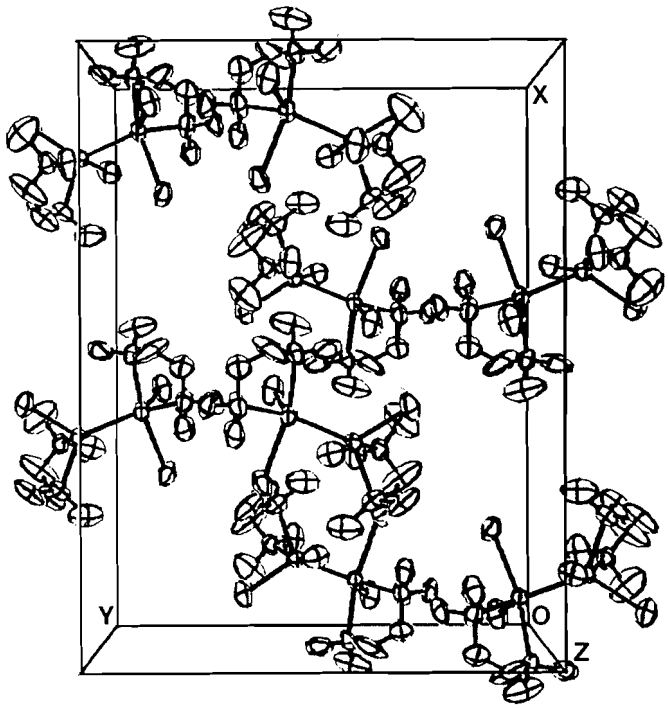

FIG. 2. The unit cell packing for $In_2Br_3I.2tmen$.

(22); and 2.271(16) and 2.288(15) Å in the oximate complex $[(CH_3)_2In(ON{=}CHC_5H_4N)]_2$ (23). With the exception of the six-coordinate $InCl_2$ (acac) (bpy) and $InCl_3.3py$, these compounds all involve indium(III) in a (distorted) trigonal–bipyramidal coordination kernel. The range of In—N bond distances in this group of five-coordinate compounds is 2.48–2.23 Å (ave. 2.31 Å), and the present results are clearly compatible with this range of values despite the different oxidation state involved.

The coordination at each indium atom is distorted trigonal bipyramidal, with an $In(In'N_2X_2)$ kernel. The equatorial plane of this kernel contains In(1), In(2), X(1), and N(1), with the In(1) atom lying 0.0537 Å off the least-squares plane and pointing towards the axial X(2) atom (see Table 4 for least-squares planes). In the second moiety the equatorial plane consists of In(2), In(1), X(3), and N(3), with In(2) 0.0463 Å off this plane and again towards the axial halogen substituent X(4). The geometrical relationship between these two moieties, shown in Fig. 1, places these two planes almost perpendicular to one another, a situation which presumably minimises the interactions between ligands on the different indium atoms. Not surprisingly, the observed angles in the $In(In'N_2X_2)$ kernel show considerable distortion from the ideal values for trigonal bipyramidal stereochemistry. No doubt both ligand–ligand interactions, and the constraint imposed by the bidentate tmen ligand, contribute to these distortions.

The geometry of the tmen ligand

The results in Table 2 show that the C—C and $C—N_{tet}$ bond distances in the coordinated tmen ligand are considerably shorter than the normal average values of 1.537(5) and 1.479(5) Å recommended for such bonds (24). The first reservation to be made is that the accuracy of these values is rather low, since most of the X-ray scattering is by the heavy indium and halogen atoms in the molecule. Such short bonds are not however unique. Maslen and Waters (25) reviewed this and related matters in 1975, and pointed out the considerable number of structures then known for which the same situation applies. A number of reports since that time have confirmed that tmen complexes show such results (e.g. the copper complexes: $[Cu(tmen)Cl_2]_2$ (26), $Cu(NO_3)_2.tmen$ (27), $Cu(ClH_2CO_2)_2.tmen$ (28), $[Cu(tmen)SO_4(H_2O)_2].H_2O_2$ (29), and the sodium complex (30) $C_5H_5Na.tmen$), but without identifying the underlying reasons. Maslen and Waters (25) conclude that such results are not due to disorder, are not due to enhanced thermal motion, and cannot be explained away as artefacts. The present results show that the phenomenon is in no way confined to transition metal complexes, but do nothing to aid in understanding the phenomenon.

Comparison with earlier work

In a previous paper (3), the vibrational spectra of $In_2Br_4.2tmen$, $In_2I_4.2tmen$, and the analogous benzene solvates, were interpreted in terms of a centrosymmetric In_2X_4 unit with coordinated bidentate tmen ligands. The only feature of this analysis which is not confirmed by the present crystallographic work concerns the In_2X_4 kernel, which is clearly not centro-symmetric. For example, the X(2)—In(1)—In(2) angle of 92.0(1)° is substantially smaller than that at In(1)—In(2)—X(3) (128.1(1)°). There seems to be no obvious rationalisation of these earlier conclusions in terms of the present results.

Acknowledgements

This work was supported by Operating Grants (to D.G.T.) from the National Sciences and Engineering Research Council of Canada. One of us (C.P.) thanks the Conselho Nacional de Desenvolvimento Científico e Tecnológico (Brasil) for the award of a scholarship.

1. A. J. CARTY and D. G. TUCK. Prog. Inorg. Chem. **19**, 245 (1975).
2. B. H. FREELAND, J. L. HENCHER, D. G. TUCK, and J. G. CONTRERAS. Inorg. Chem. **15**, 2144 (1976).
3. M. J. TAYLOR, D. G. TUCK, and L. VICTORIANO. Can. J. Chem. **60**, 690 (1982).
4. I. SINCLAIR and I. J. WORRALL. Can. J. Chem. **60**, 695 (1982).
5. K. L. BROWN and D. HALL. J. Chem. Soc. Dalton Trans. 1843 (1973).
6. M. A. KHAN, C. OLDHAM, M. J. TAYLOR, and D. G. TUCK. Inorg. Nucl. Chem. Lett. **16**, 469 (1980).

Can. J. Chem. Downloaded from www.nrcresearchpress.com by 210.87.254.5 on 09/06/12
For personal use only.

7. J. C. BEAMISH, R. W. H. SMALL, and I. J. WORRALL. Inorg. Chem. **18**, 220 (1979).
8. R. W. H. SMALL and I. J. WORRALL. Acta Crystallogr. B**38**, 2365 (1982).
9. C. PEPPE, D. G. TUCK, and L. VICTORIANO. J. Chem. Soc. Dalton Trans. 2165 (1982), and unpublished results.
10. M. A. KHAN, R. C. STEEVENSZ, D. G. TUCK, J. G. NOLTES, and P. W. R. CORFIELD. Inorg. Chem. **19**, 3407 (1980).
11. M. A. KHAN, C. PEPPE, and D. G. TUCK. Acta Crystallogr. C**39**, 1339 (1983).
12. M. A. KHAN and D. G. TUCK. Acta Crystallogr. B**36**, 803 (1982).
13. J. H. C. HOGG and W. J. DUFFIN. Acta Crystallogr. **23**, 111 (1967).
14. J. H. C. HOGG. Acta Crystallogr. B**27**, 1630 (1971).
15. J. H. C. HOGG, H. H. SUTHERLAND, and D. J. WILLIAMS. Chem. Commun. 1568 (1971).
16. L. GASTALDI, D. CARRE, and M. P. PARDO. Acta Crystallogr. B**38**, 2365 (1982).
17. H. PREUT, H. J. HAUPT, and F. HUBER. Z. Anorg. Chem. **396**, 81 (1973).
18. F. W. B. EINSTEIN and D. G. TUCK. Chem. Commun. 1182 (1970).
19. J. G. CONTRERAS and D. G. TUCK. Inorg. Chem. **11**, 2967 (1972).
20. J. G. CONTRERAS, F. W. B. EINSTEIN, and D. G. TUCK. Can. J. Chem. **52**, 3793 (1974).
21. A. J. CARTY, K. R. DYMOCK, and G. J. PALENIK. Private communication to D.G.T.
22. R. W. H. SMALL and I. J. WORRALL. Acta Crystallogr. B**38**, 932 (1982).
23. H. M. M. SHEARER, J. TWISS, and K. WADE. J. Organomet. Chem. **57**, 247 (1973).
24. L. E. SUTTON (*Editor*). Tables of interatomic distances. The Chemical Society, London. 1965.
25. H. S. MASLEN and T. N. WATERS. Coord. Chem. Rev. **17**, 137 (1975).
26. E. D. ESTES, W. E. ESTES, W. E. HATFIELD, and D. J. HODGSON. Inorg. Chem. **14**, 106 (1975).
27. S. F. PAVKOVIC, D. MILLER, and J. N. BROWN. Acta Crystallogr. B**33**, 2894 (1977).
28. M. AHLGREN, R. HAMALAI, and V. TURPEINEN. Acta Chem. Scand. A**32**, 57 (1978).
29. J. BALVICH, K. P. FIRIZZANI, S. F. PAVKOVIC, and J. N. BROWN. Inorg. Chem. **15**, 71 (1976).
30. T. AOYAGI, H. M. M. SHEARER, K. WADE, and G. WHITEHEAD. J. Organomet. Chem. **175**, 21 (1979).

Can. J. Chem. Downloaded from www.nrcresearchpress.com by 210.87.254.5 on 09/06/12
For personal use only.

Quantum chemical and statistical thermodynamic investigations of anesthetic activity. 3. The interaction between CH_4, CH_3Cl, CH_2Cl_2, $CHCl_3$, CCl_4, and an O—H···O hydrogen bond

PAVEL HOBZA
Institute of Hygiene and Epidemiology, Šrobarová 48, 100 42 Prague 10, Czechoslovakia

AND

CAMILLE SANDORFY
Département de chimie, Université de Montréal, C.P. 6210, Succ. A, Montréal (Qué.), Canada H3C 3V1

Received September 9, 1983

PAVEL HOBZA and CAMILLE SANDORFY. Can. J. Chem. **62**, 606 (1984).

The equilibrium for a water dimer (modelling an O—H···O hydrogen bond in a biomolecule) interacting with CH_4, CH_3Cl, CH_2Cl_2, $CHCl_3$, or CCl_4 is examined by quantum chemical and statistical thermodynamic means. It is shown that the presence of an acidic hydrogen in the molecule as well as its relatively high polarizability are the necessary conditions for anesthetic activity.

PAVEL HOBZA et CAMILLE SANDORFY. Can. J. Chem. **62**, 606 (1984).

Nous avons examiné, par les méthodes de la chimie quantique et de la thermodynamique statistique, l'interaction entre CH_4, CH_3Cl, CH_2Cl_2, $CHCl_3$ ou CCl_4 et la liaison hydrogène dans un dimère de la molécule d'eau. Les résultats montrent que la présence d'un hydrogène "acide" et une polarisabilité relativement élevée sont des conditions nécessaires pour qu'une molécule ait un pouvoir anesthésique appréciable.

Can. J. Chem. Downloaded from www.nrcresearchpress.com by 210.87.254.42 on 09/06/12
For personal use only.

Introduction

According to our present knowledge, anesthesia is due to temporary changes in molecular associations which insure the right structure of macromolecules (lipids and proteins) at the membrane of the nerve cell (see refs. 1, 2 for reviews). The effect of anesthetics on the ion channels and the permeability of the membrane are of particular interest (3, 4). Infrared spectroscopic studies led us to suggest that both polar and non-polar interactions are involved in the mechanisms of anesthesia. While non-polar or hydrophobic interactions can provide weak anesthetic action, potent anesthetics induce changes in polar interactions, among them associations by hydrogen bonds (H-bonds), in or around the macromolecules (5–8).

In two theoretical papers (9, 10) we investigated the perturbation of O—H···:O and N—H···:O=C< type H-bonds by a strong anesthetic, $CHCl_3$, and by CHF_3 which does not possess anesthetic potency. In conformity with this, our calculations have shown that the Gibbs free energy actually favors the "breaking" of the H-bonds and association with chloroform but not with fluoroform. The ΔG^0 in question is related to equilibria of the type

$$[1]\quad HOH\cdots OH_2 + A \overset{K_T}{\rightleftharpoons} H_2O\cdots A + H_2O$$

where A (anesthetic) is chloroform or fluoroform in our case and

$$[2]\quad \Delta G_T^0 = -RT \ln K_T$$

Conditions favoring the right hand side in [1] were found to be: (*a*) favorable changes in polar interactions in the Hartree–Fock energy, (*b*) dispersion interactions, and (*c*) favorable (i.e. relatively small) changes in interaction entropy. It was not easy, however, to sort out the various contributions by comparing two widely different systems like $CHCl_3$ and CHF_3. Therefore we decided to study the effect of the series of molecules CH_4, CH_3Cl, CH_2Cl_2, $CHCl_3$, and CCl_4 on the H-bond in the water dimer.

To a first approximation, the equilibrium constant in [1] and the change in free energy are determined by the properties of the complexes on the left and right hand sides of eq. [1]. If ΔG_T^0 of $H_2O\cdots A$ is more negative than that of $(H_2O)_2$, then A is able to break a part of the H-bonds. ΔG_T^0 is determined as the difference of an enthalpy and an entropy term:

$$[3]\quad \Delta G_T^0 = \Delta H_T^0 - T\Delta S_T^0$$

Essentially, the enthalpy term is determined by the change in internal energy, ΔE. If the change in entropy is small then the equilibrium is determined by the ΔE balance of the two complexes.

Computations

The 4-31G basis set (11) was used in all the calculations. The SCF interaction energy (ΔE^{SCF}) was determined as the difference between the energies of the geometry optimized complex and its geometry optimized subsystems. The basis set superposition error (BSSE) was evaluated at the potential energy minimum. The dispersion energy (E^D) was calculated by using the atom–atom formula:

$$[4]\quad E^D = -\sum_i \sum_j c_{ij}\, r^{-6}$$

where the summations are extended to all atoms of both molecules. The coefficients C_{ij} for H, C, O, and Cl were determined from C_6 terms of the $(H_2O)_2$ and $CCl_3H\cdots OH_2$ complexes which, in turn were evaluated by using the non-empirical Unsöld approximation (12–14). It is clear from the definition of the dispersion energy that this represents the lower limit of the actual value. (Contributions of terms of higher order to the dispersion energy are rather important.) The procedure has been described in detail in our previous publications (9, 10) as well as the standard procedure used for the calculation of the thermodynamic characteristics of the equilibria (15).

Results and discussion

Geometry

The geometries of all subsystems, optimized on the 4-31G level, are given in Fig. 1. The structures and coordinates of the

Can. J. Chem. Downloaded from www.nrcresearchpress.com by 210.87.254.42 on 09/06/12
For personal use only.

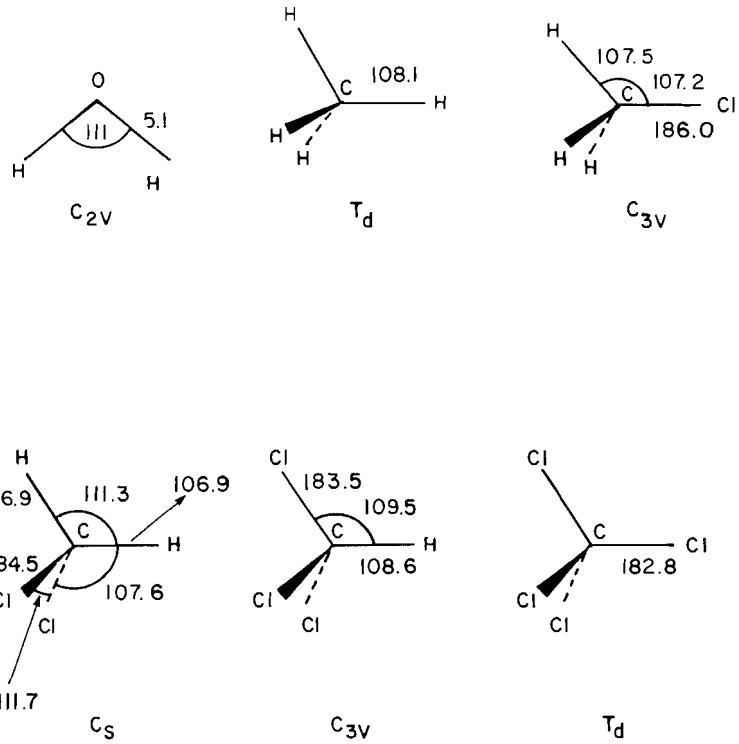

FIG. 1. Optimized 4-31G geometrical parameters for H_2O, CH_4, CH_3Cl, CH_2Cl_2, $CHCl_3$, and CCl_4: distances in pm, angles in deg.

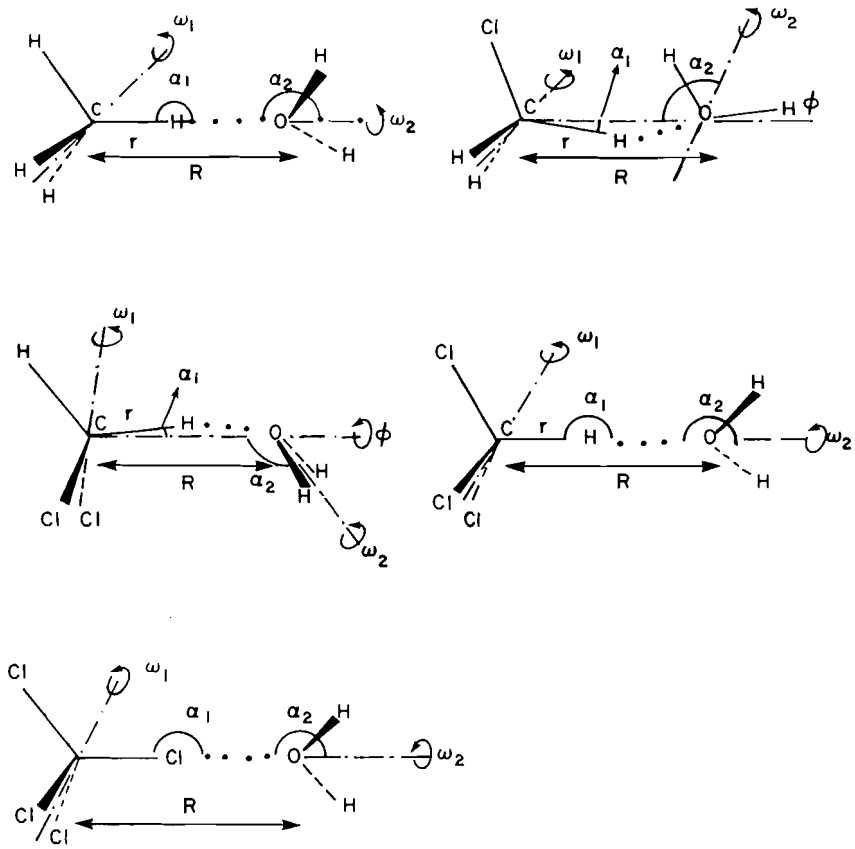

FIG. 2. Structure and coordinates of the complexes investigated (ϕ with $CClH_3 \cdots OH_2$ means out-of-plane bend of H_2O).

complexes investigated are shown in Fig. 2. The six intermolecular coordinates and the C—H intramolecular coordinate were optimized; the remaining intramolecular coordinates were kept fixed during optimization and were taken from the subsystems. The optimized bond lengths and angles are collected in Table 1. It appears from Fig. 2 and Table 1 that the H-bonds in the $CClH_3 \cdots OH_2$ complex are surprisingly non-linear. The non-linearity amounts to 29.7°; hence the complex can be char-

TABLE 1. Optimized coordinates of the complexes investigated (cf. Fig. 1); length in pm, angles in deg

Complex	Coordinates						
	P	α_1	α_2	ω_1	ω_2	ϕ	r
$CH_4\cdots OH_2$	379.1	180	180	0	[a]	—	108.1
$CClH_3\cdots OH_2$	321.5	29.7	125	0	0	0	107.5
$CCl_2H_2\cdots OH_2$	316.3	2.6	152.7	0	0	180	107.1
$CCl_3H\cdots OH_2$[b]	307.0	180	180	0	[a]	—	106.9
$CCl_4\cdots OH_2$	487.8	180	180	0	[a]	—	—

[a] Free rotation of water along the linear C—H...O bond.
[b] Taken from ref. 9.

TABLE 2. Energy characteristics of the complexes investigated (in kJ/mol)

Complex	$-\Delta E^{SCF}$	BSSE	$-E^D$	$-\Delta E^{TOT}$
$CH_4\cdots OH_2$	3.97	2.76	1.67	2.88
$CClH_3\cdots OH_2$	21.75	2.97	4.48	23.26
$CCl_2H_2\cdots OH_2$	23.53	3.35	6.78	26.96
$CCl_3H\cdots OH_2$	29.29[a]	4.10[a]	8.69	33.88
$CCl_4\cdots OH_2$	6.90	3.06	0.75	4.59

[a] Taken from ref. 9.

acterized as cyclic. The non-linearity of the H-bonds in $CCl_2H_2\cdots OH_2$ is much smaller and amounts to only 2.6°. The C—H...O bonds in $CH_4\cdots OH_2$ and $CCl_3H\cdots OH_2$ are linear. Investigating the intermolecular distances we find rather dramatic differences between the $CH_4\cdots OH_2$ and $CClH_3\cdots OH_2$ complexes, whereas further halogenation (until CCl_3H) leads only to a small decrease of R. Formation of a H-bond is characterized by a lengthening of the X-H bond; from Table 1 and Fig. 1 it is evident that only with $CCl_2H_2\cdots OH_2$ and $CCl_3H\cdots OH_2$ complexes does some lengthening of the C—H bond occur (by 0.2 and 0.3 pm).

Interaction energy

The energy characteristics are collected in Table 2. Here again the difference in ΔE^{SCF} between $CH_4\cdots OH_2$ and $CClH_3\cdots OH_2$ is much greater than that between the remaining complexes (except for $CCl_4\cdots OH_2$). Furthermore, the importance of the presence of an "acidic" hydrogen in the "anesthetic" molecule is clearly demonstrated. From the values of the 4-31G electronic charge at the hydrogen it appears that halogenation of CH_4 increases the charge rather dramatically (from 0.20 in CH_4 to 0.28, 0.35, and 0.43 in $CClH_3$, CCl_2H_2, and CCl_3H respectively).

The BSSE is almost constant for all complexes, i.e. it does not depend on the ΔE value. The constancy of the BSSE comes from the fact that with all the complexes the lowering of the energy of H_2O by the "ghost" functions of CCl_mH_n is much more important than the lowering of the energy of CCl_mH_n by the "ghost" functions of H_2O.

The dispersion energy increases upon halogenation from $CH_4\cdots OH_2$ to $CCl_3H\cdots OH_2$. The very small value of E^D with $CCl_4\cdots OH_2$ is not surprising in light of the very large intermolecular distance of the complex. It is necessary to point out here that optimizing the total interaction energy of the complex (instead of ΔE^{SCF} only) does not change either the intermolecular distance, or ΔE. From Table 2 it is further evident that compensation of BSSE and E^D is not fulfilled every time.

The values of the total interaction energy presented in Table 2 should be compared with that of $HOH\cdots OH_2$, which amounts (9) to −33.9 kJ/mol. Without the entropy term only the chloroform . . . water complex is of comparable strength to the water . . . water complex. It means that only chloroform is able to perturb the hydrogen bond in the water dimer.

Analyzing the ability of CCl_mH_n systems to break the hydrogen bonds in the water dimer, we can state: (*i*) the presence of an "acidic" hydrogen is indispensable; (*ii*) halogenation plays a favorable role in making the hydrogen more acidic as well as in increasing the polarizability of the molecule (what makes E^D of the complex more negative). The $CCl_4\cdots OH_2$ complex clearly demonstrates the high polarizability of a molecule is not enough for giving it anesthetic potency. On the other hand, the mere presence of hydrogens in a molecule is not sufficient to render it anesthetic either (e.g. CH_3Cl).

The above conclusions are based on energy characteristics only. Calculation of the ΔG term is, owing to the need to evaluate entropy (and especially of its vibrational contribution), tedious. We have shown previously (16) that the sum of vibrational frequency dependent terms (zero point energy, vibrational contribution to the entropy, and temperature dependence of enthalpy) of a H-bonded complex can be estimated on the basis of its interaction energy. Adding the rotational and translational contributions to the entropy (their evaluation is straightforward), if atomic masses and geometry of all the systems are known) we obtain an estimate of ΔG_{298} (for the quality of this estimate see ref. 16). The estimated $\Delta\Delta G_{298}$ for equilibrium [1] for A = CH_3Cl and CH_2Cl_2, respectively, amount to 13.7 and 14.1 kJ/mol. $\Delta\Delta G_{298}$ for the same equilibrium for A = $CHCl_3$, calculated previously (5), equals 2.2 kJ/mol; this value indicates that approximatively 40% of the H-bonds in the $H_2O\cdots H_2O$ are broken. The values of $\Delta\Delta G_{298}$ clearly demonstrate that CH_3Cl as well as CH_2Cl_2 are far from being able to perturb the H-bonds in the water dimer.

Conclusions

On the basis of the above analysis we can try to "design" a general anesthetic: (*i*) it must contain an "acidic" hydrogen; (*ii*) polarizability of the molecule must be large; (*iii*) polar interactions of the anesthetic molecule with a part of the target (which plays a crucial role) can be magnified if more interaction sites (both proton donor and proton acceptor) are present in the molecule simultaneously. All these conditions conform to empirical knowledge and the spectroscopic evidence related to anesthetics (5–8, 17–20).

While only one target H-bond was used in this study, the O—H...:O bond is of the strength typical of many biologically important H-bonds; it is actually stronger than the most

Can. J. Chem. Downloaded from www.nrcresearchpress.com by 210.87.254.42 on 09/06/12
For personal use only.

important N—H...:O=C$\langle$ bond. The results described in this paper give additional weight to the suggestion that molecular associations of both the polar (H-bonding) and non-polar types are important for the mechanism of anesthesia.

Acknowledgements

The authors gratefully acknowledge financial assistance from the Natural Sciences and Engineering Research Council of Canada, the Ministère de l'Education du Québec, and the Czechoslovakian Academy of Sciences.

1. R. D. KAUFMAN. Anesthesiology, **46**, 49 (1977).
2. M. J. HALSEY. *In* Anesthetic uptake and action. *Edited by* E. I. Eger. Williams and Wilson, Baltimore. 1974. pp. 45–76.
3. D. W. URRY. Proc. Natl. Acad. Sci. U.S.A. **68**, 672 (1971).
4. D. W. URRY, K. U. PRASAD, and T. L. TRAPANE. Proc. Natl. Acad. Sci. U.S.A. **79**, 390 (1982).
5. T. DI PAULO and C. SANDORFY. J. Med. Chem. **17**, 809 (1974).
6. C. SANDORFY. Anesthesiology, **48**, 357 (1978).
7. G. TRUDEAU, K. C. COLE, R. MASSUDA, and C. SANDORFY. Can. J. Chem. **56**, 1681 (1978).
8. G. TRUDEAU, J. M. DUMAS, P. DUPUIS, M. GUÉRIN, AND C. SANDORFY. Top. Curr. Chem. **93**, 91 (1980).
9. P. HOBZA, F. MULDER, and C. SANDORFY. J. Am. Chem. Soc. **103**, 1360 (1981).
10. P. HOBZA, F. MULDER, and C. SANDORFY. J. Am. Chem. Soc. **104**, 925 (1982).
11. R. DITCHFIELD, W. J. HEHRE, and J. A. POPLE. J. Chem. Phys. **54**, 724 (1971).
12. F. MULDER, M. C. VAN HEMERT, P. E. S. WORMER, and A. VAN DER AVOIRD. Theoret. Chim. Acta, **46**, 39 (1977).
13. F. MULDER and C. HUISZOON. Mol. Phys. **34**, 1215 (1977).
14. F. MULDER, G. VANDIJK, and A. VAN DER AVOIRD. Mol. Phys. **39**, 407 (1980).
15. P. CARSKY, R. ZAHRADNIK, M. URBAN, and V. KELLÖ. Collect. Czech. Chem. Commun. **43**, 1965 (1978).
16. M. M. SZCZESNIAK and P. HOBZA. J. Phys. Chem. **87**, 2608 (1983).
17. J. M. BROWN and P. A. CHALONER. Can. J. Chem. **55**, 3380 (1977).
18. L. S. KOEHLER, W. CURLEY, and K. A. KOEHLER. Mol. Pharmacol. **13**, 113 (1977).
19. R. H. DAVIES, R. D. BAGNALL, and W. G. M. JONES. Int. J. Quantum Chem. Quantum Biol. Symp. **1**, 201 (1974).
20. R. H. DAVIES, R. D. BAGNALL, W. BELL, and W. G. M. JONES. Int. J. Quantum Chem. Quantum Biol. Symp. **3**, 171 (1976).

Can. J. Chem. Downloaded from www.nrcresearchpress.com by 210.87.254.42 on 09/06/12
For personal use only.

Mechanisms in the chlorinolysis of sulfinyl chlorides

TERENCE PATRICK AHERN, MICHAEL FRANCIS HALEY, RICHARD FRANCIS LANGLER,[1] AND JUNE ELLEN TRENHOLM
Department of Chemistry, Mount Allison University, Sackville, N.B., Canada E0A 3C0

Received February 11, 1983[2]

TERENCE PATRICK AHERN, MICHAEL FRANCIS HALEY, RICHARD FRANCIS LANGLER, and JUNE ELLEN TRENHOLM. Can. J. Chem. **62**, 610 (1984).

The successful synthesis and chlorinolysis of α-mercaptodimethyl sulfone have provided additional support for our contention that Pummerer rearrangements may occur during the chlorinolyses of α-sulfonyl sulfinyl chlorides. Further exploration of chlorinolyses of α-sulfonyl systems has uncovered the first observations of CS bond cleavage during the chlorinolyses of (*i*) a sulfinyl chloride and (*ii*) a sulfinate ester.

TERENCE PATRICK AHERN, MICHAEL FRANCIS HALEY, RICHARD FRANCIS LANGLER et JUNE ELLEN TRENHOLM. Can. J. Chem. **62**, 610 (1984).

Le fait que des α-mercaptodiméthylsulfones aient pu être chlorolysées fournit une preuve additionnelle à notre suggestion que des transpositions de Pummerer peuvent se produire lors de la chlorolyse de chlorures d'α-sulfonylsulfinyles. Une étude plus poussée de chlorolyses de systèmes α-sulfonyles a permis de mettre en évidence les premières observations de rupture de liaisons C—S au cours de chlorolyses (*i*) d'un chlorure de sulfinyle et (*ii*) d'un ester sulfinate.

[Traduit par le journal]

Can. J. Chem. Downloaded from www.nrcresearchpress.com by 210.87.254.105 on 09/06/12
For personal use only.

Introduction

Some time ago (1), we reported the results of a study on the chlorinolysis of the sulfone-sulfide **1** as shown in eq. [1].

[1] $PhCH_2SCH_2SO_2CH_3 \xrightarrow[HOAc]{Cl_2/H_2O} CH_3SO_2CCl_2SO_2Cl + PhCH_2Cl$

1 **2**

Our proposal for the pathway of this reaction involved the intermediacy of the sulfenyl chloride **3***a* and the sulfinyl chloride **3***b*.

$CH_3 \cdot SO_2 \cdot CH_2 \cdot S \cdot Cl$ **3***a*

$CH_3 \cdot SO_2 \cdot CHCl \cdot SO \cdot Cl$ **3***b*

$CH_3 \cdot SO_2 \cdot CH_2 \cdot S \cdot S \cdot Ph$ **3***c*

$CH_3 \cdot SO_2 \cdot CH_2 \cdot S\ H$ **3***d*

$CH_3 \cdot S \cdot CH_2 \cdot S\ H$ **3***e*

$CH_3 \cdot SO_2 \cdot CCl_2 \cdot S \cdot O\ CH_3$ **3***f*

Subsequently, we have undertaken the synthesis of a variety of potential intermediates and intermediate precursors which resulted in the successful preparation of **3***c* (2). Chlorinolysis of **3***c*, as we have pointed out (2), is very likely to produce **3***a* and does furnish the sulfone-sulfonyl chloride **2** as we had hoped.

We wished to pursue this problem further in the hope that we could establish the intervention of an unprecedented process in the chlorinolysis of sulfinyl chlorides, viz. facile Pummerer rearrangement of a dichlorooxosulfonium cation (3*a*).

Results and discussion

Our initial efforts were focused on the preparation of the mercaptosulfone **3***d*. One of the earlier attempts is shown in eq. [2].

[2] $CH_3SCH_2Cl + AcSH \xrightarrow{Pyridine} CH_3SCH_2SAc \xrightarrow{m\text{-CPBA}} CH_3SO_2CH_2SAc$

Attempts to deacetylate the sulfone-thiolacetate with $H_2O/^-OH$, $LiAlH_4$, or $NaBH_4$ furnished complex mixtures and were abandoned. The successful conversion of the sulfide-thiolacetate into the corresponding sulfone-thiolacetate suggests that acetyl groups may have use in protecting mercaptans when peroxidic oxidation of substrates is intended to alter other functional groups.

The successful synthesis of **3***d* was accomplished as shown in Eq. [3].

[3] $CH_3SO_2CH_2SSPh + PhSH \xrightarrow[CH_2Cl_2]{Pyridine} CH_3SO_2CH_2SH + (PhS)_2$

3*c* **3***d*

The mercaptosulfone **3***d* appears to be the first known α-mercaptosulfone. As expected on the basis of the properties of the corresponding α-mercaptosulfide **3***e* (4), the oily mercaptosulfone **3***d* decomposed at room temperature depositing crystalline material which was insoluble in all common organic solvents ($t_{1/2}$ = 6 days). We presume that the crystalline material was polymeric thioformaldehyde.

Aqueous chlorinolysis of freshly prepared **3***d* produced the sulfone-sulfonyl chloride **2** in a reaction which must involve the sulfone-sulfenyl chloride **3***a* as shown in eq. [4].

[4] $CH_3SO_2CH_2SH \xrightarrow[HOAc]{Cl_2/H_2O} [CH_3SO_2CH_2SCl] \rightarrow CH_3SO_2CCl_2SO_2Cl$

3*d* **3***a* **2**

While the results shown in eq. [4] prove our contention that **3***a* would be transformed into **2** under the reaction conditions employed for the reaction shown in eq. [1], thus confirming **3***a* as a possible intermediate for that reaction, further examination of the pathway followed by **3***a* in this reaction would require the preparation and chlorinolysis ("in an anhydrous medium" (2)) of other potential intermediates (e.g. the sulfone-sulfinyl chloride **3***b*).

Early synthetic efforts aimed at **3***c* were unsuccessful until we adopted an approach which accomplished skeletal modification using a chlorinolysis step followed by a dechlorination step carried out on the appropriate ester. Consequently, we began our efforts to produce the possible sulfone-sulfinyl chlo-

[1]Author to whom correspondence should be directed at: Department of Chemistry and Chemical Engineering, Florida Institute of Technology, 150 West University Boulevard, Melbourne, Florida 32901, U.S.A.

[2]Revision received September 23, 1983.

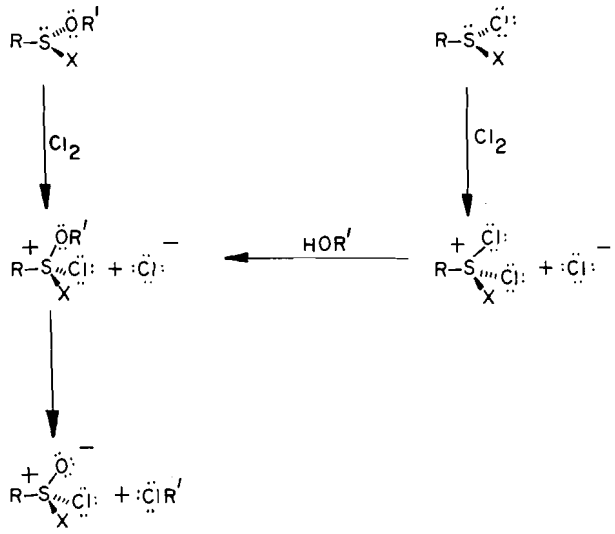

SCHEME 1

ride intermediates for the reaction in eq. [1] by preparing the sulfone-sulfinate ester **5** as shown in eq. [5].

$$[5]\quad \underset{\textbf{3}f}{CH_3SO_2CCl_2\cdot S\cdot OCH_3} \xrightarrow[CH_2Cl_2]{Cl_2} \underset{\textbf{4}}{CH_3SO_2CCl_2\cdot SO\cdot Cl} \xrightarrow{CH_3OH} \underset{\textbf{5}}{CH_3SO_2CCl_2\cdot SO\cdot OCH_3}$$

In addition to the spectroscopic evidence obtained for the structure of **4**, we have subjected it to hydrolysis which was accompanied by desulfinylation as shown in eq. [6].

$$[6]\quad \underset{\textbf{4}}{CH_3SO_2CCl_2\cdot SO\cdot Cl} + H_2O \rightarrow \underset{\textbf{6}}{CH_3SO_2CHCl_2}$$

This behaviour parallels that observed for the hydrolysis of **2** (1) and is entirely consistent with the intermediacy of a sulfinic acid which has anion stabilizing groups on C(1) (5).

While the chlorinolysis of sulfenate esters (*vide* eq. [5]) is precedented (6, 7), previous groups were unable to isolate the expected sulfinyl chlorides. Our conversion of **3***f* to **4** appears to be the first report of the successful isolation of a sulfinyl chloride from a sulfenate ester chlorinolysis. Chlorinolysis of a sulfenate ester produces an O-alkylated oxochlorosulfonium cation. Douglass and Poole (8) have produced O-alkylated oxochlorosulfonium cations by the alcoholysis of dichlorosulfonium cations. The two approaches for generating O-alkylated oxochlorosulfonium cations are depicted in Scheme 1 (X = :).

O-Alkylated dioxochlorosulfonium cations may be produced in similar manner (see Scheme 1; X = O). The usual fate of O-alkylated dioxochlorosulfonium cations involves nucleophilic attack at carbon with resultant CO bond cleavage (3*b*).

$$[7]\quad PhCH_2CH_2\cdot SO\cdot OCH_3 \xrightarrow[CH_2Cl_2]{Cl_2} PhCH_2CH_2SO_2Cl + [CH_3Cl]$$

Expecting to obtain the sulfonyl chloride **2**, we have chlorinated the sulfinate ester **5** in order to obtain some simple chemical support for the structure of **5**. The unexpected observation of CS bond cleavage in the chlorinolysis of **5** prompted us to chlorinate the sulfinyl chloride **4** which furnished a similar result, as shown in Scheme 2.

CS bond cleavage is a well-known process in the chlorinolysis of sulfoxides (3). α-Polychlorosulfoxides are particularly prone to undergo CS bond rupture pursuant to oxochlorosulfonium cation formation. Nucleophilic attack on the oxochlorosulfonium cation at the α-carbon bearing chlorine is usually the exclusive process. It is clear, however, that severe steric hindrance at the α-carbon bearing chlorine can shift some nucleophilic attack to the α′-carbon (9). A reasonably close sulfoxide relative of **4** has been shown to furnish 1,1,1-trichloro-2-thiapropane-2,2-dioxide in good yield (9) (see Scheme 3, pathway b).

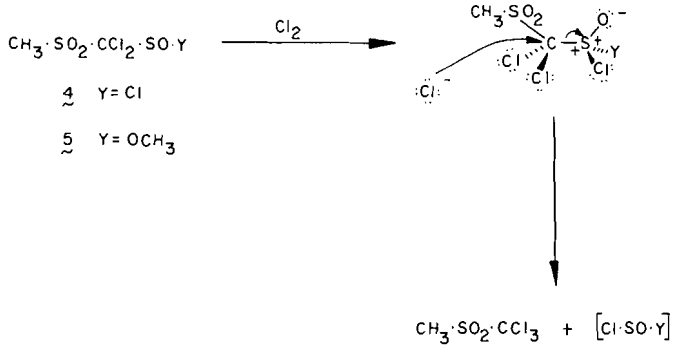

SCHEME 2

In view of the results available from sulfoxide chlorinolyses, the rupture of a CS bond during the chlorinolysis of **4**, while unprecedented, is not surprising. However, the results from the chlorinolysis of the sulfone-sulfinate ester **5** are remarkable indeed. Not only is the methyl group attached to oxygen (the usual electrophilic site in an O-alkylated dioxochlorosulfonium cation) much less crowded, but it bears a superior leaving group, viz. **2** as opposed to the $Cl\cdot SO\cdot OCH_3$ attached to the alternative electrophilic carbon. There can be no question that the trichlorosulfone is an authentic chlorinolysis product since (*i*) both hydrolysis and alcoholysis of the sulfinate ester **5** furnish the dichlorosulfone **6**, (*ii*) hydrolysis of the sulfonyl chloride **2** furnishes **6**, and (*iii*) one- to two-hour chlorinolysis of simple sulfones like **6** affords unchanged starting material (10).

We were unaware of any examination of possible reactions between sulfinyl chlorides and molecular chlorine and were thus unable to judge whether the CS bond cleavage observed during the chlorinolysis of the sulfinyl chloride **4** was a typical or unusual result. Consequently, we have prepared a series of simple sulfinyl chlorides 7*a* → 7*c* and subjected them to chlorinolysis in aprotic media.

$$\begin{array}{ll} & R\cdot SO\cdot Cl \\ 7a & R = ClCH_2— \\ 7b & R = CH_3— \\ 7c & R = PhCH_2CH_2— \end{array}$$

The chlorinolysis of chloromethanesulfinyl chloride[3] 7*a* in methylene chloride produced unchanged sulfinyl chloride quantitatively. A second run conducted in carbon tetrachloride showed no methylene chloride present in the product.

Chlorinolysis of methanesulfinyl chloride[3] 7*b* produced unchanged sulfinyl chloride along with a 13.5% yield of methanesulfonyl chloride, presumably arising from hydrolysis of the oxodichlorosulfonium cations by moisture present in the methylene chloride employed as solvent.

[3] Both chloromethansulfinyl chloride 7*a* and methanesulfinyl chloride 7*b* were produced free of the corresponding sulfonyl chlorides using our previously published method (11).

Can. J. Chem. Downloaded from www.nrcresearchpress.com by 210.87.254.105 on 09/06/12
For personal use only.

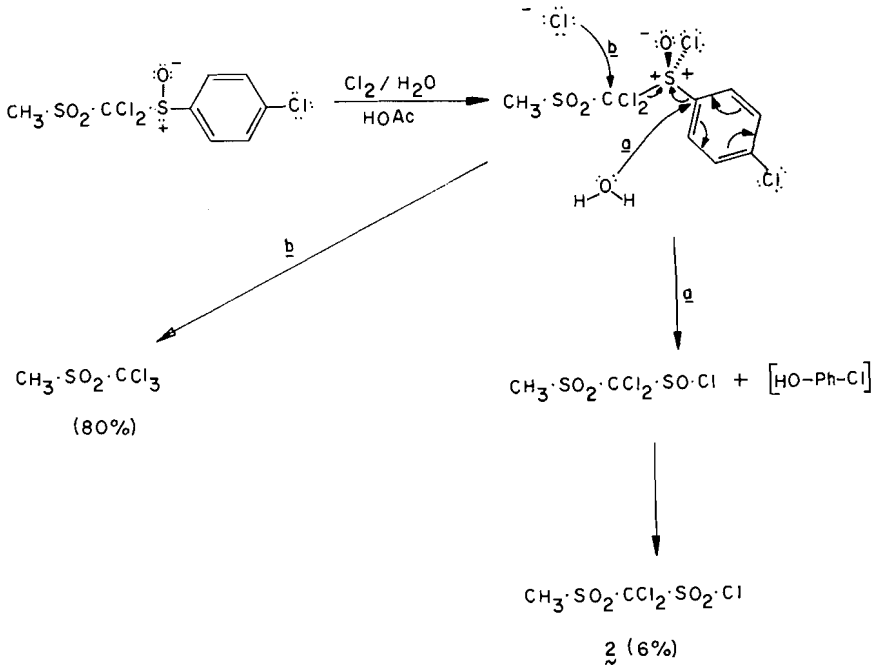

SCHEME 3

The phenethyl sulfinyl chloride 7*c* employed in our study was prepared by chlorinolysis of phenethyl thiolacetate following the procedure of Kee and Douglass (12). Hydrolysis of a sample of 7*c* prepared in this way showed it to contain ca. 20% phenethyl sulfonyl chloride. Chlorinolysis of phenethyl sulfinyl chloride 7*c* did not furnish any phenethyl chloride. The product was, in fact, ca. 50% 7*c* and ca. 50% phenethyl sulfonyl chloride.

These results indicate that the CS bond cleavage observed during the chlorinolysis of **4** is not a routine feature of sulfinyl chloride chlorinolyses.

Since our initial report of CS bond cleavage during the chlorinolyses of α-polychlorosulfoxides (13), we have been concerned about the probability that a nucleophile would be capable of attacking such severely hindered electrophilic carbon atoms. Our subsequent report (9) (see Scheme 2, Y = Ph) in which the substantially more crowded electrophilic carbon atoms in the sulfonium salts derived from α-sulfonyl-α-polychlorosulfoxides appeared to suffer nucleophilic attack, albeit more slowly, heightened our concern. In fact, on a number of occasions, referees of our papers have suggested an alternative mechanism for CS bond cleavage in these reactions (see Scheme 4). This mechanism would circumvent steric problems, although we have had serious reservations about the likelihood that the requisite ion pair formed in the cleavage step of Scheme 4 would actually form. In order to test this proposal we have carried out the following reaction.

$$[8]\quad CH_3SO_2CCl_2\cdot SO\cdot Ph + Cl_2|HCl \xrightarrow{CH_2Cl_2} CH_3SO_2CCl_3 + [CH_3SO_2CCl_2\cdot SO\cdot Cl] + ClPh$$

The absence of the dichlorosulfone, which would arise from proton capture by the carbanion pictured in Scheme 4, suggests that this mechanism is an unlikely one. Because the reaction pictured in eq. [8] is very slow (chlorination time 8 h), we have carried out a chlorination on 1,1-dichloro-2-thiapropane-2,2-dioxide.

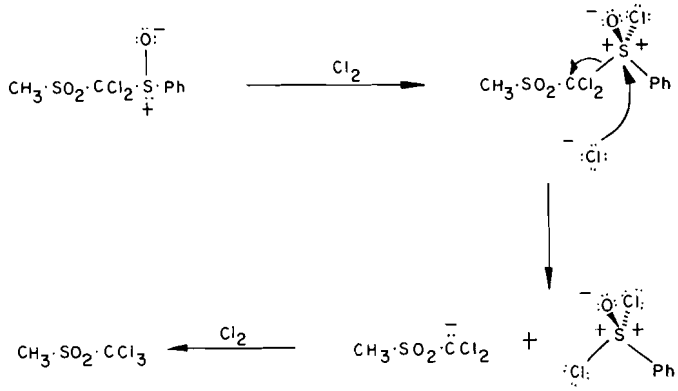

SCHEME 4

$$[9]\quad CH_3SO_2CHCl_2 + Cl_2 \xrightarrow{CH_2Cl_2} CH_3SO_2CHCl_2 + CH_3SO_2CCl_3$$
$$86\% \qquad 14\%$$

The absence of dichlorosulfone in the product mixture (eq. [8]) cannot be rationalized by assuming that it was quantitatively converted to trichlorosulfone under the reaction conditions.

The results depicted in eq. [8] are of some interest. That reaction is the first example of an α-polychlorosulfoxide chlorinolysis in which attack at the α′-carbon is the major pathway. The absence of benzenesulfinyl or benzenesulfonyl chlorides in the product mixture implicates the dichlorosulfone-sulfinyl chloride as the intermediate leading to the trichlorosulfone. Despite our dissatisfaction with the Scheme 4 mechanism, the results from the chlorinolysis of the sulfinate ester **5**, in our view, require a more complex mechanism than the simple picture presented in Scheme 2. The revised mechanism would apply to the cleavage steps in the chlorinolyses of all the α-sulfonyl systems we have studied (*vide* Schemes 2 and 3). At this stage, the most reasonable modification of the cleavage step mechanism would likely involve a complexing interaction between the incoming chloride ion and the α-sulfonyl group.

Can. J. Chem. Downloaded from www.nrcresearchpress.com by 210.87.254.105 on 09/06/12
For personal use only.

Can. J. Chem. Downloaded from www.nrcresearchpress.com by 210.87.254.105 on 09/06/12
For personal use only.

Since we have recently initiated a program of theoretical calculations designed to clarify mechanistic details for the various steps of the Sulfohaloform reaction (see ref. 14, for example), we shall defer a more detailed proposal for cleavage step transition states for α-sulfonyl substituted systems until supporting calculations can be carried out.

In conclusion, we have prepared and chlorinated α-mercaptodimethyl sulfone which has established that the sulfenyl chloride **3***a* is transformed into **2** upon aqueous chlorinolysis, as we had proposed earlier (1). The role of Pummerer rearrangements in the transformations involved in the conversion **3***a* → **2** remains to be established. The chlorinolyses of both the sulfinyl chloride **4** and the sulfinate ester **5** have revealed unprecedented CS bond cleavage for these functional groups, indicating a need to revise the simple mechanism advanced previously for CS bond rupture during chlorinolysis of α-sulfonyl sulfoxides (9).

Experimental

General

Details have been provided previously (10).

Preparation of CH_3SCH_2SAc

A solution of thioacetic S-acid (0.739 g) in dry pyridine (25 mL) was cooled and chloromethyl methyl sulfide (1.002 g) in carbon tetrachloride (2 mL) was added dropwise over 3 min. The reaction mixture was stirred at ambient temperature for 1 h. Methylene chloride (100 mL) was added and the resultant solution washed with 5% HCl (100-mL aliquots) until the aqueous pH remained acidic. The organic layer was dried and concentrated and the residue distilled at reduced pressure, affording the sulfide-thiolacetate (0.544 g, bp 78–80°C/2.4 Torr); ir ($CHCl_3$): 1695 cm^{-1}; nmr ($CDCl_3$) δ: 4.13 (2H, s), 2.46 (3H, s), and 2.26 (3H, s); ms *m/e*: 136 (M^+, 35.1%), 61 (63.7%), and 43 (100%).

Preparation of $CH_3SO_2CH_2SAc$

m-Chloroperoxybenzoic acid (85%, 3.145 g) was added to a cooled solution of the sulfide-thiolacetate (1.002 g) in chloroform (30 mL). The reaction was allowed to reach ambient temperature while stirring overnight. Methylene chloride (170 mL) was added and the resultant solution washed with 1% NaOH (two 50-mL aliquots). The organic layer was dried and concentrated, affording clean sulfone-thiolacetate (1.20 g); ir ($CHCl_3$): 1720, 1320, and 1110 cm^{-1}; nmr ($CDCl_3$) δ: 4.50 (2H, s), 3.03 (3H, s), and 2.56 (3H, s); ms *m/e*: 168 (M^+, 0.9%), 89 (13.6%), and 43 (100%).

*Preparation of $CH_3SO_2CH_2SH$ 3*d

The sulfone-disulfide **3***c* (0.200 g) (2) was dissolved in a solution containing methylene chloride (10 mL), pyridine (0.1 mL), and benzenethiol (0.200 g). The reaction mixture was stirred at ambient temperature for 2 h and the solvent evaporated. The residue was chromatographed on silica gel (10 g) employing chloroform elution (5-mL fractions). Fractions 4 and 5 contained diphenyl disulfide and unreacted benzenethiol. Fractions 7–13 contained oily α-mercaptodimethyl sulfone **3***d*[4] (0.078 g) which had ir ($CHCl_3$): 2590, 1320, and 1125 cm^{-1}; nmr ($CDCl_3$) δ: 3.83 (2H, d), 3.33 (3H, s), and 2.30 (1H, t); ms *m/e*: 126 (M^+, 23.6%), 93 (24.7%), 81 (100%), and 65 (62.5%).

*Aqueous chlorinolysis of 3*d

Mercaptosulfone **3***d* (0.100 g) was dissolved in glacial acetic acid (25 mL) and water (5 mL). Cl_2 (ca. 200 mL/min) was bubbled into the reaction mixture for 0.5 h. Methylene chloride (100 mL) and water (50 mL) were added and the layers separated. The organic layer was washed with 2.5% w/v sodium hydroxide solution (two 50-mL aliquots), dried, and concentrated. The residue was the sulfone-sulfonyl chloride **2** (0.186 g) which was identical with authentic material (1) by ir, nmr, and tlc.

Hydrolysis of 2

The dichlorosulfone-sulfonyl chloride (0.186 g) obtained from the chlorinolysis of **3***d* (described above) was dissolved in water (10 mL) and the reaction mixture refluxed for 1 h. Chloroform (200 mL) was added, and the mixture dried with $MgSO_4$ and filtered. The chloroform was evaporated, affording clean dichloromethyl methyl sulfone (0.072 g) which was identical to authentic material by ir, nmr, and mp (1).

Preparation of $CH_3SO_2CCl_2 \cdot SO \cdot Cl$ 4

The dichlorosulfone-sulfenate ester **3***f* (2) (1.045 g) was dissolved in methylene chloride (25 mL) and Cl_2 (ca. 200 mL/min) bubbled into the reaction mixture for 0.5 h. The solvent was evaporated and the crude residue recrystallized from CCl_4, affording pale yellow crystals of sulfone-sulfinyl chloride (0.637 g, mp 38–40°C). The sulfinyl chloride **4** had ir ($CHCl_3$): 1350, 1166, and 1175 cm^{-1}; λ_{max} (hexanes):[5] 226 (ε 3 488), 274 (ε 377); nmr ($CDCl_3$) δ: 3.36 (s); ms *m/e*: 79 (35.5%) and 63 (100%). *Anal.* calcd. for $C_2H_3Cl_3O_3S_2$: C 9.78, H 1.23; found: C 9.31, H 1.37.

Preparation of $CH_3SO_2CCl_2 \cdot SO \cdot OCH_3$ 5

The sulfone-sulfinyl chloride **4** (1.003 g) was dissolved in methanol (25 mL) and the reaction mixture stirred at ambient temperature for 0.5 h. The solvent was evaporated, the residue dissolved in chloroform (5 mL), and the resultant mixture filtered. The chloroform was evaporated and the residue crystallized from methanol, affording clean **5** (0.820 g, mp 56–58°C). The product had ir ($CHCl_3$): 1345, 1200, and 1150 cm^{-1}; nmr ($CDCl_3$) δ: 3.33 (3H, s) and 4.10 (3H, s); ms *m/e*: 79 (100%) and 63 (27.8%). *Anal.* calcd. for $C_3H_6Cl_2O_4S_2$: C 14.94, H 2.51; found: C 14.86, H 2.59.

Hydrolysis of $CH_3SO_2CCl_2 \cdot SO \cdot Cl$ 4

The sulfinyl chloride **4** (0.985 g) was added to distilled water (10 mL) and the reaction mixture refluxed gently for 0.5 h. The reaction mixture was homogeneous by the time reflux began. The reaction mixture was cooled to room temperature and poured into chloroform (300 mL). The chloroform was dried ($MgSO_4$) and concentrated, affording the dichlorosulfone **6** (0.535 g). After recrystallization, the dichlorosulfone **6** was shown to be identical with authentic material by ir, nmr, mp, and mixture mp.

Chlorinolysis of $CH_3SO_2CCl_2 \cdot SO \cdot OCH_3$ 5

The sulfinate ester **5** (0.991 g) was dissolved in methylene chloride (25 mL) and Cl_2 (ca. 200 mL/min) was bubbled into the solution for 1 h. The solvent was evaporated and the residue recrystallized from 95% ethanol, affording 1,1,1-trichloro-2-thiapropane-2,2-dioxide (0.464 g) which was identical with authentic material by nmr, ir, mp, and mixture mp.

Chlorinolysis of $CH_3SO_2CCl_2 \cdot SO \cdot Cl$ 4

The sulfinyl chloride **4** (1.000 g) was dissolved in methylene chloride (25 mL) and Cl_2 (ca. 200 mL/min) was bubbled into the reaction mixture for 2 h. The solvent was evaporated. The residue was recrystallized from 95% ethanol, affording 1,1,1-trichloro-2-thiapropane-2,2-dioxide (0.202 g) which was identical with authentic material by ir, nmr, and ms. The mother liquor from the recrystallization contained 1,1-dichloro-2-thiapropane-2,2-dioxide (0.210 g) and residual trichlorosulfone (0.197 g).

Thus the sulfinyl chloride had been converted to the trichlorosulfone (50% yield) by the 2-hour chlorinolysis.

Preparation of $PhCH_2CH_2SAc$

The mesylate of 2-phenyl ethanol (9.2278 g) and thioacetic S-acid (3.517 g) were added to dry pyridine (100 mL) and the reaction mixture stirred at ambient temperature for 7 days.[6] Chloroform (200

[4] This compound was too unstable for analysis, but its spectra provide unambiguous evidence for the structure.

[5] Compare with $CH_3 \cdot SO \cdot Cl$, λ_{max} (hexane): 196 (ε 6 320) and 289 (ε 600) (15).

[6] A run terminated after 3 days at room temperature afforded a mixture of thiolester (75%) and unchanged mesylate (25%).

Can. J. Chem. Downloaded from www.nrcresearchpress.com by 210.87.254.105 on 09/06/12
For personal use only.

mL) was added and the resultant mixture washed with 5% HCl (100-mL aliquots) until the aqueous pH remained acidic. The organic layer was dried ($MgSO_4$) and concentrated. The residue was rectified at reduced pressure, affording clean thiolester (5.096 g, bp 80–84°C/0.3 Torr). The product had ir ($CHCl_3$): 1695 cm^{-1}; nmr ($CDCl_3$) δ: 7.26 (5H, s), 3.00 (4H, m), and 2.30 (3H, s); ms *m/e*: 180 (M^+, 3.8%), 104 (78.2%), 91 (36.9%), and 43 (100%). *Anal.* calcd. for $C_{10}H_{12}OS$: C 66.62, H 6.70; found: C 66.83, H 6.74.

Preparation of $PhCH_2CH_2 \cdot SO \cdot Cl$ 7c

Cl_2 (ca. 200 mL/min) was bubbled into a solution of 2-phenethyl thiolacetate (5.00 g) in acetic anhydride (2.83 g) for 0.5 h. The reaction temperature was maintained just above the freezing point with an acetone/Dry Ice bath as necessary. By the end of the reaction, the mixture had taken on a persistent orange color. The reaction mixture was concentrated *in vacuo* and the residue rectified, affording impure sulfinyl chloride (1.24 g, bp 128–130°C/0.5 Torr). The sulfinyl chloride[7] had ir (CCl_4): 1155 cm^{-1}; nmr ($CDCl_3$) δ: 7.30 (5H, s) and 3.45 (4H, m).

The purity of the sulfinyl chloride sample was established as follows. A sample of the sulfinyl chloride (1.0 g) was added to a solution of glacial acetic acid (25 mL) and water (5 mL) and the reaction mixture stirred at ambient temperature for 0.5 h. Water (35 mL) was added and the resultant mixture washed with chloroform (three 50-mL aliquots). The combined organic extracts were washed with 2.5% NaOH (50-mL aliquots) until the aqueous pH remained basic. The organic layer was dried ($MgSO_4$) and concentrated. The residue was 2-phenethyl sulfonyl chloride (0.187 g) which was identical with authentic material by ir and nmr. Thus the original sulfinyl chloride sample was ca. 81% (by weight) sulfinyl chloride and 19% sulfonyl chloride.[8]

Preparation of $CH_3 \cdot SO \cdot Cl$ 7b and $ClCH_2 \cdot SO \cdot Cl$ 7a

The sulfinyl chlorides **7*a*** and **7*b*** were prepared using our published procedures (11). The sulfinyl chlorides prepared in this way were not contaminated with the corresponding sulfonyl chlorides.

Chlorinolyses of 7a, 7b, 7c

The appropriate sulfinyl chloride (1.0 g) was dissolved in methylene chloride (25 mL) and Cl_2 (ca. 200 mL/min) was bubbled into the reaction mixture for 2 h. The solvent was evaporated.

Chloromethane sulfinyl chloride **7*a*** was recovered unchanged from the chlorinolysis.

Crude product from the chlorinolysis of **7*c*** was subjected to hydrolysis in aqueous acetic acid as described under "Preparation of $PhCH_2CH_2 \cdot SO \cdot Cl$ **7*c***". Phenethyl sulfinyl chloride **7*c*** was converted into a mixture containing **7*c*** (0.450 g) and phenethyl sulfonyl chloride (0.536 g).

Methanesulfinyl chloride **7*b*** was converted into a mixture of methanesulfinyl chloride (0.688 g) and methanesulfonyl chloride (0.158 g).

Chlorinolysis of $CH_3SO_2CCl_2 \cdot SO \cdot Ph$

Run 1

The dichlorosulfone-sulfoxide (0.5582 g) was dissolved in methylene chloride (50 mL). Cl_2 (ca. 200 mL/min) and HCl (ca. 200 mL/min) were simultaneously bubbled into the reaction mixture for 8 h. The solvent was evaporated. The crude contained no 1,1-dichloro-2-thiapropane-2,2-dioxide as indicated by nmr. The crude product was chromatographed on silica gel (45 g) employing carbon tetrachloride elution (thirty-one 50-mL fractions). Fractions 13–20 were combined and concentrated, affording 1,1,1-trichloro-2-thiapropane-2,2-dioxide (0.0835 g) which was identical with authentic material by ir, nmr, and mp. Further elution with chloroform (six 50-mL fractions) furnished a mixture of unchanged dichlorosulfone-sulfoxide (0.191 g) and 1,1-dichloro-2-thiapropane-2,2-dioxide (0.038 g).[9] The identity of the dichlorosulfone was confirmed by addition of authentic material to the mixture, which increased the relative intensity of the appropriate signals in the nmr spectrum of the mixture.

Run 2

The dichlorosulfone-sulfoxide (0.5190 g) was dissolved in methylene chloride (50 mL). Cl_2 (ca. 300 mL/min) and HCl (ca. 100 mL/min) were bubbled into the reaction mixture for 8 h. The reaction mixture was evaporated to ca. 20 mL. Gas chromatography carried out on the solution indicated the presence of chlorobenzene (peak intensity increased upon addition of authentic material). The solution was concentrated. Nuclear magnetic resonance indicated a 1:1 mixture of chlorobenzene (relative intensity of chlorobenzene signal increased upon addition of authentic material) and 1,1,1-trichloro-2-thiapropane-2,2-dioxide. Reflux of the crude in water (10 mL) for 1 h did not furnish any dichlorosulfone, indicating that the chlorinolysis had gone to completion. Product was isolated by pouring the aqueous mixture into methylene chloride (500 mL), drying ($MgSO_4$), and concentrating the organic phase. The residue was recrystallized from methanol, affording 1,1,1-trichloro-2-thiapropane-2,2-dioxide (0.1714 g).

Chlorinolysis of $CH_3SO_2CHCl_2$

The dichlorosulfone (0.4799 g) was dissolved in methylene chloride (50 mL). Cl_2 (ca. 300 mL/min) was bubbled into the reaction mixture for 8 h and the solvent evaporated. The crystalline crude was a mixture of 1,1-dichloro-2-thiapropane-2,2-dioxide (86%) and 1,1,1-trichloro-2-thiapropane-2,2-dioxide (14%). Identity of the trichlorosulfone was confirmed by the addition of authentic material which increased the relative intensity of the appropriate signal in the nmr of the mixture.

Acknowledgements

The authors are indebted to Dr. J. H. Kim for running the mass spectra. We are grateful to Dalhousie University and Mount Allison University for financial support in the form of grants from their respective Research Development Funds.

1. W. R. HARDSTAFF, R. F. LANGLER, J. LEAHY, and M. J. NEWMAN. Can. J. Chem. **53**, 2664 (1975).
2. T. P. AHERN, R. F. LANGLER, and R. L. MCNEIL. Can. J. Chem. **58**, 1996 (1980).
3. (*a*) W. R. HARDSTAFF and R. F. LANGLER. *In* Sulfur in organic and inorganic chemistry. Vol. 4. *Edited by* A. Senning. M. Dekker, Inc., New York. 1982. p. 229; (*b*) p. 230.
4. M. R. ALTAMURA, T. HASSELSTROM, and L. LONG, JR. J. Org. Chem. **28**, 2438 (1963).
5. C. M. STIRLING. Int. J. Sulfur Chem. Part B, **6**, 277 (1971).
6. H. KWART, E. N. GIVENS, and C. J. COLLINS. J. Am. Chem. Soc. **91**, 5532 (1969).
7. J. G. TRAYNHAM and A. W. FOSTER. J. Am. Chem. Soc. **93**, 6216 (1971).
8. I. B. DOUGLASS and D. R. POOLE. J. Org. Chem. **22**, 536 (1957).
9. D. G. KAY, R. F. LANGLER, and J. E. TRENHOLM. Can. J. Chem. **57**, 2185 (1979).
10. J. S. GROSSERT and R. F. LANGLER. Can. J. Chem. **55**, 407 (1977).
11. J. S. GROSSERT, W. R. HARDSTAFF, and R. F. LANGLER. Can. J. Chem. **55**, 421 (1977).
12. M. L. KEE and I. B. DOUGLASS. Org. Prep. Proced. **2**, 235 (1970).
13. J. S. GROSSERT and R. F. LANGLER. Chem. Commun. 49 (1973).
14. J. L. GINSBURG and R. F. LANGLER. Can. J. Chem. **61**, 589 (1983).
15. R. F. LANGLER. Ph.D. Thesis, Dalhousie University. 1975.
16. R. F. LANGLER. Can. J. Chem. **54**, 498 (1976).

[7] The ir indicated contaminating sulfonyl chloride was present. Moderate intensity bands were present at 1385 and 1170 cm^{-1}.

[8] There is little or no hydrolysis of sulfonyl chlorides under the conditions employed. Such conditions permit the isolation of sulfonyl chlorides in high yields (16).

[9] The origin of the dichlorosulfone was very likely from hydrolysis of sulfinyl chloride **4** present in the crude.

A ^{31}P and ^{199}Hg nuclear magnetic resonance and vibrational spectroscopic study of triarylphosphine complexes of $HgCl_2$

TIM ALLMAN AND RAM G. GOEL[1]

Guelph–Waterloo Centre for Graduate Work in Chemistry, University of Guelph, Guelph, Ont., Canada N1G 2W1

Received March 1, 1983[2]

TIM ALLMAN and RAM G. GOEL. Can. J. Chem. **62**, 615 (1984).

Complexes of the type $[HgCl_2P(4\text{-}XC_6H_4)_3]_2$ and $HgCl_2(P(4\text{-}XC_6H_4)_3)_2$ (X = Me_2N, MeO, Me, H, F, Cl) have been prepared. The tertiary phosphines have similar steric requirements but vary greatly in their basicities. The vibrational spectra of the complexes were measured and each complex was found to have the expected bridging dimeric (1:1) or pseudotetrahedral monomeric (1:2 Hg/P) structure. Their ^{31}P and ^{199}Hg nmr parameters were investigated and it was found that ^1J(Hg—P) increases with increasing phosphine basicity, decreasing temperature, and decreasing sample concentration in dichloromethane solution. It is concluded that changes in the hybridisation on the P and Hg atoms may be largely responsible for the increases of ^1J(Hg—P) with increasing phosphine basicity.

TIM ALLMAN et RAM G. GOEL. Can. J. Chem. **62**, 615 (1984).

On a préparé des complexes du type $[HgCl_2P(4\text{-}XC_6H_4)_3]_2$ et $HgCl_2(P(4\text{-}XC_6H_4)_3)_2$ (X = Me_2N, MeO, Me, H, F, Cl). Les phosphines tertiaires ont des effets stériques semblables mais leurs basicités varient d'une façon considérable. On a mesuré les spectres vibrationnels des complexes et on a trouvé que chaque complexe possède la structure attendue, soit dimère ponté (1:1) ou pseudotétraèdre monomère (1:2 Hg/P). On a étudié leurs paramètres de rmn du ^{31}P et du ^{199}Hg et on a trouvé que la valeur de ^1J(Hg—P) augmente avec une augmentation de la basicité de la phosphine, une diminution de la température et une diminution de la concentration de l'échantillon en solution dans le dichlorométhane. On en conclut que des changements d'hybridisation des atomes de P et Hg sont les principaux responsables de l'augmentation de ^1J(Hg—P) avec l'augmentation de la basicité des phosphines.

[Traduit par le journal]

Can. J. Chem. Downloaded from www.nrcresearchpress.com by 210.87.254.6 on 09/06/12
For personal use only.

Introduction

Recently we reported a study in which the basicities of various tertiary phosphines were measured by titration in nitromethane (1). Most of the phosphines in the group were *para*-substituted triarylphosphines and it was shown that within this series a very wide range of basicities could be obtained.

The donor ability of the phosphine has often been used to explain observed trends in ^1J(Hg—P) (2–7). The most common trend seen in pseudotetrahedral 1:2 (Hg/P) complexes is for ^1J(Hg—P) to increase with increasing basicity of the phosphine. An unusual exception is the $[Hg(phosphine)_2](ClO_4)_2$ series (8–10), in which the coupling constant decreases markedly.

Unfortunately, while the phosphines used in most of these studies indeed had different basicities, they also had different steric requirements, thus making the interpretation of the data somewhat ambiguous. In order to isolate the electronic effects, our series of *para*-substituted triarylphosphines was used to synthesise 1:1 and 1:2 complexes of $HgCl_2$. Their vibrational and nmr spectroscopic parameters were investigated and are reported herein.

Although some of the complexes described in this study have been previously reported (5, 6) there has been little agreement about their exact ^1J(Hg—P) values, the variation in the reported values often being well beyond any expected experimental and instrumental uncertainties. For example, ^1J(Hg—P) of $HgCl_2(P(C_6H_5)_3)_2$ has been reported to be 4740 Hz (5) but is reported herein to be 4829 Hz. In order to investigate this problem, both the temperature and concentration dependences of ^1J(Hg—P) were studied. The temperature effect has already been studied by others (6, 11), who noted a linear increase in ^1J(Hg—P) with decreasing temperature. However, the variation of ^1J(Hg—P) with sample concentration has not been reported before.

Results and discussion

Vibrational spectra

Because the structures of complexes of this type have been well established, the interpretation of their vibrational spectra has become much more certain. The 1:1 complex $[HgCl_2P(C_6H_5)_3]_2$ has been found to have a chloro bridging dimeric structure (12) and the 1:2 complex $HgCl_2(P(C_6H_5)_3)_2$ is pseudotetrahedral and monomeric (13). It is isostructural with the analogous iodo complex (14). A rigorous treatment of the vibrational spectra of the $P(C_6H_5)_3$ complexes has been done previously (15). The similarity of the vibrational spectra of the complexes reported in this study shows that the structures remain the same through each series. The data are given in Tables 1 and 2.

The infrared spectra of the 1:1 complexes each contain a strong band between 270 cm^{-1} and 300 cm^{-1}. Similarly, the Raman spectra each contains a corresponding weak to strong band. These bands are assigned to the antisymmetric and symmetric terminal Hg—Cl stretching modes (16, 17). Very strong and broad ir bands, assigned to ν_b(Hg—Cl), are seen for each member of the series near 170 cm^{-1} although only two contain corresponding Raman bands and these are weak. The symmetric and antisymmetric Hg—P stretching frequencies are found, as expected, in the 130 cm^{-1} to 170 cm^{-1} region. Some of these bands are not seen because of their inherent weakness and their being hidden by the extremely broad ν_b(Hg—Cl) bands at slightly higher frequencies. Below about 110 cm^{-1} are some medium to strong bands which are assigned to skeletal deformations. Although there are several deformation modes predicted for this type of structure (17), only one fairly broad

[1] Because of the untimely death of Professor Ram G. Goel on November 8, 1982, the two consecutive papers in this volume will be the last in which he is an author. Through patience and understanding, Ram helped to generate interest and develop research skills in chemistry for many students over his 15 years at the University of Guelph. He will be deeply missed.

[2] Revision received October 18, 1983.

TABLE 1. The vibrational data of the 1:1 complexes*

Complex	ν_t(Hg—Cl) ir	ν_t(Hg—Cl) R	ν_b(Hg—Cl) ir	ν_b(Hg—Cl) R	ν(Hg—P) ir	ν(Hg—P) R	δ ir	δ R
$[HgCl_2P(4\text{-}Me_2NC_6H_4)_3]_2$	271s	268vw	163	—	—	—	89s	95vs
$[HgCl_2P(4\text{-}MeOC_6H_4)_3]_2$	287s	287m	158	160vw	—	—	107s	
$[HgCl_2P(4\text{-}MeC_6H_4)_3]_2$	285s	282m	173	—	—	168m	94m	
$[HgCl_2P(C_6H_5)_3]_2$	289s	285s	179	—	152m	156m	98s	89m
$[HgCl_2P(4\text{-}FC_6H_4)_3]_2$	281s	282s	174	172w	130w	135w	108s	110s
$[HgCl_2P(4\text{-}ClC_6H_4)_3]_2$	294s	295m	179	—	133vw	137m	91s	96s

* Samples were run as paraffin oil mulls (ir) or in glass capillaries (R). Some predicted bands were not observed either because of their weakness or their being obscured by the very strong and broad ν_b(Hg—Cl) in the ir. ν_b = bridging stretching frequency. ν_t = terminal stretching frequency. δ = unassigned deformation modes (see text).

TABLE 2. The vibrational data of the 1:2 complexes*

Complex	ν(Hg—Cl) ir	ν(Hg—Cl) R	ν(Hg—P) ir	ν(Hg—P) R	δ ir	δ R
$HgCl_2(P(4\text{-}Me_2NC_6H_4)_3)_2$	219vs	219vs	—	—	90	78
	208sh	208sh	—	—		
	215sh	—	—	—	90	
	207s					
$HgCl_2(P(4\text{-}MeOC_6H_4)_3)_2$	237s	241s	—	—	95	
	226	—	—	—		
	232sh	—	—	—	90	
	220s	—	—	—	90	
$HgCl_2(P(4\text{-}MeC_6H_4)_3)_2$	237s	237s	157w	158w	97	106
	226s	—	153w	—		
$HgCl_2(P(C_6H_5)_3)_2$	225s	225sh	136vw	136m	111	108
	215s	215s	—	—		
	226s	—	—	—	90	
$HgCl_2(P(4\text{-}FC_6H_4)_3)_2$	228vs	228s	159m	158m	91	
	216s	218sh	—	—		
	229s	—	160w	—	90	
$HgCl_2(P(4\text{-}ClC_6H_4)_3)_2$	242s	243m	149w	147sh	90	95

* The lines represent predicted frequencies that were not observed. The solid state samples were run as paraffin oil mulls. The solution spectra (underscored) were run in concentrated $CHCl_3$ solution in sealed polyethylene cells.

band is seen in those spectra where this absorption is seen at all. The most likely explanation is that the predicted bands are very close in frequency and therefore not resolved.

In the 1:2 complexes, both the symmetric and antisymmetric stretching modes are predicted to be both ir and Raman active. With the exception of the spectrum of $HgCl_2(P(4\text{-}ClC_6H_4)_3)_2$, both Hg—Cl stretching bands are clearly separated and assignable because of their strength and previously observed frequencies (16, 17). A comment on the assignment of the symmetries of the two bands is important at this point, however. We have assumed in the past that the stronger Raman band is the symmetric mode and the stronger ir band is the antisymmetric mode (16). The fact that the same band was found to be the stronger in both spectra in several cases in this study shows that this is not a valid method of assignment. The symmetries therefore remain unassigned. The frequencies observed in the 1:2 series (200 cm^{-1} to 240 cm^{-1}) are significantly lower than those observed in the 1:1 series. This is expected because of the greater competition from the extra phosphine donor. The Hg—P bands appear in the same region as before. The bands get progressively weaker as the basicity of the phosphine increases, to the point that in the spectra of $HgCl_2(P(4MeOC_6H_4)_3)_2$ and $HgCl_2(P(4\text{-}Me_2NC_6H_4)_3)_2$ there are no bands which could be reasonably assigned to these modes. Again, some low frequency bands are seen which are most likely deformation modes but further assignment is not possible for the same reasons as before. Their presence in the solution spectra confirms that they indeed arise from skeletal modes and not lattice modes. The similarity of not only the general features of the solution and solid state spectra but of their absolute frequencies indicates that the structures do not change significantly upon dissolution.

It was hoped, perhaps naively, that the systematic changes in the basicity of the phosphines would show up as trends in the vibrational spectroscopic parameters. Inspection of the data shows generally this is not the case. This is without doubt due to extensive coupling of the vibrational modes which is masking any trends which may otherwise have been present. The data do show, however, that there is consistency of structure through the two series as the phosphine is changed.

^{31}P and ^{199}Hg nuclear magnetic resonance spectra

The nmr data are given in Tables 3 and 4. The ^{31}P and ^{199}Hg nmr spectra of each 1:2 complex were run at the concentrations and temperatures given in the tables. They were dissolved in CH_2Cl_2 containing about 10% CD_2Cl_2 to provide a lock signal.

Can. J. Chem. Downloaded from www.nrcresearchpress.com by 210.87.254.6 on 09/06/12
For personal use only.

TABLE 3. Nuclear magnetic resonance data of the 1:1 complexes

Complex	δ(P) (ppm)	Δ (ppm)	^1J(Hg—P) (Hz)	Temp. (°C)
$[HgCl_2P(4\text{-}Me_2NC_6H_4)_3]_2$	33.6	45.3	7510	30
$[HgCl_2P(4\text{-}MeOC_6H_4)_3]_2$	31.5	42.1	7660	30
$[HgCl_2P(4\text{-}MeC_6H_4)_3]_2$	33.3	41.6	7500	30
$[HgCl_2P(C_6H_5)_3]_2$	34.0	40.4	7668	−60
$[HgCl_2P(4\text{-}FC_6H_4)_3]_2$	31.1	40.4	*	−60
$[HgCl_2P(4\text{-}ClC_6H_4)_3]_2$	31.8	41.0	*	−60

* Satellites were not seen because of the virtual insolubility of these complexes. The solutions were saturated but very weak.

TABLE 4. Nuclear magnetic resonance data of the 1:2 complexes*

Complex	δ(P) (ppm)	Δ (ppm)	δ(Hg) (ppm)	^1J(Hg—P) (Hz)	[Hg] (m*M*)	Temp. (°C)
$HgCl_2(P(4\text{-}Me_2NC_6H_4)_3)_2$	27.1		−426	4990	100	0
	27.1		−421	5015	100	−30
	27.1		−415	5048	100	−60
	27.0		−425	4975	50	0
	27.1		−420	5018	50	−30
	27.0	37.9	−413	5044	50	−60
	26.9		−425	4988	25	0
	27.0		−419	5036	25	−30
	27.0		−421	5068	25	−60
$HgCl_2(P(4\text{-}MeOC_6H_4)_3)_2$	25.1	35.7	−386	4942	50	−60
$HgCl_2(P(4\text{-}MeC_6H_4)_3)_2$			−381	4808	200	−30
			−383	4922	200	−60
			−380	4820	100	−30
	27.4		−384	4922	100	−60
			−380	4818	50	−30
	27.4	35.7	−383	4911	50	−60
	26.5		−378	4760	25	0
	26.9		−383	4868	25	−30
	27.7		−385	4976	25	−60
$HgCl_2(P(C_6H_5)_3)_2$	30.9	37.2	−372	4829	33†	−60
$HgCl_2(P(4\text{-}FC_6H_4)_3)_2$	28.0	37.3	−368	4880	50	−60
$HgCl_2(P(4\text{-}ClC_6H_4)_3)_2$	28.4	37.1	−364	4780	50	−60

* Samples were run at measured concentrations at the indicated temperatures in CH_2Cl_2/10% $CDCl_2$. Chemical shifts are reported with respect to 85% H_3PO_4 (^{31}P) or $(CH_3)_2Hg$ (^{199}Hg) on the delta scale. The coupling constants in the ^{31}P and ^{199}Hg spectra agreed to within 15 Hz and the numbers reported are averages of the two values.

† Saturated solution.

Because of the very low solubilities of the 1:1 complexes, they were run as saturated, but very dilute, solutions in the same solvent. Collection of their spectra at 24.4 MHz at low temperatures was judged impractical because of the time involved – about 2 days each. However, the complexes of the three most basic phosphines,[3] $P(4\text{-}Me_2NC_6H_4)_3$, $P(4\text{-}MeOC_6H_4)_3$, and $P(4\text{-}MeC_6H_4)_3$, are sufficiently non-labile to permit observation of the ^{199}Hg satellites at ambient probe temperature, about 30°C. The ambient temperature ^{31}P spectrum of $[HgCl_2\text{-}P(C_6H_5)_3]_2$ consisted of one broad peak and coupling was not observed. The 1:1 complexes of the two least basic phosphines, $P(4\text{-}FC_6H_4)_3$ and $P(4\text{-}ClC_6H_4)_3$, gave no observable signals after 200 000 pulses.

When the ^{31}P spectrum was measured at 163 MHz, the ^{199}Hg satellites in the spectrum of the $P(C_6H_5)_3$ complex were observed after about 10 000 transients were collected at −60°C. Attempts to obtain the ^{31}P spectra of $[HgCl_2P(4\text{-}FC_6H_4)_3]_2$ and $[HgCl_2P(4\text{-}ClC_6H_4)_3]_2$ at high field yielded only sharp singlets with very poor signal-to-noise ratios that did not allow the observation of the ^{199}Hg satellites.

Variation of the nuclear magnetic resonance parameters with phosphine basicity

Throughout the 1:2 series, ^1J(Hg—P) increases with increasing phosphine basicity although the values for $HgCl_2(P(C_6H_5)_3)_2$ and $HgCl_2(P(4\text{-}FC_6H_4)_3)_2$ are out of order. The coordination chemical shift, Δ, (δ complex − δ phosphine) follows ^1J(Hg—P) even to the point of the same two values being out of order. The ^{199}Hg chemical shifts show that the Hg atom becomes more shielded as the phosphine becomes more basic. As expected, the ^{199}Hg nmr spectra consisted of 1:2:1 triplets with spacing of ^1J(Hg—P).

The reasons for the trends in ^1J(Hg—P) as the phosphine or other ligands are changed have been a matter of much discussion (3–11). In Hg(II)–phosphine complexes, the expected

[3] Taken from ref. 1, the phosphines, in order of increasing basicity have pK_a values as follows: $P(4\text{-}XC_6H_4)_3$, (X = Me_2N, 8.65; MeO, 4.57; Me, 3.84; H, 2.73; F, 1.97; Cl, 1.03).

Can. J. Chem. Downloaded from www.nrcresearchpress.com by 210.87.254.6 on 09/06/12
For personal use only.

increase in the *s* electron density at the nuclei as the donor ability of the ligand is increased has usually been invoked to explain trends. However, some recent work has shown that this may not be as important as was once thought (18).

Indeed, in some Sn—Sn compounds it has been found that the *s* electon density, as reflected in the Mossbauer spectra, changes very little even though ^1J(Sn—Sn) varies greatly (19). We have previously proposed (1) that hybridisation changes, consistent with Bent's rule[4] could be responsible for the decrease in ^1J(P—H) with increasing basicity in some protonated phosphines and the same mechanism seems to be at work in a series of $P(C_6H_5)_3$ complexes: $HgX_2(P(C_6H_5)_3)_2$; X = NO_3, SCN, I, CN (20). Crystal structures of these compounds show that as X becomes more electronegative, the P—Hg—P angle opens up and the X—Hg—X angle closes. This rehybridisation, assuming only *s* and *p* orbitals are being used by Hg, is consistent with Bent's rule. That is, as X becomes more electronegative, the Hg orbitals directed towards X gain more *p* character. Therefore the orbitals bonding to the phosphines gain in their *s* character and ^1J(Hg—P) is increased.

It is reasonable to suspect that changing the basicity (electronegativity) of the phosphorus ligand in the presence of a constant X should lead to similar results. The Hg orbitals directed towards the more basic phosphines should increase their *s* character and thereby increase ^1J(Hg—P). This, of course, is consistent with the data presented in this study and in previous work. Currently, single crystal X-ray studies are underway to test this hypothesis.

The 1 : 1 complexes all have much higher coupling constants. The small bridging Cl—Hg—Cl angle in $[HgCl_2P(C_6H_5)_3]_2$ (<90°) (12) shows that there is little, if any, *s* character in these Hg orbitals. It therefore must be concentrated in the Hg—P and Hg—Cl (terminal) bonds. This helps to explain the large increase in ^1J(Hg—P) over the 1 : 2 complexes. It also indicates that because the *s* character is already concentrated in the terminal Hg orbitals, any small hybridisation changes would have little effect on the *s* character in them and therefore in these complexes ^1J(Hg—P) should be less sensitive to the basicity of the phosphine. No trend is apparent at all in the data in Table 1. This is not unexpected, however. Since the effect of substituting more electropositive groups on the phosphorus atom is to decrease the *s* character of the lone pair (and hence to decrease ^1J(Hg—P)), the rehybridisation effects on the two atoms (P and Hg) are opposite. It therefore appears that the two effects are of similar size and largely cancel whereas in the 1 : 2 series the hybridisation changes on the Hg atom are dominant.

The concentration and temperature dependence of ^1J(Hg—P)

During our work on Hg(II)–phosphine complexes it was found that, while both δ(P) and δ(Hg) were highly reproducible, ^1J(Hg—P) often varied by as much as 100 Hz. This occurred even when both nmr solutions were prepared from the same solid sample. An investigation revealed that, apart from the previously reported temperature dependence, ^1J(Hg—P) was also dependent upon the concentration of the sample.

The two complexes, $HgCl_2(P(4\text{-}MeC_6H_4)_3)_2$ and $HgCl_2(P(4\text{-}Me_2NC_6H_4)_3)_2$, were chosen for study because of their unusually high solubilities. Plots of ^1J(Hg—P) vs. temperature at various concentrations are shown in Figs. 1 and 2. They both show the familiar decrease of ^1J(Hg—P) with increasing temperature but there are significant deviations from the linearity described by Grim *et al.* (6).

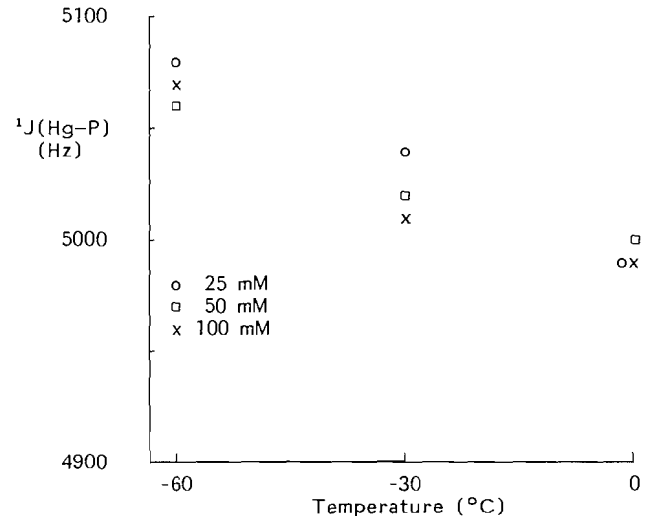

FIG. 1. Concentration and temperature dependences of ^1J(Hg—P) for $HgCl_2(P(4\text{-}Me_2NC_6H_4)_3)_2$.

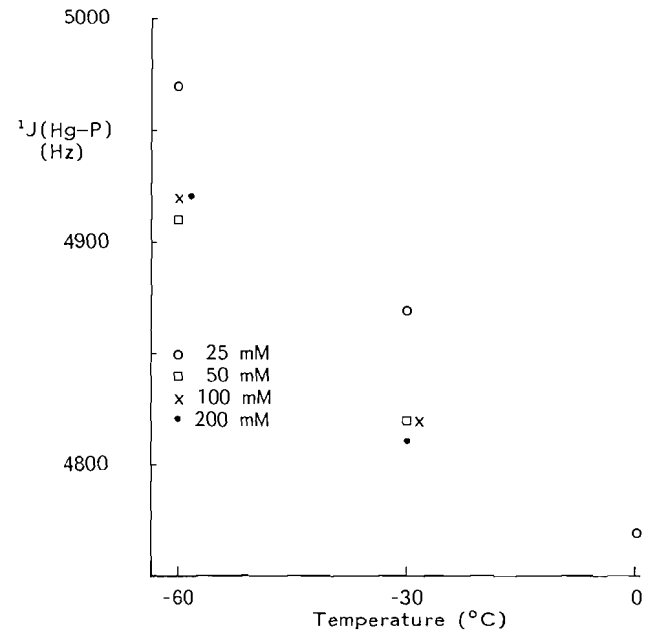

FIG. 2. Temperature and concentration dependences of ^1J(Hg—P) for $HgCl_2(P(4\text{-}MeC_6H_4)_3)_2$.

Because the ^{31}P spectra were proton decoupled, uncertainty in the sample temperature due to inductive r.f. heating from the decoupler was considered to be a possibility. Because of this, some experiments were carried out with the "phosphine thermometer" described in the experimental section. It was found that while continuous decoupling with 5.0 W of power did raise the sample temperature, there was no observable increase if the decoupler was gated, as described in the experimental section, to give an 11.3% duty cycle.

The concentration dependence appears to be greatest at low concentrations. The line for $HgCl_2(P(4\text{-}Me_2NC_6H_4)_3)_2$ at 25 mmol dm^{-3} is a large distance from the others which are almost

[4] Bent's rule predicts that the orbitals directed towards the most electropositive substituents will have the most *s* character and that the electronegative substituents will bond to orbitals with higher *p* character. See ref. 24.

Can. J. Chem. Downloaded from www.nrcresearchpress.com by 210.87.254.6 on 09/06/12
For personal use only.

TABLE 5. Analytical data of the complexes

Complex	Melting point (°C)	Elemental analysis %C found	%C (calcd.)	%H found	%H (calcd.)
$[HgCl_2P(4\text{-}Me_2NC_6H_4)_3]_2$*	281–284	43.7	(43.5)	4.8	(4.6)
$[HgCl_2P(4\text{-}MeOC_6H_4)_3]_2$	242–245	41.4	(40.4)	3.7	(3.4)
$[HgCl_2P(4\text{-}MeC_6H_4)_3]_2$	308–309 dec.	43.7	(43.8)	3.7	(3.7)
$[HgCl_2P(C_6H_5)_3]_2$	320–325 dec.	40.6	(40.5)	2.9	(2.8)
$[HgCl_2P(4\text{-}FC_6H_4)_3]_2$	275–280	37.4	(36.8)	2.1	(2.1)
$[HgCl_2P(4\text{-}ClC_6H_4)_3]_2$	300–302 dec.	35.0	(33.9)	2.1	(1.9)
$HgCl_2(P(4\text{-}Me_2NC_6H_4)_3)_2$†	280 dec.	53.2	(54.7)	5.8	(5.7)
$HgCl_2(P(4\text{-}MeOC_6H_4)_3)_2$	217–220	51.4	(51.7)	4.4	(4.3)
$HgCl_2(P(4\text{-}MeC_6H_4)_3)_2$	280–282	56.4	(57.3)	4.8	(4.8)
$HgCl_2(P(C_6H_5)_3)_2$	250–251	54.0	(54.3)	3.8	(3.8)
$HgCl_2(P(4\text{-}FC_6H_4)_3)_2$	267	48.3	(47.8)	2.8	(2.7)
$HgCl_2(P(4\text{-}ClC_6H_4)_3)_2$	120–122	43.4	(43.2)	2.8	(2.4)

*%N = 6.3 (6.3).
†%N = 8.2 (8.0).

coincident. $HgCl_2(P(4\text{-}Me_2NC_6H_4)_3)_2$ shows a smaller concentration effect.

Two reasons for the temperature effect have been put forward but they both appear untenable. Phosphine exchange (11) cannot be responsible because the ^{199}Hg satellites are sharp, sometimes at 0°C, showing that the exchange process has become slow on the nmr time scale. Yet, $^1J(Hg—P)$ continues to increase unabated 60°C below this temperature. Halogen exchange is also known to proceed (21). It was shown that when the nmr spectrum of a mixture of $HgCl_2(P(n\text{-}butyl)_3)_2$ and $HgBr_2(P(n\text{-}butyl)_3)_2$ was taken, cooling to −120°C was necessary to see three species, the starting materials and the mixed halide complex. Cooling to −50°C sufficed for the analogous $P(4\text{-}Me_2OC_6H_4)_3$ complexes. We find that a mixture of $HgBr_2(P(4\text{-}MeC_6H_4)_3)_2$ and $HgCl_2(P(4\text{-}MeC_6H_4)_3)_2$ gives a ^{31}P nmr spectrum at −40°C which shows the three species present. Again, the exchange process has become slow but the variation of $^1J(Hg—P)$ continues. Solvation almost certainly plays a role in this phenomenon but exactly what it is and why mercury has this unique property remain unclear.

Experimental

Materials

The phosphines were prepared and purified as described previously (1). Solvents and mercuric chloride were reagent grade and used as received. Analyses were performed by Guelph Chemical Laboratory, Guelph. Melting points were measured using a Gallenkamp apparatus with a calibrated thermometer. Analytical data are summarised in Table 5.

Preparation of the complexes

1:1 Complexes

The 1:1 complexes can be prepared by stirring a slurry of $HgCl_2$ in a dichloromethane solution of the phosphine and filtering off the insoluble product. However, this tends to be slow and it is difficult to tell when the reaction is complete. Therefore the following method was used. $HgCl_2$ (1 mmol) was dissolved in THF (10 mL) and added slowly to a solution of the phosphine in CH_2Cl_2 (100 mL). The complex precipitated immediately and was filtered off and dried. The yield is quantitative.

1:2 Complexes

The 1:2 complexes of all the phosphines except $P(4\text{-}ClC_6H_4)_3$ and $P(4\text{-}FC_6H_4)_3$ were prepared as follows. A solution of $HgCl_2$ (1 mmol) in THF (10 mL) was added to a solution of the phosphine (2 mmol) in CH_2Cl_2 (20 mL). The solution was reduced in volume until crystallization commenced and a small amount of Et_2O was added to precipitate the complex. The crude complex was recrystallized from CH_2Cl_2/Et_2O to give white crystalline products. The yield was about 50–60%. Attempts to prepare $HgCl_2(P(4\text{-}ClC_6H_4)_3)_2$ and $HgCl_2(P(4\text{-}FC_6H_4)_3)_2$ by this method yielded only the 1:1 complexes. Grim *et al.* (6) noted similar difficulties in trying to prepare these complexes. To prepare them, the phosphine (10 mmol) was dissolved in hot 1,2-dichloroethane (10 mL) and powdered $HgCl_2$ (1 mmol) was added. After a few minutes the solution cleared and it was allowed to cool. Stirring with a glass rod helped to initiate the crystallization of the complex along with much free phosphine. The crude product was filtered off and washed with Et_2O to leave a white crystalline product. The yield was about 70–80%.

Nuclear magnetic resonance measurements

The ^{31}P nmr spectra of the 1:1 complexes $[HgCl_2P(4\text{-}Me_2NC_6H_4)_3]_2$, $[HgCl_2P(4\text{-}MeOC_6H_4)_3]_2$, and $[HgCl_2P(4\text{-}MeC_6H_4)_3]_2$ were collected on a Bruker WP-60 nmr spectrometer operating at 24.4 MHz. The ambient probe temperature was about 30°C. The recycle time was 2 s with the decoupler being gated on during acquisition only.

The ^{31}P and ^{199}Hg nmr spectra of all the other complexes were obtained using $CH_2Cl_2/10\%$ CD_2Cl_2 solutions in non-spinning 10-mm tubes at the temperatures and concentrations given on a Bruker WH-400 nmr spectrometer. Usually the same samples were used for measurements of both nuclei. To ensure the accuracy of the temperature measurements the ^{31}P nmr spectrum of a solution of $P(C_6H_5)_3$ and $OP(C_6H_5)_3$ (0.1 mmol dm^{-3} each) in toluene was measured at each temperature (22). Because the chemical shift difference of these compounds is a linear function of temperature, the sample temperature could be found directly. Usually the temperature found this way was within 1 K of the controller's reading and this is believed to be the uncertainty in the temperature. It was found that 20 min were necessary to ensure that thermal equilibrium was reached after inserting the samples and this delay was used for all the samples. In order to prevent the precipitation of $[HgCl_2P(4\text{-}ClC_6H_4)_3]_2$ from solutions of $HgCl_2(P(4\text{-}ClC_6H_4)_3)_2$, one extra mole of phosphine was added to the solutions.

^{31}P nuclear magnetic resonance spectra

The spectra were acquired into 4K blocks. The FIDs were given an exponential line-broadening of 3 Hz and were zero filled to 8K before Fourier transformation. The sweep width used was 6024 Hz giving an acquisition time of 0.340 s and a digital resolution of 1.5 Hz. 90° (32 μs) pulses were used. The broadband decoupler was gated on during

Can. J. Chem. Downloaded from www.nrcresearchpress.com by 210.87.254.6 on 09/06/12
For personal use only.

acquisition only and a preacquisition delay was added to give a total recycle time of 3 s. The reference was 85% H_3PO_4.

^{199}Hg nuclear magnetic resonance spectra

The spectra were acquired into 4K blocks. They were given an exponential line broadening of 50 Hz and were zero filled to 8K before Fourier transformation. A sweep width of 15.151 kHz was used, giving an acquisition time of 0.135 s and a digital resolution of 3.7 Hz. 90° pulses were used with no relaxation delay. Preliminary experiments showed that use of the decoupler had no effect on the line widths (about 100–500 Hz) so the spectra were collected with no decoupling. The chemical shifts were referenced by observing internal TMS and using its absolute frequency to calculate the frequency of $(CH_3)_2Hg$ (23). Shifts are reported on the delta scale with respect to this frequency.

Vibrational measurements

The solid Raman samples were contained in melting point capillary tubes and were run on a Jarrell–Ash spectrophotometer. The 514.5 nm line of an Ar^+ laser was used for excitation and the spectra were calibrated from the known frequencies of the plasma lines. The conditions were: scan speed, 1 cm^{-1}/s; time constant, 1 s; laser power, 0.5 W; slit width, 3.0 cm^{-1}. Attempts to obtain solution Raman spectra of the most soluble complexes failed because of insufficient solubility.

All infrared spectra were obtained on a Perkin–Elmer 180 spectrometer with the far ir option. The solid samples were run as paraffin oil mulls spread on polyethylene disks. The solution spectra were obtained using sealed polyethylene cells of our own construction containing concentrated $CHCl_3$ solutions. The Hg lamp, probably because of its high uv emission, decomposed some samples so the Globar was used exclusively.

Acknowledgements

The Natural Sciences and Engineering Research Council of Canada is thanked for its support. Thanks also go to Dr. E. C. Alyea for reading the manuscript and making helpful comments. The nmr spectra were run at the South Western Ontario NMR Centre.

1. T. ALLMAN and R. G. GOEL. Can. J. Chem. **60**, 716 (1982).
2. R. L. KEITER and S. O. GRIM. Chem. Commun. 512 (1968).
3. P. S. PREGOSIN and R. W. KUNZ. NMR principles and progress. Vol. 16. Springer Verlag, New York. 1979.
4. S. O. GRIM, P. J. LUI, and R. L. KEITER. Inorg. Chem. **13**, 342 (1974).
5. E. C. ALYEA, S. A. DIAS, R. G. GOEL, W. O. OGINI, P. PILON, and D. W. MEEK. Inorg. Chem. **17**, 1697 (1978).
6. S. O. GRIM, D. P. SHAH, C. K. HAAS, J. M. RESSMER, and P. H. SMITH. Inorg. Chim. Acta, **36**, 139 (1979).
7. E. C. ALYEA and S. DIAS. Can. J. Chem. **57**, 83 (1979).
8. T. ALLMAN and R. G. GOEL. Inorg. Nucl. Chem. Lett. **15**, 199 (1979).
9. T. ALLMAN and R. G. GOEL. Can. J. Chem. **62**, 621 (1984).
10. R. COLTON and D. DAKTERNIEKS. Aust. J. Chem. **34**, 2323 (1981).
11. S. O. GRIM and D. P. SHAH. Inorg. Nucl. Chem. Lett. **14**, 105 (1978).
12. N. A. BELL, M. GOLDSTEIN, T. JONES, and I. A. NOWELL. Inorg. Chim. Acta, **43**, 87 (1980).
13. T. JONES. Ph.D. Thesis, Sheffield City Polytechnic, Pond Street, Sheffield S1 1WB, U.K.
14. L. FALTH. Chem. Scr. **9**, 71 (1976).
15. G. B. DEACON, J. H. S. GREEN, and D. J. HARRISON. Spectrochim. Acta Part A, **24**, 1921 (1968).
16. T. ALLMAN and R. G. GOEL. Spectrochim. Acta Part A, **35**, 923 (1979), and references contained therein.
17. K. NAKAMOTO. Infrared and Raman spectra of inorganic and coordination compounds. 3rd ed. Wiley, New York. 1978.
18. R. W. KUNZ. Helv. Chim. Acta, **63**, 2054 (1980).
19. T. N. MITCHELL and M. EL-BEHAIRY. Helv. Chim. Acta, **63**, 628 (1981).
20. H. B. BUERGI, R. W. KUNZ, and P. S. PREGOSIN. Inorg. Chem. **19**, 3707 (1980).
21. R. C. COLTON and D. DAKTERNIEKS. Aust. J. Chem. **33**, 955 (1980); **33**, 1463 (1980).
22. F. L. DICKERT and S. W. HELLMAN. Anal. Chem. **52**, 996 (1980).
23. R. G. KIDD and R. J. GOODFELLOW. The transition metals. *In* NMR and the periodic table. *Edited by* R. K. Harris and B. E. Mann. Academic Press, London. 1978.
24. H. A. BENT. Can. J. Chem. **38**, 1235 (1960); J. Chem. Educ. **37**, 616 (1960).

Can. J. Chem. Downloaded from www.nrcresearchpress.com by 210.87.254.6 on 09/06/12
For personal use only.

A ^{31}P and ^{199}Hg nuclear magnetic resonance and vibrational spectroscopic study of phosphine complexes of $Hg(ClO_4)_2$

TIM ALLMAN AND RAM G. GOEL[1]

Guelph–Waterloo Centre for Graduate Work in Chemistry, University of Guelph, Guelph, Ont., Canada N1G 2W1

Received May 3, 1983

TIM ALLMAN and RAM G. GOEL. Can. J. Chem. **62**, 621 (1984).

Cationic complexes of the type $[Hg(phosphine)_n](ClO_4)_2$ (n = 2, 3, 4) (phosphine = P(t-Bu)$_3$, PCy_3, P(4-$Me_2NC_6H_4$)$_3$, P(4-$MeOC_6H_4$)$_3$, P(4-MeC_6H_4)$_3$, P(3-MeC_6H_4)$_3$, P(2-MeC_6H_4)$_3$, P(4-FC_6H_4)$_3$, P(4-ClC_6H_4)$_3$) have been prepared and studied by vibrational spectroscopy in the perchlorate and low frequency regions, as well as by ^{31}P and ^{199}Hg nmr. The skeletal Hg—P frequencies have been assigned in both solution and the solid state. It was found that ^1J(Hg—P) decreases with increasing phosphine basicity and that it is also dependent upon sample concentration and temperature.

TIM ALLMAN et RAM G. GOEL. Can. J. Chem. **62**, 621 (1984).

On a préparé des complexes cationiques du type $[Hg(phosphine)_n](ClO_4)_2$ (n = 2, 3, 4) (phosphine = P(t-Bu)$_3$, PCy_3, P(4-$Me_2NC_6H_4$)$_3$, P(4-$MeOC_6H_4$)$_3$, P(4-MeC_6H_4)$_3$, P(3-MeC_6H_4)$_3$, P(2-MeC_6H_4)$_3$, P(4-FC_6H_4)$_3$ et P(4-ClC_6H_4)$_3$) et on les a étudiés par spectroscopie vibrationnelle dans les régions du perchlorate et des basses fréquences ainsi que par rmn du ^{31}P et du ^{199}Hg. On a attribué les fréquences du squelette Hg—P tant en solution qu'en phase solide. On a trouvé que la valeur de J(Hg—P) diminue avec une augmentation de la basicité des phosphines et que cette valeur varie aussi avec la température ainsi qu'avec la concentration de l'échantillon.

[Traduit par le journal]

Can. J. Chem. Downloaded from www.nrcresearchpress.com by 210.87.254.105 on 09/06/12
For personal use only.

Introduction

In phosphine complexes of Hg(II) usually both the phosphines and the anions are strongly coordinated to the metal centre. There are, however, some cationic complexes of $HgCl_2$ with trimethylphosphine in which one or both of the chloro ligands have been displaced by the phosphines (1–3). A very weakly coordinating anion will also produce cationic species and in a previous communication (4) we reported some ^{31}P nmr data on nine complexes of the general formula $[Hg(phosphine)_2](ClO_4)_2$. The most striking aspect of this series was that ^1J(Hg—P) decreased with increasing phosphine basicity, opposite the trend usually seen in Hg(II)–phosphine complexes (5).

Colton and Dakternieks (6) studied these complexes by ^{31}P and ^{199}Hg nmr but they were not characterised by other spectroscopic techniques. Most recently, the electrochemical reduction of these complexes was used in an attempt to study ligand exchange reactions (7).

In the present work, some *para*-substituted triarylphosphines which have very different basicities but similar steric requirements (8), as well as other tertiary phosphines of current interest, were used to prepare complexes of $Hg(ClO_4)_2$ in stoichiometries of 1:2, 1:3, and 1:4 (Hg/P). Their ^{31}P and ^{199}Hg nmr parameters are reported as well as their characterisation by vibrational spectroscopy in both the perchlorate and the low frequency regions.

It has been shown (5) that ^1J(Hg—P) in the $HgCl_2P_2$ series has a significant concentration dependence in addition to the previously known temperature dependence (9, 10). The $Hg(ClO_4)_2$ complexes also have this property and an investigation of this effect is presented.

[1] Because of the untimely death of Professor Ram G. Goel on November 8, 1982, the two consecutive papers in this volume will be the last in which he is an author. Through patience and understanding, Ram helped to generate interest and develop research skills in chemistry for many students over his 15 years at the University of Guelph. He will be deeply missed.

Results and discussion

Vibrational spectra and structures

Perchlorate region

In an environment of perfect tetrahedral symmetry the vibrational spectra of the perchlorate ion consist of four bands: ν_1(ν_s(Cl—O)), (A_1 symmetry); ν_2(δ(Cl—O)), (E); ν_3(ν_a(Cl—O)), (T_2); and ν_4(δ(Cl—O)) (T_2). All are Raman active. The modes ν_3 and ν_4 are also infrared active (11). Lowering the symmetry, either by coordination or by placing the ion in a site of low symmetry, causes splitting of the formerly degenerate ν_3 and ν_4 modes and the appearance of ν_1 and ν_2 in the ir spectrum.

The ir spectra of the 1:2 complexes (see Table 1) indicate that in almost every case there is a significant lowering of the perchlorate symmetry. The crystal structure of $[Hg(PCy_3)_2](ClO_4)_2$ shows that there is some Hg—O interaction even though the distance is large (12). There is significant deviation from linearity ($\angle$P—Hg—P = 170°) which was attributed to the intrusion of the anions. The loss of T_d symmetry causes the splitting of ν_3 and the appearance of ν_1 in the ir in the solid state. The structure of Pt(P(t-Bu)$_3$)$_2$ shows (13) that the phosphine completely enshrouds the metal atom. It is reasonable to assume that the Hg complex is very similar, making Hg—O interactions impossible. Yet, the ir spectrum of this complex shows a large splitting of ν_3 and both ν_1 and ν_2 are active. Clearly, band counting in the solid state spectra is not a very useful way of determining whether the anion is coordinated in these complexes. More meaningful conclusions can be drawn from the spectra run in solution. Although the conductivities of the complexes in nitromethane show that they are all 1:2 electrolytes, the solution ir spectra in CH_2Cl_2 still show a lowering of the perchlorate symmetry. This lowering of symmetry appears most in the complexes with the least basic phosphines, indicating that in these complexes there is some sort of anion–cation interaction.

The 1:3 complexes give spectra that are closer to the ideal. The ν_1 band remains active in the spectra of most of the complexes in both the solid state and in solution, but splitting of ν_3

TABLE 1. The infrared ClO_4^- frequencies of the complexes*

	ClO_4^- frequencies						
	ν_1		ν_2	ν_3		ν_4	
Phosphine	ss	soln	ss	ss	soln	ss	soln
1:2 Complexes							
$P(t\text{-}Bu)_3$	930m		460w	1045vs 1115vs	1100vs	620w	
PCy_3	930w			1060vs 1090vs	1100vs	620m	
$P(4\text{-}Me_2NC_6H_4)_3$		920vw		1100vs	1100vs	620m	
$P(4\text{-}MeOC_6H_4)_3$				1100vs	1105vs	619m	
$P(4\text{-}MeC_6H_4)_3$	925m	915w		1050vs 1140vs	1035w 1110vs	620s	
$P(3\text{-}MeC_6H_4)_3$	911m	920vw	465m	1027vs 1120vs	1030w 1110s	622s	
$P(2\text{-}MeC_6H_4)_3$	924w	910w	460m	1032vs 1098vs	1030w 1100s	623s	620w
$P(C_6H_5)_3$	924m	920w		1040vs 1110vs	1030w 1098s	620s	
$P(4\text{-}FC_6H_4)_3$	929vw	915m	480w	1060vs 1130vs	1030m 1110s	620s	
$P(4\text{-}ClC_6H_4)_3$	920w	915m	460w	1040vs 1120s	1025m 1110s	620s	
1:3 Complexes							
$P(4\text{-}Me_2NC_6H_4)_3$				1095vs	1100vs	621s	
$P(4\text{-}MeOC_6H_4)_3$	922m	915m		1095vs	1100vs	623m	620m
$P(4\text{-}MeC_6H_4)_3$	921m	910m		1090vs 1125s	1028vs 1110s	620m	622m
$P(3\text{-}MeC_6H_4)_3$	921m	910m		1095vs	1110vs	620m	622m
$P(C_6H_5)_3$	920w			1100vs	1110vs	625m	622m
$P(4\text{-}FC_6H_4)_3$		915m		1100vs	1110vs	625m	622w
$P(4\text{-}ClC_6H_4)_3$	925w	915m		1085vs	1110vs 1040vw	620m	618m
1:4 Complexes							
$P(4\text{-}Me_2NC_6H_4)_3$				1095vs	1110s	620m	620m
$P(4\text{-}MeOC_6H_4)_3$				1090vs	1110s	620m	620m
$P(4\text{-}MeC_6H_4)_3$				1085vs	1110s	620m	620m
$P(C_6H_5)_3$				1090vs	1110s	620m	620m

*The solid state (ss) spectra were run as paraffin oil mulls. Solution (soln) measurements were made on CH_2Cl_2 solutions contained in KBr cells. Absent frequencies were not observed.

is seen in only the $P(4\text{-}MeC_6H_4)_3$ and $P(4\text{-}ClC_6H_4)_3$ complexes. The crystal structure of $[Hg(P(4\text{-}MeOC_6H_4)_3)_3](ClO_4)_2$ (14) shows that there is no Hg—O interaction.

Each of the 1:4 complexes gives an infrared spectrum which is consistent with perfect tetrahedral ClO_4 symmetry in both solution and the solid state.

Low frequency region

The only studies of phosphine complexes of Hg(II) in which the anion is not coordinated to the metal have placed ν(Hg—P) near 350 cm^{-1} (1, 2). This region was examined very carefully by both ir and Raman techniques and no such bands were found in the spectra of the complexes reported herein. Because the complexes were expected to have very high symmetries, polarization measurements of the solution Raman spectra, where solubility permitted, were used to locate ν_s(Hg—P) and help to confirm the structures.

A linear P—Hg—P system ($D_{\infty h}$) should give rise to one Raman active polarized band due to ν_s(Hg—P), (Σ_g^+); one ir active band due to δ(Hg—P), (Π_u); and one ir active band due to ν_a(Hg—P), (Σ_u^+) (11). With the exception of the spectrum of $[Hg(P(4\text{-}FC_6H_4)_3)_2](ClO_4)_2$, all the spectra of the 1:2 complexes are consistent with this structure (see Table 2). For example, the solution Raman spectrum of $[Hg(P(4\text{-}Me_2NC_6H_4)_3)_2](ClO_4)_2$ has a polarized band at 129 cm^{-1} (130 cm^{-1} in the solid state) which is assigned to ν_s(Hg—P). Its solution ir spectrum contains a band at 159 cm^{-1} (ss 154 cm^{-1}) which is assigned to ν_a(Hg—P), and a broad band at 100 cm^{-1} (ss 106 cm^{-1}) which is assigned to δ(Hg—P). Similar assignments can be made for the other complexes.

The solid state ir spectrum of $[Hg(P(4\text{-}FC_6H_4)_3)_2](ClO_4)_2$ contains two skeletal bands at 168 cm^{-1} and 180 cm^{-1} and its Raman spectrum has a band at 165 cm^{-1}. The activity of both ν_s and ν_a in the ir spectrum and the correspondence of bands between the two spectra suggests a deviation from linearity in the solid state. Unfortunately the complex is not soluble enough for solution measurements. Interestingly, the spectra of $[Hg(PCy_3)_2](ClO_4)_2$, which is bent (12), are entirely consistent with the linear model.

The trigonal planar (D_{3h}) structure (which is now known for $[Hg(P(4\text{-}MeOC_6H_4)_3)_3](ClO_4)_2$) (14), should give rise to four skeletal bands. The first, ν_s(Hg—P), (A_1), is Raman active and

Can. J. Chem. Downloaded from www.nrcresearchpress.com by 210.87.254.105 on 09/06/12
For personal use only.

TABLE 2. Low frequency vibrational spectra*

Phosphine		Complexes 1:2 ν(Hg—P)		1:2 δ(Hg—P)		1:3 ν(Hg—P)	1:3 δ(Hg—P)	1:4 ν(Hg—P)	1:4 δ(Hg—P)
$P(t\text{-Bu})_3$	ir			90					
	R	130							
PCy_3	ir			88	90				
	R	145	143p						
$P(4\text{-Me}_2NC_6H_4)_3$	ir	154	159	106	100		100		80
	R	130	129p			118p			
$P(4\text{-MeOC}_6H_4)_3$	ir			100	100		100	100	
	R	143	132p	128		123p	116	116p	
$P(4\text{-MeC}_6H_4)_3$	ir	178		95			100		102
	R	166				123			
						123p		120p	
$P(3\text{-MeC}_6H_4)_3$	ir	177		100		139			
	R	148				134			
$P(2\text{-MeC}_6H_4)_3$	ir	157		100					
	R	188							
$P(C_6H_5)_3$	ir	180		80		139	100	119	
	R	161				142		130	
$P(4\text{-FC}_6H_4)_3$	ir	168, 180		90		125			
	R	165				122			
$P(4\text{-ClC}_6H_4)_3$	ir	170	164	90	80	148	85		
	R					142			
						140p			

* Solution values are underscored (CH_2Cl_2 for ir, $CHCl_3$ for R). All bands were of medium to weak intensity.

polarized. Another, ν_a(Hg—P), (E) is both Raman and ir active, as is one of the deformation modes δ (Hg—P), (E). The other deformation mode (A_2) is ir active only. Unfortunately, the bands were often very weak, especially ν_a(Hg—P), and the low solubilities often prevented solution measurements so that no single complex has an ideal set of spectra. However, taken as a group, all the essential features are there and no spectrum contained unexplainable "extra" skeletal bands. All of the 1:3 complexes are therefore assigned the trigonal planar structure found in the $P(4\text{-MeOC}_6H_4)_3$ complex.

No preliminary X-ray data are available for a 1:4 complex but the presence of the polarized Raman bands (ν_s(Hg—P), (A_1)) is strong evidence for a tetrahedral structure. In only one case is ν_a(Hg—P), (T_2) seen, but this is most likely a problem of low intensity. The deformation modes give rise to bands in the 100 cm^{-1} region as before.

There appears to be no simple trend that relates the vibrational parameters to phosphine basicity although often the highest frequencies are associated with the least basic phosphines. The sterically hindered $P(2\text{-MeC}_6H_4)_3$ ligand produces the highest value of ν_s(Hg—P) of the series. Why this occurs is not clear. The low pK_a of $P(4\text{-ClC}_6H_4)_3$ (8), along with the fact that its 1:4 complex does not form, even in solution, shows that it must be a very weak donor but it gave complexes with high ν_s(Hg—P) values. The greatest value of the spectra appears to be in their help in the structural assignments.

^{31}P and ^{199}Hg nuclear magnetic resonance spectra

The ^{31}P and ^{199}Hg data are given in Table 3. As expected, the ^{199}Hg spectra consist of 1:2:1 triplets, 1:3:3:1 quartets, and 1:4:6:4:1 quintets for the 1:2, 1:3, and 1:4 complexes respectively. The mercury chemical shift is most dependent upon the coordination number of the Hg atom with the shielding following the order 1:2 ≫ 1:4 > 1:3. There are, however, no obvious trends that relate to the basicity of the phosphine. The ^{31}P chemical shifts are also highly dependent upon the Hg coordination number with a shielding order 1:4 > 1:3 > 1:2. Neither the ^{31}P nor the ^{199}Hg chemical shift was found to vary much with either temperature or concentration.

The coupling constant, ^1J(Hg—P), decreases with increasing coordination number in a more or less linear fashion (see Fig. 1). This trend was observed in the series of trimethylphosphine complexes (1, 2) and reflects the decrease in s character of the Hg orbitals. ^1J(Hg—P) also decreases with increasing phosphine basicity although this effect diminishes as the coordination number increases.

It has been previously shown (8) that as the electron donating groups on the phosphorus atom become more electron donating, ^1J(P—X), where X is a fourth atom bonded to P, decreases. This was attributed to a lowering of the s character of the lone pair orbital. Such a rehybridisation would be in agreement with Bent's rule (15).

The Hg atom has been shown to respond similarly to electronic effects in the pseudotetrahedral HgX_2P_2 complexes (5, 16). The result of this is to increase ^1J(Hg—P) as the basicity of the phosphine increases and as the electronegativity of the anion decreases. Because the effects on ^1J(Hg—P) are opposite at the Hg and P atoms, it is apparent that the effects at mercury are dominant in determining ^1J(Hg—P).

In the cationic complexes the Hg atom cannot rehybridise in response to changes in the phosphine; the skeletal structures remain the same. Therefore only the effect of the phosphorus atom is seen and ^1J(Hg—P) decreases with increasing phosphine basicity. A plot of ^1J(Hg—P) vs. pK_a is given in Fig. 2. This gives a clue to the reason that this same trend is seen almost exclusively in complexes of transition metals with partially filled d orbitals but not in the main group of d^{10} complexes (17). The former have very highly preferred geom-

Can. J. Chem. Downloaded from www.nrcresearchpress.com by 210.87.254.105 on 09/06/12
For personal use only.

TABLE 3. ^{31}P and ^{199}Hg nmr data of the complexes*

Phosphine	δ(P) (ppm)	δ(Hg) (ppm)	^1J(Hg—P) (Hz)	[Hg] (m*M*)	Temp. (°C)
1:2 Complexes					
$P(t\text{-}Bu)_3$	122.1		3174	50	−60
PCy_3	78.7	−956	3800	50	−60
$P(4\text{-}Me_2NC_6H_4)_3$		−1244	3947	150	30
	47.8		3805	100	30
	47.8		3795		0
	47.1		3789		−30
	46.6		3769		−60
	48.5		3825	50	30
	47.8		3798		0
	47.5		3773		−30
	47.1	−1260	3716		−60
	47.8		3937	25	30
	47.5		3858		−30
	47.1		3771		−30
	46.5		3739		−60
$P(4\text{-}MeOC_6H_4)_3$		−1242	4774	400	0
		−1242	4783		−30
		−1248	4902		−60
		−1242	4767	200	0
		−1242	4782		−30
		−1247	4764		−60
	46.2		4775	100	30
	47.5	−1248	4776		0
	45.2	−1245	4765		−30
	44.8	−1248	4775		−60
	46.4		4769	50	30
	45.8		4762	50	0
	45.3		4755		−30
	44.7	−1254	4750		−60
	45.8		4760	25	0
	45.2		4756		−30
	44.9		4746		−60
$P(4\text{-}MeC_6H_4)_3$	49.8	−1241	4836	50	−60
$P(3\text{-}MeC_6H_4)_3$	51.9		4922	50	−60
$P(2\text{-}MeC_6H_4)_3$	51.9	−1141	4150	50	−60
$P(C_6H_5)_3$	47.2		5010	30	−60
$P(4\text{-}FC_6H_4)_3$	44.3		5200	50	−60
$P(4\text{-}ClC_6H_4)_3$	46.1	−1280	5329	50	30
	45.5		5321		0
	45.1		5307		−30
	44.5	−1314	5273		−60
	45.4		5291	25	0
	45.4		5280		−30
	45.4		5250		−60
1:3 Complexes					
$P(4\text{-}Me_2NC_6H_4)_3$	40.4	−542	2880	50	−60
$P(4\text{-}MeOC_6H_4)_3$	40.2	−497	3040	50	−60
$P(4\text{-}MeC_6H_4)_3$	43.3	−505	3025	50	−60
$P(3\text{-}MeC_6H_4)_3$	43.7		3077	50	−60
$P(C_6H_5)_3$	46.2		3109	50	−60
$P(4\text{-}FC_6H_4)_3$	44.0		3201	50	−60
$P(4\text{-}ClC_6H_4)_3$	42.4	−635	3269	50	−60
1:4 Complexes					
$P(4\text{-}Me_2NC_6H_4)_3$	25.6		2009	50	−60
$P(4\text{-}MeOC_6H_4)_3$		−557	2075	50	−60
	26.6	−547	2068	50	−60
$P(4\text{-}MeC_6H_4)_3$	31.4	−515	2075	50	−60
$P(3\text{-}MeC_6H_4)_3$	31.4		2082	50	−60
$P(C_6H_4)_3$	34.6		2079	50	−60

*All shifts are on the delta scale and are referenced to 85% H_3PO_4 (^{31}P) or $(CH_3)_2Hg$ (^{199}Hg). The spectra were measured at the concentrations and temperatures indicated using CH_2Cl_2/20% $CDCl_3$ as the solvent. The solution of $[Hg(P(C_6H_5)_3)_2](ClO_4)_2$ was found to be saturated at 30 m*M*. The chemical shifts are believed to be accurate to ±1 in the last digit, the coupling constants to ±15 Hz.

Can. J. Chem. Downloaded from www.nrcresearchpress.com by 210.87.254.105 on 09/06/12
For personal use only.

Can. J. Chem. Downloaded from www.nrcresearchpress.com by 210.87.254.105 on 09/06/12
For personal use only.

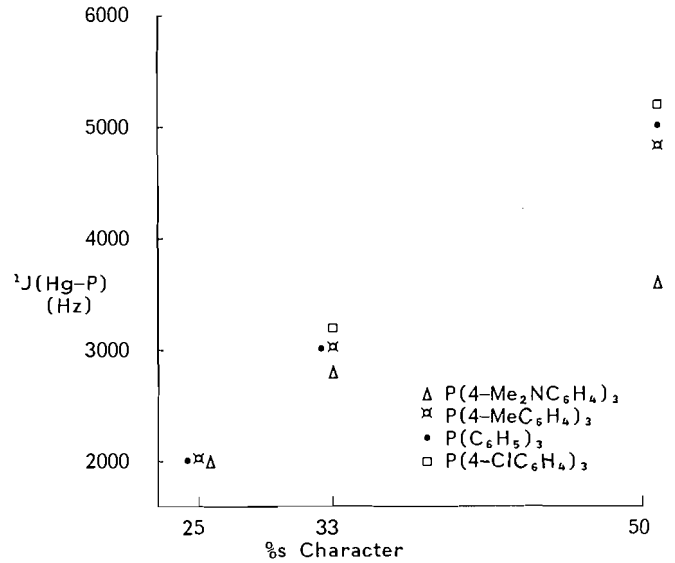

FIG. 1. A plot of ^1J(Hg—P) vs. *s* character of the Hg orbitals.

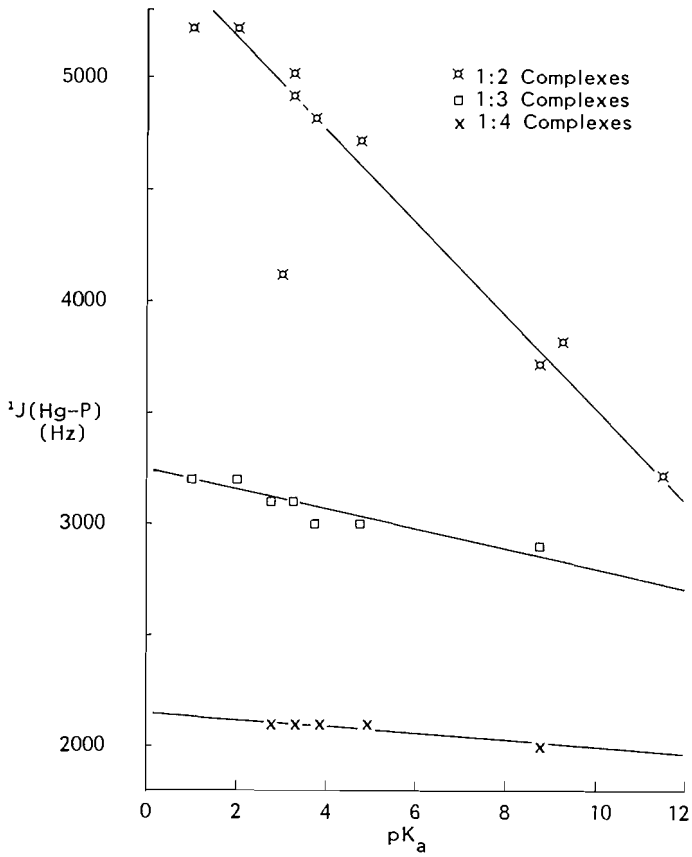

FIG. 2. A plot of ^1J(Hg—P) vs. pK_a of the phosphine.

etries, which precludes any significant hybridisation changes, while the latter have considerable flexibility.

The concentration and temperature dependences of ^{1}J(Hg—P)

The nmr parameters of phosphine complexes of the mercuric halides have been found to be both temperature and concentration dependent. Both phosphine exchange (9, 10) and halogen exchange (18) have been proposed as possible reasons for this effect. We critized these reasons as being untenable because both of these processes could be made slow on the nmr time scale by cooling without affecting the dependences (5).

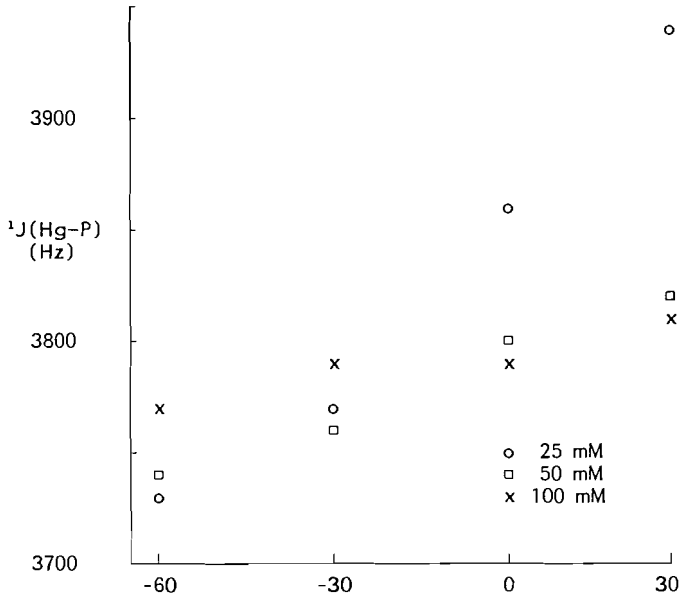

FIG. 3. Concentration and temperature dependence of ^1J(Hg—P) for $[Hg(P(4\text{-}Me_2NC_6H_4)_3)_2](ClO_4)_2$.

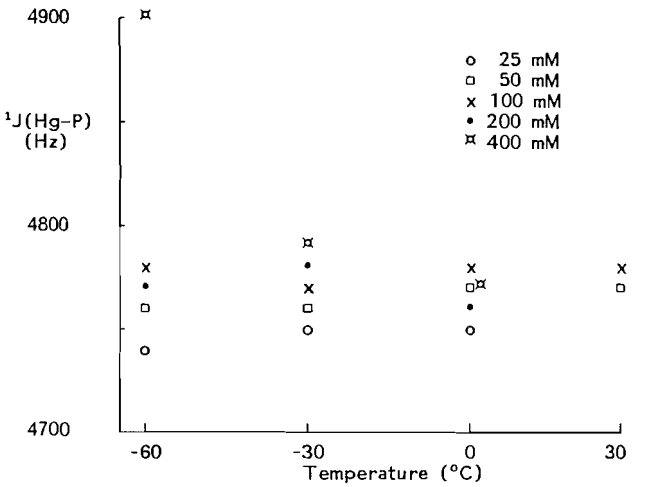

FIG. 4. Concentration and temperature dependence of ^1J(Hg—P) for $[Hg(P(4\text{-}MeOC_6H_4)_3)_2](ClO_4)_2$.

We then suggested solvation as a possibility. The data in this study confirm the above. The phosphines in these complexes exchange more slowly; coupling can be seen at 30°C for the 1:2 complexes. While the perchlorate anion probably interacts with the cations, the interaction is certainly very weak and is not expected to be significant in determining the nmr parameters. As can be seen in Figs. 3 and 4, the dependences vary with the complex and are not linear. They are also markedly different for each complex.

Experimental

Materials

The phosphines were prepared as previously reported (8). All other reagents and solvents were reagent grade and were used as received.

Preparation of the complexes

Complexes of P(t-Bu)$_3$ and P(2-MeC$_6$H$_4$)$_3$

To a solution of the phosphine (2.5 mmol) in 1:1 v/v CH_2Cl_2/ethanol (20 mL) was added solid $Hg(ClO_4)_2 \cdot 4H_2O$ (1 mmol). The solid dissolved and the solution was filtered if necessary. The complex was precipitated by the addition of diethylether. The crude products

TABLE 4. Analytical data of the complexes

Phosphine	Elemental analysis %C Found	%C (calcd.)	%H Found	%H (calcd.)	Molar conductance ohm^{-1} cm^2 mol^{-1}
1:2 Complexes					
$P(t\text{-}Bu)_3$	36.2	(35.9)	7.0	(6.8)	135
PCy_3	45.0	(45.2)	7.3	(6.9)	147
$P(4\text{-}Me_2NC_6H_4)_3$*	48.5	(48.8)	5.2	(5.1)	157
$P(4\text{-}MeOC_6H_4)_3$	45.8	(45.7)	3.6	(3.8)	162
$P(4\text{-}MeC_6H_4)_3$	49.8	(50.0)	4.8	(4.2)	123
$P(3\text{-}MeC_6H_4)_3$	50.4	(50.0)	4.8	(4.2)	148
$P(2\text{-}MeC_6H_4)_3$	50.0	(50.0)	4.5	(4.2)	166
$P(C_6H_5)_3$	46.6	(46.8)	3.2	(3.3)	145
$P(4\text{-}FC_6H_4)_3$	41.4	(41.7)	2.7	(2.5)	118
$P(4\text{-}ClC_6H_4)_3$	38.5	(38.2)	2.3	(2.1)	122
1:3 Complexes					
$P(4\text{-}Me_2NC_6H_4)_3$†	54.5	(54.9)	6.0	(5.8)	§
$P(4\text{-}MeOC_6H_4)_3$	51.3	(51.9)	4.4	(4.4)	
$P(4\text{-}MeC_6H_4)_3$	57.8	(57.7)	5.2	(5.2)	
$P(C_6H_5)_3$	55.0	(54.7)	3.8	(3.8)	
$P(4\text{-}FC_6H_4)_3$	47.2	(47.8)	2.8	(2.7)	
$P(4\text{-}ClC_6H_4)_3$	43.9	(43.3)	2.6	(2.4)	
1:4 Complexes					
$P(4\text{-}Me_2NC_6H_4)_3$‡	58.3	(58.7)	6.2	(6.2)	
$P(4\text{-}MeOC_6H_4)_3$	56.2	(55.8)	4.7	(4.7)	
$P(4\text{-}MeC_6H_4)_3$	62.4	(62.4)	5.5	(5.5)	
$P(C_6H_5)_3$	59.0	(59.5)	4.4	(4.2)	

* %N = 7.3 (7.1).
† %N = 8.3 (8.0).
‡ %N = 8.5 (8.6).
§ Addition of more phosphine to the solutions of the 1:2 complexes did not change their conductances significantly.

were recrystallized from CH_2Cl_2/hexane, using a small amount of the crude product to initiate crystallization. The white products were filtered off and dried in vacuum to remove trapped solvent. Yield = 50–60%.

This method often led to the deposition of mercury metal and badly contaminated products when used with the other phosphines. As a result, the following metathetical synthesis was used for those phosphines for which the starting material $HgCl_2P_2$ exists.

1:2 Complexes of the other phosphines

To a solution of $HgCl_2$(phosphine)$_2$ (5) (1 mmol) in CH_2Cl_2 (30 mL) was added a solution of silver perchlorate (2 mmol) in ethanol (10 mL). The AgCl was filtered off after 5 minutes stirring to yield a clear solution. The complexes were precipitated by reduction of the volume of the solution and, if necessary, the addition of hexane. They were recrystallized from CH_2Cl_2/hexane to yield crystalline products. The $P(4\text{-}Me_2NC_6H_4)_3$ complex was bright yellow. The others were white. Yield = 50–70%.

1:3 Complexes

To a solution of the appropriate 1:2 complex (1 mmol) in CH_2Cl_2 was added phosphine (2 mmol of $P(4\text{-}FC_6H_4)_3$ and $P(4\text{-}ClC_6H_4)_3$, 1 mmol of the others). The complexes were isolated as before, taking care to wash away the excess phosphine with diethylether. All were white crystalline solids except the $P(4\text{-}Me_2NC_6H_4)_3$ complex which was yellow. Yield = 60–70%.

1:4 Complexes

The complexes of all the phosphines except $P(C_6H_5)_3$ were prepared in an analogous manner but excesses of phosphine (2–6 mmol) were found to be necessary to ensure the purity of the $P(4\text{-}MeOC_6H_4)_3$ and $P(4\text{-}MeC_6H_4)_3$ complexes. Excesses of $P(4\text{-}Me_2NC_6H_4)_3$ often led to deposition of mercury metal.

Even with large excesses of phosphine, the $P(C_6H_5)_3$ complex was found by ^{31}P nmr to contain much 1:3 product. This crude mixture was added to a solution of $P(C_6H_5)_3$ (20 mmol) in 1,2-dichloroethane (5 mL) and was refluxed over a steam bath overnight.[2] A ^{31}P spectrum showed a small amount of 1:3 complex still to be present.

When excesses of phosphine were added to nmr solutions of 1:3 complexes of $P(4\text{-}FC_6H_4)_3$ and $P(4\text{-}ClC_6H_4)_3$, only peaks attributable to the 1:3 complex and free phosphine were seen. $P(3\text{-}MeC_6H_4)_3$ forms a 1:4 complex which could not be isolated. Yield = 60–80%.

Nuclear magnetic resonance measurements

Both the ^{31}P and ^{199}Hg nmr spectra were acquired on a Bruker WH-400 nmr spectrometer using conditions previously reported (5). CH_2Cl_2 containing 20% $CDCl_3$ was used as the solvent. The linewidths were typically 100–1000 Hz, with the greater values being associated with the higher concentrations. The loss in sensitivity due to line broadening often more than offset any gains expected from the increased concentrations. As a result, the times required to obtain reasonable signal-to-noise ratios tended not to increase upon dilution of the samples. About 2 000 transients were averaged for the 1:2 complexes, 4 000 for the 1:3 complexes, and 9 000 for the 1:4 complexes in order to give good S/N ratios for the weakest lines in the multiplets.

Where both ^{31}P and ^{199}Hg chemical shifts are reported, the corresponding value of ^1J(Hg—P) is the average obtained from the two spectra. The values of ^1J(Hg—P) always agreed to within 15 Hz and this is believed to be the uncertainty in the reported values.

[2] In light of the known explosion hazard of metal perchlorates in organic solvents, this is probably a dangerous procedure. It is wise therefore to shield the apparatus and to keep the reaction size small.

Can. J. Chem. Downloaded from www.nrcresearchpress.com by 210.87.254.105 on 09/06/12
For personal use only.

Vibrational measurements

The infrared spectra were measured on a Perkin–Elmer 180 spectrometer with the far-ir option. The solid samples were run as paraffin oil mulls between KBr disks in the mid-ir region or on polyethylene disks below 500 cm^{-1}. Solution measurements in the mid-ir region were made using CH_2Cl_2 solutions contained in sealed 0.2-mm NaCl cells. Far-ir solution measurements were made on $CHCl_3$ solutions in sealed 0.5-mm polyethylene cells of our own construction. Because it was found that the Hg arc source decomposed some of the samples, the Globar was used exclusively.

For Raman measurements, both the solid state and CH_2Cl_2 solution samples were contained in flame-sealed glass melting point tubes and were run on a Jarrell–Ash spectrometer. The 514.5 nm line of an argon laser was used for excitation and the spectra were calibrated from the known frequencies of the plasma lines. The conditions were: scan speed, 1 cm^{-1}/s; time constant, 1 s; laser power, 0.5 W; slit width, 3.0 cm^{-1}.

Other measurements

Elemental analyses were performed by Guelph Chemical Laboratories; the results, along with conductivity data, are given in Table 4. When melting point measurements were attempted, the complexes exploded near 200°C. Conductivities were measured in a cell with platinized Pt electrodes connected to a Yellow Springs bridge.

Acknowledgements

The Natural Sciences and Engineering Research Council of Canada is thanked for its support. Thanks also go to Dr. E. C. Alyea for reading the manuscript and making helpful comments. The nmr spectra were run at the South Western Ontario NMR centre.

1. P. L. GOGGIN, R. J. GOODFELLOW, S. R. HADDOCK, and J. G. EARY. J. Chem. Soc. Dalton Trans. 647 (1972).
2. H. SCHMIDBAUER and K. H. RATHLEIN. Chem. Ber. **106**, 2491 (1973).
3. N. A. BELL, M. GOLDSTEIN, T. JONES, and I. W. NOWELL. Inorg. Chim. Acta, **48**, 185 (1981).
4. T. ALLMAN and R. G. GOEL. J. Inorg. Nucl. Chem. Lett. **15**, 199 (1979).
5. T. ALLMAN and R. G. GOEL. Can. J. Chem. **62**, 615 (1984).
6. R. COLTON and D. DAKTERNIEKS. Aust. J. Chem. **34**, 323 (1981).
7. A. M. BOND, R. COLTON, D. DAKTERNIEKS, K. W. HANCK, and M. SVESTKA. Inorg. Chem. **22**, 236 (1983).
8. T. ALLMAN and R. G. GOEL. Can. J. Chem. **60**, 716 (1982).
9. S. O. GRIM, D. P. SHAH, C. K. HAAS, J. M. RESSMER, and P. H. SMITH. Inorg. Chim. Acta, **36**, 139 (1979).
10. S. O. GRIM and D. P. SHAH. Inorg. Nucl. Chem. Lett. **14**, 105 (1978).
11. K. NAKAMOTO. Infrared and Raman spectra of inorganic and coordination compounds. 3rd ed. Wiley, New York. 1978.
12. E. C. ALYEA, S. A. DIAS, G. FERGUSON, and M. A. KHAN. J. Chem. Res. S360, M401 (1979).
13. C. CHEIH, K. J. MOYNIHAN, and R. G. GOEL. Acta Crystallogr. Sect. B, **35**, 3060 (1979).
14. T. ALLMAN, A. L. BEAUCHAMP, and R. G. GOEL. To be published.
15. H. A. BENT. Can. J. Chem. **38**, 1235 (1960); J. Chem. Educ. **37**, 616 (1960).
16. H. B. BUERGI, R. W. KUNZ, and P. S. PREGOSIN. Inorg. Chem. **19**, 3707 (1980).
17. P. S. PREGOSIN and R. W. KUNZ. NMR principles and progress. Vol. 16. Springer Verlag, New York. 1979.
18. R. COLTON and D. DAKTERNIEKS. Aust. J. Chem. **33**, 955 (1980).

Can. J. Chem. Downloaded from www.nrcresearchpress.com by 210.87.254.105 on 09/06/12
For personal use only.

COMMUNICATIONS

Intrazeolite photochemistry. I. Phosphorescence enhancement of aromatic ketones included in silicalite.[1]

H. L. CASAL AND J. C. SCAIANO
Division of Chemistry, National Research Council of Canada, Ottawa, Ont., Canada K1A 0R6

Received October 28, 1983

H. L. CASAL and J. C. SCAIANO. Can. J. Chem. **62**, 628 (1984).

The triplet lifetime of β-phenylpropiophenone at room temperature is enhanced by ca. five orders of magnitude upon inclusion in the channels of silicalite, a hydrophobic zeolite. This behaviour is attributed to restrictions to mobility in this medium, and it is suggested that photochemical probes can provide a rather unique insight in the study of intrazeolite chemical processes.

H. L. CASAL et J. C. SCAIANO. Can. J. Chem. **62**, 628 (1984).

La vie de l'état triplet du β-phénylpropiophenone mesurée à température ambiante est approx. cinq ordres de grandeur plus longue lorsque ce composé est inclus dans des canaux de silicalite, un zéolite à caractéristiques hydrophobes. Ce comportement est attribué à des restrictions de la liberté de réorientation dans le zéolite; de même il est suggéré que les systèmes photochimiques donnent une vue unique des processus chimiques dans les zéolites.

Can. J. Chem. Downloaded from www.nrcresearchpress.com by 210.87.254.6 on 09/06/12
For personal use only.

Photochemical processes in organized media have received considerable attention during the last few years (1–3). In spite of this, and of the technological importance of zeolites, photoprocesses in zeolites have received virtually no attention; in fact, the few reports that we did find are concerned, directly or indirectly, with the cleavage of water (4, 5).

In this communication we explore the possibility of using aromatic ketones as probes of molecular mobility in zeolite cavities. Notably, we find that the lifetime of β-phenylpropiophenone (β-PP) at room temperature is enhanced by over five orders of magnitude by inclusion in silicalite cavities. At the same time, changes of this magnitude strongly suggest that photoreactions on zeolites can be expected to lead to chemical changes different from those in homogeneous or other organized media.

Silicalite (≥99% SiO_2) forms part of a class of zeolite-molecular sieves with a new topologic type of tetrahedral framework (6). The channel system of this zeolite consists of near-circular zig-zag channels which are cross-linked by elliptical straight channels. The diameter of the circular channels is 5.4 ± 0.2 Å and the free cross-section of the elliptical ones is 5.75 × 5.15 Å^2. Therefore, the limiting size for adsorption is ~6 Å at room temperature. One of the remarkable properties of this zeolite is its hydrophobicity which ensures no deactivation effect due to water.

The solution photochemistry of β-PP has been reported to involve efficient triplet deactivation involving interaction of the β-phenyl ring with the excited carbonyl group (7–9). Thus the triplet lifetime of β-PP in toluene at room temperature is ca. 1 ns (9). By contrast, propiophenone triplets have a much longer lifetime and frequently decay via reactive pathways involving hydrogen abstraction from the solvent (10). On the other hand, β-PP is photostable (9).

Silicalite S-115 (average particle size 1–2 μm), obtained from Union Carbide Canada, was calcined at 450 ± 50°C for 24 h and kept under vacuum for 12 h prior to use. The ketones studied were included in silicalite according to the following procedure: 3 g of silicalite were mixed with 80 mg of β-PP and 4 mL of 2,2,4-trimethylpentane in air at room temperature; the resulting slurry was stirred for approximately 3 h. The excess solvent was then removed by filtration and the solid washed with a further 4 mL of 2,2,4-trimethylpentane and allowed to dry in air for 10–16 h. In the case of liquid ketones, the amounts used were consistent with ~75% occupancy of the void volume of silicalite (0.19 mL/g). 2,2,4-Trimethylpentane was chosen due to its kinetic diameter (~6.5 Å) which is large enough to restrict the access of this molecule into ~6 Å channels (11).

Phosphorescence emission spectra (uncorrected, front face) were recorded using a computer-controlled Perkin-Elmer LS-5 fluorescence spectrometer. The excitation (at 254 nm) and emission bandpasses were 10 nm; the samples (under nitrogen) were contained in 3 × 7 mm Suprasil cells and an interference filter (254 nm) was placed in the excitation beam while a microscope slide was used as 300 nm emission cut-off.

Figure 1 compares the phosphorescence emission spectra of acetophenone and β-PP in silicalite (parts *A* and *B*, respectively) with that of β-PP in a methylcyclohexane glass at 77 K (Fig. 1*C*). The spectra observed are typical of aromatic ketones. The vibrational structure is evident; the differences between the spectra in parts *B* and *C* are the widths of the bands reflecting the temperature difference and the relative intensities of the bands. This latter effect seems to be also due to the temperature differences since a spectrum of β-PP in silicalite at 77 K is identical to that shown in Fig. 1*C*. The luminescence spectrum of silicalite itself was ca. 25 times weaker than those shown in Fig. 1 and no attempt was made to subtract this background. Silicalite is strongly reflecting, but does not absorb significantly in the region of interest; preliminary time-resolved diffuse reflectance measurements are consistent with these optical properties.

The initial phosphorescence lifetimes for β-PP and acetophenone in silicalite at room temperature were (0.18 ± 0.02) and (0.14 ± 0.02) ms, respectively. These values are to be compared with ca. 1 ns for β-PP at room temperature and ~1.0 ms in a methylcyclohexane glass at 77 K. We believe that the enhanced lifetime of the β-PP carbonyl triplet at room temperature is due to the steric restrictions imposed on the β-PP molecules in the channels of silicalite. Since the kinetic diameter of β-PP should be comparable to that of benzene (5.85

[1] NRCC No. 22764.

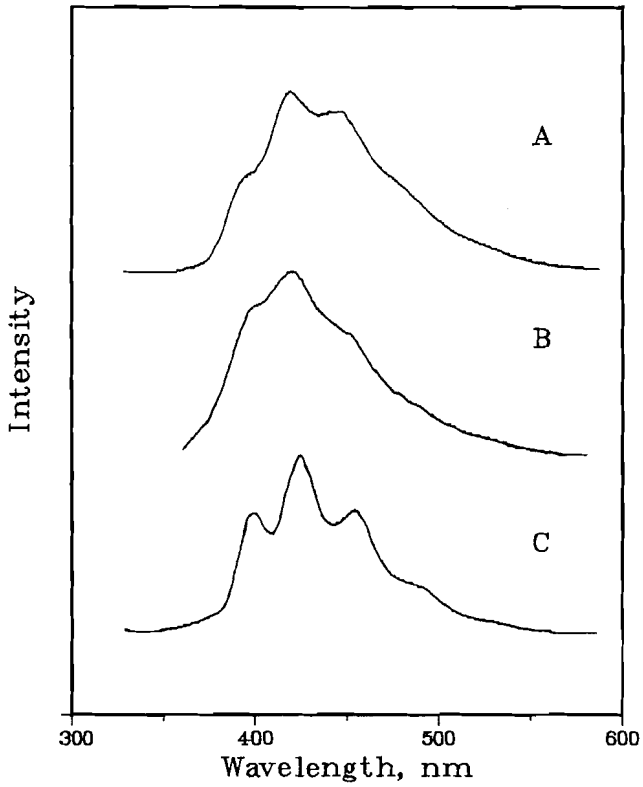

FIG. 1. Phosphorescence emission spectra (λ_{ex} = 254 nm) of *A*: acetophenone in silicalite at room temperature; *B*: β-PP in silicalite at room temperature; and *C*: β-PP in a methyl cyclohexane glass at 77 K.

Å), we can assume that β-PP has been included in the channel structure of silicalite. We suggest that the β-PP phosphorescence observed is not due to simple surface phenomena; to prove this point we subjected a sample of activated silica gel (Merck, 70–230 mesh) to the same experimental protocol with β-PP and found no phosphorescence emission comparable to that of Fig. 1*B*. We also examined a sample of β-PP adsorbed on Mordenite (Norton) which has a larger pore diameter (~9 Å) and observed no phosphorescence emission from β-PP. Thus, the phosphorescence emission of β-PP seems to depend critically on the channel dimensions of the supporting matrix.

The stabilization of triplet β-PP in the channels of silicalite can be ascribed to the impossibility of the molecule to adopt a conformation which would allow quenching by the β-phenyl group.

The channel dimension of silicalite is comparable to that found in urea inclusion complexes (12), albeit the crystal of silicalite is much more stable than urea adducts. In the case of urea inclusion adducts we found that alkanones undergo photodecomposition via the Norrish Type II mechanism and lead to a larger cyclization to fragmentation ratio than in homogeneous solution (13). We expect that included ketones in silicalite, with linear hydrocarbon chains, will also undergo photodecomposition. Indeed, we find that a sample of valerophenone included in silicalite shows increasing phosphorescence emission after uv irradiation (~300 nm), i.e., the included (non-luminescent) valerophenone is converted to acetophenone which yields strong phosphorescence emission.

Since silicalite and other zeolites are not only efficient molecular sieves or solid matrices but also very potent catalysts, further studies of the photochemical behaviour of zeolite supported molecules are expected to yield unique opportunities for understanding reaction mechanisms and provide new photocatalytic pathways.

1. J. K. THOMAS. Chem. Rev. **80**, 283 (1980); J. H. FENDLER. Acc. Chem. Res. **13**, 7 (1980).
2. K. KALYANASUNDARAM. Chem. Soc. Rev. **7**, 453 (1978).
3. N. J. TURRO, M. GRÄTZEL, and A. M. BRAUN. Angew. Chem. Int. Ed. Engl. **19**, 675 (1980); D. G. WHITTEN. Angew. Chem. Int. Ed. Engl. **82**, 937 (1978).
4. S. LEUTWYLER and E. SCHUMACHER. Chimia, **31**, 475 (1977); F. KHAN, P. YUE, L. RIZZUTI, V. AUGUGLIARO, and A. BRUCATO. Ind. Eng. Chem. Prod. Res. Dev. **22**, 238 (1983); K. CHANDRASEKARAN, T. K. FOREMAN, and D. G. WHITTEN. Nouv. J. Chim. **5**, 275 (1981).
5. W. DE WILDE, G. PEETERS, and J. H. LUNSFORD. J. Phys. Chem. **84**, 2306 (1980); L. R. FAULKNER, S. L. SUIB, C. L. RENSCHLER, J. M. GREEN, and P. R. BROS. *In* "Chemistry in Energy Production" Symposium 1980. NTIS, Springfield, 1982. pp. 99–114.
6. E. M. FLANIGEN, J. M. BENNETT, R. W. GROSE, J. P. COHEN, R. L. PATTON, R. M. KIRCHNER, and J. V. SMITH. Nature, **271**, 512 (1978).
7. F. BERGMANN and Y. HIRSHBERG. J. Am. Chem. Soc. **65**, 1429 (1943).
8. P. J. WAGNER, P. A. KELSO, A. E. KEMPPAINEN, A. HAUG, and D. R. GRABER. Mol. Photochem. **2**, 81 (1970); F. R. STERMITZ, D. E. NICODEM, V. P. MURALIDHARAN, and C. M. O'DONNELL. Mol. Photochem. **2**, 87 (1970).
9. J. C. SCAIANO, M. J. PERKINS, J. W. SHEPPARD, M. S. PLATZ, and R. L. BARCUS. J. Photochem. **21**, 137 (1983).
10. J. C. SCAIANO. J. Photochem. **2**, 81 (1973).
11. P. A. JACOBS, J. A. MARTENS, J. WEIKAMP, and H. K. BEYER. Faraday Discuss. Chem. Soc. **72**, 353 (1981).
12. L. C. FETTERLY. *In* Non-stoichiometric compounds. *Edited by* L. Mandelcorn. Academic, New York. 1964. Chapt. 8.
13. H. L. CASAL, P. DE MAYO, J. F. MIRANDA, and J. C. SCAIANO. J. Am. Chem. Soc. **105**, 5155 (1983).

Annulation via donor–acceptor reagents. An efficient total synthesis of (±)-$\Delta^{9(12)}$-capnellene

EDWARD PIERS AND VERANJA KARUNARATNE

Department of Chemistry, University of British Columbia, 2036 Main Mall, University Campus, Vancouver, B.C., Canada V6T 1Y6

Received November 25, 1983

EDWARD PIERS and VERANJA KARUNARATNE. Can. J. Chem. **62**, 629 (1984).

A short, efficient total synthesis of the racemic form of the marine sesquiterpenoid (−)-$\Delta^{9(12)}$-capnellene (**1**) is described. The key steps of the synthesis are two methylenecyclopentane annulation sequences (**14** → **16**; **22** → **24**) involving the

Can. J. Chem. Downloaded from www.nrcresearchpress.com by 210.87.254.6 on 09/06/12
For personal use only.

$CuBr \cdot Me_2S-BF_3 \cdot Et_2O$ catalyzed conjugate addition of the Grignard reagent **13** to the enones **14** and **22**, followed by intramolecular alkylation (KH, tetrahydrofuran) of the resultant adducts **15** and **23**, respectively.

EDWARD PIERS et VERANJA KARUNARATNE. Can. J. Chem. **62**, 629 (1984).

On décrit une synthèse totale qui est à la fois courte et efficace de la forme racémique du sesquiterpènoide marin, (−)-$\Delta^{9(12)}$-capnellène (**1**). Les étapes clés de la synthèse sont deux séries d'annellation de méthylènecyclopentanes (**14** → **16**; **22** → **24**) impliquant l'addition conjuguée, catalysée par le $CuBr \cdot Me_2S-BF_3 \cdot Et_2O$, du réactif de Grignard **13** aux énones **14** et **22**, qui est suivie par une alkylation intramoléculaire (KH, tétrahydrofuranne) des adduits **15** et **23** qui en résultent.

[Traduit par le journal]

Can. J. Chem. Downloaded from www.nrcresearchpress.com by 210.87.254.6 on 09/06/12
For personal use only.

The $C_{15}H_{24}$ hydrocarbon (−)-$\Delta^{9(12)}$-capnellene, isolated by Djerassi and co-workers from the soft coral *Capnella imbricata* (Quoy and Gaimard, 1833) and shown to possess the substituted tricyclo[6.3.0.$0^{2,6}$]undecane structure **1** (1), is the parent

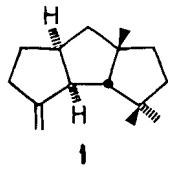

1

substance of a number of capnellane-type sesquiterpenoids (2). This structurally interesting natural product has received considerable attention from the community of synthetic organic chemists and a number of elegant syntheses of (±)-**1**, via a variety of interesting approaches, have been reported (3).

Recently, we described (4*a*) a new methylenecyclopentane annulation sequence illustrated in general terms by eq. [1] (**2** → **5** → **6**). In this process, the novel cuprate reagents **3** and **4** serve

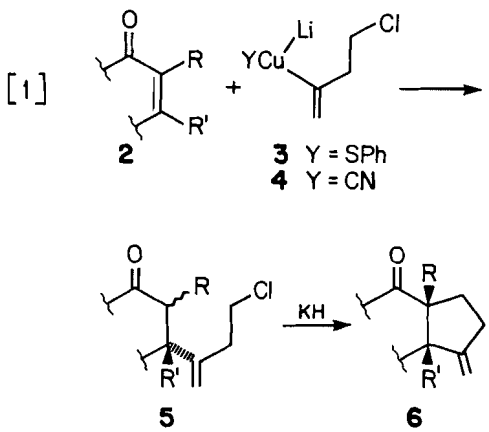

as efficient equivalents to the 1-butene d^2, a^4 synthon **7**. However, it should be recognized that suitable synthetic manipulation (e.g. hydrogenation or cyclopropanation–hydrogenation) of the carbon–carbon double bond of **7** would make reagents **3** and **4** equivalent to the synthons **8** and **9** as well. Therefore,

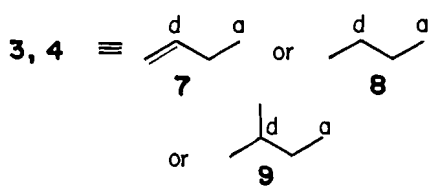

it appeared that a synthesis of (±)-$\Delta^{9(12)}$-capnellene (**1**) might be achieved expeditiously via the synthetic combination of substances equivalent to the synthons **7**, **10**, and **9**, derived from **1** by the retrosynthetic disconnections shown in eq. [2]. In such an approach, both of the "outside" five-membered rings

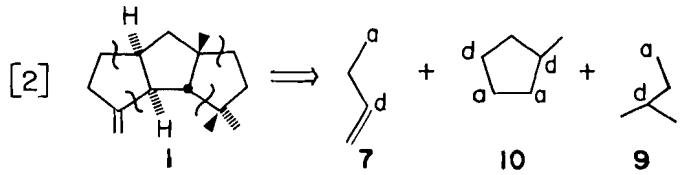

would be added to the central ring via the recently developed annulation sequence mentioned above (cf. eq. [1]).

Transmetallation (MeLi, tetrahydrofuran, −78°C) of 4-chloro-2-(trimethylstannyl)-1-butene (**11**) (4*b*, 5), followed by successive addition of anhydrous $MgBr_2$ (1.2 equiv.), $CuBr \cdot Me_2S$ (0.25 equiv.), 2-methyl-2-cyclopenten-1-one (**14**)[1] (0.83 equiv.), and $BF_3 \cdot Et_2O$ (1.0 equiv.) to the resultant solution of 4-chloro-2-lithio-1-butene (**12**) (4), afforded, after a reaction time of 2 h and suitable work-up, the chloro ketone **15** (80% yield).[2,3] Treatment of the latter substance with KH in tetrahydrofuran at room temperature provided, in 75% yield, the annulation product **16**.

Reduction of **16** ($LiAlH_4$, ether) gave the alcohols **17** (95%, mixture of epimers) which, upon reaction with $CH_2I_2-Et_2Zn$ (toluene, 50–60°C, dry air) (7), was converted into the cyclopropanes **18** (76%).[4] Hydrogenation (H_2, Pt, HOAc, room temperature) of the latter substance, followed by oxidation ($C_5H_5N \cdot CrO_3 \cdot HCl$, NaOAc, CH_2Cl_2 (8)) of the resultant mixture of alcohols **19**, afforded (81% overall) the bicyclic ketone **20**.

In order to allow for the addition of the second five-membered ring, the ketone **20** had to be converted into the corresponding enone **22**. Thus, compound **20** was transformed (Me_3SiI (9), Et_3N, CH_2Cl_2, −78°C, 15 min) into the enol ether **21** which, upon reaction with $Pd(OAc)_2$ (1 equiv.) in acetonitrile (3 h, room temperature) (10), provided the required enone **22** in 74% overall yield.

On the basis of steric considerations, conjugate addition of nucleophilic species to the enone **22** would be expected to take place from the convex side of the molecule. Indeed, subjection of **22** to reaction conditions very similar to those involved in the transformation of **14** into **15** produced a single addition product **23**, which was converted readily into the annulation product **24**

[1] We are grateful to Professor A. B. Smith III and Dr. M. D. Taylor for a generous sample of this material and for detailed procedures regarding its preparation (see ref. 6).

[2] This procedure, involving $CuBr \cdot Me_2S-BF_3 \cdot Et_2O$ catalyzed addition of the Grignard reagent **13** to the enone **14**, was more consistently successful than the corresponding additions employing the cuprate reagents **3** and **4**.

[3] All compounds reported herein exhibited spectral data in full accord with structural assignments. In addition, new compounds were fully characterized and gave satisfactory high resolution mass spectrometric molecular mass determinations.

[4] Subjection of the keto alkene **16** to similar reaction conditions gave very poor yields (~25–30%) of the corresponding keto cyclopropane.

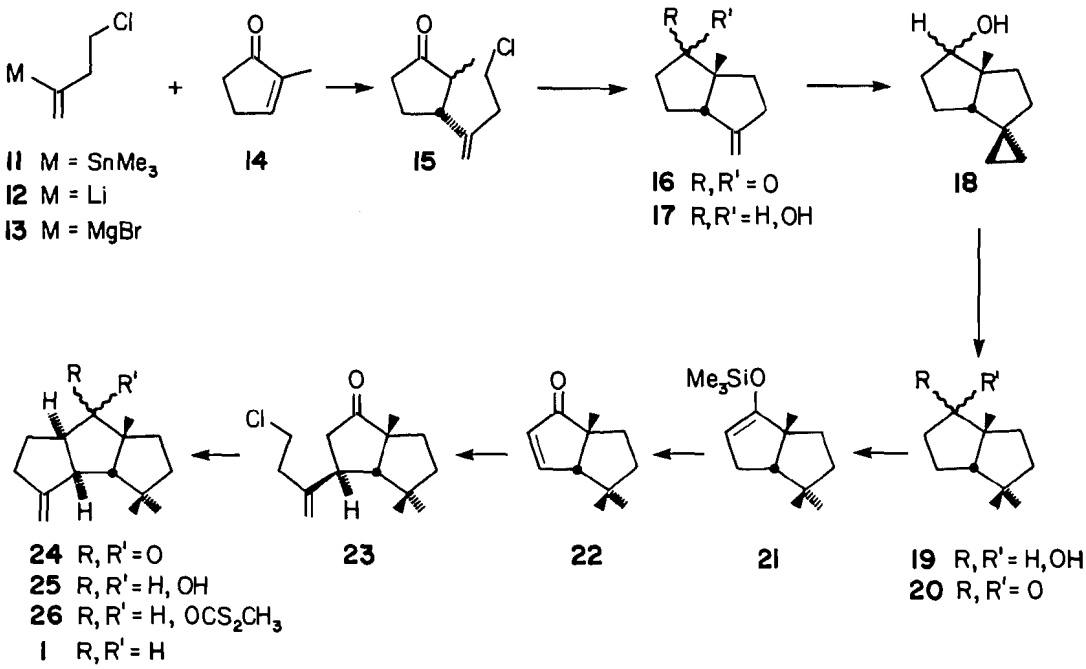

(69% from **22**). Subjection of the latter substance to reduction ($LiAlH_4$, ether), followed by deoxygenation (NaH, CS_2, MeI, tetrahydrofuran; *n*-Bu_3SnH, toluene, reflux (11)) of the resultant mixture of alcohols **25** via the methyl xanthates **26**, afforded (56% from **24**) (±)-$\Delta^{9(12)}$-capnellene (**1**). The synthetic material, purified by column chromatography and distillation, exhibited spectral data (ir, ^1H nmr) and chromatographic behavior (thin-layer and gas–liquid chromatography) identical with those of a sample of (±)-**1** obtained from Professor R. D. Little.[5]

Acknowledgement

We are grateful for financial support from the Natural Sciences and Engineering Research Council of Canada.

1. E. AYANOGLU, T. GEBREYESUS, C. M. BEECHAN, C. DJERASSI, AND M. KAISIN. Tetrahedron Lett. 1671 (1978).
2. M. KAISIN, Y. M. SHEIKH, L. J. DURHAM, C. DJERASSI, B. TURSCH, D. DALOZE, J. C. BRAEKMAN, D. LOSMAN, and R. KARLSSON. Tetrahedron Lett. 2239 (1974); Y. M. SHEIKH, G. SINGY, M. KAISIN, H. EGGERT, C. DJERASSI, B. TURSCH, D. DALOZE, and J. C. BRAEKMAN. Tetrahedron, **32**, 1171 (1976); Y. M. SHEIKH, C. DJERASSI, J. C. BRAEKMAN, D. DALOZE, M. KAISIN, B. TURSCH, and R. KARLSSON. Tetrahedron, **33**, 2115 (1977); M. KAISIN, B. TURSCH, J. P. DECLERCQ, G. GERMAIN, and M. VAN MEERSSCHE. Bull. Soc. Chim. Belg. **88**, 253 (1979).
3. R. D. LITTLE and G. L. CARROLL. Tetrahedron Lett. **22**, 4389 (1981); R. D. LITTLE, G. L. CARROLL, and J. L. PETERSEN. J. Am. Chem. Soc. **105**, 928 (1983); K. E. STEVENS and L. A. PAQUETTE. Tetrahedron Lett. **22**, 4393 (1981); W. OPPOLZER and K. BÄTTIG. Tetrahedron Lett. **23**, 4669 (1982); J. HUGUET, M. KARPF, and A. S. DREIDING. Helv. Chim. Acta, **65**, 2413 (1982); G. MEHTA, D. S. REDDY, and A. N. MURTY. J. Chem. Soc. Chem. Commun. 824 (1983).
4. E. PIERS and V. KARUNARATNE. (*a*) J. Chem. Soc. Chem. Commun. 935 (1983); (*b*) J. Org. Chem. **48**, 1774 (1983).
5. E. PIERS and J. M. CHONG. J. Chem. Soc. Chem. Commun. 934 (1983).
6. A. B. SMITH III, S. R. SCHOW, J. D. BLOOM, A. S. THOMPSON, and K. N. WINZENBERG. J. Am. Chem. Soc. **104**, 4051 (1982).
7. J. FURUKAWA, N. KAWABATA, and J. NISHIMURA. Tetrahedron, **24**, 53 (1968); S. MIYANO and H. HASHIMOTO. Chem. Commun. 1418 (1971).
8. E. J. COREY and J. W. SUGGS. Tetrahedron Lett. 2647 (1975).
9. D. E. SEITZ and L. FERREIRA. Synth. Commun. **9**, 931 (1979).
10. Y. ITO, T. HIRAO, and T. SAEGUSA. J. Org. Chem. **43**, 1011 (1978).
11. D. H. R. BARTON and S. W. MCCOMBIE. J. Chem. Soc. Perkin Trans. 1, 1574 (1975).

[5] We thank Professor Little for the sample of (±)-**1** and for copies of the ir, ^1H nmr and ^{13}C nmr spectra of this material.

Can. J. Chem. Downloaded from www.nrcresearchpress.com by 210.87.254.6 on 09/06/12
For personal use only.

Synthesis and crystal structure of tri(μ-carbonyl)bis[methyltris(1-pyrazolyl)gallato]dirhodium – benzene (1:1)

BRENDA M. LOUIE, STEVEN J. RETTIG, ALAN STORR, AND JAMES TROTTER

Department of Chemistry, University of British Columbia, 2036 Main Mall, Vancouver, B.C., Canada V6T 1Y6

Received July 11, 1983

BRENDA M. LOUIE, STEVEN J. RETTIG, ALAN STORR, and JAMES TROTTER. Can. J. Chem. **62**, 633 (1984).

The synthesis, physical properties, and crystal structure of the dirhodium species $[MeGa(N_2C_3H_3)_3]_2Rh_2(\mu\text{-}CO)_3$ containing three carbonyl bridges are reported. Crystals of tri(μ-carbonyl)bis[methyltris(1-pyrazolyl)gallato]dirhodium – benzene (1:1) are monoclinic, a = 11.660(4), b = 15.2917(7), c = 11.750(4) Å, β = 119.09(1)°, Z = 2, space group $P2_1$. The structure was solved by conventional heavy-atom techniques and was refined by full-matrix least-squares procedures to R = 0.030 and R_w = 0.033 for 2604 reflections with $I \geq 3\sigma(I)$. The molecule contains a Rh—Rh single bond of 2.5818(8) Å bridged by three CO ligands, the overall molecular symmetry being close to D_{3h}. Other important mean structural parameters are: Rh—C = 2.007(10), Rh—N = 2.181(14) Å, Rh—C—Rh = 80.1(5)°, and Rh—C—O = 140.0(7)°.

BRENDA M. LOUIE, STEVEN J. RETTIG, ALAN STORR et JAMES TROTTER. Can. J. Chem. **62**, 633 (1984).

On rapporte la synthèse, les propriétés physiques et la structure cristalline des dérivés du dirhodium $[MeGa(N_2C_3H_3)]_2$-$Rh_2(\mu\text{-}CO)_3$ contenant trois groupes carbonyles en position de ponts. Les cristaux de tri(μ-carbonyl)bis[méthyltris(pyrazolyl-1)gallato]dirhodiumbenzène (1:1) appartiennent au groupe d'espace monoclinique $P2_1$ avec a = 11,660(4), b = 15,2917(7) et c = 11,750(4) Å, β = 119,09(1)°, Z = 2. On a résolu la structure par les techniques conventionnelles de l'atome lourd et on l'a affinée par la méthode des moindres carrés (matrice entière) jusqu'a des valeurs de R = 0,030 et de R_w = 0,033 pour 2604 réflexions avec $I \geq 3\sigma(I)$. La molécule contient une liaison simple Rh—Rh de 2,5818(8) Å maintenue en position de pont par trois ligands CO, la symétrie moléculaire globale est voisine de D_{3h}. Les principaux autres paramètres strueturaux moyens sont: Rh—C = 2,007(10), Rh—N = 2,181(14) Å, Rh—C—Rh = 80,1(5)° et Rh—C—O = 140,0(7)°.

[Traduit par le journal]

Introduction

Our continuing investigations into the coordinating properties of pyrazolyl-gallate ligands have recently entered the fertile field of rhodium chemistry. Subtle differences between the cyclopentadienyl, $C_5H_5^-$, and methyltris(1-pyrazolyl)gallate, $MeGa(N_2C_3H_3)_3^-$, ligands have been discussed in a previous publication (1). The present paper extends this theme in reporting the synthesis and structure of a unique dimeric rhodium system with three bridging carbonyl groups and end-capping $MeGa(N_2C_3H_3)_3^-$ ligands, a compound having no counterpart in cyclopentadienyl rhodium carbonyl chemistry.

Experimental

Starting materials

Air-sensitive materials were handled in oxygen-free dry nitrogen. Tetrahydrofuran (THF) was dried by refluxing over sodium/benzophenone and used immediately following distillation. Benzene was dried by refluxing over molten potassium followed by distillation and methylene chloride by refluxing over P_2O_5 prior to distillation. $[Rh(CO)_2Cl]_2$ (Strem Chemicals) was sublimed *in vacuo* before use. The sodium salt of the methyltris(1-pyrazolyl)gallate ligand, $Na^+[MeGa(N_2C_3H_3)_3]^-$, was prepared as a THF solution as described earlier (1).

Synthesis of $[MeGa(N_2C_3H_3)_3]_2Rh_2(\mu\text{-}CO)_3$

The ligand, $Na^+[MeGa(N_2C_3H_3)_3]^-$ (1.790 mmol in 100 mL THF), was added to a stirred solution of $[Rh(CO)_2Cl]_2$ (0.348 g, 0.895 mmol) in 20 mL THF. The resulting mixture was refluxed for 8 h during which time the initially orange-colored solution turned lemon yellow. The mixture was filtered and the solvent allowed to evaporate slowly from the filtrate to yield a yellow product. This was recrystallized from CH_2Cl_2/C_6H_6 as lemon-yellow needles in 80% yield. The use of an excess of the gallate ligand in the reaction gave $[MeGa(N_2C_3H_3)_3]_2$-$Rh_2(\mu\text{-}CO)_3$ as the only isolable rhodium product. The analysis figures for the crystalline product indicated a 1:1 benzene solvate complex, as found in the crystal structure determination. The analysis results reported below are for the finely ground product after pumping *in vacuo* for 36 h at 45°C. *Anal.* calcd. for $[MeGa(N_2C_3H_3)_3]_2$-$Rh_2(\mu\text{-}CO)_3$: C 32.05, H 2.79, N 19.51; found: C 31.75, H 2.90, N 19.20%. ν_{CO} 1825 cm^{-1} (Nujol), 1827 cm^{-1} (CH_2Cl_2). ^1H nmr (C_6D_6; Fig. 1) τ = 9.83 s (Ga—Me), 3.88 t (pz—H^4), 2.78 d (pz—H^5), 1.93 d (pz—H^3) (τ values refer to $\tau_{C_6H_6}$ = 2.84 ppm, pz = pyrazolyl $N_2C_3H_3$, J_{HCCH} = ~2 Hz for pz protons. Assignment of pz—H^3 and pz—H^5 follows from assignment of other pyrazolyl complexes (1, 2)). The mass spectrum of the title compound showed clearly the parent ion, P^+ (28%), and a strong signal due to the $P - 2CO - 2Me^+$ ion (91%) based upon the most intense peak $N_2C_3H_4^+$ (100%).

Spectra

Mass spectra were collected on a (Kratos) AEI MS 50 spectrometer at 70 eV with an ion source temperature of 200°C. Infrared spectra were recorded on a Perkin-Elmer 598 spectrometer and the ^1H nmr spectrum on a Bruker WP80 spectrometer using FT techniques.

X-ray crystallographic analysis of tri(μ-carbonyl)bis[methyltris(1-pyrazolyl)gallato]dirhodium – benzene (1:1)

A crystal bounded by the 8 faces (followed by their distances in mm from a common origin): ±(1 0 0), 0.056, ±(0 1 0), 0.250, ±(0 0 1), 0.056, ±(1 0 −1), 0.063 was mounted in a general orientation. Unit-cell parameters were refined by least-squares on 2 sin θ/λ values for 25 reflections (2θ = 35–41°) measured on a diffractometer with Mo-Kα Radiation (λ(Kα$_1$) = 0.70930, λ(Kα$_2$) = 0.71073 Å). Crystal data at 22°C are:

$C_{29}H_{30}Ga_2N_{12}O_3Rh_2$ fw = 939.89

Monoclinic, a = 11.660(4), b = 15.2917(7), c = 11.750(4) Å, β = 119.09(1)°, V = 1830.6(9) Å^3, Z = 2, ρ_c = 1.705 g cm^{-3}, $F(0\,0\,0)$ = 928, μ(Mo-Kα) = 23.70 cm^{-1}. Absent reflections: $0k0$, k odd, space group $P2_1$ (C_2^2, No. 4) from structure analysis.

Intensities were measured with graphite-monochromated Mo-Kα radiation on an Enraf-Nonius CAD4-F diffractometer. An ω–2θ scan at 1.26–10.06° min^{-1} over a range of (0.65 + 0.35 tan θ) degrees in ω (extended by 25% on both sides for background measurement) was employed. Data were measured to 2θ = 55°. The intensities of three check reflections, measured every 3600 s throughout the data collection, remained constant to within 3%.

After data reduction,[1] an absorption correction was applied using

[1] The computer programs used include locally written programs for data processing and locally modified versions of the following: ORFLS, full-matrix least-squares, and ORFFE, function and errors, by W. R. Busing, K. O. Martin and H. A. Levy; FORDAP, Patterson and Fourier syntheses, by A. Zalkin; ORTEP II, illustrations, by C. K. Johnson.

Can. J. Chem. Downloaded from www.nrcresearchpress.com by 210.87.254.42 on 09/06/12
For personal use only.

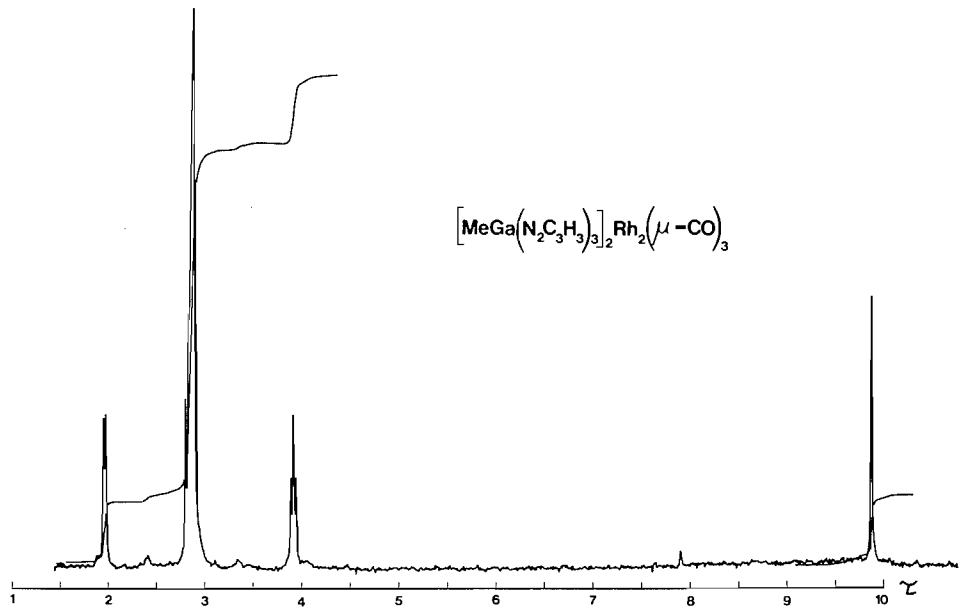

FIG. 1. ^{1}H nmr spectrum of $[MeGa(N_2C_3H_3)_3]_2Rh_2(\mu\text{-}CO)_3$.

the Gaussian integration method (3, 4). Transmission factors ranged from 0.729 to 0.789 for 96 integration points. Of the 4339 independent reflections measured, 2604 (60.0%) had intensities greater than $3\sigma(I)$ above background where $\sigma^2(I) = S + 2B + (0.04(S - B))^2$ with S = scan count and B = normalized background count.

The systematic absences allow space groups $P2_1$ or $P2_1/m$, the former being indicated by the Patterson function and verified by subsequent calculations. The coordinates of the Rh and Ga atoms were determined from the Patterson function and those of the remaining atoms from subsequent difference syntheses. Full-matrix least-squares refinement of all non-hydrogen atoms except those associated with the solvate with anisotropic thermal parameters resulted in $R = 0.046$. A difference map calculated at this point revealed a twofold disorder of the solvent benzene molecule as well as the positions of most of the hydrogen atoms. The disordered benzene was included in the refinement as two rigid groups having idealized geometry. The site occupancies were initially fixed at 0.5 and later adjusted to 0.6 and 0.4 to give nearly equal group temperature factors. Hydrogen atoms associated with the ordered complex molecule were included as fixed atoms with idealized positions (C—H = 0.97 Å, $U_H = 1.1\,U_C$ for trigonal-planar H, C—H = 0.98 Å, $U_H = 1.2\,U_C$ for methyl H). The scattering factors of ref. 5 were used for non-hydrogen atoms and those of ref. 6 for hydrogen atoms. Anomalous scattering factors from ref. 7 were used for the Rh and Ga atoms. The weighting scheme, $w = 1/\sigma^2(F)$ where $\sigma^2(F)$ is derived from the previously defined $\sigma^2(I)$, gave uniform average values of $w(|F_o| - |F_c|)^2$ over ranges of both $|F_o|$ and $\sin\theta/\lambda$ and was employed in the final stages of refinement. Unobserved reflections were not included in the refinement. Convergence was reached at $R = 0.030$ and $R_w = 0.033$ for 2604 reflections with $I \geq 3\sigma(I)$. For all 4339 reflections $R = 0.079$. The function minimized was $\Sigma w(|F_o| - |F_c|)^2$, $R = \Sigma\||F_o| - |F_c|\|/\Sigma|F_o|$ and $R_w = (\Sigma w(|F_o| - |F_c|)^2/\Sigma w|F_o|^2)^{1/2}$.

On the final cycle of refinement the mean and maximum parameter shifts corresponded to 0.04 and 0.70σ, respectively. The mean error in an observation of unit weight was 1.328. A final difference map showed a maximum residual density of 0.53 e Å^{-3} in the vicinity of the disordered solvent. The mirror-image structure refined to slightly higher values of both R and R_w. The final positional and thermal parameters appear in Tables 1 and 4[2], respectively. Measured and calculated structure factors have been placed in the Depository of Unpublished Data.[2] Calculated hydrogen coordinates and thermal parameters and rigid group parameters (Tables 5 and 6) are included as supplementary material. Selected bond distances and angles appear in Tables 2 and 3, respectively.

[2] The structure factor table, Table 4 (anisotropic thermal parameters), and other material mentioned in the text are available, at a nominal charge, from the Depository of Unpublished Data, CISTI, National Research Council of Canada, Ottawa, Ont., Canada K1A 0S2.

Results and discussion

The title compound, $[MeGa(N_2C_3H_3)_3]_2Rh_2(\mu\text{-}CO)_3$, is the first dirhodium complex containing three carbonyl bridges to be structurally characterized. The compound crystallizes as air-stable lemon-yellow needles which begin to darken in color at ~240°C. The crystals are slightly soluble in benzene and soluble in THF and CH_2Cl_2. The proton nmr spectrum (Fig. 1), the single absorption in the bridging carbonyl region and the absence of any terminal metal carbonyl bands in the ir spectrum, all indicated a very symmetrical structure for the dimeric species in solution. The crystal structure determination (see below) confirmed our predictions of a dirhodium species containing three carbonyl bridges (Fig. 2). Earlier reports (8,9) on a similar boron compound, $([HB(N_2C_3H_3)_3]_2Rh_2(CO)_3)$, suggested the possibility of a dimeric $(\mu\text{-}CO)_3$ bridged structure as found for the present title compound, but a polymeric structure, befitting the insoluble nature of the complex, was felt more likely. It is interesting to compare our findings with those reported in the related field of cyclopentadienyl rhodium carbonyl complexes. In this area the cyclopentadienyl rhodium dicarbonyl compound, $(\eta^5\text{-}C_5H_5)Rh(CO)_2$ (10), and its pentamethylcyclopentadienyl analog, $(\eta^5\text{-}C_5Me_5)Rh(CO)_2$, are quite stable at room temperature but may be converted by various techniques into a variety of associated rhodium species (11–15). In contrast the corresponding $[MeGa(N_2C_3H_3)_3]$-$Rh(CO)_2$ compound has proven to be elusive although earlier reports have mentioned the isolation of the corresponding tris(3,5-dimethylpyrazolyl)borate complex, $[HB(N_2C_5H_7)_3]$-$Rh(CO)_2$, as a stable entity (16, 17). Our attempts to prepare a gallium analog of this species, viz. $[MeGa(N_2C_5H_7)_3]Rh(CO)_2$, have so far resulted only in the appearance of the dimeric rhodium complex, $[Rh(N_2C_5H_7)(CO)_2]_2$, with bridging 3,5-dimethylpyrazolyl moieties. The cyclopentadienyl rhodium complex with the formulation directly analogous to the title compound, $(\eta^5\text{-}C_5H_5)_2Rh_2(CO)_3$, has been structurally character-

Can. J. Chem. Downloaded from www.nrcresearchpress.com by 210.87.254.42 on 09/06/12
For personal use only.

Can. J. Chem. Downloaded from www.nrcresearchpress.com by 210.87.254.42 on 09/06/12
For personal use only.

TABLE 1. Final positional (fractional × 10^4, Rh and Ga × 10^5) and isotropic thermal parameters (U × 10^3 Å^2) with estimated standard deviations in parentheses*

Atom	x	y	z	U_{eq}
Rh(1)	31098(6)	41000	15399(6)	38
Rh(2)	36143(6)	57545(5)	17658(6)	37
Ga(1)	24529(12)	18544(8)	12051(13)	62
Ga(2)	43823(12)	79708(8)	21608(11)	53
O(1)	3531(8)	4895(6)	−542(6)	72
O(2)	5500(7)	4660(4)	3989(7)	69
O(3)	1049(6)	5246(4)	1579(6)	57
N(1)	4416(7)	3100(5)	1517(7)	44
N(2)	4085(7)	2234(5)	1340(8)	53
N(3)	2716(7)	3307(5)	2855(7)	46
N(4)	2592(7)	2422(5)	2742(8)	56
N(5)	1429(7)	3500(5)	−128(8)	48
N(6)	1197(7)	2622(5)	−159(8)	50
N(7)	5416(7)	6325(5)	1981(7)	45
N(8)	5591(7)	7216(5)	2005(7)	48
N(9)	3768(8)	6559(5)	3355(7)	49
N(10)	4088(7)	7428(5)	3469(7)	53
N(11)	2438(7)	6795(5)	392(7)	42
N(12)	2778(7)	7654(5)	644(7)	49
C(1)	3479(9)	4913(6)	407(8)	45
C(2)	4573(9)	4769(5)	2973(8)	39
C(3)	2035(8)	5108(5)	1612(7)	37
C(4)	1993(14)	624(8)	973(16)	113
C(5)	4937(12)	9193(8)	2488(13)	81
C(6)	5602(9)	3168(6)	1598(10)	53
C(7)	6052(10)	2335(7)	1505(10)	52
C(8)	5080(11)	1771(7)	1348(10)	61
C(9)	2587(10)	3559(9)	3898(9)	62
C(10)	2406(13)	2822(10)	4469(12)	82
C(11)	2450(10)	2130(9)	3745(13)	82
C(12)	486(11)	3844(6)	−1145(11)	63
C(13)	−436(11)	3196(8)	−1895(10)	68
C(14)	97(10)	2446(7)	−1234(10)	61
C(15)	6447(10)	5976(7)	2006(11)	65
C(16)	7320(11)	6618(9)	2048(13)	80
C(17)	6740(10)	7378(8)	2063(10)	62
C(18)	3609(11)	6374(9)	4353(10)	70
C(19)	3799(12)	7113(8)	5107(11)	74
C(20)	4123(10)	7733(7)	4549(10)	63
C(21)	1326(9)	6758(7)	−720(9)	50
C(22)	893(10)	7582(7)	−1188(10)	58
C(23)	1795(11)	8127(7)	−343(10)	59

* U_{eq} = (1/3) trace U_{diag}.

TABLE 2. Bond lengths (Å) with estimated standard deviations in parentheses

Bond	Length (Å)	Bond	Length (Å)
Rh(1)—N(1)	2.168(7)	N(3)—C(9)	1.360(13)
Rh(1)—N(3)	2.182(7)	N(4)—C(11)	1.344(14)
Rh(1)—N(5)	2.188(7)	N(5)—N(6)	1.366(10)
Rh(1)—C(1)	2.015(9)	N(5)—C(12)	1.279(12)
Rh(1)—C(2)	2.000(9)	N(6)—C(14)	1.318(12)
Rh(1)—C(3)	2.014(8)	N(7)—N(8)	1.376(10)
Rh(2)—N(7)	2.172(7)	N(7)—C(15)	1.302(12)
Rh(2)—N(9)	2.169(7)	N(8)—C(17)	1.331(12)
Rh(2)—N(11)	2.205(7)	N(9)—N(10)	1.369(11)
Rh(2)—C(1)	1.997(9)	N(9)—C(18)	1.304(12)
Rh(2)—C(2)	1.997(8)	N(10)—C(20)	1.335(12)
Rh(2)—C(3)	2.018(9)	N(11)—N(12)	1.363(10)
Ga(1)—N(2)	1.921(8)	N(11)—C(21)	1.321(11)
Ga(1)—N(4)	1.938(9)	N(12)—C(23)	1.375(11)
Ga(1)—N(6)	1.952(8)	C(6)—C(7)	1.402(15)
Ga(1)—C(4)	1.939(12)	C(7)—C(8)	1.364(15)
Ga(2)—N(8)	1.898(8)	C(9)—C(10)	1.38(2)
Ga(2)—N(10)	1.919(8)	C(10)—C(11)	1.37(2)
Ga(2)—N(12)	1.915(8)	C(12)—C(13)	1.412(14)
Ga(2)—C(5)	1.954(13)	C(13)—C(14)	1.35(2)
O(1)—C(1)	1.146(9)	C(15)—C(16)	1.398(15)
O(2)—C(2)	1.169(10)	C(16)—C(17)	1.35(2)
O(3)—C(3)	1.151(9)	C(18)—C(19)	1.39(2)
N(1)—N(2)	1.366(11)	C(19)—C(20)	1.308(15)
N(1)—C(6)	1.343(11)	C(21)—C(22)	1.368(14)
N(2)—C(8)	1.356(12)	C(22)—C(23)	1.331(14)
N(3)—N(4)	1.361(11)	Rh(1)—Rh(2)	2.5818(8)

ized by Mills and Nice (12). It displays a markedly different geometrical arrangement, however, in that only one bridging carbonyl group is present with the other two carbonyls appearing as terminal CO ligands, one on each rhodium atom. Both the $[MeGa(N_2C_3H_3)_3]_2Rh_2(\mu\text{-}CO)_3$ and the $(\eta^5\text{-}C_5H_5)_2Rh_2(\mu\text{-}CO)(CO)_2$ complexes have a Rh—Rh single bond, in addition to the bridging ligands, holding the dimeric unit together. It is conjectured that the more sterically demanding $MeGa(N_2C_3H_3)_3^-$ ligand forces a $(\mu\text{-}CO)_3$ arrangement on $[MeGa(N_2C_3H_3)_3]_2Rh_2(\mu\text{-}CO)_3$.

Steric interactions have been held responsible for a similar terminal vs. bridging CO structural arrangement in a series of related compounds. Thus removal of CO from $(\eta^5\text{-}C_5Me_5)Rh(CO)_2$ can lead to the dirhodium complex, $(\eta^5\text{-}C_5Me_5)_2Rh_2(CO)_2$, having two bridging carbonyls and a formal double bond between the rhodium centres (14, 15). Addition of diazoalkanes to this dimeric rhodium species has led to products of two structural types depending on the R groups attached to the bridging carbene moiety. In the first type the arrangement is similar to the $(\eta^5\text{-}C_5H_5)_2Rh_2(CO)_3$ complex with a bridging carbene and two terminal CO ligands (one per Rh). In the second type, where the bridging carbene does not allow the $\eta^5\text{-}C_5Me_5$ groups to tilt from their positions at right angles to the Rh—Rh bond axis, a system containing three bridging ligands, analogous to that of $[MeGa(N_2C_3H_3)_3]_2Rh_2(\mu\text{-}CO)_3$, is observed, viz $(\eta^5\text{-}C_5Me_5)_2Rh_2(\mu\text{-}CO)_2(\mu\text{-}CR_2)$ (15).

The title compound might also be compared with other "$M_2(\mu\text{-}CO)_3$" systems such as $(\eta^5\text{-}C_5Me_5)_2Re_2(\mu\text{-}CO)_3$ (18), $(\eta^4\text{-}C_4R_4)_2Fe_2(\mu\text{-}CO)_3$ (19), and $(\eta^6\text{-}C_6H_6)_2Cr_2(\mu\text{-}CO)_3$ (20), although, rather than a single M—M bond, these three examples all require a formal M≡M triple bond for an eighteen electron configuration about the transition metal centres. Attempts to prepare the dirhenium complex, $[MeGa(N_2C_3H_3)_3]_2Re_2(\mu\text{-}CO)_3$, by uv irradiation of the complex $[MeGa(N_2C_3H_3)_3]Re(CO)_3$, have so far proven unsuccessful, unreacted starting material being recovered in high yield (21).

The crystal structure of $[MeGa(N_2C_3H_3)_3]_2Rh_2(\mu\text{-}CO)_3 \cdot C_6H_6$ consists of well separated complex and benzene solvate molecules. Although there is no crystallographically imposed molecular symmetry, the $[MeGa(N_2C_3H_3)_3]_2Rh_2(\mu\text{-}CO)_3$ molecule displays approximate D_{3h} symmetry in the solid state, consistent with the evidence discussed above for the complex in solution. There are a number of small, but statistically significant departures from this idealized symmetry (see Tables 2 and 3), but none of these are believed to be of any chemical importance. The complex features a face-shared bioctahedral geometry, the metal–metal bond resulting in a 7-coordinate capped octahedral arrangement about each Rh atom. The relevant

TABLE 3. Bond angles (deg) with estimated standard deviations in parentheses

Bonds	Angle (deg)	Bonds	Angle (deg)
N(1)—Rh(1)—N(3)	90.5(3)	N(3)—N(4)—C(11)	107.3(9)
N(1)—Rh(1)—N(5)	91.2(3)	Rh(1)—N(5)—N(6)	121.0(6)
N(1)—Rh(1)—C(1)	92.9(3)	Rh(1)—N(5)—C(12)	130.8(7)
N(1)—Rh(1)—C(2)	93.1(3)	N(6)—N(5)—C(12)	108.1(8)
N(1)—Rh(1)—C(3)	174.7(3)	Ga(1)—N(6)—N(5)	120.6(6)
N(3)—Rh(1)—N(5)	89.8(3)	Ga(1)—N(6)—C(14)	131.0(7)
N(3)—Rh(1)—C(1)	175.6(3)	N(5)—N(6)—C(14)	108.3(8)
N(3)—Rh(1)—C(2)	94.3(3)	Rh(2)—N(7)—N(8)	121.7(5)
N(3)—Rh(1)—C(3)	92.6(3)	Rh(2)—N(7)—C(15)	131.9(7)
N(5)—Rh(1)—C(1)	93.0(3)	N(8)—N(7)—C(15)	106.2(8)
N(5)—Rh(1)—C(2)	174.0(3)	Ga(2)—N(8)—N(7)	119.7(6)
N(5)—Rh(1)—C(3)	93.1(3)	Ga(2)—N(8)—C(17)	131.1(7)
C(1)—Rh(1)—C(2)	82.6(3)	N(7)—N(8)—C(17)	108.8(8)
C(1)—Rh(1)—C(3)	83.8(3)	Rh(2)—N(9)—N(10)	122.6(6)
C(2)—Rh(1)—C(3)	82.3(3)	Rh(2)—N(9)—C(18)	131.5(7)
N(7)—Rh(2)—N(9)	90.1(3)	N(10)—N(9)—C(18)	105.9(8)
N(7)—Rh(2)—N(11)	91.0(3)	Ga(2)—N(10)—N(9)	119.2(6)
N(7)—Rh(2)—C(1)	92.7(3)	Ga(2)—N(10)—C(20)	132.5(7)
N(7)—Rh(2)—C(2)	92.5(3)	N(9)—N(10)—C(20)	108.3(8)
N(7)—Rh(2)—C(3)	174.2(3)	Rh(2)—N(11)—N(12)	121.7(5)
N(9)—Rh(2)—N(11)	89.0(3)	Rh(2)—N(11)—C(21)	131.0(6)
N(9)—Rh(2)—C(1)	174.4(3)	N(12)—N(11)—C(21)	107.3(8)
N(9)—Rh(2)—C(2)	91.9(3)	Ga(2)—N(12)—N(11)	119.7(5)
N(9)—Rh(2)—C(3)	92.5(3)	Ga(2)—N(12)—C(23)	133.5(7)
N(11)—Rh(2)—C(1)	95.7(3)	N(11)—N(12)—C(23)	106.8(7)
N(11)—Rh(2)—C(2)	176.3(3)	Rh(1)—C(1)—Rh(2)	80.1(3)
N(11)—Rh(2)—C(3)	94.1(3)	Rh(1)—C(1)—O(1)	139.3(8)
C(1)—Rh(2)—C(2)	83.2(4)	Rh(2)—C(1)—O(1)	140.5(8)
C(1)—Rh(2)—C(3)	84.2(3)	Rh(1)—C(2)—Rh(2)	80.5(3)
C(2)—Rh(2)—C(3)	82.3(3)	Rh(1)—C(2)—O(2)	140.7(7)
N(2)—Ga(1)—N(4)	99.0(3)	Rh(2)—C(2)—O(2)	138.9(7)
N(2)—Ga(1)—N(6)	101.7(3)	Rh(1)—C(3)—Rh(2)	79.6(3)
N(2)—Ga(1)—C(4)	120.0(5)	Rh(1)—C(3)—O(3)	140.4(7)
N(4)—Ga(1)—N(6)	100.7(3)	Rh(2)—C(3)—O(3)	140.0(7)
N(4)—Ga(1)—C(4)	117.3(6)	N(1)—C(6)—C(7)	109.6(8)
N(6)—Ga(1)—C(4)	115.0(5)	C(6)—C(7)—C(8)	105.5(8)
N(8)—Ga(2)—N(10)	104.1(3)	N(2)—C(8)—C(7)	108.8(9)
N(8)—Ga(2)—N(12)	101.0(3)	N(3)—C(9)—C(10)	108.5(11)
N(8)—Ga(2)—C(5)	114.3(4)	C(9)—C(10)—C(11)	105.5(10)
N(10)—Ga(2)—N(12)	99.3(3)	N(4)—C(11)—C(10)	110.2(10)
N(10)—Ga(2)—C(5)	115.3(4)	N(5)—C(12)—C(13)	110.1(9)
N(12)—Ga(2)—C(5)	120.3(4)	C(12)—C(13)—C(14)	103.8(9)
Rh(1)—N(1)—N(2)	122.5(5)	N(6)—C(14)—C(13)	109.7(9)
Rh(1)—N(1)—C(6)	130.5(6)	N(7)—C(15)—C(16)	111.2(10)
N(2)—N(1)—C(6)	106.9(7)	C(15)—C(16)—C(17)	104.1(9)
Ga(1)—N(2)—N(1)	120.1(6)	N(8)—C(17)—C(16)	109.7(10)
Ga(1)—N(2)—C(8)	130.7(7)	N(9)—C(18)—C(19)	110.5(11)
N(1)—N(2)—C(8)	109.1(8)	C(18)—C(19)—C(20)	105.4(9)
Rh(1)—N(3)—N(4)	122.1(6)	N(10)—C(20)—C(19)	109.9(9)
Rh(1)—N(3)—C(9)	129.4(7)	N(11)—C(21)—C(22)	110.6(9)
N(4)—N(3)—C(9)	108.5(8)	C(21)—C(22)—C(23)	105.9(8)
Ga(1)—N(4)—N(3)	119.6(6)	N(12)—C(23)—C(22)	109.3(9)
Ga(1)—N(4)—C(11)	132.7(8)		

mean[3] geometrical parameters are: Rh—Rh = 2.5818(8), Rh—N = 2.181(14), Rh—C = 2.007(10) Å, C—Rh—C = 83.1(8), N—Rh—N = 90.3(8), C—Rh—N = 93.2(10) (*cis*) and 174.9(9) (*trans*), Rh—C—Rh = 80.1(5), and Rh—C—O = 140.0(7)°.

Cowie and Dwight, in discussing "A-frame" dirhodium species with a single bridging carbonyl ligand and a Rh—Rh single bond (22), list 2.617–2.8415 Å as a range for such single bond distances. The title complex has a Rh—Rh bond of 2.5818(8) Å, significantly shorter than the lowest values quoted and considerably shorter than the value of 2.681(2) Å observed in the singly carbonyl bridged species $(\eta^5\text{-}C_5H_5)_2Rh_2(CO)_3$ (12). The Rh—Rh and mean Rh—C(O) distances of 2.612(2) and 2.039 Å and the mean Rh—C(O)—Rh angle of 80.4° found in the carbene bridged complex $(\eta^5\text{-}C_5Me_5)_2Rh_2(\mu\text{-}CO)_2(\mu\text{-}CR_2)$ (where CR_2 = tetrabromocyclopentadienylidene) (15) may be compared to those presented here for

[3] Here and elsewhere in this report, mean values refer to weighted means with rms deviations from the mean in parentheses.

Can. J. Chem. Downloaded from www.nrcresearchpress.com by 210.87.254.42 on 09/06/12
For personal use only.

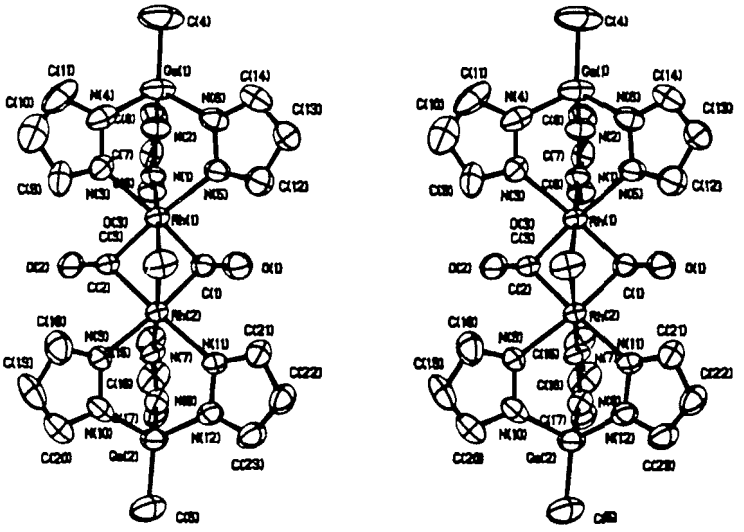

FIG. 2. Stereoscopic view of the $[MeGa(N_2C_3H_3)_3]_2Rh_2(\mu\text{-}CO)_3$ molecule. 50% probability thermal ellipsoids are shown for the non-hydrogen atoms.

$[MeGa(N_2C_3H_3)_3]_2Rh_2(\mu\text{-}CO)_3$. In this μ-carbene complex, the only other triply-bridged dirhodium complex of this type to be structurally characterized, it was argued that the strictly planar C_5Br_4 bridge forces the CO ligands into the bridging positions. The alternative structure, with a bridging carbene and one terminal CO on each Rh (as observed for R = COOMe (15)), would lead to severe steric interactions between the Me groups of the (η^5-C_5Me_5) ligands and the bromo substituents of the carbene.

The geometry of the tris(1-pyrazolyl)gallate ligand is similar to that noted previously (1, 23). All six pyrazolyl groups are planar to within experimental error, as are the three Rh_2CO moieties.

$[MeGa(N_2C_3H_3)_3]_2Rh_2(\mu\text{-}CO)_3$ remains unchanged when stirred in THF or C_6H_6 overnight in an N_2 atmosphere. However, under reflux temperatures all bridging carbonyls are lost and the dimer $[Rh(\mu\text{-}N_2C_3H_3)(CO)_2]_2$ is isolated. Similarly, stirring the title compound with PPh_3 in THF overnight effects no change in the starting materials, but refluxing the reaction mixture for 8 h produces >90% yield of the dimer $[Rh(\mu\text{-}N_2C_3H_3)(CO)(PPh_3)]_2$. Stirring $[MeGa(N_2C_3H_3)_3]_2Rh_2(\mu\text{-}CO)_3$ for 0.5 h in C_6H_6 with 2 molar equivalents of I_2 produces a deep red–orange solution from which a black solid can be isolated. Based upon ir data, this black solid contains no carbonyl groups. Preliminary experiments suggest that neither the di-iodide $[MeGa(N_2C_3H_3)_3]RhI_2$, nor the iodine bridged dimer $[MeGa(N_2C_3H_3)_3]_2Rh_2(\mu\text{-}I)_2$, are present in the reaction products. Investigations are continuing in this and related areas.

Acknowledgments

We thank the Natural Sciences and Engineering Research Council of Canada for financial support and the University of British Columbia Computing Centre for assistance.

1. K. R. BREAKELL, S. J. RETTIG, D. L. SINGBEIL, A. STORR, and J. TROTTER. Can. J. Chem. **56**, 2099 (1978).
2. P. MEAKIN, S. TROFIMENKO, and J. P. JESSON. J. Am. Chem. Soc. **94**, 5677 (1972).
3. P. COPPENS, L. LEISEROWITZ, and D. RABINOVICH. Acta Crystallogr. **18**, 1035 (1965).
4. W. R. BUSING and H. A. LEVY. Acta Crystallogr. **22**, 457 (1967).
5. D. T. CROMER and J. B. MANN. Acta Crystallogr. Sect. A, **24**, 321 (1968).
6. R. F. STEWART, E. R. DAVIDSON, and W. T. SIMPSON. J. Chem. Phys. **42**, 3175 (1965).
7. D. T. CROMER and D. LIBERMAN. J. Chem. Phys. **53**, 1891 (1970).
8. D. J. O'SULLIVAN and F. J. LALOR. J. Organomet. Chem. **65**, C47 (1974).
9. M. COCIVERA, T. J. DESMOND, G. FERGUSON, B. KAITNER, F. J. LALOR, and D. J. O'SULLIVAN. Organometallics, **1**, 1125 (1982).
10. E. O. FISCHER and K. BITTLER. Z. Naturforsch. **16b**, 225 (1961).
11. O. S. MILLS and E. F. PAULUS. J. Organomet. Chem. **10**, 331 (1967).
12. O. S. MILLS and J. P. NICE. J. Organomet. Chem. **10**, 337 (1967).
13. A. NUTTON and P. M. MAITLIS. J. Organomet. Chem. **166**, C21 (1979).
14. N. M. BOAG, M. GREEN, R. M. MILLS, G. N. PAIN, F. G. A. STONE, and P. WOODWARD. J. Chem. Soc. Chem. Commun. 1171 (1980).
15. W. A. HERRMANN, C. BAUER, J. PLANK, W. KALCHER, D. SPETH, and M. L. ZIEGLER. Angew. Chem. Int. Ed. Engl. **20**, 193 (1981).
16. S. TROFIMENKO. Inorg. Chem. **10**, 1372 (1971).
17. S. MAY, P. REINSALU, and J. POWELL. Inorg. Chem. **19**, 1582 (1980).
18. J. K. HOYANO and W. A. G. GRAHAM. J. Chem. Soc. Chem. Commun. 27 (1982).
19. S. MURAHASHI, T. MIZOGUCHI, T. HOSOKAWA, I. MORITANI, Y. KAI, M. KOHARA, N. YASUOKA, and N. KASAI. J. Chem. Soc. Chem. Commun. 563 (1974).
20. L. KNOLL, K. REISS, J. SCHAFER, and P. KLUFERS. J. Organomet. Chem. **193**, C40 (1980).
21. B. M. LOUIE and A. STORR. Unpublished results.
22. M. COWIE and S. K. DWIGHT. Inorg. Chem. **19**, 2508 (1980).
23. S. J. RETTIG, A. STORR, and J. TROTTER. Can. J. Chem. **57**, 1823 (1979).

Can. J. Chem. Downloaded from www.nrcresearchpress.com by 210.87.254.42 on 09/06/12
For personal use only.

Retroaldolisation of diacetone alcohol on Al_2O_3, $AlPO_4$, $AlPO_4-Al_2O_3$, and $AlPO_4-SiO_2$ catalysts

J. M. CAMPELO,[1] A. GARCIA, D. LUNA, AND J. M. MARINAS

Department of Organic Chemistry, Faculty of Sciences, Cordoba University, Cordoba-5, Spain

Received July 21, 1983

J. M. CAMPELO, A. GARCIA, D. LUNA, and J. M. MARINAS. Can. J. Chem. **62**, 638 (1984).

The basic properties of Al_2O_3, $AlPO_4$, $AlPO_4-Al_2O_3$, $AlPO_4-SiO_2$, and SiO_2, determined by the adsorption of acid compounds using a spectrophotometric method, were investigated. The surface concentration of basic sites varied greatly from one to another of the solid systems.

An attempt was made to relate the activity toward diacetone alcohol retroaldolisation with the surface basic properties determined by this spectrophotometric method, from the irreversible adsorption of different organic acids in cyclohexane at 298 K. It has been shown that the total basicity (vs. acrylic acid) of the catalyst is the most influential property in the retroaldolisation activity. Experimental results show a zero-order kinetics when the acid sites of the samples are blocked. Al_2O_3 shows the highest basic site concentration and the distance between the number of acid and basic sites seems to control the catalytic activity.

J. M. CAMPELO, A. GARCIA, D. LUNA et J. M. MARINAS. Can. J. Chem. **62**, 638 (1984).

On a étudié les propriétés basiques du Al_2O_3, du $AlPO_4$, du $AlPO_4-Al_2O_3$, du $AlPO_4-SiO_2$ et du SiO_2 par adsorption de composés acides en faisant appel à une méthode spectrophotométrique. La concentration des sites basiques à la surface varie beaucoup avec les systèmes solides.

On a essayé de relier l'activité vis-à-vis de la rétroaldolisation du diacétone alcool avec les propriétés basiques des surfaces telles que déterminées par cette méthode spectrophotométrique, appliquée à l'adsorption irréversible de divers acides organiques dans le cyclohexane à 298 K. On montre que la basicité totale (vs. l'acide acrylique) du catalyseur est la propriété la plus importante dans l'activité vis-à-vis la rétroaldolisation. Les résultats expérimentaux montrent une cinétique d'ordre zéro quand on bloque les sites acides des échantillons. Le Al_2O_3 possède la plus grande concentration de sites basiques et la distance entre le nombre de sites acides et basiques semble contrôler l'activité catalytique.

[Traduit par le journal]

Can. J. Chem. Downloaded from www.nrcresearchpress.com by 210.87.254.42 on 09/06/12
For personal use only.

Introduction

The acid properties of solids have been extensively studied in connection with their catalytic activity, while surface basicity has scarcely been investigated. In this sense, the retroaldolisation of diacetone alcohol (4-hydroxy-4-methyl-2-pentanone) is known to be catalyzed exclusively by bases, and the activity of catalysts in this reaction is therefore believed to be a measure of their basicity (1–6). Thus, the retroaldolisation of diacetone alcohol has been proposed as a test for basic catalysts (3, 4, 6).

Amorphous aluminium orthophosphates, $AlPO_4$, and $AlPO_4-Al_2O_3$ and $AlPO_4-SiO_2$ systems possess acid surface sites of different strengths, capable of taking part in catalytic processes, viz. dehydration, isomerization, alkylation, etc. (7–9). We have shown a correlation between the acidity and the alcohol dehydration activity, as well as the skeletal isomerization of cyclohexene (8–10).

The purpose of this work is to determine the basic properties of these solids by a spectrophotometric method already developed for the determination of acid sites, in order to attempt to correlate them to their catalytic acitivity in the retroaldolisation of diacetone alcohol.

The basicity of $AlPO_4$, $AlPO_4-Al_2O_3$, $AlPO_4-SiO_2$, Al_2O_3, and SiO_2 catalysts has been determined by the spectrophotometric method using acid compounds as titrants. Since the use of titrants with different pK_a and steric hindrance lets us obtain the total surface basicity as well as the relative number of sites accessible to adsorbed molecules, acrylic acid, phenol, and 2,6-di-*tert*-butyl-4-methylphenol were employed as titrant agents. All details concerning adsorption of probe molecules have been reported elsewhere (10–12).

The correlation between surface basicity and catalytic activity in the liquid phase retroaldolisation of diacetone alcohol is fulfilled for all catalysts examined, which leads us to the conclusion that the method described can be used for the characterization of basic properties of solid catalysts.

Experimental

Catalysts

Eight different catalysts were used: three $AlPO_4$ (Al/P = 1) that were obtained through precipitation, from aluminum chloride and phosphoric acid aqueous solutions, with aqueous ammonia (F), ethylene oxide (B), and propylene oxide (BP); a chemically pure alumina (AL) obtained by precipitation from aluminium nitrate by aqueous ammonia; a commercial silica (S) from Merck (Kieselgel 60, 70–230 mesh); two $AlPO_4-Al_2O_3$ (75:25 wt.%) systems obtained by gelification of aluminium orthophosphate with ethylene oxide (BA) and propylene oxide (BPA) on alumina AL; an $AlPO_4-SiO_2$ (20:80 wt.%) system (BS) obtained by gelification of $AlPO_4$ with ethylene oxide on silica S.

These solids, screened between 200–250 mesh, were dried at 380 K in air for 24 h, then calcined 3 h at 923 K in an electric muffle furnace, and stored in a desiccator.

Textural properties (surface area, pore volume, and main pore diameter, determined by nitrogen adsorption (BET method)) and surface acidity, determined by the spectrophotometric method (10–12), are summarized in Table 1.

Surface basicity measurement

The surface basicity was determined on the basis of the irreversible adsorption on the catalyst surface of appropriate acid substrates, following the same experimental procedure that was used previously for the determination of surface acidity (10). The adsorbates used (all from Merck, p.a.) were acrylic acid (AA, pK_a = 4.25), phenol (PH, pK_a = 9.9), and 2,6-di-*tert*-butyl-4-methylphenol (DTMPH, pK_a = 11.1). Adsorption was carried out from cyclohexane solutions (spectroscopic grade, Merck) at 298 K, and the solids were dried prior to each measurement at 390 K.

In each experiment, a freshly prepared titrant agent solution (10

[1]Author to whom correspondence may be addressed.

TABLE 1. Textural and acid properties of the catalysts

Catalyst	S^a ($m^2\ g^{-1}$)	V^b (mL g^{-1})	$\bar{d}^c$ (nm)	Acidity (μmol g^{-1})^d CY^e	PY^f	AN^g
F	181	0.40	3.6	1042	260	76
B	256	0.60	4–12	789	320	86
BP	210	0.42	2.5	732	380	124
AL	151	0.31	2.0	—	60	5
S	380	0.40	2.0	—	206	10
BA	263	0.53	3.0	620	300	35
BPA	237	0.70	2.5	684	385	35
BS	327	0.46	3.0	600	310	23

[a] Surface area.
[b] Pore volume.
[c] Main pore diameter.
[d] Uptake at equilibrium at 298 K.
[e] Cyclohexylamine as titrant, pK_a = 10.6.
[f] Pyridine as titrant, pK_a = 5.25.
[g] Aniline as titrant, pK_a = 4.6.

mL) was pipetted into a cylindrical glass tube that previously was loaded with the solid (about 0.1 g). The tube was fitted with a ground glass stopper, shaken for 1 h at constant temperature, and the concentration of the organic acid was determined spectrophotometrically.

Since the amount of titrant adsorbed on the surface of the solid was determined spectrophotometrically, the validity of the Lambert–Beer law for the solution was checked, and the sorption experiments were developed at the wavelength of the maximum absorption (λ_{max}, nm).

The time required for the system to reach the equilibrium, at constant temperature (298 K), was checked for each solid and it was never more than 45 min.

Once the adsorption remains constant, a monolayer is assumed to have been formed. The chemical interaction, acid compound – surface, may be accomplished by applying the linear transformed Langmuir adsorption isotherm:

$$[1]\quad C/X = (1/b\,X_m) + (C/X_m)$$

where C is the concentration of acid substrate in solution in equilibrium with the adsorbed substrate, b is a constant, X is the amount of adsorbed substrate per gram of basic solid, and X_m is the saturation coverage in a monolayer, which corresponds to the theoretical amount of solute adsorbed by 1.0 g of solid system, if all the basic sites are covered.

The X_m value was assumed to be the number of molecules necessary to saturate the basic sites with pK_a equal to or greater than that from the acid adsorbate used. Thus, the irreversible adsorption of the acid compound was taken as a count of basic sites corresponding to a specific pK_a.

Finally, this method let us determine the basicity of white as well as deeply coloured solids.

Catalytic activity

In all cases, the catalytic acitivity measurements were carried out in a magnetically stirred 100-mL glass reactor, at 335 ± 1 K. Reactions were accomplished with 40 mL of 0.1 *M* cyclohexane solution of diacetone alcohol (DAA) and the amount of catalyst was varied between 0.3–1.0 g (≤ 0.07 mm). The operating variables, stirring rate and particule size, were so chosen as to eliminate diffusion control on the reaction rate.

The reaction rate was obtained by following the consumption of DAA with time and, as the plots of the drop of the DAA concentration vs. time were always linear, when the acid sites were blocked, the determination of the initial slope was straightforward.

The reproducibility for different samples was checked experimentally, and the measurements were repeated 2–3 times. The relative error was approximately 10%.

The retroaldolisation of DAA was followed by gas–liquid chromatography using a stainless steel column of 2 m, packed with 10% Carbowax 20M on Chromosorb P 80/100. The temperature of the column and injector was 370 K and that of the detector was 473 K. The detected reaction products were acetone and mesityl oxide. The latter appeared only when the acid sites were not blocked.

Cyclohexane and DAA, both Merck p.a., were used without further purification.

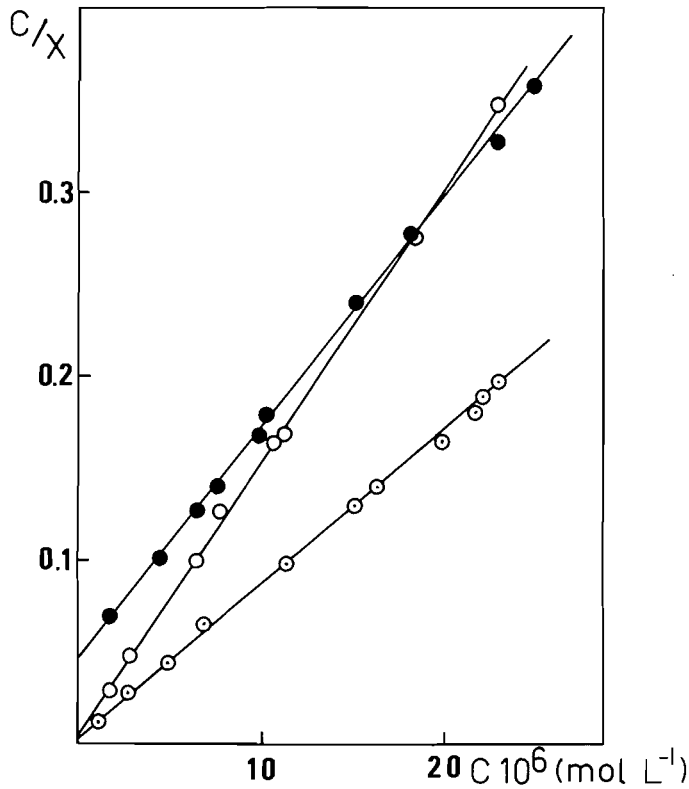

FIG. 1. Titration of F, BP, and BPA samples vs. phenol. Uptake at equilibrium and T = 298 K. (●) F; (○) BP; (⊙) BPA.

Results and discussion

Surface basicity measurement

From the plots of C/X vs. C we obtained straight lines, as can be seen in Fig. 1 where, as an example, the adsorption of PH on F, BP, and BPA samples appears so that, in all cases, the adsorption of acid titrants is consistent with the linear transformed Langmuir adsorption isotherm. Nevertheless, the adsorption is supposed to be of complex character because the surface exhibits centres of different strength, and the consistency with the Langmuir isotherm should be explained by formation of different bonds between the adsorbate and catalyst surface, which are approximately equivalent energetically, since a unique straight line is obtained.

The monolayer, X_m, was obtained from the slope of the plot C/X vs. C, and the distribution of the basic sites of various strengths on the catalyst surface are collected in Table 2. All experimental values are reproducible to within about 6% and the sequence obtained in all cases was: AA > PH > DTMPH, which is in accord with the pK_a of the titrant agent. Thus, because of their pK_a, by definition, the acrylic acid measured the total basicity of the samples. Moreover, the differences between the adsorbate values are a measure of both the number of weaker sites and the number of sites most accessible to adsorbed acid molecules, since the adsorption of DTMPH is influenced mainly by the steric effect of *t*-Bu groups.

The results obtained show that surface concentrations of

Can. J. Chem. Downloaded from www.nrcresearchpress.com by 210.87.254.42 on 09/06/12
For personal use only.

Can. J. Chem. Downloaded from www.nrcresearchpress.com by 210.87.254.42 on 09/06/12
For personal use only.

TABLE 2. Surface basic properties of the catalysts

	Basicity[a] (μmol g^{-1})		
Catalyst	AA[b]	PH[c]	DTMPH[d]
F	294	81	2.1
B	298	55	2.9
BP	474	71	2.0
AL	476	194	1.2
S	95	12	[e]
BA	327	163	1.2
BPA	518	129	1.3
BS	69	20	—

[a]Uptake at equilibrium at 298 K.
[b]Acrylic acid as titrant, $pK_a = 4.25$.
[c]Phenol as titrant, $pK_a = 9.9$.
[d]2,6-Di-*tert*-butyl-4-methylphenol as titrant, $pK_a = 11.1$.
[e]There is no adsorption of titrant agent.

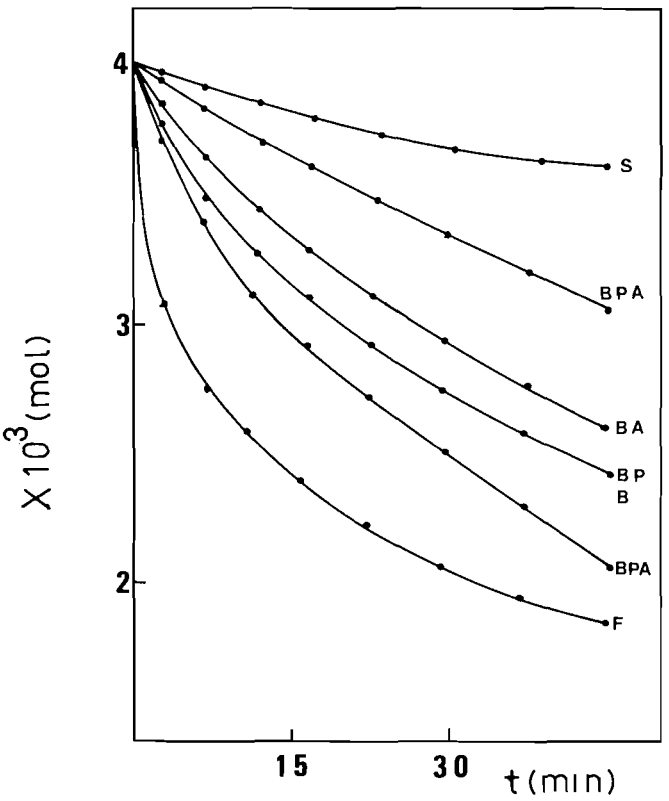

FIG. 2. Time dependence of consumption of DAA (X) in cyclohexane as solvent and at 335 K ($[DAA]_0 = 0.1$ *M*; 40 mL) with 520 mg of S, 343 mg of BPA, 524 mg of BA, 534 mg of BP, 544 mg of B, 537 mg of BPA, and 680 mg of F.

basic sites varied largely with the solid system. Thus the BP, AL, and BPA samples exhibit practically the same high total basicity (vs. acrylic acid) although the number of strong basic sites (vs. phenol) is different, the AL sample being the most basic solid.

Catalytic activity

In the catalytic action of bases in the retroaldolisation of DAA, it was found that the reaction rate is proportional to the concentration of hydroxy groups in the solutions of hydroxides in the concentration range 0.01–0.10 *M* (1). Tanabe *et al.* (2) had first applied this reaction to examining the properties of solid catalysts, beginning with the oxides of alkali earth metals (CaO, BaO, MgO, and SrO). Also, Nondek and Malek (6) chose this reaction to test the strength of basic sites on the surface of Al_2O_3, MgO, and Al_2O_3–MgO catalysts previously used in the aldol condensation of butyraldehyde (13).

It is worth mentioning that Tanabe (2) reported first-order kinetics for the retroaldolisation of DAA catalyzed by alkali earth metal oxides, while Nondek (6) found zero-order kinetics for the same reaction catalyzed by Al_2O_3, MgO, and Al_2O_3–MgO in nonpolar solvents, although for polar solvents, like 2-propanol, the kinetics of acetone formation is altered.

On the other hand, Malinowski and co-workers (14) found that, at 313 K, diacetone alcohol did not react on aluminosilicates and they attributed this result to strong acid sites of the catalysts that may hamper the retroaldolisation of DAA to acetone.

Because $AlPO_4$, Al_2O_3, SiO_2, $AlPO_4$–Al_2O_3, and $AlPO_4$–SiO_2 catalysts possess acid and basic sites capable of taking part in catalytic processes, an attempt has been made to correlate the activity to DAA retroaldolisation with the surface basicity determined by the spectrophotometric method developed by us.

In this sense, Fig. 2 shows the DAA consumption vs. time, with cyclohexane as solvent, for all catalysts studied. As can be seen, there exists a significant dependence between the solid system and its activity in the reaction of DAA.

The analysis of the reaction mixtures by means of glc shows that for the AL catalyst the only product detected was acetone, while for the remaining catalysts the reaction products were acetone and mesityl oxide, the latter appearing as a consequence of the dehydration of DAA on the acid sites of the catalysts.

The AL catalyst shows the greatest activity in the DAA retroaldolisation to acetone. Thus the distance between acidic sites and basic sites seems to control the catalytic activity. Therefore the kinetic study of the DAA retroaldolisation was carried out with the AL catalyst.

Figure 3 clearly demonstrates the independence of the reaction rate, r (mol min^{-1}), of the concentration of DAA and the dependence between the catalytic activity and the concentration of basic sites on the AL catalyst. The concentration of basic sites was varied by using different amounts of catalyst.

On the other hand, the plot of log r vs. log w, where w is the catalyst weight, is linear with a slope of 1.04, as can be seen in Fig. 4.

This result, together with those obtained with different stirring speeds where the reaction rate was independent of the stirring speed above 200 rpm, indicated that, in the range of operating variables, the reaction rates are controlled by the surface reaction and the data are free from transport influences. On the other hand, the reaction rates are zero order in DAA concentration.

During the reaction we did not observe a light brown substance deposited on the catalyst surface, reported by Tada (4) and Malinowski (5) as a consequence of the subsequent condensation reaction. This is probably because the DAA solution is so dilute.

The increase in the activity with an increasing number of basic sites leads us to conclude that the reaction proceeded in similar stages to those of aldol condensation, the proton abstraction from an undissociative adsorbed DAA molecule being the most probable rate-determining step:

Can. J. Chem. Downloaded from www.nrcresearchpress.com by 210.87.254.42 on 09/06/12
For personal use only.

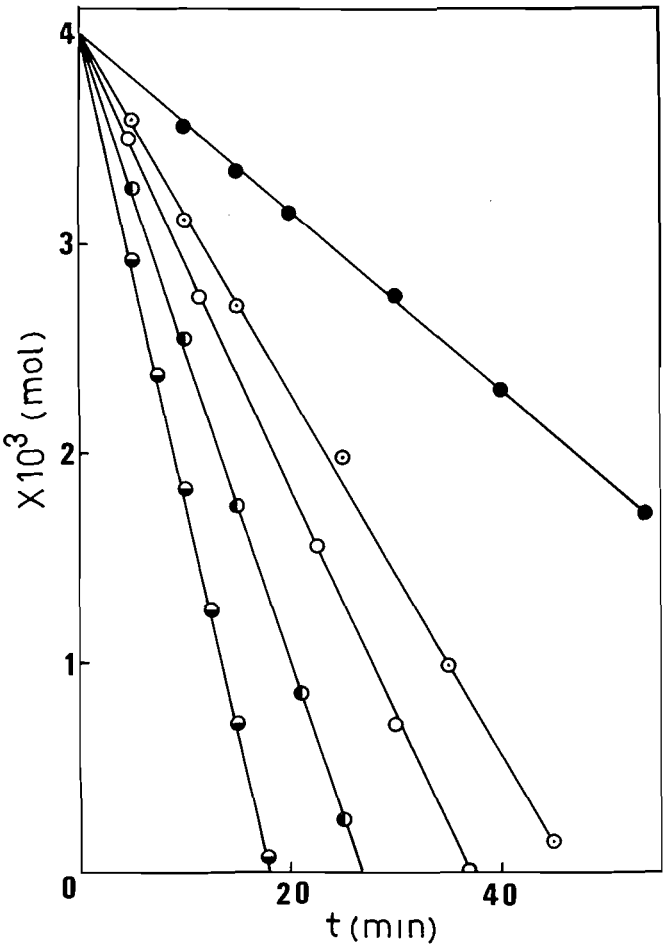

FIG. 3. Time dependence of consumption of DAA (X) as a function of AL loading ([DAA]$_0$ = 0.1 *M* in cyclohexane; 40 mL; 335 K). (●) 151 mg; (⊙) 310 mg; (○) 357 mg; (◐) 529 mg; (◒) 731 mg.

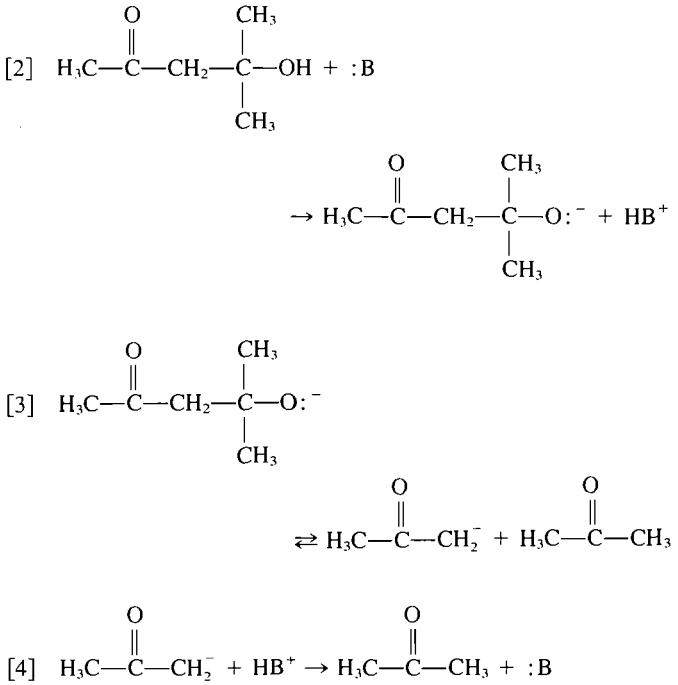

For the remaining catalysts, this reaction competes with the dehydration to mesityl oxide:

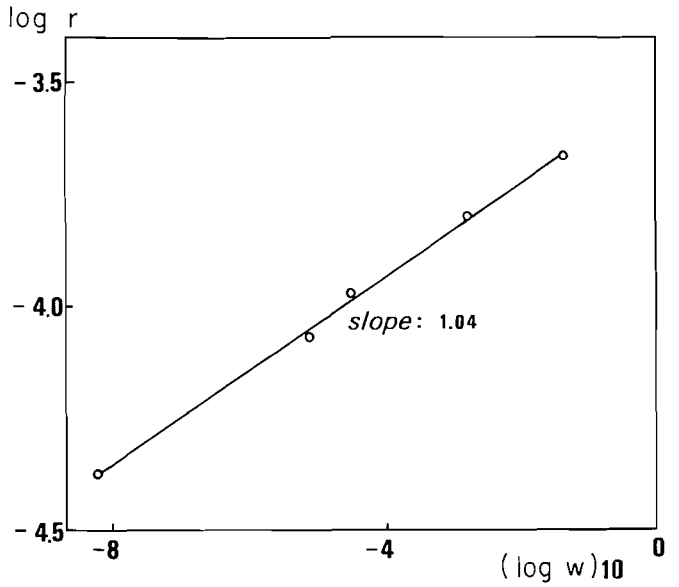

FIG. 4. Reaction order for catalyst weight.

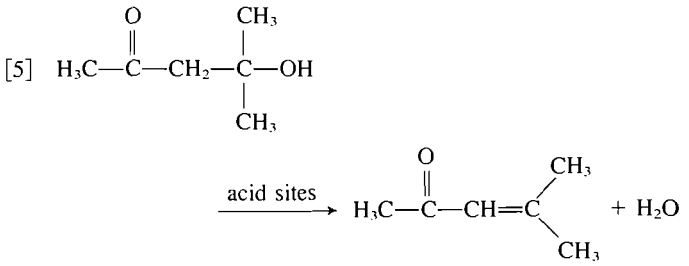

so that the consumption of DAA vs. time is not linear.

Much information about active sites can also be obtained by the blocking of the probable active sites by the adsorption of poisons associated with a simultaneous investigation of the reaction run in presence of the poisoned catalyst. In the present case, the active sites in the reaction have been identified by comparing the changes in the reaction rate of the alumina (AL) poisoned with different amounts of acrylic acid. The partial poisoning of the basic sites on the surface of the AL catalyst was performed as follows: a sample of dried catalyst was shaken in a cyclohexane solution of acrylic acid, which contained an amount of adsorbate lower than the stoichiometric amount of the surface basic sites. After 1 h, the excess of solution was removed and the solid was washed with cyclohexane. On this prepared catalyst, the retroaldolisation of DAA was carried out following the standard procedure; the results obtained are given in Table 3 and Fig. 5.

The progressive decrease of the reaction rate was parallel to the progressive increase in the acrylic acid added. Therefore there exists a significant dependence between the surface basicity measured with acrylic acid and the activity in the DAA retroaldolisation.

Furthermore, the plot of the reaction rate of DAA retroaldolisation vs. basicity of AL catalysts (vs. acrylic acid) is linear with regression coefficient above 0.99 and a slope of $1.055 \times 10^{-2}\ s^{-1}$. A "t-test" of significance shows that this is significant at a level better than 1%.

This correlation between the changes in concentration of the total surface basic sites and the activity of the reaction allows us to state unequivocally that these sites are active in the reaction.

TABLE 3. Reaction rates of DAA retroaldolisation of different AL catalysts

Catalyst	Basicity vs. acrylic acid (μmol g^{-1})	$r \times 10^{6}$ [a] (mol s^{-1} g^{-1})
AL	476	4.96
Al[b]	416	4.46
AL[b]	397	4.16
$Ni_{20}AL$[c]	498	5.31
$Ni_{20}AL$[c]	401	4.14

[a] Catalytic activity per unit weight of catalyst.
[b] AL catalysts partially poisoned with acrylic acid.
[c] Nickel supported AL catalysts at 20 wt.% Ni with different basicity vs. acrylic acid (12).

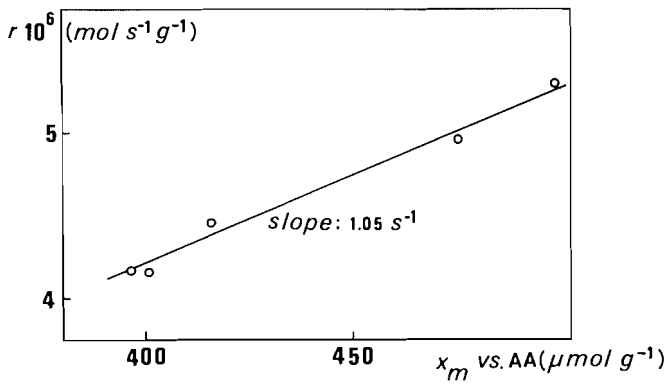

FIG. 5. Reaction rate vs. basicity of AL catalysts listed in Table 3 (basicity vs. acrylic acid).

As a consequence of the results obtained, a second step in this study was the poisoning of the acid sites on the surface of the solids, which was performed as follows: a sample of the dried catalyst was shaken in a cyclohexane solution of cyclohexylamine, which contained the adsorbate in the stoichiometric amount for the surface acid sites. After one hour, the excess of solution was removed and the catalyst was washed with cyclohexane. The retroaldolisation of DAA was then carried out on this prepared catalyst.

The rates of reaction of DAA retroaldolisation on catalysts with blocked acid sites, except AL, were independent of the concentration of DAA (Fig. 6). Thus, the retroaldolisation of DAA on all poisoned catalysts was found to follow zero-order kinetics, as in the case of the AL catalyst. The rates of reaction of retroaldolisation of DAA in this series of investigated catalysts are given in Table 4.

The changes of the reaction rates in the catalysts investigated are similar to those in the concentration of basic sites, although this relation is not linear as in the AL case, as correlations between X_m and r can exist only in a series of catalysts having the same strength of sites, since the Brönsted relationship must hold

$$[6] \quad r = G K_{diss}^{\alpha} \qquad \alpha \neq 1$$

This is valid for the AL catalysts of Table 3 where K_{diss} is more or less constant, but not for the remaining catalysts (Table 2 vs. Table 4) where acid sites of different strength are being compared.

From the intercept at the origin in the plot of C/X vs. C, we have obtained the b values that depend on the site strength. These values, although displaying a large experimental error,

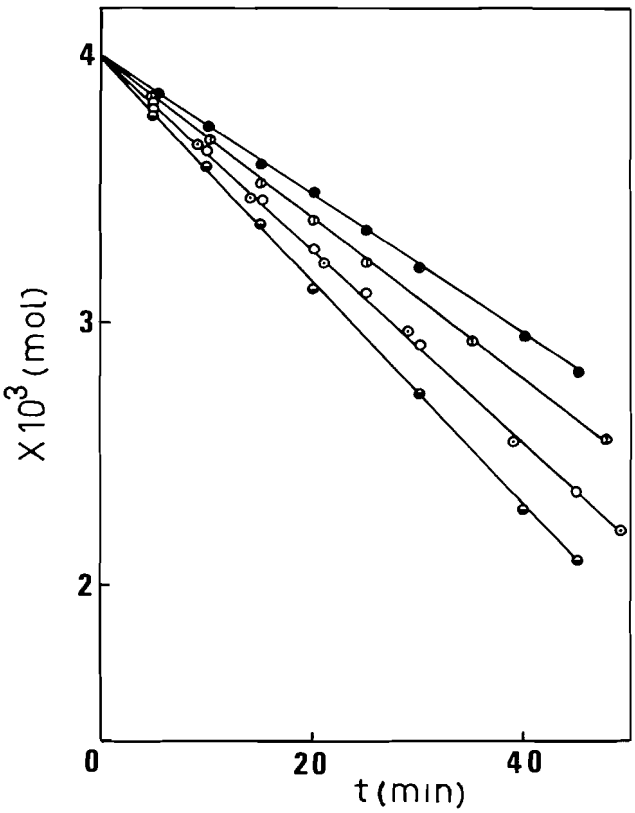

FIG. 6. Time dependence of consumption of DAA (X) for poisoned catalysts ([DAA]$_0$ = 0.1 M in cyclohexane; 40 mL; 335 K). (●) BA 258 mg; (◑) B 273 mg; (○) BPA 304 mp; (⊙) BP 325 mg; (◒) F 436 mg.

TABLE 4. Reaction rates of DAA retroaldolisation on poisoned catalysts

Catalyst	$r \times 10^{6}$ [a] (mol s^{-1} g^{-1})
F	1.63
B	1.87
BP	1.96
S	0.33
BA	1.73
BPA	2.06
BS	0.43

[a] Catalytic activity per unit weight of catalyst.

are very different from one catalyst to another. Thus, no single-line correlation for all catalysts shown in Table 4 should be obtained. Furthermore, the different porous texture of the solids may also alter the adsorption of DAA and/or the titrant agent.

However, the activity – surface basicity correlation vs. acrylic acid is better than for other titrants, especially in the case of DTMPH, which is mainly influenced by steric hindrance of t-Bu groups. Thus the total basicity seems to be mainly responsible for the retroaldolisation of DAA, the sample AL being the most active catalyst.

Conclusions

The present investigation has provided conclusive evidence

Can. J. Chem. Downloaded from www.nrcresearchpress.com by 210.87.254.42 on 09/06/12
For personal use only.

that a correlation between surface basicity of solid systems, determined by a spectrophotometric method from the irreversible adsorption of organic acids in cyclohexane solution, and their activity in the retroaldolisation of DAA is established for catalysts when their acid sites are blocked.

The poisoning of active basic sites with acrylic acid demonstrated that the total surface basicity is the predominant factor in determining the activity of the catalyst.

The results obtained lead us to the conclusion that the method described above can be used for characterization of solid bases. When the solid catalysts exhibit strong acid sites, the retroaldolisation of DAA is accompanied by the formation of mesityl oxide as a consequence of the dehydration reaction.

Acknowledgements

This work has been possible thanks to a grant of the Comision Asesora de Investigacion Cientifica y Tecnica (CAICYT), project no. 0249/81.

1. G. AKERLOF. J. Am. Chem. Soc. **49**, 2955 (1927).
2. K. TANABE, Y. FUKUDA, and S. OKAZAKI. Nippon Kagaku Kaishi, **3**, 513 (1972).
3. K. TANABE and Y. FUKUDA. React. Kinet. Catal. Lett. **1**, 21 (1974).
4. A. TADA. Bull. Chem. Soc. Jpn. **48**, 1391 (1975).
5. J. KIJENSKI and S. MALINOWSKI. Bull. Acad. Pol. Sci. Ser. Sci. Chim. **26**, 183 (1978).
6. L. NONDEK and J. MALEK. React. Kinet. Catal. Lett. **14**, 381 (1980).
7. M. A. ARAMENDIA, J. M. CAMPELO, S. ESTEBAN, C. JIMENEZ, J. M. MARINAS, and J. V. SINISTERRA. Rev. Inst. Mex. Petrol. **12**, 61 (1980).
8. J. M. CAMPELO, J. M. MARINAS, and R. PEREZ-OSSORIO. An. Quim. **74**, 86 (1978).
9. J. M. CAMPELO and J. M. MARINAS. Afinidad, **38**, 333 (1981).
10. J. M. CAMPELO, A. GARCIA, J. M. GUTIERREZ, D. LUNA, and J. M. MARINAS. Can. J. Chem. **61**, 2567 (1983).
11. J. M. MARINAS, C. JIMENEZ, J. M. CAMPELO, M. A. ARAMENDIA, V. BORAU, AND D. LUNA. Proc. 7th Symp. Iberoamerican Catal. La Plata, 1980. p. 79.
12. J. M. CAMPELO, A. GARCIA, D. LUNA, and J. M. MARINAS. Afinidad, **39**, 325 (1982).
13. L. NONDEK and J. MALEK. Chem. Prum. **30**, 30 (1980).
14. E. FEDORYNSKA, T. WOZNIEWSKI, S. MALINOWSKI, I. AHMED, and A. MADURA. J. Colloid Interface Sci. **69**, 469 (1979).

Can. J. Chem. Downloaded from www.nrcresearchpress.com by 210.87.254.42 on 09/06/12
For personal use only.

Synthesis of tri- and tetrasaccharide haptens related to the *Asialo* forms of the gangliosides G_{M2} and G_{M1}[1]

SUBRAMANIAM SABESAN AND RAYMOND U. LEMIEUX
Department of Chemistry, University of Alberta, Edmonton, Alta., Canada T6G 2G2

Received August 10, 1983

SUBRAMANIAM SABESAN and RAYMOND U. LEMIEUX. Can. J. Chem. **62**, 644 (1984).

Synthesis of βDGalNAc(1→4)βDGal(1→4)βDGlc—$O(CH_2)_8COOCH_3$ (**21**) and βDGal(1→3)βDGalNAc(1→4)βDGal-(1→4)βDGlc—$O(CH_2)_8COOCH_3$ (**33**) are presented starting from βDGal(1→4)βDGlc—$O(CH_2)_8COOCH_3$ (**1**) and D-galactose. Improvements in the preparations of D-galactal triacetate (**7**) and tri-*O*-acetyl-2-azido-2-deoxy-α-D-galacto-pyranosyl bromide (**11**) are reported. The syntheses proceeded by way of the tri-*O*-acetyl-2-deoxy-2-phthalimido-β-D-galacto-pyranosyl and 4,6-di-*O*-acetyl-3-*O*-(tetra-*O*-acetyl-β-D-galactopyranosyl)-2-deoxy-2-phthalimido-β-D-galactopyranosyl bromides (**18** and **30**), which, in turn, were prepared from the corresponding allyl glycosides (**15** and **23**). The ^{13}C chemical shifts for the tri- and tetrasaccharide portions of **21** and **33** are assigned from the chemical shifts that were observed for the carbon atoms in the disaccharides which make up these structures. The trisaccharide (**21**) only very weakly inhibited the agglutination of human A red cells by the lectin of *Dolichos biflorus*. The tetrasaccharide (**33**) was inactive.

SUBRAMANIAM SABESAN et RAYMOND U. LEMIEUX. Can. J. Chem. **62**, 644 (1984).

On propose des synthèses des βDGalNAc(1→4)βDGal(1→4)βDGlc—$O(CH_2)_8COOCH_3$ (**21**) et βDGal(1→3)βDGalNAc-(1→4)βDGal(1→4)βDGlc—$O(CH_2)_8COOCH_3$ (**33**) à partir du βDGal(1→4)βDGlc—$O(CH_2)_8COOCH_3$ (**1**) et du D-galactose. On rapporte des améliorations aux préparations du triacétate de D-galactal (**7**) et du bromure de tri-*O*-acétyl azido-2 déoxy-2 α-D-galactopyrannosyle. Les synthèses impliquent la préparation des bromures de tri-*O*-acétyl déoxy-2 phthalimido-2 β-D-galactopyrannosyle et de di-*O*-acétyl-4,6 *O*-(tétra-*O*-acétyl β-D-galactopyrannosyl)-3 déoxy-2 phthalimido-2 β-D-galacto-pyrannosyle (**18** et **30**) qui sont eux-mêmes préparés à partir des glycosides allyliques correspondants (**15** et **23**). On a attribué les déplacements chimiques du ^{13}C des portions tri- et tétrasaccharidiques des composés **21** et **33** en se basant sur les déplacements chimiques observés pour les atomes de carbones des disaccharides qui composent ces structures. Le trisaccharide (**21**) n'inhibe que très faiblement l'agglutination des cellules rouges A humaines par la lectine de *Dolichos biflorus*. Le tétrasaccharide **33** est inactif.

[Traduit par le journal]

Introduction

This paper is concerned with the synthesis of structures related to the gangliosides (1) known as G_{M2} and G_{M1} (2), compounds which are also referred to as II^3-NeuAcGgOSe$_3$ and II^3-NeuAcGgOSe$_4$ (3).

The ganglioside G_{M2} differs from G_{M1} in that it lacks the terminal βDGal residue. Treatment of these gangliosides either with neuraminidase or aqueous acids removes the acidic neuraminic acid (sialic acid) residues to provide the so-called *asialo* forms. *Asialo*-G_{M1} and *asialo*-G_{M2} are also referred to as gangliotetraosylceramide and gangliotriosylceramide, respectively (3).

The distribution of gangliosides in tissues has become a subject of major interest (4). *Asialo*-G_{M2} occurs in certain tumor cells (5) and in increased amounts in the brain in Tay Sachs disease (6). Evidence has recently been acquired (7) that the terminal disaccharide (βDGalNAc(1→4)βDGal) unit of G_{M2} occurs as a terminal unit in the human blood group Sd^a active Tamm–Horsfall urinary glycoprotein. This glycoprotein reacts with a lectin from *Dolichos biflorus* which was known to react

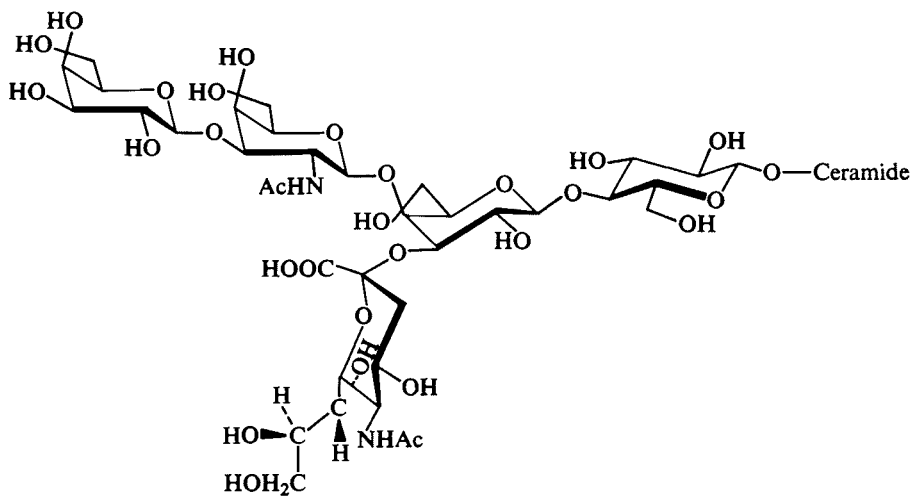

G_{M1}

βDGal(1→3)βDGalNAc(1→4)[αDNeuAc(2→3)]βDGal(1→4)βDGlc-O-ceramide

[1]Taken from a thesis by S. Sabesan presented in partial fulfillment of the Ph.D. degree, University of Alberta, 1983.

Can. J. Chem. Downloaded from www.nrcresearchpress.com by 210.87.254.5 on 09/06/12
For personal use only.

Can. J. Chem. Downloaded from www.nrcresearchpress.com by 210.87.254.5 on 09/06/12
For personal use only.

with the blood group A determinant (αDGalNAc(1→3)[αLFuc-(1→2)]βDGal) but now known (8) to react much more strongly with the Forssman determinant which terminates with an αDGalNAc(1→3)βDGalNAc(1→4)βDGal trisaccharide unit. The lectin reacts only very weakly with βDGalNAc(1→3)-βDGal(1→4)βDGal(1→4)DGlc (globoside) (8). *Asialo*-G_{M1} occurs at the surface of killer cells (9).

Since antibodies raised against the *asialo* forms of G_{M2} and G_{M1} have proven useful for the detection and distribution of these structures in tissues (see ref. 10), the methodology based on chemical synthesis of haptens suitable for the preparation of artificial antigens and immunoadsorbents (11–13) was of interest. Furthermore, it was of interest to examine the reaction of the *asialo*-G_{M2} structure with the lectin of *Dolichos biflorus* (7) and possibly other lectins with specificities related to terminal DGalNAc residues. To these ends, we report herein the synthesis of the haptens βDGalNAc(1→4)βDGal(1→4)-βDGlc—$O(CH_2)_8COOCH_3$ (**21**) and βDGal(1→3)βDGalNAc-(1→4)βDGal(1→4)βDGlc—$O(CH_2)_8COOCH_3$ (**33**). The availability of these compounds was also of interest for conformational studies based on ^1H and ^{13}C nmr measurements (14) of the carbohydrate portions of G_{M2} and G_{M1}. The results of these studies will be reported separately.

Discussion of results

The 8-methoxycarbonyloctyl β-D-lactoside (**1**) that was used as starting material had been reported by Banoub and Bundle

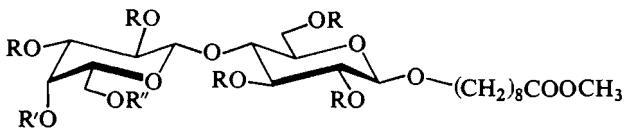

1 R = R′ = R″ = H
2 R = R′ = R″ = Ac
5 R = Ac, R′ = R″ = H
6 R = Ac, R′ = H, R″ = Bz

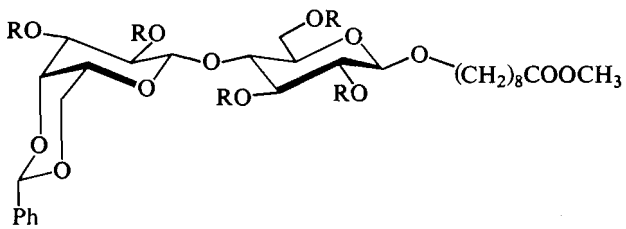

3 R = H
4 R = Ac

(15). A Koenigs–Knorr condensation using silver carbonate as promoter and followed by treatment with mercuric bromide to rearrange orthoester intermediates (detected by ^1H nmr) proved, in our hands, a more convenient procedure for the preparation of **1** which was characterized as the heptaacetate **2**. Compound **1** was converted to the diol **5** by way of the 4′,6′-O-benzylidiene derivative **3** and the acetate **4** following conventional methods (16–18). The structure of compound **3** was evident from the appearance of only one signal (at 60.31 ppm and assigned to C-6) in the region of the ^{13}C nmr spectrum characteristic for free hydroxymethyl groups in D_2O (19). The ^1H nmr spectrum for the diol **5** in DMSO-d_6 showed signals at 5.12 (doublet) and 5.05 (triplet) ppm which could be assigned to OH groups by exchange with D_2O and to arise from OH-4′ and OH-6′ by spin decoupling experiments. The preferential (20) *O*-benzoylation of the 6′-hydroxyl of **5** provided **6** in 80% yield. The ^1H nmr spectrum confirmed the composition and showed a doublet signal for OH-4′ (5.55 ppm with a spacing of 5.2 Hz) which was shown to be coupled to H-4′ at 3.98 ppm by addition of D_2O.

In order to prepare the *asialo*-G_{M2} related hapten (**21**), the 4′-alcohol (**6**) was condensed with tri-*O*-acetyl-2-deoxy-2-phthalimido-α,β-D-galactopyranosyl bromide (**18**) under the conditions developed in this laboratory (21). The yield of the blocked trisaccharide **19** was 64%. Removal of the blocking groups by way of the phthalimido compound **20** followed well-established procedures (22, 23). In the case of the phthalimido

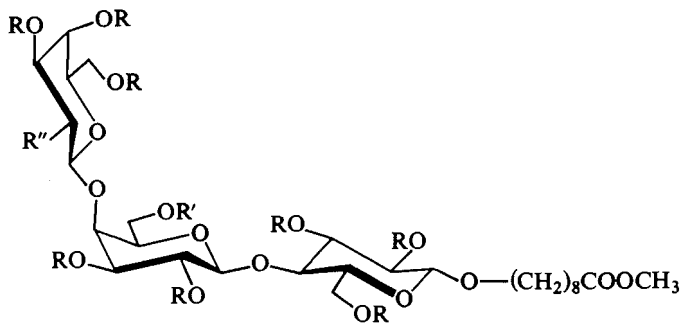

19 R = Ac, R′ = Bz, R″ = NPhth
20 R = R′ = H, R″ = NPhth
21 R = R′ = H, R″ = NHAc

compounds **19** and **20**, as expected (21), both H-1″ and H-3″ were strongly deshielded (more than 0.9 ppm to lower field than either H-1 or H-1′). The β-configuration for the newly formed glycosidic bond in **19** was evident from the ^1H nmr spectrum (H-1″ at 5.32 ppm with a spacing of 7.8 Hz). The 1″→4 linkage can be assigned since the glycosylation changed the chemical shift of H-4′ from 3.98 ppm for the alcohol **6** to 4.18 ppm for **19**. A much larger shift would have occurred had acyl migration occurred.

The preparation of the phthalimidobromide (**18**) warrants special attention. The starting material, tri-*O*-acetyl-D-galactal (**7**) could be prepared in near quantitative yield under the same buffered conditions used for the preparation of tri-*O*-acetyl-D-glucal (24) which employs a zinc–copper couple rather than the zinc-platinum couple recommended by Shafizadeh (25). Furthermore, the purity of the crude syrupy product (**7**) was estimated by ^1H nmr to be greater than 90% and this level of purity was not improved by distillation (25). As noted by Lemieux and Ratcliffe (26), the azidonitration of **7** produces an about 10% yield of the 1-acetamido compound **10**. The chromatographic separation of **10** from the 1-nitrates (**8** and **9**) complicates the preparation of the bromide **11**. It is now found that the treatment of the crude reaction mixture with Vilsmeier reagent (*N*,*N*-dimethylbromoforminium bromide (27)) rapidly converts **10** to **11**. This reaction is followed by the addition of the lithium bromide to convert the nitrates **8** and **9** into the desired bromide **11** which was isolated as a syrup by column chromatography in 40% overall yield. However, the crude syrupy bromide could be used directly for the preparation of the allyl tri-*O*-acetyl-2-azido-2-deoxy-β-D-galactopyranoside (**12**) under Koenigs–Knorr conditions to provide **12** in about 29% yield from tetra-*O*-acetyl-α-D-galactopyranosyl bromide.

The azide **12** was deacetylated to **13** prior to reduction with

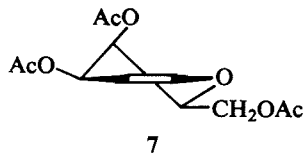

7

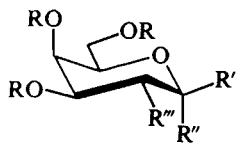

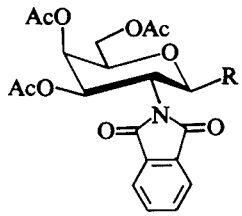

8 R = Ac, R′ = ONO_2, R″ = H, R‴ = N_3
9 R = Ac, R′ = H, R″ = ONO_2, R‴ = N_3
10 R = Ac, R′ = H, R″ = NHAc, R‴ = N_3
11 R = Ac, R′ = H, R″ = Br, R‴ = N_3
12 R = Ac, R′ = OCH_2CHCH_2, R″ = H, R‴ = N_3
13 R = H, R′ = OCH_2CHCH_2, R″ = H, R‴ = N_3
14 R = H, R′ = OCH_2CHCH_2, R″ = H, R‴ = NH_2

15 R = OCH_2CHCH_2
16 R = $OCHCHCH_3$
17 R = OH(+ α anomer)
18 R = Br

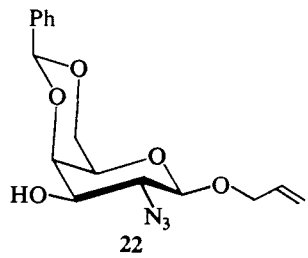

22

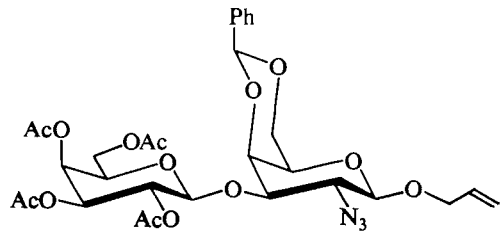

23

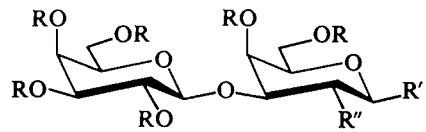

24 R = Ac, R′ = OCH_2CHCH_2, R″ = N_3
25 R = H, R′ = OCH_2CHCH_2, R″ = N_3
26 R = H, R′ = OCH_2CHCH_2, R″ = NH_2
27 R = Ac, R′ = OCH_2CHCH_2, R″ = NPhth
28 R = Ac, R′ = $OCHCHCH_3$, R″ = NPhth
29 R = Ac, R′ = OH (+ α anomer), R″ = NPhth
30 R = Ac, R′ = Br (+ α anomer), R″ = NPhth

hydrogen sulphide (28, 29) to provide the amine **14**. The crude amine was converted to the acetylated phthalimido glycoside **15** in 70% overall yield under previously reported conditions (29). Removal of the allyl group of **15** by way of the 1-propenyl intermediate (**16**) (30, 31) to provide the alcohol **17** proceeded without complication in 78% yield. The Vilsmeier bromide was used to convert **17** to the mixture of anomeric bromides **18** (29).

In view of the reliability of the so-called phthalimidobromide glycosylation reaction (32), it was decided to prepare the blocked tetrasaccharide **31** by condensation of the disaccharide phthalimidobromide **30** with the alcohol **6**.

The allyl glycoside (**13**) was condensed with α,α-dimethoxytoluene to provide the 4,6-*O*-benzylidene derivative **22** in 79% yield. The structure of this crystalline compound was evident from its ^1H nmr spectrum in pure $CDCl_3$ which displayed a doublet (8.0 Hz) for OH-3 at 2.59 ppm which caused H-3 to produce a sextet which collapsed to a quartet (spacings 3.5 and 10.0 Hz) on deuterium exchange. It is noteworthy that the signal for H-5 (3.41 ppm) appears as a broad doublet with a spacing of about 2 Hz and a half-band width of 4.4 Hz since the small couplings of H-5 appear characteristic for 4,6-*O*-benzylidene derivatives of galactopyranosides.

The condensation of **22** with tetra-*O*-acetyl-α-D-galactopyranosyl bromide to form **23** proceeded in 70% yield using the silver trifluoromethanesulfonate – *sym*-collidine complex (21). A slight deficit of the *sym*-collidine was used, as described by Garegg and Norberg (33), to ensure the rearrangement of the orthoester intermediates that normally occur. When the condensation was promoted with mercuric cyanide using toluene nitromethane as solvent (34), an about equimolar mixture of the α and β glycosides was obtained in 80% yield. The β-configuration for **23** was readily assigned since H-1′ occurred as a doublet at 4.80 ppm with spacing of 7.8 Hz.

The blocked allyl disaccharide **23** was converted to the mixture of phthalimidobromides **30** under the same conditions discussed above for the conversion of **12** to **18**. Condensation of **30** with the alcohol **6** provided **31** in 62% yield as a chromatographically pure amorphous solid. The ^1H and ^{13}C nmr spectra required a high state of purity. A comparison of the chemical shifts for H-1′, H-3′, H-4′, and H-4″ of compounds **19** and **31** show these to have a close correspondence. Since for both compounds the chemical shifts for H-4′ are identical, it is likely that these compounds do not differ in the conformational preference about the 1″→4′ glycosidic linkage. On the other hand, the chemical shifts for H-1″ were substantially different, 5.32 ppm for **19** and 5.11 ppm for **31**. However, this difference is not surprising since it is well established (21) that an equatorial phthalimido group has a strong deshielding effect on neighboring axial hydrogen atoms and, therefore, a slight change in the time-averaged orientation of the phthalimido group could cause this change in the chemical shift. In fact, a change in the orientation of the phthalimido group could cause this change in the chemical shift. In fact, a change in the orientation of the phthalimido group is to be expected (35) since the group must be in nonbonded interaction with the C-3″ substituent and, in the case of **19**, the substituent is an acetoxy group whereas, in the case of **31**, the substituent is the much bulkier acetylated β-D-galactopyranosyl group. This influence on chemical shift should also occur for the allyl glycosides **15** and **27** and, in fact, the signals for H-1 of these compounds differed in chemical shift by 0.17 ppm. A change in the orientation of the phthalimido group should also cause a change in the chemical shift of H-2″. In fact, H-2″ gave its signal at 4.53 ppm in the case of **19** but at 4.48 ppm for **31**. In the case of the allyl glycosides **15** and **27**, the change in chemical shift for H-2

Can. J. Chem. Downloaded from www.nrcresearchpress.com by 210.87.254.5 on 09/06/12
For personal use only.

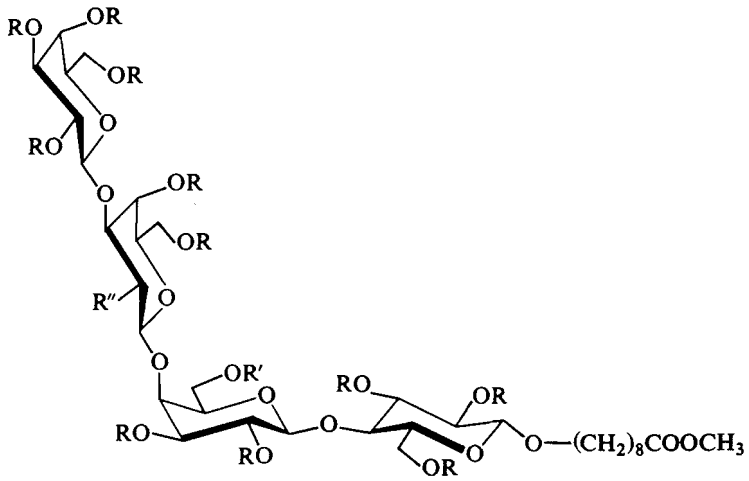

31 R = Ac, R′ = Bz, R″ = NPhth
32 R = R′ = H, R″ = NPhth
33 R = R′ = H, R″ = NHAc

was similar, namely, 0.04 ppm. The small change of 0.05 ppm as compared to the 0.20 ppm change for H-1″ atoms of **19** and **31** is not unexpected since inspection of a molecular model shows that a given rotation about the C—N bond must provide a greater increase (or greater decrease) for the distance between the neighboring carbonyl oxygen and H-1″ than for the distance between H-2″ and the other carbonyl oxygen. Lemieux and Bock (36) have discussed similar influences on chemical shift resulting from substitutions that influence the orientation of an acetamido group.

Deblocking of **31** by way of the phthalimido intermediate **32** under the usual conditions to form the free amine and followed by *N*-acetylation provided the *asialo*-G_{M1} related hapten **33** as a colorless solid with ^1H and ^{13}C nmr spectra in good general agreement with expectations for a pure substance. In order to assign ^{13}C nmr chemical shifts for the haptens **21** and **33**, the disaccharides **38** and **39** were synthesized. Table 1 contains an assignment of ^{13}C chemical shifts based on assignments for the disaccharides **1**, **38**, and **39** from the shifts observed for the

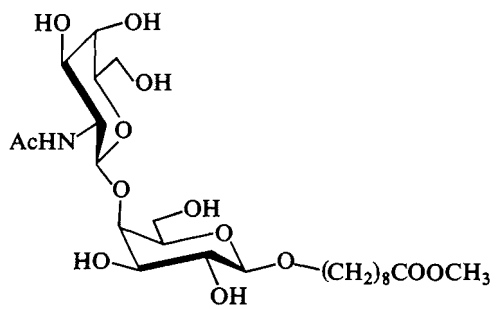

38

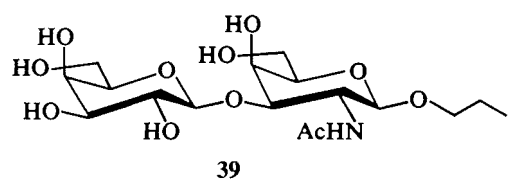

39

simple model alkyl glycosides. The chemical shifts thus assigned for the disaccharides were then used to assign the signals observed in the ^{13}C nmr spectra of **21** and **33**. Examination of Table 1 shows that excellent correspondence is obtained and these data are taken as unequivocal confirmation of the structural assignments.

Under the conditions used, the agglutination of human A red cells was completely inhibited by 16 μg of the Forssman related hapten αDGal(1→3)αDGalNAcO$(CH_2)_8COOCH_3$ (8) and by 500 μg of the A blood group related hapten αLFuc(1→2)-[αDGalNAc(1→3)]βDGalO$(CH_2)_8COOCH_3$ (37). In contrast, 3000 μg of the *asialo*-G_{M2} related hapten **21** were required. The disaccharide hapten **38** was an even weaker inhibitor (2600 μg showed only partial inhibition). The tetrasaccharide **33** was inactive.

Experimental

All solvents and reagents were purified according to standard procedures (38). Transesterifications were effected using the specified volumes of a 0.5 *M* solution of sodium methoxide in dry methanol.

Thin layer chromatograms (tlc) were performed on precoated silica gel 60-F254 plates (E. Merck. Darmstadt) and visualized by charring after spraying with 5% sulphuric acid in ethanol. For column chromatography, silica gel H (type 60) (E. Merck, Darmstadt) and distilled solvents were used and the columns were loaded in the range 1:30−1:50.

Unless otherwise stated, ^1H nmr spectra were recorded on a Bruker 360 MHz or 400 MHz at 296 K. The ^{13}C nmr spectra were recorded on a Bruker WH-200 (50.3 MHz) or WH-400 (100.6 MHz) at 305 K. For organic solvents, ^1H and ^{13}C nmr chemical shifts are in parts per million (ppm) relative to internal 1% tetramethylsilane (TMS). The ^1H chemical shifts for solutions of compounds in deuterium oxide (D_2O) are expressed relative to the HOD signal (4.81 ppm at 296 K). The ^{13}C chemical shifts were determined by using the deuterium signal as the reference. Whenever comparison of ^{13}C chemical shifts among compounds is made, the same spectrometer and temperatures were used. The melting points are uncorrected.

8-Methoxycarbonyloctyl 4-O-(β-D-galactopyranosyl)-β-D-glucopyranoside (1)

A solution of acetobromolactose (39) (72.0 g, 103 mmol) in dichloromethane (400 mL) was added to a vigorously stirred suspension of anhydrous silver carbonate (56.5 g, 206 mmol), anhydrous calcium sulphate (40 g), and 8-methoxycarbonyloctanol (40) (36.2 g, 192.5 mmol) in dichloromethane (600 mL). After 16 h, the reaction mixture was filtered through a bed of diatomaceous earth (10 g) and evaporated to a syrup which was dissolved in a mixture of toluene−nitromethane (1:1, 800 mL) containing anhydrous mercuric bromide (1.0 g). After

Can. J. Chem. Downloaded from www.nrcresearchpress.com by 210.87.254.5 on 09/06/12
For personal use only.

TABLE 1. The assignments of the ^{13}C chemical shifts* for the *Asialo*-G_{M2} and *Asialo*-G_{M1} related haptens βDGalNAc(1→4)βDGal(1→4)βDGlcO$(CH_2)_8COOCH_3$ (**21**) and βDGal(1→3)βDGalNAc(1→4)βDGal(1→4)βDGlcO-$(CH_2)_8COOCH_3$ (**33**) based on the shifts observed for the model compounds βDGlcO$(CH_2)_8COOCH_3$ (**40**), βDGalOCH_3 (**41**), βDGalNAcOCH_3 (**42**), βDGal(1→4)βDGlcO$(CH_2)_8COOCH_3$ (**1**), βDGalNAc(1→4)βDGalO$(CH_2)_8COOCH_3$ (**38**) and βDGal(1→3)βDGalNAcO$(CH_2)_2CH_3$ (**39**)

Sugar unit	Carbon atom	Chemical shifts, ppm							
		41	**42**	**40**	**1**	**38**	**39**	**21**	**33**
βDGlc	1			102.54	102.31			102.37	102.56
	2			73.40	73.14			73.16	73.36
	3			76.14	74.76			74.76	75.00
	4			69.88	78.81			79.04	79.37
	5			76.14	75.02			75.10	75.07
	6			61.06	60.45			60.53	60.81
βDGal	1′	104.08			103.22	102.80		103.34	103.52
	2′	71.00			71.25	71.16		71.45	71.20
	3′	73.05			72.85	73.08		72.90	73.20
	4′	68.94			68.84	76.15		76.48	76.53
	5′	75.36			75.62	74.29		74.78	75.00
	6′	61.23			61.27	60.61		61.03	61.24
βDGalNAc	1″		102.63			102.98	101.56	102.94	102.75
	2″		52.54			52.99	51.63	53.08	52.14
	3″		71.39			71.26	80.19	71.45	80.25
	4″		68.10			68.12	68.32	68.21	68.59
	5″		75.33			75.09	75.00	75.21	75.27
	6″		61.22			61.33	61.19	61.41	61.54
βDGal	1‴	104.08					105.06		105.16
	2‴	71.00					70.92		71.14
	3‴	73.05					72.78		73.09
	4‴	68.94					68.88		69.17
	5‴	72.36					75.26		75.51
	6‴	61.23					61.28		61.54

*Measured at 100 MHz in D_2O at 305 K with external tetramethylsilane as reference signal (0 ppm).

Can. J. Chem. Downloaded from www.nrcresearchpress.com by 210.87.254.5 on 09/06/12
For personal use only.

stirring for 24 h at 50°C, the reaction mixture was diluted with dichloromethane and washed with an aqueous potassium iodide solution and then with water. Evaporation left a colorless syrup which was extracted with cyclohexane (4 × 100 mL) to remove the excess 8-methoxycarbonyloctanol (16.0 g).

Sodium methoxide in methanol (10 mL) was added to a solution of the syrup (75.0 g) in methanol (500 mL) and the solution was stirred at room temperature for 6 h. Precipitation was completed by cooling to 0°C prior to filtration. The solid was washed with methanol and crystallized from methanol (31.2 g, 59% yield); mp 164–165°C (lit. (15) mp 159°C). The chemical shifts for H-1 and H-1′ agreed with those reported (15); ^{13}C nmr (D_2O) δ: 178.17 (C=O), 103.22 (C-1′), 102.31 (C-1), 78.81 (C-4), 75.62 (C-5′), 75.02 (C-5), 74.76 (C-3), 73.14 (C-2), 72.85 (C-3′), 71.25 (C-2′), 70.97 (aglyconic carbon), 68.84 (C-4′), 61.27 (C-6′), 60.45 (C-6), 53.22 (—COO*C*H_3), 33.97, 28.94, 28.65, 28.44, 28.39, 28.34, 25.17 and 24.51 (remaining carbons of aglycon).

8-Methoxycarbonyloctyl 2,3,6-tri-O-*acetyl-4*-O-*(2,3,4,6-tetra*-O-*acetyl-β-D-galactopyranosyl)-β-D-glucopyranoside (2)*

8-Methoxycarbonyloctyl β-lactoside (**1**) (1.0 g) was dissolved in 10 mL of pyridine – acetic anhydride (1:1) and stirred at room temperature for 24 h. The product, isolated in the usual manner (1.40 g, 90% yield), was amorphous but homogeneous by tlc; $[\alpha]_D^{25}$ −15.0° (*c* 1.33, $CHCl_3$). The ^{13}C nmr was in accord with that reported by Banoub and Bundle (15).

8-Methoxycarbonyloctyl 4-O-*(4,6*-O-*benzylidene-β-D-galactopyranosyl)-β-D-glucopyranoside (3)*

A suspension of compound **1** (24.0 g, 46.8 mmol) in acetonitrile (500 mL) was refluxed with α,α-dimethoxytoluene (14.25 g, 93.75 mmol) and *p*-toluenesulphonic acid monohydrate (50 mg) for 6 h. After neutralization with triethylamine (0.2 mL), the reaction mixture was evaporated to dryness. The residue, after extraction with *n*-hexane (3 × 50 mL) to remove the excess α,α-dimethoxytoluene, crystallized from acetonitrile (22.0 g, 78.2% yield); mp 186–188°C; $[\alpha]_D^{25}$ −32.1° (*c* 1.04, CH_3OH); ^{13}C nmr (DMSO-d_6) δ: 173.26(*C*=O), 138.46, 128.54, 127.83, 126.16 (aromatic), 102.97, 102.59 (two anomeric carbons), 99.75 (benzylic carbon), 79.03 (C-4), 75.68, 74.83, 74.78, 73.25, 71.63, 69.82, 68.69, 68.43, 66.24, 60.31 (remaining carbons of the sugar units and the aglyconic carbon), 51.02, 33.22, 29.14, 28.61, 28.53, 25.34, 24.34 (remaining carbons in aglycon). *Anal.* calcd. for $C_{29}H_{44}O_{13}$: C 57.96, H 7.38; found: C 57.69, H 7.21.

8-Methoxycarbonyloctyl 2,3,6-tri-O-*acetyl-4*-O-*(2,3-di*-O-*acetyl-4,6*-O-*benzylidene-β-D-galactopyranosyl)-β-D-glucopyranoside (4)*

A solution of compound **3** (21.0 g) in pyridine – acetic anhydride (4:1, 125 mL) containing 4-*N*,*N*-dimethylaminopyridine (10 mg) was stirred at 60°C for 12 h. It was then poured over ice (100 g) and extracted with dichloromethane (3 × 200 mL). Work-up in the usual manner left solid (28.3 g, 90% yield). The analytical sample was prepared by crystallization from ether – ethyl acetate – *n*-hexane; mp 160–162°C; $[\alpha]_D^{25}$ +32.0° (*c* 1.03, $CHCl_3$). The ^1H nmr spectrum was in general accord with expectation; ^{13}C nmr ($CDCl_3$) δ: 174.12, 170.51, 170.34, 170.27, 169.51, 168.86 (6C=O), 137.75, 129.18, 128.25, 126.3, 101.36 and 101.22 (C-1 and C-1′), 100.88 (benzylic carbon), 77.50 (C-4), 73.33, 73.06, 72.77, 72.36, 72.22, 71.89, 70.06, 69.34, 68.54, 66.63, 62.30 (remaining carbons of sugar units and aglyconic carbon), 51.32–20.40 (9 lines, carbons in aglycon and CH_3 of acetyls). *Anal.* calcd. for $C_{39}H_{54}O_{18}$: C 57.74, H 6.71; found: C 57.50, H 6.66.

8-Methoxycarbonyloctyl 2,3,6-tri-O-*acetyl-4*-O-*(2,3-di*-O-*acetyl-β-D-galactopyranosyl)-β-D-glucopyranoside (5)*

Aqueous trifluoroacetic acid (90%, 10 mL) was added to a cold

Can. J. Chem. Downloaded from www.nrcresearchpress.com by 210.87.254.5 on 09/06/12
For personal use only.

(0°C) solution of crude **4** (4.3 g) in dichloromethane (100 mL) and stirred at 0°C for 1 h. The reaction mixture was then washed with water, aqueous saturated sodium bicarbonate, and finally with water. Evaporation left a residue which was chromatographed on silica gel (100 g) using ethyl acetate – *n*-hexane – acetonitrile (2:2:1) as eluant. Evaporation of the second fraction left a solid (3.16 g, 82% yield); $[\alpha]_D^{25}$ −7.4° (*c* 1.05, $CHCl_3$); ^{1}H nmr (DMSO-d_6) δ: 5.12 (d, 1H, 4′-OH, J = 3.0 Hz), 5.05 (t, 1H, 6′-OH, J = 6 Hz), 4.88 (dd, 1H, H-2′, $J_{2',1'}$ = 7.8 Hz, $J_{2',3'}$ = 10 Hz), 4.68 (dd, 1H, H-3′, $J_{3',2'}$ = 10 Hz, $J_{3',4'}$ = 3.0 Hz), 4.62 (m, 3H, H-2, H-3, H-1), 4.47 (d, 1H, H-1′, $J_{1',2'}$ = 7.8 Hz), 4.25 (broad d, 1H, H-6a, $J_{6a,6b}$ = 12.0 Hz), 4.05 (dd, 1H, H-6b, $J_{6a,6b}$ = 12.0 Hz, $J_{6b,5}$ = 6.3 Hz), 3.90 (broad t, 1H, H-4′, J = 3.0 Hz), 3.80−3.30 (m, remaining sugar hydrogens, O—C*H*$_3$, O—C*H*$_2$ of aglycon), 2.30 (t, 2H, C*H*$_2$—COOCH$_3$, J = 8 Hz), 2.10−1.95 (15H, 5C*H*$_3$ of acetyls), 1.5−1.25 (12H, hydrogens in aglycon); ^{13}C nmr ($CDCl_3$) δ: 170.50, 170.08, 169.61, 169.41 (6C=O), 101.01, 100.60 (C-1′ and C-1), 77.23 (C-4), 74.57, 73.50, 73.46, 72.70, 71.96, 70.09, 69.84, 68.17, 62.47, 62.41 (remaining carbons of sugar units and aglyconic carbon), 51.41−20.64 (carbons in aglycon and C*H*$_3$ of acetyls).

*8-Methoxycarbonyloctyl 2,3,6-tri-*O*-acetyl-4-*O*-(2,3-di-*O*-acetyl-6-*O*-benzoyl-β-*D*-galactopyranosyl)-β-*D*-glucopyranoside (**6**)*

A solution of benzoyl chloride (0.640 g, 0.528 mL, 4.5 mmol) in dichloromethane (3 mL) was added to a cooled (−78°C) solution of compound **5** (2.96 g, 4.1 mmol) in dichloromethane (25 mL) containing anhydrous pyridine (0.363 mL, 4.5 mmol). Most of the starting diol (**5**) was consumed, as evidenced by tlc using ethyl acetate – *n*-hexane – acetonitrile (2:2:1), after stirring at −78°C for 3 h and then at −20°C for 6 h. The reaction mixture was washed with ice-cold water, ice-cold *N*-hydrochloric acid, and finally with aqueous saturated sodium bicarbonate. Solvent removal left a solid foam which was purified by flash chromatography on a column of silica gel (60.0 g) using ethyl acetate – *n*-hexane – acetonitrile (2:2.5:0.5). Evaporation of the first main fraction left a colorless foam (2.8 g, 84% yield). An analytical sample was prepared by crystallization from acetone – *n*-hexane; mp 145−146°C; $[\alpha]_D^{25}$ +1.62° (*c* 0.986, $CHCl_3$). The ^{1}H nmr spectrum was in general accord with expectation and essentially identical to that for the crude product. ^{1}H nmr (DMSO-d_6) δ: 8.04, 7.70 7.58 (m, 5H, benzoate), 5.18 (t, 1H, H-3, $J_{3,2}$ = $J_{3,4}$ = 9 Hz), 5.00 (dd, 1H, H-3′, $J_{2',1'}$ = 7.8 Hz, $J_{2',3'}$ = 10 Hz), 4.85 (dd, 1H, H-3′, $J_{3',2'}$ = 10 Hz, $J_{3',4'}$ = 3.0 Hz), 4.68 (m, 3H, H-1, H-1′, H-2), 4.48 (dd, 1H, H-6′a, $J_{6'a,5'}$ = 5.25 Hz, $J_{6'a,6'b}$ = 11.5 Hz), 4.36−4.26 (m, 2H, H-6a, H-6′b), 4.10 (dd, 1H, H-6b, $J_{6b,5}$ = 5.5 Hz, $J_{6b,6a}$ = 11.50 Hz), 4.03 (broad t, 1H, H-5′, $J_{5',6'}$ = 6.0 Hz), 3.98 (broad d, 1H, H-4′, $J_{4',3'}$ = 3.0 Hz), 3.82 (m, 1H, H-5), 3.75−3.64 (m, 5H, H-4, —O—C*H*$_3$, —O—C*H*$_2$ of aglycon), 3.43 (m, 1H, O—C*H*$_2$ of aglycon), 2.28 (t, 2H, C*H*$_2$—COOCH$_3$, J = 8.0 Hz), 2.02−1.94 (15H, 5C*H*$_3$ of acetyl), 1.5 and 1.24 (12H, hydrogens in algycon); ^{13}C nmr ($CDCl_3$) δ: 174.21, 170.39, 170.19, 169.44, 169.38, 166.40 (7C=O), 133.52, 129.74, 129.59, 128.70 (benzoate carbons), 100.75, 100.17 (C-1 and C-1′), 76.41 (C-4), 73.57, 72.80, 72.67, 72.56, 71.75, 70.13, 69.60, 66.95, 62.37, 62.18 (remaining carbons of sugar units and aglyconic carbon), 51.40−20.63 (10 lines, carbons in aglycon and C*H*$_3$ of acetyls). *Anal.* calcd. for $C_{39}H_{54}O_{19}$: C 56.65, H 6.58; found: C 56.90, H 6.64.

*3,4,6-Tri-*O*-acetyl-2-azido-2-deoxy-α-*D*-galactopyranosyl bromide (**11**)*

D-Galactal triacetate was converted by azidonitration to the product which contains compounds **8**, **9**, and **10** under the conditions reported by Lemieux and Ratcliffe (26). This crude product (45.0 g) was dissolved in dichloromethane (300 mL) and Vilsmeier bromide (27) (10.0 g, 46 mmol) was added. After the solution was stirred at 0°C for 1 h, a solution of anhydrous lithium bromide (25.0 g) in dry acetonitrile (360 mL) was added and the stirring was continued for 6 h. Work-up in the usual manner left a yellow syrup (40.0 g), a portion of which (10.0 g) was chromatographed on a column of silica gel (300 g) using ethyl acetate – *n*-hexane (3:7) as eluant. The main fraction provided material (7.0 g, 60% yield) which crystallized from diethyl ether – hexane, mp 96−98°C. The melting point and the ^{1}H nmr spectrum were in accordance with those reported by Lemieux and Ratcliffe (26).

A comparison of the ^{1}H nmr spectra indicated that the crude product was about 75% pure; ^{13}C nmr ($CDCl_3$) δ: 170.22, 169.70, 169.43 (3C=O), 89.07 (C-1), 71.53 (C-5), 69.84, 66.72 (C-4 and C-3), 60.78 (C-6), 58.75 (C-2).

*Allyl 3,4,6-tri-*O*-acetyl-2-azido-2-deoxy-β-*D*-galactopyranoside (**12**)*

A solution of the crude bromide **11** (30.0 g, 7.61 mmol) in dichloromethane (125 mL) was added slowly to a vigorously stirred suspension of anhydrous silver carbonate (20.0 g, 7.25 mmol) and anhydrous calcium sulphate (25.0 g) in allyl alcohol (200 mL). After 16 h, the reaction mixture was filtered through a bed of diatomaceous earth (10.0 g) and the filtrate was evaporated to a syrup. Chromatography on silica gel (600 g) using ethyl acetate – *n*-hexane (3:7) and evaporation of the first main fraction provided a pale yellow syrup (15.97 g, 29% based on acetobromogalactose) which appeared homogeneous by tlc; $[\alpha]_D^{25}$ −12.4° (*c* 1.5, $CHCl_3$); ^{1}H nmr ($CDCl_3$) δ: 5.96 (m, 1H, O—CH$_2$—C*H*=CH$_2$), 5.42 (m, 1H, O—CH$_2$—CH=C*H*$_2$), 5.40 (broad d, 1H, H-4, $J_{4,3}$ = 3 Hz), 5.32 (m, 1H, O—CH$_2$—CH=C*H*$_2$), 4.84 (dd, 1H, H-3, $J_{3,4}$ = 3 Hz, $J_{3,2}$ = 10.5 Hz), 4.46 (d, 1H, H-1, $J_{1,2}$ = 7.8 Hz), 4.45 and 4.24 (m, 2H, O—C*H*$_2$—CH=CH$_2$), 4.3−4.2 (m, 2H, H-6a, H-6b), 3.88 (broad t, 1H, H-5, $J_{5,6}$ = 6.75 Hz), 3.75 (dd, 1H, H-2, $J_{2,1}$ = 7.8 Hz, $J_{2,3}$ = 10.5 Hz), 2.08−2.04 (3s, 9H, C*H*$_3$ of acetyls); ^{13}C nmr ($CDCl_3$) δ: 170.30, 170.04, 169.77 (3C=O), 133.14 (O—CH$_2$—*C*H=CH$_2$), 118.25 (O—CH$_2$—CH=*C*H$_2$), 101.17 (C-1), 71.14 (C-5), 70.73, 70.64 (C-3 and C-4), 66.44 (O—*C*H$_2$—CH=CH$_2$), 61.29 (C-2), 60.93 (C-6), 20.59 (3*C*H$_3$ of acetyls). *Anal.* calcd. for $C_{15}H_{21}N_3O_{18}$: C 48.49, H 5.70, N 11.32; found: C 47.98, H 5.66, N 10.65.

*Allyl 2-azido-2-deoxy-β-*D*-galactopyranoside (**13**)*

Sodium methoxide in methanol (5 mL) was added to a solution of 3,4,6-tri-*O*-acetyl-2-azido-2-deoxy-β-D-galactopyranoside (**12**) (18.0 g) in methanol (150 mL) and stirred for 90 min. The solution was then neutralized with IRA-110 H^+ resin, decolorized with charcoal (5.0 g), and evaporated. The residue was crystallized from ethyl acetate – *n*-hexane to obtain 11.0 g (92.3%) of the product; mp 117−118°C; $[\alpha]_D^{25}$ +13.9° (*c* 0.98, CH_3OH); ^{1}H nmr (CD_3OD) δ: 6.04−5.90 (m, 1H, O—CH$_2$—C*H*=CH$_2$), 5.35 and 5.18 (m, 2H, O—CH$_2$—CH=C*H*$_2$), 4.34 (d, 1H, H-1, $J_{1,2}$ = 7.8 Hz), 3.78 (dd, 1H, H-4, $J_{4,5}$ = 1.5 Hz, $J_{4,3}$ = 3.5 Hz), 3.74 (m, 2H, H-6a, H-6b), 3.48 (m, 2H, H-2, H-5), 3.42 (dd, 1H, H-3, $J_{3,4}$ = 3.5 Hz, $J_{3,2}$ = 10.5 Hz); ^{13}C nmr (DMSO-d_6) δ: 134.37 (O—CH$_2$—*C*H=CH$_2$), 116.43 (O—CH$_2$—CH=*C*H$_2$), 100.41 (C-1), 75.20 (C-5), 71.55 (C-3), 68.80 (C-4), 67.55 (O—*C*H$_2$—CH=CH$_2$), 64.22 (C-2), 60.26 (C-6). *Anal.* calcd. for $C_9H_{15}N_3O_5$: C 44.06, H 6.16, N 17.14; found: C 43.59, H 6.21, N 17.00.

*Allyl 3,4,6-tri-*O*-acetyl-2-deoxy-2-phthalimido-β-*D*-galactopyranoside (**15**)*

A stream of hydrogen sulphide was slowly bubbled through an ice-cold solution of the azide (**13**) (14.0 g, 57.14 mmol) in pyridine (150 mL) and triethylamine (45 mL) for 4 h. The solution was then stirred at room temperature for 6 h. Evaporation left a residue which was treated with methanol−water (1:1) and the solids removed by filtration through a bed of diatomaceous earth. Solvent removal left a residue (crude **14**) which was dissolved in pyridine (50 mL). Phthalic anhydride (4.86 g, 32.83 mmol) was added and the solution was heated at 60°C for 30 min. Triethylamine (5.9 g, 57.28 mmol) and phthalic anhydride (4.86 g, 32.83 mmol) were added and the heating was continued for 2 h. Methanol (50 mL) was added and the solution was evaporated to a dry residue which was taken up in a mixture of pyridine – acetic anhydride (2:1, 60 mL) containing 4-*N*,*N*-dimethylaminopyridine (10 mg). The solution was stirred at 60°C for 24 h. Work-up in the usual manner left a solid which was purified by flash chromatography on a column of silica gel (600 g) using ethyl acetate – *n*-hexane – acetonitrile (2:2.5:0.5). Evaporation of the

Can. J. Chem. Downloaded from www.nrcresearchpress.com by 210.87.254.5 on 09/06/12
For personal use only.

main fraction left an amorphous solid (19.0 g, 70% yield) homogeneous on tlc; $[\alpha]_D^{25}$ −10.7° (*c* 1.0, $CHCl_3$); ^{1}H nmr ($CDCl_3$) δ: 7.80−7.72 (m, 4H, phthalimido), 5.8 (dd, 1H, H-3, $J_{3,2}$ = 11 Hz, $J_{3,4}$ = 3.5 Hz), 5.78−5.66 (m, 1H, O—CH_2—CH=CH_2), 5.50 (broad d, 1H, H-4, $J_{4,3}$ = 3.5 Hz), 5.35 (d, 1H, H-1, $J_{1,2}$ = 7.8 Hz), 5.14 and 5.08 (m, 2H, O—CH_2—CH=CH_2), 4.60 (dd, 1H, H-2, $J_{2,1}$ = 7.8 Hz, $J_{2,3}$ = 11.0 Hz), 4.34−4.04 (m, 5H, H-6a, H-6b, H-5, O—CH_2—CH=CH_2), 2.22, 2.1, 1.86 (3s, CH_3 of acetyls); ^{13}C nmr ($CDCl_3$) δ: 170.39, 169.79 (C=O), 134.27, 131.53, 123.78, 123.58 (aromatic carbons), 133.32 (O—CH_2—CH=CH_2), 117.84 (O—CH_2—CH=CH_2), 97.56 (C-1), 70.87, 70.17, 68.15 (C-5, C-4, C-3), 66.83 (O—CH_2—CH=CH_2), 61.50 (C-6), 51.46 (C-2), 20.70, 20.50, 20.36 ($3CH_3$—COO). *Anal.* calcd. for $C_{23}H_{25}NO_{10}$: C 58.10, H 5.30, N 2.94; found: C 57.82, H 5.30, N 2.90.

*3,4,6-Tri-*O*-acetyl-2-deoxy-2-phthalimido-*D*-galactopyranose (**17**)*

Tris-triphenylphosphine rhodium(I) chloride (300 mg, 0.32 mmol) and 1,4-diazabicyclooctane (100 mg, 1.1 mmol) were added to a solution of compound **15** (2.5 g, 5.26 mmol) in ethanol−benzene−water (7:3:1, 300 mL) and refluxed for 36 h (31). Solvent removal left a residue which was dissolved in aqueous acetone (90%, 50 mL) containing mercuric chloride (5 g) and yellow mercuric oxide (100 mg). After stirring at room temperature for 60 min, the reaction mixture was diluted with water (50 mL) and extracted with chloroform (2 × 75 mL). The chloroform layer was washed with aqueous potassium iodide (10%, 2 × 50 mL) and then with water. Evaporation left a black residue which was purified on a column of silica gel (100 g) using ethyl acetate − *n*-hexane − acetonitrile (2:2.5:0.5). Evaporation of the second and main fraction left a residue (1.88 g, 78%) which was a mixture of α and β anomers of **17** in the ratio 3:7 as estimated from the ^{1}H nmr spectrum; ^{1}H nmr ($CDCl_3$) δ: 7.90−7.70 (m, 4H, phthalimido), 6.36 (dd, H-3α, $J_{3\alpha,2\alpha}$ = 11 Hz, $J_{3\alpha,4\alpha}$ = 3.0 Hz), 5.86 (dd, H-3β, $J_{3\beta,2\beta}$ = 11 Hz, $J_{3\beta,4\beta}$ = 3.5 Hz), 5.60−5.46 (m, H-4, H-1α, H-1β), 4.84−3.06 (H-2α, H-2β, H-5, H-6a, H-6b), 1.84−2.16 (CH_3 of acetyls).

*3,4,6-Tri-*O*-acetyl-2-deoxy-2-phthalimido-β-*D*-galactopyranosyl bromide (**18**)*

Vilsmeier bromide (27) (1.31 g, 6.05 mmol) was added to an ice-cold solution of compound **17** (1.88 g, 4.32 mmol) in dichloromethane (25 mL) and stirred. *sym*-Collidine (0.802 mL, 6.05 mmol) was added dropwise to the reaction mixture. After stirring for 2 h at 0°C and 12 h at room temperature, the reaction mixture was washed with ice-cold water (15 mL), ice-cold hydrochloric acid (1 *N*, 10 mL), and finally with water. Evaporation of the solvent left a residue (1.88 g, 84% yield) containing α and β anomers of **18**. Pure β-bromide crystallized from ethyl acetate − *n*-hexane; mp 136−137°C; $[\alpha]_D^{25}$ +29.2° (*c* 0.98, $CHCl_3$); ^{1}H nmr ($CDCl_3$) δ: 7.86−7.70 (m, 4H, phthalimido), 6.36 (d, 1H, H-1, $J_{1,2}$ = 10 Hz), 5.76 (dd, 1H, H-3, $J_{3,2}$ = 11.0 Hz, $J_{3,4}$ = 3.50 Hz), 5.52 (broad d, 1H, H-4, $J_{4,3}$ = 3.50 Hz), 4.8 (dd, 1H, H-2, $J_{2,3}$ = 11 Hz, $J_{2,1}$ = 10 Hz), 4.17 (m, 3H, H-5, H-6a, H-6b), 2.28, 2.08, 1.84 (3s, CH_3 of acetyls); ^{13}C nmr ($CDCl_3$) δ: 170.27, 170.09, 169.45 (3C=O), 134.53, 131.30, 123.83 (aromatic), 78.08 (C-1), 75.88, 67.88, 66.66 (C-5, C-3, C-4), 61.38 (C-6), 54.61 (C-2), 20.64, 20.38 (CH_3 of acetyls) *Anal.* calcd. for $C_{20}H_{20}BrNO_9$: C 48.20, H 4.04, N 2.82; found: C 48.01, H 4.10, N 2.81.

*8-Methoxycarbonyloctyl 2,3,6-tri-*O*-acetyl-4-*O*-[2,3-di-*O*-acetyl-6-*O*-benzoyl-4-*O*-(3,4,6-tri-*O*-acetyl-2-deoxy-2-phthalimido-β-*D*-galactopyranosyl)-β-*D*-galactopyranosyl]-β-*D*-glucopyranoside (**19**)*

3,4,6-Tri-*O*-acetyl-2-deoxy-2-phthalimido-D-galactopyranosyl bromide (**18**) (225 mg, 0.45 mmol) in nitromethane (5 mL) was added to a solution of **6** (340 mg, 0.41 mmol), *sym*-collidine (54.4 μL, 0.411 mmol), and silver triflate (115 mg, 0.45 mmol) in dry nitromethane (5 mL) cooled to −25°C. The mixture was stirred at −25°C for 6 h and then at room temperature for 12 h. The solids that were deposited after the addition of dichloromethane (20 mL) were removed by filtration and the filtrate was washed with sodium thiosulphate solution, cold water, dilute aqueous HCl, and saturated sodium bicarbonate solution. Solvent removal and purification by preparative high pressure liquid chromatography on a column of silica gel using ethyl acetate − *n*-hexane − acetonitrile (2:2.5:0.5) provided a colorless amorphous solid (330 mg, 64.5% yield), $[\alpha]_D^{25}$ −19.9° (*c* 2.7, $CHCl_3$); ^{1}H nmr ($CDCl_3$) δ: 8.1−7.5 (m, 9H, phthalimido, benzoate), 5.92 (dd, 1H, H-3″, $J_{3'',4''}$ = 3.5 Hz, $J_{3'',2''}$ = 11 Hz), 5.44 (broad d, 1H, H-4″, $J_{4'',3''}$ = 3.5 Hz), 5.32 (d, 1H, H-1″, $J_{1'',2''}$ = 7.8 Hz), 5.15 (t, 1H, H-3, $J_{3,2}$ = $J_{3,4}$ = 10 Hz), 4.84 (m, 2H, H-2, H-3′, $J_{2,3}$ = 10 Hz, $J_{2,1}$ = 7.8 Hz, $J_{3',2'}$ = 10 Hz, $J_{3',4'}$ = 3.0 Hz), 4.70 (dd, 1H, H-6′a, $J_{6'a,6'b}$ = 11 Hz, $J_{6'a,5'}$ = 7.0 Hz), 4.53 (q, H, H-2″, $J_{2'',3''}$ = 11 Hz), 4.50 (q, H, H-2′, $J_{2',3'}$ = 10 Hz), 4.40 (m, 3H, H-6a, H-1, H-6′b), 4.28 (d, 1H, H-1′, $J_{1',2'}$ = 7.8 Hz), 4.18 (broad d, 1H, H-4′, $J_{4',3'}$ = 3.0 Hz), 4.12−3.94 (m, 4H, H-5″, H-6b, H-6″a, H-6″b), 3.8 (m, 2H, H-5′, O—CH_2 of aglycon), 3.70 (m, 4H, O—CH_3, H-4), 3.51 (m, 1H, H-5), 3.4 (m, 1H, O—CH_2 of aglycon), 2.3 (t, 2H, CH_2—$COOCH_3$, *J* = 8.0 Hz), 2.2−1.74 (8s, 24H, acetyl CH_3), 1.6 and 1.20 (12H, aglyconic hydrogens); ^{13}C nmr ($CDCl_3$) δ: 174.21 ($COOCH_3$), 170.33, 170.30, 170.27, 170.07, 169.72, 169.18, 168.59, 167.98, 167.16, 166.26, (10C=O), 134.28, 133.97, 133.44, 131.71, 129.97, 128.77, 124.58, 123.07 (phthalimido, benzoate carbons), 100.92, 100.41, 98.46 (C-1, C-1′, C-1″), 77.28 (C-4), 75.42 (C-4′), 72.89, 72.48, 72.25, 72.15, 71.83, 71.04, 70.04, 69.57, 67.49, 66.67, 62.13, 62.12, 61.41, 51.38 (remaining carbons of sugar units and the O—CH_2 of aglycon), 51.28−20.29 (12 lines, remaining carbons in aglycon, CH_3 of acetyls).

*8-Methoxycarbonyloctyl 4-*O*-[4-*O*-(2-deoxy-2-phthalimido-β-*D*-galactopyranosyl)-β-*D*-galactopyranosyl]-β-*D*-glucopyranoside (**20**)*

A freshly prepared solution of sodium methoxide in methanol (0.5 mL) was added to a solution of compound **19** (364 mg, 0.289 mmol) in methanol (20 mL) and stirred under a nitrogen atmosphere for 5 h. The reaction mixture was neutralized with dry IRA-20 H^+ resin and evaporated to a residue (220 mg, 97% yield) which was homogeneous on tlc (ethyl acetate − ethanol−water, 7:2:1); ^{1}H nmr (CD_3OD) δ: 8.0−7.7 (m, 4H, phthalimido), 5.15 (d, 1H, H-1″, $J_{1'',2''}$ = 8.0 Hz), 4.59 (dd, 1H, H-3″, $J_{3'',2''}$ = 11 Hz, $J_{3'',4''}$ = 3.50 Hz), 4.33 (dd, 1H, H-2″, $J_{2'',1''}$ = 8.0 Hz, $J_{2'',3''}$ = 11.0 Hz), 4.23−4.15 (2d, 2H, H-1, H-1′, $J_{1',2'}$ = $J_{1,2}$ = 7.8 Hz), 3.9−3.25 (m, remaining sugars and aglycons except H-2 and H-2′), 3.18 (t, 1H, H-2, $J_{2,3}$ = 9.0 Hz, $J_{1,2}$ = 7.8 Hz), 3.07 (dd, 1H, H-2′, $J_{2',1'}$ = 7.8 Hz, $J_{2',3'}$ = 9.5 Hz), 2.27 (t, 2H, CH_2COOCH_3, *J* = 8.0 Hz), 1.55 and 1.29 (12H, hydrogens in aglycon).

*8-Methoxycarbonyloctyl 4-*O*-[4-*O*-(2-acetamido-2-deoxy-β-*D*-galactopyranosyl)-β-*D*-galactopyranosyl]-β-*D*-glucopyranoside (**21**) − asialo-G_{M2} hapten*

Hydrazine (95%, 100 μL) was added to a solution of compound **20** (219 mg, 0.272 mmol) in methanol (20 mL). After refluxing for 2 h, the solution was evaporated to dryness and the residue was taken up in 11 mL of methanol − acetic anhydride (10:1). After stirring at room temperature for 3 h, the solution was taken to dryness and the residue was dissolved in ethanol−water (9:1) for application to a Biogel P-2 column. Elution with the same solvent provided a main fraction which was lyophilized to a colorless material (155 mg, 80% yield); $[\alpha]_D^{25}$ −0.1° (*c* 0.3); ^{1}H nmr (D_2O) δ: 4.58 (d, 1H, H-1″, $J_{1'',2''}$ = 9.0 Hz), 4.43, 4.39 (2d, 2H, H-1, H-1′, $J_{1',2'}$ = $J_{1,2}$ = 7.7 Hz), 4.04 (broad d, 1H, H-4′, $J_{4',3'}$ = 2.2 Hz), 4.0−3.35 (20H, remaining 15 ring hydrogens except H-2′ and H-2, O—CH_3, O—CH_2 of aglycon), 3.36 (dd, 1H, H-2′, $J_{2',1'}$ = 7.7 Hz, $J_{2',3'}$ = 9.9 Hz), 3.24 (dd, 1H, H-2, $J_{2,1}$ = 7.7 Hz, $J_{2,3}$ = 9.0 Hz), 2.4 (t, 2H, CH_2—$COOCH_3$), 2.05 (s, 3H, CH_3 of N-acetyl), 1.6 and 1.30 (12H, aglyconic hydrogens).

The ^{13}C nmr spectrum is reported in Table 1.

*Allyl 2-azido-2-deoxy-4,6-*O*-benzylidene-β-*D*-galactopyranoside (**22**)*

A solution of compound **13** (11.0 g, 44.8 mmol) in dry acetonitrile (200 mL) containing α,α-dimethoxytoluene (11.0 g, 72.3 mmol) and *p*-toluenesulphonic acid (150 mg, 0.87 mmol) was stirred at room

Can. J. Chem. Downloaded from www.nrcresearchpress.com by 210.87.254.5 on 09/06/12
For personal use only.

temperature for 16 h. The solution was then neutralized with triethylamine and evaporated to dryness. A solution of the residue in dichloromethane (150 mL) was washed with water (50 mL), dried, and evaporated to leave a pale yellow solid which was crystallized from toluene (11.8 g, 79% yield); mp 129–131°C; $[\alpha]_D^{25}$ −15.3° (*c* 1.03, $CHCl_3$); ^1H nmr ($CDCl_3$) δ: 7.48–7.34 (m, 5H, aromatic), 6.02–5.9 (m, 1H, O—CH_2—C*H*=CH_2), 5.56 (s, 1H, benzylic), 5.34 and 5.22 (m, 2H, O—CH_2—CH=CH_2), 4.44 and 4.14 (m, 3H, H-4, O—CH_2—CH=CH_2), 4.31 (m, 2H, H-1, H-6a), 4.04 (bd, *J* = 12.2 Hz, 1H, H-6b), 3.64 (dd, *J* = 8.0, 10 Hz, 1H, H-2), 3.56 (ddd, *J* = 10.0 Hz, 8.0, 3.5 Hz, 1H, H-3), 3.41 (broad s, 1H, H-5), 2.59 (d, *J* = 8.0 Hz, 1H, —O—*H*); ^{13}C nmr ($CDCl_3$) δ: 133.58 (O—CH_2*C*H=CH_2), 129–126.0 (3 lines, aromatic carbons), 117.76 (O—CH_2—CH=*C*H_2), 101.46, 100.93 (C-1, benzylic carbon), 74.61 (C-4), 71.55 (C-5), 70.23 (C-3), 69.03 (C-6), 66.56 (O—*C*H_2—CH=CH_2), 64.10 (C-2). *Anal.* calcd. for $C_{16}H_{19}N_3O_5$: C 57.62, H 5.74, N 12.61; found: C 57.48, H 5.85, N 12.58.

*Allyl 2-azido-2-deoxy-4,6-*O*-benzylidene-3-*O*-(2,3,4,6-tetra-*O*-acetyl-β-*D*-galactopyranosyl)-β-*D*-galactopyranoside (**23**)*

A solution of tetra-*O*-acetyl-α-D-galactopyranosyl bromide (41) (7.36 g, 19.7 mmol) in dry nitromethane (30 mL) was added to a cooled (−25°C) solution of the alcohol **22** (5.97 g, 17.9 mmol), silver trifluoromethanesulphonate (5.067 g, 19.7 mmol), and *sym*-collidine (2.37 mL, 17.9 mmol) in dry nitromethane (100 mL). After stirring at −25°C for 8 h, the reaction mixture was diluted with dichloromethane (200 mL) and filtered through a bed of diatomaceous earth. The filtrate was washed with water, aqueous saturated sodium bicarbonate, and finally with water. Evaporation of the solvent left a residue which was purified by flash chromatography on a column of silica gel (300 g) using ethyl acetate − *n*-hexane − acetonitrile (2:2.5:0.5). The main fraction contained a solid (8.3 g, 70% yield) which appeared homogeneous on tlc. The analytical sample was prepared by crystallization from methanol; mp 141–144°C; $[\alpha]_D^{25}$ +13.7° (*c* 0.96, $CHCl_3$). The ^1H nmr spectrum of the crude product indicated it to be essentially pure and hence it was used in following steps; ^1H nmr ($CDCl_3$) δ: 4.80 (d, 1H, H-1′, $J_{1',2'}$ = 7.8 Hz), 4.33 (d, 1H, H-1, $J_{1,2}$ = 7.8 Hz); ^{13}C nmr ($CDCl_3$) δ: 170.27, 170.10, 169.28 (4 lines expected, 3 lines observed, 4 O—*C*OCH$_3$), 137.86, 128.89, 126.31 (aromatic carbons), 133.7 (O—CH_2—*C*H=CH_2), 117.61 (O—CH_2—CH=*C*H_2), 102.32 (C-1′), 101.23 (C-1), 100.82 (benzylic), 78.63 (C-3), 75.11 (C-4), 71.03, 70.10, 69.01, 68.95, 67.17, 66.70, 62.44, 61.47 (9 lines expected, 8 lines observed, the remaining carbons of sugar units and the aglyconic carbon), 20.65, 20.52 (*C*H$_3$ of acetyls). *Anal.* calcd. for $C_{30}H_{37}N_3O_{14}$: C 54.27, H 5.62, N 6.33; found: C 54.37, H 5.72, N 6.11.

*Allyl 4,6-di-*O*-acetyl-2-azido-2-deoxy-3-*O*-(2,3,4,6-tetra-*O*-acetyl-β-*D*-galactopyranosyl)-β-*D*-galactopyranoside (**24**)*

Aqueous trifluoroacetic acid (90%, 10 mL) was added to a solution of compound **23** (5.0 g) in dichloromethane (100 mL) kept at 0°C. After stirring for 30 min, the solution was washed with ice-cold water (50 mL), aqueous saturated sodium bicarbonate, and finally with water. Solvent removal left a syrup which was dissolved in dry dichloromethane (100 mL) containing pyridine (5 mL) and acetic anhydride (5 mL). 4-*N*,*N*-Dimethylaminopyridine (10 mg) was added and the mixture was stirred at room temperature for 12 h. The reaction mixture was then washed with ice-cold hydrochloric acid (1 *N*), saturated aqueous sodium bicarbonate, and finally with water. The dried solution was evaporated to a syrup and dissolved in dichloromethane for chromatography using a short silica gel column (20 g). Evaporation of the main fraction left a solid (3.9 g, 80% yield) which appeared homogeneous on tlc; mp 111–112°C; $[\alpha]_D^{25}$ +10.0° (*c* 1.89, $CHCl_3$); ^1H nmr ($CDCl_3$) δ: 6.0–5.88 (m, 1H, O—CH_2—C*H*=CH_2), 5.4–5.22 (m, 4H, H-4, H-4′, O—CH_2—CH=CH_2), 5.15 (dd, 1H, H-2′, $J_{1',2'}$ = 7.8 Hz, $J_{2',3'}$ = 10.5 Hz), 5.0 (dd, 1H, H-3′, $J_{3',2'}$ = 10.5 Hz, $J_{3',4'}$ = 3.5 Hz), 4.71 (d, 1H, H-1′, $J_{1',2'}$ = 7.8 Hz), 4.42 (m, 1H, O—CH_2—CH=CH_2), 4.33 (d, 1H, H-1, $J_{1,2}$ = 8.0 Hz), 4.22–4.04 (m, 5H, H-6a, H-6b, H-6′a, H-6′b, O—CH_2—CH=CH_2), 3.90 (broad t, 1H, H-5′, $J_{5',6'}$ = 7.0 Hz), 3.75 (broad t, 1H, H-5, $J_{5,6}$ = 7.0 Hz), 3.64 (dd, 1H, H-2, $J_{2,1}$ = 8.0 Hz, $J_{2,3}$ = 10.0 Hz), 3.54 (dd, 1H, H-3, $J_{3,2}$ = 10.0 Hz, $J_{3,4}$ = 3.5 Hz), 2.2–2.04 (6s, 18H, C*H*$_3$—COO); ^{13}C nmr ($CDCl_3$) δ: 170.47, 170.34, 170.25, 170.07, 169.75, 159.26 (6C=O), 133.22 (O—CH_2—*C*H=CH_2), 118.09 (O—CH_2—CH=*C*H_2), 101.47, 101.00 (anomeric carbons C-1 and C-1′), 77.26 (C-3), 71.42, 70.84, 70.66, 70.47, 68.85, 68.10 (C-5, C-5′, C-3′, C-2′, C-4′, C-4), 66.83 (O—*C*H_2—CH=CH_2), 63.34 (C-2), 62.29, 61.02 (C-6, C-6′), 20.70, 20.65, 20.63, 20.53 (6 *C*H$_3$ of acetyls). *Anal.* calcd. for $C_{27}H_{37}N_3O_{16}$: C 49.16, H 5.65, N 6.37; found: C 49.27, H 5.68, N 6.27.

*Allyl 2-azido-2-deoxy-3-*O*-(β-D-galactopyranosyl)-β-D-galactopyranoside (**25**)*

Sodium methoxide in methanol (2.5 mL) was added to a solution of **24** (4.0 g) in anhydrous methanol (75 mL) and stirred at room temperature for 6 h. After neutralization with IRA-120 H^+ resin, the solution was evaporated to a residue (2.3 g, 93.5% yield) which was homogeneous on tlc (ethyl acetate − ethanol−water, 7:2:0.5). The analytical sample was prepared by crystallization from ethanol−ether; mp 168–170°C (dec.); $[\alpha]_D^{25}$ −12.0° (*c* 0.64, H_2O); ^1H nmr (D_2O) δ: 5.98 (m, 1H, O—CH_2—C*H*=CH_2), 5.34 and 5.25 (m, 2H, O—CH_2—CH=CH_2), 4.54 and 4.48 (2d, 2H, H-1′, H-1, $J_{1',2'}$ = $J_{1,2}$ = 7.8 Hz), 4.10 (dd, 1H, H-4, $J_{4,3}$ = 3.5 Hz, $J_{4,5}$ = 1.5 Hz), 3.85 (broad d, 1H, H-4′, $J_{4',3'}$ = 3.5 Hz), 3.78–3.44 (m, 10H, remaining hydrogens of sugar units); ^{13}C nmr (D_2O) δ: 133.33 (O—CH_2—*C*H=CH_2), 118.98 (O—CH_2—CH=*C*H_2), 104.44 (C-1′), 100.82 (C-1), 80.29 (C-3), 75.20 (C-5′), 75.00 (C-5), 72.69 (C-3′), 70.87 (C-2′, O—*C*H_2—CH=CH_2), 68.73 (C-4′), 68.07 (C-4), 62.77 (C-2), 61.15 and 60.96 (C-6′ and C-6).

*Allyl 2-amino-2-deoxy-3-*O*-(β-D-galactopyranosyl)-β-D-galactopyranoside (**26**)*

Hydrogen sulphide was slowly bubbled through an ice-cold solution of the crude **25** (2.3 g) in pyridine (30 mL) and triethylamine (10 mL) for 4 h. After stirring at room temperature for 12 h, the solution was taken to dryness and the residue was extracted with water. The extract was filtered through a bed of diatomaceous earth (5.0 g) and evaporated to a residue (2.3 g) which was not further purified; ^1H nmr (D_2O) δ: 6.0–5.88 (m, 1H, O—CH_2—C*H*=CH_2), 5.35 and 5.25 (m, 2H, O—CH_2—CH=CH_2), 4.50 (d, 1H, H-1′, $J_{1',2'}$ = 7.8 Hz), 4.36 (d, 1H, H-1, $J_{1,2}$ = 7.8 Hz), 4.36 and 4.18 (m, 2H, O—CH_2—CH=CH_2), 4.12 (broad d, 1H, H-4, $J_{4,3}$ = 3.50 Hz), 3.91 (broad d, 1H, H-4′, $J_{4',3'}$ = 3.5 Hz), 3.80–3.54 (m, 9H, remaining ring hydrogens except H-2), 3.0 (dd, 1H, H-2, $J_{2,1}$ = 7.8 Hz, $J_{2,3}$ = 10.0 Hz); ^{13}C nmr (D_2O) δ: 134.11 (O—CH_2—*C*H=CH_2), 119.25 (O—CH_2—CH=*C*H_2), 105.23 (C-1′), 102.90 (C-1), 83.74 (C-3), 75.59, 75.38 (C-5, C-5′), 73.17 (C-3), 71.54 (C-2), 71.14 (O—*C*H_2—CH=CH_2), 69.15 (C-4′), 68.01 (C-4), 61.56, 61.49 (C-6 and C-6′), 52.42 (C-2).

*Allyl 4,6-di-*O*-acetyl-3-*O*-(2,3,4,6-tetra-*O*-acetyl-β-D-galactopyranosyl)-2-deoxy-2-phthalimido-β-D-galactopyranoside (**27**)*

Phthalic anhydride (478 mg, 3.4 mmol) was added to a solution of the amine **26** (2.3 g, 6.0 mmol) in pyridine (20 mL). The solution was heated to 60–75°C for 20 min. Triethylamine (593 mg, 5.88 mmol) and more phthalic anhydride (478 mg, 3.4 mmol) were then added and the heating was continued for 2 h. Methanol (10 mL) was added and the solution was evaporated to a dry residue which was taken up in 15 mL of a mixture of pyridine − acetic anhydride (2:1). 4-*N*,*N*-Dimethylaminopyridine (10 mg) was added and the mixture was heated to 60°C for 12 h prior to evaporation. A solution of the residual syrup in dichloromethane (150 mL) was washed with ice-cold hydrochloric acid (1 *N*), aqueous saturated sodium carbonate, and finally with water. Solvent removal left a residue which was applied (flash chromatography) to a column of silica gel using ethyl acetate − *n*-hexane − acetonitrile (2:2:0.5). Evaporation of the first and main fraction left a solid (2.7 g, 62% yield) which appeared homogeneous on tlc. The analytical sample was prepared by crystallization from

ethanol; mp 165–166°C; $[\alpha]_D^{25}$ +16.0° (*c* 1.06, $CHCl_3$); ^1H nmr ($CDCl_3$) δ: 7.94–7.88 (m, 4H, phthalimido), 5.76–5.64 (m, 1H, O—CH_2—C*H*=CH_2), 5.50 (broad d, 1H, H-4, $J_{4,3}$ = 3.0 Hz), 5.27 (broad d, 1H, H-4′, $J_{4',3'}$ = 3.0 Hz), 5.18 (d, 1H, H-1, $J_{1,2}$ = 7.8 Hz), 5.03 (dd, 1H, H-2′, $J_{2',1'}$ = 7.8 Hz, $J_{2',3'}$ = 10.8 Hz), 5.18–5.0 (m, 2H, O—CH_2—CH=CH_2), 4.80 (dd, 1H, H-3′, $J_{3',2'}$ = 10.8 Hz, $J_{3',4'}$ = 3.0 Hz), 4.76 (dd, 1H, H-3, $J_{3,2}$ = 10.8 Hz, $J_{3,4}$ = 3.0 Hz), 4.56 (dd, 1H, H-2, $J_{2,1}$ = 7.8 Hz, $J_{2,3}$ = 10.8 Hz), 4.44 (d, 1H, H-1′, $J_{1',2'}$ = 7.8 Hz), 4.24 (dd, 1H, H-6a, $J_{6a,5}$ = 5.25 Hz, $J_{6a,6b}$ = 12.0 Hz), 4.12 (dd, 1H, H-6b, $J_{6b,5}$ = 6.75 Hz, $J_{6b,6a}$ = 12.0 Hz), 4.08–3.92 (m, 3H, H-5, H-6′a, H-6′b), 3.78 (m, 1H, H-5′), 2.22–1.54 (6s, 18H, 6CH_3 of acetyls); ^{13}C nmr ($CDCl_3$) δ: 170.54, 170.27, 170.00, 169.02 (8 lines expected, 4 lines observed, 8C=O), 134.37, 131.70, 123.72, 123.38 (phthalimido carbons), 133.43 (O—CH_2—C*H*=CH_2), 117.68 (O—CH_2—CH=CH_2), 100.72 (C-1′), 97.46 (C-1), 73.52 (C-3), 71.55 (C-5′), 70.93 (C-5), 70.85 (C-3′), 69.89 (C-2′), 68.73, 68.54 (C-4′ and C-4), 66.73 (O—CH_2—CH=CH_2), 62.47, 60.88 (C-6′ and C-6), 52.62 (C-2), 20.83, 20.76, 20.63, 20.44, 20.00 (6CH_3 of acetyls). *Anal.* calcd. for $C_{35}H_{41}NO_{18}$: C 55.05, H 5.41, N 1.83; found: C 54.98, H 5.40, N 1.85.

*4,6-Di-*O*-acetyl-3-*O*-(2,3,4,6-tetra-*O*-acetyl-β-D-galactopyranosyl)-2-deoxy-2-phthalimido-α,β-galactopyranose (**29**)*

A solution of compound **28** (1.50 g, 1.96 mmol) in ethanol–benzene–water (7:3:1, 200 mL) containing tris-triphenylphosphine rhodium(I) chloride (200 mg, 0.432 mmol) and 1,4-diazabicyclooctane (66 mg, 0.59 mmol) was refluxed for 24 h. Further processing as described for the preparation of **17** left a syrup which was applied on a short column of silica gel (30 g). Evaporation of the main fraction left a solid (1.20 g, 84.6% yield) which appeared homogeneous on tlc. The ^1H nmr spectrum was in general accord with expectation.

*4,6-Di-*O*-acetyl-3-*O*-(2,3,4,6-tetra-*O*-acetyl-β-D-galactopyranosyl)-2-deoxy-2-phthalimido-α,β-galactopyranosyl bromide (**30**)*

Vilsmeier bromide (27) (720 mg, 3.31 mmol) was added to a solution (0°C) of compound **29** (1.2 g, 1.65 mmol) in dichloromethane (15 mL). *sym*-Collidine (440 μL, 3.63 mmol) was added dropwise and the mixture was stirred at 0°C for 6 h and then at room temperature for 18 h. After washing with ice-cold water, dilute hydrochloric acid, saturated aqueous sodium bicarbonate, and finally with water, the solvent was evaporated to leave a solid (1.063 g, 82% yield) which was a mixture of the anomeric bromides; ^1H nmr ($CDCl_3$) δ: 7.87–7.6 (m, 4H, phthalimido), 6.5 (d, H-1α, $J_{1\alpha,2\alpha}$ = 3.5 Hz), 6.1 (d, H-1β, $J_{1\beta,2\beta}$ = 9.0 Hz), 5.66 (broad d, H-4α, $J_{4\alpha,3}$ = 3.0 Hz), 5.44 (broad d, H-4β, $J_{4\beta,3}$ = 3.0 Hz), 5.38 (dd, H-3α, $J_{3\alpha,2}$ = 10.5 Hz, $J_{3\alpha,4}$ = 3.0 Hz), 5.16 (broad d, H-4′β, $J_{4'\beta,3'}$ = 3.0 Hz), 4.94 (dd, H-2β, $J_{2\beta,1}$ = 9.0 Hz, $J_{2,3}$ = 10.5 Hz), 4.68 (dd, H-3′β, $J_{3'\beta,2'}$ = 10.5 Hz, $J_{3'\beta,4'}$ = 3.0 Hz), 4.60 (dd, H-3β, $J_{3\beta,2}$ = 10.5 Hz, $J_{3,4}$ = 3.0 Hz), 4.30 (d, H-1′β, $J_{1'\beta,2'}$ = 8.0 Hz), 4.26–3.66 (remaining hydrogens of sugar units), 2.18–1.60 (CH_3 of acetyls).

*8-Methoxycarbonyloctyl 2,3,6-tri-*O*-acetyl-4-*O*-[2,3-di-*O*-acetyl-6-*O*-benzoyl-4-*O*-{4,6-di-*O*-acetyl-3-*O*-(2,3,4,6-tetra-*O*-acetyl-β-D-galactopyranosyl)-2-deoxy-2-phthalimido-β-D-galactopyranosyl}-β-D-galactopyranosyl]-β-D-glucopyranoside (**31**)*

4,6-Di-*O*-acetyl-3-*O*-(2,3,4,6-tetra-*O*-acetyl-β-D-galactopyranosyl)-2-deoxy-2-phthalimido-α,β-D-galactopyranosyl bromide (**30**) (531 mg, 0.648 mmol) in nitromethane (5 mL) was added to a solution of the alcohol **6** (465 mg, 0.562 mmol), *sym*-collidine (86 μL, 0.648 mmol), and silver triflate (167 mg, 0.648 mmol) in dry nitromethane (5 mL) cooled to −25°C. The mixture was stirred at −25°C for 6 h and then at room temperature for 12 h. The solid that was deposited after the addition of dichloromethane (30 mL) was removed and the filtrate was washed with aqueous sodium thiosulphate, cold water, aqueous HCl, and then aqueous sodium bicarbonate. Solvent removal left a solid which was purified by hplc on a column of silica gel using ethyl acetate – *n*-hexane – acetonitrile (2:2:0.75). Evaporation of the second and main fraction left a solid (548 mg, 62% yield) which was homogencous on tlc; $[\alpha]_D^{25}$ −8.3° (*c* 1.6, $CHCl_3$); ^1H nmr ($CDCl_3$) δ: 8.06–7.46 (broad m, 9H, phthalimido, benzoate), 5.44 (broad d, 1H, H-4″, $J_{4'',3''}$ = 3.5 Hz), 5.24 (broad d, 1H, H-4‴, $J_{4''',3'''}$ = 3.5 Hz), 5.12 (d, 1H, H-1″, $J_{1'',2''}$ = 8.0 Hz), 5.12 (t, 1H, H-3, $J_{3,2}$ = $J_{3,4}$ = 9.0 Hz), 5.0 (dd, 1H, H-2‴, $J_{2''',1'''}$ = 8.0 Hz, $J_{2''',3'''}$ = 10.5 Hz), 4.86–4.74 (m, 4H, H-2, H-3′, H-3″, H-3‴), 4.70 (dd, 1H, H-6′a, $J_{6'a,5'}$ = 7.0 Hz, $J_{6'a,6'b}$ = 11.0 Hz), 4.53–4.30 (m, 6H, H-2″, H-2′, H-1‴, H-1, H-6a, H-6′b), 4.24 (d, 1H, H-1′, *J* = 8.0 Hz), 4.18–4.08 (m, 2H, H-4′, H-6″a), 4.03–3.86 (m, 5H, H-6‴a, H-6‴b, H-6b, H-6″b, H-5″), 3.78–3.70 (m, 3H, H-5′, H-5‴, O—CH_2 of aglycon), 3.64 (t, 1H, H-4, $J_{4,5}$ = $J_{4,3}$ = 9.0 Hz), 3.48 (m, 1H, H-5), 3.38 (m, 1H, O—CH_2 of aglycon), 2.28 (t, 2H, CH_2COOCH_3), 2.12–1.2 (45H, 11CH_3 of acetyls, 12 aglyconic hydrogens); ^{13}C nmr ($CDCl_3$) δ: 174.24, 170.59, 170.31, 170.24, 170.03, 169.94, 169.47 169.34, 169.04, 168.05, 166.92, 166.28, (15C=O, 15 lines expected, 12 lines observed), 134.50, 134.03, 133.38, 131.73, 131.61, 129.95, 129.71, 128.72, 125.22, 124.67 (phthalimido, benzoate carbons), 100.97, 100.88, 100.30, 98.37 (anomeric carbons), 75.33, 72.98, 72.83, 72.30, 72.24, 72.01, 71.74, 70.92, 70.87, 70.04, 69.48, 68.72, 68.60, 66.82, 63.26, 62.41, 62.06, 60.97, 52.51 (20 lines expected, 19 lines observed, remaining carbons of sugar units and the aglyconic carbon), 51.0–19.59 (16 lines).

*8-Methoxycarbonyloctyl 4-*O*-[4-*O*-{2-deoxy-3-*O*-(β-D-galactopyranosyl)-2-phthalimido-β-D-galactopyranosyl}-β-D-galactopyranosyl]-β-D-galactopyranoside (**32**)*

Sodium methoxide in methanol (0.5 mL) was added to a solution of compound **31** (548 mg, 0.357 mmol) in anhydrous methanol (25 mL). After stirring at room temperature under dry nitrogen atmosphere for 4 h, the solution was neutralized with IRA-120H^+ resin and evaporated to a colorless residue (350 mg, 91% yield); ^1H nmr (CD_3OD) δ: 8.1–7.81 (m, 4H, phthalimido), 5.23 (d, 1H, H-1″, $J_{1'',2''}$ = 8.0 Hz), 4.93 (dd, 1H, H-3″, $J_{3'',2''}$ = 10.0 Hz, $J_{3'',4''}$ = 3.0 Hz), 4.52–4.35 (m, 4H, H-1, H-2″, H-1′, H-1‴), 4.1–3.30 (remaining pyranose ring hydrogens and O—CH_2 of aglycon, except H-2′), 3.04 (dd, 1H, H-2′, $J_{1',2'}$ = 7.8 Hz, $J_{2',3'}$ = 9.0 Hz), 2.41 (t, 2H, CH_2COOCH_3), 1.64 and 1.33 (remaining hydrogens of aglycon).

*8-Methoxycarbonyloctyl 4-*O*-[4-*O*-{2-acetamido-2-deoxy-3-*O*-(β-D-galactopyranosyl)-β-D-galactopyranosyl}-β-D-galactopyranosyl]-β-D-glucopyranoside (**33**)*

A solution of compound **32** (350 mg, 0.357 mmol) and 95% hydrazine hydrate (~120 μL) in methanol (20 mL) was refluxed for 8 h. Solvent removal left a syrup which was redissolved in methanol (5 mL) containing acetic anhydride (1 mL) and stirred at room temperature for 3h. The solution was then evaporated to dryness and dissolved in water (5 mL). The precipitate was removed and the filtrate was concentrated to 2 mL for passage through a P-2 Biogel column by elution with water–ethanol (9:1). Lyophilization of the first and main fraction left a colorless powder (215 mg, 61.7% yield), $[\alpha]_D^{25}$ −9.2° (*c* 0.3, H_2O); ^1H nmr (D_2O) δ: 4.64 (d, 1H, H-1″, $J_{1'',2''}$ = 8.2 Hz), 4.42 (m, 3H, H-1, H-1′, H-1‴), 4.11 (broad, d, 1H, H-4′, $J_{4',3'}$ = 2.2 Hz), 4.05 (broad d, 1H, H-4″, $J_{4,3}$ = 2.2 Hz), 3.95 (dd, 1H, H-2″, $J_{2'',1''}$ = 8.0 Hz, $J_{2'',3''}$ = 10.5 Hz), 3.90–3.50 (remaining ring protons and O—CH_2 of aglycon, except H-2′ and H-2), 3.55 (dd, 1H, H-2′, $J_{2',1'}$ = 8.2 Hz, $J_{2',3'}$ = 10.1 Hz), 3.23 (dd, 1H, H-2, $J_{2,1}$ = 7.7 Hz, $J_{2,3}$ = 8.2 Hz), 2.4 (t, 2H, CH_2—COOCH_3), 2.1 (3H, CH_3 of N-acetyl), 1.68–1.38 (remaining 12H of aglycon).

The ^{13}C nmr spectrum is reported in Table 1.

*8-Methoxycarbonyloctyl 2,3-di-*O*-acetyl-4,6-*O*-benzylidene-β-D-galactopyranoside (**34**)*

A solution of 8-methoxycarbonyloctyl 4,6-*O*-benzylidene-β-D-galactopyranoside (40) (753 mg) in dichloromethane (15 mL) containing pyridine (3 mL), acetic anhydride (3 mL), and *N*,*N*-dimethylaminopyridine (10 mg) was stirred for 24 h at room temperature. Work-up in the usual manner afforded a syrup (880 mg, 98% yield) which was homogeneous as examined by tlc; ^1H nmr ($CDCl_3$) δ:

Can. J. Chem. Downloaded from www.nrcresearchpress.com by 210.87.254.5 on 09/06/12
For personal use only.

Can. J. Chem. Downloaded from www.nrcresearchpress.com by 210.87.254.5 on 09/06/12
For personal use only.

7.5–7.3 (m, 5H, aromatic), 5.50 (s, 1H, benzylic), 5.38 (dd, 1H, $J_{2,1}$ = 8.0 Hz, $J_{2,3}$ = 10.5 Hz, H-2), 4.95 (dd, 1H, $J_{3,2}$ = 10.5 Hz, $J_{3,4}$ = 3.6 Hz, H-3), 4.48 (d, 1H, $J_{1,2}$ = 8.0 Hz, H-1), 4.37 (bd, 1H, H-4), 4.33 (dd, 1H, $J_{6a,5}$ = 1.4 Hz, $J_{6a,6b}$ = 12.4 Hz, H-6a), 4.07 (dd, 1H, H-6b), 3.91 (m, 1H, O—CH_2 of aglycon), 3.66 (s, 3H, $COOCH_3$), 3.51 (d, 1H, H-5), 3.46 (m, 1H, CH_2 of aglycon), 2.29 (t, 2H, J = 7.3 Hz, CH_2—$COOCH_3$), 2.07, 2.05 (2s, 6H, $2CH_3$—COO), 1.60 and 1.29 (12H, remaining hydrogens in aglycon).

*8-Methoxycarbonyloctyl 2,3-di-*O*-acetyl-β-D-galactopyranoside (**35**)*

A solution of compound **34** (603 mg) in dichloromethane (20 mL) containing 90% aqueous trifluoroacetic acid (1.5 mL) was stirred at 0°C for 3 h. Work-up in the usual manner and the purification of the crude product on a column of silica gel afforded a colorless solid (402 mg, 80% yield).

The ^{1}H nmr was in accordance with structure **35**.

*8-Methoxycarbonyloctyl 2,3-di-*O*-acetyl-6-*O*-benzoyl-β-D-galactopyranoside (**36**)*

A solution of benzoyl chloride (332 mg, 274 μL, 2.36 mmol) in dichloromethane (1 mL) was added to a cooled (−78°C) solution of compound **35** (932 mg, 2.14 mmol) in dichloromethane (15 mL) containing anhydrous pyridine (186 μL, 2.36 mmol). After 6 h, the solution was warmed to −30°C and stirred for another 18 h. Work-up of the reaction mixture followed by purification on a column of silica gel afforded a colorless solid (725 mg, 62.7% yield); ^{1}H nmr ($CDCl_3$) δ: 8.0–7.38 (m, 5H, benzoate), 5.26 (dd, 1H, $J_{2,1}$ = 7.8 Hz, $J_{2,3}$ = 10.2 Hz, H-2), 4.99 (dd, 1H, $J_{3,4}$ = 3.1 Hz, H-3), 4.62 (dd, 1H, $J_{6a,5}$ = 6.6 Hz, $J_{6a,6b}$ = 11.2 Hz, H-6a), 4.53 (dd, 1H, $J_{6b,5}$ = 6.3 Hz, H-6b), 4.48 (d, 1H, $J_{1,2}$ = 7.8 Hz, H-1), 4.11 (dd, 1H, $J_{4,O-H}$ = 5.3 Hz, H-4), 3.90 (bt, 1H, H-5), 3.86 (m, 1H, O—CH_2 of aglycon), 3.66 (s, 3H, $COOCH_3$), 3.48 (m, 1H, O—CH_2 of aglycon), 2.40 (d, 1H, 4-O*H*), 2.29 (t, 2H, J = 7.5 Hz, CH_2COOCH_3), 2.10, 2.05 (2s, $2CH_3$—COO), 1.58 and 1.27 (m, 12H, remaining hydrogens of aglycon).

*8-Methoxycarbonyloctyl 2,3-di-*O*-acetyl-6-*O*-benzoyl-4-*O*-(3,4,6-tri-O-acetyl-2-deoxy-2-phthalimido-β-D-galactopyranosyl)-β-D-galactopyranoside (**37**)*

A solution of the phthalimidobromide **18** (437 mg, 0.87 mmol) in nitromethane (5 mL) was added to a solution of **36** (393 mg, 0.73 mmol), *sym*-collidine (105.6 mg, 0.87 mmol), and silver triflate (225 mg, 0.87 mmol) in dry nitromethane (5 mL) at −25°C. The mixture was stirred at this temperature for 12 h and then at room temperature for another 24 h. Work-up of the reaction mixture and purification on a column of silica gel afforded a colorless solid (360 mg, 48% yield); ^{1}H nmr ($CDCl_3$) δ: 8.07–7.40 (m, 9H, benzoate, phthalimido), 5.91 (dd, 1H, $J_{3',2'}$ = 11.4 Hz, $J_{3',4'}$ = 3.4 Hz), 5.45 (d, 1H, H-4′), 5.29 (d, 1H, $J_{1',2'}$ = 8.5 Hz, H-1′), 4.89 (dd, 1H, $J_{3,4}$ = 2.9 Hz, $J_{3,2}$ = 10.2 Hz, H-3), 4.72 (dd, $J_{2,1}$ = 7.8 Hz, H-2), 4.69 (dd, 1H, $J_{6a,5}$ = 5.6 Hz, $J_{6a,6b}$ = 11.5 Hz, H-6a), 4.62 (dd, 1H, H-2′), 4.45 (dd, 1H, $J_{6b,5}$ = 6.6 Hz), 4.33 (d, 1H, $J_{1,2}$ = 7.8 Hz, H-1), 4.14 (d, 1H, H-4), 4.11–3.99 (m, 3H, H-6′a, H-6′b, H-5′), 3.82 (t, 1H, H-5), 3.73 (m, 1H, O—CH_2 of aglycon), 3.66 (s, 3H, $COOCH_3$), 3.39 (m, 1H, OCH_2 of aglycon), 2.29 (t, 2H, J = 7.3 Hz, CH_2COOCH_3), 2.21–1.66 (5s, 15H, 5 CH_3COO), 1.58 and 1.25 (12H, remaining hydrogens of aglycon).

*8-Methoxycarbonyloctyl-4-*O*-(2-acetamido-2-deoxy-β-D-galactopyranosyl)-β-D-galactopyranoside (**38**)*

Removal of the *O*- and *N*-protecting groups of **37** and the *N*-acetylation of the resulting amine was accomplished under the conditions described earlier for the conversion of **19** to **21**. This afforded compound **38** in 77% overall yield. The indentity of **38** was established on the basis of comparison of ^{1}H and ^{13}C nmr data of an authentic sample of **38** provided by Dr. R. M. Ratcliffe of Chembiomed Ltd. (unpublished); ^{1}H nmr (D_2O) δ: 4.59 (d, 1H, $J_{1',2'}$ = 8.5 Hz, H-1′), 4.32 (d, 1H, $J_{1,2}$ = 8.2 Hz, H-1), 4.03 (d, $J_{4,3}$ = 2.2 Hz, H-4), 3.91–3.33 (16H, remaining hydrogens of sugar units, $COOCH_3$, OCH_2 of aglycon), 2.40 (t, 2H, CH_2—$COOCH_3$), 2.04 (s, 3H, NH($COCH_3$)), 1.61 and 1.33 (12H, remaining hydrogens of aglycon).

The ^{13}C nmr spectrum is reported in Table 1.

*n-Propyl 2-acetamido-2-deoxy-3-*O*-(β-D-galactopyranosyl)-β-D-galactopyranoside (**39**)*

A solution of compound **25** (46 mg, 0.11 mmol) in 95% ethanol (4 mL) containing palladium on carbon (10%, 10 mg) was stirred under an atmosphere of hydrogen for 3 h. The reaction mixture was filtered and evaporated to dryness. The residue (38 mg) was taken up in a mixture of methanol – acetic anhydride (10:1, 1 mL) and stirred at room temperature for 3 h. Examination of the reaction mixture at this time (EtOAc–EtOH–H_2O, 16:8:5) indicated the presence of a single compound. It was then evaporated to a dry residue which was redissolved in water and freeze-dried. This afforded a colorless material (40 mg, 0.09 mmol, 89% yield), $[\alpha]_D^{25}$ 8° (*c*, 0.09); ^{1}H nmr (D_2O) δ: 4.53 (d, 1H, $J_{1,2}$ = 10.0 Hz, H-1), 4.46 (d, $J_{1',2'}$ = 7.7 Hz, 1H, H-1′), 4.01 (dd, 1H, $J_{2,3}$ = 11.2 Hz, 1H, H-2), 3.95–3.51 (remaining sugar hydrogens and OCH_2—CH_2—CH_3), 2.02 (s, 3H, NHCO—CH_3), 1.56 (m, 2H, O—CH_2—CH_2—CH_3), 0.88 (t, J = 7.3 Hz, 3H, O—CH_2—CH_2—CH_3).

The ^{13}C nmr spectrum is presented in Table 1.

Acknowledgements

This research was supported by the Natural Sciences and Engineering Research Council of Canada (Grant A-172 to R.U.L.) and Alberta Heritage Foundation for Medical Research studentships to S.S. (1981–83). The microanalyses and many of the ^{1}H and ^{13}C nmr spectra were provided by the Analytical and Spectral Services Laboratories of this department. The inhibition study was provided by Chembiomed Ltd.

1. E. KLENK. Hoppe-Seylers Z. Physiol. Chem. **235**, 24 (1935).
2. L. SVENNERHOLM. Gangliosides. *In* Handbook of neurochemistry. Vol. III. *Edited by* A. Lajtha. Plenum Press, New York. 1970. p. 425.
3. IUPAC–IBC Commission on Biochemical Nomenclature. J. Lipid Res. **19**, 114 (1978).
4. R. W. LEDEEN. Structure and distribution of gangliosides. *In* Complex carbohydrates of nervous tissues. *Edited by* R. U. Margolis and R. K. Margolis. Plenum Press, New York. 1979. p. 1.
5. S. HAKOMORI, W. W. YOUNG, JR., and G. ROSENFELDER. Cancer Res. **37**, 1333 (1977).
6. K. SANDHOFF, K. HARRER, W. WAISSLE, and H. JATZKEWITZ. J. Neurochem. **18**, 2469 (1971).
7. A. S. R. DONALD, C. P. C. SOH, W. M. WATKINS, and W. T. J. MORGAN. Biochem. Biophys. Res. Commun. **104**, 58 (1982).
8. D. A. BAKER, S. SUGII, E. A. KABAT, R. M. RATCLIFFE, P. HERMENTIN, and R. U. LEMIEUX. Biochemistry, **22**, 2741 (1983).
9. S. HABU, H. FUKUI, K. SHIMAMURA, M. KASAI, Y. NAGAI, K. OKUMURA, and N. TAMAOKI. J. Immunol. **127**, 34 (1981).
10. C. A. SCHWARTING and A. GAJEWSKI. J. Biol. Chem. **258**, 5893 (1983), and references therein.
11. R. U. LEMIEUX, D. R. BUNDLE, and D. A. BAKER. J. Am. Chem. Soc. **97**, 4076 (1975).
12. R. U. LEMIEUX, D. R. BUNDLE, and D. A. BAKER. Can. J. Biochem. **55**, 507 (1977).
13. R. U. LEMIEUX, D. A. BAKER, W. M. WEINSTEIN, and C. M. SWITZER. Biochemistry, **20**, 199 (1981).
14. R. U. LEMIEUX. Frontiers in chemistry. *Edited by* K. H. Laidler. Pergamon Press, Oxford. 1983. p. 3.
15. J. BANOUB and D. R. BUNDLE. Can. J. Chem. **57**, 2085 (1979).
16. M. E. EVANS. Carbohydr. Res. **21**, 473 (1972).
17. A. LIPTAK, I. JODAL, and P. NANASI. Carbohydr. Res. **52**, 17 (1976).

18. D. D. COX, E. K. METZNER, and E. J. REIST. Carbohydr. Res. **63**, 139 (1978).
19. D. E. DORMAN and J. D. ROBERTS. J. Am. Chem. Soc. **93**, 4463 (1971).
20. H. PAULSEN and A. BÜNSCH. Carbohydr. Res. **100**, 143 (1982).
21. R. U. LEMIEUX, T. TAKEDA, and B. Y. CHUNG. Am. Chem. Soc. Series No. **39**, 90 (1976).
22. D. R. BUNDLE and S. JOSEPHSON. Can. J. Chem. **57**, 662 (1979).
23. R. U. LEMIEUX and M. H. BURZYNSKA. Can. J. Chem. **60**, 76 (1982).
24. W. ROTH and W. PIGMAN. Methods in carbohydrate chemistry. Vol. II. *Edited by* M. L. Wolfrom and R. L. Whistler. Academic Press, New York 1963. p. 405.
25. F. SHAFIZADEH. Methods in carbohydrate chemistry. Vol. II. *Edited by* M. L. Wolfrom and R. L. Whistler. Academic Press, New York. 1963. p. 409.
26. R. U. LEMIEUX and R. M. RATCLIFFE. Can. J. Chem. **57**, 1244 (1979).
27. D. R. HEPBURN and H. R. HUDSON. J. Chem. Soc. Perkin Trans. 1, 754 (1976).
28. T. ADACHI, Y. YAMADA, I. INOUE, and M. SANEYOSHI. Synthesis, 45 (1977).
29. R. U. LEMIEUX, S. Z. ABBAS, M. H. BURZYNSKA, and R. M. RATCLIFFE. Can. J. Chem. **60**, 63 (1982).
30. E. J. COREY and R. SUGG. J. Org. Chem. **38**, 3224 (1973).
31. R. GIGG and P. GENT. J. Chem. Soc. (C), 277 (1974).
32. R. U. LEMIEUX, S. Z. ABBAS, and B. Y. CHUNG. Can. J. Chem. **60**, 58 (1982).
33. P. GAREGG and T. NORBERG. Acta Chem. Scand. Ser. B, **33**, 116 (1979).
34. B. HELFERICH and K.-F. WENDEMEYER. Ann. **563**, 139 (1949).
35. R. U. LEMIEUX, K. BOCK, L. T. J. DELBAERE, S. KOTO, and V. S. RAO. Can. J. Chem. **58**, 631 (1980).
36. R. U. LEMIEUX and K. BOCK. Arch. Biochem. Biophys. **221**, 125 (1983).
37. R. U. LEMIEUX and R. M. RATCLIFFE. U. S. Patent No. 4,195,174 (1980).
38. D. D. PERRIN, W. L. ARMAREGO, and D. R. PERRIN. *In* Purification of laboratory compounds. Pergamon Press, London. 1966.
39. C. S. HUDSON and A. KUNZ. J. Am. Chem. Soc. **47**, 2052 (1925).
40. R. U. LEMIEUX, D. R. BUNDLE, and D. A. BAKER. U. S. Patent No. 4,137,401 (1979).
41. J. CONCHIE and G. A. LEVVY. *In* Methods in carbohydrate chemistry. Vol. II. *Edited by* M. L. Wolfrom and R. L. Whistler. Academic Press, New York. 1963. p. 335.

Can. J. Chem. Downloaded from www.nrcresearchpress.com by 210.87.254.5 on 09/06/12
For personal use only.

Electron impact mass spectrometry in a series of methyl-2-pyrimidones

ERIC PICQUENARD[1]

Laboratoire de Spectrochimie Moléculaire, Université Pierre et Marie Curie, 4 place Jussieu, 75230 Paris Cédex 05, France

AND

JACQUES RIAND AND JEAN-PIERRE BRUN

Laboratoire de Spectrochimie Infrarouge et Raman, C.N.R.S., 2 rue Henri Dunant, 94320 Thiais, France

Received July 11, 1983

ERIC PICQUENARD, JACQUES RIAND, and JEAN-PIERRE BRUN. Can. J. Chem. **62**, 655 (1984).

The fragmentation under electron impact of various methyl-2-pyrimidones is investigated. The fragmentation is markedly influenced by the methyl substituent in the 4- or 5-position and the main fragmentation pathways of the molecular ion involve the loss of carbon monoxide or methyl radical. The latter fragmentation process shows that the methyl groups are more labile in the 4- and(or) 6-position than in the 5-position. This is corroborated by the study of trideuteriomethylated analogues. One can thus distinguish by mass spectrometry the different isomers of position, 4-methyl and 5-methyl or 4,5-dimethyl and 4,6-dimethyl-2-pyrimidones.

ERIC PICQUENARD, JACQUES RIAND et JEAN-PIERRE BRUN. Can. J. Chem. **62**, 655 (1984).

On a étudié les processus de fragmentation de différentes méthylpyrimidone-2. Ceux-ci sont nettement influencés par le groupement méthyle en position 4 ou 5 sur le cycle et les fragmentations majeures de l'ion moléculaire font intervenir la perte d'une molécule neutre CO ou d'un radical méthyle. Dans ce dernier cas, les groupements méthyles en position 4 et (ou) 6 sont plus mobiles que celui en position 5, ce qui est confirmé par l'étude des dérivés trideutériométhylés. Il est alors possible de distinguer par spectrométrie de masse les différents isomères de position, méthyl-4 et méthyl-5 ou diméthyl-4,5 et diméthyl-4,6 pyrimidone-2.

Introduction

Mass spectra of 4-pyrimidones or uracil derivatives which are of great interest in connection with biologically important nucleic acids have already been examined thoroughly (1–4). However, few studies of the mass spectral behaviour of 2-pyrimidones have been reported, with the exception of one very recent work (5).

Analysis of the mass fragmentation of such compounds may provide a convenient means of structure determinations. In continuation of our previous work dealing with the methyl-2-pyrimidones (6, 7), we present results on mass spectral studies of these compounds. Those investigated are listed in Table 1. Our study of the physical properties of these compounds has led us to show that the methyl group attached to C-4 or C-6 of 2-pyrimidone undergoes hydrogen–deuterium exchange reactions in D_2O medium (6) and even in the solid phase (7). In connection with these results, we expect that studies of the fragmentation patterns could show the extent of hydrogen or methyl loss in the 4(or 6)- and 5-position. For this purpose, the 4,6-bis(trideuteriomethyl)-5-methyl-2-pyrimidone(1*D*) **7** will be used to corroborate the fragmentation process of CH_3 loss only. Furthermore, the methoxypyrimidine **9** has been studied for the sake of comparison with the *N*-methyl compound **8**.

TABLE 1. Methyl-2-pyrimidones and methoxypyrimidine studied

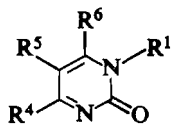

Compound	R^1	R^4	R^5	R^6
1	H	CH_3	H	H
2	H	H	CH_3	H
3	H	CH_3	CH_3	H
4	H	CH_3	H	CH_3
5	H	CH_3	CH_3	CH_3
6	H	CH_3	CD_3	CH_3
7	D	CD_3	CH_3	CD_3
8	CH_3	CH_3	CH_3	CH_3
9	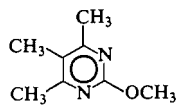			

Results and discussion

The mass spectra of methyl-2-pyrimidones show the great stability of the aromatic ring. The base peaks always correspond to the molecular ion (Table 2). Important differences between the mass spectral behaviour of these compounds and that of unsubstituted 2-pyrimidone (5) show that the fragmentation patterns are affected by the presence of a methyl group attached to the ring. As an example, the fragmentation pathways of compound **3** are outlined in Scheme 1. Transitions substantiated by an appropriate metastable peak (directly observed on the 70 eV mass spectrum) are indicated by an asterisk.

Loss of CO

A noteworthy feature of pyrimidone fragmentation is the preferential loss of carbon monoxide from the molecular ion. This loss can be characterized by the observation of a metastable ion and yields a *m/z* 82 ion for **1** and **2** and a *m/z* 96 ion for **3** and **4**. This is corroborated by exact mass measurement; the peak at *m/z* 96 in the spectrum of **3** corresponds mainly to the CO loss process ($C_5H_8N_2^{+\bullet}$, 93%) and for a minor part to another process ($C_5H_6NO^+$, 7%) which will be discussed later. This is most conveniently interpreted as arising from the keto form of the molecular ion. In agreement with this fragmentation, compounds **5** and **6** yield respectively the *m/z* 110 and

[1]Author to whom correspondence should be addressed. Present address: L.A.S.I.R., C.N.R.S., 2 rue Henri Dunant, 94320 Thiais, France.

TABLE 2. Mass spectra for compounds **1–9**. Fragment ions with respective relative intensities

	Compounds								
m/z	**1**	**2**	**3**	**4**	**5**	**6**	**7**	**8**	**9**
153								11	10
152								100	100
151									81.5
146							10		
145							100		
144							81		
143							31		
142						10.5	11		
141						100			
140						5			
139					11				
138					100			11	
137					7			81.5	5
127							20		
126						21	14		
125			9	9			5		
124			100	100				24	5
123			13.5		17			23	46
122									91.5
121									27
117							28		
116							35		
115							25		
114						6	11		
113						42	5		
112						18			
111	8	8				18			
110	100	100		5	30.5	7		11	
109	8.5	11.5	23	46	21.5			11	
107									23.5
103							7		
102							6		
101							6		
100							8.5		
99						14.5	17.5		
98						14.5	11.5		
97				6		6	6		
96			34	37	10	7		5.5	10.5
95	49.5	5	14	27	13.5	9.5			8
94								5	7
85						5			
84						5	5		
83	6	7		5.5		12.5	12.5	16.5	
82	45	37	10	11		7	6	26	9
81	10.5	11.5	8	7.5		6	6		19
80			8		7				9
75							5		
74							25.5		
73						6	68		
72						52	41		
71		5		5.5		29	16.5		
70					5.5	9.5	11.5		5.5
69	9	7	36	10	55.5	8	8		5
68	21		6.5	5	6			11	8
67	9.5			7	5.5	6	5	5	20
66	6			14					6
65									5
60	5								
59						6			
58						7	6		
57	6.5	8		9.5		25	21.5		13
56		9	9	5.5	6	27	32	39	5.5

TABLE 2. (*Concluded*)

	Compounds								
m/z	**1**	**2**	**3**	**4**	**5**	**6**	**7**	**8**	**9**
55	10	48	42	11	5.5	27	34	6	8.5
54	7	15	22.5	5.5	12.5	11.5	17	5.5	5
53		5	15.5	5	19.5	11.5	14	8.5	14.5
52	8.5	6	12		9	9.5	11.5	5	24.5
51			8		9	7	8		10.5
50			5		5.5				7
46							52		
45						8	44		
44	8.5	9	9	5.5		12.5	25		
43		7	11	9.5	5.5	28	23		
42	23.5		38.5	21.5	41	68	15	17.5	32.5
41	18	8.5	11.5	12	11.5	24	19	9	17
40	20	10	11	7	5.5	19	13		7

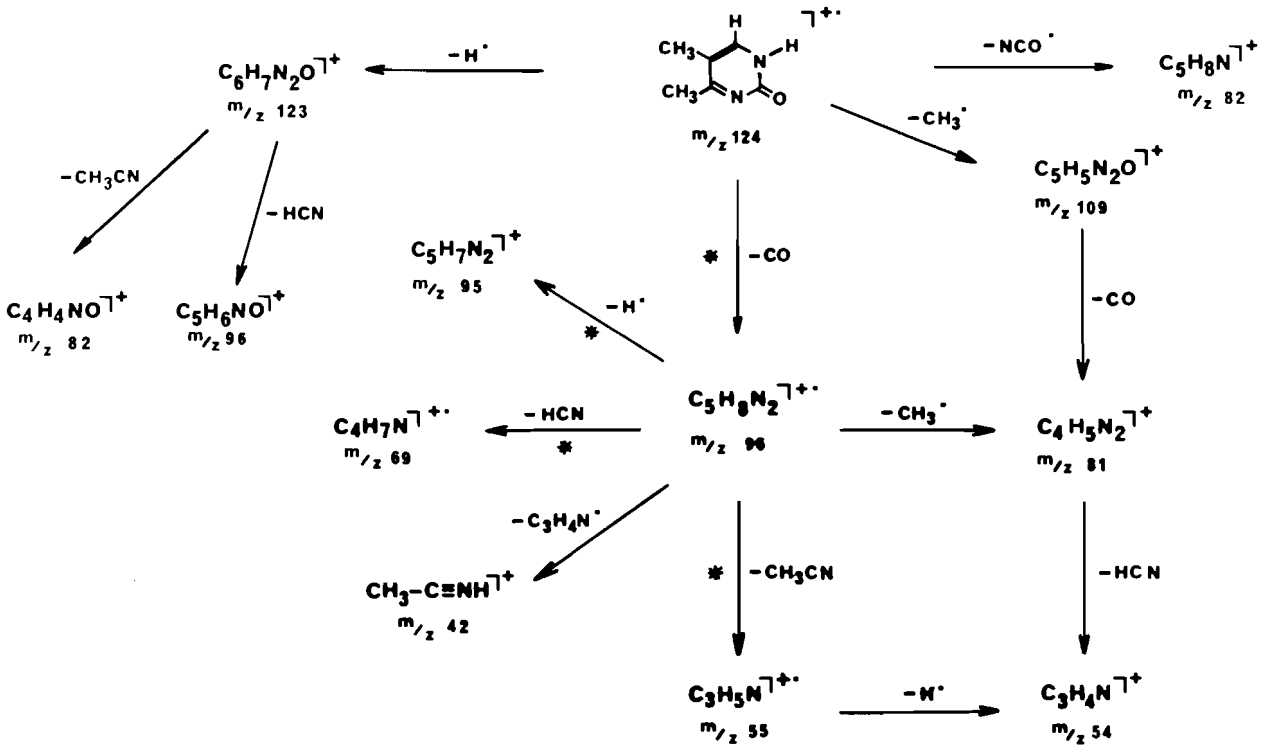

SCHEME 1. Major fragmentation processes of 4,5-dimethyl-2-pyrimidone.

113 ions. The *N*-methyl derivative **8**, in which tautomerism is prevented, displays the expected expulsion of carbon monoxide to give the *m/z* 124 ion.

This fragmentation process is of lesser importance than that observed for unsubstituted 2-pyrimidone and its *N*-methylated analogue (5) but is equivalent to the process observed for 2-methyl-4-pyrimidone and its *N*-methyl derivative (4). Therefore it appears that CO loss is a general main fragmentation process for 2- and 4-pyrimidones (2, 4, 5). The decrease in the loss of CO is then induced by the presence of the methyl group attached to the ring in the 4- or 5-position.

Loss of H·

The primary loss of H· occurs to a lesser extent for methyl-2-pyrimidones (**1** to **7**) than for unsubstituted 2-pyrimidone and is nearly negligible for compound **8**. Kazdan *et al.* (5) have concluded that this loss occurs specifically from the 4-position of unsubstituted 2-pyrimidone. Our results obtained for **3** ($M - H^{+}$: 13.5%) and **4** ($M - H^{+}$: <5%) confirm without any ambiguity that this loss occurs from the 4-position and not at all from the 5-position. Furthermore, the fragmentation study for compound **6** enables us to show that neither the loss of a hydrogen atom from the 4- or 6-methyl group nor a deuterium atom from the 5-trideuteriomethyl group is promoted. As a matter of fact, the relative intensities of $M - H^{+}$ and $M - D^{+}$ peaks for this compound are weak (5% and <5% respectively). For compound **7**, we are unable to determine the respective proportion of H loss and D loss from the 4- or 6-CD_3 groups and the 5-CH_3 group. As expected for this compound, the H/D exchange reaction occurs in the inlet and ion source, which explains the important relative intensities of $M - H^{+}$ and $M - D^{+}$ peaks compared to those of compounds **5** and **6**. Metastable peaks for these H· (D·) losses were not observed, so that no abundance measurements could be done. For 4-methyl-

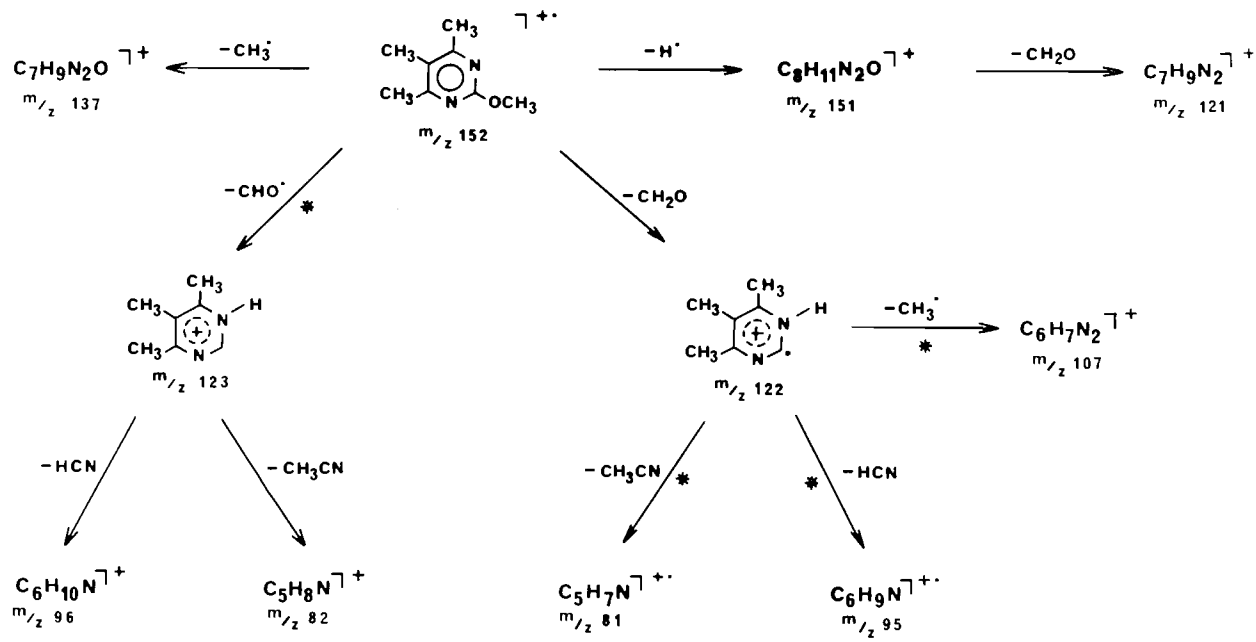

SCHEME 2. Major fragmentation processes of 2-methoxy-4,5,6-trimethylpyrimidine.

2-pyrimidone, H loss is noticeable (8.5% for the m/z 109 ion) whereas an analogous loss in the spectrum of 6-methyl-4-pyrimidone is not observed (2), which indicates the influence of the position of the carbonyl function on this fragmentation process. This can be compared with the results on the H/D exchange of methyl groups for pyrimidones, in spite of the lack of correlation. As a matter of fact, the study of isotopic exchange allows us to compare the relative mobility of methyl hydrogens in a molecule. Thus, if the 4- and (or) 6-methyl groups undergo exchange reactions in substituted 2-pyrimidones (6, 8), no exchange occurs for the methyl group in 6-methyl-4-pyrimidone.[2]

A very intense M − $H^{\cdot+}$ peak is present in the spectrum of compound **9** (Scheme 2). It has been shown that this is usual for methoxypyrimidines, the loss of a hydrogen atom coming from the methoxy group (2, 4).

Hydrogen loss is less important from the molecular ion than from the M − $CO^{\cdot+}$ ion. This last fragmentation leads to the following ions: m/z 81 for **1** and **2**, m/z 95 for **3** and **4**, and m/z 109 for **5**, with relative intensities between 10 and 27%. For compound **6**, the M − $CO^{\cdot+}$ ion loses a hydrogen and a deuterium atom to lead to the peaks at m/z 112 and 111 respectively, with the same intensity (18%). This elimination involves the 4-methyl and 5-methyl groups in the same way. For the *N*-methyl derivative **8**, the M − $CO^{\cdot+}$ ion also loses a hydrogen atom, which corresponds to the m/z 123 ion (24%).

Loss of CH_3

The loss of a methyl radical is greater for the 4- or 6-position than for the 5-position. This result enables us to distinguish unambiguously the 4-methyl-2-pyrimidone from its isomer, the 5-methyl-2-pyrimidone. The relative intensity of the M − CH_3^+ ion (m/z 95) is 49.5% for the first compound and 5% for the second one. Likewise, for dimethylated derivatives, CH_3 loss leading to the m/z 109 ion is more pronounced for 4,6-dimethyl-2-pyrimidone (46%) than for 4,5-dimethyl-2-pyrimidone (23%). Additional support for the above results comes from the spectrum of the trimethylated compound **7** in which no CH_3 loss from the 5-position is noticeable: the M − CH_3^+ ion (m/z 130) is not observed, while the relative intensity of the M − CD_3^+ ion (m/z 127) is 20%. These results are in good agreement with those obtained for dimethylpyrimidines, i.e., preferential elimination of the methyl groups attached to C-4 or C-6 rather than to C-2 or C-5 of the pyrimidine ring (9). For the 6-methylpyrimidine series, methyl loss depends on the nature of the other substituents but remains weak, especially for 2- and 4-amino substituents (2, 3).

The loss of a methyl radical from the molecular ion is greater for the *N*-methyl compound **8** than for its corresponding *N*-hydrogenated **5** (m/z 137, 81% and m/z 123, 17% respectively). Then, the ring nitrogen atom is the principal site of CH_3 loss rather than a ring carbon atom. This is similar to what is observed for dimethylaminopyrimidines. For these compounds, after the loss of the methyleneimine group, the methyl radical is expelled also from the ring nitrogen atom (10, 11). This CH_3 loss also occurs for the methoxy derivative **9**, but to a lesser extent than for **5** (Scheme 2). Such an elimination is seldom observed for methoxypyrimidines (4, 11), which is in good agreement with our results.

A CH_3 loss is also observed from the M − $CO^{\cdot+}$ ion. This loss is weaker than from the molecular ion and gives the m/z 67 ion for compounds **1** and **2**, the m/z 81 ion for **3** and **4**, and the m/z 95 ion for **5**. Exact mass measurements indicate that the m/z 81 and 95 peaks for compounds **3** and **5** respectively are solely due to the $C_4H_5N_2^+$ and $C_5H_7N_2^+$ ions. Likewise, the M − $CO^{\cdot+}$ ion of **6** can expel a CH_3 or a CD_3 radical, leading to the m/z 98 and 95 ions respectively. For the *N*-methyl derivative **8**, this fragmentation leads to a m/z 109 ion with a relative intensity weaker than for compound **5**.

Loss of HCN and CH_3CN

It has been shown that for 2-pyrimidone (5) the loss of a neutral molecule of HCN or the loss of CH_3CN for 2-methyl-4-pyrimidone (4) are the usual fragmentation processes. These processes are not significant for methyl-2-pyrimidones, since the relative intensities of the corresponding

[2] E. Piequenard, unpublished results.

ion peaks (m/z 83 ($C_4H_5NO^{\neg+\bullet}$) for compounds **1** to **4** and m/z 97 ($C_5H_7NO^{\neg+\bullet}$) for **5**) are lower than 7%. Likewise, compound **8** does not eliminate CH_3CN, no peak at m/z 111 being noticeable. Similar behaviour has been observed for the 1,2-dimethyl-4-pyrimidone (4). CH_3CN loss is then negligible compared to that of the corresponding N-hydrogenated derivative. However, such a HCN or CH_3CN loss is greater from the $M - H^{\neg+}$ and $M - CO^{\neg+\bullet}$ ions than from the molecular ion, where it is negligible. Thus, by eliminating HCN, the $M - H^{\neg+}$ ion leads to the m/z 82 ion ($C_4H_4NO^{\neg+}$) for compounds **1** and **2**, and by eliminating CH_3CN, leads to the m/z 68 ion ($C_3H_2NO^{\neg+}$) for **2**, the m/z 82 ion for **3** and **4**, and the m/z 96 ion for **5**. The relative intensities for monosubstituted compounds **1** and **2** are large (Table 2). For compound **6**, CH_3CN loss from the $M - H^{\neg+}$ and $M - D^{\neg+}$ ions leads to the m/z 99 and 98 ions respectively, with the same relative intensity (14.5%). Exact mass measurements on the m/z 96 peak for compounds **3** and **5** have been performed. For compound **5**, the contribution of the $C_5H_6NO^{\neg+}$ ion to this peak is only 33%. For compound **3**, the elimination of HCN from the $M - H^{\neg+}$ ion is a minor process since the contribution of the $C_5H_6NO^{\neg+}$ ion is only 7%.

Likewise, by loss of HCN, the $M - CO^{\neg+\bullet}$ ion generates the m/z 55 ion ($C_3H_5N^{\neg+\bullet}$) for **1** and **2** and the m/z 69 ion ($C_4H_7N^{\neg+\bullet}$) for **3**. In the spectrum of **3**, the presence of an intense peak at m/z 69 (36%) enables us to distinguish compound **3** from its isomer of position, compound **4**. By eliminating CH_3CN, the $M - CO^{\neg+\bullet}$ ion leads to the following ions: m/z 41 ($C_2H_3N^{\neg+\bullet}$) for **1**, m/z 55 ($C_3H_5N^{\neg+\bullet}$) for **3** and **4**, and m/z 69 ($C_4H_7N^{\neg+\bullet}$) for **5**, as confirmed for the last compound by exact mass measurements. The elimination of acetonitrile for deuterated derivatives, CH_3CN for **6** and CD_3CN for **7**, gives intense peaks at m/z 72(52%) and m/z 73 (68%) respectively.

Other fragmentation processes

The loss of HNCO from the molecular ion via the retro Diels–Alder mechanism is certainly, for our compounds, a minor fragmentation process, contrary to what is observed for 2-pyrimidone (5). Thus, the expected $C_5H_7N^{\neg+\bullet}$ and $C_6H_9N^{\neg+\bullet}$ ions for compounds **3** and **5** respectively do not take part in the m/z 81 and 95 peaks, as mentioned above.

The loss of a NCO radical from the molecular ion is observed as for 2-pyrimidone (5), corresponding to the peaks at m/z 68, 68, 82, 82, 96, 99, 103, and 110 respectively for compounds **1** to **8**, with weak relative intensities except for **1** (Table 2). For compound **5**, exact mass measurement shows that the corresponding ion $C_6H_{10}N^{\neg+}$ contributes to 66% of the m/z 96 peak, the other ion being $C_5H_6NO^{\neg+}$ (see above).

In the lower region of the spectra of methyl-2-pyrimidones, there are many ion peaks characteristic of pyrimidines, m/z 79, 67, 53, 52, 51, 42, and 41, among which the m/z 42 ion is largely predominant (1–5). High resolution mass measurements on compounds **3** and **5** show that the elemental composition of this last ion is $C_2H_4N^{\neg+}$ which corresponds to the acetonitrile cation; this is very usual for pyrimidines with 2-, 4-, or 6-methyl groups (4, 9). As expected, this m/z 42 ion is not observed for compound **2**. This ion comes from the molecular ion or from the $M - CO^{\neg+\bullet}$ ion, as is observed for 2-methyl-4-pyrimidone (4). For the methoxy derivative **9**, the m/z 42 ion comes either from the predominant m/z 122 ion with loss of $C_5H_6N^{\bullet}$ or from the m/z 123 ion with loss of $C_5H_7N^{\bullet}$.

2-Methoxy-4,5,6-trimethylpyrimidine

Other fragmentation processes specific for this compound will be detailed in this section. This compound can eliminate formaldehyde via the four-membered cyclic transition state to yield the large 4,5,6-pyrimidine ion (m/z 122, 91.5%), as was observed in several 4-methoxypyrimidines(2, 4). This loss is also observed from the $M - H^{\neg+}$ ion to give the m/z 121 ion. Another important process is the loss of formyl radical from the molecular ion, which yields a m/z 123 ion (46%) (Scheme 2). Elimination of acetonitrile from the molecular ion should result in the formation of a m/z 111 ion which, however, was neither detected for this compound nor for the *N*-methyl derivative **8**. However, the m/z 122 and 123 ions eliminate HCN or CH_3CN respectively to give m/z 95 and 81 ions or m/z 96 and 82 ions (Table 2). Finally, the $M - OH^{\neg+\bullet}$ ion observed for methoxybipyrimidine (11) is not obtained for compound **9**, which has a single pyrimidine ring.

The fragmentation processes for compound **9** are so characteristic of alkoxy-substituted pyrimidines that we cannot expect to obtain, with this technique, information on lactam–lactim tautomerism by comparing compound **8** with compound **9** as models for the lactam and lactim forms of **5**, respectively.

Conclusion

The detailed analysis of the mass spectra of various substituted methyl-2-pyrimidones indicates the important influence of the methyl group in the fragmentation processes of the heterocycles. This is clearly shown by the differences between the behaviour of these compounds and that reported in the literature for 2- and 4-pyrimidones. The loss of a neutral CO molecule remains a predominant fragmentation process; however, it is less so than for unsubstituted 2-pyrimidone. The loss of a methyl radical from the molecular ion is a very important fragmentation process when this methyl group is attached to C-4 or C-6, and not to C-5, of the pyrimidone ring. Then the different fragmentation behaviour, according to the substitution site, enables us to distinguish by mass spectrometry 4-methyl from 5-methyl-2-pyrimidone and 4,5-dimethyl from 4,6-dimethyl-2-pyrimidone. Finally, the loss of HCN or CH_3CN does not occur from the molecular ion but only from the $M - CO^{\neg+\bullet}$ ion.

Experimental

Syntheses of the following compounds **3** (12*a*), **4** (12*b*), **5** (6), **8** (6), and **9** (12*c*) have already been described. 5-Methyl-2-pyrimidone was obtained by two steps: commercial thymine (Aldrich Europe) by reaction with P_2S_5 yielded 4-thiothymine (13*a*), then 4-thiothymine in the presence of Raney nickel gave 5-methyl-2-pyrimidone (13*b*). The best neutralization of commercial 4-methyl-2-pyrimidone hydrochloride (Aldrich Europe) is described by Franke and Kraft (14). Syntheses of compounds **6** and **7**, deuterated analogues of **5**, are briefly described in ref. 7; full details of deuteration can be found in ref. 15. All compounds, except **7**, were purified before use by sublimation under vacuum. Isotopic purity of compound **6** (97% d_3) and compound **7** (99% d_7) was measured by mass spectrometry (10 eV). It was confirmed for **6** by infrared and ^1H nmr spectrometries. Before introduction of **7**, the inlet mass spectrometer was purged with D_2O.

The mass spectra were measured on a Hitachi–Perkin–Elmer RMU-6E simple focusing mass spectrometer operating at 70 eV with an ion source temperature of 250°C. Samples were introduced through an inlet system heated to the given temperature. Exact mass determinations were made on an AEI MS 50 instrument (Centre de Spectrochimie Organique, Université P. et M. Curie, Paris) using the peak matching technique. The relative intensities (>5%) of the ions are given in Table 2.

1. J. M. RICE, G. O. DUDEK, and M. BARBER. J. Am. Chem. Soc. **87**, 4569 (1965).
2. T. NISHIWAKI. Tetrahedron, **22**, 3117 (1966); **23**, 1153 (1967).
3. E. FALCH. Acta Chem. Scand. **24**, 137 (1970).
4. K. UNDHEIM and G. HVISTENDAHL. Acta Chem. Scand. **25**, 3227 (1971).
5. E. M. KAZDAN, R. T. B. RYE, and O. S. TEE. Can. J. Chem. **60**, 1800 (1982).
6. E. PICQUENARD and P. DIZABO. Can. J. Chem. **59**, 1270 (1981).
7. A. LAUTIÉ, E. PICQUENARD, and N. RATOVELOMANANA. Spectrochim. Acta Part A, **39**, 223 (1983).
8. T. J. BATTERHAM, D. J. BROWN, and M. N. PADDON-ROW. J. Chem. Soc. (B), 171 (1967).
9. X. HASAPIS and A. J. MACLEOD. Tetrahedron, **35**, 2087 (1979).
10. J. RIAND and J. P. BRUN. J. Heterocycl. Chem. **20**, 1187 (1983).
11. L. STREKOWSKI. Polish J. Chem. **52**, 283 (1978).
12. (*a*) S. SUGASAWA, S. YAMADA, and M. NARAHASHI. J. Pharm. Soc. Jpn. **71**, 1345 (1951); Chem. Abstr. **46**, 8034d (1952); (*b*) A. R. KATRITZKY, M. KINGSLAND, and O. S. TEE. J. Chem. Soc. (B), 1484 (1968); (*c*) A. KREUTZBERGER and U. H. TESH. J. Heterocycl. Chim. **14**, 1197 (1977).
13. (*a*) T. UEDA and J. J. FOX. J. Med. Chem. **6**, 697 (1963); (*b*) D. J. BROWN and NAGAMAKU. Aust. J. Chem. **30**, 2515 (1977).
14. W. FRANKE and R. KRAFT. Chem. Ber. **86**, 797 (1953).
15. E. PICQUENARD. Thèse de Doctorat ès Sciences. Université Pierre et Marie Curie, Paris. 1982.

The crystal and molecular structure of *syn*-9-phenyl-2,11-dithia[3,3]metacyclophane

WILLEM ANKER, KATHY A. BEVERIDGE, GORDON W. BUSHNELL, AND REGINALD H. MITCHELL[1]
Chemistry Department, University of Victoria, Victoria, B.C., Canada V8W 2Y2

Received March 9, 1983[2]

WILLEM ANKER, KATHY A. BEVERIDGE, GORDON W. BUSHNELL, and REGINALD H. MITCHELL. Can. J. Chem. **62**, 661 (1984).

The crystal structure of *syn*-9-phenyl-2,11-dithia[3,3]metacyclophane, **6**, has been determined by single crystal X-ray diffraction and refined to an *R* value of 0.0723. The crystal structure is triclinic with a = 9.573(2), b = 12.010(4), c = 8.433(2) Å, α = 108.02(2)°, β = 95.95(2)°, γ = 102.25(3)°, and the space group is $P\bar{1}$ with two molecules per cell, $D_{(meas)}$ = 1.313 g cm^{-3}, $D_{(calc)}$ = 1.306 g cm^{-3}. The bridging S atoms differ in their conformations so that the S . . . S distance is 6.391 Å. The metacyclophane rings have a distance of 3.57 Å between their centres and form a dihedral angle of 20.5°. The phenyl substituent forms an angle of 78.6° with the adjacent ring and has an *ortho* H-atom very close to the internal H-atom of the opposite ring. The phenyl substituted aromatic ring is non-planar and in a shallow boat form, the ring atoms C(11) (internal) and C(14) being 0.038(4) and 0.037(5) Å out-of-plane on the outside, the methylene C substituents are 0.212(5) and 0.199(5) Å out-of-plane on the inside. The first atom of the phenyl group is in the bowsprit position and is 0.274(4) Å above the mean plane on the outer side of the molecule. The opposite metacyclophane ring is less strained but in a similar boat form with the methylene C-atoms 0.092(4) and 0.067(6) Å to the inside. The mean bond angle at S is 103.5(2)°, the angles at C (methylene) range from 113.3(3)° to 118.0(3)°.

The variable temperature ^{1}Hmr spectra results are consistent with the *syn* conformer **6** being dominant in solution and frozen at temperatures <60°C as conformer **A**, with only relatively restricted further twisting of the biphenyl being found at ambient temperature.

WILLEM ANKER, KATHY A. BEVERIDGE, GORDON W. BUSHNELL et REGINALD H. MITCHELL. Can. J. Chem. **62**, 661 (1984).

On a déterminé la structure cristalline du phényl-9 dithia-2,11 [3,3]métacyclophane-*syn*, **6**, par diffraction de rayons-X sur un cristal unique et on l'affinée jusqu'à une valeur de *R* de 0,0723. La structure cristalline est triclinique avec a = 9,573(2), b = 12,010(4), c = 8,433(2) Å, α = 108,02(2)°, β = 95,95(2)° et γ = 102.25(3)°; le groupe d'espace est $P\bar{1}$ avec deux molécules par maille, D(mesuré) = 1,313 g/cc et D(calculé) = 1,306 g/cc. Les atomes de soufre faisant le pont sont différents dans leur conformation; leur distance S . . . S est égale à 6,391 Å. La distance entre les centres des cycles métacyclophanes est de 3,57 Å et ils forment un angle dièdre de 20,5°. Le substituant phényle forme un angle de 78,6° avec le cycle adjacent et un de ses H-*ortho* est très près d'un H interne du cycle opposé. Le cycle aromatique substitué par un phényle n'est pas plan et il existe sous une forme bateau aplatie; les atomes du cycle C(11) (interne) et C(14) sont respectivement 0,038(4) et 0,037(5) Å hors du plan vers l'extérieur alors que les C des substituants méthylènes sont respectivement 0,212(5) et 0,199(5) Å hors du plan vers l'intérieur. Le premier atome du groupement phényle est en position "beaupré"; il est à 0,274(4) Å au-dessus du plan moyen sur la face extérieure de la molécule. Le cycle métacyclophane opposé est moins tendu, mais il est aussi dans une forme bateau avec les atomes de C des méthylènes à 0,092(4) et 0,067(6) Å vers l'intérieur. L'angle moyen de liaison au niveau du S est 103,5(2)° alors que les angles au niveau du C (méthylène) varient de 113,3(3)° à 118,0(3)°.

Les spectres de rmn du proton à température variable sont en accord avec l'hypothèse que la conformation *syn* (**6**) est prépondérante en solution et qu'à des températures <60°C, le produit est figé sous la conformation **A** alors que l'on ne peut observer que des variations relativement faibles du biphényle à la température ambiante.

[Traduit par le journal]

Introduction

Higher metacyclophanes[3] do not always adopt the *anti*-stepped conformation preferred by [2,2]-metacyclophane (1). For example, we have recently shown that the dithia[3,3]-metacyclophane, **1**, exists in the crystal state as the *syn* conformer (2) while the tetrathia [4,4] metacyclophane, **2**, prefers an *anticlinal* conformation which is neither true *syn* nor *anti* from a ^{1}Hmr viewpoint (3). Indeed, ^{1}Hmr can sometimes be somewhat misleading in determining conformations, although generally reliable in extreme cases, such as **3** and **4**, where both conformers are known. However, in the case of

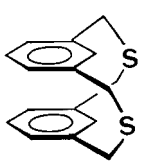

1

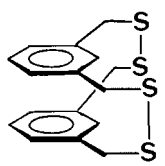

2

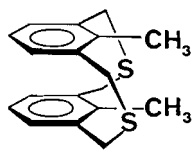

3

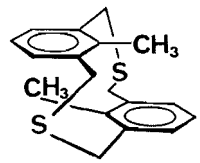

4

9-phenyl-2,11-dithia[3,3]metacyclophane, **5**, a clear distinction between the *syn* conformer **6**, in which the internal hydrogen H-18[4] would probably be shielded by the 9-phenyl substituent (depending on the angle of twist between the diphenyl unit), and the *anti* conformer **7**, in which H-18 would certainly be shielded by the opposite aryl ring, is difficult. Indeed Vogtle et al. (4) who first prepared **5** were not able to assign its stereochemistry, though they suggested that by com-

[1]Author to whom requests for reprints should be addressed.
[2]Revision received November 7, 1983.
[3]For the phane nomenclature see ref. 16.

[4]In this paper X-ray atom numbers are shown as C(21), H(31), etc.; phane atom numbering is shown as H-18, H-2, etc.

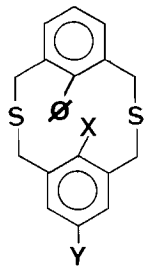

	X	Y
5	H	H
8	H	NO_2
9	H	NH_2
10	CH_3	H

parison of the chemical shift of H-18 for **5**, (δ 5.44) with that of **8** (X = H, Y = NO_2, δ 6.50, presumed *syn*) and **9** (X = H, Y = NH_2, δ 4.70, presumed *anti*), **5** is probably the *syn* con-

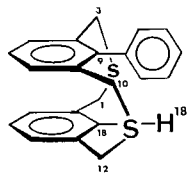

6

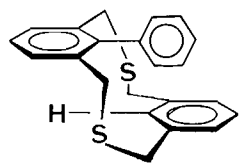

7

former **6**. Since we have studied the variable temperature ^{1}Hmr spectra of the internally methyl substituted compounds **10**, for which both *syn* and *anti* conformers exist (5), we also were interested in establishing the conformational preference of **5**, Thus in this paper we report the results of its X-ray determined crystal structure and variable temperature ^{1}Hmr results.

X-ray structure results

Experimental

Weissenberg and precession photography using CuK_α radiation gave a triclinic unit cell and approximate cell dimensions. The crystal was then transferred to a Picker 4-circle diffractometer (automated with a PDP-11/10 eomputer) on which all subsequent measurements were made. The crystal data are:

$C_{22}H_{20}S_2$ fw = 348.52

Triclinie, space group $P\bar{1}$, unit cell a = 9.573(2), b = 12.010(4), c = 8.433(2) Å, α = 108.02(2)°, β = 95.95(2)°, γ = 102.25(3)°, eell volume = 886.0(4) Å^3, $D_{(meas)}$ = 1.313 g cm^{-3} (flotation in CCl_4/*m*-xylene), $D_{(calc)}$ = 1.306 g cm^{-3}, Z = 2, absorption coeffi-cient (MoK_α) = 2.95 cm^{-1}. The colourless crystal was mounted approximately along the *b*-axis, and had dimensions 0.67 × 0.66 × 0.51 mm.

The unit cell was refined by least squares using 20 pairs of ±2θ measurements obtained by an automatic centering routine. The centering results were also used in a least-squares refinement of the diffractometer matrix. A scan of 200 steps of 0.01° in 2θ, counting for 0.25 s at each step, and two background counts of 25.0 s at each end of the scan were used for intensity measurement. A reciprocal space hemisphere ($h \geq 0$) was measured out to 2θ = 45° (2552 reflections), using Zr-filtered MoK_α radiation (λ = 0.71069 Å). Three standards (400, 060, 005) were measured after every batch of 50 reflections. The very weak reflections, for which $I < \sigma(I)$, were rejected. The Lorentz and polarization corrections were applied. There were 2117 reflections in the final dataset.

Structure determination

The SHELX-76 program (6) was used to solve and refine the crystal structure. The initial phasing was done by the centrosymmetric direct methods routine. The atomic scattering factors were for uncharged atoms (7). The development of the structure was by standard Fourier methods, using difference maps. Refinement was by least squares, minimizing $\Sigma w\Delta^2 = \Sigma w\ (||F_o| - |F_c||)^2$ where $w = 1/(\sigma^2(F) + 0.001\ F^2)$. Anisotropic temperature parameters were used for the S and C atoms. The hydrogen atoms were located by the use of a difference map and their positional and isotropic temperature parameters were refined by least squares. The scale factor and atomic parameters gave a total of 297 variables.The refinement proceeded normally and converged to R = 0.0723 and $R_w = \Sigma\Delta\sqrt{w}/\Sigma F_o\sqrt{w}$ = 0.0836, with the maximum shifts/esd being 0.100. The final difference map gave no evidence of misplaced atoms (max. 0.33 e Å^{-3}, min. −0.50 e Å^{-3}). Supplementary tables, containing the structure factors, temperature parameters, and some hydrogen atom coordinates, have been placed in the Depository for Unpublished Data.[5]

Discussion

The atomic parameters of the crystal structure are given in Table 1. The bond lengths in Table 2 are in agreement with those found previously in similar compounds (2, 3, 8). The molecular structure, shown in Fig. 1, is clearly that of the *syn* conformer, and establishes without doubt that *syn* is the preferred conformation. The reason why is less obvious, particularly since for other examples of [3,3]metacyclophanes substituted at the internal position(s), the *anti* conformer is normally thermodynamically preferred (4). In the case of the dimethyl substituted compound, for the less stable *syn* conformer **3**, the interactions between the two methyl groups must be more severe than between the methyl and opposite ring of the *anti* conformers **4**. The reverse appears to be true for the much smaller internal H substituents of **1**. Normally with the substituents (other than H), including probably even F (9), the *anti* conformer appears to be preferred (for a review, see ref. 10).

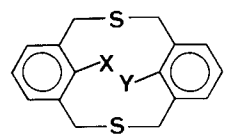

	X	Y
11	H	CH_3
12	Ø	Ø
13	Ø	CH_3

For a single substituent, the preference is not as strong; for example, **11** is reported (on ^{1}Hmr basis) to be *anti* (11). *A priori* it would be more reasonable to assume that a *syn* conformer would be more stable for **11**, since interaction between a methyl and a hydrogen substituent would not be expected to be as large as between a methyl and a ring. In fact, the $-CH_3$ signal of **11** is found at δ 2.18, which is only marginally different from those of *syn*-**3** (δ 2.54) and substantially less shielded than those of *anti*-**4** (δ 1.30) (12). The internal hydrogen atoms are shielded to δ 5.50 in contrast to those of **1** at δ 6.6 (2); however, in the *syn* conformer of **6** the signal due to H-18 appears from δ 5.5 to δ 4.6, varying with temperature (see below). Thus a definite X-ray structural assignment of **11** would be most helpful in interpreting **5**. A further complication for phenyl substituents is the interaction of the *ortho*-ring hydrogens of the 9-phenyl substituent with the methylene bridges (see ref. 5, and below). This interaction may differ in magnitude for the *syn* and *anti* conformers. For two phenyl substituents, **12**, or for one phenyl and one methyl substituent **13**, the *anti* conformers are preferred (5).

Table 3 gives selected bond angles which are of interest in showing molecular strain. The benzenoid ring angles lie in the range 120 ± 2°, and have been deposited. The angles at the

[5]Copies of these tables may be obtained, at a nominal charge, from the Depository of Unpublished Data, CISTI, National Research Council of Canada, Ottawa, Ont., Canada K1A 0S2.

TABLE 1. Atomic parameters*

Atom	x/a	y/b	z/c
S(1)	3486(1)	1054(1)	3787(1)
S(2)	−551(1)	3214(1)	−343(1)
C(1)	4515(5)	2610(4)	4197(6)
C(2)	1410(5)	3770(4)	61(6)
C(3)	−840(5)	1718(3)	−131(5)
C(4)	2011(5)	1237(5)	4931(6)
C(11)	3160(4)	3365(3)	2159(5)
C(12)	3608(4)	3399(3)	3830(5)
C(13)	3083(5)	4123(4)	5137(5)
C(14)	2146(5)	4771(4)	4832(6)
C(15)	1620(5)	4668(3)	3207(6)
C(16)	2112(4)	3953(3)	1852(5)
C(21)	3896(4)	2777(3)	749(4)
C(22)	4974(4)	3527(4)	280(5)
C(23)	5676(5)	3061(4)	−1022(5)
C(24)	5368(5)	1841(4)	−1837(5)
C(25)	4317(5)	1083(4)	−1401(6)
C(26)	3593(5)	1540(4)	−112(6)
C(31)	455(4)	1415(3)	2394(5)
C(32)	690(4)	1501(3)	4083(5)
C(33)	−335(5)	1854(4)	5023(6)
C(34)	−1537(6)	2126(4)	4321(6)
C(35)	−1704(5)	2079(4)	2660(6)
C(36)	−704(4)	1728(3)	1674(5)
H(1)	502(6)	301(4)	525(7)
H(10)	530(7)	256(5)	355(7)
H(2)	180(4)	321(4)	−81(5)
H(20)	160(6)	453(5)	−16(6)
H(3)	−20(5)	128(4)	−78(5)
H(30)	−187(6)	138(5)	−74(6)
H(4)	179(6)	50(5)	496(6)
H(40)	243(6)	192(5)	610(7)
H(13)	332(7)	412(6)	630(8)
H(14)	168(6)	526(5)	576(6)
H(15)	88(6)	498(5)	296(6)
H(22)	521(5)	438(4)	89(5)
H(23)	647(6)	368(4)	−126(6)
H(24)	581(6)	157(5)	−270(7)
H(25)	428(6)	29(6)	−178(7)
H(26)	305(10)	105(8)	46(10)
H(31)	110(5)	122(3)	181(5)
H(33)	−20(5)	199(4)	605(6)
H(34)	−232(6)	236(4)	484(6)
H(35)	−254(6)	227(4)	209(5)

*Fractional atomic coordinates × 10^3 for hydrogen atoms and × 10^4 for C and S atoms. Estimated standard deviations are given in parentheses.

TABLE 2. Bond lengths

Atoms	Length (Å)	Atoms	Length (Å)
S(1)—C(1)	1.825(5)	S(2)—C(2)	1.811(4)
S(1)—C(4)	1.804(5)	S(2)—C(3)	1.826(4)
C(1)—C(12)	1.490(6)	C(2)—C(16)	1.517(6)
C(4)—C(32)	1.528(6)	C(3)—C(36)	1.510(6)
C(11)—C(12)	1.415(5)	C(11)—C(16)	1.390(5)
C(12)—C(13)	1.389(6)	C(16)—C(15)	1.393(6)
C(13)—C(14)	1.359(7)	C(15)—C(14)	1.369(7)
C(21)—C(22)	1.395(6)	C(21)—C(26)	1.387(6)
C(22)—C(23)	1.379(6)	C(26)—C(25)	1.383(6)
C(23)—C(24)	1.362(6)	C(25)—C(24)	1.368(7)
C(31)—C(32)	1.387(6)	C(31)—C(36)	1.385(6)
C(32)—C(33)	1.379(6)	C(36)—C(35)	1.380(6)
C(33)—C(34)	1.385(7)	C(35)—C(34)	1.375(7)
C(11)—C(21)	1.509(5)		

sulphur atoms are similar to the values 104.5(3)° and 103.3(2)° found in *syn*-2,11-dithia[3,3]metacyclophanes **1** (2). The angles at the methylene C atoms are considerably larger than the ideal tetrahedral value and agree with previously determined values in similar compounds (2, 8, 13). The external angles at C(21) differ by 7.2°, showing that phenyl ring 2 is pushed outwards from the centre of molecule presumably by repulsion between H(26) and H(31). The adjacent atoms C(32) and C(4) have angles which are strained to an unusual extent.

The conformation of the C—S—S bridges differs from that found in the crystal structure of **1** (2) which has both S atoms turned outwards and back toward C(14) and C(34) giving a larger S . . . S distance of 6.974 Å. In the title compound, one of the C—S—C groups is placed in the alternative position and the S . . . S distance is thus reduced to 6.391 Å. In this process S(1) comes closer to ring 2, but the methylene H atoms on C(1) and C(4) are turned away from ring 2, and this is probably the dominant effect in determining the conformation.

The mean plane results are given in Table 4. Ring 1 is clearly nonplanar and in a shallow boat form with C(11) and C(14) at the prows and displaced to the outside of the molecule. Intramolecular close contacts involving H(26) probably promote the boat form of ring 1, and C(11) and C(14) are well to the outside of mean plane 1. The methylene C atoms C(1) and C(2) are out of mean plane 1 on the inside, to a much greater extent than C(3) and C(4) with respect to ring 3. Ring 2 is essentially planar. Ring 3 is in a very shallow boat form similar to that of ring 1, but the displacements of the six ring atoms are only marginally significant; however, the existence of a similar, but much smaller, effect on this side of the molecule seems likely.

The dihedral angle between the mean planes of rings 1 and 3 is 20.5°, and the distance between the centres of these rings is 3.57 Å, surprisingly similar to the values 20.6° and 3.50 Å found in **1** (2), considering the replacement of a small H substituent by a large phenyl. It is also remarkable that the phenyl substituent, ring 2, forms dihedral angles of 78.6° with ring 1, and 85.1° with ring 3 because this brings H(26) close to H(31). Assuming a C—H bond length of 1.07 Å and extrapolating the line from the ring centres to the C atoms we find 2.00 Å between the calculated H atom positions; alternatively the distance is 2.30 Å between observed H atom positions. The accuracy with which these H atom locations are known is low, but both figures are less than twice the van der Waals radius of 1.2 Å for hydrogen (14). However, the calculated distances between S(1) and H(26) of 2.96 Å and S(1) and H(31) of 2.71 Å are also below the sum of the van der Waals radii (3.05 Å (14)), and thus the molecule is clearly compressed in several directions.

Nuclear magnetic resonance results

Although the ^{1}Hmr spectrum of **1** has been reported (4), distinction of the *ortho*-protons H-2′,6′ of the 9-phenyl substituent could not be made because of the low (60 MHz) field used. Use of 90 and 250 MHz spectrometers and low temperature spectra enables H-2′ (and at some temperatures H-6′) to be seen clearly, as shown in Fig. 2.

At ca. 20°C, H-2′ can be observed at δ 6.67 with H-6′ at ca. δ 6.92 and with H-18 at δ 5.47. As the temperature is lowered (Fig. 2) H-2′ and H-18 both steadily move upfield, and reach δ 5.82 and δ 4.60 respectively at −100°C. The shift difference between H-2′ and H-18 stays constant (ca. 1.2 ppm) over the whole temperature range. H-6′ progressively moves into the aromatic multiplet and below −55°C cannot be clearly distin-

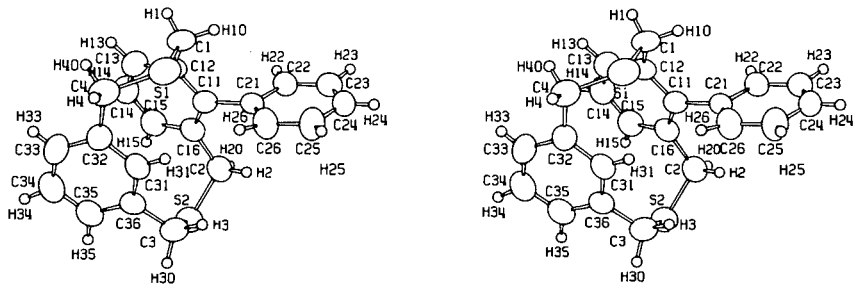

FIG. 1. A stereoscopic drawing of the molecular structure of **6** (the hydrogen atoms are shown as small spheres for clarity) the other atoms are given as thermal ellipsoids (50% probability).

TABLE 3. Selected bond angles

Atoms	Angle (deg)	Atoms	Angle (deg)
C(1)—S(1)—C(4)	103.4(2)	C(2)—S(2)—C(3)	103.6(2)
S(1)—C(1)—C(12)	113.7(3)	S(2)—C(2)—C(16)	113.3(3)
S(1)—C(4)—C(32)	118.0(3)	S(2)—C(3)—C(36)	114.7(3)
C(11)—C(21)—C(22)	117.8(3)	C(11)—C(21)—C(26)	125.0(3)
C(31)—C(32)—C(33)	117.0(4)	C(22)—C(21)—C(26)	117.2(3)
C(31)—C(32)—C(4)	123.6(4)	C(32)—C(31)—C(36)	122.7(4)

TABLE 4. Mean planes of the benzenoid rings*

(a) Coefficients of $Ax + By + Cz = D$ (Å)

Ring	A	B	C	D	χ^2
1	−0.5882	−0.8027	−0.0981	−3.9674	237.0
2	−0.6700	0.3254	−0.6673	−1.3882	18.1
3	−0.2988	−0.9141	−0.2741	−1.3896	62.8

(b) Perpendicular distances to the mean planes

Ring	Distance (Å)					
1	C(11) −0.038(4)	C(12) 0.023(4)	C(13) 0.011(5)	C(14) −0.037(5)	C(15) 0.010(4)	C(16) 0.024(4)
	S(1) 1.940(1)	S(2) 1.662(1)	C(1) 0.212(5)	C(2) 0.199(5)	C(21) −0.274(4)	C(24) −0.888(5)
2	C(11) 0.011(4)					
3	C(31) 0.020(4)	C(32) −0.013(4)	C(33) −0.004(5)	C(34) 0.019	C(35) −0.005(5)	C(36) −0.012(4)
	S(1) −0.388(1)	S(2) −1.681(1)	C(3) −0.092(4)	C(4) −0.067(6)		

(c) Angles between mean planes

1,2 = 78.6°; 2,3 = 85.1°; 1,3 = 20.5°

*Ring 1 is C(11−16), ring 2 is C(21−26), ring 3 is C(31−36).

guished even at the higher field strength. After 40°C both H-2′ and H-6′ are in the aromatic multiplet, hence the exact point at which they coalesce could not be determined accurately, although it could be estimated at ca. 60°C. We thus interpret the dynamic behavior of **6** to be analogous to *syn*-**10** (5) except that

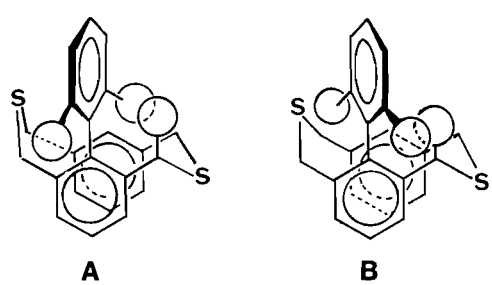

A B

for **6** T_c is ca. 60°C whereas for *syn*-**10** it is −8°C. Thus **6** exists in a relatively frozen conformation below 60°C, e.g., (**A**) rather than (**B**), although some rotation of the phenyl substituent can occur. We believe that as the temperature is lowered, the phenyl substituent rotates slightly, thereby increasing the angle between the biphenyl rings (which reaches 78.5° in the crystal). This has the effect of moving H-2′ into the shielding region between the two phane rings (15). It also probably allows the dihedral angle between the two phane rings (20° in the crystal) to increase such that H-18 likewise gets progressively more shielded. Tables S3−S6[5] give the calculated positions of the various H atoms of **6** relative to the centres of the three aromatic rings. Applying Johnson−Bovey type calculations of ring current shielding (15) to the values for H(31)[H-18], H(26)[H-2′], and H(22)[H-6′] gives the calculated ring current shielding

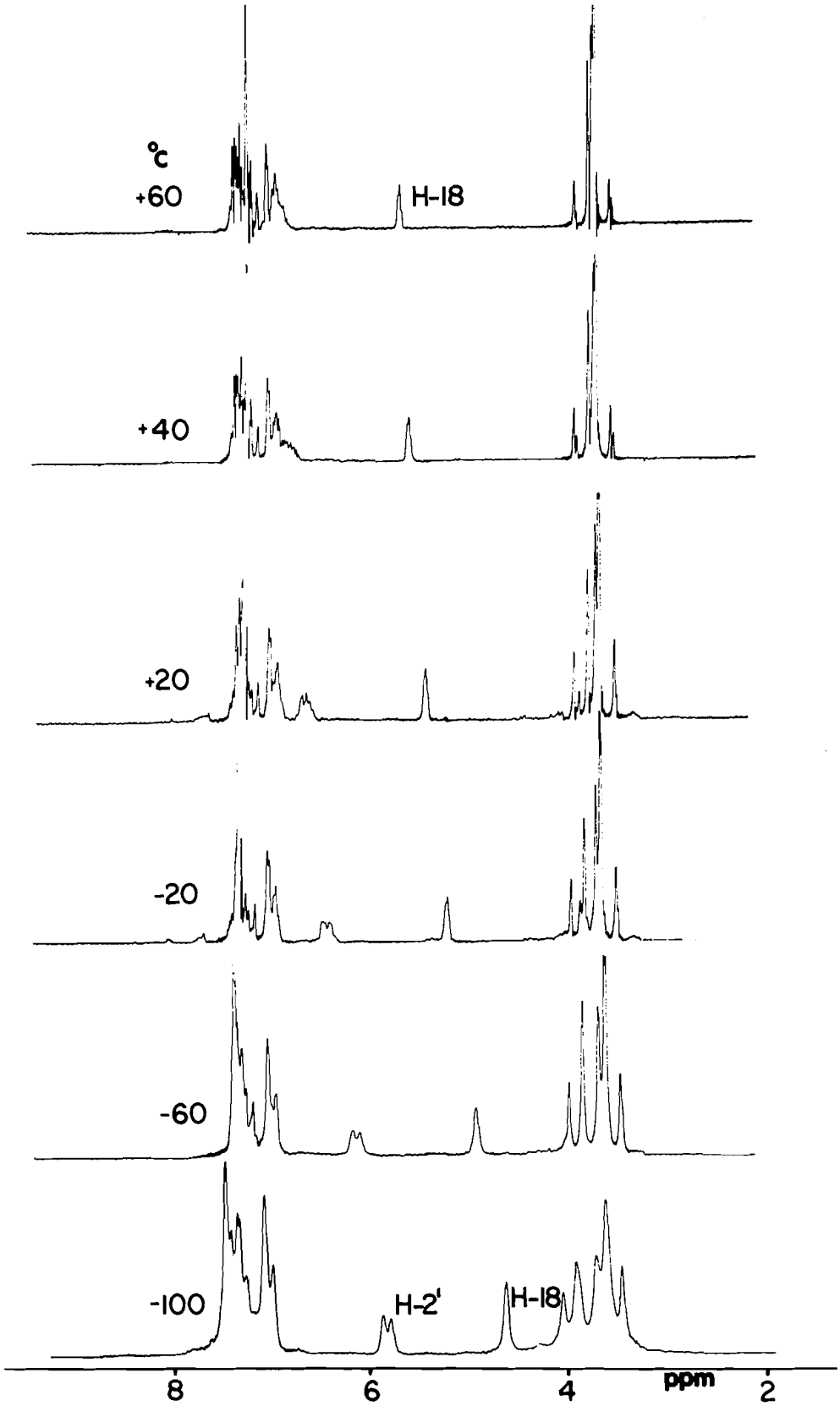

FIG. 2. Variable temperature ^{1}Hmr (90 MHz) spectrum of **6**.

(negative) or deshielding (positive) increments caused by the adjacent/opposite benzene rings (Table 5). Surprisingly good agreement between theory and experiment is obtained: H-18 is predicted to be shielded relative to H-2′ by about 1 ppm, which was found to be the case, and H-2′ is predicted to be shielded relative to H-6′, which it is, though the quantitative agreement

TABLE 5. Calculated ring current shielding (−ve) or deshielding (+ve) contributions (Δδ) (ppm) for selected H atoms of **6**

Calculated distances of H atoms from centre of rings (ring radii units) from:		H-atom 31 (X-ray) 18 (nmr)	26 (X-ray) 2′ (nmr)	22 (X-ray) 6′ (nmr)
Ring 1	$\perp r$	1.95	0.22	0.03
	$//l$	1.32	2.96	1.75
	Δδ	−0.87	+0.39	n/a
Ring 2	$\perp r$	1.22	0.00	0.23
	$//l$	2.55	1.76	3.16
	Δδ	+0.20	n/a	+0.31
Ring 3	$\perp r$	1.69	0.01	3.24
	$//l$	1.90	1.75	3.50
	Δδ	+0.23	n/a	−0.04
	ΣΔδ	−0.48	+0.51	+0.23

is not as close. This gives us considerable confidence in the assignment of stereochemistry of **5** to be *syn* in solution as well as in the crystalline state.

The disulphone of **5** has also been reported by Vogtle *et al.* (4); in that work H-18 appeared at δ 5.49, so it was assigned the *anti* conformation. However, since both H-2′ (δ 6.10) and H-6′ (δ 6.70) as well as H-18 appear at analogous positions to the signals of **6** (*syn*-**5**), it seems likely that the disulphone is also *syn*.

Sample preparation

The cyclophane **6** was prepared in a manner analogous to that of Vogtle *et al.* (4) by high dilution coupling of 2,6-bis-(mercaptomethyl)biphenyl (4,5) and α,α′-dibromo-*m*-xylene. We found that by increasing the reaction temperature to 60°C, the yield of product could be improved substantially to 40%, with mp 144°C (lit. (4) mp 134°C).

Experimental

The melting point was determined on a Kofler hot stage and is uncorrected. The ^{1}Hmr spectra were determined on a Perkin−Elmer R32 (90 MHz) or Bruker-WM250 (250 MHz) spectrometer. The ^{13}Cmr spectra were determined on the Bruker-WM250 operating at 62.9 MHz. Mass spectra were determined on a Finnigan 3300 mass spectrometer at 70 eV.

9-Phenyl-2,11-dithia[3,3]metacyclophane, syn-*5(6)*

A solution of 2,6-bis(mercaptomethyl)biphenyl (4, 5) (429 mg, 2 mmol) and α-α′-dibromo-*m*-xylene (538 mg, 2 mmol) in N_2-purged benzene (400 mL) was added dropwise over 30 h to a well-stirred solution of KOH (320 mg, 6 mmol) in N_2-purged 95% aqueous ethanol (500 mL) held at 60°C under N_2. After stirring for a further hour, the solvent was removed and the residue acidified (dilute aqueous HCl) and extracted with dichloromethane. The organic extract was washed, dried, and evaporated, and the resultant residue was pre-adsorbed on Celite and chromatographed over silica gel using pentane (500 mL) and then dichloromethane−pentane (1:9) as eluants.

Recrystallization of **6** from cyclohexane gave colourless crystals, 276 mg (40%), mp 144°C (lit. (4) mp 134°C); ^{1}Hmr (250 MHz) δ: 7.34−7.16 (m, 7H, ArH) 6.99−6.90 (m, 3H, ArH), 6.67 (dd, $J \sim 5.7$ Hz, 2.0 Hz, 1H, H-2′), 5.47 (s, 1H, H-18), 3.81 and 3.62 (AB q, $J = 12.5$ Hz, 4H, —CH_2S-), 3.74 and 3.62* (ABq, $J = 15.1$ Hz, 4H, —CH_2S—) (*at −55°C this peak moves upfield relative to the other 3.62 resonance); ^{13}Cmr δ: 143.4 (C-9), 137.7 (C-1′), 139.6, 135.0 (C-4, C-13), 130.4, 126.5 (C-5, C-14), 130.1 (C-2′), 129.5 (C-6′), 128.6 (C-18), 128.3, 127.7, 127.4 (C-6, C-15, C-4′), 127.3 (C-3′, 5′), and 35.3, 34.2 (C-1, C-3); $M^{+\cdot}$ *m/e* (relative intensity): 348 (50), 211 (19), 180 (24), and 179 (100). *Anal.* calcd. for $C_{22}H_{20}S_2$: C 75.82, H 5.78; found: C 75.70, H 5.92.

Conclusions

The stereochemistry of **5** has been found to be *syn* (i.e., **6**) both in the crystal state and in solution by X-ray and ^{1}Hmr studies respectively. This is the first reported example of an unambiguously *syn*-dithiametacyclophane with an internal substituent other than hydrogen. At temperatures below 60°C, **6** exists in a relatively frozen conformation, e.g. (**A**), where restricted rotation of the phenyl substituent occurs.

Acknowledgements

We thank the Faculty Research Committee of the University of Victoria and the Natural Sciences and Engineering Research Council of Canada for operating grants.

1. F. VOGTLE and P. NEUMANN. Angew. Chem. Int. Ed. Engl. **11**, 73 (1972).
2. W. ANKER, G. W. BUSHNELL, and R. H. MITCHELL. Can. J. Chem. **57**, 3080 (1979).
3. K. BEVERIDGE, G. W. BUSHNELL, and R. H. MITCHELL. Can. J. Chem. **61**, 1603 (1983).
4. F. VOGTLE, J. GRUTZE, R. NATSCHER, W. WIEDER, E. WEBER, and G. GRUN. Chem. Ber. **108**, 1694 (1975); K. BOCKMAN and F. VOGTLE. Chem. Ber. **114**, 1065 (1981).
5. R. H. MITCHELL and W. ANKER. Tetrahedron Lett. **22**, 5135 (1981).
6. G. M. SHELDRICK. SHELX-76 program for crystal structure determination. University of Cambridge, England. 1976 Present address: Anorganisch-Chemisches Institut der Universität Göttingen.
7. D. T. CROMER and J. T. WABER. International tables for X-ray crystallography. Vol. 4. Published for the I. U. Cr. by the Kynock Press, Birmingham, England. 1974. pp. 99, 149.
8. B. R. DAVIS and I. BERNAL. J. Chem. Soc. (B), 2307 (1971).
9. V. BOEKELHEIDE and P. H. ANDERSON. J. Org. Chem. **38**, 3928 (73); A. W. HANSON. Acta Crystallogr. Sect B, **31**, 2352 (1975).
10. R. H. MITCHELL. *In* Cyclophanes. *Edited by* P. Keehn and S. Rosenfeld. Academic Press, New York. 1983. Chapt. 4.
11. V. BOEKELHEIDE and C. H. TSAI. J. Org. Chem. **38**, 3931 (1973).
12. R. H. MITCHELL and V. BOEKELHEIDE. J. Am. Chem. Soc. **96**, 1547 (1974).
13. G. W. BUSHNELL and R. H. MITCHELL. Can. J. Chem. **60**, 362 (1982).
14. A. J. GORDON and R. A. FORD. (*Editors*). The chemist's companion. John Wiley and Sons, New York. 1972 p. 109.
15. C. E. JOHNSON and F. A. BOVEY. J. Chem. Phys. **29**, 1012 (1958); J. W. EMSLEY, F. FEENEY, and L. H. SUTCLIFFE. *In* High resolution nuclear magnetic resonance spectroscopy. Pergamon Press, Oxford. 1965 p. 595.
16. F. VOGTLE and P. NEUMANN. Tetrahedron, **26**, 5847 (1970).

Destruction des oxydes d'azote à pression atmosphérique

ODILE DESSAUX, PIERRE GOUDMAND, GÉRARD MOREAU ET BRIGITTE MUTEL

Laboratoire de Spectroscopie de la réactivité chimique. Université des Sciences et Techniques de Lille, 59655 Villeneuve d'Ascq Cedex, France

Reçu le 27 juillet 1983

ODILE DESSAUX, PIERRE GOUDMAND, GÉRARD MOREAU et BRIGITTE MUTEL. Can. J. Chem. **62**, 667 (1984).

Ce travail illustre l'intérêt de l'utilisation d'une décharge microonde pour l'amélioration du coût énergétique de destruction des oxydes d'azote par l'azote activé à pression atmosphérique. Les facteurs déterminants dans l'optimisation de ce coût sont précisés: il importe d'effectuer l'introduction de NO_x dans une zone visuellement bien limitée où la concentration en atomes d'azote est optimale, le coût énergétique de destruction de NO_x est alors très proche du coût théorique.

ODILE DESSAUX, PIERRE GOUDMAND, GÉRARD MOREAU, and BRIGITTE MUTEL. Can. J. Chem. **62**, 667 (1984).

Active nitrogen produced at atmospheric pressure by a microwave discharge is found to require less energy consumption for the decomposition of nitrogen oxides. Important parameters improving the energy cost are described: NO_x must be introduced in a visually well-limited zone where the nitrogen atom concentration is maximum, the energy cost is then nearly equal to the theoretical cost.

Can. J. Chem. Downloaded from www.nrcresearchpress.com by 210.87.254.42 on 09/06/12
For personal use only.

Introduction

Les industries de l'acide nitrique rejettent dans l'atmosphère de grandes quantités d'oxydes d'azote (NO_2, NO, N_2O). Ces rejets, souvent très localisés, ont des teneurs comprises entre 500 et 2000 ppm. Etant donnée la très grande toxicité de NO_2 et NO, le risque de pollution est très élevé à proximité de ces usines. Plusieurs méthodes sont utilisées permettant de réduire les teneurs en oxydes d'azote contenus dans les effluents gazeux avant leur rejet dans l'atmosphère (1–3).

Un procédé de destruction des oxydes d'azote basé sur la génération d'azote activé à pression atmosphérique a été mis au point au laboratoire (4). Il existe essentiellement deux agents réactifs dans l'azote activé: les atomes d'azote $N(^4S)$ et les molécules d'azote à l'état électronique fondamental vibrationnellement excité. Cette dernière espèce est impliquée dans la synthèse des oxydes d'azote selon une réaction de nature essentiellement hétérogène (5). Sa concentration décroit rapidement lorsque la pression augmente. Les atomes d'azote constituent par contre un agent destructif efficace de NO_x suivant la réaction:

$$[1] \quad N + NO_x \rightarrow N_2 + \frac{x}{2} O_2 \text{ avec } x = 1 \text{ ou } 2$$

Cette réaction est très rapide, la réaction inverse étant environ 10^{20} fois plus lente. Une décharge haute tension à pression atmosphérique (6) permet de détruire complètement les oxydes d'azote contenus dans les mélanges (N_2 + NO_x) tels que $[NO_x]/[N_2] < 1000$ ppm. Pour des teneurs supérieures, la destruction n'est que partielle (83% à 1600 ppm). D'autre part, l'énergie électrique dépensée pour la destruction d'une mole de NO est évaluée à 1,5 kW-h. Ce rendement est peu satisfaisant, l'énergie théorique nécessaire étant de 0,13 kW-h.

L'objet de ce travail est d'étudier l'incidence de l'utilisation d'un générateur de microondes sur le coût énergétique de destruction des oxydes d'azote à pression atmosphérique et de préciser les facteurs déterminants permettant d'optimiser ce coût. Les oxydes d'azote purs sont introduits dans le flux d'azote activé. La mesure des quantités de NO non détruites après leur réaction avec les atomes d'azote est effectuée pour les deux oxydes NO et NO_2 suivant des procédures expérimentales appropriées.

Procédure expérimentale

Production des atomes d'azote

Le flux d'azote circulant dans un tube de quartz de 15 mm de diamètre intérieur, est excité par une cavité résonnante conçue et réalisée au laboratoire (7) reliée à un générateur d'ondes centimétriques Thomson CSF 1211C pouvant délivrer une puissance de 1500 watts à la fréquence ν = 2450 MHz ± 25 MHz. Un wattmètre permet de contrôler les puissances incidente (P_i) et réfléchie (P_r). On désigne par $P_t = P_i - P_r$ la puissance transmise à la cavité. La connaissance de P_r est très importante car elle renseigne sur l'état de couplage de la cavité: l'adaptation est optimale lorsque P_r est minimale. L'obtention d'un plasma à pression atmosphérique nécessite $P_i \geq 300$ watts. P_r reste faible (< 40 watts) tant que P_i est ≤ 500 watts puis augmente en fonction de P_i pour $P_i > 500$ watts. La valeur P_i = 500 watts correspond donc à la valeur minimale de P_r et maximale de P_t. Le tube à décharge est refroidi à l'air comprimé. Les gaz sont directement évacués dans l'atmosphère.

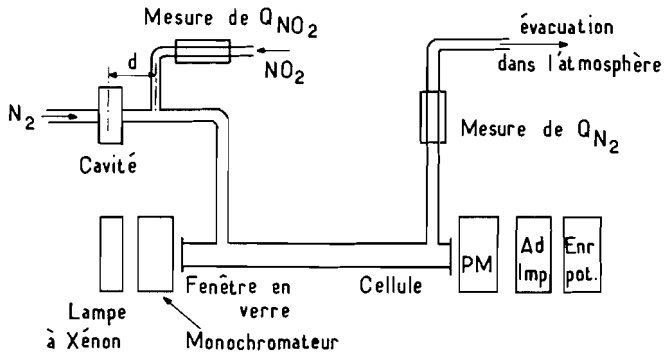

FIG. 1. Dispositif expérimental d'étude de la destruction de NO_2; d: distance entre la décharge et le conduit d'admission de NO_2; PM: photomultiplicateur; Ad Imp: adaptateur d'impédance; Enr pot: enregistreur potentiométrique.

Dosage du NO_2 détruit

Après la réaction de NO_2 avec l'azote activé, l'étude du spectre d'absorption de NO_2 permet la détection des quantités de NO_2 non détruites. Le dispositif de mesure spectroscopique utilisé est décrit dans la Fig. 1. Une lampe à Xe alimentée sous 15 volts par un générateur de courant continu éclaire la fente d'un monochromateur à réseau couvrant la gamme proche uv–visible–ir. La cellule de mesure, longue de 80 cm a un diamètre interne de 40 mm. Elle est peinte en noir afin d'éviter les lumières parasites et est munie de fenêtres en verre. Le photomultiplicateur de type RCA 1P21, dont la réponse spectrale est maximale dans la gamme 400–500 nm, est relié à un enregistreur potentiométrique.

Le spectre d'absorption de NO_2 ayant été préalablement enregistré, le monochromateur est réglé sur la bande d'absorption la plus intense située à 448 nm et la variation d'intensité de cette bande est enregistrée

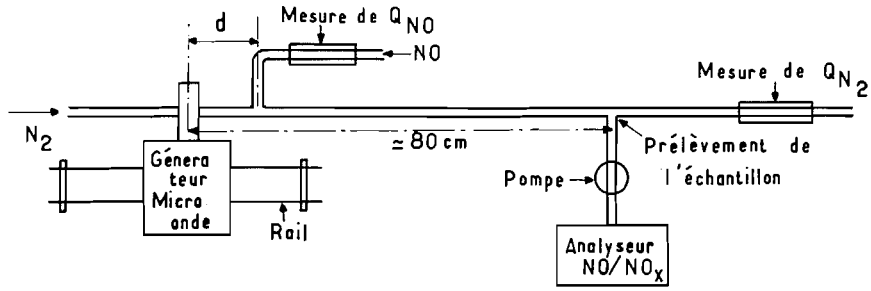

FIG. 2. Dispositif expérimental d'étude de la destruction de NO; d: distance entre la décharge et le conduit d'admission de NO.

en fonction du débit de NO_2 (Q_{NO_2}) ajouté à l'azote activé. Le débit maximal de NO_2 pouvant être décomposé par réaction avec $N(^4S)$ est noté $Q^0_{NO_2}$.

Dosage de NO détruit

La méthode utilisée consiste en un dosage "en retour" de la concentration du NO ([NO]) restant après sa réaction avec l'azote activé. Le dispositif expérimental est décrit dans la Fig. 2. [NO] est directement mesurée par un analyseur NO/NO_x Beckman modèle 951 A, basé sur le principe de la chimiluminescence de l'ozone, et dont la gamme de réponse est 0–10 000 ppm. L'échantillon est prélevé à une distance d'environ 80 cm de la décharge et est envoyé dans l'analyseur avec un débit de l'ordre de 2 L/min assuré par une pompe. Le taux de destruction τ, exprimé en %, est défini par $\tau = (ppm_i - ppm_r)/ppm_i$ où ppm_i et ppm_r désignent respectivement les teneurs du mélange en NO, exprimées en particules par million, avant et après réactions avec l'azote activé; $ppm_i = (Q_{NO} \times 10^6)/(Q_{N_2} + Q_{NO})$; Q_{NO} et Q_{N_2} désignent respectivement les débits de NO et de N_2, mesurés avec des débitmètres respectivement Rota et Brooks; ppm_r est déterminé à l'aide de l'analyseur Beckman. Les erreurs relatives $\Delta Q_{NO}/Q_{NO}$ et $\Delta ppm_r/ppm_r$ sont faibles (~1%). La mesure de Q_{N_2} effectuée à l'aide d'un débitmètre à flotteur est moins précise: $\Delta Q_{N_2}/Q_{N_2} \simeq 10\%$. L'erreur relative sur τ est de 12%.

Résultats et discussion

Le calcul du coût énergétique minimal de destruction des oxydes d'azote implique la détermination préalable des paramètres expérimentaux permettant d'optimiser d'une part, le taux de dissociation de l'azote et d'autre part, le rendement de la réaction des atomes d'azote sur NO_x, c'est-à-dire la probabilité de collision entre ces espèces. Les techniques de dosage des NO_x mises en oeuvre dans ce travail ont permis, par l'étude du débit maximal de NO_2 détruit, de préciser les conditions d'optimisation du rendement en $N(^4S)$, et par celle du taux de destruction de NO de définir les conditions favorables aux collisions $N–NO_x$.

L'azote est de qualité U, Air liquide. La distance (dénommée d, Fig. 1) entre la décharge et le conduit d'admission de NO_2 est égale à 30 mm. L'incidence sur le coût énergétique de destruction de NO_x de l'adaptation de la cavité est mise en relief en étudiant l'évolution de $Q^0_{NO_2}$ en fonction de Q_{N_2}. La cavité utilisée ne permet pas d'annuler P_r pour toutes les valeurs de Q_{N_2}, aussi la construction d'une nouvelle cavité permettant de remédier à cette insuffisance a-t-elle été entreprise postérieurement à ce travail (8). Pour la valeur $P_i = 500$ watts qui, à pression atmosphérique, correspond à la valeur minimale de P_r, la valeur du débit d'azote pour laquelle $P_r = 0$ est 700 L/h. Le tableau 1 résume l'évolution de $Q^0_{NO_2}$ en fonction de Q_{N_2} pour $P_i = 500$ watts. La valeur maximale de $Q^0_{NO_2}$ est observée pour le débit d'azote (700 L/h) pour lequel P_r s'annule. Cette optimisation de la destruction de NO_2 est attribuable essentiellement à une parfaite adaptation de la cavité (7). Aussi, la puissance incidente adoptée dans la suite du travail est-elle choisie de façon à correspondre à la valeur maximale de P_t permettant de minimiser P_r ($P_i = 500$ watts).

TABLEAU 1. Variation de $Q^0_{NO_2}$ en fonction de Q_{N_2}[a]

Q_{N_2} (L/h)	350	710	800	1240	1300	1600	1640
$Q^0_{NO_2}$ (L/h)	5,2	11	10,7	6,4	5,3	2,4	2,1

[a] $P_i = 500$ watt; $d = 30$ mm.

TABLEAU 2. Influence sur $Q^0_{NO_2}$ de la pureté de l'azote et évolution de $Q^0_{NO_2}$ après 48 h[a]

Qualité d'azote (Air liquide)	Pureté (%)	$Q^0_{NO_2}$ (L/h) $t = 0$	$Q^0_{NO_2}$ (L/h) $t = 48$ h
N 48	>99,998	19,5	
U	>99,995	22,8	13,5
R	>99,5	26	17,4

[a] $Q_{N_2} = 700$ L/h; $d = 30$ mm; $P_i = 500$ watt.

Une augmentation de la teneur en O_2 ou en H_2O dans l'azote soumis à la décharge améliore le rendement de destruction de NO_2 (Tableau 2). Ces résultats s'interprètent aisément dans le cadre d'une augmentation du taux de dissociation de la molécule d'azote en présence de traces de O_2 ou de H_2O (9). On remarque que la valeur de $Q^0_{NO_2}$ obtenue avec l'azote U: 22,8 L/h diffère de celle correspondant aux mêmes conditions expérimentales et figurant dans le tableau 1: 11 L/h. Cette divergence témoigne de l'influence d'un facteur important: l'état des parois. On observe une diminution de la quantité de NO_2 détruite au cours du temps. Les parois sont traitées à l'acide fluorhydrique dilué à 50%, puis rincées à l'eau, au méthanol et à l'éther et enfin séchées. Si cette précaution n'est pas respectée, la valeur de $Q^0_{NO_2}$ est nettement moins élevée. Dans un même tube, deux séries de mesures sont effectuées, l'une aussitôt après ce traitement, l'autre 48 heures plus tard; les résultats sont résumés dans le tableau 2. Une dégradation de l'état des parois entraîne donc une diminution de la probabilité de destruction de NO_x. Un nouveau dispositif récemment mis au point (8) permet d'éviter une telle dégradation. Dans la suite de cette étude, les tubes sont "traités" avant chaque mesure. L'azote utilisé est de qualité R.

L'influence du lieu d'adjonction de NO ou NO_2 sur l'efficacité de leur destruction a été envisagée.

Pour une puissance incidente donnée, quels que soient Q_{NO_x} et Q_{N_2} les conditions optimales de destruction de NO_x correspondent à $(30 < d < 40)$ mm. Pour des valeurs de d supérieures, on observe une décroissance rapide du taux de destruction. La figure 3 représente, en fonction de d, les évolutions de: (a) $Q^0_{NO_2}$ ($Q_{N_2} = 890$ L/h); (b) $\tau(Q_{N_2} = 700$ L/h, $Q_{NO} = 4,1$ L/h). La concentration en atomes d'azote est donc maximale et

Can. J. Chem. Downloaded from www.nrcresearchpress.com by 210.87.254.42 on 09/06/12
For personal use only.

TABLEAU 3. Variations de τ en fonction (a) de Q_{N_2} pour Q_{NO} = 25 L/h; (b) de Q_{NO} pour Q_{N_2} = 2 150 L/h[a]

	Q_{N_2} (L/h)								
	300	440	590	645	1210	1360	1630	2150	2570
Q_{NO} (L/h)	τ (%)								
15	—	—	—	—	—	—	—	16	—
20	—	—	—	—	—	—	—	26	—
25	91	87	88	86	55	47	38	35	24
30	—	—	—	—	—	—	—	40	—

[a] d = 30 mm; P_i = 500 watt.

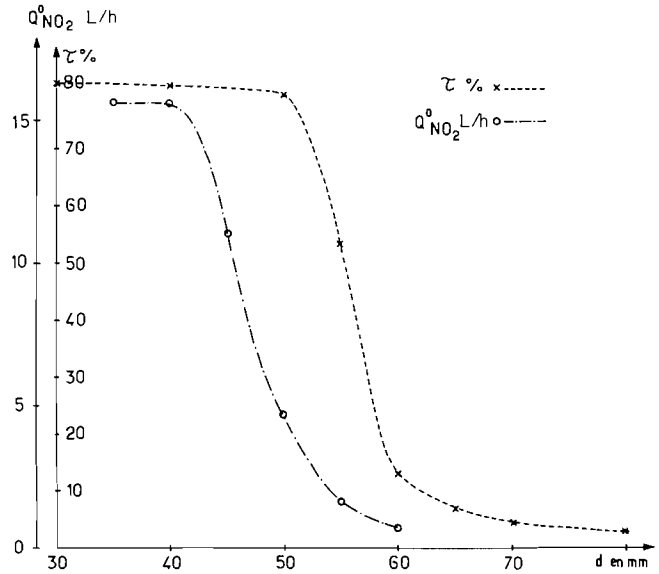

FIG. 3. Etude du débit maximal de NO_2 détruit: $Q^0_{NO_2}$ (Q_{N_2} = 890 L/h) et du taux de destruction de NO: τ (Q_{N_2} = 800 L/h, Q_{NO} = 4,1 L/h) en fonction de la distance décharge – zone d'introduction de NO_x (d); P_i = 500 watt.

constante pour ($30 < d < 40$) mm. Cette zone de concentration optimale en N(^4S) peut d'ailleurs être aisément visualisée; elle correspond à une extension du plasma, de forme conique, en dehors de la limite en aval de la cavité. Cette zone est dénommée dard. En conclusion les molécules de NO_x présentes dans le dard ont une probabilité plus élevée de rencontrer les atomes N(^4S) et donc d'être détruites. Les conditions expérimentales d'optimisation de cette probabilité de collision sont déterminées en envisageant l'influence de Q_{NO} et Q_{N_2} sur τ.

L'observation de l'evolution de τ en fonction de Q_{N_2} à Q_{NO} donné (Q_{NO} = 25 L/h) met en évidence les caractéristiques suivantes (Tableau 3): pour ($300 < Q_{N_2} < 650$) L/h, τ est approximativement constant (eu égard à la précision des mesures) et très élevé (86 à 91%); pour ($1200 < Q_{N_2} < 2600$) L/h les valeurs de τ sont beaucoup plus faibles et τ est une fonction décroissante de Q_{N_2}. L'étude n'a pu être menée pour des valeurs de débits d'azote intermédiaires ($650 < Q_{N_2} < 1200$) L/h, ppm_r étant alors >10 000 et donc non mesurable dans nos conditions expérimentales.

Dans l'hypothèse d'une répartition homogène des molécules de NO dans le milieu réactionnel, les résultats ci-dessus peuvent s'interpréter de la façon suivante. Lorsque [N(^4S)] est supérieur à [NO], τ est proportionnel à la fraction du volume total occupé par le dard et donc indépendant de Q_{NO} et Q_{N_2}. Par augmentation de Q_{N_2}, la diminution de la densité d'énergie

TABLEAU 4. Variation de τ en fonction de Q_{NO} et Q_{N_2}[a]

	Q_{N_2} (L/h)			
	300	440	590	645
Q_{NO} (L/h)	τ (%)			
10	84	81	85	82
15	87	83	86	84
20	89	86	87	85
25	91	87	88	86
30	92	90	88	87
100	96	95		

[a] d = 30 mm; P_i = 500 watt.

(P_t/Q_{N_2}) peut conduire à une valeur de [N(^4S)] inférieure à [NO] et donc à une diminution de τ. Dans le cadre de cette hypothèse postulant une répartition homogène des molécules NO on devrait également observer dans le domaine où [N(^4S)] est inférieur à [NO] une diminution de τ par augmentation de Q_{NO} à Q_{N_2} donné. Les résultats du tableau 3 font apparaître une évolution inverse et conduisent donc à rejeter l'hypothèse d'une répartition homogène de NO dans l'azote activé.

Les répartitions de NO et N(^4S) dans le milieu ne sont donc pas homogènes et τ, dont l'évolution est parallèle à celle de Q_{NO}/Q_{N_2}, représente le pourcentage de molécules de NO pénétrant dans le dard.

Les résultats précédents mettent en évidence les paramètres expérimentaux permettant d'optimiser la destruction de NO_x. Ils sont énumérés ci-après, les conditions spécifiques à la présente étude sont précisées pour chacun d'eux: la valeur de P_i doit permettre de minimiser P_r (P_i = 500 watts); présence d'impuretés oxygénées (~0,5%) dans l'azote (azote qualité R, Air liquide); il faut éviter la dégradation des parois du réacteur (l'azote est véhiculé dans des tubes récemment "traités", cf. ci-dessus); l'adjonction de NO_x doit s'effectuer dans le dard ce qui implique une contrainte d'une part sur le lieu d'adjonction de NO_x (d = 30 mm) et d'autre part sur les valeurs respectives de Q_{N_2} et Q_{NO} ($Q_{N_2} < 1000$ L/h, la condition expérimentale de détection de NO: $ppm_i < 10\,000$ suppose en outre de limiter les valeurs maximales de Q_{NO} à 30 ou 100 L/h suivant Q_{N_2}).

Les valeurs de τ pour différentes valeurs de Q_{N_2} et Q_{NO} sont reportées dans le tableau 4. Le taux de destruction maximum (Q_{N_2} = 300 L/h, Q_{NO} = 100 L/h) correspond à un coût énergétique de 0,14 kW-h/mol de NO, valeur très proche du coût théorique (0,13 kW-h/mol de NO).

La valeur optimale de $Q^0_{NO_2}$ (26 L/h) correspond à un coût énergétique de 0,43 kW-h/mol de NO_2. En réalité NO_2 n'étant jamais pur mais en équilibre avec son dimère, les valeurs de

Can. J. Chem. Downloaded from www.nrcresearchpress.com by 210.87.254.42 on 09/06/12
For personal use only.

$Q^0_{NO_2}$ sont sous-estimées et le coût énergétique est surestimé. En outre, le coût énergétique théorique de destruction de NO_2 ne peut être défini étant donné que la réaction globale de destruction de NO_2 n'est pas stoechiométrique. On peut seulement affirmer qu'il est supérieur à 0,13 kW-h/mol de NO_2.

Conclusion

L'énergie microonde permet une destruction efficace de NO_x à pression atmosphérique puisque le rendement énergétique peut être, dans certaines conditions, proche du rendement théorique. Ce travail met en relief des facteurs déterminants dans l'optimisation de cette destruction. Le dard constitue la zone préférentielle de destruction de NO_x; il convient donc d'une part de rendre son volume maximal et d'autre part, en agissant sur les valeurs respectives des débits gazeux et sur la géométrie de la chambre de mélange, d'effectuer une introduction de NO_x dans cette région fortement réactive. En outre il importe de concevoir une cavité dont les facilités d'adaptation sont telles que P_r puisse s'annuler pour les différents débits d'azote. Enfin la détérioration des parois du tube à décharge doit être minimisée. Une cavité récemment réalisée (8) permet de satisfaire à ces différents critères et laisse espérer une amélioration sensible du coût de destruction de NO_x dans une large gamme de débits gazeux.

1. M. BARNEA et P. URSU. Pollution et protection de l'atmosphère. Ed. Eyrolles (1974).
2. O. J. ADLHART, S. G. HINDIN et R. E. KENSON. Chem. Eng. Prog. **67**, 73 (1971).
3. Inform. Chim. **108**, 83 (1972).
4. O. DESSAUX, P. GOUDMAND et M. MATTOT. Brevet français ANVAR n° 228–389/D/9247 (1978).
5. B. MUTEL, O. DESSAUX et P. GOUDMAND. 6th International Symposium on Plasma Chemistry. Montréal 242 (1983).
6. M. MATTOT. Mémoire diplôme ingénieur Conservatoire National des Arts et Métiers, Lille (1978).
7. G. MOREAU. Thèse n° 1027. Université des Sciences et Techniques de Lille. (1983).
8. G. MOREAU, O. DESSAUX et P. GOUDMAND. J. Phys. E: **16**, 1160 (1983). À paraître.
9. R. R. BAKER, A. JACOB et C. A. WINKLER. Can. J. Chem. **49**, 1671 (1971).

Can. J. Chem. Downloaded from www.nrcresearchpress.com by 210.87.254.42 on 09/06/12
For personal use only.

L-Glucose. A convenient synthesis from D-glucose

WALTER A. SZAREK, GEORGE W. HAY, DOLATRAI M. VYAS,[1] EDWARD R. ISON, AND LUCJAN J. J. HRONOWSKI
Carbohydrate Research Institute and Department of Chemistry, Queen's University, Kingston, Ont., Canada K7L 3N6

Received August 31, 1983

WALTER A. SZAREK, GEORGE W. HAY, DOLATRAI M. VYAS, EDWARD R. ISON, and LUCJAN J. J. HRONOWSKI. Can. J. Chem. **62**, 671 (1984).

L-Glucose has been synthesized from D-glucose by a convenient method involving methyl 2,3-*O*-isopropylidene-β-D-gulofuranosiduronic acid (**6**) as a key intermediate. Compound **6** was converted into L-glucono-1,5-lactone (**8**), which, by a selective reduction, afforded L-glucose (**9**).

WALTER A. SZAREK, GEORGE W. HAY, DOLATRAI M. VYAS, EDWARD R. ISON et LUCJAN J. J. HRONOWSKI. Can. J. Chem. **62**, 671 (1984).

On a synthétisé de façon convenable le L-glucose à partir du D-glucose par une méthode faisant appel à l'intermédiaire de l'acide méthyle 2,3-*O*-isopropylidene-β-D-gulofuranosiduronique (**6**). On a transformé le composé **6** en L-glucono-lactone-1,5 (**8**), qui conduit par la suite au L-glucose (**9**) par une réduction sélective.

[Traduit par le journal]

Can. J. Chem. Downloaded from www.nrcresearchpress.com by 210.87.254.6 on 09/06/12
For personal use only.

Introduction

The natural sugars occur with an enormous predomination of one of the enantiomeric configurations, the other being rare or purely artificial. There is, at present, a growing interest in the study of the less-common enantiomers of the carbohydrates because of their potential organoleptic, and other biochemical, properties (1).

It has been known for more than a quarter of a century that the L-isomer of certain hexoses elicits a taste similar to, and frequently as intense as, the D-isomer (2). Although there have been claims that L-glucose occurs as a component of certain complex carbohydrates (3), the evidence is inconclusive as yet. Moreover, most studies of the metabolism of L-glucose by microorganisms have indicated that it is not metabolized (4); an enzyme catalyzing the oxidation of L-glucose has been isolated from cell-free extracts of *Pseudomonas caryophylii* IFO 13694 (5). These data suggested that certain of the enantiomers of naturally occurring sugars may be safe, effective, non-nutritive sweeteners.

The synthesis of L,L-sucrose (β-L-fructofuranosyl α-L-glucopyranoside) in this laboratory (6) permitted this hypothesis to be assessed. The compound was found to be not only indistinguishable in taste from natural sucrose (6) but also resistant to hydrolysis catalyzed by the sucrase of the jejunal brush border membrane of the hamster (7). These observations indicated that L-sugars may be useful as non-caloric or low caloric sweeteners. The need for an improved method for the synthesis of L-glucose stimulated the investigation reported below.

The first reported chemical synthesis of L-glucose was that of Fischer (8) who prepared the compound from L-arabinose by a Kiliani synthesis. Since then each of Richtmyer and Hudson (9) and Sowa (10) has published a synthesis of L-glucose starting from D-glucose by way of a chain extension and subsequent degradation. In addition, Takahata *et al.* (11) produced racemic glucose in low yield from a complex reaction of ethylene carbonate, tetrachloromethane, and sodium cyanide. However, none of these procedures has gained the relatively extensive application achieved by that of Sowden and Fischer (12) who prepared L-glucose from L-arabinose by condensation with nitromethane, hydrolysis of the 1-deoxy-1-nitroalditols, and separation of the L-mannose and L-glucose so produced. The present paper describes a new synthesis of L-glucose from D-glucose which does not involve chain extension.

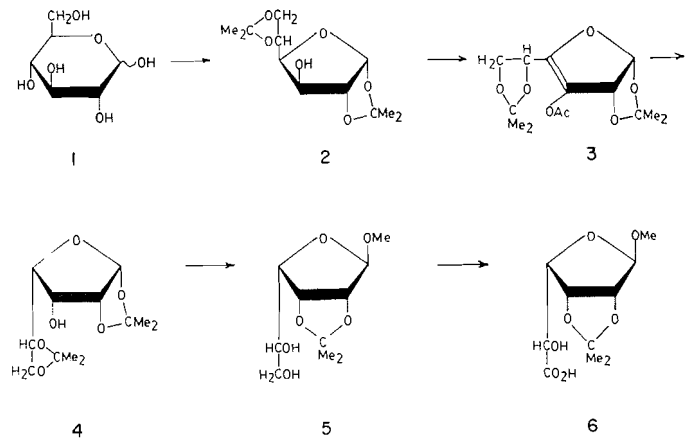

SCHEME 1

Results and discussion

The synthesis of L-glucose from D-glucose that is described in this paper involves the intermediacy of a D-glucose derivative and is an attractive one from the point of view of both the operational simplicity and the low costs of reagents.

The acid-catalysed conversion of **1** into **2** is a facile, routine method (13) which afforded the required intermediate compound (Scheme 1) in satisfactory yield. The synthesis then required the oxidation of **2** and treatment of the resultant product with acetic anhydride in pyridine to afford the enol acetate **3**, followed by reduction of **3** to give 1,2:5,6-di-*O*-isopropylidene-α-D-gulofuranose (**4**). Although **2** could be oxidized to 1,2:5,6-di-*O*-isopropylidene-α-D-*ribo*-hexofuranos-3-ulose hydrate in 95% yield using dimethylsulfoxide and acetic anhydride (14), the reduction of **3**, which was prepared from the oxidation product (15), was inhibited, presumably by traces of dimethylsulfoxide or dimethylsulfide which would poison the catalyst. Consequently, the ulose hydrate was prepared from **2** by catalytic oxidation (16) using a ruthenium tetraoxide catalyst (17), a method which gave only minor side products.

Compound **3** could be reduced quantitatively to 3-*O*-acetyl-1,2:5,6-di-*O*-isopropylidene-α-D-gulofuranose by the method

[1] Present address: Bristol Laboratories, Syracuse, NY 13201, U.S.A.

of Lemieux and Stick (18) using a palladium-on-carbon catalyst, and the product was deacetylated to afford **4**. Treatment of compound **3** with sodium borohydride gave lower yields as a result of a competing, base-catalyzed β-elimination which afforded 4,5-unsaturated compounds (15, 19). Even in buffered reaction solutions only moderate yields of product (**4**) were obtainable using sodium borohydride.

The acid-catalyzed hydrolysis of **4** to give 1,2-*O*-isopropylidene-α-D-gulofuranose was investigated. The influence of structure on the relative ease of hydrolysis of acetal rings has been well documented (20) and the conditions for the selective removal of the 5,6-*O*-isopropylidene group of such compounds as **2** (21), and the 1,2:5,6-di-*O*-isopropylidene acetals of L-idose (22) and D-allose (23), have been defined. Brimacombe *et al.* (24) have reported that the use of 70% acetic acid for the selective hydrolysis of 3-acetamido-3-deoxy-1,2:5,6-di-*O*-isopropylidene-α-D-gulofuranose gave the desired product, namely 3-acetamido-3-deoxy-1,2-*O*-isopropylidene-α-D-gulofuranose, but that it was mixed with both the starting compound and the free acetamido sugar. Similarly, it has been reported (25) that selective deacetalation of 1,2:5,6-di-*O*-isopropylidene-α-D-gulofuranose could not be achieved, but that the corresponding 3-*O*-benzyl derivative could be converted into 3-*O*-benzyl-1,2-*O*-isopropylidene-α-D-gulofuranose in 55% yield by treatment with aqueous acetic acid in 1,4-dioxane. The rationalization of these data is, at present, inadequate. A range of acidic conditions was explored in an attempt to effect the conversion of **4** into 1,2-*O*-isopropylidene-α-D-gulofuranose, but in each case the major product was the free sugar.

The high-yield conversion of D-glucose into methyl 2,3-*O*-isopropylidene-β-D-gulofuranoside (**5**) had been shown (26) to proceed through the intermediacy of methyl 2,3:5,6-di-*O*-isopropylidene-β-D-gulofuranoside. This selectivity in hydrolysis was noted (27) also in the preparation of methyl 2,3-*O*-isopropylidene-α-D-mannofuranoside from methyl 2,3:5,6-di-*O*-isopropylidene-α-D-mannofuranoside. However, methyl 2,3:5,6-di-*O*-isopropylidene-β-D-mannofuranoside was much more sensitive to acid and selective hydrolysis was unattainable (27). In the present work, the reaction of **4** with methanol, 2,2-dimethoxypropane, acetone, and hydrochloric acid produced **5** in high yield.

The catalytic oxidation of **5** to **6** was effected by the method of Perlin *et al.* (28), using a platinum-on-carbon catalyst in an aqueous reaction medium at 50°C. The pH of the reaction solution was monitored continuously and maintained at 7.5 by the addition of small increments of sodium hydrogen carbonate until a stoichiometric quantity had been utilized. Compound **6** was isolated in 91% yield as its sodium salt, and characterized by conversion (29) into its dicyclohexylammonium salt and into L-glucono-1,4-lactone. The lactone was obtained by the conversion of **6** into barium D-guluronate, which was converted, using sodium borohydride, into L-gluconic acid, the lactonization of which afforded the product. Perry and Hulyalkar (30) have established a gas–liquid chromatographic technique for the unambiguous characterization of glycono-1,4-lactones. The sample of L-glucono-1,4-lactone prepared from **6** exhibited a retention time identical to that of an authentic reference sample, obtained by way of acid-catalyzed hydrolysis of alginic acid (31), but clearly distinguishable from those of authentic samples of D-galactono-1,4-lactone, D-glucono-1,5-lactone, D-gulono-1,4-lactone, and D-mannono-1,4-lactone (32).

The synthesis now required the preparation of L-glucono-1,5-lactone (**8**) (Scheme 2). Thus, methyl 2,3-*O*-isopropylidene-β-D-gulofuranosiduronic acid (**6**) was subjected to an acid-catalyzed hydrolysis, and the resultant product (**7**) was reduced by hydrogenation over Raney nickel; from the product solution, crystalline L-glucono-1,5-lactone (**8**) was obtained by the method of crystallization described by Isbell and Frush (33) for the D-enantiomer of **8**. Catalytic reduction of **8** by the method of Glattfeld and Schimpff (34) afforded L-glucose (**9**) only in low yield. Consequently, the method of Wolfrom and Thompson (35), using sodium borohydride, was employed and a high yield of **9** was obtained. The product **9** had a melting point in agreement with that of D-glucose and exhibited the expected specific rotation; the ir and ^{1}Hmr spectra were indistinguishable from those of D-glucose. Thus, the conversion of D-glucose into L-glucose has been achieved in an unoptimized, overall yield of 12%.

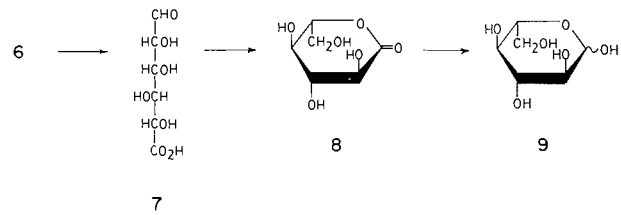

SCHEME 2

Experimental

Melting points were determined on a Fisher–Johns apparatus and are uncorrected. Optical rotations were measured with a Perkin–Elmer model 141 automatic polarimeter at 23 ± 3°C. Infrared spectra were recorded with a Beckman Acculab 6 or a Perkin–Elmer 598 spectrophotometer. The ^{1}Hmr spectra were recorded on a Bruker HX-60 (60 MHz) or a Bruker CXP-200 (200 MHz) spectrometer with tetramethylsilane (TMS) as the internal standard; chemical shifts (δ) are given in ppm downfield from TMS. Thin-layer chromatography (tlc) was performed using Merck plates precoated with silica gel 60 F-254 in the following solvent systems (v/v): (*A*) ethyl acetate – benzene, 1:1; (*B*) ethyl acetate; (*C*) 1-propanol – ethyl acetate – water, 3:1:1. The developed plates were dried and compounds located by heating the plates at ~150°C after they had been sprayed with 10% aqueous sulfuric acid containing 1% cerium sulfate and 1.5% molybdic acid.

1,2:5,6-Di-O-*isopropylidene*-α-D-*glucofuranose (2)*

The acetalation of anhydrous **1** (200 g) by the method of Stevens (13) produced **2** (160 g, 55%), mp 108–110°C; $\{\alpha\}_D$ −13.6° (*c* 2.0, $CHCl_3$) (lit. (13, 21) mp 110–111°C, $\{\alpha\}_D$ −13.5° ($CHCl_3$)).

3-O-*Acetyl-1,2:5,6-di*-O-*isopropylidene*-α-D-erythro-*hex-3-enofuranose (3)*

The oxidation of **2** (10 g) with ruthenium tetraoxide in the presence of potassium periodate (17) gave 1,2:5,6-di-*O*-isopropylidene-α-D-*ribo*-hexofuranos-3-ulose hydrate (13) (9.5 g), mp 109–110°C; $\{\alpha\}_D$ +39.5° (*c* 1.5, $CHCl_3$). The last named compound (6.1 g) was converted into **3** (15) (5.2 g, 75%), mp 62–63°C, $\{\alpha\}_D$ −32.7° (*c* 1, $CHCl_3$), by treatment with pyridine and acetic anhydride as described by Meyer zu Reckendorf (15).

1,2:5,6-Di-O-*isopropylidene*-α-D-*gulofuranose (4)*

The reduction of **3** (4.2 g) by the action of 5% palladium-on-carbon in a hydrogen atmosphere (room temperature, atmospheric pressure) (18) afforded 3-*O*-acetyl-1,2:5,6-di-*O*-isopropylidene-α-D-gulofuranose (36) (4.2 g), mp 72–74°C, $\{\alpha\}_D$ +66.5° (*c* 1.5, $CHCl_3$), a 3-g sample of which was deacetylated by stirring with Amberlite IRA-400 anion-exchange resin (OH^- form) (18) for 40 h at room temperature (~20°C) to give a quantitative yield (2.5 g) of **4** (15), mp 103–104°C; $\{\alpha\}_D$ +9.8° (*c* 2.0, $CHCl_3$).

Can. J. Chem. Downloaded from www.nrcresearchpress.com by 210.87.254.6 on 09/06/12
For personal use only.

Can. J. Chem. Downloaded from www.nrcresearchpress.com by 210.87.254.6 on 09/06/12
For personal use only.

Methyl 2,3-O-isopropylidene-β-D-gulofuranoside (5)

A solution containing **4** (500 mg) in 2,2-dimethoxypropane (1.6 mL), acetone (1.35 mL), methanol (1.35 mL), and concentrated hydrochloric acid (0.04 mL), was heated at reflux temperature for 2 h (26). The solution was cooled to room temperature, diluted with water (4 mL), and the organic solvents were removed under reduced pressure at 35°C. A white precipitate formed in the residual aqueous phase; this was dissolved by the addition of methanol (4 mL). Thin-layer chromatography of this solution revealed the presence of a new component (R_f 0.89, solvent *A*), but no **4** (R_f 0.58, solvent *A*) was detectable. Concentrated hydrochloric acid (1 mL) was added and the formation of product (R_f 0.2, solvent *A*) was monitored by tlc (~3 h at room temperature). The solution was neutralized with aqueous sodium hydrogen carbonate, concentrated to ~5 mL, and extracted with chloroform (3 × 5 mL). The aqueous layer was saturated with sodium chloride and extracted with chloroform (3 × 5 mL). The combined extracts were dried (anhydrous sodium sulfate) and evaporated to a syrup from which there were obtained 340 mg (76%) of crystalline **5** (26), mp 77–79°C (from $CHCl_3$–hexane); $\{\alpha\}_D$ −82.8° (*c* 1.2, CH_3OH).

Methyl 2,3-O-isopropylidene-β-D-gulofuranosiduronic acid (6)

To an aqueous solution (500 mL) of **5** (9.3 g) was added 10% platinum-on-carbon (0.9 g). A pH electrode was immersed in the mixture and a stream of oxygen was passed through the liquid at a rate sufficient to keep the catalyst uniformly suspended. The reaction mixture was held at 55–60°C, and the pH maintained at 7.5 by the addition, as required, of solid sodium hydrogen carbonate (2.19 g, total). After 5 h, **4** was not detectable by tlc (R_f 0.51, solvent *B*), but a new compound (R_f 0.50, solvent *C*) was observed. Evaporation of the reaction solution, after filtration, afforded 9.8 g (91%) of **6** (sodium salt), $\{\alpha\}_D$ −82.5° (*c* 1.5, H_2O); ν_{max} (KBr): 1590 (COO^-) cm^{-1}; ^{1}Hmr (60 MHz, DMSO-d_6) δ: 1.3 and 1.5 (s's, 6H, CMe_2), 3.3 (s, 3H, OMe), 3.6–4.2 (4H, H-4, H-5, 2 OH's), 4.5 (d, 1H, $J_{2,3}$ = 6 Hz, H-2), 4.7 (dd, 1H, $J_{3,4}$ = 2.5 Hz, H-3), 4.9 (s, 1H, H-1).

Compound **6** (sodium salt) decomposed before melting and was further characterized by treatment with dicyclohexylamine as described by Zissis *et al.* (29) to give **6** (dicyclohexylammonium salt), mp 158–159°C; $\{\alpha\}_D$ −45.9° (*c* 0.5, H_2O); ν_{max} (KBr): 3400 (OH), 1620, 1540 (COO^-) cm^{-1}; ^{1}Hmr (60 MHz, $CDCl_3$) δ: 1.2 and 1.4 (s's, 6H, CMe_2), 1.4–2.3 (22H, cyclohexyl protons), 1.5 (s, 3H, OMe), 4.7 (s, 1H, H-1). *Anal.* calcd. for $C_{22}H_{37}O_7$: C 51.77, H 5.62; found: C 52.01, H 5.66.

A solution of **6** (sodium salt) (650 mg) in water (5 mL) was heated on a steam bath for 3 h with Amberlite IR-120 cation-exchange resin (H^+ form) (5 mL). The resin was removed by filtration. The filtrate was neutralized with barium carbonate and evaporated to give the barium salt (540 mg) of D-guluronic acid (**7**) as a light-yellow solid, $\{\alpha\}_D$ −24.7° (*c* 2.0, H_2O); ν_{max} (KBr): 1595 (COO^-) cm^{-1}. The barium salt was converted, using sodium borohydride, into L-gluconic acid, which was then identified in the form of L-glucono-1,4-lactone by gas–liquid chromatography (see ref. 32) as described by Perry and Hulyalkar (30).

Acidification of a cold (<3°C), concentrated, aqueous solution of a sample of the sodium salt of **6** with 2 *M* hydrochloric acid yielded **6** as colorless crystals, mp 175–176°C; $\{\alpha\}_D$ −79.0° (*c* 1.01, MeOH); ^{1}Hmr (200 MHz, DMSO-d_6) δ: 1.23 and 1.36 (s's, 6H, CMe_2), 3.25 (s, 3H, OMe), 3.91 (dd, 1H, $J_{4,5}$ = 8.6 Hz, $J_{3,4}$ = 3.5 Hz, H-4), 4.08 (br d, 1H, $J_{4,5}$ = 8.6 Hz, H-5), 4.53 (d, 1H, $J_{2,3}$ = 6.0 Hz, H-2), 4.75 (dd, 1H, $J_{2,3}$ = 6.0 Hz, $J_{3,4}$ = 3.5 Hz, H-3), 4.87 (s, 1H, H-1), 5.87 (br s, 1H, exchanged in D_2O, OH), 12.59 (br s, 1H, exchanged in D_2O, CO_2H). *Anal.* calcd. for $C_{10}H_{16}O_7$: C 48.39, H 6.50; found: C 48.15, H 7.01.

L-Glucono-1,5-lactone (8)

A solution of **6** (0.516 g) in water (30 mL) was treated with Dowex 50W-X8 cation-exchange resin (H^+ form) (1 mL, 1.7 mequiv.) with constant stirring for 29 h at 60–70°C. The process was repeated with fresh resin for 17 h. The resin was removed and the filtrate evaporated to a clear, oily residue which was dissolved in water (20 mL). Alcohol-free Raney nickel (37) (0.4 mL) was added and the mixture shaken (240 cpm) in an atmosphere of hydrogen (60 psig) at room temperature for 18 h. The catalyst was removed by filtration, washed with water (30 mL), and the combined filtrate and wash solution were cooled in an ice-water bath and stirred with Dowex 50W-X8 cation-exchange resin (H^+ form) (15 mL, 27 mequiv.) for 1 h. After removal of the resin the filtrate was concentrated to 1–2 mL and treated, as described by Isbell and Frush (33) for the D series, to give **8** (254 mg, 68.5%) as colorless prisms, mp 149–151°C; $\{\alpha\}_D$ −63.6° (2 min) → −12.6° (11 h) (*c* 5, H_2O) (lit. (33) for D-enantiomer, mp 150–152°C, $\{\alpha\}_D$ +66.2° → +8.8° (24 h) (*c* 5, H_2O)).

L-Glucose (9)

Immediately following the dissolution of **8** (0.5 g) in cold (<3°C) water (5 mL), a solution of sodium borohydride (0.080 g) in water (3 mL) and 0.15 *M* sulfuric acid were added concurrently, dropwise, with stirring, over a 20-min period, in such a manner as to maintain a pH of 3–4, while keeping the temperature at <3°C (35). Five minutes after the end of the addition of sodium borohydride, 0.15 *M* sulfuric acid (0.5 mL) was added and the solution was stirred for 5 min; the solution was diluted with water to 15 mL and stirred with Amberlite IR-120 cation-exchange resin (H^+ form) (5 mL) for 15 min. The resin was removed by filtration and washed with water (3 × 5 mL). The combined filtrate and wash solutions were stirred with Amberlite IR-45 anion-exchange resin (OH^- form) (5 mL) for 1 h; the resin was removed and washed as before. The sequential treatment with fresh cation- and anion-exchange resins was repeated twice more. The solvent was evaporated and boric acid removed by distillation with an excess of dry methanol (35). The clear, oily residue was dissolved in water (0.5 mL) and the solution was diluted with methanol (5 mL) and 2-propanol (10 mL). On standing at room temperature, compound **9** was obtained (refs. 8, 12, 38) (0.270 g, 53.7%), mp 143–150°C; $\{\alpha\}_D$ −52.9° (*c* 5.48, H_2O). A second crop of **9** (0.056 g, total yield 64.8%), mp 141–148°C, was isolated from the mother liquor. The ir and ^{1}Hmr spectra were indistinguishable from those of D-glucose.

Acknowledgements

The authors are grateful to Queen's University and to the Natural Sciences and Engineering Research Council of Canada for their financial support of this work. They also wish to thank Professor H. S. Isbell for a generous, crystalline sample of L-glucono-1,5-lactone.

1. R. S. SHALLENBERGER. Zuckerindustrie, **104**, 121 (1979); A. F. HADFIELD and A. C. SARTORELLI. Carbohydr. Res. **72**, 235 (1979); D. K. MINSTER and S. M. HECHT. J. Org. Chem. **43**, 3987 (1978); G. V. LEVIN. U.S. Patent No. 4,262,032, Apr. 14, 1981, and references cited therein.
2. R. S. SHALLENBERGER, T. E. ACREE, and C. Y. LEE. Nature, **221**, 555 (1969); G. G. BIRCH, Z. LATZMER, and M. R. HOLLAWAY. Chem. Senses Flavor, **5**, 63 (1980).
3. F. POWER and F. TUTIN. Publ. Wellcome Chem. Res. Lab. **57**, 1 (1905); H. SAHA and K. CHOUDHUEY. J. Chem. Soc. **121**, 1044 (1922); J. BEEK. J. Am. Chem. Soc. **63**, 1483 (1941); J. BEEK. J. Res. Natl. Bur. Stand. **27**, 507 (1941).
4. J. BRUNTON, W. H. HORNER, and G. A. RUSS. J. Biol. Chem. **242**, 813 (1967); H. RUDNEY. Science, **92**, 112 (1940).
5. K.-I. SASAJIMA and A. J. SINSKEY. Biochim. Biphys. Acta, **571**, 120 (1979).
6. W. A. SZAREK and J. K. N. JONES. U.S. Patent No. 4,207,413, June 10, 1980.
7. P. K. DINDA, I. T. BECK, W. A. SZAREK, G. W. HAY, E. R. ISON, and D. M. VYAS. Can. J. Physiol. Pharm. **60**, 652 (1982).
8. E. FISCHER. Ber. **22**, 2204 (1889); **23**, 930, 2618 (1890).
9. N. K. RICHTMYER and C. S. HUDSON. J. Am. Chem. Soc. **64**, 1609 (1942).
10. W. SOWA. Can. J. Chem. **47**, 3931 (1969).

11. K. TAKAHATA, T. KUNIEDO, and T. TAKIZAWA. Chem. Pharm. Bull. **23**, 3017 (1975).
12. J. C. SOWDEN and H. O. L. FISCHER. J. Am. Chem. Soc. **69**, 1963 (1947).
13. J. D. STEVENS. Methods Carbohydr. Chem. **6**, 123 (1972).
14. W. SOWA and G. H. S. THOMAS. Can. J. Chem. **44**, 836 (1966).
15. W. MEYER ZU RECKENDORF. Angew. Chem. Int. Ed. Engl. **6**, 177 (1967); Methods Carbohydr. Chem. **6**, 129 (1972).
16. V. M. PARIKH and J. K. N. JONES. Can. J. Chem. **43**, 3452 (1965); B. T. LAWTON, W. A. SZAREK, and J. K. N. JONES. Carbohydr. Res. **10**, 456 (1969).
17. P. J. BENYON, P. M. COLLINS, P. T. DOGANGES, and W. G. OVEREND. J. Chem. Soc. C, 1131 (1966).
18. R. U. LEMIEUX and R. V. STICK. Aust. J. Chem. **28**, 1799 (1975).
19. W. MEYER ZU RECKENDORF and J. C. JOCHIMS. Ber. **102**, 4199 (1969).
20. A. H. HAINES. Adv. Carbohydr. Chem. Biochem. **39**, 13 (1981).
21. O. TH. SCHMIDT. Methods Carbohydr. Chem. **2**, 318 (1963).
22. R. SCHAFFER. Natl. Bur. Stand. U.S. Tech. Note, **427**, 60 (1967).
23. O. THEANDER. Acta Chem. Scand. **18**, 2209 (1964).
24. J. S. BRIMACOMBE, A. M. MOFTI, and M. STACEY. Carbohydr. Res. **16**, 303 (1971).
25. H. KUZUHARA, H. TERAYAMA, H. OHRUI, and S. EMOTO. Carbohydr. Res. **20**, 165 (1971).
26. L. M. LERNER. J. Org. Chem. **40**, 2401 (1975).
27. M. H. RANDALL. Carbohydr. Res. **11**, 173 (1969).
28. A. S. PERLIN, B. CASU, G. R. SANDERSON, and J. TSE. Carbohydr. Res. **21**, 123 (1972).
29. E. ZISSIS, H. W. DIEHL, and H. G. FLETCHER, JR. Carbohydr. Res. **26**, 323 (1973).
30. M. B. PERRY and R. K. HULYALKAR. Can. J. Biochem. **43**, 573 (1965).
31. F. G. FISCHER and H. DÖRFEL. Hoppe-Seyler's Z. Physiol. Chem. **302**, 186 (1955).
32. E. R. ISON. Ph.D. Thesis, Queen's University, Kingston. 1982.
33. H. S. ISBELL and H. L. FRUSH. J. Res. Natl. Bur. Stand. **11**, 649 (1933).
34. J. W. E. GLATTFELD and G. W. SCHIMPFF. J. Am. Chem. Soc. **57**, 2204 (1935).
35. M. L. WOLFROM and A. THOMPSON. Methods Carbohydr. Chem. **2**, 65 (1963).
36. K. N. SLESSOR and A. S. TRACEY. Can. J. Chem. **47**, 3989 (1969).
37. A. A. PAVLIC and H. ADKINS. J. Am. Chem. Soc. **68**, 1471 (1941).
38. J. C. SOWDEN. Methods Carbohydr. Chem. **1**, 132 (1962).

Can. J. Chem. Downloaded from www.nrcresearchpress.com by 210.87.254.6 on 09/06/12
For personal use only.

Gas phase negative ion chemistry of alkylchloroformates. A convenient method for bimolecular generation of chloride ion adducts and determination of chloride affinities from ion cyclotron resonance thermal equilibrium measurements

J. W. LARSON[1] AND T. B. MCMAHON

Department of Chemistry, University of New Brunswick, Fredericton, N.B., Canada E3B 6E2

Received August 25, 1983

J. W. LARSON and T. B. MCMAHON. Can. J. Chem. **62**, 675 (1984).

A new method for production of chloride ion adducts, MCl^-, via a sequence of bimolecular ion molecule reactions involving chloroformate esters is described. These reactions have been used in trapped-ion ion cyclotron resonance thermal equilibrium studies to determine the relative chloride ion affinities of twenty compounds with Cl^- binding energies in the range 10–25 kcal mol^{-1}. The present results are found to be in good agreement with chloride affinities obtained by other methods. The resulting chloride affinity scale establishes a convenient framework for the systematic investigation of effects of molecular structure and chemical properties on the binding energy of Cl^- to both Lewis and Brønsted acids.

J. W. LARSON et T. B. MCMAHON. Can. J. Chem. **62**, 675 (1984).

On décrit une nouvelle méthode de produire des adduits d'ions chlorures, MCl^-, par le biais d'une série de réactions bimoléculaires ion-molécule impliquant des esters chloroformates. On a utilisé ces réactions pour effectuer des études d'équilibre thermique par ions piégés grâce à la résonance ionique dans un cyclotron; ces études ont été réalisées afin de déterminer les affinités relatives de l'ion chlorure pour vingt composés dans lesquels les énergies de liaison du chlorure varient de 10 à 25 kcal/mol. On trouve que nos résultats sont en bon accord avec les valeurs obtenues par d'autres méthodes pour les affinités du chlorure. L'échelle d'affinité de chlorure qui en résulte établit un modèle pour l'étude systématique des effets de structure moléculaire et des propriétés chimiques sur l'énergie de liaison du chlorure avec des acides de Lewis et de Brønsted.

[Traduit par le journal]

Introduction

The development of methods for studying ion molecule thermochemistry in the gas phase has resulted in important contributions to a number of areas of chemistry (1). The gas phase acidities and basicities of molecules (2–7) have been extensively studied and have led to a better understanding of the intrinsic factors affecting molecular acid–base properties as opposed to those relating to solvation phenomena. In addition, the direct study of solvation of cations and anions (8–11) has further shown the utility of gas phase data in explaining both chemical and physical interactions affecting solution processes.

The study of binding of anions to neutral molecules (12–18) has proven particularly useful. In addition to increasing the understanding of basic factors affecting stability of hydrogen bonds and structural factors influencing binding of anions to Lewis acids, a number of new anions have been generated in the gas phase with sufficiently great apparent stability to predict the probable ability to synthesize them in condensed phase (16–21). The potential of anion affinity data as a guide in engineering the molecular structure of compounds analogous to crown ethers and cryptates is another motivation for this laboratory's past interest in fluoride affinities (16, 17, 21) and the present work on chloride ion binding energetics of neutral molecules.

The ability to carry out ICR thermal equilibrium measurements of chloride affinities for a wide range of molecules at low pressure is dependent on three factors: (*i*) there must be a compound capable of producing a chloride ion adduct of some molecule either by dissociative electron attachment or by a sequence of bimolecular reactions; (*ii*) the compound used to generate primary chloride ions adducts in the system must itself have a sufficiently low Cl^- binding energy so that formation of Cl^- adducts of this compound does not interfere with generation of other desired adducts; (*iii*) there must exist at least one compound for which accurate thermochemical data for Cl^- attachment is available.

The first of these conditions is met by several compounds already described in the literature. Riveros *et al.* (22, 23) have demonstrated that $ClCO^-$ may be generated by dissociative electron attachment to Cl_2CO and this ion subsequently transfers Cl^- to species as weakly acidic as xenon and methylchloride. The cross section for $ClCO^-$ production is, however, exceedingly low, necessitating the use of high Cl_2CO pressures and thus rendering the ICR trapping experiment inoperative. Brauman (24) has shown that $CF_3Cl^{\cdot -}$ may be generated from CF_3COCl and this ion again acts as a facile Cl^- transfer agent. Our attempts to use CF_3COCl as a source of Cl^- adducts failed, again due to the exceedingly low cross section for $CF_3Cl^{\cdot -}$ production. The SO_2Cl^- ion has been shown by Sullivan and Beauchamp (18) to be readily generated by dissociative electron attachment to SO_2Cl_2 and SO_2ClF. In addition, mixtures of SF_6 and HCl have been shown to lead to the facile production of $FHCl^-$ (25) which subsequently acts as a Cl^- donor to compounds binding Cl^- more strongly than does HF. Unfortunately, these latter two methods for producing Cl^- donors, as well as the previous two (already unacceptable for our purposes), fail to satisfy the second condition. Each of the compounds involved, Cl_2CO, CF_3COCl, SO_2, SO_2Cl_2, SO_2ClF, and HCl, binds Cl^- more strongly than most of the substrates which we wished to examine. The final condition, availability of absolute Cl^- binding thermochemistry, is met for several compounds using high pressure mass spectrometric (HPMS) methods. Very recently, Kebarle (15) has examined clustering equilibria, eq. [1], for a variety of compounds and examined the effect of molecular structure, gas phase acidity, and charge distribution on the enthalpy of Cl^- binding, ΔH^0_1.

[1] $\quad RH + Cl^- \rightarrow RHCl^-$

[1]On sabbatical leave from Marshall University, Huntington, WV, U.S.A.

Can. J. Chem. Downloaded from www.nrcresearchpress.com by 210.87.254.105 on 09/06/12
For personal use only.

Can. J. Chem. Downloaded from www.nrcresearchpress.com by 210.87.254.105 on 09/06/12
For personal use only.

These data provide convenient anchor points for the construction of our ladder of ICR thermal equilibrium Cl^- transfer measurements, eq. [2].

[2] $R_1HCl^- + R_2H \rightleftharpoons R_2HCl^- + R_1H$

In the present work, we wish to report a new class of compounds, chloroformate esters, which satisfy the conditions above for convenient generation of Cl^- adducts for use in ICR thermal equilibrium experiments. These new reagents have been used to generate a scale of Cl^- binding energetics for ten new compounds, chosen because of their availability, volatility, chemical inertness, and low tendency to be absorbed on surfaces. These compounds thus provide ideal reference species for determination of chloride affinities of all other compounds with Cl^- binding energies between those of benzene and formic acid. These new compounds also fill gaps in the chloride affinity scale not yet filled by the HPMS experiments, such that no new compound in this range would have a chloride affinity more than 1 kcal mol^{-1} from these reference species.

Experimental

All experiments were conducted at ambient temperature using an ICR spectrometer of basic Varian V-5900 design extensively modified to permit ion-trapping experiments (26). Details of design and operation of both conventional and trapped-ion ICR experiments have been described in detail previously (27, 28).

Methylchloroformate, ethylchloroformate, and ethylthiochloroformate were obtained from ICN Pharmaceuticals Inc. All other liquid materials were commercial samples of highest purity obtainable. Gases used were obtained from Matheson Canada Ltd. (sulfurdioxide, methylchloride, hydrogenchloride, and fluoroform), P.C.R. Inc. (phosphorous trifluoride, pentafluoroethane, *t*-butylfluoride and pentafluoroacetone), and Alfa Products Inc. (triethylborane). Hydrogen cyanide was prepared by condensing gaseous HCl into a concentrated aqueous solution of KCN. All samples were used following degassing by several freeze–pump–thaw cycles.

Results and discussion

1. Negative ion chemistry of chloroformate esters

Dissociative attachment of electrons to methylchloroformate and ethylchloroformate produces only Cl^-, eq. [3].

[3] $e^- + ClCO_2R \rightarrow Cl^- + RCO_2^{\cdot}$

Subsequent reaction of Cl^- with the neutral esters yields $ClCO_2^-$ via an apparent nucleophilic displacement reaction, eq. [4].

[4] $Cl^- + ClCO_2R \rightarrow ClCO_2^- + RCl$

The observed rate constants for this reaction were 1.1×10^{-10} cm^3 $molecule^{-1}$ s^{-1} for the methyl ester and 0.8×10^{-10} cm^3 $molecule^{-1}$ s^{-1} for the ethyl ester. Variation of relative negative ionic abundances with trapping time is shown in Fig. 1 for ethylchloroformate. As seen from this figure, in the absence of any other chloride acceptor molecules, the $ClCO_2^-$ reacts further with the neutral ester to generate a dichloroalkoxide ion, eq. [5].

[5] $ClCO_2^- + ClCO_2R \rightarrow Cl_2C(OR)O^- + CO_2$

The rate constant for this reaction is roughly 1.5×10^{-10} cm^3 $molecule^{-1}$ s^{-1} for both the methyl and ethyl esters.

Double resonance experiments revealed that $^{35}Cl^-$ is reactively coupled to both $^{35}ClCO_2^-$ and $^{37}ClCO_2^-$ with similar results for $^{37}Cl^-$. This result is consistent with either direct S_N2 attack at the α carbon of the ester alkyl group, or intermediate

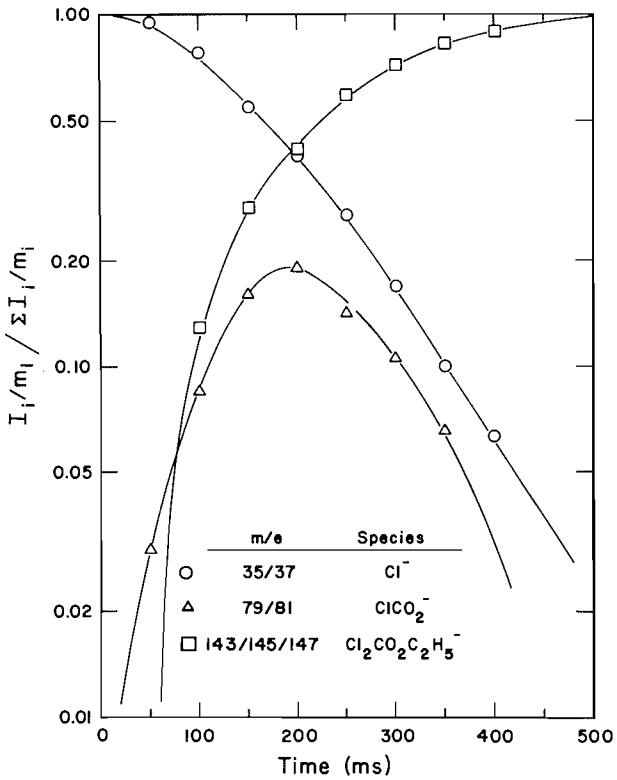

FIG. 1. Variation of relative negative ionic abundances with reaction time for $ClCO_2C_2H_5$ at 2.4×10^{-6} Torr following a 5 ms, 70 eV electron beam pulse.

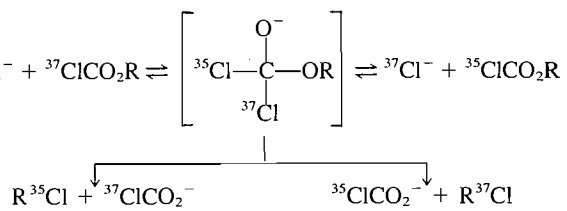

SCHEME 1

formation of a dichloroalkoxide ion followed by dissociation to $ClCO_2^-$ and RCl, Scheme 1. In this case, halide interchange very probably also occurs via formation of this intermediate complex. It is estimated that roughly 5% of encounters of Cl^- with $ClCO_2R$ lead to $ClCO_2^-$ production.

Reaction of F^- in mixtures of NF_3 and chloroformate esters also yield $ClCO_2^-$, eq. [6].

[6] $F^- + ClCO_2R \rightarrow ClCO_2^- + RF$

Reaction with Br^- showed no observable reaction products.

In the presence of an additional chloride acceptor molecule, M, with Cl^- binding energy in excess of that for either CO_2 or $ClCO_2R$, a Cl^- transfer is readily observed to yield a new chloride adduct, eqs. [7] and [8].

[7] $ClCO_2^- + M \rightarrow MCl^- + CO_2$

[8] $Cl_2CO_2R^- + M \rightarrow MCl^- + ClCO_2R$

A typical result is that shown in Fig. 2 for a mixture of fluoroform, CF_3H, and methylchloroformate.

For compounds with chloride affinities between those of CO_2 and the chloroformate esters, eq. [7] competes favourably with eq. [5] when the relative pressure of M is greater than that of

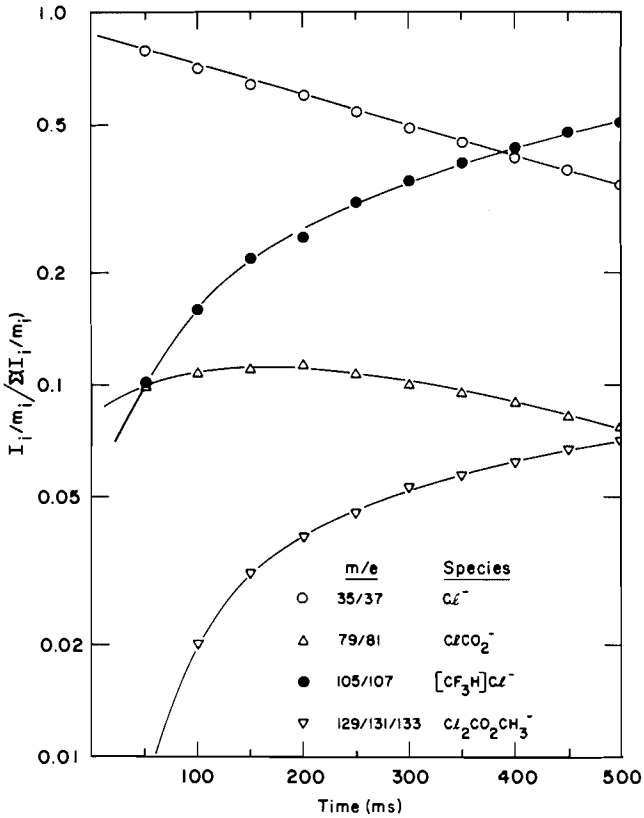

FIG. 2. Variation of relative negative ionic abundances with reaction time for a 1:1 mixture of $ClCO_2CH_3$:CHF_3 at 1.2×10^{-6} Torr total pressure following a 5 ms, 70 eV electron beam pulse.

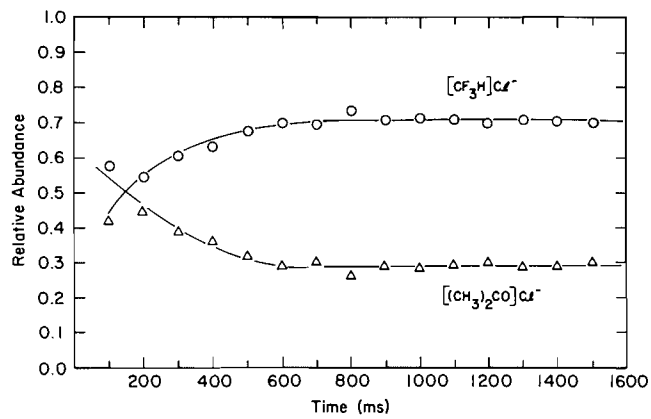

FIG. 3. Variation of relative negative ionic abundances with reaction time for a 2.7:1:5.5 mixture of $ClCO_2CH_3$:CHF_3:$(CH_3)_2CO$ at a total pressure of 2.4×10^{-6} Torr following a 5 ms, 70 eV electron beam pulse.

$ClCO_2R$. In this way Cl^- transfer could be observed to compounds such as cyclohexane and ethylene, both of which bind Cl^- less strongly than does benzene. No Cl^- transfer could be observed, however, to Xe or CO, placing the chloride affinity of CO_2 between benzene and xenon. This is consistent with the chloride affinity of benzene determined in the present work and elsewhere (15), the chloride affinity of CO_2 determined by Keesee, Lee, and Castleman (29) as 8.0 kcal mol^{-1}, and the chloride affinity of Xe estimated by Riveros *et al.* (23) to be 7.5 kcal mol^{-1}.

2. Chloride ion transfer equilibrium measurements

A quantitative scale of chloride affinities has been established from a series of multiple overlap chloride transfer equilibrium measurements. A typical chloride transfer equilibrium is shown in Fig. 3 for a mixture of acetone and fluoroform of accurately known partial pressure ratio in the presence of methylchloroformate. The equilibrium constant for eq. [9] may

[9] $CF_3HCl^- + (CH_3)_2CO \rightleftharpoons [(CH_3)_2CO]Cl^- + CF_3H$

then be determined from the observed steady-state ionic abundances and the known neutral pressure ratio. In general, the chloride exchange reactions were established by time-delayed ion ejection experiments to be an order of magnitude faster than the formation of $ClCO_2^-$ via eq. [4]. As a result, equilibrium steady-state was readily achieved within 300 ms of initial ion formation.

Although attainment of a persistent steady-state was taken to be the initial indication that thermal equilibrium had been established, this was confirmed by a number of other routes: (*i*) a calculated equilibrium constant that was invariant to changes in neutral pressure ratio and to total pressure; (*ii*) multiple overlap experiments which gave the difference in free energy of attachment of Cl^- for any two compounds by at least two independent paths; (*iii*) double resonance and ion ejection experiments carried out at long reaction times to verify the occurrence of reaction in both forward and reverse directions and in some cases to obtain rate constants. This last condition was particularly important in confirming equilibria in compounds with chloride affinities less than methylchloroformate. In cases where competing chloride transfer to methylchloroformate was especially severe, no quantitative conclusions regarding the binding energies of these low chloride affinity species were drawn.

Standard free energy changes for each of the chloride transfer equilibria observed may be calculated from eq. [10].

[10] $\Delta G_2^0 = -RT \ln K_{eq}$

These values are reported in Table 1. The uncertainty associated with each of these ΔG_2^0 values is at maximum ± 0.2 kcal mol^{-1}. The value for free energy of binding of Cl^- to *tert*-butanol of 11.1 kcal mol^{-1} (12, 13, 15) has been adopted as the primary reference standard for the chloride binding energy scale since this value is roughly in the middle of the scale of chloride affinities and since the value for free energy of binding has remained unchanged after repeated measurements by HPMS. The free energy of binding of Cl^- for each of the compounds studied, ΔG_{11}^0, is thus obtained from the value of

[11] $MCl^- \rightarrow M + Cl^-$

ΔG_2^0 relative to 11.1 kcal mol^{-1} for t-C_4H_9OH. These values are also summarized in Table 1. For the most part, values of ΔG_{11}^0 obtained in the present work agree within ± 0.4 kcal mol^{-1} with those obtained by other methods. This uncertainty is well within the combined uncertainties of the individual techniques.

Fehsenfeld and Ferguson (30) have determined ΔG_{12}^0 from measurements of the forward and reverse rate constants for eq. [12] in a flowing afterglow apparatus. Their value of

[12] $Cl^- \cdots HOH + SO_2 \rightleftharpoons ClSO_2^- + H_2O$

6.0 kcal mol^{-1} is in excellent agreement with our present one of 6.5 kcal mol^{-1}, especially considering the experimental difficulty associated with measurement of the extremely slow rate of the reverse reaction. The value of ΔG_{11}^0 for SO_2 of 14.7 kcal mol^{-1} obtained by us is also in excellent agreement with that of

Can. J. Chem. Downloaded from www.nrcresearchpress.com by 210.87.254.105 on 09/06/12
For personal use only.

TABLE 1. Standard free energies, entropies, and enthalpies of chloride ion binding for selected compounds at 258 K

M	ΔG_2^0 (kcal mol^{-1})	ΔG_{11}^0 (kcal mol^{-1})	ΔS_{11}^0 (cal mol^{-1} °K^{-1})	ΔH_{11}^0 (kcal mol^{-1})
HCO_2H	1.7, 1.2	18.4,[a] 20.1,[b] 25.4[c]	24.1	25.6,[a] 27.4,[b] 37.2[c]
BEt_3	0.9, 2.1	17.2[a]	22.0	23.8[a]
CH_3CO_2H	0.7	16.7,[a] 17.3,[b] 15.8[c]	24.0	23.9,[a] 21.6[b]
CF_3COCF_2H	0.3	16.3[a]	23.9	23.4[a]
HCl	1.1, 1.6	16.0,[a] 16.7[d]	23.5	23.1,[a] 23.7[d]
SO_2	0.7	14.7,[a] 14.2,[e] 14.9[f]	20.8	20.9,[a] 21.8[f]
HCN	0.9	13.9[a]	23.7	21.0[a]
FCH_2CH_2OH	1.9, 1.1	13.0[a]	25.0	20.5[a]
CF_3CF_2H	0.7	11.8[a]	23.3	18.8[a]
t-BuOH	1.2	(11.1)[b,c]	23.4	18.1,[a] 19.2,[b] 14.2[c]
MeOH	0.1	9.9,[a] 9.8[b,c]	22.9	16.8,[a] 14.1[c]
CF_3H	0.5, 1.3	9.8[a]	22.9	16.7[a]
PF_3	1.0, 1.6	9.2[a]	21.0	15.5[a]
H_2O	0.1	8.4,[a] 8.2,[b] 9.0,[i] 8.8[h]	20.1	14.4,[a] 13.1,[b] 14.9,[i] 14.8
Me_2CO	1.1	8.2,[a] 7.9[b]	19.7	14.1,[a] 13.7[b]
$ClCO_2Me$	0.7	7.8[a]	21.0	14.1[a]
t-BuF	0.9, 0.2, 0.6	7.1[a]	20.8	13.3[a]
ϕCl		6.9,[a] 6.5[b]	22.4	13.6[a]
MeCl	1.3	6.1,[a] 4.1[g]	20.5	12.2,[a] 8.7[g]
C_6H_6		4.8,[a] 3.8[b]	17.1	9.9[a]

[a]This work.
[b]Reference 15.
[c]Reference 13.
[d]Reference 14.
[e]Reference 30.
[f]Reference 29.
[g]Reference 36.
[h]Reference 32.
[i]Reference 31.

14.9 kcal mol^{-1} obtained by Keesee and Castleman (31) in a temperature dependent study of clustering equilibria of Cl^- with SO_2. In addition, our value of 8.4 kcal mol^{-1} for ΔG_{11}^0 for H_2O is in excellent agreement with that of Kebarle and co-workers (15) of 8.2 kcal mol^{-1} from an HPMS temperature dependent study of clustering equilibria, and in reasonable agreement with the values of 8.8 kcal mol^{-1} and 9.0 kcal mol^{-1} obtained by Burdett and Heyhurst (32) and Keesee and Castleman (31) respectively. Excellent agreement between our work and that of Kebarle and co-workers (15) is also obtained for ΔG_{11}^0 values for chlorobenzene, acetone, and methanol, and good agreement for data for HCl and acetic acid. The single case where serious disagreement between the present data and other studies of clustering equilibria occurs is for formic acid. In early work, Yamdagni and Kebarle (13) reported a value of ΔG_{11}^0 of 25.4 kcal mol^{-1} employing neat formic acid. However, in a more recent study (15), this value has been revised to 20.1 kcal mol^{-1} using formic acid as a constituent in methane bath gas. This value is still somewhat larger than the presently obtained value of 18.4 kcal mol^{-1}. Given the known tendency of formic acid to undergo pyrolysis (33) at the highest temperatures employed in the HPMS study, it may be that partial decomposition of formic acid is occurring above 600 K leading to an erroneous van't Hoff plot. We thus believe the ICR value for formic acid is more reliable.

Entropies of association, ΔS_{11}^0, for hydrogen bonded chloride adducts were calculated by a statistical thermodynamic method derived previously (34) using eq. [13].

$$[13]\quad \Delta S_{11}^0 = R\left(8.98 + 1.5 \ln \Delta H_{11}^0 - 2 \ln l + \ln \frac{\sigma_{MCl^-}}{\sigma_M}\right) + \Delta S_v'$$

The enthalpy change ΔH_{11}^0 is obtained by successive iterations using ΔG_{11}^0 and calculated ΔS_{11}^0 values; l, the hydrogen bond distance is estimated from *ab initio* calculations; σ is the symmetry number of the molecule or ion; and $\Delta S_v'$ is a small negative correction to ΔS_{11}^0 due to low frequency vibrations of hydrogen bonded species using formulae for classical oscillators. The value of ΔS_{11}^0 for SO_2Cl^- was calculated using the

Can. J. Chem. Downloaded from www.nrcresearchpress.com by 210.87.254.105 on 09/06/12
For personal use only.

known vibrational frequencies (35) and estimated bond distances while values for PF_3Cl^- and $ClB(Et)_3^-$ were estimated from similar compounds. These entropy values are all also summarized in Table 1. In addition the enthalpy changes, ΔH^0_{11} determined from the experimental ΔG^0_{11} values and calculated ΔS^0_{11} values are included in Table 1.

Conclusions

The experiments described above provide the methodology for the convenient generation of chloride ion adducts of both Lewis and Brønsted acids at low pressures via bimolecular reaction sequences. The quantitative scale of chloride ion binding energetics developed provides a convenient series of reference compounds relative to which chloride affinities of most common organic and inorganic species may be readily determined. We are currently in the process of determining chloride affinities of a wide variety of compounds in order to determine intrinsic factors affecting hydrogen bond strengths and anion binding energies.

Acknowledgement

Generous financial support from the Natural Sciences and Engineering Research Council of Canada is gratefully acknowledged.

1. P. KEBARLE. Ann. Rev. Phys. Chem. **28**, 445 (1977).
2. J. F. WOLF, R. H. STALEY, I. KOPPEL, M. TAAGEPERA, R. T. McIVER, JR., J. L. BEAUCHAMP, and R. W. TAFT. J. Am. Chem. Soc. **99**, 5417 (1977).
3. D. H. AUE and M. T. BOWERS. *In* Gas phase ion chemistry. Vol. 2. *Edited by* M. T. Bowers. Academic Press, New York. 1979.
4. J. E. BARTMESS and R. T. McIVER, JR. *In* Gas phase ion chemistry. Vol. 2. *Edited by* M. T. Bowers. Academic Press, New York. 1979.
5. T. B. McMAHON and P. KEBARLE. J. Am. Chem. Soc. **98**, 3399 (1976).
6. T. B. McMAHON and P. KEBARLE. J. Am. Chem. Soc. **99**, 2222 (1977).
7. E. M. ARNETT, F. M. JONES, M. TAAGEPERA, W. G. HENDERSON, J. L. BEAUCHAMP, D. HOLTZ, and R. W. TAFT. J. Am. Chem. Soc. **94**, 4724 (1972).
8. I. DZIDIC and P. KEBARLE. J. Phys. Chem. **74**, 1466 (1970).
9. M. ARSHADI, R. YAMADAGNI, and P. KEBARLE. J. Phys. Chem. **74**, 1475 (1970).
10. W. R. DAVIDSON, J. SUNNER, and P. KEBARLE. J. Am. Chem. Soc. **101**, 1675 (1979).
11. J. W. LARSON and T. B. McMAHON. J. Am. Chem. Soc. **104**, 6255 (1982).
12. P. KEBARLE, W. R. DAVIDSON, M. FRENCH, J. B. CUMMING, and T. B. McMAHON. Faraday Discuss. Chem. Soc. **64**, 220 (1978).
13. R. YAMDAGNI and P. KEBARLE. J. Am. Chem. Soc. **93**, 7139 (1971).
14. R. YAMDAGNI and P. KEBARLE. Can. J. Chem. **52**, 2449 (1974).
15. M. A. FRENCH, S. IKUTA, and P. KEBARLE. Can. J. Chem. **60**, 1907 (1982).
16. T. B. McMAHON and C. J. NORTHCOTT. Can. J. Chem. **56**, 1069 (1978).
17. J. W. LARSON and T. B. McMAHON. J. Am. Chem. Soc. **104**, 5848 (1982).
18. S. A. SULLIVAN and J. L. BEAUCHAMP. Int. J. Mass Spectrom. Ion Phys. **28**, 69 (1976).
19. B. S. AULT. J. Phys. Chem. **84**, 3448 (1980).
20. B. S. AULT. Acc. Chem. Res. **15**, 103 (1982).
21. J. W. LARSON and T. B. McMAHON. J. Am. Chem. Soc. **105**, 2944 (1983).
22. J. M. RIVEROS. Adv. Mass Spectrom. **6**, 277 (1974).
23. J. M. RIVEROS, P. W. TIEDEMAN, and A. C. BREDA. Chem. Phys. Lett. **20**, 345 (1973).
24. W. N. OLMSTEAD and J. I. BRAUMANN. J. Am. Chem. Soc. **99**, 4219 (1977).
25. M. S. FOSTER and J. L. BEAUCHAMP. Chem. Phys. Lett. **31**, 479 (1975).
26. T. B. McMAHON and J. L. BEAUCHAMP. Rev. Sci. Instrum. **43**, 509 (1973).
27. T. A. LEHMAN and M. M. BURSEY. Ion cyclotron resonance spectroscopy. Wiley-Interscience, New York. 1976.
28. J. L. BEAUCHAMP. Ann. Rev. Phys. Chem. **22**, 517 (1971).
29. R. G. KEESEE, N. LEE, and A. W. CASTLEMAN, JR. J. Chem. Phys. **73**, 2195 (1980).
30. F. C. FEHSENFELD and E. E. FERGUSON. J. Chem. Phys. **61**, 3181 (1974).
31. R. G. KEESEE and A. W. CASTLEMAN, JR. Chem. Phys. Lett. **74**, 139 (1980).
32. N. A. BURDETT and A. N. HEYHURST. J. Chem. Soc. Faraday Trans. I **78**, 2997 (1982).
33. C. HINSHELWOOD. Proc. R. Soc. A**255**, 444 (1960).
34. J. W. LARSON and T. B. McMAHON. J. Phys. Chem. Submitted for publication.
35. D. F. BUROW. Inorg. Chem. **11**, 573 (1972).
36. R. C. DOUGHERTY, J. DALTON, and J. D. ROBERTS. Org. Mass Spectrom. **8**, 77 (1974).

Can. J. Chem. Downloaded from www.nrcresearchpress.com by 210.87.254.105 on 09/06/12
For personal use only.

Étude théorique de la structure du phosphate d'isaxonine

JEAN-PIERRE MONTI
Laboratoire de Biophysique, Faculté de Pharmacie, 27 Boul. J. Moulin, 13385 Marseille Cedex 5, France
MARCEL SARRAZIN[1]
Laboratoire de Physique Pharmaceutique, Faculté de Pharmacie, 27 Boul. J. Moulin, 13385 Marseille Cedex 5, France
ET
PIERRE BROUANT
Laboratoire de Chimie Thérapeutique, Faculté de Pharmacie, 27 Boul. J. Moulin, 13385 Marseille Cedex 5, France

Reçu le 8 juillet 1983

JEAN-PIERRE MONTI, MARCEL SARRAZIN et PIERRE BROUANT. Can. J. Chem. **62**, 680 (1984).

Les auteurs étudient les protonations du phosphate d'isaxonine au moyen des méthodes quantiques CNDO/2 et CNDO/S et comparent les résultats théoriques aux résultats expérimentaux publiés précédemment. Les indices de Wiberg et les pourcentages de caractère *S* calculés à partir des populations électroniques permettent de prévoir correctement les variations des longueurs et des angles de liaisons ainsi que les valeurs des constantes de couplage $J_{^{13}C-H}$. Enfin, le calcul de la constante d'écran conduit à une bonne prédiction des variations des déplacements chimiques des protons lors des protonations de la molécule.

JEAN-PIERRE MONTI, MARCEL SARRAZIN, and PIERRE BROUANT. Can. J. Chem. **62**, 680 (1984).

Protonations of isaxonine phosphate are studied by performing CNDO/2 and CNDO/S molecular orbital calculations. Results are compared with previously published data. Wiberg's bond indices and *S* character percentages calculated using electronic populations are shown to correctly predict variations of bond lengths and bond angles as well as $J_{^{13}C-H}$ coupling constants. A good prediction of proton chemical shift variations using a calculation of the screening constant was obtained.

Can. J. Chem. Downloaded from www.nrcresearchpress.com by 210.87.254.6 on 09/06/12
For personal use only.

Introduction

Récemment est apparue une nouvelle molécule, le phosphate d'isaxonine (isopropyl amine pyrimidine phosphate; IAPP), spécifiquement neurotrope et susceptible de favoriser la croissance et la régénération des neurones (1). Cette activité parait liée à une augmentation de la synthèse de la tubuline ou à une accélération de sa polymérisation (2).

L'isaxonine est actuellement la seule molécule présentant cette propriété, ce qui lui a permis d'être utilisé dans le traitement de certaines neuropathies. Une première étude par des méthodes spectrales (3) nous a déjà permis de mieux connaître la réactivité de l'isaxonine en solution. Cependant, il nous a paru nécessaire, dans un deuxième temps, de faire appel aux méthodes de calcul de la chimie théorique afin de préciser la structure et la réactivité de cette molécule.

Ceci nous amenera à vérifier la qualité des résultats théoriques par comparaison avec les résultats expérimentaux obtenus précédemment (3).

I. Méthodes théoriques et géométrie

Nous avons appliqué les méthodes quantiques CNDO/2 de Pople *et al.* (4, 5) et CNDO/S de Del Bene et Jaffe (6) sans interaction de configuration, et avec leur paramétrisation originale. Ces deux méthodes, compte tenu du niveau d'approximation, conduisent à de bons résultats qualitatifs. Cependant, un type de paramétrisation ne peut, en général, rendre compte quantitativement de plusieurs grandeurs à la fois. En effet, les propriétés moléculaires où les orbitales π jouent un rôle prépondérant sont mieux décrites par la CNDO/S, alors que la répartition électronique au voisinage des atomes d'hydrogène est meilleure à l'aide de la CNDO/2 (7).

En l'absence de résultats expérimentaux en phase non condensée (microondes, diffraction électronique), nous avons utilisé pour le calcul de l'isaxonine base (IAP) la géométrie du cycle amino-2 pyrimidine déterminée par Scheinbeim et Schempp (8) en phase solide au moyen des rayons X.

La valeur de la constante de couplage $^3J_{NH-CH}$ égale à 8,0 Hz (3), nous a amené à adopter un angle diédre entre les liaisons N—H et C—H de 155°, valeur calculée en utilisant une relation de type Karplus (9).

Pour les deux groupements méthyles nous avons utilisé des angles et des longueurs de liaisons habituels (10).

Les spectres rmn montrent que les deux atomes d'azote intracycliques sont suceptibles d'être protonés et font apparaître le rôle joué par la taille du substituant alkyle (3). De ce fait, nous avons choisi d'effectuer le calcul des formes monoprotonée en N_1 (IAPP) et diprotonée en N_1 et N_3 (IAPDP) en adoptant des longueurs de liaison N^+—H égales à 1,083 Å (10).

La numérotation et le système d'axes employés dans les calculs sont donnés dans la figure 1.

II. Résultats et discussion

1. *Les énergies des niveaux occupés*

En l'absence de résultats expérimentaux quant aux potentiels d'ionisation de l'isaxonine, nous avons choisi de comparer nos résultats théoriques avec les potentiels d'ionisation obtenus pour la pyrimidine, expérimentalement (11) et par une méthode *ab initio* STO-3G (12).

En effet, la présence de la chaîne alkyle ne doit perturber que faiblement l'énergie des niveaux supérieurs, essentiellement de symétrie *n* ou π.

Les énergies des dernières orbitales moléculaires occupées sont présentées dans la figure 2.

On note tout d'abord le bon accord entre le classement des niveaux de la méthode CNDO/S et celui de la méthode *ab initio:* $\pi_3 < n_A < \pi_2 < n_S$. De plus ces deux méthodes conduisent à des coefficients des fonctions d'onde peu différents. Comparativement aux valeurs du premier potentiel d'ionisation (P.I.) (8,98 eV en STO-3G et 9,58 eV en CNDO/S), on observe une augmentation de la stabilité des niveaux n_A, π_2 et n_S de

[1]Auteur à qui la correspondance doit être envoyée.

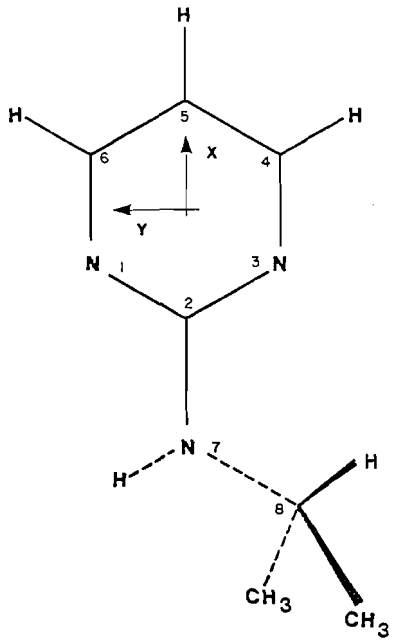

FIG. 1. Structure moléculaire de l'isaxonine (IAP) et numérotation employée.

l'IAP, alors que les différences d'énergie de ces niveaux sont conservées. Notons que pour la molécule d'IAP, calculée en CNDO/S, l'orbitale dans laquelle intervient principalement le doublet libre de l'azote N_7 est située entre les niveaux π_2 et n_S.

Le méthode CNDO/2 fournit des résultats indiquant une stabilisation apparemment plus forte des niveaux ($P.I._{\pi_3}$ = 11,10 eV), tout en perturbant leur ordre: $\pi_3 < n_A < n_S < \pi_2 < \pi$.

Ainsi la méthode CNDO/S conduit à des résultats plus proches de ceux obtenus pour la pyrimidine à l'aide de la méthode *ab initio*. Cependant cette dernière méthode ne permettait pas de rendre compte de l'ordre expérimental des potentiels d'ionisation de la pyrimidine: $n_A < \pi_3 < n_S < \pi_2$. Du fait de sa paramétrisation qui déstabilise les niveaux π, la CNDO/S ne donne pas non plus le classement attendu pour la molécule d'IAP, tout en conduisant à des valeurs des énergies plus cohérentes que celles obtenues par CNDO/2.

2. *Les charges électroniques et les grandeurs associées*

(a) *Les charges électroniques*

Le tableau 1 regroupe les valeurs des charges électroniques des atomes de l'IAP, l'IAPP et de l'IAPDP calculées par les méthodes CNDO/2 et CNDO/S. La protonation sur les atomes d'azote intracycliques est confirmée par les valeurs des densités de charge en N_1, N_3, et N_7. En effet, les deux méthodes de calcul attribuent pour la forme non protonée les charges électroniques les plus élevées aux atomes N_1 et N_3. Mais ces deux valeurs, peu différentes, ne permettent pas de prévoir le site de la protonation. Cependant, le calcul effectué sur les formes monoprotonée en N_1 et monoprotonée en N_3 montre que cette dernière est la moins stable, ce qui donne du poids à l'hypothèse de la protonation sur l'atome d'azote intracyclique le moins encombré. De plus, la formation de la liaison N^+—H s'accompagne d'une diminution de la densité de charge de l'azote, diminution qui est le reflet de la transformation du doublet libre de l'hétéroatome en l'orbitale σ de la liaison N^+—H.

Les protonations successives entrainent la diminution des charges totales de tous les protons à l'exception de celle de l'hydrogène 8 de la forme IAPDP. Cette variation des charges est en bon accord avec les déblindages observés en rmn pour tous les protons lorsque l'on passe de la forme IAP non protonée à la forme IAPP monoprotonée puis à la forme IAPDP diprotonée (3). En effet, pour des séries homogènes de molécules, il est classique de considérer que la constante d'écran des protons dépend essentiellement du terme diamagnétique, lui même proportionnel à la densité électronique du noyau (13). A une diminution de la densité électronique correspond alors une diminution de la constante d'écran ce qui traduit bien le déblindage observé par rmn pour chacun des protons.

L'examen du tableau 1 fait également apparaître une diminution de la charge totale de chacun des atomes de carbone aromatique lors des protonations successives. Cette diminution, notable pour les carbones C_2, C_4 ou C_6 (de l'ordre de −0,060 en CNDO/2 et −0,080 en CNDO/S), est nettement plus faible pour le carbone C_5 (de l'ordre de −0,013 en CNDO/2 et −0,036 en CNDO/S). Des effets analogues ont déjà été mis en évidence par Pugmire *et al.* (14) dans le cas de la pyrimidine en utilisant la méthode EHT ou dans le cas d'hétérocycles azotés apparentés par la méthode CNDO-SCF-MO (15, 16). Mais contrairement aux protons, dans le cas des atomes de carbone, il est plus difficile de relier ces variations des charges aux variations des déplacements chimiques. En effet, il n'est plus possible de négliger l'effet des orbitales *p* donc du terme paramagnétique de la constante d'écran dont le calcul fait intervenir les populations de liaison entre les atomes voisins. Nous discuterons de la validité des approximations mises en oeuvre pour ce calcul dans le paragraphe se rapportant aux déplacements chimiques des atomes de carbone.

(b) *Les déplacements chimiques des protons*

Il est classique d'essayer de corréler le déplacement chimique des protons avec les charges électroniques des atomes qui les portent. Dans notre cas, la corrélation étendue à tous les protons n'est pas significative, tant en CNDO/2 (r = 0,467) qu'en CNDO/S (r = 0,678). Par contre, la corrélation est d'une bonne qualité si l'on considère seulement les protons de l'hétérocycle (r = 0,969 en CNDO/2; r = 0,984 en CNDO/S) pour lesquels l'effet des charges sur les déplacements chimiques provient essentiellement des charges π (r = 0,964 en CNDO/2; r = 0,974 en CNDO/S).

L'impossibilité de corréler les déplacements chimiques de tous les protons avec les densités de charge provient du fait que celles-ci n'interviennent que pour une part dans l'expression de la constante d'écran (17–20).

$$[1] \quad \sigma_{ppm} = \sigma_q + \sigma_{CC} + \sigma_{CE} + \sigma_A + \sigma_{solv.}$$

où σ_q est l'effet dû aux charges, σ_{CC} l'effet dû au courant de cycle, σ_{CE} l'effet dû aux doublets non partagés, σ_A l'effet dû à l'anisotropie des hétéroatomes et enfin $\sigma_{solv.}$ est l'effet dû à la solvatation. Nous avons utilisé pour le calcul de chacune de ces contributions les expressions classiques suivantes (21–25):

$$[2] \quad \sigma_q = 12{,}5 \sum_i \frac{\Delta q_i \cos\theta_i}{R_i^2} - 17{,}0 \left(\sum_i \frac{\Delta q_i}{R_i^2} \right)^2$$

où Δq_i: excès de charge p_z sur l'atome i; R_i: distance H$\cdots i$; θ_i: angle C—H$\cdots i$.

$$[3] \quad \sigma_{CC} = \frac{12(2Z_N^2 - \rho_N)}{a(\rho_N^2 + Z_N^2)^{5/2}}$$

où a: rayon moyen du cycle; ρ_N et Z_N: coordonnées cylindriques

Can. J. Chem. Downloaded from www.nrcresearchpress.com by 210.87.254.6 on 09/06/12
For personal use only.

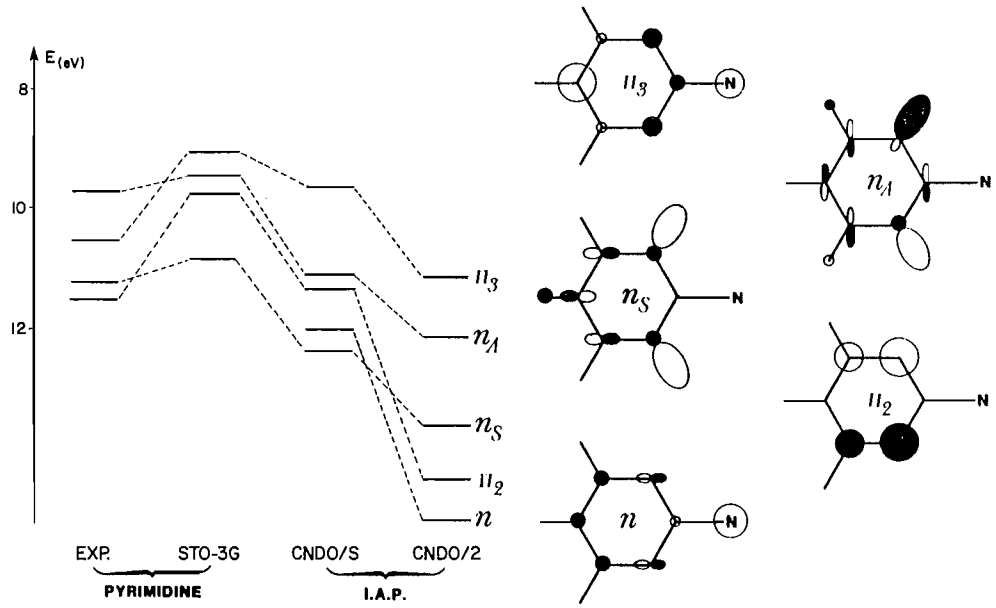

FIG. 2. Comparaison entre les valeurs des potentiels d'ionisation de l'IAP et de la pyrimidine et diagramme des orbitales moléculaires correspondantes de l'IAP.

TABLEAU 1. Densités de charge totale et densités de charge dans l-orbitale p_z

	IAP				IAPP				IAPDP			
	CNDO/2		CNDO/S		CNDO/2		CNDO/S		CNDO/2		CNDO/S	
Atomes	$Q_{Tot.}$	Q_{p_z}	$Q_{Tot.}$	Q_{p_z}	$Q_{Tot.}$	Q_{p_z}	$Q_{Tot.}$	Q_{p_z}	$Q_{Tot.}$	Q_{p_z}	$Q_{Tot.}$	Q_{p_z}
N_1	5,248	1,195	5,315	1,304	5,073	1,513	5,109	1,657	5,073	1,511	5,091	1,649
C_2	3,674	0,860	3,691	0,773	3,614	0,802	3,588	0,698	3,562	0,784	3,511	0,655
N_3	5,247	1,195	5,314	1,303	5,194	1,204	5,283	1,314	5,076	1,509	5,097	1,643
C_4	3,852	0,887	3,883	0,802	3,806	0,846	3,812	0,768	3,725	0,718	3,726	0,627
C_5	4,106	1,116	4,079	1,132	4,084	1,092	4,040	1,090	4,080	1,097	4,006	1,080
C_6	3,853	0,887	3,885	0,802	3,784	0,772	3,783	0,658	3,726	0,718	3,729	0,626
H_4	1,012		0,941		0,945		0,902		0,893		0,860	
H_5	1,000		0,979		0,930		0,934		0,867		0,896	
H_6	1,012		0,941		0,950		0,898		0,894		0,861	
N_7	5,223	1,779	5,239	1,820	5,191	1,707	5,209	1,758	5,153	1,616	5,164	1,675
C_8	3,861	1,004	3,933	1,026	3,858	1,034	3,931	1,044	3,867	1,050	3,936	1,053
C*(CH_3)	4,031	1,007	4,065	1,011	4,037	1,004	4,057	1,006	4,043	1,008	4,049	1,006
H_7	0,883		0,862		0,856		0,845		0,808		0,813	
H_8	1,010		0,959		0,992		0,952		0,999		0,958	
H*(CH_3)	0,993		0,975		0,974		0,966		0,954		0,956	

* Valeurs moyennes.

du proton par rapport au centre du cercle (en unité de rayon).

$$[4] \quad \sigma_{CE} = -2{,}7 \times 10^{-12} \frac{\mu}{R^3} (3 \cos \phi_1 \cos \phi_2 - \cos \phi_3)$$

où ϕ_1: angle entre le moment dipolaire $\vec{\mu}$ dû au doublet libre de l'azote et la direction N···H; ϕ_2: angle entre N···H et la liaison C—H; ϕ_3: angle entre $\vec{\mu}$ et C—H.

$$[5] \quad \sigma_A = \frac{1}{3NR^3} \sum_i \chi_i (1 - 3 \cos^2 \theta_i)$$

où χ_i: composantes de la susceptibilité magnétique moléculaire de l'hétéroatome; θ_i: angle entre la direction i et la direction N···H.

$$[6] \quad \sigma_{solv.} = -2{,}7 \times 10^{-12} \frac{2(\epsilon - 1)(n^2 - 1)}{3(2\epsilon + n^2)\alpha} \mu \cos \theta$$

où ϵ: constante diélectrique du solvant; n: indice de réfraction du soluté; α: polarisabilité du soluté; θ: angle entre $\vec{\mu}$ et la liaison C—H.

Nous avons rapporté dans la figure 3 les déplacements chimiques expérimentaux en fonction des constantes calculées à partir des résultats de la CNDO/S. Cette figure nous a conduit encore une fois à considérer séparement les protons de l'hétérocycle de ceux de la chaîne isopropylamine. On obtient alors les relations linéaires suivantes:

$$\delta_{H_{cycle}} = -0{,}36\,\sigma + 6{,}44 \qquad r = 0{,}990$$

$$\delta_{H_{chaîne}} = -0{,}96\,\sigma + 2{,}38 \qquad r = 0{,}973$$

Les valeurs des coefficients de corrélation, plus élevées que précedemment, notamment dans le cas des protons de la chaîne pour lesquels aucune relation significative n'avait été obtenue, traduisent l'amélioration dûe à l'introduction des termes σ_{CC},

Can. J. Chem. Downloaded from www.nrcresearchpress.com by 210.87.254.6 on 09/06/12
For personal use only.

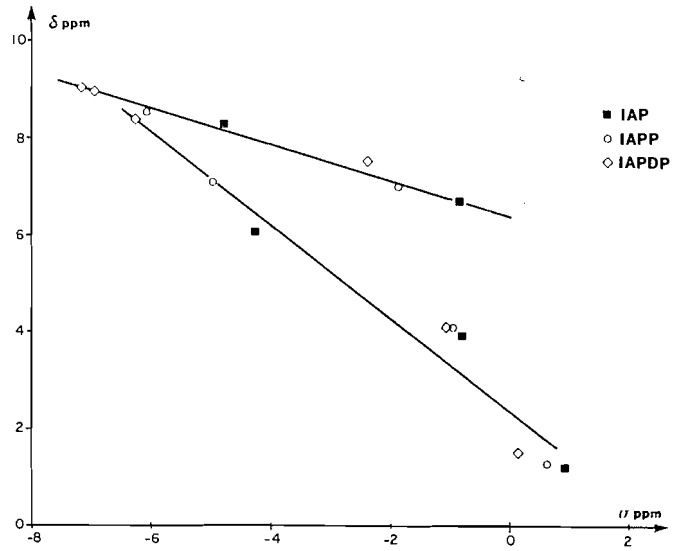

FIG. 3. Correlation entre les déplacements chimiques expérimentaux des protons et les constantes d'écran calculées (CNDO/S).

σ_{CE}, σ_A, $\sigma_{solv.}$.

Ainsi, seul le calcul de tous les termes de la constante d'écran conduit pour les deux classes de protons à une excellente estimation des déplacements chimiques et de leurs variations lors des protonations successives de la molécule d'IAP.

Notons enfin que les résultats obtenus à partir des calculs de la méthode CNDO/2 sont voisins mais que les regressions sont moins significatives.

(c) *Les déplacements chimiques des carbones*

Dans un premier temps, nous avons essayé d'établir des relations classiques entre les déplacements chimiques et les charges électroniques des carbones. Aucune de ces relations ne s'est révélée significative.

Nous avons alors envisagé un calcul plus élaboré de la constante d'écran qui peut être décomposée en une somme de termes (26, 27):

$$[7] \quad \sigma = \sigma_{dia} + \sigma_{para} + \sigma_A + \sigma_{solv.}$$

où σ_{dia} et σ_{para} sont respectivement les contributions diamagnétiques et paramagnétiques de l'atome considéré, σ_A est la contribution due à l'anisotropie des atomes voisins et $\sigma_{solv.}$ est la contribution due au solvant.

Là encore, les calculs n'ont pas permis d'obtenir de relations fortement significatives tant pour les atomes de carbone aromatique que pour les atomes de carbone aliphatique. ($r < 0{,}94$ en CNDO/S). Cet échec semble provenir du terme paramagnétique dont la contribution est prépondérante (28). En effet, la protonation de l'atome d'azote conduit à une diminution des populations des liaisons engagées par celui-ci. Ceci a pour effet de diminuer la valeur du terme d'écran paramagnétique (16). De plus la protonation élimine les niveaux de basse énergie associés aux doublets libres des atomes d'azote ce qui augmente l'énergie moyenne d'excitation et diminue encore la contribution paramagnétique (16, 17). Ces deux effets conduisent à prévoir pour tous les atomes de carbone un déplacement vers les champs forts consécutif à la protonation. Le calcul rend bien compte du blindage observé pour les carbones de l'IAPP mais il n'est pas vérifié expérimentalement dans le cas des carbones C_4, C_5 et C_6 de la molécule diprotonée IAPDP ni dans le cas des carbones C_8 des formes IAPP et IAPDP pour lesquels on observe un déplacement vers les champs faibles lors des protonations (3).

Il faut noter que Fliszar *et al.* (29) ont montré que, dans une série de molécules aromatiques, les charges σ et π varient en sens contraire. À ces variations sont associées des variations des déplacements chimiques, une diminution de la charge σ se traduisant par un effet de blindage. Les résultats portés dans le tableau 1 et inteprétés selon les conclusions de Fliszar (29) nous permettent de prédire qualitativement le blindage du carbone C_2 lors des deux protonations et le blindage du carbone C_4 lors de la première protonation puis son déblindage lors de la seconde. Cependant, il n'est pas possible de rendre compte des déplacements chimiques des carbones C_5 et C_6.

Au contraire, dans le cas de carbones sp^3, à l'augmentation de la densité de charge de l'orbitale $2s$ correspond un déplacement vers les champs faibles (29). Dans ces conditions les variations de la charge de l'orbitale $2s$ des carbones des groupements méthyl et du carbone C_8 (Tableau 2) permettent de prédire qualitativement le blindage observé pour les premiers et le déblindage observé pour le dernier lors des protonations.

3. *Les liaisons et les grandeurs associées*

(a) *Les indices de liaison*

Plusieurs indices de liaison ont été proposés par les auteurs afin de rendre compte des liaisons dans les molécules (30–32). Nous avons pour notre part choisi d'utiliser l'indice de Wiberg (30) dont l'application peut être étendue au calcul de l'hybridation (33). Dans le cas d'une liaison A—B, l'indice W_{AB} est égal à la somme des carrés des populations électroniques $P_{\mu\nu}$, où les orbitales atomiques μ et ν appartiennent aux atomes A et B.

$$[8] \quad W_{AB} = \sum_{\mu \in A} \sum_{\nu \in B} P_{\mu\nu}^2$$

Les valeurs des indices de liaison de l'IAP, l'IAPP et l'IAPDP calculées en utilisant les populations électroniques de la CNDO/S sont données dans le tableau 3. La comparaison des indices des liaisons C—C et C—N permet de constater que la valeur la plus faible est obtenue pour la liaison N_7—C_8 et que cette valeur diminue encore lors des protonations du cycle pyrimidique. Il est difficile de relier la valeur d'un indice qui reflète la stabilité intrinsèque d'une liaison (34, 35) avec l'énergie requise pour rompre celle-ci en spectrométrie de masse. Toutefois, l'énergie de chacune des liaisons est un des facteurs intervenant dans la production des différents fragments (36). Aussi, sans vouloir en tirer de règles générales, nous constaterons simplement que les valeurs faibles de l'indice de Wiberg pour les liaisons N_7—C_8 vont de pair avec la possibilité de rupture de ces liaisons mise en évidence par spectrométrie de masse pour l'IAP et l'IAPP (3).

La déstabilisation de cette liaison va de pair avec le gain de stabilité de la liaison C_2—N_7. En effet, pour l'IAP, la valeur de l'indice de la liaison C_2—N_7, intermédiaire entre celles d'une liaison σ et celle d'une liaison π, traduit la faible conjugaison du doublet libre de l'azote N_7. Cette valeur se trouve très fortement accrue par les deux protonations. L'augmentation du caractère π est bien retrouvée experimentalement. En effet, les spectres rmn montent que la libre rotation autour de la liaison C_2—N_7 de l'IAP, ralentie par la première protonation, est empêchée dans le cas de la molécule d'IAPDP (3).

L'analyse des indices des liaisons du cycle pyrimidique permet ainsi de noter l'augmentation de la valeur obtenue pour la liaison entre le carbone en position *ortho* et le carbone en

Can. J. Chem. Downloaded from www.nrcresearchpress.com by 210.87.254.6 on 09/06/12
For personal use only.

TABLEAU 2. Densités de charge dans l'orbitale 2*s*

	IAP		IAPP		IAPDP	
Atomes	CNDO/2	CNDO/S	CNDO/2	CNDO/S	CNDO/2	CNDO/S
C_8	0,962	1,002	0,966	1,005	0,975	1,011
C* (CH_3)	1,028	1,022	1,027	1,020	1,027	1,019

* Valeurs moyennes.

TABLEAU 3. Indices de liaison W_{AB} calculés à partir des résultats de la méthode CNDO/S

Liaisons	IAP	IAPP	IAPDP
N_1—H		0,9453	0,9291
N_3—H			0,9146
C_4—H	0,9827	0,9782	0,9697
C_5—H	0,9859	0,9816	0,9750
C_6—H	0,9842	0,9764	0,9697
N_7—H	0,9675	0,9601	0,9497
C_8—H	0,9833	0,9842	0,9797
N_1—C_2	1,3542	1,2036	1,2175
C_2—N_3	1,3524	1,3563	1,2188
N_3—C_4	1,4061	1,4047	1,2139
C_4—C_5	1,4365	1,3349	1,4561
C_5—C_6	1,4360	1,5720	1,4562
C_6—N_1	1,4069	1,2012	1,2135
C_2—N_7	1,1215	1,1945	1,3531
N_7—C_8	0,9726	0,9493	0,9288
C_8—Me	1,0809	1,0041	0,9970

position *meta* de l'azote protoné, ce qui traduit le raccourcissement de cette liaison. De plus, la formation de la liaison N^+—H s'accompagne d'une perte partielle de la conjugaison des liaisons engagées par l'atome d'azote et de la liaison entre le carbone *méta* et le carbone *para*, donc d'un allongement de celles ci, comme en témoigne la diminution des valeurs des indices de ces liaisons.

Ces effets mis en évidence par la méthode CNDO/S ont déjà été observés dans le cas de la protonation de la purine, experimentalement au moyen des rayons X (37) et théoriquement par un calcul CNDO-SCF-MO (15, 16).

Les résultats obtenus à partir des populations électroniques de la CNDO/2 conduisent aux mêmes conclusions.

À des modifications des longueurs de liaisons lors des protonations correspondent des modifications des angles internucléaires et interorbitaux.

(b) *Les angles interorbitaux*

Dans le cas d'une liaison de type sp_2 entre les atomes A et B, le rapport des populations électroniques:

$$[9] \quad S_{A\to B} = \frac{\sum_{\nu} P^2_{2s_A - \nu_B}}{\sum_{\nu} (P^2_{2s_A - \nu_B} + P^2_{2px_A - \nu_B} + P^2_{2py_A - \nu_B})}$$

est une mesure du pourcentage du caractère *S* de l'orbitale hybride centrée sur A et dirigée vers B (33). Connaissant les pourcentages $S_{A\to B}$ et $S_{A\to C}$ on peut alors calculer l'angle interorbital η_{B-A-C} en utilisant la formule (38):

$$[10] \quad \cos \eta_{B-A-C} = -\frac{S_{A\to B} \times S_{A\to C}}{(1 - S_{A\to B})(1 - S_{A\to C})}$$

Seules les valeurs correspondant à la géométrie de l'hétérocycle, qui présentent les plus fortes variations, sont reportées dans le tableau 4.

TABLEAU 4. Angles interorbitaux du cycle pyrimidique calculés à partir des résultats de la méthode CNDO/S

Angles	IAP	IAPP	IAPDP
N_1—C_2—N_3	122,2	121,5	121,1
C_2—N_3—C_4	113,3	110,7	120,0
N_3—C_4—C_5	120,5	119,9	119,3
C_4—C_5—C_6	122,0	120,9	120,0
C_5—C_6—N_1	120,5	119,8	119,3
C_6—N_1—C_2	111,4	121,2	120,3

On observe principalement une augmentation de l'angle interorbital porté par l'atome d'azote protoné. Une variation analogue de l'angle internucléaire C—N—C de la purine a été mise en évidence théoriquement par la méthode MNDO (39) et expérimentalement au moyen des rayons X (37).

Les valeurs calculées pour les angles portés par les atomes de carbone laissent supposer une tendance à la fermeture lors des protonations. Bien qu'ici cette variation soit faible, elle a été observée dans le cas de l'angle internucléaire N—C—C de la pyrimidine (39).

(c) *Les constantes de couplage* J^{13}_{C-H}

En première approximation, la constante de couplage entre les spins nucléaires d'un atome de carbone ^{13}C et d'un atome d'hydrogène qui lui est lié est directement proportionnelle au pourcentage de caractère *S* de l'orbitale hybride assurant la liaison (40). Cependant, de nombreux auteurs ont montré qu'un terme constant, corrigeant certaines approximations, devait être soustrait afin d'obtenir une bonne concordance entre les valeurs expérimentales et les valeurs calculées (41–44).

Les pourcentages de caractères *S* calculés utilisant la relation (33):

$$[11] \quad S_{C-H} = \frac{P^2_{2S_C - S_H}}{\sum_{\nu \epsilon C} P^2_{\nu - S_H}}$$

ont été corrélés aux valeurs expérimentales de J_{C-H}.

La méthode des moindres carrés conduit aux relations linéaires:

$$J_{C-H_{exp.}} = 709\, S_{C-H} - 41 \qquad r = 0{,}976$$

dans le cas de la CNDO/2, et

$$J_{C-H_{exp.}} = 685\, S_{C-H} - 38 \qquad r = 0{,}983$$

dans le cas de la CNDO/S (Fig. 4).

Les paramètres des deux relations sont trés proches de ceux obtenus dans le cas de travaux similaires utilisant la méthode INDO et un calcul plus élaboré des constantes de couplage (45) on une méthode adoptant le critère du recouvrement maximal (46, 47).

Can. J. Chem. Downloaded from www.nrcresearchpress.com by 210.87.254.6 on 09/06/12
For personal use only.

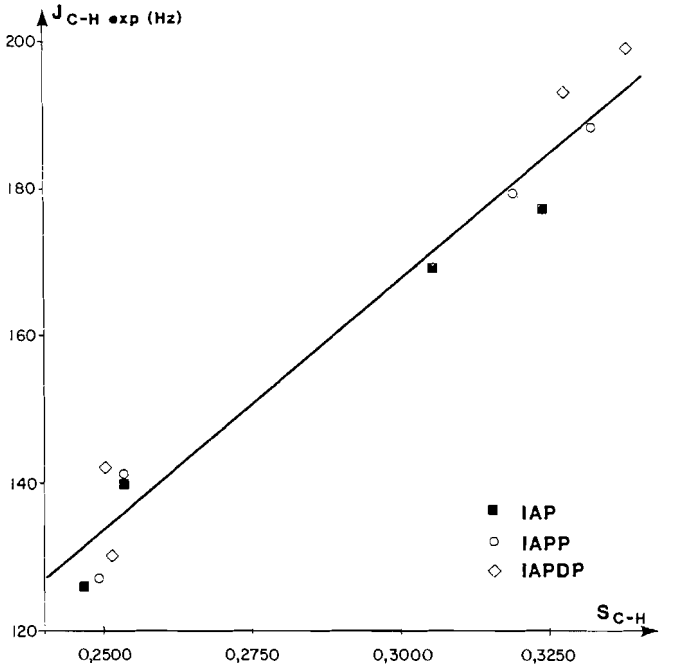

FIG. 4. Correlation entre les constantes de couplages $J_{^{13}C-H}$ expérimentales et les pourcentages de caractère S calculés (CNDO/S).

L'augmentation des valeurs expérimentales des constantes de couplage lors des protonations, plus marquée pour les liaisons C—H de l'hétérocycle, est bien traduite par les deux relations. Elle peut être attribuée sans ambiguité à une augmentation du caractère S consécutive aux variations de la géométrie et au transfert des charges électroniques que nous avons précédemment mis en évidence.

Conclusions

Aucune des méthodes CNDO n'a permis de rendre compte de l'énergie des niveaux électroniques correspondant aux doublets libres des atomes d'azote. L'échec provient de l'incapacité des deux méthodes à décrire les électrons des doublets libres.

L'analyse des charges électroniques montre qu'à leurs variations lors des protonations correspondent des modifications des déplacements chimiques des protons. Ces résultats expérimentaux ont été bien rendus par un calcul de la constante d'écran.

Il n'a pas été possible, dans le cas des atomes de carbone de rendre compte des déplacements chimiques par le calcul. Il convient de noter qu'une comparaison des variations des densités de charge permet de prédire avec succés les déplacements chimiques de la majorité des atomes de carbone.

Les deux protonations successives de la molécule d'IAP augmentent la stabilité de la liaison C_2—N_7 et déstabilisent la liaison N_7—C_8. Les valeurs des indices de liaison ont permis de vérifier et de préciser les résultats expérimentaux obtenus (3).

De plus, le calcul des pourcentages de caractère S a fait apparaître l'augmentation de l'angle interorbital C—N—C lors de la protonation de l'atome d'azote et a permis de rendre compte des valeurs des constantes de couplage $J_{^{13}C-H}$.

Enfin si en général les deux paramétrisations de la méthode CNDO, appliquées à la géométrie adoptée, conduisent à des résultats théoriques qualitativement peu différents, on peut noter que la méthode CNDO/S s'est révélée mieux adaptée au calcul des grandeurs associées aux charges ou aux pourcentages de caractère S.

Ainsi notre travail nous a conduit à une meilleure connaissance de la structure électronique et de la géométrie de l'isaxonine en solution et à définir les domaines d'application de la CNDO dans l'étude de cette molécule. Cette premiére approche de la réactivité de l'isaxonine va nous permettre, dans un second temps, de mieux appréhender l'activité biologique de cette molécule.

Remerciements

Nous tenons à exprimer nos remerciements à Monsieur le Professeur A. Crevat pour les discussions fructueuses que nous avons eues et le soutien constant qu'il nous a apporté. Nous remercions également Monsieur H. Bouteille et Mademoiselle S. Lorenzi pour leur collaboration technique.

1. T. TARRADE et A. HUGELIN. Neurosci. Lett. **1**, 545 (1978).
2. R. COELHO et M. ISTIN. Nouv. Presse Méd. **16**, 1227 (1982).
3. J. P. MONTI, D. BRAGUER, A. CREVAT et A. MURISASCO. À paraître.
4. J. A. POPLE, D. P. SANTRY et G. A. SEGAL. J. Chem. Phys. **43**, S129 (1965).
5. J. A. POPLE et G. A. SEGAL. J. Chem. Phys. **43**, 5236 (1965); **44**, 3286 (1966).
6. J. DEL BENE et H. H. JAFFE. J. Chem. Phys. **48**, 1807 (1968); **48**, 4050 (1968); **49**, 1221 (1968).
7. M. RAJZMANN. Thèse de Doctorat d'Etat, Marseille, 1973.
8. J. SCHEINBEIM et E. SCHEMPP. Acta Crystallogr. Sect. B, **32**, 607 (1976).
9. K. WUTHRICH. NMR in biological research: peptides and proteins. North Holland Pub. Comp., Amsterdam. 1976. p. 76.
10. L. E. SUTTON. Tables of interatomic distances and configurations in molecules and ions. Publ. No. 11. Chem. Soc., London. 1958.
11. W. VON NIESSEN, G. H. F. DIERCKSEN et L. S. CEDERBAUM. Chem. Phys. **41**, 113 (1979).
12. V. BARONE, C. LAULETTI, F. LELJ, M. N. PIANCASTELLI et N. RUSSO. J. Am. Chem. Soc. **104**, 4571 (1982).
13. M. L. MARTIN et G. J. MARTIN. Manuel de résonance magnétique nucléaire. Azoulay Ed., Paris. 1971. p. 34.
14. R. J. PUGMIRE et D. M. GRANT. J. Am. Chem. Soc. **90**, 697 (1968).
15. R. J. PUGMIRE et D. M. GRANT. J. Am. Chem. Soc. **93**, 1880 (1971).
16. R. J. PUGMIRE, M. J. ROBINS, D. M. GRANT et R. K. ROBINS. J. Am. Chem. Soc. **93**, 1887 (1971).
17. A. SAIKA et C. P. SLICHTER. J. Chem. Phys. **22**, 26 (1954).
18. J. A. POPLE, W. G. SCHNEIDER et H. J. BERNSTEIN. High resolution nuclear magnetic resonance. McGraw–Hill, New York. 1959.
19. J. A. POPLE. J. Chem. Phys. **37**, 53 (1962).
20. H. M. MCCONNEL. J. Chem. Phys. **27**, 226 (1957).
21. M. P. SCHWEIZER, S. I. CHAN, G. K. HELMKAMP et P. O. P. TS'O. J. Am. Chem. Soc. **86**, 696 (1964).
22. D. E. O'REILLY. Prog. Nucl. Magn. Reson. Spectrosc. **2**, 27 (1967).
23. A. D. BUCKINGHAM. Can. J. Chem. **38**, 300 (1960).
24. V. M. S. GIL et J. N. MURREL. Trans. Faraday Soc. **60**, 248 (1964).
25. L. ONSAGER. J. Am. Chem. Soc. **58**, 1486 (1936).
26. G. J. MARTIN, M. L. MARTIN et S. ODIOT. Org. Magn. Reson. **7**, 2 (1975), et réf. citées.
27. W. ADAM, A. GRIMISON et G. RODRIGUEZ. J. Chem. Phys. **50**, 645 (1969).
28. M. KARPLUS et J. A. POPLE. J. Chem. Phys. **38**, 2803 (1963).
29. S. FLISZAR, G. CARDINAL et M. T. BERALDIN. J. Am. Chem.

Can. J. Chem. Downloaded from www.nrcresearchpress.com by 210.87.254.6 on 09/06/12
For personal use only.

Soc. **104**, 5287 (1982), et réf. citées.
30. K. B. WIBERG. Tetrahedron, **24**, 1083 (1967).
31. S. EHRENSON et S. SELTZER. Theor. Chim. Acta, **20**, 17 (1971).
32. R. L. FLURRY, JR., D. BREEN et D. L. HOWLAND. Theor. Chim. Acta, **20**, 371 (1971).
33. C. TRINDLE et O. SINANOGLU. J. Am. Chem. Soc. **91**, 853 (1969); **91**, 4054 (1969).
34. D. R. ARMSTRONG, P. G. PERKINS et J. J. P. STEWART. J. Chem. Soc. Dalton Trans. 838 (1976).
35. V. P. ZHUKOV et V. A. GUBANOV. J. Mol. Struct. **28**, 247 (1975).
36. F. W. MCLAFFERTY. Spectrographie de masse. Ediscience, Paris. 1969.
37. H. STERNGLANZ et C. E. BUGG. J. Cryst. Mol. Struct. **8**, 268 (1978).
38. D. W. DAVIS. Chem. Commun. **12**, 258 (1965).
39. M. SCHUMACHER et H. GUNTHER. J. Am. Chem. Soc. **104**, 4167 (1982).
40. N. MULLER et D. E. PRITCHARD. J. Chem. Phys. **31**, 768 (1959); **31**, 1471 (1959).
41. Z. B. MAKSIC, M. ECKERT-MAKSIC et M. RANDIC.Theor. Chim. Acta, **22**, 70 (1971).
42. M. D. NEWTON, J. M. SCHULMAN et M. M. MANUS. J. Am. Chem. Soc. **96**, 17 (1974).
43. J. M. SCHULMAN et M. D. NEWTON. J. Am. Chem. Soc. **96**, 6295 (1974).
44. H. P. FIGEYS, P. GEERLINGS, P. RAEYMAEKERS, G. VAN LOMMEN et N. DEFAY. Tetrahedron, **31**, 1731 (1975).
45. G. E. MACIEL, J. W. MCIVER, N. S. OSTLUND et J. A. POPLE. J. Am. Chem. Soc. **92**, 1 (1970).
46. M. RANDIC, Z. MEIC et A. RUBCIC. Tetrahedron, **28**, 565 (1972).
47. Z. B. MAKSIC et M. RANDIC. J. Am. Chem. Soc. **95**, 6522 (1973).

Can. J. Chem. Downloaded from www.nrcresearchpress.com by 210.87.254.6 on 09/06/12
For personal use only.

N,N-Linked biazoles. III. MNDO calculations on the conformation of *N,N*-linked biazoles and their quaternary salts

MARIA LUISA CASTELLANOS, SANTIAGO OLIVELLA, AND NURIA ROCA
Departament de Quimica Organica, Facultat de Quimica, Universitat de Barcelona, Barcelona-28, Spain

AND

JAVIER DE MENDOZA[1] AND JOSÉ ELGUERO
Departamento de Química Orgánica, Facultad de Ciencias, Universidad Autónoma de Madrid, Madrid-34, Spain

Received July 28, 1983

MARIA LUISA CASTELLANOS, SANTIAGO OLIVELLA, NURIA ROCA, JAVIER DE MENDOZA, and JOSÉ ELGUERO. Can. J. Chem. **62**, 687 (1984).

A theoretical study of fourteen *N,N*-linked biazoles has been carried out using the MNDO method with full optimization of the geometries. The variation of energy as a function of the conformation around the central *N*—*N* bond shows in all cases the higher stability of the orthogonal or near-orthogonal form. The contribution of the three main types of "*ortho*" interactions (H...H, N̈...N̈, and H...N̈) and the effect of quaternization have been evaluated. Of the electronic properties calculated, one must emphasize the excellent agreement of dipole moments with experimental values.

MARIA LUISA CASTELLANOS, SANTIAGO OLIVELLA, NURIA ROCA, JAVIER DE MENDOZA et JOSÉ ELGUERO. Can. J. Chem. **62**, 687 (1984).

Une étude théorique de quatorze *N,N*-biazoles a été conduite en utilisant la méthode MNDO avec optimisation complète de la géométrie. La variation de l'énergie en fonction de la conformation autour de la liaison centrale *N*—*N* montre dans tous les cas la plus grande stabilité des formes orthogonales ou proches de l'orthogonalité. La contribution des trois types d'interactions "*ortho*" (H...H, N̈...N̈ et H...N̈) a été évaluée, ainsi que l'effet de la quaternarisation. Parmi les propriétés électroniques calculées on note l'excellent accord des moments dipolaires avec les valeurs expérimentales.

Can. J. Chem. Downloaded from www.nrcresearchpress.com by 210.87.254.42 on 09/06/12
For personal use only.

Introduction

Conformation about a single bond linking two aromatic rings, i.e., about a C_{sp^2}—C_{sp^2} bond, has been extensively studied in biphenyl derivatives (atropoisomerism) (1–5). These studies, both experimental and theoretical, have been extended to heterocyclic derivatives, like phenylpyridines and bipyridines (6–11). However, the case of a single bond of the N_{sp^2}—C_{sp^2} type connecting two aromatic rings (*N*-phenylazoles) has received much less attention, and only two theoretical studies have been published: one by Galasso and Alti (12) on *N*-phenylpyrrole, and another by Avignon, Bouscasse, and Elguero (13) on eight *N*-arylazoles. The E.H.T. method was used in both calculations.

The third general case, a single bond between two N_{sp^2}—N_{sp^2} atoms belonging to neutral aromatic rings can be found only in *N,N*-linked biazoles (14, 15). To the best of our knowledge, only 1,1′-bipyrrole has been calculated by Galasso (16) and by Flitsch, Rademacher and co-workers in order to assign its photoelectron spectrum (17). In the former paper, the E.H.T. method was again used, but in the latter the authors adopted the MNDO/2 approximation. Both concluded that an angle of twist of 90° between rings was about 13 kJ/mol more stable than a coplanar conformation.

The present paper deals with this original class of heterocyclic derivatives. The following fourteen compounds have been studied:

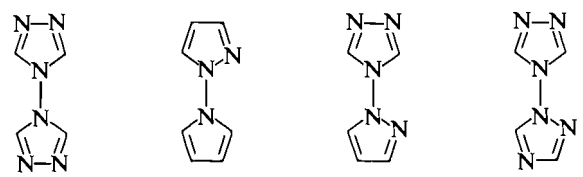

1 **2** **3** **4**

[1]To whom all correspondence should be addressed.

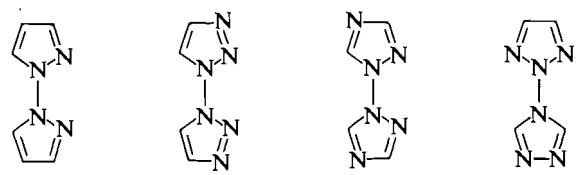

5 **6** **7** **8**

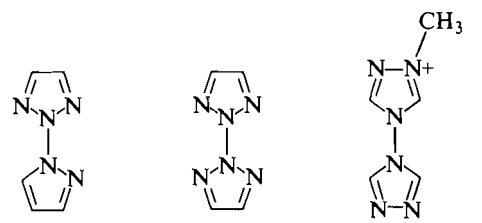

9 **10** **11**

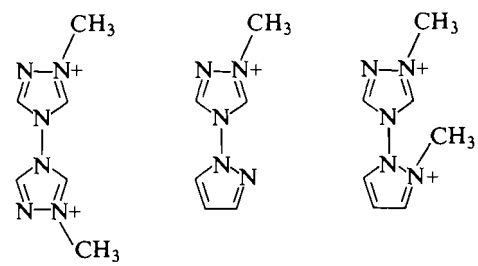

12 **13** **14**

Calculations

The calculations were performed using the LCAO-MO-SCF MNDO method with standard parameters (18). All equilibrium geometries were determined by minimizing the total energy with respect to the geometrical variables using the Davidon–Fletcher–Powell (DFP) algorithm (19, 20). All computations were carried out on the UNIVAC 1108 computer of the C.P.D. of "Ministerio de Educación y Ciencia (Madrid)", using a

TABLE 1.

Compound	Dihedral angle (deg)	Internuclear 1–2	2–3	3–4	4–5	5–1	1–6	6–7	7–8	8–9	9–10
1	0	1.417	1.343	1.321	1.343	1.417	1.352	1.417	1.343	1.321	1.343
	30	1.417	1.342	1.323	1.342	1.417	1.349	1.417	1.342	1.323	1.342
	45	1.417	1.342	1.325	1.342	1.417	1.346	1.417	1.342	1.325	1.342
	60	1.417	1.341	1.326	1.341	1.417	1.343	1.417	1.341	1.326	1.341
	90	1.419	1.340	1.326	1.340	1.419	1.341	1.419	1.340	1.326	1.340
2	0	1.343	1.353	1.353	1.393	1.414	1.357	1.408	1.391	1.441	1.391
	90	1.346	1.349	1.344	1.389	1.416	1.348	1.410	1.390	1.441	1.390
3	0	1.416	1.344	1.322	1.343	1.416	1.355	1.344	1.352	1.440	1.390
	30	1.417	1.343	1.323	1.342	1.417	1.352	1.345	1.350	1.446	1.390
	45	1.416	1.343	1.324	1.342	1.416	1.349	1.346	1.350	1.443	1.388
	60	1.416	1.342	1.325	1.341	1.417	1.347	1.347	1.349	1.445	1.387
	90	1.417	1.341	1.326	1.341	1.417	1.345	1.347	1.348	1.446	1.386
4	0	1.417	1.340	1.324	1.340	1.417	1.353	1.347	1.349	1.395	1.340
	90	1.419	1.337	1.329	1.337	1.419	1.343	1.350	1.346	1.402	1.337
5	0	1.343	1.352	1.440	1.389	1.418	1.359	1.343	1.352	1.440	1.389
	30	1.342	1.351	1.441	1.389	1.418	1.356	1.342	1.351	1.441	1.389
	60	1.343	1.349	1.445	1.388	1.418	1.351	1.343	1.349	1.445	1.388
	90	1.346	1.348	1.446	1.388	1.419	1.348	1.346	1.348	1.446	1.388
	107.76	1.347	1.349	1.444	1.388	1.417	1.349	1.347	1.349	1.444	1.388
	120	1.345	1.351	1.443	1.390	1.417	1.349	1.345	1.351	1.443	1.390
	150	1.344	1.352	1.439	1.393	1.415	1.357	1.344	1.352	1.439	1.393
	180	1.344	1.352	1.439	1.392	1.416	1.358	1.344	1.352	1.439	1.392
6	0	1.357	1.261	1.409	1.388	1.420	1.353	1.357	1.261	1.409	1.388
	90	1.359	1.258	1.415	1.385	1.421	1.343	1.359	1.258	1.415	1.385
	180	1.357	1.262	1.408	1.390	1.417	1.352	1.357	1.262	1.408	1.390
7	0	1.347	1.348	1.399	1.334	1.420	1.355	1.347	1.348	1.399	1.334
	90	1.357	1.341	1.407	1.329	1.426	1.350	1.357	1.341	1.407	1.329
	180	1.348	1.347	1.398	1.337	1.417	1.354	1.348	1.347	1.398	1.337
8	0	1.341	1.350	1.450	1.350	1.341	1.353	1.418	1.341	1.325	1.341
	90	1.343	1.348	1.450	1.348	1.343	1.380	1.380	1.348	1.325	1.348
9	0	1.342	1.354	1.446	1.354	1.342	1.357	1.347	1.350	1.443	1.388
	90	1.343	1.347	1.456	1.347	1.343	1.350	1.347	1.348	1.446	1.388
10	0	1.344	1.351	1.445	1.351	1.344	1.356	1.344	1.351	1.445	1.351
	90	1.346	1.346	1.445	1.346	1.346	1.348	1.346	1.346	1.445	1.346
11	0	1.383	1.372	1.343	1.337	1.427	1.352	1.435	1.331	1.332	1.332
	90	1.393	1.369	1.348	1.336	1.430	1.342	1.435	1.332	1.335	1.330
12	0	1.404	1.360	1.345	1.330	1.451	1.360	1.404	1.360	1.345	1.330
	90	1.408	1.358	1.351	1.330	1.447	1.348	1.408	1.358	1.351	1.330
	180	1.404	1.361	1.346	1.330	1.450	1.360	1.404	1.361	1.346	1.330
13	0	1.389	1.376	1.344	1.337	1.426	1.353	1.358	1.341	1.456	1.381
	90	1.389	1.369	1.350	1.337	1.427	1.345	1.360	1.340	1.460	1.378
	180	1.386	1.374	1.341	1.340	1.429	1.352	1.358	1.341	1.457	1.379
14	0	1.401	1.365	1.343	1.331	1.444	1.367	1.376	1.388	1.421	1.395
	90	1.410	1.358	1.352	1.329	1.443	1.345	1.377	1.381	1.430	1.393
	180	1.408	1.360	1.343	1.333	1.438	1.367	1.377	1.385	1.425	1.392

locally modified version (by S.O.) of the original MNDO program.[2]

[2]M. J. S. Dewar and W. Thiel. Private communication to S.O.

Results and discussion

1. Geometries

The calculated geometries for compounds **1**–**14** at different dihedral angles between rings (we have taken arbitrarily $\theta = 0°$

Can. J. Chem. Downloaded from www.nrcresearchpress.com by 210.87.254.42 on 09/06/12
For personal use only.

Internuclear distances (Å)

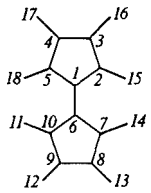

distance												
10–6	*2–15*	*3–16*	*4–17*	*5–18*	*7–14*	*8–13*	*9–12*	*10–11*	*14–15*	*18–11*	*18–14*	*11–15*
1.417	1.083			1.083	1.083			1.083	2.446	2.446		
1.417	1.083			1.083	1.083			1.083				
1.417	1.083			1.083	1.083			1.083				
1.417	1.083			1.083	1.083			1.083				
1.419	1.083			1.083	1.083			1.083				
1.408	1.083	1.081	1.081	1.083		1.085	1.080	1.082		2.356		
1.410	1.082	1.080	1.080	1.082		1.084	1.079	1.081				
1.417	1.084			1.082		1.084	1.079	1.080		2.435		
1.415	1.084			1.081		1.084	1.079	1.081				
1.419	1.083			1.082		1.084	1.079	1.081				
1.420	1.083			1.082		1.084	1.079	1.081				
1.421	1.083			1.083		1.084	1.079	1.082				
1.416	1.084			1.082		1.086		1.084		2.517		
1.418	1.084			1.084		1.084		1.084				
1.418		1.084	1.079	1.080		1.084	1.079	1.080		2.370		
1.418		1.084	1.079	1.081		1.084	1.079	1.081				
1.418		1.084	1.079	1.081		1.084	1.079	1.081				
1.419		1.084	1.079	1.081		1.084	1.079	1.081				
1.417		1.084	1.078	1.081		1.084	1.078	1.081				
1.417		1.084	1.079	1.081		1.084	1.079	1.081				
1.415		1.084	1.079	1.082		1.084	1.079	1.082				
1.416		1.084	1.079	1.082		1.084	1.079	1.082				
1.420			1.081	1.079			1.081	1.079		2.465		
1.421			1.081	1.080			1.081	1.080				
1.417			1.081	1.081			1.081	1.081				
1.419		1.087		1.083		1.087		1.083		2.516		
1.426		1.086		1.084		1.086		1.085				
1.417		1.086		1.085		1.086		1.085				
1.418		1.082	1.082		1.083			1.083				
1.380		1.082	1.082		1.083			1.083				
1.421		1.082	1.082			1.084	1.079	1.081				
1.417		1.082	1.082			1.085	1.079	1.080				
1.344		1.082	1.082			1.082	1.082					
1.346		1.082	1.082			1.082	1.082					
1.435	1.090	1.505		1.089	1.083			1.083	2.447	2.429		
1.436	1.091	1.506		1.090	1.084			1.084				
1.451	1.091	1.523		1.088	1.091	1.523		1.088	2.452	2.264		
1.447	1.093	1.522		1.093	1.093	1.522		1.093				
1.450	1.092	1.523		1.087	1.092	1.523		1.087			2.358	2.358
1.433	1.092			1.088		1.087	1.082	1.080		2.473		
1.435	1.091			1.091		1.087	1.081	1.081				
1.435	1.089			1.091		1.086	1.082	1.080				2.491
1.428	1.088	1.520		1.091	1.507	1.093	1.088	1.087		2.175		
1.426	1.094	1.517		1.091	1.508	1.093	1.087	1.088				
1.428	1.095	1.519		1.091	1.511	1.094	1.087	1.088				2.191

the planar conformation represented in the above formula) are described in Tables 1 and 2. The only compound in the series with a known experimental geometry is 4,4′-bi-1,2,4-triazole, **1**, for which a crystalline structure has been determined by Domiano (21). In the crystal, **1** shows an angle of twist of 91.9° between the two triazolyl moieties. The differences in bond lengths and bond angles with our calculations at any conformation are indeed small: maximum deviation in bond length

Can. J. Chem. Downloaded from www.nrcresearchpress.com by 210.87.254.42 on 09/06/12
For personal use only.

Can. J. Chem. Downloaded from www.nrcresearchpress.com by 210.87.254.42 on 09/06/12
For personal use only.

TABLE 2. Bond

Compound	Dihedral angle (deg)	*1*	*2*	*3*	*4*	*5*	*6*	*7*
1	0	106.93	110.35	110.35	127.28	127.28	106.93	110.35
	30	106.89	110.33	110.33	127.26	127.26	106.89	110.33
	45	106.84	110.33	110.33	127.84	127.84	106.84	110.33
	60	106.85	110.36	110.36	127.17	127.17	106.85	110.36
	90	106.58	110.49	110.49	127.07	127.07	106.58	110.49
2	0	107.75	107.89	107.89	126.11	119.12	105.86	110.48
	90	106.94	108.24	108.24	125.15	120.11	105.55	110.66
3	0	106.69	110.52	110.22	127.17	118.96	105.92	110.29
	30	106.51	110.61	110.27	126.98	119.13	105.91	110.16
	45	106.57	110.53	110.25	127.21	119.40	105.64	110.42
	60	106.56	110.55	110.27	127.18	119.60	105.56	110.60
	90	106.57	110.54	110.29	127.07	119.76	105.51	110.49
4	0	106.73	110.45	110.45	127.22	119.66	104.06	112.54
	90	106.75	110.41	110.41	127.17	120.53	103.90	112.66
5	0	105.68	110.61	106.09	119.98	119.98	105.68	110.61
	30	105.65	110.65	106.07	120.14	120.14	105.65	110.65
	60	105.47	110.61	106.18	120.11	120.11	105.47	110.61
	90	105.30	110.83	106.09	119.83	119.83	105.30	110.83
	107.76	105.17	110.97	105.97	119.61	119.61	105.17	110.97
	120	105.62	110.44	106.31	119.61	119.61	105.62	110.44
	150	105.70	110.41	106.31	118.83	118.83	105.70	110.41
	180	105.70	110.41	106.31	118.83	118.83	105.70	110.41
6	0	108.46	110.74	107.74	121.31	121.31	108.46	110.74
	90	108.28	110.76	107.82	121.46	121.47	108.28	110.76
	180	108.48	110.56	107.93	120.84	120.84	108.48	110.56
7	0	103.90	112.75	105.56	120.83	120.83	103.90	112.75
	90	104.16	112.82	105.53	121.47	117.59	104.16	112.82
	180	103.77	112.74	105.71	119.39	119.42	103.77	112.74
8	0	104.01	107.86	107.86	121.82	127.11	106.52	110.52
	90	103.82	107.99	107.99	121.81	126.86	106.64	110.22
9	0	103.64	108.03	108.03	121.15	121.15	103.64	108.03
	90	103.68	107.96	107.96	120.76	120.76	105.54	110.62
10	0	103.80	108.06	108.06	121.86	121.86	103.80	108.06
	90	103.68	108.06	108.06	121.71	121.71	103.68	108.06
11	0	105.19	111.58	108.27	126.13	127.72	106.65	110.73
	90	104.63	111.84	108.58	125.66	126.91	105.96	111.04
12	0	104.97	111.95	109.50	126.46	126.46	104.97	111.95
	90	104.23	112.37	109.35	125.86	125.86	104.23	112.37
	180	104.93	111.94	109.47	125.49	125.49	104.93	111.94
13	0	105.00	111.54	108.30	125.40	117.63	105.56	110.39
	90	104.90	111.67	108.31	125.69	118.09	105.03	110.78
	180	104.91	111.90	108.18	126.62	117.28	105.68	110.24
14	0	106.02	111.27	109.03	130.78	126.64	107.35	109.59
	90	105.19	111.30	109.89	126.20	122.77	106.85	109.30
	180	105.95	111.31	109.13	122.85	125.87	107.42	109.63

lies within a range of ±0.15 Å, and bond angles do not deviate more than 3.3°. The rest of values of Tables 1 and 2 must be taken as normal for these kinds of heterocycles, and are not appreciably distorted by a twist in conformation. In every case, however, the N—N bond linking both heterocycles is slightly shortened (by c.a. 0.01 Å) at $\theta = 90°$ with respect to any of the planar conformations.

The effect of quaternization (compounds **11**–**14**) in bond angles and distances, although small in absolute terms, causes enough distortion to the whole *N*-methylated ring as to make significant the variation of internuclear distances between the hydrogen atoms situated "*ortho*" to the N—N bonded nitrogen in each of the rings with respect to the same atoms on the neighbouring ring in the planar conformations. For example, in the monocation **13** ($\theta = 0°$), the distance between the two hydrogen atoms situated more distant to the methyl groups

angles (deg)

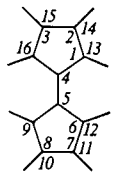

Angle at									
8	*9*	*10*	*11*	*12*	*13*	*14*	*15*	*16*	Methyl H—C—H
110.35	127.08			127.08	127.08			127.08	
110.33	127.52			127.52	127.52			127.52	
110.33	127.24			127.24	127.24			127.24	
110.36	128.07			128.07	128.07			128.07	
110.49	128.37			128.37	128.37			128.37	
106.05	131.32	126.50	121.42		126.20	126.11	126.00	126.20	
106.11	132.86	126.15	121.65		126.47	125.88	125.88	126.47	
106.36	131.76	126.25	121.41		127.49			127.14	
106.32	132.14	126.13	121.82		127.91			127.57	
106.42	132.58	126.04	121.58		128.05			127.90	
106.22	132.83	125.94	121.65		128.21			128.11	
106.49	133.03	125.86	121.67		128.34			128.27	
105.68	127.44		124.57		127.69			127.41	
105.67	128.40		124.80		128.40			128.40	
106.09	131.32	126.39	121.36			121.36	126.39	131.32	
106.07	131.89	126.31	121.42			121.42	126.31	131.89	
106.18	132.66	126.18	121.58			121.58	126.18	132.66	
106.09	132.91	126.08	121.59			121.59	126.08	132.91	
105.97	132.59	126.28	121.46			121.46	126.28	132.59	
106.31	132.39	126.11	121.59			121.59	126.11	132.39	
106.31	131.91	126.29	121.37			121.37	126.29	131.91	
106.31	131.90	126.30	121.37			121.37	126.30	131.90	
107.74	132.94	121.19					121.19	132.94	
107.82	134.18	120.81					120.81	134.18	
107.93	133.36	121.12					121.12	133.36	
105.56	127.46		124.48			124.48		127.46	
105.54	128.51		124.98			124.98		128.51	
105.71	128.01		124.51			124.51		128.01	
110.52	127.83			127.83		126.03	126.10		
110.22	128.11			128.11		123.12	128.89		
108.03	132.00	126.18	121.32			122.87	129.10		
106.17	132.57	126.10	121.84			126.03	126.03		
108.06		129.19	122.75			122.75	129.19		
108.06		127.33	124.60			124.60	127.33		
110.98	127.55			127.60	126.59	127.88		126.21	108.67
111.09	129.10			129.25	128.22	127.99		127.84	108.74
109.50	131.97		128.52	126.81	126.81	128.52		131.97	108.07
109.35	131.97		128.31	128.64	128.64	128.31		131.97	108.10
109.47	131.97		128.38	126.79	126.79	128.38		131.97	108.07
107.08	133.10	125.37	121.92		127.00	127.76		126.43	108.21
106.94	134.10	125.42	122.03		127.92	128.12		127.50	108.11
107.26	133.02	124.99	122.06		126.84	127.56		126.74	108.23
106.58	129.46	126.39	121.86	122.69	124.72	128.48		125.36	108.57
107.34	132.46	125.77	122.09	126.64	128.00	129.18		128.07	108.61
106.34	129.87	126.42	121.88	122.58	125.42	128.93		124.10	108.48

(those labelled *11* and *18* in Table 1) is 0.18 Å *shorter* than the same distance in the neutral molecule **1**. No such effect is observed in the distance between the hydrogen atoms situated at the same side of the methyl groups (labelled as *14* and *15*), which remains essentially unchanged with respect to the neutral molecule. The same effect, though even more pronounced, is found in compound **14** ($\theta = 0°$): the H...H distance (labels *11* and *18* in Table 1) is reduced by 0.26 Å in comparison with the neutral compound **3**. Finally, in compound **14**, at $\theta = 180°$ (labelled atoms *14* and *15*), the shortening is about 0.24 Å.

2. Energies

All molecules are found to be more stable at conformations near orthogonality, as values of heats of formation clearly indicate (Table 3). In those molecules having a plane of symmetry at 90° (**1**–**4**, and **8**–**11**), the energy minima correspond

Can. J. Chem. Downloaded from www.nrcresearchpress.com by 210.87.254.42 on 09/06/12
For personal use only.

Can. J. Chem. Downloaded from www.nrcresearchpress.com by 210.87.254.42 on 09/06/12
For personal use only.

TABLE 3. Heat of formation, ionization potential, dipolar

Compound	Dihedral angle (deg)	ΔH_f (kJ/mol)	Ionization potential (eV)	Dipolar moment (D)	I
1	0	521.187	10.840	0.00	5.150
	30	512.431	10.843	0.00	5.155
	45	505.182	10.837	0.01	5.160
	60	499.026	10.823	0.01	5.165
	90	493.736	10.815	0.00	5.172
2	0	490.661	8.905	1.93	5.091
	90	470.774	8.880	2.23	5.101
3	0	520.179	9.960	5.23	5.142
	30	514.153	10.030	5.26	5.145
	45	509.002	10.146	5.30	5.146
	60	504.758	10.255	5.32	5.150
	90	501.332	10.348	5.35	5.153
4	0	516.928	10.520	3.12	5.150
	90	498.524	10.618	3.26	5.162
5	0	543.625	9.186	3.57	5.050
	30	535.555	9.294	3.52	5.054
	60	522.424	9.604	3.31	5.062
	90	514.930	9.927	2.85	5.069
	107.76	513.642	9.749	2.45	5.067
	120	514.241	9.589	2.11	5.061
	150	519.084	9.289	1.13	5.051
	180	522.578	9.169	0.00	5.049
6	0	579.697	10.229	6.34	5.094
	90	554.437	10.578	4.75	5.112
	180	562.228	10.229	0.00	5.091
7	0	533.157	10.072	2.08	5.079
	90	504.591	10.694	1.57	5.117
	180	508.382	10.044	0.00	5.080
8	0	557.485	10.242	5.55	4.993
	90	552.068	10.377	5.78	5.032
9	0	574.727	9.391	1.96	4.983
	90	559.694	9.978	2.17	5.010
10	0	621.491	9.648	0.00	4.989
	90	604.397	10.584	0.00	5.005
11	0	1248.807			5.066
	90	1219.441			5.101
12	0	2270.020			5.159
	90	2228.992			5.183
	180	2267.148			5.160
13	0	1202.723			5.058
	90	1190.062			5.076
	180	1209.718			5.050
14	0	2329.719			5.133
	90	2257.761			5.171
	180	2328.224			5.133

*N-Methyl carbon atoms: 3.785 ± 0.014.

moment, and total charges on ring atoms of *N*,*N*′-biazoles

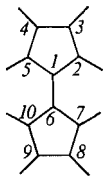

Total charges on ring atoms*								
2	*3*	*4*	*5*	*6*	*7*	*8*	*9*	*10*
3.966	5.112	5.112	3.966	5.150	3.966	5.112	5.112	3.966
3.963	5.113	5.113	3.963	5.155	5.963	5.113	5.113	3.963
3.961	5.114	5.114	3.961	5.160	3.961	5.114	5.115	3.961
3.957	5.117	5.115	3.957	5.166	3.957	5.116	5.116	3.957
3.954	5.117	5.117	3.954	5.172	3.954	5.117	5.117	3.954
3.972	4.114	4.109	4.038	5.046	5.122	4.045	4.168	3.982
3.997	4.129	4.125	3.999	5.078	5.098	4.048	4.170	3.967
3.930	5.137	5.114	3.985	5.058	5.121	4.032	4.158	3.975
3.931	5.137	5.116	3.979	5.065	5.115	4.033	4.160	3.972
3.933	5.135	5.118	3.974	5.073	5.108	4.035	4.160	3.969
3.936	5.133	5.120	3.966	5.081	5.103	4.036	4.160	3.966
3.949	5.128	5.126	3.949	5.087	5.097	4.037	4.161	3.962
3.924	5.132	5.109	3.981	5.081	5.137	3.978	5.236	3.892
3.945	5.122	5.122	3.945	5.105	5.115	3.982	5.240	3.879
5.067	4.059	4.156	3.995	5.050	5.067	4.059	4.156	3.995
5.070	4.058	4.157	3.990	5.054	5.070	4.058	4.157	3.990
5.078	4.052	4.162	3.975	5.062	5.078	4.052	4.162	3.975
5.091	4.045	4.169	3.956	5.069	5.091	4.045	4.169	3.956
5.102	4.042	4.174	3.947	5.067	5.102	4.042	4.174	3.947
5.112	4.039	4.178	3.945	5.061	5.112	4.039	4.177	3.945
5.132	4.035	4.183	3.940	5.051	5.132	4.035	4.183	3.940
5.138	4.033	4.185	3.939	5.049	5.138	4.033	4.185	3.939
4.933	5.123	4.091	4.017	5.094	4.933	5.123	4.091	4.017
4.952	5.115	4.103	3.983	5.112	4.952	5.115	4.103	3.983
4.995	5.109	4.115	3.968	5.091	4.995	5.109	4.115	3.968
5.079	4.000	5.231	3.908	5.079	5.079	4.000	5.231	3.908
5.131	3.977	5.251	3.847	5.088	5.127	3.965	5.244	3.860
5.152	3.974	5.253	3.855	5.080	5.152	3.974	5.253	3.855
5.083	4.079	4.079	5.082	5.148	3.940	5.127	5.127	3.940
5.062	4.078	4.078	5.062	5.126	3.941	5.132	5.116	3.953
5.040	4.100	4.079	5.099	5.059	5.077	4.045	4.171	3.953
5.055	4.089	4.088	5.053	5.060	5.085	4.039	4.169	3.947
5.050	4.088	4.088	5.050	4.989	5.050	4.088	4.088	5.050
5.046	4.084	4.082	5.045	5.005	5.046	4.084	4.082	5.045
3.797	5.142	5.044	3.879	5.225	3.948	5.049	5.057	3.931
3.769	5.141	5.059	3.854	5.246	3.934	5.061	5.062	3.933
3.776	5.103	5.007	3.829	5.159	3.776	5.103	5.007	3.829
3.753	5.109	5.016	3.828	5.183	3.753	5.109	5.016	3.828
3.760	5.109	5.002	3.842	5.160	3.760	5.109	5.002	3.842
3.763	5.165	5.050	3.892	5.135	5.138	3.963	4.113	3.941
3.761	5.152	5.068	3.850	5.164	5.102	3.981	4.113	3.948
3.818	5.147	5.065	3.849	5.137	5.116	3.969	4.105	3.957
3.775	5.107	5.006	3.861	5.065	9.163	3.778	4.108	3.812
3.756	5.104	5.029	3.834	5.097	5.162	3.767	4.123	3.795
3.778	5.102	5.013	3.858	5.066	5.148	3.783	4.099	3.834

Can. J. Chem. Downloaded from www.nrcresearchpress.com by 210.87.254.42 on 09/06/12
For personal use only.

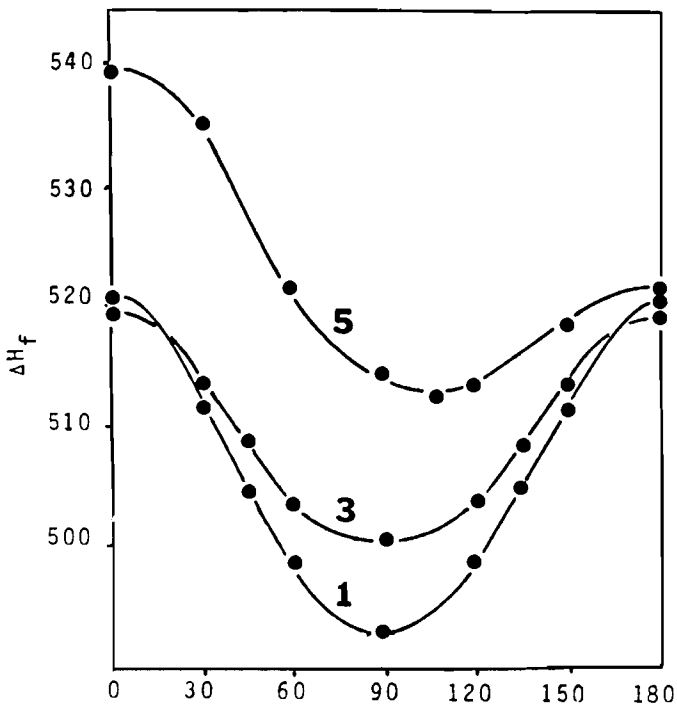

FIG. 1. Plot of energy (kJ mol^{-1}) vs. angle of twist in 4,4′-bi-1,2,4-triazole (**1**), 4-(1-pyrazolyl)-1,2,4-triazole (**3**), and 1,1′-bipyrazole (**5**).

to that angle of twist. There is no reason, however, for the same situation to hold for less symmetric compounds (**5**–**7** and **12**–**14**). For example, 1,1′-bipyrazole, **5**, shows an energy minimum at 107.76°. A plot of energy vs. angle of twist can be drawn for compounds such as **1**, **3**, and **5**, calculated for a large enough number of dihedral angles[3] (Fig. 1).

The scarce experimental data available for *N*,*N*-linked biazoles are also in good agreement with an orthogonal conformation of both rings. We have already mentioned the crystallographic data of 4,4′-bi-1,2,4-triazole, **1** (21). From the splittings of the π_2-ionizations of the photoelectron spectrum of 1,1′-bipyrrole it has been also concluded that this compound has the most stable conformation at 90° (17).

Thus the preference for a perpendicular or quasi perpendicular conformation seems to be quite general for this family of compounds, and has no equivalent in other series, like biphenyls, bipyridines, or phenylazoles. In particular, *N*-phenylpyrrole shows a minimum at an angle of twist of about 40° (12). On the other hand, calculations on 2,2′-bipyridine revealed the existence of two minima, the lower one corresponding to an "*anti*" conformation (both nitrogen atoms 180° apart from each other) in agreement with experimental evidence, and the other situated *not* at θ = 0°, but in a "*cisoid*" conformation, at an angle of 35° (7). This behaviour can be interpreted as a compromise between coplanarity, favored by the conjugation across the bond linking the rings together, and the repulsive interaction of the two lone pairs of the heteroatoms.

In addition to the differences in conjugation, another factor must be taken into account when comparing biphenyles, *N*-phenylazoles, and *N*,*N*-linked biazoles: the shortening of the interannular distance, C—C, 1.48 Å (7), C—N, 1.40 Å (13), and N—N, 1.36 Å (this work).

3. Interactions at the planar conformations

The presence of a singular minimum of energy, far from the planar conformations, makes *N*,*N*-linked biazoles particularly suitable models for the study of internuclear interactions in five-membered dimers. The three main interactions to be considered are those arising from (*i*) pairs of hydrogen atoms situated "*ortho*" at each ring (H...H interactions), (*ii*) pairs of electrons of the nitrogen atoms (N̈...N̈ interactions), and (*iii*) hydrogen atoms of one ring interacting with lone pairs of the other ring (H...N̈ interactions).

Since the planar conformations can be associated with transition states (see Fig. 1), the energy differences between the most stable conformation (θ = 90°, or some value near this) and maxima at 0° and 180°, can be directly related to the magnitude of the interaction. According to the number and type of existing interactions, the neutral molecules **1**–**10** can be classified into seven groups, **A**–**G** (Table 4).

The only representative compound with two H...H interactions is 4,4′-bi-1,2,4-triazole, **1**. The calculated energy barrier (difference of heat of formation between the conformations at 0° and 90°) is 27.45 kJ/mol. That gives a value of about 13.7 kJ/mol for the H...H interaction. At the other end of the table, compound **10** represents an example of two N̈...N̈ interactions. The calculated barrier gives now a value of 8.54 kJ/mol for a single interaction of this type.

The concordance of these values with those found for the rest of situations in Table 4 is far from being perfect, however. For example, compounds **5**–**7** (at θ = 0°), having one H...H and one N̈...N̈ interaction each (group **C**) show too high barriers in comparison with the prediction from the above values (c.a. 22.24 kJ/mol). On the other hand, the value for a H...N̈ interaction deduced in groups **B** and **F** by subtraction of 13.7 and 8.54 kJ/mol, respectively, lies betwen 4.7 and 6.49 kJ/mol, which is also too high if we compare it with the value derived from groups **D** and **E**, where only H...N̈ interactions exist. We do not have a single explanation for these differences, but must note that the presence of other factors may influence the magnitude of the barriers. In particular, the effect of other heteroatoms situated at the β positions can be relevant in this discussion. A multilinear regression analysis with the whole set of values in Table 4 gives a mean value for each interaction, namely 15.4 kJ/mol for H...H, 10.3 kJ/mol for N̈...N̈, and 3.2 kJ/mol for H...N̈.

Although these values, when applied additively, deviate in some cases from those calculated for each particular compound, they afford an order of magnitude that can explain, for example, the lower barriers at 180° than at 0° for compounds **5**, **6**, and **7**. In other words, it explains that the "preference" of two nitrogen lone-pairs is to be "*anti*" to each other (θ = 180°), a situation that closely parallels the results found in 2,2′-bipyridine.

The effect of quaternization on the magnitude of the interactions can be discussed only in compounds **11**–**13**, since the steric effect of the methyl groups situated "*ortho*" in the pyrazolyl moiety of compound **14** largely determines the height of the barrier. In bitriazoles **11** and **12**, the barriers are 29.37 (**11**), 41.03 (**12**, θ = 0°), and 38.16 (**12**, θ = 180°) kJ/mol. These high values, especially in the case of the dication **12**, indicate a progressive destabilization of the planar conformations as the number of positive charges is increased from the neutral mole-

[3]For compound **1**, the points fit the equation ΔH_f = 493.7 (±0.2) + 4.8 (±0.6) cos θ + 22.5 (±0.6) $\cos^3$ θ, r = 0.9999.

Can. J. Chem. Downloaded from www.nrcresearchpress.com by 210.87.254.42 on 09/06/12
For personal use only.

TABLE 4. Interactions between "*ortho* substituents" at the planar conformations

Group	Type and number of interactions H...H	N...N	H...N	Representative compounds in the series	$\Delta E^{\ddagger}$ (kJ mol^{-1})
A 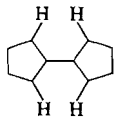	2	0	0	**1** (θ = 0° and 180°)	27.45
B 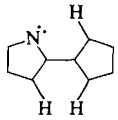	1	0	1	**2** (θ = 0° and 180°) **3** (θ = 0° and 180°) **4** (θ = 0° and 180°)	19.89 18.85 18.40
C 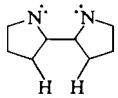	1	1	0	**5** (θ = 0°) **6** (θ = 0°) **7** (θ = 0°)	28.69 25.26 28.57
D 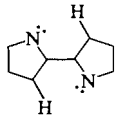	0	0	2	**5** (θ = 180°) **6** (θ = 180°) **7** (θ = 180°)	7.65 7.79 3.79
E 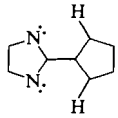	0	0	2	**8** (θ = 0° and 180°)	5.42
F 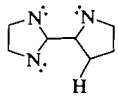	0	1	1	**9** (θ = 0° and 180°)	15.03
G 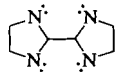	0	2	0	**10** (θ = 0° and 180°)	17.09

cule. Moreover, the distortion in the geometry of the triazolyl cation with respect to the neutral species, which causes the H...H distance to be shorter and, therefore, the interaction to be greater, can also explain the magnitude of the effect.

4. Electronic properties

The ionization potentials, dipole moments, and total charges on ring atoms of compounds **1**−**14**, in all the conformations studied, are listed on Table 3. The overall electronic distribution of the molecules is well reflected in the values of their dipole moments.

The agreement of the MNDO calculations with the experimental data available is quite good, and much better than the values calculated by the CNDO/2 approach (14). For example, the experimental values for 1-(1-pyrrolyl)pyrazole, **2**, and 4-(1-pyrazolyl)-1,2,4-triazole, **3** (2.04 and 5.33 D, respectively), are very close to the calculated values at 90° for the same compounds (Table 3). We must then conclude that dipole moments, measured experimentally and calculated by MNDO at different dihedral angles, can be used as a tool for the prediction of the preferred conformation of *N*,*N*-linked biazoles, especially when the calculated values show large differences between 0° and 180°.

1. E. L. ELIEL. Stereochemistry of carbon compounds, McGraw Hill, New York, NY. 1962. p. 156.
2. B. TINLAND. J. Mol. Struct. **3**, 161 (1969).
3. A. GOLEBIEWSKI and A. PARCZEWSKI. Z. Naturforsch. A. **25**, 1710 (1970).
4. J. RAYEZ and J. J. DANNENBERG. Chem. Phys. Lett. **41**, 492 (1976).
5. M. M. MESTECHKIN, V. N. POLTAVETS, V. E. UMANSKII, G. E. VAIMAN, and A. V. LUZANOV. Theor. Eksp. Khim. **13**, 321 (1977); Chem. Abstr. **87**, 167378 (1977).
6. G. FAVINI. Gazz. Chim. Ital. **94**, 1287 (1964).
7. V. GALASSO, G. DE ALTI, and A. BIGOTTO. Tetrahedron, **27**, 991 (1971).
8. S. P. SHINA. Rev. Roum. Chim. **18**, 777 (1973).
9. A. B. BOLOTIN, V. A. BOLOTIN, and V. GINEITITE. Usp. Kvantovoi Khim. Kvantovoi Biol., Tr. Mezhdunar. Konf. **2**, 40 (1978); Chem. Abstr. **95**, 145704 (1981).
10. V. A. BOLOTIN and A. B. BOLOTIN. Liet. Fiz. Rinkinys **19**, 195 (1979); Chem. Abstr. **91**, 74129 (1979).
11. R. BENEDIX, P. BIRNER, F. BIRNSTOCK, H. HENNIG, and H. J. HOFMANN. J. Mol. Struct. **51**, 99 (1979).
12. V. GALASSO and G. DE ALTI. Tetrahedron, **27**, 4947 (1971).
13. T. AVIGNON, L. BOUSCASSE, and J. ELGUERO. Tetrahedron, **34**, 1139 (1978).
14. J. DE MENDOZA, M. L. CASTELLANOS, J. P. FAYET, M. C. VERTUT, and J. ELGUERO. J. Chem. Res. (S) 50 (1980).
15. J. DE MENDOZA, C. MILLAN, and P. RULL. J. Chem. Soc. Perkin Trans. 1, 403 (1981).
16. V. GALASSO and N. TRINAJSTIC. Tetrahedron, **28**, 4419 (1972).
17. W. FLITSCH, H. PEETERS, W. SCHULTEN, and P. RADEMACHER. Tetrahedron, **34**, 2301 (1978).
18. M. J. S. DEWAR and W. THIEL. J. Am. Chem. Soc. **99**, 4899 (1977).
19. W. C. DAVIDON. A. E. C. Res. Develop. Rep. ANL 5990 (1959).
20. R. FLETCHER and M. J. D. POWELL. Comput. J. **6**, 163 (1963).
21. P. DOMIANO. Cryst. Struct. Commun. **6**, 503 (1977).

Can. J. Chem. Downloaded from www.nrcresearchpress.com by 210.87.254.42 on 09/06/12
For personal use only.

Crystal and molecular structure and ^{31}P and ^{195}Pt nmr spectroscopy of $[Pt_3S_2(PMe_2Ph)_6][BEt_4]_2$; a trinuclear complex containing triply-bridging sulphide ligands

GORDON WILLIAM BUSHNELL,[1] KEITH ROGER DIXON,[1] REIKO ONO, AND ALAN PIDCOCK[2]
Department of Chemistry, University of Victoria, Victoria, B.C., Canada V8W 2Y2

Received June 30, 1983

GORDON WILLIAM BUSHNELL, KEITH ROGER DIXON, REIKO ONO, and ALAN PIDCOCK. Can. J. Chem. **62**, 696 (1984).

An X-ray diffraction study of $[Pt_3S_2(PMe_2Ph)_6][BEt_4]_2$ shows that it crystallises in the monoclinic space group, $C2/c$, with a = 15.447(2), b = 18.033(3), c = 26.505(5) Å, β = 96.73(2)°. The cation consists of three, distorted, square-planar *cis*-$PtS_2(PMe_2Ph)_2$ moieties combined by sharing of the two sulphur atoms to produce a central Pt_3S_2 unit with C_2 symmetry and Pt—Pt distances of 3.182(1) Å (one edge) and 3.108(1) Å (two edges). Complete analysis and computer simulation of $^{31}P\{^1H\}$ and $^{195}Pt\{^1H\}$ nuclear magnetic resonance spectra give values for ^1J(Pt—P), 3202 Hz; ^3J(Pt—P), −25 Hz; and ^2J(Pt—Pt), 476 Hz. The structure is compared with previous results for analogous Ni and Pd complexes and the structural and nmr parameters are discussed with reference to the possibility of metal−metal interactions.

GORDON WILLIAM BUSHNELL, KEITH ROGER DIXON, REIKO ONO et ALAN PIDCOCK. Can. J. Chem. **62**, 696 (1984).

Une étude par diffraction des rayons-X du $[Pt_3S_2(PMe_2Ph)_6][BEt_4]_2$ montre que ce produit cristallise dans le groupe d'espace monoclinique, $C2/c$, avec a = 15,447(2), b = 18,033(3), c = 26,505(5) Å, β = 96,73(2)°. Le cation comporte trois groupes déformés, plan-carré de $PtS_2(PMe_2Ph)_2$-*cis* combinés par le partage des deux atomes de soufre pour produire une unité centrale de Pt_3S_2 possédant une symétrie C_2 et des distances Pt—Pt de 3,182(1) Å (un côté) et de 3,108(1) Å (deux côtés). Une analyse complète et une simulation par ordinateur des spectres de RMN du $^{31}P\{^1H\}$ et $^{195}Pt\{^1H\}$ permet de déterminer les valeurs de ^1J(Pt—P) (3202 Hz), ^3J(Pt—P) (−25 Hz) et ^2J(Pt—Pt) (476 Hz). On compare cette structure avec celles déterminées antérieurement pour des complexes analogues du Ni et du Pd; on discute des paramètres rmn et structuraux pour évaluer l'existence d'interactions métal−métal.

[Traduit par le journal]

Can. J. Chem. Downloaded from www.nrcresearchpress.com by 210.87.254.42 on 09/06/12
For personal use only.

Introduction

Complexes in which an M_3 triangle is capped by two sulphide ligands to form an approximately trigonal bipyramidal M_3S_2 unit are relatively common among the later transition elements. The metal−metal distances vary widely, from strongly bonded examples such as the $[Co_3S_2(\eta^5\text{-}C_5H_5)_3]^+$ cation (1), Co—Co 2.474(2) and 2.649(1) Å, through intermediate cases such as $[Ni_3S_2(\eta^5\text{-}C_5H_5)_3]$ (2), Ni—Ni 2.801(5) Å, to distances over 3 Å as found in the $[Pd_3S_2(PMe_3)_6]^{2+}$ cation (3). There is also a dichotomy between complexes having three approximately equal metal−metal distances and those in which one distance differs significantly from the other two. An extreme example of the latter type is $[Fe_3S_2(CO)_9]$, where two edges of the metal triangle are clearly bonding distances, 2.60 Å, and the third is non-bonding 3.37 Å(4). A more subtle example is the $[Co_3S_2(\eta^2\text{-}C_5H_5)_3]^+$ cation mentioned above which has one short edge, 2.474(2) Å, and two long edges, 2.649(1) Å, and forms an interesting contrast to the neutral molecule, $[Co_3S_2(\eta^5\text{-}C_5H_3)_3]$, in which the metal triangle is approximately equilateral, 2.687(3) Å(1). In these more subtle examples, especially cases such as $[Pd_3S_2(PMe_3)_6]^{2+}$ where very long metal−metal distances are involved (see below), it is difficult to say whether the asymmetry is due to some fundamental molecular factor or merely to packing and crystal symmetry effects.

In view of the above considerations the $[Pt_3S_2(PMe_2Ph)_6]^{2+}$ cation represents an interesting opportunity to complete a comparative study of analogous complexes for all three members of a transition metal triad. The cation was prepared in 1970 by reaction of sodium sulphide with *cis*-$[PtCl_2(PMe_2Ph)_2]$ and a trinuclear structure proposed on the basis of ^1H nmr evidence (5). Recent papers have reported diffraction studies of the analogous $[Ni_3S_2(PEt_3)_6]^{2+}$ (6) and $[Pd_3S_2(PMe_3)_6]^{2+}$ (3) cations, the former having three approximately equal metal−metal distances (2.91(3) Å) and the latter one short (3.011(2) Å) and two long (3.144(3), 3.178(2) Å), but the platinum structure has not been confirmed by an X-ray study. Moreover, the presence of the spin-1/2 ^{31}P (abundance, 100%) and ^{195}Pt (abundance, 33.8%) nuclei presents the possibility of a detailed nmr study of the solution structure with parameters such as ^2J(Pt—Pt) and ^3J(Pt—P) available as probes of the metal−metal interaction. In the present paper we report such a dual study, with complete $^{31}P\{^1H\}$ and $^{195}Pt\{^1H\}$ nmr and X-ray diffraction characterization of the complex, $[Pt_3S_2(PMe_2Ph)_6][BEt_4]_2$.

Experimental

(a) Synthesis

The synthesis of $[Pt_3S_2(PMe_2Ph)_6][BF_4]_2$ was conducted under an atmosphere of dry nitrogen using tetrahydrofuran (THF) which had been dried and deoxygenated by reflux over potassium/benzophenone. Sublimed sulphur was obtained from Matheson, Coleman and Bell and $Li[BHEt_3]$ from Aldrich as a 1 *M* solution in THF. *cis*-$[PtCl_2(PMe_2Ph)_2]$ was prepared as previously described (7). Microanalysis was by the Canadian Microanalytical Service, Vancouver, B.C.

A solution (8 mL, 1 *M*) of $Li[BHEt_3]$ in THF was added dropwise to a stirred slurry of sulphur (0.12 g, 3.7 mmol) in THF. After 15 min the resulting clear yellow solution of Li_2S (8) was added dropwise to a stirred suspension of *cis*-$[PtCl_2(PMe_2Ph_2]$ (2.0 g, 3.7 mmol) in nitrogen-purged ethanol (70 mL). After stirring for 3 h, the resulting yellow solid was collected by filtration, washed with water and ethanol, and recrystallized twice from CH_2Cl_2/EtOH to yield $[Pt_3S_2(PMe_2Ph)_6][BEt_4]_2$ as air stable, pale yellow crystals (1.8 g, 1.0 mmol, mp 147−150°C). *Anal.* calcd. for $C_{64}H_{106}B_2P_6Pt_3S_2$: C 44.3, H 6.2, S 3.7; found: C 44.3, H 6.0, S 4.2.

(b) Nuclear magnetic resonance

Phosphorus-31 and platinum-195 nmr spectra were recorded in CD_2Cl_2 solution at 101.3 and 53.5 MHz respectively, using a Bruker

[1]Authors to whom correspondence should be addressed.
[2]Permanent address: School of Chemistry and Molecular Sciences, University of Sussex, Falmer, Brighton, BN1 9QJ, U.K.

Can. J. Chem. Downloaded from www.nrcresearchpress.com by 210.87.254.42 on 09/06/12
For personal use only.

WP250 Fourier transform spectrometer locked to the solvent deuterium resonance. Protons were decoupled by broad band ("noise") irradiation at appropriate frequencies. ^{31}P chemical shifts were measured relative to external $P(OMe)_3$ and are reported in ppm relative to 85% H_3PO_4 using a conversion factor of +141 ppm. Positive values are downfield of the reference. ^{195}Pt chemical shifts (Ξ) are reported in MHz standardised to $[Si(CH_3)_4]$ at 100 MHz. Simulated nmr spectra were calculated on an IBM 3031 computer and plotted on a Calcomp 1039 plotter. The programmes used were a locally constructed package based on the UEAITR and NMRPLOT programmes from the literature (9, 10).

(c) X-Ray diffraction

Crystals of $[Pt_3S_2(PMe_2Ph)_6][BEt_4]_2$ suitable for study by X-ray diffraction were prepared by solvent diffusion. A sample was dissolved in dichloromethane in a small tube and an equal volume of ethanol placed carefully on top to form a double layer. Crystallization occurred as the solvents mixed over a period of ~15 h.

Preliminary photographic work was done using Weissenberg and precession cameras with CuKα radiation. The crystals were monoclinic, space group $C2/c$ (No. 15), a = 15.447(2), b = 18.033(3), c = 26.505(5) Å, β = 96.73(2)°, V_{cell} = 7332(2) Å^3, D_{calcd} = 1.569 g cm^{-3} for $C_{64}H_{106}B_2P_6Pt_3S_2$, M = 1732.4, D_{meas} = 1.568 g cm^{-3} (flotation in CCl_4/*m*-xylene), asymmetric unit = 1/2 molecule. The pale yellow crystal (0.37 × 0.46 × 0.38 mm) was mounted in a capillary tube and measurements were done at 23°C on a Picker 4-circle diffractometer automated with a PDP-11/10 computer. The unit cell was refined by least squares using 13 pairs of centering measurements (±2θ). Intensity measurements were done over a hemisphere and out to 2θ = 40° (7289 reflections) using MoKα radiation (λ = 0.71069 Å). The scans were 160 steps of 0.01° in 2θ counting for 0.25 s per step, and background counting was for 20 s at each end. Absorption corrections were applied by numerical integration using a 10 × 10 × 10 Gaussian grid, μ = 62.22 cm^{-1}, transmission range 0.048–0.160. Lorentz and polarisation corrections were applied and equivalent reflections were averaged to give a file containing 3427 independent reflections.

The crystal structure was found and refined using the SHELX-76 program package supplied by Dr. G. M. Sheldrick (11). The atomic scattering factors used were those contained in the program, with the addition of the Pt curve (12). The solution was by centrosymmetric direct methods, and the refinement by Fourier methods and least squares minimizing $\Sigma w(|F_o| - |F_c|)^2$. The weights were obtained from counting statistics using $w = 1/(\sigma^2(F) + 0.001F^2)$. All atoms were treated anisotropically and convergence was attained with a maximum (shift/esd) ratio of 0.055. The residuals were R = 0.0545 and $R_w = (\Sigma w\Delta^2/\Sigma wF_o^2)^{1/2}$ = 0.0641. The final difference map had a maximum of 2.08 e Å^{-3} and a minimum of −0.79 e Å^{-3}, but gave no indication that any material had been overlooked. The hydrogen atom positions were not determined. Supplementary tables containing structure factors, anisotropic temperature parameters, selected inter- and intra-molecular distances and mean plane results have been deposited.[3]

Results

(a) Synthesis

The complexes $[Pt_3S_2(PMe_2Ph)_6][X]_2$, X = ClO_4^-, BF_4^-, or BPh_4^-, had been previously synthesized by Chatt and Mingos (5) using the reaction of *cis*-$[PtCl_2(PMe_2Ph)_2]$ with sodium sulphide followed by treatment with $HClO_4$, HBF_4, or $NaBPh_4$ as appropriate. The yields were, however, very low (~10%) and the structure of the cation was not fully characterised prior to this work. We have used the method of Gladysz *et al.* (8) to generate Li_2S *in situ* by reduction of elemental sulphur with $Li[BHEt_3]$ and find that the resulting solution, which also contains BEt_3, reacts with *cis*-$[PtCl_2(PMe_2Ph)_2]$ to give the trinuclear complex in high yield (>80%).

TABLE 1. Fractional atomic coordinates and temperature parameters*

Atom	x/a	y/b	z/c	U_{eq}
Pt(1)	50149(3)	64742(3)	30872(2)	524(2)
Pt(2)	50000(0)	49346(4)	25000(0)	488(3)
S(1)	5983(2)	5939(2)	2558(1)	51(1)
P(1)	6158(2)	6894(2)	3633(1)	62(1)
P(2)	3944(2)	6935(2)	3511(1)	64(1)
P(3)	3846(2)	4152(2)	2455(1)	62(1)
C(11)	6598(11)	6180(8)	4072(5)	77(6)
C(12)	7415(10)	6269(9)	4359(6)	87(7)
C(13)	7685(12)	5706(11)	4701(6)	105(8)
C(14)	7184(15)	5076(11)	4772(7)	111(9)
C(15)	6357(14)	4995(10)	4493(7)	109(9)
C(16)	6058(11)	5561(8)	4133(5)	87(7)
C(17)	6031(9)	7711(7)	4049(5)	79(6)
C(18)	7102(9)	7195(9)	3314(5)	89(6)
C(21)	4004(8)	7941(7)	3554(5)	64(5)
C(22)	4283(9)	8315(9)	3142(6)	79(6)
C(23)	4339(10)	9074(11)	3152(7)	101(8)
C(24)	4117(11)	9470(10)	3612(9)	112(9)
C(25)	3872(13)	9069(10)	4008(6)	99(8)
C(26)	3811(10)	8317(8)	3987(5)	78(6)
C(27)	2837(9)	6771(9)	3226(6)	98(7)
C(28)	3969(12)	6580(8)	4167(5)	97(7)
C(31)	3137(10)	4387(8)	2939(5)	71(6)
C(32)	2311(11)	4656(11)	2807(6)	102(8)
C(33)	1800(13)	4807(13)	3214(11)	144(12)
C(34)	2153(18)	4682(12)	3717(10)	132(12)
C(35)	2968(18)	4439(11)	3834(8)	145(12)
C(36)	3485(12)	4261(9)	3444(6)	104(8)
C(37)	3153(10)	4223(9)	1844(5)	85(6)
C(38)	3955(10)	3148(8)	2548(6)	95(7)
B(1)	4694(12)	2032(9)	812(5)	74(7)
C(1)	5229(11)	2309(9)	347(5)	92(7)
C(2)	5782(12)	3004(10)	444(6)	117(8)
C(3)	4092(10)	2711(8)	1007(6)	90(7)
C(4)	3379(12)	2994(10)	615(7)	116(8)
C(5)	5442(12)	1802(11)	1288(6)	113(8)
C(6)	5048(14)	1432(10)	1758(6)	121(10)
C(7)	4021(11)	1338(8)	608(6)	91(7)
C(8)	4500(11)	654(9)	437(6)	106(8)

*Estimated standard deviations are given in parentheses. Coordinates ×10^n where n = 5, 4, 4, 4, 4 for Pt, S, P, C, and B. Temperature parameters ×10^n where n = 4, 3, 3, 3, 3 for Pt, S, P, C, and B. U_{eq} = the equivalent isotropic temperature parameter; $U_{eq} = (1/3)\Sigma_i\Sigma_j U_{ij}a_i^*a_j^*(a_i.a_j)$; $T = \exp[-(8\pi^2U_{iso} \times \sin^2\theta/\lambda^2)]$.

(b) Crystal and molecular structure

The $[Pt_3S_2(PMe_2Ph)_6]^{2+}$ cation and the two $[BEt_4]^-$ anions exist as discrete entities in the crystal. A stereoscopic view of the cation structure is shown in Fig. 1 which also gives the atom labelling scheme and the thermal vibration ellipsoids. The fractional atomic coordinates, interatomic distances, and bond angles are given in Tables 1–3, respectively. The asymmetric unit is one half of the formula unit.

The structure of the cation is best described as three, distorted, square-planar *cis*-$PtS_2(PMe_2Ph)_2$ moieties combined together by sharing of the two sulphur atoms. This creates a central Pt_3S_2 unit which has a crystallographic C_2 symmetry axis passing through Pt(2) and the mid-point of Pt(1)—Pt(1)′. Thus the three platinum atoms form an isosceles triangle with

[3]Copies are available upon request, at a nominal charge, from the Depository of Unpublished Data, CISTI, National Research Council of Canada, Ottawa, Ont., Canada K1A 0S2.

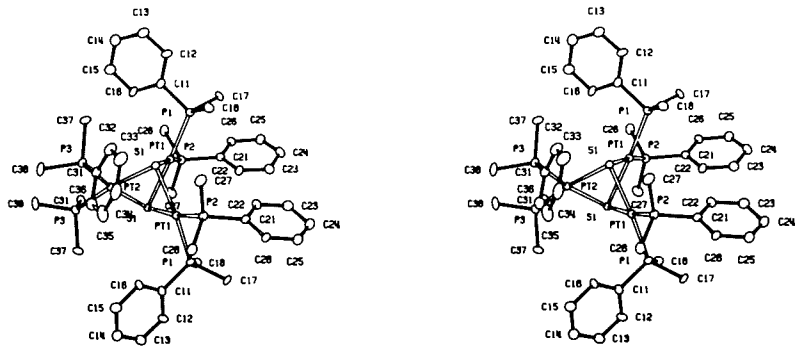

FIG. 1. A stereoscopic view of the $[Pt_3S_2(PMe_2Ph)_6]^{2+}$ ion. A phenyl ring C(32)—C(36) at the back of the molecule has been omitted for clarity.

TABLE 2. Interatomic distances (Å)*

Atoms	Distance	Atoms	Distance
Pt(2)—Pt(1)	3.182(1)	Pt(1)—Pt(1′)	3.108(1)
S(1)—Pt(1)	2.372(3)	S(1)—Pt(2)	2.358(3)
P(1)—Pt(1)	2.278(3)	P(3)—Pt(2)	2.265(3)
P(2)—Pt(1)	2.264(3)		
C(11)—P(1)	1.813(15)	C(21)—P(2)	1.819(14)
C(17)—P(1)	1.866(13)	C(27)—P(2)	1.810(16)
C(18)—P(1)	1.849(14)	C(28)—P(2)	1.849(14)
C(31)—P(3)	1.833(13)	C(38)—P(3)	1.832(15)
C(37)—P(3)	1.839(13)		
C(12)—C(11)	1.404(21)	C(14)—C(13)	1.400(24)
C(16)—C(11)	1.413(21)	C(15)—C(14)	1.406(25)
C(13)—C(12)	1.392(22)	C(16)—C(15)	1.437(21)
C(22)—C(21)	1.396(18)	C(24)—C(23)	1.488(24)
C(26)—C(21)	1.395(17)	C(25)—C(24)	1.363(23)
C(23)—C(22)	1.372(22)	C(26)—C(25)	1.362(21)
C(32)—C(31)	1.372(21)	C(34)—C(33)	1.397(29)
C(36)—C(31)	1.401(20)	C(35)—C(34)	1.334(31)
C(33)—C(32)	1.435(26)	C(36)—C(35)	1.415(22)
C(1)—B(1)	1.639(20)	C(5)—B(1)	1.661(24)
C(3)—B(1)	1.656(21)	C(7)—B(1)	1.675(23)
C(2)—C(1)	1.522(20)	C(6)—C(5)	1.597(23)
C(4)—C(3)	1.511(23)	C(8)—C(7)	1.533(21)

*Estimated standard deviations are given in parentheses.

metal−metal distances 3.182(1) Å for Pt(2)—Pt(1) and 3.108(1) Å for Pt(1)—Pt(1)′. The angle between the square planes of Pt(1) and Pt(2) is 121.8° and that between the square planes of Pt(1) and Pt(1)′ is 116.4°. The principal distortion of the square planes is compression of the S—Pt—S angles to 79.0(1)° at Pt(1) and 79.6(1)° at Pt(2), accompanied by widening of the P—Pt—P angles to 96.9(1)° and 103.0(2)°, respectively. These distortions are very similar to those reported previously for the $[Ni_3S_2(PEt_3)_6]^{2+}$ and $[Pd_3S_2(PMe_3)_6]^{2+}$ cations. There is also some distortion of the Pt(2) coordination from planarity ($\chi^2 = \sum_i p_i^2/\sigma^2(p_i) = 352$ over 5 atoms), probably caused by steric repulsion between C(38) and C(38′), 3.267 Å. The coordination around Pt(1) is much more closely planar ($\chi^2 = 50$). The platinum−sulphur bond lengths are all closely similar and average 2.365(3) Å, which is in accord with the metal−sulphur distances in the nickel (2.11−2.23 Å) (6) and palladium (2.312−2.358 Å) (3) analogues, and is also closely comparable with other platinum−sulphur distances where the sulphur is *trans* to phosphorus, both in mononuclear complexes containing terminal RS groups (13) and in RS-bridged trinuclear complexes (14, 15).

The PMe_2Ph groups are placed so that the phenyl group is on one side of the Pt square plane, one methyl is on the opposite side, and the third methyl is close to the Pt coordination plane. Evidence of steric repulsion of these in-plane methyl groups is seen in the Pt—P—C angles which are 116.2°, 120.7°, and 123.3° for C(17), C(27), and C(38), respectively, much larger than the other values in the range 110.5−113.8°. The disparity in the three wider angle values can be understood in terms of the various interactions involved (see Fig. 1). Adjacent (*cis*) PMe_2Ph groups have their phenyl groups on opposite sides of the appropriate coordination planes.

The tetraethylborate anion has angles at boron which are within 5° of the ideal tetrahedral value, and angles at the inner carbon atoms which are slightly larger (mean 114.7°), presumably owing to a steric effect similar to that observed in NEt_4^+ (16).

(c) Nuclear magnetic resonance

For the purposes of analysis of the $^{31}P\{^1H\}$ and $^{195}Pt\{^1H\}$ nmr spectra of the title compound, we may assume that the $Pt_3P_6S_2$ core effectively possesses D_{3h} symmetry in solution. It is then necessary to consider spectra due to four different isotopomers:

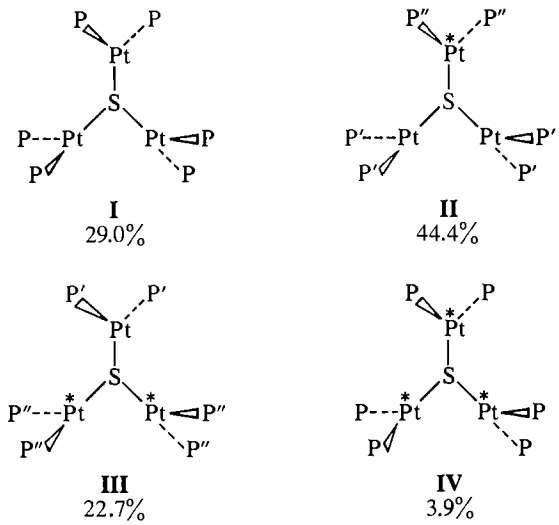

*Denotes magnetically active platinum-195

A fully rigorous treatment of these spectra would require the analysis of some rather complex spin systems, involving up to nine magnetically non-equivalent nuclei (see Appendix). Fortunately, considerable simplification is possible by introducing the assumption that $^4J(P—P)$ is effectively zero. Previous re-

Can. J. Chem. Downloaded from www.nrcresearchpress.com by 210.87.254.42 on 09/06/12
For personal use only.

TABLE 3. Bond angles (deg)*

Atoms	Angle	Atoms	Angle
Pt(1)—S(1)—Pt(1′)	81.9(1)	Pt(2)—S(1)—Pt(1)	84.6(1)
S(1)—Pt(1)—S(1′)	79.0(1)	S(1)—Pt(2)—S(1′)	79.6(1)
P(2)—Pt(1)—P(1)	96.9(1)	P(3)—Pt(2)—P(3′)	103.0(2)
P(1)—Pt(1)—S(1)	90.8(1)	P(2)—Pt(1)—S(1)	172.2(1)
P(3)—Pt(2)—S(1)	168.2(1)	P(2)—Pt(1)—Pt(2)	126.8(1)
P(1)—Pt(1)—Pt(2)	124.2(1)	P(3)—Pt(2)—Pt(1)	122.0(1)
Pt(1)—Pt(2)—Pt(1′)	58.47(5)	Pt(2)—Pt(1)—Pt(1′)	60.76(4)
C(11)—P(1)—Pt(1)	112.1(6)	C(18)—P(1)—Pt(1)	113.7(5)
C(17)—P(1)—Pt(1)	120.7(5)	C(27)—P(2)—Pt(1)	116.2(5)
C(21)—P(2)—Pt(1)	111.2(4)	C(28)—P(2)—Pt(1)	113.8(6)
C(31)—P(3)—Pt(2)	110.5(4)	C(37)—P(3)—Pt(2)	112.1(5)
C(38)—P(3)—Pt(2)	123.3(5)	C(27)—P(2)—C(21)	103.2(7)
C(17)—P(1)—C(11)	103.8(7)	C(28)—P(2)—C(21)	106.9(6)
C(18)—P(1)—C(11)	104.2(7)	C(28)—P(2)—C(27)	104.6(8)
C(18)—P(1)—C(17)	100.5(7)	C(38)—P(3)—C(31)	100.8(6)
C(37)—P(3)—C(31)	105.5(7)	C(38)—P(3)—C(37)	102.8(7)
C(12)—C(11)—P(1)	120.8(13)	C(22)—C(21)—P(2)	116.8(10)
C(16)—C(11)—P(1)	116.9(12)	C(26)—C(21)—P(2)	121.5(11)
C(32)—C(31)—P(3)	121.2(12)	C(36)—C(31)—P(3)	116.0(12)
C(16)—C(11)—C(12)	122.2(14)	C(15)—C(14)—C(13)	119.7(18)
C(13)—C(12)—C(11)	116.8(16)	C(16)—C(15)—C(14)	118.5(18)
C(14)—C(13)—C(12)	123.5(17)	C(15)—C(16)—C(11)	119.3(16)
C(26)—C(21)—C(22)	121.7(14)	C(25)—C(24)—C(23)	119.2(17)
C(23)—C(22)—C(21)	119.5(15)	C(26)—C(25)—C(24)	121.5(16)
C(24)—C(23)—C(22)	118.3(16)	C(25)—C(26)—C(21)	119.8(14)
C(36)—C(31)—C(32)	122.8(13)	C(35)—C(34)—C(33)	121.8(20)
C(33)—C(32)—C(31)	116.9(18)	C(36)—C(35)—C(34)	120.2(23)
C(34)—C(33)—C(32)	119.9(20)	C(35)—C(36)—C(31)	118.3(19)
C(3)—B(1)—C(1)	111.2(12)	C(7)—B(1)—C(1)	109.5(12)
C(5)—B(1)—C(1)	106.2(13)	C(7)—B(1)—C(3)	107.6(13)
C(5)—B(1)—C(3)	108.3(12)	C(7)—B(1)—C(5)	114.1(13)
C(2)—C(1)—B(1)	116.5(12)	C(6)—C(5)—B(1)	113.7(15)
C(4)—C(3)—B(1)	115.2(13)	C(8)—C(7)—B(1)	113.2(13)

*Estimated standard deviations are given in parentheses.

Can. J. Chem. Downloaded from www.nrcresearchpress.com by 210.87.254.42 on 09/06/12
For personal use only.

sults (14, 17, 18) would lead to the expectation of a very small value (<5 Hz) for the coupling and, since the observed spectra have linewidths ca. 10 Hz (^{31}P) and ca. 90 Hz (^{195}Pt), such a small coupling will not affect the analysis. This assumption leads to effective magnetic equivalence of the geminal phosphorus atoms (for example, the pair labelled P″ in isotopomer **II**) and to a considerable simplification of the spin systems (see Appendix). Also, at the effective signal/noise of the observed spectra it is not necessary to consider the very low abundance isotopomer **IV** in the analysis, although its contribution has been included in the final computer simulations.

With the adoption of these assumptions, we proceeded with an analytical solution of the ^{31}P{^{1}H} spectrum as detailed below. The correctness of the analysis was then confirmed by direct use of the derived parameters in a successful simulation of the ^{195}Pt{^{1}H} spectrum. The spectra are shown in Figs. 2 and 3 together with the computer simulations and the derived parameters are collected in Table 4.

(i) $^{31}P\{^{1}H\}$ spectrum. In Fig. 2 the intense central resonance (line 6) is clearly due to isotopomer **I**. Moreover, because of the very different magnitudes of ^{1}J(Pt—P) and ^{3}J(Pt—P) and the effectively zero value of ^{4}J(P—P), the P′ and P″ regions of the spectrum of isotopomer **II** are essentially independent. Each consists of a doublet, as is illustrated by the computer simulation, and the values of ^{1}J(Pt—P) 3201.4 Hz and ^{3}J(Pt—P) 25.2 Hz can be directly measured as the separations of lines 2 and 10, and 5 and 7, respectively.

A similar independence pertains for isotopomer **III** but the P′ region is expected to lie under the other central peaks and is not resolved. With the assumptions outlined above, the P″ region is effectively the A part of an $A_2XX'A_2'$ spin system which, in the limit of small J(AA′), i.e. ^{4}J(P—P), will be identical with the A part of an AXX′A′ system. We have previously treated this last system in detail for dinuclear platinum and palladium complexes of phosphorus ligands (17) and the same methods may be applied to the present example. In general the A region may be divided into two components: (*a*) a strong doublet of separation $2K$, (*b*) two symmetrical quartets, which are mutually coincident when $|J(XX')| \gg |J(AA')|$, a condition which is met in the present case since $|^{2}J(Pt—Pt)| \gg |^{4}J(P—P)|$. The line positions of the coincident quartets relative to δ(A) are given by $\pm\{S \pm (S^2 + L^2)^{1/2}\}$ and the secondary parameters are defined as follows:

$$2K = J(AX) + J(AX') = {}^{1}J(Pt—P) + {}^{3}J(Pt—P)$$

$$2L = J(AX) - J(AX') = {}^{1}J(Pt—P) - {}^{3}J(Pt—P)$$

$$2S \simeq J(XX') \simeq {}^{2}J(Pt—Pt)$$

In the present case the major doublet is easily assigned as lines 3 and 9, separation 3176.4 Hz, and the coincident quartets to lines 1, 4, 8, and 11, which are positioned at ±1394.1 and ±1869.8 Hz relative to δ(P).

The magnitudes of ^{1}J(Pt—P) and ^{3}J(Pt—P) obtained from isotopomer **II** suggest 3226.6 or 3176.2 Hz as the possible

Can. J. Chem. Downloaded from www.nrcresearchpress.com by 210.87.254.42 on 09/06/12
For personal use only.

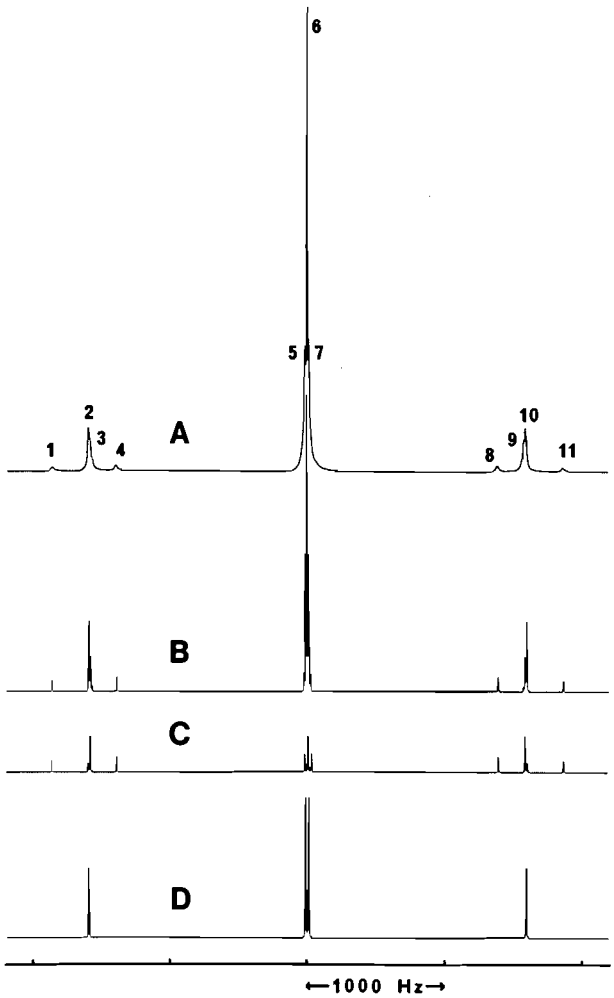

FIG. 2. $^{31}P\{^1H\}$ nmr spectra of the $[Pt_3S_2(PMe_2Ph)_6]^{2+}$ ion at 101.3 MHz. (*A*) Observed spectrum; (*B*) computer simulation of the composite spectrum produced by summation of contributions from isotopomers **I**, **II**, **III**, and **IV**; (*C*) computer simulation of the contribution from isotopomer **III**; (*D*) computer simulation of the contribution from isotopomer **II**.

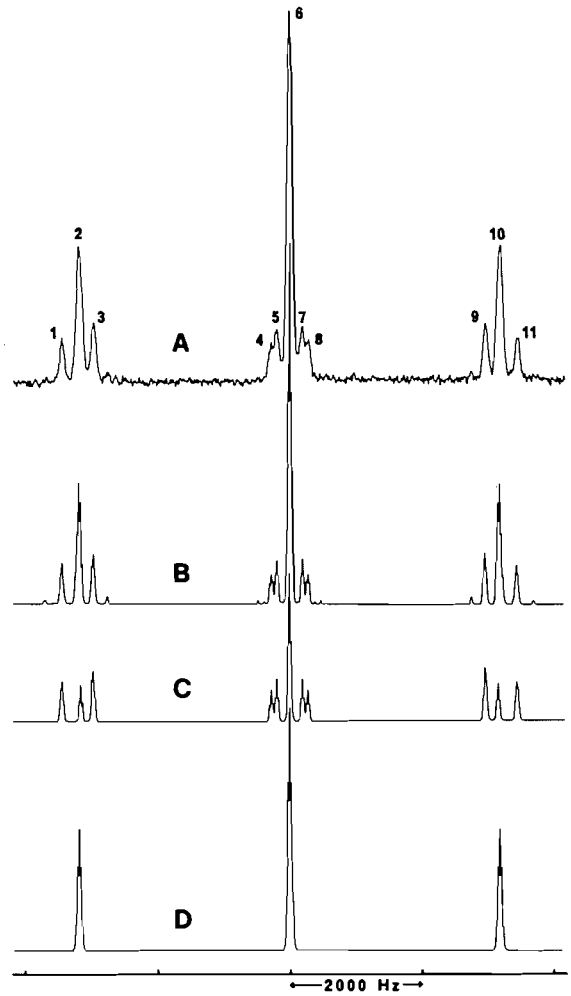

FIG. 3. $^{195}Pt\{^1H\}$ nmr spectra of the $[Pt_3S_2(PMe_2Ph)_6]^{2+}$ ion at 53.5 MHz. (*A*) Observed spectrum; (*B*) computer simulation of the composite spectrum produced by summation of contributions from isotopomers **II**, **III**, and **IV**; (*C*) computer simulation of the contribution from isotopomer **III**; (*D*) computer simulation of the contribution from isotopomer **II**.

TABLE 4. Nuclear magnetic resonance parameters for the $[Pt_3S_2(PMe_2Ph)_6]^{2+}$ cation

Chemical shift	Value	Coupling constant	Value (Hz)
^{31}P (ppm)	−16.7	^1J(Pt—P)	3202
		^3J(Pt—P)	−25
^{195}Pt (Ξ, MHz)	21.404075	^2J(Pt—Pt)	476
		^4J(P—P)	<5

values for $2K$ depending on the relative signs of the direct and indirect couplings. Thus the measured value of $2K$ establishes ^3J(Pt—P) as opposite in sign to ^1J(Pt—P) and presumably negative since directly bonded Pt—P couplings are known to be positive (19). Moreover, substitution of the positions of lines 1, 4, 8, and 11 into the above relationships leads to 3229.0 Hz as the value of $2L$, in excellent agreement with the 3226.6 Hz which the values of ^1J(Pt—P) and ^3J(Pt—P) would predict. Finally, the line positions 1, 4, 8, and 11 lead to a value of 475.7 Hz for $2S$, in excellent agreement with the 476.6 Hz obtained by measurement of ^2J(Pt—Pt) in the platinum spectrum (see below). This result also confirms our assumption of an essentially zero value for ^4J(P—P) since the quartets are coincident and $2S \simeq {}^2J$(Pt—Pt) only when ^4J(P—P) can be neglected (17).

(ii) $^{195}Pt\{^1H\}$ spectrum. The spectrum of isotopomer **II** is expected to consist basically of a triplet due to coupling of the single magnetically active platinum with the two directly bonded phosphorus nuclei. Assignment of lines 2, 6 and 10 (see Fig. 3) to this triplet gives a value of 3201.8 Hz for ^1J(Pt—P), in excellent agreement with the value derived from the ^{31}P spectrum. The width at half-height of line 6 is ~90 Hz and hence further splitting of the triplet due to ^3J(Pt—P), −25.2 Hz, is evidently not resolved. Assuming as before that ^4J(P—P) is unimportant, the remaining lines in the $^{195}Pt\{^1H\}$ spectrum should be assignable as the X region of an $A_2A_2'A_2''XX'$ spin system due to isotopomer **III**. All the couplings (except ^4J(P—P) which is assumed zero) are known from analysis of the $^{31}P\{^1H\}$ spectrum and can be used in a computer simulation of the $^{195}Pt\{^1H\}$ spectrum. The results of this simulation are shown in Fig. 3. The fit to the observed spectrum is excellent and the correctness of the analysis for the

TABLE 5. Metal–metal distances in $[M_3S_2L_6]^{2+}$ cations

Cation	M—M distances (Å)	Space group	R	Reference
$[Ni_3S_2(PEt_3)_6]^{2+}$	2.96(2), 2.88(2), 2.89(3)	$P2_1/a$	0.18	6
$[Pd_3S_2(PMe_3)_6]^{2+}$	3.011(2), 3.178(2), 3.144(2)	$P2_1/c$	0.102	3
$[Pt_3S_2(PMe_2Ph)_6]^{2+}$	3.108(1), 3.182(1)	$C2/c$	0.0545	This work

$^{31}P\{^1H\}$ spectrum is thus confirmed. It is noteworthy for the purposes of simple interpretation that the separations of lines 1 and 3, 4 and 7, 5 and 8, and 9 and 11 are all approximately equal to ^2J(Pt—Pt) and yield an average value of 476.6 Hz, again confirming the value derived from the $^{31}P\{^1H\}$ spectrum. The simulations also confirm the negative, relative sign of ^3J(Pt—P) since only this sign combination leads to the observed splitting of lines 4 and 5, and 7 and 8. The spectra are insensitive to the choice of relative sign for ^2J(Pt—Pt).

Discussion

The shortest, well-determined, platinum–platinum bond lengths appear to be those in the bridged complexes, $[Pt_2(SO_4)_2(OSMe_2)_2]^{2-}$, 2.471 (1) Å, and $[Pt_2(HPO_4)_4(H_2O)_2]^{2-}$, 2.486 (2) Å, where there is a formal single bond between Pt^{III} centres (20, 21). However, a very wide range of Pt—Pt lengths has been reported and it is clear that significant interactions persist at much longer distances. In cluster complexes containing Pt_3 triangles, distances in the range 2.6–2.8 Å are generally found (22, 23). In α-pyridone blue (24), and in related complexes containing two Pt atoms bridged by pyrimidine bases (25), values up to 2.98 Å have been considered short enough to suggest metal–metal bonding. A correlation between partial oxidation states and the resonating valence bond theory of metals has shown that some weak interactions may persist to about 3.2 Å (26), and SCF-Xα-SW calculations on $[Rh_2Cl_2(CO)_4]$ have suggested a metal–metal interaction as the explanation for the "bent" structure (27). This last example is especially relevant to the present situation since the Rh—Rh distance is 3.12 Å and the metal–metal bonding, actually a subtle effect caused by mixing of d_{z^2} character into a bonding d_{xz}—d_{xz} combination, is proposed to account for an observed dihedral angle of 124° between the two Rh square planes (27). Both the dihedral and the metal–metal distance are similar to those found here for $[Pt_3S_2(PMe_2Ph)_6]^{2+}$ and it is therefore clear that, although the distances in the present complex, 3.108(1) and 3.182(1) Å, are certainly too long to imply formal bonding, the possibility of weak interactions sufficient to influence the core geometry cannot be discounted. For example, for a three atom cluster in the point group D_{3h} there are two sets of orbitals of symmetry e' and one set of symmetry e'' which are cluster valence orbitals, near to the LUMO level and derived from s and p atomic orbitals (28). A Jahn–Teller type distortion involving these double degenerate levels could account for the main features of the observed structures.

The alternative point of view is that any metal-to-metal interactions are weak enough that low energy external forces, such as crystal packing, suffice to produce variations in metal-to-metal distances. The available crystallographic data are given in Table 5. The nickel structure is not accurate enough for detailed bond length comparisons. The palladium structure is based on a large set of intensity measurements and, although not fully refined, indicates three significantly different metal–metal distances, one considerably shorter than the other two. This does suggest that influences external to the Pd_3S_2 core are having an effect, despite the minimal steric requirements of the PMe_3 ligands. In the platinum compound with its bulkier PMe_2Ph ligands, the intramolecular distances C(27)—C(33), 3.89 Å, and C(37)—C(16), 3.84 Å, give a possible explanation for the long Pt(1)—Pt(2) distance since they are counteracted only by C(18)—C(27), 4.16 Å, C(22)—C(22′), 4.27 Å, and C(23)—C(23′), 4.22 Å.

The nmr spectra were analyzed in terms of D_{3h} symmetry for the $Pt_3S_2P_6$ core rather than the C_2 symmetry suggested by the X-ray work. This could reflect a truly more symmetrical structure in solution or could be due to dynamic interchange between C_2 structures, possibilities which would be difficult to distinguish even with extensive low temperature studies. This problem notwithstanding, the nmr parameters remain a potential source of information on bonding interactions. Unfortunately, the J(Pt—Pt) value (476 Hz) is of little assistance. It is consistent with previous results for thio-bridged dinuclear compounds (18, 29) but it is known that in general J(Pt—Pt) coupling constants show no correlation with Pt—Pt distance or even with the presence or absence of a metal–metal bond (29). However, there is evidence that longer range couplings are increased when metal–metal bonds are present. Thus, in complexes containing the grouping **1**, both ^{3-4}J(P—P) and ^{2-3}J(Pt—P) are markedly dependent on the Pt—Pt interaction.

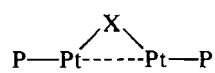

1

In dinuclear complexes bridged by chloro (18), phosphido (17, 18, 30), and thiolato (14, 18) groups there is essentially no question of significant metal–metal interaction and both ^4J(P—P), <5 Hz, and ^3J(Pt—P), 7–63 Hz, are of small magnitude. By contrast, magnitudes in trinuclear clusters, where the geometry is essentially similar but there is a metal–metal bond, are much larger: ^3J(P—P), 20–160 Hz; ^2J(Pt—P), 120–519 Hz (17, 23, 31, 32). Clearly the values for the present complex, ^4J(P—P) < 5 Hz, ^3J(Pt—P) = −25 Hz, fall into the non metal–metal bonded ranges.

Overall, it appears to be most satisfactory to regard the $[Pt_3S_2(PMe_2Ph)_6]^{2+}$ cation, and its Ni and Pd analogues, as formed from three 16 electron square planes joined by sharing of the sulphide ligands. The crystal packing and metal–metal bonding arguments are not mutually exclusive and both may contribute to the slight deviations from trigonal symmetry, but it seems unlikely that the latter is an important component of the primary bonding.

1. P. D. FRISCH and L. F. DAHL. J. Am. Chem. Soc. **94**, 5082 (1972).
2. H. VAHRENKAMP, V. A. UCHTMAN, and L. F. DAHL. J. Am. Chem. Soc. **90**, 3272 (1968).
3. H. WERNER, W. BERTLEFF, and U. SCHUBERT. Inorg. Chim. Acta, **43**, 199 (1980).

Can. J. Chem. Downloaded from www.nrcresearchpress.com by 210.87.254.42 on 09/06/12
For personal use only.

4. C. H. WEI and L. F. DAHL. Inorg. Chem. **4**, 493 (1965).
5. J. CHATT and D. M. P. MINGOS. J. Chem. Soc. A, 1243 (1970).
6. C. A. GHILARDI, S. MIDOLLINI, and L. SACCONI. Inorg. Chim. Acta, **31**, L431 (1978).
7. J. M. JENKINS and B. L. SHAW. J. Chem. Soc. A, 770 (1966).
8. J. A. GLADYSZ, V. K. WONG, and B. S. JICK. Tetrahedron, **35**, 2329 (1979).
9. R. B. JOHANNSEN, J. A. FERRETI, and R. K. HARRIS. J. Magn. Reson. **3**, 84 (1970).
10. J. D. SWALEN. *In* Computer programmes for chemistry. Vol. I. *Edited by* D. F. Detar. W. A. Benjamin, New York. 1968.
11. G. SHELDRICK. SHELX-76 program manual. Inorganic Chemistry Institute of Gottingen University, Fed. Rep. of Germany.
12. D. T. CROMER and J. T. WABER. International tables for X-ray crystallography. Vol. 4. The Kynoch Press, Birmingham, England. 1974. pp. 99, 149.
13. J. W. GOSSELINK, G. VAN KOTEN, A. M. F. BROUWERS, and O. OVERBEEK. J. Chem. Soc. Dalton Trans. 342 (1981).
14. P. H. BIRD, U. SIRIWARDANE, R. D. LAI, and A. SHAVER. Can. J. Chem. **60**, 2075 (1982).
15. M. C. HALL, J. A. J. JARVIS, B. T. KILBOURN, and P. G. OWSTON. J. Chem. Soc. Dalton Trans. 1544 (1972).
16. G. W. BUSHNELL, A. PIDCOCK, and M. A. R. SMITH. J. Chem. Soc. Dalton Trans. 572 (1975).
17. J. B. BRANDON and K. R. DIXON. Can. J. Chem. **59**, 1188 (1981).
18. C. EABORN, K. J. ODELL, and A. PIDCOCK. J. Organomet. Chem. **170**, 105 (1979).
19. W. MCFARLANE. J. Chem. Soc. A, 1922 (1967).
20. F. A. COTTON, L. R. FALVELLO, and S. HAN. Inorg. Chem. **21**, 2889 (1982).
21. F. A. COTTON, L. R. FALVELLO, and S. HAN. Inorg. Chem. **21**, 1709 (1982).
22. A. ALBINATI. Inorg. Chim. Acta, **22**, L31 (1977); A. ALBINATI, G. CARTURAN, and A. MUSCO. Inorg. Chim. Acta, **16**, L3 (1976); J. C. CALABRESE, L. F. DAHL, P. CHINI, G. LONGONI, and S. MARTINENGO. J. Am. Chem. Soc. **96**, 2614 (1974); Y. YAMAMOTO, H. YAMAZAKI, and T. SAKURAI. J. Am. Chem. Soc. **104**, 2329 (1982); D. G. EVANS, G. R. HUGHES, D. M. P. MINGOS, J. M. BASSETT, and A. J. WELCH. J. Chem. Soc. Chem. Commun. 1255 (1980).
23. P. L. BELLON, A. CERIOTTI, F. DEMARTIN, G. LONGONI, and B. T. HEATON. J. Chem. Soc. Dalton Trans. 1671 (1982).
24. J. K. BARTON, D. J. SZALDA, H. N. RABINOWITZ, J. V. WASZCZAK, and S. J. LIPPARD. J. Am. Chem. Soc. **101**, 1434 (1979).
25. R. FAGGIANI, B. LIPPERT, C. J. L. LOCK, and R. A. SPERANZINI. J. Am. Chem. Soc. **103**, 1111 (1981); C. J. L. LOCK, H. J. PERESIE, B. ROSENBERG, and G. TURNER. J. Am. Chem. Soc. **100**, 3371 (1978); B. LIPPERT and D. NEUGEBAUER. Inorg. Chem. **21**, 451 (1982).
26. A. H. REIS, JR. and S. W. PETERSON. Inorg. Chem. **15**, 3186 (1976).
27. J. G. NORMAN, JR. and D. J. GMUR. J. Am. Chem. Soc. **99**, 1446 (1977).
28. J. W. LAUHER. J. Am. Chem. Soc. **100**, 5305 (1978).
29. N. M. BOAG, J. BROWNING, C. CROCKER, P. L. GOGGIN, R. J. GOODFELLOW, M. MURRAY, and J. L. SPENCER. J. Chem. Res. S, 228 (1978).
30. A. J. CARTY, F. HARTSTOCK, and N. J. TAYLOR. Inorg. Chem. **21**, 1349 (1982).
31. A. MOOR, P. S. PREGOSIN, and L. M. VENANZI. Inorg. Chim. Acta, **61**, 135 (1982); A. MOOR, P. S. PREGOSIN, and L. M. VENANZI. Inorg. Chim. Acta, **48**, 153 (1981).
32. K. R. DIXON and A. D. RATTRAY. Inorg. Chem. **17**, 1099 (1978).
33. C. W. HAIGH. J. Chem. Soc. A, 1682 (1970).

Appendix

The use of existing standard nomenclature to describe the spin systems involved in these isotopomers is not entirely straightforward. For example, **II**, **III**, and **IV** could be described as AA′A″A‴A⁗A⁗′X, AA′A″A‴A⁗A⁗′XX′, and AA′A″A‴A⁗A⁗′XX′X″, respectively. This is accurate but not especially helpful since specification of all the coupling constants is necessary to make apparent the symmetry of the systems. The more recent symmetry related nomenclature proposed by Haigh (33) (and now in common use) gives an elegant representation of **IV** as an $[[A]_2X]_3$ system, but is unable to deal with **II** or **III** because these contain isochronous, magnetically non-equivalent nuclei which are not related by a symmetry element. Although this situation is of common occurrence in isotopomers, the nomenclature makes no provision for it and introduction of a distinctive symbol (an asterisk is here proposed) is necessary for a really useful description. Thus, using inner brackets to represent the symmetry plane containing the three Pt atoms and outer brackets for the C_2 axis, we obtain $[[A]_2A^*]_2X$ as a description of the spin system in isotopomer **II**. There are several possible choices for **III** but the most concise is probably $[A[A^*]_2X]_2$, where the brackets have the same significance as for **II**. In the interests of consistency, A* in both cases refers to phosphorus directly bonded to magnetically active platinum but this choice is not essential to the description.

The analysis in the main text has been simplified by assuming that ^4J(P—P) is zero. This is effectively the same as assuming magnetic equivalence of phosphorus atoms which are related by the plane of symmetry containing the three Pt atoms. Under these conditions, isotopomers **II**, **III**, and **IV** could be represented as $[A_2]_2A^*{}_2X$, $A_2[A^*{}_2X]_2$, and $[A_2X]_3$ respectively. Brackets in the first two cases represent the C_2 axis and in the last example represent the C_3 axis.

Can. J. Chem. Downloaded from www.nrcresearchpress.com by 210.87.254.42 on 09/06/12
For personal use only.

Solvent and temperature dependence of absorption and phosphorescence of *trans*-diisothiocyanate (bis)ethylenediaminechromium(III) ion[1]

COOPER H. LANGFORD[2] AND THOMAS M. SCHEAR

Department of Chemistry and Canadian Picosecond Flash Photolysis Centre, Concordia University, 1455 de Maisonneuve W., Montreal, P.Q., Canada H3G 1M8

Received August 9, 1983

COOPER H. LANGFORD and THOMAS M. SCHEAR. Can. J. Chem. **62**, 703 (1984).

An unusual case of absorption and fluorescence bands shifting in the same direction as solvent varies is reported. Solvent shifts in the quartet absorption maximum and doublet or phosphorescence emission maximum of *trans*-$Cren_2(NCS)_2^+$ ion are related to the Gutmann solvent donor number. The correlation is discussed in terms of solvent effects on the vibrations identified as responsible for the vibronic transitions and are in agreement with Hollebone's notion of "vibronic" intersystem crossing. The activation parameters for decay of phosphorescence in eight solvents correlate by a Barclay–Butler plot and are consistent with the possibility of a single common dominant mechanism for the *T*-dependent decay path. They do not, however, depend on solvent donor numbers as quantum yields for substitution do. Therefore, they offered no new support for the notion that the pathway is by chemical reaction. The activation parameters also fail to correlate with solvent fluidity.

COOPER H. LANGFORD et THOMAS M. SCHEAR. Can. J. Chem. **62**, 703 (1984).

On rapporte un cas inusité où les bandes d'absorption et de fluorescence se déplacent dans la même direction lorsqu'on fait varier le solvant. On a établi une relation entre le nombre donneur de Gutman relatif aux solvants et les déplacements dus aux solvants dans le quartet d'absorption maximale ainsi que l'émission maximale double ou de phosphorescence de l'ion $Cren_2(NCS)_2^+$-*trans*. On discute de la corrélation en termes d'effets de solvant sur les vibrations que l'on a identifiées comme responsables des transitions vibroniques et ils sont en bon accord avec la notion de Hollebone concernant les croisements entre systèmes vibroniques. Une bonne corrélation entre les paramètres d'activation pour la disparition de la phosphorescence dans huit solvants peut être établie grâce à une courbe de Barclay–Butler et ces paramètres sont en accord avec la possibilité d'un seul mécanisme commun dominant pour les voies de disparition de la phosphorescence qui dépendent de *T*. Ils ne dépendent toutefois pas des nombres donneurs des solvants comme c'est le cas pour les rendements quantiques pour la substitution. Ils n'offrent donc aucun support pour la notion que la voie est une réaction chimique. Il n'existe pas non plus de corrélation entre les paramètres d'activation et la fluidité du solvant.

[Traduit par le journal]

Introduction

Despite the common notion that the ligand field bands in the spectra of transition metal complexes are insensitive to solvent, there have been several interesting discussions of solvent effects on the decay of the phosphorescent doublet state of Cr(III) complexes (1–4). In particular, some authors (2) have felt that trends identified in solvent effects were best interpreted in terms of a photosubstitution pathway as the dominant mode of relaxation, whereas others (1, 3) have tended to regard back intersystem crossing to the quartet as the dominant pathway of relaxation of the doublet (i.e. the doublet fate is analogous to delayed fluorescence). A third possible path is, of course, direct "intersystem crossing" to the quartet ground state.

The complex ion *trans*-$Cren_2(NCS)_2^+$ shows a particularly simple and dramatic dependence of photoreaction quantum yield on solvents. The yields are linearly related to a "nucleophilicity" correlated parameter, the Gutmann donor number (5).

Since the factor, which has led both to the suggestion of a dominant reactive decay of the doublet and to the suggestion of a dominant back intersystem crossing process, is the relatively high apparent activation energy for decay of the doublet, it seemed useful to see if this activation energy also correlated with a single solvent parameter. An affirmative result could lend considerable support to the claims that one decay mechanism is dominant.

Experimental

Materials

The solvents used included spectrograde reagent CH_3OH, CH_3NO_2, CH_3CN, $(CH_3)_2CO$, dimethylsulfoxide (DMSO), *N*,*N*-dimethylformamide (DMF), and $(CH_3CO)_2O$ used without further purifications. Water was distilled and deionized.

The complex was prepared from $Cren_3(SCN)_3$ (6). A quantity of reagent grade chromium(III) sulfate was dried to the pentahydrate as indicated by water insolubility. A sample of 0.137 mol were mixed with 0.898 mol of ethylene diamine (98%) and refluxed at 105°C. A period of 4–5 h of manual agitation is necessary as the mixture tends to solidify. Once the mixture is dark brown, agitation is no longer necessary and refluxing is continued for an additional 20 h. The product is yellow–brown (yield 115 g). $[Cren_3]_2(SO_4)_3$ is converted to the chloride by dissolution in a mixture of 18 mL concentrated HCl and 110 mL of H_2O which was preheated to 65°C. The hot solution is quickly filtered into an ice-cold solution of 96 mL concentrated HCl mixed with 160 mL of 95% ethanol. The yellow solid is collected after about 30 min and washed with absolute ethanol and ether (yield 72 g). The $Cren_3Cl_3$ is dissolved in 225 mL of water at 60°C NH_4NCS (87 g) is dissolved in 100 mL of water and added. The resulting solution is held in an ice bath for 30 min to precipitate $[Cren_3](SCN)_3$ which is collected and washed with absolute ethanol and ether. Yield is 57 g, 49% based on $Cr_2(SO_4)_3 \cdot 5H_2O$.

trans-$[Cren_2(NCS)_2]SCN$ was prepared by heating 10 g of finely powdered $Cren_3(SCN)_3$ in an oven at a carefully controlled temperature of 130–134°C. The mass, spread thinly on a plate, is broken up every hour. When 16% of the weight has been lost the reaction is deemed suitably complete. The crude thiocyanate salt (8.4 g) is warmed with 120 mL of concentrated HCl (45–55°C) until evolution of HSCN is almost complete. The hot mixture is filtered quickly and the filtrate is held at 5°C for 30 min to complete precipitation. The resulting product, *trans*-$[Cren_2(NCS)_2]Cl$, is washed well and recrystallized from a minimum amount of hot water (yield 2.3 g). Parameters of the visible spectrum are given in Table 1. These param-

[1]We thank the Natural Sciences and Engineering Research Council of Canada and Formation des Chercheurs et Action Concertée du Québec for financial support.

[2]To whom correspondence should be addressed.

Can. J. Chem. Downloaded from www.nrcresearchpress.com by 210.87.254.40 on 09/06/12
For personal use only.

TABLE 1. Spectroscopic parameters and solvent characteristics (all data at 25.0°C)

Solvent	DN[a]	I/η[b]	Absorption max. (cm^{-1})	ϵ (M^{-1} cm^{-1})[c]	Emission max. (cm^{-1})
CH_3NO_2	2.7	1.61	20 330	93.2	13 620
$(CH_3CO)_2O$	10.5	1.28	20 410	88.1	13 680
CH_3CN	14.1	2.90	20 450	92.6	13.660
$(CH_3)_2CO$	17.0	3.17	20 330	91.0	13 680
CH_3OH	19.0	1.83	20 330	92.6	13 680
DMF	26.6	1.26	20 490	82.3	13 760
DMSO	29.8	0.505	20 530	83.0	13 770
H_2O	33.0	1.12	20 580	85.6	13 790

[a]The donor number (13*a*).
[b]$1/\eta$ is reciprocal of solvent viscosity in reciprocal centripoise from ref. 13(*b*)
[c]Molar extinction coefficient in reciprocal molar concentration cm^{-1}.

eters (7) and the ir spectrum (8) are in good agreement with literature values.

The chloride salt was used in studies in H_2O, DMF, DMSO, and CH_3OH. It was converted to the perchlorate salt for use in CH_3NO_2, CH_3CN, $(CH_3)_2CO$, and $(CH_3CO)_2O$ by recrystallization with 70% $HClO_4$.

Spectroscopy

Absorption spectra were obtained on a Perkin-Elmer 552. Emission spectra were recorded on a Perkin-Elmer MPF-44B equipped with a differential corrected spectra unit. Temperature control of samples was achieved by circulating either hot water or refrigerated ethylene glycol through the cell holder. The exact temperature of the solution was monitored by placing a precise thermometer in a cell of the same solvent placed in the spectrophotometer sample cell holder ($T \pm 0.1$°C).

A temperature dependence run was initiated by a half-hour warm-up period. The concentration of the complex was always in the range of $3.00-7.00 \times 10^{-4}$ *M* where emission intensity was linear in concentration. Care was taken to avoid suspended scattering matter in the solutions. The solution and the *T* monitor cell were mounted in two positions of the sample holder. When *T* had stabilized (~30 min), emission was monitored as a function of time at the wavelength maximum shown in Table 1. Corrected spectra indicate that the excitation maximum matches the absorption maximum. Excitation wavelength was set at 492 nm throughout. At temperatures below room temperature, a stream of dry N_2 was used to prevent fogging. After a point was complete, the shutters were closed and solutions were replaced from the stock. Generally, 10 to 15 temperatures were investigated for each run. Since values used for study of *T* dependence are relative to others within one solvent, instrument parameters were optimized for each solvent.

Results

Spectroscopic parameters and solvent characteristics at 25°C are collected in Table 1. It is clear that there is a measurable change in positions of the absorption and emission ligand field band maxima with solvent. The values in the table are precise (not necessarily absolutely accurate) to ± 25 cm^{-1}. There is a correlation that is "statistically significant" (95%) between increasing energy of both transitions and increasing Gutmann donor number (correlation coefficients: $R_{abs} = 0.78$, $R_{em} = 0.95$). But donor number (DN) is not indicated to be the dominant solvent characteristic controlling measurable differences. DN and fluidity give a reasonable model. (Multiple regression $R^2 = 0.697$, significant at 94%, *but* standard error of estimate 60 cm^{-1} or greater than 2×25.)

In more comprehensive temperature-dependence studies than this (down to 77 K), two distinct regions of temperature dependence of phosphorescence intensity are seen to be well

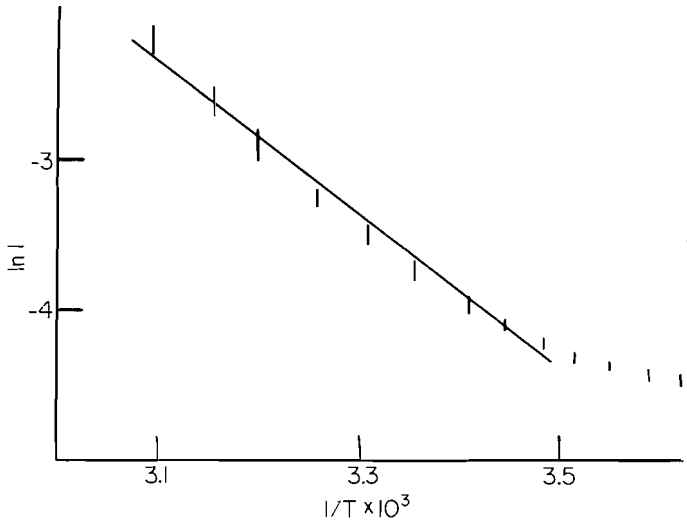

FIG. 1. Plot of (natural log emission intensity)$^{-1}$ (log I^{-1}) vs. reciprocal absolute *T* in CH_3OH.

defined (9, 10). From 77 K to above 200 K, phosphorescence intensity is independent of temperature but quantum yields of emission are well below unity (9, 10). This region reveals the radiationless deactivation from the lowest vibrational level of the doublet state by a weak coupling mechanism. At higher temperature, the phosphorescence intensity decreases with increasing temperature in a manner consistent with the Arrhenius equation. In the present study, an effort was made to ensure that deviation from the Arrhenius slope at lower temperature where the temperature-independent mechanism becomes important was not ignored. This was done by fitting the higher temperature points to a straight line by eye and being careful to determine if lower temperature points deviated significantly from the line. Where they did, an appropriate small number of low temperature points were excluded from consideration and the remaining points were fitted to a straight line Arrhenius relation by linear regression using eq. [1].

$$[1] \quad \ln (1/I) = \ln A - E_a/RT$$

Two typical cases are shown in Figs. 1 and 2. In the case of CH_3CN shown in Fig. 1, five points were excluded from the linear regression as indicating contributions of the temperature-independent mechanism. In the case of DMSO shown in Fig. 2, no points were excluded from the linear regression. Temperature dependence parameters for all solvents as obtained from the linear regression are collected in Table 2. The activa-

Can. J. Chem. Downloaded from www.nrcresearchpress.com by 210.87.254.40 on 09/06/12
For personal use only.

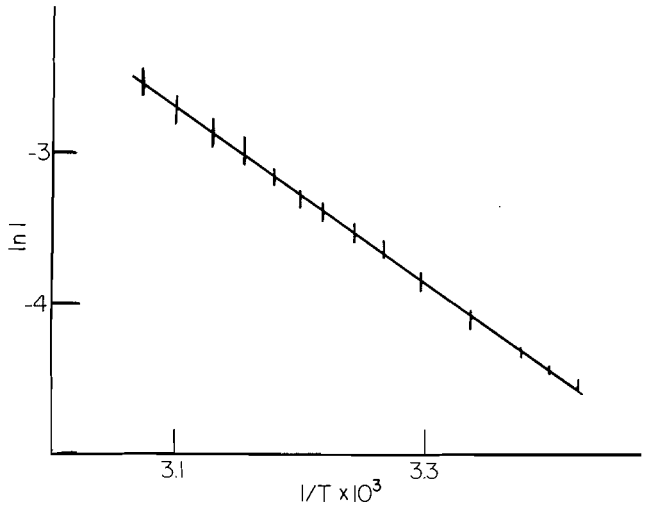

FIG. 2. Plot of (natural log of emission intensity)$^{-1}$ (log I^{-1}) vs. reciprocal absolute T in DMSO.

TABLE 2. Activation parameters for phosphorescence of *trans*-$Cren_2(NCS)_2^+$

Solvent	E_{app} (kcal mol^{-1})[a]	ln A[b]	r^2[c]
CH_3NO_2	9.8(2)	12.7	0.990
$(CH_3CO)_2O$	11.7(2)	16.2	0.988
CH_3CN	10.5(2)	13.9	0.990
$(CH_3)_2CO$	8.8(2)	11.4	0.970
CH_3OH	13.6(3)	20.0	0.998
DMF	7.0(2)	8.0	0.998
DMSO	11.5(2)	15.3	0.998
H_2O	12.4(4)	17.7	0.992

[a]Apparent activation energies from eq. [1] fits. Numbers in parentheses indicate the number of independent T-dependence studies run on each solvent.
[b]ln A from eq. [1] fits.
[c]r^2 test of goodness-of-linear-regression fits.

tion parameters in Table 2 deviate from some values reported earlier for water (1, 2). This is attributed to the exclusion here of some low temperature points from the Arrhenius equation linear fit.

Discussion

The original purpose of this study was to use the complex for which a simple relation between solvent and photochemical reactivity had been established by Cusumano and Langford to search support for Adamson's hypothesis of "reactive" doublet relaxation via analysis of the large activation energies. As will be seen in section 2 below, no such unequivocal evidence was forthcoming. In the process, we noticed another point of considerable interest. Contrary to the common case where solvent effects alter absorption and luminescence band positions in *opposite* directions (because the solvent is equilibrated around the ground state in the first case and around the excited in the second), we find luminescence and absorption shifting in the *same* direction with solvent. This strongly suggests *dynamic* effects. We cannot give a full account of this very interesting phenomenon but section 1 provides some initial speculations which may help to orient research on the problems.

1. Solvent shifts

The wavelength shift in the position of the absorption maximum of the spin-allowed band indicates that solvents affect the vibronic processes which relax the Laporte forbidden character of the $d-d$ transition. We can make some speculative remarks which show how this could arise. In the case of $Cr(OH_2)_6^{3+}$, Hollebone *et al.* have shown that the t_{1u} "buckle" vibration is involved in the quartet–quartet transition (11). It appears that the potential surface of this type of vibration is sensitive, at least in part, to the donor number of the solvent. The shift to higher energy with higher donor number could arise if the force constant increased with donor number and the absorption maximum remained at about the fifth term in the vibrational progression where it is found in $Cr(OH_2)_6^{3+}$. The shift to lower energy paralleling fluidity has a less evident origin.

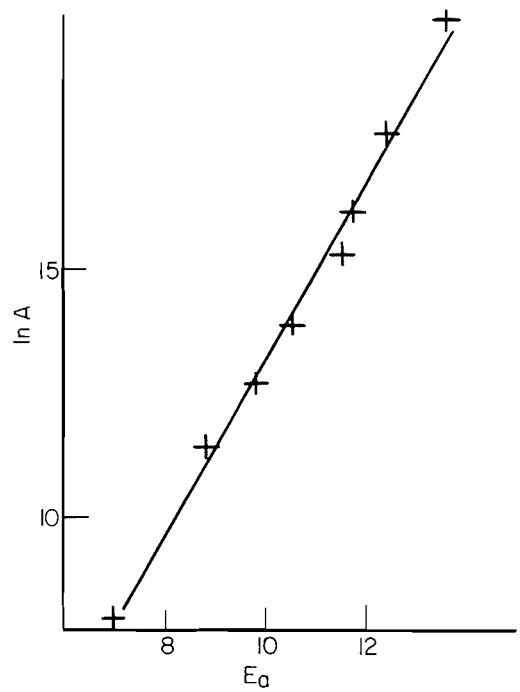

FIG. 3. Barclay–Butler plot of parameters of Arrhenius equation from Table 2.

The details of the solvent effects on the absorption maximum and our speculative explanations are not as important as the interesting *parallel* between the solvent dependence of the absorption maximum and the emission maximum. The weakness of spin–orbit coupling in Cr(III) has caused some puzzles with respect to the efficiency of intersystem crossing from the excited quartet to the excited doublet. Hollebone *et al.* (11) have recently shown that angular momentum may be associated with vibrational basis functions by subduction from spherical symmetry just as it is in the case of electronic basis functions. Consequently, the analysis of Hollebone *et al.* suggests that the quartet and doublet of an octahedral Cr(III) complex couple via an asymmetric stretch t_{1u} vibration if the maximum remains at the same vibrational state. This provides a consistent explanation for the otherwise surprising observations of a common trend between absorption where solvent is in an equilibrium arrangement around the ground state and emission where solvent is in an equilibrium configuration around the excited state. It is significant that solvent dependence supports the vibronic mechanism of intersystem crossing.

2. Temperature dependence

We now turn to the less speculative and more immediately significant part of this work. Figure 3 shows a Barclay–Butler

Can. J. Chem. Downloaded from www.nrcresearchpress.com by 210.87.254.40 on 09/06/12
For personal use only.

plot (enthalpy–entropy correlation) which gives some support to the notion that the temperature-dependent mechanism for non-radiative relaxation of the doublet is the same in all the solvents. However, neither the values of E_a nor ln A correlate with donor numbers (this is evident without a plot). Thus, the support sought for the idea that the T-dependent pathway is reactive is not found. In contrast to the close relation of SCN^- substitution quantum yield to donor number, no simple correlation emerged here. Looking in another direction, it is also interesting that no simple correlation is found with solvent fluidity (reciprocal of viscosity) which seemed to control substitution yield in $[Cr(NH_3)_2(NCS)_4]^-$ (5).

The final question is to ask whether the results support the model in which back intersystem crossing dominates the doublet relaxation pathways. Two points are mildly favourable. The Barclay–Butler plot suggests that a single relaxation may well dominate throughout. As well, the low temperature behaviour suggests a weak coupling pathway for the direct radiationless decay of the doublet so that attention is directed to the search for an alternative mechanism for the temperature dependent path. The energetics are consistent. The splitting in absorption between the states labelled ^4T and ^2E in O_h symmetry is near 19 kcal mol^{-1}. But the large Stokes shifts of quartet fluorescence observed for those few complexes which are fluorescent (12) suggest that vibrationally relaxed quartet levels are much closer to the doublets. In fact, the best estimates of the location of the zero–zero band in the present compound comes from Adamson's suggestion (12) that it is at the point in the absorption band where intensity is 5% of the maximum or from the MCD analysis of the vibrational progression of $Cr(OH_2)_6^{3+}$ in water at 25°C by Hollebone *et al.* (11). These make it feasible to assign the E_a values here to the barrier to back intersystem crossing. However, it must be stated that the evidence favouring back intersystem crossing as a dominant mechanism for doublet relaxation remains quite weak.

1. N. A. P. KANE-MAGUIRE and C. H. LANGFORD. J. Chem. Soc. Chem. Commun. 895 (1971).
2. A. R. GUTIERREZ and A. W. ADAMSON. J. Phys. Chem. **82**, 902 (1978).
3. S. C. PYKE, M. OGERSAWARA, L. KEVAN, and J. F. ENDICOTT. J. Phys. Chem. **82**, 302 (1978).
4. C. F. C. WONG and A. D. KIRK. Can. J. Chem. **54**, 3794 (1976).
5. M. CUSUMANO and C. H. LANGFORD. Inorg. Chem. **17**, 2222 (1978).
6. G. G. SCHLESSINGER. Inorganic laboratory preparations. Chemical Publishing Co. New York. 1962.
7. W. A. BAKER and M. G. PHILLIPS. Inorg. Chem. **5**, 1042 (1966).
8. J. A. MCLEAN. J. Inorg. Nucl. Chem. **26**, 1245 (1964).
9. S. R. ALLSOPP, A. COX, T. J. KEMP, W. J. REED, S. SOOTERO, and O. TRAVERSO. J. Chem. Soc. Faraday I, **76**, 162 (1980).
10. K. KUHN, F. WASGESTIAN, and H. KUPTA. J. Phys. Chem. **85**, 665 (1981).
11. B. R. HOLLEBONE, C. H. LANGFORD, and N. SERPONE. Coord. Chem. Rev. **39**, 181 (1981).
12. A. W. ADAMSON. Prog. Inorg. Chem. **17**, 1 (1972).
13. (*a*) V. GUTMANN. Electrochim. Acta, **21**, 661 (1976); (*b*) CRC handbook of chemistry and physics, 61st ed. CRC Press, Cleveland, OH 1980.

Can. J. Chem. Downloaded from www.nrcresearchpress.com by 210.87.254.40 on 09/06/12
For personal use only.

The theory of regular solutions applied to molar excess enthalpies and volumes of binary mixtures containing stannic bromide

S. K. SURI[1] AND R. C. MAHESHWARI

Chemistry Department, Indian Institute of Technology, New Delhi — 110016, India

Received May 9, 1983

S. K. SURI and R. C. MAHESHWARI. Can. J. Chem. **62**, 707 (1984).

The molar excess enthalpies, H_m^E, at 313.15 K and molar excess volumes, V_m^E, at 303.15, 308.15, and 313.15 K for the binary mixtures of stannic bromide with benzene, cyclohexane, and tetrachloromethane have been determined. Both H_m^E and V_m^E for the three sets of binary mixtures are positive over the entire range of composition. The experimental results have been compared with those predicted by regular solution theory. It is observed that H_m^E calculated for regular solutions are highly sensitive to the estimation of C_{12}. The calculated V_m^E are in good agreement with the experimental data if it is assumed that $(\partial E/\partial P)_T = 0$; and the ratio of the internal pressures to the cohesive energy density are the same for unmixed and the mixed components.

S. K. SURI et R. C. MAHESHWARI. Can. J. Chem. **62**, 707 (1984).

On a determiné les enthalpies molaires en excès, H_m^E à 313,15 K et les volumes molaires en excès, V_m^E, à 303,15, 308,15 et 313,15 K de mélanges binaires de bromure stannique avec le benzène, le cyclohexane et le tétrachlorométhane. Les valeurs de H_m^E et de V_m^E sont positives pour les trois mélanges dans tout l'intervalle des compositions. On a comparé les résultats expérimentaux avec ceux prévues par la théorie des solutions régulières. On observe que les valeurs de H_m^E calculées pour des solutions régulières sont fortement influencées par l'évaluation de C_{12}. Les valeurs de V_m^E calculées sont en bon accord avec les données expérimentales si l'on admet que $(\partial E/\partial P)_T = 0$ et que les rapports des pressions internes sur la densité d'énergie de cohésion sont les mêmes pour les composants sous formes de mélanges ou non mélangés.

[Traduit par le journal]

Can. J. Chem. Downloaded from www.nrcresearchpress.com by 210.87.254.5 on 09/06/12
For personal use only.

Introduction

In our earlier studies (1, 2), we have reported the solubilities and partial molar volumes of arsenic, antimony, bismuth, and stannic bromides in various non-polar organic solvents. It was observed that the behaviour of these bromide solutions conform to the broader theories of non-electrolytes solutions proposed by Hildebrand and co-workers (3, 4). As an extension to our investigation on such solutions, we have measured the molar excess enthalpies (H_m^E) and molar excess volumes (V_m^E) of the binary mixtures of stannic bromide with benzene, cyclohexane, and tetrachloromethane. Attempts have been made to compare our results with those predicted by Hildebrand's regular solution model to see if the excess functions for these solutions can be described within the framework of this theory.

Experimental

Stannic bromide was synthesised by refluxing a slight excess of tin metal (A. R. Grade) with bromine in tetrachloromethane media till the solution was no longer coloured brown. The solution was filtered hot, the solvent distilled off, and the residue distilled over the metal *in vacuo*. The sample obtained was crystallised from anhydrous tetrachloromethane and dried at ~300 K under reduced pressure for an extended period of time. It was stored in brown bottles in a desiccator. Analytical reagent grade benzene, cyclohexane, and tetrachloromethane were purified according to standard procedures (5) and subjected to fractional distillation immediately before use. Some measured physical properties of the liquids have been compared with the literature values (6–12) in Table 1.

The molar excess enthalpies were determined in the calorimeter used in our earlier studies (13). The maximum uncertainty in the H_m^E data reported here is estimated to be around 2% for very small heat exchange.

The molar excess volumes have been calculated from the experimental densities of the binary mixtures determined pycnometrically. We preferred this method for the estimation of V_m^E over the direct dilatometric measurements because of the chemically aggressive nature of stannic bromide towards the blocking fluid mercury. The details of pycnometer used and experimental procedure for the preparation of solutions and measurement of densities have been described earlier (11). The maximum uncertainty in molar excess volumes is expected to be less than 0.010 $cm^3\ mol^{-1}$.

[1]To whom all correspondence should be addressed.

Results and discussion

The experimental results for H_m^E and V_m^E are represented graphically in Figs. 1 and 2, respectively. Each set of data were fitted by the method of unweighed least-squares to a polynomial of the form

$$[1] \quad X_m^E = x_1 x_2 \sum_{i=0}^{n-1} C_i (x_1 - x_2)^{i-1}$$

where X_m^E is either H_m^E or V_m^E and x_1 and x_2 are the mole fractions of stannic bromide and the organic component, respectively. The values of the coefficients for each function are given in Table 2 along with the standard deviation $\sigma(X_m^E)$. Since the standard deviation for all sets of data is of the same order of magnitude, as the estimated uncertainty in the respective experimental results, eq. [1] can be taken to represent the experimental results.

It is observed from Fig. 1 that H_m^E for the three sets of binary mixtures are positive over the entire composition range and show a maximum at $x_i \simeq 0.4$. The H_m^E for the benzene solution as estimated from freezing point data at eutectic point (i.e. 174.15 K and $x_1 = 0.371$) has been reported to be $1071 \pm 523\ J\ mol^{-1}$ (14). The uncertainty reported in this value renders any comment about it difficult. To the best of our knowledge, there is no other literature report on the molar enthalpies of mixing for these mixtures to compare our results.

All three sets of binary mixtures exhibited expansion on mixing over the entire composition range with the V_m^E maxima around $x_1 \simeq 0.4$ (Fig. 2). V_m^E is found to be large for solutions containing benzene, and cyclohexane as compared to those containing tetrachloromethane. The $(\partial V_m^E/\partial T)_P$ was positive for binary mixtures containing tetrachloromethane and nega-

TABLE 1. Some physical properties of liquids used[a]

Liquid	Freezing temperature (K)	Refractive index at 313.15 K	Density, g cm^{-3} at 303.15 K	308.15 K	313.15 K	318.15 K	323.15 K
$SnBr_4$	302.4 (302.55)[6]	1.6562	3.3358	3.3212 (3.34)[7]	3.3061	3.2917	3.2771
C_6H_6	278.75 (278.68)[8]	1.4888 (1.4882)[8b]	0.86818 (0.86825)[8]	0.86225 (0.86296)[8]	0.85731 (0.85760)[8]	0.85203 (0.85220)[9]	0.84684 (0.8468)[8]
c-C_6H_{12}	279.80 (279.70)[8]	1.4149 (1.4154)	0.76893 (0.7693)[8]	0.76409 (0.7646)[10]	0.76008 (0.75953)[11]	0.75528 (0.7550)[10]	0.75042
CCl_4	—	1.4475 (1.4481)[8b]	1.57480 (1.57456)[8]	1.56535 (1.55478)[8]	1.55571 (1.55498)[8]	1.54589 (1.5457)[12]	1.53603 (1.53611)[8]

[a]Values in parentheses show the literature values, reference numbers appear in superscript.
[b]Extrapolated values.

Can. J. Chem. Downloaded from www.nrcresearchpress.com by 210.87.254.5 on 09/06/12
For personal use only.

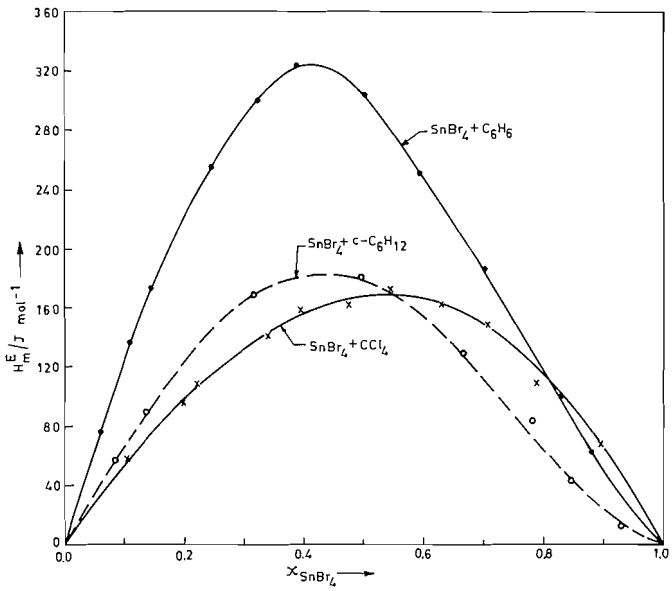

FIG. 1. Molar excess enthalpies, H_m^E, as a function of composition for the binary mixtures at 313.15 K.

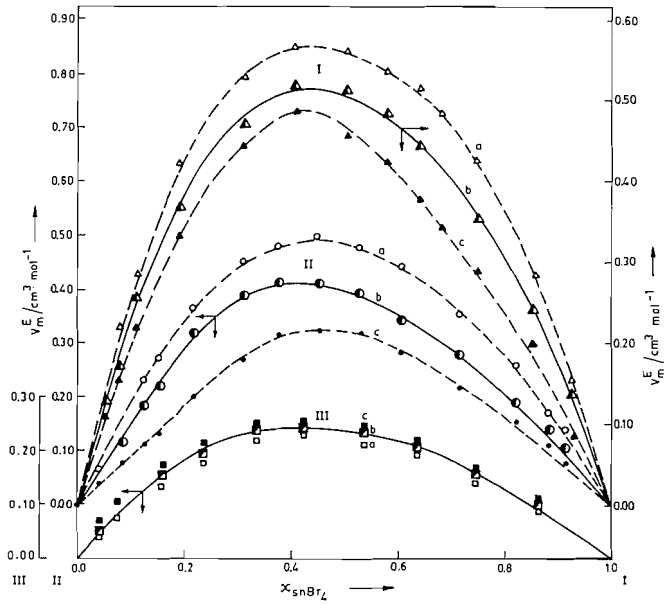

FIG. 2. Molar excess volumes, V_m^E, as a function of composition for the binary mixtures.

tive for the other two sets of binary mixtures. The V_m^E for the binary mixture of stannic bromide and tetrachloromethane at 308.15 K and $x_1 = 0.467$ reported by Hildebrand and Carter (15) is 0.002 cm^3 mol^{-1} higher than the one obtained by eq. [1] using the constants given in Table 2. We are not aware of any other volumetric studies on these binary mixtures.

It is observed that the magnitude of both H_m^E and V_m^E decreases as the ionization potential of the organic component increases.

The experimental H_m^E values were converted to respective molar excess energies at constant volume using the thermodynamic relationship (16)

$$[2] \quad E_m^E = H_m^E - T\frac{\alpha_m}{\beta_m} V_m^E$$

where α_m and β_m are the coefficients of thermal expansion and isothermal compressibilities for the binary mixtures, respectively. For the purpose of our calculations, these parameters were estimated from the data for pure components (Table 3) assuming additivity on volume fraction basis. The E_m^E values so obtained have been compared with those corresponding to a regular solution calculated using the expression (3)

$$[3] \quad E_m^E = (x_1 v_1 + x_2 v_2)(C_{11} + C_{22} - 2C_{12})\phi_1\phi_2$$

where ϕ_i and V_i are the volume fractions and molar volumes for the component molecules and the cohesive energy densities, C_{ii}, are given by

$$[4] \quad C_{ii} = \delta_i^2 = (\Delta H_i^{vap} - RT)/V_i$$

δ_i being the solubility parameter. The term C_{12} in eq. [3] was eliminated using the Berthalot relationship

$$[5] \quad C_{12} = (C_{11}C_{22})^{1/2}$$

It is observed from Fig. 3 that while for benzene solutions the experimental E_m^E values are ~4–5 times higher than those predicted from eq. [3], for the other two sets of binary mixtures these were significantly lower (~one-third of eq. [3] values for cyclohexane solutions and ~two-thirds for tetrachloromethane solutions).

In order to investigate the effect of geometric mean assumption (eq. [6]), the unlike interaction parameter, C_{12}, was estimated following Kohler (16):

$$[6] \quad C_{12} = \frac{16P_1P_2}{V_1V_2(V_1^{1/3} + V_2^{1/3})^3}\frac{\mu_1\mu_2}{\mu_1 + \mu_2}$$

TABLE 2. Coefficients and standard error (σ) for representation of excess functions of the binary mixtures by eq. [1]

System (1) + (2)	Function[a]	T (K)	C_0	C_1	C_2	C_3	σ
$SnBr_4 + C_6H_6$	H_m^E	313.15	1208.3	−649.9	−323.5	259.2	4.6
	V_m^E	303.15	2.2585	−0.303	0.652	−0.212	0.004
		308.15	2.0333	−0.462	0.306	0.116	0.006
		313.15	1.8454	−0.728	−0.043	0.353	0.007
$SnBr_4 + c\text{-}C_6H_{12}$	H_m^E	313.15	723.1	−282.8	−326.5	−45.9	2.4
	V_m^E	303.15	1.9572	−0.533	−0.116	0.501	0.004
		308.15	1.6062	−0.758	−0.174	0.946	0.006
		313.15	1.2785	−0.292	−0.513	0.586	0.007
$SnBr_4 + CCl_4$	H_m^E	313.15	674.4	100.4	−28.5	−78.2	4.0
	V_m^E	303.15	0.8914	−0.285	—	0.150	0.004
		308.15	0.9704[c]	−0.268	−0.020	0.024	0.003
		313.15	0.9893	−0.222	0.263	−0.219	0.005

[a]Units: H_m^E, J mol^{-1}; V_m^E, cm^3 mol^{-1}.

TABLE 3. Parameters of pure components at 313.15 K

Parameter	$SnBr_4$	C_6H_6	$c\text{-}C_6H_{12}$	CCl_4
$C_p(l)$ (J deg^{-1} mol^{-1})	165.4[a]	—	—	—
$C_p(g)$ (J deg^{-1} mol^{-1})	103.4[19]	—	—	—
V (cm^3 mol^{-1})	132.58[b]	91.11[b]	110.72[b]	98.89[b]
$\alpha \times 10^4$	8.92[b]	11.92[b]	11.60[b]	12.51[b]
ΔH^{vap} (kJ mol^{-1})	51.98[c]	33.03[c]	32.25[c]	31.91[c]
δ_i (eq. [4])/(J cm^3)$^{1/2}$	19.30	18.30	16.34	17.22
IP (eV)	—	9.24[7]	9.80[7]	11.47[7]
$\beta \times 10^{10}$ (m^2 N^{-1})	8.00[d]	11.05[7]	12.56[7]	11.96[7]
$P \times 10^{24}$ (eq. [7]) (cm^3 mol^{-1})	19.31	10.41	11.00	11.19
$\mu \times 10^{-52}$ (eq. [8]) (J mol^{-1})	232.5	233.6	300.3	229.1

[a]Average of $C_p(l)$ for $SnCl_4$ = 163.1 J deg^{-1} mol^{-1} (17) and SnI_4 = 167.7 J deg^{-1} mol^{-1} (18).
[b]From data in Table 1.
[c]Extrapolated values.
[d]Assumed to be the same as that of $SnCl_4$ (20).

where

$$[7] \quad P_i = \frac{3}{4\pi N}\frac{\epsilon_i - 1}{\epsilon_i + 2}V_i$$

and

$$[8] \quad \mu_i \frac{C_{ii}V_i^3}{P_i^3}$$

ϵ and N being the dielectric constant and Avogadro's number, respectively. In deriving eq. [6], it has been assumed that the interactions between unlike molecules occur between point centres only. The C_{12} values obtained from eqs. [5] and [6] have been compared with those required to fit the experimental results in Table 4. Though both approaches offer a good estimate of C_{12}, it is observed that an uncertainty of ~1% in its estimation propagates an appreciable difference in the evaluation of E_m^E using eq. [3]. The deviations from geometic mean law have been explained using an empirical binary coefficient, l_{12}, defined by (4)

$$[9] \quad C_{12} = (1 - l_{12})(C_{11}C_{22})^{1/2}$$

For the three binary mixtures containing stannic bromide, we found l_{12} to be dependent on composition. It increased with an increase in the mole fraction of stannic bromide for tetrachloromethane solutions and decreased for benzene and for cyclohexane solutions (Fig. 4). The sign and magnitude of l_{12} for these mixtures cannot be explained on the basis of intermolecular interactions and/or difference in shapes of the component molecules (4).

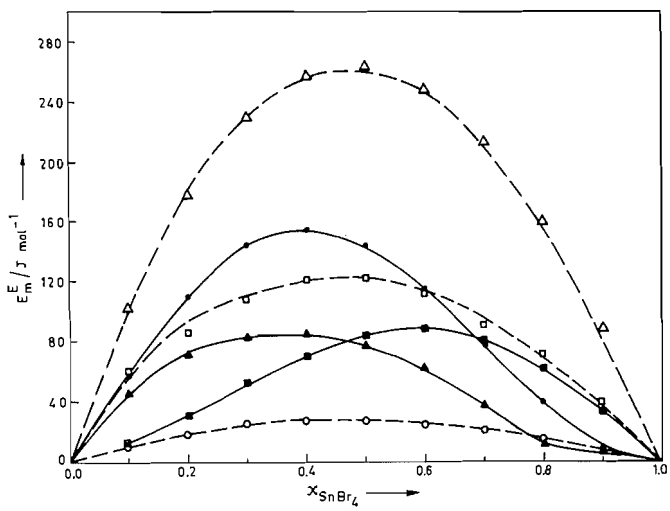

FIG. 3. Comparison of experimental molar excess energies, E_m^E, at 313.15 K with those obtained by eq. [3].

It is established that in the absence of electron−donor,

Can. J. Chem. Downloaded from www.nrcresearchpress.com by 210.87.254.5 on 09/06/12
For personal use only.

TABLE 4. Unlike interaction parameters, C_{12} (J mol^{-1}) at 313.15 K

System (*1*) + (*2*)	C_{12} from eq. [5]	C_{12} from eq. [6]	C_{12} required to fit experimental data
$SnBr_4$ + C_6H_6	353.2	350.8	351.4±0.7
$SnBr_4$ + c-C_6H_{12}	315.4	312.6	318.5±0.8
$SnBr_4$ + CCl_4	332.3	331.0	333.1±0.7

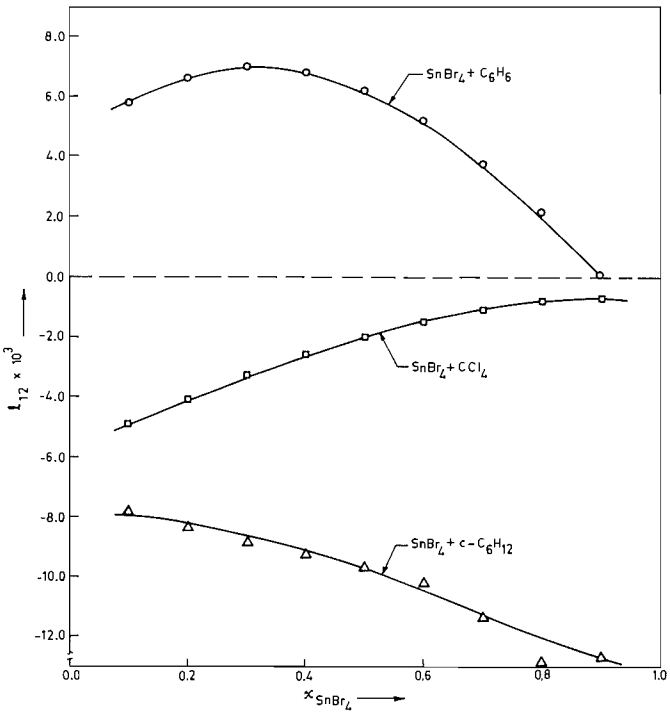

FIG. 4. Dependence of the empirical binary co-efficient, l_{12}, on composition at 313.15 K.

−acceptor interactions, normal liquids ordinarily expand on mixing (4). The V_m^E for all the three sets of binary mixtures under investigation exhibited a volume fraction dependence given by the expression

$$[10] \quad V_m^E = k\phi_1\phi_2$$

indicating that these systems approximate to regular solutions. We observed a linear correlation between k and ΔH_2^{vap} or $(\Delta H_1^{vap} - \Delta H_2^{vap})/(\Delta H_1^{vap} + \Delta H_2^{vap})$. At 313.15 K, the numerical value of k were 1.90 ± 0.03, 1.23 ± 0.04, and 1.05 ± 0.05 cm^3 mol^{-1} for benzene, cyclohexane, and tetrachloromethane solutions, respectively. The organic component having higher ΔH^{vap} exhibited higher k and hence higher V_m^E (for stannic bromide solutions). For V_m^E, Scott derived the expression (3, 21):

$$[11] \quad V_m^E = \eta_m\beta_m G_P^E \qquad (i)$$

$$- T(\partial S_v^E/\partial P)_T \qquad (ii)$$

$$- (\eta_m\beta_m E_m - x_1\eta_1\beta_1 E_1 - x_2\eta_2\beta_2 E_2) \qquad (iii)$$

$$- \eta_m\beta_m T S_v^E \qquad (iv)$$

where η_m is the ratio of internal pressure to the cohesive energy density for the mixture. He observed that the contributions from terms (*ii*) and (*iii*) of eq. [11] approximately cancel each other. If we assume the same to hold good for the binary mixtures under investigation, the apparent volumetric effects

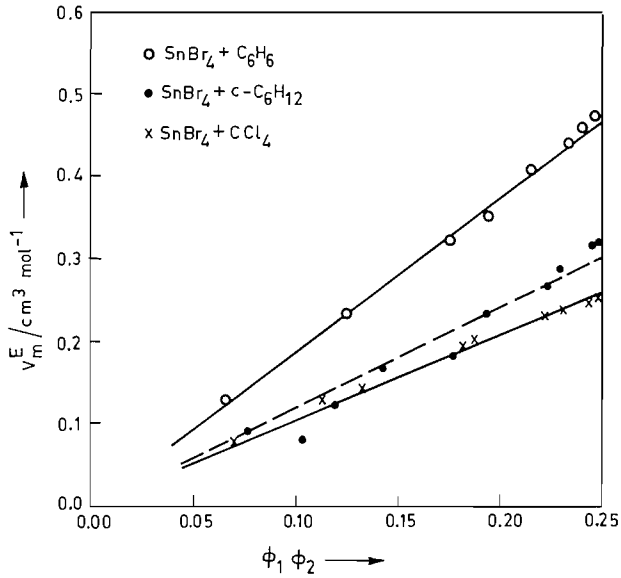

FIG. 5. V_m^E for the binary mixtures at 313.15 K plotted against the product of the volume fractions of component molecules $\phi_1\phi_2$.

TABLE 5. Contribution of terms (*i*) and (*iv*) of eq. [11] to the molar excess volumes of binary mixtures of equimolar composition at 313.15 K

System	Terms of eq. [11] (cm^3 mol^{-1}) (*i*)	(*iv*)	(*i*) + (*iv*)	V_m^E (exptl) (cm^3 mol^{-1})
$SnBr_4$ + C_6H_6	0.273	0.133	0.406	0.461
$SnBr_4$ + c-C_6H_{12}	0.187	0.085	0.272	0.320
$SnBr_4$ + CCl_4	0.150	0.079	0.229	0.247

TABLE 6. Comparison of $(\alpha_m/\delta_{m^2})T$ with experimental (V_m^E/H_m^E) at equimolar concentration and 313.15 K

System	$\frac{\alpha_m}{\delta_{m^2}}T \times 10^4$ (cm^3 J^{-1})	$\frac{V_m^E}{H_m^E} \times 10^4$ (cm^3 J^{-1})
$SnBr_4$ + C_6H_6	9.0	15.3
$SnBr_4$ + c-C_6H_{12}	10.2	17.7
$SnBr_4$ + CCl_4	9.2	15.3

show an excellent agreement with the one predicted by eq. [11] (Table 5). Various researchers (21) proposed an approximate formula equivalent to the first term of eq. [11] for V_m^E. For stannic bromide solutions, this by itself could reproduce neither the magnitude nor the shape of the experimental molar excess volumes. It was observed (Table 6) that for the three sets of binary mixtures, the experimental (V_m^E/H_m^E) are ~70% higher than α_m^T/δ_m^2, where $\delta_m^2 = \delta_1\delta_2$. This leads us to the conclusion that the volumetric effects in these mixtures arise from similar phenomena.

Acknowledgement

The authors wish to express their gratitude to Dr. K. K. G. Menon, Research Director, Hindustan Lever Research Centre, for providing secretarial facilities for the preparation of this manuscript.

Can. J. Chem. Downloaded from www.nrcresearchpress.com by 210.87.254.5 on 09/06/12
For personal use only.

1. R. C. MAHESHWARI, S. K. SURI, and V. RAMAKRISHNA. J. Inorg. Nucl. Chem. **36**, 1809 (1974).
2. R. C. MAHESHWARI, S. K. SURI, and V. RAMAKRISHNA. J. Inorg. Nucl. Chem. **37**, 1937 (1975).
3. J. H. HILDEBRAND and R. L. SCOTT. Regular solutions. Prentice-Hall, New Jersey. 1962.
4. J. H. HILDEBRAND, R. L. SCOTT, and J. M. PRAUSNITZ. Regular and related solutions. Van Nostrand, N.Y. 1970.
5. J. A. RIDDICK and W. B. BUNGER (*Editors*). Technique of organic chemistry. Vol. II. Organic solvents 3rd ed. Wiley-Interscience 1970.
6. J. J. KEAVNEY and N. O. SMITH. J. Phys. Chem. **64**, 737 (1960).
7. R. C. WEAST (*Editor*). Handbook of chemistry and physics. 61st ed. CRC Press Inc., Florida, 1980–81.
8. J. TIMMERMANS (*Editor*). Physicochemical constants of pure organic compounds. Vols. I and II. Elsevier, Amsterdam. 1965.
9. M. DIAZ'PENA and G. TARDAJOS. J. Chem. Thermodyn. **10**, 19 (1978).
10. M. B. EWING and K. N. MARSH. J. Chem. Thermodyn. **6**, 395 (1974).
11. R. C. MAHESHWARI, S. K. SURI, and U. S. TEWARI. J. Chem. Eng. Data, **24**, 237 (1979).
12. R. P. TOMLINS and M. ADAMSON. J. Chem. Thermodyn. **6**, 757 (1974).
13. S. K. SURI and R. C. MAHESHWARI. J. Chem. Thermodyn. **12**, 1191 (1980).
14. A. F. KAPUSTINSKU and YU. M. KESSLER. Izvest. Akad. Nauk SSSR, Otdel, Khim. Nauk. **10**, 889 (1956).
15. J. H. HILDEBRAND and J. M. CARTER. J. Am. Chem. Soc. **54**, 3592 (1932).
16. I. A. MCLURE, J. E. BENNETT, A. E. P. WATSON, and G. C. BENSON. J. Phys. Chem. **69**, 2759 (1965).
17. International critical tables. Vol. 5. 1929. p. 106.
18. G. R. NEGISHI. J. Am. Chem. Soc. **58**, 2293 (1936).
19. M. KH. KARAPET'YANTS and M. L. KARAPET'YANTS (*Editors*). Handbook of thermodynamic constants of inorganic compounds. Israel Program for Scientific Translation. 1966.
20. H. SACKMANN and A. BOEZEK. Z. Physik-Chem. **29**, 329 (1961).
21. R. BATTINO. Chem. Rev. **71**, 5 (1971).

Can. J. Chem. Downloaded from www.nrcresearchpress.com by 210.87.254.5 on 09/06/12
For personal use only.

Synthetic and kinetic studies of the reversible addition of a bridging NSN fragment to the electron-rich heterocycles $(R_2PN)(SN)_2$ (R = Me, Ph, F)

NEIL BURFORD, TRISTRAM CHIVERS,[1] RICHARD T. OAKLEY,[2] AND TOM OSWALD
Department of Chemistry, The University of Calgary, Calgary, Alta., Canada T2N 1N4

Received September 26, 1983

NEIL BURFORD, TRISTRAM CHIVERS, RICHARD T. OAKLEY, and TOM OSWALD. Can. J. Chem. **62**, 712 (1984).

The oxidative addition of Cl_2 (using SO_2Cl_2) to the six-membered ring $(R_2PN)(SN)_2$ (R = Me, Ph) produces the mixed phosphazene–thiazyl heterocycles, $(R_2PN)(NSCl)_2$, which react with $Me_3SiNSNSiMe_3$ to give the bicyclic compounds $R_2PS_3N_5$. The latter undergo thermal decomposition, at ca. 100°C in toluene, via reductive elimination of an NSN unit to regenerate $(R_2PN)(SN)_2$ in high yield. Kinetic measurements of this process, using ^{31}P nmr spectroscopy, yield an activation energy of 102.4 ± 6.0 kJ mol^{-1} for the release of the NSN fragment from $Me_2PS_3N_5$. The thermolysis route has been used to prepare the thermally unstable $(F_2PN)(SN)_2$, characterized as a 1:1 adduct with norbornadiene.

NEIL BURFORD, TRISTRAM CHIVERS, RICHARD T. OAKLEY et TOM OSWALD. Can. J. Chem. **62**, 712 (1984).

L'addition oxydative du chlore (utilisant le SO_2Cl_2) aux cycles à six chaînons $(R_2PN)(SN)_2$ (R = Me, Ph) conduit aux hétérocycles mixtes phosphazène–thiazyles $(R_2PN)(NSCl)_2$ qui réagissent avec le $Me_3SiNSNSiMe_3$ pour donner les composés bicycliques $R_2PS_3N_5$. Ces derniers subissent une décomposition thermique, à environ 100°C dans le toluène, via une élimination réductrice d'une unité de NSN pour regénérer le $(R_2PN)(SN)_2$ avec un bon rendement. Des mesures cinétiques de ce processus, faisant appel à la spectroscopie RMN du ^{31}P, ont permis de déterminer que l'énergie d'activation, pour l'élimination du fragment NSN à partir du $Me_2PS_3N_5$ s'établit à 102,4 ± 6,0 kJ/mol. On a utilisé la voie de la thermolyse pour préparer le composé $(F_2PN)(SN)_2$ qui est thermiquement instable et que l'on a caractérisé sous forme d'adduit 1:1 avec le norbornadiène.

[Traduit par le journal]

Can. J. Chem. Downloaded from www.nrcresearchpress.com by 210.87.254.6 on 09/06/12
For personal use only.

Introduction

We have recently reported the preparation and the molecular and electronic structure of π-electron-rich heterocycles containing the PS_2N_3 ring, **1** (R = Me, Ph), which undergo a reversible cycloaddition reaction with norbornadiene (NBD) (1). In the adduct, **2**, the olefin is symmetrically bound to the sulfur atoms of **1**, a mode of addition which has been explained by the primarily sulfur-based character of the HOMO and LUMO of **1** (1). We now report that **1** (R = Me, Ph) undergoes oxidative addition reactions with halogenating agents, e.g., SO_2Cl_2, to give $(R_2PN)(NSCl)_2$, **3**, which is converted to the bicyclic compound $R_2PS_3N_5$, **4**, on treatment with $Me_3SiNSNSiMe_3$ (2).

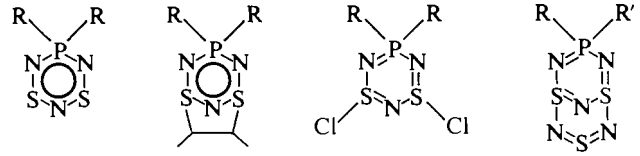

1 **2** **3** **4**

Derivatives of **4** (R = R′ = F; R = Ph, R′ = F) have previously been prepared by the reaction of $Me_3SiNSNSiMe_3$ with PF_5 (3, 4) (or $PhPF_4$ (4, 5)) and their thermal decomposition in benzene at ca. 70°C was reported to give the radical anion N_2S^- on the basis of a five line esr spectrum (4, 6).[3] We find, however, that the thermolysis of **4** (R = Ph, Me) regenerates **1** in high yield via the reductive elimination of a neutral NSN unit. The latter molecule has never been characterized but it is a frequent reaction fragment in cyclothiazene chemistry.[4] We have carried out a kinetic study of this decomposition, using ^{31}P nmr spectroscopy, in order to determine the activation energy for the release of NSN and we have used the thermolysis of **4** (R = R′ = F) to prepare the previously unknown difluoro derivative, **1** (R = F), as an adduct with NBD (**2**, R = F).[5]

Experimental

Reagents and general procedures

Solvents were dried (toluene (sodium) and acetonitrile (CaH_2 and P_2O_5)) and freshly distilled before use. All reactions were conducted under an atmosphere of nitrogen (99.98% purity passed through Ridox and silica gel).

Sulfuryl chloride (Aldrich) was freshly distilled before use and phosphorus pentafluoride (Penwalt) was used as received. The following reagents were prepared by the literature procedures: $Me_3SiNSNSiMe_3$ (8), $(R_2PN)(SN)_2$ (R = Me, Ph) (1), and $F_2PS_3N_5$ (4). The latter reagent was purified by sublimation (10^{-3} Torr) onto a cold finger (0°C).

Instrumentation

Infrared spectra (4000–250 cm^{-1}) were recorded as Nujol mulls (CsI windows) on a Perkin-Elmer 467 grating spectrophotometer, Ultraviolet–visible spectra were obtained using a Cary 15 instrument. All nmr spectra were recorded with a Varian XL-200 spectrometer using the following references: ^1H and ^{13}C (internal Me_4Si), ^{19}F (external CF_3COOH), ^{31}P (external 85% H_3PO_4). Chemical analyses were performed by MHW Laboratories, Phoenix, AZ.

Preparation of $(Ph_2PN)(NSCl)_2$

Sulfuryl chloride (0.7 mmol) was added dropwise, by syringe, to a stirred solution of $(Ph_2PN)(SN)_2$ (0.20 g, 0.7 mmol) in acetonitrile (20 mL). The purple solution turned yellow immediately. The volume of the mixture was reduced to 10 mL by removal of solvent *in vacuo*. The solution was cooled to −20°C and a few moisture-sensitive, yellow–orange crystals of $(Ph_2PN)(NSCl)_2$ were deposited. *Anal.*

[1]To whom correspondence should be addressed.

[2]Present address: Department of Chemistry, University of Guelph, Guelph, Ont., Canada N1G 3G5.

[3]The observed esr spectrum establishes that the radical contains two nitrogen atoms but *does not* define the number of sulfur atoms, which could be more than one.

[4]The most stable arrangement of two nitrogen and one sulfur atoms is linear NNS ($C_{\infty v}$) (7).

[5]The related heterocycles **1** (R = CF_3, C_2F_5) have recently been prepared by the reaction of $R_2PN(SiMe_3)_2$ with $S_3N_2Cl_2$ and the NBD adduct of the CF_3 derivative has been structurally characterized by X-ray crystallography (H. W. Roesky, J. Lucas, M. Noltemeyer, and G. M. Sheldrick. Private communication).

Can. J. Chem. Downloaded from www.nrcresearchpress.com by 210.87.254.6 on 09/06/12
For personal use only.

calcd. for $C_{12}H_{10}Cl_2N_3PS_2$: C 39.79, H 2.78, N 11.60, Cl 19.57; found: C 40.39, H 3.32, N 11.78, Cl 19.89. Infrared (major bands): 1440(vs), 1125(vs), 1074(vs), 1028(m), 1000(m), 898(vs), 756(m), 737(vs), 692(s), 637(m), 543(vs), 499(s), 416(s), 311(m), 299(m) cm^{-1}.

Preparation of $Ph_2PS_3N_5$

Sulfuryl chloride (1.0 mmol) was added dropwise, by syringe, to a stirred solution of $(Ph_2PN)(SN)_2$ (0.30 g, 1.0 mmol). A solution of $Me_3SiNSNSiMe_3$ (0.21 g, 1.0 mmol) in acetonitrile (10 mL) was slowly added to the resulting yellow solution, which became orange–red. The volume of the solvent was reduced to 10 mL by removal of solvent *in vacuo* and, on cooling to −30°C, orange needles were obtained. Recrystallization from acetonitrile gave orange–brown crystals of $Ph_2PS_3N_5$ (0.25 g, 0.7 mmol). *Anal.* calcd. for $C_{12}H_{10}N_5PS_3$: C 41.00, H 2.87, N 19.92, S 27.35: found: C 40.93, H 3.35, N 20.09, S 26.73. Infrared (major bands): 1440(s), 1130(s), 1116(s), 1091(vs), 1076(s), 991(m), 809(s), 724(s), 697(m), 687(m), 567(s), 504(s), 468(m) cm^{-1}. $\{^1H\}$ ^{31}P nmr ($CDCl_3$) δ: −21.3 ppm.

Preparation of $Me_2PS_3N_5$

Sulfuryl chloride (1.5 mmol) was added dropwise, by syringe, to a solution of freshly sublimed $(Me_2PN)(SN)_2$ (0.24 g, 1.4 mmol) in acetonitrile (20 mL). The resulting yellow–green slurry was filtered to remove a small amount of a pale brown solid. A solution of $Me_3SiNSNSiMe_3$ (0.31 g, 1.5 mmol) in acetonitrile (15 mL) was added dropwise to the yellow filtrate which immediately became red–brown. Removal of solvent *in vacuo* gave a red–brown oil which was recrystallized from acetonitrile to give shiny brown crystals of $Me_2PS_3N_5$ (0.13 g, 0.6 mmol). Infrared: 1410(m), 1295(vs), 1090(vs), 1070(vs), 980(vs), 948(vs), 920(vs), 870(vs), 797(s), 756(m), 722(vs), 713(vs), 680(s), 635(s), 580(vs), 540(vs), 475(vs), 418(vs), 382(vs), 270(m) cm^{-1}. $\{^1H\}$ ^{31}P nmr ($CDCl_3$) δ: −4.4 ppm. Satisfactory elemental analyses could not be obtained due to the thermal instability of $Me_2PS_3N_5$.

Thermal decomposition of $Ph_2PS_3N_5$

A solution of $Ph_2PS_3N_5$ (0.20 g, 0.60 mmol) in toluene (25 mL) was heated at reflux for 3 h. The resulting purple solution was reduced in volume to ca. 10 mL, by removal of solvent *in vacuo*, and eluted down a Bio Beads S-X8 chromatography column (30 × 500 mm). Two bands, purple and yellow, were observed. The purple fraction was collected and solvent was removed *in vacuo* to give $(Ph_2PN)(SN)_2$ (0.12 g, 0.40 mmol) after recrystallization from acetonitrile. The yellow fraction contained a very small amount of S_4N_4 (ir spectrum) (9).

Thermal decomposition of $Me_2PS_3N_5$

A solution of $Me_2PS_3N_5$ (0.25 g, 1.0 mmol) in toluene (25 mL) was heated at reflux for 2 h. The resulting red–purple solution was reduced in volume to ca. 10 mL and eluted down a Bio Beads S-X8 chromatography column (30 × 500 mm) to give yellow (S_4N_4) and purple fractions. Removal of solvent from the latter fraction gave a purple oil from which purple crystals of $(Me_2PN)(SN)_2$ (ir spectrum) (1) were obtained by sublimation onto a cold finger (0°C). An accurate yield could not be obtained due to the thermal instability of the product.

Preparation of $(F_2PN)(SN)_2$ by the thermal decomposition of $F_2PS_3N_5$

A solution of $F_2PS_3N_5$ (0.10 g, 0.4 mmol) in Nujol (5 mL) was placed in a flask connected to the vacuum line via an empty flask cooled in liquid nitrogen. The system was evacuated and the Nujol solution was warmed to ca. 90°C using an oil bath. The yellow solution quickly became blue–green and a very volatile blue product condensed in the liquid nitrogen-cooled flask. After 3 h, the product was allowed to warm up to room temperature to give $(F_2PN)(SN)_2$ as a thermally unstable blue oil, λ_{max} (CH_2Cl_2, 23°C) 573 and 410 nm; ^{31}P nmr ($CDCl_3$) δ: −7.6 ppm, J_{PF} = 1055 Hz. ^{19}F nmr δ: −22.2 ppm. $(F_2PN)(SN)_2$ was also characterized as an adduct with norbornadiene (NBD).

Preparation of $(F_2PN)(SN)_2 \cdot C_7H_8$

A slight excess of norbornadiene was added dropwise to a solution of $(F_2PN)(SN)_2$ in diethyl ether. The purple solution became colorless immediately and a white precipitate was deposited. The crude product was crystallized from CH_3CN/CH_2Cl_2 containing norbornadiene to give an almost quantitative yield of $(F_2PN)(SN)_2 \cdot C_7H_8$. *Anal.* calcd. for $C_7H_8F_2N_3PS_2$: C 31.46, H 3.02, N 15.72; found: C 31.02, H 3.11, N 15.07. ^1H nmr ($CDCl_3$) δ: 1.32, 1.80 (AB, 10.0), 3.33, (t, 1.8), 4.66 (d, 1.6), 6.40; $\{^1H\}$ ^{13}C nmr ($CDCl_3$) δ: 41.1, 43.9, 85.0, 139.2; ^{19}F nmr ($CDCl_3$) δ: −43.8, −79.4 ppm. ($^1J_{PF}$ = 1001 Hz; $^2J_{FF}$ = 82.0 Hz).

^{31}P nmr spectroscopic monitoring of the thermal decomposition of $R_2PS_3N_5$

A flask containing a solution of $Ph_2PS_3N_5$ (0.30 g) in toluene (20 mL) was placed in a warm oil bath (95–100°C). Five minutes were allowed for the solution to reach the temperature of the oil bath and then samples were taken by syringe at regular intervals during a 100 min period. These samples were immediately cooled and their ^{31}P nmr spectra (500 scans) were recorded at −60°C. A similar procedure was used to monitor the thermal decomposition of $Me_2PS_3N_5$.

Kinetic measurements[6]

All solutions were handled in a dry, inert atmosphere. To determine the order of the reaction, solutions of various concentrations were obtained by dilution of a stock solution of $Ph_2PS_3N_5$ (0.1 *M*) in toluene at 23°C using a syringe. The reaction rates at different temperatures were measured by adding a known weight of $Ph_2PS_3N_5$ to each of five aliquots of toluene to give a 0.01 *M* solution. Temperatures were accurate to ±0.5°C. Samples were removed from the reaction vessels at suitable intervals, placed in an nmr tube, and cooled rapidly to −60°C to quench the reaction. The formation of $(Ph_2PN)(SN)_2$ was followed by the ^{31}P nmr spectrum and the amount present at a given time was determined from the percentage of the total area of the two peaks due to **1** and **4**.

Results and discussion

Preparation of $(Ph_2PN)(NSCl)_2$, 3 (R = Ph)

The eight π-electron heterocycle **1** reacts instantaneously with SO_2Cl_2 (as a source of Cl_2) to give $(R_2PN)(NSCl)_2$, **3** (R = Ph), as yellow, moisture-sensitive crystals characterized by chemical analyses and infrared spectroscopy. The reactions of **1** with Br_2 or I_2 also occur readily but the oily products could not be obtained pure. The heterocycle **3** can be considered as a hybrid of the well-known cyclotriphosphazene, $(Ph_2PN)_3$, and cyclotrithiazyl chloride, $(NSCl)_3$, ring systems and is the missing member of the series $(Ph_2PN)_{3-x}(NSCl)_x$ (x = 0–3). The other mixed phosphazene–thiazyl six-membered ring $(Ph_2PN)_2(NSCl)$ was recently prepared by the reaction of Ph_2PCl with S_4N_4 (3:1 molar ratio) in acetonitrile (10).

Preparation of the bicyclic compounds $R_2PS_3N_5$, 4

In view of the unusual range of reactions observed for $(Ph_2PN)_2(NSX)$ derivatives (10–13) the bifunctional nature of **3** offers interesting synthetic possibilities. We have found that the reaction of **3** with $Me_3SiNSNSiMe_3$ produces the bicyclic compounds **4** in good yields (cf. $Cl_3S_3N_3 + Me_3SiNSNSiMe_3 \rightarrow S_4N_5Cl + 2Me_3SiCl$) (14). The preparation of **4** from **3** supports a structure for **3** in which each sulfur is attached to one chlorine substituent. However, it is not possible to conclude that these substituents adopt a *cis* configuration in **3** based on this evidence. For example, it is known that the reaction of $Me_3SiNSNSiMe_3$ with 1,5-$Cl_2S_4N_4$, in which the chlorine at-

[6]Complete set of data may be obtained upon request, at a nominal charge, from the Depository of Unpublished Data, CISTI, National Research Council of Canada, Ottawa, Ont., Canada K1A 0S2.

Can. J. Chem. Downloaded from www.nrcresearchpress.com by 210.87.254.6 on 09/06/12
For personal use only.

oms are in *exo*, *endo* positions, produces S_5N_6 in which the NSN bridge enforces an *endo*, *endo* configuration (15). Thus it is possible for inversion to occur at sulfur in these metathetical reactions of bifunctional cyclothiazyl halides. However, the chlorine substituents are on the same side of the ring in the related six-membered heterocycles, $(Me_2NCN)(NSCl)_2$ (16) and $[(NSO_2)(NSCl)_2]^-$ (17), and an all *cis* geometry is found for $(NSCl)_3$ (18).

We also attempted to prepare **4** by the reaction of R_2PCl_3 (R = Me, Ph) with $Me_3SiNSNSiMe_3$. The ^{31}P nmr spectra of the reaction mixtures revealed the presence of many phosphorus-containing products, including **4**, which could not be separated as a pure compound. The reaction of $Me_3SiNSNSiMe_3$ with PCl_5 produces the six-membered ring $(Cl_2PN)_2(ClSN)$ (19). Thus the preparation of **4** from $Me_3SiNSNSiMe_3$ and phosphorus(V) reagents appears to be limited to the use of PF_5 (3, 4) or $PhPF_4$ (4).

Thermal decomposition of $R_2PS_3N_5$

A notable structural feature of **4** (R = R′ = F) is the relative length of the S—N bonds (1.69 Å) connecting the NSN unit (d(S—N) = 1.55 Å) to the six-membered $R_2PS_2N_3$ ring (average d(S—N) = 1.61 Å). This suggests a tendency to thermal breakdown of **4** via loss of an NSN unit, a process which is known to occur readily for many sulfur–nitrogen heterocycles (e.g. $S_4N_5^- \xrightarrow{-N_2S} S_3N_3^-$) (20).

We have monitored the thermolysis of **4** (R = Me, Ph) in toluene at ca. 100°C by ^{31}P nmr spectroscopy. The singlet due to **4** is gradually replaced by another singlet at lower field attributed to **1**. This conversion is complete after ca. 1.5 h and no other phosphorus-containing products can be detected in the ^{31}P nmr spectrum. In the case of **4** (R = Ph), the product **1** was isolated in ca. 70% yield. Thus the thermal breakdown of **4** must involve loss of a neutral NSN fragment, which has a low energy barrier to decomposition to N_2 and S (estimated to be 15–25 kcal for linear NSN ($D_{\infty h}$) and 9–15 kcal for bent (90°) NSN (C_{2v}) (7*a*)). The isolation of small amounts of S_4N_4 suggests that an alternative decomposition pathway exists for **4**, which may account for the formation of N_2S_x in sufficient concentration to be detected by its esr spectrum (4, 6).[3]

From an electronic point of view the reductive elimination of an NSN fragment from **4** can be understood in the same context as the reversible cycloaddition of norbornadiene to **2** (1). In essence, the NSN unit represents an isolobal analogue of a simple olefin. The N—N $\sigma(4a_1)$ and $\sigma^*(3b_2)$ orbitals of NSN (C_{2v}) (7*a*) are of the correct symmetry to interact with the LUMO and HOMO of **1**, respectively. Figure 1 illustrates the Hartree–Fock–Slater energy levels for the two reaction products (using $H_2PS_2N_3$ as a model for **1**) and correlates the interacting frontier orbitals.

Kinetic measurements

The formation of **1** (R = Ph) from **4** (R = R′ = Ph) as a function of temperature was followed by ^{31}P nmr spectroscopy. At 100°C the reductive elimination was found to follow first order kinetics with the rate constants being independent of the initial concentration of **4**. These simple kinetics are due to the rapid decomposition of NSN (7*a*) which precludes the second order back reaction. The rate constants, k, for the process

$$R_2PS_3N_5 \xrightarrow{k} (R_2PN)(SN)_2 + NSN$$

were obtained from the slopes of the first order kinetic plots in Fig. 2. Using the Arrhenius equation, a plot of ln k vs. T^{-1} (Fig. 3) yielded an activation energy of 102.4 ± 6.0 kJ mol^{-1} for the reductive elimination reaction. We have been unable to find similar data for S—N compounds with which to compare this value.

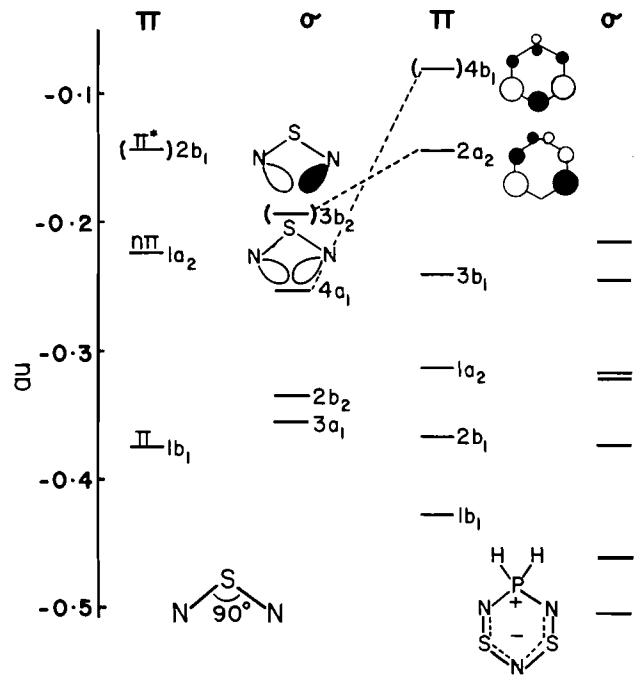

FIG. 1. Frontier orbitals of NSN (with NSN = 90°) and $H_2PS_2N_3$ taken from refs. 7*a* and 1, respectively. For clarity, the σ and π orbitals are separated. Virtual orbitals are indicated with parentheses ( ).

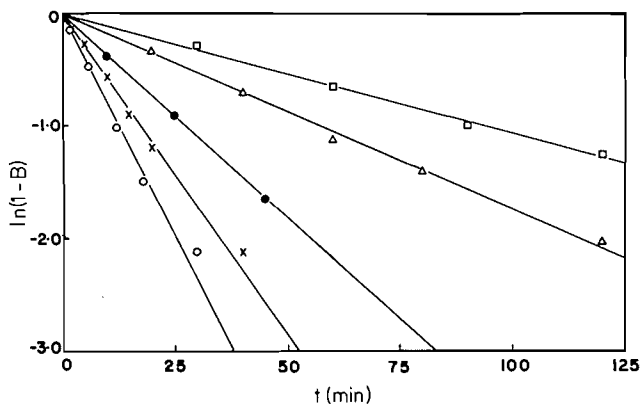

FIG. 2. Plots of ln $(1 - B)$ vs. time at various temperatures for the thermolysis of **4** (R = R′ = Ph); B = $[(Ph_2PN)(SN)_2]/[(Ph_2PN)(SN)_2 + (Ph_2PS_3N_5)]$ (see Experimental section); □, 86°C; △, 92°C; ●, 98°C; ×, 102°C; ○, 110°C.

Preparation of $(F_2PN)(SN)_2$ and $(F_2PN)(SN)_2 \cdot NBD$

The thermal decomposition of **4** (R = R′ = F) in Nujol at ca. 100°C produces **1** (R = F) as a volatile blue oil, which exhibits a strong visible absorption band at 573 nm, characteristic of cyclophosphadithiatriazenes and attributed to the π*HOMO → π*LUMO transition (1). The availability of a range of molecules (**1**, R = Me, Ph, PhO, F) provides a unique opportunity to examine the effects of different substituents R on the energy of this π* → π* transition. In the π-electron precise cyclophosphazenes, $(R_2PN)_x$, the HOMO (π) → LUMO (π*) transition occurs below 200 nm, so that substituent effects are

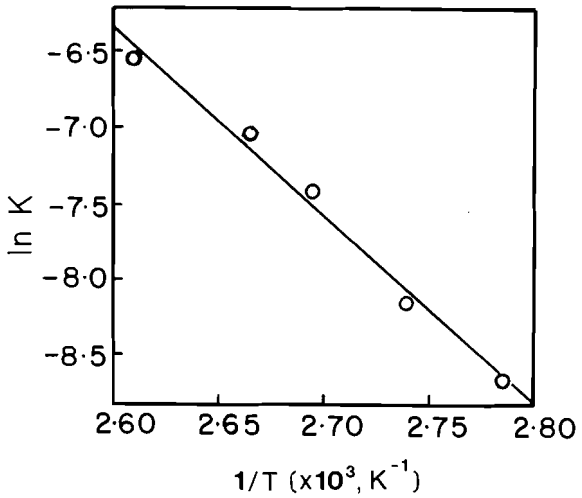

FIG. 3. Plot of $\ln k$ vs. $1/T$ for the thermolysis of **4** (R = R′ = Ph).

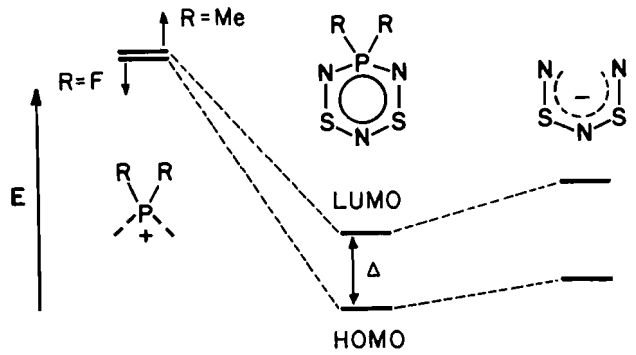

FIG. 4. Effect of exocyclic ligands attached to phosphorus on the HOMO−LUMO separation (△) of $(R_2PN)(SN)_2$.

not easily assessed. To the extent that the participation of $3d$ orbitals on phosphorus is important in describing the electronic structure of **1**, the involvement will be most pronounced in systems containing electronegative ligands (e.g. R = F, OPh). As indicated in Fig. 4, all orbitals will be stabilized under these circumstances, but the effect will be greater for the LUMO than the HOMO. Hence the bathochromic shift observed for R = F, OPh (λ_{max} 573 and 583 nm) relative to R = Me, Ph (λ_{max} 543 and 550 nm) finds a satisfactory correlation with the expected trend in the excitation energies.

In distinct contrast to **1** (R = Ph), which is a crystalline solid stable towards air, heat, and water, the fluoro derivative (**1**, R = F) is very moisture-sensitive and decomposes within ca. 1 h at 22°C under nitrogen. It can, however, be conveniently stored as a readily formed, crystalline adduct with norbornadiene (**2**, R = F). The ^1H and ^{13}C nmr spectra of this adduct closely resemble those reported for **2** (R = Ph (1), CF_3)[5] for which X-ray structural determinations have established an S,S mode of addition.

The values of the ^{19}F nmr chemical shift (−22.2 ppm) and J_{P-F} (1055 Hz) for **1** (R = F) are fairly typical for fluorocyclophosphazenes (21). The ^{19}F nmr spectrum of **2** (R = F) shows non-equivalent fluorine atoms as was found for the methyl substituents in **2** (R = Me) (1).

Conclusion

The bicyclic compounds $R_2PS_3N_5$ (R = Me, Ph) have been prepared from $(R_2PN)(SN)_2$, **1**, via a two-step synthesis involving the oxidative addition of Cl_2 followed by treatment with $Me_3SiNSNSiMe_3$. The thermolysis of these bicyclic systems regenerates the six-membered rings via reductive elimination of NSN, a process which is similar to the reversible cycloaddition of olefins to **1** in terms of frontier orbital concepts.

Acknowledgements

We thank the Natural Sciences and Engineering Research Council of Canada and the Alberta Research Council (postgraduate scholarship to N.B.) for financial support. The assistance of Dr. R. Yamdagni with the ^{31}P nmr experiments is gratefully acknowledged.

1. N. BURFORD, T. CHIVERS, R. T. OAKLEY, A. W. CORDES, and P. N. SWEPSTON. J. Chem. Soc. Chem. Commun. 1204 (1980); N. BURFORD, T. CHIVERS, A. W. CORDES, W. G. LAIDLAW, M. C. NOBLE, R. T. OAKLEY, and P. N. SWEPSTON. J. Am. Chem. Soc. **104**, 1282 (1982).
2. T. CHIVERS and R. T. OAKLEY. Top. Curr. Chem. **102**, 117 (1982).
3. H. W. ROESKY and O. PETERSEN. Angew. Chem. Int. Ed. Engl. **12**, 415 (1973).
4. R. APPEL, I. RUPPERT, R. MILKER, and V. BASTIAN. Chem. Ber. **107**, 380 (1974).
5. J. WEISS. Acta Crystallogr. Sect. B, **33**, 2272 (1974).
6. D. CHAPMAN and A. G. MASSEY. Trans. Faraday Soc. **58**, 1291 (1962).
7. (*a*) W. G. LAIDLAW and M. TRSIC. Inorg. Chem. **20**, 1792 (1981); (*b*) M. P. S. COLLINS and B. J. DUKE. J. Chem. Soc. Dalton Trans. 277 (1978).
8. O. J. SCHERER and R. WEISS. Z. Naturforsch. **25**b, 1486 (1970).
9. M. VILLENA-BLANCO and W. L. JOLLY. Inorg. Synth. **9**, 98 (1967).
10. T. CHIVERS, M. N. S. RAO, and J. F. RICHARDSON. J. Chem. Soc. Chem. Commun. 982 (1982).
11. T. CHIVERS, M. N. S. RAO, and J. F. RICHARDSON. J. Chem. Soc. Chem. Commun. 186 (1983).
12. T. CHIVERS, M. N. S. RAO, and J. F. RICHARDSON. J. Chem. Soc. Chem. Commun. 700 (1983).
13. T. CHIVERS, M. N. S. RAO, and J. F. RICHARDSON. J. Chem. Soc. Chem. Commun. 702 (1983).
14. T. CHIVERS and L. FIELDING. J. Chem. Soc. Chem. Commun. 212 (1978); T. CHIVERS, L. FIELDING, W. G. LAIDLAW, and M. TRSIC. Inorg. Chem. **18**, 3379 (1979).
15. W. S. SHELDRICK, M. N. S. RAO, and H. W. ROESKY. Inorg. Chem. **19**, 538 (1980).
16. H. W. ROESKY, P. SCHÄFER, M. NOLTEMEYER, and G. M. SHELDRICK. Z. Naturforsch. **38**b, 347 (1983).
17. R. T. OAKLEY, M. SHEVALIER, A. W. CORDES, and W. L. PENNINGTON. 184th Am. Chem. Soc. Meeting, Kansas City, Abstract INORG 86 (1982).
18. G. A. WIEGERS and A. VOS. Acta Crystallogr. **20**, 192 (1966).
19. S. POHL, O. PETERSEN, and H. W. ROESKY. Chem. Ber. **112**, 1545 (1979).
20. T. CHIVERS and R. T. OAKLEY. J. Chem. Soc. Chem. Commun. 752 (1979); T. CHIVERS, W. G. LAIDLAW, R. T. OAKLEY, and M. TRSIC. J. Am. Chem. Soc. **102**, 5573 (1980).
21. T. CHIVERS and N. L. PADDOCK. Inorg. Chem. **11**, 848 (1972); T. CHIVERS, R. T. OAKLEY, and N. L. PADDOCK. J. Chem. Soc. A, 2324 (1970).

Can. J. Chem. Downloaded from www.nrcresearchpress.com by 210.87.254.6 on 09/06/12
For personal use only.

Simulation of edge effects in electroanalytical experiments by orthogonal collocation. Part 4. Application to voltammetric experiments

JOHN F. CASSIDY and STANLEY PONS[1]
Department of Chemistry, University of Utah, Salt Lake City, UT 84112, U.S.A.

A. SCOTT HINMAN
Department of Chemistry, University of Calgary, Calgary, Alta., Canada T2N 1N4

AND

BERND SPEISER
Institut für Organische Chemie, Universität Tübingen, auf der Morgenstelle 18, D-7400 Tübingen, West Germany

Received August 2, 1983

JOHN F. CASSIDY, STANLEY PONS, A. SCOTT HINMAN, and BERND SPEISER. Can. J. Chem. **62**, 716 (1984).

Orthogonal collocation is used to simulate cyclic voltammograms that are influenced by non-linear diffusion due to edge effects at small disc electrodes.

JOHN F. CASSIDY, STANLEY PONS, A. SCOTT HINMAN et BERND SPEISER. Can. J. Chem. **62**, 716 (1984).

On utilise une "collocation" orthogonale pour simuler des voltagrammes cycliques influencés par de la diffusion qui n'est pas linéaire à cause d'effets d'arête sur des petites électrodes en forme de disques.

[Traduit par le journal]

Can. J. Chem. Downloaded from www.nrcresearchpress.com by 210.87.254.6 on 09/06/12
For personal use only.

Introduction

In this paper, the general theory derived in Part 2 of this series is implemented, and the effect of edge diffusion on the cyclic voltammetric response at very small electrodes is examined. The use of very small electrodes for cyclic voltammetric experiments has usually been limited to specialized investigations, for example, in neurochemical studies (1, 2). There are obvious advantages in using very small electrodes. In theory, the ratio of the faradaic to the double layer charging current increases with decreasing electrode area. Small electrodes are suited for experiments where available volumes of analyte are limited. In general, several effects have been observed in various systems as the electrode size was reduced. Thus increased faradaic peak separation (3), little or no reverse sweep currents (4, 5), and a steady-state current plateau (6) have been observed. In the case of a small hanging mercury drop electrode, anomalous behavior was observed when the reduced species was soluble in the mercury drop (7–9). The resulting ratio of the reverse peak current to the forward peak current was found to be greater than one.

Examination of the so-called "edge-effect" has been carried out for chronoamperometric experiments (10, 11). The analysis by various workers has led to a correction term σ to the Cottrell equation

$$[1] \quad i = nFAC^0\left(\frac{D}{\pi t}\right)^{1/2}\left[1 + \sigma\left(\frac{Dt}{r_0^2}\right)^{1/2}\right]$$

where r_0 is the electrode radius, and σ varies between 1.772 and 2.257 (11, 12). Using implicit finite difference methods, Heinze developed an analogous equation for the cyclic voltammetric response with contribution from edge effects (6):

$$[2] \quad \chi_{total} = \chi_{i,d}(at) + \rho(at)\sqrt{\beta'}/\sqrt{\pi}$$

with $\beta' = D/ar_0^2$, $a = nFv/RT$, v = sweep rate. $\chi_{i,d}(at)$ is the planar diffusion current function and the second term is the radial diffusion current function. In this work, we give the results for the voltammetric response in terms of the efficient orthogonal collocation technique (13, 14), the results of which, in many cases, are exact.

The term "very small electrodes" (e.g. 3–300 μm radius (5)) is used herein to differentiate them from microelectrodes, diffusion to which is purely hemispherical. The case examined here is that where the amount of hemispherical diffusion to a planar disk electrode is large enough to cause significant departure in the response from semi-infinite linear diffusion theory. Extensions to the two limiting cases will be discussed.

The solution of the non-linear partial differential equations describing this case has been treated in Part 2 (15). The general method is the simulation of the concentration profiles in the diffusion layer by approximate trial functions in distance whose time-dependent coefficients are selected by weighted residual techniques such that the differential equation is satisfied at chosen fixed (collocation) points in the distance coordinate. These points are also chosen purposely as the roots of orthogonal polynomials, combinations of which best approximate the expected profiles and the boundary conditions. The model used herein accounts for planar and lateral diffusion. As has been pointed out (16), it is a simple matter to add homogeneous reactions to the overall scheme once the basic model is developed. The reliability and accuracy of the model have been verified in Part 3 (17) of the series, where the chronoamperometric response was simulated.

Theory

The full description of the theory is given in Part 2, (15) and is briefly summarized here. The mechanism considered was an EC type:

$$[3] \quad A \underset{+ne^-}{\overset{-ne^-}{\rightleftharpoons}} B \qquad E^\circ$$

$$[4] \quad B \rightarrow C \qquad k$$

In this paper, we will not consider the effects of [4], i.e. we let $\alpha = 0$ and the electrode geometry is a planar disk electrode of radius r_0, flush mounted in an insulating cylinder. The diffusion coefficients D_i for all of the species are assumed to be equal, even though the treatment is only slightly different if

[1]To whom all correspondence should be addressed.

Can. J. Chem. Downloaded from www.nrcresearchpress.com by 210.87.254.6 on 09/06/12
For personal use only.

different D_i are used (13). For this system, the current density will not be homogeneous across the electrode surface, but will be greater near the edges due to additional diffusion to the edge from the region over the insulator. Dimensionless diffusion equations describing the model are

$$[5]\quad \frac{\partial c^*_{A_1}}{\partial T'} = \beta\frac{\partial^2 c^*_{A_1}}{\partial X^2} + \frac{\beta'}{R}\frac{\partial c^*_{A_1}}{\partial R} + \beta'\frac{\partial^2 c^*_{A_1}}{\partial R^2}$$

$$[6]\quad \frac{\partial c^*_{B_1}}{\partial T'} = \beta\frac{\partial^2 c^*_{B_1}}{\partial X^2} + \frac{\beta'}{R}\frac{\partial c^*_{B_1}}{\partial R} + \beta'\frac{\partial^2 c^*_{B_1}}{\partial R^2} - \alpha c^*_{B_1}$$

$$[7]\quad \frac{\partial c^*_{C_1}}{\partial T'} = \beta\frac{\partial^2 c^*_{C_1}}{\partial X^2} + \frac{\beta'}{R}\frac{\partial c^*_{C_1}}{\partial R} + \beta'\frac{\partial^2 c^*_{C_1}}{\partial R^2} - \alpha c^*_{C_1}$$

where the subscript 1 denotes the concentrations above the electrode surface. A similar set of equations exists for the area above the insulator.

The terms in the equations are:

$$[8]\quad \beta = \frac{D}{aL^2},\ \beta' = \frac{D}{ar_0^2},\ \beta'' = \frac{D}{a(M - r_0)^2},\ \alpha = \frac{k}{a},\ c^* = \frac{c}{c^0_A}$$

where $a = nFv/RT$. L represents that distance out in solution above the electrode where no diffusion occurs and M the radial distance out into solution from the center of the electrode where no diffusion occurs. These terms need to be included to normalize the equations later to a (0, 1) distance coordinate so that Legendre polynomials might be used to represent the concentration solutions (15, 17). r_0 is the radius of the electrode and the other terms have their usual significance.

The constant β' is a quantity given by experimental parameters. For simplicity herein we let $\beta = \beta''$. This is a sensible approximation since both L and M are $\gg r_0$. The choice of β may be optimized by various procedures already described (18, 19). β in essence defines a "window" on the diffusion phenomena. If β is too small, the diffusion layer will be small compared to the collocation point span, and it will be poorly simulated or missed entirely. If, on the other hand, β is chosen too large, then the diffusion effects may be present at L or M and the boundary conditions will be violated. This is the intuitive reason for optimization of β values. The procedure for optimization depends on the integration method used for solution of the set of differential equations. Each such integration method will have a corresponding set of stability and accuracy criteria which vary significantly from method to method. In the Hammings predictor–corrector method used herein, the stability criterion (20) takes the form

$$[9]\quad h \le \frac{0.65}{|f_y|}$$

where h is the independent variable stepwidth chosen for the integration, and f_y is the Jacobian or derivative of the differential equation $f(x,y)$ with respect to the independent variable at each point of interest. Thus, accuracy and curve shape relax as h is made very small, whereas unstable oscillation will occur if h is too large.

The corresponding first-order differential equations for the problem (Part 2 (15)) are:

$$[10]\quad \left.\frac{dc^*_{A1}}{dT'}\right|_{X_i,R_k} = \beta\left\{-\frac{B_{i,1}\theta_{A/B}S_\lambda(T')}{A_{1,1}[1+\theta_{A/B}S_\lambda(T')]}\left[A_{1,N_x+2} + \sum_{j=2}^{N_x+1} A_{1,j}[c^*_{A1}(X_j,R_k,T') + c^*_{B1}(X_j,R_k,T')]\right] + B_{i,N_x+2} + \sum_{j=2}^{N_x+1} B_{i,j}c^*_{A1}(X_j,R_k,T')\right\}$$
$$+ \frac{\beta'}{G_1}\left\{\sqrt{\frac{\beta''}{\beta'}}I_{1,k}C'_{N_R+2,1} + \sum_{l=2}^{N_R+1}\left[J_{l,k}\left(\sqrt{\frac{\beta''}{\beta'}}C'_{1,1} - C_{N_R+2,N_R+2}\right) - I_{1,k}C_{l,N_R+2} + I_{l,k}C_{1,N_R+2}\right]c^*_{A1}(X_i,R_l,T')\right.$$
$$\left. + \sum_{l=2}^{N_{R'}+1}\sqrt{\frac{\beta''}{\beta'}}I_{1,k}C'_{l,1}\,c^*_{A2}(X_i,R'_l,T')\right\}$$

$$[11]\quad \left.\frac{dc^*_{B1}}{dT'}\right|_{X_i,R_k} = \beta\left\{-\frac{B_{i,1}}{A_{1,1}[1+\theta_{A/B}S_\lambda(T')]}\left[A_{1,N_x+2} + \sum_{j=2}^{N_x+1} A_{1,j}[c^*_{A1}(X_j,R_k,T') + c^*_{B1}(X_j,R_k,T')]\right] + \sum_{j=2}^{N_x+1} B_{i,j}c^*_{B1}(X_j,R_k,T')\right\}$$
$$+ \frac{\beta'}{G_1}\left\{\sum_{l=2}^{N_R+1}\left[J_{l,k}\left(\sqrt{\frac{\beta''}{\beta'}}C'_{1,1} - C_{N_R+2,N_R+2}\right) - I_{1,k}C_{l,N_R+2} + I_{l,k}C_{1,N_R+2}\right]c^*_{B1}(X_i,R_l,T') + \sum_{l=2}^{N_{R'}+1}\sqrt{\frac{\beta''}{\beta'}}I_{1,k}C'_{l,1}c^*_{B2}(X_i,R'_l,T')\right\} - \alpha c^*_{B1}$$

$$[12]\quad \left.\frac{dc^*_{A2}}{dT'}\right|_{X_i,R'_k} = \frac{\beta}{A_{1,1}}\left\{K_{i,N_x+2} + \sum_{j=2}^{N_x+1} K_{i,j}c^*_{A2}(X_j,R'_k,T')\right\} + \frac{\beta''}{G_1}\left\{L'_{N_{R'}+2,k} + \sum_{l=2}^{N_R+1} F'_{1,k}H_l c^*_{A1}(X_i,R_l,T') + \sum_{l=2}^{N_{R'}+1} L'_{l,k}c^*_{A2}(X_i,R'_l,T')\right\}$$

$$[13]\quad \left.\frac{dc^*_{B2}}{dT'}\right|_{X_i,R'_k} = \frac{\beta}{A_{1,1}}\left\{\sum_{j=2}^{N_x+1} K_{i,j}c^*_{B2}(X_j,R'_k,T') + \frac{\beta''}{G_1}\sum_{l=2}^{N_R+1} F'_{1,k}H_l c^*_{B1}(X_i,R_l,T') + \sum_{l=2}^{N_{R'}+1} L'_{l,k}c^*_{B2}(X_i,R'_l,T')\right\} - \alpha c^*_{B2}$$

The A_i, B_i, C_i, F_i, G_i, H_i, J_i, K_i, and L_i are discretization matrix elements which have been defined previously (15, 17).

The Jacobians of each of these expressions are

$$[14]\quad f_1 = \frac{\partial}{\partial c^*_{A_1}}\left(\frac{dc^*_{A_1}}{dT'}\right);\qquad f_2 = \frac{\partial}{\partial c^*_{B_1}}\left(\frac{dc^*_{B_1}}{dT'}\right)$$

$$f_3 = \frac{\partial}{\partial c^*_{A_2}}\left(\frac{dc^*_{A_2}}{dT'}\right);\qquad f_4 = \frac{\partial}{\partial c^*_{B_2}}\left(\frac{dc^*_{B_2}}{dT'}\right)$$

We then specify the two limiting cases at $S_\lambda(T') = 1$ (at the beginning of the experiment), and $S_\lambda(T') = 0$ (at the end of the experiment). Thus there are six total conditions to be treated by the iteration procedure described previously (14, 19) so that the optimum value of β for a given steplength is obtained.

Results and discussion

The program was first tested under conditions of semiinfinite linear diffusion and the resulting values of the current function

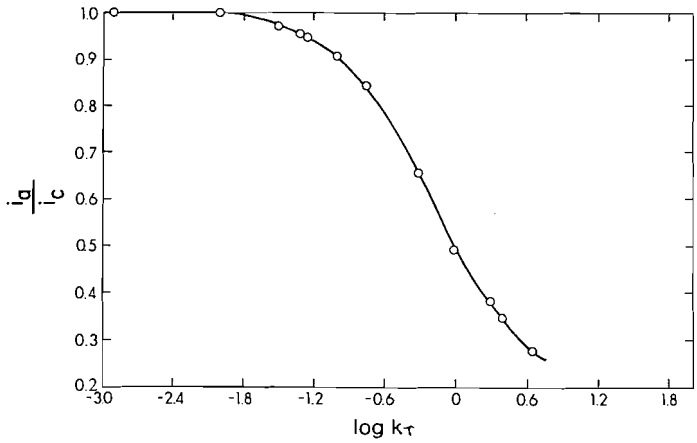

FIG. 1. Ratio of peak currents as a function of log ($k\tau$) curve from Nicholson and Shain; points calculated at $\beta' = 10^{-6}$ and β optimized at 0.01089.

$\chi(at)$ compared well with those of Nicholson and Shain (21) ($\chi(at) = 0.44627$ at $\beta' = 10^{-10}$, $\beta = 0.05$, and $\Delta E_p = 0.057$ V). Various combinations of α and switching potentials were used to vary the parameter log ($k\tau$) where τ is the time between E° and E_λ governed by the scan rate, and k is the homogeneous rate constant for the follow-up reaction. The results are shown in Fig. 1. This verifies the consistency of the model at low values of β'. For any value of β' chosen, the corresponding value of β is optimized by iteration and it makes little difference what original value of β is input since rapid convergence to the optimum value is manifested.

The general shape of the voltammograms may be predicted with reference to the factor β. When β is small, the corresponding value of L is large and the radius is small with respect to L. Thus the factor

$$[15] \quad \beta' = \left[\frac{D}{\left(\frac{nFv}{RT}\right) r_0^2}\right]$$

contributes more to the current function and we reach a steady state at faster times.

If, on the other hand, β is large then L is small relative to r_0 so that the spherical diffusion effects are less and more classical voltammogram is expected. The ratio $\sqrt{\beta/\beta'}$ equals r_0/L and the effect of this factor on the shape and magnitude of the current function are shown in Fig. 2. Curves *a* and *b* are calculated for the case when β is not optimized. Thus they have the appearance of voltammograms from microelectrodes. However, r_0 for curve *a* is 113 μm whereas for curve *c* is 9 μm ($D_0 = 10^{-6}$ cm^2/s, $v = 1$ V/s). The effect of optimizing the parameter β for curve *c* is the scaling down of the surrounding dimensions to accommodate the small radius. Thus the voltammogram has a classical shape. This does not occur physically and for very small radii a voltammogram of the form *a* is observed which can be easily simulated with the appropriate value of β.

Figure 3 shows the effect of β' on the current function. At small values of β' the classical value of 0.4463 is obtained. At large values there is an asymptotic approach to hemispherical diffusion values.

Anomalous forward/reverse peak current ratios have been observed at small hanging mercury drop electrodes. Beyerlein and Nicholson (7) have pointed out that these are caused by

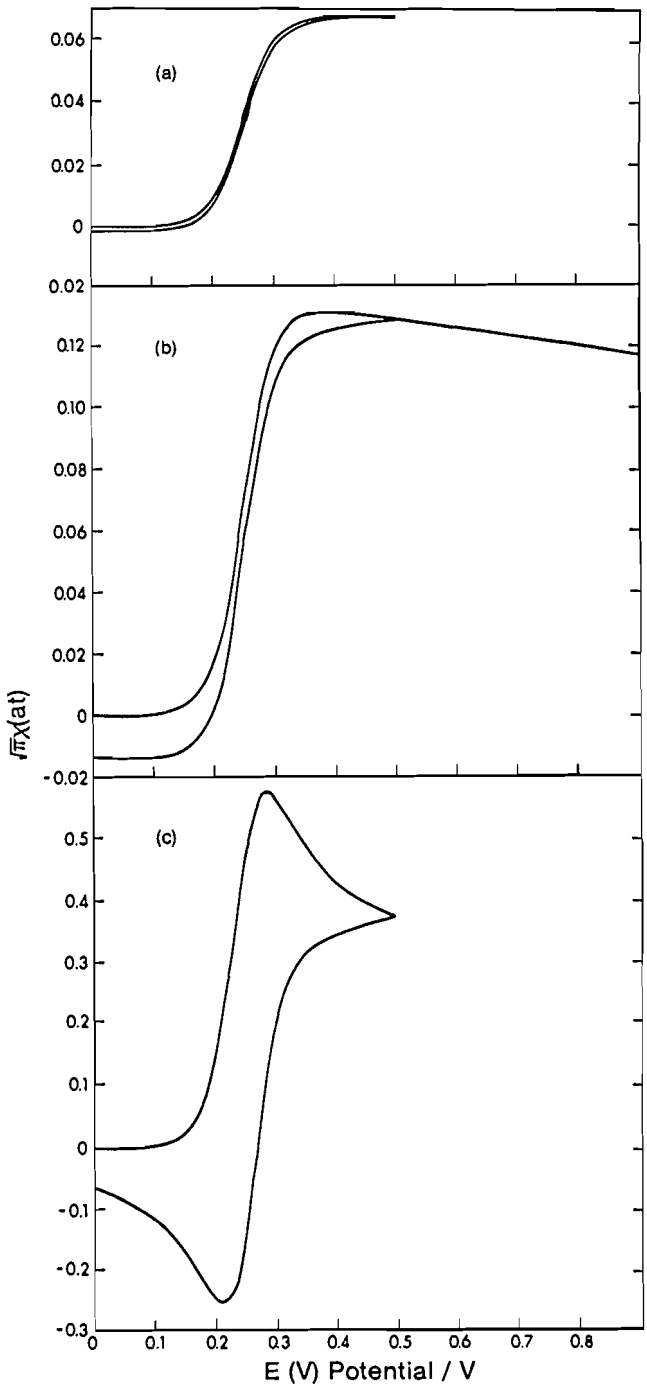

FIG. 2. Curve *a*: $\beta = 2.5 \times 10^{-6}$, $\beta' = 2 \times 10^{-4}$, $r_0/L = 0.112$. Curve *b*: $\beta = 10^{-5}$, $\beta' = 2 \times 10^{-4}$, $r_0/L = 0.223$. Curve *c*: $\beta = 0.0081$, $\beta' = 0.03162$, $r_0/L = 0.506$. (β optimized).

both sphericity and amalgam formation and have demonstrated the dependance of the magnitude on $\sqrt{\beta'}$. Guminski and Galus (8) developed an experimental equation for the resulting ratio

$$[16] \quad \frac{i_{pf}}{i_{pr}} = \left[1 + 3.2\sqrt{\frac{D_{red}(E_{pc} - E_\lambda)}{vr_0^2}}\right]$$

The spherical correction obviously becomes less at large drop sizes and/or high sweep rates.

Galus has presented a spherical correction equation for small planar disks (22)

Can. J. Chem. Downloaded from www.nrcresearchpress.com by 210.87.254.6 on 09/06/12
For personal use only.

Can. J. Chem. Downloaded from www.nrcresearchpress.com by 210.87.254.6 on 09/06/12
For personal use only.

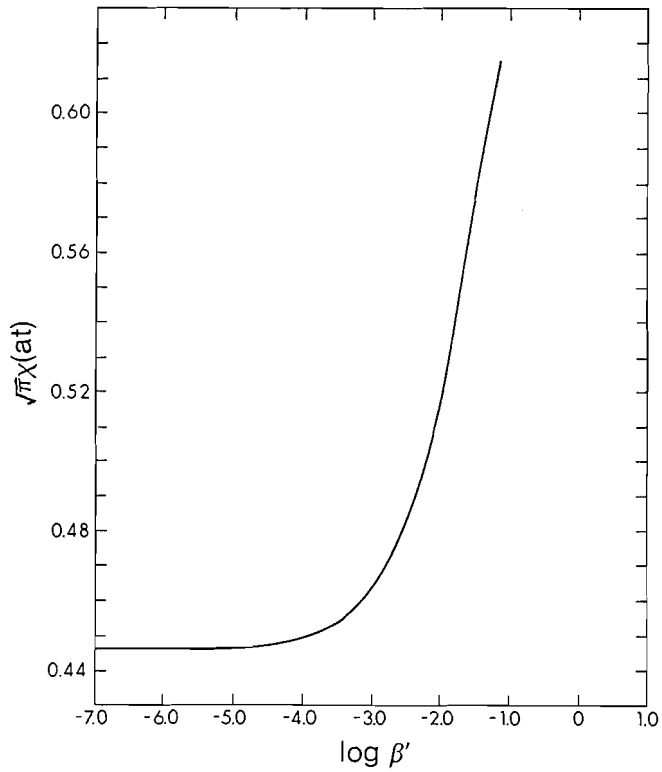

FIG. 3. Effect of β' on the magnitude of peak current function (β optimized).

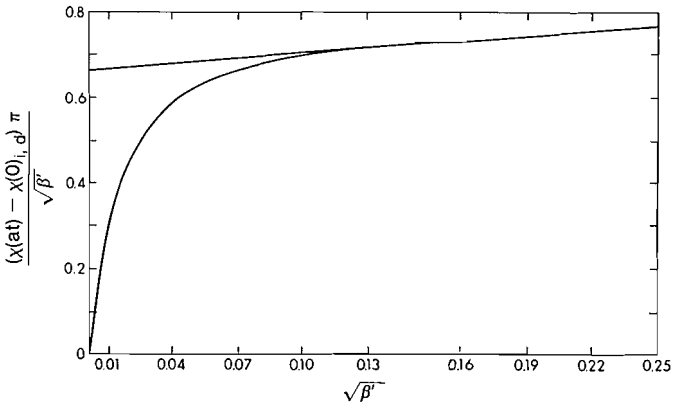

FIG. 4. Plot of $\pi(\chi - \chi_{id})/\sqrt{\beta'}$ against $\sqrt{\beta'}$ showing the transition between the two limiting cases of semi-infinite linear diffusion and hemispherical diffusion.

$$[17] \quad \frac{i_{pf}}{i_{pr}} = \{1 + Q'\sqrt{\beta'}\}$$

Q' was estimated as 0.92 by oxidizing ferrocyanide at a graphite paste planar disk electrode (r_0 = 81 μm). At low scan rates, however, there was no reverse current observable.

In the model presented herein for small planar disks there is no evidence for departure from the current ratio of unity due to edge effects. In practice, it is probably true that the small but not negligible charging current contributes to the observed results.

Beyerlein and Nicholson (7) have presented an equation for the current function at a hanging mercury drop electrode in terms of a linear combination of planar and spherical components:

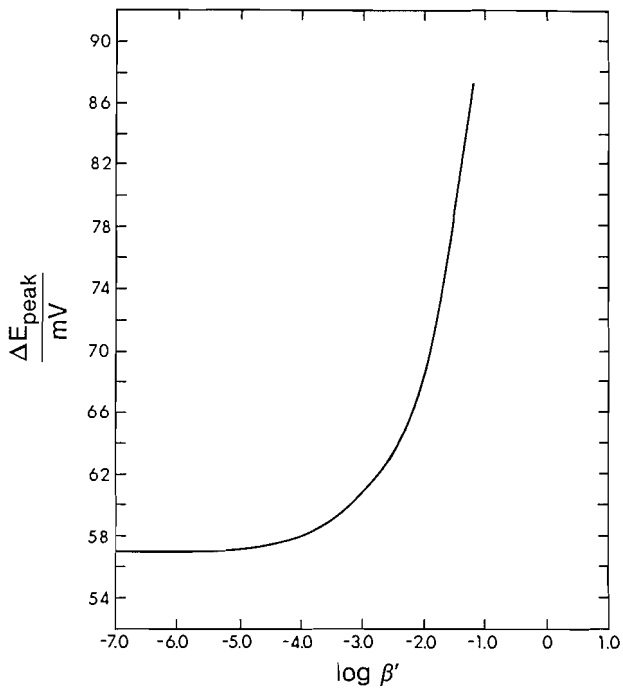

FIG. 5. Working curve for determining D from ΔE where $\beta' = D/ar_0^2$ ($a = nFv/RT$) (β optimized; T = 25°C).

$$[18] \quad \chi(at) = \chi(0)_{i,d} + A\beta' + B\sqrt{\beta'}$$

If the equation is rearranged, it is seen that a plot of

$$[19] \quad \frac{\chi(at) - \chi(0)_{i,d}}{\sqrt{\beta'}}$$

vs. $\sqrt{\beta'}$ should yield a straight line for a system having spherical diffusion contribution. It is seen in Fig. 4 that such a plot constructed with the present model leads to an intercept, when extrapolation is made from large β' values (small r_0). This intercept is equivalent to the value obtained by Beyerlein and Nicholson for a peak current function value. This indicates the model is correctly providing currents consistent with pure hemispherical diffusion at large values of β'.

Recently an expression for the current in the following form was proposed (23):

$$[20] \quad i(t) = i_{i,d}(t) + \frac{i_1(t)}{r_0} + \frac{i_2(t)}{r_0^2}t + \ldots.$$

the second term being found analytically in the case of the potential scan. The calculated value for B from the first two terms compares well with that of Beyerlein and Nicholson (7).

It is observed that, as different values of the integration stepwidth h were chosen, the product of the optimized value of β and h is a constant. The reason for this becomes clear as the following points are considered. We assume that the diffusion layer thickness δ

$$[21] \quad \delta^2 = \pi D\Delta t$$

has grown to some value after some time interval Δt. It is noted again that L^2 is related to δ^2 through the definition of β. Thus any change in Δt by a factor Q' implies a necessary $1/Q'$ factor change in β to preserve the relative values of δ and L. This, of course, is true only at the optimized β value for a given h. Thus if an optimized β, h pair is known, it is unnecessary to re-optimize β if a new value of h is used, or conversely, it is

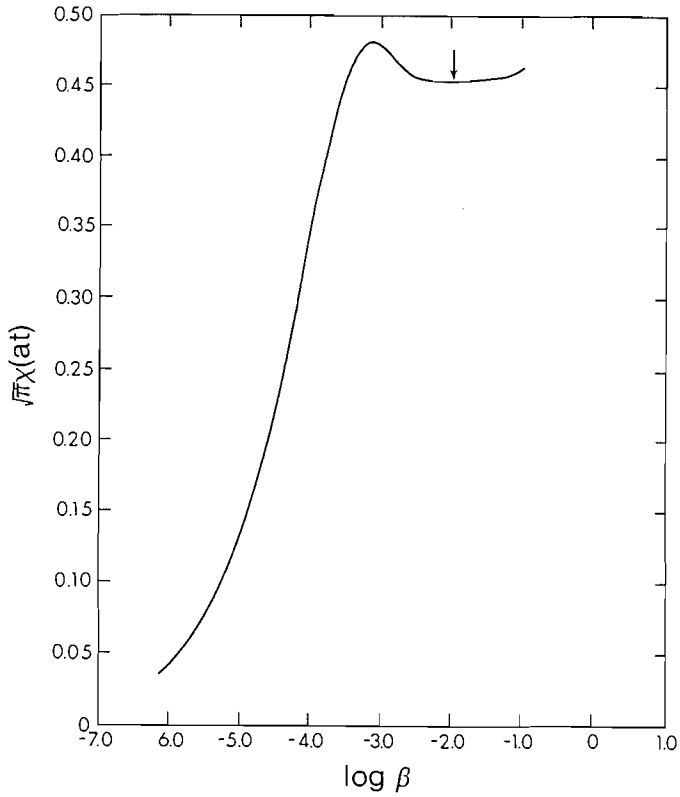

FIG. 6. The effect of changing the parameter β on the current function.

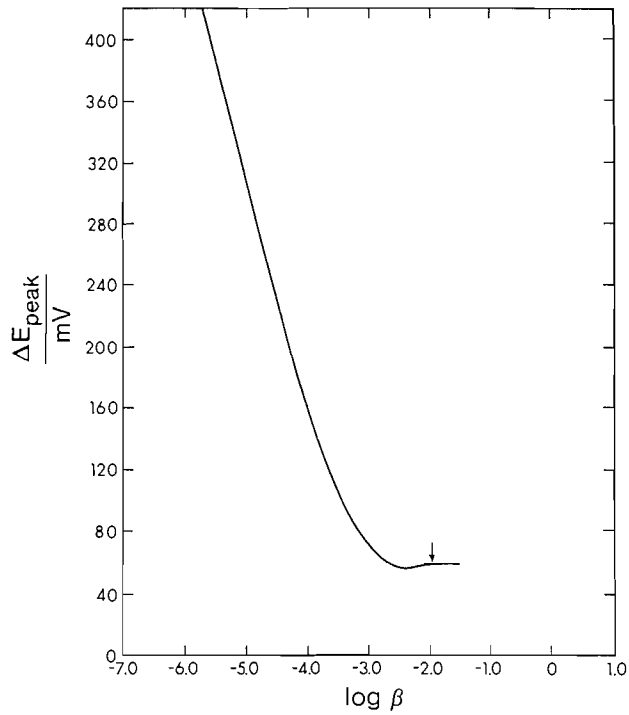

FIG. 7. The effect of changing β on the peak separation.

unnecessary to calculate a new h by trial and error if it is desired to use a specific value of β.

The model also provides a convenient method for obtaining diffusion coefficients or n values. Such a working curve is presented in Fig. 5. The predicted change in ΔE_p is plotted vs. log β′. The diffusion coefficient is then given by

$$[22] \quad D = \frac{\beta' n F v r_0^2}{RT}$$

where β′ is obtained at the observed value of ΔE_p on the working curve.

Figures 6 and 7 demonstrate the effect on the current function and peak separation of changing the value of the parameter β for a given value of β′. The optimized values of β are indicated.

Acknowledgement

The authors thank the Office of Naval Research, Washington, DC, for support of part of this work.

1. A. G. EWING, M. A. DAYTON, and R. M. WIGHTMAN. Anal. Chem. **53**, 1842 (1981).
2. R. M. WIGHTMAN. Anal. Chem. **53**, 1125A (1981).
3. R. LINES and V. D. PARKER. Acta Chem. Scand. B**31**, 369 (1977).
4. M. A. DAYTON, J. C. BROWN, K. J. STUTTS, and R. M. WIGHTMAN. Anal. Chem. **52**, 946 (1980).
5. Z. GALUS, J. O. SCHENK, and R. N. ADAMS. J. Electroanal. Chem. **135**, 1 (1982).
6. J. HEINZE. Ber. Bunsenges. Phys. Chem. **85**, 1096 (1981).
7. F. H. BEYERLEIN and R. S. NICHOLSON. Anal. Chem. **44**, 1647 (1972).
8. C. GUMINSKI and Z. GALUS. Rocz. Chem. **43**, 2147 (1969).
9. J. E. SPELL and R. H. PHILP, JR. Anal. Chem. **51**, 2287 (1979).
10. K. B. OLDHAM. J. Electroanal. Chem. **122**, 1 (1981).
11. K. AOKI, and J. OSTERYOUNG. J. Electroanal. Chem. **122**, 19 (1981).
12. J. HEINZE. J. Electroanal. Chem. **124**, 73 (1981).
13. S. PONS. Can. J. Chem. **59**, 1538 (1981).
14. B. SPEISER, S. PONS, and A. RIEKER. Electrochim. Acta, **27**, 1171 (1982).
15. B. SPEISER and S. PONS. Can. J. Chem. **60**, 2463 (1982).
16. B. SPEISER and A. RIEKER. J. Electroanal. Chem. **102**, 1 (1979).
17. B. SPEISER and S. PONS. Can. J. Chem. **61**, 156 (1983).
18. L. F. WHITING, and P. W. CARR. J. Electroanal. Chem. **81**, 1 (1977).
19. B. SPEISER. J. Electroanal. Chem. **110**, 69 (1980).
20. A. RALSTON. *In* Mathematical methods for digital computers. *Edited by* A. H. Ralston and H. S. Wilf. Wiley, New York, London. 1960. p. 95.
21. R. S. NICHOLSON and I. SHAIN. Anal. Chem. **36**, 706 (1964).
22. Z. GALUS, J. O. SCHENK, and R. N. ADAMS. J. Electroanal. Chem. **135**, 1 (1982).
23. J. GOODISMAN. J. Electroanal. Chem. **144**, 33 (1983).

Can. J. Chem. Downloaded from www.nrcresearchpress.com by 210.87.254.6 on 09/06/12
For personal use only.

Ferene — a new spectrophotometric reagent for iron

DOUGLAS J. HENNESSY AND GARY R. REID
Diagnostic Chemicals Limited, Charlottetown, P.E.I., Canada C1A 4H5

AND

FRANK E. SMITH[1] AND STEPHEN L. THOMPSON
Chemistry Department, University of Prince Edward Island, Charlottetown, P.E.I., Canada C1A 4P3

Received June 10, 1983

DOUGLAS J. HENNESSY, GARY R. REID, FRANK E. SMITH, and STEPHEN L. THOMPSON. Can. J. Chem. **62**, 721 (1984).

Ferene iron reagent, 3-(2-pyridyl)-5,6-bis(2-(5-furyl sulfonic acid)-1,2,4-triazine, disodium salt, monohydrate, has been synthesized and characterized. Results of a study of its complex formation with iron(II) including λ_{max}, ϵ_{max}, and log K values are reported.

DOUGLAS J. HENNESSY, GARY R. REID, FRANK E. SMITH et STEPHEN L. THOMPSON. Can. J. Chem. **62**, 721 (1984).

On a synthétisé et caractérisé le ferène: le sel de (pyridyl-2)-3-bis-5,6-(furyl-2-acide sulfonique-5)-triazine-1,2,4-disodium monohydraté. On rapporte les résultats de l'étude de la formation d'un complexe avec le fer(II), parmi lesquels on retrouve les valeurs de λ_{max}, ϵ_{max} et log K.

[Traduit par le journal]

Introduction

Bidentate chelating agents containing the α-diimine or ferroin group have been used for many years as chromogenic reagents for the determination of iron and copper (1–5). A major step forward in the development of reagents of this type came with a discovery by Case and Smith and their respective coworkers (6–8). They found that the incorporation of phenyl groups in positions *para* to the ferroin group led to greatly enhanced absorption by the metal chelates, resulting in considerable improvements in the sensitivity of the resulting reagents. Following this discovery, the widely used reagents bathophenanthroline (6, 7), bathocuproine (9), terrosite (10), PPDT (11), and PDT (12) were introduced. These phenyl-substituted compounds and their metal chelates all suffer from the disadvantage of having very low solubilities in water. This makes them unsuitable for use in the rapid, highly automated procedures necessary for dealing with large numbers of samples.

The sulfonation of bathophenanthroline by Trinder (13) led to a water soluble derivative which retained the favourable chromogenic characteristics of the parent compound even after sulfonation. Subsequently, the sulfonated, water-soluble derivatives of bathocuproine (14), PDT (15), and terrosite (16, 17) have all been reported, as well as those of a series of new phenyl-substituted triazines recently synthesized by Case (18, 19). The chromophoric enhancement observed in the phenyl-substituted reagents is presumably a result of the phenyl groups acting in such a way as to favor the charge transfer process which causes the intense colors of the iron(II) and copper(I) complexes. This being the case, it was considered that the introduction of furyl groups into the chelating molecules might well lead to a similar chromophoric enhancement. The compound 3-(2-pyridyl)-5,6-bis(2-furyl)-1,2,4-triazine containing two furyl groups was therefore synthesized. Sulfonation of this triazine has led to the isolation of a new, highly sensitive and water-soluble colorimetric reagent for iron, the disodium salt of 3-(2-pyridyl)-5,6-bis(2-(5-furyl sulfonic acid))-1,2,4-triazine, hereafter referred to as Ferene (Fig. 1).

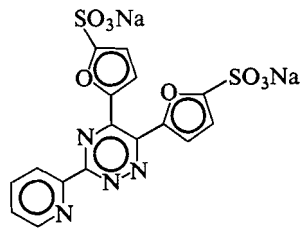

FIG. 1. Structure of Ferene.

Ferene reacts with iron(II) to form a stable, deep blue complex which is also very soluble in water. This new reagent constitutes an attractive alternative to the commonly used Ferrozine for the determination of serum iron.

Experimental

Synthesis of 3-(2-pyridyl)-5,6-bis(2-furyl)-1,2,4-triazine

To a stirred suspension of 16 g (0.84 mol) of furyl in 130 mL of isopropyl alcohol heated to 60°C, 13 g (0.96 mol) of picolinamidrazone (20) (called 2-pyridyl hydrazidine in the reference) was added portion-wise over a period of 5 min. The stirring at 60°C was continued for 1/2 h. The solid product obtained by filtration and washing with water was suspended in 140 mL of 0.06 *N* hydrochloric acid. After stirring for 2½ h the slurry was filtered. The product was washed with water, then with hexane, and was air dried. Melting point, 155–157°C. *Anal.* calcd. for $C_{16}H_{10}N_4O_2$: C 66.21, H 3.47, N 19.31; found: C 66.16, H 3.45, N 19.24.

Synthesis of the monosodium salt of 3-(2-pyridyl)-5,6-bis(2-(5-furyl sulfonic acid)-1,2,4-triazine

To 22 mL of 30% fuming sulfuric acid heated to 60°C, 16.5 g (0.57 mol) of the triazine was added portion-wise with stirring so that the temperature remained at 65 ± 3°C. The mixture was then warmed to 75°C for 3/4 h after which it was poured cautiously into 44 mL of stirred water. With the resulting solution at 60°C, 90 mL of 25% aqueous sodium chloride at the same temperature was added with stirring. After standing overnight under refrigeration, the solid product was collected by filtration, then washed with 3 × 35 mL of 10% aqueous sodium chloride and 2 × 35 mL of 70% aqueous ethanol, after which it was air dried.

Synthesis of the disodium salt of 3-(2-pyridyl)-5,6-bis(2-(5-furyl sulfonic acid)-1,2,4-triazine (Ferene)

The air-dried monosodium salt was suspended in 13 mL of water

[1] To whom correspondence should be addressed. Present address: Chemistry Department, Laurentian University, Sudbury, Ont., Canada P3E 2C6.

Can. J. Chem. Downloaded from www.nrcresearchpress.com by 210.87.254.40 on 09/06/12
For personal use only.

Can. J. Chem. Downloaded from www.nrcresearchpress.com by 210.87.254.40 on 09/06/12
For personal use only.

and with stirring brought to pH 8.5 by careful addition of 50% aqueous sodium hydroxide. The mixture was warmed to 70°C, filtered, brought again to 70°C, and then 75 mL of boiling ethanol added. After standing overnight under refrigeration the product was collected by filtration and washed with small amounts of ethanol and methanol. Recrystallization by solution in two parts of hot water followed by addition of seven parts of boiling ethanol with subsequent refrigeration yielded 15.2 g of bright yellow crystalline Ferene. After drying for several hours at 110°C, Ferene was obtained as the yellow monohydrate. *Anal.* calcd. for $C_{16}H_8N_4O_8S_2Na_2 . H_2O$: C 37.51, H 1.97, N 10.93, S 12.51; found: C 37.41, H 1.94, N 10.83, S 12.32.

The ^1H nmr spectrum of Ferene shows absorptions typical of pyridine ring protons along with four other aromatic protons, in two coupled pairs. The narrow range spectrum shows the couplings to be 3.54 and 3.42 Hz, typical of 3–4 couplings in furans, but much larger than 2–3 couplings, or any cross-ring coupling. We therefore conclude that the sulfonation has taken place in the 2-positions of both furyl rings, as indicated in Fig. 1. This assignment is supported by the ^{13}C nmr spectrum, which shows absorptions due to four protonated furyl carbon atoms at between 110 and 120 ppm, indicating that the furyl protons occupy the 3- and 4-positions in each ring, and confirming that sulfonation has occurred in the 2-positions.

Characterization of the Ferene–iron(II) complex

Reagents

Stock iron solution — A typical stock iron solution (1.79×10^{-4} *M*) was prepared by taking 10 mL of an atomic absorption standard (1 mg/mL, Fisher Scientific Co.) and 50 mL of the reducing agent, and making up to 1 L with distilled water.

Iron complexing reagent — A typical stock Ferene solution (6.38×10^{-4} *M*) was prepared by dissolving 0.35 g of Ferene (Diagnostic Chemicals Limited) in distilled water, adding 50 mL of the acetate buffer, and making up to 1 L with distilled water.

Iron standards — The standards were prepared by making serial dilutions of the stock iron solution in 100 mL volumetric flasks topped to the mark with distilled water.

Acetate buffer — The acetate buffer was prepared by dissolving 61.2 g (1 mol) of acetic acid and 82.0 g (1 mol) of sodium acetate in distilled water, and making up to 1 L.

Reducing agent — A 10% solution of hydroxylamine hydrochloride was prepared by dissolving 100 g of the material in 900 mL of distilled water.

Apparatus

A Cary Model 210 spectrophotometer was used for the absorbance measurements; cells were 1 cm (TSL). A Fisher model 620 pH meter with glass and calomel electrodes was used for the pH measurements.

Determination of conditional formation constant

To determine the conditional formation constant of the Ferene–iron complex, two types of runs were carried out. In the first, the concentration of Ferene was varied while the concentration of iron was held constant, and in the second, the conditions were reversed.

In the series where the concentration of the ligand was varied, stock solutions of iron (4×10^{-4} *M*, containing 50 mL of reducing agent solution per L) and Ferene (5×10^{-4} *M*, containing 50 mL of acetate buffer solution per L) were prepared as described above. To each of a series of 100 mL flasks was added 10 mL of stock iron solution, followed by a varying amount (5 – 80 mL) of stock Ferene solution. The flasks were topped up to the mark with distilled water. A second series was run with 5 mL of iron solution, and 5–40 mL of Ferene solution in each flask, topped to the mark with distilled water.

In the runs where the iron concentration was varied, the stock Ferene solution was 1.2×10^{-3} *M* (with 50 mL acetate buffer solution per L) and the stock iron solution was 1.25×10^{-4} *M* (with 50 mL of reducing agent solution per L). To each 100 mL flask was added 10 mL of the stock Ferene solution, followed by a varying amount (10–80 mL) of the stock iron solution. The flasks were made up to the mark with distilled water.

All absorbance readings were taken after allowing 5 min for the colour of the complex to fully develop.

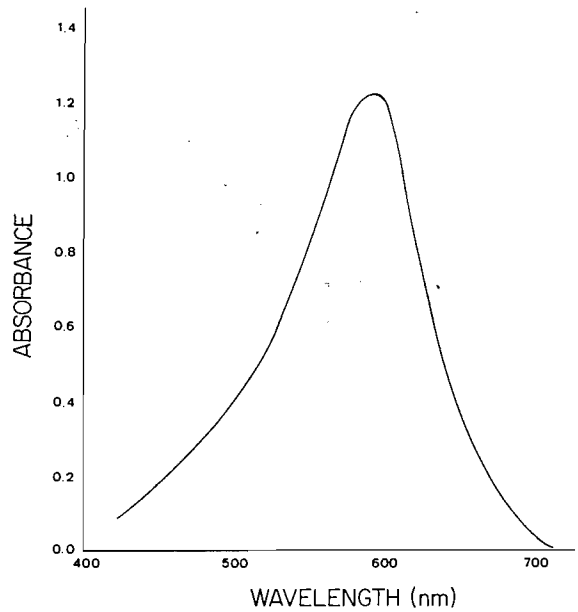

FIG. 2. Visible absorption spectrum of ferrous complex of Ferene.

Determination of log *K* (ie. log β_3) values were made as described by Gibbs (21).

Continuous variations study

A continuous variations series with a total concentration of 1.79×10^{-4} *M* was performed. Ferene and iron solutions of equal concentration (1.79×10^{-4} *M*) were combined such that the total volume was always 100 mL, i.e., 90 mL Ferene solution and 10 mL iron solution; 80 mL Ferene solution and 20 mL iron solution, etc. Again, a period of about 5 min was allowed to ensure full color development of the complex in each instance.

Variation of absorbance with pH

This was carried out in the manner described by Gibbs (21).

Several solutions, each having a total volume of 100 mL, were made up to contain 15 mL of 10^{-3} *M* Ferene, 5 mL of 5×10^{-4} *M* iron, 2 mL of 1 *M* reducing agent, and 5 mL of 2 *M* acetate buffer solution. The amount of acid (1 *M* HCl) or base (1 *M* NaOH) added to each flask was varied so as to give a broad range of pH values. The remainder of each flask was filled to the mark with distilled water. A period of 15 min was allowed for full color development of the various solutions, at which time absorbance readings were taken on the spectrophotometer at 593 nm.

Results and discussion

The visible absorption spectrum of the iron(II) complex of Ferene exhibits a single sharp peak with a maximum absorbance at 593 nm (Fig. 2). At this wavelength, the molar absorptivity is 34 500 L cm^{-1} mol^{-1} and the Beer–Lambert law is obeyed up to iron concentrations of 15 mg/L (a 1 mm cell was used for the highly concentrated solutions).

The Ferene molecule would be expected to behave as a bidentate chelating agent, probably via the pyridyl and 2-triazine nitrogen atoms, like the Ferrozine molecule (15, 21). However, with the presence of the oxygen atoms in the furyl rings, there is also the possibility that Ferene could behave as a planar tridentate chelating agent via the pyridyl nitrogen, the 4-triazine nitrogen, and a furyl oxygen atom. If this were to be the case, then a *bis* rather than a *tris* iron(II) complex would be formed. The results of the continuous variations study (Fig. 3) show that the maximum absorbance occurs at a point corresponding to a value of the mole fraction for iron of 0.25, indicating that a *tris* Ferene iron(II) complex is formed. This

TABLE 1. Determination of the conditional formation constant for the tris(Ferene)iron(II) complex (FeL_3^{2+})

Conditions	Fe^{2+}:L ratio	$[FeL_3^{2+}]^a$	$[Fe^{2+}]^b$	$[L]^c$	$\log_{10} K^d$
$[Fe^{2+}]$ constant (4.48×10^{-5} *M*) ([L] varied)	1:3	3.91×10^{-5} *M*	0.57×10^{-5} *M*	1.71×10^{-5} *M*	15.1
$[Fe^{2+}]$ constant (2.24×10^{-5} *M*) ([L] varied)	1:3	1.65×10^{-5} *M*	0.59×10^{-5} *M*	1.77×10^{-5} *M*	14.7
[L] constant (1.2×10^{-4} *M*) ($[Fe^{2+}]$ varied)	1:3	3.42×10^{-5} *M*	0.58×10^{-5} *M*	1.74×10^{-5} *M*	15.0
Continuous variations (both [L] and $[Fe^{2+}]$ varied)	1:3	3.76×10^{-5} *M*	0.72×10^{-5} *M*	2.12×10^{-5} *M*	14.7
				Mean value =	14.9

[a] Calculated using $\epsilon_{max} = 34\,500$ L cm^{-1} mol^{-1}.
[b] $[Fe^{2+}] = [Fe^{2+}]_{initial} - [FeL_3^{2+}]$.
[c] $[L] = [L]_{initial} - 3[FeL_3^{2+}]$.
[d] $K = [FeL_3^{2+}]/[Fe^{2+}][L]^3$.

Can. J. Chem. Downloaded from www.nrcresearchpress.com by 210.87.254.40 on 09/06/12
For personal use only.

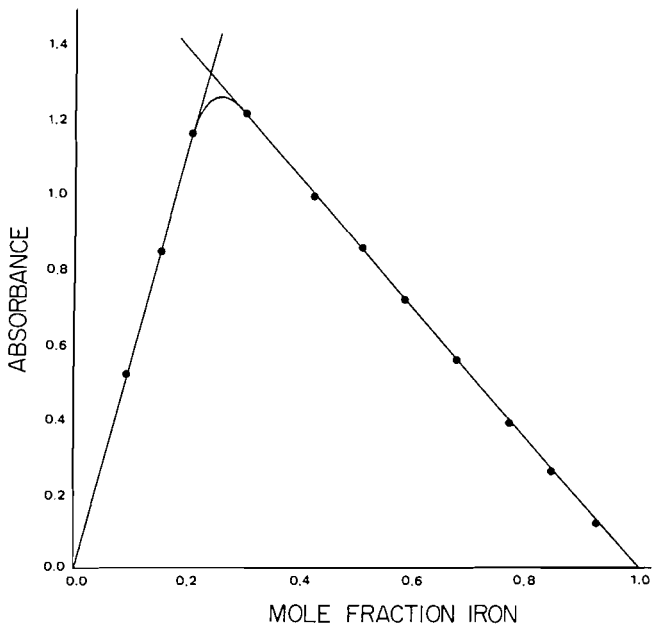

FIG. 3. Continuous variations of Ferene and iron concentrations keeping a constant total concentration of 1.79×10^{-4} *M*.

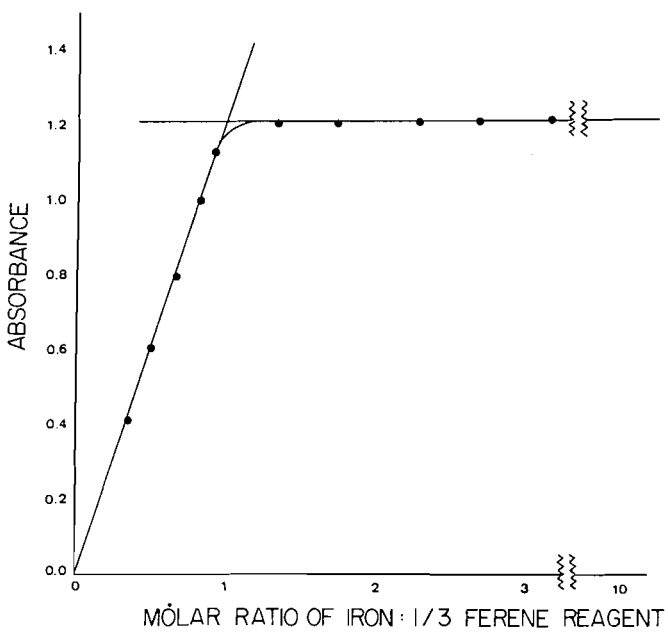

FIG. 4. Variation of iron concentration with Ferene concentration held constant.

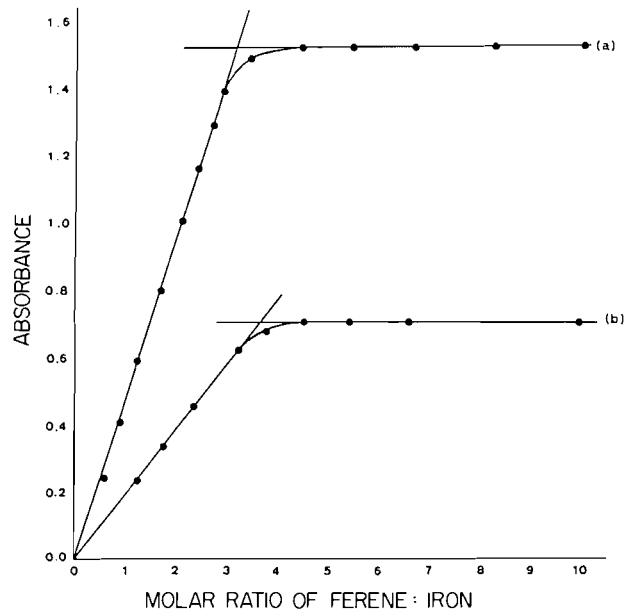

FIG. 5. Variation of Ferene concentration with iron concentration held constant at 4.48×10^{-5} *M* for *a* and 2.24×10^{-5} *M* for *b*.

confirms that Ferene behaves as a bidentate rather than a tridentate chelating agent under these conditions.

Spectrophotometric titration experiments were carried out with the iron concentration held at two different constant values, and also with the Ferene concentration held constant. The results of these experiments are summarized in Figs. 4 and 5. In each case, confirmation of the 3:1 Ferene:iron ratio present in the complex was obtained. Furthermore, since excess reagent was required for complete complex formation to be achieved, it was possible to evaluate *K*, the conditional formation constant, by straightforward means. The concentrations measured and the log *K* values obtained are given in Table 1. The mean log *K* value obtained was 14.9. This may be compared with the values reported for: bipyridine, 16.4–17.6; 1,10-phenanthroline, 20.2–21.5, and Ferrozine, 15.6 (21, 22).

The intense blue color of the Ferene–iron(II) complex was found to be fully developed within 3 min at 25°C, over a pH range of 2–7.5 in acetate buffer (Fig. 6). This is virtually the same range as reported for formation of the Ferrozine–iron(II) complex in acetate buffer (21). Thus it would seem that a pH range of 3–6 could be relied on to give the best test results.

Apart from iron, the only metal normally present in serum which forms a coloured complex with Ferene is copper. Inter-

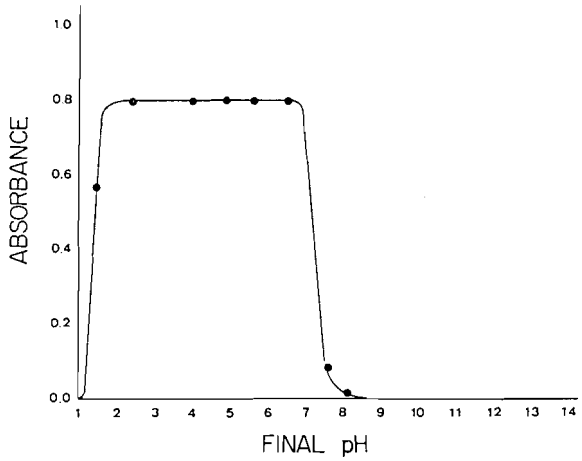

FIG. 6. Effect of pH on formation of ferrous complex of Ferene.

ference studies with Na^+, K^+, Ca^{2+}, Mg^{2+}, Hg^{2+}, and Pb^{2+} have shown that the presence of these ions, even in concentrations as high as 100 mg/L, has no effect on iron determinations using Ferene (26). Copper interference with Ferene is similar to that reported for Ferrozine (27) and may be suppressed in a similar way. The effects of copper interference can be almost entirely eliminated by the addition of thiourea, which preferentially binds the copper in a copper(I) complex (26).

Ferene is one of the most sensitive colorimetric reagents for iron(II) yet reported. Both the reagent itself and its iron(II) complex are highly water soluble, making Ferene very suitable for completely automated analyses on a practical scale. Two reports on such uses have already appeared (23, 24), and there will doubtless be many more in the future. Ferene has been used as the basis of a kit for determination of serum iron since 1979 (25).

Acknowledgement

The authors wish to thank the Natural Sciences and Engineering Research Council of Canada for financial support.

1. G. F. SMITH and F. P. RICHTER. Phenanthroline and substituted phenanthroline indicators. The G. Frederick Smith Chemical Co., Columbus, OH. 1944.
2. A. A. SCHILT. Analytical applications of 1,10-phenanthroline and related compounds. Pergamon Press, New York, NY. 1969.
3. B. ZAK and N. RESSLER. Anal. Chem. **28**, 1158 (1956).
4. N. RESSLER and B. ZAK. Am. J. Clin. Pathol. **27**, 219 (1957).
5. B. ZAK. Clin. Chim. Acta, **2**, 328 (1958).
6. F. H. CASE. J. Org. Chem. **16**, 1541 (1951).
7. A. F. SMITH, W. H. MCCURDY, JR., and H. DIEHL. Analyst, **77**, 418 (1952).
8. F. H. CASE and E. KOFT. J. Am. Chem. Soc. **81**, 905 (1959).
9. H. DIEHL, G. F. SMITH, A. A. SCHILT, and L. MCBRIDE. The copper reagents cuproine, neocuproine, bathocuproine. 2nd ed. The G. Frederick Smith Chemical Co., Columbus, OH. 1972.
10. A. A. SCHILT and G. F. SMITH. Anal. Chim. Acta, **15**, 567 (1956).
11. A. A. SCHILT and W. C. HOYLE. Anal. Chem. **39**, 114 (1967).
12. A. A. SCHILT and P. J. TAYLOR. Anal. Chem. **42**, 220 (1970).
13. P. TRINDER. J. Clin. Pathol. **9**, 170 (1956).
14. D. BLAIR and H. DIEHL. Talanta, **7**, 163 (1961).
15. L. L. STOOKEY. Anal. Chem. **42**, 779 (1970).
16. B. ZAK, E. EPSTEIN, and E. S. BAGINSKI. Microchem. J. **14**, 155 (1969).
17. B. ZAK, E. S. BAGINSKI, E. EPSTEIN, and L. WEINER. Clin. Chim. Acta, **29**, 77 (1970).
18. F. H. CASE. J. Heterocycl. Chem. **7**, 1001 (1970).
19. G. L. TRAISTER and A. A. SCHILT. Anal. Chem. **48**, 1216 (1976).
20. F. H. CASE. J. Org. Chem. **30**, 931 (1965).
21. C. R. GIBBS. Anal. Chem. **48**, 1197 (1976).
22. L. G. SILLEN and A. E. MARTELL. Stability constants of metal-ion complexes. 2nd ed. The Chemical Society, London. 1964.
23. J. D. ARTISS, D. R. STRANDBERG, and B. ZAK. Microchem. J. **28**, 275 (1983).
24. T. HIGGINS. Clin. Chem. **27**, 1619 (1981).
25. Diagnostic Chemicals Ltd., Charlottetown, P.E.I., Canada. Catalogue Number 1522.
26. J. GAUDIN. The determination of serum iron and total iron binding capacity. Diagnostic Chemicals Ltd., Charlottetown, P.E.I., Canada.
27. J. R. DUFFY and J. GAUDIN. Clin. Biochem. **10**, 122, 1977.

Can. J. Chem. Downloaded from www.nrcresearchpress.com by 210.87.254.40 on 09/06/12
For personal use only.

Hydrogen bonding in the crystal structures of the adducts between 1-phenyl-3,5-dimethylpyrazole with oxalic and perchloric acids

J. ZUKERMAN-SCHPECTOR, E. E. CASTELLANO, AND G. OLIVA

Instituto de Física e Química de São Carlos, Universidade de São Paulo, Caixa Postal 369, 13560 São Carlos, SP, Brazil

AND

A. C. MASSABNI AND A. DERBLI PINTO

Instituto de Química de Araraquara (UNESP), Caixa Postal 174, 14800 Araraquara, SP, Brazil

Received July 22, 1983

J. ZUKERMAN-SCHPECTOR, E. E. CASTELLANO, G. OLIVA, A. C. MASSABNI, and A. DERBLI PINTO. Can. J. Chem. **62**, 725 (1984).

The crystal structures of the title compounds have been determined from diffractometric X-ray data and refined by full-matrix least-squares to final *R* factors of 0.057 and 0.071 for the oxalic and perchloric adducts respectively.

The space groups and cell dimensions are: (oxalic) $C2/c$, $a = 16.516(3)$, $b = 11.685(2)$, $c = 12.587(3)$ Å, $\beta = 107.11(2)°$ with $Z = 4$; (perchloric) *Pbca*, $a = 16.204(3)$, $b = 15.329(6)$, $c = 10.296(3)$ Å with $Z = 8$.

In both structures the complex is stabilized by a strong hydrogen bond between the N(2) of the 1-phenyl-3,5-dimethylpyrazole (PDMP) group and an oxygen of the acid. In the oxalic adduct the PDMP group is neutral and the N(2) atom acts as a proton acceptor, while in the perchloric complex the PDMP group is positively charged with the N(2) atom acting as a proton donor.

J. ZUKERMAN-SCHPECTOR, E. E. CASTELLANO, G. OLIVA, A. C. MASSABNI et A. DERBLI PINTO. Can. J. Chem. **62**, 725 (1984).

On a déterminé les structures cristallines des composés mentionnés dans le titre en faisant appel à des données de diffraction de rayons-X affinées par le méthode des moindres carrés (matrice complète) jusqu'à des valeurs finales de *R* de 0,057 et 0,071 respectivement pour les adduits oxalique et perchlorique.

Les groups d'espace et les dimensions cellulaires sont: (oxalique) $C2/c$, $a = 16,516(3)$, $b = 11,685(2)$ et $c = 12,587(3)$ Å, $\beta = 107,11(2)°$ avec $Z = 4$; (perchlorique) *Pbca*, $a = 16,204(3)$, $b = 15,329(6)$ et $c = 10,296(3)$ Å avec $Z = 8$.

Dans chacune des structures, le complexe est stabilisé par une liaison hydrogène forte entre le N(2) du groupement phényl-1 diméthyl-3,5 pyrazole (PDMP) et un oxygène de l'acide. Dans l'adduit oxalique, le groupement PDMP est neutre et l'atome N(2) agit comme accepteur de proton alors que dans le complexe perchlorique le groupement PDMP est chargé positivement avec un atome N(2) agissant comme donneur de proton.

[Traduit par le journal]

Can. J. Chem. Downloaded from www.nrcresearchpress.com by 210.87.254.6 on 09/06/12
For personal use only.

Introduction

The structure of 1-phenyl-3,5-dimethylpyrazole (PDMP) has been determined in some metal complexes (1–4) where it appears as a neutral group. In the adduct with nitric acid (5) it has been found to be positively charged, forming a strong ionic complex with the nitrate anion. In this system, the ions are hydrogen-bonded, with the N(2) atom of the PDMP group acting as a proton donor and one of the anion oxygens acting as acceptor.

When complexed with different acids, it is conceivable that the net charge of the PDMP group could depend on the ionic strength of the acid, i.e. that the N(2) atom may behave as a donor or as an acceptor in the hydrogen bonding interactions. To investigate this point, the crystal structure determination of the title compounds, in which PDMP has been complexed with a strong and a weak acid, has been undertaken.

Experimental

Synthesis

$(PDMP)_2 . C_2O_4H_2$

A solution of oxalic acid in ethanol was added to a hot solution of PDMP in ketone so that the final molar proportion was 2:1 (base:acid). The solution was stirred for 10 min and after cooling a small volume of petroleum ether (bp 60–80°C) was added. Crystals were obtained by slow evaporation of the solution at room temperature.

$[PDMPH]^+ClO_4^-$

A solution of perchloric acid was added to a boiling solution of PDMP in ketone to obtain a final molar proportion of 1:1. The solution was continuously stirred and evaporated to half its original volume. The same volume of petroleum ether (bp 60–80°C) was then added. Crystals were obtained by slow evaporation of this solution at room temperature.

Structural solution and refinements

Crystal data are given in Table 1. Intensities were measured on an Enraf-Nonius CAD-4 diffractometer by the $\omega-2\theta$ scan technique, with scan rates determined from fast prescans on each reflection, using graphite monochromated MoKα ($\lambda = 0.71073$ Å) radiation. The intensities of two standard reflections were essentially constant over the duration of both experiments. Data were corrected for Lorentz and polarization effects. The perchlorate data were also corrected for absorption by the method of Busing and Levy (7) (minimum and maximum transmission factors are 0.9737 and 0.9591).

The $(PDMP)_2 . C_2O_4H_2$ structure was solved using MULTAN-80 (6) and the $[PDMPH]^+ClO_4^-$ structure with SHELX-76 (7). Both structures were refined by full-matrix least-squares with the SHELX-76 (7) system of programs. The usual sequence of isotropic and anisotropic refinement, using unit weights, was followed. After convergency all H-atoms were located from a difference Fourier synthesis and assigned, in both cases, a common isotropic temperature factor of 5.0 Å^2. Further anisotropic refinement for the non-hydrogen atoms and with the methyl groups set as rigid groups was carried out. During the process of refinement of the $[PDMPH]^+ClO_4^-$ considerable apparent thermal motion of the O atoms of the perchlorate ion was revealed. The final weighting schemes used are described in Table 1. In both

[1]Complete set of data may be obtained at a nominal charge, upon request, from the Depository of Unpublished Data, CISTI, National Research Council of Canada, Ottawa, Ont., Canada K1A 0S2.

Can. J. Chem. Downloaded from www.nrcresearchpress.com by 210.87.254.6 on 09/06/12
For personal use only.

TABLE 1. Summary of data collection and processing parameters

Parameter	Value	
	$(PDMP)_2 \cdot C_2O_4H_2$	$[PDMPH]^+ClO_4^-$
Molecular formula	$C_{24}H_{26}N_4O_4$	$C_{11}H_{13}N_2O_4Cl$
Molecular weight	434.5	272.7
Space group	$C2/c$	$Pbca$
Cell constants	a = 16.516(3)	16.204(5) Å
	b = 11.685(2)	15.329(6)
	c = 12.587(3)	10.296(3)
	β = 107.11(2)°	
	V = 2322(2)	2557(3) Å^3
Molecules per cell	Z = 4	8
Density (calcd)	ρ = 1.24	1.42 g·cm^{-3}
Crystal size (approximate)	0.4 × 0.4 × 0.25	0.4 × 0.25 × 0.02 mm
Absorption coefficient	μ = 0.5	2.6 cm^{-1}
Collection range	$0° < \theta < 23°$	$0° < \theta < 22°$
Scan width	0.8 + 0.35 tan θ	0.8 + 0.35 tan θ
Scan rate	6.6 to 15	33 to 40 deg min^{-1}
Total data collected	3547	2051
Data with $I > 3\sigma(I)$	906	
Data with $I > 2\sigma(I)$		750
$R = \Sigma\|\|F_o\| - \|F_c\|\|/\Sigma\|F_o\|$	0.057	0.071
$R_w = \|\Sigma w(\|F_o\| - \|F_c\|)^2/\Sigma w\|F_o\|^2\|^{1/2}$	0.060	0.069
Weights	$1.0/\sigma^2(F_o) + 0.02011F_o^2$	$1.0/\sigma^2(F_o) + 0.00031F_o^2$

TABLE 2. Atomic coordinates and calculated isotropic temperature factors with esd's in parentheses for $(PDMP)_2 \cdot C_2O_4H_2$. The standard deviations of B_{iso} were calculated as $\sigma(B_{iso}) = \sum_{ij} T_{ij}\,(B_{ij})$

Atom	X/A	Y/B	Z/C	B_{iso} (Å^2)
N(1)	0.7550(2)	0.1351(3)	0.6327(3)	3.8(1)
N(2)	0.6689(2)	0.1349(3)	0.5877(3)	3.9(1)
O(1)	0.5597(2)	0.1614(2)	0.7034(3)	4.5(1)
O(2)	0.5501(2)	0.3507(3)	0.6798(3)	5.3(1)
C(1)	0.6539(3)	0.0963(3)	0.4842(4)	4.2(1)
C(2)	0.7307(3)	0.0731(3)	0.4632(4)	4.5(2)
C(3)	0.7946(3)	0.0990(3)	0.5576(4)	4.0(1)
C(4)	0.8880(3)	0.0944(5)	0.5802(5)	5.6(2)
C(5)	0.5670(4)	0.0822(5)	0.4101(5)	6.1(2)
C(6)	0.7911(3)	0.1784(3)	0.7425(3)	3.4(1)
C(7)	0.8579(3)	0.1232(4)	0.8161(4)	4.6(2)
C(8)	0.8921(4)	0.1668(5)	0.9218(4)	5.5(2)
C(9)	0.8574(4)	0.2630(5)	0.9536(5)	5.8(2)
C(10)	0.7904(3)	0.3160(4)	0.8817(4)	5.1(2)
C(11)	0.7566(3)	0.2571(4)	0.7744(4)	4.0(1)
C(12)	0.5314(3)	0.2627(4)	0.7156(3)	3.5(1)

TABLE 3. Atomic coordinates and calculated isotropic temperature factors with esd's in parentheses for $[PDMPH]^+ClO_4^-$. The standard deviation of B_{iso} was calculated as $\sigma(B_{iso}) = \sum_{ij} T_{ij}\,(B_{ij})$

Atom	X/A	Y/B	Z/C	B_{iso} (Å^2)
N(1)	0.2568(5)	0.1362(6)	0.7967(8)	3.1(3)
N(2)	0.1893(6)	0.1198(6)	0.8686(9)	3.4(3)
C(1)	0.1267(7)	0.0967(7)	0.791(1)	3.6(5)
C(2)	0.1565(8)	0.0956(7)	0.667(1)	3.9(5)
C(3)	0.2382(7)	0.1202(8)	0.671(1)	3.4(4)
C(4)	0.2992(7)	0.1272(9)	0.566(1)	5.3(5)
C(5)	0.0432(7)	0.0764(9)	0.847(1)	5.8(6)
C(6)	0.3331(7)	0.1592(7)	0.856(1)	3.2(4)
C(7)	0.3732(7)	0.2328(9)	0.812(1)	4.6(6)
C(8)	0.4480(8)	0.2555(9)	0.867(2)	5.3(6)
C(9)	0.4789(8)	0.207(1)	0.965(2)	5.4(7)
C(10)	0.4395(9)	0.137(1)	1.010(1)	5.7(7)
C(11)	0.3627(8)	0.1099(9)	0.957(1)	4.6(5)
Cl	0.1626(2)	0.1213(2)	1.2320(3)	4.1(1)
O(1)	0.2280(7)	0.0707(7)	1.263(1)	12.5(7)
O(2)	0.0980(7)	0.0742(8)	1.196(2)	16.1(9)
O(3)	0.1456(7)	0.1819(7)	1.329(1)	9.5(5)
O(4)	0.1848(9)	0.1739(7)	1.128(1)	13.0(8)

cases refinement was considered complete when the shifts/esd ratios were less than 0.01. Bonded H-atom scattering factors (8) and complex neutral scattering factors (9, 10) for the remaining atoms were employed. A final difference Fourier map showed no features of chemical significance. Measured and calculated structure factors, anisotropic thermal parameters for non-hydrogen atoms and H-atom parameters have been deposited.[1]

Atomic coordinates, together with calculated isotropic temperature factors, are given in Tables 2 and 3, where the expression for B_{iso} is of the form:

$$B_{iso} = \frac{1}{3}\sum_{ij} T_{ij} B_{ij}$$

where T_{ij} are the elements of the metric tensor and B_{ij} are the elements of the thermal tensor usually obtained by least-squares refinement (11).

Discussion

The oxalic acid molecule is sited on a center of symmetry; its crystallographic independent moiety and a neighbour PDMP group are depicted in Fig. 1, which also shows intramolecular bond distances and atomic numbering. Angles between non-hydrogen bonded atoms are given in Table 4. The phenyl and pyrazole rings and the COOH group are planar to within experimental accuracy. Least-squares planes referred to the conventional orthogonalized coordinates; deviations of atoms from the planes and dihedral angles are given in Table 5. The OH group is in the *syn*-planar conformation; the overall geometry of the acid is in good agreement with the averages reported in an exhaustive study of carboxylic acids made by Leiserowitz (12).

Even though corrected for absorption, the perchlorate adduct

TABLE 4. Angles between non-hydrogen bonded atoms with esd in parentheses

Bonds	Angle (deg) $(PDMP)_2 \cdot C_2O_4H_2$	Angle (deg) $[PDMPH]^+ClO_4^-$
C(3)—N(1)—N(2)	111.5(3)	108.2(9)
C(6)—N(1)—N(2)	119.2(3)	121.1(8)
C(6)—N(1)—C(3)	129.1(4)	130.5(9)
C(1)—N(2)—N(1)	106.1(3)	109.4(9)
C(2)—C(1)—N(2)	109.3(4)	107(1)
C(5)—C(1)—N(2)	121.6(4)	120(1)
C(5)—C(1)—C(2)	129.1(4)	133(1)
C(3)—C(2)—C(1)	107.8(4)	108(1)
C(2)—C(3)—N(1)	105.3(4)	107(1)
C(4)—C(3)—N(1)	124.1(4)	123(1)
C(4)—C(3)—C(2)	130.6(4)	130(1)
C(7)—C(6)—N(1)	120.6(4)	118(1)
C(11)—C(6)—N(1)	118.8(4)	119(1)
C(11)—C(6)—C(7)	120.6(4)	122(1)
C(8)—C(7)—C(6)	119.7(5)	119(1)
C(9)—C(8)—C(7)	119.9(5)	120(1)
C(10)—C(9)—C(8)	120.3(5)	122(1)
C(11)—C(10)—C(9)	120.6(5)	122(1)
C(10)—C(11)—C(6)	118.9(5)	116(1)
O(1)—C(12)—O(2)	126.7(4)	—
O(1)—Cl—O(2)	—	108(1)
O(1)—Cl—O(3)	—	102.5(7)
O(1)—Cl—O(4)	—	108.3(8)
O(2)—Cl—O(3)	—	114.1(8)
O(2)—Cl—O(4)	—	111.9(7)
O(3)—Cl—O(4)	—	111.7(7)

data did not allow a structure analysis as precise as that of the previous structure.This is due to a somewhat high thermal disorder, as shown by the oxygen's *B* values given in Table 3 and by the smaller number of independent observed reflections, with the consequence that the standard deviations of bond distances and angles are rather large, as expected after Cruickshank (13). The perchlorate complex is depicted in Fig. 2, which also shows intramolecular bond distances and atom labeling. Angles between non-hydrogen bonded atoms are given in Table 4. The phenyl and pyrazole rings are planar, to within experimental accuracy, as can be seen in Table 5. The perchlorate anion is in an approximate tetrahedral configuration with a mean C—O distance of 1.36 Å, somewhat shorter than expected (14), due to the fact that the high apparent thermal motion causes the distance between the mean atomic positions to be less than the corresponding mean interatomic separation, which is the quantity of chemical significance (15).

In both structures the complex is stabilized by a strong hydrogen bond. The relevant parameters are given in Table 6. It can be seen from this table that in the oxalic complex, the N(2) atom acts as a proton acceptor while in the perchlorate complex it acts as a donor. This fact is reflected in the geometric configuration of the pyrazole ring. In the oxalic case the C(2)—C(3) distance is shorter than the C(1)—C(2) as expected in neutral pyrazole (1, 16, 17). In the perchlorate case where the two nitrogen atoms behave as pyrrolic, the C(2)—C(3) distance is essentially identical to the C(1)—C(2) as it was found in $[PDMPH]^+NO_3^-$(5). As has been pointed out (5), this is to be expected due to the fact that the dihedral angle (56.2° in the present case) between benzene and pyrazole rings does not favour a strong $\pi-\pi$ interaction between them.

TABLE 5.
(*a*) Least-squares planes and deviations of atoms from them[a]

Plane 1[c]			Plane 2[c]			Plane 3[c]	
	Distance (Å)			Distance (Å)			Distance (Å)
Atom	A[b]	B[b]	Atom	A[b]	B[b]	Atom	A[b]
N(1)	−0.004	0.011	C(6)	0.001	0.015	C(12)	−0.006
N(2)	0.004	−0.013	C(7)	−0.009	−0.013	O(1)	0.007
C(1)	−0.003	0.009	C(8)	0.009	0.003	O(2)	0.003
C(2)	0.000	−0.003	C(9)	−0.002	0.003	H(01)	−0.004
C(3)	0.003	−0.005	C(10)	−0.006	−0.001	N(2)*	0.065
C(4)*	0.054	0.015	C(11)	0.006	−0.008		
C(5)*	−0.013	−0.055	N(1)*	−0.011	0.019		
C(6)*	0.066	−0.052					

(*b*) Dihedral angle

Plane	Plane	Dihedral angle (deg)
1*A*	2*A*	42.9
1*A*	3*A*	85.0
2*A*	3*A*	−78.5
1*B*	2*B*	52.6

[a]Atoms marked with asterisks were not included in the calculation of the plane.
[b]A corresponds to the $(PDMP)_2 \cdot C_2O_4H_2$ compound and B corresponds to the $[PDMP]^+ClO_4^-$ complex.
[c]Plane 1*A*: $0.1257X + 0.9389Y - 0.3203Z - 0.3261 = 0$; plane 2*A*: $0.7579X + 0.5713Y - 0.3151Z - 6.1938 = 0$; plane 3*A*: $-0.5180X - 0.1272Y - 0.8459Z + 10.8395 = 0$; plane 1*B*: $-0.2707X + 0.9568Y - 0.1064Z + 0.0120 = 0$; plane 2*B*: $0.4863X - 0.5707Y - 0.6617Z + 4.6148 = 0$.

Can. J. Chem. Downloaded from www.nrcresearchpress.com by 210.87.254.6 on 09/06/12
For personal use only.

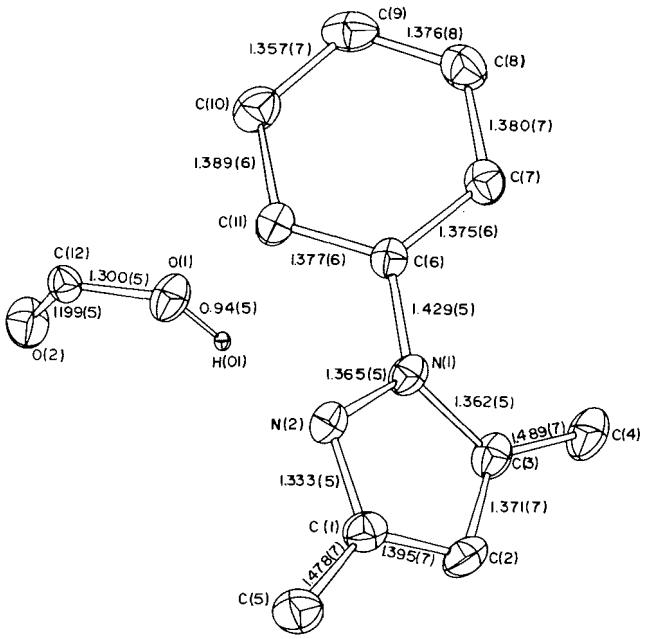

FIG. 1. The crystallographic independent moiety of $(PDMP)_2 \cdot C_2O_4H_2$ showing the bond distances (Å) with esd in parentheses and numbering scheme. The thermal ellipsoids are 45% equiprobability envelopes, the hydrogen atom is a sphere of arbitrary diameter.

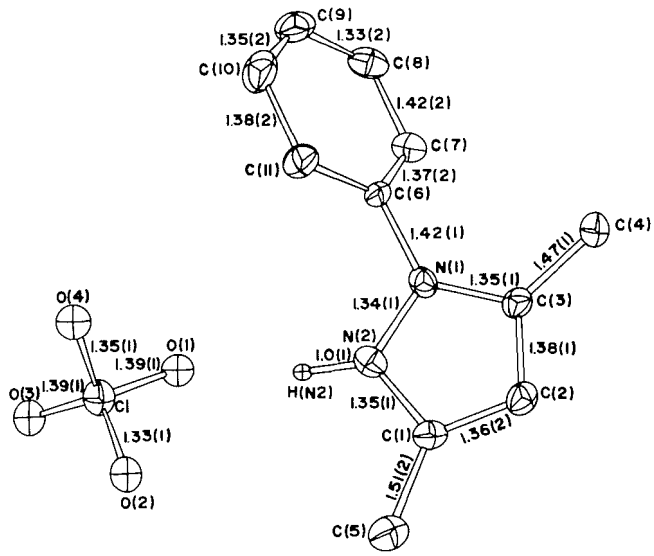

FIG. 2. The $[PDMPH]^+ClO_4^-$ compound, showing the bond distances (Å) with esd in parentheses and numbering scheme. The thermal ellipsoids are 45% equiprobability envelopes except the H and O atoms which are spheres of arbitrary diameter.

TABLE 6. Distances (Å) and angles (deg) involving hydrogen bonds

Parameter	Value	
	$(PDMP)_2 \cdot C_2O_4H_2$	$[PDMPH]^+ClO_4^-$
i	N(2)	N(2)
j	H(01)	H(N2)
k	O(1)	O(1)
D_{ij}	1.717	1.0
D_{jk}	0.94	1.86
D_{ik}	2.560	2.80
$\angle ijk$	151.3	178

1. R. H. P. FRANCISCO, Y. P. MASCARENHAS, and J. R. LECHAT. Acta Crystallogr. B**35**, 177 (1979).
2. R. H. P. FRANCISCO, J. R. LECHAT, and Y. P MASCARENHAS. Acta Crystallogr. B**35**, 1468 (1979).
3. R. H. P. FRANCISCO, J. R. LECHAT, A. C. MASSABNI, C. B. MELIOS, and M. MOLINA. J. Coord. Chem. **10**, 149 (1980).
4. A. M. G. DIAS RODRIGUES, Y. P. MASCARENHAS, and M. M. RODRIGUES. Acta Crystallogr. B**36**, 159 (1980).
5. J. ZUKERMAN-SCHPECTOR, E. E. CASTELLANO, A. C. MASSABNI, and A. DERBLI PINTO. Can. J Chem. **60**, 97 (1982).
6. P. MAIN, S. E. HULL, L. LESINGER, G. GERMAIN, J. DECLERCQ, and M. M. WOOLFSON. MULTAN 80. A system of computer programs for the automatic solution of crystal structures from X-ray diffraction data. Universities of York, England, and Louvain, Belgium. 1980.
7. G. M. SHELDRICK. SHELX-76 program for crystal structure determination. University of Cambridge, England. 1976.
8. R. F. STEWART, E. R. DAVIDSON, and W. T. SIMPSON. J. Chem. Phys. **42**, 3175 (1965).
9. D. T. CROMER and D. LIBERMAN. J. Chem. Phys. **53**, 1981 (1970).
10. D. T. CROMER and B. MANN. Acta Crystallogr. A**24**, 321 (1968).
11. W. C. HAMILTON. Acta Crystallogr. **12**, 609 (1959).
12. L. LEISEROWITZ. Acta Crystallogr. B**32**, 775 (1976).
13. D. W. J. CRUICKSHANK. Acta Crystallogr. **13**, 774 (1960).
14. M. R. TRUTER, D. W. CRUICKSHANK, and G. A. JEFFREY. Acta Crystallogr. **13**, 855 (1960).
15. C. K. JOHNSON. Crystallographic computing. *Edited by* F. R. Ahmed. pp. 207–219. Copenhagen. Munksgaard. 1970. pp. 207–219.
16. T. LA COUR and S. E. RASMUSSEN. Acta Chem. Scand. **27**, 1845 (1973).
17. E. N. MASLEN, J. R. CANNON, A. H. WHITE, and A. C. WILLIS. J. Chem. Soc. Perkin II, 1298 (1974).

Can. J. Chem. Downloaded from www.nrcresearchpress.com by 210.87.254.6 on 09/06/12
For personal use only.

Kinetics and mechanism of disproportionation and ferricyanide oxidation of the 10-methylacridinium cation in aqueous base

JOHN W. BUNTING AND GLENN M. KAUFFMAN[1]
Department of Chemistry, University of Toronto, Toronto, Ont., Canada M5S 1A1

Received October 5, 1983

JOHN W. BUNTING and GLENN M. KAUFFMAN. Can. J. Chem. **62**, 729 (1984).

The kinetics of disproportionation and ferricyanide ion oxidation of the 10-methylacridinium cation have been measured spectrophotometrically over the pH range 9–14 in 20% CH_3CN – 80% H_2O (v/v) and ionic strength 1.0 at 25°C. Disproportionation is kinetically second-order in total acridine species. The pH–rate profile is consistent with the rate-determining reaction of one acridinium cation with the pseudobase alkoxide anion derived from a second acridinium cation. Ferricyanide ion oxidation is kinetically first-order in each of ferricyanide ion and total acridine species. The pH–rate profile requires three distinct pathways for the ferricyanide ion oxidation of the 10-methylacridinium cation. For pH < 9.7, rate-determining attack of ferricyanide ion on the neutral pseudobase predominates, while for pH > 12.8 the predominant oxidation pathway involves reaction of ferricyanide ion with the pseudobase alkoxide ion. Between pH 9.7 and 12.8, the major oxidation pathway involves initial disproportionation of the acridinium cation followed by ferricyanide ion oxidation of the 9,10-dihydro-10-methylacridine product. This latter route accounts for a maximum of 69% of the total ferricyanide ion oxidation at pH 11.1.

JOHN W. BUNTING et GLENN M. KAUFFMAN. Can. J. Chem. **62**, 729 (1984).

Faisant appel à une méthode spectrophotométrique et opérant à 25°C, à une force ionique de 1,0 et à des pH allant de 9 à 14 dans des solutions à 20% (v/v) d'acétonitrile dans l'eau, on a mesuré les cinétiques de disproportionation et d'oxydation par l'ion ferricyanure du cation méthyl-10 acridinium. La disproportionation est cinétiquement du deuxième ordre en espèces acridines totales. Le profil de la courbe pH/vitesse est en accord avec une réaction impliquant, comme étape déterminante, la réaction d'un cation acridinium avec un anion alcoolate pseudobase qui serait dérivé d'un deuxième cation acridinium. L'oxydation par l'ion ferricyanure est du premier ordre à la fois en ion ferricyanure et en espèces acridines totales. Le profil de la courbe pH/vitesse requiert trois voies distinctes pour l'oxydation du cation méthyl-10 acridinium par l'ion ferricyanure. A des pH < 9,7, l'étape déterminante implique principalement l'attaque d'un ion ferricyanure sur une pseudobase neutre alors qu'à des pH > 12,8, la voie d'oxydation prédominante implique une réaction de l'ion ferricyanure sur un ion alcoolate de la pseudobase. A des pH allant de 9,7 à 12,8, la voie majeure d'oxydation implique une disproportionation initiale du cation acridinium qui est suivie par une oxydation, par l'ion ferricyanure, de la dihydro-9,10 méthyl-10 acridine qui est produite. A un pH de 11,1, cette dernière voie rend compte de 69% de l'oxydation totale due à l'ion ferricyanure.

[Traduit par le journal]

Heteroaromatic cations have long been known to undergo both a disproportionation reaction and oxidation by ferricyanide ion in basic aqueous solutions (1). The ferricyanide oxidation is of some synthetic utility and has become known as the Decker Oxidation (2). Although both of these reactions have been known for over 90 years, it is only recently that there has been any attempt to characterize their mechanisms via kinetic studies. A detailed kinetic study of the ferricyanide ion oxidation is now available for 5-nitroisoquinolinium cations (3), while the disproportionation mechanism has been investigated via a "crossed disproportionation" involving two isoquinolinium cations bearing different substituents (4). For both disproportionation and ferricyanide oxidation, it has been concluded that the rate-determining transition state involves hydride abstraction from the alkoxide ion that is obtained upon deprotonation of the appropriate isoquinoline pseudobase species.

Acridinium cations are of some historical interest in this area, since they were among the first group of heteroaromatic cations for which these two reactions were recognised (5–7). Furthermore, the pseudobases derived from acridinium cations are formally 1,4-dihydropyridine derivatives rather than the 1,2-dihydropyridines that are produced upon pseudobase formation from isoquinolinium cations. Acridinium cations therefore provide a suitable system for further exploring the generality of the mechanisms of disproportionation and ferricyanide oxidation that have been indicated for the isoquinolinium cations. For acridinium cations, disproportionation (eq. [1]) occurs readily in dilute aqueous base (7), and so this system provides the opportunity for a mechanistic comparison of a true disproportionation with the "crossed disproportionation" that is currently the best studied example of this class of reaction (4). Clark and Bakavoli (8) have shown by deuterium labelling experiments that disproportionation of the 10-methylacridinium cation occurs via direct transfer of the hydrogen nucleus between the C-9 atoms of the two acridine moieties without exchange with solvent protons.

[1] 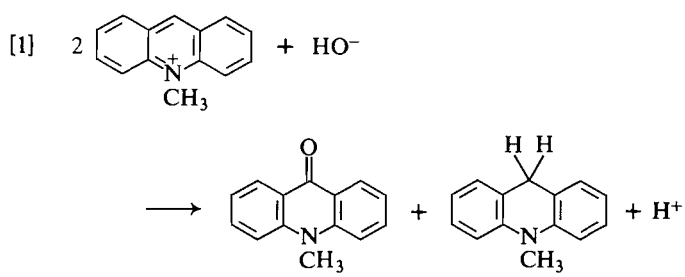

In the current work we report a detailed kinetic study of the disproportionation (eq. [1]) and ferricyanide oxidation (eq. [2]) of the 10-methylacridinium cation over the range pH 9–14. In general we find that the mechanistic details of these reactions in the acridine system are analogous to those deduced earlier in the 5-nitroisoquinoline series. However, in the more weakly basic solutions, the reduction of ferricyanide ion may also proceed via the reaction of ferricyanide with 9,10-dihydro-10-methylacridine (10-methylacridan) which is a product of the disproportionation reaction.

[1]Permanent address: Department of Chemistry, Eastern Mennonite College, Harrisonburg, VA 22801, U.S.A.

Can. J. Chem. Downloaded from www.nrcresearchpress.com by 210.87.254.5 on 09/06/12
For personal use only.

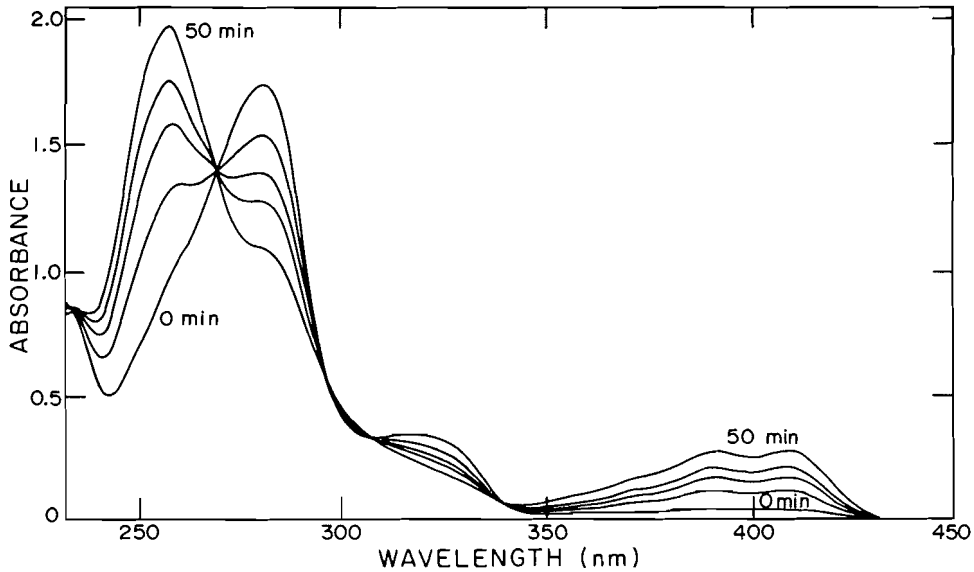

FIG. 1. Disproportionation of the 10-methylacridinium cation (1.0 mM in 1-mm cell) at pH 12.0. Spectra determined at: 0, 10, 20, 30, 50 minutes.

[2] 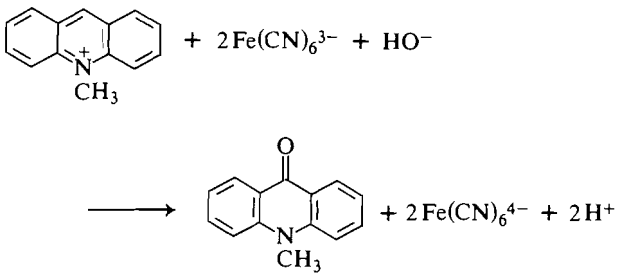

Experimental

10-Methylacridinium chloride

Acridine was methylated with dimethyl sulfate, and the methylsulfate salt was converted to the chloride as described by Albert (9).

Reagents and solvents

The following chemicals were all used in ACS Reagent Grade purity: $K_3Fe(CN)_6$, $K_4Fe(CN)_6$, KCl, KOH, Na_2CO_3, $Na_2B_4O_7$, HCl, and CH_3CN. All kinetic studies were carried out in 20% CH_3CN − 80% H_2O (v/v) adjusted to ionic strength 1.0 (KCl + buffer). Standard solutions of KOH were used as buffers for pH > 11, while lower pH buffers were prepared by appropriate neutralization of Na_2CO_3 or $Na_2B_4O_7$ solutions with hydrochloric acid. It was noted that pH-meter calibration with a standard aqueous pH 10 buffer solution led to pH readings that were uniformly 0.28 pH units too high relative to the known hydroxide ion concentration for standard KOH solutions (pH 11−13) in this mixed solvent reaction medium. In order to provide a uniform pH scale for carbonate and borate buffers and standard hydroxide solutions we have therefore chosen to calibrate the pH meter using a reading of 9.72 for the standard aqueous pH 10 buffer.

Kinetic studies

All kinetic studies were carried out spectrophotometrically in the above standard reaction medium at 25°C, by recording the time-dependence of the absorbance at 409 nm on a Cary 210 spectrophotometer in cells of either 1-cm or 1-mm path length. Extinction coefficients measured for the various species in this solvent are, 10-methylacridinium cation: 3700 M^{-1} cm^{-1}; ferricyanide ion: 1000 $M^{-1}cm^{-1}$; 10-methyl-9-acridone: 8300 $M^{-1}cm^{-1}$; all other species: 0. Absorbance vs. time data were recorded over 75% (very slow reactions) to greater than 90% reaction, and were digitized into approximately 20 data points and fitted to standard second-order kinetic equations. Such data were linear over the above reaction regions (see Fig. 2), although the ferricyanide ion oxidations showed some curvature in these fits at very long reaction times due to a slow decomposition of ferricyanide ion in very basic solutions. Second-order rate constants were evaluated from least-squares slopes of these kinetic plots.

Results

Disproportionation

The time-dependence of the electronic absorption spectrum of the 10-methylacridinium cation at pH 12 in 20% CH_3CN − 80% H_2O is shown in Fig. 1. Other workers (7, 8) have isolated 10-methyl-9-acridone and 9,10-dihydro-10-methylacridine (10-methylacridan) as the only products obtained from basic aqueous solutions of this cation. The spectral changes observed in Fig. 1 are quite consistent with this result. At pH 12, the 10-methylacridinium cation (pK_{R^+} = 10.01 in aqueous solution at 25°C (10)) is present essentially completely as its pseudobase, 9,10-dihydro-9-hydroxy-10-methylacridine, having λ_{max} = 280 nm, which corresponds to the initial spectrum in Fig. 1. The final spectrum in Fig. 1 is similar, but not identical, to that of 10-methyl-9-acridone in this solvent (λ_{max}(log ϵ) = 257(4.79), 391(3.92), 409(3.92)), but the intensity of each of these maxima corresponds to only 0.5 mole of acridone product per mole of acridinium cation initially present, consistent with the stoichiometry of eq. [1]. The other product, 9,10-dihydro-10-methylacridine has λ_{max}(log ϵ) = 286(4.05) in the current solvent. This peak is so much weaker than that at 257 nm in the acridone spectrum that it appears only as a shoulder in the vicinity of 280 nm in the product spectrum. We have shown that the disproportionation product spectrum is identical with that of a genuine 1:1 mixture of these two reaction products.

Rates of acridine pseudobase disproportionation were measured spectrophotometrically from the time-dependent increase in absorbance at 409 nm which is a measure of 10-methyl-9-acridone product formation. Such absorbance increases proved to be kinetically second-order (Fig. 2) in the total concentration of reactant acridine species for all solutions in the pH range 9−14. Second-order rate constants (k_{dis}) are independent of total acridine species concentration (Table 1).

Can. J. Chem. Downloaded from www.nrcresearchpress.com by 210.87.254.5 on 09/06/12
For personal use only.

Can. J. Chem. Downloaded from www.nrcresearchpress.com by 210.87.254.5 on 09/06/12
For personal use only.

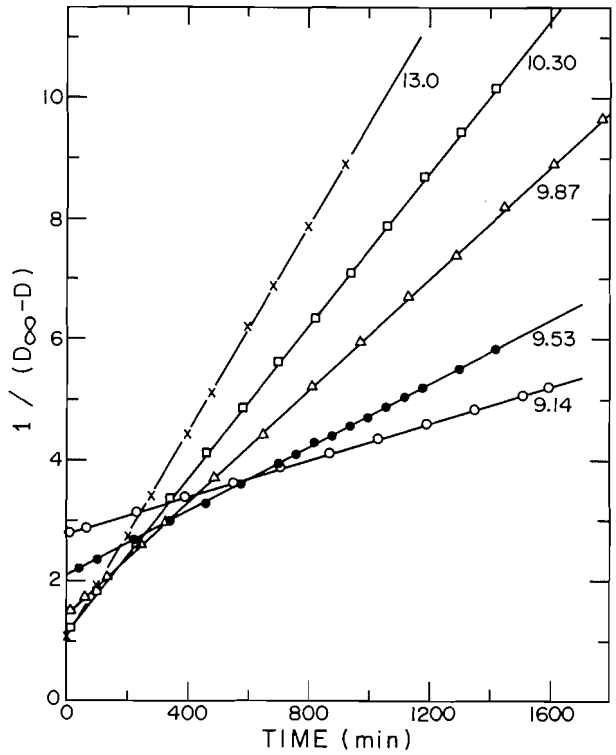

FIG. 2. Second-order kinetic plots for disproportionation of the 10-methylacridinium cation (0.25 mM) at various pH as shown. D represents absorbance at time t during the course of the reaction, and D_∞ is the absorbance of the product; all data at 409 nm. Variation in the ordinate intercept arises from differing cation/pseudobase ratios at low pH.

TABLE 1. Second-order rate constants for the disproportionation of the 10-methylacridinium cation[a]

pH	$[A_T]$, mM	k_{dis}, M^{-1} s^{-1}
13.03	0.0487	0.565
	0.243	0.592
	0.487	0.583
10.30	0.102	0.307
	0.256	0.303
	0.511	0.312

[a]In 20% CH_3CN – 80% H_2O, ionic strength 1.0, 25°C.

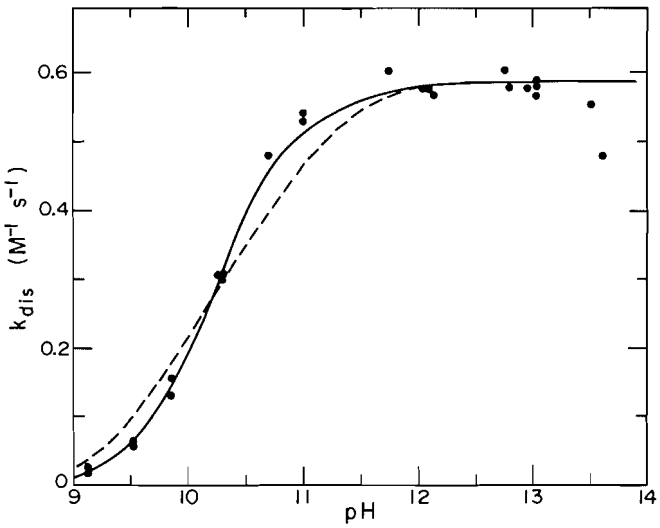

FIG. 3. The pH-dependence of k_{dis}. Broken line represents a titration curve for pK 10.3. Solid line calculated according to eq. [5] using the parameters in the text.

The pH-dependence of these second-order rate constants is displayed in Fig. 3, and suggests that the pseudobase species is more reactive towards disproportionation than the acridinium cation. However, the apparently sigmoidal curve in the region pH 9–12 is not simply a titration curve of an acid of pK 10. Attempts to fit these data to a titration curve give the best fit indicated by the broken line in Fig. 3 which is based on an acid ionization of pK 10.3. This broken line is, at best, a poor fit to the data. Furthermore, since the reaction is kinetically second-order in acridine species, any simple interpretation in terms of the pseudobase as the reactive species would require construction of a mechanism in which two molecules of the pseudobase are involved in (or appear prior to) the rate-determining transition state. We have been unable to conceive of any such disproportionation mechanism that would be chemically reasonable.

In an earlier study (4) of a "crossed disproportionation", it was shown that the alkoxide ion that is derived from the pseudobase of the 2-benzyl-5-nitroisoquinolinium cation acts as hydride donor towards the 2-methylisoquinolinium cation. An analogous mechanism can be postulated in the current 10-methylacridinium cation disproportionation. Thus, a rate-determining reaction of the pseudobase alkoxide ion **2** with acridinium cation would be consistent with the overall kinetically second-order reaction that is observed. Such a mechanism would have the rate law:

$$[3] \quad d[P]/dt = k_1[AO^-][A^+] = k_{dis}[A_T]^2$$

where $[A_T]$ represents the total concentration of all reactant acridine species, and A^+ and AO^- represent the acridinium cation and pseudobase alkoxide ion respectively. Thus:

$$[4] \quad k_{dis} = \frac{k_1}{(1 + [H^+]/K_{RO^-} + [H^+]^2/K_{R^+}K_{RO^-})(1 + K_{R^+}/[H^+] + K_{R^+}K_{RO^-}/[H^+]^2)}$$

where K_{RO^-} represents the acid ionization constant of the pseudobase **1** to give its alkoxide ion conjugate base **2**.

Equation [4] predicts that k_{dis} should pass through a maximum value at pH = $(pK_{R^+} + pK_{RO^-})/2$. The pH profile in Fig. 3 does seem to indicate that k_{dis} is decreasing in the most basic solutions that are readily investigated. However, it should be noted that data at pH > 13.5 may possibly be influenced by specific ion effects as chloride ion is replaced by hydroxide ion

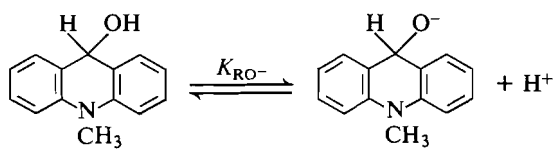

1 **2**

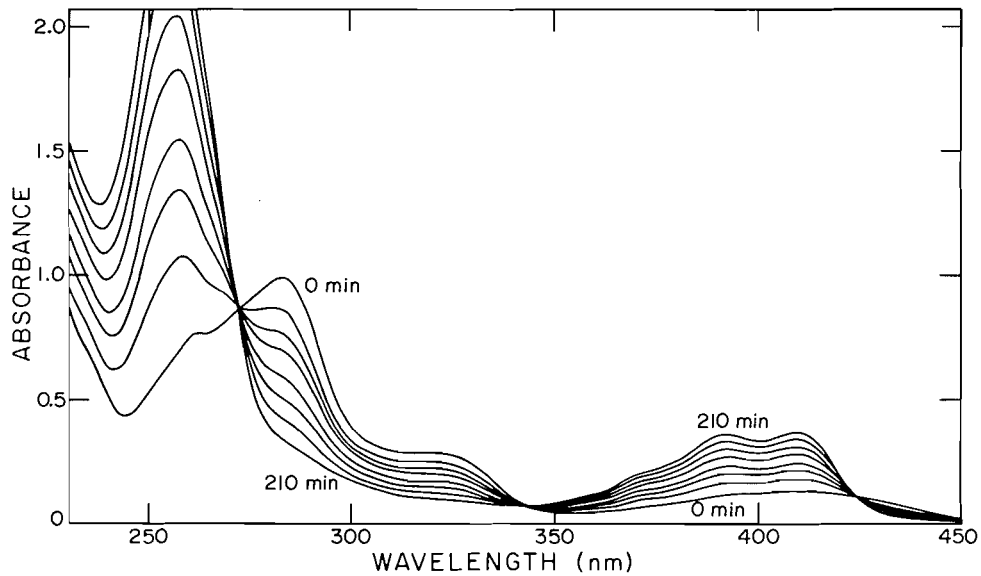

FIG. 4. Reaction of ferricyanide ion (1.0 mM) with the 10-methylacridinium cation (0.5 mM) at pH 13.0 (1-mm cell). Spectra determined at: 0, 10, 20, 30, 50, 80, 120, 210 minutes.

in order to maintain constant ionic strength in these basic solutions.

The pseudobase **1** is a secondary alcohol containing no strongly acidifying substituents. Thus pK_{RO^-} is certainly expected to be greater than 14. Takahashi *et al.* (11) have estimated that diphenylmethanol (benzhydrol) should have pK_a = 15.34. Alternatively, suitable modification of the dependence of pK_a on σ^* reported by Ballinger and Long (12) for primary alcohols allows an estimate of pK_a = 14.9 for benzhydrol. These values are in reasonable agreement and should be reasonably close to the pK_{RO^-} value for the pseudobase **1**. Thus the assumption $K_{RO^-} \ll [H^+]$ should be valid throughout the pH range in Fig. 3. Under this assumption, eq. [4] becomes:

$$[5] \quad k_{dis} = \frac{k_1 K_{RO^-}}{[H^+](1 + [H^+]/K_{R^+})(1 + K_{R^+}/[H^+])}$$

When the data in Fig. 3 are fitted to eq. [5] by an iterative curve-fitting procedure, the parameters $k_1K_{RO^-}$ = 8.0 (± 0.2) × 10^{-11} s^{-1} and K_{R^+} = 1.35 (± 0.04) × 10^{-10} M are obtained. This latter parameter corresponds to pK_{R^+} = 9.87 and is in reasonable agreement with pK_{R^+} = 10.01 reported for this cation in aqueous solution at ionic strength 0.1 (10). The curve in Fig. 3 is drawn using eq. [5] and these parameters which produce a reasonable fit to the experimental data as judged by an average deviation of only 5% between calculated and experimental data points. As a further test of these parameters it can be noted that for $[H^+] \ll K_{R^+}$, eq. [5] simplifies to $k_{dis} = k_1K_{RO^-}/K_{R^+}$. This condition certainly holds for pH 12–13.5, for which k_{dis} appears to be pH-independent (Fig. 3). The average experimental value of k_{dis} in this region is 0.58 ± 0.02 which is in good agreement with the value of 0.59 calculated from the ratio of the above two parameters.

Ferricyanide oxidation

The time-dependence of the electronic absorption spectrum of a mixture of 10-methylacridinium cation and potassium ferricyanide in 1:2 molar ratio (i.e. stoichiometric ratio according to eq. [2]) at pH 13 is shown in Fig. 4. The final spectrum shown is essentially that of 10-methyl-9-acridone at the same concentration as the original acridinium cation. Ferrocyanide ion, the other reaction product, absorbs only weakly in this spectral region.

Rates of ferricyanide ion oxidation of the 10-methylacridinium cation were evaluated at 409 nm and proved to be kinetically first-order in each of ferricyanide ion and total acridine reactant species present. Second-order rate constants (k_{ox}) at several concentrations of each species in stoichiometric ratio are shown in Table 2. These rate constants appear to be unaffected by the presence of significant initial concentrations of ferrocyanide ion (Table 2). The pH–rate profile for k_{ox} is shown in Fig. 5.

In the region pH 9–12.5, k_{ox} for ferricyanide ion oxidation in Fig. 5 is of similar magnitude, although not identical, to k_{dis} for the disproportionation reaction in Fig. 3. Thus in this region the disproportionation reaction competes with the ferricyanide ion oxidation of the 10-methylacridinium cation. One of the products of disproportionation, namely 10-methyl-9-acridone, is identical to the ferricyanide ion oxidation product, and we have observed that the second disproportionation product, 9,10-dihydro-10-methylacridine, is itself readily susceptible to ferricyanide ion oxidation. We will report later on the kinetics of this latter oxidation which formally regenerates the acridinium cation. Thus the sequence of reactions shown in Scheme 1 exists.

The overall stoichiometry of the combined reactions in Scheme 1 is identical to that shown in eq. [2] for the usually assumed mechanism of direct ferricyanide ion attack upon the pseudobase. Provided the ferricyanide ion oxidation of 9,10-dihydro-10-methylacridine is faster than the rate of disproportionation, the overall rate of ferricyanide oxidation via these two pathways is then given by:

$$[6] \quad d[P]/dt = k_{dis}[A_T]^2 + k_{Fe}[Fe(CN)_6^{3-}][A_T]$$

For stoichiometric ratio of reactants, $[A_T] = [Fe(CN)_6^{3-}]/2$, and:

$$[7] \quad d[P]/dt = (k_{dis}/2 + k_{Fe})[Fe(CN)_6^{3-}][A_T] = k_{ox}[Fe(CN)_6^{3-}][A_T]$$

Thus:

Can. J. Chem. Downloaded from www.nrcresearchpress.com by 210.87.254.5 on 09/06/12
For personal use only.

TABLE 2. Second-order rate constants for the oxidation of the 10-methylacridinium cation by ferricyanide ion[a]

pH	$[A_T]$, m*M*	$[Fe(CN)_6^{3-}]$, m*M*	$[Fe(CN)_6^{4-}]$, m*M*	k_{ox}, M^{-1} s^{-1}
13.61	0.0954	0.191	0	2.10
	0.110	0.220	0	2.43
	0.204	0.408	0	2.21
13.09	0.102	0.204	0	1.05
	0.202	0.404	0	0.85
	0.202	0.404	0.40	0.87
12.38	0.102	0.204	0	0.532
	0.205	0.410	0	0.535
10.12	0.202	0.404	0	0.222
	0.202	0.404	0.40	0.215
9.89	0.143	0.286[b]	0	0.131
	0.143	0.286[c]	0	0.139
	0.143	0.286[d]	0	0.147

[a]In 20% CH_3CN − 80% H_2O, ionic strength 1.0, 25°C.
[b]In 0.04 *M* carbonate buffer.
[c]In 0.08 *M* carbonate buffer.
[d]In 0.16 *M* carbonate buffer.

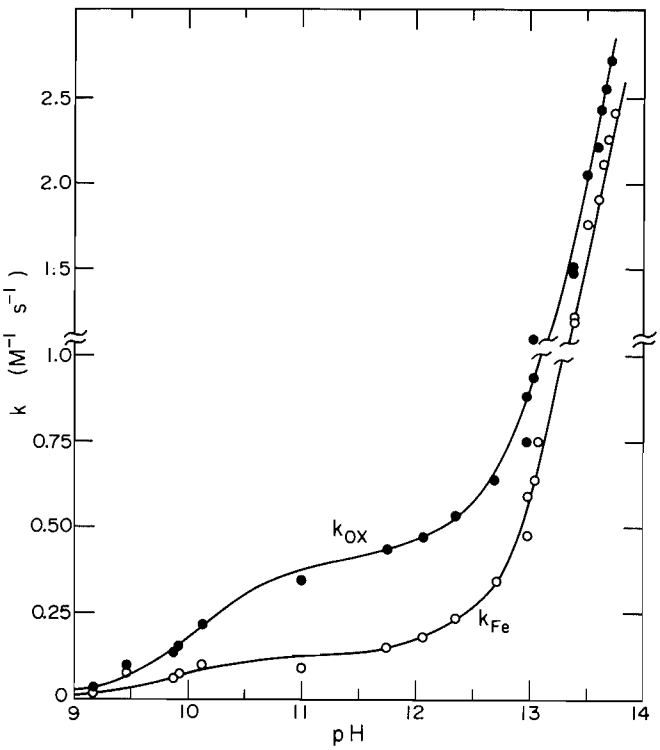

FIG. 5. The pH-dependence of k_{ox} and k_{Fe}. The k_{ox} curve is calculated as $k_{Fe} + k_{dis}/2$ using eqs. [5] and [11] and the parameters in the text. The k_{Fe} data points are calculated from eq. [8], while the k_{Fe} line is calculated from eq. [11].

$$[8] \quad k_{Fe} = k_{ox} - k_{dis}/2$$

The pH-dependence of k_{Fe} calculated from eq. [8], making use of experimental values of k_{ox} and values of k_{dis} calculated from eq. [5], is included in Fig. 5. In the region pH 9−10, k_{ox} is larger than k_{dis}, and so it is clear that the pathway shown in Scheme 1 cannot account for the complete rate of ferricyanide ion oxidation of the 10-methylacridinium cation in this region, nor in the region pH 10−12 where k_{Fe} is smaller than the rate of disproportionation, but is not insignificant. Above pH 12, k_{Fe} begins to increase dramatically with increasing pH, with the rate of ferricyanide ion oxidation becoming much faster than the rate of disproportionation in the most basic solutions.

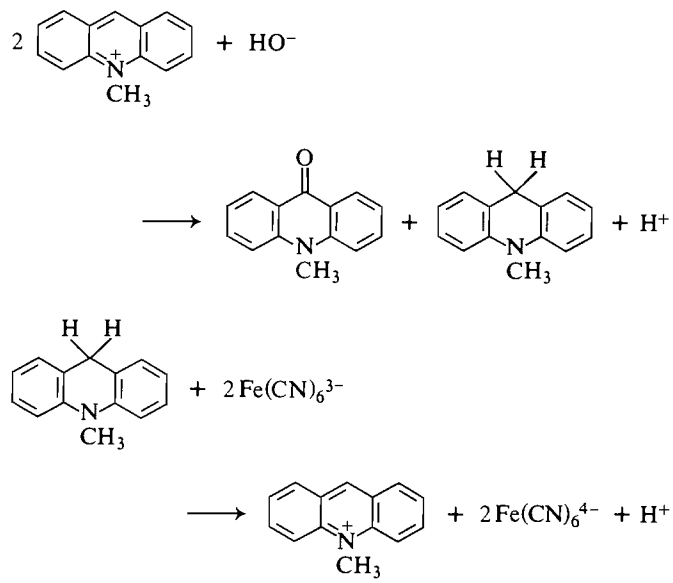

SCHEME 1

The pH-dependence of k_{Fe} in Fig. 5 suggests that direct ferricyanide oxidation can occur either via the pseudobase (**1**) or its conjugate base alkoxide ion (**2**). Thus:

$$[9] \quad d[P]/dt = k_2[Fe(CN)_6^{3-}][AOH] + k_3[Fe(CN)_6^{3-}][AO^-] = k_{Fe}[Fe(CN)_6^{3-}][A_T]$$

Therefore, using K_{R^+} and K_{RO^-} as defined above:

$$[10] \quad k_{Fe} = \frac{k_2 + k_3K_{RO^-}/[H^+]}{[H^+]/K_{R^+} + 1 + K_{RO^-}/[H^+]}$$

For $K_{RO^-} \ll [H^+]$, eq. [10] becomes:

$$[11] \quad k_{Fe} = \frac{k_2 + k_3K_{RO^-}/[H^+]}{[H^+]/K_{R^+} + 1}$$

Attempts to fit eq. [11] to the data for k_{Fe} in Fig. 5 by evaluating the three parameters k_2, $k_3K_{RO^-}$, and K_{R^+} by an

Can. J. Chem. Downloaded from www.nrcresearchpress.com by 210.87.254.5 on 09/06/12
For personal use only.

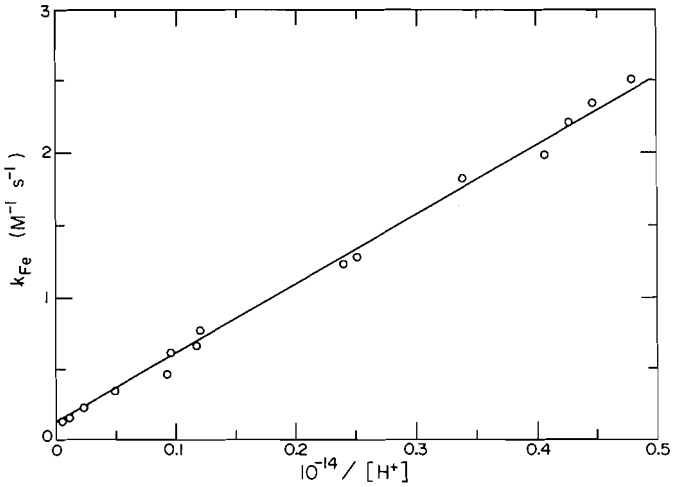

FIG. 6. Variation of k_{Fe} with $1/[H^+]$ as in eq. [12].

iterative curve-fitting routine gave fits which were relatively insensitive to the value of K_{R^+}. This result can be traced to the fact that the values of k_{Fe} at pH values in the vicinity of pK_{R^+} are quite small relative to k_{Fe} at high pH. We have therefore fixed K_{R^+} at 1.35×10^{-10} M as determined above for the disproportionation reaction, and have obtained the best fit using the other two parameters. When this is done, the values $k_2 = 0.12 \pm 0.02$ M^{-1} s^{-1} and $k_3K_{RO^-} = 4.7 (\pm 0.2) \times 10^{-14}$ s^{-1} are obtained. The curves through the data points for k_{Fe} and k_{ox} in Fig. 5 make use of these parameters and eq. [11] and fit the data with an average deviation of 8% from the experimental data points.

The condition $K_{RO^-} \ll [H^+]$ is further supported by the following analysis. For $[H^+] \ll K_{R^+}$ (i.e. pH > 12), eq. [11] may be further simplified to:

$$[12] \quad k_{Fe} = k_2 + k_3K_{RO^-}/[H^+]$$

A plot of k_{Fe} vs. $1/[H^+]$ is shown in Fig. 6 for pH > 12. This plot is quite linear, and of slope $4.8 (\pm 0.2) \times 10^{-14}$ s^{-1}, which is in good agreement with the value of $k_3K_{RO^-}$ reported above for a fit to the complete data in the range pH 9–13.7. Significant deviations from linearity would be expected for the data at high pH in Fig. 6 if the condition $K_{RO^-} \ll [H^+]$ did not hold.

Discussion

The pH-dependence of the disproportionation reaction of the 10-methylacridinium cation in basic solution is quite consistent with the reaction occurring between the pseudobase alkoxide ion and acridinium cation. Clark and Bakavoli (8) have established that this disproportionation occurs with direct transfer of a hydrogen atom from C-9 of one acridine species (alkoxide ion) to C-9 of the other acridine species (acridinium cation) without exchange with solvent protons. Thus the one-step direct hydride transfer shown in Scheme 2 is consistent with the experimental data, although we cannot rule out kinetically equivalent mechanisms involving one-electron transfer steps ($e^- + H^\cdot$ or $e^- + H^+ + e^-$) provided that the hydrogen transfer step in such a mechanism occurs within a radical pair cage intermediate. We note that the "crossed disproportionation" previously studied for two isoquinolinium cations is only consistent with the direct hydride transfer mechanism (4). However, in view of the uncertainty (13–17) surrounding the mechanisms of other reactions which involve formal hydride transfers to or from acridine derivatives, we cannot unambiguously

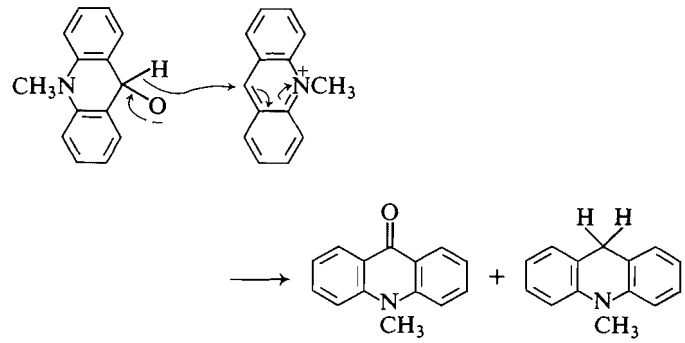

SCHEME 2

establish the direct one-step hydride transfer for the acridinium cation disproportionation at the present time. We also note that a general base-catalyzed termolecular process, involving hydroxide ion, neutral pseudobase, and acridinium cation, is kinetically equivalent to Scheme 2. Such a mechanism seems less likely, however, in view of the lack of any buffer catalysis in carbonate buffers of several different concentrations for either the disproportionation or ferricyanide ion oxidation reactions (Table 2).

The above kinetic analysis of the pH profile for k_{dis} gives only the parameter $k_1K_{RO^-}$. Evaluation of k_1 requires the value of pK_{RO^-} which lies outside the pH range of the current investigation. However, the use of $pK_{RO^-} = 15.34$ estimated for benzyhydrol (11), allows the estimation of $k_1 = 1.8 \times 10^5$ M^{-1} s^{-1}. This value indicates that the acridine pseudobase alkoxide ion is far more reactive as a hydride donor towards the 10-methylacridinium cation than either 1-benzyl-1,4-dihydronicotinamide (second-order rate constant 400 M^{-1} s^{-1} (13))[2] or 9,10-dihydro-10-methylacridine (0.051 M^{-1} s^{-1} in acetonitrile at 30°C (14)).

The base-catalyzed oxidation of 5-nitroisoquinolinium cations by ferricyanide ion has been established to occur via a mechanism which is kinetically first-order in each of ferricyanide ion and the pseudobase alkoxide ion (3). A similar reaction predominates in the ferricyanide ion oxidation of the 10-methylacridinium cation in the most basic solutions investigated (k_3 in eq. [9]). However, in more dilute base two further pathways for ferricyanide ion oxidation have been identified in the current work. One of these pathways is kinetically first-order in each of ferricyanide ion and neutral pseudobase (k_2 in eq. [9]), while the other occurs via an initial disproportionation as outlined in Scheme 1. The relative importance of each of these pathways over the pH range 9–14 is indicated in Fig. 7. Below pH 9.7 the k_2 path predominates, while above pH 12.8 the k_3 path becomes the major oxidation route. In the pH 9.7–12.8 region, the predominant ferricyanide ion oxidation route for the 10-methylacridinium cation occurs via initial disproportionation as outlined in Scheme 1, with the maximum contribution from this route reaching 69% at pH 11.1.

It is clear that the neutral pseudobase is much less susceptible to oxidation by ferricyanide ion than is the pseudobase alkoxide ion. A quantitative estimate of the relative reactivities of these two species can be made by using $k_3K_{RO^-} = 4.7 \times 10^{-14}$ M^{-1}

[2]Unless otherwise indicated, all comparisons of rate constants in this discussion involve data obtained under the same experimental conditions, namely in 20% CH_3CN – 80% H_2O, ionic strength 1.0, at 25°C.

Can. J. Chem. Downloaded from www.nrcresearchpress.com by 210.87.254.5 on 09/06/12
For personal use only.

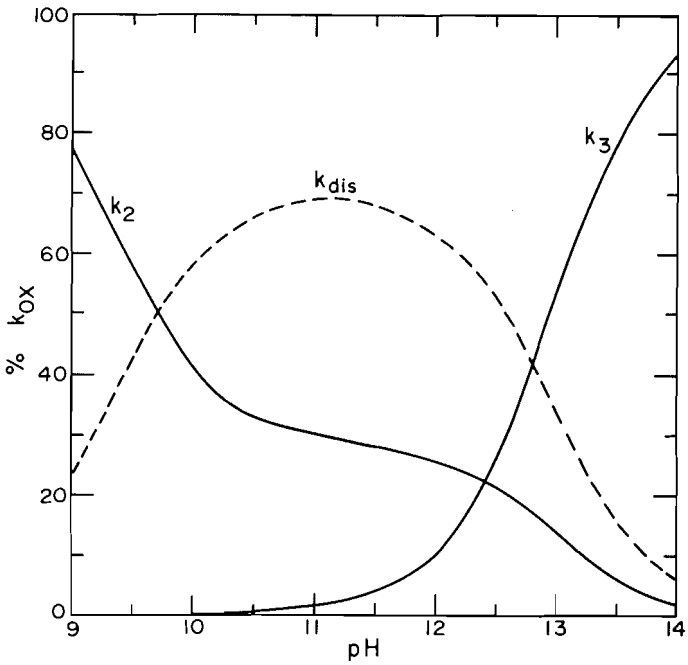

FIG. 7. Variation of contributions (as percentages) to k_{ox} from the k_2, k_3, and k_{dis} routes for pH 9–14.

s^{-1} and the estimated value of $pK_{RO^-} = 15.34$. Thus the value of k_3 can be estimated to be 100 M^{-1} s^{-1}, and the ratio $k_3/k_2 = 800$ is obtained.

This $k_3 = 100\ M^{-1}\ s^{-1}$ is only slightly smaller than the second-order rate constant of 238 M^{-1} s^{-1} found (3) for reaction of the pseudobase alkoxide ion of the 2-benzyl-5-nitroisoquinolinium cation with ferricyanide ion. This latter reaction is only readily interpretable (3) as involving hydride abstraction from the alkoxide ion by ferricyanide. An analogous interpretation for k_3 for the acridine alkoxide ion requires only 2-fold lower reactivity for the acridine system than for the 5-nitroisoquinoline system. The only related reaction that we are aware of that allows a similar comparison of reactivity is the loss of hydroxide ion from the pseudobases to regenerate these heteroaromatic cations. In this case the 2-benzyl-5-nitroisoquinoline system is over 2000-fold more reactive than the 10-methylacridine species (10, 17). On this basis it seems unlikely that both the above pseudobase alkoxide ion oxidations involve hydride abstraction by ferricyanide ion, although it is difficult to assess the possible role of steric differences in these reactions. The enhanced reactivity in the acridine system would seem to point towards a mechanism other than direct hydride abstraction in this case. An analogous enhanced reactivity (almost 40 000-fold relative to isoquinolinium cations) in the reduction of acridinium cations by 1,4-dihydronicotinamides has been noted (13), and has been suggested as being due to the occurrence of one of the kinetically equivalent one-electron mechanisms for hydride transfer in the acridine case. It should be noted that acridanyl radicals seem to be readily accessible from both acridinium cations and 9,10-dihydroacridines (13, 19–26).

It is also of interest to compare the relative reactivities of the acridine pseudobase alkoxide ion towards ferricyanide ion (k_3) and towards the 10-methylacridinium cation (k_1). This comparison can be made without an explicit value for K_{RO^-}, and gives $k_1/k_3 = 1700$. Thus the 10-methylacridinium cation is 1700-fold more reactive than ferricyanide ion for the oxidation of the alkoxide ion to the acridone. While this is an interesting observation, it is complicated by the fact that while one reaction involves a monoanion and a monocation, the other involves a monoanion reacting with a trianion. A much lower selectivity between the 10-methylacridinium cation and the ferricyanide ion as oxidants is obtained if one compares their relative reactivities for the oxidation of a neutral molecule such as 1-benzyl-1,4-dihydronicotinamide. In an unpublished study we have obtained a second-order rate constant of 30 M^{-1} s^{-1} for ferricyanide ion oxidation of the latter compound (20% CH_3CN – 80% H_2O, ionic strength 1, 25°C). Comparison of this value with the second-order rate constant of 400 M^{-1} s^{-1} for the oxidation of 1-benzyl-1,4-dihydronicotinamide by the 10-methylacridinium cation (13) indicates that the 10-methylacridinium cation is only 13-fold more reactive than ferricyanide ion in the oxidation of this neutral molecule.

Acknowledgement

We appreciate the support of this work through an Operating Grant to J.W.B. from the Natural Sciences and Engineering Research Council of Canada.

1. J. W. BUNTING. Adv. Heterocycl. Chem. **25**, 1 (1979).
2. E. A. PRILL and S. M. MCELVAIN. Org. Synth. Coll. Vol. **2**, 419 (1943).
3. J. W. BUNTING, P. A. LEE-YOUNG, and D. J. NORRIS. J. Org. Chem. **43**, 1132 (1978).
4. J. W. BUNTING and S. H. KABIR. J. Org. Chem. **43**, 3662 (1978).
5. H. DECKER. Chem. Ber. **24**, 690 (1891).
6. H. DECKER. J. Prakt. Chem. **45**, 161 (1892).
7. A. PICTET and E. PATRY. Chem. Ber. **35**, 2534 (1902).
8. J. CLARK and M. BAKAVOLI. J. Chem. Soc. Perkin Trans. 1, 1966 (1977).
9. A. ALBERT. The acridines. 2nd ed. Edward Arnold Ltd., London. 1966. p. 343.
10. J. W. BUNTING and W. G. MEATHREL. Can. J. Chem. **51**, 1965 (1973).
11. S. TAKAHASHI, L. A. COHEN, H. K. MILLER, and E. G. PEAKE. J. Org. Chem. **36**, 1205 (1971).
12. P. BALLINGER and F. A. LONG. J. Am. Chem. Soc. **82**, 795 (1960).
13. J. W. BUNTING, V. S. F. CHEW, G. CHU, N. P. FITZGERALD, A. GUNASEKARA, and H. T. P. OH. Bioorg. Chem. In press.
14. M. F. POWELL and T. C. BRUICE. J. Am. Chem. Soc. **104**, 5834 (1982).
15. M. F. POWELL and T. C. BRUICE. J. Am. Chem. Soc. **105**, 7139 (1983).
16. A. K. COLTER, G. SAITO, and F. J. SHAROM. Can. J. Chem. **55**, 2741 (1977).
17. A. VAN LAAR, H. J. VAN RAMESDONK, and J. W. VERHOEVEN. Recl. Trav. Chim. Pay-Bas, **102**, 157 (1983).
18. J. W. BUNTING and D. J. NORRIS. J. Am. Chem. Soc. **99**, 1189 (1977).
19. G. SAITO and A. K. COLTER. Tetrahedron Lett. 3325 (1977).
20. K. S. PETERS, E. PANG, and J. RUDZKI. J. Am. Chem. Soc. **104**, 5535 (1982).
21. C. C. LAI and A. K. COLTER. J. Chem. Soc. Chem. Commun. 1115 (1980).
22. E. G. JANZEN, J. B. PICKETT, J. W. HAPP, and W. DEANGELIS. J. Org. Chem. **35**, 88 (1970).
23. J. W. HAPP and E. G. JANZEN. J. Org. Chem. **35**, 96 (1970).
24. P. NETA. J. Phys. Chem. **83**, 3096 (1979).
25. E. AHLBERG, O. HAMMERICH, and V. D. PARKER. J. Am. Chem. Soc. **103**, 844 (1981).
26. R. E. BALLARD, J. JONES, and E. SUTHERLAND. Tetrahedron Lett. **23**, 3677 (1982).

Can. J. Chem. Downloaded from www.nrcresearchpress.com by 210.87.254.5 on 09/06/12
For personal use only.

Calcul des intensités des transitions laser dans $^{12}C^{16}O_2$ et ses molécules isotopiques

PHILIPPE MILLIE
Département de Physico-chimie, CEN/Saclay, 91191 Gif-sur-Yvette-Cedex, France

Reçu le 8 juillet 1983

PHILIPPE MILLIE. Can. J. Chem. **62**, 736 (1984).

Les intensités des raies lasers à 9 et 10 μm de $^{12}C^{16}O_2$ et ses molécules isotopiques sont calculées théoriquement. Les fonctions d'ondes vibrationnelles sont obtenues par diagonalisation directe à partir d'une fonction potentiel determinée antérieurement. Une comparaison avec les valeurs expérimentales est présentée. Le rôle de l'anharmonicité électrique est discuté ainsi que les erreurs dues à la méthode de transformation de contact dans le calcul des niveaux d'énergie.

PHILIPPE MILLIE. Can. J. Chem. **62**, 736 (1984).

The laser emission-line intensities of $^{12}C^{16}O_2$ and several isotopes were theoretically calculated. The vibrational wave functions were obtained to a direct diagonalization by utilizing a previously known potential function. These values are compared to the experimental ones. The effect of electrical anharmonicity is discussed. The validity of the contact transformation method is briefly analyzed.

Can. J. Chem. Downloaded from www.nrcresearchpress.com by 210.87.254.6 on 09/06/12
For personal use only.

Introduction

Les lasers CO_2 constituent encore une des seules sources de rayonnement cohérent de puissance dans l'infra-rouge. Pour en augmenter l'accordabilité ou couvrir des domaines que ne permet pas d'atteindre l'isotope usuel $^{12}C^{16}O_2$, l'attention s'est portée depuis quelques années sur la possibilité de lasers "isotopiques". Ainsi, fonctionnent déjà ceux utilisant les molécules $^{12}C^{18}O_2$, $^{13}C^{16}O_2$ et $^{12}C^{16}O^{18}O$ (1). Or, la possibilité d'obtenir un effect laser et le gain qu'on peut escompter sont étroitement liés aux moments dipolaires de transition (1). Si certains sont connus expérimentalement, il n'en est pas de même pour les molécules isotopiques les moins abondantes (2).

Par ailleurs, d'un point de vue théorique, le calcul précis de tels moments dipolaires exige la détermination de très bonnes fonctions d'ondes, donc l'utilisation d'une fonction potentielle la meilleure possible. A notre connaissance, aucun calcul n'a utilisé jusqu'à présent la fonction potentielle déterminée par A. Chedin (3), dont la convergence est très bonne et où le terme du troisième ordre par rapport au potentiel harmonique qui joue un rôle non négligeable dans le couplage de Fermi a été explicitement introduit contrairement aux déterminations antérieures (4, 5). Sa valeur a été testée aussi bien en ce qui concerne les constantes moléculaires sur des transitions jusqu'alors inobservées (6, 7) que sur l'analyse des intensités Raman des raies laser d'un certain nombre de molécules isotopiques (8).

Enfin, comme on le verra par la suite, cette étude permet de comparer la méthode de la transformation de contact à la méthode "brutale" de diagonalisation et de discuter de leurs mérites respectifs.

I. Obtention des fonctions d'ondes

1. *Nécessité de fonctions d'ondes précises*

Les deux transitions impliquées sont les transitions (0, 0°, 1) → I et (0, 0°, 1) → II, où I et II sont, en première approximation, des combinaisons linéaires des états harmoniques (1, 0°, 0) et (0, 2°, 0) entre lesquels existe un très fort couplage de Fermi (ν_1 correspond à l'allongement symétrique Σ_g^+, ν_3 à l'allongement dissymétrique Σ_u^+ et ν_2 au bending de symétrie π_u). L'opérateur moment dipolaire de transition est lui-même de symétrie Σ_u et peut s'écrire à l'ordre zéro $\mu = aQ_3$ (où Q_3 est la coordonnée normale sans dimension associée au mode ν_3). On voit que si on ne tient compte que du couplage de Fermi et qu'on néglige l'anharmonicité du moment dipolaire, on trouve des intensités nulles: ces deux transitions ne sont permises que grâce aux anharmonicités mécaniques et électriques (9) et la détermination de leurs intensités exige donc des fonctions d'ondes précises.

2. *Méthode utilisée*

Elle consiste simplement à écrire les fonctions d'ondes comme somme de produits des fonctions harmoniques et donc à diagonaliser l'opérateur énergie cinétique + potentiel harmonique + potentiel anharmonique dans cette base. Nous avons négligé l'interaction rotation−vibration, ce qui semble raisonnable pour des niveaux vibrationnels aussi bas, compte tenu par ailleurs de la précision du potentiel utilisé (cf. *infra*) et de la complexité que son introduction entraîne pour le calcul. Dans ces conditions, pour les molécules symétriques, la matrice à diagonaliser se scinde en deux sous-matrices correspondant aux états de symétrie Σ_g^+ $[n_1\nu_1, 2n_2\nu_2, 2n_3\nu_3]$ et $\Sigma_u^+[n_1\nu_1, 2n_2\nu_2, (2n_3 + 1)\nu_3]$.

3. *Etude de la convergence*

La qualité de la fonction d'onde obtenue dépend bien entendu de la dimension de la base utilisée. Pour éviter tout arbitraire, il semble qu'une bonne façon de procéder soit d'étudier comment varient les valeurs propres, c'est à dire les énergies des niveaux vibrationnels, en fonction de la dimension de la base. Pour cela, on effectue la diagonalisation en agrandissant progressivement la base utilisée (méthode des matrices "emboîtées"): on sait que, dans ces conditions, les différentes valeurs propres tendent, de façon monotone et par valeur supérieure, vers leur valeur limite pour une dimension infinie (10). Deux critères ont été retenus pour cet agrandissement: un critère énergétique d'un part, et le fait que l'on doive diagonaliser ensemble tous les états correspondant à une même valeur $(2\nu_1 + \nu_2)$ à cause du couplage de Fermi, d'autre part. On trouvera dans l'annexe I, les bases utilisées dans le cas des molécules symétriques.

L'examen de la table 1 montre clairement que l'énergie d'un niveau donné se stabilise à partir d'un certaine dimension, dimension d'autant plus élevée que le niveau étudié est plus haut en énergie. Dans notre cas, on a convergence du niveau fondamental et des niveaux I et II (construits sur 1, 0°, 0 et 0, 2°, 0) à partir de la dimension 34. Au total, en base 90, l'énergie des dix premiers niveaux a convergé à mieux que 0,1 cm^{-1} près. Il en résulte que les vraies observables, c'est à dire les niveaux d'énergies rapportées au niveau fondamental, ont aussi convergé avec une précision quasiment identique. Les mêmes constatations pourraient être faites pour la symétrie Σ_u^+.

Can. J. Chem. Downloaded from www.nrcresearchpress.com by 210.87.254.6 on 09/06/12
For personal use only.

Ajoutons qu'en supposant, ce qui est raisonnable, que le niveau fondamental converge au moins aussi vite que les autres, on obtient ainsi des valeurs des niveaux d'énergies rapportées au fondamental qui sont supérieures aux énergies que l'on obtiendrait en diagonalisant une matrice infinie.

Une étude similaire, quoique moins poussée, a été effectuée dans le cas des molécules non symétriques. En effet, il n'y a plus séparation en Σ_g^+ et Σ_u^+ et, pour obtenir des résultats de qualité similaire, il faudrait diagonaliser des matrices de dimension environ 200. L'étude du cas symétrique montrant qu'en fait, une convergence raisonnable est atteinte des la dimension 34 pour les niveaux qui nous intéressent, on peut penser qu'une dimension de l'ordre de 92 est amplement suffisante, ce que confirme l'examen de la table 2. Il faut, cependant, noter que les critères pour agrandir progressivement la base sont nettement moins clairs que précédemment. Si les termes de couplage anharmonique, nuls dans le cas des molécules symétriques, sont très petits devant les autres, il est clair qu'il faut simplement juxtaposer les bases utilisées précédemment pour les cas Σ_g^+ et Σ_u^+. C'est le principe utilisé pour les bases 20, 48 et 68 (respectivement égales à 10 + 10, 24 + 24, 34 + 34). Si, par contre, tous les termes de couplage sont du même ordre, le critère énergétique est prépondérant; c'est lui que l'on a utilisé au moins en partie pour passer de la base 68 à la base 92 (ceci explique qu'il y ait plus de niveaux de type (v_1, v_2, 0) que de type (v_1, v_2, 1) ayant convergé).

4. *Comparaison avec la méthode de transformation de contact*

La méthode de la transformation de contact consiste, par des changements de base appropriés, à annuler certains éléments de matrice non-diagonaux du potentiel. Ceci revient, en fait, à diagonaliser une matrice infinie par perturbation, puis à diagonaliser par une méthode exacte l'interaction de Fermi (voir par example référence 11). Si cette méthode semble de loin la plus praticable pour extraire un potentiel de données expérimentales, par contre, à cause notamment de la très grande valeur de la constante de couplage anharmonique k_{133} ($\sim$250 cm^{-1}), l'erreur introduite par le traitement de perturbation peut être importante et augmente de façon significative avec le nombre quantique v_3 (voir table 15 de la référence 3). Les différences entre les énergies expérimentales et les énergies obtenues par diagonalisation directe ont été rassemblées dans la table 3. Les erreurs sont de l'ordre de 0,5 à 1.2%, sont significativement plus grandes pour les niveaux (v_1, v_2,- 1) que pour les niveaux (v_1, v_2, 0) et augmentent avec ($2v_1 + v_2$). Il en résulte que l'erreur sur la fonction potentielle est du même ordre de grandeur et ce résultat peut justifier dans une certaine mesure le fait de négliger l'interaction rotation–vibration.

Au total, la méthode de la transformation de contact semble supérieure à celle de la diagonalisation directe, au moins en ce qui concerne CO_2 (11), mais elle a le désavantage de ne pas fournir directement les fonctions d'onde.

II. Calcul des forces oscillatrices de transition

1. *Expressions théoriques*

La force oscillatrice d'une transition donnée entre deux états vibrationnels φ_i et φ_j est donnée par:

$$f = \langle \varphi_i | M | \varphi_j \rangle^2$$

où M est l'opérateur de moment dipolaire.

Cet opérateur M peut lui-même être développé en série en fonction des coordonnées normales sans dimension tandis que

TABLE 1. Etude de la convergence des états Σ_g^+ les plus bas: cas de $^{12}C^{16}O_2$. Valeurs propres (en cm^{-1}) en prenant pour origine l'énergie de l'état fondamental dans l'approximation harmonique

	(0, 0°, 0)	(1, 0°, 0) II	(1, 0°, 0) I	(2, 0°, 0) III	(2, 0°, 0) II	(2, 0°, 0) I	(3, 0°, 0) IV	(3, 0°, 0) III	(3, 0°, 0) II	(3, 0°, 0) I	(0, 0°, 2)
Base 10	−9,620	1278,900	1383,735	2552,510	2679,854	2802,188	3824,219	4017,200	4181,943	4270,936	
Base 24	−12,282	1276,080	1379,528	2539,461	2665,282	2789,240	3789,977	3951,650	4073,174	4228,004	4689,470
Base 34	−12,323	1272,358	1375,430	2538,848	2664,465	2788,575	3784,173	3939,324	4060,597	4217,378	4679,335
Base 52	−12,329	1272,212	1375,260	2534,231	2657,924	2783,412	3777,940	3930,667	4051,915	4210,794	4677,200
Base 69	−12,329	1272,195	1375,253	2534,189	2657,867	2783,377	3777,677	3929,238	4050,532	4210,399	4661,604
Base 90	−12,336	1272,193	1375,233	2534,151	2657,759	2783,311	3777,581	3929,067	4050,385	4210,330	4657,437

TABLE 2. Etude de la convergence des états Σ^+ dans le cas d'une molécule non symétrique: cas $^{12}C^{16}O^{18}O$

	(0,0°, 0)	(1, 0°, 0) II	(1, 0°, 0) I	(0, 0°, 1)	(2, 0°, 0) III	(2, 0°, 0) II	(2, 0°, 0) I	(1, 0°, 1) II	(1, 0°, 1) I
Base 20	−9,363	1254,315	1360,187	2327,354	2506,393	2622,338	2760,535	3576,084	3682,390
Base 48	−11,942	1250,918	1356,876	2319,439	2493,092	2608,308	2748,833	3568,810	3672,877
Base 68	−11,982	1246,993	1353,243	2318,622	2492,517	2607,528	2748,155	3557,544	3661,332
Base 92	−11,985	1246,830	1353,129	2318,577	2487,658	2602,013	2743,855	3555,600	3659,661

TABLE 3. Valeurs (en cm^{-1}) de ($E_{\text{expérmental}} - E_{\text{théorique}}$). Pour les niveaux couplés par résonance de Fermi, seule cette différence moyennée sur le multiplet est indiquée

$v_1 + v_2/2$	v_3	$^{12}C^{16}O_2$	$^{13}C^{16}O_2$	$^{14}C^{16}O_2$	$^{12}C^{18}O_2$	$^{13}C^{18}O_2$	$^{12}C^{16}O^{17}O$	$^{12}C^{17}O^{18}O$	$^{12}C^{16}O^{18}O$	$^{13}C^{16}O^{17}O$	$^{13}O^{16}O^{18}O$
1	0	0,75	0,75	0,75	0,66	0,66	0,70	0,68	0,66	0,70	0,68
2	0	1,46	1,46	—	1,28	1,28	—	—	—	—	—
3	0	1,94	1,96	—	1,69	—	—	—	—	—	—
0	1	1,73	1,71	1,69	1,54	1,52	1,62	1,53	1,56	1,61	1,53
1	1	4,09	4,06	—	3,62	3,59	3,64	3,44	3,52	3,64	3,52
2	1	6,35	6,31	—	5,60	—	—	—	—	—	—
3	1	7,62	7,60	—	—	—	—	—	—	—	—

TABLE 4. Convergence des moments dipolaires de transition: cas de $^{12}C^{16}O_2$

Paramètres	Base 10	Base 24	Base 34	Base 52	Base 69	Base 90
$\langle 0, 0°, 1\|Q_3\|1, 0°, 0^{II}\rangle$	0,057517	0,081461	0,085660	0,086087	0,086267	0,086291
$\langle 0, 0°, 1\|Q_1Q_3\|1, 0°, 0^{II}\rangle$	0,369298	0,385585	0,397438	0,398830	0,398984	0,399053
$\langle 0, 0°, 1\|Q_3\|1, 0°, 0^{I}\rangle$	0,071327	0,100203	0,101398	0,101552	0,101753	0,101785
$\langle 0, 0°, 1\|Q_1Q_3\|1, 0°, 0^{I}\rangle$	0,363447	0,362327	0,365311	0,365585	0,365628	0,365708
$\left[\frac{\langle 0, 0°, 1\|Q_3\|1, 0°, 0^{I}\rangle}{\langle 0, 0°, 1\|Q_3\|1, 0°, 0^{II}\rangle}\right]^2$	1,5378	1,5131	1,4012	1,3916	1,3912	1,3914

φ_i et φ_j sont obtenues comme des sommes de produits de fonctions harmoniques.

Dans le cas des transitions laser qui sont des transitions parallèles, M peut donc s'écrire:

$$M = \lambda_1(a_3Q_3 + a_1Q_1) + \lambda_2(a_{13}Q_1Q_3 + a_{11}Q_1^2 + a_{33}Q_3^2) + \ldots$$

Par ailleurs, pour une molécule linéaire triatomique XYZ, on peut écrire, au premier ordre, si X et Z sont deux isotopes:

$$M = \frac{\partial M}{\partial r}(\Delta X + \Delta Z - 2\Delta Y)$$

où ΔX, ΔY et ΔZ sont les déplacements suivant l'axe internucléaire des trois atomes.

On peut exprimer $\Delta X + \Delta Z - 2\Delta Y$ en fonction des coordonnées normales sans dimension: $\Delta X + \Delta Z - 2\Delta Y = b_3Q_3 + b_1Q_1$, où b_3 et b_1 sont fonctions de l'isotope considéré alors que $\partial M/\partial r$ est une caractéristique de la molécule étudiée.

Dans le cas où $X \equiv Z$, $a_1 = a_{11} = a_{33} = 0$. Dans le cas non-symétrique, on a donc a_{11}, $a_{33} \ll a_{13}$ et on peut négliger leur contribution (voir aussi la référence 12). Par contre, on ne peut négliger, a priori, le terme $\lambda_2a_{13}Q_1Q_3$ devant le terme $\lambda_1a_3Q_3$: si les différentes études antérieures (12 − 16) montrent que $-0,05 < \lambda_2a_{13}/\lambda_1a_3 < 0,0$, par contre il est évident que:

$$\langle\varphi_i|Q_1Q_3|\varphi_j\rangle \gg \langle\varphi_i|Q_3|\varphi_j\rangle$$

pour ce qui concerne les transitions lasers. Comme nous ne nous intéressons qu'aux intensités de ces transitions rapportées à celles de $^{12}C^{16}O_2$, les seuls coefficients à déterminer sont $a_3 \equiv b_3$ et $a_1 \equiv b_1$ que l'on trouvera rassemblés dans l'annexe. Le terme correctif $\lambda_2a_{13}/\lambda_1a_3$ sera pris comme un paramètre, supposé en première approximation indépendant de l'isotope.

2. *Etude de la convergence*

Comme dans le cas des énergies, nous avons étudié la variation des éléments de matrice des opérateurs Q_3, Q_1 et Q_1Q_3 en fonction de la dimension de la base utilisée. Les résultats sont rassemblés dans la table 4 pour $^{12}C^{16}O_2$ et la table 5 pour $^{12}C^{16}O^{18}O$. Comme on pouvait s'y attendre, les éléments de matrice convergent beaucoup moins vite que les énergies car le test est beaucoup plus sévère et basé directement sur la qualité des fonctions vibrationnelles obtenues. On obtient une précision supérieure à 1% avec une base 90 dans le cas des molécules symétriques, de l'ordre de 1% avec une base 92 pour les non-symétriques sauf pour les éléments de matrice de Q_1 qui dépendent beaucoup des tout petits coefficients dans le développement de la fonction vibrationnelle (erreur d'environ 3%). Au total, cependant, compte tenu de la précision des valeurs expérimentales et de l'imprécision sur l'anharmonicité du moment dipolaire, la convergence peut être considérée comme suffisante.

3. *Discussion des résultats*

Sont rassemblés dans la table 6, un certain nombre de résultats théoriques et expérimentaux concernant les moments dipolaires des deux transitions laser pour l'isotope $^{12}C^{16}O_2$. Le critère retenu est le rapport des forces oscillatrices des deux transitions calculé pour trois valeurs du rapport $K = \lambda_2a_{13}/\lambda_1a_3$: 0,0, −0,03 et −0,05.

On voit que, bien que les valeurs théoriques ne diffèrent guère entre elles de plus de 10%, l'écart sur le rapport des forces oscillatrices peut être considérable et seules permettent d'encadrer les résultats expérimentaux les valeurs de la réfé-

Can. J. Chem. Downloaded from www.nrcresearchpress.com by 210.87.254.6 on 09/06/12
For personal use only.

TABLE 5. Convergence des moments dipolaires de transition: cas de $^{12}C^{16}O^{18}O$

Paramètres	Base 20	Base 48	Base 68	Base 92
$\langle 0, 0°, 1\|Q_3\|1, 0°, 0^{II}\rangle$	0,067112	0,094035	0,098239	0,098634
$\langle 0, 0°, 1\|Q_1\|1, 0°, 0^{II}\rangle$	−0,007770	−0,007949	−0,007672	−0,008071
$\langle 0, 0°, 1\|Q_3 + b_1/b_3 Q_1\|1, 0°, 0^{II}\rangle$	0,067194	0,094120	0,098320	0,098720
$\langle 0, 0°, 1\|Q_1 Q_3\|1, 0°, 0^{II}\rangle$	0.415154	0,430687	0,442475	0,443719
$\langle 0, 0°, 1\|Q_3\|1, 0°, 0^{I}\rangle$	0,063168	0,087978	0,088637	0,088723
$\langle 0, 0°, 1\|Q_1\|1, 0°, 0^{I}\rangle$	−0,005795	−0,006179	−0,006037	−0,006244
$\langle 0, 0°, 1\|Q_3 + b_1/b_3 Q_1\|1, 0°, 0^{I}\rangle$	0,063230	0,088044	0,088702	0,088768
$\langle 0, 0°, 1\|Q_1 Q_3\|1, 0°, 0^{I}\rangle$	0,310037	0,306973	0,308524	0,308578
$\left[\frac{\langle 0, 0°, 1\|Q_3 + b_1/b_3 Q_1\|1, 0°, 0^{I}\rangle}{\langle 0, 0°, 1\|Q_3 + b_1/b_3 Q_1\|1, 0°, 0^{II}\rangle}\right]^2$	0,8855	0,8751	0,8139	0,8085

TABLE 6. Valeurs expérimentales et théoriques des forces oscillatrices: cas de $^{12}C^{16}O_2$

Paramètres	Réf. 13	Réf. 16	Réf. 14	Ce travail	Expérience
$\langle 0, 0°, 1\|Q_3\|1, 0°, 0^{II}\rangle$	0,0708	0,0857	0,079	0,0863	
$\langle 0, 0°, 1\|Q_1 Q_3\|1, 0°, 0^{II}\rangle$	0,3457	0,4003	0,384	0,3990	
$\langle 0, 0°, 1\|Q_3\|1, 0°, 0^{I}\rangle$	0,1089	0,0994	0,104	0,1018	
$\langle 0, 0°, 1\|Q_1 Q_3\|1, 0°, 0^{I}\rangle$	0,4084	0,3617	0,359	0,3657	
R,* $K = 0,0$	2,366	1,344	1,733	1,391	1,387[2]
R, $K = -0,03$	2,560	1,443	1,870	1,493	1,391[16]
R, $K = -0,05$	2,735	1,532	2,050	1,584	1,414[14]

* $R = \left[\frac{\langle 00°1\|Q_3 + KQ_1Q_3\|10°0^{I}\rangle}{\langle 00°1\|Q_3 + KQ_1Q_3\|10°0^{II}\rangle}\right]^2$

TABLE 7. Comparaison avec l'expérience pour un certain nombre de molécules isotopiques

Paramètres*	$^{12}C^{16}O_2$	$^{13}C^{16}O_2$	$^{12}C^{16}O^{17}O$	$^{12}C^{16}O^{18}O$	$^{12}C^{18}O_2$
R_{exp}	1,40	3,11	1,19	1,24(?)	0,4
R_{th}†	1,39−1,58	3,07−3,58	1,05−1,19	0,81−0,92	0,50−0,57
$R1_{exp}$		0,63	0,80	0,96	
$R1_{th}$†		0,54−0,51	1,15−1,16	1,29−1,31	
$R2_{exp}$		1,42	0,68	0,86	
$R2_{th}$†		1,18−1,15	0,86−0,87	0,75−0,76	

*R_{exp} tiré des données de la réf. 2; R: même signification que dans la table 6; $R1$: force oscillatrice de la transition $(1, 0°, 0)^{II} \rightarrow (0, 0°, 1)$ rapportée à $^{12}C^{16}O_2$; $R2$: force oscillatrice de la transition $(1, 0°, 0)^{I} \rightarrow (0, 0°, 1)$ rapportée à $^{12}C^{16}O_2$.

†Les deux valeurs indiquées correspondent respectivement à $K = 0$ et $K = -0,05$.

TABLE 8. Valeurs théoriques des forces oscillatrices pour l'ensemble des isotopes étudiées (R, $R1$, $R2$: même signification que pour la table 7)

Paramètres	$^{12}C^{16}O_2$	$^{12}C^{17}O_2$	$^{12}C^{18}O_2$	$^{13}C^{16}O_2$	$^{13}C^{17}O_2$	$^{13}C^{18}O_2$	$^{14}C^{16}O_2$	$^{12}C^{16}O^{17}O$	$^{12}C^{17}O^{18}O$	$^{12}C^{16}O^{18}O$	$^{13}C^{16}O^{17}O$	$^{13}C^{16}O^{18}O$
R $K = 0$	1,39	0,80	0,50	3,07	1,68	0,97	6,35	1,05	0,63	0,81	2,27	1,71
$K = -0,05$	1,58	0,91	0,57	3,58	1,92	1,10	7,73	1,19	0,71	0,92	2,62	1,96
$R1$ $K = 0$	1,0	1,30	1,53	0,54	0,79	1,06	0,27	1,15	1,42	1,29	0,66	0,78
$K = -0,05$	1,0	1,33	1,58	0,51	0,78	1,06	0,25	1,16	1,45	1,31	0,63	0,77
$R2$ $K = 0$	1,0	0,75	0,55	1,18	0,96	0,74	1,25	0,86	0,64	0,75	1,07	0,96
$K = -0,05$	1,0	0,76	0,57	1,15	0,95	0,74	1,20	0,87	0,66	0,76	1,05	0,95

rence 16 et celles de ce travail.

Ce bon accord avec l'expérience est aussi valable pour d'autres isotopes (voir table 7), compte tenu du fait que la valeur expérimentale tirée des tables Geisa (2) pour $^{12}C^{16}O^{18}O$ nous semble entachée d'une erreur importante. On peut remarquer en effet, que la valeur expérimentale de R diminue régulièrement de $^{12}C^{16}O_2$ à $^{12}C^{18}O_2$, comme d'ailleurs la valeur théorique, sauf pour $^{12}C^{16}O^{18}O$. L'accord est nettement moins bon en ce qui concerne les forces oscillatrices des deux transitions laser rapportées à celles de $^{12}C^{16}O_2$ et il ne nous semble pas simple de départager entre les erreurs dues aux approximations faites dans ce travail et les erreurs expérimentales. Au total, cependant, on doit pouvoir accorder une assez grande confiance aux résultats théoriques obtenus pour d'autres iso-

Can. J. Chem. Downloaded from www.nrcresearchpress.com by 210.87.254.6 on 09/06/12
For personal use only.

topes qui sont rassemblés dans la table 8 et qui permettent de déceler quelles seront les transitions sur lesquelles on peut espérer obtenir un effet laser.

Conclusion

On a montré que les erreurs dues à l'emploi de la méthode de transformation de contact pour la détermination de la fonction potentielle à partir des valeurs expérimentales se traduisent, au niveau des énergies calculées, par une erreur relative de l'ordre de $1°/_{oo}$. L'emploi d'un bon potentiel est tout à fait crucial en ce qui concerne la détermination théorique des moments dipolaires de transition. Le potentiel déterminé dans la référence 3 donne des résultats en bon accord avec l'expérience en ce qui concerne les intensités des raies laser. L'anharmonicité électrique joue un rôle considérable dans le rapport des intensités des deux transitions laser; il joue, par contre, un rôle négligeable en ce qui concerne les intensités de ces deux raies pour les molécules isotopiques à condition de les rapporter à celles de l'isotope $^{12}C^{16}O_2$.

Remerciements

Je tiens à remercier Messieurs A. Chedin, B. Levy et G. Salvetat pour les nombreuses discussions que nous avons pu avoir, Messieurs Weulersse et Botter pour avoir attiré mon attention sur l'intérêt du problème et Madame Vinh pour m'avoir facilité l'accès du centre de calcul de l'ENSJF.

1. M. Silver, T. S. Hartwick et M. J. Posakony. J. Appl. Phys. **41**, 4566 (1970).
2. A. Chedin, N. Husson, N. A. Scott, I. Cohen-Hallaleh et A. Berroir. Tables Geisa. Laboratoire de Météorologie dynamique du CNRS. Notes internes n° 108, 113 et 116 (1982).
3. A. Chedin. J. Mol. Spectrosc. **76**, 430 (1979).
4. P. K. L. Yin. Appl. Opt. **8**, 997 (1969).
5. I. Suzuki. J. Mol. Spectrosc. **25**, 479 (1968).
6. A. Baldacci, C. P. Rinsland, M. A. H. Smith et K. Narahari Rao. J. Mol. Spectrosc **94**, 351 (1982).
7. M. L. Hoke et J. H. Shaw. Appl. Opt. **21**, 935 (1982); **22**, 328 (1983).
8. H. Finsterhölzl. Ber. Bunsenges. Phys. Chem. **86**, 797 (1982).
9. K. G. Brown et W. B. Person. J. Chem. Phys. **65**, 2367 (1976).
10. J. K. McDonald. Phys. Rev. **43**, 830 (1933).
11. M. Lacy. Mol. Phys. **45**, 253 (1982).
12. R. Akhmedzhanov et M. O. Bulanin. Opt. Spectrosc. (USSR) **44**, 45 (1978).
13. H. Statz, C. L. Tang et G. F. Koster. J. Appl. Phys. **37**, 4278 (1966).
14. I. Suzuki. J. Mol. Spectrosc **80**, 12 (1980).
15. A. N. Garand. Thèse 3ème cycle, Université Pierre et Marie Curie, Paris (Juil. 1972).
16. J. Borde. Thèse de Doctorat d'Etat, Université Pierre et Marie Curie, Paris (Mai 1975).

Annexe 1

Bases utilisées dans le cas des molécules symétriques. Cas des niveaux Σ_g^+. Les bases pour les niveaux Σ_u^+ s'obtiennent en ajoutant un quantum dans le mode Σ_u^+.

Base de dimension 10: (0, 0°, 0), (1, 0°, 0), (0, 2°, 0), (2, 0°, 0), (1, 2°, 0), (0, 4°, 0), (3, 0°, 0), (2, 2°, 0), (1, 4°, 0), (0, 6°, 0).

Base de dimension 24 = base 10 + (4, 0°, 0), . . . (0, 8°, 0), (5, 0°, 0) . . . (0, 10°, 0), (0, 0°, 2), (1, 0°, 2), (0, 2°, 2).

Base de dimension 34 = base 24 + (6, 0°, 0),. . . (0, 12°, 0), (2, 0°, 2), . . . (0, 4°, 2).

Base de dimension 52 = base 34 + (7, 0°, 0),. . . (0, 14°, 0), (3, 0°, 2), . . . (0, 6°, 2), (4, 0°, 2), . . . (0, 8°, 2), (0, 0°, 4).

Base de dimension 69 = Base 52 + (8, 0°, 0),. . .(0, 16°, 0), (5, 0°, 2), . . . (0, 10°, 2), (1, 0°, 4), (0, 2°, 4).

Base de dimension 90 = Base 69 + (9, 0°, 0), . . . (0, 18°, 0), (6, 0°, 2), . . . (0, 12°, 2), (2, 0°, 4), . . . (0, 4°, 4), (0, 0°, 6).

Annexe II

Coefficients b_3 et b_1 du développement $\Delta X + \Delta Z - 2\Delta Y = b_3 Q_3 + b_1 Q_1$

	b_3	b_1		b_3	b_1
$^{12}C^{16}O_2$	0,677004	0,0	$^{14}C^{16}O_2$	0,640871	0,0
$^{12}C^{17}O_2$	0,671550	0,0	$^{12}C^{16}O^{17}O$	0,674270	−0.003834
$^{12}C^{18}O_2$	0,666667	0,0	$^{12}C^{17}O^{18}O$	0,669105	−0,003314
$^{13}C^{16}O_2$	0,657794	0,0	$^{12}C^{16}O^{18}O$	0,671816	−0,007149
$^{13}C^{17}O_2$	0,652180	0,0	$^{13}C^{16}O^{17}O$	0,654979	−0,004160
$^{13}C^{18}O_2$	0,647149	0,0	$^{13}C^{16}O^{18}O$	0,652446	−0,007744

Can. J. Chem. Downloaded from www.nrcresearchpress.com by 210.87.254.6 on 09/06/12
For personal use only.

Open-chain nitrogen compounds. Part V. Hydroxymethyltriazenes: synthesis of some new alkyl homologues of the anti-tumour 3-methyl-3-hydroxymethyltriazenes and preparation of the derived acetoxymethyl-, benzoyloxymethyl-, and methoxymethyltriazenes

CHANTAL M. HEMENS, HARTFORD W. MANNING, KEITH VAUGHAN,[1] RONALD J. LAFRANCE, AND YORK TANG
Department of Chemistry, Saint Mary's University, Halifax, N.S., Canada B3H 3C3

Received August 16, 1983

CHANTAL M. HEMENS, HARTFORD W. MANNING, KEITH VAUGHAN, RONALD J. LAFRANCE, and YORK TANG. Can. J. Chem. **62**, 741 (1984).

The synthesis of some new 1-aryl-3-alkyl-3-hydroxymethyltriazenes is described. The method of coupling a diazonium salt with an alkylamine/formaldehyde mixture has been extended to (a) some diazonium ions with *para* substituents other than —M groups, (b) those with substituents in the *ortho* position, and (c) to homologous alkylamines (e.g. ethylamine, propylamine, etc.). Hydroxymethyltriazenes can also be prepared by the reaction of a 1-aryl-3-methyltriazene with formaldehyde. Several new derivatives of the hydroxymethyl function have been prepared. Reaction with acetic anhydride or benzoyl chloride in pyridine affords respectively the acetoxymethyl- and benzoyloxymethyl-triazenes; the acetates and benzoates react readily with methanol to give the novel methoxymethyltriazenes. This is the first report of a series of dialkyltriazenes with an ether linkage in the α position. An ether of this type has also been obtained directly from the diazonium fluoroborate salt by coupling with a mixture of benzylamine and formaldehyde in ethanolic solution.

CHANTAL M. HEMENS, HARTFORD W. MANNING, KEITH VAUGHAN, RONALD J. LAFRANCE et YORK TANG. Can. J. Chem. **62**, 741 (1984).

On décrit la synthèse de quelques nouveaux aryl-1 alkyl-3 hydroxyméthyl-3 triazènes. On a élargi les possibilités offertes par la méthode de couplage d'un sel de diazonium avec un mélange alkylamine/formaldéhyde de façon à inclure (a) quelques ions diazonium portant des substituants en *para* qui soient différents de —M, (b) ceux portant des substituants en position *ortho* et (c) les alkylamines homologues (comme l'éthylamine, la propylamine, etc.). On peut aussi préparer les hydroxyméthyltriazènes par réaction d'un aryl-1 méthyl-3 triazène avec le formaldéhyde. On a aussi préparé plusieurs nouveaux dérivés de la fonction hydroxyméthyle. Les réactions avec l'anhydride acétique ou le chlorure de benzoyle dans la pyridine conduisent respectivement aux acétoxyméthyl- et benzoyloxyméthyl-triazènes; les acétates et benzoates réagissent facilement avec le méthanol pour conduire à les nouveaux méthoxyméthyltriazènes. Ceci constitue la première publication relative à une série de dialkyltriazènes portant une liaison éther en position α. On a aussi pu obtenir ce type d'éther directement à partir d'un sel fluoroborate de diazonium par couplage avec un mélange de benzylamine et de formaldéhyde en solution dans l'éthanol.
[Traduit par le journal]

Introduction

1-Aryl-3-alkyl-3-hydroxymethyltriazenes (**1**) have been a subject of interest in recent chemical and pharmacological literature. The biological importance of these molecules stems from their assumed role in the metabolism of the anti-tumour dimethyltriazenes; the hydroxymethyltriazene **1** is the oxidative intermediate en route to the proposed active metabolite, the monomethyltriazene, Ar.N=N—NHMe (1). The potential anti-neoplastic property of the hydroxymethyltriazenes has stimulated activity aimed at devising methods for their synthesis. The reaction of an arenediazonium salt with a mixture of methylamine and formaldehyde has been shown (2) to afford crystalline hydroxymethyltriazenes, which are surprisingly stable and possess significant anti-tumour activity (3).

Recent studies (4, 5) have shown that the diazonium coupling reaction with methylamine/formaldehyde mixtures is more complex. The hydroxymethyltriazene **1** is not always the only product and frequently a significant yield of a second compound, a bis(1-aryl-3-methyltriazen-3-ylmethyl-)methylamine **2**, is obtained. The formation of these novel heptazanonadienes arouses some intriguing speculation regarding the equilibrium species present in the formaldehyde/methylamine solution and is the subject of the following paper in this series. In this paper, we report an investigation of further aspects of the synthesis of the hydroxymethyltriazenes, in which variations of the 3-alkyl and 1-aryl moieties have been explored. In addition, we have studied the derivatization of the hydroxymethyltriazene functional group as acetate and benzoate esters and alkyl ethers; these derivatives may be useful as pro-drugs for the anti-tumour hydroxymethyltriazenes.

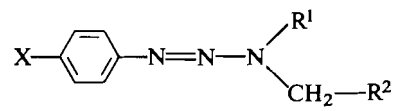

1 R^1 = alkyl, R^2 = OH
3 R^1 = Me, R^2 = OAc
4 R^1 = Me, R^2 = OCOPh
5 R^1 = Me, R^2 = OMe
6 R^1 = CH_2Ph, R^2 = O—Et, X = CN
7 R^1 = Me, R^2 = CN

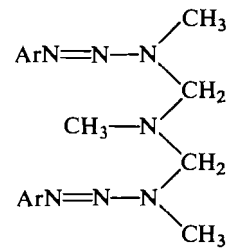

2

Discussion

The first objective of this study was to establish that the synthesis of 3-methyl-3-hydroxymethyltriazenes first described by us (2) is extendable to other 3-alkyl homologues. An aqueous solution of a diazonium chloride, in which the aryl group carries a strongly electron-withdrawing substituent in the *para* position, reacts readily with a mixture of formaldehyde and methylamine or ethylamine to afford a good yield of the corresponding hydroxymethyltriazene. The minimum molar proportion of formaldehyde/alkylamine required for optimum hydroxymethyl triazene yield is approximately 15:1; below this ratio appreciable amounts of the corresponding bis-triazene **2** may be produced (5, 6). In the synthesis of these 3-methyl- and 3-ethyltriazenes, there was no apparent difference in the yield

[1] Author to whom correspondence may be addressed.

Can. J. Chem. Downloaded from www.nrcresearchpress.com by 210.87.254.42 on 09/06/12
For personal use only.

TABLE 1(a). Physical data of the 1-aryl-3-alkyl-3-hydroxymethyltriazenes (**1**)

No.	X	R^1	Method	Yield (%)	Melting point (°C)	Solvent	Infrared (cm^{-1})
1*a*	COOMe	n-Pr	B	10	72–76	Ether/pet.ether	3450 (OH)
			C	35			1700 (C=O)
1*b*	COOMe	n-Bu	B	34	Oil	—	3450 (OH)
			E	20			1720 (C=O)
1*c*	COOEt	Et	A	45	44–48	Hexane	3430 (OH)
							1725 (C=O)
1*d*	CN	n-Pr	E	86	Oil	—	3390 (OH)
							2230 (CN)
1*e*	CN	n-Bu	B	59	Oil	—	3460 (OH)
			E	20			2230 (CN)
1*f*	Ac	Et	A	39	81–86	Hexane/benzene	3350 (OH)
							1660 (C=O)
1*g*	NO_2	Me	A	57	103–104	Ether/$CHCl_3$	3370 (OH)
1*h*	NO_2	Et	A	55	84–90 (dec.)	dec.	3450 (OH)
1*i*	NO_2	n-Pr	E	34	Oil	—	3400 (OH)
1*j*†	CF_3	Me		15	47	Ether/pet. ether	3350 (OH)
1*k*	SO_2NH_2	Me	A	0.04	179–180.5	*	3250 (OH)
1*l*	Br	Me	D	77	72.5–74	Ether/pet. ether	3330 (OH)
1*m*	*o*-CF_3	Me	A	75	58–59	Hexane	3240 (OH)
1*n*	*o*-CN	Me	A	60	81–82.5	Hexane/benzene	3440 (OH)
							2235 (CN)

*The crude product was washed with methanol to remove impurities, which resulted in a low yield of a pure product.

†Triazene **1***j* was prepared by the method of Iley and co-workers (4); the reaction was carried out at −15°C and the diazonium salt was neutralized before mixing.

TABLE 1(b). The H-1 nuclear magnetic resonance spectra (ppm)

No.	Solvent*	Arom.	CH_2	OH	R	X
1*a*	X	7.3–8.1	5.13 (d)	—	1.0 (t)	3.9 (s, OMe)
					1.75 (m)	
					3.8 (t)	
1*b*	X	7.3–8.1	5.2 (br, s)	—	0.95 (t)	3.9 (s, OMe)
					1.1–1.9 (m)	
					3.8 (t)	
1*c*	X	7.4–8.2	5.2 (br, s)	—	1.3 (t)	1.4 (t)
					3.95 (q)	4.4 (q)
1*d*	X	7.6	5.2 (br, s)	—	1.0 (t)	—
					1.7 (m)	
					3.8 (t)	
1*e*	X	7.55	5.2 (br, s)	—	0.97 (t)	—
					1.1–1.9 (m)	
					3.8 (t)	
1*f*	Y	7.6–8.1	5.23 (br, s)	—	1.35 (t)	2.6 (s, Ac)
					3.9 (q)	
1*g*	Y	7.5–8.4	5.18 (d)	6.5 (t)	3.23 (s)	—
1*h*	X	7.4–8.3	5.2 (d)	1.7 (br)	1.35 (t)	—
					3.9 (q)	
1*i*	X	7.4–8.3	5.2 (br, s)	—	1.0 (t)	—
					1.73 (m)	
					3.83 (t)	
1*j*	Y	7.4–7.9	5.17 (d)	6.4 (t)	3.2 (s)	—
1*k*	Y	7.0–7.8	5.1 (d)	—	3.03 (s)	—
1*l*	X	7.2–7.6	5.2 (d)	—	3.3 (s)	—
1*m*	Y	7.4–7.9	5.13 (br, s)	6.36	3.13 (s)	—
1*n*	Y	7.2–7.9	5.2 (s)	6.5 (br)	3.23 (s)	—

*Solvent: X = deuteriochloroform; Y = DMSO-d_6.

between neutralization before or after mixing the diazonium salt with the carbinolamine solution. Several new triazenes in the 3-methyl- and 3-ethyl series are reported in Table 1.

When this method was extended to the 3-n-propyl- and 3-n-butyl-3-hydroxymethyltriazene, some minor modifications to the procedure were necessary. Formaldehyde solution reacts

Can. J. Chem. Downloaded from www.nrcresearchpress.com by 210.87.254.42 on 09/06/12
For personal use only.

Can. J. Chem. Downloaded from www.nrcresearchpress.com by 210.87.254.42 on 09/06/12
For personal use only.

somewhat vigorously with propylamine and butylamine and the formation of an oil as a separate layer is frequently evident. Several modifications have been attempted in order to facilitate reaction of these mixtures with the diazonium salt, as follows: (a) the alkylamine/formaldehyde mixture is stirred vigorously so that the oil is dispersed during the addition of the diazonium salt; or (b) the alkylamine/formaldehyde mixture is diluted with the minimum volume of absolute methanol required to create a single layer prior to mixing with the diazonium salt solution; or (c) the alkylamine is dissolved in water, acidified to pH 2, mixed with formaldehyde, then with the diazonium salt, and finally neutralized to pH 7–8. The 3-n-propyl- and 3-n-butyl-3-hydroxymethyltriazenes were isolated initially as oils, some of which produced crystals on standing.

When the procedures described above were applied to the reaction of diazonium salts without a —M group in the *para* position, such as *p*-bromobenzene diazonium chloride, the hydroxymethyltriazene was not the only major product. A significant yield of the *p*-bromophenyl bis-triazene was obtained, along with the hydroxymethyltriazene, when the ratio of formaldehyde to methylamine is in the range 5:1 to 15:1. The optimum yield of the *p*-bromophenyl-3-hydroxymethyltriazene is obtained by coupling the diazonium salt with a 50:1 formaldehyde/methylamine mixture and by slow neutralization of the mixture. The effect of the formaldehyde/methylamine ratio on the yields of the two products has been studied in more detail and is described in the following paper (6), wherein the implications of these observations to the mechanism of formation are discussed.

It has been claimed that the use of the arenediazonium fluoroborate, in place of the chloride, may improve the method of hydroxymethyltriazene synthesis (7). Although it has now been shown (4, 5) that the products described by these authors are in fact bis-triazenes, we have explored the potential of the fluoroborate method and in general there is no real advantage to this method. However, in extending the hydroxymethyltriazene synthesis to the n-propyl analogues, the products are frequently oils which are not easy to purify. In method E (see experimental), the diazonium fluoroborate is employed and the propylamine is used in the form of the hydrochloride salt; this combination, together with careful control of pH, affords relatively clean 3-propyl-3-hydroxymethyl triazenes.

In addition to studying the extension of the hydroxymethyl triazene synthesis to 3-alkyl homologues and to substituents in the aryl group which are not —M in character, we have also explored the effect of relocation of the aryl substituent to the *ortho* position. This has not turned out to be a trivial modification. It had previously been shown that location of the COOMe group in the *ortho* position gives an unstable hydroxymethyltriazene, which decomposes by loss of formaldehyde and cyclization of the methyl *o*-3-methyltriazenobenzoate to a benzotriazinone (2, 3). However, reaction of *o*-trifluoromethylbenzene diazonium chloride with methylamine/formaldehyde by method A gives an excellent yield of the hydroxymethyltriazene, which is quite stable. The reaction has also been extended successfully to the *o*-cyanophenyl-3-hydroxymethyltriazene.

Kolar et al. have reported (8, 9) that hydroxymethyltriazenes may be prepared by reaction of the monomethyltriazene (Ar.N=N—NH—Me) with formaldehyde, but have not elaborated on the general application of the method, which may be a useful entry to hydroxymethyltriazenes not accessible by the route described here (such as those with electron-donating groups in the aryl moiety). Accordingly, a sample of the 1-*p*-cyanophenyl-3-methyltriazene was prepared (10) and was found to react in suspension in aqueous formaldehyde at 0°C very readily to afford an excellent yield of 1-*p*-cyanophenyl-3-hydroxymethyl-3-methyltriazene (**1** X = CN, R = Me), which was identical with a sample prepared by Method A. This method is now being explored more extensively in this laboratory and will be reported more fully at a later date.

Characterization of the hydroxymethyltriazenes listed in Table 1 is based on infrared and nmr spectroscopy and on comparison with previously reported data on the 3-methyl analogues (3). The presence of the OH stretching band in the range 3250–3460 cm^{-1} is diagnostic for the *N*-hydroxymethyl group. The nmr spectra compare favourably with previous observations; the hydroxyl proton is not always observed in deuteriochloroform, but is usually clearly observed in solution in DMSO-d_6. The methylene protons of the hydroxymethyl group are always seen at ca. 5.2 ppm; coupling to the hydroxylic proton is often observed, resulting in a broad doublet appearance of the methylene singlet, which collapses after addition of deuterium oxide. An obvious but important observation in the nmr spectrum is to confirm the incorporation of the appropriate alkyl group at N-3.

The mass spectrum of 1-*p*-bromophenyl-3-hydroxymethyl-3-methyltriazene (**1***l*) does not show the molecular ion at *m/e* 243/245, but does show a fragmentation pattern consistent with the presence of a single bromine atom in the hydroxymethyltriazene molecule. Loss of the formaldehyde unit is indicated by a pair of fragments at *m/e* 213/215 with relative intensities close to 1:1, and further loss of the *N*-methyl group by fragments at *m/e* 198/200. There are also strong peaks in the mass spectrum of **1***l* arising from the *p*-bromobenzenediazonium ion (*m/e* 183/185) and the *p*-bromophenyl cation (*m/e* 155/157). These fragmentations are consistent with the behaviour of other triazenes which can undergo fragmentation via the monomethyltriazene (3).

Several new derivatives of the hydroxymethyltriazene functionality have now been synthesized. The reaction of the hydroxymethyltriazenes with benzoyl chloride in pyridine, first reported for the 1-*p*-methoxycarbonylphenyltriazene (**1** X = COOMe, R = Me) by us (2), has now been extended to other substituents and a series of 3-benzoyloxymethyltriazenes ("benzoates") **4** has been characterized (Table 3). These derivatives are not always easy to crystallize and do not usually have sharp melting points, even after several recrystallizations; the products appear to be spectroscopically pure. A much better series of derivatives are the 3-acetoxymethyltriazenes ("acetates") (**3**) (Table 2), which are readily obtained by reaction of the hydroxymethyltriazene with acetic anhydride in pyridine and are sharply-melting crystalline compounds. The use of pyridine as a solvent is essential in these preparations, since it neutralizes the acidic by-products of the reactions which otherwise would cause degradation of the triazenes.

The acetates and benzoates are characterized by ir and nmr spectroscopy. Hydroxyl group absorption bands are absent in the ir spectra; the acetates exhibit C=O stretch at 1735–1755 cm^{-1} and the benzoates at ca. 1720 cm^{-1}. In the nmr spectra, the *N*-methylene group produces a signal at ca. 6.1 ppm in the benzoates and 5.8 ppm in the acetates, compared to 5.2 ppm for the analogous protons in the hydroxymethyltriazenes. Other signals in the nmr are consistent with the assigned structures (see Tables 2 and 3).

Recrystallization of the acetates and benzoates was carried

Can. J. Chem. Downloaded from www.nrcresearchpress.com by 210.87.254.42 on 09/06/12
For personal use only.

TABLE 2. Physical and spectroscopic data of the 1-aryl-3-methyl-3-acetoxymethyltriazenes (**3**)

						Ultraviolet*		^{1}H nmr (ppm) in $CDCl_3$				
No.	X	Yield (%)	Melting Point (°C)	Solvent	Infrared (cm^{-1})	λ_{max} (nm)	ϵ	Arom. AA′BB′	CH_2	Ac	N—CH_3	X
3*a*	COOMe	92	61–61.5	Pet. ether	1705 (C=O) 1735 (C=O)	310 (sh) 293 222	19 300 22 970 10 215	7.45–8.2	5.83	2.1	3.3	3.93 (s, O—Me)
3*b*	CN	91	89–91	Ether/ pet. ether	1735 (C=O) 2220 (CN)	310 (sh) 295 223	19 870 22 713 11 214	7.33–7.8	5.84	2.1	3.3	—
3*c*	$CONH_2$	32	115–120		1730 (C=O) 1745 (C=O)			7.45–8.0	5.9	2.2	3.4	—
3*d*	NO_2	45	95–97	Ether/ $CHCl_3$	1340 (NO_2) 1510 (NO_2) 1755 (C=O)	344 230	17 250 7 663	7.45–8.35	5.75	2.14	3.29	—
3*e*	Ac	63	59–60	Ether/ pet. ether	1735 (C=O) 1745 (C=O) (sh)	320 (sh 301 224	19 120 22 311 10 302	7.32–8.05	5.79	2.05	3.24	2.54 (s, Ac-aryl)
3*f*	Br	28	34–36	—	1745 (C=O)	310 (sh) 280 219	14 603 24 040 11 339	7.35–7.6	5.75	2.15	3.25	—

* Ultraviolet spectra were recorded in acetonitrile.

TABLE 3. Physical and spectroscopic data of the 1-aryl-3-methyl-3-benzoyloxymethyltriazenes (**4**)

						Ultraviolet*		^{1}H nmr (ppm) in $CDCl_3$			
No.	X	Yield (%)	Melting Point (°C)	Solvent	Infrared (cm^{-1})	λ_{max} (nm)	ϵ	Arom.	CH_2	CH3	X
4*a*	COOMe†	73	88–89	Pet. ether	1695 (C=O) 1710 (C=O)	300 224	15 251 8 733	7.4–8.2	6.1	3.34	3.91 (s, O—Me)
4*b*	COOEt	50	66–68	Ether/ pet. ether	1700 (C=O) 1720 (C=O)	320 (sh) 295 227	16 680 22 145 21 178	7.35–8.15	6.05	3.35	1.40 (t) 4.35 (q)
4*c*	CN	67	74–78	Ether/ $CHCl_3$	1720 (C=O) 2220 (CN)	300 (sh) 288 225	20 460 26 580 21 670	7.35–8.15	6.11	3.39	—
4*d*	Ac	28	65–69	Ether/ pet. ether	1665 (C=O) 1675 (C=O)	320 (sh) 293 227	24 660 31 320 26 965	7.45–8.2	6.15	3.4	2.6 (s, Me—(C=O)
4*e*	Br	47	43–50	—	1739 (C=O)			7.35–8.2	6.1	3.35	—

* See Table 2.
† See ref. 3.

Can. J. Chem. Downloaded from www.nrcresearchpress.com by 210.87.254.42 on 09/06/12
For personal use only.

out in non-protic solvents since it was found that both types of ester derivative react with alcohols. The products of these reactions were not the expected products of a simple transesterification, i.e. the hydroxymethyltriazene and methyl acetate or benzoate. The products were clearly identified as the methyl ethers **5**, and the reaction was shown to be general for a number of aryl substituents (Table 4). These are the first examples of triazene derivatives with an ether function in the α position of one of the alkyl groups to be reported. Structural assignment is based on the absence of OH and acetoxy- or benzoyloxy-carbonyl absorption in the ir and on the nmr spectra. The ether linkage is clearly indicated by an *O*-methyl signal at 3.2 ppm, almost coincident with the *N*-methyl signal at 3.3 ppm; the *N*-methylene signal is at 5.15 ppm, which is very similar to the methylene signal of the hydroxymethyltriazenes.

The structures of all the acetates, benzoates, and methyl ethers reported here have been confirmed by C-13 nmr spectroscopy (Table 5). The chemical shift of the *N*-methylene carbon appears at 78–79 ppm in the acetates, benzoates, and hydroxymethyltriazenes, but is shifted slightly downfield to 86.5 ppm in the methyl ethers. The *N*-methyl carbon is found at 33–34 ppm in all series and the *O*-methyl carbon of the ethers appears at 55.7 ppm.

The mechanism of formation of the methyl ethers is most likely that represented in Scheme 1. The triazene N-3 nitrogen is capable of using its electron lone-pair to displace the acetate or benzoate leaving group affording the intermediate methylene-triazenium ion **8**. Reaction of **8** with methanol then leads to the methyl ether. The solvating capability of the alcohol might also facilitate the initial ionization. This type of reaction has not so far been observed with the hydroxymethyltriazene itself; no ether formation is evident when hydroxymethyltriazenes are treated with methanol. Evidently the electron lone-pair push from N-3 is not sufficient to eject the hydroxyl group; derivatization to the acetate or benzoate changes the nature of the leaving group so that formation of **8** is facilitated. The observed reaction of **8** with methanol suggests that similar reactions of the acetoxymethyltriazenes with different nucleophiles could lead to the synthesis of other α-substituted alkyltriazenes, e.g. the α-cyanomethyltriazenes **7**.

The possible intermediate existence of the triazenium ion **8** has important implications to the understanding of the metabolism and pharmacology of a wide range of drugs and xenobiotic molecules. The formation of carbinolamines from substituted amines has been proposed to take place during the intermediary oxidative metabolism of a number of drugs (11). The carbinolamines are thought to exist in equilibrium with iminium ions (12), analogous to the intermediate **8**. Studies on the oxidative metabolism of nicotine, benzylpyrrolidine, methapyrilene, and phencyclidine have provided strong evidence for the formation of electrophilic iminium ions through characterization of the corresponding α-cyano adducts formed by their in vitro reaction with nucleophilic cyanide ion (13). In chemical studies, *N*-nitrosoimminium ions have been invoked as intermediates in the formation of α-acetoxy-*N*-nitrosamines from the corresponding nitrosamino acids (14); the acetoxynitrosamines, which are very close structural analogues of the acetoxyalkyltriazenes reported here, have proven to be invaluable as model compounds in metabolism studies of the carcinogenic dimethylnitrosamines (15). The acetoxyalkyltriazenes similarly should be useful as model compounds for the metabolites of the anti-tumour dimethyltriazenes. A signifi-

TABLE 4. Physical and spectroscopic data of the 1-aryl-3-methyl-3-methoxymethyltriazenes (**5**)

No.	X	Method	Yield (%)	Melting Point (°C)	Solvent	Infrared (cm^{-1})	Ultraviolet* λ_{max}	Ultraviolet* ε	^{1}H nmr (ppm) in $CDCl_3$ Arom.	CH_2	N-Me	O-Me	X
5*a*	COOMe	A	90	79–81	Ether/ pet. ether	1730 (C=O)	310 (sh)	21 920	7.35–8.2	5.15	3.3	3.2	3.85 (s, O—Me)
		B	70				300	23 170					
							224	10 754					
5*b*	CN	A	57	Oil	—	2220 (CN)	310 (sh)	18 650	7.4–7.75	5.15	3.3	3.2	—
		B	79				300	19 207					
							224	9 790					
5*c*	NO_2	A	53	38–40	Ether/ $CHCl_3$		350	18 252	7.35–8.25	5.15	3.3	3.2	—
							257	5 966					
							234	8 711					
5*d*	Ac	A	72	55–56	Ether/ $CHCl_3$	1670 (C=O)	318	19 785	7.35–8.1	5.1	3.3	3.2	2.55 (s, Ac)
							226	9 650					
5*e*	Br	A	92	Oil	—		310 (sh)	15 100	7.35–7.6	5.15	3.3	3.2	—
							281	21 828					
							219	11 183					

* See Table 2.

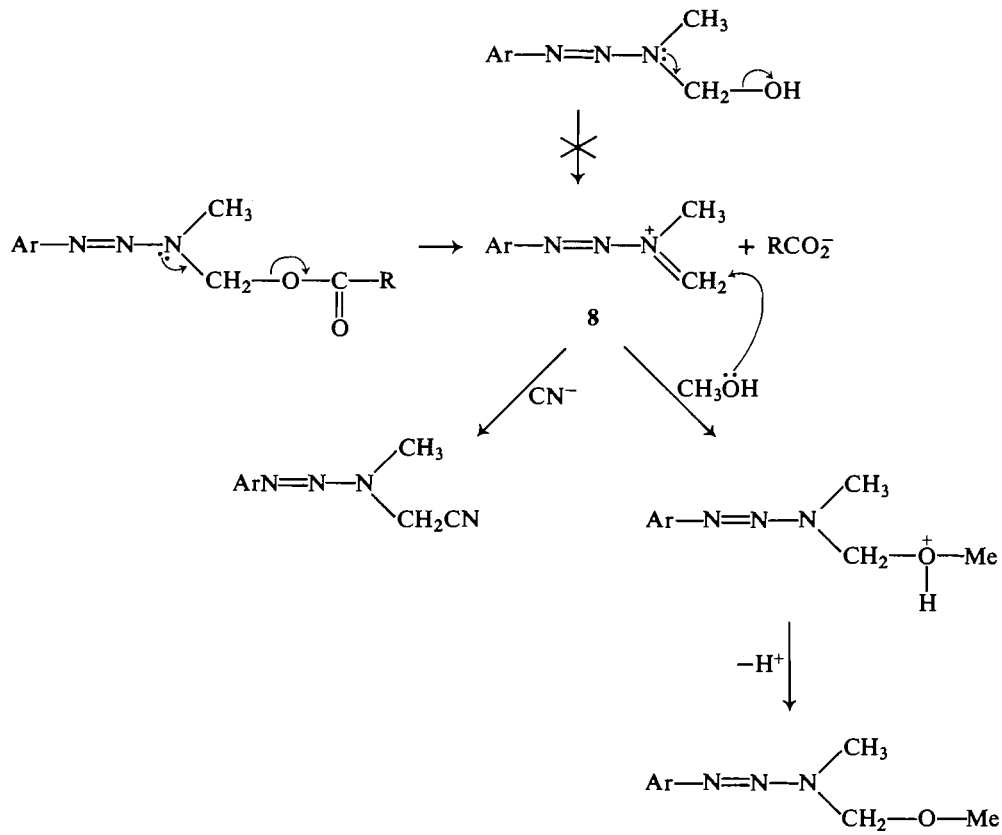

SCHEME 1

cant advantage of the triazene series for such experiments is the relative stability of the hydroxymethyltriazenes shown in our studies; the analogous hydroxymethylnitrosamines have been shown to have very short half-lives (several seconds) under physiological conditions (16).

The results reported here show clearly that the iminium ion type of intermediate, such as **8**, cannot be formed directly from the carbinolamine, which cannot follow this pathway directly because of the poor leaving-group character of the hydroxide ion. In the triazene system the reaction is facilitated by chemical conversion to the acetate leaving group; in metabolism experiments, the carbinolamine OH must be conjugated in some form to facilitate the formation of an iminium ion. Thus, we suggest that the contention that carbinolamines give rise to iminium ions during metabolism without some modification to the α-hydroxyamine functional group should be reconsidered.

The success of the reaction of the acetates with methanol as a synthetic method for the methoxymethyltriazenes encouraged us to search for other approaches to ethers of this type. If it is possible to generate triazenium ions of type **8** in non-aqueous media, then it should be possible to trap such species with a variety of agents such as alcohols. This approach has been successful in the synthesis of α-alkoxyalkylnitrosamines by nitrosation of the carbinolamine ether, generated *in situ* from a mixture of the alkylamine, aldehyde, alcohol, and acetic acid (17). Accordingly the *p*-cyanobenzenediazonium fluoroborate was reacted with a mixture of benzylamine, hydrochloric acid, formaldehyde, and ethanol, and the mixture neutralized with pyridine. Purification of the product by repeated column chromatography afforded a substance which had the nmr spectrum corresponding to the 3-benzyl-3-ethoxymethyltriazene (**6**). The success of this reaction is very encouraging for further study as a synthetic method for new types of α-oxidized alkyltriazenes and is now being investigated for general application.

Experimental

Melting points were determined on a Koffler hot-stage apparatus, calibrated with Fisher thermetric standards. Infrared spectra were recorded with liquid films or Nujol mulls on Perkin–Elmer 299 and 1330 spectrophotometers. Proton magnetic resonance spectra were recorded on a Varian EM360 spectrometer and uv spectra recorded with a Unicam SP8-400 spectrophotometer. Mass spectra were obtained with a Dupont CEC-104 medium resolution spectrometer and carbon-13 spectra were recorded at 90 MHz on the Nicolet 360 NB spectrometer.

1-Aryl-3-alkyl-3-hydroxymethyltriazenes (1)

Method A

This method, which has been described in a previous report (3), is applicable to the synthesis of 3-methyl- and 3-ethyl-3-hydroxymethyltriazenes with a —M substituent in the aryl group. An aqueous solution of the arenediazonium chloride was coupled with a mixture of formaldehyde and methylamine or ethylamine, and neutralized with aqueous sodium bicarbonate to afford the solid hydroxymethyltriazene. New hydroxymethyltriazenes obtained by this method are shown in Table 1.

Method B

This method is a modification of Method A and is applicable to the synthesis of 3-n-propyl and 3-n-butyl-3-hydroxymethyltriazenes with a —M substituent in the aryl group. The appropriate arylamine (13 mmol) was diazotized in hydrochloric acid with sodium nitrite. The alkylamine, either n-propyl- or n-butylamine (13 mmol), was mixed with 37% aqueous formaldehyde (10.6 g, 130 mmol), whereupon a separate oily layer was observed. The mixture was stirred vigorously, so that the oil was dispersed throughout the aqueous layer, while the cold arenediazonium salt solution was added dropwise. After stirring for 0.25 h, the brown oil which had formed was extracted into chloro-

Can. J. Chem. Downloaded from www.nrcresearchpress.com by 210.87.254.42 on 09/06/12
For personal use only.

Can. J. Chem. Downloaded from www.nrcresearchpress.com by 210.87.254.42 on 09/06/12
For personal use only.

form. Evaporation of the dried chloroform extract afforded the crude hydroxymethyltriazene, usually as an oil; purification was achieved in most cases by trituration and recrystallization. The triazenes obtained in this way are shown in Table 1.

Method C

This method is identical to Method B for propyl- and butylamine with a minor modification; after mixing the alkylamine and the formaldehyde solution, the mixture was treated with the minimum volume of methanol required to dissolve the carbinolamine and give a homogeneous mixture. This solution was then added to the diazonium salt solution and the reaction completed as described in Method B.

Method D

This method is applicable to the synthesis of hydroxymethyltriazenes with substituents in the aryl group which are not strongly electron withdrawing. The preparation of the *p*-bromo derivative will be described in detail to illustrate the procedure.

p-Bromoaniline (2.25 g, 13 mmol) was dissolved in hydrochloric acid (4.0 mL concentrated HCl + 26 mL water) and diazotized at 0°C with sodium nitrite (1.0 g) in water over a period of 1 hour. The solution was filtered and the clear filtrate was treated with a pre-cooled mixture of 40% aqueous methylamine (1.02 g) and 37% aqueous formaldehyde (53.2 g) over a period of 15 min. The pH was adjusted to 6–7 by the addition of saturated sodium bicarbonate and the mixture stirred for a further 15 min before raising the pH to 7.5–8.0 with bicarbonate. The mixture was stirred until precipitation was complete (up to 1 h) and the product filtered, dried, and recrystallized from petroleum ether to afford the 1-*p*-bromophenyl-3-methyl-3-hydroxymethyltriazene (2.5 g, 77%), mp 72.5–74°C.

Method E

Propylamine (0.9 g) was dissolved in water (10 mL), acidified to pH 2 with concentrated hydrochloric acid, and mixed with 37% aqueous formaldehyde (16.7 g). The propylamine/formaldehyde mixture was added to a suspension of the *p*-nitro- or *p*-cyanobenzenediazonium fluoroborate (10 mmol) in water (25 mL). The combined mixture was cooled to 0°C and rendered slightly basic (pH ~8) with saturated sodium bicarbonate solution (approximately 10 mL). After stirring for 0.5 h, the precipitate was filtered, dissolved in ether, separated from a water layer, dried over anhydrous magnesium sulphate, and evaporated to give an oil. The nmr spectra indicated that the products were clean samples of the 1-*p*-cyanophenyl- and 1-*p*-nitrophenyl-3-hydroxymethyl-3-n-propyltriazenes. The cyano derivative seems to be stable under refrigeration, but the nitro compound decomposed at room temperature giving off a gas.

*Reaction of 1-*p*-cyanophenyl-3-methyltriazene with formaldehyde*

1-*p*-Cyanophenyl-3-methyltriazene was prepared by reaction of *p*-cyanobenzene diazonium chloride with methylamine, according to our published method (10). The monomethyltriazene (0.7 g) was suspended in water (20 mL) at 0°C and 37% aqueous formaldehyde (17.7 g) was added to the suspension. The mixture was stirred for 6 h and the insoluble product filtered and dried to afford 1-*p*-cyanophenyl-3-hydroxymethyl-3-methyltriazene (**1**, X = CN, R = Me) (0.69 g, 83%), which was identical (ir, nmr, and mp) with an authentic sample prepared by Method A described above.

1-Aryl-3-methyl-3-acetoxymethyltriazenes (3)

General procedure

1-Aryl-3-methyl-3-hydroxymethyltriazene (1.6 mmol) was dissolved in anhydrous, redistilled pyridine (1.33 mL). Freshly distilled acetic anhydride (0.24 mL) was added slowly to the stirred pyridine solution, and the mixture stirred in an ice-bath for one hour. The clear solution was poured over crushed ice (3.0 g) and stirred for 0.5 h. (In some cases, the pyridine solution was filtered prior to the treatment with ice to remove insoluble material.) The product usually appeared as a precipitate in the aqueous pyridine and was separated by filtration, washing with cold water, drying overnight under vacuum, and recrystallization from an appropriate solvent mixture to afford the triazene acetate. Yields, physical and spectroscopic data are given in Table 2.

TABLE 5. Carbon-13 chemical shifts in $CDCl_3$ for the triazenes *p*-X—C_6H_4—N=N—N(CH_3)—CH_2OR

No.	X	R	C-1	C-2,6	C-3,5	C-4	N—CH_3	N—CH_2	O—C(=O)	O_2C—CH_3	CH_2OCH_3	Other
1*g*	NO_2	H	155.45	120.88	124.89	144.36	33.39	78.49	—	—	—	—
1*l*	Br	H	149.39	118.00	122.41	131.78	32.99	77.99	—	—	—	—
3*a*	CO_2Me	$COCH_3$	153.09	121.07	130.54	128.17	34.58	78.94	170.74	20.92	—	54.04 $COOCH_3$ 166.83 $COOCH_3$
3*b*	CN	$COCH_3$	152.77	121.86	133.02	109.78	34.62	78.72	170.59	20.89	—	119.03 *C*N
3*d*	NO_2	$COCH_3$	154.38	121.64	124.70	145.96	34.73	78.70	170.58	20.88	—	—
3*e*	$COCH_3$	$COCH_3$	153.15	121.23	129.41	135.27	34.56	78.70	170.71	20.92	—	26.615 CH_3CO 197.368 CH_3CO
5*b*	CN	CH_3	153.51	121.51	133.01	108.96	33.44	86.57	—	—	55.69	119.21 *C*N
5*d*	$COCH_3$	CH_3	153.94	120.88	129.45	134.70	33.31	86.52	—	—	55.63	26.58 $COCH_3$ 197.38 $COCH_3$
4*d*	$COCH_3$	COPh	153.11	121.12	130.56	128.29	34.52	79.43	—	—	—	129.79 C-2′,6′ 129.42 C-1′ 128.43 C-3′,5′ 133.40 C-4′ 166.82 Ph*C*=O

*1-Aryl-3-methyl-3-benzoyloxymethyltriazenes (**4**)*

General procedure

The hydroxymethyltriazene (4.5 mmol) was dissolved in dry pyridine (4.0 mL) at room temperature in a vessel fitted with a drying tube. Freshly distilled benzoyl chloride (0.66 g) was added to the pyridine solution, slowly with stirring; the mixture was stirred in an ice-bath for 1 h, filtered by gravity, and the clear filtrate poured onto crushed ice (8.3 g). A precipitate was usually observed at once; after stirring in the cold for up to 0.5 h the product was filtered, dried, and recrystallized to afford the benzoate. Yields, physical and spectroscopic data are given in Table 3.

*1-Aryl-3-methyl-3-methoxymethyltriazenes (**5**)*

Method A. General procedure

The 3-acetoxymethyltriazene (0.2 g) was dissolved in absolute methanol (5.0 mL) and stirred at room temperature until the reaction was complete. The reactions were followed by tlc on silica gel with 50:50 ether/petroleum ether as the mobile phase. The reaction time varied with the aryl substituent as follows: X = CN, 23 h; X = Ac, 18 h; X = nitro, 48 h; X = COOMe, 6 h; X = Br, 2.5 h. After completion of the reaction, the methanol was evaporated *in vacuo* and the residue dissolved in ether (30 mL). The ether solution was washed successively with aqueous sodium bicarbonate (5 mL of a saturated solution + 15 mL of water), water (20 mL), and saturated sodium chloride (20 mL), then dried over anhydrous sodium sulphate before evaporation *in vacuo* to afford the pure methyl ethers. The products were usually oils, except in the case of the *p*-methoxycarbonyl- and *p*-acetyl derivatives, which crystallized readily. Yields, physical and spectral data are given in Table 4.

Method B. General procedure

The procedure described in Method A above was followed exactly using the 3-benzoyloxymethyltriazene instead of the acetate as the starting material. The reaction times were as follows: X = CN, 26 h; X = COOMe, 21 h. Yields and other data are given in Table 4.

*1-*p*-Cyanophenyl-3-benzyl-3-ethoxymethyltriazene (**6**)*

Benzylamine (0.55 g) was dissolved in absolute ethanol (10 mL), acidified with an equivalent quantity of concentrated hydrochloric acid, and mixed with 37% aqueous formaldehyde (8.3 g). The *p*-cyanobenzenediazonium fluoroborate (5 mmol) was dissolved in absolute ethanol (50 mL) and added slowly to the stirred ethanolic benzylamine/formaldehyde mixture. The clear solution was cooled to 0°C and neutralized with pyridine (1.0 mL). The ethanol was removed under vacuum, the residue was diluted with water and extracted with ether. The residue from the dried ether extract was a dark oil (1.0 g), which was purified by column chromatography on 60/200 mesh Hi-flosil (80 g). Elution with 15% chloroform in hexane gave an oil (0.80 g), which was rechromatographed on the same adsorbent; elution with 25% chloroform in petroleum ether gave the pure ethoxymethyltriazene (oil, 0.50 g, 35%), nmr spectrum (deuteriochloroform): 1.2(t), 3.5(q), 5.05(s), 5.2(s), and 7.0–7.9(m) ppm.

Acknowledgements

The authors are grateful to the Natural Sciences and Engineering Research Council of Canada for a research grant (to K.V.), and to Dalhousie University Chemistry Department and Dr. J.S. Grossert for mass spectra. The C-13 nmr spectra were recorded on the Nicolet 360 spectrometer of the Atlantic Region Magnetic Resonance Centre at Dalhousie University.

1. A. GESCHER, J. A. HICKMAN, R. J. SIMMONDS, M. F. G. STEVENS, and K. VAUGHAN. Biochem. Pharmacol. **30**, 89 (1981).
2. A. GESCHER, J. A. HICKMAN, R. J. SIMMONDS, M. F. G. STEVENS, and K. VAUGHAN. Tetrahedron Lett. 5041 (1978).
3. K. VAUGHAN, Y. TANG, G. LLANOS, J. K. HORTON, R. J. SIMMONDS, J. A. HICKMAN, and M. G. F. STEVENS. J. Med. Chem. In press.
4. S. C. CHENG, M. L. DE S. FERNANDES, J. ILEY, and M. E. N. ROSA. J. Chem. Res.(S), 108 (1983).
5. R. J. LAFRANCE, Y. TANG, K. VAUGHAN, and D. L. HOOPER. Chem. Commun. 721 (1983).
6. H. W. MANNING, Y. TANG, C. M. HEMENS, R. J. LAFRANCE, and K. VAUGHAN. Can. J. Chem. **62**, 000 (1984).
7. M. JULLIARD, G. VERNIN, and J. METZGER. Synthesis, 116 (1980).
8. G. F. KOLAR, K. MAURER, and M. WILDSCHUTTE. Cancer Letters, **10**, 235 (1980).
9. G. F. KOLAR. Triazenes. *In* Chemical carcinogens. 2nd ed. American Chemical Society Monograph Series, No. 173. In press.
10. T. P. AHERN, H. FONG, and K. VAUGHAN. Can. J. Chem. **55**, 1701 (1977).
11. B. TESTA and P. JENNER. Drug metabolism – chemical and biochemical aspects. Marcel Dekker, New York. 1976. p. 82.
12. D. BEKE. Adv. Heterocycl. Chem. **1**, 167 (1963).
13. D. P. WARD, A. J. TREVOR, A. KALIR, J. D. ADAMS, T. A. BAILLIE, and N. CASTAGNOLI. Drug Metab. Dispos. **10**, 690 (1982), and references therein.
14. J. E. SAAVEDRA. J. Org. Chem. **44**, 4511 (1979).
15. J. E. BALDWIN, A. SCOTT, S. E. BRANZ, S. R. TANNENBAUM, and L. GREEN. J. Org. Chem. **43**, 2427 (1978).
16. M. MOCHIZUKI, T. ANJO, and M. OKADA. Tetrahedron Lett. **21**, 3693 (1980).
17. J. E. SAAVEDRA. J. Org. Chem. **48**, 2388 (1983).

Can. J. Chem. Downloaded from www.nrcresearchpress.com by 210.87.254.42 on 09/06/12
For personal use only.

Open-chain nitrogen compounds. Part VI. The formation of bis(1-aryl-3-methyltriazen-3-ylmethyl) methylamines in the reaction of diazonium ions with mixtures of formaldehyde and methylamine

HARTFORD W. MANNING, CHANTAL M. HEMENS, RONALD J. LAFRANCE, YORK TANG, AND KEITH VAUGHAN[1]
Department of Chemistry, Saint Mary's University, Halifax, N.S., Canada B3H 3C3

Received August 16, 1983

HARTFORD W. MANNING, CHANTAL M. HEMENS, RONALD J. LAFRANCE, YORK TANG, and KEITH VAUGHAN. Can. J. Chem. **62**, 749 (1984).

The synthesis of a series of *N,N*-bis(1-aryl-3-methyltriazen-3-ylmethyl) methylamines from coupling diazonium salts with mixtures of methylamine and formaldehyde is described. These novel bis-triazenes, or heptazanonadienes, have significant anti-tumour activity against the TLX5 lymphoma in mouse. The mechanism of formation of these triazenes is discussed with reference to the implication to the presumed equilibria taking place in the methylamine/formaldehyde solution. The formation of the bis-triazene is usually accompanied by the formation of a 3-hydroxymethyltriazene, and it has been shown that the hydroxymethyltriazene can be transformed into the bis-triazene. The proportions of the two products are strongly influenced by the relative amounts of methylamine and formaldehyde. Coupling the *p*-bromobenzenediazonium salt to a 1:1 methylamine/formaldehyde mixture affords mainly the bis-triazene, whereas a 1:50 mixture gives almost totally the hydroxymethyl triazene. These results suggest that the two triazenes arise from diazonium coupling to different species in the amine/formaldehyde mixture; this hypothesis is supported by the formation of identical product mixtures from coupling the diazonium ion with (a) a 1:1 $MeNH_2/CH_2O$ mixture, and (b) the cyclic trimer of the carbinolamine $MeNHCH_2OH$, and by the identification of a minor product from the reaction of *p*-chlorobenzenediazonium fluoroborate with $MeNH_2/CH_2O$ as bis(1-*p*-chlorophenyl-3-methyltriazen-3-yl) methane.

HARTFORD W. MANNING, CHANTAL M. HEMENS, RONALD J. LAFRANCE, YORK TANG et KEITH VAUGHAN. Can. J. Chem. **62**, 749 (1984).

On décrit la synthèse d'une série de *N,N*-bis-(aryl-1 méthyl-3 triazène-3 ylméthyl) méthylamines provenant du couplage de sels de diazonium avec des mélanges de méthylamine et de formaldéhyde. Ces nouveaux bis-triazènes ou heptazanonadiènes ont une activité anti-tumorale importante contre les lymphomes TLX5 chez la souris. On discute du mécanisme de formation de ces triazènes en se référant à l'implication possible de l'équilibre qui est sensé s'établir dans une solution de méthylamine/formaldéhyde. La formation du bis-triazène est habituellement accompagnée par la formation de l'hydroxyméthyl-3 triazène et on a montré que l'hydroxyméthyltriazène peut être transformé en bis-triazène. Les proportions des deux produits sont fortement influencées par les quantités relatives de méthylamine et de formaldéhyde. Le couplage du sel de *p*-bromobenzènediazonium avec un mélange 1:1 de méthylamine/formaldéhyde conduit presqu'exclusivement au bis-triazène alors qu'un mélange 1:50 fournit presque complètement l'hydroxyméthyltriazène. Ces résultats suggèrent que ces deux triazènes proviennent d'un couplage du diazonium avec diverses espèces présentes dans un mélange amine/formaldéhyde; cette hypothèse est supportée par le fait qu'il y a formation de mélanges identiques de produits lorsqu'on couple l'ion diazonium avec (a) un mélange 1:1 d'amine et de formaldéhyde et (b) le trimère cyclique de la carbinolamine $MeNHCH_2OH$ ainsi que par le fait que l'on a pu identifier un produit mineur de la réaction du fluoroborate de *p*-chlorobenzènediazonium avec un mélange de $MeNH_2/CH_2O$; ce produit est le bis(*p*-chlorophényl-1 méthyl-3 triazène-3 yl) méthane.

[Traduit par le journal]

Can. J. Chem. Downloaded from www.nrcresearchpress.com by 210.87.254.105 on 09/06/12
For personal use only.

Introduction

The reaction of diazonium ions with mixtures of formaldehyde and methylamine has been the subject of considerable interest in the recent literature. The importance of this reaction stems in part from the potential pharmacological significance of the expected products, the 3-hydroxymethyl-3-methyl-1-aryltriazenes (**2**), which have been postulated as metabolites of the anti-tumour dimethyltriazenes ($ArN{=}N{-}NMe_2$) (1). In addition to the anticipated biological activity of such hydroxymethyltriazenes, there is considerable interest in the chemistry of the diazonium coupling reaction with the carbinolamine, $RNHCH_2OH$, which may be generated *in situ* from the amine and formaldehyde.

The synthesis and characterization of stable hydroxymethyltriazenes were reported first by us in 1978 (2). The hydroxymethyltriazenes were formed in good yield when a solution of a diazonium chloride, with —M substituents in the aryl group, was treated with an aqueous solution of methylamine and formaldehyde, the latter being in large excess. Subsequently, a minor variation of our method was published by Julliard *et al.* (3); the latter group employed the diazonium fluoroborate (instead of the chloride) and claimed that this modification afforded hydroxymethyltriazenes with other than —M substituents (e.g. Cl and Br). Concurrent reinvestigations of this reaction by Iley and co-workers (4) and by us (5) have shown that the diazonium coupling reaction with methylamine/formaldehyde solutions affords mixtures of **2** and a novel type of bis-triazene, the heptazanonadienes **1**, and

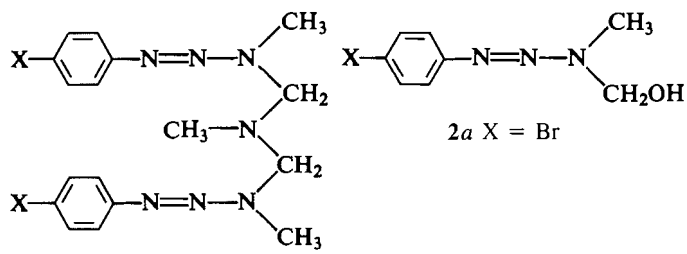

2*a* X = Br

1*a* X = Br
b X = Cl
c X = NO_2
d X = CN
e X = CF_3
f X = COOEt
g X = $COCH_3$

[1]Author to whom correspondence may be addressed.

Can. J. Chem. Downloaded from www.nrcresearchpress.com by 210.87.254.105 on 09/06/12
For personal use only.

TABLE 1. Physical data, yields, and spectroscopic data of the bis-triazenes (**1**)

No.	X	Method	Molar ratio ArN_2^+	Molar ratio $MeNH_2$	Molar ratio CH_2O	Yield (%)	Melting point (°C)	Solvent	^{1}H nmr (ppm) in CDl_3 Arom. AA'BB'	CH_2	CH_3(N-5)	CH_3(N-3, 7)	X	Solvent
1*a*	Br	A	1	1	1	36	126–128	Ether	7.3–7.6	4.63(s)	2.43(s)	3.23(s)	—	$CDCl_3$
1*b*	Cl	A	1	1.5	18	17	116	Ether	7.36	4.63(s)	2.40(s)	3.23(s)	—	$CDCl_3$
1*c*	NO_2	B	1	1	4	30	134–136	Ether/$CHCl_3$	7.5–8.2	4.73(s)	2.48(s)	3.31(s)	—	$CDCl_3$
1*d*	CN	B	1	8	31	20	123–124	Ether	7.6–7.7	4.73(s)	2.46(s)	3.32(s)	—	$CDCl_3$
1*e*	CF_3	A	1	1.5	7	14	86–88	Ether/pet. ether	7.6–7.8	4.80(s)	2.40(s)	3.25(s)	—	DMSO-d_6
1*f*	COOEt	A	1	2.6	23	15	Oil	—	7.4–8.2	4.65(s)	2.40(s)	3.37(s)	1.4(t) 4.3(q)	DMSO-d_6
1*g*	$COCH_3$	A	1	6	3.5	15	85–87	EtOH	7.4–8.1	4.7	2.43(s)	3.30(s)	2.60(s)	$CDCl_3$

that the products described by Julliard *et al.* (3) are of type **1**, not **2**.

This paper gives a more detailed account of the synthesis of the bis-triazenes **1** reported in a preliminary communication (5) and reports some new evidence which provides an insight into the mechanism of formation of the triazenes of types **1** and **2**.

Discussion

The reaction of diazonium ions with mixtures of methylamine and formaldehyde affords the bis-triazenes **1**, in addition to the hydroxymethyltriazenes **2**. In the preceding paper in this series (6), the synthesis and chemistry of the hydroxymethyltriazenes **2** were explored, whereas in this paper the emphasis is on the conditions for synthesis of **1** and on the mechanism whereby **1** is produced. In the preparation of the bis-triazenes, the ratio of formaldehyde/methylamine required for optimum yield varies from 1:2 to 12:1 and is dependent on the substituent in the aryl group (see details in Table 1). In most cases the optimum yield was obtained using the diazonium chloride method, but in two instances, the *p*-nitro- and *p*-cyanobenzenediazonium fluoroborates gave good yields. In all cases, the bis-triazenes had to be separated from the hydroxymethyltriazene. This was achieved by recrystallization from an appropriate solvent; the bis-triazene invariably recrystallized in the first crop and two or three crystallizations were sufficient to remove the hydroxymethyltriazene. Details of yields, and physical properties, are given in Table 1.

The characterization of the bis-triazenes is based on spectroscopic evidence. Absence of OH absorption in the ir spectra confirms that these products are not hydroxymethyltriazenes. The nmr spectra clearly indicate the presence of two types of *N*-methyl proton at 3.2–3.3 ppm (6 protons for N-3 and N-7 methyl groups) and at 2.4–2.5 ppm (3 protons for N-5 methyl), and the *N*-methylene protons at 4.63–4.73 ppm. Detailed nmr data are shown in Table 1. The structure of the *p*-chloro, *p*-bromo-, and *p*-cyanophenyl bis-triazenes was confirmed by ^{13}C nmr spectroscopy (see Table 2). The presence of two *N*-methyl signals at ca. 34 and 37 ppm, and the methylene signal at ca. 74 ppm, confirms the bis-triazene structure. The bis-triazene structure was also confirmed by mass spectroscopy and elemental analysis. The mass spectra of the bis-*p*-chlorophenyltriazene (**1***b*) (see Table 3) show the molecular ion at 393/395/397, showing clearly the presence of two chlorine atoms in the molecule. The principal fragments in the spectrum occur at *m/e* 225/227 and 169/171, each containing a single chlorine atom, and suggesting that the major fragmentation of the bis-triazene occurs at the N3—C4 bond. Analogous fragmentation is seen in the mass spectrum of the *p*-bromo analogue (**1***a*), indicated by the fragments at *m/e* 269/271 and 213/215.

Thus the structure of these novel bis-triazenes (**1**), or "heptazanonadienes", has been established beyond doubt and corroborates the observations reported by Iley and co-workers (4). However, the mechanism of formation of the bis-triazenes has not been clearly established in previous reports (4, 5) and the elucidation of this mechanism became a principal objective of this study. It seemed logical that the diazonium coupling reaction provides a means to establish the nature of the dominant species in the methylamine/formaldehyde mixtures; the identification of the products of this coupling reaction might serve as a "probe" for determining the position of equilibrium

TABLE 2. Carbon-13 nmr data of bis-triazenes in $CDCl_3$ (ppm)

No.	X	Me(N-3 + N-7)	Me(N-5)	CH_2	Arom.
1*b*	Cl	37.6	34.4	74.2	121.9, 128.9, 131.1, 149.2
1*a*	Br	37.6	34.4	74.2	119.0, 122.3, 131.8, 149.6
1*d*	CN*	37.5	34.6	74.6	119.3, 121.3, 133.0, 153.7

*CN signal at 108.5 ppm.

TABLE 3. Mass spectral data (*m/e*) of the bis-triazene (**1***b*) $(Cl.C_6H_4N)=N-NCH_3-CH_2)_2NCH_3$

m/e	Relative intensity	Assignment
397	0.06	M^+
395	0.23	
393	0.35	
353	0.47	
351	2.35	
349	3.5	
326	0.8	$ArN=N-NCH_3-CH_2NCH_3-Ar]^{+\cdot}$
324	4.7	
322	7.0	
227	32	$ArN_3(CH_3)-CH_2-N^+=CH_2$
225	94	CH_3
212	5.3	$ArN_3CH_2-N=CH_2]^{+\cdot}$
210	13	CH_3
182	15	
171	34	$ArN_3HCH_3]^{+\cdot}$
169	86	
154	10	
141	93	
139	100	

(Ar = *p*-chlorophenyl)

in the mixture.[2]

A possible mechanism to account for the formation of the triazenes **1** and **2**, shown in Scheme 1, has been proposed by other workers (4). This is an attractive scheme because of its simplicity; direct coupling to the carbinolamine ($RNHCH_2OH$), generated *in situ*, affords the protonated methyloltriazene **3** which might readily deprotonate to give product **2**, or undergo dehydration to give the reactive intermediate "methylenetriazenium" species **4**. The latter species is an essential element in this route to **1** and would be expected to react with any free methylamine to give the triazene **5** which could then couple to a second unit of **4** to give the observed bis-triazene **1**. However, there are several objections to this proposal, not least of which is the absence of triazenes of type **5** in the reaction mixtures.

An important factor in the proposed scheme is that the conversion of **3** → **2** is not reversible (4), although the reverse reaction **2** → **3** should be a facile protonation in aqueous solution. The evidence for this proposal is that **2** does not interconvert to **1** under the conditions of the reaction (4). However,

[2]This is true only if *either* coupling to each species occurs at the same rate (which is a reasonable assumption) *or* coupling to each species is at least an order of magnitude faster than the rates at which they interconvert.

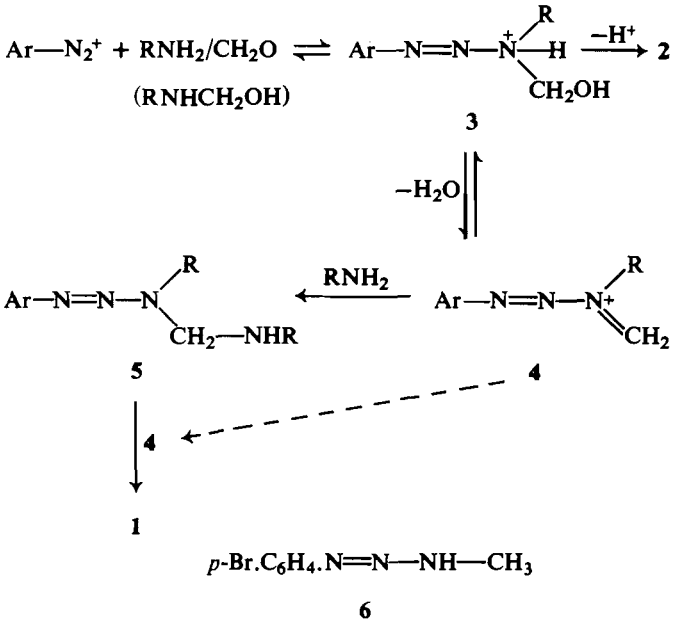

SCHEME 1

we have found that the hydroxymethyltriazene **2***a* can be converted to the bis-triazene **1***a* under certain conditions, but not vice versa. When **2***a* was treated with a dilute solution of methylamine/formaldehyde (1:5 molar ratio), no reaction occurred. However, reaction of **2***a* with a 1:1 methylamine/formaldehyde mixture, at a concentration equivalent to the reaction conditions used for the synthesis of **1***a*, afforded a mixture of the two triazenes **1***a* and **2***a*; the proportion of the two products was similar to the mixture obtained when the diazonium salt was treated with a 1:1 mixture of methylamine/formaldehyde. Reaction of **2***a* with methylamine alone affords only the monomethyltriazene **6** in high yield; Cheng and Iley have recently shown that this reaction is an excellent general method for the synthesis of monomethyltriazenes (7).

Perhaps the most convincing argument against the mechanism in Scheme 1 is that there is evidently no free methylamine in the formaldehyde/methylamine mixtures, since there is no evidence for formation of the monomethyltriazene in the diazonium coupling reaction. An essential component of Scheme 1 is the reaction of **4** with *free* methylamine to give **5**, the immediate precursor of the bis-triazene in this scheme.

An alternative mechanism is shown in Scheme 2 and involves a series of complex equilibria which are known to exist in mixtures of aldehydes and amines. This complex subject has been extensively reviewed (8). The first step is the addition of the amine to the carbonyl group to produce the α-hydroxyamine ("carbinolamine") **7**, which is usually not capable of isolation and may react by dehydration to give the Schiff base **8**. Either **7** or **8** may be involved in further condensation steps to give more complex species as shown in Scheme

Can. J. Chem. Downloaded from www.nrcresearchpress.com by 210.87.254.105 on 09/06/12
For personal use only.

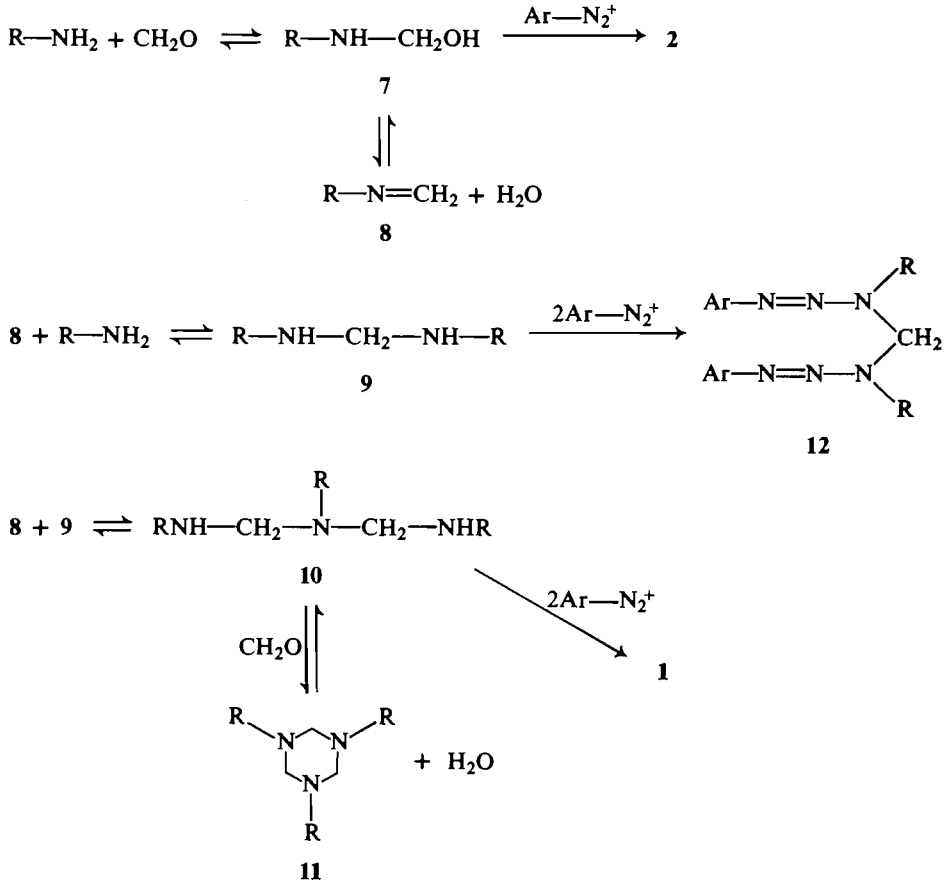

SCHEME 2

TABLE 4. The effect of the methylamine/formaldehyde ratio on the coupling reaction with *p*-bromo and *p*-cyano-benzenediazonium chlorides

Ratio of moles of reagents used			*p*-Bromo			*p*-Cyano-		
			Total yield	Mole fraction of products		Total yield	Mole fraction of products	
ArN_2^+	$MeNH_2$	CH_2O	(%)	**2***a*	**1***a*	%	**2**(X = CN)	**1***d*
1	1	50	77	0.99	<0.01	79	1.00	0
1	1	25	74	0.95	0.05	83	1.00	0
1	1	10	63	0.73	0.27	83	0.94	0.06
1	1	5	51.5	0.49	0.51	88	0.85	0.15
1	1	1	43	0.19	0.81	89	0.62	0.38

2, such as the bis-alkylaminomethane **9** and the bis-(alkylaminomethyl) alkylamine **10**. Further condensation of **10** with formaldehyde gives cyclic trimer **11**; a significant question is whether or not the latter step is reversible.

Faced with the multitude of species in Scheme 2, it is not surprising that a diazonium coupling reaction with methylamine/formaldehyde mixtures leads to more than one product. Indeed it is surprising that only two products arise, since there are three species in the scheme which could couple with a diazonium ion to give stable triazenes. There is no doubt that the hydroxymethyltriazene **2** arises from coupling to the carbinolamine **7**, and bis-diazonium coupling to **10** would afford the bis-triazene, **1**. The intermediate species **9** should also be capable of diazonium coupling to afford the bis-triazenylmethane **12**.

A test of the mechanism in Scheme 2 would be to determine the effect of the methylamine/formaldehyde ratio on the proportions of the product **1** and **2** obtained, since it is reasonable to expect that a higher methylamine/formaldehyde ratio should favour the bis-triazene. Indeed, we have found this to be the case. The *p*-bromobenzenediazonium chloride was treated with mixtures of formaldehyde/methylamine ranging from 50:1 to 1:1 in composition. The relative yields of **1***a* and **2***a* are easily measured from the relative integrals of the methylene group protons at ca. 4.7 and 5.2. The results are shown in Table 4. It is clear that the yield of **1***a* goes down and of **2***a* goes up as the amount of formaldehyde decreases. We have shown that this is not a dilution effect by carrying out the experiment with the 1:10 ratio, diluted to the same volume as the 1:50 experiment; essentially the same yield and molar ratio were observed.

Can. J. Chem. Downloaded from www.nrcresearchpress.com by 210.87.254.105 on 09/06/12
For personal use only.

TABLE 5. In vivo anti-tumour activity of the bis-triazenes against the TLX5 lymphoma

Compound No.	Max ILS (% T/C)	Optimal dose (mg/kg; five daily doses)
1*b*	190	160
1*d*	150	80

The same trend was observed when the series of experiments was carried out with the *p*-cyanobenzenediazonium salt (Table 4). However, it is significant that the yield of bis-triazene, at a given ratio of methylamine/formaldehyde, is much lower when the substituent is a cyano group than when it is a bromo group, which corroborates our previous observation (2) that the formation of hydroxymethyltriazenes is favoured by —M groups in the aryl moiety. The results in Table 4 unequivocally show that the coupling reaction is influenced quite strongly by the methylamine/formaldehyde ratio and thus is convincing evidence in favour of the mechanism proposed in Scheme 2.

It has been suggested (4) that the mechanism proposed in Scheme 2 is unlikely to be involved in the formation of bis-triazenes since the end product of this equilibrium is the cyclic trimer **11** which cannot couple to the diazonium ion. The crucial question is whether the final step leading to **11** is reversible. Accordingly, a sample of the cyclic trimer was prepared by distillation of the methylamine/formaldehyde mixture over solid KOH(8). Compound **11** was treated in aqueous solution with the *p*-cyanobenzenediazonium salt; the product was a mixture of the hydroxymethyltriazene (**2**, X = CN) and the bis-triazene **1***d*, and had almost the same composition as the mixture obtained from reaction of the same diazonium salt with a 1:1 mixture of methylamine and formaldehyde. These results clearly show (a) that the equilibrium in Scheme 2 is valid, (b) that the same equilibrium mixture arises either when methylamine and formaldehyde are mixed 1:1 or when the cyclic trimer (**11**) is dissolved in water, and (c) that the mechanism of the formation of the bis-triazenes **1** most likely involves reaction of **10** with the diazonium ion.

Further evidence for the mechanism in Scheme 2 was provided by the reaction of *p*-chlorobenzenediazonium fluoroborate with a 10:1 mixture of formaldehyde/methylamine. The major product, not surprisingly, was the bis-triazene (**1***b*), but a minor product (0.5% yield) was isolated from the residue in the recrystallization mother liquor and was identified from its nmr spectrum as the bis-(triazenyl) methane (**12**, Ar = *p*-chlorophenyl). The nmr spectrum shows two equivalent *N*-methyl groups at 3.15 ppm and a single methylene group at 5.65 ppm, in addition to the protons of two equivalent aromatic rings. Although this is the only example of a triazene of type **12** that we have obtained, its formation implies that the bis-(alkylamino) methane **9** is a minor constituent of the equilibrium mixture from methylamine/formaldehyde and is further strong evidence for the mechanism in Scheme 2.

The mechanism proposed in Scheme 2 also explains the experimental observation that **2***a* reacts with a methylamine/formaldehyde mixture to give the bis-triazene **1***a*. Under protic conditions, the hydroxymethyltriazene should behave like a dialkyltriazene and protonate at N-3 (9), thereby catalyzing fragmentation to the diazonium ion and the carbinolamine (**7**), which then exists in equilibrium with all the species in Scheme 2, including **10**. Reaction of the diazonium salt with **10** affords the bis-triazene (eq. [1]):

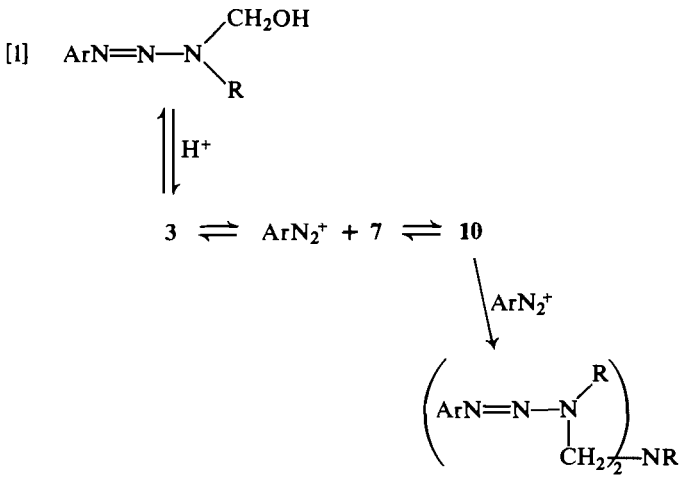

In addition to the fascinating chemistry of the bis-triazenes, their pharmacological properties are worthy of investigation because of their structural similarity to the anti-tumour dimethyltriazenes (1). Julliard *et al.* (3) did record that these products, although mis-identified as triazenes of type **2**, did not have significant activity in vitro. This observation is not surprising; compounds of type **1** should be anti-tumour agents, but will require metabolic activation to exhibit a cytotoxic effect in vitro. Two of the compounds in the bis-triazene series (**1***b* and **1***d*) have been tested against the TLX5 lymphoma in vivo, according to a published method (10), and have comparable activity (Table 5) to other methylalkyltriazenes.

Experimental

Melting points were determined on a Koffler hot-stage apparatus, calibrated with Fisher thermetric standards. Infrared spectra were recorded with liquid films in Nujol mulls on Perkin—Elmer 299 and 1330 spectrophotometers. Proton magnetic resonance speetra were recorded on a Varian EM360 spectrometer and mass spectra were obtained with a Dupont CEC-104 medium resolution spectrometer.

N,N-*Bis(1-aryl-3-methyltriazen-3-ylmethyl) methylamines. General procedure*

Method A

The appropriate arylamine (6.5 mmol) was dissolved in hydrochloric acid (2 mL concentrated HCl + 13 mL water) and diazotized at 0°C with sodium nitrite (0.5 g) in water. The diazonium salt solution is then treated with a mixture of 40% aqueous methylamine and 37% aqueous formaldehyde; the proportions of aqueous methylamine and formaldehyde necessary for optimal yield of bis-triazene depended on the substituent present in the aryl group of the diazonium salt (see Table 1). After stirring for 15 min in the cold, the mixture was neutralized rapidly with saturated sodium bicarbonate and stirring continued until precipitation of the product was complete. The product was then either filtered, if the solid was sufficiently crystalline to be handled in this way, or, in those cases when the precipitate was sticky and gummy, it was extracted into chloroform. Work-up of the product by immediate recrystallization in the case of solids or by trituration and recrystallization in the case of chloroform residues afforded pure crystalline bistriazenes. Yields and physical data are shown in Table 1.

Method B

This method is identical to Method A except that the diazonium fluoroborate is used in place of the chloride.

Effect of methylamine/formaldehyde ratio on the coupling reaction with p-*bromobenzenediazonium chloride*

For the purpose of this experiment, the *p*-bromoaniline (0.013 mol) was diazotized at 0°C in hydrochloric acid (4 mL concentrated

Can. J. Chem. Downloaded from www.nrcresearchpress.com by 210.87.254.105 on 09/06/12
For personal use only.

HCl + 26 mL water) with sodium nitrite (1.0 g) in water. The diazonium salt solution was treated with a pre-cooled mixture of 40% aqueous methylamine and 37% formaldehyde over a period of 15 min and the pH was then adjusted to 6–7 by the addition of saturated sodium bicarbonate. The mixture was stirred for 10–15 min, then adjusted to pH 7.5–8.0 with saturated $NaHCO_3$ and stirred until precipitation and/or formation of oil was complete. The product was separated by either filtration or extraction into chloroform, depending on the general condition (varying from a flocculent white precipitate to a sticky semi-solid mass). The composition of the product mixture was determined from the nmr spectrum by measurement of the relative integration of the *N*-methylene protons at ca. 5.15 and 4.7 ppm. The results of these experiments are shown in Table 4.

Effect of the methylamine/formaldehyde ratio on the coupling reaction with p-*cyanobenzenediazonium chloride*

A solution of *p*-aminobenzonitrile (0.77 g, 6.5 mmol) in hydrochloric acid (2.0 mL of concentrated HCl + 13.0 mL water) was diazotized at 0°C with sodium nitrite (0.5 g) in water over a period of 1.5 h. The solution was filtered and the appropriate mixture of 40% aqueous methylamine and 37% aqueous formaldehyde was added to the clear filtrate, which was stirred for a further 0.5 h at 0°C. The pH of the mixture was then raised to ~7 with saturated sodium bicarbonate and the solid product isolated by vacuum filtration. After drying in a vacuum desiccator, the composition of the product was determined from the nmr spectrum in deuteriochloroform. The results of these experiments are shown in Table 4.

*Bis(1-*p*-chlorophenyl-3-methyltriazen-3-yl) methane (**12**, Ar = p-Cl.$C_6H_4^-$)*

p-Chlorobenzenediazonium fluoroborate (0.03 mol) was dissolved in water (70 mL) at room temperature and added to a premixed solution of 40% aqueous methylamine (1.55 g) and 37% aqueous formaldehyde (15.5 g). The mixture was neutralized with saturated sodium carbonate and an immediate reaction was observed giving a reddish brown oil, which was extracted into $CHCl_3$. Evaporation of the dried chloroform extract gave 3.7 g of crude product, which was recrystallized from ether to give the bis(1-*p*-chlorophenyl-3-methyltriazen-3-ylmethyl) methylamine (**1***b*) (0.8 g, 14%). Evaporation of the ether mother liquors from recrystallization gave an oil. After several days standing, a small quantity of crystalline substance grew in the oil; separation of this product and washing with hexane afforded the bis(1-*p*-chlorophenyl-3-methyltriazen-3-yl) methane (50 mg, 0.5%), mp 124–126°C; nmr ($CDCl_3$): 3.15 (s, 6H, N—Me), 5.65 (s, 2H, N—CH_2—N), and 7.4 (m, 8H, aromatic) ppm.

*Reaction of 1-*p*-bromophenyl-3-hydroxymethyl-3-methyltriazene with formaldehyde/methylamine*

The hydroxymethyltriazene (**2***a*) (0.25 g) was suspended in a mixture of 40% aqueous methylamine (80 mg) and 37% aqueous formaldehyde (85 mg) with water (5.0 mL) and stirred at room temperature for three days. The insoluble material was recovered by filtration and was identified by the nmr spectrum as a mixture of the hydroxymethyltriazene (**2***a*, 45%) and the bis-triazene (**1***a*) (34%). Total yield = 0.2 g.

*Reaction of 1-*p*-bromophenyl-3-hydroxymethyl-3-methyltriazene with methylamine*

The hydroxymethyltriazene (**2***a*) (100 mg) was added to a solution of 40% aqueous methylamine (34 mg) in water (5.0 mL) and the suspension stirred for 2 days at room temperature. The insoluble solid was filtered and dried to afford a pure sample of 1-*p*-bromophenyl-3-methyltriazene (74 mg, 84%), mp 86°C (lit. (11) mp 86–87°C).

*1,3,5-Trimethylhexahydro-1,3,5-triazine (**11**, R = Me)*

37% Aqueous formaldehyde (16.2 g), 40% aqueous methylamine (20.9 g), and solid sodium hydroxide (8 g) were mixed and refluxed for 4 h. The mixture was cooled to room temperature and extracted with chloroform. Evaporation of the dried chloroform extracts gave the triazine (**11**, R = Me) (8.3 g, 96%) as a yellow oil; nmr ($CDCl_3$): 2.3 (s, 3H) and 3.2 (s, 2H) ppm.

Reaction of 1,3,5-trimethylhexahydro-1,3,5-triazine with p-*cyanobenzenediazonium chloride*

p-Aminobenzonitrile (0.005 mol) was diazotized in hydrochloric acid with sodium nitrite at 0°C. The trimethylhexahydrotriazine (0.65 g) was added directly to the diazonium salt solution and the mixture stirred in the cold for 2 h. The insoluble solid was filtered and dried to give a mixture of the bis-triazene (**1***d*) (14%) and the hydroxymethyltriazene (**2**, X = CN) (32%), total yield 0.45 g.

Acknowledgements

The authors are grateful to the Natural Sciences and Engineering Research Council of Canada for a research grant (to K.V.), to Dalhousie University Chemistry Department and Dr. J. S. Grossert for mass spectra, and to the Cancer Chemotherapy Research Group of the Pharmacy Department, University of Aston in Birmingham, U.K. for anti-tumour evaluations. The 90 MHz ^{13}C nmr spectra were recorded on the Nicolet 360 spectrometer of the Atlantic Region Magnetic Resonance Centre at Dalhousie University.

1. T. A. CONNORS, P. M. GODDARD, K. MERAI, W. C. J. ROSS, and D. E. V. WILMAN. Biochem. Pharmacol. **25**, 241 (1976).
2. A. GESHER, J. A. HICKMAN, R. J. SIMMONDS, M. F. G. STEVENS, and K. VAUGHAN. Tetrahedron Lett. 5041 (1978).
3. M. JULLIARD, G. VERNIN, and J. METZGER. Synthesis, 116 (1980).
4. S. C. CHENG, M. L. DE S. FERNANDES, J. ILEY, and M. E. N. ROSA. J. Chem. Res. (S), 108 (1983).
5. R. J. LAFRANCE, Y. TANG, K. VAUGHAN, and D. L. HOOPER. Chem. Commun. 721 (1983).
6. C. M. HEMENS, H. W. MANNING, K. VAUGHAN, R. J. LAFRANCE, and Y. TANG. Can. J. Chem. **62**, 741 (1984).
7. S. C. CHENG and J. ILEY. J. Chem. Res. (S). 320 (1983).
8. M. M. SPRUNG, Chem. Rev. **26**, 297 (1940).
9. V. ZVERINA and M. MATRKA. Chem. Listy, **63**, 55 (1969).
10. A. GESCHER, J. A. HICKMAN, R. J. SIMMONDS, M. F. G. STEVENS, and K. VAUGHAN. Biochem. Pharmacol. **30**, 89 (1981).
11. M. REMES, J. DIVIS, V. ZVERINA, J. MARHOLD, and M. MATRKA. Cesk. Farm. **21**, 442 (1972).

Can. J. Chem. Downloaded from www.nrcresearchpress.com by 210.87.254.105 on 09/06/12
For personal use only.

Preparation and characterization of some ruthenium(II) porphyrins containing tertiary phosphine axial ligands, including the crystal structure of (octaethylporphinato)bis(triphenylphosphine)ruthenium(II)

SARA ARIEL, DAVID DOLPHIN,[1] GEORGE DOMAZETIS, BRIAN R. JAMES,[1] TAK W. LEUNG, STEVEN J. RETTIG, JAMES TROTTER, AND GREGORY M. WILLIAMS

Department of Chemistry, University of British Columbia, Vancouver, B.C., Canada V6T 1Y6

Received August 24, 1983

SARA ARIEL, DAVID DOLPHIN, GEORGE DOMAZETIS, BRIAN R. JAMES, TAK W. LEUNG, STEVEN J. RETTIG, JAMES TROTTER, and GREGORY M. WILLIAMS. Can. J. Chem. **62**, 755 (1984).

The ruthenium(II) porphyrin complex $Ru(OEP)(PPh_3)_2$ (OEP = the dianion of octaethylporphyrin) has been prepared from Ru(OEP)(CO)EtOH, and the X-ray crystal structure determined; as expected, the six-coordinate ruthenium is situated in the porphyrin plane and has two axial phosphine ligands. Synthesized also from the carbonyl(ethanol) precursors were the corresponding tris(*p*-methoxyphenyl)phosphine complex, and the $Ru(TPP)L_2$ (TPP = the dianion of tetraphenylporphyrin, L = PPh_3, $P(p\text{-}CH_3OC_6H_4)_3$, P^nBu_3) and $Ru(TPP)(CO)PPh_3$ complexes. Optical and ^1H nmr data are presented for the complexes in solution. In some cases dissociation of a phosphine ligand to generate five-coordinate species occurs and this has been studied quantitatively in toluene at 20°C for the $Ru(OEP)L_2$ and $Ru(TPP)L_2$ systems.

SARA ARIEL, DAVID DOLPHIN, GEORGE DOMAZETIS, BRIAN R. JAMES, TAK W. LEUNG, STEVEN J. RETTIG, JAMES TROTTER et GREGORY M. WILLIAMS. Can. J. Chem. **62**, 755 (1984).

On a préparé les complexes ruthénium(II)–porphyrines, $Ru(OEP)(PPH_3)_2$ (OEP = le dianion de l'octaéthylporphyrine), à partir du Ru(OEP)(CO)EtOH et on a déterminé leur structure par diffraction des rayons-X; comme ou pouvait le prévoir, le ruthénium est hexacoordonné, il se trouve dans le plan de la porphyrine et deux ligands phosphines lui sont attachés en position axiale. Partant des précurseurs carbonyles(éthanol) appropriés, on a aussi synthétisé les complexes tris(*p*-méthoxyphényl)-phosphines correspondants ainsi que les complexes $Ru(TPP)L_2$ (TPP = le dianion de la tétraphénylporphyrine et L = PPh_3, $P(p\text{-}MeOC_6H_4)_3$ ou P^nBu_3) et $Ru(TPP)(CO)PPh_3$. On rapporte des données optiques et de rmn du proton relativement à ces complexes en solutions. Dans quelques cas, il se produit une dissociation d'un ligand phosphine et il y a génération d'espèces pentacoordonnées; on a étudié ces réactions quantitativement en solution dans le toluène à 20°C en utilisant les systèmes $Ru(OEP)L_2$ et $Ru(TPP)L_2$ comme exemples.

[Traduit par le journal]

Introduction

Our continuing interest in, and development of, ruthenium porphyrin chemistry (1) led us to discover that ruthenium(II) porphyrins containing tertiary phosphines as axial ligands were efficient catalysts for the decarbonylation of aldehydes (2), as well as for oxidation of substrates such as phosphines and sulfides by molecular oxygen through generation of hydrogen peroxide (3). The complexes also undergo two successive one-electron electrochemical oxidations to yield first a ruthenium(III) bisphosphine cation and then a ruthenium(III) π-cation radical (4).

We report here the details of the preparation and characterization of some of the ruthenium porphyrin – tertiary phosphine complexes, including the X-ray structure of $Ru(OEP)(PPh_3)_2$.[2] The dissociative equilibrium involving the loss of a phosphine ligand from the $Ru(porp)L_2$, L = PPh_3, $P(p\text{-}CH_3OC_6H_4)_3$, complexes in toluene solution is also considered. Other groups (5, 6) have described the synthesis of $Ru(TPP)(PPh_3)_2$, but the reported solution optical spectral data did not make allowance for the dissociation of phosphine.

Experimental

The solvents (toluene, heptane, hexane, MeOH, EtOH, 2-(2-methoxyethoxy)ethanol, CH_2Cl_2) were spectroscopic grade and were distilled prior to use, the CH_2Cl_2 being distilled from CaH_2. All manipulations, including preparation of the complexes, were carried out under an atmosphere of argon with the use of Schlenk techniques. Optical spectra were recorded on a Cary 17D that could be thermostatted, infrared on a Perkin Elmer 598, and ^1H nmr spectra on a Varian XL-100 operating in the Fourier transform mode. Mass spectral data were taken on a Kratos-AEI MS 902, source temperature 220–240°C, direct insertion probe, electron energy 70 eV.

The ruthenium was obtained as $RuCl_3 \cdot 3H_2O$ from Johnson, Matthey Ltd.; $Ru_3(CO)_{12}$ was either purchased from Strem Chemicals or synthesized according to a literature method from the trichloride (7). H_2TPP (8), H_2OEP (9), and the Ru(porp)(CO)EtOH precursors via $Ru_3(CO)_{12}$ were prepared according to literature procedures (4, 10). A method of synthesizing the carbonyl(ethanol) precursors directly from $RuCl_3 \cdot 3H_2O$ is described below.[3] The phosphines were Strem products: PPh_3 and $P(p\text{-}CH_3OC_6H_4)_3$ were recrystallized from ethanol, while P^nBu_3 was distilled at reduced pressure and stored under Ar. Microanalyses were performed by Mr. P. Borda of this department and by the Canadian Microanalytical Service Ltd.

Preparation of complexes

The yields in the synthetic procedures described below for the phosphine complexes were always >80%.

Ru(porp)(CO)EtOH from $RuCl_3 \cdot 3H_2O$

$RuCl_3 \cdot 3H_2O$ (0.5 g, 1.9 mmol) and H_2(porp) (0.5 g, 0.8–0.9 mmol) were refluxed in 2-(2-methoxyethoxy)ethanol (200 mL) overnight under a CO stream. After removing ~90% of the solvent by vacuum distillation and cooling to room temperature, EtOH (20 mL) was added and the solution stirred for 30 min. Some product (~300 mg) precipitated and was collected. The ethanol was evaporated off from the filtrate, and CH_2Cl_2 (50 mL) added; the resulting solution was extracted with H_2O (4 × 50 mL) and the CH_2Cl_2 layer dried with

[1]Authors to whom correspondence should be addressed.

[2]Ligand abbreviations used: porp = dianion of octaethylporphyrin (OEP) or tetraphenylporphyrin (TPP); dpm = bis(diphenylphosphine)methane, dpe = 1,2-bis(diphenylphosphino)ethane, diop = 2,3-*o*-isopropylidene-2,3-dihydroxy-1,4-bis(diphenylphosphino)-butane; DMSO = dimethylsulfoxide.

[3]The synthetic procedure was based on one first used in Collman's group (11).

Can. J. Chem. Downloaded from www.nrcresearchpress.com by 210.87.254.5 on 09/06/12
For personal use only.

Can. J. Chem. Downloaded from www.nrcresearchpress.com by 210.87.254.5 on 09/06/12
For personal use only.

TABLE 1. Optical spectral data for some ruthenium(II) porphyrin – tertiary phosphine species in CH_2Cl_2 solution

Complex	λ_{max} nm (log ϵ)
Ru(OEP)$(PPh_3)_2$[a]	530 (4.01), 512 (4.02), 420 (5.30), 355 (4.55)
Ru(OEP)(PPh_3)[b]	520 (4.57), 395 (5.40), 350 (4.61)
Ru(OEP)$\{P(p\text{-}CH_3OC_6H_4)_3\}_2$[a]	533 (4.03), 505 (4.03), 396 (5.40)
Ru(OEP)$\{P(p\text{-}CH_3OC_6H_4)_3\}$[b]	530 (4.50), 424 (5.43), 355 (4.70)
Ru(TPP)$(PPh_3)_2$[a]	555 sh (3.84), 515 (4.02), 433 (5.32)
Ru(TPP)(PPh_3)[b]	508 (4.02), 422 (5.39)
Ru(TPP)$\{P(p\text{-}CH_3OC_6H_4)_3\}_2$[a]	555 sh (3.92), 520 (4.10), 435 (5.30)
Ru(TPP)$\{P(p\text{-}CH_3OC_6H_4)_3\}$[b]	518 (4.20), 413 (5.36)
Ru(TPP)$(P^nBu_3)_2$	559 (3.56), 525 (3.82), 478 (3.40), 437 (5.12), 399 (4.38), 354 (4.38)
Ru(TPP)(CO)PPh_3[a]	573 (3.92), 535 (4.38), 418 (5.34)
Ru(TPP)(CO)[b]	533 (4.20), 413 (5.36)

[a]In presence of excess phosphine (see text).
[b]Measured using ~ 10^{-6} *M* solutions Ru(porp)L_2, L = phosphine, or Ru(TPP)(CO)(PPh_3).

TABLE 2. ^{1}H nmr data for some ruthenium(II) porphyrin – tertiary phosphine complexes in $CDCl_3$ at 20°C

Complex	Chemical shifts, ppm downfield from TMS
Ru(OEP)$(PPh_3)_2$	1.70 (t, CH_3), 3.68 (q, CH_2), 4.02 (d, *o*-H), 6.2–6.8 (m, *m*- and *p*-H), 8.80 (s, meso-H)
Ru(OEP)(CO)PPh_3[a]	1.75 (t, CH_3), 3.63 (m, CH_2),[b] 3.80 (m, *o*-H), 6.31 (m, *m*-H), 6.67 (t, *p*-H), 9.60 (s, meso-H)
Ru(OEP)$\{P(p\text{-}CH_3OC_6H_4)_3\}_2$	1.71 (t, CH_3), 3.60 (s, OCH_3), 3.63 (q, CH_2), 3.88 (d, *o*-H), 5.87 (d, *m*-H), 8.73 (s, meso-H)
Ru(TPP)$(PPh_3)_2$	4.25 (d, *o*-H), 6.3–7.0 (m, *m*- and *p*-H), 7.60 (br s, porphyrin phenyl), 8.11 (s, pyrrole-H)
Ru(TPP)(CO)(PPh_3)	4.08 (m, *o*-H), 6.4–7.0 (m, *m*- and *p*-H), 7.5–8.3 (m, porphyrin phenyl), 8.50 (s, pyrrole-H)
Ru(TPP)$(P^nBu_3)_2$	0.15–0.50 (m, ^{n}Bu), 8.2 (br s, porphyrin phenyl), 8.90 (s, pyrrole-H)
Ru(TPP)$\{P(p\text{-}CH_3OC_6H_4)_3\}_2$	3.53 (s, OCH_3), 4.13 (d, *o*-H), 6.00 (d, *m*-H), 7.53 (br s, porphyrin phenyl), 8.01 (s, pyrrole-H)

[a]The synthesis and optical spectra of this complex were presented in ref. 4.
[b]At 400 MHz, the multiplet is resolved into a 12-line multiplet.

$MgSO_4$, filtered, and evaporated to dryness. The solid crude products were combined and purified by column chromatography (grade III alumina, Merck) using 1:1 CH_2Cl_2/EtOH as elutant (~20% yield).

Ru(OEP)$(PPh_3)_2$

Ru(OEP)(CO)EtOH (0.5 g, 0.71 mmol) and PPh_3 (2.0 g, 7.6 mmol) were dissolved in 150 mL toluene and the solution refluxed for 24 h. After removal of solvent, the product was recrystallized from 1:5 CH_2Cl_2/MeOH three times. Crystals suitable for X-ray work were obtained by layering a concentrated solution in CH_2Cl_2 with heptane. *Anal.* calcd. for $C_{72}H_{74}N_4P_2Ru$: C 74.60, H 6.46, N 4.84, P 5.35; found: C 74.00, H 6.37, N 4.55, P 5.5. *Mass spec.*: *M/e* 896 (100), Ru(OEP)$(PPh_3)^+$; 634 (80), Ru(OEP)$^+$.

Ru(TPP)$(PPh_3)_2$

This complex was prepared from Ru(TPP)(CO)EtOH by the procedure described above for the OEP analogue. *Anal.* calcd. for $C_{80}H_{58}N_4P_2Ru$: C 77.59, H 4.72, N 4.52, P 5.00; found: C 77.29, H 4.84, N 4.35, P 5.10. *Mass spec.*: *M/e* 976 (80), Ru(TPP)$(PPh_3)^+$; 714 (100), Ru(TPP)$^+$.

Ru(TPP)(CO)PPh_3

Ru(TPP)(CO)EtOH (0.4 g, 0.56 mmol) and PPh_3 (0.2 g, 0.76 mmol) were stirred in 30 mL CH_2Cl_2 for 1 h. After reducing the volume to 5 mL, 25 mL hexane were added and the solution reduced in volume and cooled by passing Ar over the solution. The product dropped out as purple crystals that were collected by filtration. *Anal.* calcd. for $C_{63}H_{43}N_4OPRu$: C 75.36, H 4.32, N 5.58; found: C 75.17, H 4.18, N 5.35. *Mass spec.*: *M/e*: 1004 (1), Ru(TPP)(CO)PPh_3^+; 976 (90), Ru(TPP)$(PPh_3)^+$; 742 (50), Ru(TPP)(CO)$^+$; 714 (100), Ru(TPP)$^+$. *Infrared*: ν_{CO} 1956 cm^{-1} (Nujol).

Ru(TPP)$\{P(p\text{-}CH_3OC_6H_4)_3\}_2$

Ru(TPP)(CO)EtOH (0.3 g, 0.42 mmol) and $P(p\text{-}CH_3OC_6H_4)_3$ (0.4 g, 1.1 mmol) were refluxed in 150 mL toluene for 24 h. On slowly removing the solvent at room temperature, the product crystallized out eventually leaving a colourless solution; the crystals, which were then collected, washed with ethanol and air-dried, contained a toluene solvate molecule. *Anal.* calcd. for $C_{86}H_{69}O_6N_4P_2Ru \cdot C_7H_8$: C 73.94, H 5.13, N 3.71, P 4.10; found: C 74.69, H 4.82, N 4.27, P 4.0.

Ru(OEP)$\{P(p\text{-}CH_3OC_6H_4)_3\}_2$

This complex was prepared from Ru(OEP)(CO)EtOH by the procedure described above for the TPP analogue. *Anal.* calcd. for $C_{78}H_{86}N_4P_2O_6Ru$: C 69.98, H 6.48, N 4.19; found: C 69.66, H 6.39, N 4.23.

Ru(TPP)$(P^nBu_3)_2$

This complex was prepared from Ru(TPP)(CO)EtOH and excess phosphine on the scale used, and with the procedure described earlier (4), for the OEP analogue. *Anal.* calcd. for $C_{68}H_{82}N_4P_2Ru$: C 73.03, H 7.38, N 5.01, P 5.54; found: C 71.97, H 7.39, N 4.94, P 6.1. *Mass spec.*: *M/e* 1118 (1), Ru(TPP)$(P^nBu_3)_2^+$; 916 (100), Ru(TPP)$(P^nBu_3)^+$; 714 (90), Ru(TPP)$^+$.

The optical and ^{1}H nmr spectra data for the complexes are given in Tables 1 and 2, respectively.

Can. J. Chem. Downloaded from www.nrcresearchpress.com by 210.87.254.5 on 09/06/12
For personal use only.

Equilibrium constant measurements

Equilibrium constants for phosphine dissociation in toluene solution, eq. [1], were measured by a spectrophotometric titration technique using a standard 1-cm optical cell fitted with a serum cap.

$$[1]\quad \mathrm{Ru(porp)L_2} \overset{K}{\rightleftharpoons} \mathrm{Ru(porp)L} + \mathrm{L}; \qquad \mathrm{L} = \text{phosphine}$$

In sufficiently dilute solution ($\leq 10^{-6}$ *M*), the six-coordinate complexes dissociate completely as evidenced by a single band in the Soret region that on addition of aliquots (μL) of 10^{-2} *M* phosphine in toluene, subsequently decreases in intensity with concomitant formation of a new Soret band at higher wavelengths. Phosphine added in sufficient excess ($\geq 10^{-2}$ *M*) generates the limiting spectrum of the six-coordinate species.

The data were fitted to the equation

$$[2]\quad \log\{[\mathrm{Ru(porp)L_2}]/[\mathrm{Ru(porp)L}]\} = \log[\mathrm{L}] - \log K$$

using $(A - A_0)/(A_\infty - A)$ to calculate the concentration ratio, where A_0 and A_∞ are the absorbances for the five- and six-coordinate species, respectively, and A is the absorbance at any intermediate added phosphine concentration. Values of log *K* were determined from the intercept of the line (least-squares method) for a plot of log $(A - A_0/A_\infty - A)$ vs. log [L]; the slopes were 1.0 ± 0.1, consistent with a simple ligand association according to eq. [1]. Values of *K* were independent of the wavelength used, but were most conveniently determined from data at the wavelength of a Soret maximum. Equilibrium [1] was evident also in CH_2Cl_2 solution over similar complex and ligand concentration ranges.

X-ray crystallographic analysis

A dark red single crystal of $Ru(OEP)(PPh_3)_2$ was mounted on an Enraf-Nonius CAD4-F diffractometer in a non-specific orientation. Final unit cell parameters were refined by least-squares on 2 sin θ/λ values for 25 reflections having 30° < 2θ < 39° measured with MoKα$_1$ radiation (λ = 0.70930 Å); cell reduction revealed no higher symmetry. Crystal data (at 22°C) were:

$C_{72}H_{74}N_4P_2Ru$ fw = 1158.4

a = 12.139(2), b = 12.120(2), c = 20.878(4) Å; α = 86.51(1), β = 86.25(1), γ = 79.90(1)°; space group $P\bar{1}$; V = 3013(1) Å^3, Z = 2, D_c = 1.277 g cm^{-3}, μ(MoKα) = 3.04 cm^{-1}.

Intensities were measured with graphite-monochromatized MoKα radiation. An ω−2θ scan at 0.7−10.1° min^{-1} was employed over a range of (0.55 + 0.35 tan θ) degrees in ω (extended by 25% on both sides for background measurements). Data were collected for ±*h*, ±*k*, *l* for 0° < 2θ < 50°; the aperture used was (2.0 + tan θ) × 4 mm, 173 mm from the crystal. Three reflections (613, 36$\bar{1}$, $\bar{1}$17) were monitored every hour of exposure time for random intensity fluctuations (±2%), and were recentered every 150 reflections for orientation control. A total of 9163 independent reflections was measured, with 5697 having intensities greater than 1.5σ(I) ($\sigma^2(I) = S + 2B + [0.04(S-B)]^2$ with S = scan count and B = background count); these were employed in the structure solution and refinement procedure using the SHELX computer program (12). The indices for boundary planes (10 faces) were {011}, {01$\bar{1}$}, {10$\bar{1}$}, {001}, and {101}, with distances from crystal centre of 0.17, 0.17, 0.20, 0.10 and 0.17 mm.

The coordinates of the Ru and P atoms were determined from the Patterson function and those of the remaining non-hydrogen atoms from a subsequent difference Fourier map. There are two independent half molecules, A and B, in the asymmetric unit, and in each of these the Ru atom coincides with a crystallographic inversion centre. Two ethyl groups in molecule B are disordered, with the methyl carbon atoms each distributed over two sites, C(32), C(32′) and C(34), C(34′); these four disordered C atoms were refined isotropically. All other non-hydrogen atoms were refined anisotropically. Refinement of atomic parameters was carried out using block-diagonal least-squares techniques on F, minimizing the function $\Sigma w(|F_o| - |F_c|)^2$ where $w = 1/\sigma^2(F_o)$. Neutral-atom scattering factors were taken from ref. 13.

Four vinyl hydrogens, H(23) and H(28) of molecules A and B, were located in a difference Fourier map. No attempt was made to locate the remaining H atoms; these were included at "ideal" positions, recalculated after each cycle of the refinement, and their isotropic thermal parameters were refined. Methyl hydrogen atoms, except for the disordered methyl groups that were kept fixed, were each refined as a rigid group possessing a local C_3-symmetry.

Convergence was reached at R = 0.0454 and R_w = 0.0372 for the 5697 reflections and 820 variables. Final positional and equivalent thermal parameters (U_{eq} = (1/3) trace U) for the non-hydrogen atoms are listed in Table 3, while the anisotropic thermal parameters are given in Table 4.[4] The calculated hydrogen atom positional and isotropic thermal parameters are given in Table 5.[4]

Bond lengths and angles for the non-hydrogen atoms appear in Tables 6 and 7, respectively, while those involving the H atoms are given in Tables 8 and 9.[4] Measured and calculated structure factors have been placed in the Depository of Unpublished Data.

Results and discussion

The bis(tertiary phosphine) complexes were readily synthesized in high yields from the carbonyl(ethanol) precursors and excess phosphine (up to 10:1) by a reflux procedure in toluene; in the case of the more basic P^nBu_3 systems (4), a room temperature treatment, preferably in CH_2Cl_2, is sufficient to effect the substitution process. The photolysis procedure required to effect replacement of the carbonyl by nitrogen- and oxygen-donors is not necessary (1, 15). Earlier syntheses of $Ru(TPP)(PPh_3)_2$ (5, 6) had used a thermal procedure (refluxing benzene or CH_2Cl_2 at room temperature), but we found that the use of a higher temperature gave better yields. Replacement of the ethanol only from the carbonyl(ethanol) complex by a phosphine to give, for example, $Ru(TPP)(CO)PPh_3$ is readily accomplished at room temperature using a slight excess of the phosphine. The direct synthesis of the Ru(porp)(CO)EtOH precursors from $RuCl_3 \cdot 3H_2O$ is convenient and obviates the use of $Ru_3(CO)_{12}$ as an intermediate, but the overall yield based on the trichloride is greater via the two-stage procedure (40 vs. 20%).

Structure description

The crystal structure of $Ru(OEP)(PPh_3)_2$ reveals an inversion centre at the ruthenium which is thus constrained to be in the plane of the four nitrogens of the octaethylporphinato (OEP) ligand. The two axial PPh_3 ligands complete the essentially octahedral coordination of the metal. Figure 1 shows the atomic numbering scheme of the molecule, while Fig. 2 shows a stereoscopic packing drawing. The molecular conformation of the ethyl groups within OEP structures generally, including Ru species, has been considered usually to depend on molecular packing within the crystal (14, 15), but the disorder noted in the present bis(phosphine) complex and some recent work on $[Ru(OEP)(OH)]_2O$ (16) suggest a more random choice of upward or downward from the pyrrole planes.

The structure of $Ru(OEP)(PPh_3)_2$ is the second one reported for a bis(phosphine) of a Ru(II) porphyrin, the earlier on of $Ru(TPP)(dpm)_2$ containing monodentate dpm ligands also coming from these laboratories (17). The only other six-coordinate Ru(II) porphyrin structures of which we are aware are those of $Ru(OEP)py_2$ (15), Ru(TPP)(CO)py (18), and Ru(TPP)(CO)(EtOH) (10). The average Ru—P distance of 2.428 Å found in the present structure is typical for *trans* P

[4]The structure factor table and Tables 4, 5, 8, and 9 are available, at a nominal charge, from the Depository of Unpublished Data, CISTI, National Research Council of Canada, Ottawa, Ont., Canada K1A 0S2.

TABLE 3. Atomic coordinates ($\times 10^4$) and thermal parameters ($Å^2 \times 10^3$) with esd's in parentheses

Atom	x/a	y/b	z/c	U_{eq}	Atom	x/a	y/b	z/c	U_{eq}
		Molecule A					Molecule B		
Ru(1)	0	0	0	25	Ru(1)	5000	5000	5000	30
P(1)	469(1)	1438(1)	−756(<1)	30	P(1)	5922(1)	4289(1)	4009(<1)	36
N(1)	−1702(2)	526(3)	−32(1)	28	N(1)	5595(3)	3532(3)	5500(1)	35
N(2)	24(2)	986(3)	757(1)	28	N(2)	3541(2)	4418(3)	4882(1)	30
C(1)	1296(3)	877(3)	−1457(2)	35	C(1)	6536(4)	5369(4)	3525(2)	42
C(2)	2429(4)	453(4)	−1450(2)	43	C(2)	7562(4)	5656(4)	3642(2)	56
C(3)	3009(5)	−81(4)	−1975(3)	61	C(3)	7972(5)	6500(5)	3248(3)	80
C(4)	2427(6)	−206(5)	−2508(3)	74	C(4)	7371(7)	7058(6)	2774(3)	99
C(5)	1305(5)	187(5)	−2519(2)	70	C(5)	6328(6)	6826(5)	2676(3)	90
C(6)	730(4)	727(4)	−2001(2)	50	C(6)	5923(5)	5976(5)	3048(2)	67
C(7)	1271(3)	2473(3)	−441(2)	35	C(7)	7048(4)	3075(4)	4095(2)	43
C(8)	736(4)	3123(4)	46(2)	52	C(8)	6743(5)	2106(5)	4352(3)	81
C(9)	1225(5)	3952(5)	286(3)	66	C(9)	7470(6)	1120(5)	4405(3)	99
C(10)	2262(5)	4130(5)	61(3)	78	C(10)	8593(7)	1096(6)	4234(3)	99
C(11)	2806(5)	3493(5)	−436(3)	79	C(11)	8935(5)	2051(7)	3948(4)	100
C(12)	2318(4)	2675(4)	−688(2)	56	C(12)	8167(4)	3031(5)	3885(3)	77
C(13)	−554(3)	2556(4)	−1174(2)	37	C(13)	5231(3)	3721(4)	3372(2)	43
C(14)	−1691(4)	2618(5)	−1087(3)	76	C(14)	4142(4)	3594(5)	3409(2)	69
C(15)	−2430(5)	3484(5)	−1399(3)	91	C(15)	3688(5)	3155(6)	2897(3)	98
C(16)	−2019(5)	4245(5)	−1798(3)	75	C(16)	4323(4)	2868(5)	2353(3)	81
C(17)	−889(5)	4202(5)	−1889(3)	76	C(17)	5418(4)	2988(6)	2316(3)	94
C(18)	−169(4)	3370(5)	−1575(2)	63	C(18)	5852(4)	3413(6)	2814(2)	87
C(19)	−2395(3)	189(3)	−448(2)	29	C(19)	6622(3)	3255(4)	5757(2)	43
C(20)	−3533(3)	789(3)	−328(2)	32	C(20)	6729(4)	2150(4)	6067(2)	61
C(21)	−3508(3)	1481(3)	160(2)	34	C(21)	5773(4)	1755(4)	5990(3)	68
C(22)	−2350(3)	1312(3)	344(2)	30	C(22)	5062(4)	2624(4)	5621(2)	46
C(23)	−1945(3)	1835(4)	825(2)	33	C(23)	4021(4)	2568(4)	5407(2)	49
C(24)	−863(3)	1695(3)	1034(2)	31	C(24)	3311(3)	3375(4)	5069(2)	38
C(25)	−495(3)	2236(3)	1563(2)	34	C(25)	2203(3)	3280(4)	4869(2)	45
C(26)	613(3)	1869(3)	1591(2)	34	C(26)	1774(3)	4279(4)	4578(2)	40
C(27)	950(3)	1089(3)	1084(2)	30	C(27)	2620(3)	4988(4)	4586(2)	38
C(28)	2032(3)	557(3)	925(2)	31	C(28)	2558(3)	6057(4)	4295(2)	44
C(29)	1406(4)	2125(4)	2064(2)	47	C(29)	676(3)	4598(4)	4259(2)	48
C(30)	1650(5)	1202(5)	2581(3)	80	C(30)	798(4)	4403(5)	3540(2)	71
C(31)	−1252(4)	3049(4)	1982(2)	51	C(31)	1660(4)	2242(5)	4975(3)	77
C(32)	−1597(5)	4204(5)	1667(3)	83	C(32)[a]	1897	1474	4498	76(4)[b]
C(33)	−4456(3)	2274(4)	462(2)	45	C(32′)[a]	958	2057	5523	76(5)[b]
C(34)	−4413(4)	3511(4)	286(3)	75	C(33)	5461(5)	604(6)	6212(4)	142
C(35)	−4510(3)	668(4)	−714(2)	40	C(34)[a]	4974	372	6794	145(7)[b]
C(36)	−4554(4)	1385(5)	−1337(2)	69	C(34′)[a]	5597	−330	5856	145(9)[b]
					C(35)	7818(7)	1543(6)	6373(4)	124
					C(36)	7810(9)	1965(8)	6981(5)	193

[a]Disordered methyls; occupancy ratio is 44(1)/56(1) for the individual pairs: C(32)/C(32′) and C(34′)/C(34).
[b]The carbon atoms of the disordered methyl groups: C(32), C(32′), C(34), and C(34′) were refined isotropically.

Can. J. Chem. Downloaded from www.nrcresearchpress.com by 210.87.254.5 on 09/06/12
For personal use only.

atoms on Ru(II) (17), and the mean P—C distance of 1.84 Å is also normal. The average Ru—N distance (2.050 Å) corresponds to those reported in other ruthenium(II)–porphyrin complexes (10, 15–17), and the geometry of the OEP ligand is as expected (14, 16).

The finding that the $Ru(OEP)(PPh_3)_2$ complex dissociates a triphenylphosphine ligand in dilute solution (see below), which has implications in catalysis (1–3), may be a common property of low-spin ruthenium(II) species containing essentially *trans* phosphine ligands with Ru—P distances of greater than about 2.40 Å (for example, as with $RuCl_2(PPh_3)_3$ (19, 20)), while related complexes such as $RuHCl(PPh_3)_3$ and $RuHCl(diop)_2$ with somewhat shorter *trans* Ru—P distances (in the range 2.329–2.393 Å (21, 22) do not measurably dissociate (23). A somewhat long Ru—N_{py} bond of 2.193 Å within Ru(TPP)(CO)py has been similarly considered to reflect enhanced lability of the pyridine ligand in this complex compared to that in $Ru(OEP)py_2$, where Ru—N_{py} = 2.10 Å (15, 18).

Solution species

As described in the Experimental section, noted spectral changes on adding phosphine to dilute solutions of the $Ru(porp)L_2$ complexes were consistent with a dissociation equilibrium (eq. [1]). Figure 3 shows the spectral changes observed for the spectrophotometric titration for the $Ru(OEP)(PPh_3)_2/PPh_3$ system in toluene at 20°C and the inset log–log plot shows the excellent agreement with analysis according to eq. [2]. The data do not analyze for dimer formation (eq. [3]), although such metal–metal bonded dimers are known (24, 25); further, the electronic spectra of the dimers (24) are quite different to those of the suggested five-coordinate species (Fig.3, Table 1).

[3] $2Ru(porp)L_2 \rightleftharpoons [Ru(porp)L_n]_2 + (4 - 2n)L; \qquad n = 0, 1$

Can. J. Chem. Downloaded from www.nrcresearchpress.com by 210.87.254.5 on 09/06/12
For personal use only.

The existence of the five-coordinate Ru(porp)(CO) complexes seems well substantiated (10), and thus the lower wavelength Soret maximum of the spectrophotometric titration data (Fig. 3) is assigned to the Ru(OEP)(PPh_3) species; the familiar two-peak maxima of the low spin, six-coordinate, bis(ligand) species in the 500−600 nm region (1, 4, 10, 26) is replaced by a somewhat broader, single, and more intense band (Fig. 3, Table 1). The spectra of the bis(phosphine) complexes, therefore, in general will be concentration dependent; visible spectra reported previously for Ru(TPP)(PPh_3)$_2$ correspond more closely to that of the five-coordinate species, although the concentrations used were not stated (5, 6).

The abscissa intercept of Fig. 3 (inset) gives $K = 1.2 \times 10^{-5}$ M. For the tris(*p*-methoxyphenyl)phosphine system, $K = 5 \times 10^{-6}$ M, while the corresponding values for the TPP systems were 1.35×10^{-4} M (PPh_3) and 3.7×10^{-6} M (P(*p*-$CH_3OC_6H_4$)$_3$). Excellent data were obtained for all four systems, and the values are considered accurate to ±15%. Because tri-*n*-butylphosphine is a required cocatalyst in the decarbonylation of aldehydes using the Ru(TPP)(PPh_3)$_2$ complex (2), equilibria [1] with L = P^{n}Bu$_3$ were studied also. The bis(tri-*n*-butylphosphine) complexes of the TPP and OEP systems at $<10^{-6}$ M gave spectra of the six-coordinate species only (Table 1, and Table 1 in ref. 4, respectively) implying much smaller dissociation constants ($<10^{-8}$ M); the much higher basicity of the trialkylphosphines compared to triphenylphospine (>7 pK_a units (27)) readily accounts for this difference, but steric factors could be as important. Within either porphyrin system, the less basic PPh_3 compared to P(*p*-$CH_3OC_6H_4$)$_3$, by ~2 pK_a units (27), accounts for larger K values with the PPh_3 system, although the factors differ considerably (~2.5 and ~35 for the OEP and TPP systems, respectively). The difference in porphyrin basicities is one factor (OEP, pK_a ~ 6; TPP, pK_a ~ 3 (28)), and while normally within a related series of porphyrins (such as TPP derivatives containing *p*-substituents on the phenyl rings), axial ligand binding is enhanced with decreasing porphyrin basicity (28, 29), this has not been established for porphyrins as diverse as OEP and TPP, where contacts with the phenyl or ethyl groups on TPP and OEP, respectively, may also be important. Limited data on binding of a single amine ligand to four-coordinate cobalt(II) porphyrins show little difference in the binding constants for OEP and TPP systems (28). In the present Ru systems (a five- to six-coordinate equilibrium), the P(*p*-$CH_3OC_6H_4$)$_3$ ligand binds to much the same extent with both porphyrin systems, while PPh_3 binds more strongly (×10) to the more basic OEP system. Within these four systems, steric factors should be of little consequence; differences in solvation by toluene of the five- and six-coordinate species and the ligand could certainly play a role (30). The factors affecting axial ligand binding to metalloporphyrins are many and complex (particularly π-bonding effects); further data on the ruthenium systems are essential for a better understanding of equilibria such as [1], but the individual K values are important in estimating catalytic potential of the systems where the concentration of the 16*e* five-coordinate species is likely to be essential, for example, in abstracting CO from aldehydes with concomitant formation of Ru(porp)(CO)L (2). Dilute solutions of the (carbonyl)phosphine complex Ru(TPP)(CO)PPh_3 similarly show dissociation of the phosphine ligand and reveal the spectrum of Ru(TPP)(CO), that is formed also in dilute solutions of the ethanol precursor Ru(TPP)(CO)EtOH (10). The spectrum of the six-coordinate (carbonyl)phosphine is generated in the presence of excess phosphine (Table 1); the dissociation equilibrium was not studied quantitatively but is of the order of 2×10^{-6} M in toluene at room temperature.

TABLE 6. Bond lengths (Å) with esd's in parentheses

Bond	Length	
	Molecule A	Molecule B
P(1)—Ru(1)	2.438(<1)	2.419(<1)
N(1)—Ru(1)	2.057(3)	2.049(3)
N(2)—Ru(1)	2.044(3)	2.052(3)
C(1)—P(1)	1.837(4)	1.836(5)
C(7)—P(1)	1.845(5)	1.834(4)
C(13)—P(1)	1.853(4)	1.845(5)
C(2)—C(1)	1.381(6)	1.392(7)
C(3)—C(2)	1.393(7)	1.411(9)
C(4)—C(3)	1.386(9)	1.345(10)
C(5)—C(4)	1.363(9)	1.375(12)
C(6)—C(5)	1.384(7)	1.391(9)
C(6)—C(1)	1.402(7)	1.379(7)
C(8)—C(7)	1.382(6)	1.360(8)
C(9)—C(8)	1.387(8)	1.359(9)
C(10)—C(9)	1.363(9)	1.382(11)
C(11)—C(10)	1.392(9)	1.385(11)
C(12)—C(11)	1.386(9)	1.381(9)
C(12)—C(7)	1.396(6)	1.393(7)
C(14)—C(13)	1.371(7)	1.354(7)
C(15)—C(14)	1.411(8)	1.405(9)
C(16)—C(15)	1.345(9)	1.358(8)
C(17)—C(16)	1.365(9)	1.359(8)
C(18)—C(17)	1.377(7)	1.361(9)
C(18)—C(13)	1.379(7)	1.381(7)
C(19)—N(1)	1.374(5)	1.368(5)
C(20)—C(19)	1.458(5)	1.440(7)
C(21)—C(20)	1.364(6)	1.354(8)
C(22)—C(21)	1.458(5)	1.454(6)
C(22)—N(1)	1.376(5)	1.375(6)
C(23)—C(22)	1.379(6)	1.381(7)
C(24)—C(23)	1.389(6)	1.378(6)
C(24)—N(2)	1.374(5)	1.459(6)
C(25)—C(24)	1.452(6)	1.371(6)
C(26)—C(25)	1.344(5)	1.355(6)
C(27)—C(26)	1.453(6)	1.452(7)
C(27)—N(2)	1.380(5)	1.370(5)
C(28)—C(27)	1.388(5)	1.389(6)
C(28)—C(19*)[a]	1.383(5)	1.401(6)
C(29)—C(26)	1.504(6)	1.507(6)
C(30)—C(29)	1.512(7)	1.528(7)
C(31)—C(25)	1.505(6)	1.517(8)
C(32)—C(31)	1.512(7)	1.387(6)
C(32′)—C(31)	—	1.411(6)
C(33)—C(21)	1.496(5)	1.546(9)
C(34)—C(33)	1.530(7)	1.352(8)
C(34′)—C(33)	—	1.372(8)
C(35)—C(20)	1.509(6)	1.552(9)
C(36)—C(35)	1.518(7)	1.395(13)

[a]C(19*) is related to C(19) by the inversion centre.

In relation to the catalysis, the reactions of six-coordinate Ru(porp)L_2 complexes generally (L = phosphine, CH_3CN, THF, etc.) with gas molecules such as CO, and sometimes O_2 (3), go via the dissociative mechanism shown in eq. [4] (1, 31−34), exactly analogous to corresponding Fe(II) systems (28, 35).

$$[4]\quad \text{Ru(porp)L}_2 \underset{k_{-1},\ +\text{L}}{\overset{k_1,\ -\text{L}}{\rightleftharpoons}} \text{Ru(porp)L} \underset{k_{-2},\ -\text{gas}}{\overset{k_2,\ \text{gas}}{\rightleftharpoons}} \text{Ru(porp)(gas)L}$$

Standard kinetic analysis of such systems allows for deter-

TABLE 7. Bond angles (deg) with esd's in parentheses

Bonds	Angle		Bonds	Angle	
	Molecule A	Molecule B		Molecule A	Molecule B
N(1)—Ru(1)—P(1)	94.2(1)	91.5(1)	C(16)—C(15)—C(14)	120.0(5)	120.9(5)
N(2)—Ru(1)—P(1)	91.0(1)	94.7(1)	C(17)—C(16)—C(15)	120.2(5)	118.8(6)
N(1)—Ru(1)—N(2)	89.9(1)	89.6(1)	C(18)—C(17)—C(16)	119.8(5)	119.9(5)
C(1)—P(1)—Ru(1)	110.4(1)	111.9(1)	C(17)—C(18)—C(13)	121.9(5)	122.9(5)
C(7)—P(1)—Ru(1)	116.1(1)	115.8(1)	C(20)—C(19)—N(1)	109.2(3)	109.6(4)
C(13)—P(1)—Ru(1)	125.5(1)	125.2(1)	C(21)—C(20)—C(19)	107.3(3)	107.6(4)
C(7)—P(1)—C(1)	106.6(2)	106.3(2)	C(35)—C(20)—C(19)	124.0(4)	123.2(5)
C(13)—P(1)—C(1)	99.3(2)	99.1(2)	C(35)—C(20)—C(21)	128.7(3)	129.0(5)
C(13)—P(1)—C(7)	96.4(2)	95.7(2)	C(22)—C(21)—C(20)	106.7(3)	106.6(4)
C(19)—N(1)—Ru(1)	126.4(2)	126.2(3)	C(33)—C(21)—C(20)	128.4(4)	129.0(5)
C(22)—N(1)—Ru(1)	126.2(3)	126.8(3)	C(33)—C(21)—C(22)	124.9(4)	124.4(5)
C(22)—N(1)—C(19)	107.3(3)	106.9(3)	C(21)—C(22)—N(1)	109.5(3)	109.3(4)
C(24)—N(2)—Ru(1)	127.3(3)	126.7(2)	C(23)—C(22)—N(1)	124.0(3)	123.9(4)
C(27)—N(2)—Ru(1)	126.5(2)	126.6(3)	C(23)—C(22)—C(21)	126.4(3)	126.8(4)
C(27)—N(2)—C(24)	106.2(3)	106.7(3)	C(24)—C(23)—C(22)	129.3(4)	128.8(5)
C(2)—C(1)—P(1)	123.0(3)	123.1(3)	C(23)—C(24)—N(2)	123.1(4)	124.1(4)
C(6)—C(1)—P(1)	118.3(3)	118.7(4)	C(25)—C(24)—N(2)	110.0(3)	109.4(3)
C(6)—C(1)—C(2)	118.3(4)	118.1(5)	C(25)—C(24)—C(23)	126.9(3)	126.4(4)
C(3)—C(2)—C(1)	121.4(4)	119.5(5)	C(26)—C(25)—C(24)	106.9(3)	107.1(4)
C(4)—C(3)—C(2)	119.0(5)	121.2(7)	C(31)—C(25)—C(24)	124.4(4)	125.2(4)
C(5)—C(4)—C(3)	120.5(5)	119.9(7)	C(31)—C(25)—C(26)	128.7(4)	127.7(4)
C(6)—C(5)—C(4)	120.6(5)	119.7(6)	C(27)—C(26)—C(25)	107.5(4)	106.7(4)
C(5)—C(6)—C(1)	120.3(5)	121.5(6)	C(29)—C(26)—C(25)	129.2(4)	128.1(4)
C(8)—C(7)—P(1)	116.1(3)	116.6(4)	C(29)—C(26)—C(27)	123.2(3)	125.1(4)
C(12)—C(7)—P(1)	125.5(3)	126.2(4)	C(26)—C(27)—N(2)	109.4(3)	110.1(4)
C(12)—C(7)—C(8)	118.2(5)	117.1(5)	C(28)—C(27)—N(2)	124.2(4)	124.0(4)
C(9)—C(8)—C(7)	121.1(5)	123.2(6)	C(28)—C(27)—C(26)	126.4(4)	125.8(4)
C(10)—C(9)—C(8)	121.0(5)	119.5(7)	C(30)—C(29)—C(26)	112.5(4)	112.3(3)
C(11)—C(10)—C(9)	118.7(6)	119.1(6)	C(32)—C(31)—C(25)	114.4(4)	115.8(4)
C(12)—C(11)—C(10)	120.9(6)	119.6(6)	C(32′)—C(31)—C(25)	—	122.8(4)
C(11)—C(12)—C(7)	120.1(5)	121.1(6)	C(34)—C(33)—C(21)	113.8(4)	124.5(6)
C(14)—C(13)—P(1)	123.4(4)	124.5(4)	C(34′)—C(33)—C(21)	—	126.5(6)
C(18)—C(13)—P(1)	119.2(3)	118.5(4)	C(34′)—C(33)—C(34)	—	109.0(5)
C(18)—C(13)—C(14)	117.3(4)	117.0(5)	C(36)—C(35)—C(20)	112.5(4)	106.5(6)
C(15)—C(14)—C(13)	120.7(5)	120.5(5)			

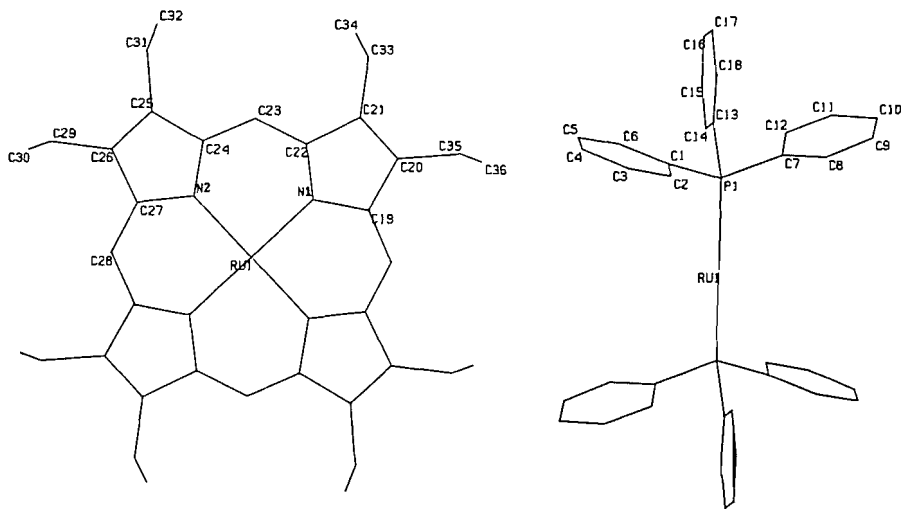

FIG. 1. The atomic numbering scheme for the $Ru(OEP)(PPh_3)_2$ molecule.

mination of the rate constants k_1, k_{-2}, and the ratio k_{-1}/k_2 (28); independent measurement of K (i.e. k_1/k_{-1}), as discussed above, thus provides for evaluation of both k_{-1} and k_2. Factors affecting the fixing of the gas molecule at the Ru centre can thus be better elucidated. These kinetic studies, presently described in the theses of Walker and Tarpey (33, 34), will be published later.

Exposure to air of solutions of the bis(phosphine) complexes

Can. J. Chem. Downloaded from www.nrcresearchpress.com by 210.87.254.5 on 09/06/12
For personal use only.

Can. J. Chem. Downloaded from www.nrcresearchpress.com by 210.87.254.5 on 09/06/12
For personal use only.

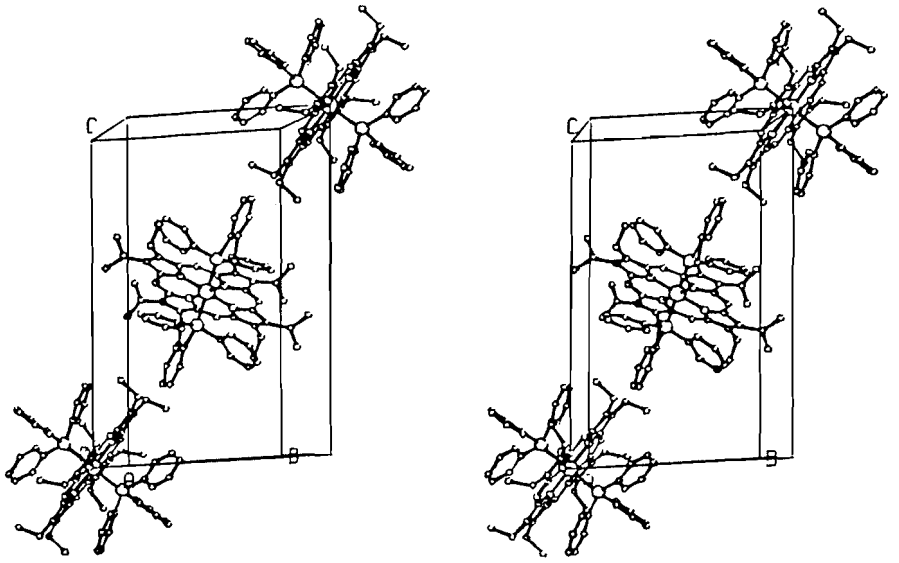

FIG. 2. Stereoscopic view of the unit cell contents (both positions are shown for disordered carbon atoms in molecule B).

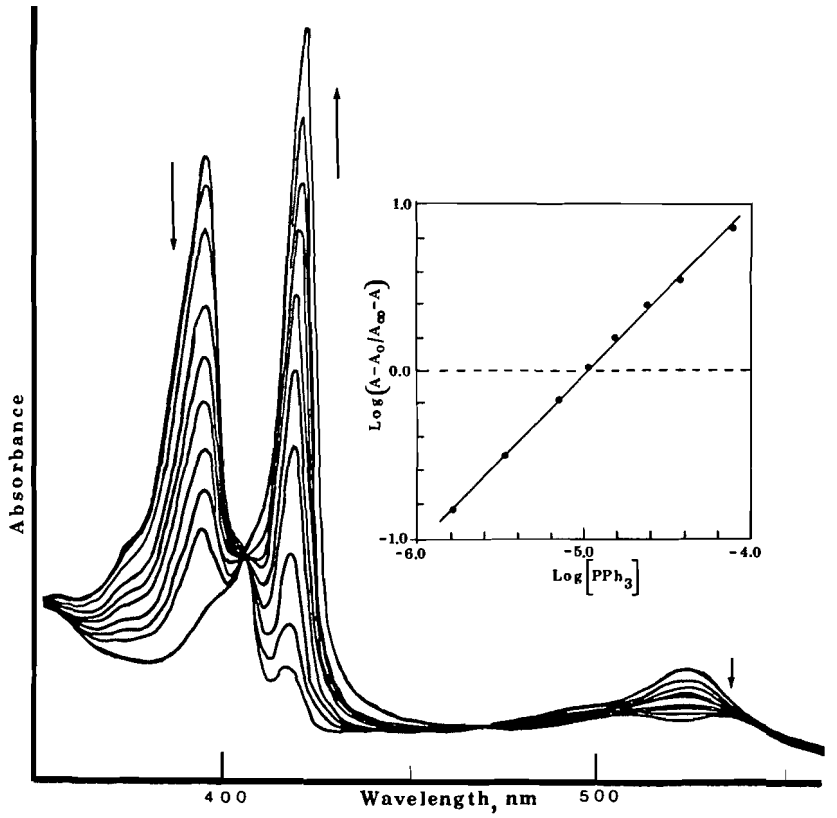

FIG. 3. Spectrophotometric titration for the $Ru(OEP)(PPh_3)_2/PPh_3$ system. Addition of the PPh_3 to $\sim 10^{-6}$ *M* of $Ru(OEP)(PPh_3)_2$ gives conversion from the five-coordinate (λ_{max} 395 nm) to six-coordinate species (λ_{max} 420 nm); absorbance (*A*) measured at 420 nm. Inset shows the log/log plot according to eq. [2].

led to slow generation over a few days of the ruthenium(IV) μ-oxo dimer $[Ru(porp)(OH)]_2O$, as evidenced by the uv/vis spectrum (16, 24).

Evidence has been presented elsewhere for dissociation of a phosphine from $Ru(OEP)(CO)PPh_3$ (4) and $Ru(OEP)(dpe)_2$ (17, 36) complexes in non-coordinating solvents such as toluene or CH_2Cl_2. Dissolution of the bis(monodentatephosphine) complexes, including the *n*-butylphosphine complex, in these solvents containing a few percent by volume of a coordinating solvent such as DMSO or CH_3CN generated a six-coordinate type spectrum that was slightly blue-shifted from that of the bis(phosphine) species. The species present is almost certainly Ru(porp)(phosphine)(coordinating solvent). In the case of adding $Ru(OEP)(P^nBu_3)_2$ to CH_2Cl_2 containing ~0.3 *M* DMSO, the species generated (λ_{max} at 406 nm) would be Ru(OEP)(P^nBu_3) (DMSO); support for this is that the same spectrum is generated on reducing solutions of $Ru(OEP)(P^nBu_3)Br$ (4) by borohydride or superoxide in DMSO solution, and that

upon further treatment with excess P^nBu_3 the spectrum of Ru(OEP)(P^nBu_3)$_2$ is regenerated via a clean isosbestic system. The spectrum of Ru(OEP)(DMSO)$_2$ (15) is not generated at any stage.

The ^{1}H nmr data were measured using solution of the complexes at $10^{-2}-10^{-1}$ *M*, when the only detectable species are the six-coordinate bis(phosphine) or carbonyl(phosphine) species (Table 2). Based on fairly extensive literature data for OEP and TPP complexes including Ru systems (6, 10, 15, 24, 36, 37), the shifts are typical for diamagnetic species and are readily assigned. The symmetry of the bis(phosphine) species is revealed by the equivalence of corresponding protons on the two axial ligands, for example, the *o*-hydrogens of the PPh_3 and P(*p*-$CH_3OC_6H_4$)$_3$ ligands (the shifts are at relatively high field, (3.8−4.2)δ, due to the ring current effect exerted by the porphyrin; the *m*- and *p*-hydrogens are similarly shifted but less so, (5.8−7.0)δ). In the symmetrical OEP complexes, the methylene protons of the ethyl groups appear as the expected quartet. The asymmetry present in the Ru(OEP)(CO)(PPh_3) complex leads to the methylene protons becoming diastereotopic and their detection as an ABX_3 pattern within the ethyl group (24, 36); the 12-line multiplet detected at 400 MHz is essentially identical to one reported previously for a [Nb(OEP)]$_2$(μ-O)$_3$ complex (38). The asymmetry in the Ru(TPP)(CO)(PPh_3) complex is probably reflected in the resonances of the porphyrin phenyl ring; in the symmetrical bis(phosphine) complexes, the *o*-, *m*-, and *p*-protons appear as slightly broadened singlets at ~7.6δ for the two triarylphosphine systems, and at 8.2 δ for the P^nBu_3 system, while the carbonyl derivative gives a complex pattern at (7.5−8.3)δ.

Concluding remarks

Details for the synthesis of some bis(tertiary phosphine) and carbonyl(tertiary phosphine) of Ru(II) are presented, together with their characterization by uv/vis and ^{1}H nmr spectra. The crystal structure of Ru(OEP)(PPh_3)$_2$ is reported also. Several of the complexes have been reported in previous papers from this laboratory dealing with their catalytic and redox chemistry (2−4, 31, 36), but in most cases details of their syntheses and characterization were not presented. The quantitative determination of the equilibrium constants for phosphine dissociation from the bis(phosphine) complexes is critical for an understanding of their solution chemistry, which is currently being developed.

Acknowledgements

This work, a contribution from the Bioinorganic Chemistry Group, was supported by grants from the Natural Sciences and Engineering Research Council of Canada, and the United States Institutes of Health (AM 17989). We also thank Johnson, Matthey Ltd. for the loan of ruthenium, and the University of British Columbia Computing Centre for assistance.

1. B. R. JAMES, A. W. ADDISON, M. CAIRNS, D. DOLPHIN, N. P. FARRELL, D. R. PAULSON, and S. WALKER. *In* Fundamental research in homogeneous catalysis. Vol. 3. *Edited by* M. Tsutsui. Plenum Press, New York. 1979. p. 751.
2. G. DOMAZETIS, B. R. JAMES, B. TARPEY, and D. DOLPHIN. Am. Chem. Soc. Symp. Ser. No. 152, 243 (1981).
3. B. R. JAMES, S. R. MIKKELSEN, T. W. LEUNG, G. M. WILLIAMS, and R. WONG. Inorg. Chim. Acta. In press.
4. M. BARLEY, J. Y. BECKER, G. DOMAZETIS, D. DOLPHIN, and B. R. JAMES. Can. J. Chem. **61**, 2389 (1983).
5. B. C. CHOW and I. A. COHEN. Bioinorg. Chem. **1**, 57 (1971).
6. T. BOSCHI, G. BONTEMPELLI, and G. A. MAZZOCCHIN. Inorg. Chim. Acta, **37**, 155 (1979).
7. A. MANTOVANI and S. CENINI. Inorg. Synth. **16**, 47 (1976).
8. A. D. ADLER, F. R. LONGO, J. D. FINARELLI, J. GOLDMACHER, J. ASSOUP, and L. KORSAKOFF. J. Org. Chem. **32**, 476 (1967).
9. J. B. PAINE, W. B. KIRSHNER, D. W. MOSKOWITZ, and D. DOLPHIN. J. Org. Chem. **41**, 3857 (1976).
10. J. J. BONNET, S. S. EATON, G. R. EATON, R. H. HOLM, and J. A. IBERS. J. Am. Chem. Soc. **95**, 2141 (1973).
11. T. J. COLLINS. Private communication.
12. G. M. SHELDRICK. SHELX (1976). Program for crystal structure determination, University of Cambridge.
13. International tables for X-ray crystallography. Vol. IV. Kynock Press, Birmingham, England. 1974. p. 99.
14. H. MASUDA, T. TAGA, K. OSAKI, H. SUGIMOTO, Z-I. YOSHIDA, and H. OGOSHI. Inorg. Chem. **19**, 950 (1980).
15. F. R. HOPF, T. P. O'BRIEN, W. R. SCHEIDT, and D. G. WHITTEN. J. Am. Chem. Soc. **97**, 277 (1975).
16. H. MASUDA, T. TAGA, K. OSAKI, H. SUGIMOTO, M. MORI, and H. OGOSHI. J. Am. Chem. Soc. **103**, 2199 (1981).
17. R. G. BALL, G. DOMAZETIS, D. DOLPHIN, B. R. JAMES, and J. TROTTER. Inorg. Chem. **20**, 1556 (1981), and references therein.
18. R. G. LITTLE and J. A. IBERS. J. Am. Chem. Soc. **95**, 8583 (1973).
19. B. R. JAMES, L. K. THOMPSON, and D. K. W. WANG. Inorg. Chim. Acta, **29**, L237 (1978).
20. S. J. LAPLACA and J. A. IBERS. Inorg. Chem. **4**, 778 (1965).
21. A. C. SKAPSKI and P. G. H. TROUGHTON. Chem. Commun. 1230 (1968).
22. R. G. BALL and J. TROTTER. Inorg. Chem. **20**, 261 (1981).
23. B. R. JAMES. Adv. Organomet. Chem. **17**, 319 (1979).
24. J. P. COLLMAN, C. E. BARNES, T. J. COLLINS, P. J. BROTHERS, J. GALLUCCI, and J. A. IBERS. J. Am. Chem. Soc. **103**, 7031 (1981).
25. P. N. SWEPSTON and J. A. IBERS. Am. Crystallographic Assoc. Meeting Mar. 1983. Univ. of Missouri, Abstract PB23.
26. A. ANTIPAS, J. W. BUCHLER, M. GOUTERMAN, and P. D. SMITH. J. Am. Chem. Soc. **100**, 3015 (1978).
27. T. ALLMAN and R. G. GOEL. Can. J. Chem. **60**, 716 (1982).
28. B. R. JAMES. *In* The porphyrins. Vol. V. *Edited by* D. Dolphin. Academic Press, New York. 1978. p. 205.
29. D. W. SMITH. Ph.D. dissertation. University of British Columbia. 1980.
30. F. A. WALKER. J. Am. Chem. Soc. **95**, 1150 (1973).
31. G. DOMAZETIS, B. TARPEY, D. DOLPHIN, and B. R. JAMES. J. Chem. Soc. Chem. Commun. 939 (1980).
32. N. P. FARRELL, D. DOLPHIN, and B. R. JAMES. J. Am. Chem. Soc. **100**, 324 (1978).
33. S. G. WALKER. M.Sc. thesis. University of British Columbia. 1980.
34. B. TARPEY. M.Sc. thesis. University of British Columbia. 1982.
35. J. MARTINSON, M. MILLER, D. TROJAN, and D. A. SWEIGART. Inorg. Chem. **19**, 2162 (1980).
36. G. DOMAZETIS, B. R. JAMES, and D. DOLPHIN. Inorg. Chim. Acta, **54**, L47 (1981).
37. T. R. JANSON and J. J. KATZ. *In* The porphyrins. Vol. IV. *Edited by* D. Dolphin. Academic Press, New York. 1978. p. 1.
38. C. LECOMTE, J. PROTAS, R. GUILARD, B. FLINIAUX, and P. FOURNARI. J. Chem. Soc. Dalton, 1306 (1979).

Can. J. Chem. Downloaded from www.nrcresearchpress.com by 210.87.254.5 on 09/06/12
For personal use only.

N-acylglycine dithioesters form enethiolates near pH 9[1]

H. LEE, P. R. CAREY, AND A. C. STORER
Division of Biological Sciences, National Research Council of Canada, Ottawa, Ont., Canada K1A 0R6

Received September 26, 1983

H. LEE, P. R. CAREY, and A. C. STORER, Can. J. Chem. **62**, 763 (1984).

It is demonstrated that *N*-acylglycine ethyl dithioesters have fairly acidic α-CH protons, and that ionization leads to the formation of enethiolate anions. For example, the pK_a's of *N*-benzoyl- and *N*-(β-phenylpropionyl)glycine ethyl dithioesters are 9.04 and 9.62, respectively. *N*-acylglycine papain dithioesters are formed during the papain catalyzed hydrolysis of the corresponding methyl thionoesters. However, for the papain dithioesters, no evidence was found for the formation of enethiolate anions.

H. LEE, P. R. CAREY et A. C. STORER. Can. J. Chem. **62**, 763 (1984).

On a démontré que les protons α-CH des dithioesters d'éthyle et de *N*-acylglycine sont assez acides et que leur ionisation conduit à la formation d'anions ènethiolates. Par exemple, les pK_a des dithioesters d'éthyle et soit de *N*-benzoyl- ou de *N*-(β-phénylpropionyl)-glycine sont respectivement 9,04 et 9,62. Les dithioesters de papaine et de *N*-acylglycine se forment lors de l'hydrolyse catalysée par la papaine des thionoesters méthyliques correspondants. Toutefois, on n'a pas pu mettre en évidence de formation d'anions ènethiolates avec les dithioesters de papaine.

[Traduit par le journal]

Can. J. Chem. Downloaded from www.nrcresearchpress.com by 210.87.254.40 on 09/06/12
For personal use only.

Introduction

The present work originates in our resonance Raman, kinetic, and X-ray crystallographic studies of *N*-acylglycine papain dithioesters and their corresponding model compounds (1). The papain catalysed hydrolysis of *N*-acylglycine thionoesters proceeds via the formation of a dithioacyl enzyme intermediate which may be monitored by either spectrophotometry or resonance Raman (RR) spectroscopy (2). The use of the RR spectra to elucidate the events occurring in the enzyme's active site requires an in-depth understanding of the RR specroscopy and the chemistry of dithioesters. To this end there have been several spectroscopic (3, 4), kinetic (5), and X-ray crystallographic (6) studies on model dithioesters of varying degrees of complexity. In one recent kinetic study (5), concerning the hydrolysis of simple dialkyl dithioesters (e.g. ethyl dithioacetate), it was shown that hydrolysis is in competition with a second process. It was suggested that, due to the high acidity of the α-CH protons, this second process most probably involves the formation of a quasi-stable enethiolate anion. However, since the evidence presented was entirely kinetic, it was impossible to rule out completely the alternative explanation that the second process is due to the formation of a stabilized tetrahedral intermediate. One objective of the present work was to see if the hydrolysis of *N*-acylglycine dithioesters exhibits similar kinetic behaviour to that of the simple dithioesters. Moreover, unlike the simple dithioester case, we are able to use RR data to identify the quasi-stable intermediates formed during the hydrolysis of *N*-benzoylglycine ethyl dithioester (I) and *N*-(β-phenylpropionyl)glycine ethyl dithioester (II).

Finally, we use the RR spectroscopic information gained on model *N*-acylglycine dithioesters to search for evidence of α-CH ionization in the glycine portion of *N*-acylglycine papain dithioester intermediates.

Experimental

The dithioesters and their isotopically substituted analogues were synthesized as described in refs. 3 and 4. The reactions of the dithioesters in borate buffer pH 8.5–10.5 were monitored using a Cary 219 spectrophotometer. Plots of log ($OD_\infty - OD_t$) against time were linear for >90% of the reaction and the rate constants were obtained by a linear least-squares treatment of the data. At higher pH's the hydroxide ion concentration was varied by making direct additions of a standard NaOH solution to the reaction mixture, using distilled, deionized water throughout. For the buffered solutions the [OH^-] values were calculated from the measured pH, whereas for the unbuffered solutions the [OH^-] values were obtained by adding a known quantity of the standard NaOH solution. No attempt was made to keep the ionic strength constant due to the complex variation in buffer ionic strength with pH and the modest range of ionic strength used. Because of the higher rate of reaction above pH 10.5, the absorption changes were monitored using a Cantech (Winnipeg, Canada) stopped-flow spectrometer. This instrument was coupled to a PET microcomputer via a transient recorder. The transmission changes were <5% and the data (256 data points with 8-bit resolution) were fitted to a single exponential decay using a non-linear least-squares procedure (7). Dithioester I was monitored at 360 nm and dithioester II at 295 nm. All reactions were carried out at 20°C. The RR spectra were obtained using 324 nm Kr^+ laser excitation and a diode array based detection system described previously (4, 8).

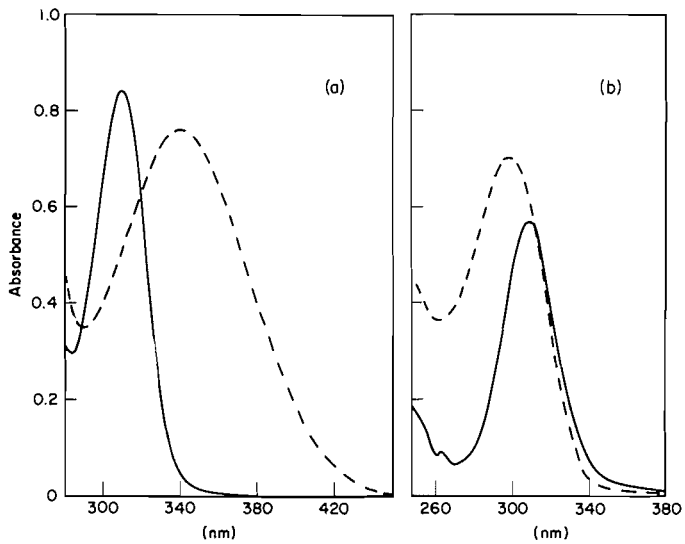

FIG. 1. Absorption spectra of (a) *N*-benzoylglycine ethyl dithioester (I) (8.4×10^{-5} *M*, 1-cm cell) and (b) *N*-(β-phenylpropionyl)glycine ethyl dithioester (II) (5.3×10^{-5} *M*, 1-cm cell) at pH 7 (———) and in 0.01 *N* NaOH (– – –).

Results and discussion

Figures 1(a) and (b) show absorption spectral changes that

[1]NRCC No. 22861.

occur on placing the *N*-acyl glycine dithioesters in 0.01 *N* NaOH solution. For dithioester I there is a red shift in the near uv peak from 308 nm to 340 nm, whereas for dithioester II there is a blue shift in the peak from 308 nm to 298 nm. The spectral changes are complete within a few seconds. The shifted peaks then decay away in a second process that takes several hours ($t_{1/2} \simeq 5$ h). These biphasic spectral changes are comparable with those observed for simple dialkyl dithioesters (5). In the case of the dialkyl dithioesters a rapid spectral change is observed as a new form of the dithioester is reversibly produced at high pH and that is followed by a slow spectral change as the residual dithioester hydrolyses irreversibly:[2]

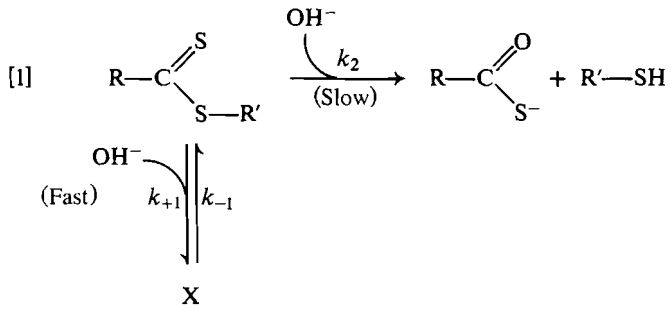

For dithioesters I and II the initial rapid spectral changes can also be shown to be reversible, since on changing the pH to neutral the spectrum reverts to that of the original dithioester. Therefore for dithioesters I and II the scheme proposed for the dialkyl dithioesters is believed to apply also. Provided the base concentration is far in excess of the dithioester concentration, the rate constant (k_{meas}) defining the initial equilibration process is:

$$[2] \quad k_{meas} = k_{-1} + k_{+1} \cdot b$$

where b = hydroxide ion concentration (see ref. 5 for more details). The rapid spectral shifts were followed, in the 10-m*M* to 200-m*M* range of hydroxide concentration, using a stopped-flow spectrometer. A typical trace is shown in Fig. 2 for dithioester I, and a plot of k_{meas} against b is shown in Fig. 3 for

[2]An alternative suggestion put forward by a referee is that the slow spectral change may not be due to hydrolysis of the residual dithioester but rather an elimination–addition mechanism involving the enethiolate, i.e.

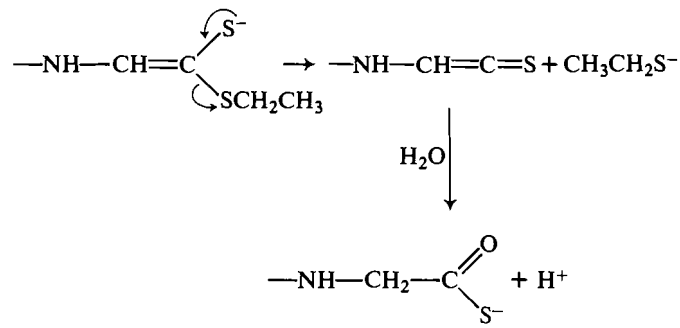

The data presently available cannot distinguish between the two possibilities although the authors prefer the simple hydrolysis mechanism. This preference is based on the fact that in order for the alternative mechanism to make a significant contribution to the rate of disappearance of the dithioester, the rate of hydrolysis of dithioesters must be much slower than that of esters and thioesters rather than just 6- to 8-fold slower as suggested in ref. 5.

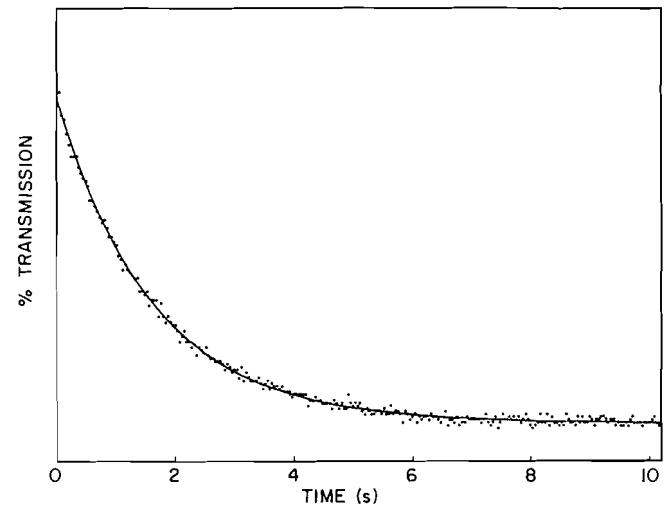

FIG. 2. Stopped flow trace of 5 μ*M* dithioester (I) in 39.2 m*M* NaOH monitored at 360 nm. The total transmission change is <5%. The solid line represents the best fit of the data to a single exponential function using a non-linear least-squares fitting procedure (7).

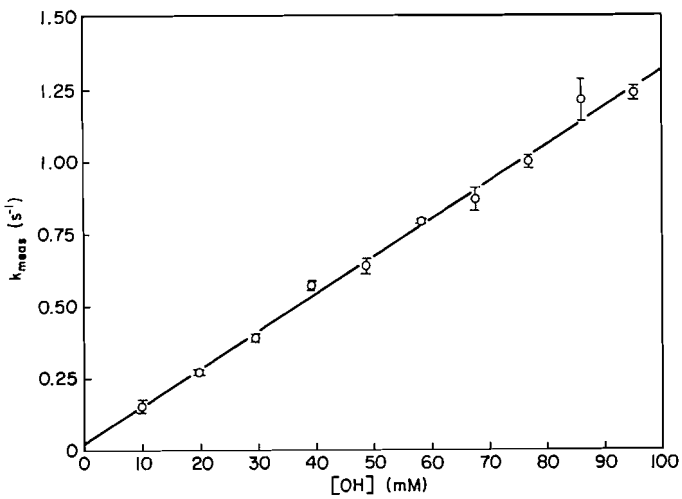

FIG. 3. Plot of k_{meas} against b ([OH^-]) for dithioester (II); k_{meas} values are the averages of at least three determinations and the error bars represent the standard deviations. The solid line represents a linear least-squares fit to the data weighted according to their standard deviations.

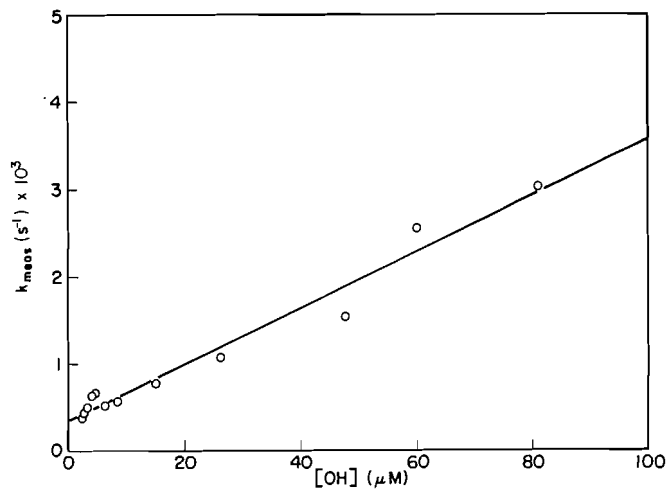

FIG. 4. Plot of k_{meas} against b ([OH^-]) for dithioester (I) obtained in 50 m*M* borate buffer. The solid line represents an unweighted linear least-squares fit to the data.

Can. J. Chem. Downloaded from www.nrcresearchpress.com by 210.87.254.40 on 09/06/12
For personal use only.

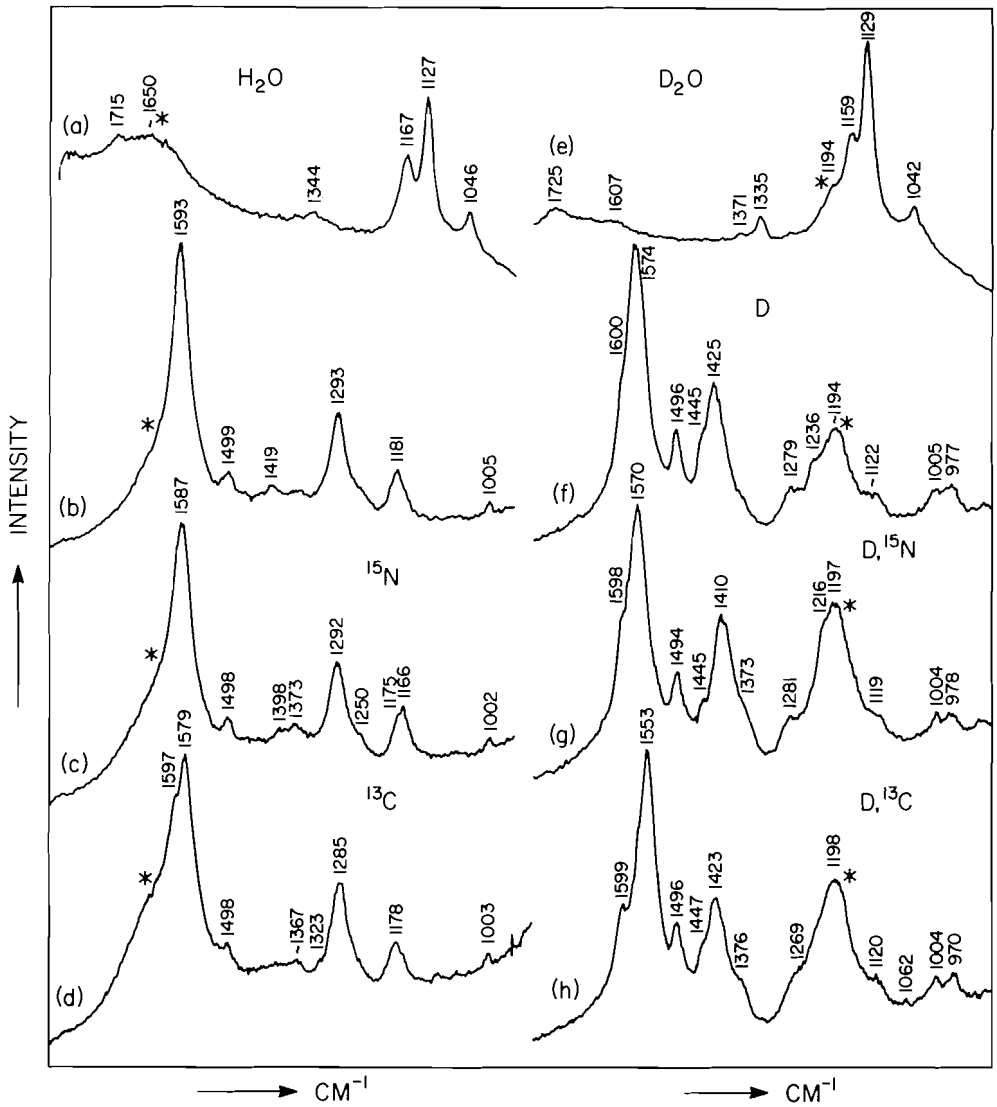

FIG. 5. Resonance Raman spectra of 4×10^{-4} *M* *N*-benzoylglycine ethyl dithioester (I) near neutral pH in H_2O (a) and neutral pD in D_2O (e), at high pH (b–d) or pD (f–h). Isotopic substitutions ^{15}N and $^{13}C{=}S$ are indicated on figure. Each spectrum was obtained using 80 mW of 324 nm Kr^+ excitation, spectral slit 12 cm^{-1}, 1 min total acquisition (4 s × 15). H_2O or D_2O contribution marked by an asterisk.

dithioester II. The error bars represent the standard deviations of the data points which are the averages of at least three determinations. The line was obtained by a linear least-squares analysis of the data weighted according to the standard deviations. From the slopes of the plots, values for k_{+1} of 15.81 ± 0.03 M^{-1} s^{-1} and 12.91 ± 0.03 M^{-1} s^{-1} were obtained for dithioesters I and II, respectively. These values are approximately one order of magnitude greater than the value of 1.36 M^{-1} s^{-1} obtained for ethyl dithioacetate (5). Although values for k_{-1} can also be obtained from the plots they are not reliable since accurate intercept values (Fig. 3) cannot be obtained with the range of concentrations used. In order to determine k_{-1} more accurately, the reactions were also monitored, using a spectrophotometer in the pH range 8.5–10.5 using 50 m*M* borate buffer. Under these conditions, since *b* does not vary appreciably with time, eq. [2] still applies. The data for dithioester I are shown in Fig. 4.

The values of k_{+1} are 32.2 ± 1.9 M^{-1} s^{-1} and 23.0 ± 1.1 M^{-1} s^{-1} for I and II, respectively, approximately twice the values obtained in the absence of borate. This difference could possibly be due to the different methods of obtaining the $[OH^-]$ concentrations or possibly some degree of buffer catalysis. The values of k_{-1} are 0.35 (±0.06) ± 10^{-3} s^{-1} and 0.95 (±0.13) × 10^{-3} s^{-1} for I and II, respectively. From the k_{+1} and k_{-1} values obtained in borate buffer it is possible to calculate pK_a's of 9.04 and 9.62 for dithioesters I and II, respectively. These pK_a values are unusually low for the α-CH of a depsipeptide but can be rationalized on the basis that the α-CH protons of dithioesters are more acidic than those of the corresponding esters or thiolesters (5, 9, 10). The fairly slow rates of proton transfer from the dithioesters to hydroxide (k_{+1}) are within the range normally encountered for carbon acids, i.e. the comparable rates for acetone and acetylacetone are 0.27 and 4×10^4 M^{-1} s^{-1}, respectively (11).

The identity of species X in eq. [1] can be established with reasonable probability from the RR data. Figures 5 and 6 compare the neutral- and high-pH RR spectra of I and II, respectively, along with the RR spectra of various isotopically-substituted forms at high pH. There are major spectral changes upon going to high pH; the characteristic intense RR bands of the neutral species in the 600 (data not shown) and 1150 cm^{-1} regions (3, 4) are replaced by a dominant feature near 1600

Can. J. Chem. Downloaded from www.nrcresearchpress.com by 210.87.254.40 on 09/06/12
For personal use only.

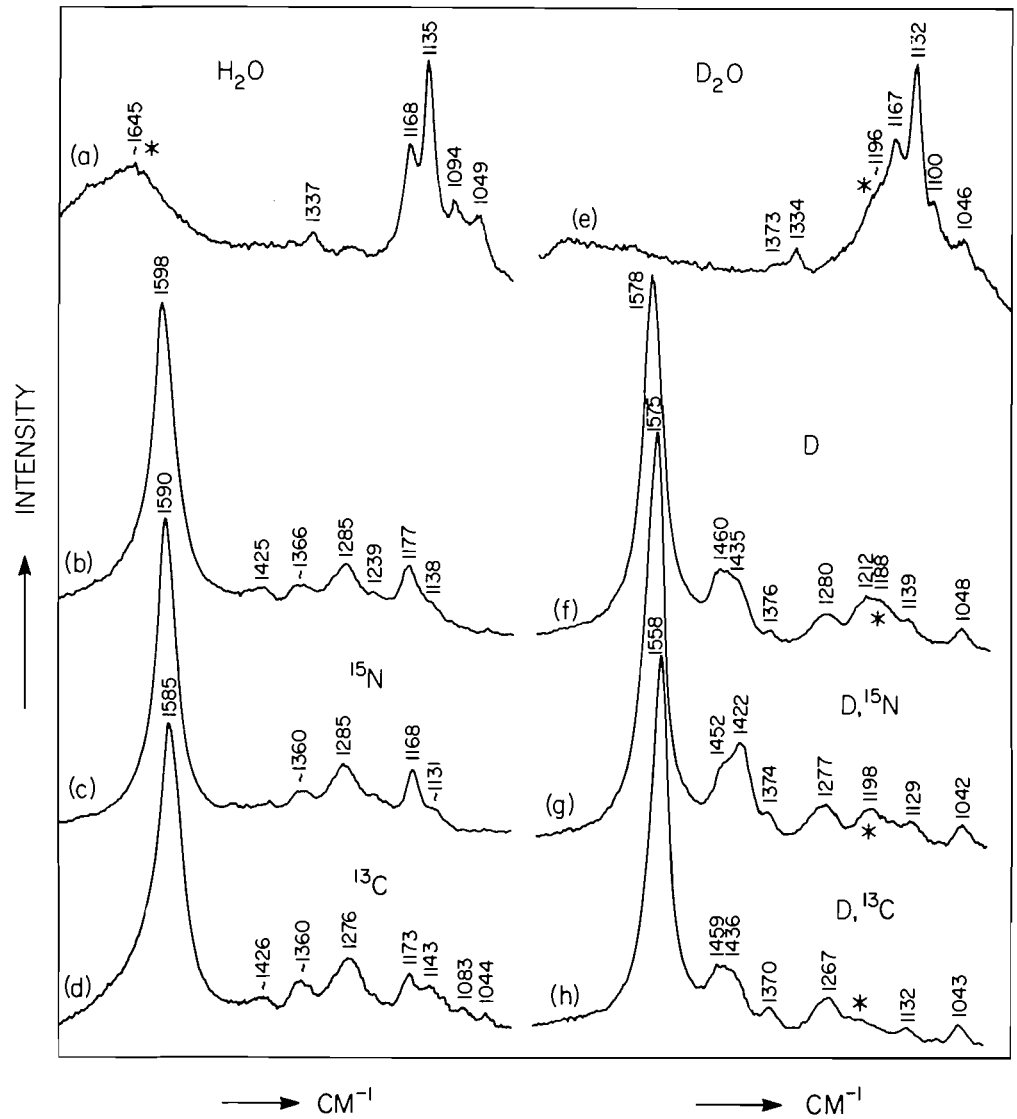

FIG. 6. Resonance Raman spectra of 10^{-3} *M* *N*-(β-phenylpropionyl)glycine ethyl dithioester (II) near neutral pH in H_2O (a) and neutral pD in D_2O (e), at high pH (b–d) or pD (f–h). Isotopic substutitons ^{15}N and $^{13}C{=}S$ are indicated on figure. Conditions as for Fig. 5. H_2O or D_2O contribution marked by an asterisk.

cm^{-1} at high pH. Isotopic substitution demonstrates that the latter feature is not due to a localized mode. Upon ^{15}N or ^{13}C (C=S) replacement the intense band shifts to lower frequency by 6 and 14 cm^{-1}, respectively for I; and by 8 and 13 cm^{-1}, respectively, for II. The position of the band, near 1600 cm^{-1}, suggests that the mode possesses double bond character but the relatively low sensitivity to ^{13}C replacement, taken with the ^{15}N results, suggests that the mode is delocalized through the glycine linkages. These findings are consistent with the species X being an enethiolate of the type:

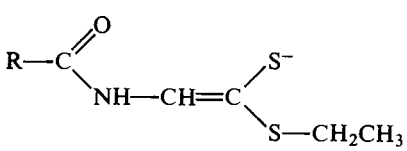

Thus, although *N*-acylglycine dithioesters are quite stable at neutral pH in the thione form (in contrast to thioketones which enolize readily if there is an α-H present), they deprotonate above pH ≃ 9.5 to form a stable enethiolate.

Further evidence for the enethiolate can be found in the spectra of the deuterated compounds. The enethiolate form has two labile hydrogens (i.e. the amide and vinyl hydrogens). In NaOD solution both are exchanged for deuterons. The mode near 1600 cm^{-1} for I and II shows a 20 cm^{-1} shift upon deuteration. In general, the C=C stretching mode of a vinyl group is sensitive to the C-deuteration because of vibrational mixing with the CH in-plane rocking mode (12). The 20 cm^{-1} shift of the 1600 cm^{-1} mode is comparable with that reported for the $C_9{=}C_{10}$ stretch of all-*trans* retinal (13). Thus, the deuteration results support the assignment of the intense 1600 cm^{-1} peak to a delocalized double bond stretching motion having some $\nu_{C=C}$ character.

Several other peaks in the high-pH RR spectra are sensitive to isotopic substitution. Features near 1290 cm^{-1} for both I and II are sensitive to ^{13}C, but not ^{15}N, replacement. The bands near 1180 cm^{-1} are sensitive to ^{15}N substitution in both compounds. In NaOD/D_2O, weak to medium bands appear near 1430 cm^{-1} for both I and II, and these bands shift upon ^{15}N substitution. It is possible that the latter bands possess some amide II′

Can. J. Chem. Downloaded from www.nrcresearchpress.com by 210.87.254.40 on 09/06/12
For personal use only.

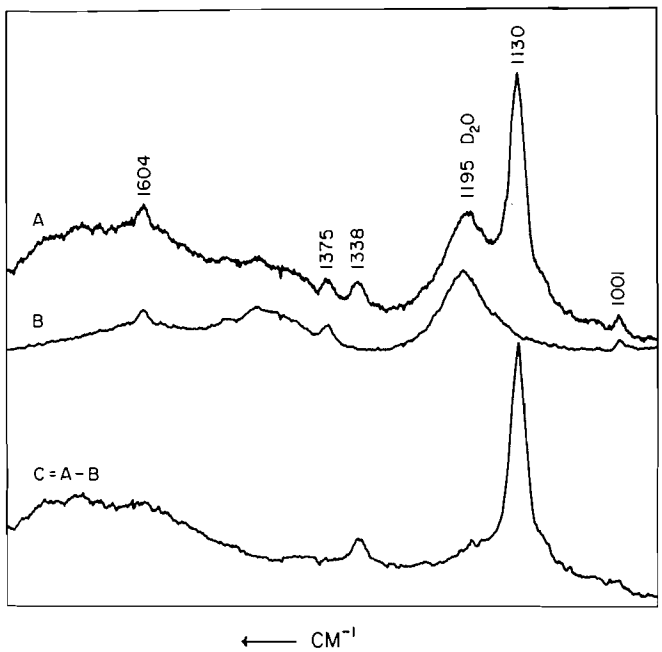

FIG. 7. Resonance Raman spectra of reaction mixture containing (A) *N*-benzoylglycine dithioacyl papain in D_2O at pD 9.2, (B) substrate alone, and (C) B subtracted from A. Conditions are given in ref. 15.

character but given the unknown nature of the force field for the enethiolate species we do not feel confident in assigning any band except the most intense feature near 1600 cm^{-1}.

Strong support for electron delocalization is seen in the RR spectra of compound I. The high-pH spectra in Fig. 5 have phenyl ring modes around 1000 cm^{-1} and 1500 cm^{-1} (14) along with a shoulder near 1600 cm^{-1} which is also due to a ring mode. Equivalent features are not seen in the high-pH spectra of compound II (Fig. 6). The appearance of the phenyl modes for I indicates that the π-electrons are delocalized throughout the acyl group and that the phenyl ring is, at least to a degree, part of the chromophore:

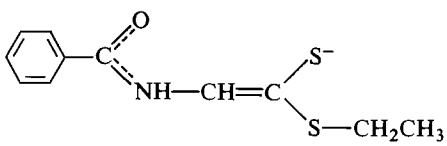

For the dithioester II, the phenyl ring is insulated from the conjugated amide–enethiolate system by two methylene groups and the phenyl group is not part of the chromophore. This difference is reflected in the frequencies of the band near 1600 cm^{-1} of the two enethiolates in that for any isotopomer the frequency, for I, is always a few wavenumbers lower, as a consequence of the greater electron delocalization, than that for II. The presence of the conjugated systems also explains the increasing red shift in λ_{max} for the series of enethiolates formed from ethyl dithioacetate (258 nm) (5), dithioester II (298 nm), and dithioester I (340 nm) since the degree of conjugation involving the enethiolate increases throughout the series. In addition, part of the variation in the α-CH pK_a's (12.5, 9.62, 9.04 for the same series) can be explained on the same basis, with increasing conjugation leading to a decrease in pK_a, since the anions formed are stabilized to a greater extent.

N-acylglycine dithioesters are formed in the active site of papain during the catalysed hydrolysis of *N*-acylglycine thionoesters (1) and it is of interest to search for the possible ionization of the glycine α-hydrogens in this environment. Thus, the intense enethiolate RR feature at approximately 1600 cm^{-1} was used as a marker in an attempt to detect the presence of an enethiolate anion form in a dithioacyl enzyme population. For the enzyme work, D_2O solutions were used in order to eliminate the possibility of the broad H_2O peak at 1650 cm^{-1} (Figs. 5 and 6) obscuring weak dithioacyl enzyme features. We were able to detect dithioacyl papain RR features at pD 9.2 (due to the decrease in activity and increase in instability of the enzyme at high pH (pD), higher values were not tried). At this pD the model dithioester I would be ca. 70% in the enethiolate form. However, as shown in Fig. 7, no peak at or around 1600 cm^{-1} ascribable to an enethiolate could be detected in the RR spectrum of *N*-benzoyl glycine dithioacyl papain. Although a weak peak at 1604 cm^{-1} was observed, this peak, based on its isotopic insensitivity and its presence in substrate spectra obtained in the absence of enzyme, was assigned to a benzene ring mode of the substrate which is present in the reaction mixture at relatively high concentrations. The absence of any enethiolate features in the dithioacyl papain spectra can be due to one or more of the following reasons: (*i*) based on the solution kinetics at pH 9.2, the uncatalysed rate of enethiolate formation would be approximately 10^2 times slower than the catalysed deacylation rate of the dithioacyl enzyme (unpublished work, this laboratory); (*ii*) in the enzyme's active site the pK_a of the α-CH protons may be very different from the value in solution (the α-CH acidity of ethyl dithioacetate is environment dependent (5)); and (*iii*) the geometry of the active site may be such that it is sterically difficult for the acyl group to undergo the conformational change associated with the ionization of the α-CH protons. Whatever the reason, it may be concluded that there is no significant ionization of the dithioacyl groups in the intermediates formed during the papain catalysed hydrolysis of *N*-acylglycine thionoesters.

Acknowledgement

We are grateful to Dr. Y. Ozaki for assistance in some preliminary studies.

1. P. R. CAREY, and A. C. STORER. Acc. Chem. Res. In press.
2. A. C. STORER, W. F. MURPHY, and P. R. CAREY. J. Biol. Chem. **254**, 3163 (1979).
3. A. C. STORER, Y. OZAKI, and P. R. CAREY. Can. J. Chem. **60**, 199 (1982).
4. H. LEE, A. C. STORER, and P. R. CAREY. Biochemistry, **22**, 4781 (1983).
5. A. C. STORER. Can. J. Chem. **61**, 1440 (1983).
6. C. P. HUBER, Y. OZAKI, D. H. PLIURA, A. C. STORER, and P. R. CAREY. Biochemistry, **21**, 3109 (1982).
7. D. W. MARQUARDT. J. Soc. Ind. Appl. Math. **11**, 431 (1963).
8. P. R. CAREY and L. R. SANS CARTIER. J. Raman Spectrosc. **14**, 271 (1983).
9. A. THUILLIER and J. VIALLE. Bull. Soc. Chim. Fr. 2182 (1963).
10. B. V. KURGANE, M. T. BRAKMANE, Y. P. STRADYN, and S. A. GILLER. Zh. Org. Khim. **11**, 926 (1975).
11. M. EIGEN. Angew. Chem. Int. Ed. Engl. **3**, 1 (1964).
12. N. B. COLTHUP, L. H. DALY, and S. E. WIBERLEY. Introduction to infrared and Raman spectroscopy. Academic Press, New York. 1975. p. 246.
13. B. CURRY, A. BROEK, J. LUGTENBURG, and R. MATHIES. J. Am. Chem. Soc. **104**, 5274 (1982).
14. H. SHINDO and J. HIRAISHI. J. Raman Spectrosc. **12**, 194 (1982).
15. A. C. STORER, H. LEE, and P. R. CAREY. Biochemistry, **22**, 4789 (1983).

Can. J. Chem. Downloaded from www.nrcresearchpress.com by 210.87.254.40 on 09/06/12
For personal use only.

The electrochemical reduction of *N*-fluorourethans in acetonitrile. The generation of carbethoxynitrene[1,2]

JEAN LESSARD[3] AND DENIS BÉRUBÉ[4]

Département de chimie, Université de Sherbrooke, Sherbrooke (Qué.), Canada J1K 2R1

Received August 18, 1983

JEAN LESSARD and DENIS BÉRUBÉ. Can. J. Chem. **62**, 768 (1984).

The electrochemical reduction of *N*-fluoro-*N*-methylurethan (**1***a*) and *N*-fluorourethan (**2***a*) in acetonitrile generates the amide anion and a fluoride ion. Both the fluoride and the amide anion can react with the starting *N*-fluoroamide either as bases or as nucleophiles. Many products are formed and the coulometric results are low (0.5 to 0.7 F/mol). In the case of NFU (**2***a*), abstraction of the proton on nitrogen both by the urethan anion and the fluoride anion generates the conjugate base EtOCONF (**7**) which immediately undergoes α-elimination of the fluoride ion to give carbethoxynitrene (**11**). This nitrene was generated also by treating NFU (**2***a*) with a base such as triethylamine or lithium hydride. The α-elimination of F^- from EtOCONF is much easier than the α-climination of Cl^- from EtOCONCl.

JEAN LESSARD et DENIS BÉRUBÉ. Can. J. Chem. **62**, 768 (1984).

La réduction électrochimique du *N*-fluoro-*N*-méthyluréthane (**1***a*) et du *N*-fluorouréthane (**2***a*) conduit à l'anion d'amide et à l'ion fluorure. Ces deux anions peuvent réagir avec le *N*-fluoroamide de départ comme bases ou comme nucléophiles, ce qui engendre de nombreux produits et des coulométries observées faibles (0,5 à 0,7 F/mol). Dans le cas du NFU (**2***a*), l'anion de l'uréthane et l'ion fluorure arrachent le proton de l'azote pour former la base conjuguée EtOCONF (**7**) qui perd immédiatement l'ion fluorure (élimination α) en donnant le carbéthoxynitrène (**11**). Ce nitrène est obtenu également en traitant le NFU (**2***a*) par une base telle la triéthylamine ou l'hydrure de lithium. L'élimination α de F^- à partir de EtOCONF est beaucoup plus facile que l'élimination α de Cl^- à partir de EtOCONCl.

We have recently reported (1) that the electrochemical reduction of *N*-bromo- and *N*-chloroamides (ZCONRX) in acetonitrile leads to the amide anion (eq. [1]). In the case of *N*-halo-*N*-alkyl(aryl)amides, the amide anion abstracts a proton from the medium to give the parent amide and strong bases or nucleophiles (eq. [2]) which react with the starting *N*-haloamide to regenerate the amide anion (eq. [3]).

[1] $ZCONRX + 2e^- \rightarrow ZCO\bar{N}R + X^-$

[2] $ZCO\bar{N}R + SH \rightarrow ZCONHR + S^-$

[3] $ZCONRX + S^- \rightarrow ZCO\bar{N}R + SX$

In the case of *N*-halo-*N*-hydroamides (R = H), the amide anion reacts with an incoming *N*-halo-*N*-hydroamide molecule to give the parent amide and the conjugate base of the *N*-haloamide (eq. [4], father–son protonation). If water is present in the double layer, the conjugate base can be reduced to the parent amide (eq. [5]).

[4] $ZCO\bar{N}H + ZCONHX \rightarrow ZCONH_2 + ZCO\bar{N}X$

[5] $ZCO\bar{N}X + 2\,H_2O + 2e^- \rightarrow ZCONH_2 + 2\,HO^- + X^-$

This paper reports on the electrochemical reduction of *N*-fluoro-*N*-methylurethan (NFMU) (**1***a*) and *N*-fluorourethan (NFU) (**2***a*) and on their reaction with bases. These *N*-fluorourethans are compared to their *N*-chloro analogues, *N*-chloro-*N*-methylurethan (NCMU) (**1***b*) and *N*-chlorourethan (NCU) (**2***b*), studied previously (1).

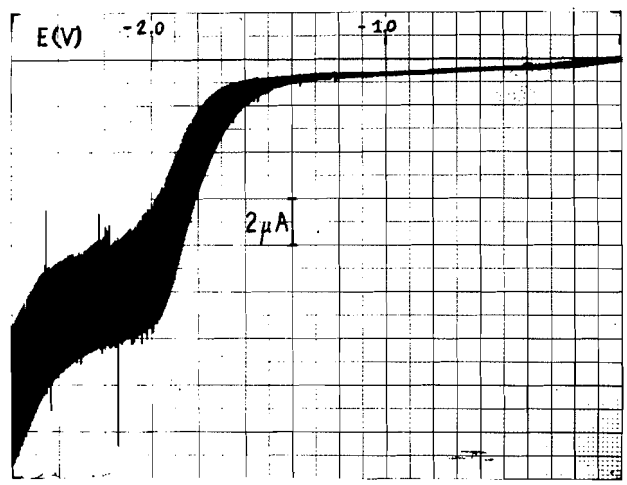

FIG. 1. Polarogram of NFMU (**1***a*) (1.52 m*M*) in acetonitrile–TEAP (0.1 *M*) (sweep rate: 10 mV/s; t = 0.5 s).

Results and discussion

N-*Fluoro*-N-*methylurethan (1*a*)*

In acetonitrile containing tetraethylammonium perchlorate (TEAP) 0.1 *M* as supporting electrolyte,[5] the polarogram of **1***a* (Fig. 1) shows one irreversible (αn value of 0.25–0.28) and diffusion-controlled reduction wave at $E_{1/2}$ = −1.75 V vs. a saturated calomel electrode (sce).[6] An N—F bond is stronger than an N—Cl bond (2) and, indeed, **1***a* is more difficult to reduce than its *N*-chloro analogue **1***b* by about 1.4–1.6 V (1).

Both NFMU (**1***a*) and NCMU (**1***b*) are consumed by secondary reactions during their electrochemical reduction as shown by low coulometric n values: 0.66 F/mol for **1***a*; 0.49–0.57 F/mol for **1***b* (1). These secondary reactions are minimized or

[1] Part III in the series "Electroreduction of *N*-haloamides". For part II, see ref. 1.

[2] Taken from the Ph.D. Thesis of D. Bérubé, Université de Sherbrooke, Sherbrooke, Québec, 1979.

[3] Author to whom correspondence should be addressed.

[4] NRCC (1977–1978) and Ministère de l'Education du Québec (1975–1976) predoctorate fellow. Present address: Chemistry Division, National Research Council of Canada, Ottawa, Ont., Canada K1A 0R6.

[5] Unless specified otherwise, the acetonitrile–TEAP (0.1 *M*) contains about 0.2% of water (0.1 *M*).

[6] All the potentials reported in this paper were measured with respect to an aqueous saturated calomel electrode (sce).

Can. J. Chem. Downloaded from www.nrcresearchpress.com by 210.87.254.40 on 09/06/12
For personal use only.

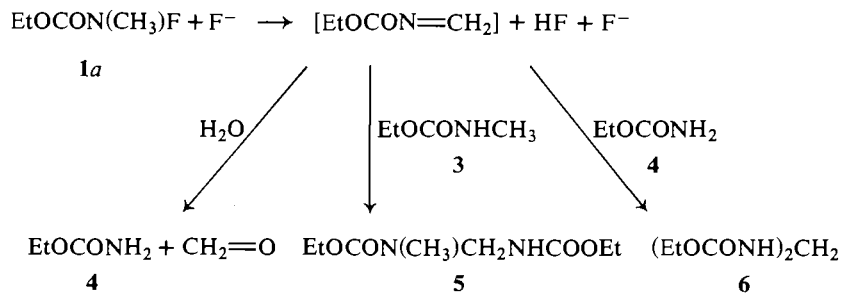

SCHEME 1

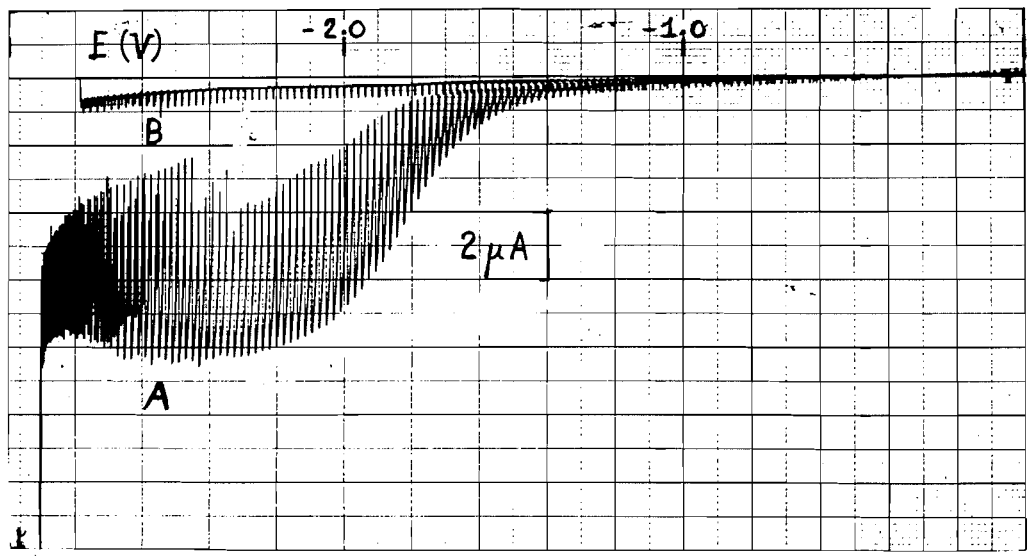

FIG. 2. Curve A: polarogram of NFU (**2***a*) (2.21 m*M*) in acetonitrile–TEAP (0.1 *M*) (sweep rate: 10 mV/s; t = 2 s); curve B: acetonitrile–TEAP (0.1 *M*) (background current).

suppressed in the presence of acetic acid: coulometries of 1.8 F/mol or higher; increase of 30–36% of the limiting current of the polarographic wave(s).[7] Controlled potential electrolysis of NCMU (**1***b*) gave *N*-methylurethan (**3**) in high yield (90%) and reaction [3] has been suggested to be responsible for the low n values (1). In the case of NFMU (**1***a*), other reactions must be involved since the controlled potential electrolysis gave both *N*-methylurethan (**3**) and urethan (**4**) in 26% and 25% yields, respectively, together with about 1% each of the amidals **5** and **6** (Scheme 1); polymers were formed also, according to ^{1}H nmr spectroscopy. The parent amide **3** comes from reduction of the N—F bond (eq. [1]) followed by abstraction of a proton from the medium by the anion of *N*-methylurethan (eq. [2]). The formation of urethan and of amidals **5** and **6** can be accounted for by the reactions shown in Scheme 1. The reactions of NFMU (**1***a*) with tetraethylammonium fluoride (TEAF) in acetonitrile gave 22% of urethan but no amidals were detected. Reactions such as reaction [6] could be partly responsible for the low material balance in both the electrochemical reduction of **1***a* and its reaction with TEAF. Analysis of the cathode and anode compartments for fluoride ions after exhaustive electrolysis of **1***a* gave 70%. Polarographic analysis showed the disappearance of the NFMU wave and the appearance of a

[6] $\underset{\mathbf{1}a}{\mathrm{EtOCON(CH_3)F}} + 2\ \mathrm{F^-} \rightarrow \mathrm{COF_2} + \mathrm{CH_3\bar{N}F} + \mathrm{EtO^-}$

wave at $E_{1/2} = -2.4$ V with a limiting current corresponding to about 15% of that of the NFMU wave of the initial solution. This wave probably corresponds to the reduction of amides.

N-*Fluorourethan* (*2*a)

Voltammetry

The polarogram of NFU (**2***a*) in acetonitrile–TEAP (0.1 *M*) (Fig. 2) shows one irreversible (αn = 0.20–0.23) and diffusion controlled wave at $E_{1/2} = -1.81$ V. The close similarity of the reduction potentials ($E_{1/2}$) and transfer coefficients (αn) for NFU (**2***a*) and NFMU (**1***a*) strongly suggests that the N—F bond (eq. [7]), and not the N—H bond of NFU (eq. [8]), is reduced. This is confirmed by the absence of hydrogen evolution during the preparative electrolysis of NFU on mercury

[7] $\underset{\mathbf{2}a}{\mathrm{EtOCONHF}} + 2\ \mathrm{e^-} \rightarrow \mathrm{EtOC\bar{O}NH} + \mathrm{F^-}$

[8] $\underset{\mathbf{2}a}{\mathrm{EtOCONHF}} + \mathrm{e^-} \rightarrow \mathrm{EtOC\bar{O}NF^-} + \tfrac{1}{2}\ \mathrm{H_2}$

and on platinum. Thus although (*i*) NFU (pK_a = 5.69 in water) is more acidic than NCU (pK_a = 8.02) (3), and (*ii*) an N—F bond is more difficult to reduce than an N—Cl bond, the reduction of NFU involves the cleavage of the *N*-halogen bond (eqs. [1] and [7]) as with the other *N*-halo-*N*-hydroamides

[7] The time scale of a polarographic experiment is much shorter than that of a coulometric determination. Therefore secondary reactions consuming the *N*-fluorourethans **1***a* and **1***b* that are slower than the dropping time should have no influence on the polarographic limiting current but do have an influence on the coulometric n value.

Can. J. Chem. Downloaded from www.nrcresearchpress.com by 210.87.254.40 on 09/06/12
For personal use only.

studied (1). Also, as for NCU (**2***b*) and the other *N*-halo-*N*-hydroamides (1), reaction [7] must be followed by reaction [9] (see eq. [4], father–son protonation).

[9] $\underset{\mathbf{2}a}{EtOCO\bar{N}H} + \underset{\mathbf{4}}{EtOCONHF} \rightarrow \underset{\mathbf{4}}{ETOCONH_2} + \underset{\mathbf{7}}{EtOCO\bar{N}F}$

The addition of 1 equiv. or more of acetic acid causes a small change of αn (0.25–0.28) and a 55% increase of the limiting current of the NFU polarographic wave. With *N*-chloro- and *N*-bromo-*N*-hydroamides (1), a 100% increase of the first polarographic wave (eq. [1], R = H) was observed in the presence of 1 equiv. or more of acetic acid because all the *N*-haloamide reaching the electrode is reduced whereas, in a neutral medium, 50% only is reduced due to the father–son protonation [4]. In the case of NFU, the fluoride ion is a base strong enough to abstract a proton from NFU (see the section entitled *Reaction with bases*) and, therefore, two father–son protonations (eqs. [9] and [10]) can follow the reduction step (eq. [7]). The sum of reactions [7], [9], and [10] gives [11] according to which 33% only of the NFU reaching the electrode should be reduced. Assuming that, in the presence of 1 equiv.

[10] $\underset{\mathbf{2}a}{EtOCONHF} + F^- \rightarrow \underset{\mathbf{7}}{EtOCO\bar{N}F} + HF$

[11] $3\ \underset{\mathbf{2}a}{EtOCONHF} + 2\ e^- \rightarrow \underset{\mathbf{4}}{EtOCONH_2} + 2\ \underset{\mathbf{7}}{EtOCO\bar{N}F} + HF$

of acetic acid or more, the father–son protonation [9] is suppressed[8] (replaced by protonation [12]) but not the father–son protonation [10], reaction [13] (the sum of reactions [7], [12], and [10]) is obtained. According to eq. [13], 50% of the NFU reaching the electrode should be reduced, which is 1.5 times more (50% increase) than in a neutral medium. These figures agree quite well with the observed 55% increase of the limiting current with the addition of acetic acid (see above).[9]

[12] $\underset{\mathbf{4}}{EtOCO\bar{N}H} + AcOH \rightarrow \underset{\mathbf{4}}{EtOCONH_2} + AcO^-$

[13] $\underset{\mathbf{2}a}{2\ EtOCONHF} + AcOH + 2\ e^- \rightarrow \underset{\mathbf{4}}{EtOCONH_2} + \underset{\mathbf{7}}{EtOCO\bar{N}F} + HF + AcO^-$

The cyclic voltammogram of NFU on mercury is shown in Fig. 3. The peak corresponding to the reduction of NFU is at −2.0 V. The reversible system with E_{eq} = 0.0 V corresponds to the oxidation of mercury in the presence of anions. There are two small reduction peaks at −0.2 V (shoulder, reduction of **14**, Scheme 2) and −0.7 V (reduction of **12**, Scheme 2). On a platinum electrode (Fig. 4), the reduction peak of NFU appears between −1.25 and −1.4 V, there is an oxidation peak at −0.1 V (unidentified), and a small reduction peak at −0.5 V

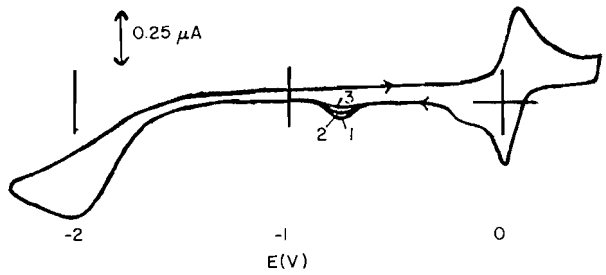

FIG. 3. Cyclic voltammogram of NFU (**2***a*) (0.25 m*M*) in acetonitrile–TEAP (0.1 *M*) on a hanging mercury drop electrode (sweep rate: 100 mV/S); three consecutive scans.

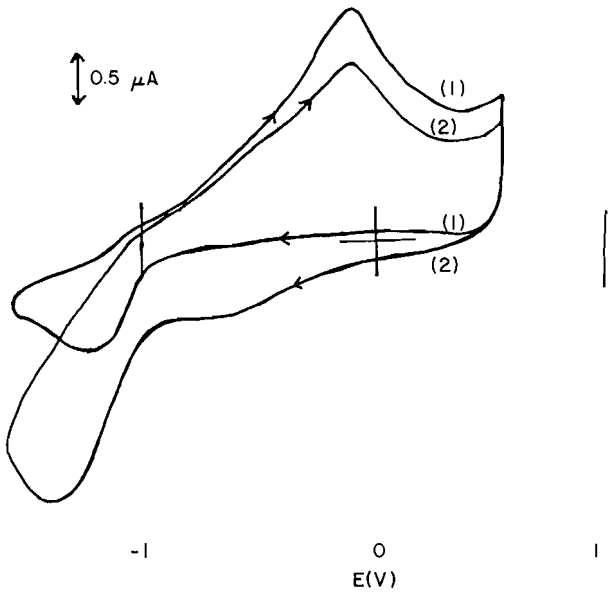

FIG. 4. Cyclic voltammogram of NFU (**2***a*) (0.3 m*M*) on platinum in acetonitrile–TEAP (0.1 *M*). For the oxidation scans, the sweep rate was 10 V/S. For the reduction scans, the sweep rates were (1) 1 V/s; (2) 10 V/S.

(reduction of **12**, Scheme 2). On a rotating disc platinum electrode (ω = 600 rpm, sweep rate = 5 mV/s), the half-wave potential for the reduction of NFU is −1.0 V.[10]

Controlled potential electrolyses

The results are summarized in Table 1. In a neutral medium, the controlled potential electrolysis of NFU (**2***a*) requires between 0.6 and 0.7 F/mol (electrolyses 1 and 3) in agreement with eq. [11]. According to eq. [13], the electrolysis should require 1 F/mol in the presence of 0.5 equiv. or more of acetic acid and the coulometric results (electrolysis 2) do agree with eq. [13].

However, the analysis of products (see Table 1) showed that the situation is far more complex than that described by eqs.

[8] In water, the acetate ion (pK_a = 4.74) is a stronger base than the fluoride ion (pK_a = 3.18) and we have to assume that the order of relative basicities remains the same in acetonitrile–TEAP (0.1 *M*) or/and in the double layer.

[9] In order to suppress the father–son protonation [10], we tried trifluoracetic acid and pyridinium perchlorate. Unfortunately these acids are more easily reduced ($E_{1/2}$ = −1.70 V and −1.30 V respectively) than NFU. The polarographic wave of acetic acid appears at −2.3 V.

[10] Usually, electron-transfer reactions at a solid electrode are slower (are less reversible) and potentials are more negative than at a mercury electrode (4). The slowness of electron transfer was recently ascribed to the partial blocking of the surface of the solid electrode (5). In our case, the potentials are less negative at a platinum electrode. No electrochemical pretreatment of the electrode (5) was made. The electrode was polished before each use on a Buehler Carbimet 600 abrasive paper.

Can. J. Chem. Downloaded from www.nrcresearchpress.com by 210.87.254.40 on 09/06/12
For personal use only.

Can. J. Chem. Downloaded from www.nrcresearchpress.com by 210.87.254.40 on 09/06/12
For personal use only.

[11] and [13]. The material balance is low.[11] The yield of urethan (**4**) is much lower than that predicted by eqs. [11] and [13]. In fact, in electrolyses 1 and 3, the urethan present in the starting NFU is consumed: about 1 mol% in electrolysis 1 and up to 11 mol% in electrolysis 3. The yield of inorganic fluoride is somewhat higher than predicted: 46% (neutral medium, electrolysis 1) compared to 33% predicted by eq. [11]. The complexity of the reaction is due to the very facile α-elimination of the fluoride ion from the conjugate base **7** to give the reactive carbethoxynitrene (**11**) (eq. [14]) (see also the reaction of NFU with bases) and could be due also the reactivity of NFU and some of the electrolysis products towards nucleophiles.[12]

[14] $\underset{\mathbf{7}}{EtOCO\bar{N}F} \rightarrow \underset{\mathbf{11}}{EtOCO\ddot{N}:} + F^-$

The oxadiazole **8** arises from 1,3-dipolar cycloaddition of carbethoxynitrene (**11**) to acetonitrile (eq. [18] and ref. 6). Smith

[18] $\underset{\mathbf{11}}{EtOC(O^-)=N^+} + CH_3CN \rightarrow$ 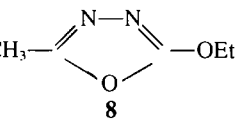

8

[11] In addition to the products shown in Table 1, the vpc and thin-layer chromatographic (tlc) analysis showed the presence of at least eight other products formed in small amounts and not identified. Furthermore, TEAP was removed by extraction with water and some of the electrolysis products might be more soluble in water than in ether. Finally, volatile products were probably lost when removing ether in the rotatory evaporator.

[12] For instance, the nucleophilic addition of fluoride ions to NFU could lead to the reactive carbonyl fluoride and the $\bar{N}HF$ anion (eq. [15]); the nucleophilic reaction of urethan or its anion with NFU could lead to the azamalonate **10** (eq. [16]). However, fluoramine could not be detected (eqs. [15] and [16]). Furthermore, in the electrochemical reduction of NFMU (**1***a*) discussed in the preceding section, ethyl *N*-methylazamalonate (**17**), which could have been formed by nucleophilic addition of *N*-methylurethan or its anion to NFMU (eq. [17]), was not detected.

[15] $\underset{\mathbf{2}a}{EtOCONHF} + 2\ F^- \rightarrow$

$COF_2 + EtO^- + \bar{N}HF$ → $:\ddot{N}H + F^-$; SH → $NH_2F + S^-$

[16] $\underset{\mathbf{2}a}{EtOCO\bar{N}H} + EtOCONHF \rightarrow$

$\underset{\mathbf{10}}{(ETOCO)_2NH} + \bar{N}HF$ → $:\ddot{N}H + F^-$; SH → $NH_2F + S^-$

[17] $\underset{\mathbf{1}a}{EtOCO\bar{N}CH_3} + EtOCON(CH_3)F \rightarrow$

$(EtOCO)_2NCH_3 + \bar{N}FCH_3$

17

not detected

TABLE 1. Controlled potential electrolyses of NFU (**2***a*) in acetonitrile–TEAP (0.1 *M*)[a]

Electrolysis No.	$[NFU]_0$[b] (m*M*)	Working electrode	[AcOH] (m*M*)	$-E$[c] (V)	n_{app} (F/mol)	Iodometry[d] (%)	Yield of products[e] (%) EtOCONH₂ **4**	**8**	(EtOCONH)₂ **9**	(EtOCO)₂NH **10**
1	71	Hg	0	1.9	0.60	11.9	0[f]	9	25	10
2	68	Hg	38	1.9	0.98	0.0	15	~4[g]	23	8
3	37	Pt	0	1.0	0.72	0.0	0[h]	9	47	2

[a] The electrolyses were carried out at room temperature using a magnesium auxiliary electrode and were stopped when no more NFU was left according to polarographic analysis.
[b] The sample of NFU contained 10.5 mol% of urethan in electrolysis 1 and 2 and 21 mol% in electrolysis 3.
[c] *E* vs. sce.
[d] Iodometric titration at the end of the electrolysis.
[e] By vpc unless indicated otherwise.
[f] Recovery of 86% of the urethan present in the starting NFU.
[g] By ^1H nmr.
[h] Recovery of 43% of the urethan present in the starting NFU.

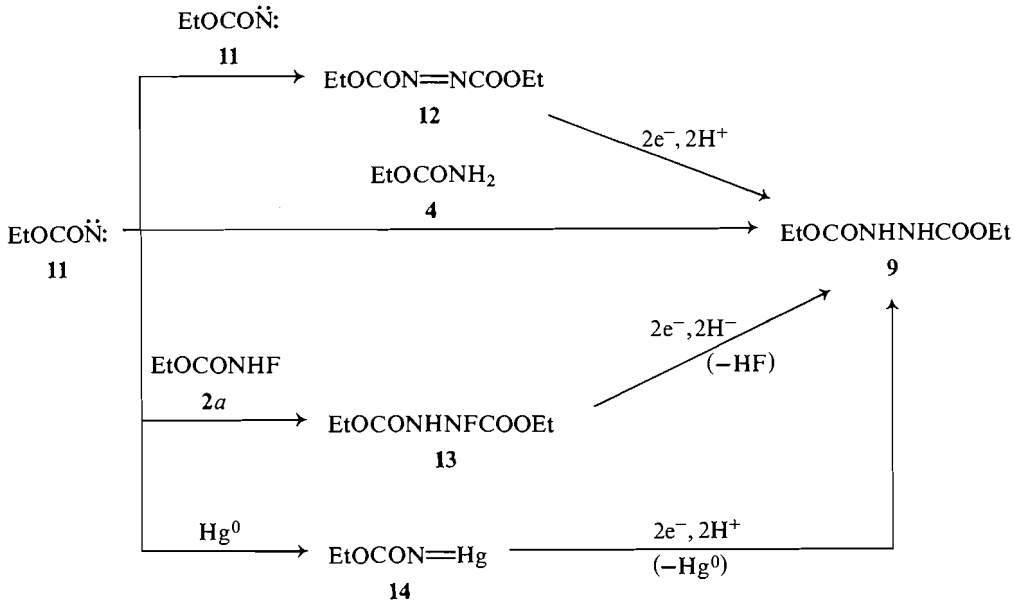

SCHEME 2

and Rogers (7) have shown that oxadiazoles are reduced electrochemically to saturated and ring-opened products in dimethylformamide in the presence of a proton donor. The oxadiazole **8** shows two polarographic waves in acetonitrile–TEAP (0.2 *M*) ($(E_{1/2})_1$ = −1.61 V and $(E_{1/2})_2$ = −2.5 V) and it should be reduced at the electrolysis potential (−1.9 V) until no more NFU, acting as the proton donor, is available. Oxadiazole **8** could be consumed also by the fluoride ions produced during the electrolysis, NFU acting again as an acid. Thus, oxadiazole **8** reacts with tetraethylammonium fluoride (TEAF) provided an acid is present.[13]

Four plausible routes for the formation of diethyl hydrazodicarboxylate (**9**) are shown in Scheme 2. The coupling of two carbethoxynitrenes (**11**) leads to diethyl azodicarboxylate (**12**) $E_{1/2}$ = −0.5 V, which is then reduced to **9** at the electrolysis potential (−1.9 V). In the cyclic voltammograms of NFU, the peak at −0.7 V on a mercury electrode (Fig. 3) and the peak at −0.5 V on a platinum electrode (Fig. 4) are attributed to the azo compound **12**.[14] Further evidence for the intermediacy of **12** comes from its formation in the reaction of NFU with bases (see below). The hydrazo derivative **9** can be formed also by insertion of carbethoxynitrene (**11**) into an N—H bond of urethan. This reaction would account for the consumption of the urethan present in the starting NFU during the electrolyses carried out in a neutral medium (Table 1, electrolyses 1 and 3). The insertion of **11** into the N—H bond of NFU would give **13** which should then be reduced to **9**. Finally, the reaction of carbethoxynitrene (**11**) with mercury followed by reduction of the organomercuric derivative **14** represents another route to **9** (Scheme 2). The shoulder at −0.2 V in the cyclic voltammogram of NFU on mercury (Fig. 1) can be attributed to **14**; this peak is absent when a platinum electrode is used (Fig. 2).

[13] Oxadiazole **8** did not react with TEAF in acetonitrile. However, the addition of sulfuric acid (0.5 mol per mol of **8**) led to the complete disappearance of **8** after 4 h.

[14] The controlled potential reduction of diethyl azodicarboxylate (**12**) on mercury at −0.7 V in acetonitrile–TEAP (0.1 *M*) gave diethyl hydrazodicarboxylate (**9**) in a 41% yield.

In order to confirm the formation of carbethoxynitrene (**11**) as an intermediate, the electrolysis of NFU was carried out at −1.9 V in the presence of cyclohexene (cyclohexene/acetonitrile–TEAP (0.1 *M*) = 0.5): the aziridine **15** and

15 **16**

N-cyclohexenylurethan (**16**) were obtained in 5.4% and 0.6% yield (vpc) respectively. The other products identified were urethan (20%) and diethyl hydrazodicarboxylate (**9**) (20%). The oxadiazole **8** and the azamalonate **10** were not detected. The iodometric analysis gave 9.4%.

The origin of the iodometric activity at the end of the electrolyses is discussed below.

Reaction with bases

The reaction of NFU (**2***a*) with bases (eq. [19]) is followed by loss of fluoride ion to form carbethoxynitrene (**11**) (eq. [14]). The α-elimination of the fluoride ion must be quite facile. Indeed, aliquots taken immediately after mixing NFU

[19] $EtOCONHF + B^- \rightleftarrows EtOCO\bar{N}F + BH$

with one equivalent of base in acetonitrile and analysed by polarography did not contain any NFU. The following bases did react with NFU: triethylamine, lithium hydride, tetraethylammonium fluoride, and lithium trichloroacetate. Surprisingly pyridine, which is more basic (pK_a = 5.29) than the trichloroacetate ion (pK_a = 0.65) in water, did not react with NFU.

Since the fluoride ion can act as a base and is generated in reaction [14], a catalytic amount of base should have been sufficient to cause the complete reaction of NFU (chain reaction). However, for the reaction of NFU with TEAF in acetonitrile, 0.75 equivalent of TEAF was needed to cause the complete disappearance of NFU (polarography). Some fluoride ions must be consumed in competitive reactions and/or react with HF to give the HF_2^- anion, which then would not be basic enough to abstract a proton from NFU. Also, the fact that lithium chloroacetate reacts with NFU shows that the acetate

Can. J. Chem. Downloaded from www.nrcresearchpress.com by 210.87.254.40 on 09/06/12
For personal use only.

Can. J. Chem. Downloaded from www.nrcresearchpress.com by 210.87.254.40 on 09/06/12
For personal use only.

ion should induce the decomposition of NFU. Therefore in order to account for the polarographic and coulometric behavior of NFU (see eq. [13]), the reaction of the acetate ion with NFU must be relatively slow.

A comparison between controlled potential electrolyses of NFU (Table 1) and its reaction with bases in acetonitrile (Table 2), with and without added cyclohexene, shows that essentially the same products are obtained.[11] In the reaction with bases, the iodometric activity could be due to the formation of diethyl *N*-fluoro-hydrazodicarboxylate (**13**) resulting from the insertion of carbethoxynitrene (**11**) into the N—H bond of NFU (Scheme 2). The iodometric activity at the end of the electrolyses (Table 1) cannot be due to **13** since it should be reduced to **9** (Scheme 2). Furthermore, the iodometric activity is present only when the electrolyses are carried out on mercury and in a neutral medium. The presence of the organomercuric compound **14** arising from the reaction of carbethoxynitrene (**11**) with mercury (Scheme 2) could be responsible for the iodometric activity and for the presence of a polarographic wave at ca. 0 V after completion of the electrolyses. We believe that the reduction of **14** requires a proton donor. In a neutral medium, NFU would act as the proton donor (eq. [20]). Since side reactions (see [15] and [17]) are consuming NFU during the electrolyses, a substantial amount of **14** could still be present (Table 1, entry 1) when all the NFU has disappeared (polarographic analysis).

[20] $\underset{\mathbf{14}}{\text{EtOCONHg}} + \underset{\mathbf{2}a}{\text{EtOCONHF}} + 2\,e^- \rightarrow \underset{\mathbf{4}}{\text{EtOCONH}_2} + 2\,\underset{\mathbf{7}}{\text{EtOCO}\bar{\text{N}}\text{F}}$

When NFU was treated with triethylamine in acetonitrile in the presence of mercury (Table 2, entry 2), the polarographic wave at 0 V attributed to the organomercuric derivative **14** (see above) did appear (Fig. 5) whereas that of NFU disappeared. The same wave was observed also when carbethoxynitrene (**11**) was generated from *N*-paranitrobenzenesulfonoxyurethan (**18**) and triethylamine (6) in acetonitrile and in the presence of mercury. In order to account for the low iodometric activity, we propose the protonolysis of **14** by NFU (eq. [21]).

[21] $\underset{\mathbf{14}}{\text{EtOCONHg}} + 2\,\underset{\mathbf{2}a}{\text{EtOCONHF}} \rightarrow \underset{\mathbf{4}}{\text{EtOCONH}_2} + 2\,\underset{\mathbf{7}}{\text{EtOCO}\bar{\text{N}}\text{F}} + \text{Hg}^{2+}$

We have compared the reaction of NFU and that of *N*-paranitrobenzenesulfonoxyurethan (**18**) with triethylamine in cyclohexene. The results are recorded in Table 3. The main feature is the nearly identical ratio of insertion (**16**) to addition (**15**): 0.15 with **2***a*, 0.17 with **18** (8). This ratio is close to that observed in the electrochemical reduction of NFU in acetonitrile in the presence of cyclohexene: **16**/**15** = 0.11. However, when NFU was reacted with triethylamine and cyclohexene in acetonitrile, the insertion-to-addition ratio was much higher: **16**/**15** = 1.1 (Table 2, entry 3). This higher ratio (or the lower yield of aziridine **15**) is due to the reaction of aziridine **15** with triethylammonium fluoride which was shown to give *trans-N*-(2-fluorocyclohexyl)urethan (**19**) and *trans-N*-(2-acetamidocyclohexyl)urethan (**20**) (Scheme 3).

If one compares the reaction of NFU and the reaction of *N*-paranitrobenzenesulfonoxyurethan (**18**) with triethylamine in acetonitrile, the yield of oxadiazole **8** is much higher with **18**

TABLE 2. Reaction of NFU (**2***a*) with bases[a]

Entry No.	Base	Solvent	Iodometry[b] (%)	Yield of products[c] (%)					
				8	$(EtOCONH)_2$ **9**	$(EtOCO)_2NH$ **10**	$(EtOCN{=})_2$ **12**	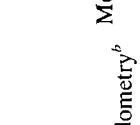 **15**	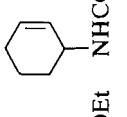 **16**
1	Et_3N	CH_3CN	2	1.3	29				
2	Et_3N	CH_3CN–TEAP (0.1 *M*)/Hg	2	0.4	34	1	7		
3	Et_3N	CH_3CN–TEAP (0.1 *M*)/cyclohexene	3	2	14			1.6	1.8
4	LiH	CH_3CN	5	11			6		

[a] The reactions were carried out at room temperature under a nitrogen atmosphere and were followed by polarography and iodometry. The sample of NFU used contained between 10 to 20 mol% of urethan.
[b] Iodometric titration after the disappearance of NFU (polarography).
[c] By vpc. The content of urethan (**4**) of the reaction product was less than in the starting NFU (see the Experimental).

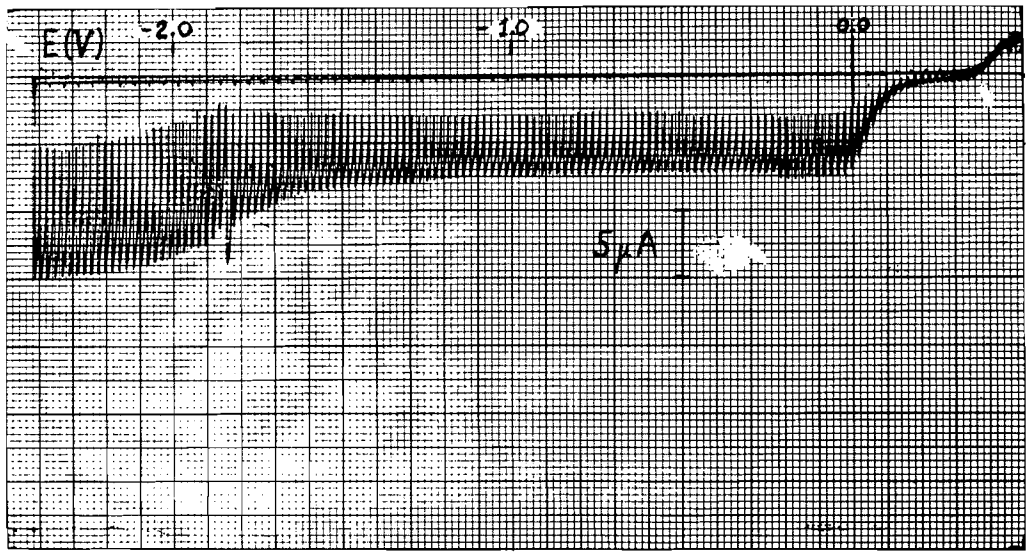

FIG. 5. Polarogram of a solution of NFU (**2***a*) in acetonitrile–TEAP (0.1 *M*) stirred in the presence of mercury and triethylamine (0.05 equiv.) for 8 h.

TABLE 3. Generation of carbethoxynitrene (**11**) from NFU (**2***a*) and *N*-paranitrobenzenesulfonoxyurethan (**18**)[a]

	Yield of products[b] (%)			
	$(EtOCONH)_2$	$(EtOCON{=})_2$	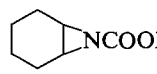	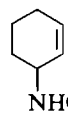
Starting material	**9**	**12**	**15**	**16**
2*a*[c]	5	5	9.4	1.4
18[d]	3.8		12	2

[a] Reactions carried out in cyclohexene as solvent with triethylamine (1 equiv.).
[b] By vpc. The urethan content of the product was 4%.
[c] The NFU contained 10.5 mol% of urethan.
[d] Taken from ref. 8.

(32%) than with NFU (1.3%, Table 2, entry 1). This is most probably due to the reaction of oxadiazole **8** with triethylammonium fluoride when carbethoxynitrene (**11**) is generated from NFU. Indeed, polarography did show the complete disappearance of **8** after 4 h when **8** was treated with triethylammonium fluoride in acetonitrile.

α-Elimination of fluoride ion

The α-elimination of a fluoride ion has been proposed to explain the decomposition of difluoramine in the presence of a base and the formation of difluorodiazene (eq. [22]) (9). It is noteworthy that the α-elimination of a chloride ion is much

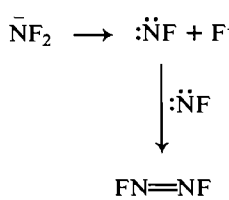

[22]

more difficult. The decomposition of the lithium salt of *N*-chlorourethan in acetonitrile is a slow process and no oxadiazole **8** could be detected. The same observation holds for the conjugate base of NCU generated electrochemically (1). When NCU, in cyclohexene, was treated with triethylamine, no aziridine **15** nor *N*-cyclohexenylurethan (**16**) could be detected. The *cis* 1,2-adduct **21** and the *trans* 1,2-adduct **22** were isolated in 14% and 4% yield respectively and the *cis*-to-*trans* ratio suggests that they could result from a radical chain reaction of NCU with cyclohexene (10). Recently, Torimoto *et al.* (11) have obtained the compound **23** from the thermolysis (50–70°C) of the sodium salt of NCU in dioxane and they gave evidence that **23** results from a radical chain reaction.

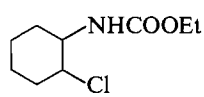

21

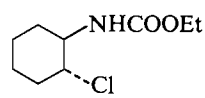

22

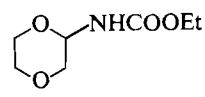

23

The more facile α-elimination of a fluoride ion from —N̄—F as compared to that of a chloride ion from —N̄—Cl could be explained by electron delocalization into the *d* orbitals of the chlorine atom (—N=Cl⁻) and by a stronger repulsion between the 2*p* electrons of nitrogen and those of fluorine than between the 2*p* electrons of nitrogen and the 3*p* electrons of chlorine. The same explanation would hold for the relative acidity of fluoroform (pK_a = 25.5), chloroform (pK_a = 15), and bromoform (pK_a = 9) (12).

Can. J. Chem. Downloaded from www.nrcresearchpress.com by 210.87.254.40 on 09/06/12
For personal use only.

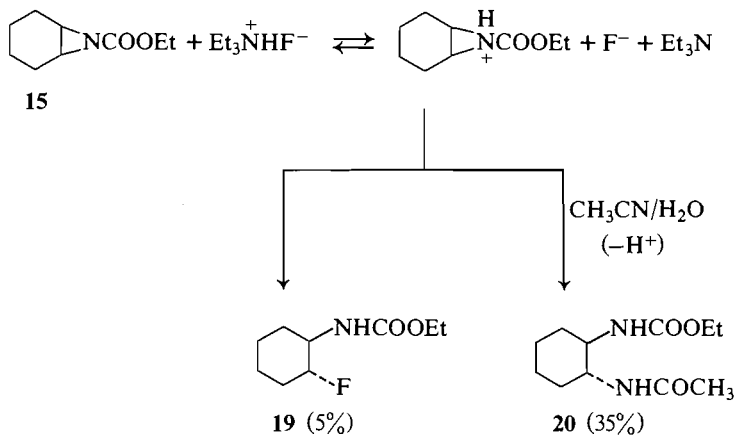

SCHEME 3

Experimental

The pertinent information concerning *acetonitrile, electrolytes, and the electrochemical instrumentation and methods* has been given in ref. 1. The general information concerning the analysis of products is the same as that given in refs. 1 and 13.

N-*Fluorourethan* (**2**a)

A mixture of fluorine (20%) and nitrogen (80%) was bubbled through a solution of urethan (25 g, 0.28 mmol) in water (350 mL) (14). The reaction was followed by ^{1}H nmr and stopped when the ratio of NFU (*t* at 1.36 ppm) to ethanol reached a maximum value (6.5 h). Some urethan was left. Nitrogen was bubbled through the reaction mixture for 15 min. It was extracted with methylene chloride (8 × 50 mL). The organic phases were kept overnight over sodium fluoride in the refrigerator, then dried over sodium sulfate. Evaporation of the solvent followed by distillation gave N-*fluorourethan* (**2***a*), bp 95–98°C (20 Torr) (93% active fluorine by iodometry, 16% yield); δ ($CDCl_3$): 1.36 (t, J = 7 Hz), 4.46 (q, J = 7 Hz), and 10.35 (d, J = 56 Hz) ppm.

N-*Fluoro*-N-*methylurethan* (**1**a)

N-Fluorourethan (4.5 g, 88% active fluorine, 37 mmol) in ether (25 mL) was treated with diazomethane (100 mL of a 3% solution in ether, 3 g, 71 mmol) until cessation of nitrogen evolution. The excess of diazomethane was removed with a stream of nitrogen. Ether was distilled, methylene chloride (50 mL) was added, and the mixture was washed with brine. The solvent was distilled and the residue was purified by distillation to give N-*fluoro*-N-*methylurethan* (**1***a*), bp 50°C (20 Torr) (1.5 g, 33%). It was identical (ir and ^{1}H nmr) to a sample prepared by the method of Grakauskas and Baum (15); ν_{max} ($CHCl_3$): 1750 and 1725 cm^{-1}; δ ($CDCl_3$): 1.30 (t, J = 7 Hz), 3.31 (d, J = 28 Hz), and 4.22 (q, J = 7 Hz) ppm.

Authentic samples

The preparation of *N*-methyl-*N,N'*-methylene-*bis*-urethan (amidal **5**) has been described in ref. 10 and that of diethyl azamalonate (**10**) and diethyl *N*-methylazamalonate (**17**) in ref. 1.

N,N'-*Methylene-bis-urethan (amidal* **6***)*

This compound was prepared from urethan, formaldehyde, and hydrochloric acid (16), mp 128–129°C (lit. (16) mp 131°C); ν_{max} ($CHCl_3$): 3470, 1710, and 1495 cm^{-1}; δ ($CDCl_3$): 1.23 (t, J = 7 Hz), 4.13 (q, J = 7 Hz), 4.48 (t, J = 7 Hz), and 5.85 (m) ppm; *m/e*: 190 (M^+).

2-Ethoxy-5-methyl-1,3,4-oxadiazole (8)

N-Paranitrobenzenesulfonoxyurethan (**18**) was prepared according to the method of Lwowski and Maricich (8), mp 114–115°C (lit. (8) mp 116°C) (43% yield). To a solution of **18** (5 g, 17.3 mmol), in acetonitrile (50 mL) under a nitrogen atmosphere, triethylamine (1.8 g, 17.8 mmol) was added dropwise (20 min). The mixture was stirred at room temperature for 1.5 h and the solvent was removed in a rotatory evaporator. The residue was dissolved in methylene chloride (50 mL) and the solution was washed with ice-cold water (2 × 25 mL), then dried over sodium sulfate. The solvent was evaporated and the resulting oil was purified by preparative vpc (OS-138, 15%; 150°C) to give the *oxadiazole* **8** as a colorless liquid; ν_{max} ($CHCl_3$): 1630, 1580, and 1225 cm^{-1}; δ ($CDCl_3$): 1.49 (t, J = 7 Hz), 2.43 (s), and 4.62 (t, J = 7 Hz) ppm; *m/e*: 128 (M^+). The yield determined by analytical vpc was 32%.

Diethyl hydrazodicarboxylate (9)

This compound was prepared according to an Organic Synthesis procedure (17), mp 133–134°C (lit. (17) mp 131–133°C); ν_{max} ($CHCl_3$): 3410, 1730, and 1490 cm^{-1}; δ ($CDCl_3$): 1.30 (t, J = 7 Hz), 4.31 (q, J = 7 Hz), and 6.62 (broad s) ppm; *m/e*: 176 (M^+).

7-Carbethoxy-7-aza-bicyclo[4.1.0]heptane (aziridine **15***)*

This compound was prepared from cyclohexene and iodine isocyanate according to the method described by Hassner *et al.* (18) with a yield of 43%, bp 94°C (20 Torr); δ ($CDCl_3$): 1.28 (t, J = 7 Hz), 1.90 (m, 4H), 2.70 (m, 2H), and 4.23 (q, J = 7 Hz) ppm; *m/e*: 169 (M^+).

N-*(2-Cyclohexenyl)urethan (16)*

This compound was prepared from 3-bromocyclohexene according to the method described by Lwowski and Mattingly (19) and was purified by vpc (OS-138, 15%; 200°C); ν_{max} ($CHCl_3$): 3450, 1710, and 1500 cm^{-1}; δ ($CDCl_3$): 1.24 (t, J = 7 Hz, 3H), 4.22 (m + q, J = 7 Hz, 3H), 4.80 (m, NH), and 5.87 (m, 2H) ppm; *m/e*: 169 (M^+).

Mass electrolyses

These were carried out under a nitrogen atmosphere as described in ref. 1. All the products were identified with respect to authentic samples by ir and ^{1}H nmr spectroscopy, vpc, and/or tlc. A few electrolyses are described below.

Reduction of N-*fluoro*-N-*methylurethan* (**1**a)

NMFU (**1***a*) (483 mg, 3.91 mmol) was added to the cathode compartment containing 150 mL of a 0.1 *M* solution of TEAP in acetonitrile. The anode compartment contained 25 mL of the 0.1 *M* electrolyte solution. A potential of −1.9 V (Hg cathode) (i_0 = 1.65 mA/cm^2) was applied until the current reached a near zero value (4 h, 249 C). The polarographic analysis showed the complete disappearance of **1***a* and a new wave at $E_{1/2}$ = −2.4 V (its limiting current did correspond to about 20% of the limiting current of the starting solution). The anolyte was filtered to remove the magnesium fluoride. The anolyte and catholyte were combined and the solvent was evaporated. Water was added and the resulting mixture extracted with ether. The organic phase was dried, then concentrated in a rotatory evaporator. The resulting solution was transferred into a 50-mL volumetric flask. The vpc analysis (OS-138, 15%; 110°C) gave 26% of *N*-methylurethan, 25% of urethan, 1% of amidal **5**, and 1% of amidal **6**. An aliquot was separated by preparative vpc for comparison to authentic samples.

Reduction of N-*fluorourethan* (**2**a) *in the presence of cyclohexene*

NFU (**2***a*) (510 mg, 85% active fluorine, 4.05 mmol) and cyclohexene (50 mL) were added to the cathode compartment containing

Can. J. Chem. Downloaded from www.nrcresearchpress.com by 210.87.254.40 on 09/06/12
For personal use only.

Can. J. Chem. Downloaded from www.nrcresearchpress.com by 210.87.254.40 on 09/06/12
For personal use only.

100 mL of the 0.1 *M* electrolyte solution. The anode compartment contained 25 mL of the electrolyte solution. A potential of −1.9 V (Hg cathode) was applied for 5 h ($i \simeq 0$, 344 C). After the usual work-up (see above), the vpc analysis gave 20% urethan (**4**) (corresponding to the amount present in the starting solution), 20% diethyl hydrazodicarboxylate (**9**), 5.4% of aziridine **15**, 0.6% of *N*-(2-cyclohexenyl)urethan (**16**), and about 1% each of oxadiazole **8** and azamalonate **10**.

Reduction of diethyl azodicarboxylate (12)

Diethyl azodicarboxylate (**12**) (635 mg, 3.65 mmol) in 50 mL of acetonitrile–TEAP 0.1 *M* (the anodic compartment contained 25 mL) was reduced at −0.7 V for 0.5 h (102 C). During the electrolysis, the solution became yellow and a gas was evolved. The usual work-up was followed by continuous extraction with methylene chloride. The ^{1}H nmr of the crude product (301 mg) showed that it consisted essentially of diethyl hydrazodicarboxylate (**9**) (41% yield by vpc; OS-138, 15%, 200°C). After recrystallization, it proved identical to the authentic sample.

Reactions with fluoride ions

All reactions were carried out at room temperature and under nitrogen.

N-*Fluoro*-N-*methylurethan (1*a*) and tetraethylammonium fluoride (TEAF)*

To NFMU (242 mg, 2.0 mmol) in acetonitrile–TEAP (0.1 *M*) (10 mL) was added dropwise a 0.5 *M* solution of TEAF in acetonitrile (2.3 mL, 1.15 mmol). A polarogram taken after 4.5 h showed that half of the NFMU had disappeared. An additional 2.3 mL of the TEAF solution (total amount: 2.3 mmol) was added and the mixture stirred at room temperature. A polarogram taken after 24 h showed the presence of 10% of NFMU and a new wave at $E_{1/2} = -2.4$ V. After 40 h no more NFMU was left. The amount of fluoride ion determined with a lanthanum fluoride electrode was 2.3 mmol. The reaction was repeated on a smaller scale (0.71 mmol) and TEAF (1.09 mmol) was added rapidly. The reaction was followed by vpc (UCON-2000, 80°C). After 1 h the reaction was almost complete and after 4 h, no NFMU was left. Water (10 mL) was added and the mixture extracted with methylene chloride (4 × 50 mL). After the usual work-up, the crude product (33 mg) was analysed by ^{1}H nmr and vpc. The sole product identified was urethan (**4**) (22%). No amidal **5** nor amidal **6** could be detected by vpc. The ^{1}H nmr spectrum of the crude product showed absorptions corresponding to those of amidals **5** and **6** but they were probably due to the presence of polymers.

N-*Fluorourethan (2*a*) and TEAF*

To NFU (314 mg, 85% active fluorine, 2.49 mmol) in acetonitrile (10 mL) a 0.53 *M* solution of TEAF (4.7 mL, 2.49 mmol) was added very slowly (24 h). The reaction was followed by polarography. The solvent was evaporated. Water (25 mL) was added and the mixture was extracted with ether (4 × 50 mL). After the usual work-up, the ^{1}H nmr spectrum of the crude product showed the presence of urethan (**4**), oxadiazole **8**, and diethyl hydrazodicarboxylate (**9**) as the main products. Their yields were not determined.

Oxadiazole 8 and triethylammonium fluoride

In a polarographic cell containing 10 mL of acetonitrile–TEAP (0.1 *M*), oxadiazole **8** (15 mg, 0.117 mmol) was treated with a 0.5 *M* solution of Et_3NHF in acetonitrile (0.3 mL, 0.15 mmol). After 4 h the oxadiazole waves ($E_{1/2} = -1.61$ V and −2.5 V) had disappeared.

Oxadiazole 8 and TEAF

In a polarographic cell containing 10 mL of acetonitrile–TEAP (0.1 *M*), oxadiazole **8** (15 mg, 0.117 mmol) was treated with a 0.53 *M* solution of TEAF in acetonitrile (0.2 mL, 1.06 mmol). After 0.5 h, no change was observed in the polarogram. A 66 m*M* solution of sulfuric acid was added (1.1 mL, 0.073 mmol). After 1 h, there was about 25% oxadiazole **8** left and it had disappeared completely after 4 h.

Aziridine 15 and triethylammonium fluoride

Triethylamine (511 mg, 5.06 mmol) in acetonitrile–TEAP (0.1 *M*) (50 mL) was treated with anhydrous HF. The excess HF was removed with a stream of nitrogen. The aziridine **15** (852 mg, 5.04 mmol) in acetonitrile (20 mL) was added slowly (80 min) to the previous solution. After 7.5 h, the solvent was evaporated. Ether (50 mL) was added. The solids were removed by filtration and the solution was washed with saturated sodium bicarbonate (15 mL). The residue (506 mg) obtained after the usual work-up was separated by plc on silica gel (methylene chloride – ether 1:1) to give two main fractions. The less polar fraction (50 mg) consisted of trans N-*(2-fluorocyclohexyl)-urethan* (**19**), mp 62–65°C (5%); ν_{max} ($CHCl_3$): 3440, 1720, and 1510 cm^{-1}; δ ($CDCl_3$): 1.26 (t, J = 7 Hz), 3.8 (m, $H_1 + H_2$), 4.21 (q, J = 7 Hz), and 5.00 (m, H_2 + NH) ppm; m/e: 189 (M^+).

The other fraction (408 mg) consisted of trans N-*(2-acetamidocyclohexyl)urethan* (**20**), mp 133–135°C (35%). It was recrystallized from ether–cyclohexane (1:1) to afford the analytical sample, mp 136.5–137°C (lit. (20) mp 134–135°C); ν_{max} ($CHCl_3$): 3440, 3340, 1705, 1665, and 1510 cm^{-1}; δ ($CDCl_3$): 1.26 (t, J = 7 Hz), 1.99 (s), 3.58 (m, $H_1 + H_2$), 4.20 (q, J = 7 Hz), 5.56 (m, NH), and 6.66 (m, NH) ppm; m/e: 228 (M^+). *Anal.* calcd. for $C_{11}H_{20}N_2O_3$: C 57.87, H 8.83; found: C 57.71, H 9.12.

Reactions with bases

All reactions were carried out under a nitrogen atmosphere at room temperature.

N-*Fluorourethan (2*a*) and triethylamine in acetonitrile*

To a solution of NFU (500 mg, 91% active fluorine, 4.25 mmol) in acetonitrile (15 mL) was added a solution of triethylamine (516 mg, 5.11 mmol) in acetonitrile (10 mL). The reaction mixture became yellow as soon as triethylamine was added and no more NFU was present (polarography) as soon as the addition of triethylamine was completed. After 1 h, the iodometric activity was 2%. The solvent was evaporated and the residue was dissolved in methylene chloride (50 mL) and washed with water (2 × 25 mL). The aqueous layers were combined and continuously extracted with methylene chloride (36 h). The organic phases were dried and the solvent was evaporated. The ^{1}H nmr spectrum of the crude product showed the presence of urethan (**4**), oxadiazole (**8**), and diethyl hydrazodicarboxylate (**9**). The yields determined by vpc (OS-138, 15%) are given in Table 2, entry 1. The urethan content was 7 mol% compared to 12 mol% in the starting NFU.

N-*Fluorourethan (2*a*) and triethylamine in acetonitrile–TEAP (0.1* M*) in the presence of mercury*

To NFU (524 mg, 85% active fluorine, 4.16 mmol) in mercury (25 g) in acetonitrile–TEAP (0.1 *M*) (100 mL), a solution of triethylamine (451 mg, 4.47 mmol) in acetonitrile (10 mL) was added over 10 min (yellow solution). The polarogram showed the absence of NFU and a wave at ca. 0 V. After 1.5 h (2% iodometric activity) hydrochloric acid (25 mL of a 5% solution) was added (the reaction mixture became colorless). Mercury was decanted, was washed with acetonitrile, and the solvent was evaporated. Water (50 mL) was added and continuously extracted with ether (36 h). The crude product was analysed by vpc and the yields are given in Table 2, entry 2. The urethan content was 20 mol% compared to 21 mol% in the starting NFU.

N-*Fluorourethan (2*a*) and triethylamine in acetonitrile–TEAP (0.1* M*) in the presence of cyclohexene*

Triethylamine (418 mg, 4.14 mmol) in acetonitrile (5 mL) was added over 25 min to a solution of NFU (483 mg, 92% active fluorine, 4.15 mmol) in cyclohexene (10 mL) and acetonitrile–TEAP (0.1 *M*) (20 mL). After 1.5 h (3% iodometric activity), the solution was concentrated to ca. 5 mL and ether (100 mL) was added. The solution was washed with saturated aqueous sodium bicarbonate, dried, then concentrated. The yields determined by vpc analysis are given in Table 2, entry 3. The urethan content was 2.5 mol% compared to 10.5 mol% in the starting NFU.

N-*Fluorourethan (2*a*) and triethylamine in cyclohexene*

Triethylamine (561 mg, 5.55 mmol) in cyclohexene (5 mL) was added dropwise (50 min) to a solution of NFU (643 mg, 92% active fluorine, 5.53 mmol) in cyclohexene (25 mL). Two phases were

formed. After 1.5 h, ether (75 mL) was added (homogeneous solution) and the solution washed with saturated sodium bicarbonate. After the usual work-up, the yields were determined by vpc (OS-138) and are given in Table 3. The urethan content was 4 mol% compared to 10.5 mol% in the starting NFU.

N-Fluorourethan (2a) and lithium hydride in acetonitrile

To lithium hydride (200 mg, 29 mmol) in acetonitrile (10 mL), NFU (9 mL of a 15.3 m*M* solution, 1.38 mmol) was added slowly (1.5 h). The reaction mixture was stirred until the cessation of hydrogen evolution (12 h). The iodometric activity was 5%. After filtration and solvent evaporation, water (50 mL) was added and the mixture extracted with ether (2 × 25 mL). The yields (vpc, OS-138) are given in Table 2, entry 4. The urethan content was 6% compared to 12% in the starting NFU.

N-Chlorourethan (2b) and triethylamine in the presence of cyclohexene

Triethylamine (597 mg, 5.91 mmol) in methylene chloride (10 mL) was added dropwise (45 min) to a solution of NCU (800 mg, 91% active chlorine, 5.89 mmol) in cyclohexene (20 mL) and methylene chloride (20 mL). After 10 h, a white precipitate was formed and the iodometric activity was 7%. The reaction mixture was washed with 5% hydrochloric acid (2 × 25 mL), then with water (25 mL). After the usual work-up, the crude product (554 mg) was separated by plc on silica gel (hexane–ether 3:1) to afford cis *N-(2-chlorocyclohexyl)urethan* (**21**), mp 52–54°C (lit. (21) mp 57.5–58°C) (178 mg, 14%), identical to an authentic sample (22), and trans *N-(2-chlorocyclohexyl)urethan* (**22**), mp 82–85°C (lit. (23) mp 96°C) (54 mg, 4%), identical to an authentic sample (22).

Acknowledgements

We are grateful to the "Ministère de l'Education du Québec" and to the Natural Sciences and Engineering Research Council of Canada for financial assistance.

1. D. BÉRUBÉ and J. LESSARD. Can. J. Chem. **60**, 1127 (1982).
2. T. L. COTTRELL. The strengths of chemical bonds. Butterworths Publications Ltd., London. 1958. p. 278.
3. H. MÉNARD and J. LESSARD. J. Chem. Eng. Data, **23**, 64 (1978).
4. D. A. CORRIGAN and D. H. EVANS. J. Electroanal. Chem. **106**, 287 (1980).
5. C. AMATORE, J. M. SAVÉANT, and D. TESSIER. J. Electroanal. Chem. **146**, 37 (1983).
6. W. LWOWSKI. Tetrahedron Lett. 2497 (1964).
7. G. L. SMITH and J. W. ROGERS. J. Electrochem. Soc. **118**, 1089 (1971).
8. W. LWOWSKI and T. MARICICH. J. Am. Chem. Soc. **87**, 3630 (1965).
9. K. J. MARTIN. J. Am. Chem. Soc. **87**, 394 (1965).
10. J. LESSARD, M. MONDON, and D. TOUCHARD. Can. J. Chem. **59**, 431 (1981).
11. N. TORIMOTO, T. SHINGAKI, and T. NAGAI. J. Org. Chem. **44**, 636 (1979).
12. M. HUDLICKY. Chemistry of organic fluorine compounds. 2nd ed. John Wiley and Sons, New York. 1976. p. 548.
13. D. BÉRUBÉ, J. CAZA, F. M. KIMMERLE, and J. LESSARD. Can. J. Chem. **53**, 3060 (1975).
14. R. E. BANKS, R. N. HASZELDINE, and J. P. LALU. J. Chem. Soc. (C), 1514 (1966).
15. V. GRAKAUSKAS and K. BAUM. J. Am. Chem. Soc. **91**, 1679 (1969).
16. R. C. BRIAN and A. H. LAMBERTON. J. Chem. Soc. 1633 (1949); E. E. GILBERT. Synthesis, 30 (1972).
17. N. NABJOHN. Org. Synth. Coll. Vol. IV. John Wiley and Sons. New York. 1956. p. 237.
18. A. HASSNER, M. E. LORBER, and C. HEATCOCK. J. Org. Chem. **32**, 540 (1967); **30**, 1748 (1965).
19. W. LWOWSKI and T. M. MATTINGLY. J. Am. Chem. Soc. **87**, 1947 (1965).
20. T. HIYAMA, H. KOIDE, S. FUJITA, and H. NOZAKI. Tetrahedron, **29**, 3137 (1973).
21. K. SCHRAGE. Tetrahedron Lett. 5795 (1966).
22. H. DRIGUEZ, J. M. PATON, and J. LESSARD. Can. J. Chem. **55**, 700 (1977).
23. T. FOGLIA and D. SWERN. J. Org. Chem. **31**, 3625 (1966).

Can. J. Chem. Downloaded from www.nrcresearchpress.com by 210.87.254.40 on 09/06/12
For personal use only.

Alkaloids of *Aconitum columbianum* Nutt.[1]

VITO BOIDO,[2] OLIVER E. EDWARDS, KASHMIRI L. HANDA,[3] RALPH J. KOLT, AND KOZIPARAMBIL K. PURUSHOTHAMAN[4]

Division of Chemistry, National Research Council of Canada, Ottawa, Ont., Canada K1A 0R6

Received August 26, 1983

VITO BOIDO, OLIVER E. EDWARDS, KASHMIRI L. HANDA, RALPH J. KOLT, and KOZIPARAMBIL K. PURUSHOTHAMAN. Can. J. Chem. **62**, 778 (1984).

The most abundant readily isolated alkaloids of the aerial portion of *Aconitum columbianum* Nutt. were found to be talatisamine and cammaconine. New spectral data for known derivatives of these alkaloids and descriptions of new derivatives are presented. Less abundant alkaloids identified included the known ones sachaconitine, talatizidine, isotalatizidine, and 14-*O*-acetyltalatisamine, and the new ones 8-*O*-methyltalatisamine and a tetrahydroxymonomethoxy alkaloid, columbianine, with the same oxygenation pattern and stereochemistry as cammaconine.

VITO BOIDO, OLIVER E. EDWARDS, KASHMIRI L. HANDA, RALPH J. KOLT et KOZIPARAMBIL K. PURUSHOTHAMAN. Can. J. Chem. **62**, 778 (1984).

On a trouvé que, parmi les alcaloïdes facilement isolables de la portion aérienne du *Aconitum columbianum* Nutt., les plus abondants sont la talatisamine et la cammaconine. On rapporte de nouvelles données spectrales de dérivés connus de ces alcaloïdes ainsi que la description de nouveaux dérivés. Parmi les alcaloïdes moins abondants, on a pu identifier la sachaconitine, la talatizidine, l'isotalatizidine et la *O*-acétyl-14 talatisamine qui étaient déjà connus en plus de deux nouveaux alcaloïdes, la *O*-méthyl-8 talatisamine et un dérivé tétrahydroxymonométhoxy de l'alcaloïde columbianine qui possède la même stéréochimie et le même arrangement d'oxydation que la cammaconine.

[Traduit par le journal]

There are only two native Canadian aconites, *A. columbianum* Nutt. which grows in central British Columbia, and *A. delphinipholium* D. C. which grows at medium altitudes in the Rocky Mountains of Alberta. The alkaloids of the latter have been the subject of recent study (1), but those of *A. columbianum* only received brief attention years ago by Beath (2).

The aerial portions of the plant, collected just before flowering, were found to contain around 0.45% of alkaloids (of air-dried weight).

The two principal bases were methoxylated hexacyclic bases with *N*-ethyl groups. Oxidation studies showed that they both had a tertiary hydroxyl group and that the major difference between them was the presence of a primary hydroxyl group in one, and the corresponding methyl ether in the other. This was confirmed by conversion of both to the identical tetramethoxy compound (**2**). Both alkaloids could be fully acetylated under forcing conditions, and the resulting acetates underwent the "pyro" reaction characteristic of the aconine[5] family of diterpenoid alkaloids (4). Finally, their mass spectra had *M*-31 as base peak, characteristic of the aconite alkaloids with a 1-methoxyl group.

From its formula ($C_{24}H_{39}NO_5$), melting point, and the above evidence it appeared that the less polar base was talatisamine **1** whose structure had been assigned by the Yunusovs (5). This was confirmed by comparison kindly made by Professor Yunusov, who also sent a reference sample. The structure and stereochemistry of this alkaloid has been confirmed by total synthesis by Wiesner *et al.* (6).

The main more-polar base thus had structure **5**, isomeric with that originally assigned to cammaconine (7) but identical to that attributed to the base from hydrolysis of aconorine (8). Comparison of samples established the identity of our alkaloid with this hydrolytic base.[6] However, recent work (9) has revised the structure of cammaconine to **5**. Identity with our alkaloid was suggested by comparison of ^{13}C nmr spectra. The identity of a pentamethyl ether **3**, prepared from talatisamine and our alkaloid, with one prepared by Mollov and co-workers[7] (7) from cammaconine confirmed this. Since the name cammaconine was assigned first, the name columbianine (8) which we had tentatively given to our alkaloid has been transferred to a new monomethoxy base described below. It follows that aconorine (8) is 18-*O*-(*N*-acetylanthranoyl) cammaconine.

We were able to prepare a didehydroxocammaconine (**6**) which must be the same as the "diketolactam" prepared by Mollov's group (7). They were unable to detect the formyl group of this derivative, which may well be due to its hydration. We observed just such a phenomenon in a transformation product of lycoctonine, which was also a formylacetamide (10). We sublimed **6** under high vacuum. This may have dehydrated a hydrate (marked rise in melting point) so that the aldehyde proton was observable.

The minor alkaloids from *A. columbianum* were partly separated by chromatography on alumina and preparative thin-layer chromatography on silica gel plates. The alkaloids identified in this way were talatizidine (**10**), isotalatizidine (**11**), 14-*O*-acetyltalatisamine (**4**), and the new ones, 8-*O*-methyltalatisamine (**12**) and the very polar columbianine (**14**). Sachaconitine (**9**) was only obtained as its derivatives oxosachaconitine (**9***a*) and 14-dehydrooxosachaconitine, obtained by separation of permanganate oxidation products from mixtures rich in the alkaloid.[8]

[1]Issued as NRCC No. 22875.

[2]Postdoctoral Fellow of the Consiglio Nazionale delle Ricerche (Rome).

[3]Columbo Plan Research Fellow.

[4]N.R.C. Postdoctoral Fellow.

[5]The term "aconine" is used to denote the sub-family of hexacyclic C_{19} diterpenoid alkaloids having 7-hydrogen and 8-oxygen substituents, while the lycoctonine sub-family (3) has oxygen functions on both C-7 and C-8.

[6]We thank Professors M.S. and S. Yu. Yunusov for this comparison.

[7]We thank Professor Mollov for a reference sample of the ether.

[8]We have so far been unable to obtain reference samples of sachaconitine or its derivatives.

Can. J. Chem. Downloaded from www.nrcresearchpress.com by 210.87.254.105 on 09/06/12
For personal use only.

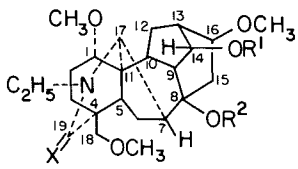

1 $R^1 = R^2 = H$ $X = H_2$
1*a* $R^1 = R^2 = H$ $X = O$
2 $R^1 = CH_3$ $R^2 = H$ $X = H_2$
3 $R^1 = R^2 = CH_3$ $X = H_2$
4 $R^1 = Ac$ $R^2 = H$ $X = H_2$

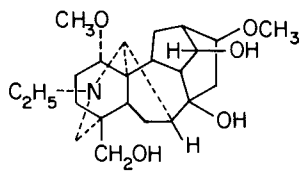

5

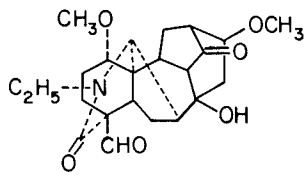

6

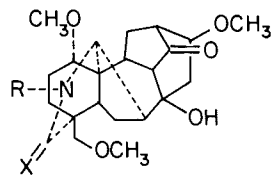

7 $R = C_2H_5$ $X = H_2$
7*a* $R = C_2H_5$ $X = O$
8 $R = CHO$ $X = H_2$

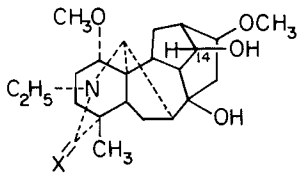

9 $X = H_2$
9*a* $X = O$

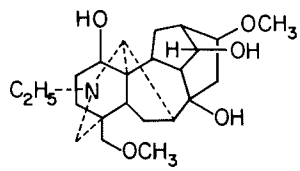

10

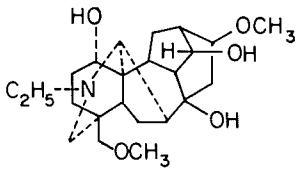

11

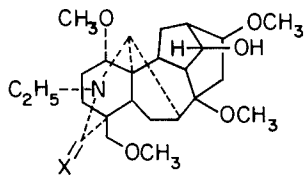

12 $X = H_2$
12*a* $X = O$

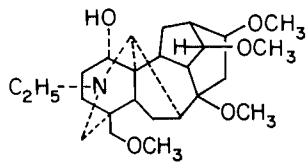

13

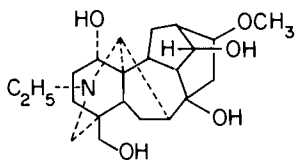

14

Columbianine had mp 202–205°C and $[\alpha]_D$ −6° in ethanol. Its mass spectrum had $M - 17$ as its base peak, showing that a 1-hydroxyl group was present. This and its ^{13}C nmr spectrum (Table 1) suggested that it was 1-des-*O*-methylcammaconine. Methylation of the base gave the hitherto unknown tetramethyl ether **13** (8,14-di-*O*-methylisotalatizidine), while more vigorous methylation gave the same pentamethyl ether that had been obtained from cammaconine and talatisamine. Thus columbianine had structure **14**. It is conceivable that before the polarity and low solubility in organic solvents of bases like columbianine was recognized, much was lost on columns and in aqueous solution.

Oxidation of mixtures of minor alkaloids with permanganate in wet acetone containing acetic acid gave *N*-desethyl-*N*-formyl derivatives of several bases in addition to the simple lactams. However, there was no ^1H nmr evidence for the presence of *N*-methyl alkaloids. We conclude that oxidative removal of the *N*-ethyl groups followed by formylation was the source of these formyl derivatives. Pelletier *et al.* have recently produced strong evidence for this phenomenon (11). However, the very rapid oxidation of C_{19} diterpenoid alkaloids by permanganate in 50% aqueous acetone gave nearly clean lactams (12), so should be used for analogous studies. As was found by Katsui and Hasegawa (13) for sachaconitine, the *N*-desethyl bases were by-products of these oxidations.

New derivatives of talatisamine characterized in this work were 14-dehydrotalatisamine (**7**), and *N*-desethyl-*N*-formyl-14-dehydrotalatisamine (**8**) and its 14-*O*-methyl ether **2** (1,14-dimethylisotalatizidine). New well-characterized derivatives of cammaconine were its triacetate and demethoxyisopyrocammaconine.

The ^{13}C nmr shifts for the bases recorded in Table 1 are based on multiplicities, correlations with other bases in our laboratory, and the extensive correlations by Jones and Benn (14) and by Pelletier and co-workers (9). The spectra of a few lactams have been recorded previously (12, 15) but many more are

Can. J. Chem. Downloaded from www.nrcresearchpress.com by 210.87.254.105 on 09/06/12
For personal use only.

TABLE 1. Carbon-13 chemical shifts of bases

Carbon, multiplicity	1*	2*	3*	4*	10	11	12*	13*	14
1 d	86.1	85.5	85.6	85.7	68.8	72.7	85.5	72.5	72.4
2 t	26.4	27.0	27.2	26.7	27.4	28.8	26.5	27.4	26.5
3 t	33.2	33.2	33.2	33.2	30.7	30.6	33.0	30.5	29.9
4 s	39.0	38.8	38.8	38.9	38.6	37.8	38.8	37.6	38.1
5 d	46.3†	46.6	46.6†	46.8	39.5	42.2	46.5†	41.5	41.4
6 t	25.5	25.9	24.9	25.7	24.9	25.6	24.2	24.9	24.8
7 d	46.3	46.0	40.5	46.4	41.6	45.5	40.2	39.5	45.3
8 s	72.9	74.1	78.2	73.7	74.0	74.2	78.3	78.8	74.2
9 d	47.6	47.5	46.2†	45.9†	46.9	47.4	46.0†	44.7	46.8
10 d	46.2†	46.0	43.9	45.5†	44.8	44.8	46.4†	43.1	44.2
11 s	49.0	49.1	49.6	49.1	49.5	49.1	49.0	49.8	48.8
12 t	28.2	29.9	29.9	28.8	29.1	27.8	28.9	30.1	28.5
13 d	38.6	37.9	39.8	36.2	39.6	40.7	38.8	39.3	40.3
14 d	75.8	85.0	84.6	77.2	75.9	76.3	75.4	84.9	75.9
15 t	39.3	42.7	35.9	41.9	41.8	43.1	33.7	36.6	42.3
16 d	82.8	83.1	84.3	82.5	82.3	82.6	82.7	84.2	82.0
17 d	62.7	62.1	61.5	62.0	63.9	64.1	62.5	63.2	64.1
18 t	79.8	79.9	80.1	79.9	79.5	79.3	79.9	79.4	68.3
19 t	53.8	53.8	53.9	53.9	53.4	56.9	53.6	57.2	56.4
N—CH_2	49.6	49.4	49.3	49.5	49.1	48.6	49.4	48.5	48.6
CH_3	13.8	13.8	13.8	13.8	13.5	13.2	13.7	13.1	13.1
1′	55.7	55.6	55.7	55.7	—	—	55.7	—	—
8′	—	—	48.1	—	—	—	47.9	48.2	—
14′	—	57.4	57.4	—	—	—	—	57.3	—
16′	56.1	55.9	55.9	56.0	56.4	55.9	55.8	56.0	56.5
18′	59.2	59.2	59.2	59.2	59.5	59.1	59.1	59.1	—
CH_3CO	—	—	—	20.9	—	—	—	—	—

*In C_6D_6.
†Values interchangeable in the column.

Can. J. Chem. Downloaded from www.nrcresearchpress.com by 210.87.254.105 on 09/06/12
For personal use only.

listed in Table 2. The use of C_6D_6 as solvent in recording spectra of bases is recommended since reaction with deuteriochloroform often occurs during long runs. In the case of columbianine and talatizidine, however, low solubility precluded the use of C_6D_6. The major modification of the assignments made previously for related alkaloids (9, 16) is in those for C-9 and C-13. This was done to fit the expected downfield shift (6–8 ppm) when the 14-hydroxyl was transformed to a carbonyl. This modification of the assignments by Pelletier and co-workers had previously been suggested by Sakai *et al.* (17). A few chemical shift differences are noteworthy. The transition from hydroxyl to methoxyl on C-8 produces an upfield shift for C-7 of 6 ppm (β effect). The oxidation of the 19-methylene to a carbonyl giving the oxo compounds had its major effect on the N—CH_2 group (8 ppm upfield), C-4 (12 ppm downfield), and C-18 (5 ppm upfield).

Based on biogenetic postulates and the natural occurrence of the C_{19} alkaloids of the aconine sub-family,[5] it is possible to suggest a sequence for the introduction of oxygen functions in their biosynthesis.[9] The ubiquitous 8-oxygen is very probably introduced during formation of the 7,17 bond from a precursor with a 7,8 double bond (4a) and the 14-oxygen is introduced when one carbon of the original C_{20} skeleton is removed. Thus both must appear at an early stage in the biosynthesis. The nearly universal 16-oxygen must also appear early, followed by the very common one on C-1. An 18-oxygen is common, and is probably introduced next. A 6-oxygen is missing in the alkaloids of many aconite species, indicating the absence or suppression of the requisite enzyme system. It appears likely that it is introduced late in the biosynthesis.

On the same grounds, it appears that methylation of the oxygens is in the sequence 16, 6 and 18, 1, then 14. The rare 8-methoxyl probably arises from participation of methanol instead of the more common water or acetic acid in the formation of the 7,17 bond (4a).

Experimental

Infrared spectra were taken in dichloromethane solutions unless otherwise stated. The ^1H nmr spectra were taken of solutions in deuteriochloroform unless otherwise stated. Preparative plate separations were done on 20 cm × 20 cm 1000-μ SiO_2 plates with fluorescent indicator. The ^1H nmr spectra were obtained at 80 MHz and ^{13}C nmr spectra at 20.15 MHz on a Bruker WP-80 FT spectrometer. Rotations were determined at room temperature (25 ± 2°C).

Aconitum Columbianium *Nutt.*

Aerial portions of *A. columbianium* collected just before flowering in central British Columbia were air-dried, then ground. The extractives were obtained by soaking in 95% ethanol, followed by percolation until little was extracted. The ethanol solution was evaporated under reduced pressure, then the residue separated into neutral, basic, and acidic components. In this way 11.8 kg dried plant yielded a large neutral fraction, 53 g alkaloids (0.45%), and 19 g of acids (0.16%).

The crude alkaloid mixture was separated into two fractions by dissolving it in an excess of dilute sulfuric acid, raising the pH to 7 by addition of sodium carbonate, extracting the less polar bases (fraction A) with dichloromethane, then taking the aqueous layers to pH 11 and extracting the more polar bases (fraction B) with dichloromethane.

Fraction A crystallized in part from ether giving talatisamine. The

[9]H. Hikino and co-workers have used similar arguments based on the alkaloid content of *A. carmichaeli* (18).

Can. J. Chem. Downloaded from www.nrcresearchpress.com by 210.87.254.105 on 09/06/12
For personal use only.

TABLE 2. Carbon-13 chemical shifts of amides*

Carbon, multiplicity	A	B	C	D	E	F	G
1 d	84.1	84.0	83.6	83.9	84.3	83.5	83.0
2 t	26.4	26.4	26.0	26.5	26.2	25.0	25.0
3 t	31.1	31.0	31.0	31.1	35.5	32.2	32.0
4 s	50.8	50.7	50.6	50.7	47.0	37.8	37.8
5 d	52.9	52.2	48.0	52.0	52.1	52.5	47.9
6 t	26.1	26.0	25.3	26.2	27.4	24.6	24.1
7 d	43.5	43.3	43.6	43.0	49.2	45.7	45.1
8 s	71.7	81.5	76.4	85.7	81.6	82.0	77.3
9 d	46.0	54.4	44.9	51.3	54.7	54.5	45.5
10 d	46.0	46.1	45.9	46.1	46.2	46.2	45.9
11 s	47.4	47.4	47.7	47.5	47.7	48.4	48.2
12 t	27.1	24.6	27.4	24.2	24.7	24.7	27.3
13 d	37.3	44.1	37.2	44.1	44.3	43.8	37.9
14 d	75.3	214.2(s)	74.9	214.8(s)	214.0(s)	214.2(s)	74.9
15 t	37.2	35.9	31.0	31.8	36.2	37.0	32.4
16 d	82.2	85.0	81.9	84.6	84.9	85.1	82.0
17 d	61.8	62.4	61.9	61.7	62.7	60.7	60.0
18 t	75.1	74.7	75.2	74.9	22.1(q)	79.1	78.4
19 s	171.7	171.5	171.7	171.6	173.6	44.2(t)	43.8(t)
$N-CH_2$	41.4	41.4	41.4	41.4	41.6	162.5(d)	162.3(d)
CH_3	13.1	13.1	13.1	13.1	13.2	—	—
1′	55.8	55.8	55.7	55.7	55.8	55.8	55.8
8′	—	—	48.4	51.1	—	—	48.5
16′	56.6	56.1	56.5	56.1	56.1	56.1	56.5
18′	59.5	59.4	59.5	59.5	—	59.5	59.5

*Legend for Table 2: A, oxotalatisamine (**1***a*); B, 14-dehydrooxotalatisamine (**7***a*); C, 8-*O*-methyloxotalatisamine (**12***a*); D, 14-dehydro-8-*O*-methyloxotalatisamine (**12***a*, 14-carbonyl); E, 14-dehydrooxosachaconitine (**9***a*, 14-carbonyl); F, *N*-desethyl-*N*-formyl-14-dehydrotalatisamine (**8**; ref. 16); G, *N*-desethyl-*N*-formyl-8-*O*-methyltalatisamine (**12**, *N*-formyl).

bases in the mother liquors were partially separated by adsorption on a 20-fold ratio of neutral alumina (activity III). Benzene–ether mixtures eluted 14-*O*-acetyltalatisamine followed by a mixture of bases. Ether eluted talatisamine, and 2% methanol in ether eluted more talatisamine and other bases. Finally methanol containing ammonia eluted a fraction containing talatizidine and isotalatizidine.

Fraction B crystallized in part from aqueous methanol giving a hydrate of cammaconine, mp 88–95°C. The bases from the mother liquor were adsorbed on a 10-fold ratio of neutral alumina (Act IV). Benzene eluted much talatisamine and other less polar bases, while methanol in chloroform eluted fractions rich in cammaconine followed by a fraction rich in columbianine.

Non-crystalline mixtures of less polar bases from A and B were further separated on a 20-fold ratio of alumina (Act IV). Only 8-*O*-methyltalatisamine (eluted with 25% dichloromethane in benzene) and more talatisamine (1% methanol in chloroform) were obtained in a reasonable state of purity. No crystalline perchlorate, hydrochloride, or hydriodide could be obtained from these base mixtures. Hence resort was made to oxidation with permanganate, with hope of separating lactams. The use of permanganate in acetone containing 5–10% water and 1% acetic acid was a poor choice. Mixtures of lactams, keto-lactams, *N*-desethyl-*N*-formyl derivatives, and *N*-desethyl bases were obtained. The neutral products were then oxidized with Jones' reagent in acetone giving keto lactams and *N*-formyl ketones. Oxidation by permanganate in 50% aqueous acetone, however, was rapid under controlled conditions (see oxidation of cammaconine, ref. 12) and mixtures of the lactams and *N*-desethyl bases were the major products. The neutral products were separated on silica gel plates using 5% methanol in chloroform. In this way 8-*O*-methyl-14-dehydroxotalatisamine, *N*-desethyl-*N*-formyl-14-dehydrooxotalatisamine, oxosachaconitine, and 14-dehydrooxosachaconitine were isolated and characterized.

Talatizidine, isotalatizidine, and columbianine were isolated by purification of the appropriate fractions (see above) on silica gel plates using 7% methanol and 10% diethylamine in benzene for development.

The yield of talatisamine was approximately 0.06% and cammaconine 0.05% of the dry weight of plant. The other bases were less abundant and yields were not obtained. It is likely that much polyhydroxy base was lost during extractions and chromatography.

Cammaconine

The initially-observed hydrate, mp 88–95°C, when dried, crystallized from methanol as rods, mp 136–138°C (lit. (7) mp 135.7°C) and had $[\alpha]_D$ 0° (*c*, 1.0 in chloroform) and pK_a 9.55 in 50% methanol. It gave a hydriodide, mp 225–227°C. *Anal.* calcd. for $C_{23}H_{36}INO_5$: C 51.78, H 6.80, N 2.63; found: C 51.70, H 6.93, N 2.65.

*14,18-Didehydrooxocammaconine (**6**)*

Oxocammaconine (100 mg) was dissolved in 3 mL of pyridine. To this was added the complex from 80 mg of chromium trioxide and 1 mL of pyridine. The mixture was stirred for 18 h at room temperature, then evaporated to near dryness *in vacuo*. Crushed ice was added, then sulfur dioxide bubbled through the solution until it became green. The products were extracted into chloroform, then this was washed with dilute sodium carbonate solution. The neutral product from the chloroform (96 mg) crystallized from benzene–hexane. It melted at 194–196°C. This was sublimed at 175°C, 1×10^{-5} Torr. It then melted at 218°C and had ν_{max}: 3400, 1755, 1725 cm^{-1}. Its ^1H nmr spectrum had signals at δ: 10.15 (1H, s), 3.35 (6H, s), and 1.23 (3H, t, J = 7 Hz). *Anal.* calcd. for $C_{23}H_{31}NO_6$: C 66.16, H 7.48; found: C 65.62, H 7.42. This is undoubtedly identical to the "diketolactam", mp 194–195°C of Mollov and co-workers (7).

Cammaconine triacetate

A mixture of 300 mg of cammaconine, 150 mg of *p*-toluenesulfonic acid, and 3 mL of acetic anhydride was heated at 100°C for 1 h. The

Can. J. Chem. Downloaded from www.nrcresearchpress.com by 210.87.254.105 on 09/06/12
For personal use only.

product was adsorbed onto 7 g of neutral alumina, activity III, from benzene. Benzene eluted 280 mg of ester which crystallized from hexane. The triacetate had mp 105–107°C. It gave ^{1}H nmr signals at δ: 4.84 (1H, t, J = 5 Hz), 3.80 (2H, s), 3.34 and 3.30 (3H singlets), 2.05, 2.04 and 1.95 (3H singlets), and 1.05 (3H, t, J = 7 Hz). *Anal.* calcd. for $C_{29}H_{43}NO_8$: C 65.27, H 8.12; found: C 65.33, H 8.11.

Pyrolysis of cammaconine triacetate

The triacetate was heated at 210–230°C under 10 Torr during 5 min, by which time bubbling had stopped. The product was dissolved in chloroform, washed with a small volume of sodium carbonate solution, dried, and the solvent removed. The residue was distilled at 215°C, 1×10^{-4} Torr. It gave ^{1}H nmr signals at δ: 5.9 (1H, m), 4.75 (1H, t), 3.86 (2H, s), 3.30 and 3.18 (3H singlets), 2.06 and 2.00 (3H singlets), and 1.04 (3H, t, J = 7 Hz). *Anal.* calcd. for $C_{27}H_{39}NO_6$: C 68.47, H 8.30; found: C 68.81, H 8.51.

Demethoxyisopyrocammaconine

Pyrocammaconine (50 mg) in 10 mL of ether was stirred overnight with 200 mg of lithium aluminum hydride. The excess reagent was destroyed with methanol, then a small amount of water was added. The ether was decanted from the solids, and these were extracted thoroughly with dichloromethane. The 33 mg of product was dissolved in chloroform and filtered through a short bed of activity IV alumina. After removal of the chloroform, the product crystallized from solution in acetone–hexane giving 12 mg, mp 194–198°C. It had ^{1}H nmr signals at δ: 5.8 (2H, br, m), 4.1 (1H, br), 3.29 (3H, s), 1.08 (3H, t, J = 7 Hz). *Anal.* calcd. for $C_{22}H_{33}NO_3$: *Mol. Wt.* 359; C 73.50, H 9.25; found: C 73.34, H 9.05. Its mass spectrum gave M^+ 359 and the base peak at 328 (M − 31).

*Talatisamine (**1**)*

This crystallized from ether as small prisms. It could be recrystallized from acetone–hexane or methanol giving prisms with mp 142–143°C. In an evacuated capillary it had mp 148°C and showed no mp depression with a sample with mp 148.5°C (evacuated capillary) obtained from S. Yu. Yunusov (5). It had $[\alpha]_D$ 0° (c, 1.0 in ethanol) and pK_a 9.05 in 50% methanol. Its hydrochloride, hydriodide, or perchlorate would not crystallize readily. The base gave ^{1}H nmr signals at δ: 4.81 (1H, d, J = 5 Hz, OH), 4.29 (1H, t, J = 5 Hz), 3.68 (1H, s, OH), 3.44, 3.38, 3.34 (3H singlets), and 1.07 (3H, t, J = 7 Hz).

*Talatisamine 14-O-acetate (**4**)*

Talatisamine was slowly acetylated in 1 : 1 acetic anhydride – pyridine. After 20 h reaction was complete. The amorphous product (ref. 5 reports mp 97°C) gave ^{1}H nmr signals at δ: 4.82 (1H, t, J = 5 Hz), 3.29, 3.27 and 3.23 (3H singlets), 2.05 (3H, s), and 1.06 (3H, t, J = 7 Hz) (see ref. 14). Its mass spectrum had M^+ 463.2793 ($C_{26}H_{41}NO_6$ requires 463.2934) and a base peak at m/e 432 (M − 31).

Talatisamine diacetate

Talatisamine (150 mg) in 4 mL of acetic anhydride containing 75 mg of *p*-toluenesulfonic acid hydrate was heated at 95°C for two hours. The crude product was adsorbed on 3 g of alumina (Act. III). The diacetate was rapidly eluted with benzene. It crystallized from hexane, mp 120–122°C (ref. 5 gives mp 122–123°C). It gave ^{1}H nmr signals of δ: 4.80 (1H, t, J = 5 Hz), 3.32, 3.29, 3.28 (3H singlets), 2.02, 1.94 (3H singlets), and 1.06 (3H, t, J = 7 Hz). It lost acetic acid when heated at 150°C *in vacuo* to give a mixture of pyro and isopyro compounds (see also ref. 5).

*14-Dehydrotalatisamine (**7**)*

Twenty-five mg of chromium trioxide was added to a stirred solution of 85 mg of talatisamine in 1 mL of acetic acid. After 4 h at room temperature the solution was evaporated under reduced pressure, then the residue was dissolved in 1 *N* sulfuric acid. A chloroform extraction removed traces of neutral and acidic products, after which the solution was made basic with sodium carbonate. The bases extracted into dichloromethane weighed 80 mg. This was adsorbed on 1.8 g of neutral alumina (Act. III). The base eluted with benzene (48 mg) crystallized from benzene–hexane giving 25 mg, mp 124–127°C. This had ν_{max}: 3300 and 1750 cm^{-1} and had a pK_a in 50% methanol of 8.1. *Anal.* calcd. for $C_{24}H_{37}NO_5$: C 68.70, H 8.89; found: C 68.70, H 8.75.

*14-Dehydrooxotalatisamine (**7**a)*

A solution of 0.30 g of talatisamine in 8 mL of pyridine was added to a solution of 1.2 g of chromium trioxide in 12 mL of dry pyridine. The mixture was stirred for 16 h at room temperature. The excess chromium trioxide was reduced by sulfur dioxide, then the pyridine was removed under reduced pressure. The residue was dissolved in cold 2 *N* sulfuric acid, then extracted with dichloromethane (4 × 20 mL). The organic layers were washed with water, then sodium bicarbonate solution. The dichloromethane was removed, leaving 240 mg of gum which crystallized from acetone–hexane. This was separated on two silica gel plates (10% methanol in chloroform) into 14-dehydrooxotalatisamine (R_f 0.56) and *N*-desethyl-*N*-formyl-14-dehydrotalatisamine (**8** R_f 0.3, see below). The lactam crystallized from acetone–hexane as laths, mp 195–198°C. It had ν_{max}: 3575, 1752, and 1631 cm^{-1} and $[\alpha]_D$ −41°C (c, 0.66). It gave ^{1}H nmr signals at δ: 3.92 (1H, br, s), 3.59 (1H, s), 3.33 (9H, br, s), and 1.19 (3H, t, J = 7 Hz). *Anal.* calcd. for $C_{24}H_{35}NO_6$: C 66.49, H 8.14; found: C 66.36, H 7.99.

*Oxotalatisamine (**1**a)*

14-Dehydrooxotalatisamine was reduced with excess sodium borohydride in methanol. The product crystallized from acetone as rods, mp 196–198°C (lit. (5) mp 197–200°C); ν_{max} ($CHCl_3$): 1619 cm^{-1}; $[\alpha]_D$ −42°C (c, 1.09 in ethanol). Its ^{1}H nmr spectrum had signals at δ: 4.98 (1H, d, J = 4.4 Hz, OH), 3.73 (1H, s), 3.60 (probably 2H, s), 3.37, 3.33 and 3.24 (3H singlets), 1.6 (3H, t, J = 7 Hz).

N-*Desethyl*-N-*formyl-14-dehydrotalatisamine (**8**)*

This product from the chromium trioxide – pyridine oxidation of talatisamine (see above) crystallized from acetone. It had mp 270°C and ν_{max}: 3580, 1752, and 1662 cm^{-1}. Its ^{1}H nmr spectrum had signals at δ: 8.0 (1H, s), 4.33 (1H, s), 3.89 (br, 2H, s), 3.30, 3.27 and 3.24 (3H singlets). *Anal.* calcd. for $C_{23}H_{33}NO_6$: C 65.85, H 7.93, N 3.34; found: C 65.81, H 7.79, N 3.29.

*8-O-Methyltalatisamine (**12**)*

This was obtained as a new alkaloid from *A. columbianum*. A reference sample was obtained by reduction of 8-*O*-methyloxotalatisamine by lithium aluminium hydride in refluxing dioxane. It gave ^{1}H nmr signals at δ: 4.10 (1H, br, t), 3.17, 3.14, 3.08 and 2.96 (3H singlets), 2.89 (probably 2H, s), and 1.05 (3H, t, J = 7 Hz). Its mass spectrum had peaks at m/e: 435.3046 (5%, M^+), 406.0 (7%), 405 (41%), and 404.0 (100%). M^+ calcd. for $C_{25}H_{41}NO_5$: 435.2985.

*8-O-Methyloxotalatisamine (**12**a)*

This was obtained by oxidation of alkaloid fractions rich in 8-*O*-methyltalatisamine using permanganate in 50% acetone or by reduction of 14-dehydro-8-*O*-methyloxotalatisamine by sodium borohydride in methanol. It was purified on silica gel plates using 5% methanol in chloroform (R_f 0.5). It was not obtained crystalline. It had ν_{max}: 3480 and 1629 cm^{-1} and gave ^{1}H nmr signals at δ: 3.86 (1H, OH), 3.56 (2H, s), 3.38, 3.33, 3.25 and 3.14 (3H singlets), and 1.15 (3H, t, J = 7 Hz). Its mass spectrum had peaks at m/e: 450.1 (6%), 449.2771 (19%, M^+), 435.1 (27%), and 434.1 (100%). M^+ calcd. for $C_{25}H_{39}NO_6$: 449.2777.

*8-O-Methyl-14-dehydrooxotalatisamine (**12**a, 14-carbonyl)*

This was obtained by oxidation of alkaloid fractions rich in 8-*O*-methyltalatisamine by permanganate in acetone containing 10% water and 1% acetic acid, followed by Jones oxidation in acetone, or by methylation of 14-dehydrooxotalatisamine (see below). It crystallized from acetone–hexane as rods, mp 156–158°C. It had ν_{max}: 1755 and 1632 cm^{-1} and gave ^{1}H nmr signals (80 MHz) at δ: 3.84 (1H, s), 3.58 (2H, s), 3.34, 3.32, 3.29 and 3.24 (3H singlets), and 1.1 (3H, t, J = 7 Hz). *Anal.* calcd. for $C_{25}H_{37}NO_6$: C 67.09, H 8.33, N 3.13; found: C 66.92, H 8.50, N 3.24.

Can. J. Chem. Downloaded from www.nrcresearchpress.com by 210.87.254.105 on 09/06/12
For personal use only.

N-*Desethyl*-N-*formyl*-8-O-*methyltalatisamine* (**12**, *NCHO*)

This product of oxidation of 8-*O*-methyltalatisamine by permanganate in acetone (containing 10% water and 1% acetic acid) ran just behind 8-*O*-methyloxotalatisamine on silica gel plates (5% methanol in chloroform). It crystallized from acetone–hexane as prisms or needles, mp 197°C. It had ν_{max}: 3500 and 1658 cm^{-1} and gave ^1H nmr signals at δ: 7.96 (1H, s), 3.35, 3.27, 3.16 and 3.10 (3H singlets). Its mass spectrum gave peaks at *m/e*: 436(33), 435.2617(100, M^+), 420(13), 405(42), 404(80), 403(39), etc. M^+ calcd. for $C_{24}H_{37}NO_6$: 435.2622.

Methylation of 14-dehydrooxotalatisamine (**7**a)

A solution of the keto lactam **7***a* (61 mg) in 2 mL of dry peroxide-free dimethoxyethane was added to 126 mg of sodium hydride. After addition of 2 mL of methyl iodide the mixture was stirred under argon for 18 h. It was then filtered and evaporated to dryness under reduced pressure. Water was added to the residue, and the product extracted into dichloromethane. The nearly pure 8-*O*-methyl compound was separated from impurities on a silica gel plate using 5% methanol in chloroform. The 63 mg of product had mp 158°C and had spectra identical to those of the corresponding product (**12***a*) from the new alkaloid **12**.

Methylation of cammaconine

A mixture of 200 mg of cammaconine, 225 mg of sodium hydride, and 1.4 mL of methyl iodide in 10 mL of dioxane was refluxed under nitrogen for 7.5 h. The suspension was filtered through Celite and the filtrate evaporated. The residue was distributed between 1 *N* hydrochloric solution, then the bases extracted into dichloromethane. The 204 mg of product was extracted with hexane, giving 110 mg of non-polar ethers. This was adsorbed on 3.3 g of Act I neutral alumina. Hexane–ether (4:1) eluted 11 mg, rich in pentamethoxy compound. This solvent and hexane–ether (1:1) eluted 53 mg of tetramethyl ether which crystallized readily from pentane.

Methylation of talatisamine

Methylation of 200 mg of talatisamine as for cammaconine, followed by alumina chromatography, gave 30 mg rich in pentamethoxy compound and 84 mg of nearly pure tetramethyl ether. The early eluates from several runs were remethylated to enrich the pentamethoxy content.

14,18-Di-O-*methylcammaconine = 14*-O-*methyltalatisamine* (**2**)

This crystallized from pentane as rectangular plates with mp 103–105°C. It showed no mp depression with the tetramethoxy compound from talatisamine and their X-ray powder patterns, mass spectra, and ^1H nmr spectra were identical. The ether **2** gave ^1H nmr signals at δ: 3.71 (1H, t), 3.39, 3.30, 3.29 and 3.26 (3H singlets), and 1.06 (3H, t, J = 7 Hz). *Anal.* calcd. for $C_{25}H_{41}NO_5$: *Mol. Wt.* 435; C 68.93, H 9.49, N 3.22; found: C 68.51, H 9.47, N 3.29. Its mass spectrum had *m/e*: 435 (M^+) and 404 (M − 31, base peak).

8,14,18-Tri-O-*methylcammaconine = 8,14-Di*-O-*methyltalatisamine* (**3**)

The pentamethyl ether-rich fractions from cammaconine and talatisamine were purified by chromatography on activity I alumina (40-fold) from which the ether was eluted with 1:1 benzene–hexane. It crystallized from aqueous methanol as flat needles, mp 103–114°C. The ether **3** gave ^1H nmr signals at δ: 3.36 (6H, s), 3.30, 3.27 and 3.13 (3H singlets), and 1.06 (3H, s, J = 7 Hz). In C_6D_6 it gave signals at δ: 3.44, 3.20, 3.15, 3.10 and 3.095 (3H singlets) and 1.075 (3H, t, J = 7 Hz). Its mass spectrum had *m/e* 449 (M^+) and the base peak *m/e* 418 (M − 31). M^+ calcd. for $C_{26}H_{43}NO_5$: 449. A sample of fully methylated cammaconine kindly sent by Professor N. V. Mollov crystallized from aqueous methanol, mp 103–107°C. Its mixture mp with the above pentamethoxy compound was 103–114°C, and the mass spectra and X-ray powder patterns were identical.

Columbianine **14**

The most polar base from *A. columbianum* that was characterized crystallized from methanol, mp 202–205°C, and had $[\alpha]_D$ −6° (*c*, 0.5 in ethanol). It gave ^1H nmr signals at δ: 4.22 (1H, t, J = 4.5 Hz), 3.73 (1H, br, s), 3.34 (3H, s), 2.81 (1H, s), and 1.12 (3H, t, J = 7 Hz). *Anal.* calcd. for $C_{22}H_{35}NO_5$: *Mol. Wt.* 393: C 67.14, H 8.97, N 3.56; found: C 66.98, H 8.83, N 3.69. Its mass spectrum had *m/e* 393 (M^+) and 376 (M − 17).

Methylation of columbianine

A mixture of 54 mg of columbianine, 200 mg of sodium hydride, and 1 mL of methyl iodide in 7 mL of dioxane was refluxed under argon for 4 h, then left for 48 h at room temperature. After work-up as for cammaconine, the product was purified on a 1000-μ SiO_2 plate using 10:1 benzene–diethylamine for development. The main zone gave 35 mg of tetramethoxy base **13** (8,14,18-tri-*O*-methylcolumbianine). Repetition of the above experiment on 30 mg of columbianine but refluxing for 17 h gave 20 mg of pentamethoxy base which proved identical (^1H nmr, ^{13}C nmr) to 8,14-di-*O*-methyltalatisamine (**3**).

8,14,18-Tri-O-*methylcolumbianine* (**13**)

This new tetramethoxy base from the methylation of columbianine gave ^1H nmr signals at δ: 3.37 (6H, s), 3.32 and 3.15 (3H singlets), and 1.12 (3H, s, J = 7 Hz). Its mass spectrum gave *m/e*: 435.2997 (M^+) and 418.2958 (base peak, M − 17). M^+ calcd. for $C_{25}H_{41}NO_5$: 435.2985.

14-Dehydrooxosachaconitine (**9**a, *14-carbonyl*)

This crystallized as small plates from acetone, mp 235–236°C (recrystallized as rods before melting). It had $[\alpha]_D$ −30° (*c*, 0.69 in ethanol) and ν_{max}: 3570, 1751, and 1633 cm^{-1}. It gave ^1H nmr signals at δ: 3.93 (1H, s), 3.34 and 3.30 (3H singlets), 1.20 (3H, t, J = 7 Hz), and 1.17 (3H, s). Reference 13 gives mp 239°C and $[\alpha]_D$ +35.7° (note the reversed sign).

Oxosachaconitine (**9**a)

14-Dehydrooxosachaconitine was reduced by excess sodium borohydride in methanol. The product crystallized as laths from acetone–hexane, mp 197–199°C; $[\alpha]_D$ −35° (*c*, 0.36 in ethanol). Its ^1H nmr spectrum had signals at δ: 4.04 (1H, d, J = 4 Hz, OH), 4.18 (1H, m), 3.71 (1H, s, OH), 3.60 (1H, s), 3.38 and 3.24 (3H singlets), and 1.17 3H, t, J = 7 Hz). Its mass spectrum had peaks at *m/e*: 405.2518 (M^+), 390 (M − 15), 376, 375, 374, 373 (base peak, M − 32). M^+ calcd. for $C_{23}H_{35}NO_5$: 405.2515. Reference 13 gives mp 196°C and $[\alpha]_D$ −37.8°.

Acknowledgements

We wish to thank Professors N. M. Mollov, S. W. Pelletier, K. Wiesner, and M. S. and S. Yu. Yunusov for reference samples, Mr. H. Seguin for microanalyses, Dr. M. Przybylska for the X-ray powder pattern comparisons, and Dr. C. Kazakoff of the Ottawa–Carleton Mass Spectrometry Center for mass spectra. The help of Mrs. O. E. Edwards, Sr. and Mr. D. Edwards in collecting and drying plant material is gratefully acknowledged.

1. V. N. Aiyar, P. W. Codding, K. A. Kerr, M. H. Benn, and A. J. Jones. Tetrahedron Lett. 483 (1981).
2. O. A. Beath. J. Am. Pharm. Assoc. **15**, 265 (1926).
3. L. Marion and M. Przybylska. Can. J. Chem. **34**, 185 (1956); O. E. Edwards and M. Przybylska. Can. J. Chem. **60**: 2661 (1982).
4. (*a*) O. E. Edwards. Chem. Commun. 318 (1965); (*b*) S. W. Pelletier and L. H. Keith. *In* The alkaloids. Vol. 12. *Edited by* R. H. F. Manske. Academic Press, New York. 1970. p. 2.
5. M. S. Yunusov and S. Yu. Yunusov. Khim. Prir. Soedin. **6**, 90 (1970); Chem. Nat. Compounds (USSR), **6**, 85 (1970).
6. K. Wiesner, T. Y. R. Tsai, K. Huber, S. E. Bolton, and R. Vlahov. J. Am. Chem. Soc. **96**, 4990 (1974).
7. M. A. Khaimova, M. D. Palamareva, N. M. Mollov, and V. P. Krestev. Tetrahedron, **27**, 819 (1971).
8. V. A. Tel'nov, M. S. Yunusov, S. Yu. Yunusov, and B. Sh. Ibragimov. Khim. Prir. Soedin. **11**, 814 (1975); Chem. Nat.

Compounds (USSR), **11**, 83 (1975).
9. (*a*) N. V. MODY, S. W. PELLETIER, and N. M. MOLLOV. Heterocycles, **14**, 1751 (1980); (*b*) J. FINER-MOORE, N. V. MODY, S. W. PELLETIER, N. A. B. GRAY, C. W. CRANDELL, and D. H. SMITH. J. Org. Chem. **46**, 3399 (1981).
10. O. E. EDWARDS. Can. J. Chem. **59**, 3039 (1981).
11. S. W. PELLETIER, J. A. GLINSKI, and N. V. MODY. J. Am. Chem. Soc. **104**, 4676 (1982).
12. O. E. EDWARDS, R. J. KOLT, and K. K. PURUSHOTHAMAN. Can. J. Chem. **61**, 1194 (1983).
13. N. KATSUI and G. HASEGAWA. Bull. Chem. Soc. Jpn. **33**, 1037 (1960).
14. A. J. JONES and M. H. BENN. Can. J. Chem. **51**, 486 (1973).
15. S. W. PELLETIER, N. V. MODY, Z. DJARMATI, and S. D. LAJSIĆ. J. Org. Chem. **41**, 3042 (1976).
16. S. W. PELLETIER, N. V. MODY, R. S. SAWHNEY, and J. BHATTACHARYYA. Heterocycles, **7**, 327 (1977); S. W. PELLETIER, N. V. MODY, and N. KATSUI. Tetrahedron Lett. 4027 (1977); S. W. PELLETIER and Z. DJARMATI. J. Am. Chem. Soc. **98**, 2626 (1976).
17. S. SAKAI, H. TAKAYAMA, and T. OKAMOTO. Yakugaku Zasshi, **99**, 647 (1979).
18. C. KONNO, M. SHIRASAKA, and H. HIKINO. J. Nat. Prod. **45**, 128 (1982).

Can. J. Chem. Downloaded from www.nrcresearchpress.com by 210.87.254.105 on 09/06/12
For personal use only.

Surface reactions and catalysis at *alcohol vapour/3d transition metal oxide* interfaces at $T \leq 475$ K. Part I. Dehydration and dehydrogenation of isopropanol over V_2O_5 and V_2O_3

JOSEPH CUNNINGHAM, MOHAMMAD ILYAS, AND JOHN NUNAN
Chemistry Department, University College, Cork, Ireland

Received April 15, 1983

JOSEPH CUNNINGHAM, MOHAMMAD ILYAS, and JOHN NUNAN. Can. J. Chem. **62**, 785 (1984).

Pseudo steady-state conversions of alcohol vapours observed in a differential flow microcatalytic reactor provide the basis for comparing catalytic activities for a minor dehydrogenation ($-H_2$) process and for a dominant dehydration ($-H_2O$) process over both oxygenated and deoxygenated *alcohol vapour/vanadium oxide* interfaces. Effects of surface pre-reduction or pre-oxidation upon sample activity and ir spectra are consistent with an involvement of quadrivalent vanadium in the surface sites responsible for ($-H_2$) and ($-H_2O$) activities. Different sensitivities towards poisoning by phenol point to important differences in the environment of V^{IV} in the ($-H_2$) and ($-H_2O$) sites. Observations by ir and X-ray diffraction show extensive reduction by alcohol vapour at deoxygenated, but not at oxygenated interfaces.

JOSEPH CUNNINGHAM, MOHAMMAD ILYAS et JOHN NUNAN. Can. J. Chem. **62**, 785 (1984).

On utilise les conversions à un pseudo état stationnaire de vapeurs alcooliques dans un réacteur microcatalytique à flux différentiel comme base pour comparer les activités catalytiques pour un processus de déshydrogénation mineur ($-H_2$) et pour un processus déshydratation ($-H_2O$) majeur sur des interfaces *vapeur d'alcool/oxyde de vanadium* oxygénées ainsi que désoxygénées. Les effets de pré-réduction ou de pré-oxydation de la surface sur l'activité des échantillons et les spectres ir sont en accord avec une implication de vanadium quadrivalent dans les sites de surface responsables des activités ($-H_2$) et ($-H_2O$). Des différences de sensibilités vis-à-vis l'empoisonnement par le phénol suggèrent qu'il existe de grandes différences dans l'environnement du V^{IV} dans les sites responsables de ($-H_2$) et ($-H_2O$). Des observations par ir et par diffraction des rayons X montrent qu'il se produit une réduction importante des interfaces désoxygénées par les vapeurs d'alcool; ce n'est pas le cas au niveau des interfaces oxygénées.

[Traduit par le journal]

Can. J. Chem. Downloaded from www.nrcresearchpress.com by 210.87.254.40 on 09/06/12
For personal use only.

Introduction

The following features of catalytic activity identified in published work with oxides of 3*d*-transition metals prompted the work to be described in this series of papers: (*i*) indications that oxygen content at the oxide surfaces can vary in a complex manner with temperature and with oxygen overpressure (1–3); (*ii*) results from these and other laboratories showing that the activity and/or selectivity of some pure unsupported oxides for dehydration ($-H_2O$) and/or dehydrogenation ($-H_2$) of secondary alcohols could be strongly altered by prior reduction or oxidation of the oxide surface (4); (*iii*) proposals that sustained high catalytic activity attainable for oxidative catalytic processes over various oxides in the presence of gaseous oxygen can involve reaction and removal of lattice oxygen in an initial step followed by fast re-oxidation by gaseous oxygen of metal oxide sites reduced in the first step (5–7), e.g.

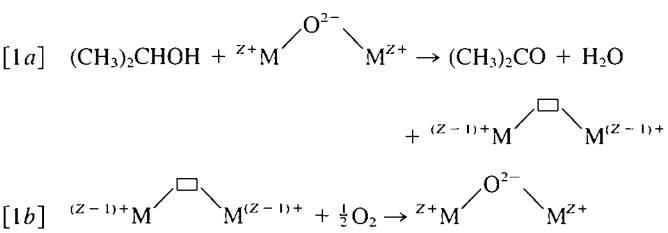

[1*a*] $(CH_3)_2CHOH + {}^{Z+}M(O^{2-})M^{Z+} \rightarrow (CH_3)_2CO + H_2O + {}^{(Z-1)+}M(\square)M^{(Z-1)+}$

[1*b*] ${}^{(Z-1)+}M(\square)M^{(Z-1)+} + \tfrac{1}{2}O_2 \rightarrow {}^{Z+}M(O^{2-})M^{Z+}$

and (*iv*) evidence for some cases, such as Mn_2O_3 or V_2O_5, that surface redox processes may be effectively restricted to the topmost surface layers (8) — provided that suitably moderate temperatures could be utilised. Interesting possibilities which emerge from the foregoing and which have come under mainly kinetic study in the work to be described in this series of papers include the following: (*A*) Identification of moderate oxygen overpressures capable of contribution added surface oxygen species sufficient to drive surface reoxidation similar to [1*b*] but insufficient to favour processes of type [1*c*] or [1*d*].

[1*c*] $O_{2(ads)} + M_{(s)}^{(Z-1)+} \rightarrow O_{2(ads)}^{-} + M_s^{Z+}$

[1*d*] $O_{2(ads)} + (CH_3)_2CHOH_{ads} \rightarrow (CH_3)_2CO + H_2O_2$

(*B*) Identification of moderate temperature conditions such that surface reduction–oxidation cycles (c.f. eq. [1*a*] followed by [1*b*] or [1*c*]) may be restricted to topmost surface layers, thereby allowing the underlying bulk oxide to remain in a chemically and structurally unaltered state. Results in the present paper will show that this latter possibility is not realised in V_2O_5 due to extensive reduction of the bulk by isopropanol even at 400 K. Interesting effects relevant to possibility (*A*) do, however, emerge in the present study for oxygenated isopropanol/vanadium oxide systems.

Experimental

Materials

Spectrochemically pure (>99.99%) V_2O_5 powder (surface area 2.6 $m^2\ g^{-1}$) was used as supplied (Spex), as also was reagent grade V_2O_3 (Ventron). Isopropanol was Aristar grade and *t*-butanol reagent grade which were absorbed onto a column of molecular sieve pellets and the purified vapour extracted therefrom by a flow of argon carrier gas. Prior to contact with alcohol vapour, the metal oxide powders were preheated either in a flow of argon alone (to remove surface water), or in a flow of argon admixed with oxygen in order also to preoxidize the surface when that was desired. Usually such pretreatments were at the temperature of subsequent reaction. However, when extensive surface dehydroxylation was required, samples were pretreated for 16 h at 675 K either in argon alone (which also yielded some pre-reduction of the surface) or in a 1 : 1 flow of argon plus oxygen (which yielded well pre-oxidised surfaces). When extensive surface pre-reduction was required this was achieved by heating in a flow of 3% H_2 in N_2 at 675 K. Bulk reduction of V_2O_5 to V_2O_3 was accomplished (9) by heating in a flow of pure H_2 at 873 K.

Can. J. Chem. Downloaded from www.nrcresearchpress.com by 210.87.254.40 on 09/06/12
For personal use only.

Procedures

Observations were made in a continuous reactant flow (c.r.f.) mode and involved the establishment of a continuous flow of argon carrier gas, *plus* alcohol vapour at a set pressure (*plus* O_2 whenever required), through the preconditioned sample at a fixed reaction temperature in the range 375–475 K. In this c.r.f. mode a gas-sampling valve was utilised intermittently to sample exit gases from the reactor at desired intervals and pass them to a gas chromatograph for analysis using a flame ionization detector. The minimum feasible exposures of samples to alcohol vapour were moderately high in this c.r.f. mode, e.g. net exposure of 200 molecules per surface ion pair (m/s.i.p.) when a sample of exit gases was extracted after only 10 min continuous flow. Net yields of $(-H_2O)$ or $(-H_2)$ products could be calculated as turnover per surface ion pair (t/s.i.p.) from known total flow times and rates of conversion evaluated from samples analysed over that time. Blank runs with the empty reactor pretreated in identical fashion to that used for studying reaction with metal oxide in the reactor were made in all cases. Any minor conversions observed with the blanks have been taken into account in arriving at the corrected values for the rates of $(-H_2O)$ and $(-H_2)$ processes catalysed by the vanadium oxide surfaces. Linearity of plots of yield vs. reciprocal of the flow rate was also checked for both the $(-H_2O)$ and $(-H_2)$ processes in order to confirm that reaction on the surface was the rate limiting process — rather than diffusional limitation in arrival of reactant(s) or departure of product(s).

Surface areas were evaluated from measurement of N_2 adsorption at 77 K with a vacuum microbalance and BET plots. The rather small surface areas found in this way (2.6 $m^2 g^{-1}$ for V_2O_5) militated against adequate transmission of ir through self supporting discs and it was necessary to disperse appropriately pretreated samples into KBr discs for ir examination.

Results and discussion

1. Parallel $(-H_2O)$ and $(-H_2)$ from isopropanol on V_2O_5

Data taken previously in the c.r.f. mode at 395 K, with non-oxygenated isopropanol as reactant over a high-purity oxide of initial stoichiometry V_2O_5, were reported elsewhere (4) and established unusually high initial $(-H_2O)$ activity for conversion to propene with selectivity ~95%. Although selectivity for $(-H_2)$ was only ~5%, that did correspond to substantial and accurately measurable steady-state rates of conversion to acetone. A progressive decay with time was observed in that earlier work for both $(-H_2O)$ and $(-H_2)$ activities of V_2O_5 at 395 K in the c.r.f. mode whilst the net yield of propene increased to t/s.i.p. ~10 in the absence of $O_{2(g)}$. Similar rapidly-decaying activity profiles were again observed at 410 and 395 K in the present study. One general view of declining activity profiles of the type shown in Fig. 1 for temperatures ca. 400 K would be: (*i*) that active sites present in topmost layers of V_2O_5 experienced non-selective and partially reversible degradation of both $(-H_2O)$ and $(-H_2)$ activities whilst net yield for the latter process increased to t/s.i.p. ~10; and (*ii*) that such non-selective degradation involved decreases in oxidation state of vanadium at certain sites in the surface layer(s) (e.g. cf. eq. [1*a*]). This was examined here by the introduction of oxygen at various pressures into the reactant flow in a set of experiments prompted in part by a report (8) that the re-oxidation sequence depicted in reaction [2] could be restricted to surface layers of V_2O_5 if temperature was limited to <475 K.

$$[2]\quad V^{III} \xrightarrow[E_{act} = 6.3\ kJ]{+O_2} V^{IV} \xrightarrow[E_{act} = 21\ kJ]{+O_2} V^{V}$$

In efforts to evaluate the influence of oxygen upon *steady-state* activities, the V_2O_5 catalyst was first brought to its steady-state (working) activity in a flow of isopropanol alone, then oxygen

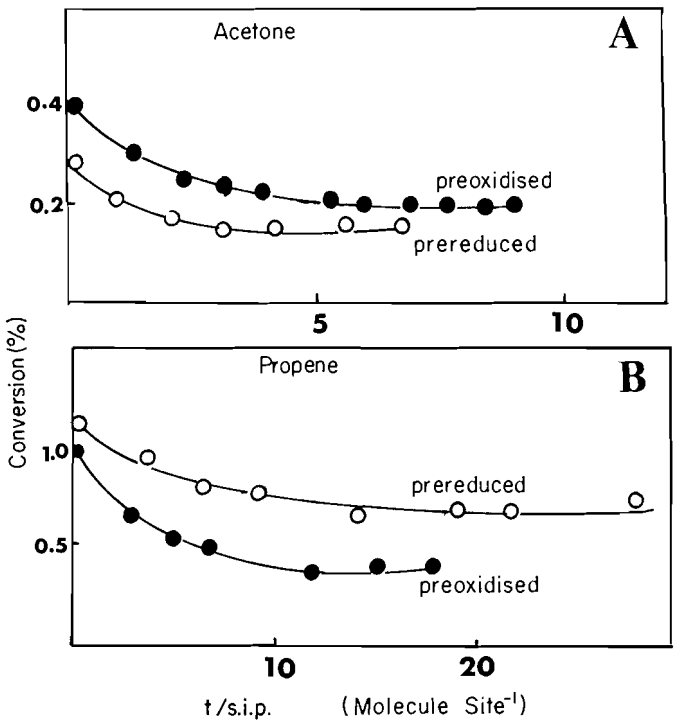

FIG. 1. Declining $(-H_2)$ and $(-H_2O)$ activity profiles for deoxygenated $(CH_3)_2CHOH/V_2O_5$ at 395 K. Results were obtained from rates measured after various contact times but are related in this plot to net yield expressed as turnover per surface ion pair (t/s.i.p.). The V_2O_5 surfaces had been either preoxidised in O_2 at 673 K (data points ●) or midly prereduced in argon at 673 K (data points ○). Plots *A* and *B* represent activity for dehydrogenation to acetone and dehydration to propene, respectively.

was introduced at a selected low pressure, which was maintained until a new altered steady-state activity was reached, whereupon the oxygen pressure was altered to a new value and another steady-state value was measured. Figure 2*A* summarises results demonstrating the manner in which the enhancing effects of oxygen upon steady-state rates of $(-H_2)$ and $(-H_2O)$ conversions varied with P_{O_2}. Rapid enhancement is apparent for both the $(-H_2)$ and $(-H_2O)$ activities in the 20 to 50 Torr pressure range for P_{O_2} and would be consistent with progressive reversal by oxygen of an extensive initial surface reduction experienced by the V_2O_5 sample in the flow of deoxygenated isopropanol (see below). Figure 2*A* also shows a lack of additional enhancing effect, rather indeed a small decline in activity, as P_{O_2} increased to values >150 Torr. Overall the dependence of P_{O_2} would be qualitatively consistent with [2] on the basis that low P_{O_2} promoted $V^{III} \rightarrow V^{IV}$ whilst higher pressures of O_2 further oxidise $V^{IV} \rightarrow V^{V}$, thereby causing maximum surface concentration of V^{IV} to occur at $P_{O_2} \sim 50$ Torr. Also consistent with the idea of an oxygen-sensitive, dynamic steady-state concentration of V^{IV} at the surface of the working catalyst were observations made upon changes in activity when gas-phase O_2 was suddenly removed from or reintroduced into the reactant flow. These are summarised in Fig. 2*B*; both parts of which show that activity dropped when gas-phase oxygen was removed from the flow of oxygenated alcohol vapour over the vanadium oxide catalyst having initially the stoichiometry of V_2O_5. The initial segments of both plots in Fig. 2*B* demonstrate that, — unlike preoxidized V_2O_5 material which had shown an initial rapid decay in $(-H_2)$ activity (cf. Fig. 1*A*) when exposed to deoxygenated alcohol vapour — preoxidized

Can. J. Chem. Downloaded from www.nrcresearchpress.com by 210.87.254.40 on 09/06/12
For personal use only.

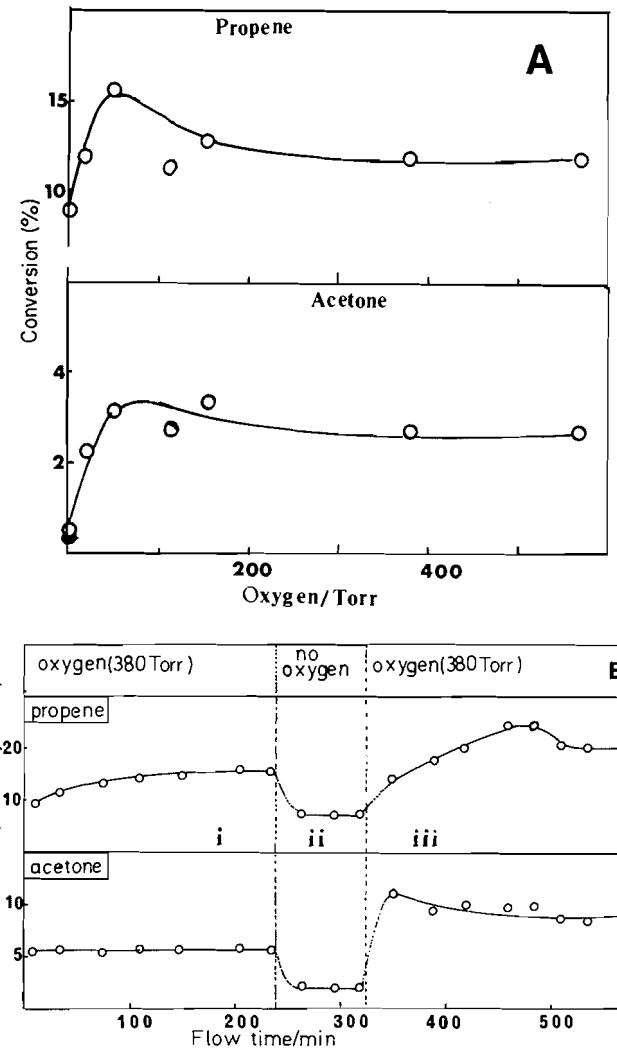

FIG. 2. Enhancing effects of oxygen upon activity of V_2O_5 at 433 K. (*A*): enhancing effects observed upon steady-state ($-H_2$) and ($-H_2O$) activities when indicated pressures of O_2 were admixed with 20 Torr of $(CH_3)_2CHOH$ in the c.r.f. procedure over V_2O_5. (*B*): (*i*) stable ($-H_2$) activity and slightly rising ($-H_2O$) activity observed with 380 Torr O_2 admixed with 20 Torr $(CH_3)_2CHOH$ up to 240 min; (*ii*) diminished activity when O_2 removed; (*iii*) enhanced activities upon re-introducing O_2.

V_2O_5 which was maintained instead of a premixed flow of isopropanol *plus* O_2 showed almost no decay in activity. The final segments of the plots in Fig. 2*B* show that when O_2 was introduced following a temporary interruption, activities for both ($-H_2O$) and ($-H_2$) processes were again increased. Enhancement of *both* the ($-H_2O$) and ($-H_2$) activity of V_2O_5 towards isopropanol through the operation of sample re-oxidation processes was thus clearly established for the $[(CH_3)_2CHOH + O_2]$–V_2O_5 interfaces and appeared consistent with oxygen enhancement of the dynamic surface concentration of V^{IV}.

A diligent search was made for appearance of new products which might be expected in the oxygenated system, and particularly for acetaldehyde which might arise from V_2O_5-catalysed attack by oxygen upon propene (10), or upon a surface isopropoxy radical formed by homolytic rupture of the vanadium–oxygen bond of a chemisorbed isopropoxide ion (11). Even at the high sensitivity of the f.i.d., however, no

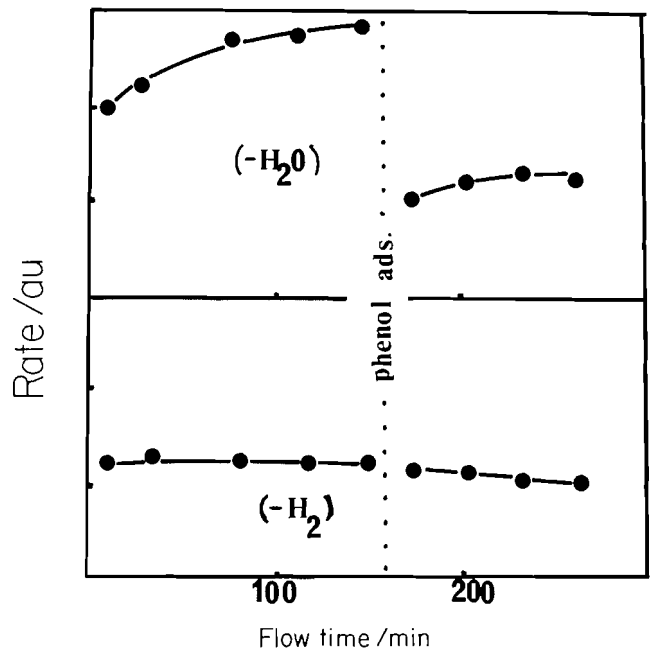

FIG. 3. Selective inhibition of dehydration upon exposure to phenol vapour at an oxygenated $(CH_3)_2CHOH/V_2O_5$ interface in the c.r.f. mode at 433 K.

measurable amounts of acetaldehyde were detected in the exit gases for the oxygenated $(CH_3)_2CHOH/V_2O_5$ system at temperatures to 433 K. The following additional experiments lent added confidence that the absence of significant CH_3CHO from the $(CH_3)_2CHOH/V_2O_5$ system was a real effect rather than an experimental artifact: (*i*) when acetaldehyde pulses were injected into the reactor, swept over the V_2O_5 catalyst, and analysed by gc in the normal manner, they were readily detected; (*ii*) independent checks made by mass spectrometric sampling from a closed glass reactor containing $(CH_3)_2CHOH$ at 10 Torr over V_2O_5 at 475 K confirmed that propene was the major gas-phase product (ca. 95%), accompanied by smaller but readily measurable yield of acetone, but that no detectable gas-phase acetaldehyde resulted from isopropanol over either preoxidized or mildly prereduced V_2O_5 or when 10 Torr of O_2 was present together with isopropanol vapour. It was concluded that, even for the oxygenated systems, acetone and propene remained the only significant hydrocarbon products at the moderate temperature employed here.

Experiments were made to test whether the oxygen-enhanced ($-H_2O$) and ($-H_2$) activities would respond in the c.r.f. mode to preadsorption of phenol in similar fashion to that noted previously (4) for deoxygenated $(CH_3)_2CHOH/V_2O_5$ in a pulsed mode, viz. that phenol poisoned ($-H_2O$), but not ($-H_2$), activity. Our new results for the oxygenated system in c.r.f. mode are presented in Fig. 3 and show a much stronger poisoning effect of phenol adsorption upon the oxygen-enhanced ($-H_2O$) activity than upon oxygen-enhanced ($-H_2$) activity. The main implication to be drawn from our combined phenol-poisoning results is that different sites continued to be responsible for ($-H_2O$) and ($-H_2$) activities in the presence of oxygen — as was also the case in the deoxygenated system. On the other hand, the parallel behaviour noted above for the ($-H_2O$) and ($-H_2$) activities in respect of initially rapid decline in deoxygenated conditions (cf. Fig. 1*A*), and of oxygen enhancement in steady-state rates (cf. Fig. 2*A*), point towards involvement of quadrivalent vanadium in each type of site.

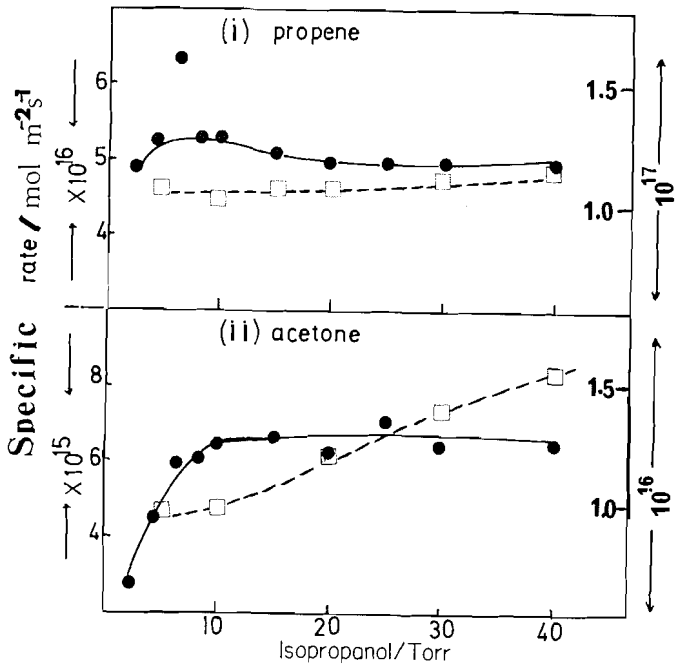

FIG. 4. Alcohol pressure dependence of steady-state, specific rates of conversion to $(-H_2O)$ or to $(-H_2)$ products at over V_2O_5 (molecules m^{-2} min^{-1}). Comparison of deoxygenated (unbroken plots, left hand scale) with oxygenated (dashed plots; right hand scale) for dehydration (part *i*) and dehydrogenation (part *ii*), respectively.

Various dual-site models could be envisaged featuring V^{IV} in both sites, but with important differences in its local environment for the sites active for $(-H_2O)$ and $(-H_2)$, e.g. $(V^{IV}-O)$ surface ion-pairs acting as acid–base type catalytic sites to promote E_2-type dehydration, but $V^{IV}-V^{IV}$ pairs (12) at surface-defect locations, acting to promote E1-type dehydrogenation. Efforts to discriminate between various dual-site models by electron spin resonance were unsuccessful since the unsupported oxides in their working catalytic state gave a very broad unresolved resonance.

Differences of detail shown in Fig. 4 between the alcohol pressure dependence of steady-state rates of $(-H_2O)$ and $(-H_2)$ conversions for oxygenated and deoxygenated $(CH_3)_2CHOH/V_2O_5$ systems lend support to the idea of important differences in the sites responsible for the two processes. Thus the comparison attempted in Fig. 4*A* for alcohol pressure dependence of $(-H_2O)$ activities for the oxygenated and deoxygenated systems (cf. broken and unbroken plots) indicate little or no dependence upon P_{ROH} and could be consistent with an approach to saturation coverage of $(V^{IV}-O)$ ion-pair sites for dehydration across the alcohol pressure range 2–40 Torr. The $(-H_2)$ type activity, on the other hand, continued to rise with alcohol pressure across the range 10 to 40 Torr in systems oxygenated by 380 Torr of O_2 (cf. broken line in Fig. 4*B*) whilst little dependence of the $(-H_2)$ rate was evidenced by the deoxygenated systems across that pressure range.

One final point in favour of an acid–base type, ion-pair site for $(-H_2O)$ activity emerged from a comparison made at 408 K between the steady-state $(-H_2O)$ activities displayed in the c.r.f. mode by identically pretreated samples of V_2O_5 towards *t*-butanol, isopropanol, and isobutanol. This yielded the following values when expressed as molecules m^{-2} s^{-1}: 4.2×10^{17} for $(CH_3)_3COH$, 4.7×10^{15} for $(CH_3)_2CHOH$, and 3.8×10^{13} for $(CH_3)_2CHCH_2OH$. These exhibit the order expected if ease of formation/stability of the corresponding carbonium ion via loss of the alcoholic-OH group were important for the $(-H_2O)$ activity.

2. Oxygen enhancement on V_2O_3

It could be argued on the basis of eq. [2] and ideas outlined above: (*i*) that if the pure sesquioxide, V_2O_3, were used negligible catalytic activity for $(-H_2O)$ or $(-H_2)$ would be expected and (*ii*) that exposure to oxygen in appropriate conditions might lead to surface oxidation. Alternative hypotheses by which gaseous oxygen could promote V^{III} oxidation were envisaged as in reactions [3] or [4]. The former envisaged non-dissociative adsorption of oxygen which then became involved in diatomic form both in surface oxidation and oxidative dehydrogenation:

$$[3a] \quad O_{2(g)} \rightleftharpoons O_{2(ads)}$$

$$[3b] \quad V_s^{III} + O_{2(ads)} \rightarrow (V_s^{IV} \text{ - - - } O_2^-)_s$$

$$[3c] \quad (V_s^{IV} \text{ - - - } O_2^-) + (CH_3)_2CHOH_{(ads)} \rightarrow V_s^{III} + H_2O_2 + (CH_3)_2CO$$

The alternative hypothesis, based upon dissociative chemisorption of oxygen and involvement of the monatomic oxygen fragments in both surface oxidation and oxidative dehydrogenation, was envisaged as follows:

$$[4a] \quad \tfrac{1}{2}O_{2(g)} \rightleftharpoons O_{(ads)}$$

$$[4b] \quad O_{(ads)} + 2V^{III} \rightarrow O_s^{2-} + 2V^{IV}$$

$$[4c] \quad 2V^{IV} + O_s^{2-} + (CH_3)_2CHOH \rightarrow 2V^{III} + H_2O + (CH_3)_2CO$$

Experiments were first made to test whether prolonged prereduction of V_2O_5 by H_2 in conditions which have been reported to yield the sesquioxide (9) would result in negligible $(-H_2)$ activity. This was confirmed with deoxygenated isopropanol at temperatures up to 433 K over V_2O_5 pre-reduced to V_2O_3 at 873 K. Negligible $(-H_2)$ or $(-H_2O)$ activity was also confirmed upon loading commercially available V_2O_3 into the reactor, pretreating in non-oxidising conditions, and testing with deoxygenated isopropanol up to 433 K (cf. Fig. 5*A*). Data to test the alternative hypotheses given in reactions [3] and [4] were sought by comparing the steady-state rates of the elimination reactions as progressively increasing pressures of oxygen were introduced into the flow of argon whilst maintaining a constant pressure of isopropanol over the sesquioxide materials at 433 K. Results confirming the progressive enhancement of steady-state $(-H_2)$ and $(-H_2O)$ activities as P_{O_2} increased are shown in Fig. 5*B*. Inspection of the possible mechanism represented by reaction [3] for oxygen-enhancement of $(-H_2)$ activity readily reveals one limiting case in which steps [3*b*] and [3*c*] are rate-limiting whilst [3*a*] is in rapid equilibrium. Then the equilibrium surface coverage, θ_{O_2}, by non-dissociatively chemisorbed oxygen can well be approximated by eq. [3*d*], provided also that alcohol reactants and products do not compete for the same sites as oxygen.

$$[3d] \quad \theta_{O_2} \simeq KP_{O_2}/(1 + KP_{O_2})$$

The condition for dynamic steady-state surface concentration of $(V^{IV} \text{ - - - } O_2^-)_s$ in this limiting case may then be approximated by

$$[3e] \quad k_{3b}\theta_{O_2} V^{III} \simeq k_{3c}\theta_{(V^{IV} \cdots O_2^-)} \theta_{ROH}$$

from which it is clear that the steady-state surface concen-

Can. J. Chem. Downloaded from www.nrcresearchpress.com by 210.87.254.40 on 09/06/12
For personal use only.

Can. J. Chem. Downloaded from www.nrcresearchpress.com by 210.87.254.40 on 09/06/12
For personal use only.

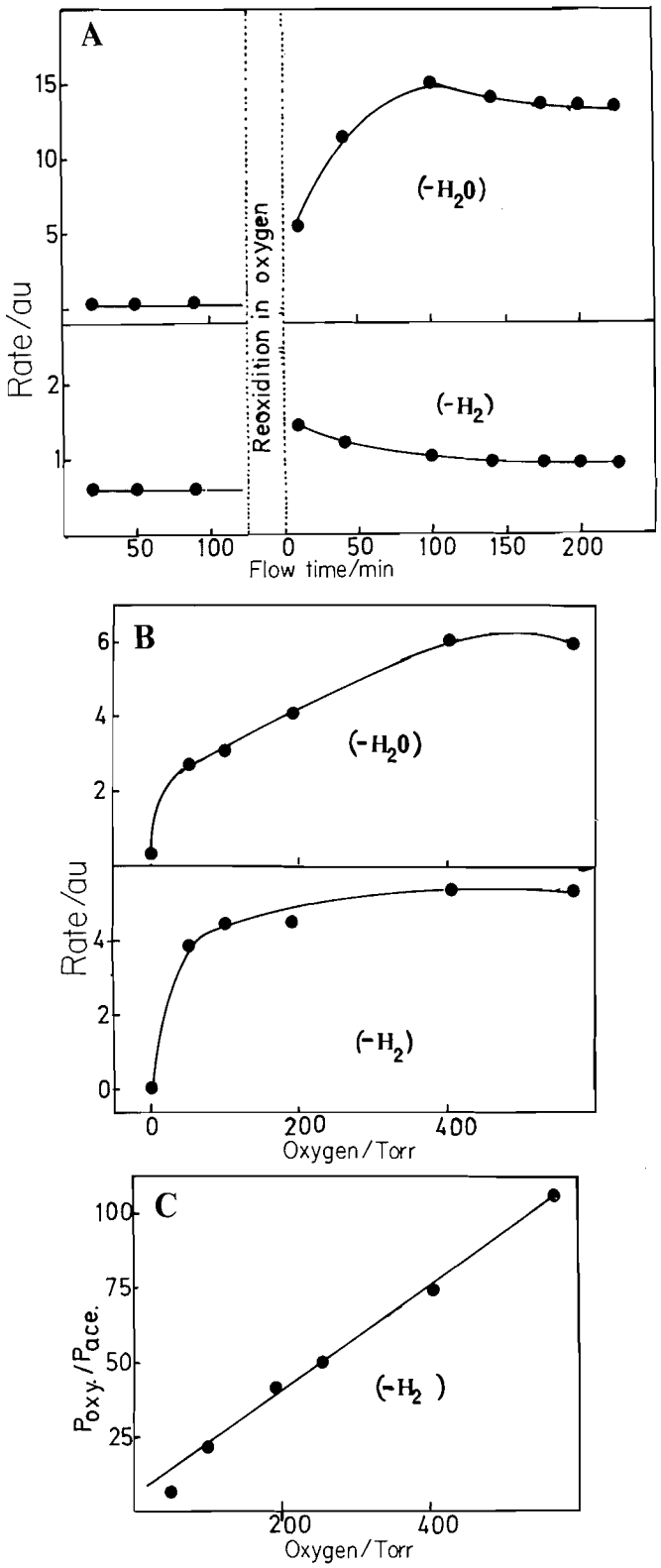

FIG. 5. Data obtained in c.r.f. mode over vanadium sesquioxide and illustrating: (*A*) initially low ($-H_2$) and ($-H_2O$) activities up to 100 min over deoxygenated $(CH_3)_2CHOH/V_2O_3$ at 433 K, but enhancement of activities subsequent to the sample being oxidised in O_2 for 3 h at 873 K; (*B*) enhancing effects of indicated pressures of P_{O_2} upon steady-state ($-H_2O$) and ($-H_2$) activities at 433 K; (*C*) linearization achieved at P_{O_2} 50 to 550 Torr by plotting inverse of steady-state ($-H_2$) rate, (expressed by $P_{acetone}$), in manner appropriate for θ_{O_2} and the rate of acetone production increasing with P_{O_2} according to $\theta_{O_2} = KP_{O_2}/(1 + KP_{O_2})$.

trations of V^{IV} and V^{III} species are influenced by the surface coverage by alcohol species. Under conditions of fixed alcohol pressure and surface coverage, however, the influence of P_{O_2} originates mainly from the θ_{O_2} term in [3*e*] and thus from eq. [3*d*]. An appropriate graphical test showing a degree of consistency with this kinetic analysis is represented in Fig. 5*C* for the data from Fig. 5*B* on oxygen-enhanced steady-state ($-H_2$) activities at 433 K. The least-squares regression co-efficient (0.984) for linearization in the manner of Fig. 5*C* was significantly better than that obtained (0.855) in the linearization of the same data based upon reaction [4] and the involvement of dissociatively chemisorbed oxygen in surface oxidation and alcohol dehydrogenation. (i.e. assumptions similar to those applied above to reaction [3] are readily shown to lead, in the case of reaction [4] to a dependence of rate upon $\theta_{O^\cdot}$ which should be well approximated by $\theta_{O^\cdot} \simeq KP_{O_2}^{1/2}/(1 + KP_{O_2}^{1/2})$ but that was less successful as a basis for linearizing the data). The significance of the somewhat better agreement of the oxygen-enhanced steady-state ($-H_2$) rates with non-dissociative oxygen adsorption should not be exaggerated, however, in view of (*i*) known difficulties of kinetic analysis when diatomic and monatomic oxygen species are simultaneously present on oxide surfaces and (*ii*) insufficiency of our data for a rigorous kinetic test of P_{O_2}-dependence.

3. *Structure studies*

The question of whether opposing processes of catalyst reduction by alcohol and reoxidation by O_2 over vanadium oxides were restricted to surface regions, or whether they caused major modifications of the vanadium oxide bonding and crystal structure down to great depths within the solid, were examined by observing changes brought about in the ir spectra and X-ray diffraction patterns when flows of alcohol and/or O_2 were established over preoxidised V_2O_5 (*Ar + O_2 at 675 K*). The ir spectra shown in Fig. 6*A* demonstrate that, whilst a flow of isopropanol alone over the sample at 435 K caused marked ir changes in the range 1000–600 cm^{-1} relative to V_2O_5 preoxidised at 675 K, no such changes occurred whenever 380 Torr of O_2 was admixed with 40 Torr of isopropanol. These differences once again lend support to an efficient reoxidising role of gas-phase O_2. In terms of detailed ir spectra reported by Frederickson and Hausen (13) for V_2O_3, V_2O_4, and V_2O_5, the predominance of ir at ca. 1020 cm^{-1} and 825 cm^{-1} in spectra *A* and *B* of Fig. 6 indicate persistence of a mainly V_2O_5-type oxide in samples exposed to O_2 only, or to O_2 admixed with isopropanol. Alterations of the spectrum to that in 6*C* after exposure to alcohol vapour alone at 350 K — viz. appearance of a strong band at ca. 900 cm^{-1}, a weaker narrow band at 850 cm^{-1} and a broad absorbance at 750 cm^{-1} — would be consistent with predominance of V_2O_4 in the surface regions examined by the ir beam. (It is worth noting that our spectrum for V_2O_3, like that reported by Frederickson and Hausen, gave no significant absorbance at the values just assigned to V_2O_4, but rather lacked any absorbances standing out well against a generally low transmittance.)

Comparisons of X-ray diffraction patterns yielded similar conclusions to the ir studies, viz. that diffraction lines from V_2O_5 predominated for preoxidised V_2O_5 (*O_2, 675 K*) and for V_2O_5 maintained in a flow of O_2 + isopropanol at 350 K, whereas diffraction lines characteristic of V_2O_4 were clearly distinguishable in vanadium oxide treated only with alcohol vapour at 375 K. Thus, it became clear from both the ir and X-ray diffraction studies that treatment with isopropanol alone,

Can. J. Chem. Downloaded from www.nrcresearchpress.com by 210.87.254.40 on 09/06/12
For personal use only.

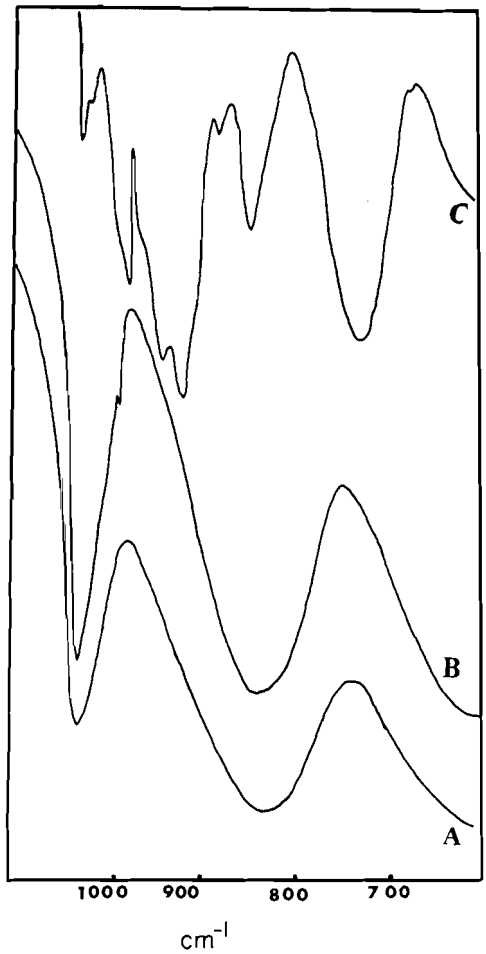

FIG. 6. Infrared spectra of V_2O_5. *A*, V_2O_5 treated in O_2 flow at 673 K overnight, then cooled down to room temperature in O_2; *B*, sample after passing isopropanol + O_2 (40:380 Torr) at 433 K for 7 h, then cooled down to room temperature to argon; *C*, sample after treating in isopropanol (40 Torr) + argon for 7 h, then cooled down to room temperature in argon flow. After cooling to room temperature the V_2O_5 samples were mixed with KBr.

even at 375 K, produced V_2O_4 to depths much greater than the topmost few layers of oxide. Conversely, the absence of any V_2O_4 discernible by ir or X-ray when O_2 was present together with the alcohol vapour, supports the occurrence of a fast and efficient re-oxidation process in the presence of $P_{O_2} \sim 380$ Torr even at the moderate temperatures here employed.

4. Kinetic parameters at vacuum/V_2O_5 and $(CH_3)_2CHOH$/V_2O_5 interfaces

Comparisons of the rates of loss of oxygen from the surface with rates of the $(-H_2O)$ and $(-H_2)$ processes in the same temperature range provide evidence that the latter could not have arisen from spontaneous breakdown of the V_2O_5 lattice at the reaction temperature and subsequent attack by oxygen fragments upon adsorbed alcohol. Thus the rate of loss of oxygen at 435 K, as evaluated by downward extrapolation of weight loss vs. outgassing temperature data taken with a vacuum microbalance, corresponded to ca. one monolayer equivalent h^{-1} whereas the net yield of $(-H_2O)$ and $(-H_2)$ products from isopropanol during one hour of reaction at 435 K corresponded to 260 and 50 monolayer equivalents, respectively. Further indications of involvement of other activated processes in elimination reactions at the surface came from large differences between an activation energy of ca. 20 kJ mol^{-1} estimated for surface lattice breakdown (from the vacuum microbalance data) and activation energy values of 84 ± 3 for $(-H_2O)$ and 59 ± 4 kJ mol^{-1} for $(-H_2)$. These were obtained for deoxygenated isopropanol from linear Arrhenius plots of steady-state rate data over the temperature range 375 to 475 K but activation energies obtained in similar fashion for the corresponding oxygenated systems were 105 ± 5 and 83 ± 4 kJ mol^{-1}. The increase in E_{act} (by ca. 20 kJ mol^{-1} in each case) upon oxygenation provides evidence for operation of an additional activated step involving oxygen. However, as already noted, propene and acetone continued to be the sole significant products and rates of their production were increased in the oxygenated system. The proportionate oxygen-induced increases in pre-exponential terms necessary to compensate for the increased E_{act} values and so achieve the rate increases observed at 433 K corresponded to $e^{7.1}$ for the $(-H_2O)$ and $e^{7.4}$ for the $(-H_2)$ process. Such increases are qualitatively consistent with the roles deduced earlier for sites containing quadrivalent vanadium and for oxygen in promoting their dynamic surface concentrations (cf. eqs. [3] and [4]). It is interesting that the increase of ca. 20 kJ mol^{-1} in E_{act} in each case corresponds to what could be expected if removal of oxygen from V_2O_5 were the additional activated step (e.g. in the manner of eq. [1*a*]).

Acknowledgements

The authors are grateful to Dr. J. L. G. Fierro (Madrid) and J. Tobin (Cork) for making the vacuum-microbalance and mass-spectrometric measurements, respectively, and to University College, Cork, for financial support.

1. E. F. McCarthy, D. G. Klissurski, and R. A. Ross. J. Catal. **26**, 380 (1972).
2. A. Bielanski and J. Haber. Catal. Rev. **19**, 1 (1979).
3. B. Grzybowska, Y. Barbaux, and J. P. Bonnelle. J. Chem. Res. S, 48 (1981).
4. (*a*) J. Cunningham, B. K. Hodnett, M. Ilyas, J. P. Tobin, and E. L. Leahy. Faraday Discuss. Chem. Soc. **52**, 301 (1981); (*b*) K. J. Miller and J.-L. Wu. J. Catal. **27**, 60 (1972).
5. (*a*) P. Mars and D. W. van Krevelen. Chem. Eng. Sci. Spec. Suppl. **3**, 41 (1954). (*b*) D. B. Dadybarjor, S. S. Jewur, E. Ruchenstein. Catal. Rev. **19**, 293 (1979).
6. I. S. Jaswal, R. F. Mann, J. A. Juusola, and J. Downie. Can. J. Chem. Eng. **47**, 284 (1969).
7. J. A. Juusola, R. F. Mann, and J. Downie. J. Catal. **17**, 106 (1970).
8. A. Bielanski, V. Dyrek, and E. Sirwicka. J. Catal. **66**, 316 (1980).
9. P. J. Hammett. Private communication.
10. P. Pichat, J.-M. Herrmann, J. Disdier, and M.-N. Mozzanega. J. Phys. Chem. **83**, 3122 (1979).
11. J. K. Kochi. Organometallic mechanisms and catalysis. Academic Press. 1978.
12. D. R. Chabrabarty, M. Rajyalakshmi, and A. B. Biswas. Proc. Indian Acad. Sci. Chem. Sci. **89**, 131 (1980).
13. L. D. Frederickson and D. M. Hausen. Anal. Chem. **35**, 818 (1963).

Metal-catalyzed rearrangements of allylic esters[1,2]

A. C. OEHLSCHLAGER, P. MISHRA, AND S. DHAMI
Department of Chemistry, Simon Fraser University, Burnaby, B.C., Canada V5A 1S6

Received May 20, 1983[3]

A. C. OEHLSCHLAGER, P. MISHRA, and S. DHAMI. Can. J. Chem. **62**, 791 (1984).

It has been shown that $Pd(CH_3CN)_2Cl_2$ catalyzes the rearrangement of allylic esters. Carbamates rearrange more rapidly than acetates which in turn rearrange more rapidly than carbonates. Allylic carbamates are more rapidly isomerized by $Pd(CH_3CN)_2Cl_2$ than by $Hg(OCOCF_3)_2$. The rearrangement proceeds well except in cases where the central carbon of the allylic system is fully substituted.

In contrast to the reported rearrangement of allylic carbamates by Hg^{2+} and previous reports of Pd^{2+}-catalyzed rearrangements of allylic esters, this work showed the latter are extremely *E* specific; thus, *E* allylic acetates yield equilibrium mixtures free of *Z* allylic isomers, under conditions in which *Z* allylic acetates are unreactive. This *E* specificity is applied to stereospecific 1,3-diene synthesis from bis *E,Z*-allylic acetates.

A. C. OEHLSCHLAGER, P. MISHRA et S. DHAMI. Can. J. Chem. **62**, 791 (1984).

On a démontré que le $Pd(CH_3CN)_2Cl_2$ catalyse la transposition des esters allyliques. Les carbamates se transposent plus rapidement que les acétates qui se transposent à leur tour plus rapidement que les carbonates. Les carbamates allyliques sont isomérisés plus rapidement par le $Pd(CH_3CN)_2Cl_2$ que par le $Hg(OCOCF_3)_2$. La transposition se produit facilement dans tous les cas excepté lorsque le carbone central du système allylique est complètement substitué.

Par opposition aux transpositions des carbamates allyliques par le Hg^{2+} et des transpositions des esters allyliques catalysées par le Pd^{2+} qui ont été rapportées antérieurement, on démontre dans le présent travail que ces dernières réactions sont extrèmement spécifiques aux isomères *E*; ainsi, les acétates allyliques *E* fournissent des mélanges à l'équilibre qui ne contiennent pas d'isomères allyliques *Z* dans des conditions où les acétates allyliques *Z* ne sont pas réactifs. On a appliqué cette spécificité *E* à une synthèse stéréospécifique des dienes-1,3 à partir de bis-acétates allyliques-*E,Z*.

[Traduit par le journal]

Introduction

Soft electrophilic metal ions dramatically catalyze rearrangement of allylic esters (1), 1,5-dienes (2), and *S*-allylthioimidates (3). The catalyst systems that have received most attention are based on mercuric(II) and palladium(II) salts.

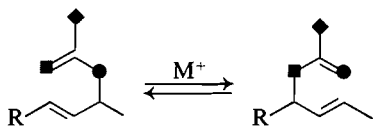

Mercuric trifluoroacetate has been shown to be a particularly effective catalyst for rearrangement of allylic *N,N*-dimethyl carbamic esters (**1***a*–**3***a*) at room temperature (1*a*).

The lack of formation of an amine product and the inversion of the allylic fragment which is observed in the rearrangement of thionocarbamates were considered to be consistent with a mechanism in which the mercury(II) catalyst interacted with the carbon–carbon π-bond to promote intramolecular cyclization to yield a 1,3-dioxanium ion intermediate **4***a* (1*a*).

Organic soluble palladium salts (especially $Pd(CH_3C{\equiv}N)_2Cl_2$) catalyze the rearrangement of allylic acetates at room temperature (1*b*–*e*, 4).

These reactions produce mixtures except when the allylic π-bond in one isomer is conjugated or where relief of steric compression (3° acetate → 1° acetate) attends the rearrangement (1*b*, 4). The most compelling evidence that the palladium-catalyzed process involves transfer of the acetate via a 1,3-dioxanium intermediate (**4***b*, Scheme 1) is the complete retention of optical purity in the palladium(II)-catalyzed rearrangement of the chiral allylic acetate **5** to **6** (4*a*).

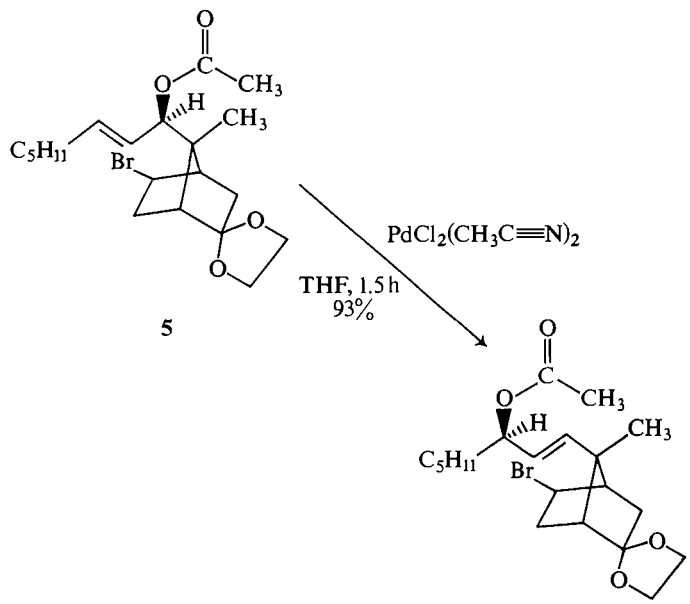

5 **6**

A similarly striking transfer of chirality occurs in the palladium(II)-catalyzed rearrangement of 1,5-dienes and is consistent with a similar cyclization-induced rearrangement mechanism (2).

The present investigation was undertaken to extend the metal ion-catalyzed rearrangement to cyclic and bicyclic terpenoid allylic esters and investigate the selectivity for rearrangement of *E* allylic esters vs. *Z* allylic esters. Since such selectivity was observed, we pursued selective dienylacetate synthesis via this route. In the course of this investigation we also found palladium(II) more facile than mercury(II) catalysis of carbamates.

[1] Research supported by the Natural Sciences and Engineering Research Council of Canada, Operating Grant No. A3881.

[2] Preliminary Communication, 65th Canadian Chemical Conference, Toronto. May, 1982. Abstr. OR 7-5.

[3] Revision received October 4, 1983.

Can. J. Chem. Downloaded from www.nrcresearchpress.com by 210.87.254.6 on 09/06/12
For personal use only.

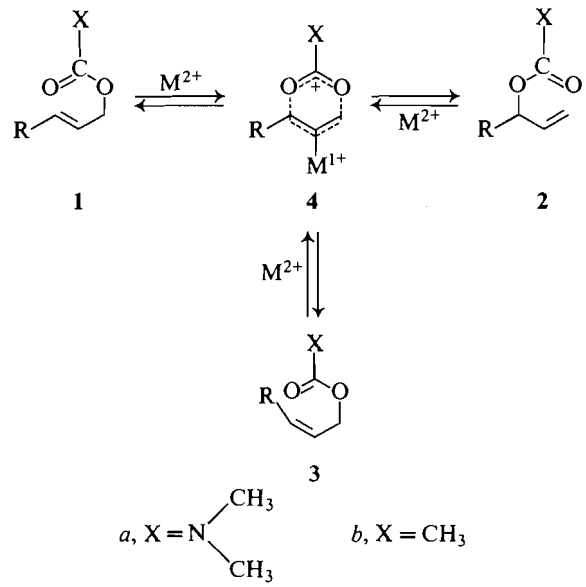

SCHEME 1

Results and discussion

Reaction of several straight chain and cyclic allylic esters with bis(acetonitrile)palladium(II)chloride gave equilibrium mixtures of allylic isomers, usually in less than ten minutes at room temperature. Table 1 gives the examples studied. Although acyclic (e.g., **7**, **8**, **10**, **11**, **12**, **28**, and **30**) and cyclic (**14**, **15**, **17**, **22**, **24**, and **25**) esters underwent facile reaction, we were unable to induce rearrangement in cyclic acetate **16** and bicyclic esters **19**–**21**. Heating of these latter reactions to reflux (THF) resulted in formation of palladium metal and gave no rearrangement. In an effort to keep the palladium catalyst in the oxidized state, we repeated the rearrangement of **19** (X = CH_3) and **20** with $PdCl_2(CH_3CN)_2$ in the presence of one equivalent (per acetate) of cupric chloride. These conditions resulted in formation of many chlorinated products. Use of $LiPdCl_3$ in acetic acid (1*c*) also gave no rearrangement of esters **19**–**21**. Overman et al. (2) noted palladium(II)-catalyzed Cope rearrangements of 1,5-dienes failed in systems substituted at both positions 2 and 5 (2). Similarly, palladium(II)-catalyzed 3,3-sigmatropic rearrangement of *S*-allylthioimidates failed when there was a substituent at position 2 of the allyl group (3).

The failure of the palladium(II) catalyst to induce rearrangement in these systems is probably due to steric requirements of the presumed intermediate (**4**). It is also probable that systems requiring formation of a tertiary carbon–palladium bond suffer metal hydride elimination more easily than those in which a secondary carbon–palladium bond is involved. That this latter condition is important can be gauged from the ease of rearrangement of **24** and **25** compared to **16**. During work using alkyl–rhodium(I) complexes to alkylate acid chlorides, Hegedus *et al.* (5) noted a greater tendency of secondary carbon–rhodium systems to suffer β hydride elimination compared to primary carbon–rhodium systems.

In an effort to circumvent the sluggishness of rearrangement of bicyclic esters **19**–**21**, we examined the effect of metal ion and ester structure on the rates of rearrangement in those systems where the rates of rearrangement were amenable to time course analysis by glpc. Thus we examined the effect of metal ion on the rate of rearrangement of carbamates **12** and **17**. The palladium(II) catalyst is superior to mercuric trifluoroacetate

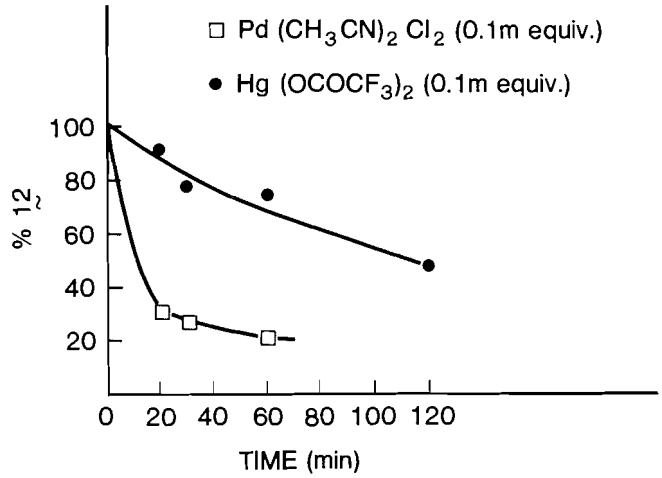

FIG. 1. Palladium(II) vs. mercury(II) catalysis of carbamate **12** in THF at 31°C.

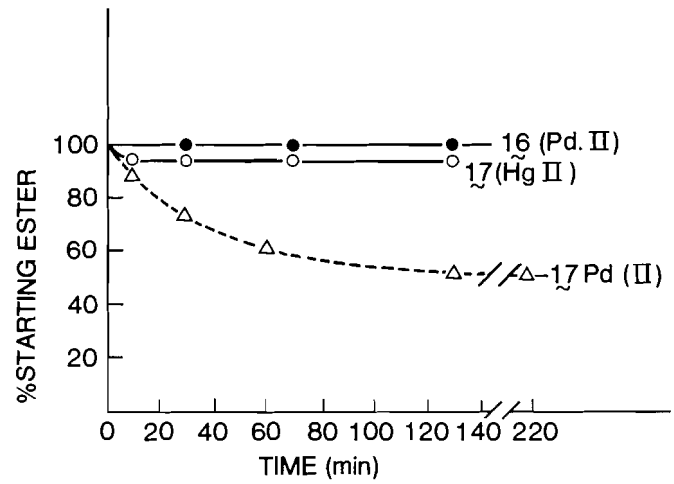

FIG. 2. Palladium(II)-catalyzed rearrangement of acetate **16** and carbamate **17** (THF, 31°C, 0.1 *M* equiv. PdII) and mercury(II)-catalyzed rearrangement of carbamate **17** (THF, 31°C, 0.1 *M* equiv. HgII).

for this rearrangement (Figs. 1 and 2). The relative rates of palladium(II)-catalyzed rearrangement of allylic carbamates, acetates, and carbonates (Figs. 2 and 3) were found to be those expected (carbamates > acetates, **17** > **16**, and acetates > carbonates, **7** > **10**; **8** > **11**) if the reaction proceeds via a cyclization-induced rearrangement involving an intermediate such as **4**. In such a mechanism the better the "X" group stabilizes the positive charge on the ester carbonyl carbon, the faster the rearrangement.

The above suggests that palladium(II)-catalyzed rearrangement of allylic carbamates offers the best chance of achieving allylic rearrangement under mild conditions in hindered systems such as **19**. We attempted rearrangement of both α and β isomers of **19** (X = $N(CH_3)_2$) using $Pd(CH_3C{\equiv}N)_2Cl_2$ without success.

The rate of palladium(II)-catalyzed rearrangement of *Z* acetate **9** is very slow compared to the *E* isomer **8** and allylic isomer **7** (Fig. 3). The formation of **9** is not observed to any significant extent during the equilibration of **7** or **8**. These observations, coupled with evidence that palladium(II)-catalyzed rearrangement of 1,5-dienes (2) proceeds via a cyclization-induced rearrangement involving an intermediate

Can. J. Chem. Downloaded from www.nrcresearchpress.com by 210.87.254.6 on 09/06/12
For personal use only.

TABLE 1. Palladium(II)-catalyzed allylic ester rearrangements

Starting material	Equiv. of $PdCl_2(CH_3CN)_2$ (solvent, time)	Products (ratio) (yield)
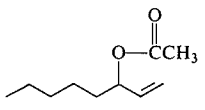 **7**	0.03 (THF, 0.5 h)	**7/8/9** (1:2.3:0.03) (86%)
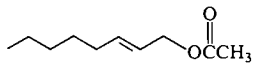 **8**	0.04 (THF, 0.5 h)	**7/8/9** (1:2.3:0.03) (quant.)
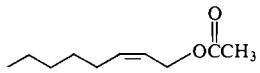 **9**	0.04 (THF, 2h)	**7/8/9** (1:5:116) (97%)
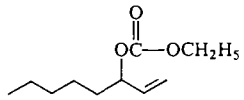 **10**	0.04 (THF, 0.5 h)	**10/11** (1.7:1) (82%)
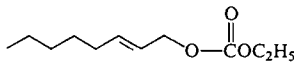 **11**	0.04 (THF, 2 h)	**10/11** (2.0:1) (94%)
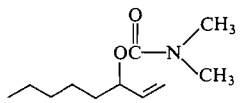 **12**	0.1 (THF, 1 h)	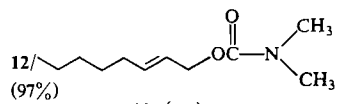 **12**/(97%) **13** (1:2)
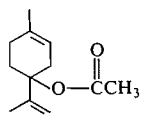 **14**	0.08 (THF, 2 h)	**14/15** (1:10) (88%)
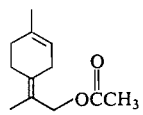 **15**	0.08 (THF, 2 h)	**14/15** (1:22) (91%)
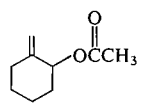 **16**	0.08 (THF, 18 h)	No rearrangement
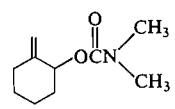 **17**	0.1 (THF, 18 h)	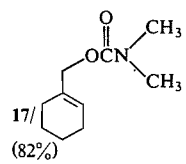 **17**/(82%) **18** (57:42)
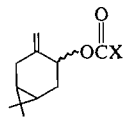 X = CH_3, $N(CH_3)_2$ **19**	0.08 (THF, 18 h)	No rearrangement

Can. J. Chem. Downloaded from www.nrcresearchpress.com by 210.87.254.6 on 09/06/12
For personal use only.

TABLE 1. (*Concluded*)

Starting material	Equiv. of $PdCl_2(CH_3CN)_2$ (solvent, time)	Products (ratio) (yield)
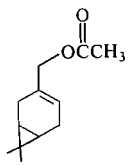 **20**	0.08 (THF, 18 h)	No rearrangement
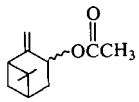 **21**	0.08 (THF, 12 h)	No rearrangement
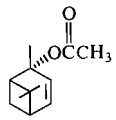 **22**	0.10 (THF, 2.5 h)	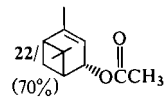 **22**/**23** (7:3) (70%)
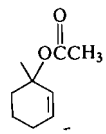 **24**	0.10 (THF, 0.5 h)	**24/25** (1:22) (70%)
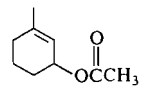 **25**	0.10 (THF, 5 h)	**24/25** (1:22) (80%)
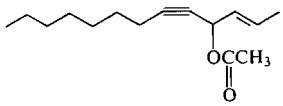 **26**	0.09 (THF, 12 h)	No rearrangement
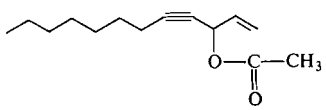 **27**	0.09 (THF, 12 h)	No rearrangement
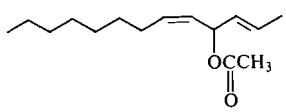 **28**	0.08 (THF, 2 h)	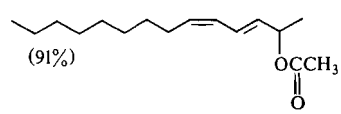 (91%) **29**
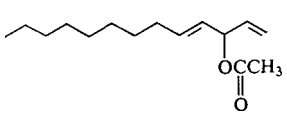 **30**	0.08 (THF, 2 h)	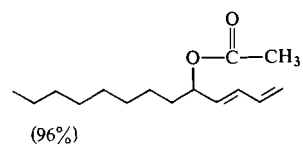 (96%) **31**

similar to **4**, lead us to suggest that in the present process, both addition and elimination of palladium (**1**, **3**, **2**–**4**) are subject to rigid stereochemical bias. Thus, if we presume a 1,3-dioxanium ion (**4**) with a chair conformation is formed via *trans* addition of palladium(II) and the carbonyl oxygen to the carbon π-bond of a *Z* allylic ester (e.g. **9**, R^1 = H; R^2 = alkyl), unfavorable axial interactions occur for substituents at C1 (R^1, R^3). These interactions do not occur when *E* allylic esters (e.g. **8**, R^1 = alkyl, R^2 = H) react with palladium(II) to form the dioxanium intermediate. Possible mechanisms for $Z \rightarrow E$ isom-

Can. J. Chem. Downloaded from www.nrcresearchpress.com by 210.87.254.6 on 09/06/12
For personal use only.

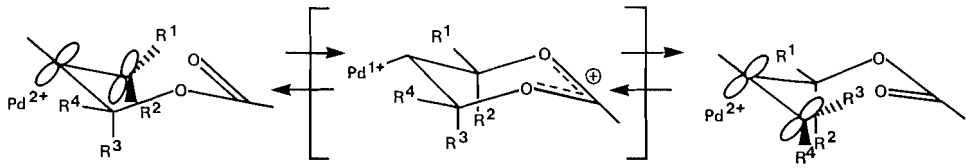

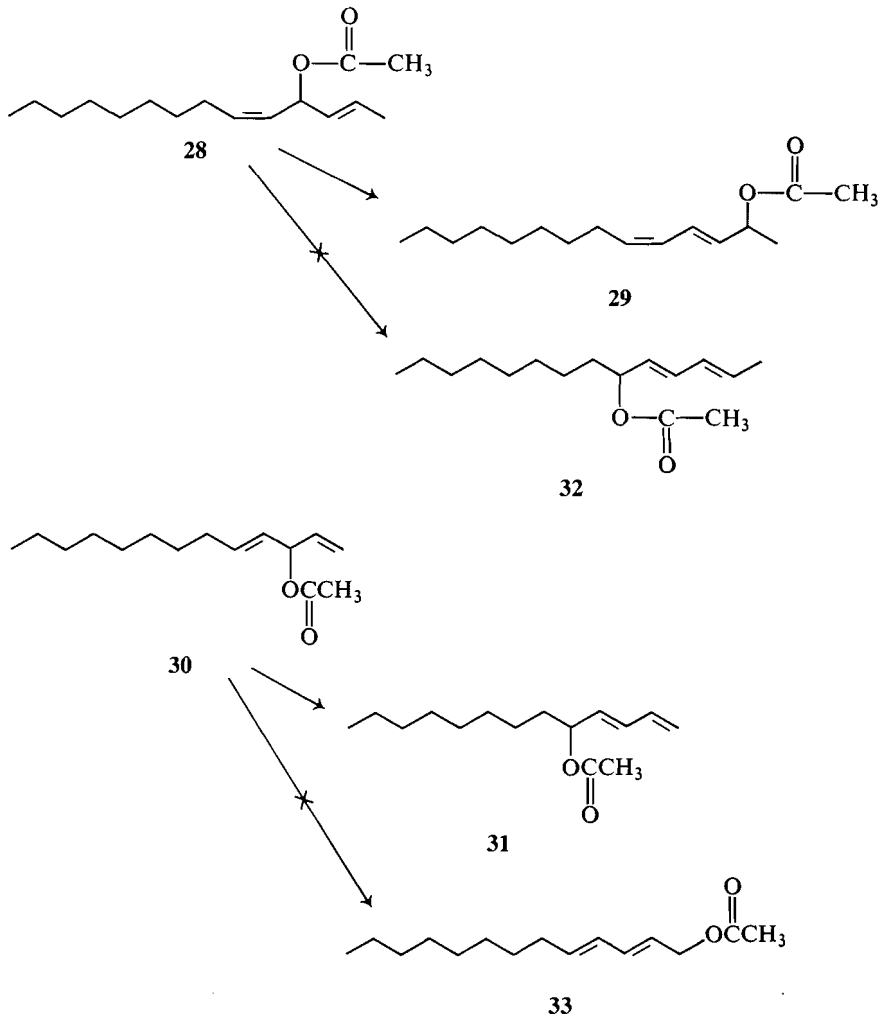

erization are by (*a*) rotation around the C2—C3 bond of the 1,3-dioxanium intermediate or (*b*) equilibration with the terminal vinyl isomer which returns to form either *E*(fast) or *Z*(slow).[4] Comparison of the *Z*/*E* ratio (1:99) obtained in the palladium(II)-catalyzed rearrangement of **8** with the *Z*/*E* ratio (12:88) reported for mercuric(II) ion-catalyzed rearrangement of analogous allylic carbamates (1*a*) reveals either (*a*) that the palladium(II)-catalyzed reaction is significantly more selective for the *E* isomer or (*b*) that equilibrium was obtained with mercuric(II) ion but not palladium(II).

The differential rate of palladium(II)-catalyzed rearrangements of *Z* and *E* allylic acetates can be employed to generate specific dienyl acetates (1*f*). Thus, **28** smoothly rearranges to **29** to the exclusion of **32**. The allylic acetate **30** smoothly rearranges to **31** and not **33**. The mildness of these reactions, coupled with their high selectivity, makes their use in synthesis a decided advantage.

[4] Suggested by Professor Overman.

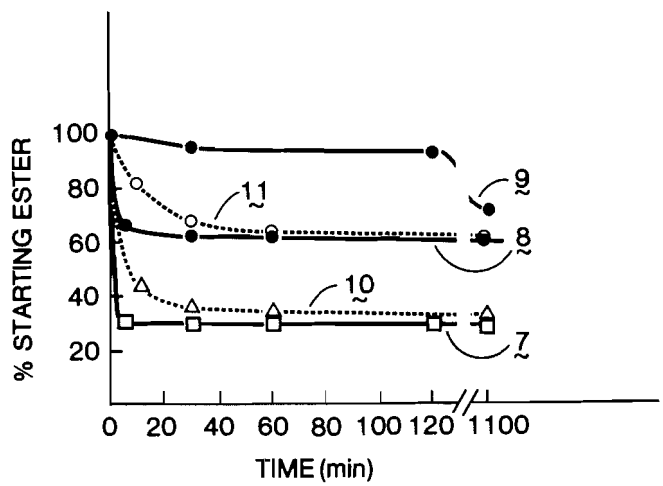

FIG. 3. Palladium(II)-catalyzed rearrangements of acetates and carbamates (THF, 31°C, 0.08 *M* equiv. Pd^{2+}).

Can. J. Chem. Downloaded from www.nrcresearchpress.com by 210.87.254.6 on 09/06/12
For personal use only.

Can. J. Chem. Downloaded from www.nrcresearchpress.com by 210.87.254.6 on 09/06/12
For personal use only.

Experimental

The nmr spectra were recorded on Varian EM360 and Bruker WM400 spectrometers. Unit resolution mass spectra were obtained using a Hewlett–Packard 5985B GC/MS/DS system operating at 70 eV. High resolution mass spectra were obtained on an MS-50 by Dr. G. Eigendorf at the University of British Columbia.

Ester preparation

Alcohols (3–6 mmol) were stirred with 5 mL dry pyridine and 5 mL acetic anhydride, or molar equivalents of ethyl chlorocarbonate at room temperature for 1 (1° alcohols) to 3 (3° alcohols) days. The reactions were quenched with 10 mL H_2O and extracted with three 15-mL portions of ether. The ether was washed with 25 mL 5% HCl, 25 mL 5% $NaHCO_3$, and finally, 25 mL H_2O. The ether was dried over anhydrous $MgSO_4$, filtered, concentrated, and the products distilled *in vacuo*. In the case of acetylation of **24**, the reaction was 50% complete after 18 days. It was worked up as above and the acetate purified by preparative tlc (SiO_2; 1:9 EtOAc/hexane).

Acetates **7** (6), **8** (6, 7), **9** (7), **14** (8), **15** (9), **16** (10), **21** (11), **24** (12), and **25** (13) have been previously reported.

The α- and β-alcohol precursors of **19** were prepared by rearrangement of carene α- and β-epoxides with tri-isobutyl aluminum (14). The α-isomer has been previously reported (15), as has the alcohol precursor of **20** (16).

Carbonate **10** was formed in 49% yield, bp (0.5 Torr) 27–31°C; ^{1}Hmr ($CDCl_3$) δ: 0.87 (t, 3H), 1.27 (t, 3H), 1.17–1.56 (m, 8H), 4.17 (q, 2H), 5.4 (m, 4H). *Exact Mass* calcd. for $C_{11}H_{20}O_3$: $(M - C_4H_9)^+$, 144.0785; found (ms): 144.0793.

Carbonate **11** was formed in 55% yield, bp (0.5 Torr) 29–32°C; ^{1}Hmr ($CDCl_3$) δ: 0.88 (t, 3H), 1.35 (t, 3H), 1.25–1.42 (m, 6H), 2.16 (q, 2H), 4.20 (q, 2H), 4.78 (q, 2H), 5.62 (m, 1H), 5.84 (m, 1H). *Exact Mass* calcd. for $C_{11}H_{20}O_3$: M^+, 200.1412; found (ms) 200.1409.

Carbamate **12** was prepared (1*a*) in 94% yield, bp (0.1 Torr) 55–56°C; ^{1}Hmr ($CDCl_3$) δ: 0.95 (t, 3H), 1.3–1.7 (m, 8H), 2.95 (s, 6H), 5.1–5.5 (m, 2H), 5.6–6.3 (m, 1H). *Exact Mass* calcd. for $C_{11}H_{21}O_2N$: M^+, 199.1572; found (ms): 199.1571.

Carbamate **17** was prepared (1*a*) in 76% yield, bp (0.1 Torr) 62–63°C; ^{1}Hmr ($CDCl_3$) δ: 1.2–2.4 (m, 8H), 2.83 (s, 6H), 4.68 (m, 2H), 5.33 (m, 1H). *Exact Mass* calcd. for $C_{10}H_{17}O_2N$: M^+, 183.1260; found (ms): 183.1258.

Carbamate **19** (α isomer) was prepared (1*a*) in 66% yield, bp (0.1 Torr) 72–77°C; ^{1}Hmr ($CDCl_3$) δ: 0.97 (s, 3H), 1.08 (s, 3H), 0.8–2.7 (m, 6H), 3.00 (s, 6H), 4.93 (m, 2H), 5.11 (t, 1H). *Exact Mass* calcd. for $C_{13}H_{21}O_2N$: M^+, 223.1572; found (ms): 223.1564.

Carbamate **19** (β isomer) was prepared (1*a*) in 20% yield, bp (0.05 Torr) 74–78°C; ^{1}Hmr ($CDCl_3$) δ: 0.90 (s, 6H), 0.5–2.7 (m, 6H), 3.0 (s, 6H), 4.63 (m, 2H), 4.93 (m, 1H). *Exact Mass* calcd. for $C_{13}H_{21}O_2N$: M^+, 223.1572; found (ms): 223.1595.

The isomeric purity of each ester was verified by glass capillary glpc on a 15 m × 0.21 mm id methyl silicone column; in each instance (except **24**) the esters were >95% isomerically pure. Acetate **24** rearranged slowly to **25** on standing. Its isomeric purity was ≈80% for the reactions reported in Table 1.

General procedure for bis(acetonitrile)palladium(II)chloride rearrangements

(a) *Preparative scale*

Solutions (0.2–0.3 *M*) of ester in dry THF under argon were treated with 0.03–0.1 molar equivalents of $Pd(CH_3CN)_2Cl_2$. The reactions were stirred for 30 min to several days as indicated in Table 1, concentrated to ≈1/5 the original volume under a stream of nitrogen, and filtered through a short column of silica using an ether wash. The filtrate was concentrated (N_2) and subjected to vacuum distillation. Isomer ratios changed very little (<5%) before and after distillation. The isomer ratios and yields reported in Table 1 were determined on distilled product.

Rearrangement of 0.2 g **12** by $Pd(CH_3CN)_2Cl_2$ gave 0.198 g distilled product (bp (0.1 Torr) 54–62°C) which was a 1:2 mixture of **12** and (*E*)-2-octen-1-yl *N*,*N*-dimethylcarbamate (**13**). The two carbamates were separated by preparative tlc on Silica Gel G (0.5 mm × 20 cm × 20 cm plates) containing 20% $AgNO_3$ using hexane/ethyl acetate, 95:5, as the development solvent (development four times). Carbamate **12** was isolated from the R_f 0.21–0.30 band and **13** from the R_f 0.36–0.52 band by elution of each band with ether. Carbamate **13** had bp (0.1 Torr) 56–60°C; ^{1}Hmr ($CDCl_3$) δ: 0.92 (t, 3H), 1.33 (m, 6H), 2.1 (m, 2H), 2.93 (s, 6H), 4.53 (d, 2H), 5.66 (octet, 2H). *Exact Mass* calcd. for $C_{11}H_{21}O_2N$: M^+, 199.1572; found (ms): 199.1577.

Rearrangement of 0.2 g carbamate **17** with $Pd(CH_3C{\equiv}N)_2Cl_2$ gave 0.164 g distilled product (bp (0.1 Torr) 59–60°C) which was a 57:42 mixture of **17** and 1-cyclohexene-1-methanol *N*,*N*-dimethylcarbamate (**18**) respectively. The two carbamates were separated by preparative tlc on Silica Gel G with 20% $AgNO_3$ using hexane/ethyl acetate, 90:10, as the development solvent (double development). Carbamate **17** was recovered from the R_f 0.17–0.29 band and the allylic isomer from the R_f 0.32–0.45 band by elution of each band with ether. The latter carbamate gave bp (0.1 Torr) 54–58°C; ^{1}Hmr ($CDCl_3$) δ: 1.4–2.2 (m, 8H), 2.98 (s, 6H), 4.48 (s, 2H), 5.73 (m, 1H). *Exact Mass* calcd. for $C_{10}H_{17}O_2N$: M^+, 183.1260; found (ms): 183.1264.

(b) *Analytical scale*

The kinetic data in Figs. 1–3 were obtained on 0.1 *M* solutions of esters in dry THF (≈5 mL). Solutions were treated with stock solutions of dodecane and, subsequently, either 0.1 *M* $Pd(CH_3C{\equiv}N)_2Cl_2$ or $Hg(OCOCF_3)_2$ in dry THF. (The entire addition operation was performed under argon.) Each reaction was kept at 31 ± 1°C in a water bath (under argon). Samples were withdrawn and passed through short alumina columns (≈1 cm × 0.75 cm diameter) which were washed with 2 mL ether. The filtrates were analyzed by glpc (methyl silicone 30 m × 0.21 mm id fused silica capillary column, HP5880A glpc unit.) Electronically-integrated peak areas were corrected for relative responses determined for dodecane–ester solutions prepared independently and passed through alumina prior to analysis.

Preparation of (E)-*tetradec-2-en-5-yn-4-ol,* **26**

Dec-1-ynyl lithium (dec-1-yne, 6.9 g, 0.05 mol; 20.8 mL, 2.4 *M* butyl lithium) in 100 mL of THF was treated with freshly-distilled crotonaldehyde (3.85 g, 0.05 mol) at 0° to 15°C (17). The reaction was warmed over 30 min to room temperature and worked up as described for the preparation of tridec-1-en-4-yn-3-ol below. Distillation gave 8.5 g, 82% yield, bp (0.15 Torr) 94–95°C; ^{1}Hmr ($CDCl_3$) δ: 0.87 (t, 3H), 1.28 (m, 12H), 1.7 (m, 12H), 1.71 (m, 2H), 1.71 (d, 3H), 2.2 (m, 1H), 4.77 (m, 1H), 5.5–6.0 (m, 2H).

Acetylation gave 92% (*E*)-tetradec-2-en-5-yn-4-yl acetate, **26**, bp (0.1 Torr) 103–104°C; ^{1}Hmr ($CDCl_3$) δ: 0.88 (t, 3H), 1.27 (m, 12H), 1.72 (d, 3H), 2.03 (s, 3H), 2.20 (m, 2H), 5.30–6.30 (m, 3H).

Preparation of (E, Z)-*tetradec-2,5-dien-4-yl acetate,* **28**

To 1 g of $Ni(OAc)_2 \cdot 4H_2O$ in 50 mL ethanol under H_2 purge was added 5 mL of a solution prepared by filtering the solution from 1 g $NaBH_4$ in 24 mL ethanol and 1.25 mL 2 *N* NaOH (18). After H_2 evolution had ceased (≈15–20 min), 0.7 mL ethylenediamine was added, followed by 0.354 g (1.7 mmol) of (*E*)-tetradec-2-en-5-yl-4-ol. After 1.5 h the reaction was stopped by addition of 75 mL 20% NaCl and extracted into three 75-mL portions of ether. The ether was dried over anhydrous $MgSO_4$, filtered, concentrated *in vacuo*, and distilled (bulb-to-bulb), bp (0.2 Torr) 85–89°C, to give 0.28 g, 78% yield; ^{1}Hmr ($CDCl_3$) δ: 0.87 (t, 3H), 1.27 (br s, 12H), 1.50 (d, 3H), 1.71 (s, 1H, exch.), 2.07 (m, 2H), 4.90 (m, 1H), 5.5 (m, 4H). Acetylation gave **28**, 97%, bp (0.2 Torr) 106–107°C; ^{1}Hmr ($CDCl_3$, 400 MHz) δ: 0.86 (t, 3H, CH_3), 1.24 (m, 12H, CH_2), 1.69 (d, 3H, J = 7.2 Hz, CH_3—C=), 2.02 (s, 3H, Ac), 2.12 (br q, 2H, $J \simeq 7 \pm 1$ Hz, CH_2—C=), 5.36 (q, 1H, J = 8, 12 Hz, vinyl, A), 5.47 (q of d, 1H, J = 2.8, 16 Hz, vinyl, B), 5.55 (d of t, 1H, J = 6.4, 6.4, 12 Hz, vinyl, C), 5.73 (sextet, 1H, vinyl, D), 5.94 (br q, 1H, $J \cong 6, 8$ Hz, C*H*—O). *Exact Mass* calcd. for $C_{16}H_{28}O_2$: M^+, 252.2089; found (ms): 252.2090.

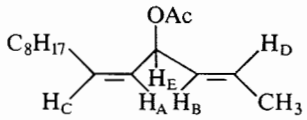

Rearrangement of (E,Z)-*tetradeca-2,5-dien-4-yl acetate,* ***28***

A 0.2 *M* solution of **28** in dry THF was treated with 0.8 mmol equiv. $Pd(CH_3C{\equiv}N)_2Cl_2$ for 2 h at room temperature. The usual work-up gave 91% distilled product (bp (0.1 Torr) 72–76°C) which gave one major (>95% by glpc) acetate (**29**), ^{1}Hmr ($CDCl_3$, 400 MHz) δ: 0.84 (t, 3H, CH_3), 1.23 (m, 12H, CH_2), 1.29 (d, 3H, J = 7.2 Hz, O—CH—CH_3), 2.00 (s, 3H, Ac), 2.13 (q, 2H, J = 7 Hz, CH_2—C═), 5.4 (m, 2H, vinyl, B, C*H*O), 5.58 (q, 1H, J = 7, 16 Hz, vinyl, C), 5.90 (5, 1H, J = 11.6 Hz, vinyl, D), 6.48 (q, 1H, J = 11.6, 16 Hz, vinyl, E). *Exact Mass* calcd. for $C_{16}H_{28}O_2$: M^+, 252.2089; found (ms): 252.2085.

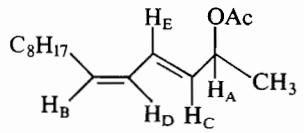

Preparation of tridec-1-en-4-yn-3-yl acetate, ***27***

Dec-1-ynyl lithium (6.9 g; 0.05 *M* dec-1-yne, 20.8 mL 2.4 *M* butyl lithium) in 100 mL THF was treated at 0° to −15°C with 2.8 g (0.05 mol) freshly-distilled acrolein in 10 mL dry THF. The reaction was stirred 30 min at 0°C, then warmed to room temperature (17). The reaction was quenched with 50 mL of aqueous NH_4Cl and extracted with three 50-mL portions of ether. The ether was dried over anhydrous $MgSO_4$, filtered, concentrated *in vacuo*, and the concentrate distilled to yield 8.05 g (83%) tridec-1-en-4-yl-3-ol, bp (0.2 Torr) 88–90°C; ^{1}Hmr ($CDCl_3$) δ: 0.73 (t, 3H), 1.30 (m, 12H), 2.23 (m, 3H), 4.9 (m, 1H), 5.23 (d of t, 1H), 5.57 (m, 1H), 6.05 (d of q, 1H).

Acetylation gave tridec-1-en-4-yn-3-yl acetate (**27**) in 84% yield, bp (0.1 Torr) 90–91°C; ^{1}Hmr ($CDCl_3$) δ: 0.72 (t, 3H), 1.27 (m, 12H), 2.08 (s, 3H), 2.22 (m, 2H), 5.1–6.0 (m, 4H). *Exact Mass* calcd. for $C_{15}H_{24}O_2$: M^+, 236.1776; found (ms): 236.1778.

Preparation of (E)-*trideca-1,4-dien-3-yl acetate,* ***30***

Tridec-1-en-4-yn-3-ol (1.5 g, 7.7 mmol) was treated with $LiAlH_4$ (0.58 g, 15 mmol) in ether/THF at reflux for 22 h (17). The reaction was quenched by addition of ethyl acetate and worked up by sequential addition of 50 mL 20% NaOH, extraction with three 50-mL portions of ether, drying of the ether over anhydrous Na_2CO_3, filtration, concentration *in vacuo*, and vacuum distillation (bp (0.05 Torr) 78–82°C) to yield 1.36 g (90%) (*E*)-trideca-1,4-dien-3-ol; ^{1}Hmr ($CDCl_3$) δ: 0.87 (t, 3H), 1.25 (m, 12H), 2.00 (m, 2H), 4.52 (5, 1H), 4.70 (s, 1H), 5.0–6.0 (m, 5H); ms (rel. int.): 178(4%), 83(100%), 79(29%), 70(51%), 55(38%).

Acetylation gave (*E*)-trideca-1,4-dien-3-yl acetate (**30**) in 94% yield, bp (0.05 Torr) 75–78°C; ^{1}Hmr ($CDCl_3$) δ: 0.87 (t, 3H), 1.2–2.0 (m, 14H), 2.02 (s, 3H), 5.05 (d of t, J = 10, 1.5, 1.5 Hz, H_A), 5.14 (d of t, J = 17, 1.5, 1.5 Hz, H_B), 5.34 (dd, J = 15, 7 Hz, H_E), 5.51 (br t, $J \approx 7$ Hz, H_D), 5.65 (d of t, J = 15, 7, 7 Hz, H_F), 5.72 (m, J = 17, 10, 6 Hz, H_C). *Exact Mass* calcd. for $C_{15}H_{26}O_2$: M^+, 238.1933; found (ms): 238.1935.

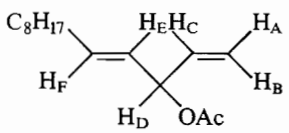

Rearrangement of (E)-*trideca-1,4-dien-3-yl acetate,* ***30***

A 0.2 *M* solution of **30** in dry THF was treated with 0.08 mol equiv. $Pd(CH_3CN)_2Cl_2$ for 2 h at room temperature. The usual work-up gave 96% **31**, bp (0.05 Torr) 65–70°C (bulb-to-bulb) (>97% one isomer by glpc); ^{1}Hmr ($CDCl_3$) δ: 0.87 (t, 3H), 1.25–1.67 (m, 14H), 2.03 (s, 3H), 5.07 (dd, J = 10, 2 Hz, H_A), 5.19 (dd, J = 15, 2 Hz, H_B), 5.22 (g, J = 6.8 Hz, H_F), 5.57 (dd, J = 15, 6.8 Hz, H_E); 6.21 (m, H_CH_D). *Exact Mass* calcd. for $C_{15}H_{26}O_2$: M^+, 238.1933; found (ms): 238.1933.

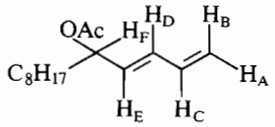

1. (*a*) L. E. OVERMAN, C. B. CAMPBELL, and F. M. KNOLL. J. Am. Chem. Soc. **100**, 4822 (1978); (*b*) L. E. OVERMAN and F. M. KNOLL. Tetrahedron Lett. 321 (1979); (*c*) P. M. HENRY. J. Am. Chem. Soc. **94**, 5200 (1971); (*d*) J. TSUJI, U. HIROAKI, Y. KOBAYASHI, and H. OKUMOTO. Tetrahedron Lett. 2573 (1981). (*e*) I. SHIMIZU, T. YAMADA, and J. TSUJI. Tetrahedron Lett. 3199 (1980); (*f*) B. T. GOLDING, C. PIERPOINT, and R. ANEJA. J. Chem. Soc. Chem. Commun. 1030 (1981).
2. L. E. OVERMAN and F. M. KNOLL. J. Am. Chem. Soc. **102**, 865 (1980); L. E. OVERMAN and E. J. JACOBSEN. J. Am. Chem. Soc. **104**, 7225 (1982).
3. Y. TAMARU, M. KAGOTANI, and Z. YOSHIDA. J. Org. Chem. **45**, 5223 (1980).
4. (*a*) P. A. GRIECO, T. TAKIGAWA, S. L. BONGERS, and H. TANAKA. J. Am. Chem. Soc. **102**, 7587 (1980); (*b*) P. A. GRIECO, P. A. TUTHILL, and H. L. SHAM. J. Org. Chem. **46**, 5005 (1981).
5. L. S. HEGEDUS, P. M. KENDALL, S. M. LO, and J. R. SHEATS. J. Am. Chem. Soc. **97**, 5448 (1975).
6. J. TSUJI, K. TSURUOKA, and K. YAMAMOTO. Bull. Chem. Soc. Jpn. **49**, 1701 (1976).
7. J. KOCHI and H. E. MAINS. J. Org. Chem. **30**, 1862 (1965).
8. A. F. THOMAS and W. BUCHER. Helv. Chim. Acta, **53**, 771 (1970).
9. E. KLEIN and W. ROJAHN. Dragoco Rep. **14**, 139 (1967).
10. K. KIKUKAWA, K. SAKAI, K. ASCADA, and T. MATSUDA. J. Organomet. Chem. **77**, 131 (1974).
11. R. N. MOORE, C. GOLUMBIC, and G. S. FISHER. J. Am. Chem. Soc. **78**, 1173 (1956).
12. A.-M. MANDROU, P. POTIN, and R. WYLDE-LACHAZETTE. Bull. Soc. Chim. Fr. 1546 (1962).
13. M. I. BOWMAN, C. C. KETTERER, and G. DINGA. J. Org. Chem. **17**, 563 (1952).
14. P. TEISSEIRE, A. GALFAE, M. PLATTIER, P. ROULLIER, and B. CORBIER. Recherches, **16**, 119 (1967).
15. K. GOLLNICK, S. SCHROETER, G. OHLOFF, G. SCHADE, and G. O. SCHENCK. Justus Liebigs Ann. Chem. **687**, 14 (1965).
16. K. GOLLNICK and G. SCHADE. Tetrahedron, **22**, 133 (1966).
17. L. BRANDSMA. Preparative acetylenic chemistry. Elsevier Publishing Company, Amsterdam, London, New York. 1971.
18. C. A. BROWN and V. K. AHUJA. J. Chem. Soc. Chem. Commun. 553 (1973).

Can. J. Chem. Downloaded from www.nrcresearchpress.com by 210.87.254.6 on 09/06/12
For personal use only.

The preparation, spectral properties, structures, and base-induced cleavage reactions of some α-halo-β-ketosulfones

J. STUART GROSSERT,[1] PRAMOD K. DUBEY, GLEN H. GILL, T. STANLEY CAMERON,[1] AND PATRICK A. GARDNER
Department of Chemistry, Dalhousie University, Halifax, N.S., Canada B3H 4J3

Received March 28, 1983[2]

J. STUART GROSSERT, PRAMOD K. DUBEY, GLEN H. GILL, T. STANLEY CAMERON, and PATRICK A. GARDNER. Can. J. Chem. **62**, 798 (1984).

The halogenation of β-ketosulfones such as α-methylsulfonylacetophenone (**1**) and benzenesulfonylacetone (**10**) can be effected with sulfuryl chloride or pyridinium bromide perbromide. Regiochemical control can be achieved by control of stoichiometry and/or the reaction conditions. Detailed ^1H and ^{13}C nmr, and mass spectra are recorded for a series of halogenated β-ketosulfones, together with structures by X-ray crystallography for **1**, 2-chloro-2-methylsulfonyl-1-phenylethanone (**2**), chloromethyl methyl sulfone (**4**), and α-chloroacetophenone (**21**). Results from these studies are used to suggest a reason for the difficulty associated with substitution reactions of α-halosulfones.

J. STUART GROSSERT, PRAMOD K. DUBEY, GLEN H. GILL, T. STANLEY CAMERON et PATRICK A. GARDNER. Can. J. Chem. **62**, 798 (1984).

L'halogénation des β-cétosulfones comme l'α-méthylsulfonylacétophénone (**1**) et la benzènsulfonylacétone (**10**) peut être effectuée avec le chlorure de sulfuryle ou le perbromure du bromure de pyridinium. On peut exercer un contrôle régiochimique en controlant la stoichiométrie et/ou les conditions de la réaction. On a enregistré des spectres détaillés de la rmn du proton et du carbone-13 ainsi que les spectres de masse d'une série de β-cétosulfones; de plus, faisant appel à la diffraction des rayons-X, on a déterminé les structures de **1**, de la chloro-2 méthylsulfonyl-2 phényléthanone (**2**), de la chlorométhyl méthyl sulfone (**4**) et de l'α-chloroacétophénone (**21**). On utilise les résultats de ces études pour suggérer une raison pour la difficulté associée aux réactions de substitutions des α-halosulfones.

[Traduit par le journal]

Can. J. Chem. Downloaded from www.nrcresearchpress.com by 210.87.254.6 on 09/06/12
For personal use only.

Introduction

The chemistry of β-ketosulfones has not been explored in detail and much of the reported chemistry involves the incorporation of the functionality into directed alkylation sequences from which the sulfone is later discarded (1–4). Even less has been reported on derivatives such as α-halo-β-ketosulfones (5–7). A systematic study of these functionalities could be useful; for example, it could provide information about halogenation of ketones with an adjacent sulfonyl group which would complement traditional studies on halogenation reactions of ketones with an adjacent electron-withdrawing group (8). However, the potential of these functionalities as precursors of α-sulfenylated-β-ketosulfones was of particular interest to us.

In this paper we report on the controlled halogenation of two β-ketosulfones together with the alkaline cleavage reactions of the resulting α-halo-β-ketosulfones. The range of polyfunctional sulfones obtained in this study forms a useful series in which to study spectroscopic properties and we have, in addition, determined crystal structures of certain selected compounds by X-ray diffraction techniques. In subsequent papers we will describe reactions of α-halo-β-ketosulfones with nucleophiles having varying degrees of hardness on the HSAB scale,[3] and report on direct sulfenylation reactions to give α-sulfenylated-β-ketosulfones (9).

Results and discussion

Preparations and reactions

The present study has focussed on the chemistry of two known, structurally isomeric β-ketosulfones, **1** and **10**. These were chosen partly for their convenience of preparation, but also to represent the two possible extremes in structure of β-ketosulfones, namely a ketone with α-hydrogens only between the ketone and sulfonyl groups (**1**) and a ketone with hydrogens both in such a position and also in a methyl group α′ to a ketone (**10**).

Monohalogenation of the methylene in **1** was readily achieved using either sulfuryl chloride or pyridinium bromide perbromide, in either neutral or acidic reaction media. The products, provided stoichiometry was controlled, were either the known monochloro compound, **2**, or the previously unreported monobromo compound, **3**. Compound **2** has been prepared previously by Bohlmann and Haffer, using a different route (7). Both **2** and **3** possess a relatively strongly-acidic

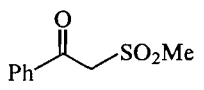

1

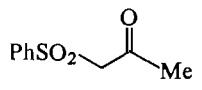

10

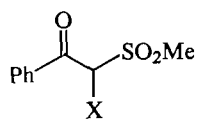

2 X = Cl
3 X = Br

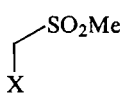

4 X = Cl
5 X = Br

methine proton that is easily abstracted by triethylamine in deuterochloroform solution. Deuterium oxide exchange of these methine protons in a basic solution was extremely rapid but did not occur in deuterochloroform containing ca. 20% trifluoroacetic acid, even after 48 hours at room temperature. Careful examination by ^{13}C nmr yielded no detectable enol formation in an acidic medium and, furthermore, infrared spectroscopy showed no sign of enolization in either chloroform solution or a potassium bromide pellet, the two spectra being

[1] Authors to whom correspondence may be addressed; correspondence regarding the X-ray crystallography should be directed to T.S.C.

[2] Revision received November 24, 1983.

[3] Preliminary results were presented to the 64th Canadian Chemical Conference in Halifax, N.S., June 1980.

Can. J. Chem. Downloaded from www.nrcresearchpress.com by 210.87.254.6 on 09/06/12
For personal use only.

quite similar. Similar deuterium oxide exchange of the methylene protons in **1** was observed. Halogenation of ketones in neutral or acidic media proceeds by way of reaction between the enol and a source of positive halogen (8, 10). Hence when **1** is halogenated in this manner, enolization of **2** or **3** does not occur, and further halogenation is thus not possible.

We have examined reactions of **2** and **3** involving attack by hydroxide or alkoxides, and found that in both cases reactions are exclusively at the carbonyl with subsequent displacement of the halosulfonyl carbon. This reaction has potential as a synthesis of halomethylsulfones (RSO_2CH_2X or RSO_2CHX_2, X = Cl or Br), although the dibromomethyl sulfones tended to be readily reduced to monobromoethyl compounds. Thus, for example, aqueous alkaline hydrolysis of **2** gave the known (11) chloromethyl methyl sulfone (**4**) and benzoic acid, whereas ethanolic sodium ethoxide alcoholysis gave **4** and ethyl benzoate. Similar reactions with **3** gave **5** and benzoic acid or ethyl benzoate.

Dichlorination of **1** was accomplished readily with sulfuryl chloride in a basic reaction medium to give **6** which was accessible also by similar chlorination of **2**. Saponification of **6** gave **7** and benzoic acid only, no traces of **4** being detectable. Dibromination of **1** gave the expected dibromo-β-ketosulfone (**8**)

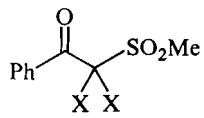

6 X = Cl
8 X = Br

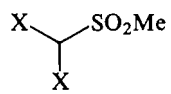

7 X = Cl
9 X = Br

together with a small amount of the dibromosulfone **9**. This small amount of **9** was most likely formed by hydrolysis of **8** during work-up of the reaction. Aqueous alkaline treatment of the reaction products resulted in both hydrolysis and reduction, with **5** being the only isolable sulfone product; it is known that α,α-dibromosulfones are readily reduced (12). We have found that compounds such as **4**, **5**, and dimethyl sulfone have appreciable water solubility, which complicated their isolation in high yields during work-up of reactions from the saponification process.

Halogenation of **1**, under the conditions we have employed, was possible only at a single center. By contrast, halogenation of **10** presented a more interesting problem for regiocontrol of reaction. Bromination of **10** with one mole equivalent of pyridinium bromide perbromide in dichloromethane – acetic acid led to the formation, in high yield, of the previously unreported, crystalline α′ monobromo compound, **11**. By changing the solvent to pyridine–dichloromethane, either compounds **12** (α-monobromo) or **14** (α,α-dibromo) could be obtained, depending on the reaction stoichiometry. Spectral characterization of these was followed by cold aqueous alkaline hydrolysis to the respective brominated phenyl sulfones, $PhSO_2CH_2Br$ (**13**) and **15**, although **14** always yielded a mixture of **15** and its reduction product **13**. It should be noted that both the tribromo- and triiodomethyl phenyl sulfones have been reported (13), apparently as stable products, from haloform reactions on **10**.

Chlorination of **10** with sulfuryl chloride has been reported previously (14) as yielding α-chloro-α-phenylsulfonylacetone (**16**). We have been unable to obtain **16** in a pure form; the best chlorination conditions involved chlorination with sulfuryl chloride in acetic acid – methylene chloride and the products were shown by nmr spectroscopy to be **16**, always contaminated with about 20% of its regioisomer, **17**. Chlorination of **10** in the presence of triethylamine gave the unstable dichlorocompound **18**, which could be saponified readily to dichloromethyl phenyl sulfone (**19**).

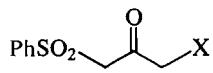

11 X = Br
17 X = Cl

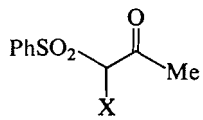

12 X = Br
16 X = Cl

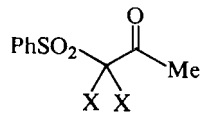

14 X = Br
18 X = Cl

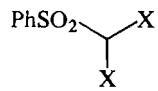

15 X = Br
19 X = Cl

These reactions demonstrate clearly that the sulfonyl group exerts a powerful directing effect on the course of β-ketosulfone reactions. The regiochemistry of halogenation parallels that of α-haloketones (8). In addition, the α-halo-β-ketosulfones show a strongly electrophilic carbonyl group and the major reaction that we have described is the alkoxide-induced cleavage of the C_α—CO bond, undoubtedly due to the stabilization of $^-$:CHCl.SO_2R which is a good leaving group. This trend is evident even in **1**, which is slowly hydrolyzed in alkaline solution. It has been shown previously (15) that α-halosulfones are reduced by attack of alkoxide at halogen. In all the cases described here, except **14**, the α-halo-β-ketosulfones were attacked at the carbonyl rather than at halogen and were cleaved, but were not reduced. Precise delineation of the relative activation energies for these competing reactions remains to be made.

Mass spectra

Although some of the compounds reported in this paper have been described previously, they have invariably not been fully characterized by modern spectroscopic techniques. Exceptions are the β-ketosulfone (**1**) and its monochloro derivative (**2**), mass spectra for which have been reported by Bohlmann and Haffer (7). The fragmentation patterns of compounds **4**, **5**, **7**, and **9** are all similar and are in agreement with the fragmentations of simple sulfones (16).

The mass spectra of **11** and **12** are similar to those of **1**–**3** in that predominant fragmentations occur either by McLafferty rearrangement or by α-cleavage, in this latter case, however, to $PhSO_2]^+$ as compared to $PhCO]^+$ for **1**–**3**, indicative of the controlling influence exerted by the phenyl group. These fragmentations are outlined in Scheme 1. It is interesting to note that ions of *m/z* 94 were not observed in these spectra, which indicates that the rearrangement processes operating in simple phenylsulfonyl sulfones (16) are not important in these compounds.

Nuclear magnetic resonance spectra

The ^{1}H nmr spectra of these compounds were all quite routine, especially in that the observed chemical shifts all fall within the ranges normally expected. The methylsulfonyl compounds **1**–**3** showed 4-bond, proton–proton couplings of less than 1 Hz across the sulfonyl group. This has been observed previously in similar cases (17, 18). These couplings are appar-

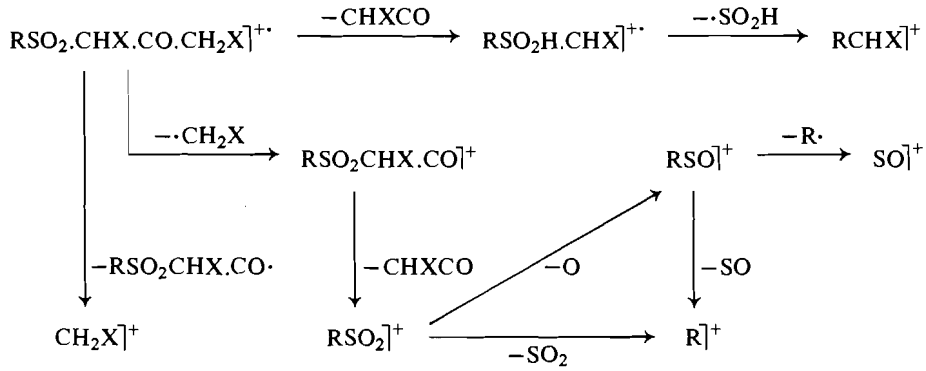

SCHEME 1

TABLE 1. The ^{13}C nuclear magnetic resonance spectral parameters of substituted sulfones and β-ketosulfones*

Compound	δ CH_3	δ CH_2	δ CH	δ CO
$CH_3SO_2CH_3$, **20**	42.33	—	—	—
$ClCH_2SO_2CH_3$, **4**	37.45 (q of t)† ($^1J_{CH}$ = 139.2 Hz)‡	56.65 (t of q) ($^1J_{CH}$ = 160.2 Hz)§	—	—
$BrCH_2SO_2CH_3$, **5**	37.79 (q) ($^1J_{CH}$ = 139.1 Hz)	42.40 (t) ($^1J_{CH}$ = 160.4 Hz)	—	—
$Cl_2CH.SO_2CH_3$, **7**	34.42 (q) ($^1J_{CH}$ = 140.4 Hz)	—	78.45 (d) ($^1J_{CH}$ = 185.1 Hz)	—
$PhCO.CH_2SO_2CH_3$, **1**‡‡	41.62 (q) ($^1J_{CH}$ = 139.2 Hz	60.97 (t) ($^1J_{CH}$ = 137.1 Hz)	—	189.10
$PhCO.CHCl.SO_2CH_3$, **2**	36.73 ($^1J_{CH}$ = 139.9 Hz)	—	68.23 (d) ($^1J_{CH}$ = 157.5 Hz)	187.23
$PhCO.CCl_2.SO_2CH_3$, **6**¶	37.61	—	—	185.16
$PhCO.CHBr.SO_2CH_3$, **3**	37.58 (q of d) ($^1J_{CH}$ = 140.4 Hz)§	—	55.82 (d) ($^1J_{CH}$ = 156.9 Hz)	187.59
$PhSO_2.CH_2.COCH_3$, **10**‡‡	31.18	67.39	—	**
$PhSO_2.CH_2.COCH_2Br$, **11**	—	—SO_2CH_2— 63.94 (t) —CH_2Br 34.18 (t)	—	**
$PhSO_2.CH_2.COCH_2Cl$, **17**	—	—SO_2CH_2— 63.87 (t) —CH_2Cl 48.64 (t)	—	190.01
$PhSO_2.CHCl.COCH_3$, **16**	27.97 (q)	—	75.90 (d)	193.60

* The chemical shifts are reported with respect to TMS, δ($^{13}CDCl_3$) = 76.90 (23).
† Abbreviations: d = doublet; q = quartet; t = triplet.
‡ $^3J_{CH}$ = 0.4 Hz.
§ $^3J_{CH}$ = 0.7 Hz.
‡‡ All aryl carbons exhibited absorptions within the expected range (ref. 20, pp. 375–376 and refs. therein) of chemical shifts.
¶ The quarternary carbon bearing two chlorine atoms was observed at δ 92.08.
** Not observed.

ently dependent on the oxidation level of the sulfur atom, as we have not observed them to be present across sulfenyl sulfur atoms (19). Also of note is the remarkably precise chemical shift coincidence of the two methylene sets in **17**, although this is an agreement with a Strehlow-type calculation of chemical shifts (20) using a value of $S(\delta) = 2.0$ for a $PhSO_2$ group at position 2.

Whenever possible, ^{13}C nmr spectra of the compounds described were measured also, although in some cases compounds were not sufficiently stable to permit accumulation of an adequate number of transients. Parameters from these spectra, which were recorded under conditions described previously (19), are given in Table 1. The chemical shifts of carbons in all the compounds studied fall within acceptable ranges but several observations are noteworthy.

The series provides for interesting comparisons of γ-effects in acyclic compounds, and these are highlighted in Table 2. The values observed for Δδ are intermediate between those reported (21) for acyclic and for rigid cyclic compounds. For example, the motionally averaged γ-effect for an acyclic chlorine is a 4-ppm upfield shift (21), whereas γ-*gauche* effects for chlorine range from −6.88 ppm[4] on methylene carbons in conformationally rigid cyclohexanes (21) to −5.72 ppm for the axial methyl and −3.45 ppm for the equatorial methyl in

[4] The negative sign denotes an upfield shift.

Can. J. Chem. Downloaded from www.nrcresearchpress.com by 210.87.254.6 on 09/06/12
For personal use only.

TABLE 2. γ-Effects in the ^{13}C chemical shifts of certain methyl sulfones and ketones

Compound		δ CH_3	Δδ
$CH_3SO_2CH_3$	**20**	42.33	—
$BrCH_2SO_2CH_3$	**5**	37.79	−4.54
$ClCH_2SO_2CH_3$	**4**	37.45	−4.88
$Cl_2CHSO_2CH_3$	**7**	34.32	−6.01
$PhCO.CH_2SO_2CH_3$	**1**	41.62	−0.71
$PhCO.CHBr.SO_2CH_3$	**3**	37.58	−4.04*
$PhCO.CHCl.SO_2CH_3$	**2**	36.73	−4.89*
$PhCO.CCl_2.SO_2CH_3$	**6**	37.62	−4.00*
$PhSO_2.CH_2.COCH_3$	**10**	31.18	—
$PhSO_2.CHCl.COCH_3$	**16**	27.97	−3.21

*With respect to the chemical shift of the methyl carbon in **1**.

2-chloro-1,1-dimethylcyclohexane (22). These authors caution that whereas distinctions between *gauche* and *anti* geometries can be made using γ-shielding effects, there is no general, precise correlation between the γ-effect and dihedral angles. From the magnitude of the effects exhibited by **2** and **4**, it is likely that the methyls and chlorines are largely in a *gauche* orientation, which are the conformations adopted by **2** and **4** in the solid state (*vide infra*). Similar conclusions concerning both the solid- and liquid-state conformations of sulfones with polar groups in the α-position have been reached by Engberts, Exner, and Vos (23). Study of a model of **2** leads to the conclusion that the solid-state conformation is likely to be adopted by the molecule (at least in solutions of low or moderate polarity) due to the considerable steric demands by the benzoyl and sulfonyl groups. One might then expect the γ-effect in **6** to parallel that in **7**, yet such is not the case, indicating again (22) that the origins of the effect do not lend themselves to simple explanations. Finally, it is reasonable to assume a smaller steric demand by a carbonyl group versus a sulfonyl group, with a resulting greater freedom of rotation likely in **16** versus **2**; the γ-effect in **16** is 1.68 ppm less than that in **2**.

Also of interest in this series of compounds are the chemical shifts of the carbonyl carbons. Using acetophenone as a base model for **1**, we have observed an upfield shift of −9.0 ppm due to the replacement of a hydrogen atom by a methylsulfonyl group.[5] The carbonyl absorption in α-chloroacetophenone (**21**) is at δ 190.9 (24), which therefore shows an upfield shift of −7.2 ppm due to the replacement of a hydrogen by a chlorine. As seen in Table 1, further halogenation (compounds **2**, **3**, and **6**) results in further upfield shifting of the carbonyl absorption, albeit not in a linear manner.

It was possible in a number of cases to record the ^{13}C nmr spectra under conditions of gated decoupling. From these spectra, values for $^1J_{CH}$ were measured and are recorded in Table 1. The values obtained are in general agreement with trends recorded in the literature (ref. 20, pp. 375–376 and references therein). We had previously reported sizeable 3-bond carbon–proton couplings across sulfenyl sulfur (19). Such couplings have apparently not been reported across sulfonyl groups and we have not observed them previously. However, by careful recording of spectra and data processing using the spectrometer computer, we were able to observe small, 3-bond proton–carbon couplings for both the methyl and methylene carbons in **4**, and for the methyl carbon only in **3**. The observation of these long-range couplings, the origins of which are complex (21), is of interest but their value is limited by their small magnitude and the consequent difficulties of observing them.

Structural studies

Only a few structures of acyclic sulfones with a polar group in the α position have been determined (23, 25–28). Given this fact and the complexities of nucleophilic displacement reactions in these compounds (*vide infra*), we wished to determine structural parameters for some of the compounds made available by this study. In particular, a comparison of solid-state and solution structural parameters for **2** was thought to be worth obtaining, with a long-term view of potential correlations between such sulfone structures and their reactivity.

Structures were determined for $PhCOCH_2SO_2Me$ (**1**), for its α-chlorinated derivative, **2**, and for the hydrolysis product of **2**, CH_2ClSO_2Me (**4**). The structure of α-chloroacetophenone ($PhCOCH_2Cl$) (**21**) was also included in order to compare bond distances, bond angles, and torsional angles involving the benzoyl group when the sulfonyl group is not present. Preparation of the crystals is described under Experimental.[6] Crystal data of the four compounds are presented in Table 3, dimensions of the molecules are given in Table 4; pictures of the molecules are shown in Figs. 1 to 4, selected torsional angles are given in Fig. 5, and the packing of the molecules in their unit cells is given in Figs. 6–9.[7]

A CAD-4 four-circle diffractometer with an $\omega/2\theta$ scan was used for all crystals to establish unit-cell dimensions and to collect intensities. Since α-chloroacetophenone proved to be unstable at room temperature, intensities for this crystal alone were collected at −140°C. Reflection data were reduced by routine procedures which are described in ref. 29. Lorenz, polarization, but not absorption corrections were applied; two reflections were omitted from the data for compound **4** because of extinction. Scattering factors were taken from ref. 30.

Partial structures were determined from the *E*-maps in each case, using direct centrosymmetric methods for compounds **2** and **4** and by applying the multisolution tangent formula for compounds **1** and **21**. Other atoms were found on subsequent Fourier maps. Full matrix least-squares refinements ($\omega\Delta F^2$ = min) were carred out with anisotropic temperature factors on the non-hydrogen atoms and isotropic temperature factors on the hydrogens. The SHELX 76 system was used for all calculations (31).

The structure of α-chloroacetophenone (**21**) was reported in 1966 (32) based on 327 visually estimated intensities. A poor *R* value of 0.16 prompted us to repeat the structure determination at −140°C. This gave similar cell parameters and the same space group but a different arrangement of the molecules in the unit cell. We were unable to confirm the structure as reported in 1966 since adequate reflection data could not be obtained at room temperature.

Molecular geometries

The principal bond distances, bond angles, and torsional

[5] We have measured δCO in acetophenone as 198.1 ppm.

[6] A commercial sample of **21** (Aldrich) was recrystallized to constant mp (54–55°C).

[7] A complete list of atomic parameters, distances, angles, and torsional angles (Table 4), a list of structure factors (Tables 5–8), and unit cell packing diagrams (Figs. 6–9) are available from the Depository of Unpublished Data, CISTI, National Research Council of Canada, Ottawa, Ont., Canada K1A 0S2.

Can. J. Chem. Downloaded from www.nrcresearchpress.com by 210.87.254.6 on 09/06/12
For personal use only.

Can. J. Chem. Downloaded from www.nrcresearchpress.com by 210.87.254.6 on 09/06/12
For personal use only.

TABLE 3. Crystal data for $PhCOCH_2SO_2Me$ (**1**), $PhCOCHClSO_2Me$ (**2**), $ClCH_2SO_2Me$ (**4**), and $PhCOCH_2Cl$ (**21**)

	Compound			
Parameter	$PhCOCH_2SO_2Me$	$PhCOCHClSO_2Me$	$ClCH_2SO_2Me$	$PhCOCH_2Cl$
Formula weight	198.24	232.68	128.57	154.60
a, Å	9.242(3)	8.566(2)	5.162(2)	4.034(5)
b, Å	5.231(2)	8.354(2)	7.130(1)	9.54(2)
c, Å	9.622(3)	14.767(2)	7.151(2)	18.999(9)
α, deg			101.59(3)	
β, deg	92.42(3)	104.34(2)	89.42(4)	
γ, deg			92.97(1)	
Z	2	4	2	4
V, Å^3	464.8	1023.8	257.5	730.9
d, g.cm^{-3}	1.42	1.51	1.66	1.41
Space group	$P2_1$	$P2_1/a$	$P\bar{1}$	$P2_12_12_1$
F(000)	208	480	264	320
μ*	2.67	4.91	18.50	3.88
Reflections:				
counted	969	1857	904	1216
unique	914	1788	712	1024
used	811 (>3 esd)	812 (>3 esd)	376 (>3 esd)	436 (>1 esd)
Temperature	20°C ± 1°	20°C ± 1°	20°C ± 1°	−140°C ± 5°
p†	0.012680	0.013045	0.005556	0.060639
R	0.038	0.031	0.046	0.096
R_w	0.035	0.031	0.043	0.094

*MoK_α (λ = 0.70926 Å).
†Weight = $[\sigma^2(F) + pF^2]$.

TABLE 4. Bond lengths,* bond angles,† and torsional angles† for $PhCOCH_2SO_2Me$ (**1**), $PhCOCHClSO_2Me$ (**2**), $ClCH_2SO_2Me$ (**4**), and $PhCOCH_2Cl$ (**21**) (refer to Fig. 5)

	Compound			
Bonds	$PhCOCH_2SO_2Me$	$PhCOCHClSO_2Me$	$ClCH_2SO_2Me$	$PhCOCH_2Cl$‡
S—C_α	1.787(4)	1.815(4)	1.781(9)	
S—Me	1.759(4)	1.760(5)	1.765(9)	
S—O_1	1.425(3)	1.434(3)	1.424(7)	
S—O_2	1.441(3)	1.430(4)	1.445(8)	
C_α—C_β	1.525(5)	1.553(6)		1.55(3)‡
C_α—Cl		1.754(4)	1.761(8)	1.70(3)‡
C_β—Ph	1.474(5)	1.473(6)		1.43(3)‡
C_β—O	1.216(5)	1.203(6)		1.20(3)‡
Angles				
Me—S—C_α	104.7(2)	104.1(2)	105.2(5)	
S—C_α—C_β	112.3(3)	109.2(3)		
S—C_α—Cl		108.8(2)	111.6(5)	
C_α—C_β—Ph	119.9(3)	118.0(4)		119(2)‡
C_α—C_β—O	117.8(3)	118.8(4)		118(2)‡
Cl—C_α—C_β		112.3(3)		114(2)‡
O—S—O	118.3(2)	118.2(2)	119.1(4)	
Torsional angles				
Me—S—C_α—C_β	−72.9(3)	−172.6(3)		
Me—S—C_α—Cl		64.5(3)	−59.4(6)	
S—C_α—C_β—O	80.0(3)	−92.4(4)		
S—C_α—C_β—Ph	−98.6(3)	86.1(4)		
Cl—C_α—C_β—Ph		−153.1(3)		177(2)‡

*Bond lengths are reported in Å.
†Bond and torsional angles are reported in degrees.
‡C_α for this compound is defined as the chloromethyl carbon, and C_β as the carbonyl carbon.

Can. J. Chem. Downloaded from www.nrcresearchpress.com by 210.87.254.6 on 09/06/12
For personal use only.

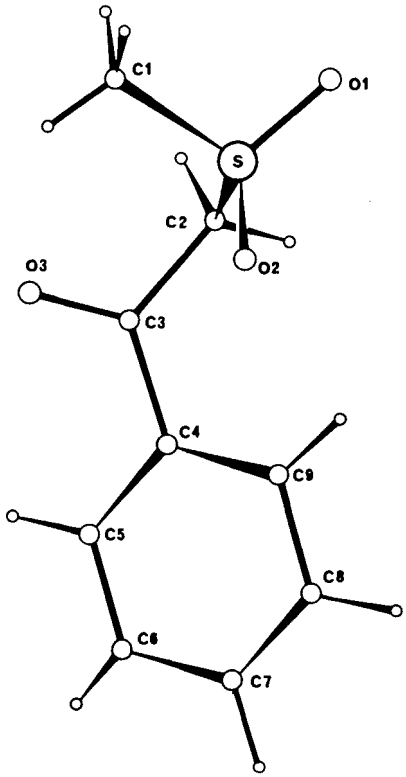

FIG. 1. The crystal structure of $PhCO.CH_2SO_2CH_3$, (**1**).

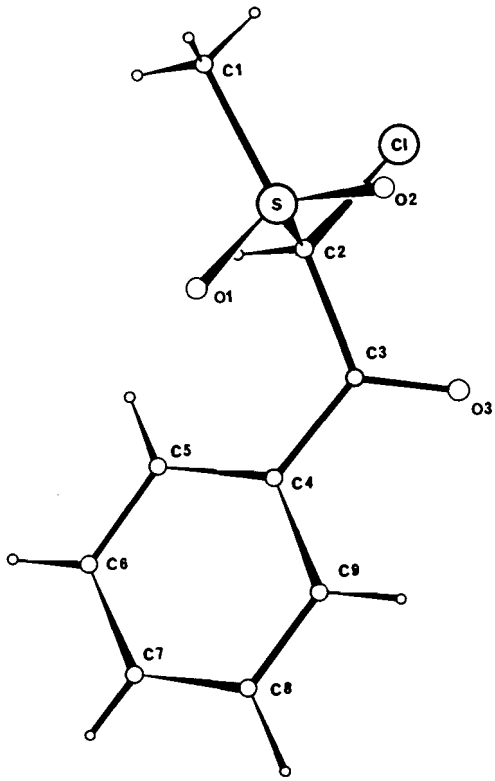

FIG. 2. The crystal structure of $PhCO.CHCl.SO_2CH_3$, (**2**).

angles are listed in Table 4 and presented graphically in Fig. 5. The main features can be summarized as follows.

The S—C_α distances in compounds **1**, **2**, and **4** are 1.787(4), 1.815(4), and 1.781(9) Å. The lengthening of this bond in **2** is a consequence of the substitution of hydrogen by the electron-withdrawing chlorine, which also causes the C_α—C_β bond to be longer in **2** than in **1** (1.525(5), **1**; 1.553(6) Å, **2**). The S—C_α bond in **4** should be shorter than that of **2**, since **4** lacks the benzoyl group, but it should be longer than the S—C bond in dimethyl sulfone (**20**) (1.774(3) Å) (26); the S—C_α distance observed in **4** (1.781(9) Å) falls within this range but it could not be determined very accurately. The C—Cl distances in **2**, **4**, and **21**, 1.754(4), 1.761(8), and 1.70(3) respectively, are not significantly different and compare with those in vinyl chloride (1.728(7) Å) and methyl chloride (1.784(3) Å) (33), both values having been determined by electron diffraction techniques. The S—Me distances in **1**, **2**, and **4** (1.759(4), 1.760(5), 1.765(9) Å) are equivalent and similar to a previously reported compound (34), yet possibly significantly shorter than those observed in dimethyl sulfone (1.774(3) Å) (26). The structural results for **21** gave a clear picture of the molecular conformation in the crystalline state (Fig. 5), but the molecular dimensions could not be determined sufficiently accurately to merit detailed comment.

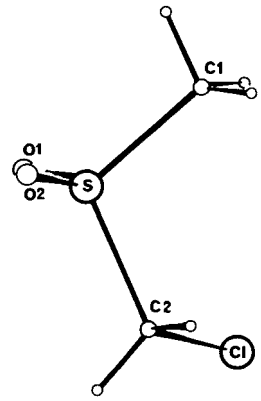

FIG. 3. The crystal structure of $ClCH_2SO_2CH_3$, (**4**).

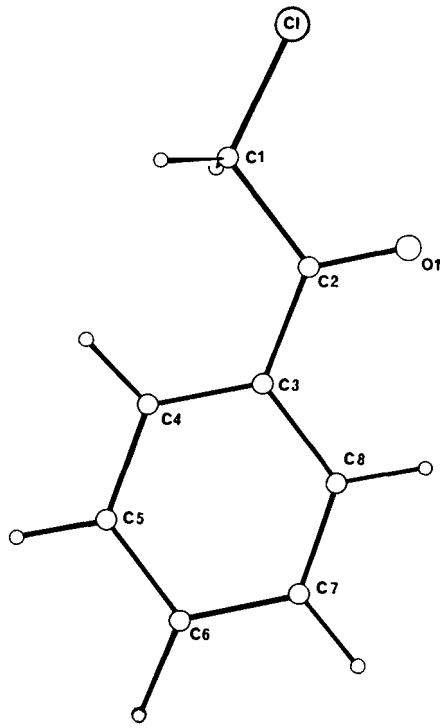

FIG. 4. The crystal structure of $PhCO.CH_2Cl$, (**21**).

Can. J. Chem. Downloaded from www.nrcresearchpress.com by 210.87.254.6 on 09/06/12
For personal use only.

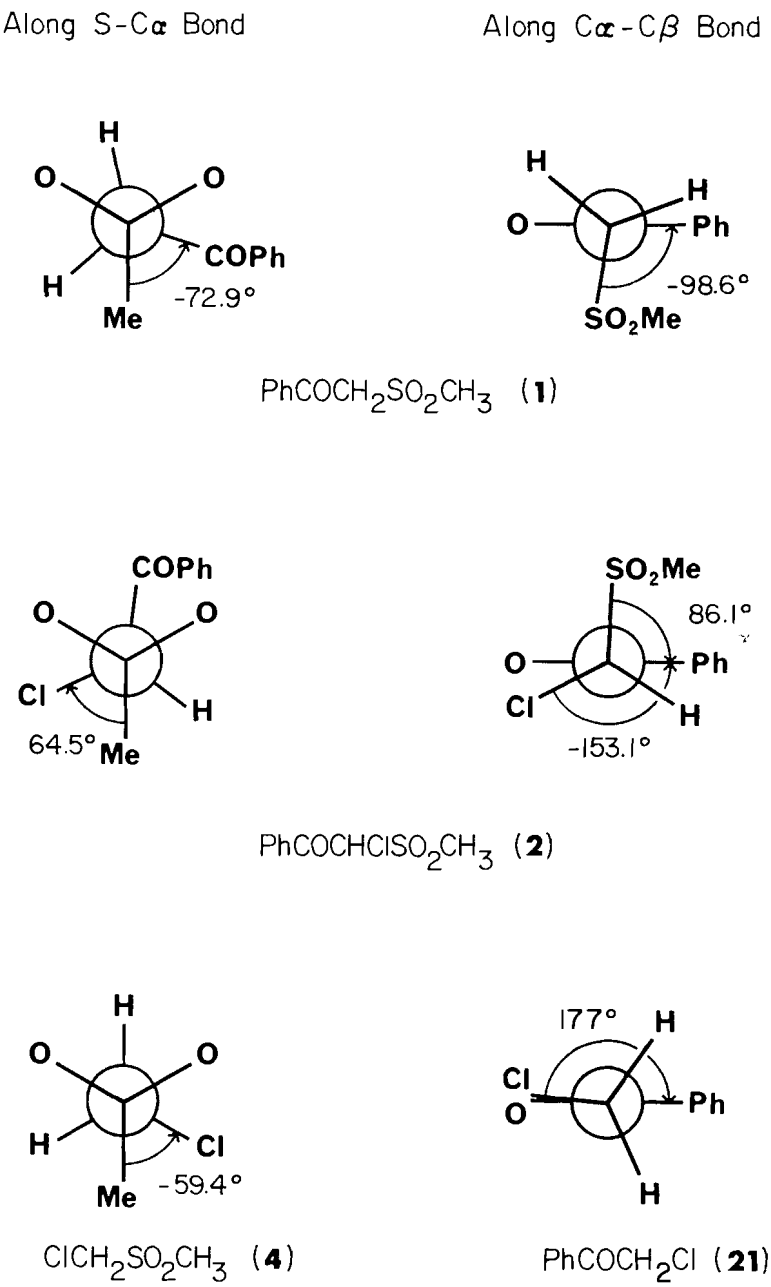

FIG. 5. Torsional angles for $PhCOCH_2SO_2CH_3$ (**1**), $PhCOCHClSO_2CH_3$ (**2**), $ClCH_2SO_2CH_3$ (**4**) and $PhCOCH_2Cl$ (**21**).

The two S—O distances in a sulfone are normally equivalent (23, 26–28, 34, 35), the mean of some reported values being 1.439(14) Å, (26). The S—O distances in **1**, **2**, and **4** range from 1.425(3) to 1.445(8) with a mean of 1.433(8). The two S—O distances in **1** are significantly different, although the causes of this are obscure.

The electron-withdrawing property of the chlorine atom also shows in a slight closure of the $S—C_\alpha—C_\beta$ angle from 112.3(3)° in **1** to 109.2(3)° in **2**; the same effect is less marked at the $C_\alpha—C_\beta—Ph$ angle which decreases slightly from 119.9(3) to 118.0(4)°. Loss of the benzoyl group from the α-chloro-β-ketosulfone (**2**) increases the angle between chlorine and sulfur at the α-carbon: the $S—C_\alpha—Cl$ angle in **4** was 111.6(5)° as compared to 108.8(2)° in **2**. Electron repulsion also explains an apparent widening of the $Cl—C_\alpha—C_\beta$ angle of 112.3(3)° when the methylsulfonyl group in **2** is replaced by a hydrogen, although the 114(2)° figure for α-chloroacetophenone (**21**) is not very precise.

The compounds **1**, **2**, **4** comprise a series that permits useful structural comparisons to be made between sulfonyl groups with polar substituents at an α-carbon. These results can then be compared with those from the carbonyl compound, **21**. Two α-bromosulfones have been reported as having a bromine *gauche* to both sulfonyl oxygens (25). However, sulfones with a polar group at C_α usually adopt a conformation in the crystalline state in which the polar group is *gauche* to only one of the sulfonyl oxygens (23, 27, 28, 34). Dipole moment evidence by Exner and Engberts suggests that this same conformation is predominant in solution (the *gauche* effect) although in such molecules the causes of this phenomenon are obviously more complex than in simple molecules like 1,2-dihaloethanes or dialkyl disulfides (23). It was thus gratifying to find that the methyl group and chlorine in both **2** and **4** were in a *gauche* orientation about the $S—C_\alpha$ bond (Fig. 5). This same con-

Can. J. Chem. Downloaded from www.nrcresearchpress.com by 210.87.254.6 on 09/06/12
For personal use only.

formation was apparently predominant in solutions of these molecules (*vide supra*).

A more subtle conformational effect was observed by examining the S—C_α—C_β—Ph torsional angles[7] in **1** and **2** and comparing these with the Cl—C—C—Ph angle in **21** (Fig. 5). It was found that the chloro and carbonyl groups in **21** were almost synperiplanar; such conformations of α-haloketones have been studied by infrared spectroscopy (36). Presumably this synperiplanar arrangement of the chloro and carbonyl groups derives from the fact that the electron density in the carbonyl group is rather different from that in a polar group involving only σ bonds. Furthermore, since the phenyl and carbonyl groups must be coplanar, a *gauche* orientation of the carbonyl and chlorine in **21** would produce severe nonbonded repulsion between a hydrogen of the chloromethyl group and one of the *ortho* hydrogens on the phenyl ring. The corresponding projection of **1** was quite different from that of **21**, reflecting the much greater bulk of a methylsulfonyl versus a chloro group. The S—C_α—C_β—Ph angle in **2** was 12.5° less than the corresponding angle in **1**, thus permitting the chloro and carbonyl groups to be in closer proximity to each other.

Conclusions

A consideration of the above conformational effects offers the possibility of some intriguing speculation concerning the fact that the intermolecular displacement of a leaving group from a carbon adjacent to a sulfonyl group is a difficult and often complex process (2, 15, 37, 38). Among displacement reactions, a small number of efficient substitutions involving the reaction of thiolate anions with chloromethyl sulfones are known (15, 39), but the mechanism of these substitution reactions has not been unequivocally established. More commonly, nucleophiles reduce α-halosulfones which must require attack at halogen rather than at carbon. This is in contrast to α-haloketones which generally (37, 40), although not always (41), undergo facile nucleophilic substitution reactions at carbon. A regular S_N2-type mechanism has only been demonstrated to operate when sulfones with exceptionally powerful adjacent leaving groups (triflate and $-N_2^+$) are attacked by nucleophiles (42).

If the predominant conformation of an α-halosulfone is that in which the halogen is *gauche* to only one of the sulfonyl oxygens, then the other oxygen must be *anti*. Thus the trajectory of attack at carbon by a nucleophile must approach close to this other oxygen, and furthermore the nucleophile must pass parallel to the polar S—O bond (see Fig. 10). Such a conformation and trajectory would undoubtedly result in a greater activation energy for an S_N2-type displacement in α-halosulfones as compared to one, for example, in alkyl halides.[8] In fact, if the activation energy for attack at carbon becomes sufficiently large, substitution reactions would then preferentially occur in a two-step process, initiated by attack at halogen.[9] Since thiolate anions are the only nucleophiles that have been reported to give substitution products from α-halosulfones, it is indeed likely that attack at halogen rather than at carbon is the lower energy pathway. We are actively engaged in studies to cast light on these speculations.

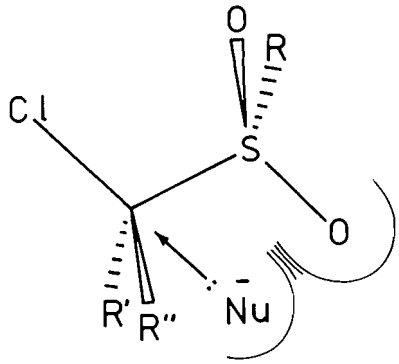

FIG. 10. The postulated path of attack by a nucleophile on carbon in an α-halosulfone.

Experimental

General

Thin-layer chromatographic analyses were carried out on Eastman silica sheets, containing a fluorescent indicator, and developed with EtOAc–ligroin, bp 40–60°C (1:1) or i-PrOH – toluene (1:9). Infrared spectra were run in chloroform solution on a P-E 237 spectrometer. Other details have been reported previously (19). All ^{13}C spectral results are collected in Table 1; conditions for recording spectra have been reported previously (19).

Preparation of 2-methylsulfonyl-1-phenylethanone, 1

This preparation was carried out with ethyl benzoate (50 mmol), sodium hydride (100 mmol), and dimethyl sulfone (100 mmol) using the procedure developed by Corey and Chaykovsky (44). Residual amounts of dimethyl sulfone were removed by washing the final dichloromethane extract thoroughly with water to give **1** in 85% yield. After 2 recrystallizations (toluene), **1** was tlc pure and had mp 106–107°C (lit. (45) mp 107.5–108°C, (3) mp 104–106°C); ir: 3030 (m), 1670 (s), 1590 (m), 1320 (vs), 1155 (s); ^1H nmr, δ: 3.15 (3H, t, J = 0.8 Hz), 4.60 (2H, q, J = 0.8 Hz), 7.43–8.07 (m, 5H).

Preparation of 2-chloro-2-methylsulfonyl-1-phenylethanone, 2

Sulfuryl chloride (1.6 mL, 20 mmol) was dropped into an ice-cold solution of **1** (3.96 g, 20 mmol) in CH_2Cl_2 (25 mL), which was then stirred for 4 h at 25°C. Rotary evaporation gave a crude solid, a CH_2Cl_2 solution of which was washed (water, 5% $NaHCO_3$, water), dried, and evaporated to give **2** (3.95 g, 86%). Two recrystallizations (ether) gave the pure **2**, mp 103–104°C (lit. (7) mp 105°C); ir: 3040 (w), 3015 (w), 2985 (m), 2940 (w), 1690 (s), 1590 (m), 1315 (s), 1130 (s); ^1H nmr δ: 3.22 (3H, d, J = 0.7 Hz), 5.98 (1H, q, J = 0.7 Hz) 7.53–8.08 (5H, m); ms, *m/z*: 234 (1.0), 232 (2.4), 156 (2), 154 (6), 127 (11), 125 (31), 106 (42), 105 (100), 90 (9), 89 (20), 78 (22), 77 (100), 63 (26), 51 (73).

Preparation of 2-bromo-2-methylsulfonyl-1-phenylethanone, 3

A solution of **1** (3.96 g, 20 mmol) in CH_2Cl_2 (100 mL) was added to a solution of pyridinium bromide perbromide ($PyHBr_3$) (7.00 g, 22 mmol) in CH_2Cl_2 (600 mL) and glacial HOAc(50 mL). After stirring (4 h at 25°C), the solution was washed and worked up (as above for **2**) to give **3** (5.0 g, 90%). Two recrystallizations (ether) gave **3** as prisms, mp 90–91°C; ir: 3040 (m) 1680 (vs), 1590 (m), 1320 (vs), 1270 (vs); ^1H nmr, δ: 3.35 (3H, s), 6.13 (1H, s), 7.5–8.2 (5H, m); ms, *m/z*: 278(1) 276(1) $M^{+\cdot}$, 198(1.5), 171(3), 169(3), 106(10), 105(100), 90(5), 89(4), 79(2), 77(26), 63(27). *Anal.* calcd. for $C_9H_9BrO_3S$: C 39.01, H 3.27, Br 28.8, S 11.57%; found: C 38.93, H 3.27, Br 27.7, S 11.14%.

Hydrolyses of 2 or 3 in aqueous alkali

A mixture of either **2** or **3** (10 mmol) and 10% aqueous NaOH (100 mL) was stirred at room temperature for 2 h. Extraction with

[8] It should be noted that these speculations assume reaction through the major conformer. Obviously, the Curtin–Hammett principle (43) needs to be considered in making such a postulation.

[9] This possibility has been considered previously (15), but ruled out due to the high reactivity of α-sulfonyl carbanions with hydroxylic solvents. However, it is possible for reaction between the α-sulfonyl carbanions and the intermediate sulfenyl halide to occur before the latter has diffused out of the solvent cage.

CH_2Cl_2 (3 × 50 mL) gave, after routine processing, chloromethyl methyl sulfone, **4** (0.86 g, 68% from **2**) or bromomethyl methyl sulfone **5** (1.20 g, 70% from **3**); **4** had mp (from ether) 56°C (lit. (11) mp 57.2–58.2°C); ^{1}H nmr ($CDCl_3$) δ: 3.07 (s, 3H), 4.50 (s, 2H); **5** had mp (from ether) 34°C (lit. (46) mp 35°C); ^{1}H nmr ($CDCl_3$) δ: 3.17 (s, 3H), 4.48 (s, 2H); ms, *m/z*: 174 (7), 172 (7), 159 (4), 157 (4), 95 (88), 93 (97), 79 (11), 63 (100), 48 (11), 45 (12). The aqueous alkaline solutions from these reactions were acidified (HCl); routine processing gave pure (by ^{1}H nmr) benzoic acid (1.01 g, 82% from **2**; 1.03 g, 83% from **3**) which was recrystallized for comparison with an authentic sample.

*Reaction of **1** with sulfuryl chloride – triethylamine*

Sulfuryl chloride (0.32 mL, 4 mmol) was cautiously dropped into an ice-cooled solution of **1** (396 mg, 2 mmol) and Et_3N (0.6 mL, 4 mmol) in CH_2Cl_2 (25 mL). The solution was allowed to warm to room temperature and was then stirred for 12 h. Work-up, as described for the preparation of **2**, gave oily 2,2-dichloro-2-methylsulfonyl-1-phenylethanone, **6**, 490 mg (91%); ^{1}H nmr ($CDCl_3$) δ: 3.47 (s, 3H), 7.4–8.4 (m, 5H); the mass spectrum could not be recorded as the spectrum changed continually with time as the compound decomposed under electron impact.

Aqueous alkaline hydrolysis of the crude **6**, as described above, gave benzoic acid (184 mg, 82%) and dichloromethyl methyl sulfone, **7** (0.266 g, 88%); mp (ex CCl_4) 69–71°C (lit. (11) mp 72.0–72.3°C); ir: 3030 (m), 2960 (w), 2940 (w), 1340 (vs), 1330 (sh); ^{1}H nmr ($CDCl_3$) δ: 3.20 (s, 3H), 6.23 (s, 1H); ms, *m/z*: 164 (3.8), 162 (5.0), 149 (12), 147 (16), 85 (648), 83 (1000), 79 (102), 63 (143), 48 (372).

*Reaction of **1** with pyridinium bromide perbromide – pyridine*

A solution of **1** (396 mg, 2 mmol), and dry pyridine (2 mL) in CH_2Cl_2 (25 mL) was added slowly to $PyHBr_3$ (1.32 g, 4.13 mmol) in CH_2Cl_2 (50 mL). The mixture was stirred at 25°C for 12 h and then worked up as described for **2** to give an unstable crude product (567 mg, 88%) that was a mixture of **8** (0.58 mmol) and **9** (1.17 mmol) in a ratio of 1:2 respectively, from ^{1}H nmr ($CDCl_3$) δ: 3.30 (s, $Br_2CHSO_2CH_3$), 3.37 (s, $PhCOCBr_2SO_2CH_3$), 6.30 (s, $Br_2CHSO_2CH_3$), 7.47–8.47 (m, 5H). The total crude mixture was hydrolyzed in aqueous alkali as described above to give benzoic acid (87 mg, 0.71 mmol, 61% based on **8**) as the only alkali-soluble product and **5** (132 mg, 43% based on **8** and **9**) as the only isolable neutral product.

*Preparation of 1-methyl-2-phenylsulfonylethanone, **10***

Sodium benzenesulfinate and chloroacetone were reacted (47) in refluxing ethanol to give **10**, which was crystallized from ether to give plates, mp 53.3–55°C (lit. (47) mp 57–58°C); ir: 3030 (m), 1715 (s), 1585 (w), 1445 (m), 1325 (s), 1230 (s); ^{1}H nmr ($CDCl_3$) δ: 2.40 (s, 3H), 4.15 (s, 2H), 7.55–7.96 (m, 5H); ms, *m/z*: 198 (7), 156 (13), 141 (20), 134 (45), 125 (13), 91 (39), 77 (100).

*Preparation of 1-bromomethyl-2-phenylsulfonylethanone, **11***

A solution of **10** (396 mg, 2 mmol) in CH_2Cl_2 (10 mL) was added to a solution of $PyHBr_3$ (700 mg, 2.2 mmol) in CH_2Cl_2 (60 mL) and glacial acetic acid (10 mL). After stirring the orange-red solution at 25°C for 5 h, work-up as described above gave **11** (500 mg, 90%), mp (colourless needles from ether) 90.0–90.5°C; ir: 3030 (m), 2940 (w), 1730 (s), 1580 (w), 1330 (s), 1300 (sh); ^{1}H nmr ($CDCl_3$) δ: 4.16 (s, SO_2—CH_2—CO—), 4.41 (s, —CH_2Br), 7.6–8.2 (m, 5H); ms, *m/z*: 278 (3), 276 (3), 214 (1), 212 (1), 197 (6), 183 (16), 141 (49), 125 (9), 95 (3), 93 (3), 91 (6), 77 (100), 51 (41), 42 (11).

*Preparation of 2-bromo-1-methyl-2-phenylsulfonylethanone, **12***

Bromination of **10** (2 mmol) with $PyHBr_3$ (2.2 mmol) in CH_2Cl_2 (60 mL) containing pyridine (2 mL) gave **12** (503 mg, 90%) as a brown oil which could not be purified, ^{1}H nmr ($CDCl_3$) δ: 2.60 (s, 3H), 5.18 (s, 1H), 7.6–8.2 (m, 5H); ms, *m/z*: 278 (13), 276 (13), 236 (18), 234 (18), 171 (5), 169 (5), 141 (44), 125 (7), 77 (100).

Hydrolysis of **12** in aqueous alkali (*vide supra*) gave bromomethyl phenyl sulfone, **13** (390 mg, 91%), mp (ether–hexane) 49–50°C (lit. (48) mp 50–52°C); ^{1}H nmr ($CDCl_3$) δ: 4.50 (s, 2H), 7.60–8.27 (m, 5H).

*Preparation of 2,2-dibromo-1-methyl-2-phenylsulfonylethanone, **14***

Bromination of **10** (2 mmol) with $PyHBr_3$ (4.4 mmol) in CH_2Cl_2 (60 mL) and pyridine (2 mL) gave **14** (677 mg, 95%) as an unstable brown-tinged syrup; ^{1}H nmr ($CDCl_3$) δ: 2.78 (s, 3H), 7.47–8.17 (m, 5H); $M^{+\cdot}$ at *m/z* 358, 356, and 354 (39:87:41).

Hydrolysis of this oil in aqueous alkali (same conditions as above) gave a mixture of **13** and **15** (510 mg) in a ratio of 56:44 (by nmr); ^{1}H nmr ($CDCl_3$) δ: 4.50 (s, —CH_2Br), 6.33 (s, —$CHBr_2$), 7.62–8.62 (m, 5H).

*Reaction of **10** with sulfuryl chloride in dichloromethane – acetic acid*

Sulfuryl chloride (0.2 mL, 2.5 mmol) was dropped into an ice-cold solution of **10** (396 mg, 2 mmol) in CH_2Cl_2–HOAc (20 mL, 1:1). After stirring at 25°C for 4 h the reaction mixture was worked up as before to give an oily mixture of products (430 mg) which consisted of **16** and **17** (9:2, by nmr); ^{1}H nmr ($CDCl_3$) δ: 2.55 (s, —$COCH_3$), 4.42 (s, —CH_2—CO—CH_2Cl), 5.22 (s, —SO_2—$CHCl$—CO—), 7.25–8.25 (m, 5H).

*Preparation of 2,2-dichloro-1-methyl-2-phenylsulfonylethanone, **18***

An ice-cold solution of **10** (2 mmol) in CH_2Cl_2 (30 mL), containing Et_3N (0.6 mL, 4 mmol) was chlorinated for 3 h with SO_2Cl_2 (0.32 mL, 4 mmol). Work-up as before gave **18** as an unstable, brown-tinged oil (509 mg, 95%), ^{1}H nmr ($CDCl_3$) δ: 2.73 (s, 3H), 7.55–8.12 (m, 5H).

The crude **18** was hydrolyzed with aqueous alkali (*vide supra*) to give dichloromethyl phenyl sulfone, **19** (331 mg, 77%), mp (CH_2Cl_2–hexane) 79–81°C (lit. (49) mp 81.5–83.0°C); ^{1}H nmr ($CDCl_3$) δ: 6.10 (s, 1H), 7.5–8.1 (m, 5H); ms, *m/z*: 226 (0.8), 224 (1.1), 191 (0.5), 189 (0.8), 162 (2.0), 160 (4.0), 156 (3), 141 (54), 125 (9), 85 (6), 83 (9), 77 (100).

Acknowledgements

We thank the Natural Sciences and Engineering Research Council of Canada for financial support (to J.S.G. and T.S.C.) and an undergraduate summer award (to G.H.G.). The Government of India awarded a scholarship for overseas study (to P.K.D.), Dr. D. L. Hooper kindly provided nmr spectra, and K. Jochem gave technical assistance.

1. P. D. MAGNUS. Tetrahedron, **33**, 2019 (1977).
2. T. DURST. *In* Comprehensive organic chemistry. Vol. 3. *Edited by* D. N. Jones. Pergamon, Oxford. 1979. pp. 197–213.
3. H. O. HOUSE and J. K. LARSON. J. Org. Chem. **33**, 61 (1968).
4. B. M. TROST and J. E. VINCENT. J. Am. Chem. Soc. **102**, 5680 (1980); B. M. TROST and B. R. ADAMS. J. Am. Chem. Soc. **105**, 4849 (1983).
5. D. DILLER and F. BERGMANN. J. Org. Chem. **37**, 2147 (1972).
6. J. FICINI and G. STORK. Bull. Soc. Chim. Fr. 723 (1964).
7. F. BOHLMANN and G. HAFFER. Chem. Ber. **102**, 4017 (1969).
8. A. J. WARING. *In* Comprehensive organic chemistry. Vol. 1. *Edited by* J. F. Stoddart. Pergamon, Oxford. 1979. pp. 1036–1039.
9. J. S. GROSSERT and P. K. DUBEY. J. Chem. Soc. Chem. Commun. 1183 (1982).
10. L. F. FIESER and M. FIESER. Reagents for organic synthesis. **1**, 967 (1967); **5**, 568 (1975).
11. W. E. TRUCE, B. H. BIRUM, and E. T. MCBEE. J. Am. Chem. Soc. **74**, 3594 (1952).
12. L. A. PAQUETTE. Org. React. **25**, 28 (1977); F. G. BORDWELL, E. B. HOYT, JR., B. B. JARVIS, and J. M. WILLIAMS, JR. J. Org. Chem. **33**, 2030 (1968).
13. P. DEL BUTTERO and S. MAIORANA. Gazz. Chim. Ital. **103**, 809 (1973).
14. L. CHIODINI, L. GARANTI, and G. ZECCHI. Synthesis, 603 (1978).
15. F. G. BORDWELL and B. B. JARVIS. J. Org. Chem. **33**, 1182 (1968).
16. J. H. BOWIE, D. H. WILLIAMS, S.-O. LAWESSON, J. O. MADSEN, C. NOLDE, and G. SCHROLL. Tetrahedron, **22**, 3515 (1966);

Can. J. Chem. Downloaded from www.nrcresearchpress.com by 210.87.254.6 on 09/06/12
For personal use only.

R. A. KHMEL'NITSKII and YU. A. EFREMOV. Russ. Chem. Rev. **46**, 46 (1977).
17. J. S. GROSSERT and M. M. BHARADWAJ. J. Chem. Soc. Chem. Commun. 144 (1974).
18. J. S. GROSSERT, M. M. BHARADWAJ, R. F. LANGLER, T. S. CAMERON, and R. E. CORDES. Can. J. Chem. **56**, 1183 (1978).
19. J. S. GROSSERT, D. L. HOOPER, and W. N. NEAVES. Can. J. Chem. **59**, 326 (1981).
20. H. GÜNTHER. NMR spectroscopy. Wiley, New York. 1980. pp. 95–96.
21. F. W. WEHRLI and T. WIRTHLIN. Interpretation of carbon-13 NMR spectra. Heyden, London. 1976. Chapt. 2.
22. J. B. LAMBERT and A. R. VAGENAS. Org. Magn. Reson. **17**, 265 (1981); **17**, 270 (1981).
23. R. J. J. VISSER, A. VOS, and J. B. F. N. ENGBERTS. J. Chem. Soc. Perkin Trans. 2, 634 (1978); O. EXNER and J. F. B. N. ENGBERTS. Collect. Czech. Chem. Commun. **44**, 3378 (1979), and references therein.
24. SPECTRUM #295. *In* Selected ^{13}C nuclear magnetic resonance spectral data. Thermodynamics Research Center Data Project, Texas A and M University, College Station, Texas. Oct. 31, 1976.
25. F. G. BORDWELL and E. DOOMES. J. Org. Chem. **39**, 2526 (1974).
26. I. HARGITTAI. Sulphone molecular structures (Lecture Notes in Chemistry, #6). Springer Verlag, Berlin. 1978.
27. G. D. ANDREETTI, G. BOCELLI, and P. SGARABOTTO. Cryst. Struct. Commun. **2**, 519 (1973).
28. W. SAENGER and C. H. SCHWALBE. J. Org. Chem. **36**, 3401 (1971).
29. T. S. CAMERON and R. E. CORDES. Acta Crystallogr. Sect. B, **35**, 748 (1979).
30. INTERNATIONAL TABLES FOR X-RAY CRYSTALLOGRAPHY. Vol. III. The Kynoch Press, Birmingham, England. 1962.
31. G. SHELDRICK. X-ray system report. University Chemical Laboratory, Lensfield Road, Cambridge, England. 1976.
32. Y. BARRANS and J.-J. MAISSEU. C. R. Acad. Sci. Ser. C, **262**, 91 (1966).
33. R. C. IVEY and M. I. DAVIS. J. Chem. Phys. **57**, 1909 (1972); L. S. BARTELL and L. O. BROCKWAY. J. Chem. Phys. **23**, 1860 (1955).
34. J. S. GROSSERT, M. M. BHARADWAJ, J. B. FAUGHT, and A. TERZIS. Can. J. Chem. **58**, 1106 (1980).
35. R. J. BOYD and J. P. SZABO. Can. J. Chem. **60**, 730 (1982).
36. L. J. BELLAMY. The infrared spectra of complex molecules. 3rd ed. Chapman and Hall, London. 1975. pp. 157–159.
37. F. G. BORDWELL and W. T. BRANNEN, JR. J. Am. Chem. Soc. **86**, 4645 (1964).
38. B. B. JARVIS and P. E. NICHOLAS. J. Org. Chem. **45**, 2265 (1980).
39. P. ROBSON, P. R. H. SPEAKMAN, and D. G. STEWART. J. Chem. Soc. (C), 2180 (1968); R. F. LANGLER and J. A. PINCOCK. Can. J. Chem. **55**, 2316 (1977); D. G. KAY; R. F. LANGLER, and J. E. TRENHOLM. Can. J. Chem. **57**, 2185 (1979), and references therein.
40. W. FORSTER and R. M. LAIRD. J. Chem. Soc. Perkin Trans. 2, 135 (1982); T. H. LOWRY and K. S. RICHARDSON. Mechanism and theory in organic chemistry. 2nd ed. Harper and Row, New York. 1981. p. 347.
41. A. HALVORSEN and J. SONGSTAD. J. Chem. Soc. Chem. Commun. 327 (1978); R. SESHADRI, W. J. PEGG, and M. ISRAEL. J. Org. Chem. **46**, 2596 (1981).
42. A. BRUGGINK, B. ZWANENBURG, and J. B. F. N. ENGBERTS. Tetrahedron, **27**, 4571 (1971); K. HOVIUS and J. B. F. N. ENGBERTS. Tetrahedron Lett. 2477 (1972).
43. J. I. SEEMAN. Chem. Rev. **83**, 84 (1983).
44. E. J. COREY and M. CHAYKOVSKY. J. Am. Chem. Soc. **87**, 1345 (1965).
45. W. E. TRUCE and R. H. KNOSPE. J. Am. Chem. Soc. **77**, 5063 (1955).
46. H. BÖHME, H. FISCHER, and R. FRANK. Justus Liebigs Ann. Chem. **563**, 54 (1949).
47. R. OTTO and W. OTTO. J. Prakt. Chem. [2]**36**, 401 (1887); cf. Beilsteins Handbuch der organischen Chemie, VI, 307 (1923); D. F. TAVARES, W. I. O'SULLIVAN, and C. R. HAUSER. J. Org. Chem. **27**, 1251 (1962); R. L. CRUMBIE, B. S. DEOL, J. E. NEMORIN, and D. D. RIDLEY. Austr. J. Chem. **31**, 1965 (1978).
48. A. N. NESMEYANOV, D. N. KRAVTSOV, B. A. FAINGOR, and L. I. PETROVSKAYA. Izv. Akad. Nauk SSR, Ser. Khim (3), **534** (1968); Chem. Abstr. **69**, 67507 p. (1968).
49. W. MIDDELBOS, J. STRATING, and B. ZWANENBURG. Tetrahedron Lett. 351 (1971).

Can. J. Chem. Downloaded from www.nrcresearchpress.com by 210.87.254.6 on 09/06/12
For personal use only.

Spectroscopic and structural studies of some bisdithiocarbamates and cyclic thiones

THOMAS C. W. MAK

Department of Chemistry, The Chinese University of Hong Kong, Shatin, New Territories, Hong Kong

AND

KHALID S. JASIM AND CHUNG CHIEH

Guelph–Waterloo Centre for Graduate Work in Chemistry, University of Waterloo, Waterloo, Ont., Canada N2L 3G1

Received July 6, 1983

THOMAS C. W. MAK, KHALID S. JASIM, and CHUNG CHIEH. Can. J. Chem. **62**, 808 (1984).

The syntheses of bisdithiocarbamates from diamines and CS_2 are described, and possible complications in these reactions explained. Ethylenebisdithiocarbamate was prepared from ethylenediamine and CS_2 in basic solution, but the same reaction using *o*-phenylenediamine led to a cyclization product, *o*-phenyleneimidazolidine-2-thione or benzimidazolidine-2-thione. In these reactions, if slightly insufficient amounts of CS_2 are used, bisdithiocarbamates will not be formed; instead, the cyclization reactions will occur, leading to the formation of thiones. Crystallographic studies were carried out for disodium ethylenebisdithiocarbamate and imidazolidine-2-thione or ethylenethiourea. The hexahydrate crystals of the former, $Na_2[S_2CNHCH_2CH_2NHCS_2]\cdot 6H_2O$, F.W. 364.42, are triclinic with a = 5.766(1), b = 7.212(1), c = 10.074(1) Å, α = 88.53(1), β = 98.41(1), γ = 105.50(1)°, V = 399.3(1) Å^3, and Z = 1. The structure was determined from 2259 unique reflections, (2θ[Mo-Kα] < 65°) to an R factor of 0.022. The bisdithiocarbamate ion has a center of symmetry between the two CH_2 groups, and therefore the two NCS_2^{2-} groups are separated as far apart as possible. Each Na^+ ion is octahedrally surrounded by five water molecules with Na...O distances ranging from 2.373 to 2.446 Å, and a sulphur atom of the thiocarbamate group with Na...S = 3.060 Å. The two C—S bonds of the CS_2^- group are 1.710(1) and 1.727(1) Å, and ∠SCS = 121.9(1)°. Crystals of imidazolidine-2-thione, $(CH_2NH)_2CS$, are monoclinic, with a = 5.800(1), b = 14.516(3), c = 5.780(1) Å, β = 101.33(2)°, V = 477.2(2) Å^3, and Z = 4. This structure, first determined thirty years ago, has been refined by full-matrix least-squares to R = 0.031, using 975 new Mo-Kα data.

THOMAS C. W. MAK, KHALID S. JASIM et CHUNG CHIEH. Can. J. Chem. **62**, 808 (1984).

On décrit des synthèses de bisdithiocarbamates à partir de diamines et de sulfure de carbone; on explique certaines complications possibles dans ces réactions. On a préparé l'éthylènebisdithiocarbamate à partir de l'éthylènediamine et du sulfure de carbone en milieu alcalin; toutefois, la même réaction appliquée à l'*o*-phénylènediamine conduit à un produit de cyclisation, l'*o*-phénylèneimidazolidinethione-2 ou benzimidazolidinethione-2. Dans ces réactions, si on utilise une quantité légèrement déficiente de sulfure de carbone, les bisdithiocarbamates ne se forment pas; les réactions de cyclisation se produiront alors de préférence et il y aura formation des thiones. On a effectué des études cristallographiques sur l'éthylènebisdithiocarbamate de disodium et sur l'imidazolidinethione-2 ou éthylène thiourée. Les cristaux hexahydratés du premier, $Na_2[S_2CNHCH_2CH_2NHCS_2]\cdot 6H_2O$, P.M. = 364,42, sont tricliniques, a = 5,766(1), b = 7,212(1), c = 10,074(1) Å, α = 88,53(1), β = 98,41(1), γ = 105,50(1)°, V = 399,3(1) Å^3 et Z = 1. On a affinée la structure jusqu'à une valeur de R = 0,022 pour 2259 réflexions uniques (2θ[Mo-Kα] < 65°). L'ion bisdithiocarbamate a un centre de symétrie entre les deux groupements méthylènes et la séparation entre les deux groupements NCS_2^{2-} est donc maximale. Chaque cation de sodium est entouré du façon octaédrique par cinq molécules d'eau (les distances Na...O varient de 2,373 à 2,446 Å) et par un atome de soufre du groupement thiocarbamate (distance Na...S = 3,060 Å). Les longueurs des deux liaisons C—S du groupement CS_2^- sont respectivement 1,710(1) et 1,727(1) Å alors que ∠SCS = 121,9(1)°. Les cristaux de l'imidazolidinethione-2, $(CH_2NH)_2CS$, sont monocliniques, a = 5,800(1), b = 14,516(3), c = 5,780(1) Å, β = 101,33(2)°, V = 477,2(2) Å^3 et Z = 4. Cette structure, qui a été déterminée pour la première fois il y a trente ans, a été affinée par la méthode des moindres carrés (matrices complètes) jusqu'à une valeur de R = 0,031 en faisant appel à 975 nouvelles données Mo-Kα.

[Traduit par le journal]

Introduction

Although the reaction of ethylenediamine with CS_2 was reported by Hofmann in 1872 (1), the disodium salt of ethylenebisdithiocarbamate, Na_2(Hbisdtc), was not prepared in the pure state until 1943 (2), and its crystal and molecular structure has not been elucidated till now. Shah and Jones (3) claimed the preparation of *o*-phenylenebisdithiocarbamate from the reaction of *o*-phenylenediamine, CS_2, and NaOH; however, neither elemental analysis nor spectroscopic data for this compound was reported. We tried the same reaction, but failed to obtain the bisdithiocarbamate; instead, the reaction always gave a thione as a cyclization by-product.

The formation of thiones from similar reactions of diamine and CS_2 in acidic medium has been reported (4), but we found that the cyclization reactions can be promoted purely by putting insufficient amounts of CS_2 in the reaction flasks in basic media. The production of *N,N'*-dimethylimidazolidine-2-thione has been observed under various conditions (5) and its structure has been determined (6).

This paper reports the first structure determination of a bisdithiocarbamate. The crystal structure of imidazolidine-2-thione, commonly known as ethylenethiourea, was determined by Wheatley (7) in 1953 by means of successive three-dimensional differential syntheses, using photographic data when electronic computers were in their infancy; however, the structure was determined carefully and accurately, to an R of 0.12. It would be interesting to compare results obtained then with those based on least-squares refinement using new diffractometer data.

Our attempt to prepare various bisdithiocarbamates has led to an improvement of the synthetic method and a better understanding of their chemistry. The lack of success in the preparation of a bisdithiocarbamate from *o*-phenylenediamine and CS_2 in an alkaline solution will be explained.

Experimental

Infrared spectra were recorded as 2% KBr and CsBr disks on the

Can. J. Chem. Downloaded from www.nrcresearchpress.com by 210.87.254.105 on 09/06/12
For personal use only.

TABLE 1. Crystal data and parameters pertaining to structural analyses

Molecular formula	$Na_2[S_2CNHCH_2]_2 \cdot 6H_2O$	$(CH_2NH)_2CS$
Molecular weight	364.42	102.15
Cell constants	a = 5.766(1)	a = 5.800(1) [5.774](7)
	b = 7.212(1)	b = 14.516(3) [14.540]
	c = 10.074(1)	c = 5.780(1) [5.801]
	α = 88.53°(1)	
	β = 98.41°(1)	β = 101.33°(2) [101.3°]
	γ = 105.50°(1)	
	V = 399.3(1)	V = 477.2(2)
	Z = 1	Z = 4
Density (calcd.)	1.516 g cm^{-3}	1.422 g cm^{-3}
Density (measured)	1.518 g cm^{-3}	1.417 g cm^{-3}
Space group	$P1$	$p2_1/c$
Radiation	Graphite-monochromatized MoKα, λ = 0.71069 Å	
Absorption coefficient	6.38 cm^{-1}	4.90 cm^{-1}
Mean μr	0.13	0.10
Transmission factors	0.689–0.836	0.785–0.953
Scan type and speed	ω–2θ; 2.02–8.37 deg min^{-1}	
Scan range	1° below Kα_1 to 1° above Kα_2	
Background counting	Stationary counts for one-half of scan time at each end of scan	
2θ max	65°	54°
Unique data measured	2259	1016
Observed data with $\|F\| > 3\sigma(\|F\|)$ used in analysis, n	2134	975
Number of variables, p	109	73
$R = \Sigma\|\|F_o\| - \|F_c\|\|/\Sigma\|F_o\|$	0.022	0.031
Weighting scheme	$w = [\sigma^2(F) + 0.0002\,\sigma\|F\|^2]^{-1}$	
$R_w = [\Sigma w(\|F_o\| - \|F_c\|)^2/\Sigma w\|F_o\|^2]^{1/2}$	0.035	0.047
$S = [\Sigma w(\|F_o\| - \|F_c\|)^2/(n-p)]^{1/2}$	1.88	2.57
Highest residual peak	0.29 e $Å^{-3}$	0.31 e $Å^{-3}$
Crystal size	0.24 × 0.38 × 0.40 mm	0.20 × 0.40 × 0.45
No. of very strong reflections omitted from analyses	5	2

following instruments: Beckman Acculab 10, and Perkin–Elmer 457 and 180. The ^1H and ^{13}C nmr spectra were recorded on a Brüker WP-80 FT nmr spectrometer. Elemental analyses were carried out by Guelph Chemical Laboratories Ltd. Reagent grade chemicals were used without further purification except where specified.

Prepartion of disodium ethylenebisdithiocarbamate

Disodium ethylenebisdithiocarbamate was prepared by a modification of the literature method (8) by adding CS_2 drop-wise to a basic solution of ethylenediamine. The reaction mixture was stirred for three hours in a water bath at 308–318 K, cooled to room temperature, and separated into two layers by the addition of excess acetone. The top acetone layer was discarded; the lower one was stirred again with additional acetone until crystallization occurred. The liquid phase was decanted and reserved, whereas the solid residue was dissolved in a minimum amount of water and again treated with acetone. This treatment was repeated 5 to 10 times until a colorless or pale yellow solution was obtained from which slow evaporation yielded colorless plate-like crystals of $Na_2(Hbisdtc) \cdot 6H_2O$. Some white particles suspended in the acetone wash were collected and subsequently shown to be identical to the sample from crystallization. Since we have determined the crystal structure, no elemental analysis was performed. The ^1H nmr (80 MHz, D_2O) consisted of δ: 3.71 (CH_2, s) ppm and the ^{13}C nmr (80 MHz, D_2O), δ: 49.10 (CH_2) and 214.69 (CS_2) ppm.

Preparation of imidazolidine-2-thione

Imidazolidine-2-thione was prepared according to the method for its *N,N'*-dimethyl analogue, as described in ref. 5. The ^1H nmr (80 MHz, D_2O) consisted of δ: 3.62 (CH_2, s) ppm and ^{13}C nmr δ: 46.42 (CH_2) ppm in acetone-d_6 and 47.01 ppm in D_2O.

Attempts to prepare disodium o*-phenylenebisdithiocarbamate*

Attempts to prepare *o*-phenylenebisdithiocarbamate by the same method (3) were not successful. Application of the modified procedure used for the ethylenebisdithiocarbamate also failed to produce the desired compound. In prolonged reactions, a white powder was obtained and identified as Na_2CO_3. A detailed account of these reactions will be given later (see Results and discussion).

Preparation of benzimidazolidine-2-thione

When 8 mL (0.13 mol) CS_2 was added dropwise to a mixture of 13.5 g (0.125 mol) of *o*-phenylenediamine and 5 g (0.125 mol) of NaOH in 200 mL of water at room temperature, in a three-necked flask equipped with dropping funnel and a mercury-sealed condenser, during a period of 30 min, there was a visible but slow reaction. The temperature was then slowly increased to 303–313 K while stirring continued, but the reaction rate was not much faster and eventually the temperature was raised to a gentle reflux for 30 min. The solid formed was filtered, washed with water, and dried under vacuum over silica gel. The ^1H nmr (80 MHz, acetone-d_6) showed δ: 7.22 (CH), 7.20 (CH), 2.85 (NH) ppm, and ^{13}C (80 MHz, acetone-d_6) δ: 110.14 (CH), 123.20 (CH), 133.27 (C), and 170.67 (CS) ppm. *Anal.* calcd. for $C_7H_6N_2S$: C 56.00, H 4.00, N 18.67; found: C 55.98, H 4.14, N 18.35.

Crystallographic studies

As crystals of disodium ethylenebisdithiocarbamate hexahydrate, $Na_2(S_2CNHCH_2CH_2NHCS_2) \cdot 6H_2O$, rapidly turn opaque in air, a specimen for diffraction work was sealed in a Lindemann glass capillary. Suitable crystals of the two compounds were selected and then centered on a Nicolet R3m automatic diffractometer. The determinations of the crystal class, orientation matrix, and accurate cell dimensions were performed according to standard procedures (9). Crystal data and parameters used in the structural determination are given in Table 1.

Normalized structure factors were calculated from $|F_o|$ values and

Can. J. Chem. Downloaded from www.nrcresearchpress.com by 210.87.254.105 on 09/06/12
For personal use only.

Can. J. Chem. Downloaded from www.nrcresearchpress.com by 210.87.254.105 on 09/06/12
For personal use only.

TABLE 2. Atom coordinates ($\times 10^4$) and temperature factors ($Å^2 \times 10^3$) of $Na_2(Hbisdtc)\cdot 6H_2O$

Atom	x	y	z	U
Na	2364(1)	−4467(1)	4084(1)	36(1)*
S(1)	−4253(1)	−3322(1)	1069(1)	32(1)*
S(2)	−4217(1)	−681(1)	3336(1)	29(1)*
C(1)	−3358(2)	−1095(1)	1822(1)	24(1)*
N	−2012(2)	374(1)	1215(1)	29(1)*
C(2)	−1195(2)	279(2)	−78(1)	31(1)*
O(1)	4079(2)	−3856(1)	6331(1)	39(1)*
O(2)	−75(2)	−2713(1)	4917(1)	37(1)*
O(3)	257(2)	−5370(1)	1854(1)	41(1)*
HN	−1521(28)	1374(23)	1577(16)	40
H(C21)	−983(27)	1562(21)	−499(15)	40
H(C22)	−2464(28)	−634(22)	−596(15)	40
H(O22)	4956(32)	−2761(25)	6466(17)	50
H(O12)	4440(31)	−4488(26)	6989(18)	50
H(O21)	809(30)	−1876(23)	5448(18)	50
H(O22)	−1016(31)	−2165(23)	4513(18)	50
H(O31)	−697(32)	−4811(25)	1522(18)	50
HO32)	1229(33)	−5082(26)	1480(18)	50

*Equivalent isotropic U defined as one-third of the trace of the orthogonalized U_{ij} tensor.

TABLE 3. Atom coordinates ($\times 10^4$) and thermal parameters ($Å^2 \times 10^3$) for $[(CH_2)NH]_2CS$

Atom	x	y	z	U
S	2739(1)	1141(1)	4560(1)	46(1)*
C(1)	448(3)	1191(1)	2246(3)	35(1)*
C(2)	−1919(3)	1674(1)	−1269(3)	46(1)*
C(3)	−3173(3)	911(3)	−191(3)	45(1)*
N(1)	279(2)	1765(1)	428(2)	46(1)*
N(2)	−1475(3)	676(1)	1938(3)	53(1)*
HC(21)	−2837(33)	2253(16)	−1470(38)	60
HC(22)	−1653(32)	1504(15)	−2778(39)	60
HC(31)	−4686(39)	1121(13)	204(42)	60
HC(32)	−3373(34)	346(15)	−1252(38)	60
HN(1)	1237(37)	2144(15)	366(36)	60
HN(2)	−1651(35)	294(15)	2835(38)	60

*Equivalent isotropic U defined as one-third of the trace of the orthogonalized U_{ij} tensor.

the statistical distributions of the $|E|$ values for both compounds were consistent with those of centrosymmetric crystals. Both structures were solved by direct method and the positions of the non-hydrogen atoms were found from the E-maps. The coordinates and anisotropic temperature factors were then refined by full-matrix least-squares methods, using the SHELXTL program package (10, 11) on a General Corporation Nova 3/12 minicomputer. All hydrogen atoms appeared on a difference map; they were assigned isotropic thermal parameters and their positions were varied in the least-squares cycles. Analytic expressions of neutral-atom scattering factors (12, 13) were employed. Atomic parameters for the two compounds are given in Tables 2 and 3 respectively.[1]

Results and discussion

Disodium ethylenebisdithiocarbamate, $Na_2(Hbisdtc)$, is very soluble in water but only sparingly so in dry acetone, dichloromethane, chloroform, and ethanol. The solubility difference in water and acetone was fully exploited in the separation of $Na_2(Hbisdtc)$ from the reaction mixture which contained an excess of NaOH. The dried solid sample is very unstable and decomposes at room temperature, 295 K, to isothiocyanate. After a day, its ir spectrum exhibits the two characteristic bands of isothiocyanate: N=C=S at 2080 cm^{-1} and C=N at 1620 cm^{-1} (14). Imidazolidine-2-thione and benzimidazolidine-2-thione are insoluble in benezene, toluene, and aliphatic hydrocarbons, but are soluble in chlorinated solvents, ethanol, and acetone. In water, the solubility of the former increases rapidly with temperature, whereas the latter is insoluble in both cold and hot water.

The two thiones are thermally very stable; samples heated at temperatures ranging from 293 to 513 K showed no change in their ir spectra. Heating of $Na_2(Hbisdtc)$ accelerated its decomposition to isothiocyanate, rather than to thione as in the case of its group IIB metal complexes (15).

The low yield (50–60%) of $Na_2(Hbisdtc)$ is probably due to the following reasons. (*a*) In basic medium, the alkali metal dithiocarbamates formed from primary amines may decompose according to the reaction:

$$(CH_2—NH—CS_2Na)_2 \rightarrow (CH_2—NCS)_2 + H_2S + Na_2S$$

(*b*) During the course of the reaction, the sulphide ion S^{2-} resulting from (*a*) reacts with CS_2:

$$Na_2S + CS_2 \rightarrow Na_2CS_3$$

thereby reducing its availability for bisdithiocarbamate production. The formation of Na_2CS_3 can easily be seen from its orange colour in the reaction mixture.

We were not able to prepare *o*-phenylenebisdithiocarbamate by the method of reference (3), nor by the modified procedure used for $Na_2(Hbisdtc)$. In all preparative attempts in a nitrogen atmosphere, benzimidazolidine-2-thione and Na_2CS_3 were the products. The instability may be due to the constrained proximity of the two NCS_2^- groups leading to the cyclization:

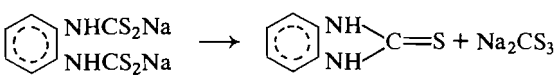

The release of the S^{2-} species is obvious from the odor released during the reaction, and from the subsequent lead acetate paper test. If the reaction mixture is exposed to air for a prolonged period, the Na_2CS_3 so formed is hydrolyzed to Na_2CO_3, by the reaction (15):

$$2Na_2CS_3 + 2H_2O + O_2 \rightarrow Na_2CO_3 + Na_2S_2O_3 + CS_2 + H_2S$$

We expected the white powder in the mixture to be the bisdithiocarbamate, but elemental and spectroscopic analyses confirmed it as Na_2CO_3. The imidazolidine-2-thione was identified by its ir and nmr spectra.

Selected ir and Raman bands for three thiones and two bisdithiocarbamates are given in Table 4. Assignments of these bands were made with reference to the literature (16, 17). The N—H stretching frequencies in $CHCl_3$ are higher by about 210 cm^{-1} than those observed in the solid state, due to the presence of hydrogen bondings. For $Na_2(Hbisdtc)\cdot 6H_2O$, the N—H stretching came close to that of the hydrated water molecules and the assignment became ambiguous. On the whole, the RN—C stretching frequencies are lower for compounds with a methyl or phenylene group attached to the N than those with a H atom. The same is also observed for the C=S stretching for the thiones, but the reverse is observed for the C=S symmetric or asymmetric stretching frequencies for the bisdithiocarba-

[1] A complete set of data is available, at a nominal charge, from the Depository of Unpublished Data, CISTI, National Research Council of Canada, Ottawa, Ont., Canada K1A 0S2.

TABLE 4. Selected infrared and Raman absorption bands*

Compound	ν(N—H)		ν(RN—C)		ν_s(C—S)		ν_a(C—S)	
	$CHCl_3$	Solid state	ir	Raman	ir	Raman	ir	Raman
Na_2(Hbisdtc)·$6H_2O$	3250	3190 s, sh	1500 s, b	1495 s	1040 s	1045 s	560 vb	610 m
					950 s	945 s	$\Delta \approx 50$	
Na_2(Mebisdtc)			1475 s, b	1475 s	1070 s	1015 s	575 s	590 m
					968 s	933 s	535 s	570 s
$(CH_2NH)_2CS$	3440 s	3230 s, b	1510 s, b	1510 s	510 s			
$(C_6H_4)(NH)_2CS$	3340 s	3150 s	1475 s, b	1450 s	487 s			
		3090 s, sh						
$(CH_2NMe)_2CS$			1515 s, b		510 s			

*s, strong; b, broad; m, medium; v, very; sh, shoulder.

TABLE 5. Bond lengths and angles for Na_2(Hbisdtc)·$6H_2O$

Bond	Length (Å)	Bond	Angle (°)
(a) Bisdithiocarbamate dianion			
C(1)—S(1)	1.710(1)	S(1)—C(1)—S(2)	121.9(1)
C(1)—S(2)	1.727(1)	S(1)—C(1)—N	119.4(1)
C(1)—N	1.328(1)	S(2)—C(1)—N	118.7(1)
N—H(N)	0.780(2)	C(1)—N—C(2)	125.5(1)
N—C(2)	1.458(2)	C(1)—N—H(N)	120.0(1)
C(2)—C(2)*	1.522(3)	C(2)—N—H(N)	115.0(1)
		N—C(2)—C(2)*	111.5(1)
(b) Coordination geometry around the Na^+ ion			
Na...O(1)	2.446(1)	O(1)—Na—O(3)	173.5(1)
Na...O(2)	2.373(1)	O(2)*—Na—S(2)*	169.4(1)
Na...O(3)	2.409(1)	O(1)*—Na—O(2)	168.9(1)
Na...O(1)*	2.410(1)	O(1)—Na—O(2)	83.6(1)
Na...O(2)*	2.396(1)	O(1)—Na—O(2)*	83.9(1)
Na...S(1)*	3.060(2)	O(1)—Na—O(1)*	85.2(1)
		O(1)—Na—S(2)*	85.5(1)
Na...Na*	3.421(1)	O(3)—Na—O(2)	102.5(1)
Na...Na*	3.574(1)	O(3)—Na—O(2)*	93.8(1)
		O(3)—Na—O(1)*	88.7(1)
Na—O(1)—Na*	94.8(1)	O(3)—Na—S(2)*	96.8(1)
Na—O(2)—Na*	91.7(1)	O(2)—Na—O(2)*	88.3(1)
		O(2)—Na—S(2)*	89.6(1)
		O(1)*—Na—O(2)*	90.4(1)
		O(1)*—Na—S(2)*	89.6(1)

*Symmetry related atoms.

mates. The presence of a doublet in the C=S stretching region in both the ir and Raman spectra of bisdithiocarbamates is a good indication that the C=S bonds are different in the CS_2^- group, and this is confirmed by the structural results.

Although the structures of many dithiocarbamates have been reported (18, 19), the configuration of ethylenebisdithiocarbamate, especially in its alkali metal salt, is of particular interest as it may change upon complexation with metal ions. The present study reveals that the Hbisdtc anion is centrosymmetric and the two NCS_2^- groups are separated as much as possible, an expected conformation. The bond lengths and angles for the bifunctional anion and other relevant data are given in Table 5, and an ORTEP plot of the anion is shown in Fig. 1. The two C—S bond lengths are significantly different, C(1)—S(1) 1.710(1), and C(1)—S(2) 1.727(1) Å. The difference may be a result of the weak interaction of Na...S(2) = 3.060 Å, but there is no close Na...S(1) contact in the crystal. Thus it is not surprising that two bands for C=S stretching were observed. This feature is also found in the crystal structure of dimethylammonium dimethyldithiocarbamate (18), in which the two C—S bonds are 1.706 and 1.715 Å. In this compound, the sulphur atom with two strong S...H—N hydrogen bonds has a longer distance than the one with one strong, and one weak S...H—N hydrogen bonds. Similar asymmetric bonding modes have also been observed in $Cu(S_2CN(CH_3)_2)_2$ (20) and other dithiocarbamate complexes (21).

Even though distorted, each sodium ion is surrounded octahedrally by the oxygen atoms of five water molecules at distances ranging from 2.373 to 2.446 Å, and by a sulfur atom from the dithiocarbamate with Na...S(2) = 3.060 Å. Two water molecules are bridged between two Na^+ ions, rather symmetrically, and the Na...O...Na angles are 91.7 and 94.8° respectively; see Table 5. The Na^+ ions are thus linked together forming chains with neighboring Na...Na distances of 3.421 and 3.574 Å. A packing diagram showing this relationship is given in Fig. 2.

The bond distances and angles for imidazolidine-2-thione

Can. J. Chem. Downloaded from www.nrcresearchpress.com by 210.87.254.105 on 09/06/12
For personal use only.

Can. J. Chem. Downloaded from www.nrcresearchpress.com by 210.87.254.105 on 09/06/12
For personal use only.

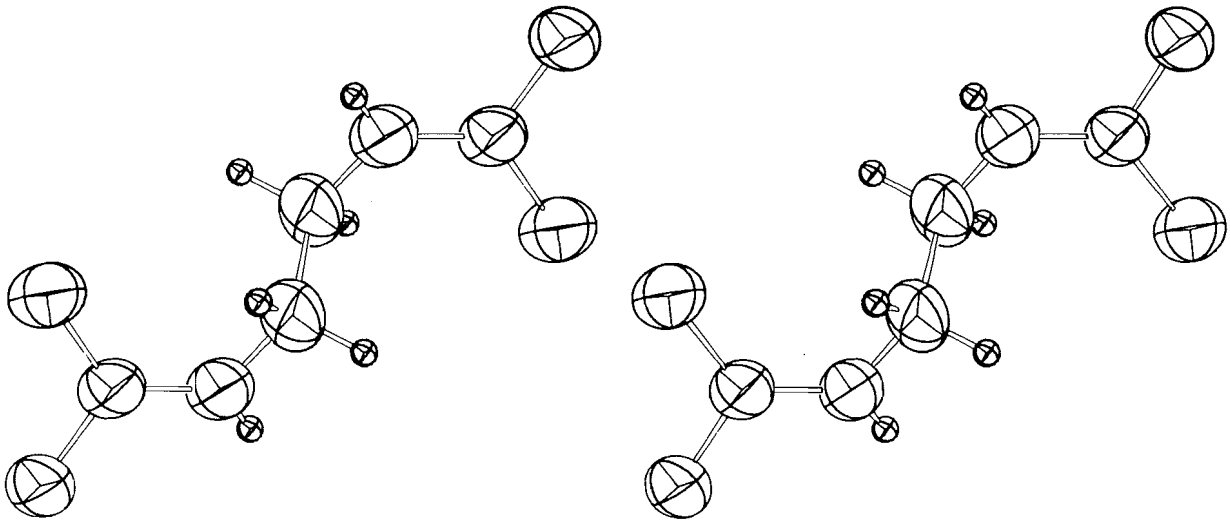

FIG. 1. An ORTEP plot of the ethylenebisdithiocarbamate ion.

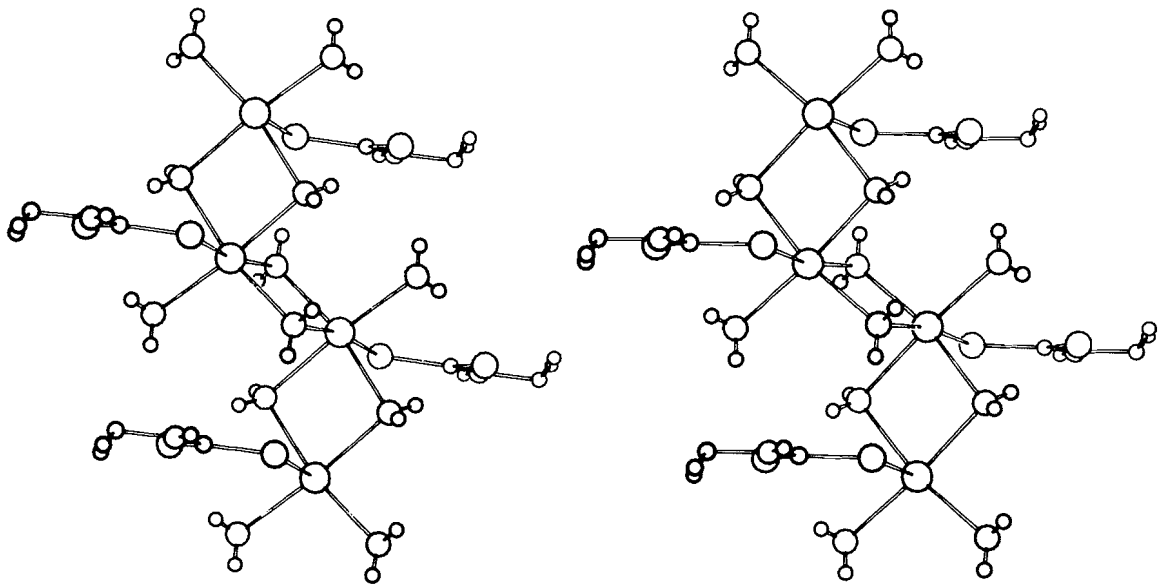

FIG. 2. Packing diagram showing the coordination around the sodium ion for $Na_2(Hbisdtc)\cdot 6H_2O$.

TABLE 6. Comparison of bond lengths (Å) and angles (°) for imidazolidine-2-thione

Bond	This work	Wheatley (7)
Lengths:		
C(1)—S	1.692(1)	1.708
C(1)—N(1)	1.330(2)	1.315
C(1)—N(2)	1.325(2)	1.328
mean	1.328	1.322
C(2)—N(1)	1.454(2)	1.480
C(3)—N(2)	1.457(2)	1.461
mean	1.456	1.470
C(2)—C(3)	1.524(3)	1.536
Angles:		
SC(1)N(1)	125.2(1)	123.5
SC(1)N(2)	126.3(1)	126.2
N(1)C(1)N(2)	108.6(1)	110.2
C(1)N(1)C(2)	113.2(1)	112.8
C(1)N(2)C(3)	113.1(1)	112.3
N(1)C(2)C(3)	102.5(1)	103.0
N(2)C(3)C(2)	102.6(1)	101.8

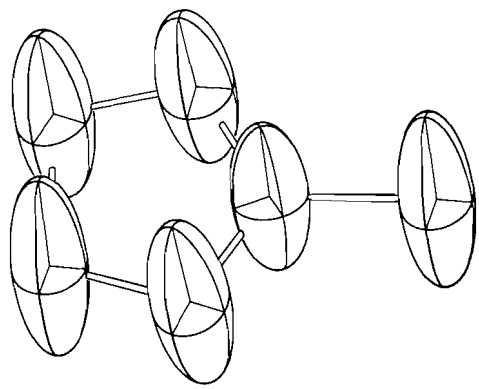

FIG. 3. An ORTEP plot of the imidazolidine-2-thione molecule. The hydrogen atoms have been excluded for clarity.

resulting from the full-matrix least-squares refinement (this work) and from differential analysis (7) are compared in Table 6. Our more accurate parameters may be of some interest in theoretical studies relating to bond order charge density calculations (22) for this simple cyclic thione. An ORTEP plot of the

molecule excluding the hydrogen atoms is shown in Fig. 3. The longest axes of the thermal ellipsoids for all non-hydrogen atoms point in the direction normal to the plane of the molecule, indicating that there is considerable molecular thermal motion in the crystal. A detailed description of this structure can be found in ref. 7.

Acknowledgement

This work was supported by the Natural Sciences and Engineering Research Council of Canada.

1. A. W. HOFMANN. Ber. **5**, 240 (1872).
2. A. E. DIMOND, J. W. HENBERGER, and J. G. HORSFALL. Phytopathology, **33**, 1095 (1943).
3. A. M. SHAH and J. W. JONES. J. Am. Pharm. Assoc. **47**, 399 (1958).
4. C. F. H. ALLEN, C. O. EDENS, and J. VAN ALLEN. Org. Synth. Coll. Vol. **111**. 6th ed. *Edited by* E. C. Horning. 1967. p. 394.
5. G. D. THORN and R. A. LUDWIG. Can. J. Chem. **32**, 872 (1954).
6. C. CHIEH and S. K. CHEUNG. Can. J. Chem. **61**, 211 (1983).
7. P. J. WHEATLEY. Acta. Crystallogr. **6**, 369 (1953).
8. H. L. KLOPPING and VAN DER KERK. Recl. Trav. Chim. Pays-Bas, **70**, 949 (1951).
9. R. A. SPARKS. *In* Crystallographic computing techniques. *Edited by* F. R. Ahmed. Munksgaard, Copenhagen. 1976. p. 452.
10. SHELXTL User manual. Revision 3A. Nicolet XRD Corporation, Fremont. 1982.
11. G. M. SHELDRICK. *In* Computational crystallography. *Edited by* D. Sayre. Oxford University Press, New York. 1982. p. 506.
12. D. T. CROMER and J. B. MANN. Acta Crystallogr. Sect. A, **24**, 321 (1968).
13. International tables for X-ray crystallography. Vol. 4, Kynoch Press, Birmingham. 1973. p. 99.
14. R. A. LUDWIG, G. D. THORN, and C. H. UNWIN. Can. J. Bot. **33**, 42 (1955).
15. K. S. JASIM and C. CHIEH. Inorg. Chim. Acta. Submitted.
16. F. A. DEVILLANOVA and G. VERANI. J. Inorg. Nucl. Chem. **42**, 623 (1980).
17. R. SHUNMUGAM and D. N. SATHYANARYANA. J. Coord. Chem. **12**, 151 (1983).
18. A. WAHLBERG. Acta Crystallogr. Sect. B, **34**, 3392 (1978).
19. A. WAHLBERG. Acta Chem. Scand. Ser. A, **30**, 433 (1978).
20. F. W. B. EINSTEIN and J. S. FIELD. Acta Crystallogr. Sect. B, **30**, 2928 (1974).
21. C. CHIEH and S. K. CHEUNG. Can. J. Chem. **59**, 2746 (1981).
22. M. J. JANSEN. Recl. Trav. Chim. Pays-Bas, **79**, 1066 (1960).

Can. J. Chem. Downloaded from www.nrcresearchpress.com by 210.87.254.105 on 09/06/12
For personal use only.

Vapor-phase charge-transfer complexes. 12. Dimethyl ether – iodine

S. J. Lo and M. Tamres
Department of Chemistry, University of Michigan, Ann Arbor, MI 48109, U.S.A.

Received June 6, 1983

S. J. Lo and M. Tamres. Can. J. Chem. **62**, 814 (1984).

Both a modified Benesi–Hildebrand method and the constant activity method were used to study the spectral and thermodynamic properties of the dimethyl ether – iodine complex in the vapor phase and in *n*-heptane solution. Comparison is made of these results with those for the diethyl ether – iodine complex. The solvent effects on ether – iodine, a relatively weak complex, are compared with those on stronger complexes.

S. J. Lo et M. Tamres. Can. J. Chem. **62**, 814 (1984).

On a utilisé la méthode modifiée de Benesi–Hildebrand ainsi que la méthode d'activité constante pour étudier les propriétés spectrales et thermodynamiques du complexe iode – éther méthylique en phase vapeur ainsi qu'en solution dans le *n*-heptane. On a fait une comparaison de ces résultats avec ceux obtenus pour le complexe iode – éther éthylique. On compare les effets de solvant sur le complexe iode – éther, un complexe relativement faible, avec ceux observés avec des complexes plus forts.
[Traduit par le journal]

Can. J. Chem. Downloaded from www.nrcresearchpress.com by 210.87.254.5 on 09/06/12
For personal use only.

Introduction

There is very little in the literature on the characterization of the spectral and thermodynamic properties of iodine complexes with ethers in the vapor phase. Only the complex with diethyl ether (1–6) has been studied rather thoroughly while that with furan (7) has been studied partially.

The present work reports an extensive study of the dimethyl ether – iodine complex in the vapor phase and in *n*-heptane solution using both the conventional (modified Benesi–Hildebrand) method (8–10) and the constant activity method (11–13).

Experimental

Material

The purification of iodine and the synthesis of tetramethylammonium pentaiodide and of tetramethylammonium enneaiodide have been described elsewhere (14–16).

n-Heptane (Eastman Spectro Grade) and dimethyl ether (Matheson) were used without further purification.

Apparatus and procedures

Spectral measurements were made with a Cary 14 spectrophotometer. Experimental details of the apparatus and of the procedures used to study the complexes in the vapor phase and in solution have been presented in earlier papers (17–21) (and in the thesis of S. J. Lo (22)). The handling of gaseous reagents also has been described (23).

Calculations

The pertinent equations for donor (D) interaction with an acceptor (A) to form a complex (C) are summarized as follows (24).

(1). For the conventional (modified Benesi–Hildebrand) method:

$$[1]\quad \frac{D_0 l A_0}{\mathrm{ABS}} = \frac{D_0 + A_0}{\epsilon_c} + \frac{1}{K_c \epsilon_c} - \frac{\mathrm{ABS}}{l \epsilon_c^2}$$

Here K_c is the equilibrium constant, D_0 and A_0 are the initial concentrations of donor and acceptor, l is the cell path, ABS is absorbance, and ϵ_c is the molar absorptivity (corrected for the contribution of free donor and free acceptor). For weak complexes, such as ether – iodine, the last term may be dropped (25, 26).

(2). For the constant activity method, the iodine concentration was controlled by the equilibrium between tetramethylammonium polyiodides.

$$[2]\quad 1/2\ \mathrm{TMAI_9}\ (\mathrm{solid}) \rightleftarrows 1/2\ \mathrm{TMAI_5}\ (\mathrm{solid}) + \mathrm{I_2}\ (\mathrm{vapor})$$

and

$$[3]\quad \mathrm{TMAI_5}\ (\mathrm{solid}) \rightleftarrows \mathrm{TMAI_3}\ (\mathrm{solid}) + \mathrm{I_2}\ (\mathrm{solution})$$

In the usual case of using a large excess of donor, the equation which applies is

$$[4]\quad \mathrm{ABS} = K_c \epsilon_c l D_0 [\mathrm{I_2}]_{0,T}$$

where $[\mathrm{I_2}]_{0,T}$ is the fixed iodine concentration at equilibrium for eq. [2] or [3] at temperature T.

Taking the logarithm of eq. [4] and differentiating with respect to $1/T$ gives for the vapor phase

$$[5]\quad \frac{\Delta E_c^0}{2.303\,R} = \frac{\mathrm{d}\log K_c + \mathrm{d}\log \epsilon_c}{\mathrm{d}(1/T)} = \frac{\mathrm{d}\log \mathrm{ABS}}{\mathrm{d}(1/T)} - \frac{\mathrm{d}\log [\mathrm{I_2}]_{0,T}}{\mathrm{d}(1/T)}$$

and for the solution phase

$$[6]\quad \frac{\Delta H_c^0}{2.303\,R} = \frac{\mathrm{d}\log K_c + \mathrm{d}\log \epsilon_c}{\mathrm{d}(1/T)} = \frac{\mathrm{d}\log \mathrm{ABS}}{\mathrm{d}(1/T)} - \frac{\mathrm{d}\log [\mathrm{I_2}]_{0,T}}{\mathrm{d}(1/T)} - \frac{\mathrm{d}\log D_0}{\mathrm{d}(1/T)}$$

ΔE_c^0 is the change in internal energy of complexation, and ΔH_c^0 is the heat of complexation. They can be determined from plots of (*a*) log K_c vs. $1/T$, (*b*) log $K_c \epsilon_c$ vs. $1/T$ (assuming constancy in ϵ over the temperature range), and (*c*) log ABS vs. $1/T$ (provided the other terms in eqs. [5] and [6] are determined separately). The last method allows determination of ΔE_c^0 or ΔH_c^0 from just a single mixture of donor and acceptor (19, 27). The method also is applicable in the conventional study provided $D_0 \gg A_0 \gg C$, so that $[A_0 - C]$ does not vary greatly over the temperature range, as is the case for weak complexes (6).

Results

Results of a study via the conventional method in the vapor phase are shown in Fig. 1 for the ultraviolet region. The charge-transfer band, with a peak at 222.5 nm, decreased in intensity as the temperature increased. A regression analysis of a plot of log ABS (at the band maximum) versus $1/T$ (Fig. 2) gave a ΔE_c^0 value of -4.27 ± 0.2 kcal mol^{-1} (correlation constant 0.999). The low equilibrium constant for this system made it impossible to separate the terms in the $K_c \epsilon_{max}^{CT}$ product by the usual procedure according to the criteria established by Person (28) and others (26, 29, 30).

Two experiments were performed using the constant activity method with $\mathrm{TMAI_9/TMAI_5}$ as the iodine source. The dimethyl ether concentrations were 0.0332 *M* and 0.0340 *M* in 100-cm cells. The complex was studied over the relatively low temperature range of 49°C to 73°C because the free iodine concentration at higher temperatures causes the slit width to open rapidly in the visible region. The entire spectrum from

Can. J. Chem. Downloaded from www.nrcresearchpress.com by 210.87.254.5 on 09/06/12
For personal use only.

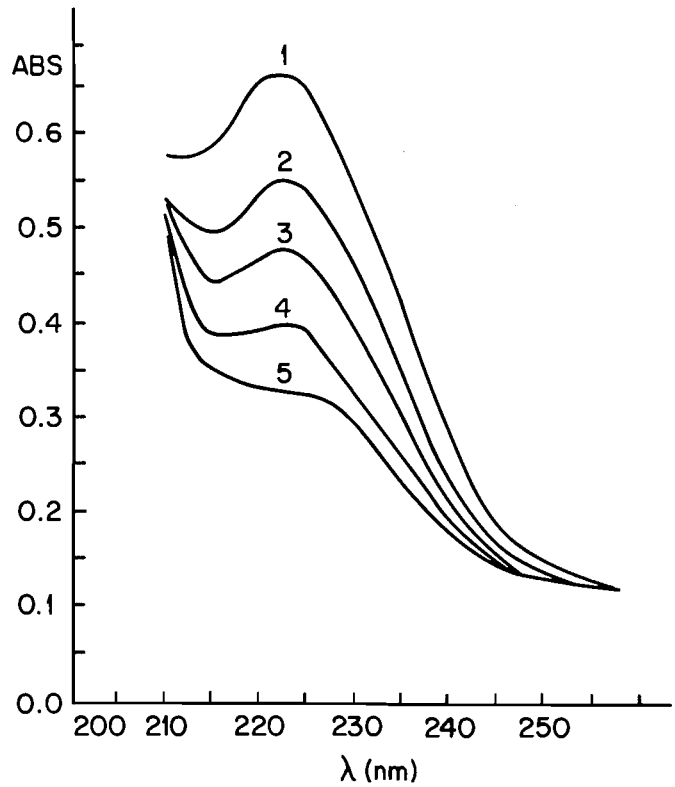

FIG. 1. The temperature dependence of the vapor-phase charge-transfer band of dimethyl ether ($3.41 \times 10^{-2} M$) and iodine ($3.259 \times 10^{-5} M$); λ_{max}^{CT} = 222.5 nm; cell path = 100 cm: (1) 60°C; (2) 70°C; (3) 78°C; (4) 88°C; (5) 100°C.

200 nm to 500 nm is shown in Fig. 3 at 53°C, 60°C, and 69°C. The charge-transfer band maximum occurred at 222.5 nm, as was obtained also by the conventional method. Just as had been reported in the literature for the diethyl ether donor (5, 19), the dimethyl ether donor gave a complexed visible iodine band spectrum which appeared to level off in the vicinity of 500 nm. The spectrum could not be studied above 500 nm due to the onset of the vibrational band structure of iodine. The maximum was obtained by extrapolating the absorbance data in the continuum region (from 450–497.5 nm) assuming a Gaussian band shape and using a computer program similar to that of Fraser and Suzuki (31–34). The complexed visible iodine band maximum was determined to occur at 495 ± 3 nm. (For the diethyl ether – iodine complex, the extrapolated band maximum occurred at 509 ± 3 nm (5, 19).)

Data for the temperature dependence of the absorbance at the charge-transfer band maximum and the complexed visible iodine band maximum are shown in Table 1, along with $K_c\epsilon_{max}^{CT}$, $K_c\epsilon_{max}^{BS}$, and the $\epsilon_{max}^{CT}/\epsilon_{max}^{BS}$ ratio. The $K_c\epsilon_{max}^{CT}$ and $K_c\epsilon_{max}^{BS}$ products were calculated from eq. [4]. The average $\epsilon_{max}^{CT}/\epsilon_{max}^{BS}$ ratio was 5.3. The variation in this ratio at the different temperatures is probably due to small instrument fluctuations in the low absorbance in the visible region.

From the temperature dependence of log ABS and the saturation pressure curve for the equilibrium, 1/2 $TMAI_9 \rightleftarrows$ 1/2 $TMAI_5 + I_2$, the ΔE_c^0 can be calculated using eq. [5]. The ΔE_{sat} for this polyiodide system in the vapor phase was determined by Tamres and Bhat (19) to be -13.65 ± 0.09 kcal mol^{-1}. The log ABS at 222.5 nm in the ultraviolet spectral region, and at the extrapolated value at 495 nm in the visible spectral region, were plotted versus $1/T$ as shown in Fig. 4. A regression

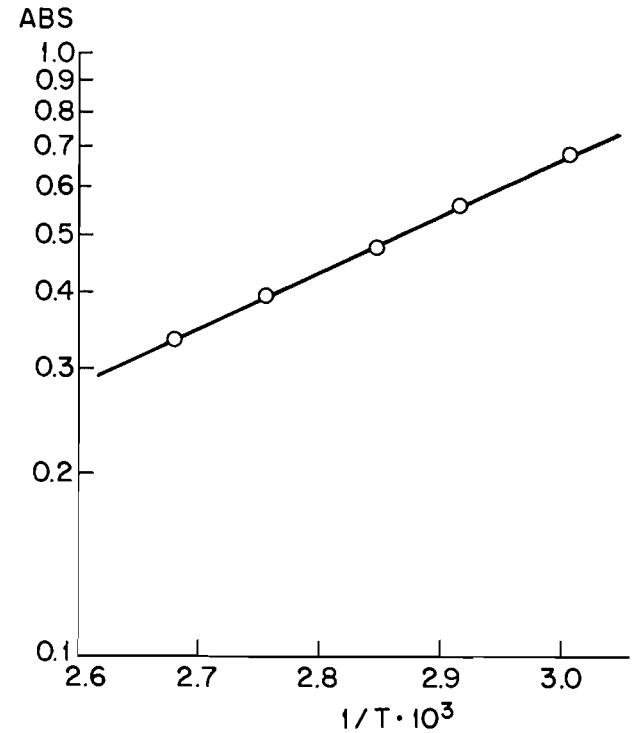

FIG. 2. Semilog plot of the temperature dependence of absorbance for dimethyl ether ($3.41 \times 10^{-2} M$) and iodine ($3.259 \times 10^{-5} M$) in the vapor phase at λ_{max}^{CT} = 222.5 nm; cell path = 100 cm.

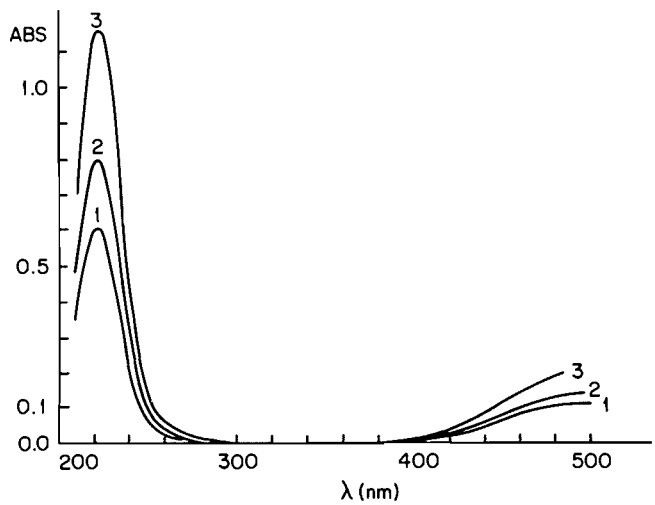

FIG. 3. The charge-transfer band and complexed visible iodine band of the dimethyl ether – iodine complex in the vapor phase: cell path = 100 cm; $[(CH_3)_2O] = 3.40 \times 10^{-2} M$; (1) 53°C, $[I_2] = 2.11 \times 10^{-5} M$; (2) 60°C, $[I_2] = 3.28 \times 10^{-5} M$; (3) 69°C, $[I_2] = 6.05 \times 10^{-5} M$. This is a difference spectrum with $TMAI_9/TMAI_5$ in the sample and reference cells.

analysis of these data, corrected for ΔE_{sat}, gave a ΔE_c^0 of -4.72 ± 0.7 kcal mol^{-1} at 222.5 nm and a value of -5.58 ± 0.5 kcal mol^{-1} at λ_{max}^{BS} at 495 nm. The ΔE_c^0 obtained from the data at 495 nm is probably less accurate for three reasons. First, the very low absorbance in the visible region makes the data more sensitive to baseline shifts. Second, the ultraviolet absorbance was read at the charge-transfer band maximum, while the visible absorbance was an extrapolated value. Third, the large free iodine absorption causes the slits on the spectrophotometer to open appreciably in the visible region from 480–500 nm.

TABLE 1. Temperature dependence study[a] of dimethyl ether[b] – iodine by the constant activity method in the vapor phase ($TMAI_9/TMAI_5$ = iodine source)

T(°C)	$[I_2]$ ($M \times 10^5$)	Corrected absorbance,[c] CT band	Corrected absorbance,[d] complexed visible iodine band	$K_c\epsilon_{max}^{CT} \times 10^{-3}$[e] ($M^{-2}$ cm^{-1})	$K_c\epsilon_{max}^{BS} \times 10^{-3}$[e] ($M^{-2}$ cm^{-1})	$\epsilon_{max}^{CT}/\epsilon_{max}^{BS}$
49	1.62	0.504	0.102	9.15	1.85	4.95
53	2.11	0.616	0.121	8.59	1.69	5.08
60	3.28	0.793	0.147	7.11	1.31	5.43
62.5	3.83	0.881	0.165	6.77	1.27	5.33
69	5.65	1.166	0.208	6.07	1.08	5.61
73	7.13	1.336	0.243	5.51	1.00	5.50

[a] In a 100-cm cell.
[b] $[(CH_3)_2O] = 0.0340\ M$.
[c] Using a 0–2.0 absorbance scale, readings taken at 222.5 nm.
[d] Using a 0–0.2 absorbance scale. readings extrapolated to the values at 495 nm.
[e] Calculated using eq. [4].

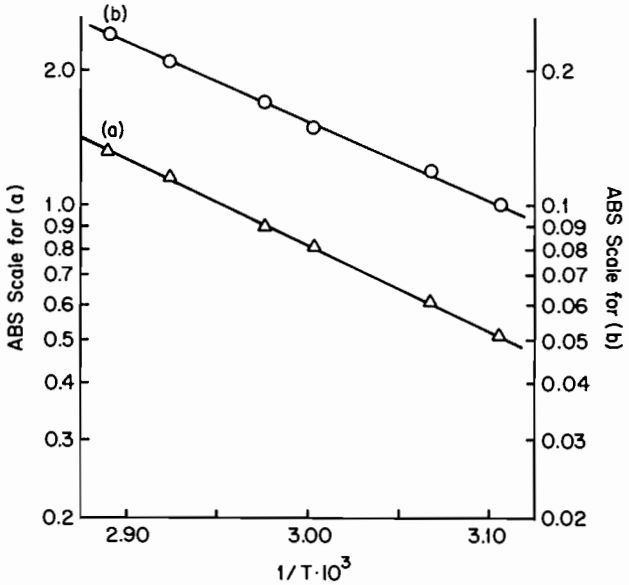

FIG. 4. A semilog plot of the temperature dependence of absorbance for dimethyl ether ($3.40 \times 10^{-2}\ M$) and iodine (from $TMAI_9/TMAI_5$) in the vapor phase; cell path = 100 cm; (a) absorbance at 222.5 nm; (b) absorbance at λ_{max}^{BS} (extrapolation to 495 nm).

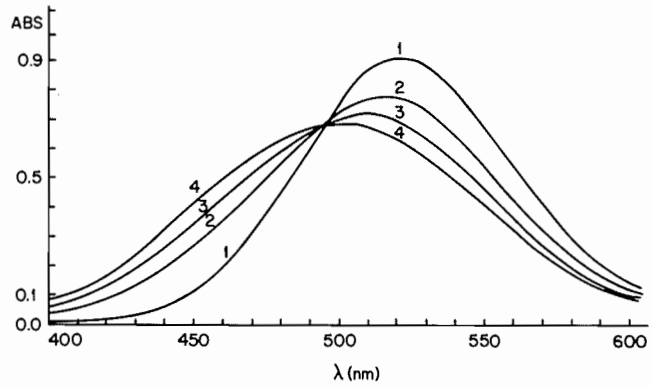

FIG. 5. The visible spectra for the dimethyl ether – iodine complex at 24.4°C in *n*-heptane; isosbestic point at 494 nm; cell path = 1.000 cm; $[I_2] = 1.001 \times 10^{-3}\ M$; $[(CH_3)_2O]$ increases $1 < 2 < 3 < 4$.

The properties of the complex also were studied in solution. The isosbestic point for the dimethyl ether – iodine complex in the visible spectral region was determined at 24.4°C in *n*-heptane using 1.000-cm glass-stoppered silica cells. An iodine solution ($1.001 \times 10^{-3}\ M$) was placed in the sample cell and its spectrum was run (curve 1 in Fig. 5). An unknown quantity of dimethyl ether was then bubbled directly into the 1.000-cm cell. The spectrum of this solution was scanned (Fig. 5, curve 2). This procedure was repeated two more times yielding curves 3 and 4, respectively. The isosbestic point occurred at 494 ± 1 nm. A molar absorptivity of 679 ± 17 M^{-1} cm^{-1} was calculated from the absorbance of the initial iodine solution at this wavelength. Precise determination of the wavelength of the isosbestic point was difficult because some solvent and iodine might have been lost through evaporation each time dimethyl ether was bubbled into the cell.

Results also were obtained in solution via the constant activity method. Approximately 0.08 g of $TMAI_5/TMAI_3$ was placed in matched Teflon-stoppered silica cells 2.00 cm in length. Rubber caps were placed over the Teflon stoppers to minimize evaporation of ether, iodine, and *n*-heptane. Dimethyl ether was bubbled directly into the sample cell three times. After each addition the difference spectrum was run in the ultraviolet and visible regions. The spectrum of the complex at 24.4°C in *n*-heptane is shown in Fig. 6. Curves 1, 2, and 3 show the increase in complex concentration as the dimethyl ether concentration is increased. The ether concentration was not determined for this experiment (although this was done approximately in one experiment to be discussed). The charge-transfer band maximum occurred at 239 nm, while the complexed visible iodine band maximum occurred at ~474 nm. The $\epsilon_{max}^{CT}/\epsilon_{max}^{BS}$ ratio was calculated to be 7.51, 7.42, and 7.35 for curves 1 through 3, respectively. Since the isosbestic point (494 ± 1 nm) and the molar absorptivity (679 M^{-1} cm^{-1}) at this wavelength are known for the dimethyl ether – iodine complex, the individual ϵ_{max}^{CT} and ϵ_{max}^{BS} values can be calculated. Data for ABS^{iso}, ABS^{CT}, and ABS^{BS} for each of the three curves in Fig. 6 are listed in Table 2 along with the ϵ_{max}^{CT} and ϵ_{max}^{BS} results. The average ϵ_{max}^{CT} and ϵ_{max}^{BS} values are 6150 M^{-1} cm^{-1} and 828 M^{-1} cm^{-1}, respectively.

The constant activity method enables the heat of complexation, ΔH_c^0, to be determined from the temperature dependence of the absorbance of a single mixture of donor and polyiodide via eq. [6]. The energy value obtained from a plot of log ABS versus $1/T$ must be corrected for the d log $[D]_0$/d$(1/T)$ term, which represents the density change of the solution with temperature, and for the saturation pressure curve of the polyiodide

Can. J. Chem. Downloaded from www.nrcresearchpress.com by 210.87.254.5 on 09/06/12
For personal use only.

TABLE 2. Absorbance data[a, b] and molar absorptivities for the charge-transfer and complexed visible iodine band maxima of the dimethyl ether – iodine complex in *n*-heptane ($TMAI_5/TMAI_3$ = iodine source)

Run[c]	ABS^{iso} (494 nm)	ABS^{CT} (239 nm)	ABS^{BS} (474 nm)	$\epsilon_{I_2}^{iso\,d}$ (M^{-1} cm^{-1})	ϵ_{max}^{CT} (M^{-1} cm^{-1})	ϵ_{max}^{BS} (M^{-1} cm^{-1})
1	0.098	0.901	0.120	679	6250	832
2	0.140	1.276	0.172	679	6190	835
3	0.205	1.816	0.247	679	6020	819

[a] Using 2.00-cm cells.
[b] Temperature = 24.4°C.
[c] Run refers to Fig. 6.
[d] Calculated from an iodine solution of known concentration.

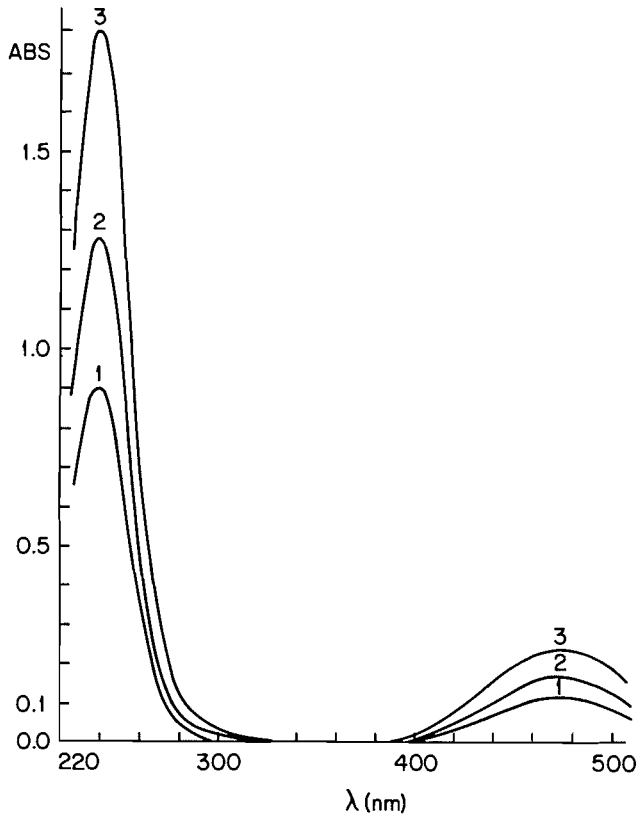

FIG. 6. The charge-transfer band and complexed visible iodine band of the dimethyl ether – iodine complex at 24.5°C in *n*-heptane; cell path = 2.00 cm: $[I_2] = 1.97 \times 10^{-4} M$, $[(CH_3)_2O]$ increases 1 < 2 < 3. These are difference spectra with $TMAI_5/TMAI_3$ in the sample and reference cells.

(i.e., the d log $[I_2]_{0,T}$/d(1/T) term). For a dilute solution, the value for d log $[D]_0$/d(1/T) corresponds to the density change of the solvent with temperature, which for *n*-heptane (35) is −0.22 kcal mol^{-1}. Tse (31) has determined the heat of solution for $TMAI_5/TMAI_3$ in *n*-heptane to be 8.18 ± 0.14 kcal mol^{-1}. A preliminary experiment was run to test the effect of the volatility of the donor in determining the enthalpy of the dimethyl ether – iodine complex. Solutions were made up at room temperature in matched Beckman 1.000-cm glass-stoppered cells. A short time was allowed for equilibrium and the absorbance was recorded at 24.4°C. The system then was cooled to 9.6°C whence, after allowing twenty-four hours for equilibration, the complex spectrum was recorded. Returning the system to 24.4°C showed that the absorbance had diminished, indicating some of the ether had evaporated. Thus, the system was studied at only two temperatures. The procedure adopted is based on the assumption that the ether probably evaporates from the cell at the same rate during the heating and cooling stages, if the time elapsed for each stage is the same. Thus, the enthalpy should be the average of those obtained from the two stages. This is tantamount to using the absorbance at 9.6°C and the average absorbance at 24.4°C at the start and end of the experiment. The average absorbance read at the charge-transfer band maximum was 0.767 at 24.4°C, while the absorbance was 1.086 at 9.6°C. This gives an uncorrected ΔH of 3.93 kcal mol^{-1}. Subtracting the corrections for the density change of the solvent (35) with temperature (−0.22 kcal mol^{-1}), along with the heat of solution for $TMAI_5/TMAI_3$ (8.18 ± 0.14 kcal mol^{-1}) (31), yields a heat of complexation for the dimethyl ether – iodine complex in *n*-heptane of −4.0 kcal mol^{-1}. This value is probably good to ±0.5 kcal mol^{-1}.

Calculation of the equilibrium constant of the dimethyl ether – iodine complex requires that the initial concentration of dimethyl ether be determined. This was done in one experiment using a Finnigan gc mass spectrometer. Immediately after the uv–visible spectrum of the solution was run, it was decanted from the excess polyiodide in the cell and poured into a small glass tube covered with a rubber septum. Using a micro syringe, very small quantities of the solution were injected into the gc mass spectrometer and the relative percentage of ether and *n*-heptane was analyzed. The technique was standardized using a solution of known concentration of diethyl ether in *n*-heptane. The percentages were determined to be good within ±1% from the analysis of several injections into the mass spectrometer. The average of all the percentages was taken as the concentration of the dimethyl ether (0.339 M).

From the absorbance at the isosbestic point and using eq. [4] the equilibrium constant was determined to be 3.0 M^{-1} at 25°C. This value establishes the order of magnitude for the equilibrium constant. However, a 1% change in the analysis of a solution containing 2% dimethyl ether leads to a 50% change in the equilibrium constant.

Discussion

The complete spectral and thermodynamic properties of the iodine complexes with diethyl ether and with dimethyl ether are summarized in Table 3. The effect of the solvent on the properties of these relatively weak complexes is apparent by comparing the data in the vapor phase with the data in *n*-heptane solution. To facilitate comparison with the solvent effect on a relatively strong complex, literature data are included in Table 3 for trimethylamine – sulfur dioxide (36).

The results for the ether – iodine complexes contrast in several ways with those for the corresponding sulfide–iodine

Can. J. Chem. Downloaded from www.nrcresearchpress.com by 210.87.254.5 on 09/06/12
For personal use only.

Can. J. Chem. Downloaded from www.nrcresearchpress.com by 210.87.254.5 on 09/06/12
For personal use only.

TABLE 3. Spectral and thermodynamic properties of ether – iodine and trimethylamine – sulfur dioxide[a] complexes in the vapor phase and in solution[b, c]

	Dimethyl ether – iodine		Diethyl ether – iodine		$(CH_3)_3N-SO_2$	
	Vapor[d]	*n*-Heptane[d]	Vapor[e]	*n*-Heptane	Vapor[f]	*n*-Heptane[f]
Spectral, CT band:						
λ_{max} (nm)	222.5	239	234[g]	252[h]	276	273
ϵ_{max} (M^{-1} cm^{-1})		6150 ± 100[i]	2850[j]	5480[l]	5700 ± 350[i]	5000 ± 40[i, m]
			2500[j]		(39.7°C)	(40.3°C)
			(2100 ± 400)[g, k]			
$\Delta\bar{\nu}_{1/2}{}^n$ (cm^{-1})	5500	5700	6600[g]	6900[o]	5500	6550[p]
					(39.7°C)	(40.3°C)
f^q		0.164	0.053[g]	0.168[o]	0.212	0.221
μ^r_{mn} (Debye)		2.88	1.6[g]	2.99[o]	3.53	3.58
$K_c\epsilon_{max}$ (M^{-2} cm^{-1})	3400[s]	4700[s]	2940[g]	1340[l, s]	1.938×10^6	1.381×10^7
(t, °C)	(100°C)	(100°C)	(100°C)	(100°C)	(25°C)	(25°C)
	5510		6700[j]	5480[l, s]		
	(73°C)		(63.6°C)	(25°C)		
	9150	18 000[t]	6200[j]	7120[l]		
	(49°C)	(25°C)	(59.8°C)	(15°C)		
	16 500[s]		13 400[g, s]			
	(25°C)		(25°C)			
Spectral, visible I_2 band:						
λ_{max} (nm)	495	474	509[j]	470[h]		
ϵ_{max} (M^{-1} cm^{-1})		828 ± 20[i]	870[i]	852[h]		
			750[i]			
$\Delta\bar{\nu}_{1/2}{}^n$ (cm^{-1})	4540	3820	4500[j]	3910[h]		
f^q		0.014	0.0169[j]	0.0144[h]		
μ^r_{mn} (Debye)		1.2	1.35[j]	1.20[h]		
$K_c\epsilon_{max}$ (M^{-2} cm^{-1})	580[s]	640[s]	890[u]	210[u]		
(t, °C)	(100°C)	(100°C)	(100°C)	(100°C)		
	1000					
	(73°C)					
	1850	2450[t]	4060[u]	850[u]		
	(49°C)	(25°C)	(25°C)	(25°C)		
	3500[s]			830[v]		
	(25°C)			(25°C)		
f^{CT}/f^{BS}		12	3.1	12		
$\epsilon^{CT}_{max}/\epsilon^{BS}_{max}$	5.3	7.4	3.3	6.4		

Can. J. Chem. Downloaded from www.nrcresearchpress.com by 210.87.254.5 on 09/06/12
For personal use only.

TABLE 3. (*Concluded*)

	Dimethyl ether – iodine		Diethyl ether – iodine		$(CH_3)_3N-SO_2$	
	Vapor[d]	*n*-Heptane[d]	Vapor[e]	*n*-Heptane	Vapor[f]	*n*-Heptane[f]
Thermodynamic:						
K_c (M^{-1})		3.0 ± 1.5[w]	4.35 ± 0.30[i,x]	1.0	340 ± 35[i,s]	2550 ± 50[i]
(t, °C)		(25°C)	(35°C)	(25°C)	(25°C)	(25°C)
			(6.4 ± 1.2)[g,k]	1.3		
			(25°C)	(15°C)		
$-\Delta E_c^0$ (kcal mol^{-1})	4.7 ± 0.7		4.3 ± 0.3[y]		9.1	
$-\Delta H_c^0$ (kcal mol^{-1})	5.3 ± 0.7	4.0 ± 0.5[z]	4.9 ± 0.3[y]	4.2 ± 0.2[l]	9.7 ± 0.4[i]	11.0 ± 0.3[i]
$-\Delta S_c^0$ (cal mol^{-1} deg^{-1})		11.2	10.7	14.1	21.0 ± 1.0[i]	21.4 ± 0.9[i]

[a] Literature data for trimethylamine – sulfur dioxide are included to facilitate comparison of solvent effects on weak and strong complexes.
[b] Standard state of 1 M.
[c] Error limits at 95% confidence level.
[d] Present study.
[e] From this laboratory; ref. 2.
[f] Reference 36.
[g] References 1 and 56.
[h] References 11 and 38.
[i] Standard error.
[j] Reference 4.
[k] Some question as to the reliability in separating terms in the $K_c\epsilon^{CT}$ product.
[l] Reference 37.
[m] Average value over temperature range 12.9 to 40.3°C is 5340 L mol^{-1} cm^{-1}.
[n] Half-width; difference in $\bar{\nu}$ at half the maximum intensity on the high- and low-energy side of the band, or twice the difference between the band peak and half of the maximum on (1) the low-energy side of the CT band for $(CH_3)_2O-I_2$ in both phases and for $(C_2H_5)_2O-I_2$ in the vapor phase, or (2) the high-energy side of the BS band for both ether–I_2 complexes in the vapor phase.
[o] Reference 6.
[p] Average value over temperature range 12.9 to 40.3°C is 6200 cm^{-1}.
[q] Oscillator strength (ref. 54*c*).
[r] Electronic transition dipole (ref. 54*c*).
[s] Extrapolated value.
[t] Based on a value of $K_c = 3.0\ M^{-1}$ at 25°C which may be in error by 50% (see text).
[u] Based on the value of $K_c\epsilon_{max}^{CT}$ and $\epsilon_{max}^{CT}/\epsilon_{max}^{BS}$ ratio.
[v] Direct evaluation from ref. 14 after converting K_x (the equilibrium constant in units of mole fraction) to K_c via the relation $K_c = K_x V_0$, where V_0 is the molar volume of *n*-heptane.
[w] Large error limits (see text).
[x] Isopiestic method, ref. 3.
[y] References 5 and 31.
[z] Estimated error limits (see text).

Can. J. Chem. Downloaded from www.nrcresearchpress.com by 210.87.254.5 on 09/06/12
For personal use only.

complexes (see preceding paper (24)). Comparison of the spectral and thermodynamic properties (such as K_c and $K_c\epsilon_{max}^{CT}$) indicated that diethyl sulfide is a stronger donor towards iodine than dimethyl sulfide. The situation is less clear-cut for the dimethyl ether – I_2 and diethyl ether – I_2 complexes. Comparison of their properties shows that the former probably is the stronger complex. Even allowing for a 50% error in determining K_c at 25°C for $(CH_3)_2O-I_2$ in *n*-heptane, the value is greater than that reported for $(C_2H_5)_2O-I_2$ under the same conditions. The $K_c\epsilon_{max}^{CT}$ product, both in the vapor phase and in *n*-heptane, is larger for the $(CH_3)_2O-I_2$ complex, as is also the $K_c\epsilon_{max}^{BS}$ product in solution. Only for $K_c\epsilon_{max}^{BS}$ in the vapor phase, does the value seem slightly larger for $(C_2H_5)_2O-I_2$. (Extrapolated results have to be compared with some caution because of the slightly different ΔE_c^0 and ΔH_c^0 values.)

One factor which could influence the strength of interaction is the dipole moment of the donor. The dipole moment for dimethyl ether (1.30 Debye) is greater than that for diethyl ether (1.15 Debye), whereas this is not the case for the sulfides (1.5 Debye for dimethyl sulfide and 1.54 Debye for diethyl sulfide) (39). Another factor is the inductive effect, i.e., ethyl substituents increase donor strength relative to methyl substituents. For the dimethyl and diethyl ethers, these two effects operate in opposing directions, which may make their donor ability more comparable. For the sulfides, both factors favor diethyl versus dimethyl sulfide.

It may be noted that, on comparing dissociation constants, dimethyl ether forms a stronger adduct with boron trifluoride in the vapor phase than does diethyl ether (40), while the reverse is true for the corresponding sulfides (41). Drago *et al.* (42–45) have developed a four-parameter equation for the enthalpy of adduct formation

$$\Delta H = E_A E_B + C_A C_B$$

where E and C are electrostatic and covalent parameters, respectively, for the acceptor (A) and the donor (base B). For the $(C_2H_5)_2O-I_2$ adduct, the experimental ΔH and calculated ΔH are the same (46), but for $(C_2H_5)_2O-BF_3$ the calculated value of 14.8 kcal mol^{-1} is larger (46) than the experimental value (of 11.9 kcal mol^{-1}) (47). Drago *et al.* have used this difference as a measure of a steric effect.

A linear correlation has been reported (48) for the enthalpy of adduct formation of diethyl ether, tetrahydrofuran, and tetrahydropyran with iodine in *n*-heptane solution and that of the same donors with BF_3 in the vapor phase. The point for dimethyl ether – iodine and dimethyl ether – boron trifluoride would fall on the line if the value for the enthalpy of complexation with iodine were 4.5 kcal mol^{-1}. The value of 4.0 kcal mol^{-1} cited in Table 3 is in reasonable agreement considering the crudeness of the determination.

Another point of contrast between the iodine complexes with ethers and with sulfides (24) is in the effect of *n*-heptane on their molar absorptivities. For both types of complexes, ϵ_{max}^{CT} is enhanced in solution relative to the vapor phase. However, the effect on ϵ_{max}^{BS} is quite different. There is very little effect of the solvent on ϵ_{max}^{BS} for ether–I_2, but the presence of the solvent approximately doubles the value of ϵ_{max}^{BS} for sulfide–I_2. As a consequence, the $\epsilon_{max}^{CT}/\epsilon_{max}^{BS}$ ratio is higher in the vapor phase relative to the solution phase for sulfide–I_2, but is the reverse for ether–I_2.

From the data so far available (6), it appears that the magnitude and even the direction of the solvent effect on the change in thermodynamic and spectral properties (e.g., K_c, ΔH_c^0, and λ_{max}^{CT}) depend on the strength of complexation, as may be seen by comparing the data in Table 3. The sulfide–iodine complexes are intermediate in strength between those of ether – iodine and of trimethylamine – sulfur dioxide, and the solvent effect is observed to be intermediate as well (24). A solvent cage model (49) seems to account satisfactorily for many of the effects observed (24). The solvent cage effect has been likened to pressure effects on these complexes (49, 50). A study by Suzuki and co-workers (51, 52) of the effect of pressure on complexes of varying strength in *n*-heptane parallels the changes observed between the solution and vapor phases. Thus, with an increase in pressure from 1 to 3300 bar, λ_{max}^{CT} for the iodine complexes of the relatively weak donors benzene, toluene, mesitylene, and diethyl ether was red shifted. For iodine complexes with donors of intermediate strength, hexamethylbenzene, diethyl sulfide, and diethyl selenide, the initial increase in pressure caused red shifts, but increasing the pressure still further reversed the trend and caused blue shifts. For strong complexes of iodine with triethylamine, tri-*n*-propylamine, and tri-*n*-butylamine, only blue shifts were observed as the pressure increased. Suzuki and co-workers (52) conclude that their observations could be interpreted by a sum of two effects: (1) increased polarity of the solvent with pressure which always causes a red shift, and (2) decreased intermolecular distance with pressure which contributes a red shift in a weak complex and a blue shift in a strong one. The latter explanation, proposed by Offen and Nakashima (53), is based on the relative importance of the terms Δ^2, $\beta_0\beta_1$, and S_{01} for weak and strong complexes in the Mulliken equation (54*a*).

$$h\nu^{CT} = \sqrt{\frac{\Delta^2 + 4\beta_0\beta_1}{1 - S_{01}^2}}$$

Suzuki and co-workers (55) have also examined the effect of increasing pressure on the visible iodine band for its complexes with diethyl ether, diethyl sulfide, and diethyl selenide in *n*-heptane solution. In each case, an increase in pressure produced a greater blue shift in the visible iodine band. Pressure increase enhanced the molar absorptivity of the complexed visible iodine band for the diethyl sulfide – iodine and the diethyl selenide – iodine complexes, but gave no enhancement for diethyl ether – iodine. These results confirm the finding of the solvent effect on these complexes when the phase is changed from vapor to solution. The lack of solvent enhancement of the molar absorptivity of the blue-shifted iodine band in complexes with donors containing oxygen (ethers (14) and alcohols (21, 31)) remains an anomaly (54*b*).

1. F. T. LANG and R. L. STRONG. J. Am. Chem. Soc. **87**, 2345 (1965).
2. J. GRUNDNES, M. TAMRES, and S. N. BHAT. J. Phys. Chem. **75**, 3682 (1971).
3. J. GRUNDNES, S. D. CHRISTIAN, and V. CHEAM. Acta Chem. Scand. **24**, 1836 (1970).
4. M. TAMRES and S. N. BHAT. J. Am. Chem. Soc. **95**, 2516 (1973).
5. H. C. TSE and M. TAMRES. J. Phys. Chem. **81**, 1977 (1977).
6. M. TAMRES. Molecular complexes. Vol. 1. *Edited by* R. Foster. Paul Elek Ltd., London. 1973. Chapt. 2.
7. E. I. GINNS and R. L. STRONG. J. Phys. Chem. **71**, 3059 (1967).
8. R. FOSTER. Organic charge-transfer complexes. Academic Press, New York. (1969).
9. H. A. BENESI and J. H. HILDEBRAND. J. Am. Chem. Soc. **71**, 2703 (1949).

10. R. L. SCOTT. Rec. Trav. Chim. Pays-Bas, **75**, 787 (1956).
11. J. D. CHILDS. Ph.D. Thesis, University of Oklahoma, Norman, Oklahoma. 1971.
12. J. D. CHILDS, S. D. CHRISTIAN, J. GRUNDNES, and S. R. ROACH. Acta Chem. Scand. **25**, 1679 (1971).
13. J. D. CHILDS, S. D. CHRISTIAN, and J. GRUNDNES. J. Am. Chem. Soc. **94**, 5657 (1972).
14. M. BRANDON, M. TAMRES, and S. SEARLES, JR. J. Am. Chem. Soc. **82**, 2129 (1960).
15. F. D. CHATTAWAY and G. HOYLE. J. Chem. Soc. **123**, 654 (1923).
16. A. I. POPOV and R. E. BUCKLES. Inorg. Synth. **5**, 172 (1957).
17. M. KROLL. J. Am. Chem. Soc. **90**, 1097 (1968).
18. M. TAMRES and S. N. BHAT. J. Am. Chem. Soc. **94**, 2577 (1972).
19. M. TAMRES and S. N. BHAT. J. Am. Chem. Soc. **95**, 2516 (1973).
20. M. TAMRES and J. GRUNDNES. J. Am. Chem. Soc. **93**, 801 (1971).
21. H. C. TSE and M. TAMRES. J. Phys. Chem. **81**, 1367 (1977).
22. S. J. LO. Ph.D. Thesis, The University of Michigan, Ann Arbor, Michigan. 1981.
23. S. N. BHAT, M. TAMRES, and M. S. RAHAMAN. J. Phys. Chem. **77**, 2756 (1973).
24. S. J. LO and M. TAMRES. Can. J. Chem. **61**, 1933 (1983).
25. M. TAMRES. J. Phys. Chem. **65**, 654 (1961).
26. R. A. LABUDDE and M. TAMRES. J. Phys. Chem. **74**, 4009 (1970).
27. M. TAMRES and J. YARWOOD. Spectroscopy and structure of molecular complexes. *Edited by* J. Yarwood. Plenum Press, New York. 1973. Chapt. 3.
28. W. B. PERSON. J. Am. Chem. Soc. **87**, 167 (1965).
29. D. A. DERANLEAU. J. Am. Chem. Soc. **91**, 4044 (1969).
30. P. R. HAMMOND. J. Chem. Soc. 479 (1964).
31. H. C. TSE. Ph.D. Thesis, The University of Michigan, Ann Arbor, Michigan. 1976.
32. R. D. B. FRASER and E. SUZUKI. Anal. Chem. **38**, 1770 (1966).
33. R. D. B. FRASER and E. SUZUKI. Anal. Chem. **41**, 37 (1969).
34. R. D. B. FRASER and E. SUZUKI. Physical principles and techniques in protein chemistry. *Edited by* S. J. Leach. Academic Press, New York, NY. 1973. Part C, Chapt. 21.
35. J. TIMMERMANS. Physico-chemical constants of pure organic compounds. Elsevier Publishing Co., New York, NY. 1950.
36. J. GRUNDNES and S. D. CHRISTIAN. J. Am. Chem. Soc. **90**, 2239 (1968).
37. M. BRANDON and M. TAMRES. J. Am. Chem. Soc. **82**, 2134 (1960).
38. H. TSUBOMURA and R. LANG. J. Am. Chem. Soc. **83**, 2085 (1961).
39. R. D. NELSON, JR., DAVID R. LIDE, JR., and ARTHUR A. MARYOTT. Selected values of electric dipole moments for molecules in the gas phase. Published as part of the National Data Reference Series, National Bureau of Standards (NSRDS-NBS 10). Issued September 1, 1967.
40. D. E. MCLAUGHLIN and M. TAMRES. J. Am. Chem. Soc. **82**, 5618 (1960).
41. H. L. MORRIS, N. I. KULEVSKY, M. TAMRES, and S. SEARLES, JR. Inorg. Chem. **5**, 124 (1966).
42. R. S. DRAGO and B. B. WAYLAND. J. Am. Chem. Soc. **87**, 3571 (1965).
43. R. S. DRAGO, G. C. VOGEL, and T. E. NEEDHAM. J. Am. Chem. Soc. **93**, 6014 (1971).
44. R. S. DRAGO. Struct. Bonding (Berlin) **15**, 73 (1973).
45. R. S. DRAGO. J. Chem. Educ. **51**, 300 (1974).
46. R. PAETZOLD. Z. Chem. **15**, 377 (1975).
47. D. E. MCLAUGHLIN and M. TAMRES. J. Am. Chem. Soc. **82**, 5618 (1960).
48. D. E. MCLAUGHLIN, M. TAMRES, and S. SEARLES, JR. J. Am. Chem. Soc. **82**, 5621 (1960).
49. J. PROCHOROW and A. TRAMER. J. Chem. Phys. **44**, 4545 (1966).
50. P. J. TROTTER. J. Am. Chem. Soc. **88**, 5721 (1966).
51. S. SAWAMURA, Y. TANIGUCHI, and K. SUZUKI. Bull. Chem. Soc. Jpn. **52**, 284 (1979).
52. S. SAWAMURA, Y. TANIGUCHI, and K. SUZUKI. Bull. Chem. Soc. Jpn. **52**, 3511 (1979).
53. H. W. OFFEN and T. T. NAKASHIMA. J. Chem. Phys. **47**, 4446 (1967).
54. R. S. MULLIKEN and W. B. PERSON. Molecular complexes: a lecture and reprint volume. Wiley–Interscience, New York. 1969: (*a*) Chapt. 2; (*b*) p. 158; (*c*) Chapt. 3.
55. S. SAWAMURA, Y. TANIGUCHI, and K. SUZUKI. Bull. Chem. Soc. Jpn. **52**, 281 (1979).
56. F. T. LANG. Ph.D. Thesis, Rennselaer Polytechnic Institute, Troy, NY. 1964.

Can. J. Chem. Downloaded from www.nrcresearchpress.com by 210.87.254.5 on 09/06/12
For personal use only.

Oxidation of *trans*-[RhCl(CO)(PPh_2R)$_2$] (R = Et, Pr^i, CH_2SPh) with $HgCl_2$ to form rhodium–mercury bonded complexes, and complexes of mercury(II) with phosphinoalkylthioethers or dithioethers

ALAN R. SANGER

Alberta Research Council, 11315 - 87 Avenue, Edmonton, Alta., Canada T6G 2C2

Received August 25, 1983

ALAN R. SANGER. Can. J. Chem. **62**, 822 (1984).

Mononuclear complexes of Hg^{II} of 1:1 stoicheiometry are formed with the chelating ligands $Ph_2P(CH_2)_nSPh$ (n = 1, 2) or $(PhS)_2(CH_2)_n$ (n = 1–4). In contrast to the behaviour of *trans*-[RhCl(CO)(PPh_3)$_2$], reactions of *trans*-[RhCl(CO)(PPh_2R)$_2$] (R = Et, Pr^i, or CH_2SPh) with $HgCl_2$ give the corresponding oxidative addition complexes [$RhCl_2$(HgCl)(CO)(PPh_2R)$_2$]. For [$RhCl_2$(HgCl)(CO)(PPh_2CH_2SPh)$_2$] the pendant thioether groups coordinate to mercury. Reactions of $HgCl_2$ with [MCl_2(Ph_2PCH_2SPh)$_2$] (M = Pd, Pt) give the corresponding heterodinuclear, Ph_2PCH_2SPh bridged complexes, [$MHgCl_4$(μ-Ph_2PCH_2SPh)$_2$]. The ^{199}Hg nmr spectrum of [$RhCl_2$(HgCl)(CO)($PEtPh_2$)$_2$] has been obtained, and the first value for $^1J(^{103}Rh—^{199}Hg)$ has been measured.

ALAN R. SANGER. Can. J. Chem. **62**, 822 (1984).

Le Hg^{II} forme des complexes mononucléaires de stoichiométrie 1:1 avec les ligands chélatants $Ph_2P(CH_2)_nSPh$ (n = 1, 2) ou $(PhS)_2(CH_2)_n$ (n = 1 à 4). Par opposition avec le comportement du [RhCl(CO)(PPh_3)$_2$-*trans*, les réactions du [RhCl(CO)(PPh_2R)$_2$]-*trans* (R = Et, Pr^i ou CH_2SPh) avec le $HgCl_2$ conduisent aux complexes d'addition oxydative correspondants [$RhCl_2$(HgCl)(CO)(PPh_2R_2)]. Dans le cas du [$RhCl_2$(HgCl)(CO)(PPh_2CH_2SPh)$_2$], les groupes thioéthers se coordonnent au mercure. Les réactions du $HgCl_2$ avec le [MCl_2(Ph_2PCH_2SPh)$_2$] (M = Pd, Pt) conduisent aux complexes hétérodinucléaires correspondants pontés par Ph_2PCH_2SPh, [$MHgCl_4$(μ-Ph_2PCH_2SPh)$_2$]. On a déterminé les spectres rmn du ^{199}Hg du [$RhCl_2$(HgCl)(CO)($PEtPh_2$)$_2$] et on a mesuré la première valeur de $^1J(^{103}Rh—^{199}Hg)$.

[Traduit par le journal]

Can. J. Chem. Downloaded from www.nrcresearchpress.com by 210.87.254.5 on 09/06/12
For personal use only.

Introduction

Synthetic and structural aspects of the chemistry of complexes containing bonds between dissimilar metal atoms are of continuing interest (1, 2). A series of heterobinuclear complexes has been described in which the metal atoms are bridged by either bis(diphenylphosphino)methane (3) or 2-(diphenylphosphino)pyridine ligands (4), and in some of these complexes there exists a metal–metal bond. The catalytic utility of heteropolynuclear materials may differ significantly from that of materials containing one of the metals alone (e.g. refs. 5–7).

The reactions of mercury(II) complexes with complexes of transition metals are various (2). When the transition metal complex is electron-rich it may act as a Lewis base, forming a donor–acceptor complex with a mercury complex, e.g. [RhCp(cod)·$HgCl_2$] (8). When the transition metal complex is less basic, and amenable to oxidation, oxidative addition (e.g. eq. [1]) (9), which can include ligand exchange (e.g. eq. [2]) (10) or oxidative elimination (e.g. eq. [3]) (11), may occur.

[1] $IrCl(CO)(PPh_3)_2 + HgCl_2 \rightarrow IrCl_2(HgCl)(CO)(PPh_3)_2$

[2] $[RhCl(nbd)]_2 + 2Hg(Pr^iNCHNPr^i)_2 \rightarrow [Rh(nbd)(Pr^iNCHNPr^i)HgCl]_2$

[3] $Fe(CO)_3(PPh_3)_2 + HgCl_2 \rightarrow FeCl(HgCl)(CO)_2(PPh_3)_2 + CO$

Oxidation of *trans*-[$IrCl(CO)(PPh_3)_2$] by mercury(II) halides or pseudohalides is facile, but similar reactions of *trans*-[RhCl(CO)(PPh_3)$_2$] do not occur (9). Indeed, very few reactions are known in which complexes of rhodium are oxidized by complexes of mercury(II) (2). Nevertheless, a series of Rh—Hg bonded complexes and the cluster complex [$Hg_6Rh_4(PMe_3)_{12}$] have been synthesized by alternate routes (2, 12, 13).

Herein the reactions of $HgCl_2$ with complexes of rhodium(I) containing phosphines more basic than PPh_3 will be described. In some cases the complexes of mercury(II) halides with the pertinent phosphines were previously unknown, and so they too will be described.

Experimental

All reactions were carried out under ambient conditions in dry solvents under an atmosphere of nitrogen or carbon monoxide. The ligands Ph_2PCH_2SPh (14) and $Ph_2PCH_2CH_2SPh$ (15) and the complexes *trans*-[RhCl(CO)(PR_3)$_2$] (R_3 = $EtPh_2$, Pr^iPh_2, $Ph_2(CH_2SPh)$, or $Ph_2(CH_2CH_2SPh)$) (14, 16) were prepared according to published procedures. Spectra were obtained using the following instruments: ir, Perkin-Elmer 283; nmr, Brüker WP80. The ^{199}Hg nmr spectrum was determined by Brüker Spectrospin, Canada Ltd., Milton, Ontario, using a 200 MHz instrument.

The following examples illustrate the preparative procedures.

Example 1: synthesis of [$HgCl_2$(Ph_2PCH_2SPh)]

Under an atmosphere of nitrogen $HgCl_2$ (0.154 g, 0.567 mmol) and Ph_2PCH_2SPh (0.172 g, 0.558 mmol) were successively added to stirred acetone (20 mL) to form a colourless solution. The solution was allowed to stand under a stream of nitrogen for 30 min, during which the solvent partially evaporated, and then was filtered to give, as white crystals [$HgCl_2$(Ph_2PCH_2SPh)] (0.263 g, 81%).

Analytical and spectroscopic data for this and other complexes of mercury with phosphinoalkylthioethers or dithioethers are in Table 1.

Example 2: reaction of $HgCl_2$ with trans-*[RhCl(CO)(Ph_2PCH_2SPh)$_2$]*

Under an atmosphere of carbon monoxide $HgCl_2$ (0.168 g, 0.619 mmol) was added to a suspension of *trans*-[RhCl(CO)(Ph_2PCH_2SPh)$_2$] (0.480 g, 0.613 mmol) in acetone (40 mL) to rapidly form initially an orange solution and subsequently a white precipitate. The mixture was stirred (15 min) and then filtered to give [$RhCl_2$(HgCl)(CO)(Ph_2PCH_2SPh)$_2$] as white crystals. Subsequent further evaporation of solvent gave additional material (total yield 76%).

Analytical and spectroscopic data for this and other Hg—Rh bonded complexes are in Table 2.

Example 3: reaction of $HgCl_2$ with trans-*[RhCl(CO)($Ph_2PCH_2CH_2SPh$)$_2$]*

Under an atmosphere of nitrogen $HgCl_2$(0.075 g, 0.276 mmol) was added to a suspension of *trans*-[RhCl(CO)($Ph_2PCH_2CH_2SPh$)$_2$] (0.210

TABLE 1. Complexes of $HgCl_2$ or HgI_2

Complex	Analysis[a] C	H	M[b]	^{31}P nmr[c] δ_p	$^1J(^{199}Hg—^{31}P)$	Comments
$[HgCl_2(Ph_2PCH_2SPh)]$	40.26	3.14	617	36.2	7664	
	(39.35)	(2.96)	(580)			
$[HgCl_2(Ph_2PCH_2CH_2SPh)]$	40.40	3.24	729	29.9	7618	
	(40.45)	(3.22)	(594)			
$[HgI_2(Ph_2PCH_2SPh)]$	29.99	2.29	512	9.0	4980	
	(29.92)	(2.25)	(763)			
$[HgI_2(Ph_2PCH_2CH_2SPh)]$	30.62	2.47	781	15.0	4738	
	(30.92)	(2.47)	(777)			
$[HgCl_2(PhSCH_2SPh)]$	28.04	2.08	392			
	(30.99)	(2.40)	(504)			
$[HgCl_2(PhSCH_2CH_2SPh)]$	32.76	2.92	331			
	(32.47)	(2.72)	(518)			
$[HgCl_2(PhS(CH_2)_3SPh)]$	34.40	3.14	382			Soft crystals
	(33.87)	(3.03)	(532)			
$[HgCl_2(PhS(CH_2)_4SPh)]$	36.10	3.53	403			
	(35.19)	(3.32)	(546)			

[a]Calculated values in parentheses.
[b]Osmometry, in CH_2Br_2.
[c]^{1}H decoupled; chemical shifts in ppm downfield from 85% H_3PO_4; coupling constants in Hz; solutions in CD_2Cl_2 at −50°C.

TABLE 2. Rhodium complexes

Complex	Analysis[a] C	H	Cl	M[d]	Infrared[b] ν(CO)	ν(M—Cl)	^{31}P nmr[c] δ_p	J(RhP)	J(HgP)
trans-$[RhCl(CO)(PEtPh_2)_2]$	(ref. 16)				1955	297	28.1	122	—
$[RhCl_2(HgCl)(CO)(PEtPh_2)_2]$[e]	40.01	3.73	13.09	722	2044	307, 298	22.9	75.7	337
	(40.20)	(3.49)	(12.28)	(866)		250			
trans-$[RhCl(CO)(Ph_2PCH_2SPh)_2]$	(ref. 14)				1957	291	24.2	123	—
$[RhCl_2(HgCl)(CO)(Ph_2PCH_2SPh)_2]$[f]	44.83	3.48		922	2042	325, 295,	23.0	77.5	306
	(44.42)	(3.25)		(1055)		272			
"$RhCl_2(HgCl)(CO)(PPr\ Ph_2)_2$"?	(see text)						15.6	76.3	360
$[RhCl_2(HgCl)(Ph_2PCH_2CH_2SPh)_2]$[g]	48.16	3.99	11.16		—	290	43.0	107	—
	(46.66)	(3.63)	(10.07)				25.0		n.o.

[a]Calculated values in parentheses.
[b]Nujol mulls; values in wavenumbers.
[c]^{1}H decoupled, solution in CD_2Cl_2, −50°C; chemical shifts in ppm downfield from 85% H_3PO_4; coupling constants in Hz.
[d]Osmometry in CH_2Br_2.
[e]$^1J(^{103}Rh—^{199}Hg)$ 426 Hz.
[f]Λ_M 2.2 S cm^{-1} mol^{-1}, 0.58 × 10^{-3} *M* solution in acetone.
[g]S, 6.85; contaminated with a small amount of $[RhCl_3(Ph_2PCH_2CH_2SPh)_2]$.

g, 0.259 mmol) in acetone (30 mL) to initially form a deep yellow solution. The mixture was stirred (1 h) during which a yellow precipitate formed. The precipitate was removed by filtration and dried under vacuum to give a pale orange powder (0.073 g) which has not yet been identified. The mother liquor was allowed to evaporate to dryness under nitrogen, and the golden mass so formed was taken up in dichloromethane (1 mL) to form a golden–orange solution and leave, as a grey residue, a trace of mercury, identified by X-ray fluorescence analysis. The solution was diluted with diethylether to form, as a yellow powder, $[RhCl_2(HgCl)(Ph_2PCH_2CH_2SPh)_2]$ (0.107 g, 39%), contaminated with a small amount of $[RhCl_3(Ph_2PCH_2CH_2SPh)_2]$.

Results and discussion

(A) Complexes of Mercury (II) with $Ph_2P(CH_2)_nSPh$ (n = 1, 2)

Under an atmosphere of nitrogen equimolar amounts of either $HgCl_2$ or HgI_2 and either Ph_2PCH_2SPh or $Ph_2PCH_2CH_2SPh$ were dissolved in acetone. Slow evaporation of the solvent gave the complexes $[HgX_2 \cdot PR_3]$ as white crystals. The complexes were characterized by elemental analysis, molecular weight, and ir and ^{31}P nmr spectroscopy (Table 1). In each case the complexes are mononuclear. All ^{31}P nmr spectroscopic parameters are of value similar to those expected for a 1:1 tertiary phosphine complex; the values of $^1J(^{199}Hg—^{31}P)$ for 2:1 complexes $[HgX_2(PR_3)_2]$ are universally lower than those for the corresponding, usually dinuclear, 1:1 complexes, $[Hg_2X_2(\mu\text{-}X)_2(PR_3)_2]$ (17). The above complexes must therefore contain $Ph_2P(CH_2)_nSPh$ (n = 1, 2) as bidentate (P, S), chelating ligands. However, the interaction of the thioether function with the mercury centre must be relatively weak to have such a slight influence on the value of ^1J(Hg—P). Complexes of mercury halides with the dithioethers $(PhS)_2(CH_2)_n$ (n = 1–4) are formed, but molecular weight determinations indicate facile dissociation in solution in either acetone or dibromomethane (Table 1). I have been unable to isolate complexes of the dithioethers (n = 5, 6), either because they are extremely labile or because the product is an oil which is different to manipulate.

Can. J. Chem. Downloaded from www.nrcresearchpress.com by 210.87.254.5 on 09/06/12
For personal use only.

Can. J. Chem. Downloaded from www.nrcresearchpress.com by 210.87.254.5 on 09/06/12
For personal use only.

(B) Reactions of $HgCl_2$ with complexes of rhodium(I)

In contrast to the lack of reaction of $HgCl_2$ with *trans*-[$RhCl(CO)(PPh_3)_2$], and in reactions analogous to those of iridium complexes, an acetone solution of either *trans*-[$RhCl(CO)(PEtPh_2)_2$] or *trans*-[$RhCl(CO)(PPh_2CH_2SPh)_2$] reacted with $HgCl_2$ under an atmosphere of CO to form a 1:1 oxidative addition complex [$RhCl_2(HgCl)(CO)(PR_3)_2$] (Table 2). Slow evaporation of the solvent under a stream of CO gave the product as yellow (PR_3 = $PEtPh_2$) or white (PR_3 = Ph_2PCH_2SPh) crystals. Traces of green impurity were due to decomposition to Hg and [$RhCl_3(CO)(Ph_2PR)_2$] and could be removed by recrystallization.

The ir spectrum of [$RhCl_2(HgCl)(CO)(Ph_2PCH_2SPh_2)$] exhibits three metal–chlorine bands at 325, 295, and 272 cm^{-1}. A strong band at 2040 cm^{-1} is appropriate for a carbonyl ligand in an oxidized complex. There is only one environment for phosphorus in the ^{31}P nmr spectrum of the complex, which at 300 K shows only a broad doublet (δ_p 23.0 ppm (versus 85% H_3PO_4); $^1J(^{103}Rh—^{31}P)$ 77.5 Hz). At 223 K the spectrum is sharper, and $^{199}Hg—^{31}P$ coupling is observed (δ_p 23.2 ppm; ^1J(Rh—P) 76.3 Hz; ^2J(Hg—P) 306 Hz). The value of the Rh—P coupling constant is also appropriate for Rh in a higher oxidation state than that of the starting material (^1J(Rh—P) 125.7 Hz) (14). The Hg—P coupling constant is considerably lower than ^1J(Hg—P) for tertiary phosphine complexes of Hg^{II} (e.g. ref. 17), and is therefore appropriately assigned as a two-bond coupling constant. The complex is a nonelectrolyte in acetone solution.

The ^{199}Hg nmr spectrum of [$RhCl_2(HgCl)(CO)(PEtPh_2)_2$] consists of a doublet of triplets. The rhodium–mercury coupling constant is 426 Hz.This represents the first such value determined, and so no conclusions can be drawn from its magnitude.

The ir and nmr parameters of each product are consistent with a complex with mutually *trans* phosphine ligands and *cis* chloro ligands. For the Rh—Hg bonded complex containing $PEtPh_2$ ligands the ^{31}P chemical shift is +5.2 ppm (upfield) from that of the parent Rh^I complex (Table 2). For the Ph_2PCH_2SPh complexes the corresponding difference is only +1.2 ppm. For each Rh—Hg bonded complex three metal–chlorine bands are observed in the ir spectrum, but the positions of the bands are very different (Table 2). These comparisons indicate that, although the structures of the complexes are similar about rhodium, a significant difference exists. The ligand Ph_2PCH_2SPh is capable of bridging two similar nuclei (14, 18). Dithioether complexes of $HgCl_2$ have been made (Table 1). Consequently, the differences between the above products are possibly due to coordination of the thioether function of the Ph_2PCH_2SPh ligands to the mercury centre (Fig. 1). The $PEtPh_2$ complex will be similar, but without coordination of pendant ligands to Hg.

If this postulate is correct, the difference in change in ^{31}P chemical shift could be due to a "ring contribution" (19) of approximately +4 ppm for the Ph_2PCH_2SPh complex. However, this value is so small that it cannot be considered as strong evidence.

Although the formation of Hg—S bonds may stabilize the product in Fig. 1, it is doubtful that the presence of the pendant thioether groups alone will promote oxidative addition of $HgCl_2$ to *trans*-[$RhCl(CO)(Ph_2PCH_2SPh)_2$]. The successful synthesis of the analogous $PEtPh_2$ complex indicates that the reaction is favoured by the presence in the parent rhodium complex of phosphine ligands which are both less bulky and more basic.

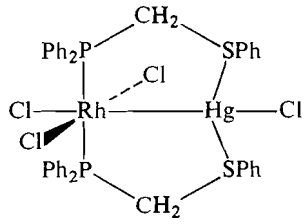

FIG. 1. Structure of [$RhCl_2(HgCl)(CO)(Ph_2PCH_2SPh)_2$].

In contrast to the above phenomena the reaction of $HgCl_2$ with *trans*[$RhCl(CO)(PPr^iPh_2)_2$] gave [$HgCl_2(PPr^iPh_2)]_2$ as the only pure, isolable product. The phosphine ligands are sufficiently basic that oxidative addition of $HgCl_2$ should be favoured, but the high steric requirements of PPr^iPh_2 mitigate against formation of a stable, six-coordinate rhodium complex (20). The reaction was repeated in acetone and the solvent was allowed to evaporate off completely to leave a mass which was then triturated under ethanol to give an orange powder. The ^{31}P nmr spectrum of a dichloromethane solution of this powder showed signals due to *trans*-[$RhCl(CO)(PPr^iPh_2)_2$], [$HgCl_2(PPr^iPh_2)]_2$, some minor components, and a new species. The parameters of the new species (δ_p 15.6 ppm; ^1J(Rh—P) 86.3 Hz; ^2J(Hg—P) 360 Hz) are sufficiently similar to the above oxidative addition products to suggest that they are due to [$RhCl_2(HgCl)(CO)(PPr^iPh_2)_2$], but no such complex has been isolated.

The reaction of equimolar amounts of $HgCl_2$ and *trans*-[$RhCl(CO)(Ph_2PCH_2CH_2SPh)_2$] in acetone gave a yellow precipitate which was not the starting material, [$HgCl_2(Ph_2CH_2CH_2SPh)$] (Table 1), or [$RhCl(CO)(Ph_2PCH_2CH_2SPh)$] (14). Although the material analyzed approximately as a 1:1 addition product of the reagents, the spectra indicated the presence of more than one product. The material showed *two* carbonyl bands of similar intensity in the ir spectrum (2040 and 1972 cm^{-1}), but, surprisingly, no band of significant intensity that could be assigned as a metal–chlorine stretch. The ^{31}P nmr of a dichloromethane solution of the products showed a singlet (δ_p 31.4 ppm), and a doublet (δ_p 43.1 ppm; ^1J(Rh—P) 107 Hz). There was also a broad minor doublet (δ_p 52.8 ppm; J, 107 Hz) downfield from the major doublet.

Evaporation of the solvent from the mother liquor from the above reaction gave [$RhCl_2(HgCl)(Ph_2PCH_2CH_2SPh)_2$] contaminated with a small amount of [$RhCl_3(Ph_2PCH_2CH_2SPh)_2$], as shown by the elemental analysis (Table 2). This impurity arises by elimination of mercury, which was separated as metal in trace amounts. The structure of [$RhCl_2(HgCl)(Ph_2PCH_2CH_2SPh)_2$] has not yet become clear. The ir spectrum shows no carbonyl band, and the only band (250–400 cm^{-1}) is a relatively weak feature at 290 cm^{-1}. The ^{31}P nmr of a solution in dichloromethane exhibits two major signals, a doublet (δ_p 43.0 ppm, ^1J(Rh—P) 107 Hz) and a broad singlet (δ_p 25.0 ppm) of equal intensity, and a minor signal due to the impurity. These data indicate that only one half of the phosphine ligands in this material are coordinated to Rh. It is interesting to note that the doublet in this spectrum is virtually identical with the doublet in the spectrum of the major, precipitated, product of this reaction.

(C) Reactions of [$MCl_2(Ph_2PCH_2SPh)_2$] (M = Pd, Pt) with $HgCl_2$

Neither [$MCl_2(Ph_2PCH_2SPh)_2$] (M = Pd, Pt) nor $HgCl_2$ is very soluble in acetone, and $HgCl_2$ is of very low solubility in

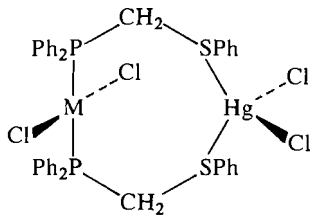

FIG. 2. Structure of $[MCl_2(\mu\text{-}Ph_2PCH_2SPh)_2HgCl_2]$ (M = Pd, Pt).

dichloromethane. However, a 1:1 mixture of either the palladium or platinum complex with $HgCl_2$ dissolves readily in a 1:1 mixture of these solvents to form a golden-yellow (Pd) or pale yellow (Pt) solution. In the case of the palladium complex, slow evaporation of the solvents gave yellow crystals which analyzed[1] as $[HgPdCl_4(Ph_2PCH_2SPh)_2]$, but for platinum the product was a pale yellow intractable oil.

The ir spectrum of the product containing palladium differed from that of the parent complex. The ^{31}P nmr spectrum exhibited one major signal (δ_p 30.4 ppm), which did not show coupling to ^{199}Hg, and which was not due to the starting material (δ_p 16.5 ppm).[2] Although the chemical shift is close to the value for $[PdCl_2(Ph_2PCH_2SPh)]_4$ (δ_p 30.7 ppm) (14), the elemental analysis is not correct for this material, and no $[HgCl_2(Ph_2PCH_2SPh)]$ (Table 1) is formed.

Attempts to obtain crystalline materials from the oily platinum product by recrystallization from various solvents such as acetone or diethylether gave only the parent platinum complex. The ^{31}P nmr of a dichloromethane solution prepared from equimolar amounts of $[PtCl_2(Ph_2PCH_2SPh)_2]$ and $HgCl_2$ exhibited signals due to only one species (δ_p 8.6 ppm; ^1J(Pt—P) 3750 Hz) which was neither the starting material (δ_p 8.1 ppm; ^1J(Pt—P) 3691 Hz) (14) nor $[HgCl_2(Ph_2PCH_2SPh)]$ (Table 1).

On the basis of the above evidence, and by analogy with complexes of Pd^{II} or Pt^{II} and Hg^{II}, bridged by two $Ph_2PCH_2PPh_2$ ligands (3), it is tentatively proposed that heterobinuclear complexes of Pd^{II} or Pt^{II} with Hg^{II} are formed which are bridged by Ph_2PCH_2SPh ligands, and that the phosphine groups coordinate to Pd or Pt (^{31}P nmr) and the thioether groups coordinate to Hg, $[MCl_2(\mu\text{-}Ph_2PCH_2SPh)_2HgCl_2]$ (M = Pd, Pt) (Fig. 2). The products are, therefore, effectively dithioether complexes of Hg^{II}, similar to those in Table 1. The Hg—S bonds are relatively labile as demonstrated by the molecular weight of the palladium product in dibromomethane (*M*, 794; calculated: 1066), and the reformation of the parent complex on treatment of the oily platinum product with donor solvents. Alternative structures of the form $[HgCl_2 \cdot MCl_2(Ph_2PCH_2SPh)_2]$ (M = Pd, Pt) are unprecedented for palladium or platinum, although similar donor–acceptor complexes are known for other metals (2).

[1]*Anal.* calcd. for $[HgPdCl_4(Ph_2PCH_2SPh)_2]$: C 42.83, H 3.22; found: C 43.74, H 3.65.

[2]The chemical shift for this complex was incorrectly reported as +43.5 ppm in ref. 14.

Acknowledgements

I thank Brüker Spectrospin, Canada Ltd. for obtaining the ^{199}Hg nmr, and for permission to publish the results.

1. (*a*) D. L. KEPERT and K. VRIEZE. *In* Comprehensive inorganic chemistry. Vol. 4. *Edited by* J. C. Bailar, Jr., H. J. Emeleus, Sir R. Nyholm, and A. F. Trotman-Dickenson. Pergamon Press, Oxford. 1973, Chapt. 47; (*b*) A. T. T. HSIEH and M. J. MAYS. *In* I. T. P. Internat. Rev. Science, Inorg. Chem. Series 1. Vol. 6. Butterworth, London. 1972.
2. SIR G. WILKINSON, F. G. A. STONE, and E. W. ABEL (*Editors*). Comprehensive organometallic chemistry. Vol. 6. Pergamon Press, Oxford, 1982. Chapt. 40–43.
3. W. C. MCDONALD, P. G. PRINGLE, and B. L. SHAW. J. Chem. Soc. Chem. Commun. 861 (1982); P. G. PRINGLE and B. L. SHAW. J. Chem. Soc. Chem. Commun. 956 (1982); D. M. MCEWAN, P. G. PRINGLE, and B. L. SHAW. 1240 (1982); C. R. LANGRICK, P. G. PRINGLE, and B. L. SHAW. Inorg. Chim. Acta, **76**, L263 (1983).
4. J. P. FARR, M. M. OLMSTEAD, and A. L. BALCH. Inorg. Chem. **22**, 1229 (1983) and references therein.
5. G. DOYLE. J. Mol. Catal. **18**, 251 (1983).
6. J. F. KNIFTON. J. Chem. Soc. Chem. Commun. 729 (1983).
7. M. ICHIKAWA. J. Catal. **59**, 67 (1979).
8. D. J. COOK, J. L. DAWES, and R. D. W. KEMMITT. J. Chem. Soc. A, 1547 (1967).
9. R. S. NYHOLM and K. VRIEZE. J. Chem. Soc. 5337 (1965).
10. D. M. ADAMS, D. J. COOK, and R. D. W. KEMMITT. Nature, London, **205**, 589 (1965).
11. P. I. VANVLIET, M. KOKKES, G. VAN KOTEN, and K. VRIEZE. J. Organomet. Chem. **187**, 413 (1980).
12. R. S. NYHOLM and K. VRIEZE. J. Chem. Soc. 5331 (1965); A. SACCO, R. UGO, and A. MOLES. J. Chem. Soc. A, 1670 (1966).
13. R. A. JONES, F. M. REAL, G. WILKINSON, A. M. R. GALAS, and M. B. HURSTHOUSE. J. Chem. Soc. Dalton, 126 (1981).
14. A. R. SANGER. Can. J. Chem. **61**, 2214 (1983).
15. D. L. DUBOIS, W. H. MYERS, and D. W. MEEK. J. Chem. Soc. Dalton, 1011 (1975).
16. A. R. SANGER. J. Chem. Soc. Dalton, 120 (1977).
17. S. O. GRIM, P. J. LUI, and R. L. KEITER. Inorg. Chem. **13**, 342 (1974); E. C. ALYEA and S. A. DIAS. Can. J. Chem. **57**, 83 (1979); T. ALLMAN, R. G. GOEL, and P. PILON. Can. J. Chem. **57**, 91 (1979); R. G. GOEL, W. P. HENRY, and W. O. OGINI. Can. J. Chem. **57**, 762 (1979); E. C. ALYEA, S. DIAS, G. FERGUSON, and M. KHAN. Can. J. Chem. **57**, 2217 (1979); H. B. BUERGHI, R. W. KUNZ, and P. S. PREGOSIN. Inorg. Chem. **19**, 3707 (1980); E. C. ALYEA, S. A. DAIS, R. G. GOEL, W. O. OGINI, P. PILON, and D. W. MEEK. Inorg. Chem. **17**, 1697 (1978); N. A. BELL, M. GOLDSTEIN, T. JONES, and I. W. NOWELL. J. Chem. Soc. Chem. Commun. 1039 (1976).
18. A. R. SANGER, C. G. LOBE, and J. E. WEINER-FEDORAK. Inorg. Chim. Acta Lett. **51**, L123 (1983).
19. P. E. GARROU. Chem. Rev. **81**, 229 (1981).
20. C. A. TOLMAN. Chem. Rev. **77**, 313 (1977).

Can. J. Chem. Downloaded from www.nrcresearchpress.com by 210.87.254.5 on 09/06/12
For personal use only.

COMMUNICATION

Shikimic acids from furan; methods of stereocontrolled access to 3,4,5-trioxygenated cyclohexenes

D. RAJAPAKSA, B. A. KEAY, AND R. RODRIGO[1]

Department of Chemistry, Guelph–Waterloo Centre for Graduate Work in Chemistry, University of Waterloo, Waterloo, Ont., Canada N2L 3G1

Received August 12, 1983

D. RAJAPAKSA, B. A. KEAY, and R. RODRIGO. Can. J. Chem. **62**, 826 (1984).

Oxabicycloheptenes **1** and **2** are converted to 3,4,5-oxygenated cyclohexenes by stereocontrolled hydroxylations and epoxidations coupled with reverse-Michael cleavage of the oxabicyclo system. Three epimers of shikimic acid are synthesized by these methods.

D. RAJAPAKSA, B. A. KEAY et R. RODRIGO. Can. J. Chem. **62**, 826 (1984).

On a transformé les oxabicycloheptènes **1** et **2** en cyclohexènes oxygénés en positions-3,4,5 grâce à des hydroxylations et des époxydations stéréocontrolées couplées à une scission de type rétro-Michael du système oxabicyclique. On a synthétisé trois épimères de l'acide shikimique par ces méthodes.

[Traduit par le journal]

In a current paper (1) we report the general occurrence of some 5-*endo-trig* reversals of 7-oxabicyclo[2.2.1]heptenes and provide a stereoelectronic rationale for the violations of Baldwin's Rules (2) observed in these cases. The reverse-Michael reactions (1, 3) of such compounds, coupled with standard epoxidations and hydroxylations, offer significant opportunities for the generation of multi-oxygenated cyclohexenes with virtually complete control of stereochemistry. We illustrate herein the application of these procedures to the efficient synthesis of some shikimic acids (4).[2]

Oxabicycloheptenes **1** and **2**, easily obtained from furan (5), were employed as starting materials. Conversion (1) of cyanide **2** to cyclohexadiene **3** followed by osmylation (osmium tetroxide/pyridine) produced diol **4** with complete regio and stereoselectivity. There is little doubt that the bulky TBDMS group is responsible for directing hydroxylation from the lower face of the 3,4 double bond. The synthesis of (±) shikimic acid **5** was then completed by the standard procedures of desilylation (tetrabutylammonium fluoride/THF) and alkaline hydrolysis in 31% overall yield from **2**.

If the osmylation is conducted before the reverse-Michael fission, the stereochemistry of the *cis*-diol function thereby introduced is reversed and 5-epishikimic acid should result. Accordingly, bicyclo ester **1** was osmylated as before and the resulting *exo*-diols **6** converted to the acetonides **7**. Reverse-Michael cleavage of the latter (LDA, THF, 0°C) provided the expected cyclohexenol **8** (86%). Hydrolysis of the acetonide (aqueous acetic acid, 16 h, 20°C) and saponification produced (±) 5-epishikimic acid **9** in 39% overall yield from **1**. This epimer of shikimic acid has not been previously synthesized but its methyl ester (6) and a related triacetate **10** are known (7). Hydrolysis of the acetonide **8**, as before, and acetylation confirmed the identity (^{1}Hmr) and stereochemistry of our product.

Expoxidations of the double bond similarly timed can produce the other two isomers to shikimic acid. Thus *exo*-epoxides **11** obtained by MCPBA treatment of **1** reacted with LDA at −78°C to afford a 1:1 mixture of two products (86%). These were separated by distillation and identified as epoxycyclohexenol **12** (bp 110°C/0.05 Torr) and cyclopropane **13** (bp 92–100°C/0.05 Torr). The former has recently been con-

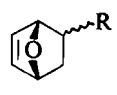

1 (R = CO_2Me)
2 (R = CN)

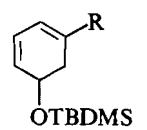

3 (R = CN)
15 (R = CO_2Me)

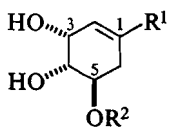

4 (R^1 = CN, R^2 = TBDMS)
5 (R^1 = CO_2H, R^2 = H)

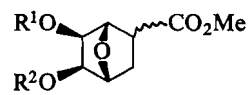

6 (R^1 = R^2 = H)
7 (R^1 + R^2 = CMe_2)

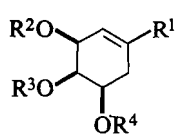

8 (R^1 = CO_2Me, R^2 = R^3 = CMe_2, R^4 = H)
9 (R^1 = CO_2H, R^2 = R^3 = R^4 = H)
10 (R^1 = CO_2Me, R^2 = R^3 = R^4 = Ac)

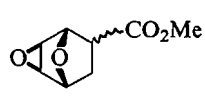

11

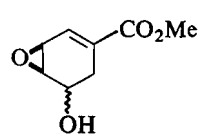

12 (β-OH)
14 (α-OH)

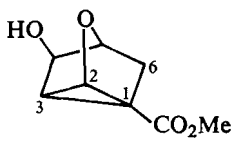

13

[1] Author to whom correspondence may be addressed.

[2] Shikimic acid and related metabolites have recently been the focus of much synthetic interest. For a review, see ref. 4*a*; for later work, see ref. 4*b*.

Can. J. Chem. Downloaded from www.nrcresearchpress.com by 210.87.254.6 on 09/06/12
For personal use only.

verted (8) into (±) methyl 4-epishikimate. Epoxidation of the diene **15** (1) with MCPBA and CH_2Cl_2 (73%), followed by desilylation (tetrabutylammonium fluoride), provided a 7:1 mixture (400 MHz ^{1}Hmr) of **14** and **12**. The former has recently been isolated and synthesised (9).[3]

We are proceeding with our experiments to convert **14** into the all-*trans* 3-epishikimic acid and to employ these techniques in the synthesis of other shikimate related metabolites.[4]

Acknowledgements

We thank the Natural Sciences and Engineering Research Council of Canada for support of this work.

1. B. A. KEAY, D. RAJAPAKSA, and R. RODRIGO. Can. J. Chem. In press.
2. J. E. BALDWIN. J. Chem. Soc. Chem. Commun. 734 (1976); J. E. BALDWIN, J. CUTTING, W. DUPONT, L. KRUSE, L. SILBERMAN, and R. C. THOMAS. J. Chem. Soc. Chem. Commun. 736 (1976).
3. B. A. KEAY and R. RODRIGO. Can. J. Chem. **61**, 637 (1983).
4. (*a*) B. GANEM. Tetrahedron, **34**, 3353 (1978); (*b*) K. E. COBLENS, V. B. MURALIDHARAN and B. GANEM. J. Org. Chem. **47**, 5041 (1982); R. H. SCHLESSINGER and A. LOPES. J. Org. Chem. **46**, 5252 (1981); M. KOREEDA and M. A. CIUFOLINI. J. Am. Chem. Soc. **104**, 2308 (1982); D. A. MCGOWAN and G. A. BERCHTOLD. J. Am. Chem. Soc. **104**, 1153 (1982); B. GANEM. N. IKOTA, V. B. MURALIDHARAN, W. S. WADE, S. D. YOUNG, and Y. YULIMOTO. J. Am. Chem. Soc. **104**, 6787 (1982); G. W. J. FLEET and T. K. M. SHING. J. Chem. Soc. Chem. Commun. 849 (1983).
5. W. L. NELSON, D. R. ALLEN, and F. F. VINCENZI. J. Med. Chem. **14**, 698 (1971); F. KIENZLE. Helv. Chim. Acta, **58**, 1180 (1975); W. G. DAUBEN and H. O. KRABBENHOFT. J. Am. Chem. Soc. **98**, 1992 (1976); F. BRION. Tetrahedron Lett. 5299 (1982).
6. R. GREWE and S. KERSTEN. Chem. Ber., **100**, 2546 (1967).
7. T. ETHERINGTON, R. B. HERBERT, F. G. HOLLIMAN, and J. B. SHERIDAN. J. Chem. Soc. Perkin Trans. 1, 2416 (1979).
8. D. A. MCGOWAN and G. A. BERCHTOLD. J. Am. Chem. Soc. **104**, 7036 (1982).
9. T. FEX, J. TROFAST, and B. WICKBERG. Acta Chem. Scand. Ser. B, **35**, 91 (1981).

[3] We are grateful to a referee for calling our attention to this paper and to ref. 6.

[4] All compounds prepared in this study provided analytical and (or) spectroscopic data consistent with the assigned structures. Full details will be published later.

Can. J. Chem. Downloaded from www.nrcresearchpress.com by 210.87.254.6 on 09/06/12
For personal use only.

Intramolecular alkylation of cyclopentenones: a general route to conjoint ring systems

KAZIMIERZ ANTCZAK,[1] JOHN F. KINGSTON, SANDRA J. ALWARD, AND ALEX G. FALLIS
Department of Chemistry, Memorial University of Newfoundland, St. John's, Nfld., Canada A1B 3X7

Received July 13, 1983

KAZIMIERZ ANTCZAK, JOHN F. KINGSTON, SANDRA J. ALWARD, and ALEX G. FALLIS. Can. J. Chem. **62**, 829 (1984).

The intramolecular alkylation of several bromo- and epoxy-2-methylcyclopentenones, **18**–**23** and **33**, are described. In all cases, except **33**, alkylative cyclization occurs at the γ′ position to the conjoint ring systems **25**–**31**. The "blocked" bromide **33** (γ′ geminal dimethyl substituent) cyclizes to the fused ring hydrindenones **35** and/or **34** depending upon conditions. Enolate anion generation from 3-ethyl-2-methyl-2-cyclopentenone (**36**) with various bases (KH, LDA, Et_3N) is described and the anion populations determined by quenching with chlorotrimethylsilane to afford the enol ethers **39**–**41**. The intramolecular alkylations are discussed.

KAZIMIERZ ANTCZAK, JOHN F. KINGSTON, SANDRA J. ALWARD et ALEX G. FALLIS. Can. J. Chem. **62**, 829 (1984).

On décrit l'alkylation intramoléculaire de plusieurs bromo- et époxy-méthyl-2 cyclopenténones (**18**–**23** et **33**). Dans tous les cas, excepté **33**, la cyclisation alkylative se produit en position γ′ pour conduire aux systèmes cycliques conjoints **25** à **31**. Le bromure **33** "bloqué" (par un *gem*-diméthyle en γ′) se cyclise pour conduire aux cycles condensés hydrindénones **35** et/ou **34** suivant les conditions expérimentales. On décrit la génération de l'anion énolate de l'éthyl-3 méthyl-2 cyclopentène-2 one (**36**) en faisant appel à diverses bases (KH, LDA, Et_3N) et on a déterminé les populations d'anions en les piégeant avec le chlorotriméthylsilane pour obtenir les éthers énoliques **39** à **41**. On discute des alkylations intramoléculaires.
[Traduit par le journal]

Can. J. Chem. Downloaded from www.nrcresearchpress.com by 210.87.254.5 on 09/06/12
For personal use only.

Introduction

Interest in polycyclopentanoid natural products has stimulated the development of new methodology for the construction of condensed five-membered ring systems (1). The synthesis of functionalized bicyclo[3.3.0]octane synthons (2) for the elaboration of more complex targets has received particular attention, since the preparation of simple systems has proven particularly challenging (3). We wished to develop a general intramolecular alkylation sequence to these and related rings, such as the diverse ring assemblies found in cuparanes, trichothecanes, and guaianolides based on the internal cyclization of cyclopentenones.

Previous studies (4) with α,β-unsaturated ketones have established that kinetically controlled formation of the α′ enolate anion results from treatment with strong nonnucleophilic bases under aprotic conditions. Intermolecular alkylation then affords the α′ alkylation product provided anion equilibration is relatively slow. In contrast, equilibrating conditions (protic solvent) favour thermodynamic control so that alkylation at the α-carbon generally results. In addition to the effect of the base–solvent combination, the balance between competing pathways in intramolecular alkylation is influenced by the nature of the electrophile and the length of the sidechain. This is exemplified by the octalones **1** and **2** studied by Piers *et al.* (5) (Scheme 1). They found that the product distribution (α′ = **3**, α = **4**, γ = **5**) could be partially controlled by the reaction conditions. Thus the α′ and α products predominated for $n = 3$, whereas for $n = 1$ only the γ and α products were encountered. Johnson and Vajs (6) found that the related cyclohexenone **6** afforded only α alkylation product **7** with potassium *tert*-butoxide (*t*BuOH), whereas conditions which facilitated proton transfer (KOH, H_2O, dimethyl sulfoxide) gave the γ alkylation product **8**.

In contrast to cyclohexenones, enolate anion generation and intramolecular alkylation of cyclopentenones have received much less attention. However, Cargill and Jackson (7) demonstrated that treatment of **9** with potassium *tert*-butoxide (*t*BuOH) resulted in selective formation of the α′ product **10**.

Clearly, substrate structure and the experimental conditions have a significant influence on the site of intramolecular alkylation of α,β-unsaturated cycloenones. As Scheme 2 illustrates, intramolecular alkylation of **11** could afford a complex product mixture. Excluding α′ and O-alkylated products, both of which are improbable due to the anti-Bredt olefins which would result, the most likely bicyclic systems are **F** to **I**. If the initial enolate is **A** or **B** it may be regarded as a masked cyclopentadiene and treatment with a second mole of strong base should generate **D** to give a different product ratio.

A variety of dianion systems have been gainfully employed in synthesis (8) and cyclopentenones appear to satisfy the general criteria for generation of a dianion species. However, with the exception of a methoxyindanone example (9), a report of some reactions of the dianions from 3-isobutoxy-2-cyclopentenones (10), and the *in situ* generation of the dianion of 3-methyl-2-cyclopentenone in an early hydroxyferrocene preparation (11), their potential as versatile synthetic intermediates remains unexplored.

Our initial investigations into the behaviour of a series of 3-substituted 2-methyl-2-cyclopentenones and their internal alkylation with bromides and epoxides are reported herein. These results provide a general entry into conjoint[2] ring systems (**I**) such as those found in bazzanene (**12**) and cuprenenol (**13**), as well as related β-cyclopropyl cyclopentenones, which are useful synthetic intermediates for cyclopentane ring annulation (12). At present, direct entry to fused cyclopentane ring systems (**F**, **G**) is feasible only in certain cases such as that leading to **34**. No spiro products (**H**) were encountered.

Preparation of cyclopentenones

The substrates required for this study were prepared by alkyl

[1]On leave from the Department of Chemistry, Merchant Marine Academy, Gdynia, Poland.

[2]IUPAC Rule A-5.1. states that two or more cyclic systems (single rings or fused systems) which are directly joined to each other by double or single bonds are named "ring assemblies". This is a very broad definition and we feel there is merit in having a simple descriptive class name to describe two or more cyclic systems joined directly by a single bond so they are neither fused nor bridged rings but "conjoint rings".

Can. J. Chem. Downloaded from www.nrcresearchpress.com by 210.87.254.5 on 09/06/12
For personal use only.

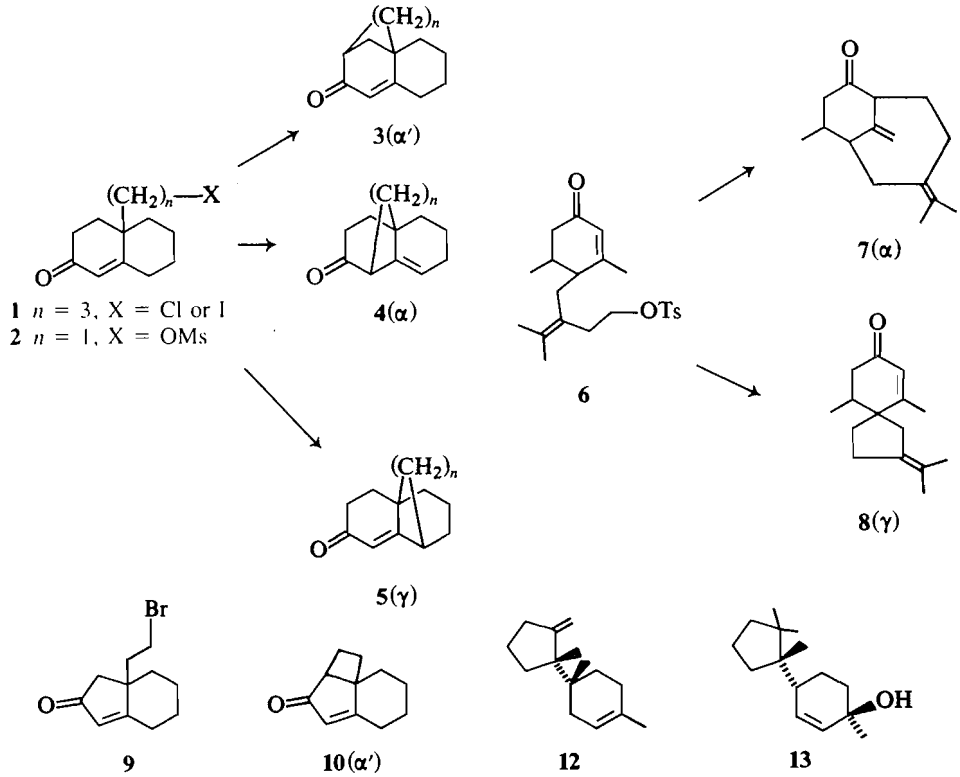

SCHEME 1

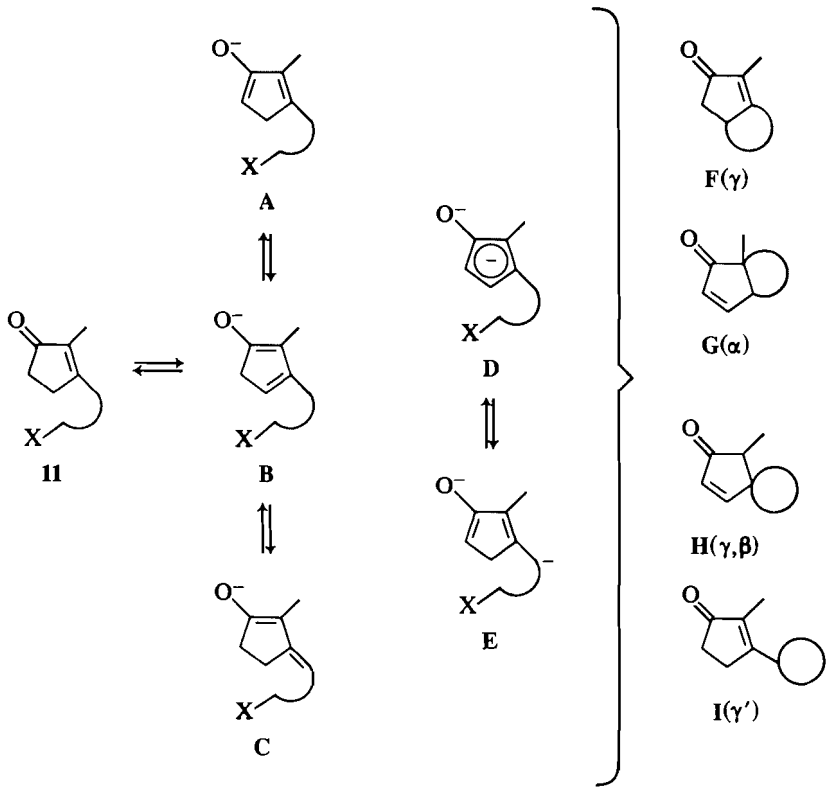

SCHEME 2

lithium addition of the requisite sidechain to the enol ether **14** followed by aqueous acid work-up as outlined in Scheme 3. The resulting dienones **15** to **17** afforded the bromides **18** to **20** regioselectively in good yields (87–93%) upon treatment with $HBr/ZnBr_2$ in acetic acid. Selective epoxidation of the terminal olefins with *m*-chloroperbenzoic acid in chloroform proceeded cleanly to give **21** to **23** (70–75%). In similar fashion the γ′-dimethylated bromide **33** was synthesized, as were authentic samples of the related 3-substituted cyclopentenones **27**, **36–38**.

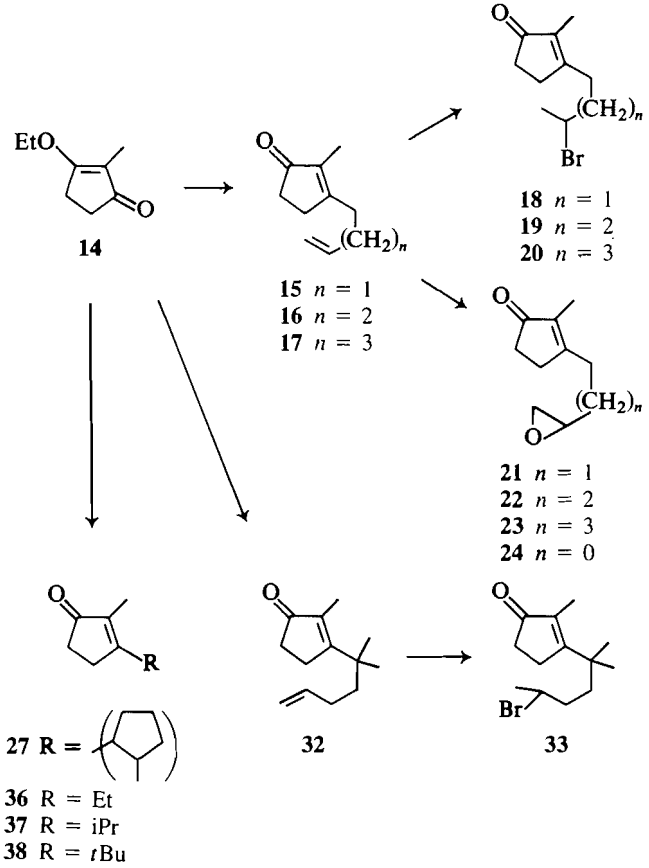

SCHEME 3

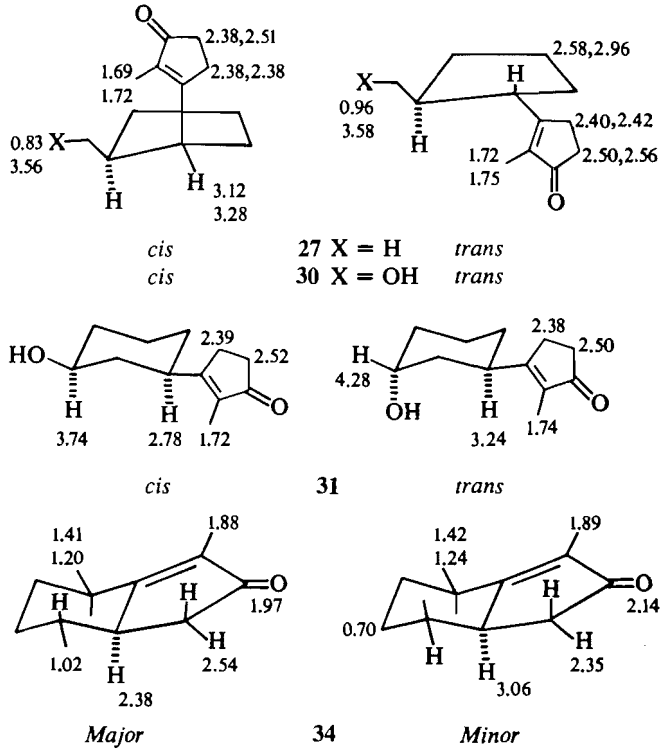

SCHEME 4

Results

Intramolecular alkylations

Table 1 summarizes the results from the intramolecular alkylation of the bromides **18**–**20** and the epoxides **21**–**23**. Except for entry 12, which proved inert to cyclization, all the products were conjoint ring systems of type **I**. The course of these cyclizations, using potassium hydride, was independent of chain length and leaving group. The structures were established on the basis of their spectral features and, in the case of **27**, by comparison with an authentic sample. The ^{1}H nmr features for **27**, **30**, and **31** are summarized in Scheme 4. Generally, axial protons resonate at higher field (~0.5 ppm) than equatorial protons and methyl signals are often significantly shifted by olefinic anisotropic effects (e.g, the *syn* and *anti* bridge methyls, δ 0.72 and 1.23 in β-pinene). This information combined with the observation that "authentic" **27** (entry 5) possessed a different major isomer to entry 3 permitted the assignment of the *cis* stereochemistry to the product with the pseudo-equatorial *tert*-allylic proton. In addition, the secondary methyl group appears to be slightly shielded by the cyclopentenone moiety. The stereochemical differences between the isomers of **31** were assigned on the basis of ^{1}H nmr (400 MHz) spectra and relevant decoupling experiments.

In addition to their synthetic utility for the introduction of hydroxyl functionality, the epoxides provided a probe for Baldwin's rules (13) in cyclizations of this type. In principle these oxiranes may be opened from either end as a result of either an *exo*- or *endo*-tet displacement. In practice the *endo* mode was only encountered with the longer sidechain present in **23** which allowed intramolecular attack of the epoxide at both ends. At the other extreme, **24** did not cyclize but opened to the allylic alcohol 3-(3-hydroxyprop-1-enyl)-2-methyl-2-cyclopentenone. For **22** there was insufficient freedom in the sidechain to achieve the necessary geometry for ring opening, although **21** cyclized to a single *trans* isomer. The failure of **22** to react thus differs from related epoxy-nitriles which afforded cyclobutanes as the preferred product (14*a*; for a discussion, see ref. 14*b*).

Bromide **33** was examined in order to ascertain if fused ring formation was feasible, once γ′ anion formation was blocked. As anticipated, it afforded a 70% yield of the fused ring system **34** (type **F**) with potassium hydride. The major isomer has the stereochemistry depicted (Scheme 4), in which the *tert*-allylic proton appears as a complex multiplet at δ 2.38 (400 MHz) ($W_{1/2}$ = 25 Hz) coupled to the two cyclopentane α protons (J = 4, 2.5 Hz) and the adjacent axial proton (J = 11 Hz). In the minor isomer this proton is shifted to lower field δ 3.06 ($W_{1/2}$ = 17 Hz), appearing as a complex multiplet from overlapping coupling with the three adjacent protons (J = 7, 2.5, and 5 Hz). The secondary methyl group lies in the shielding cone of the π system and is therefore shifted upfield (δ 0.70 vs. 1.02), while in each case the vinyl methyl signal appears as a doublet due to coupling (J = 1.8 Hz) with the *tert*-allylic proton.

In contrast to the behaviour of potassium hydride, it has been well established (4, 5) that lithium diisopropylamide (LDA) results in kinetically controlled deprotonation at the α′ position. Thus, under conditions where anion equilibration is slow, no internal alkylation should occur with bromides **20** and **33** upon treatment with LDA. This was confirmed experimentally (entries 6 and 15). Increasing the polarity of the medium (added hexamethylphosphoramide, HMPA) facilitated anion equilibration resulting in the conjoint product (entry 7). However, 2 molar equivalents of LDA promoted elimination (entries 8 and 9), implying that a dianion of type **E** was reluctant to cyclize. Treatment of the blocked system **33** with 2 molar

Can. J. Chem. Downloaded from www.nrcresearchpress.com by 210.87.254.5 on 09/06/12
For personal use only.

TABLE 1. Intramolecular alkylation products

Entry	Substrate	Conditions*	Product yield (*cis*/*trans*)			
	Bromide		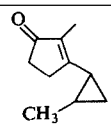 **25**	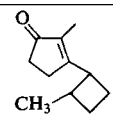 **26**	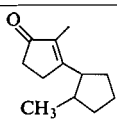 **27**	Elimination products
1	**18**	KH(1.1 equiv.) DME 22°C	95% (1:2)	—	—	—
2	**19**	KH(1.1 equiv.) DME 85°C	—	60% (1:4)	—	—
3	**20**	KH(1.1 equiv.) DME 22°C	—	—	81% (2:1)	—
4	**20**	KH(2.2 equiv.) DME 22°C	—	—	65% (1:1)	—
5	Direct synthesis from **14** and 1-bromo-2-methylcyclopentane				35% (1:20)	—
6	**20**	LDA(1.1 equiv.) DME or THF −78° → 22°C	—	—	0%	—
7	**20**	LDA(1.1 equiv.) DME/HMPA(5:2) −78° → 22°C	—	—	85% (1:4)	—
8	**20**	LDA(2.2 equiv.) DME −78° → 22°C	—	—	0%	~10%
9	**20**	LDA(2.2 equiv.) DME/HMPA(5:2) −78° → 22°C	—	—	0%	~80%
10	**20**	NaOH(1.1 equiv.) DMSO/H_2O (7.5:2.5) 22°C	—	—	99% (1:1)	—
	Epoxide		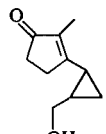 **28**	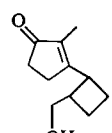 **29**	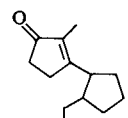 **30**	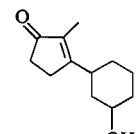 **31**
11	**21**	KH(1.1 equiv.) THF 22°C	60% (0:1)	—	—	—
12	**22**	KH(1.1 equiv.) Various	—	No reaction	—	—
13	**23**	KH(1.1 equiv.) THF 22°C	—	—	19% (1:11)	41% (19:7)
	"Blocked" bromide		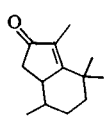 **34**	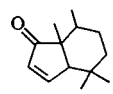 **35**	Elimination products	
14	**33**	KH(1.1 equiv.) DME 22°C	70% (10:1)	—	~10%	
15	**33**	LDA(1.1 equiv.) DME −78° → 22°C	0%	0%	—	
16	**33**	LDA(2.2 equiv.) DME −78° → 22°C	66%	30%	4%	

*DME = 1,2-dimethoxyethane; THF = tetrahydrofuran; LDA = lithium diisopropylamide; HMPA = hexamethylphosphoramide; DMSO = dimethylsulfoxide.

Can. J. Chem. Downloaded from www.nrcresearchpress.com by 210.87.254.5 on 09/06/12
For personal use only.

TABLE 2. Enolate anion quenching of 3-ethyl-2-methyl-2-cyclopentenone (**36**)

Entry	Conditions*	Product distribution		
		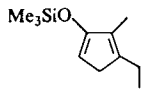	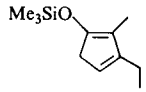	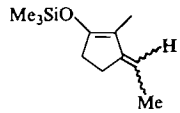
		39	**40**	**41**
1	LDA(1.1 equiv.) DME TMSCl, Et_3N $-78° \rightarrow 22°C$	83% (~5:1)		—
2	KH(1.1 equiv.) DME TMSCl, Et_3N $0° \rightarrow 22°C$	—	—	41%
3	Et_3N, $ZnCl_2$ Benzene TMSCl 22°C	66% (~4:1)		—

*TMSCl = Me_3SiCl; LDA = lithium diisopropylamide; DME = 1,2-dimethoxyethane.

equivalents of LDA afforded the γ alkylation product **34** (type **F**) and the α alkylation product **35** (type **G**) from the dianion **D**. Finally, proton transfer conditions (NaOH, H_2O, dimethyl sulfoxide) which favour enolate anion equilibration should parallel the pattern for potassium hydride, as was found (entry 10).

*Alkylation of 3-ethyl-2-methyl-2-cyclopentenone (**36**)*

In order to further establish the generality of the cyclopentenone anion reactions described above, the behaviour of 3-ethyl-2-methyl-2-cyclopentenone (**36**) with chlorotrimethylsilane and different bases was investigated. Quenching experiments provide a useful comparison of enolate anion populations even though equilibration competes with alkylation and with saturated cyclic ketones the ratio may be affected by the nature of the enol ether (15).

Table 2 summarizes the results. It was significant that the single exocyclic enol ether **41** was formed with potassium hydride whereas LDA and triethylamine/zinc chloride both afforded only the endocyclic species **39** and **40** (interconverting via a 1,5-sigmatropic rearrangement) and none of **41**. The latter result was surprising since some of the thermodynamic enol was expected, although this result was analogous to the results of Snowden (16). Apparently under these conditions quenching was more rapid than equilibration.

Unfortunately, intermolecular alkylation of **36** with methyl iodide and potassium hydride in dimethoxyethane was not selective and afforded a mixture of **36**, **37**, and **38** which may also contain some α′ alkylation product. This mixture could not be fully resolved but the structures were established by spectral comparison with authentic samples.

Discussion

The competition between the rate of enolate anion equilibration and their intramolecular alkylation is important in understanding these reactions. Scheme 2 provides a framework for the various pathways.

Lithium enolates equilibrate slowly and internal α′ alkylation of the kinetically generated enolate anion **A** is inhibited by the incorporation of a bridgehead double bond. However, under equilibrating conditions cyclization from anion **C** to the conjoint ring system **I** occurs readily. Apparently cyclization from **B** to the fused ring system **F** is less rapid (facile) and cannot compete. Similarly, generation of the α alkylation product **G** from either enolate **B** or **C** is disfavoured.

In comparison with the lithium salts potassium enolates equilibrate rapidly. It is not entirely clear whether the α′ or γ′ proton is abstracted preferentially but the experimental result is consistent with the preferential formation of enolate anion **C** either directly or by rapid equilibration. Consistent with the Curtin–Hammett principle (17)[3] cyclization to **I** must be slower than equilibration but anion **C** itself cyclizes faster than the other enolates.

The "blocked" system **33** permits the behaviour of the enolate anions **A** and **B** to be distinguished. As above, direct cyclization from **A** does not occur but generation of **B** with potassium hydride proceeds to the γ alkylation product **F** since the preferred pathway to **I** is no longer available.

Generation of the dianion intermediate **D** in the "blocked" bromide **33** affords the fused ring systems **F** and **G** (~2:1) representing γ and α alkylation respectively. Apparently the transition state leading to the spiro system **H** is of higher energy and thus cannot compete.

Conclusions

These studies have established that the preferred mode of intramolecular alkylation of compounds **18** to **23** is to the conjoint ring products arising from γ′ alkylation. When this pathway was blocked, the fused ring system from γ alkylation resulted. Fused ring products corresponding to α alkylation were only encountered from dianion intermediates in which the γ′ site was blocked. Thus some control over the product distribution may be exercised by variation of the experimental conditions and judicious choice of substrate.

The use of enol ethers via a cyclopentadiene anion inter-

[3]This principle applies when two or more isomers in rapid equilibrium react so that each isomer gives a unique product. The ratio of these products is independent of the relative energies of the original isomers and depends only on the relative energy levels of the transition states leading to these products provided the activation energy for product formation is large compared to that for isomerization.

Can. J. Chem. Downloaded from www.nrcresearchpress.com by 210.87.254.5 on 09/06/12
For personal use only.

mediate should allow selective generation of fused ring skeletons. We are currently examining this possibility as well as alternative applications of cyclopentenones to natural product total synthesis.

Experimental

Melting points were determined in capillary tubes with a Thomas–Hoover Uni-Melt apparatus, or a Fischer–Johns melting point apparatus and are uncorrected. Infrared spectra were recorded on a Perkin–Elmer 237B or 451 grating spectrophotometer, and were calibrated with the 2850 and 1601 cm^{-1} bands of polystyrene film. Ultraviolet spectra were recorded on a Perkin–Elmer 202 uv–visible spectrophotometer and were calibrated with a 279.4 nm band of a Holmium oxide filter. Proton magnetic resonance spectra were measured at 80 MHz with a Bruker model WP 80 spectrometer employing a chloroform lock or at 60 MHz with a Varian model EM 360 spectrometer or at 400 MHz with a Bruker WH 400 spectrometer at the University of Alberta. Signal positions are reported in ppm downfield from tetramethylsilane (δ scale) as an internal standard; the number of protons, multiplicity, coupling constants, and proton assignments are indicated in parentheses. Mass spectra were determined on a V.G. Micromass 7070 HS instrument using an ionization energy of 70 electron volts. Gas–liquid chromatographic analyses were conducted on a Hewlett Packard 402B chromatograph equipped with a column (3 m × 6 mm, id) containing 1.5% OV-17 supported on Gas Chrom Q using helium as the carrier gas. Thin-layer chromatographic analyses were carried out on commercial precoated silica gel plates with fluorescent indicator (Eastman Kodak silica gel 13181). Preparative thin-layer chromatography was conducted on 20 × 20 cm glass plates coated with silica gel $PF_{254+366}$ type 60 (E. Merck). Flash chromatography using BDH silica gel Kieselgel 60, 230–400 mesh was employed for all column chromatography.

Solutions in organic solvents were dried over anhydrous magnesium sulphate and stripped of solvent with a Büchi rotary evaporator connected to a water aspirator. Unless otherwise indicated all reactions were conducted under argon.

6-Bromohexene

Potassium *tert*-butoxide (50 g, 0.45 mol) was suspended in anhydrous tetrahydrofuran (THF) (400 mL) containing 18-crown-6 ether (1 g, Aldrich) and to this stirred, refluxing suspension 1-chloro-6-hydroxyhexane (20.4 g, 0.15 mol, Aldrich) in THF (50 mL) was added dropwise over 0.85 h. Reflux was continued for 1 h after addition was complete, the reaction mixture was concentrated, and hexane added. The mixture was washed with water, the aqueous layer extracted with hexane (3 × 50 mL), the combined organic layers dried and filtered, and the product distilled, bp 62–63°C/12 Torr (lit. (19) bp 57–58°C/15 Torr) to give 6-hexenol, 11 g (72%).

To a solution of triphenylphosphine (28.8 g, 0.11 mol) in dry benzene (90 mL), mechanically stirred and cooled in an ice bath, bromine (16.8 g, 0.105 mol) was added dropwise. The resulting suspension of Ph_3PBr_2 was stirred at 22°C (1 h), pyridine (8.7 g, 0.11 mol) added, the stirred mixture recooled to 0°C, and 6-hexenol (10 g, 0.10 mol) in benzene (20 mL) added dropwise. After addition was complete, the ice bath was removed and stirring was continued for a further 5 h at 22°C. Petroleum ether (300 mL) was added, the flask cooled in the freezer to precipitate triphenylphosphine oxide, the mixture filtered, concentrated, and the bromide purified by distillation, bp 73–74°C/58 Torr (lit. (18) bp 47–51°C/16 Torr) to give the bromide, 13.04 g (80%).

5-Bromopentene was prepared in 73% yield from 5-pentenol (Aldrich) by an analogous procedure, bp 74–76°C/160 Torr (lit. (19) bp 127–129°C/770 Torr).

Preparation of olefins ***15–17***

3-(3-Butenyl)-2-methyl-2-cyclopentenone ***(15)***

Enol ether **14** (19, 20) (7.0 g, 0.05 mol) was dissolved in anhydrous ether (200 mL) in a 500-mL three-necked flask containing 2% sodium in lithium alloy (0.8 g) and equipped with a nitrogen inlet tube, condenser, and pressure-equalizing dropping funnel. The flask was immersed in an ultrasonic bath (21) and 4-bromobutene (7.43 g, 0.055 mol, Aldrich), dissolved in anhydrous ether (70 mL), added dropwise to the exothermic reaction. After 3 h the residual alloy was removed by filtration, the ethereal solution washed with 3 *N* hydrochloric acid, saturated aqueous Na_2CO_3, and brine, then dried, filtered, concentrated, and chromatographed (petroleum ether/ether, 10:1) to give **15** (5.1 g, 68%); ir (film): 1685 (C=O), 1630 (C=C) cm^{-1}; ^1H nmr (CCl_4) δ: 1.61 (3H, s, CH_3C=C), 1.8–2.6 (8H), 4.81 (1H, br s, CH=C), 5.02 (1H, br d, J = 4.5 Hz, CH=C), 5.3–6.0 (1H, m, CH=C). *Exact Mass* calcd. for $C_{10}H_{14}O$: 150.1044; found: 150.1041.

3-(4-Pentenyl)-2-methyl-2-cyclopentenone ***(16)*** was prepared from 5-bromopentene and **14** in similar fashion in 64% yield; ir (KBr): 1698 (C=O), 1645 (C=C) cm^{-1}; ^1H nmr (CCl_4) δ: 1.61 (3H, s, CH_3C=C), 1.7–2.6 (10H), 4.78 (1H, br s, CH=C), 4.99 (1H, br d, J = 4 Hz, CH=C), 5.3–6.1 (1H, m, CH=C). *Exact Mass* calcd. for $C_{11}H_{16}O$: 164.1201; found: 164.1202.

3-(5-Hexenyl)-2-methyl-2-cyclopentenone ***(17)*** was prepared from 6-bromohexene and **14** as above in 65% yield; ir (film): 1690 (C=O), 1645 (C=C) cm^{-1}; ^1H nmr (CCl_4) δ: 1.60 (1H, s, CH_3C=C), 1.8–2.7 (10H), 4.80 (1H, br s, CH=C), 5.00 (1H, m, CH=C), 5.35–6.1 (1H, m, CH=C); (400 MHz, $CDCl_3$) δ: 1.45 (2H, m, CH_2), 1.55 (2H, m, J = 6.5 Hz, CH_2), 1.70 (3H, t, J = 1.8 Hz, CH_3—C=C), 2.10 (2H, m, J = 6.5, ~1 Hz, CH_2), 2.39 (2H, m, J = 1.8 Hz, CH_2—C=C), 2.44 (2H, t, J = 6.5 Hz, CH_2—C=C), 2.51 (2H, br s, CH_2—C=O), 4.99 (1H, m, J = 10.5, 2.5, 1Hz, CH=C), 5.04 (1H, m, J = 17.5, 2.5, 1Hz, CH=C), 5.82 (1H, m, J = 17.5, 10.5, 6.5 Hz, CH=C).

3-(1,1-Dimethyl-4-pentenyl)-2-methyl-2-cyclopentenone ***(32)*** was prepared from the lithium derivative of 5-bromo-5-methylhexene (itself obtained by Grignard addition of MeMgCl to 5-hexen-2-one (Aldrich) and treatment with PBr_3) and **14** in 35% yield; ir (film): 1685 (C=O), 1645, 1620 (C=C) cm^{-1}; ^1H nmr (CCl_4) δ: 1.28 (6H, s, $(CH_3)_2C$), 1.79 (3H, s, CH_3C=C), 4.79 (1H, br s, CH=C), 5.01 (1H, br d, J = 5 Hz, CH=C), 5.3–6.1 (1H, m, CH=C). *Exact Mass* calcd. for $C_{13}H_{20}O$: 192.1514; found: 192.1521.

Preparation of bromides ***18–20, 33***

The appropriate olefin (0.025 mol) was added to a 2.2 *M* solution (40 mL) of HBr in acetic acid to which $ZnBr_2$ (0.5 g) had been added and the reaction mixture stirred in the dark, at 22°C for 15 h. The mixture was poured into ice-water (150 mL), extracted with ether, the ethereal extracts washed with saturated aqueous Na_2CO_3 until basic, then with brine, dried, filtered, concentrated, and chromatographed (petroleum ether/ether, 2:1 → 1:1) to give the bromides **18–20** and **33** in 87%, 93%, 90%, and 88% yield, respectively.

3-(3-Bromobutyl)-2-methyl-2-cyclopentenone ***(18)***, ir (film): 1685 (C=O), 1640 (C=C) cm^{-1}; ^1H nmr (CCl_4) δ: 1.65 (3H, d, J = 7 Hz, CH_3CH), 1.78 (3H, s, CH_3—C=C), 4.02 (1H, sextet, J = 7 Hz, CHBr). *Exact Mass* calcd. for $C_{10}H_{15}BrO$: 230.0307; found: 230.0299.

3-(4-Bromopentyl)-2-methyl-2-cyclopentenone ***(19)***, ir (film): 1685 (C=O), 1640 (C=C) cm^{-1}; ^1H nmr (CCl_4) δ: 1.69 (3H, br s, CH_3CH), 1.81 (3H, s, CH_3—C=C), 4.17 (1H, br sextet, J ~ 6 Hz, CHBr).

3-(5-Bromohexyl)-2-methyl-2-cyclopentenone ***(20)***, ir (film): 1685 (C=O), 1640 (C=C) cm^{-1}; ^1H nmr (CCl_4) δ: 1.60 (1H, br s, CH_3CH), 1.75 (3H, s, CH_3—C=C), 4.27 (1H, sextet, J = 6.5 Hz, CHBr).

3-(4-Bromo-1,1-dimethylpentyl)-2-methyl-2-cyclopentenone ***(33)***, ir (film): 1685 (C=O), 1620 (C=C) cm^{-1}; ^1H nmr (80 MHz, CCl_4) δ: 1.27 (6H, s, $(CH_3)_2C$), 1.72 (3H, d, J = 6.5 Hz, CH_3—CH), 1.87 (3H, t, J = 1.5 Hz, CH_3—C=C), 2.35 (2H, m, CH_2—C=C), 2.51 (2H, m, CH_2—C=O), 4.13 (1H, sextet, J = 6 Hz, CHBr).

Preparation of epoxides ***21–23***

The appropriate olefin (0.02 mol) in dichloromethane (40 mL) to which *m*-chloroperbenzoic acid (5 g, 80%, 0.023 mol, Aldrich) had

Can. J. Chem. Downloaded from www.nrcresearchpress.com by 210.87.254.5 on 09/06/12
For personal use only.

Can. J. Chem. Downloaded from www.nrcresearchpress.com by 210.87.254.5 on 09/06/12
For personal use only.

been added was stirred for 15 h at room temperature. 10% Aqueous sodium thiosulfate (10 mL) was added and stirring continued for a further 10 min. Ether (150 mL) was added and the organic material washed with saturated aqueous sodium carbonate. After ether extraction of the aqueous layer, the combined extracts were dried, filtered, and chromatographed (petroleum ether/ether, 2:1 → 1:1) to give the epoxides **21**–**23** as viscous oils in 70, 75, and 79% yields.

3-(3,4-Epoxybutyl)-2-methyl-2-cyclopentenone (21), ir (film): 1705, 1685 (C=O), 1640 (C=C) cm^{-1}; ^1H nmr (CCl_4) δ: 1.60 (3H, s, CH_3C=C). *Exact Mass* calcd. for $C_{10}H_{14}O_2$: 166.0994; found: 166.0988.

3-(4,5-Epoxypentyl)-2-methyl-2-cyclopentenone (22), ir (film): 1708, 1685 (C=O), 1640 (C=C) cm^{-1}; ^1H nmr (80 MHz, CCl_4) δ: 1.65 (3H, s, CH_3—C=C), 1.68 (4H, br s, CH_2CH_2), 2.40 (6H, m, CH_2C=), 2.6–3.1 (3H, m, CH(O)CH_2). *Exact Mass* calcd. for $C_{11}H_{16}O_2$: 180.1150; found: 180.1147.

3-(5,6-Epoxyhexyl)-2-methyl-2-cyclopentenone (23), ir (film): 1708, 1685 (C=O), 1640 (C=C) cm^{-1}; ^1H nmr (CCl_4) δ: 1.51 and 1.59 (9H, br s, CH_3C=C and CH_2's), 2–3 (9H, complex). *Exact Mass* calcd. for $C_{12}H_{18}O_2$: 194.1307; found: 194.1311.

Cyclization studies of bromides 18–20, 33

Potassium hydride (0.24 g, 2.1 mol, 35% oil suspension, Aldrich) was suspended in anhydrous dimethoxyethane (DME) under nitrogen, cooled in an ice bath, and stirred magnetically. The appropriate bromide (2 mmol) dissolved in DME (5 mL) was added dropwise and after ~10 min at 0°C the reaction was stirred at 22°C for 1–15 h, diluted with ether, and washed with saturated aqueous ammonium chloride. The aqueous layer was extracted with ether (2×) and the combined ether fractions dried, filtered, concentrated, and chromatographed (petroleum ether/ether 4:1 → 2:1) to give the conjoint ring systems **25** and **27** in yields of 95% and 81%, respectively. The preparation of **26** (60%) required 0.5 h at 0°C and 10 minutes reflux. Bromide **33** afforded **34** (70%) as a 10:1 isomeric mixture accompanied by ~10% elimination to olefins. Isomers were separated by hplc.

3-(2-Methylcyclopropyl)-2-methyl-2-cyclopentenone (25), ir (film): 1735, 1690 (C=O), 1650 (C=C) cm^{-1}; ^1H nmr (80 MHz, $CDCl_3$) δ: 0.80 (1H, m, cyclopropyl H), 1.0–1.35 (5H, br s, cyclopropyl H, CH_3CH), 1.68 (1H, m, cyclopropyl H), 1.75 (3H, t, J = 1.8 Hz, CH_3—C=C), 2.0–2.4 (4H, complex); (400 MHz (*cis*), $CDCl_3$) δ: 0.70 (1H, m, J = 7, 8 Hz, cyclopropyl H), 1.05 (3H, d, J = 7 Hz, CH_3—CH), 1.10 (1H, m, J = 8, 1.5 Hz, cyclopropyl H), 1.38 (1H, m, J = 7, 8 Hz, cyclopropyl $CHCH_3$), 1.81 (3H, t, J = 1.8 Hz, CH_3C=C), 1.85 (1H, m, J = 8 Hz, cyclopropyl CH—C=C), 2.39 (4H, m, O=C—CH_2CH_2—C=C); (400 MHz (*trans*), $CDCl_3$) δ: 0.82 (1H, m, J = 8, 5 Hz, cyclopropyl H), 1.10 (1H, m, J = 8, 5 Hz, cyclopropyl H), 1.22 (3H, d, J = 6 Hz, CH_3CH), 1.30 (1H, m, J = 8, 6, 5 Hz, cyclopropyl $CHCH_3$), 1.75 (1H, m, J = 8, 5 Hz, cyclopropyl CH—C=C), 1.80 (3H, t, J = 1.8 Hz, CH_3—C=C), 2.15 (2H, m, CH_2—C=O), 2.40 (2H, m, CH_2—C=C). *Exact Mass* calcd. for $C_{10}H_{14}O$: 150.1044; found: 150.1044.

3-(2-Ethylcyclobutyl)-2-methyl-2-cyclopentenone (26), ir (film): 1735, 1690 (C=O), 1640 (C=C) cm^{-1}; ^1H nmr ($CDCl_3$) δ: 1.01 (3H, overlapping d, J = 6.5 Hz, CH_3CH), 1.59 (3H, br s, CH_3C=C), 2.91 (1H, m, J ~ 7 Hz, CH—C=C); (400 MHz, $CDCl_3$) δ: 1.02 (3H, d, J = 6.5 Hz, CH_3CH), 1.61 (3H, t, J = 1.8 Hz, CH_3—C=C), 1.96 (5H, complex, CH_2), 2.30 (2H, m, CH_2—C=C), 2.50 (2H, br s, O=C—CH_2), 3.00 (1H, m, J = 7.5 Hz, allylic CH). *Exact Mass* calcd. for $C_{11}H_{16}O$: 164.1201; found: 164.1204.

3-(2-Methylcyclopentyl)-2-methyl-2-cyclopentenone (27), ir (film): 1695 (C=O), 1640 (C=C) cm^{-1}; ^1H nmr (CCl_4) δ: 0.80, 0.98 (3H, overlapping d, J = 6.5 Hz, CH_3CH), 1.61 (3H, br s, CH_3C=C), 3.14 (1H, m, J ~ 7, CH—C=C); (400 MHz (*cis*), $CDCl_3$) δ: 0.83 (3H, d, J = 7 Hz, CH_3CH), 1.69 (3H, t, J = 1.8 Hz, CH_3C=C), 2.38 (4H, complex, O=C—CH_2CH_2—C=C), 3.12 (1H, m, J ~ 8 Hz, allylic H); (400 MHz (*trans*), $CDCl_3$) δ: 0.96 (3H, d, J = 6.5 Hz, CH_3CH), 1.33 (1H, m, CH_2), 1.67 (1H, m, CH_2), 1.72 (3H, t, J = 1.8 Hz, CH_3—C=C), 1.74 (1H, m, CH_2), 1.87 (2H, m, CH_2), 1.96 (2H, m, CH_2), 2.40 (2H, m, J ~ 5 Hz, CH_2—C=C), 2.50 (2H, m, O=C—CH_2), 2.58 (1H, m, J = 8.5 Hz, allylic H). *Exact Mass* calcd. for $C_{12}H_{18}O$: 178.1358; found: 178.1362.

2,2,5,9-Tetramethylbicyclo[4.3.0]non-9-en-8-one (34), ir (film): 1700 (C=O), 1625 (C=C) cm^{-1}; ^1H nmr (400 MHz (major), $CDCl_3$) δ: 1.02 (3H, d, J = 6 Hz, CH_3CH), 1.16 (1H, m, CH_2), 1.20 (3H, s, CH_3), 1.41 (3H, s, CH_3), 1.88 (3H, d, J = 1.8 Hz, CH_3—C=C), 1.97 (1H, dd, J = 18.5, 2.5 Hz, O=C—CH_2C), 2.38 (1H, m, J = 11, 4, 2.5, 1.8 Hz, $W_{1/2}$ = 25 Hz, CH—C=), 2.54 (1H, dd, J = 18.5, 6.5 Hz, O=C—CH_2). *Exact Mass* calcd. for $C_{13}H_{20}O$: 192.1514; found: 192.1499; ir (film): 1700 (C=O), 1625 (C=C) cm^{-1}; ^1H nmr (400 MHz (minor)) δ: 0.70 (3H, d, J = 6 Hz, CH_3CH), 1.24 (3H, s, CH_3), 1.36 (1H, m, J = 14, 4 Hz, CH_2), 1.42 (3H, s, CH_3), 1.54 (1H, m, CH_2), 1.75 (1H, m, J = 14, 4 Hz, CH_2), 1.89 (3H, d, J = 1.8 Hz, CH_3—C=C), 1.97 (1H, m, CH_2), 2.14 (1H, m, J = 9.5, 1Hz, O=C—CH_2), 2.20 (1H, m, CH_2), 2.36 (1H, m, J = 19, 7 Hz, O=C—CH_2), 3.06 (1H, m, J = 7, 5, 2.5, 1.8 Hz, $W_{1/2}$ = 17 Hz, CH—C=C). *Exact Mass* calcd. for $C_{13}H_{20}O$: 192.1514; found: 192.1538.

Cyclization studies with lithium diisopropyl amide (LDA) were conducted as follows. LDA was generated at −78°C and the appropriate ketohalide added. The reaction mixture after 5 min at −78°C was allowed to warm to room temperature (22°C) and the progress of the reaction monitored by tlc.

Bromide 20

LDA (1.1 equiv.) in DME or THF gave recovered **20**.

LDA (1.1 equiv.) in DME/HMPA (5:2) afforded ketone **27** (85%).

LDA (2.2. equiv.) in DME caused some elimination (~10%) and gave recovered **20**.

LDA (2.2 equiv.) in DME/HMPA (5:2) gave only elimination products.

Bromide 33

LDA (1.1 equiv.) in DME gave recovered **33**.

LDA (2.2 equiv.) in DME after chromatography (petroleum ether/ether, 5:1) afforded **34** (66%), olefins (4%), and 1,2,5,5-tetramethylbicyclo[4.3.0]non-7-en-9-one (**35**) (30%); ir (film): 1705 (C=O) cm^{-1}; ^1H nmr (CCl_4) δ: 0.82 (6H, overlapping CH_3, CH_3C, CH_3CH), 1.04 (3H, s, CH_3—C), 1.08 (3H, s, CH_3—C), 6.18 (1H, m, C=CH—C=O), 7.38 (1H, m, CH=C—C=O).

Based on the conditions of Johnson and Vajs (6), cyclization of **20** was also examined. The bromide **20** (0.259 g, 1 mmol) in dimethyl sulfoxide (3.75 mL) and water (1.25 mL) containing NaOH (52 mg) was stirred at room temperature under N_2 for 2 h. The reaction mixture was diluted with petroleum ether, extracted, washed with water, dried, filtered, and concentrated to give the conjoint product **27**, 0.180 g (99%) as a 1:1 isomeric mixture.

Cyclization of epoxides 21–23

Potassium hydride (0.24 g, 2.1 mmol, 35% oil suspension, Aldrich) was suspended in anhydrous tetrahydrofuran (THF) under nitrogen, cooled in an ice bath, and stirred magnetically. The appropriate epoxide (2 mmol) dissolved in THF (5 mL) was added dropwise and after 20 min at 0°C the reaction was stirred at 22°C for 15 h, diluted with ether, and washed with saturated aqueous ammonium chloride solution. The aqueous layer was extracted with ether (3×), and the combined ether fractions were dried, filtered, concentrated, and chromatographed (ether/2-propanol, 1:0 → 95:5) to give the cyclized alcohol(s) in 60% yield. A single *trans* isomer was formed in the case of **28**, while **30** and **31** occurred in 1:11 and 19:7 *cis*/*trans* ratios, respectively. No conditions were found for effective cyclization of **22**.

3-[(2-Hydroxymethyl)cyclopropyl]-2-methyl-2-cyclopentenone (28), ir (film): 3300–3500 (br, OH), 1680 (C=O), 1630 (C=C) cm^{-1}; ^1H nmr (80 MHz) ($CDCl_3$) δ: 0.85–1.22 (m, CH_3 and cyclopropyl H), 1.80 (3H, t, J = 1.8 Hz, CH_3—C=C), 3.60 (2H, m, J ~ 6, 2 Hz, CH_2—O); (400 MHz, $CDCl_3$) δ: 1.00 (1H, m, J = 7, 4.5 Hz, cyclopropyl H), 1.14 (1H, m, cyclopropyl H), 1.55 (1H, m, cyclopropyl H), 1.78 (3H, t, J = 1.8 Hz, CH_3—C=C), 1.94 (1H, m, J = 4.5 Hz,

Can. J. Chem. Downloaded from www.nrcresearchpress.com by 210.87.254.5 on 09/06/12
For personal use only.

allylic cyclopropyl H), 2.18 (2H, br, O=C—CH_2), 2.33 (2H, m, J ~ 5, 2.5 Hz, CH_2C=C), 3.64 (2H, m, J ~ 6 Hz, CH_2—O). *Exact Mass* calcd. for $C_{10}H_{14}O_2$: 166.0994; found: 166.0991.

3-[(2-Hydroxymethyl)cyclopentyl]-2-methyl-2-cyclopentenone (30) (trans), ir (CCl_4): 3610 (sh, OH), 3410 (br, OH), 1685 (C=O), 1635 (C=C) cm^{-1}; ^1H nmr (80 MHz, $CDCl_3$) δ: 1.70 (3H, t, J = 1.8 Hz, CH_3C=C), 2.2–2.6 (4H, complex, CH_2—C=C), 2.88 (1H, m, CH—C=C), 3.53 (2H, m, J ~ 5.5 Hz, CH_2—O); (400 MHz, $CDCl_3$) δ: 1.62 (2H, m, CH_2), 1.73 (2H, m, CH_2), 1.75 (3H, t, J = 1.8 Hz, CH_3—C=C), 1.96 (2H, m, CH_2), 2.20 (1H, m, J = 8.5 Hz, CH—CH_2OH), 2.42 (2H, m, CH_2—C=C), 2.56 (2H, br, O=C—CH_2), 2.96 (1H, m, J = 8.5, CH—C=C), 3.58 (2H, m, J = 5.5 Hz, CH_2O). *Exact Mass* calcd. for $C_{12}H_{18}O_2$: 194.1307; found: 194.1305; (*cis*), ^1H nmr ($CDCl_3$ 80 MHz) δ: 1.73 (3H, t, J = 1.8 Hz, CH_3—C=C), 2.43 (4H, br m, O=C—CH_2CH_2—C=C), 2.88 (1H, m, CH—C=C), 3.46 (2H, m, J ~ 6 Hz, CH_2—O); (400 MHz, $CDCl_3$) δ: 1.72 (3H, t, J = 1.8 Hz, CH_3—C=C), 2.38 (2H, m, CH_2—C=C), 2.51 (2H, m, O=C—CH_2), 3.28 (1H, m, CH—C=C), 3.56 (2H, m, J = 5.5 Hz, CH_2—O).

3-(3-Hydroxycyclohexyl)-2-methyl-2-cyclopentenone (31) (cis), mp 59–62°C; ir (CCl_4): 3590 (OH), 3400 (br, OH), 1685 (C=O), 1640 (C=C) cm^{-1}; ^1H nmr (80 MHz, $CDCl_3$) δ: 1.69 (3H, t, J = 1.8 Hz, CH_3—C=C), 2.38 (4H, br m, O=C—CH_2CH_2—C=C), 2.75 (1H, m, CH—C=C), 3.69 (1H, m, CH—O); (400 MHz, $CDCl_3$) δ: 1.35 (4H, m, CH_2), 1.63 (1H, m, J = 12, 3 Hz, CH_2), 1.72 (3H, t, J = 1.8 Hz, CH_3—C=C), 1.94 (2H, m, J = 11, 3 Hz, CH_2), 2.08 (1H, d of m, J = 12 Hz, CH_2), 2.39 (2H, m, CH_2—C=C), 2.52 (2H, m, O=C—CH_2), 2.78 (1H, m, J = 12, 3 Hz, CH—C=C), 3.74 (1H, m, J = 11, 3 Hz, CH—O). *Exact Mass* calcd. for $C_{12}H_{18}O_2$: 194.1307; found: 194.1311; (*trans*), mp 87–89°C; ir (CCl_4): 3610 (OH), 3460 (br, OH), 1690 (C=O), 1640 (C=C) cm^{-1}; ^1H nmr (80 MHz) ($CDCl_3$) δ: 1.71 (3H, t, J = 1.8 Hz, CH_3C=C), 2.38 (4H, br m, O=C—CH_2CH_2—C=C), 3.21 (1H, m, CH—C=C), 4.22 (1H, m, CH—O); (400 MHz, $CDCl_3$) δ: 1.41 (2H, m, CH_2), 1.65 (4H, m, CH_2), 1.74 (3H, t, J = 1.8 Hz, CH_3—C=C), 1.85 (2H, m, CH_2), 2.38 (2H, m, J = 4 Hz, CH_2—C=C), 2.50 (2H, br m, O=C—CH_2), 3.24 (1H, m, J = 12, 3 Hz, CH—C=C), 4.28 (1H, m, J = 2.5 Hz, CH—O). *Exact Mass* calcd. for $C_{12}H_{18}O_2$: 194.1307; found: 194.1301.

Preparation of substituted cyclopentenones 27, 36, 37, 38

The procedure was identical to the one outlined above for the preparation of olefins **15–17** from enol ether **14**.

For the preparation of authentic **27**, the requisite bromide (2-methylbromocyclopentane) was synthesized from cyclopentanone by addition of methyl lithium, acid-catalyzed elimination to methylcyclopentene, followed by HBr addition. The sample of **27** prepared in this manner (35%) was a 1:20 *cis/trans* isomeric mixture.

Ketone **36**, bp 45–47°C/0.2 Torr was obtained in 82% using an excess (3 *M*) of bromoethane; ir (film): 1690 (C=O), 1640 (C=C) cm^{-1}; ^1H nmr (CCl_4) δ: 1.52 (3H, t, J = 7 Hz, CH_3—CH_2), 1.62 (3H, s, CH_3C=C), 2.27 (2H, m, CH_2—C=C), 2.45 (2H, m, CH_2—C=O).

An authentic sample of 3-isopropyl-2-methyl-2-cyclopentenone (**37**) was prepared in 63% yield with an excess (3 *M*) of 2-bromopropane; ir (film): 1690 (C=O), 1640 (C=C) cm^{-1}; ^1H nmr (CCl_4) δ: 1.15 (6H, d, J = 7 Hz, $(CH_3)_2CH$), 1.60 (3H, s, CH_3—C=C), 2.33 (2H, CH_2—C=C), 2.48 (2H, CH_2—C=O), 3.03 (1H, septet, J = 7 Hz, H—$C(CH_3)_2$).

An authentic sample of 3-*tert*-butyl-2-methyl-2-cyclopentenone **38**, bp 114–122°C/10 Torr was prepared in 53% yield from commercial *tert*-butyllithium; ir (film): 1700 (C=O), 1620 (C=C) cm^{-1}; ^1H nmr (CCl_4) δ: 1.25 (9H, s, $(CH_3)_3C$), 1.77 (3H, t, J ~ 1.5 Hz, CH_3C=C), 2.20 (2H, m, CH_2—C=C), 2.52 (2H, m, CH_2—C=O). *Exact Mass* calcd. for $C_{10}H_{16}O$: 152.1201; found: 152.1204.

Quenching studies: preparation of silyl enol ethers 39–41

A. *LDA/DME method*

Ketone **36** (0.62 g, 0.5 mmol) in DME (5 mL) was added dropwise to LDA (6.5 mmol) in DME (5 mL) at −78°C followed by rapid addition of a DME (10 mL) solution containing triethylamine (0.7 mL, 5 mmol) and chlorotrimethylsilane (2 mL, 15 mmol). After 20 min at −78°C the reaction mixture was allowed to warm to room temperature (22°C), the solvents removed, and the residue distilled (bp 50–51°C/0.5 Torr) to give the endocyclic enol ethers, 0.78 g (83%), **39** and **40** (~5:1, glc); ir (film): 1645 (C=C), 1140 (C—O) cm^{-1}; ^1H nmr (CCl_4) δ: 0.30 (9H, s, $(CH_3)_3$—Si), 1.11 (3H, t, J = 7 Hz, CH_3—CH_2), 1.77 (3H, s, CH_3—C=C), 2.37 (2H, overlapping q, J = 7 Hz, CH_2—CH_3), 2.72 (2H, m, J ~ 2 Hz, =C—CH_2—C=), 4.98 (major), 5.33 (minor) (1H, m, J ~ 2 Hz, CH=C).

B. *$Me_3SiCl/NEt_3/ZnCl_2$ based on the method of Danishefsky and Kitahara (22)*

Zinc chloride (30 mg) and triethylamine (2.5 g) were dissolved in benzene, and chlorotrimethylsilane (4 mL) and ketone **36** (1.24 g, 10 mmol) added. The reaction was stirred under nitrogen for 15 h at 22°C, diluted with hexane, filtered, concentrated, and distilled to give 1.72 g (66%) of the endocyclic enol ethers **39** and **40** (~4:1, glc).

C. *KH/DME method*

Potassium hydride (0.350 g, 8 mmol, 35% oil dispersion, Aldrich) was washed with petroleum ether to remove the oil and DME (5 mL) added. The resulting stirred suspension was cooled in an ice bath and a DME solution (3 mL) of ketone **36** (0.62 g, 5 mmol) added dropwise, followed by a solution of chlorotrimethylsilane (2 mL, 15 mmol) and triethylamine (0.3 mL, 3 mmol) dissolved in DME (5 mL). After 5 min at 0°C and 0.5 h at 22°C the reaction was concentrated, hexane added, the resulting precipitates removed by filtration, and the product distilled, bp 48–50°C/0.5 Torr, to give **41**, 0.4 g (41%); ^1H nmr (CCl_4) δ: 0.19 (9H, s, $(CH_3)_3$—Si), 1.51 (3H, br s, CH_3—CH=C), 1.64 (3H, br s, CH_3—C=C), 2.32 (4H, m, O=C—CH_2CH_2—C=C), 4.88 (1H, br q, J = 6.5 Hz, CH=C).

D. *Intermolecular alkylation with methyl iodide*

Potassium hydride (0.38 g, 3.3 mmol, 35% oil dispersion, Aldrich) was washed with petroleum ether to remove the oil and DME (10 mL) added. The resulting stirred suspension was cooled to −78°C and a DME solution (3 mL) of ketone **36** (0.372 g, 3 mmol) added dropwise, followed by a solution of methyl iodide (0.43 g, 3 mmol) dissolved in DME (1 mL). The reaction was allowed to warm to 22°C, quenched with saturated aqueous ammonium chloride solution, extracted with ether, dried, concentrated, and chromatographed (petroleum ether/ether, 2:1) to give three fractions: 0.126 g (**36**); 0.072 g (mostly **37**); 0.036 g (**37**, **38**, and probably some 3-ethyl-2,5-dimethyl-2-cyclopentenone). The mixtures were not further resolved by glc but comparison of their ^1H nmr spectra with those of authentic samples established their identity.

Acknowledgements

We are grateful to Memorial University of Newfoundland and the Natural Sciences and Engineering Research Council of Canada for financial support of this research; B. Gregory for high resolution mass spectra; H. J. Liu (University of Alberta) for 400 MHz ^1H nmr spectra; and the referees for their constructive comments.

1. L. A. PAQUETTE. Fortschr. Chem. Forsch. **79**, 43 (1979).
2. L. A. PAQUETTE, E. FARKAS, and R. GALEMMO. J. Org. Chem. **46**, 5434 (1981); B. M. TROST and D. P. CURRAN. J. Am. Chem. Soc. **102**, 5699 (1980); M. L. QUESADA, R. H. SCHLESSINGER, and W. H. PARSONS. J. Org. Chem. **43**, 3968 (1978).
3. D. K. KLIPA and H. HART. J. Org. Chem. **46**, 2816 (1981); N. E. SCHORE and M. C. CROUDACE. J. Org. Chem. **46**, 5436 (1981); A. SMITH III, B. TODER, S. BRANCA, and R. K. DIETER. J. Am. Chem. Soc. **103**, 1996 (1981).
4. R. A. LEE, C. MCANDREWS, K. M. PATEL, and W. REUSCH. Tetrahedron Lett. 965 (1973); K. M. PATEL and W. REUSCH. J. Org. Chem. **40**, 1504 (1975); M. L. QUESADA, R. H. SCHLESSINGER, and W. H. PARSONS. J. Org. Chem. **43**, 3968

(1978); J. D'ANGELO. Tetrahedron, **32**, 2979 (1976); N. W. ATWATER. J. Am. Chem. Soc. **82**, 2847 (1960); H. J. RINGOLD and G. ROSENKRANTZ. J. Org. Chem. **22**, 602 (1957); G. STORK and R. L. DANHEISER. J. Org. Chem. **38**, 1775 (1973); G. STORK, G. A. KRANS, and G. A. GARCIA. J. Org. Chem. **39**, 3459 (1974); L. NEDELEC, J. C. GASC, and R. BUCOURT. Tetrahedron, **30**, 3263 (1974).

5. E. PIERS, M. ZBOZNY, and D. C. WIGFIELD. Can. J. Chem. **57**, 1064 (1979).
6. A. P. JOHNSON and V. VAJS. Chem. Commun. 817 (1979).
7. R. L. CARGILL and T. E. JACKSON. J. Org. Chem. **38**, 2125 (1973).
8. J. C. STOWELL. Carbanions in organic synthesis. Wiley, New York, NY. 1979. p. 10.
9. B. M. TROST and L. H. LATIMER. J. Org. Chem. **42**, 3212 (1977).
10. M. KOREEDA, Y. LIANG, and H. AKAG. Chem. Commun. 449 (1979); M. KOREEDA and S. G. MISLANKAR. Abstract ORGN 182, 185th American Chemical Society National Meeting, Seattle, Washington. March 20–25, 1983; J. Am. Chem. Soc. **105**, 7203 (1983).
11. R. E. BENSON and R. V. LINDSEY, JR. J. Am. Chem. Soc. **79**, 5471 (1957).
12. E. PIERS, J. BANVILLE, C. K. LAU, and I. NAGAKURA. Can. J. Chem. **60**, 2965 (1982).
13. J. E. BALDWIN. Chem. Commun. 734 (1976); J. E. BALDWIN, R. C. THOMAS, L. I. KRUSE, and L. SILBERMAN. J. Org. Chem. **42**, 3846 (1977).
14. (*a*) G. STORK and J. F. COHEN. J. Am. Chem. Soc. **96**, 5270 (1974); (*b*) P. DESLONGCHAMPS. Stereoelectronic effects in organic chemistry. Pergamon Press, Oxford. 1983. pp. 166–172.
15. H. O. HOUSE, L. J. CZUBA, M. GALL, and H. D. OLMSTEAD. J. Org. Chem. **34**, 2324 (1969); H. O. HOUSE, M. GALL, and H. D. OLMSTEAD. J. Org. Chem. **36**, 2361 (1971).
16. R. L. SNOWDEN. Tetrahedron Lett. **22**, 97 (1981).
17. E. L. ELIEL, N. L. ALLINGER, S. J. ANGYAL, and G. A. MORRISON. Conformational analysis. Wiley, New York, NY. 1965. p. 28; L. P. HAMMET. Physical Organic Chemistry, 2nd ed. McGraw–Hill Book Co., New York, NY. 1970. pp. 119–120.
18. R. E. LEYDE, E. WITT, and J. C. PATTISON. J. Org. Chem. **21**, 61 (1956).
19. C. L. WILSON. J. Chem. Soc. 48 (1945).
20. S. J. ALWARD and A. G. FALLIS. Can. J. Chem. **62**, 121 (1984).
21. J. L. LUCHE and J. C. DAMIANO. J. Am. Chem. Soc. **102**, 7926 (1980).
22. S. DANISHEFSKY and T. KITAHARA. J. Am. Chem. Soc. **96**, 7807 (1974).

Can. J. Chem. Downloaded from www.nrcresearchpress.com by 210.87.254.5 on 09/06/12
For personal use only.

Structural studies of organoboron compounds. XVI.[1] Preparation and crystal and molecular structures of 4,4-dimethyl-2,5,5-triphenyl-1,3-dioxa-4-azonia-2-bora-5-boratacyclopentane and 4,4,5,5-tetramethyl-2,2-diphenyl-1,3-dioxa-4-azonia-2-boratacyclopentane

W. KLIEGEL AND H.-W. MOTZKUS

Institut für Pharmazeutische Chemie der Technischen Universität Braunschweig, 3300 Braunschweig, Beethovenstraße 55, Bundesrepublik Deutschland

AND

STEVEN J. RETTIG AND JAMES TROTTER

Department of Chemistry, University of British Columbia, 2036 Main Mall, Vancouver, B.C. Canada V6T 1Y6

Received February 23, 1983[2]

W. KLIEGEL, H.-W. MOTZKUS, STEVEN J. RETTIG, and JAMES TROTTER. Can. J. Chem. **62**, 838 (1984).

Details of the synthesis, physical properties, and molecular structures of 4,4-dimethyl-2,5,5-triphenyl-1,3-dioxa-4-azonia-2-bora-5-boratacyclopentane, **4**, and 4,4,5,5-tetramethyl-2,2-diphenyl-1,3-dioxa-4-azonia-2-boratacyclopentane, **5**, are reported. Crystals of **4** are triclinic, a = 9.841(2), b = 14.722(3), c = 6.6701(12) Å, α = 86.79(1), β = 102.95(1), γ = 93.89(1)°, Z = 2, space group $P\bar{1}$; and those of **5** are monoclinic, a = 14.9164(12), b = 6.4732(3), c = 18.2248(15) Å, β = 117.263(3)°, Z = 4, space group Cc. Both structures were solved by direct methods and were refined by full-matrix least-squares procedures to final R values of 0.032 and 0.035 for 1456 and 1649 observed reflections, respectively. Molecules of **4** contain non-planar BOBON rings with an unusually long N(sp^3)—B(sp^3) distance of 1.728(3) Å and in **5** there is a long N(sp^3)—C(sp^3) bond of 1.591(3) Å. These structural features are ascribed to steric hindrance.

W. KLIEGEL, H.-W. MOTZKUS, STEVEN J. RETTIG et JAMES TROTTER. Can. J. Chem. **62**, 838 (1984).

On rapporte les détails relatifs à la synthèse, aux propriétés physiques et aux structures moléculaires du diméthyl-4,4 triphényl-2,5,5 dioxa-1,3 azonia-4 bora-2 borata-5 cyclopentane (**4**) et du tétraméthyl-4,4,5,5 diphényl-2,2 dioxa-1,3 azonia-4 borata-2 cyclopentane (**5**). Les cristaux de **4** sont tricliniques, a = 9,841(2), b = 14,722(3), c = 6,6701(12) Å, α = 86,79(1), β = 102,95(1), γ = 93,89(1)°, Z = 2, groupe d'espace $P\bar{1}$; ceux de **5** sont monocliniques, a = 14,9164(12), b = 6,4732(3), c = 18,2248(15) Å, β = 117,263(3)°, Z = 4, groupe d'espace Cc. On a résolu les deux structures par des méthodes directes et on les a affinées par la méthode des moindres carrés (matrices complètes) jusqu'à des valeurs finales respectives de R de 0,032 et 0,035 pour 1456 et 1649 réflexions observées. Les molécules de **4** comportent des cycles BOBON qui ne sont pas plans et qui contiennent des liaisons N(sp^3)—B(sp^3) qui sont anormalement longues (1,728(3) Å); dans **5**, il existe une liaison N(sp^3)—C(sp^3) qui est longue (1,591(3) Å). On attribue ces caractéristiques à l'empêchement stérique.

[Traduit par le journal]

Introduction

It is known (1) that *O*-acylation of *N,N*-dialkylhydroxylamines by organoboron compounds leads to *N,N*-dialkylaminoxyboranes. In solution these compounds exist both as monomeric "BON" compounds and as dimeric "BONBON" compounds, depending on steric requirements and the interaction between the N- and B-substituents. The product **2** of the acylation of *N-N*-dimethylhydroxylamine, **1**, with diphenylborinic acid derivatives Ph_2B—X (e.g. X = $OBPh_2$) was trapped by reaction with phenylboronic acid or with acetone. The resulting 1:1 adducts of the "monomeric" form of **2** with phenylboronoxide[3] and with acetone show elemental analyses consistent with the proposed structures **3**–**6**. ^{1}H nmr spectra and reactions with diphenylcarbazone (2) indicate the presence of intact Ph_2B moieties and hydrolysis followed by oxidation of the liberated *N,N*-dimethylhydroxylamine with triphenyltetrazolium chloride (3) indicates the presence of intact N—O bonds in both of the 1:1 adducts.

The phenylboronoxide adduct can be described by the structures **3** or **4**, both of which are consistent with the chemical and spectral data for the isolated material. Both forms contain diphenylborinic acid and phenylboronic acid residues in anhydridic linkage as well as a hydrolytically separable *N,N*-dimethylhydroxylamine moiety. The form **3**, favored on steric grounds, corresponds to the diphenylboron chelates of *N,N*-dimethylhydroxylamine–aldehyde adducts (4), the structure of this type of compound having been confirmed by the X-ray crystallographic analysis of the representative example **8** (5). The alternate form **4** resembles the diphenylborinates of amino-alcohols, for which intramolecular N→B coordination has been established by X-ray analyses of a number of examples (6–9), as well as comparable oxime derivatives such as **7** which also contain N→B coordinative bonds (10). The mass spectrum of the phenylboronoxide adduct, which shows a molecular ion of low intensity, does not unambiguously indicate either **3** or **4**. Prominent fragments such as $(M - Ph)^+$, $(M - PhBO)^+$, or $(M - Ph_2BO)^+$ are consistent with either form. An X-ray crystallographic study was undertaken in order to resolve this ambiguity.

A very similar problem arises with the acetone adduct, for which the two alternative structures **5** and **6** come into question. An identical compound was also isolated during an attempted recrystallization of **3**/**4** from acetone. Structure **5** is analogous to the well established (5) diphenylboron chelate type **8**. The form **6** can otherwise be regarded as a carba-analog of **4**, considering the exchange of the boronate ester group for the acetal group. However, the similarity of the components in the synthesis of **8** and in that of the acetone derivative supports the

[1]Previous paper in this series: ref. 9.

[2]Revision received November 4, 1983.

[3]The anhydride of phenylboronic acid ("phenylboronoxide") exists only as a trimeric triphenylboroxin, $(PhBO)_3$, under normal conditions.

Can. J. Chem. Downloaded from www.nrcresearchpress.com by 210.87.254.6 on 09/06/12
For personal use only.

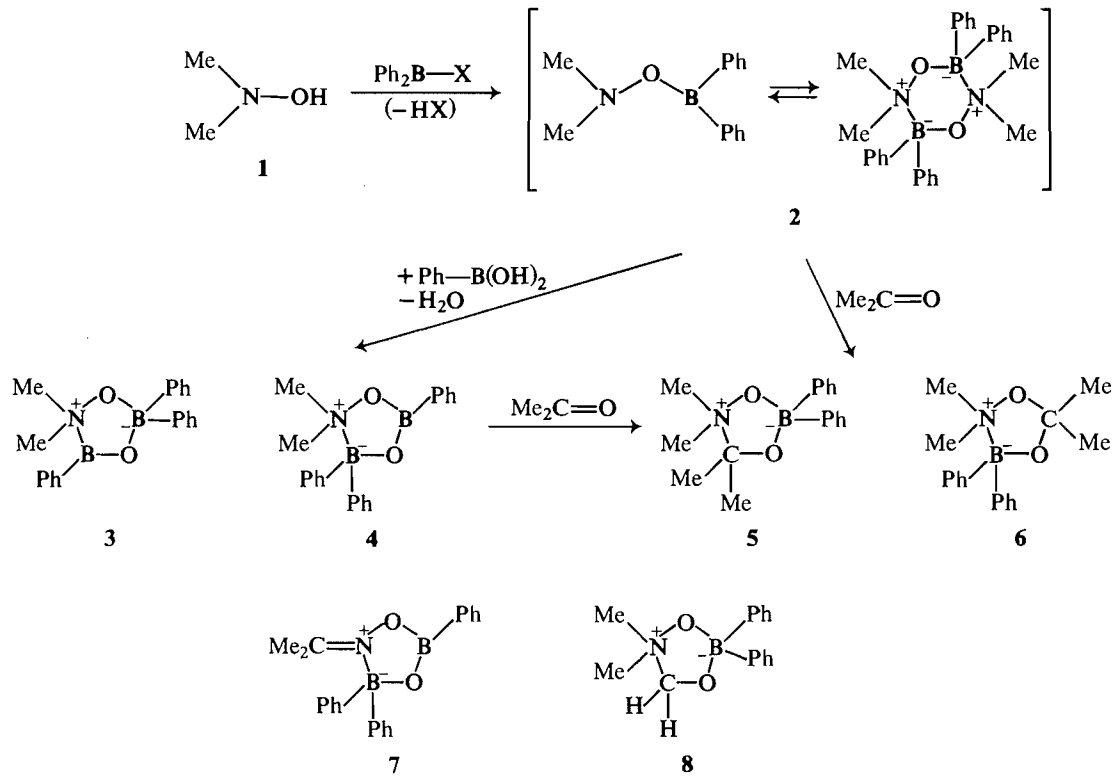

chelate structure **5**.

For both ring systems, **5** and **6**, a considerable steric strain can be expected to influence the stability of the compound. The mass spectrum does not register a peak corresponding to the molecular ion. Typical fragments are $(M - Me_2CO)^+$, $(M - Me_2CO - O)^+$, $(Ph_2BO)^+$, and $(Ph_2B)^+$. An x-ray crystallographic analysis of this compound was undertaken in order to verify the structure **5** and to assess the structural differences between this compound and the more stable derivative **8**.

Experimental

4,4-Dimethyl-2,5,5-triphenyl-1,3-dioxa-4-azonia-2-bora-5-boratacyclopentane, 4

Method A

To a solution of *N,N*-dimethylhydroxylamine hydrochloride (0.49 g, 5 mmol) in 1 *M* NaOH (5 mL), oxybis(diphenylborane) (0.87 g, 2.5 mmol) was added. After shaking this mixture with chloroform (30 mL), the organic phase was separated and the chloroform removed *in vacuo*. The remaining oil was dissolved in ethanol (10 mL). After dissolving phenylboronic acid (0.61 g, 5 mmol) in this solution, crystallization of a white substance began at room temperature. The product was recrystallized from ethanol. Yield: 1.29 g (78%). Mp 103°C.

Method B

N,N-Dimethylhydroxylamine hydrochloride (0.49 g, 5 mmol), oxybis(diphenylborane) (0.87 g, 2.5 mmol), and phenylboronic acid (0.61 g, 5 mmol) were disolved in ethanol (10 mL). This solution was then carefully underlayed with 1 *M* NaOH (5 mL), avoiding mixture. At the interface between the two layers, white crystals began to grow at room temperature which were analytically pure after washing with ethanol. Yield: 1.09 g (65%). This substance is shown to be identical to that synthesized by method A by mp and ir spectrum.

Anal. calcd. for $C_{20}H_{21}B_2NO_2$ (fw = 329.0): C 73.01, H 6.43, B 6.57, N 4.26; found: C 72.62, H 6.43, B 6.24, N 4.60. ^{1}H nmr (90 MHz, $CDCl_3$/TMS): δ(ppm) = 2.76 (s, NMe_2), 7.1–8.1 (m, BPh_2, BPh). Mass spectrum (70 eV): *m/e* (% relative intensity) = 329(3, M^+), 312(3, $[PhBO]_3$), 284(4), 268(1), 252(100, M − Ph), 237(1), 225(3, M − PhBO), 209(7, M − $PhBO_2$), 181(12, Ph_2BO), 174(15), 165(68, Ph_2B), 154(54), 148(60, M − Ph_2BO), 132(34), 113(12), 105(51, PhBOH), 91(39), 77(49), 70(20), 58(22), 53(42), 44(49).

The substance gives a positive blue color reaction with diphenylcarbazone (2) in methanolic solution. An ethanolic solution of the substance and crystals of triphenyltetrazolium chloride gives a deep red color reaction upon addition of aqueous NaOH (3). Crystals suitable for X-ray analysis were obtained according to method B.

4,4,5,5-Tetramethyl-2,2-diphenyl-1,3-dioxa-4-azonia-2-boratacyclopentane, 5

Oxybis(diphenylborane) (0.87 g, 2.5 mmol) and *N,N*-dimethylhydroxylamine hydrochloride (0.49 g, 5 mmol) were suspended in acetone (15 mL). After the addition of 1 *M* NaOH (5 mL) white crystals began to precipitate at room temperature. The substance was recrystallized from acetone. Yield: 1.33 g (94%). Mp 142–143°C.

Anal. calcd. for $C_{17}H_{22}BNO_2$ (fw = 283.2): C 72.11, H 7.83, N 4.95; found: C 71.85, H 7.86, N 4.94. ^{1}H nmr (90 MHz, $CDCl_3$/TMS): δ (ppm) = 2.17 (s, CMe_2), 2.62 and 2.82 (s, 5H and s, 1H, NMe_2), 7.2–7.9 (m, BPh_2). Mass spectrum (70 eV): *m/e* (relative intensity) = 312(5, $[PhBO]_3$), 252(96, M − Me_2CO), 209(11, M − Me_2CO − O), 195(3), 185(45, Ph_2BO), 165(100, Ph_2B), 154(4), 148(56, M − Me_2CO − Ph), 137(34), 132(45, M − Me_2CO − O − Ph), 121(64), 113(33), 105(43, PhBOH), 91(39), 77(68), 58(32), 51(45), 43(52).

The substance gives a positive blue color reaction with diphenylcarbazone and a red color reaction with triphenyltetrazolium chloride similar to compound **4**. Compound **5** was also obtained by recrystallization of **4** from acetone. Crystals of **5** suitable for X-ray analysis were obtained by recrystallization from acetone.

X-ray crystallographic analyses

4,4-Dimethyl-2,5,5-triphenyl-1,3-dioxa-4-azonia-2-bora-5-boratacyclopentane, 4

A crystal bounded by the six faces (followed by their distances in mm from a common origin): ±(1 0 0), 0.050, ±(0 1 0), 0.131, ±(0 1 2), 0.213 was mounted in a general orientation. Unit-cell parameters were refined by least-squares on 2 sin θ/λ values for 25

Can. J. Chem. Downloaded from www.nrcresearchpress.com by 210.87.254.6 on 09/06/12
For personal use only.

Can. J. Chem. Downloaded from www.nrcresearchpress.com by 210.87.254.6 on 09/06/12
For personal use only.

reflections ($2\theta = 30-40°$) measured on a diffractometer with Mo-Kα Radiation ($\lambda(K\alpha_1) = 0.70930$, $\lambda(K\alpha_2) = 0.71359$ Å). Crystal data at 22°C are:

$C_{20}H_{21}B_2NO_2$ fw = 329.0

Triclinic, $a = 9.841(2)$, $b = 14.722(3)$, $c = 6.6701(12)$ Å, $\alpha = 86.79(1)$, $\beta = 102.95(1)$, $\gamma = 93.89(1)°$, $V = 938.8(3)$ Å^3, $Z = 2$, $\rho_c = 1.164$ g cm^{-3}, $F(000) = 348$, μ(Mo-Kα) = 0.68 cm^{-1}. Absent reflections: none, space group $P\bar{1}$ (C_i^1, No. 2) from structure analysis.

Intensities were measured with graphite-monochromated Mo-Kα radiation on an Enraf-Nonius CAD4-F diffractometer. An $\omega-2\theta$ scan at 1.06–10.06° min^{-1} over a range of $(0.65 + 0.35 \tan\theta)$ degrees in ω (extended by 25% on both sides for background measurement) was employed. Data were measured to $2\theta = 51°$. The intensities of three check reflections, measured every 3600 s throughout the data collection, remained constant to within 3%.

Of the 3474 independent reflections measured and processed,[4] 1456 (42%) had intensities greater than $3\sigma(I)$ above background where $\sigma^2(I) = S + 2B + (0.04(S - B))^2$ with S = scan count and B = normalized background count. The structure was solved by direct methods, the positions of all non-hydrogen atoms being determined from an E-map. After full-matrix least-squares refinement of the non-hydrogen atoms with anisotropic thermal parameters to $R = 0.084$, all 21 hydrogen atoms were positioned from a difference map and were subsequently included in the refinement with isotropic thermal parameters. The scattering factors of ref. 11 were used for non-hydrogen atoms and those of ref. 12 for hydrogen atoms. The weighting scheme, $w = 1/\sigma^2(F)$ where $\sigma^2(F)$ is derived from the previously defined $\sigma^2(I)$, gave uniform average values of $w(|F_o| - |F_c|)^2$ over ranges of both $|F_o|$ and $\sin\theta/\lambda$ and was employed in the final stages of refinement. Unobserved reflections were not included in the refinement. Convergence was reached at $R = 0.032$ and $R_w = 0.036$ for 1456 reflections with $I \geq 3\sigma(I)$. For all 3474 reflections $R = 0.130$. The function minimized was $\Sigma w(|F_o| - |F_c|)^2$, $R = \Sigma||F_o| - |F_c||/\Sigma|F_o|$ and $R_w = (\Sigma w(|F_o| - |F_c|)^2/\Sigma w|F_o|^2)^{1/2}$.

On the final cycle of refinement the mean and maximum parameter shifts corresponded to 0.07 and 0.51σ, respectively. The mean error in an observation of unit weight was 1.630. A final difference map showed no unusual features. The final positional and thermal parameters appear in Tables 1 and 2[5] respectively. Measured and calculated structure factors have been placed in the Depository of Unpublished Data.[5]

4,4,5,5-Tetramethyl-2,2-diphenyl-1,3-dioxa-4-azonia-2-boratacyclopentane, ***5***

Experimental details are as above except where noted. The crystal employed for data collection was bounded by the 10 faces (followed by their distances in mm from a common origin): ±(1 1 0), 0.213, ±(1 0 −1), 0.188, ±(1 −1 0), 0.250, ±(0 0 1), 0.325, (−1 0 0), 0.250, and (−1 −1 1), 0.238. Crystal data are as follows:

$C_{17}H_{22}BNO_2$ fw = 283.2

Monoclinic, $a = 14.9164(12)$, $b = 6.4732(3)$, $c = 18.2248(15)$ Å, $\beta = 117.263(3)°$, $V = 1564.2(2)$ Å^3, $Z = 4$, $\rho_c = 1.202$ g cm^{-3}, $F(000) = 608$, μ(Mo-Kα) = 0.74 cm^{-1}. Absent reflections: hkl, $h + k$ odd, and $h0l$, l odd, space group Cc (C_s^4, No. 9) assumed on the basis of the number of molecules in the unit cell.

An $\omega-2\theta$ scan at 1.68–10.06° min^{-1} over a range of $(0.85 + 0.35 \tan\theta)°$ in ω was employed. Of 2261 independent reflections measured (to $2\theta = 60°$), 1649 (73%) had intensities greater than $3\sigma(I)$ above background. The intensities of the check reflections remained constant to within 2%.

The structure was solved by direct methods, all non-hydrogen atoms being located from an E-map. After refinement of the non-hydrogen atoms with anisotropic thermal parameters to $R = 0.065$, all 22 hydrogen atoms were positioned from a difference map and were refined with isotropic thermal parameters in subsequent least-squares cycles. Convergence was reached at $R = 0.035$ and $R_w = 0.041$ for 1649 observed reflections, for all 2261 reflections $R = 0.053$. The mean and maximum parameter shifts on the final cycle of refinement corresponded to 0.08 and 0.70σ, respectively, the maximum shift being associated with the y coordinate of H(3c). The mean error in an observation of unit weight was 1.846.

Analysis of thermal motion

The thermal motion in both structures (Figs. 1 and 2) has been analysed in terms of the rigid-body modes of translation, libration, and screw-motion (13). The rms errors in the U_{ij} (derived from the least-squares analyses) are 0.0009 and 0.0012 Å^2 for **4** and **5** respectively. In each case analysis of the entire molecule indicated significant independent motion of various fragments which were separately analysed (rms $\Delta U_{ij} = 0.0007-0.0038$ Å^2). The appropriate bond distances have been corrected for libration (13, 14), using shape parameters q^2 of 0.08 for all atoms involved. Corrected bond lengths appear in Table 3 along with the uncorrected values; corrected bond angles do not differ by more than 1σ from the uncorrected values given in Table 4. Intra-annular torsion angles defining the conformations of chelate rings are listed in Table 5. Bond lengths and angles involving hydrogen and a complete listing of torsion angles (Tables 6–8) are included as supplementary material.

Results and discussion

The X-ray analyses show that the "phenylboronoxide" and acetone adducts of **2** have the structures **4** and **5**, respectively. The crystal structure of **4** consists of discrete molecules separated by normal van der Waals distances, and that of **5** consists of molecules each linked to two others (related by translations along b) by weak C—H···O interactions (C(16)—H(16b) ···O(1) (x, 1 + y, z), H···O = 2.46(4), C···O = 3.411(4) Å, C—H···O = 159(2)°).

The five-membered BOBON ring in **4**, unlike the essentially planar analogs in **7** (10) and **9** (15), is significantly non-planar and has a distorted B(2)–envelope conformation (see Table 5). The phenyl ring bonded to the trigonal planar boron atom is twisted out of the B(1) coordination plane by 7.1°, this value being similar to those observed for other derivatives of phenylboronic acid (10, and references therein). The non-planarity of the five-membered heterocycle results from steric interactions between the adjacent Ph_2B and Me_2N moieties, which would be in an eclipsed conformation with respect to the N—B bond if the ring were planar. The strain is also relieved by a considerable lengthening of the N—B bond to 1.728(3) Å,[6] compared with a mean[7] value of 1.654(1) Å for compounds **10** (R = H) (6–8), 1.630(3) Å in L-prolinatodiphenylboron **11** (16),

[4]The computer programs used include locally written programs for data processing and locally modified versions of the following: MULTAN 80, multisolution program by P. Main, S. J. Fiske, S. E. Hull, L. Lessinger, G. Germain, J. P. Declercq, and M. M. Woolfson; ORFLS, full-matrix least-squares, and ORFFE, function and errors, by W. R. Busing, K. O. Martin and H. A. Levy; FORDAP, Patterson and Fourier synthesis, by A. Zalkin; ORTEP II, illustrations, by C. K. Johnson.

[5]The structure factor table, Table 2 (anisotropic thermal parameters) and other material mentioned in the text are available, at a nominal charge, from the Depository of Unpublished Data, CISTI, National Research Council of Canada, Ottawa, Ont., Canada K1A 0S2.

[6]Libration-corrected bond lengths (esd's assumed equal to those of the uncorrected values) are employed throughout the discussion. All distances compared to those reported here have been similarly treated except those for compound **12**, the structure of which was determined at 87 K.

[7]Here and elsewhere in this report mean values refer to weighted means with rms deviations from the mean in parentheses.

TABLE 1. Final positional (fractional) and isotropic thermal parameters ($U \times 10^3$ Å^2) with estimated standard deviations in parentheses

Atom	x	y	z	U_{eq}/U_{iso}	Atom	x	y	z	U_{eq}/U_{iso}
	4 ($\times 10^4$, H $\times 10^3$)					**5** ($\times 10^5$, H $\times 10^4$)			
O(1)	6835(2)	3378(1)	4680(3)	64	O(1)	44630	3586(20)	50170	38
O(2)	5730(2)	3189(1)	7400(2)	51	O(2)	49208(16)	37499(21)	48558(14)	39
N	5892(2)	2575(1)	4213(3)	55	N	41033(19)	38210(30)	50359(16)	46
C(1)	4714(4)	2897(3)	2567(5)	80	C(1)	36215(21)	15999(32)	47566(17)	39
C(2)	6681(4)	1915(3)	3392(6)	81	C(2)	30130(26)	15200(51)	38266(20)	59
C(3)	7419(3)	4602(2)	7317(4)	62	C(3)	29907(27)	9832(51)	51698(25)	60
C(4)	7384(4)	4893(2)	9257(6)	82	C(4)	63272(19)	10778(30)	57600(16)	36
C(5)	8160(5)	5663(2)	10054(8)	104	C(5)	70230(21)	26265(42)	61733(19)	47
C(6)	8974(5)	6141(3)	8895(10)	114	C(6)	79184(24)	22427(49)	68758(20)	59
C(7)	9034(5)	5882(3)	6987(10)	120	C(7)	81374(24)	2706(47)	71908(19)	57
C(8)	8257(4)	5110(2)	6222(7)	93	C(8)	74715(24)	−13080(46)	67976(18)	54
C(9)	6561(2)	1587(1)	7846(3)	42	C(9)	65815(22)	−9052(41)	60858(18)	45
C(10)	6183(3)	706(2)	8481(4)	51	C(10)	53938(18)	9913(31)	41094(15)	34
C(11)	7118(3)	151(2)	9765(4)	58	C(11)	52469(20)	−9941(35)	37718(17)	44
C(12)	8478(3)	461(2)	10470(4)	61	C(12)	53724(23)	−14187(45)	30744(17)	52
C(13)	8905(3)	1320(2)	9872(4)	63	C(13)	56555(22)	1226(46)	27013(17)	53
C(14)	7959(2)	1869(2)	8604(4)	55	C(14)	58115(21)	20868(42)	30216(17)	49
C(15)	3857(2)	1926(2)	6113(3)	47	C(15)	56753(19)	25140(37)	37135(16)	41
C(16)	2897(3)	2380(2)	6877(4)	57	C(16)	34240(26)	55416(47)	45550(27)	67
C(17)	1509(3)	2088(2)	6557(5)	72	C(17)	44943(32)	41249(56)	59433(21)	66
C(18)	1022(3)	1343(2)	5419(5)	75	B	52878(20)	15149(35)	49360(17)	33
C(19)	1921(3)	868(2)	4633(5)	69	H(2a)	2375(40)	2231(69)	3624(31)	96(13)
C(20)	3317(3)	1157(2)	4986(4)	59	H(2b)	2862(27)	−17(55)	3670(20)	64(9)
B(1)	6599(3)	3712(2)	6506(5)	54	H(2c)	3482(24)	2039(47)	3586(19)	59(7)
B(2)	5457(3)	2273(2)	6525(4)	44	H(3a)	2505(30)	2005(60)	5096(24)	69(10)
H(1a)	515(3)	321(2)	132(5)	97(9)	H(3b)	3409(32)	852(55)	5773(27)	81(11)
H(1b)	409(3)	237(2)	209(4)	94(10)	H(3c)	2822(25)	−428(61)	5032(20)	67(10)
H(1c)	425(3)	336(2)	319(4)	85(11)	H(5)	6963(28)	3711(59)	5951(23)	68(11)
H(2a)	761(4)	177(2)	438(5)	114(12)	H(6)	8395(29)	3476(51)	7180(22)	63(8)
H(2b)	686(3)	223(2)	218(5)	89(10)	H(7)	8774(29)	75(52)	7663(23)	66(8)
H(2c)	607(4)	141(2)	296(5)	114(13)	H(8)	7602(21)	−2668(49)	6971(19)	49(7)
H(4)	670(3)	455(2)	1008(5)	106(12)	H(9)	6164(24)	−1863(55)	5910(18)	55(8)
H(5)	820(4)	590(3)	1152(7)	150(15)	H(11)	5039(23)	−2099(48)	4029(18)	54(8)
H(6)	948(4)	667(3)	927(5)	124(14)	H(12)	5363(22)	−2688(54)	2927(19)	54(8)
H(7)	958(4)	621(3)	610(7)	165(18)	H(13)	5760(23)	−64(47)	2216(21)	61(8)
H(8)	836(3)	492(2)	490(5)	98(12)	H(14)	5985(23)	3153(52)	2740(18)	57(8)
H(10)	519(2)	48(1)	804(3)	47(6)	H(15)	5810(25)	3900(56)	3911(19)	60(9)
H(11)	681(2)	−46(2)	1017(4)	72(8)	H(16a)	2890(40)	5342(86)	4739(37)	133(16)
H(12)	914(2)	10(1)	1129(4)	61(7)	H(16b)	3782(26)	6834(54)	4839(19)	56(8)
H(13)	986(3)	157(2)	1040(4)	80(8)	H(16c)	3283(34)	5055(65)	3992(30)	82(12)
H(14)	829(2)	249(2)	822(3)	60(7)	H(17a)	3977(31)	4326(57)	6068(24)	73(9)
H(16)	323(3)	292(2)	759(4)	72(8)	H(17b)	4873(38)	5337(76)	6025(27)	90(13)
H(17)	92(3)	246(2)	709(4)	86(10)	H(17c)	4940(36)	2885(69)	6230(30)	87(12)
H(18)	7(3)	116(2)	515(4)	68(8)					
H(19)	164(3)	32(2)	378(4)	85(9)					
H(20)	399(3)	81(1)	443(4)	66(8)					

*Equivalent U = (1/3) trace (diagonalized U).

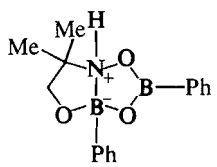

9

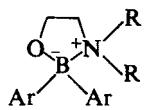

10

R = H; Ar = C_6H_5, *p*-FC_6H_4, *p*-$CH_3C_6H_4$
R = Me; Ar = C_6H_5

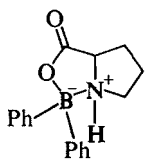

11

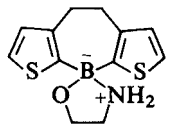

12

1.635(3) in **12** (17), 1.676(4) Å in the closely related azomethene derivative **7** (10), 1.692(2) Å in the pyroboronate complex **9** (15), and 1.691(2) Å for the sterically hindered bond in **10** (Ar = Ph, R = Me) (9). It was noted previously (10) that despite significant differences between corresponding bond lengths, the sums of bond lengths in the planar BOBON rings of **7** and **9** are identical. In **4** those bonds in the stable —B—O—B(Ph)O— moiety are equal in length (within experimental error) to those in **7**, while both bonds involving nitrogen are significantly longer than those in **7** and **9**. As in **7** and **9**, there is the characteristic short anhydridic O—B(sp^2) bond (1.340(3) Å), indicative of a strong π-interaction. The mean B(sp^3)—C and B(sp^2)—C distances (1.605(11) and 1.553(4) Å) are normal and essentially equal to those in **7**

Can. J. Chem. Downloaded from www.nrcresearchpress.com by 210.87.254.6 on 09/06/12
For personal use only.

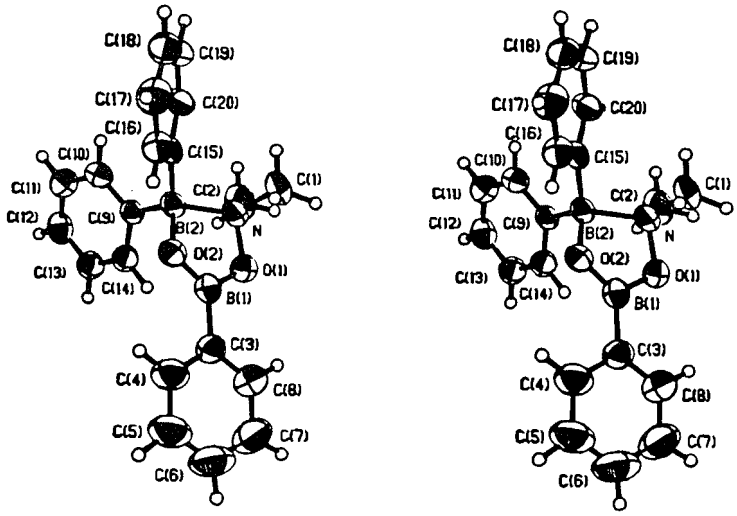

FIG. 1. Stereoscopic view of 4,4-dimethyl-2,5-5-triphenyl-1,3-dioxa-4-azonia-2-bora-5-boratacyclopentane. 50% probability thermal ellipsoids are shown for the non-hydrogen atoms; hydrogen atoms have been assigned arbitrarily small thermal parameters for the sake of clarity.

TABLE 3. Bond lengths (Å) with estimated standard deviations in parentheses

	Length			Length	
Bond	Uncorr.	Corr.	Bond	Uncorr.	Corr.
			4		
O(1)—N	1.457(2)	1.467	C(9)—C(10)	1.395(3)	1.403
O(2)—B(1)	1.410(3)	1.422	C(9)—C(14)	1.398(3)	1.406
O(2)—B(1)	1.329(3)	1.340	C(9)—B(2)	1.612(3)	1.615
O(2)—B(2)	1.483(3)	1.487	C(10)—C(11)	1.385(3)	1.388
N—C(1)	1.491(3)	1.504	C(11)—C(12)	1.371(3)	1.379
N—C(2)	1.483(4)	1.496	C(12)—C(13)	1.372(4)	1.380
N—B(2)	1.717(3)	1.728	C(13)—C(14)	1.381(4)	1.384
C(3)—C(4)	1.394(4)	1.406	C(15)—C(16)	1.392(3)	1.402
C(3)—C(8)	1.378(4)	1.389	C(15)—C(20)	1.402(3)	1.408
C(3)—B(1)	1.549(4)	1.553	C(15)—B(2)	1.591(3)	1.594
C(4)—C(5)	1.385(4)	1.388	C(16)—C(17)	1.377(4)	1.381
C(5)—C(6)	1.370(6)	1.382	C(17)—C(18)	1.367(4)	1.374
C(6)—C(7)	1.364(6)	1.375	C(18)—C(19)	1.370(4)	1.380
C(7)—C(8)	1.381(5)	1.385	C(19)—C(20)	1.382(4)	1.386
			5		
O(1)—C(1)	1.379(3)	1.387	C(5)—C(6)	1.385(4)	1.389
O(1)—B	1.504(3)	1.507	C(6)—C(7)	1.376(5)	1.384
O(2)—N	1.401(2)	1.410	C(7)—C(8)	1.376(4)	1.384
O(2)—B	1.530(3)	1.534	C(8)—C(9)	1.391(4)	1.395
N—C(1)	1.584(3)	1.591	C(10)—C(11)	1.398(3)	1.405
N—C(16)	1.491(3)	1.500	C(10)—C(15)	1.395(3)	1.401
N—C(17)	1.493(4)	1.505	C(10)—B	1.621(3)	1.624
C(1)—C(2)	1.513(4)	1.524	C(11)—C(12)	1.394(3)	1.398
C(1)—C(3)	1.504(3)	1.511	C(12)—C(13)	1.378(4)	1.384
C(4)—C(5)	1.390(3)	1.399	C(13)—C(14)	1.374(4)	1.381
C(4)—C(9)	1.392(3)	1.400	C(14)—C(15)	1.394(3)	1.397
C(4)—B	1.614(3)	1.618			

(1.603(1) and 1.548(5) Å).

The five-membered BOCNO ring in **5** has a distorted C(1)—envelope conformation in which both O(1) and B lie on the same side of the NCO(2) plane. In **8** the corresponding ring has a distorted O(1)—envelope conformation with C(1) and N on the same side of the OBO plane. The conformational change allows for partial staggering of the methyl groups about the C(1)—N bond, analogous to the situation in **4**. The C(1)—N bond is lengthened to 1.591(3) Å as a result of the steric hindrance, the corresponding distance in **8** being 1.505(10) Å. This increase in the C(1)—N distance is compensated by a shortening of the B—O(2) bond from 1.556(8) Å in **8** to 1.534(3) Å in **5**, the remaining bond lengths in the five-membered heterocyclic rings of **5** and **8** being equal within experimental error. The N(sp^3)—Me bond lengths in both **5** and **8** assume normal values of about 1.50 Å. The bond angles in the five-membered ring also show evidence of the steric strain; the angles at N, C(1), and O(1) being 102.12(15),

Can. J. Chem. Downloaded from www.nrcresearchpress.com by 210.87.254.6 on 09/06/12
For personal use only.

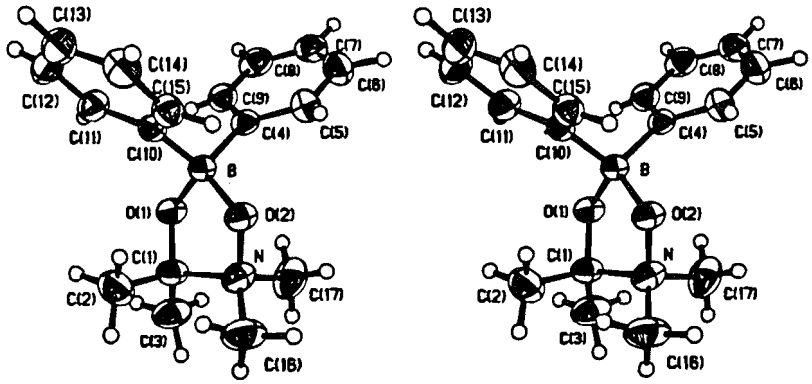

FIG. 2. Stereoscopic view of 4,4,5,5-tetramethyl-2,2-diphenyl-1,3-dioxa-4-azonia-2-boratacyclopentane. 50% probability thermal ellipsoids are shown for the non-hydrogen atoms; hydrogen atoms have been assigned arbitrarily small thermal parameters for the sake of clarity.

TABLE 4. Bond angles (deg) with estimatated standard deviations in parentheses

Bonds	Angle (deg)	Bonds	Angle (deg)
		4	
N—O(1)—B(1)	106.5(2)	C(11)—C(12)—C(13)	119.3(3)
B(1)—O(2)—B(2)	111.8(2)	C(12)—C(13)—C(14)	119.9(3)
O(1)—N—C(1)	104.6(2)	C(9)—C(14)—C(13)	123.0(3)
O(1)—N—C(2)	106.0(2)	C(16)—C(15)—C(20)	115.7(2)
O(1)—N—B(2)	103.32(14)	C(16)—C(15)—B(2)	121.0(2)
C(1)—N—C(2)	110.3(3)	C(20)—C(15)—B(2)	123.3(2)
C(1)—N—B(2)	114.6(2)	C(15)—C(16)—C(17)	122.1(3)
C(2)—N—B(2)	116.6(2)	C(16)—C(17)—C(18)	120.3(3)
C(4)—C(3)—C(8)	117.4(3)	C(17)—C(18)—C(19)	120.1(3)
C(4)—C(3)—B(1)	120.3(3)	C(18)—C(19)—C(20)	119.4(3)
C(8)—C(3)—B(1)	122.2(3)	C(15)—C(20)—C(19)	122.5(3)
C(3)—C(4)—C(5)	121.4(4)	O(1)—B(1)—O(2)	115.0(2)
C(4)—C(5)—C(6)	118.7(5)	O(1)—B(1)—C(3)	117.8(2)
C(5)—C(6)—C(7)	121.9(4)	O(2)—B(1)—C(3)	127.1(3)
C(6)—C(7)—C(8)	118.6(5)	O(2)—B(2)—N	96.8(2)
C(3)—C(8)—C(7)	122.1(5)	O(2)—B(2)—C(9)	109.5(2)
C(10)—C(9)—C(14)	114.8(2)	O(2)—B(2)—C(15)	113.3(2)
C(10)—C(9)—B(2)	123.3(2)	N—B(2)—C(9)	110.0(2)
C(14)—C(9)—B(2)	121.7(2)	N—B(2)—C(15)	109.1(2)
C(9)—C(10)—C(11)	122.7(2)	C(9)—B(2)—C(15)	116.4(2)
C(10)—C(11)—C(12)	120.2(3)		
		5	
C(1)—O(1)—B	109.44(14)	C(5)—C(6)—C(7)	119.7(3)
N—O(2)—B	108.69(15)	C(6)—C(7)—C(8)	119.7(2)
O(2)—N—C(1)	102.14(15)	C(7)—C(8)—C(9)	120.0(3)
O(2)—N—C(16)	108.5(2)	C(4)—C(9)—C(8)	121.9(3)
O(2)—N—C(17)	108.9(2)	C(11)—C(10)—C(15)	116.5(2)
C(1)—N—C(16)	113.8(2)	C(11)—C(10)—B	122.6(2)
C(1)—N—C(17)	111.4(2)	C(15)—C(10)—B	120.9(2)
C(16)—N—C(17)	111.6(3)	C(10)—C(11)—C(12)	121.5(2)
O(1)—C(1)—N	102.2(2)	C(11)—C(12)—C(13)	120.4(2)
O(1)—C(1)—C(2)	110.5(2)	C(12)—C(13)—C(14)	119.4(2)
O(1)—C(1)—C(3)	110.7(2)	C(13)—C(14)—C(15)	120.1(2)
N—C(1)—C(2)	110.0(2)	C(10)—C(15)—C(14)	122.1(2)
N—C(1)—C(3)	112.1(2)	O(1)—B—O(2)	101.94(14)
C(2)—C(1)—C(3)	111.1(2)	O(1)—B—C(4)	107.6(2)
C(5)—C(4)—C(9)	116.4(2)	O(1)—B—C(10)	114.8(2)
C(5)—C(4)—B	122.5(2)	O(2)—B—C(4)	113.8(2)
C(9)—C(4)—B	121.1(2)	O(2)—B—C(10)	106.98(15)
C(4)—C(5)—C(6)	122.4(2)	C(4)—B—(10)	111.5(2)

102.2(2), and 109.44(14)° in **5** compared with values of 105.0(4), 105.7(6), and 103.8(4)° in **8**. These findings are consistent with the lower stability of **5** relative to that of **8**, the former decomposing relatively quickly in solution.

The O—B distances in **5** (1.507(3) and 1.534(3) Å) may be compared to those in other compounds with Ph_2BO_2 groups: 1.506(7) and 1.556(8) Å in **8**, 1.500(4) and 1.574(4) Å in **13** (18), 1.552(2) and 1.548(2) Å in **14** (19), 1.530(2)−1.547(2)

Can. J. Chem. Downloaded from www.nrcresearchpress.com by 210.87.254.6 on 09/06/12
For personal use only.

TABLE 5. Intra-annular torsion angles (deg), standard deviations in parentheses

Atoms	Value (deg)
4	
B(1)—O(1)—N—B(2)	−19.1(2)
O(1)—N—B(2)—O(2)	24.4(2)
B(1)—O(2)—B(2)—N	−22.2(2)
B(2)—O(2)—B(1)—O(1)	12.9(3)
N—O(1)—B(1)—O(2)	6.1(3)
5	
B—O(1)—C(1)—N	−34.3(2)
O(2)—N—C(1)—O(1)	39.7(2)
B—O(2)—N—C(1)	−29.6(2)
N—O(2)—B—O(1)	10.3(2)
C(1)—O(1)—B—O(2)	17.0(2)

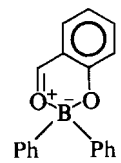

13

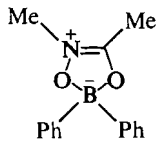

14

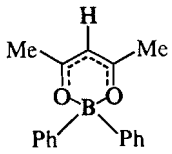

15

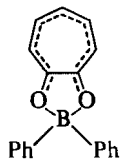

16

Å in **15** (20), and 1.544(2) and 1.565(2) Å in **16** (20). The B—C distances and the substituent-induced geometrical distortions of the phenyl rings in both **4** and **5** are as expected (21). The C(9) and C(15) phenyl rings of **4** and the C(4) phenyl ring of **5** are slightly, but significantly, non-planar (χ^2 = 10.6–18.7) although deviations of atoms from the respective mean planes do not exceed ±0.009(3) Å.

Acknowledgments

We thank the Natural Sciences and Engineering Research Council of Canada for financial support and the University of British Columbia Computing Centre for assistance. We are grateful to the Institut für Organische Chemie der Technischen Universität Braunschweig for running the mass spectra.

1. A. SINGH, V. D. GUPTA, G. SRIVASTAVA, and R. C. MEHROTRA. J. Organomet. Chem. **64**, 145 (1974).
2. R. NEU. Z. Anal. Chem. **142**, 335 (1954); **176**, 343 (1960).
3. G. ZINNER and W. KLIEGEL. Arch. Pharm. (Weinheim, Ger.) **299**, 166 (1966).
4. W. KLIEGEL. Z. Chem. **9**, 112 (1969).
5. S. J. RETTIG, J. TROTTER, and W. KLIEGEL. Can. J. Chem. **52**, 2531 (1974).
6. S. J. RETTIG and J. TROTTER. Can. J. Chem. **51**, 1288 (1973).
7. S. J. RETTIG and J. TROTTER. Acta Crystallogr. Sect. B, **30**, 2139 (1974).
8. S. J. RETTIG and J. TROTTER. Can. J. Chem. **54**, 3130 (1976).
9. S. J. RETTIG and J. TROTTER. Can. J. Chem. **61**, 2334 (1983).
10. W. KLIEGEL, D. NANNINGA, S. J. RETTIG, and J. TROTTER. Can. J. Chem. **61**, 2329 (1983).
11. D. T. CROMER and J. B. MANN. Acta Crystallogr. Sect. A, **24**, 321 (1968).
12. R. F. STEWART, E. R. DAVIDSON, and W. T. SIMPSON. J. Chem. Phys. **42**, 3175 (1965).
13. V. SCHOMAKER and K. N. TRUEBLOOD. Acta Crystallogr. Sect. B, **24**, 63 (1968).
14. D. W. J. CRUICKSHANK. Acta Crystallogr. **9**, 747 (1956); **9**, 754 (1956); **14**, 896 (1961).
15. S. J. RETTIG, J. TROTTER, W. KLIEGEL, and H. BECKER. Can. J. Chem. **54**, 3142 (1976).
16. S. J. RETTIG and J. TROTTER. Can. J. Chem. **55**, 958 (1977).
17. I. CYNKIER and H. HOPE. Acta Crystallogr. Sect. B, **34**, 2990 (1978).
18. S. J. RETTIG and J. TROTTER. Can. J. Chem. **54**, 1168 (1976).
19. S. J. RETTIG, J. TROTTER, W. KLIEGEL, and D. NANNINGA. Can. J. Chem. **56**, 1676 (1978).
20. S. J. RETTIG and J. TROTTER. Can. J. Chem. **60**, 2957 (1982).
21. A. DOMENICANO, A. VACIAGO, and C. A. COULSON. Acta Crystallogr. Sect. B, **31**, 221 (1975); **31**, 1630 (1975).

Can. J. Chem. Downloaded from www.nrcresearchpress.com by 210.87.254.6 on 09/06/12
For personal use only.

Structural studies of organoboron compounds. XVII.[1] Preparation and crystal and molecular structure of 3*a*-methyl-2,4,9*a*-triphenyl-1,2,3*a*,4,9,9*a*-hexahydro-1,3,9-trioxa-3*a*-azonia-2-bora-9*a*-boratacyclopenta[*b*]naphthalene

W. KLIEGEL AND D. NANNINGA

Institut für Pharmazeutische Chemie, der Technischen Universität Braunschweig, 3300 Braunschweig, Beethovenstraße 55, Bundesrepublik Deutschland

AND

STEVEN J. RETTIG AND JAMES TROTTER

Department of Chemistry, University of British Columbia, 2036 Main Mall, Vancouver, B.C., Canada V6T 1Y6

Received May 4, 1983[2]

W. KLIEGEL, D. NANNINGA, STEVEN J. RETTIG, and JAMES TROTTER. Can. J. Chem. **62**, 845 (1984).

The title compound was prepared by the reaction of 8-methyl-6,6-diphenyl-5,7-dioxa-8-azonia-6-borata-6,7-dihydro-5*H*-benzocycloheptene (**1**) with phenylboronic acid. Crystals of 3*a*-methyl-2,4,9*a*-triphenyl-1,2,3*a*,4,9,9*a*-hexahydro-1,3,9-trioxa-3*a*-azonia-2-bora-9*a*-boratacyclopenta[*b*]naphthalene are monoclinic, a = 11.8548(4), b = 22.7837(4), c = 8.5457(3) Å, β = 106.952(2)°, Z = 4, space group $P2_1/n$. The structure was solved by direct methods and was refined by full-matrix least-squares procedures to R = 0.040 and R_w = 0.047 for 2970 reflections with $I \geq 3\sigma(I)$. The molecule was found to be a formal addition product between **1** and PhBO which had undergone a 1,4-shift of a phenyl group from boron to carbon. The backbone of the molecule consists of a folded system of three fused rings. The structure contains the longest known B(sp^3)—N(sp^3) bond, 1.759(2) Å.

W. KLIEGEL, D. NANNINGA, STEVEN J. RETTIG et JAMES TROTTER. Can. J. Chem. **62**, 845 (1984).

On a préparé le composé mentionné dans le titre en faisant réagir de l'acide phénylboronique avec le méthyl-8 diphényl-6,6 dioxa-5,7 azonia-8 borata-6 dihydro-6,7 5*H*-benzocycloheptène (**1**). Les cristaux du méthyl-3*a* triphényl-2,4,9*a* hexahydro-1,2,3*a*,4,9,9*a* trioxa-1,3,9 azonia-3*a* bora-2 borata-9*a* cyclopenta[*b*]naphtalène sont monocliniques, a = 11,8548(4), b = 22,7837(4), c = 8,5457(3) Å, β = 106,952(2)°, Z = 4, groupe d'espace $P2_1/n$. On a résolu la structure par des méthodes directes et on l'a affinée par la méthode des moindres carrés (matrices complètes) jusqu'à des valeurs de R = 0,040 et R_w = 0,047 pour 2970 réflexions avec $I \geq 3\sigma(I)$. On a trouvé que la molécule est le produit d'addition formelle entre **1** et PhBO qui a subi une transposition 1,4 du groupement phényle du bore au carbone. La base de la molécule comporte un système replié de trois cycles condensés. La structure comporte la liaison $B(sp^3)$—N(sp^3) la plus longue connue, 1,759(2) Å.

[Traduit par le journal]

Introduction

By heating the diphenylboron chelate **1** of *N*-methylsalicylaldonitrone (1) (which contains a seven-membered chelate ring) with $PhB(OH)_2$ in refluxing benzene with the continuous removal of water, a crystalline reaction product is formed. The elemental composition of this product corresponds to an addition compound of **1** + PhBO. Infrared and ^{1}H nmr data indicate the loss of the nitrone function of **1**. The characteristic C=N$^+$ absorption of **1** at 1650 cm^{-1} (1) disappears after the addition of PhBO, and the low-field resonance signal of the proton ($^\alpha$H) identifying the nitrone group (δ ~ 8 ppm) is shifted to higher field by more than 2 ppm. At first sight this indicates a 1:1 adduct of "phenylboronoxide" (Ph—B=O) to **1** which could have the structure **2** as a result of a 1,3-dipolar cycloaddition of "phenylboronoxide" to the nitrone group of **1**, or the isomeric structure **3**.[3] The five-membered BONCO ring structure of **3**

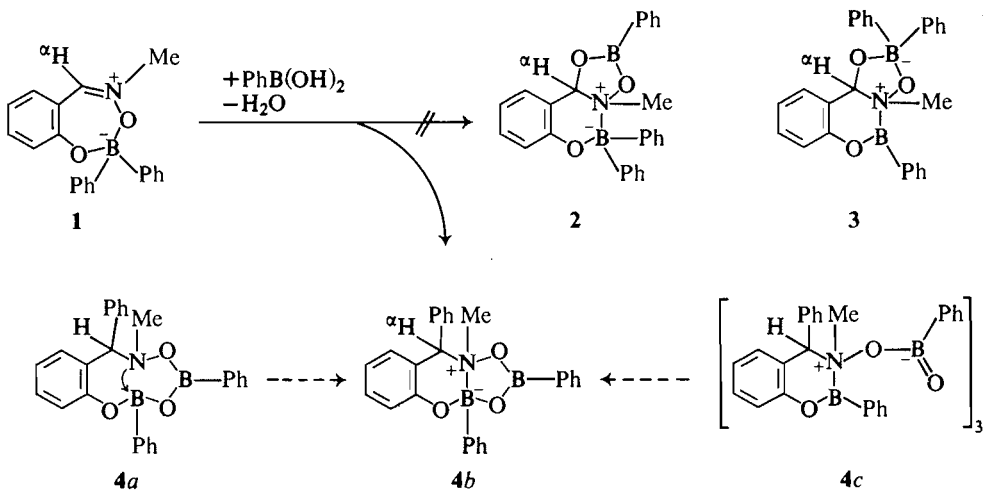

[1]Previous paper in this series: ref. 3.

[2]Revision received November 3, 1983.

[3]The anhydride of phenylboronic acid ('phenylboronoxide') exists only as a trimeric triphenylboroxine, $(PhBO)_3$, under normal conditions.

Can. J. Chem. Downloaded from www.nrcresearchpress.com by 210.87.254.42 on 09/06/12
For personal use only.

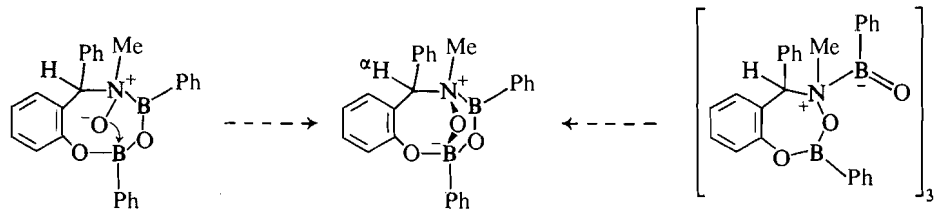

4d **4e** **4f**

resembles the well-known (2, 3) BONCO ring systems of similar cyclic B,N-betaines. However, after careful purification of the adduct by repeated recrystallizations, a negative color reaction with diphenylcarbazone (4) precluded the presence of an intact diphenylboron moiety in this new compound.

It is known (5, 6) that triphenylborane adducts of nitrones undergo thermal rearrangement during which one of the phenyl groups shifts from boron to the alkylidene carbon atom of the nitrone function. This 1,4-shift results in the formation of phenylalkylaminoxydiphenylboranes (cf. **5** → **6**). If this type

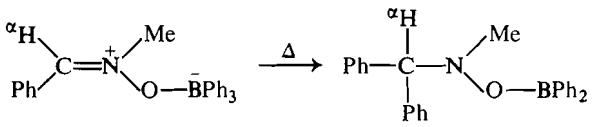

5 **6**

of rearrangement were to occur in the case of the diphenylboron chelate **1**, the alternate structures **4***a*–*f* could arise from thermal rearrangement during the insertion of a PhBO moiety. Comparison of the ^{1}H nmr data of **5** and **6** (5) with those of **1** (1) and the addition/rearrangement compound **4** shows parallels in the upfield shifts of the H and CH_3 proton resonance signals, demonstrating the transformation of the $^{\alpha}HC{=}NCH_3$ moiety into an $^{\alpha}HC{-}NCH_3$ grouping (see Table 1).

The bicyclic structures **4***a* and **4***d* can be excluded *a priori* on the basis of unfavorable ring sizes as well as the potential for transannular coordinative bonding. The adducts **4***c* and **4***f* should exist only in trimeric forms (as boroxine derivatives),[4] but could also undergo intramolecular coordination to produce **4***b* and **4***e*, respectively. Since chemical methods did not allow an unambiguous structure assignment, an X-ray crystallographic analysis has been undertaken in order to determine which of the isomeric structures, especially **4***b* or **4***e*, represents that of the adduct.

Experimental

3a-Methyl-2,4-9a-triphenyl-1,2,3a,4,9,9a-hexahydro-1,3,9-trioxa-3a-azonia-2-bora-9a-boratacyclopenta[b]naphthalene, **4***b*

8-Methyl-6,6-diphenyl-5,7-dioxa-8-azonia-6-borata-6,7-dihydro-5*H*-benzocycloheptene, **1**, prepared as described previously (1) (0.63 g, 2 mmol) and phenylboronic acid (0.25 g, 2 mmol) were heated in refluxing benzene, using a Dean-Stark trap for the continuous removal of water. The solution was refluxed for 14 h and then cooled. Upon the addition of petroleum ether, 0.82 g (92% yield) of colorless crystals precipitated and were subsequently recrystallized from dioxane/hexane or from cyclohexane, mp 192°C. *Anal.* calcd. for $C_{26}H_{23}B_2NO_3$ (fw 419.0): C 74.51, H 5.53, B 5.16, N 3.34; found: C 74.17, H 5.49, B 5.41, N 3.34. ^{1}H nmr ($CDCl_3$/TMS): δ (ppm) = 2.36 (s, CH_3), 6.63–8.0 (m, 3 C_6H_5, C_6H_4).

[4]An example of Lewis-base adducts to boroxines is the crystalline addition compound of three equivalents of *N*-methylbenzaldonitrone and one equivalent of triphenylboroxine which dissociates in solution upon warming (7).

TABLE 1. Comparison of ^{1}H nmr data of **1**/**4** and **5**/**6** (in $CDCl_3$/TMS)

	Chemical shift (δ, ppm)			
Compound*	$^{\alpha}H{-}C{=}N{-}CH_3$		$^{\alpha}H{-}C{-}N{-}CH_3$	
1 (1)	~8†	3.86		
4			5.36	2.36
5 (5)	~8†	3.73		
6 (5)			4.72	2.72

*Reference number in parentheses.
†Signal overlapped by signals of phenyl protons.

X-ray crystallographic analysis

A crystal bounded by the six faces (followed by their distance in mm from a common origin): ±(1 1 0), 0.100, ±(1 −1 0), 0.096, ±(1 1 −1), 0.150 was mounted in a general orientation. Unit-cell parameters were refined by least-squares on 2 sin θ/λ values for 25 reflections (2θ = 80–101°) measured on a diffractometer with Cu-Kα Radiation (λ(Kα$_1$) = 1.54056, λ(Kα$_2$) = 1.54439 Å). Crystal data at 22°C are:

$C_{26}H_{23}B_2NO_3$ fw = 419.10

Monoclinic, a = 11.8548(4), b = 22.7837(4), c = 8.5457(3) Å, β = 106.952(2)°, V = 2207.9(1) Å^3, Z = 4, ρ_c = 1.261 g cm^{-3}, F(000) = 880, μ(Cu-Kα) = 6.02 cm^{-1}. Absent reflections: $h0l$, $h + l$ odd, and $0k0$, k odd uniquely indicate the space group $P2_1/n$ [non-standard setting of $P2_1/c$, C_{2h}^5, No. 14, equivalent positions: ±(x, y, z; 1/2 − x, 1/2 + y, 1/2 − z)].

Intensities were measured with graphite-monochromated Cu −Kα radiation on an Enraf-Nonius CAD4-F diffractometer. An ω–2θ scan at 0.86–10.06° min^{-1} over a range of (0.80 + 0.15 tan θ) degrees in ω (extended by 25% on both sides for background measurement) was employed. Data were measured to 2θ = 150°. The intensities of three check reflections, measured every 3600 s throughout the data collection, showed only small random fluctuations. After data reduction,[5] an absorption correction was applied using the Gaussian integration method (8, 9). Transmission factors ranged from 0.820 to 0.920 for 96 integration points. Of the 4557 independent reflections measured, 2970 (65.2%) had intensities greater than 3σ(I) above background where $\sigma^2(I) = S + 2B + (0.04(S - B))^2$ with S = scan count and B = normalized background count.

The structure was initially solved and refined using a data set collected with Mo radiation (1681 observed data from 5043 independent reflections to 2θ = 55°). The structure was solved by direct methods, the coordinates of all non-hydrogen atoms being determined from an E-map. After full-matrix least-squares refinement of the non-hydrogen atoms with anisotropic thermal parameters to R = 0.076, all 23 hydrogen atoms were located from a difference map and were

[5]The computer programs used include locally written programs for data processing and locally modified versions of the following: MULTAN 80, multisolution program by P. Main, S. J. Fiske, S. E. Hull, L. Lessinger, G. Germain, J. P. Declercq, and M. M. Woolfson; ORFLS, full-matrix least-squares, and ORFFE, function and errors, by W. R. Busing, K. O. Martin and H. A. Levy; FORDAP, Patterson and Fourier syntheses, by A. Zalkin; ORTEP II, illustrations, by C. K. Johnson.

Can. J. Chem. Downloaded from www.nrcresearchpress.com by 210.87.254.42 on 09/06/12
For personal use only.

Can. J. Chem. Downloaded from www.nrcresearchpress.com by 210.87.254.42 on 09/06/12
For personal use only.

refined with isotropic thermal parameters in subsequent least-squares cycles. The structure was refined to $R = 0.032$ and $R_w = 0.033$ for 1681 reflections. In order to improve the data/parameter ratio a second set of data was collected using a different crystal and Cu radiation (see above). The refinement was continued employing the more extensive data set. The scattering factors of ref. 10 were used for non-hydrogen atoms and those of ref. 11 for hydrogen atoms. The weighting scheme, $w = 1/\sigma^2(F)$ where $\sigma^2(F)$ is derived from the previously defined $\sigma^2(I)$, gave uniform average values of $w(|F_o| - |F_c|)^2$ over ranges of both $|F_o|$ and $\sin\theta/\lambda$ and was employed in the final stages of refinement. Unobserved reflections were not included in the refinement. Convergence was reached at $R = 0.040$ and $R_w = 0.047$ for 2970 reflections with $I \geq 3\sigma(I)$. For all 4557 reflections $R = 0.085$. The function minimized was $\sum w(|F_o| - |F_c|)^2$, $R = \sum||F_o| - |F_c||/\sum|F_o|$ and $R_w = (\sum w(|F_o| - |F_c|)^2/\sum w|F_o|^2)^{1/2}$.

On the final cycle of refinement the mean and maximum parameter shifts corresponded to 0.02 and 0.33σ, respectively. The mean error in an observation of unit weight was 2.073. A final difference map was essentially featureless, the largest fluctuations being -0.24 and $+0.14$ e Å^{-3}.

The esd's of the refined parameters for the Cu data were found to be generally about 1/3 less than those for the Mo data set. The results presented below are thus based on the refinement employing the data set collected with Cu radiation. A half-normal probability plot for the atomic coordinates of all atoms derived from the two refinements has been deposited.[6] This plot shows a unit slope and zero intercept, indicating correctly estimated standard deviations and an absence of systematic errors for both analyses. There are no statistically significant deviations between corresponding derived parameters (i.e. bond lengths, angles, etc.) for the two refinements of the structure. The final positional and thermal parameters appear in Tables 2 and 3 respectively. Measured and calculated structure factors have been placed in the Depository of Unpublished Data.[6]

The ellipsoids of thermal motion for the non-hydrogen atoms are shown in Fig. 1. The thermal motion has been analysed in terms of the rigid-body modes of translation, libration, and screw motion (12). The rms standard error in the temperature factors σU_{ij} (derived from the least-squares analysis) is 0.0010 Å^2. Analysis of all 32 non-hydrogen atoms indicated significant independent motion of segments of the molecule. Five smaller groups were separately anaysed: C(7)Ph, B(1)Ph, B(2)Ph, O(1)C(1−7), and the 10-atom group consisting of the two heterocyclic rings plus C(8) (rms ΔU_{ij} = 0.0015, 0.0012, 0.0017, 0.0015, and 0.0029 Å^2, respectively). The appropriate bond distances have been corrected for libration (12, 13), using shape parameters q^2 of 0.08 for all atoms involved. Corrected bond lengths appear in Table 4 along with the uncorrected values; corrected bond angles do not differ by more than 1σ from the uncorrected values given in Table 5. Intra-annular torsion angles defining the conformations of five- and six-membered heterocyclic rings are listed in Table 6. Bond lengths and angles involving hydrogen and a complete listing of torsion angles (Tables 7−9) are included as supplementary material.

Results and discussion

The X-ray analysis shows that the addition product has the structure **4***b*. The 1,4-shift of the phenyl group from boron to carbon, similar to that noted for 1:1 triphenylborane−nitrone adducts (5, 6), is confirmed. The crystal structure of **4***b* consists of discrete molecules separated by normal van der Waals distances.

The backbone of the molecule consists of a system of three fused rings; the central six-membered C_3OBN ring has a distorted boat conformation (see Table 6). The five-membered heterocycle is *cis*-fused to the central ring at adjacent pseudo-equatorial positions, resulting in a marked folding of the fused-ring system, the angle between normals to the mean planes of the terminal rings being 71.9(2)°.

TABLE 2. Final positional (fractional × 10^5, H × 10^4) and isotropic thermal parameters ($U \times 10^3$ Å^2) with estimated standard deviations in parentheses

Atom	x	y	z	U_{eq}*/U_{iso}
O(1)	47650(9)	3318(5)	24358(14)	40
O(2)	52404(10)	18067(4)	37147(13)	41
O(3)	45840(10)	13121(5)	12533(13)	41
N	48387(11)	12500(5)	41710(15)	35
C(1)	59730(14)	3405(7)	28104(20)	38
C(2)	66071(13)	6646(7)	41614(19)	37
C(3)	78353(15)	6767(8)	45446(23)	47
C(4)	84001(18)	3596(10)	36056(26)	57
C(5)	77561(18)	259(9)	22985(26)	56
C(6)	65384(17)	164(8)	18916(24)	49
C(7)	59092(13)	9189(6)	52329(18)	35
C(8)	40192(17)	13972(9)	51271(25)	48
C(9)	65924(14)	12645(7)	67193(19)	38
C(10)	65434(15)	10884(8)	82536(20)	43
C(11)	71440(18)	13990(9)	96477(24)	54
C(12)	77944(18)	18856(10)	95084(27)	61
C(13)	78653(18)	20585(9)	80049(28)	60
C(14)	72755(16)	17526(8)	66064(24)	50
C(15)	28101(14)	8470(7)	18716(19)	38
C(16)	20814(15)	12711(8)	9212(23)	49
C(17)	8581(17)	12239(10)	4799(26)	58
C(18)	3412(17)	7479(10)	9749(25)	55
C(19)	10366(17)	3227(9)	19182(26)	54
C(20)	22569(15)	3721(8)	23610(24)	47
C(21)	53989(15)	23645(8)	12421(21)	43
C(22)	61526(21)	27811(8)	21803(26)	60
C(23)	64214(25)	32933(10)	14946(32)	73
C(24)	59327(22)	34022(11)	−1225(34)	75
C(25)	51999(23)	29906(14)	−10845(34)	93
C(26)	49313(21)	24784(11)	−4041(28)	71
B(1)	41998(16)	8979(8)	22948(22)	37
B(2)	50688(16)	17981(8)	20248(23)	39
H(3)	8294(18)	903(9)	5529(26)	59(6)
H(4)	9298(22)	375(10)	3929(28)	67(7)
H(5)	8142(22)	−192(11)	1589(31)	92(8)
H(6)	6099(19)	−229(10)	982(29)	68(6)
H(7)	5536(15)	582(7)	5647(20)	37(4)
H(8a)	3742(17)	1001(9)	5453(24)	57(6)
H(8b)	3349(18)	1610(9)	4387(25)	54(5)
H(8c)	4452(21)	1646(11)	6003(30)	75(7)
H(10)	6082(18)	717(9)	8333(23)	55(5)
H(11)	7102(17)	1255(9)	10662(27)	59(6)
H(12)	8221(20)	2094(10)	10475(28)	75(7)
H(13)	8323(21)	2411(12)	7954(28)	92(8)
H(14)	7333(17)	1874(9)	5533(25)	61(6)
H(16)	2442(18)	1612(10)	544(26)	65(6)
H(17)	390(21)	1538(10)	−224(30)	79(7)
H(18)	−519(22)	721(9)	703(28)	73(7)
H(19)	673(19)	−15(10)	2336(26)	71(7)
H(20)	2709(17)	49(10)	2987(25)	63(6)
H(22)	6528(21)	2703(10)	3392(31)	80(7)
H(23)	6948(27)	3589(14)	2215(37)	116(10)
H(24)	6159(24)	3776(12)	−602(34)	101(9)
H(25)	4851(21)	3092(11)	−2304(30)	96(8)
H(26)	4437(28)	2221(15)	−1118(39)	123(12)

*U_{eq} = (1/3) trace U_{diag}.

[6]The structure factor table, Table 3 (anisotropic thermal parameters) and other material mentioned in the text are available, at a nominal charge, from the Depository of Unpublished Data, CISTI, National Research Council of Canada, Ottawa, Ont., Canada K1A 0S2.

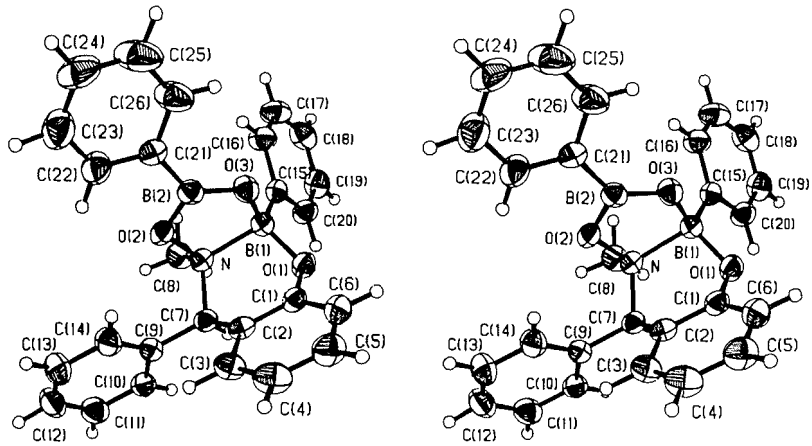

FIG. 1. Stereoscopic view of 3*a*-methyl-2,4,9*a*-triphenyl-1,2,3*a*,4,9,9*a*-hexahydro-1,3,9-trioxa-3*a*-azonia-2-bora-9*a*-boratacyclopenta[*b*]-naphthalene. 50% probability thermal ellipsoids are shown for the non-hydrogen atoms; hydrogen atoms have been assigned arbitrarily small thermal parameters for the sake of clarity.

TABLE 4. Bond lengths (Å) with estimated standard deviations in parentheses

	Length			Length	
Bond	Uncorr.	Corr.	Bond	Uncorr.	Corr.
O(1)—C(1)	1.373(2)	1.377	C(10)—C(11)	1.390(3)	1.394
O(1)—B(1)	1.442(2)	1.445	C(11)—C(12)	1.375(3)	1.381
O(2)—N	1.448(2)	1.451	C(12)—C(13)	1.370(3)	1.377
O(2)—B(2)	1.399(2)	1.401	C(13)—C(14)	1.384(3)	1.388
O(3)—B(1)	1.458(2)	1.461	C(15)—C(16)	1.389(2)	1.398
O(3)—B(2)	1.331(2)	1.334	C(15)—C(20)	1.391(2)	1.399
N —C(7)	1.527(2)	1.529	C(15)—B(1)	1.585(2)	1.587
N —C(8)	1.479(2)	1.482	C(16)—C(17)	1.392(3)	1.395
N —B(1)	1.755(2)	1.759	C(17)—C(18)	1.372(3)	1.379
C(1)—C(2)	1.392(2)	1.397	C(18)—C(19)	1.371(3)	1.380
C(1)—C(6)	1.385(2)	1.388	C(19)—C(20)	1.389(2)	1.392
C(2)—C(3)	1.396(2)	1.401	C(21)—C(22)	1.387(3)	1.401
C(2)—C(7)	1.517(2)	1.520	C(21)—C(26)	1.378(3)	1.396
C(3)—C(4)	1.388(3)	1.391	C(21)—B(2)	1.555(2)	1.559
C(4)—C(5)	1.383(3)	1.387	C(22)—C(23)	1.384(3)	1.388
C(5)—C(6)	1.383(3)	1.387	C(23)—C(24)	1.356(4)	1.375
C(7)—C(9)	1.513(2)	1.516	C(24)—C(25)	1.376(4)	1.389
C(9)—C(10)	1.389(2)	1.396	C(25)—C(26)	1.382(3)	1.386
C(9)—C(14)	1.395(2)	1.402			

The five-membered BOBON ring in **4***b* is significantly non-planar, having a flattened B(1)-envelope conformation. In the less sterically demanding molecules **7** (14) and **8** (3), the analogous rings are essentially planar while that in the monocyclic compound **9** (15) is markedly non-planar. Steric interactions between the B-phenyl and N-methyl groups of **9** are minimized by a combination of torsional twisting about the B—N bond (O—B—N—O = 24.4(2)°) and lengthening of that bond to 1.728(3) Å, longer than any previously reported B(sp^3)—N(sp^3) distance (ref. 15, and references therein). Torsional freedom about the B—N bond in **4***b* is constrained by the occurrence of this bond at the junction of two rings (O—B—N—O = 9.0(2)°). The presence of the N-methyl group limits the possible orientations of the C(7)- and B(1)-phenyl rings, which interact sterically with O(2) and O(3) of the BOBON ring, respectively (O(2)···C(14) = 2.910(2) and O(3)···C(16) = 2.898(2) Å). The strain in **4***b* is thus relieved by an even greater lengthening of the B—N bond (to 1.759(2) Å) than that observed in **9**, as well as a significant increase in the N—C(7) distance (to 1.529(2) Å from the expected value of 1.48 Å). Other distances in the five-membered ring, including the characteristic short anhydridic B(sp^2)—O bond length of 1.334(2) Å, are similar to those in **7**, **8**, and **9**. The bond lengths involving the tetrahedrally coordinated boron atom, with the exception of the B—N distance discussed above, are essentially the same as the corresponding distances in **7** (14).

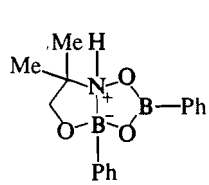

7

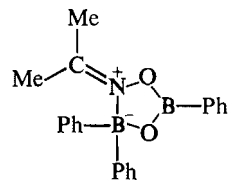

8

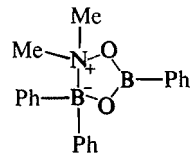

9

The trigonally coordinated boron atom B(2) is displaced 0.024(2) Å from the plane of its substituents. The phenyl ring bonded to B(2) is twisted out of the B(2) coordination plane by 19.1°, this value being in the range normally observed for derivatives of phenylboronic acid (refs. 3, 15, and references

Can. J. Chem. Downloaded from www.nrcresearchpress.com by 210.87.254.42 on 09/06/12
For personal use only.

TABLE 5. Bond angles (deg) with estimated standard deviations in parentheses

Bonds	Angle (deg)	Bonds	Angle (deg)
C(1)—O(1)—B(1)	115.73(12)	C(12)—C(13)—C(14)	120.8(2)
N —O(2)—B(2)	107.80(11)	C(9)—C(14)—C(13)	119.9(2)
B(1)—O(3)—B(2)	113.75(13)	C(16)—C(15)—C(20)	116.70(15)
O(2)—N —C(7)	108.13(11)	C(16)—C(15)—B(1)	120.70(15)
O(2)—N —C(8)	105.72(12)	C(20)—C(15)—B(1)	122.55(14)
O(2)—N —B(1)	104.05(10)	C(15)—C(16)—C(17)	121.7(2)
C(7)—N —C(8)	110.47(13)	C(16)—C(17)—C(18)	120.1(2)
C(7)—N —B(1)	112.31(11)	C(17)—C(18)—C(19)	119.6(2)
C(8)—N —B(1)	115.50(13)	C(18)—C(19)—C(20)	120.2(2)
O(1)—C(1)—C(2)	118.37(14)	C(15)—C(20)—C(19)	121.7(2)
O(1)—C(1)—C(6)	120.29(15)	C(22)—C(21)—C(26)	117.4(2)
C(2)—C(1)—C(6)	121.30(15)	C(22)—C(21)—B(2)	121.3(2)
C(1)—C(2)—C(3)	118.62(15)	C(26)—C(21)—B(2)	121.2(2)
C(1)—C(2)—C(7)	116.47(13)	C(21)—C(22)—C(23)	121.4(2)
C(3)—C(2)—C(7)	124.47(15)	C(22)—C(23)—C(24)	120.2(2)
C(2)—C(3)—C(4)	120.0(2)	C(23)—C(24)—C(25)	119.5(2)
C(3)—C(4)—C(5)	120.5(2)	C(24)—C(25)—C(26)	120.5(2)
C(4)—C(5)—C(6)	120.1(2)	C(21)—C(26)—C(25)	121.0(2)
C(1)—C(6)—C(5)	119.4(2)	O(1)—B(1)—O(3)	114.18(13)
N —C(7)—C(2)	109.57(12)	O(1)—B(1)—N	105.44(12)
N —C(7)—C(9)	112.99(12)	O(1)—B(1)—C(15)	112.36(13)
C(2)—C(7)—C(9)	116.93(13)	O(3)—B(1)—N	97.67(11)
C(7)—C(9)—C(10)	118.87(14)	O(3)—B(1)—C(15)	113.39(13)
C(7)—C(9)—C(14)	122.41(14)	N —B(1)—C(15)	112.64(12)
C(10)—C(9)—C(14)	118.72(15)	O(2)—B(2)—O(3)	115.79(15)
C(9)—C(10)—C(11)	120.7(2)	O(2)—B(2)—C(21)	116.97(15)
C(10)—C(11)—C(12)	119.8(2)	O(3)—B(2)—C(21)	127.2(2)
C(11)—C(12)—C(13)	120.2(2)		

TABLE 6. Intra-annular torsion angles (deg) standard deviations in parentheses

Atoms	Value (deg)
B(1)—O(1)—C(1)—C(2)	52.2(2)
O(1)—C(1)—C(2)—C(7)	7.5(2)
C(1)—C(2)—C(7)—N	−50.7(2)
B(1)—N —C(7)—C(2)	37.96(15)
C(7)—N —B(1)—O(1)	10.09(15)
C(1)—O(1)—B(1)—N	−56.6(2)
B(2)—O(2)—N —B(1)	−6.33(14)
O(2)—N —B(1)—O(3)	9.02(13)
B(2)—O(3)—B(1)—N	−9.0(2)
N —O(2)—B(2)—O(3)	1.0(2)
B(1)—O(3)—B(2)—O(2)	6.3(2)

therein). The C(1)—C(6), C(9)—C(14), and C(21)—C(26) rings are slightly, but significantly, non-planar (χ^2 = 158.0, 58.7, and 42.8; maximum deviations 0.012(2), 0.009(2), and 0.012(3) Å, respectively); C(15)—C(20) ring is planar within experimental error. The atom C(7) is considerably displaced (0.223(2) Å) from the C(1)—C(6) mean plane. The substituent induced geometrical distortions of the phenyl rings are as expected (16).

Acknowledgments

We thank the Natural Sciences and Engineering Research Council of Canada for financial support and the University of British Columbia Computing Centre for assistance.

1. W. KLIEGEL and D. NANNINGA. J. Organomet. Chem. **243**, 373 (1983).
2. S. J. RETTIG and J. TROTTER. Can. J. Chem. **52**, 2531 (1974).
3. W. KLIEGEL, H.-W. MOTZKUS, S. J. RETTIG, and J. TROTTER. Can. J. Chem. **62**, 838 (1984).
4. R. NEU. Z. Anal. Chem. **142**, 335 (1954); **176**, 343 (1960).
5. P. PAETZOLD and G. SCHIMMEL. Z. Naturforsch. **35***b*, 568 (1980).
6. W. KLIEGEL and D. NANNINGA. Unpublished results.
7. P. PAETZOLD, G. WEBER, R. REINARDS, H. FENRICH, and K.-H. SOCKEL. Forschungsber. Landes Nordrhein-Westfalen Nr. 2476, Westdeutscher Verlag, Opladen. 1975.
8. P. COPPENS, L. LEISEROWITZ, and D. RABINOVICH. Acta Crystallogr. **18**, 1035 (1965).
9. W. R. BUSING and H. A. LEVY. Acta Crystallogr. **22**, 457 (1967).
10. D. T. CROMER and J. B. MANN. Acta Crystallogr. Sect. A, **24**, 321 (1968).
11. R. F. STEWART, E. R. DAVIDSON, and W. T. SIMPSON. J. Chem. Phys. **42**, 3175 (1965).
12. V. SCHOMAKER and K. N. TRUEBLOOD. Acta Crystallogr. Sect. B, **24**, 63 (1968).
13. D. W. J. CRUICKSHANK. Acta Crystallogr. **9**, 747 (1956); **9**, 754 (1956); **14**, 896 (1976).
14. S. J. RETTIG, J. TROTTER, W. KLIEGEL, and H. BECKER. Can. J. Chem. **54**, 3142 (1976).
15. W. KLIEGEL, D. NANNINGA, S. J. RETTIG, and J. TROTTER. Can. J. Chem. **61**, 2329 (1982).
16. A. DOMENICANO, A. VACIAGO, and C. A. COULSON. Acta Crystallogr. Sect. B, **31**, 221 (1975); **31**, 1630 (1975).

Can. J. Chem. Downloaded from www.nrcresearchpress.com by 210.87.254.42 on 09/06/12
For personal use only.

The crystal structure of tris-2,2′-bipyridinium nitrate hexanitratothorate(IV), $[(C_{10}H_8N_2H)_3NO_3][Th(NO_3)_6]$

MASOOD A. KHAN, N. KUMAR, AND DENNIS G. TUCK[1]

Department of Chemistry, University of Windsor, Windsor, Ont., Canada N9B 3P4

Received August 4, 1983

MASOOD A. KHAN, N. KUMAR, and DENNIS G. TUCK. Can. J. Chem. **62**, 850 (1984).

The title compound was prepared by the addition of 2,2′bipyridine (bpy) to an electrochemically prepared solution of thorium(IV) nitrate in tri-*n*-butyl phosphate. The structure has been established by a complete three-dimensional X-ray diffraction study. The compound crystallises in the space group $P\bar{1}$, with a = 9.300(2) Å, b = 14.161(3) Å, c = 17.037(4) Å, α = 108.79(2)°, β = 95.77(2)°, γ = 102.88(2)°, V = 2034(1) Å^3. Diffraction intensities were collected with a Syntex $P2_1$ automated diffractometer using MoKα radiation. The structure was solved by the heavy atom method and refined by block-matrix least-squares calculations to the final discrepancy indices R_F = 0.029 and R_{WF} = 0.031 for 5783 observed reflections ($2\theta_{max}$ = 50°). The structure of the $[Th(NO_3)_6]^{2-}$ anion is described as a nonsymmetric distorted icosahedron in which symmetric bidentate nitrato ligands occupy all the available sites. Three $bpyH^+$ cations are hydrogen-bonded to a nitrate ion to form the unusual $[(bpyH)_3NO_3]^{2+}$ cation.

MASOOD A. KHAN, N. KUMAR et DENNIS G. TUCK. Can. J. Chem. **62**, 850 (1984).

On a préparé le composé mentionné dans le titre en ajoutant de la bipyridine-2,2′ (bpy) à une solution de nitrate de thorium(IV) dans du phosphate de tri-*n*-butyle qui a été préparée électrochimiquement. On a établi la structure par une étude tridimensionnelle complète effectuée grâce à la diffraction des rayons-X. Le composé cristallise dans le groupe d'espace $P\bar{1}$ avec a = 9,300(2), b = 14,161(3), c = 17,037 Å, α = 108,79(2), β = 95,77(2), γ = 102,88(2)°, V = 2034(1) Å^3. On a mesuré les intensités à l'aide d'un diffractomètre automatique Syntex $P2_1$ en utilisant la radiation MoKα. On a résolu la structure par la méthode de l'atome lourd et on l'a affinée par la méthode des moindres carrés (matrices diagonales) jusqu'à des valeurs de R_F = 0,029 et R_{WF} = 0,031 pour 5783 réflexions observées ($2\theta_{max}$ = 50°). On peut décrire la structure de l'anion $[Th(NO_3)_6]^{2-}$ comme étant celle d'un eicosaèdre déformé et non symétrique dans lequel les ligands nitrato bidentates symétriques occupent tous les sites disponibles. Les trois cations $bpyH^+$ sont liés par des ponts hydrogènes avec une ion nitrate et ils forment un cation inhabituel de $[(bpyH)_3NO_3]^{2+}$.

[Traduit par le journal]

Introduction

Nitrato complexes of actinide elements play an important role in the separation chemistry of these elements, and the literature contains a number of reports of synthetic studies (1). There is less information on the detailed stereochemistry of these interesting compounds, in which the matter of unusually high coordination numbers is of importance. In the course of studies of the electrochemical synthesis of thorium complexes by the oxidation of the metal in non-aqueous media (2, 3), we obtained the unusual title compound, whose crystal structure has now been established by X-ray diffraction crystallography. The lattice consists of $[Th(NO_3)_6]^{2-}$ anions and monopositive 2,2′-bipyridinium cations, which are hydrogen bonded to an uncomplexed nitrate ion to give the unusual $[(bpyH)_3NO_3]^{2+}$ unit.

There have been three previous reports (4–6) of structural determinations involving the $[Th(NO_3)_6]^{2-}$ anion, and we discuss the details of these below. The analogous hexanitratocerate(IV) anion has also been studied (7), as has thorium(IV) nitrate pentahydrate, for which both X-ray (8) and neutron diffraction (9) results are available.

Experimental

Preparative

The electrochemical procedures were essentially those described in earlier papers from this laboratory (2, 3, 10). The solution phase consisted of 20 cm^3 of a 3.65 *M* solution of nitric acid in tri-*n*-butyl phosphate prepared by liquid–liquid equilibration (11). A disc of thorium metal (0.8 cm diameter, 0.2 cm thick) suspended on a platinum wire formed the anode and a platinum foil (1 × 1 cm^2) on a second platinum wire was the cathode. An applied voltage of 2 V from a Coutant LQ 50/50 dc power supply gave an initial current of 10 mA; electrolysis for a period of 8 h resulted in the dissolution of 0.154 g of thorium metal. The electrodes were then removed from the cell, and a solution of 0.42 g 2,2′-bipyridine (bpy) in ethanol (10 cm^3) added. The mixture was stirred for 2 h at room temperature, after which the volume was reduced by about 30% by pumping *in vacuo*. The white solid which was thrown out of solution was collected, washed with diethyl ether, and recrystallised from 1:1 (v/v) acetone/toluene. *Anal.* calcd. for $C_{30}H_{27}N_{13}O_{21}Th$: Th 20.3; found (EDTA titration): Th 20.8. Yield 80%, based on thorium dissolved.

A detailed discussion of this and other direct electrochemical syntheses of thorium nitrate complexes, including the choice of solvent, will be given elsewhere (12).

Crystallographic analysis

A colourless prismatic-shaped crystal of the title compound mounted directly on a thin-glass fiber with its axis parallel to the long dimension was used to obtain both the cell dimensions and the intensities. All data were obtained at room temperature on a Syntex $P2_1$ diffractometer following the procedure described elsewhere (13). The space group $P\bar{1}$ was assumed and confirmed by this analysis. The crystal was stable during data collection and the intensities of three monitor reflections did not change significantly. The data were corrected for Lorentz and polarization effects and an analytical absorption correction was also applied.

The structure was solved by sharpened Patterson and Fourier methods. The structure was refined by the block-matrix least-squares method in two blocks. The positional and anisotropic temperature coordinates for the thorium atom, and an overall scale factor, were refined in each block; the first matrix contained, in addition, the positional and anisotropic coordinates for all seven nitrate groups, while the second contained the positional and isotropic temperature coordinates for the $bpyH^+$ cations. Convergence was achieved in ten cycles to R = 0.032. A difference Fourier synthesis then showed electron density maxima in some of the plausible hydrogen atom locations. All C—H hydrogen atoms were included in the subsequent refinement in the idealized positions, with C—H = 0.95 Å, and were

[1] To whom all correspondence should be addressed.

Can. J. Chem. Downloaded from www.nrcresearchpress.com by 210.87.254.42 on 09/06/12
For personal use only.

Can. J. Chem. Downloaded from www.nrcresearchpress.com by 210.87.254.42 on 09/06/12
For personal use only.

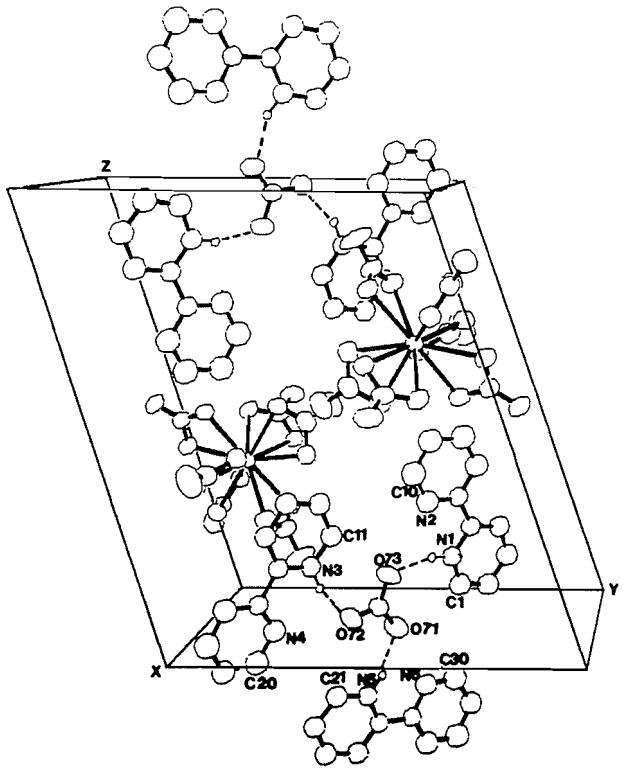

FIG. 1. Unit cell packing of $[(bpyH)_3NO_3][Th(NO_3)_6]$. Hydrogen bonds are shown by dotted lines. The symmetry-equivalent positions for bipyridinium cations with labels N1/N2 are $1-x, 1-y, 1-z$; with N3/N4 x, y, z; and with N5/N6 $x, y, z-1$.

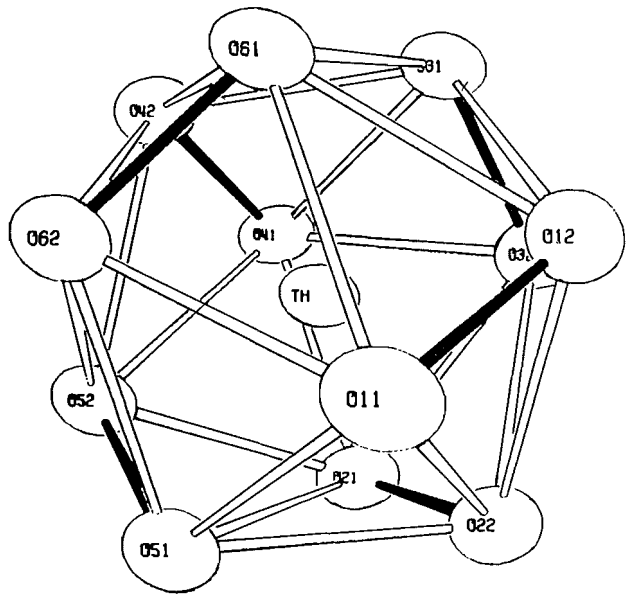

FIG. 2. ThO_{12} polyhedron, showing approximate C_2 symmetry.

constrained to ride on the appropriate carbon atoms with individual isotropic temperature factors which were refined for each hydrogen atom. Six cycles of refinement gave an R-value = 0.030, and the difference map showed peaks for H(N1) and H(N3) atoms (see Figs. 1 and 2 for nomenclature). The H(N5) atom was assumed to be on N(5), both because of its position, and because the distance from the O(71) atom seemed appropriate for the formation of a hydrogen bond (see below). These three hydrogen atoms were also included in the subsequent refinement in the idealized positions (N—H = 0.95 Å).

TABLE 1. Summary of crystal data, intensity collections, and structural refinement for $C_{30}H_{27}N_{13}O_{21}Th$, $[(bpyH)_3NO_3][Th(NO_3)_6]$

Cell constants	a = 9.300(2) Å, b = 14.161(3) Å, c = 17.037(4) Å, α = 108.79(2)°, β = 95.77(2)°, γ = 102.88(2)°
Cell volume	2034(1) Å^3
Space group	$P\bar{1}$ (No. 2)
Z	2
M_r	1137.65
ρ(calcd)	1.857 g cm^{-3}
Absorption coefficient	μ = 35.7 cm^{-1}
Crystal dimensions	0.30 × 0.23 × 0.19 mm
Radiation	MoK_α (λ = 0.71069 Å)
Min/max absorption correction	1.803/2.172
2θ angle	4–50°
Scan type	coupled θ (crystal)/2 θ (counter)
Scan width	$K_{\alpha 1}$ − 1° to $K_{\alpha 2}$ + 1°
Scan speed	2.02–4.88°/min
Background time/scan time	0.5
Total reflections measured	7197
Unique average data	5783[$F_o^2 > 3\sigma(F_o)^2$]
No. of parameters (NP)	262, 181, blocked, see text
$R = (\Sigma\Delta/\Sigma\lvert F_o\rvert)$	0.029
$R_w = [\Sigma w\Delta^2/\Sigma wF_o^2]^{1/2}$	0.031

The refinement converged to six more cycles, with the final R = 0.029 and the final R_w = 0.031. The weighting scheme employed was $w = 1/[\sigma^2(F) + 0.001F^2]$. In the final cycle of refinement all shifts were less than 0.1 esd, and a final difference synthesis had no significant features, the maximum peak being ~0.7 e Å^{-3} and close to the thorium atom.

Scattering factors for all non-hydrogen atoms, including the anomalous dispersion correction terms ($\Delta f'$) and ($\Delta f''$) for thorium, were taken from ref. 14, and for the hydrogen atoms from ref. 15. All calculations were carried out on the IBM 3031 computer with the programmes CHECK, PROC, ABSORB, SHELX 77, XANADU, and ORTEP (16).

The cell constants and other related crystal data are given in Table 1. The atomic coordinates are given in Table 2, and the interatomic distances and angles are listed in Tables 3 and 4. Tables of hydrogen coordinates, anisotropic thermal parameters, and observed and calculated structure factor amplitudes are available as supplementary data.[2]

Results and discussion

Previous studies of $[Th(NO_3)_6]^{2-}$

As noted in the Introduction, there have been three previous reports of structural determinations of the $[Th(NO_3)_6]^{2-}$ anion. The earliest of these (4), based on the photographic recording of 152 reflections, with R = 0.124, established that the thorium atom is surrounded by an irregular icosahedron in which oxygen atoms of bidentate nitrate ligands occupy all the available sites. The average Th—O distance was reported to be 2.63 Å, with the range 2.50–2.80 Å. The thorium atom was placed in a centrosymmetric position because of crystallographic requirements, so that the polyhedron is also centrosymmetric.

Alcock and co-workers (5) identified the $[Th(NO_3)_6]^{2-}$ anion in a complex lattice also containing the $[Th(NO_3)_3(Me_3PO)_4]^+$ cation. The geometry of the anion is again described as icosahedral, but with the thorium atom in a non-centric position (R = 0.090; Th—O (ave) = 2.61 Å). Studies of the related ionic complex $[Th(NO_3)_3(tdpo)_4]_2[Th(NO_3)_6]$ (tdpo = tris(dimethyl-

[2] Complete set of data may be obtained upon request, at a nominal charge, from the Depository of Unpublished Data, CISTI, National Research Council of Canada, Ottawa, Ont., Canada K1A 0S2.

TABLE 2. Atomic coordinates for $[(bpyH)_3NO_3][Th(NO_3)_6]$

Atom	x/a	y/b	z/c	U_{eq}[a]/U (Å^2 × 10^3)	Atom	x/a	y/b	z/c	U_{eq}/U (Å^2 × 10^3)
Th	0.15353(2)	0.16887(1)	0.32959(1)	41.4(1)	C(1)	0.8572(7)	0.3682(5)	0.9654(4)	70(2)
O(11)	0.2573(5)	0.3208(3)	0.4703(2)	63(2)	C(2)	0.9435(8)	0.3055(5)	0.9784(5)	72(2)
O(12)	0.2812(4)	0.3604(3)	0.3592(2)	59(2)	C(3)	0.9556(8)	0.2264(5)	0.9090(4)	72(2)
O(13)	0.3306(6)	0.4826(3)	0.4834(3)	98(4)	C(4)	0.8827(7)	0.2111(5)	0.8292(4)	66(1)
O(21)	0.3249(4)	0.0488(3)	0.2914(2)	55(2)	C(5)	0.7981(6)	0.2766(4)	0.8176(3)	53(1)
O(22)	0.4387(4)	0.2062(3)	0.3692(2)	58(2)	C(6)	0.7208(6)	0.2721(4)	0.7367(3)	53(1)
O(23)	0.5655(5)	0.0933(4)	0.3318(4)	106(4)	C(7)	0.7152(8)	0.1949(6)	0.6621(4)	76(2)
O(31)	0.0692(4)	0.2254(3)	0.2074(2)	56(2)	C(8)	0.6489(8)	0.1970(6)	0.5879(5)	85(2)
O(32)	0.2848(4)	0.1928(3)	0.2079(2)	57(2)	C(9)	0.5849(8)	0.2763(5)	0.5896(5)	79(2)
O(33)	0.1885(6)	0.2317(5)	0.1057(3)	98(4)	C(10)	0.5925(9)	0.3498(6)	0.6670(5)	85(2)
O(41)	0.0530(4)	0.0140(3)	0.1912(2)	53(2)	C(11)	0.5271(7)	0.4028(5)	0.2050(4)	63(1)
O(42)	−0.1208(4)	0.0704(3)	0.2509(2)	56(2)	C(12)	0.5868(7)	0.4128(5)	0.2859(4)	64(1)
O(43)	−0.1807(5)	−0.0623(3)	0.1328(3)	70(3)	C(13)	0.6652(7)	0.3448(5)	0.2968(4)	65(1)
O(51)	0.2270(4)	0.1129(3)	0.4526(2)	56(2)	C(14)	0.6851(7)	0.2691(5)	0.2268(4)	60(1)
O(52)	0.0581(5)	−0.0043(3)	0.3515(2)	58(2)	C(15)	0.6256(6)	0.2602(4)	0.1471(3)	53(1)
O(53)	0.1316(6)	−0.0376(3)	0.4619(3)	77(3)	C(16)	0.6362(6)	0.1818(4)	0.0676(3)	50(1)
O(61)	−0.0281(4)	0.2802(3)	0.3608(2)	55(2)	C(17)	0.7194(8)	0.1134(5)	0.0685(5)	73(2)
O(62)	−0.0341(5)	0.1780(3)	0.4311(2)	60(2)	C(18)	0.7219(9)	0.0393(6)	−0.0084(5)	84(2)
O(63)	−0.1701(5)	0.2872(4)	0.4550(3)	75(3)	C(19)	0.6460(7)	0.0392(5)	−0.0800(4)	69(2)
O(71)	0.2716(7)	0.4448(4)	−0.0447(3)	97(4)	C(20)	0.5684(8)	0.1121(5)	−0.0740(5)	77(2)
O(72)	0.4030(7)	0.3595(4)	−0.0018(3)	96(4)	C(21)	0.3326(7)	0.2377(5)	0.8042(4)	64(1)
O(73)	0.3416(7)	0.4837(4)	0.0883(3)	105(4)	C(22)	0.3374(7)	0.1537(5)	0.7359(4)	65(1)
N(10)	0.2924(6)	0.3916(4)	0.4391(3)	62(3)	C(23)	0.2681(7)	0.1432(5)	0.6577(4)	68(2)
N(20)	0.4487(6)	0.1147(4)	0.3309(3)	60(3)	C(24)	0.1960(7)	0.2145(5)	0.6469(4)	64(1)
N(30)	0.1812(6)	0.2176(4)	0.1708(3)	57(3)	C(25)	0.1907(6)	0.2973(4)	0.7157(3)	51(1)
N(40)	−0.0867(5)	0.0038(3)	0.1894(3)	52(3)	C(26)	0.1130(6)	0.3756(4)	0.7134(3)	50(1)
N(50)	0.1389(6)	0.0215(4)	0.4239(3)	54(3)	C(27)	0.0523(8)	0.3816(5)	0.6394(5)	75(2)
N(60)	−0.0829(5)	0.2492(4)	0.4172(3)	54(3)	C(28)	−0.0233(9)	0.4567(6)	0.6409(5)	85(2)
N(70)	0.3393(7)	0.4291(4)	0.0138(3)	71(3)	C(29)	−0.0308(7)	0.5240(5)	0.7179(4)	72(2)
N(1)	0.7892(5)	0.3533(4)	0.8877(3)	58(1)	C(30)	0.0336(8)	0.5139(6)	0.7898(5)	80(2)
N(2)	0.6594(6)	0.3491(4)	0.7402(3)	72(1)					
N(3)	0.5482(5)	0.3286(3)	0.1390(3)	54(1)					
N(4)	0.5624(6)	0.1831(4)	−0.0030(3)	66(1)					
N(5)	0.2606(5)	0.3052(3)	0.7928(3)	55(1)					
N(6)	0.1072(6)	0.4423(4)	0.7890(3)	66(1)					

[a] U_{eq} for the first 29 atoms is calculated from the refined anisotropic thermal parameters (deposited) ($U_{eq} = (1/3)\sum_{i=1}^{3}(\text{rmsd})_i^2$, rmsd values are taken from ORTEP output, esd's are mean esd values of U_{11}, U_{22}, and U_{33}).

amido)phosphine oxide) by English *et al.* (6) lead to a description of two different anionic sites; in this analysis (R = 0.138; Th—O (ave) 2.60 Å), the thorium coordination was described as involving six octahedrally-sited bidentate nitrate groups, and the deviation of the N—Th—N angles from the required value of 90° was reportedly less than 3°.

Structure of $[Th(NO_3)_6]^{2-}$

The present work is fortunately based on more reliable methods than those available to Sćavnicar and Prodić (4), and the structural analysis is not affected by disorder problems, or by poor quality data as in the other studies noted (5, 6). The present work therefore allows the structural features of the $[Th(NO_3)_6]^{2-}$ anion to be identified with greater certainty than was previously possible.

The fundamental geometry of the coordination kernel of the anion is that of a distorted icosahedron, essentially as reported by Sćavnicar and Prodić (4), with twelve isosceles and eight equilateral triangles forming the surface of the polyhedron (Fig. 2). The approximate symmetry of the icosahedron is C_2, in contrast to the asymmetry reported earlier (4, 6). The structure is clearly not octahedral (c.f. ref. 6), as demonstrated by the N—Th—N angles in Table 4. Figure 2 shows the ThO_{12} polyhedron, with solid lines indicating short O---O contacts (2.154(2) Å) arising from chelating nitrato groups, and double lines showing the longer ones (2.86(2) Å).

The distortions within the ThO_{12} icosahedron are established not so much by the Th—O bond lengths, which lie randomly in the range 2.540(4)–2.602(3) Å (ave 2.567 Å), as by the O—Th—O angles. If one considers a regular ThO_{12} icosahedron, and identifies a specific oxygen atom, then the O—Th—O angles will be 63.5° (five such), 116.5° (five such), and 180° (one such). The results in Table 4 show that these values are not found. In discussing the experimental results, it is convenient (and accurate) to divide the oxygen atoms into two sets, labelled O(i1) and O(i2) (i = 1–6). The immediate environment of a specific oxygen atom in each of these two sets is such that the short O—O contacts are parallel to each other in the first set, but approximately perpendicular in the second.

The O—Th—O angles associated with each type of oxygen atom are set out in Table 4. For O(i1), the angles fall into values grouped around 49.6° (six), 67.5° (eighteen), 112.2° (eighteen), 131.5 (six), and 177.6° (three), where the numbers in parentheses are the total number of such angles within the icosahedron. For the O(i2) atoms, the associated O(i2)—Th—O angles are grouped around average values of

Can. J. Chem. Downloaded from www.nrcresearchpress.com by 210.87.254.42 on 09/06/12
For personal use only.

TABLE 3. Interatomic distances (Å) with estimated standard deviations for $[(bpyH)_3NO_3][Th(NO_3)_6]$

Atoms	Distance	Atoms	Distance	Atoms	Distance	Atoms	Distance
(i) $[TH(NO_3)_6]^{2-}$				*(iii) 2,2-Bipyridinium cation*			
Th—O(11)	2.568(3)	Th—O(12)	2.566(4)	N(1)—C(1)	1.338(9)	N(2)—C(10)	1.340(10)
Th—O(21)	2.562(4)	Th—O(22)	2.560(4)	N(1)—C(5)	1.355(7)	N(2)—C(6)	1.327(9)
Th—O(31)	2.572(4)	Th—O(32)	2.585(4)	N(3)—C(11)	1.335(7)	N(4)—C(20)	1.316(8)
Th—O(41)	2.560(3)	Th—O(42)	2.602(3)	N(3)—C(15)	1.361(8)	N(4)—C(16)	1.330(8)
Th—O(51)	2.551(4)	Th—O(52)	2.573(4)	N(5)—C(21)	1.333(9)	N(6)—C(26)	1.344(7)
Th—O(61)	2.540(4)	Th—O(62)	2.573(4)	N(5)—C(25)	1.364(8)	N(6)—C(30)	1.341(11)
N(10)—O(11)	1.275(8)	N(20)—O(21)	1.268(5)	C(1)—C(2)	1.376(11)	C(2)—C(3)	1.376(9)
N(10)—O(12)	1.272(7)	N(20)—O(22)	1.279(7)	C(3)—C(4)	1.385(10)	C(4)—C(5)	1.389(10)
N(10)—N(13)	1.214(6)	N(20)—O(23)	1.191(8)	C(5)—C(6)	1.464(8)	C(6)—C(7)	1.371(8)
N(30)—O(31)	1.274(7)	N(40)—O(41)	1.270(6)	C(7)—C(8)	1.361(12)	C(8)—C(9)	1.378(13)
N(30)—O(32)	1.273(7)	N(40)—O(42)	1.284(6)	C(9)—C(10)	1.375(10)	C(11)—C(12)	1.382(9)
N(30)—O(33)	1.195(8)	N(40)—O(43)	1.207(5)	C(12)—C(13)	1.376(11)	C(13)—C(14)	1.383(8)
N(50)—O(51)	1.275(6)	N(60)—O(61)	1.284(7)	C(14)—C(15)	1.369(9)	C(15)—C(16)	1.478(7)
N(50)—O(52)	1.274(6)	N(60)—O(62)	1.272(8)	C(16)—C(17)	1.371(10)	C(17)—C(18)	1.395(10)
N(50)—O(53)	1.207(8)	N(61)—O(63)	1.200(7)	C(18)—C(19)	1.346(11)	C(19)—C(20)	1.371(11)
				C(21)—C(22)	1.383(8)	C(22)—C(23)	1.367(10)
(ii) Nitrate ion				C(23)—C(24)	1.379(11)	C(24)—C(25)	1.379(8)
				C(25)—C(26)	1.461(9)	C(26)—C(27)	1.366(10)
N(70)—O(71)	1.232(8)	N(70)—O(72)	1.232(9)	C(27)—C(28)	1.395(12)	C(28)—C(29)	1.370(10)
N(70)—O(73)	1.252(6)			C(29)—C(30)	1.372(12)		
				(iv) Hydrogen bonding			
				H(N1)—O(73)	1.876	H(N3)—O(72)	1.937
				H(N5)—O(71)	1.900	N(1)—O(73)	2.778(9)
				N(3)—O(72)	2.838(9)	N(5)—O(71)	2.813(9)

TABLE 4. Bond angles (deg)[a] for $[(bpyH)_3NO_3][Th(NO_3)_6]$

(*i*) Thorium oxygen polyhedra

O(*i*1)—Th—O	Angle	Mean angle[b]	Range	Number in group
O(11)—Th—O(12)	49.7(1)	49.6(1)	49.4–49.7	6
O(11)—Th—O(22)	69.1(1)	67.5(12)	65.1–69.6	18
O(11)—Th—O(51)	66.5(1)			
O(11)—Th—O(61)	69.6(1)			
O(11)—Th—O(62)	67.7(1)			
O(11)—Th—O(21)	113.6(1)	112.2(12)	109.9–114.5	18
O(11)—Th—O(31)	113.2(1)			
O(11)—Th—O(32)	113.4(1)			
O(11)—Th—O(52)	112.0(1)			
O(11)—Th—O(42)	131.2(1)	131.5(16)	129.5–133.5	6
O(11)—Th—O(41)	178.3(1)	177.6(8)	176.7–178.3	3

O(*i*2)—Th—O	Angle	Mean angle[b]	Range	Number in group
O(12)—Th—O(22)	69.6(1)	67.8(9)	66.6–69.6	18
O(12)—Th—O(31)	68.4(1)			
O(12)—Th—O(32)	68.5(1)			
O(12)—Th—O(61)	68.0(1)			
O(12)—Th—O(62)	102.9(1)	102.4(5)	101.9–102.9	3
O(12)—Th—O(21)	114.5(1)	112.0(14)	109.9–114.5	12
O(12)—Th—O(51)	112.2(1)			
O(12)—Th—O(42)	125.6(1)	125.9(6)	125.5–126.6	3
O(12)—Th—O(41)	131.6(1)	131.5(16)	129.5–133.5	6
O(12)—Th—O(52)	161.3(1)	160.2(12)	159.0–161.3	3

[a] Estimated standard deviations in parentheses.

[b] Estimated standard deviations on average values are calculated from the "scatter formula": $\sigma = [\Sigma(d_i - \bar{d})^2/(N-1)]^{1/2}$, where d_i is the ith and $\bar{d}$ is the mean of N equal measurements.

Can. J. Chem. Downloaded from www.nrcresearchpress.com by 210.87.254.42 on 09/06/12
For personal use only.

TABLE 4. (*Concluded*)

(*ii*) N—Th—N

Bonds	Angle	Bonds	Angle
N(10)—Th—N(20)	93.9(1)	N(10)—Th—N(30)	91.8(1)
N(10)—Th—N(40)	150.6(1)	N(10)—Th—N(50)	113.7(1)
N(10)—Th—N(60)	72.1(1)	N(20)—Th—N(30)	91.2(1)
N(20)—Th—N(40)	110.9(1)	N(20)—Th—N(50)	74.1(1)
N(20)—Th—N(60)	152.1(1)	N(30)—Th—N(40)	72.8(1)
N(30)—Th—N(50)	150.9(1)	N(30)—Th—N(60)	112.8(1)
N(40)—Th—N(50)	89.0(1)	N(40)—Th—N(60)	90.5(1)
N(50)—Th—N(60)	90.2(1)		

(*iii*) Nitrato ligand

Bonds	Angle	Bonds	Angle
O(11)—N(10)—O(12)	115.8(4)	O(21)—N(20)—O(22)	114.9(5)
O(11)—N(10)—O(13)	121.3(5)	O(21)—N(20)—O(23)	122.7(5)
O(12)—N(10)—O(13)	122.9(6)	O(22)—N(20)—O(23)	122.4(4)
O(31)—N(30)—O(32)	115.6(5)	O(41)—N(40)—O(42)	115.4(3)
O(31)—N(30)—O(33)	122.4(6)	O(41)—N(40)—O(43)	122.3(5)
O(32)—N(30)—O(33)	122.0(6)	O(42)—N(40)—O(43)	122.3(5)
O(51)—N(50)—O(52)	115.4(5)	O(61)—N(60)—O(62)	114.8(5)
O(51)—N(50)—O(53)	123.0(4)	O(61)—N(60)—O(63)	121.8(6)
O(52)—N(50)—O(53)	121.6(4)	O(62)—N(60)—O(63)	123.3(5)

(*iv*) Nitrate ion

Bonds	Angle	Bonds	Angle
O(71)—N(70)—N(72)	119.6(5)	O(71)—N(70)—N(73)	119.6(6)
O(72)—N(70)—N(73)	120.8(6)		

(*v*) 2,2′-Bipyridinium cation

Bonds	Angle	Bonds	Angle
C(1)—N(1)—C(5)	123.4(6)	C(6)—N(2)—C(10)	117.2(6)
N(1)—C(1)—C(2)	120.9(6)	N(1)—C(5)—C(4)	116.8(5)
N(1)—C(5)—C(6)	117.0(6)	C(4)—C(5)—C(6)	126.2(5)
N(2)—C(6)—C(5)	115.5(5)	N(2)—C(6)—C(7)	122.2(6)
C(5)—C(6)—C(7)	122.3(6)	N(2)—C(10)—C(9)	124.0(8)
C(11)—N(3)—C(15)	123.0(5)	C(16)—N(4)—C(20)	116.7(6)
N(3)—C(11)—C(12)	119.6(6)	N(3)—C(15)—C(14)	118.0(5)
N(3)—C(15)—C(16)	116.0(5)	C(14)—C(15)—C(16)	126.0(6)
N(4)—C(16)—C(15)	116.2(6)	N(14)—C(16)—C(17)	123.3(5)
C(15)—C(16)—C(17)	120.6(6)	N(4)—C(20)—C(19)	124.7(7)
C(21)—N(5)—C(26)	123.4(5)	C(26)—N(6)—C(30)	117.5(6)
N(5)—C(21)—C(22)	120.0(6)	N(5)—C(25)—C(24)	117.3(6)
N(5)—C(25)—C(26)	117.1(4)	C(24)—C(25)—C(26)	125.6(6)
N(6)—C(26)—C(25)	115.6(5)	N(6)—C(26)—C(27)	122.2(6)
C(25)—C(26)—C(27)	122.2(6)	N(6)—C(30)—C(29)	123.4(7)
Mean (of 18) C—C—C	119.6(12)	Range 117.5–121.1	

(*vi*) Hydrogen bonding

Bonds	Angle	Bonds	Angle
O(73)—H(N1)—N(1)	158	O(72)—H(N3)—N(3)	158
O(71)—H(N5)—N(5)	160		

67.8°, 102.4°, 112.0°, 125.9°, 131.5°, and 160.2°. Table 4 gives the number of examples contributing to each group, the range of values, and the mean angle.

Nitrato ligand

Although there are significant differences in the Th—O bond distances to the nitrato ligands of the anion, and especially for nitrates 3–6, the average difference in bond length between the N(*i*)—O(*i*1) and N(*i*)—O(*i*2) bonds is 0.001 Å, in keeping with the limits quoted by Addison *et al.* (17) for symmetrical bidentate nitrate. The average lengths of the N(*i*)—O(*i*1), N(*i*)—O(*i*2) and N(*i*)—O(*i*3) bonds are

Can. J. Chem. Downloaded from www.nrcresearchpress.com by 210.87.254.42 on 09/06/12
For personal use only.

1.274(6), 1.275(5), and 1.202(9) Å, very close to those previously reported (4, 5) for $[Th(NO_3)_6]^{2-}$ and $Th(NO_3)_4(H_2O)_3 \cdot 2H_2O$ (6), and for the analogous cerium(IV) anion (7) $[Ce(NO_3)_6]^{2-}$. The average O—N—O angles are 115.3(4)°, 122.2(6)°, and 122.4(6)°, again similar to previously reported values. Following the arguments of Addison *et al.* (17), and Hester and Grossman (18), one concludes that the total valence bond order in the nitrato ligand is 3.9.

The 2,2′-bipyridinium cation and the $[bpyH)_3NO_3]^{2+}$ complex

Monoprotonated 2,2′-bipyridinium cations have been identified in three earlier crystal structure studies (19, 21). The present work, like that of earlier authors, shows that in the crystal lattice, the cation adopts a configuration in which two nitrogen atoms are *syn*, in contrast to the *anti* stereochemistry found in the neutral molecule (22), and in the diprotonated cation (23). The rings of the monopositive cation are both planar, but the *syn* conformation is apparently stablized by a slight twisting about the C—C axis, producing dihedral angles of 6.6, 4.3, and 7.8°.

The N—C and C—C bond lengths in the present structure are consistent with those reported for 2,2′-bipyridine (22), the 2,2′-bipyridinium cation (19), and coordinated 2,2′-bipyridine (19, 24, 25). There are some significant differences between the protonated and non-protonated rings, as noted previously by Figgis *et al.* (19). The most significant points are an increased C—N—C angle at the protonated nitrogen atoms N(1), N(3), and N(5), and a corresponding decrease in the angles at adjacent carbon atoms C(1), C(11), C(21). It is interesting that the geometry of the coordinated ligand is generally closer to that of the neutral compound, or to that of the non-protonated ring of the monopositive cation, than to the protonated C_5H_4N moiety of the cation.

The nitrate ion N(70), O(71,72,73) in the lattice is essentially trigonal (average angle 120.0(7)°, average N—O bond length 1.239(11) Å) and planar. The bond length is similar to other reported distances for ionic nitrate (e.g. ref. 26). Each oxygen atom is hydrogen-bonded to the N—H^+ function of a 2,2′-bipyridinium molecule, with an average O--H--N distances of 2.810 Å, typical of such bonds (27). The hydrogen atom can be identified at an average distance of 1.90 Å from oxygen in this bond.

The effect of this hydrogen bonding is to produce the unusual cationic complex $[(bpyH)NO_3]^{2+}$ in the lattice. This unit has approximate C_3 symmetry (see Fig. 1). Attempts to investigate the stability of this cation in solution have so far proved inconclusive, largely because of the lack of a suitable solvent. It is not unreasonable to conclude that the stability of the lattice of the title compound is maximised by the formation of a large dipositive cationic unit which acts as the counterion for $[Th(NO_3)_6]^{2-}$.

Acknowledgement

This work was supported in part by Operating Grants (to D.G.T.) from the Natural Sciences and Engineering Research Council of Canada.

1. D. BROWN. Comprehensive inorganic chemistry. Vol. 5. *Edited by* A. F. Trotman-Dickenson. Pergamon Press, Oxford. 1973. p. 151.
2. N. KUMAR and D. G. TUCK. Can. J. Chem. **60**, 2579 (1982).
3. N. KUMAR and D. G. TUCK. Inorg. Chem. **22**, 1951 (1983).
4. S. SCAVNICAR and B. PRODIC. Acta Crystallogr. **18**, 698 (1965).
5. N. W. ALCOCK, S. ESPERAS, K. W. BAGNALL, and W. HSIAN-YUN. J. Chem. Soc. Dalton Trans. 638 (1978).
6. R. P. ENGLISH, J. G. H. DU PREEZ, L. R. NASSIMBENI, and C. P. J. VAN VUUREN. S.-Afr. Tydskr. Chem. **32**, 119 (1979).
7. (*a*) A. ZALKIN, J. D. FORRESTER, and D. H. TEMPLETON. J. Chem. Phys. **39**, 2881 (1963); (*b*) T. A. BEINEKE and J. DELGAUDIO. Inorg. Chem. **7**, 715 (1968).
8. T. VEKI, A. ZALKIN, and D. H. TEMPLETON. Acta Crystallogr. **20**, 386 (1966).
9. J. C. TAYLOR, M. H. MUELLER, and R. L. HITTERMAN. Acta Crystallogr. **20**, 842 (1966).
10. C. OLDHAM and D. G. TUCK. J. Chem. Ed. **59**, 420 (1982).
11. D. G. TUCK. J. Chem. Soc. 2783 (1958).
12. N. KUMAR and D. G. TUCK. Unpublished results.
13. M. A. KHAN, R. C. STEEVENSZ, D. G. TUCK, J. G. NOLTES, and P. W. R. CORFIELD. Inorg. Chem. **19**, 3407 (1980).
14. J. A. IBERS and W. C. HAMILTON. (*Editors*). International tables for X-ray crystallography. Vol. IV. Kynoch Press: Birmingham, England. 1974. pp. 99, 149.
15. R. F. STEWART, E. R. DAVIDSON, and W. T. SIMPSON. J. Chem. Phys. **42**, 3175 (1965).
16. (*a*) P. W. R. CORFIELD. CHECK, A programme to calculate the scaling factors for data. Wayne State University. 1979; (*b*) W. SCHMONSEES. PROC, A programme for data reduction (1972); (*c*) D. H. TEMPLETON and L. TEMPLETON. ABSORB, An analytical absorption correction programme. Univ. of California, Berkeley. 1973; (*d*) G. M. SHELDRICK. SHELX 77, A programme for crystal structure determination. Univ. of Cambridge, England. 1977; (*e*) P. J. ROBERTS AND G. M. SHELDRICK. XANADU, A programme for crystallographic calculations. Univ. of Cambridge, England. 1975; (*f*) C. K. JOHNSON. ORTEP. Report ORNL-3794. Oak Ridge National Laboratory, TN. 1965.
17. C. C. ADDISON, N. LOGAN, S. C. WALLWORK, and C. D. GARNER. Q. Rev. Chem. Soc. **25**, 289 (1971).
18. R. E. HESTER and W. E. L. GROSSMAN. Inorg. Chem. **5**, 1308 (1966).
19. B. N. FIGGIS, B. W. SKELTON, and A. H. WHITE. Aust. J. Chem. **31**, 57 (1978).
20. G. J. GAINSFORD, R. J. DELLACA, and W. T. ROBINSON. Acta Crystallogr. A**25**, 580 (1969).
21. J. L. LIPKOWSKI, P. SGARABOTTO, and G. D. ANDREETTI. Cryst. Struct. Commun. **5**, 931 (1976).
22. L. L. MERRITT and E. D. SCHROEDER. Acta Crystallogr. **9**, 801 (1956).
23. K. NAKATSU, H. YOSHIOKA, M. MATSUI, S. KODA, and S. OOI. Acta Crystallogr. A**28**, S24 (1972).
24. J. L. HENCHER, M. A. KHAN, F. F. SAID, R. SIELER, and D. G. TUCK. Inorg. Chem. **21**, 2787 (1982).
25. M. A. KHAN and D. G. TUCK. Acta Crystallogr. B**37**, 1409 (1981).
26. N. W. ALCOCK and W. D. HARRISON. J. Chem. Soc. Dalton Trans. 1421 (1982).
27. S. N. VINOGRADOV and R. H. LINNELL. Hydrogen bonding. Van Nostrand Reinhold Company, New York. 1971. p. 177.

Can. J. Chem. Downloaded from www.nrcresearchpress.com by 210.87.254.42 on 09/06/12
For personal use only.

Dissolution enthalpy of NaI in water–alcohol mixtures at 288.15 and 308.15 K. Enthalpy of interaction in electrolyte–alcohol–water systems

HENRYK PIEKARSKI, ALINA PIEKARSKA, AND STEFANIA TANIEWSKA-OSIŃSKA
Institute of Physical Chemistry, University of Łódź, Łódź, ul. Nowotki 18, 91-416, Poland

Received May 2, 1983

HENRYK PIEKARSKI, ALINA PIEKARSKA, and STEFANIA TANIEWSKA-OSIŃSKA. Can. J. Chem. **62**, 856 (1984).

The enthalpy of NaI solution was determined in water mixtures with methanol, ethanol, propanol, and isopropanol in the entire range of mixed-solvent concentration at 288.15 and 308.15 K, and in water mixtures with *s*-butanol and *tert*-butanol in the range of 0–5 mol% alcohol at 308.15 K. The dependence of $\bar{C}^0_{p_2}$ on solvent composition was studied. The enthalpic pair interaction coefficients h_{EN} for NaI–alcohol in water and NaI–water in alcohols were determined, and the effect of temperature on h_{EN} values in the systems under study was analyzed.

HENRYK PIEKARSKI, ALINA PIEKARSKA et STEFANIA TANIEWSKA-OSIŃSKA. Can. J. Chem. **62**, 856 (1984).

On a déterminé l'enthalpie de solutions de NaI dans des mélanges aqueux de méthanol, d'éthanol, de propanol et d'isopropanol dans l'intervalle complet de concentration des solvants mixtes à 288,15 et à 308,15 K et également dans des mélanges aqueux de *s*-butanol et de *tert*-butanol à des concentrations allant de 0 à 5 mol% d'alcool à 308,15 K. On a étudié l'effet de la composition du solvant sur la valeur de $\bar{C}^0_{p_2}$. On a déterminé les coefficients enthalpiques des paires d'interaction, h_{EN}, pour NaI–alcool dans l'eau et NaI–eau dans des alcools et on a analysé l'effet de la température sur les valeurs de h_{EN} dans les systèmes étudiés.

[Traduit par le journal]

Can. J. Chem. Downloaded from www.nrcresearchpress.com by 210.87.254.5 on 09/06/12
For personal use only.

Introduction

While calorimetric investigations of electrolyte solutions in water – aliphatic alcohols have often been conducted at various laboratories, there is little data on the effect of temperature on the thermochemical properties of electrolyte–alcohol–water systems in the whole range of mixed-solvent composition (1). In view of this we decided to measure the enthalpy of NaI solution in methanol, ethanol, propanol, and isopropanol mixtures with water over the entire range of mixed-solvent concentration at 288.15 K and 308.15 K. We have also determined the enthalpy of NaI solution in *s*-butanol and *tert*-butanol mixtures with water at 308.15 K in the range of a few mol% of alcohol. Sodium iodide had been used previously as an electrolyte because of its good solubility in the systems under investigation and, consequently, we had at our disposal substantial material for comparison.

Experimental

Materials

Sodium iodide, analytically pure (JT Baker Chemicals B.V., Holland); solvents methanol, ethanol, propanol, isopropanol, all analytically pure (POCh Gliwice, Poland); and *s*-butanol and *tert*-butanol, A.R. (Reanal, Hungary), were purified and dried using the procedure described in an earlier paper (2).

Apparatus and method of measurement

The measurements of solution enthalpies were made using an "isoperibol" calorimeter. The calorimeter and the method of measurement have been described in an earlier report (3). Six to eight experimental runs were performed for each composition of mixed solvent. The range of electrolyte concentration was 0.003–0.015 mol/kg of solvent. The uncertainties in the measured enthalpies did not exceed ±0.5% of the measured value.

Results and discussion

Solution enthalpy

The measured enthalpies of solution were extrapolated to infinite dilution by the method of Criss and Cobble (4). The dielectric permittivity and the density of water–alcohol mixture were adopted from the literature (5, 6). The standard enthalpies of NaI solution in all mixtures under study are collected in Tables 1 and 2. As an example, Fig. 1 illustrates the effect of temperature on the shape of the $\Delta H^0 = f(x)$ NaI plot in water–ethanol mixtures. As can be seen from these data, the plot of ΔH^0 for NaI in water–alcohol mixture under investigation exhibits a maximum in the range of small alcohol content. A similar maximum of ΔH^0 has been observed in all electrolyte–water–alcohol systems studied thus far. It is assumed that this maximum is connected with the structure-making or -stabilizing effect of the added alcohol on water (7–10). Previous research (1–3) as well as the results of the present study suggest that the position of the maximum of ΔH^0 depends on the size of the alcohol molecule (Tables 1, 2). As the molecular size increases, the maximum shifts towards

TABLE 1. Standard enthalpies of NaI solution in water–alcohol mixtures at 288.15 K

X_{alc} (mol%)	ΔH^0 (J mol^{-1})[a]			
	Methanol	Ethanol	Propanol	Isopropanol
0	−6 505	−6 505	−6 505	−6 505
1	−6 090	−5 710	−5 480	−5 175
2	−5 690	−4 920	−4 435	−3 870
4	−4 870	−3 365	−2 385	−1 310
5	−4 500	−2 600	−1 380	−70
6	—	−1 875	−420	+1 160
8	−3 450	−420	−420	+2 160
10	−2 890	+630	−1 460	+1 670
12	—	+780	—	+920
15	−2 090	+150	−4 020	−620
20	—	—	—	−3 490
30	−4 440	−5 650	−11 090	−8 490
50	−8 490	−12 180	−16 320	−16 480
70	−14 480	−15 100	−19 750	−22 430
80	−18 870	−16 860	−21 325	−24 155
90	−24 460	−19 600	−22 800	−25 770
95	−27 300	−21 480	−23 500	−26 540
100	−31 420	−24 015	−24 180	−27 280
	−32 160[b]	−24 400[b]		

[a]Estimated uncertainties in the extrapolated standard enthalpies: in water-rich region: ±50 J mol^{-1}; in alcohol-rich region ±100 J mol^{-1}.
[b]Interpolated values from the literature data at 283.15 K and 298.15 K (11).

TABLE 2. Standard enthalpies of NaI solution in water–alcohol mixtures at 308.15 K

X_{alc} (mol%)	ΔH^0 (J mol^{-1})[a]					
	Methanol	Ethanol	Propanol	Isopropanol	*s*-Butanol	*tert*-Butanol
0	−8 660	−8 660	−8 660	−8 660	−8 660	−8 660
1	−8 370	−8 110	−7 940	−7 800	−7 530	−7 450
2	−8 140	−7 575	−7 220	−6 955	−6 520	−6 400
3	—	—	—	—	−5 610	—
4	−7 675	−6 510	−5 800	−5 300	−4 800	−4 790
5	−7 440	−6 020	−5 095	−4 490		
6	—	−5 550	−4 400	−3 690		
8	−6 920	−4 540	−4 820	−3 445		
10	−6 530	−4 160	−6 550	−4 150		
12	—	−4 180	—	−4 950		
15	−6 065	−4 910	−9 200	−6 400		
20	—	—	—	− 8 930		
30	−8 140	−9 870	−15 500	−13 300		
50	−11 550	−15 690	−19 920	−20 100		
70	−16 880	−17 655	−22 510	−24 890		
80	−20 960	−18 950	−23 665	−26 380		
90	−26 150	−21 550	−24 750	−27 610		
100	−32 760	−25 440	−25 770	−28 580		

[a]Estimated uncertainties in the extrapolated standard enthalpies: in water-rich region ±50 J mol^{-1}, in alcohol-rich region ±100 J mol^{-1}.

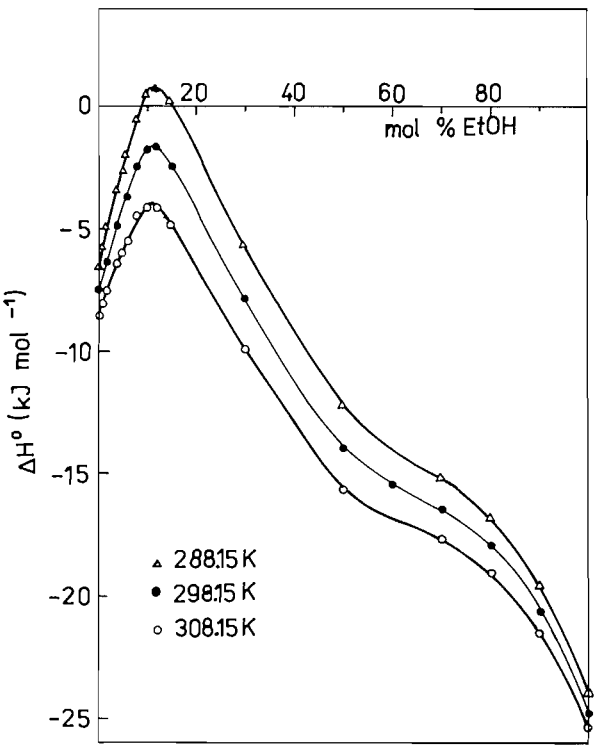

FIG. 1. Standard dissolution enthalpy ΔH^0 of NaI in water–ethanol mixtures as a function of mol% ethanol. (Data for T = 298.15 K are taken from ref. 2).

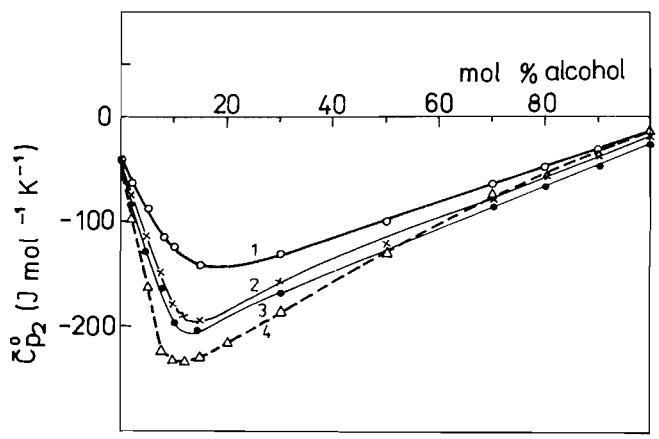

FIG. 2. Partial molar heat capacity $\bar{C}^0_{p_2}$ of NaI in water–alcohols mixtures vs. solvent composition (1–methanol, 2-ethanol, 3-propanol, 4-isopropanol).

smaller alcohol content in the mixture.

An analysis of the results obtained shows that in all mixtures under investigation, in the temperature range 288.15–308.15 K, the standard enthalpy of NaI solution becomes more exothermic as the temperature increases, with the shape of $\Delta H^0 = f(x)$ isotherms remaining essentially unchanged. The only effect that is observed is the lowering and flattening of the maximum of ΔH^0, but its position does not change. The standard enthalpies of NaI solution determined in this study made it possible to calculate the molar specific heat of NaI in infinitely dilute solution $\bar{C}^0_{p_2}$ in all mixtures under study (Fig. 2).

$$[1]\quad \frac{d\Delta H^0}{dT} = \Delta C^0_p = \bar{C}^0_{p_2} - C_{p_{cryst.}}$$

where $C_{p_{cryst.}}$ is molar heat of crystalline electrolyte. It follows from the data obtained that in all systems under investigation $\bar{C}^0_{p_2}$ NaI is negative in all mixed solvent composition over the entire temperature studied. The $\bar{C}^0_{p_2} = f(x)$ curves exhibit a minimum in the range of small alcohol content, and its position and depth depend on the kind of alcohol. As the size of the alcohol molecule increases, this minimum becomes deeper and shifts towards lower alcohol content. The position of the minimum of $\bar{C}^0_{p_2}$ approximately corresponds to the position of the ΔH^0 maximum. Further increase in alcohol content beyond the minimum produces a gradual increase in $\bar{C}^0_{p_2}$. In alcohol-rich mixtures, the $\bar{C}^0_{p_2} = f(x)$ curves for different water–alcohol mixture lie close to one another.

The presence of the $\bar{C}^0_{p_2}$ minimum seems to favour the view of the maximum ordering of the water–alcohol mixture, with composition corresponding to maximum standard enthalpy of

Can. J. Chem. Downloaded from www.nrcresearchpress.com by 210.87.254.5 on 09/06/12
For personal use only.

TABLE 3. NaI-nonelectrolyte pair interaction coefficients h_{EN} in water solution at several temperatures

	h_{EN} (J kg mol^{-2})		
Nonelectrolyte	288.15 K	298.15 K[a]	308.15 K
Methanol	+193	+157	+126
Ethanol	+360	+298	+248
Propanol	+467	+395	+326
Isopropanol	+603	+509	+385
s-Butanol	—	+643	+525
tert-Butanol	—	+720	+574
Formamide	−393[b]	−348[b]	−266[b]
DMF	−235[b]	−212[b]	−183[b]
DMSO		−314[b]	
THF		+172[b]	
Acetone		−46[b]	

[a]Data taken from ref 2.
[b]The values calculated from literature data: formamide and DMF (15), DMSO (16), THF (17), acetone (18).

TABLE 4. NaI−water pair interaction coefficients h_{EN} in alcoholic solution at several temperatures

	h_{EN} (J kg mol^{-2})		
Solvent	288.15 K	298.15 K[a]	308.15 K
Methanol	+607	+583	+572
Ethanol	+573	+551	+523
Propanol	+200	+177	+148
Isopropanol	+219	+173	+126
Isobutanol		−1370	
s-Butanol		−1420	

[a]The values calculated from literature data (2, 3).

NaI solution in these mixtures. The increase in $\bar{C}^0_{p_2}$ NaI beyond the minimum is probably related to the breaking of the maximum ordered structure of the mixture with increasing alcohol content. Mixed water−alcohol associates may be present in the intermediate composition range of the mixture. In the temperature range studied, the structure of the pure alcohol may also be less sensitive to a change in temperature than the maximum-ordered structure which corresponds to the minimum $\bar{C}^0_{p_2}$. The calculated value[1] of $\bar{C}^0_{p_2}$. NaI in water, −54.2 J K^{-1} mol^{-1} is in fair agreement with that obtained in the same way by Mishchenko *et al.* (−59.5 J K^{-1} mol^{-1}) (12) but it differs considerably from the value −76.5 J K^{-1} mol^{-1} determined by the direct method of Desnoyers *et al.* (13). The discrepancy must be a result of an error in the solution enthalpy measurement and in the extrapolation to infinite dilution on the values of the coefficient $d\Delta H^0/dT$.

Enthalpic pair interaction coefficients

As is well known, quantitative determination of the interaction of solute molecules in three-component systems can be conveniently expressed in pair, triplet, etc., interaction coefficients, as proposed by McMillan-Mayer (14). For this reason we thought it advisable to calculate, on the basis of the data obtained, enthalpic pair interaction coefficients for NaI−nonelectrolyte in water and for NaI−water in the nonaqueous solutions studied.

The h_{EN} coefficients calculated by the method described in the previous paper (2) are collected in Tables 3 and 4. To permit comparison enthalpic pair interaction coefficients for other nonelectrolyte−NaI pairs calculated on the basis of literature data (15−18) are also included. It has to be pointed out that the h_{EN} coefficients listed in the table constitute, in each case, the "mean ionic" pair interaction coefficients, or, more precisely, in the case of 1−1 electrolyte (E), they correspond to half the sum of the enthalpic effect of the interaction between the molecule of the given nonelectrolyte (N) and the cation (K^+) and the anion (A^-):

$$[2] \quad h_{EN} = \frac{1}{2}[h(K^+A^-—N)] = \frac{1}{2}[h(K^+—N) + h(A^-—N)]$$

It follows from the data presented in Table 3 that the positive coefficients h_{EN} are for pairs in which the nonelectrolytes are aliphatic alcohols, known as water structure-making or -stabilizing substances. In the case of the remaining nonelectrolytes, with the exception of THF, the pair interaction coefficients for NaI−nonelectrolyte are negative for reasons not fully understood. It seems, however, that the observed difference in the sign of the h_{EN} coefficient is connected with the different effect of the molecule of the above-mentioned two nonelectrolyte groups on the structure of water.

In an earlier study (2), a linear correlation was obtained between h_{EN} for NaI−alcohol pairs in water and the polarizability of alcohol molecule. An analysis of the h_{EN} values for NaI−alcohol in water obtained in this study as well as those reported in the above-mentioned paper has further shown that there is also a linear dependence of h_{EN} and the reciprocal of the dielectric permittivity of the alcohol $1/\epsilon$ (Fig. 3). This is somewhat surprising, for in contradistinction to polarizability (α), which is a molecular quantity, dielectric permittivity (ϵ) is related to a number of molecules. There exists, to be sure, a nonlinear dependence between α and ϵ, but the "structure" of pure liquid substance plays a significant role in it.

The values of the coefficient h_{EN} for electrolyte−alcohol in water in the temperature range 288.15−308.15 K (Table 3) lead to the conclusion that the strongest interactions between ions and alcohol molecules in water take place in the system containing methanol, possibly because of the small size of the methanol molecules and their similarity to water molecules. In view of the fact that in water solutions, alcohol molecules with large alkyl radicals may undergo hydrophobic hydration, ion−

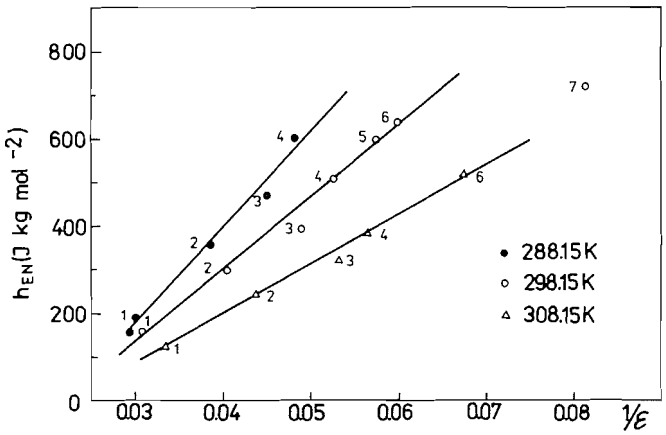

FIG. 3. Dependence of the enthalpic pair interaction coefficients of NaI−alcohol in water solutions on reciprocal of the alcohol dielectric permittivity (1-methanol, 2-ethanol, 3-propanol, 4-isopropanol, 5-isobutanol, 6-*s*-butanol, 7-*tert*-butanol).

[1] $C_{p\,\text{cryst. NaI}} = 54.31$ J K^{-1} mol^{-1}.

Can. J. Chem. Downloaded from www.nrcresearchpress.com by 210.87.254.5 on 09/06/12
For personal use only.

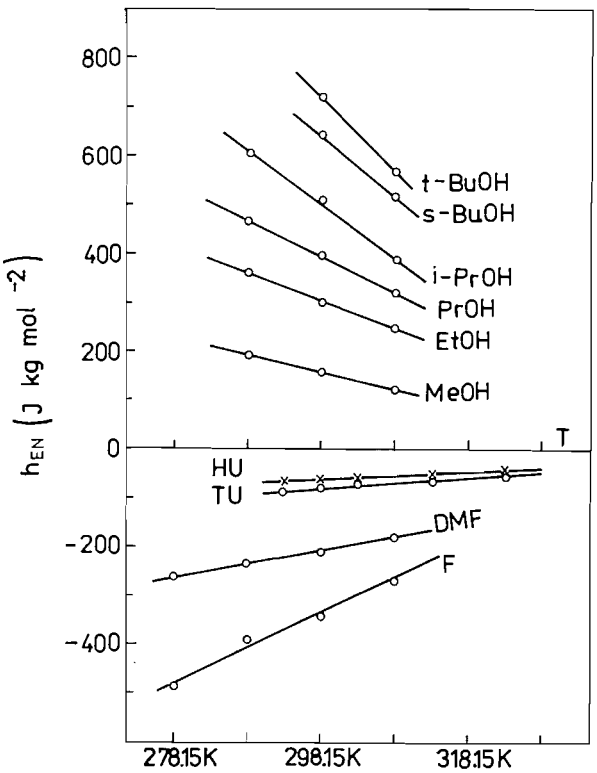

FIG. 4. Temperature dependence of enthalpic pair interaction coefficients for NaI–nonelectrolyte pairs in water solution. A kind of the nonelectrolyte is marked in the graph. The data for NaI–hydroxyurea (HU) and NaI–thiourea (TU) pairs are taken from the literature (17).

TABLE 5. Heat capacity pair interaction coefficients C_{EN}

		C_{EN} (J kg mol^{-2} K^{-1})	
Solvent	Nonelectrolyte	NaI	NaCl[a]
Water	Methanol	−3.4	−3.5
	Ethanol	−5.6	−6.0
	Propanol	−7.0	−7.0
	Isopropanol	−10.9	
	Butanol		−7.5
	s-Butanol	−11.8	
	tert-Butanol	−14.6	
	Formamide	+6.5	
	DMF	+2.5	
Methanol	Water	−1.7	
Ethanol		−2.5	
Propanol		−2.6	
Isopropanol		−4.6	

[a]From ref. 20.

alcohol interactions become weaker as the size of the alcohol molecule increases. As a result, the endothermicity of the coefficient h_{EN} also increases. The values of the pair interaction coefficient h_{EN} for NaI–water in alcohols (Table 4) suggest that the weakest ion–water interaction takes place in methanol solution. This may be related to the strong solvation of both ions and water molecules by methanol molecules.

Among the systems under investigation, the strongest electrolyte–water interaction takes place in butanol solutions, where the enthalpic pair interaction coefficients h_{EN} have high negative values.

The effect of temperature on the pair interaction coefficient h_{EN} for NaI–alcohol in water is presented in Fig. 4, which also includes h_{EN} data for other electrolyte–nonelectrolyte–water systems calculated on the basis of literature data (15) or adopted from other studies (19). As can be seen, with increasing temperature the h_{EN} values for all systems studied, both the positive and the negative ones, tend to zero. In quantitative terms, the effect of temperature on the values of h_{EN} can be presented by means of function C_{EN} defined by equation

$$[3] \quad h_{EN}(T_2) = h_{EN}(T_1) + C_{EN}(T_2 - T_1)$$

The calculated mean values of C_{EN} for NaI–alcohol and NaI–water in the temperature range 288.15 to 308.15 K are collected in Table 5. For the sake of comparison C_{EN} values for NaCl–alcohol pairs in water adopted from Perron *et al.* (20) are also included. As can be seen from the results above, the C_{EN} coefficients for the investigated electrolyte–alcohol pairs in water have negative values. The larger the alcohol molecule, the more negative the C_{EN} values. It seems that the above findings cannot be accounted for until more work is done on other electrolytes and/or on three-component systems containing, in addition to the electrolyte, two nonaqueous solvents. Appropriate studies are in progress.

1. G. A. KRESTOV. Thermodynamics of ionic processes in solutions. Khimiya, Leningrad, 1973.
2. H. PIEKARSKI. Can. J. Chem. **61**, 2203 (1983).
3. S. TANIEWSKA-OSIŃSKA and H. PIEKARSKI. J. Solution Chem. **7**, 891 (1978).
4. C. M. CRISS and J. W. COBBLE. J. Am. Chem. Soc. **83**, 3223 (1961).
5. J. TIMMERMANS. The physico-chemical constants of binary systems in concentrated solutions. Interscience Publishing Co. Inc., New York. 1959.
6. G. AKERLÖF. J. Am. Chem. Soc. **54**, 4125 (1932).
7. G. NEMETHY. Ann. Ist. Super. Sanita. **6**, 487 (1970).
8. O. YA. SAMOILOV. Zhur. Strukt. Khim. **7**, 15 (1964); **7**, 175 (1964).
9. G. NEMETHY and H. A. SHERAGA. J. Phys. Chem. **66**, 1773 (1962).
10. K. P. MISHCHENKO and G. M. POLTORATSKII. Problems of thermodynamics and structure of aqueous and nonaqueous electrolyte solutions. Plenum Publishing Corp., New York. 1972.
11. V. P. KOROLEV, A. M. KOLKER, and G. A. KRESTOV. Izv. VUZ. SSSR, Khim. Khim. Tekhnol. **20**, 997 (1977).
12. I. I. LONKEVICH, K. P. MISHCHENKO, and S. V. SHADSKII. Zhur. Obshch. Khim. **39**, 1210 (1969).
13. J. E. DESNOYERS, C. DE VISSER, G. PERRON, and P. PICKER. J. Solution Chem. **5**, 605 (1976).
14. W. G. MCMILLAN, JR. and J. E. MAYER. J. Chem. Phys. **13**, 276 (1945).
15. S. TANIEWSKA-OSIŃSKA and A. PIEKARSKA. Bull. Acad. Pol. Sci. Ser. Sci. Chim. **26**, 612 (1978).
16. R. FUCHS and C. P. HAGAN. J. Phys. Chem. **77**, 1797 (1973).
17. S. TANIEWSKA-OSIŃSKA, B. PIESTRZYŃSKA, and R. ŁOGWINIENKO. Can. J. Chem. **58**, 1584 (1980).
18. J. MOKRZAN. Private communication.
19. B. PAŁECZ. Thesis. University of Łódź, Łódź. Poland. 1982.
20. G. PERRON, D. JOLY, J. E. DESNOYERS, L. AVEDIKIAN, and J.-P. MOREL. Can. J. Chem. **56**, 552 (1978).

Can. J. Chem. Downloaded from www.nrcresearchpress.com by 210.87.254.5 on 09/06/12
For personal use only.

The vibrational spectra, crystal and molecular structure of bis(acetonitrile)dichloroplatinum(II)

F. D. ROCHON AND R. MELANSON

Département de chimie, Université du Québec à Montréal, C.P. 8888, Succ. A, Montréal (Qué.), H3C 3P8

AND

H. E. HOWARD-LOCK, C. J. L. LOCK, AND G. TURNER

Institute for Materials Research, McMaster University, Hamilton, Ont., Canada L8S 4M1

Received November 16, 1982[1]

F. D. ROCHON, R. MELANSON, H. E. HOWARD-LOCK, C. J. L. LOCK, and G. TURNER. Can. J. Chem. **62**, 860 (1984).

The crystal structure of $Pt(CH_3CN)_2Cl_2$ has been determined twice independently. The compound is the *cis* isomer. It crystallizes in the monoclinic $P2_1/c$ space group, a = 6.660(3) [6.668(4)], b = 12.500(7) [12.519(8)], c = 10.277(6) [10.308(5)] Å, β = 105.42(4) [105.41(4)]°, V = 824.7(8) [829.6(9)] Å^3. The structure was refined by full-matrix least-squares analysis to a conventional R factor of 0.054 [0.058] and R_w = 0.053 [0.057] for 1578 [1226] observed reflections. The coordination is square planar with bond lengths (Pt—N = 1.98(1), 1.98(1) [1.95(2), 1.99(2)] Å and Pt—Cl = 2.264(4), 2.263(3) [2.270(6), 2.277(5)] Å) slightly shorter than normal. The N—C bonds are 1.10(2), 1.11(2) [1.11(3), 1.16(2)] Å. The C—CH_3 bonds are shorter than normal single bonds (1.48(2), 1.45(2) [1.49(3), 1.45(3)] Å and the N—C—C framework is almost linear. Infrared (4000–100 cm^{-1}) and Raman (4000–60 cm^{-1}) spectra of the crystalline solid have been measured and assigned; the vibrational spectra confirm the *cis* structure. A rough molecular force constant analysis based on a *cis*-planar C_{2v} skeleton (ignoring H atoms) was carried out and aided in the vibrational assignments. The ν(Pt—Cl) bands occur at 362 and 333 cm^{-1}; the ν(Pt—N) bands occur at 463 and 408 cm^{-1}, and show strong coupling with the PtNC deformations.

F. D. ROCHON, R. MELANSON, H. E. HOWARD-LOCK, C. J. L. LOCK et G. TURNER. Can. J. Chem. **62**, 860 (1984).

La structure cristalline de $[Pt(CH_3CN)_2Cl_2]$ a été déterminée indépendamment par deux groupes de chercheurs. Le composé est l'isomère *cis*. Le cristal appartient au système monoclinique et le groupe d'espace $P2_1/c$. Les paramètres de maille sont a = 6,600(3) [6,668(4)], b = 12,500(7) [12,519(8)], c = 10,277(6) [10,308(5)] Å, β = 105,42(4) [105,41(4)]° et V = 824,7(8) [829,6(9)] Å^3. La structure a été affinée par moindres carrés à matrice entière jusqu'à un facteur R = 0,054 [0,058] et R_w = 0,053 [0,057] pour 1578 [1226] réflections observées. La coordination autour de l'atome de platine est un plan carré, avec les liens Pt—N (1,98(1), 1,98(1) [1,95(2), 1,99(2)] Å) et Pt—Cl (2,264(4), 2,263(3) [2,270(6), 2,277(5)] Å) légèrement plus courts que des liens normaux. Les liens N—C sont 1,10(2), 1,11(2) [1,11(3), 1,16(2)] Å et les liens C—CH_3 sont plus courts (1,48(2), 1,45(2) [1,49(3), 1,45(3)] Å) que des liens simples normaux. Les ligands acétonitriles sont presque linéaires. Les spectres infrarouges (4000–100 cm^{-1}) et Raman (4000–60 cm^{-1}) du composé à l'état solide ont été mesurés et l'attribution en a été faite. Les spectres vibrationels ont confirmé la structure *cis*. Une analyse approximative des constantes de force basée sur le squelette *cis* plan carré C_{2v} (en négligeant les atomes H) a été faite et utilisée pour l'attribution des bandes. Les vibrations ν(Pt—Cl) absorbent à 362 et 333 cm^{-1}; celles ν(Pt—N) à 463 et 408 cm^{-1}, et montrent un couplage avec les déformations PtNC.

Introduction

Certain platinum complexes have been shown to be potent antitumor agents (1) and more recently it has been suggested that "platinum blues" might act as useful second generation platinum anti-tumor drugs (2). These "platinum blues" are obtained from the reaction of pyrimidines with *cis*-dichlorodiammineplatinum(II) (2) and also from the reaction of platinum(II) complexes with carbohydrates (3). Lippard *et al.* (4) have prepared a "platinum blue" with α-pyridone units bridging pairs of platinum atoms, which also each have two *cis*-ammine groups coordinated to them.

$Pt(CH_3CN)_2Cl_2$ was first prepared by Hoffmann and Bugge in 1907 (5) and platinum blue or "platinblau" was the name originally assigned to the intense blue colour obtained when $Pt(CH_3CN)_2Cl_2$ was treated with aqueous silver nitrate, and the resulting solution allowed to stand in air (6). It was postulated that "platinblau" was an acetamide complex of platinum, the acetamide being obtained by insertion of water into coordinated acetonitrile (7). Brown *et al.* (8) determined that the reaction product of $Pt(CH_3CN)_2Cl_2$ and molten trimethylacetamide had a *trans* stereochemistry. They implied that this product was a typical "platinblau" complex. The reaction of $Pt(CH_3CN)_2Cl_2$ with ammonia also gives a product with a *trans* stereochemistry (9). $Pt(CH_3CN)_2Cl_2$ prepared in the usual manner (5) has been postulated, however, to be the *cis* complex. Lebedenskii and Golovnya (10) assigned the *cis* configuration to the compound, based on its chemical reactions. In 1964, Gillard and Wilkinson (7) suggested that the infrared data of the compound were consistent with the *cis* structure. Walton (11*a*) measured the infrared spectra of the complexes $[M(RCN)_2Cl_2]$ (M = Pt, Pd and R = methyl and phenyl) and showed that $[Pd(RCN)_2Cl_2]$ were the *trans* isomers while $[Pt(RCN)_2Cl_2]$ were the *cis* isomers. In order to characterize all the compounds involved in these reactions we have used X-ray crystallographic methods. The crystal structure of $[Pt(CH_3CN)_2Cl_2]$ was determined, independently in Montreal and in Hamilton. We became aware of this when one of us (C.J.L.L.) was asked to referee the work of the other (F.D.R.). It seemed appropriate to present the work in a joint paper. Of the data reported here, the first values refer to the work in Montreal and the latter values [in square brackets] refer to the work in Hamilton.[2]

Experiments

Preparation of bis(acetonitrile)dichloroplatinum(II), cis-[Pt(CH$_3$CN)$_2$Cl$_2$]

The title compound was prepared by the standard method (5).

[1] Revision received November 18, 1983.

[2] This manuscript is based on two manuscripts received by Can. J. Chem. on August 10, 1982 (F. D. R. and R. M.) and on September 1, 1982 (H. E. H. L., C. J. L. L., and G. T.).

Can. J. Chem. Downloaded from www.nrcresearchpress.com by 210.87.254.105 on 09/06/12
For personal use only.

Can. J. Chem. Downloaded from www.nrcresearchpress.com by 210.87.254.105 on 09/06/12
For personal use only.

Crystals were grown from water at room temperature [by evaporation of the mother liquor at 5°C]. The ^{15}N-enriched derivative was prepared by reaction of 95.2 atom % ^{15}N-enriched CH_3CN (MSD Isotope) with K_2PtCl_4 in H_2O.

Vibrational spectra and other experiments

X-ray powder diffraction showed that the compound obtained consisted of a single product. The powder pattern could be indexed on the basis of the cell obtained from the single crystal sample.

Vibrational spectra were obtained for normal and ^{15}N-enriched ligand and complex. Infrared spectra were obtained on Perkin Elmer Model 521 and 283 spectrometers, from KBr discs in the range 4000–200 cm^{-1}, and on a Nicolet Model 7199 Ft-IR spectrometer from Nujol mulls in polyethylene plates in the range 500–100 cm^{-1}. Spectra were calibrated with indene and polystyrene. Raman spectra were obtained from crystalline samples on Coderg PHO and Spex 14018 spectrometers, the exciting radiation being the 6417 Å (and 5145 Å) line of a Spectra-Physics Model 164-02 Krypton (and Argon) ion laser. The spectrometer was calibrated with a neon lamp; the wavenumber readout was constant to ±1 cm^{-1}. The vibrational spectra could be assigned on the basis of a *cis* complex. These spectra are reported in Table 5. There was no difference in the spectra of samples obtained from several different preparations of the title compound. The samples obtained readily gave the deep blue "platinblau" colour on treatment with aqueous silver nitrate solution.

Collection of diffraction data

The crystal used for the X-ray study had nine faces and approximate dimensions 0.20 × 0.20 × 0.30 mm [irregular yellow parallelepiped, ground to a cylinder 0.40 mm long × 0.18 mm in diameter]. A set of precession photographs indicated the monoclinic $P2_1/c$ space group. The cell parameters were obtained by least-squares refinement from the setting angles of 15 automatically centred reflections on a Syntex P$\bar{1}$ diffractometer using graphite-monochromatized MoKα radiation. Crystal data are as follows:

$PtCl_2C_4H_6N_2$ mw = 348.10

Monoclinic $P2_1/c$, a = 6.660(3) [6.668(4)], b = 12.500(7) [12.519(8)], c = 10.277(6) [10.308(5)] Å, β = 105.42(4) [105.41(4)]°, V = 824.7(8) [829.6(9)] Å^3, Z = 4, D_x = 2.803 g cm^{-3}, D_m = 2.80(2) [2.79(1)] g cm^{-3} (flotation), λ(MoKα) = 0.71069 Å, μ(MoKα) = 184.5 cm^{-1}, and T = 295 [295] K.

A total of 2417 [1775] independent reflections were measured in the range $2\theta < 60°$ [55°] by the $2\theta/\theta$ scan technique using MoKα radiation. The scan rate was 1° [4°] (2θ) min^{-1} for most reflections, but rates as high as 24° [24°]/min^{-1} were selected for strong reflections by the autocollection program. A 2θ scan range of 1° below $K\alpha_1$ and 1° above $K\alpha_2$ was chosen. The background time to scan time ratio was 0.50. During the data collection three [one] standard reflections, measured after every 47 [49] reflections, showed intensity fluctuations within ±3% [±1.6%] of their mean values.

The 1578 [1226] reflections with $I > 2.5\sigma(I)$ [$3\sigma(I)$] were considered observed, where $\sigma(I)$ was calculated as already described (12, 13). An absorption correction based on the equations of the crystal faces was applied to all reflections. The transmission factors varied from 0.042 to 0.107 [0.050 to 0.075]. The data were then corrected for the Lorentz and polarization effects. The scattering factors of Cromer and Waber (14) were used. The anomalous dispersion terms (15) of Pt and Cl were included in the calculations.

Solution of the structure

The Pt atom was easily located from the three-dimensional Patterson map. The positions of all the other atoms were obtained by structure-factor and Fourier-map calculations. The refinement of the parameters was done by full-matrix least-squares methods. In the early stages of refinement, unit weight was assigned to all the reflections. Later individual weights $w = 1/\sigma^2(F)$ were applied. The refinement of the scale factor, the coordinates, and anisotropic temperature factors of all atoms converged to $R = \Sigma||F_o| - |F_c||/\Sigma|F_o| = 0.054$ [0.058] and $R_w = [\Sigma w(|F_o| - |F_c|)^2/\Sigma|F_o|^2]^{1/2} = 0.053$ [0.057]. The final residual electron density map showed a few peaks as high as 1.5 e Å^{-3} [0.58 e Å^{-3}] in the very close environment of the platinum atom.

The calculations were carried out with a Cyber 73 [Cyber 170/730] computer and the programs used have already been described (12, 13).[3]

Discussion

The refined atomic parameters are listed in Table 1. A list of the anisotropic temperature factors is available.[3] A labelled diagram of the molecule is shown in Fig. 1. The bond lengths and the bond angles are shown in Table 2.

The two structural determinations agree very well in all aspects. Most parameters agree to better than 2σ ($\sigma = (\sigma_1^2 + \sigma_2^2)^{1/2}$) and the only values which are significantly different are V (4σ), Cl(2)—Pt—N(2) (6σ), N(1)—Pt—N(2) (3.2σ), N(1) y coordinate (5σ), and C(3) y coordinate (4.7σ). Even the temperature factors agree well. The errors are slightly lower for the Montreal structure; this is probably caused by the greater number of observed reflections, partly from the larger cut-off value of 2θ and partly because of the lower value of significance used to define an observed reflection.

As expected, the coordination around the platinum atom is square planar. The angles around the Pt atom are close to the expected 90 and 180°. The weighted best plane was calculated through the five atoms. The deviations from this plane are: Pt, −0.0001(5); Cl(1), −0.004(4); Cl(2), 0.006(4); N(1), −0.037(12); and N(2), 0.063(10) Å. One acetonitrile ligand is slightly above the platinum plane while the second ligand is below the platinum plane. The deviations of the other atoms from the plane are: C(1), −0.14(1); C(2), −0.20(1); C(3), 0.21(1); and C(4), 0.41(1) Å.

The compound is the *cis*-isomer as predicted by infrared spectroscopy. The Pt—Cl bonds are 2.264 [2.270(6)] and 2.263(3) [2.277(5)] Å. They seem shorter than normal bonds (2.29–2.30 Å). The *trans* influence of CH_3CN seems therefore smaller than the one of amines, halides, and sulfoxides.

The *trans*-effect of acetonitrile is not well known but it should be fairly high because of the high multiplicity of the C—N bond. We have studied the reactions between $K[Pt(CH_3CN)Cl_3]$ and pyridine (py) and between $K[Pt(py)Cl_3]$ and acetonitrile. We have found the following reactions:

$$K[Pt(py)Cl_3] + CH_3CN \xrightarrow[3\ h]{H_2O} \textit{cis}\text{-}[Pt(CH_3CN)(py)Cl_2]$$

$$K[Pt(CH_3CN)Cl_3] + py \xrightarrow{H_2O} \textit{trans}\text{-}[Pt(CH_3CN)(py)Cl_2]$$

Because Cl^- has a higher *trans* effect than pyridine, only *cis*-$[Pt(CH_3CN)(py)Cl_2]$ is formed in the first reaction. The ir spectrum of this product showed two ν_{Pt-Cl} vibrations at 339 and 349 cm^{-1}. In the second reaction, the *trans* isomer is first formed. It has one ν_{Pt-Cl} vibration at 330 cm^{-1}. These results indicate that the *trans* effect of acetonitrile is greater than the *trans* effect of chlorine. It is generally believed than ligands containing multiple bonds have a high *trans* effect but their *trans* influence is not well known. In the compound *mer*-$[Os(CH_3CN)Cl_3(PPh_3)_2]$, the Os—Cl bond in *trans* position to CH_3CN is equal in length to the other two Os—Cl bonds *trans* to each other (16). But in octahedral complexes, the *trans*

[3] Lists of structure factors and anisotropic thermal parameters are available, at a nominal charge, from the Depository of Unpublished Data, CISTI, National Research Council of Canada, Ottawa, Ont., Canada K1A 0S2.

TABLE 1. Positional parameters, with their esd's and temperature factors ($Å^2$) (all $\times 10^3$)

Atom	x		y		z		U_{eq}*	
Pt	198.33(8)	[198.72(10)]	223.90(4)	[223.74(6)]	222.01(5)	[721.91(6)]†	33.2	[34.9(4)]
Cl(1)	438.2(6)	[437.9(5)]	291.5(3)	[290.4(4)]	124.3(4)	[622.7(5)]	54	[54(3)]
Cl(2)	129.4(6)	[130.2(8)]	389.7(3)	[390.8(4)]	287.3(4)	[786.2(5)]	47	[49(3)]
N(1)	−6(2)	[−2(3)]	162.5(8)	[169(1)]	310(1)	[812(1)]	45	[47(10)]
N(2)	252(2)	[253(3)]	79.7(9)	[80(1)]	159(1)	[657(2)]	37	[47(10)]
C(1)	−112(2)	[−112(3)]	131(1)	[133(2)]	367(1)	[864(2)]	42	[47(11)]
C(2)	−260(2)	[−259(3)]	85(1)	[87(2)]	436(2)	[935(2)]	48	[58(14)]
C(3)	272(2)	[274(2)]	2(1)	[−3(1)]	112(1)	[612(2)]	35	[31(9)]
C(4)	298(2)	[298(2)]	−101(1)	[−103(2)]	52(1)	[548(2)]	43	[46(11)]

* $U_{eq} = (1/3)(U_{11} + U_{22} + U_{33} + 2U_{13}\cos\beta)$.
† z parameters for the Hamilton crystal have an origin shift of 0.5 compared to the Montreal crystal.

TABLE 2. Bond distances (Å) and angles (deg)

Bond	Distance		Bonds	Angle	
Pt—Cl(1)	2.264(4)	[2.270(6)]	Cl(1)—Pt—Cl(2)	90.7(1)	[90.7(2)]
Pt—Cl(2)	2.263(3)	[2.277(5)]	Cl(1)—Pt—N(1)	178.6(4)	[178.2(4)]
Pt—N(1)	1.977(12)	[1.95(2)]	Cl(1)—Pt—N(2)	89.0(3)	[88.2(6)]
Pt—N(2)	1.981(11)	[1.99(2)]	Cl(2)—Pt—N(1)	90.1(4)	[88.1(5)]
N(1)—C(1)	1.102(19)	[1.11(3)]	Cl(2)—Pt—N(2)	178.0(3)	[177.4(5)]
N(2)—C(3)	1.113(16)	[1.16(2)]	N(1)—Pt—N(2)	90.2(5)	[93.0(2)]
C(1)—C(2)	1.480(21)	[1.49(3)]	Pt—N(1)—C(1)	175(1)	[177(2)]
C(3)—C(4)	1.449(17)	[1.45(3)]	Pt—N(2)—C(3)	174(1)	[175(2)]
			N(1)—C(1)—C(2)	177(1)	[179(1)]
			N(2)—C(3)—C(4)	179(1)	[177(2)]

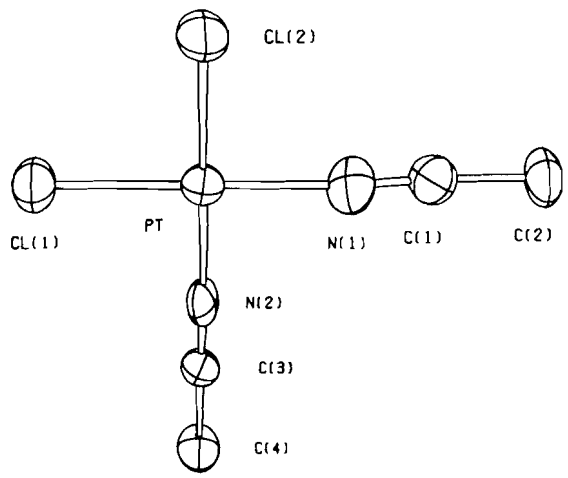

FIG. 1. Labelled diagram of the molecule *cis*-$[Pt(CH_3CN)_2Cl_2]$ (the hydrogen atoms are not drawn).

effect is much less important than in square planar compounds. It might be similar for the *trans* influence.

The acetonitrile ligands are bonded to platinum through the lone-pair of electrons on the nitrogen atom. The Pt—N bonds are 1.977(12) [1.95(2)] and 1.981(11) [1.99(2)] Å. These distances are probably slightly shorter than the normal Pt—N(amine) bonds (17, 18). This is the first structure determination of a compound where acetonitrile is bonded to platinum. Acetonitrile is expected to accept electron density from the metal, much like CO and other unsaturated ligands which possess available empty π orbitals. Infrared spectroscopic studies of $[Pt(CH_3CN)_2Cl_2]$ (11*a*) have shown that the N≡C bond is strengthened upon coordination to platinum rather than weakened as in conventional metal carbonyl complexes. However, the results of crystallographic studies of compounds containing CH_3CN are not very conclusive. Table 3 summarizes several recent crystal structures containing CH_3CN, either free as a molecule of crystallization or bonded to a metal. The structure of acetonitrile has been determined in 1955 (19) by electron diffraction, but the standard deviations are high. A better geometry was calculated from rotational spectra by Costain (20). It is interesting to observe that CH_3CN seems to have almost the same structure, whether it is coordinated to a metal or free as a molecule of crystallization. In *cis*-$[Pt(CH_3CN)_2Cl_2]$, the C—N bonds are 1.102(19) [1.11(3)] and 1.113(16) [1.16(2)] Å while the C—C bonds are shorter (1.449(17) [1.45(3)] and 1.480(21) [1.49(3)] Å) than normal single bonds, as observed in other CH_3CN crystal structures. In structures where the CH_3CN is not bound to the metal (i.e. "lattice" CH_3CN), the average C—N and C—CH_3 bonds are 1.14 and 1.42 Å (Table 3). These values are not very precise since most of the published structures have high standard deviations. Many of them contain disordered CH_3CN molecules. In structures where the CH_3CN is bound to the metal, the thermal motion is reduced and more precise results are obtained. The average C—N and C—CH_3 bonds in the metal-bonded CH_3CN structures are 1.13 and 1.45 Å. These results are in the right direction, assuming a stronger C—N bond and a weaker C—CH_3 bond upon coordination as suggested by infrared spectroscopy. But at the moment, we are not sure if the observed differences are significant.

The Pt—N—C bond angles 175(1) [177(2)] and 174(1) [175(2)]° deviate slightly from 180° as do the analogous angles for most other M—$NCCH_3$ complexes listed in Table 3. The nonlinearity of the Pt—N—C moiety is probably due, as suggested previously (41), to the use of partial sp^2 character by the donor nitrogen atom. The acetonitrile ligands are linear 177(1) [179(1)] and 179(1) [177(2)]° as in most other published struc-

Can. J. Chem. Downloaded from www.nrcresearchpress.com by 210.87.254.105 on 09/06/12
For personal use only.

TABLE 3. Published CH_3CN crystal structures

Compound	Distance (Å) N—C	Distance (Å) C—CH_3	Angle M—N—C	Angle N—C—CH_3	Reference
Free CH_3CN					
CH_3CN (electron diffraction)	1.155(30)	1.465(20)			19
(rotational spectra)	1.15710	1.45836		180	20
$Rh_2(mhp)_4(C_3H_4N_2 . 0.5\ CH_3CN$	1.07(2)	1.50(2)		180	21
$Os_2(hp)_4Cl_2 . 2CH_3CN$	1.19(5)	1.45(5)		175(6)	22
	1.12(4)	1.40(5)		171(5)	
$[PtCl_2(cyclophosphazene)] . CH_3CN$	1.06(6)	1.48(4)		171(3)	23
$[Co(C_{24}H_{24}N_4)(C_5H_5N)]PF_6 . CH_3CN$	1.089(8)	1.412(12)		173.3(12)	24
$[Fe_2(C_9H_8N_2O)(CO)_6] . CH_3CN$	1.123(5)	1.445(6)		179.3(6)	25
$[Ta(C_5H_5)_2(dnpe)]Cl . CH_3CN$	1.123(10)	1.427(10)		177.7(8)	26
$[Co(P(OCH_2)_3CMe)_5][Co(NO_3)_3(CH_3CN)] . 2CH_3CN$	1.18(3)	1.36(3)			27
	1.18(2)	1.40(2)			
$[Pd(CNMe)_4](TCNQ)_4 . 2CH_3CN$	1.167(17)	1.336(15)		163(2)	28
$[Co(PMe_3)_3(C_2H_4)(CH_3CN)]BPh_4 . CH_3CN$	1.23(2)	1.38(2)			29
Bonded CH_3CN					
cis-$[PtCl_2(CH_3CN)_2$	1.102(19)	1.480(21)	175(1)	177(1)	This work
	1.113(16)	1.449(17)	174(1)	179(1)	
$Rh_2(mhp)_4(CH_3CN)$	1.12(1)	1.38(1)	165(1)	178(2)	21
$[CuIAsPh_3(CH_3CN)]_2$	1.125(6)	1.479(7)	176.0(3)	179.6(5)	30
mer-$[OsCl_3(CH_3CN)(PPh_3)_2]$	1.121(9)	1.454(10)	177.2(6)	179.6(9)	17
$[Pd(CH_3CN)_2(C_3H_5)]_2B_{10}Br_{10} . C_6H_6$	1.16(2)	1.47(2)		177	31
$[Fe(TIM)(CH_3CN)_2]BF_6$	1.121(2)	1.461(4)			32
$[Fe(TIM)(CH_3CN)(CO)]BF_6$	1.128(4)	1.453(5)			33
$[Fe(C_5H_5)(dppe)(CH_3CN)]BPh_4$	1.139(9)	1.431(10)	171.9(5)	176.9(8)	34
$[Co(CH_3CN)_2(C_{14}H_{24}N_8O_2]^{3+}$	1.13(2)	1.43(2)		178.5(16)	35
	1.12(2)	1.47(2)			
$[Co(CH_3CN)_2((C_2H_5OC(O)CH)_2)_2]$	1.13(1)	1.49(1)	171(3)	178(7)	36
	1.14(1)	1.47(1)	168(2)	179(19)	
$[Co(P(OCH_2)_3CMe)_5][Co(NO_3)_3(CH_3CN)] . 2CH_3CN$	1.156(11)	1.477(19)	174.0(11)	178.8(15)	27
$[Ni(CH_3CN)((C_2H_5OC(O)CH)_2)_2]$	1.129(6)	1.46(1)	178(8)	178(7)	37
$[BeCl_2(CH_3CN)_2$	1.131(3)	1.439(3)	171.7(2)	178.7(2)	38
$[Co(PMe_3)_3(C_2H_4)(CH_3CN)]BPh_4 . CH_3CN$	1.134(9)	1.45(1)	177.3(6)		29
$[Co(CH_3CN)_2(POMe_3)_4](BPh_4)_2$	1.117(8)	1.451(10)	171.4(4)		39
$[Co(CH_3CN)(Ph—C\equiv C—Ph)(PMe_3)_3]BPh_4$	1.135(6)	1.450(7)	174.1(4)	177.4(5)	40

tures (Table 3).

The packing of the molecules within the cell is shown in Fig. 2. The molecules lie in layers roughly parallel to the 102 planes and thus the distance between layers is about 3.6 Å. The forces within the plane and between the planes are primarily van der Waals, although the molecules are oriented to give dipole–dipole interactions between translationally equivalent molecules in the *b* direction. There is one contact shorter than the sum of the van der Waals radii. The intermolecular distance C(2) . . . Cl(1) is 3.497 Å and the angle C(1)—C(2) . . . Cl(1) is 130.7(9) and may indicate very weak hydrogen bonding.

The vibrational spectra of $PtCl_2(CH_3CN)_2$ have been recorded previously (11) but only one or two bands have been reported. We have recorded complete (4000–60 cm^{-1}) infrared and Raman spectra. Many of the vibrations were assigned by comparison with spectra of similar compounds, but an aid to the assignments, particularly of the Pt—N stretches, was a rough force constant analysis.

For the purpose of carrying out the force constant analysis only the symmetry of the heavier skeleton of the complex was considered and the CH_3 groups were treated as discrete units. This skeleton was assumed to be planar with C_{2v} symmetry, with the C_2 axis parallel to the *z*-axis of the Cartesian coordinates. The skeleton contains nine atoms and has 21 normal modes of vibration. It was further assumed that the C—C≡N—Pt chains are rectilinear and that the adjacent angles around the Pt atom in the *yz* plane are all 90°. By standard group theoretical methods it can be shown that the number of normal modes of each symmetry species is $8a_1$, $3a_2$, $7b_1$, and $3b_2$. These modes are all Raman-allowed and all except the a_2 modes are infrared-allowed. The numberings, symmetry, and approximate description of the normal modes

Can. J. Chem. Downloaded from www.nrcresearchpress.com by 210.87.254.105 on 09/06/12
For personal use only.

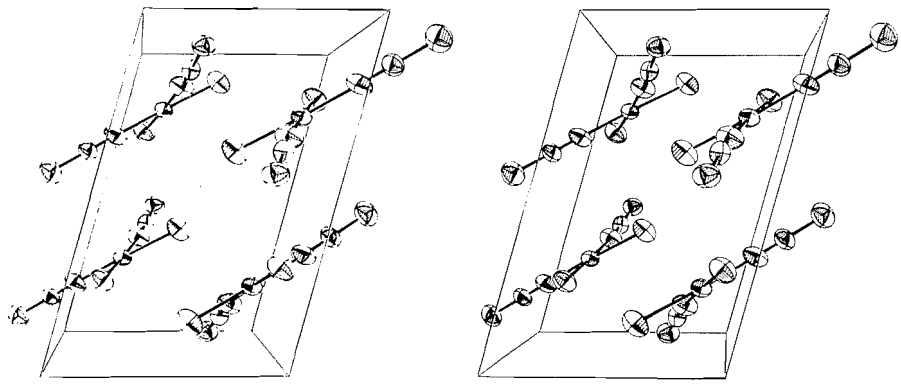

FIG. 2. The packing of the molecules within the unit cell. ***a*** and ***c**** are parallel to the bottom and side of the page respectively, and the view is down ***b***.

TABLE 4. Description of normal modes and symmetry coordinates for the C_{2v} planar unit Cl_2—Pt—$(NC—C)_2$

Normal mode	A_1	Description	Normal mode	B_1	Description
ν_1	$S_1 = r_{46} + r_{57}$	$\nu_{C\equiv N}$	ν_{12}	$S_{12} = r_{46} - r_{57}$	$\nu_{C\equiv N}$
ν_2	$S_2 = r_{68} + r_{79}$	ν_{C-C}	ν_{13}	$S_{13} = r_{68} - r_{79}$	ν_{C-C}
ν_3	$S_3 = r_{14} + r_{15}$	ν_{Pt-N}	ν_{14}	$S_{14} = r_{14} - r_{15}$	ν_{Pt-N}
ν_4	$S_4 = \alpha_{468} + \alpha_{579}$	$\delta_{C-C\equiv N}$	ν_{15}	$S_{15} = \alpha_{468} - \alpha_{579}$	$\delta_{N\equiv C-C}$
ν_5	$S_5 = \alpha_{146} + \alpha_{157}$	δ_{Pt-N-C}	ν_{16}	$S_{16} = \alpha_{146} - \alpha_{157}$	δ_{Pt-N-C}
ν_6	$S_6 = r_{12} + r_{13}$	ν_{Pt-Cl}	ν_{17}	$S_{17} = r_{12} - r_{13}$	ν_{Pt-Cl}
ν_7	$S_7 = \alpha_{415} + \alpha_{312}$	δ_{N-Pt-N}	ν_{18}	$S_{18} = \alpha_{314} - \alpha_{512}$	$\delta_{Cl-Pt-N}$
ν_8	$S_8 = \alpha_{415} - \alpha_{312}$	$\delta_{Cl-Pt-Cl}$			
Normal mode	A_2	Description	Normal mode	B_2	Description
ν_9	$S_9 = \beta_{468} - \beta_{579}$	$\pi_{N\equiv C-C}$	ν_{19}	$S_{19} = \beta_{468} + \beta_{579}$	$\pi_{N\equiv C-C}$
ν_{10}	$S_{10} = \beta_{146} - \beta_{157}$	$\pi_{Pt-N\equiv C}$	ν_{20}	$S_{20} = \beta_{146} + \beta_{157}$	π_{Pt-N-C}
ν_{11}	$S_{11} = \beta_{214} - \beta_{315}$	$\pi_{Cl-Pt-N}$	ν_{21}	$S_{21} = \beta_{214} + \beta_{315}$	$\pi_{Cl-Pt-N}$

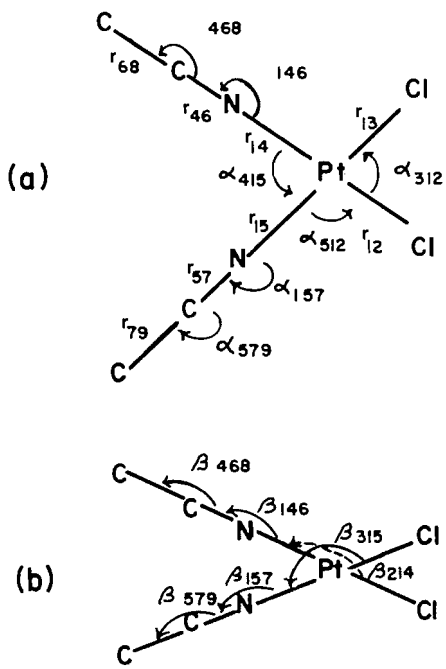

FIG. 3. Internal coordinates for the $Cl_2Pt(NCC)_2$ entity, (*a*) in-plane and (*b*) out-of-plane.

are shown in Table 4.

The numberings of the internal coordinates are indicated in Fig. 3. The *r*'s are bond-stretching deformations, the α's are in-plane angle deformations, and the β's are out-of-plane angle deformations. Even if the angles at Pt were not 90°, most likely α_{314} would be equal to α_{512}. (Table 2 shows that the angles α_{312}, α_{314}, α_{512}, α_{415} are close to 90°.) The redundancy condition $\alpha_{312} + 2\alpha_{314} + \alpha_{415} = 360°$ holds for the in-plane bends, and therefore α_{314} and α_{512} were not used as independent coordinates. The symmetry coordinates for the skeletal unit are also listed in Table 4.

Choice of interaction force constants

The limited number of observed frequencies limits the number of interaction constants which can be chosen. It seems reasonable to assume that the interactions between adjacent bonds, e.g. C—C and C≡N, will be greater than interactions between non-adjacent bonds, e.g., the two C≡N bonds. When one works through the symmetrization algebra, however, the force constant for the a_1 C≡N stretching vibration F_{a_1} is distinguished from that for the b_1 vibration F_{b_1} by the C≡N, C≡N interaction; that is (ignoring other terms),

[1] $F_{a_1}, \nu_{C\equiv N} = F_{C\equiv N} + F_{C\equiv N, C\equiv N} + F_{C\equiv N, C-C}$

[2] $F_{b_1}, \nu_{C\equiv N} = F_{C\equiv N} - F_{C\equiv N, C\equiv N} + F_{C\equiv N, C-C}$

$F_{C\equiv N, C-C}$ may be much larger than $F_{C\equiv N, C\equiv N}$, but it does not

Can. J. Chem. Downloaded from www.nrcresearchpress.com by 210.87.254.105 on 09/06/12
For personal use only.

TABLE 5. Vibrational wavenumbers and assignments for *cis*-$Pt(CH_3CN)_2Cl_2$ bands in cm^{-1}

Normal complex		^{15}N-enriched complex		
Infrared*	Raman†	Infrared*	Raman†	Assignment‡
3290 w		3257 w		
3252 w		3221 w		
			2993, 41	
2970		2970	2963, 138	ν_a(CH)
2923		2922	2925, 193	ν_s(CH)
2909			2903, 100	
	2348, 50			
	2339, 154		2325	
2332.8	2333, 192	2312.5	2310, 165	ν_1(C≡N), a_1
			2296, 193	
			2287, 441	
	2327, 50			
2304.7	2310, 108	2282.10	2281, 234	ν_{12}(C≡N), b_1
	2300, 50			
1440 sh		1441 sh		
1408 s	1410, 23		1410, 34	$\delta_a(CH_3)$
	1401 sh	1407 s	1401 sh	$\delta_a(CH_3)$
1385 ms		1384 ms		
	1370, 69		1370, 125	$\delta_s(CH_3)$
1353	1354, 46	1355	1354, 97	$\delta_s(CH_3)$
	1123, 20		1123	$r(CH_3)$
1030	1034, 35	1029.6	1032, 41	ν_2(C—C), a_1
1020 sh	1017, 10		1018, 10	ν_{13}(C—C), b_1
	978, 35		965, 96	
960 w	963, 85	949 w	953, 124	$r(CH_3)$
	960, 66		950, 83	
673		668		2 × 338
626		615		$\nu_5 + \nu_8$
463, 20		453, 17		ν_3(Pt—N), a_1
440, 25	440, 73	430, 20	430, 62	ν_5(PtNC), a_1
431, 60		423, 35		ν_{16}(PtNC), b_1
417.3, 25	417, 35	410, 15	410, 55	δ(NCC)
408, 60	408, 40	401, 30	402, 50	ν_{14}(Pt—N), b_1
403 sh	403, 58	397 sh	397, 60	
	387, 54		380, 90	δNCC
362(353,348), 250	367(357,349), 92	362(353,348), 250	362(357,349),83	ν_6(Pt—Cl), a_1 isotope effect 9:6:1
	338(332), 31		338(332), 55	ν_{17}(Pt—Cl), b_1
			298, 8	
302 m	290, 4		290, 8	
277		264 w		
	254, 12	252 m	252, 12	
230 ms		230 ms		ν_7, δ(NPtN), a_1
227	228, 13		225, 15	
203 ms	203, 31		199, 30	
177 m	176, 66	173 w	175, 62	ν_8, δClPtCl, a_1
170 m	166, 12		167, 15	
		160 m		
151				
128 m	125, 100	125 m	125, 100	
121 m	118, 80	120 m	118, 62	
	98, 2		100, 15	δNPtCl
	88, 4		90, 12	
	73, 77		70, 73	

*Infrared intensities: s = strong, m = medium, w = weak, v = very, sh = shoulder; numerical values in arbitrary units relative to 362 cm^{-1} band = 250.

†Raman shifts $\Delta\nu$ in cm^{-1}; intensities in arbitrary units relative to 125 cm^{-1} band = 100.

‡Assignments: ν = stretching, δ = deformation, r = rock, s = symmetric, a = antisymmetric; a_1, b_1, a_2, b_2 are symmetry species (C_{2v}) for the skeleton $Pt(NCC)_2Cl_2$.

differentiate between the two frequencies governed by the two different force constants described by eqs. [1] and [2]; hence $F_{C\equiv N.C\equiv N}$ cannot be ignored.

These two frequencies occur at 2333 and 2305 cm^{-1}, and so $F_{C\equiv N.C\equiv N}$ is about 1.0% of $F_{C\equiv N}$ (i.e. ~0.20). $F_{C\equiv N.C-C}$ will of course contribute to the mean position of both $\nu_{C\equiv N}$ and ν_{C-C}. Similarly, $F_{C\equiv N.Pt-N}$ will contribute to the position of ν_{Pt-N}, and $F_{Pt-N.Pt-Cl}$ to the position of ν_{Pt-Cl}.

Can. J. Chem. Downloaded from www.nrcresearchpress.com by 210.87.254.105 on 09/06/12
For personal use only.

Can. J. Chem. Downloaded from www.nrcresearchpress.com by 210.87.254.105 on 09/06/12
For personal use only.

TABLE 6. Force constants used in normal coordinate analysis of $Pt(NCC)_2Cl_2$*

Index	Force constant†	Original value (mdyn Å^{-1})	Refined value (mdyn Å^{-1})
1	F_{PtCl}	2.620	2.251
2	$F'_{PtCl,PtCl}$	0.100	0.196
3	F_{PtN}	3.050	4.050
4	$F'_{PtN,PtN}$	0.100	0.402
5	F_{CN}	18.580	18.400
6	$F'_{CN,CN}$	0.138	0.196
7	F_{CC}	4.970	4.830
8	$F'_{CC,CC}$	0.0760	0.004
9	F_{ClPtCl}	0.470	0.291
10	F_{NPtN}	0.630	0.318
11	F_{PtNC}	0.150	0.098
12	F_{NCC}	0.299	0.093
13	$F_{PtNC\perp}$	0.100	0.153
14	$F_{NCC\perp}$	0.100	0.041
15	$F_{NPtCl\perp}$	0.050	0.092

*F' denotes interaction force constants for coordinates at 90° (F_2, F_4, F_6, F_8).
† $\perp$ denotes force constants for out-of-plane coordinates (F_{13}, F_{14}, F_{15}).

There is no simple way of describing the bending motions around the N_2PtCl_2 core because each motion contains some change in the Cl—Pt—N angles: it seems reasonable, however, to expect that for some motions either the Cl—Pt—Cl or the N—Pt—N contribution will dominate. Two bending motions which move a common bond may be expected to show a greater interaction than others. For example, of the a_1 deformations, ν_4 and ν_5 will interact with each other as will ν_5 and ν_7. Of the a_2 twisting deformations ν_9 and ν_{10} will interact, as will ν_{10} and ν_{11}. Of the b_1 deformations, ν_{15} and ν_{16} will interact, as will ν_{16} and ν_{18}; and of the b_2 deformations, ν_{19} and ν_{20} will interact, as will ν_{19} and ν_{21}.

Without the use of more isotopically substituted species the number of observed frequencies is limited, and therefore certain arbitrary but reasonable assumptions in the selection of interaction and bending force constants were required and are summarized here: (*1*) Where an interaction exists between the stretching force constants for two adjacent bonds, such as $F_{C\equiv N}$, F_{C-C}, then this interaction was assigned a value of 5% of the lower of the two force constants. Thus if $F_{C\equiv N} = 18$ mdyn Å^{-1} and $F_{C-C} \approx 5$ mdyn Å^{-1}, then $F_{C\equiv N,C-C} \approx 0.25$ mdyn Å^{-1}. An exception was made for $F_{C\equiv N,Pt-N}$, (2.5% of F_{Pt-N}), since the C≡N and Pt—N stretching vibrations have a large frequency difference. It was found for $ReO_2(CN)_4^{3-}$ that the lower force constant for the adjacent bonds Re—C and C≡N was $F_{Re-C} = 2.4$ mdyn Å^{-1}, and that $F_{CN,Re-C}$ was 0.06 mdyn Å^{-1}; the latter constant seemed surprisingly small, but the frequency difference was large for the two stretching vibrations C≡N and Re—C (42). (*2*) For simplicity in treating the deformations around the N_2PtCl_2 core the number of bending force constants was restricted to two: F_{N-Pt-N} and $F_{Cl-Pt-Cl}$. The b_1 mode then has a force constant $\frac{1}{2}[F_{N-Pt-N} - F_{Cl-Pt-Cl}]$. The interaction force constants between different adjacent bending coordinates were set at zero for the a_1 and b_1 blocks, and 2.5–5% for the a_2 and b_2 blocks. The interaction force constant of a bending coordinate with itself was set equal to 2.5% that is, $F_{Pt-N-C,Pt-N-C} = 0.025\,F_{Pt-N-C}$.

The Raman spectrum of CH_3CN has been discussed by Herzberg (43). CH_3CN is transparent between 1124 and 918, 918 and 380, and below 380 cm^{-1}; many bands for the complex fall in these "windows"; also bands below 380 cm^{-1} result from various Pt—N and Pt—Cl deformations.

TABLE 7. Comparison of observed and calculated vibrational wave numbers, cm^{-1}

	$Pt(NCC)_2Cl_2$*		^{15}N-enriched $Pt(NCC)_2Cl_2$*	
Mode	Observed	Calculated	Observed	Calculated
A_1	2333	2339.8	2312	2306.2
	1034	1040.2	1032	1028.4
	463	459.4	453	455.5
	431	428	423	419.5
	362	362.0	362	361.9
	225	216.1	220	214.0
	175	171.9	175	171.7
	—	49.6	—	49.6
B_1	2305	2308.8	2282	2276.4
	1020	1022.7	1018	1011.5
	440	445.2	430	438.0
	408	405.5	401	401.0
	333	332.8	333	332.3
	203	206.9	199	205.6
	73	69.9	70	69.7
A_2	387	388.3	380	380.1
	118	114.4	118	113.2
	73	56.8	70	56.8
B_2	407	408.4	401	399
	125	132.7	125	132.0
	73	67.7	70	67.5

*Observed wavenumbers for $Pt(CH_3CN)_2Cl_2$ and calculated wavenumbers for the skeleton $Pt(NCC)_2Cl_2$.

Computations for the force constant analysis were carried out as described previously (42). The force constants of the $Pt(NCC)_2Cl_2$ entity were refined from 20 observed vibrational frequencies. The trial and refined force constants are listed in Table 6. A comparison of observed and calculated frequencies is shown in Table 7. There is excellent agreement, the largest single difference being ~4% (ν_6) and the average difference <2% for the a_1 and b_1 blocks. The agreement is slightly poorer for the a_2 and b_2 blocks. The potential energy distribution is shown in Table 8. The distribution for the ^{15}N species was the same within the error limits and is not listed here. The high degree of coupling is evident for the in-plane vibrations ν_3 and ν_4; ν_{11} and ν_{12} and ν_6 and ν_{14}. The out-of-plane angle deformations are also highly coupled, especially δNCC and δNPtCl. Figure 4 shows the spectra in the region 465–325 cm^{-1} with the inset showing the νC≡N region.

Coordination through the lone pair on nitrogen always increases the C≡N frequency because of kinematic coupling and the ionic character of the C—N bond (44, 45). The title complex shows the expected increase in ν(C≡N): 2249 cm^{-1} (ligand), 2332 cm^{-1} (complex).

The frequencies 1124 cm^{-1} and 380 cm^{-1} in CH_3CN belong to the two degenerate vibrations of the linear system (H_3)—C—C≡N, the former being mainly a CH_3 rocking vibration, and the latter a C—C≡N bending vibration. For the platinum complex, bands at 1123 and 384 cm^{-1} were observed by us in the Raman spectrum, and are assigned to similar vibrational motions.

The bands at 1034 and 1020 cm^{-1} are assigned to the in-phase and out-of-phase C—C stretching vibrations, $\nu_2(a_1)$ and $\nu_{13}(b_1)$. In free CH_3CN the C—C vibration is at 918 cm^{-1}, in

TABLE 8. Potential energy distribution for $Pt(NCC)_2Cl_2$

Vibration		Contribution (%) of force constants, $F_i (i = 1-15)$											
Mode	Assignment	F_1	F_2	F_3	F_4	F_5	F_6	F_7	F_8	F_9	F_{10}	F_{11}	F_{12}
A_1	ν_1			3.0	0.4	87.3	0.9	8.3					
	ν_2			15.6	1.6	3.6		79.1					
	ν_3	7.2	0.8	47.9	4.7	5.3		8.5		0.7	10.2	8.4	6.2
	ν_4	0.6		17.7	1.7	1.9		2.8			19.5	27.8	27.8
	ν_5	83.0	7.0	6.2	0.6	0.8		1.1		0.3		0.3	0.6
	ν_6	0.6		0.3						1.9	52.8		44.3
	ν_7	0.4		0.2						97.0	1.1		1.0
	ν_8										16.5	63.6	19.8
B_1	ν_9			3.0	−0.4	89.6	−1.0	8.8					
	ν_{10}			15.4	−1.6	4.9		81.4					
	ν_{11}	3.9	−0.4	19.4	−1.9	1.5		2.2		12.3	14.0	27.5	21.3
	ν_{12}	4.0	−0.4	66.0	−6.5	4.6		6.8		1.6	1.8	10.6	11.6
	ν_{13}	99.9	−8.5	6.6	−0.6	0.6		0.8				0.4	0.8
	ν_{14}	1.5	−0.1	0.7	−0.1					25.1	28.7		44.0
	ν_{15}	0.1								6.1	7.0	64.8	21.9

Vibration				
Mode	Assignment	F_{13}	F_{14}	F_{15}
A_2	ν_{16}	73.1	19.2	7.7
	ν_{17}	3.2	57.4	39.4
	ν_{18}	23.8	23.9	52.2
B_2	ν_{19}	74.1	16.7	9.2
	ν_{20}	0.1	42.4	57.5
	ν_{21}	25.9	41.4	32.7

C_2H_6 it is at 993 cm^{-1}, and CH_3OH has the C—O vibration at 1034 cm^{-1}.

The frequencies of Pt—N and Pt—Cl stretching vibrations have been discussed by numerous authors. Studies of Pt(IV) and Pt(II) complexes containing a variety of ligands have been made (46–51). There is a considerable variation in bond lengths and bond strengths.

Hendra (46) studied the Raman spectrum of *trans*-$Pt(NH_3)_2Cl_2$ in the region 0–600 cm^{-1} and found that the symmetric metal–nitrogen mode had a higher frequency than the asymmetric mode, while the metal–halogen vibrations showed the more common asymmetric > symmetric frequency. He noted that the force constant equations do not allow for this characteristic, and therefore the Pt—N force constant was calculated on the basis of each mode separately; an average value was 2.4 mdyn $Å^{-1}$. Nolan and James (47, 48) found the highest observed ν(Pt—N) to be the symmetric one for several chloro ammine complexes of Pt(IV). Their range for ν(Pt—N) was 516–568 cm^{-1} with one low intensity band at 600 cm^{-1}.

Typical Pt—N force constants collected in Nakamoto's recent book (52) are in the range 2.0–3.8 mdyn $Å^{-1}$. A calculated ν(Pt—N) for a relatively low force constant of 2.0 would be 600 cm^{-1}, on the assumption of a relatively weak bond. Because the Pt—N distances of the title compound lie at the lower end of the range of Pt—N distances we infer that the Pt—N bond is stronger than most other Pt—N bonds and indeed the force constant analysis gives 4.05 mdyn $Å^{-1}$.

It seems reasonable, therefore, to assign a fairly high frequency to ν(Pt—N) and at first consideration one might expect it to fall in the higher portion of the 500–700 cm^{-1} region. The CCN group, however, has about the same mass as Cl, and there seems to be such strong coupling that ν(Pt—N) is lost as a pure vibration, and the mode observed is a motion of the whole CCN group against Pt. The force constant analysis shows these interactions and the bands at 463 and 408 cm^{-1} have the highest contribution of ν(Pt—N) but are coupled with δPtNC, δNPtN, and δCCN. These three deformations combine to produce a high frequency mode which is largely δPtNC and a very low frequency mode which has a contribution of all three (which may be pictured as an accordian-like deformation of the whole skeleton). In scanning the low frequency region at a higher laser power (~500 mW) we observed very weak broad bands at 618 and 583 cm^{-1} which coincide with infrared bands at 620 and 580 cm^{-1}. We assign these to combinations.

Although this complex is an unusual one for ν(Pt—N) assignments, it seems that most authors have assigned much too low a frequency to the ν(Pt—N) mode. Before the discovery of the chemotherapeutic uses of platinum complexes, the interest in *cis*- and *trans*-Pt(II) complexes was concentrated on metal–halogen vibrations, rather than the metal–nitrogen ones. Also the frequency ranges previously observed were restricted: Hendra's Raman frequency shifts covered the region 600 cm^{-1} and below (46); Adams *et al.* (50) infrared spectra covered 170–460 cm^{-1}. Walton (11*b*) reporting infrared spectra in the 500–200 cm^{-1} region observed no bands >350 cm^{-1} which could be assigned to ν(Pt—N) modes and suggested that these modes occur below 200 cm^{-1}. Meester (51) also made some very low ν(Pt—N) assignments. A low polarizability change in the Pt—N bond has made observations of Raman scattering difficult and it may well be that electronic spectra or resonance Raman spectra will provide more data in future work.

It has been found in *cis*-$[PtCl_2L_2]$ type complexes that the position of ν(Pt—Cl) is directly related to the *trans* effect of

Can. J. Chem. Downloaded from www.nrcresearchpress.com by 210.87.254.105 on 09/06/12
For personal use only.

Can. J. Chem. Downloaded from www.nrcresearchpress.com by 210.87.254.105 on 09/06/12
For personal use only.

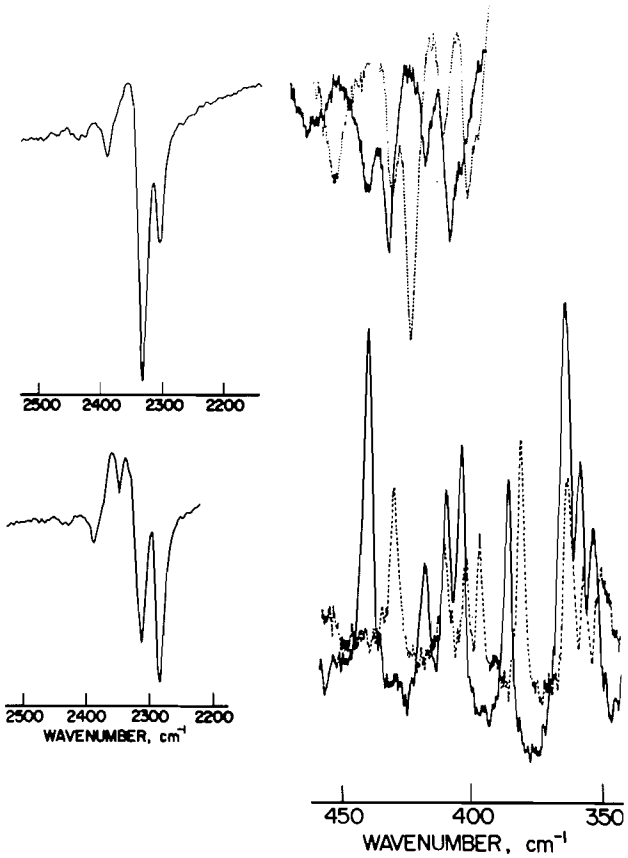

FIG. 4. The vibrational spectra of $Pt(CH_3CN)_2Cl_2$, 470–325 cm^{-1}. Upper, infrared of KBr pellet; lower, Raman of solid. Solid line, normal complex; dashed line, ^{15}N-enriched complex. Inset: infrared of KBr pellet, 2500–2200 cm^{-1}: upper, normal complex; lower, ^{15}N-enriched complex.

the ligand L. Assignments for ν_{Pt-Cl} wave number range 320–360 cm^{-1} are typical. The observation here of two ν(Pt—Cl) bands in both Raman and infrared is consistent with the *cis* configuration. In the *trans* compounds there is a single Pt—Cl mode observed in the 330–335 cm^{-1} region. The expected Cl isotope effect is a splitting into three components of relative intensity 9:6:1 which is most likely to be seen on the a_1 band. This effect was observed by us for the Raman band at 358 cm^{-1}.

Simple geometric considerations show that for a *cis* configuration the separation between symmetric and asymmetric frequencies is a function of angle. The asymmetric frequency is higher, and the maximum spread of symmetric and asymmetric frequencies is for angles of 180°, e.g. C—C≡N. The separation becomes smaller as the angle decreases until at 90° the two frequencies are the same. The symmetric frequency becomes higher than the asymmetric frequency for a bond angle of 60°. This is just a result of the geometry change, and does not depend on force constants (53). In the title compound the Cl—Pt—Cl bond angle is 90.7°, the large difference in frequencies (25 cm^{-1}) is likely caused by very strong Pt—Cl coupling with consequent strong interaction force constants. Indeed, the Pt—Cl interaction was found to be ~7% of the primary Pt—Cl force constant.

All *trans*-$PtCl_2XY$ complexes show two bands in the infrared and Raman at about 130 and 160 cm^{-1}. These are assigned to Pt—Cl deformation modes (46). In this work we observe bands at 125 and 175 cm^{-1} which are so assigned.

N—Pt—N deformations are generally close to 250 cm^{-1}. We assign the broad bands centred at 230 cm^{-1} in the infrared to some or all of these modes.

The remaining deformations are C—C≡N and C≡N—Pt which we assign to the observed frequencies 387, 407 cm^{-1} (C—C≡N) and 431, 440 cm^{-1} (C≡N—Pt). There is a reasonable comparison for the latter with the $ReO_2(CN)_4^{3-}$ complex (470, 434 cm^{-1} for δRe—C≡N) (42).

The assumption that the CH_3 groups can be treated as discrete units seems to be an adequate one, since there is no evidence for interaction of the CH_3 vibrations with other vibrations. It is still possible, however, to assign the vibrations of the CH_3 groups, since they fall into characteristic regions of the spectrum. Both stretches and deformations are motions which are well localized within the CH_3 groups. These are listed in Table 5 with descriptions, but without mode numberings.

Acknowledgements

The authors are grateful to the Natural Sciences and Engineering Research Council of Canada, to the Ministère de l'Education (FCAC), to McMaster University Science and Engineering Research Board, and to the National Cancer Institute of Canada for financial support.

1. Papers in J. Clin. Hematol. and Oncol. **7** (1) and **7** (2), 1977; papers presented at the 3rd International Conference on Platinum Coordination Complexes in Cancer Chemotherapy, Dallas, Texas. October 1976.
2. S. K. AGGARWAL, R. W. WAGNER, P. K. MCALLISTER, and B. ROSENBERG. Proc. Natl. Acad. Sci. **72**, 928 (1975).
3. M. ESHAQUE, M. J. MCKAY, and T. THEOPHANIDES. J. Clin. Hematol. Oncol. **7**, 338 (1977).
4. J. K. BARTON, H. N. RABINOWITZ, D. J. SZALDA, and S. J. LIPPARD. J. Am. Chem. Soc. **99**, 2827 (1977).
5. K. A. HOFFMANN and G. BUGGE. Ber. **40**, 1772 (1907).
6. K. A. HOFFMANN and G. BUGGE. Ber. **41**, 312 (1908).
7. R. D. GILLARD and G. WILKINSON. J. Chem. Soc. 2835 (1964).
8. D. B. BROWN, R. D. BURBANK, and M. B. ROBIN. J. Am. Chem. Soc. **91**, 2895 (1969); **90**, 5621 (1968).
9. N. C. STEPHENSON. J. Inorg. Nucl. Chem. **24**, 801 (1962).
10. V. V. LEBEDINSKII and V. A. GOLOVNYA. Izvest. Sekt. Platiny, **18**, 38 (1945); **21**, 32 (1948).
11. R. A. WALTON. (*a*) Spectrochim. Acta, **21**, 1795 (1965); (*b*) Can. J. Chem. **44**, 1480 (1966).
12. R. MELANSON and F. D. ROCHON. Can. J. Chem. **53**, 2371 (1975).
13. R. P. HUGHES, N. KRISHNAMACHARI, C. J. L. LOCK, J. POWELL, and G. TURNER. Inorg. Chem. **16**, 314 (1977).
14. D. T. CROMER and J. T. WABER. Acta Crystallogr. **18**, 104 (1965).
15. D. T. CROMER. Acta Crystallogr. **18**, 17 (1965).
16. R. L. PARKES, N. C. PAYNE, and E. O. SHERMAN. Can. J. Chem. **58**, 1042 (1980).
17. C. J. L. LOCK and M. ZVAGULIS. Inorg. Chem. **20**, 1817 (1981).
18. C. J. L. LOCK, R. A. SPERANZINI, and M. ZVAGULIS. Acta Crystallogr. B**36**, 1789 (1980).
19. M. D. DANFORD and R. L. LIVINGSTON. J. Am. Chem. Soc. **77**, 2944 (1955).
20. C. C. COSTAIN. J. Chem. Phys. **29**, 864 (1968).
21. F. A. COTTON and T. R. FELTHOUSE. Inorg. Chem. **20**, 584 (1981).
22. F. A. COTTON and J. L. THOMPSON. J. Am. Chem. Soc. **102**, 6437 (1980).
23. J. P. O'BRIEN, R. W. ALLEN, and H. R. ALLCOCK. Inorg. Chem. **18**, 2230 (1979).

24. M. C. WEISS, G. C. GORDON, and V. L. GOEDKEN. J. Am. Chem. Soc. **101**, 857 (1979).
25. G. DETTLAF, U. BEHRENS, T. EICHER, and E. WEISS. J. Organomet. Chem. **152**, 203 (1978).
26. B. M. FOXMAN, T. J. MCNEESE, and S. S. WREFORD. Inorg. Chem. **17**, 2311 (1978).
27. J. O. ALBRIGHT, J. C. CLARDY, and J. G. VERKADE. Inorg. Chem. **16**, 1575 (1977).
28. S. Z. GOLDBERG, R. EISENBERG, J. S. MILLER, and A. J. EPSTEIN. J. Am. Chem. Soc. **98**, 5173 (1976).
29. A. L. BEAUCHAMP, M. J. OLIVIER, M. DARTIGUENAVE, Y. DARTIGUENAVE, and B. CAPELLE. J. Am. Chem. Soc. **104**, 3891 (1982).
30. M. R. CHURCHILL and J. R. MISSERT. Inorg. Chem. **20**, 619 (1981).
31. G. A. KUKINA, V. S. SERGIENKO, YU. L. GAFT, I. A. ZAKHAROVA, and M. A. PARAI-KOSHITS. Inorg. Chim. Acta, **45**, L257 (1980).
32. H. W. SMITH, B. D. SANTASIERO, and E. C. LINGAFELTER. Cryst. Struct. Commun. **8**, 49 (1979).
33. L. E. MCCANDLISH, B. D. SANTARSIERO, N. J. ROSE, and E. C. LINGAFELTER. Acta Crystallogr. B**35**, 3053 (1979).
34. P. E. RILEY, C. E. CAPSHEW, R. PETTIT, and R. E. DAVIS. Inorg. Chem. **17**, 408 (1978).
35. S. M. PENG and V. L. GOEDKEN. Inorg. Chem. **17**, 820 (1978).
36. G. AGNES, I. W. BASSI, C. BENEDICENTI, R. INTRITO, M. CALCATERRA, and C. SANTINI. J. Organomet. Chem. **129**, 401 (1977).
37. I. W. BASSI and M. CALCATERRA. J. Organomet. Chem. **110**, 129 (1976).
38. C. CHAVANT, J. C. DARAN, Y. JEANNIN, G. KAUFMANN, and J. MACCORDICK. Inorg. Chim. Acta, **14**, 281 (1975).
39. A. L. BEAUCHAMP, M. J. OLIVIER, M. DARTIGUENAVE, Y. DARTIGUENAVE, and B. CAPELLE. Private communication.
40. A. L. BEAUCHAMP, M. DARTIGUENAVE, Y. DARTIGUENAVE, and B. CAPELLE. J. Am. Chem. Soc. **105**, 4662 (1983).
41. F. A. COTTON and S. J. LIPPARD. Inorg. Chem. **5**, 416 (1966).
42. H. E. HOWARD-LOCK, C. J. L. LOCK, and G. TURNER. Spectrochim. Acta, **38**A (12) 1283 (1982).
43. G. HERZBERG. Infrared and Raman spectra, D. van Nostrand Co. Inc., New Jersey. 1962.
44. R. H. WALTON. Q. Rev. **19** (2), 126 (1965).
45. T. WEIL, L. SPAULDING, and M. ORCHIN. J. Coord. Chem. **1**, 25 (1971).
46. P. J. HENDRA. Spectrochim. Acta, **23**A, 1275, 1967.
47. M. J. NOLAN and D. W. JAMES. J. Raman Spectrosc. **1**, 259 (1973).
48. D. W. JAMES and M. J. NOLAN. J. Raman Spectrosc. **1**, 271 (1973).
49. H. POULET, P. DELORME, and J. P. MATHIEU. Spectrochim. Acta, **20**, 1855 (1964).
50. D. M. ADAMS, J. CHATT, J. GERRATT, and A. D. WESTLAND. J. Chem. Soc. 734 (1964).
51. M. A. M. MEESTER. Inorg. Chim. Acta, **14**, 25 (1975).
52. K. NAKAMOTO. Infrared and Raman spectra of inorganic and coordination compounds. 3rd ed. John Wiley and Sons, New York. 1978.
53. N. B. COLTHUP, L. H. DALY, and S. E. WIBERLEY. Introduction to infrared and Raman spectroscopy. Academic Press, New York. 1964. p. 183.

Can. J. Chem. Downloaded from www.nrcresearchpress.com by 210.87.254.105 on 09/06/12
For personal use only.

Gas chromatography − mass spectrometry of osulose derivatives: *O*-trimethylsilyl, *O*-acetyl, *O*-isopropylidene, methyl glycosides, and 1,1-dimethyl acetals

PEDRO ANTONIO GARCÍA RUIZ, INMACULADA CARTAGENA TRAVESEDO, AND ANTONIO SOLER MARTINEZ
Department of Organic Chemistry, Faculty of Science, University of Murcia, Murcia, Spain

Received October 21, 1982[1]

PEDRO ANTONIO GARCÍA RUIZ, INMACULADA CARTAGENA TRAVESEDO, and ANTONIO SOLER MARTINEZ. Can. J. Chem. **62**, 870 (1984).

Structure determination of the *O*-trimethylsilyl, *O*-acetyl, and *O*-isopropylidene derivatives of some hexosuloses, pentosuloses, and one tetrosulose, as well as their methyl glycosides and 1,1-dimethyl acetals has been achieved by gas chromatography − mass spectrometry.

By study based on the qualitative and quantitative differences in the 36 derivatives obtained, and their analogues prepared from tetradeuterio methanol and/or hexadeuterio acetone, and comparison with results reported in the literature, criteria for the unambiguous determination of the structural grouping are proposed. The relative abundance of each compound when the osulose forms more than one isomeric derivative in the same reaction, as well as chromatographic data for the isolated products, are reported.

PEDRO ANTONIO GARCÍA RUIZ, INMACULADA CARTAGENA TRAVESEDO et ANTONIO SOLER MARTINEZ. Can. J. Chem. **62**, 870 (1984).

Faisant appel à la chromatographie en phase gazeuse couplée à la spectrométrie de masse, on a déterminé la structure des dérivés *O*-triméthylsilyl, *O*-acétyl et *O*-isopropylidène des quelques hexosuloses, pentosuloses et d'un tétrosulose ainsi que de leurs glucosides de méthyle et de leurs diméthyl-1,1 acétals.

En se basant, d'une part, sur les différences qualitatives et quantitatives observées dans les 36 dérivés obtenus et dans leurs analogues préparés à partir du tétradeutéro méthanol et/ou de l'hexadeutéro acétone et, d'autre part, sur une comparaison avec les résultats rapportés dans la littérature, on propose des critères pour la détermination non-ambigue des caractéristiques de structure. On rapporte aussi les données chromatographiques pour les produits isolés ainsi que les abondances relatives de chaque composé formé lorsque les osuloses forment plus d'un dérivé isomère dans la même réaction.

[Traduit par le journal]

Can. J. Chem. Downloaded from www.nrcresearchpress.com by 210.87.254.40 on 09/06/12
For personal use only.

Introduction

Although, glc−ms is a powerful tool for the structural elucidation (1) of the sugars, and analyses of some of the volatile derivatives of aldoses (2) and ketoses (3) that have been reported, until now no efficient method for the determination of the volatile derivatives of the osuloses has been published.

The present paper describes studies by electron impact mass spectrometry of four types of volatile derivatives of eight osuloses. These were the isopropylidene acetals, trimethylsilyl ethers, and acetate esters of the free sugars, and the isopropylidene acetals of the methyl glycosides.

Results and discussion

The derivatives detected and identified by gas chromatography, their relative retention times, and the relative abundance of each compound when the osulose forms more than one derivative in the same reaction, have been summarized in Tables 1 and 2.

The assignment of structure was made on the basis of the presence or absence of certain fragments characteristic of the structures of the ring types (4). The hydrogen contribution of the substituents in the fragments was confirmed by the relation between their m/e elevation and the number of hydrogen atoms changed by preparation of deuterated analogues (5).

Because the spectra of diastereoisomeric sugars differ only in the intensity of particular peaks (4), only one of them is discussed in detail (i.e., of the compounds **3**, **7**, and **13**, only compound **3** is discussed). The corresponding data for all of the compounds listed in Table 1 are available in the Journal's Depository of Supplementary Material.[2] The characteristic peaks of the general types of structural groupings will be discussed in the following sections.

A. *The molecular weight determination*

O-*Isopropylidene derivatives*

No molecular ions can be observed with the acetonides, but an intense $M^{+\cdot} - 15$ species (formed by the loss of one methyl group in the isopropylidene moiety to give an oxonium ion (6)) makes possible an easy calculation of the molecular weight. Further decompositon of $M^{+\cdot} - 15$ occurs by the loss of 58 (acetone), 60 (acetic acid), and 58 + 60 mass units. These fragments are found in the spectra of all the di-*O*-isopropylidene derivatives (3). The tri-*O*-isopropylidene derivatives show, in addition, peaks at $M^{+\cdot} - 15 - 58 - 58$; $M^{+\cdot} - 15 - 58 - 58 - 60$; $M^{+\cdot} - 58$; $M^{+\cdot} - 58 - 58$; $M^{+\cdot} + 1 - 58 - 58 - 58$; and $M^{+\cdot} + 1$.

The presence of many other linkages leads to a noticeable $M^{+\cdot} + 1$ peak. This small peak is easily recognized on the original record (7), especially when easily fragmented groups such as —OH or —$CH(OMe)_2$, linked to the ring, are absent.

For the mono-*O*-isopropylidene derivatives, the loss of acetone from the $M^{+\cdot} - 15$ species is not possible, because it requires an intact second isopropylidene moiety; peaks corresponding to $M^{+\cdot} - 15 - 58$ and $M^{+\cdot} - 15 - 60$ are absent in the spectrum (7). Only occasionally is the $M^{+\cdot} - 15 - 60$ species formed by several derivatives.

All the isopropylidene derivatives show two abundant fragments of lower mass, at m/e 59 (m/e 65 for the compounds from hexadeuterio acetone), corresponding to the protonated acetone ion, and at m/e 43 (m/e 46 for the compounds from hexadeuterio acetone) due to Me—CO^+; this is often the base peak.

The molecular weight and the most characteristic ions are summarized in Table 3A. This table shows, moreover, the m/e of the fragments for the analogous compounds prepared from

[1]Revision received December 5, 1983.

[2]This data is available, at a nominal charge, from the Depository of Unpublished Data, CISTI, National Research Council of Canada, Ottawa, Ont., Canada K1A 0S2.

TABLE 1. Identified osulose derivatives

Compound number	Substituents	Ring size
Parent osulose: D-*arabino* hexos-2-ulose		
1	2,3:4,5-Di-*O*-isopropylidene	2,6-Pyranose
2	2,3:4,5-Di-*O*-isopropylidene; 1,1-dimethyl acetal	2,6-Pyranose
3	1,2:2,3:5,6-Tri-*O*-isopropylidene	1,4-Furanose
4	2,3:5,6-Di-*O*-isopropylidene; methyl glycoside	1,4-Furanose
5	2,3,4,6-Tetra-*O*-trimethylsilyl	2,5-Furanose
6	2,3,4,6-Tetra-*O*-acetyl	2,5-Furanose
Parent osulose: D-*lyxo* hexos-2-ulose		
7	1,2:2,3:5,6-Tri-*O*-isopropylidene	1,4-Furanose
8	4,6-*O*-Isopropylidene; methyl glycoside	2,5-Furanose
9	4,6-*O*-Isopropylidene- methyl glycoside; 1,1-dimethyl acetal	2,5-Furanose
10	2,3,4,6-Tetra-*O*-trimethylsilyl	2,5-Furanose
11	1,3,5,6-Tetra-*O*-trimethylsilyl	1,4-Furanose
12	1,3,5,6-Tetra-*O*-acetyl	1,4-Furanose
Parent osulose: L-*xylo* hexos-2-ulose		
13	1,2:2,3:5,6-Tri-*O*-isopropylidene	1,4-Furanose
14	2,3,4,6-Tetra-*O*-trimethylsilyl	2,5-Furanose
Parent osulose: 6-deoxy-L-*arabino* hexos-2-ulose		
15	1,2:2,3-Di-*O*-isopropylidene	1,5-Pyranose
16	2,3-*O*-Isopropylidene	2,5-Furanose
17	2,3-*O*-Isopropylidene; 1,1-dimethyl acetal	2,5-Furanose
18	2,3,4-Tri-*O*-trimethylsilyl	2,5-Furanose
19–20	2,3,4-Tri-*O*-acetyl	2,5-Furanose
Parent osulose: D-*erythro* pentos-2-ulose		
21	1,2:3,4-Di-*O*-isopropylidene	1,5-Pyranose
22	3,4-*O*-Isopropylidene	2,5-Furanose
23	3,4-*O*-Isopropylidene; methyl glycoside	2,5-Furanose
Parent osulose: D-*erythro* hexos-2-ulose		
24	3,4-*O*-Isopropylidene; 1,1-dimethyl acetal	2,5-Furanose
25	3,4-*O*-Isopropylidene; methyl glycoside; 1,1-dimethyl acetal	2,5-Furanose
26	2,3,4-Tri-*O*-trimethylsilyl	2,5-Furanose
27	1,3,5-Tri-*O*-acetyl	1,4-Furanose
28	2,3,4-Tri-*O*-acetyl	2,5-Furanose
Parent osulose: L-*erythro* pentos-2-ulose		
29	3,4-*O*-Isopropylidene; 1,1-dimethyl acetal	2,5-Furanose
30	2,3,4-Tri-*O*-trimethylsilyl	2,5-Furanose
31–32	2,3,4-Tri-*O*-acetyl	2,5-Furanose
Parent osulose: D-*threo* pentos-2-ulose		
33	2,3-*O*-Isopropylidene	2,5-Furanose
34	1,3,5-Tri-*O*-trimethylsilyl	1,4-Furanose
Parent osulose: D-*glycero* tetros-2-ulose		
35	1,2:2,3-Di-*O*-isopropylidene	1,4-Furanose
Pentose: D-erythrose		
36	2,3-*O*-Isopropylidene	1,4-Furanose

hexadeuterio acetone and tetradeuterio methanol which are in agreement with the hydrogen contribution of the substituents in the fragments: e.g., for compound **1**, the $(M - 15)^+$ ion (corresponding to the loss of one Me group from the acetone) increases their m/e by nine mass units in the deuterated analogue, as should be expected for a di-*O*-isopropylidene derivative.

O-*Trimethylsilyl derivatives*

The mass spectra show very weak peaks for the molecular ions and more abundant peaks at $(M - 15)^+$, $(M - 15 - 90)^+$, $(M - 15 - 90 - 90)^+$, $(M - 73)^+$, and $(M - 89)^+$ as are characteristic of the TMS derivatives of the sugars (8) (see Table 3B) which occur through the loss of the Me (15), $SiMe_3$ (73), $OSiMe_3$ (89), and $HOSiMe_3$ (90) groups.

O-*Acetyl derivatives*

According to the literature data for discerning the molecular ions (6, 9, 10), the acetates show peaks at $M + 43$; $M + 1$; $M - 43$; $M - 59$; $M - 43 - 59$; and $M - 59 - 60$ through loss of the acetyl (43), acetic acid (59), and acetate anion (60) (see Table 3C).

The molecular weight is also confirmed on the basis of all the fragments obtained from $M^{+\cdot}$ by loss of characteristic groups such as CH_2OR or CHO.

B. *The ring type determination*

The different pyranoid or furanoid forms may be distinguished on the basis of low m/e cyclic fragments. Thus, the fragment at m/e 99 (3, 7, 9, 11) is relatively abundant in the 2,5-furanoses, the 1,5-pyranoses, and the 1,4-furanoses. The

Can. J. Chem. Downloaded from www.nrcresearchpress.com by 210.87.254.40 on 09/06/12
For personal use only.

TABLE 2. Osulose derivatives and their chromatographic data

Parent osulose	Compound	Molecular weight	T values[a] SE-30	T values[a] SE-52	AB[b]
		Isopropylidenation products			
Hexosuloses					
D-*arabino*	**1**	258	0.63	0.61	33
	3	316	0.93	0.97	67
D-*lyxo*	**7**	316	0.98	0.92	100
L-*xylo*	**13**	316	0.96	0.98	100
6-Deoxy-L-*arabino*	**15**	260	0.59	0.72	37
Pentosuloses					
D-*erythro*	**22**	188	0.45	0.58	64
	21	246	0.69	0.64	36
D-*threo*	**33**	188	0.56	0.70	100
Tetrosulose					
D-*glycero*	**35**	216	0.31	0.36	100
Aldotetrose					
D-*erythrose*	**36**		0.14	0.15	100
		Methanolysis and isopropylidenation products			
Hexosuloses					
D-*arabino*	**1**	258	—	0.61	10
	2	304	—	0.75	61
	4	290	—	0.95	29
D-*lyxo*	**8**	232	0.86	0.89	44
	9	278	0.91	0.93	56
6-Deoxy-L-*arabino*	**17**	248	0.61	0.70	100
Pentosuloses					
D-*erythro*	**23**	202	0.28	0.42	43
	24	234	0.60	0.69	23
	25	248	0.48	0.59	34
L-*erythro*	**29**	234	0.71	0.75	100
		Trimethylsilyl ethers			
Hexos-2-uloses					
D-*arabino*	**5**	466	0.86	0.85	100
L-*xylo*	**14**	466	1.12	1.19	100
D-*lyxo*	**10**	466	1.20	0.99	45
D-*lyxo*	**11**	466	1.34	1.16	55
6-Deoxy-L-*arabino*	**18**	378	0.60	0.51	100
Pentos-2-uloses					
D-*erythro*	**26**	364	0.61	0.50	100
D-*threo*	**34**	364	0.82	—	100
L-*erythro*	**30**	364	0.69	0.78	100
		Acetates			
Hexos-2-uloses					
D-*arabino*	**6**	389	1.18	—	100
D-*lyxo*	**12**	389	1.59	—	100
6-Deoxy-L-*arabino*	**19**	331	0.62	—	83
	20	331	0.64	—	17
Pentos-2-uloses					
L-*erythro*	**31**	317	0.75	—	46
	32	317	0.79	—	54
D-*erythro*	**27**	317	0.66	—	52
	28	317	0.69	—	48

[a]Relative retention times: for isopropylidenation and methanolysis and isopropylidenation products, relative to 2,3:5,6-di-*O*-isopropylidene-D-mannose. For trimethylsilyl ethers, relative to 1,2,3,4,6-pentatrimethylsilyl-α-D-glucopyranose. For acetates, relative to 1,2,3,4,6-pentaacetyl-D-glucopyranose.

[b]Relative abundances (%) by the Bartlet and Schmidt method (47).

ion at m/e 69 (7, 12, 13) (protonated furan) is always present in all derivatives of the hex- and pentosuloses and, in spite of their higher abundance in the furanose forms, is not indicative of the ring type.

Furthermore, fragments at m/e 69, m/e 157 (for the acetates (6, 9, 11, 14), m/e 319 (or its equivalent for the trimethylsilyl derivatives (8, 15, 16)), m/e 217 (greater than m/e 204 for the trimethylsilyl derivatives (15, 16, 17)), and m/e 83 (for the 6-deoxy-hexosulose isopropylidene derivatives (5)) are more abundant in the furanoses.

Can. J. Chem. Downloaded from www.nrcresearchpress.com by 210.87.254.40 on 09/06/12
For personal use only.

TABLE 3A. The characteristic fragments in the determination of the molecular weight of some *O*-isopropylidene derivatives, (*m/e* for the analogues prepared from hexadeuterio acetone) *m/e* (% relative intensity); base peak *m/e* 43

Ions	Compounds		
	1	**3**	**8**
$(M + 1)^+$	(272)259(0.20)	(336)317(0.01)	
$(M - 15)^+$	(252)243(11.80)	(316)301(3.0)	(220)217(1.60)
$(M - 15 - 58)^+$	(188)185(1.90)	(252)243(3.60)	(155)155(11.30)
$(M - 15 - 58 - 58)^+$		(188)185(16.0)	
$(M - 15 - 58 - 60)^+$	(125)125(9.60)		
$(M - 15 - 60)$			(155)155(0.30)
$(M - 58)^+$		(270)258(0.30)	

TABLE 3B. The characteristic fragments in the determination of the molecular weight of some *O*-trimethylsilyl derivatives, *m/e* (% relative intensity); base peak *m/e* 73

Ions	Compounds		
	5	**18**	**30**
$M^{+\cdot}$	466(0.25)	378(—)	364(0.11)
$(M - 15)^{+\cdot}$	451(1.21)	363(1.01)	349(0.1)
$(M - 15 - 90)^{+\cdot}$	361(0.98)	273(2.11)	259(1.6)
$(M - 15 - 90 - 90)^{+\cdot}$	271(4.70)	183(2.30)	169(1.06)
$(M - 73)^{+\cdot}$	393(0.27)	305(13.3)	291(1.31)
$(M - 89)^{+\cdot}$	377(25.5)	289(72.89)	275(0.95)

TABLE 3C. The characteristic fragments in the determination of the molecular weight of some *O*-acetyl derivatives, *m/e* (% relative intensity); base peak *m/e* 43

Ions	Compounds		
	6	**19**	**27**
$(M + 43)^{+\cdot}$	389(11.0)	331(0.10)	317(—)
$(M + 1)^{+\cdot}$	347(12.1)	289(—)	275(1.3)
$(M - 43)^{+\cdot}$	303(11.3)	245(0.32)	321(5.3)
$(M - 59)^{+\cdot}$	287(18.3)	229(—)	215(11.5)
$(M - 43 - 59)^{+\cdot}$	244(4.62)	186(12.57)	172(9.12)
$(M - 59 - 60)^{+\cdot}$	227(2.61)	169(—)	155(—)

The most marked characteristic differences, which provide a firm basis for distinguishing between ring types, are the positions and intensities of peaks corresponding to the fragments formed by fission of the side chains or groups connected to the carbon α to the ring oxygen (6−9). These fragmentations are discussed below for the most characteristic X groups, and all the investigated compounds show abundant peaks at $M^{+\cdot} - X$ and their corresponding series, as has been indicated (3, 9).

C. *The formyl group determination*

It has been shown for the aldehydo derivatives of sugars that the most intense peaks are formed by cleavage of the C_1—C_2 bond with the subsequent loss of the Me, ROH, R_2O, and other typical fragments (3, 9, 13). For example, in the aldehydo acetates the fragments of a series arise from the fission of the formyl group (—CHO) (20 mass units) and subsequent elimination of Ac_2O (102 mass units), AcOH (60 mass units), and ketene (42 mass units) (13, 18).

All the investigated compounds containing the CHO group (as revealed in Table 4) show the following fragments.

O-Isopropylidene derivatives: $M^{+\cdot} - 29$ ($M^{+\cdot}$ − CHO) and $M^{+\cdot} - 29 - 58$ ($M^{+\cdot}$ − CHO − Me_2CO) which show the expected *m/e* in the deuterio analogues.

O-Trimethylsilyl derivatives: $M^{+\cdot} - 29$; $M^{+\cdot} - 29 - 28 - 1$ ($M^{+\cdot}$ − CHO − CO − H^+); $M^{+\cdot} - 29 - 89 - 15$ ($M^{+\cdot}$ − CHO − $OSiMe_3$ − Me); and $M^{+\cdot} - 29 - 103$ ($M^{+\cdot}$ − CHO − CH_2 − $OSiMe_3$).

O-Acetyl derivatives: $M^{+\cdot} - 29$; $M^{+\cdot} - 29 - 59$ ($M^{+\cdot}$ − CHO − MeCOO·); $M^{+\cdot} - 29 - 42$ ($M^{+\cdot}$ − CHO − CH_2CO); $M^{+\cdot} - 29 - 42 - 60$($M^{+\cdot}$ − CHO − CH_2CO − MeCOOH); and *m/e* 100 (MeCOOCHCO).

Furthermore, fragments such as *m/e* 57 (CHO—CO^+), *m/e* 69 (protonated furan), and *m/e* 73 (MeO^+=CH—CHO), have been reported to be characteristic of the formyl group (2, 9, 14), but their presence does not establish the presence of the formyl group because each peak may be obtained by other routes.

D. *The formyl dimethyl acetal group determination*

In the spectra of compounds **2**, **9**, **17**, **24**, **25**, and **29**, the most intense peaks are formed by cleavage of the C_1—C_2 bond, as occurs with the aldehydo dithioacetals (19). This series is represented by the ions *m/e* 75 (MeOCH=OMe) (9, 20) (which usually is the base peak), $M^{+\cdot} - 58 - 75$, and $M^{+\cdot} - 75$.

Furthermore, the presence of this group produces two other series of fragments. The loss of one of the methoxyl groups as MeO· (*m/e* 31) (5) and the subsequent elimination of acetone gives the ions $M^{+\cdot} - 31$, $M^{+\cdot} - 31 - 58$ and $M^{+\cdot} - 31 - 58 - 58$. On the other hand, the loss of Me—OH—Me (*m/e* 47) and acetone produces the ions at $M^{+\cdot} - 47$, $M^{+\cdot} - 47 - 58$, and *m/e* 47.

As revealed in Tables 5A and 5B, the observed *m/e* values of the deuterio analogues are in agreement with the loss of these groups. For the peak at *m/e* 47, as revealed in Tables 5A and 5B, the major contribution to this fragment is provided by the two methyl groups of the $CH(OMe)_2$ unit; because the MeOH was replaced by CD_3—OD, their series shifted by six *m/e* units.

E. *The CH_2OR group determination*

Analogously, the loss of the substituent α to the ring oxygen (the CH_2OR group) with the formation of the $M^{+\cdot} - CH_2OR$ ions and the loss of the CHO—CH_2OR group, are indicative of this group (6, 8−11, 14). As shown in Table 6A, the trimethylsilyl derivatives give fragments at *m/e* 103, $M^{+\cdot} - 103$, *m/e* 133, and $M^{+\cdot} - 132$, and the acetates at *m/e* 73, $M^{+\cdot} - 60 - 73$ and $M^{+\cdot} - 102$, in accordance with the expected fragmentations for structures which contain the CH_2OR group.

F. *The CHOR—CH_2OR group determination*

The most characteristic fragmentation process for the com-

Can. J. Chem. Downloaded from www.nrcresearchpress.com by 210.87.254.40 on 09/06/12
For personal use only.

Can. J. Chem. Downloaded from www.nrcresearchpress.com by 210.87.254.40 on 09/06/12
For personal use only.

TABLE 4. Some characteristic ions in the formyl group determination (*m/e* for the analogues prepared from hexadeuterio acetone), *m/e* (% relative intensity)

Ions	Compounds		
	O-Isopropylidene derivatives		
	1	**8**	**23**
$(M - 29)^{+\cdot}$	(241)229(10.3)	(209)205(4.1)	(179)173(85.3)
$(M - 29 - 58)^{+\cdot}$	(177)171(16.6)	(145)145(6.7)	(115)115(13.3)
	O-Trimethylsilyl derivatives		
	5	**18**	**30**
$(M - 29)^{+\cdot}$	437(1.81)	349(1.98)	335(0.3)
$(M - 29 - 28 - 1)^{+\cdot}$	408(0.2)	320(—)	306(—)
$(M - 29 - 15 - 89)^{+\cdot}$	333(—)	245(4.11)	231(1.37)
$(M - 29 - 103)^{+\cdot}$	334(1.53)	—	—
	O-Acetyl derivatives		
	6	**19**	**28**
$(M - 29)^{+\cdot}$	317(9.10)	259(0.51)	245(6.32)
$(M - 29 - 59)^{+\cdot}$	258(0.25)		186(0.23)
$(M - 29 - 42)^{+\cdot}$	275(6.51)	217(0.71)	203(12.7)
$(M - 29 - 42 - 60)^{+\cdot}$	215(3.55)	157(54.28)	
m/e 100	(6.0)	(31.14)	(13.3)

TABLE 5A. Some characteristic fragments in the formyl dimethyl acetal group determination, (*m/e* for the analogue prepared from hexadeuterio acetone) *m/e* (% relative intensity)

Ions	Compounds		
	9	**24**	**25**
$(M - 75)^{+\cdot}$	(209)203(15.9)	(165)159(1.8)	(179)173(15.9)
$(M - 75 - 58)^{+\cdot}$	(145)145(12.5)	(101)101(5.5)	(115)115(2.3)
$(M - 47)^{+\cdot}$	(237)231(13.3)	(193)187(1.9)	(207)201(0.3)
$(M - 47 - 58)^{+\cdot}$	(173)173(3.8)	(129)129(0.5)	(143)143(0.9)
$(M - 31)^{+\cdot}$	(253)247(1.0)	(209)203(0.8)	(223)217(1.3)
$(M - 31 - 58)^{+\cdot}$	(189)189(2.1)	(145)145(2.5)	(159)159(1.7)
m/e 75	75(100)	75(68.9)	75(72.7)
m/e 47	47(30.8)	47(32.5)	47(45.5)

TABLE 5B. Some characteristic fragments in the dimethyl acetal group determination for the compound **2** (as in Table 1)[a]

Ions	A	B	C	D	E
m/e 75	75	75	81	81	100
$M^{+\cdot} - 75$	229	241	229	241	32.1
$M^{+\cdot} - 75 - 58$	171	177	171	177	31.3
$M^{+\cdot} - 47$	257	269–266	257–260	269	3.0
$M^{+\cdot} - 47 - 58$	199	205	199–202	205	1.8
$M^{+\cdot} - 31$	273	285	276	288	1.1
$M^{+\cdot} - 31 - 58$	215	221	218	224	15.0
m/e 47	47	47	53	53	22.6

[a]A: *m/e*; B: *m/e* for the analogue prepared from hexadeuterio acetone; C: *m/e* for the analogue prepared from tetradeuterio methanol; D: *m/e* for the analogue prepared from hexadeuterio acetone and tetradeuterio methanol; E: % relative intensity.

pound with this group is the cleavage of the C_4—C_5 bond (7) resulting in the fragments at *m/e* 205 for the trimethylsilyl derivatives (8) or at *m/e* 145 for the acetates (9, 10) (Table 6B), and their fragment series.

Compound **11** shows fragments at *m/e* 205, $M^{+\cdot} - 205$, $M^{+\cdot} - 205 - 15$, and *m/e* 115 (*m/e* 205 − 90) whereas the acetylated compound **12** shows peaks at *m/e* 145, $M^{+\cdot} - 145$, $M^{+\cdot} - 145 - 42$, $M^{+\cdot} - 145 - 60 - 42$, *m/e* 103, and *m/e* 85, as expected.

G. *The methoxyl group on the methyl glycosides*

The degradation of methyl glycosides (20) proceeds through elimination of MeO· (fragment which is unstable and produces only a small peak at *m/e* 31) (ref. 9) and the subsequent elimination of acetone to give the $M^{+\cdot} - 31$ and $M^{+\cdot} - 31 - 58$ peaks. The loss of MeOHMe (*m/e* 47) produces small peaks at *m/e* 47, $M^{+\cdot} - 47 - 58$ because only one of the Me groups of the *m/e* 47 is derived from the glycoside, whereas the other is derived from the isopropylidene group.

In addition, other fragments which contain the OCH_3 group, such as the *m/e* 73 (MeO=CH—CHO) (21, 24) and *m/e* 113 (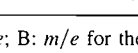 —CH=$\overset{+}{O}$—Me), have been observed. Table 7 shows the *m/e*, relative abundances, and the *m/e* of the deuterio analogues (in accordance with the preceding losses).

H. *The free hydroxyl group determination*

The study of the *O*-isopropylidene derivatives bearing a free OH group showed, as expected, the fragmentation series $M^{+\cdot} - 1$, $M^{+\cdot} - 1 - 58$, $M^{+\cdot} - 17$, and $M^{+\cdot} - 17 - 58$ ($M^{+\cdot} - OH - Me_2CO$). Compounds **4**, **21**, **22**, **24**, **29**, and **36** have more intense $M^{+\cdot} - 1$ and $M^{+\cdot} - 17$ peaks due to the attachment of the OH to the C_1 or C_2 rather than to some other carbon atom (5). The fragments are listed in Table 7.

I. *The 5,6-O-isopropylidene structural unit*

The most characteristic fragmentation process for the com-

TABLE 6A. Some characteristic fragments in the CH_2OR group determination[a]

	O-TMS derivatives				*O*-Acetyl derivatives			
	5		**34**		**6**		**27**	
Ions	A	B	A	B	A	B	A	B
CH_2OR	103	20.6	103	15.9	73	3.17	73	100
M − (CH_2OR)	363	0.58	261	0.3	273	6.25	201	8.4
O=CH—CH_2OR	133	19.6	133	10.8				
M − (O=CH—CH_2OR)	334	1.53			244	4.62	172	9.12
M − (CH_2OR) − (ROH)					213	1.5		

[a]A = *m/e*; B = % relative intensity.

TABLE 6B. Some characteristic fragments in the CHOR—CH_2OR group determination, *m/e* (% relative intensity)

	Compounds	
Ions	**11**	**12**
CH_2OR	103(45.9)	
CHOR—CH_2OR	205(9.8)	145(2.60)
M − (CHOR—CH_2OR)	261(0.8)	201(4.67)
(CHOR—CH_2OR) − OR	115(11.1)	
(CHOR—CH_2OR) − ROH		85(3.60)
(CHOR—CH_2OR) − CH_2CO		103(9.17)
M − (CHOR—CH_2OR) − (CH_2CO)		159(3.71)

pounds with this structural unit is the cleavage of the C_4—C_5 bond (7) resulting in the fragments at *m/e* 101 (very intense peak shifted to *m/e* 107 in the acetone deuterated analogues (6)), $M^{+\cdot} - 101$, $M^{+\cdot} - 101 - 15$, and $M^{+\cdot} - 130 - 15$. These peaks are listed in Table 8A.

Other characteristic fragments of the compounds with this structural unit are the *m/e* 129 (shifted to *m/e* 136 in the deuterated analogues, and which seem to represent the cleavage of the C_3—C_4 and O—C_1 bonds (7)), *m/e* 117 (with shift to *m/e* 123 in the deuterated analogues (7)), *m/e* 115 (with shift to *m/e* 118 (3)), and *m/e* 72 ($\cdot CH_2$—O=CMe_2 with shift to *m/e* 78 (3, 7, 11)).

Furthermore, other fragments typical of *O*-isopropylidene derivatives are also present but in reduced relative intensity, because of the competitive cleavage of the C_4—C_5 bond (7).

J. *The 4,6-O-isopropylidene structural unit*

As in the compounds of the preceding structural unit, compounds **8** and **9** show fragments at *m/e* 101, 115, and 129 which must proceed from a rearrangement (9). Characteristic of this structural unit (7, 19, 22) are abundant peaks at *m/e* 72, *m/e* 113 (Me_2C—O—CH=CH—CHO shifted by 119 (7, 9) in deuterated analogues), *m/e* 85 (shifted by 88), *m/e* 71 (shifted by 74), and *m/e* 117, as shown in Table 8B.

K. *Other O-isopropylidene structural units*

For the *O*-isopropylidene derivatives that do not contain structural units equivalent to those discussed in sections I or J, the C_4—C_5 fragmentation to give such ions is impossible (3, 23).

These *O*-isopropylidene derivatives give a characteristic peak at *m/e* 85 (shifted by 88 in deuterated analogues).

L. *The Me group of the 6-deoxy-osulose derivatives*

For the acetates, the fragments at $M^{+\cdot} - 15$, $M^{+\cdot} - 15 - 29$, $M^{+\cdot} - 15 - 60$, $M^{+\cdot} - 15 - 60 - 60$, $M^{+\cdot} - 15 - 42$, and $M^{+\cdot} - 15 - 60 - 42$ make possible its assignment for the compounds **19** and **20** by criteria analogous to those employed in the preceding structural unit (see Table 8C).

M. *Fragmentation data and elimination of alternative structure*

In the preceding sections (A to L) the molecular weight and the presence of the characteristic groups and structural units were determined unambiguously in the compounds studied. This determination makes possible the assignment of structure, because alternative structures (for example, another ring type) should have (a) lower molecular weight (for compound **3** the 2,5-furanose or the 2,6-pyranose is not possible for a tri-*O*-isopropylidene derivative), or (b) other groups (for compound **5** the 1,4-furanose should give peaks corresponding to the CH_2OR—CHOR—group), or (c) the absence of the characteristic peaks of some groups (for compound **5** in the 1,4-furanose, the peaks for a CHO group should be absent), or (d) the absence of the characteristic peaks of the assigned structure (for compound **5**, the characteristic peaks of the furanose ring should be absent in the alternative pyranose rings).

With respect to the latter, although the mass spectra provide strong evidence for the assigned structures, these assignments have been verified for compounds **1** (24−26) and **3** (27) and all the bibliographic results were consistent with the assigned structures for the TMS and acetate derivatives (24, 28−31), and with the conclusion that the substrate was an osulose or other sugar *O*-isopropylidene derivative which contains formyl (24−26, 32, 33), formyl dimethyl acetal (30, 34, 35), and methoxyl groups (35), the 5,6-*O*-isopropylidene structural unit (27, 36, 37),or ring types (24 to 37) as assigned in the present paper.

Experimental

Starting products

The monosaccharides were obtained commercially: D-glucose anhydrous, Fluka A. G. Puriss p.a., Ref. 49140; D-galactose, Fluka A. G. Puriss p.a., Ref. 48260; L-sorbose, Fluka A. G. Puriss p.a., Ref. 85542; L-rhamnose monohydr., Fluka A. G. Puriss p.a., Ref. 83650; D-ribose, Fluka A. G. Puriss p.a., Ref. 83860; L-arabinose, Fluka A. G. Puriss p.a., Ref. 10840; D-xylose, Fluka A. G. Puriss p.a., Ref. 95730; D-erythrose, Fluka A. G. Pract., Ref. 45681.

The hex- (38), pent- (39) and tetrosuloses (40) were prepared from the monosaccharides, according to literature methods. D-*Arabino* hexos-2-ulose: mp 103.3°C (dec.); uv λ_{max}: 245 nm and 279 nm. *Anal.* calcd. for $C_6H_{12}O_7$: C 36.73, H 6.12; found: C 37.38, H 6.14. D-*lyxo* hexos-2-ulose: mp 89.9°C (dec.); uv λ_{max}: 220 nm and 275 nm. *Anal.* found: C 36.01, H 5.92. L-*xylo* hexos-2-ulose: mp 92.1°C (dec.); uv λ_{max}: 218 nm and 282 nm. *Anal.* found: C 36.41, H 5.84. 6-Deoxy-L-*arabino* hexos-2-ulose: *Anal.* calcd. for $C_6H_{12}O_6$: C 40.0, H 6.66; found: C 39.2, H 6.53. D-*erythro* pentos-2-ulose: *Anal.* calcd. for $C_5H_{10}O_6$: C 36.14, H 6.02; found: C 36.0, H 5.91. L-*erythro* pentos-2-ulose: *Anal.* found: C 35.91, H 5.86. D-*threo* pentos-2-ulose: uv

Can. J. Chem. Downloaded from www.nrcresearchpress.com by 210.87.254.40 on 09/06/12
For personal use only.

TABLE 7. Some characteristic fragments in the *O*-isopropylidene derivatives with an OMe group, (*m/e* for the analogues prepared from hexadeuterio acetone) *m/e* (% relative intensity)

Ions	Compounds 4	8	23
$(M - OMe)^{+\cdot}$	(271)259(2.1)	(207)201(2.6)	(177)171(56.7)
$(M - (OMe) - (Me_2CO))^{+\cdot}$	(207)201(4.2)	(143)143(16.6)	(113)113(8.3)
$(M - (OMe) - 2(Me_2CO))^{+\cdot}$	(149)149(0.1)		
$(M - (OH) - Me)^{+\cdot}$	(50) 47(0.6)	(50) 47(3.6)	(50) 47(4.1)
$(M - (MeOHMe))^{+\cdot}$	(252)243(1.6)	(188)185(2.7)	(158)155(1.6)

TABLE 8A. Some characteristic fragments in the 5,6-*O*-isopropylidene structural unit, (*m/e* of the analogues prepared from hexadeuterio acetone) *m/e* (% relative intensity)

Ions	Compounds 3	4
m/e 101	(107)101(23.1)	(107)101(60.4)
$(M - 101)^{+\cdot}$	(227)215(0.6)	(195)189(2.5)
$(M - 101 - 15)^{+\cdot}$	(209)200(1.8)	(177)174(16.0)
$(M - 130 - 15)^{+\cdot}$	(180)171(1.7)	(180)171(1.2)
m/e 129	(135)129(2.9)	(135)129(40.4)
m/e 117	(123)117(7.0)	(123)117(10.1)
m/e 115	(118)115(7.3)	(118)115(12.2)
m/e 72	(78) 72(12.5)	(78) 72(50.8)

TABLE 8B. Some characteristic fragments in the 4,6-*O*-isopropylidene structural unit, (*m/e* for the analogues prepared from hexadeuterio acetone) *m/e* (% relative intensity)

Ions	Compounds 8	9
m/e 71	(74) 71(20.5)	(74) 71(20.5)
m/e 72	(78) 72(13.8)	(78) 74(19.1)
m/e 85	(88) 85(50.4)	(88) 85(62.2)
m/e 101	(107)101(5.7)	(107)101(16.7)
m/e 113	(119)113(7.1)	(119)113(35.1)
m/e 115	(118)115(13.1)	(118)115(12.5)
m/e 117	(123)117(4.1)	(123)117(14.2)
m/e 129	(135)129(7.5)	(135)129(18.6)

TABLE 8C. Some characteristic fragments in the Me group of the 6-deoxy-*O*-isopropylidene derivatives, *m/e* (% relative intensity)

Ions	Compound 19
$(M - 15)^{+\cdot}$	273(2.4)
$(M - 15 - 29)^{+\cdot}$	244(1.25)
$(M - 15 - 60)^{+\cdot}$	213(1.6)
$(M - 15 - 60 - 60)^{+\cdot}$	153(11.42)
$(M - 15 - 60 - 42)^{+\cdot}$	171(3.71)
$(M - 15 - 42)^{+\cdot}$	231(42.0)

λ_{max}: 230 nm and 279 nm. *Anal.* found: C 35.96, H 5.89. D-*glycero* tetrosulose: *Anal.* calcd. for $C_4H_8O_5$: C 35.29, H 5.88; found: C 35.01, H 5.76.

Preparation of osulose derivatives

The *O*-isopropylidene derivatives were prepared by the acetone (and acetone-d_6) – sulphuric acid method (41, 42). The methyl glycosides and 1,1-dimethyl acetals were prepared from methanol (and methanol-d_4) (43). The acetates were prepared by the acetic anhydride – sodium acetate method (44). The literature method was modified only for the preparation of the trimethylsilyl derivatives (45), the solvent (pyridine) being replaced by *N,N*-dimethyl formamide (33, 46).

Analytical methods

Gas–liquid chromatography was performed on a Perkin–Elmer F-30 gas chromatograph equipped with a flame-ionization detector and coiled stainless columns (6 ft × 1/8 in.) packed with 3% SE-30 and SE-52 on Chromosorb W HP 80–100. Nitrogen was used as the carrier gas, at a flow rate of the 30 mL/min. The temperature of the oven was programmed from 100–275°C at 2°C/min.

The determination of the relative abundances of each compound when the osulose formed more than one derivative in the same reaction was made by glc (47).

For the glc–ms analyses, a Hewlett–Packard 5980 A gas chromatograph was used in combination with a Hewlett–Packard 5710 A mass spectrometer, operating at 70 eV under the same conditions as described above for glc, although the carrier gas was helium in this case.

1. V. KOVACIK, V. MIHALOV, and P. KOVAC. Carbohydr. Res. **88**, 189 (1982).
2. S. MORGENLIE. Carbohydr. Res. **41**, 285 (1975).
3. S. MORGENLIE. Carbohydr. Res. **80**, 215 (1980).
4. N. K. KOCHETKOV and O. S. CHIZKOV. *In* Methods in carbohydrate chemistry. Vol. VI. *Edited by* R. L. Whistler and J. BeMiller. Academic Press Inc., New York. 1972. pp. 540–553.
5. H. W. KIRCHER. *In* Methods in carbohydrate chemistry. Vol. I. *Edited by* R. L. Whistler and M. L. Wolfrom. Academic Press Inc., New York. 1962. p. 13.
6. D. C. DEJONGH and K. BIEMANN. J. Am. Chem. Soc. **86**, 64 (1964).
7. H. BUDZIKIEWICZ, C. DJERASSI, and D. WILLIAMS. Structure elucidation of natural products by mass spectrometry. Vol. II. Holden–Day Inc., London. 1964. pp. 203–240.
8. D. C. DEJONGH, T. RADFORD, J. D. HRIBAR, S. HANESSIAN, M. BIWBER, G. DAWSON, and C. C. SWEELEY. J. Am. Chem. Soc. **91**, 1728 (1969).
9. N. K. KOCHETKOV and O. S. CHIZHOV. Adv. Carbohydr. Chem. **21**, 39 (1966).
10. F. JANSSON and B. LINDBERG. Carbohydr. Res. **86**, 278 (1960).
11. A. ROSENTHAL. Carbohydr. Res. **8**, 61 (1968).
12. K. HEYNS and H. SCHARMAN. Carbohydr. Res. **1**, 371 (1966).
13. J. SZAFRANEK, A. WISNIEWSKI, and P. VOUROS. Carbohydr. Res. **30**, 11 (1977).
14. T. FUJIWARA and K. ARAI. Carbohydr. Res. **87**, 11 (1980).
15. N. K. KOCHETKOV, O. S. CHIZHOV, and N. V. MOLODTSOV. Tetrahedron, **24**, 5587 (1968).
16. J. F. KENNEDY and S. M. ROBERTSON. Carbohydr. Res. **58**, 1 (1978).
17. O. LOUGREN and S. SVENSON. Adv. Carbohydr. Chem. Biochem. **29**, 42 (1974).

Can. J. Chem. Downloaded from www.nrcresearchpress.com by 210.87.254.40 on 09/06/12
For personal use only.

18. D. C. DEJONGH. J. Org. Chem. **30**, 453 (1965).
19. D. C. DEJONGH. J. Am. Chem. Soc. **86**, 3149 (1964).
20. N. K. KOCHETKOV and O. S. CHIZHOV. Tetrahedron, **21**, 55 (1965).
21. K. HEINS and D. MULLER. Tetrahedron, **21**, 2029 (1965).
22. R. F. BRADY, JR. Adv. Carbohydr. Chem. Biochem. **26**, 197 (1971).
23. O. S. CHIZHOV, L. S. GOLOVIKINA, and N. S. WULFSON. Carbohydr. Res. **6**, 138 (1968).
24. R. W. BINKLEY. J. Org. Chem. **42**, 1216 (1977).
25. R. F. BRADY, JR. Carbohydr. Res. **15**, 35 (1970).
26. R. E. ARRICK, D. C. BAKER, and D. D. HORTON. Carbohydr. Res. **26**, 441 (1973).
27. S. BAYNE, G. A. COLLIS, and H. A. FEWARWE. J. Chem. Soc. 2766 (1952).
28. G. M. GREE, D. M. MACKIE, and A. S. PERLIN. Can. J. Chem. **47**, 511 (1969).
29. D. M. MACKIE and A. S. PERLIN. Carbohydr. Res. **24**, 67 (1972).
30. G. J. R. CHITTENDEN. Carbohydr. Res. **11**, 424 (1969).
31. K. MAURER. Ber. **62**, 332 (1929); Ber. **63**, 25 (1930).
32. N. TAKEO, M. FUJISAKU, and H. TADAMITSU. Chem. Abstr. **82**, 140436 (1975).
33. S. BAYNE and J. A. FEWSTER. Adv. Carbohydr. Chem. **11**, 43 (1965).
34. A. HASEGAWA and M. KISO. Carbohydr. Res. **79**, 265 (1980).
35. A. ASSARSSON and O. THEANDER. Acta Chem. Scand. **17**, 47 (1963).
36. K. JAMES, A. R. TATCHELL, and P. L. RAY. J. Chem. Soc. (C), 2681 (1967).
37. K. BISCHOFBERGER, S. J. EITELMAN, and A. JORDAN. Carbohydr. Res. **74**, 145 (1979).
38. S. BAYNE. *In* Methods in carbohydrate chemistry. Vol. II. *Edited by* R. L. Whistler and M. L. Wolfrom. Academic Press Inc., New York. 1963. pp. 421–423.
39. E. C. TAYLOR and P. A. JACOBI. J. Am. Chem. Soc. **98**, 2305 (1976).
40. D. J. WALTON. Can. J. Chem. **47**, 3483 (1969).
41. K. FREUNDENBERG and R. M. HIXON. Ber. **56**, 2119 (1923).
42. K. FREUNDENBERG and A. WOLF. Ber. **60**, 232 (1927).
43. S. COFFEY. *In* Rodd's chemistry of carbon compounds. Vol. I-F. Elsevier, New York. 1967. pp. 324–325.
44. M. L. WOLFROM and A. THOMPSON. *In* Methods in carbohydrate chemistry. Vol. II. *Edited by* R. L. Whistler and M. L. Wolfrom. Academic Press Inc., New York. 1963. p. 212.
45. C. C. SWEELEY, R. BENTLEY, M. MAKITA, and W. W. WELLS. J. Am. Chem. Soc. **85**, 2497 (1963).
46. W. C. ELLIS. J. Chromatogr. **41**, 325 (1969).
47. J. C. BARTLET and D. M. SMITH. Can. J. Chem. **38**, 2057 (1960).

Can. J. Chem. Downloaded from www.nrcresearchpress.com by 210.87.254.40 on 09/06/12
For personal use only.

Capacités calorifiques, volumes, expansibilités et compressibilités des solutions aqueuses concentrées de LiOH, NaOH et KOH

ALAIN H. ROUX,[1] GÉRALD PERRON ET JACQUES E. DESNOYERS[2]

Département de chimie, Université de Sherbrooke, Sherbrooke (Qué.), Canada J1K 2R1

Reçu le 15 août 1983

ALAIN H. ROUX, GÉRALD PERRON et JACQUES E. DESNOYERS. Can. J. Chem. **62**, 878 (1984).

Les masses volumiques et capacités calorifiques de solutions aqueuses d'hydroxydes alcalins ont été mesurées entre 4 et 55°C à l'aide d'un densimètre à tube vibrant et d'un microcalorimètre dynamique. Le domaine de concentration étudié est respectivement de 0,04 à 3,8 mol kg^{-1} pour LiOH, 0,02 à 10,9 mol kg^{-1} pour NaOH et 0,02 à 15,5 mol kg^{-1} pour KOH. Les volumes et capacités calorifiques molaires partiels ($\bar{V}_2$, $\bar{C}_{p,2}$) ont été calculés par dérivation des équations analytiques obtenues à l'aide d'une méthode de moindres carrés appliquée aux grandeurs molaires apparentes (V_ϕ, $C_{p,\phi}$) en fonction de la molalité. De l'influence de la température sur les grandeurs molaires apparentes à une concentration donnée, nous avons déduit les expansibilités molaires apparentes E_ϕ et $(\partial C_{p,\phi}/\partial T)_P$. Les vitesses ultrasonores ont aussi été mesurées à 25°C pour NaOH dans le domaine des faibles concentrations et ont été utilisées pour calculer les compressibilités et les capacités calorifiques molaires partielles à volume constant dans l'état standard. Les données présentées ont été comparées avec les valeurs de la littérature. La dépendance avec la concentration des propriétés des solutions d'hydroxydes est semblable à celle des autres électrolytes 1:1 bien que les déviations à la loi limite de Debye–Hückel soient plus grandes.

ALAIN H. ROUX, GÉRALD PERRON, and JACQUES E. DESNOYERS. Can. J. Chem. **62**, 878 (1984).

The densities and heat capacities of various alkali hydroxides were measured in water with a vibrating tube densimeter and a flow microcalorimeter in the temperature range 4 to 55°C. The concentration ranges investigated were respectively: 0.04 to 3.8 mol kg^{-1} for LiOH, 0.02 to 10.9 mol kg^{-1} for NaOH, and 0.02 to 15.5 mol kg^{-1} for KOH. The partial molar volumes ($\bar{V}_2$) and heat capacities ($\bar{C}_{p,2}$) were calculated from the least-squares fit of the apparent molar quantities (V_ϕ and $C_{p,\phi}$) as a function of molalities. From the temperature dependence of these functions the apparent molar expansibilities (E_ϕ) and $(\partial C_{p,\phi}/\partial T)_P$ were derived. The ultrasonic velocities were also measured for the dilute solutions of NaOH at 25°C, and can be used to calculate the standard partial molar compressibilities and isochoric heat capacities. The present data were compared with literature values. The general trends as a function of concentration are similar to those of other 1:1 electrolytes even though the deviations from the Debye–Hückel theory are larger.

Introduction

L'étude des propriétés des solutions aqueuses d'hydroxydes alcalins aux fortes concentrations présente un intérêt certain lié en particulier au domaine de l'énergie électrochimique (1). Ces systèmes sont aussi importants au point de vue fondamental car il n'est pas encore clairement établi quel rôle l'interaction particulière entre l'ion OH^- et H_2O peut avoir sur les interactions soluté–soluté aux fortes concentrations (2). Ainsi, l'influence de la concentration des hydroxydes alcalins sur les réactions d'hydrolyse de diverses molécules organiques se traduit par un effet catalytique observé depuis longtemps (3–7). Finalement, les théories des solutions concentrées d'électrolytes ont été développées surtout pour les solutions d'électrolytes simples comme NaCl (8–10) où la solvatation joue un rôle beaucoup moins important que dans le cas des hydroxydes alcalins.

Lors de l'étude des solutions concentrées, une bonne connaissance des fonctions thermodynamiques est nécessaire pour améliorer notre compréhension des interactions ion–solvent et ion–ion et pour prédire l'influence de la température et de la pression sur ces systèmes. La plupart des études réalisées sur un grand domaine de température sont assez anciennes (11) et souvent les études plus récentes, sauf exception (12), ne concernent que le domaine dilué ou un domaine limité en température. Il nous a donc paru utile, avec l'avènement d'instrumentation moderne, d'effectuer une étude assez complète des volumes et capacités calorifiques des hydroxydes alcalins sur une gamme étendue de concentration et de température. Nous avons aussi déterminé les compressibilités isentropiques aux faibles concentrations de soude à 25°C de façon à obtenir les capacités calorifiques à volume constant dans l'état standard.

Méthode expérimentale

Les mesures de masse volumique ont été effectuées à l'aide d'un densimètre Picker à tube vibrant fonctionnant en écoulement continu (Sodev, modèle 01D) dont le principe et les performances sont bien connus (13). Les mesures de capacités calorifiques volumiques ont été réalisées à l'aide d'un microcalorimètre différentiel à écoulement Sodev déjà décrit dans la littérature (14, 15). La régulation thermique est stable à ±0,001°C et la température de mesure a été contrôlée à 0,01°C au moyen d'un thermomètre à quartz (Hewlett–Packard).

Les compressibilités ont été évaluées à partir de mesures de vitesses ultrasonores déterminées à l'aide de la technique "sing around" (Nusonic modèle 6105). La technique (16) et la cellule (17) ont déjà été décrites. L'étalonnage de l'appareil a été réalisé à partir des valeurs de référence pour l'eau obtenues par Delgrosso et Mader (18).

Les produits utilisés ont $LiOH \cdot H_2O$ solide (Baker certified), une solution 10 *N* NaOH (Fisher certified) et une solution 40% de KOH (Fisher Certified). Toutes les solutions one été préparées par pesée, soit directement soit à partir d'une solution mère elle-même préparée par pesée. Dans tous les cas on a utilisé de l'eau distillée et déionisée, dégazée sous vide pour éviter toute carbonation des solutions d'hydroxydes ainsi que toute formation de bulles. Les solutions ont été conservées sous atmosphère d'azote en récipient plastique étanche.

Les solutions mères ont été dosées par conductométrie à l'aide d'une solution étalon de HCl (Analar), elle-même dosée par conductométrie avec une solution de nitrate d'argent préparée par pesée à partir du sel anhydre pur.

Résultats

Les résultats de volumes et de capacités calorifiques sont exprimés en quantités molaires apparentes V_ϕ (cm^3 mol^{-1})

[1]Laboratoire de Thermodynamique et cinétique chimique, Université de Clermont-Ferrand 2, 63170 Aubière, France.

[2]Institut National de Recherche Scientifique, C.P. 7500, Ste-Foy (Qué.), Canada G1V 4C7.

Can. J. Chem. Downloaded from www.nrcresearchpress.com by 210.87.254.40 on 09/06/12
For personal use only.

Can. J. Chem. Downloaded from www.nrcresearchpress.com by 210.87.254.40 on 09/06/12
For personal use only.

$$[1] \quad V_\phi = \frac{M}{d} - \frac{10^3(d - d_0)}{mdd_0}$$

et $C_{p,\phi}$ (J K^{-1} mol^{-1})

$$[2] \quad C_{p,\phi} = Mc_p + 10^3 (c_p - c_{p,0})/m$$

où M (g mol^{-1}) est la masse moléculaire, d et d_0 (g cm^{-3}) les masses volumiques de la solution et du solvant, c_p et $c_{p,0}$ (J K^{-1} g^{-1}) les capacités calorifiques massiques de la solution et du solvant et m est la molalité (mol kg^{-1}) de la solution. La différence des capacités calorifiques massiques $c_p - c_{p,0}$ a été calculée à partir des capacités calorifiques volumiques σ et σ_0 et des masses volumiques.

$$[3] \quad c_p - c_{p,0} = c_{p,0} \left\{ \frac{\sigma - \sigma_0}{\sigma} + 1 \right\} \frac{d}{d_0} - c_{p,0}$$

Les valeurs de référence pour l'eau pure sont celles de Kell pour d_0 (19) et Stimson pour $c_{p,0}$ (20), soit

T (K)	d_0 (g cm^{-3})	$c_{p,0}$ (J K^{-1} g^{-1})
277,15	0,999972	4,2045
283,15	0,999700	4,1919
298,15	0,997045	4,1793
313,15	0,992716	4,1783
328,15	0,985695	4,1821

Les compressibilités isentropiques β_S (bar^{-1}) sont obtenues à partir de la masse volumique (g/cm^3) et de la vitesse u (cm s^{-1}), par la relation usuelle

$$[4] \quad \beta_S = \frac{10^6}{d\,u^2}$$

et la grandeur molaire $K_{S,\phi} = -(\partial V_\phi/\partial P)_T$ (cm^3 bar^{-1} mol^{-1}) par

$$[5] \quad K_{S,\phi} = V_\phi\beta_S + 10^3 (\beta_S - \beta_{S,0})/md_0$$

Les résultats obtenus sont donnés aux Tableaux 1 et 2.

Traitement des données

Les grandeurs molaires apparentes Y_ϕ d'un électrolyte en fonction de la molalité sont généralement représentées sous forme d'un développement limité en $m^{1/2}$ de la forme

$$[6] \quad Y_\phi = \bar{Y}_2^\theta + A_Y m^{1/2} + B_Y m + C_Y m^{3/2} + \ldots$$

où $\bar{Y}_2^\theta$ est la grandeur molaire partielle standard (dilution infinie) du soluté. Des coefficients de la série, seul le premier, A_Y, peut être calculé à partir de la théorie de Debye–Hückel. Plusieurs auteurs ont développé d'autres expressions, pour les solutions concentrées, entre autres Guggenheim (21) et Pitzer (22), qui conviennent bien pour les solutions d'électrolytes simples et requièrent donc moins de paramètres ajustables. Dans le cas des hydroxydes alcalins, les déviations à la loi limite de Debye–Hückel sont grandes et le même nombre de paramètres ajustables est généralement nécessaire quelque soit la relation utilisée. Aussi, nous nous en sommes tenus à l'équation la plus simple, c'est-à-dire à la relation [6].

Au Tableau 3 on trouve les valeurs des paramètres de l'éq. [6] obtenues à l'aide d'une méthode de moindres carrés. Le paramètre A_Y a été fixé aux valeurs prédites par la théorie de Debye–Hückel, celles calculées auparavant (23) pour les volumes et les capacités calorifiques. Nous avons remarqué que si on considère plutôt A_Y comme une variable dans l'analyse par moindres carrés on utilise parfois moins de paramètres dans l'éq. [6] mais l'écart quadratique est souvent du même ordre de grandeur et les valeurs standard, extrapolées à dilution infinie, diffèrent rarement de plus de 0,2 cm^3 mol^{-1} pour les volumes et de 3 J K^{-1} mol^{-1} pour les capacités calorifiques. Il est toutefois préférable de toujours utiliser l'éq. [6] avec A_Y prédit car c'est dans ce cas que nous obtiendrons le paramètre $\bar{Y}_2^\theta$ le plus fiable (24).

A partir de l'équation de lissage et des paramètres figurant au Tableau 3, il est possible de calculer les grandeurs molaires partielles du soluté $\bar{Y}_2$;

$$[7] \quad \bar{Y}_2 = Y_\phi + m\partial Y_\phi/\partial m$$

Nous pouvons aussi calculer, à partir des volumes et des capacités calorifiques à diverses températures, les expansibilités molaires apparentes $E_\phi = (\partial V_\phi/\partial T)_P$ et les valeurs de $(\partial C_{p,\phi}/\partial T)_P$. Pour cela, les valeurs de V_ϕ et $C_{p,\phi}$ sont calculées à des molalités fixes et exprimées en fonction de la température par la relation polynomiale suivante:

$$[8] \quad Y_\phi(T) = Y_\phi(T_0) + A(T - T_0) + B(T^2 - T_0^2) + C(T^3 - T_0^3)$$

où T_0 est la température de référence, habituellement 298,15 K. Ensuite, par dérivation de cette relation on obtient les valeurs de E_ϕ et de $(\partial C_{p,\phi}/\partial T)_P$ aux températures choisies. On peut remarquer qu'il existe un écart sensible (de quelques pourcents) entre les valeurs issues de cette formulation et l'approximation habituelle $E_\phi \simeq \Delta V_\phi/\Delta T$. Ces grandeurs apparentes ont aussi été lissées au moyen de l'éq. [6] et les paramètres obtenus pour NaOH et KOH sont résumés au Tableau 4.

Les compressibilités isentropiques de NaOH ont aussi été exprimées au moyen de l'éq. [6] et la relation obtenue est 10^4 $K_{S,\phi} = -82{,}01\ (\pm 0{,}29) + 2{,}555\ m^{1/2} + 9{,}892\ (\pm 2{,}312)\ m$, l'écart quadratique étant de $0{,}24 \times 10^4$ cm^{-3} bar^{-1} mol^{-1}. En combinant $\bar{K}_{S,2}^\theta$ avec $\bar{C}_{P,2}^\theta$ et $\bar{E}_2^\theta$ on peut calculer les compressibilités isothermes $\bar{K}_2^\theta$ et les capacités calorifiques isochores à partir des relations suivantes:

$$[9] \quad \bar{K}_2^\theta = \bar{K}_{S,2}^\theta + \frac{2\alpha_0 T}{\sigma_0}\bar{E}_2^\theta - \frac{\alpha_0^2 T}{\sigma_0^2}\bar{C}_{P,2}^\theta$$

et

$$[10] \quad \bar{C}_{V,2}^\theta = \bar{C}_{P,2}^\theta - \frac{2\alpha_0 T}{\beta_{T,0}}\bar{E}_2^\theta + \frac{\alpha_0^2 T}{\beta_{T,0}^2}\bar{K}_2^\theta$$

où α_0 est le coefficient de dilatation thermique (K^{-1}), $\beta_{T,0}$ la compressibilite isotherme (bar^{-1}) et σ_0 la capacité calorifique volumique (J K^{-1} cm^{-3}) de l'eau à la température T_0. Les deux derniers termes des relations [9] et [10] doivent être multipliés par, 0,1 pour obtenir les bonnes unités. Les valeurs de $\bar{K}_2^\theta$ et $\bar{C}_{V,2}^\theta$ sont respectivement $-78{,}35 \times 10^{-4}$ cm^3 bar^{-1} mol^{-1}, $-137{,}6$ J K^{-1} mol^{-1}.

Comparaison des résultats

Comme règle générale l'accord entre nos résultats et les valeurs de la littérature est assez bon aux concentrations élevées. Les divergences sont plus grandes aux faibles concentrations où les incertitudes expérimentales sont généralement accentuées. Nos comparaisons se feront donc surtout pour les quantités standard où l'incertitude est maximum.

Can. J. Chem. Downloaded from www.nrcresearchpress.com by 210.87.254.40 on 09/06/12
For personal use only.

TABLEAU 1. Volumes et capacités calorifiques apparentes molaires d'hydroxydes alcalins en solution aqueuse à différentes températures: m (mol kg^{-1}), $10^3\,\Delta d$ (g cm^{-3}), V_ϕ (cm^3 mol^{-1}), $10^3\,\Delta\sigma/\sigma_0$, $C_{p,\phi}$ (J K^{-1} mol^{-1})

	LiOH	25°C		
0.04485	1.276	- 4.59	- 0.53	- 68.2
0.04517	1.279	- 4.45		
0.09855	2.782	- 4.36	- 1.12	- 65.8
0.10012	2.808	- 4.18		
0.19485	5.384	- 3.75	- 2.03	- 59.2
0.19769	5.460	- 3.74		
0.2885	7.901	- 3.50		
0.2909	7.977	- 3.54	- 2.79	- 54.8
0.4763	12.872	- 3.12	- 3.85	- 46.8
0.4892	13.204	- 3.08		
0.4919	13.265	- 3.07	- 3.96	- 46.4
0.9831	25.669	- 2.19	- 5.11	- 30.8
1.9571	49.036	- 1.13	- 2.23	- 9.4
2.841	68.751	- 0.30	4.87	5.9
3.793	88.680	0.46	15.86	19.4
	LiOH	55°C		
0.10012	2.758	- 4.05	- 0.55	- 39.6
0.19769	5.409	- 3.85	- 0.81	- 33.0
0.2885	7.771	- 3.40	- 0.67	- 23.7
0.4919	13.014	- 2.90	- 0.28	- 14.3
0.9831	25.170	- 2.00	1.68	- 1.1
1.9571	48.127	- 0.97	9.87	17.1
2.841	67.817	- 0.25	20.82	29.6
3.793	87.164	0.59	35.06	41.2
	NaOH	4°C		
0.02035	0.992	- 8.76	- 0.84	-211.1
0.03045	1.485	- 8.74	- 1.19	-200.3
0.04054	1.970	- 8.59	- 1.63	-205.1
0.05078	2.461	- 8.44	- 2.06	-205.7
0.06058	2.935	- 8.43	- 2.45	-205.4
0.08075	3.901	- 8.28	- 3.16	-199.3
0.10144	4.889	- 8.16	- 3.91	-196.1
0.3042	14.390	- 7.20	- 10.01	-168.3
0.5067	23.630	- 6.48	- 14.49	-147.1
1.0126	45.820	- 5.02		
1.0158	45.947	- 5.01	- 20.45	-105.3
2.020	86.901	- 2.78	- 19.18	- 51.4
3.026	124.540	- 1.03	- 9.54	- 17.6
5.027	191.208	1.65	17.05	21.3
7.532	262.516	4.08	50.58	46.2
10.880	340.774	6.47	82.27	61.2
	NaOH	10°C		
0.02035	0.956	- 7.02	- 0.66	-165.5
0.03045	1.431	- 7.01	- 0.94	-159.0
0.04054	1.905	- 6.99	- 1.26	-159.8
0.05078	2.383	- 6.93	- 1.53	-155.4
0.06058	2.839	- 6.87	- 1.82	-154.3
0.08075	3.770	- 6.68	- 2.36	-150.6
0.10144	4.728	- 6.59	- 2.93	-148.6
0.3042	13.969	- 5.85	- 7.66	-129.9
0.5067	22.976	- 5.24	- 10.94	-112.2
	NaOH	10°C		
1.0126	44.669	- 3.95		
1.0158	44.794	- 3.94	- 15.16	- 78.8
2.020	85.035	- 1.95	- 12.31	- 33.6
3.026	122.199	- 0.35	- 2.14	- 4.4
5.027	188.408	2.11	26.01	30.8
7.532	259.387	4.41	61.51	53.8
10.880	337.320	6.72	97.58	68.5
	NaOH	25°C		
0.03855*	1.730	- 5.02	- 0.59*	- 84.3
0.06815*	3.059	- 5.03	- 1.09*	- 87.6
0.09652*	4.292	- 4.60	- 1.52*	- 84.8
0.14477*	6.407	- 4.37	- 2.16*	- 80.6
0.19197*	8.449	- 4.12	- 2.73*	- 76.6
0.3945*	17.163	- 3.59	- 4.72*	- 64.9
0.4934*	21.342	- 3.33	- 5.45*	- 59.9
0.5027	21.735	- 3.31	- 5.61	- 60.4
0.9996	42.196	- 2.25	- 7.09	- 38.9
1.0006*	42.245	- 2.26	- 6.88*	- 38.7
2.032	82.253	- 0.56	- 1.91	- 6.2
3.098	120.610	0.86	10.12	17.3
5.256	190.188	3.12	42.97	47.7
7.422	250.656	4.91	78.58	66.3
10.880	330.727	7.16	126.2	82.1
	NaOH	40°C		
0.03727	1.618	- 3.80	- 0.41	- 61.4
0.06069	2.626	- 3.63	- 0.60	- 56.5
0.08169	3.521	- 3.45	- 0.77	- 53.6
0.09978	4.291	- 3.36	- 0.94	- 53.3
0.10000	4.314	- 3.49		
0.10144	4.369	- 3.42	- 0.94	- 52.9
0.3042	12.906	- 2.74	- 2.26	- 42.3
0.5067	21.250	- 2.24	- 3.03	- 34.3
1.0094	41.405	- 1.30	- 2.88	- 17.3
1.0126	41.590	- 1.35	- 2.85	- 17.4
1.0158	41.665	- 1.30	- 2.88	- 17.2
2.020	79.876	0.14	3.56	7.9
3.026	115.773	1.30	15.26	26.5
5.027	179.916	3.35	46.29	53.0
7.532	249.450	5.33	89.71	73.9
10.880	326.036	7.43	139.00	88.5
	NaOH	55°C		
0.1005	4.218	- 2.60	- 0.72	- 40.9
0.2028	8.459	- 2.32	- 1.07	- 31.6
0.3007	12.468	- 2.07	- 1.38	- 27.7
0.5063	20.776	- 1.62	- 1.59	- 19.8
1.0146	40.754	- 0.73	- 0.50	- 5.1
2.027	78.552	0.65	6.96	17.06
3.026	113.460	1.79	18.85	33.5
5.045	177.641	3.68	51.03	58.2
7.494	245.059	5.54	95.08	78.1
10.893	322.162	7.64	146.6	92.4
	KOH	4°C		
0.02032	1.091	2.42	- 1.16	-229.6
0.04087	2.193	2.44	- 2.34	-230.2
0.06173	3.315	2.41	- 3.38	-220.1
0.08157	4.378	2.43	- 4.50	-221.9
0.10222	5.474	2.55	- 5.57	-218.6
0.2018	10.728	2.91	- 10.52	-207.2
0.3035	16.014	3.29	- 15.19	-196.9
0.5122	26.679	3.92	- 23.85	-179.7
1.0068	51.004	5.18	- 40.17	-146.8
1.0132	51.301	5.21	- 40.50	-147.0
2.019	97.259	7.23	- 62.63	-101.9
3.542	159.551	9.54	- 83.18	- 62.0
4.972	211.659	11.17	- 99.84	- 42.1
7.541	293.673	13.27	-104.65	- 8.4
10.254	367.043	14.86	-103.95	13.4
15.510	480.659	16.96	- 99.19	37.4
	KOH	10°C		
0.02032	1.079	3.00	- 0.94	-181.1
0.04087	2.150	3.48	- 1.88	-178.1
0.06173	3.242	3.56	- 2.91	-182.5
0.08157	4.279	3.62	- 3.81	-180.6
0.10222	5.365	3.59	- 4.70	-177.9
0.2018	10.481	4.11	- 8.87	-167.1
0.3035	15.653	4.45	- 12.93	-160.3
0.5122	26.095	5.02	- 20.41	-146.5
1.0068	50.002	6.13	- 35.37	-122.5
1.0132	50.288	6.15	- 35.59	-122.4
2.019	95.628	7.97	- 56.51	- 85.8
3.542	157.407	10.07	- 76.92	- 52.1
4.972	209.212	11.60	- 88.97	- 30.7
7.541	290.908	13.58	- 98.57	- 3.5
10.254	364.005	15.106	- 98.30	16.89
15.510	477.299	17.147	- 94.15	39.65
	KOH	25°C		
0.02032	1.039	4.84		
0.04087	2.074	5.23		
0.05172	2.617	5.36	- 1.79	-122.6
0.06173	3.118	5.45		
0.08157	4.112	5.54		
0.1022	5.147	5.60		
0.1056	5.312	5.63	- 3.58	-118.4
0.2018	10.074	5.99		
0.2084	10.387	6.07	- 6.82	-111.6
0.3035	15.051	6.29		
0.3115	15.439	6.32	- 9.86	-106.2
0.5122	25.109	6.79		
0.5199	25.486	6.79	- 15.63	- 97.8
1.0068	48.225	7.72		
1.0132	48.521	7.73		
1.0140	48.558	7.73	- 27.47	- 81.9
1.0175	48.721	7.73	- 27.55	- 81.8
2.019	92.728	9.22		
2.025	92.959	9.23	- 45.76	- 57.8
3.508	152.240	10.95	- 63.73	- 33.2
3.542	153.454	11.00		
4.940	203.785	12.27	- 75.50	- 16.6
4.972	204.626	12.34		
7.427	282.393	14.05	- 85.20	5.6
7.541	285.633	14.13		
10.244	357.995	15.54	- 87.12	23.6
10.254	358.453	15.53		
15.510	470.673	17.49	- 85.09	43.8
	KOH	40°C		
0.02032	1.024	5.37	- 0.59	- 98.7
0.04087	2.034	5.98	- 1.19	- 96.7
0.06173	3.062	6.14	- 1.77	- 94.5
0.08157	4.030	6.34	- 2.30	- 91.4
0.2018	9.848	6.91	- 5.51	- 85.7
0.3035	14.708	7.21	- 8.08	- 81.5
0.5122	24.555	7.67	- 12.95	- 74.3
1.0068	47.248	8.48	- 23.33	- 62.5
1.0132	47.508	8.51	- 23.51	- 62.5
2.019	91.053	9.84	- 39.65	- 42.9
3.542	151.142	11.46	- 56.94	- 22.4
4.972	202.157	12.67	- 67.45	- 7.7
7.541	282.446	14.40	- 77.47	12.2
10.254	354.553	15.79	- 80.11	27.6
15.510	446.423	17.69	- 80.39	45.8
	KOH	55°C		
0.10558	5.120	6.98		
0.2084	10.007	7.42	- 5.06	- 70.8
0.3115	14.895	7.60	- 7.40	- 68.3
0.5199	24.615	8.00	- 11.69	- 61.7
1.0140	46.946	8.85	- 20.50	- 48.8
1.0175	47.111	8.85	- 20.51	- 48.7
2.019	90.164	10.04	- 34.83	- 32.2
2.025	90.410	10.04	- 35.33	- 33.1
3.508	148.503	11.61	- 50.66	- 15.0
4.940	199.438	12.78	- 60.73	- 1.9
7.427	277.256	14.44	- 70.01	15.9
10.244	351.987	15.89	- 73.29	30.8
15.510	463.604	17.79	- 75.96	47.3

TABLEAU 2. Compressibilités isentropiques molaires apparentes de NaOH dans l'eau à 25°C

$m \times 10^3$ (mol/kg)	Δu (m/s)	$10^3 K_{S,\phi}$ (cm^3 bar^{-1} l mol^{-1})
0,7055	0,065	−7,779
1,4129	0,135	−7,996
2,8162	0,279	−8,200
4,2184	0,419	−8,204
5,6166	0,557	−8,196
7,0110	0,697	−8,208
10,480	1,041	−8,201
13,925	1,384	−8,197
17,346	1,728	−8,202
20,744	2,067	−8,200
27,470	2,735	−8,182
33,247	3,319	−8,189
46,860	4,670	−8,158
60,439	6,000	−8,117
73,984	7,333	−8,088
87,495	8,658	−8,060
100,97	9,976	−8,034
134,52	13,259	−7,977
167,86	16,528	−7,929
233,92	22,945	−7,828
299,17	29,272	−7,739
360,80	35,246	−7,661

(a) *Volumes*

Peu de résultats permettent une comparaison avec LiOH. La valeur un peu ancienne de Gucker (25), $\bar{V}_2^0 = 6{,}0$ cm^3 mol^{-1} à 25°C, diffère notablement de la présente valeur, −5,06 cm^3 mol^{-1}.

Beaucoup plus de résultats sont disponibles pour NaOH. Sur un large domaine de concentration nous avons pu comparer nos données avec celles d'Akerloff et Kegeles (26). Aux concentrations élevées l'écart est faible, tandis qu'à 1 *m*, à 40°C l'écart est de 0,25 cm^3 mol^{-1}, et à 10°C de 0,62 cm^3 mol^{-1}. Par contre, pour les valeurs à dilution infinie à 40 et 10°C, ces auteurs obtiennent −4,94 et −8,16 alors que nous avons évalué −4,16 et −7,37 cm^3 mol^{-1} en bon accord avec Allred et Woolley (27) qui retiennent −4,30 et −7,54. A 25°C, notre valeur −5,26 cm^3 mol^{-1} se compare bien avec celles de Millero *et al.* (28), −5,20; Hepler *et al.* (29), −5,25; Swarin et Curran (30), −5,42; Allred et Woolley (27), −5,37; mais moins bien avec les résultats de Bodansky et Kauzmann (31), −4,60; de Lanman et Mair (32), −6,48; de Gucker (33), −6,7; de Owen et Brinkley (34), −6,8; de Hamann et Lin (35), −6,8; et d'Akerloff et Kegeles (26), −5,94.

Dans le cas de KOH nous pouvons constater un excellent accord, 0,1 cm^3 mol^{-1}, entre nos valeurs et celles d'Akerloff et Bender (36) sur toute la gamme de concentration et de température où les résultats peuvent être comparés. Seules les valeurs extrapolées à dilution infinie divergent. Respectivement à 40 et 10°C ces auteurs ont déterminé 5,05 et 1,86 alors que nous avons déterminé 5,72 et 2,98 cm^3 mol^{-1}. A 25°C, nous obtenons 4,83 en mauvais accord avec 3,4 de Owens et Brinkely (34), 3,6 de Fajans et Johnson (37) et 2,9 de Gucker (33).

En général, les différences les plus notables sont observées pour les valeurs à dilution infinie si on compare nos résultats avec ceux de travaux anciens. Ceci provient à la fois de la précision des techniques utilisées pour le domaine dilué et de la procédure d'extrapolation qui ne tenait pas compte de la pente limite de Debye−Hückel.

L'application de la règle d'additivité pour $\bar{V}_2^0$ permet d'effectuer un test de cohérence et aussi de juger de la précision (reproductibilité) des résultats. Par exemple la différence

$$\Delta V^0_{K^+-Na^+} = \bar{V}_2^0\,(KOH) - \bar{V}_2^0\,(NaOH)$$

à 25°C est 10,09 cm^3 mol^{-1}, en bon accord avec les valeurs suggérées par Millero (24), 10,2; et par Desnoyers *et al.* (38), 10,25; mais en moins bon accord avec la valeur moyenne 10,7 obtenue par Roux *et al.* (50). De la même manière $\Delta V^0_{Na^+-Li^+}$ est −0,20 pour les hydroxydes en bon accord avec les résultats de Redlich et Rosenfeld (39), −0,14; Vaslow (40), −0,36; Desnoyers *et al.* (38), −0,29, pour d'autres anions communs.

(b) *Expansibilités*

Il est assez difficile de comparer nos résultats pour E_ϕ obtenus à partir de l'éq. [8] avec les valeurs de la littérature car la plupart des auteurs ont calculé cette quantité à partir de $\Delta V_\phi/\Delta T$ pour des intervalles de température assez grands. Malgré ceci, l'accord est excellent pour NaOH et KOH entre nos résultats et ceux d'Akerloff (26, 36) dans le domaine concentré, l'écart s'accentuant aux faibles concentrations. A 25°C, notre valeur pour NaOH, $\bar{E}_2^0 = 0{,}096$ cm^3 mol^{-1} K^{-1} est en accord satisfaisant avec celle de Allred et Woolley (27), 0,108.

(c) *Capacités calorifiques*

Dans tous les cas, nos résultats sont en excellent accord avec les valeurs repertoriées par Parker (41) pour les concentrations supérieures à 1 *m*. Par contre, l'écart s'accroît lorsque la concentration diminue pour atteindre un maximum à dilution infinie. Ceci provient du manque de précision des techniques antérieurement à 1965 et de la méthode d'extrapolation. Il est donc préférable de comparer $\bar{C}^0_{p,2}$ seulement avec les valeurs récentes. Pour NaOH à 25°C, notre valeur, −97,4 J K^{-1} mol^{-1}, se compare avec celles de Singh *et al.* (42), −96,2; Allred et Woolley (27), −100,5 Desnoyers *et al.* (15), −94,6. A 10 et 40°C, Allred et Woolley (27) obtiennent −167,4 et −67,3 tandis que nous avons −164,8 et −65,8 J K^{-1} mol^{-1}.

Une meilleure idée de la précision peut être obtenue par le principe d'additivité. Notre valeur pour $\Delta C^0_{P,K^+-Na^+} = -33{,}1$ J K^{-1} mol^{-1} est en accord raisonable avec les valeurs suggérées par Desnoyers *et al.* (15), −30; par Singh *et al.* (42), −30,8, par Roux *et al.* (50), −26. Les valeurs obtenues pour $\Delta C^0_{P,Na^+-Li^+} = -19{,}5$ J K^{-1} mol^{-1}, sont en excellent accord avec les valeurs suggérées par Desnoyers *et al.* (15), −19.

(d) $(\partial C_{p,\phi}/\partial T)_P$

L'accord avec les valeurs déduites du répertoire de Parker (41) est bon aux concentrations élevées seulement. A dilution infinie, notre valeur pour NaOH, 3,0 J K^{-2} mol^{-1} est en bon accord avec celle d'Allred et Woolley (27), 3,3.

(e) *Compressibilité*

Seule la soude a été étudiée dans le domaine dilué. La valeur à dilution infinie, $\bar{K}^0_{S,2} = -82{,}0 \times 10^4$ cm^3 bar^{-1} mol^{-1}, est en excellent accord avec la valeur de Millero *et al.* (43), $-82{,}8 \times 10^{-4}$ et en moins bon accord avec celles de Mathieson et Conway (44), $-85{,}3 \times 10^{-4}$ et Allan et Lee (45), −86,8.

Par additivité on peut obtenir les valeurs pour LiOH et KOH. A partir des valeurs de Millero *et al.* (43) par $\Delta K^0_{S,Na^+-Li^+}$ et $\Delta K^0_{S,K^+-Na^+}$ on en déduit.

$$\bar{K}^0_{S,LiOH} = -68{,}9 \times 10^{-4}\ cm^3\ bar^{-1}\ mol^{-1}$$

$$\bar{K}^0_{S,KOH} = -76{,}4 \times 10^{-4}\ cm^3\ bar^{-1}\ mol^{-1}$$

Can. J. Chem. Downloaded from www.nrcresearchpress.com by 210.87.254.40 on 09/06/12
For personal use only.

TABLEAU 3. Paramètres de lissage de l'équation [6] pour les volumes et capacités calorifiques molaires apparents de LiOH, NaOH et KOH dans l'eau (N: nombre de points expérimentaux; σ: écart quadratique moyen

Paramètres	Température 4°C	10°C	25°C	40°C	55°C
			NaOH		
$\bar{V}_2^\theta$	−8,971 ±0,016	−7,366 ± 0,015	−5,259 ±0,019	−4,158 ± 0,016	−3,393 ±0,023
A_V	1,512	1,612	1,865	2,131	2,418
B_V	3,793 ±0,115	2,423 ± 0,047	1,492 ±0,056	0,7925 ± 0,0198	−0,2533 ±0,1434
C_V	−1,715 ±0,148	−0,7095 ± 0,0347	−0,3846 ±0,040	−0,1131 ± 0,0062	0,6997 ±0,1730
D_V	+0,3719 ±0,0629	0,06650± 0,0646	0,03241±0,00728		−0,2670 ±0,0704
E_V	−0,0340 ±0,00868				0,03152±0,00941
σ	0,018	0,028	0,030	0,041	0,021
N	13	13	13	15	10
			NaOH		
$\bar{C}_{p,2}^\theta$	−218,22 ±0,52	−164,81 ± 0,53	−97,40 ±0,30	−65,77 ±0,27	−52,65 ±0,48
A_C	22,163	25,229	28,95	33,805	39,390
B_C	173,64 ±4,13	86,72 ± 7,76	45,92 ±0,90	19,86 ±0,83	10,93 ±0,49
C_C	−107,67 ±5,23	−15,82 ±14,87	−17,78 ±0,63	−5,515 ±0,614	−2,889 ±0,150
D_C	26,43 ±2,20	−16,97 ±10,63	1,879 ±0,116	0,2063 ±0,1142	
E_C	−2,425 ±0,300	7,495 ± 3,279			
F_C		−0,8856 ± 0,3662			
σ	0,80	0,62	0,47	0,51	0,89
N	12	12	13	14	10
			KOH		
$\bar{V}_2^\theta$	1,840 ±0,018	2,983 ± 0,023	4,917 ±0,011	5,721 ±0,043	6,254 ±0,038
A_V	1,512	1,612	1,865	2,131	2,418
B_V	2,329 ±0,092	2,116 ± 0,054	1,224 ±0,025	0,8029 ±0,0954	−0,2145 ±0,1605
C_V	−0,4812 ±0,0984	−0,6168 ± 0,0333	−0,3033 ±0,0153	−0,1823 ±0,0582	0,4849 ±0,1678
D_V	−0,04018±0,03510	0,05268±0,005156	0,01976±0,00240	0,009418±0,008973	−0,1627 ±0,0590
E_V	0,01278±0,00406				0,01569±0,00677
σ	0,028	0,045	0,018	0,077	0,042
N	14	14	26	13	13
			KOH		
$\bar{C}_{p,2}^\theta$	−235,54 ±1,11	−192,53 ±0,48	−130,52 ±0,22	−102,58 ±0,28	−90,09 ±0,33
A_C	22,163	24,229	28,95	33,805	39,39
B_C	125,14 ±5,79	83,84 ±2,52	32,93 ±1,05	9,072 ±0,626	1,900 ±0,233
C_C	−75,78 ±6,20	−47,73 ±2,70	−16,57 ±1,11	−2,654 ±0,382	−0,7690 ±0,0600
D_C	18,42 ±2,22	11,03 ±0,96	3,470 ±0,395	0,1522 ±0,0588	
E_C	−1,644 ±0,256	−0,9516 ±0,116	−0,2882 ±0,0455		
σ	1,748	0,76	0,30	0,51	0,63
N	14	14	13	13	12
			LiOH		
$\bar{V}_2^\theta$			−5,062 ±0,107		−5,047 ±0,096
A_V			1,865		2,418
B_V			3,848 ±1,433		1,988 ±0,635
C_V			−5,059 ±2,879		−1,859 ±0,719
D_V			2,710 ±1,960		0,4946 ±0,2117
E_V			−0,5115 ±0,4398		
σ			0,070		0,080
N			13		8
			LiOH		
$\bar{C}_{p,2}^\theta$			−77,87 ±0,46		−59,40 ±3,02
A_C			28,95		39,39
B_C			41,32 ±5,74		110,13 ±38,45
C_C			−35,38 ±11,11		−160,93 ±73,34
D_C			15,03 ±7,40		87,13 ±48,26
E_C			−2,521 ±1,633		−16,36 ±10,56
σ			0,23		1,44
N			9		8

Can. J. Chem. Downloaded from www.nrcresearchpress.com by 210.87.254.40 on 09/06/12
For personal use only.

TABLEAU 4. Paramètres de lissage pur les expansibilités et $(\partial C_{p,\phi}/\partial T)_P$ de NaOH et de KOH dans l'eau

	NaOH			KOH		
Paramètres	10°C	25°C	40°C	10°C	25°C	40°C
$\bar{E}_2^\theta$	0,2153	0,09641	0,04850	0,1745	0,08306	0,03769
A_E	0,01663	0,01705	0,01838	0,01663	0,01705	0,01838
B_E	−0,1467	−0,04003	−0,03656	−0,05768	−0,03656	−0,04597
C_E	0,09473	0,006169	0,01576	0,005303	0,01069	0,02725
D_E	−0,02661	0,002736	−0,002840	0,005248	−0,000814	−0,006970
E_E	0,002856	−0,000614	0,000189	−0,000955	−0,0000233	0,000660
$(\partial \bar{C}_{p,2}^\theta/\partial T)_P$	7,05	3,03	1,08	5,89	2,74	1,13
$A_{C'}$	0,330	0,312	0,340	0,330	0,312	0,340
$B_{C'}$	−8,035	−2,262	−0,3180	−2,523	−1,016	−0,223
$C_{C'}$	6,037	0,9535	−0,3614	0,5022	0,1870	0,0213
$D_{C'}$	−1,766	−0,06567	0,2556	−0,04333	−0,01541	−0,000959
$E_{C'}$	0,18689	−0,01381	−0,04046	0,001293	0,000447	0,0000154

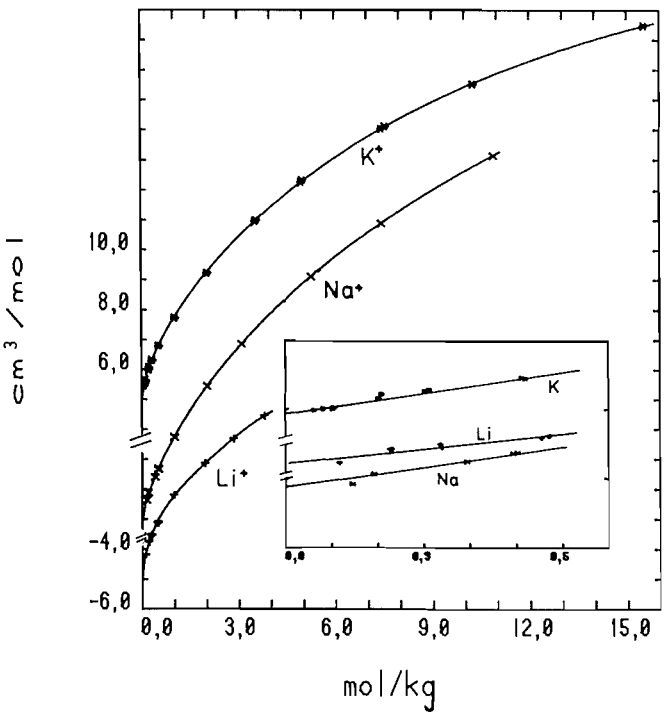

FIG. 1. Volumes molaires apparents en fonction de la concentration: LiOH(+), NaOH(×) et KOH(*) à 25°C. L'ordonnée dans l'insertion est $V_\phi - A_v m^{1/2}$.

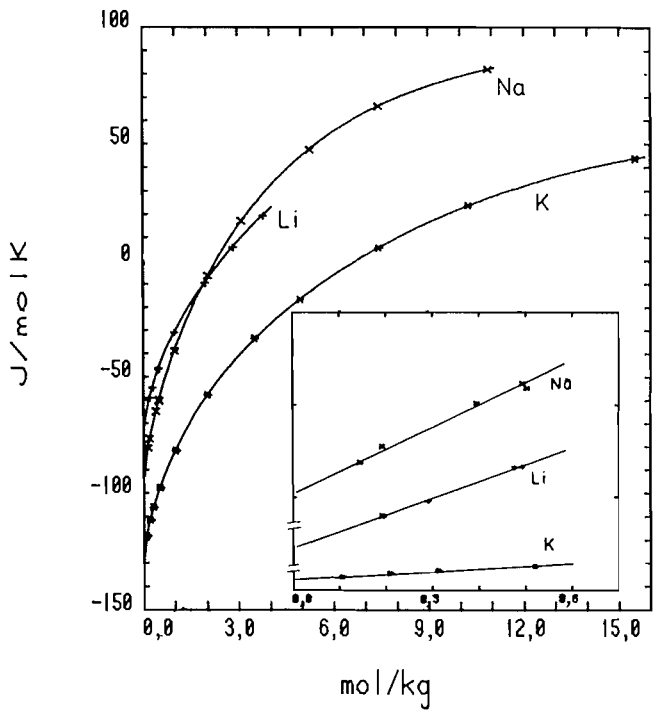

FIG. 2. Capacités calorifiques molaires apparentes en fonction de la concentration: LiOH(+), NaOH(×) et KOH(*) à 25°C. L'ordonnée dans l'insertion est $C_{p,\phi} - A_c m^{1/2}$.

Discussion

Les différentes quantités thermodynamiques Y_ϕ varient d'une façon assez régulière en fonction de la molalité tel qu'on peut le voir aux figures 1 et 2 pour les volumes et les capacités calorifiques à 25°C. Les écarts à la loi limite de la théorie de Debye–Hückel sont positifs aux faibles molalités et d'autant plus importants que la température est basse comme on le voit avec NaOH (Fig. 3). Aux fortes concentrations, les valeurs de $C_{p,\phi}$ varient assez peu avec la température.

Ces résultats suggèrent donc que NaOH est fortement briseur de structure aux basses concentrations et basses températures ($\bar{C}_{p,2}^\theta$ très négatif). Les interactions soluté–soluté vont dans la direction d'une diminution de cette solvatation. Aux concentrations plus élevées que 5 mol kg^{-1} la solution ressemble plutôt à un sel fondu hydraté où les effets structuraux ont complètement disparu. Les variations avec la température aux fortes concentrations viennent probablement de facteurs plus macroscopiques tels que la constante diélectrique du milieu. Cette explication des changements de capacité calorifique avec la température n'est pas en contradiction avec la forte hydratation qu'on reconnaît généralement aux ions OH^- tant dans la phase gazeuse (46) qu'en solution (47, 48). L'effet briseur de structure s'additionne à l'hydratation hydrophile. Contrairement aux propriétés telles que les enthalpies et entropies d'hydratation, ou les coefficients B de viscosité, $\bar{C}_{p,2}^\theta$ est peu sensible à la solvatation hydrophile mais dépend beaucoup des effets structuraux (49).

Les quantités molaires partielles, $\bar{V}_2$, $\bar{C}_{p,2}$ et $\bar{E}_2$, et apparentes, E_ϕ et $\partial C_{p,\phi}/\partial T$, sont représentées en fonction de la molalité en NaOH dans l'eau à 25°C à la figure 4. Alors que $\bar{V}_2$ augmente régulièrement, les autres fonctions ont plutôt tendance à plafonner aux concentrations élevées. Les légers

Can. J. Chem. Downloaded from www.nrcresearchpress.com by 210.87.254.40 on 09/06/12
For personal use only.

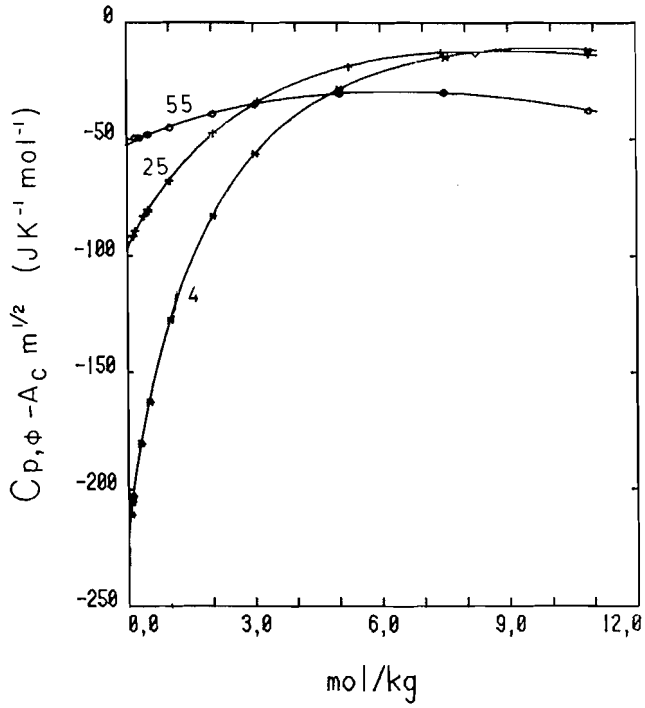

FIG. 3. Déviations à la loi limite de la théorie de Debye–Hückel pour les capacités calorifiques de NaOH à différentes températures: 4(*), 25(+) et 55(○)°C.

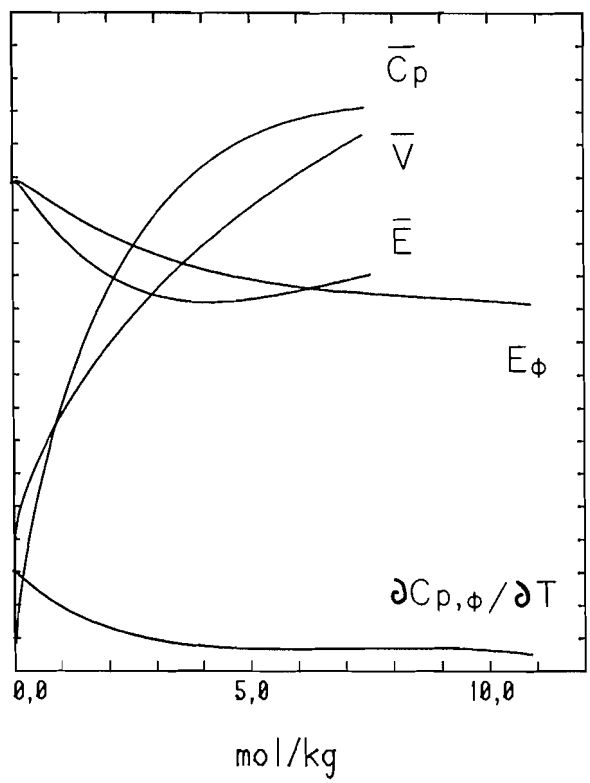

FIG. 4. Comparaison des quantités molaires partielles ou apparentes pour NaOH à 25°C: $\bar{V}$(cm^3 mol^{-1}), $\bar{C}_p$(J K^{-1} mol^{-1}), $\bar{E}$(cm^3 mol^{-1} K^{-1}), E_ϕ(cm^3 mol^{-1} K^{-1}), $\partial C_{p,\phi}/\partial T$ (J K^{-2} mol^{-1}).

changements de pentes pour E_ϕ et $\partial C_{p,\phi}/\partial T$ aux concentrations supérieures à 7,5 mol kg^{-1} ne sont pas significatives et proviennent fort probablement du lissage des données de V_ϕ et $C_{p,\phi}$ en fonction de la température. Ici encore l'allure de toutes ces quantités ressemble à celles des électrolytes 1:1 et ne montre aucune anomalie pour ces systèmes.

Remerciements

Nous sommes reconnaissants au Conseil de recherches en sciences naturelles et en génie du Canada et au ministère de l'Education du Québec (programme d'échange France–Québec) qui nous ont permis de réaliser ce travail.

1. D. M. DRAZIC et C. S. HAO. Electrochim. Acta, **27**, 1409 (1982).
2. W. GOOD. Electrochim. Acta, **12**, 1031 (1967).
3. S. S. BIECHLER et R. W. TAFT. J. Am. Chem. Soc. **79**, 4927 (1957).
4. F. KEZDY et A. BRUYLANTS. Bull. Soc. Chim. Belg. **69**, 602 (1960).
5. P. PAPOFF et P. G. ZAMBONIN. Talenta, **14**, 581 (1967).
6. R. M. POLLACK et M. L. BENDER. J. Am. Chem. Soc. **92**, 7190 (1970).
7. A. H. ROUX. Thèse de Doctorat d'Etat, Université de Clermont Ferrand, France (1975); A. H. ROUX et A. VIALLARD. J. Chem. Res. (S) 232 (1977); (M) 2626 (1977); A. ROUX, G. PERRON, P. PICKER et J. E. DESNOYERS. J. Solution Chem. **9**, 59 (1980).
8. A. LOSURDO, E. M. ALZOLA et F. J. MILLERO. J. Chem. Thermodyn. **14**, 649 (1982).
9. L. F. SYLVESTER et K. S. PITZER. J. Phys. Chem. **81**, 1822 (1977).
10. L. F. SYLVESTER et K. S. PITZER. J. Solution Chem. **7**, 327 (1978).
11. D. S. MAGOWAN et R. N. GOLDBERG. Natl. Bur. Stand. Spec. Publ. 537 (1979).
12. P. RIPOCHE et M. ROLIN. Bull. Soc. Chim. Fr. 375 (1980); 380 (1980).
13. P. PICKER, E. TREMBLAY et C. JOLICOEUR. J. Solution Chem. **3**, 377 (1984).
14. P. PICKER, P. A. LEDUC, P. R. PHILIP et J. E. DESNOYERS. J. Chem. Thermodyn. **3**, 631 (1971).
15. J. E. DESNOYERS, C. DEVISSER, G. PERRON et P. PICKER. J. Solution Chem. **5**, 605 (1976).
16. R. GARNSEY, R. MAHONEY et T. A. LITOVITZ. J. Chem. Phys. **64**, 2073 (1964).
17. I. DAVIDSON, G. PERRON et J. E. DESNOYERS. Can. J. Chem. **59**, 2212 (1981).
18. V. A. DELGROSSO et C. W. MADER. J. Acoust. Soc. Am. **52**, 1442 (1972).
19. G. S. KELL. *Dans* Water – a comprehensive treatise. *Edité par* F. Franks. Plenum Press, New York. 1972.
20. H. F. STIMSON. Am. J. Phys. **23**, 614 (1955).
21. G. N. LEWIS et M. RANDALL. Thermodynamics. *Revisé par* K. S. Pitzer et L. Brewer. McGraw–Hill, New York. 1961.
22. K. S. PITZER. Acc. Chem. Res. **10**, 371 (1977).
23. G. PERRON, N. DESROSIERS et J. E. DESNOYERS. Can. J. Chem. **54**, 2163 (1976).
24. F. J. MILLERO. *Dans* Water and aqueous solutions: structure, thermodynamics and transport properties. *Edité par* R. A. Horne. Wiley Interscience, New York. 1972.
25. F. T. GUCKER. Chem. Rev. **13**, 111 (1933).
26. G. AKERLOFF et G. KEGELES. J Am. Chem. Soc. **61**, 1027 (1981).
27. G. C. ALLRED et E. M. WOOLLEY. J. Chem. Thermodyn. **13**, 309 (1981).
28. F. J. MILLERO, E. V. HOFF et L. KAHN. J. Solution Chem. **1**, 309 (1972).
29. L. G. HEPLER, J. M. STOKES et R. H. STOKES. Trans. Faraday Soc. **61**, 20 (1965).
30. S. J. SWARIN et D. J. CURRAN. J. Chem. Thermodyn. **10**, 381 (1978).
31. A. BODANSZKY et W. KAUZMANN. J. Phys. Chem. **66**, 177 (1962).

Can. J. Chem. Downloaded from www.nrcresearchpress.com by 210.87.254.40 on 09/06/12
For personal use only.

32. E. H. LANMAN et B. J. MAIR. J. Am. Chem. Soc. **56**, 390 (1934).
33. F. T. GUCKER. J. Phys. Chem. **38**, 307 (1934).
34. B. B. OWEN et S. R. BRINKLEY. Chem. Rev. **29**, 461 (1941).
35. S. D. HAMANN et S. C. LIM. Aust. J. Chem. **7**, 329 (1954).
36. G. AKERLOFF et P. BENDER. J. Am. Chem. Soc. **63**, 1085 (1941).
37. K. FAJANS et O. JOHNSON. J. Am. Chem. Soc. **64**, 668 (1942).
38. J. E. DESNOYERS, M. AREL, G. PERRON et C. JOLICOEUR. J. Phys. Chem. **73**, 3346 (1969).
39. O. REDLICH et P. ROSENFELD. Z. Elektrochem. **37**, 705 (1931).
40. F. VASLOW. J. Phys. Chem. **70**, 2286 (1966).
41. W. B. PARKER. *Dans* Thermal properties of aqueous uni–univalent electrolytes. National Bureau of Standards. Ref. Data Series, NBS 2, Washington, DC. 1965.
42. P. P. SINGH, E. M. WOOLLEY, K. G. MCCURDY et L. G. HEPLER. Can. J. Chem. **54**, 3315 (1976).
43. F. J. MILLERO, G. K. WARD et P. CHETIRKIN. J. Acoust. Soc. Am. **61**, 1491 (1977).
44. J. G. MATHIESON et B. E. CONWAY. J. Solution Chem. **3**, 455 (1974).
45. D. S. ALLAN et W. H. LEE. J. Chem. Soc. **A**, 5 (1966).
46. M. ARSHADI et P. KEBARLE. J. Phys. Chem. **74**, 1483 (1970).
47 D. F. C. MORRIS. Electrochim. Acta, **27**, 1487 (1982).
48. D. J. P. OUT et J. M. LOS. J. Solution Chem. **9**, 19 (1980).
49. J. E. DESNOYERS et C. JOLICOEUR. Treatise in electrochemistry. Vol. 5. *Edité par* J. O'M. Bockris, E. Yeager et B. E. Conway. Plenum Press, New York. 1983. p. 1.
50. A. ROUX, G. M. MUSBALLY, G. PERRON, J. E. DESNOYERS, P. P. SINGH, E. M. WOOLLEY et L. G. HEPLER. Can. J. Chem. **56**, 24 (1978).

Can. J. Chem. Downloaded from www.nrcresearchpress.com by 210.87.254.40 on 09/06/12
For personal use only.

The formation of 3,4,6,tri-*O*-benzyl-2,5-anhydro-L-iditol from 2,3,4,6-tetra-*O*-benzyl-D-glucopyranose. Intramolecular displacement of a secondary mesyloxy group by a benzyloxy group, in the presence of cesium propionate

VANGA S. RAO AND ARTHUR S. PERLIN
Department of Chemistry, McGill University, Montreal, P.Q., Canada H3C 3G1

Received May 31, 1983[1]

VANGA S. RAO and ARTHUR S. PERLIN. Can. J. Chem. **62**, 886 (1984).

The reaction between 2,3,4,6-tetra-*O*-benzyl-1,5-di-*O*-mesyl-D-glucitol and cesium propionate in dimethylformamide at 100°C leads to an almost quantitative conversion into 3,4,6-tri-*O*-benzyl-1-*O*-propionyl-2,5-anhydro-L-iditol. Closure of the anhydro ring appears to entail anchimeric assistance by the 2-*O*-benzyl substituent in an S_N2 displacement at C-5, leading to an inversion at the latter position. Probable contributors to the marked regio- and stereoselectivity observed for the reaction are a unique property of cesium propionate as compared with other carboxylate salts, large differences in rate between competing reactions, and a geometry highly favorable to an intramolecular displacement process. Conformational properties of 2,5-anhydro-L-iditol, as well as of isomeric 2,5-anhydro-D-mannitol, are described, based on nmr evidence.

VANGA S. RAO et ARTHUR S. PERLIN. Can. J. Chem. **62**, 886 (1984).

La réaction du tétra-*O*-benzyl-2,3,4,6 di-*O*-mésyl-1,5 D-glucitol avec le propionate de césium dans le diméthylformamide à 100°C conduit à une conversion presque quantitative en tri-*O*-benzyl-3,4,6-*O*-propionyl-1 anhydro-2,5 L-iditol. La fermeture du cycle anhydro semble impliquer une assistance anchimérique du substituant *O*-benzyl-2 au cours d'une substitution S_N2 en C-5; ceci conduit à une inversion de configuration dans cette position. Les principales causes des régio- et stéréo-sélectivités remarquables notées au cours de cette réaction sont probablement (a) une propriété unique du propionate de césium comparée aux autres sels carboxyliques, (b) de grandes différences dans les vitesses des réactions qui sont en compétition et (c) une géométrie hautement favorable à une réaction de substitution intramoléculaire. Utilisant des données de rmn, on décrit les propriétés conformationnelles de l'anhydro-2,5 L-iditol et de l'anhydro-2,5 D-mannitol qui lui est isomère.

[Traduit par le journal]

Introduction

Earlier (1), in examining possibilities for a facile and convenient synthesis of L-idose, we attempted to use potassium superoxide as an oxygen nucleophile in a reaction with 2,3,4,6-tetra-*O*-benzyl-1,5-di-*O*-mesyl-D-glucitol (**1**). Rather

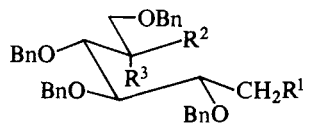

1, $R^1 = R^2 = OSO_2CH_3$; $R^3 = H$
2, $R^1 = R^3 = OH$; $R^2 = H$
4, $R^1 = OCOC_2H_5$; $R^2 = OSO_2CH_3$; $R^3 = H$

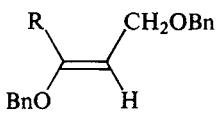

3, R = $(CHOBn)_2CH_2OH$(L-threo)

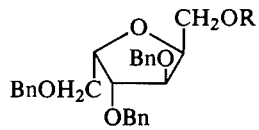

5, R = COC_2H_5
6, R = H

than the expected S_N2 displacement product, **2**, a novel regio- and stereoselectively formed olefin,[2] **3**, was obtained in an intramolecularly initiated elimination process. Our continuing search for a suitable oxygen nucleophile now encompasses the use of cesium carboxylates (2) in dimethylformamide as a possible means for the introduction of a hydroxy substituent by intermolecular S_N2 nucleophilic substitution.

Results and discussion

Cesium propionate, prepared from cesium carbonate and propionic acid in methanol, was selected. If this compound were to displace both of the mesyloxy substituents of **1**, then, after ester hydrolysis, the desired product (**2**) should be obtained. In fact, however, the reaction of **1** with cesium propionate in DMF at 50–60°C for 2 days in a nitrogen atmosphere gave about a 90% yield of a compound characterized as a monopropionate (**4**), admixed with ~10% of **5**, the identification of which will be described later. The ^1H nmr spectrum of **4** (Table 1) contained a quartet at δ 2.29 and a triplet at δ 1.12, attributable to the $—CH_2$ and $—CH_3$ groups, respectively, of a propionyloxy moiety at C-1, and a singlet at δ 2.93 characteristic of the CH_3 resonance of a mesyloxy substituent. The relative positions of the sulfonate and propionate ester groups were inferred indirectly from the following information, dealing with the formation and characterization of compound **5**.

At a reaction temperature of 90–100°C, product **5** was formed in almost quantitative yield. The ^{13}C nmr spectrum of the product (Table 2) showed resonances at δ 174.19 (—O—*C*=O), 138.48, 138.05, 137.78 (*ipso*, phenyl), 81.94, 81.46 (characteristic of the C-4 resonance (4) of a furanoid ring, substituted by an alkyl group), 68.22, 63.22 ($—CH_2—$O), 27.51, and 15.32 ($—CH_2$ and $—CH_3$ of an $—OCOCH_2CH_3$ group). These data suggested that a furanoid ring had been formed from **1** as the result of a concomitant loss of both a mesyloxy and a benzyloxy group, and substitution of the other mesyloxy group by a propionate moiety.

When the crude reaction mixture was subjected to methanolysis catalysed by sodium methoxide, the product (**6**) gave

[1] Revision received December 5, 1983.

[2] When the characterization of **3** was reported (1), the location of the double bond was clearly evident, whereas its geometric configuration was unknown. Nevertheless, based on the mechanism postulated for its formation, olefin **3** was expected to be the *E*-isomer. Additional support for this assignment has been found, since then, in ^{13}C chemical shift similarities between **3** and 1,5-di-*O*-acetyl-2,4,6-tri-*O*-benzyl-2-dehydro-3-deoxy-D-*erythro*-hex-2-(*E*)-enitol (for boron assisted departure of a benzyloxy group, see ref. 3), which is viewed as evidence that the substitution patterns on the carbon atoms of the latter and of **3** are analogous.

Can. J. Chem. Downloaded from www.nrcresearchpress.com by 210.87.254.5 on 09/06/12
For personal use only.

Can. J. Chem. Downloaded from www.nrcresearchpress.com by 210.87.254.5 on 09/06/12
For personal use only.

TABLE 1. Proton chemical shifts (δ) and spacings (Hz, in parenthesis) for compounds **1**, **4**, **6**, **7**, **8**, **9**, and **10**

Compound (solvent)	H-1 ($J_{1,2}$; $J_{1',2}$)	H-1′ ($J_{1,1'}$)	H-2 ($J_{2,3}$)	H-3 ($J_{3,4}$)	H-4 ($J_{4,5}$)	H-5 ($J_{5,6}$)	H-6 ($J_{5,6'}$)	H-6′ ($J_{6,6'}$)	Others
1 ($CDCl_3$)	4.46 (2.7; 7.2)	4.24 (11.1)	3.89 (5.1)	3.69 (5.1)	4.03 (3.0)	5.02 (3.0)	3.85 (7.2)	3.75 (11.1)	4.45 (s), 4.54 (s), 4.55, 4.66 (AB, J = 11.4), 4.61, 4.74 (AB, J = 11.4), OCH_2Ph; 2.93 (s), OSO_2CH_3
4 ($CDCl_3$)	4.40 (3.6: 6.6)	4.18 (12.3)	~3.87 (5.4)	3.74 (5.4)	4.08 (2.7)	5.04 (2.7)	3.89 (7.3)	3.78 (11.1)	4.46 (s), 4.65 (s) 4.57, 4.67 (AB, J = 11.7), 4.68, 4.77 (AB, J = 11.1), OCH_2Ph; 2.29 (q, CH_2), 1.12 (t, CH_3), $OCOCH_2CH_3$
6 ($CDCl_3$)	3.84 (5.4; 4.8)	3.76 (12.0)	4.25 (5.0)	4.09 (1.8)	4.07 (4.0)	4.37 (5.9)	3.73 (6.2)	3.69 (9.7)	4.38, 4.55 (AB, J = 11.9), 4.50, 4.54 (AB, J = 12.0), 4.52, 4.60 (AB, J = 12.0), OCH_2Ph
7 (D_2O)	3.58 (4.64: 6.84)	3.51 (11.73)	4.04[a] (3.3)	4.01[a] —	4.01 (3.3)	4.04 (4.64)	3.58 (6.84)	3.51 (11.73)	—
9 ($CDCl_3$)	4.22 (5.17; 6.61)	4.15 (11.64)	4.50 (3.91)	5.37 —	5.37 (3.91)	4.50 (5.17)	4.22 (6.61)	4.15 (11.64)	2.08 (s, CH_3), 2.11 (S, CH_3), $OCOCH_3$
8 (D_2O)	3.58 (3.2; 5.4)	3.49 (12.4)	3.70 (7.3)	3.86 —	3.86 (7.3)	3.70 (3.2)	3.58 (5.4)	3.49 (12.4)	—
10 ($CDCl_3$) (C_6D_6)	4.26 4.25	4.26 4.25	4.26 4.25	5.17 5.29	5.17 5.29	4.26 4.25	4.26 4.25	4.26 4.25	2.11 (s, CH_3), $OCOCH_3$ 1.55 (s, CH_3), 1.67 (s, CH_3), $OCOCH_3$

[a] Interchangeable.

TABLE 2. Carbon-13 chemical shifts (δ) for compounds **5**, **7**, **8**, **9**, and **10**

Compound (solvent)	C-1	C-2	C-3	C-4	C-5	C-6	Others
5 ($CDCl_3$)	63.22	81.94[a]	79.25, 78.06 73.58, 72.56 72.40[b]		81.46[a]	68.22	15.32 (CH_3), 27.51 (CH_2), 174.19 (—C=O), $OCOCH_2CH_3$; 127.74, 128.39, 128.55 (phenyl), 137.78, 138.05, 138.48 (*ipso*-phenyl)
7 (D_2O)	60.91	81.25	77.47	77.47	81.25	60.91	—
9 ($CDCl_3$)	61.88	~78.44	75.85	75.85	~78.44	61.88	20.61, 20.82 (CH_3), 169.34, 170.58 (—C=O), $OCOCH_3$
(C_6D_6)	61.93	77.36	76.12	76.12	77.36	61.93	19.91, 20.28 (CH_3), 168.91, 169.82 (—C=O), $OCOCH_3$
8 (D_2O)	62.15	83.30	77.40	77.40	83.30	62.15	—
10 ($CDCl_3$)	63.23	81.24	78.33	78.33	81.24	63.23	20.77 (2 × CH_3), 169.93, 170.63 (—C=O), $OCOCH_3$

[a] Interchangeable.
[b] These include three resonances from 3 × OCH_2Ph groups.

a ^1H nmr spectrum (Table 1) that showed the presence of a hydroxymethyl group (δ 3.84, 3.76), two methylene protons at δ 3.73 and 3.69, and three AB quartets characteristic of the methylene groups of benzyloxy substituents. Reesterification of **6** with Ac_2O in pyridine shifted the resonances at δ 3.84 and 3.76 to δ ~4.4 and 4.2, respectively, confirming that the original propionyloxy group was present on a primary carbon atom. Catalytic transfer hydrogenation (5) of **6** with 10% Pd–C and formic acid in methanol removed the *O*-benzyl substituents, giving **7**. Identification of the latter was made by comparison of its nmr spectra (Tables 1 and 2) with those of appropriate, known, sugar derivatives.

The ^1H nmr spectrum of **7** contains signals at δ 3.58 (dd), 3.51 (dd), characteristic of the AB part of an ABX spin system, and a complex multiplet centered at δ 4.02. The latter signal was converted, by simultaneous irradiation of the signals at δ 3.58 and 3.51, into an AB quartet with chemical shifts of δ 4.04 and 4.01. The ^{13}C spectrum contains only three resonances, i.e., at δ 81.25, 77.47, and 60.91. These data indicate that there are four types of protons attached to three different types of carbon atoms, one of which is primary (δ 60.91), and

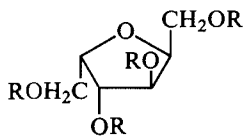

7, R = H
9, R = Ac

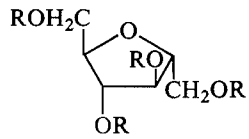

8, R = H
10, R = Ac

that the molecule possesses C_2 symmetry. Also, as mentioned, the nmr data for **5** indicated the presence of a furanoid ring structure. Hence, if the configuration at C-3 and C-4 of **1** had been preserved in the product, only two structures, namely 2,5-anhydro-L-iditol (**7**) and 2,5-anhydro-D-mannitol (**8**), can accommodate the spectral data. Acetylation of the anhydroalditol resulted in deshielding appropriate to the assignments given for its ^1H nmr spectrum (compare **7** and **9**, Table 1), and both the ^1H and ^{13}C (Table 2) data for **9** demonstrate once again the symmetrical nature of the compound. Confirmatory evidence for the structure of **7** comes from the fact that its ^{13}C nmr spectrum corresponds fully to published data (6) for 2,5-anhydroiditol, and that **7** exhibits a *positive* optical rotation.

Can. J. Chem. Downloaded from www.nrcresearchpress.com by 210.87.254.5 on 09/06/12
For personal use only.

The mass spectrum of the acetylated derivative (**9**) showed the occurrence of mass units at 375 and 333, whereas the calculated molecular weight of **9** is 332. Hence, the peak at 333 must have been due to $M + H^+$, indicating that the molecule undergoes self chemical ionization. Similarly, the peak at 375 must have arisen from self chemical ionization due to an acetyl cation (CH_3CO^+),[3] resulting in a ($M + CH_3CO^+$) ion, i.e., 375. Furthermore, the ratio 375:333 increased with an increase in temperature and the source pressure, results that are consistent with the notion overall that the molecule has a molecular ion ($M^{+\cdot}$) of 332 and hence a molecular weight of 332.

In order to add further to the structural elucidation of **7**, and also to gain some insight into its conformational behavior and that of furanoid ring compounds having a diastereomeric relationship with it, 2,5-anhydro-D-mannitol (**8**) was prepared by a known method (7) and its ^1H nmr and ^{13}C nmr data were compared with those of **7**. The ^{13}C nmr data for **8** (Table 2) agree well with those already published (6). This is taken as additional confirmatory evidence that, in the reaction between **1** and cesium propionate in DMF, at elevated temperatures, the product formed is 1-*O*-propionyl-3,4,6-tri-*O*-benzyl-2,5-anhydro-L-iditol (**5**), rather than the *manno* isomer.

A comparison of the ^1H nmr chemical shifts of **7** and **8** indicates that when a *cis* relationship exists between the —CH_2OH and —OH groups at C-2 and C-3, as in **7**, as compared with their *trans* arrangement, as in **8**, then the protons (H-2, H-3) attached to the carbon atoms bearing these substituents appear at lower field, i.e., at δ 4.01 and 4.04 in **7** vs. δ 3.70 and 3.86 in **8**. The same trend is also observed for their acetylated derivatives. On the other hand, the opposite trend is found in their carbon chemical shifts (6), i.e., the C-2 resonance of **8** is at lower field (δ 83.3) than the corresponding shift in **7** (δ 81.25). The C-1 shifts also are in the same direction, although the shift difference is smaller, whereas the C-3 shifts are virtually unchanged.

The diastereotopic exocyclic methylene protons (H-1, 1′) of **8** show differential coupling with H-2, indicating a preferential rotamer population around the C-1—C-2 bond. The combination of couplings of 3.2 Hz and 5.4 Hz suggests a contribution of rotamers **B** and either **A** or **C**, not both **A** and **C**. Although a basis for choosing between **A** and **C** is not obvious, the

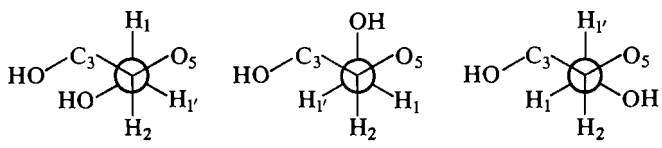

A **B** **C**

magnitude of the couplings observed suggests (8) an analogy with the rotamer population around the C_5—C_6 fragment in D-glucopyranose and its derivatives. The apparent[4] large coupling constant (7.3 Hz) between H-2 and H-3 requires these protons to be nearly *anti* to each other, and also suggests a

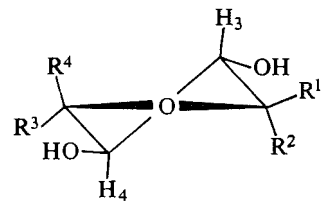

D, $R^1 = R^3 = CH_2OH$; $R^2 = R^4 = H$
G, $R^1 = R^3 = H$; $R^2 = R^4 = CH_2OH$

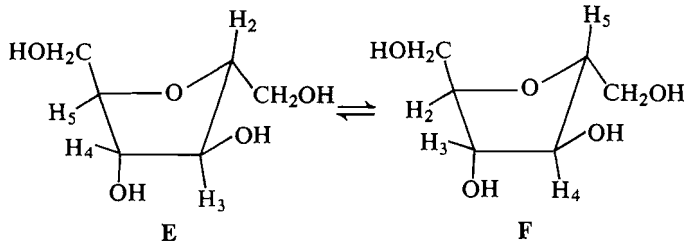

E **F**

conformational preference for the five-membered furanoid ring in its envelope-twist pseudorotational itinerary (for an excellent overview, see ref. 9). Such conformations may be realized either in a twist form **D** ($^3T_4$) or two rapidly interconverting envelope forms **E** and **F** (^2E and ^5E). These ring conformations also facilitate a high population of rotamer **B**, by flexing the carbon atom (C-2) bearing the —CH_2OH group so that this moiety is farther away from the ring atoms, and also of rotamer **C**. In these ring conformations, rotamer **A** may, indeed, be destabilized due to a *semi* 1,3-parallel interaction between the primary hydroxyl group and the OH-3 group. If this analysis is valid, then the downfield methylene signal with smaller coupling (3.2 Hz) may tentatively be assigned (8) to the proton having the pro-*R* configuration, and the upfield signal with larger coupling (5.4 Hz) to that having the opposite configuration (pro-*S*).

The methylene proton (H-1, 1′) couplings with H-2 in **7** are 4.6 and 6.8 Hz. Although their magnitude is larger than for **8**, the differential nature of these couplings requires an inhomogeneous mixture of rotamers **A**, **B**, and **C** to be present. Hence, this situation appears similar to that of the rotamer population around the C-5—C-6 fragment in D-galactopyranose (8). As to the ring conformation, the observed small coupling between H-2 and H-3 (3.3 Hz) is not as informative as for **8**, although it readily serves to distinguish **7** from **8**. Because of the *cis* disposition of the substituents on C-2 and C-3, a twist about the C-2—C-3 bond is anticipated, and hence the same two envelopes and the corresponding twist ring (**G**) conformation as deduced for **8** may well accommodate the steric requirements of **7**.

The formation of anhydride **5** from **1** and cesium propionate deserves comment.[5] As already noted, product **5** was not obtained earlier (1) in the reaction of **1** with potassium superoxide. Furthermore, it has not been detected in other experiments (unpublished) employing potassium acetate, sodium acetate, or sodium benzoate. Consequently, in yielding **5** as the *sole* product, cesium propionate shows remarkably distinctive behaviour which, we expect, is due to the highly polarizable cesium ion rather than the propionate moiety.

In the sickle conformation (10) of **1** (or of intermediate **4**),

[3] Attributable to the formation of an acetyl cation and/or the elements of acetic acid as a normal step in the fragmentation pathway (O. Mamer, private communication).

[4] In the ^1H nmr spectrum of **8**, the H-3 signal, instead of giving a doublet, actually showed 6 lines characteristic of combination lines arising from *virtual* coupling. The $J_{3,4}$ value calculated was 8.9 Hz. The high rms error (0.35) obtained was due to imperfect matching between the experimental and calculated spectrum of the H-2 resonance, although the matching of the H-3 resonance was excellent.

[5] We are indebted to the referees for a very helpful discussion of this matter.

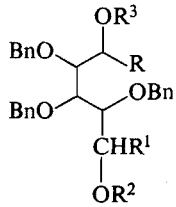

1, R = $C(6)H_2OBn$; R^1 = H; R^2 = R^3 = mesyl

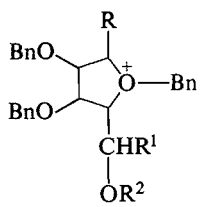

11

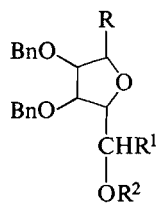

5, R = $C(6)H_2OBn$; R^1 = H; R^2 = propionate

12, R = R^1 = H; R^2 = R^3 = tosyl

13

14, R = R^1 = H; R^2 = tosyl

the 2-*O*-benzyl group appears to be suitably positioned[6] to displace the 5-*O*-mesyl group in an S_N2 fashion, causing an inversion of configuration at C-5, as depicted by the sequence **1** → **11** → **5**. This possibility is supported by observations (11) on anhydro-ring formation during the solvolysis of 1,5-di-*O*-tosyl-2,3,4-tri-*O*-benzyl-pentitols. For example, the D-*xylo* isomer (**12**), when heated under reflux in 95% ethanol, yielded 1,4-anhydro-2,3-di-*O*-benzyl-5-*O*-tosyl-DL-xylitol (**14**) and benzyl tosylate. As shown (11) by kinetic evidence, there was anchimeric assistance of the *O*-tosyl displacement step by the 4(or 2)-*O*-benzyl group, indicating that the transformation involved such an intermediate as **13**.

Aside from these apparent analogies, however, the reactions of **1** and **12** differ notably in that the ring-closure to give **14** occurred at a primary carbon atom, whereas a secondary position was involved in the formation of **5**. Presumably, because ethanol is a relatively poor nucleophile, the displacement of the 1-*O*-tosyl group of **12** favored participation by the 4-*O*-benzyl group (and the 5-*O*-tosyl by the 2-*O*-benzyl). By contrast, the 1-*O*-mesyl substituent of **1**, as seen by the initial, selective, formation of monoproprionate **4**, was far more amenable to displacement by the strongly nucleophilic cesium propionate than to an intramoleuclar attack by its 4-*O*-benzyl group. Consequently, there was a complete reversal in the comparative effectiveness of cesium propionate and the (2)-*O*-benzyl group in displacing the 5-*O*-mesyl substituent of **1**.

This combination of contrast and analogy may be explained in terms of relative rates. That is, the rate of displacement of the 1-*O*-mesyl group of **1** by cesium propionate is far higher than is the rate for participation of the 4-*O*-benzyl group, whereas the solvolysis of the 1-*O*-tosyl group of **12** does not compete effectively with participation by its 4-*O*-benzyl group. In the displacement of the 5-*O*-mesyl substituent of **1**, however, the propionate anion acts as a much less efficient nucleophile than the intramolecular 2-*O*-benzyl, towards secondary carbon-5. An analogous situation does not apply for **12**, which contains only primary *O*-sulfonyl groups. Consequently, the outcome of reactions such as these may vary not only with the experimental conditions, but from compound to compound and, possibly, with configuration as well, because the latter might determine the relative ease of achieving an intermediary orientation favorable for neighboring-group participation by an *O*-benzyl group.

Experimental

Solutions were evaporated below 40°C under diminished pressure. Solvents were dried by conventional procedures (methanol over magnesium methoxide, dimethyl formamide over barium oxide, and pyridine over sodium hydroxide), distilled, and stored over molecular sieves (Type 4A). Cesium carbonate and propionic acid were obtained from Aldrich Chemicals, and 2,3,4,6-tetra-*O*-benzyl-D-glucopyranose from Pfanstiehl Laboratories (Waukegan, IL). Eastman Chromagram sheets of silica gel with fluorescent indicators were used for thin-layer chromatography. Proton magnetic spectra were recorded with a Varian XL-200, or a Bruker WH-400, with the aid of homonuclear decoupling. Chemical shifts (δ) are reported with reference to tetramethylsilane with $CDCl_3$ as solvent, and HOD (δ 4.61) with D_2O as solvent. Carbon-13 nmr spectra were recorded with a Bruker WH-90 spectrometer. The theoretical proton nmr spectrum of compound **8** was calculated using ITRCAL program (Nicolet Instrument Corporation) on a B-NC 12 model minicomputer (Bruker Data System). Carbon-13 chemical shifts are reported with reference to tetramethylsilane, with $CDCl_3$ as the solvent, or to methanol (CH_3OH, δ 49.8) with D_2O as the solvent. Mass spectra were obtained with an LKB 9000 spectrometer at an ion source of 70 eV.

Cesium propionate

To a stirred solution of cesium carbonate (3.3 g, 10 mmol) in dry methanol (80 mL) was added, through a septum, a solution of propionic acid (2.2 g, 30 mmol) in the same solvent (20 mL). After stirring at room temperature for 3 h, the solution was evaporated and the residue (white powder) was washed three times with dry ether (3 × 100 mL). Due to the extremely hygroscopic nature of the cesium propionate, washing was carried out by serum capping the flask and removing the supernatant liquid with the aid of a double-tipped needle under nitrogen pressure.[7] The white solid residue was dried in vacuum at ~40°C for several hours.

*2,3,4,6-Tetra-*O*-benzyl-1,5-di-*O*-mesyl-D-glucitol (1)*

The title compound was prepared according to a procedure already described (1). That is, 1,3,4,5-tetra-*O*-benzyl-L-gulitol, obtained by reduction of 2,3,4,6-tetra-*O*-benzyl-D-glucopyranose with sodium borohydride in 7:3 tetrahydrofuran–water, was di-*O*-mesylated with methanesulfonyl chloride in pyridine to afford **1**. The ^1H nmr data are given in Table 1.

*2,3,4,6-Tetra-*O*-benzyl-1-*O*-propionyl-5-*O*-mesyl-D-glucitol (4)*

To a vigorously stirred solution of cesium propionate (0.68 g, weighed under dry nitrogen) in dry dimethylformamide (30 mL) under nitrogen was added a solution of **1** (0.25 g) in the same solvent (4 mL) through a serum cap. The mixture was heated to ~60°C, at which time a clear solution was obtained, and maintained at that temperature for ~48 h. Then it was poured into ice water (400 mL) saturated with sodium chloride, extracted with chloroform, and the extract was washed successively with cold 10% hydrochloric acid, sodium hydrogen carbonate, and water, dried (anhydrous sodium sulfate), and evaporated to a syrupy residue (0.24 g). The ^1H nmr data are given in Table 1.

[6] By contrast, in the zigzag conformation, the O-2 and O-4 benzyl groups, as well as the substituents on C-3 and C-5, should all involve destabilizing 1,3 parallel interactions.

[7] Extreme care must be taken that the needle is not blocked by fine solid particles during this procedure. Alternatively, the powder may be washed on a filter under a nitrogen atmosphere.

Can. J. Chem. Downloaded from www.nrcresearchpress.com by 210.87.254.5 on 09/06/12
For personal use only.

1-O-Propionyl-3,4,6-tri-O-benzyl-2,5-anhydro-L-iditol (5)

An analogous reaction was carried out with 0.66 g of cesium propionate in dry dimethylformamide (30 mL) and **1** (0.5 g) in the same solvent (8 mL) at ~100°C for ~48 h under dry nitrogen. Following the work-up procedure, as described for **4**, a syrupy product consisting of a single component (tlc and nmr evidence) was isolated (yield, 0.39 g). The ^{13}C nmr data are given in Table 2.

1-O-Acetyl-3,4,6-tri-O-benzyl-2,5-anhydro-L-iditol (6)

Product **5** was subjected to methanolysis with sodium methoxide in dry methanol, the solution was neutralized with IR 120 (H^+) ion-exchange resin, the suspension was filtered, and evaporation of the filtrate gave **6**. The ^1H nmr data are presented in Table 1.

Compound **6** was acetylated with 1:2 acetate anhydride – pyridine to afford the title compound. The ^1H nmr data ($CDCl_3$) δ: 4.60 and 4.51 (AB, 2H, OCH_2, J_{gem} 12.0 Hz), 4.53 and 4.48 (AB, 2H, OCH_2, J_{gem} 12.1 Hz), 4.60 and 4.51 (AB, 2H, OCH_2, J_{gem} 12.1 Hz), 4.39–4.31 (m, 3H, H-1, 2, 5), 4.20 (dd, H-1′, $J_{1',2}$ 8.65, $J_{1,1'}$ 12.5 Hz), 4.03 or 3.99 (dd, 2H, H-3, H-4, $J_{3,4}$ 1.3, $J_{4,5}$ 3.8 Hz), 3.73 (dd, H-6, $J_{5,6}$ 6.5, $J_{6,6'}$ 9.6 Hz), 3.69 (dd, H-6′, $J_{5,6'}$ 6.1 Hz), 2.04 (s, 3H, CH_3).

1,3,4,6-Tetra-O-acetyl-2,5-anhydro-L-iditol (9)

Removal of the *O*-benzyl groups from **6** by catalytic transfer hydrogenolysis with 10% Pd–C/formic acid/methanol (5) yielded 2,5-anhydro-L-iditol (**7**); $[\alpha]_D^{25}$ +6.4 (*c* 1.1, H_2O) (lit. (12) $[\alpha]_D$ +9.7). The ^1H nmr data are given in Table 1. Compound **7** was acetylated with 1:2 acetic anhydride – pyridine to afford **9**. The ^1H nmr data are given in Table 1. Mass spectrum, *m/z*: 333 (1.8, $M + 1$), 259 (5.6, $M - CH_2OAc$), 145 (25.7, $AcOCH_2 - \overset{+}{C}HOAc$ or triacetoxonium ion (13)), 119 (15.7, $CH_3—\overset{H}{\overset{|}{O}}—\overset{+}{O}=CH_2CH_2OAc$), 103 (17.2, AcO – $\overset{+}{C}H_2CHOH$ or diacetoxonium ion (13)), 85 (86.3, 145 – HOAc or), 83 (99.8, 84 – 1), 43 (83.4, $CH_3\overset{+}{C}O$).

1,3,4,6-Tetra-O-acetyl-2,5-anhydro-D-mannitol (10)

Following a literature procedure (7), 2-amino-2-deoxy-D-glucose hydrochloride was subjected to deamination and ring contraction with sodium nitrate in acetic acid to afford 2,5-anhydro-D-mannose, which was immediately reduced with sodium borohydride to give 2,5-anhydro-D-mannitol (**8**). Acetylation of **8** with acetic anhydride in pyridine gave the title compound (**10**). The ^1H and ^{13}C nmr data for **8** and **10** are given in Tables 1 and 2, respectively.

Acknowledgments

Generous support by the Natural Sciences and Engineering Research Council of Canada is acknowledged with thanks. We are especially grateful to Dr. O. Mamer for assistance in interpreting the mass spectra. The 400 MHz ^1H nmr spectra were recorded by P. V. M. Tan at Laboratoire Régional de RMN à Haut Champ, Université de Montréal.

1. V. S. RAO and A. S. PERLIN. Can. J. Chem. **59**, 333 (1981).
2. W. H. KRUIZINGA, B. STRIJTVEEN, and R. M. KELLOGG. J. Org. Chem. **46**, 4321 (1981), and references cited.
3. V. S. RAO and A. S. PERLIN. J. Org. Chem. **47**, 3265 (1982).
4. J. B. STOTHERS. Carbon-13 NMR spectroscopy. Academic Press, New York. 1972. p. 467.
5. V. S. RAO and A. S. PERLIN. Carbohydr. Res. **83**, 175 (1980).
6. L. QUE, JR. and G. R. GRAY. Biochemistry, **13**, 146 (1974).
7. D. HORTON and K. D. PHILIPS. Carbohydr. Res. **30**, 367 (1973).
8. A. DE BRUYN and M. ANTEUNIS. Carbohydr. Res. **47**, 311 (1976); R. U. LEMIEUX and J. D. STEVENS. Can. J. Chem. **43**, 2059 (1965).
9. J. F. STODDART. Stereochemistry of carbohydrates. Wiley–Interscience, New York. 1971. p. 97.
10. P. L. DURETTE and D. HORTON. Adv. Carbohydr. Chem. Biochem. **26**, 49 (1971).
11. G. R. GRAY, F. C. HARTMAN, and R. BARKER. J. Org. Chem. **30**, 2020 (1965).
12. L. VARGHA and E. KASZTREINER. Chem. Ber. **93**, 1608 (1960).
13. K. BIEMANN, D. C. DEJONGH, and H. K. SCHNOES. J. Am. Chem. Soc. **85**, 1763 (1963).

Can. J. Chem. Downloaded from www.nrcresearchpress.com by 210.87.254.5 on 09/06/12
For personal use only.

Structure and magnetic exchange in poly-bis(μ-dialkylphosphinato)copper(II) compounds

JOHN S. HAYNES, KATHERINE W. OLIVER, STEVEN J. RETTIG, ROBERT C. THOMPSON, AND JAMES TROTTER
Department of Chemistry, University of British Columbia, 2036 Main Mall, Vancouver, B.C., Canada V6T 1Y6

Received October 12, 1983

JOHN S. HAYNES, KATHERINE W. OLIVER, STEVEN J. RETTIG, ROBERT C. THOMPSON, and JAMES TROTTER. Can. J. Chem. **62**, 891 (1984).

The preparation, magnetic and thermal properties, electronic and infrared spectra, and molecular structure of poly-bis(μ-di-*n*-hexylphosphinato)copper(II) are described. Crystals of the compound are triclinic, a = 9.800(3), b = 12.336(6), c = 13.352(8) Å, α = 88.53(3), β = 74.02(4), γ = 82.33(3)°, Z = 2, space group $P\bar{1}$. The structure was solved by Patterson and Fourier syntheses and was refined by full-matrix least-squares procedures to R = 0.045 and R_w = 0.056 for 3095 reflections with $I \geq 3\sigma(I)$. The crystal structure of $Cu[(n\text{-}C_6H_{13})_2PO_2]_2$ consists of well-separated infinite chains of centrosymmetric spiro-fused eight-membered rings propagating along the crystallographic a axis.

The magnetic susceptibility of $Cu[(n\text{-}C_6H_{13})_2PO_2]_2$ was studied over the temperature range 4.2 to 300 K. The compound shows ferromagnetic behaviour and the data have been successfully analyzed according to the isotropic Heisenberg model for linear chains with g = 2.16 and J = 2.58 cm^{-1}. For comparison, the magnetic susceptibilities of $Cu[(C_2H_5)_2PO_2]_2$ and $Cu[(n\text{-}C_4H_9)_2PO_2]_2$ have also been measured over the range 4.2 to 300 K. The butyl derivative shows ferromagnetic exchange with g = 2.16 and J = 2.22 cm^{-1} while the ethyl derivative is antiferromagnetic with g = 2.19 and $-J$ = 1.27 cm^{-1}. The structural details of all three compounds are examined in the light of the differing magnetic properties.

JOHN S. HAYNES, KATHERINE W. OLIVER, STEVEN J. RETTIG, ROBERT C. THOMPSON et JAMES TROTTER. Can. J. Chem. **62**, 891 (1984).

On décrit les propriétés magnétiques et thermales, les spectres électronique et infrarouge, et la structure moléculaire de poly-bis(μ-di-*n*-hexyle phosphinato) cuivre(II). Les cristaux sont tricliniques, a = 9,800(3), b = 12,336(6), c = 13,352(8) Å, α = 88,53(3), β = 74,02(4), γ = 82,33(3)°, Z = 2, groupe d'espace $P\bar{1}$. On a résolu la structure par les synthèses de Patterson et de Fourier et on l'a affinée par la méthode des moindres carrés (matrice entière) jusqu'à des valeurs de R = 0,045 et R_w = 0,056 pour 3095 réflexions avec $I \geq 3\sigma(I)$. La structure du cristal de $Cu[(n\text{-}C_6H_{13})_2PO_2]_2$ consiste en chaînons, infinis et bien séparés, des cycles de huit membres, centrosymmetriques et spiro-fusées, qui sont propagés suivant l'axe c.

On a étudié la susceptibilité magnétique dans l'intervalle de température de 4.2 à 300 K. La composé présente les propriétés ferromagnétiques et on a analysé les données d'après la modèle isotropique de Heisenberg pour les chaînons linéaires, avec g = 2,16 et J = 2,58 cm^{-1}. Par comparaison, les susceptibilités magnétiques de $Cu[(C_2H_5)_2PO_2]_2$ et de $Cu[(n\text{-}C_4H_9)_2PO_2]_2$ ont été mesurés aussi dans l'intervalle 4,2 à 300 K. Le dérivatif butylique exhibe l'échange ferromagnétique, avec g = 2,16 et J = 2,22 cm^{-1}, tandis que le dérivatif éthylé est antiferromagnétique avec g = 2,19 et $-J$ = 1,27 cm^{-1}. On a examiné les particularités structurales de tous les trois composés en vue des propriétés magnétiques différentes.

Introduction

Single crystal X-ray diffraction studies on $Cu[(C_2H_5)_2PO_2]_2$ (1) and $Cu[(n\text{-}C_4H_9)_2PO_2]_2$ (2) have shown them to be polymeric with well-separated infinite chains of copper atoms (flattened tetrahedral coordination geometries) linked by double phosphinate bridges. Interest in the magnetic properties of these materials has been expressed because of the possibility of the propagation of magnetic exchange via the O—P—O bridges (1, 2); however, because of the lack of magnetic susceptibility studies to cryogenic temperatures no clear evidence concerning exchange was obtained prior to the present work. We report here magnetic susceptibility studies over the range from room temperature to 4.2 K. As alluded to earlier (3), it is not possible to predict at the present time the nature of the exchange in systems such as these. Indeed, it was interesting to note in the present work that, in spite of their structural similarities, the ethyl and *n*-butyl derivatives exhibit magnetic exchange coupling (albeit weak in both cases) of opposite sign.

In the course of our studies on the synthesis, structure, and properties of copper(II) phosphinates generally we obtained one other compound, the *n*-hexyl derivative, in crystalline form suitable for X-ray structure determination. The structure and magnetic properties of this material were also studied here in order to explore magneto-structural correlations in these systems more fully.

Experimental

Syntheses

Poly-bis(μ-di-*n*-butylphosphinato)copper(II), $Cu[(n\text{-}C_4H_9)_2PO_2]_2$, and poly-bis(μ-di-*n*-hexylphosphinato)copper(II), $Cu[(n\text{-}C_6H_{13})_2PO_2]_2$, were prepared by the reaction of copper(II) sulfate pentahydrate with the appropriate acid, neutralized with slightly less than a stoichiometric amount of sodium hydroxide. The preparation of poly-bis(μ-diethylphosphinato)copper(II), $Cu[(C_2H_5)_2PO_2]_2$, has been reported previously (1).

Di-*n*-hexylphosphinic acid was synthesized by the peroxide catalyzed addition of hypophosphorous acid to 1-hexene (4). A solution of the acid (5.7 mmol) in 3:1 ethanol:water was neutralized with aqueous sodium hydroxide (5.6 mmol) and an aqueous solution of copper(II) sulfate (2.8 mmol) was added dropwise with stirring. Precipitation began almost immediately and after the addition of the copper solution was complete, an equivalent volume (500 mL) of water was added to the reaction mixture (this prevents the formation of the blue–green sulfate co-polymer) and the resultant solution was stirred overnight. The blue precipitate was separated by filtration, washed with water, then ethanol, yielding pure $Cu[(n\text{-}C_6H_{13})_2PO_2]_2$ (77% yield). *Anal.* calcd. for $CuC_{24}H_{52}P_2O_4$: Cu 11.98, C 54.37, H 9.89; found: Cu 12.04, C 54.24, H 9.88. Crystals of $Cu[(n\text{-}C_6H_{13})_2PO_2]_2$ suitable for crystallographic studies were obtained by slow evaporation of a solution in 60–90° petroleum ether.

Di-*n*-butylphosphinic acid was prepared following the procedure of Kasolapoff and Watson (5), with the exception that the oxidation of the intermediate di-*n*-butylphosphite, $(n\text{-}C_4H_9)_2POH$, was accom-

Can. J. Chem. Downloaded from www.nrcresearchpress.com by 210.87.254.5 on 09/06/12
For personal use only.

Can. J. Chem. Downloaded from www.nrcresearchpress.com by 210.87.254.5 on 09/06/12
For personal use only.

plished with aqueous potassium permanganate rather than hydrogen peroxide and the final product was recrystallized from acetone rather than benzene. An aqueous solution of copper(II) sulfate (8.0 mmol) was added slowly, with stirring, to an aqueous solution of the partially neutralized acid (16.0 mmol acid; 15.9 mmol sodium hydroxide). After the addition of approximately one half of the copper solution, a blue solid began to precipitate. After the addition was complete the mixture was stirred for 1.5 h; the solid was then separated by filtration and washed with cold water. Additional product was obtained by concentrating the filtrate under vacuum. Total yield was 90%. *Anal.* calcd. for $CuC_{16}H_{36}P_2O_4$: Cu 15.20, C 45.98, H 8.68; found: Cu 15.23, C 45.80, H 8.60.

Carbon and hydrogen were determined by P. Borda of the Department of Chemistry, The University of British Columbia. Copper was determined by EDTA titration.

Solubilities

Qualitative solubility tests show $Cu[(n\text{-}C_4H_9)_2PO_2]_2$ to be soluble (in excess of 0.1 g in 100 mL) in water and chloroform, slightly soluble in methanol, ethanol, and dichloromethane, and insoluble in acetone, carbon tetrachloride, benzene, and petroleum ether. $Cu[(n\text{-}C_6H_{13})_2PO_2]_2$ is soluble in dichloromethane, chloroform, carbon tetrachloride, and petroleum ether, slightly soluble in benzene and ethanol, and insoluble in water, methanol, and acetone.

Differential scanning calorimetry (DSC)

$Cu[(C_2H_5)_2PO_2]_2$ exhibits a reversible endothermic phase transition (ΔH = 24 J g^{-1}) at 128.1°C, followed by reversible melting at 240.0°C (ΔH = 41 J g^{-1}); the compound oxidatively decomposes above 280°C. $Cu[(n\text{-}C_4H_9)_2PO_2]_2$ undergoes a reversible endothermic phase transition at 130.4°C (ΔH = 14 J g^{-1}), melts at 155.1°C (ΔH = 64 J g^{-1}) and oxidatively decomposes above 235°C. $Cu[(n\text{-}C_6H_{13})_2PO_2]_2$ melts at 108.8°C (ΔH = 75 J g^{-1}) and oxidatively decomposes above 250°C.

The DSC studies were made using a Mettler DSC 20 cell and a Mettler TC 10 TA Processor.

Infrared spectra

$Cu[(n\text{-}C_4H_9)_2PO_2]_2$. Data for the range 1400 to 300 cm^{-1}: 1304 m, 1276 w, 1223 m, 1204 w sh, 1162 vs, 1096 w sh, 1057 s, 1043 w sh, 1035 w sh, 904 m, 892 w sh, 806 s, 780 vw, 772 w, 745 w, 725 m, 545 s, 517 m, 428 vw, 420 vw, 362 m, 322 w. (w = weak, m = medium, s = strong, v,= very, br = broad, sh = shoulder.)

$Cu[(n\text{-}C_6H_{13})_2PO_2]_2$. Data for the range 1400 to 300 cm^{-1}: 1317 w, 1289 w, 1259 m, 1238 w, 1205 w, 1113 vs, 1061 s sh, 1039 s, 975 vw, 963 vw, 891 w, 880 vw, 865 w, 856 w sh, 803 s, 777 vw sh, 751 vw, 722 m, 709 w sh, 551 s, 514 m, 480 vw sh, 442 m, 401 m, 380 vw sh, 361 m, 339 m sh. (abbreviations as above.)

Infrared spectra were obtained on samples mulled in Nujol and pressed between KRS-5 plates (Harshaw Chemical Co). The infrared spectrophotometer was a Perkin-Elmer model 598.

Electronic spectra

Electronic spectra of Nujol mulls were obtained using a Cary 14 spectrophotometer (range 3 800 to 30 000 cm^{-1}). $Cu[(n\text{-}C_4H_9)_2PO_2]_2$ and $Cu[(n\text{-}C_6H_{13})_2PO_2]_2$ exhibit broad absorption bands centered at 11 500 cm^{-1} and 11 600 cm^{-1}, with shoulders at 13 200 and 13 300 cm^{-1}, respectively.

Magnetic susceptibilities

Variable temperature magnetic susceptibility measurements over the range 125 to 4.2 K were made using a Princeton Applied Research Model 155 Vibrating Sample Magnetometer, internally calibrated with ultrapure nickel metal. Temperature equilibration was obtained using a Janis Research Company Model 153 cryostat and a Princeton Applied Research Model 152 cryogenic temperature controller with a gallium arsenide diode temperature sensor.

Temperature measurement was achieved with a chromel vs. Au − 0.02% Fe thermocouple (6) located in the sample holder immediately above the sample. The thermocouple was calibrated using the known susceptibility versus temperature dependence of tetramethylethylenediammonium tetrachlorocuprate(II) and checked with mercury tetrathiocyanatocobaltate(II) (7). From the scatter in data points for four separate calibration runs the temperatures are estimated to be accurate to ±1% over the range studied.

The calibration was checked further by immersing the sample rod with thermocouple directly into liquid helium, oxygen, and nitrogen and the measured temperatures agreed with expected values to within the error of measurement. Thermocouple potentials were measured using a Fluke 8200 A digital voltmeter.

A Walker-Magnion model L75BF electromagnet and model HS 1050 power supply provided magnetic fields up to 10 000 G. Measurements were normally obtained with a field of 9625 G with checks for field dependence of magnetic susceptibilities using several or all of the following values: 1280, 2549, 3850, 5251, 6200, 7501, 8520, 9225, and 9625 G. None of the samples studied in the present work gave evidence of field dependence. Magnetic fields were set to an accuracy of 0.5% and measured using a F. W. Bell Inc. Model 620 Gaussmeter.

Samples weighing approximately 100 mg were placed in gelatin capsules attached to a Kel-F holder. The sample holder was attached to the drive rod which had been modified as recommended by Drake and Hatfield (8) so as to reduce the diamagnetic background and to allow for the passage of the thermocouple leads. Corrections were applied for the background diamagnetism of the sample holder. Magnetic susceptibilities were corrected for the diamagnetism of all atoms (155×10^{-6}, 215×10^{-6}, and 344×10^{-6} cm^3 mol^{-1} for the ethyl, *n*-butyl, and *n*-hexyl derivatives, respectively) and the temperature independent paramagnetism (60×10^{-6} cm^3 mol^{-1}) of copper(II).

Variable temperature magnetic susceptibility measurements over the range 300−80 K were made using Gouy equipment described elsewhere (9).

X-ray crystallographic analysis of $Cu[(n\text{-}C_6H_{13})_2PO_2]_2$

Selection of a crystal suitable for X-ray analysis proved to be a difficult task. The elongated, very thin plates could not be cleaved in any direction except parallel to the long axis of the crystal. The smaller specimens were found to be somewhat bowed, necessitating the use of a sufficiently thick crystal. Of the many crystals examined by X-ray photographs, only one was deemed suitable for data collection. This crystal (bounded by the six faces (followed by their distances in mm from a common origin): ±(100), 0.35, ±(010), 0.20, ±(001), 0.03) was mounted in a general orientation. Unit-cell parameters were refined by least-squares on 2 sin θ/λ values for 25 reflections measured on a diffractometer with MoKα radiation ($\lambda(K\alpha_1)$ = 0.70930, $\lambda(K\alpha_2)$ = 0.71359 Å). Crystal data at 22°C are:

$C_{24}H_{52}CuO_4P_2$ fw = 530.17

Triclinic, a = 9.800(3), b = 12.336(6), c = 13.352(8) Å, α = 88.53(3), β = 74.02(4), γ = 82.33(3)°, V = 1538(1) $Å^3$, Z = 2, ρ_c = 1.145 g cm^{-1}, $F(000)$ = 574, μ(MoKα) = 8.4 cm^{-1}. Absent reflections: none, space group $P\bar{1}$ (C_i^1, No. 2, reduced cell) from structure analysis.

Intensities were measured with graphite-monochromatized MoKα radiation on an Enraf-Nonius CAD4-F diffractometer. An ω−2θ scan at 1.44−10.06° min^{-1} over a range of (0.75 + 0.35 tan θ)° in ω (extended by 25% on both sides for background measurement) was employed. Data were measured to 2θ = 55°. The intensities of three check reflections, monitored every hour throughout the data collection, remained constant to within ±4%. After data reduction,[1] an absorption correction was applied using the Gaussian integration method (10, 11). Transmission factors ranged from 0.765 to 0.921 for 96 sampling points. Of the 7040 independent reflections measured,

[1]The computer programs used include locally written programs for data processing and locally modified versions of the following: ORFLS, full-matrix least-squares, and ORFFE, function and errors, by W. R. Busing, K. O. Martin, and H. A. Levy; FORDAP, Patterson and Fourier syntheses, by A. Zalkin; ORTEP II, illustrations, by C. K. Johnson.

Can. J. Chem. Downloaded from www.nrcresearchpress.com by 210.87.254.5 on 09/06/12
For personal use only.

TABLE 1. Final positional (fractional × 10^4, Cu and P × 10^5) and isotropic thermal parameters ($U \times 10^3$ Å^2) with estimated standard deviations in parentheses

Atom	x	y	z	U_{eq}*
Cu	25661(5)	48080(4)	48964(4)	62
P(1)	3754(11)	55705(10)	35525(10)	67
P(2)	47367(10)	41029(9)	62447(10)	62
O(1)	1297(3)	4768(2)	4045(2)	70
O(2)	−1194(3)	5415(3)	3819(2)	80
O(3)	4140(2)	4029(2)	5320(2)	65
O(4)	6325(2)	4192(2)	5973(2)	69
C(1)	532(5)	6936(4)	3863(4)	85
C(2)	−361(6)	7827(4)	3400(5)	100
C(3)	−182(7)	8966(5)	3650(6)	128
C(4)	−1035(8)	9888(6)	3246(7)	159
C(5)	−841(11)	11021(6)	3519(9)	197
C(6)	−1726(13)	11886(8)	3312(9)	227
C(7)	1043(5)	5385(4)	2157(4)	84
C(8)	976(6)	4272(6)	1784(6)	116
C(9)	1534(8)	4035(9)	656(7)	159
C(10)	1387(21)	2922(19)	332(17)	323
C(11)	1796(22)	2358(17)	−192(23)	381
C(12)	1580(14)	1233(12)	−416(11)	277
C(13)	4485(5)	2866(4)	6980(4)	79
C(14)	5263(6)	1849(4)	6367(5)	95
C(15)	5157(7)	810(4)	6975(5)	113
C(16)	5961(8)	−205(5)	6396(6)	132
C(17)	5930(9)	−1212(6)	6995(7)	161
C(18)	6681(10)	−2194(6)	6427(7)	171
C(19)	3772(4)	5221(4)	7065(4)	79
C(20)	4298(5)	5428(4)	8024(5)	93
C(21)	3480(7)	6422(5)	8639(5)	116
C(22)	3951(9)	6710(7)	9557(6)	149
C(23)	3035(13)	7744(11)	10122(8)	233
C(24)	3328(16)	8108(16)	10869(13)	327

*U_{eq} = (1/3) trace u_{diag}.

3095 had intensities greater than $3\sigma(I)$ above background where $\sigma^2(I) = S + 2B + (0.04(S - B))^2$ with S = scan count and B = normalized background count.

The centrosymmetric space group $P\bar{1}$ was indicated both by the E-statistics and by the Patterson function. The coordinates of the Cu and P atoms were determined by conventional heavy-atom techniques, and those of the remaining non-hydrogen atoms from subsequent difference maps. Refinement of all non-hydrogen atoms with anisotropic thermal parameters resulted in $R = 0.058$. The last two or three atoms of each n-hexyl group display high degrees of thermal motion and are not particularly well-defined. Although the possibility of disorder was considered (in particular for the C(10)—C(12) fragment), no clearcut secondary positions for these atoms were in evidence. The refinement was continued with the assumption that these terminal n-hexyl fragments are not disordered but are subject to excessive thermal motion. Hydrogen atoms were included as fixed atoms in idealized positions (C—H = 0.98 Å, staggered methyl groups, B = 1.1 × value for bonded C atom) in subsequent cycles of refinement, the coordinates and thermal parameters for hydrogen atoms being recalculated after each least-squares cycle. The scattering factors and anomalous scattering terms for Cu and P were taken from ref. 12. The weighting scheme, $w = 1/\sigma^2(F)$ where $\sigma^2(F)$ is derived from the previously defined $\sigma^2(I)$, gave uniform average values of $w(|F_o| - |F_c|)^2$ over ranges of both $|F_o|$ and sin θ/λ and was employed in the final stages of refinement. Convergence was reached at $R = 0.045$ and $R_w = 0.056$ for 3095 reflections with $I \geq 3\sigma(I)$. The function minimized was $\Sigma w(|F_o| - |F_c|)^2$, $R = \Sigma||F_o| - |F_c||/\Sigma|F_o|$, $R_w = (\Sigma w(|F_o| - |F_c|)^2/\Sigma w|F_o|^2)^{1/2}$.

On the final cycle of refinement the mean and maximum parameter shifts corresponded to 0.04 and 0.38 σ, respectively. The mean error

TABLE 2. Bond lengths (Å) with estimated standard deviations in parentheses*

Bond	Length (Å)	Bond	Length (Å)
Cu —O(1)	1.907(3)	C(5)—C(6)	1.366(11)
Cu —O(3)	1.932(2)	C(7)—C(8)	1.488(8)
Cu —O(2)′	1.902(3)	C(8)—C(9)	1.479(9)
Cu —O(4)″	1.896(3)	C(9)—C(10)	1.48(2)
P(1)—O(1)	1.521(3)	C(10)—C(11)	0.97(2)
P(1)—O(2)	1.514(3)	C(11)—C(12)	1.48(2)
P(1)—C(1)	1.779(5)	C(13)—C(14)	1.521(7)
P(1)—C(7)	1.807(5)	C(14)—C(15)	1.498(7)
P(2)—O(3)	1.513(3)	C(15)—C(16)	1.507(8)
P(2)—O(4)	1.515(2)	C(16)—C(17)	1.459(9)
P(2)—C(13)	1.798(4)	C(17)—C(18)	1.455(10)
P(2)—C(19)	1.789(5)	C(19)—C(20)	1.543(7)
C(1)—C(2)	1.547(6)	C(20)—C(21)	1.510(8)
C(2)—C(3)	1.493(8)	C(21)—C(22)	1.488(9)
C(3)—C(4)	1.510(8)	C(22)—C(23)	1.553(13)
C(4)—C(5)	1.500(10)	C(23)—C(24)	1.221(14)

*Here and elsewhere in this report primed and double-primed atoms have coordinates related to those in Table 1 by the symmetry operations $-x$, $1 - y$, $1 - z$, and $1 - x$, $1 - y$, $1 - z$, respectively.

in an observation of unit weight was 2.232. A final difference map was essentially featureless, the largest residual density (+0.45 e Å^{-3}) being located near P(2). The final positional and thermal parameters for the non-hydrogen atoms appear in Tables 1 and 6[2], respectively. Calculated hydrogen coordinates and thermal parameters are given in Table 5.[2] Bond distances, bond angles, and intra-annular torsion angles are given in Tables 2–4. A complete listing of torsion angles (Table 7) and the measured and calculated structure factors have been placed in the Depository of Unpublished Data.[2]

Results and discussion

The crystal structure of Cu[(n-C_6H_{13})$_2$$PO_2$]$_2$

Atom labelling in the asymmetric unit is shown in Fig. 1. The crystal structure of Cu[(n-C_6H_{13})$_2$$PO_2$]$_2$ consists of well-separated infinite chains of centrosymmetric spiro-fused eight-membered rings propagating along the crystallographic a axis (see Fig. 2). The overall structure is very similar to those observed for the ethyl (1) and n-butyl (2) derivatives. There are a number of small but significant differences between the three structures which are discussed below in relation to the electronic spectra and magnetic properties of these compounds. The anomalous geometrical parameters for the n-hexyl groups (Tables 2 and 3) result from the large degree of thermal motion noted above.

Electronic spectra

The X-ray crystal structures of all three of the compounds considered here reveal the copper atoms to be in compressed tetrahedral environments of four oxygens with approximate D_{2d} symmetry. Earlier (1) we assigned the spectrum of Cu[(C_2H_5)$_2$$PO_2$]$_2$ to a crystal field model (13) involving the crystal field parameters Dq and Cp and a distortion parameter α (half the largest O—Cu—O bond angle). The CuO_4 chromophores in the n-butyl and n-hexyl derivatives are slightly less compressed than in the ethyl derivative (α = 74.3, 73.3, and 73.0° for the ethyl, n-butyl, and n-hexyl derivatives, respectively, from the X-ray data). Assuming the same Dq and Cp

[2]Complete set of data is available, at a nominal charge, from the Depository of Unpublished Data, CISTI, National Research Council of Canada, Ottawa, Ont., Canada K1A 0S2.

TABLE 3. Bond angles (deg) with estimated standard deviations in parentheses

Bonds	Angle (deg)	Bonds	Angle (deg)
O(1)—Cu —O(3)	145.43(14)	P(2)—O(4)—Cu″	130.5(2)
O(1)—Cu —O(2)′	95.96(11)	P(1)—C(1)—C(2)	115.2(4)
O(1)—Cu —O(4)″	94.04(12)	C(1)—C(2)—C(3)	114.1(5)
O(3)—Cu —O(2)′	94.14(12)	C(2)—C(3)—C(4)	117.7(6)
O(3)—Cu —O(4)″	95.39(10)	C(3)—C(4)—C(5)	116.3(7)
O(2)′—Cu —O(4)″	146.71(14)	C(4)—C(5)—C(6)	119.4(9)
O(1)—P(1)—O(2)	116.0(2)	P(1)—C(7)—C(8)	114.3(4)
O(1)—P(1)—C(1)	110.5(2)	C(7)—C(8)—C(9)	118.2(7)
O(1)—P(1)—C(7)	107.1(2)	C(8)—C(9)—C(10)	115.4(12)
O(2)—P(1)—C(1)	108.7(2)	C(9)—C(10)—C(11)	144(3)
O(2)—P(1)—C(7)	105.7(2)	C(10)—C(11)—C(12)	139(3)
C(1)—P(1)—C(7)	108.5(3)	P(2)—C(13)—C(14)	113.4(4)
O(3)—P(2)—O(4)	115.0(2)	C(13)—C(14)—C(15)	114.9(5)
O(3)—P(2)—C(13)	108.2(2)	C(14)—C(15)—C(16)	116.0(6)
O(3)—P(2)—C(19)	109.6(2)	C(15)—C(16)—C(17)	116.5(7)
O(4)—P(2)—C(13)	105.4(2)	C(16)—C(17)—C(18)	116.4(8)
O(4)—P(2)—C(19)	110.0(2)	P(2)—C(19)—C(20)	115.7(3)
C(13)—P(2)—C(19)	108.2(2)	C(19)—C(20)—C(21)	112.2(5)
Cu —O(1)—P(1)	138.2(2)	C(20)—C(21)—C(22)	116.0(6)
P(1) —O(2)—Cu′	132.4(2)	C(21)—C(22)—C(23)	111.2(8)
Cu —O(3)—P(2)	134.5(2)	C(22)—C(23)—C(24)	118.9(14)

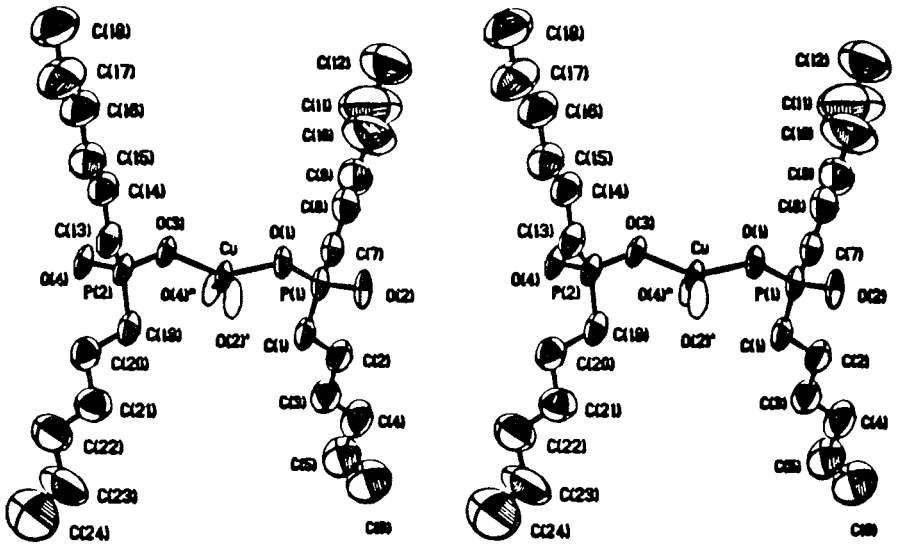

FIG. 1. Stereoview of $Cu[(n\text{-}C_6H_{13})_2PO_2]_2$ showing the atom numbering scheme and the coordination about Cu. 25% probability thermal ellipsoids are shown.

TABLE 4. Intra-annular torsion angles (deg) standard deviations in parentheses

Atoms	Value (deg)
O(2)′—Cu —O(1)—P(1)	96.7(3)
O(2)—P(1)—O(1)—Cu	−124.3(3)
O(1)—P(1)—O(2)—Cu′	47.3(3)
O(1)—Cu —O(2)′—P(1)′	−0.1(3)
O(4)″—Cu —O(3)—P(2)	95.1(2)
O(4)—P(2)—O(3)—Cu	−128.2(2)
O(3)—P(2)—O(4)—Cu″	54.1(3)
O(3)—Cu —O(4)″—P(2)″	2.0(3)

values as derived for the ethyl compound (1665 and 1800 cm^{-1}, respectively) and employing an α value of 73° yields predicted energies of 11 500, 11 800, and 13 900 cm^{-1} for the $^2B_2 \rightarrow {}^2A_1$, ^2E, and $^2B_1$ transitions. This is in excellent agreement with the observed spectra for the *n*-butyl and *n*-hexyl compounds, assuming as before (1) that the observed band at 11 500 and 11 600 cm^{-1} is assigned to the unresolved $^2B_2 \rightarrow {}^2A_1$, ^2E transition with the shoulder assigned to the $^2B_2 \rightarrow {}^2B_1$ transition. It is not too surprising that there is no detectable difference in the crystal field parameters for the different R_2PO_2 groups with differences in the electronic spectra arising primarily from small differences in the coordination geometries.

Infrared spectra

A complete listing of observed frequencies (1400 to 300 cm^{-1}) for both $Cu[(n\text{-}C_4H_9)_2PO_2]_2$ and $Cu[(n\text{-}C_6H_{13})_2PO_2]_2$ is given in the Experimental section. A partial assignment made as described previously (1) identifies the antisymmetric and symmetric PO_2 stretching frequencies at 1116 and 1057 cm^{-1},

Can. J. Chem. Downloaded from www.nrcresearchpress.com by 210.87.254.5 on 09/06/12
For personal use only.

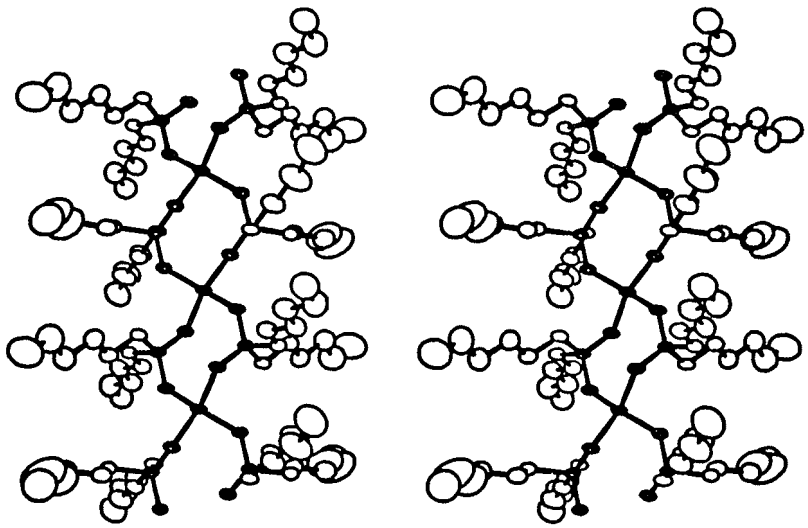

FIG. 2. Stereoview of the polymeric structure of $Cu[(n\text{-}C_6H_{13})_2PO_2]_2$.

respectively, for the butyl derivative and 1113 and 1039 cm^{-1}, respectively, for the hexyl derivative (14). Bands at 806 and 725 cm^{-1} in the butyl compound and 803 and 722 cm^{-1} in the hexylphosphinate are tentatively assigned to the antisymmetric and symmetric PC_2 vibrations (15), with bands in the 510–550 cm^{-1} range assigned to angle bending of both PC_2 and PO_2 groups (16). The medium intensity bands near 360 cm^{-1} in both compounds probably arise primarily from Cu—O stretching (1).

Magnetic properties

Magnetic susceptibilities, measured over the range 300 to 4.2 K, are given in Table 8 and the magnetic moments are plotted in Fig 3. While the data show virtually no temperature dependence from 300 to 100 K, significant dependencies are seen at lower temperatures, particularly below 10 K, for all three compounds.

The magnetic properties of $Cu[(C_2H_5)_2PO_2]_2$ suggest weak antiferromagnetic coupling. In view of the known structure of this material (1), the magnetic data were analyzed according to the isotropic Heinsberg model for linear chains. Employing the polynomial expression developed by Hall (17, 18) for the magnetic susceptibility, the best fit to the data was found with the parameters $J = -1.27$ cm^{-1} and $g = 2.19$ (rms deviation in the magnetic susceptibility is 12×10^{-6} cm^3 mol^{-1}). The data are plotted as magnetic moment against temperature in Fig. 3(*a*) where the solid line is calculated from theory using the best fit values of g and J. The criterion for best fit is that set of parameters which give the minimum value of the rms deviation. The accuracy to which the value of J is measured by this analysis is considered to be ±10% or better (agreement between theory and experiment for a 10% variation in J is illustrated in Fig. 4(*a*)) while g is considered accurate to about ±2% (see Fig. 4(*b*)).

Both $Cu[(n\text{-}C_4H_9)_2PO_2]_2$ and $Cu[(n\text{-}C_6H_{13})_2PO_2]_2$ exhibit increasing magnetic moments with decreasing temperature at low temperatures indicative of ferromagnetic coupling. Employing the polynomial expression of Baker *et al.* (18, 19) for the isotropic Heisenberg model for ferromagnetically coupled chains, the best fits to the magnetic susceptibility data gave g values of 2.16 for both compounds and J values of +2.22 and +2.58 for the butyl- and hexyl-derivatives, respectively (rms deviations were 18×10^{-6} and 13×10^{-6} cm^3 mol^{-1} for the butyl and hexyl derivatives, respectively). The data are plotted as magnetic moments in Fig 3(*b*) and 3(*c*); the lines are calculated from theory employing the best fit g and J values.

The excellent agreement between experiment and theory for the magnetic properties of chains of $S = 1/2$ ions supports the conclusion that in all three compounds studied here intrachain coupling dominates and there are no significant interchain magnetic interactions. This is not too surprising considering the large separations of the Cu—O—P—O—Cu backbones in neighbouring chains and the mutual insulation of the chains provided by the alkyl groups attached to phosphorus. The shortest intrachain copper–copper distances are of the order of 5 Å, too large, probably, for direct metal–metal interactions and requiring, therefore, a superexchange mechanism for the exchange. In view of the observation of antiferromagnetically coupled metal centres in the ethyl derivative and ferromagnetically coupled centres in the other two, we examined the structural details of the eight-membered $Cu(R_2PO_2)_2Cu$ rings closely for a possible explanation.

There are only relatively minor differences in the structural details of the inorganic backbones of the three compounds studied here. The ethyl derivative has slightly longer copper–copper distances (4.9555(8) and 5.0245(8)[3] Å (1) versus 4.938(2) for the butyl derivative (2) and 4.9277(8) and 4.9310(8) Å for the hexyl compound). The CuO_4 chromophore is slightly more planar in the ethyl compound than in the other two. The average values of the two large O—Cu—O angles are 148.6, 146.5, and 146.1° for the ethyl, butyl, and hexyl derivatives, respectively. Two crystallographically distinct eight-membered rings containing the copper atoms are seen for each compound. Very little difference in bond angles and lengths is seen from compound to compound. Total path lengths for superexchange, obtained by summing the appropriate bond lengths, are within experimental error, the same for all three compounds. All rings are distinctly puckered. The torsion angles have been given for the ethyl(1) and hexyl derivatives (Table 4) and a measure of the total deviation from planarity is the average of the absolute values of these angles. The average values of the torsion angles for the two rings in the ethyl derivative are 70.59 and 70.39°, and are slightly greater

[3]This distance was inadvertently omitted in ref. 1.

Can. J. Chem. Downloaded from www.nrcresearchpress.com by 210.87.254.5 on 09/06/12
For personal use only.

Can. J. Chem. Downloaded from www.nrcresearchpress.com by 210.87.254.5 on 09/06/12
For personal use only.

TABLE 8. Magnetic susceptibilities

T (K)	$10^6\chi_M$ (cm^3 mol^{-1})	T (K)	$10^6\chi_M$ (cm^3 mol^{-1})	T (K)	$10^6\chi_M$ (cm^3 mol^{-1})	T (K)	$10^6\chi_M$ (cm^3 mol^{-1})	T (K)	$10^6\chi_M$ (cm^3 mol^{-1})	T (K)	$10^6\chi_M$ (cm^3 mol^{-1})
	$Cu[(C_2H_5)_2PO_2]_2$				$Cu[(n\text{-}C_4H_9)_2PO_2]_2$				$Cu[(n\text{-}C_6H_{13})_2PO_2]_2$		
4.20	62 430	28.4	14 790	4.20	177 600	36.1	13 150	4.25	185 340	36.2	13 210
4.55	60 960	31.0	13 570	4.65	159 340	39.5	11 900	4.73	158 630	39.9	11 930
5.05	57 940	33.7	12 530	4.88	147 790	42.8	10 960	5.07	144 030	43.0	11 010
5.49	55 510	36.1	11 680	5.58	124 590	48.3	9 620	6.08	113 080	48.3	9 620
6.09	53 020	39.4	10 780	5.90	113 630	54.6	8 420	6.82	95 400	54.7	8 400
6.88	48 950	42.6	9 980	6.90	92 110	60.8	7 560	7.99	78 300	60.9	7 590
7.80	44 680	48.0	8 910	7.85	72 220	70.4	6 570	9.15	66 360	70.4	6 540
8.82	40 810	54.5	7 860	8.95	66 800	80.5	5 630	10.1	59 640	82.0	5 670
9.90	37 310	60.6	7 220	9.80	59 540	82.1	5 540	11.0	53 260	92.1	5 040
10.85	34 400	70.3	6 250	10.95	51 550	92.2	4 940	11.7	48 510	100.0	4 580
11.8	31 800	81.8	5 410	11.8	47 040	100.5	4 510	12.6	43 580	110.5	4 110
13.1	29 850	91.8	4 810	12.6	43 260	110.3	4 080	13.8	39 810	123.9	3 590
13.8	28 180	100.5	4 390	13.65	39 400	124.7	3 610	16.15	33 090	129.9	3 470
14.6	26 660	110.7	3 970	14.8	35 960	128.8	3 540	18.0	29 030	145.6	3 080
16.1	24 570	125.1	3 510	16.65	30 970	152.3	2 960	19.4	25 320	179.4	2 490
16.8	23 350	129.3	3 400	18.7	26 980	179.1	2 560	22.35	22 370	202.4	2 190
17.9	22 250	154.1	2 850	20.4	24 440	203.8	2 210	25.5	19 470	228.8	1 960
18.7	21 290	179.1	2 450	22.15	22 300	228.5	1 950	28.2	17 440	253.9	1 730
19.4	20 520	203.3	2 180	25.2	19 460	254.6	1 790	31.1	15 590	279.4	1 590
20.4	19 590	230.0	1 910	28.2	17 270	279.4	1 620	33.8	14 250	304.7	1 450
21.35	18 800	253.9	1 720	31.1	15 510	304.1	1 510				
21.9	18 290	278.5	1 570	33.8	14 090						
25.2	16 340	304.1	1 430								

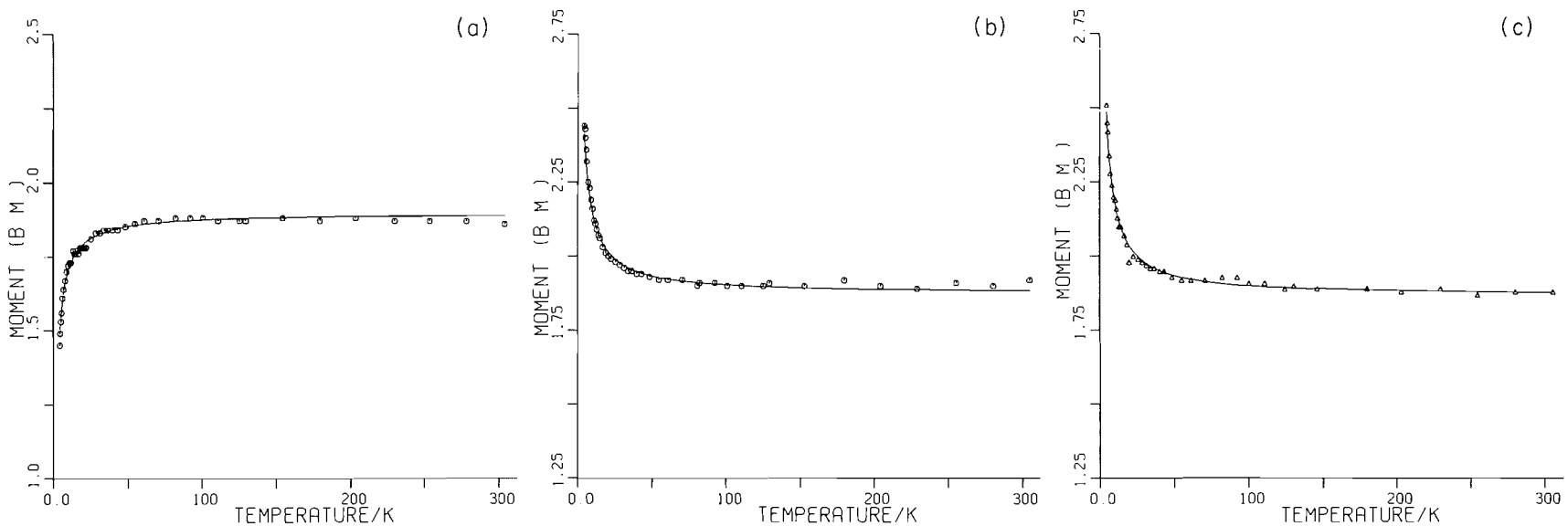

FIG. 3. Magnetic moment vs. temperature plots. Solid lines are calculated from theory using the best fit values of g and J (see text). (*a*) $Cu[(C_2H_5)_2PO_2]_2$, (*b*) $Cu[(n\text{-}C_4H_9)_2PO_2]_2$, (*c*) $Cu[(n\text{-}C_6H_{13})_2PO_2]_2$.

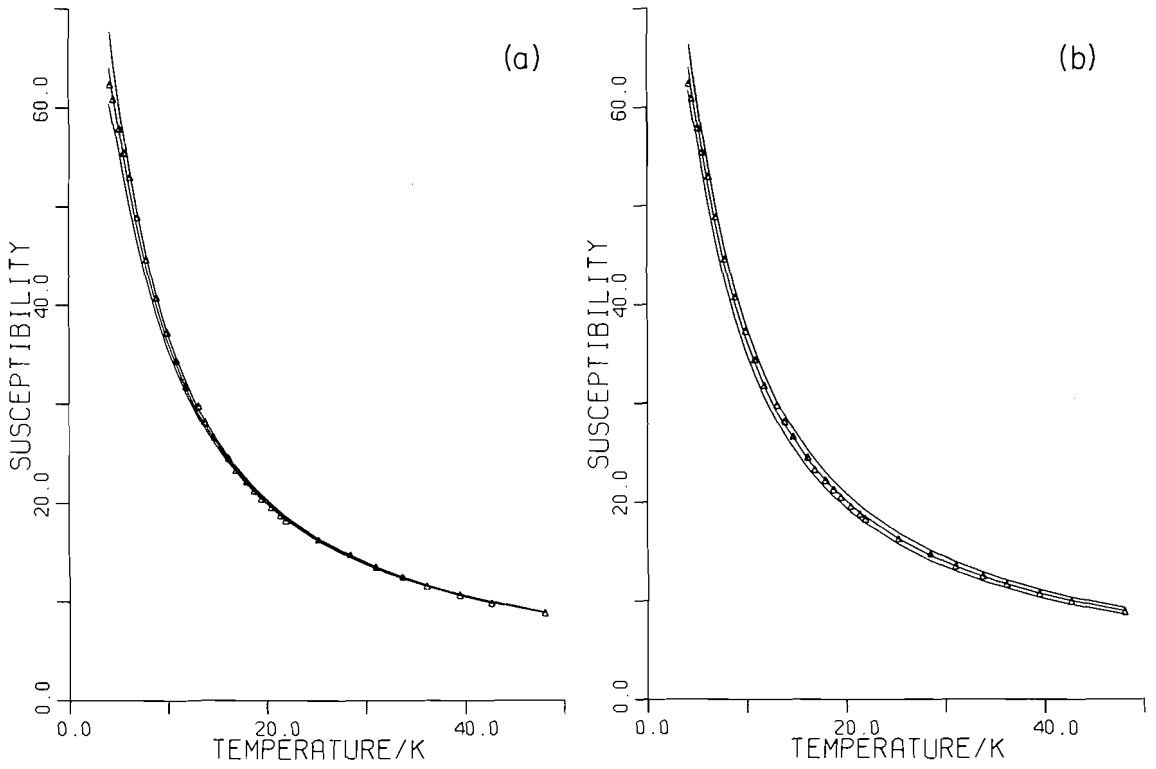

FIG. 4. Magnetic susceptibility $10^3\chi_M$ ($cm^3\ mol^{-1}$) vs. temperature plots for $Cu[(C_2H_5)_2PO_2]_2$. (*a*) Solid lines are calculated for $g = 2.19$ and, from top to bottom, $-J = 1.14, 1.27, 1.39$. (*b*) Solid lines are calculated for $-J = 1.27$ and, from top to bottom, $g = 2.23, 2.19, 2.15$.

than the values of 67.10 and 69.85° calculated for the hexyl derivative (the corresponding mean deviations (Å) from the mean planes are 0.247, 0.242; 0.214, and 0.235 respectively). Finally we note interesting structural differences involving the alkyl groups, in particular structural conformation involving the α-carbons. In both the butyl and hexyl derivatives each phosporus has one α-carbon on which the hydrogens are staggered with respect to a P—O bond, and one on which the hydrogens are staggered with respect to a P—C bond. This has the effect of orienting both alkyl groups in an axial configuration with respect to the eight-membered ring. In the ethyl derivative, on the other hand, one of the rings has alkyl group orientations as seen for the other derivatives, while in the other ring both alkyl groups on each phosphorus have α-carbons with hydrogens staggered with respect to P—O bonds. The effect is to orient one of the alkyl groups axial to this ring and the other equatorial in the ethyl derivative. The orientations of the alkyl groups relative to the eight-membered rings affect the nature of the interchain packing and this in turn may cause some of the small differences seen in the bonding parameters of the inorganic backbone.

In summary, small but significant intrachain magnetic exchange coupling is observed in the diethyl, di-*n*-butyl, and di-*n*-hexylphosphinates of copper(II). It is possible that both antiferromagnetic and ferromagnetic routes for superexchange (20) are available in all three compounds with the observed behaviour dependent on which route dominates for a particular compound. The ethyl derivative has the flattest CuO_4 chromophore, the longest copper–copper distance (through space) and the most-puckered eight-membered rings. Any or all of these structural features may enhance the antiferromagnetic over the ferromagnetic route, thus accounting for the overall antiferromagnetic exchange observed for this compound. It is important to note that one of these structural features, namely the CuO_4 stereochemistry, has been correlated previously with the nature of magnetic exchange in copper compounds. It has long been noted that in binuclear copper(II) complexes distortion from a tetrahedral to a planar environment results in increased antiferromagnetic coupling (21, 22).

Acknowledgements

We thank the Natural Sciences and Engineering Research Council of Canada for financial support, which included an equipment grant for the purchase of the vibrating sample magnetometer, and the University of British Columbia Computing Centre for assistance. The NSERC Research Committee, U.B.C., is thanked for a grant to purchase the DSC equipment. K.W.O. also thanks the U.B.C. Graduate Scholarship Committee and NSERC for scholarship awards. The authors thank D. H. Jones for valuable assistance with the magnetic moment computations.

1. K. W. OLIVER, S. J. RETTIG, R. C. THOMPSON, and J. TROTTER. Can. J. Chem. **60**, 2017 (1982).
2. R. CINI, P. COLAMARINO, P. L. ORIOLI, L. S. SMITH, P. R. NEWMAN, H. D. GILLMAN, and P. NANNELLI. Inorg. Chem. **16**, 3223 (1977).
3. S. L. LAMBERT, T. R. FELTHOUSE, and D. N. HENDRICKSON. Inorg. Chim. Acta, **29**, L223 (1978).
4. D. F. PEPPARD, G. W. MASON, and S. LEWEY. J. Inorg. Nucl. Chem. **27**, 2065 (1965).
5. G. M. KOSOLAPOFF and R. M. WATSON. J. Am. Chem. Soc. **73**, 4101 (1951).
6. L. L. SPARKS and R. L. POWELL. J. Res. Natl. Bur. Stand. **76A**, 263 (1972).
7. D. B. BROWN, V. H. CRAWFORD, J. W. HALL, and W. E. HATFIELD. J. Phys. Chem. **81**, 1303 (1977).

Can. J. Chem. Downloaded from www.nrcresearchpress.com by 210.87.254.5 on 09/06/12
For personal use only.

8. R. F. DRAKE and W. E. HATFIELD. Rev. Sci. Instrum. **45**, 858 (1974).
9. H. C. CLARK and R. J. O'BRIEN. Can. J. Chem. **39**, 1030 (1961).
10. P. COPPENS, L. LEISEROWITZ, and D. RABINOVICH. Acta Crystallogr. **18**, 1035 (1965).
11. W. R. BUSING and H. A. LEVY. Acta Crystallogr. **22**, 457 (1967).
12. International tables for X-ray crystallography. Vol. 4. Kynoch Press, Birmingham. 1974.
13. M. GERLOCH and R. C. SLADE. Ligand-field parameters. The University Press, Cambridge. 1973.
14. E. A. ROBINSON. Can. J. Chem. **41**, 173 (1963).
15. P. J. CHRISTEN, L. M. VAN DER LINDE, and F. N. HOUGE. Rec. Trav. Chim. **78**, 161 (1959).
16. R. A. NYQUIST. J. Mol. Struct. **2**, 111 (1968).
17. J. W. HALL, Ph.D. Thesis, University of North Carolina. 1977.
18. W. E. ESTES, W. E. HATFIELD, J. A. C. VAN OOIJEN, and J. REEDIJK. J. Chem. Soc. Dalton, 2121 (1980).
19. G. A. BAKER, JR., G. S. RUSHBROOK, and H. E. GILBERT. Phys. Rev. A**135**, 1272 (1964).
20. A. P. GINSBERG. Inorg. Chim. Acta Rev. 45 (1971).
21. R. J. BUTCHER and E. SINN. Inorg. Chem. **15**, 1604 (1976).
22. M. MELNIK. Coord. Chem. Rev. **42**, 259 (1982).

Can. J. Chem. Downloaded from www.nrcresearchpress.com by 210.87.254.5 on 09/06/12
For personal use only.

Primary kinetic isotope effect in the gas phase photochlorination of ethyl chloride-1-d_1

JAN NIEDZIELSKI,[1] T. YANO,[2] AND E. TSCHUIKOW-ROUX[3]
Department of Chemistry, University of Calgary, Calgary, Alta., Canada T2N 1N4

Received October 12, 1983

JAN NIEDZIELSKI, T. YANO, and E. TSCHUIKOW-ROUX. Can. J. Chem. **62**, 899 (1984).

The abstraction of hydrogen/deuterium from CH_3CHDCl by ground state chlorine atoms produced photolytically from Cl_2 has been investigated at temperatures betwen 280 and 368 K. The relative rates for the internal competition

$$CH_3CHDCl + Cl \rightarrow CH_3CDCl + HCl \quad k_H$$
$$\rightarrow CH_3CHCl + DCl \quad k_D$$

are found to conform to an Arrhenius rate law:

$$k_D/k_H = (0.865 \pm 0.025) \exp[(-133 \pm 7)/T]$$

These data, taken together with the external competition results for the C_2H_5Cl/CH_3CHDCl system, in conjunction with the competitive results using CH_4 as a primary reference, have yielded the rate constants ($cm^3\ s^{-1}$):

$$k_H = (1.20 \pm 0.04) \times 10^{-11} \exp[-(480 \pm 20)/T]$$

$$k_D = (1.04 \pm 0.04) \times 10^{-11} \exp[-(613 \pm 20)/T]$$

The relatively weak primary kinetic isotope effect, k_H/k_D, decreases with increasing temperature from 1.85_5 at 280 K to 1.66 at 365 K. The results are compared with those obtained based on the BEBO method. While both the trend and the magnitude of the kinetic isotope effect are satisfactorily predicted, the activation energy is not.

JAN NIEDZIELSKI, T. YANO et E. TSCHUIKOW-ROUX. Can. J. Chem. **62**, 899 (1984).

Opérant entre 280 et 368 K, on a étudié l'enlèvement de hydrogène/deutérium du CH_3CHDCl par des atomes de chlore à l'état fondamental qui sont générés photochimiquement à partir du chlore. On a trouvé que les vitesses relatives pour la compétition interne

$$CH_3CHDCl + Cl \rightarrow CH_3CDCl + HCl \quad k_H$$
$$\rightarrow CH_3CHCl + DCl \quad k_D$$

sont en accord avec la loi de vitesse d'Arrhenius:

$$k_D/k_H = (0{,}865 \pm 0{,}025) \exp[(-133 \pm 7)/T]$$

Utilisant ces données de concert avec les résultats de compétition externe obtenus avec le système C_2H_5Cl/CH_3CHDCl et en conjonction avec les résultats compétitifs obtenus en utilisant le méthane comme référence primaire, on peut en déduire les constantes de vitesses ($cm^3\ s^{-1}$):

$$k_H = (1{,}20 \pm 0{,}04) \times 10^{-11} \exp[-(480 \pm 20)/T]$$

$$k_D = (1{,}04 \pm 0{,}04) \times 10^{-11} \exp[-(613 \pm 20)/T]$$

L'effet isotopique cinétique primaire, k_H/k_D, est relativement faible et il diminue avec une augmentation de la température; il passe de $1{,}85_5$ à 280 K à 1,66 à 365 K. On compare les résultats obtenus avec ceux obtenus en se basant sur la méthode BEBO. Même si on prédit correctement tant l'amplitude que l'évolution de l'effet isotopique cinétique, il n'est pas possible de prédire l'énergie d'activation.

[Traduit par le journal]

Introduction

In a recent paper from this laboratory (1) the photochlorination of gaseous ethyl chloride and ethyl chloride-d_5 was examined. Kinetic data on the hydrogen and deuterium atom abstraction by photochemically generated chlorine atoms were obtained, and the magnitude of the overall kinetic isotope effect was established. In the present work these studies are extended to the photochlorination of ethyl chloride-1-d_1. Our aim is twofold: firstly, to determine accurately the primary kinetic isotope effect and the absolute rate parameters by way of a suitable reference reaction, and, secondly, to compare these values with those predicted using semiempirical schemes applicable to metathetical atom transfer reactions. Of these, the most widely used is the bond energy – bond order (BEBO) method (2, 3) based on Johnston's concept of bond order conservation (4). The approach is purely empirical, and the necessary input data are drawn entirely from structural, non-kinetic information. Although the BEBO method is too crude to account for the fine points of the experiment, the general trends can usually be pointed out correctly. In the case of several classes of reactions to which abstractions by chlorine atoms belong, the BEBO method is known to fail (3, 5). Generally, activation energies can be calculated to within 1 or 2 kcal/mol compared with the experimental data, whereas abstractions of hydrogen by chlorine atoms are predicted to have activation energies much higher than those observed, frequently by 6–7 kcal/mol. If the reactant is a chlorinated hydrocarbon, as in the present

[1]Permanent address: Department of Chemistry, Warsaw University, Warsaw, Poland.

[2]Present address: Hitotsubashi University, Kunitachi,Tokyo, Japan.

[3]To whom all correspondence should be addressed.

Can. J. Chem. Downloaded from www.nrcresearchpress.com by 210.87.254.6 on 09/06/12
For personal use only.

Can. J. Chem. Downloaded from www.nrcresearchpress.com by 210.87.254.6 on 09/06/12
For personal use only.

case, the reasons for the failure of the BEBO method may be sought in terms of non-bonding interactions between the attacking chlorine atom and the bound chlorine in the molecule, as suggested by Johnston and Goldfinger (6). While activation energies are known to be highly sensitive to non-bonding interactions the kinetic isotope effects are not. In the latter case, the potential energy field around the atom being transferred and the atomic masses involved are the crucial factors. An extensive study of kinetic isotope effects in the photochlorination of hydrogen, methane, methyl chloride, and ethane was reported by Chiltz *et al.* (7). The BEBO method was applied to calculate activation energies, kinetic isotope rate constant ratios, and their temperature coefficients, but met only with partial success. Although the calculations broadly fitted the experimental temperature dependence of the kinetic isotope effects, no unique set of adjustable BEBO parameters could be assigned which would quantitatively predict all the experimental data. Clyne and Walker (8), using improved experimental data for the pairs CH_4/CD_4 and $CHCl_3/CDCl_3$, obtained a better, albeit still not completely satisfactory, fit with the theory. Recently, the necessity to update the original BEBO parameters has been emphasized (9–11). New calculations should incorporate the refinements in potential parameters for rate gas clusters, the revision of the numerical factor in Pauling's bond length – bond order rule, and new assessments of the magnitude of triplet repulsions. In the present paper we reexamine whether or not the updated BEBO version will provide a reasonable description of the kinetic isotope effects in the chlorination of ethyl chlorides.

Experimental

The apparatus, light source, and experimental procedure have been described previously (1). Photolyses were carried out over the temperature range 7–95°C using filtered visible light centered at 424 nm. The only products observed were 1,1- and 1,2-dichloroethanes. Analyses were performed by gas chromatography in the first instance,and the determination of the contribution of the deuterated dichloroethanes to the total yield was accomplished by coupled gc/ms (computer-controlled Hewlett-Packard, Model HP-5992A) which featured a standard selected ion monitor program. The parent peaks were monitored at a source pressure of ca. 10^{-6} Torr to prevent the occurrence of ion–molecule reactions.

For each dichloroethane three different parent peaks were observed, reflecting the natural isotopic abundance of $^{35}Cl_2$, $^{35}Cl^{37}Cl$, and $^{37}Cl_2$ in the molecules. The abundance of peaks corresponding to the $^{37}Cl_2$ moiety, i.e., m/e = 102 for $C_2H_4Cl_2$ and m/e = 103 for C_2H_3DCl were small, hence a greater scatter in the experimental results occurred and these data were rejected. Only four peaks were therefore monitored: 98, 99, 100, and 101. Ideally, the peak ratios 98/99 and 100/101 should be identical, and both yield the contribution of the deuterated species to the total yield of either 1,1- or 1,2-dichloroethane. However, the parent ions were always found to be accompanied by some fragment ions. For example, to apply the appropriate corrections to each of the m/e = 98 and m/e = 100 ion abundances for the presence of the peaks 99 and 101, respectively, the cracking patterns of all four products involved (CH_3CHCl_2, CH_3CDCl_2, CH_2ClCH_2Cl, $CH_2ClCHDCl$) were determined (Table 1). In the case of normal dichloroethanes, the results obtained using both authentic samples, and the products of the photochlorination of pure ethyl chloride under our experimental conditions were in satisfactory agreement. Since commercial samples of the monodeuterated dichloroethanes were not available to us, the 1,2-dichloroethane-d_1 ($CH_2ClCHDCl$) was manufactured by the photochlorination of ethyl chloride-1-d_1 (CH_3CHDCl) and isolated by gas chromatography. Similarly, 1,1-dichloroethane-1-d_1 (CH_3CDCl_2) was obtained from the photolysis of ethyl chloride-1,1-d_2 (CH_3CD_2Cl).

TABLE 1. Mass spectral cracking patterns of normal and monodeuterated dichloroethanes[a]

	Intensity for m/e =			
Dichlorethane	98	99	100	101
CH_3CHCl_2	100	6.9±0.3	84.9±0.5	1.8±0.2
CH_2ClCH_2Cl	100	3.8±0.8	87.0±0.5	1.8±0.4
$CH_2ClCHDCl$	8.1±0.4	100	11.2±0.2	94.7±0.3
CH_3CDCl_2	5.4±0.6	100	7.8±0.2	90.0±0.3

[a]The error limits are ±1σ.

Parenthetically, it may be noted that all the cracking patterns determined here showed some dependence on the operating parameters of the mass spectrometer. Therefore, every series of experiments, including all the necessary calibrations, was completed under unchanged conditions. The reliability of these procedures was checked by introducing a known mixture of CH_3CH_2Cl and CH_3CHDCl into the ion source. The composition of the mixture was reproduced accurately to within 1%.

Ethyl chloride-1-d_1 (Merck, Sharp and Dohme) 99% D was thoroughly purified by bulb-to-bulb vacuum distillations until the level of impurities, mainly ethylene and methyl chloride, was approximately three orders of magnitude smaller than the amounts of products. The peak intensities for m/e = 64 ($C_2H_5{}^{35}Cl$) and m/e = 53 ($CD_2{}^{37}Cl$) were negligible; however, a detailed examination of the mass spectral cracking pattern revealed that the compound was contaminated with about 1% of CH_2DCH_2Cl. Ordinary ethyl chloride and chlorine (Matheson) were purified as described previously (1).

Results and discussion

Experimental results

The photochlorination of CH_3CHDCl has been investigated over the range of temperatures 7–95°C at total pressures of about 21 Torr. The reagent was used in about twenty-fold excess over chlorine which insures that the prevailing chain termination is by radical–radical combination (1). Light intensities and photolysis times were kept sufficiently low to prevent the formation of detectable amounts of secondary photochlorination products. The pertinent rate laws, as well as the verification of the long chain assumption, have been presented elsewhere (1).

Under these conditions the relevant processes are the three abstraction reactions

[1] $CH_3CHDCl + Cl \rightarrow CH_3CDCl + HCl$

[2] $\rightarrow CH_3CHCl + DCl$

[3] $\rightarrow CH_2CHDCl + HCl$

followed by

[4] $R + Cl_2 \rightarrow RCl + Cl$

where R denotes any of the chloroethyl radicals formed in reactions [1]–[3]. It should be noted that the radicals R are thermal and hence can neither decompose nor undergo any internal rearrangement prior to reaction with Cl_2. It can also be readily shown that, for low conversions, other side reactions, viz., hydrogen/deuterium and/or chlorine exchange, or the abstraction of H or D from the product hydrogen halides, are of no importance (1, 12). The sequence of reactions [1]–[4] leads to the formation of three final products: CH_3CDCl_2 (reaction [1]), CH_3CHCl_2 (reaction [2]), and $CH_2ClCHDCl$ (reaction [3]).

For internal competition and long chains, the product ratio

TABLE 2. Relative Arrhenius parameters for H/D abstraction by chlorine atoms obtained from gc/ms experiments[a,b]

Competitors	A/A' Parameter	A/A' Value	$(E' - E)/R$ (K) Parameter	$(E' - E)/R$ (K) Value	m/e[c]
Internal competition					
CH_3CHDCl/CH_3CHDCl	(A_2/A_1)	0.917±0.024	$(E_1 - E_2)$	−132±9	98/99
		0.865±0.015		−134±6	100/101
External competition					
CH_3CH_2Cl/CH_3CHDCl	(A_6/A_1)	2.121±0.054	$(E_1 - E_6)$	66±9	99/98
		1.806±0.066		61±12	101/100
CH_3CH_2Cl/CH_3CHDCl	(A_7/A_3)	0.799±0.019	$(E_3 - E_7)$	40±8	99/98
		0.838±0.005		20±1	101/100

[a]Stated uncertainty limits are ±1σ. Both precision of analyses and error involved in the determination of correction factors for detector sensitivity are accounted for.
[b]Statistical *A*-factor ratio (*not* reduced on a per atom basis).
[c]Ion peaks monitored.

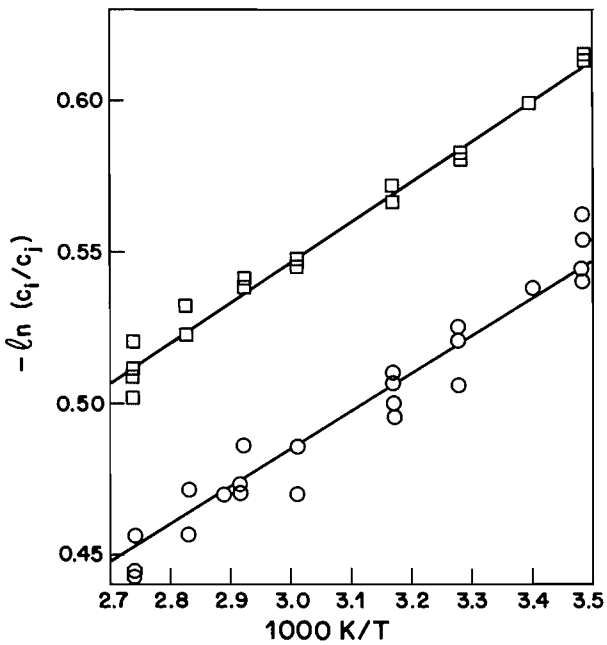

FIG. 1. Temperature dependence of the rate ratios for internal competition: based on gc/ms measurements; $c_i/c_j = [CH_3CHCl_2]/[CH_3CDCl_2]$; circles: 98/99 ions monitored; squares: 100/101 ions monitored.

determines the rate constant ratio for the abstraction reaction directly (1)

$$\frac{k}{k'} = \frac{[RCl]}{[R'Cl]}$$

For reactions [1] and [2] the rate constant ratio k_1/k_2 yields the magnitude of the primary kinetic isotope effect, i.e., the effect associated with the C—H and C—D bonds being broken. Since the task of separating the CH_3CDCl_2 and CH_3CHCl_2 pair cannot be achieved by gas-chromatography alone, the photolysis products were subjected to gc/ms analysis. The results are shown in Fig. 1 and the plots are linear.

Although on theoretical grounds a strictly Arrhenius behaviour is not to be expected, as has been observed in the chlorination of methane in the temperature range 200−500 K (13, 14), over the narrower range of temperatures covered in this study no deviations from linearity are apparent. From the slopes and intercepts, using a least-squares treatment, we obtain the relative Arrhenius parameters presented in Table 2. The precision of the measurements is on the level of 2−4% but, unfortunately, the overall accuracy is worse, due to the occurrence of a significant systematic error which is evidenced by the inequality of the results obtained using m/e = 99/98 and 101/100 monitoring. The lack of agreement is especially striking in the case of the *A*-factors (Table 2). Apparently some experimental artefacts are operative because the errors involved in the determinations of the mass spectral cracking patterns are too small to account for this difference. On the other hand, the discrepancies in the differences in activation energies are within the stated error limits.

In order to obtain the absolute Arrhenius parameters for k_1 and k_2, reaction [3] can be used, in principle, as an internal standard. To this end the ratio $c_i/c_j = (CH_3CDCl_2 + CH_3CHCl_2)/CH_2ClCHDCl$ was measured by gas chromatography and its temperature dependence was established. As shown in Fig. 2 over the temperature range 7−95°C the plot is also linear, and satisfies the following expression:

$$[5] \quad \ln [(k_1 + k_2)/k_3] = -0.114 \pm 0.05 + (361 \pm 16)/T$$

where the stated uncertainty limits are one standard deviation and account for both, the experimental precision, and for the systematic errors due to uncertainties in the calibration coefficients for the gc detector sensitivity towards 1,1- and 1,2-dichloroethanes. This relative correction factor was determined previously (12) as: $[CH_3CHCl_2] = (1.057 \pm 0.013) \times [CH_2ClCH_2Cl]$. However, any small differences in the detector response towards monodeuterated dichloroethanes were not taken into account.

Although the Arrhenius-like parameters given by eq. [5] are devoid of simple physical meaning they provide a numerical means for arithmetical material balancing. Using the k_1/k_2 values determined by the gc/ms analysis in conjunction with eq. [5], the temperature dependence of k_1/k_3 and k_2/k_3 can be calculated, which, in turn, would yield absolute Arrhenius parameters for k_1 and k_2 based on those for k_3 established previously (12). However, the problem of choosing between the two values presented in Table 2 for A_2/A_1 would still not be solved. Therefore, supplementary external competition experi-

Can. J. Chem. Downloaded from www.nrcresearchpress.com by 210.87.254.6 on 09/06/12
For personal use only.

Can. J. Chem. Downloaded from www.nrcresearchpress.com by 210.87.254.6 on 09/06/12
For personal use only.

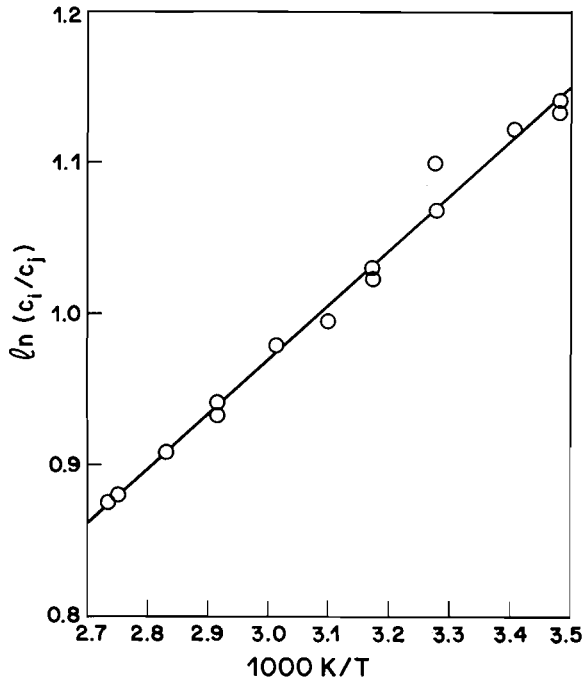

FIG. 2. Temperature dependence of the product ratios for internal competition; c_i/c_j = ([CH_3CDCl_2] + [CH_3CHCl_2])/[$CH_2ClHDCl$].

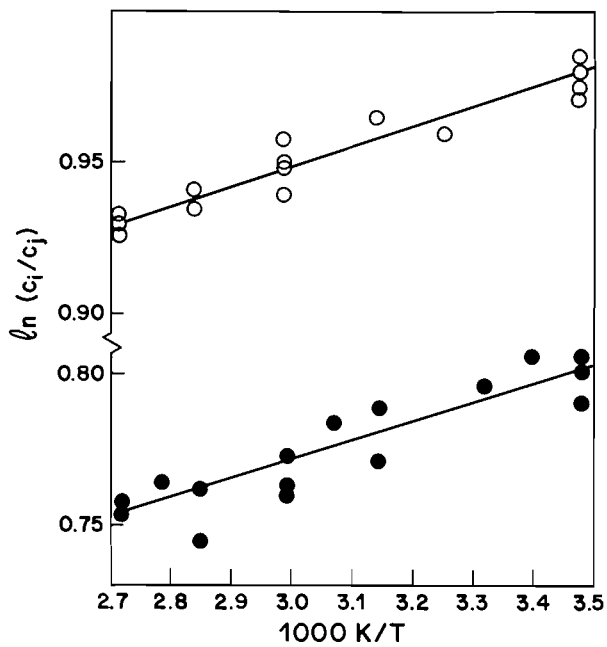

FIG. 3. Temperature dependence of the rate ratios for external competition in the system CH_3CHDCl/CH_3CH_2Cl based on gc/ms measurements; c_i/c_j = [CH_3CDCl_2]/[CH_3CHCl_2]; open circles: 99/98 ions monitored; full circles: 101/100 ions monitored. The concentration of CH_3CHCl_2 refers to the contribution from reaction [6].

ments were performed using C_2H_5Cl as a secondary standard, serving as a check for the internal self-consistency of the results. The presence of C_2H_5Cl as competitor introduces two additional reactions

[6] $CH_3CH_2Cl + Cl \rightarrow CH_3CHCl + HCl$

[7] $\rightarrow CH_2CH_2Cl + HCl$

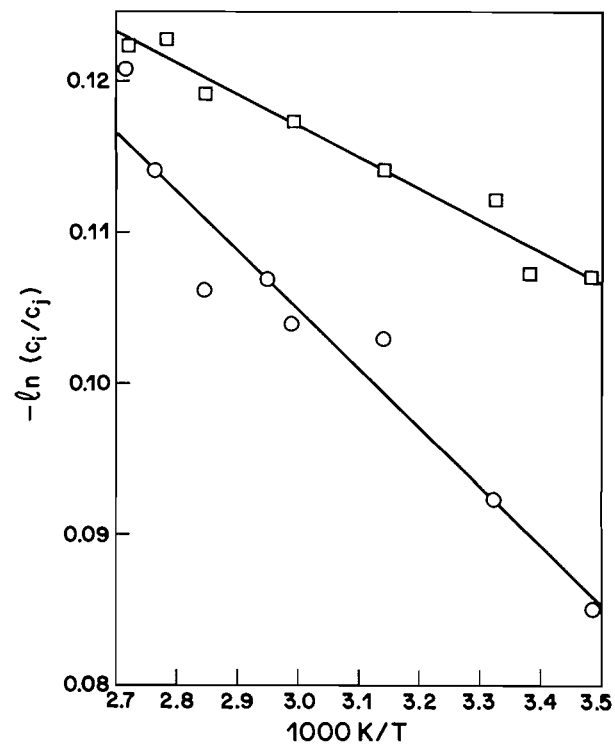

FIG. 4. Temperature dependence of the rate ratios for external competition in the system CH_3CHDCl/CH_3CH_2Cl; c_i/c_j = [$CH_2ClCHDCl$]/[CH_2ClCH_2Cl]; circles: 99/98 ions monitored; squares: 101/100 ions monitored.

which, coupled with reactions [1]–[3], yield altogether four different dichloroethane products. For competitive photochlorination of CH_3CHDCl (RH) with a reference compound CH_3CH_2Cl (R′H) the rate constant ratio, in terms of the product yields up to moderate conversions (~30%), is given by (15):

$$\frac{k}{k_r} = \frac{[RCl]\,[R'H]_m}{[R'Cl]\,[RH]_m}$$

where the subscript m refers to the mean reactant concentration. This equation holds also in the case of simultaneous internal competition against an external standard for each identifiable chlorination product. Under the experimental conditions used, the conversion with respect to both RH and R′H was so low that no noticeable loss in accuracy was introduced by using the initial rather than the mean concentrations.

Furthermore, it was hoped that the use of C_2H_5Cl as an external standard would yield data on the secondary kinetic isotope effects: an effect of the first kind resulting from the difference in the residual isotopic composition at the carbon atom undergoing C—H/C—D bond rupture (CH_3CH_2Cl/CH_3CHDCl), and an effect of the second kind due to isotopic substitution in the vicinal group (CH_3CH_2Cl/CH_3CHDCl).

The products of the photolysis of the (CH_3CH_2Cl/CH_3CHDCl) system were also analyzed by both the gc and gc/ms methods. The gc/ms results for the pairs CH_3CHCl_2/CH_3CDCl_2 and CH_2ClCH_2Cl/$CH_2ClCHDCl$ are shown in Figs. 3 and 4, respectively, and included in Table 2. As previously, the discrepancies between the values obtained using m/e = 99/98 and 101/00 monitoring are outside the limits of experimental precision. For purposes of cross-checking, the data based on the gc analysis are plotted in Fig. 5. The linear plot obeys the expression:

TABLE 3. Preferred relative Arrhenius parameters for H/D abstraction by chlorine atoms[a]

Competitors RH/R'H	A/A'		$(E' - E)/R$ (K)	
	Parameter	Value	Parameter	Value
External competition				
I CH_3CH_2Cl/CH_4[b]		1.422±0.026		1113.5±3.0
II CH_3CH_2Cl/CH_3CHDCl	(A_6/A_1)	1.965±0.052	$(E_1 - E_6)$	63±20
III CH_3CH_2Cl/CH_3CHDCl	(A_7/A_3)	0.838±0.015	$(E_3 - E_7)$	30±20
Internal competition				
IV CH_3CH_2Cl/CH_3CH_2Cl[b]	(A_6/A_7)	1.099±0.015	$(E_7 - E_6)$	429.2±1.8
V CH_3CHDCl/CH_2CHDCl	(A_2/A_1)	0.865±0.025	$(E_1 - E_2)$	−133±7
VI CH_3CHDCl/CH_3CHDCl	(A_1/A_3)	0.488±0.026	$(E_3 - E_1)$	410±26
VII CH_3CHDCl/CH_3CHDCl	(A_2/A_3)	0.422±0.022	$(E_3 - E_2)$	277±8

[a]Except for processes marked (*b*) stated uncertainty limits are based on evaluations which maximize errors.
[b]Reference 12.

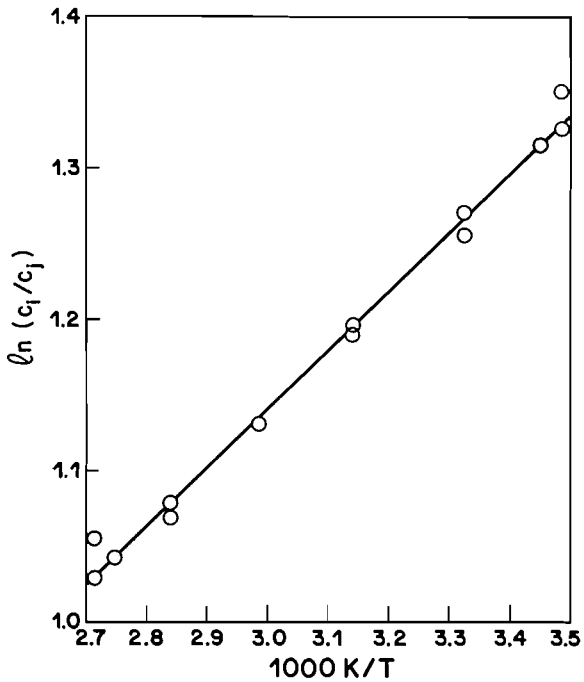

FIG. 5. Temperature dependence of the product ratios for external competition in the system CH_3CHDCl/CH_3CH_2Cl; c_i/c_j = $([CH_3CDCl_2] + [CH_3CHCl_2])/([CH_2ClCHDCl] + [CH_2ClCH_2Cl])$.

$$[8] \quad \ln [(k_1 + k_2 + k_6)/(k_3 + k_7)] = -0.027 \pm 0.04 + (389 \pm 13)/T$$

Three checks for the internal self-consistency of the results are now available, and can be of some assistance in the task of choosing the more reliable values. Using $A_2/A_1 = 0.865$ (Table 2) and eq. [5], $A_1/A_3 = 0.488$ may be obtained. This value, coupled with $A_6/A_1 = 1.806$ (Table 2) and $A_6/A_7 = 1.099$ (taken from ref. 12) leads to $A_7/A_3 = 0.802$ in good agreement with the values $A_7/A_3 = 0.799$ and 0.838 reported in Table 2. Similarly $E_3 - E_7 = 46.8/R$ K can be calculated, which is in reasonable agreement with the independent value of $39.6/R$ reported in Table 2. Another check for self-consistency involves the use of eq. [8]. For example, at a temperature of 300 K the gc data represented by this equation give ln $[(k_1 + k_2 + k_6)/(k_3 + k_7)] = 1.27 \pm 0.047$, in agreement with an independent value of 1.29 based on the evaluation of $(k_1 + k_2)/k_3$, k_6/k_7, k_6/k_1, and k_2/k_3 at 300 K. Another independent value, k_7/k_3, may be included for comparison; the value for ln $[(k_1 + k_2 + k_6)/(k_3 + k_7)]$ becomes 1.16 which is still satisfactory.

TABLE 4. Absolute Arrhenius parameters for[a] H/D-atom abstraction from ethyl chlorides by chlorine atoms

Reactant	Reaction	$10^{11} \times (A/cm^3s^{-1})$	$E_a/(cal\ mol^{-1})$
CH_3CH_2Cl	[6]	2.35±0.04	829±6
CH_3CHDCl	[1]	1.20±0.04[b]	954±40[b]
CH_3CHDCl	[2]	1.04±0.04[b]	1218±40[b]
CH_3CH_2Cl	[7]	2.13±0.05	1682±6
CH_3CHDCl	[3]	2.54±0.46	1742±40

[a]The uncertainties in the Arrhenius parameters for the reference reaction [9] are not taken into account.
[b]Preferred values, see text.

Even though these tests are not very sensitive they do provide some useful clues, and, based on these, the preferred values for the relative Arrhenius parameters are assembled in Table 3. Also included in Table 3 are the Arrhenius parameters for the competitive photochlorination of C_2H_5Cl against methane (12), which make it possible to calculate the absolute Arrhenius parameters as shown in Table 4. The choice of CH_4 as a reference, as well as the choice of the absolute rate constant value ($cm^3\ s^{-1}$) for the chlorination of methane reported by Keyser (16).

$$[9] \quad k_{CH_4} = (1.64 \pm 0.32) \times 10^{-11} \exp [-(1530 \pm 68)/T]$$

have been discussed previously (1). The uncertainty limits of the reference reaction are of necessity not included in the data presented in Table 4.

Of the five sets of data reported in Table 3 that are concerned with CH_3CHDCl (II, III, V−VII), two,VI and VII, are interrelated. Using either one and the remaining four sets of data to assess the parameters shown in Table 4, we obtain two different sets of Arrhenius parameters for processes [1] and [2]. The differences are small, e.g., for reaction [1] the pre-exponential factors are 1.20 and 1.11×10^{-11} $cm^3\ s^{-1}$ while the activation energies are 954 and 1021 cal mol^{-1}, respectively. The former values are preferred because they pass the test for self-consistency better. Also the values of the secondary kinetic isotope effects calculated using the latter parameters are too large.

Can. J. Chem. Downloaded from www.nrcresearchpress.com by 210.87.254.6 on 09/06/12
For personal use only.

TABLE 5. Primary kinetic isotope effect (CH_3CHDCl/CH_3CHDCl)

T (K)	k_H/k_D (expt)	k_H/k_D[a] (calcd)	$\frac{k_H/k_D \text{ (expt)}}{k_H/k_D \text{ (calcd)}}$	k_H/k_D[b] (calcd)	k_H/k_D[c] (calcd)
280	1.85_5	1.13 (1.21)	1.65	2.15	1.96_5
290	1.83	1.14 (1.22)	1.60_5	2.12	1.94
300	1.80	1.15 (1.23)	1.56_5	2.09	1.89
320	1.75	1.17 (1.24_5)	1.50	2.03	1.85_5
340	1.71	1.19 (1.25_5)	1.44	1.97	1.79_5
365	1.66	1.21 (1.27)	1.37	1.90_5	1.76

[a]Based on updated BEBO method (see text). Values in parentheses are based on original BEBO formulation (2). In both cases contribution from quantum mechanical tunnelling is ignored.
[b]Includes tunnelling correction based on Bell's truncated parabola (3, 30).
[c]Includes tunnelling correction based on unsymmetrical Eckart barrier (3).

Based on the data presented in Table 4 both primary and secondary kinetic isotope effects can be determined over the range of temperatures covered in these studies. Experimental values for the primary effect, k_H/k_D, at selected temperatures, are shown in Table 5. These determinations are based on internal competition experiments exclusively, and the overall accuracy is assessed to be about 4%. Both the magnitude of this effect and the decreasing trend with increasing temperature agree very well with our previous data on ethyl chloride-d_5 (1). However, the secondary kinetic isotope effects are based on external competition experiments, thus additional errors are involved and the overall accuracy deteriorates to an estimated ±10%. This accuracy is not adequate to establish the existence of an effect, much less its magnitude or temperature dependence. Therefore, numerical values are not reported. Still, the results for these effects are reasonable, and, within the limits of experimental error, are close to unity as expected. Hence our confidence in the reliability of the primary effects, determined more accurately, is much enhanced.

BEBO calculations

The bond energy – bond order (BEBO) method was used to calculate both the kinetic isotope effect (kie) and the activation energy for the abstraction of secondary hydrogen by Cl atoms from ethyl chloride. As has been noted earlier, although the BEBO method has been usually fairly successful for a large number of reactions in predicting activation energies and kie values (17–19), perhaps the worst disagreement between theory and experiment is encountered in the case of hydrogen abstraction by chlorine atoms. For instance, both the magnitude and the trend in activation energy with the heat of reaction for chlorine atom attack in chloromethanes and chloroethanes is predicted, contrary to experiments (6). Furthermore, the chlorination of C_2H_6/C_2D_6 is one of the few examples of the failure of the BEBO method for the calculation of kie (3, 7). In the case of ethyl chloride the situation might have been expected to be even worse based on the arguments of Johnston and Goldfinger (6) that the preferential attraction of the chlorine atom by the bound chlorine may result in collision complexes of the form C—Cl---Cl superseding those of the form C—H---Cl to the extent that in the case of a molecule such as $CHCl_3$ a hydrogen atom transfer complex may never be formed. Nevertheless, we thought it worthwhile to examine whether the failure of the BEBO method, when applied to this class of reactions, could be remedied by updating the input parameters as has been recently recommended (10, 11). However, no attempt was made to *adjust* parameters so as to achieve an exact fit of experiment with theory.

The derivation of the BEBO theory has been lucidly presented by Johnston (3). The main feature in the formulation is that the path of minimum potential energy for reaction lies along the line of constant bond-order ($n_1 + n_2 = 1$). Accordingly, for a hydrogen transfer process

$$AH + B \rightarrow A\text{---}H\text{---}B \rightarrow A + BH$$

the potential energy of the system is given by

$$[10] \quad V = D_{1s}(1 - n^{p_1}) - D_{2s}(1 - n)^{p_2} + D_{3s}B(n - n^2)^{\gamma}[1 + B(n - n^2)^{\gamma}]$$

where n is the progress variable ranging from 1 to 0; D_{1s}, D_{2s}, D_{3s} are single bond energies of AH, BH, and AB, respectively, and the constants p_1, p_2, B, and γ are non-adjustable parameters which can be calculated by combining empirical correlations and spectroscopic data for reactant and product molecules. Since the cited changes affect these input parameters their definitions are briefly reviewed:

$$[11] \quad B = f \exp(-\beta \Delta R_s)$$

$$[12] \quad \gamma = a\beta$$

where β is a function of the force constant and bond dissociation energy between end atoms ($\beta = (F/2D_0)^{1/2}$), and ΔR_s relates to single bond lengths ($\Delta R_s = R_{1s} + R_{2s} - R_{3s}$). The factor f in eq. [11], which can be traced to the modified Sato triplet function (3), was taken as 1/2 in the original formulation. More recently, Zavitsas (20) has shown that $f = 0.45$ gives a value for the triplet repulsive term which is more consistent with a value obtained based on variational calculations, and this value has been adopted by Gilliom (11) and here. In eq. [12] the factor a is the constant in Pauling's formula relating bond length to bond order

$$[13] \quad R_n = R_s - a \ln n$$

When the bond lengths are expressed in Ångstrom units the original Pauling value of a is 0.26. This numerical value is a subject of some controversy. Refinements in the values of bond lengths for C—C, C=C, and C≡C led Gilliom (10) to redetermine the constant as $a = 0.28$. A similar value of 0.277 was suggested by Marschoff and Jatem (21) and an even higher value of 0.30 by Burton *et al.* (22). According to a generalization of the Pauling equation developed by Agmon (23) the value of a ceases to be constant and depends on the equilibrium separation of atoms. In our calculations we have adopted Gilliom's value.

The partial bond index p which appears in the "bonding" terms in eq. [10] is evaluated by combining Pauling's rule, eq. [13], with Johnston's correlation for bond energy – bond order (2, 3)

$$[14] \quad D_n = D_s n^p$$

for a value of n corresponding to a noble-gas diatomic cluster ($n \rightarrow x$)

$$[15] \quad p = a[\ln (D_s/D_x)]/(R_x - R_s)$$

where D_x is the depth of the attractive potential, and R_x is the

Can. J. Chem. Downloaded from www.nrcresearchpress.com by 210.87.254.6 on 09/06/12
For personal use only.

TABLE 6. Input parameters for BEBO calculations

Bond	D_0^0 (kcal/mol)	ω (cm^{-1})	D_e (kcal/mol)	R_s (Å)	F (dyn/cm)	Noble gas cluster Bond	D_x (cal/mol)	R_x (Å)	p
CH_3CClH—H	95.7	2990.5	100.0	1.091	5.2×10^5	He—Ne	45.4	29.7	1.147
Cl—H	102.2	2899	106.4	1.274	5.163×10^5	He—Ar	58.36	3.47	0.958
C—Cl	77.3	681	78.3	1.76	3.44×10^5				

internuclear distance for the rare gas "molecule" in the same row of the periodic table as the interacting atoms. In the original evaluation of the p parameters Lennard-Jones potentials were used (3). More recently, both Jordan and Kaufman in their criticism of BEBO (9), and Gilliom in his modification of the method (10), utilized the rare gas intermolecular potentials obtained from molecular beam differential elastic scattering measurements by Lee and co-workers (24, 25). However, Lee's values are no longer tenable; further measurements with improved techniques yielded significantly different results (26, 27). We have adopted the following values: for He—Ne a well depth of $D_x = 45.4$ cal mol^{-1} and $R_x = 2.97$ Å (26); for He—Ar, $D_x = 58.4$ cal mol^{-1} and $R_x = 3.47$ Å (27). Other input parameters are collected in Table 6.

Using these data, the potential function V, eq. [10], was evaluated point by point for values of n from 1 to 0 at increments of 0.01. The maximum value of V, which corresponds to the potential energy of activation, was found at $n^* = 0.53$, $V^* = 6.59$ kcal/mol. The potential energy of activation exceeds the experimental activation energy by about 5.5 kcal/mol. Corrections for zero point energies do not alter the situation significantly. The use of other values for Pauling's constant (22, 23) resulted in even higher values for V^*. The conclusion which must be drawn is that the updating of the input parameters did not result in any improvement in the BEBO prediction of the activation energy for this system. It has been pointed out (28) that the BEBO calculations are quite sensitive to the adopted values of the p parameters. However, for the C—H and H—Cl bonds these values are, respectively, slightly above and below unity, and no reasonable adjustments for the rare gas intermolecular potentials can significantly alter the calculated V^* value. The contribution of the partial bonds is relatively small and negative in the present case, and V^* is mainly determined by the end atom triplet repulsion, the evaluation of which is the most arbitrary part of the theory, as pointed out by Jordan and Kaufman (9). Finally, we note that Johnston's prescription (3) that the theory will fail if the zero-point energy of the bond being broken exceeds the potential energy of activation holds true in this case.

Kinetic isotope effect calculations were based on a linear three-atom activated complex model which is both simple and adequate (29). Once the value of n^* is determined, all the needed parameters for a vibrational analysis are available. Two sets of vibrational frequencies are listed in Table 7. The first set represents the values obtained using the updated BEBO parameters; the values in parentheses were calculated using the original parameters of Johnston and Parr (2). Since for H and D transfer the reactants are identical, the expression for kie has the simple form (3)

$$[16] \quad k_H/k_D = (\nu^*\Gamma^*\Pi\Gamma)_H\dagger/(\nu^*\Gamma^*\Pi\Gamma)_D\dagger$$

where ν^* denotes the imaginary frequency associated with the reaction coordinate, $\Gamma = x/\sinh x$ where $x = h\nu/2kT$ and Γ^*

TABLE 7. Vibrational frequencies (cm^{-1}) for activated complexes[a,b]

Parameter	CH_3CDCl—H—Cl	CH_3CHCl—D—Cl
Reaction coordinate	1299.4 i (1179 i)	965.3 i (861 i)
Stretch	328.9 (317)	315.6 (317)
Bends (2)	404.9 (426)	288 (349)

[a]Based on linear three-atom model.
[b]Values in parentheses are calculated according to original prescription of Johnston and Parr (2).

is a tunnelling correction. The calculated values of k_H/k_D, with and without the tunnelling correction, are listed in Table 5. A comparison with the experimental data shows that the uncorrected values of $(k_H/k_D)_{calcd}$, column 3, are lower than experimentally determined, and, moreover, show an inverse temperature dependence. Column 4 shows the corresponding ratio and would provide a measure of the tunnelling contribution, if the calculated maximum along the potential energy path were a good representation of the locus of the activated complex. The theoretical evaluation of the quantum tunnelling correction is not straightforward. However, simple model calculations can readily be made. For small degrees of tunnelling, the correction for an inverted parabolic barrier has been given by Bell (30).

$$[17] \quad \Gamma^* = |x^*|/\sin x^*$$

where $|x^*| = h|\nu^*|/2kT$. Equation [17] is applicable when the reaction coordinate is separable, $|x^*| < \pi$. For H-atom transfer at room temperature this condition is not met, and application of eq. [17] overestimates the tunnelling effect (column 5, Table 5). However, it does restore the observed decreasing trend in the values of k_H/k_D with temperature. A more appropriate correction for these exothermic processes is provided by considering an unsymmetrical Eckart potential for which the barrier penetration factors, Γ^*, have been evaluated and tabulated by Johnston (3) as a function of dimensionless parameters. The information needed to use this table can be obtained from the activation and zero point energies, the enthalpy of the reaction, and the imaginary frequencies of the activated complex. Corrected k_H/k_D values based on the Eckart potential are listed in column 6 of Table 5. The agreement with the experimental data is markedly improved, both with respect to the magnitude (within ~6%) and temperature dependence. However, this agreement may be fortuitous. The three atom model for the transition state alone is expected to cause deviations on the level of 10%. In a recent series of papers Garrett and Truhlar (31–33) have recommended a canonical variational theory rather than the conventional transition state theory for practical computations of gas-phase reaction rate constants. As far as kinetic isotope effects are concerned they suggest a more

Can. J. Chem. Downloaded from www.nrcresearchpress.com by 210.87.254.6 on 09/06/12
For personal use only.

sophisticated treatment involving not only mass differences but also differences in force constants and bond distances, based on arguments that the location of the transition state may depend strongly on isotopic substitution. Therefore, no more is claimed for the BEBO method presented here other than it is simple and does corroborate the experimental data on the kinetic isotope effect if not the activation energy.

Acknowledgement

The continued support of the Natural Sciences and Engineering Research Council of Canada is gratefully acknowledged.

1. E. TSCHUIKOW-ROUX, T. YANO, and J. NIEDZIELSKI. J. Phys. Chem. In press.
2. H. S. JOHNSTON and C. PARR. J. Am. Chem. Soc. **85**, 2544 (1963).
3. H. S. JOHNSTON. Gas phase reaction rate theory. Ronald Press, New York. 1966.
4. H. S. JOHNSTON. Adv. Chem. Phys. **3**, 131 (1960).
5. R. L. BROWN and A. H. LAUFER. J. Phys. Chem. **85**, 3826 (1981).
6. H. S. JOHNSTON and P. GOLDFINGER. J. Chem. Phys. **37**, 700 (1962).
7. G. CHILTZ, R. ECKLING, P. GOLDFINGER, G. HUYBRECHTS, H. S. JOHNSTON, L. MEYERS, and G. VERBEKE. J. Chem. Phys. **38**, 1053 (1963).
8. M. A. A. CLYNE and R. F. WALKER. J. Chem. Soc. Faraday Trans. I, **69**, 1547 (1973).
9. R. M. JORDAN and F. KAUFMAN. J. Chem. Phys. **63**, 1691 (1975).
10. R. D. GILLIOM. J. Chem. Phys. **65**, 3027 (1976).
11. R. D. GILLIOM. J. Am. Chem. Soc. **99**, 8399 (1977).
12. J. NIEDZIELSKI, E. TSCHUIKOW-ROUX, and T. YANO. Int. J. Chem. Kinet. In press.
13. M. S. ZAHNISER, B. M. BERQUIST, and F. KAUFMAN. Int. J. Chem. Kinet. **10**, 15 (1978).
14. D. A. WHYTOCK, J. H. LEE, J. V. MICHAEL, W. A. PAYNE, and L. J. STIEF. J. Chem. Phys. **66**, 2690 (1977).
15. G. C. FETTIS and J. H. KNOX. In Progress in reaction kinetics. Vol. 2. *Edited by* G. Porter. Pergamon Press and Macmillan, New York. 1964.
16. L. F. KEYSER. J. Chem. Phys. **69**, 214 (1978).
17. I. W. M. SMITH. Kinetics and dynamics of elementary gas reactions. Butterworths, London. 1980. p. 45.
18. D. G. TRUHLAR. J. Am. Chem. Soc. **94**, 7584 (1972).
19. O. KAFRI and M. J. BERRY. Faraday Discuss. Chem. Soc. **62**, 127 (1977).
20. A. A. ZAVITSAS. J. Am. Chem. Soc. **94**, 2779 (1972).
21. C. M. MARSCHOFF and A. JATEM. Chem. Phys. Lett. **56**, 35 (1978).
22. G. W. BURTON, L. B. SIMS, J. C. WILSON, and A. FRY. J. Am. Chem. Soc. **99**, 3371 (1977).
23. N. AGMON. Chem. Phys. Lett. **45**, 343 (1977).
24. C. H. CHEN, P. E. SISKA, and Y. T. LEE. J. Chem. Phys. **59**, 601 (1973).
25. A. L. J. BURGMANS, J. M. FARRAR, and Y. T. LEE. J. Chem. Phys. **64**, 1345 (1976).
26. R. P. GERBER, M. SHAPIRO, U. BUCK, and J. SCHLEUSENER. Phys. Rev. Lett. **41**, 23b (1978).
27. R. A. AZIZ, P. W. RILEY, U. BUCK, G. MANIKE, J. SCHLEUSENER, G. SCOLES, and U. VALBUSA. J. Chem. Phys. **71**, 2637 (1979).
28. D. A. DIXON and D. R. HERSCHBACH. Faraday Discuss. Chem. Soc. **62**, 166 (1977).
29. T. E. SHARP and H. S. JOHNSTON. J. Chem. Phys. **37**, 1541 (1962).
30. R. P. BELL. Trans. Faraday Soc. **55**, 1 (1959).
31. B. C. GARRETT and D. G. TRUHLAR. J. Am. Chem. Soc. **101**, 5207 (1979).
32. B. C. GARRETT and D. G. TRUHLAR. J. Am. Chem. Soc. **101**, 4534 (1979).
31. B. C. GARRETT and D. G. TRUHLAR. J. Am. Chem. Soc. **101**, 2559 (1980).

Can. J. Chem. Downloaded from www.nrcresearchpress.com by 210.87.254.6 on 09/06/12
For personal use only.

The proton activating factor and its application to acid and base catalysis of aldehyde hydration

ROSS STEWART
Department of Chemistry, University of British Columbia, Vancouver, B.C., Canada V6T 1Y6

Received October 12, 1983

ROSS STEWART. Can. J. Chem. **62**, 907 (1984).

The data of McClelland and Coe for the general acid and general base catalyzed hydration of a series of substituted benzaldehydes has been analyzed in terms of the proton activating factor, *paf*, and concepts related thereto. Although the latter were derived for use with prototropic systems, the present work shows that they have application to nucleophilic addition as well. Three conclusions emerge from the analysis. 1. Alternative means of calculating *paf* from buffer catalytic data that were previously derived on theoretical grounds can be used in practice to give essentially the same results. 2. The mechanism of the general acid catalyzed pathway for aldehyde hydration is that favoured by McClelland and Coe and by Jencks, to wit the class (e) mechanism, rather than the class (n) mechanism. 3. Electron-withdrawing groups in the benzaldehyde ring cause the disparity between the contributions of alternative, kinetically equivalent, pathways for the uncatalyzed reaction to become greater.

ROSS STEWART. Can. J. Chem. **62**, 907 (1984).

Les données de McClelland et Coe concernant l'hydratation, soumise à une catalyse générale des acides et des bases, d'une série de benzaldéhydes substitués ont été analysées en termes du facteur activant des protons, *fap*, et de concepts qui lui sont reliés. Quoique ces derniers ont été développés pour utilisation avec des systèmes prototropiques, le présent travail démontre qu'ils ont aussi des applications dans le domaine des additions nucléophiles. Il ressort trois conclusions de notre analyse. 1. Les méthodes alternatives de calculer *fap* à partir de données catalytiques tamponnées, que l'on a antérieurement dérivées sur des bases théoriques, peuvent être utilisées en pratique pour donner essentiellement les mêmes résultats. 2. Le mécanisme impliquant le chemin de catalyse acide générale pour l'hydratation de l'aldéhyde est celui favorisé par McClelland et Coe et par Jencks, à savoir le mécanisme de classe (e) plutôt que le mécanisme de classe (n). 3. Les groupes électro-affinitaires attachés au benzaldéhyde favorisent les contributions des voies alternatives, mais cinétiquement équivalentes, pour la réaction qui n'est pas catalysée.

[Traduit par le journal]

Can. J. Chem. Downloaded from www.nrcresearchpress.com by 210.87.254.105 on 09/06/12
For personal use only.

Introduction

There are two important classes of organic reactions that are subject to acid and base catalysis. One of these is the prototropic process in which a proton is removed from one location in a molecule and transferred to a second location (unless some other process intervenes). Enolization and the transformations for which it is the first step (many condensations, oxidations, and other processes) typify the prototropic reaction. One way of analyzing such reactions is in terms of the proton activating factor *paf*, a term introduced by Stewart and Srinivasan to indicate the degree of activation that results from protonation of the substrate molecule (1–3). Consider a molecule Z undergoing enolization (or enolate anion formation) as a result of attack by a base A^- on Z or on its conjugate acid ZH^+ (eq. [1]). The quotient of the rate constants, k'/k, the proton activating factor, can be obtained using eq. [2], where k_{HA} and k_{A^-} are the experimental catalytic coefficients, and K_{ZH^+} and K_{HA} are the acidity constants of the substrate and the catalyzing buffer acid HA, respectively.

[1] $$\begin{array}{ll} Z + A^- & \xrightarrow{\;k\;} \\ \downarrow\uparrow & \qquad \text{products or reactive intermediates} \\ ZH^+ + A^- & \xrightarrow{\;k'\;} \end{array}$$

[2] $$paf = \frac{k'}{k} = \frac{k_{HA} K_{ZH^+}}{k_A - K_{HA}}$$

In the absence of buffer acids the same process can be brought about by a water molecule or an hydroxide ion filling the role of the general base, in which case the *deprotonating factor, dpf*, becomes pertinent. It represents the degree of activation brought about by removal of a proton from the base.

It has been found that *paf* varies enormously in size, depending on various characteristics of the reaction and the substrate, but in all cases examined it is considerably less, often by a very large factor, than *dpf*. That is, removing a proton from the base is more effective than adding a proton to the substrate, which is to be expected since the proton removed from the base comes from the atom that is the basic centre, whereas the proton added to the substrate takes a position that is merely adjacent to the reaction centre (eq. [3]). In the case of acetone, *dpf/paf* is greater than 10^3 (2).

[3] 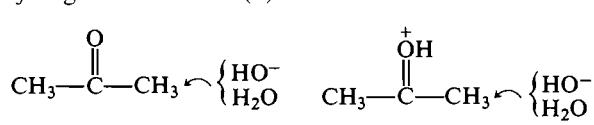

The second major class of organic reactions that is subject to general acid and base catalysis involves reactions at carbonyl centres. A recent paper by McClelland and Coe (4) describes a detailed study of such a reaction, the hydration of aromatic aldehydes catalyzed by general acids and bases (eq. [4]). Their work provides sufficient kinetic data to enable the reaction and its component steps to be scrutinized in a way similar to that previously employed with prototropic processes.

[4] $ArCHO + H_2O \rightleftharpoons ArCH(OH)_2$

There are three points of interest that emerge from the present study. The first is a check of the equivalence of alternative means of determining *paf* that had been previously described. The second is an examination of the alternative routes, known as mechanisms (e) and (n) (4, 5), for the general acid catalyzed pathways in the light of the magnitude of the *paf* and *dpf* values that are calculated herein. The third is concerned with the width of the valley in the plot of log *k* against pH in the absence of buffers, and the significance of this quantity in terms of alternative reaction pathways.

TABLE 1. Basicity constants for benzaldehydes and the apparent *paf* values for their hydration in various buffers calculated using eq. [2] and the catalytic coefficients reported in ref. 4[a]

Substituted benzaldehyde	$-pK_{BH^+}$	$paf^{app} \times 10^9$ Buffer acids					
		Acetic	Formic	β-Chloropropionic	Methoxyacetic	Chloroacetic	Cyanoacetic
3,5-$(NO_2)_2$	6.65	23	11	32	13	9.1	7.0
3-NO_2,4-Cl	5.48	4.5	1.9	2.9	1.3	1.9	1.2
4-NO_2	5.35	3.8	1.7	3.7	2.1	2.1	1.8
3-NO_2	5.28	4.4	1.9	1.9	2.5	2.0	—
4-CF_3	4.89	2.4	1.2	2.4	2.5	—	—
3-Cl	4.59	2.0	1.3	1.9	1.8	—	—
4-Cl	4.11	1.1	0.9	1.2	—	—	—

[a]The catalytic coefficients for the buffer acids and anions reported in Table 1 of ref. 4 refer to the sum of the rate constants for hydration and dehydration; however, they can be used directly to calculate *paf* for hydration as can be seen by combining eq. [7] of ref. 4 with eq. [2] herein.

Alternative means of determining *paf*

In order to determine *paf* using eq. [2] the basicity constant of the aldehyde, pK_{ZH^+}, needs to be known (eq. [5]).

[5] $ArCHOH^+ \rightleftharpoons ArCHO + H^+$

The pK_{ZH^+} values of the aldehydes have been calculated as follows. Edward and Wong (6) have determined the pK values of a number of oxygen bases using characteristic vector analysis and the Bunnett–Olsen equation; their value for benzaldehyde is −3.91. (This value suggests that aromatic aldehydes are more basic than had hitherto been believed; use of earlier values would simply exacerbate the *paf/dpf* anomaly described in the next section and reinforce the mechanistic conclusions reached therein.) The pK_{ZH^+} values for substituted benzaldehydes were calculated using the Hammett equation (7), σ^+ values, and the ρ value of −1.85 determined earlier by Stewart and Yates (8). In view of what is now known about the behaviour of acidity functions, their reported ρ value may be too large (9–11). However, any errors introduced to the calculations by use of an incorrect ρ will only have a significant effect on the least basic aldehydes considered herein and will not seriously affect the conclusions to be drawn. Table 1 lists the pK_{ZH^+} values for the seven aldehydes and the apparent *paf* values calculated for each of them using eq. [2] and the catalytic data for the six neutral acids reported by McClelland and Coe.

It will be seen from the discussion in the next section that the principal general acid catalyzed route does not appear to involve protonation of the substrate, unlike the prototropy case. Hence, the *paf* calculated here is more correctly designated as an *apparent paf* (paf^{app}) and we have done so in Table 1. (The same equations can be used to calculate *paf* and paf^{app} since the alternative routes considered below are kinetically equivalent, with parallel lines on the left hand side of plots such as that shown in Fig. 1.)

The relative contributions that the components of an acid–base pair make to a general acid–base reaction of the type shown in eq. [1] depend on three factors: the pH, the basicity of the substrate, and the pK of the buffer acid. In general, for a series of buffer acids, a plot of log k_{HA} and log k_{A^-} against pK_{HA} will give two intersecting straight lines, whose slopes depend on the Bronsted α and β values. Such a plot is shown in Fig. 1 for 3,5-dinitrobenzaldehyde and the six buffer acids under consideration. We have shown previously that the dissociation constant of a hypothetical buffer whose pK

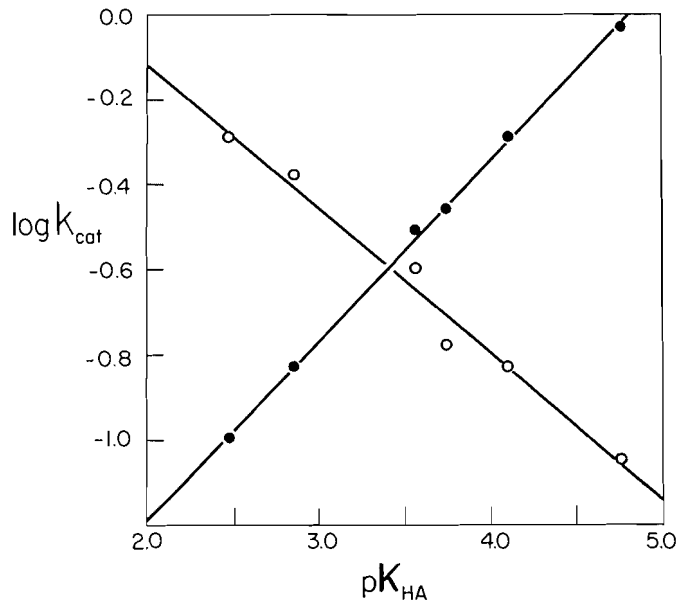

FIG. 1. A plot of the logarithm of the catalytic coefficients for the hydration of 3,5-dinitrobenzaldehyde against acidity constants of the buffer acids; buffer acid catalysis (open circles), buffer anion catalysis (filled circles). Data from ref. 4.

corresponds to the pH of intersection should be equal to K_{ZH^+}/paf (2). Thus, *paf* can be calculated by taking K at the point of intersection of plots such as that in Fig. 1 and multiplying by K_{ZH^+} of the substrate. This has been done for each of the six aldehydes, and the values are given in Table 2 together with the average of each set of values reported in Table 1. It can be seen that there is good correspondence between the numbers determined in these two ways. (As, indeed, there should be, since the two methods derive from the same assumptions regarding the mechanism of the acid and base catalyzed processes.)

The *paf* for any one compound will be independent of the identity of the buffer pair provided the sum of the Bronsted α and β coefficients is unity (2). The work of McClelland and Coe shows that this condition is not quite met in the present cases and is doubtless the cause of the drift to higher *paf* values that can be seen in Table 1 as the strength of the buffer acids declines.

Mechanism of the general acid catalyzed pathway

Simplified versions of the two routes considered by Jencks

Can. J. Chem. Downloaded from www.nrcresearchpress.com by 210.87.254.105 on 09/06/12
For personal use only.

and co-workers (5) and by McClelland and Coe (4) for the general acid catalyzed hydration of aldehydes are shown in eq. [6] for the class (e) and class (n) mechanisms. Both these groups favour the class (e) mechanism.

[6] 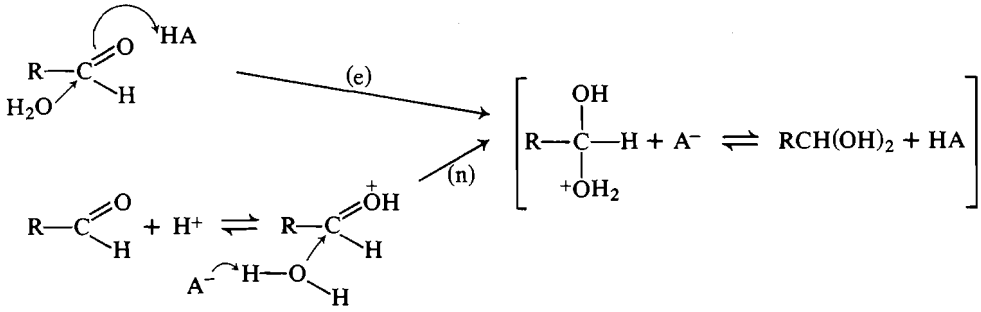

either donation of a proton to the carbonyl group (class (e)) or removal of a proton from the water molecule (class (n)).

We have calculated *dpf* for the present compounds from the data of McClelland and Coe for the water and hydroxide catalyzed rates, and the values are listed in Table 2. It can be seen that without exception *dpf* is smaller than the *paf* that is calculated on the assumption that the class (n) route prevails, that is, that the aldehyde is protonated in a pre-equilibrium step in a way that is analogous to that found in enolization processes. The *dpf* has always been found to be much larger than *paf* in other systems, suggesting that the actual rate of the class (n) route is considerably less than the rate determined experimentally. Hence we conclude that the class (e) reaction must be providing a more favourable route to products than that provided by the class (n) reaction, in agreement with the conclusions of Jencks and McClelland.

It should be pointed out that the true *paf* might well be greater for a carbonyl reaction than for an enolization process since the site of protonation in the former case is closer to the atom being attacked by the nucleophile or base. However, it seems very unlikely that such activation would actually be greater than that produced by deprotonating the attacking nucleophile.

It is generally agreed that the general base catalyzed route for aldehyde hydration follows the course shown in eq. [7], making it similar to the general base catalyzed pathway for enolization (eq. [8]).

[7] 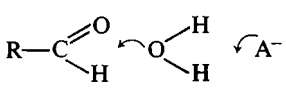

[8] 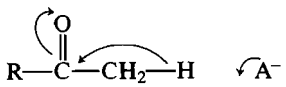

It might be expected that *dpf* would be similar in the two kinds of reactions and this is indeed the case. The *dpf* values found for the enolization of ketones are in the range of 10^8 to 10^{10} (2); the values found herein are of the order of 10^9.

Alternative pathways for the uncatalyzed reaction

There are two kinetically equivalent pathways for the uncatalyzed enolization of a compound Z; they are $Z + H_2O$ and $ZH^+ + HO^-$. For ideal systems we have shown that the ratio of their rates (though not which is greater) is a function of the

The (e)/(n) designation was introduced by Jencks (5*b*) to distinguish the sites of catalysis in additions of nucleophiles to carbonyl and like groups. In the case of general acid catalysis of aldehyde hydration, the rate-controlling step can involve

width of the flat valley[1] found at the bottom of the curve when buffer-free rates are plotted against pH (3)[2]. (An ideal system is one in which *paf* and *dpf* are independent of the ionic state of the base and the substrate.) As has been shown, the nucleophilic process examined herein is somewhat more complicated in that the acid catalyzed rate responsible for the left hand part of the pH–rate profile appears to involve a water molecule reacting with the complexed species $Z \cdot H_3O^+$ rather than with the fully protonated species ZH^+. Regardless of mechanism, the distance apart of the flat valley's extremities depends on the quantity $k^2_{H_2O}/k_{H^+}k_{HO^-}$ and the data of McClelland and Coe reveal that this quantity increases steadily as the electron-withdrawing character of the group in the benzaldehyde ring increases. For 3,5-dinitrobenzaldehyde it is some 440 times greater than for the 4-chloro compound, meaning that the valley is some 2.7 pH units (log 440 = 2.7) wider than that of the 4-chloro compound. If the water catalyzed reaction is analogous to that for buffer acids, then its mechanism is that shown in eq. [9], rather than those shown in eqs. [10*a*], or [10*b*], which both involve attack by hydroxide ion on the activated substrate.

TABLE 2. Comparison of *dpf* and paf^{app} for the hydration of substituted benzaldehydes

Substituted benzaldehyde	$dpf \times 10^9$	$paf^{app} \times 10^9$ Method 1[a]	$paf^{app} \times 10^9$ Method 2[b]
3,5-$(NO_2)_2$	0.79	10	15
3-NO_2, 4-Cl	0.70	4.3	2.3
4-NO_2	0.84	2.0	2.6
3-NO_2	0.72	2.4	2.1
4-CF_3	0.67	2.0	2.1
3-Cl	0.69	1.7	1.8
4-Cl	0.52	1.8	1.0

[a] Using the point of intersection of plots of log k_{HA} and log k_{A^-} against pK_{HA} of the buffer acids (see Fig. 1) and multiplying by K_{ZH^+}.
[b] Average values taken from Table 1.

[1] The term *plateau* has sometimes been used to describe this region of the curve, but *valley* would appear to have better geographical antecedents.
[2] A corrected statement regarding the valley's limits appears in ref. 12.

Can. J. Chem. Downloaded from www.nrcresearchpress.com by 210.87.254.105 on 09/06/12
For personal use only.

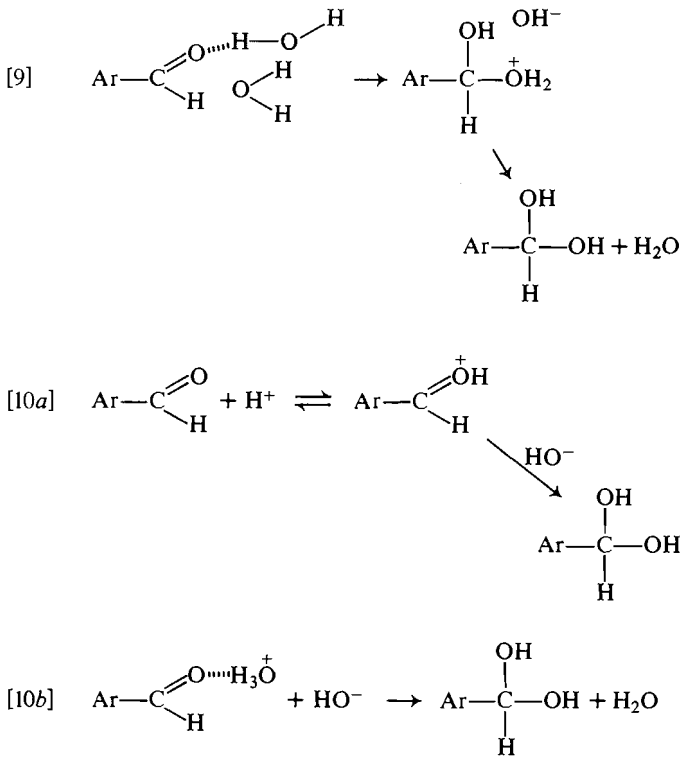

Reactions [10*a*] and [10*b*], which can be assumed to be minor pathways, will have similar responses to changes in aldehyde basicity and so one can use the effect of ring substituents on the quantity $k^2_{H_2O}/k_{H^+}k_{HO^-}$ (which strictly speaking applies only to systems that are ideal and that follow routes [9] and [10*a*]) as a measure of the relative importance of the major and minor routes. This treatment shows that an increase in the electron-withdrawing character of the aldehyde's substituents causes the contribution of the minor routes to diminish even further. Conversely, electron-donating groups, which increase the concentration of the aldehyde conjugate acid, can be expected to increase markedly the contribution of route [10*a*] (and presumably [10*b*]), and, indeed, the latter might be expected to make significant contributions to the uncatalyzed reaction in such cases. A plot of log $(k^2_{H_2O}/k_{H^+}k_{HO^-})$ against σ, the Hammett substituent parameter (7, 13), gives a straight line of slope 2.05, correlation coefficient 0.995 (Fig. 2). The substantial slope indicates how sensitive the rate ratio for the two uncatalyzed routes [9] and [10] is to the electronic effect of ring substituents.

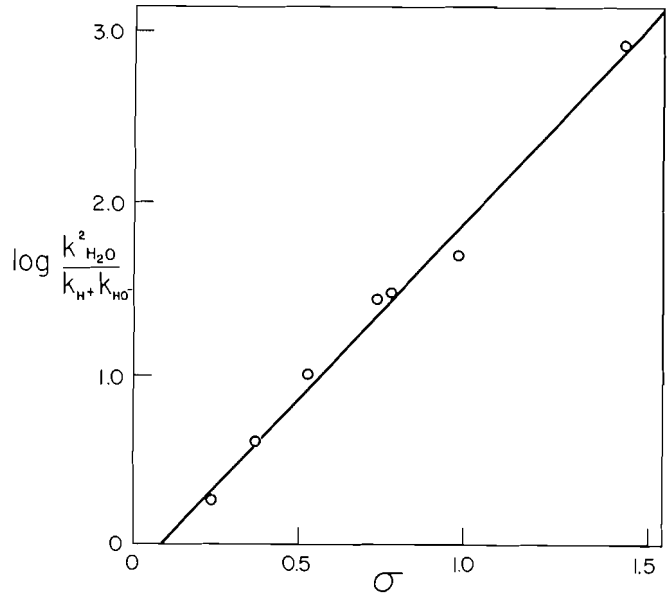

FIG. 2. A plot of log $k^2_{H_2O}/k_{H^+}k_{HO^-}$ (data from ref. 4) against the Hammett substituent constant ρ (values from ref. 13) for the hydration of substituted benzaldehydes.

1. R. SRINIVASAN and R. STEWART. Can. J. Chem. **53**, 224 (1975).
2. R. STEWART and R. SRINIVASAN. Acc. Chem. Res. **11**, 271 (1978).
3. R. STEWART and R. SRINIVASAN. Can. J. Chem. **59**, 957 (1981).
4. R. A. MCCLELLAND and M. COE. J. Am. Chem. Soc. **105**, 2718 (1983).
5. (*a*) L. H. FUNDERBURK, L. ALDWIN, and W. P. JENCKS. J. Am. Chem. Soc. **100**, 5444 (1978); (*b*) W. P. JENCKS. Acc. Chem. Res. **9**, 425 (1976).
6. J. T. EDWARD and S. C. WONG. J. Am. Chem. Soc. **99**, 4229 (1977).
7. C. D. JOHNSON. The Hammett equation. Cambridge University Press. 1976.
8. R. STEWART and K. YATES. Can. J. Chem. **37**, 664 (1959).
9. C. H. ROCHESTER. Acidity functions. Academic Press, London. 1970.
10. R. A. COX and K. YATES. Can. J. Chem. **61**, 2225 (1983).
11. T. G. BONNER and J. PHILLIPS. J. Chem. Soc. (B), 650 (1966).
12. R. STEWART and R. SRINIVASAN. Can. J. Chem. **59**, 3318 (1981).
13. D. D. PERRIN, B. DEMPSEY, and E. P. SERJEANT. pK_a Prediction for organic acids and bases. Chapman and Hall, London. 1981.

Can. J. Chem. Downloaded from www.nrcresearchpress.com by 210.87.254.105 on 09/06/12
For personal use only.

Structures cristallines des (±) oxy-2β bis(bromo-3α phényl-5β tétrahydrofuranne), (±) oxy-2β bis(bromo-3α méthyl-4α phényl-5β tétrahydrofuranne) et (±) oxy-2β bis(bromo-3α (triméthyl-2′,4′,6′ phényl)-5β tétrahydrofuranne)

GILBERT DANA, ESTERA TOUBOUL ET MARTHA MORALES-RIOS

Laboratoire de Stéréochimie Réactionnelle, Université Pierre et Marie Curie, Bâtiment F, 8, rue Cuvier, 75230 Paris Cedex 05, France

ET

MICHÈLE PHILOCHE-LEVISALLES ET CLAUDETTE BOIS

Laboratoire de Chimie Structurale des Matériaux, Université Pierre et Marie Curie, Bâtiment F, 8, rue Cuvier, 75230 Paris Cedex 05, France

Reçu le 16 juin 1983

GILBERT DANA, ESTERA TOUBOUL, MARTHA MORALES-RIOS, MICHÈLE PHILOCHE-LEVISALLES et CLAUDETTE BOIS. Can. J. Chem. **62**, 911 (1984).

Les trois éthers A, B et C formés aux cours de l'hydrolyse des dérivés dibromés tétrahydrofuranniques **1** ont une structure racémique. Dans les trois cas, la sélectivité de la réaction correspond donc à une association entre énantiomères de même configuration absolue. Dans les trois molécules étudiées, le cycle tétrahydrofurannique a une conformation caractérisée notamment par des groupes polaires en 2 (effet anomère) et en 3 diaxiaux et un groupe aromatique d'autant plus équatorial qu'il est volumineux.

GILBERT DANA, ESTERA TOUBOUL, MARTHA MORALES-RIOS, MICHÈLE PHILOCHE-LEVISALLES, and CLAUDETTE BOIS. Can. J. Chem. **62**, 911 (1984).

The three ethers A, B, and C formed during the hydrolysis of dibrominated tetrahydrofuran derivatives **1** are racemic. In all three cases, the reaction selectivity corresponds to an association between enantiomers of the same absolute configuration. In the three molecules studied, the tetrahydrofuran ring assumes a conformation characterized by polar groups in the 2-position (anomeric effect) and in the 3-position being diaxial and by the bulky aromatic group being equatorial.

[Journal translation]

Can. J. Chem. Downloaded from www.nrcresearchpress.com by 210.87.254.105 on 09/06/12
For personal use only.

L'hydrolyse des dérivés dibromés racémiques de type **1** conduit à des hémiacétals bromés **2** accompagnés d'une quantité parfois importante (30 à 50%) d'un éther bis-tétrahydrofurannique **3** sous forme d'un isomère pur ou largement prédominant.

[1] 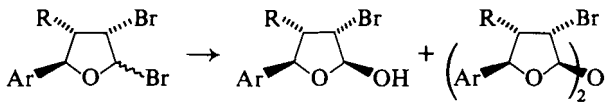

1 **2** **3**

La rmn du proton ou du ^{13}C ne nous a pas permis de déterminer s'il s'agit de l'isomère **3** *méso* ou **3** *dl*.

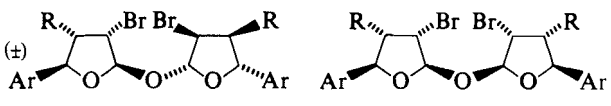

3 *dl* **3** *méso*

L'étude du mécanisme de la reconnaissance énantiomérique (1) au cours de cette réaction nécessitant la connaissance de la structure du produit formé, nous avons entrepris sa détermination par diffraction de rayons X, dans trois cas:

composé A: Ar = C_6H_5, R = H;

composé B: Ar = C_6H_5, R = CH_3;

composé C: Ar = $(CH_3)_3C_6H_2$, R = H.

Par ailleurs, ce travail conduit à la connaissance de la conformation des cycles tétrahydrofuranniques correspondants, utile pour une étude en cours des propriétés des bromhydrines **2** et de leurs dérivés.

Partie expérimentale

Les monocristaux ont été obtenus par évaporation lente de solutions dans l'éther de pétrole léger à température ambiante.

Les mesures ont été faites sur un diffractomètre automatique quatre cercles Philips PW 1100, à monochromateur de graphite, en utilisant la radiation MoKα (0,7107 Å). Les réflexions ont été enregistrées dans un intervalle $2° < \theta < 25°$, avec une vitesse de balayage en $\omega/2\theta$ de 0,05° s^{-1} et une amplitude de balayage de 1,2° + 0,3° tg θ. Le fond continu a été mesuré de part et d'autre de chaque tache. L'enregistrement d'une tache de référence toutes les 120 minutes a permis de vérifier que le cristal ne s'altérait pas. Les paramètres de la maille ont été obtenus par affinement à partir des angles de 25 réflexions.

L'enregistrement des composés B et C a été fait à température ambiante. Celui de B a été refait à 233 K pour tenter d'obtenir un plus grand nombre de données utilisables pour les affinements, mais les résultats furent similaires. L'enregistrement de A a été effectué directement à 233 K.

Les intensités ont été corrigées des facteurs de Lorentz et de polarisation. Pour les corrections d'absorption une tentative a été faite pour la première structure étudiée (B), sans apporter d'amélioration notable. A notre avis, la difficulté du problème réside plutôt dans le trop grand nombre de réflexions faibles (mesurées avec trop peu de précision). Cette correction d'absorption n'a donc pas été faite pour les deux structures suivantes. Les structures ont été résolues, par interprétation de la fonction de Patterson qui a permis la localisation du brome. Une série de Fourier "différence" a fait alors apparaître les autres atomes lourds. Les coordonnées de ces atomes ont été affinées (leur agitation thermique étant supposée anisotrope). Les atomes d'hydrogène ont tous pu être placés sur une série de Fourier différence; leurs coordonnées ont été affinées (pour A et B) et on leur a attribué

Can. J. Chem. Downloaded from www.nrcresearchpress.com by 210.87.254.105 on 09/06/12
For personal use only.

Données cristallographiques

Paramètres	Composé A	Composé B	Composé C
Formule	$C_{20}H_{20}O_3Br_2$	$C_{22}H_{24}O_3Br_2$	$C_{26}H_{32}O_3Br_2$
PM	468	496	552
Fusion	109°C	160°C	216°C
Syst. crist.	Monoclinique	Quadratique	Orthorhombique
a (Å)	16,644(5)	15,135(5)	19,315(8)
b (Å)	6,089(3)	—	14,311(6)
c (Å)	19,807(7)	9,301(4)	9,267(4)
β (°)	108,7(1)	—	—
V (Å^3)	1901	2130	2562
Z	4	4	4
D_c (g cm^{-3})	1,63	1,55	1,43
Groupe spatial	$P2_1/n$	$P4_2/n$	$Pccn$
μ (mm^{-1})	4,52	4,05	3,37
Dimension crist. (mm)	0,2 × 0,2 × 0,5	0,4 × 0,5 × 0,7	0,3 × 0,3 × 0,7
Réflexions observables	3797	2130	2587
Réflexions conservées	2267	1124	1156
Critère d'exclusion	$F < 2\sigma(F)$	$F < 2\sigma(F)$	$F < 2\sigma(F)$
R	0,065	0,052	0,052
R_w	0,068	0,058	0,056

TABLEAU 1. Coordonnées atomiques (composé A)

Atome	x/a	y/b	z/c	$B_{eq.}$
Br(1)	−0,1601(1)	0,5126(2)	0,2537(1)	4,4
O(1)	−0,0403(3)	0,2762(9)	0,1689(3)	2,5
C(2)	−0,0377(5)	0,2102(14)	0,2385(4)	2,8
C(3)	−0,1285(5)	0,2116(14)	0,2365(4)	3,1
C(4)	−0,1763(5)	0,1360(15)	0,1614(4)	3,0
C(5)	−0,1238(4)	0,2381(13)	0,1184(4)	2,4
C(51)	−0,1195(5)	0,0869(14)	0,0575(4)	2,5
C(52)	−0,1582(6)	0,1556(16)	−0,0125(4)	3,6
C(53)	−0,1546(7)	0,0188(21)	−0,0677(5)	5,1
C(54)	−0,1126(7)	−0,1729(20)	−0,0543(5)	5,4
C(55)	−0,0746(6)	−0,2423(17)	0,0150(5)	4,7
C(56)	−0,0786(5)	−0,1106(16)	0,0705(4)	3,6
O(2)	−0,0105(3)	−0,0122(10)	0,2525(3)	2,8
Br′(1)	0,1805(1)	−0,3932(2)	0,2340(1)	4,1
O′(1)	0,1306(3)	0,0412(9)	0,3205(3)	3,0
C′(2)	0,0761(5)	−0,0498(13)	0,2569(4)	2,8
C′(3)	0,0840(5)	−0,2938(14)	0,2625(4)	3,0
C′(4)	0,1033(5)	−0,3327(14)	0,3433(4)	3,0
C′(5)	0,1545(5)	−0,1275(14)	0,3758(4)	2,6
C′(51)	0,1420(5)	−0,0503(14)	0,4448(4)	2,6
C′(52)	0,1768(6)	−0,1777(15)	0,5051(4)	3,7
C′(53)	0,1633(6)	−0,1171(19)	0,5685(5)	5,0
C′(54)	0,1179(6)	0,0649(17)	0,5730(5)	4,4
C′(55)	0,0862(6)	0,1924(17)	0,5127(5)	5,1
C′(56)	0,0961(6)	0,1314(16)	0,4477(5)	3,9

un facteur d'agitation thermique isotrope, égal au B équivalent de l'atome porteur. L'affinement a été poursuivi jusqu'à ce que les variations des paramètres soient toutes inférieures à 0,05 fois l'écart type. Les dernières séries-différences ne laissent alors apparaître que des résidus de 0,4 e Å^{-3}. En ce qui concerne C, le nombre insuffisant de réflexions conservées en fonction du critère $F > 2\sigma(F)$ n'a pas permis d'affiner leurs coordonnées; de plus les pics correspondant aux atomes d'hydrogène des groupes méthyle étaient diffus, en raison sans doute du grand nombre de ces groupes et de leur rotation quasi-libre.

Les affinements par la méthode des moindres carrés ont été réalisés à l'aide du programme AFFINE adapté de ORXFLS (2), utilisant une matrice complète. Les réflexions ont été pondérées par un facteur $\omega = 1/\sigma^2(F)$. On a tenu compte de la correction de dispersion anomale (partie réelle) pour le brome.

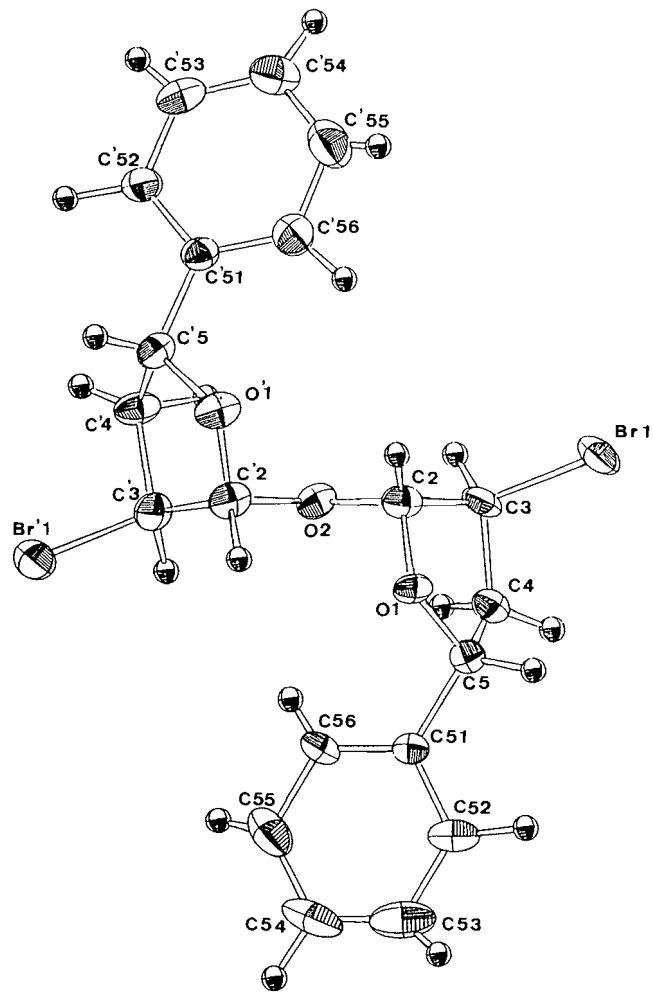

FIG. 1. Vue en perspective du composé A indiquant la numérotation des atomes.

Les tableaux 1, 2 et 3 donnent les coordonnées atomiques respectivement pour les composés A, B et C ainsi que leurs écarts types.

Notons que pour le composé B (groupe $P4_2/n$) nous avons choisi l'origine sur un centre d'inversion. Les tableaux des amplitudes des

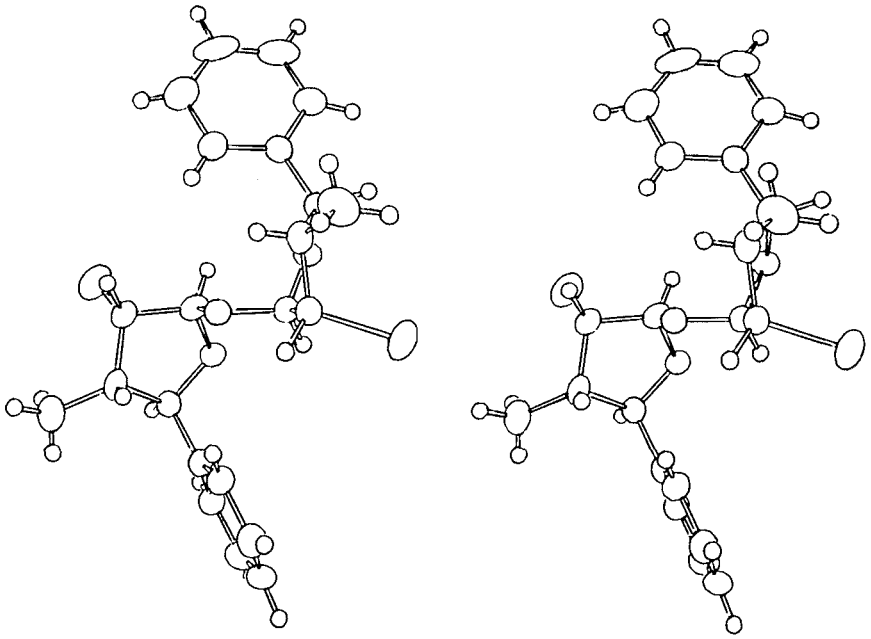

FIG. 2. Vue stéréoscopique du composé B, montrant les orientations équatoriales ou axiales des substituants des cycles tétrahydrofuranniques, et l'orientation relative des différents cycles.

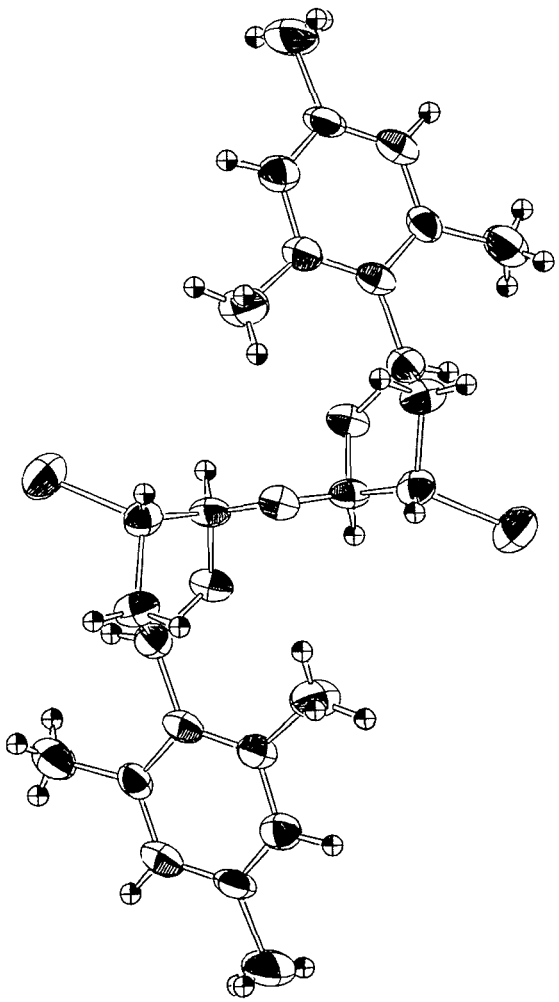

FIG. 3. Vue en perspective du composé C.

TABLEAU 2. Coordonnées atomiques (composé B)

Atome	x/a	y/b	z/c	$B_{eq.}$
Br(1)	0,4875(1)	0,2276(1)	0,3826(1)	5,6
O(1)	0,6693(2)	0,3303(2)	0,4777(4)	3,3
O(2)	0,75	0,25	0,3070(5)	3,2
C(2)	0,6709(4)	0,2541(4)	0,3925(6)	3,4
C(3)	0,5958(4)	0,2637(4)	0,2848(6)	3,3
C(4)	0,5997(4)	0,3619(4)	0,2536(6)	3,3
C(41)	0,5200(5)	0,4042(5)	0,1836(8)	3,3
C(5)	0,6259(4)	0,4017(4)	0,3993(6)	5,3
C(51)	0,6877(4)	0,4803(4)	0,3916(6)	3,1
C(52)	0,7618(4)	0,4821(4)	0,3037(7)	4,0
C(53)	0,8162(4)	0,5561(5)	0,3003(8)	5,2
C(54)	0,7976(5)	0,6263(4)	0,3906(9)	6,2
C(55)	0,7265(4)	0,6250(4)	0,4808(8)	5,7
C(56)	0,6705(4)	0,5523(4)	0,4811(7)	4,2

facteurs de structure, des coordonnées des atomes d'hydrogène, et des facteurs d'agitation thermique anisotrope sont disponibles.[1]

Résultats et discussion

Les structures des 3 composés sont constituées de molécules discrètes, liées entre elles par des forces de van der Waals. Pour B et C, la molécule a une symétrie C_2, l'atome O(2) occupant une position spéciale ($\frac{1}{4}$, $\frac{3}{4}$, z) sur un axe binaire.

Pour A, les deux fragments de la molécule sont symétriquement indépendants, cependant on peut observer aussi une symétrie C_2 très approximative (fig. 1). Les figures 1, 2 et 3 tracées à l'aide du programme ORTEP (3) représentent les molécules et donnent la numérotation des atomes; les ellipsoïdes correspondent à une probabilité de présence de 40% et les tailles des atomes d'hydrogène sont arbitraires, la molécule du composé C est projetée sur un plan perpendiculaire à

[1] On peut les obtenir à un prix nominal en s'adressant au Dépôt de données non publiées, ICIST, Conseil National de recherches du Canada, Ottawa, Ont., Canada K1A 0S2.

Can. J. Chem. Downloaded from www.nrcresearchpress.com by 210.87.254.105 on 09/06/12
For personal use only.

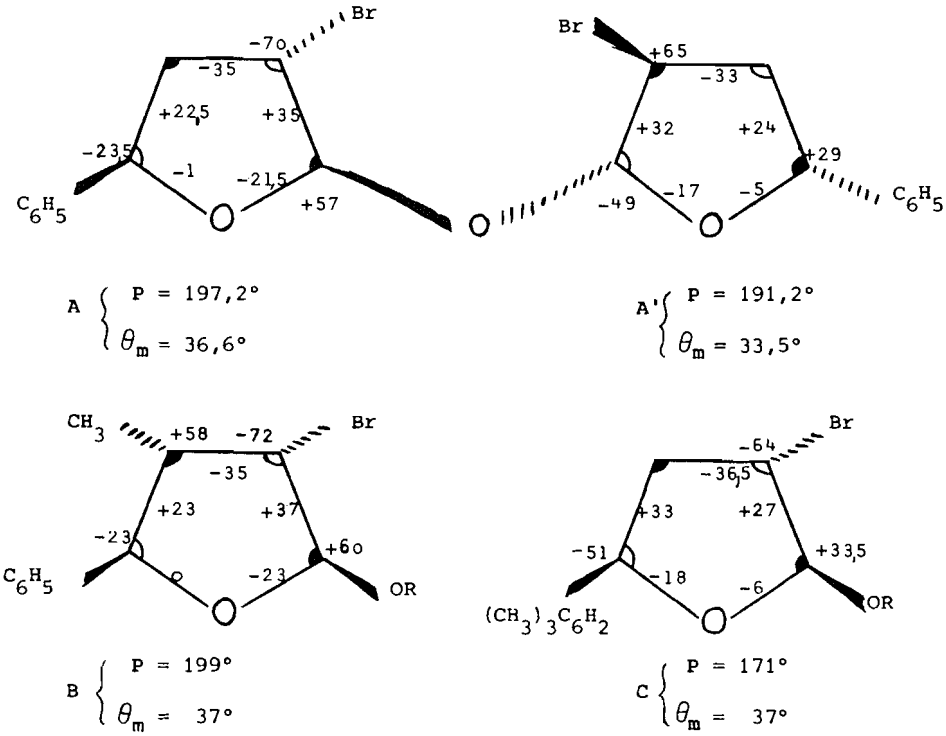

FIG. 4. Analyse conformationnelle des cycles tétrahydrofuranniques: angles dièdres, caractère axial des substituants (8) et paramètres de pseudorotation (6, 7).

TABLEAU 3. Coordonnées atomiques (composé C)

Atome	*x/a*	*y/b*	*z/c*	B_{eq}
Br(1)	0,2235(1)	1,0248(1)	0,0569(1)	7,1
O(1)	0,3201(2)	0,8321(4)	0,1599(5)	3,8
O(2)	0,2500	0,7500	−0,0030(7)	3,5
C(2)	0,2570(4)	0,8317(5)	0,0804(8)	3,7
C(3)	0,2614(4)	0,9104(5)	−0,0278(8)	4,1
C(4)	0,3402(4)	0,9201(6)	−0,0532(10)	4,6
C(5)	0,3678(4)	0,9008(6)	0,0961(9)	4,1
C(51)	0,4423(4)	0,8680(6)	0,1127(8)	3,8
C(52)	0,4651(4)	0,7826(5)	0,0611(10)	4,2
C(53)	0,5346(4)	0,7565(7)	0,0841(10)	4,8
C(54)	0,5791(4)	0,8108(6)	0,1639(11)	4,9
C(55)	0,5565(4)	0,8958(7)	0,2135(10)	4,9
C(56)	0,4889(4)	0,9257(5)	0,1884(9)	4,0
C(521)	0,4203(4)	0,7127(7)	−0,0159(11)	6,5
C(541)	0,6525(5)	0,7742(8)	0,1911(15)	8,5
C(561)	0,4686(4)	1,0207(7)	0,2440(12)	6,3

son axe binaire, la molécule de A sur un plan perpendiculaire à O(2)M (M est le milieu de C(2)—C′(2)).

Le tableau 4 donne les principales distances et les angles de valence pour les trois composés. Bien que certaines liaisons équivalentes présentent des différences notables, celles-ci ne sont pas significatives, compte tenu des écarts types.

Le tableau 5 donne les dièdres entre les substituants comportant un atome lourd, aussi que les angles de ces substituants avec le plan moyen tétrahydrofurannique T. Les angles de torsion de ce cycle sont donnés dans la figure 4.

Il apparaît dans les trois cas examinés que l'isomère formé dans la réaction 1 est le produit **3** racémique et non pas *méso*, c'est à dire que la duplication deshydratante ne se produit qu'entre substrats de même configuration absolue. Une étude plus détaillée de cette énantiosélectivité est en cours.

L'étude conformationnelle des cycles pentagonaux connaît actuellement un grand développement utilisant le concept de pseudorotation (4–6).

En désignant par θ_1, θ_2 . . . les dièdres C3—C4, C2—C3, O1—C2 . . . , on évalue (6) la phase de pseudorotation P par:

$$\operatorname{tg} P = \frac{\theta_3 + \theta_5 - \theta_2 - \theta_4}{3{,}08\ \theta_1}$$

et le gauchissement du cycle θ_m par $\theta_m = \theta_1/\cos P$.

Nous pouvons alors comparer la conformation des cycles tétrahydrofuranniques dans les trois structures étudiées. Dans la fig. 4, nous avons représenté les 4 cycles obtenus pour A, A′, B et C en utilisant les dièdres des liaisons des cycles et le caractère axial des substituants (8) (pour les valeurs positives, le substituant axial est vers l'avant; le caractère axial est réputé faible pour une valeur absolue inférieure à 30 ou 40°).

1. *Gauchissement du cycle* θ_m

On peut remarquer que le puckering θ_m du cycle tétrahydrofurannique des molécules B, C et de la première partie du composé A est de l'ordre de 37° alors qu'il n'est que de 33,5° pour la deuxième partie de A (partie primée des tableaux).

Ce cycle est donc plus aplati que les trois autres. En recherchant les distances courtes entre atomes non liés, nous avons remarqué que la distance de deux bromes appartenant aux parties A′ de deux molécules voisines est de 3,75 Å, ce qui est légèrement inférieur à la somme (2 × 1,95 Å) des rayons de van der Waals de deux bromes. Une telle compression dans l'empilement moléculaire ne se retrouve pas pour les autres cycles. On peut penser que le faible puckering du cycle A′ résulte de l'écrasement de cette partie de la molécule et la valeur θ_m = 37° apparaît comme la valeur normale pour les molécules de cette étude. Cet écrasement se manifeste également par la rotation du cycle benzénique dont l'angle α avec T (tableau 5) se réduit à 50° alors qu'il est de 78 à 88° dans les

Can. J. Chem. Downloaded from www.nrcresearchpress.com by 210.87.254.105 on 09/06/12
For personal use only.

Can. J. Chem. Downloaded from www.nrcresearchpress.com by 210.87.254.105 on 09/06/12
For personal use only.

TABLEAU 4. Principales distances (Å) et principaux angles de liaison (°)

	Composé			
Liaison	A	A′	B	C
O(1)—C(2)	1,423(10)	1,409(9)	1,400(7)	1,424(8)
C(2)—C(3)	1,500(13)	1,492(12)	1,522(8)	1,510(11)
C(3)—C(4)	1,516(10)	1,546(12)	1,516(8)	1,545(11)
C(4)—C(5)	1,533(13)	1,532(11)	1,535(8)	1,508(12)
C(5)—O(1)	1,448(8)	1,460(9)	1,460(7)	1,472(8)
C(2)—O(2)	1,427(10)	1,433(10)	1,439(6)	1,409(8)
C(3)—Br(1)	1,966(9)	1,960(10)	1,953(5)	1,958(8)
C(4)—C(41)	—	—	1,512(9)	—
C(5)—C(51)	1,537(12)	1,521(12)	1,514(8)	1,522(11)
C—C moyen‡	1,375(14)	1,380(14)	1,385(9)	1,390(11)
C(2)—O(1)—C(5)	110,4(6)	109,6(6)	109,6(4)	109,3(5)
O(1)—C(2)—C(3)	104,8(6)	108,0(6)	106,3(4)	107,0(6)
O(1)—C(2)—O(2)	111,4(7)	109,8(7)	111,3(4)	111,7(5)
C(3)—C(2)—O(2)	105,4(7)	103,1(7)	105,1(5)	105,0(6)
C(2)—C(3)—C(4)	103,4(7)	102,3(7)	101,0(4)	102,9(6)
C(2)—C(3)—Br(1)	108,9(6)	110,3(6)	107,0(4)	109,6(5)
Br(1)—C(3)—C(4)	111,6(5)	109,4(5)	113,3(4)	110,8(5)
C(3)—C(4)—C(5)	102,0(6)	102,3(7)	103,0(4)	101,1(7)
C(3)—C(4)—C(41)	—	—	117,9(5)	—
C(41)—C(4)—C(5)	—	—	114,8(5)	—
C(4)—C(5)—O(1)	105,8(6)	106,1(5)	105,4(4)	105,6(6)
C(4)—C(5)—C(51)	111,8(7)	114,3(7)	115,2(5)	118,9(7)
C(51)—C(5)—O(1)	111,2(6)	111,9(7)	109,1(4)	110,2(6)
C(2)—O(2)—C(2)*	114,4(6)	—	112,9(6)*	113,4(8)†
Angle moyen‡	120,0(9)	120,0(9)	120,0(6)	120,0(7)

* Opération de symétrie, $\frac{1}{2} - x, \frac{1}{2} - y, z$.
† Opération de symétrie, $\frac{1}{2} - x, \frac{3}{2} - y, z$.
‡ Valeurs moyennes pour le noyau benzénique.

TABLEAU 5. (a) Dièdres des substituants lourds*

	Composé			
	A	A′	B	C
Br(1)—C(3)—C(2)—O(1)	−83,5(6)	−84,8(7)	−81,8(7)	−90,8(6)
Br(1)—C(3)—C(2)—O(2)	158,9(7)	159,0(5)	160,1(3)	150,4(4)
C(4)—C(3)—C(2)—O(2)	−82,3(7)	−84,6(7)	−81,1(7)	−91,6(6)
Br(1)—C(3)—C(4)—C(41)	—	—	48,7(5)	—
Br(1)—C(3)—C(4)—C(5)	81,9(7)	84,1(7)	78,8(7)	80,5(7)
C(2)—C(3)—C(4)—C(41)	—	—	−162,9(5)	—
O(1)—C(5)—C(4)—C(41)	—	—	−152,4(5)	—
C(51)—C(5)—C(4)—C(41)	—	—	−87,3(7)	—
C(51)—C(5)—C(4)—C(3)	143,8(7)	147,6(7)	143,3(5)	157,7(7)

(b) Angles des substituants avec le plan moyen T du THF

	Composé			
	A	A′	B	C
Plan Ar – plan T (α)	78,5(7)	50,7(8)	87,9(7)	78,6(7)
Liaison C(2)—O(2) avec T (β)	77,4(7)	77,0(7)	78,6(7)	68,6(7)
Liaison C(3)—Br(1) avec T (γ)	81,7(7)	80,3(7)	82,2(7)	79,4(7)
Liaison C(5)—C(51) avec T (δ)	43,1(8)	37,7(8)	41,6(8)	26,6(8)

* Les dièdres du cycle sont donnés dans la figure 4.

trois autres cas. De plus la densité de A est particulièrement élevée (1,63 g/cm^3) comparée à celles des deux autres composés et sa température de fusion (109°C) bien plus basse.

2. *Phase de pseudorotation* P

Notons la grande analogie des conformations entre le premier cycle A et le cycle B (même forme enveloppe avec $P = 198° \pm 1°$). (Le cycle A′ en raison de ses tensions particulières se rapproche plutôt d'une forme twist.)

Le groupe aromatique y occupe une position à peine équatoriale et ce n'est pas le groupe anomère (9) (—OR en 2) qui

occupe la position la plus axiale, mais le brome en 3 (cf. figures 1, 2, 3 et angles β et γ du tableau 5). Pour B, on note que le méthyle occupe la position d'un hydrogène équatorial de A et n'introduit pas de nouvelle tension dans le cycle (même valeur P et θ_m pour A et B). Tout au plus, peut-on noter que l'angle α du plan du benzène avec le plan moyen du tétrahydrofurannique (tableau 5) augmente en présence du méthyle et les deux plans deviennent presque perpendiculaires (α = 78°5 pour A devient 87°9 pour B).

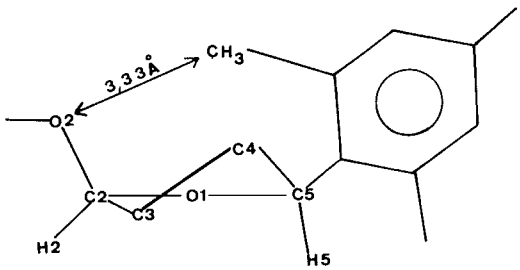

Dans le cas du composé C, le groupe aromatique, plus volumineux, occupe une position plus nettement équatoriale. Mais ceci semble obtenu au détriment du caractère axial de l'oxygène anomère (voir également l'angle β, tableau 5). On peut en effet noter que les méthyles *ortho* du groupe mésitylène exercent une pression sur l'oxygène O(2) qui entraine à la fois le groupe aromatique dans une position plus équatoriale et le groupe anomère dans une position moins axiale; la distance O(2)—C(521) n'est en effet que de 3,33 Å, c'est-à-dire à peine égale à la somme des rayons de van der Waals de l'oxygène (1,40 Å) et du méthyle (2 Å).

Toutefois l'angle α entre les plans des deux cycles reste identique à celui trouvé pour A (78,6°).

1. H. WYNBERG et B. FERINGA. Tetrahedron, **32**, 2831 (1976).
2. W. R. BUSING, K. O. MARTIN et H. A. LEVY. Report ORNL-TM 305. Oak Ridge National Laboratory, Oak Ridge, TN. 1962.
3. C. K. JOHNSON. Report ORNL-3794. Oak Ridge National Laboratory, Oak Ridge, TN. 1965.
4. C. ALTONA et M. SUNDARALINGAM. J. Am. Chem. Soc. **94**, 8205 (1972).
5. D. CREMER et J. A. POPLE. J. Am. Chem. Soc. **97**, 1358 (1975).
6. D. CREMER et J. A. POPLE. J. Am. Chem. Soc. **97**, 1354 (1975).
7. C. A. G. HAASNOOT, F. A. A. M. DE LEEUW, H. M. P. DE LEEUW et C. ALTONA. Org. Magn. Reson. **15**, 43 (1981).
8. R. BUCOURT. Bull. Soc. Chim. Fr. 2080 (1964).
9. P. DESLONGCHAMPS, D. D. ROWAN, N. POTHIER, G. SAUVÉ et J. SAUNDERS. Can. J. Chem. **59**, 1105 (1981).

Can. J. Chem. Downloaded from www.nrcresearchpress.com by 210.87.254.105 on 09/06/12
For personal use only.

Reduction of benzylideneacetone derivatives with Pd/SiO_2-AlPO_4 as catalyst and cyclohexene as hydrogen donor

A. ALBA, A. ARAMENDIA, V. BORAU, A. GARCIA-RASO, C. JIMENEZ, AND J. M. MARINAS[1]

Department of Organic Chemistry, Faculty of Sciences, Córdoba University, Córdoba-5, Spain

Received October 4, 1983

A. ALBA, A. ARAMENDIA, V. BORAU, A. GARCIA-RASO, C. JIMENEZ, and J. M. MARINAS. Can. J. Chem. **62**, 917 (1984).

The hydrogen transfer reduction of benzylideneacetone derivatives *p*-X-C_6H_4—CH=CH—CO—R (X = —OCH_3, H; R = C_6H_5, alkyl, OR, OH) using cyclohexene as hydrogen donor has been studied. The selective reduction of the C=C bond is observed and the effects of the nature of X and R, solvent, catalyst, and reaction temperature on the initial reaction rate are analyzed. In all cases, and for any substrate or catalyst, the reaction is first-order with respect to the hydrogen donor and acceptor.

A. ALBA, A. ARAMENDIA, V. BORAU, A. GARCIA-RASO, C. JIMENEZ et J. M. MARINAS. Can. J. Chem. **62**, 917 (1984).

Utilisant le cyclohexène comme donneur d'hydrogène, on a étudié la réduction par transfert d'hydrogène des dérivés de la benzylidèneacétone *p*-X-C_6H_4—CH=CH—CO—R (X = —OCH_3, H; R = C_6H_5, alkyl, OR, OH). On a observé une réduction sélective de la liaison C=C et on analyse les effets de la nature de X et de R, du solvant, du catalyseur et de la température de la réaction sur la vitesse initiale de la réaction. Dans tous les cas et pour tous les substrats ou catalyseurs, la réaction est du premier ordre par rapport au donneur d'hydrogène et à l'accepteur.

[Traduit par le journal]

Introduction

Hydrogen transfer reduction of organic compounds is one of the most rapidly developing areas of organic synthesis (1). The process can be homogeneously (2, 3) or heterogeneously (4, 5) catalyzed. The process has some advantages with respect to classical hydrogenation, such as the simplicity of the method and apparatus necessary. Moreover, the reactions are carried out at atmospheric pressure and usually at low temperatures, avoiding the use of gaseous hydrogen. We have recently shown the usefulness of catalysts obtained by supporting palladium on $AlPO_4$, $AlPO_4-SiO_2$, and $AlPO_4-Al_2O_3$ in the hydrogen transfer reduction of organic functional groups using different hydrogen donors, e.g., reduction of aromatic nitro compounds using cyclohexene (6), or formic acid/triethylamine (7) as hydrogen donors, or the selective reduction of the C=C bond of α,β-unsaturated carbonyl compounds using $HCOOH/NEt_3$ (8).

In the present paper the reduction of different benzylidene derivatives by hydrogen transfer, using cyclohexene as a hydrogen source and different catalysts obtained by supporting Pd on commercial silica or $AlPO_4-SiO_2$ supports, is described.

Experimental

Fixed amounts of hydrogen acceptor (benzylidene derivative), hydrogen donor (cyclohexene), and catalyst (see below) are introduced in a three-necked flask equipped with a thermometer, a refluxing refrigerant, and a rubber subseal. The flask is immersed in a silicone oil bath electrically heated to maintain a vigorous reflux of the reaction mixture while magnetically stirred (720 rpm). Samples are periodically withdrawn through the rubber subseal with a syringe and analyzed during the reaction.

The benzylidene derivatives have been synthesized by methods published elsewhere (9, 10). Cyclohexene was from Merck, ref. 802824, and was distilled immediately before use. Solvents were from Merck or Fluka.

Catalysts

The catalysts have been synthesized in our laboratories. Table 1 collects some physicochemical properties of the catalysts. Support S was a commercial silica (Merck ref. 7734), while supports PM2, F72, 72P, EL, and E correspond to 80:20 by weight SiO_2-AlPO_4 mixtures gelled in different organic media. Their syntheses have been reported in ref. 11. Particles sizes between 70–230 mesh were used.

TABLE 1. Physicochemical characteristics[a] of the supports of the Pd catalysts

Support	Gelling medium	$S_{esp} \pm 15$ (m^2/g)	$V_p \pm 0.05$ (mL/g)	I.P.
E	Ethylene oxide	395	0.56	3.4
EL[b]	Ethylene oxide	420	0.58	3.8
PM2	Propylene oxide	465	0.56	4.3
72P[c]	Propylene oxide	410	0.56	4.0
F72	Ammoniacal	310	0.52	3.2
S	Commercial (Merck)	395	0.55	1.0[d]
F	Ammoniacal	156	0.49	3.2

[a] S_{esp}: specific surface area by the BET method; V_p: total pore volume; I.P.: zero point of charge, as measured following Brunelle (12).
[b] The gel is air-dried and then washed with isopropyl alcohol.
[c] The gel is ripened with isopropyl alcohol for 15 days.
[d] According to Brunelle (12).

Two different methods were used to support the palladium: ionic exchange for palladium content lower than 1% and impregnation for those catalysts with more than 1% palladium content.

Taking into account the zero point charge of the supports (Table 1), $[Pd(NH_3)_4]^{2+}$ was chosen as the metallic precursor, being incorporated following a method previously described (7). On the other hand, for those catalysts obtained by impregnation, $Na_2(PdCl_4)$ (precursor M) and $Pd(NH_3)_4Cl_2$ (precursor N) were used. When naming the catalysts, "C" and "NC" indicate if calcination has or has not been, respectively, carried out before reduction, following a thermal treatment (with air instead of hydrogen) similar to that used for reduction. The initial and final reduction temperatures (in °C) are indicated in brackets in the name of the catalyst. Reduction was carried out in a flow of hydrogen (60 mL min^{-1}) at a linear heating rate of 1°C min^{-1} up to the final reduction temperature, which was maintained for 5 min, and then cooling to room temperature.

The metallic content in the catalysts was measured by atomic absorption using a Perkin–Elmer model 370 spectrometer. The metallic dispersion was determined by CO adsorption in a conventional gravimetric system for the low-loaded catalysts, while X-ray diffraction was also used for those having a metal loading between 3–5%,

[1] All correspondence concerning this paper should be addressed to: Prof. J. M. Marinas Rubio, Dpto. Química Orgánica, Facultad de Ciencias, Universidad de Córdoba, Avda. Medina Azahara, s/n, Córdoba-5 (España).

Can. J. Chem. Downloaded from www.nrcresearchpress.com by 210.87.254.40 on 09/06/12
For personal use only.

TABLE 2. Effect of the solvent on the reduction rate of benzylideneacetone[a]

Solvent	μ (Debyes)[b]	T_b (°C)[c]	X (% ½ h)[d]	X (% 1 h)	$10^3 \times r_0$ (mol h^{-1})[e]
Toluene	0.37	111	18.9	33.1	0.94
m-Xylene	0.48	140	29.2	56.5	1.46
Cumene	0.65	153	29.2	62.5	1.46
t-Butylbenzene	0.70	169	40.1	90.6	2.05
Dimethylformamide	3.82	153	43.1	100.0	2.15
Anisole	1.38	154	25.0	45.3	1.25
Tetrahydrofuran	1.63	55	8.7	23.2	0.43
o-Xylene	0.68	144	39.1	100.0	1.95

[a] Moles of benzylideneacetone: 2.5×10^{-3}; moles of cyclohexene: 2.95×10^{-2}; solvent: 5 mL; metal: 15×10^{-3} g (Pd EL_5N (50–300)C).
[b] μ: dipolar moment of the solvent at 25°C.
[c] T_b: boiling temperature of the solvent.
[d] X (% ½ h), X (% 1 h): conversion after ½ and 1 h reaction, respectively.
[e] r_0: initial reduction rate.

TABLE 3. Effect of the support, for ion-exchanged catalysts, on the reduction rate of benzylideneacetone[a]

Catalyst	$\bar{d}$ (Å)[b]	$10^3 \times r_0$ (mol/h g_{Pd})[c]	$10^5 \times r_0'$ (mol/h m_{Pd}^{-2})[d]	X (% 8 h)[e]
Pd $EL_{0.75}$ (50–300)C	38	6.0	4.6	2.9
Pd $PM2_{0.74}$ (50–300)C	31	6.7	4.2	3.2
Pd $72P_{0.74}$ (50–300)C	30	8.9	5.3	4.3
Pd $F72_{0.77}$ (50–300)C	32	8.8	5.6	4.2
Pd $S_{0.68}$ (50–300)C	18	18.5	6.6	8.8
Pd $F_{0.97}$ (50–320)C	36	4.8	3.4	2.3

[a] Moles of benzylideneacetone: 5.0×10^{-3}; moles of cyclohexene: 5.9×10^{-2}; temperature: 100°C; catalyst: equivalent to 3×10^{-3} g metal.
[b] $\bar{d}$: average metallic particle diameter (Å) as measured by CO chemisorption (9).
[c] r_0: initial reduction rate of the C=C bond (mol h^{-1} g_{Pd}^{-1}).
[d] r_0': initial reduction rate of the C=C bond (mol h^{-1} m_{Pd}^{-2}).
[e] X (% 8 h): conversion of benzylideneacetone to 4-phenyl-2-butanone, in wt. %, after 8 h reaction.

following a method previously described (13), with a Philips 1130/00/60 instrument. In the palladium-rich samples a good agreement between CO adsorption and X-ray diffraction results was observed, this last technique being faster.

Blank experiments

These were carried out to check that, under the experimental conditions here used, the reaction was not diffusion-controlled. Moreover, blank runs indicate a lack of activity in the absence of metallic phase, even in the presence of the pure support.

Analysis of the products

The analysis of the products was carried out by gas chromatography using a Hewlett–Packard model 5830 A instrument provided with a flame ionization detector, and a Perkin–Elmer model 2025/7 liquid chromatograph with a C-8 column using a 75:25 (by volume) CH_3OH/H_2O mixture as carrier when analyzing 4-nitrochalcone.

Mass and infrared spectra of the products were recorded with a Hewlett–Packard 5992 B ms–gc instrument and a Perkin–Elmer 599 B spectrophotometer coupled to a data station, respectively. The data for reaction rates (in mol/h $g_{Pd} \times 10^3$) shown in the tables correspond to the average value of three experiments. The upper limit of the error found was 2×10^{-4}, therefore all the data displayed are significant.

Results

Effect of the solvent

As shown in Table 2, when polar or high boiling point solvents are used, the reduction rate of the C=C bond of benzylideneacetone is increased.

Effect of the catalyst

The effect of several parameters of the catalyst on the reduction rate of benzylideneacetone has been studied, and the corresponding results have been summarized in Tables 3 to 6. Thus, the effect of the nature of the support (Table 3), the nature of the support and of the reduction process (Table 4), the nature of the starting palladium salt and the reduction process (Table 5), and the promoting effect of Ag and Pt on the catalytic activity of Pd (Table 6) have been studied; in this last case, the amounts of Ag or Pt correspond to 0.3% (w/w) of the total palladium content.

Effect of the nature of X and R on the reduction rate of the C=C bond

The substances to be reduced were of the type

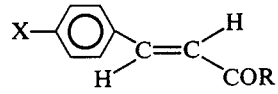

In all cases, a 100% selectivity towards reduction of the C=C bond has been achieved.

Conversions after 3 hours reaction for 17 different substrates have been collected in Table 7, as well as the initial reduction rate given in mol h^{-1} g_{Pd}^{-1} (r_0) and mol h^{-1} m_{Pd}^{-2} (r_0'). As shown in this table, both X and R play an important role in the reduction rate. Because of its *para* position from the C=C

Can. J. Chem. Downloaded from www.nrcresearchpress.com by 210.87.254.40 on 09/06/12
For personal use only.

TABLE 4. Effect of the support and the reduction conditions of the metallic precursor[a]

Catalyst	$\bar{d}$ (Å)	$10^3 \times r_0$ (mol/h g_{Pd})	$10^5 \times r'_0$ (mol/h m^2_{Pd})	X (% 1 h)	X (% 8 h)
Pd EL_5N (50–300)C	78	19.6	30.6	5.9	34.5
Pd $F72_5N$ (50–300)C	81	12.0	19.3	3.6	14.7
Pd E_5M (50–300)C	52	37.0	38.5	11.1	100.0
Pd E_5M (50–400)C	71	10.6	15.1	3.2	29.4
Pd E_5M 300C[b]	88	9.3	16.3	2.8	20.3
Pd E_5N 300C[b]	92	9.6	17.7	2.9	19.5
Pd C_5[c]	79	9.3	14.7	2.8	18.8

[a] Moles of benzylideneacetone: 5.0×10^{-3}; moles of cyclohexene: 5.9×10^{-2}; temperature: 100 °C; catalyst: 15×10^{-3} g metal; $\bar{d}$: average metallic particle diameter (Å); r_0: initial reduction rate of the C=C bond (mol h^{-1} g^{-1}_{Pd}); r'_0: initial reduction rate of the C=C bond (mol h^{-1} m^{-2}_{Pd}); X (% 1 h), X (% 8 h): conversion of benzylideneacetone to 4-phenyl-2-butanone, in wt. %, after 1 and 8 h reaction.
[b] These catalysts were reduced at 300°C in 60 mL min^{-1} for 2 h.
[c] Pd C_5: commercial catalyst, Fluka, ref. 75992.

TABLE 5. Effect of the precursor salt and its reduction process[a]

Catalyst	$\bar{d}$ (Å)	$10^3 \times r_0$ (mol/h g_{Pd})	$10^5 \times r'_0$ (mol/h m^2_{Pd})	X (% 1 h)	X (% 8 h)
Pd $F72_3M$ (50–300)NC	90	9.0	16.0	2.7	12.9
Pd $F72_3M$ (100–240)NC	90	10.3	18.3	3.1	13.7
Pd $F72_3M$ (100–240)C	20	39.6	15.8	11.9	66.9
Pd $F72_3N$ (50–300)NC	38	19.5	15.0	5.9	29.1
Pd $F72_3N$ (100–240)NC	50	20.0	20.0	6.0	29.4
Pd $F72_3N$ (100–240)C	67	18.6	24.8	5.6	37.9

[a] See footnote *a*, Table 4.

TABLE 6. Effect of Ag and Pt on the reduction rate of benzylideneacetone[a]

Catalyst	Promoter	$\bar{d}$ (Å)	$10^3 \times r_0$ (mol/h g_{Pd})	$10^5 \times r'_0$ (mol/h m^2_{Pd})	X (% 1 h)	X (% 8 h)
Pd $F72_3M$ (100–240)C	—	20	39.6	15.8	11.9	66.9
Pd $F72_3M$ (100–240)C	0.3% Ag	66	11.6	15.2	3.5	9.8
Pd $F72_3M$ (100–240)C	0.3% Pt	50	24.6	24.6	7.4	35.8
Pd $F72_3N$ (100–240)NC	—	50	20.0	20.0	6.0	29.4
Pd $F72_3N$ (100–240)NC	0.3% Ag	70	19.3	26.8	5.8	23.0
Pd $F72_3N$ (100–240)NC	0.3% Pt	50	24.3	24.3	7.3	38.0

[a] See footnote *a*, Table 4.

moiety, it can be safely assumed that group X has no steric effect, but rather electronic, on the reduction rate. So, if X = OCH_3 (electron-donating substituent) the reduction rate is increased, while for X = NO_2 (electron acceptor) the reduction rate is sharply decreased. The opposite results have been reported by Beaupére *et al.* (14) when reducing similar substrates with alcohol and $RhH(PPh_3)_4$ as a catalyst, thus suggesting in our case a cationic polar intermediate. Regarding R, it seems to play an electronic and/or steric effect on the reduction of the C=C bond. So, for R = alkyl substituents, the reduction rate decreases in the order i-Bu > n-Bu > *t*-Bu. It should be noted that while the stretching O—H mode of free phenol is recorded at 3603 cm^{-1}, when associated with *p*-X—C_6H_4—CH=CH—CO—R substrates (R = i-Bu, n-Bu, *t*-Bu), the ν_{O-H} band is recorded at 3371, 3397, and 3404 cm^{-1}, respectively, this order being the same as that for the reduction rate, thus indicating the importance of steric effects on the reduction rate.

For linear alkyl substituents (methyl to butyl), the initial reduction rate increases with the length of the hydrocarbon chain, decreasing for n-pentyl; this fact can be due to an increase in the initial reduction rate with the +I electron donor ability of R, while for the pentyl-substituted substrate the steric hindrance predominates over the electronic effect.

When R is changed to phenyl, methyl or *tert*-butyl, the reduction rate increases in the order Ph < Me < *t*-Bu, while for the corresponding benzylidene derivatives the half-wave potentials (15) are −1.35, −1.58, and −1.63 V, respectively, i.e., the lower the half-wave potential, the slower the reduction rate, thus suggesting that the rate-determining step for reduction may be the transference of a proton from cyclohexene to the substrate.

It is worthy of note that, for homogeneous hydrogen transfer reduction of benzylidene derivatives similar to those here studied, Beaupére *et al.* (14) have reported that the reduction rate decreases when R is changed in the order Me > Ph > *t*-Bu, opposite to that here reported (related to the reduction half-wave potentials) and related to the shift of the ν_{O-H} band of phenol when associated with the carbonyl group of the benzylidene derivatives to be reduced; thus these authors conclude that R has a steric effect on the reduction rate.

Can. J. Chem. Downloaded from www.nrcresearchpress.com by 210.87.254.40 on 09/06/12
For personal use only.

TABLE 7. Hydrogenation of benzylidene derivatives of the type p-X—C_6H_4—CH=CH—CO—R[a]

R	X	Product	$10^3 \times r_0$ (mol/h g_{Pd})	$10^3 \times r'_0$ (mol/h m^{-2}_{Pd})	X (% 3 h)
CH_3	H	$C_6H_5CH_2CH_2COCH_3$	16.4	0.13	2.3
Et	H	$C_6H_5CH_2CH_2COEt$	31.6	0.24	6.0
nPr	H	$C_6H_5CH_2CH_2COPr$-n	103.2	0.79	19.6
iBu	H	$C_6H_5CH_2CH_2COBu$-i	165.4	1.27	36.2
tBu	H	$C_6H_5CH_2CH_2COBu$-t	43.4	0.33	9.7
nBu	H	$C_6H_5CH_2CH_2COBu$-n	105.6	0.81	22.9
nPe	H	$C_6H_5CH_2CH_2COPe$-n	77.4	0.59	12.2
C_6H_5	H	$C_6H_5CH_2CH_2COC_6H_5$	11.7	0.09	1.1
OH	H	$C_6H_5CH_2CH_2COOH$	44.6	0.34	8.8
OCH_3	H	$C_6H_5CH_2CH_2COOCH_3$	30.5	0.23	5.7
OEt	H	$C_6H_5CH_2CH_2COOEt$	48.1	0.37	9.1
Et	OCH_3	p-$CH_3OC_6H_4CH_2CH_2COEt$	336.7	2.59	95.0
nPr	OCH_3	p-$CH_3OC_6H_4CH_2CH_2COPr$-n	369.6	2.84	94.9
nBu	OCH_3	p-$CH_3OC_6H_4CH_2CH_2COBu$-n	865.9	6.66	100.0
iBu	OCH_3	p-$CH_3OC_6H_4CH_2CH_2COBu$-i	323.8	2.49	94.5
nPe	OCH_3	p-$CH_3OC_6H_4CH_2CH_2COPe$-n	822.5	6.33	100.0
iPe	OCH_3	p-$CH_3OC_6H_4CH_2CH_2COPe$-i	450.6	3.47	100.0
C_6H_5	NO_2	p-$O_2NC_6H_4CH_2CH_2COC_6H_5$	—	—	<0.2

[a]Moles of cyclohexene: 5.9×10^{-2}; moles of substrate: 1.76×10^{-3}; temperature: 100°C; catalyst: 1.5×10^{-3} g metal (Pd $EL_{0.75}$ (50–300)C); r_0: initial reduction rate of the C=C bond (mol h^{-1} g^{-1}_{Pd}); r'_0: initial reduction rate of the C=C bond (mol h^{-1} m^{-2}_{Pd}); X (% 3 h): conversion after 3 h reaction, in wt.%.

Kinetics of the reduction

The experimental results conform to a kinetic equation typical of a first-order process with respect to both the donor and the acceptor. An identical kinetic expression has been found for all α,β-unsaturated ketones studied, regardless of the catalyst used.

Discussion and conclusions

As the hydrogenation rate is enhanced when the dielectric constant of the solvent is increased, it can be concluded that the process takes place through polar intermediates. On the other hand, as the reduction rate of the C=C bond depends on the nature of both X and R, a 1,4 reduction mechanism can be claimed, the rate-determining step seeming to be the proton transfer from the donor (cyclohexene) to the substrate to be reduced.

The reduction takes place under mild conditions and with a yield close to 100% when operating under the following conditions: 2.5×10^{-3} moles of substrate, 5.9×10^{-2} moles of cyclohexene, and 0.30 g of catalyst with 5% Pd.

The full selectivity towards reduction of the C=C bond and the ease of separation by distillation of the non-oxidized reactive (cyclohexene) as well as its oxidized form (benzene) make this method very useful in obtaining saturated carbonyl compounds from the corresponding α,β-unsaturated compounds.

Finally, it should be noted that the catalyst can be repeatedly used, with no activity loss, after being washed and dried in vacuum.

The difference in activity of the catalysts may be attributed to the following.

1. Differences in the particle size of the catalyst.
2. Changes in the number of active sites of the catalyst or in the surface morphology (16, 17).
3. Alterations in metal–support interactions (18–21).

The influence of the last two factors is rather difficult to assess. With regard to the nature of the catalyst, the largest activity is obtained when the content of silica is increased in the ion-exchanged catalysts (Table 3), as a consequence of the enhanced metallic dispersion. However, the palladium particles are markedly sintered by treatments above 300°C (Table 4), as checked by X-ray diffraction, thus leading to a lower activity.

The most active catalysts are those prepared using $Na_2(PdCl_4)$ as the precursor salt, probably because of an enhanced dispersion of Pd in the presence of sodium. However, no promoting effect of Pt or Ag is observed, as these metals lead to a worse dispersion of Pd. Calcination of the catalyst before reduction yields better results, especially for catalysts obtained from $Na_2(PdCl_4)$.

Acknowledgement

This study has been carried out with a grant from the "Comision Asesora de Investigacion Cientifica y Tecnica", Project number: 0291/82.

1. G. BRIEGER and T. J. NESTRICK. Chem. Rev. **74**, 567 (1974).
2. Y. SASSON and J. BLUM. J. Org. Chem. **40**, 1887 (1975).
3. J. WATANABE, T. OTA, and J. TSUJI. Chem. Lett. 1585 (1980).
4. M. FERLES, O. KOCIAN, and S. RADL. Collect. Czech. Chem. Commun. **43**, 1628 (1978).
5. N. A. CORTESE and R. F. HECK. J. Org. Chem. **43**, 3985 (1978).
6. M. A. ARAMENDIA, V. BORAU, C. JIMENEZ, and J. M. MARINAS. Rev. Roum. Chim. **27**, 753 (1982).
7. M. A. ARAMENDIA, M. S. CLIMENT, C. JIMENEZ, and J. M. MARINAS. React. Kinet. Catal. Lett. **14**, 489 (1980).
8. M. A. ARAMENDIA, V. BORAU, C. JIMENEZ, and J. M. MARINAS. Appl. Catal. In press.
9. A. GARCIA-RASO, B. CAMPANER, J. V. SINISTERRA, and J. M. MARINAS. An. Quim. **78**, 112 (1982).
10. A. GARCIA-RASO, B. CAMPANER, J. V. SINISTERRA, and J. M. MARINAS. An. Quim. **77**, 222 (1981).
11. C. JIMENEZ, J. M. MARINAS, J. V. SINISTERRA, and V. BORAU. An. Quim. **73**, 561 (1977).
12. J. R. BRUNELLE. Pure Appl. Chem. **50**, 1211 (1978).
13. M. A. ARAMENDIA, V. BORAU, C. JIMENEZ, J. M. MARINAS, and J. A. PAJARES. J. Catal. **78**, 188 (1982).

Can. J. Chem. Downloaded from www.nrcresearchpress.com by 210.87.254.40 on 09/06/12
For personal use only.

14. D. BEAUPÉRE, P. BAUER, and R. UZAN. Can. J. Chem. **57**, 218 (1979).
15. J. P. SEGUIN, D. BEAUPÉRE, P. BAUER, and R. UZAN. Bull. Soc. Chim. Fr. 168 (1974).
16. A. Y. GWATHMEY and R. E. CUNNINGHAN. Adv. Catal. **10**, 57 (1968).
17. M. BOUDART. Proc. VIth Internat. Cong. Catal. Vol. I. London. 1976. p. 1.
18. R. T. K. BAKER, E. B. PRESTRIDGE, and R. L. GARTEN. J. Catal. **59**, 293 (1979).
19. R. L. MOSS, D. POPE, B. J. DAVIS, and B. H. EDWARDS. J. Catal. **58**, 206 (1979).
20. P. MERIAUDEAU, O. H. ELLESTEAD, M. DUFAUX, and C. NACCACHE. J. Catal. **75**, 243 (1982).
21. M. A. VANNICE and R. L. GARTEN. J. Catal. **63**, 255 (1980).

Can. J. Chem. Downloaded from www.nrcresearchpress.com by 210.87.254.40 on 09/06/12
For personal use only.

An *ab initio* molecular orbital study of isomers on the $C_2NH_5^{+\cdot}$ and C_2NH_5 surfaces

MIN H. LIEN
Department of Chemistry, National Chung-Hsing University, Taichung, Taiwan 400

AND

ALAN C. HOPKINSON
Department of Chemistry, York University, Downsview, Ont., Canada M3J 1P3

Received July 26, 1983

MIN H. LIEN and ALAN C. HOPKINSON. Can. J. Chem. **62**, 922 (1984).

The structures and relative energies of seven possible $C_2NH_5^{+\cdot}$ isomers have been calculated using *ab initio* molecular orbital theory. Structure optimisations have been performed with a 4-31G basis set, using both the restricted (RHF) and unrestricted (UHF) Hartree–Fock methods. The optimum geometries were then used for single point calculations using the 6-31G* basis set. The relative energies are **1** < **7** < **5** < **3** ≈ **2** ≈ **6** < **4**. This order is the same, with the exception of **6**, as for isomers on the $C_2H_4O^{+\cdot}$ surface and the relative energies are very similar to those on the $C_2H_4O^{+\cdot}$ surface. The structures of the radical cations $C_2NH_5^{+\cdot}$ are compared with those of the neutral molecules C_2NH_5.

MIN H. LIEN et ALAN C. HOPKINSON. Can. J. Chem. **62**, 922 (1984).

Faisant appel à la théorie *ab initio* des orbitales moléculaires, on a calculé les structures et les énergies relatives des sept isomères possibles pour le $C_2NH_5^{+\cdot}$. On a optimisé les structures à l'aide d'une base 4-31G et en utilisant les méthodes restraintes (RHF) et non-restraintes (UHF) de Hartree–Fock. On a ensuite utilisé les géométries optimales pour faire des calculs en un point unique à l'aide d'une base 6-31G*. Les énergies relatives sont dans l'ordre **1** < **7** < **5** < **3** ≈ **2** ≈ **6** < **4**. A l'exception de **6**, l'ordre est le même que pour les isomères sur la surface de $C_2H_4O^{+\cdot}$ et les énergies relatives sont très semblables à celles sur la surface de $C_2H_4O^{+\cdot}$. On compare les structures des radicaux cations $C_2NH_5^{+\cdot}$ avec celles des molécules neutres C_2NH_5.

[Traduit par le journal]

There has been considerable experimental (1–4) and theoretical (5, 6) work on the structures, stabilities, and relative energies of various isomers on the $C_2H_4O^{+\cdot}$ energy hypersurface. The isoelectronic $C_2NH_5^{+\cdot}$ species is one of the principal ions in the mass spectra of nitrogen-containing compounds and five different isomers (**1** – **5**) have been identified (7, 8). Deuterium labelling studies have established **5** to be the base peak for pyrrolidine and both **3** and **5** are produced from

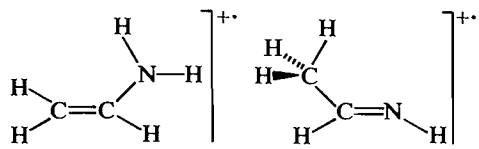

1 **2**

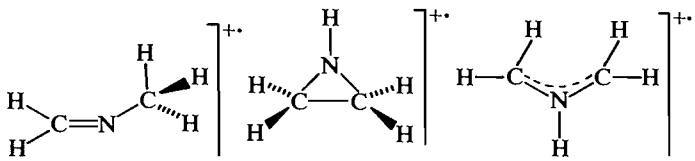

3 **4** **5**

piperidine (9). From metastable ion studies different ions, given structures **1**, **2**, **3**, and **4** and/or **5**, were shown to retain their structural identities prior to fragmentation by loss of hydrogen atom (7), and subsequent studies (8) using collision-induced dissociation have established that **5** is the dominant ion, with **4** being produced only from aziridine. Ion **2** (or its *cis*-isomer **6**) has also been reported as a minor product in the laser photolysis of methylamine (10), but no structural information was provided.

The transient nature of these ions precludes a detailed experimental study of their structures and even the relative energies of these ions are not known. We now report an *ab initio* molecular orbital study of the $C_2NH_5^{+\cdot}$ energy hypersurface in which we determine the relative energies of isomers **1** → **6** and we also report details of their structures. All structures were found to be at minima on the surface and an additional structure, **7**, not previously mentioned in the literature was found to be at the second lowest minimum. Initally all structures were subjected to geometry optimisation at the 4-31G (11) level of theory using the unrestricted Hartree–Fock method (UHF). However, spin contamination created a problem with structures **1** and **7** and we therefore decided to use the restricted Hartree–Fock method (RHF).

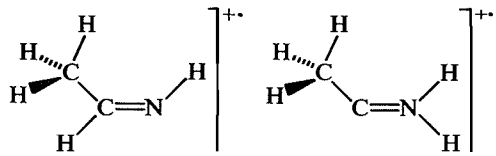

6 **7**

All calculations were performed with the MONSTERGAUSS program (12) using the optimally conditioned optimisation algorithm (13) for geometry optimisations. In all the molecular species the norm of the gradient vector was less than 5×10^{-4} mdyn at convergence, a condition which usually produces bond lengths and angles within 0.0001 Å and 0.01°, respectively, of the true optimum value (14). Single calculations were performed at the 6-31G* (15, 16) level of theory, using the 4-31G optimised geometry and we denote these results by the label 6-31G*//4-31G.

Results and discussion

After preliminary studies at the STO-3G level all radical cations were subjected to complete geometry optimisation in C_s symmetry using the 4-31G basis set. Two of the ions, **4** and **5**, were found to be planar and to belong to the C_{2v} point group. Geometries were also optimised for the neutral molecules

Can. J. Chem. Downloaded from www.nrcresearchpress.com by 210.87.254.5 on 09/06/12
For personal use only.

Can. J. Chem. Downloaded from www.nrcresearchpress.com by 210.87.254.5 on 09/06/12
For personal use only.

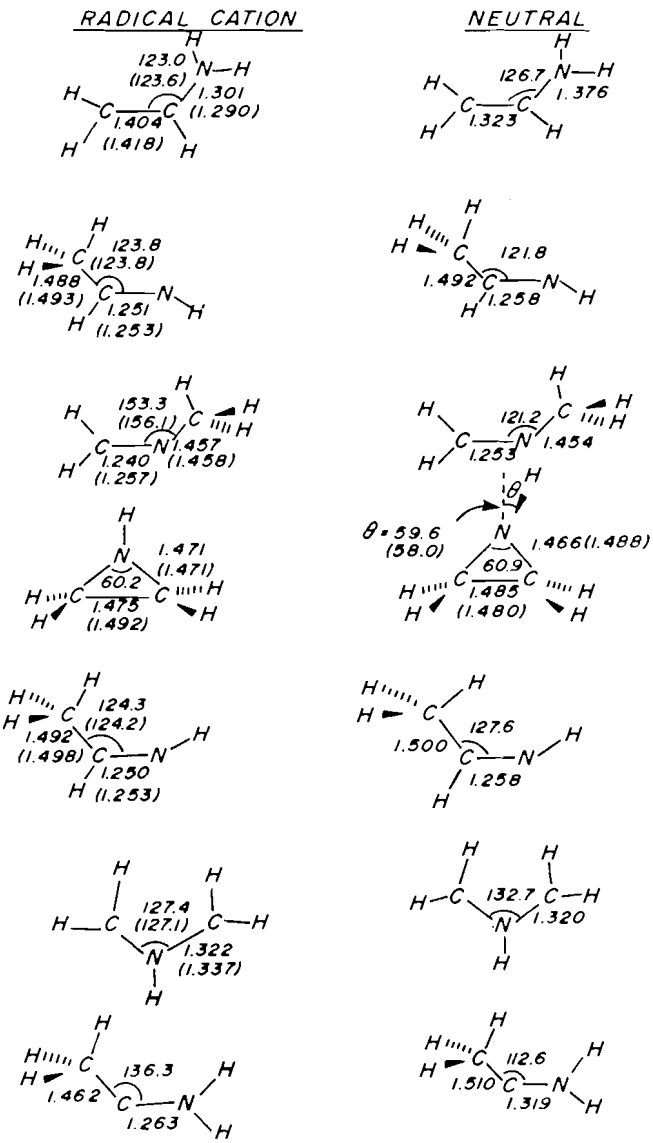

FIG. 1. Geometries for isomers of $C_2NH_5^{+\cdot}$ and C_2H_5N. All bond lengths are in Ångstroms and angles are in degrees. For the cations values in parentheses are from UHF calculations. For aziridine the numbers in parentheses are experimental values from ref. 22.

formed by addition of an electron to the radical cations. The optimum geometries for the radical cations and the corresponding neutrals are given in Fig. 1. For the sake of simplicity only the bond lengths and bond angles associated with bonding between "heavy atoms" are given. Geometry optimisations were performed with both the RHF and UHF methods for the radical cations and the latter are given in parentheses on the structures. There is satisfactory agreement between the structures provided by the two open shell methods.

Comparison of the geometries of cations with the corresponding neutral molecules shows most bond lengths to be slightly shorter in the cations. Major structural changes occur either in the bond from which an electron is removed or in the bond angles around nitrogen when an electron is removed from the lone pair on nitrogen. In **1** a π-electron is removed from aminoethylene resulting in an increase in the C—C bond length and a slight decrease in the C—N bond. Radical cation **1**, then, is best described in valence bond terminology by the canonical structures **1***a* and **1***b*.

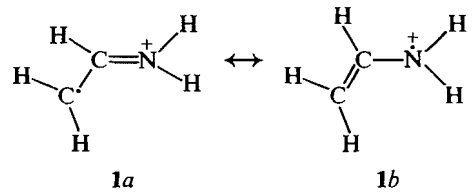

1*a* **1***b*

Ions **2**, **3**, **6** are formed by removal of an electron from the nitrogen lone pair. In these σ-radicals the bond lengths are only slightly changed but the bond angles at nitrogen are much larger than those in the corresponding neutral compounds (149.0° compared with 115.6° in **2**, 156.1° compared with 121.2° in **3**, and 149.5° compared with 115.7° in **6**).

The inversion barrier in the neutral aziridine molecule is 49 kJ mol^{-1} at the 4-31G//4-31G level and removal of an electron from the nitrogen lone pair is expected to decrease this barrier. In fact, radical cation **4** is found to be planar at nitrogen. Ring-opening of **4** to give **5** is an exothermic process but structure **4** was found to have no imaginary vibrational frequencies and this ion then is at a minimum on the $C_2NH_5^{+\cdot}$ energy hypersurface.

Methyl groups usually eclipse double bonds (17) and only eclipsing structures were examined for **2**, **3**, and **6**. Ions **6** and **2** are *cis* and *trans* isomers about C=N and the *trans* isomer is very slightly lower in energy (0.5 0.8 kJ mol^{-1}) at all three levels of calculation (Table 1).

In radical cation **5** the barrier to rotation of one methylene group is very low (8 kJ mol^{-1} at 4-31G//4-31G and 7 kJ mol^{-1} at 6-31G*//4-31G). The perpendicular ion has a short C—N bond (1.267 Å) for the in-plane methylene group and a long C—N bond (1.450 Å) for the out-of-plane methylene. This perpendicular radical cation then is best described by the canonical structure **5**a, where the unpaired electron is on the

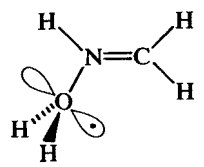

5*a*

carbon of the rotating methylene group (the unpaired spin density on C is 0.98 at the 6-31G*//4-31G level).

The isoelectronic allyl radical also has a low barrier to rotation (18 kJ mol^{-1} from MINDO/3 (18) and 25.0 kJ mol^{-1} at the 4-31G//4-31G level (19)). As in **5***a* the allyl radical has one long bond (1.475 Å) and one short bond (1.319 Å) at the 4-31G//4-31G level.

The neutral compound corresponding to structure **5** is an imine ylide. Geometry optimisations on this molecule showed it to belong to the C_{2v} point group, with a structure very similar to that of the radical cation and not to be a zwitterion (i.e., *not* **5***a* with the unpaired electron replaced by a lone pair). No valence bond structure can be drawn for this symmetrical molecule and it is therefore not surprising that this molecule is by far the highest energy species on the C_2NH_5 energy hypersurface.

In radical cation **7**, the methyl group preferentially eclipses the carbon–nitrogen bond but the barrier to rotation is very low (2 kJ mol^{-1} at 4-31G//4-31G and 3 kJ mol^{-1} at 6-31G*//4-31G). In this σ-radical the C—N distance (1.263 Å) is approximately that found for a double bond and the C—C dis-

TABLE 1. Total energies (hartrees) and energies (kJ mol^{-1}) relative to **1** for $C_2H_5N^{+\cdot}$

Structure	Point group	4-31G//4-31G UHF	4-31G//4-31G RHF	6-31G*//4-31G RHF	Energies relative to **1** at 6-31G*//4-31G
1	C_s	—	−132.62899	−132.81657	0
2	C_s	−132.58683	−132.58090	−132.77075	120
3	C_s	−132.58636	−132.57675	−132.77079	120
4	C_{2v}	−132.54765	−132.54327	−132.74261	194
5	C_{2v}	−132.61662	−132.59407	−132.78484	83
6	C_s	−132.58665	−132.58068	−132.77045	121
7	C_s	—	−132.60136	−132.78899	72

tance (1.462 Å) is intermediate between a single and a double bond. Most of the spin (0.92 at the 6-31G*//4-31G level) is located on the central carbon atom. The charges are +0.23 on CH_3, +0.55 on the carbene C, and +0.22 on NH_2 and the ion is best described in valence bond terminology by structures *7a* and *7b*.

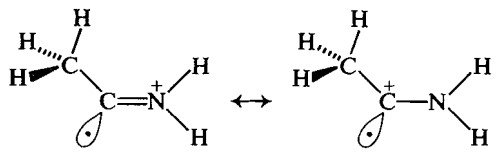

7a *7b*

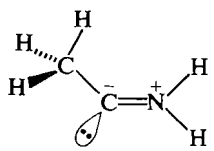

7c

The neutral molecule corresponding to **7** is an α-aminocarbene. In this structure the C—C (1.510 Å) and C—N (1.319 Å) bonds are both longer than in the radical cation, but the latter is much shorter than a single C—N bond (1.47 Å (20). Clearly then there is some π-donation from the nitrogen lone pair to the electron-deficient carbon and the α-aminocarbene has some zwitterionic character (structure *7c*). These conclusions are supported by the π-populations on N (1.72e) and on the carbene C (0.30e). However, the net-charge on the amino group is −0.17 and that on the carbene carbon +0.27, and the molecule is best represented by a carbene structure rather than by the zwitterionic structure *7c*.

On both the C_2NH_5 and the $C_2NH_5^{+\cdot}$ energy hypersurfaces the aminoethylene structure has the lowest energy (Tables 1 and 2). On the C_2NH_5 surface aziridine and molecules **5** and **7**, for which it is not possible to draw neutral structures, are all high in energy but the other molecules all have similar but lower energies. However, on the $C_2NH_5^{+\cdot}$ surface the energies of the radical cations are more widely separated with the cyclic ion again being the highest but **5** and **7** now being the two lowest above **1**.

The relative energies of the radical cations given in Table 1 are basis set dependent and all decrease on going from the 4-31G//4-31G to the 6-31G*//4-31G level. Polarisation functions are particularly important in cyclic structures and **4** is improved the most by the improvement in basis set. Inclusion of correlation energy is beyond the scope of the present investigation but this would also be expected to further decrease the energy differences and to be most significant for the cyclic

TABLE 2. Total energies (hartrees) for isomers on C_2NH_5 surface and energies (kJ mol^{-1}) relative to aminoethylene

Structure	Point group	4-31G//4-31G	Energies relative to aminoethylene at 4-31G//4-31G
1[a]	C_s	−132.87521	0
2	C_s	−132.87182	9
3	C_s	−132.85699	48
4 (pyr)	C_s	−132.82390	135
4 (planar)	C_{2v}	−132.80500	184
5	C_{2v}	−132.78337	241
6	C_s	−132.87060	12
7	C_s	−132.82640	128

[a]The amino group was assumed to be planar.

structures. For example, in a recent study (21) of carbocations the allyl cation was found to be more stable than the cyclopropyl cation by 37.8 kcal mol^{-1} at the 6-31G**//6-31G level but inclusion of correlation energy decreased the difference to 35.6 kcal mol^{-1} (at the MP4(DSQ)//6-31G* level).

Comparison of the relative energies of isomers for the isoelectronic $C_2NH_5^{+\cdot}$ and $C_2H_4O^{+\cdot}$ surfaces revealed that the corresponding isomers (NH replacing O) are, with one exception, in the same order (**1** < **7** < **5** < **3** ≈ **2** ≈ **6** < **4**) and the energy differences are also remarkably similar. The one exception is the radical cation derived from acetaldehyde, $CH_3CHO^{+\cdot}$, which is 52 kJ mol^{-1} less stable than the vinyl alcohol radical cation, whereas the analogous $CH_3CHNH^{+\cdot}$ is 121 kJ mol^{-1} less stable than the aminoethylene ion.

Summary

The structures of seven isomers on the $C_2NH_5^{+\cdot}$ energy hypersurface were determined with both the RHF and UHF methods and there is good agreement in the calculated structures. Similar good agreement was found between the two methods for the isoelectronic $C_2H_4O^{+\cdot}$ species.

Five isomeric cations, **1**, **2**, **3**, **4**, and **5** have been shown experimentally to retain their identity in the gas phase and, of these, molecular orbital calculations show **1** to have the lowest energy. One other structure, **7**, which is not known experimentally, is lower in energy than all other isomers except **1**. Radical cation **7** could form **1** by a 1,2-hydrogen shift but **7** was found to be at a minimum on the surface. Similarly, the aziridine radical cation **4** can ring open to give **5**, and **3** can also yield **5** via a 1,2-hydrogen shift. However, the calculations show both **3** and **4** to be at minima on the surface. No attempt was made here to investigate the barriers to intramolecular rearrangement but ring opening of the oxirane radical cation was previously shown to have a high barrier.

Can. J. Chem. Downloaded from www.nrcresearchpress.com by 210.87.254.5 on 09/06/12
For personal use only.

Acknowledgements

We thank the Natural Sciences and Engineering Research Council of Canada for financial support and York University Computer Centre for generous allotments of computer time.

1. C. C. VAN DE SANDE and F. W. MCLAFFERTY. J. Am. Chem. Soc. **97**, 4613 (1975).
2. J. L. HOLMES and J. K. TERLOUW. Can. J. Chem. **53**, 2076 (1975).
3. J. L. HOLMES, J. K. TERLOUW, and F. P. LOSSING. J. Phys. Chem. **80**, 2860 (1976).
4. W. J. BOUMA, J. K. MACLEOD, and L. RADOM. J. Chem. Soc. Chem. Commun. 724 (1978).
5. W. J. BOUMA, J. K. MACLEOD, and L. RADOM. Nouveau J. Chem. **2**, 439 (1978).
6. W. J. BOUMA, J. K. MACLEOD, and L. RADOM. J. Am. Chem. Soc. **101**, 5540 (1979).
7. J. L. HOLMES and J. K. TERLOUW. Can. J. Chem. **54**, 1007 (1976).
8. A. MAQUESTIAU, Y. VAN HAVERBEKE, R. FLAMMANG, and A. MENU. Bull. Soc. Chim. Belg. **88**, 53 (1979).
9. A. M. DUFFIELD, H. BUDZIKIEWICZ, D. H. WILLIAMS, and C. DJERASSI. J. Am. Chem. Soc. **87**, 810 (1965).
10. N. NISHI, H. SHINOHARA, and I. HANAZAKI. Chem. Phys. Lett. **73**, 473 (1980).
11. R. DITCHFIELD, W. J. HEHRE, and J. A. POPLE. J. Chem. Phys. **54**, 724 (1971).
12. M. R. PETERSON and R. A. POIRIER. MONSTERGAUSS. University of Toronto. 1980.
13. W. C. DAVIDON. Math. Programming, **9**, 1 (1975).
14. T. J. ZIELINSKI, R. A. POIRIER, M. R. PETERSON, and I. G. CSIZMADIA. J. Comp. Chem. **3**, 477 (1982).
15. W. J. HEHRE, R. DITCHFIELD, and J. A. POPLE. J. Chem. Phys. **56**, 2257 (1973).
16. P. C. HARIHARAN and J. A. POPLE. Theoret. Chim. Acta, **28**, 213 (1973).
17. F. BERNARDI, A. BOTTONI, and G. TONACHINI. J. Chem. Soc. Perkin Trans. **2**, 15 (1983).
18. R. C. BINGHAM, M. J. S. DEWAR, and D. H. LO. J. Am. Chem. Soc. **97**, 1294 (1975).
19. A. C. HOPKINSON and M. J. LIEN. Unpublished work.
20. J. A. POPLE and D. L. BEVERIDGE. *In* Approximate molecular orbital theory. McGraw-Hill. 1970. p. 111.
21. K. RAGHAVACHARI, R. A. WHITESIDE, J. A. POPLE, and P. v. R. SCHLEYER. J. Am. Chem Soc. **103**, 5649 (1981).
22. T. TURNER, V. C. FIORA and V. M. KENDRICK. J. Chem. Phys. **23**, 1966 (1955).

Can. J. Chem. Downloaded from www.nrcresearchpress.com by 210.87.254.5 on 09/06/12
For personal use only.

Comparative extraction studies of potassium phenoxide, *p*-nitrophenoxide, and picrate into methylene chloride by macrocyclic crown ether and cryptand complexing agents

E. BUNCEL AND H. S. SHIN
Department of Chemistry, Queen's University, Kingston, Ont., Canada K7L 3N6

AND

R. A. B. BANNARD AND J. G. PURDON
Chemical Defence Section, Defence Research Establishment Ottawa, Shirley Bay, Ottawa, Ont., Canada K1A 0Z4

Received August 11, 1983

E. BUNCEL, H. S. SHIN, R. A. B. BANNARD, and J. G. PURDON. Can. J. Chem. **62**, 926 (1984).

The results of a comparative extraction study of potassium phenoxide, *p*-nitrophenoxide, and picrate, from aqueous medium into methylene chloride in the presence of crown ether and cryptand complexing agents, are reported. The efficiency of extraction varies extremely widely with the nature of the anion and the ligand. An analysis of the results in terms of constituent equilibrium constants, and the factors which influence these, is presented. The significance of the results to other areas including phase transfer catalysis is pointed out.

E. BUNCEL, H. S. SHIN, R. A. B. BANNARD et J. G. PURDON. Can. J. Chem. **62**, 926 (1984).

On rapporte les résultats obtenus lors d'une étude effectuée en vue de comparer les possibilités relatives d'extraire du phénolate, du *p*-nitrophénolate et du picrate de potassium contenus dans des phases aqueuses par du chlorure de méthylène en présence d'éthers couronnes et d'agents complexants cryptants. L'efficacité des extractions varie considérablement suivant la nature de l'anion et du ligand. On présente une analyse des résultats en termes de constantes d'équilibre des constituants et des facteurs qui les influencent. On met en relief l'importance de ces résultats pour d'autres domaines comme la catalyse par transfert de phase.

[Traduit par le journal]

Can. J. Chem. Downloaded from www.nrcresearchpress.com by 210.87.254.40 on 09/06/12
For personal use only.

As part of a continuing study on the effect of complexing agents on reactivity (1), we have previously reported on the results of a detailed extraction study of potassium *p*-nitrophenoxide into a variety of organic solvents by crown ether and cryptand complexing agents (2). The results of that study, when compared with some literature data pertaining to picrate as the counterion, showed interesting and major differences for the two cases. A systematic study was hence undertaken which would allow us to compare the series potassium phenoxide, *p*-nitrophenoxide, and picrate in their extraction characteristics into common organic solvents by macrocyclic agents. As well, the results for potassium phenoxide could be of further interest since phenoxide ion is a commonly employed nucleophile in reactivity studies.

Ever since the discovery of the crown ethers by Pederson (3*a*) and his development of the picrate extraction method for measuring their complexation abilities (3*b*,*c*), extraction procedures have been frequently used to assess the complexing properties of newly synthesized macrocyclic ligands (4–10). This is because many of the synthetic macrocycles are very sparingly soluble in aqueous solution and studies of the complexing equilibria in a single organic phase are correspondingly difficult to carry out. Picrate anion has generally been used in such studies as the counterion, presumably because of its relative ease of transport into nonaqueous media and convenient spectral properties.

In this study we consider ligand–solvent systems for which the partitioning of both the ligands and complexed salts between the two phases can be determined, while information on the complexing properties in aqueous solution is already available. This permits a much more detailed analysis of the overall extraction process in terms of the constituent equilibria that are involved. The influence of the anion on the extraction process, from aqueous medium into methylene chloride, as a typical nonpolar organic solvent, has been studied by using the series phenoxide, *p*-nitrophenoxide, and picrate. The nature of the counterion is shown to have a dramatic effect on the ease of extraction of the potassium salts by the different complexing agents.

TABLE 1. Stability constants in water (K_s) and distribution constants (K_{dc}) between aqueous phase and methylene chloride for the macrocyclic ligands

Ligand	$K_s(M^{-1})$ H_2O	K_{dc} CH_2Cl_2
DC-18-C-6	$10^{2\,a}$	2.0×10^{3}
DB-18-C-6	44.7^{b}	$>10^{4\,e}$
18-C-6	$1.15\times10^{2\,c}$	5.0
(2,2,2)	$2.5\times10^{5\,d}$	5.0

[a]Reference 11.
[b]Reference 12.
[c]Reference 13.
[d]Reference 14.
[e]Lower limit for K_{dc} using the experimental method (4).

Results

The extraction studies with potassium phenoxide, *p*-nitrophenoxide, and picrate, from aqueous medium into methylene chloride, were performed using dicyclohexano-18-crown-6 ether (DC-18-C-6), dibenzo-18-crown-6 ether (DB-18-C-6), 18-crown-6-ether (18-C-6), and [2.2.2]cryptand (2,2,2) as the complexing agents. The stability constants (K_s) of K^+ with these ligands in water are known (Table 1). The distribution constants (K_{dc}) of the ligands between the aqueous and organic phase were determined using the method described by Frensdorff (4) and are included in Table 1.

The spectrophotometrically determined percent extraction values for the potassium aryloxide salts are given in Table 2. These results were obtained under optimized conditions of concentration of ArO^-, K^+ (introduced as ArOH and KOH, respectively), and complexing agent (see Experimental and

TABLE 2. Equilibrium constants and percent extraction by complexing agents for potassium phenoxide, *p*-nitrophenoxide, and picrate between aqueous phase and methylene chloride[a,b]

Complexing agent (C)	ArO^- (X^-)	% Extr.	K_e' (M^{-2})	K_e (M^{-2})	K_{dcs} (M^{-1})
DC-18-C-6	PhO^-	5.6	0.43	0.45	9.0
	p-NO_2PhO^-	88.0	157	161	3.2×10^3
	$PicO^-$	98.9	1.8×10^6	1.8×10^6	8.4×10^7
DB-18-C-6	PhO^-	1.8	0.18	0.18	41.9
	p-NO_2PhO^-	9.0	3.4	3.5	770
	$PicO^-$	87.0	1.6×10^5	1.7×10^5	3.7×10^7
18-C-6	PhO^-	5.2	0.54	13.7	0.60
	p-NO_2PhO^-	34.8	9.4	82.8	3.6
	$PicO^-$	96.0	7.3×10^5	1.1×10^6	4.9×10^4
(2,2,2)	PhO^-	58.8	22	1.1×10^6	21.0
	p-NO_2PhO^-	99.9	2.9×10^4	1.1×10^8	2.3×10^3
	$PicO^-$	>99.9	$>1.6\times10^7$	$>1.5\times10^{10}$	$>3.9\times10^5$

[a]See text for definition of K_e', K_e, and K_{dcs}.
[b]Concentrations of ArO^-, KOH, and C pertaining to the percent extraction values in this table are given in Table 3.

TABLE 3. Initial concentrations of complexing agent, aryloxide, and potassium ions in extraction experiments

Complexing agent (C)	ArO^- (X^-)	% Extr.	[ArOH] (M)	[KOH] (M)	[C] (M)
DC-18-C-6	PhO^-	5.6	5.26×10^{-2}	1.00	0.140
	p-NO_2PhO^-	88.0	4.65×10^{-2}	0.25	0.263
	$PicO^-$	98.9	5.30×10^{-4}	0.01	5.67×10^{-3}
DB-18-C-6	PhO^-	1.8	5.37×10^{-2}	1.00	0.103
	p-NO_2PhO^-	9.0	4.82×10^{-2}	0.25	0.123
	$PicO^-$	87.0	5.30×10^{-4}	0.01	4.85×10^{-3}
18-C-6	PhO^-	5.2	5.26×10^{-2}	1.00	0.105
	p-NO_2PhO^-	34.8	4.65×10^{-2}	0.25	0.260
	$PicO^-$	96.0	5.21×10^{-4}	0.01	4.00×10^{-3}
(2,2,2)	PhO^-	58.8	5.26×10^{-2}	1.00	9.76×10^{-2}
	p-NO_2PhO^-	99.9	4.68×10^{-2}	0.13	9.77×10^{-2}
	$PicO^-$	>99.9	5.10×10^{-4}	0.01	3.90×10^{-3}

Table 3). Equilibrium constants, as defined in the following section, were calculated according to the method given in the Appendix. The results are presented in Table 2.

Discussion

1. *Extraction efficiencies*

The results in Table 2 clearly point to the relative extraction order for the three anions as picrate > *p*-nitrophenoxide > phenoxide, which holds for all four ligands studied. This relative order remains valid even though standard conditions in the three sets of experiments could not be maintained owing to the very large differences in ease of extraction of these anions (e.g. in the picrate systems very much smaller concentrations of both ligand and salt had to be used compared to the phenoxide systems).

2. *Analysis of equilibria*

A more quantitative analysis of the data requires detailed consideration of the various equilibria that are involved in these systems (15, 16). This in turn reveals certain fundamental relationships which tend to be obscured when viewing only percentages of extraction, as a result of the interplay of several constituent factors which contribute to this overall result.

A pictorial representation of the possible equilibria involved in this system is given in Scheme 1, which expands on the earlier treatment given by Frensdorff (4), while introducing also a more systematic nomenclature for the various equilibria involved.

Not included in this scheme is the possibility of dissociation of the ion pairs M^+X^- in the organic phase into the free ions $M^+ + X^-$, or the dissociation of the complexed ion pairs MC^+X^- in the organic phase into $MC^+ + X^-$. The assumption that $(M^+X^-)_{org}$ does not dissociate into the free ions is probably valid for nonpolar organic solvents. It is considered that this assumption, as well as that $(MC^+X^-)_{org}$ does not dissociate, will not affect the overall conclusions regarding the trends observed (see below).

The equilibrium constants in Scheme 1 are defined as: K_s: stability constant for complex formation in aqueous phase; K_{ds}: distribution constant of salt between aqueous and organic phases; K_{dc}: distribution constant of complexing agent between aqueous and organic phases; K_{dcs}: distribution constant of complexed salt between aqueous and organic phases; K_a: equilibrium constant for complexation of salt in organic phase.

Can. J. Chem. Downloaded from www.nrcresearchpress.com by 210.87.254.40 on 09/06/12
For personal use only.

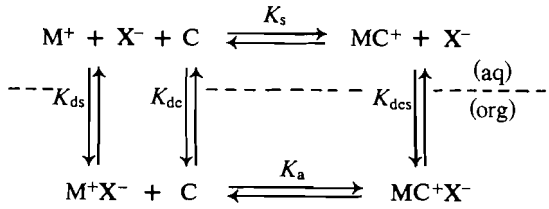

SCHEME 1

The algebraic expressions for the respective equilibrium constants are given in eqs. 1–5.[1]

$$[1] \quad K_s = \frac{[MC^+]_{aq}}{[M^+]_{aq}\,[C]_{aq}}$$

$$[2] \quad K_{ds} = \frac{[M^+X^-]_{org}}{[M^+]_{aq}\,[X^-]_{aq}}$$

$$[3] \quad K_{dc} = \frac{[C]_{org}}{[C]_{aq}}$$

$$[4] \quad K_{dcs} = \frac{[MC^+X^-]_{org}}{[MC^+]_{aq}\,[X^-]_{aq}}$$

$$[5] \quad K_a = \frac{[MC^+X^-]_{org}}{[M^+X^-]_{org}\,[C]_{org}}$$

Of the above equilibrium constants, only four are independent quantities. Also, K_s, K_{ds}, and K_{dc} can be measured independently of the ligand extraction experiments.

Previous studies of extraction equilibria have included discussion (3, 4, 15) of the extraction equilibrium constant, K_e, as defined by eq. [6]:

$$[6] \quad K_e = \frac{[MC^+X^-]_{org}}{[M^+]_{aq}\,[X^-]_{aq}\,[C]_{org}}$$

K_e provides a practical measure of the extraction efficiency of a given ligand for a particular salt from the aqueous to the organic phase. However, K_e values only relate directly to the extraction percentages in systems where the ligand is effectively confined to the organic phase. It will be seen that this is not the case for 18-C-6 and [2,2,2] in the present work.

Scheme 1 entails seven different species in equilibrium. The concentrations of the various species at equilibrium can be evaluated using the stoichiometric relationships [7]–[9],

$$[7] \quad [C]_{tot} = [C]_{aq} + [C]_{org} + [MC^+]_{aq} + [MC^+X^-]_{org}$$

$$[8] \quad [M^+]_{tot} = [M^+]_{aq} + [MC^+]_{aq} + [M^+X^-]_{org} + [MC^+X^-]_{org}$$

$$[9] \quad [X^-]_{tot} = [X^-]_{aq} + [M^+X^-]_{org} + [MC^+X^-]_{org}$$

together with the measured equilibrium concentration of $(X^-)_{aq}$ and the known equilibrium constants K_s, K_{ds}, and K_{dc} (eqs. [1]–[3]). In the present system, K_{ds} values were too small to be measurable; correspondingly, K_a values are too large in this system to be meaningfully discussed. An iterative procedure, as described in the Appendix, was used to derive the various calculable quantities.

It is useful to define a further equilibrium constant, K_e'. For many systems considered in the literature, the extent of partition of the ligand into the aqueous phase is small and has often been neglected. Hence these literature values strictly refer to an "equilibrium constant", K_e', defined by eq. [10]:

$$[10] \quad K_e' = \frac{[MC^+X^-]_{org}}{[M^+]'_{aq}\,[X^-]_{aq}\,[C]'_{org}}$$

where $[M^+]'_{aq}$ and $[C]'_{org}$ are the total concentrations of M^+ and C exclusive of $[MC^+X^-]_{org}$. Thus:

$$[M^+]'_{aq} = [M^+]_{total} - [MC^+X^-]_{org}$$

$$[C]'_{org} = [C]_{total} - [MC^+X^-]_{org}$$

This assumes that $[C]_{aq}$ and $[MC^+]_{aq}$ are negligibly small. K_e' values can then readily be calculated (Table 2).

3. *Evaluation of results*

(a) *Comparison of* K_e *and* K_e' *values*

The values of these two equilibrium constants are expected to agree under the conditions that (*i*) the partition of the ligand into the aqueous phase is small (K_{dc} large), and (*ii*) the stability constants (K_s) of the aqueous complexes are small.

The results in Table 1 show that these conditions are met for the DC-18-C-6 and DB-18-C-6 complexes of all three anions. On the other hand, large differences between K_e and K_e' are found for the 18-C-6 complexes and especially for the (2,2,2) complexes (note that K_e/K_e' ratios vary by up to 10^5). For the latter, this is the result of moderate partitioning of the free ligand into the aqueous solution in conjunction with very strong complex formation in aqueous solution (Table 1).

The effects are much smaller for picrate extraction by 18-C-6 because the total concentrations of K^+ and C used were sufficiently low that the concentrations of KC^+ and C in the aqueous phase were relatively low. On the other hand, for (2,2,2) where the stability constant is much larger, the overall effect is still important so that K_e and K_e' differ appreciably.

(b) *Absolute* K_e *values*

Inspection of the K_e values reveals the order DB-18-C-6 < DC-18-C-6 < 18-C-6 ≪ (2,2,2), which holds for all three anions. While this is in the same order as the percentage extracted values, the K_e values greatly exaggerate the apparent extraction efficiency of (2,2,2) relative to the other ligands. This is essentially because the concentration of (2,2,2) in the organic phase represents only a small fraction of the total (2,2,2) present in the system; thus (2,2,2) partitions efficiently into the aqueous phase and complexes avidly with K^+. (Note that in eq. [6], $[C]_{org}$ is extremely small for (2,2,2) because any (2,2,2) not in the form of $(MC^+X^-)_{org}$ is almost completely partitioned into the aqueous phase.)

(c) *The ligand effect on* K_{dcs} *values*

The overall order of K_e values suggests that (2,2,2) is by far the most effective ligand in terms of extracting the salt from the aqueous into the organic phase. However, if we focus on the transfer of the complexed salt MC^+X^- across the phase boundary, a different picture emerges. Thus the K_{dcs} results show in fact that DC-18-C-6, DB-18-C-6, and (2,2,2) are comparable in effectiveness, and significantly more effective than 18-C-6

[1] It is recognized that the expressions for the various equilibrium constants should strictly contain activity terms in place of concentrations as given in the present treatment. The practice of using concentration terms in extraction studies of this type, in common with other authors (e.g. refs. 5, 6, 8, 9), stems in part from the scarcity of data concerning activity coefficients for the majority of the systems investigated. However, in order to test the assumptions employed, we have carried out sample calculations for different concentrations of the aryloxide, potassium hydroxide, and complexing agent used. The resulting K_e values generally showed satisfactory agreement, indicating the overall validity of the methods employed.

Can. J. Chem. Downloaded from www.nrcresearchpress.com by 210.87.254.40 on 09/06/12
For personal use only.

Can. J. Chem. Downloaded from www.nrcresearchpress.com by 210.87.254.40 on 09/06/12
For personal use only.

in extraction ability.

Two factors should largely govern the ease of transfer of the complexed cation into the organic phase: (*i*) the "organic" nature or hydrophobicity of the ligand, and (*ii*) the extent to which the solvent molecules have been shed from the cation's solvation sphere on complexation. Compared with DC-18-C-6 and DB-18-C-6, (2,2,2) can be considered as less hydrophobic (cf. K_{dc} values, Table 2), but the 3-dimensional nature of the ligand cavity in (2,2,2) should be much more effective in excluding direct cation–solvent interactions. The net effect of these two factors appears to be a roughly equal degree of transfer of the complexed cation. On the other hand, 18-C-6 is less hydrophobic than DC-18-C-6 and DB-18-C-6, and it also allows cation–solvent interactions to persist, at least in part, in the complex. Hence the 18-C-6 complexed cation has a much greater tendency to remain in the aqueous phase, as judged by the K_{dcs} value.

(d) *The anion effect on* K_e *and* K_{dcs}

Increasing charge dispersal in the series phenoxide → *p*-nitrophenoxide → picrate has a dramatic effect on K_e and K_{dcs} values, as clearly shown in Table 2. This must predominantly reflect the relative free energies of transfer of the respective anions from aqueous to the nonpolar media employed. In the absence of ion-pair formation in the organic phase, relative K_{dcs} values for the different anions should be independent of the complexing agent involved. However, ion-pair formation in the organic phase will tend to reduce the differences in transfer of the anions. Thus the relative stabilization of the anions in the organic solvent through ion-pair formation should be in the order phenoxide > *p*-nitrophenoxide > picrate. This stabilization through ion-pair formation will also be expected to be greatest for 18-C-6 relative to the other ligands, as discussed above. Some evidence for this is seen through comparison of K_e and K_{dcs} values for DC-18-C-6 and 18-C-6. Thus for example, K_{dcs} (picrate)/K_{dcs} (phenoxide) = 1×10^7 for DC-18-C-6 and 1×10^5 for 18-C-6.

4. *Significance to other areas including phase transfer catalysis*

The present results show also that the effective range of reactivities of different anions that can be achieved through a phase transfer (17) type of experiment is much lower than might be expected from a consideration of the relative reactivities of the anions in a pure organic solvent. For example, comparing phenoxide with picrate, although the intrinsic reactivity of phenoxide ion as a nucleophile is very much greater, the concentrations that can be achieved in the organic phase are very much smaller than those of picrate. This results in a levelling effect on the overall capabilities of the two ions to react in a phase transfer system. Similar comments should also apply to other series of related anionic nucleophiles or bases.

Experimental

Materials

The macrocyclic ligands were purchased from BDH, Aldrich, Merck, or Parish Chemical Co. and used as received. The organic solvents were purified, dried, and distilled. Phenol and *p*-nitrophenol were reagent grade. Picric acid was recrystallized from ethanol.

Extraction procedure

A standard aqueous solution of the potassium aryloxide was prepared from the phenol and a standard KOH solution, the latter being in excess. A standard solution of the ligand in a particular organic solvent was also prepared. Equal volumes (1 mL) of the two solutions were placed in a small glass-stoppered test tube and after thorough mixing on a Vortex mixer for 1 min were allowed to stand for phase separation to occur; alternatively separation was effected by centrifugation. The equilibrium concentrations of aryloxide in both phases were determined after appropriate dilution using a Beckman DU-8 spectrophotometer. In the phenoxide experiments, following extraction the organic phase was diluted with 2 mL of 20% methanolic tetramethylammonium hydroxide solution in order to prevent a slow conversion of phenoxide ion to phenol on standing. This, however, was not required in the case of the *p*-nitrophenoxide and picrate ion extractions. The measured value of the aryloxide concentration in the organic phase, and the value obtained by difference before and after extraction of the aqueous solution, agreed satisfactorily. A "blank" extraction in the absence of ligand was also performed for evaluation of the distribution constant K_{ds}. There was no detectable dissolution of the potassium aryloxides in methylene chloride in the absence of the macrocyclic ligands, i.e. K_{ds} is negligibly small in these cases.

Details of the concentrations of reagents used, corresponding to the results in Table 2, are given in Table 3. The percent extraction values given are the mean of two determinations which usually agreed within ±2%.

K_{dc} values were determined spectrophotometrically using the procedure described by Frensdorff (4).

Acknowledgements

The authors thank Dr. B. G. Cox for helpful discussions. This research was supported by Supply and Services Canada, Department of National Defence (Contract No. 2SU79-00255).

1. E. BUNCEL and B. C. MENON. J. Am. Chem. Soc. **99**, 4457 (1977).
2. E. BUNCEL, H. S. SHIN, R. A. B. BANNARD, and J. G. PURDON. Abstracts, Fifth Symposium on Macrocyclic Compounds, Provo, Utah. 1981.
3. (*a*) C. J. PEDERSON. J. Am. Chem. Soc. **89**, 2495 (1967); **89**, 7017 (1967); (*b*) Fed. Proc. Fed. Am. Soc. Exp. Biol. **27**, 1305 (1968); (*c*) J. Am. Chem. Soc. **92**, 391 (1970).
4. H. K. FRENSDORFF. J. Am. Chem. Soc. **93**, 4684 (1971).
5. J. M. TIMKO, S. S. MOORE, D. M. WALBA, P. C. HIBERTY, and D. J. CRAM. J. Am. Chem. Soc. **99**, 4207 (1977).
6. H. NAKAMURA, M. TAKAGI, and K. UENO. Anal. Chem. **52**, 1668 (1980).
7. I. M. KOLTHOFF. Can. J. Chem. **59**, 1548 (1981).
8. Y. TAKEDA. Bull. Chem. Soc. Jpn. **54**, 526 (1981).
9. Y. HASEGAWA, H. WAKABAYASHI, M. SAKUMA, and T. SEKINE. Bull. Chem. Soc. Jpn. **54**, 2427 (1981).
10. T. MIYAZAKI, S. YANAGIDA, A. ITOH, and M. OKAHARA. Bull. Chem. Soc. Jpn. **55**, 2005 (1982).
11. R. M. IZATT, J. H. RYTTING, D. P. NELSON, B. L. HAYMORE, and J. J. CHRISTENSEN. Science, **164**, 443 (1969).
12. E. SHCHORI, N. NAE, and J. JAGUR-GRODZINSKI. J. Chem. Soc. Dalton Trans. 2381 (1975).
13. J. M. LEHN and J. P. SAUVAGE. Chem. Commun. 440 (1971).
14. R. M. IZATT, R. E. TERRY, B. L. HAYMORE, L. D. HANSEN, N. K. DALLEY, A. G. AVONDET, and J. J. CHRISTENSEN, J. Am. Chem. Soc. **98**, 7620 (1976).
15. F. DEJONG and D. N. REINHOUDT. Adv. Phys. Org. Chem. **17**, 279 (1980).
16. B. G. COX, J. GARCIA-ROSAS, and H. SCHNEIDER. J. Am. Chem. Soc. **103**, 1384 (1981).
17. C. M. STARKS and C. LIOTTA. Phase transfer catalysis. Academic Press, New York. 1978.

Appendix

In the present systems K^+ is in excess over the other species involved in the various equilibria represented in Scheme 1 (see Table 3). Also the amount of salt extracted in the absence of complexing agent is extremely small and can be neglected.

Therefore, as a starting point in the iteration, we take the following:

$$[K^+X^-]_{org} = 0$$

$$[A1] \quad [K^+]'_{aq} = [K^+]_{total} - [KC^+X^-]_{org}$$

It then follows that

$$[KC^+X^-]_{org} = [X^-]_{total} - [X^-]_{aq}$$

and hence

$$[A2] \quad [C]'_{org} = [C]_{total} - [KC^+X^-]_{org} = [C]_{org} + [C]_{aq} + [KC^+]_{aq}$$

From eq. [3],

$$[C]_{aq} = [C]_{org}/K_{dc}$$

and from eq. [1],

$$[KC^+]_{aq} = K_s[K^+]_{aq}[C]_{aq} = K_s[K^+]_{aq}[C]_{org}/K_{dc}$$

Substitution for $[C]_{aq}$ and $[KC^+]_{aq}$ in eq. [A2] gives

$$[A3] \quad [C]_{org} = \frac{[C]'_{org}}{1 + 1/K_{dc} + K_s[K^+]_{aq}/K_{dc}}$$

Substitution for $[K^+]'_{aq}$ from eq. [A1] gives $[C]_{org}$, and hence $[C]_{aq}$ (eq. [3]) and $[KC^+]_{aq}$ (eq. [A2]).

A second estimate of $[K^+]_{aq}$ is then made from the expression

$$[A4] \quad [K^+]_{aq} = [K^+]_{total} - [KC^+X^-]_{org} - [KC^+]_{aq}$$

This is substituted into eq. [A3] giving new estimates of $[C]_{org}$, $[C]_{aq}$, and $[KC^+]_{aq}$ and hence of $[K^+]_{aq}$ from eq. [A4] using the new value of $[KC^+]_{aq}$. The process is repeated until the values converge. At this stage, concentrations of all species required for calculation of K_c and K_{dcs} have been obtained. Convergence within reasonable limits (<2%) usually occurs after about 2–3 iterative cycles.

Can. J. Chem. Downloaded from www.nrcresearchpress.com by 210.87.254.40 on 09/06/12
For personal use only.

Transposition des cations radicaux aminés en spectrométrie de masse

HENRI EDOUARD AUDIER, JEAN PIERRE DENHEZ, ARIELLE MILLIET ET GEORGES SOZZI
Laboratoire de Synthèse Organique, Ecole Polytechnique, 91128 Palaiseau Cedex, France

Reçu le 11 juillet 1983

Ce travail est dédicacé au Professeur E. Lederer à l'occasion de son 75ème anniversaire

HENRI EDOUARD AUDIER, JEAN PIERRE DENHEZ, ARIELLE MILLIET et GEORGES SOZZI. Can. J. Chem. **62**, 931 (1984).

Il est montré en spectrométrie de masse, que les cations radicaux de faible énergie interne des alkylamines substituées en position 2, s'isomérisent au travers d'intermédiaires constitués par des cyclopropanes ionisés, liés à une molécule d'ammoniac. Ce processus est induit par le transfert sur l'azote d'un hydrogène de la chaîne situé en position 3. L'ouverture et la dissociation de ces complexes conduisent à des ions fragments m/z 44, 58 et 72 de structure $[CH_3(CH_2)_nCH\ NH_2]$. Le mécanisme de leur formation est démontré par les données des spectres MIKE de composés marqués, soit au ^{13}C, soit au deutérium. Les résultats expérimentaux sont en accord avec ceux précédemment obtenus par Gross et coll. qui ont étudié les produits de fragmentation du complexe résultant de la réaction entre une molécule d'ammoniac et des cyclopropanes substitués ionisés, en phase gazeuse.

HENRI EDOUARD AUDIER, JEAN PIERRE DENHEZ, ARIELLE MILLIET, and GEORGES SOZZI. Can. J. Chem. **62**, 931 (1984).

It is demonstrated in mass spectrometry that alkylamines substituted at C2 and containing weak internal energy isomerize in the gas phase into intermediary ions composed of ionized cyclopropanes complexed with an ammonia molecule. This process is induced by a C3 hydrogen shift on the nitrogen atom. After opening of the cyclopropane, the dissociation of these complexes leads to m/z 44, 58, and 72 ions having $[CH_3(CH_2)_nCH\ NH_2]$ structures. The mechanism of their formation is demonstrated by the MIKE spectra of ^{13}C and deuterium labelled compounds. The experimental results are in good agreement with those described by Gross *et al.*, who studied the fragmentation of the complexes formed during the reaction between substituted ionized cyclopropanes and ammonia in the gas phase.

Can. J. Chem. Downloaded from www.nrcresearchpress.com by 210.87.254.40 on 09/06/12
For personal use only.

Introduction

Dans un travail préliminaire, un mécanisme de transposition des chaînes alkylées a été proposé (1) pour expliquer la fragmentation en phase gazeuse de cations radicaux organiques de faible énergie interne.

Ce mode de réarrangement (schéma 1) a été mis en évidence lors de l'étude des éthers (1, 2), des benzoates d'alkyle (3) et de l'acide isopentaoïque (4).

Il est induit par le transfert d'un hydrogène de la chaîne sur la fonction présente dans la molécule, conduisant à un intermédiaire dans lequel un ion cyclopropanique substitué est lié à une molécule neutre.

Le même mode de transposition est observé pour les amines. Alors qu'à 70 eV, le spectre de masse des ions aminés $[R—CH_2—NH_2]^{+\cdot}$ ne présente qu'un seul pic très intense: m/z 30 (CH_2—NH_2), ce pic est le plus souvent absent du spectre MIKE dès lors que la longueur de la chaîne excède trois carbones (1, 5–7). Des pics intenses apparaissent à m/z 44, 58, 72, etc... Ils correspondent à des ions plus substitués et donc plus stables dont la formation implique une transposition préalable de la molécule.

Ainsi la décomposition métastable de l'isoamylamine (1) conduit à l'obtention d'un ion fragment abondant m/z 58 de structure $[(CH_3)_2—C^+—NH_2]$ (8) dont la formation a été expliquée par le mécanisme représenté schéma 2.

Afin de vérifier la validité et la généralité de ce mécanisme, les amines alkylées et substituées en position 2 ont été étudiées dans ce travail (**1** à **5**, schéma 3).

Résultats et interprétation

1. *Données expérimentales*

(a) Les spectres MIKE des ions **1** à **5** (tableau 1) présentent: des ions correspondant à l'élimination d'un radical (m/z 44, 58, 72 et m/z 30 dans le seul cas de **1**) qui sont généralement intenses; des ions découlant de la perte d'une molécule d'alcène dès lors que la chaîne principale contient cinq carbones au moins (ions m/z 59 et 73 dans les amines **3** et **5**); des ions m/z 32, $[CH_3—NH_3]^+$ de faible abondance; enfin des ions $[M - NH_3]^+$ dont l'étude est rendue difficile par la présence fréquente d'ions situés à une unité de masse inférieure et dont l'origine n'a pu être précisée.

(b) Les spectres ont été comparés à ceux d'amines isomères. Seuls ont été rapportés les résultats relatifs aux amines **6** à **10** à cinq atomes de carbone, isomères de **2**. Tous ces spectres diffèrent fondamentalement de celui de **2**, ce qui indique que cette amine ne s'isomérise pas en une forme moléculaire ionisée avant dissociation.

(c) Tous les pics correspondant à la perte d'un radical sont fins, les valeurs de $T_{0.5}$ étant faibles et inférieures à 0,020 eV (tableau 2).

(d) Les structures des ions m/z 44 et 58 ont déjà fait l'objet d'une étude particulière (8). Dans le cas des amines **1** à **4**, l'ion m/z 44 a toujours la structure $[CH_3—CH—NH_2]^+$ et l'ion m/z 58: $[CH_3—CH_2—CH—NH_2]^+$.

(e) Enfin de nombreux composés marqués ont été préparés (tableaux 3, 4 et 5).

2. *Les spectres MIKE des composés **1** à **5** et de leurs dérivés marqués sont en accord avec le mécanisme d'isomérisation proposé*

Ruptures simples et réarrangements

Le comportement de l'isobutylamine **1** se distingue nettement de celui des homologues supérieurs **2** à **5**: le pic m/z 30 est très intense dans le spectre MIKE de **1** (tableau 1); il est totalement déplacé à m/z 32 pour l'isobutylamine 1,1-d_2 et correspond donc à une rupture simple; et les pics m/z 44 et 58 sont de très faible intensité.

Par contre l'absence de pic m/z 30 dans les spectres MIKE des amines **2** à **5** (tableau 1), l'élimination totale des hydrogènes en position 1 lors de la formation des ions m/z 44 notamment (tableaux 3, 4 et 5) prouvent qu'il y a réarrangement des ions moléculaires avant leur dissociation.

En particulier, les spectres MIKE des amines isomères **3** et **4** présentent des pics intenses aux mêmes unités de masse avec des valeurs de $T_{0.5}$ très proches. Seules les intensités respectives

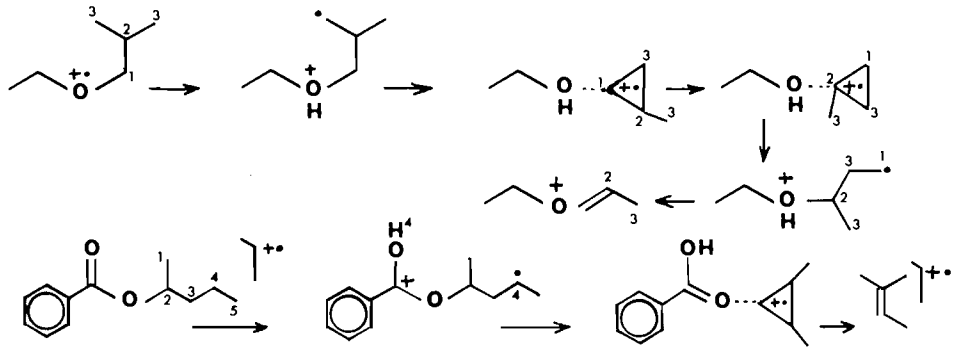

SCHÉMA 1

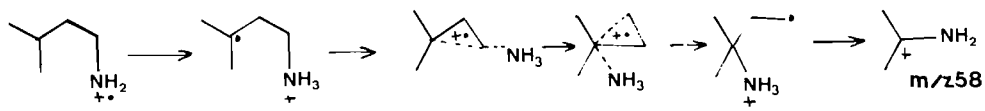

SCHÉMA 2

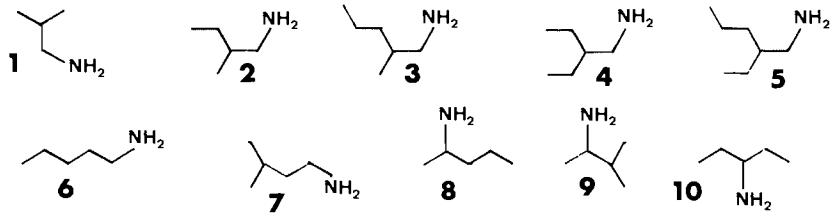

SCHÉMA 3

TABLEAU 1. Spectres MIKE des composés **1** à **10** (intensités relatives)

	m/z																				
Composé	30	31	32	43	44	45	55	56	57	58	59	69	70	72	73	83	84	86	87	97	98
1	60	<1	1	—	9	—	22	7	—	<1	—	—	—	—	—	—	—	—	—	—	—
2	0,5	2	8	—	28	1,5	—	—	—	38	4	11,5	6	1	—	—	—	—	—	—	—
3	0,5	—	4	—	19	—	—	—	—	32,5	23,5	—	—	8,5	—	—	11,5	—	0,5	—	—
4	—	—	6	—	24	—	—	—	—	14	1	—	—	38	1	—	16	—		—	—
5	—	—	—	—	2	—	—	—	—	7	—	—	—	10	7	—	—	26	—	2,5	45,5
6	13,5	—	—	—	25	52,5	—	—	—	4	—	0,5	1,5	3	—	—	—	—	—	—	—
7	—	—	—	—	—	—	—	—	—	57	11	2	28	2	—	—	—	—	—	—	—
8	1	1,5	—	36	19	1	—	—	—	1	—	8,5	5	27,5	—	—	—	—	—	—	—
9	1	0,5	—	26	1	2	—	—	—	—	—	44	25	0,5	—	—	—	—	—	—	—
10	1	3	—	—	3	2	—	—	49	15	3	17	5	3	—	—	—	—	—	—	—

TABLEAU 2. Valeurs de *T* (meV) pour les transitions M → *m/z* 44, *m/z* 58, *m/z* 72

	T (meV)		
Composé	*m/z* 44	*m/z* 58	*m/z* 72
1	6	—	—
2	15	19	—
3	14,5	14,5	17,5
4	14,5	16	17,5
8	2,5	—	—
10	—	6	—

des pics et notamment l'existence d'un pic important à *m/z* 59 pour **3**, permettent de différencier les deux spectres. Ces observations suggèrent l'existence d'intermédiaires de fragmentation communs.

Mécanisme de réarrangement de la méthyl-2 pentylamine ***3***

La fragmentation de l'amine **3** est précédée d'un échange des hydrogènes du groupe NH_2 (tableau 3: **3***a*). Toutefois cet échange n'implique pas les hydrogènes en position 1 (**3***b*) ou 2 (**3***c*); la même observation a déjà été faite pour les amines linéaires (7). Les hydrogènes portés par le C3′ ne s'échangent que lentement; par contre, ceux portés par les groupes CH_2 sont nettement impliqués (**3***e*). C'est donc par la migration sur l'azote de l'un des hydrogènes échangeable que débute la fragmentation; cette première étape conduit aux ions *a*, *b* et *c* (schéma 4).

Les ions *a* et *b* conduisent aux formes *d* dans lesquelles un ion cyclopropane ionisé est lié à une molécule d'ammoniac. Ces entités s'isomérisent par fixation de NH_3 sur un carbone substitué du cyclopropane qui s'ouvre pour donner les ions intermédiaires de type *e* dont la dissociation conduit aux ions

Can. J. Chem. Downloaded from www.nrcresearchpress.com by 210.87.254.40 on 09/06/12
For personal use only.

Can. J. Chem. Downloaded from www.nrcresearchpress.com by 210.87.254.40 on 09/06/12
For personal use only.

fragments m/z 44, 58 et 72 (schéma 4).

Les mécanismes de formation de ces fragments sont confirmés par l'étude des spectres des composés spécifiquement marqués (tableau 3). (*i*) La formation de l'ion m/z 44, de structure $[CH_3—CH—NH_2]^+$ (8), se produit avec rétention des hydrogènes du C2 (**3***c*) et du groupe CH_3 en position 3′ (**3***d*, **3***f* et **3***g*) mais avec élimination des hydrogènes du C1 (**3***b*), ce qui est conforme au mécanisme proposé. (*ii*) Le pic m/z 72 est déplacé à m/z 74 pour le composé **3***b*, à m/z 73 pour **3***c* et **3***f*, à m/z 75 pour **3***d* et **3***g*, ce dont rend compte le schéma 4. (*iii*) Enfin, conformément à ce schéma, l'ion m/z 58, de structure $[CH_3—CH_2—CH—NH_2]^+$ (8), a deux origines. Pour 20% environ (tableau 3) cet ion se forme à partir de *a* avec élimination des hydrogènes portés par les carbones C1, C2 et C3′. La fraction dominante de l'ion m/z 58 découle de *b*: selon ce mécanisme, l'ion est déplacé à m/z 59 pour **3***c* et **3***f*, à 60 pour **3***b* et à 61 pour **3***d* et **3***g*.

Dans les dérivés marqués pour lesquels il y a échange d'hydrogène avant isomérisation, les résultats expérimentaux ont été comparés à ceux d'un calcul statistique en supposant l'échange rapide d'atomes d'hydrogène portés par le groupe NH_2 avec les quatre portés par les groupes CH_2 en positions 3 et 4. Un tel calcul revient à rechercher par exemple dans le dérivé **3***a*, les intensités respectives des pics m/z 44, 45 et 46 en considérant un système H_4D_2 (9) avec rétention de deux de ces atomes dans l'ion comme le prévoit le mécanisme proposé. Les bonnes corrélations obtenues pour les dérivés **3***a* (H_4D_2) et **3***e* (H_4D_2 avec rétention du groupe CD_3) confirment que l'échange des hydrogènes en 3 et 4 est facile et celui des hydrogènes en 3′ beaucoup plus lent (tableau 3).

Enfin l'ion *c* ne saurait être précurseur des ions fragments étudiés: en effet, la fixation de NH_3 sur le carbone 4 à partir de *c* conduirait à un ion m/z 44 contenant les carbones 4 et 5, ce qu'infirment les spectres des dérivés marqués. Par contre, par rupture simple, *c* donne l'ion m/z 59 (schéma 4).

*Intermédiaires de fragmentation communs à la méthyl-2 pentylamine **3** et à l'éthyl-2 butylamine **4***

Du fait de son caractère symétrique, la fragmentation de l'amine **4** est plus simple (schéma 5). Le transfert d'un hydrogène de la position 3 sur l'azote conduit au complexe d_1, puis après isomérisation à d_2 et d_3.

Les ions m/z 44, 58 et 72 découlent des ruptures de d_2 et d_3. Les intermédiaires d_1, d_2 et d_3 sont identiques à ceux formés à partir de l'amine **3** (schémas 4 et 5): l'identité des valeurs de $T_{0,5}$ pour les ions m/z 44 et 72 (tableau 2) dans les spectres de **3** et **4** témoigne de l'existence de ces intermédiaires communs.

Les composés marqués (tableau 4) corroborent le mécanisme: il y a élimination des H1 et H2 lors de la formation de l'ion m/z 44, rétention de ces hydrogènes lors de celle de l'ion m/z 72 et élimination des H1 lors de celle de l'ion m/z 58. Il y a par ailleurs échange rapide des H3 et H4 avec ceux du groupe NH_2 avant isomérisation.

Les comportements de **3** et **4** se distinguent toutefois sur deux points: (*i*) le pic m/z 58 est nettement plus intense dans le spectre de **3**: comme il a été montré, la fraction principale de ce pic provient dans ce composé de la fragmentation de l'ion *b* qui ne peut se former à partir de **4** (schéma 4); l'élimination d'alcène est une fragmentation importante pour l'amine **3** (m/z 59, $[M - C_3H_6]^+$) alors que le pic correspondant m/z 73 $[M - C_2H_4]^+$ est pratiquement inexistant dans le spectre de **4**. La plus grande stabilité de la molécule de propène par rapport à celle d'éthylène serait à l'origine de ce phénomène.

TABLEAU 3. Déplacement des pics dans les spectres des dérivés marqués de **3** (entre parenthèses: les répartitions statistiques calculées – voir texte)

Dérivé		*m/z*																
		44	45	46	47	48	49	58	59	60	61	62	63	64	72	73	74	75	76	77
3		100	—	—	—	—	—	58	42	—	—	—	—	—	100	—	—	—	—	—
3*a*	*N,N-d*$_2$	43	51	6	—	—	—	20	35	37	8	—	—	—	15	53	32	—	—	—
		(40)	(53)	(7)	—	—	—	—	—	—	—	—	—	—	—	—	—	—	—	—
3*b*	1,1-*d*$_2$	98	2	—	—	—	—	11[b]	6	41[c]	42[a]	—	—	—	—	8	92	—	—	—
3*c*	2-*d*$_1$	—	100	—	—	—	—	13[b]	45[c]	43	—	—	—	—	—	100	—	—	—	—
3*d*	3′,3′,3′-*d*$_3$	—	—	4	96	—	—	18[b]	1	2	40[c]	39[a]	—	—	—	—	5	95	—	—
3*e*	3,3,3′,3′,3′-*d*$_5$	—	—	2	42	51	5	—	2	11	28	31	24	5	—	—	—	11	47	42
					(40)	(53)	(7)													
3*f*	3′-^{13}C	5	95	—	—	—	—	15[b]	44[c]	41[a]	—	—	—	—	5	95	—	—	—	—
3*g*	1,1-*d*$_2$,3′-^{13}C	4	95	1	—	—	—	11[b]	2	6	39[c]	42[a]	—	—	—	—	14	86	—	—

[a] Pic provenant du déplacement de m/z 59.
[b] Pic provenant de m/z 58 avec élimination de H1, H2 et H3′.
[c] Pic provenant de m/z 58 avec rétention des mêmes atomes (voir texte).

TABLEAU 4. Déplacement des pics dans les spectres MIKE des dérivés marqués de **4**

Dérivé		*m/z* 44	45	46	47	48	58	59	60	61	62	63	72	73	74	75	76	77
4		100	—	—	—	—	94	6	—	—	—	—	98	2	—	—	—	—
4*a*	*N,N*-d_2	20	54	26	—	—	11	50	38	2	—	—	13	51	36	—	—	—
4*b*	1,1-d_2	100	—	—	—	—	89	2	3	6	—	—	—	—	94	6	—	—
4*c*	1,1,2-d_3	100	—	—	—	—	—	93	4	2	—	—	—	—	—	99	1	—
4*d*	3,3-d_2	25	49	27	—	—	9	50	41	—	—	—	21	45	34	—	—	—
4*e*	3,3,3′,3′-d_4	1	20	48	28	3	1	7	37	43	11	1	1	15	43	34	6	1
4*f*	*N,N*,3,3-d_4	3	24	44	25	4	1	9	34	40	14	2	1	16	38	34	10	1

TABLEAU 5. Déplacement des pics dans les spectres MIKE des dérivés marqués de **2**

Dérivé		*m/z* 44	45	46	47	48	49	58	59	60	61	62	63
2		93	7	—	—	—	—	92	8	—	—	—	—
2*a*	*N,N*-d_2	18	40	42	—	—	—	42	48	8	2	—	—
2*b*	1,1-d_2	94	4	3	—	—	—	—	2	94	4	—	—
2*c*	2-d_1	41	57	2	—	—	—	20[a]	79	1	—	—	—
2*d*	3′,3′,3′-d_3	32	8	5	45	9	—	—	1	2	97	—	—
2*g*	3,3,3′,3′,3′-d_5	—	8	35	23	29	5	—	—	2	50	44	4
2*e*	3′-^{13}C	43	53	4	—	—	—	6	91	3	—	—	—
2*f*	3,3-d_2	19	40	41	—	—	—	45	45	9	1	—	—
2*h*	*N,N*,3,3-d_4	4	25	23	25	23	—	17	52	25	5	1	—

[a] Ce pic, beaucoup plus fin, correspond très probablement à une impureté qui n'a pu être éliminée.

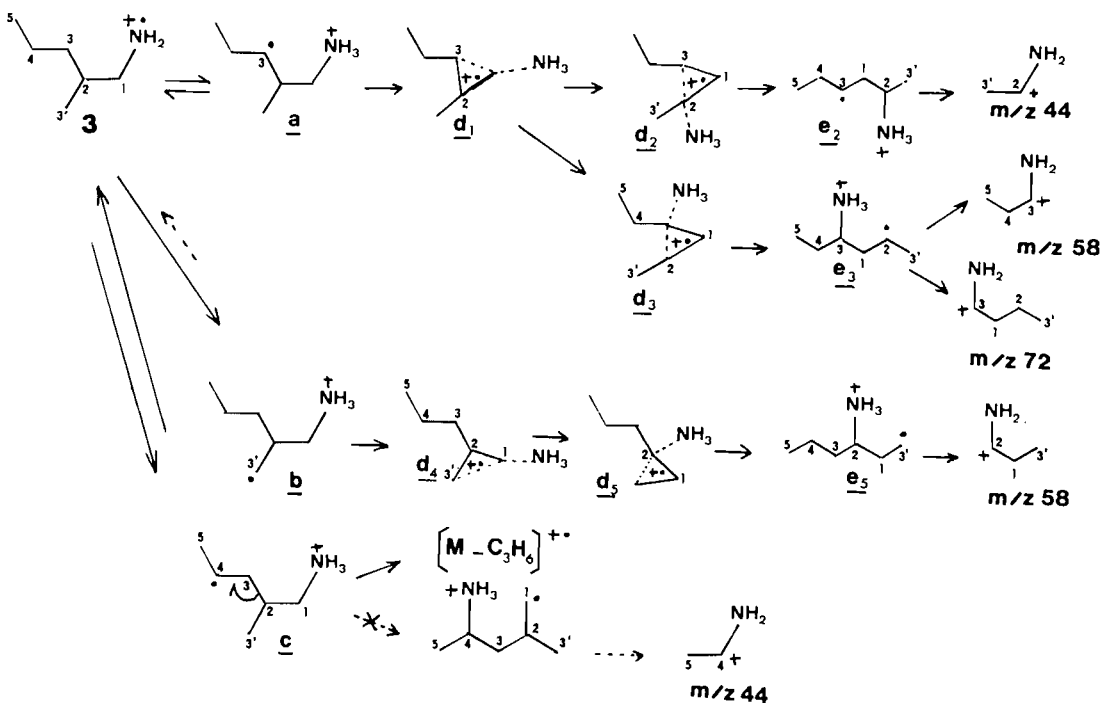

SCHÉMA 4

L'ensemble de ces données permet de conclure que **3** et **4** se fragmentent au travers des intermédiaires communs d_1, d_2 et d_3 et que les réactions **3** ou **4** → *d* ne sont pas réversibles.

La méthyl-2 butylamine **2** *conduit à un intermédiaire dans lequel les carbones en positions 3 et 4 jouent un rôle symétrique*

Les composés marqués (tableau 5) de la méthyl-2 butylamine **2** montrent tout d'abord que les modes d'échange des hydrogènes sont les mêmes que ceux déjà décrits: absence de participation des H1 et H2, échange lent des H3′ primaires, échange rapide des H3 secondaires (comparaison des spectres de **2***a* et **2***f*).

Le transfert d'un H3 ou d'un H3′ conduit aux ions *h* et *i* puis aux formes cyclopropaniques *j*.

Dans le mécanisme proposé, l'ion j_1 étant symétrique doit

Can. J. Chem. Downloaded from www.nrcresearchpress.com by 210.87.254.40 on 09/06/12
For personal use only.

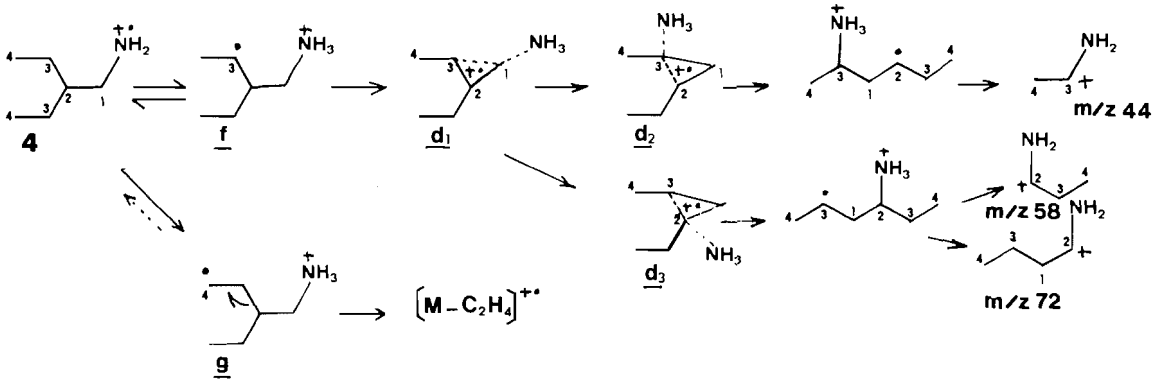

SCHÉMA 5

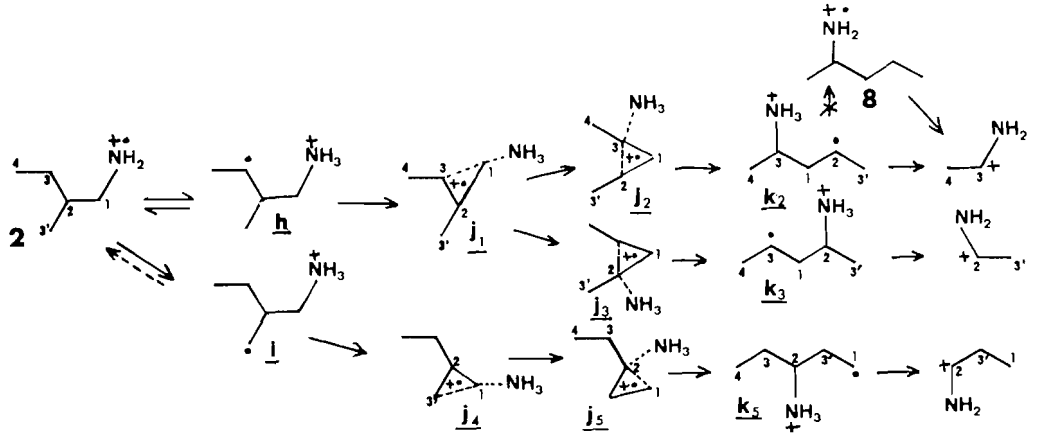

SCHÉMA 6

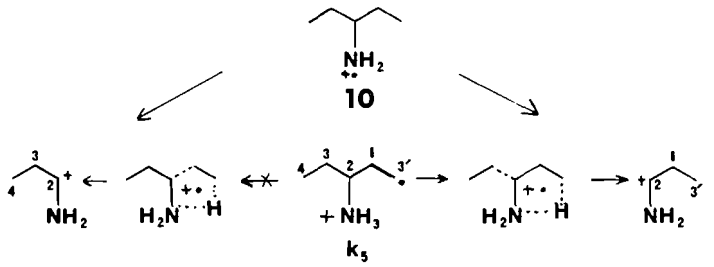

SCHÉMA 7

conduire après isomérisation à deux ions m/z 44 de structure $CH_3—\overset{+}{C}H—NH_2$ (8) contenant des carbones placés différemment dans l'ion moléculaire initial (schéma 6).

Conformément à ce schéma, le pic m/z 44 est déplacé environ pour moitié[1] à m/z 45 dans les spectres des dérivés **2***c* et **2***e* et m/z 47 pour **2***d* tandis que les H1 sont éliminés (**2***b*) (tableau 5).

La formation de l'ion m/z 58 $CH_3CH_2—\overset{+}{C}H—NH_2$ (8) est induite par le transfert sur l'azote d'un hydrogène en 3′ (schéma 6): il y a bien rétention des H1, H2 et H3′ (tableau 5).

Afin de préciser le mécanisme conduisant à la dissociation de **2**, le spectre de **2** a été comparé à ceux des isomères **8**, **9** et **10**. Le spectre de **8** comme celui de **9** présente un pic intense m/z 43 (tableau 1) lié à l'élimination d'une molécule de propane (10). Ce pic est totalement absent dans le spectre de **2**: il n'y a pas isomérisation $k_2 \rightarrow$ **8** ou **9**. La formation de l'ion m/z 44 à partir de k_2 résulte donc de la rupture d'une liaison C—C concertée avec le transfert sur le radical d'un hydrogène du groupe NH_3 (schéma 6).

De même le spectre de **10** (schéma 6) présente un pic m/z 57 lié à l'élimination d'éthane, phénomène qui n'est pas observé pour l'amine **2** (tableau 1). L'absence d'isomérisation $k_5 \rightarrow$ **10** est confirmée par les spectres des composés marqués: si un tel processus avait lieu avant formation de l'ion m/z 58, celui-ci ne conserverait que la moitié des H1 et des H3′, ce qui n'est pas le cas (schéma 7).

Deux types de facteur déterminent le mode de fragmentation des ions *k* (ou des ions *e* provenant de **3** et **4**): (*i*) la nature du radical élininé n'est pas sans incidence sur le processus. Ainsi un radical méthyle s'élimine difficilement: les pics $[M - CH_3]^+$ sont très généralement de faible intensité ou inexistants dans les dérivés **1** à **5**; (*ii*) quand un ion de type *k* est susceptible d'éliminer deux radicaux identiques mais suivant des états de transition différents ($[C_2H_5]^•$ à partir de k_5 par exemple: schéma

[1] La présence d'un pic de faible intensité m/z 45 dont l'origine n'a pu être précisée rend difficile une appréciation exacte du taux de déplacement de l'ion m/z 44.

Can. J. Chem. Downloaded from www.nrcresearchpress.com by 210.87.254.40 on 09/06/12
For personal use only.

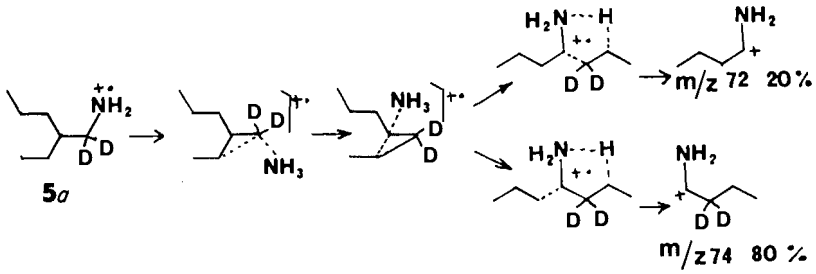

SCHÉMA 8

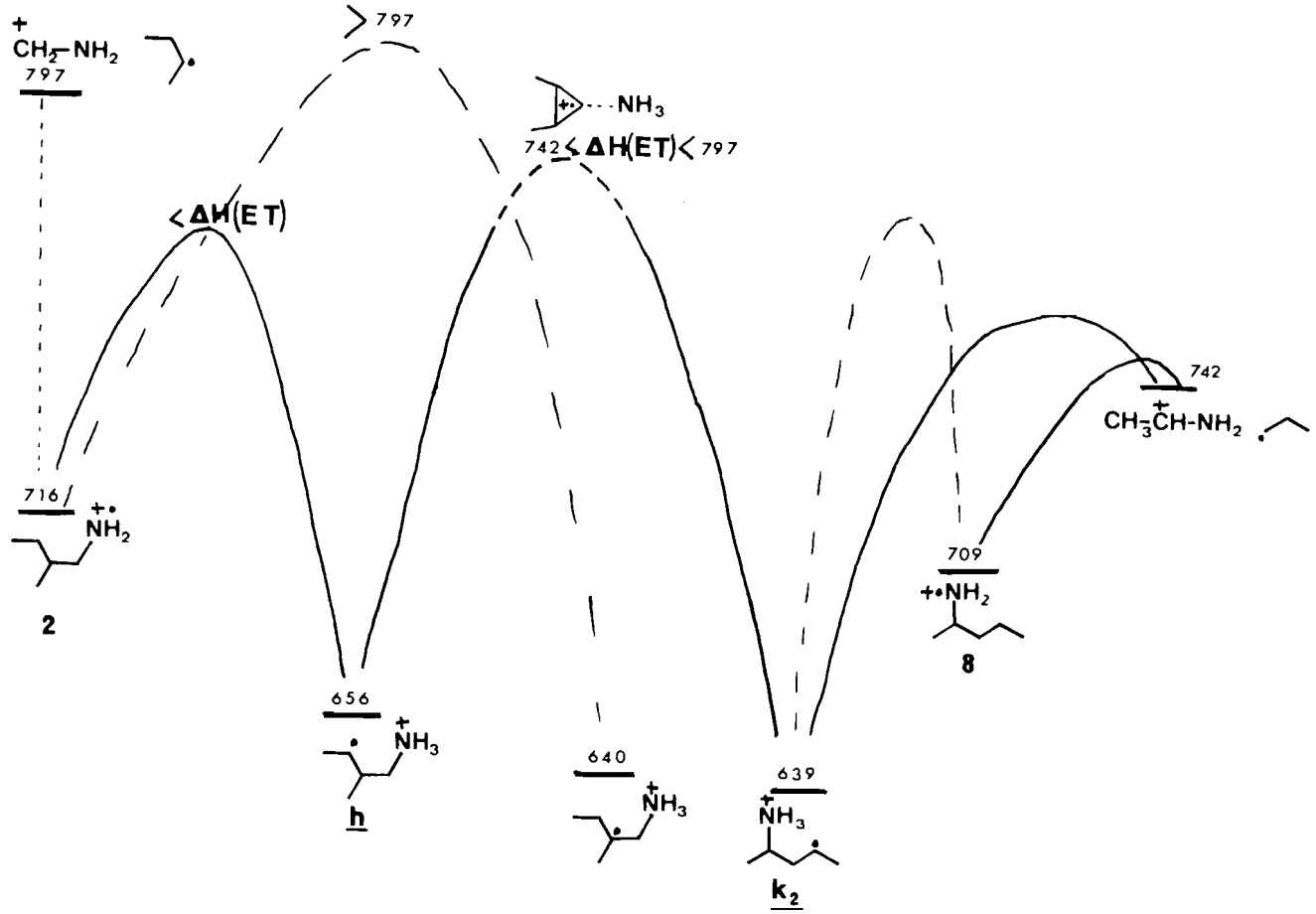

FIG. 1. Profil réactionnel de fragmentation de l'amine **2**. Les ΔH_f sont exprimés en kJ mol^{-1}.

7), il y a rétention dans l'ion de la chaîne portant initialement le radical.

Dans le but de vérifier le caractère général de la sélectivité de ce mode de rupture, l'amine **5** a été étudiée. Le spectre de ce composé présente un pic m/z 72 qui est déplacé pour 80% à 74 dans le spectre de sont dérivé bideutérié en position 1, **5***a*: schéma 8.

Discussion

(a) *Les ions* m/z *44, 58 ou 72 sont plus substitués donc plus stables que l'ion* m/z *30*, $\overset{+}{C}H_2$—NH_2 (fig. 1). Lossing *et al.* (11) ont en effet mis en évidence une différence de 88 kJ mol^{-1} entre le ΔH_f de $\overset{+}{C}H_2$—NH_2 (744 kJ mol^{-1}) et celui de l'ion CH_3—$\overset{+}{C}H$—NH_2 (656 kJ mol^{-1}).

Dans ces conditions, alors que la rupture simple **2** → $[30]^+$ nécessite 81 kJ (voir partie expérimentale), le ΔH_f correspondant à l'état final de l'ion m/z 44 est situé 26 kJ seulement au-dessus du ΔH_f de l'ion moléculaire **2**.

(b) *La première étape de la fragmentation – la protonation de l'azote par un hydrogène de la chaîne – est fortement exothermique*. Ainsi le ΔH_f de l'ion *h* (656 kJ mol^{-1}) est 60 kJ mol^{-1} plus faible que celui de l'ion **2** dont il provient.

Le ΔH_f de l'état de transition conduisant à l'ion m/z 30 étant au moins égal à 797 kJ mol^{-1}, les isomérisations de *h* conduisant à un ion stable et dont l'énergie critique est inférieure à 141 kJ seront observées (fig. 1).

Toutefois, même si ΔH_f (*h*) < ΔH_f (**2**), la réaction de protonation de l'azote présente une énergie critique qui dépend de la nature et de la position de l'hydrogène transféré. Il apparaît notamment que les migrations des hydrogènes en positions 1 et 2 ne s'effectuent pas (tableau 5).

L'étude de la formation du pic m/z 30 dans l'isobutylamine **1** explique cette constation. Ce pic est totalement déplacé à m/z 32 dans le dérivé bideutérié en position 1 et demeure à m/z 30 dans le composé 2-d_1. L'énergie critique nécessaire à des trans-

Can. J. Chem. Downloaded from www.nrcresearchpress.com by 210.87.254.40 on 09/06/12
For personal use only.

Can. J. Chem. Downloaded from www.nrcresearchpress.com by 210.87.254.40 on 09/06/12
For personal use only.

ferts et échanges de ces hydrogènes est donc supérieure à l'énergie de la rupture **1** → $[30]^+$, soit 85 kJ. Ces transferts ne peuvent donc être observés lors de la formation des ions m/z 44, 58, ou 72 dans les amines **2** à **5**.

(c) *Des formes intermédiaires ou des états de transition de type cyclopropanique ont été proposés pour expliquer la fragmentation de nombreux composés:* alcènes (12–14), alcanes (15), acides et esters (16, 17) dérivés phénoliques (18), etc. . .

Par ailleurs, l'existence de formes stables dans lesquelles un ion $[C_nH_{2n}]^+$ de structure éthylénique, carbénique ou cyclopropanique est lié à une molécule d'eau ou d'ammoniac a été montrée (19–24). Quand l'entité C_nH_{2n} a une structure éthylénique ou carbénique, ces formes stables ont des ΔH_f souvent inférieurs à ceux des alcools et amines isomères. Il n'existe par contre pas de données thermodynamiques quant aux complexes cyclopropaniques proposés dans ce travail.

Toutefois les données expérimentales indiquent que les réactions donnant ces intermédiaires constituent une barrière dans le processus d'isomérisation.

Tout d'abord ces réactions sont irréversibles. En effet, dans l'hypothèse d'une réversibilité de la réaction $h \rightleftarrows j$ (schéma 6), l'ion m/z 58 formé à partir de **2** contiendrait – fut-ce partiellement – le carbone en position quatre, ce qui est contraire aux données expérimentales (tableau 5, schéma 6). Les différences de comportement de **3** et **4** déjà évoquées vont dans le même sens.

Par ailleurs, alors que dans les amines **2**, **3** et **4**, les hydrogènes en position 3 s'échangent statistiquement avant formation de l'ion m/z 44, l'échange de ces mêmes hydrogènes est très lent avant formation du même ion m/z 44 dans la 3,3-d_2 heptylamine.

Ceci montre que l'énergie critique nécessaire à la formation de l'ion m/z 44 au travers d'une forme cyclopropanique est supérieure à celle nécessaire à sa formation à partir des amines linéaires pour lesquelles l'intermédiaire proposé est constitué par un ion alcène lié à une molécule de NH_3 (7).

Enfin la stabilité du complexe intermédiaire proposé dépend nécessairement du nombre et de la nature des substituants du cyclopropane. Il est connu en effet (25) que l'énergie d'ionisation du méthyl-cylopropane est supérieure à celle de l'éthyl-cyclopropane et plus encore à celle d'un diméthyl-cyclopropane.

Dans le cas de l'isobutylamine **1**, l'intermédiaire de transposition donnant l'ion m/z 44 est précisément le méthyl-cyclopropane ionisé lié à NH_3 moins stable que les complexes cyclopropaniques formés à partir des homologues supérieurs.

Cette observation peut expliquer la faible intensité de l'ion m/z 44 et corrélativement l'abondance de l'ion m/z 30 découlant de la rupture simple de **1**.

Conclusion

Un mode général d'isomérisation en phase gazeuse des cations aminés a été mis en évidence dans ce travail sur la base de nombreuses données expérimentales.

Le mécanisme proposé est en accord avec les résultats obtenus par Gross et Lin (26) qui ont étudié à 15 et 25 eV les fragmentations des complexes formés par action d'un ion cyclopropane substitué et d'une molécule de NH_3: un ion m/z 44 est observé quand un carbone du cyclopropane est substitué par un groupe méthyle, un ion m/z 58 est formé quand l'un des carbones porte, soit un groupe éthyle, soit deux groupes méthyles.

D'autres travaux sur la fragmentation des amines sont en cours afin de préciser si les "complexes" proposés dans ce travail constituent des formes métastables ayant une certaine durée de vie ou ne sont simplement que des états de transition.

Partie expérimentale

Les ΔH_f des radicaux propyle (86 kJ), isopropyle (73 kJ) et *sec*-butyle (53 kJ) figurent dans les tables (25).

Le ΔH_f (**2**) = 716 kJ mol^{-1} a été calculé à partir du ΔH_f de la molécule neutre (−120 kJ mol^{-1}) déterminée par la méthode de Benson (25) et de l'énergie d'ionisation de l'isobutylamine, soit 8,70 eV (25).

Le même calcul et les mêmes sources conduisent à ΔH_f (**1**) = 732 kJ mol^{-1} et à ΔH_f (**8**) = 709 kJ mol^{-1}.

Les ΔH_f [$\overset{+}{C}H_2$—NH_2] = 744 kJ mol^{-1} et ΔH_f [CH_3—$\overset{+}{C}H$—NH_2] = 656 kJ mol^{-1} ont été déterminés par Lossing *et al.* (11).

Le ΔH_f (*h*) = 653 kJ mol^{-1} est calculé à partir du ΔH_f de la méthyl-2 butylamine (−120 kJ mol^{-1}) de l'affinité protonique (27) de l'isobutylamine (932 kJ mol^{-1}) et de l'énergie de dissociation d'une liaison CH—H (28).

Les spectres MIKE ont éte réalisés sur un appareil VG.ZAB.2F. Les valeurs de $T_{0.5}$ ont été déterminées à partir de la largeur à mi-hauteur des pics après correction liée à la largeur du faisceau principal.

Les composés marqués ont été préparés suivant des procédés classiques: alkylation en α des nitriles, réduction par $AlLiD_4$, etc. . .

1. H. E. AUDIER et A. MILLIET. Int. J. Mass Spectrom. Ion Phys. **47**, 475 (1983).
2. H. E. AUDIER, G. BOUCHOUX, Y. HOPPILLIARD et A. MILLIET. Org. Mass Spectrom. **17**, 382 (1982).
3. H. E. AUDIER et A. MILLIET. Org. Mass Spectrom. **15**, 477 (1980).
4. H. E. AUDIER et G. SOZZI. Soumis pour publication.
5. S. HAMMERUM. Tetrahedron Lett. **22**, 157 (1981).
6. S. HAMMERUM, J. B. CHRISTENSEN, H. EGSGAARD, E. LARSEN, P. J. DERRICK et K. F. DONCHI. Int. J. Mass Spectrom. Ion Phys. **47**, 351 (1983).
7. H. E. AUDIER, A. MILLIET et J. P. DENHEZ. Org. Mass Spectrom. **18**, 131 (1983).
8. H. E. AUDIER, A. MILLIET, G. SOZZI et J. P. DENHEZ. Org. Mass Spectrom. Sous presse.
9. R. G. COOKS, J. H. BEYNON, R. M. CAPRIOLI et G. R. LESTER. Metastable ions. Elsevier, Amsterdam. 1973. p. 257.
10. S. HAMMERUM, K. F. DONCHI et P. J. DERRICK. Int. J. Mass Spectrom. Ion Phys. **47**, 347 (1983).
11. F. P. LOSSING, Y. T. LAM et A. MACCOLL. Can. J. Chem. **59**, 2228 (1981).
12. A. HARRISON et P. P. DYMERSKI. Org. Mass Spectrom. **12**, 703 (1977).
13. M. S. H. LIN et A. G. HARRISON. Can. J. Chem. **52**, 1813 (1974).
14. A. HARRISON et K. R. LAREDOUTE. 9th International Mass Spectrometry Conference, Vienna (Austria). 1982.
15. M. YAMAMOTO, T. TAKEUCHI et K. NISHIMOTO. Int. J. Mass Spectrom. Ion Phys. **46**, 239 (1983).
16. D. J. MCADOO et D. N. WITIAK. Org. Mass Spectrom. **13**, 499 (1978).
17. P. H. HEMBERGER, J. C. KLEINGELD, K. LEVSEN, N. MAINZER, A. MANDELBAUM, N. M. M. NIBBERING, H. SCHWARZ, R. WEBER, A. WEISZ et C. WESDEMIOTIS. J. Am. Chem. Soc. **102**, 3736 (1980).
18. C. B. THEISSLING et N. M. M. NIBBERING. Adv. Mass Spectrom. **7**, 1287 (1978).
19. J. L. HOLMES, F. P. LOSSING, J. K. TERLOUW et P. C. BURGERS. 9th International Mass Spectrometry Conference, Vienna (Austria). 1982.
20. P. C. BURGERS, J. K. TERLOUW et J. L. HOLMES. Org. Mass Spectrom. **17**, 369 (1982).
21. J. K. TERLOUW, W. HEERMA et G. DIJKSTRA. Int. J. Mass Spec-

trom. Ion Phys. **47**, 147 (1983).
22. J. L. HOLMES, F. P. LOSSING, J. K. TERLOUW et P. C. BURGERS. J. Am. Chem. Soc. **104**, 2931 (1982).
23. H. M. ROSENSTOCK, K. DRAXL, B. W. STEINER et J. T. HERRON. J. Phys. Chem. Ref. Data, **6**, (1977).
24. W. J. BOUMA, J. M. DAWES et L. RADOM. Org. Mass Spectrom. **18**, 12 (1983).
25. S. W. BENSON. Thermochemical kinetics. J. Wiley, New York 1968.
26. M. L. GROSS et P. H. LIN. Org. Mass Spectrom. **9**, 1194 (1974).
27. R. WALDER et J. L. FRANKLIN. Int. J. Mass Spectrom. Ion Phys. **36**, 85 (1980).
28. J. A. KERR. Chem. Rev. **66**, 465 (1966).

Can. J. Chem. Downloaded from www.nrcresearchpress.com by 210.87.254.40 on 09/06/12
For personal use only.

Addition d'ylures d'azométhine aux méthoxycarbonyl cyclopentènes et cyclohexènes benzocondensés. Diastéréosélectivité de la cycloaddition

JOËL VEBREL

Laboratoire de Chimie appliquée, Faculté des Sciences et Techniques de Besançon, Route de Gray, 25030 Besançon Cédex, France

ET

DANIELLE GRÉE ET ROBERT CARRIÉ

Groupe de Physicochimie Structurale, Université de Rennes, E.R.A. C.N.R.S., N° 389, Avenue du Général Leclerc, 35042 Rennes Cédex, France

Reçu le 5 août 1983

JOËL VEBREL, DANIELLE GRÉE et ROBERT CARRIÉ. Can. J. Chem. **62**, 939 (1984).

Les ylures d'azométhine s'additionnent d'une manière stéréospécifique aux méthoxycarbonyl-3 dihydro-1,2 naphtalènes substitués en 1 ou 2. La diastéréospécificité de la réaction est discutée. Le comportement des méthoxycarbonyl-2 ou -3 indènes et du méthoxycarbonyl-4 dihydro-1,2 naphtalène est également étudié.

JOËL VEBREL, DANIELLE GRÉE, and ROBERT CARRIÉ. Can. J. Chem. **62**, 939 (1984).

Azomethine ylids add stereospecifically to 3-methoxycarbonyl-1-2-dihydronaphthalenes substituted in the 1 or 2 position. The diastereospecificity of the reaction is discussed. The behaviour of 2- or 3-methoxycarbonyl indenes and of 4-methoxycarbonyl-1,2-dihydronaphthalene is also studied.

Can. J. Chem. Downloaded from www.nrcresearchpress.com by 210.87.254.40 on 09/06/12
For personal use only.

Dans le cadre d'une étude de la diastéréosélectivité des réactions de cycloaddition dipolaire-1,3 l'addition d'ylures d'azométhine résultant de l'ouverture thermique d'aziridines aux méthoxycarbonyl-3 dihydro-1,2 naphtalènes monosubstitués en 1 ou 2 (composés **1**) a été étudiée.

L'objet essentiel de ce travail était de préciser si la diastéréospécificité observée lors de ces réactions avec les azides (2) (dipôles de la classe propargyl allénique (1) persistait avec les dipôles de la classe allylique tels que les ylures d'azométhine.

En outre, les recherches entreprises ont permis de préciser la réactivité dipolarophilique des oléfines bicycliques **1**, et des composés apparentés dihydro-1,2 naphtaléniques et indéniques **2**, **3** et **4** vis à vis des ylures d'azométhine et notamment d'établir l'orientation de l'addition.

I. Obtention d'ylures d'azométhine et addition aux composés ethyléniques

Depuis les travaux de Padwa et Hamilton (3), Heine *et al.* (4), Huisgen et collaborateurs (5, 6), il est connu que certaines aziridines sont susceptibles de s'ouvrir photochimiquement ou thermiquement entre les atomes de carbone cycliques. L'aziridine est en équilibre avec l'ylure d'azométhine ainsi formé.

Lors de nos recherches les ylures d'azométhine **5***a* et **5***b* proviennent de l'ouverture des aziridines **6***a* et **6***b* préparées à partir des oléfines **7***a* et **7***b* selon le schéma 1.

L'aziridine **6***a* est obtenue quantitativement par thermolyse de la triazoline **8***a* (15 à 20 min à 170°C) sous atmosphère d'azote sec (7*a*). L'aziridine **6***b* résulte de la décomposition thermique de la triazoline **8***b* (8) dans les mêmes conditions. L'équilibre entre l'aziridine **6***a* et l'ylure d'azométhine correspondant **5***a* intervient dès la température ambiante (7 à 10). L'aziridine **6***b* n'est en équilibre avec l'ylure correspondant **5***b* qu'à plus haute température. L'existence de **5***b* a été mise en évidence dans le xylène bouillant (8).

Etudiant l'addition de l'ylure d'azométhine **5***a* résultant de l'ouverture thermique de l'aziridine **6***a* à diverses oléfines monoactivées, Texier et Carrié (7) remarquent que l'orientation de l'addition dépend de la stéréochimie de l'oléfine. Le cinnamate de méthyle et le cinnamonitrile *cis* conduisent chacun à deux pyrrolidines résultant d'une addition dans les deux sens alors qu'un seul cycloadduit est obtenu avec les oléfines *trans*. Pour celles-ci l'orientation unique se fait de telle sorte que le carbone nucléophile du dipôle se lie au carbone électrophile du dipolarophile (11).

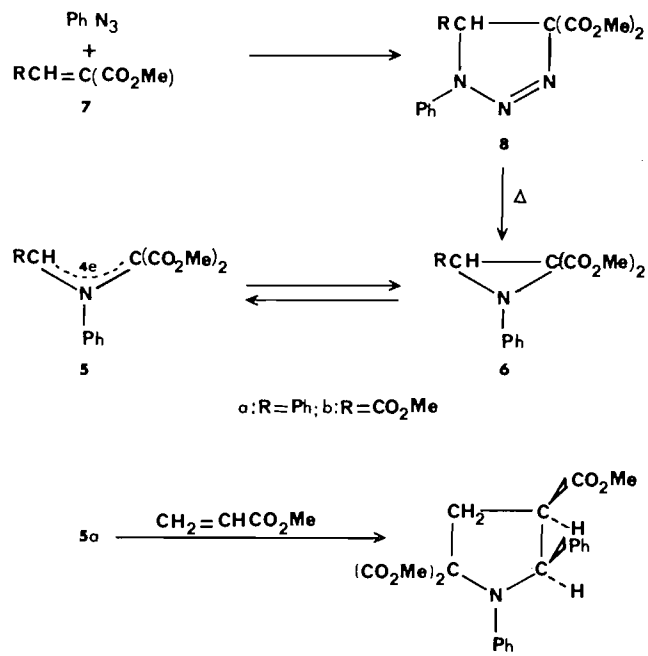

SCHÉMA 1

L'importance des facteurs stériques intervenant lors de l'approche du dipolarophile par le dipôle et déterminant la stéréochimie des cycloadduits a été soulignée (12). Cependant les travaux de Texier et Carrié (13) montrent qu'il convient de tenir compte des effets orbitalaires. Ainsi, lors de la réaction de **5***a* avec l'acrylate de méthyle l'approche des deux réactifs (supposés dans des plans pratiquement parallèles) est telle que le phényle lié au carbone du dipôle se place sous le groupement ester du dipolarophile (obtention d'un adduit *cis*, schéma 1).

TABLEAU 1. Obtention des pyrrolidines **9** à **13**. Conditions opératoires. Rendements

Pyrrolidines	n	R	X	R^1	R^2	Température de réaction (°C)	Durée de la réaction (h)	Rdt (%)[a]
9*a*	2	Ph	CO_2Me	—	—	160–165	48	96
9*a*	2	Ph	CN	—	—	160–165	30	92
9*b*	2	CO_2Me	CO_2Me	—	—	135–140	36	89
10*a*	1	Ph	CO_2Me	—	—	160–165	40	92
10*b*	1	CO_2Me	CO_2Me	—	—	135–140	24	95
11*a*	1	Ph	—	—	—	160–165	24	87
11*b*	1	CO_2Me	—	—	—	160–165	24	89
12*b*	2	CO_2Me	—	—	—	160–165	24	78[b]
13*a*	—	Ph	—	Me	H	160–165	72	70[c]
13*a*	—	Ph	—	Ph	H	160–165	72	75[d]
13*b*	—	CO_2Me	—	Me	H	160–165	28	70[c]
13*a*	—	Ph	—	H	Me	160–165	72	72[e]
13*a*	—	Ph	—	H	Ph	160–165	72	80[e]
13*b*	—	CO_2Me	—	H	Me	160–165	28	85[e]

[a]Rendement en produit pur.
[b]Environ 5% de l'oléfine de départ n'ont pas réagi (rmn).
[c]Environ 10% de l'oléfine de départ sont mis en évidence à l'aide de la chromatographie.
[d]8% d'oléfine n'ont pas réagi (chromatographie).
[e]Moins de 5% d'oléfine restante (chromatographie).

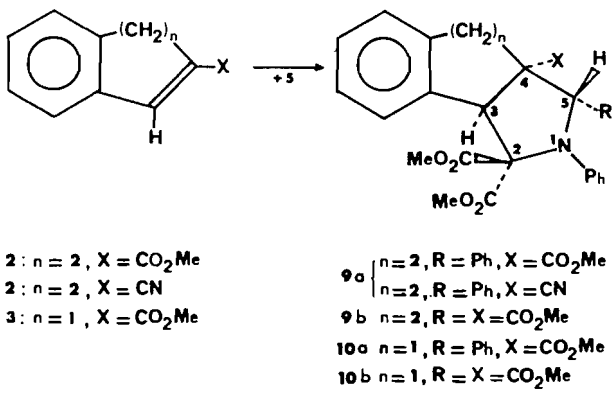

SCHÉMA 2

Les influences orbitalaires qui en résultent ont été discutées en détail avec d'autres dipôles comme les nitrones et les esters nitroniques (14); elles sont suffisamment importantes pour supplanter l'effet stérique attendu. Des comportement analogues ont été observés avec d'autres oléfines *Z* activées (8).

Lors de ce travail, les cycloadditions aux dipolarophiles **1** à **4** sont conduites en milieu anhydre sous atmosphère d'azote en solution dans le xylène ou le mésitylène bouillant, les réactifs étant en proportion équimoléculaires. Les conditions expérimentales et les rendements des pyrrolidines **9** à **13** obtenues sont précisés dans le tableau 1.

II. Addition des ylures d'azométhine 5 aux composés indéniques et dihydronaphtaléniques 2 et 3

Les différentes réactions (Schéma 2) s'effectuent avec des rendements pratiquement quantitatifs.

On constate (Tableau 1) que le dipolarophile indénique manifeste, avec le même ylure d'azométhine, une plus grande réactivité que son homologue dihydronaphtalénique.

Les principales caractéristiques spectroscopiques des pyrrolidines obtenues (ir, rmn ^1H) sont données dans le tableau 2.

L'examen du tableau 2 met en évidence les points importants suivants: l'addition est unidirectionnelle et son orientation est en accord avec celle que laissent prévoir les données de la littérature (7). Les signaux des protons H_3 et H_5 des pyrrolidines **9** et **10** sont en effet des singulets.

Il est connu qu'en série pyrrolidinique (13) les protons d'un groupement ester sont nettement blindés par un phényle en *cis* (blindage minimum de 0,3 à 0,4 ppm), lorsque ces deux groupements sont portés par des carbones vicinaux.

L'examen des données relatives aux composés **9***a* et **10***a* (R = Ph, X = CO_2Me) montre que les protons de deux groupements esters sont blindés, ce qui laisse penser que l'ester porté par le carbone 4 (X = CO_2Me) est en *cis* du phényle substituant le carbone 5 (R = Ph). Les données relatives au composé **9***a* (X = CN) dont les méthyles d'un seul groupement ester sont blindés, confirment l'attribution de la stéréochimie précédente.

La stéréochimie des composés **9***b* et **10***b* (R = CO_2Me) n'est pas établie. Elle est supposée être analogue à celle des composés **9***a* et **10***a*.

III. Addition de l'ylure d'azométhine 5 aux composés indénique et dihydronaphtalénique 4

Il nous a paru intéressant de comparer le comportement des composés **2** et **3** avec celui des dipolarophiles **4** isomères différant des précédents par la position du groupement ester. Les réactions suivantes (Schéma 3) ont été effectuées.

Les rendements sont excellents sauf pour **12***b* (Tableau 1). Dans ce cas le rendement n'est pas optimisé.

Les principales caractéristiques ir et rmn ^1H des pyrrolidines obtenues **11** et **12** sont données dans le tableau 3. L'analyse du spectre de rmn du composé **11***a* s'est révélée délicate et a nécessité des découplages de spin.

L'orientation de l'addition est parfaitement établie. Le proton H_5 est un doublet résultant du couplage ^3J avec H_4. Ces deux protons sont donc portés par deux carbones vicinaux. La littérature (7, 11) laissait prévoir l'orientation inverse. La compréhension des résultats nécessiterait une étude théorique délicate étant donné que les ylures d'azométhine ne sont pas isolables et par suite leurs géométries ne sont pas connues.

Si les données de rmn sont en accord avec les structures proposées, la configuration relative des carbones 4 et 5 ne peut être précisée avec certitude. Toutefois, la faible valeur obser-

Can. J. Chem. Downloaded from www.nrcresearchpress.com by 210.87.254.40 on 09/06/12
For personal use only.

TABLEAU 2. Caractéristiques spectroscopiques ir et de rmn (100 MHz) des pyrrolidines **9** et **10**

N°	n	X	R	Infrarouge (KBr) ν(C=O) (cm^{-1})	Résonance magnétique nucléaire ^1H ($CDCl_3$, TMS) δ H_3 et H_5	$\delta_{CO_2CH_3}$	$\delta(CH_2)_n$	δ (Protons benzéniques)
9*a*	2	CO_2Me	Ph	1724, 1735, 1746	5,02 (1H, s) 5,36 (1H, s)	3,10 3,92	2,3–3,0 (4H, m)	6,5–7,6 (m)
9*a*	2	CN	Ph	1725, 1742[a]	4,96 (1H, s) 5,02 (1H, s)	3,04 3,85	2,0–3,0 (4H, m)	6,5–7,5 (m)
9*b*	2	CO_2Me	CO_2Me	1730, 1736, 1742, 1752	4,68 (1H, s) 5,30 (1H, s)	3,10 3,60 3,67 3,81	1,6–2,7 (4H, m)	6,6–7,8 (m)
10*a*	1	CO_2Me	Ph	1720, 1733, 1744	5,20 (2H, s)[b]	3,00 3,08 4,04	Système AB 3,60 (A) ^2J = 16 Hz 3,84 (B)	6,4–7,6 (m)
10*b*	1	CO_2Me	CO_2Me	1722, 1732, 1746, 1752	4,90 (1H, s) 5,22 (1H, s)	2,92 3,60 3,80	3,48 (2H, s)	6,5–7,4 (m)

[a] ν(C≡N): 2230 cm^{-1}.
[b] Lorsque le spectre est enregistré dans C_6D_6 on mesure δ = 5,28 (1H, s) et δ = 5,44 (1H, s).

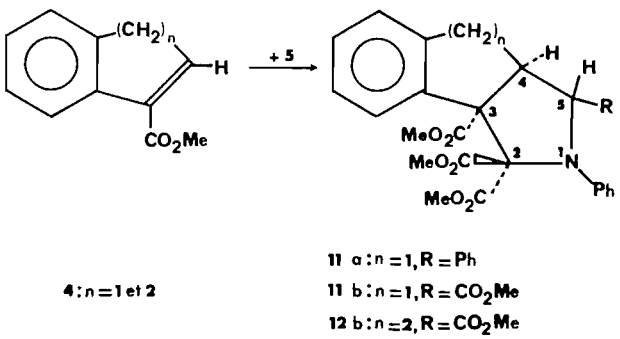

SCHÉMA 3

vée pour le couplage ^3J entre H_4 et H_5 pour **12***b* (3,9 Hz) semble indiquer que ces deux hydrogènes sont en *trans*.

IV. Addition de l'ylure d'azométhine 5a à quelques composés dihydronaphtaléniques substitués 1

Le comportement des méthoxycarbonyl dihydro-1,2 naphtalènes **1** substitués en α ($R^1 \neq H$, $R^2 = H$) et en β ($R^1 = H$, $R^2 \neq H$) a été étudié. Comme nous l'avons indiqué le but essentiel poursuivi était de voir si la diastéréospécificité constatée lors de la cycloaddition des azides (2) aux dipolarophiles **1**, s'observait également avec les ylures d'azométhine.

Chaque dipolarophile étudié conduit à une seule pyrrolidine. La réaction est à la fois régio et diastéréospécifique. Les réactions effectuées figurent au schéma 4.

Les rendements (rmn du produit brut) sont excellents; cependant l'examen du tableau 1 montre que l'introduction d'un substituant R^1 ou $R^2 \neq H$ diminue considérablement la vitesse de cycloaddition. Remarque: Toutes ces cycloadditions conduisent à *une seule pyrrolidine* (isolable) contrairement à ce que nous avons publié (15) en discutant uniquement le spectre de rmn ^1H du produit brut de la réaction.

Les principales données spectroscopiques (ir et rmn ^1H) des pyrrolidines obtenues **13** figurent au tableau 4. (Les caractéristiques des protons aromatiques entre 6,40 et 7,90 ppm ne sont pas précisées.)

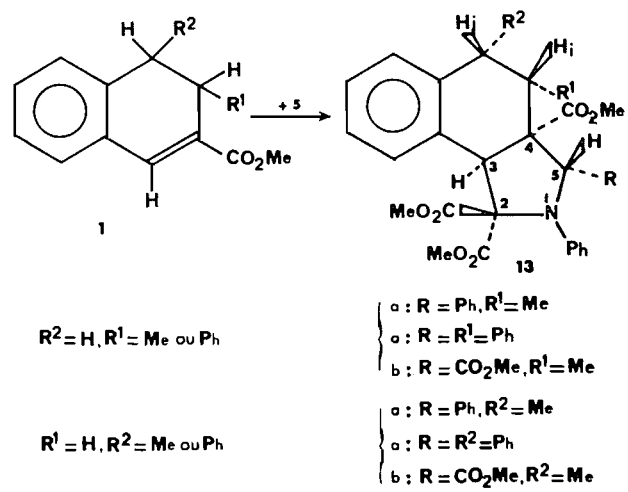

SCHÉMA 4

L'orientation de l'addition est déterminée sans ambiguité, les protons H_3 et H_5 n'étant pas couplés.

La rmn ^1H ne permet pas d'établir la stéréochimie des pyrrolidines. Cependant, un certain nombre de précisions intéressantes peuvent être apportées lorsque R = Ph.

(a) Les protons de deux des trois groupements esters sont fortement blindés ce qui donne la configuration relative des carbones 4 et 5 (ester et R = Ph en *cis*).

(b) L'enregistrement des spectres des composés **13** à haut champ (270 MHz) permet une analyse au premier ordre et l'examen des constantes de couplage des protons du carbocycle benzocondensé fournit des renseignements conformationnels intéressants: quelle que soit la nature de R^1 (Me ou Ph) des composés **13***a*, R = Ph, R^2 = H, le proton H_i n'est jamais fortement couplé avec H_j et R^2 ce qui exclut un couplage de type *trans* diaxial supérieur généralement à 10 Hz. Le substituant R^1 (Me ou Ph) occupe donc préférentiellement une position pseudo axiale. Lorsque R^2 = Me ou Ph, R = Ph, R^1 = H (composés **13***a*, le proton H_j est couplé sensiblement de la même façon avec R^1 et H_i ($5,0 < J < 7,5$) ce qui lui confère

Can. J. Chem. Downloaded from www.nrcresearchpress.com by 210.87.254.40 on 09/06/12
For personal use only.

TABLEAU 3. Caractéristiques spectroscopiques des pyrrolidines **11** et **12**

N°	Infra-rouge (KBr), ν(C=O) (cm^{-1})	Résonance magnétique nucléaire ^1H (C_6D_6), δ[a] CH_2 cycliques (J)	H_4 (J)	H_5 (J)	CO_2CH_3	Protons benzéniques
		Système AB				
	1720	4,89 (1H, d)	3,82 (dd)		3,14	
11*a*	1730	4,65 (1H, dd)	(^3J = 7,1 et	4,93 (d)	3,32	6,5–7,8 (m)
	1750	($^2J_{AB}$ = 7,4, ^3J = 7,1)	$^3J_{H_4H_5}$ = 6,9)	(^3J = 6,9)	3,51	
	1722				3,00	
	1730	3,9–4,2	3,2–3,4	4,55 (d)	3,33	
11*b*	1748	(2H, m)	(1H, m)	(^3J = 6,1)	3,36	6,6–7,6 (m)
	1760				3,54	
	1725				3,07	
	1738			4,69 (d)	3,62	
12*b*	1750	2,1–3,5 (5H) m		(^3J = 3,9)	3,73	6,6–7,9 (m)
	1765				3,81	

[a]Spectres de rmn protonique enregistrés par un appareil WP 80 Bruker (transformée de Fourier).

TABLEAU 4. Caractéristiques spectroscopiques des pyrrolidines **13**

R	R^1	R^2	Infra-rouge (KBr) ν(C=O)	Résonance magnétique nucléaire ^1H ($CDCl_3$) δ et J $\delta(H_i)$	$\delta(R^1 = H)$	$\delta(H_j)$	$J(H_iR^1)$	$J(H_iH_j)$	$J(H_jR^1)$	$\delta(R^2)$ (J)	$\delta(H_3)$ et $\delta(H_5)$	$\delta(CO_2CH_3)$
			1725									2,80
Ph	H	Me[a]	1730	1,92	2,57	3,05	14,0	7,5	5,0	1,24 (7,0)	5,09 5,24	3,04
			1745									3,94
			1725									2,67
Ph	H	Ph[a]	1738	2,41	2,91	4,26	14,0	6,0	6,2	—	5,07	2,89
			1755								5,38	3,97
			1715									3,05
CO_2Me	H	Me	1720			2,20 à 3,10 (m) – 1,14 (6,5)					4,66	3,65
			1735								5,38	3,66
			1750									3,79

R	R^1	R^2	ν(C=O)	$\delta(H_i)$	$\delta(R^2 = H)$	$\delta(H_j)$	$J(H_iR^2)$	$J(H_iH_j)$	$J(H_jR^1)$	$\delta(R^1)$ (J)	$\delta(H_3)$ et $\delta(H_5)$	$\delta(CO_2CH_3)$
			1722									2,76
Ph	Me	H[a]	1738	2,62	3,18	2,48	4,0	6,8	16,5	0,95 (6,8)	5,20 5,29	2,98
			1750									3,96
			1712									2,76
Ph	Ph	H[a]	1738	3,84	3,32	2,99	4,5	8,0	16,5	—	5,44 5,52	2,92
			1762									3,98
			1725									3,05
CO_2Me	Me	H	1730			2,40 à 3,00 (m) – 1,18 (6,4)					5,07	3,60
			1741								5,30	3,67
			1750									3,80

[a]Spectres de ces composés enregistrés à 270 MHz (Bruker, δ/HMDS) et à 100 MHz (JEOL MHz 100) pour les autres pyrrolidines (δ/TMS).

une position pseudo équatoriale préférentielle et implique que le substituant R^2 soit pseudo axial.

V. Diastéréospécificité de la cycloaddition

(a) Détermination de la stéréochimie des cycloadduits

La discussion nécessite la connaissance de la stéréochimie des pyrrolidines. La structure des composés **13***a*, R = Ph, R^1 = H, R^2 = Me et **13***a*, R = Ph, R^1 = Me, R^2 = H, a été déterminée à l'aide de la diffraction des rayons-X par l'équipe du Professeur Meinnel que nous remercions (16). Les figures 1 et 2 permettent de discuter cette stéréochimie.

Les structures obtenues montrent sans ambiguité que le méthyle substituant le cycle à six chaînons est en *cis* du groupement ester lié au même cycle. On remarque comme l'analyse rmn le laissait supposer que ce méthyle R^1 ou R^2 est dans les deux cas en position pseudo axiale.

(b) Discussion de la diastéréosélectivité

Les résultats observés avec les azides sont confirmés (2) et les interprétations avancées restent valables.

Les dipolarophiles **1**, $R^1 \neq H$, R^2 = H et **1**, R^1 = H, $R^2 \neq H$ adoptent des conformations privilégiées pour lesquelles les substituants R^1 ou R^2 sont en position pseudo axiale (2). Lors d'une cycloaddition, les réactifs sont en général supposés s'approcher dans deux plans parallèles. Le dipôle attaque la face du dipolarophile *anti* par rapport aux substituants R^1 ou

Can. J. Chem. Downloaded from www.nrcresearchpress.com by 210.87.254.40 on 09/06/12
For personal use only.

Can. J. Chem. Downloaded from www.nrcresearchpress.com by 210.87.254.40 on 09/06/12
For personal use only.

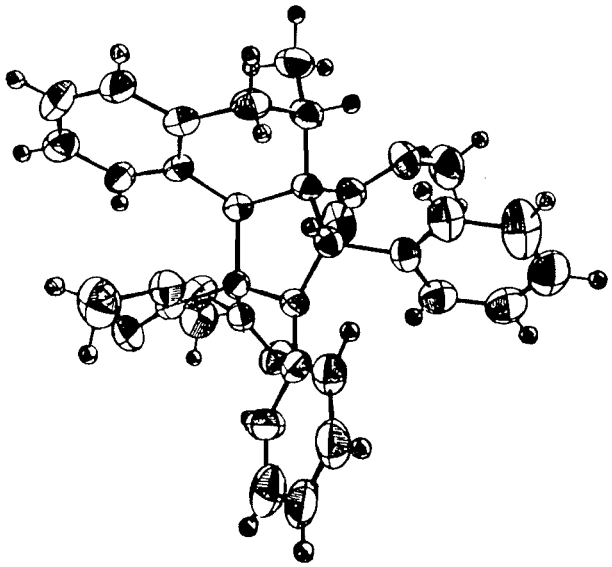

FIG. 1. Pyrrolidine **13***a* (R = Ph, R^1 = Me, R^2 = H).

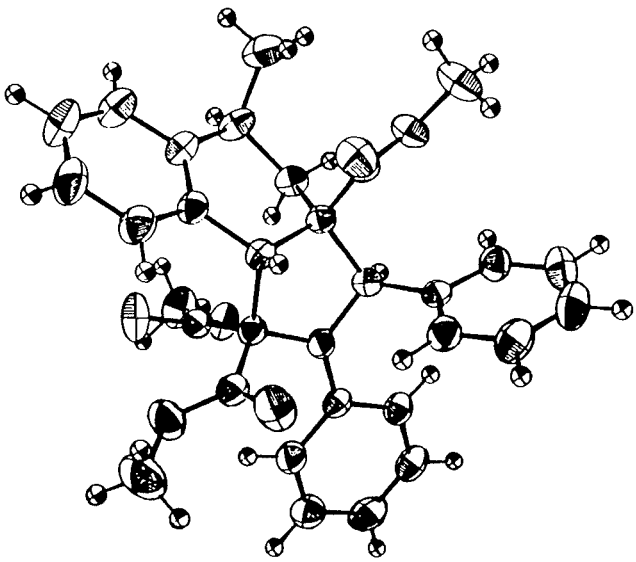

FIG. 2. Pyrrolidine **13***a* (R = Ph, R^1 = H, R^2 = Me).

R^2 qu'ils soient en α (Fig. 3) ou en β (Fig. 4) de l'insaturation.

Le dipôle approche la face la moins encombrée de l'oléfine conduisant aux adduits **13** (groupement ester du dipolarophile en *cis* des substituants R^1 ou R^2).

Les conclusions tirées des recherches conduites avec les azides semblent donc généralisables. La conformation du dipolarophile a une influence déterminante sur la diastéréochimie de la réaction. L'étude expérimentale et théorique de l'addition du diazométhane est actuellement en cours.

Partie expérimentale

Les spectres de rmn ont été enregistrés soit à l'aide d'un appareil à onde continue (JEOL MH, 100 MHz) soit avec un appareil à transformée de Fourier (Bruker WP 80 DS, 80MHz pour ^{1}H et 20,115 MHz pour ^{13}C et Bruker WH 270 (270 MHz pour ^{1}H)). Les caractéristiques infra-rouge sont obtenues à l'aide d'un spectrophotomètre Perkin–Elmer, modèle 325; les liquides sont examinés sous forme de films, les composés solides sont pastillés dans KBr. Les spectres de masse sont enregistrés en utilisant un appareil Varian mat 311 (Centre de Mesures Physiques de Rennes) avec une source à

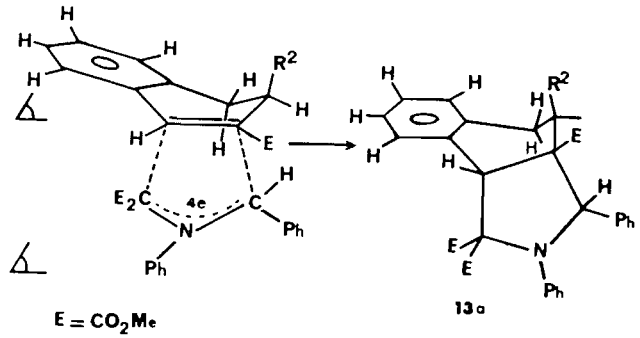

FIG. 3.

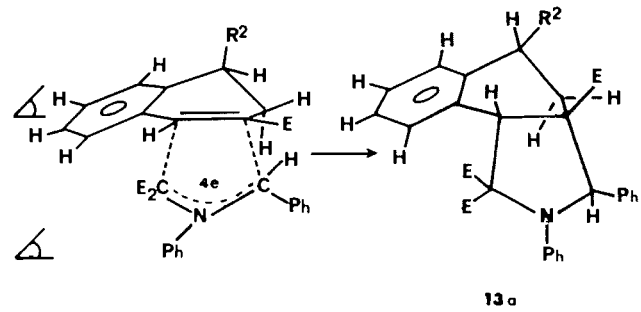

FIG. 4.

impact électronique; l'énergie du faisceau électronique est 70 eV, l'intensité du courant d'émission 300 μA et la tension d'accélération des ions 3 kV. Les points de fusion sont pris à l'aide d'un banc chauffant Kofler et les analyses élémentaires effectuées par le Service Central de Microanalyses du C.N.R.S.

I. Synthèses des dipolarophiles

A l'exception du cyano-3 dihydro-1,2 naphtalène obtenu selon la technique décrite par Julia (17), la synthèse des dipolarophiles a été décrite précédemment (18).

II. Synthèse des triazolines 8

(a) Oléfines RCH=C(CO$_2$Me)$_2$ 7

La méthode de Allen et Sprangler (19) est utilisée pour la préparation du benzylidène malonate de méthyle. Lorsque R = CO_2Me, à la méthode de House *et al.* (20) modifiée par Hall et Ykman (21), nous avons préféré la technique de Ouali *et al.* (22) qui donne d'excellents rendements (95%).

(b) Triazolines 8

Le phénylazide et le composé éthylénique sont mélangés en quantités équimoléculaires. Le mélange est maintenu sans solvant à 60°C pendant un mois pour **8***a* (7*b*) ou à 40°C pendant 15 jours pour **8***b* (8). Composé **8***a*, Rdt 70% F, 172°C (MeOH); rmn ($CDCl_3$) δ: 5,90 (s, 1H), 3,18 (s, 3H), 3,88 (s, 3H). Composé *8b*, Rdt 44%, F 118°C (MeOH); rmn ($CDCl_3$) δ: 5,45 (s, 1H), 4,00 (s, 3H), 3,94 (s, 3H), 3,79 (s, 3H).

III. Synthèse des pyrrolidines

(a) Modes opératoires généraux

Procédure A

Le mélange équimoléculaire de triazoline **8***a* et de dipolarophile dissous dans 20 cm^3 de mésitylène anhydre est porté progressivement à 160–165°C sous atmosphère d'azote. Une coloration caractéristique de l'ylure d'azométhine (rose d'abord, rouge violacé ensuite) se développe. La thermolyse s'accompagne d'un intense dégagement gazeux. Lorsque celui-ci a cessé (30 à 45 min), on porte alors à reflux du mésitylène (160–165°C). Les temps de réaction sont compris entre 24 et 72 h. Après refroidissement, le mésitylène est distillé sous pression réduite. Le résidu huileux est repris avec un peu d'éther qui provoque

Can. J. Chem. Downloaded from www.nrcresearchpress.com by 210.87.254.40 on 09/06/12
For personal use only.

la cristallisation de la pyrrolidine. Dans le cas contraire, le produit brut huileux est chromatographié.

Procédure B

Il consiste à remplacer le mésitylène par le xylène dont la température d'ébullition est suffisante pour assurer une thermolyse rapide de la triazoline **8***b* (la thermolyse commence dès 110–115°C). La solution d'aziridine **6***b* en équilibre avec l'ylure d'azométhine **5***b* a une coloration jaune très caractéristique. Après distillation du solvant et addition d'une petite quantité d'éther la pyrrolidine cristallise.

Composé **9***a*, $n = 2$, R = Ph, X = CO_2Me. Procédure A. Rdt 96%; F 162–163°C (méthanol). *Anal.* calc. pour $C_{30}H_{29}NO_6$: C 72,13, H 5,85, N 2,80; trouvée: C 72,3, H 5,9, N 2,8.

Composé **9***a*, $n = 2$, R = Ph, X = CN. Procédure A. Rdt 92%; F 186–187°C (méthanol). *Anal.* calc. pour $C_{29}H_{26}N_2O_4$: C 74,68, H 5,58, N 6,01; trouvée: C 74,4, H 5,5, N 6,1.

Composé **9***b*, $n = 2$, R = X = CO_2Me. Procédure B. Rdt 89%; F 89–90°C (éther–hexane). *Anal.* calc. pour $C_{26}H_{27}NO_8$: C 64,86, H 5,61, N 2,91; trouvée: C 64,6, H 5,7, N 2,9.

Composé **10***a*, $n = 1$, R = Ph, X = CO_2Me. Procédure A. Rdt 92%; F 188–189°C (méthanol). *Anal.* calc. pour $C_{29}H_{27}NO_6$: C 71,74, H 5,61, N 2,89; trouvée: C 71,7, H 5,4, N 3,1.

Composé **10***b*, $n = 1$, R = X = CO_2Me. Procédure B. Rdt 95%; F 161–162°C (méthanol). *Anal.* calc. pour $C_{25}H_{25}NO_8$: C 64,24, H 5,37, N 2,99; trouvée: C 64,4, H 5,4, N 2,9.

Composé **11***a*, $n = 1$, R = Ph. Procédure A. Le résidu (huile rougeâtre), après distillation du mésitylène, est chromatographié sur gel de silice (230–400 mesh; éluant: cyclohexane–éther, 50:50). Rdt 87%; F 201–202°C (méthanol). *Anal.* calc. pour $C_{29}H_{27}NO_6$: C 71,75, H 5,61, N 2,89; trouvée: C 71,8, H 5,7, N 2,8.

Composé **11***b*, $n = 1$, R = CO_2Me. Procédure A. Après élimination du mésitylène le résidu est chromatographié sur gel de silice (70–230 mesh; éluant: cyclohexane éther, 50:50). Rdt 89%; F 134–135°C (éthanol à 95°C). *Anal.* calc. pour $C_{25}H_{25}NO_8$: C 64,24, H 5,37, N 2,99; trouvée: C 64,0, H 5,4, N 3,0.

Composé **12***b*, $n = 2$, R = CO_2Me. Procédure A. Le solvant éliminé, l'huile rougeâtre résiduelle est chromatographiée sur gel de silice (230–400 mesh; éluant: cyclohexane–éther, 50:50). Rdt 78%; F 124–125°C (éthanol à 95°C). *Anal.* calc. pour $C_{26}H_{27}NO_8$: C 64,86, H 5,61, N 2,91; trouvée: C 64,6, H 5,7, N 2,9. Lors de la chromatographie on isole environ 5% d'aziridine **6***b* (huile) caractérisée à l'aide de la rmn (8) ^1H (TMS, C_6D_6) δ: 3,94 (H cyclique), 3,06, 3,39 et 3,60 (CO_2CH_3).

Composé **13***a*, R = Ph, R^1 = Me, R^2 = H. Procédure A. Purification par chromatographie sur gel de silice (230–400 mesh; éluant: hexane–éther, 60:40). Rdt 70%; F 158–159°C (méthanol). Spectrométrie de masse, masse moléculaire calc. pour $C_{31}H_{31}NO_6$: 513,215; trouvée: 513,213. Les cristaux étudiés à l'aide de la diffraction des rayons X (16) sont obtenus par cristallisation lente à 0°C d'une solution de pyrrolidine pure dans le mélange méthanol–acétone (95:5).

Composé **13***a*, R = Ph, R^1 = Ph, R^2 = H. Procédure A. On dissout dans le mélange acétone – éther éthylique (60:40) le résidu obtenu après distillation du mésitylène. La pyrrolidine cristallise lentement au réfrigérateur. Rdt 75%; F 232–233°C (mélange acétone – éther éthylique, 50:50). Spectrométrie de masse, masse moléculaire calc. pour $C_{36}H_{33}NO_6$: 575,231; trouvée: 575,227.

Composé **13***b*, R = CO_2Me, R^1 = Me, R^2 = H. Procédure A. Après élimination du mésitylène l'huile jaune orangée résiduelle est chromatographiée sur gel de silice (70–230 mesh; éluant: cyclohexane–éther, 50:50). Rdt. 70%; F 135–136°C (éthanol à 95°C). Spectrométrie de masse, masse moléculaire calc. pour $C_{27}H_{29}NO_8$: 495,189; trouvée: 495,188. La chromatographie permet d'isoler sous forme d'huile environ 10% d'aziridine **6***b* qui est caractérisée par son spectre de rmn ^1H.

Composé **13***a*, R = Ph, R^1 = H, R^2 = Me. Procédure A. On ajoute une petite quantité d'éther éthylique à l'huile jaune obtenue après distillation du mésitylène. Par refroidissement à 0°C, la pyrrolidine cristallise en partie. Les eaux mères de filtration sont chromatographiées sur gel de silice (230–400 mesh; éluant: hexane–éther, 60:40). Rdt 72%; F 158–159°C (méthanol). Spectrométrie de masse, masse moléculaire calc. pour $C_{31}H_{31}NO_6$: 513,215; trouvée: 513,213. Les cristaux étudiés à l'aide de la diffraction des rayons X (16) sont obtenus par cristallisation lente à 0°C d'une solution de pyrrolidine pure dans un mélange méthanol–acétone (95:5).

Composé **13***a*, R = Ph, R^1 = H, R^2 = Ph. Procédure A. L'huile rouge épaisse obtenue après élimination du mésitylène est chromatographiée sur gel de silice (230–400 mesh; éluant: hexane – éther éthylique, 60:40). Rdt 80%; F 186–187°C (mélange hexane – éther éthylique, 60:40). *Anal.* calc. pour $C_{36}N_{33}NO_6$: C 75,13, H 5,74, N 2,43; trouvée: C 74,9, H 5,8, N 2,4.

Composé **13***b*, R = CO_2Me, R^1 = H, R^2 = Me. Procédure A. Après élimination du mésitylène, il reste une huile rouge-orangée qui est chromatographiée sur gel de silice (70–230 mesh; éluant cyclohexane – éther éthylique, 50:50). Rdt 85%; F 180–181°C (éthanol à 95°C). *Anal.* calc. pour $C_{27}H_{29}NO_8$: C 65,45, H 5,86, N 2,83; trouvée: C 65,3, H 5,9, N 2,7. Lors de la chromatographie on isole environ 5% d'aziridine **6***b* caractérisée par son spectre de rmn ^1H.

1. R. HUISGEN. J. Org. Chem. **33**, 2291 (1968).
2. J. VEBREL et R. CARRIÉ. Tetrahedron. **39**, 4163 (1983).
3. A. PADWA et L. HAMILTON. Tetrahedron Lett. 4363 (1965); A. PADWA et L. HAMILTON. J. Heterocycl. Chem. **4**, 118 (1967).
4. H. HEINE et R. PEAVY. Tetrahedron Lett. 3125 (1965); H. HEINE, R. PEAVY et A. DURBETAKI. J. Org. Chem. **31**, 3924 (1966).
5. R. HUISGEN, R. GRASHEY et E. STEINGRÜBER. Tetrahedron Lett. 1441 (1963).
6. R. HUISGEN, W. SCHEER, G. SZEIMIES et H. HUBER. Tetrahedron Lett. 397 (1966); R. HUISGEN, W. SCHEER et H. HUBER. J. Am. Chem. Soc. **89**, 1753 (1967); R. HUISGEN. Helv. Chim. Acta, **254**, 2421 (1967).
7. (*a*) F. TEXIER et R. CARRIÉ. Tetrahedron Lett. 823 (1969); (*b*) F. TEXIER. Thèse de Doctorat d'Etat, Rennes, 1970; (*c*) F. TEXIER et R. CARRIÉ. Bull. Soc. Chim. Fr. 4119 (1971); 258 (1972); 2373 (1972); 2381 (1972); 3437 (1973).
8. M. VAULTIER. Thèse de Doctorat d'Etat, Rennes, 1977.
9. M. VAULTIER, R. DANION-BOUGOT, D. DANION, J. HAMELIN et R. CARRIÉ. Tetrahedron Lett. 1923 (1973).
10. J. PERROCHEAU. Thèse de 3ème Cycle, Rennes, 1979.
11. M. VAULTIER, R. DANION-BOUGOT, D. DANION, J. HAMELIN et R. CARRIÉ. Tetrahedron Lett. 2883 (1973); C. R. Acad. Sci. Ser. C. **277**, 1041 (1973); **280**, 213 (1975); J. Org. Chem. **40**, 2990 (1975); Bull. Soc. Chim. Fr. 1537 (1976); M. VAULTIER et R. CARRIÉ. Tetrahedron, **32**, 2525 (1976); **35**, 1357 (1979).
12. (*a*) R. HUISGEN, W. SCHEER et H. MADER. Angew. Chem. Int. Ed. Engl. **8**, 602 (1969); (*b*) R. HUISGEN, W. SCHEER, H. MADER et E. BRUNN. Angew. Chem. Int. Ed. Engl. **8**, 604 (1969); (*c*) R. HUISGEN et H. MADER. Angew. Chem. Int. Ed. Engl. **8**, 604 (1969).
13. F. TEXIER et R. CARRIÉ. Bull. Soc. Chim. Fr. 310 (1974).
14. R. GRÉE, M. JOUCLA, F. TONNARD, J. HAMELIN et R. CARRIÉ. 4ème Congr. Int. de Chimie Hétérocyclique, Salt Lake City, U.S.A., Juillet 1973; M. JOUCLA, F. TONNARD, D. GRÉE et J. HAMELIN. J. Chem. Res (S), 240 (1978).
15. J. VEBREL, E. CERUTTI et R. CARRIÉ. C. R. Acad. Sci. Ser. C, **288**, 265 (1979).
16. L. TOUPET et J. C. MESSAGER. Acta Crystallogr. C **39**, 750 (1983).
17. S. JULIA. Ann. Chim. **7**, 129 (1952).
18. J. VEBREL et R. CARRIÉ. Bull. Soc. Chim. Fr. II, 116 (1982); 161 (1982).
19. C. F. ALLEN et F. W. SPRANGLER. Org. Synth. **25**, 42 (1949).
20. H. O. HOUSE, F. J. SAUTER, W. G. KENYON et J. J. RIEHL. J. Org. Chem. **33**, 957 (1968).
21. H. K. HALL et P. YKMAN. J. Am. Chem. Soc. **97**, 800 (1975).
22. M. S. OUALI, M. VAULTIER et R. CARRIÉ. Synthesis, 626 (1977).

Low-temperature infrared study of ammonium carbamate formation

I. C. HISATSUNE

Department of Chemistry, 152 Davey Laboratory, The Pennsylvania State University, University Park, PA 16802, U.S.A.

Received September 6, 1983

I. C. HISATSUNE. Can. J. Chem. **62**, 945 (1984).

Two types of infrared spectra observed during the formation of ammonium carbamate $NH_4^+NH_2CO_2^-$ from the reaction of NH_3 and CO_2 in the solid state at low temperatures have been re-examined. These spectra had been assigned previously to amorphous and crystalline ammonium carbamate but the present data suggest their origins to be $NH_4^+NH_2CO_2^-$ and its unstable precursor $(NH_3)_2CO_2$ in which CO_2 is bent. Spectra of amorphous and crystalline ammonium carbamate have been distinguished by comparing the systems NH_3/CO_2 and $NH_3/CO_2/H_2O$. Hydrogen ion transfer in the diammoniates occurred at about $-80°C$ for NH_3/CO_2 and about $-40°C$ for ND_3/CO_2.

I. C. HISATSUNE. Can. J. Chem. **62**, 945 (1984).

On a réétudié deux types de spectres infrarouges observés au cours de la formation du carbamate d'ammonium, $NH_4^+NH_2CO_2^-$, par réaction de l'ammoniac et de l'anhydride carbonique à l'état solide et à basse température. Au cours des travaux antérieurs, ces spectres avaient été attribués aux formes amorphes et cristallines du carbamate d'ammonium; toutefois, les nouvelles données suggèrent qu'ils sont dus au $NH_4^+NH_2CO_2^-$ et à son précurseur instable, $(NH_3)_2CO_2$, dans lesquels le CO_2 serait déformé. On a pu distinguer les formes amorphe et cristalline du carbamate d'ammonium en les comparant aux systèmes NH_3/CO_2 et $NH_3/CO_2/H_2O$. Il se produit un transfert d'ions hydrogènes dans les diammoniates à environ $-80°C$ pour NH_3/CO_2 et à environ $-40°C$ pour ND_3/CO_2.

[Traduit par le journal]

Introduction

It was reported earlier (1) that in acid–base reactions involving hydrogen-bonded solids, proton-transfer occurs at temperatures significantly above the boiling point of liquid nitrogen. Hence, such reactions can be studied conveniently in conventional, liquid-nitrogen cooled, low-temperature infrared cells. In the present investigation, the same experimental technique was used to examine the formation of ammonium carbamate from ammonia and carbon dioxide in the solid state at low temperatures. This interesting system had been studied previously by Frasco (2) who observed two kinds of infrared spectra. The origin of one type of spectrum was attributed to an amorphous solid ammonium carbamate since this species was the first to be formed at $-78°C$. Warming of this initial species to $-25°C$ gave rise to the second type of spectrum which was assigned to crystalline ammonium carbamate $NH_4^+NH_2CO_2^-$. Results from the present investigation indicate that this interpretation must be modified.

Experimental

Ammonia and carbon dioxide gases were from the Matheson Co., and they were distilled or sublimed, respectively, under reduced temperature and pressure into gas storage bulbs. Ammonia-d_3 from Merck, Sharp, and Dohme of Canada, Ltd., was degassed and then used directly.

A liquid-nitrogen cooled, low-temperature cell described before (3) was used to record the infrared spectra of the samples. Spectra were taken on Perkin-Elmer Model 521 or 621 grating spectrophotometers.

Results and discussion

According to the top spectra in Figs. 1 and 2 and in agreement with an earlier observation of Frasco (2), no products were formed when mixtures of ammonia and carbon dioxide gases were condensed on an infrared window cooled at $-190°C$. Broad peaks present in the $1400-1600\ cm^{-1}$ region in these initial scans are due to solid ammonia and not to any products. However, warming of these matrices to about $-160°C$ and above caused new absorption peaks to appear. Reactions giving rise to these new peaks were evidently over by about $-130°C$. The middle spectra in Figs. 1 and 2 illustrate the changes caused by these warming sequences, and their peak frequencies are summarized in Table 1 (columns 2 and 3). The present spectra are similar to those identified as Type I by Frasco (2) although he reported no frequency values.

Additional changes in the spectra of NH_3/CO_2 and ND_3/CO_2 matrices occurred when sample temperatures reached near $-80°C$ and $-40°C$, respectively. Most notably, the peak at 3370(2510) cm^{-1} disappeared and new peaks appeared at 3475(2600), 3310(2430), 1485(1072), 1265(915), 1040(~810), 728(~700), and 460(342) cm^{-1} where values in parentheses are for the ND_3/CO_2 system. These new spectra (Figs. 1 and 2) and their peak frequencies (Table 1) are essentially the same as those from the Type II species in the work of Frasco (2). No further changes in these spectra were observed until about 0°C when the samples began to sublime off the infrared window and absorption bands of gaseous ammonia became visible.

The source of Type II spectra had been proposed by Frasco (2) to be a crystalline ammonium carbamate $NH_4^+NH_2CO_2^-$. The present work provides additional support for this interpretation. During the formation of this product as evidenced by the changes described in the preceding paragraph, continued annealing of a sample caused single peaks in the spectrum to change into multiplets characteristic of amorphous to crystalline phase changes. Such multiplets were observed at 3120/3010, 2830/2750, 1485/1464/1447, 745/728, 580/567, and 512/460 cm^{-1}. Since water was expected to stabilize the amorphous phase through hydrogen-bond formation (1), several mixtures of $NH_3/H_2O/CO_2$ with NH_3/H_2O mole ratios ranging from one to two were also examined. These systems gave complex spectra due to the presence of ammonia hydrates and low yields of the carbamate since the reactivity of NH_3 was reduced and sufficient CO_2 could not be maintained in the matrix at the reaction temperatures. However, in such matrices, the multiplet bands all appeared as single peaks even at temperatures where the samples began to sublime off the infrared window. The spectra of these amorphous samples were also distinct from those of the initial reaction product (central spectra, Figs. 1 and 2). In particular, the spectra of amorphous ammonium carbamate always showed a pair of peaks at 3460

Can. J. Chem. Downloaded from www.nrcresearchpress.com by 210.87.254.6 on 09/06/12
For personal use only.

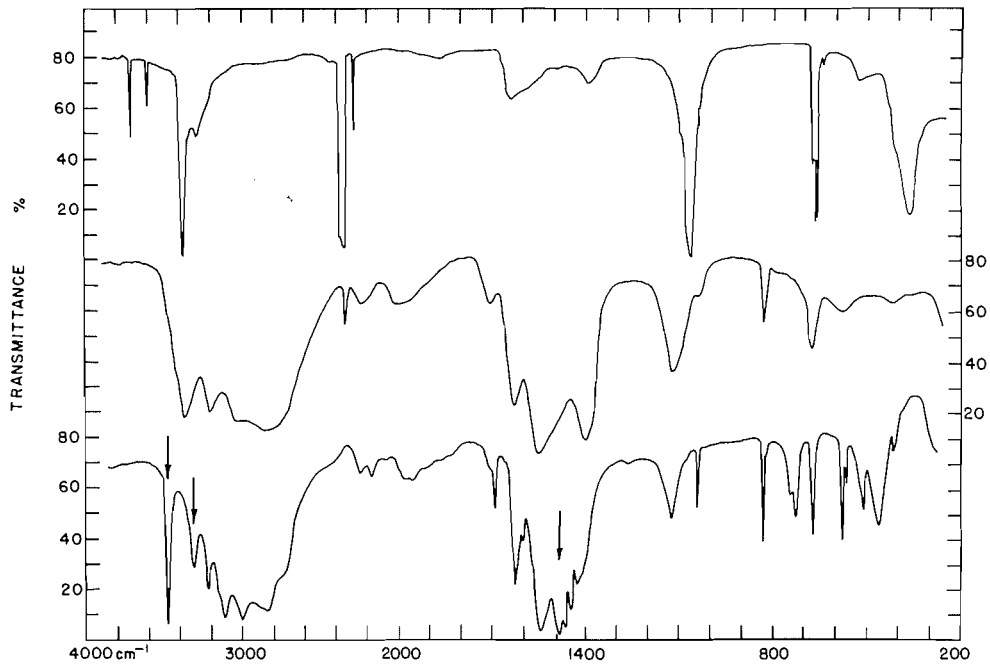

FIG. 1. Infrared spectra of NH_3/CO_2 = 3.0 system at −190°C. Top spectrum, initial; central spectrum, after warming to −100°C; lower spectrum, after warming to −25°C. Arrows indicate characteristic $\nu(NH_2)$ and $\delta(NH_4^+)$ absorption bands.

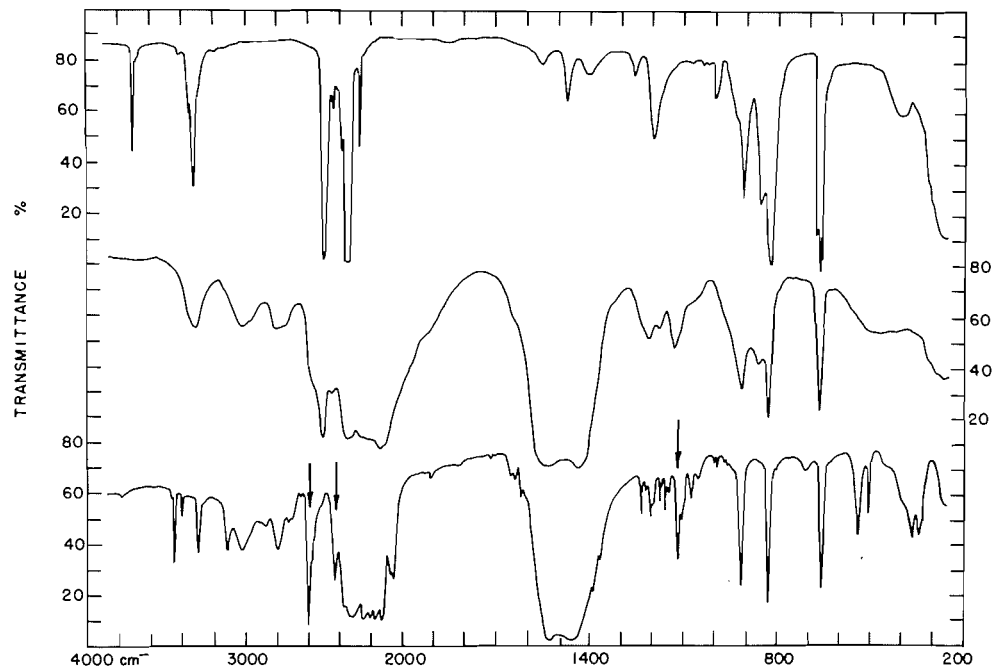

FIG. 2. Infrared spectra of ND_3/CO_2 = 2.0 system at −190°C. Top spectrum, initial; central spectrum, after warming to −75°C; lower spectrum, after warming to −40°C. Arrows indicate characteristic $\nu(ND_2)$ and $\delta(ND_4^+)$ absorption bands.

and 3300 cm^{-1} as well as a broad single peak at about 1470 cm^{-1}. Corresponding peaks in the crystalline sample are identified in Table 1 and in Figs. 1 and 2. Other peaks in the amorphous spectra were at ~3000, 1680, 1620, 1530, 1110, 826, ~730, 665, 570, and ~460 cm^{-1}.

If the Type I species is not an amorphous ammonium carbamate as was originally suggested (2), then it must be an unstable precursor of the final reaction product. Since several unstable ammoniates of water (4) and of sulfur dioxide (5) are known, it is reasonable to expect this precursor to be an ammoniate of CO_2. In view of the ease (−80°C for NH_3 and −40°C for ND_3) with which proton-transfer took place to change this precursor into the final product, this complex must be $(NH_3)_2CO_2$. Here, the two ammonia molecules may not be equivalent just as in the case of $(NH_3)_2H_2O$ (4, 6). One NH_3 may be forming an NC bond causing the carbon dioxide molecule to be bent and giving rise to intense $\nu(CO_2)$ bands at 1545 and 1400 cm^{-1}. The second NH_3 molecule, on the other hand, may be only hydrogen-bonded to an oxygen atom of CO_2. According to the temperature dependence study, both isotopic diammoniates are formed at about −160°C, but there is a significant isotope effect in the transformation of this complex

Can. J. Chem. Downloaded from www.nrcresearchpress.com by 210.87.254.6 on 09/06/12
For personal use only.

TABLE 1. Infrared spectra of ammonium carbamate and its precursor at −190°C (cm^{-1} units)

Assignments[a]	$(NH_3)_2CO_2$	$(ND_3)_2CO_2$	$NH_4^+NH_2CO_2^-$	$NH_4^+ND_2CO_2^-$	Assignments[a]
			3475[b]	2600[b]	$\nu_a(NH_2)$
$\nu_a(NH_3)$	3370	2510			
			3310[b]	2430[b]	$\nu_s(NH_2)$
$\nu_s(NH_3)$	3220	~2340	3220	~2330	
			3120	2250	
	~3030	~2240			
			3010	2183	$\nu(NH_4^+)$
	~2850	~2140	~2830	2125	
			~2750	~2070	
	~2240	~1650	2240		
			2170		
	~1975		~1970		
	~1710		1680		
				1232	
$\delta_a(NH_3)$	1625	1210	1625	1200	$\delta(NH_2)$
		~1180			
				1174	$\delta(NH_4^+)$
				1158	
				1150	
$\nu_a(CO_2)$	1545	1530	1545	1527	$\nu_a(CO_2)$
	~1490				
			1485[b]	1072[b]	$\delta(NH_4^+)$
			1464	~1052	
			1447		
$\nu_s(CO_2)$	1400	1435	1425	~1450	$\nu_s(CO_2)$
				1390	
				1367	
				1000	
				990	
			1265	915	$\rho(NH_2)$
ν(CN)	1120	1130	1122	1117	ν_tCN)
		~1080		~1100	
$\delta_s(NH_3)$		910			
			1040	~810	$\omega(NH_2)$
$\delta_s(NH_3)$		860			
$\omega(CO_2)$	830	827	832	826	$\omega(CO_2)$
			745		
			728	~700	$\rho(CO_2)$
$\delta(CO_2)$	680	665	670	657	$\delta(CO_2)$
$\tau(CO_2)$	~580	~500	580	537	$\tau(CO_2)$
			567	510	
				~440	
				~390	
			512	364	
			460	342	$L(NH_4^+)$

[a] ν_a = antisymmetric stretch, ν_s = symmetric stretch, δ = deformation, ω = wag, ρ = rock, τ = torsion, and L = lattice.

[b] These peaks are identified by arrows in Figs. 1 and 2.

to the carbamate. Water (1, 4) and sulfur dioxide (5) also form mono-and di-ammoniate complexes.

Tentative assignments of the fundamental modes of carbon dioxide diammoniate and ammonium carbamate are summarized in Table 1. The assignments for the carbamate follow those of Frasco (2) with minor modifications. In ND_3 system, bands were observed at 810 and 915 cm^{-1} whereas Frasco reported bands at 748 and 968 cm^{-1}. A transient band was detected at 970 cm^{-1} as well as at 2440, 880, 870, 622, 538, 510, 470, and 410 cm^{-1} when an ND_3/CO_2 system was warmed to −50°C, but it disappeared at −40°C when the sample changed to the carbamate. In order to identify bands due to isotopic dilution, H_2O was condensed on top of several samples of ND_3/CO_2 and exchange reactions were followed as these samples were allowed to warm to 0°C several times. Exchange reactions did occur in these samples, but the bands listed in Table 1 under the deuterium species did not appear to change their relative intensities. Hence, peaks of deuterium species with no hydrogen counter-parts listed in Table 1 presumably have their corresponding hydrogen peaks hidden by other strong bands in the spectra. Finally, the ease with which an ionic $NH_4^+NH_2CO_2^-$ sublimes at room temperature into NH_3 and CO_2 is reminiscent of room temperature sublimations of ionic $(NH_4)_2SO_3$ into NH_3, H_2O, and SO_2 (5) and of ionic $NO_2^+NO_3^-$ into gaseous N_2O_5 (7). All of these ionic solids can be pumped off readily at room temperature. Their infrared spectra, so far, have not provided any clues as to why these salts sublime so readily.

Can. J. Chem. Downloaded from www.nrcresearchpress.com by 210.87.254.6 on 09/06/12
For personal use only.

1. T. HUSTON, I. C. HISATSUNE, and J. HEICKLEN. Can. J. Chem. **61**, 2077 (1983).
2. D. L. FRASCO. J. Chem. Phys. **41**, 2134 (1964).
3. L. A. HULL, I. C. HISATSUNE, and J. HEICKLEN. J. Am. Chem. Soc. **94**, 4856 (1972).
4. J. E. BERTIE and M. M. MORRISON. J. Chem. Phys. **73**, 4832 (1980).
5. I. C. HISATSUNE and J. HEICKLEN. Can. J. Chem. **53**, 2646 (1975).
6. W. J. SIEMONS and D. H. TEMPLETON. Acta Crystallogr. **7**, 194 (1954).
7. I. C. HISATSUNE, J. P. DEVLIN, and Y. WADA. Spectrochim. Acta, **18**, 1641 (1962).

Can. J. Chem. Downloaded from www.nrcresearchpress.com by 210.87.254.6 on 09/06/12
For personal use only.

Thermodynamic properties of binary mixtures containing ketones. VIII. Heat capacities and volumes of some *n*-alkanone + *n*-alkane mixtures at 298.15 K[1]

JEAN-PIERRE E. GROLIER
Laboratoire de Thermodynamique et Cinétique Chimique (ERA CNRS 1005), Université de Clermont-Ferrand 2, F-63170 Aubière, France

AND

GEORGE C. BENSON
Division of Chemistry, National Research Council of Canada, Ottawa, Ont., Canada K1A 0R6

Received November 14, 1983

JEAN-PIERRE E. GROLIER and GEORGE C. BENSON. Can. J. Chem. **62**, 949 (1984).

Excess molar volumes, V_m^E, and excess molar heat capacities at constant pressure, $C_{p,m}^E$, have been obtained for some *n*-alkanone + *n*-alkane mixtures at 298.15 K from density and volumetric heat capacity measurements using liquid-flow techniques. The $C_{p,m}^E$ data are much more accurate than those estimated from the temperature dependence of other thermodynamic properties (excess free energies and/or excess enthalpies). The rather *unusual* composition dependence of the excess heat capacities — two minima, or W-shape curves — is most likely due to cooperative induced conformational molecular "arrangements" in these mixtures.

JEAN-PIERRE E. GROLIER et GEORGE C. BENSON. Can. J. Chem. **62**, 949 (1984).

Les volumes d'excès, V_m^E, et les capacités calorifiques d'excès, $C_{p,m}^E$, ont été obtenus pour quelques mélanges *n*-alcanone + *n*-alcane à 298.15 K à partir de mesures des densités et des capacités calorifiques volumiques, à l'aide de techniques à écoulement de liquide. Les valeurs de $C_{p,m}^E$ ainsi obtenues sont beaucoup plus précises que celles estimées à partir de la variation, avec la température, d'autres propriétés thermodynamiques (enthalpies libres d'excès et/ou enthalpies d'excès). La variation avec la concentration des capacités calorifiques d'excès se manifeste par des formes de courbe tout à fait *inhabituelles* — deux minima ou forme en W —, ce qui traduit probablement des "arrangements" moléculaires par effets conformationnels coopératifs et induits, dans ces mélanges.

Can. J. Chem. Downloaded from www.nrcresearchpress.com by 210.87.254.42 on 09/06/12
For personal use only.

Binary *n*-alkanone + *n*-alkane mixtures have been investigated fairly extensively from a thermodynamic point of view. For our part, we have measured a number of heats of mixing, and recently we published two review papers (1, 2) analysing the information available in the literature about the thermodynamic properties of this class of mixtures in terms of a quasi-chemical group contribution model. Surprisingly, no data could be found for their heat capacities. This lack of information, and our interest in binary liquid mixtures having an *n*-alkane as one component and a simple organic compound as the other, prompted us to investigate the excess molar heat capacity at constant pressure, $C_{p,m}^E$, of *n*-alkanone + *n*-alkane mixtures. $C_{p,m}^E$ is of importance since it is related to the structures of the pure component liquids and their variation when the liquids are mixed.

The present paper reports $C_{p,m}^E$ and excess molar volumes, V_m^E, both at 298.15 K, for binary mixtures of methylethylketone (MEK, or 2-butanone) with *n*-heptane, *n*-dodecane, and *n*-tetradecane, and of diethylketone (DEK, or 3-pentanone) with *n*-heptane. In addition, V_m^E is reported for MEK + *n*-decane at 298.15 K.

Experimental

Component liquids

Sources of the primary materials were as follows: methylethylketone and diethylketone (Certified Grade reagents) from Fisher Scientific Co., *n*-heptane (stated purity ≥ 99.5 mol%), *n*-decane (stated purity ≥ 99 mol%), *n*-dodecane (stated purity ≥99 mol%), and *n*-tetradecane (stated purity ≥ 99.5 mol%) from Fluka. The two ketones were purified chromatographically using a column packed with Chromosorb P (60/80 mesh) containing 25 mass % Apiezon L. The alkanes were used without further purification. Prior to the experimental measurements, the component liquids were carefully dried with molecular sieve beads (Union Carbide Type 4A) from Fluka.

Density and heat capacity measurements

Binary mixtures were prepared by weighing. Densities, ρ, of the pure liquids and their mixtures were determined with a vibrating-tube densimeter (3) from Sodev (Model 02D). Before each series of measurements, the instrument was calibrated using a vacuum and degassed doubly distilled water: ρ(298.15 K) = 997.047 kg m^{-3} (4). Excess molar volumes

$$[1]\quad V_m^E = V_m - xV_1 - (1-x)V_2$$

were obtained from the density ρ of the mixture according to the relation

$$[2]\quad V_m^E = xM_1(\rho^{-1} - \rho_1^{-1}) + (1-x)M_2(\rho^{-1} - \rho_2^{-1})$$

where V_i, M_i, and ρ_i denote respectively the molar volume, molar mass, and density of pure component i (1 for *n*-alkanone, 2 for *n*-alkane), and x is the mole fraction of *n*-alkanone.

Heat capacities per unit volume, $C_{p,m}/V_m$, were determined with a Picker flow microcalorimeter (5, 6) from Setaram using the stepwise procedure (6, 7). Excess molar isobaric heat capacities were calculated from the molar heat capacities, $C_{p,m}$, for the mixture, and $C_{p,i}$ for the components using the equation

$$[3]\quad C_{p,m}^E = C_{p,m} - xC_{p,1} - (1-x)C_{p,2}$$

Details of the experimental techniques and of the accuracy attainable for non-electrolyte mixtures may be found in previous publications; see, for example, refs. 7 and 8.

Results and discussion

Experimental results for the pure substances are summarized in Table 1, where some literature values (9–17) are given for comparison. Although small discrepancies are evident between the results from different sources, the overall agreement is satisfactory and attests to the reliability of our experimental techniques.

[1] NRCC No. 22772. This work is a contribution to the TOM project (ref. 32).

TABLE 1. Densities ρ and molar isobaric heat capacities $C_{p,m}$ of component liquids at 298.15 K

Liquid	ρ (kg m^{-3})		$C_{p,m}$ (J K^{-1} mol^{-1})	
	Experimental	Literature	Experimental	Literature
n-Heptane	679.42	679.46[a]		224.781[b]
n-Decane	726.11	726.35[a]		
n-Dodecane	745.39	745.18[c]	375.26	375.97 (11), 375.70 (12), 374.82 (13)
n-Tetradecane	759.20	759.20[c]	436.40	438.48 (11), 433.86 (12), 436.52 (14)
2-Butanone	799.66	799.7[d]	157.91	158.6 (16), 157.8 (17)
3-Pentanone	809.45	809.45[d]	190.30	190.95[e] 191.0 (16), 190.1 (17), 189.6 (17)

[a] Reference 9, see Table 23-2-(1.101)-*a*, p. 1, dated October 31, 1977.
[b] This value from Fortier *et al.* (10) was adopted for the *n*-heptane used as the ultimate reference liquid in all our heat capacity measurements.
[c] Reference 9, see Table 23-2-(1.101)-*a*, p. 2, dated October 31, 1976.
[d] Reference 15, see Table 23-2-1-(1.1130)-*a*, dated December 31, 1965.
[e] Reference 15, see Table 23-2-1-(1.2020)-*vc*, p. 3, dated June 30, 1982.

TABLE 2. Excess molar volumes, V_m^E, and excess molar isobaric heat capacities, $C_{p,m}^E$, for some *n*-alkanone + *n*-alkane mixtures at 298.15 K

x	V_m^E (cm^3 mol^{-1})	$C_{p,m}^E$ (J K^{-1} mol^{-1})	x	V_m^E (cm^3 mol^{-1})	$C_{p,m}^E$ (J K^{-1} mol^{-1})
xCH$_3$COC$_2$H$_5$ + (1 − x)C$_7$H$_{16}$			xCH$_3$COC$_2$H$_5$ + (1 − x)C$_{10}$H$_{22}$		
0.0928	0.3482	0.24$_8$	0.1076	0.3985	
0.2140	0.6202	0.82$_8$	0.2138	0.6602	
0.3005	0.7334	1.29$_6$	0.3285	0.8495	
0.3925	0.7951	1.77$_4$	0.3747	0.8912	
0.4932	0.8049	1.80$_8$	0.5005	0.9532	
0.5671	0.7801	1.70$_0$	0.6136	0.9256	
0.6907	0.6685	1.28$_4$	0.6948	0.8500	
0.7820	0.5379		0.7926	0.6891	
0.7827	0.5275	0.90$_4$	0.8850	0.4619	
0.8929	0.3069	0.43$_9$			
xCH$_3$COC$_2$H$_5$ + (1 − x)C$_{12}$H$_{26}$			xCH$_3$COC$_2$H$_5$ + (1 − x)C$_{14}$H$_{30}$		
0.0931	0.3516	−0.58$_1$	0.0956	0.3582	−0.86$_3$
0.1677	0.5595	−0.32$_3$	0.1990	0.6326	−0.85$_2$
0.2993	0.8277	0.33$_3$	0.2915	0.8268	−0.53$_6$
0.3988	0.9418	0.80$_0$	0.3786	0.9537	−0.15$_0$
0.4928	0.9995	1.14$_5$	0.4936	1.0397	0.31$_9$
0.6234	0.9724	1.25$_3$	0.5797	1.0379	0.55$_3$
0.6833	0.9265	1.14$_8$	0.6870	0.9729	0.64$_4$
0.7870	0.7703	0.77$_8$	0.7847	0.8274	0.36$_5$
0.8863	0.5121	0.22$_9$	0.8937	0.5310	−0.04$_0$
xC$_2$H$_5$COC$_2$H$_5$ + (1 − x)C$_7$H$_{16}$					
0.0772	0.2183	−0.10$_6$			
0.1772	0.3926	0.18$_8$			
0.2866	0.4936	0.63$_3$			
0.3801	0.5299	0.84$_1$			
0.4768	0.5231	0.96$_1$			
0.5904	0.4819	0.88$_9$			
0.6931	0.4074	0.73$_6$			
0.7852	0.3264	0.51$_2$			
0.8741	0.1992	0.30$_9$			

V_m^E and $C_{p,m}^E$ for the mixtures are listed in Table 2. Graphical representations of these results are shown in Figs. 1–3. For each mixture, the excess quantities were fitted by the method of unweighted least-squares with a smoothing polynomial of the type

$$[4] \quad Q^E = x(1 - x) \sum_{i=0}^{n-1} A_i(1 - 2x)^i$$

where Q^E is either V_m^E/(cm^3 mol^{-1}) or $C_{p,m}^E$/(J K^{-1} mol^{-1}). The coefficients A_i and the corresponding standard deviations $s(Q^E)$ are given in Table 3. These coefficients were used to calculate the curves shown in Figs. 1–3.

As expected from the excess molar enthalpies (18), the excess molar volumes (Fig. 1) for MEK with *n*-alkanes are more positive than for DEK with the corresponding *n*-alkane. Also, for a given *n*-alkanone, the excess molar volumes become more positive as the length of the *n*-alkane increases.

The only V_m^E data at 298.15 K found in the literature are those

Can. J. Chem. Downloaded from www.nrcresearchpress.com by 210.87.254.42 on 09/06/12
For personal use only.

Can. J. Chem. Downloaded from www.nrcresearchpress.com by 210.87.254.42 on 09/06/12
For personal use only.

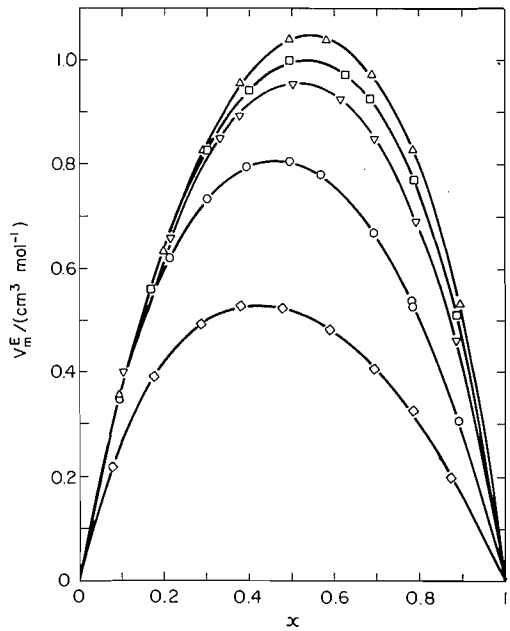

FIG. 1. Experimental excess molar volumes, V_m^E, at 298.15 K for $x CH_3COC_2H_5 + (1 - x)C_nH_{2n+2}$: ○, $n = 7$; ▽, $n = 10$; □, $n = 12$; △, $n = 14$; and for $xC_2H_5COC_2H_5 + (1 - x)C_7H_{16}$: ◇. The curves were calculated from eq. [4] with coefficients from Table 3.

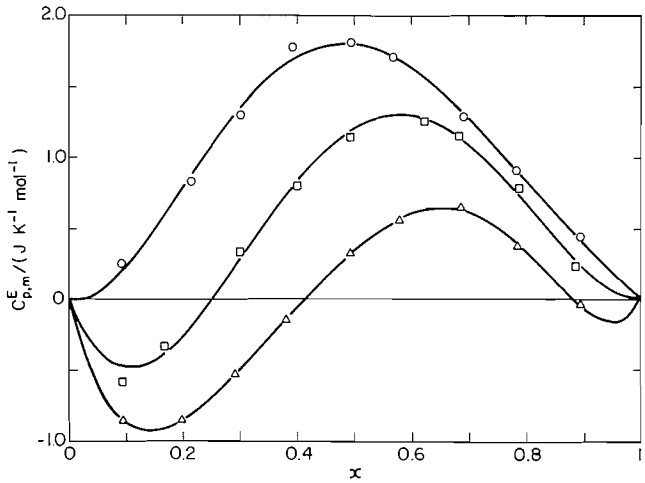

FIG. 2. Experimental excess molar isobaric heat capacities, $C_{p,m}^E$, at 298.15 K for $x CH_3COC_2H_5 + (1 - x)C_nH_{2n+2}$: ○, $n = 7$; □, $n = 12$; △, $n = 14$. The curves were calculated from eq. [4] with coefficients from Table 3.

of Rhim *et al.* (19) and Dusart *et al.* (20) for MEK + *n*-heptane, and those of Messow *et al.* (21) for MEK + *n*-dodecane. Rhim *et al.* obtained V_m^E from pyconometric measurements of densities; Dusart *et al.* used a vibrating-tube densimeter similar to ours. A comparison with these two sets of data is given in Fig. 4, where deviations from the representation of our results for MEK + *n*-heptane by eq. [4] are plotted. In general, the results of Rhim *et al.* are lower than ours with deviations of more than 5% occurring for $x > 0.7$. On the other hand, the V_m^E reported by Dusart *et al.* are higher than our results, particularly for $x < 0.5$. The V_m^E curve reported by Messow *et al.* (21) for MEK + *n*-dodecane (not shown here) falls below our curve and corresponds to relatively large deviations from our results over most of the concentration range.

No direct measurements of excess molar heat capacities

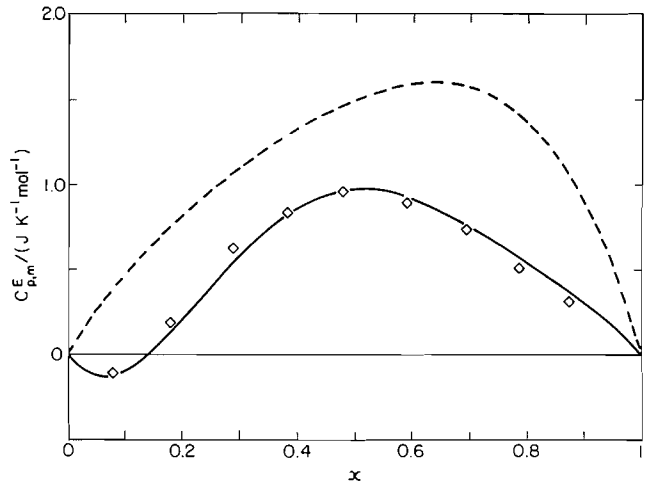

FIG. 3. Experimental excess molar isobaric heat capacities, $C_{p,m}^E$, at 298.15 K for $xC_2H_5COC_2H_5 + (1 - x)C_7H_{16}$: ◇. The full curve was calculated from eq. [4] with coefficients from Table 3. The broken curve represents $(\partial H_m^E/\partial T)_p = C_{p,m}^E$ at 298.15 K, estimated from the H_m^E data of Geiseler and Köhler (22).

could be found for any of the systems investigated here. However, Geiseler and Köhler (22) measured excess molar enthalpies, H_m^E, of DEK + *n*-heptane at 10 K intervals from 283.15 to 313.15 K. From their results we estimated values of $(\partial H_m^E/\partial T)_p = C_{p,m}^E$ at 298.15 K. These give no indication of a sigmoid variation with concentration (see Fig. 3) and are almost two times larger than our experimental results. This is not unexpected in view of the small number and scatter of the primary H_m^E data. It is well established that direct calorimetric measurements of $C_{p,m}^E$ generally yield much more accurate results than those estimated from the temperature variation of H_m^E. In the latter case, results of comparable accuracy are obtained only when using H_m^E data of the highest quality.

Estimation of $C_{p,m}^E$ from a combination of H_m^E data and excess molar free energies, G_m^E, was also investigated. Following the method outlined by Van Ness (23), we used two sets of G_m^E data and one set of H_m^E data, each at a different temperature, T_i. Assuming that $C_{p,m}^E$ is independent of temperature, it can be shown that

$$[5]\quad C_{p,m}^E = \frac{\dfrac{G_m^E(T_1)}{T_1} - \dfrac{G_m^E(T_2)}{T_2} + H_m^E(T_3)\left(\dfrac{1}{T_2} - \dfrac{1}{T_1}\right)}{\ln\left(\dfrac{T_2}{T_1}\right) + T_3\left(\dfrac{1}{T_2} - \dfrac{1}{T_1}\right)}$$

Data are available in the literature for the G_m^E of MEK + *n*-heptane (24, 25), of MEK + *n*-dodecane (21, 26) and of DEK + *n*-heptane (22). Unfortunately they are at temperatures from 20 to 55 K above 298.15 K. The data used for H_m^E at 298.15 K (21, 27, 28) are relatively more reliable, but estimates of $C_{p,m}^E$ obtained from eq. [5] are unrealistic; thus for an equimolar mixture $C_{p,m}^E$ $(x = 0.5)$/(J K^{-1} mol^{-1}) = −34.8, 3.0, and −3.2 for the three systems, respectively, as compared to 1.80, 1.20, and 0.97 calculated from eq. [4].

The most interesting and intriguing feature of the present results is the unusual composition dependence of $C_{p,m}^E$. A broad positive maximum is observed in the central range of concentration with a point of inflexion on each side of this range. These two inflexions eventually become two distinct minima when the chain length of the *n*-alkane is increased. This behav-

TABLE 3. Coefficients, A_i, and standard deviations, s, for least-squares representations of V^E_m and $C^E_{p,m}$ by eq. [4]

	Q^E	A_0	A_1	A_2	A_3	A_4	$s(Q^E)$
$x CH_3COC_2H_5$							
$+ (1-x) C_7H_{16}$	V^E_m/(cm^3 mol^{-1})	3.2118	0.4140	0.6402	0.2342		0.003_9
	$C^E_{p,m}$/(J K^{-1} mol^{-1})	7.194	1.002	−5.946	−3.347		0.05_7
$+ (1-x) C_{10}H_{22}$	V^E_m/(cm^3 mol^{-1})	3.8090	−0.2202	0.8254			0.004_5
$+ (1-x) C_{12}H_{26}$	V^E_m/(cm^3 mol^{-1})	3.9823	−0.4162	0.9812	−0.3488		0.004_4
	$C^E_{p,m}$/(J K^{-1} mol^{-1})	4.810	−4.812	−9.827			0.06_5
$+ (1-x) C_{14}H_{30}$	V^E_m/(cm^3 mol^{-1})	4.1631	−0.6034	0.5805	−0.5745	0.8434	0.003_7
	$C^E_{p,m}$/(J K^{-1} mol^{-1})	1.370	−6.893	−5.845	2.037	−6.998	0.01_7
$x C_2H_5COC_2H_5$							
$+ (1-x) C_7H_{16}$	V^E_m/(cm^3 mol^{-1})	2.0763	0.5291	0.5091	0.2719		0.004_6
	$C^E_{p,m}$/(J K^{-1} mol^{-1})	3.880	0.319	−4.230	−3.896		0.02_3

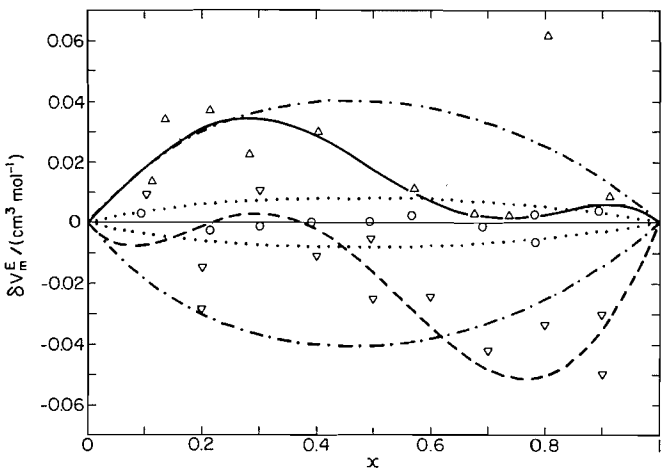

FIG. 4. Comparison of excess molar volumes, V^E_m, at 298.15 K for $x CH_3COC_2H_5 + (1-x) C_7H_{16}$. Plot shows $\delta V^E_m = V^E_m$(expt.) − V^E_m (eq. [4]): ○, present results; ▽ and - - -, Rhim *et al.* (19); △ and ——, Dusart *et al.* (20). The curves ··· and ·-·-· indicate deviations of ±1% and ±5%, respectively.

ior, more pronounced in the case of MEK (Fig. 2) than DEK (Fig. 3), is reported here for the first time for mixtures containing *n*-alkanones. The present results, as well as those reported recently for other mixtures showing a similar composition dependence of $C^E_{p,m}$, provide evidence of possible cooperative induced conformational "arrangements" in mixtures of certain types of molecules with aliphatic hydrocarbons. Previously $C^E_{p,m}$ curves with two minima were observed for 1,4-dioxane + *n*-alkane mixtures (14, 29); the two minima were more marked for longer *n*-alkanes (as for the present mixtures) and the more prominent minimum was situated at small mole fractions of the cyclic ether. A W-shaped $C^E_{p,m}$ curve was also observed for 2,5,8-trioxanonane + *n*-heptane mixtures (30), the more prominent minimum again being situated at small mole fractions of the ether. In addition, similar behavior was reported for 1,4-dioxane + cyclohexane mixtures (31) but was not observed for oxane + cyclohexane (31). In the former mixture, the more prominent minimum again occurs at small mole fractions of the cyclic ether.

A more detailed discussion will be possible when other different organic liquids have been studied in mixtures containing an *n*-alkane or cyclohexane. The present $C^E_{p,m}$ data will be useful for a reevaluation of the energy parameters used for calculating the main thermodynamic properties of *n*-alkanone containing mixtures in terms of the general quasi-chemical group contribution theory (1, 2, 32).

Acknowledgment

We are indebted to Mr. C. J. Halpin for purifying the ketones used in this investigation.

1. H. V. KEHIAIAN, J.-P. E. GROLIER, M.-R. KECHAVARZ, and G. C. BENSON. Fluid Phase Equilib. **5**, 159 (1981).
2. H. V. KEHIAIAN, J.-P. E. GROLIER, M.-R. KECHAVARZ, G. C. BENSON, O. KIYOHARA, and Y. P. HANDA. Fluid Phase Equilib. **7**, 95 (1981).
3. P. PICKER, E. TREMBLAY, and C. JOLICOEUR. J. Solution Chem. **3**, 377 (1974).
4. G. S. KELL. J. Chem. Eng. Data, **20**, 97 (1975).
5. P. PICKER, P.-A. LEDUC, P. R. PHILIP, and J. E. DESNOYERS. J. Chem. Thermodyn. **3**, 631 (1971).
6. J.-P. E. GROLIER, G. C. BENSON, and P. PICKER. J. Chem. Eng. Data, **20**, 243 (1975).
7. J.-L. FORTIER, and G. C. BENSON. J. Chem. Thermodyn. **8**, 411 (1976).
8. J.-P. E. GROLIER, E. WILHELM, and M. H. HAMEDI. Ber. Bunsenges. Phys. Chem. **82**, 1282 (1978).
9. Selected values of properties of hydrocarbons and related compounds. Thermodynamics Research Center Hydrocarbon Project. Thermodynamics Research Center, Texas A & M University, College Station, Texas.
10. J.-L. FORTIER, G. C. BENSON, and P. PICKER. J. Chem. Thermodyn. **8**, 289 (1976).
11. J. F. MESSERLY, G. B. GUTHRIE, S. S. TODD, and H. L. FINKE. J. Chem. Eng. Data, **12**, 338 (1967).
12. J.-P. E. GROLIER and A. FARADJZADEH. Int. Data Ser. Selec. Data Mixts. Ser. A, 136 (1979); 137 (1979).
13. J.-P. E. GROLIER, A. INGLESE, A. H. ROUX, and E. WILHELM. Ber. Bunsenges. Phys. Chem. **85**, 768 (1981).
14. J.-P. E. GROLIER, A. INGLESE, and E. WILHELM. J. Chem. Thermodyn. To be published.
15. Selected values of properties of chemical compounds. Thermodynamics Research Center Data Project. Thermodynamics Research Center, Texas A & M University, College Station, Texas.
16. R. J. L. ANDON, J. F. COUNSELL, and J. F. MARTIN. J. Chem. Soc. A, 1894 (1968).
17. R. FUCHS. Can. J. Chem. **58**, 2305 (1980).
18. O. KIYOHARA, G. C. BENSON, and J.-P. E. GROLIER. J. Chem. Thermodyn. **9**, 315 (1977).
19. J. N. RHIM, S. S. PARK, and H. C. LEE. Hwahak Konghak, **11**, 41 (1973).
20. O. DUSART, C. PIEKARSKI, S. PIEKARSKI, and A. VIALLARD. J.

Can. J. Chem. Downloaded from www.nrcresearchpress.com by 210.87.254.42 on 09/06/12
For personal use only.

Chim. Phys. **73**, 837 (1976).
21. U. MESSOW, U. DOYÉ, and D. KUCHENBECKER. Z. Phys. Chem. Leipzig, **259**, 664 (1978).
22. G. GEISELER, and H. KÖHLER. Ber. Bunsenges. Phys. Chem. **72**, 697 (1968).
23. H. C. VAN NESS. Ind. Eng. Chem. **59**(9), 33 (1967).
24. V. YU. ARISTOVICH, A. G. MORACHEVSKII, and I. I. SABYLIN. J. Appl. Chem. USSR, **38**, 2633 (1965); G. C. BENSON. Int. Data Ser. Selec. Data Mixts. Ser. A 34 (1980).
25. M. TAKEO, K. NISHII, T. NITTA, and T. KATAYAMA. Fluid Phase Equilib. **3**, 123 (1979).
26. G. C. BENSON. Int. Data Ser. Selec. Data Mixts. Ser. A 38 (1980).
27. O. KIYOHARA, Y. P. HANDA, and G. C. BENSON. J. Chem. Thermodyn. **11**, 453 (1979); G. C. BENSON, and Y. P. HANDA. Int. Data Ser. Selec. Data Mixts. Ser. A, 68 (1980); 78 (1980).
28. U. MESSOW, U. DOYÉ, and D. KUCHENBECKER. Int. Data Ser. Selec. Data Mixts. Ser. A 17 (1980).
29. A. INGLESE, E. WILHELM, and J.-P. E. GROLIER. 37th Annual Calorimetry Conference, Snowbird, Utah, U.S.A., 22–25 July 1982. Paper No. 54.
30. F. KIMURA, P. J. D'ARCY, M. E. SUGAMORI, and G. C. BENSON. Thermochim. Acta, **64**, 149 (1983).
31. A. INGLESE, J.-P. E. GROLIER, and E. WILHELM. Fluid Phase Equilib. To be published.
32. H. V. KEHIAIAN, J.-P. E. GROLIER, and G. C. BENSON. J. Chim. Phys. **75**, 1031 (1978).

Can. J. Chem. Downloaded from www.nrcresearchpress.com by 210.87.254.42 on 09/06/12
For personal use only.

Kinetics and isotope effects of the proton transfer reactions between 1-(4-nitrophenyl)-1-nitroethane to phenyltetramethylguanidine in dipolar aprotic solvents

ARNOLD JARCZEWSKI AND PRZEMYSLAW PRUSZYNSKI
Department of Chemistry, Adam Mickiewicz University, Poznan, Poland

AND

MOHAMMED KAZI AND KENNETH T. LEFFEK
Department of Chemistry, Dalhousie University, Halifax, N.S. Canada B3H 4H6

Received October 31, 1983

ARNOLD JARCZEWSKI, PRZEMYSLAW PRUSZYNSKI, MOHAMMED KAZI and, KENNETH T. LEFFEK. Can. J. Chem. **62**, 954 (1984).

The carbon acid 1-(4-nitrophenyl)-1-nitroethane reacts with phenyltetramethylguanidine in the aprotic solvents acetonitrile, benzonitrile, and chlorobenzene in a bimolecular proton transfer reaction. The primary isotope effects, k_H/k_D, for these reactions at 25°C are 8.5 ± 0.4, 6.1 ± 0.4, and 16 in acetonitrile, benzonitrile, and chlorobenzene respectively. The magnitude of the isotope effects on the enthalpy of activation ($\Delta H_D^{\ddagger} - \Delta H_H^{\ddagger}$) are 2.3 ± 0.2, 1.6 ± 0.7, and 4.2 ± 0.6 kcal mol^{-1}, which indicates a contribution from proton tunnelling to the reaction rate of the normal substrate.

ARNOLD JARCZEWSKI, PRZEMYSLAW PRUSZYNSKI, MOHAMMED KAZI et KENNETH T. LEFFEK. Can. J. Chem. **62**, 954 (1984).

La carbone acide du (nitro-4 phényl)-1 nitro-1 éthane réagit avec la phényltétraméthylguanidine dans les solvants aprotiques, acétonitrile, benzonitrile et chlorobenzène, par une réaction de transfert de proton bimoléculaire. Les effets isotopiques primaires, k_H/k_D, pour ces réactions effectuées à 25°C sont respectivement 8,5 ± 0,4, 6,1 ± 0,4 et 16 pour les réactions dans l'acétonitrile, le benzonitrile et le chlorobenzène. Les amplitudes des effets isotopiques sur l'enthalpie d'activation ($\Delta H_D^{\ddagger} - \Delta H_H^{\ddagger}$) sont 2,3 ± 0,2, 1,6 ± 0,7 et 4,2 ± 0,6 kcal/mol; ceci indique qu'il y a une contribution de l'effet tunnel du proton à la vitesse de réaction du substrat normal.

[Traduit par le journal]

Introduction

Proton transfer reactions from carbon acids to bases of various strength and steric hindrance in polar aprotic solvents show considerably smaller values of the primary kinetic isotope effect, k_H/k_D, relative to those found in nonpolar solvents (1, 2). This was attributed (1, 2) to an increase in the effective mass of the transferred proton in the polar solvents, reflecting the motion of large solvent molecules in the reaction path from the initial to the transition state, particularly for ionogenic reactions with more ordered transition states than initial states. However, the value of k_H/k_D found for such systems frequently exceeded the standard value of 7 which is predicted by the assumption of the complete loss of the carbon–hydrogen stretching vibration during the activation process. This was interpreted as a significant contribution from tunnelling to the reaction rate (1–13).

In a case where the steric hindrance to proton abstraction was very great, the reaction between 1-(4-nitrophenyl)-1-nitroethane with the strong base, 2,7-dimethoxy-1,8-bis(dimethylamino)naphthalene, first-order kinetics were observed with no dependence on the base concentration (11). This was explained as a two-step proton transfer reaction to the highly hindered base where the first step, the ionization of the carbon acid, was rate determining.

For the reaction of 1-(4-nitrophenyl)-1-nitroethane and the base phenyltetramethylguanidine (PTMG), which involves appreciable but not excessive steric crowding in the base molecule, it was expected to show second-order kinetics and large isotopic rate ratios arising from a narrow potential energy barrier. Phenyltetramethylguanidine is a weaker base than tetramethylguanidine and there is no hydrogen atom present at the nitrogen of the imino group to allow the isotopic "scrambling effect" observed by Rogne (4), who asserted that the reversibility of the proton–deuteron transfer reaction in the case of the reaction of the deuterated carbon acid with normal TMG was the cause of the very high values of k_H/k_D found for several reactions with TMG base. Therefore, the present investigation attempts to provide a measure of the isotope effects free from this uncertainty, with an enhanced contribution from steric hindrance of the base to the isotope effect. The carbon acid 1-(4-nitrophenyl)-1-nitroethane is very similar to the 4-nitrophenylnitromethane used by Caldin and Mateo (1, 2) and by Rogne and co-workers (4–7), except that the additional methyl group adds to the steric hindrance to proton transfer, so this system serves as a general check of the extensive studies carried out with the methane acid.

Results and discussion

The reaction of 1-(4-nitrophenyl)-1-nitroethane with phenyltetramethylguanidine in chlorobenzene, acetonitrile, and benzonitrile solvent gives a product with a single absorption peak at λ_{max} 478 nm, 525 nm, and 520 nm respectively. These maxima show the same type of solvent dependence as observed by Caldin and Mateo (1) for the proton transfer from 4-nitrophenylnitromethane, and the position of the maximum in acetonitrile is very similar to our previous studies of proton transfers from the ethane to other nitrogen bases in the same solvent (11, 12). The equilibrium constants, K, and molar absorptivity, ϵ, were determined by fitting the change in optical density, O.D., with base concentration [B], to eq. [1]

$$[1] \quad [A]/O.D. = 1/K\epsilon[B] + 1/\epsilon$$

The acid concentration, [A] was maintained constant at a level very much smaller than the base [B]. Equation [1] is derived with the assumption that the product is an ion-pair. Good linear plots of [A]/O.D. vs. 1/[B] were obtained, indicating that the reaction is well represented by eq. [2].

Can. J. Chem. Downloaded from www.nrcresearchpress.com by 210.87.254.42 on 09/06/12
For personal use only.

[2] 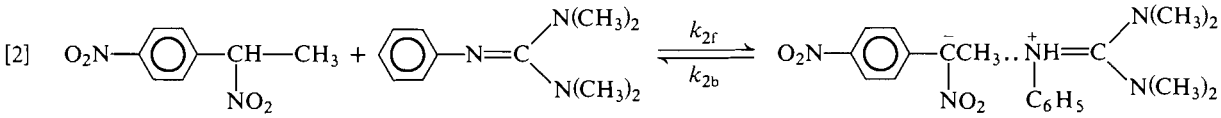

The intercept of the plots yielded a molar absorptivity, ϵ, of 10 000 $dm^3\ mol^{-1}\ cm^{-1}$ and the slopes gave equilibrium constants for the reaction at 20°C of 3 $dm^3\ mol^{-1}$ in chlorobenzene, 40 $dm^3\ mol^{-1}$ in benzonitrile, and 300 $dm^3\ mol^{-1}$ in acetonitrile. These equilibrium constants are smaller than those observed for the same acid reacting with 1,8-diazabicyclo-[5.4.0]undec-7-ene (DBU) which has a K about 50 times larger in acetonitrile solvent (12), reflecting the fact that PTMG is a weaker base than DBU.

The rate constants for the reaction of 1-(4-nitrophenyl)-nitroethane and its deuterated analogue with PTMG in the three solvents are shown in Table 1, together with the isotopic rate ratios. The second-order rate constants were the calculated slopes of plots of the pseudo first-order rate constant k_{obs}, versus base concentration. The second-order rate constants were obtained by a linear least-squares calculation and are quoted with their standard deviations. The observed rate constants were a function of base concentration according to eq. [3] except for the deuterated substrate in chlorobenzene

$$[3]\quad k_{obs} = k_f[B] + k_b$$

solvent, where the experimentally determined relationship was eq. [4].

$$[4]\quad k_{obs} = k_f[B]$$

Melander and Saunders (14) have shown that eq. [4] may be derived for the deuteron transfer when the concentration of exchangeable protons is large compared to the initial concentration of the carbon acid. Under these conditions the reverse reaction of the carbanion to produce the deuterated carbon acid may be neglected. This situation may apply in the present reactions when the equilibrium constant is small and when even a very small amount of adventitious moisture will be sufficient to bring about complete and rapid exchange of the deuterium in the carbanion ion-pair. Even with the greatest care to exclude adventitious moisture, it was not possible to observe in chlorobenzene the dependence shown in eq. [3]. Thus, the rate constant for the reverse reaction could not be determined, although the deuterium exchange does not affect the determination of the rate constant for the forward reaction.

The second-order rate constant for the normal substrate in chlorobenzene solvent is very difficult to determine with precision. Since the equilibrium constant in this solvent is only 3 $dm^3\ mol^{-1}$, the slope of the plot of k_{obsH} vs. base concentration is small and the intercept (k_b) is comparatively large. The values of k_{obsH} therefore change very slowly with base concentration, so that the ±2% precision (at best) of the stopped-flow spectrophotometer yields a scatter in k_{obsH} which is reflected in a very large standard deviation in k_{fH}. This problem does not exist for the deuterated substrate which follows eq. [4]. The rate ratios, k_K/k_D, in chlorobenzene solvent are believed to be reliable to about ±3.

Since the equilibrium constant in the other two solvents is larger, the effect of deuterium exchange is not so pronounced. However, a test of its importance may be made by comparing the equilibrium constants, determined by k_f/k_b for the normal and deuterated substrate. If these differ by more than a few percent, exchange is indicated.

If exchange is negligible, eq. [3] is obeyed and the ratio k_f/k_b gives the true equilibrium constant. If exchange is taking place, then k_{obs} will follow neither eq. [3] nor eq. [4] but some combination of the two. In this case the k_b value will be spuriously low for the deuterated compound. The results in Table 1 show that in acetonitrile k_f/k_b for the normal compound is 320 at 20°C, in good agreement with the value of 300 from the equilibrium measurements, whereas k_f/k_b for the deuterated substrate is 660. Thus it is concluded that the k_{bD} values contain a significant error due to deuterium exchange. The good agreement between the value of k_f/k_b for the normal substrate and the K determined from equilibrium measurements shows that eq. [2] is a good description of the reaction, i.e. decomposition of the ion-pair product other than to substrate and base is negligibly small.

In benzonitrile solvent, k_f/k_b for the protium substrate is 44 at 20°C, in good agreement with K determined from equilibrium measurements. However, k_f/k_b for the deuterated analogue is abnormally low.

The reaction in all three solvents is second-order, indicating that phenyltetramethylguanidine is not sufficiently sterically hindered to bring about the first-order kinetics observed with 2,7-dimethoxy-1,8-bis(dimethyl-amino)naphthalene (11).

The kinetic isotope effects confirm that the proton transfer is rate determining, although the rate ratios do not follow the expected order with respect to solvent polarity (1). Large isotope effects are expected in solvents of low polarity, but benzonitrile, while less polar than acetonitrile, shows a slightly smaller isotopic rate ratio. The reaction does show a large effect, k_H/k_D about 16 to 25°C, in chlorobenzene. However, this value is much smaller than the 50 ± 8 observed by Caldin and Mateo (1) for the reaction 4-nitrophenylnitromethane with tetramethylguanidine in chlorobenzene. The value of 16 at 25° is generally in agreement with the maximum values observed by Rogne and co-workers for various reactions (4–7, 15).

The activation parameters derived from the rate constants collected in Table 1 are shown in Table 2. The enthalpy of activation is largest in benzonitrile and smallest in chlorobenzene solvent, an effect which is overcompensated by the entropies of activation so that the second order rate constant is also largest in benzonitrile and smallest in chlorobenzene. It is not possible to account for this behaviour from these data above, but it is interesting to note that Caldin and Mateo found the same qualitative relation in these three solvents for $\Delta H^{\ddagger}$ and also observed a rate reversal between acetonitrile and benzonitrile, for the reaction 4-nitrophenylnitromethane and tetramethylguanidine (1). Their more extensive study of solvent dependence showed that the above observations were scatter within a general semiquantitative correlation of the rate constants (and $\Delta H^{\ddagger}$) with the dielectric constant of the solvent.

Although the isotopic rate ratios are smaller than those observed by Caldin and Mateo (1), the isotope effects on the enthalpy of activation are about the same, within experimental error. Thus it is concluded that tunnelling is important in the proton transfer from 1-(4-nitrophenyl)-1-nitroethane, as it is in proton transfer from 4-nitrophenylnitromethane.

Thus nearly all of the general observations of the kinetics of

Can. J. Chem. Downloaded from www.nrcresearchpress.com by 210.87.254.42 on 09/06/12
For personal use only.

Can. J. Chem. Downloaded from www.nrcresearchpress.com by 210.87.254.42 on 09/06/12
For personal use only.

TABLE 1. Rate constants for the reaction of 1-(4-nitrophenyl)-1-nitroethane with phentyltetramethylguanidine

(a) Acetonitrile solvent Temp (°C)	10^3 [Base] (M)	$10^2 k_{obs}$ (s^{-1})	k_f(dm^3 mol^{-1} s^{-1})	$10^2 k_b$ (s^{-1})	k_H/k_D
(*i*) $NO_2C_6H_4$ $CH(CH_3)NO_2$					
5	4.3–17.2	1.7–4.7	2.3±0.1	0.6±0.1	
10	4.3–17.2	2.2–5.9	2.85±0.1	0.9±0.8	
15	4.3–17.2	2.8–7.6	3.7±0.2	1.1±0.2	
20	4.3–17.2	3.5–9.4	4.5±0.2	1.4±0.2	
25	4.3–17.2	4.4–11.9	5.7±0.2	1.0±0.3	
30	4.3–17.2	5.6–14.8	7.1±0.3	2.3±0.3	
(*ii*) $NO_2C_6H_4CD(CH_3)NO_2$					
5	3.8–15.2	0.43–0.66	0.20±0.01	0.35±0.01	11.5±0.7
10	3.8–15.2	0.56–0.68	0.28±0.01	0.45±0.01	10.1±0.6
15	3.8–15.2	0.74–1.2	0.39±0.01	0.59±0.01	9.5±0.5
20	3.8–15.2	0.95–1.5	0.50±0.01	0.76±0.01	9.1±0.4
25	3.8–15.2	1.2–2.0	0.68±0.01	0.97±0.01	8.5±0.4
30	3.8–15.2	1.6–2.6	0.88±0.01	1.22±0.03	8.3±0.4

(b) Benzonitrile solvent Temp (°C)	10^3 [Base] (M)	k_{obs} (s^{-1})	k_f(dm^3 mol^{-1} s^{-1})	k_b (s^{-1})	k_H/k_D
(*i*) $NO_2C_6C_4CH(CH_3)NO_2$					
10	5.4–21.2	0.12–0.21	5.4±0.4	0.09±0.01	
15	5.4–21.2	0.18–0.28	6.2±0.2	0.15±0.01	
20	5.4–21.2	0.25–0.39	8.9±0.4	0.20±0.06	
25	5.4–21.2	0.34–0.53	12.1±0.3	0.28±0.06	
30	5.4–21.2	0.42–0.74	19.8±0.6	0.33±0.03	
35	5.4–21.2	0.64–1.03	24.0±0.6	0.51±0.09	
40	5.4–21.2	0.88–1.39	31.4±0.2	0.71±0.01	
(*ii*) $NO_2C_6H_4CD(CH_3)NO_2$					
15	5.8–23.2	0.063–0.080	0.99±0.04	0.06±0.01	6.3±0.3
20	5.8–23.2	0.091–0.11	1.38±0.07	0.08±0.01	6.5±0.5
25	5.8–23.2	0.013–0.16	1.98±0.11	0.12±0.01	6.1±0.4
30	5.8–23.2	0.18–0.23	2.97±0.05	0.16±0.01	6.6±0.2
35	5.8–23.2	0.25–0.32	4.01±0.15	0.23±0.01	6.0±0.3

(c) Chlorobenzene solvent Temp (°C)	10^3 [Base] (M)	k_{obs} (s^{-1})	k_f(dm^3 mol^{-1} s^{-1})	k_b (s^{-1})	k_H/k_D
(*i*) $NO_2C_6H_4CH(CH_3)NO_2$					
10	1.7–8.5	0.33–0.40	1.3±0.5	0.29	
15	1.7–8.5	0.45–0.55	1.6±0.5	0.41	
20	1.7–8.5	0.58–0.69	1.65±0.5	0.56	
25	1.7–8.5	0.81–0.97	1.9±0.8	0.83	
(*ii*) $NO_2C_6H_4CD(CH_3)NO_2$					
5	2.9–9.8	0.0016–0.0041	0.049±0.003	—	
10	2.9–9.8	0.0019–0.0052	0.055±0.001	—	24
15	2.9–9.8	0.0021–0.0065	0.069±0.005	—	23
20	2.9–9.8	0.0027–0.0090	0.090±0.005	—	18
25	2.9–9.8	0.0030–0.0110	0.115±0.006	—	16

the proton transfer from 4-nitrophenylnitromethane to TMG found by Caldin and Mateo (1) have closely parallel features in the present study. The major exception is the very large primary kinetic isotope effect, k_H/k_D up to 50, observed in chlorobenzene and other solvents of low polarity. Rogne and co-workers (7) have reported a k_H/k_D of 13.7 ± 0.4 at 25°C for 4-nitrophenylnitromethane and PTMG in toluene and Kresge and Powell found 14.2 ± 0.2 and 13.8 ± 0.2 at 25°C for the same acid reacting in toluene with TMG and PTMG respectively (9), calculated from a primary tritium isotope effect. If the later rate constant measurements of Caldin *et al.* (10) are interpreted according to eq. [4] derived by Melander and Saunders (14), a good fit is obtained which yields a significantly higher value of k_D and a lower k_H/k_D by about 30%. Such a reinterpretation, on the reasonable assumption that deuterium exchange cannot be avoided, would reduce the isotope effect reported by Caldin and Mateo from a k_H/k_D of 45 to about 30.

Notwithstanding this, the present study clearly confirms the reports of Rogne and co-workers (7) and Kresge and Powell (9) that primary deuterium isotope effects of these nitroalkanes reacting with guanidine bases in solvents of low polarity are only slightly larger than those in more polar solvents.

TABLE 2. Activation parameters for the reaction of 1-(4-nitrophenyl)-1-nitroethane and phenyltetramethylguanidine

	Acetonitrile		Benzonitrile		Chlorobenzene	
Parameter	H-transfer	D-transfer	H-transfer	D-transfer	H-transfer	D-transfer
$\Delta H^{\ddagger}$ (kcal mol^{-1})	7.0±0.1	9.3±0.1	10.4±0.6	12.0±0.3	3.0±0.5	7.2±0.3
$\Delta S^{\ddagger}$ (cal mol deg^{-1})	−31.5±0.3	−28.2±0.4	−18.4±2	−16.9±1	−47.2±2	−38.7±1
$\Delta H_D^{\ddagger} - \Delta H_D^{\ddagger}$ (kcal mol^{-1})	2.3±0.2		1.6±0.7		4.2±0.6	
$\Delta S_D^{\ddagger} - \Delta S_D^{\ddagger}$ (cal mol^{1} deg^{-1})	3.3±0.6		1.5±2.3		8.5±2.3	

TABLE 3. Run # 54; temperature 25.0°C; initial concentration $NO_2C_6H_4CD(CH_3)NO_2 = 3.6 \times 10^{-4}$ *M*; initial concentration of base = 2.94×10^{-2}; solvent chlorobenzene

Time (min)	x_1[a]	x_2
0.0	0.111	0.513
1.5	0.223	0.525
3.0	0.305	0.533
4.5	0.366	0.538
6.0	0.408	0.542
7.5	0.441	0.545
9.0	0.467	0.547
10.5	0.484	0.548
12.0	0.500	0.549

$k_1 = 2.98 \times 10^{-3}$ s^{1} (by Guggenheim analysis)
Cor. coeff. 0.9995

[a] x_1 and x_2 are readings from the chart paper in arbitrary units.

Experiments

Materials

1-(4-Nitrophenyl)-1-nitroethane and its α-deuterated analogue were prepared as previously described (11).

The solvents were prepared by standard methods (1), carefully dried, and distilled. They were always purified immediately before use in the kinetic runs.

Phenyltetramethylguanidine was prepared by the method of Bredereck and Bredereck (16) using tetramethylurea, $POCl_3$, and aniline. The reaction was carried out in benzene solvent.

Equilibrium constant measurements

The absorbance at equilibrium for a series of reaction mixtures with constant acid concentration and various base concentrations, always in large excess, was determined using uv−vis spectrophotometers fitted with thermostated cells. The results fitted eq. [1] and did not fit the analogous equation derived on the assumption that the product exists as free ions.

Kinetic measurements

The kinetic measurements were carried out under pseudo first-order conditions with the base concentration in large excess. The solutions of the carbon acid and the deuterated carbon acid were always freshly prepared using freshly distilled solvent and were kept under a nitrogen atmosphere. The reaction rates were measured with a stopped-flow spectrophotometer using the standard technique previously described (17) except for the reaction in chlorobenzene solvent for which a standard spectrophotometer was used with a slave pen recorder. A sample run is given in Table 3. The kinetic runs were analyzed by the Guggenheim method (18), except that the runs in chlorobenzene were also analyzed using the infinity readings. Generally, the rate constants obtained from the two methods differed by a few percent, although there was no systematic variation. The rate constants quoted are those obtained by the Guggenheim method.

Acknowledgement

The authors are grateful for financial support by the Natural Sciences and Engineering Research Council of Canada.

1. E. F. CALDIN and S. MATEO. J. Chem. Soc. Faraday Trans. 1, **71**, 1876 (1975).
2. E. F. CALDIN and S. MATEO. J. Chem. Soc. Chem. Commun. 854 (1973).
3. E. F. CALDIN and S. MATEO. J. Chem. Soc. Faraday Trans. 1, **72**, 112 (1976).
4. O. ROGNE. Acta Chem. Scand. Ser. A, **32**, 559 (1978).
5. E. F. CALDIN, O. ROGNE, and C. J. WILSON. J. Chem. Soc. Faraday Trans. 1, **74**, 1796 (1978).
6. E. F. CALDIN and O. ROGNE. J. Chem. Soc. Faraday Trans. 1, **74**, 2065 (1978).
7. I. HEGGEN, J. LINDSTROM, and O. ROGNE. J. Chem. Soc. Faraday Trans. 1, **74**, 1263 (1978).
8. A. JARCZEWSKI, P. PRUSZYNSKI, and K. T. LEFFEK. Can. J. Chem. **57**, 669 (1979).
9. A. J. KRESGE and M. F. POWELL. J. Am. Chem. Soc. **103**, 201 (1981).
10. E. F. CALDIN, S. MATEO, and P. WARRICK. J. Am. Chem. Soc. **103**, 202 (1981).
11. K. T. LEFFEK and P. PRUSZYNSKI. Can. J. Chem. **59**, 3034 (1981).
12. K. T. LEFFEK and P. PRUSZYNSKI. Can. J. Chem. **60**, 1692 (1982).
13. A. JARCZEWSKI, P. PRUSZYNSKI, and K. T. LEFFEK. Can. J. Chem. **61**, 2029 (1983).
14. L. MELANDER and W. H. SAUNDERS. Reaction rates of isotopic molecules. Wiley, New York. 1980. Chapt. 10.
15. J. H. BLANCH and O. ROGNE. J. Chem. Soc. Faraday Trans. 1, **74**, 1254 (1978).
16. H. BREDERECK and K. BREDERECK. Ber. **94**, 2278 (1961).
17. A. JARCZEWSKI and K. T. LEFFEK. Can. J. Chem. **50**, 24 (1972).
18. E. A. GUGGENHEIM. Philos. Mag. **2**, 538 (1926).

Can. J. Chem. Downloaded from www.nrcresearchpress.com by 210.87.254.42 on 09/06/12
For personal use only.

An infrared study of water–ion interactions in perfluorosulfonate (Nafion) membranes[1]

SYLVIO QUEZADO[2] AND JAN C. T. KWAK
Department of Chemistry, Dalhousie University, Halifax, N.S., Canada B3H 4J3

AND

MICHAEL FALK
Atlantic Research Laboratory, National Research Council of Canada, Halifax, N.S., Canada B3H 3Z1

Received August 30, 1983

SYLVIO QUEZADO, JAN C. T. KWAK, and MICHAEL FALK. Can. J. Chem. **62**, 958 (1984).

We have studied the infrared spectra of Nafion membranes in twenty different cationic forms, in order to characterize the water–anion–cation interactions at low water contents. Spectra in the OH stretching region and in the H—O—H bending region allow the distinction between hydrogen-bonded and non-hydrogen-bonded water molecules, and yield information on the mode of attachment of water molecules to the anion–cation pairs. When there is a good match between the Lewis acid strength of the cation and the Lewis base strength of the anion, ion pairs are relatively stable and water molecules tend to attach on the outside. When the acid strength of the cation and the base strength of the anion are mismatched, as is the case for small cations of high charge or for large cations of low charge, water molecules tend to be inserted between the ion pairs even at the lowest water contents.

SYLVIO QUEZADO, JAN C. T. KWAK et MICHAEL FALK. Can. J. Chem. **62**, 958 (1984).

Nous avons étudié les spectres infrarouge de vingt formes cationiques différentes de membranes de Nafion, afin de caractériser les interactions eau–anion–cation à basses teneurs d'eau. Les spectres dans la région des vibrations de valence OH et aussi dans la région des vibrations de déformation H—O—H nous permettent de distinguer entre les molécules d'eau liées et non-liées par liaison hydrogène et de constater le mode d'attachement de H_2O aux paires d'ions. Quand il y a équilibre entre l'acidité Lewis du cation et la basicité Lewis de l'anion, les paires anion–cation sont relativement stables et les molécules d'eau tendent à s'attacher à l'extérieur. Quand il y a déséquilibre, comme dans le cas de petits cations de haute charge ou de gros cations de faible charge, les molécules d'eau tendent à s'introduire entre le cation et l'anion.

Can. J. Chem. Downloaded from www.nrcresearchpress.com by 210.87.254.42 on 09/06/12
For personal use only.

Introduction

Nafion is an ion-containing polymer whose physical properties are of considerable interest in connection with the use of Nafion membranes as electrochemical separators and ion-exchangers (1). Nafion consists of a perfluorinated polyethylene backbone with pendant ether-linked side-chains terminating with a sulfonate group, $—O—CF_2—CF_2—SO_3—M^+$, where M^+ represents an exchangeable cation. Water penetrates Nafion easily and resides within the ionic regions, the equilibrium water content being dependent on the nature of the cation, pre-treatment of the sample, and water activity of the surroundings (2).

The Nafion–water system offers an opportunity of examining water–ion interactions by infrared spectroscopy because (unlike in the spectra of other ion-containing polymers (3, 4)) in the Nafion spectrum the OH stretching fundamentals of the hydrogen-bonded and non-hydrogen-bonded protons of water are particularly clearly separated. This has been demonstrated in an earlier paper (5) in which the OH stretching absorption of water in Nafion has been shown to consist of distinct sub-bands corresponding to the bonded and non-bonded protons, the latter being well separated to high wavenumbers under the influence of the fluorocarbon medium. Those observations yielded information about the local environment of the water molecules and the geometry of the hydrated ion clusters (5, 6). Preliminary infrared studies of perfluorocarboxylate membranes have shown that, as in the Nafion spectrum, the bonded and non-bonded protons give rise to well-separated OH stretching bands (7).

We have now extended our infrared study to include Nafion membranes with a variety of counterions of charge one, two, and three. Our main concern has been to characterize the water–ion interactions at very low water contents. In the nearly dry membrane, when not more than one water molecule is associated with an ion pair, two principal modes of attachment may occur: the water molecules may be *inserted* between the cation and the anion (or between the cation and a pair of anions) as in Fig. 1*a*, or they may be *attached* to the cation–anion pair without disrupting the cation–anion bond as in Fig. 1*b* or 1*c*. At higher water contents the insertion mode must prevail, leading eventually to a complete dissociation of all ion pairs, in analogy with the dilute solutions of electrolytes. At low water contents, however, local situations may be present involving either *insertion* (*a*) or *attachment* without insertion (*b* or *c*), depending on the relative affinity of the cations, anions, and water molecules for one another. In the case of insertion both water protons would be hydrogen bonded, while in the case of attachment one or both protons might be exposed to the fluorocarbon medium. This situation may be expected to give rise to spectroscopically distinguishable doubly-bonded, singly-bonded, and non-bonded water molecules. With this expectation we have examined the trends that occur in the spectrum of water at low water content when the nature, size, and charge of the counterion in Nafion is varied.

Experimental

The Nafion membranes used were of type 142 E, which corresponds to a thickness of 51 μm and equivalent weight of 1400 g per mol of SO_3^-. The samples were supplied by the manufacturer (Du Pont de Nemours and Co.) in the acid form. In accordance with a standard procedure, the samples were boiled in distilled water for half an hour, neutralized by immersion in aqueous salt solution of the desired cation for another half an hour, rinsed in distilled water, wiped with filter

[1] NRCC No. 22915.

[2] On leave from the Departamento de Física, Universidade Federal da Paraíba, 58100 Campina Grande-Pb, Brazil.

Can. J. Chem. Downloaded from www.nrcresearchpress.com by 210.87.254.42 on 09/06/12
For personal use only.

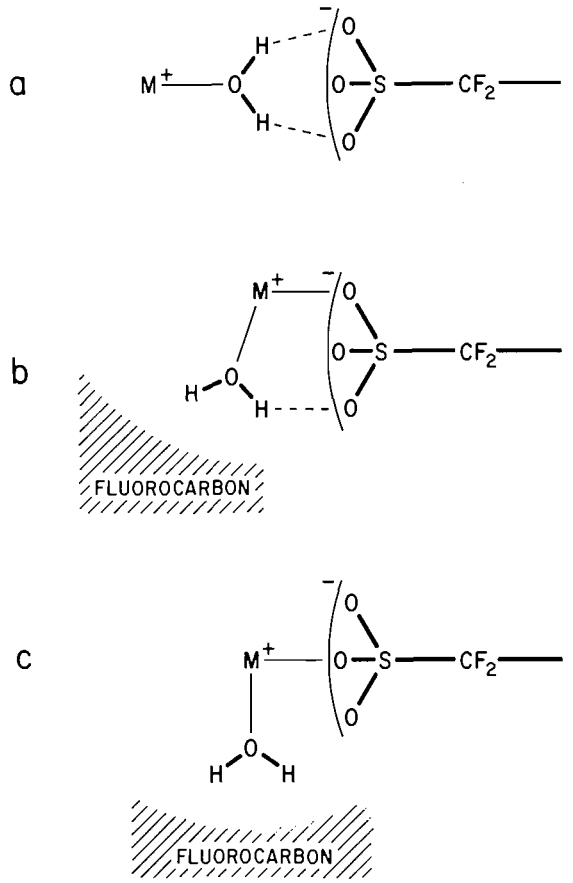

FIG. 1. Possible modes of attachment of water to cations and anions in Nafion (diagrammatic). *a*, two hydrogen bonds (these bonds may be to two different anions); *b*, one hydrogen bond; *c*, no hydrogen bond.

paper, and stored in stoppered glass containers. Completeness of cation exchange was verified by the disappearance of the infrared absorption bands of the acid form of Nafion (6).

Infrared spectra corresponding to Figs. 2, 3, and 10 and Tables 1 and 2 were measured on a Perkin-Elmer grating infrared spectrophotometer model 180. In these measurements the water content was controlled by placing the sample in a closed chamber through which moist air with a controlled H_2O/D_2O ratio was circulated. For D_2O measurements a matching undeuterated sample was placed in the reference beam to compensate the absorption at about 2360 cm^{-1} due to an overtone of the C—F stretching mode.

All other infrared spectra were measured in the range 4000–800 cm^{-1} on a Bomem DA3.02 Fourier transform infrared spectrophotometer. Usually 64 interferograms were coadded, which required about 1.5 min, and the Fourier transform was calculated at an apodized resolution of 2 cm^{-1}. Peak wavenumbers were measured visually on the video display by using the cursor position. The membranes were placed inside the sample compartment which was then evacuated. Different evacuation times were used to obtain different water contents. Examination of successive spectra confirmed that the water content of the samples remained very nearly constant during the coadding of interferograms.

Water content was calculated from the band area of the HOH bending fundamental (6). Low water contents for the salts of the divalent and trivalent cations could only be achieved by heating the samples in vacuum at 100°C to 160°C for periods of 24 h or longer.

Results and discussion

OH stretching of HDO at low water contents

Spectra of isotopically dilute HDO were studied for the five alkali metal salts and four alkaline earth metal salts of Nafion listed in Table 1. Figure 2 shows the region of the OH stretching fundamental for the five alkali metal salts at low water content. All five spectra can be seen to contain two bands, *A* at 3680 ± 10 cm^{-1} and *B* at 3522 ± 8 cm^{-1}. Their halfwidths are of the order of 200 cm^{-1} for band *B* and 25 cm^{-1} for band *A*, values typical for hydrogen-bonded and non-hydrogen-bonded OH protons in condensed phases, respectively.[3] Spectra of Mg, Ca, Sr, and Ba salts of Nafion (not shown) are very similar, with the relative intensity of band *A* greater than for the Li salt. The positions of bands *A* and *B* (Table 1) differ only slightly from Li to Cs and again from Mg to Ba. The intensity ratio of the two bands, on the other hand, varies considerably: relative intensity of band *A* increases in the series Cs to Li and increases still further for the alkaline earth salts.

TABLE 1. Observed peak positions (cm^{-1}) in the OH stretching region of the spectrum of isotopically diluted HDO (85% D, 15% H) in the alkali and alkaline earth metal salts of Nafion at low water content (about 1 water molecule per $—SO_3^-$)

Counterion	Band A	Band B
Li^+	3692 ± 2	3520 ± 2
Na^+	3670 ± 10	3522 ± 2
K^+	3680 ± 5	3530 ± 5
Rb^+	3680 ± 5	3520 ± 5
Cs^+	3685 ± 5	3517 ± 5
Mg^{2+}	3688 ± 4	3480 ± 10
Ca^{2+}	3684 ± 2	3486 ± 6
Sr^{2+}	3680 ± 4	3510 ± 6
Ba^{2+}	3676 ± 4	3510 ± 5

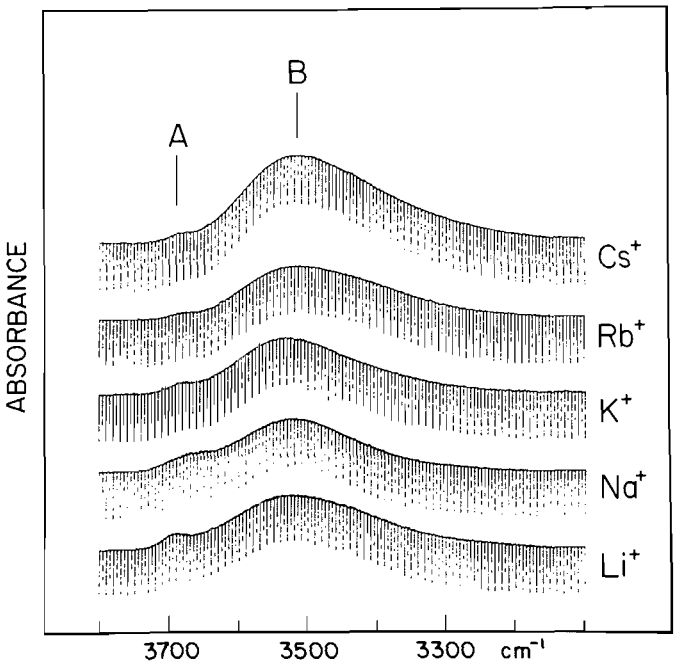

FIG. 2. The OH stretching region of HDO in the spectra of the alkali metal salts of Nafion (85% D, 15% H). Water content: about 1 molecule per $—SO_3^-$.

[3] Band *A* in the spectrum of the sodium salt has a halfwidth of about 45 cm^{-1}, appreciably greater than any of the others. The reason for this is not clear.

TABLE 2. Observed peak positions (cm^{-1}) in the OD stetching region of the spectrum of D_2O in the alkali and four alkaline earth metal salts of Nafion at low water content (about 1 water molecule per $-SO_3^-$), Bu_4N^+ salt included

Counterion	ν_3(AA)	ν_A(AB)	ν_1(AA)	ν_3(BB)	ν_B(AB)	ν_1(BB)
Li^+	2740 ± 5	2710 ± 10	2657 ± 5	[a]	2587 ± 5	[a]
Na^+	2740 ± 15	2710 ± 5	[b]	2650 ± 5	2575 ± 5[f]	[c]
K^+	[d]	2725 ± 5	[d]	2655 ± 5	[c]	2575 ± 5
Rb^+	[d]	2725 ± 5	[d]	2643 ± 5	[c]	2580 ± 5
Cs^+	[d]	2730 ± 5	[d]	2632 ± 5	[c]	2576 ± 5
Bu_4N^+	[d]	2732 ± 5	[d]	2662 ± 5	[c]	2568 ± 5
Mg^{2+}	2760 ± 5	2726 ± 5	2640 ± 10	[a]	2530 ± 5	[a]
Ca^{2+}	2760 ± 5	2734 ± 5	2648 ± 2	[a]	2552 ± 5	[a]
Sr^{2+}	2760 ± 5	2726 ± 5	2648 ± 4	[a]	2568 ± 5	[a]
Ba^{2+}	2760 ± 5	2732 ± 5	2644 ± 4	[a]	2570 ± 5	[a]

[a] Not observed due to low population of BB species.
[b] Not observed due to overlap with ν_3(BB).
[c] Not observed due to overlap with ν_B(AB).
[d] Not observed due to low population of AA species.
[e] Not observed due to overlap with ν_1(BB).
[f] Position uncertain due to overlap with ν_1(BB).

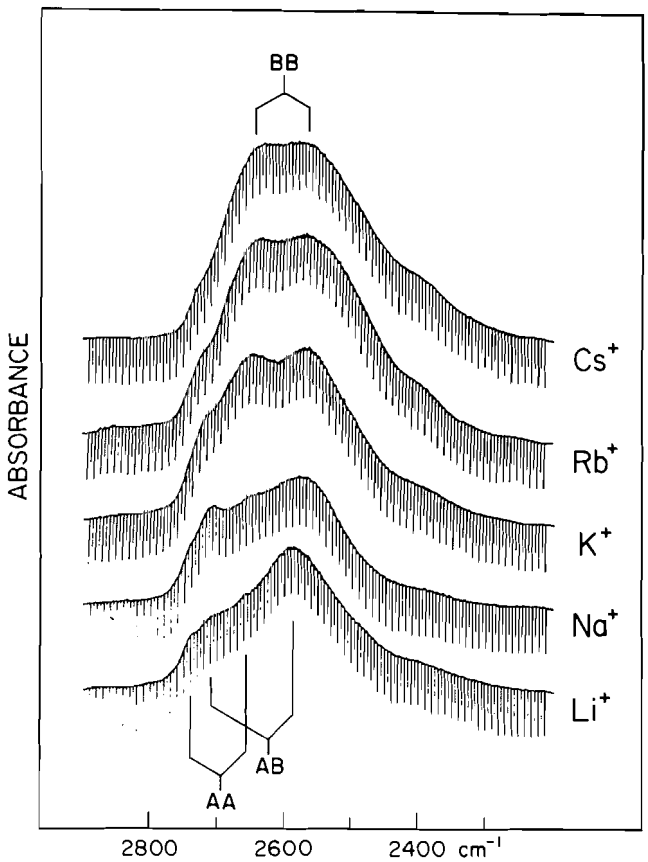

FIG. 3. The OD stretching region of D_2O in the spectra of alkali metal salts of Nafion. Water content and H/D ratio as in Fig. 2.

In the following, as in ref. 5, we shall associate band *A* with the protons exposed to the fluorocarbon medium, OH . . . CF_2, and band *B* with the protons participating in O—H . . . O hydrogen bonds. At low water contents the hydrogen-bond acceptors must be preponderantly the oxygen atoms of the sulfonate anions.

Assignment of H_2O and D_2O stretching fundamentals

As discussed in ref. 5, spectra of H_2O and D_2O in Nafion salts in the region of the stretching fundamentals are more complex than the corresponding spectra of HDO. Assuming the existence of two spectroscopically distinct proton environments, A and B, there should be three types of water molecules, labelled AA, BB, and AB, and these should give rise to six stretching fundamentals: ν_3(AA) and ν_1(AA); ν_3(BB) and ν_1(BB); ν_A(AB) and ν_B(AB).[4]

The wavenumbers of these six bands should be related to those of the corresponding A and B bands of HDO as indicated in Fig. 6 of ref. 5. Because of band overlap and low populations of some water species, the six stretching fundamentals are never resolved completely in any one spectrum. However, a consistent set of assignments of the observed H_2O stretching bands can be made with the use of (*i*) HDO, D_2O, and H_2O spectra of each Nafion salt, (*ii*) spectral trends upon increasing the water content, and (*iii*) low-temperature spectra.

The spectra of H_2O and D_2O in the stretching region contain a contribution from the overtone of the bending vibration, $2\nu_2$, present as a shoulder at about 2400 cm^{-1} for D_2O and 3250 cm^{-1} for H_2O.

The OD stretching fundamental of D_2O at low water content

The positions of the observed bands in the spectra of D_2O in the five alkali metal salts and four of the alkaline earth metal salts of Nafion, at low water content, and their assignments in terms of AA, AB, and BB species of water are recorded in Table 2. Relative intensities of the AA, AB, and BB bands vary considerably from Li to Cs (Fig. 3). The spectrum of the Cs salt is dominated by the BB bands. These bands diminish in intensity in the series Cs, Rb, K, Na, Li. In the spectra of the Na and Li salts the AA and AB bands have become appreciably intense.

Stretching bands in the spectra of Mg, Ca, Sr, and Ba salts of Nafion (not shown) resemble those of the Li salt, with an even higher relative intensity of the AB bands. The differences between the spectral profiles in the series Mg to Ba are minor.

[4] The two stretching fundamentals of AB molecules were designated ν_1(AB) and ν_3(AB) in refs. 5 and 6. The present designation, ν_A(AB) and ν_B(AB), seems more appropriate, since the two vibration modes lie close in wavenumber to the ν_A and ν_B modes of HDO and should correspond largely to motions of the A proton and B proton, respectively.

Can. J. Chem. Downloaded from www.nrcresearchpress.com by 210.87.254.42 on 09/06/12
For personal use only.

TABLE 3. Observed peak positions (cm^{-1}) in the OH stretching region of H_2O in different salts of Nafion

Counterion	$H_2O/—SO_3^-$	ν_3(AA)	ν_A(AB)	ν_1(AA)	ν_3(BB)	ν_B(AB)	ν_1(BB)
Li^+	0.61	3725 ± 15[a]	3710 ± 4	3647 ± 2	[b]	3543 ± 10	[b]
Na^+	0.64	3715 ± 10	3668 ± 4	[c]	[b]	3538 ± 8	[b]
K^+	0.64	3715 ± 15[i]	3682 ± 4	[c]	[d]	3520 ± 5[f]	[e]
Rb^+	0.61	3710 ± 20[i]	3682 ± 5	[c]	[d]	3527 ± 8[f]	[e]
Cs^+	0.58	3712 ± 20[i]	3683 ± 6	[c]	[d]	3518 ± 8[f]	[e]
Bu_4N^+	0.60	[c]	3680 ± 4	[c]	3586 ± 10	3503 ± 20[f]	[e]
Be^{2+}	0.86	[c]	3680 ± 4	[c]	[d]	3240 ± 15[f]	[e]
Mg^{2+}	0.70	[g]	3697 ± 3	3628 ± 8	3550 ± 20	3475 ± 10[f]	[e]
Ca^{2+}	0.67	[g]	3698 ± 3	3623 ± 5	3550 ± 20	3465 ± 10[f]	[e]
Sr^{2+}	0.79	[g]	3710 ± 3	3620 ± 5	[d]	3480 ± 12[f]	[e]
Ba^{2+}	0.85	[g]	3697 ± 4	3612 ± 5	[d]	3493 ± 15[f]	[e]
Mn^{2+}	0.59	[g]	3684 ± 3	3618 ± 10	3530 ± 15	3455 ± 6[f]	[e]
Co^{2+}	0.63	[g]	3673 ± 3	3610 ± 10	3510 ± 20	3440 ± 10[f]	[e]
Ni^{2+}	0.91	[g]	3668 ± 3	3605 ± 10	3500 ± 15	3440 ± 10[f]	[e]
Cu^{2+}	0.62	[c]	3650 ± 4	[c]	[d]	3360 ± 8	[e]
Zn^{2+}	0.65	[g]	3672 ± 3	3600 ± 15	[d]	3438 ± 8[f]	[e]
Al^{3+}	1.2	[c]	3660 ± 4	[c]	[d]	3230 ± 15[f]	[e]
Sc^{3+}	1.4	3700 ± 10	3670 ± 6	[h]	[d]	3410 ± 20[f]	[e]
Y^{3+}	1.2	[g]	3678 ± 3	3610 ± 10	[d]	3480 ± 15[f]	[e]
La^{3+}	1.3	[g]	3675 ± 3	3610 ± 10	[d]	3470 ± 6[f]	[e]

[a] Resolved only at low temperature.
[b] Not observed due to low population of BB species.
[c] Not observed due to low population of AA species.
[d] Not resolved due to overlap with ν_1(BB) and ν_B(AB).
[e] Not resolved due to overlap with ν_3(BB) and ν_B(AB).
[f] Position uncertain due to overlap (see footnotes *d* and *e*).
[g] Not resolved due to overlap with ν_A(AB).
[h] Not resolved due to overlap with ν_B(AB).
[i] Observed clearly only at very low water contents (0.05 $H_2O/—SO_3^-$).

The OH stretching of H_2O at low water content

Spectra of Nafion salts in the OH stretching region of H_2O resemble the corresponding spectra of D_2O, except that the $\nu_3 - \nu_1$ wavenumber splitting is smaller for H_2O.[5] Because of smaller splitting, the bands due to ν_1(AA) and ν_3(AA) are closer together and in most cases overlap with ν_A(AB) to yield a single unresolved absorption band. Similarly, ν_1(BB) and ν_3(BB), together with ν_B(AB), tend to yield one unresolved band. On the other hand, ν_1(AA), which in the D_2O stretching spectra of most Nafion salts tends to coincide with ν_3(BB), lies some 70 cm^{-1} above ν_3(BB) in the corresponding H_2O spectra. As a result, for H_2O the three A bands, i.e., ν_3(AA), ν_A(AB), and ν_1(AA), lie above 3650 cm^{-1}, while the three B bands, i.e., ν_3(BB), ν_B(AB), and ν_1(BB), tend to lie below 3650 cm^{-1}. In this way the A and B band systems overlap much less for H_2O than for D_2O. Consequently, the relative integrated intensity contributions of the three A bands may be roughly estimated from the ratio

[1] **A** = (band area above 3650 cm^{-1})/(total band area)

The positions of the observed bands in the spectrum of H_2O at low water contents for the different salts of Nafion are recorded in Table 3, with band assignments in terms of the AA/AB/BB model.

The spectra of alkali metal salts of Nafion in the OH stretching region of H_2O at low water contents are shown in Fig. 4 (top left). As also observed for HDO and D_2O spectra of this series, the intensity of the A region of the spectrum (above 3650 cm^{-1}) decreases gradually from Li to Cs, while the intensity of the B region (below 3650 cm^{-1}) increases substantially. In addition, the H_2O spectra, like the corresponding D_2O spectra, indicate a rather large variation in the relative contributions of AA, AB, and BB absorptions along the series. The spectrum of the Cs salt has an intense BB absorption (unresolved ν_1 and ν_3), with only a small admixture of AB and an even smaller contribution of AA. The relative intensity of AB bands increases from Cs to Li. AA bands first become clearly visible in the spectrum of the Na salt and become fairly intense in the Li salt. Only the high-wavenumber ν_3(AA) band is observed in the spectrum of the Na salt while the low-wavenumber ν_1(AA) band shows up more clearly in the spectrum of the Li salt.

Figure 4 (top right) shows the spectra of four alkaline earth metal salts of Nafion in the OH stretching region of H_2O. The overall intensity of the A region in these spectra is appreciably greater than in the Li salt and the major contributor to the spectrum appears to be the AB molecules. A small, relatively sharp band at about 3620 ± 10 cm^{-1}, assigned to ν_1(AA), indicates a small contribution of AA molecules, increasing somewhat along the series from Mg to Ba. A broader band at about 3550 ± 20 cm^{-1} assigned to ν_3(BB) decreases from Mg to Ca, then increases again from Ca to Ba, indicating that the population of BB molecules may pass through a minimum. The spectrum of the Be salt of Nafion differs considerably from that of the other salts of this group and will be described below.

Figure 4 (bottom left) shows the spectra of divalent transition metal salts (Mn, Co, Ni, Cu, and Zn) of Nafion in the OH stretching region of H_2O. The spectra of Mn, Co, and Ni salts resemble closely those of the Mg–Ba series. The two major bands are due to ν_A(AB) and ν_B(AB), with much smaller bands near 3610 cm^{-1} and 3510 cm^{-1} assigned to ν_1(AA) and ν_3(BB), respectively, indicating appreciable contribution of the AA and

[5] In the vapor state $\nu_3 - \nu_1$ = 2788.1 − 2671.5 = 116.6 cm^{-1} for D_2O and 3755.8 − 3656.7 = 99.1 cm^{-1} for H_2O (8).

Can. J. Chem. Downloaded from www.nrcresearchpress.com by 210.87.254.42 on 09/06/12
For personal use only.

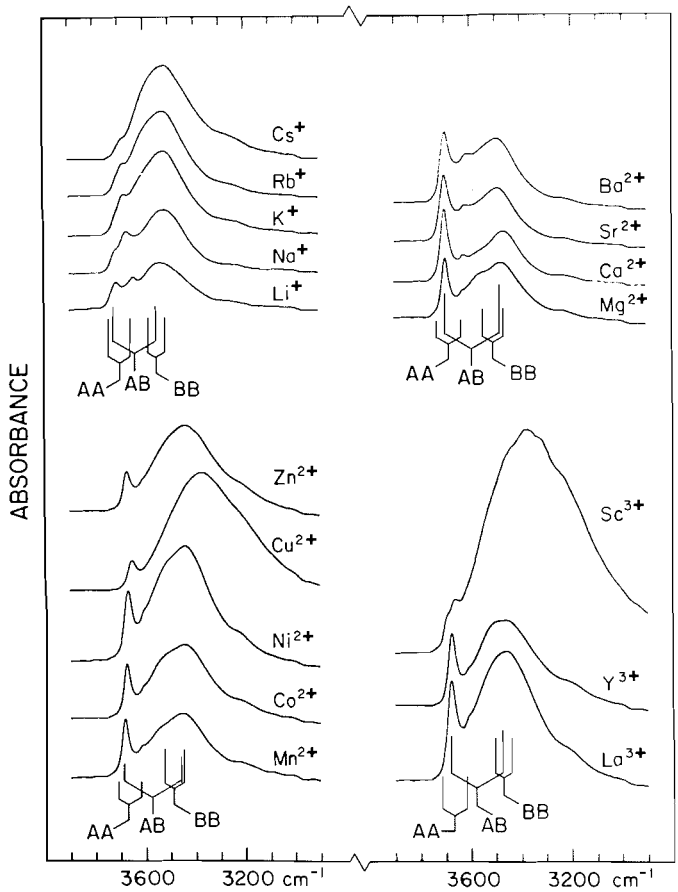

FIG. 4. The OH stretching region of H_2O in the spectra of different salts of Nafion. Water content mostly below 1 $H_2O/—SO_3^-$ (see Table 3).

BB molecules as well. The spectrum of the Zn salt shows a somewhat less intense A region and a much less intense ν_1(AA) band, while the spectrum of the Cu salt shows an even less intense ν_A(AB) band and no detectable ν_1(AA). Thus in the case of the Cu salt all the water molecules appear to be of type AB and BB. The ν_A(AB) band of the Cu salt is over 20 cm^{-1} below that in the spectra of other divalent metal salts. At the same time the center of the B absorption region, probably largely made up of ν_B(BB), centered at 3360 cm^{-1}, lies some 80 cm^{-1} below those in the spectra of the other divalent metal salts. This indicates substantially stronger hydrogen bonding, implying a stronger polarization of H_2O by the Cu^{2+} ion.

The spectra of trivalent Sc, Y, and La salts of Nafion in the OH stretching region of H_2O are shown in Fig. 4 (bottom right). The spectra of Y and La salts resemble those of the divalent salts such as Mg and Mn, the major contributor being AB molecules. That of the Sc salt, on the other hand, is distinctive in that the A region is of very low intensity and in that it contains two small bands of comparable low intensities at about 3700 cm^{-1} and 3670 cm^{-1}, assigned to ν_3(AA) and ν_A(AB). This is the only case in which AA and AB molecules appear to be present in nearly equal proportions.

The spectra of Be and Al salts of Nafion in the OH stretching region of H_2O are shown in Fig. 5. These spectra resemble each other and differ from those of the other salts in that the A region is of exceedingly low intensity, only about 2% of the total band area, and the B region is shifted to much lower wavenumbers, 3240 and 3230 cm^{-1}, respectively, for Be and Al. This attests

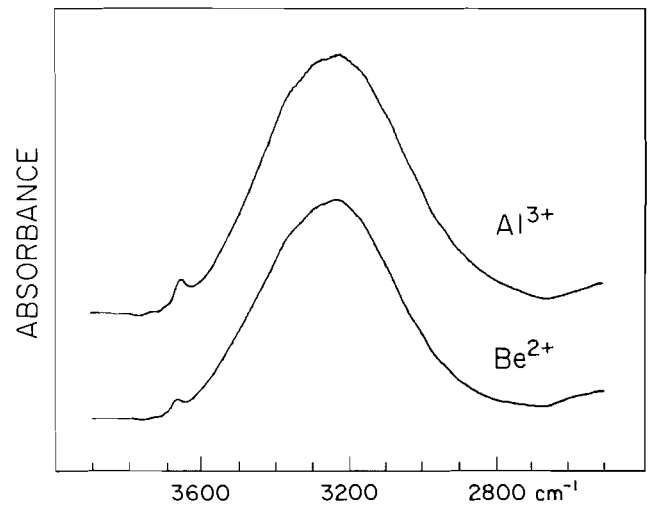

FIG. 5. The OH stretching region of H_2O in the spectra of Al and Be salts of Nafion.

to very strong hydrogen bonding brought about by a strong polarization of H_2O by these two cations.

Spectral changes with varying water content

The spectra described in the preceding sections are those corresponding to low water content, in most cases below 1 $H_2O/—SO_3^-$. Spectra obtained at still lower water contents, down to 0.1 $H_2O/—SO_3^-$ are not appreciably different. We therefore believe that our results correspond closely to the ultimate behaviour of isolated water molecules interacting with anion–cation pairs.

Changes which occur upon increasing the water content of the membranes are the same for all Nafion salts and involve increased intensity of the absorption in the hydrogen-bonded region of the spectrum, below 3650 cm^{-1}, relative to the absorption in the non-hydrogen-bonded region, above 3650 cm^{-1}. This is illustrated for the H_2O spectrum of the Li salt of Nafion in Fig. 6. It can be seen that the B region of the spectrum increases rapidly with respect to the A region. AA bands, detectable at lower water contents, become submerged at higher water contents and BB bands dominate the spectrum.

The HOH bending fundamental

An interesting finding of the present study is that for several salts of Nafion the bending fundamental of H_2O resolves into two components which clearly correspond to water molecules in structurally distinct environments. Such resolution is very rarely observed for systems containing several types of water molecules[6] and confirms that water in Nafion occurs in widely different bonding environments.

Spectra of the Li and La salts of Nafion, representative of those for which the bending fundamental resolves into a doublet, are shown for different water contents in Fig. 7. At low water contents the low-wavenumber component, *L* (at 1616 cm^{-1} for Li and 1606 cm^{-1} for La), accounts for most of the band intensity in the case of La and about one-third in the case of Li. In either case its intensity increases less rapidly with increasing water content than that of the high-wavenumber

[6] For example, in the spectra of aqueous solutions of electrolytes the bending fundamental is an unresolved singlet even in cases where the stretching fundamental is resolved into widely separated bands as with perchlorates and fluoroborates (10, 11).

Can. J. Chem. Downloaded from www.nrcresearchpress.com by 210.87.254.42 on 09/06/12
For personal use only.

Can. J. Chem. Downloaded from www.nrcresearchpress.com by 210.87.254.42 on 09/06/12
For personal use only.

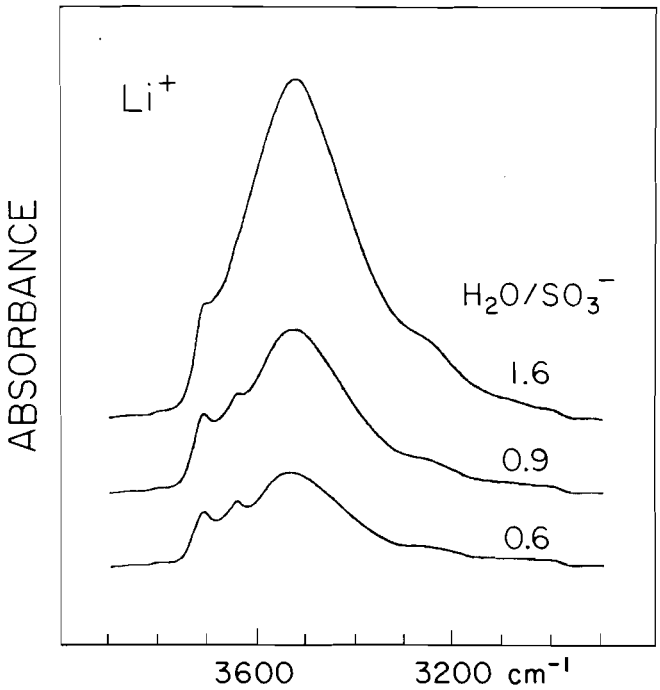

FIG. 6. The OH stretching region of H_2O in the spectra of Li salt of Nafion at different water contents.

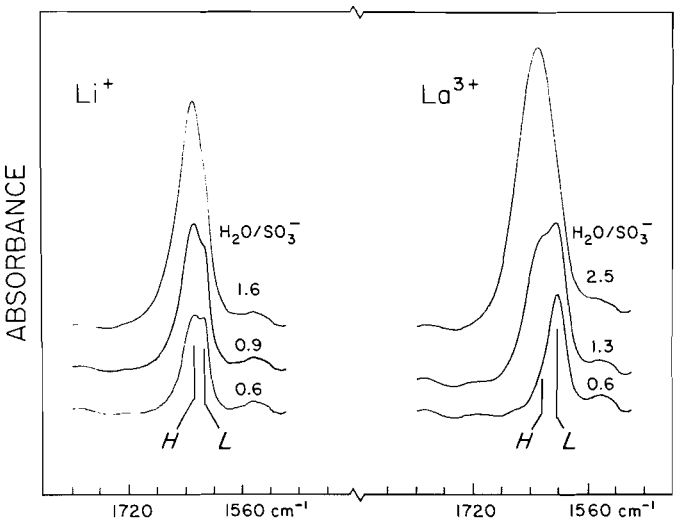

FIG. 7. The HOH bending fundamental region of H_2O in spectra of Li and La salts of Nafion at different water contents.

component, *H* (1629 cm^{-1} for Li and 1625 cm^{-1} for La), which becomes the dominant feature at high water contents. It is clear that *H* originates in more strongly hydrogen-bonded water molecules and *L* in less strongly hydrogen-bonded water molecules for the following reasons:

(*i*) Hydrogen bonding is known to raise the wavenumber of the bending fundamental of water just as it lowers the wavenumber of the stretching fundamental (9).

(*ii*) The bandwidth of component *H* is larger than that of component *L*, a characteristic of more strongly hydrogen-bonded systems.

(*iii*) Lowering the temperature (cf. Fig. 10) shifts *L* to lower wavenumbers and *H* to higher wavenumbers, as expected from the observation that strong hydrogen bonds (which tend to be

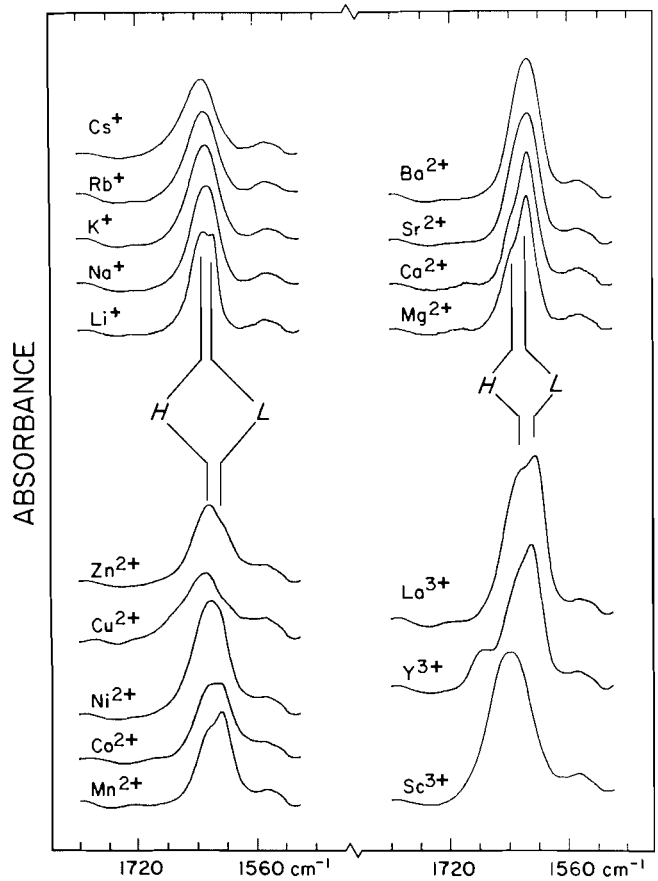

FIG. 8. The HOH bending fundamental region of H_2O in the spectra of different salts of Nafion (water content as in Table 4).

linear (12)) are strengthened at lower temperatures, while weak hydrogen bonds (which tend to be bent (12)) are weakened at lower temperatures (13).

(*iv*) At different water contents the relative areas of components *H* and *L* vary roughly in proportion to the relative band areas of water species BB and AB, respectively, in the region of the stretching fundamental.

We therefore provisionally assign component *H* to the fully hydrogen-bonded BB molecules and component *L* to the partially bonded AB molecules with a possible contribution of the non-hydrogen-bonded AA molecules. This leaves open the question why bands due to AA and AB molecules are not resolved. In the spectra of most Nafion salts studied by us the population of AA species is small, but at least in the case of the Li salt AA bands in the OH stretching region are fairly intense so that AA population must be significant. Possibly the bending fundamental of AA is not very far separated from that of AB.

In nine of the cases studied, the HOH bending fundamental did not resolve into a doublet at any water content. Lowering of temperature down to 10 K did not bring about band resolution.[7] In all cases the overall band center shifted to higher wavenumbers with increasing water content, the increase being largest for Cs and smallest for Na. This behaviour is consistent with the unresolved component *H*, corresponding to hydrogen-

[7] The bandwidths in the OH stretching and HOH bending region showed only a minor decrease from 300 K to 10 K, indicating that the factors responsible for the bandwidth are not dynamic in nature, but are probably due to a distribution of local environments of the H_2O molecule.

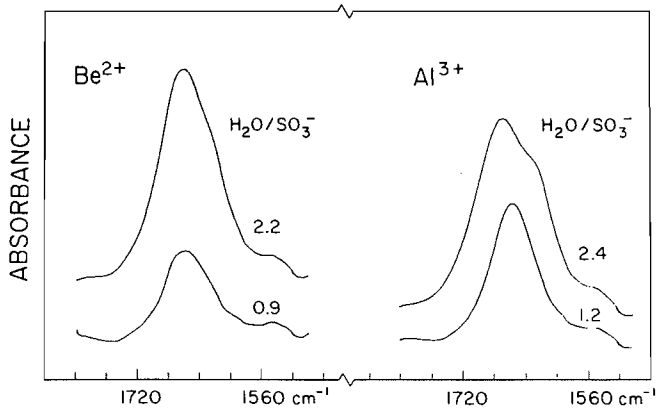

FIG. 9. The HOH bending fundamental region of H_2O in the spectra of Be (left) and Al (right) salts of Nafion at different water contents.

bonded water molecules, increasing with increasing water content in the same manner as for Li and La salts.

Spectra in the HOH bending region are shown in Fig. 8 (top left) for the five alkali metal salts of Nafion at low water content. Only the spectrum of the Li salt exhibits a resolved doublet; those of Na through Cs show broad bands, centered at 1625 cm^{-1} to 1632 cm^{-1}, which we interpret as unresolved doublets.

In the spectra of the alkaline earth salts of Nafion, shown in Fig. 8 (top right), the bending fundamental at low water content resolves into two components in the case of Mg and Ca salts, but remains unresolved for the Sr and Ba salts. For Mg and Ca, the low wavenumber component, at about 1614 cm^{-1}, is the major contributor to the band intensity at low water contents. This is consistent with the conclusion from the OH stretching spectral region that AB is the major species. Again, the relative intensity of the high-wavenumber component increases with increasing water content for Mg and Ca salts, while for Sr and Ba salts the unresolved band shifts gradually to higher wavenumbers, indicating a similar underlying increase in the proportion of the hydrogen-bonded water molecules.

The spectrum of the Be salt of Nafion is different from those of the other alkaline earth salts. Only one broad band is observed in the region of the HOH bending, centered at the unusually high wavenumber, 1660 cm^{-1} (Fig. 9, left). This clearly corresponds to strongly hydrogen bonded water molecules, and is consistent with the unusually low wavenumber of the H_2O stretching fundamental at about 3200 cm^{-1}, and the very low incidence of the incompletely hydrogen-bonded molecules — deduced from the spectrum in the OH stretching region. The center of the band at 1660 cm^{-1} is considerably above the wavenumber of the bending fundamental in pure liquid water at room temperature (about 1640 cm^{-1}). At higher water contents a new distinct band appears at about 1630 cm^{-1}. This band must be due to fully hydrogen-bonded water molecules in the outer hydration shell of the Be ion and no longer strongly polarized by the cation.

The spectra of the Nafion salts of the divalent transition metals Mn, Co, Ni, and Zn all show doublets in the HOH bending region at low water content, resolved to varying extent as shown in Fig. 8 (bottom left). In all of these the high-wavenumber component becomes more prominent at higher water contents. Relative intensity of the low-wavenumber component correlates with that of the ν_A(AB) band in the stretching region; it is dominant in the spectrum of the Mn salt and

TABLE 4. Observed peak positions (cm^{-1}) of bands *H* and *L* and area fraction[a] **L** from the spectra of the HOH bending fundamental of H_2O in Nafion; water content same as in Table 3

Counterion	*H*	*L*	Area fraction **L**
Li^+	1629 ± 3	1616 ± 1	0.25
Na^+	1625 ± 3[b]		
K^+	1627 ± 3[b]		
Rb^+	1629 ± 3[b]		
Cs^+	1632 ± 4[b]		
Bu_4N^+	1632 ± 4[b]		
Be^{2+}	1662 ± 4	1621 ± 10[c]	
Mg^{2+}	1632 ± 4	1614 ± 1	0.64
Ca^{2+}	1632 ± 6	1614 ± 2	0.67
Sr^{2+}		1614 ± 2[b]	
Ba^{2+}		1614 ± 2[b]	
Mn^{2+}	1621 ± 4	1606 ± 3	0.53
Co^{2+}	1623 ± 4	1609 ± 4	0.39
Ni^{2+}	1622 ± 4	1607 ± 8	0.30
Cu^{2+}	1628 ± 4		
Zn^{2+}	1624 ± 4	1604 ± 8	
Al^{3+}	1657 ± 2	1627 ± 6[c]	
Sc^{3+}	1639 ± 5[b]		
Y^{3+}	1630 ± 8	1609 ± 2	
La^{3+}	1625 ± 6	1605 ± 2	0.39

[a] Obtained from deconvoluted spectra by [2].
[b] Band not resolved.
[c] Observed only at higher water contents (see Fig. 9).

decreases in the series Mn/Co/Ni/Zn. The spectra of the Cu salt do not resemble the rest of this series; the bending fundamental is broader, the high-wavenumber component higher, and the low-wavenumber component lower than for Mn.

At low water contents the Sc salt, whose spectrum in the stretching region showed a dominant BB band, exhibits only the *H* band in the bending region (Fig. 8, bottom right). On the other hand, the Y and La salts which show large AB bands in the OH stretching region, exhibit doublets in the HOH bending region, with the *L* component dominant.

The spectra of the Al salt in the H—O—H bending region (Fig. 9, right) resemble closely those of the Be salt, again in agreement with their general resemblance in the OH stretching region.

Resolution enhancement by Fourier self-deconvolution

Because of severe band overlap it was difficult to estimate the band areas of *H* and *L* components directly even in the 11 cases where they were partly resolved in the original spectra. In order to calculate these areas we have enhanced the resolution by Fourier self-deconvolution (14). This procedure, known to preserve the band areas of individual components, diminished band overlap and thus minimized the experimental error in the area measurements. In order to diminish the error arising from the small residual band overlap, the area fraction **L** of the low-wavenumber component was obtained from the deconvolved spectra as follows:

$$[2] \quad \mathbf{L} = I_L/(I_L + I_H)$$

where I_L is the band area below the peak position of band *L* and I_H is the band area above the peak position of band *H*. **L** values are recorded in column 4 of Table 4.

For most of the nine salts with unresolved HOH bending fundamentals a clear-cut decomposition into components could

Can. J. Chem. Downloaded from www.nrcresearchpress.com by 210.87.254.42 on 09/06/12
For personal use only.

Can. J. Chem. Downloaded from www.nrcresearchpress.com by 210.87.254.42 on 09/06/12
For personal use only.

TABLE 5. Properties of some counterions

Counterion	Lewis acid strength	Area fraction **A**	Rough estimates of population fractions		
			AA	AB	BB
Li^+	0.22	0.19	15	25	60
Na^+	0.16	0.17	12	20	68
K^+	0.13	0.12	8	15	77
Rb^+	0.10	0.10	5	10	85
Cs^+	0.08	0.06	0	5	95
Bu_4N^+	0.03	0.04	0	3	97
Be^{2+}	0.50	0.02	0	5	95
Mg^{2+}	0.36	0.17	5	50	45
Ca^{2+}	0.29	0.24	7	60	33
Sr^{2+}	0.24	0.24	15	55	30
Ba^{2+}	0.20	0.22	15	50	35
Mn^{2+}	0.36	0.12	5	50	45
Co^{2+}	0.40	0.17	5	40	55
Ni^{2+}	0.50	0.15	3	30	67
Cu^{2+}	0.45	0.05	0	10	90
Zn^{2+}	0.36	0.12	2	18	80
Al^{3+}	0.63	0.02	0	5	95
Sc^{3+}	0.50	0.03	2	3	95
Y^{3+}	0.45	0.13	10	30	60
La^{3+}	0.40	0.13	10	30	60

not be achieved by self-deconvolution. One exception was the spectrum of the Na salt, in which the original singlet at 1625 cm^{-1} upon self-deconvolution yielded a doublet at 1632 and 1614 cm^{-1}.

Band areas and populations of AA, AB, and BB species

The difficulties of calculating the populations of the molecular species of water in Nafion from the observed intensities of the infrared absorption bands in the OH stretching region are of three types:

(*i*) *Inadequacy of the model*. The three-species AA–AB–BB model oversimplifies the real situation in the Nafion–water system. The observed components may be themselves a mixture of further unresolved components, so that a continuum-type model might in fact be more appropriate for some purposes.

(*ii*) *Band overlap* makes it difficult to estimate the areas belonging to the individual bands. Attempts to enhance the resolution by means of Fourier self-deconvolution were not successful because of widely different widths of A and B component bands.

(*iii*) *Uncertain absorptivities*. Bands B, which originate in the hydrogen-bonded OH groups are probably at least four times as intense per oscillator as bands A (5). The exact absorptivities of the AA, AB, and BB bands are not known and could be to some extent variable: absorptivities tend to increase with decreasing wavenumbers of OH stretching, and there are considerable differences between the positions of the maxima of the B bands in the spectra of the different Nafion salts (cf. Table 3).

In view of (*ii*) and (*iii*) it is not possible to calculate very accurately the populations of AA, AB, and BB species from the intensities of the corresponding H_2O absorption bands, even within the framework of the three-species model. However, we have been able to derive rough estimates of the population fractions and these are tabulated in columns 4–6 of Table 5. These values were obtained from visually estimated relative band intensities, assuming that the integrated absorptivities of

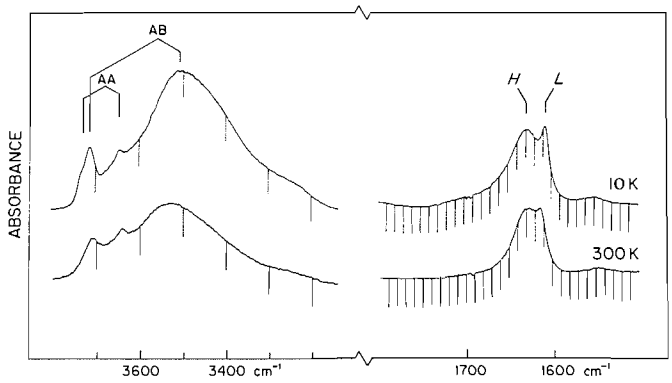

FIG. 10. The OH stretching region (left) and HOH bending fundamental region (right) of H_2O in the spectra of Li salt of Nafion. Temperatures: 10 K (top spectra) and 300 K (bottom spectra).

ν_3(AA), ν_1(AA), and ν_A(AB) are roughly equal. The necessary scaling was accomplished by assuming that AB population fractions are approximately equal to the area fraction **L** for those seven salts for which this quantity could be calculated (Table 4). This procedure was intended to ensure that the numbers within each column correctly reflect the trends for the increasing or decreasing populations of each species, even though the numbers along rows may be in error. The trends observed in this manner coincide with those set by the area fraction **A** defined by [1] and obtained directly from the spectra (column 3 in Table 5).

Mode of attachment of the water molecule to anion–cation pairs

Our results, tabulated in columns 3–6 of Table 5, show that at low water content different cationic forms of Nafion are characterized by widely different porportions of water molecules in configurations AA, AB, and BB. With the Al and Cs salts we see almost exclusively the BB configuration, while in the Ca salt the AB configuration dominates. This is interpreted to indicate that in the Al and Cs salts the water molecule is predominantly inserted between the cation and anion as depicted in Fig. 1*a*, while in the Ca salt the water molecule attaches to the ion pair largely without insertion, as in Fig. 1*b* and *c*. The results for the 20 cationic forms studied appear at first puzzling, as the trends do not simply follow the variation of ionic radius: for the monovalent cations the BB fraction *increases* with increasing ion size, but it *decreases* for the trivalent cations, while for divalent cations it varies irregularly. However, the trends we observe must reflect the tendency of an isolated water molecule to enter between an anion and a cation, and this must depend fairly specifically on anion–cation affinity. The property of anions and cations which is most intimately connected with such affinity is the *Lewis acid strength* of the cation and the *Lewis base strength* of the anion (15). The base strength of the sulfonate anion in Nafion can be approximated by that for the sulfonate anion in $CF_3SO_3^-$ salts, 0.27 ± 0.02 units (16). The best match and hence the greatest anion–cation affinity would be expected for those cations whose acid strength is also around 0.27.

The values of acid strength for the cations used in the present study are recorded in column 2 of Table 5. When the area fraction **A** (column 3) is plotted against the Lewis acid strength of the cation (Fig. 11), a clear pattern emerges: a maximum in the value of fraction **A**, indicating a minimum of water insertion between anion and cation, appears at acid strength of

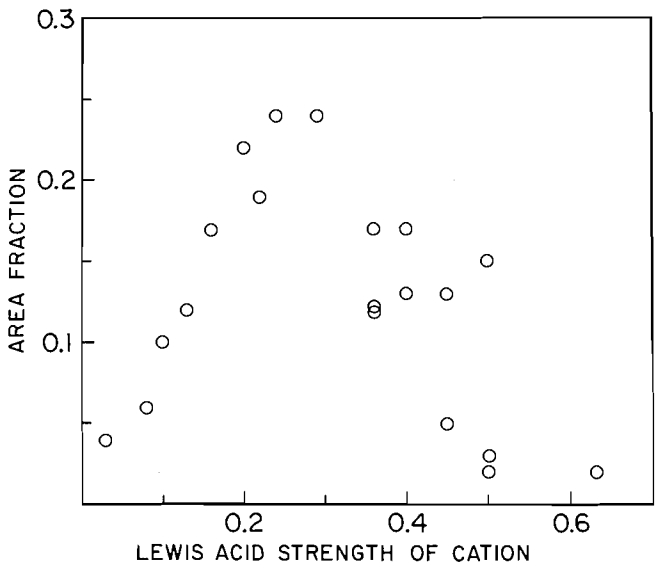

FIG. 11. Plot of the area fraction **A** against the Lewis acid strength of the cation.

about 0.26 ± 0.02 units, corresponding to the estimated base strength of the sulfonate anion in Nafion. On either side of this maximum, **A** fraction falls off rapidly, indicating increasing occurrence of insertion. Large deviations from a smooth plot are largely due to the transition-metal cations, for which highly variable acid strengths are encountered (15, 16). Very similar plots are obtained when the population fractions of columns 4–6 of Table 5 are plotted against the cation acid strength, with AA population showing a maximum at Li (acid strength ~0.22), AB population showing a maximum at Ca (acid strength ~0.30), and the BB population passing through a minimum at Sr (acid strength ~0.24).

The following picture emerges: when the anion–cation pair is relatively stable, which tends to happen when there is a good match between the acid strength of the cation and the base strength of the anion, water molecules are not inserted between the anion and the cation, but tend to be attached on the outside. When, on the other hand, the ion-pair is mismatched, there is a strong tendency for the water molecule to be inserted. Lewis acid and base strengths of cations and anions appear to be a good indicator of their affinity for each other and of the resistance of cation–anion pairs to disruption by water molecules.

Acknowledgements

S.Q. wishes to acknowledge a post-graduate fellowship from the Conselho Nacional de Desenvolvimento Científico e Technológico-CNPq. Helpful discussions with Professor I. D. Brown and Professor W. J. Kauzmann are gratefully acknowledged.

1. W. GROT. Chem. Ing. Tech. **50**, 299 (1978).
2. A. EISENBERG and H. L. YEAGER (*Editors*). Perfluorinated ionomer membranes. Am. Chem. Soc. Symposium Ser. 180. Washington, D.C. 1982.
3. G. ZUNDEL. Hydration and intermolecular interactions. Academic Press, New York. 1969.
4. L. Y. LEVY, M. MUZZI, and H. D. HURWITZ. J. Chem. Soc. Faraday Trans. I, **78**, 17 (1982).
5. M. FALK. Can. J. Chem. **58**, 1495 (1980).
6. M. FALK. *In* Perfluorinated ionomer membranes. Chapt. 7.
7. H. L. YEAGER, Z. TWARDOWSKI, and L. M. CLARKE. J. Electrochem. Soc. **129**, 324 (1982).
8. W. S. BENEDICT, N. GAILAR, and E. K. PLYER. J. Chem. Phys. **24**, 1139 (1956).
9. M. FALK. Spectrochim. Acta. **40**A, 43 (1984).
10. G. BRINK and M. FALK. Can. J. Chem. **48**, 3019 (1970).
11. S. QUEZADO and M. FALK. Unpublished results.
12. I. D. BROWN. Acta Crystallogr. A**32**, 24 (1976).
13. O. KNOP, W. J. WESTERHAUS, and M. FALK. Can. J. Chem. **58**, 270 (1980).
14. J. K. KAUPPINEN, D. J. MOFFATT, H. MANTSCH, and D. G. CAMERON. Appl. Spectrosc. **35**, 271 (1981).
15. I. D. BROWN. Structure and bonding in crystals. Vol. II. Academic Press, New York. 1981. Chapt. 14.
16. I. D. BROWN. Private communication.

Can. J. Chem. Downloaded from www.nrcresearchpress.com by 210.87.254.42 on 09/06/12
For personal use only.

Synthesis and properties of a series of linked porphyrin–quinone molecules designed as models of the reaction centre in photosynthesis[1]

TE-FU HO, ALAN R. MCINTOSH, AND ALAN C. WEEDON[2]

Photochemistry Unit, Department of Chemistry, The University of Western Ontario, London, Ont., Canada N6A 5B7

Received June 28, 1983[3]

TE-FU HO, ALAN R. MCINTOSH, and ALAN C. WEEDON. Can. J. Chem. **62**, 967 (1984).

The synthesis of the covalently linked porphyrin–quinone compounds **4***a*, **4***b*, and **4***c* is described. The structures of the linked compounds and their precursors in the synthetic route are established by ultraviolet/visible absorption spectroscopy, ^{1}H nmr, ir, and mass spectroseopy. Some of the photophysical properties of the compounds prepared are reported with reference to their use as models of the reaction centre in photosynthesis.

TE-FU HO, ALAN R. MCINTOSH et ALAN C. WEEDON. Can. J. Chem. **62**, 967 (1984).

On décrit la synthèse des composés **4***a*, **4***b* et **4***c* qui sont des porphyrines liées d'une façon covalente avec des quinones. Les structures des composés liés ainsi que celles de leurs précurseurs ont été établies par spectroscopie d'absorption ultraviolette–visible, par rmn du ^{1}H, par ir et par spectroscopie de masse. On rapporte quelques propriétés photophysiques des composés préparés en relation avec leur utilisation comme modèles du centre réactionnel de la photosynthèse.

[Traduit par le journal]

Can. J. Chem. Downloaded from www.nrcresearchpress.com by 210.87.254.5 on 09/06/12
For personal use only.

Introduction

The primary photochemical process in green plant photosynthesis is transfer of an electron from a photoexcited chlorophyll donor to an acceptor (ultimately a benzoquinone derivative in many cases), these two species being held together in close proximity in a reaction centre protein. Very little is known about the structural requirements for orientation of the components in the electron transfer reaction *in vivo* and there has recently been much interest in attempts to mimic the electron transfer process in model systems. These investigations include the preparation of covalently linked chlorophyll chromophores (1), of capped, bridged, and cofacially linked porphyrins (2–5), and of other molecules which are capable of light induced intramolecular electron transfer (6–10).

We wished to gain an understanding of the structural and electronic factors governing the efficiency of electron transfer between a photo-excited molecule and an adjacent acceptor molecule, and also of the factors affecting the rate of the subsequent back electron transfer in the radical ion pair generated. To this end, compounds have been prepared in this laboratory (11), using the method of Kong and Loach (6), which consist of a tetraarylporphyrin attached by a covalent linkage of variable length to a benzoquinone (compounds **4***d*, **4***e*, and **4***f*). The epr spectra produced when these compounds are irradiated with visible light suggest that the porphyrin transfers an electron to the benzoquinone to generate a radical ion pair. At low temperatures this charge separated species is stable, while at higher temperatures it reverts to the neutral, linked porphyrin–benzoquinone precursor, suggesting that an activation barrier for back electron transfer exists (11).

Studies of the photophysical properties of these compounds have been hindered by the hydrolytic instability of the diester linkage between the porphyrin and the benzoquinone. This problem is especially acute, as we wish to investigate light induced electron transfer in these molecules (which possess surfactant properties) in monolayer assemblies in aqueous systems where conformational mobility of the linkage between porphyrin and benzoquinone is minimized. To solve this problem, we embarked upon a program aimed at synthesizing a series of compounds analogous to **4***d*–**4***f* where the ester linkages are replaced by hydrolytically more stable amide functions. In addition, it was hoped that the linkage between the porphyrin and quinone would be made more rigid, with respect to conformational mobility, in consequence of the greater double bond character of the carbon to heteroatom bond in the amide functions as compared to the ester functions. We describe here the synthesis and some properties of the compounds **4***a*–**4***c* in which a porphyrin and a benzoquinone are linked together via two amide bonds and a methylene chain of variable length.

Results and discussion

The synthetic sequence leading to compounds **4***a* to **4***c* is shown in Scheme 1 and will be described below for the 1,3-diaminopropane linked molecule **4***b*. Commercially available 2,5-dimethoxyphenylacetic acid was converted to its methyl ester and treated with a large excess of 1,3-diaminopropane to yield the amide **1***b*. Preparation of **1***b* by direct acylation of the diamine with 2,5-dimethoxyphenylacetyl chloride was found to be unsatisfactory; under all conditions examined, including standard Schotten–Bauman conditions and addition of the acid chloride to excess diamine in organic solvents, the major product was the diacylated compound *N,N'*-di(2,5-dimethoxyphenylacetyl)-1,3-diaminopropane.

The structure of **1***b* was readily confirmed by the ^{1}H nmr spectrum which exhibited signals ascribable to the primary amine, secondary amide, and methylene protons. The compound was further characterized by conversion to its *N*-acetylated derivative.

The porphyrin 5-(*p*-carboxyphenyl)-10,15,20-tri(*p*-tolyl)-porphyrin ("PCO_2H") was prepared by the condensation of pyrrole with a mixture of *p*-tolualdehyde and 4-carboxybenzaldehyde in refluxing propionic acid, followed by chromatographic separation of the mono- and polycarboxyporphyrins obtained (12). The monocarboxyporphyrin was converted to its acid chloride ("PCOCl") with thionyl chloride and treated with the amine **1***b* in the presence of pyridine to give the porphyrin–dimethoxybenzene linked compound **2***b*, which was purified by chromatography.

The ^{1}H nmr spectrum of the linked compound **2***b* is shown in Fig. 1. Despite the fact that 54 hydrogen atoms are present

[1] Contribution number 308 from the Photochemistry Unit, The University of Western Ontario, London, Ontario.

[2] Author to whom correspondence may be addressed.

[3] Revision received December 13, 1983.

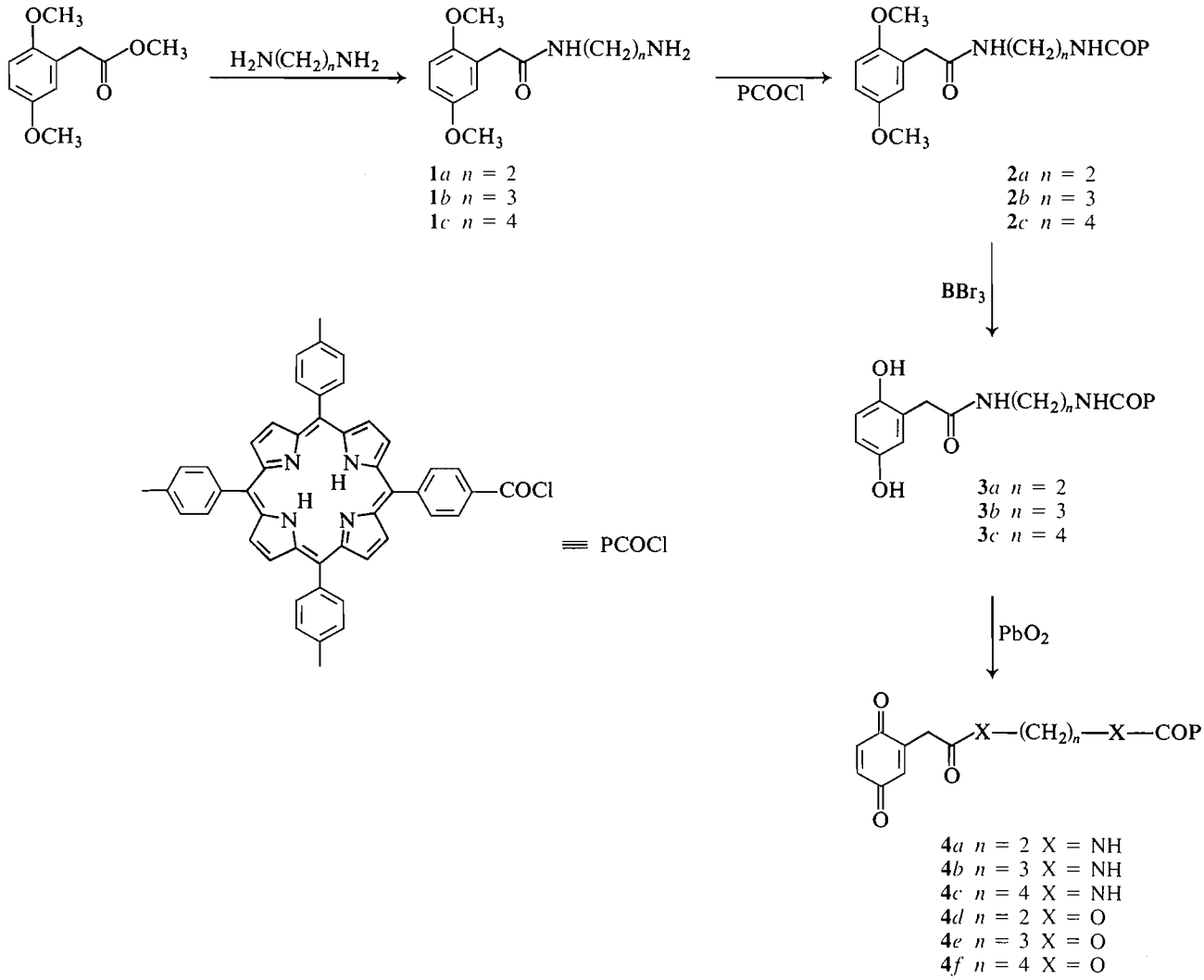

SCHEME 1

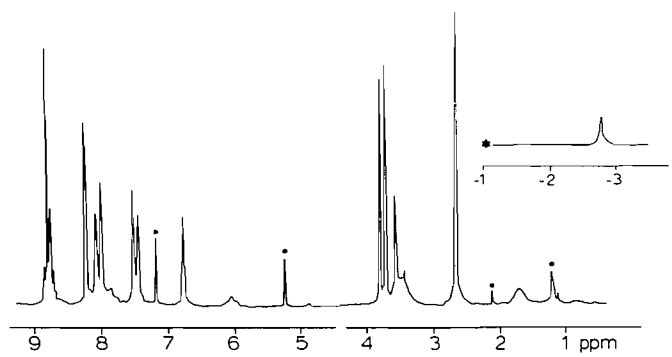

FIG. 1. The ^{1}H nmr spectrum (100 MHz) of **2***b* in $CDCl_3$. Peaks marked by asterisks are impurities in the solvent. The inset shows the porphyrin NH protons.

in the molecule, the environments of nonequivalent positions are sufficiently different and isolated that the protons appear over a chemical shift range of 12 ppm with minimal coupling and can all be easily distinguished. The highly shielded protons on the porphyrin nitrogen atoms appear at −2.8 ppm while those on the β-positions of the pyrrolic rings are highly deshielded and appear at ca. 8.8 ppm. The tolyl ring protons are visible as an AA′BB′ system at 7.4–8.2 ppm and the corresponding methyl groups are at 2.68 ppm. The aromatic protons on the linking phenyl of **2***b* resonate at 8.35 ppm and those on the dimethoxybenzene at 6.75 ppm. The secondary amide protons show as a broadened signal at 6.1 ppm and the methylenes of the propane linkage at 1.6–2.0 and 3.3–3.6 ppm. The methoxyl groups of the protected hydroquinone and the adjacent benzylic protons are also observed clearly at 3.75, 3.72, and 3.64 ppm, respectively.

The ultraviolet/visible spectrum of **2***b* exhibits the characteristic porphyrin Q-bands in the visible region and the more intense Soret band at 420 nm (Table 1). The absorption spectrum confirms that the porphyrin in **2***b* is metal-free and nonprotonated. Porphyrins are excellent metal scavengers and are also weak bases; unless pretreated with base, chlorinated organic solvents often contain sufficient hydrochloric acid to produce appreciable amounts of diprotonated porphyrin, and silica gel used for preparative thin layer chromatography contains sufficient metal ions (mainly zinc silicate, present as a fluorescor) to produce large quantities of metal centred porphyrins. Such contamination is readily detected chromatographically and by inspection of the absorption spectrum (see below, and Table 2.)

Conversion of the dimethoxybenzene portion of **2***b* to the corresponding hydroquinone was achieved by treatment with

Can. J. Chem. Downloaded from www.nrcresearchpress.com by 210.87.254.5 on 09/06/12
For personal use only.

TABLE 1. Ultraviolet/visible absorption spectra of linked porphyrins in methylene chloride

Compound	Soret band ($\epsilon \times 10^{-5}$)	Q-bands ($\epsilon \times 10^{-3}$)			
2*a*	419 (4.5)	515 (18)	552 (9.4)	592 (5.4)	646 (4.7)
2*b*	419 (4.4)	515 (17)	552 (8.6)	591 (5.3)	646 (4.3)
2*c*	419 (5.0)	515 (17.5)	552 (8.9)	591 (5.1)	646 (4.5)
4*a**	421 (3.9)	518 (19)	553 (8.2)	593 (5.7)	649 (5.0)
4*b**	421 (4.2)	518 (20.8)	553 (8.5)	593 (6.1)	649 (5.3)
4*c**	420 (4.5)	517 (19)	551 (9.9)	591 (5.9)	646 (5.2)

*Measured using samples of **4** containing up to 25% **3**. The latter causes minimal perturbation of the spectra (see Fig. 2 and text).

TABLE 2. Ultraviolet/visible absorption spectra of dications of linked porphyrins in methylene chloride – methanol (96:4)

Compound	λ_{max}, nm ($\epsilon \times 10^{-4}$)	
2*a*	443 (37.6)	665 (5.23)
2*b*	443 (34.0)	665 (4.15)
2*c*	443 (47.0)	665 (6.06)
3*a*	447 (30.7)	670 (4.56)
3*b*	447.5 (26.1)	672 (4.07)
3*c*	447 —	670 —

boron tribromide at low temperature under standard conditions (13). This step proceeded much more cleanly than with the corresponding ester linked analogue where substantial ester cleavage occurred. The hydroquinone **3***b* obtained by this route was relatively unstable, as has previously been observed for these compounds (5), and was contaminated with the quinone **4***b* (see below); the compound could be purified by chromatography to give a homogeneous sample for rapid spectroscopic analysis, but attempts to obtain microanalytical data were unsuccessful. The ^{1}H nmr spectrum of **3***b* confirmed that the desired transformation had occurred. In particular, the methoxyl groups present in **2***b* were absent from the spectrum of **3***b* and the hydroquinone ring protons appeared as a multiplet with peaks at 6.76 and 6.72 ppm (Fig. 3a), which compares well with the spectrum obtained of methylhydroquinone in the same solvent where a multiplet with peaks at 6.70 and 6.64 ppm was observed.

Oxidation of the hydroquinone **3***b* to the corresponding quinone **4***b* could be achieved under mild conditions using high potential quinone oxidants such as dichlorodicyanobenzoquinone (DDQ). However, purification of product, particularly removal of the products of DDQ reduction by **3***b*, was difficult and it was found preferable to achieve the transformation of **3***b* to **4***b* by two-phase oxidation of **3***b* using a suspension of lead dioxide in methylene chloride (5, 14). In this way essentially quantitative conversion of **3***b* to **4***b* could be achieved and the excess oxidant and its reduction products removed by filtration, obviating the need for chromatographic purification of the quinone. The course of the oxidation was conveniently followed by uv/visible spectroscopy; as oxidation proceeded, the quinone absorption at 246 nm increased to a maximum while a weak band at 300 nm assigned to the hydroquinone chromophore decreased. The visible (porphyrin Q-bands) and near uv (porphyrin Soret band) regions of the absorption spectrum indicated that the porphyrin was unaffected during oxidation and, in particular, did not incorporate a metal atom. Figure 2 shows these transformations for the oxidation of **3***b* to **4***b*. The extinction coefficients at 246 and 300 nm were determined for **3***b* and **4***b* and, using the values obtained, it was determined that samples of **3***b* direct from the boron tribromide mediated cleavage of **2***b* contained approximately 25% of **4***b* and 75% of **3***b*.

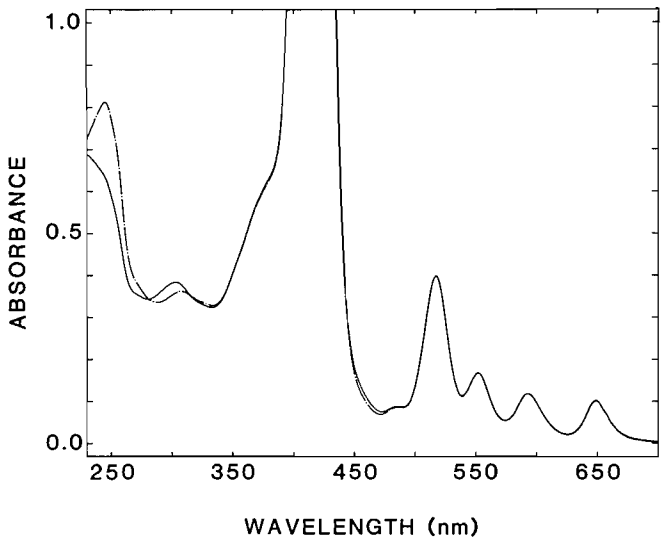

FIG. 2. Ultraviolet/visible absorption spectra showing the transformation **3***b* to **4***b*. Solid line, **3***b*; broken line, **4***b*.

The ^{1}H nmr spectrum of **4***b* was similar to that of its precursor **3***b*. The major difference is in the signals assigned to the aromatic ring protons and these are shown in Fig. 3. In Fig. 3(a) the hydroquinone ring protons of **3***b* are seen at 6.76 and 6.72 ppm; Fig. 3(b) shows the spectrum of the same sample after incomplete oxidation with lead dioxide, where the quinone ring protons are seen at 6.84 ppm superimposed upon the remaining hydroquinone signals. The linked porphyrin–quinone **4***b* was also found to be relatively unstable; on standing, it slowly reverted to the hydroquinone **3***b*. This transformation is shown in Fig. 3(c) and is in contrast to the observations of Ganesh and Sanders (5) who have reported finding that a quinone capped porphyrin was stable, but that the hydroquinone precursor was unstable with respect to formation of what was tentatively identified as a semiquinone species. An analogous semiquinone species has not been observed for either **3***b* or **4***b*; in particular, no epr signal was found which could be ascribed to the semiquinone form.

The linked porphyrin–quinone molecules **4***a*, **4***b*, and **4***c* were chosen as synthetic targets in order to study the effect of separation of the two chromophores upon the efficiency of light induced intramolecular charge transfer. Prior to such a study it is necessary to determine if there is any ground state interaction of the chromophores, either intramolecularly or intermolecularly. To this end the optical properties of the precursors **2***a*–**2***c*, **3***a*–**3***c*, and the quinones **4***a*–**4***c* were studied.

The visible and near uv spectra of these compounds are shown in Table 1. Spectra were recorded in dichloromethane with the addition of 4% methanol to achieve sufficient solubility over a range of 10^{-4} to 10^{-6} *M*. Under these conditions the Beer–Lambert Law was obeyed, suggesting that the compounds are monomeric and not subject to aggregation. The

Can. J. Chem. Downloaded from www.nrcresearchpress.com by 210.87.254.5 on 09/06/12
For personal use only.

Can. J. Chem. Downloaded from www.nrcresearchpress.com by 210.87.254.5 on 09/06/12
For personal use only.

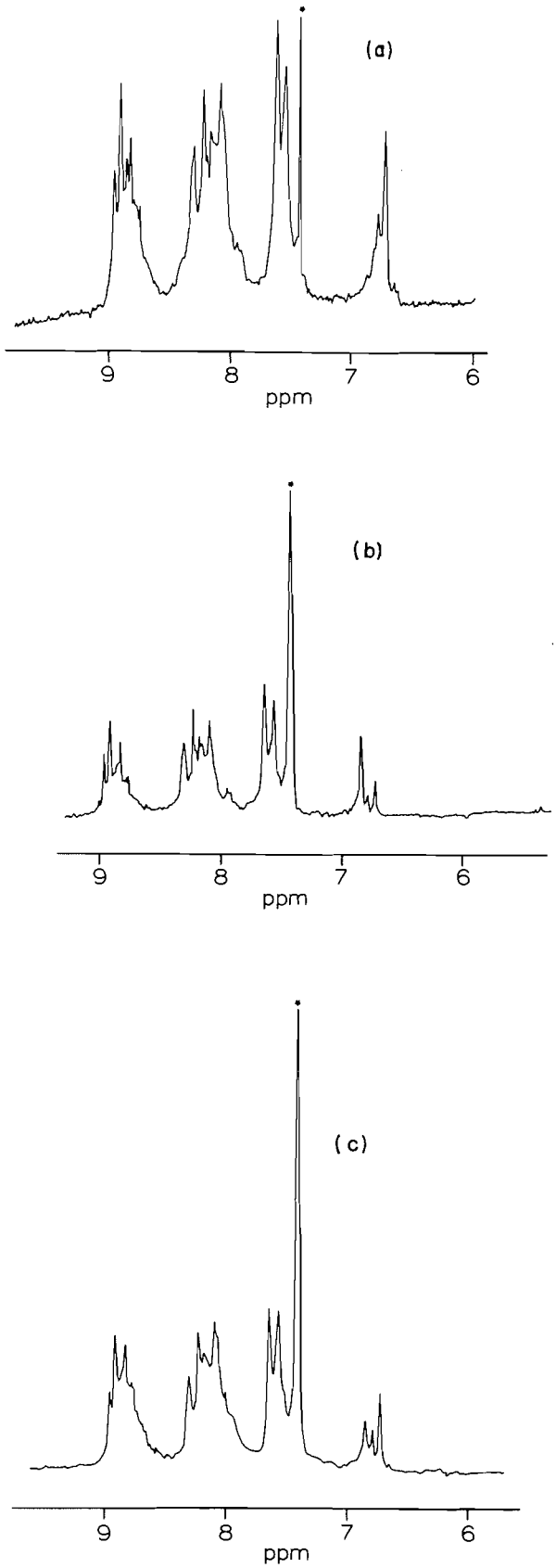

FIG. 3. Partial ^{1}H nmr spectra showing the transformation **3***b* to **4***b*. The asterisk marks residual protium in $CDCl_3$. (a) Aromatic region for hydroquinone **3***b*. (b) Aromatic region following ca. 70% oxidation to **4***b*. (c) Same as (b) after standing overnight.

spectra were also recorded in the presence of 1% trifluoroacetic acid; under these conditions the porphyrin exists as its dication and this results in a bathochromic shift of the Soret band and the Q-bands of the porphyrin with one of the latter increasing greatly in intensity. The spectra of the dications are given in Table 2.

The absorption spectra of the linked porphyrin–dimethoxybenzene compounds **2***a*, **2***b*, and **2***c* were essentially identical and all show the presence of a normal porphyrin chromophore, indicating that no strong interaction exists between the two halves of the molecule. This is illustrated in Fig. 4(a) where the absorption spectra of the porphyrin–dimethoxybenzene compound **2***b* in the Soret band region is shown superimposed upon the spectrum of 5-(*p*-carboxyphenyl)-10,15,20-tri(*p*-tolyl)porphyrin. The absorption spectrum of the porphyrin–hydroquinone molecule **3***c*, in which the two chromophores are linked by 1,4-diaminobutane, is also normal, indicating no intramolecular interaction. However, the spectra of **3***a* and **3***b* are perturbed, with the bands showing a slight bathochromic shift. In addition, the Soret band exhibits substantial broadening. This is illustrated in Fig. 4(b) where the absorption spectra of the linked porphyrin–hydroquinones **3***a*, **3***b*, and **3***c* are shown superimposed upon each other. These effects suggest that, with the shorter linkages present in **3***a* and **3***b*, there is an interaction between the porphyrin and the hydroquinone chromophores in the ground state which is not possible in **3***c*, presumably because the longer linkage prevents adoption of the required conformation. That the interaction does not occur for the porphyrin–dimethoxybenzene linked molecules **2***a*–**2***c* may be due to steric interference by the methyl groups present.

The absorption spectra of the linked porphyrin–benzoquinones **4***a*–**4***c* were essentially identical to those of their precursors **3***a*–**3***c* apart from changes in the bands assigned to benzoquinone at shorter wavelength, discussed above. Thus the postulated intramolecular interaction giving rise to a bathochromic shift of the Soret band in **3***a* and **3***b* is also present in **4***a* and **4***b* but not **4***c*.

The fluorescence spectra of 5-(*p*-carboxyphenyl)-10,15,20-tri(*p*-tolyl)porphyrin and of compounds **2** and **3**, and **4** were also recorded. The fluorescence data for compounds **2** and **3** are given in Table 3, and the fluorescence spectra for the unlinked porphyrin and for compounds **3***b* and **4***b* are shown in Fig. 5. From Fig. 5 it can be seen that excitation of the Soret band (420 nm) of the porphyrins **3***b* and **4***b* produces normal porphyrin fluorescence, while excitation at longer wavelength (440 nm) produces a fluorescence which is red shifted. This effect is not observed for the unlinked porphyrin. This may reflect excitation of different conformers of the linked porphyrins with irradiation at longer wavelength preferentially exciting the conformation in which the two ends of the molecule are interacting and which gives rise to the bathochromic shift observed in the absorption spectrum. Fluorescence quantum yields were also determined for compounds **2***b*, **3***b*, and **4***b* relative to tetraphenylporphyrin (Table 4). The values obtained suggest that some quenching of the singlet excited state is occurring, but since the quantum yield is reduced for **3***b* as well as for **4***b* this may arise from an interaction between the two chromophores in the molecule which is perturbing the rate of intersystem crossing rather than from electron transfer quenching.

The results of a more detailed study of the photophysical properties of these molecules which support the above conclusions and demonstrate light induced intramolecular electron transfer in compounds **4***a*–*c* will be reported elsewhere.

Can. J. Chem. Downloaded from www.nrcresearchpress.com by 210.87.254.5 on 09/06/12
For personal use only.

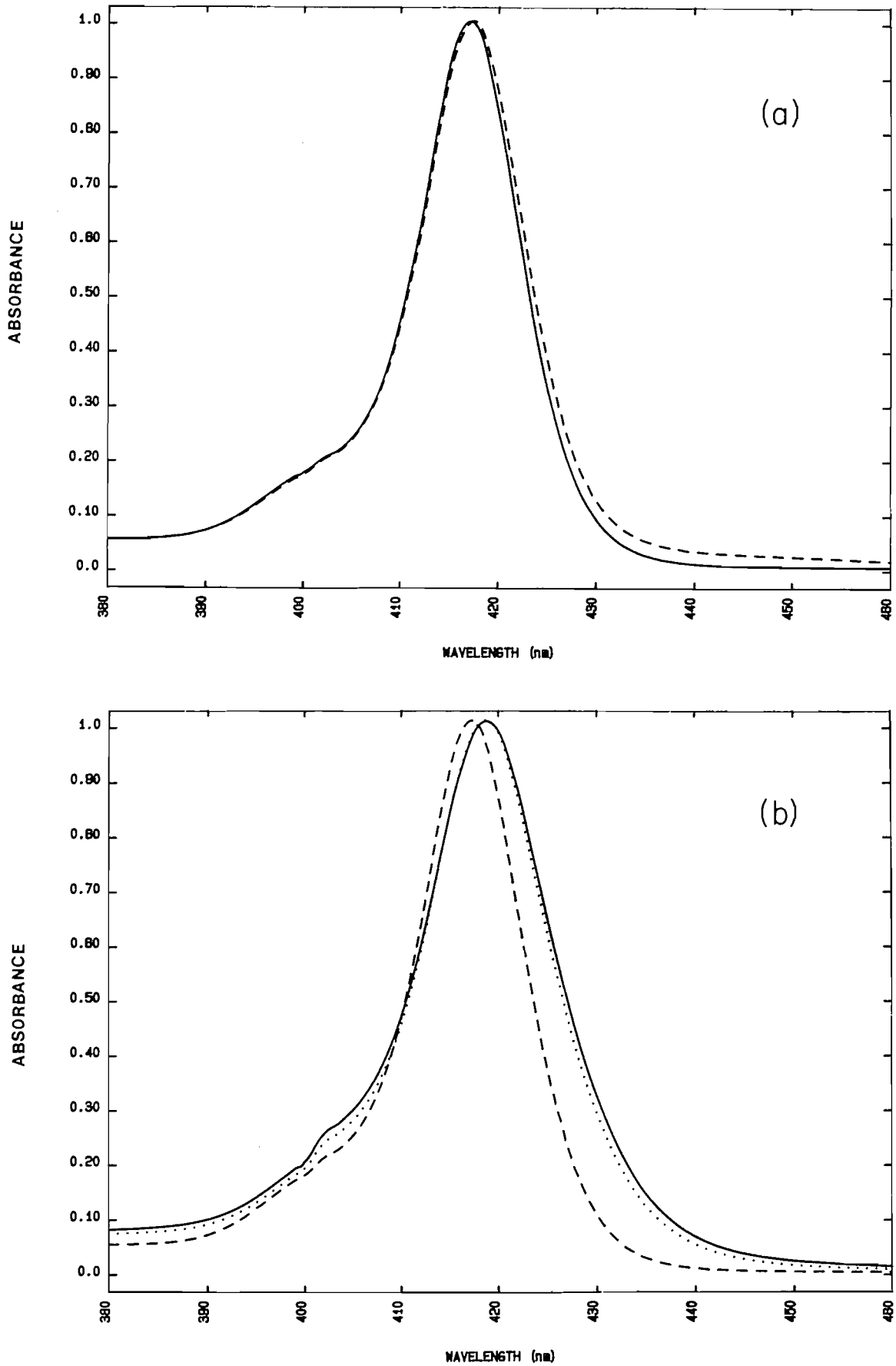

FIG. 4. Ultraviolet absorption spectra for linked porphyrins in methylene chloride. (a) Solid line, 5-(*p*-carboxyphenyl)-10,15,20-tri(*p*-tolyl)porphyrin ("PCO_2H"); broken line, **2***b*. (b) Dotted line, **3***a*; solid line, **3***b*; broken line, **3***c*.

TABLE 3. Fluorescence data for linked porphyrins and their dications in methylene chloride

Compound	Free base (nm)		Dication (nm)		
2*a*	651	717	700	763	(shoulder)
2*b*	651	717	695	763	(shoulder)
2*c*	651	717	700	763	(shoulder)
3*a*	652	717	698	763	(shoulder)
3*b*	653	717	702	763	(shoulder)
3*c*	653	717	700	763	(shoulder)

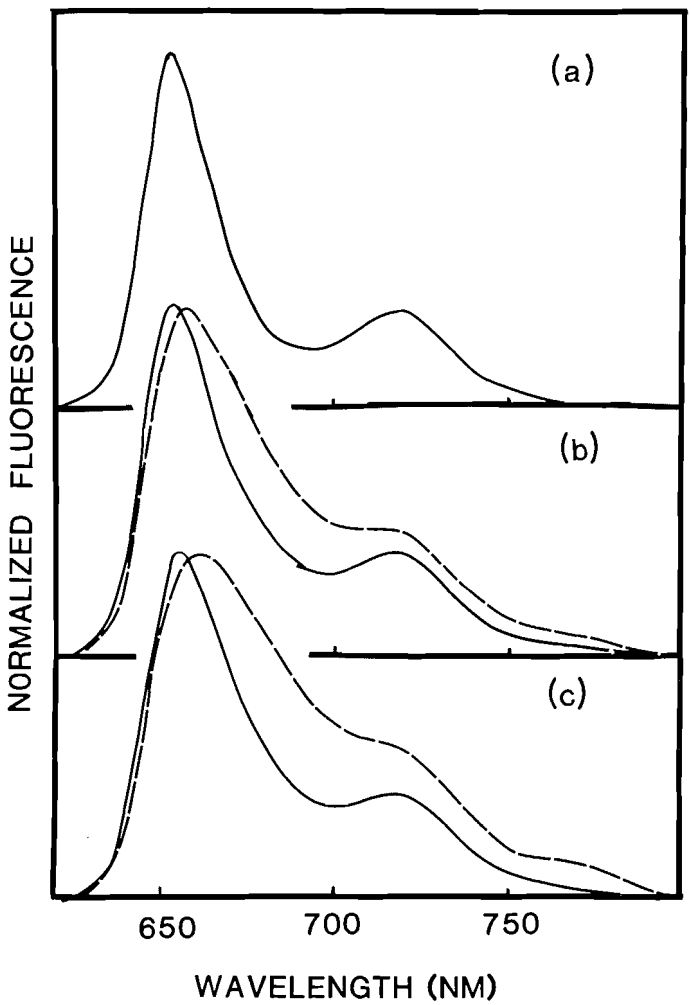

FIG. 5. Normalized fluorescence for linked porphyrin in methylene chloride. (a) 5-(*p*-Carboxyphenyl)-10,15,20-tri(*p*-tolyl)porphyrin. Excitation at 420 nm and 440 nm. (b) Fluorescence spectrum of **3***b*. Solid line, excitation at 420 nm; broken line, excitation at 440 nm. (c) Fluorescence spectrum of **4***b*. Solid line, excitation at 420 nm; broken line, excitation at 440 nm.

Experimental

The ^{1}H nmr spectra were recorded on a Varian T-60 or Varian XL-100 instrument with tetramethylsilane as internal standard. The uv/visible absorption spectra were recorded on a Cary 219 spectrometer and fluorescence spectra were recorded on a Perkin–Elmer MPF-4 fluorescence spectrometer in 1.00 cm cells using low optical density solutions of porphyrin in methylene chloride. Elemental analyses were performed by Guelph Chemical Laboratories Ltd., Guelph, Ontario.

TABLE 4. Quantum yields of fluorescence for air saturated solutions of linked porphyrin in methylene chloride*

Compound	ϕ_f
2*b*	0.11
3*b*	0.06
4*b*	0.03

* Measured using *meso*-tetraphenylporphyrin as a standard and assuming a quantum yield of 0.11 for this compound (15).

Analytical and preparative thin layer chromatography of porphyrin containing compounds was performed using Polygram Sil-N-HR silica gel from Macherey–Nagel to avoid incorporation of metal ions used as fluorescors in other brands. Porphyrins were handled in subdued light and stored in darkness to avoid self-sensitized photooxidation. Melting points of all linked porphyrin compounds were found to be greater than 300°C.

Methyl 2,5-dimethoxyphenylacetate

A solution of 2,5-dimethoxyphenylacetic acid (4 g, 0.02 mol), dimethylsulphate (3.8 g, 0.03 mol), and potassium carbonate (5.5 g, 0.04 mol) in anhydrous acetone (200 mL) was refluxed under nitrogen for 5 h. After cooling, filtration to remove inorganic salts, and evaporation, a residue was obtained which was purified by column chromatography on silica gel using methylene chloride as eluent. The material so obtained was recrystallized from chloroform – petroleum ether to give **2** (3.4 g, 80%) which had mp 40°C (lit. (16) mp 44°C).

N-*(2,5-Dimethoxyphenylacetyl)-1,2-diaminoethane*, **1***a*

Methyl 2,5-dimethoxyphenylacetate (0.5 g, 2.38 mmol) was stirred in ethylenediamine (2.5 mL) at room temperature for 2 days. Excess amine was removed under reduced pressure and the residue was chromatographed on silica gel using methanol containing concentrated aqueous ammonia (98:2) as eluent to yield **1***a* (70%), mp 91°C; ir (Nujol): 3330–3295, 1650, 1550, 1230 cm^{-1}; uv (MeOH): 296 (ϵ = 3 800), 227 (ϵ = 8 000) nm; ^{1}H nmr ($CDCl_3$): 1.61 (s, 2H, exch.), 2.6–3.0 (m, 2H), 3.0–3.4 (m, 2H), 3.47 (s, 2H), 3.72 (two singlets almost superimposed, 6H), 6.2 (bs, 1H, exch.), 6.77 (s, 3H) ppm; *m/e*: 238 (M^+), 178, 151. *Mol. Wt.* calcd. for $C_{12}H_{18}N_2O_3$: 238.1317; found: 238.1315.

N-*(2,5-Dimethoxyphenylacetyl)-1,3-diaminopropane*, **1***b*

Compound **1***b* was prepared in an analogous manner to **1***a* in 70% yield and had similar ir and uv spectra. For **1***b*, mp 68°C; ^{1}H nmr ($CDCl_3$): 1.4–1.78 (m, 4H), 2.65 (m, 2H), 3.13–3.43 (m, 2H), 3.47 (s, 2H), 3.73 (two singlets, almost superimposed, 6H), 6.2 (bs, 1H), 6.7 (s, 3H) ppm; *m/e*: 252 (M^+), 178, 151. *Mol. Wt.* calcd. for $C_{13}H_{20}N_2O_3$: 252.1471; found: 252.1466.

N-*(2,5-Dimethoxyphenylacetyl)-1,4-diaminopropane*, **1***c*

Compound **1***c* was prepared in an analogous manner to **1***a* in 65% yield and had similar ir and uv spectra. For **1***c*, mp 80°C; ^{1}H nmr ($CDCl_3$): 1.25–1.6 (m, 4H), 1.45 (s, 2H, exch.), 2.4–2.8 (m, 2H), 2.9–3.33 (m, 2H), 3.47 (s, 2H), 3.73 (two singlets, 6H), 6.1 (bs, 1H), 6.7 (s, 3H) ppm; *m/e*: 266 (M^+), 178, 151. *Mol. Wt.* calcd. for $C_{14}H_{22}N_2O_3$: 266.1630; found: 266.1634.

N,N′-*Di-(2,5-dimethoxyphenylacetyl)-1,2-diaminoethane*

2,5-Dimethoxyphenylacetic acid (0.5 g) was dissolved in a mixture of benzene (50 mL) and thionyl chloride (6 mL) and refluxed for 1 h. The solvents were evaporated and the residue was added to a solution of ethylene diamine (1 mL) in 10% aqueous sodium hydroxide (10 mL) and the mixture was shaken vigorously for 15 min. Dilution with water (30 mL), filtration, and purification of the product by chromatography (silica gel, methanol–chloroform, 5:95) gave 0.38 g (79%) of the diamide which had mp 138°C; ir (Nujol): 3295, 1650,

Can. J. Chem. Downloaded from www.nrcresearchpress.com by 210.87.254.5 on 09/06/12
For personal use only.

Can. J. Chem. Downloaded from www.nrcresearchpress.com by 210.87.254.5 on 09/06/12
For personal use only.

1550, 1230 cm^{-1}; ^1H nmr ($CDCl_3$): 3.2–3.3 (m, 4H), 3.46 (s, 4H), 3.68, 3.73 (two singlets, 12H), 6.1 (b, 2H), 6.76 (s, 6H) ppm; *m/e*: 416 (M^+).

N,N′-*Di-(2,5-dimethoxyphenylacetyl)-1,3-diaminopropane*

The diamide was prepared as above in 72% yield and had mp 118°C; ^1H nmr ($CDCl_3$): 1.2–1.7 (m, 2H), 3.0–3.3 (m, 4H), 3.47 (s, 4H), 3.7 (two singlets, 12H), 6.2 (b, 2H), 6.75 (s, 6H) ppm; *m/e*: 430 (M^+).

N,N′-*Di-(2,5-dimethoxyphenylacetyl)-1,4-diaminobutane*

The diamide was prepared as above in 63% yield and had mp 135°C; ^1H nmr ($CDCl_3$): 1.2–1.55 (m, 4H), 3.0–3.3 (m, 4H), 3.47 (s, 4H), 3.73 (two singlets, 12H), 6.0 (b, 2H), 6.77 (s, 6H) ppm; *m/e*: 444 (M^+).

N-*Acetyl*-N′-*(2,5-dimethoxyphenylacetyl)-1,3-diaminopropane*

The acetylation was performed using acetyl chloride as above to give the product in 85% yield and had ^1H nmr ($CDCl_3$): 1.4–1.78 (m, 2H), 1.95 (s, 3H), 3.0–3.4 (m, 4H), 3.47 (s, 2H), 3.7 (2 singlets, 6H), 6.2 (b, 2H), 6.77 (s, 3H) ppm.

N-*(2,5-Dimethoxyphenylacetyl)*-N′-*(5*-p-*benzoyl-10,15,20-tri*-p-*tolylporphyrin)-1,2-diaminoethane*, **2**a

The unsymmetrically substituted porphyrin 5-*p*-carboxyphenyl-10,15,20-tri-*p*-tolylporphyrin (12) (0.25 g, 0.36 mmol) was dissolved in thionyl chloride (25 mL) and the solution was refluxed under nitrogen for 1 h. The excess thionyl chloride was removed by evaporation under vacuum to yield the crude acid chloride, as its green hydrochloride salt. This material was dissolved in methylene chloride (20 mL) and the solution was added dropwise to an ice-cooled, stirred solution of the amine **3***a* (0.5 g, 2.1 mmol) in methylene chloride (30 mL) containing pyridine (1 mL). After the addition was complete the solution was stirred at room temperature overnight. The reaction mixture was diluted with chloroform (200 mL) and washed with water (3 × 50 mL), dried (Na_2SO_4), and evaporated to give a purple solid which was chromatographed on a column of silica gel using chloroform and then chloroform–methanol (98:2) as eluent. The major component was further purified by preparative thin layer chromatography on silica gel (chloroform–hexane–methanol, 70:26:4) to give the product **2***a* in 45% yield. This material had mp > 300°C; ir (Nujol): 3260–3340, 1665, 1545, 1225, 1038 cm^{-1}; ^1H nmr ($CDCl_3$): −2.8 (bs, 2H, exch.), 2.7 (s, 9H), 3.4–3.6 (m, 4H), 3.62 (s, 2H), 3.68 (s, 3H), 3.82 (s, 3H), 6.3 (bs, 2H, exch.), 6.76–6.88 (m, 3H), 7.58–7.48 (d, 6H), 8.0–8.12 (d, 6H), 8.22–8.34 (m, 4H), 8.75–8.91 (m, 8H) ppm; *m/e*: 920 (M^+). *Anal.* calcd. for $C_{60}H_{52}N_6O_4$: C 78.24, H 5.69, N 9.12%; found: C 78.36, H 5.74, N 9.20%.

N-*(2,5-Dimethoxyphenylacetyl)*-N′-*(5*-p-*benzoyl-10,15,20-tri*-p-*tolylporphyrin)-1,3-diaminopropane*, **2**b

This compound was prepared in an analogous manner to compound **2***a* in 40% yield and had mp > 300°C; ir (Nujol): 3260–3340, 1665, 1636, 1550, 1230 cm^{-1}; ^1H nmr ($CDCl_3$): 1.6–2.0 (m, 2H), 2.68 (s, 9H), 3.3–3.64 (m, 4H), 3.64 (s, 2H), 3.72 (s, 3H), 3.75 (s, 3H), 6.1 (bs, 2H, exch.), 6.76–6.73 (m, 3H), 7.45–7.55 (d, 6H), 8.02–8.12 (d, 6H), 8.34–8.39 (m, 4H), 8.75–8.91 (m, 8H) ppm. *Anal.* calcd. for $C_{61}H_{54}N_6O_4$: C 78.35, H. 5.82, N 8.99%; found: C 78.28, H 5.85, N 9.01%.

N-*(2,5-Dimethoxyphenylacetyl)*-N′-*(5*-p-*benzoyl-10,15,20-tri*-p-*tolylporphyrin)-1,4-diaminobutane*, **2**c

This compound was prepared in an analogous manner to compound **2***a* in 50% yield and had mp > 300°C; ir (Nujol): 3260–3330, 1665, 1640, 1550, 1230 cm^{-1}; ^1H nmr ($CDCl_3$): 1.6–2.0 (m, 4H), 2.68 (s, 9H), 3.3–3.7 (m, 4H), 3.64 (s, 2H), 3.72 (s, 3H), 3.75 (s, 3H), 6.1 (bs, 2H), 6.73–6.76 (m, 3H), 7.45–7.55 (d, 6H), 8.0–8.12 (d, 6H), 8.25 (m, 4H), 8.75–8.91 (m, 8H) ppm. *Anal.* calcd. for $C_{62}H_{56}N_6O_4$: C 78.46, H 5.95, N 8.85%; found: C 78.32, H 6.00, N 8.68%.

N-*(2,5-Dihydroxyphenylacetyl)*-N′-*(5*-p-*benzoyl-10,15,20-tri*-p-*tolylporphyrin)-1,2-diaminoethane*, **3**a

Compound **2***a* (0.202 g, 0.2 mmol) in methylene chloride (30 mL) was cooled in an acetone – Dry Ice bath and the solution was maintained under a blanket of dry nitrogen. Boron tribromide (2.9 g) in methylene chloride (8 mL) was added dropwise with stirring and, at completion of the addition, the mixture was stirred for a further 3 h at −70°C before being allowed to warm to 0°C. Water (15 mL) was added dropwise and the organic phase was washed with aqueous saturated sodium bicarbonate (2 × 100 mL) and water (2 × 100 mL), dried (sodium sulphate), and evaporated to give a residue which was purified by column chromatography on silica gel and then by preparative thin layer chromatography on silica gel using chloroform–methanol (97:3) to give **3***a* in 20% yield. This material had mp > 300°C and ^1H nmr ($CDCl_3$ + CD_3OD): 2.68 (s, 9H), 3.4–3.6 (m, 4H), 3.63 (s, 2H), 6.6–7.0 (m, 3H), 7.53 (d, 6H), 8.08 (d, 6H), 8.04–8.31 (m, 4H), 8.88 (m, 8H) ppm.

N-*(2,5-Dihydroxyphenylacetyl)*-N′-*(5*-p-*benzoyl-10,15,20-tri*-p-*tolylporphyrin)-1,3-diaminopropane*, **3**b

This compound was prepared from **2***b* in the same manner, and in similar yield as for **3***a*. For **3***b*, mp > 300°C; ^1H nmr ($CDCl_3$ + $(CD_3)_2SO$): −2.85 (bs, 2H), 2.7 (s, 9H), 3.3–3.63 (m, 4H), 3.63 (s, 2H), 6.58–6.78 (m, 3H), 7.51 (d, 6H), 8.05 (d, 6H), 8.30 (m, 4H), 8.7–8.92 (m, 8H), 9.12 (bs, 2H) ppm.

N-*(2,5-Dihydroxyphenylacetyl)*-N′-*(5*-p-*benzoyl-10,15,20-tri*-p-*tolylporphyrin)-1,4-diaminobutane*, **3**c

This compound was prepared from **2***c* in the same manner and in similar yield as for **3***a*. For **3***c*, mp > 300°C; ^1H nmr ($CDCl_3$ + CD_3OD): 1.53–1.66 (m, 4H), 2.68 (s, 9H), 3.1–3.5 (m, 4H), 3.45 (s, 2H), 6.5–7.0 (m, 3H), 7.44 (d, 6H), 8.10 (d, 6H), 8.05–8.22 (m, 4H), 8.83 (m, 8H) ppm.

Procedure for oxidation of hydroquinones **3**a–c *to quinones* **4**a–c

The hydroquinone **3** (1 mg) in chloroform (3 mL) was stirred with excess lead dioxide (150 mg) at room temperature for 10 min and then filtered. Removal of solvent from the filtrate gave the quinone **4**. In the case of **3***b*, the oxidation was judged to be quantitative, based upon uv and ^1H nmr spectroscopy. In the cases of **3***a* and **3***c* the product quinones were contaminated with ca. 25% of the hydroquinone precursors. Attempted further purification of the quinones led to reversal of the oxidation and increased hydroquinone contamination. The spectral data for **4** are given in Table 1 and Figs. 2 and 3.

Acknowledgement

This work was supported by a Strategic Grant in Energy from the Natural Sciences and Engineering Research Council of Canada.

1. S. G. Boxer and G. L. Closs. J. Am. Chem. Soc. **98**, 5406 (1976).
2. J. Almog, J. E. Baldwin, R. L. Dyer, and M. Peters. J. Am. Chem. Soc. **97**, 226 (1975).
3. C. K. Chang. J. Am. Chem. Soc. **99**, 2819 (1977).
4. N. E. Kagan, D. Mauzerall, and R. B. Merrifield. J. Am. Chem. Soc. **99**, 5484 (1977).
5. K. N. Ganesh and J. K. M. Sanders. J. Chem. Soc. Perkin Trans. 1, 1611 (1982).
6. J. L. Y. Kong and P. A. Loach. J. Heterocycl. Chem. **17**, 737 (1980).
7. I. Tabushi, N. Koga, and M. Yanagita. Tetrahedron Lett. 257 (1979).
8. S. Nishitani, N. Kurata, Y. Sakata, S. Misumi, M. Migita, T. Okada, and N. Mataga. Tetrahedron Lett. 2099 (1981).
9. M. Migita, T. Okada, N. Mataga, S. Nishitani, N. Kurata, Y. Sakata, and S. Misumi. Chem. Phys. Lett. **84**, 263 (1981).
10. T. L. Netzel, M. A. Bergkamp, C. K. Chang, and J. Dalton. J. Photochem. **17**, 451 (1981).
11. T.-F. Ho, A. R. McIntosh, and J. R. Bolton. Nature, **286**, 254 (1980).

12. J. A. ANTON, J. KONG, and P. A. LOACH. J. Heterocycl. Chem. **13**, 717 (1976).
13. J. F. W. MCOHMIE and M. L. WATTS. Chem. Ind. 1658 (1963).
14. R. KUHN and I. HAMMER. Chem. Ber. **83**, 413 (1950).
15. P. G. SEYBOLD and M. GOUTERMANN. J. Mol. Spectrosc. **31**, 113 (1969).
16. R. W. BOST and C. A. HOWE. J. Am. Chem. Soc. **74**, 257 (1952).

Can. J. Chem. Downloaded from www.nrcresearchpress.com by 210.87.254.5 on 09/06/12
For personal use only.

Some chemical and analytical aspects of polysaccharide modifications. IV.[1] Electron spin resonance studies of nitroxide-labelled chitin and chitosan derivatives[2]

MANSSUR YALPANI[3] AND LAURANCE D. HALL

Department of Chemistry, University of British Columbia, Vancouver, B.C., Canada V6T 1W5

Received September 14, 1983

MANSSUR YALPANI and LAURANCE D. HALL. Can. J. Chem. **62**, 975 (1984).

Nitroxide spin labels have been attached to chitin, chitosan, and their derivatives in order to investigate the solution and gel characteristics of these polymers. Thus, chitin was nonselectively acylated using the chloroacetamide label **3** to afford the corresponding nitroxide derivative **4**. Selective and nonselective labelling of chitosan was accomplished either via reductive alkylation using the keto label **5** and sodium cyanoborohydride or via a chitosan sulfate intermediate using labels **3** or **5**. Two branched water soluble chitosan derivatives, carrying C-6 oxidized, terminal galactose side chains were selectively labelled by reductive amination using the amine label **13** to yield derivatives **14** and **15**. Motional correlation values of the covalently-linked nitroxide moieties were shown to reflect the nature of the linkage between spin label and polymer, as well as structural differences between the branch residues of derivatives **14** and **15**. The spin-probe – spin-label method was employed to demonstrate structural heterogeneities for the chitosan derivatives **7** and **15**.

MANSSUR YALPANI et LAURANCE D. HALL. Can. J. Chem. **62**, 975 (1984).

Dans le but d'étudier les caractéristiques de ces polymères en solution et sous forme de gel, on a attaché des marqueurs de spin de type nitroxyde à la chitine, au chitosane et à leurs dérivés. Ainsi, on a acylé la chitine d'une façon qui n'est pas sélective, en utilisant le marqueur chloroacétamide **3** pour obtenir le dérivé nitroxyde **4** correspondant. On a réalisé le marquage sélectif et non sélectif du chitosane soit par une alkylation réductrice en utilisant soit le cétomarqueur **5** et le cyanoborohydrure de sodium soit via l'intermédiaire du sulfate de chitosane en utilisant les marqueurs **3** ou **5**. Utilisant le marqueur aminé **13** qui conduit aux dérivés **14** et **15** par amination réductrice, on a marqué de façon sélective deux dérivés du chitosane qui sont solubles dans l'eau et qui portent comme chaînes latérales des unités terminales de galactose oxydé en C-6. On montre que les valeurs de corrélation de mouvement des unités nitroxydes liées par des liaisons covalentes réflètent la nature de la liaison entre le marqueur de spin et le polymère ainsi que les différences structurales entre les unités ramifiées des dérivés **14** et **15**. On a utilisé la méthode du marqueur de spin/sonde de spin pour démontrer les hétérogénéités structurales des dérivés **7** et **15** du chitosane.

[Traduit par le journal]

Can. J. Chem. Downloaded from www.nrcresearchpress.com by 210.87.254.40 on 09/06/12
For personal use only.

Introduction

The current interest in the development of new chitin- and chitosan-derived products for a diverse range of applications (1) is reflected in increasing efforts to establish a better understanding of the fundamental physical characteristics of these vastly abundant and inexpensive biopolymers. Chitin and chitosan and their derivatives are distinguished from most other polysaccharides by several unique features such as, for example, their solution and gel behaviour. However, many of their properties are not yet thoroughly evaluated, mainly due to their intractability. Several studies have recently explored the shape and molecular properties of these aminopolysaccharides. Buffington and Stevens (2) have concluded from circular dichroism data that inter- rather than intra-molecular interactions between *N*-acetyl groups play an important factor in the gel formation of chitan and chitin. Hirano *et al.* (3) have observed pronounced changes in specific rotation of chitosan during Schiff's base formation and the attendant gelation process. More recently, Komai and co-workers (4) have studied the molecular motions of a spin-probe in films of various acylchitins, while Aleksandrova *et al.* (5) have examined the segmental mobility of chitosan using the spin-labelling technique. We have previously employed nitroxide labels to demonstrate the formation of inclusion complexes for a branched chitosan derivative (6).

As part of a general programme of nmr (7) and esr (8) studies of native and derivatized polysaccharides, and in continuation of our development of new, water soluble products derived from chitin and chitosan (6, 9), we were interested in establishing facile methods for the preparation of new types of chitin/chitosan derivatives which would exhibit a range of solubility and gelling characteristics. We report here on the synthesis and characterization of various nitroxide spin-labelled aminopolysaccharide derivatives.

Results and discussion

Syntheses

Spin labelling of chitin, **1**, was accomplished by pretreatment of the solid material with dimethyl sulfoxide and aqueous sodium hydroxide, followed by nonselective acylation using 4-chloroacetamido-2,2,6,6-tetramethylpiperidine-1-oxy-1, **3**, to produce the labelled derivative **4**. The degree of substitution (d.s.) was low (0.04), but suitable for our subsequent experiments. It was found that derivative **4** swelled to a limited extent in aqueous or alcohol suspensions.

Several unsuccessful attempts were made to selectively spin label chitin under homogeneous conditions by reductive alkylation of the residual free amine groups with 4-oxy-2,2,6,6-

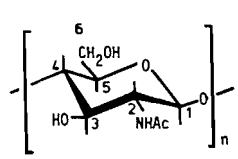

1

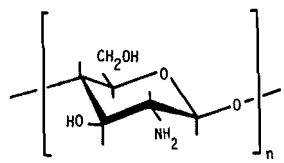

2

[1] For Part III, see ref. 6.

[2] Aspects of this work were presented at the 28th IUPAC Congress, Vancouver, August 16–22, 1982.

[3] Present address: B.C. Research, Chemical Technology Division, 3650 Wesbrook Mall, Vancouver, British Columbia, Canada V6S 2L2.

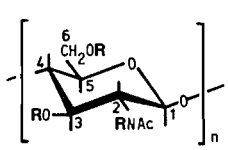

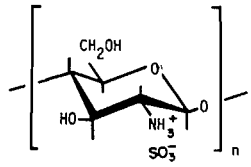

4 R = H, 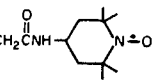

8

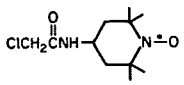

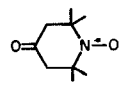

3

5

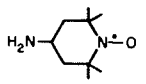

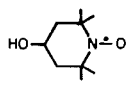

13

6

tetramethylpiperidine-1-oxyl, **5**, using sodium cyanoborohydride and the lithium chloride – dimethylacetamide solvent system (10).

Reductive alkylation of chitosan, on the other hand, proceeded smoothly using the keto label **5** and methanol – aqueous acetic acid as solvent to afford a product **7** (d.s. 0.1) which gelled considerably in methanol or aqueous media. Chitosan could alternatively be spin labelled via the *N*-sulfate derivative **8**, exploiting the fact that the latter is moderately soluble in water at elevated temperatures. Thus, labelling of derivative **8** using nitroxides **3** and **5** readily afforded the corresponding derivatives **9** (d.s. 0.5) and **10** (d.s. 0.45), respectively. Both of these derivatives formed gels in aqueous solution at low concentrations (ca. 3% w/v).

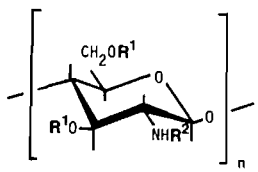

9 $R^1, R^2 = H$, 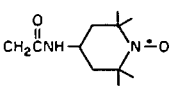

7,10 $R^1 = H; R^2 =$ 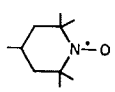

In an alternative approach to the synthesis of labelled, water soluble compounds, we employed the branched chitosan derivatives **11** and **12** which were available from another study (6, 9). The selective labelling of these derivatives at terminal positions of their side chains was readily accomplished by activation of the C-6 hydroxyl function of the pendant D-galactose residues via oxidation with Galactose Oxidase (E.C.1.1.3.9.) (6). The resultant C-6 aldehyde derivatives were reductively aminated, using 4-amino-2,2,6,6-tetramethylpiperidine-1-oxyl (**13**) to yield the corresponding labelled products **14** (d.s. 0.35) and **15** (d.s. 0.15), respectively. Derivatives **14** and **15** were both freely soluble in water, forming viscous solutions at low concentrations, which added further interest to studies of their esr spectra.

Electron spin resonance

Spin label experiments

The esr spectra of the spin-labelled chitin and chitosan derivatives revealed a number of interesting spectral characteristics, as illustrated in Figs. 1 and 2. The chitin derivative **4** (Fig. 1A), for example, was found to enjoy a greater freedom of rotational reorientation than the various chitosan derivatives, its motional correlation time, τ_c, (2 ns) being about an order of magnitude smaller. This presumably derives from the fact that the chitin derivative, in contrast to the latter, was labelled under essentially heterogeneous reaction conditions. The difference in treatment seems to have led not only to a lower overall level of substitution in derivative **4**, but also to a concentration of labels only at the more accessible surface of the solid particles. The tumbling rate of these labels would be determined only by their degree of rotational freedom about their acetamide linkage to the polymer, with the latter making no motional contribution on the esr time scale (i.e. $\tau_c > 100$ ns). It is reasonable that these readily solvated spin labels should also be more mobile than those attached to the chitosan derivatives, whose overall tumbling rate includes a motional component from the polymer chains within a gel matrix or solution aggregate. That the proposed relation between solvation and nitroxide tumbling

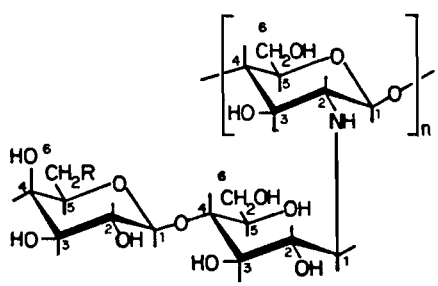

11 R = OH

14 R = NH 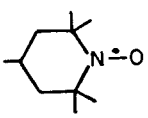

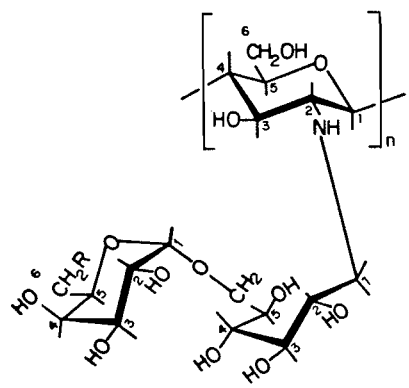

12 R = OH

15 R = NH 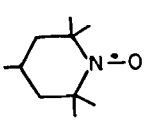

Can. J. Chem. Downloaded from www.nrcresearchpress.com by 210.87.254.40 on 09/06/12
For personal use only.

Can. J. Chem. Downloaded from www.nrcresearchpress.com by 210.87.254.40 on 09/06/12
For personal use only.

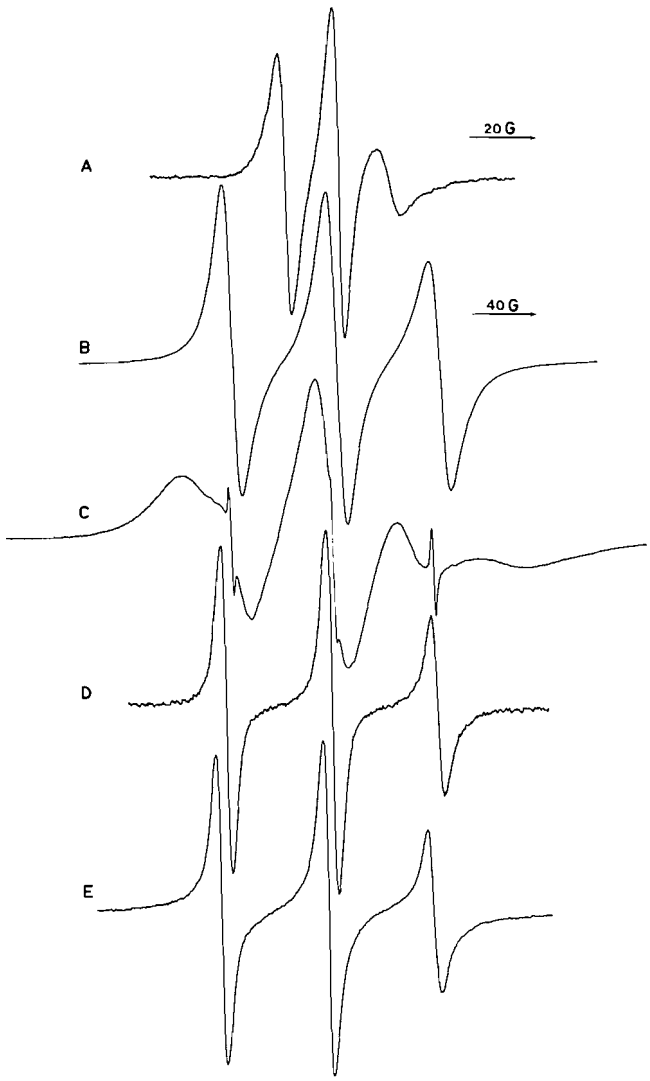

FIG. 1. Ambient temperature esr spectra of derivatives (A) **4**; (B) **9**; (C) **10**; (D) **14**; and (E) **15** in aqueous solution.

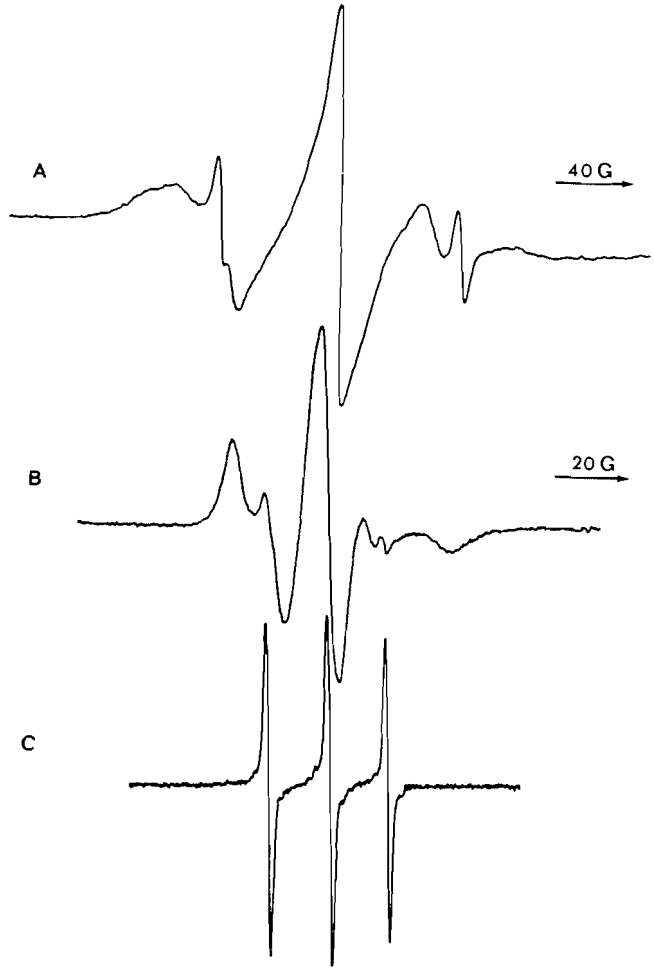

FIG. 2. Ambient temperature esr spectra of gels of derivative **7** in solvent cycle experiment: (A) in aqueous suspension; (B) in methanol suspension; (C) aqueous suspension; see text for discussion.

rate exists is also supported by the fact that the use of a somewhat less polar solvent (methanol) resulted in increases in the A_z component and in the width of the low-field line of derivative **4**.

Within the series of labelled chitosan products, the esr spectra of derivatives **9**, **14**, and **15** (Figs. 1B, D, E) displayed similar spectral lineshapes consisting of single component triplets which were indicative of moderately rapid rotational motions. The correlation time values of these derivatives ranged between 35 and 70 ns. Derivatives **7** (Fig. 2) and **10** (Fig. 1C) exhibited multicomponent esr spectra, as will be discussed below; their complex lineshape precluded τ_c determinations.

Interestingly, a comparison of Figs. 1B and 1C reveals that derivative **10** is much more immobilized than derivative **9**, with the former displaying solid-like characteristics, and the latter an almost isotropic spectrum, despite the fact that both products were obtained from the same chitosan sulfate precursor and that they were substituted to about the same extent. It would therefore be reasonable to assume that the spectral differences are attributable to structural distinctions. For derivative **10**, the keto spin label is attached to only one specific site, i.e. the amine function, whereas derivative **9** is also randomly labelled at both the primary and secondary alcohol functions. Thus, nitroxide moieties linked to the C-6 position of derivative **9** would enjoy a greater motional freedom than those attached to the 2-amine functions of derivative **10**. An additional contribution to the mobility of **9** derives from the four-bond acetamide linkage which constitutes a spacer group between the paramagnetic centre and the polymer.

Similar arguments appear to apply to the marked difference in the τ_c values of derivatives **14** (68 ns) and **15** (43 ns), which presumably arises from the different types of linkages involved. The melibiityl derivative **15** contains α-1,6-linked, six-carbon acyclic D-glucityl moieties, whereas the lactityl derivative **14** has β-1,4-linked, four-carbon D-glucityl moieties with additional two-carbon residues at C-4. The more extended side-chains of derivative **15** could give rise to a more ordered, sterically less restricted polymer solution structure, whereas the branched side-chains of derivative **14** would tend to lead to a more disordered conformation in which the nitroxide moieties enjoy relatively smaller motional freedom due to entanglement of the side chains. These conclusions were also supported by the results of previous SEM (scanning electron microscopy) studies of the diamagnetic, solid precursors (11).

Gels of derivative **7** in water exhibited a complex esr spectrum (Fig. 2A) consisting of an immobilized component with a split high-field signal and a superimposed mobile nitroxide signal. The presence of the latter signal, even after extensive

Can. J. Chem. Downloaded from www.nrcresearchpress.com by 210.87.254.40 on 09/06/12
For personal use only.

washing of the material, could be attributed to either an unbound, physically trapped, or to a bound, but very mobile nitroxide sub-population. The esr spectrum of derivative **7** appeared to consequently indicate the presence of at least two nitroxide populations residing in sites which were accessible to different degrees to solvent.

Further experiments were conducted to confirm the above implications and to exclude the possibility that the observed esr lineshape arose from a single isotropically tumbling nitroxide population.

First, gels of derivative **7**, dispersed in methanol instead of water, gave esr spectra with similarly complex lineshapes in which there was a proportionally smaller presence of the more mobile nitroxide component (see Fig. 2B). Second, when a sample of derivative **7** was subjected to an experiment in which the supernatant solvent was successively replaced (water–methanol–water) over periods of two weeks, a drastic redistribution of the spectral components was observed. The mobile nitroxide population was found to predominate over a less mobile, barely detectable one (Fig. 2C) on completion of the solvent cycle, indicating a gradual structural reorganization of the gel into an assembly in which the spin labels were more accessible to solvent. It should be noted that these spectral changes were not associated with an apparent softening or dissolution of the gel; while the gel seemed to retain its rigidity, we did notice an almost two-fold increase in its macroscopic volume in the last transition of the solvent cycle. This volume expansion could, at least partially, account for the observed enhancement of the nitroxide mobility.

Selective broadening experiments

Previous workers (12–17) have demonstrated the utility of paramagnetic "probe" ions, such as transition metal ions, which lead to exchange broadening of the esr lines of spin labels, both in solution and attached to macromolecules, and thereby provide valuable structural information. While, for instance, such probe ions cause line broadening of *free* nitroxides in solution beyond the detection limit, any residual spectra obtained for *polymer-bound* spin labels are indicative of some form of steric hindrance which interferes in the rapid exchange between at least a certain fraction of the bound nitroxides and the probe ions in solution. We therefore employed the spin-probe – spin-label method (13) in order to confirm our previous evidence for structural heterogeneities in the chitosan derivatives.

The line width of the nitroxide esr signal of the free hydroxyl label **6** in solution increased rapidly with increasing nickel sulphate concentration, with no signal being detectable above 3 m*M* $Ni(H_2O)_6^{2+}$ concentrations. In contrast, the branched chitosan derivative **15**, for example, produced a more complex pattern with a residual signal being observable even at tenfold higher nickel ion concentrations, although reduced in intensity by approximately two orders of magnitude in comparison with the signal obtained in the absence of metal ion.

Figure 3 illustrates the probe-induced line broadening of label **6** and of derivatives **7** and **15** in terms of the dependency of the increase in peak-to-peak width of the centre field line $[\Delta\omega_0(C) - \Delta\omega_0(O)]$ on paramagnetic ion concentration. At low nickel concentrations, a rapid, linear increase in the line broadening of derivatives **7** and **15** was observed, while the probe seemed to exert little or no influence at concentrations above 10 m*M*. The nonlinear features in Figs. 3B and 3C confirm (13) the presence of nitroxide sub-populations in derivatives **7**

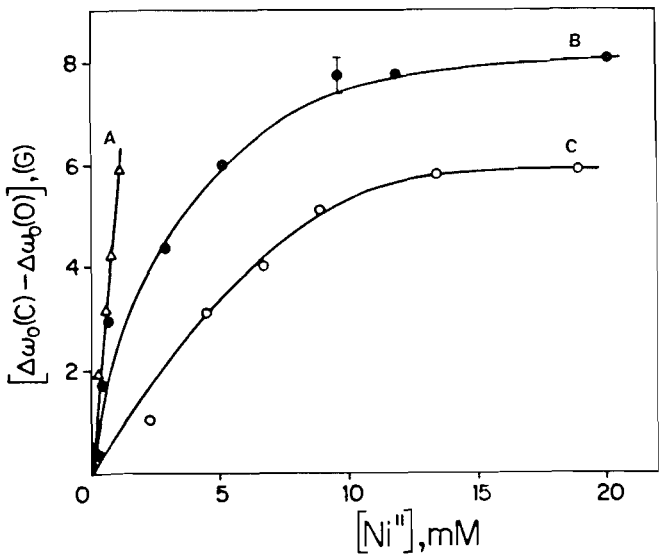

FIG. 3. Broadening of centre field line width as a function of added nickel sulfate for (A) hydroxyl spin label **6**; (B) derivative **15**; and (C) derivative **7** in aqueous solution.

and **15**, which seemed to be unaffected by the paramagnetic probe ions in solution.

It should be noted that similar phenomena were also found for derivative **10**, which showed a residual esr spectrum at nickel concentrations of up to 26 m*M*. However, its unresolved lineshape at higher probe ion concentrations precluded line broadening determination in this case. The observation of structural microenvironments for derivative **10** is not surprising in light of its close structural similarity to the chitosan derivative **7**. It is also not unexpected that the esr spectrum of derivative **9**, in contrast to that of **10**, was broadened beyond detection limits in the presence of only 4 m*M* nickel, since this finding is consistent with the previously discussed mobility differences between derivatives **9** and **10**. Similarly, derivative **14** lost its residual esr spectrum at six-fold lower (5 m*M*) probe ion concentrations than its analogue **15**, confirming previously indicated structural distinctions.[4,5] If our aforementioned arguments about the respective structures of derivatives **14** and **15** are valid, the selective broadening results could tentatively be interpreted as an indication that the proposed, more regular structure of derivative **15** gives rise, by way of intra- or intermolecular associations, to an organized type of solution structure, which is unattainable by derivative **14** on account of its structural irregularities. Clearly, a more detailed explanation of the nature of these solution structures, as well as the site variations for derivative **15**, requires complementary spectroscopic evidence.

Conclusions

The generally mild reaction conditions of the spin-labelling procedures described here and the, in some instances, some-

[4] Selective broadening experiments were not conducted for the chitin derivative **4** in view of its limited swelling capacity.

[5] Throughout these experiments, we found no evidence of interference from nickel chelation by the polymers. This is presumably a result of the relatively short experimental time scale involved (minutes) which would be insufficient for any substantial chelation to occur (23). The high nickel ion concentrations employed would additionally offset any effects from this source.

Can. J. Chem. Downloaded from www.nrcresearchpress.com by 210.87.254.40 on 09/06/12
For personal use only.

what laborious synthetic approach involving, for example, activated or intermediate polymer species, were imposed by considerations of both the acid lability of the nitroxide moieties and the requisite ultimate physical state (solution, gel, or solid) of the resulting chitin and chitosan derivatives. These methods complement our previously reported fluorescent labelling (18) and other selective derivatization (6, 9) procedures for chitin and chitosan, which together provide a versatile array of synthetic techniques for further evaluations of the physical properties of these biopolymers. These methods have facilitated, for the first time, spectroscopic studies of chitosan and its derivatives in both the solution and gel form in *aqueous* medium, whereas previous investigations involved either chitosan films suspended in organic solvents (4) or solutions in aqueous organic acids (3, 5).

It has been demonstrated that spin labelling provides a useful and sensitive analytical tool for studying molecular solution parameters of chitin and chitosan. Thus, the solvation and swelling of the polymer matrices were reflected in the variation in correlation times, similar to observations from previous studies with spin-labelled polystyrene (19) and agarose (16).

It is noteworthy that the τ_c values of our chitosan derivatives are of the same order of magnitude as that found by Aleksandrova *et al.* (5) for chitosan in acetic acid solution (14.5 ns). Perhaps the most interesting result of our esr study is the observation of structural heterogeneities for the chitosan derivatives which seem to arise from the nature of the respective solution and gel structures.

These features may be of significance for understanding certain chitosan solution and other properties, such as its metal chelation performance. Precedence for the presence of such structural microenvironments, with restricted solute and solvent accessibilities, exists for other polysaccharides, such as for cellulose (17) and agarose (16). It should be noted, however, that the selective labelling methods employed for derivatives **7** and **15** have the distinct advantage of eliminating a potential source of confusion in the interpretation of site variations, namely product mixtures arising from nonselective derivatization methods (16, 17).

Experimental

General methods and materials

The esr spectra were recorded at X-band with a Varian E-3 instrument. Correlation times for rotational reorientation were determined using the quadratic term of the ratio-of-heights method of McConnell and co-workers (20), assuming isotropic nitroxide tumbling. No computer simulation of spectra was performed, since only estimates for relative comparisons were required here. All esr spectra were obtained in aqueous solution or dispersion (ca. 5% w/v, pH 7), unless indicated otherwise. All other esr methods have been previously described (8).

Elemental microanalyses were performed by Mr. P. Borda of the Microanalytical Laboratory, Department of Chemistry, University of British Columbia.

Chitosan (from shrimp shells, ca. 15% *N*-acetylated) and chitin (from crab shells, ca. 10% *N*-deacetylated; both previously characterized (6)) were purchased from Sigma and used without further purification. The chemical derivation reactions of chitosan resulted in a slight reduction of the residual *N*-acetyl content (6). Sodium cyanoborohydride, 4-amino-2,2,6,6-tetramethylpiperidine-1-oxyl, and 4-oxo-2,2,6,6-tetramethylpiperidine-1-oxyl were purchased from Aldrich Chemical Co. The other spin labels, 4-hydroxy-2,2,6,6-tetramethylpiperidine-1-oxyl and 4-chloroacetamido-2,2,6,6-tetramethylpiperidine-1-oxyl, were synthesized using the method of McConnell (22).

*Preparation of [4-acetamido-2,2,6,6-tetramethylpiperidine-1-oxyl] chitin, **4***

Chitin (180 mg, 0.85 mmol) was soaked in methyl sulfoxide (15 mL) for 48 h, then filtered and suspended in aqueous (65%) NaOH solution (40 mL) for 1 h, after which the alkali chitin was filtered, pressed, and resuspended in isopropanol (25 mL). A solution of the label **3** (250 mg, 0.92 mmol) was added with stirring. After 2 h, the product was filtered, washed (water 100 mL, methanol 150 mL), and dried. The product had d.s. 0.04. *Anal.* calcd. for $[(C_8H_{13}NO_5)_{0.96}(C_{19}H_{32}N_3O_7)_{0.04}]\cdot 0.47\ H_2O$: C 45.77, H 6.70, N 6.83; found: C 45.58, H 6.45, N 6.78.

Attempted reductive amination: chitin (1 g, 4.72 mmol) was dissolved in a mixture containing 3.6% (w/v) LiCl and dimethylacetamide (DMAC) (40 mL) and the undissolved material was separated by filtration through glass wool. To the filtrate was added a solution of keto spin label **5** (3.6 g, 21 mmol) in DMAC (10 mL) and $NaCNBH_3$ (2 g, 33 mmol). The reaction mixture was warmed (50°C) for 24 h, after which aqueous methanol (70 mL) was added to separate the product out as a gel. The product was found to contain no bound label.

Preparation of [4-N-(2,2,6,6-tetramethylpiperidine-1-oxyl)] chitosan, 7

Chitosan (250 mg, 1.5 mmol) was dissolved in 10% aqueous acetic acid (50 mL) and precipitated by addition of an aqueous ammonium sulfate solution. The precipitated chitosan sulfate (21) was collected by centrifugation, and then suspended in phosphate buffer (20 mL, pH 6.5). The solution was heated to 50°C to dissolve the sulfate salt upon which keto spin label **5** (340 mg, 2.0 mmol) and $NaCNBH_3$ (0.44 g, 7.2 mmol) were added with stirring. The reaction mixture was kept at 50°C for 5 h, then aqueous sodium hydroxide solution was added to precipitate the product at slightly alkaline pH. The product, **7**, had a d.s. 0.45. *Anal.* calcd. for $[(C_8H_{13}NO_5)_{0.10}(C_6H_{12}NO_7S)_{0.45}(C_{15}H_{27}N_2O_5)_{0.45}]\cdot 0.6\ H_2O$: C 43.63, H 7.17, N 7.20; found: C 43.55, H 6.99, N 7.44.

The spin labelling was also attempted by reacting chitosan with spin label in 2 *M* aqueous pyridine and 1% aqueous acetic acid, resulting, however, in a much lower yield.

*Preparation of [4-acetamido-2,2,6,6-tetramethylpiperidine-1-oxyl] chitosan, **9***

The labelling was carried out via the chitosan sulfate intermediate (200 mg, 0.8 mmol) described above, which was dissolved in hot water (20 mL, adjusted to pH 6.5). A solution of 4-chloroacetamido-2,2,6,6-tetramethylpiperidine-1-oxyl, **3** (176 mg, 1 mmol), in 65% aqueous acetone (2 mL) was added with stirring and the reaction mixture was kept at 40–50°C for 6 h, at which time gelation occurred. The gel was separated, washed consecutively with water, ethanol, acetone, and ether, and then dried; the product had d.s. 0.25. *Anal.* calcd. for $[(C_8H_{13}NO_5)_{0.1}(C_6H_{12}NO_7S)_{0.65}(C_{17}H_{30}N_3O_6)_{0.25}]\cdot 1.2\ H_2O$: C 36.73, H 6.55, N 7.18; found: C 36.60, H 6.49, N 7.14.

The same reaction carried out in the presence of 4-dimethylaminopyridine catalyst (100 mg, 0.8 mmol) gave a product with greater d.s. (0.5). *Anal.* calcd. for $[(C_8H_{13}NO_5)_{0.1}(C_6H_{12}NO_7S)_{0.4}(C_{17}H_{30}N_3O_6)_{0.5}]\cdot 1.35\ H_2O$: C 42.87, H 7.32, N 8.55; found: C 42.64, H 7.28, N 8.88.

*Preparation of [4-N-(2,2,6,6-tetramethylpiperidine-1-oxyl)] chitosan, **10***

Chitosan (500 mg, 3 mmol) was dissolved in a mixture (1:1) of methanol and 0.4% aqueous acetic acid (50 mL) to which was added, with stirring, a solution of 4-oxy-2,2,6,6-tetramethylpiperidine-1-oxyl, **5**, (1.0 g, 5.8 mmol) and $NaCNBH_3$ (0.9 g, 15 mmol) in methanol (10 mL). The solution was stirred for 12 h, at which point a soft white gel had formed. The product had a d.s. 0.1. *Anal.* calcd. for $[(C_8H_{13}NO_5)_{0.02}(C_6H_{11}NO_4)_{0.88}(C_{15}H_{27}N_2O_7)_{0.10}]\cdot 0.49\ H_2O$: C 44.72, H 7.38, N 8.27; found: C 44.47, H 7.10, N 8.15.

*Preparation of spin-labelled, branched chitosan derivatives **14** and **15***

(a) The C-6′ aldehydo lactityl chitosan derivative (43 mg, 0.06

mequiv. galactose) obtained from derivative **11** (6), was suspended in aqueous methanol (15 mL) to which was added a solution of amine spin label **13** (150 mg, 0.9 mmol) and $NaCNBH_3$ (0.1 g, 2 mmol) in the same solvent (5 mL). The amination was carried out for 12 h and the product, **14**, was purified by dialysis (3 d); esr double integration gave a d.s. ~0.35 (the microanalytical results could not be exactly matched with a molecular formula; found: C 40.82, H 6.53, N 3.87).

(b) The C-6′ aldehydo melibiityl chitosan derivative (58 mg, 0.08 mequiv. galactose) obtained from derivative **12** (6), was treated as above, yielding a product (**15**) with d.s. ~0.15 (from esr); (found: C 41.47, H 6.77, N 9.32).

Acknowledgements

This work was supported by the Natural Sciences and Engineering Research Council of Canada via operating grants to L.D.H. (A 1905), and via an industrial research fellowship to M.Y.

1. P. R. AUSTIN, C. J. BRINE, J. E. CASTLE, and J. P. ZIKAKIS. Science, **212**, 749 (1981); R. A. A. MUZZARELLI. Chitin. Pergamon Press, Oxford. 1977.
2. L. A. BUFFINGTON and E. S. STEVENS. J. Am. Chem. Soc. **101**, 5159 (1979).
3. S. HIRANO, N. MATSUDA, O. MIURA, and H. IWAKI. Carbohydr. Res. **71**, 339 (1979).
4. K. KAIFU, T. KOMAI, and A. TSUTSUMI. Polymer J. **14**, 803 (1982).
5. T. A. ALEKSANDROVA, A. M. VASSERMAN, A. I. GAMZAZADE, S. V. ROGOZHIN, I. A. SIMENEL, and V. P. TIMOFEER. Vysokomol. Soedin. Ser. B, **25**, 219 (1983); Chem. Abstr. **98**, 162738x, 1983.
6. M. YALPANI and L. D. HALL. Macromolecules. In press.
7. L. D. HALL and M. YALPANI. Carbohydr. Res. **91**, C1 (1981).
8. M. YALPANI and L. D. HALL. Can. J. Chem. **59**, 3105 (1981); M. YALPANI and L. D. HALL. J. Polym. Sci. Polym. Chem. Ed. **20**, 3399 (1982).
9. L. D. HALL and M. YALPANI. J. Chem. Soc. Chem. Commun. 1153 (1980).
10. C. L. MCCORMICK and D. K. LICHATOWICH. J. Polym. Sci. Polym. Lett. Ed. **17**, 479 (1979).
11. L. D. HALL, M. YALPANI, and N. YALPANI. Biopolymers, **20**, 1413 (1981).
12. E. ODGAARD, T. B. MELO, and T. HENRIKSEN. J. Magn. Reson. **18**, 436 (1975); G. I. LIKHTENSTEIN. Adv. Mol. Relaxation Interact. Processes, **10**, 47 (1977).
13. G. I. LIKHTENSTEIN. Spin labels in molecular biology. Nauka, Moscow. 1974.
14. J. S. HYDE, H. M. SWARTZ, and W. E. ANTHOLINE. *In* Spin labelling II. *Edited by* L. J. Berliner. Academic Press, New York. 1979. p. 71.
15. J. D. APLIN and L. D. HALL. Eur. J. Biochem. **110**, 295 (1980).
16. J. D. APLIN and L. D. HALL. Carbohydr. Res. **75**, 17 (1979).
17. L. D. HALL and J. D. APLIN. J. Am. Chem. Soc. **100**, 1934 (1978), and references cited therein; F. SUNDHOLM, B. WESTERMARK, and E. G. ROZANTSEV. Acta Chem. Scand. Ser. A, **34**, 177 (1980).
18. M. YALPANI and L. D. HALL. Can. J. Chem. **59**, 2934 (1981).
19. S. L. REGEN. J. Am. Chem. Soc. **97**, 3108 (1975).
20. H. W. WIEN, J. D. MORRISETT, and H. M. MCCONNELL. Biochemistry, **11**, 3707 (1972).
21. M. S. MASRI, V. G. RANDALL, and W. L. STANLEY. *In* Proc. 1st Int. Conf. Chitin/Chitosan, Cambridge, MA, U.S.A. *Edited by* R. A. A. Muzzarelli and E. R. Pariser. 1978. p. 364.
22. T. J. STONE, T. BUCKMAN, P. L. NORDIO, and H. M. MCCONNELL. Proc. Natl. Acad. Sci. U.S.A. **54**, 1010 (1965).
23. L. D. HALL and M. YALPANI. Carbohydr. Res. **83**, C5 (1980).

Can. J. Chem. Downloaded from www.nrcresearchpress.com by 210.87.254.40 on 09/06/12
For personal use only.

An approximate absolute ^{33}S nuclear magnetic shielding scale

RODERICK E. WASYLISHEN,[1] CHUCK CONNOR,[2] AND JAN O. FRIEDRICH[2]
Department of Chemistry, Dalhousie University, Halifax, N.S., Canada B3H 4J3

Received October 6, 1983

RODERICK E. WASYLISHEN, CHUCK CONNOR, and JAN O. FRIEDRICH. Can. J. Chem. **62**, 981 (1984).

Sulfur-33 chemical shifts have been measured for a number of simple compounds, e.g. SF_6, $HFSO_3$, X_2SO_2, SO_2, Cl_2SO, CH_3SH, H_2S, and OCS, which have not been previously reported. Our results indicate that the range of ^{33}S chemical shifts is approximately 1000 ppm, slightly less than that observed for ^{17}O and approximately one half the range reported for ^{77}Se. Using the ^{33}S nuclear spin-rotation constant of OCS measured by molecular-beam electric resonance and Flygare's procedure, an absolute ^{33}S shielding constant of 843 ± 12 ppm is calculated for OCS, permitting an approximate absolute shielding scale to be proposed for this nucleus.

RODERICK E. WASYLISHEN, CHUCK CONNOR et JAN O. FRIEDRICH. Can. J. Chem. **62**, 981 (1984).

On a mesuré les déplacements chimiques du soufre-33 d'un certain nombre de composés simples (comme le SF_6, le $HFSO_3$, le X_2SO_2, le SO_2, le Cl_2SO, le CH_3SH, le H_2S et le OCS) qui n'avaient pas été étudiés antérieurement. Nos résultats indiquent que les déplacements chimiques du ^{33}S s'étalent sur environ 1000 ppm; cette valeur n'est que légèrement inférieure aux valeurs observées pour le ^{17}O et n'est approximativement que la moitié de la valeur rapportée pour le ^{77}Se. En utilisant la constante de rotation de spin nucléaire du ^{33}S du OCS mesurée par résonance électrique de faisceau moléculaire et par la méthode de Flygare, on peut calculer que la constante de blindage du ^{33}S du OCS est égale à 843 ± 12 ppm; ceci permet de proposer une échelle absolue et approximative du blindage provoqué par ce noyau.

[Traduit par le journal]

Can. J. Chem. Downloaded from www.nrcresearchpress.com by 210.87.254.105 on 09/06/12
For personal use only.

Introduction

In most nmr studies one measures a difference in Larmor resonance frequencies between some nucleus of interest, ν_i, and that of a reference compound containing the same isotopic species, ν_{ref}. It is then customary to define the chemical shift of i using eq. [1].

$$[1] \quad \delta = \frac{\nu_i - \nu_{ref}}{\nu_{ref}} \times 10^6$$

Since $\nu_i = \gamma/2\pi(1 - \sigma_i)B_0$, the chemical shift can be expressed in terms of shielding or screening constants, σ's (eq. [2]).

$$[2] \quad \delta = \frac{\sigma_{ref} - \sigma_i}{1 - \sigma_{ref}} \cong \sigma_{ref} - \sigma_i$$

Although it is generally possible to measure differences in shielding constants very accurately, often to better than 0.1 ppm, a knowledge of their absolute value is a much more difficult problem (1). If the absolute value of σ is known for any compound of a particular isotopic species, it is then possible, in principle, to establish an absolute nuclear shielding scale. The procedure of establishing an *approximate* absolute ^{33}S chemical shielding scale is outlined below (under theory) and the ^{33}S chemical shifts of several relatively simple compounds are reported.

Sulfur-33 has a natural abundance of 0.76%, a nuclear spin of 3/2, and relatively large quadrupole moment, -5.5×10^{-30} m^2 (2). In the absence of a symmetric electric field gradient at the nucleus, the large quadrupole moment generally leads to electric quadrupole coupling constants in the range of 20 to 50 MHz (3), hence very efficient nuclear spin relaxation with concomitant broad resonances. For ^{33}S, the line width at half maximum height is given by eq. [3], where all symbols have their usual meaning (4).

$$[3] \quad \nu_{1/2} = \frac{2}{5}\pi\,(1 + \eta^2/3)\,(e^2qQ/h)^2\,\tau_{eff}$$

This represents a lower limit on the line width. The potential of ^{33}S nmr in structural chemical studies was first explored by Retcofsky and Friedel (5). Subsequently Lutz and co-workers (6–9) have determined accurate ^{33}S chemical shifts for a few simple compounds and have suggested that the ^{33}S resonance of the sulfate anion serve as a ^{33}S nmr reference (6). More recently, ^{33}S nmr studies of some simple sulfones and sulfonic acids have been reported (10, 11).

Theory

The nuclear shielding tensor, σ_{ij}, is generally expressed as a sum of two terms of opposite sign, the so-called diamagnetic and paramagnetic terms (ref. 4, Chapt. 6). In isotropic solution nmr studies one measures a quantity related to the average value of σ_{ij}, hence

$$[4] \quad \sigma_{av} = \sigma^d_{av} + \sigma^p_{av}$$

Flygare and co-workers (12–15) have shown that for a nucleus S in a molecule the diamagnetic term can be approximated by eq. [5]

$$[5] \quad \sigma^d_{av}(S) \simeq \sigma^d_{av}\,(\text{free atom}) + \frac{e^2}{3mc^2}\sum_n \frac{Z_n}{r_n}$$

where σ^d_{av} (free atom), the diamagnetic shielding in the free atom obtained from atomic Hartree–Fock functions, is 1050.5 ppm for sulfur (16), Z_A is the atomic number of the n^{th} nucleus ($n \neq S$), and r_n is the distance between n and S. The paramagnetic term in eq. [4] is closely related to the nuclear spin-rotation constant, for a linear molecule,

$$[6] \quad \sigma^p_{av}(S) = \left(\frac{2\pi e}{3mhc}\right) R_\perp I_\perp - \frac{e^2}{3mc^2}\sum_n \frac{Z_n}{r_n}$$

where $R_\perp = M_\perp/g_S\mu_0$ and $M_\perp/h$ is the nuclear spin rotation constant in Hz, μ_0 is the nuclear magneton, $g_S(^{33}S) = 0.429$ (6), and $I_\perp$ is the moment of inertia. Note that the nuclear contribution to $\sigma^d_{av} + \sigma^p_{av}$ is zero. For ^{33}S, the only spin-rotation

[1] Author to whom all correspondence should be directed.

[2] Holder of a 1982 NSERC summer undergraduate research assistantship.

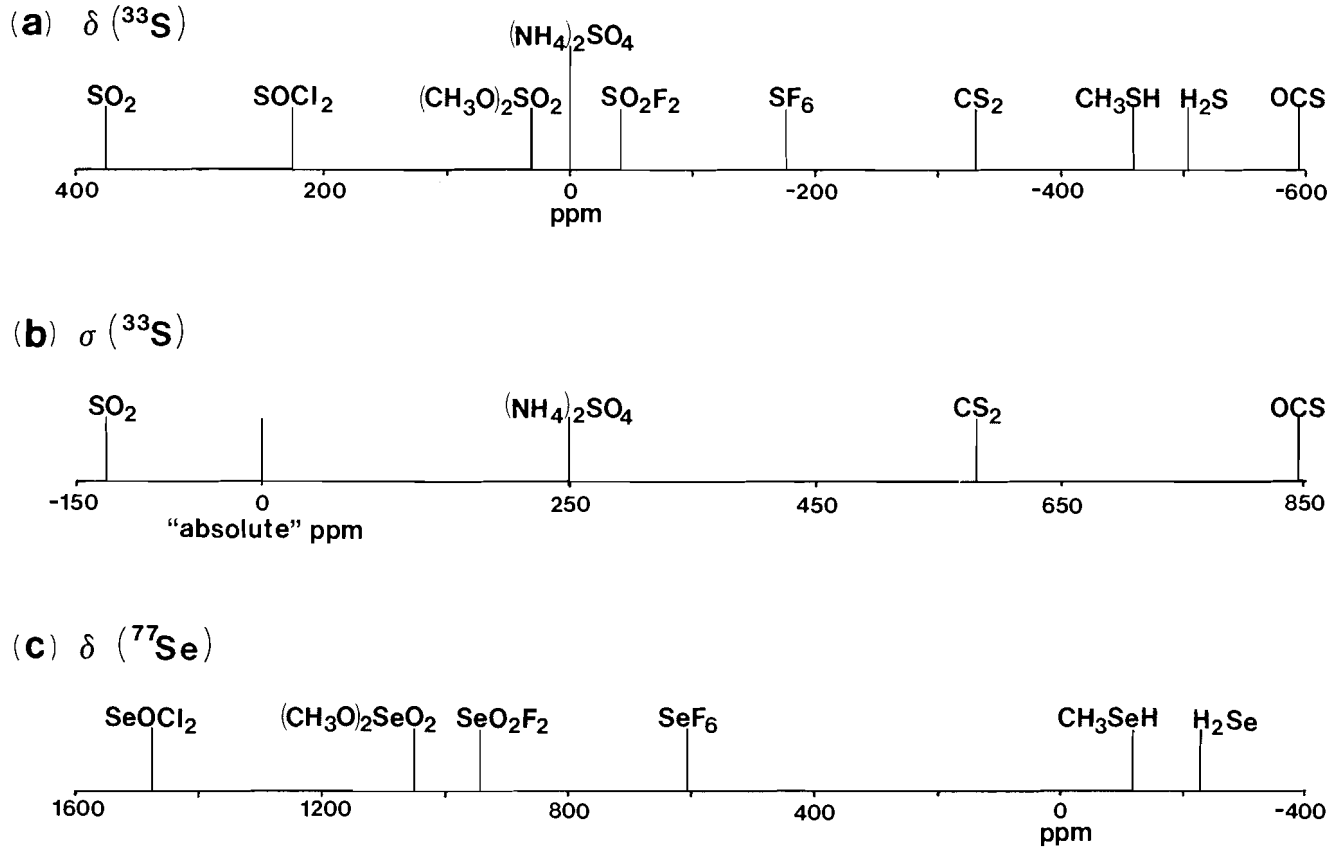

FIG. 1. (a) Sulfur-33 nmr chemical shifts with respect to 4 *m* $(NH_4)_2SO_4$; positive values are to high frequency of the reference; (b) an approximate absolute ^{33}S nmr chemical shielding scale, see text; (c) ^{77}Se nmr chemical shifts with respect to $(CH_3)_2Se$, ref. 21.

constant we are aware of is that of OCS. For the ground vibrational state $M_\perp/h$ = 870 ± 50 Hz (17). Substitution into eq. [5] and [6] gives σ_{av} = 843 ± 12 ppm. This of course is the average ^{33}S nuclear shielding constant of an isolated OCS molecule in the ground vibrational state.

Experimental

All ^{33}S nmr measurements were carried out at 27.7 MHz on a Nicolet 360 (B_0 = 8.480 T) using a broad-band (16 to 56 MHz variable temperature 10-mm probe. The probe was tuned and matched for each sample. The $\pi/2$ pulse width was approximately 45 μs. Neat samples of H_2S, CH_3SH, OCS, SF_6, SO_2, and SO_2F_2 from Matheson were prepared on a gas rack by condensing each of the above gases in thick walled 10-mm od nmr tubes. The nmr samples of SO_2Cl_2, $SOCl_2$, and $HFSO_3$ were prepared in an inert atmosphere.

Results and discussion

(i). *General features of the ^{33}S nuclear magnetic resonance spectra*

The results of this study are summarized in Table 1 and Fig. 1(a). With the exception of SF_6, $(NH_4)_2SO_4$, and sulfolane (tetramethylene sulfone (**I**)), the ^{33}S nmr line widths at half-height were significantly greater than 100 Hz but less than 2

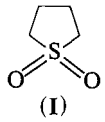

(**I**)

kHz. The sharpest lines ($\nu_{1/2}$ < 1 Hz) were observed for SF_6 at 295 K where the central line had an apparent T_1 of 10 ± 2 s! The

TABLE 1. ^{33}S nuclear magnetic resonance frequencies[a, b]

Compound	ν	Δσ
$(NH_4)_2SO_4$, 4 *m* in H_2O	27,716,302 ± 1 Hz	0.0 ppm
CS_2	27,707,100 ± 50	−332.0 ± 2
OCS	27,699,843 ± 50	−593.8 ± 2
SF_6	27,711,406 ± 1	−176.6 ± 0.1
H_2S	27,702,360 ± 50	−503.0 ± 2
CH_3SH	27,703,600 ± 50	−458.3 ± 2
O_2SCl_2	27,715,063 ± 50	−44.7 ± 2
O_2SF_2 (−50°C)	27,715,170 ± 50	−40.8 ± 2
$O_2S(OCH_3)_2$	27,717,194 ± 50	+32.2 ± 2
SO_2	27,726,692 ± 50	374.9 ± 2
$SOCl_2$	27,722,520 ± 500	224 ± 20
H_2SO_4 ~5 *M*	27,716,058 ± 25	−8.8 ± 1
$HFSO_3$	27,715,680 ± 100	−22.4 ± 3
Sulfolane	27,717,343 ± 2	37.6 ± 0.2
Isothiazole	27,717,790 ± 500	53.7 ± 20
ZnS (powder)	—	−562 ± 1[d]
$(NH_4)_2S_2O_3$, 4 *m* in H_2O	—	34.5 ± 0.2[e]
K_2MoS_4, 1.1 *m* in H_2O	—	33.4 ± 1.6[e]

[a] Field in which the ^1H nmr respoance of liquid TMS is 361,077,305 ± 1 Hz.
[b] Neat liquids at 295 ± 1 K unless otherwise indicated.
[c] $^1J(^{33}S, ^{19}F)$ = 251.6 ± 0.2 Hz.
[d] Reference 9 with respect to 4.0 *m* Cs_2SO_4 at 298 ± 2 K.
[e] Reference 7.

spectrum, a seven line multiplet ($^1J(^{33}S, ^{19}F)$ = 251.8 ± 0.2 Hz), is shown in Fig. 2. This value of *J* is in good agreement with the value obtained from an early ^{19}F nmr study (18). Scalar couplings involving ^{33}S and ^1H or ^{19}F were not directly observable in any of the other compounds studied, presumably be-

Can. J. Chem. Downloaded from www.nrcresearchpress.com by 210.87.254.105 on 09/06/12
For personal use only.

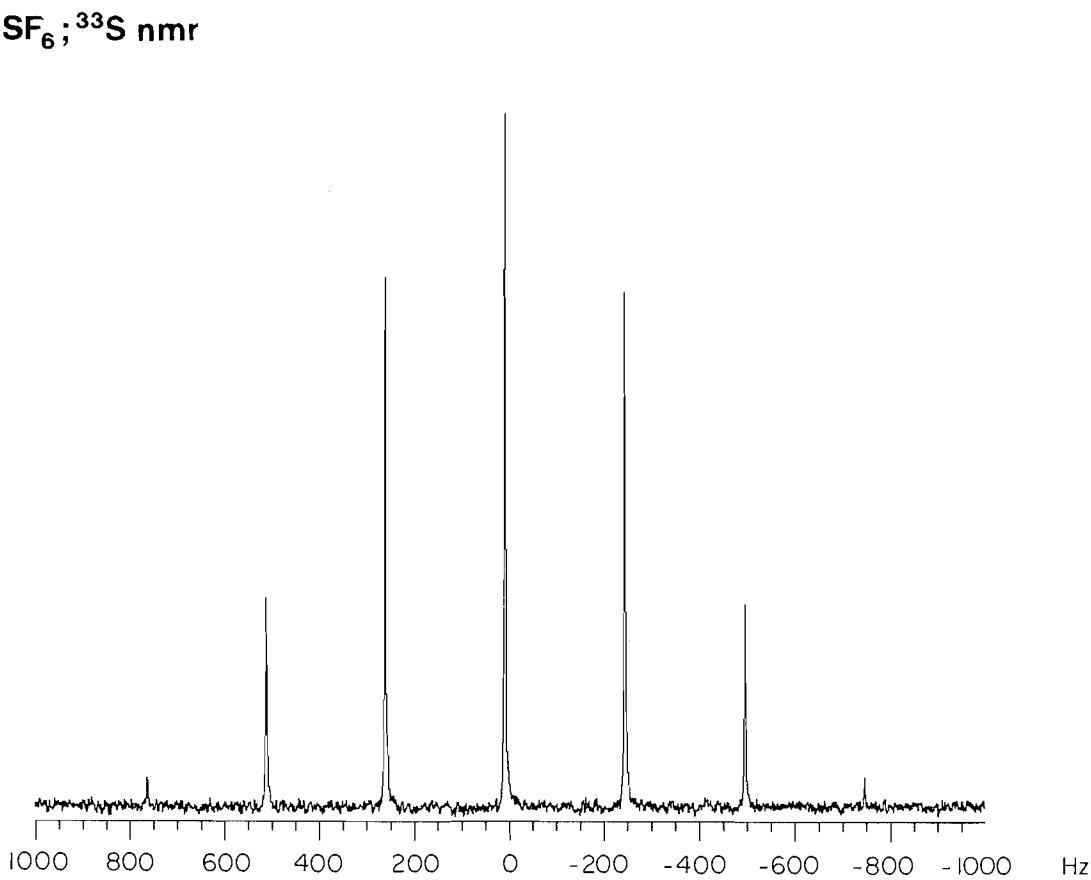

FIG. 2. The ^{33}S nmr spectrum of neat liquid SF_6 at 295 K.

cause the natural line widths are substantially greater than the spin–spin couplings. A ^{33}S nmr spectrum more typical of those obtained for the compounds listed in Table 1 is that of OCS, Fig. 3. Approximately 5.5 min were required to obtain this spectrum (3200 scans, acquisition time of 0.1024 s, and line broadening of 25 Hz). Substituting the ^{33}S nuclear quadrupole coupling constant, 29.12 MHz (17), and the observed line width, 440 ± 50 Hz, into eq. [3] implies a rotational correlation time of 0.41 ps for OCS. This is significantly shorter than the value, 1.3 ps, reported for liquid CS_2 at 288 K (19).

(ii). *Relative chemical shifts*

The ^{33}S chemical shift of SO_2 is 340 ppm to higher frequency than that of any other sulfur resonance previously investigated. The central ^{17}O of ozone which is structurally analogous to the ^{33}S of SO_2 is also highly deshielded relative to $^{17}OH_2$ (20), 1032 ppm. On the basis of the data in Fig. 1, the chemical shift range of ^{33}S is less than 1000 ppm, which is slightly less than the ^{17}O chemical shift range (20*b*). The ^{77}Se chemical shift range (21) is much larger than that of ^{33}S and ^{17}O. In Fig. 1(c) the ^{77}Se chemical shifts of several compounds with respect to $(CH_3)_2Se$ are given; note that the scale used to express the relative ^{77}Se chemical shifts is double that used for the ^{33}S shifts. The close correspondence between the relative ^{33}S and ^{77}Se chemical shifts in analogous compounds is quite striking. For example, the ^{33}S resonance of SF_6 is approximately 325 ppm to high frequency of H_2S and 400 ppm to low frequency of $SOCl_2$; similarly, the ^{77}Se resonance of SeF_6 is approximately 836 ppm to high frequency of H_2Se and 890 ppm to low frequency of $SeOCl_2$ (21).

The relative chemical shift ranges for ^{17}O, ^{33}S, and ^{77}Se are analogous to those reported for the group IV nuclides, ^{13}C, ^{29}Si, and ^{73}Ge. Silicon has a chemical shift range of approximately 400 ppm, smaller than carbon (22), but germanium has a chemical shift range of at least 1200 ppm, much greater than either carbon or silicon. Similarly, the chemical shift range of ^{31}P, ~600 ppm, is less than that of N, ~1000 ppm; unfortunately the large quadrupole moment of ^{75}As severely limits the range of As compounds which can be investigated (23). On moving across the second row elements there is a definite increase in the range of chemical shift; Si (400 ppm), P (600 ppm), and S (1000 ppm).

The replacement of a hydrogen in H_2S by a methyl group leads to a high frequency ^{33}S nmr shift of 44.7 ± 2 ppm; the corresponding ^{77}Se shift in H_2Se relative to CH_3SeH is 110 ppm (21*b*). Because of hydrogen bonding effects, these values are probably dependent on solvent (21*c*).

(iii) *An absolute ^{33}S shielding scale*

In order to establish an absolute ^{33}S nmr shielding scale, we must assume that the gas to liquid chemical shifts are similar for our primary reference (OCS) and any other sulfur compound, S. Typically, the nucleus becomes more shielded on going from the gas to liquid phase and the magnitude of the shift appears to be related to the chemical shift range of that particular isotope (24). Attempts to measure the ^{33}S nmr resonance frequency of OCS in the gas phase (8.8 atm) have been unsuccessful to date. For the ^{17}O nucleus of OCS, we have observed a gas to liquid shift of −4.9 ppm (greater shielding in the gas phase). The ^{17}O and ^{33}S chemical shift ranges are both similar (1000 ppm), thus gas to liquid ^{33}S chemical shifts are probably generally small and eq. [7] is a good approximation.

Can. J. Chem. Downloaded from www.nrcresearchpress.com by 210.87.254.105 on 09/06/12
For personal use only.

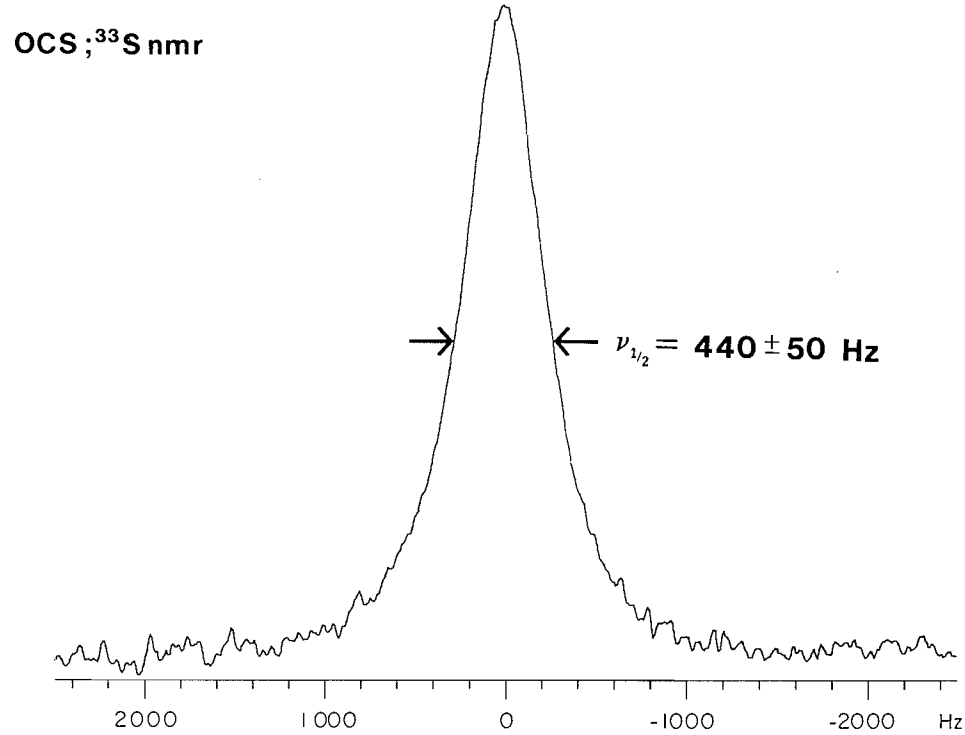

FIG. 3. The ^{33}S nmr spectrum of neat liquid OCS at 295 K.

[7] $\sigma_e^S \simeq \sigma_0^{OCS} + \sigma^S$ (liq. T) $- \sigma^{OCS}$ (liq. T)

Here σ_e^S is the average absolute shielding of nucleus S for the equilibrium configuration, and σ_0^{OCS} is the average absolute shielding of an isolated OCS molecule, +843 ppm. The absolute ^{33}S scale is sketched in Fig. 1(b); σ is 249 ppm and 581 ppm for 4 *m* ($(NH_4)_2SO_4$ and CS_2, respectively, two common ^{33}S nmr references.

Few theoretical calculations of ^{33}S shielding constants have been reported (25, 26). The most recent calculations by Ridard *et al.* (26) use a pseudo-potential technique. For the ^{33}S nucleus of H_2S they calculate the following average shielding constants: σ^d = 1062.4 ppm, σ^p = −327.8 ppm, and σ = 734.6 ppm;[3] using the data in Table 1 and eq. [7], σ = 752 ppm. Considering the error in σ_0^{OCS} and the assumptions in applying eq. [7], the agreement is excellent.

Further ^{33}S nuclear spin-rotation constants and nuclear shielding calculations will be necessary to test the reliability of the scale proposed here. Nevertheless the results in Table 1 expand our knowledge of ^{33}S chemical shielding and represent a first step in establishing a ^{33}S shielding scale. We believe that ^{33}S will become a more important nucleus for chemists as nmr pulse programmers and probe designs improve, particularly if studies are carried out at high applied magnetic fields.

Acknowledgements

All sulphur-33 nmr spectra were obtained at the Atlantic Regional NMR Center. We are grateful to NSERC for financial support in helping establish and maintain this center and for operating (R.E.W.) and summer assistantship (C.C. and J.F.) grants.

[3] NOTE ADDED IN PROOF: More recent calculations by Höller and Lischka (27) yield σ = 721 ppm for H_2S.

1. C. J. JAMESON, A. K. JAMESON, and P. M. BURRELL. J. Chem. Phys. **73**, 6013 (1980).
2. G. H. FULLER. Phys. Ref. Chem. Data, **5**, 835 (1976).
3. E. A. C. LUKEN. Nuclear quadrupole coupling constants. Academic Press, New York. 1969.
4. A. ABRAGAM. The principles of nuclear magnetism. Oxford University Press, London. 1961.
5. H. L. RETCOFSKY and R. A. FRIEDEL. J. Am. Chem. Soc. **94**, 6579 (1972).
6. O. LUTZ, A. NOLLE, and A. SCHWENK. Z. Naturforsch. Teil A, **28**, 1370 (1973).
7. O. LUTZ, W. NEPPLE, and A. NOLLE. Z. Naturforsch. Teil A, **31**, 978 (1976).
8. P. KRONECK, O. LUTZ, and A. NOLLE. Z. Naturforsch. Teil A, **35**, 226 (1980).
9. M. HALLER, W. E. HERTLER, O. LUTZ, and A. NOLLE. Solid State Commun. **33**, 1051 (1981).
10. R. FAURE, E. J. VINCENT, J. M. RUIZ, and L. LENA. Org. Magn. Reson. **15**, 401 (1981).
11. D. L. HARRIS and S. A. EVANS. J. Org. Chem. **47**, 3355 (1982).
12. W. H. FLYGARE and J. GOODISMAN. J. Chem. Phys. **49**, 3122 (1968).
13. T. D. GIERKE and W. H. FLYGARE. J. Am. Chem. Soc. **94**, 7277 (1972).
14. W. H. FLYGARE. Chem. Rev. **74**, 653 (1974).
15. W. H. FLYGARE. Molecular structure and dynamics. Prentice–Hall, Inc., Englewood Cliffs, NJ. 1978. Section 6–9.
16. G. MALLI and C. FROESE. Int. J. Quant. Chem. **15**, 95 (1967).
17. J. M. L. J. REINARTZ and A. DYMANUS. Chem. Phys. Lett. **24**, 346 (1974).
18. P. T. INGLEFIELD and L. W. REEVES. J. Chem. Phys. **40**, 2425 (1964).
19. R. R. VOLD, S. W. SPARKS, and R. L. VOLD. J. Magn. Reson. **30**, 497 (1978).
20. (*a*) I. J. SOLOMON, J. N. KEITH, A. J. KACMAREK, and J. K. RAMSEY. J. Am. Chem. Soc. **90**, 5408 (1968); (*b*) J.-P. KINTZINGER. *In* NMR – basic principles and progress. Vol. 17. *Edited by* P. Diehl, E. Fluck, and R. Kosfeld. Springer Verlag, New York. 1981.

Can. J. Chem. Downloaded from www.nrcresearchpress.com by 210.87.254.105 on 09/06/12
For personal use only.

21. (*a*) C. MCFARLANE and W. MCFARLANE. *In* NMR and the periodic table. *Edited by* R. K. Harris and B. E. Mann. Academic Press, New York. 1978. pp. 402–409; (*b*) W. MCFARLANE and R. J. WOOD. J. Chem. Soc. Dalton Trans. 1397 (1972); (*c*) J. D. ODOM, W. H. DAWSON, and P. D. ELLIS. J. Am. Chem. Soc. **101**, 5815 (1979).
22. R. K. HARRIS, J. D. KENNEDY, and W. MCFARLANE. *In* NMR and the periodic table. *Edited by* R. K. Harris and B. E. Mann. Academic Press, New York. 1978. pp. 309–342.
23. B. E. MANN. *In* NMR and the periodic table. *Edited by* R. K. Harris and B. E. Mann. Academic Press, New York. 1978. pp. 96–105.
24. C. J. JAMESON. Bull. Magn. Reson. **3**, 3 (1980).
25. S. ROTHENBERG, R. H. YOUNG, and H. F. SCHAEFER III. J. Am. Chem. Soc. **92**, 3243 (1970).
26. J. RIDARD, B. LEVY, and PH. MILLIE. Mol. Phys. **36**, 1025 (1978).
27. R. HÖLLER and H. LISCHKA. Mol. Phys. **41**, 1041 (1980).

Can. J. Chem. Downloaded from www.nrcresearchpress.com by 210.87.254.105 on 09/06/12
For personal use only.

Vapour pressure and thermodynamic data for the binary liquid mixture of pyridine and sulphur dioxide

C. L. GARDNER and R. W. DAY

Defence Research Establishment Ottawa, Ottawa, Ont., Canada K1A 0Z4

Received September 8, 1983

C. L. GARDNER and R. W. DAY. Can. J. Chem. **62**, 986 (1984).

Solubility and nmr data are presented for the pyridine – sulphur dioxide system. The data have been analyzed to determine partial vapour pressures, activity coefficients, and thermodynamic functions. The results indicate that a 1:1 complex of pyridine and SO_2 is formed in these solutions.

C. L. GARDNER et R. W. DAY. Can. J. Chem. **62**, 986 (1984).

On rapporte des données relatives à la solubilité et à rmn du système pyridine – dioxyde de soufre. On a analysé les données pour déterminer les tensions de vapeur partielles, les coefficients d'activité et les fonctions thermodynamiques. Les résultats indiquent que, dans ces solutions, il y a formation d'un complexe 1:1 entre la pyridine et le SO_2.

[Traduit par le journal]

Can. J. Chem. Downloaded from www.nrcresearchpress.com by 210.87.254.105 on 09/06/12
For personal use only.

1. Introduction

In recent years a number of high energy density battery systems using lithium as the anodic material have been introduced. Among these, the lithium – sulphur dioxide system has been one of the most successful. The electrolyte in this battery consists (1) of a mixture of sulphur dioxide, acetonitrile, and a lithium salt, usually lithium bromide. While this electrolyte offers exceptional performance, under certain conditions, reaction of excess lithium with the acetonitrile can lead to the formation of relatively large amounts of lithium cyanide (2). In addition, the solubility of sulphur dioxide in acetonitrile is not as high as in other solvents (3) and, as a result, the internal pressure in lithium – sulphur dioxide cells is relatively high.

In our laboratory, we have initiated studies of alternative electrolyte systems that offer improved safety. In this regard, a detailed study of the sulphur dioxide/*N*-methyl-2pyrrolidinone system has been published (4). In this paper we report solubility results for the pyridine – sulphur dioxide system while results of Raman spectroscopic studies will be reported in the near future (5).

The formation of relatively strong addition compounds between nitrogen bases and sulphur dioxide is well known (6). It was suggested as early as 1935 (7) that a compound of pyridine with sulphur dioxide existed at low temperatures. The phase equilibrium of pyridine and the picolines with sulphur dioxide was studied by Hoffman and Van der Werf (8). These results showed clearly that a 1:1 addition compound was formed between sulphur dioxide and pyridine. The system has also been examined by dielectric measurement (9) and more recently by Raman spectroscopy (5, 10, 11). These studies show clearly that the complex formed between pyridine and sulphur dioxide is charge transfer in nature.

Vapour pressure and calorimetric data for the solution of sulphur dioxide in pyridine given by Benoit and Milanova (3) show pyridine to be an excellent solvent for sulphur dioxide. The work reported in this paper extends the solubility work of Benoit and Milanova to higher pressures, enabling the range of complex formation in this solution to be examined in more detail and thermodynamic excess functions to be determined.

2. Experimental

The pyridine (Fisher centified ACS) was vacuum distilled (40 kPa at about 40°C) from a calcium hydride slurry. Samples of pyridine were tested for water content on a Perkin Elmer Sigma 3 gas chromatograph using a Poropack QS column on a thermal conductivity detector. The results indicated the water content to be about 14 ppm. The distilled solvent was stored in an argon atmosphere in a Vacuum Atmospheres glove box. All manipulations were carried out under anhydrous conditions. The purified liquid was loaded into the solubility flask in the glove box and degassed immediately before use on the vacuum line by several freeze–pump–thaw cycles. Matheson anhydrous SO_2 was used for the measurements without further purification.

Gas solubility measurements were made by introducing a known amount of SO_2 gas (measured using a gas burette) to a known amount of pyridine (typically of the order of 0.5 g) and noting the pressure above the solution after equilibration which normally took about 1 h. The solubility flask was thermostatted to better than ±0.5°C using a constant temperature bath. The solution was stirred constantly using a small magnetic stirrer. The pressure above the solution was measured using a mercury manometer. Corrections to the mass of SO_2 dissolved were made assuming the gas in the space above the solution to follow the ideal gas equation of state.

Nuclear magnetic resonance spectra were recorded on a Varian T-60 spectrometer at 308 K. The samples for the nmr were prepared gravimetrically in the glove box by bubbling SO_2 into a known weight of pyridine. A thermoelectric cooler was used to cool the pyridine as the SO_2 was added since a significant amount of heat was liberated during the dissolution process. The samples were sealed in nmr tubes with screw caps and Teflon sealers to prevent loss of SO_2. Spectra were recorded soon (usually the same day) after preparation. Loss of SO_2 through Teflon sealers was negligible during this period.

The samples were run with an external standard of *N*,*N*-dimethyl formamide (DMF), sealed in a capillary tube, which was inserted into each nmr tube. DMF was chosen since it offered a peak adjacent to the peak due to the *ortho* protons in the pyridine and provided a convenient reference.

3. Results and discussion

The total vapour pressures for mixtures of sulphur dioxide and pyridine at six temperatures are listed in Table 1 and illustrated in Fig. 1. From Fig. 1, it is seen that the system shows a large negative deviation from Raoult's law.

Partial vapour pressures, P_{SO_2} and P_{py}, of the sulphur dioxide and the pyridine were obtained using a method similar to that described in refs. 4, 12, and 13. In this method it is assumed that the excess free energy of mixing, ΔG^e_{mix}, can be expressed as the polynomial

$$\Delta G^e_{mix} = RTX_{SO_2}X_{py} \sum_{i=1}^{n} C_i(X_{SO_2} - X_{py})^{i-1}$$

From the relationship

Can. J. Chem. Downloaded from www.nrcresearchpress.com by 210.87.254.105 on 09/06/12
For personal use only.

TABLE 1. Vapour pressures and thermodynamic properties for mixtures of pyridine and sulphur dioxide

X_{SO_2}*	Total pressure (kPa) Observed	Total pressure (kPa) Calculated	Activity coefficients γ_{SO_2}	Activity coefficients γ_{py}	$-\Delta G^{e}_{mix}$† (kJ mol^{-1})	Association constant K (M^{-1})
			T = 273 K			
0.000	0.64	0.64	—	1.000	0.00	
0.207	0.96	0.75	0.004	1.226	2.23	425
0.368	2.35	1.60	0.024	0.566	3.93	152
0.470	6.72	7.20	0.098	0.206	4.38	113
0.532	16.50	16.61	0.201	0.099	4.39	—
0.583	29.73	29.28	0.323	0.048	4.25	—
0.619	40.87	41.09	0.427	0.036	4.07	—
1.000	155.24	155.24	1.000	—	0.00	
			T = 278 K			
0.000	0.75	0.75	—	1.000	0.00	
0.264	1.92	2.09	0.037	0.451	3.36	55
0.350	3.52	3.56	0.051	0.390	3.82	61
0.379	3.67	4.38	0.059	0.358	3.95	64
0.415	6.45	6.02	0.075	0.305	4.08	67
0.466	11.73	10.47	0.118	0.213	4.20	80
0.511	20.29	18.60	0.192	0.134	4.22	150
0.519	18.05	20.81	0.211	0.121	4.21	199
0.571	43.83	43.50	0.402	0.056	4.06	—
1.000	189.36	189.36	1.000	—	0.00	
			T = 283 K			
0.000	1.04	1.04	—	1.000	0.00	
0.156	1.71	1.62	0.018	1.093	1.28	79
0.282	3.15	2.43	0.026	0.968	2.47	86
0.294	2.77	2.60	0.028	0.939	2.56	84
0.375	5.79	5.21	0.056	0.669	3.14	65
0.436	9.23	10.17	0.099	0.450	3.43	62
0.472	14.96	15.43	0.140	0.335	3.53	70
0.517	25.69	25.41	0.214	0.223	3.58	158
0.556	39.42	39.73	0.303	0.149	3.55	—
0.593	55.01	55.40	0.407	0.100	3.46	—
1.000	229.07	229.07	1.000	—	0.00	
			T = 288 K			
0.000	1.53	1.53	—	1.000	0.00	
0.145	2.19	2.17	0.026	0.879	1.54	54
0.211	2.88	3.00	0.035	0.823	2.07	48
0.283	4.51	4.31	0.045	0.756	2.59	48
0.378	8.21	8.04	0.072	0.595	3.16	51
0.406	9.57	10.12	0.086	0.528	3.29	53
0.445	14.82	14.49	0.116	0.425	3.44	57
0.517	30.56	30.58	0.214	0.239	3.56	158
0.549	43.27	43.27	0.286	0.172	3.55	—
1.000	274.98	274.98	1.000	—	0.00	
			T = 293 K			
0.000	2.05	2.05	—	1.000		
0.078	2.64	2.85	0.037	1.009	0.61	31
0.147	3.44	3.48	0.036	1.012	1.17	38
0.159	3.52	3.61	0.036	1.010	1.26	39
0.253	6.08	5.39	0.048	0.933	1.99	40
0.289	6.51	6.69	0.057	0.871	2.24	39
0.371	12.43	12.47	0.095	0.679	2.72	35
0.442	22.93	23.67	0.160	0.476	2.99	36
0.493	38.42	37.57	0.230	0.344	3.08	48
0.537	55.54	55.82	0.316	0.246	3.09	126
1.000	327.74	327.43	1.000	—	0.00	
			T = 298K			
0.000	2.67	2.67	—	1.000	0.00	
0.154	4.40	4.46	0.039	0.952	1.34	36
0.160	4.64	4.57	0.039	0.949	1.39	36
0.307	9.63	9.63	0.068	0.795	2.44	35
0.420	21.81	21.81	0.128	0.551	2.99	37
0.486	37.94	37.94	0.198	0.385	3.17	54
1.000	388.03	388.03	1.000	—	0.00	

* Mole fraction of SO_2.
† Gibbs excess free energy of mixing.

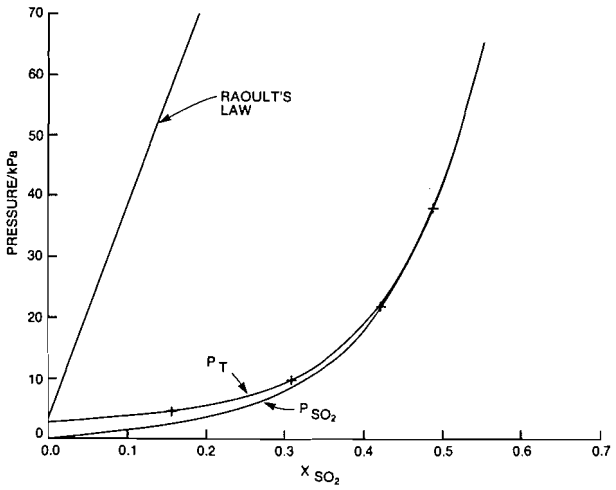

FIG. 1. Total pressure and partial vapour pressure of SO_2 above a pyridine–SO_2 solution at 25°C.

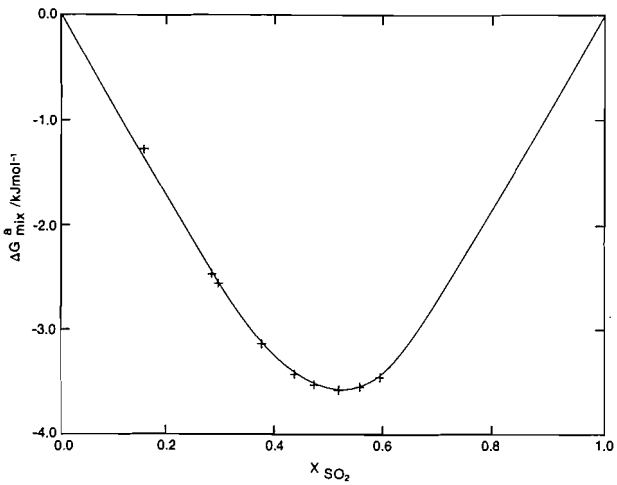

FIG. 2. Excess Gibb's free energy of mixing for a pyridine–SO_2 solution at 15°C.

$$\Delta G^e_{mix} = -RT\{X_{SO_2} \ln \gamma_{SO_2} + X_{py} \ln \gamma_{py}\}$$

and the Gibbs–Duhem equation

$$X_{SO_2} \, d \ln \gamma_{SO_2} + X_{py} \, d \ln \gamma_{py} = 0$$

the activity coefficients can be expressed as

$$\ln \gamma_{SO_2} = X^2_{py}\left\{C_1 + \sum_{i=2}^{n} C_i(2iX_{SO_2} - 1)(X_{SO_2} - X_{py})^{i-2}\right\}$$

and

$$\ln \gamma_{py} = X^2_{SO_2}\left\{C_1 + \sum_{i=2}^{n} C_i(1 - 2iX_{py})(X_{SO_2} - X_{py})^{i-2}\right\}$$

The number of parameters, n, used to fit the vapour pressure data using a non-linear least-squares method, at the six temperatures was chosen to be four. Trials were done using from two to six parameters. For the low number of data points, six parameters proved to be too high. The use of only two parameters did not produce a good fit. The use of four parameters was a compromise between a good fit and a forced fit since the number of parameters did not usually approach the number of data points. The partial vapour pressures, activity coefficients for each component, and excess free energies of mixing, ΔG^e_{mix}, obtained from these calculations are included in Table 1. The excess enthalpy and entropy of mixing, ΔH^e_{mix} and ΔS^e_{mix}, can be obtained from the data for ΔG^e_{mix} at different temperatures. The values obtained for ΔH^e_{mix} and ΔS^e_{mix} for a mole fraction of SO_2 of 0.5 are -19.9 ± 2.5 kJ mol^{-1} and -54.7 ± 9.3 J K^{-1} mol^{-1}, respectively.

Figure 2 shows ΔG^e_{mix} as a function of solution composition at 15°C. At all temperatures ΔG^e_{mix} is a minimum at a mole fraction of 0.5 ± 0.05. These results support previous Raman spectroscopic (10, 11) and phase equilibrium (8) studies that suggest the formation of a 1:1 addition compound in mixtures pyridine and sulphur dioxide.

When two components of a binary mixture form a complex, a simple equilibrium equation of the form

$$A + B \overset{K}{\rightleftharpoons} AB$$

can be used. As discussed by Prausnitz (14), it can be shown from a simple chemical theory of binary solutions that complex formation causes negative deviations from Raoult's law and results in a minimum in ΔG^e_{mix} at $X_A = 0.5$. The equilibrium constant K can be related to the activity coefficients of SO_2, using the relationship

$$\gamma_{SO_2} = \{kX_{SO_2} - 2 + 2(1 - kX_{SO_2}X_{py})^{1/2}\}/kX^2_{SO_2}$$

where

$$k = 4K/(K + 1)$$

By rearrangement, it can be shown that

$$k = (2A + B)/A^3$$

where

$$A = (X^2_{SO_2}\gamma_{SO_2} - X_{SO_2})/2$$

and

$$B = X_{SO_2}X_{py}$$

Values of K obtained by this procedure are tabulated in Table 1. These values are reasonably consistent up to a mole fraction of SO_2 of about 0.5. At higher mole fractions the procedure breaks down (in some cases K becomes negative).

The inconsistency in K values that is observed at high mole fractions may be the result of the formation of other complexes in solution. Laser Raman spectroscopic results of Adams and Dierker (5) have shown evidence for the formation of a 2:1 SO_2 to pyridine complex at mole fractions of 0.45 and above.

Nuclear magnetic resonance spectroscopy was also used to study the formation of complexes in the mixtures of SO_2 and pyridine. The addition of SO_2 to pyridine causes an upfield shift of the resonance due to the ortho protons. Using DMF as a reference, the successive chemical shifts of the *ortho* protons of the pyridine were recorded for a number of samples containing increasing amounts of SO_2. The upfield shift of the *ortho* protons can be attributed to the formation of the Py.SO_2 addition complex. Assuming rapid equilibrium, the field position will be a weighted average of the resonances for free and complexed pyridine. The data were treated using Job's method (15) and the Job's plot is illustrated in Fig. 3. The maximum observed in the Job's plot at 0.5 indicates that the 1:1 Py.SO_2 complex is the major species formed in this solution.

As described in the paper of Adams, Kruus, and Patraboy (4), the solubility data can also be used to obtain the free energy of solution from the relation

Can. J. Chem. Downloaded from www.nrcresearchpress.com by 210.87.254.105 on 09/06/12
For personal use only.

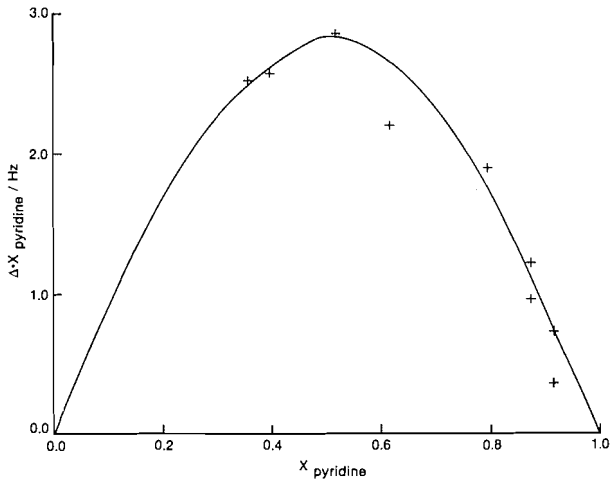

FIG. 3. Job plot for the pyridine–SO_2 system at 35°C. $\Delta = \partial_{\text{pyridine}} - \partial_{\text{obs}}$. Experimental values for *ortho* protons.

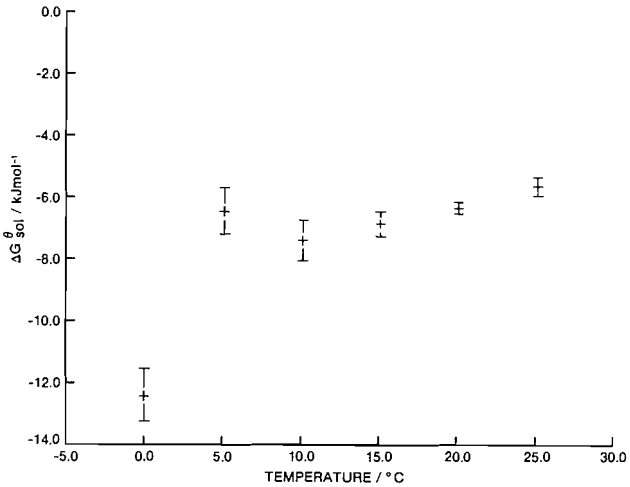

FIG. 4. $\Delta G^{\theta}_{\text{sol}}$ for SO_2 in pyridine as a function of temperature.

$$\Delta G_{\text{sol}} = -RT \ln K_c$$

where $K_c = X_{SO_2}/P_{SO_2}$. The free energy of solution at infinite dilution, $\Delta G^{\theta}_{\text{sol}}$, is obtained by extrapolating the data for ΔG_{sol} to $X_{SO_2} = 0$. The value of $\Delta G^{\theta}_{\text{sol}}$ was obtained by using a least-squares method to fit a quadratic curve to the experimental data. Because a relatively long extrapolation is required there is considerable uncertainty in the values obtained.

This uncertainty is especially high at low temperatures because the pressures being measured are very small at low mole fractions and could not be determined accurately with the apparatus used. Figure 4 shows $\Delta G^{\theta}_{\text{sol}}$ as a function of temperature.

The enthalpy and entropy of solutions can be obtained using the relationships

$$\Delta H^{\theta}_{\text{sol}} = \partial(\Delta G^{\theta}_{\text{sol}}/T)/\partial(1/T)$$

and

$$\Delta S^{\theta}_{\text{sol}} = -\partial(\Delta G^{\theta}_{\text{sol}})/\partial T$$

Because the error in $\Delta G^{\theta}_{\text{sol}}$ is considerably greater at the lower temperature than at the higher temperatures, a weighted least squares method (16) was used to fit the data. Using this method one obtains values of $\Delta H^{\theta}_{\text{sol}} = -54.6 \pm 6.6$ kJ mol^{-1} and $\Delta S^{\theta}_{\text{sol}} = -166 \pm 23$ J K^{-1} mol^{-1}. If only the four high temperature points are used, values of $\Delta H^{\theta}_{\text{sol}} = -51.6 \pm 5$ kJ mol^{-1} and $\Delta S^{\theta}_{\text{sol}} = -148 \pm 17$ J K^{-1} mol^{-1} are obtained using a simple least-squares fit. These values can be compared with the values of $\Delta H^{\theta}_{\text{sol}} = -48.5$ kJ mol^{-1} and $\Delta S^{\theta}_{\text{sol}} = -142.7$ J K^{-1} mol^{-1} obtained by Benoit and Milanova (3).

4. Conclusions

Solubility and nmr studies have shown clearly that a relatively strong 1:1 complex is formed when SO_2 is dissolved in pyridine. These results are in agreement with phase equilibrium (8) and Raman spectroscopic studies (11). The solubility data has been analyzed to determine partial vapour pressures, activity coefficients, and thermodynamic functions for binary mixtures of SO_2 in pyridine.

5. Acknowledgements

The authors wish to thank T. Patraboy, W. A. Adams, and P. Kruus for helpful advice.

1. R. V. MOSHTEV and P. ZLATILOVA. Electrochim. Acta, **27**, 1107 (1982).
2. G. DI MASI and J. CHRISTOPULOS. Proc. 28th Power Sources Symposium. 1978. p. 179.
3. R. L. BENOIT and E. MILANOVA. Can. J. Chem. **57**, 1319 (1979).
4. W. A. ADAMS, P. KRUUS, and T. J. PATRABOY. Can. J. Chem. **61**, 37 (1983).
5. W. A. ADAMS and L. DIERKER. Unpublished results.
6. L. C. BATEMAN, E. D. HUGHES, and C. K. INGOLD. J. Chem. Soc. 243 (1944).
7. A. E. HILL and T. B. FITZGERALD. J. Am. Chem. Soc. **57**, 250 (1935).
8. K. R. HOFFMAN and C. A. VAN DER WERF. J. Am. Chem. Soc. **68**, 997 (1946).
9. J. A. MOEDE and C. CURRAN. J. Am. Chem. Soc. **71**, 852 (1949).
10. A. TRAMER. Bull. Acad. Pol. Sci. Cl III, **4**, 355 (1956); **5**, 501 (1957); **5**, 509 (1957).
11. Z. PAWELKA, G. MAES, and TH. ZEEGERS-HUYSKENS. J. Phys. Chem. **85**, 3431 (1981).
12. J. W. LORIMER, B. C. SMITH, and G. H. SMITH. J. Chem. Soc. Faraday Trans. 1, **71**, 2232 (1975).
13. T. J. PATRABOY. B.Sc. Honours Report. Carleton University, Ottawa. 1981.
14. J. M. PRAUSNITZ. Molecular thermodynamics of fluid-phase equilibria. Prentice-Hall Inc., Englewood Cliff, NJ. 1969.
15. G. H. NANCOLLAS. Interactions in electrolyte solutions. Elsevier Publishing Co., Amsterdam. 1966. p. 90.
16. P. R. BEVINGTON. Data reduction and error analysis for the physical sciences. McGraw Hill Inc., New York. 1969. p. 118.

Can. J. Chem. Downloaded from www.nrcresearchpress.com by 210.87.254.105 on 09/06/12
For personal use only.

Effects of added cations on rate enhancements for the nickel(II)−PADA reaction in micellar solutions

JOANNE R. HICKS AND VINCENT C. REINSBOROUGH
Chemistry Department, Mount Allison University, Sackville, N.B., Canada E0A 3C0

Received October 17, 1983

JOANNE R. HICKS and VINCENT C. REINSBOROUGH. Can. J. Chem. **62**, 990 (1984).

Rate enhancements of the Ni^{2+}−PADA bidentate formation reaction have been obtained at 25.0°C in anionic micellar solutions with added electrolyte. Sodium dodecylsulfate, sodium octanesulfonate, and sodium octylsulfate were the surfactants employed and Na^+, Ca^{2+}, and Mg^{2+} were the added cations. Kinetic analyses revealed that the chief effect in leading to a decreased rate enhancement with salt present was a lowering of the surface potential manifested by an increase in the reaction volume. The binding of the Ni^{2+} ion to the micelles showed little change beyond an initial drop with the lowest Na^+ addition with sodium dodecylsulfate. The binding of the hydrophobic reagent PADA decreased more gradually but not sufficiently to account for the reduction in rate enhancements. In the presence of Ca^{2+} or Mg^{2+} ions, the rate enhancements and the kinetic parameters did not show unusual behaviour except that Mg^{2+} ion appeared to be slightly more effective in excluding Ni^{2+} ion from the micellar surface region. The sphere-to-rod micellar transformation that occurs at 0.4 mol dm^{-3} Na^+ does not have a pronounced effect on the micellar surface region.

JOANNE R. HICKS et VINCENT C. REINSBOROUGH. Can. J. Chem. **62**, 990 (1984).

Opérant à 25°C, dans une solution micellaire anionique contenant un électrolyte ajouté, on a déterminé les accroissements de vitesse de réaction pour la formation du bidentate Ni^{2+}−PADA. Les agents de surface utilisés sont les dodécylsulfate, octylsulfonate et octylsulfate de sodium et les cations ajoutés sont les ions Na^+, Ca^{2+} et Mg^{2+}. Les analyses cinétiques ont révélé que l'effet principal conduisant à une diminution de l'accroissement de vitesse avec le sel présent est un abaissement du potentiel de surface qui se manifeste par une augmentation du volume de la réaction. Avec le dodécylsulfate de sodium, la liaison de l'ion Ni^{2+} avec les micelles ne change pas beaucoup au delà d'une chute initiale avec la plus faible addition de Na^+. La liaison du réactif hydrophobe PADA décroit plus graduellement mais pas suffisamment pour intervenir dans la diminution des accroissements de vitesse. En présence des ions Ca^{2+} ou Mg^{2+}, les accroissements de vitesse et les paramètres cinétiques ne révèlent pas de comportement inhabituel à l'exception des ions Mg^{2+} qui semblent légèrement plus efficaces dans l'exclusion des ions Ni^{2+} de la région de la surface micellaire. La transformation micellaire de la forme sphère à la forme de bâtonnet qui se produit à une concentration en ion Na^+ de 0,4 mol dm^{-3} n'a pas d'effet marqué sur la région de la surface micellaire.

[Traduit par le journal]

Can. J. Chem. Downloaded from www.nrcresearchpress.com by 210.87.254.42 on 09/06/12
For personal use only.

Introduction

Added salt generally decreases micellar rate enhancements (1−3). The extra counterions can effectively compete with ionic reagents for micellar sites, thus lowering the surface potential. This decrease in rate occurs despite the increase in aggregation number which accompanies salt addition and which by itself should favour greater solubilization of hydrophobic reagents to give larger rate enhancements. The bidentate formation reaction that occurs with $Ni^{2+}_{(aq)}$ and pyridine-2-azo-*p*-dimethylaniline (PADA) involves both an ionic and a hydrophobic reagent and the kinetic model developed by Robinson and co-workers (3, 4) from Berezin's original concept (5) allows the influence of each reagent on the pronounced rate enhancements to be evaluated separately and quantitatively. This reaction is then well suited for such a kinetic analysis whereby the effects of added salt on rate enhancements might be better understood in terms of each reagent's contribution. This reaction can also serve kinetically as a probe of the micellar surface region (6) and, in this context, should shed light on any changes occurring in the surface region as the micelles undergo structural changes on salt addition. Thus, the main purposes of this project were to discover why basically rate enhancements in micellar solutions decreased with salt additions when one reagent was ionic and the other hydrophobic and how the micellar surface region was affected by the sphere-to-rod transition that occurs in salt-doped surfactant solutions.

Experimental

The kinetic rate constants (k_{obs}) for the Ni^{2+}−PADA reaction were measured at pH 7.8−8.0 by the stopped-flow technique under pseudo-first order conditions (usually 1.0×10^{-3} mol dm^{-3} Ni^{2+} and 1×10^{-5} mol dm^{-3} PADA). Details of the method and apparatus are given elsewhere (4, 6, 7). Activation energies for the reaction were measured in $NaNO_3$-doped solutions to ensure that the rate-determining step was still the ejection of water from hydrated Ni^{2+} ion. The results were always confirmatory.

Salt additions were made with nitrates rather than chlorides since the latter complexed with $Ni^{2+}_{(aq)}$ in the time range of the stopped-flow determinations (dead-time was approximately 3 ms).

Chemicals were supplied by Sigma Chemicals (sodium octanesulfonate and PADA), Fisher Scientific (sodium octylsulfate and the inorganic salts) and BDH (specially pure sodium dodecylsulfate). They were used without further purification.

Results and discussion

In the presence of anionic micelles, the Ni^{2+}−PADA reaction takes place in two media, bulk water and the surface region of the micelles. In the latter, the two reagents are preferentially adsorbed, one electrostatically and the other chiefly by hydrophobic attraction. Any rate enhancement that is observed in micellar solution will depend on how strongly each reagent is bound to the micelle where sheer proximity of the two ensures a faster reaction rate. If one reagent is very weakly bound to the micelle, the rate enhancement will not be pronounced no matter how strongly the other reagent is partitioning into the micelle. The kinetic expression that embodies all of this quantitatively at constant pH is the following (8, 9):

$$[1] \quad k_{obs} = k_1^m[Ni^{2+}]/(CV_s\{1 + (CK_{Ni})^{-1}\}\{1 + (CK_{PADA})^{-1}\}) + k_{-1}^m$$

where k_{obs} is the observed first-order rate constant; k_1^m and k_{-1}^m,

Can. J. Chem. Downloaded from www.nrcresearchpress.com by 210.87.254.42 on 09/06/12
For personal use only.

the forward and backward rate constants for the reaction on the micelle surface; C, the surfactant concentration in the micelles in mol dm^{-3}; K_{Ni} and K_{PADA}, the binding constants for each reagent to the micelles; and V_s, the reaction volume in dm^3 per mole of surfactant. The kinetics of the reaction occurring in the bulk water phase is given by a similar equation. However, since the observed kinetic trace was analyzed only for the faster pseudo-first order rate constant, eq. [1] need only be considered.

Approximating k_1^m and k_{-1}^m by the corresponding rate constants in water has been shown to be reasonable (3, 10) and has even been invoked in alcoholic micellar systems (11). This assumption is difficult to test directly since all the quantities in eq. [1] cannot be independently obtained experimentally. However, the continued adequacy of this equation to represent micellar rate enhancements quantitatively and, in particular, to yield reasonable V_s values (the only quantity that is as yet inaccessible to experimental verification) argues for the validity of the approximation. An additional re-assurance in the present case is that the activation energy for the probe reaction is unaltered from the water situation when salt is introduced to the micellar systems.

The partitioning or binding constant, K_{PADA}, is defined as $[PADA]_M/C[PADA]_W$ where the two PADA concentrations are those for the micellar and aqueous "phases". K_{Ni} is similarly expressed. These constants can be obtained independently of the kinetic data. For example, K_{PADA} can be determined through solubility measurements (4, 8, 9) and K_{Ni} by the murexide technique (12, 13). For short-chained surfactants especially, the murexide technique is open to much uncertainty because estimates of the activity coefficients are necessary. Consequently, it is more convenient and as accurate to obtain K_{Ni} by computer-fitting the k_{obs} data to eq. [1] using K_{PADA} values from solubility measurements with V_s as variable also.

The reaction volume cannot yet be independently measured. Berezin (5) approximated V_s by the molar volume of the surfactant. In the pseudo-phase ion exchange model for micellar catalysis, the reaction is assumed to occur only in the Stern layer of the micelle which for sodium dodecylsulfate is 0.14 dm^3 mol^{-1} or about half the molar volume (2). This strictly defined reaction volume, issuing from a model that precludes much flexibility and dynamism in micelle structure, cannot easily accommodate k_{obs} data for short-chained surfactants where V_s values are often two to three times the molar volume (8, 9). This may be at the heart of recently reported "failures" of the pseudo-phase model (14, 15). We prefer to allow V_s to seek its own value in accordance with eq. [1] where, with surfactants of medium chain length (about 12 carbons) or greater, the Berezin estimate of the molar volume is invariably found. Given the present dynamic view of micelles where monomers are continually partially popping out into the solution (16), a reaction volume for a micellar surface becomes difficult to define especially where a hydrophobic reagent may be deeply embedded in the core of the micelle.

The k_{obs} data are more conveniently plotted as k_1^{app}/k_1^w where k_1^{app} is the apparent rate constant (coefficient of $[Ni^{2+}]$ in eq. [1]). This ratio of rate constants (R) is a direct measure of the rate enhancement achieved in the presence of micelles. The value of k_1^w increases with increasing ionic strength from 1.20 $\pm$ 0.05 $\times$ 10^3 dm^3 mol^{-1} s^{-1} with no added salt to 1.78 $\pm$ 0.05 $\times$ 10^3 dm^3 mol^{-1} s^{-1} at 0.80 mol dm^{-3} $NaNO_3$.

In Fig. 1 are shown the R values for sodium dodecylsulfate (SLS) solutions for the probe reaction at 25.0°C for $NaNO_3$ additions in the range 0.10–0.80 mol dm^{-3}. The maximum in

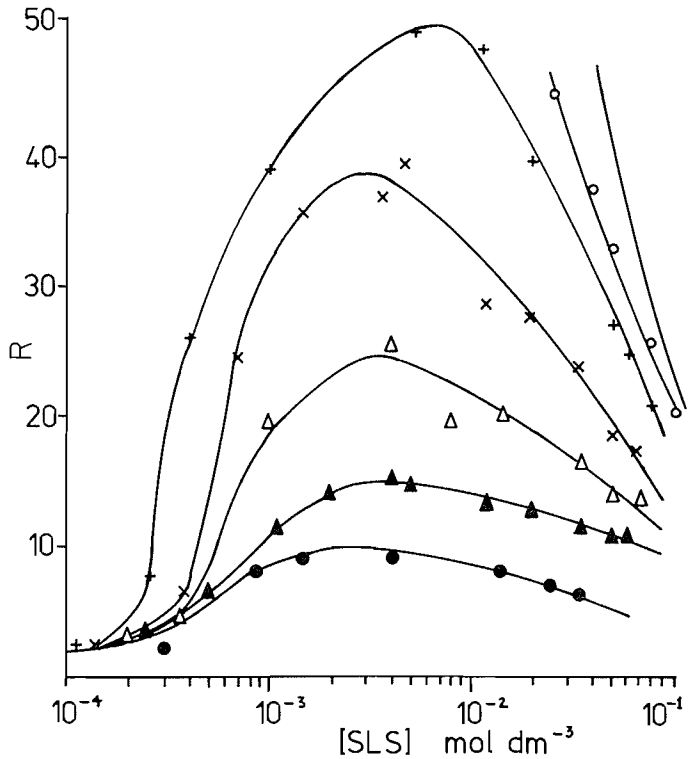

FIG. 1. Rate enhancements (R) in SLS solutions with added salt: ○, 0.10 mol dm^{-3} Na^+; +, 0.20 mol dm^{-3} Na^+; ×, 0.30 mol dm^{-3}; △, 0.40 mol dm^{-3} Na^+; ▲, 0.60 mol dm^{-3} Na^+; ●, 0.80 mol dm^{-3} Na^+. The top line to the right is the pure solution curve.

the R curve for 0.10 mol dm^{-3} $NaNO_3$ additions was inaccessible to the stopped-flow apparatus but could be sketched for the other salt additions. It is clear that added electrolyte strongly depresses the rate enhancements with the maximum in R in the presence of 0.80 mol dm^{-3} $NaNO_3$ being only 1% of the corresponding R for pure SLS. Salt additions also shifted the critical micelle concentrations (CMC) and the maximum value of R to progressively lower concentrations.

Complete kinetic analyses according to eq. [1] were conducted on each of the systems depicted in Fig. 1 and the resulting fitted values of K_{Ni} and V_s along with the K_{PADA} values obtained through solubility measurements were listed in Table 1.

The major change that apparently occurs in Na^+ ion addition in SLS solutions is an increase in the volume of reaction (see Fig. 2). Little change from the molar volume of SLS ($\approx$0.3 dm^3 mol^{-1}) occurs until 0.2–0.3 mol dm^{-3} Na^+ is present but then V_s increases quite markedly until at 0.8 mol dm^{-3}, V_s is 10 times the pure surfactant value. It is well known that salt addition causes an increase in aggregation number in SLS micellar solutions (17–20) and that, around 0.4 mol dm^{-3} in Na^+ ion, the spherical SLS micelles become rod-like in structure (17, 18, 21). A case can be made from Fig. 2 for a structural change of some sort in the 0.2–0.4 mol dm^{-3} Na^+ region. It is not clear, however, how V_s should be affected by changes in aggregation number and in structure. V_s values increase on descending a homologous series of surfactants until, with the most weakly forming ones, V_s values are several times the molar volumes of the surfactants themselves (8, 9). In this same direction, micellar surface potentials rapidly decrease. Zachariasse *et al.* (22) have noted that the surface polarity of SLS micelles changes only slightly to 0.25 mol dm^{-3} Na^+ ion

TABLE 1. Rate enhancement parameters for anionic surfactants with added salt

Surfactant	Added cation (mol dm^{-3})	K_{PADA} (dm^3 mol^{-1})	K_{Ni} (dm^3 mol^{-1})	V_s (dm^3 mol^{-1})
SLS	—	2800	650	0.29
	0.10 Na^+	800	40	0.35
	0.20 Na^+	600	41	0.48
	0.30 Na^+	530	50	0.74
	0.40 Na^+	440	53	1.07
	0.60 Na^+	370	55	1.78
	0.80 Na^+	310	60	2.84
SOSO	—	160	22	0.70
	0.10 Na^+	150	26	0.62
	0.50 Na^+	80	26	1.29
SOS	—	300	11	0.55
	0.50 Na^+	210	16	1.32
	0.05 Ca^{2+}	200	12	0.55
	0.10 Ca^{2+}	180	14	0.82
	0.10 Mg^{2+}	180	6	0.48

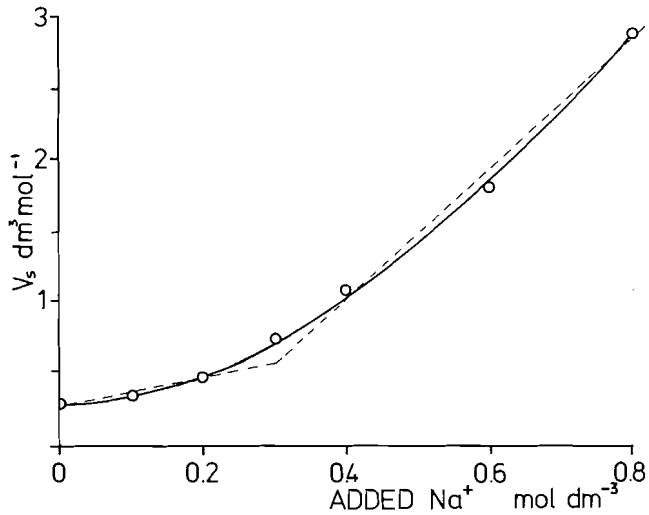

FIG. 2. Reaction volumes (V_s) in SLS solutions with varying amounts of added Na^+ ion.

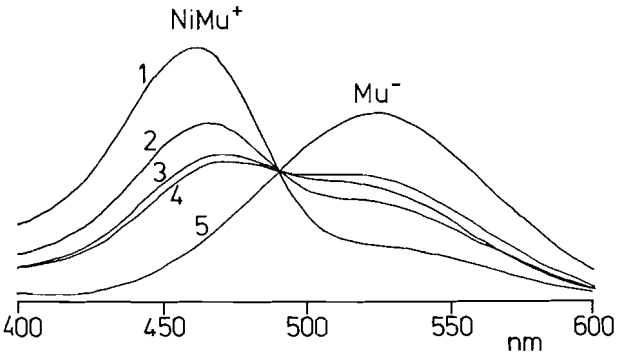

FIG. 3. Spectra of Ni^{2+} and murexide ion (Mu^-) in salt-doped SLS solutions at 25.0°C. $[Mu^-] = 2.10 \times 10^{-5}$ mol dm^{-3} and $[Ni^{2+}] = 2 \times 10^{-3}$ mol dm^{-3}. pH = 3.9 − 4.2. (*1*) No additives, (*2*) 0.20 mol dm^{-3} Na^+, (*3*) 0.05 mol dm^{-3} SLS and 0.40 mol dm^{-3} Na^+, (*4*) 0.05 mol dm^{-3} SLS and 0.02 mol dm^{-3} Na^+, and (*5*) 0.05 mol dm^{-3} SLS with no added salt.

followed by a rapid decrease with further salt additions. V_s is a measure of the volume per mole of surfactant accessible to reaction so that the product CV_s defines the volume fraction of the solution in which the probe reaction occurs. The lowered surface potential will result in the reactant species being less closely bound in the micellar surface region which will then extend further into the solution. The reactants on the surface will have been effectively diluted and the rate enhancements will not be as pronounced as with surfactant in water alone.

The increase in V_s is accompanied by changes in K_{Ni} and K_{PADA} which act in the same direction on the rate enhancements. These are undoubtedly inter-related and influenced by the decrease in micellar surface potential. K_{Ni} is most obviously affected with the Ni^{2+} ion being less attracted into the micellar surface region. The first Na^+ ion addition of 0.10 mol dm^{-3} reduces K_{Ni} to less than 10% of its value in pure SLS solutions (Table 1) but further Na^+ ion additions do not further change K_{Ni}. The two positively charged ions compete for surface sites and the presence of 0.10 mol dm^{-3} Na^+ ion with 10^{-3} mol dm^{-3} Ni^{2+} ion radically lowers the Ni^{2+} ion concentration in the surface region. Increasing the salt content further causes little further change in K_{Ni}, in part due to the compensating increase in V_S.

This was tested by examining Ni^{2+} − murexide spectra in various salt-doped SLS solutions. One such series of spectra is given in Fig. 3. With no SLS present, $NiMu^+$ is the predominant species in the visible spectrum (460 nm) but, in micellar SLS solutions, the Ni^{2+} ion is adsorbed into the micellar surface region, reversing the $NiMu^+$ equilibrium, and essentially only the Mu^- peak at 525 nm is found. Adding 0.02 mol dm^{-3} $NaNO_3$ to the latter system dramatically restores the equilibrium to an intermediate position. Of course, in 0.02 mol dm^{-3} Na^+ ion solution, the ratio of Na^+ ion to Ni^{2+} ion is at least 20 to 1 (augmented slightly by Na^+ ions from the surfactant) so that the Na^+ ion despite its lower charge competes successfully for surface sites. This sharp drop in K_{Ni} with low salt additions of only 0.10 mol dm^{-3} Na^+ ion is thus not unreasonable. The spectra for the two Na^+ ion solutions are almost the same confirming that K_{Ni} undergoes little further change with increasing salt additions.

The solubility data from PADA and hence K_{PADA} reveal that the hydrophobic reagent is bound less strongly to micelles with increasing Na^+ ion solution content. This decrease in K_{PADA}, which is much smoother and less dramatic than with K_{Ni}, may

Can. J. Chem. Downloaded from www.nrcresearchpress.com by 210.87.254.42 on 09/06/12
For personal use only.

Can. J. Chem. Downloaded from www.nrcresearchpress.com by 210.87.254.42 on 09/06/12
For personal use only.

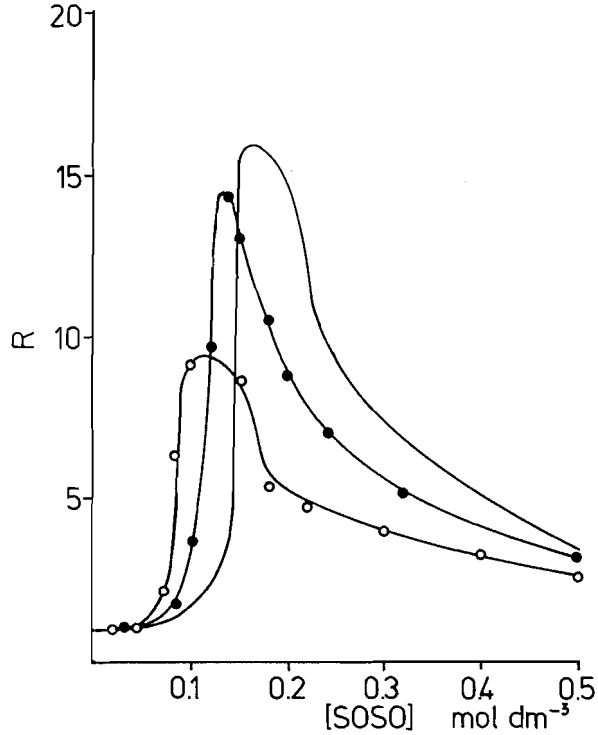

FIG. 4. Rate enhancements (R) for SOSO solutions with added Na^+: ●, 0.10 mol dm^{-3}; ○, 0.50 mol dm^{-3}. The top curve is the pure SOSO curve.

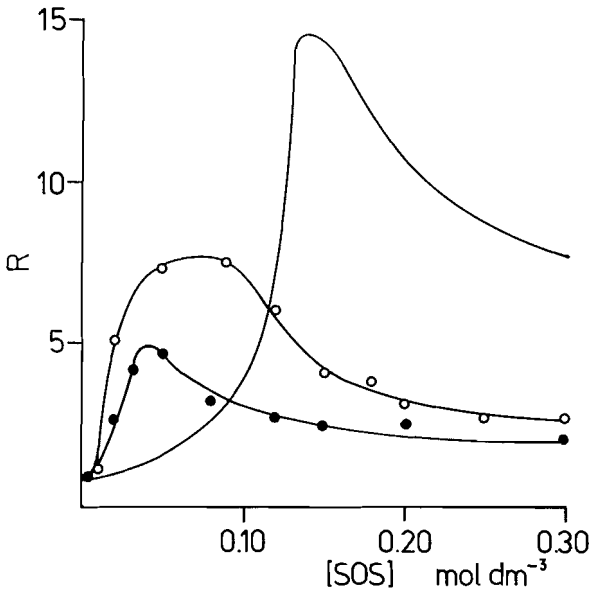

FIG. 5. Rate enhancements (R) for SOS solutions with added Na^+: ○, 0.20 mol dm^{-3}; ●, 0.50 mol dm^{-3}. The top curve is the pure SOS curve.

simply be an activity coefficient effect with some input from the decreased surface polarity since PADA is slightly polar.

Rate enhancements were also measured in salt-doped sodium octanesulfonate (SOSO) and sodium octylsulphate (SOS) micellar solutions. These short-chained surfactants have high CMC values and thus contribute substantial Na^+ ion amounts, often in excess of the added electrolyte, to the total Na^+ ion concentration. Thus, the near constant ionic strength situation that prevailed in salt-doped SLS micellar systems does not hold here. Nevertheless, the results are informative in a comparative sense since the rate enhancements in the pure and salt-doped short-chained surfactant systems were measured under the same conditions.

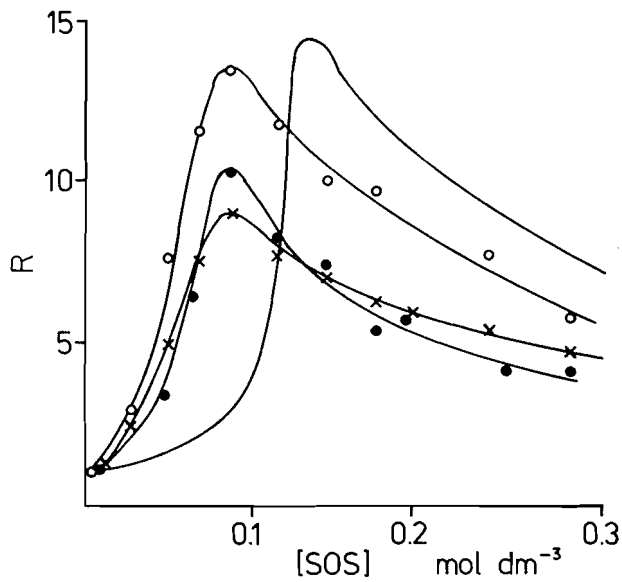

FIG. 6. Rate enhancements (R) for SOS solutions with added Ca^{2+} and Mg^{2+}: ○, 0.05 mol dm^{-3} Ca^{2+}; ●, 0.10 mol dm^{-3} Ca^{2+}; ×, 0.10 mol dm^{-3} Mg^{2+}. The top curve is the pure SOS curve.

Figures 4 and 5 show the rate enhancements for the Ni^{2+}–PADA reactions in SOSO and SOS solutions with added Na^+ ion. The R curves were similar in behavior to the salt-doped SLS system. The complete kinetic analysis was performed with representative salt systems for each surfactant and the values of the parameters displayed the same trends as with SLS solutions (Table 1). For example, with 0.50 mol dm^{-3} $NaNO_3$ in SOSO solutions, K_{PADA} declined a third from the pure solution value, K_{Ni} remained the same and V_s increased threefold. The binding of Ni^{2+} in pure SOS micellar solutions is already weak due to the 100-fold excess of Na^+ ion from the surfactant itself. In this respect there is a difference from the SLS system because further additions of Na^+ ion through $NaNO_3$ to SOS solutions will have little further effect on K_{Ni} while even small Na^+ ion additions of the order of 0.02 mol dm^{-3} causes K_{Ni} in SLS solutions to plunge from the pure solution value to a relatively constant value.

Calcium and magnesium additions were also made to micellar SOS solutions. Raman spectra studies had indicated that Ca^{2+} ion but not Mg^{2+} nor Na^+ ion binds to the sulfate head group of the micellar surfactant (23). If this complexing evidence in Raman time (ca. 10^{-10} s) were to persist in stopped-flow time (10^{-3} s), then negative charge centres in the micellar surface region would be eliminated to produce considerably lower rate enhancements with Ca^{2+} ion than with either of the other two ions. The R curves for two Ca^{2+} ion and one Mg^{2+} ion series of additions to SOS are shown in Fig. 6. Complete kinetic analyses were conducted on all three and the resulting parameters listed in Table 1. It is clear that Ca^{2+} ion has no more effect on R than Na^+ ion of double the concentration or Mg^{2+} ion. Either the complexation rates of Ca^{2+} with the sulfate head group are more rapid than can be seen in the stopped-flow technique or else the lowering of the surface potential induced by foreign cations is not determined by whether an actual bond forms with micellar charge centres.

Magnesium ion appears to influence the rate enhancements in slightly different fashion than either Ca^{2+} ion or Na^{+} ion. The kinetic analysis reveals that K_{Ni} is about half the pure solutions value with Mg^{2+} ion present and V_s is relatively unchanged. Apparently, the greater charge density of unhydrated Mg^{2+} ions over either Ca^{2+} and Ni^{2+} ions which are roughly the same size gives Mg^{2+} ion a competitive edge over Ni^{2+} ions for surface sites that Ca^{2+} ions do not enjoy.

Acknowledgement

Financial aid from the Natural Sciences and Engineering Research Council of Canada made this research possible.

1. J. H. FENDLER and E. J. FENDLER. Catalysis in micellar and macromolecular systems. Academic Press, New York. 1975. p. 91.
2. C. A. BUNTON and L. S. ROMSTED. *In* Solution behaviour of surfactants. *Edited by* K. L. Mittal and E. J. Fendler. Plenum Press, New York. 1982. p. 975.
3. A. D. JAMES and B. H. ROBINSON. J. Chem. Soc. Faraday Trans. 1, **74**, 10 (1978).
4. V. C. REINSBOROUGH and B. H. ROBINSON. J. Chem. Soc. Faraday Trans. 1, **75**, 2395 (1979).
5. K. MARTINEK, A. K. YATSIMIRSKI, A. V. LEVASHOV, and I. V. BEREZIN. *In* Micellization, solubilization and microemulsions. Vol. 2. *Edited by* K. L. Mittal. Plenum Press, New York. 1977. p. 489.
6. J. R. HICKS and V. C. REINSBOROUGH. *In* Surfactants in solution. *Edited by* K. L. Mittal and B. Lindman. Plenum Press, New York. In press.
7. B. H. ROBINSON, N. C. WHITE, and C. MATEO. Adv. Mol. Relaxation Processes. **7**, 321 (1975).
8. P. D. I. FLETCHER and V. C. REINSBOROUGH. Can. J. Chem. **59**, 1361 (1981).
9. J. R. HICKS and V. C. REINSBOROUGH. Aust. J. Chem. **35**, 15 (1982).
10. B. H. ROBINSON and N. C. WHITE. J. Chem. Soc. Faraday Trans. 1, **74**, 2625 (1978).
11. P. D. I. FLETCHER and B. H. ROBINSON. J. Chem. Soc. Faraday Trans. 1, **79**, 1959 (1983).
12. M. FISCHER, W. KNOCHE, B. H. ROBINSON, and J. WEDDERBURN. J. Chem. Soc. Faraday Trans. 1, **75**, 119 (1979).
13. M. FISCHER, W. KNOCHE, P. D. I. FLETCHER, B. H. ROBINSON, and N. C. WHITE. Colloid Polym. Sci. **258**, 733 (1980).
14. T. J. BROXTON and D. B. SANGO. Aust. J. Chem. **36**, 711 (1983).
15. F. NOME, A. F. RUBIRA, C. FRANCO, and L. G. IONESCU. J. Phys. Chem. **86**, 1881 (1982).
16. G. E. A. ANIANSSON. J. Phys. Chem. **82**, 2805 (1978).
17. N. A. MAZER, G. B. BENEDEK, and M. C. CAREY. J. Phys. Chem. **80**, 1075 (1976).
18. C. Y. YOUNG, P. J. MISSEL, N. A. MAZER, G. B. BENEDEK, and M. C. CAREY. J. Phys. Chem. **82**, 1375 (1978).
19. P. LIANOS and R. ZANA. J. Colloid Interface Sci. **84**, 100 (1981).
20. M. ALMGREN and J.-E. LÖFROTH. J. Colloid Interface Sci. **81**, 486 (1981).
21. N. A. MAZER and G. OLOFSSON. J. Phys. Chem. **86**, 4584 (1982).
22. K. A. ZACHARIASSE, N. V. PHUC, and B. KOZANKIEWICZ. J. Phys. Chem. **85**, 2676 (1981).
23. M. H. BROOKER, D. J. JOBE, and V. C. REINSBOROUGH. J. Chem. Soc. Faraday Trans. 1. In press.

Can. J. Chem. Downloaded from www.nrcresearchpress.com by 210.87.254.42 on 09/06/12
For personal use only.

Protonation de l'adénine, de la purine et de l'adénosine en milieu acide fort[1]

ROBERT L. BENOIT ET MONIQUE FRÉCHETTE
Département de chimie, Université de Montréal, C. P. 6210, Succ. A, Montréal (Qué.), Canada H3C 3V1

Reçu le 29 août 1983

ROBERT L. BENOIT et MONIQUE FRÉCHETTE. Can. J. Chem. **62**, 995 (1984).

Faisant suite à une valeur proposée pour l'enthalpie de seconde protonation de l'adénine, on a étudié par ealorimétrie et spectroscopie rmn la protonation des bases B biologiquement importantes: adénine, purine, adénosine, et incidemment, celle de l'imidazole et de l'amino-3 pyridine. Les chaleurs de dissolution des bases solides et les déplacements chimiques de leurs protons et carbones-13 ont été déterminés en fonction des concentrations des acides $HClO_4$ et H_2SO_4. Nos résultats démontrent que contrairement à une utilisation antérieure, un effet de milieu important rend impossible l'emploi des données calorimétriques pour calculer les fonctions thermodynamiques des réactions de protonation. D'un autre côté, les données de carbone-13 ont été interprétées avec succès en utilisant la méthode de Cox et Yates dite "excess acidity". Les valeurs obtenues pour $pK_{BH_2^{2+}}$ et $pK_{BH_3^{3+}}$ sont respectivement: adénine −0,43, −4,23, purine −1,66, < −6, adénosine −1,4 avec hydrolyse du glucoside. Les sites de protonation ont été confirmés comme étant essentiellement sur le cycle imidazole pour la seconde protonation et sur le cycle pyrimidine (N-3) pour la troisième.

ROBERT L. BENOIT and MONIQUE FRÉCHETTE. Can. J. Chem. **62**, 995 (1984).

In view of a previously proposed enthalpy value for the second protonation of adenine, a calorimetric and nmr spectroscopic study has been made of the protonation of biologically important bases B: adenine, purine, adenosine and, incidentally, that of imidazole and 3-amino pyridine. Heats of solution of the solid bases, and their carbon-13 and proton chemical shifts were determined as a function of $HClO_4$ and H_2SO_4 concentration. Our results demonstrate that, contrary to previous usage, a strong medium effect precludes the use of the calorimetric results to calculate the thermodynamic functions for the protonation reactions. On the other hand, the carbon-13 nmr data are successfully interpreted on the basis of the Cox and Yates excess acidity method. The values obtained for $pK_{BH_2^{2+}}$ and $pK_{BH_3^{3+}}$ are, respectively: adenine −0.43, −4.23, purine −1.66, < −6, adenosine −1.4 with hydrolytic cleavage of the glycosidic bond. The protonation sites are confirmed as being essentially on the imidazole ring for the second protonation and on the pyrimidine ring (N-3) for the third one.

L'adénine, une base importante dans les systèmes biologiques, et particulièrement ses réactions avec le proton et les ions métalliques ont fait l'objet de nombreuses études. Le caractère basique des 3 azotes hétérocycliques, N-1, N-3 et N-7 a été mis en évidence ainsi que des relations complexes entre les basicités relatives de ces 3 azotes et la nature de l'acide de Lewis. Avec le proton en solution diluée, l'adénine (amino-6 purine) réagit en N-1 (1, 2) et les caractéristiques thermodynamiques associées à cette réaction de protonation sont connues: pK_1 = 4,19 et $\Delta H_1 = -21{,}2$ kJ mol^{-1} (3).

La molécule d'adénine avec ses trois sites basiques peut aussi réagir successivement avec plusieurs ions H^+. Ainsi, des sels d'adénine diprotonée (N-1 et N-7) (4) ont été caractérisés par cristallographie aux rayons-X. Dans les solvants non-aqueux acides HCF_3CO_2 et HSO_3F, Wagner et von Philipsborn (5) ont identifié par rmn du proton à différentes températures, les cations diprotonés (N-1 et N-7) et triprotonés (N-1, N-7 et N-3) respectivement. En solution aqueuse, Budo et Tomasz (6) ont utilisé les faibles différences spectrales dans l'uv pour calculer une valeur $pK = -0{,}35$ pour le cation diprotoné. La seule étude calorimétrique concernant les seconde et troisième protonations de l'adénine est, à notre connaissance, l'étude de Kilday (7) en milieu HCl concentré. Cet auteur propose pour l'enthalpie ΔH_2 une valeur de +7,9 kJ mol^{-1} et suggère la possibilité d'une troisième protonation pour des concentrations de HCl supérieures à 5 *M*.

Dans notre travail, nous avons cherché à caractériser plus précisément les deuxième et troisième étapes de protonation de l'adénine. Nous avons d'abord évalué les résultats calorimétriques et l'interprétation de Kilday en déterminant, comme cet auteur, la chaleur de dissolution de l'adénine solide dans des solutions concentrées d'acide mais en utilisant $HClO_4$ et H_2SO_4. Devant les difficultés d'interprétation de nos résultats et notre mise en question des conclusions de Kilday, nous avons alors procédé à une étude de la protonation de l'adénine dans $HClO_4$ et H_2SO_4 concentrés par spectroscopies rmn du proton et du carbone-13. Afin d'évaluer la validité des méthodes calorimétriques et spectroscopiques de détermination de pK en milieu acide fort, nous avons étudié par ces deux méthodes le comportement de l'imidazole, pK = 7,2 (8) et la seconde protonation de l'amino-3 pyridine dont le pK_2 (−1,4) a déjà été établi par spectroscopie uv (9).

Nous avons aussi étendu notre étude en examinant par les mêmes méthodes la protonation de deux autres composés voisins de l'adénine, l'adénosine et la purine. Aucune donnée thermodynamique ne semble disponible pour l'adénosine, mais pour la purine Schumacher et Günther (10) ont tout récemment évalué le pK du cation diprotoné (N-1 et N-7/N-9) à −1,5 à partir des faibles variations des constantes de couplage du ^{13}C et ^1H dans D_2SO_4.

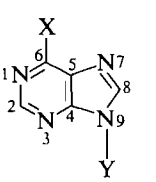

Adénine (Ade): X = NH_2, Y = H
Adénosine (Ado): X = NH_2, Y = D-ribose
Purine (Pur): X = H, Y = H

Partie expérimentale

Réactifs

L'adénine et l'adénosine (Aldrich) et la purine (Sigma) ont été utilisées sans purification ultérieure. Le titrage acidimétrique des bases par une solution de $HClO_4$ dans l'acide acétique indique une pureté de 99,5 ± 0,5%. L'amino-3 pyridine et l'imidazole (Aldrich) ont été recristallisés et séchés, ils titrent 99,9 ± 0,3%.

Les solutions aqueuses de HCl, $HClO_4$ et H_2SO_4 ont été préparées par dilution de solutions de concentrations connues. Les solutions de $NaClO_4$ ont été obtenues par neutralisation de solutions de $HClO_4$

[1] Partiellement présenté au Minisymposium de Chimie Organique Physique, Montréal, 1–3 octobre 1982.

Can. J. Chem. Downloaded from www.nrcresearchpress.com by 210.87.254.6 on 09/06/12
For personal use only.

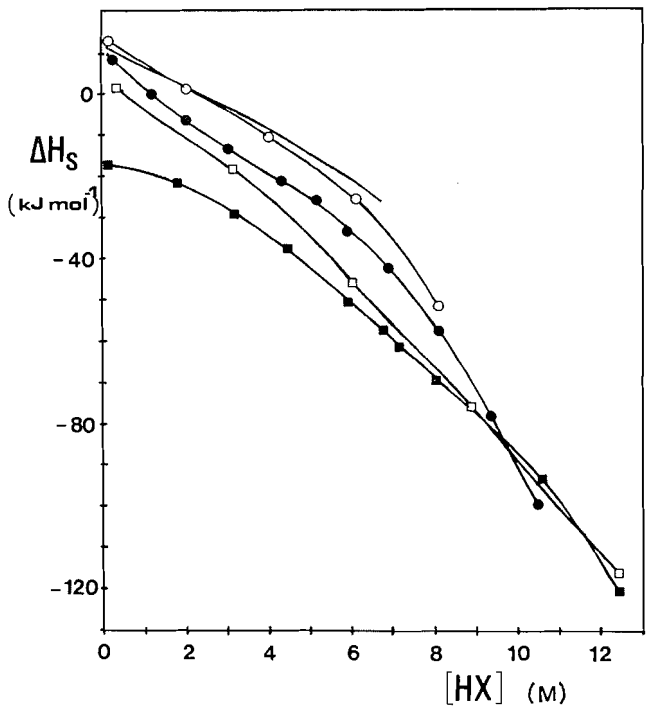

FIG. 1. Chaleurs de dissolution, ΔH_s, de l'Ade, l'Ado et l'Ampy en fonction de la concentration d'acide, [HX]. Ade–HCl (—), Ade–$HClO_4$ (●), Ade–H_2SO_4 (□), Ado–$HClO_4$ (○), Ampy–H_2SO_4 (■).

titrées par Na_2CO_3 (McArthur) jusque pH = 6, les solutions ont été filtrées puis diluées.

Mesures

Calorimétrie

Les chaleurs de dissolution de poids connus (0,035–0,125 g) des bases solides dans 100 mL de solutions d'acides de concentrations connues ont été mesurées à 25,00 ± 0,01°C avec un calorimètre isopéribolique LKB (modèle 8721-1). Le système calorimétrique précédemment décrit (11) a été légèrement modifié. La cellule utilisée est de 100 mL. La thermistance de 2000 Ω constitue l'une des branches du pont de Wheatstone. Le circuit électrique est alimenté par une source de courant constant (300 ou 500 μA). Le signal du détecteur de zéro (Keithley 155) après passage par un diviseur de potentiel, est enregistré sur un appareil Tacussel EPLI. La résistance chauffante de calibration (50 Ω) est alimentée par une source de tension stabilisée (Tacussel PRT 500 LC) et le temps de chauffage est mesuré avec un chronomètre (Precision Scientific) commandé par un interrupteur double. La tension aux bornes de la résistance est lue sur un multimètre digital (Keithley 179). Le calcul des quantités de chaleur est fait comme précédemment (11). Les performances du calorimètre ont été évaluées en mesurant la chaleur de neutralisation du THAM solide dans HCl aqueux 0,10 *M*. Les valeurs obtenues correspondent aux données de la littérature à mieux de 0,5% (12).

Résonance magnétique nucléaire

Les spectres rmn du carbone-13 ont été obtenus à 20,2 MHz sur un appareil Bruker WP-80. Les concentrations d'adénine, adénosine, purine, imidazole et amino-3 pyridine dans les solutions aqueuses de $HClO_4$ et H_2SO_4 et dans HCF_3CO_2 sont comprises entre 0,2 et 0,7 *M*. Les déplacements chimiques des carbones-13 sont mesurés par rapport au dioxanne en référence externe et rapportés au tétraméthylsilane en donnant aux carbones du dioxanne un déplacement de 67,40 ppm. Quelques mesures ont été effectuées à 100,6 MHz avec le spectromètre Bruker WH-400 sur des solutions 0,10 *M* d'adénine.

Les spectres rmn du proton ont été enregistrés à 90,0 MHz sur un appareil Bruker WH-90. Les déplacements chmiques ont été mesurés par rapport aux CH_3 du DSS ($(CH_3)_3Si(CH_2)_3SO_3^-Na^+$) en référence

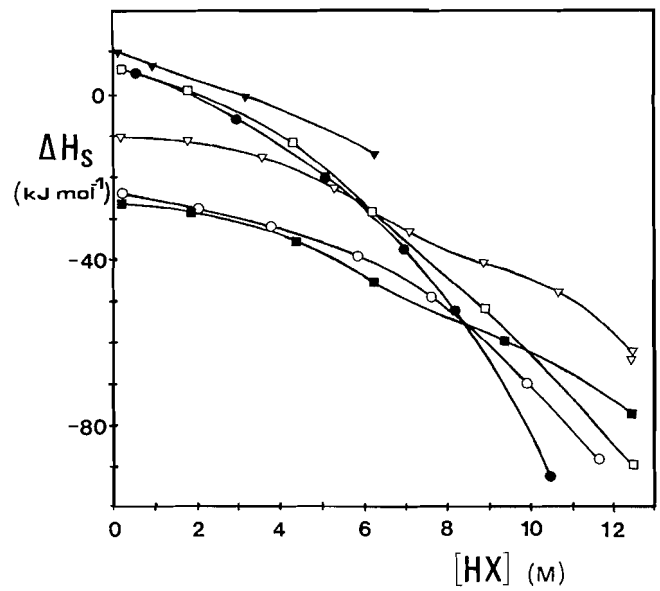

FIG. 2. Chaleurs de dissolution, ΔH_s, de la Pur, l'Imid et le Benzimid en fonction de la concentration d'acide, [HX]. Pur–HCl (▲), Pur–$HClO_4$ (●), Pur–H_2SO_4 (□), Imid–$HClO_4$ (○), Imid–H_2SO_4 (■), Benzimid–H_2SO_4 (△).

interne. Les valeurs des déplacements sont rapportées au TMS en prenant des valeurs identiques nulles pour les protons de CH_3 du DSS et ceux du TMS (13).

Résultats

Calorimétrie

Nous avons déterminé les chaleurs de dissolution de l'adénine (Ade) dans H_2SO_4 et $HClO_4$, celles de l'adénosine (Ado) dans $HClO_4$ et celles de l'amino-3 pyridine (Ampy) dans H_2SO_4. Les enthalpies molaires de dissolution ΔH_s sont portées en fonction des concentrations molaires des acides dans la figure 1. Les valeurs obtenues par Kilday pour l'Ade en milieu HCl sont aussi données à titre de comparaison. La figure 2 reflète les résultats relatifs à la purine (Pur) dans HCl, $HClO_4$ et H_2SO_4, à l'imidazole (Imid) dans $HClO_4$ et H_2SO_4 et au benzimidazole (Benzimid) dans H_2SO_4. L'effet de la concentration de l'adénine (6 valeurs entre $2,2 \times 10^{-3}$ et $1,7 \times 10^{-2}$ *M*) a été étudié à deux niveaux de concentration de $HClO_4$, 2,02 *M* et 0,20 *M*. On a obtenu respectivement pour les enthalpies molaires de dissolution des valeurs indépendantes de la concentration $-6,87 \pm 0,30$ kJ mol^{-1} ($r = 0,9998$) et $+8,55 \pm 0,20$ kJ mol^{-1} ($r = 0,9996$). Ces résultats nous ont fait conclure que compte tenu de la précision des mesures, les enthalpies calculées peuvent être assimilées aux valeurs à dilution infinie. Une série de mesures de ΔH_s de l'Ade a aussi été effectuée avec des solutions de concentration constante 1,113 *M* en $HClO_4$ mais variables en $NaClO_4$. En augmentant la concentration de $NaClO_4$ jusqu'à 6,38 *M*, les valeurs de ΔH_s passent graduellement de −0.6 à −18,0 kJ mol^{-1}. Ces variations font entrevoir un effet de milieu important sur la protonation de l'Ade.

Résonance magnétique nucléaire

Les spectres rmn du proton et du carbone-13 ont été pris pour l'Ade dans des solutions de $HClO_4$ aux acidités moyennes et de H_2SO_4 aux fortes acidités étant donné les solubilités limitées des sels, (bisulfates et perchlorates), dans certains domaines d'acidités. Les concentrations d'acides libres [HX] en solution

Can. J. Chem. Downloaded from www.nrcresearchpress.com by 210.87.254.6 on 09/06/12
For personal use only.

Can. J. Chem. Downloaded from www.nrcresearchpress.com by 210.87.254.6 on 09/06/12
For personal use only.

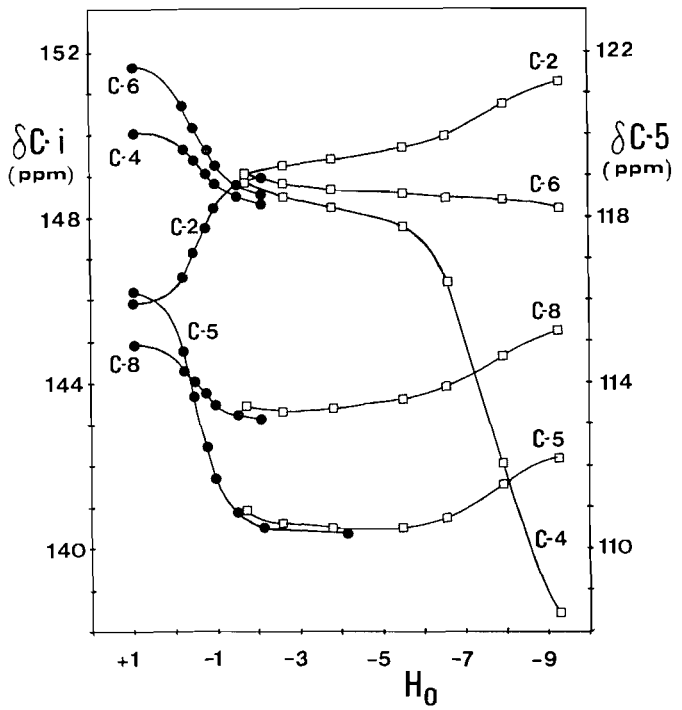

FIG. 3. Déplacements chimiques des carbones-13 de l'Ade, δC-*i*, en fonction de H_0 dans $HClO_4$ et H_2SO_4. Ade–$HClO_4$ (●), Ade–H_2SO_4 (□). [Ade] = 0,10 *M* à 0,71 *M*.

ont été calculées en retranchant des concentrations initiales *n* fois les concentrations des espèces BH_n^{n+} formées dans les réactions de protonation de l'Ade. Ces dernières concentrations ont été obtenues à partir des concentrations de la base et du rapport *I* déduit des déplacements chimiques δ observés et des δ limites pour les espèces BH_n^{n+} (éq. [2]). Les valeurs des fonctions d'acidité H_0, H_+ et H_A ont alors été déduites des valeurs de [HX] en utilisant les données dans la littérature (14–16, 17, 18–20). L'attribution des cinq carbones de l'adénine a été faite sur la base des données de la littérature (21) et de résultats en milieu DMSO[2] et vérifiée avec les spectres de découplage off-resonance. On a représenté Fig. 3 les courbes d'allure sigmoïde donnant les δ des 5 carbones de l'adénine en fonction de H_0. Les courbes correspondant aux solutions dans H_2SO_4 et $HClO_4$ sont déplacées d'environ 0,3 ppm, celles pour H_2SO_4 étant à des champs plus faibles.

Les résultats correspondants pour la purine en milieu H_2SO_4 sont donnés à la Fig. 4. Les spectres sont enregistrés rapidement pour éviter une certaine décomposition dans les milieux d'acidité intermédiaire (0,5–4 *M*). Les déplacements chimiques des carbones-13 de l'amino-3 pyridine et de l'imidazole dans H_2SO_4 sont donnés à la Fig. 5 en fonction des valeurs de H_0. Pour l'Ampy, l'attribution du carbone C-3 dont le signal apparaît à des champs nettement plus faibles, est faite avec le spectre découplé. Une étude plus poussée serait nécessaire pour identifier les autres carbones et n'entre pas dans le cadre des objectifs poursuivis ici. Les spectres de l'adénosine représentés Fig. 6 ont été pris en deça d'une heure afin de minimiser la réaction d'hydrolyse de ce nucléoside (22) et la dégradation du D-ribose, réactions de plus en plus notables lorsque l'acidité croît. Pour une concentration de $H_2SO_4 \geq 10{,}7$ *M*, le spectre de l'adénosine n'a pu être obtenu. Les produits de l'hydrolyse, adénine et D-ribose, ont été facilement identifiés par comparaison des spectres rmn dans les mêmes milieux acides. Les carbones sont attribués à partir des valeurs obtenues pour l'adénosine monoprotonée par l'acide picrique dans le Me_2SO[2], de données de la littérature (23) et des spectres découplés. Les courbes des déplacements chimiques des protons H-2 et H-8 de l'adénine en fonction de H_0 pour les acides $HClO_4$ et H_2SO_4, ont aussi une allure sigmoïde. On remarque toutefois un effet de milieu important, les valeurs de δ en milieu H_2SO_4 étant décalées d'environ 0,5 ppm vers les champs plus forts par rapport aux valeurs en milieu $HClO_4$ (Fig. 7).

[2] D. Boulet et M. Fréchette. Résultats non-publiés.

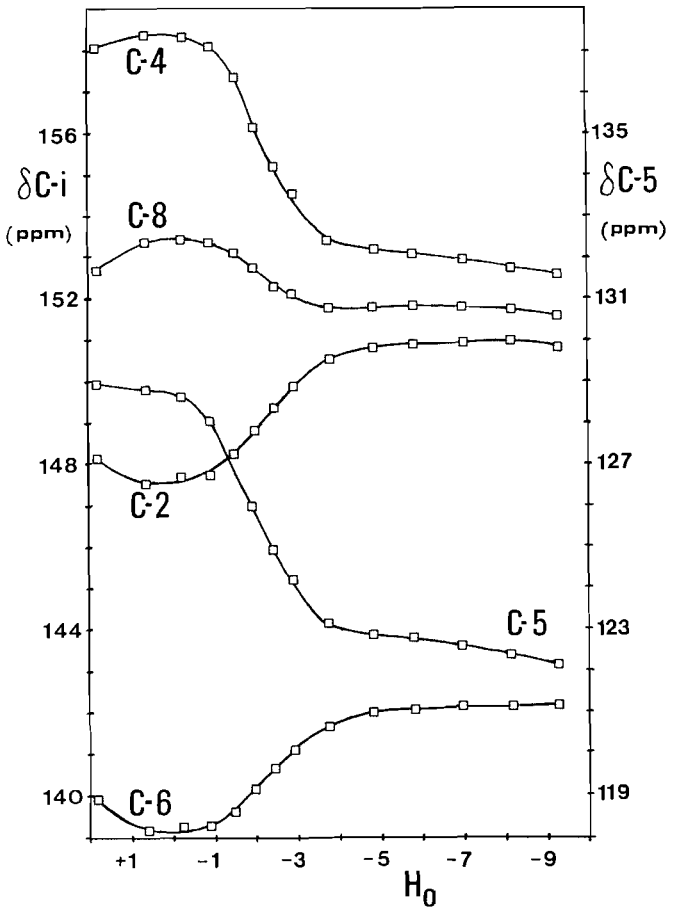

FIG. 4. Déplacements chimiques des carbones-13 de la Pur, δC-*i*, en fonction de H_0 dans H_2SO_4. [Pur] = 0,29 *M* à 0,51 *M*.

Dans le domaine de concentration des bases étudiées (0,1–0,7 *M*) (les intervalles étant précisés dans les légendes des Fig. 3 à 6), on n'a pas noté d'effet de concentration sur les valeurs des déplacements chimiques. Les points expérimentaux se placent bien sur les courbes sigmoïdes et leurs composantes horizontales. Read et Goldstein (24) ont aussi remarqué qu'avec la purine l'effet de concentration de la base sur les déplacements du proton disparaît lorsque la base est protonée.

Le calcul des $pK_{BH_n^{n+}}$ des espèces BH_n^{n+} ($n = 2,3$) à partir des résultats de rmn présente des difficultés, tout d'abord au niveau du choix de la fonction d'acidité H_i qui convient. Ce point est illustré au Tableau 1 où sont rassemblées les valeurs des pK_n et pentes m_n obtenues pour l'Ampy (pK_2) et l'Ade (pK_2 et pK_3) à partir des graphiques des différentes fonctions H_0, H_+, H_A en fonction de log *I*. Ces graphiques sont basés sur l'équation:

$$[1] \quad H_i = pK_n - m_n \log \frac{|BH_n^{n+}|}{|BH_{n-1}^{(n-1)+}|} = pK_n - m_n \log I$$

Can. J. Chem. Downloaded from www.nrcresearchpress.com by 210.87.254.6 on 09/06/12
For personal use only.

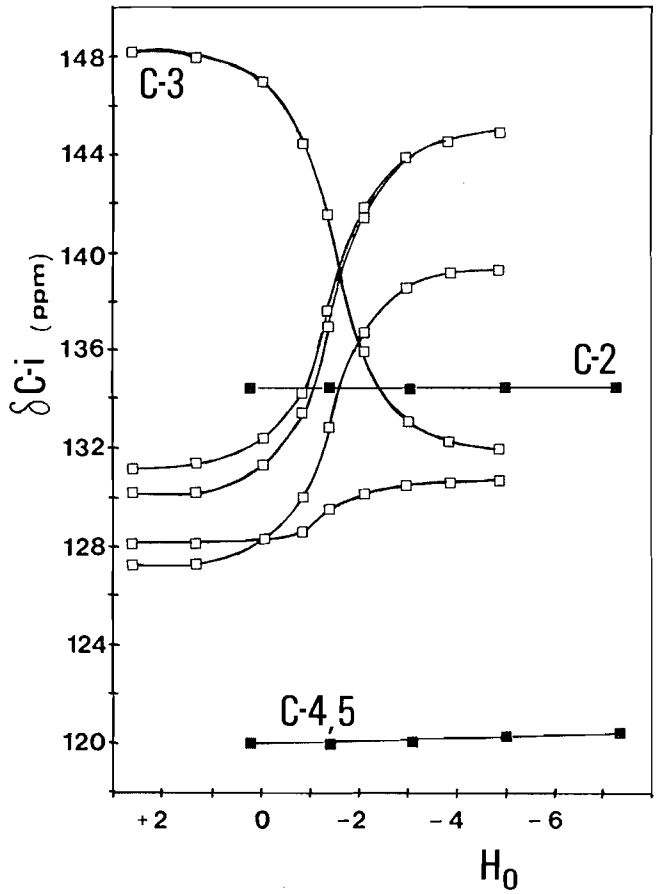

FIG. 5. Déplacements chimiques des carbones-13 de l'Ampy et l'Imid, δC-*i*, en fonction de H_0 dans H_2SO_4. Ampy (□), Imid (■). [Ampy] = 0,30 *M* à 0,45 *M* et [Imid] = 0,39 *M* à 0,73 *M*.

où les rapports *I* des concentrations des espèces BH_n^{n+} et $BH_{n-1}^{(n-1)+}$ sont obtenus à partir des valeurs de δ et celles des δ limites pour les deux espèces:

$$[2] \quad I = \frac{|BH_n^{n+}|}{|BH_{n-1}^{(n-1)+}|} = \frac{\delta - \delta_{BH_n^{(n-1)+}}}{\delta_{BH_n^{n+}} - \delta}$$

Dans une certaine mesure pour contourner le problème du choix des fonctions d'acidité H_i, d'autres méthodes générales de calcul des pK_n ont été proposées en particulier par Bunnett et Olsen (25) et récemment par Cox et Yates (26). Cette dernière méthode dite "excess acidity method" est basée sur la résolution de l'équation

$$[3] \quad \log I - \log C_{H^+} = m^* X + pK_n$$

Les valeurs de *X* et $\log C_{H^+}$ sont connues, indépendemment de la base utilisée pour un acide donné en concentration donnée (27). Log *I* est déduit de nos résultats de rmn tel qu'indiqué plus haut. Un programme permet alors d'ajuster les paramètres inconnus m^* et pK_n. Les résultats sont consignés dans le Tableau 2.

Discussion

La comparaison des résultats obtenus pour la protonation des bases Ade, Pur, Ado et Ampy en rmn et en calorimétrie met en évidence des différences essentielles. D'un côté les courbes donnant les déplacements, δ, des carbones-13 en fonction de

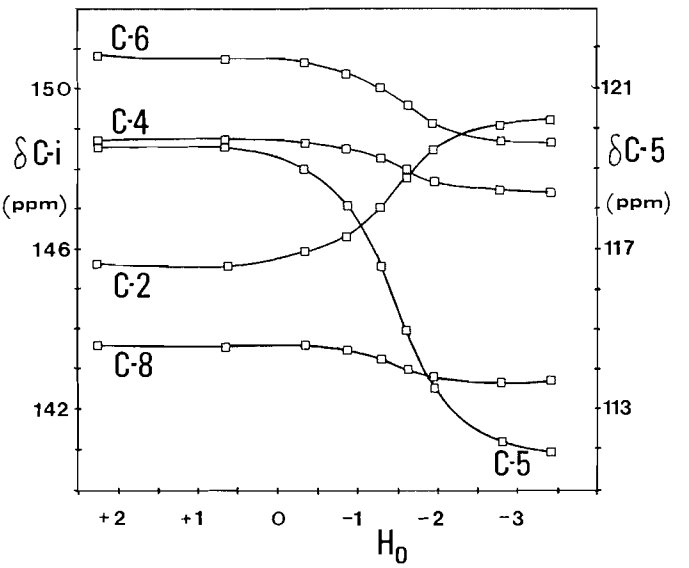

FIG. 6. Déplacements chimiques des carbones-13 de l'Ado, δC-*i*, en fonction de H_0 dans H_2SO_4. [Ado] = 0,38 *M* a 0,78 *M*.

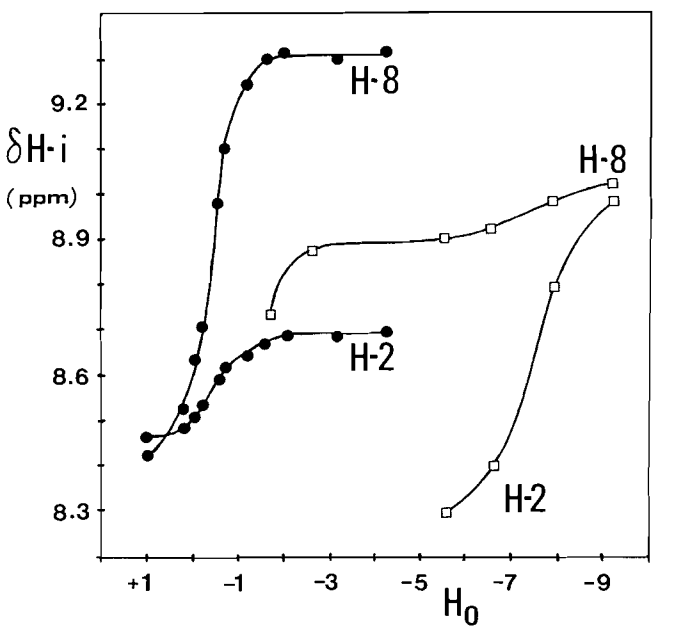

FIG. 7. Déplacements chimiques des protons de l'Ade, δH-*i*, en fonction de H_0 dans $HClO_4$ et H_2SO_4. Ade–$HClO_4$ (●), Ade–H_2SO_4 (□). [Ade] = 0,10 *M* à 0,71 *M*.

H_0 (Fig. 3–6) ont l'allure sigmoïde attendue des réactions de protonation. Par contre, les courbes de la chaleur de dissolution, ΔH_s, des bases en fonction de H_0 (ou de la concentration d'acide, Fig. 1, 2) ne réflètent qu'une exothermicité croissante alors que l'on devrait avoir aussi des courbes sigmoïdes analogues à celle obtenue en fonction du pH ($2 < pH < 6$) pour la première protonation de l'Ade (3). Les résultats inattendus de calorimétrie s'expliquent en considérant le cas plus simple de la base imidazole, B ($pK_{BH^+} = 7,2$ (8)). On note Fig. 5 que les variations des δ des carbones C-4, 5 de l'imidazole sont inférieures à 0,5 ppm entre $+0,2 > H_0 > -9,4$ (soit 0,5 *M* < H_2SO_4 < 17,2 *M*) et celles du C-2 sont négligeables. Ces résultats nous font conclure que dans le domaine d'acidité considéré, d'une part il n'y a pas de réaction de protonation additionnelle de l'ion imidazolium, BH^+, et d'au-

Can. J. Chem. Downloaded from www.nrcresearchpress.com by 210.87.254.6 on 09/06/12
For personal use only.

TABLEAU 1. $pK_{BH_n^{n+}}$ et pentes m_n correspondant aux fonctions d'acidité, H_0, H_+, H_A

B	H_i	$pK_{BH_2^{2+}}$	m_2	$pK_{BH_3^{3+}}$	m_3
Ampy	H_0	−1,55	1,30		
	H_+	−1,76	1,30		
	H_A	−1,30	1,06		
Ade	H_0	−0,51	0,89	−7,6	1,8
	H_+	—	—	−5,5	0,35
	H_A	−0,41	0,71	−4,7	0,98

TABLEAU 2. $pK_{BH_n^{n+}}$ suivant la méthode Cox–Yates

B	$pK_{BH_2^{2+}}$	$pK_{BH_3^{3+}}$
Ampy	−1,23	
Ade	−0,43	−4,23
Ado	−1,48	Hydrolyse
Pur	−1,66	< −6

tre part que l'effet de milieu sur les δ des carbones-13 est très faible. Par contre, en dépit de cette absence de protonation additionnelle de BH^+, la chaleur de dissolution ΔH_s de l'imidazole change de façon continue et considérable avec la concentration de $HClO_4$ et H_2SO_4 (Fig. 2). Ainsi ΔH_s qui est de −24,3 kJ mol^{-1} dans $HClO_4$ 0,20 *M* (en excellent accord avec la valeur de −24,0 kJ mol^{-1} dans HCl 0,20 *M* (28)) passe à −88,7 kJ mol^{-1} dans $HClO_4$ 11,65 *M*. On doit donc conclure à un effet du milieu extrêmement important, −64,4 kJ mol^{-1}, sur le ΔH_s de la réaction de protonation de l'imidazole,

[4] $B(c) + H^+ClO_4^- = BH^+ClO_4^-$

Nous avons alors cherché à évaluer les contributions respectives des variations d'enthalpie de $H^+ClO_4^-$ et $BH^+ClO_4^-$ à l'effet du milieu sur la réaction [4]. On déduit de [4] que lorsque l'on passe par exemple d'un premier milieu dilué, tel que $HClO_4$ 0,20 *M*, à un second milieu concentré, tel que $HClO_4$ 11,65 *M*, la variation de ΔH_s est égale à la différence des enthalpies de transfert ΔH_t d'une mole de $BH^+ClO_4^-$ et de $H^+ClO_4^-$ du milieu concentré au milieu dilué.

[5] $\delta\Delta H_s = \Delta H_t(BH^+ClO_4^-) - \Delta H_t(H^+ClO_4^-)$

On calcule qu'avec ces deux milieux, d'après les données de la littérature (29), $\Delta H_t(H^+ClO_4^-) = -41{,}8$ kJ mol^{-1}, il reste donc pour $\Delta H_t(BH^+ClO_4^-)$ −64,4 + 41,8 soit −22,6 kJ mol^{-1}. En d'autres termes, le passage de ΔH_s de −24,3 kJ mol^{-1} dans $HClO_4$ 0,20 *M* (chaleur de solution de B, +12,8 kJ mol^{-1}, plus chaleur de protonation de B, −37,1 kJ mol^{-1}) à −88,7 kJ mol^{-1} dans $HClO_4$ 11,65 *M* est due pour 65% à la chaleur de transfert d'une mole de $H^+ClO_4^-$ d'un milieu à l'autre et pour 35% à celle d'une mole de $BH^+ClO_4^-$. On peut aussi réécrire [5]

[6] $\delta\Delta H_s = \Delta H_t(BH^+) - \Delta H_t(H^+)$

Cette équation relie cette fois le ΔH_s aux enthalpies de transfert ioniques de BH^+ et H^+ entre deux milieux, la contribution importante étant vraisemblablement celle de H^+. L'équation [6] montre aussi que des variations analogues de ΔH_s doivent se retrouver avec les autres acides concentrés utilisés HCl et H_2SO_4. Ainsi, et cette fois dans le cas de l'adénine, lorsque l'on passe de HCl 0,10 *M* à HCl 6,6 *M*, les concentrations limites utilisées par Kilday (7) pour obtenir ΔH_2, l'enthalpie de la seconde protonation de l'adénine, on calcule $\Delta H_t(H^+Cl^-) = -16{,}7$ kJ mol^{-1}. Ceci signifie que lorsque la chaleur de dissolution de l'adénine solide passe de +10,8 kJ mol^{-1} dans HCl 0,10 *M* à −25,3 kJ mol^{-1} dans HCl 6,6 *M* (7), la diminution de −36,1 kJ mol^{-1} inclut déjà une contribution majeure de −33,4 kJ mol^{-1} due au seul transfert de 2 moles de H^+Cl^-, l'Ade étant diprotonée à cette acidité. Nous avons d'ailleurs essayé de corriger les valeurs expérimentales de ΔH_s obtenues par Kilday entre HCl 0,10 et 6,6 *M* en retranchant les contributions dues au seul transfert de H^+Cl^-, le nombre de moles de HCl transféré étant calculé d'après $pK_2 = -0{,}43$. Les ΔH_s ainsi corrigés portés en fonction de H_0 ont donné une courbe d'allure sigmoïde. On a alors calculé à partir de ces valeurs $\Delta H_2 = -3{,}7$ kJ mol^{-1} pour la réaction

[7] $BH^+Cl^- + H^+Cl^- = BH_2^{2+}(Cl^-)_2$

Toutefois en répétant le même processus avec nos valeurs de ΔH_s en milieux $HClO_4$ et H_2SO_4, on a obtenu pour ΔH_2 des valeurs totalement différentes. Apparemment les contributions opposées de $\Delta H_t(BH^+X^-)$ et $\Delta H_t(BH_2^{2+}(X^-)_2)$ (où $X^- = Cl^-$, ClO_4^-, HSO_4^-) qui restent incluses dans les valeurs ainsi calculées de ΔH_2 ne se compensent pas. En conclusion, non seulement il n'est pas possible d'atteindre un ΔH_2 valable en corrigeant seulement pour le transfert de l'acide, mais aussi la valeur de +7,9 kJ mol^{-1} calculée par Kilday sans correction aucune, est à rejeter totalement.

Passons maintenant aux résultats de rmn. Les très faibles variations des valeurs des déplacements chimiques, δ, des carbones-13 de l'imidazole dans H_2SO_4 (Fig. 5) laissent prévoir un effet de milieu négligeable pour les autres bases étudiées. On n'a d'ailleurs décelé par la méthode Cox–Yates qu'un très faible effet de milieu pour la purine et aucun effet pour l'adénine et l'adénosine.[3] Le calcul des $pK_{BH_n^{n+}}$ est ainsi facilité. Comparons d'abord nos valeurs de pK_2 de l'amino-3 pyridine données au Tableau 1 avec la valeur de −1,43 obtenue par spectroscopie uv (9) mais sans tenir compte d'un effet de milieu possible. En considérant le choix de la fonction d'acidité, on aurait pu penser à priori que la fonction H_+ convenait mieux pour la deuxième protonation de l'Ampy mais la valeur correspondante de la pente, $m_2 = 1{,}30$, est élevée. De plus, Brignell *et al.* (9) dans leur étude uv ont utilisé la fonction H_0 et obtenu une pente de 1,08. Avec H_0 notre pente est $m_2 = 1{,}30$ mais par contre avec H_A dont le choix est moins justifiable nous obtenons une valeur $m_2 = 1{,}06$ plus satisfaisante. Pour éviter ce problème de sélection de fonction d'acidité, nous avons utilisé la méthode Cox–Yates pour calculer les p*K* retenus au Tableau 2. Notre valeur de $pK_{BH_2^{2+}} = -0{,}43$ pour l'adénine est en bon accord avec la valeur −0,35 trouvée par spectroscopie uv (6). Quant à la valeur correspondante pour la purine, −1,66, elle se compare favorablement à la récente valeur −1,5 estimée à partir de données sur $^1J(^{13}C,^1H)$ dans D_2SO_4 (10). On note que les différences des valeurs des p*K*, $pK_{BH_2^{2+}} - pK_{BH^+}$ sont d'environ −4,5 unités tandis que $pK_{BH_3^{3+}} - pK_{BH^+}$ est de −8,3 unités. Comme les p*K* correspondant aux deux protonations d'une pyrimidine voisine l'amino-4 diméthyl-2,6 pyrimidine (7,0 et −1,7)[2] diffèrent de −8,7, les p*K* obtenus suggèrent que la seconde protonation des bases B se fait sur le cycle imidazole et la troisième sur le cycle pyrimidine.

Examinons pour terminer l'incidence de nos résultats de rmn sur le choix des sites de protonation des bases Ade, Pur et Ado et les attributions faites antérieurement. La première protonation de l'Ado et de l'Ade en N-1 est bien établie (1, 2) et

[3] R. A. Cox. Communication personnelle.

Can. J. Chem. Downloaded from www.nrcresearchpress.com by 210.87.254.6 on 09/06/12
For personal use only.

celle de la Pur sur le même azote a été confirmée par spectroscopie rmn du proton (24) puis du carbone-13 (30). Notre choix du site de la seconde protonation des bases est fait en comparant les variations des déplacements chimiques des carbones observés lors du passage de BH^+ à BH_2^{2+} aux données obtenues pour la protonation du benzimidazole (28). Les déplacements chimiques des carbones correspondants, pour l'Ade, Pur, Ado d'une part et le benzimidazole d'autre part sont tous dans le même sens, celui du C-6 de la purine mis à part. Cette comparaison nous fait mettre la seconde protonation de l'Ado, Ade et Pur sur le cycle imidazole, c'est-à-dire en N-7 (Ado) et N-7/N-9 (Ade, Pur) compte tenu de la présence de tautomères pour B (31). La protonation de N-7 est en accord avec l'effet α noté par Pugmire et Grant (30). Ces auteurs ont observé que les carbones situés en α des sites de protonation d'hétérocycles azotés se déplaçaient vers les champs forts lors de la protonation. Les variations des C-5 et C-8 adjacents à N-7 sont bien dans le sens prévu par cette règle et une protonation en N-3 conduirait à un déplacement du C-2 inverse de celui qui est observé. La seconde protonation de l'Ade et Pur sur le cycle imidazole est aussi en accord avec les conclusions atteintes par d'autres chercheurs en interprétant d'une part la variation des constantes de couplage spin–spin ^{13}C, ^1H dans des milieux D_2SO_4 (10) et d'autre part les spectres rmn du proton dans HCF_3CO_2 (TFA), HSO_3F et HSO_3F–SbF_5–SO_2 à 27, −20 et −55°C (5). Toutefois Wagner et von Philipsborn (5) supposent la présence exclusive dans le TFA des espèces $AdeH_2^{2+}$ et $PurH^+$ respectivement. En comparant nos valeurs des déplacements du ^{13}C dans le TFA et les solutions de $HClO_4$ et H_2SO_4, nous avons déduit que dans le TFA on avait $AdeH_2^{2+}/AdeH^+ = 4:1$ et $PurH_2^{2+}/PurH^+ = 1:2$; les valeurs de ces rapports sont confirmés pour l'Ade par nos données en rmn du proton sur Δ(H-8) − (H-2) et pour la Pur par les résultats de Schumacher et Günther (10).

Quant au site de la troisième protonation de l'Ade, nous l'avons placé en N-3 sur le cycle pyrimidine en comparant les variations des déplacements chimiques des carbones de l'Ade et du cycle pyrimidine de l'amino-4 diméthyl-2,6 pyrimidine (Adp) lors des protonations successives. Les carbones C-4 et C-5 de l'Ade se déplacent vers les champs forts et faibles respectivement comme les carbones correspondants de l'Adp (C-6 et C-5) lors de la première protonation en position N-1 (32) tandis que le carbone C-2 de l'Ade, entre deux azotes protonés, est déplacé vers les champs faibles comme le C-2 de l'Adp lors de sa deuxième protonation. Notre attribution du site de la troisième protonation à N-3 est aussi conforme à celle de Wagner et von Philipsborn (5).

Finalement, dans le cas de l'Ade les variations des déplacements des deux protons H-2 et H-8 (Fig. 7) sont en accord avec la deuxième protonation en N-7/N-9 et la troisième en N-3, les déplacements des protons en α des sites de protonation, respectivement H-8 et H-2, montrent les plus grandes variations. La figure 7 complémente aussi utilement le schéma donné par les auteurs précités (5) pour illustrer le double "croisement" des valeurs des déplacements de H-2 et H-8 lorsqu'en augmentant l'acidité du milieu, ils passent de l'Ade (H_2O) ($\delta_{H\text{-}2} > \delta_{H\text{-}8}$) à $AdeH_2^{2+}$ (TFA) ($\delta_{H\text{-}2} < \delta_{H\text{-}8}$) puis à $AdeH_3^{3+}$ (HSO_3F) ($\delta_{H\text{-}2} > \delta_{H\text{-}8}$). Les valeurs de H-2 (8,98 ppm) < H-8 (9,02 ppm) à la Fig. 7 pour notre milieu le plus acide (H_0 = −9,3, H_2SO_4 17,0 *M*) ne correspondant qu'à $AdeH_3^{3+}/AdeH_2^{2+} = 87:13$, on a calculé pour $AdeH_3^{3+}$ H-2 (9,08 ppm) > H-8 (9,04 ppm), c'est-à-dire une différence de 0,04 ppm en accord satisfaisant avec les 0,09 ppm observés dans HSO_3F ($H_0 \sim -15$). L'attribution à H-2 du proton apparaissant au champ le plus faible dans ce milieu est ainsi correcte (5).

Remerciements

Nous remercions le Conseil de recherches en sciences naturelles et en génie du Canada pour son aide financière. Nos remerciements vont aussi au Professeur K. Yates pour l'intérêt qu'il a porté à ce travail et au Dr. R. A. Cox qui a très aimablement calculé les constantes d'acidité avec son programme.

1. R. M. Izatt, J. J. Christensen et J. H. Rytting. Chem. Rev. **71**, 439 (1971).
2. N. C. Gonnella, H. Nakanishi, J. B. Holtwick, D. S. Horowitz, K. Kanamori, N. J. Leonard et J. D. Roberts. J. Am. Chem. Soc. **105**, 2050 (1983).
3. S. Zimmer et R. Biltonen. J. Sol. Chem. **1**, 291 (1972).
4. T. J. Kistenmacher et T. Shigematsu. Acta Crystallogr. Sect. B, **30**, 1528 (1974).
5. R. Wagner et W. von Philipsborn. Helv. Chim. Acta, **54**, 1543 (1971).
6. G. Budo et J. Tomasz. Acta Biochim. Biophys. Acad. Sci. Hung. **9**, 217 (1974).
7. M. V. Kilday. J. Res. Natl. Bur. Stand. (U.S.) **83**, 347 (1978).
8. F. Marsicano et R. D. Hancock. J. Chem. Soc. Dalton Trans. 228 (1978).
9. P. J. Brignell, C. D. Johnson, A. R. Katritzky, N. Shakir, H. O. Tarhan et G. Walker. J. Chem. Soc. (B) 1233 (1967).
10. M. Schumacher et H. Günther. J. Am. Chem. Soc. **104**, 4167 (1982).
11. R. L. Benoit, M. Rinfret et R. Domain. Inorg. Chem. **11**, 2603 (1972).
12. J. O. Öjelund et I. Wadsö. J. Chem. Thermodyn. **1**, 111 (1969).
13. R. J. Abraham et P. Loftus. Proton and carbon-13 NMR spectroscopy. Heyden, London. 1980. p. 14.
14. C. D. Johnson, A. R. Katritzky et S. A. Shapiro. J. Am. Chem. Soc. **91**, 6654 (1969).
15. K. Yates et H. Wai. J. Am. Chem. Soc. **86**, 5408 (1964).
16. M. A. Paul et F. A. Long. Chem. Rev. **57**, 1 (1957).
17. P. Vetešnik, J. Bielavský et M. Večeřa. Collect. Czech. Chem. Commun. **33**, 1687 (1968).
18. K. Yates, J. B. Stevens et A. R. Katritzky. Can. J. Chem. **42**, 1957 (1964).
19. G. D. Frederick et C. D. Poulter. J. Am. Chem. Soc. **97**, 1797 (1975).
20. K. Yates, H. Wai, G. Welch et R. A. McClelland. J. Am. Chem. Soc. **95**, 418 (1973).
21. E. Breitmaier et W. Voelter. Tetrahedron, **30**, 3941 (1974).
22. J. A. Zoltewicz, D. F. Clark, T. W. Sharpless et G. Grahe. J. Am. Chem. Soc. **92**, 1741 (1970).
23. A. J. Jones, D. M. Grant, M. W. Winkely et R. K. Robins. J. Am. Chem. Soc. **92**, 4079 (1970).
24. J. M. Read, Jr. et J. H. Goldstein. J. Am. Chem. Soc. **87**, 3440 (1965).
25. J. F. Bunnett et F. P. Olsen. Can. J. Chem. **44**, 1899 (1966).
26. R. A. Cox et K. Yates. Can. J. Chem. **59**, 1560 (1981), et références incluses.
27. R. A. Cox et K. Yates. J. Am. Chem. Soc. **100**, 3861 (1978).
28. I. Wadsö. Acta Chem. Scand. **16**, 479 (1962).
29. D. R. Bidinosti et W. J. Biermann. Can. J. Chem. **34**, 1591 (1956).
30. R. J. Pugmire et D. M. Grant. J. Am. Chem. Soc. **93**, 1880 (1971).
31. M. Th. Chenon, R. J. Pugmire, D. M. Grant, R. P. Panzica et L. B. Townsend. J. Am. Chem. Soc. **97**, 4639 (1975).
32. J. Riand, M. Th. Chenon et N. Lumbroso-Bader. J. Am. Chem. Soc. **99**, 6838 (1977).

COMMUNICATION

Surface photochemistry: use of spiropyrans as indicators of surface polarity

PAUL DE MAYO, ALI SAFARZADEH-AMIRI, AND S. KING WONG

Photochemistry Unit, Department of Chemistry, The University of Western Ontario, London, Ont., Canada N6A 5B7

Received December 2, 1983

PAUL DE MAYO, ALI SAFARZADEH-AMIRI, and S. KING WONG. Can. J. Chem. **62**, 1001 (1984).

The position of the long wavelength absorption band in the spectrum of a spiropyran is sensitive to solvent polarity. This property has been used to determine the polarity of the silica gel surface.

PAUL DE MAYO, ALI SAFARZADEH-AMIRI et S. KING WONG. Can. J. Chem. **62**, 1001 (1984).

La position de la bande d'absorption à une longueur d'onde élevée, dans le spectre d'un spiropyranne, est sensible à la polarité du solvant. On a utilisé cette propriété pour déterminer la polarité de la surface du gel de silice.

[Traduit par le journal]

Can. J. Chem. Downloaded from www.nrcresearchpress.com by 210.87.254.40 on 09/06/12
For personal use only.

Recently there has been a burst of activity in several laboratories as regards the investigation of the photochemistry (see ref. 1 for a recent review, ref. 2) and photophysics (3, 4) of organic molecules adsorbed on solid oxide supports. The purpose has been two-fold: to use these techniques to learn about the adsorbent surface, and to use the surface properties to induce new photochemistry. Amongst the surface properties of general importance is polarity, and we describe here a technique for its determination on dry and hydrated silica gel surfaces.

Solvatochromic dyes, such as 1-alkylpyridinium iodides and pyridinium-*N*-phenol betaines (for a review, see ref. 5) have been used successfully as indicators of solvent polarity by measuring the shift of the long wavelength absorption band as a function of solvent polarity. The oscillator strength of this transition is small and, in solvents of high polarity, appears as a shoulder on a much stronger absorption band and is ill-resolved; moreover, the substances are very unstable on dry silica gel and cannot be used. Pyrene (E_p), a recent candidate, when used fluorimetrically (6) suffers from insensitivity to hydrogen-bonding, evidently a critical weakness on a hydroxylated surface. Indolinobenzospiropyrans (e.g. **1**) in their open, coloured, forms (e.g. **2**) are sensitive to solvent polarity:[1] the intense, well-resolved long wavelength absorption band moves to higher energy with increasing solvent polarity. The transition energies (E_{sp}) of **2** in a variety of solvents are given in Table 1, and a plot of E_{sp} against the well-established E_T (5) is shown in Fig. 1. Evidently, the correlation between E_{sp} and E_T is very satisfactory.

To test the use of the spiropyran **1** on silica gel, the gel was first dehydrated (720°C/5 h) *in vacuo* which reduced the concentration of silanols from 5–6/nm^2 to ca. 2/nm^2 (7, 8), and the surface modified by the addition of various amounts of water (Table 2). The resultant hydrolysis of strained siloxane bonds and the regeneration of silanol functions plus the presence of physisorbed water should render the surface more polar.[2] That this is so is indicated in Table 2. The surface with isolated, unsolvated (8, 9) silanol functions had an E_{sp} close to that of MeOH/H_2O (40:60), whilst the most polar surface, that of silica gel equilibrated with the atmosphere was close to that of MeOH/H_2O (30:70) whether the silica gel was pre-heated or not.

TABLE 1. The position of λ_{max} and transition energies of spiropyran (E_{sp}) and the E_T[a] values for several solvents

Solvents		λ_{max} (nm)	E_{sp} (kcal/mol)	E_T (kcal/mol)[b]
CH_3OH/H_2O	30:70	498	57.4	58.4[c]
	40:60	517	55.3	58.9[c]
	50:50	525	54.5	57.6[c]
C_2H_5OH/H_2O	50:50	537	53.2	54.6[c]
	80:20	545	52.6	53.6
CH_3OH		545	52.6	55.5
C_2H_5OH		548	52.2	51.9
1-Propanol		557	51.3	50.7
1-Butanol		567	50.4	50.2
Ethyleneglycol		542	52.7	56.3
Cyclohexanol		560	51.1	[d]
Acetonitrile		569	50.3	46
Acetone		576	49.6	42.2
1,2-Dichloroethane		588	48.6	41.9
Chlorobenzene		584 and 614	48.9 and 46.6	37.4
Benzene		585 and 622	48.9 and 46.0	34.5

[a] From ref. 5.
[b] Using 1-(4-hydroxy-3,5-diphenylphenyl)-2,4,6-triphenylpyridinium betaine.
[c] Obtained with the aid of E_T values of 1-(*p*-hydroxyphenyl)-2,4,6-triphenylpyridinium betaine and conversion to scale in *b*.
[d] Could not be measured.

[1] A detailed discussion of all aspects of the chemistry of these substances is contained in ref. 11.

[2] After modification of the surface, the dye (0.5 mg/g SiO_2) in benzene was transferred and the benzene removed *in vacuo*. The silica gel was then transferred to a 1 mm cuvette, the absorption being measured on the "dry" powder, and the entire operation being performed in a closed system. The sequence of the steps is critical. An application of Kosower's *Z* to a silica gel slurry has been reported (10).

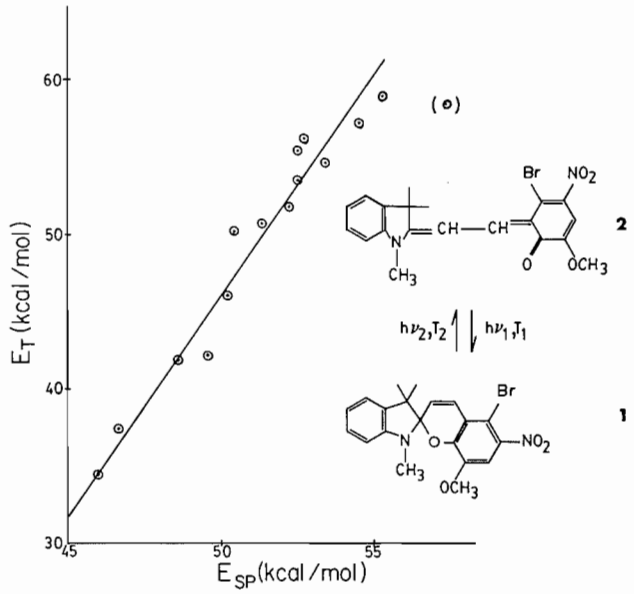

FIG. 1. Plot of E_T vs. E_{sp}. The solid line is the least-squares fit of the data points to a straight line excluding the point in the parenthesis ($r = 0.98$).

TABLE 2. Variation of E_{sp} of **2** on treated silica gel[a]

E_{sp} (kcal/mol)	λ_{max} (nm)	Treatment[b] (mol/g SiO_2)
54.5	525	4.2×10^{-4} 1-decanol
54.9	521	—
55.2	518	2.8×10^{-4}
55.4	516	5.6×10^{-4} H_2O
56.1	510	1.1×10^{-3} H_2O
56.5	506	2.2×10^{-3} H_2O
56.9	502	[c]
56.9	502	[d]

[a] The silica gel was 35–70 mesh (EM reagents).
[b] All specimens except *d* where heated 5 h in vacuum at 700°C.
[c] Equilibrated with atmosphere.
[d] Equilibrated with the atmosphere without heating.

The addition of alcohols should lead to alcoholysis and physisorption, both of which, because of the hydrophobic hydrocarbon "tails", should render the surface less polar. The observations were again in accord with expectation (Table 2). Addition of 1-decanol decreased the surface polarity in comparison to that of silica gel without any coadsorbent and its polarity was similar to that of MeOH/H_2O (50:50 mixture).

Acknowledgement

The authors are grateful to Dr. R. C. Bertelson for a sample of **1**. It is available from Chroma Chemicals Inc. (Dayton, Ohio).

1. P. DE MAYO. Pure App. Chem. **54**, 1623 (1982).
2. D. AVNIR, L. J. JOHNSTON, P. DE MAYO, and S. K. WONG. J. Chem. Soc. Chem. Commun. 958 (1981); D. AVNIR, P. DE MAYO, and I. ONO. J. Chem. Soc. Chem. Commun. 1109 (1978); P. DE MAYO, A. NAKAMURA, P. W. K. TSANG, and S. K. WONG. J. Am. Chem. Soc. **104**, 6824 (1982); R. L. JACKSON and M. R. TRUSHHEIM. J. Am. Chem. Soc. **104**, 6590 (1982).
3. K. HARA, P. DE MAYO, W. R. WARE, A. C. WEEDON, G. S. K. WONG, and K. C. WU. Chem. Phys. Lett. **69**, 105 (1980); R. K. BAUER, P. DE MAYO, W. R. WARE, and K. C. WU. J. Phys. Chem. **86**, 3781 (1982); R. K. BAUER, R. BORENSTEIN, P. DE MAYO, K. OKADA, M. RAFALSKA, W. R. WARE, and K. C. WU. J. Am. Chem. Soc. **104**, 4635 (1982) and references therein; R. K. BAUER, P. DE MAYO, K. OKADA, W. R. WARE, and K. C. WU. J. Phys. Chem. **87**, 460 (1983).
4. C. FRANCIS, J. LIN, and L. A. SINGER. Chem. Phys. Lett. **94**, 162 (1983); G. BECK and J. K. THOMAS. Chem. Phys. Lett. **94**, 553 (1983); N. NAKASHIMA and D. PHILLIPS. Chem. Phys. Lett. **97**, 337 (1983); R. W. KESSLER and F. WILKINSON. J. Chem. Soc. Faraday Trans. 1, **77**, 309 (1981); D. OELKRUG and M. RADJAIPOUR. Z. Phys. Chem. **123**, 163 (1980).
5. C. REICHARDT. Angew Chem. Int. Ed. **4**, 29 (1965).
6. D. C. DONG and M. A. WINNIK. Photochem. Photobiol. **35**, 17 (1982); K. KALYANASUNDARAM and J. K. THOMAS. J. Am. Chem. Soc. **99**, 2039 (1977).
7. J. J. FRIPIAT and J. UYTTERHOEVEN. J. Phys. Chem. **66**, 800 (1962).
8. D. W. SINDORF and G. E. MACIEL. J. Am. Chem. Soc. **105**, 1487 (1983).
9. A. V. KISELEV and V. I. LYGIN. Infrared spectra of surface compounds. J. Wiley and Sons, New York. 1975.
10. T. R. EVANS, A. F. TOTH, and P. A. LEERMAKERS. J. Am. Chem. Soc. **89**, 5060 (1967).
11. R. C. BERTELSON. *In* Photochromism. *Edited by* G. H. Brown. John Wiley and Sons, New York. 1971. Chapt. 2.

Can. J. Chem. Downloaded from www.nrcresearchpress.com by 210.87.254.40 on 09/06/12
For personal use only.

Synthesis, spectroscopic, and magnetic studies of new alkoxy and allied bimetallic derivatives of nickel(II) with aluminium

R. C. MEHROTRA[1] AND JAGVIR SINGH
Chemical Laboratories, University of Rajasthan, Jaipur-302004, India

Received June 24, 1983

R. C. MEHROTRA and JAGVIR SINGH. Can. J. Chem. **62**, 1003 (1984).

Nickel(II) tetraisopropoxyaluminate undergoes alcoholysis reactions with various alcohols and acetylacetone to yield products with the composition: $Ni[Al(OR)_4]_2$ (when ROH = methanol, ethanol, 2,2,2-trifluoroethanol, 2,2,2-trichloroethanol, *n*-butanol, and 1,3-dichloro-2-propanol); $Ni[Al(O\text{-}i\text{-}Pr)(O\text{-}t\text{-}Bu)_3]_2$ (with tertiary butyl alcohol); $Ni[Al(O\text{-}i\text{-}Pr)_2(O\text{-}t\text{-}Am)_2]_2$ (with tertiary amyl alcohol); and $Ni[Al(O\text{-}i\text{-}Pr)_2(acac)_2]$ (with acetylacetone). On the basis of their visible reflectance and infrared spectra along with molecular weights and magnetic susceptibilities, and octahedral geometry is tentatively suggested for these complexes in the solid state with indications of an equilibrium between tetrahedral and octahedral forms in solution. The alkoxy ligands have also been fitted into the spectrochemical and nephelauxetic series.

R. C. MEHROTRA et JAGVIR SINGH. Can. J. Chem. **62**, 1003 (1984).

Le tétraisopropylate d'aluminium et de nickel(II) subit des réactions d'alcoolyse avec divers alcools et avec l'acétylacétone qui conduisent, suivant les conditions, aux produits de compositions suivantes: $Ni[Al(OR)_4]_2$ (quand ROH = méthanol, éthanol, trifluoro-2,2,2 éthanol, trichloro-2,2,2 éthanol, *n*-butanol et dichloro-1,3 propanol-2); $Ni[Al(O\text{-}i\text{-}Pr)(O\text{-}t\text{-}Bu)_3]_2$ (avec l'alcool butylique tertiaire); $Ni[Al(O\text{-}i\text{-}Pr)_2(O\text{-}t\text{-}Am)_2]_2$ (avec l'alcool amylique tertiaire) et $Ni[Al(O\text{-}i\text{-}Pr)_2(acac)_2]_2$ (avec l'acétylacétone). En se basant sur leurs spectres de réflectance visible et sur leurs spectres infrarouges ainsi que sur leurs poids moléculaires et sur leurs susceptibilités magnétiques, on suggère qu'à l'état solide, ces complexes existent sous une géométrie octaédrique; il y a des indications à l'effet qu'en solution, il existerait un équilibre entre les formes tétraédriques et octaédriques. On a aussi ajusté les ligands alcoolates dans les séries spectrochimiques et néphélauxétiques.

[Traduit par le journal]

Can. J. Chem. Downloaded from www.nrcresearchpress.com by 210.87.254.42 on 09/06/12
For personal use only.

Introduction

Although the simple alkoxides (1–4) of the later "3*d*" metals including nickel are insoluble, polymeric, and non-volatile in nature, a number of bimetallic isopropoxides of these metals have been reported (5, 6) in recent years as soluble monomeric volatile products with the general formula, $M[Al(O\text{-}i\text{-}Pr)_4]_n$ where $n = 3$, when M = Cr(III) or Fe(III) and $n = 2$, when M = Mn(II), Fe(II), Co(II), Ni(II), or Cu(II) by reacting their anhydrous chlorides (or their benzene soluble adducts) with potassium tetraisopropoxyaluminate in isopropanol–benzene medium in the required stoichiometric ratios. A few bimetallic alkoxides of nickel(II), $Ni[Al(OR)_4]_2$ (where R = CH_3, C_2H_5, $n\text{-}C_3H_7$, $n\text{-}C_4H_9$) have also been reported more recently by Stumpp and co-workers (7) employing a different technique.

Except for some steric factors (8) in cases of highly ramified alcohols, the alkoxides of non-transition and earlier transition metals undergo facile alcoholysis reactions (1). By contrast, recent studies on the alcoholysis reactions of simple alkoxides of later "3*d*" metals have shown interesting features including specificity in certain directions (6). For example, the primary alkoxides $Ni(OR)_2$ do not appear to undergo alcoholysis with secondary, tertiary, and higher primary alcohols even under favourable conditions. Nickel isopropoxide, on the other hand, undergoes facile interchange with primary alcohols, but does not react with tertiary or other secondary alcohols. These interesting differences have been correlated with changes in the stereochemistry of nickel(II) in combination with different types of alkoxy groups (9). In view of these differences a study of alcoholysis reactions of bimetallic alkoxides of nickel appeared to be of considerable interest.

Compared with simple alkoxides, the bimetallic nickel tetraisopropoxyaluminate appears to undergo facile alcoholysis reactions which are controlled under certain conditions by steric factors only. We, therefore, describe here our results on the synthesis of a variety of bimetallic alkoxides, $Ni[Al(OR)_4]_2$, by the alcoholysis of $Ni[Al(O\text{-}i\text{-}Pr)_4]_2$ and a study of their physicochemical properties with a view to elucidate their structural features.

[1] To whom all correspondence should be addressed.

Results and discussion

1. Synthetic studies

Alcoholysis reactions of $Ni[Al(O\text{-}i\text{-}Pr)_4]_2$ have been carried out with various alcohols and acetylacetone. In the cases of methanol, ethanol, and 2,2,2-trifluoroethanol, the bimetallic isopropoxide was refluxed with large excess of the alcohol for 2–3 h. In all other cases, the reaction mixture of $Ni[Al(O\text{-}i\text{-}Pr)_4]_2$ with the alcohol in benzene was refluxed under a fractionating column and the progress of the reaction was followed by estimation of isopropanol collected in the azeotrope (Table 1). Like methoxides (simple as well as bimetallic) in a number of other cases, $Ni[Al(OMe)_4]_2$ (a yellowish green solid) is insoluble in organic solvents and is non-volatile. $Ni[Al(OEt)_4]_2$ is a purple viscous liquid which can be distilled under reduced pressure; it is insoluble in benzene but dissolves in ethanol (monomeric). Other tetraalkoxyaluminates of nickel synthesised during the course of these investigations (Table 1) are volatile and dissolve in benzene also.

The reactions with excess of tertiary butyl and amyl alcohols result in only partial replacement of the isopropoxy groups of $Ni[Al(O\text{-}i\text{-}Pr)_4]_2$ with the formation of monomeric soluble volatile products, $Ni[Al(O\text{-}t\text{-}Bu)_3(O\text{-}i\text{-}Pr)]_2$ and $Ni[Al(O\text{-}t\text{-}Am)_2(O\text{-}i\text{-}Pr)_2]_2$, respectively:

$$Ni[Al(O\text{-}i\text{-}Pr)_4]_2 \xrightarrow{t\text{-BuOH}} Ni[Al(O\text{-}i\text{-}Pr)(O\text{-}t\text{-}Bu)_3]_2 + 6i\text{-PrOH}$$

$$\xrightarrow{t\text{-AmOH}} Ni[Al(O\text{-}i\text{-}Pr)_2(O\text{-}t\text{-}Am)_2]_2 + 4i\text{-PrOH}$$

Reactions of $Ni[Al(O\text{-}i\text{-}Pr)_4]_2$ with acetylacetone (Hacac) have been carried out in 1:4 and 1:8 molar ratios in benzene

Can. J. Chem. Downloaded from www.nrcresearchpress.com by 210.87.254.42 on 09/06/12
For personal use only.

TABLE 1. Reactions of nickel aluminium isopropoxide with various alcohols and acetylacetone

1	*2*	*3*	*4*	*5*	*6*	*7*	*8*	*9*	*10*
Serial No.	$Ni[Al(O\text{-}i\text{-}Pr)_4]_2$ (g)	Reagent used (g) (mol.)	Isopropanol liberated, found (calcd) (g)	Nature of the distilled product (Yield % of the distilled product)	Volatility (°C/mm)	Analysis, found (calcd)			Mol. wt., found (calcd)
						Ni	Al	OR	
1	3.04	Methanol ~20 ml (Excess)	—	$Ni[Al(OMe)_4]_2$ (99) Yellowish green powder insoluble in benzene	—	16.59 (16.28)	15.24 (15.96)	67.03 (68.76)	—
2	3.37	Ethanol ~20 ml (Excess)	—	$Ni[Al(OEt)_4]_2$ (62) Purple viscous liquid	150/0.6	11.97 (12.42)	11.92 (11.41)	75.05 (76.16)	495+ (473)
3	3.18	2,2,2-Trifluoro ethanol ~8.0 g (Excess)	—	$Ni[Al(OCH_2CF_3)_4]_2$ (65) Purple viscous liquid	115/0.6	5.56 (6.49)	6.20 (5.96)	—	—
4	3.43	2,2,2-Trichloro ethanol (8 mol)	2.80 (2.82)	$Ni[Al(OCH_2CCl_3)_4]_2$ (98) Blackish brown sticky compound	Decomposed at 250/0.6	5.02 (4.52)	4.75 (4.15)	—	—
5	3.12	*n*-Butanol ~35 ml (Excess)	2.54 (2.57)	$Ni[Al(O\text{-}n\text{-}Bu)_4]_2$ (24) Light pinkish viscous compound	170/0.6	8.73 (8.42)	7.98 (7.74)	—	735 (698)
6	1.87	1,3-Dichloro-2-propanol 3.31 g (8 mol)	1.50 (1.53)	$Ni[Al\{OCH(CH_2Cl)_2\}_4]_2$ (99) Brownish black solid	Decomposed at 270/0.6	5.47 (5.17)	5.02 (4.75)	—	—
7	3.14	*t*-Butanol ~40 ml (Excess)	1.90 (1.93)	$Ni[Al(O\text{-}i\text{-}Pr)(O\text{-}t\text{-}Bu)_3]_2$ (69) Purple powder	*140–150/0.6	8.92 (8.77)	7.80 (8.06)	16.88 (17.65)	691 (670)
8	2.28	*t*-Pentanol ~45 mol (Excess)	0.92 (0.94)	$Ni[Al(O\text{-}i\text{-}Pr)_2(O\text{-}t\text{-}Am)_2]_2$ (36) Purple semi-solid	*185/0.8	8.54 (8.42)	7.77 (7.73)	—	760
9	3.46	Acetylacetone 2.42 g (4 mol)	1.41 (1.42)	$Ni[Al(O\text{-}i\text{-}Pr)_2(acac)_2]_2$ (45) Brown pinkish solid	†240–260/0.6	8.15 (7.88)	7.52 (7.24)	—	708 (745)
10	2.55	Acetylacetone 3.50 g (8 mol)	1.96 (2.09)	$Ni[Al(acac)_4]_2$ (78) Light green solid	‡150–170/0.6	6.96 (6.48)	8.72 (5.96)	—	357 (906)

* Sublimed.
† Molecular weight in ethanol medium.
‡ Disproportionation.

Can. J. Chem. Downloaded from www.nrcresearchpress.com by 210.87.254.42 on 09/06/12
For personal use only.

and can be represented as below:

$$Ni[Al(O\text{-}i\text{-}Pr)_4]_2 \xrightarrow{4Hacac} Ni[Al(O\text{-}i\text{-}Pr)_2(acac)]_2 + 4i\text{-}PrOH$$

$$\xrightarrow{8Hacac} Ni[(acac)_2 + 2Al(acac)_3 + 8i\text{-}PrOH$$

The product $Ni[Al(O\text{-}i\text{-}Pr)_2(acac)_2]_2$ could be sublimed and its molecular weight in benzene corresponded to the formula weight; it can, therefore, be represented by the structure:

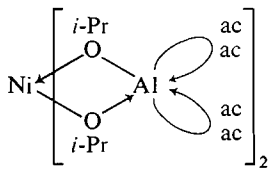

Magnetic studies

Magnetic moments of these derivatives, $Ni[Al(OR)_4]_2$, have been measured at room temperature. Values of the magnetic moments for all these derivatives fall in the range 3.28 to 3.47 BM, which correspond to two unpaired spins anticipated for both tetrahedral and octahedral geometries (10). The low temperature magnetic susceptibility measurements in the range 80 to 300 K have been made for $Ni[Al(O\text{-}i\text{-}Pr)_4]_2$ and the moments are found to be practically independent of temperature. This behaviour is indicative of octahedral geometry (9) for the complex. The plot of $1/\chi_M$ (corr.) versus T gives a straight line with the value of θ as 0 K.

Spectroscopic studies

Infrared spectra

The infrared spectra (4000–400 cm^{-1}) of all the nickel(II) bimetallic alkoxides exhibit the characteristic frequencies for alkoxy groups, aluminium–oxygen, and nickel–oxygen bands.

Electronic spectra

The data for the electronic spectra of the products are summarised in Table 2. The observed bands in the regions of 12 790 – 14 860 and 23 255 – 25 455 cm^{-1} have been assigned to the transitions ν_2, $[^3A_{2g} \rightarrow {}^3T_{1g}(F)]$ and ν_3, $[^3A_{2g} \rightarrow {}^3T_{1g}(P)]$, respectively, for octahedral nickel(II) species. As ν_1, $[^3A_{2g} \rightarrow {}^3T_{2g}(F)]$ which represents $10Dq$, could not be observed under the experimental conditions employed. The values of ν_1 as well as that of Racah parameter β (column 8) were calculated by the equations given by Underhill and Billings (11):

$$340Dq^2 - 18(\nu_2 + \nu_3)Dq + \nu_2\nu_3 = 0$$

$$15B = \nu_2 + \nu_3 - 30Dq$$

In addition to the above, another band in the range 17 095 to 19 340 cm^{-1} has been observed in the spectra of a few derivatives and this has been ascribed to the transition ν_3, $[^3T_1 \rightarrow {}^3T_1(P)]$ of tetrahedral nickel(II).

In view of the observed (1, 5, 12) bidentate nature of the ligand $[Al(OR)_4]^-$, the monomeric bimetallic nickel aluminium alkoxides, $Ni[Al(OR)_4]_2$, could be expected to be tetrahedral compounds in which both aluminium as well as nickel atoms exhibit tetrahedral geometry. However, physicochemical characteristics of these monomeric nickel(II) bimetallic derivatives appear to show a tendency of nickel to acquire an octahedral geometry, indicating the possibility that in such situations, $[Al(OR)_4]^-$ may act as a tridentate ligand:

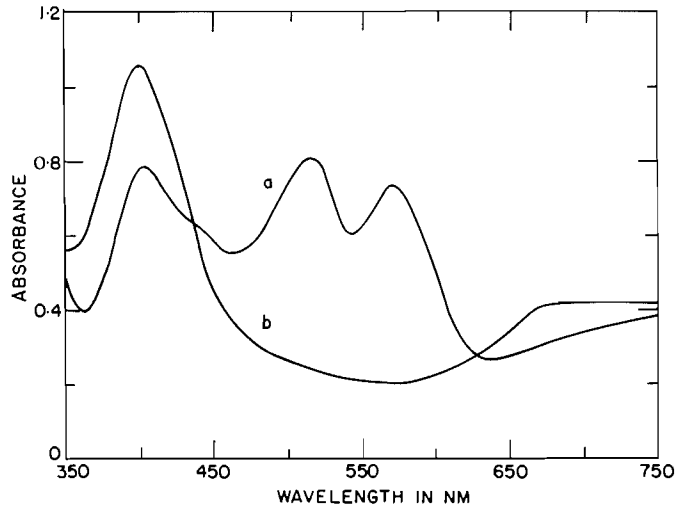

FIG. 1. Visible spectra of $Ni[Al(OEt)_4]_2$ in (*a*) Nujol and (*b*) ethanol.

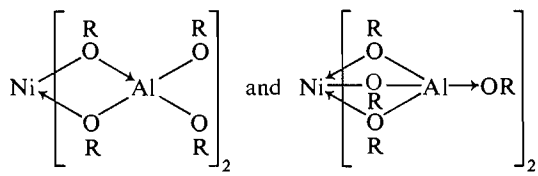

Tetrahedral Octahedral

The above tendency to attain octahedral geometry appears to increase as the alkoxy groups become smaller and less ramified. For example, $Ni[Al(OMe)_4]_2$ shows only two bands at 13 985 and 25 445 cm^{-1}, characteristic of Ni(II) in an octahedral geometry. The spectra of $Ni[Al(OEt)_4]_2$ and $Ni[Al(O\text{-}i\text{-}Pr)_4]_2$, on the other hand, show increasing proportions of tetrahedral nickel species in equilibrium with octahedral forms.

On dissolving purple–green $Ni[Al(OEt)_4]_2$ in ethanol, a pinkish solution is obtained and the bands due to tetrahedral molecules disappear (Fig. 1, Table 2). A plausible explanation for this could be that the coordination of solvent ethanol molecules converts the tetrahedral species into octahedral ones. The spectra of $Ni[Al(O\text{-}i\text{-}Pr)_4]_2$ in film and in benzene solution are almost identical, showing bands (Table 2) characteristic of both octahedral and tetrahedral forms. In isopropanol solution, the spectrum of $Ni[Al(O\text{-}i\text{-}Pr)_4]_2$ indicates a greater intensity of octahedral bands in comparison to the tetrahedral ones. This can again be tentatively explained by the coordination of isopropanol molecules which, however, appears to be partial due to steric factors. The spectrum of $Ni[Al(O\text{-}i\text{-}Pr)_4]_2$ was, therefore, recorded in a stronger donor ligand solvent pyridine, in which case, as expected, the conversion to octahedral form shown below:

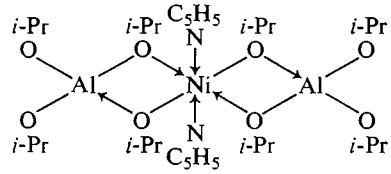

appears to be complete as shown by disappearance of tetrahedral bands (Table 2) in the spectrum.

The spectra of mixed tertiary butoxy and tertiary amyloxy

Can. J. Chem. Downloaded from www.nrcresearchpress.com by 210.87.254.42 on 09/06/12
For personal use only.

TABLE 2. Electronic spectra of bimetallic alkoxides and allied derivatives of nickel with aluminium

1	*2*	*3*	*4*	*5*	*6*	*7*	*8*	*9*	*10*
			Octahedral						Tetrahedral
Serial No.	Compound	Medium	$^3A_{2g} \rightarrow {}^3T_{2g}(F)$ (ν_1)*	$^3A_{2g} \rightarrow {}^3T_{1g}(F)$ (ν_2)	$^3A_{2g} \rightarrow {}^3T_{1g}(P)$ (ν_3)	Dq (cm^{-1})	B (cm^{-1})	β_{35}	$^3T_1 \rightarrow {}^3T_1(P)$ ($\nu_{3'}$)
1	$Ni[Al(OMe)_4]_2$	(*a*) Nujol	8 380	13 985	25 445	838	953	0.91	—
2	$Ni[Al(OEt)_4]_2$	(*a*) Nujol	9 028	14 705	24 690	903	821	0.79	17 480 19 340
		(*b*) EtOH	8 334	13 890	25 000	833	926	0.89	
3	$Ni[Al(O\text{-}n\text{-}Bu)_4]_2$	(*a*) Film	8 988	14 860	25 975	899	925	0.89	—
		(*b*) *n*-BuOH	9 115	14 925	25 380	911	865	0.83	—
4	$Ni[Al(O\text{-}i\text{-}Pr)_4]_2$	(*a*) Film	9 226	13 605	23 810	823	849	0.82	17 390 19 230
		(*b*) Benzene	9 005	12 790	23 640	900	629	0.60	17 390 19 050
		(*c*) *i*-PrOH	8 950	14 470	23 925	895	770	0.74	17 095 19 120
		(*d*) Pyridine	9 125	14 815	24 690	912	809	0.78	—
5	$Ni[Al(O\text{-}i\text{-}Pr)(O\text{-}t\text{-}Bu)_3]_2$	(*a*) Benzene	7 365	12 390	23 255	736	904	0.87	17 390 18 650
6	$Ni[Al(O\text{-}i\text{-}Pr)_2(O\text{-}t\text{-}Am)_2]_2$	(*a*) Benzene	7 254	12 240	23 365	725	923	0.88	17 380 18 690
7	$Ni[Al(OCH_3CF_3)_4]_2$	(*a*) Benzene	9 104	14 705	24 270	910	778	0.75	17 390 19 050
8	$Ni[Al(O\text{-}i\text{-}Pr)_2(acac)_2]_2$	(*a*) Benzene	7 690	12 930	23 810	769	908	0.87	17 390 18 975
9	$Ni[Al(acac)_4]_2$	(*a*) Benzene	9 917	15 550	24 690	992	699	0.67	—

*Calculated.

Can. J. Chem. Downloaded from www.nrcresearchpress.com by 210.87.254.42 on 09/06/12
For personal use only.

derivatives (columns 5 and 6 in Table 2) show comparatively more predominant bands due to tetrahedral forms as could be expected from the steric factors of more ramified tertiary alkyl groups. The spectrum of $Ni[Al(O\text{-}i\text{-}Pr_2(acac)_2]_2$ again depicts bands characteristic of an octahedral as well as a tetrahedral form, which appears to be much more predominant. The spectrum of the product with the composition $Ni[Al(acac)_4]_2$ is almost identical with that of the pure octahedral $Ni(acac)_2$ (13), and shows it to be a mixture of $Ni(acac)_2$ and $Al(acac)_3$.

Ligand field parameters for nickel(II) derivatives

From the spectroscopic data, various spectroscopic parameters like ligand field energy (10 *Dq*), Racah interelectronic-repulsion parameter (*B*), and covalency factor (β_{35}) have been calculated (Table 2). It is observed that the values of ν_1 (10 *Dq*), ν_2, and ν_3 transitions change markedly from the methoxide to ethoxide derivative but those for ethoxide and butoxide are almost similar. These values, however, show a marked decrease from *n*-butoxide to isopropoxide derivatives. Similarly there is a marked decrease in the values of ν_1 (10 *Dq*) from the isopropoxide to the tertiary butoxide derivative which is almost of same order as that of the tertiary amyloxide derivative. The values of Racah interelectronic repulsion parameter (*B*) obtained in these bimetallic alkoxides of nickel(II) are below the free ion value (1041 cm^{-1}) which are indicative of considerable covalent nature of the metal–ligand bond.

Spectrochemical and nephelauxetic series

The values of ligand field parameters (10 *Dq*) and (β_{35}) for alkoxy ligands can be fitted into the following spectrochemical and nephelauxetic series (14), respectively:

$$\underset{(680)}{Br^-} < \underset{(720)}{Cl^-} < \underset{(725)}{F^-} < \underset{(830)}{C_2H_5O^-} < \underset{(840)}{CH_3O^-} < \underset{(850)}{H_2O} < \underset{(895)}{i\text{-}C_3H_7O^-} < \underset{(910)}{n\text{-}C_4H_9O^-} < \underset{(1080)}{NH_3}$$

$$\underset{(0.92)}{F^-} > \underset{(0.91)}{CH_3O^-} > \underset{(0.89)}{H_2O} \simeq \underset{(0.89)}{C_2H_5O^-} > \underset{(0.84)}{NH_3} > \underset{(0.83)}{n\text{-}C_4H_9O^-} > \underset{(0.79)}{Cl^-} > \underset{(0.74)}{i\text{-}C_3H_7O^-} > \underset{(0.73)}{Br^-}$$

Experimental section

To avoid hydrolysis of starting materials as well as products, stringent precautions were taken to exclude moisture throughout the experimental work.

Hydrated $NiCl_2$ (B.D.H.) was made anhydrous by heating it carefully in an atmosphere of dry hydrogen chloride gas. Aluminium isopropoxide, $Al(O\text{-}i\text{-}Pr)_3$, was prepared (15) from aluminium foil and distilled (95°/0.5 mm) before use. Benzene and alcohols were dried according to the standard literature procedures. 2,2,2-Trifluoroethanol (Aldrich), 2,2,2-trichloroethanol (Aldrich), and 1,3-dichloro-2-propanol (Aldrich) were used after distillation.

Aluminium in the bimetallic compounds of nickel and aluminium was estimated as oxinate after removing nickel as nickel dimethylglyoximate. Isopropanol in the azeotrope was determined by a chromate oxidimetric method (8).

A semi-micro ebulliometer (Gallenkamp) with thermistor sensing was used for molecular weight determinations. The magnetic susceptibility measurements were carried out by Gouy Method.

Reactions of nickel aluminium isopropoxide, $Ni[Al(O\text{-}i\text{-}Pr)_4]_2$ with methanol, ethanol, and 2,2,2-trifluoroethanol

The benzene solution of $Ni[Al(O\text{-}i\text{-}Pr)_4]_2$ is refluxed with alcohol (methanol, ethanol, or 2,2,2-trifluoroethanol in excess) for 2–3 h and benzene and unreacted alcohol were removed from the reaction mixture under reduced pressure. The products thus obtained were finally dried at 30°/1 mm and analyzed. Synthetic and analytical data of these reactions are given in Table 1.

Reactions of $Ni[Al(O\text{-}i\text{-}Pr)_4]_2$ with n-butyl, tertiary butyl, and amyl alcohols, 2,2,2-trichloroethanol, and 1,3-dibromo-2-propanol

The reactions of $Ni[Al(O\text{-}i\text{-}Pr)_4]_2$ with *n*-butyl, tertiary butyl, and amyl alcohols, 2,2,2-trichloroethanol, and 1,3-dibromo-2-propanol have been carried out by heating a mixture of $Ni[Al(O\text{-}i\text{-}Pr)_4]_2$ and alcohol in benzene followed by azeotropic removal of liberated isopropanol. The completion of the reactions could be known by estimating the isopropanol content of the azeotrope quantitatively. When temperature became constant at 80°C, excess of solvent was removed under reduced pressure and the products were purified by distillation. With tertiary butyl and amyl alcohols, the amounts of isopropanol liberated as well as the analysis of the end products isolated corresponded to $Ni[Al(O\text{-}i\text{-}Pr)(O\text{-}t\text{-}Bu)_3]_2$ and $Ni[Al(O\text{-}i\text{-}Pr)_2(O\text{-}t\text{-}Am)_2]_2$, respectively. No further replacements of isopropoxy group with tertiary butoxy and amyloxy groups were possible even after a prolonged reflux (~5 h). The details of these reactions are shown in Table 1.

Reactions of $Ni[Al(O\text{-}i\text{-}Pr)_4]_2$ with acetylacetone in 1:4 and 1:8 molar ratio

Reactions of $Ni[Al(O\text{-}i\text{-}Pr)_4]_2$ with acetylacetone were carried out in benzene in 1:4 and 1:8 molar ratios. Calculated amount of acetylacetone was added to the benzene solution of $Ni[Al(O\text{-}i\text{-}Pr)_4]_2$ and contents were refluxed for ~10 h with the fractionation of the liberated isopropanol between 72–80°C. Completion of the reaction was checked by estimation of the amount of isopropanol in the azeotrope. Excess solvent was stripped off under reduced pressure. The pure compound $Ni[Al(O\text{-}i\text{-}Pr)_2(acac)_2]_2$ was isolated by distillation under reduced pressure, whereas $Ni[Al(acac)_4]_2$ was disproportionated into $Ni(acac)_2$ and $Al(acac)_3$ on attempted distillation. Other details of the reactions are given in Table 1.

Acknowledgements

One of the authors (J.V.S.) wishes to thank the University Grants Commission, New Delhi, for financial support.

1. D. C. BRADLEY, D. P. GAUR, and R. C. MEHROTRA. Metal alkoxides. Academic Press, London. 1978.
2. D. A. BROWN, D. CUNNINGHAM, and W. K. GLASS. J. Chem. Soc. 1563 (1968).
3. R. C. MEHROTRA, P. C. BHARARA, and B. P. BARANWAL. Transition Metal Chem. **2**, 204 (1977).
4. J. V. SINGH, B. P. BARANWAL, and R. C. MEHROTRA. Z. Anorg. Allgem. Chem. **477**, 235 (1981).
5. J. V. SINGH, N. C. JAIN, and R. C. MEHROTRA. Synth. React. Inorg. Metal-Org. Chem. **9**, 79 (1979).
6. R. C. MEHROTRA. Coordination chemistry-21. Pergamon, New York. 1981. pp. 113–125.
7. E. STUMPP and U. HILLEBRAND. Z. Naturforsch. **34**b, 262 (1979).
8. R. C. MEHROTRA. J. Ind. Chem. Soc. **30**, 585 (1953); **31**, 85 (1954).
9. B. P. BARANWAL and R. C. MEHROTRA. Aust. J. Chem. **33**, 37 (1980).
10. B. N. FIGGIS and J. LEWIS. Prog. Inorg. Chem. **6**, 37 (1964).
11. A. E. UNDERHILL and D. E. BILLING. Nature, London, **210**, 834 (1966).
12. J. V. SINGH and R. C. MEHROTRA. J. Ind. Chem. Soc. **54**, 109 (1977).
13. G. J. BULLEN, R. MASON, and P. PAULING. Inorg. Chem. **4**, 456 (1965).
14. A. B. P. LEVER. Inorganic electronic spectroscopy. Elsevier, London. 1968.
15. A. I. VOGEL. A text book of practical organic chemistry. Longman, London. 1973.

Excess heat capacities and excess volumes of tetraalkyltin compounds: $SnR_4 + SnR'_4$. Effect of correlations of molecular orientations and steric hindrance. Part 1

BERNARD RIEDL AND GENEVIÈVE DELMAS
Department of Chemistry, University of Quebec at Montreal, Montreal, P.Q., Canada H3C 3P8

Received July 4, 1983

BERNARD RIEDL and GENEVIÈVE DELMAS. Can. J. Chem. **62**, 1008 (1984).

A Picker flow calorimeter has been used to obtain molar excess capacities (c_p^E) through the concentration range at 25°C for the systems $SnR_4 + SnR'_4$ where R is the alkyl group C_nH_{2n+1} ($n = 1, 2, 3, 4, 8, 12$). Excess volumes have also been measured for the mixtures. Two contributions to c_p^E and v^E were investigated: those associated with disordering the long alkyl chains and with steric hindrance. The steric hindrance contribution has been found to occur for molecules having a highly substituted central atom. The sign of this contribution is negative in h^E and positive in c_p^E, indicative of an ordering or loss of mobility for the molecules going from pure liquid to solution. The c_p^E results confirm the more sterically hindered character of the ethyl and propyl derivatives already found with h^E. The separation of the disorder and steric contribution is possible in systems involving long-chain compounds. It is found that the orientational order contribution diminishes more slowly with temperature than the steric hindrance effect. The trend of v^E in the series is reasonably well predicted by the Prigogine–Patterson–Flory theory.

BERNARD RIEDL et GENEVIÈVE DELMAS. Can. J. Chem. **62**, 1008 (1984).

Opérant à 25°C, sur un large éventail de concentrations et utilisant un calorimètre à écoulement du type Picker, on a déterminé les capacités molaires en excès (c_p^E) des systèmes $SnR_4 + SnR'_4$ où R est un groupe alkyle du type C_nH_{2n+1} ($n = 1, 2, 3, 4, 8, 12$). On a également mesuré les volumes molaires en excès de ces mélanges. On a évalué deux contributions au c_p^E et au v^E soit celle associée au désordre apporté par les longues chaînes alkylées ainsi que celle due à l'encombrement stérique. On a trouvé que la contribution due à l'encombrement stérique se manifeste dans les molécules ayant un atome central très substitué. Cette contribution a un signe négatif pour h^E et un signe positif pour c_p^E; ceci indique la présence d'un agencement spécial ou une perte de mobilité pour les molécules passant du liquide pur à la solution. Les résultats pour c_p^E confirment les conclusions qui découlent de h^E à l'effet que les dérivés éthyliques et propyliques sont stériquement plus encombrés. Il est possible de séparer la contribution relative au désordre et de la contribution stérique dans les systèmes impliquant des composés à longue chaîne. On a trouvé que la contribution due à l'ordre orientationel diminue plus lentement avec la température que l'effet dû à l'encombrement stérique. La tendance de v^E dans la série peut être prévue de façon raisonnable par la théorie de Prigogine–Patterson–Flory.

[Traduit par le journal]

Introduction

This work is part of an investigation of the effect of the molecular shape on the thermodynamic properties of mixtures. The SnR_4 ($R = C_nH_{2n+1}$) molecules are convenient for this purpose since the gradual lengthening of the R group will transform the molecular shape from globular to star-shape without significantly changing the chemical nature. Furthermore, the presence of a tetrasubstituted Sn central atom gives the molecule some special features similar to those in carbon compounds (for example, $C(C_2H_5)_4$ or 3,3-diethyl pentane (DEP)). Heats of mixing of the $SnR_4 + SnR'_4$ compounds (1) as well as those of SnR_4 with linear and branched alkanes (2, 3) have given a coherent picture of the orientational order in long chain alkane-like compounds. Orientational order occurring in the pure compounds (A) may be partially preserved if the second component (B) is also ordered (3). On the contrary, globular (B) molecules destroy the order in A and this disordering process is associated with a large endothermic heat. Excess volumes (4) and excess viscosities (5, 6) of mixtures involving SnR_4 compounds have been obtained and compared with theoretical predictions using recent data on equation of state parameters (7) of the SnR_4 liquids. The order of pure liquids diminishes rapidly with increasing temperature as does the corresponding contribution to h^E (8–10).

Since unexpected values of h^E have been found in many systems involving some molecules whose central atom is highly substituted (10–13), a new negative contribution to the heats of mixing, h^E (steric hindrance), has been suggested. This contribution has also been called "condensation" contribution by Patterson (13–15) and "coupling of torsional oscillations" contribution by de Ligny (16). The term condensation is in line with the negative sign of the heat, interpreted as a reduction of the mobility of the flexible —CH_2—CH_2— segments (and possibly of the other component) after mixing. In the series of differently substituted hexanes, heptanes, octanes, the extent of steric hindrance of the pure compounds has been related (16) to the mean number of *gauche* configurations, Z_g (17). The steric hindrance contribution is smaller in trialkylamine series (8, 12, 18) but large in polymeric solutions (19).

In previous work, the heats of mixing were written as the sum of four different contributions:

$$[1]\quad h^E(\text{exp}) = h^E(\text{chem}) + h^E(\text{f.v.}) + h^E(\text{dis.}) + h^E(\text{ster. hindr.})$$

where f.v. stands for free volume, dis. stands for disorder, and ster. hindr. for steric hindrance.

This equation was found to be a convenient way to describe the heats even if there is no proof that these contributions are independent and additive.

Similarly, c_p^E may be written in the same format:

$$[2]\quad c_p^E(\text{exp}) = c_p^E(\text{chem}) + c_p^E(\text{f.v.}) + c_p^E(\text{dis.}) + c_p^E(\text{ster. hindr.})$$

where c_p^E(chem) and c_p^E(f.v.) refer, respectively, to the contributions coming from force field and free volume difference and c_p^E(dis.) and c_p^E(ster. hindr.) from the disordering and steric hindrance contributions that we are focussing on in the present work.

Can. J. Chem. Downloaded from www.nrcresearchpress.com by 210.87.254.42 on 09/06/12
For personal use only.

TABLE 1. Expected signs of h^E, v^E, and c_p^E for the different contributions

Parameter	Force field difference	Free volume difference	Disordering	Sterical hindrance
h^E	$+^a$	$-^{b,d}$	+	−
Change of h^E when T increases	Little change	More −	Less +	Less −
c_p^E	About 0	$-^{b,d}$	−	+
v^E	+	$-^{b,c,d}$	+	−

[a] In non-polar systems.
[b] Depends mostly on the difference in expansion coefficients.
[c] Depends also on the relative cohesive energy of the two components.
[d] Values have been calculated in ref. 1 for h^E, in Tables 3 and 4 for c_p^E and v^E.

Can. J. Chem. Downloaded from www.nrcresearchpress.com by 210.87.254.42 on 09/06/12
For personal use only.

Signs of h^E *and* c_p^E

The excess heat capacity $c_p^E = dh^E/dT$ may be used to separate the different contributions to the heats or at least to detect the dominant one. For non-polar systems, the normal sign of h^E is positive and that of c_p^E is usually negative but small. However, when h^E is due to the destruction of order, c_p^E is expected to be large and negative since the orientational order diminishes rapidly when T increases. The facts that the steric hindrance contribution is linked with the mobility of the molecule, and that it is found to increase with a low free volume second component (8) and the direct determination of h^E(ster. hindr.) with temperature (13) all indicate that this contribution, like h^E(dis.), diminishes with temperature. Fortunately, since h^E(ster. hindr.) is exothermic, c_p^E(ster. hindr.) is expected to be positive, a feature which will assist the separation of the contributions to c_p^E. Table 1 gives a summary of the above considerations.

In the present work, excess volumes and heat capacities have been measured at 25°C for the fourteen $SnR_4 + SnR_4'$ systems listed in Table 2. The aim was mainly to confirm the steric hindrance character of the propyl and ethyl derivatives and support the validity of the separation of the contributions as proposed for the h^E. A comparison will be made between the stability with temperature of the correlations of molecular orientations in the SnR_4 molecules and the alkanes (14). In the following text, the names of the SnR_4 will be shortened to $SnMe_4$, $SnEt_4$, etc. as listed in Table 3.

Experimental section

Materials

The tetraalkyltin derivatives were prepared by the Organisch Chemical Instituut (Utrecht) except for $SnDodec_4$ which has been obtained from Inorganic Chem. Corp. (Sun Valley, Calif.). Density and gas chromatography were used to test their purity. The latter, as given by a Hewlett Packard 5730A gas chromatograph was 99.8% or more for five compounds and 98.6 and 97.4% for $SnPr_4$ and br-C_{16}, respectively (Table 3). For non-volatile compounds such as $SnOct_4$ and $SnDodec_4$, the largest difference in density with those previously measured (1, 8) was 7×10^{-4} g cm^{-3}.

Apparatus

Excess heat capacities were obtained at 25°C throughout the concentration range using the Picker flow calorimeter (Techneurop, Montreal, and Setaram, Lyon) as described previously (20). For more viscous solutions, the cross section of the tubing was increased from 0.5 to 1.0 mm^2. Densities have been measured with an Anton-Paar precision densitometer (Fisher Co.) described elsewhere (5). *Precision and accuracy*: for the reference system c-C_6 + n-C_{16}, the present c_p^E values are within 0.02 J K^{-1} mol^{-1} of the published data. For a given system, the reproducibility of the measurements which include solution density and heat capacity data is about the same. For the $SnDodec_4$ systems, the reproducibility is poorer (0.1 to 0.2 J K^{-1} mol^{-1}) due to the high viscosity of the solutions. For each system, the number of points made and the mean square standard deviation have been added in the table.

Physicochemical constants and calculated parameters

Table 3 gives the densities, thermal expansion coefficients, and thermal pressure coefficients (γ) of the SnR_4 compounds. The parameters necessary to calculate the equation of state terms in h^E, v^E, and c_p^E such as P^*, V^*, are also listed. V^* is the core volume or volume at 0 K. The details of the calculations and, in particular, the equations for the free volume contribution to h^E, c_p^E, and v^E and the interaction energy parameters X_{12} are given in the Appendix.

Molecular shape

The molecular surface-to-volume ratios used in the Prigogine–Patterson–Flory theory can be obtained from models. A cylindrical model for the linear alkanes (n-C_7 to n-C_{16}) gives s values between 1.0 and 0.9 Å^{-1}. For $SnMe_4$ a spherical model gives $s = 0.96$. A combination of the two models gives s values between 0.82 and 0.86 for the SnR_4 compounds ($2 \leq n \leq 12$).

Results and discussion

The c_p^E and v^E values are represented by the Redlich–Kister equations:

$$c_p^E = x_1 x_2 \sum_{i=0}^{2} C_i (x_1 - x_2)^i$$

$$v^E = x_1 x_2 \sum_{i=0}^{2} B_i (x_1 - x_2)^i \quad [3]$$

The concentrations, the values at the maximum, and the values of the constants B_i, C_i are listed in Tables 2 and 4. The B_i, C_i parameters have been omitted for systems involving the dodecyl component due to the lack of precision caused by the high viscosity of $SnDodecyl_4$.

In Table 2, the systems are divided into two groups: six systems made of globular SnR_4 are listed in the type-A group for which h^E(dis.) $\simeq c_p^E$(dis.) = 0 and eight systems are in the type-B group for which the disordering of $SnOct_4$ and $SnDodec_4$ brings a large disordering contribution in h^E and c_p^E.

The X_{12} interchange energy parameter calculated from the experimental heats from which the free volume contribution has been subtracted, corresponds to the sum of the three other contributions. A negative value of X_{12} is an indication of the importance of the steric hindrance contribution since it is the only contribution which gives negative heats apart from the free volume one. For the mixture of globular molecules (A systems), X_{12} is found negative for only one system, $SnEt_4 + SnPr_4$

Can. J. Chem. Downloaded from www.nrcresearchpress.com by 210.87.254.42 on 09/06/12
For personal use only.

TABLE 2. Excess heat capacities, c_p^E for the $SnR_4 + SnR'_4$ systems at the concentration x_1 of the maximum; the C_i parameters are the coefficients of the Redlich–Kister equation; c_p^E(f.v.) has been calculated at the same concentration

Class	Component: (1)	(2)	c_p^E(exp) ($J K^{-1} mol^{-1}$)	x_1	C_0 ($J K^{-1} mol^{-1}$)	C_1 ($J K^{-1} mol^{-1}$)	C_2 ($J K^{-1} mol^{-1}$)	$(c_p^E)_v \times 10^{2\,b}$ ($J cm^{-3} K^{-1}$)	c_p^E(f.v.) ($J mol^{-1} K^{-1}$)	c_p^E(exp) − c_p^E(f.v.) ($J mol^{-1} K^{-1}$)	$\sigma(\ )^c$
A^a	$SnMe_4$	+ $SnEt_4$	−0.29	0.65	−1.185	0.322	−0.129	−0.23	−0.23	−0.06	0.04(5)
	$SnMe_4$	+ $SnPr_4$	−0.44	0.58	−1.838	−1.059	1.181	−0.31	−0.62	0.18	0.05(5)
	$SnMe_4$	+ $SnBut_4$	−0.31	0.46	−1.224	−0.905	—	−0.20	−0.88	0.57	0.01(5)
	$SnEt_4$	+ $SnPr_4$	0.51	0.58	2.083	0.863	−1.143	0.28	−0.08	0.59	0.03(5)
	$SnEt_4$	+ $SnBut_4$	−0.32	0.69	−1.098	−1.513	—	−0.16	−0.19	−0.13	0.05(3)
	$SnPr_4$	+ $SnBut_4$	−0.18	0.55	−0.778	−0.0878	−0.386	−0.08	−0.05	−0.13	0.03(5)
B^a	$SnMe_4$	+ $SnOct_4$	−4.15	0.51	−17.092	−4.333	+5.242	−1.55	−1.06	−1.69	0.28(5)
	$SnMe_4$	+ $SnDodec_4$	−5.03					−2.69	−1.07	−3.96	(7)[d]
	$SnEt_4$	+ $SnOct_4$	−1.21	0.78	−4.213	−4.540		−0.50	−0.26	−0.95	0.16(3)
	$SnEt_4$	+ $SnDodec_4$	−2.87					−1.10	−0.32	−2.55	(8)[d]
	$SnPr_4$	+ $SnOct_4$	−0.50	0.65	−1.779	−1.217		−0.17	−0.05	−0.45	0.05(3)
	$SnPr_4$	+ $SnDodec_4$	−1.43					−0.43	−0.09	−1.34	(7)[d]
	$SnBut_4$	+ $SnOct_4$	−1.97	0.55	−8.689	−0.976	9.036	−0.56	0.06	−1.91	0.12(5)
	$SnBut_4$	+ $SnDodec_4$	−4.90					−1.24	−0.12	−4.78	

[a] In class A, the c_p^E values are small due to the absence of long-chain molecules and the destruction of the orientational order prevalent in class B systems.
[b] c_p^E per cm^3 for comparison of systems with different V^*, as used in Fig. 1.
[c] Number of experimental points in parentheses.
[d] In separate runs, more points are made in solutions rich in the less viscous component.

TABLE 3. Physicochemical data[a] (d, α, γ) equation of state parameters (p^*, V^*)[b] and shape factors (s) for the pure compounds, SnR_4

Compound	$d_{25°C}$ (g cm^{-3})	$10^3\ \alpha_{25°C}$ (K^{-1})	$\gamma^{25°C}$ (J cm^{-3} K^{-1})	P^* (J cm^{-3})	V^* (cm^3 mol^{-1})	$s = S/v^{c}$ (Å^{-1})	Purity[c] (%)
$SnMe_4$	1.2805	1.28	0.809	409	106.7	0.96	99.8
$SnEt_4$	1.1955	1.00	0.977	454	158.6	0.86	99.9
$SnProp_4$	1.0992	0.89	1.071	579	215.8	0.84	98.6
$SnBut_4$	1.0456	0.818	1.006	439	275.6	0.83	99.9
$SnOct_4$	0.9571	0.790	—	445[d]	496.4	0.83	—
$SnDodec_4$	0.9170	0.767	1.107	473	724.7	0.82	—

[a] Reference 8.
[b] See Appendix.
[c] See text.
[d] Interpolated.
[e] Using a Hewlet-Packard 5730A gas chromatograph, with a polydimethyl siloxane column (OV-101), set at $T = T_E - 20$ K where T_E is the boiling point of the solvent.

(tenth column of Table 4). This is not surprising since a small positive h^E(chem) must occur in the mixtures of lighter SnR_4. The advantage of the c_p^E is indeed to allow a finer separation of the contributions as will be seen later. On the type-B systems, the large irregularities in the series of h^E or X_{12} were interpreted as an indication of sizeable steric hindrance contributions.

Two of the contributions to c_p^E in eq. [2] will not come into the discussion. On the one hand, the c_p^E(chem) are negligible for two reasons: the similarity in force field of these molecules and the lack of variation with temperature of h^E(chem) and, on the other hand, the c_p^E(f.v.) which can be calculated. By assuming c_p^E(chem) = 0, eq. [3] becomes, for the type-B systems:

$$[4]\quad c_p^E(\text{exp}) - c_p^E(\text{f.v.}) = c_p^E(\text{dis.}) + c_p^E(\text{ster. hindr.})$$

while, for the type-A group mixtures, it reduces to:

$$[5]\quad c_p^E(\text{exp}) - c_p^E(\text{f.v.}) = c_p^E(\text{ster. hindr.})$$

The free volume contribution to c_p^E has been listed in the eighth column of Table 2. (See Appendix for the expression.) The last column is $c_p^E - c_p^E$(f.v.). For six systems out of the fourteen, the c_p^E(f.v.) is less than 5% of the experimental value.

The signs of the c_p^E(exp) listed in Table 2 are all negative except for the system $SnEt_4 + SnPr_4$. This means that for all the other systems, the free volume and disordering contributions combine to mask the steric hindrance term, if there is one, as was the case with h^E.

Mixtures of globular SnR_4: (type-A systems)

For the $SnEt_4 + SnPr_4$ system, the positive c_p^E gives the same information as h^E, i.e., dominance of a steric hindrance contribution. For four other systems, the subtraction of c_p^E(f.v.) gives values of the difference inferior to 0.2 J K^{-1} mol^{-1} so that no special comment is necessary on such small values which must be the combination of several small effects as were the small (<60 J mol^{-1}) h^E. The c_p^E measurements may have revealed a steric hindrance contribution on the $SnMe_4 + SnBut_4$ system since c_p^E(exp) − c_p^E(f.v.) is +0.57. However, one must be careful in this conclusion for the following reason. Many indications have been gathered (1–3, 21) on a large variety of systems, showing that the free volume term calculated is too large for important free volume differences between the components with the consequence of an increased X_{12} for these systems. Similar errors in the calculated c_p^E(f.v.) would generate positive values of c_p^E(exp) − c_p^E(f.v.) which would not have a physical meaning in terms of steric hindrance. Although it is not unlikely that the calculated c_p^E(f.v.) are not as much overestimated as the h^E(f.v.), it is only possible to say that the steric hindrance may indeed occur for this system but that it is not very large. Fortunately, on the type-B group containing the $SnOct_4$ and $SnDodec_4$ molecules made of long —CH_2—CH_2— sequences which can be disordered, the steric hindrance contribution will be seen without ambiguity.

Mixtures of globular + linear SnR_4: (type-B systems)

In order to compare the experimental values for the different systems, c_p^E(exp) per cm^3 at the maximum of the concentration range for the different systems have been plotted in the bottom part of Fig. 1 versus the core volume of the second component. A line is drawn through the points for the $SnOct_4$ and another for the $SnDodec_4$ results.

$$[6]\quad (c_p^E)_v = c_p^E \text{ per cm}^3 = c_p^E \text{ per mole}/(x_1 V_1^* + x_2 V_2^*)$$

The same plot is given in the top part of Fig. 1, using h_v^E, the experimental heat of mixing per cm^3 defined in the same way as $(c_p^E)_v$.

The characteristic features of these SnR_4 mixtures given by this figure are the following: (*1*) The $(c_p^E)_v$ are large and negative and increase between $SnOct_4$ and $SnDodec_4$. (*2*) The irregularities observed in h_v^E with $SnEt_4$ and $SnPr_4$ and interpreted as due to an extra exothermic steric hindrance contribution for these two components, are seen on the $(c_p^E)_v$ and correspond to a positive term as expected. (*3*) The $(c_p^E)_v$ curves are mirror images of the h_v^E indicating probably that, in each case, one contribution, that of disordering the long chains, is dominant.

Variation of the steric hindrance contribution with the size of the alkyl group SnR_4

When the length of the alkyl group becomes greater the influence of the central crowded atom along the chain and towards the second component in solution is likely to diminish so that the steric hindrance contribution decreases also. However, since the steric hindrance effect has been shown (19,21) to increase for low free volume of the sterically hindered component, one can expect the size of the steric hindrance contribution to be lower for the volatile SnR_4. Consequently, the apparently maximum effect with $SnPr_4$ is then not unreasonable. Furthermore, $SnMe_4$ may fail to give a steric hindrance contribution on mixing (or give a lower one than $SnEt_4$ and $SnPr_4$) not only for its large free volume but also because of the shielding effect of the four bulky methyl groups which prevent the second component to come near enough to the central atom.

Can. J. Chem. Downloaded from www.nrcresearchpress.com by 210.87.254.42 on 09/06/12
For personal use only.

Can. J. Chem. Downloaded from www.nrcresearchpress.com by 210.87.254.42 on 09/06/12
For personal use only.

TABLE 4. Excess volumes v^E for the $SnR_4 + SnR'_4$ systems at the concentration x_1 of the maximum; the B_i parameters are the coefficients of the Redlich–Kister equation, v^E and $X_{12}s_1^{-1}$ have been calculated at the same concentration

Class	Component (1)	Component (2)	v^E ($cm^3\ mol^{-1}$)	x_1	B_0[d]	B_1[d]	B_2[d]	v^E(calcd)[d]	$v^E(h^E)$[d]	$v^E(P^*)$[d]	v^E(f.v.)[d]	$X_{12}s_1^{-1}$[e]	σ( )[b]
A[a]	$SnMe_4$	+ $SnEt_4$	−0.38	0.55	−1.55	−0.42	−0.17	−0.314	0.010	−0.180	−0.144	0.32	0.00(5)
	$SnMe_4$	+ $SnPr_4$	−0.31	0.61	−1.20	−0.53	0.01	−0.640	0.077	−0.417	−0.300	1.71	0.01(5)
	$SnMe_4$	+ $SnBut_4$	−0.47	0.65	−1.74	−0.89	−0.14	−0.652	0.101	−0.255	−0.498	3.82	0.01(5)
	$SnEt_4$	+ $SnPr_4$	−0.02	0.65	−0.05	−0.06	−0.037	−0.106	−0.012	−0.057	−0.036	−0.35	0.00(4)
	$SnEt_4$	+ $SnBut_4$	0.04	0.42	0.16	−0.03	0.00	−0.005	0.042	0.066	−0.114	1.20	0.00(5)
	$SnPr_4$	+ $SnBut_4$	0.03	0.46	0.11	−0.01	−0.01	0.072	0.014	−0.079	−0.021	0.33	0.00(5)
B[a]	$SnMe_4$	+ $SnOct_4$	−0.73	0.70	−2.44	−2.35	−1.58	−1.180	0.316	−0.816	−0.683	9.40	0.04(5)
	$SnMe_4$	+ $SnDodec_4$	−0.91	0.80	−2.23	−2.10	−5.43	−1.030	0.536	−0.783	−0.785	17.1	0.06(4)
	$SnEt_4$	+ $SnOct_4$	0.13	0.53	0.51	−1.09	−0.24	−0.227	0.157	−0.196	−0.187	3.40	0.00(6)
	$SnEt_4$	+ $SnDodec_4$	0.66	0.70	3.07	−1.52	0.864	−0.121	0.302	−0.155	−0.268	4.70	0.01(6)
	$SnPr_4$	+ $SnOct_4$	−0.14	0.51	−0.52	−0.32	0.19	0.121	0.201	−0.025	−0.055	1.40	0.01(5)
	$SnPr_4$	+ $SnDodec_4$	−0.12	0.70[c]	—	—	—	0.177	0.243	0.018	−0.084	3.50	— (6)
	$SnBut_4$	+ $SnOct_4$	0.22	0.50	0.86	0.01	0.166	0.163	0.156	0.012	−0.005	1.90	0.01(6)
	$SnBut_4$	+ $SnDodec_4$	0.28	0.55	1.09	0.28	−0.68	0.246	0.338	−0.078	−0.014	4.20	0.01(6)

[a] For $SnEt_4$, $SnPr_4$, and $SnBut_4$, the $s_1^{-1}X_{12}$ are smaller than quoted in ref. 1 because the cylindrical model (8) rather than the spherical model has been used to calculate s_1.
[b] Number of experimental points.
[c] *S*-shape curve with a positive maximum at $x_1 = 0.30$ of 0.08 $cm^3\ mol^{-1}$.
[d] In $cm^{-3}\ mol^{-1}$.
[e] In $J\ cm^{-3}\ Å^{-1}$.

Can. J. Chem. Downloaded from www.nrcresearchpress.com by 210.87.254.42 on 09/06/12
For personal use only.

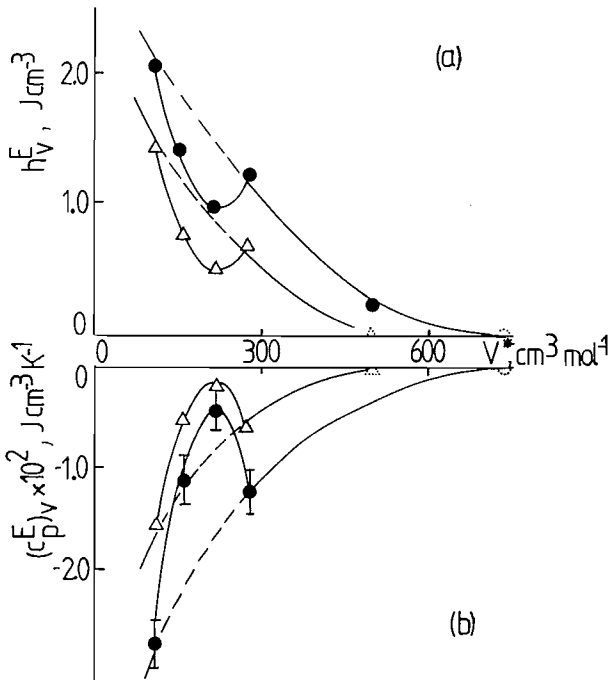

FIG. 1. Excess heats in J cm^{-3} (curve *a*) and excess heat capacities in J cm^{-3} K^{-1} (curve *b*) for $SnOct_4$ (△) and $SnDodec_4$ (●) mixed with $SnMe_4$, $SnEt_4$, $SnPr_4$, $SnBut_4$ plotted against the core volume V^* of the smaller SnR_4. The main contribution comes from the disordering of the long chain giving positive h^E and negative c_p^E. The difference between the curves and the dotted lines corresponds to the extra steric hindrance contribution with $SnEt_4$, and $SnPr_4$ ($h^E < 0$ and $c_p^E > 0$) plotted in Fig. 2 (curve *a*).

1. Quantitative evaluation of the disordering contribution c_p^E(dis.)

Because of the more negative values of c_p^E for the four systems $SnMe_4$ and $SnBut_4$ mixed with the dodecyl and octyl derivatives, the assumption will be made for these four systems that:

$$c_p^E(\text{exp}) - c_p^E(\text{f.v.}) = c_p^E(\text{dis.})$$
$$h_p^E(\text{exp}) - h^E(\text{f.v.}) = h^E(\text{dis.}) \quad [7]$$

2. Temperature variation of the order in long chain liquids

If the order is assumed to diminish exponentially with temperature, the disordering contribution of h^E and c_p^E can be written (14):

$$h^E(\text{dis.}) = h_0 \exp(-T/\tau)$$
$$c_p^E(\text{dis.}) = \frac{h_0}{\tau} \exp(-T/\tau) \quad [8]$$
$$h^E(\text{dis.})/c_p^E(\text{dis.}) = -\tau$$

One would then expect a linear relationship between h^E(dis.) and c_p^E(dis.). Such a relationship has indeed been found for the four systems cited above with a characteristic temperature τ of 120 K as shown in Fig. 2.

However, instead of plotting the disordering contribution as defined in eq. [7], the h^E(exp) and c_p^E(exp) have been used directly. We make this choice because of the likely dominance of one contribution; the four points lie reasonably well on a straight line and it extrapolates to 0. Due to the large calculated free volume contributions to h^E (−100 J mol^{-1}) and c_p^E (1.0 J K^{-1} mol^{-1}) in the $SnMe_4$ systems, there may be as much error subtracting the free volume terms as ignoring them. The difference between the characteristic temperatures 50 K for n-C_{16} and 120 K for $SnOct_4$ and $SnDodec_4$ is quite reasonable. At equal free volume, one would expect the order of a chain of the SnR_4 to be stabilized by the order of the three others and by the large mass of the compounds. Consequently, when the temperature increases the order would disappear more slowly than that of the worm-like alkane chains. The method to find h^E(dis.) which could appear arbitrary seems to be justified by the results which compare well with h^E(dis.) found for linear alkanes (8, 12, 14).

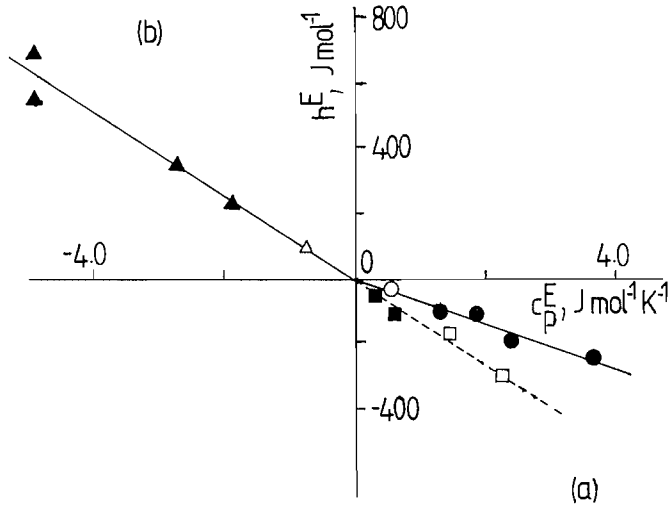

FIG. 2. Correlation between the h^E and c_p^E for the steric hindrance contribution (curve *a*) and the disordering contribution (curve *b*), of $SnOct_4$ and $SnDodec_4$ mixed with $SnMe_4$ and $SnBut_4$ (▲) and with $SnEt_4$ and $SnPr_4$ (●). From eq. [8] the characteristic temperatures are found to be 120 K and 70–80 K for the disordering and steric hindrance effects, respectively. In the disorder quadrant, the point corresponding unexpectedly to the $SnEt_4$ + br-C_{16} system (△) has been added (Part 2, to be published). In the steric hindrance part, two values in the literature on the systems 3,3-DEP + n-C_9 and n-C_{16} (□), have been plotted for comparison as well as two systems presented in part 2, $SnPr_4$ and $SnBut_4$ + br-C_{16}. (■). Direct experimental data for the $SnEt_4$ + $SnPr_4$ system (○).

Analysis of the steric hindrance contribution

The systems involving long-chain components will again be used to evaluate the magnitude of the steric hindrance contribution. In Fig. 1, the two points on the peak of the dodecyl curve (●) and the two points on that of the octyl curve (△) corresponding to the c_p^E values in mixtures with the ethyl and propyl derivatives will be considered. The difference between the experimental value and the expected value on the dotted line will be assumed to represent the steric hindrance contribution for these four systems. The values per mole obtained after multiplying by the molar volume at the concentration of the maximum are, respectively, in J K^{-1} mol^{-1}, 1.3 and 1.8 for $SnEt_4$ and $SnPr_4$ mixed with $SnOct_4$ and 2.4 and 3.6 for the same mixed with $SnDodec_4$. Other ways of obtaining the expected value without steric hindrance such as interpolating a plot of c_p^E versus α rather than c_p^E versus V^* or using the molar c_p^E would give c_p^E(ster. hindr.) within 0.1 to 0.2 J K^{-1} mol^{-1} of the ones listed above. On the lower part of Fig. 2, the points c_p^E(ster. hindr.) have been plotted versus h^E(ster. hindr.) which was obtained in ref. 1 using a procedure similar to that described above for c_p^E(ster. hindr.). The alignment of the four

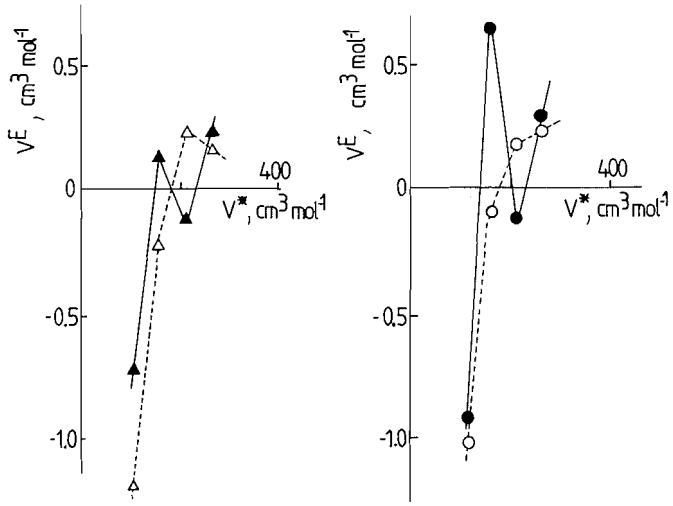

FIG. 3. v^E(exp) for the systems $SnOct_4$ (▲) and $SnDodec_4$ (●) + $SnMe_4$, $SnEt_4$, $SnPr_4$, and $SnBut_4$ plotted against the core volume V^* of the smaller SnR_4 compounds. The dotted lines correspond to the calculated values. With these two compounds, as with others (18), the v^E values in the $SnEt_4$ mixtures are unexpectedly high.

points with the origin and with the point obtained directly (○, $SnEt_4$ + $SnPr_4$ system) gives some confidence in the validity of the method of evaluation of a specific contribution. The c_p^E(ster. hindr.) are positive as expected from an exothermic contribution to the heats which becomes less important when the temperature is raised. With the same assumption as that made for the temperature dependence of order (eq. [8]), the characteristic temperature is found to be between 70 and 80 K for the steric hindrance effect compared to 120 K for the disorder one.

The corresponding steric hindrance contributions for two other systems whose components are rather similar in shape with the present ones have been plotted on Fig. 1*b*. They are 3,3-DEP (or CEt_4) mixed with *n*-C_9 and *n*-C_{16} (9, 10). There, the separation of the steric contribution has been done by subtracting the values obtained with 3,3-DEP from those obtained with an isomer 2,2,5-trimethylhexane which is considered much less or not at all sterically hindered. This effect is found to be of similar magnitude in the two series, their differences in slope and characteristic temperatures may have several origins. It may be due to the difference in shape of the ordered molecules, i.e. *n*-C_{16} and $SnDodec_4$ or a difference in steric hindrance due to the central atoms, C for DEP and Sn for $SnEt_4$ and $SnPr_4$ respectively. Probably, the procedures of separation used in the two series, which cannot be identical since non-sterically hindered isomers of the SnR_4 do not exist, may introduce some difference in the characteristic temperature.

Excess volumes

As verified over a large number of systems (4, 15, 18) the Prigogine–Patterson–Flory theory with the van der Waals model can successfully predict v^E for non-polar or polar mixtures due in part to the fact that the experimental h^E is included in the calculation. Table 2 gives the overall v^E results and Fig. 3 the comparison between v^E(exp) and v^E(calcd) for the type-B systems.

Type-A systems

v^E(exp) − v^E(calcd) is less than 0.1 cm^3 mol^{-1} for four of the six systems in this group. Columns 6 to 9 give the details of the three contributions to v^E(calcd). The negative v^E are due mainly to the contraction on mixing of the lighter SnR_4 when mixed with a less volatile compound. For the second and third systems, v^E is found to be too large because of the $v^E(P^*)$ term whose negative contribution adds to $v^E(\tilde{v})$. On similar systems (18), $v^E(P^*) = (\tilde{v}_1 - \tilde{v}_2)\,(P_1^* - P_2^*)$ also appeared overestimated for relatively large differences in $\tilde{v}$ or in P^* of the two components.

Type-B systems

The dotted lines in Fig. 3 give the calculated v^E, at the maximum, for eight systems. For the two larger order-breakers, $SnPr_4$ and $SnBut_4$, the disordering of the octyl and dodecyl chains is at the origin of the dominant positive contribution while the difference of free volumes contributes to the negative v^E for the more volatile SnR_4. The general trend of the experimental results is well predicted. However, the two systems involving $SnPr_4$ and the two with $SnEt_4$ present interesting large difference between v^E(calcd) and v^E(exp). The more negative v^E(exp) when a sterically hindered compound is mixed with a long chain has been found previously (4) with two highly branched alkanes, probably reflecting the diminution of mobility due to steric hindrance. The result obtained for the system $SnEt_4$ + $SnDodec_4$ is completely anomalous since it is found to be 0.66 cm^3 mol^{-1} while the predicted value is 0.12 cm^3 mol^{-1}. A similar high positive value is seen in the $SnEt_4$ + $SnOct_4$ system although the anomaly is less pronounced. The result seems less eccentric when other v^E measurements on mixtures involving $SnEt_4$ (Part 2, to be published, and ref. 18*b*) also show unexpected positive v^E. But for the other systems, h^E is also positive or more positive than expected. The present system constitutes then an interesting and rare case where the v^E shows an anomaly not yet seen on the heats.

In the SnR_4 + SnR_4' mixtures, the experimental results on c_p^E confirm the interpretation of the h^E in terms of free volume, disordering and steric hindrance contributions and, in particular, of the greater importance of the latter in the $SnEt_4$ and $SnPr_4$ systems when the second component is a long flexible —CH_2—CH_2— chain.

Acknowledgment

The financial support of the Natural Sciences and Engineering Research Council of Canada is gratefully acknowledged.

1. G. DELMAS and NG. T. THANH. J. Phys. Chem. **81**, 1730 (1977).
2. S. TURRELL and G. DELMAS. J. Chem. Soc. Faraday I, **70**, 572 (1974).
3. G. DELMAS and NG. T. THANH. J. Chem. Soc. Faraday I, **71**, 1172 (1975).
4. G. DELMAS, P. DE SAINT-ROMAIN, and P. PURVES. J. Chem. Soc. Faraday I, **71**, 118 (1975).
5. G. DELMAS, P. PURVES, and P. DE SAINT-ROMAIN. J. Phys. Chem. **79**, 1970, (1975).
6. C. JAMBON and G. DELMAS. Can. J. Chem. **55**, 1360 (1977).
7. R. PHILIPPE, M. COUCHON, and G. DELMAS. Can. J. Chem. **56**, 370 (1978).
8. R. PHILIPPE, H. P. NGUYEN, and G. DELMAS. Can. J. Chem. **56**, 2856 (1978).
9. M. CROUCHER and D. PATTERSON. J. Chem. Soc. Faraday II, **70**, 1479 (1974).
10. P. TANCRÈDE, P. BOTHOREL, and D. PATTERSON. J. Chem. Soc. Faraday II, **73**, 29 (1977).
11. P. TANCRÈDE, P. BOTHOREL, P. DE SAINT-ROMAIN, and D. PATTERSON. J. Chem. Soc. Faraday II, **73**, 15 (1977).

Can. J. Chem. Downloaded from www.nrcresearchpress.com by 210.87.254.42 on 09/06/12
For personal use only.

12. R. PHILIPPE, G. DELMAS, and P. N. HONG. Can. J. Chem. **57**, 517 (1979).
13. P. DE SAINT-ROMAIN, H. TRA VAN, and D. PATTERSON. J. Chem. Soc. Faraday I, **75**, 1708 (1979).
14. S. N. BATTACHARYYA and D. PATTERSON. J. Solution Chem. **9**, 247 (1980).
15. (*a*) H. TRAVAN and D. PATTERSON. J. Solution Chem. **11**, 793 (1982). (*b*) M. COSTAS and D. PATTERSON. J. Solution Chem. **11**, 807 (1982).
16. C. L. DE LIGNY and W. E. HAMMERS. J. Solution Chem. **7**, 155 (1978).
17. G. MANN. Tetrahedron, **23**, 3375 (1967).
18. (*a*) B. RIEDL and G. DELMAS. Can. J. Chem. **61**, 1876 (1983); (*b*) H. P. NGUYEN, B. RIEDL, and G. DELMAS. Can. J. Chem. **61**, 1885 (1983).
19. H. P. NGUYEN and G. DELMAS. Macromolecules, **12**, 746 (1979).
20. P. TANCRÈDE, L. V. LAM, P. PICKER, and D. PATTERSON. J. Chem. Soc. Faraday II, **70**, 1465 (1974).
21. P. TANCRÈDE and G. DELMAS. European Polymer J. **9**, 199 (1973).
22. G. DELMAS and D. PATTERSON. Discuss. Faraday Soc. **49**, 98 (1970).

Appendix

Calculation of the free volume terms

$h^E(f.v.)$ *and* $X_{12}s_1^{-1}$

The free volume term depends only on the difference between the reduced volume of the pure components. We apply a developed (22) form of the Prigogine–Flory theory which separates the interactional and free volume contributions. The free volume contribution h^E(f.v.) is defined as:

$$[A1]\quad h^E(\text{f.v.})/(x_1U_1^* + x_2U_2^*) = \tilde{c}_p(\tilde{T}_u)\,(\psi_1\tilde{T}_1 + \psi_2\tilde{T}_2 - \tilde{T}_u)$$

Here $\tilde{T}_u$ is the average reduced temperature for the solution appropriate to the energy $\tilde{U}$ and is defined by:

$$\tilde{U}(\tilde{T}_u) = \psi_1\tilde{U}(\tilde{T}_1) + \psi_2\tilde{U}(\tilde{T}_2)$$

With the van der Waals model, $\tilde{U}(\tilde{T}_u) = -1/\tilde{v}$, so that the volume corresponding to $\tilde{T}_u$ is $1/\tilde{v}_u = \psi_1/\tilde{v}_1 + \psi_2/\tilde{v}_2$, where $\psi_1 = x_1U_1^*/(x_1U_1^* + x_2/U_2^*)$. In this model, the reduced volume of the pure components is obtained from their expansion coefficients α and $\tilde{v}^{1/3} = [(4/3)\alpha T + 1]/(\alpha T + 1)$. The reduced temperature is calculated from the reduced volume and $\tilde{T} = \tilde{v}^{-1}(1 - \tilde{v}^{-1/3})$. Also $\tilde{c}_p(\tilde{T}_u) = [(4/3)\tilde{v}_u^{-1/3} - 1]^{-1}$ and $U^* = P^*V^*$ and $P^* = \gamma\tilde{v}^2T$ where γ is the thermal pressure coefficient. Equation [A1] does not depend on the surface-to-volume ratio. In the Flory terminology, the interactional contribution, which is the difference between the experimental value of the heat and the free volume contribution, is expressed through the X_{12} parameter. In the present form, X_{12} is obtained by eq. [A2]

$$[A2]\quad h^E(\text{exp}) - h^E(\text{f.v.})/(x_1U_1^* + x_2U_2^*) = (X_{12}/P_1^*)\,\theta_2\psi_1 f(\tilde{v})$$

The term $f(\tilde{v})$ $(= (\tilde{v}^{-1} + T\tilde{c}_p))$ is not very different from 1. ψ_1 and θ_2 ($\theta_2 = x_2V^*s_2/(x_1V_1^*s_1 + x_2V_2^*s_2)$) are used rather than the mole fractions. The units of X_{12} are in energy per cm^3. The parameter $X_{12}s_1^{-1}$ is independent of the choice of 1 or 2 as a second component, i.e. $X_{12}s_1^{-1} = X_{21}s_2^{-1}$. The left side of eq. [A2] does not depend on the surface-to-volume ratio s_1 and s_2 while X_{12} and θ_2 do to some extent. $X_{12}s_1^{-1}$ also relies very little on s_1 and s_2. The core volume, V^*, is obtained from the molar volume V and $\tilde{V} = V/V^*$.

c_p^E(*f.v.*)

It is given by the equation:

$$[A3]\quad c_p^E = \tilde{c}_{p,s}[x_1(U_1^*/T_1^*) + x_2(U_2^*/T_2^*)] - x_1\tilde{c}_{p1}(U_1^*/T_1^*) - x_2\tilde{c}_{p2}(U_2^*/T_2^*)$$

The reduced volume of the solution $\tilde{v}_s$ used to calculate $\tilde{c}_{p,s}$ is obtained from the solution reduced temperature $\tilde{T}_s$ defined as an energy average.

$$\tilde{T}_s = (\psi_1\tilde{T}_1 + \psi_2\tilde{T}_2)\,(1 - X_{12}\psi_1\theta_2/P_1^*)$$

The X_{12} term has not a large effect on $\tilde{T}_s$ in the present systems.

v^E

The excess volume can be written using the van der Waals model:

$$[A4]\quad \frac{v^E}{x_1V_1^* + x_2V_2^*} = \tilde{T}_v\frac{\partial\tilde{v}}{\partial\tilde{T}_v}\psi_1\theta_2(X_{12}/P_1^*) + (\tilde{v}_1 - \tilde{v}_2)\,(\psi_1 - \phi_1) - \frac{1}{2}\left(\frac{\tilde{v}_1 - \tilde{v}_2}{\partial\tilde{v}/\partial\tilde{T}_v}\right)^2\frac{\partial^2\tilde{v}}{\partial\tilde{T}_v^2}\{\psi_1\psi_2 + (\psi_1 - \theta_1)^2\}$$

here $\tilde{v}_v = \phi_1\tilde{v}_1 + \phi_2\tilde{v}_2$ and $\tilde{T}_v$ corresponds to $\tilde{v}_v$. By developing the second term in eq. [A4] we can show that $\psi_1 - \phi_1$ varies as $P_1^* - P_2^*$. The first term of eq. [A4] is $v^E(h^E)$, the second $v^E(P^*)$, and the last v^E(f.v.) as listed in Table 4.

Can. J. Chem. Downloaded from www.nrcresearchpress.com by 210.87.254.42 on 09/06/12
For personal use only.

Reactions between Ni(II) and $NaBH_3CN$ in the presence of bidentate phosphines

DAVID G. HOLAH, ALAN N. HUGHES, AND NAZRUL I. KHAN
Department of Chemistry, Lakehead University, Thunder Bay, Ont., Canada P7B 5E1

Received September 6, 1983

DAVID G. HOLAH, ALAN N. HUGHES, and NAZRUL I. KHAN. Can. J. Chem. **62**, 1016 (1984).

Reactions between Ni(II) and $NaBH_3CN$ in the presence of $Ph_2P(CH_2)_nPPh_2$ (n = 1, Dppm; n = 2, Diphos) have been studied. With Dppm, the main products are Ni(I)–CN–Dppm complexes and the nature of the actual product formed depends critically upon the reaction conditions. With Diphos, the products mainly involve coordinated BH_3CN^- in Ni(II)–Diphos complexes. Evidence from ^{31}P nmr and ir spectra are used to support proposed structural assignments.

DAVID G. HOLAH, ALAN N. HUGHES et NAZRUL I. KHAN. Can. J. Chem. **62**, 1016 (1984).

On a étudié les réactions entre le Ni(II) et le $NaBH_3CN$ en présence de $Ph_2P(CH_2)_nPPh_2$ (n = 1, Dppm; n = 2, Diphos). Avec le Dppm, les produits principaux sont des complexes de Ni(I)–CN–Dppm et la nature exacte des produits formés dépend d'une façon critique des conditions de la réaction. Avec le Diphos, les produits impliquent principalement des anions BH_3CN^- coordonnés à des complexes de Ni(II)–Diphos. On a utilisé des données des spectres de rmn du ^{31}P et des spectres ir pour proposer des attributions de structure.

[Traduit par le journal]

Can. J. Chem. Downloaded from www.nrcresearchpress.com by 210.87.254.40 on 09/06/12
For personal use only.

Introduction

Reactions between transition metal ions and $NaBH_4$ in the presence of tertiary phosphines are rapid, making it difficult to isolate intermediate products (1). $NaBH_3CN$ is a milder reducing agent (2) and, therefore, similar reactions (and reductions) should proceed more slowly, making it easier to isolate products of both a terminal and intermediate type. This paper presents the results of studies on reactions between Ni(II) and $NaBH_3CN$ in the presence of the bis(diphenylphosphino)alkanes $Ph_2P(CH_2)_nPPh_2$ (n = 1, Dppm; n = 2, Diphos). These bidentate phosphines were chosen because an earlier study (1) showed that in reactions of Ni(II) with $NaBH_4$ in the presence of similar bidentate phosphines, minor variations in phosphine ligand structure cause major variations in final product type. Further examples of both known modes of coordination of $NaBH_3CN$ (metal–$NCBH_3$ and metal–$NCB(H_2)H$–metal) will be reported.

Experimental

Materials

The phosphines were obtained from Strem Chemicals Inc. and used without further purification. $NaBH_3CN$ and $NaBD_3CN$ (98% isotopic purity) were obtained from the Aldrich Chemical Company and the Alfa Division of the Ventron Corporation respectively, and were stored over $CaCl_2$. $NaBH_3C^{15}N$ was synthesized from $NaC^{15}N$ (purchased from Stohler Isotope Chemicals) and a borane–tetrahydrofuran solution (Aldrich) in a manner similar to that reported (3) for the preparation of $NaBH_3CN$: $\nu_{C^{15}N}$2152 ($\nu_{C^{14}N}$2179 cm^{-1}). *Anal.* calcd. for $NaBH_3C^{15}N$: C 18.2, H 4.6, N 21.3; found: C 18.3, H 4.6, N 20.6.

All solvents were reagent grade and were purified by distillation and degassed with oxygen-free dry nitrogen before being stored over type 4A molecular sieves in a glove box.

Analyses and measurements

All air-sensitive samples were properly protected from atmospheric oxidation or hydrolysis during weighing or data collection. Microanalytical data for nitrogen, carbon, and hydrogen were acquired on a Perkin Elmer model 240 Analyser, using, where necessary, V_2O_5 as a combustion aid. Chloride analyses were determined by the Mohr titration method. The ir spectra of the samples were recorded on Beckman IR-12 and IR-4250 spectrophotometers (calibrated periodically with a polystyrene reference film) as Nujol mulls pressed between NaCl plates (600–4000 cm^{-1}) or between polyethylene plates (200–600 cm^{-1}). A Bruker WP-80 Fourier transform instrument equipped with an automatic temperature control device (B-VT 1000) was used to record ^1H and proton-decoupled ^{31}P nmr spectra at 80 MHz and 32.3 MHz, respectively. The chemical shifts were measured relative to internal tetramethylsilane (TMS) and external H_3PO_4 for ^1H and ^{31}P respectively and are positive if downfield from the reference signal.

X-ray powder diffraction measurements, electronic reflectance spectra, mass spectra, magnetic moments, and electrical conductivities were recorded as previously described (1).

Molecular weights were determined in $CHCl_3$ solution at 45°C using a Knauer Vapour Pressure Osmometer calibrated with Benzil in benzene at 45°C and the accuracy was checked periodically by measurement of the molecular weight of pentaerythrityl tetrastearate.

Syntheses

Unless otherwise specified, all synthetic work was carried out under a flow of pure nitrogen in a glove box. In general, an ethanolic solution of $NaBH_3CN$ was added to a mixture of Ni(II) chloride or perchlorate (dissolved in ethanol) and the phosphine (dissolved in toluene or benzene). Yields were generally in the 25–35% range. As the formation of some products depends rather critically on reaction conditions, complete details will be given for each synthesis. Some ir data are recorded in this section, and some later in the "Results and discussion" section.

(Cyanotrihydroborato)bis[bis(diphenylphosphino)methane]-nickel(II) perchlorate, $[Ni(BH_3CN)(Dppm)_2]ClO_4$

An ethanolic solution (20 mL) of $NaBH_3CN$ (0.10 g, 1.59 mmol) was added dropwise over a period of 2 min to a stirred mixture of $Ni(ClO_4)_2 \cdot 6H_2O$ (0.3 g, 0.82 mmol) and Dppm (0.63 g, 1.63 mmol) in benzene/ethanol (1:1, 20 mL). One drop of $NaBH_3CN$ solution turned the reaction mixture instantly from yellow to brown and upon complete addition of the $NaBH_3CN$, the solution was filtered, yielding a brown solid. This was washed with benzene (~10 mL), ethanol (~10 mL), and n-hexane (~5 mL) before drying under reduced pressure. It is soluble in CH_2Cl_2, THF, DMF, and acetone but it decomposes in all solvents within 30 min. The complex was therefore purified by precipitation from CH_2Cl_2 by very rapid addition of n-hexane and dried under reduced pressure for 12 h. This complex is air stable in the solid state. The analogous reaction has also been carried out with $NaBD_3CN$. *Anal.* calcd. for $[Ni(BH_3CN)(Dppm)_2]ClO_4$: C 63.3, H 4.9, N 1.4; found: C 62.9, H 5.2, N 1.4; ^{31}P nmr (CH_2Cl_2) δ −62.75.

(Cyanotrihydroborato)(cyano)bis[bis(diphenylphosphino)-methane]dinickel(I), $Ni_2(BH_3CN)(CN)(Dppm)_2 \cdot 0.5EtOH$

$Ni(ClO_4)_2 \cdot 6H_2O$ (0.3 g, 0.82 mmol) and Dppm (0.63 g, 1.63 mmol) were mixed in ethanol (40 mL) and this immediately precipitated a yellow solid. An ethanolic solution (20 mL) of $NaBH_3CN$ (0.4

Can. J. Chem. Downloaded from www.nrcresearchpress.com by 210.87.254.40 on 09/06/12
For personal use only.

g, 6.30 mmol) was added dropwise to the stirred yellow suspension over a period of 10 min during which the mixture changed first to brown, then to light green, and finally to deep green. The mixture was stirred for a further 3 h and the greenish brown solid which precipitated was filtered off, washed with ethanol (~10 mL) and *n*-hexane (~10 mL), and dried under reduced pressure for several hours. The complex dissolves to give green solutions in EtOH, CH_3OH, CH_2Cl_2, THF, benzene, and CH_3CN, but it decomposes to give light brown solutions within a few minutes. This colour changes to violet after a few hours. Purification by recrystallization was therefore not possible but was effected by washing the crude product with small amounts of cold ethanol followed by benzene. Similar reactions using $NaBD_3CN$ and $NaBH_3C^{15}N$ produced the appropriately labelled complex. The complex is air stable and the synthesis is reproducible. *Anal.* calcd. for $Ni_2(BH_3CN)(CN)(Dppm)_2 \cdot 0.5EtOH$: C 65.3, H 5.1, N 2.9; found: C 65.4, H 5.2, N 2.8; ^1H nmr ($CDCl_3$) EtOH at δ 1.25(t), 3.75(q); integration EtOH:Dppm = 1:4; ^{31}P nmr (EtOH) δ +29.30, +28.42. The ethanol could not be removed even by pumping at 10^{-6} Torr for several hours.

The same complex was also synthesized from $NiCl_2 \cdot 6H_2O$ as follows. A solution of $NaBH_3CN$ (0.079 g, 1.25 mmol) in ethanol (20 mL) was added over a period of 2 min to a stirred mixture containing $NiCl_2 \cdot 6H_2O$ (0.15 g, 0.63 mmol) and Dppm (0.52 g, 1.35 mmol) in ethanol (40 mL). The pink solution immediately turned green upon addition of the $NaBH_3CN$ and the mixture was allowed to stir for 3 h. The resulting solid was separated and purified as discussed above.

Bis(cyano)tris[bis(diphenylphosphino)methane]dinickel(I), $Ni_2(CN)_2(Dppm)_3 \cdot 4EtOH$

This deep green crystalline solid was obtained in low yield from the filtrates of the two reactions described above after they were allowed to stand at room temperature for 48 h. The crystals were filtered off, washed with ethanol (~10 mL), and dried under reduced pressure for 24 h. The product is soluble in EtOH, CH_2Cl_2, benzene, THF, MeOH, and DMF to give, initially, a deep green solution, which, after 24 h, turned to a deep violet, although the EtOH and MeOH solutions seemed the most stable. This compound is air stable in the solid state. Labelled complexes were also prepared using $NaBD_3CN$ and $NaBH_3C^{15}N$. *Anal.* calcd. for $Ni_2(CN)_2(Dppm)_3 \cdot 4EtOH$: C 67.8, H 6.0, N 1.9; found: C 67.5, H 5.1, N 1.9. ^1H nmr ($CDCl_3$) EtOH at δ 1.25(t), 3.75(q); integration EtOH:Dppm = 4:3. This ethanol was retained after drying under reduced pressure (10^{-6} Torr) for 24 h. ^{31}P nmr (EtOH) δ +15.98(s).

In addition, when the time that the above reaction mixtures were allowed to stir at room temperature was increased from 3 to 17 h, $Ni_2(CN)_2(Dppm)_3 \cdot 4EtOH$ was separated directly from the reaction mixture as the major product.

Bis(cyano)bis[bis(diphenylphosphino)methane]dinickel(I), $Ni_2(CN)_2(Dppm)_2 \cdot EtOH$ and $Ni_2(CN)_2(Dppm)_2 \cdot C_6H_6$

(a) From $Ni(ClO_4)_2 \cdot 6H_2O$. To a stirred suspension containing $Ni(ClO_4)_2 \cdot 6H_2O$ (0.3 g, 0.8 mmol) and Dppm (0.63 g, 1.63 mmol) in ethanol (20 mL), a solution of $NaBH_3CN$ (0.05 g, 0.79 mmol) in ethanol (10 mL) was added dropwise over a period of 2 min. The mixture was stirred at room temperature for a further 22 h during which time a pinkish yellow solid precipitated. This was filtered off and the deep violet filtrate concentrated under reduced pressure to yield violet crystals. It was necessary to recrystallize several times from ethanol, methanol, or benzene to obtain a pure product, as the ethanol or benzene solvate. The same product was prepared using $NaBD_3CN$ and the ^{15}N-labelled complexes were prepared in a similar manner using $NaBH_3C^{15}N$.

The complex has some air stability and is soluble in all common solvents, with slow decomposition over about 48 h. Thereafter the solutions turn brown. *Anal.* calcd. for $Ni_2(CN)_2(Dppm)_2 \cdot EtOH$: C 65.9, H 5.1, N 2.8; found: C 65.9, H 4.9, N 2.7. ^1H nmr ($CDCl_3$) EtOH at δ 1.25(t), 3.75(q); integration EtOH:Dppm = 1:2; ^{31}P nmr (EtOH) δ 1.4(s). *Anal.* calcd. for $Ni_2(CN)_2(Dppm)_2 \cdot C_6H_6$: C 68.5, H 4.9, N 2.8; found: C 68.5, H 5.0, N 2.7. The presence of benzene was confirmed by mass spectrometry. The solvent molecules were retained after pumping (10^{-6} Torr) for 24 h.

(b) From $NiCl_2 \cdot 6H_2O$. An ethanolic solution (20 mL) of $NaBH_3CN$ (0.316 g, 5.02 mmol) was added over a period of 5 min to a stirred mixture of $NiCl_2 \cdot 6H_2O$ (0.15 g, 0.63 mmol) and Dppm (0.519 g, 1.35 mmol) in ethanol (40 mL) and the mixture stirred for 1 h at 77°C. The solution was then stirred at room temperature for a further 4 h, during which time a small amount of purple solid was formed. This was filtered off, washed with a little ethanol and *n*-hexane, and purified as above.

Hydridobis[bis(1,2-diphenylphosphino)ethane]nickel(II) perchlorate or cyanotrihydroborate, $[NiH(Diphos)_2]X$, $X = ClO_4^-$, BH_3CN^-

(a) $X = ClO_4^-$. $NaBH_3CN$ (0.26 g, 4.07 mmol) in ethanol (20 mL) was added dropwise over a period of 15 min to a stirred mixture of $Ni(ClO_4)_2 \cdot 6H_2O$ (0.75 g, 2.05 mmol) in toluene/ethanol (10 mL, 1:1) and Diphos (2.45 g, 6.15 mmol) in toluene (20 mL). The mixture was stirred for 21 h at room temperature and the orange–red precipitate was filtered off, washed with toluene (~5 mL), ethanol (~5 mL), and *n*-hexane (~5 mL), and then dried under reduced pressure for several hours. More product was obtained from the red filtrate after several days at room temperature. The complex is air stable and soluble in CH_2Cl_2, $CHCl_3$, THF, DMF, and acetone to give solutions which are stable for up to 12 h. The complex was identified as the known (1) species, $[NiH(Diphos)_2]ClO_4$; ^1H nmr ($CDCl_3$) δ −13.1(quintet), J_{PH} = 5.6 Hz; ^{31}P nmr ($CHCl_3$), δ 44.95; ir, ν_{Ni-H}, 1950 cm^{-1}.

(b) $X = BH_3CN^-$. From the wine-red filtrate of the reaction mixture described in (*a*) below, a wine-red crystalline solid was separated by filtration after 24 h at room temperature, washed with ethanol (~5 mL) and *n*-hexane, and then dried under reduced pressure for several hours. The product was precipitated from CH_2Cl_2 with addition of *n*-hexane (1:1). Solutions in CH_2Cl_2, THF, $CHCl_3$, DMF, and acetone are stable for 24 h. The solid is air stable. $[NiD(Diphos)_2]BD_3CN$ was synthesized using $NaBD_3CN$. *Anal.* calcd. for $[NiH(Diphos)_2](BH_3CN)$: C 71.1, H 5.8, N 1.6; found: C 71.1, H 5.8, N 1.6; ^1H nmr ($CDCl_3$) δ −13.1(quintet), J_{PH} 5.6 Hz; ^{31}P nmr ($CHCl_3$) δ 44.95(s); ir ν_{CN} 2179, ν_{BH} 2330(s), 2290(w, sh), ν_{NiH} 1950 cm^{-1}.

Tris(cyanotrihydroborato)bis[bis(1,2-diphenylphosphino)-ethane]dinickel(II)chloride or perchlorate, $[Ni_2(BH_3CN)_3(Diphos)_2]X$ where $X = Cl^-$ or ClO_4^-

(a) $X = ClO_4^-$. To a stirred yellow mixture of $Ni(ClO_4)_2 \cdot 6H_2O$ (0.98 g, 2.68 mmol) in ethanol (20 mL) and Diphos (1.96 g, 4.92 mmol) in ethanol (20 mL) was added $NaBH_3CN$ (1.5 g, 23.8 mmol) in ethanol (20 mL) over a period of 2 min. The mixture was stirred for a further 30 min and the yellow solid, which deposited, was filtered off and washed with ethanol (~10 mL) and *n*-hexane (~10 mL). Work-up of the wine-red filtrate is described in (*b*) above. The crude product was reprecipitated from CH_2Cl_2 with rapid addition of *n*-hexane followed by drying under reduced pressure. The complex produces yellow solutions in CH_2Cl_2, $CHCl_3$, and THF but decomposes and turns brown in all solvents fairly rapidly. Immediate decomposition occurs in DMF. A synthesis of the deuterated complex using $NaBD_3CN$ was also carried out. *Anal.* calcd. for $[Ni_2(BH_3CN)_3(Diphos)_2]ClO_4$: C 61.4, H 5.3, N 3.9; found: C 61.8, H 5.3, N 4.1. ^{31}P nmr (CH_2Cl_2) δ 63.30.

(b) $X = Cl^-$. $NiCl_2 \cdot 6H_2O$ (0.5 g, 2.10 mmol) and Diphos (1.67 g, 4.20 mmol) were mixed in ethanol (20 mL) and to the stirred pink solution an ethanolic solution (10 mL) of $NaBH_3CN$ (0.224 g, 3.57 mmol) was added dropwise over a period of 4 min. The mixture was stirred for 3 h at room temperature and the yellow precipitate separated and purified as described for the ClO_4^- salt. The deuterated complex was prepared from $NaBD_3CN$. *Anal.* calcd. for $[Ni_2(BH_3CN)_3(Diphos)_2]Cl$: C 61.7, H 5.3, N 3.9, Cl 3.3; found: C 61.7, H 5.3, N 4.0, Cl 3.3. ^{31}P nmr (CH_2Cl_2) δ 63.30(s).

Alternatively, the chloride product can be obtained from the following reaction in which much larger amounts of $NaBH_3CN$ are used.

$NaBH_3CN$ (0.93 g, 14.71 mmol) in ethanol (10 mL) was added dropwise over a period of 5 min to a stirred mixture of $NiCl_2 \cdot 6H_2O$

Can. J. Chem. Downloaded from www.nrcresearchpress.com by 210.87.254.40 on 09/06/12
For personal use only.

(0.5 g, 2.10 mmol) and Diphos (1.64 g, 4.20 mmol) in ethanol (20 mL). The mixture was stirred for 4.5 h and the yellow solid was separated and purified as above.

Dichlorobis(cyanotrihydroborato)tetrakis[bis(1,2-diphenylphosphino)ethane]dinickel(II), $Ni_2Cl_2(BH_3CN)_2(Diphos)_4$

To a stirred mixture of $NiCl_2 \cdot 6H_2O$ (0.5 g, 2.10 mmol) in ethanol (20 mL) and Diphos (1.67 g, 4.20 mmol) in ethanol (20 mL) was added $NaBH_3CN$ (0.925 g, 14.72 mmol) in ethanol (20 mL) over a period of 10 min. The mixture was stirred for 48 h, during which time the initial brown colour changed to orange (after 18 h), then to green (after 36 h), and finally to greenish yellow. A greenish yellow solid was filtered off, washed with ethanol (~10 mL) and *n*-hexane (~5 mL), and dried under reduced pressure for 24 h. The product is soluble in CH_2Cl_2, $CHCl_3$, THF, and DMF and the resulting solutions are stable for several hours. The crude product was purified by reprecipitation from CH_2Cl_2 with addition of *n*-hexane. The addition of *n*-hexane had to be such as to maintain a constant volume of solution and a constant time interval between the additions, otherwise decomposition occurred. The complex is air stable in the solid state. *Anal.* calcd. for $Ni_2Cl_2(BH_3CN)_2(Diphos)_4$: C 68.4, H 5.5, N 1.5, Cl 4.9; found: C 68.5, H 5.5, N 1.5, Cl 4.8. ^{31}P nmr (CH_2Cl_2) δ 29.34, 28.03; mol. wt. ($CHCl_3$) calcd. 1860; found 1845.

Dichlorobis(cyanotrihydroborato)bis[bis(1,2-diphenylphosphino)ethane]dinickel(II), $Ni_2Cl_2(BH_3CN)_2(Diphos)_2 \cdot EtOH$

An ethanolic solution (20 mL) of $NaBH_3CN$ (0.93 g, 14.72 mmol) was added dropwise over a period of 5 min to a stirred mixture of $NiCl_2 \cdot 6H_2O$ (0.5 g, 2.10 mmol) and Diphos (1.67 g, 4.20 mmol) in ethanol (40 mL). The brown mixture was then heated at 55°C for a further 30 min and then filtered. This produced solid $Ni(Diphos)_2$ and a dark brown filtrate which, after 5 days at 0°C, produced brown crystals. These were filtered off, washed with ethanol (~10 mL) and *n*-hexane (~5 mL), and then dried under reduced pressure for several hours. The solid was recrystallized from CH_2Cl_2 with slow addition of *n*-hexane and is soluble in CH_2Cl_2, $CHCl_3$, and THF with some solution stability. The solid is stable in air. An identical synthesis using $NaBD_3CN$ has also been carried out. *Anal.* calcd. for $Ni_2Cl_2(BH_3CN)_2(Diphos)_2 \cdot EtOH$: C 60.5, H 5.4, N 2.5, Cl 6.7; found: C 60.7, H 5.5, N 2.4, Cl 6.6. ^1H nmr ($CDCl_3$) EtOH at δ 1.25(t), 3.75(q); integration EtOH:Diphos 1:2; ir, ν_{OH} from EtOH 3360(b) cm^{-1}; ^{31}P nmr (CH_2Cl_2) δ 43.86.

Bis[bis(1,2-diphenylphosphino)ethane]nickel(0), $Ni(Diphos)_2$

This known (4) complex has been isolated in varying amounts from almost all filtrates of the reactions described for Diphos, but the yield increases in the higher temperature reactions.

Results and discussion

As expected, it has proved possible to isolate and identify a range of products from Ni(II)–phosphine–$NaBH_3CN$ reactions provided careful attention is paid to the reactant ratios, the rate of addition of $NaBH_3CN$, and the time of the reaction. Of particular interest is the mode of co-ordination of the BH_3CN^- group in those products which contain this group and the frequency of the B—H stretching mode is of fundamental importance in determining this. Of the five known examples of metal—BH_3CN^- complexes where the mode of BH_3CN^- coordination has been determined by crystallographic methods, three, $(Me_5Dien)Cu(BH_3CN)_2$ (5), $CoH(BH_3CN)(PPh_3)_3$ (6), and $Cu_2(BH_3CN)_2(Diphos)_3$ (7), have metal—$NCBH_3$ arrangements with B—H stretching frequencies in the range 2330–2346 cm^{-1} (2320 cm^{-1} in $NaBH_3CN$). On the other hand, two complexes, $[trenNi(BH_3CN)]_2^{2+}$ (8) and $[Cu(BH_3CN)(PPh_3)_2]_2$ (9), are binuclear species containing two bridging metal—HBH_2CN—metal linkages with analogous B—H_t frequencies in the significantly different 2376–2380 cm^{-1} range. In addition, these dimeric compounds show M—H—B bridging modes underlying the ν_{CN} region at ~2200 cm^{-1}. These ir differences between monodentate and bridging BH_3CN^- have been discussed elsewhere (8) and will be utilized in structural assignments of some of the new complexes reported here.

Dppm complexes

The most significant aspect of the Ni(II)–Dppm–$NaBH_3CN$ reactions is that Ni(II) is rapidly reduced to Ni(I), accompanied by cleavage of the B—C bond to produce Ni—CN complexes. This can be prevented only, it seems, by stopping the reaction very shortly after the addition of the $NaBH_3CN$. Thus, the brown $[Ni(BH_3CN)(Dppm)_2]ClO_4$ is formed under conditions where the Ni:Dppm:$NaBH_3CN$ ratio of 1:2:2 was adjusted to keep a relatively small excess of BH_3CN^- and the time allowed for the reaction was only 2 min. In fact, the formation of this complex is particularly sensitive to these factors. The solid must be filtered off immediately and is stable only for short periods (30 min) in solvents. The presence of ionic perchlorate in the solid complex is confirmed by the strong broad peak at 1100 cm^{-1} in the ir spectrum. Involvement of the CN group in coordination is shown by the position of the CN stretching frequency at 2190 cm^{-1} (a shift of 11 cm^{-1} from 2179 cm^{-1} in the spectrum of $NaBH_3CN$), and in the B—H region, the strong BH_t absorption appears at 2320 cm^{-1} with a weak shoulder at 2265 cm^{-1}. In the deuterated complex the B—D frequency occurs, as expected from isotopic shift calculations, at 1755 cm^{-1}. All these data are strong evidence for the presence of Ni—$NCBH_3$ type of coordination in this complex. ^{31}P nmr spectra in methylene chloride, run immediately on freshly prepared samples, show a strong peak at δ −62.75. The P atoms are clearly equivalent in solution and the position of the signal is consistent with chelating Dppm ligands since the structurally related $PtCl_2(Dppm)_2$ (10) shows δ ^{31}P at −64.3. In addition, there is a weak signal at δ −34 in the ^{31}P spectrum which increases in intensity with time while the −62.75 signal decreases to disappear completely after several hours. This decomposition can be represented as:

$$[Ni(BH_3CN)(Dppm)_2]^+ \rightarrow [Ni(Dppm)_2]^{2+}$$

since the ^{31}P nmr spectrum of $Ni(Dppm)_2(ClO_4)_2$ (formed by reacting $Ni(ClO_4)_2$ with Dppm) shows a singlet at δ −34. All the available evidence, therefore, is consistent with a five-coordinated Ni(II) ion with chelating ligands and N-bound BH_3CN^-.

When either the reaction time, the amount of $NaBH_3CN$, or the temperature is increased, three interrelated Ni(I) complexes are produced. Very careful adjustments to reaction conditions are necessary in order to isolate pure species, which have been characterized as the greenish-brown $Ni_2(BH_3CN)(CN)(Dppm)_2 \cdot 0.5EtOH$, the deep green crystalline $Ni_2(CN)_2(Dppm)_3 \cdot 4EtOH$, and the violet crystalline $Ni_2(CN)_2(Dppm)_2 \cdot S$ (S = EtOH or benzene). The first two complexes are very difficult to isolate, as they are slowly converted into the violet compound in solution. Thus, while coordinated BH_3CN^- seems reasonably stable in the Ni(II)/Dppm system (as in $[Ni(BH_3CN)(Dppm)_2]ClO_4$ described above), cyanide abstraction from coordinating BH_3CN^- occurs very readily when Ni(II) is reduced to Ni(I). In order to assign unambiguously the important ir bands in these Ni(I) complexes, the deuterium and ^{15}N-labelled species were also synthesized. All complexes retained ethanol (even after extensive drying under reduced pressure), the amount of which was established

Can. J. Chem. Downloaded from www.nrcresearchpress.com by 210.87.254.40 on 09/06/12
For personal use only.

from ^{1}H nmr spectra (experimental). Extensive decomposition of the complexes occurs in $CDCl_3$ and estimation was simply made on the basis of the ratio of aromatic : ethanol protons. The presence of the ethanol was also clear from broad OH bands at ~3400 cm^{-1} in the ir spectra of the complexes.

The ir spectrum of $Ni_2(BH_3CN)(CN)(Dppm)_2 \cdot 0.5EtOH$ shows three major peaks in the 2000–2400 cm^{-1} region at 2020, 2190, and 2320 (with a weak shoulder at 2265 cm^{-1}). The 2320 cm^{-1} peak shifts to 1755 cm^{-1} on deuteration and is therefore ν_{B-H}, in the position consistent with non-involvement of the hydrogens in coordination. The sharp peak at 2190 cm^{-1} is the ν_{CN} associated with the BH_3CN group and its position supports a Ni—$NCBH_3$ arrangement. This peak shifts to 2155 cm^{-1} in the ^{15}N-labelled species. The remaining sharp peak at 2020 cm^{-1} is consistent with a terminal Ni—CN group; it shifts to 1990 cm^{-1} when labelled with ^{15}N, as expected. The ir evidence is therefore consistent with the proposed formulation. It should be noted that although the C≡N stretching frequency is rather low for a metal cyanide (normally, *ca.* 2080–2100), it has been observed (11) that cyanides of metals in lower than normal oxidation states do show these vibrations at lower values.

The ir spectrum of $Ni_2(CN)_2(Dppm)_3 \cdot 4EtOH$ in the same region shows only a sharp peak at 2020 cm^{-1} and a weak peak at 2110 cm^{-1}. These shift to 1970 and 2070, respectively, when labelled with ^{15}N and confirm their assignment as terminal Ni—CN frequencies. Similarly, the ir spectrum of the violet crystals shows a single peak at 1975 cm^{-1} which shifts to 1940 cm^{-1} when labelled with ^{15}N. (Several recrystallizations are necessary to remove traces of a Ni—H impurity, ν_{Ni-H} 1987 cm^{-1}, which vanishes on deuteration.) Thus both complexes have Ni—CN groups present. Attempts were made to determine the molecular weight in chloroform solution of the relatively stable violet complex. However, while a molecular weight in good agreement with a dimeric formulation was obtained, ^{1}H nmr examination of a chloroform solution of the complex over a time period similar to that required for molecular weight measurements showed that sufficient decomposition occurs to render the molecular weight results unreliable.

The interrelationship among the three complexes is seen in ^{31}P nmr studies. $Ni_2(BH_3CN)(CN)(Dppm)_2 \cdot 0.5EtOH$, which in ethanol has two peaks at δ 29.30 and 28.42 of approximately equal area (29.56 and 28.48 in methanol), clearly has two sets of very similar but not identical P atoms. The position of the signals is more consistent with bridging rather than chelating Dppm (10) ligands and the structure of the complex is probably best represented as **1**. However, the apparent simplicity of the ^{31}P spectra requires some discussion.

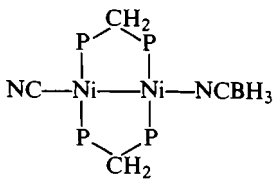

1

Structure **1** would be expected to show P—P coupling by analogy with similar unsymmetrical Pt(I) dimeric systems in the literature (12) and the simplicity of the ^{31}P spectrum could indicate the presence of two distinct compounds in roughly equal amounts. That this is almost certainly not the case is shown by the fact that if a sample pure enough to show only these two peaks in the ^{31}P spectrum is allowed to undergo solution decomposition in the strict absence of oxygen, only one phosphorus-containing product (the violet complex mentioned above and discussed further below) is obtained in significant quantity as shown by the ^{31}P nmr spectrum.

Considering now the coupling problem, the expected coupling pattern for **1** could be AA′BB′ by analogy with related Pt(I) complexes (12) but could be as simple as AB if coupling between non-equivalent P atoms occurs only through the carbon backbone and not the two metal centres. This suggests that the two peaks observed could be the inner two lines of an AB pattern for the situation where $^2J_{P-P}$ is fairly large and signal separation is small as in the case here. Computer-simulated spectra (Bruker ITRCAL program) show that for the signal-to-noise ratios (dictated by the solution instability of the complex) and line broadening observed in the real spectrum, the outer two lines of such an AB pattern would probably not be observable if $^2J_{P-P}$ were significantly greater than about 35 Hz. A search of the literature shows (12, 13) that in similar Pt(I) complexes, $^2J_{P-P}$ values of greater than 40 Hz are quite normal. Unfortunately, spectra with better signal-to-noise ratios could not be obtained because of the rapid decomposition of the complex in solution.

Within a very short time, the intensities of these two peaks observed in the ^{31}P spectrum of $Ni_2(BH_3CN)(CN)(Dppm)_3 \cdot 0.5EtOH$ decrease and a new sharp signal appears at δ 1.4. Eventually the two peaks disappear completely, and the solution turns violet in colour. The spectrum of the pure violet complex $Ni_2(CN)_2(Dppm)_2 \cdot EtOH$ shows this same signal at δ 1.4 and it appears that the interconversion takes place by loss of BH_3 from the former complex. However, the upfield shift of ~27 ppm suggests that a major structural change accompanies the interconversion, the δ 1.4 signal being more consistent with chelating Dppm (10). The most reasonable structure for the violet crystals, therefore, appears to be **2** containing two tetrahedral Ni(I) atoms thereby rendering the P atoms equivalent

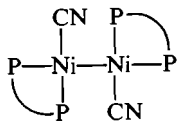

2

as indicated by the ^{31}P spectrum. In this context, it is interesting to note that there appears to be only one other chelate Dppm complex of a tetrahedral metal ion in the literature (14).

There are many examples of the alternative phosphine-bridged type of structure in the literature and this is particularly true for Pt(I) systems (15) for which δ ^{31}P are close to 0 (16). Since it appears that Ni(I) species of comparable structure would be expected (10) to show ^{31}P shifts at about 15 ppm to lower field, the phosphine-bridged alternative to **2** can probably be ruled out.

The ^{31}P spectrum of a freshly prepared deep green solution of $Ni_2(CN)_2(Dppm)_3 \cdot 4EtOH$ shows a single peak at δ = 15.98, but the intensity of this decreases rapidly with time and new signals appear at δ 1.4 (violet complex) and −21 (free phosphine). Again, the solution turns violet as the interconversion takes place and, as expected from the stoichiometries of the two complexes, free Dppm would be expected as one of the products of the interconversion. The position of the signal at δ 15.98 is, on the basis of the above argument, probably more

consistent with bridging Dppm ligands as in the five-coordinate species **3**.

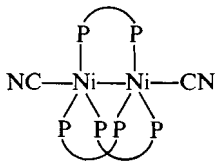

3

This raises the question of why two CN vibrations are observed in the ir spectrum of **3**. They are 90 cm^{-1} apart and this separation, together with the fact that the lower frequency peak is much more intense, suggests that these absorptions represent symmetrical and asymmetrical vibrations. Unfortunately, neither of the compounds formulated as **2** and **3** forms sufficiently good crystals for X-ray work.

Further evidence for interconversions between these complexes was obtained from additional ^{31}P studies. Solutions of both $Ni_2(BH_3CN)(CN)(Dppm_2 \cdot 0.5EtOH$ and $Ni_2(CN)_2(Dppm)_2 \cdot EtOH$ in the presence of added Dppm show the appearance of weak signals at δ 16, suggesting the formation of a small amount of $Ni_2(CN)_2(Dppm)_3 \cdot 4EtOH$ although many other signals, including some which indicate the formation of complexes containing monodentate Dppm, also appear in the spectra upon addition of free Dppm. These interconversion reactions are summarized below.

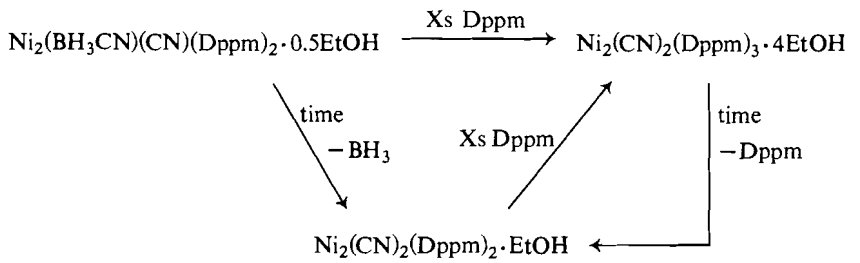

One last comment regarding these Ni(I) complexes should be made. Thus, ^1H nmr spectra might be considered to be helpful in establishing the bridging or chelating nature of the Dppm ligand since criteria have been established for similar Pt complexes which allow this distinction (16, 17). However, this is based upon the coupling of ^{195}Pt with the PCH_2P protons of the ligand and would not apply to Ni complexes. A literature survey shows that chemical shifts of the CH_2 protons of bridging or chelating Dppm are quite similar and would therefore offer little information here. Nevertheless, attempts were made to record ^1H spectra on very freshly prepared samples in C_6D_6 and $CDCl_3$. Two of the complexes decomposed so rapidly that no data could be obtained. The violet complex showed more stability and spectra in C_6D_6 showed the PCH_2P protons as a broad unresolved signal centred on δ 4.3. No further information was obtainable from proton spectra.

Diphos complexes

In marked contrast to the Dppm products, products from similar Diphos reactions are exclusively Ni(II) or Ni(0) complexes. The latter, in the form of $Ni(Diphos)_2$, occurs in most reactions but only in significant yields when reaction mixtures are heated or when large amounts of $NaBH_3CN$ are used for longer times. No Ni–CN–Diphos species has been identified, although reproducible evidence for such a product was obtained from $NiCl_2$/Diphos/$NaBH_3CN$ (1:2:7 mole ratios) reactions over 17 h. This product is isolated in low yields as an extremely air-sensitive yellow solid, the major product of the reactions being $Ni(Diphos)_2$. The occurrence of coordinated BH_3CN^- in the products of these reactions is common and the formation of particular compounds appears to depend more on whether $NiCl_2$ or $Ni(ClO_4)_2$ is used as a starting material rather than on such factors as the amount of BH_3CN^-, its rate of addition, or the solvent. Without X-ray diffraction, the formulation of structures for some of these complex products was difficult.

The $[NiH(Diphos)_2]^+$ cation is well-known (1) and is formed here as the ClO_4^- (1) and BH_3CN^- (minor product) salts from reactions between $Ni(ClO_4)_2$/Diphos and $NaBH_3CN$ where small and large amounts of $NaBH_3CN$ respectively are used. ^{31}P and ^1H (upfield of TMS) nmr spectra for the two complexes are identical, and the ir spectrum of the BH_3CN^- salt is entirely consistent with ionic BH_3CN^-.

The yellow, diamagnetic, and isomorphous solids $[Ni_2(BH_3CN)_3(Diphos)_2]^+X^-$ (X = Cl^- or ClO_4^-) are formed from short time reactions involving Ni(II) chloride or perchlorate. In fact, the perchlorate salt is the major product in the reaction leading to the above BH_3CN^- salt. These products decompose rapidly in solution but can be reprecipitated rapidly from CH_2Cl_2 to achieve purification. In the ir spectra, a broad peak at 1100 cm^{-1} confirms the presence of ionic ClO_4^- in one of the complexes, and the absence of an absorption in the 200–400 cm^{-1} region of the spectrum of the chloride complex is consistent with ionic Cl^-. Both complexes have a single sharp peak at 2207 cm^{-1} due to $\nu_{C\equiv N}$, the shift of 28 cm^{-1} from $NaBH_3CN$ being indicative of Ni–$NCBH_3$ interaction. There is also a strong, broad absorption in the 2360–2370 cm^{-1} region (with weak shoulders) due to terminal ν_{B-H}, and this position is strongly indicative of Ni–HBH_2CN interaction as discussed earlier. Indeed, the stoichiometry of the complex alone strongly suggests three bridging BH_3CN^- groupings. The peak appears at 1770 cm^{-1} in the deuterated complexes as has been observed for similar bridged structures (8, 9). There is no peak which can be assigned to the Ni–H–B group analogous to the very broad band observed in the 2000–2200 cm^{-1} region seen in the confirmed bridging structures mentioned earlier although there is evidence of underlying weak peaks, which vanish on deuteration, in this region. Freshly prepared solutions of the chloride (4×10^{-3} *M*) in $CHCl_3$ conduct electricity at room temperature (11 ohm^{-1} cm^2 mol^{-1}) although with a conductivity less than expected for a 1:1 electrolyte. This value decreases rapidly with time as the solution changes colour from yellow to brown (see later).

^{31}P nmr spectra in CH_2Cl_2 of both compounds show, initially, a sharp signal at δ 63.3, indicating the presence of equivalent P atoms in Diphos units acting as chelating (10) ligands

Can. J. Chem. Downloaded from www.nrcresearchpress.com by 210.87.254.40 on 09/06/12
For personal use only.

Can. J. Chem. Downloaded from www.nrcresearchpress.com by 210.87.254.40 on 09/06/12
For personal use only.

to Ni. Considering this, and the ir data, the molecule must have a high degree of symmetry, and the most reasonable structure would be as shown in **4** which contains three bridging BH_3CN^- groups. Normally, in such bridging structures, the bridges are arranged in a head-to-tail manner (8, 9). However, in this case,

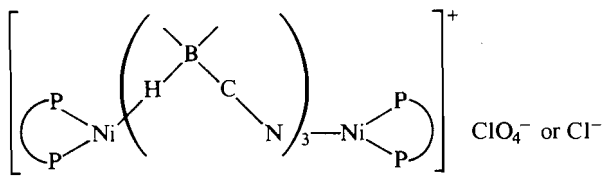

4

at least two bridges would have to be head-to-head giving some asymmetry to the system. This might be expected to lead to two ^{31}P signals in the nmr spectrum. However, as discussed below, one BH_3CN^- bridge is fairly readily displaced in a spontaneous reaction and it may well be that some fluxionality of the bridging BH_3CN^- units is allowed in solution giving rise to equivalent P atoms.

There are two further Diphos complexes which arise from these reactions and for which, due to conflicting data, definite structural assignments have not been possible. Thus, the δ 63.3 signal in the ^{31}P spectrum disappears completely after 48 h as the yellow compounds gradually decompose to new brown species each with a sharp signal at δ 44. Small amounts of solid could be isolated only from the chloride solution. This same compound, analyzing reproducibly over several preparations as $Ni_2Cl_2(BH_3CN)_2(Diphos)_2 \cdot EtOH$ (^{31}P nmr δ 44), is better prepared (along with $Ni(Diphos)_2$) from reactions between $NiCl_2$, Diphos, and $NaBH_3CN$ after 30 min under reflux. Air-stable, brown, poorly formed crystals slowly precipitate from the filtrate over a 5-day period and these can be recrystallized from CH_2Cl_2. The solution stability allowed molecular weight measurements which indicate a dimeric structure. The chloride appears to be covalently bound since the complex is a non-electrolyte in CH_2Cl_2. This would also account for the fact that the solution decomposition of the precursor $[Ni_2(BH_3CN)_3(Diphos)_2]^+Cl^-$ is accompanied by a rapid decrease in conductivity. The ^{31}P shift and the ir spectrum (ν_{B-H} 2370, 2290sh, ν_{B-D} 1770, $\nu_{C\equiv N}$ 2207 cm^{-1}) suggest the presence of chelating Diphos (10) and bridging BH_3CN^- and the structure might therefore be **5**.

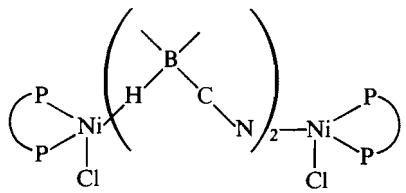

5

However, questions such as why the decomposition of **4** (ClO_4^-) leads to the same (δ 44) nmr signal and what the other products of decomposition (having no detectable ^{31}P signal) are remain unanswered but may be resolved if attempts to obtain crystals of **5** suitable for X-ray work are successful.

The second complex of uncertain structure is produced from reactions between $NiCl_2$, Diphos, and $NaBH_3CN$ (1:2:7) over long periods (48 h). After a series of colour changes, the air- and solution-stable, diamagnetic $Ni_2(BH_3CN)_2(Diphos)_4Cl_2$ is formed. The dimeric nature of this is again strongly suggested by molecular weight data and the compound is a non-electrolyte in CH_2Cl_2. These results are consistent only with non-ionic chlorines. (No similar compound was observed (^{31}P nmr) in reactions with $Ni(ClO_4)_2$.) The infrared spectrum is consistent with terminal $Ni-NCBH_3$ groups, with peaks at 2330 (ν_{B-H}) [1755 (ν_{B-D})] and 2200 cm^{-1} ($\nu_{C\equiv N}$). The ^{31}P nmr spectrum shows peaks at δ = 29.34 and 30.03, the two peaks being of approximately equal area but with the lower field peak broadened and rounded and the higher field peak sharp and intense. The chemical shifts are small for chelating Diphos (although much depends upon the coordination number of the metal and the number of coordinated ligands (10)) and the best that can be said at present is that the structure possibly contains bridging Diphos units and terminal BH_3CN groups.

It is clear that these reactions are closely related to similar reactions involving $NaBH_4$ (1) in that Dppm and Diphos behave in a fundamentally different way. The former results in the formation of mostly Ni(I) complexes and the latter forms Ni(II) and Ni(0). This is presumably related to the different bites of the two ligands and the propensity of Dppm to act primarily as a bridging ligand. Just how interaction of Dppm with Ni(II) (and Cu(I) (7)) leads to such ready production of cyanides is not yet clear. Certainly, with Diphos, much more forcing conditions are needed for only small amounts of cyanide complex production.

The only reasonable interpretation of data for several BH_3CN^- complexes involves this group acting as a bridging ligand which, it is hoped, will be confirmed by X-ray crystallography. It is, however, disturbing that no ν_{M-H-B} of comparable intensity to those seen previously (8, 9) has been observed.

Acknowledgements

We thank the Natural Sciences and Engineering Research Council of Canada for financial support.

1. D. G. HOLAH, A. N. HUGHES, B. C. HUI, and C. T. KAN. Can. J. Chem. **56**, 2552 (1978).
2. R. O. HUTCHINS and N. R. NATALE. Organic preparations and procedures. Int. **11**, 201 (1979).
3. B. C. HUI. Inorg. Chem. **19**, 3185 (1980).
4. J. CHATT, F. A. HART, and H. R. WATSON. J. Chem. Soc. 2537 (1962).
5. B. G. SEGAL and S. J. LIPPARD. Inorg. Chem. **13**, 822 (1974).
6. R. J. BARTON, D. G. HOLAH, S. HU, A. N. HUGHES, S. I. KHAN, and B. E. ROBERTSON. Inorg. Chem. In press.
7. D. G. HOLAH, A. N. HUGHES, C. KAYDEN, K. W. MORSE, and M. SHIMOI. Inorg. Chem. To be published.
8. B. G. SEGAL and S. J. LIPPARD. Inorg. Chem. **16**, 1623 (1977).
9. K. M. MELMED, T. LI, J. J. MAYERLE, and S. J. LIPPARD. J. Am. Chem. Soc. **96**, 69 (1974).
10. P. E. GARROU. Chem. Rev. **81**, 229 (1981).
11. K. NAKAMOTO. Infrared and Raman spectra of inorganic and coordination compounds. 3rd ed. Wiley–Interscience, New York. 1980.
12. M. P. BROWN, R. J. PUDDEPHATT, M. RASHIDI, and K. R. SEDDON. J. Chem. Soc. Dalton Trans. 1540 (1978).
13. M. P. BROWN, J. R. FISHER, S. J. FRANKLIN, R. J. PUDDEPHATT, and K. R. SEDDON. J. Organomet. Chem. **161**, C46 (1978).
14. K. K. CHOW and C. A. MCAULIFFE. Inorg. Chim. Acta, **14**, 121 (1975).
15. P. G. PRINGLE and B. L. SHAW. J. Chem. Soc. Chem. Commun. 81 (1982).
16. M. P. BROWN, R. J. PUDDEPHATT, M. RASHIDI, and K. R. SEDDON. J. Chem. Soc. Dalton Trans. 951 (1977).
17. M. P. BROWN, R. J. PUDDEPHATT, and M. RASHIDI. Inorg. Chim. Acta, **19**, L33 (1976).

Pyrolysis products of 1-(1-phenylcyclohexyl)piperidine (PCP)

RODNEY W. BEAVER AND LOUIS A. JONES[1]

Department of Chemistry, North Carolina State University, Raleigh, NC 27650, U.S.A.

Received September 9, 1983

RODNEY W. BEAVER and LOUIS A. JONES. Can. J. Chem. **62**, 1022 (1984).

PCP was pyrolyzed in air at 400°, 600°, and 800°C and the yield of HCN produced was barely detectable at 400°C, 2.3% at 600°C, and 5.1% at 800°C. Gas chromatography (gc) and gc/mass spectrometry (gc/ms) showed the only pyrolysis products produced at 400°C to be phenylcyclohexane and 1-phenylcyclohexene with 60–70% of the PCP recovered. Only trace amounts of PCP survived the 600°C pyrolysis, the majority of the pyroproducts being polynuclear aromatics (PNAs) with three or fewer rings. The 800°C pyrolysis yielded minor amounts of four-ring PNAs, the remainder being similar to the 600°C products but differing in the relative amounts. Minor amounts of aza-arenes were produced in the 600°C and 800°C pyrolyses and separation techniques are described.

RODNEY W. BEAVER et LOUIS A. JONES. Can. J. Chem. **62**, 1022 (1984).

On a effectué la pyrolyse de la PCP dans l'air à des températures de 400, 600 et 800°C; les rendements en HCN, qui sont à peine détectables à 400°C, sont respectivement de 2,3% et 5,1% à 600 et 800°C. A l'aide de la chromatographie en phase gazeuse (cpg) et de la cpg/spectrométrie de masse (cpg/sm), on a pu montrer que les seuls produits de pyrolyse à 400°C sont le phénylcyclohexane et le phényl-1 cyclohexène alors que l'on récupère 60–70% de la PCP. Il n'y a que des traces de PCP qui survivent à la pyrolyse à 600°C; la majorité des produits formés sont des composés aromatiques polycondensés (APC) comportant au maximum trois cycles. Les pyrolyses à 800°C conduisent à de faibles quantités de composés APC comportant quatre cycles; le reste des produits est qualitativement le même quoique l'on peut observer des différences au point de vue quantitatif. Au cours des pyrolyses à 600 et à 800°C, il se produit de faibles quantités d'aza-arènes; on décrit les techniques de séparation.

[Traduit par le journal]

Can. J. Chem. Downloaded from www.nrcresearchpress.com by 210.87.254.105 on 09/06/12
For personal use only.

Introduction

The illicit drug 1-(1-phenylcyclohexyl)piperidine (PCP, **1**) is a popular drug of abuse, frequently ingested by smoking PCP-impregnated cigarettes (1, 2). Although the variable effects of PCP use have been well-documented (3), no detailed studies have been carried out on the pyrolysis of PCP and conceivably the high-temperature degradation or rearrangement products could contribute to the physiological activity of "smoked" PCP.

In a recent study of these products, Freeman and Martin (1) recovered an average of ca. 40% PCP in the mainstream smoke of parsley cigarettes containing 3–50 mg of tritiated PCP.HCl/cigarette. The only pyrolysis product identified was 1-phenylcyclohexene (**2**), present in the smoke condensate in nearly equimolar concentrations with PCP. Cook *et al.* (2) pyrolyzed 1-(1-phenyl-3-^{3}H cyclohexyl)piperidine.HCl in air at 300, 600, and 800°C by inserting a quartz boat containing ca. 30 mg of the test compound into a horizontal tube furnace and pyrolyzing until all the drug had disappeared from the boat (30 seconds to 5 minutes). Reportedly, >93% of the radioactivity was contained in 1-phenylcyclohexene (**2**) at all temperatures, while for the free base pyrolyzed at 300°C, 57.8% of the recovered radioactivity was found in undecomposed **1** and 34.3% as **2**. The presence of unlabelled piperidine was noted. No other pyrolysis products were reported. The smoke condensate from tritiated (phenyl-3-^{3}H) **1** and PCP.HCl laced parsley cigarettes was similarly studied and 57–59% of the radiolabel was found in the surviving PCP with the remaining 36–41% in **2**.

We chose to study the pyrolysis of pure **1** at temperatures approximating those of the burning zone of a cigarette to determine if the pyrolysis products could be responsible for the variable effects attributed to its use (3). It was felt that the smoke condensates obtained from parsley cigarettes (1, 2) could have been complicated by the large number of compounds originating from the pyrolysis of parsley itself, thus masking the occurrence of other compounds, while the quartz boat pyrolysis method (2) could have allowed unpyrolyzed **1** to distill from the heated pyrolysis zone before being fully subjected to the desired temperature. In our studies, pure **1** was pyrolyzed in an apparatus designed to assure maximum exposure of the test compound to the desired temperature and the pyrolyzate thus produced was separated and analyzed. We now wish to report the results of this study.

Results and discussion

The pyrolysis of approximately 9 g of rigorously purified PCP, synthesized as described by Kalir *et al.* (4), was carried out in a packed, vertically mounted tube and the pyrolyzate collected in a series of three traps: T1, a cold trap; T2, an aqueous acid trap; and T3, an aqueous base trap.

Triplicate samples of PCP were pyrolyzed at 400, 600, and 800°C with average mass yields (T1) of 92.5%, 75.5%, and 41.0% respectively, the 800°C temperature chosen to approximate the maximum burning zone temperature of a cigarette (5). The contents of T1 were analyzed for PCP and its degradation products, while T3 was examined to determine the amount of HCN produced in the pyrolysis (6). The intermediate trap T2 contained aqueous HCl to trap the minor amounts of volatile amines but was not characterized since it contained less than 5% of the pyrolyzate yield (*vide infra*).

After sample pyrolysis had been completed, the cold bath of T1 was removed and the trap gently warmed while the entire apparatus was still being swept with air to insure that any HCN condensed in T1 (bp HCN = 26°C) (7) would be swept into T3 containing a known amount of NaOH. The presence of cyanide in T3 was qualitatively determined via the Prussian blue test (8) and quantification was accomplished by the method of Barakat *et al.* (9). The mean yield for the 800°C pyrolyses was 4.6%, equivalent to 51 mg of HCN per 10 g of PCP, while at 600°C the mean yield of 2.1% corresponded to 23.3 mg of HCN per 10 g of PCP. No HCN was detected in the 400°C pyrolyzate.

[1] Author to whom correspondence may be addressed.

TABLE 1. Preliminary fractionation scheme for silica gel clean-up of 600 and 800°C PCP pyrolyzate

Fraction number	Eluent	Compound class eluted	600°C yield	800°C yield
1	100% Hexane	Alkanes	0	0
2	1:1 Hexane–benzene	Alkanes and alkenes	0.1%	0
3	100% Hexane–benzene	Aromatic hydrocarbons with 3 or fewer rings	97%	95%
4	100% CH_2Cl_2	Aromatic hydrocarbons with more than 3 rings	1.0%	2.0%
5	2:1 CH_2Cl_2–methanol	Aromatic hydrocarbons (>3 rings) and oxygenated aromatics	0.1%	0.1%
6	1:2 CH_2Cl_2–methanol	Aza-arenes and bases	0.1%	0.1%
7	100% Methanol	Aza-arenes and bases	1.0%	1.5%

The pyrolytic generation of HCN from nitrogen-containing organic compounds has been studied by Johnson and Kang (10) who also found that the amount of HCN increased substantially with temperature. Piperidine was shown to yield 33% HCN at 700°C, 47% HCN at 800°C, and 62% HCN at 1000°C. Substantially lower yields of HCN were obtained in our study of the *N*-substituted piperidine of PCP, in accord with Johnson and Kang (10) who found that pyrrolidine gave a 95% yield of HCN at 1000°C, while at the same temperature *N*-methyl pyrrolidine produced only 35% HCN. They proposed that HCN was generated from pyrrolidine. With the *N*-methyl derivative, however, the preferred cleavage to the methyl radical and the pyrrolidine radical subsequently yielded methane and the Δ^1-pyrroline, the latter compound producing HCN in reduced yield (10). The analogous reaction of PCP could initially yield the relatively stable benzylic radical (**3**) and the piperidyl *N*-radical:

[1] 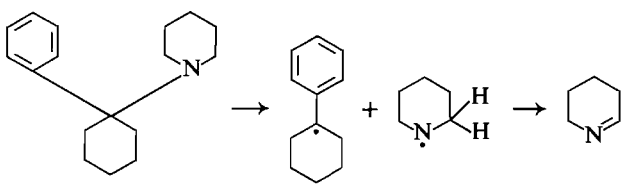

1 **3** **4**

Structure **3** conveniently accounts for some other observed pyrolysis products of PCP (*vide infra*), while **4** gives rise to HCN.

Despite the well-known toxicity of HCN (11), it is unlikely that the level of production contributes significantly to the toxic effects of PCP. A typical PCP-laced cigarette containing 50 mg of PCP (1) would yield only about 0.3 mg of HCN if all of the PCP were subjected to 800°C and presuming the maximum yield of approximately 5% was realized. A standard tobacco cigarette yields as much as 3–5 mg of HCN from the burning of the tobacco alone (6).

The cooled trap (T1) contained a brown to back vile-smelling semi-solid after each pyrolysis and the amount of pyrolyzate produced decreased with increasing temperature, indicative of more complete degradation of the PCP and its pyrolysis products at higher temperatures. Badger *et al.* (12) reported similar results in the pyrolysis of n-butylbenzene and noted that, at 400°C, n-butylbenzene gave ca. 85% pyrolyzates, while at 800°C this yield decreased to less than 10%.

The 400°C pyrolyzate collected in T1 proved to consist of three major components. Gas chromatographic/ms analysis and co-injection of authentic samples on a capillary gc column showed these compounds to be PCP (**1**), range 58.0–73.4%; 1-phenylcyclohexene (**2**), range 21.4–34.4%; and phenylcyclohexane (**5**), range 1.3–9.2%. Piperidine was not detected under the gc conditions used and is presumed not to have survived the pyrolysis (*vide infra*).

The previously postulated phenylcyclohexyl radical (**3**) from eq. [1] can account for the formation of both **2** and **5** as shown in eq. [2]:

[2] 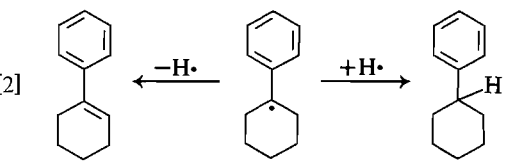

2 **3** **5**

That more of **2** is generated is not unexpected, due to the enhanced stability acquired through the conjugated system produced. It should be noted that PCP has been shown to decompose to **2** at temperatures as low as 250°C with no evidence of **5** (13) and two additional elimination pathways appear reasonable to account for the amounts of **2** produced. First, similar to the mechanism proposed for the radical-induced β-elimination of phosphoranyl radicals (14), is the attack of the piperidinyl radical (eq. [1]) on **1** (eq. [3]), while the second possibility involves the internal *syn*-β-elimination of **1** to give **2** and piperidine, analogous to the pyrolytically induced Ei *cis*-elimination of esters, alkyl halides, and amine salts (15). In either case, the generated piperidine would proceed to generate HCN (10) and the precursor for butadiene.

[3] 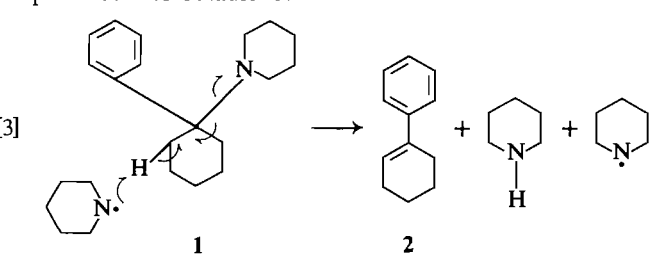

1 **2**

The 600 and 800°C pyrolyzates were substantially more complex than those obtained at 400°C and, before gc/ms or capillary column gc analysis could be undertaken, necessitated a preliminary silica gel fractionation with increasingly polar solvents to give the compound class separation (16) and approximate yields shown in Table 1. These individual fractions

Can. J. Chem. Downloaded from www.nrcresearchpress.com by 210.87.254.105 on 09/06/12
For personal use only.

Can. J. Chem. Downloaded from www.nrcresearchpress.com by 210.87.254.105 on 09/06/12
For personal use only.

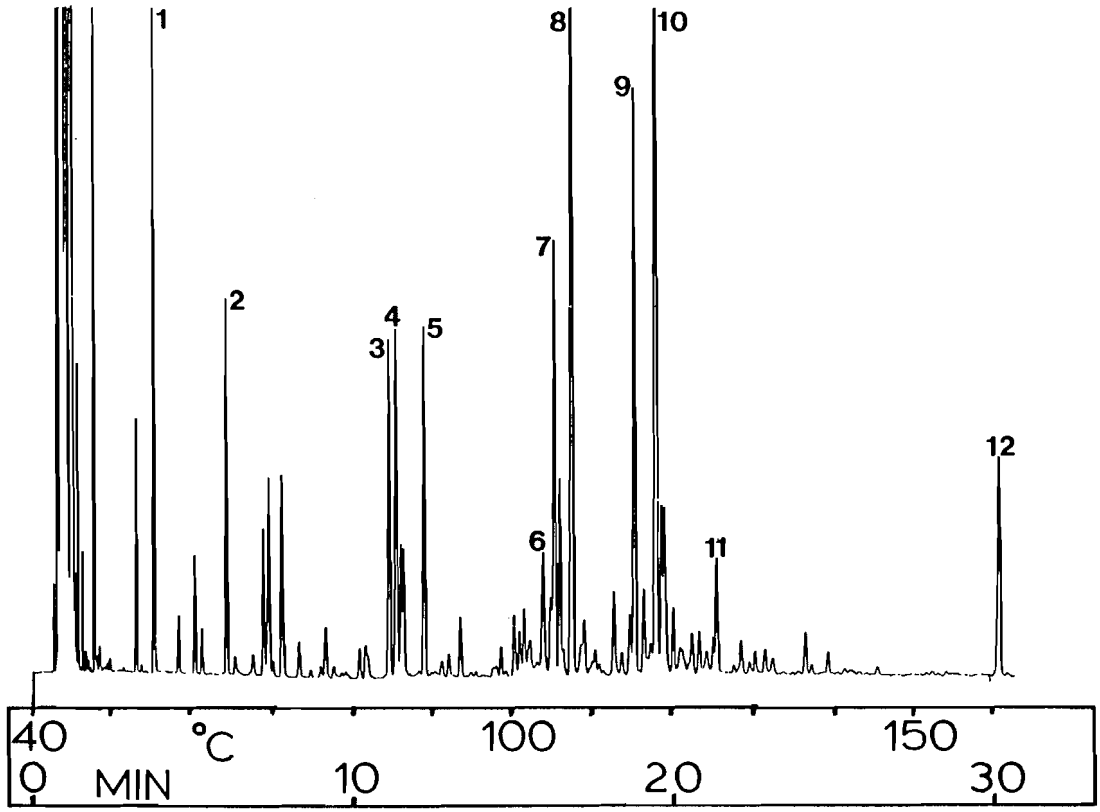

FIG. 1. The gas chromatogram of silica gel Fraction 3, 600°C PCP pyrolyzate, 12-m SP-2100 fused silica capillary column. Numbers refer to compounds in Table 1.

TABLE 2. Compounds present in fraction 3 of the 600°C and 800°C PCP pyrolyzates

	600°C Pyrolysis		800°C Pyrolysis	
Compound	RI_{exp}/RI_{std}[a]	Rel. area % (FID response)[b]	RI_{exp}/RI_{std}	Rel. area % (FID response)[b]
Styrene	1.003	3.9 (1)	0.991	9.3 (1)
α-Methyl styrene	1.003	<1.0 (2)	0.996	3.2 (2)
Propynyl benzene	Not present	—	—[c]	9.4 (3)
x-Methyl [1]-indene	—[c]	3.9 (3)	—[c]	−1.2 (4)
y-Methyl [1]-indene	—[c]	4.1 (4)	—[c]	
Naphthalene	1.000	4.2 (5)	1.000	35.6 (5)
2-Methyl naphthalene	1.000	1.6 (6)	0.999	4.1 (6)
1-Methyl naphthalene	1.000	6.3 (7)	0.991	4.9 (7)
Phenylcyclohexane	0.999	9.7 (8)	Not present	—
Biphenyl	1.000	8.5 (9)	0.999	9.7 (8)
1-Phenylcyclohexene	1.000	14.5 (10)	Not present	—
Acenaphthene	1.000	<1.0 (11)	Not present	—
Phenanthrene	Not present	(12)	1.000	3.2 (9)
Anthracene	Not present	—	0.999	0.8 (10)

[a] Retention Index experimental/Retention Index standard, average of three or more determinations.
[b] Numbers in parenthesis refer to numbered gc peaks in Fig. 1 (SP-2100 capillary column), Fig. 2(SE-52 capillary column) respectively.
[c] Mass spectral library match >98% but no standards available.

were examined by gc/ms and preliminary compound identity was based on matching the mass spectra obtained for selected peaks with those obtained by a computer assisted mass spectral library search. Positive peak identification required the combination of mass spectral library match (>97%) with high-resolution chromatographic retention data (17*a*) (i.e. capillary gc) and relied on the retention index system designed specifically by Novotny and co-workers for programmed temperature capillary gc conditions (18) for relative retention time identification.

Capillary column gc of the individual fractions (Table 1) of the 600°C pyrolysis showed that only Fraction 3 (polynuclear aromatics) and Fraction 7 (aza-arenes and bases) contained detectable gc peaks. The chromatograms of Fraction 3 obtained from each of the triplicate 600°C pyrolyses gave the same peak pattern (Fig. 1) with essentially the same relative peak in-

Can. J. Chem. Downloaded from www.nrcresearchpress.com by 210.87.254.105 on 09/06/12
For personal use only.

tensities and demonstrated the excellent reproducibility of the silica gel fractionation/gc separation procedure. Predictably, gc/ms analysis of these samples indicated that all of the peaks from Fraction 3 were due to aromatic hydrocarbons (16) (identified in Table 2). One internal standard, naphthalene, was present in the pyrolyzate while the second, phenanthrene, was not present and was added to the samples as a retention index standard.

Fraction 7, the aza-arene/base fraction from the silica gel clean-up of the 600°C pyrolyzate, gave an extremely complex chromatogram constituting only a minor portion (<1%) of the total pyrolyzate (based on FID responses for equal injection volumes). Due to the complexity of the sample, accurate retention index measurements and "clean" mass spectra proved difficult to obtain but methylpyridines, methylquinolines, and methylisoquinolines were tentatively identified. A very small amount of PCP (confirmed by co-injection of authentic PCP) also proved to be present.

After subjecting the 800°C PCP pyrolyzate to the silica gel clean-up (Table 1), each fraction was examined by gc and Fig. 2 illustrates the easily reproducible capillary gas chromatogram obtained for Fraction 3 of an 800°C pyrolyzate. Table 2 lists the identities of the numbered peaks in Fig. 2 which were confirmed by gc and gc/ms. These results suggest that anthracene and phenanthrene are produced at the expense of phenylcyclohexene (**2**) and phenylcyclohexane (**5**), since these aromatics become present while **2** and **5** disappeared.

Fractions 4 and 5 were found to contain very low levels of polynuclear aromatics with 4 or more rings. These included pyrene, fluoranthene, and chrysene while Fraction 6 contained 1-napthylacetonitrile, phenanthridine, acridine, 1-cyanonaphthalene, and 2-cyanonaphthalene.

The chromatogram of the aza-arene/base fraction, Fraction 7, from the 800°C pyrolyzates was even more complex than the corresponding fraction from the 600°C pyrolyzates and necessitated further simplification of the mixture. Novotny and coworkers (19) reported the synthesis and use of an alkyl-amino bonded silica in the hplc (high performance liquid chromatography) fractionation of the basic fraction of marijuana smoke condensate. Fraction 7 was further separated on a hplc column packed with this prepared (19) alkyl-amino bonded phase and repetitive injections provided sufficient sample for gc and gc/ms analyses. Identified were benzo[*h*]quinoline, 2-phenylquinoline, and a methylphenylquinoline.

As previously noted, Fraction 3 obtained from the silica gel clean-up (Table 2) of the 600°C and 800°C pyrolyses contained aromatic hydrocarbons with fewer than three fused rings and gc detector response indicated that more than 95% of the pyroproducts were contained in this fraction. Minor nitrogen-containing aromatic compounds found in Fraction 7 included the tentatively identified methylpyridines, methyl quinolines, and isoquinolines, and, more confidently (gc/ms) identified, phenanthridine with some cyanonaphthalenes and 1-naphthylacetonitrile. It would appear, therefore, that the major pyrolytic pathway involves the formation of stable polyaromatic compounds, the heterocyclic compounds originating from a less favored pathway. The work of Badger and Kimber in their definitive mechanistic studies on the pyrolysis of arylalkenes, accounts for the pyrogenesis of the arenes identified and requires butadiene as their precursor (20). The pyrolysis of butadiene itself has been reported to yield ethylbenzene and styrene as well as naphthalene and tetralin (21). In the results reported herein, the origin of butadiene is proposed to derive from the piperidyl moiety (as in eq. [3]) as well as from the cyclohexyl group. The increase in naphthalene and absence of 1-phenylcyclohexene (**2**) in the 800°C pyrolysis (Table 2) would appear to support the increased generation of butadiene with increased temperature.

The enhanced generation of the nitrogen-containing aromatics with increasing pyrolysis temperature can be accounted for by the reaction of piperidine and butadiene (eq. [4]) analogous to that reported for piperidine with terminal olefines (22). Subsequent ring closure, aromatization, and further butadiene/quinoline coupling produces acridine and phenanthridine similar to the polynuclear aromatic pyrogenesis described by Badger and Kimber (20). The relatively low concentration of these heteroaromatic compounds can be accounted for by noting that the HCN generation increased with increasing temperature, thus decreasing the piperidyl moiety concentration.

[4]

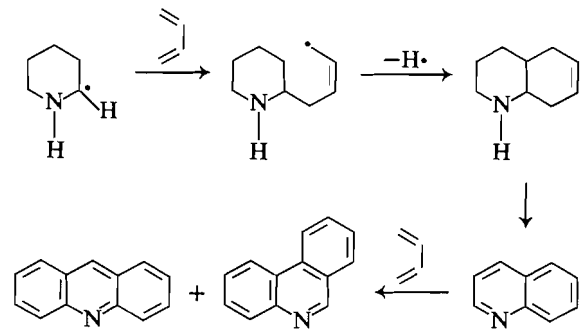

In conclusion, the major pyrolysis products of PCP obtained at 400, 600, and 800°C have been identified. Except for the PCP found in the 400 and 600°C pyrolyzates, no compounds analogous to PCP were detected which would be expected to result in hallucinogenic or other PCP-like activity, although many of the pyrolysis products identified are known to be toxic and/or carcinogenic (17*b*).

Experimental

Pyrolysis apparatus and procedure

A 55 cm × 28-cm id Vycor tube (Fisher) was fitted with a very coarse quartz frit (Type T08, Porosity 00; Heraeus–Amersil, Sayreville, NJ) 11 cm from the bottom, upon which was deposited an 8-cm deep bed of quartz chips, consisting of 6 mm × 6 mm Type T08 quartz rods (Heraeus–Amersil). The top of the Vycor tube was fitted with a quartz female 14/20 joint to which was fitted a male 14/20 quartz joint equipped with a side-arm gas inlet and septum adapter. The Vycor pyrolysis tube was vertically mounted in a Hoskins Tube Furnace (FD303A) such that the quartz frit was located 11 cm from the bottom end of the furnace. The temperature was controlled by a variable transformer and monitored by an indicating pyrometer with a Chromel/Alumel thermocouple (Fisher 13-902) molded into a 28/15 standard joint which fitted a mating joint located on the pyrolysis tube 12 cm below the oven. When inserted into the tube, the end of the thermocouple was 0.5 mm below the quartz frit. Prior to each pyrolysis the oven was brought to temperature with the thermocouple in place and allowed to equilibrate for 2–3 hours, after which the thermocouple was removed and the joint sealed. The oven temperature was determined to be homogeneous throughout. Traps were constructed of 40-mm Pyrex O-ring joints and were sealed with Buna-N O-rings. The entire system was sealed when the injection septum was in place and the O-ring joints clamped. Trap 1 (T1) was located directly beneath the oven and was cooled in a Dry Ice/$CHCl_3$ bath; T1 was connected to Trap 2 (T2), which contained 10% HCl (aqueous), and which in turn was connected to Trap 3 (T3) containing 200.0 mL

Can. J. Chem. Downloaded from www.nrcresearchpress.com by 210.87.254.105 on 09/06/12
For personal use only.

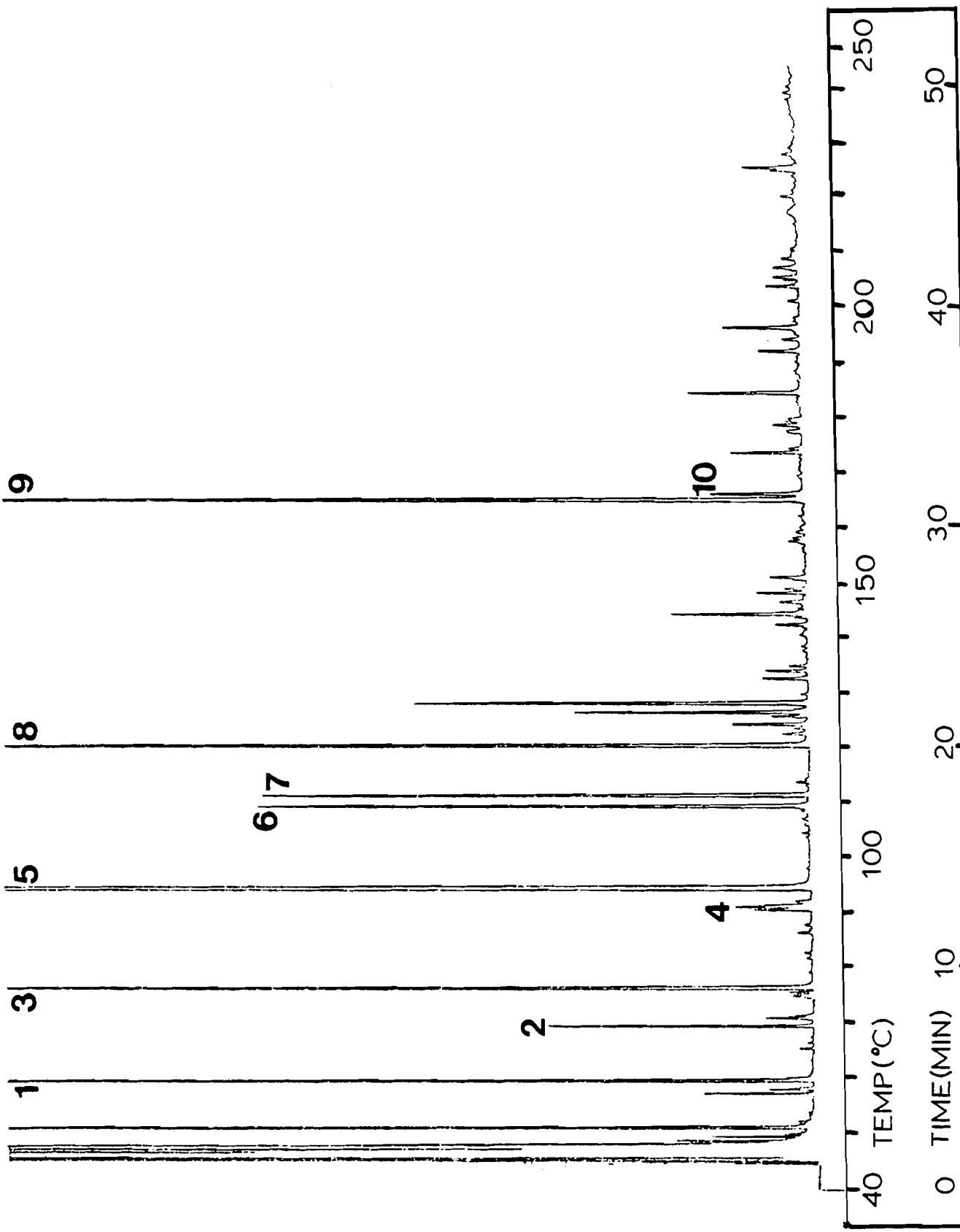

FIG. 2. The gas chromatogram of silica gel Fraction 3, 800°C PCP pyrolyzate, 12-m SE-52 fused silica column. Numbers refer to compounds in Table 1.

Can. J. Chem. Downloaded from www.nrcresearchpress.com by 210.87.254.105 on 09/06/12
For personal use only.

of 0.5 *M* aqueous NaOH.

In all pyrolyses, the apparatus was swept with breathing grade air at a flow rate of 40 ± 2 mL/min during sample introduction. Triply vacuum-distilled PCP (bp of third distillate = 127°C at 0.8 Torr) was prepared according to the method of Kalir *et al.* (4) and approximately 9 g of the gently warmed, liquefied PCP was dripped onto the quartz beads (syringe, ca. 10 drops/min) such that the entire sample was introduced in 30 ± 3 minutes. Following the pyrolysis, the apparatus was allowed to cool and the cold bath removed from T1 which was subsequently gently warmed (ca. 40°C) with continued air flow to assure that any HCN condensed in T1 would be swept into T3. T1 and T3 were then examined as described below.

Determination of cyanide

A 10.00-mL aliquot of T3 (total volume T3 = 200.0 mL) was removed and buffered with 50.0 mL of aqueous 0.1 *M* NaH_2PO_4. Cyanide was determined according to the method of Baraket *et al.* (9) using freshly prepared 0.01*XXX M* aqueous n-bromosuccinimide (NBS) for the 800°C pyrolyses and 0.005*XXX M* NBS for the 600°C pyrolyses.

Gas chromatography

All gas chromatography (gc) was carried out on a Hewlett–Packard 5880A instrument equipped with a flame ionization detector and a Level IV microprocessor which allowed for the measurement of retention times to the thousandth of a minute. Gas chromatographic analyses utilized temperature programming from 40 to 250°C or 40 to 280°C at 4°C/min. Helium (zero grade) was used as a carrier gas at a flow rate of 0.8 mL/min. Injections were split 1 : 00 with an injection volume of 1 μL. Columns were 12-meter fused silica capillary columns (0.2-mm id) deactivated with Carbowax 20M and coated with either SP-2100 (methyl silicone) or SE-52 (5% phenyl methyl silicone). Retention indices were calculated by the method of Novotny and co-workers (18) as previously described. Standards were obtained from various commercial sources and were purified where necessary.

Gas chromatography/mass spectrometry

All gc/ms analyses were carried out on a Hewlett–Packard 5985B instrument equipped with a 25-meter SP-2100 fused silica capillary column programmed from 40 to 250°C at 4°C/min. The spectrometer used a Probability Based Search routine (23) to search the EPA–NIH mass spectral data base (24).

Pyrolyzate fractionation on silica gel

Silica gel (70–230 mesh) was slurried in hexane and slurry packed to a depth of 6 cm in a 1-cm diameter glass column equipped with a Teflon stopcock. All solvents were either commercial distilled-in-glass or were redistilled in this laboratory. Fractionation was carried out by carefully placing ca. 50 mg of pyrolyzate on top of the silica bed and pipetting 4 mL of successively more polar solvents into the column (see Table 1). Fractions of 4 mL were collected in chromic acid washed vials equipped with Teflon lined septum caps. After initial gc and gc/ms runs to determine their presence in the pyrolyzate, retention index standards (naphthalene, phenanthrene, chrysene) were spiked into the fractions and triplicate gc runs made for retention index calculations. Crude weights were obtained by evaporating one of the separation sequences to dryness and weighing (Table 1).

Preparation of and chromatography with alkyl-amine bonded silica

The reaction of 25 g of *N*-(2-aminoethyl-3-aminopropyl)trimethoxysilane, $(H_2N(CH_2)_2NH(CH_2)_3Si(OEt_3)$ (Alfa Products, Danvers, MA) with hydrated silica gel was carried out as described (19) and analysis of the product showed the alkyl-amino bonded silica to contain 5.1% C and 2.6% N by weight. A 60 cm long × 7.8-mm id hplc column was packed with the above described alkyl-amino silica (ca. 20 g required) using the "tap-fill" method (25). With 100% heptane at a flow rate of 9.9 mL/min and nitrobenzene as the solute ($k' = 1.5$), the column was found to exhibit 500 theoretical plates.

Fraction 7 from the silica gel clean-up of the 800°C pyrolyzate was reduced from 4 mL to dryness and made up to 1 mL with 3.5% CH_2Cl_2 in heptane. Five injections of 200 μL each of this solution were made onto the above hplc column with a mobile phase of 3.5% CH_2Cl_2 in heptane at a flow rate of 3.5 mL/min. Fractions were collected as follows: Fraction A, 22 mL; Fraction B, 5 mL; Fraction C, 15 mL; Fraction D, 10 mL; Fraction E, 20 mL. After combining Fraction A from each injection, the solvent was removed by rotary evaporation, the sample transferred to a 1-mL cone-tipped vial with 5 × 200 μL of CH_2Cl_2, and the $CHCl_2$ reduced to 50 μL under a gentle stream of N_2. Injections of 1 μL of this 50-μL solution were used for the gc analysis.

Acknowledgment

The financial assistance of the N.I.H. Biomedical Research Grant RR07071 is gratefully acknowledged.

1. A. S. FREEMAN and B. R. MARTIN. Pharm. Sci. **70**, 1002 (1981).
2. C. E. COOK, D. R. BRINE, G. D. QUIN, M. E. WALL, M. PEREZ-REYES, and S. R. DIGUISEPPI. Life Sci. **29**, 1967 (1981).
3. D. A. LABIANCA. J. Chem. Ed. **58**, 664 (1981).
4. A. KALIR, H. EDERY, Z. PELAH, D. BALDERMAN, and G. PORATH. J. Med. Chem. **12**, 413 (1969).
5. E. B. HIGMAN, R. F. SEERSON, R. F. ARRENDALE, and O. T. CHORTYK. J. Agric. Food Chem. **25**, 120 (1977).
6. W. T. SMITH, JR., S. P. CHEN, and J. M. PATTERSON. Tob. Sci. **14**, 50 (1975).
7. R. C. WEAST (*Editor*). Handbook of chemistry and physics. 59th ed. CRC Press, Boca Raton, FL. 1978. p. B-123.
8. R. L. SHRINER, R. C. FUSON, and D. Y. CURTIN. The systematic identification of organic compounds. 5th ed. John Wiley and Sons, New York. 1964. pp. 63–64.
9. M. Z. BARAKAT, M. SHAKER, and N. NAQUIB. Microchem. J. **11**, 485 (1966).
10. W. R. JOHNSON and J. C. KANG. J. Org. Chem. **36**, 189 (1971).
11. M. WINDHOLZ (*Editor*). The Merck index. 9th ed. Merck and Co., Inc., Rahway, NJ. Entry 4688.
12. G. M. BADGER, R. W. L. KIMBER, and J. NOVOTNY. Aust. J. Chem. **17**, 778 (1964).
13. D. C. K. LIN, A. F. FENTIMAN, JR., R. L. FOLTZ, R. D. FORNEY, JR., and I. SUNSHINE. Biomed. Mass Spectrom. **2**, 206 (1975).
14. R. S. DAVIDSON. Tetrahedron, **25**, 3383 (1969).
15. J. MARCH. Advanced organic chemistry, reactions, mechanisms, and structures. 2nd ed. McGraw Hill Book Co., New York, NY. 1977. p. 917 and references therein.
16. M.-L. YU and R. A. HITES. Anal. Chem. **53**, 951 (1981).
17. (*a*) M. L. LEE, M. V. NOVOTNY, and K. D. BARTLE. Analytical chemistry of polycyclic aromatic compounds. Academic Press, New York. 1981. p. 242; (*b*) pp. 50–57.
18. M. L. LEE, D. L. VASSILAROS, C. M. WHITE, and M. NOVOTNY. Anal. Chem. **51**, 768 (1979).
19. F. MERLI, M. NOVOTNY, and M. L. LEE. J. Chromatogr. **199**, 371 (1980).
20. G. M. BADGER and R. W. L. KIMBER. J. Chem. Soc. 2746 (1960), and references therein.
21. C. WEIZMANN, V. HENRI, and E. BERGMANN. Ind. Eng. Chem. **43**, 2312 (1951); 2318 (1951); 2325 (1951).
22. W. H. URRY, O. O. JUVELAND, and F. W. STACEY. J. Am. Chem. Soc. **74**, 6155 (1952); **80**, 3322 (1958).
23. HP5985-B software manual, GC/MS data system. Hewlett–Packard, Palo Alto, CA. 1980. Appendix B.
24. S. R. HELLER and G. W. A. MILNE. EPA–NIH mass spectral data base. U.S. Government Printing Office. Washington, DC. 1978.
25. L. R. SNYDER and J. J. KIRKLAND. Introduction to modern liquid chromatography. 2nd ed. John Wiley and Sons, New York. 1979. p. 207.

Electrochemical reduction of quinoxalino[2,3-*b*]quinoxaline: a revised mechanism

JOSEPH ARMAND AND LINE BOULARES
Laboratoire de Physicochimie des Solutions, ENSCP 11, rue Pierre et Marie Curie, 75 231 Paris Cedex 05, France

CHRISTIAN BELLEC
Laboratoire de Chimie des Hétérocycles, Université Pierre et Marie Curie, 4 place Jussieu, 75 230 Paris Cedex 05, France

CLAUDETTE BOIS AND MICHÈLE PHILOCHE-LEVISALLES
Laboratoire de Chimie Systématique, Université Pierre et Marie Curie, 4 place Jussieu, 75 230 Paris Cedex 05, France

AND

JEAN PINSON
Laboratoire d'Electrochimie, Université de Paris, 7, 2 place Jussieu, 75 251 Paris Cedex 05, France

Received July 29, 1983

JOSEPH ARMAND, LINE BOULARES, CHRISTIAN BELLEC, CLAUDETTE BOIS, MICHÈLE PHILOCHE-LEVISALLES, and JEAN PINSON. Can. J. Chem. **62**, 1028 (1984).

The electrochemical reduction of fluoflavine **2** gives compound **9** to which we had previously assigned a hexahydroquinoxalino[2,3-*b*]quinoxaline structure. A crystallographic study of a diacetylated derivative of **9** shows that **9** is in fact 2-(*o*-aminoanilinomethyl)benzimidazole. This result permits us to propose a detailed reduction mechanism for **2** and its diacetyl derivative **25**.

JOSEPH ARMAND, LINE BOULARES, CHRISTIAN BELLEC, CLAUDETTE BOIS, MICHÈLE PHILOCHE-LEVISALLES et JEAN PINSON. Can. J. Chem. **62**, 1028 (1984).

La réduction électrochimique de la fluoflavine **2** conduit à un composé **9** auquel nous avions attribué la structure d'une hexahydroquinoxalino[2,3-*b*]quinoxaline. Une étude cristallographique d'un dérivé diacétylé de **9** montre que **9** est en réalité le 2-(*o*-aminoanilinomethyl)benzimidazole. Ce résultat nous permet de proposer des mécanismes de réduction détaillés pour **2** et son dérivé diacétylé **25**.

Can. J. Chem. Downloaded from www.nrcresearchpress.com by 210.87.254.6 on 09/06/12
For personal use only.

In a preceding paper (1) dealing with the electrochemical reduction of quinoxalino[2,3-*b*]quinoxaline and its derivatives, we have shown that the 5,12-dihydro derivative **2** — known as fluoflavine — is reduced in acidic medium through a $4F$/mol process into **9** to which we had assigned the structure 5,5*a*,6,11,11*a*,12-hexahydroquinoxalino[2,3-*b*]quinoxaline. In order to establish the conformation of **9** we carried out a crystallographic study of **9′**, a diacetyl derivative of **9**. The structure of **9′** is shown in Fig. 1. It shows that **9** is in fact 2-(*o*-aminoanilinomethyl)benzimidazole, a compound as yet unknown. The nmr spectrum of **9**(1) is in agreement with this structure. Indeed, the aromatic protons of *o*-phenylene diamine appear as a singlet at 6.75 ppm and that of 2-methylbenzimidazole as an AA′BB′ pattern between 7.4 and 7.85 ppm. In the case of **9** the aromatic protons appear as two multiplets, one of them between 6.4 and 6.7 ppm and the other between 7 and 7.8 ppm (AA′BB′ pattern).

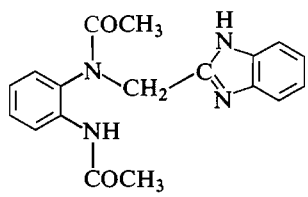

9′

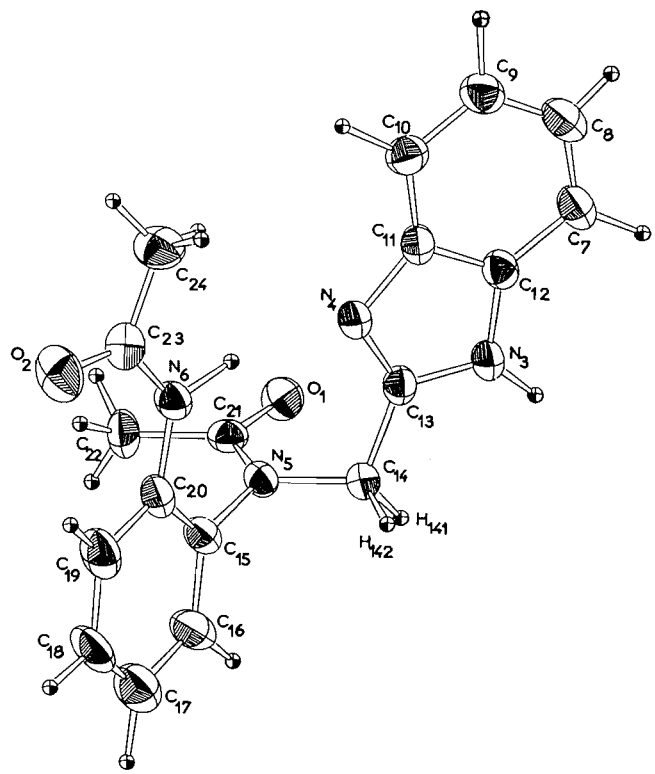

FIG. 1. ORTEP diagram of the crystal structure of **9′**.

Reduction mechanism

Reduction of 2 in acidic medium

Scheme 1 shows a possible reduction mechanism leading to **9**. The first step leads to the tetrahydro derivative **11**, which is in agreement with the results of cyclic voltammetry (1). The next step, the isomerisation of **11** into **12**, is frequently observed in 1,4-dihydroquinoxalines (2) or 1,4-dihydropyrazines (3, 4). The hydration of the C=N double bond leading to **32**

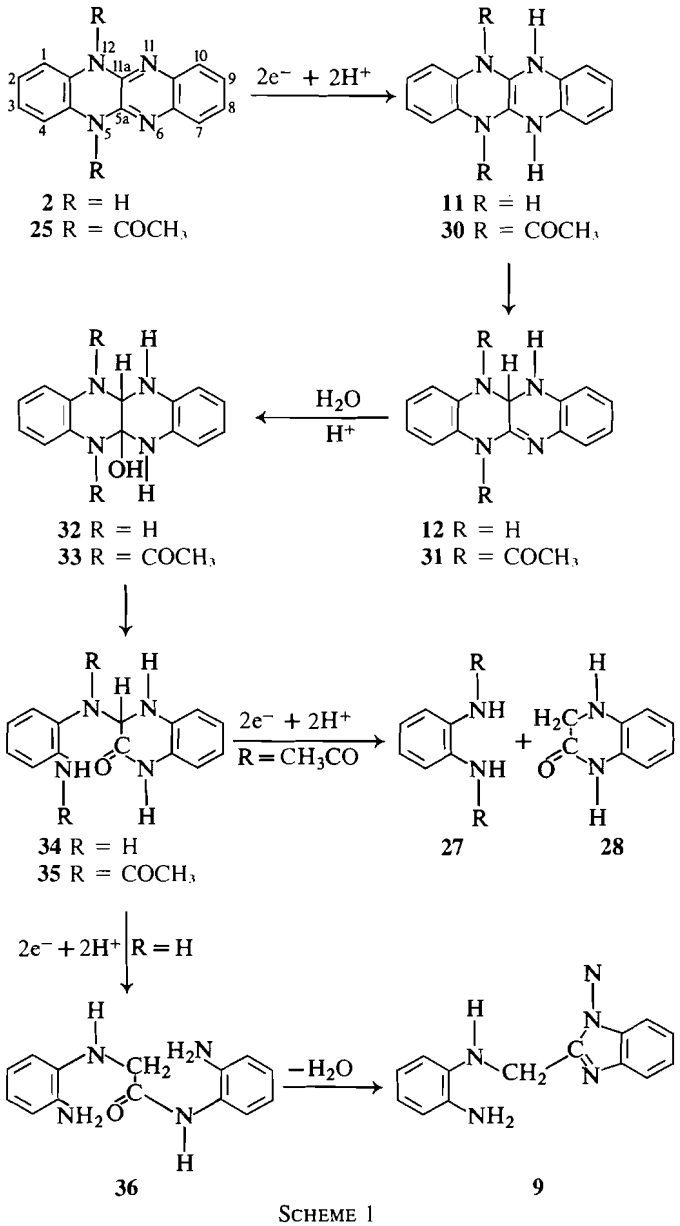

SCHEME 1

is an often encountered reaction during the electrochemical reduction (5*a*) and oxidation (5*b*) of pteridines and during the oxidation of uric acid (5*c*). The next step is an hydrolytic cleavage of the C_{5a}—N_5 bond, giving **34** which is further electrochemically reduced into **36**. This electrochemical reduction involving the cleavage of C_{11a}—N_{11} bond is analogous to that of α-aminoketones. It is indeed well established (6–8) that α-aminoketones are electrochemically reduced according to

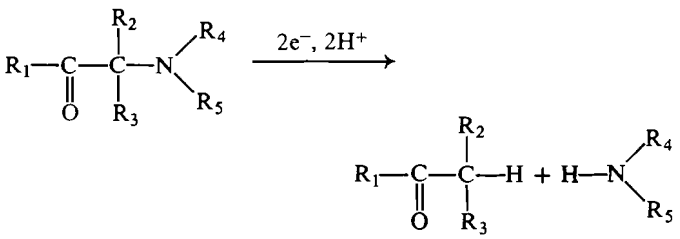

The last step, the cyclization of **36** into **9**, is similar to the formation of 2-methyl benzimidazole from *N*-acetyl-*o*-phenylenediamine (9).

TABLE 1. Positional parameters ($\times 10^4$) and isotropic thermal parameters* with esd's in parentheses for **9'**

Atom	*X*	*Y*	*Z*	B_{iso} (Å^2)
O(1)	8119(2)	5079(3)	213(2)	3.9
O(2)	5567(2)	−1647(3)	−291(2)	5.6
N(3)	10440(2)	2614(4)	333(2)	3.3
N(5)	7796(2)	3116(3)	−774(2)	2.9
N(4)	8960(2)	1267(4)	570(2)	3.3
N(6)	6842(2)	266(4)	−329(2)	3.4
C(14)	8942(3)	2873(5)	−811(2)	3.5
C(12)	10646(3)	1811(4)	1126(2)	3.2
C(15)	7089(3)	2305(4)	−1406(2)	3.1
C(24)	6789(3)	−1347(5)	966(3)	4.9
C(11)	9726(3)	984(4)	1271(2)	3.1
C(20)	6603(3)	905(5)	−1185(2)	3.5
C(22)	6299(3)	4510(5)	−195(3)	4.2
C(16)	6915(3)	2963(5)	−2247(2)	4.4
C(13)	9423(3)	2229(4)	47(2)	3.0
C(19)	5909(3)	144(5)	−1827(3)	4.8
C(18)	5756(3)	867(6)	−2671(3)	5.4
C(10)	9665(3)	50(5)	2028(2)	3.9
C(8)	11470(3)	849(5)	2465(3)	4.5
C(21)	7467(3)	4270(4)	−236(2)	3.1
C(9)	10559(3)	3(5)	2623(2)	4.3
C(7)	11552(3)	1780(5)	1720(3)	4.0
C(23)	6332(3)	−939(5)	56(3)	3.8
C(17)	6241(3)	2243(6)	−2892(3)	5.3
H(19)	5580	−1180	−1700	4.8
H(16)	7350	4100	−2420	4.4
H(13)	5240	260	−3110	5.4
H(3)	10960	3510	90	3.3
H(7)	12280	2430	1550	4.0
H(8)	12040	700	2900	4.5
H(9)	10580	−880	3240	4.3
H(241)	7250	−410	1230	4.9
H(242)	7260	−2340	940	4.9
H(243)	6300	−1910	1350	4.9
H(221)	5810	3520	−210	4.2
H(222)	5910	5160	−590	4.2
H(223)	6040	4940	410	4.2
H(141)	9350	4010	−1040	3.5
H(142)	9170	1990	−1320	3.5
H(10)	8950	−880	2200	3.9
H(6)	7530	710	100	3.4
H(17)	6070	2870	−3540	5.3

*B_{iso} for the non-H atoms is calculated by the expression: $B_{iso} = (4/3)\ \Sigma_i\Sigma_j\beta_{ij}(a_i a_j)$.

Reduction of 5,12-diacetyl-5,12-dihydroquinoxalino[2,3-b]-quinoxaline, 25

Scheme 1 also rationalizes the formation of **27** and **28** by electrochemical reduction of **25**. The first four steps are common to **2** and **25**; they lead to **34** in the case of **2** and to **35** in the case of **25**. As stated above, the electrochemical reduction of α-aminoketones in acidic medium leads to the cleavage of the C—N bond. In the case of **34** and **35** there are two C—N bonds on carbon C_{11a}. As **27** and **28** are obtained from **35** the reduction must involve the cleavage of the C_{11a}—N_{12} bond. This means that replacing R = H by R = $COCH_3$ on N_{12} favours the cleavage of C_{11a}—N_{12} bond at the expense of the C_{11a}—N_{11} bond.

As a whole, Scheme 1 presents quite an original mechanism in the quinoxaline series, leading to the unexpected compound **9**.

Can. J. Chem. Downloaded from www.nrcresearchpress.com by 210.87.254.6 on 09/06/12
For personal use only.

Can. J. Chem. Downloaded from www.nrcresearchpress.com by 210.87.254.6 on 09/06/12
For personal use only.

Experimental section

The crystals of **9′**, a diacetyl derivative of **9**, are obtained by slow evaporation of a methanolic solution of **10** the triacetyl derivative of **9** (1). In methanol, the triacetyl derivative **10** loses an acetyl group; the thorough evaporation of the methanolic solution leaves only the diacetyl derivative **9′** with the following ^{1}H nmr spectrum (DMSO-d_6): $\rangle$N—$COCH_3$, $NHCOCH_3$: two singlets at 1.66 and 2.30 ppm (2 × 3H); CH_2: two doublets centered at 4.52 and 5.36 ppm (2 × 1H); aromatic protons: multiplet, 7−8.2 ppm (8H); N_1H: singlet 12.6 ppm exchanged with D_2O (1H).

Crystallographic study of 9′

Crystal data are as follows:

$C_{18}H_{18}N_4O_2$ fw = 322

Monoclinic, a = 12.660(2), b = 8.466(2), c = 15.172(3) Å, β = 94.21(1)°, V = 1621.8 Å^3, Z = 4, ρ_c = 1.32 g cm^{-3}, ρ_0 = 1.32(2) g cm^{-3} (20°C), MoK$_\alpha$ λ = 0.7107 Å, μ = 0.93 cm^{-1}.

Preliminary X-ray photographs showed the following systematic absences: $h0l$, $l = 2n + 1$, $0k0$, $k = 2n + 1$; a statistical analysis of the intensity data indicated the centrosymmetric space group $P2_1/c$. A crystal (0.35 × 0.75 × 0.25 mm) was mounted with the b axis parallel to the ϕ axis of a Philips automated diffractometer equipped with a graphite monochromator. The intensities of all reflections having 2θ less than 50° were measured using the variable $\omega-2\theta$ scan technique. During the course of the data collection three standard reflections were measured every 54 reflections. A total of 1743 independent reflections was measured, 1353 of which had $I > 4\sigma(I)$. The data were reduced to $|F_o|$ by the routine procedure. Lorentz and polarization but no absorption or extinction corrections were applied.The scattering factors for neutral atoms were taken from ref. 10. The structure was determined by direct methods (MULTAN) (11) and refined by large block least squares $\Sigma\omega(F_o - |F_c|)^2$ = minimum with $\omega = 1/\sigma^2$. The refinement with anisotropic thermal parameters on the non-hydrogen atoms converged to R = 0.084. At this stage, a difference Fourier map revealing the positions of all the hydrogen atoms was calculated; refinement of their positional parameters was carried out using the thermal parameters of the corresponding heavy atoms at the end of isotropic refinement. The refinement converged with R = 0.057 and R_w = 0.056.

Positional parameters and isotropic thermal parameters are given in Table 1. Tables of bond lengths (Table 2), bond angles (Table 3), temperature factors (Table 4), and observed and calculated structure factor amplitudes were put in the Depository of Unpublished Data.[1]

Acknowledgement

The technical help of Mrs. Th. Quenot is gratefully acknowledged.

1. J. ARMAND, L. BOULARES, C. BELLEC, and J. PINSON. Can. J. Chem. **60**, 2797 (1982).
2. J. PINSON and J. ARMAND. Coll. Czech Chem. Commun. **36**, 585 (1971).
3. L. N. KLATT and R. L. ROUSEFF. J. Am. Chem. Soc. **94**, 7295 (1972).
4. J. ARMAND, K. CHEKIR, and J. PINSON. Can. J. Chem. **52**, 3971 (1974).
5. (*a*) G. DRYHURST. Electrochemistry of biological molecules. Academic Press, New York. 1977. p. 331; (*b*) D. EGE-SERPKENCI and G. DRYHURST. J. Electroanal. Chem. Interfacial Electrochem. **141**, 175 (1982); (*c*) R. N. GOYAL, A. BRAJER-TOTH, and G. DRYHURST. J. Electroanal. Chem. Interfacial Electrochem. **131**, 181 (1982); R. N. GOYAL, A. BRAJER-TOTH, G. DRYHURST, and N. T. NGUYEN. J. Electroanal. Chem. Interfacial Electrochem. **141**, 39 (1982).
6. H. LUND. Acta Chem. Scand. **14**, 1927 (1960).
7. P. ZUMAN and V. HORAK. Coll. Czech. Chem. Commun. **26**, 176 (1961).
8. J. ARMAND and L. BOULARES. Bull. Soc. Chim. Fr. 711 (1975).
9. M. A. PHILLIPS. J. Chem. Soc. 176 (1928).
10. International Tables for X-ray crystallography. Vol. IV. The Kynoch Press, Birmingham, England. 1974.
11. G. GERMAIN, P. MAIN, and M. M. WOOLFSON. Acta Crystallogr. A**27**, 268 (1971)

[1]A complete set of tabular data is available, at a nominal charge, from the Depository of Unpublished Data, CISTI, National Research Council of Canada, Ottawa, Ont., Canada K1A 0S2.

Biphasic hydrogenation of olefins, dienes, and α,β-unsaturated carbonyl compounds catalyzed by the dimer of chloro(1,5-hexadiene)rhodium

KRZYSZTOF R. JANUSZKIEWICZ AND HOWARD ALPER[1]

Ottawa–Carleton Institute for Research and Graduate Studies in Chemistry, Department of Chemistry, University of Ottawa, Ottawa, Ont., Canada K1N 9B4

Received October 24, 1983

KRZYSZTOF R. JANUSZKIEWICZ and HOWARD ALPER. Can. J. Chem. **62**, 1031 (1984).

Olefins, dienes, and trienes can be hydrogenated in an aqueous–organic two-phase medium using the dimer of chloro-(1,5-hexadiene)rhodium as the catalyst. Selective reduction of the double bond of α,β-unsaturated carbonyls occurs in high yields. These reactions occur at room temperatures and atmospheric pressure, and are simple to work-up.

KRZYSZTOF R. JANUSZKIEWICZ et HOWARD ALPER. Can. J. Chem. **62**, 1031 (1984).

Opérant dans un milieu aqueux–organique en deux phases, on peut hydrogéner des oléfines, des dièmes et des triènes en utilisant le dimère du chloro[hexadiène-1,5]rhodium comme catalyseur. On peut réaliser, avec d'excellents rendements, la réduction sélective des doubles liaisons des composés carbonylés non-conjugués en α,β.

[Traduit par le journal]

Can. J. Chem. Downloaded from www.nrcresearchpress.com by 210.87.254.42 on 09/06/12
For personal use only.

Recently, we described the hydrogenation of aromatic hydrocarbons and heterocyclic compounds using the dimer of chloro(1,5-hexadiene)rhodium ((1,5-HDRhCl)$_2$) as the metal catalyst, cetyltrimethylammonium bromide (CTAB) or tetrabutylammonium hydrogen sulfate (THS) as the phase transfer catalyst, with benzene, hexane, or methylene chloride used as the organic phase, and a buffer solution of pH 7.6 as the aqueous phase. This authentic phase transfer reaction occurs under remarkably mild conditions (room temperature, 1 atm) (1). We now wish to report the application of this process to the reduction of olefins, dienes, trienes, and α,β-unsaturated ketones and aldehydes.

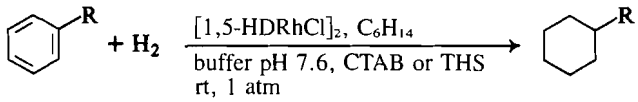

When *p*-methoxystyrene was reacted for 7 h, as described above (hexane as the organic phase), *p*-ethylanisole was formed in quantitative yield. Reduction of the arene ring occurs, but only after an extended period of reaction (48 h). In contrast to arene hydrogenation, the reduction of the double bond of *p*-methoxystyrene, and of other olefins, dienes, and α,β-unsaturated carbonyls does *not* require a phase transfer agent. In other words, these are biphasic and not phase transfer reactions.

In Table 1 are listed results for the hydrogenation of olefins. There are several noteworthy features of these reactions. First, an olefin can be hydrogenated in the presence of bromide (6-bromo-1-hexene). Second, while the three double bonds of methyl linolenate are reduced in a facile manner, cycloheptatriene affords cycloheptene as the major product and no reaction occurs with 5-methyl-1,3,6-heptatriene possibly because the double bonds are strongly complexed to rhodium. Third, non-conjugated and conjugated dienes experience partial or complete reduction.

It was previously demonstrated that cyclohexene is hydrogenated more readily than 1,3- or 1,4-cyclohexadiene which in turn is more easily reduced than benzene (1). The stereochemistry of hydrogenation of cyclohexenes was examined using a series of isomeric dimethylcyclohexenes. Although these reductions were not stereospecific, they did show *cis* selectivity, the highest being realized for the tetrasubstituted olefin, 1,2-dimethylcyclohexene (7.3/1.0 *cis/trans*-1,2-dimethylcyclohexane). The clear preference for *cis*-dimethylcyclohexanes from 1,6- and 1,3-dimethylcyclohexenes is probably a consequence of the allylic methyl group of the rhodium complex of the olefin, in each case, existing in an axial or pseudo-axial conformation. For 1,4-dimethylcyclohexene there is no allylic methyl substituent and hence little discrimination. These stereochemical results are similar, but not identical, to those observed with rhodium in *t*-butanol(2). The reactivity and stereochemistry are clearly different from the hydrogenation of dimethylcyclohexenes effected with rhodium on carbon (3), or with Wilkinson's catalyst (4). These observations are in accord with experiments indicating that the biphasic process is heterogeneous as far as the metal species is concerned (i.e., a highly active form of colloidal rhodium) (5).

α,β-Unsaturated ketones can be selectively hydrogenated to saturated carbonyl compounds using similar reaction conditions to those described for olefins. Fine yields of products were obtained (Table 2) and the reactions can be followed very simply using thin layer chromatography (tlc), appropriate developing solvents,and a 5% solution of vanillin (in 96% H_2SO_4) for visualization (Table 3). Reactions were usually faster when hexane was used as the organic phase instead of benzene. These reactions are quite facile for substrates containing a disubstituted or trisubstituted double bond (2-cyclohexen-1-one, 3-penten-2-one, 3-methyl-2-cyclopenten-1-one), *provided* the carbonyl group is not attached to a fully substituted unsaturated carbon atom (e.g., 1-acetyl-1-cyclohexene) in which case a much slower reaction occurred. In addition, conjugation of a phenyl group with the α,β-unsaturated carbonyl unit (4-phenyl-3-buten-2-one) slows down the reaction appreciably when compared with an alkyl analog.

The principal product formed from the room temperature hydrogenation of cinnamaldehyde is hydrocinnamaldehyde. The latter can also be obtained using Wilkinson's catalyst, but drastic conditions are required (6). Elevated temperatures and/or pressures are usually necessary for the reduction of α,β-unsaturated aldehydes by rhodium on alumina (7, 8).

Finally, while the reduction of arene hardly occurs (4%) using water instead of the buffer as the aqueous phase, the hydrogenation of α,β-unsaturated ketones still takes place, but at a reduced rate. Specifically, the reduction of 2-cyclo-

[1] To whom all correspondence should be addressed.

Can. J. Chem. Downloaded from www.nrcresearchpress.com by 210.87.254.42 on 09/06/12
For personal use only.

TABLE 1. Hydrogenation of olefins, dienes, and trienes

Reactant	Organic phase[a]	Reaction time (h)	Products[b]	Yield (%)
p-Methoxystyrene	A	7	*p*-Ethylanisole	100
6-Bromo-1-hexene	A	4	1-Bromohexane	78
1,6-Dimethylcyclohexene	B	13	1,2-Dimethylcyclohexane (3.0:1.0 *cis*:*trans*)	70
1,2-Dimethylcyclohexene	B	6	1,2-Dimethylcyclohexane (7.3:1.0 *cis*:*trans*)	79
1,3-Dimethylcyclohexene	B	8	1,3-Dimethylcyclohexane (3.75:1.00 *cis*:*trans*)	80
1,4-Dimethylcyclohexene	B	9	1,4-Dimethylcyclohexane (3.0:2.0 *cis*:*trans*)	84
1,4-Octadiene	B	4	4-octene, *n*-octane (1:1)	100
	B	7	*n*-octane	67
1,4-Diphenyl-1,3-butadiene	C	20	1,4-Diphenylbutane	91
2,3-Dimethyl-1,3-butadiene	B	2	2,3-Dimethyl-2-butene	27
			2,3-Dimethyl-1-butene	22
			2,3-Dimethylbutane	25
Cycloheptatriene	B	31	Cycloheptene	46
			Cycloheptane	9
Methyl linolenate	A	9	Methyl stearate	100
5-Methyl-1,3,6-heptatriene	A or B	20	No reaction	—

[a] A = C_6H_{14}; B = neat; C = benzene.
[b] Products were identified by comparison of spectral (ir, nmr (^1H, ^{13}C), ms) and physical data with those for authentic materials.

TABLE 2. Hydrogenation of α,β-unsaturated carbonyl compounds

Reactant	Organic phase[a]	Reaction time (h)	Products[b]	Yield (%)
2-Cyclohexen-1-one	A or B	1.25	Cyclohexanone	91
1-Acetyl-1-cyclohexene	A	14	Acetylcyclohexane	80
	B	26	Acetylcyclohexane	86
3-Methyl-2-cyclopenten-1-one	A	1.5	3-Methylcyclopentanone	67
	B	5.5	3-Methylcyclopentanone	61
Santonin	B	24	1,2-Dihydrosantonin	100
$PhCH{=}CHCOCH_3$	A	39	$PhCH_2CH_2COCH_3$	90
$CH_3CH{=}CHCOCH_3$	A	3.0	$C_3H_7COCH_3$	71
$PhCH{=}CHCHO$	A	20	$PhCH_2CH_2CHO$	68
			$PhCH{=}CHCH_2OH$	14
			$Ph(CH_2)_2CH_2OH$	12

[a] A = C_6H_{14}; B = C_6H_6.
[b] Products were identified by comparison of spectral and physical data with those for authentic materials.

TABLE 3. Monitoring the hydrogenation of α,β-unsaturated carbonyls on tlc using 5% vanillin in sulfuric acid (96%)[a]

	Color[b]		R_f	
Reactant	Reactant	Product	Reactant	Product
2-Cyclohexen-1-one	Blue	Green	0.33	0.49
1-Acetyl-1-cyclohexene	Red	Blue	0.47	0.51
3-Methyl-2-cyclopenten-1-one	Brown	Green	0.33	0.62
$PhCH{=}CHCOCH_3$	Red	Blue	0.16	0.26
$PhCH{=}CHCHO$	Grey	Violet	0.46	0.57

[a] Developing solvent mixture was 3:1 C_6H_6/ether (except cinnamaldehyde where a 5:1 C_6H_6/ether ratio was used).
[b] Color refers to the color of the spot on the tlc plate.

hexen-1-one in benzene using buffer (75 min) is essentially twice as fast when compared with water. The one-phase reaction (i.e., using benzene only) is considerably slower than the buffer process, requiring more than 7 h to reach completion.

In conclusion, the biphasic rhodium(I) catalyzed hydrogenation of olefins, dienes, and α,β-unsaturated carbonyl compounds occurs under very gentle conditions, affording reduced products in good yields. Execution and work-up of these reac-

tions are remarkably simple. This method compares favorably with other biphasic and phase transfer hydrogenation reactions (9, 10).

Experimental

General procedures for the biphasic hydrogenation of unsaturated hydrocarbons and α,β-unsaturated carbonyl compounds

To the organic phase (15 mL) was added $(1,5\text{-HDRhCl})_2$ (0.028 g, 0.063 mmol) and then a buffer solution of pH 7.6. After 1 min, the substrate (6.25 mmol) was added, followed by an additional 5 mL of the organic phase. Hydrogen was bubbled through the stirred solution at room temperature and atmospheric pressure until reaction was complete (see Tables 1 and 2 for reaction times). The phases were separated, the aqueous phase was extracted with hexane or benzene (10 mL), and the combined organic phase was dried ($MgSO_4$), concentrated by rotary evaporation, and pure products were isolated by chromatography or distillation.

In the event that the reactant also functions as the organic phase, one adds 56 mg (0.126 mmol) of $(1,5\text{-HDRhCl})_2$ to 25 mmol of the substrate, followed by 3 mL of the buffer solution of pH 7.5.

Acknowledgement

We are grateful to British Petroleum for support of this research.

1. K. R. JANUSZKIEWICZ and H. ALPER. Organometallics, **2**, 1055 (1983).
2. S. NISHIMURA, H. SAKAMOTO, and T. OZAWA. Chem. Lett. 855 (1973).
3. S. MITSUI, S. IMAIZUMI, A. NAMBU, and Y. SENDA. J. Catal. **36**, 333 (1975).
4. A. S. HUSSEY and Y. TAKEUCHI. J. Org. Chem. **35**, 643 (1970); A. S. HUSSEY and Y. TAKEUCHI. J. Am. Chem. Soc. **91**, 672 (1969).
5. K. R. JANUSZKIEWICZ and H. ALPER. Unpublished results.
6. T. MIZOROKI, K. SEKI, S. MEGURO, and A. OZAKI. Bull. Chem. Soc. Jpn. **50**, 2148 (1977).
7. E. UCCIANI AND L. TANGUAY. Compt. Rend. **284**C, 577 (1977).
8. D. V. SOKOL'SKII, A. M. PAK, L. D. ROZMANOVA, and S. M. TURGANBAEVA. Zh. Org. Khim. 77 (1977).
9. H. ALPER. Adv. Organomet. Chem. **19**, 183 (1981).
10. F. JOO and Z. TOTH. J. Mol. Catal. **8**, 369 (1980).

Can. J. Chem. Downloaded from www.nrcresearchpress.com by 210.87.254.42 on 09/06/12
For personal use only.

The conformational properties of the gangliosides G_{M2} and G_{M1} based on ^1H and ^{13}C nuclear magnetic resonance studies

SUBRAMANIAM SABESAN,[1] KLAUS BOCK,[2] AND RAYMOND U. LEMIEUX
Department of Chemistry, University of Alberta, Edmonton, Alta., Canada T6G 2G2

Received October 18, 1983

SUBRAMANIAM SABESAN, KLAUS BOCK, and RAYMOND U. LEMIEUX. Can. J. Chem. **62**, 1034 (1984).

A comparison of the ^1H and ^{13}C nmr parameters for the disaccharide derivatives βDGal(1→4)βDGlcO$(CH_2)_8COOCH_3$ (**1**), βDGalNAc(1→4)βDGalO$(CH_2)_8COOCH_3$ (**2**), and βDGal(1→3)βDGalNAcO$(CH_2)_2CH_3$ (**3**) allowed assignments of the signals observed for the *asialo*-G_{M2}- and *asialo*-G_{M1}-related synthetic haptens, βDGalNAc(1→4)βDGal(1→4)βDGlcO$(CH_2)_8COOCH_3$ (**4**) and βDGal(1→3)βDGalNAc(1→4)βDGal(1→4)βDGlcO$(CH_2)_8COOCH_3$ (**5**). ^1H nuclear Overhauser enhancement studies confirmed the conformational preferences for **2** and **3** predicted by HSEA calculation. Comparison of the ^1H and ^{13}C spectra indicate that these preferences and that previously known for the lactoside (**1**) are closely maintained in the haptens **4** and **5**. HSEA calculation indicates that the methyl group of methyl *N*-acetyl-α-D-neuraminic acid (**10**) prefers the orientation wherein the carboxyl group is near *anti*-periplanar to the methyl group. However, this orientation was not confirmed by saturation of the methyl group since no enhancement of either Ha-3 or He-3 was observed. On the other hand, saturation of Ha-3^e of the αDNeuAc unit of the G_{M1}-related pentasaccharide, βDGal(1→3)βDGalNAc(1→4)[αDNeuAc(2→3)]-βDGal(1→4)α,βDGlc, caused strong enhancement of the signal for the aglyconic hydrogen, H-3^b of the βDGal(1→4) unit. This observation, along with those of other nuclear Overhauser experiments, established that this pentasaccharide has the carboxyl group *anti*-periplanar to C-3^b. Furthermore, the C-7^e to C-9^e chain of the αDNeuAc unit adopts nearly the same conformation for the compound in aqueous solution as exists for *N*-acetylneuraminic acid in the crystalline state. The HSEA calculation indicates important attractive interaction between this chain and the βDGalNAc unit of the aglycon. These conlcusions were extended to the G_{M2} and G_{M1} gangliosides by the comparison of chemical shift data. In these compounds, the carboxyl group projects over the hydrophobic α-side of the βDGalNAc unit and the polar OH-4^e, NAc-5^e, OH-7^e groups project over the hydrophobic β-side of the lactose unit. Comments are made on the possible bearing of these topographical features on certain biological properties of gangliosides.

SUBRAMANIAM SABESAN, KLAUS BOCK et RAYMOND U. LEMIEUX. Can. J. Chem. **62**, 1034 (1984).

Une comparaison des paramètres de la rmn du ^1H et du ^{13}C des dérivés suivants de dissaccharides βDGal(1→4)βDGlcO$(CH_2)_8COOCH_3$ (**1**), βDGalNAc(1→4)βDGalO$(CH_2)_8COOCH_3$ (**2**) et βDGal(1→3)βDGalNAcO$(CH_2)_2CH_3$ (**3**) a permis de faire une attribution des signaux observés pour les haptènes de synthèse *asialo*-G_{M2} et l'*asialo* G_{M1} qui leur sont reliés soit les βDGalNAc(1→4)βDGal(1→4)βDGlcO$(CH_2)_8COOCH_3$ (**4**) et βDGal(1→3)βDGalNAc(1→4)βDGal(1→4)βDGlcO$(CH_2)_8$-$COOCH_3$ (**5**). Des études d'augmentation par effet Overhauser nucléaire du ^1H confirment les préférences conformationnelles qui avaient été prédites par des calculs HSEA pour les composés **2** et **3**. Une comparaison des spectres rmn du ^1H et du ^{13}C indique que ces préférences et celle qui avait été déterminée antérieurement pour le lactoside **1** sont bien maintenues dans les haptènes **4** et **5**. Les calculs HSEA indiquent que dans son orientation préférentielle, le groupe méthyle de l'acide méthyl *N*-acétyl α-D-neuraminique (**10**) est presque *anti* périplanaire par rapport au groupe carboxylique. Cependant cette orientation n'est pas confirmée par la saturation du groupe méthyle puisqu'on n'observe pas d'accroissement de Ha-3 ou de He-3. Par ailleurs, la saturation du Ha-3^e de l'unité αDNeuAc du pentasaccharide apparenté au G_{M1}, βDGal(1→3)βDGalNAc(1→4)[αD-NeuAc(2→3)]]βDGal(1→4)α,βDGlc, provoque un fort acroissement du signal de l'hydrogène aglyconique, H-3^b, de l'unité βDGal(1→4). Cette observation ainsi que celles d'autres expériences d'effet nucléaire Overhauser établissent que dans ce pentasaccharide le groupe carboxylique est *anti* périplanaire par rapport à C-3^b. De plus, en solution aqueuse, la chaîne C-7^e à C-9^e de l'unité αDNeuAc adopte pratiquement la même conformation que celle de l'acide *N*-acétylneuraminique à l'état cristallin. Des calculs HSEA indiquent qu'il existe une interaction attractive importante entre cette chaîne et l'unité βDGalNAc de l'aglycone. On a étendu ces conclusions aux gangliosides G_{M2} et G_{M1} par comparaison des données de déplacement chimique. Dans ces composés, le groupe carboxyle se retrouve au-dessus du côté α hydrophobe de l'unité βDGalNAc et les groupes polaires OH-4^e NAc-5^e, OH-7^e se retrouvent au-dessus du côté β hydrophobe de l'unité lactose. On discute de l'incidence possible de ces caractéristiques topographiques sur certaines propriétés biologiques des gangliosides.
[Traduit par le journal]

Introduction

Sillerud and Yu (1) have recently published a comparison of the ^{13}C nmr spectra of the ganglioside G_{M1} with those of *asialo*-G_{M1} and the G_{M1}-pentasaccharide. The earlier literature was reviewed and the interest in sialic acid-containing, cell-surface glycolipids was outlined.

More recently, Koerner *et al.* (2*a*) have reported the use of homonuclear two-dimensional spin-echo *J*-correlated ^1H nmr spectroscopy for the determination of the compositions and anomeric configurations of the gangliosides G_{M4}, G_{M3}, G_{M2}, and G_{M1}. Although these studies were conducted using dimethyl-d_6 sulfoxide as solvent, of particular interest to our present contribution is their observation of long range effects on chemical shifts of the βDGalNAc unit arising from the introduction of the αDNeuAc group at the 3-position of the βDGal(1→4) unit of both G_{M2} and G_{M1}. The occurrence of these specific through-space interactions between the αDNeuAc and βDGalNAc units was taken as an indication that some secondary structure involving these two units stabilizes their conformational preference. In a second paper, Koener *et al.* (2*b*) applied two-dimensional nuclear Overhauser coupling studies to confirm the primary structures of these gangliosides. Inter-residue couplings were observed which were shown to allow

[1] Taken in part from a thesis presented in partial fulfillment of the Ph.D. degree, 1983. Present address: Department of Biological Chemistry, UCLA School of Medicine, Center for Health Sciences, Los Angeles, CA 90024, U.S.A.

[2] Department of Organic Chemistry, The Technical University of Denmark, DK-2800 Lyngby, Denmark.

Can. J. Chem. Downloaded from www.nrcresearchpress.com by 210.87.254.5 on 09/06/12
For personal use only.

Can. J. Chem. Downloaded from www.nrcresearchpress.com by 210.87.254.5 on 09/06/12
For personal use only.

the complete sequencing of these oligosaccharides. It was suggested that quantitative experiments may limit the range of possible secondary structures.

We have recently reported (3) the syntheses of both the trisaccharide unit of *asialo*-G_{M2} and the tetrasaccharide unit of *asialo*-G_{M1} in the form of haptens wherein the aglycon is the potential linking arm $(CH_2)_8COOCH_3$ (4). In G_{M2} and G_{M1}, these neutral core structures form the aglycon of the sialic acid known as *N*-acetyl-D-neuraminic acid (NeuAc) (5). It is well established that these occur as the α-D-glycosides wherein the carboxyl group is in axial orientation at C-2 of the αDNeuAc group (6).

In this communication, we report a reinvestigation of the ^{13}C nmr spectra of G_{M1} (**8**) and the G_{M1}-oligosaccharide (**9**) and extend these studies to include the ^{13}C nmr spectrum of the G_{M2}-oligosaccharide (**7**). In addition, we report the first detailed ^1H nmr study of the G_{M1}-oligosaccharide (**9**) including ^1H nuclear Overhauser enhancement experiments in the difference mode (7) on this and related compounds that firmly establish its conformational preference in aqueous solution. The results obtained are shown to be in agreement with the molecular model for G_{M1} predicted by hard-sphere, *exo*-anomeric (HSEA) calculations (8).

Discussion

HSEA calculations were conducted in the usual manner (8) to estimate the conformational preference for the oligosaccharide portion of *asialo*-G_{M1}. Since all the interactions are between only two sugar units about each of the three intersugar glycosidic bonds, the calculations were first made for the three constituent disaccharide units, namely, βDGal^b(1→4)βDGlc^a (**1**), βDGalNAc^c(1→4)βDGal^b (**2**), and βDGal^d(1→3)βDGalNAc^c (**3**).[3] As expected, the results did not change when the calculations were made using the intact tetrasaccharide. The results of these calculations are presented in Fig. 1. These ϕ^H and ψ^H values for the core tetrasaccharide were then maintained throughout the calculations to assess the orientation of the αDNeuAc unit at position 3 of the βDGal^b(1→4) unit of the ganglioside G_{M1}.

In order to calculate the orientation of the αDNeuAc unit, the atomic coordinates for this unit were synthesized from the crystal structure of *N*-acetyl-β-D-neuraminic acid dihydrate provided by Flippen (9). The synthesis involved only the exchange of the carboxyl and hydroxyl groups at C-2 while preserving the same bond lengths (C—O = 1.400 Å and C—C = 1.531 Å). The lengths of the two carbon-to-oxygen bonds in the carboxylate group were taken as 1.198 Å. Hard-sphere calculations for the conformers arising from rotation about the carboxylate (C-1—O^{A}O^B) to C-2 bond indicated a preference for the orientation that sets a torsion angle of +80° for C—O^A and −100° for C—O^B with the C-2^c to O-2^c bond of the αDNeuAc unit. This orientation was maintained throughout the calculations that followed, setting the C-2^c—O—C-3^b (τ) bond angle at 117° (10). This αDNeuAc unit (attached to O-3^b of the core neutral tetrasaccharide) was then rotated, at 5° intervals, about the C-2^c—O-3^b bond to change the $\phi^{C\text{-}1^c,C\text{-}3^b}$ torsion angle after having set the $\psi^{H\text{-}3^b,C\text{-}2^c}$ torsion angle. The calculation (8) was then repeated setting this angle at 5° intervals through the 360° range. These calculations suggested the existence of only two energy minima which were separated by 4.38 kcal/mol in favor of conformer A as presented in Table 1. Examination of Table 2 shows that conformer A is favored over conformer B about equally for reasons of lesser forces of repulsion and greater forces of attraction between the αDNeuAc unit and the βDGalNAc(1→4)βDGal portion of the aglycon. The repulsive non-bonded interactions indicated for conformer A are listed in Table 2. The interaction of HA-6^c of the βDGalNAc unit with O-9^c of the αDNeuAc unit arises because no effort was made to minimize the conformational energy of conformer A by rotation about the C-8^c to C-9^c bond. This rather hard interaction does highlight the fact that this HSEA-favored conformer places the C-7^c to C-9^c side chain of the αDNeuAc unit in close proximity to the βDGalNAc(1→4) unit (c). The possible bearing of this orientation on the stability of conformer A can be judged from the attractive interactions listed in Table 2. Only attractive interactions of 10 cal and over are included, in order to limit the list. It is noteworthy, however, that there were a total of 1026 attractive interactions involving the αDNeuAc unit for a total of −8.33 kcal/mol, in contrast to the 205 attractive interactions which total −6.04 kcal/mol presented in Table 2. With specific regard to possible involvement of the C-7^c to C-9^c side chain of the αDNeuAc unit, the HSEA calculation shows a total of 178 attractive interactions with the βDGalNAc unit which contribute to the stabilization of conformer A by −2.01 kcal/mol. Of these, 57 have values of 10 cal or more, distributed as follows (atom (number of interactions) calories): C-7^c (7) −95; O-7^c (2) −20; C-8^c (9) −285; O-8^c (4) −95; H-8^c (11) −435; C-9^c (10) −289; O-9^c (7) −243; HA-9^c (2) −21; HB-9^c (5) −149; for a total of −1.63 kcal/mol. Thus, as pointed out by Salem (11), a large number of weak but multipoint van der Waals forces between large complementary surfaces can add to a large attractive force. Certainly, these play an important role in establishing conformational preferences by HSEA calculation (12). It is noteworthy in this regard that hard interactions between atoms in van der Waals conflict are much more sensitive to errors in the geometry imposed on the molecule from crystal data than are the attractive forces. As will be seen below, the HSEA calculation placed G_{M1} in a conformer that proved to be in fine accord with the ^1H nmr data obtained for the pentasaccharide portion of this ganglioside.

We have recently reported (3) the synthesis of the haptens βDGalNAc(1→4)βDGal(1→4)βDGlcOR (**4**) and βDGal(1→3)βDGalNAc(1→4)βDGal(1→4)βDGlcOR (**5**) wherein R = $(CH_2)_8COOCH_3$. These compounds are related to the *asialo*-forms of the gangliosides G_{M2} (**6**) and G_{M1} (**8**), respectively. Following the trivial nomenclature introduced by Sillerud and Yu (1), these haptens are referred to as ASG_{M2}-Hp (**4**) and ASG_{M1}-Hp (**5**). The preparation of the component disaccharide units of **5** as simple glycosides, namely, compounds **1**–**3** of Table 3, was also reported. The assignments of the ^1H chemical shifts presented in Table 3 for these disaccharides were in general agreement with expectations based on the ^1H nmr spectral assignments for the component sugar units as methyl β-D-hexopyranosides (7). The nmr parameters given in Table 3 for the haptens **4** and **5** could then be based on these assignments. It is of interest in this regard to compare the spectra for compounds **1**–**5** which are reproduced in Fig. 1. In all cases, the assignments were confirmed by spin-decoupling experiments. In view of the coupling constants listed, there can be no doubt that the pyranose rings are all held in the $^4C_1$ conformation. In view of the generally good agreements in chemical shifts, the conclusion is drawn that the conformational

[3] These sugar units will be labelled a, b, c, and d as shown throughout this discussion.

Can. J. Chem. Downloaded from www.nrcresearchpress.com by 210.87.254.5 on 09/06/12
For personal use only.

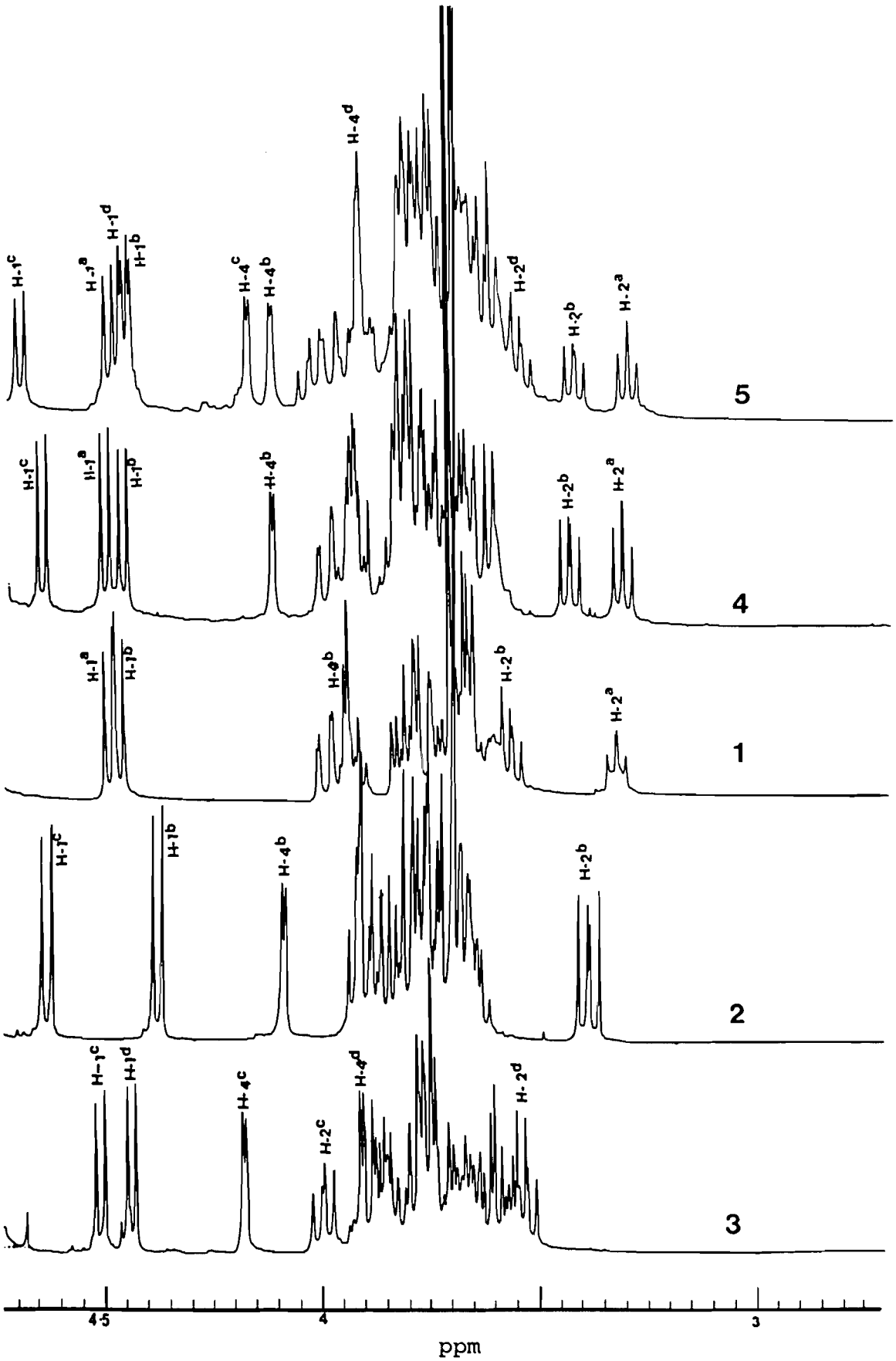

FIG. 1. A comparison of the ^{1}H nmr spectra (400 MHz) for the compounds βDGal(1→4)βDGlcOR (**1**), βDGalNAc(1→4)βDGalOR (**2**), βDGal(1→3)GalNAcOPr(**3**), βDGalNAc(1→4)βDGal(1→4)βDGlcOR (**4**), and βDGal(1→3)βDGalNAc(1→4)βDGal(1→4)βDGlcOR(**5**) (R = $(CH_2)_8COOCH_3$) in D_2O. The chemical shifts and spacings that could be determined are reported in Table 3.

TABLE 1. The HSEA conformer* for the oligosaccharide portion of the ganglioside G_{M1} (βDGal^d(1→3)βDGalNAc^c(1→4)[αDNeuAc^e-(2→3)]βDGal^b(1→4)βDGlc^{a}OCer)

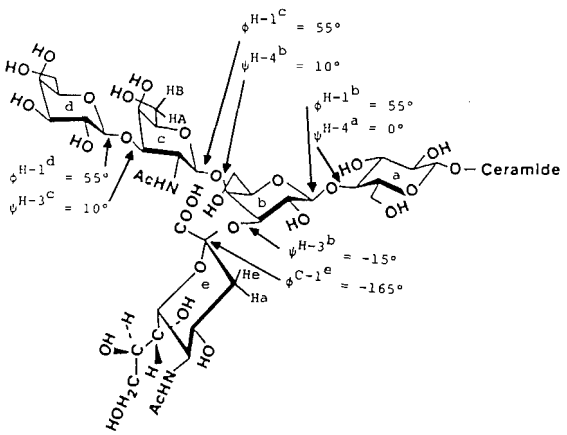

Internuclear distances (Å)			
From H-1^d	From H-1^c	From H-1^b	From Ha-3^e†
H-3^c, 2.46	H-4^b, 2.46	H-4^a, 2.44	H-3^b, 2.05
H-4^c, 4.21	H-3^b, 4.00	H-3^a, 4.49	H-4^b, 4.13
H-2^c, 3.81	H-5^b, 4.75	H-5^a, 3.91	H-3^e, 1.79
H-2^d, 3.06	H-2^c, 3.06	H-2^b, 3.06	H-5^e, 2.58
H-3^d, 2.57	H-3^c, 2.60	H-3^b, 2.57	
H-5^d, 2.28	H-5^c, 2.41	H-5^b, 2.28	

* For each glycosidic bond, the φ torsion angle is that defined by the bond of the atom designated in superscript to the anomeric carbon and the neighboring aglyconic carbon to glycosidic oxygen bond. The ψ torsion angle is that defined by the bond of the hydrogen indicated in superscript and the neighboring anomeric carbon to glycosidic oxygen bond.

† From He-3^e; H-3^b, 2.28; and H-4^e, 2.44.

preferences for the glycosidic linkages of **4** and **5** are those for the component disaccharides. As will be seen below, the preferences in the case of the disaccharide compounds **2** and **3**, suggested by HSEA calculation (Table 1), were well confirmed by the nuclear Overhauser experiments.

In view of the internuclear distances listed in Table 1, saturation of H-1^b of compound **1** should cause enhancements of H-4^a, H-2^b, H-3^b, and H-5^b. However, because of the nearly identical chemical shifts (13) for H-4^a and H-3^a and for H-3^b and H-5^b, all of which are strongly coupled to vicinal hydrogens, the results obtained from these experiments provided no useful information on the magnitude of the enhancement of the signal for H-4^a. Thus, the torsion angles $\phi^{H-1^b}/\psi^{H-4^a}$ = 55°/0° rest on the results of the HSEA calculation which are supported by studies of closely related structures (10) and are confirmed by the H-1^b—^{13}C-4^a and H-4^a—^{13}C-1^b coupling constants for methyl β-lactoside (13). In contrast, saturation of H-1^c of compound **2** provided useful results. In view of the internuclear distances provided by the HSEA model given in Table 1, the signals for H-4^b, H-2^c, H-3^c, and H-5^c should be enhanced. However, except for the signal for H-4^b, these signals are overlapped by other signals and the difference spectrum showed some residue of positive signals arising from hydrogens other than H-2^c, H-3^c, and H-5^c. Thus, their relative enhancements could not be determined with precision. However, an 8% positive enhancement was found for H-4^b, a result which is in accord with the HSEA conformer A. Enhancements of approximately 4% were found for H-2^c and H-3^c, and likely greater than 4% for H-5^c. The nOe experiments were highly successful for the disaccharide derivative **3**. In this case, saturation of H-1^d resulted in enhancements of H-3^c (9%), H-2^d (7%), and H-3^d + H-5^d (17%). These results are in good accord with the conformational preferences given in Table 1.

Two of the conformers for methyl αDNeuAc that result from changes in the orientation of the methoxy group and the conformation of the C-7—C-9 side chain are displayed by formulae **10***a* and **10***b*. HSEA calculation, to estimate the preferred

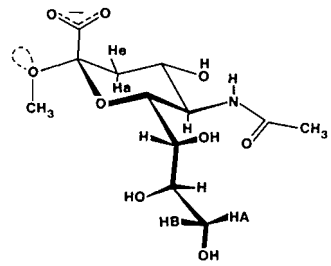

10*a*

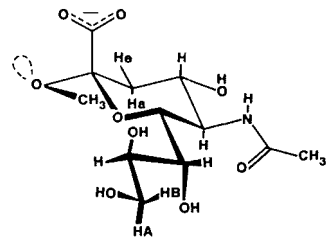

10*b*

orientation about the anomeric center of the αDNeuAc unit of G_{M1}, placed the oligosaccharide aglycon in the *syn*-axial-like orientation to Ha-3^e (i.e., C-1^e *anti*-periplanar to C-3^b) and similar to the orientation shown for the methyl group in structure **10***a*. However, HSEA calculation also placed the methyl group of **10** in the orientation shown in **10***a* and not that in **10***b* which is normally found for methyl aldopyranosides (14). Since saturation of the methyl group of **10** caused no observable enhancement of the signals for either Ha-3 or He-3 (Table 3), as may have occurred for conformation **10***a*, this indication was not confirmed. As will be seen below, the remarkable orientation of the aglycon in G_{M1} that is predicted by HSEA calculation received unequivocal experimental justification.

As mentioned above, the conformation for the αDNeuAc unit of G_{M1} was taken as that for *N*-acetyl-β-D-neuraminic acid in the crystalline state except that the orientation of the carboxyl and hydroxyl groups at C-2 were interchanged. Thus, the orientation for the C-7—C-9 group shown in **10***b* was maintained, rather than the conformational preference suggested by Czarniecki and Thornton (15). This latter conformation is presented in **10***a* in order to display that H-5 is in close proximity (2.3 Å) to H-8. Therefore, in this conformation, saturation of H-5 should enhance the signal for H-8. However, this could not be ascertained since the difference in chemical shifts for these hydrogens was too small (0.07 ppm) for the experiment using methyl αDNeuAc. However, in the case of *N*-acetyl-β-D-neuraminic acid, the difference in the chemical shifts (0.18 ppm) for H-5 and H-8 was sufficient, but no enhancement of H-8 (at 3.75 ppm) was observed on saturation of H-5 (at 3.93 ppm). It seemed possible, therefore, that this acid has the same conformation in aqueous solution as in the crystalline state where H-5 and H-8 are separated by 4.528 Å. This possibility was reinforced by the observation that saturation of H-5 caused enhancement not only of the *syn*-axial Ha-3 but also of H-7 at 3.56 ppm. Indeed, the crystalline structure for β-D-neuraminic acid has H-5 and H-7 separated by only 3.016 Å. In the light of these observations, H-5 of methyl αDNeuAc (**10**) was saturated and, in fact, an enhancement of H-7 was observed similar in intensity to that observed for the β-acid. Thus, there remains no doubt that the conformational preference suggested by Thornton and co-workers (15, 16) and which has gained widespread acceptance (17–19) should be abandoned for sialoside

Can. J. Chem. Downloaded from www.nrcresearchpress.com by 210.87.254.5 on 09/06/12
For personal use only.

TABLE 2. The conformational preference of the αNeuAc unit of G_{M1} and G_{M2} as assessed by HSEA calculation

Conformer A

$\phi^{C\text{-}1^e} = -165°$, $\psi^{H\text{-}3^b} = -15°$

$(4.58 - 8.33)^{HS} + 0.21^{E\Lambda} = -3.54^{HSE\Lambda}$ kcal/mol

Conformer B

$\phi^{C\text{-}1^e} = -75°$, $\psi^{H\text{-}3^b} = 10°$

$(6.64 - 6.44)^{HS} + 0.64^{E\Lambda} = 0.84^{HSE\Lambda}$ kcal/mol

Conformer A

Repulsive non-bonded interactions

Atoms interacting	Internuclear distance, Å	Energy, kcal/mol
HA-6^e – O-9^e	2.378	0.44
C-3^b – C-3^e	3.062	0.31
C-3^b – O-6^e	2.668	0.98
C-3^b – Ha-3^e	2.719	0.13
C-4^b – C-2^e	3.330	0.02
C-4^b – O-6^e	3.054	0.08
H-3^b – C-2^e	2.399	1.05
H-3^b – C-3^e	2.655	0.22
H-3^b – O-6^e	2.394	0.40
H-3^b – Ha-3^e	2.045	0.70
H-4^b – O-6^e	2.458	0.25
		Total 4.58

Attractive interactions (>10 cal/mol) with the αDNeuAc unit

βDGal Unit (b)			βDGalNAc Unit (c)		
Atom	Number	Total energy (cal/mol)	Atom	Number	Total energy (cal/mol)
C-1	4	−101	C-1	13	−412
C-2	10	−382	C-2	5	−98
C-3	14	−532	C-4	4	−49
C-4	16	−459	C-5	12	−347
C-5	10	−200	C-6	7	−232
C-6	4	−50	C-8	1	−16
O-2	8	−300	N-2	3	−90
O-6	8	−156	O-1	8	−219
H-1	3	−38	O-5	12	−262
H-2	4	−73	O-6	5	−142
H-3	11	−350	H-1	11	−416
H-4	12	−466	H-3	2	−32
H-5	3	−55	H-5	9	−277
			HA*-6	7	−259
			HB*-6	2	−33
Totals	104	−3,153		101	−2,884

*HA is *syn*-clinal to H-5 and HB is *anti*-periplanar.

units in their conformational ground states. Instead, the original proposal by Brown *et al.* (20), which is now confirmed, should be adopted.

In order to test the validity of the HSEA conformer for G_{M2} (**6**) and G_{M1} (**8**), the oligosaccharides $G_{M2}OS$ (**7**) and $G_{M1}OS$ (**9**) were prepared in the usual manner by mild base degradation of the products of ozonolysis (21). No effort was made to purify these oligosaccharides since the ^1H nmr spectra (that for $G_{M1}OS$ is reproduced in Fig. 2) required the crude preparation to be of sufficient purity for the present investigation. The signal assignments presented in Table 3 for $G_{M2}OS$ (**7**) were made on the basis of simple inspections and confirmed by appropriate spin-decoupling experiments. The pentasaccharide $G_{M1}OS$ (**9**), was chosen for the more detailed ^1H nmr examination. In this case, a number of signals which could not be assigned directly were assigned using nuclear Overhauser enhancements. The chemical shifts and coupling constants derived from these experiments are reported in Table 3. The signal for H-7^e was overlapped in the case of $G_{M1}OS$ (**9**) but clearly visible as a quartet at 3.52 ppm (spacings 2.2 and 11 Hz) in the spectrum for $G_{M2}OS$ (**7**). Since the signal for H-7^e was at 3.59 ppm (spacings 1.6 and 9.3 Hz) for methyl αDNeuAc (**10**), it is apparent that the two NeuAc residues do not differ appreciably in their conformational preferences for the C-7 and C-9 side chain. These

Can. J. Chem. Downloaded from www.nrcresearchpress.com by 210.87.254.5 on 09/06/12
For personal use only.

Can. J. Chem. Downloaded from www.nrcresearchpress.com by 210.87.254.5 on 09/06/12
For personal use only.

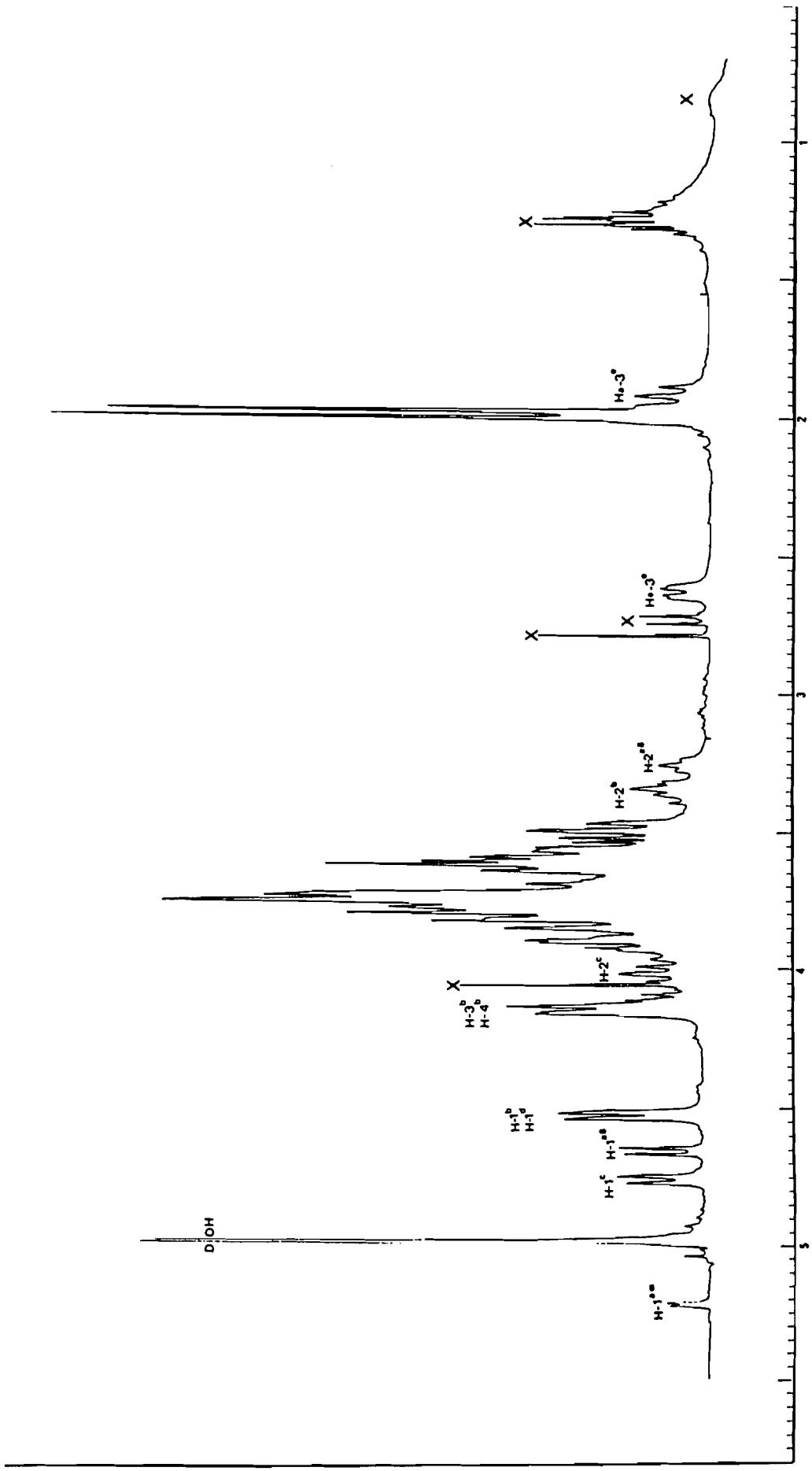

FIG. 2. The ^1H nmr spectrum in D_2O for the crude $G_{M1}OS$ (**9**) used in the studies reported in Table 3. The signals marked "X" arise from water-soluble chloroform nonextractable impurities.

TABLE 3. ^{1}H chemical shifts and vicinal coupling constants for oligosaccharides related to the gangliosides G_{M2} and G_{M1}

Hydrogen atom	Chemical shift, (spacing, Hz)						
	βDGal(1→4) βDGlcOR (**1**)	βDGalNAc(1→4) βDGalOR (**2**)	βDGal(1→3) βDGalNAcOPr (**3**)	ASG_{M2}-Hp (**4**)	$G_{M2}OS$ (**7**)	ASG_{M1}-Hp (**5**)	$G_{M1}OS$ (**9**)
H-1[a], α				—	5.25 (3.8)	—	5.22 (3.9)
H-1[a], β	4.43 (8.0)	—	—	4.43 (7.7)	4.70 (8.0)	4.43 (7.7)	4.67 (8.0)
H-2[a], β	3.25	—	—	3.24 (8.5)	3.30	3.24 (8.2)	3.27 (9.7)
H-1[b]	4.40 (7.7)	4.32 (8.2)	—	4.39 (7.7)	4.57 (8.2)	4.39 (8.2)	4.54 (7.8)
H-2[b]	3.49 (9.9)	3.33 (9.9)	—	3.36 (9.9)	3.39	3.35 (10.1)	3.35 (~10)
H-3[b]	—	—	—	—	4.19	—	~4.15*
H-4[b]	—	4.03 (2.2)	—	4.04 (2.2)	4.16	4.05 (2.2)	~4.15*
H-1[c]	—	4.59 (8.5)	4.53 (8.5)	4.58 (9.0)	4.76 (8.5)	4.64 (8.2)	4.77 (8.1)
H-2[c]	—	3.85	4.01 (10.1)	3.89		3.95	4.02 (10.2)
H-3[c]	—	3.73 (~3.5, 10.5)*	3.88 (10.1)*	—	—	—	3.82 (2.8, 10.8)*
H-4[c]	—	3.85	4.19	3.88	—	4.11	—
H-5[c]	—	~3.65*	—	—	—	—	3.76*
NAc-2[c]	—	2.06	2.05	2.08	2.06	2.04	2.02
H-1[d]	—	—	4.46 (7.7)	—	—	4.40 (7.7)	4.54 (7.6)
H-2[d]	—	—	3.54 (10.9)	—	—	3.47	3.51 (10.0)
H-3[d]	—	—	3.64 (~3, 10)*	—	—	—	—
H-4[d]	—	—	3.93	—	—	3.85	—
H-5[d]	—	—	3.67*	—	—	—	—
		Me αDNeuAc (**10**)					
H-3e[e]		2.72 (4.4, −12)			2.68 (4.1, −12)		2.65 (3.9, −12)
H-3a[e]		1.64 (~12)			1.99 (12)		1.96 (12)
H-4[e]		3.67 (10.3)*			—		3.78* (octet)
H-5[e]		3.81 (10.3)*			3.85 (10.3)		3.88 (10, 10)*
H-6[e]		3.71 (1.6)			—		—
H-7[e]		3.59 (9.3)			3.52 (2.2, 11)		—
H-8[e]		~3.88 (—, 6.3[B])			—		—
HA-9[e]		~3.88 (−12.2[AB])			—		—
HB-9[e]		3.64			3.58 (6.6, 11.8)		—
OCH_3		3.34			—		—
NAc-5[e]		2.04			2.04		2.00

*Located by nuclear Overhauser enhancements.

observations support the conformation used in the HSEA calculation for G_{M1}.

Nuclear Overhauser experiments were conducted to investigate the hydrogen environments of Ha-3[e], H-1[e], and He-3[e] in the pentasaccharide $G_{M1}OS$ (**9**). Also, an experiment was performed wherein H-3[b] and H-4[b], which have near identical chemical shifts, were simultaneously saturated. The results obtained proved to be in fine agreement with expectations based on the HSEA model (Table 1). All the enhancements were negative, as would be expected (7), since such a large polar molecule in water should be tumbling slowly and anisotropically as seems likely from the ^{13}C nmr spectrum for $G_{M1}OS$ (1).

1. *Saturation of Ha-3[e]*

The percentages of the enhancements relative to the signal for Ha-3[e] could not be measured since the signal is overlapped by the signals for the two acetamido groups. However, signals were enhanced that definitely could be assigned to H-3[b], He-3[e], and H-5[e] at the positions given in Table 3. The relative intensities of these signals were 1:1.25:~1, respectively. The strong enhancement of H-3[b] (relative to the geminal He-3[e]) is particularly noteworthy since this enhancement alone eliminates conformer B wherein Ha-3[e] and H-3[b] are separated by 4.221 Å. Only extremely weak enhancement was observed for H-4[b] as compared with H-3[b] and, therefore, Ha-3[e] does not reside between H-3[b] and H-4[b] but only in close proximity to H-3[b] as predicted by the HSEA calculations for conformer A.

2. *Saturation of He-3[e]*

The signal for He-3[e] was well disposed for an nOe experiment. For conformer A, the nucleus of this hydrogen is separated from H-3[b] by 3.378 Å. Consequently, saturation of He-3[e] would be expected not to enhance H-3[b] appreciably. In fact, relative to the strong enhancements found for Ha-3[e] and H-4[e], the enhancement of H-3[b] was barely discernible at the noise level and could not be measured.

3. *Simultaneous saturation of H-3[b] and H-4[b]*

On the basis of conformer A, saturation of H-3[b] should enhance Ha-3[e] (2.045 Å), H-5[e] (3.350Å), H-1[b] (2.565 Å), H-5[b] (2.502 Å), and H-2[b] (3.050 Å); and saturation of H-4[b] should enhance H-5[b] (2.468 Å), HB-6[b] (3.133Å), and H-1[e] (2.460 Å). In fact, the experiment led to strong, readily assigned enhancements of the signals for Ha-3[e], H-1[b], H-2[b], and H-1[e]. The relative enhancements of these signals were ~0.5:0.7:0.8:1, respectively. Other enhancements occurred in the region 3.40–4.00 ppm but these could not be assigned because of overlap and also because the saturation undoubtedly affected atoms, including H-2[c] at 4.02 ppm, other than H-3[b] and H-4[b].

Can. J. Chem. Downloaded from www.nrcresearchpress.com by 210.87.254.5 on 09/06/12
For personal use only.

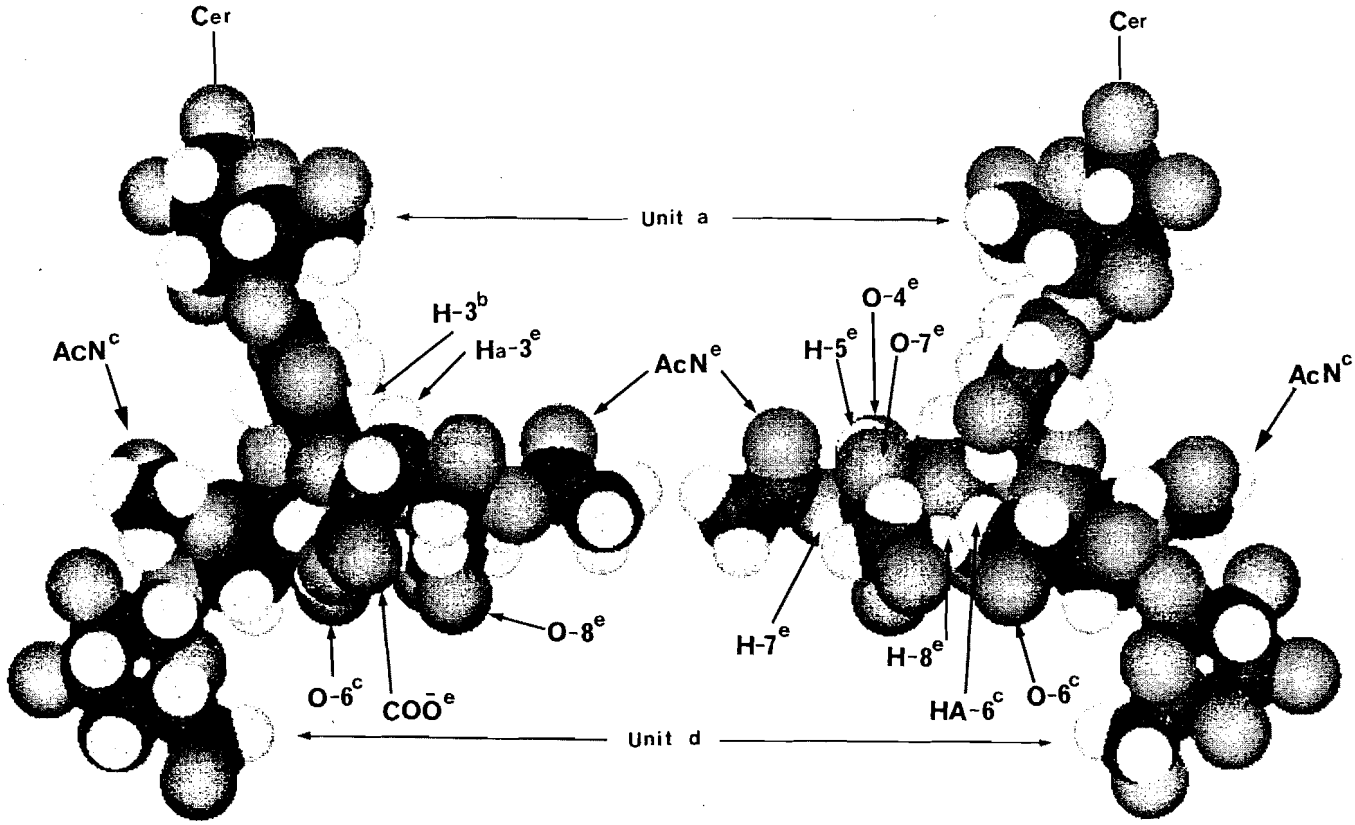

FIG. 3. Computer-drawn conformer A (Table 1) showing both sides for the oligosaccharide portion of G_{M1}. The hydrogen atoms of the hydroxyl groups are not shown. Note that H-3^b/Ha-3^e and HA-6^c/H-8^e are in van der Waals contact, that the carboxyl group ($C\bar{O}O^e$) extends toward the lipophilic side of the c-d unit, that the NC=O^e, OH-4^e, and OH-7^e groups extend toward the lipophilic side of the a-b unit, and that H-5^e and H-7^e define a torsion angle of near 120°. Note, for example, that, although O-6^c may appear to be close to the carboxyl group in one projection, the other shows that it is in fact on the other side of the molecule. The construction of a model using these projections for reference is recommended.

4. *Saturation of H-1^c*

As expected from the internuclear distances given in Table 1, this experiment caused enhancements of H-4^b, H-2^c, H-3^c, and H-5^c which provided the assignments of the chemical shifts reported in Table 3, except for H-2^c which could be assigned by spin-decoupling of H-1^c. The spacings in the enhanced signals at 3.82 ppm allowed its assignment to H-3^c with confidence. The enhancement at 4.15 ppm was then assigned to H-4^b and it followed that the enhanced signal at 3.76 ppm arose from H-5^c.

Consideration of the ^{1}H chemical shifts presented in Table 3 clearly suggests that the conformation of the core tetrasaccharide present in G_{M1}OS (**9**) is very similar to that in the hapten **5**. This matter will be discussed in more detail below in connection with the ^{13}C nmr data presented in Tables 4 and 5. At this point, it is of interest to examine the computer-drawn CPK model for the pentasaccharide portion of G_{M1} shown in Fig. 3. The main purpose of this drawing is to enable the reader to readily construct a CPK space-filling model for conformer A. However, the drawing helps to highlight a number of topographical features of interest to receptor binding specificities exhibited by G_{M1} and related receptor molecules. Examination of the model shows that the carboxylate group is extended near a large lipophilic region which involves the α-sides of both the c (βDGalNAc) and d (βDGal) units. Thus, it can be expected that the introduction of the αDNeuAc unit at position 3^b of *asialo*-G_{M1} strongly changes a region of *asialo*-G_{M1} which can be expected to express an immunodominant role (22). This, likely, is behind the reason why *anti-asialo*-G_{M1} antibodies do not react with G_{M1} (23). In contrast to the lipophilic α-side, the β-side of the βDGal(1→3)βDGalNAc unit is strongly hydrophilic and an engagement of a receptor with this side of the molecule would encounter ten polar groups of which six are hydroxyl groups. It is noteworthy in these regards that we have found (unpublished results) in several instances that the combining sites of antibodies and lectins bind large lipophilic areas of oligosaccharides that then terminate in a cluster of two or three hydroxyl groups. It is considered that the cluster of hydroxyl groups interacts with a polar grouping at the periphery of the combining site and that this interaction is mainly to provide high specificity to the binding reaction. The establishment of multipoint van der Waals attractions, involving the lipophilic region of the oligosaccharide with nonpolar regions of amino acids that form the combining site, could in principle provide the main driving force leading to complex stability (22). These considerations are noteworthy since evidently the juxtaposition in G_{M1} of the highly polar carboxylate group near the α-side of the βDGal(1→3)βDGalNAc unit provides a similar situation to the cluster of hydroxyl groups mentioned above. Similar considerations apply to the lipophilic β-sides of the βDGal(1→4)βDGlc unit of G_{M1}. Consideration of the projection in Fig. 3 shows that this side is guarded by the 4- and

Can. J. Chem. Downloaded from www.nrcresearchpress.com by 210.87.254.5 on 09/06/12
For personal use only.

TABLE 4. Assignments of the ^{13}C chemical shifts* for βDGalNAc(1→4)βDGal(1→4)βDGlcOR† (ASG_{M2}-Hp, **4**) and βDGal(1→3)βDGalNAc(1→4)βDGal(1→4)βDGlcOR† (ASG_{M1}-Hp, **5**) based on the shifts observed for βDGal(1→4)βDGlcOR (**1**), βDGalNAc(1→4)βDGalOR (**2**), and βDGal(1→3)βDGalNAcO$(CH_2)_2CH_3$ (**3**) and the comparison of the shifts for **5** with those reported (1) for *Asialo*-G_{M1}

		Chemical shifts, ppm						
Sugar unit	Carbon atom	**1**	**2**	**3**	ASG_{M2}-Hp **4**	ASG_{M1}-Hp **5**	ASG_{M1} (C)	$\delta_C - \delta_5$
βDGlc	1a	102.31			102.37	102.56	103.34	0.78
	2a	73.14			73.16	73.36	74.09	0.73
	3a	74.76			74.76	75.00	75.57	0.57
	4a	78.81			79.04	79.37	80.18	0.81
	5a	75.02			75.10	75.27	75.95	0.68
	6a	60.45			60.53	60.81	61.33	0.52
βDGal	1b	103.22	102.80		103.34	103.52	103.77	0.25(0.92)
	2b	71.25	71.16		71.45	71.67	72.22‡	0.55
	3b	72.85	73.08		72.90	73.09	[73.87]§	0.78
	4b	68.84	76.15		76.48	76.53	76.92	0.39
	5b	75.62	74.29		74.78	75.00	75.73	0.73
	6b	61.27	60.61		61.03	61.24	62.14	0.90
βDGalNAc	1c		102.98	101.56	102.94	102.75	104.44	1.69(1.02)
	2c		52.99	51.63	53.08	52.14	52.84	0.70
	3c		71.26	80.19	71.45	80.25	81.23	0.98
	4c		68.12	68.32	68.21	68.59	69.18	0.59
	5c		75.09	75.00	75.21	75.07	75.57	0.50
	6c		61.33	61.19	61.41	61.54	61.41	−0.13
	N—C=O				175.29	175.30	175.70	0.40
	CH_3				22.76	22.97	23.45	0.48
βDGal	1d			105.06		105.16	105.90	0.74
	2d			70.92		71.25	71.96	0.71
	3d			72.78		73.20	[74.09]§	0.89
	4d			68.88		69.17	69.80	0.63
	5d			75.26		75.51	76.13	0.62
	6d			61.28		61.54	62.14	0.60

* See the experimental section for details.
† R = $(CH_2)_8COOCH_3$.
‡ This signal was assigned twice, which is not in agreement with the published spectrum (1).
§ Reassigned on the basis of the published spectrum (1).

7-hydroxyl groups of the αDNeuAc unit along with the polar carbonyl oxygen of the acetamido group which projects between these two hydroxyl groups. The recent finding (24) that haemagglutinin glycoproteins of influenza virus membranes (which differ in recognizing either αDNeuAc(2→3)βDGal-(1→4)βDGlc (G_{M3}) or αDNeuAc(2→6)βDGal(1→4)βDGlc linkages) differ only in the single substitution of glutamine for leucine may be related to this feature, which is expected (by HSEA calculation) to persist in the ganglioside G_{M3}. It is the G_{M3} structure that reacts with the receptor site which contains the glutamine unit, but not with the receptor site formed by the protein wherein the glutamine unit is replaced by a leucine unit. Evidently, the carboxamido group of the glutamine unit, through an ability to displace water and bind to the above-mentioned hydrated polar grouping, may be allowed to penetrate and thereby gain access to the nonpolar side of the βDGal(1→4)βDGlc unit for an expression of short range van der Waals forces of attraction. On the other hand, the nonpolar isobutyl group of leucine is not expected to readily penetrate the hydrated polar region to come close enough for effective interaction.

Although we have not examined the conformational preference for αDNeuAc^c(2→6)βDGal^b experimentally, HSEA calculations were made based on the assumption that the ω torsion angle H-5^b/O-6^b is +60° as appears demanded for the conformer of βDGal(1→4)βDGlcNAc(1→6)βDGal that is bound by the monoclonal *anti*-I Ma antibody (25). Based on this assumption, two minima are indicated; namely, $\phi^{C\text{-}1^c}/\psi^{HA\text{-}6^a}$ = −70°/5° (1.09 kcal/mol) and −170°/5° (−0.02 kcal/mol). We expect, however, that the energy difference is in fact much greater, since the −70°/5° conformer brings HB-6^b in close proximity to the carboxylate group which must be strongly hydrated, and therefore expresses an effective volume greater than that used in the calculation. We have discussed this matter in relation to the conformational preference exhibited by βDGal(1→4)βDGlcNAc(1→6)6-*SC*CH_3-βDGal (26). It is noteworthy that the preferred conformer (−170°/5°) has HA-6^b in contact with Ha-3^c, much as was found for G_{M1}, and, therefore, an nOe-test for this conformational preference is indicated. The conformer (−170°/5° and ω = 60°) places the carboxyl group much in the mean of the plane defined by the pyranose rings of the βDGal(1→4)βDGlc unit of αDNeuAc(2→6)βDGal(1→4)βDGlc and on the side where it is to be expected (25) that OH-3^a of the βDGlc unit is intramolecularly hydrogen bonded to O-5^b of the βDGal unit.

With reference to Table 4, the assignments of the ^{13}C chemical shifts to the haptens **4** and **5**, on the basis of those found for the component disaccharide units present in compounds **1**–**3**, are straightforward. That essentially the same chemical shifts, when applicable, are found throughout, is in accord with

Can. J. Chem. Downloaded from www.nrcresearchpress.com by 210.87.254.5 on 09/06/12
For personal use only.

TABLE 5. ^{13}C nuclear magnetic resonance chemical shifts for the ganglioside G_{M1} (**8**) and the oligosaccharides βDGalNAc(1→4)[αDNeuAc-(2→3)]βDGal(1→4)α,βDGlc ($G_{M2}OS$, **7**) and βDGal(1→3)βDGalNAc(1→4)[αDNeuAc(2→3)]βDGal(1→4)α,βDGlc ($G_{M1}OS$, **9**)

Carbon atom	$G_{M2}OS$ (**7**)	$G_{M1}OS$ (**9**)	$G_{M1}OS$ (A)*	G_{M1} (**8**)	G_{M1} (B)*	$\delta_A - \delta_9$	$\delta_B - \delta_8$	$\delta_5 - \delta_8$†	
1a	96.10	96.11	96.61	102.92	103.47	0.50	0.55	0.36	
2a	74.09	74.11	74.59	73.56	74.11	0.48	0.55	0.01	
3a	74.70	74.71	75.19	74.75	75.24	0.48	0.49	0.25	
4a	78.93	78.95	79.35	79.38	79.83	0.40	0.45	−0.01	
5a	75.10	75.12	75.60	75.23	75.76	0.48	0.53	0.04	
6a	60.49	60.51	60.96	60.71	61.09	0.45	0.38	0.10	
1b	102.94	102.93	103.36	103.20	103.47§	0.43	0.27	0.32	
2b	70.33	70.34	70.81	70.31	70.85	0.47	0.54	1.36	
3b	77.50	77.48	75.19	77.93	75.24	−2.29 (0.47)	−2.69 (0.41)	−4.84	
4b	75.04	74.71	77.95 (A)	74.75	78.34 (D)	3.24 (0.48)	3.59 (0.49)	1.78	
5b	74.37	74.43	74.92	74.48	75.00	0.49	0.52	0.52	
6b	60.91	60.98	61.97	61.05	61.90	0.99 (0.52)	0.85 (0.44)	0.19	
1c	103.07	102.83	103.36	102.92	103.47	0.53	0.55	−0.17	
2c	52.68	51.52	52.47 (B)	51.50	52.84 (E)	0.95 (0.49)	1.34 (0.56)	0.64	
3c	71.65	80.70	81.17	80.91	81.58	0.47	0.67	−0.66	
4c	68.13	68.25	68.73	68.30	68.75	0.48	0.45	0.29	
5c	74.70	74.71	75.19	75.23	75.76	0.48	0.53	−0.16	
6c	61.47	61.43	61.50	61.37	61.49	0.07 (0.54)	0.12 (0.53)	0.17	
N—C=O	175.15	175.08	175.62	174.98	175.65	0.54	0.67	0.30	
CH_3	22.95	22.96	23.45 (C)	23.18	23.45 (F)	0.49	0.27	−0.21	
1d	—	105.04	105.57	105.07	105.60	0.53	0.53	0.09	
2d	—	71.05	71.54	71.14	71.77	0.49	0.63	0.11	
3d	—	72.86	73.35	73.99	73.65	0.49	0.66	0.21	
4d	—	68.96	69.44	68.92	69.26	0.48	0.34	0.25	
5d	—	75.23	75.72	75.23	75.76	0.49	0.53	0.28	
6d	—	61.29	61.77	61.37	61.90	0.48	0.53	0.17	
								Me αDNeuAc‡ (**10**)	$\delta_8 - \delta_{10}$
1e	174.40	174.40	174.93	174.46	174.84	0.53	0.38	173.67	0.79
2e	101.95	101.95	102.46	102.24	102.66	0.51	0.42	100.99	1.25
3e	37.36	37.38	37.84	37.20	37.90	0.46	0.70	40.38	−3.18
4e	69.00	69.01	(69.44)‖	69.03	69.26	0.43	0.23	68.56	0.47
5e	51.96	51.98	52.01	52.21	52.06	0.03 (0.49)	−0.15 (0.63)	52.21	0
6e	73.40	73.42	73.88	73.18	73.65	0.47	0.47	72.86	0.32
7e	68.37	68.39	68.86	68.52	69.26	0.47	0.74	68.49	0.03
8e	72.58	72.58	73.04	72.55	73.03	0.46	0.48	71.94	0.61
9e	63.18	63.19	63.66	63.34	63.89	0.47	0.55	62.94	0.40
N—C=O	175.39	175.40	175.92	175.37	175.65	0.52	0.28	175.39	−0.02
CH_3	22.39	22.42	22.94	22.65	22.86	0.52	0.21	22.30	0.35

* Published by Sillerud and Yu (1).
† See Table 4 for the chemical shifts for compound **5**.
‡ Sodium salt.
§ Occurred in an ill-defined band (1).
‖ Reassignment based on published spectrum (1).

the prediction based on HSEA calculation. Exact correspondence is not expected since the degrees of freedom for the flexing of the various pyranose rings will not be constant and this must influence ^{13}C chemical shifts. Our assignments are compared with those reported by Sillerud and Yu (1) for *asialo*-G_{M1}. Considering that the measurements were made at different temperatures and that the compounds differ greatly in the nature of the aglycons, the agreement is excellent. We would only suggest that the assignments for C-1^b and C-1^c be interchanged. Since we have high confidence in the assignments for the hapten **5**, these are compared in Table 5 to those for $G_{M1}OS$ (**9**) and G_{M1} (**8**).

The ^{13}C chemical shifts for G_{M1} (**8**) and $G_{M1}OS$ (**9**) that we determined at 90.56 MHz and 30°C are compared in Table 5 with those reported by Sillerud and Yu (1) at 50.3 MHz and 20°C. Also, the ^{13}C chemical shifts for $G_{M2}OS$ are reported. As noted in Table 5, we recommend a number of changes in assignment. Change A is mandatory since we have already shown (10) that glycosylation at a position neighboring to one that is already glycosylated leads to less deshielding of the new aglyconic carbon than is normally observed, but to a shielding of the aglyconic carbon at the neighboring position. Thus C-4^b, which is at 76.53 ppm in the hapten **5**, should be shielded on introducing the αDNeuAc group at O-3^b. Therefore, its signal must be at 74.71 and not 77.48 ppm. Our other suggested changes (B and C, Table 5) are based on the observation (note the $\delta_A - \delta_9$ values in brackets) that to do so would bring the data into much better overall agreement. The lack of agreement

Can. J. Chem. Downloaded from www.nrcresearchpress.com by 210.87.254.5 on 09/06/12
For personal use only.

Can. J. Chem. Downloaded from www.nrcresearchpress.com by 210.87.254.5 on 09/06/12
For personal use only.

between our assignment of the ^{13}C chemical shifts for G_{M1} and those reported by Sillerud and Yu is quite remarkable. As seen in Table 5 from the $\delta_B - \delta_8$ values presented in brackets, a much better agreement would be reached on the basis of the changes (D, E, and F) shown. The change D is for the reasons discussed above in relation to the effect of branching. Changes E and F are less secure but are considered appropriate. The $\delta_5 - \delta_8$ values listed in Table 5 only represent the best match between those observed for G_{M1} (**8**) and those assigned in Table 4 for the hapten **5** (ASG_{M1}-Hp). The assignment of the signal at 79.38 ppm for C-4[a] of G_{M1} appears required, as is the assignment of the signal at 79.37 ppm for C-4[a] of the hapten **5**. Thus, on this basis, it might appear that all the ^{13}C atoms of the βDGlc unit would have nearly the same chemical shifts for both **5** and **8**. However, the data do not allow this to be the case and it must be concluded that the aglycons have an influence on the ^{13}C chemical shifts of the βDGlc unit. In fact, this would not be surprising since the ceramide aglycon of G_{M1} is known to lead to micelle formation when G_{M1} is dissolved in water. That the anchoring of the oligosaccharide portion of G_{M1} to a lipid surface would cause a change in the ^{13}C chemical shifts for the first sugar unit, as compared with when the substance is in true solution, would not be surprising. That this effect would not be as important for the terminal βDGal(1→3) unit would be expected and, indeed, it was possible to assign ^{13}C chemical shifts, which produce much more constant $\delta_5 - \delta_8$ values, to this unit. The values for the βDGal(1→4) (b unit) are in general accord with expectation, in that introduction of the αDNeuAc unit at C-3[b] of this unit should lead to deshielding of this atom, but shielding of C-4[b] and likely C-2[b], as is assigned in Table 5. The effect of this substitution on the ^{13}C chemical shifts of the other carbon atoms of the b unit, as well as those of the c unit, cannot be predicted with a high level of confidence. Nevertheless, as seen in Table 5, our assignments for the c unit indicate that the substitution has a considerable effect on the ^{13}C chemical shifts for atoms in this neighboring unit. This effect would not be surprising since our conformational analysis, based on HSEA calculation, indicates that the βDGalNAc unit is extensively and rather strongly bonded through secondary forces of attraction to the αDNeuAc unit. This interaction would be expected to alter the ^{13}C chemical shifts of both the βDGalNAc and the αDNeuAc units. That the latter is the case is apparent from the $\delta_8 - \delta_{10}$ values listed in Table 5 for the atoms C-6[c] to C-9[c]. Indeed, the contrast of these values with those for the $\delta_5 - \delta_8$ values for the terminal d unit of G_{M1} lends support to the conclusion reached by the HSEA calculation that the αDNeuAc unit of G_{M1} is strongly attracted to the βDGalNAc(1→4)βDGal unit of the core tetrasaccharide. As was stated above, Koerner *et al.* (2*b*) surmised an attraction between the αDNeuAc and βDGalNAc units of G_{M2} and G_{M1}. In this connection, it was suggested that dipole-charge, hydrophobic, hydrogen-bond, and counter-ion interactions or combinations of these possibilities are responsible for such secondary structure. We contend that the van der Waals forces of attraction commented upon with reference to Table 2 essentially provide the driving force for the presence of this secondary structure.

Experimental

Methods

The ^1H nmr spectra were conducted in 5-mm degassed and sealed tubes containing the compound (near 0.02 *M*) after exchanging three times with D_2O and dissolution in pure D_2O. Either a Bruker WP-360 or WH-400 spectrometer (360 and 400 MHz, respectively) with 32K points (Aspect 2000 computer) was used. The nuclear Overhauser experiments were performed in the difference mode (27) with a power level of 35 db below 0.2 W. The chemical shifts are relative to the signal for DOH at 4.81 ppm at 296 K for all compounds except for $G_{M2}OS$ (**7**) and $G_{M1}OS$ (**9**) where the spectra were measured at 178 K (δ_{DOH} = 4.99 ppm).

The ^{13}C nmr spectra were measured using the same solutions as for the ^1H nmr measuremetns and the above-mentioned spectrometers operating at 90.56 and 100.63 MHz, respectively, at 303 K. A relaxation delay of 0.5 s was used between 90° pulses. A line broadening factor of 0.5 Hz was introduced before the Fourier transformation of the free induction decay. The chemical shifts are relative to external tetramethylsilane using the deuterium lock of the spectrometer, which set the ^{13}C chemical shift of dioxane in D_2O at 66.88 ppm at 303 K (28).

The atomic coordinates for the a, b, c, d, and e units used in the HSEA calculations were taken from the crystal structures for gentiobiose (29), methyl β-D-galactopyranoside (30), *N*-acetyl-β-D-galactosamine (31), and *N*-acetyl-β-D-neuraminic acid (9).

$G_{M2}OS$ (7) and $G_{M1}OS$ (9)

Samples (32) of G_{M1} (27 mg) and G_{M2} (15 mg)[4] were treated with ozone as described by Wiegandt and Bücking (21). In each case, the ozonide was decomposed with dimethyl sulfide and the solution was evaporated to dryness. The residue was dissolved in a 5% solution of triethylamine in methanol and the solution was kept at 4°C for 24 h. After solvent removal, the residue was triturated with water (5 × 5 mL) and the solution was filtered using a 0.22 μm millipore filter (Millipore Corporation, Bedford, MA, U.S.A.). Freeze-drying left a colorless solid which was redissolved in water (1 mL) for passage through a column of Amberlite IRA-120(H^+) resin (1.0 g). After neutralization with sodium bicarbonate, the solution was freeze-dried to a colorless solid. The ^1H nmr of $G_{M1}OS$ (see Fig. 2) showed the product to be contaminated by material which produced signals at the positions shown. Since these impurities could not be removed by extraction with chloroform, no further purification was attempted.

Acknowledgements

This research was supported by a grant (A172 to R.U.L.) from the Natural Sciences and Engineering Research Council of Canada and studentships to S.S. from the Alberta Heritage Foundation for Medical Research. We are indebted to Dr. Ole Hindsgaul and Mr. Glenn Bigam for valuable assistance.

1. L. O. SILLERUD and R. K. YU. Carbohydr. Res. **113**, 173 (1983).
2. T. A. W. KOERNER, JR., J. H. PRESTEGARD, P. C. DAMOU, and R. K. YU. Biochemistry, **22**, (*a*) 2676 (1983); (*b*) 2687 (1983).
3. S. SABESAN and R. U. LEMIEUX. Can. J. Chem. **62**, 644 (1984).
4. R. U. LEMIEUX, D. A. BAKER, W. M. WEINSTEIN, and C. M. SWITZER. Biochemistry, **20**, 199 (1981).
5. IUPAC–IBC Commission on Biochemical Nomenclature, J. Lipid. Res. **19**, 114 (1978).
6. S.-S. NG and J. A. DAIN. *In* Biological roles of sialic acid. *Edited by* A. Rosenberg and C.-L. Schengrund. Plenum Press, New York. 1976. p. 75.
7. K. BOCK and H. THØGERSEN. Annu. Rep. NMR Spectrosc. **13**, 7 (1982).
8. H. THØGERSEN, R. U. LEMIEUX, K. BOCK, and B. MEYER. Can. J. Chem. **60**, 44 (1982).
9. J. L. FLIPPEN. Acta Crystallogr. Sect. B, **29**, 1881 (1973).
10. R. U. LEMIEUX, K. BOCK, L. T. J. DELBAERE, S. KOTO, and V. S. RAO. Can. J. Chem. **58**, 631 (1980).
11. L. SALEM. *In* Electronic aspects of biochemistry. *Edited by* B. Pullman. Academic Press, New York. 1964. p. 293.

[4] We are grateful to Dr. S. K. Kundu for generous gifts of these valuable compounds.

12. R. U. LEMIEUX and K. BOCK. Arch. Biochem. Biophys. **220**, 125 (1983).
13. M. L. HAYES, A. S. SERIANNI, and R. BARKER. Carbohydr. Res. **100**, 87 (1982).
14. R. U. LEMIEUX, S. KOTO, and D. VOISIN. ACS Symposium Series, No. 87. 1979. Chapt. 2. p. 17.
15. M. F. CZARNIECKI and E. R. THORNTON. J. Am. Chem. Soc. **99**, 8273 (1977).
16. P. L. HARRIS and E. R. THORNTON. J. Am. Chem. Soc. **100**, 6738 (1978).
17. R. SCHAUER, R. W. VEH, M. SANDER, A. P. CORFIELD, and H. WIEGANDT. *In* Structure and function of gangliosides. *Edited by* L. Svennerholm, P. Mandel, H. Dreyfus, and P.-F. Urban. Plenum Press, New York. 1980. pp. 291–293.
18. K. C. LESKAWA and A. ROSENBERG. *In* Structure and function of gangliosides. *Edited by* L. Svennerholm, P. Mandel, H. Dreyfus, and P.-F. Urban. Plenum Press, New York. 1980. p. 133.
19. R. SCHAUER. Adv. Carbohydr. Chem. Biochem. **40**, 169 (1982).
20. E. B. BROWN, W. S. BREY, JR., and W. WELTNER, JR. Biochim. Biophys. Acta, **399**, 124 (1975).
21. H. WIEGANDT and H. W. BÜCKING. Eur. J. Biochem. **15**, 287 (1970).
22. R. U. Lemieux. *In* Frontiers in chemistry. *Edited by* K. J. Laidler. Pergamon Press, Oxford. 1982. p. 21.
23. M. NAIKI, D. M. MARCUS, and R. LEDEEN. J. Immunol. **113**, 84 (1974).
24. G. N. ROGERS, J. C. PAULSON, R. S. DANIELS, J. J. SKEHEL, I. A. WILSON, and D. C. WILEY. Nature, **304**, 76 (1983).
25. E. A. KABAT, J. LIAO, M. H. BURZYNSKA, T. C. WONG, H. THØGERSEN, and R. U. LEMIEUX. Mol. Immunol. **18**, 873 (1981).
26. R. U. LEMIEUX, T. C. WONG, and H. THØGERSEN. Can. J. Chem. **60**, 81 (1982).
27. R. RICHARZ and K. WÜTHRICH. J. Magn. Reson. **30**, 147 (1978).
28. L.-Å. FRANSSON, T. N. HUCKERBY, and I. A. NIEDUSZYNSKI. Biochem. J. **175**, 302 (1978).
29. DE F. ARENE, A. NEUMAN, and F. LONGCHAMBON. C. R. Acad. Sci. Paris, **288**, 331 (1979).
30. S. TAKAGI and G. A. JEFFREY. Acta Crystallogr. Sect. B, **35**, 902 (1979).
31. W. T. WINTER, S. ARNOTT, D. H. ISAAC, and E. D. T. ATKINS. J. Mol. Biol. **125**, 1 (1978).
32. S. K. KUNDU and S. K. ROY. J. Lipid Res. **19**, 390 (1978).

Can. J. Chem. Downloaded from www.nrcresearchpress.com by 210.87.254.5 on 09/06/12
For personal use only.

Pyrrole chemistry. XXVII. 2,3,4-Trisubstituted pyrroles and a second synthesis of porphobilinogen from pyrrole

KURT FABER, HUGH J. ANDERSON,[1] CHARLES E. LOADER, AND ANNETTE S. DALEY
Department of Chemistry, Memorial University of Newfoundland, St. John's, Nfld., Canada A1B 3X7

Received November 8, 1983

KURT FABER, HUGH J. ANDERSON, CHARLES E. LOADER, and ANNETTE S. DALEY. Can. J. Chem. **62**, 1046 (1984).

Changes in some of the key intermediates and procedures used in our earlier total synthesis of porphobilinogen from pyrrole that improve the yield to 11% are reported. Ethyl pyrrole-3-acetate was formylated by the Vilsmeier–Haack method and then iodinated. The desired 2,3,4-substituted pyrrole isomer was isolated in moderate yield and, after conversion of iodide to acrylate and aldehyde to aldoxime, reduction and work-up afforded porphobilinogen lactam ethyl ester. Hydrolysis of the latter gave porphobilinogen in ten steps from pyrrole.

KURT FABER, HUGH J. ANDERSON, CHARLES E. LOADER et ANNETTE S. DALEY. Can. J. Chem. **62**, 1046 (1984).

Grâce à des changements dans quelques intermédiaires clés et dans quelques-unes des procédures utilisées dans notre synthèse totale antérieure du porphobilinogène à partir du pyrrole, il est possible d'améliorer le rendement à 11%. On a formylé le pyrroleacétate-3 d'éthyle par la méthode de Vilsmeier–Haack et on l'a alors iodé. L'isomère désiré du pyrrole substitué en 2,3,4 est isolé avec un rendement modéré; après conversion de l'iodure en acrylate, et de l'aldéhyde en aldoxime, une réduction et une extraction permettent d'isoler l'ester éthylique de la lactame du porphobilinogène. L'hydrolyse de ce dernier conduit au porphobilinogène en dix étapes à partir du pyrrole.

[Traduit par le journal]

Can. J. Chem. Downloaded from www.nrcresearchpress.com by 210.87.254.105 on 09/06/12
For personal use only.

We have recently reported a total synthesis of porphobilinogen (**1**), the precursor of naturally occurring porphyrins and corrins, in nine steps from pyrrole with an overall yield of about 6% (1). In that synthesis, reduction of the cyanide group led to the partial reduction of the pyrrole ring and was a major factor in reducing the yield. Attempts to develop a better procedure for this reduction, using as a model the readily available 4-carbethoxyvinylpyrrole-2-carbonitrile (see the experimental section), failed. The model appeared more susceptible to ring reduction than the porphobilinogen precursor itself under most conditions.

A variation on the earlier synthesis provides both a marked increase in the overall yield of porphobilinogen and also further demonstrates the versatility of this approach to the synthesis of 2,3,4-trisubstituted pyrroles, a type sometimes used as porphyrin building blocks (2). The steps by which a labelled carbon or nitrogen atom could be introduced into the eventual aminomethyl side chain are also simplified.

A general outline of this approach is given in Scheme 1, and follows the philosophy outlined in the earlier paper (1). The aldoxime rather than the cyanide group was used as a precursor to the aminomethyl side chain and the lactam ethyl ester of porphobilinogen (**2**) was the desired final intermediate.

This synthetic approach began, as did the earlier one, with the preparation of ethyl pyrrole-3-acetate (**3**) in three steps from pyrrole (1). Attempts to improve this synthesis by using the Wilgerodt–Kindler rearrangement of the readily available (3, 4) 3-acetyl-1-phenylsulfonylpyrrole failed. Although the rearrangement was successful, the yield of the corresponding morpholide:

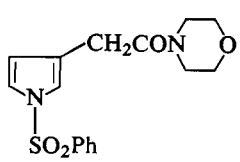

was low and this approach was not pursued.

A variety of methods are available for the introduction of the aldehyde group onto the pyrrole nucleus (5). However, the acetic ester side chain in the starting material **3** made acidic conditions undesirable. The method of Clezy *et al.* using trifluoroacetic acid and ethyl orthoformate (6) gave a mixture that showed the presence of the two isomeric aldehyde products, but during work-up a good deal of decomposition occurred. When a catalytic amount of *p*-toluenesulfonic acid was used in place of trifluoroacetic acid, there was still extensive loss of material through polymerization and(or) decomposition. The Vilsmeier–Haack procedure, with dimethylformamide (DMF) and oxalyl chloride as the formylating agent (7), gave an excellent yield of the formylated 3-acetic ester, but the ratio of 2-substitution to 5-substitution was 40:60 at 0°C and unsatisfactory. Lowering the temperature improved this ratio, but at about −20°C the reaction ceased. Inverse addition of the reagents had only a slight effect. The addition of one equivalent of hexamethylphosphoric triamide improved the ratio of the desired 2- (**4**) over the undesired 5-isomer (**5**) to 60:40 at −26°C. For comparison, the Vilsmeier–Haack formylation of 3-methylpyrrole gave a 4:1 ratio of 2- and 5-substitution (8, 9). The combination of the steric and electronic effects of the acetic ester group results in the less favorable ratio, as in the cyanation of the 3-acetic ester (1). Mild hydrolysis of the iminium salt did not hydrolyze the ester group and conversion to the aldehyde product was excellent.

The isomeric aldehydes **4** and **5** could be separated by flash chromatography with less difficulty than the corresponding

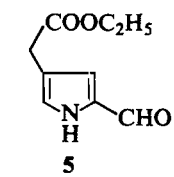

5

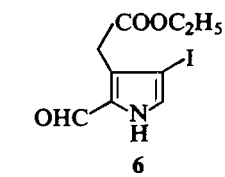

6

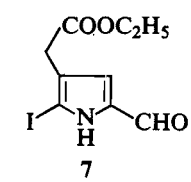

7

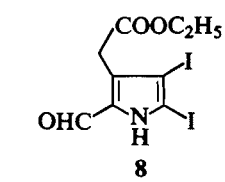

8

[1] Author to whom all correspondence should be addressed.

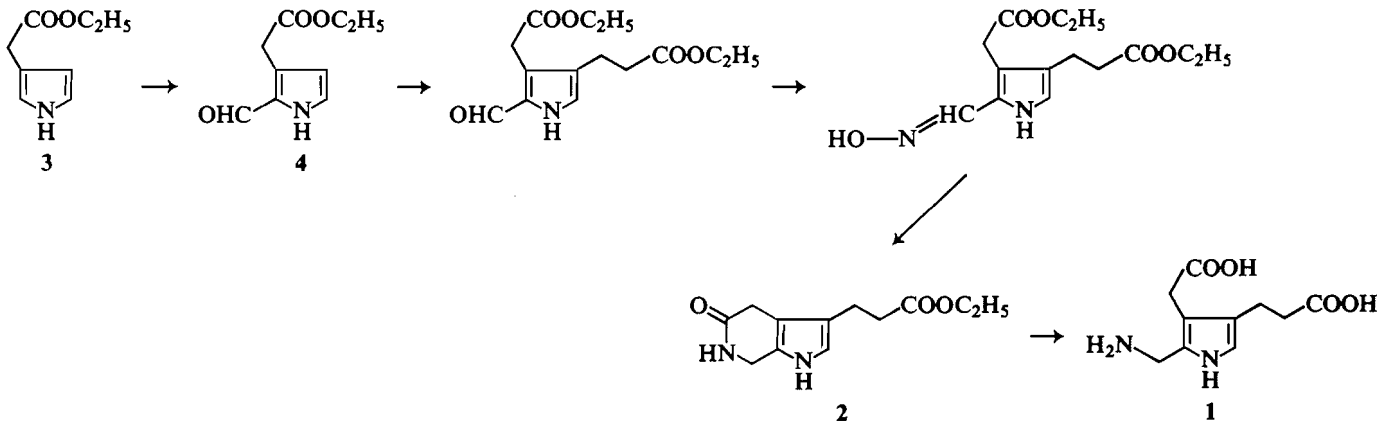

SCHEME 1

nitriles, which required medium pressure liquid chromatography (1). After the initial isolation, purification, and identification, the yields were found to be 59.5% **4** and 37% **5**.

The decarbonylation of the undesired aldehyde **5** using palladized charcoal to give back the starting material **3** for the Vilsmeier–Haack reaction afforded only a 50% yield, in contrast to the almost quantitative yield obtained for the decarbonylation of the corresponding glyoxalate. For this reason, and because the separation of the mixture of isomeric aldehydes was tedious, this procedure was not used to recover the starting material, **3**.

As with the isomeric nitriles (1), the iodination of the reaction product mixture of **4** and **5**, using the iodine/iodic acid (4:1 ratio) method (10), led to a mixture of three compounds (**6**, **7**, and **8**). The desired ethyl 4-iodo-2-formylpyrrole-3-acetate (**6**) could now be easily separated and thus obtained in two steps from the 3-acetic ester, **3**, in a 52.6% yield.

The acidic proton on the pyrrole nitrogen was expected to interfere with the Heck reaction (1, 11, 12) and was replaced by a benzoyl group by the phase-transfer benzoylation of **6**, giving **9**. When compound **9** was condensed with ethyl acrylate an excellent yield of a mixture of products with (**10**), and without (**11**), the *N*-benzoyl group was obtained. More cleavage of the benzoyl group was evident than with corresponding

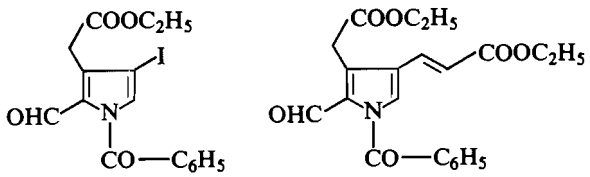

9 **10**

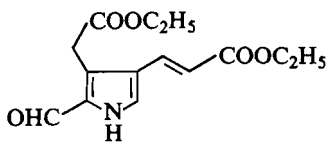

11

nitrile derivative (1). The *N*-benzoyl does not impart any added stability to the reduced material (1) and was conveniently removed during work-up of the Heck reaction product by treatment with ammonia; thus **11** became the only product from the reaction.

The ethyl ester of porphobilinogen lactam (**2**) is stable and gives porphobilinogen in excellent yield on hydrolysis (1). Attempts to obtain this compound directly by the reductive amination of **11** gave the alcohol and only a trace of the desired lactam ester (**2**). Similarly, when the reductive amination was attempted on the model compound, ethyl 2-formylpyrrole-3-acetate (**4**), alcohol formation predominated over lactam formation. In addition, some decarbonylation to the 3-acetic ester (**3**) took place. It appears that in both cases the equilibrium (13, 14) between the aldehyde and the intermediate carbinolamine or imine was unfavorable. While it is possible that a small change in pH might improve the operation, the conventional procedure was used, despite the extra step involved. Thus, **11** was converted to its oxime **12** (88% yield) using a mostly ethanolic solution of hydroxylamine at room temperature rather than the refluxing aqueous solutions used by earlier workers (15–17). The tlc, ir, and nmr properties of the product and those of the known isomeric pyrrole-2-aldoximes showed that the *syn*-isomer was the major isomer in **12**.

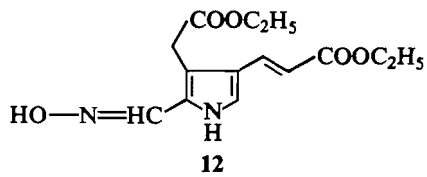

12

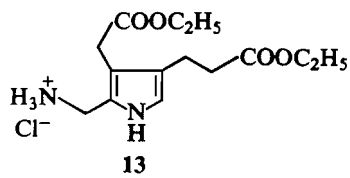

13

In our previous synthesis (1), platinum oxide catalysis was necessary to reduce the nitrile group. However, reduction of the pyrrole ring lowered the yield of the product substantially. The aldoxime was expected to be more easily reduced to the aminomethyl group than the nitrile. The palladium black catalyzed reduction of **12**, under the same conditions (ethanolic ammonia) used to hydrogenate the corresponding nitrile, failed to give porphobilinogen lactam ester but the starting material was used up. The conditions used and the higher R_f of the major component suggested that the product was possibly the ester of the byproduct of unknown structure reported by Arsenault and MacDonald (16) during reduction of their 2-oxime-3-acetic acid-4-propanoic acid when the solvent was aqueous ammonia. The instability of this product prevented further investigation. Reduction over palladium black in a slightly acidic ethanol solution gave the ammonium salt (**13**), which was easily converted without isolation to the desired lactam ester by treatment

Can. J. Chem. Downloaded from www.nrcresearchpress.com by 210.87.254.105 on 09/06/12
For personal use only.

Can. J. Chem. Downloaded from www.nrcresearchpress.com by 210.87.254.105 on 09/06/12
For personal use only.

with ethanolic sodium ethoxide. This procedure was a slightly modified version of the MacDonald route (15) which used a similar oxime of a pyrrole containing a propanoic rather than acrylic ester side chain. The yield of the lactam ethyl ester **2** from the oxime **12**, identical to a sample from the earlier nitrile route, was about 80%. As this lactam ester had already been hydrolyzed to porphobilinogen (**1**), the above sequence constitutes another total synthesis of that compound in ten steps from pyrrole with an overall yield of 11%.

Experimental

Melting points are uncorrected. Elemental analyses were by Atlantic Microlabs, GA, U.S.A. The ir spectra were recorded on a Perkin–Elmer 237B grating spectrophotometer as KBr discs, unless otherwise stated. The ^{1}H nmr spectra (nmr) were determined using a Varian EM 360 or a Bruker WP-80 instrument and are expressed in ppm (δ values) relative to tetramethylsilane as internal reference in $CDCl_3$, unless otherwise stated. Mass spectra were recorded on a VG Micromass 7070HS spectrometer. The ^{13}C nmr spectra were determined at 20.122 MHz in $CDCl_3$ on a Bruker WP-80 Fourier transform instrument. All solvents were dried and distilled before use. Throughout, the term "petroleum" refers to the fraction of bp 30–60°C. The term "hexanes" refers to a mixture of isomers bp 65.8–69.0°C (Fisher Scientific). Flash chromatography (18) was carried out using "Baker Analyzed" silica gel for flash chromatography.

Formylation of ethyl pyrrole-3-acetate (3)

The Vilsmeier–Haack complex was generated by adding oxalyl chloride, (1.265 g, 9.97 mmol) in dichloromethane (25 mL) to a cooled (0°C) solution of DMF (0.765 g, 10.5 mmol) in dichloromethane (25 mL) over 10 min, and then the reaction mixture was stirred at 0°C for 15 min and at room temperature for a further 15 min. The complex was then cooled to between −10 and −15°C and hexamethylphosphoric triamide (1.85 g, 10.3 mmol) in dichloromethane (25 mL) was added slowly, keeping the temperature below −10°C. The solution was then cooled to about −30°C and ethyl pyrrole-3-acetate (**3**) (1.02 g, 6.65 mmol) in dichloromethane (50 mL) was added over 30 min. The temperature was then allowed to rise and was held at −26°C for 30 min and then at 0°C for a further 30 min. Thin-layer chromatography showed absence of starting material, and an aqueous solution of sodium acetate (125 mL, 1 mol L^{-1}) was added dropwise at 0°C, followed by vigorous stirring for 1 h at room temperature. The layers were separated, the aqueous layer was saturated with NaCl and then extracted 4 times with dichloromethane (50-mL portions). The organic layers were combined, dried ($MgSO_4$), and the solvent was removed.

I. The crude product was separated by flash chromatography on silica gel using hexanes/ether (elution gradient 4:1, rising to 2:1). The following were obtained in order of elution.

(a) *Ethyl 2-formylpyrrole-4-acetate* (**5**) (450 mg, 37.3%), mp 62.5°C from hexanes/dichloromethane; ir: 1650, 1730, 2900, 2975, 3150 cm^{-1}; nmr δ: 1.28 (3H, t, —CH_3, J = 7 Hz), 3.52 (2H, s, CH_2COO), 4.15 (2H, q, —CH_2—CH_3, J = 7 Hz), 6.93 (1H, m, 3-H), 7.05 (1H, m, 5-H), 9.38 (1H, s, —CHO) 10.5 (1H, b, NH); m/z = 181. *Anal.* calcd. for $C_9H_{11}NO_3$: C 59.66, H 6.16, N 7.73; found: C 59.72, H 6.16, N 7.73.

(b) *Ethyl 2-formylpyrrole-3-acetate* (**4**) (718 mg, 59.5%), mp 59.0°C from hexanes/dichloromethane; ir: 1625, 1730, 2975, 3250 cm^{-1}; nmr δ: 1.25 (3H, t, —CH_3, J = 7 Hz), 3.78 (2H, s, —CH_2COO), 4.15 (2H, q, —CH_2—CH_3, J = 7 Hz), 6.23 (1H, m, 4-H), 7.03 (1H, m, 5-H), 9.60 (1H, s, —CHO), 10.7 (1H, b, NH); m/z = 181. *Anal.* calcd. for $C_9H_{11}NO_3$: C 59.66, H 6.12, N 7.73; found: C 59.53, H 6.15, N 7.69.

II. On a preparative scale, the isomer mixture of **4** and **5** could be freed of hexamethylphosphoric triamide by flash chromatography on a short column using hexanes/ether (2:1). This mixture was then iodinated as follows.

Iodination of the mixture of aldehydes of ethyl pyrrole-3-acetate (4 and 5)

The mixture of aldehyde esters **4** and **5** from II above (1.02 g, 5.62 mmol), iodic acid (198 mg, 1.123 mmol), and iodine (570 mg, 4.49 mmol) in CCl_4 (40 mL) water (1.2 mL), acetic acid (2.8 mL), and sulfuric acid (0.1 mL, concentrated) was stirred vigorously under nitrogen at room temperature for 24 h. The reaction mixture was diluted with dichloromethane (100 mL), the organic layer separated, washed with aqueous sodium thiosulfate (50 mL, saturated), aqueous sodium hydrogen carbonate (50 mL, 5%), saturated aqueous NaCl, and dried ($MgSO_4$). The product mixture from the rotary evaporation was flash chromatographed using an elution gradient of hexanes/ether (3:1) rising to ether as solvent. The following were obtained in order of elution.

(a) *Ethyl 2-formyl-5-iodopyrrole-4-acetate* (**7**) (452 mg, 26.1%), mp 98.5°C from hexanes/dichloromethane; ir: 1625, 1700, 3150 cm^{-1}; nmr δ: 1.30 (3H, t, —CH_3, J = 7 Hz), 3.48 (2H, s, —CH_2COO), 4.23 (2H, q, —CH_2—CH_3, J = 7 Hz), 6.95 (1H, d, 3-H, $J_{1,3}$ = 1.2 Hz), 9.33 (1H, s, —CHO), 10.4 (1H, b, NH); m/z = 307. *Anal.* calcd. for $C_9H_{10}INO_3$: C 35.20, H 3.28, N 4.56; found: C 35.13, H 3.27, N 4.50.

(b) *Ethyl 2-formyl-4,5-diiodopyrrole-3-acetate* (**8**) (25.2 mg, 3%), mp 147.5°C from hexanes/dichloromethane; ir: 1650, 1720, 3175, 3400 cm^{-1}; nmr δ: 1.30 (3H, t, —CH_3, J = 7 Hz), 3.80 (2H, s, —CH_2COO), 4.20 (2H, q, —CH_2—CH_3, J = 7 Hz), 9.38 (1H, s, —CHO); m/z: = 433. *Anal.* calcd. for $C_9H_9I_2NO_3$: C 24.96, H 2.10, N 3.24; found: C 25.15, H 2.12, N 3.21.

(c) *Ethyl 2-formyl-4-iodopyrrole-3-acetate* (**6**) (937 mg, 54.2%), mp 86.5°C from hexanes/dichloromethane; ir: 1670, 1720, 3300 cm^{-1}; nmr δ: 1.30 (3H, t, —CH_3, J = 7 Hz), 3.78 (2H, s, —CH_2COO), 4.25 (2H, q, —CH_2—CH_3, J = 7 Hz), 7.14 (1H, d, 5-H, $J_{1,4}$ = 1.4 Hz), 9.60 (1H, s, —CHO), 10.55 (1H, b, NH); m/z = 307. *Anal.* calcd. for $C_9H_{10}INO_3$: C 35.20, H 3.28, N 4.56; found: C 35.08, H 3.29, N 4.53.

Ethyl 1-benzoyl-2-formyl-4-iodopyrrole-3-acetate (9)

Benzoyl chloride (422 mg, 3 mmol) in dichloromethane (5 mL) was added dropwise over 30 min to a well-stirred and cooled (ice bath) mixture of ethyl 2-formyl-4-iodopyrrole-3-acetate (**6**) (614 mg, 2 mmol), powdered NaOH (136 mg, 3.4 mmol), and tetrabutylammonium hydrogen sulfate (34 mg, 0.1 mmol) in dichloromethane (15 mL) under N_2, then stirred at 0°C for an additional 2 h. The reaction mixture was filtered through Celite, washing with several portions of dichloromethane. The combined organic layer was washed with saturated aqueous NaCl and dried ($MgSO_4$). Evaporation of the solvent[2] afforded a crude product which was flash chromatographed using hexanes/ether (3:1) as eluent to give pure ethyl 1-benzoyl-2-formyl-4-iodopyrrole-3-acetate (**9**) (752 mg, 91.5%), mp 106.5–107°C (hexanes/dichloromethane); ir: 1640, 1700, 1725, 2950, 3100, 3350 cm^{-1}; nmr δ: 1.30 (3H, t, —CH_3, J = 7 Hz), 3.90 (2H, s, CH_2COO), 4.18 (2H, q, —CH_2—CH_3, J = 7 Hz), 7.21 (1H, s, 5-H), 7.5–7.9 (5H, m, phenyl H), 10.05 (1H, s, —CHO); m/z = 411. *Anal.* calcd. for $C_{16}H_{14}INO_4$: C 46.73, H 3.43, N 3.41; found: C 46.78, H 3.47, N 3.41.

Ethyl 2-formyl-4-carbethoxyvinylpyrrole-3-acetate (11)

A mixture of ethyl 1-benzoyl-2-formyl-4-iodopyrrole-3-acetate (**9**) (123 mg, 0.3 mmol), freshly distilled triethylamine (46 mg, 0.45 mmol), ethyl acrylate (45 mg, 0.45 mmol), palladium(II) acetate (2 mg), and acetonitrile (1 mL), was placed in a heavy walled Pyrex tube, sealed at one end and fitted with a Teflon cap. The tube was flushed with dry N_2 and the cap fitted tightly, then inserted into a stirred and preheated (99–100°C) oil bath. The reaction mixture was stirred at that temperature for 40 min, then cooled to room temperature

[2] Note: This product sublimes slowly in a rotary evaporator (45°C, 6 Torr).

Can. J. Chem. Downloaded from www.nrcresearchpress.com by 210.87.254.105 on 09/06/12
For personal use only.

and taken up in dichloromethane (15 mL).[3] This solution was washed with dilute aqueous HCl (0.5 mol L^{-1}); saturated aqueous NaCl, and dried ($MgSO_4$). Evaporation of the volatiles gave a crude product that was flash chromatographed using an elution gradient of hexanes/ether (1 : 1) rising to pure ether as solvent. The following were obtained in order of elution.

(a) *Ethyl 1-benzoyl-2-formyl-4-carbethoxyvinylpyrrole-3-acetate* (**10**) (35 mg, 30.5%), mp 126.5°C from hexanes/dichloromethane; ir: 1630, 1650, 1700, 1710, 1730, 3400 cm^{-1}; nmr δ: 1.28 (6H, t, —C*H*$_3$, J = 7 Hz), 4.02 (2H, s, —C*H*$_2$COO), 4.14 (2H, q, —C*H*$_2$—CH$_3$, J = 7 Hz), 4.16 (2H, q, —C*H*$_2$—CH$_3$, J = 7 Hz), 6.10 (1H, d, CH=C*H*, J = 16 Hz), 7.3 (1H, m, 5-H), 7.60 (1H, d, C*H*=CH, J = 16 Hz), 7.45–7.85 (5H, m, phenyl H), 10.01 (1H, s, —CHO). *Mol. Wt.* (high resolution ms) calcd. for $C_{21}H_{21}NO_6$: 383.13689; found: 383.1362.

(b) *Ethyl 2-formyl-4-carbethoxyvinylpyrrole-3-acetate* (**11**) (52 mg, 62.2%), mp 91°C from hexanes/dichloromethane; ir: 1625, 1680, 1725, 2950, 3230 cm^{-1}; nmr δ: 1.25 (3H, t, —C*H*$_3$, J = 7 Hz), 1.32 (3H, t, —C*H*$_3$, J = 7 Hz), 3.88 (2H, s, —C*H*$_2$COO), 4.19 (2H, q, —C*H*$_2$—CH$_3$, J = 7 Hz), 4.25 (2H, q, —C*H*$_2$—CH$_3$, J = 7 Hz), 6.18 (1H, d, CH=C*H*, J = 16 Hz), 7.40 (1H, m, 5-H), 7.61 (1H, d, C*H*=CH, J = 16 Hz), 9.70 (1H, s, —CHO), 10.35 (1H, b, NH). *Mol. wt.* (high resolution ms) calcd. for $C_{14}H_{17}NO_5$: 279.11066; found: 279.1102.

Ethyl 2-[(hydroxyimino)methyl]-4-carbethoxyvinylpyrrole-3-acetate (12) (oxime of 11)

Finely powdered hydroxylammonium chloride (1.5 g) was suspended in dry ethanol (25 mL) and titrated with aqueous NaOH (10 mol L^{-1}) to about pH 6. The NaCl was filtered and the clear solution kept under N_2 for use.

The aldehyde diester (**11**) (121 mg, 0.433 mol), in dry ethanol (5 mL), was treated with a solution of hydroxylamine (0.75 mL, 0.65 mmol) and stirred under N_2 at room temperature for 1.5 h. Then a further amount of the hydroxylamine solution (0.5 mL, 0.43 mmol) was added and, after 30 min stirring, tlc showed complete reaction. The solution was diluted with water (30 mL), the pH adjusted (if necessary) to near 7, then ethanol was removed under reduced pressure (bath temperature about 35°C). After 2 h of refrigeration the oxime was recovered by filtration. The mother liquors were concentrated and refrigerated to give a second crop of oxime. The total recovery of aldoxime diester, **12**, was 113 mg (88%), mp 117.5–118°C from toluene; ir: 1650, 1700, 2900, 3300 cm^{-1}; nmr[4] δ: 1.29 (3H, t, —CH$_3$, J = 7 Hz), 1.35 (3H, t, —CH$_3$, J = 7 Hz), 3.68 (2H, s, —CH$_2$COO), 4.17 (2H, q, —C*H*$_2$CH$_3$, J = 7 Hz), 4.26 (2H, q, —C*H*$_2$CH$_3$, J = 7 Hz), 6.13 (1H, d, CH=C*H*, J = 16 Hz), 7.11 (1H, m, 5-H), 7.63 (1H, d, C*H*=CH, J = 16 Hz), 8.10 (1H, s, —CH=N), 9.4 (1H, b, NH); m/z = 294. *Anal.* calcd. for $C_{14}H_{18}N_2O_5$: C 57.13, H 6.16, N 9.52; found: C 56.98, H 6.18, N 9.47.

*Ethyl 4,5,6,7-tetrahydro-5-oxo-1*H*-pyrrolo-[2,3,c]pyridine-3-propanoate (2)* (porphobilinogen lactam ethyl ester)

An aqueous solution of 1 mol L^{-1} HCl (0.136 mL, 0.136 mmol) was added to the aldoxime diester **12** (40 mg, 0.136 mmol) in dry ethanol (20 mL). Hydrogenation took place at room temperature and atmospheric pressure over palladium black (10 mg) until about 3.1 molar equivalents had been taken up (1.5 to 2 h). The bright yellow solution was filtered from the catalyst, cooled to 0°C, and sodium ethoxide (0.75 mL of a solution of 138 mg Na in 20 mL ethanol) was added to bring the pH to about 8. After stirring 1 h at room temperature in the dark, the solution was brought to pH 5–6 with glacial acetic acid and evaporated under reduced pressure (bath temperature 40°C) until first cloudiness. The mixture was quickly warmed to redissolve the precipitate and refrigerated overnight.[5] The white precipitate was collected and washed with dry ether to give pure porphobilinogen lactam ethyl ester (**2**). A second crop was obtained by further evaporation and refrigeration of the mother liquor. Total yield 25.5 mg (79%), mp 248°C, mixture mp with the product from the earlier route (1), was undepressed. Proton spectra were identical; m/z = 236.

1-Benzoyl-4-iodopyrrole-2-carbonitrile

A mixture of 4-iodopyrrole-2-carbonitrile (1) (2.18 g, 10 mmol), sodium hydroxide powder (0.66 g, 170 mmol), and tetrabutylammonium hydrogen sulfate (0.17 g, 0.50 mmol) in 15 mL of dichloromethane was cooled in an ice bath. A solution of benzoyl chloride (2.10 g, 15 mmol) in dichloromethane was added dropwise over 30 min. The reaction mixture was stirred at the same temperature (ice bath) for 60 min. Dichloromethane (20 mL) was then added, and the organic extract was washed with water (1 × 20 mL), saturated brine (1 × 20 mL), and dried ($MgSO_4$). The solvent was removed, and the pale green solid product was recrystallized from dichloromethane/petroleum to give 1-benzoyl-4-iodopyrrole-2-carbonitrile (2.52 g, 78%), mp 171–172°C; ir: 1715, 2230 cm^{-1}; nmr δ: 7.65 (5H, m), 7.28 (1H, d), 7.15 (1H, d). *Anal.* calcd. for $C_{12}H_7IN_2O$: C 44.75, H 2.19, H 8.70; found: C 44.79, H 2.24, N 8.69.

1-Benzoyl-4-carbethoxyvinylpyrrole-2-carbonitrile and 4-carbethoxyvinylpyrrole-2-carbonitrile

A mixture of 1-benzoyl-4-iodopyrrole-2-carbonitrile (500 mg, 1.6 mmol), palladium(II) acetate (8 mg), triethylamine (260 mg, 2.6 mmol), ethyl acrylate (230 mg, 2.3 mmol), and CH_3CN (1 mL) was stirred and heated at 100°C for 30 min as described above. Following work-up, the crude product was found by ^1H nmr to contain about a 60:40 mixture of 1-benzoyl-4-carbethoxyvinylpyrrole-2-carbonitrile and 4-carbethoxyvinylpyrrole-2-carbonitrile. Conversion to the crude product mixture was about 75%. Flash chromatography gave the following in order of elution.

(a) *1-Benzoyl-4-carbethoxyvinylpyrrole-2-carbonitrile*, mp 138–139°C after sublimation; nmr δ: 1.30 (3H, t, J = 7 Hz), 4.23 (2H, q, J = 7 Hz), 6.23 (1H, d, J = 16 Hz), 7.2–7.8 (8H, m). *Mol. Wt.* (high resolution ms) calcd. for $C_{17}H_{14}N_2O_3$: 294.10044; found: 294.0996.

(b) *4-Carbethoxyvinylpyrrole-2-carbonitrile*, mp 136–137°C after sublimation; nmr δ: 1.32 (3H, t, J = 7 Hz), 4.25 (2H, q, J = 7 Hz), 6.17 (1H, d, J = 16 Hz), 7.07 (1H, m), 7.20 (1H, m), 7.56 (1H, d, J = 16 Hz). *Anal.* calcd. for $C_{10}H_{10}N_2O_2$: C 63.15, H 5.30, N 14.73; found: C 63.01, H 5.31, N 14.70.

Acknowledgements

We gratefully acknowledge the financial assistance of the Memorial University of Newfoundland and the Natural Sciences and Engineering Research Council of Canada, and also of Employment and Immigration Canada for a Summer Internship (ASD). We also thank Dr. Brian Gregory for high resolution mass spectra and Mr. Avery Earle for Fourier transform nmr.

1. B. J. DEMOPOULOS, H. J. ANDERSON, C. E. LOADER, and K. FABER. Can. J. Chem. **61**, 2415 (1983).
2. J. B. PAINE III. *In* The porphyrins. Vol. 1A. *Edited by* D. Dolphin. Academic Press, New York, San Francisco, London. 1978. pp. 101–163.
3. R. X. XU, H. J. ANDERSON, N. J. GOGAN, C. E. LOADER, and ROBERT MCDONALD. Tetrahedron Lett. **22**, 4899 (1981).

[3] Note: If cleavage of the benzoyl group is desired, the dichloromethane solution is saturated with gaseous NH_3 and stirred in a closed flask for 1.5 h at room temperature. The solution is then washed with brine, dried ($MgSO_4$), and evaporated. Flash chromatography with ether as solvent gives **11** only, with no loss of material.

[4] Note: Major isomer shifts only; minor isomer is about 10%. Vinylic protons also differ in the two isomers.

[5] Note: It is important to refrigerate for an extended time to obtain the best recovery.

4. J. ROKACH, P. HAMEL, M. KAKUSHIMA, and G. H. SMITH. Tetrahedron Lett. **22**, 4901 (1981).
5. A. GOSSAUER. Die Chemie der Pyrrole. Springer Verlag, New York, Berlin, Heidelberg. 1974. pp. 289–297.
6. P. S. CLEZY, C. J. R. FOOKES, and A. J. LIEPA. Aust. J. Chem. **25**, 1979 (1972).
7. G. H. BARNETT, H. J. ANDERSON, and C. E. LOADER. Can. J. Chem. **58**, 409 (1980).
8. R. L. HINMAN and S. T. THEODOROPULOS. J. Org. Chem. **28**, 352 (1963).
9. J. ELGUERO, R. JAQUIER, and B. SHIMIZU. Bull. Soc. Chim. Fr. 2823 (1969).
10. M. FARNIER and P. FOURNARI. C. R. Acad. Sci. Ser. C, **273**, 919 (1971); Bull. Soc. Chim. Fr. 351 (1973).
11. W. C. FRANK, Y. C. KIM, and R. F. HECK. J. Org. Chem. **43**, 2947 (1978).
12. A. J. CHALK and S. A. MAGENNIS. J. Org. Chem. **41**, 1206 (1976).
13. M. FREIFELDER. Practical catalytic hydrogenation. Wiley–Interscience, New York. 1971. pp. 356–358.
14. P. N. RYLANDER. Catalytic reduction over platinum metals. Academic Press, New York. 1967. pp. 291–303.
15. G. UFER, S. S. TJOA, and S. F. MACDONALD. Can. J. Chem. **56**, 2437 (1978).
16. G. P. ARSENAULT and S. F. MACDONALD. Can. J. Chem. **39**, 2043 (1961).
17. A. H. JACKSON and S. F. MACDONALD. Can. J. Chem. **35**, 715 (1957).
18. W. C. STILL, M. KAHN, and A. MITRA. J. Org. Chem. **43**, 2923 (1978).

Can. J. Chem. Downloaded from www.nrcresearchpress.com by 210.87.254.105 on 09/06/12
For personal use only.

Conductance studies in amide–water mixtures. VI. Nitrates of sodium, potassium, and ammonium in *N,N*-dimethylformamide–water mixtures at 25°C

LAL BAHADUR AND M. V. RAMANAMURTI

Department of Chemistry, Faculty of Science, Banaras Hindu University, Varanasi-221005, India

Received July 14, 1983

LAL BAHADUR and M. V. RAMANAMURTI. Can. J. Chem. **62**, 1051 (1984).

Conductance data for the nitrates of sodium, potassium, and ammonium in *N,N*-dimethylformamide (DMF) – water mixtures ($74.39 \geq D \geq 36.11$) at 25°C are reported for the concentration range 0.0003–0.06 mol dm^{-3}. Also densities, viscosities, and dielectric constants of the solvent mixture (DMF–water) are reported at the same temperature. The data have been analysed by the Fuoss (1978) equation excluding the term α. The existence of a maximum in the viscosity at a 1:3 mol ratio of DMF and water is attributed to the formation of a solvated complex $DMF.3H_2O$. The Walden products for all the three salts pass through a maximum while the equivalent conductances show a minimum with the change of DMF content in the solvent mixtures. In any given solvent mixture, the limiting equivalent conductances show the trend $NaNO_3 < KNO_3 < NH_4NO_3$. The existence of a maximum in Walden product is attributed to the dehydration of ions due to presence of the cosolvent (DMF). For all the three salts, the association constant was negligible ($K_A < 10$) in all the solvent mixtures studied.

LAL BAHADUR et M. V. RAMANAMURTI. Can. J. Chem. **62**, 1051 (1984).

Opérant à 25°C, dans des mélanges de *N,N*-diméthylformamide (DMF) – eau ($74{,}39 \geq D \geq 36{,}11$) et à des concentrations allant de 0,0003 à 0,06 mol dm^{-3}, on a mesuré les conductivités des nitrates de sodium, de potassium et d'ammonium. On rapporte aussi, à la même température, les densités, les viscosités et les constantes diélectriques des mélanges de solvants (DMF–eau). On a analysé les données à l'aide de l'équation de Fuoss (1978) en excluant le terme α. C'est à la formation d'un complexe solvaté $DMF.3H_2O$ qu'on attribue la présence d'un maximum dans la viscosité à un rapport molaire de 1:3 de DMF et d'eau. Les produits de Walden, pour les trois sels, passent par un maximum alors que les conductivités équivalentes présentent un minimum avec une variation de la concentration de DMF dans les mélanges de solvants. Dans chacun des mélanges de solvants, les conductivités limites équivalentes varient dans l'ordre suivant: $NaNO_3 < KNO_3 < NH_4NO_3$. On attribue la présence d'un maximum dans le produit de Walden à la déshydratation des ions due à la présence du cosolvant (DMF). Pour les trois sels, la constante d'association est négligeable ($K_A < 10$) pour tous les mélanges de solvants étudiés.

[Traduit par le journal]

Introduction

In our previous works (1–5) in this series of investigations it has been observed that the conductance behaviour of electrolyte solutions in formamide–water (F–H_2O) mixtures (1, 5) is quite different from that observed in *N,N*-dimethylformamide–water (DMF–H_2O) (2) and *N,N*-dimethylacetamide–water (DMA–H_2O) mixtures (3, 4). For salts studied in DMF–H_2O and DMA–H_2O mixtures, Walden product – solvent composition curves show maxima at nearly the same solvent composition (~10 mol% amide). However, for salts studied in F–H_2O mixtures, entirely different trend in Walden product was observed (5). In F–H_2O mixtures, tetralkylammonium bromides showed maxima in Walden product at ~70 mol% formamide solvent composition while cesium bromide does not show any such maximum and in the case of lithium bromide a minimum in Walden product was observed with the change in solvent composition. Apart from this, some unsatisfactory results were obtained in these investigations regarding the distance parameter R. In some cases, it was found that R does not vary systematically with solvent properties while in other cases, almost constant values of R were obtained (5). These R's are physically meaningless, since they are less than the sum of the crystallographic radii of the constituent ions of the electrolyte.

These observations gave the stimulus to study some more electrolytes in aqueous binary mixtures of amides with particular interest to see the trend in Walden product and distance parameter with the variation of solvent composition. This is, therefore, a continuation of an attempt to generalize or categorize, if possible, the observations and to draw some definite conclusions.

The present paper contains the conductance data for the nitrates of sodium, potassium, and ammonium in DMF–H_2O mixtures at 25°C covering the whole range of solvent composition. Solvent properties like densities, viscosities, and dielectric constants (6) are also reported.

Experimental

Water, potassium chloride, and *N,N*-dimethylformamide were purified as described earlier (2). Potassium nitrate, sodium nitrate, and ammonium nitrates (all A.R., B.D.H.) were recrystallized twice from conductivity water. Samples were dried and stored over phosphorus pentoxide under vacuum.

All the experimental techniques and procedures for the measurements of density and viscosity of the solvent mixtures and conductance of electrolyte solution have been described in detail previously (2). Dielectric constants of the solvent mixtures were taken from the literature (6).

Result and discussion

In Table 1 densities, ρ, viscosities, η, and dielectric constants (6), D, of DMF–H_2O mixtures are reported at 25°C. Equivalent conductance, Λ, of electrolyte solutions as a function of concentration, c, is given in Table 2 for sodium nitrate, potassium nitrate, and ammonium nitrate in DMF–H_2O mixture of different concentrations at 25°C. For a given set of conductance data (c_j, Λ_j; $j = 1, n$), three adjustable parameters Λ_0, K_A, and R were obtained by solving the following equations:

$$[1] \quad \Lambda = \nu[\Lambda_0(1 + RX) + EL]$$

$$[2] \quad \nu = 1 - K_A c \nu^2 f^2$$

$$[3] \quad -\ln f = \beta\kappa/2(1 + \kappa R)$$

Here R is the cosphere diameter (7) and RX and EL are the relaxation and hydrodynamic terms, respectively, derived by

Can. J. Chem. Downloaded from www.nrcresearchpress.com by 210.87.254.5 on 09/06/12
For personal use only.

TABLE 1. Properties of the solvent mixtures (DMF–H_2O) at 25°C

DMF (mol%)	D*	ρ (g/mL)	η (10^{-2} P)
0	78.39	0.99707	0.8903
10	71.24	0.9973	1.7552
30	58.06	0.9923	2.4998
40	53.06	0.9848	2.2548
50	48.89	0.9766	1.8791
70	43.09	0.9631	1.3078
100	36.71	0.9439	0.8020

* Values taken from the literature (9).

Fuoss (8). Other terms have their usual meaning. Although the expressions used here for *RX* and *EL* were the same as those derived by Fuoss (8) in his 1978 version of concentration–conductance equations, the introduction of a new term α, as suggested by Fuoss (8), and consequently the replacements of ν by $[1 - \alpha(1 - \nu)]$ in eq. [1] and K_A by $K_R/(1 - \alpha)$ in eq. [2] have been avoided here as in our previous publications (3–5). The reason for this has already been given (5). The detailed method of analysis of the data has been described elsewhere (3). Various parameters thus derived from the conductance data are summarized in Table 3.

The viscosity of the solvent mixture (DMF–H_2O) increases rapidly with increasing DMF content to a maximum of nearly 2.8 times the viscosity of water and decreases afterwards with slow rate (Fig. 1). The maximum in η corresponds to ~25 mol% DMF, possibly indicating the maximum amount of structuredness in this binary mixture at 1:3 mole ratio of DMF and water, respectively. Assarsson and Eirich (9) have also observed maximum in η at the same composition of various other dialkylamide–water mixtures. In aqueous *N,N*-dimethylformamide of this composition, an extreme of several other properties of solutions has also been reported (10–13). The present observation clearly indicates the strong structure formation between DMF and water molecules, probably through hydrogen bonding, and a maximum in η can be attributed to the formation of the solvated complex DMF.$3H_2O$. These are in agreement with the findings of other workers (6, 9, 12, 14) who have studied the same solvent mixture through other properties. From the curve η vs. solvent composition, it is clear that the effect of the addition of DMF to water is more pronounced than that of the addition of water to DMF as indicated by the rate of change of viscosity. A similar conclusion was drawn by Visser and Somsen (14) on the basis of their study of heat capacities of DMF–water mixtures. Also the comparison of present observation at 25°C with what has already been reported (2) at 35°C indicates that the percentage composition corresponding to maximum viscosity and the nature of the viscosity curve are not affected by the change in temperature from 25 to 35°C.

The variation of limiting equivalent conductance, Λ_0, with the solvent composition for $NaNO_3$, KNO_3, and NH_4NO_3 in DMF–H_2O mixtures at 25°C is represented in Fig. 1. The values of Λ_0 for the three salts in pure water (15, 16) and DMF (16) are taken from the literature. The limiting equivalent conductance decreases with the corresponding increase in viscosity of the solvent mixture, but it is evident that these variations do not compensate each other to give the Walden product a constant value (Fig. 2). As well, the maximum in viscosity does not coincide with the observed minimum in Λ_0 (Fig. 1). This means that the percentage composition of the solvent for maximum η does not agree with the same for minimum conductance. This indicates the simultaneous control of the other factors on Λ_0 along with the hydrodynamic viscous force which in turn affects the speed of ions. It is obvious that the dielectric constant is not involved in affecting the values of Λ_0 since it controls the ionization which is expected to be complete at zero (limiting) concentration. The shift of minimum in Λ_0 towards the richer region in DMF can partially be explained on the basis of ion–solvent interactions. Since water molecules are smaller than DMF molecules, the hydrodynamic entity of an ion solvated with water will be smaller than a DMF-solvated one provided the solvation numbers are almost the same. Consequently, the mobility of solvated ion in DMF-rich region will be smaller than in water-rich region, resulting in further decrease in Λ_0 in DMF-rich region, as observed. This can also be interpreted as a preferential solvation of ions by DMF. The limiting equivalent conductance, Λ_0, varies in the order $NH_4NO_3 > KNO_3 > NaNO_3$ in any given solvent mixture. For the evaluation of ionic conductances, data for limiting transport numbers of the constituent ions of these electrolytes are not available in DMF–water mixtures and the method proposed by Gill (17) also was not found to be satisfactory for the present systems. However, by applying Kohlrausch's law it can safely be concluded that the independent ionic mobilities of the respective cations also change in the same order, viz., $NH_4^+ > K^+ > Na^+$ since the anion (NO_3^-) is the same. Now, the comparison of this trend in mobility with the crystallographic size of ions, which is in the order (18, 19) $NH_4^+ > K^+ > Na^+$, shows that the larger the size of the bare ion, the greater its ionic mobility; this is contrary to expectation. However, it is well known that these ions do not exist as bare ions in solutions but are solvated. The trend of variation of ionic mobilities should, therefore, indicate the relative actual sizes of ions as they exist in solutions concerned. In other words, the sizes of these cations as they exist in solution follow the order $Na^+ > K^+ > NH_4^+$, which should indicate the extent of solvation, i.e., Na^+ is the most solvated and NH_4^+, the least. This can be attributed to the charge density of these cations which varies in the order $Na^+ > K^+ > NH_4^+$ because their size (18, 19) varies in reverse order. Thus the ion having maximum charge density (Na^+) will be the most solvated while the ion having minimum charge density (NH_4^+) will be the least solvated. Similar trend has been reported (20) in other solvents also.

The variation of the Walden product with solvent composition is shown in Fig. 2. It passes through a maximum at nearly 15 mol% DMF and then decreases rapidly with the increase in DMF content in the solvent mixtures. Nearly twofold variation in Walden product was observed. This large variation in Walden product also indicates strong ion–solvent interaction in the system under study as concluded from the shift of minimum in Λ_0 from the point corresponding to maximum η towards the region rich in DMF (Fig. 1).

That the Walden product varies with the composition of mixed polar solvents is now well established. Several significant reasons were suggested for this variation and their mathematical treatments have also been given by different workers (21–33) from time to time especially during the last two decades. A critical assessment of all these various existing theories regarding ion–solvent interactions clearly indicates that even the latest theory fails to predict (or explain) the experimental results satisfactorily though a few "selected" systems apparently seem to respond. In such circumstances, it is, therefore, desirable that before looking for a better theory, all existing theories should be thoroughly tested for a variety of electrolyte

Can. J. Chem. Downloaded from www.nrcresearchpress.com by 210.87.254.5 on 09/06/12
For personal use only.

TABLE 2. Conductance data in DMF–water system at 25°C

Sodium nitrate		Potassium nitrate		Ammonium nitrate	
$c/10^{-4}$ mol dm^{-3}	Λ/S cm^2 mol^{-1}	$c/10^{-4}$ mol dm^{-3}	Λ/S cm^2 mol^{-1}	$c/10^{-4}$ mol dm^{-3}	Λ/S cm^2 mol^{-1}
		10 mol% DMF			
574.343	63.29	536.001	74.62	555.081	72.79
487.322	63.79	477.694	75.04	470.984	73.50
389.071	64.38	381.383	75.58	376.021	74.32
337.102	64.75	331.271	75.79	324.011	74.91
277.264	65.30	271.792	76.31	267.972	75.60
219.113	65.89	271.302	76.82	217.902	76.28
148.903	66.78	145.961	77.50	181.813	76.81
113.701	67.40	103.104	78.28	143.913	77.47
77.433	68.08	66.593	79.05	108.121	78.19
49.023	68.80			78.162	78.92
		30 mol% DMF			
324.015	40.81	320.502	45.36	287.731	44.05
268.935	40.92	278.311	45.55	233.501	44.58
225.003	41.05	225.013	45.82	190.402	45.17
175.301	41.38	188.701	46.08	144.002	45.85
126.812	41.82	146.403	46.41	112.435	46.42
94.091	42.24	108.105	46.81	88.361	46.92
57.762	42.85	71.582	47.26	61.462	47.61
38.445	43.36	43.832	47.76	42.460	48.21
22.842	43.80	27.042	48.11	25.021	48.92
13.991	44.17			15.521	49.49
		40 mol% DMF			
252.802	39.70	210.251	43.60	256.023	42.20
207.511	39.92	176.902	43.89	217.315	42.61
162.903	40.17	139.319	44.23	175.301	43.18
123.721	40.50	112.403	44.61	136.921	43.78
88.362	40.91	81.002	45.10	100.322	44.55
58.992	41.38	52.701	45.67	67.892	45.36
40.463	41.78	32.491	46.24	44.635	46.20
24.402	42.21	19.362	46.71	27.463	46.95
15.211	42.56	9.475	47.22	16.810	47.60
8.413	42.89			8.880	48.25
		50 mol% DMF			
195.502	41.60	191.623	44.69	196.056	44.42
162.413	42.00	161.315	44.99	164.402	44.93
134.600	42.38	133.701	45.28	136.921	45.47
110.315	42.81	104.802	45.63	107.200	46.15
84.262	43.40	76.743	46.08	80.652	46.64
56.601	44.05	51.845	46.54	53.293	47.73
44.962	44.71	34.812	47.02	36.031	48.43
25.010	45.43	21.162	47.56	21.531	49.16
14.902	46.07	10.243	48.27	12.251	49.84
7.509	46.70	4.841	48.90	5.762	50.53
		70 mol% DMF			
121.015	50.01	135.102	50.80	121.004	53.18
100.031	50.62	121.011	51.25	97.231	54.12
80.652	51.33	27.632	52.19	76.032	55.22
40.206	53.38	77.442	53.06	57.153	56.34
26.423	54.40	55.951	54.16	35.760	57.98
17.141	55.23	37.702	55.28	23.235	59.20
9.004	56.26	24.601	56.40	13.103	60.56
4.843	57.00	12.961	57.64	6.763	61.80
—	—	5.475	58.82	3.245	62.62

Can. J. Chem. Downloaded from www.nrcresearchpress.com by 210.87.254.5 on 09/06/12
For personal use only.

TABLE 3. Conductance parameters

DMF (mol%)	D	Λ_0	K_A	$K^*_{A(range)}$	R	$R^*_{(range)}$	$\beta/2$	σ (%)	$\Lambda_0\eta$
				Sodium nitrate					
0	78.39	121.55	—	—	—	—	—	—	1.080
10	71.24	72.18 ± 0.04	0.55	0.30–0.78	4.25	3.54–5.10	3.93	0.036	1.267
30	58.06	45.58 ± 0.05	0.00	0.00–0.50	4.50	4.50–5.54	4.83	0.205	1.139
40	53.06	44.21 ± 0.02	0.30	0.00–0.77	6.81	6.17–8.00	5.28	0.071	0.997
50	48.89	48.27 ± 0.03	1.35	0.34–2.80	3.80	2.95–5.21	5.73	0.100	0.907
70	43.09	59.02 ± 0.01	5.90	5.50–7.10	4.84	7.70–5.89	6.50	0.037	0.772
100	36.71	87.20	—	—	—	—	—	—	0.699
				Potassium nitrate					
0	78.39	145.11	—	—	—	—	—	—	1.292
10	71.24	82.83 ± 0.11	0.39	0.00–0.64	5.70	4.07–7.17	3.93	0.081	1.452
30	58.06	50.08 ± 0.04	0.87	0.70–1.08	8.50	7.64–9.54	4.83	0.055	1.253
40	53.06	48.68 ± 0.03	1.70	1.20–2.14	7.61	6.41–8.92	5.28	0.056	1.098
50	48.89	50.05 ± 0.02	0.00	0.00–1.24	5.79	5.75–7.90	5.73	0.109	0.940
70	43.09	61.02 ± 0.02	11.40	11.05–11.70	9.52	8.80–10.16	6.50	0.035	0.798
100	36.71	88.10	—	—	—	—	—	—	0.701
				Ammonium nitrate					
0	78.39	144.89	—	—	—	—	—	—	1.290
10	71.24	83.55 ± 0.05	1.50	1.38–1.60	5.86	5.20–6.40	3.93	0.027	1.466
30	58.06	51.24 ± 0.02	2.20	1.54–2.90	3.16	2.46–4.23	4.83	0.067	1.281
40	53.06	49.69 ± 0.01	2.65	1.50–3.78	3.15	2.25–4.59	5.28	0.137	1.120
50	48.89	52.02 ± 0.02	4.80	0.00–5.80	6.39	1.95–8.44	5.73	0.117	0.977
70	43.09	64.39 ± 0.02	10.50	8.20–12.60	4.22	2.88–6.00	6.50	0.091	0.842
100	36.71	96.00	—	—	—	—	—	—	0.764

*$X_{(range)}$ (X being K_A or R) corresponds to $\sigma \leq 1.1\sigma_{min}$ and other values correspond to $\sigma = \sigma_{min}$.

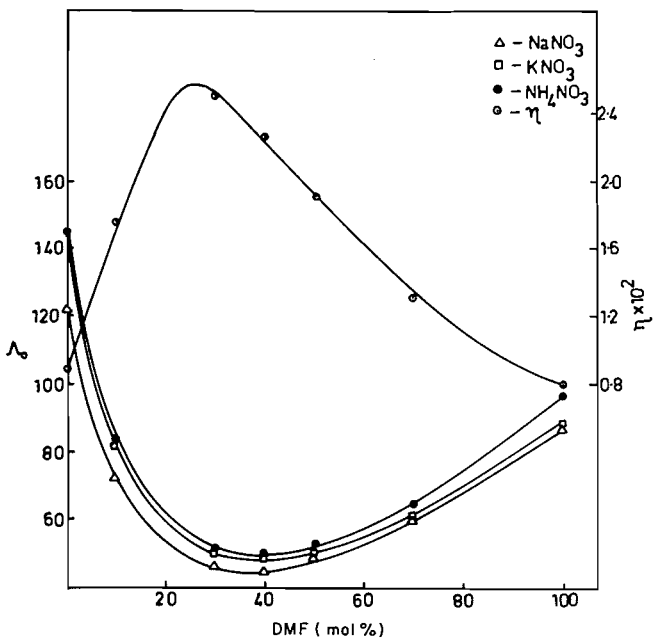

FIG. 1. Variation of viscosity of the solvent, η, and limiting equivalent conductance, Λ_0, with composition of the solvent mixtures.

solutions. We then assess to see if we can find the one theory closest to experimental results for most of the systems so far studied. Then and only then attempts should be made to improve that theory as far as possible. This will be the main object of our future publication and it is the reason for our not testing any one of the existing theories, say even the latest one, here for the limited systems presented in this paper.

Because of reasons mentioned above, it seems difficult at this stage to compare theoretically predicted values of mobility of ions, and in turn Walden product, $\Lambda_0\eta$, with that obtained experimentally. Some plausible interpretations can be given for the qualitative variation of Walden product with solvent composition for the systems in the present work. From Fig. 2 it is clear that the maximum in Walden product is obtained in all the three salts and the height of the maximum from the point corresponding to pure water as solvent is not the same for different salts. But this height shows a trend $NH_4NO_3 \approx KNO_3 < NaNO_3$. If we consider the Λ_0 values in water as the measure of structure breaking effect of the ions, we find the order for cations (anion, NO_3^-, being the same) $NH_4^+ \approx K^+ > Na^+$. If the excess mobility (i.e., maximum in Walden product) is due to a structure-breaking effect of the ions, the magnitude of this effect (i.e., the height of maximum from the point corresponding to pure water as solvent) should follow the order $NH_4^+ \approx K^+ > Na^+$, which is the reverse of the order observed (Fig. 2). Thus the existence and the magnitude of the excess mobility can not be simultaneously explained on the basis of structure-breaking effect of ions. Alternatively, both can be explained on the basis of dehydration of ions due to cosolvent (DMF). Let us consider first the electrolyte in water and then the addition of DMF. The presence of DMF molecules may cause the dehydration of ions giving excess mobility of ions producing a maximum in Walden product in the water-rich region. Moreover, ions may also be solvated with the second component (DMF) of the solvent mixture. This effect will increase with increasing DMF content in the solvent mixture. Thus dehydration of ions will be more effective in the water-rich region giving excess mobility of ions while the solvation of ions with DMF molecules will be more effective in the DMF-rich region, resulting in further decrease of Walden product. This explains the variation of Walden product with solvent composition. Since the maximum in Walden product exists due to dehydration of ions, the height of maximum, therefore, will depend

Can. J. Chem. Downloaded from www.nrcresearchpress.com by 210.87.254.5 on 09/06/12
For personal use only.

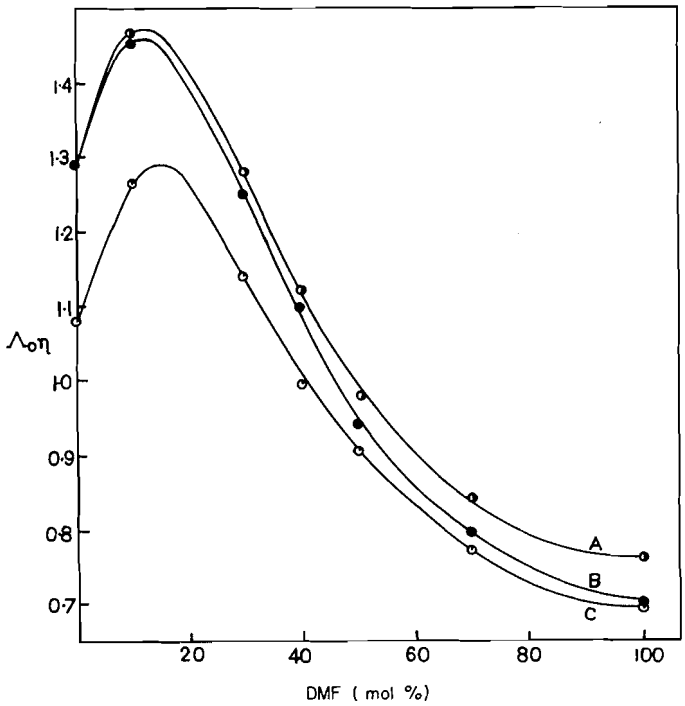

FIG. 2. Variation of Walden product with composition of the solvent mixtures. *A*, NH_4NO_3; *B*, KNO_3; *C*, $NaNO_3$.

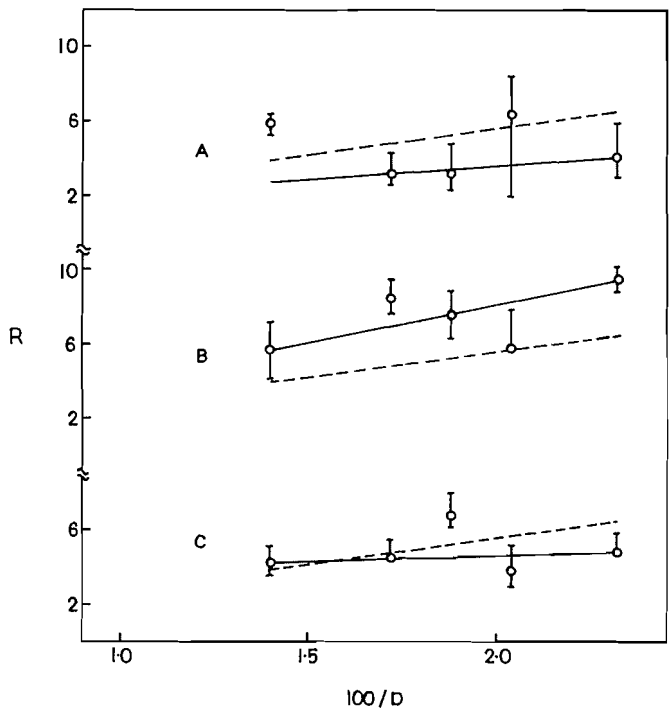

FIG. 3. Variation of pairing radius *R* with reciprocal of the dielectric constant of the solvent mixtures. *A*, NH_4NO_3; *B*, KNO_3; *C*, $NaNO_3$. Dotted line represents $\beta/2$.

upon the extent of dehydration of ions. Now dehydration will be more effective in case of more hydrated ion. Hydration of cations (anion being the same) follows the order $NH_4^+ \approx K^+ < Na^+$ (on the basis of Λ_0 values in water), so the order of dehydration and consequently the order of the height of maximum in Walden product should be the same, as was observed. A similar idea was successfully applied in other electrolytes also (2). Kay and co-workers (34, 35) also explained the existence of similar maxima in Walden product for different electrolytes in other aqueous binary mixtures on the basis of similar mechanism while they proposed salting-out effect in their recent work (36).

Association constants for all the systems are practically negligible (i.e., $K_A < 10$). So the numerical values of K_A should not be taken seriously. One can only conclude that all three electrolytes exist as free ions in the solvent mixtures. This is expected also because dielectric constants of solvent mixtures are fairly high ($36.7 \leq D \leq 78.39$). It is a general practice that $K_A < 10$ is neglected. However, recently Fuoss and co-workers (37) attempted to find the physical significance, rather than the mathematical parameter only, of an association constant even if it was less than 10. They were not able to arrive at any useful conclusion. Variation of the pairing radius *R* with reciprocal of the dielectric constant of the solvent mixture is shown in Fig. 3 for different salts. The dotted line shows the variation of Bjerrum radius ($\beta/2$). Perpendicular lines in this plot show the limits of *R* values corresponding to $\sigma \leq 1.1\sigma_{min}$ and circles correspond to best values (i.e., $\sigma = \sigma_{min}$). An attempt has been made to draw the best possible curves shown by solid lines to show the variation of *R* with $1/D$. However, due to the wider ranges of acceptable *R* values (which reproduce data within $1.1\sigma_{min}$) these lines should not be taken too seriously. Consequently, it is difficult to draw any definite conclusion.

Thus, on the basis of our present as well as previous works (2–4) it can be concluded here that the Walden product for different salts studied in aqueous binary mixtures of DMA and DMF varies systematically with solvent composition, showing a maximum corresponding to the solvent mixture containing 10–15 mol% amide, unlike the behaviour observed in F–H_2O mixture (5) where no similar trend was observed with different electrolytes. Thus, it will require further extensive study to arrive at any general conclusion about the conductance behaviour of various electrolytes in aqueous binary mixtures of different amides (non, mono, and dialkylated). Some more systems are under study and results will appear in future papers.

Acknowledgements

We thank Professor R. M. Fuoss for invaluable help in making his computer programs available, the Head of the Department of Chemistry, Banaras Hindu University, for providing the necessary facilities, and C.S.I.R., Government of India, for granting a Junior Research Fellowship to one of the authors (L.B.).

1. M. V. RAMANAMURTI and L. BAHADUR. Indian J. Chem. **14A**, 1015 (1976).
2. D. SINGH, L. BAHADUR, and M. V. RAMANAMURTI. J. Solution Chem. **6**, 703 (1977).
3. M. V. RAMANAMURTI and L. BAHADUR. Electrochim. Acta, **25**, 601 (1980).
4. L. BAHADUR and M. V. RAMANAMURTI. J. Chem. Soc. Faraday Trans. I, **76**, 1409 (1980).
5. L. BAHADUR and M. V. RAMANAMURTI. J. Electrochem. Soc. **128**(2), 339 (1981).
6. P. ROHDEWALD and M. MÖLDNER. J. Phys. Chem. **77**, 373 (1973).
7. (*a*) R. M. FUOSS. J. Phys. Chem. **79**, 525 (1975); (*b*) C. F. MATTINA and R. M. FUOSS. J. Phys. Chem. **79**, 1604 (1975).
8. R. M. FUOSS. Proc. Natl. Acad. Sci. USA, **75**, 16 (1978); J. Phys. Chem. **82**, 2427 (1978).
9. P. ASSARSSON and F. R. EIRICH. J. Phys. Chem. **72**, 2710 (1968).

Can. J. Chem. Downloaded from www.nrcresearchpress.com by 210.87.254.5 on 09/06/12
For personal use only.

10. T. ONCESCU and E. JURCONI. Ev. Roum. Chim. **16**, 1033 (1971).
11. Z. KOZLOWSKY. Soc. Sci. Lods. Acta Chim. **16**, 17 (1971).
12. S. SAPHON and H. J. BITTRICH. Z. Phys. Chem. Leipzig. **252**, 113 (1973).
13. C. DE VISSER and G. SOMSEN. J. Solution Chem. **3**, 847 (1974); J. Phys. Chem. **78**, 1719 (1974).
14. C. DE VISSER and G. SOMSEN. Z. Phys. Chem. N.F; **92**, 159 (1974).
15. B. E. CONWAY. Electrochemical data. Elsevier Publishing Co., New York. 1952.
16. J. E. PRUE and P. J. SHERRINGTON. Trans. Faraday Soc. **57**, 1795 (1961).
17. D. S. GILL. J. Chem. Soc. Faraday Trans. I, **77**, 751 (1981).
18. R. A. ROBINSON and R. H. STOKES. Electrolyte solutions. Butterworth's Scientific Publishers, London. 1959.
19. L. PAULING. The nature of the chemical bond. 3rd ed. Cornell University Press, Ithaca. 1960.
20. (*a*) P. H. TEWARI and G. P. JOHARI. J. Phys. Chem. **65**, 512 (1963); (*b*) R. C. PAUL, J. P. SINGLA, D. S. GILL, and S. P. NARULA. Indian J. Chem. **9**, 981 (1971); (*c*) ref. 18, p. 331.
21. R. M. FUOSS. Proc. Natl. Acad. Sci. USA, **45**, 807 (1959).
22. R. H. BOYD. J. Chem. Phys. **35**, 1281 (1961); **39**, 2376 (1963).
23. R. ZWANZIG. J. Chem. Phys. **38**, 1603 (1963).
24. D. F. T. TUAN and R. M. FUOSS. J. Phys. Chem. **67**, 1343 (1963).
25. A. D'APRANO and R. M. FUOSS. J. Phys. Chem. **67**, 1704 (1963); **67**, 1722 (1963).
26. R. ZWANZIG. J. Chem. Phys. **52**, 3625 (1970).
27. P. HEMMES. J. Phys. Chem. **78**, 907 (1974).
28. A. D'APRANO and R. M. FUOSS. J. Solution Chem. **4**, 175 (1975).
29. (*a*) J. HUBBARD and L. ONSAGER. J. Chem. Phys. **67**, 4850 (1977); (*b*) J. B. HUBBARD. J. Chem. Phys. **68**, 1649 (1978).
30. P. G. WOLYNES. J. Chem. Phys. **68**, 473 (1978).
31. D. F. EVANS, T. TOMINAGA, J. B. HUBBARD, and P. G. WOLYNES. J. Phys. Chem. **83**, 2669 (1979).
32. J. H. CHEN and S. A. ADELMAN. J. Chem. Phys. **72**, 2819 (1980).
33. J. B. HUBBARD and R. F. KAYSER. J. Chem. Phys. **74**, 3535 (1981).
34. T. L. BROADWATER and R. L. KAY. J. Phys. Chem. **74**, 3802 (1970).
35. R. L. KAY and T. L. BROADWATER. Electrochim. Acta, **16**, 664 (1971).
36. R. L. KAY and T. L. BROADWATER. J. Solution Chem. **5**, 57 (1976).
37. A. D'APRANO, J. KOMIYAMA, and R. M. FUOSS. J. Solution Chem. **5**, 279 (1976).

Can. J. Chem. Downloaded from www.nrcresearchpress.com by 210.87.254.5 on 09/06/12
For personal use only.

Rhodium(I) complexes containing bidentate pyrazolylgallate ligands. X-ray crystal structures of $[Me_2Gapz_2]Rh(COD)$, $[Rh(\mu\text{-}3,5\text{-}Me_2pz)(CO)_2]_2$, and $[Rh(\mu\text{-}3,5\text{-}Me_2pz)(COD)]_2$

BRENDA M. LOUIE, STEVEN J. RETTIG, ALAN STORR, AND JAMES TROTTER

Department of Chemistry, University of British Columbia, 2036 Main Mall, Vancouver, B.C., Canada V6T 1Y6

Received October 19, 1983

BRENDA M. LOUIE, STEVEN J. RETTIG, ALAN STORR, and JAMES TROTTER. Can. J. Chem. **62**, 1057 (1984).

The synthesis and characterization of the complexes $[Me_2Gapz_2]Rh(LL)$ (where LL = COD, $(CO)_2$, $(PPh_3)_2$, or $(PPh_3)(CO)$), incorporating the bidentate, chelating, dimethylbis(1-pyrazolyl)gallate ligand are described. Non-rigidity in solution has been demonstrated by ^1H nmr studies for some of the complexes. A crystal structure determination of the COD complex has confirmed the boat conformation for the Ga—(N—N)$_2$—Rh six-membered ring in this complex in the solid state. In addition, the solid state structures of the 3,5-dimethylpyrazolyl bridged dirhodium complexes $[Rh(\mu\text{-}3,5\text{-}Me_2pz)(CO)_2]_2$ and $[Rh(\mu\text{-}3,5\text{-}Me_2pz)(COD)]_2$ have been determined. Crystals of $[Me_2Gapz_2]Rh(COD)$ are orthorhombic, a = 22.7447(8), b = 11.9776(5), c = 6.4635(3) Å, Z = 4, space group *Pnma*; those of $[Rh(\mu\text{-}3,5\text{-}Me_2pz)(CO)_2]_2$ are monoclinic, a = 8.7403(6), b = 16.3594(6), c = 25.434(2) Å, β = 95.286(3)°, Z = 8, space group $P2_1/c$; and those of $[Rh(\mu\text{-}3,5\text{-}Me_2pz)(COD)]_2$ are triclinic, a = 10.350(2), b = 11.401(2), c = 12.355(2) Å, α = 112.485(7), β = 99.394(9), γ = 105.387(8)°, Z = 2, space group $P\bar{1}$. All three structures were solved by conventional heavy atom techniques and were refined by full-matrix least-squares procedures to final conventional R values of 0.026, 0.024, and 0.037 for 1824, 5135, and 6109 reflections with $I \geq 3\sigma(I)$, respectively. In each case the Rh atoms have distorted square planar coordination geometry. Important mean structural parameters are Rh—N = 2.087(2), Rh—C = 2.129(2), Rh···Ga = 3.5527(5) Å for $[Me_2Gapz_2]Rh(COD)$; Rh—N = 2.063(6), Rh—CO = 1.852(9), Rh···Rh = 3.262(4) Å for $[Rh(\mu\text{-}3,5\text{-}Me_2pz)(CO)_2]_2$; and Rh—N = 2.084(1), Rh—C = 2.131(7), Rh···Rh = 3.1538(3) Å for $[Rh(\mu\text{-}3,5\text{-}Me_2pz)(COD)]_2$.

BRENDA M. LOUIE, STEVEN J. RETTIG, ALAN STORR et JAMES TROTTER. Can. J. Chem. **62**, 1057 (1984).

On décrit la synthèse et la caractérisation de complexes $[Me_2Gapz_2]Rh(LL)$ (où LL = COD, $(CO)_2$, $(PPh_3)_2$ ou (PPh_3) (CO)) incorporant le ligand chélatant bidenté diméthylbis(pyrazolyl-1) gallate. Pour certain de ces complexes, on a démontré l'absence de rigidité en solution grâce à des études de rmn du ^1H. Une détermination de la structure du cristal du complexe avec le COD confirme la conformation bateau, à l'état solide, du cycle à 6 chaînons Ga—(N—N)$_2$—Rh de ce complexe. De plus, on a déterminé les structures, à l'état solide, des complexes pontés du diméthyl-3,5 pyrazolyl dirhodium, $[Rh(\mu\text{-}Me_2\text{-}3,5pz)(CO)_2]_2$ et $[Rh(\mu\text{-}Me_2\text{-}3,5\ pz)(COD)]_2$. Les cristaux du $[Me_2Gapz_2]Rh(COD)$ sont orthorhombiques et appartiennent au groupe d'espace *Pnma* avec a = 22,7447(8), b = 11,9776(5), c = 6,4635(3) Å, Z = 4. Ceux de $[Rh(\mu\text{-}Me_2\text{-}3,5\ pz)(CO)_2]_2$ sont monocliniques avec a = 8,7403(6), b = 16,3594(6), c = 25,434(2) Å, β = 95,286(3)°, Z = 8 et groupe d'espace $P2_1/c$; et ceux de $[Rh(\mu\text{-}Me_2\text{-}3,5\ pz)(COD)]_2$ sont tricliniques, groupe d'espace $P\bar{1}$, avec a = 10,350(2), b = 11,401(2), c = 12,355(2) Å, α = 112,484(7), β = 99,394(9), γ = 105,387(8)° et Z = 2. On a résolu les trois structures par les techniques conventionnelles des atomes lourds et on les a affinées par la méthode des moindres carrés (matrice entière) jusqu'à des valeurs finales de R = 0,026, 0,024 et 0,037 pour respectivement 1824, 5135 et 6109 réflexions avec $I \geq 3\sigma(I)$. Dans chaque cas, les atomes de Rh ont une géométrie de coordination plan carré déformée. Les paramètres structuraux moyens importants sont: Rh—N = 2,087(2), Rh—C = 2,129(2), Rh···Ga = 3,5527(5) Å pour le $[Me_2Gapz_2]Rh(COD)$; Rh—N = 2,063(6), Rh—CO = 1,852(9), Rh···Rh = 3,262(4) Å pour le $[Rh(\mu\text{-}Me_2\text{-}3,5\ pz)(CO)_2]_2$; et Rh—N = 2,084(1), Rh—C = 2,131(7), Rh···Rh = 3,1538(3) Å pour le $[Rh(\mu\text{-}Me_2\text{-}3,5\ pz)(COD)]_2$.

[Traduit par le journal]

Introduction

As part of an ongoing study of pyrazolylgallate ligands our attention has recently focussed on the reactivity of the bidentate ligands, $[Me_2Gapz_2]^-$ and $[Me_2Ga(3,5\text{-}Me_2pz)_2]^-$ (where pz = pyrazolyl, $N_2C_3H_3$, and 3,5-Me_2pz = 3,5-dimethylpyrazolyl, $N_2C_5H_7$) (1–6), towards selected Rh(I) complexes. The new compounds $[Me_2Gapz_2]Rh(CO)_2$, $[Me_2Gapz_2]Rh(CO)(PPh_3)$, $[Me_2Gapz_2]Rh(PPh_3)_2$, and $[Me_2Gapz_2]Rh(COD)$ (COD = 1,5-cyclooctadiene) have been synthesized and shown to be non-rigid in solution by variable temperature ^1H nmr studies. Attempts to prepare analogous complexes using the $[Me_2Ga(3,5\text{-}Me_2pz)_2]^-$ ligand resulted only in the isolation of the bridged dimeric species $[Rh(\mu\text{-}3,5\text{-}Me_2pz)(CO)_2]_2$ and $[Rh(\mu\text{-}3,5\text{-}Me_2pz)(COD)]_2$. X-ray crystallographic analyses of the latter two complexes and that of the $[Me_2Gapz_2]Rh(COD)$ compound are reported.

Experimental

Starting materials

Air-sensitive materials were handled in oxygen-free dry nitrogen. Tetrahydrofuran (THF) was dried by refluxing over sodium/benzophenone and used immediately following distillation. Benzene was dried by refluxing over molten potassium followed by distillation and methylene chloride by refluxing over P_2O_5 prior to distillation. $[Rh(CO)_2Cl]_2$ (Strem Chemicals) was sublimed *in vacuo* before use. $[Rh(COD)Cl]_2$ (Strem Chemicals), $Rh(PPh_3)_3Cl$ (Strem Chemicals), and PPh_3 (MCB) were used as supplied. The sodium salts of the two gallium ligands, $[Me_2Gapz_2]^-$ and $[Me_2Ga(3,5\text{-}Me_2pz)_2]^-$, were prepared as THF solutions as described earlier (1).

Preparation of $[Me_2Gapz_2]Rh(CO)_2$

Two molar equivalents of $Na^+[Me_2Gapz_2]^-$ in THF were added dropwise to a stirred solution of $[Rh(CO)_2Cl]_2$ (0.330 g, 0.849 mmol) in 75 mL THF held at 0°C. The resulting mixture was allowed to warm to room temperature and then stirred overnight. The mixture was filtered and solvent removed *in vacuo* from the orange filtrate to leave an orange oil. Attempted crystallization of this product from methylene chloride and/or benzene resulted only in the recovery of the orange oil which darkened if exposed to air. ^1H nmr and ir data for the complex are reported in Table 1. The mass spectrum (Varian MAT CH4B spectrometer 70 eV, probe at room temperature) of the compound showed a weak signal due to the parent ion, P^+ (1%), with the strongest signals corresponding to the P − Me^+ (100%) ion followed

Can. J. Chem. Downloaded from www.nrcresearchpress.com by 210.87.254.42 on 09/06/12
For personal use only.

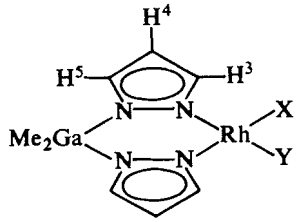

TABLE 1. Physical data for the complexes Me_2Ga

X	Y	Analysis (%) found (calcd.) C	H	N	^{1}H nmr τ(ppm)* GaMe	H^3	H^4	H^5	Other	ν_{CO} (cm^{-1}) Cyclohexane	Nujol
CO	CO				9.73s	2.68d	4.01t	2.71d		2088	2085
										2020	2018
CO	PPh_3	51.27	4.34	9.10	9.53s	2.16d	3.88t	†	2.51m, 2.99m	1995	1993
		(51.72	4.31	8.94)		†	4.32t	†	(PPh_3)		
PPh_3	PPh_3	61.00	4.93	6.28	8.75s, br	2.56d	4.40t	2.95d	2.31m, 3.15m	—	—
		(61.35	4.91	6.50)	9.73s, br				(PPh_3)		
COD		43.11	5.39	12.51	9.50s	2.56d	3.96t	2.72d	6.07s, br; 7.73m	—	—
		(43.18	5.40	12.59)					8.48m (COD)		

*τ values refer to $\tau_{C_6H_6}$ = 2.84 ppm.

† Obscured by PPh_3 multiplets. s = singlet, d = doublet, t = triplet, m = multiplet. $J_{HCCH} \simeq 2$ Hz for pz protons. Assignment of pzH^3 and pzH^5 follows from assignment of other pyrazolyl complexes (7, 8).

by signals corresponding to ions resulting from successive loss of CO ligands viz P − Me − CO^+ (50%) and P − Me − $2CO^+$ (53%).

Preparation of [Me_2Gapz_2]Rh(CO)PPh_3

PPh_3 (0.175 g, 0.668 mmol) dissolved in 25 mL benzene was added to [Me_2Gapz_2]$Rh(CO)_2$ (0.25 g, 0.636 mmol) in 25 mL of the same solvent at room temperature. The color of the solution lightened from deep orange to orange–yellow with rapid evolution of CO. After stirring the reaction mixture for 5 min the solvent was removed *in vacuo* to yield the product as an orange–yellow powder in 90% yield, mp 130–131°C. Table 1 collects selected physical data. The mass spectrum (AEI MS50 spectrometer 70 eV, probe temperature 170°C) again displayed a weak signal due to the parent ion P^+ (1%) with stronger signals arising from P − Me^+ (40%), P − Me − CO^+ (33%), and PPh_3^+ (100%).

Preparation of [Me_2Gapz_2]Rh(PPh_3)$_2$

$Rh(PPh_3)_3Cl$ (0.379 g, 0.410 mmol) was stirred in 75 mL C_6H_6 and an equimolar amount of $Na^+[Me_2Gapz_2]^-$ ligand in 10 mL THF added. The reaction mixture was stirred for 3 days at room temperature and then filtered. Evaporation of the solvents from the filtrate left a yellow–orange powder. Free PPh_3 was sublimed from this material under vacuum at 70°C to leave the desired product in 93% yield, mp 127–129°C. Elemental analysis figures and selected ^{1}H nmr data are recorded in Table 1. The mass spectrum (AEI MS50 spectrometer, 70 eV, probe temperature 150°C) contained signals corresponding to the parent ion, P^+ (4%), P − Me^+ (1%), P − Me − PPh_3^+ (17%), and PPh_3^+ (100%).

Preparation of [Me_2Gapz_2]Rh(COD)

Two molar equivalents of $Na^+[Me_2Gapz_2]^-$ in THF were added to $[Rh(COD)Cl]_2$ (0.314 g, 0.637 mmol) in THF at 0°C. The reaction mixture was allowed to warm to room temperature and then stirred for approximately 6 h. The solvent was then removed *in vacuo* and the remaining yellow–orange residue extracted in a minimum amount of benzene and filtered. Slow evaporation of the benzene gave initially orange crystals of the dimer $[Rh(\mu\text{-pz})(COD)]_2$. The lemon yellow solution remaining, on further concentration, produced yellow crystals of the desired product in 40% yield, mp 105–106°C (the residue obtained on complete evaporation of the benzene solvent was shown to be primarily the dimer $[Me_2Ga(\mu\text{-pz})]_2$). The mass spectrum (Varian MAT CH4B spectrometer, 70 eV, probe temperature 80°C) of the desired product showed the presence of the parent ion P^+ (11%) with the strongest signal arising from the P − Me^+ ion (100%). Elemental analyses and ^{1}H nmr data for the complex are reported in Table 1.

Spectra

Infrared spectra were recorded on a Perkin-Elmer 598 spectrometer and ^{1}H nmr spectra on a Bruker WP-80 or Varian XL-100 instrument using FT techniques.

X-ray crystallographic analyses

[Dimethylbis(1-pyrazolyl)gallato-N^2,$N^{2'}$](1,5-cyclooctadiene)-rhodium(I)

A crystal bounded by the 10 faces (followed by their distances in mm from a common origin): (2 − 1 0), 0.138, (−1 1 2), 0.175, ±(1 0 0), 0.188, ±(1 0 −2), 0.200, ±(1 1 0), 0.150, (−3 2 0), 0.138, (−1 −1 −1), 0.163 was mounted in a general orientation. Unit-cell parameters were refined by least-squares on 2 sin θ/λ values for 25 reflections (2θ = 40–49°) measured on a diffractometer with Mo-Kα radiation (λ($K\alpha_1$) = 0.70930, λ($K\alpha_2$) = 0.71073 Å). Crystal data at 22°C are as follows:

$C_{16}H_{24}GaN_4Rh$ fw = 445.02

Orthorhombic, a = 22.7447(8), b = 11.9776(5), c = 6.4635(3) Å, V = 1760.8(1) Å^3, Z = 4, ρ_c = 1.679 g cm^{-3}, F(000) = 896, μ(Mo-Kα) = 24.5 cm^{-1}. Absent reflections: 0kl, $k + l$ odd, and hk0, h odd, space group *Pnma* (D_{2h}^{16}, No. 62) from structure analysis.

Intensities were measured with graphite-monochromatized Mo-Kα radiation on an Enraf-Nonius CAD4-F diffractometer. An ω-2θ scan at 1.34–10.06° min^{-1} over a range of (0.65 + 0.35 tan θ) degrees in ω (extended by 25% on both sides for background measurement) was employed. Data were measured to 2θ = 60°. The intensities of three check reflections, measured every 3600 s throughout the data collection, showed only minor random fluctuations. After data reduction,[1] an absorption correction was applied using the Gaussian integration method (9, 10). Transmission factors ranged from 0.430 to 0.558 for 128 integration points. Of the 2660 independent reflections measured, 1824 (68.6%) had intensities greater than 3σ(I) above back-

[1] The computer programs used include locally written programs for data processing and locally modified versions of the following: ORFLS, full-matrix least-squares, and ORFFE, function and errors, by W. R. Busing, K. O. Martin and H. A. Levy; FORDAP, Patterson and Fourier syntheses, by A. Zalkin; ORTEP II, illustrations, by C. K. Johnson.

Can. J. Chem. Downloaded from www.nrcresearchpress.com by 210.87.254.42 on 09/06/12
For personal use only.

Can. J. Chem. Downloaded from www.nrcresearchpress.com by 210.87.254.42 on 09/06/12
For personal use only.

ground where $\sigma^2(I) = S + 2B + (0.04(S - B))^2$ with S = scan count and B = normalized background count.

The centrosymmetric space group *Pnma* was indicated by both the Patterson function and the *E*-statistics. The coordinates of the heavy atoms were determined from the Patterson function and those of the remaining non-hydrogen atoms from a subsequent difference map. After full-matrix least-squares refinement of the non-hydrogen atoms with anisotropic thermal parameters to $R = 0.036$, a difference map revealed the positions of all 13 unique hydrogen atoms. The methyl and methylene hydrogen atoms were found not to refine satisfactorily and were fixed in idealized positions (C—H = 0.98 Å, recalculated after each least-squares cycle) in the final stages of refinement. The remaining H atoms were refined with isotropic thermal parameters. The scattering factors of ref. 11 were used for non-hydrogen atoms and those of ref. 12 for hydrogen atoms. Anomalous scattering factors from ref. 13 were used for the Rh and Ga atoms. The weighting scheme, $w = 1/\sigma^2(F)$ where $\sigma^2(F)$ is derived from the previously defined $\sigma^2(I)$, gave uniform average values of $w(|F_o| - |F_c|)^2$ over ranges of both $|F_o|$ and $\sin\theta/\lambda$ and was employed in the final stages of refinement. Unobserved reflections were not included in the refinement. Convergence was reached at $R = 0.026$ and $R_w = 0.034$ for 1824 reflections with $I \geq 3\sigma(I)$. For all 2660 reflections $R = 0.055$. The function minimized was $\Sigma w(|F_o| - |F_c|)^2$, $R = \Sigma||F_o| - |F_c||/\Sigma|F_o|$ and $R_w = (\Sigma w(|F_o| - |F_c|)^2/\Sigma w|F_o|^2)^{1/2}$.

On the final cycle of refinement the mean and maximum parameter shifts corresponded to 0.006 and 0.045σ, respectively. The mean error in an observation of unit weight was 1.441. A final difference map showed a maximum fluctuation of +0.50 e Å^{-3} in the vicinity of C(3). The final positional and thermal parameters appear in Tables 2 and 7,[2] respectively. Measured and calculated structure factors have been placed in the Depository of Unpublished Data.[2]

Bis(μ-3,5-dimethylpyrazolyl-N,N')-bis[dicarbonylrhodium(I)]

Experimental details are as above except where noted. The six bounding faces of the crystal used for data collection were (0 −1 1), 0.144, ±(1 0 0), 0.150, (0 1 −3), 0.144, ±(0 1 1), 0.100 mm. Crystal data are as follows:

$C_{14}H_{14}N_4O_4Rh_2$ fw = 508.10

Monoclinic, a = 8.7403(6), b = 16.3594(6), c = 25.434(2) Å, β = 95.286(3)°, V = 3621.2(4) Å^3, Z = 8, ρ_c = 1.864 g cm^{-3}, $F(000)$ = 1984, μ(Mo-Kα) = 18.2 cm^{-1}. Absent reflections: $0k0$, k odd, and $h0l$, l odd, uniquely indicate the space group $P2_1/c$ (C_{2h}^5, No. 14).

An ω−2θ scan at 0.87−10.06° min^{-1} over a range of (0.50 + 0.35 tan θ)° in ω was employed. Of the 8281 independent reflections measured, 5135 had intensities greater than $3\sigma(I)$ above background and were employed in the solution and refinement of the structure. Transmission factors ranged from 0.607 to 0.727 for 108 sampling points.

The coordinates of the four independent Rh atoms were determined from the Patterson function and those of the remaining non-hydrogen atoms from a subsequent difference map. After full-matrix least-squares refinement of the non-hydrogen atoms to $R = 0.038$, a difference map gave the positions of all H atoms, which were placed in idealized locations and included as fixed atoms in subsequent calculations. An isotropic type I extinction correction (Thornley−Nelmes definition of mosaic anisotropy with a Lorentzian distribution) was applied (14−16). The final value of g was 7.8(3) × 10^4. Convergence was reached at $R = 0.024$ and $R_w = 0.030$ for 5135 observed reflections, for all 8281 reflections, $R = 0.065$. The mean and maximum parameter shifts on the final cycle of refinement corresponded to 0.08 and 0.44σ respectively, and the mean error in an observation of unit weight was 1.475. The largest peak on the final difference map corresponded to 0.40 e Å^{-3}.

Bis(μ-3,5-dimethylpyrazolyl-N,N')-bis[(1,5-cyclooctadiene)-rhodium(I)]

The eight bounding faces of the crystal used for data collection were: ±(1 −1 0), 0.109, ±(1 0 −1), 0.121, ±(0 1 −1), 0.071, ±(3 2 6), 0.175 mm. Crystal data are as follows:

$C_{26}H_{38}N_4Rh_2$ fw = 612.42

Triclinic, a = 10.350(2), b = 11.401(2), c = 12.355(2) Å, α = 112.485(7), β = 99.394(9), γ = 105.387(8)°, V = 1240.2(3) Å^3, Z = 2, ρ_c = 1.640 g cm^{-3}, $F(000)$ = 624, μ(Mo-Kα) = 13.3 cm^{-1}. Absent reflections: none, space group $P\bar{1}$ (C_i^1, No. 2, reduced cell) from structure analysis.

An ω−2θ scan at 1.26−10.06° min^{-1} in ω was employed. Of the 8919 independent reflections measured (to 2θ = 60°), 6109 had intensities greater than $3\sigma(I)$. Transmission factors ranged from 0.744 to 0.840 for 96 sampling points.

The centrosymmetric space group $P\bar{1}$ was indicated both by the *E*-statistics and by the Patterson function, from which the heavy atom coordinates were determined. The C and N coordinates were determined from a subsequent difference map. After refinement of all non-hydrogen atoms with anisotropic thermal parameters to R = 0.043, a difference map revealed the positions of all H atoms. As in the case of [Me_2Gapz_2]Rh(COD), the COD methylene H atoms did not refine well and were included as fixed atoms in idealized positions, the remaining H atoms being refined with isotropic thermal parameters. The structure was refined to $R = 0.037$ and $R_w = 0.045$ for 6109 observed reflections, for all 8919 reflections $R = 0.065$. The mean and maximum parameter shifts on the final cycle of refinement corresponded to 0.04 and 0.78σ (the latter for a hydrogen coordinate) respectively, and the mean error in an observation of unit weight was 1.918. A final difference map showed maximum fluctuations of ±1.2 e Å^{-3} near the Rh atoms and ±0.40 e Å^{-3} elsewhere.

Analysis of thermal motion

The thermal motion in all three structures (Fig. 2) has been analysed in terms of the rigid-body modes of translation, libration, and screw motion (17). The rms errors in the U_{ij} (derived from the least-squares analyses) are 0.0016, 0.0024, and 0.0020 Å^2 respectively for the three compounds. The analyses carried out were as follows (rms ΔU_{ij} Å^2 in parentheses): RhGapz (0.0015), GaC_2N_2 (0.0020), and Rh(COD) (0.0041) for [Me_2Gapz_2]Rh(COD); N_2C_5 (0.0019, 0.0016, 0.0014, 0.0014), corrections for $N_2Rh(CO)_2$ approximated from the analysis of the entire molecules (0.0070, 0.0072) of [Rh(μ-3,5-Me_2pz)-$(CO)_2]_2$; all but uncoordinated COD carbons (0.0039), corrections involving COD methylene carbons approximated from two Rh(COD) (0.0052, 0.0090) for [Rh(μ-3,5-Me_2pz)(COD)]$_2$. The appropriate bond distances have been corrected for libration (17, 18), using shape parameters q^2 of 0.08 for all atoms involved. Corrected bond lengths appear in Table 3 along with the uncorrected values; corrected bond angles do not differ by more than 1σ from the uncorrected values given in Table 4. Intra-annular torsion angles defining the conformations of the M_2N_4 and COD rings are listed in Table 5. Calculated hydrogen coordinates and thermal parameters (Table 6) are included as supplementary material.

Results and discussion

There have been a number of reports dealing with Rh(I) complexes containing polypyrazolyl borate ligands such as [R_2Bpz_2]$^-$ (where R = H, Et, or pz) (19−27). The majority of these complexes incorporate bidentate ligands and display a square planar Rh environment, although a few examples have been reported which contain tridentate borate ligands and a 5-coordinate Rh metal centre. The present paper deals with a number of Rh(I) complexes incorporating the [Me_2Gapz_2]$^-$ ligand.

The complex [Me_2Gapz_2]Rh(CO)$_2$ has been isolated as an orange liquid which darkens in color when exposed to air. It can be compared to the similar boron complexes, [R_2Bpz_2]Rh(CO)$_2$ (R = H (20, 21) or Et (22)), in that it displays

[2] The structure factor table, Table 7 (anisotropic thermal parameters), and other material mentioned in the text are available, at a nominal charge, from the Depository of Unpublished Data, CISTI, National Research Council of Canada, Ottawa, Canada K1A 0S2.

TABLE 2. Final positional (fractional × 10^5, H × 10^4) and isotropic thermal parameters (U × 10^3 Å^2)* with estimated standard deviations in parentheses

Atom	x	y	z	U_{eq}/U_{iso}	Atom	x	y	z	U_{eq}/U_{iso}
				$(Me_2Gapz_2)Rh(COD)$					
Rh	32615(1)	25000	41763(4)	31	C(6)	26408(21)	19010(33)	81523(54)	80
Ga	48002(2)	25000	51219(7)	41	C(7)	37325(13)	3659(24)	19171(47)	48
N(1)	38313(9)	12665(18)	30875(32)	38	C(8)	42523(14)	−2042(27)	15633(55)	54
N(2)	44214(9)	12832(20)	35002(37)	41	C(9)	46667(13)	3892(26)	26005(49)	50
C(1)	44855(21)	25000	79366(69)	53	H(4)	2605(12)	844(24)	3588(46)	35(8)
C(2)	56386(19)	25000	43500(87)	67	H(5)	3168(12)	780(27)	6246(42)	40(8)
C(3)	19746(16)	19086(31)	39941(75)	79	H(7)	3309(12)	224(26)	1335(47)	37(7)
C(4)	25535(13)	13386(24)	43567(51)	45	H(8)	4337(15)	−805(31)	929(47)	55(10)
C(5)	28524(14)	13421(24)	62133(45)	47	H(9)	5092(16)	269(28)	2607(54)	65(10)
				$[Rh(\mu\text{-}3,5\text{-}Me_2pz)(CO)_2]_2$ (O, N, and C × 10^4)					
Rh(1)	56576(4)	48213(2)	24567(1)	46	C(13)	6978(6)	4027(4)	1279(2)	82
Rh(2)	19890(4)	51407(2)	21641(1)	47	C(14)	1287(6)	4653(4)	795(2)	78
Rh(3)	43754(3)	64024(2)	45547(1)	45	O(5)	3515(5)	4943(3)	3889(2)	102
Rh(4)	80195(3)	67660(2)	48485(1)	44	O(6)	2740(5)	5712(3)	5430(1)	93
O(1)	7070(4)	5227(2)	3542(1)	78	O(7)	10090(4)	5565(2)	4390(1)	79
O(2)	7702(5)	6034(3)	2007(2)	91	O(8)	9476(5)	6356(3)	5921(1)	96
O(3)	245(4)	5728(3)	3046(2)	97	N(5)	5559(4)	6914(2)	3971(1)	45
O(4)	1232(5)	6664(2)	1551(2)	90	N(6)	7078(3)	7080(2)	4104(1)	43
N(1)	4153(4)	3991(2)	2739(1)	48	N(7)	4959(4)	7426(2)	5008(1)	45
N(2)	2607(4)	4109(2)	2593(1)	49	N(8)	6484(3)	7577(2)	5136(1)	45
N(3)	4736(4)	4526(2)	1704(1)	51	C(15)	3851(5)	5500(3)	4138(2)	64
N(4)	3214(4)	4694(2)	1574(1)	49	C(16)	3367(5)	5967(3)	5095(2)	60
C(1)	6527(5)	5081(3)	3136(2)	55	C(17)	9313(5)	6030(3)	4563(2)	55
C(2)	6933(5)	5577(3)	2179(2)	60	C(18)	8904(5)	6507(3)	5519(2)	62
C(3)	900(5)	5507(3)	2709(2)	64	C(19)	5242(5)	7087(3)	3458(2)	52
C(4)	1496(5)	6081(3)	1781(2)	58	C(20)	6546(5)	7371(3)	3258(2)	56
C(5)	4296(5)	3360(3)	3074(2)	55	C(21)	7695(5)	7345(2)	3669(2)	49
C(6)	2851(6)	3066(3)	3142(2)	64	C(22)	4147(5)	7985(3)	5245(2)	51
C(7)	1828(5)	3541(3)	2840(2)	59	C(23)	5141(6)	8512(3)	5525(2)	57
C(8)	5332(5)	4253(3)	1267(2)	57	C(24)	6606(5)	8237(3)	5447(1)	49
C(9)	4179(6)	4249(3)	857(2)	62	C(25)	3664(6)	6958(4)	3181(2)	80
C(10)	2880(5)	4526(3)	1058(2)	56	C(26)	9339(6)	7583(3)	3686(2)	70
C(11)	5823(7)	3061(4)	3310(2)	81	C(27)	2421(6)	7979(4)	5182(2)	74
C(12)	108(6)	3508(4)	2754(2)	83	C(28)	8151(6)	8582(3)	5640(2)	69
				$[Rh(\mu\text{-}3,5\text{-}Me_2pz)(COD)]_2$ (N and C × 10^4, H × 10^3)					
Rh(1)	20633(2)	14584(2)	32507(2)	29	C(22)	3741(6)	5800(5)	1572(5)	71
Rh(2)	22756(2)	36018(2)	21988(2)	31	C(23)	3945(4)	5400(4)	2592(4)	51
N(1)	157(3)	1417(3)	2340(2)	33	C(24)	4505(4)	4435(4)	2604(4)	48
N(2)	242(3)	2315(2)	1843(2)	32	C(25)	5021(4)	3660(5)	1571(5)	64
N(3)	2254(3)	3385(2)	4509(2)	32	C(26)	3919(5)	2493(6)	504(4)	76
N(4)	2281(3)	4285(2)	4025(2)	33	H(2)	−301(4)	119(3)	157(3)	29(8)
C(1)	−1191(3)	870(3)	2269(3)	36	H(5)	138(4)	570(4)	639(4)	42(10)
C(2)	−1988(3)	1411(4)	1719(3)	39	H(7a)	−245(7)	−9(6)	303(6)	102(20)
C(3)	−1046(3)	2322(3)	1476(3)	34	H(7b)	−167(7)	−100(7)	234(6)	107(22)
C(4)	1976(3)	3887(3)	5586(3)	36	H(7c)	−85(5)	12(5)	357(4)	58(12)
C(5)	1831(4)	5122(4)	5804(3)	41	H(8a)	−67(6)	401(6)	131(6)	95(20)
C(6)	2015(3)	5335(3)	4799(3)	35	H(8b)	−132(5)	300(4)	3(4)	59(12)
C(7)	−1638(5)	−87(5)	2812(4)	52	H(8c)	−235(4)	336(4)	105(4)	43(10)
C(8)	−1329(5)	3241(4)	948(4)	47	H(9a)	109(8)	350(8)	682(7)	138(27)
C(9)	1822(5)	3132(5)	6343(4)	52	H(9b)	128(4)	206(4)	569(4)	46(10)
C(10)	1885(5)	6465(4)	4518(5)	49	H(9c)	272(5)	321(5)	681(4)	60(13)
C(11)	4235(4)	1803(4)	3907(3)	42	H(10a)	280(7)	705(7)	476(6)	108(22)
C(12)	3485(4)	1183(4)	4508(3)	42	H(10b)	146(6)	624(6)	379(5)	72(17)
C(13)	3109(6)	−317(5)	4192(5)	70	H(10c)	126(6)	691(6)	480(6)	92(18)
C(14)	1859(6)	−1254(5)	3161(6)	76	H(11)	475(4)	280(4)	440(3)	32(8)
C(15)	1386(4)	−693(3)	2298(3)	44	H(12)	348(4)	181(4)	525(4)	42(10)
C(16)	2207(4)	−138(4)	1704(3)	45	H(15)	40(4)	−100(3)	197(3)	29(8)
C(17)	3720(5)	−84(5)	1807(5)	70	H(16)	178(4)	−14(4)	106(3)	31(9)
C(18)	4786(4)	1093(5)	2907(4)	62	H(19)	185(5)	161(5)	21(4)	58(13)
C(19)	2442(4)	2439(4)	440(3)	47	H(20)	116(6)	326(5)	24(5)	64(15)
C(20)	1945(5)	3409(5)	388(4)	50	H(23)	401(5)	592(5)	320(5)	67(15)
C(21)	2823(8)	4683(6)	361(6)	96	H(24)	480(4)	448(4)	342(4)	40(10)

* U_{eq} = (1/3) trace U_{diag}.

Can. J. Chem. Downloaded from www.nrcresearchpress.com by 210.87.254.42 on 09/06/12
For personal use only.

TABLE 3. Bond lengths (Å) with estimated standard deviations in parentheses*

Bond	Length		Bond	Length	
	Uncorr.	Corr.		Uncorr.	Corr.
			$(Me_2Gapz_2)Rh(COD)$		
Rh —N(1)	2.087(2)	2.090	N(2)—C(9)	1.340(3)	1.342
Rh —C(4)	2.131(3)	2.146	C(3)—C(4)	1.502(5)	1.516
Rh —C(5)	2.127(3)	2.140	C(3)—C(3)′	1.417(7)	1.423
Ga —N(2)	1.991(2)	1.996	C(4)—C(5)	1.379(4)	1.395
Ga —C(1)	1.955(4)	1.963	C(5)—C(6)	1.500(4)	1.511
Ga —C(2)	1.971(4)	1.978	C(6)—C(6)′	1.435(8)	1.441
N(1)—N(2)	1.369(3)	1.371	C(7)—C(8)	1.384(4)	1.386
N(1)—C(7)	1.337(3)	1.339	C(8)—C(9)	1.358(4)	1.360
			$[Rh(\mu\text{-}3,5\text{-}Me_2pz)(CO)_2]_2$		
Rh(1)—N(1)	2.065(3)	2.071	C(5)—C(6)	1.377(7)	1.384
Rh(1)—N(3)	2.064(3)	2.070	C(5)—C(11)	1.494(7)	1.500
Rh(1)—C(1)	1.872(5)	1.876	C(6)—C(7)	1.366(7)	1.374
Rh(1)—C(2)	1.847(5)	1.851	C(7)—C(12)	1.500(7)	1.505
Rh(2)—N(2)	2.054(3)	2.060	C(8)—C(9)	1.381(7)	1.390
Rh(2)—N(4)	2.057(3)	2.063	C(8)—C(13)	1.483(7)	1.489
Rh(2)—C(3)	1.851(5)	1.853	C(9)—C(10)	1.365(6)	1.374
Rh(2)—C(4)	1.850(5)	1.853	C(10)—C(14)	1.503(7)	1.509
Rh(3)—N(5)	2.064(3)	2.069	O(5)—C(15)	1.132(6)	1.134
Rh(3)—N(7)	2.071(3)	2.076	O(6)—C(16)	1.136(5)	1.138
Rh(3)—C(15)	1.850(5)	1.854	O(7)—C(17)	1.135(5)	1.138
Rh(3)—C(16)	1.842(5)	1.846	O(8)—C(18)	1.124(5)	1.128
Rh(4)—N(6)	2.059(3)	2.065	N(5)—N(6)	1.367(4)	1.374
Rh(4)—N(8)	2.068(3)	2.073	N(5)—C(19)	1.339(5)	1.349
Rh(4)—C(17)	1.846(5)	1.848	N(6)—C(21)	1.346(5)	1.356
Rh(4)—C(18)	1.855(5)	1.857	N(7)—N(8)	1.365(4)	1.371
O(1)—C(1)	1.122(5)	1.123	N(7)—C(22)	1.335(5)	1.342
O(2)—C(2)	1.122(5)	1.123	N(8)—C(24)	1.337(5)	1.344
O(3)—C(3)	1.135(5)	1.139	C(19)—C(20)	1.370(6)	1.378
O(4)—C(4)	1.132(6)	1.136	C(19)—C(25)	1.505(6)	1.511
N(1)—N(2)	1.381(5)	1.389	C(20)—C(21)	1.382(6)	1.391
N(1)—C(5)	1.337(5)	1.346	C(21)—C(26)	1.486(6)	1.491
N(2)—C(7)	1.342(5)	1.350	C(22)—C(23)	1.375(6)	1.382
N(3)—N(4)	1.369(5)	1.377	C(22)—C(27)	1.502(6)	1.507
N(3)—C(8)	1.348(5)	1.359	C(23)—C(24)	1.388(6)	1.395
N(4)—C(10)	1.346(5)	1.358	C(24)—C(28)	1.504(6)	1.509
			$[Rh(\mu\text{-}3,5\text{-}Me_2pz)(COD)]_2$		
Rh(1)—N(1)	2.084(3)	2.087	C(3)—C(8)	1.495(5)	1.496
Rh(1)—N(3)	2.083(2)	2.086	C(4)—C(5)	1.382(5)	1.384
Rh(1)—C(11)	2.135(3)	2.136	C(4)—C(9)	1.495(5)	1.495
Rh(1)—C(12)	2.133(3)	2.134	C(5)—C(6)	1.385(5)	1.387
Rh(1)—C(15)	2.122(3)	2.123	C(6)—C(10)	1.488(5)	1.489
Rh(1)—C(16)	2.136(3)	2.138	C(11)—C(12)	1.397(5)	1.408
Rh(2)—N(2)	2.084(2)	2.087	C(11)—C(18)	1.489(5)	1.502
Rh(2)—N(4)	2.085(2)	2.088	C(12)—C(13)	1.521(6)	1.534
Rh(2)—C(19)	2.132(3)	2.134	C(13)—C(14)	1.458(8)	1.466
Rh(2)—C(20)	2.123(4)	2.124	C(14)—C(15)	1.518(6)	1.530
Rh(2)—C(23)	2.123(3)	2.124	C(15)—C(16)	1.391(5)	1.404
Rh(2)—C(24)	2.139(3)	2.141	C(16)—C(17)	1.533(6)	1.545
N(1)—N(2)	1.373(3)	1.376	C(17)—C(18)	1.481(7)	1.489
N(1)—C(1)	1.342(4)	1.344	C(19)—C(20)	1.355(6)	1.365
N(2)—C(3)	1.339(4)	1.341	C(19)—C(26)	1.502(6)	1.510
N(3)—N(4)	1.368(3)	1.371	C(20)—C(21)	1.511(7)	1.519
N(3)—C(4)	1.345(4)	1.347	C(21)—C(22)	1.483(8)	1.490
N(4)—C(6)	1.345(4)	1.347	C(22)—C(23)	1.499(6)	1.513
C(1)—C(2)	1.389(5)	1.391	C(23)—C(24)	1.376(6)	1.386
C(1)—C(7)	1.499(5)	1.499	C(24)—C(25)	1.518(6)	1.530
C(2)—C(3)	1.384(5)	1.386	C(25)—C(26)	1.474(7)	1.480

* Here and elsewhere in this report primed atoms have coordinates related to those in Table 2 by the symmetry operation x, $1/2 - y$, z.

Can. J. Chem. Downloaded from www.nrcresearchpress.com by 210.87.254.42 on 09/06/12
For personal use only.

Can. J. Chem. Downloaded from www.nrcresearchpress.com by 210.87.254.42 on 09/06/12
For personal use only.

TABLE 4. Bond angles (deg) with estimated standard deviations in parentheses

Bonds	Angle (deg)	Bonds	Angle (deg)	Bonds	Angle (deg)	Bonds	Angle (deg)
			$(Me_2Gapz_2)Rh(COD)$				
N(1)—Rh —C(4)	91.46(10)	N(2)—N(1)—C(7)	106.7(2)	C(5)—Rh —C(5)′	81.4(2)	Rh —C(5)—C(6)	111.5(2)
N(1)—Rh —C(5)	91.08(10)	Ga —N(2)—N(1)	122.5(2)	N(2)—Ga —C(1)	109.35(11)	C(4)—C(5)—C(6)	124.8(3)
N(1)—Rh —N(1)′	90.11(12)	Ga —N(2)—C(9)	129.3(2)	N(2)—Ga —C(2)	106.58(12)	C(5)—C(6)—C(6)′	116.5(2)
N(1)—Rh —C(4)′	161.72(11)	N(1)—N(2)—C(9)	108.2(2)	N(2)—Ga —N(2)′	94.09(14)	N(1)—C(7)—C(8)	110.4(3)
N(1)—Rh —C(5)′	160.38(11)	Rh —C(4)—C(3)	110.9(2)	C(1)—Ga —C(2)	126.1(2)	C(7)—C(8)—C(9)	104.7(3)
C(4)—Rh —C(5)	37.80(12)	Rh —C(4)—C(5)	70.9(2)	Rh —N(1)—N(2)	122.2(2)	N(2)—C(9)—C(8)	110.1(2)
C(4)—Rh —C(4)′	81.5(2)	C(3)—C(4)—C(5)	124.5(3)	Rh —N(1)—C(7)	131.1(2)		
C(4)—Rh —C(5)′	93.51(11)	Rh —C(5)—C(4)	71.3(2)				
			$[Rh(\mu\text{-}3,5\text{-}Me_2pz)(CO)_2]_2$				
N(1)—Rh(1)—N(3)	87.79(13)	C(6)—C(5)—C(11)	129.1(4)	N(8)—Rh(4)—C(17)	176.96(15)	Rh(4)—N(8)—N(7)	116.8(2)
N(1)—Rh(1)—C(1)	92.6(2)	C(5)—C(6)—C(7)	106.9(4)	N(8)—Rh(4)—C(18)	92.9(2)	Rh(4)—N(8)—C(24)	135.1(3)
N(1)—Rh(1)—C(2)	177.3(2)	N(2)—C(7)—C(6)	108.8(4)	C(17)—Rh(4)—C(18)	89.7(2)	N(7)—N(8)—C(24)	108.0(3)
N(3)—Rh(1)—C(1)	179.0(2)	N(2)—C(7)—C(12)	120.1(4)	Rh(1)—N(1)—N(2)	116.9(2)	Rh(3)—C(15)—O(5)	178.8(4)
N(3)—Rh(1)—C(2)	90.0(2)	C(6)—C(7)—C(12)	131.1(5)	Rh(1)—N(1)—C(5)	134.8(3)	Rh(3)—C(16)—O(6)	178.8(5)
C(1)—Rh(1)—C(2)	89.6(2)	N(3)—C(8)—C(9)	108.3(4)	N(2)—N(1)—C(5)	108.1(3)	Rh(4)—C(17)—O(7)	178.6(4)
N(2)—Rh(2)—N(4)	88.07(13)	N(3)—C(8)—C(13)	120.9(4)	Rh(2)—N(2)—N(1)	117.4(2)	Rh(4)—C(18)—O(8)	178.2(5)
N(2)—Rh(2)—C(3)	89.8(2)	C(9)—C(8)—C(13)	130.8(4)	Rh(2)—N(2)—C(7)	134.2(3)	N(5)—C(19)—C(20)	109.2(4)
N(2)—Rh(2)—C(4)	178.2(2)	C(8)—C(9)—C(10)	106.9(4)	N(1)—N(2)—C(7)	107.6(3)	N(5)—C(19)—C(25)	121.6(4)
N(4)—Rh(2)—C(3)	177.9(2)	N(4)—C(10)—C(9)	108.6(4)	Rh(1)—N(3)—N(4)	117.7(2)	C(20)—C(19)—C(25)	129.2(4)
N(4)—Rh(2)—C(4)	91.3(2)	N(4)—C(10)—C(14)	121.0(4)	Rh(1)—N(3)—C(8)	134.1(3)	C(19)—C(20)—C(21)	106.3(4)
C(3)—Rh(2)—C(4)	90.8(2)	C(9)—C(10)—C(14)	130.4(4)	N(4)—N(3)—C(8)	107.9(3)	N(6)—C(21)—C(20)	108.3(4)
N(5)—Rh(3)—N(7)	87.63(12)	Rh(3)—N(5)—N(6)	116.2(2)	Rh(2)—N(4)—N(3)	117.0(2)	N(6)—C(21)—C(26)	121.4(4)
N(5)—Rh(3)—C(15)	91.5(2)	Rh(3)—N(5)—C(19)	135.6(3)	Rh(2)—N(4)—C(10)	134.7(3)	C(20)—C(21)—C(26)	130.3(4)
N(5)—Rh(3)—C(16)	177.8(2)	N(6)—N(5)—C(19)	108.0(3)	N(3)—N(4)—C(10)	108.3(3)	N(7)—C(22)—C(23)	109.0(4)
N(7)—Rh(3)—C(15)	178.9(2)	Rh(4)—N(6)—N(5)	118.4(2)	Rh(1)—C(1)—O(1)	178.7(4)	N(7)—C(22)—C(27)	121.1(4)
N(7)—Rh(3)—C(16)	90.4(2)	Rh(4)—N(6)—C(21)	132.8(3)	Rh(1)—C(2)—O(2)	179.5(4)	C(23)—C(22)—C(27)	129.8(4)
C(15)—Rh(3)—C(16)	90.5(2)	N(5)—N(6)—C(21)	108.3(3)	Rh(2)—C(3)—O(3)	179.2(5)	C(22)—C(23)—C(24)	105.7(4)
N(6)—Rh(4)—N(8)	86.97(12)	Rh(3)—N(7)—N(8)	117.6(2)	Rh(2)—C(4)—O(4)	178.1(4)	N(8)—C(24)—C(23)	108.8(4)
N(6)—Rh(4)—C(17)	90.5(2)	Rh(3)—N(7)—C(22)	133.8(3)	N(1)—C(5)—C(6)	108.4(4)	N(8)—C(24)—C(28)	121.1(4)
N(6)—Rh(4)—C(18)	178.5(2)	N(8)—N(7)—C(22)	108.5(3)	N(1)—C(5)—C(11)	122.4(4)	C(23)—C(24)—C(28)	130.1(4)
			$[Rh(\mu\text{-}3,5\text{-}Me_2pz)(COD)]_2$				
N(1)—Rh(1)—N(3)	84.45(10)	C(2)—C(1)—C(7)	129.1(3)	N(4)—Rh(2)—C(23)	92.66(13)	C(14)—C(15)—C(16)	125.9(4)
N(1)—Rh(1)—C(11)	163.86(12)	C(1)—C(2)—C(3)	105.6(3)	N(4)—Rh(2)—C(24)	95.35(13)	Rh(1)—C(16)—C(15)	70.4(2)
N(1)—Rh(1)—C(12)	157.85(12)	N(2)—C(3)—C(2)	109.0(3)	C(19)—Rh(2)—C(20)	37.1(2)	Rh(1)—C(16)—C(17)	112.4(3)
N(1)—Rh(1)—C(15)	90.70(12)	N(2)—C(3)—C(8)	122.9(3)	C(19)—Rh(2)—C(23)	95.2(2)	C(15)—C(16)—C(17)	122.8(4)
N(1)—Rh(1)—C(16)	95.34(13)	C(2)—C(3)—C(8)	128.1(3)	C(19)—Rh(2)—C(24)	81.6(2)	C(16)—C(17)—C(18)	114.4(3)
N(3)—Rh(1)—C(11)	93.55(12)	N(3)—C(4)—C(5)	109.1(3)	C(20)—Rh(2)—C(23)	82.2(2)	C(11)—C(18)—C(17)	115.6(3)
N(3)—Rh(1)—C(12)	94.74(12)	N(3)—C(4)—C(9)	122.1(3)	C(20)—Rh(2)—C(24)	92.2(2)	Rh(2)—C(19)—C(20)	71.0(2)
N(3)—Rh(1)—C(15)	160.08(12)	C(5)—C(4)—C(9)	128.8(3)	C(23)—Rh(2)—C(24)	37.7(2)	Rh(2)—C(19)—C(26)	111.6(3)
N(3)—Rh(1)—C(16)	161.51(13)	C(4)—C(5)—C(6)	105.9(3)	Rh(1)—N(1)—N(2)	116.0(2)	C(20)—C(19)—C(26)	125.2(4)
C(11)—Rh(1)—C(12)	38.21(14)	N(4)—C(6)—C(5)	108.7(3)	Rh(1)—N(1)—C(1)	135.2(2)	Rh(2)—C(20)—C(19)	71.8(2)
C(11)—Rh(1)—C(15)	96.27(14)	N(4)—C(6)—C(10)	122.5(3)	N(2)—N(1)—C(1)	107.8(2)	Rh(2)—C(20)—C(21)	112.0(3)
C(11)—Rh(1)—C(16)	81.52(15)	C(5)—C(6)—C(10)	128.7(3)	Rh(2)—N(2)—N(1)	114.5(2)	C(19)—C(20)—C(21)	123.5(5)
C(12)—Rh(1)—C(15)	82.56(14)	Rh(1)—C(11)—C(12)	70.8(2)	Rh(2)—N(2)—C(3)	135.0(2)	C(20)—C(21)—C(22)	115.3(4)
C(12)—Rh(1)—C(16)	92.30(15)	Rh(1)—C(11)—C(18)	112.2(3)	N(1)—N(2)—C(3)	108.5(2)	C(21)—C(22)—C(23)	115.3(4)
C(15)—Rh(1)—C(16)	38.14(15)	C(12)—C(11)—C(18)	124.5(4)	Rh(1)—N(3)—N(4)	114.1(2)	Rh(2)—C(23)—C(22)	111.0(3)
N(2)—Rh(2)—N(4)	83.87(10)	Rh(1)—C(12)—C(11)	71.0(2)	Rh(1)—N(3)—C(4)	134.9(2)	Rh(2)—C(23)—C(24)	71.8(2)
N(2)—Rh(2)—C(19)	94.04(13)	Rh(1)—C(12)—C(13)	110.8(3)	N(4)—N(3)—C(4)	108.0(2)	C(22)—C(23)—C(24)	125.1(4)
N(2)—Rh(2)—C(20)	94.11(14)	C(11)—C(12)—C(13)	123.5(4)	Rh(2)—N(4)—N(3)	116.5(2)	Rh(2)—C(24)—C(23)	70.5(2)
N(2)—Rh(2)—C(23)	159.05(14)	C(12)—C(13)—C(14)	116.1(4)	Rh(2)—N(4)—C(6)	133.4(2)	Rh(2)—C(24)—C(25)	112.3(3)
N(2)—Rh(2)—C(24)	163.12(13)	C(13)—C(14)—C(15)	115.1(4)	N(3)—N(4)—C(6)	108.4(2)	C(23)—C(24)—C(25)	123.2(4)
N(4)—Rh(2)—C(19)	162.40(13)	Rh(1)—C(15)—C(14)	109.9(3)	N(1)—C(1)—C(2)	109.1(3)	C(24)—C(25)—C(26)	115.2(3)
N(4)—Rh(2)—C(20)	160.28(14)	Rh(1)—C(15)—C(16)	71.5(2)	N(1)—C(1)—C(7)	121.6(3)	C(19)—C(26)—C(25)	115.6(4)

Can. J. Chem. Downloaded from www.nrcresearchpress.com by 210.87.254.42 on 09/06/12
For personal use only.

two strong ν_{CO} bands in its ir spectrum and equivalent pyrazolyl groups in its ^{1}H nmr spectrum, both consistent with a square planar arrangement about the Rh(I) metal centre. The dicarbonyl derivative reacts readily with PPh_3 to yield an air-stable solid in which just one carbonyl group is replaced by the phosphine ligand, $[Me_2Gapz_2]Rh(CO)(PPh_3)$. The ^{1}H nmr of this complex indicates two different pyrazolyl groups as expected. The cyclooctadiene (COD) complex, $[Me_2Gapz_2]$-Rh(COD), has been isolated as air-stable yellow crystals and again shows two equivalent pz groups in its ^{1}H nmr spectrum. Interestingly the "Me_2Ga" moiety in each of the above three complexes displays but one sharp singlet in the ^{1}H nmr spectra at room temperature (see Table 1 and Figs. 1 and 2). This would suggest either a planar geometry for the Ga—(N—N)$_2$—Rh six-membered rings in solution or a rapidly inverting boat conformation viz:

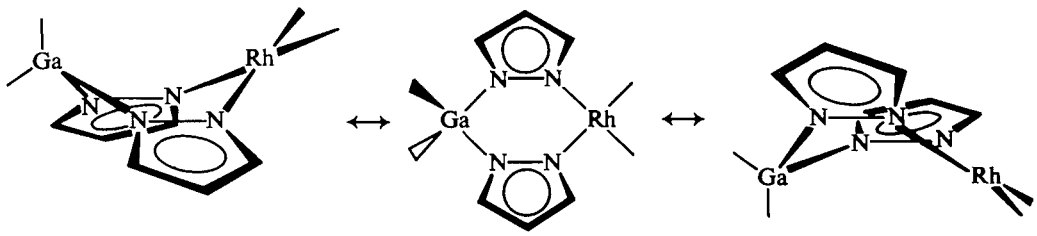

Molecular models indicate that the favored structure should be the boat conformation and to probe the solution behaviour of the complexes, low temperature ^{1}H nmr studies on the $[Me_2Gapz_2]Rh(CO)(PPh_3)$ and $[Me_2Gapz_2]Rh(COD)$ compounds were carried out (Figs. 1 and 2). As expected, the single "$GaMe_2$" signal observed at room temperature for each of these compounds collapses as the temperature is lowered and eventually appears as two singlets. This is accompanied by a shift in the signals due to the pyrazolyl protons as can be clearly seen in Fig. 1. In addition the spectra of the COD complex (Fig. 2) show a splitting of the signals due to the protons on the COD ligand at the lower temperatures, particularly noticeable for the olefinic protons closest to the Rh atom at around 5.8 τ. These observations are consistent with a fluxional behaviour in solution at room temperature giving an average planar Ga—(N—N)$_2$—Rh ring as shown above. A similar mechanism has been proposed for the observed fluxional behaviour in solution of the complexes $[Me_2Ga(3,5\text{-}Me_2pz)_2]Ni(\eta^3\text{-}C_3H_5)$ (5) and $[Me_2Gapz_2]_2Ni$ (3). In both these species at higher temperatures a single "$GaMe_2$" resonance is observed but on cooling the solution this signal broadens, collapses, and is replaced by two singlets at lower temperatures consistent with static boat conformations for the Ga—(N—N)$_2$—Ni six-membered rings at these temperatures.

The puckered nature of the Ga—(N—N)$_2$—Rh six-membered ring in the complex $[Me_2Gapz_2]Rh(COD)$ has been clearly demonstrated in the solid state by a crystal structure determination (see below). It is interesting to compare $[Me_2Gapz_2]Rh(COD)$ with the recently reported compound $B(pz)_4Rh(COD)$ (24, 25). For the latter, in the solid state, a crystallographic study has determined that the Rh(I) centre is four-coordinate with two pz groups bridging the B and Rh atoms while the other two pz groups occupy the remaining tetrahedral positions about the B atom. Interestingly, a proton nmr study indicates that all the pz groups are equivalent at room temperature, but at lower temperatures the pz groups are indicated to be of two types in the ratio of 3:1. In this complex it is proposed that all four pz groups exchange in solution at room temperature via a pentacoordinate trispyrazolyl borate rhodium intermediate.

The complex $[Me_2Gapz_2]Rh(PPh_3)_2$ has been prepared by the reaction of the $[Me_2Gapz_2]^-$ ligand with Wilkinson's catalyst, $Rh(PPh_3)_3Cl$. For this complex the room temperature ^{1}H nmr spectrum, in either C_6D_6 or d_6-acetone, shows two broad signals in the "$GaMe_2$" region of the spectrum, suggesting that the fluxional process observed for the three complexes discussed above is somewhat less facile for the present compound. The presence of the two bulky phosphine ligands on the Rh atom might be expected to hinder the fluxional process but varying the temperature of the solutions did lead to the expected changes in the ^{1}H nmr spectra. Thus cooling the solutions caused a significant sharpening of the signals due to the "$GaMe_2$" protons whereas warming the solutions caused further broadening of these signals.

The phosphine complexes prepared in this study, $[Me_2Gapz_2]Rh(CO)(PPh_3)$ and $[Me_2Gapz_2]Rh(PPh_3)_2$, have been investigated as potential catalysts for the hydrogenation of olefins (cyclohexene or 1-hexene) in benzene solution at room temperature. No hydrogen uptake by the olefins was observed in any of the experiments.

Our attempts to prepare the analogous complexes containing the $[Me_2Ga(3,5\text{-}Me_2pz)_2]^-$ ligand were thwarted by the facile formation of the dimer species, $[Rh(\mu\text{-}3,5\text{-}Me_2pz)(CO)_2]_2$ and $[Rh(\mu\text{-}3,5\text{-}Me_2pz)(COD)]_2$. It is speculated that disproportionation of the gallate ligand is occurring and that this is enhanced by the ready incorporation of the pyrazolyl moieties so produced into the very stable bridged Rh dinuclear species. For example:

$$2\ Na^+[Me_2Ga(3,5\text{-}Me_2pz)_2]^- + [Rh(COD)Cl]_2 \rightarrow$$

$$[Me_2Ga(\mu\text{-}3,5\text{-}Me_2pz)]_2 + [Rh(\mu\text{-}3,5\text{-}Me_2pz)(COD)]_2 + 2\ NaCl$$

Corroborative evidence for this proposal comes with the isolation of the bridged gallium dimer species $[Me_2Ga(\mu\text{-}3,5\text{-}Me_2pz)]_2$ (28) from the reaction products.

The rhodium(I) dimers $[Rh(\mu\text{-}3,5\text{-}Me_2pz)(CO)_2]_2$ and $[Rh(\mu\text{-}3,5\text{-}Me_2pz)(COD)]_2$ were first synthesized some years ago by Trofimenko (19) using a more direct synthetic route. The Rh(I) dimers isolated in this study gave analytical and physical data (ir, ^{1}H nmr) in agreement with those reported earlier by Trofimenko (19) and by Banditelli *et al.* (29). The exquisite crystalline nature of these dimers and the general paucity of structural data in the literature on this type of complex (Uson *et al.* have reported the structure of the dimer

Can. J. Chem. Downloaded from www.nrcresearchpress.com by 210.87.254.42 on 09/06/12
For personal use only.

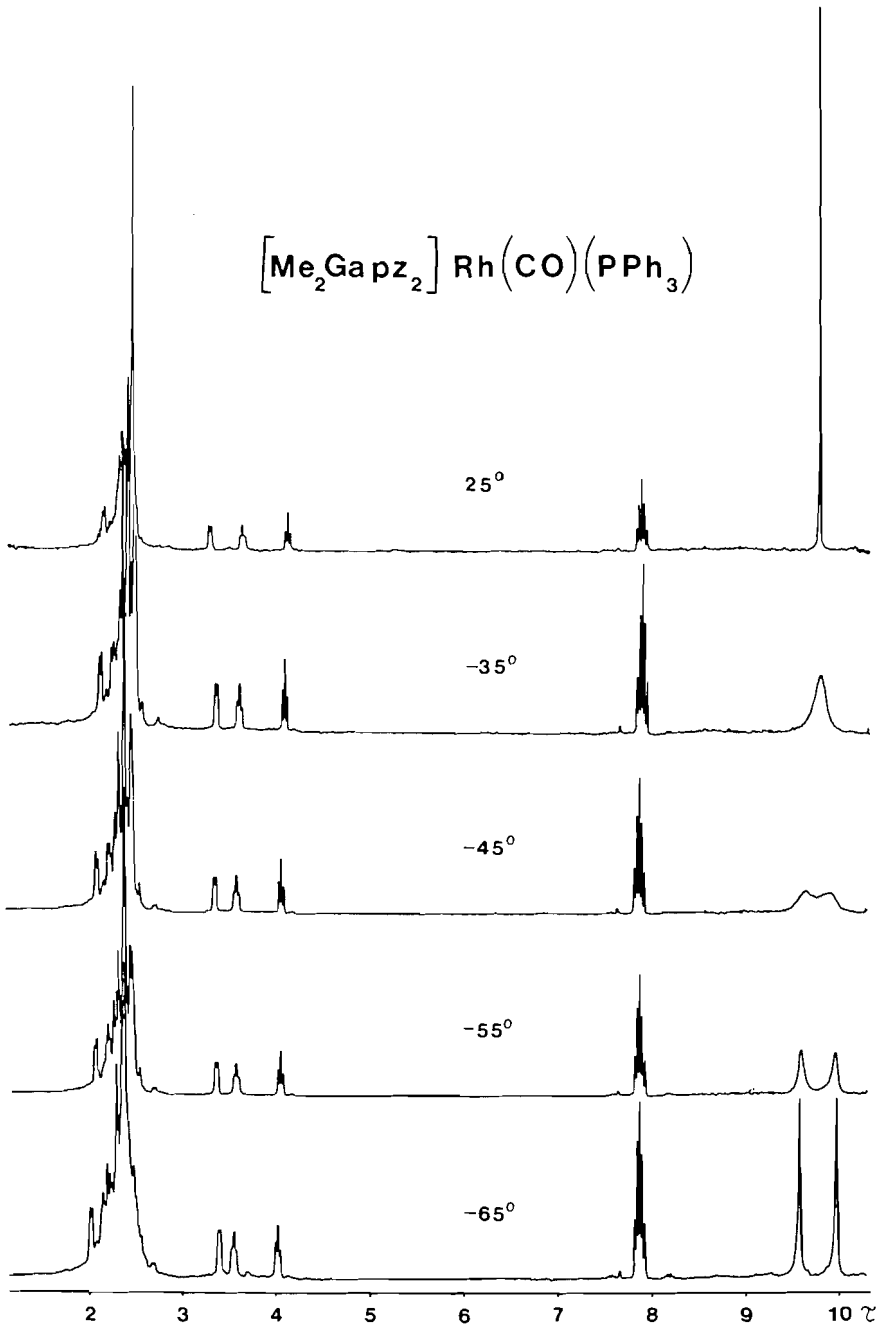

FIG. 1. Low temperature ^{1}H nmr spectra of $[Me_2Gapz_2]Rh(CO)(PPh_3)$ in d_6-acetone.

$[Rh(\mu\text{-}pz)(CO)(P(OPh)_3)]_2$ (30)) prompted us to perform X-ray crystallographic analyses of these two complexes.

Crystal structures of $[Me_2Gapz_2]Rh(COD)$, $[Rh(\mu\text{-}3,5\text{-}Me_2pz)(CO)_2]_2$, and $[Rh(\mu\text{-}3,5\text{-}Me_2pz)(COD)]_2$

Each of the three structures consists of discrete molecules (Fig. 3) separated by normal van der Waals distances. In all three compounds the Rh(I) atoms are in distorted square planar environments. The mean[3] bond lengths involving Rh (Rh—C = 2.129(2), Rh—N = 2.087(2) Å in $[Me_2Gapz_2]Rh(COD)$; Rh—CO = 1.852(9), Rh—N = 2.063(6) Å in $[Rh(\mu\text{-}3,5\text{-}Me_2pz)(CO)_2]_2$; and Rh—C = 2.131(7), Rh—N = 2.084(1) Å in $[Rh(\mu\text{-}3,5\text{-}Me_2pz)(COD)]_2$) are internally consistent and in good agreement with those reported for related molecules (24, 30, and references cited therein). The Rh—N distances in the carbonyl complex are significantly shorter than those in the two COD complexes. Other bond lengths and bond angles in the three structures (Tables 3 and 4) are normal. The pyrazolyl rings are all planar within experimental error or very nearly so, the maximum deviation of any ring atom from the respective N_2C_3 mean plane being 0.010(4) Å.

The central feature of each of the three structures reported here is the boat conformation of the six-membered Rh—(N—N)$_2$—M (M = Ga or Rh) ring. As can be seen by inspection of the intraannular torsion angles in Table 5, these

[3] Here and elsewhere in this report mean values refer to weighted means with rms deviations from the mean in parentheses.

Can. J. Chem. Downloaded from www.nrcresearchpress.com by 210.87.254.42 on 09/06/12
For personal use only.

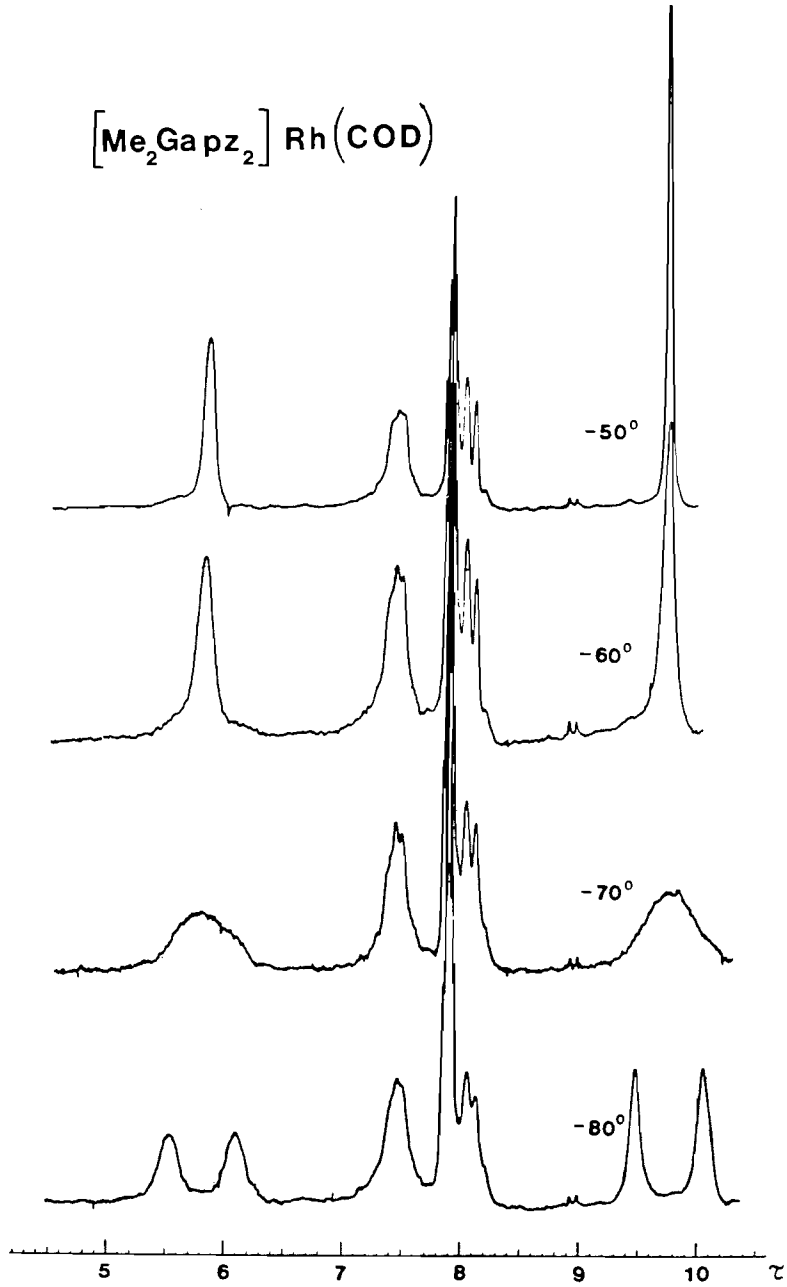

FIG. 2. Low temperature ^{1}H nmr spectra of $[Me_2Gapz_2]Rh(COD)$ in d_6-acetone.

rings differ substantially between the three molecules. This fundamental structural difference is related to the markedly different steric requirements of the ligands.

In the heterobinuclear complex $[Me_2Gapz_2]Rh(COD)$, which possesses exact C_s (mirror) symmetry, folding of the $RhGaN_4$ ring results primarily from steric interaction between the pyrazolyl and COD moieties (H(4)···H(7) = 2.29(4) Å). The Rh···Ga distance is 3.5527(5) Å, the dihedral angle between the pyrazolyl mean planes 114.1°, the maximum deviation from the RhN_2M_2 mean plane (M = midpoint of C=C) 0.016(3) Å, and the deviations of the metal atoms from the pyrazolyl mean plane 0.0124(2) Å for Rh and 0.0748(4) Å for Ga. The folding of the central six-membered ring in $[Me_2Gapz_2]Rh(COD)$ is greater than that observed in the compounds $B(pz)_4Rh(COD)$ and $B(pz)_4Rh(NBD)$ (NBD = norbornadiene) (24) in which ring folding is hindered by steric interaction of the coordinated olefin with the pseudoaxial, nonbridging, pyrazolyl group on the boron atom.

Each of the crystallographically independent (but virtually identical) molecules of $[Rh(\mu\text{-}3,5\text{-}Me_2pz)(CO)_2]_2$ and the $[Rh(\mu\text{-}3,5\text{-}Me_2pz)(COD)]_2$ molecule display approximate C_{2v} symmetry in the solid state. In both of these compounds steric interactions between the bridging 3,5-Me_2pz ligand and the terminal ligands result in folding of the Rh—(N—N)$_2$—Rh rings, the latter compound showing the greatest strain. The resulting cross-ring Rh···Rh distances (mean 3.262(4) Å for the carbonyl and 3.1538(3) Å for the COD complex), although significantly shorter than the Rh···Rh distance of 3.568 Å quoted by Uson *et al.* for $[Rh(\mu\text{-pz})(CO)(P(OPh)_3]_2$ (30), are nevertheless not supportive of any direct bonding interactions between the two Rh metal centres (31). It is interesting to compare these findings with the recently reported structures of

Can. J. Chem. Downloaded from www.nrcresearchpress.com by 210.87.254.42 on 09/06/12
For personal use only.

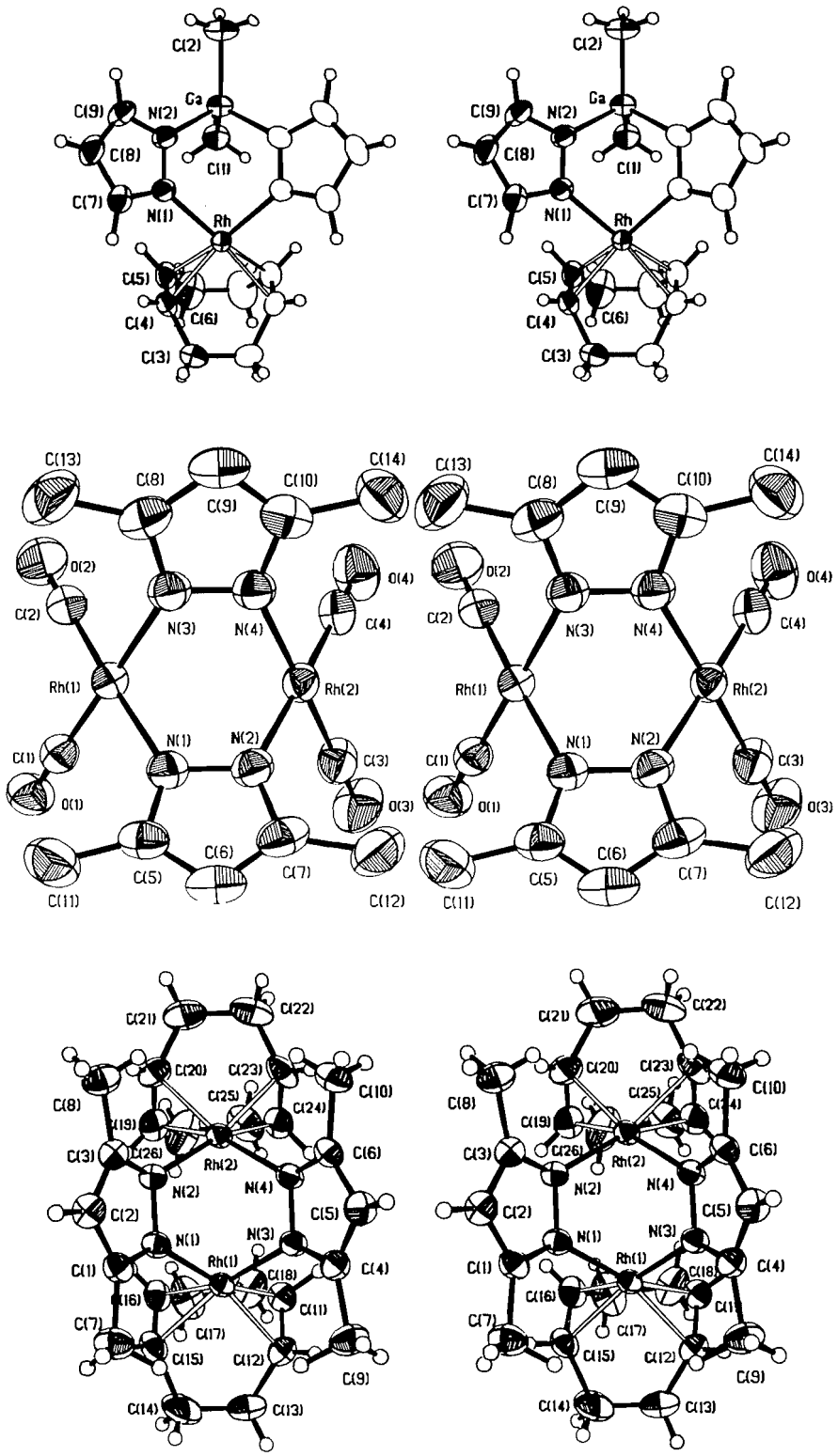

FIG. 3. Stereoscopic views of the $[Me_2Gapz_2]Rh(COD)$ (top), $[Rh(\mu\text{-}3,5\text{-}Me_2pz)(CO)_2]_2$ (middle), and $[Rh(\mu\text{-}3,5\text{-}Me_2pz)(COD)]_2$ (bottom) molecules; 50% probability thermal ellipsoids are shown for the non-hydrogen atoms.

the pyrazolyl-bridged iridium dimers $[Ir(\mu\text{-}pz)(COD)]_2$ (32) and $[Ir(\mu\text{-}pz)(CO)(PPh_3)]_2$ (33) (Ir···Ir = 3.216 and 3.162(2) Å respectively) which were postulated to possess some degree of direct metal–metal interaction. The structure of the former Ir complex is very similar to that of $[Rh(\mu\text{-}3,5\text{-}Me_2pz)(COD)]_2$ while that of the latter differs markedly in the degree of folding and hence the M···M distance from the $Rh(P(OPh)_3)$ analog (30), presumably as a result of the different steric requirements of the PPh_3 and $P(OPh)_3$ ligands.

The Rh(I) dimers $[Rh(\mu\text{-}3,5\text{-}Me_2pz)(CO)_2]_2$ and $[Rh(\mu\text{-}3,5\text{-}Me_2pz)(COD)]_2$ both show a greater degree of strain than $[Me_2Gapz_2]Rh(COD)$. Dihedral angles between the pyrazolyl mean planes are 110.9 and 70.0°, maximum deviations from the Rh coordination planes 0.037(5) and 0.074(4) Å, and mean

TABLE 5. Intraannular torsion angles (deg) standard deviations in parentheses

Atoms	Value (deg)
$(Me_2Gapz_2)Rh(COD)$*	
N(1)′—Rh—N(1)—N(2)	49.1(2)
Rh—N(1)—N(2)—Ga	−1.4(3)
N(2)′—Ga—N(2)—N(1)	−48.7(2)
C(4)—C(3)—C(3)′—C(4)′	0
C(3)′—C(3)—C(4)—C(5)	69.2(3)
C(3)—C(4)—C(5)—C(6)	0.9(5)
C(4)—C(5)—C(6)—C(6)′	−70.0(3)
C(5)—C(6)—C(6)′—C(5)′	0
$[Rh(\mu\text{-}3,5\text{-}Me_2pz)(CO)_2]_2$	
N(3)—Rh(1)—N(1)—N(2)	−56.8(3)
Rh(1)—N(1)—N(2)—Rh(2)	−4.8(3)
N(4)—Rh(2)—N(2)—N(1)	63.3(3)
N(2)—Rh(2)—N(4)—N(3)	−57.3(3)
Rh(1)—N(3)—N(4)—Rh(2)	−4.6(4)
N(1)—Rh(1)—N(3)—N(4)	63.0(3)
N(7)—Rh(3)—N(5)—N(6)	58.8(3)
Rh(3)—N(5)—N(6)—Rh(4)	2.3(4)
N(8)—Rh(4)—N(6)—N(5)	−62.4(3)
N(6)—Rh(4)—N(8)—N(7)	59.8(3)
Rh(3)—N(7)—N(8)—Rh(4)	0.8(4)
N(5)—Rh(3)—N(7)—N(8)	−61.2(3)
$[Rh(\mu\text{-}3,5\text{-}Me_2pz)(COD)]_2$	
N(3)—Rh(1)—N(1)—N(2)	67.2(2)
Rh(1)—N(1)—N(2)—Rh(2)	−3.2(2)
N(4)—Rh(2)—N(2)—N(1)	−62.1(2)
N(2)—Rh(2)—N(4)—N(3)	68.0(2)
Rh(1)—N(3)—N(4)—Rh(2)	−4.3(3)
N(1)—Rh(1)—N(3)—N(4)	−61.5(2)
C(18)—C(11)—C(12)—C(13)	−1.4(6)
C(11)—C(12)—C(13)—C(14)	−82.9(6)
C(12)—C(13)—C(14)—C(15)	19.3(7)
C(13)—C(14)—C(15)—C(16)	54.9(7)
C(14)—C(15)—C(16)—C(17)	3.0(6)
C(15)—C(16)—C(17)—C(18)	−83.8(5)
C(16)—C(17)—C(18)—C(11)	17.0(6)
C(12)—C(11)—C(18)—C(17)	59.0(6)
C(26)—C(19)—C(20)—C(21)	1.3(6)
C(19)—C(20)—C(21)—C(22)	−81.6(7)
C(20)—C(21)—C(22)—C(23)	14.7(8)
C(21)—C(22)—C(23)—C(24)	59.4(7)
C(22)—C(23)—C(24)—C(25)	1.1(6)
C(23)—C(24)—C(25)—C(26)	−81.1(5)
C(24)—C(25)—C(26)—C(19)	14.7(7)
C(20)—C(19)—C(26)—C(25)	59.7(6)

* Mirror-related torsion angles have the opposite sign.

deviations of Rh from the pyrazolyl mean planes 0.136 and 0.416 Å, respectively, for the two molecules. The dihedral angles between the two metal coordination planes of 78.7° for the carbonyl complex and 71.7° for the COD complex are the smallest yet reported for this type of dinuclear Rh complex.

Acknowledgments

We thank the Natural Sciences and Engineering Research Council of Canada for financial support and the University of British Columbia Computing Centre for assistance.

1. K. R. BREAKELL, D. J. PATMORE, and A. STORR. J. Chem. Soc. Dalton Trans. 749 (1975).
2. D. J. PATMORE, D. F. RENDLE, A. STORR, and J. TROTTER. J. Chem. Soc. Dalton Trans. 718 (1975).
3. F. G. HERRING, D. J. PATMORE, and A. STORR. J. Chem. Soc. Dalton Trans. 711 (1975).
4. D. F. RENDLE, A. STORR, and J. TROTTER. J. Chem. Soc. Dalton Trans. 176 (1975).
5. K. S. CHONG, S. J. RETTIG, A. STORR, and J. TROTTER. Can. J. Chem. **59**, 996 (1981).
6. S. E. ANSLOW, K. S. CHONG, S. J. RETTIG, A. STORR, and J. TROTTER. Can. J. Chem. **59**, 3173 (1981).
7. K. R. BREAKELL, S. J. RETTIG, D. L. SINGBEIL, A. STORR, and J. TROTTER. Can. J. Chem. **56**, 2099 (1978).
8. P. MEAKEN, S. TROFIMENKO, and J. P. JESSON. J. Am. Chem. Soc. **94**, 5677 (1972).
9. P. COPPENS, L. LEISEROWITZ, and D. RABINOVICH. Acta Crystallogr. **18**, 1035 (1965).
10. W. R. BUSING and H. A. LEVY. Acta Crystallogr. **22**, 457 (1967).
11. D. T. CROMER and J. B. MANN. Acta Crystallogr. Sect. A, **24**, 321 (1968).
12. R. F. STEWART, E. R. DAVIDSON, and W. T. SIMPSON. J. Chem. Phys. **42**, 3175 (1965).
13. D. T. CROMER and D. LIBERMAN. J. Chem. Phys. **53**, 1891 (1970).
14. P. J. BECKER AND P. COPPENS. Acta Crystallogr. Sect. A, **30**, 129 (1974); **30**, 148 (1974); **31**, 417 (1975).
15. P. COPPENS and W. C. HAMILTON. Acta Crystallogr. Sect. A, **26**, 71 (1970).
16. F. R. THORNLEY and R. J. NELMES. Acta Crystallogr. Sect. A, **30**, 748 (1974).
17. V. SCHOMAKER and K. N. TRUEBLOOD. Acta Crystallogr. Sect. B, **24**, 63 (1968).
18. D. W. J. CRUICKSHANK. Acta Crystallogr. **9**, 747 (1956); **9**, 754 (1956); **14**, 896 (1961).
19. S. TROFIMENKO. Inorg. Chem. **10**, 1372 (1971).
20. R. B. KING and A. BOND. J. Organomet. Chem. **73**, 115 (1974).
21. F. BONATI, G. MINGHETTI, and G. BANDITELLI. J. Organomet. Chem. **87**, 365 (1975).
22. H. C. CLARK and S. GOEL. J. Organomet. Chem. **165**, 383 (1979).
23. M. COCIVERA, T. J. DESMOND, G. FERGUSON, B. KAITNER, F. J. LALOR, and D. J. O'SULLIVAN. Organometallics, **1**, 1125 (1982).
24. M. COCIVERA, G. FERGUSON, B. KAITNER, F. J. LALOR, D. J. O'SULLIVAN, M. PARVEZ, and B. RUHL. Organometallics, **1**, 1132 (1982).
25. M. COCIVERA, G. FERGUSON, F. J. LALOR, and P. SZCZECINSKI. Organometallics, **1**, 1139 (1982).
26. N. F. BORKETT and M. I. BRUCE. J. Organomet. Chem. **65**, C51 (1974).
27. S. MAY, P. REINSALU, and J. POWELL. Inorg. Chem. **19**, 1582 (1980).
28. D. F. RENDLE, A. STORR, and J. TROTTER. Can. J. Chem. **53**, 2944 (1975).
29. G. BANDITELLI, A. L. BANDINI, F. BONATI, and G. MINGHETTI. J. Organomet. Chem. **218**, 229 (1981).
30. R. USON, L. A. ORO, M. A. CIRIANO, M. T. PINILLOS, A. TIRIPICCHIO, and M. CARMELLINI. J. Organomet. Chem. **205**, 247 (1981).
31. M. COWIE and S. K. DWIGHT. Inorg. Chem. **19**, 2508 (1980).
32. A. W. COLEMAN, D. T. EADIE, S. R. STOBART, M. J. ZAWOROTKO, and J. L. ATWOOD. J. Am. Chem. Soc. **104**, 922 (1982).
33. K. A. BEVERIDGE, G. W. BUSHNELL, K. R. DIXON, D. T. EADIE, and S. R. STOBART. J. Am. Chem. Soc. **104**, 920 (1982).

Can. J. Chem. Downloaded from www.nrcresearchpress.com by 210.87.254.42 on 09/06/12
For personal use only.

Hydrolysis of trioxaadamantane ortho esters. I. Dialkoxycarbocation – ortho ester equilibrium and acidity function

ROBERT A. MCCLELLAND AND PATRICK W. K. LAM

Department of Chemistry, University of Toronto, Scarborough Campus, Scarborough, Ont., Canada M1C 1A4

Received November 9, 1983

ROBERT A. MCCLELLAND and PATRICK W. K. LAM. Can. J. Chem. **62**, 1068 (1984).

3-Aryl-2,4,10-trioxaadamantane ortho esters (T) undergo a rapid equilibration with a ring-opened dioxan-2-ylium ion (DH^+) prior to hydrolysis to product (a 1,3,5-cyclohexanetriol monobenzoate). The cation is stable in concentrated H_2SO_4 solutions where it has been characterized by nmr spectroscopy. It is observed using uv spectroscopy in dilute acids, and the ratio $[DH^+]/[T]$ at equilibrium has been measured as a function of acidity. Reversibility of the ring opening is established by the pattern of plots of cation absorbance versus acid concentration and by the observation that solutions containing cation on neutralization or dilution yield ortho ester, not hydrolysis product. Equilibrium constants for the reaction $DH^+ \rightleftharpoons T + H^+$ have been measured by obtaining the acidity function H_T for this system. The effects of the aromatic substituent and the steepness of the acidity function plot versus acid concentration are interpreted in terms of a strong intramolecular interaction in the cation between the cationic center and the hydroxyl oxygen.

ROBERT A. MCCLELLAND et PATRICK W. K. LAM. Can. J. Can. J. Chem. **62**, 1068 (1984).

Les ortho esters (T), aryl-3 trioxaadamantane-2,4,10, subissent un équilibre rapide avec le cycle ouvert, l'ion dioxannyl-2 ium (DH^+), avant leur hydrolyse en produit (un monobenzoate du cyclohexanetriol-1,3,5). Le cation est stable dans des solutions concentrées d'acide sulfurique dans lesquelles il a été caractérisé par spectroscopie rmn. Faisant appel à la spectroscopie uv, il est possible de l'observer en solutions acides diluées et on a mesuré le rapport $[DH^+]/[T]$ à l'équilibre en fonction de l'acidité. On a établi que l'ouverture du cycle est réversible en se basant sur l'allure des courbes d'absorption du cation en fonction de la concentration d'acide et aussi par l'observation que, lors de leur neutralisation ou de leur dilution, des solutions contenant du cation conduisent à des ortho esters plutôt qu'à des produits d'hydrolyse. On a mesuré les constantes d'équilibre pour la réaction $DH^+ \rightleftharpoons T + H^+$ en obtenant la fonction d'acidité, H_T, pour ce système. On a interprété les effets des substituants aromatiques et la forte pente de la courbe de la fonction d'acidité en fonction de la concentration en faisant appel à une forte interaction moléculaire entre le centre cationique et l'oxygène hydroxylique dans le cation.

[Traduit par le journal]

Equations [1]–[3] depict the three-stage reaction mechanism now accepted (1, 2) for the hydrolysis of an ortho ester.

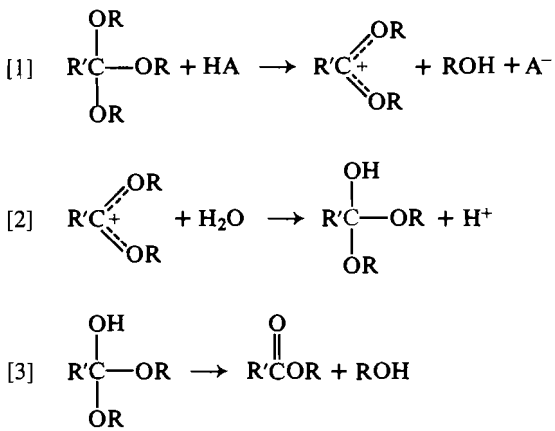

Although the first reaction stage is in principle reversible, hydrolyses are usually carried out in a large excess of water, and under these conditions the probability is low that the cation once formed will undergo the back reaction with the small amount of alcohol being released. This situation could be different with cyclic systems, where a ring opens in the first stage. Here the reverse is an intramolecular ring closure, and this could in principle compete with water addition, even with water as solvent. Such a reversible ring opening has been suggested with cyclic acetals as the explanation behind their diminished hydrolytic reactivity (3). Evidence for reversibility has been obtained in two instances (4, 5), although in both cases the rates of water addition and the ring closure were quite similar.

The subject of this paper is the 2,4,10-trioxaadamantane (T) system. These ortho esters are ideally set up for a reversible

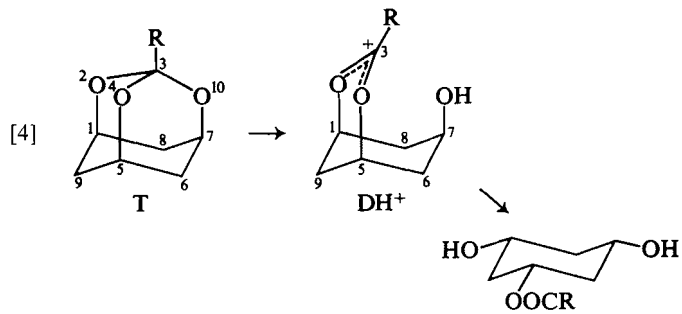

ring opening since the departing hydroxyl group is forced to remain in close proximity to the cationic center. Lamaty, Moreau and co-workers (6, 7) were the first to suggest that pronounced reversibility does occur. Their suggestion was based on three kinetic observations: enormously retarded (10^6–10^9) rates of hydrolysis compared with those of acyclic analogs, negative entropies of activation, and a substituent effect, $k(3\text{-H}) > k(3\text{-CH}_3)$, opposite to that expected for rate-limiting cation formation. We have reported (8) in preliminary form verification of reversibility, in the actual observation of the 1,3-dioxan-2-ylium ion DH^+ in equilibrium with ortho ester. Although oxocarbocations can be isolated as stable salts or solutions (9) or observed as transient intermediates (2, 10–12), this represents the first example where equilibration with an acetal or ortho ester precursor is involved. We have now carried out a detailed study of the system. In this paper we discuss the quantitative aspects of the ring-opening equilibrium. The next paper presents a kinetic analysis of the overall hydrolysis.

Can. J. Chem. Downloaded from www.nrcresearchpress.com by 210.87.254.105 on 09/06/12
For personal use only.

Can. J. Chem. Downloaded from www.nrcresearchpress.com by 210.87.254.105 on 09/06/12
For personal use only.

Experimental

Materials

Substituted trimethyl orthobenzoates were prepared using the benzanilide acetal procedure recently reported by us (13). Compounds prepared, overall yield, and bp are as follows: trimethyl 4-methoxyorthobenzoate, 75%, 85°C/0.3 Torr; trimethyl 4-methylorthobenzoate, 75%, 80°C/0.3 Torr; trimethyl 4-chloroorthobenzoate, 70%, 90°C/0.3 Torr; trimethyl 3-chloroorthobenzoate, 91%, 69°C/0.3 Torr; trimethyl 4-nitroorthobenzoate, 78%, mp 56–57°C. The 2,4,10-trioxaadamantanes were prepared by exchange of the trimethyl ortho ester and cyclohexane-1β,3β,5β-triol (14), using the procedure of Stetter and Steinacker (15). Purification involved recrystallization from methanol. Despite several attempts using various conditions, the procedure failed with trimethyl 4-methoxyorthobenzoate, the major product being the methyl ester of 4-methoxybenzoic acid. The following lists the 3-substitutent, the temperature employed in the exchange, yield, melting point, ^{1}H nmr spectral data for the 3-aryl substituent, and analytical data. The nmr spectra were recorded in $CDCl_3$, $(CH_3)_4Si$ reference. The ^{1}H nmr associated with the trioxaadamantane portion was the same in every case, δ: 4.5–4.6 (3H, wide singlet, H1, H5, H7), 2.75 (3H, d, H6e, H8e, H9e), 1.75 (3H, d, H6a, H8a, H9a).

3-(4-Methylphenyl)-2,4,10-trioxaadamantane: 45°C, 65%, 177–178°C; δ: 7.56 (2H, d, ArH), 7.08 (2H, d, ArH), 2.32 (3H, s, CH_3). *Anal.* calcd. for $C_{14}H_{16}O_3$: C 72.39, H 6.94; found: C 72.51, H 7.11.

3-Phenyl-2,4,10-trioxaadamantane: 25°C, 82%, 176–177°C (lit. (12) mp 176–177°C); δ: 7.5–7.8 (2H, m, ArH), 7.1–7.3 (3H, m, ArH); ^{13}C nmr ($CDCl_3$, $(CH_3)_4Si$), δ: 139.6, 129.0, 128.0, 125.1, 108.9 (C3), 68.9 (C1, C5, C7), 33.0 (C6, C8, C9).

3-(4-Chlorophenyl)-2,4,10-trioxaadamantane: 10°C, 62%, 149–150°C; δ: 7.72 (2H, d, ArH), 7.31 (2H, d, ArH). *Anal.* calcd. for $C_{13}H_{13}O_3Cl$: C 61.79, H 5.19; found: C 61.73, H 5.12.

3-(3-Chlorophenyl)-2,4,10-trioxaadamantane: 5°C, 71%, 135–136°C'; δ: 7.1–7.7 (4H, m). *Anal.* calcd. for $C_{13}H_{13}O_3Cl$: C 61.79, H 5.19; found: C 61.95, H 5.26.

3-(4-Nitrophenyl)-2,4,10-trioxaadamantane: 0°C, 45%, 231.5–233°C; δ: 8.18 (2H, d, ArH), 7.76 (2H, d, ArH). *Anal.* calcd. for $C_{13}H_{13}O_5N$: C 59.31, H 4.98; found: C 59.21, H 4.87.

The cations DH^+ were prepared as stable solutions in 80–100% H_2SO_4 or D_2SO_4 by the slow addition of the solid ortho ester to the stirred acid solution cooled in an ice bath. The nmr spectra were recorded in D_2SO_4 with external $(CH_3)_4Si$ as standard. Chemical shift values (uncorrected for bulk susceptibility differences) recorded for the cation DH^+ with R = phenyl in 75% D_2SO_4 are as follows: ^{1}H nmr, δ: 8.1–8.3 (2H, m, *ortho* ArH), 7.5–7.8 (3H, m, *meta* + *para* ArH), 5.75 (2H, wide singlet, H1, H5), 5.35 (1H, wide singlet, H7), 3.3 (2H, d, H6e, H8e), 2.2–2.6 (4H, m, H9e, H6a, H8a, H9a); ^{13}C nmr, δ: 188.8 (C3), 149.4, 141.2, 139.4, 132.6 (all phenyl), 90.0 (2C, C1, C5), 84.4 (1C, C7), 43.1 (2C, C6, C8), 35.8 (1C, C9).

Cation – ortho ester equilibrium constants

Measurements were performed on a Unicam SP 1800 ultraviolet spectrophotometer equipped with a thermostatically controlled cell-block at 25.0 ± 0.1°C. A methanolic solution of the trioxaadamantane (5.0 μL) was injected into 2.5 mL of the thermostatted acid solution to give final concentrations of approximately 10^{-4} molar ortho ester. The absorbance was recorded at the λ_{max} of the cation DH^+ (4-$CH_3C_6H_4$, 283 nm; C_6H_5, 260 nm; 4-ClC_6H_4, 286 nm; 3-ClC_6H_4, 267 nm; 4-$NO_2C_6H_4$, 272 nm). The plot of absorbance versus time was extrapolated to zero time (time of mixing) to provide the absorbance of the solution before any hydrolysis had occurred.

Results and discussion

Cation identification

Solutions of dialkoxycarbocations can usually be obtained by addition of ortho esters to concentrated sulfuric acid (9, 16–19), taking advantage of the low nucleophilicity of the medium to stabilize the cation. This is true also in the present case, with the cations DH^+ being easily characterized by nmr spectroscopy. Figures 1 and 2 show ^{13}C nmr spectra of 3-phenyl-2,4,10-trioxaadamantane in $CDCl_3$ and 75% D_2SO_4 respectively. The symmetry in the ortho ester results in only three signals, in addition to those associated with the 3-substituent. This symmetry is reduced when the cation forms and this appears as a splitting of the signals due to $C_{6,8,9}$ and to $C_{1,5,7}$ into two signals each in a 2:1 ratio. A large downfield shift in the signal due to the C_3 carbon also occurs. The ^{1}H nmr spectrum of this solution is also consistent with the cation structure (see Experimental), although the complexity of the signals makes the analysis more difficult. The ester product can be ruled out as being responsible for the concentrated acid spectra. This product is obtained in more dilute acids (less than 50% H_2SO_4), and it does have the same number of ^{13}C nmr signals as the cation, but their positions are very different.

Three other comments can be made regarding these concentrated acid solutions. (*i*) The cations DH^+ can tolerate a sizeable amount of water and remain stable in the solution; for instance, the spectrum in Fig. 2 is unchanged after one week. In contrast, other dialkoxycarbocations are stable only in very concentrated acids. The phenyldimethoxycarbocation, for example, is stable above 95% H_2SO_4, but its half-life in 75% H_2SO_4 is only 1 s (18). (*ii*) There is perhaps some indication of a diprotonated species, that is, protonation of the hydroxyl oxygen of DH^+. As the acid concentration is increased from 75% D_2SO_4 to 100% D_2SO_4, the spectral pattern remains unchanged but there are some changes in the relative chemical shifts. A particularly significant change is observed in the relative positions of the two signals due to $C_{1,5}$ and C_7, with the C_7 signal moving downfield at higher acidity. (*iii*) The observation of separate signals for $C_{1,5}$ and C_7 and for $C_{6,8}$ and C_9 indicates that there is no scrambling on the nmr time scale. This could occur by ring closure of the cation to the trioxaadamantane followed by ring opening in another direction. Interestingly, the temperature-jump kinetic measurements (accompanying paper) show that in dilute acids ring closure would be sufficiently rapid (half-lives of 10^{-5} to 10^{-4} s) for this isomerization to be observed in the nmr as a coalescence for signals. The cations unfortunately are not stable enough in these solutions for ^{13}C nmr spectra to be obtained. The slowing down of the ring closure in more concentrated acids may in part be associated with the protonation of the OH group. More importantly in our opinion it represents a requirement for an additional water molecule, functioning as a base to remove the OH proton as the ring closes. The requirement for this base

[5] 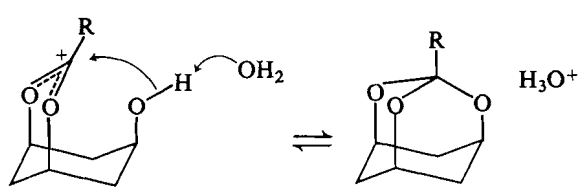

is also seen in the addition of water to protonated esters (20) and dialkoxycarbocations (19). The rates of these reactions fall off considerably more rapidly with increased acid concentration than is expected on the basis of the decrease in water activity, slopes of log k versus log a_{H_2O} being two and greater. This is interpreted (19, 20) in terms of a mechanism in which, in addition to the water molecule which acts as a nucleophile, a second water is present to remove the proton.

Can. J. Chem. Downloaded from www.nrcresearchpress.com by 210.87.254.105 on 09/06/12
For personal use only.

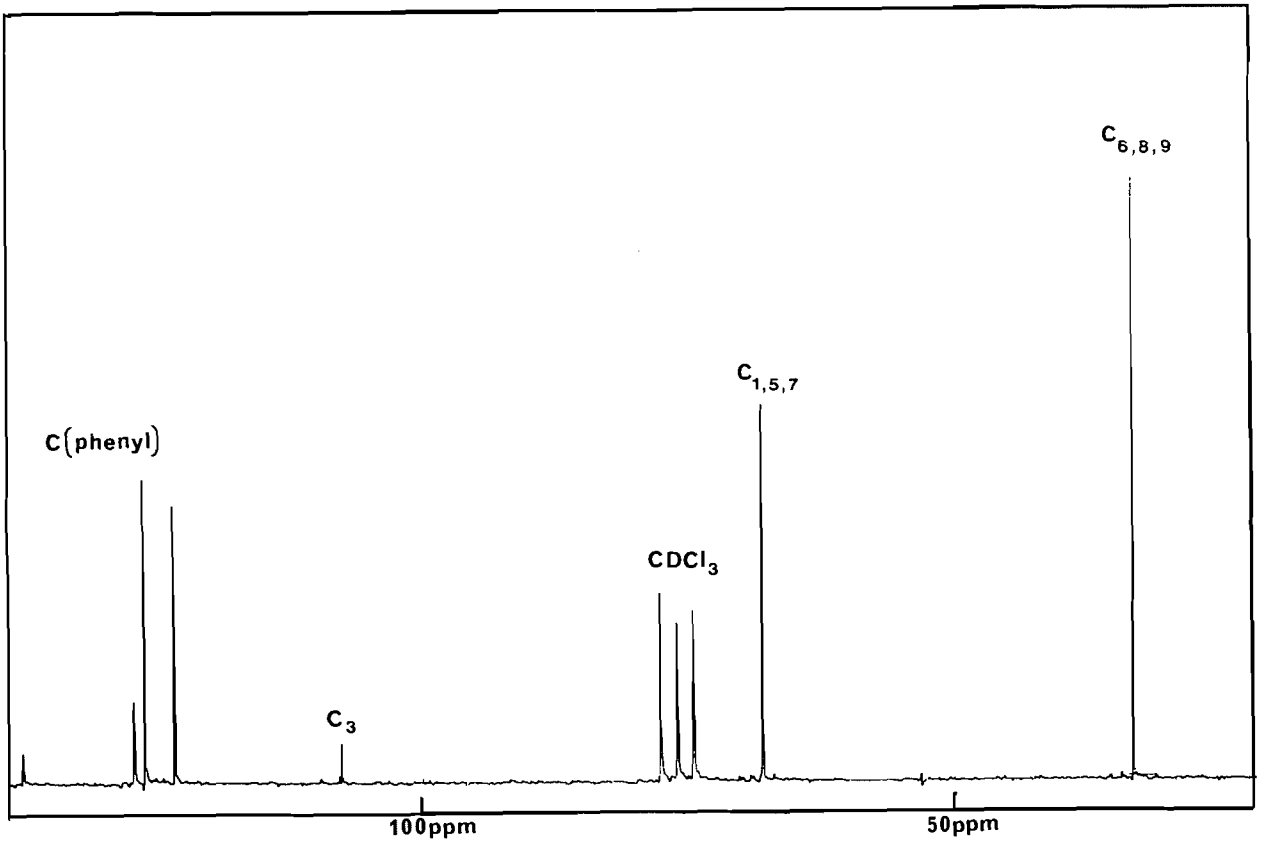

FIG. 1. The ^{13}C nmr spectrum of 3-phenyl-2,4,10-trioxaadamantane in $CDCl_3$, with $(CH_3)_4Si$ internal reference.

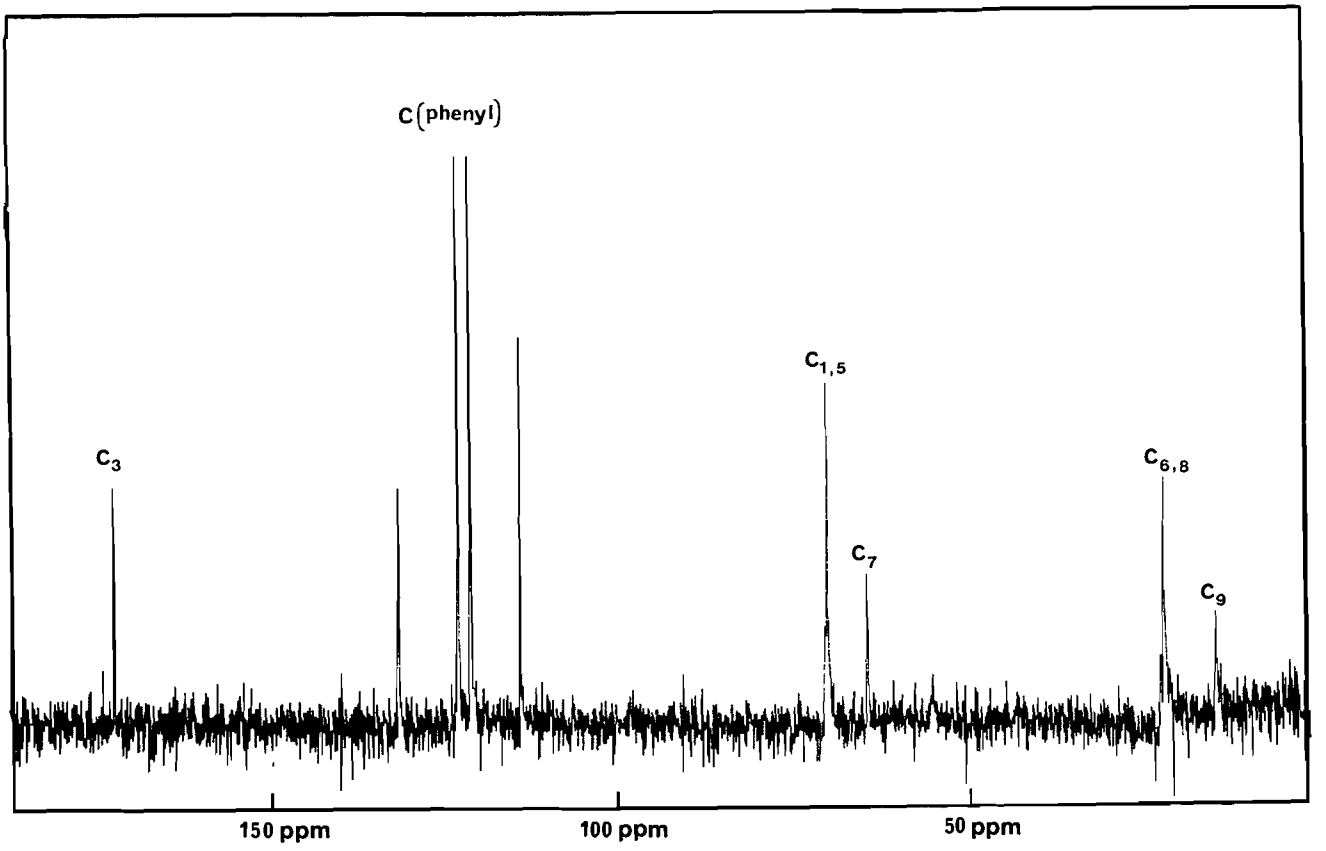

FIG. 2. The ^{13}C nmr spectrum of 3-phenyl-2,4,10-trioxaadamantane in 75% D_2SO_4, with $(CH_3)_4Si$ external reference.

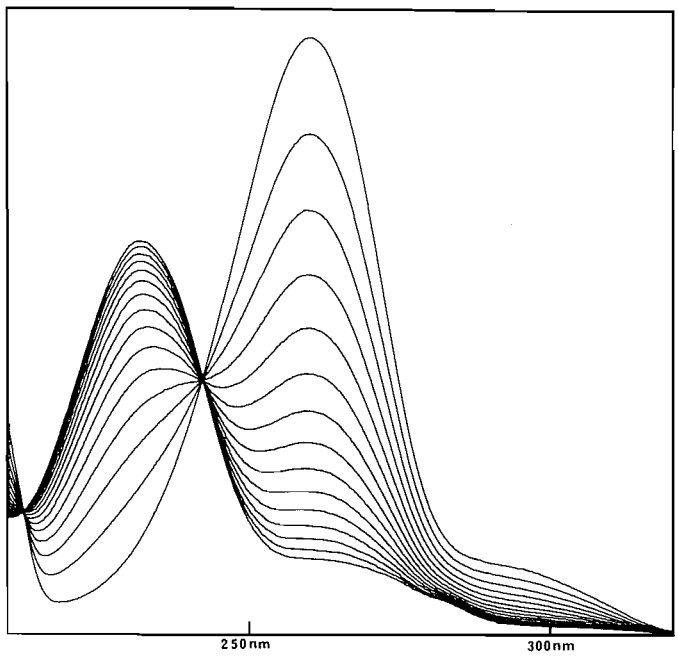

FIG. 3. The uv spectral change for 3-phenyl-2,4,10-trioxaadamantane in 35% H_2SO_4, showing the conversion of the cation DH^+ to ester product. Spectra were recorded at 10-min intervals.

Reversible ring opening

The cations DH^+ can also be observed in more dilute acids, but they are less stable here and have been identified using uv spectroscopy. 3-Phenyl-2,4,10-trioxaadamantane itself exhibits little uv absorbance at wavelengths above 220 nm, except for weak absorbance near 260 nm associated with the benzene chromophore. Hydrolysis in dilute acids (pH > 1) results in the appearance of a strong absorbance with λ_{max} at 232 nm. This new peak is due to the benzoate ester product, and the behavior here is typical of a benzoic acid ortho ester derivative (2, 21–23). What makes the trioxaadamantane very different, however, is the behavior in slightly more concentrated acids, where a new peak with λ_{max} at 260 nm appears (Fig. 3). This peak can be assigned to the cation DH^+ with R = phenyl. The same absorbance is found in more concentrated acids where the cation can be characterized by nmr spectroscopy, as just discussed. Spectra with λ_{max} near 260 nm are also observed with other phenyl substituted dialkoxycarbocations (2, 18, 19, 23). The other trioxaadamantanes also produce cations in moderately concentrated acids (see Experimental for λ_{max}).

The appearance of the cation in these acids is extremely rapid, too rapid in fact to be observed even with stopped-flow spectroscopy. That is, the formation of the cation signal is complete within the stopped-flow dead-time (2 ms) when a neutral aqueous solution of trioxaadamantane is mixed with aqueous H_2SO_4. As shown in Fig. 3, the cation signal slowly disappears, accompanied by the appearance at the same rate of the ester peak at 232 nm. The rate of this reaction varies with acidity, passing through a maximum around 20–30% H_2SO_4. At the maximum the half-life is about 6 min.

A further significant observation is that the relative amount of cation which is produced in the rapid reaction increases with acidity, eventually reaching a maximum value. This is shown in Fig. 4, which plots the initial absorbance at the λ_{max} of the cation for three trioxaadamantanes. "Initial" in this context refers to an extrapolation to zero time on a conventional uv

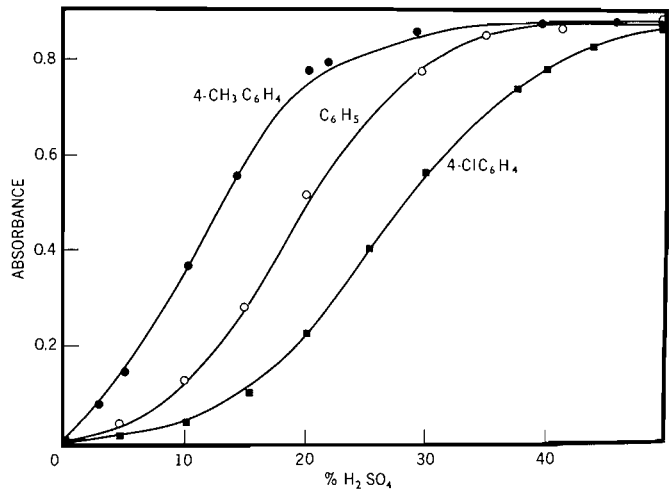

FIG. 4. Initial cation absorbance for solutions of 3-aryl-2,4,10-trioxaadamantanes in aqueous H_2SO_4. Wavelengths: 4-$CH_3C_6H_4$, 283 nm; C_6H_5, 260 nm; 4-ClC_6H_4, 286 nm. The concentration of trioxaadamantane in each system was constant (about 5×10^{-5} mol/L.

spectrophotometer. This represents a situation where cation formation is complete but the subsequent reaction which produces ester has not yet commenced.The sigmoidal shaped curves in Fig. 4 are typical of a system undergoing acid–base equilibration. They suggest that what is being observed is the acid-dependent equilibration of trioxaadamantane and ortho ester. That this process is rapid compared to the further reaction

$$[6] \quad DH^+ \rightleftharpoons T + H^+$$

of the cation to give ester is obvious from the rates of the uv spectral changes, as just discussed. The reversibility of the cation formation is evident from the uv spectral behavior. Moreover, if acid solutions are diluted or neutralized, trioxaadamantane is produced, not ester.

Equilibrium constants and acidity function

The equilibrium in question here has the form of a weak organic base being converted to a conjugate acid in moderately concentrated acids, and it can be analyzed using the acidity function method (24). The ratio of cation to trioxaadamantane, the "ionization ratio", has been calculated from the sigmoidal curves using the standard method (24),

$$[7] \quad \frac{[DH^+]}{[T]} = \frac{A - A_0}{A_a - A}$$

where A, A_0, and A_a represent absorbance values in the acid in question, water, and 60–90% H_2SO_4, respectively. A listing of absorbance and ionization ratio data is given in Table S1.[1] The thermodynamic dissociation constant is defined as

$$[8] \quad K_{DH^+} = \frac{a_{H^+} a_T}{a_{DH^+}}$$

where activities refer to water as the standard state. In the usual way (24), the value of this constant for the 4-methylphenyl compound has been obtained by extrapolation of the quantity $[H^+][T]/[DH^+]$ to zero acid concentration. Values for the other

[1]Supplementary material is available, at a nominal charge, from the Depository of Unpublished Data, CISTI, National Research Council of Canada, Ottawa, Ontario, Canada K1A 0S2.

Can. J. Chem. Downloaded from www.nrcresearchpress.com by 210.87.254.105 on 09/06/12
For personal use only.

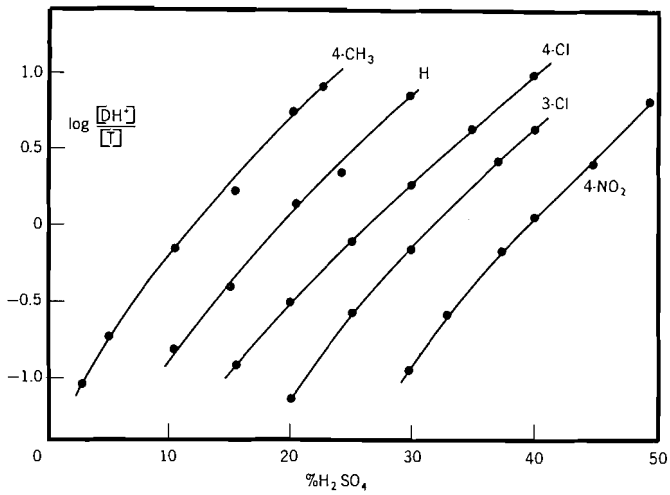

FIG. 5. The logarithm of the ionization ratio $[DH^+]/[T]$ as a function of sulfuric acid concentration.

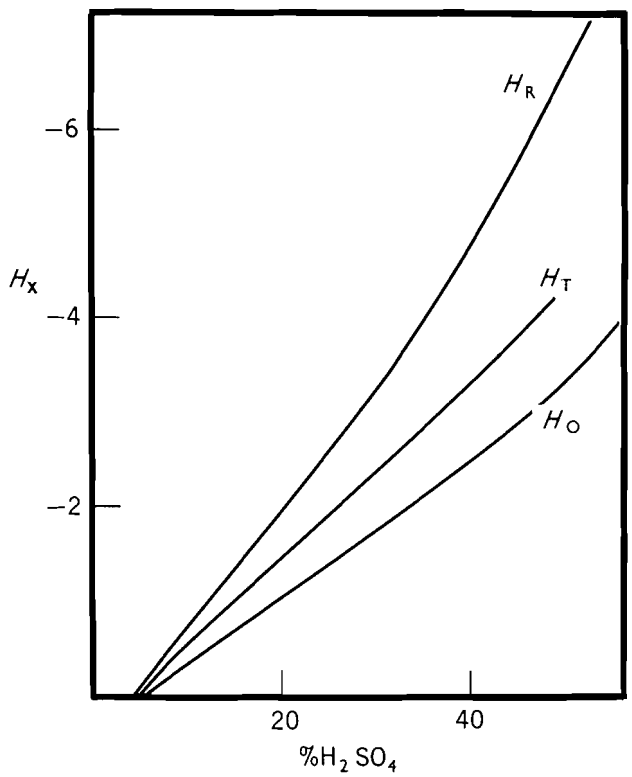

FIG. 6. Acidity functions in aqueous sulfuric acid. Values for H_R, H_T, and H_0 from ref. 25.

ortho esters have then been obtained using the overlap method (24). As seen in Fig. 5, the overlap and parallelism between successive ionization ratio curves is good. Values of pK_{DH^+} obtained in this way are listed in Table 1. The acidity function for this system is defined as

$$[9] \quad H_T = -\log \frac{a_{H^+} f_T}{f_{DH^+}}$$

This has been calculated as $H_T = pK_{DH^+} - \log [DH^+]/[T]$. Values are listed in Table 2, and displayed graphically as a function of acid concentration in Fig. 6.

This represents the first time when the equilibrium constants for conversion of an ortho ester to its dialkoxycarbocation have been measured directly under hydrolytic conditions. Values for trimethyl orthobenzoates (eqs. [10], [11]) have been indirectly

$$[10] \quad \overset{+}{\text{ArC}}(\text{OMe})_2 + \text{MeOH} \underset{k_r}{\overset{k_f}{\rightleftharpoons}} \text{ArC}(\text{OMe})_3 + \text{H}^+$$

$$[11] \quad K_{DH^+} = \frac{[\text{ArC}(\text{OMe})_3][\text{H}^+]}{[\text{ArC}(\text{OMe})_2{}^+][\text{MeOH}]} = \frac{k_f}{k_r}$$

estimated (19) as the ratio k_f/k_r. The k_r value is measured; the k_f value is calculated as $k(H_2O)/55$ where $k(H_2O)$ represents the rate constant for cation hydration estimated by extrapolation to water of rate measurements made in concentrated H_2SO_4. Figure 7 shows Hammett plots for the two systems. Although the actual pK values are quite similar, there is a significant difference in the ρ values. This may reflect a strong interaction between the hydroxyl oxygen and cationic center in the trioxaadamantane system. Such an interaction would delocalize positive charge, so that the effect of aromatic substituents would be attenuated.

[12]

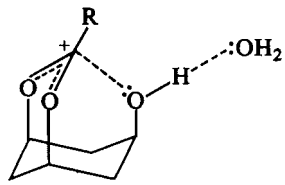

The acidity dependence of the equilibrium as seen in the H_T acidity function provides further evidence for this interaction. It is now well established (26) that the steepness of acidity functions in plots of the acidity function versus acid concentration is determined mainly by the solvation requirements of the charged species involved. At one extreme lies the H_R acidity function with a very steep dependence arising because triarylcarbocations, being large and delocalized, require very little solvation. At the other extreme the alcohol acidity function H_{ROH} has a very shallow dependency (27), reflecting the strong solvation of the protonated alcohol through hydrogen bonding of the O^+—H···OH type. The H_T acidity function represents what in principle is an intramolecular analog of the triarylcarbocation−triarylcarbinol equilibrium. It is interesting, therefore, that its dependency on acidity is not nearly as

TABLE 1. Dissociation constants for the equilibration of 3-aryl-2,4,10-trioxaadamantanes and their ring-opened dioxanylium ion forms

Aromatic substituent	pK_{DH^+}
4-CH_3	−0.77
H	−1.19
4-Cl	−2.00
3-Cl	−2.47
4-NO_2	−3.24

TABLE 2. Values of the H_T acidity function

% H_2SO_4	H_T	% H_2SO_4	H_T
4	+0.07	28	−2.20
8	−0.36	32	−2.58
12	−0.72	36	−2.94
16	−1.10	40	−3.32
20	−1.47	44	−3.71
24	−1.82	48	−4.12

Can. J. Chem. Downloaded from www.nrcresearchpress.com by 210.87.254.105 on 09/06/12
For personal use only.

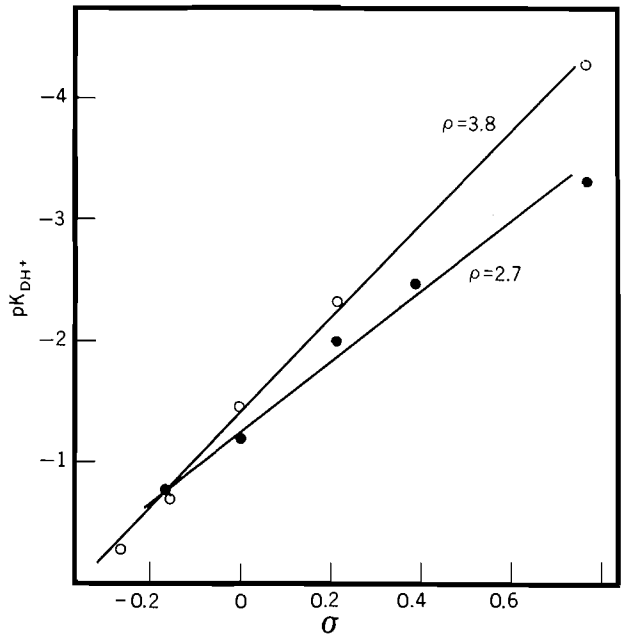

FIG. 7. Hammett plots for equilibrium constants for conversion of ortho esters to dialkoxycarbocations. (●) 3-aryl-2,4,10-trioxadamtanes; (○) trimethyl orthobenzoates.

steep, suggesting a much greater solvation in the dioxan-2-ylium cation. The interaction pictured in [12] would place some positive charge on the hydroxyl oxygen. This could result in the cation having some of the characteristics of a protonated alcohol or ether, with a relatively strong hydrogen bond between the OH group and a solvent water molecule. This would cause the acidity function to rise less steeply.

Evidence that a strong intramolecular interaction should exist comes from a crystal structure of a carbonate analog (28). The distance between the carbonyl carbon and hydroxyl

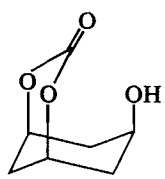

oxygen in this molecule is only 2.93 Å, less than the sum of the van der Waals radii of these groups.

Acknowledgements

Continued financial support of the Natural Sciences and Engineering Research Council of Canada is gratefully acknowledged.

1. E. H. CORDES and H. G. BULL. Chem. Rev. **74**, 581 (1974).
2. M. AHMAD, R. G. BERGSTROM, M. J. CASHEN, Y. CHIANG, A. J. KRESGE, R. A. McCLELLAND, and M. F. POWELL. J. Am. Chem. Soc. **101**, 2669 (1979).
3. A. V. WILLI. *In* Comprehensive chemical kinetics. Vol. 8. *Edited by* C. H. Bamford and C. F. H. Tipper. Elsevier, Amsterdam. 1977. pp. 49–52.
4. B. CAPON and M. I. PAGE. Chem. Commun. 1443 (1970).
5. R. A. McCLELLAND, M. AHMAD, and G. MANDRAPILIAS. J. Am. Chem. Soc. **101**, 970 (1979).
6. O. BOUAB, G. LAMATY, and C. MOREAU. J. Chem. Soc. Chem. Commun. 678 (1978).
7. O. BOUAB, G. LAMATY, C. MOREAU, O. POMARES, P. DESLONGCHAMPS, and L. RUEST. Can. J. Chem. **58**, 567 (1980).
8. P. W. K. LAM and R. A. McCLELLAND. J. Chem. Soc. Chem. Commun. 883 (1980).
9. H. PERST. Oxonium ions in organic chemistry. Academic Press, New York. 1971.
10. R. A. McCLELLAND and M. AHAMD. J. Am. Chem. Soc. **100**, 7027 (1978).
11. R. A. McCLELLAND, R. SOMANI, and A. J. KRESGE. Can. J. Chem. **57**, 2260 (1979).
12. R. A. McCLELLAND and M. ALIBHAI. Can. J. Chem. **59**, 1169 (1981).
13. R. A. McCLELLAND, G. PATEL, and P. W. K. LAM. J. Org. Chem. **46**, 1011 (1981).
14. H. STETTER and K. H. STEINACKER. Chem. Ber. **85**, 453 (1952); P. N. STRONG and J. F. W. KEANA. J. Org. Chem. **40**, 956 (1975).
15. H. STETTER and K. H. STEINACKER. Chem. Ber. **86**, 970 (1953); **87**, 205 (1954).
16. B. G. RAMSAY and R. W. TAFT. J. Am. Chem. Soc. **88**, 3058 (1966).
17. D. BRUCK and M. RABINOVITZ. J. Chem. Soc. Perkin Trans. 2, 1656 (1975).
18. R. A. McCLELLAND and M. AHMAD. J. Am. Chem. Soc. **99**, 5356 (1977).
19. R. A. McCLELLAND and M. AHMAD. J. Am. Chem. Soc. **100**, 7031 (1978).
20. K. YATES and R. A. McCLELLAND. J. Am. Chem. Soc. **89**, 2686 (1967); K. YATES. Acc. Chem. Res. **4**, 136 (1971).
21. H. G. BULL, K. KOEHLER, T. C. PLETCHER, J. J. ORTIZ, and E. H. CORDES. J. Am. Chem. Soc. **93**, 3002 (1971).
22. Y. CHIANG, A. J. KRESGE, P. SALOMAA, and C. I. YOUNG. J. Am. Chem. Soc. **96**, 4494 (1974).
23. R. A. McCLELLAND, S. GEDGE, and J. BOHONEK. J. Org. Chem. **46**, 886 (1981).
24. C. H. ROCHESTER. Acidity functions. Academic Press, London. 1970.
25. R. H. BOYD. *In* Solute–solvent interactions. *Edited by* J. F. Coetzee and C. D. Ritchie. Marcel Dekker, New York. 1969. pp. 97–218.
26. K. YATES and R. A. McCLELLAND. Prog. Phys. Org. Chem. **11**, 327 (1974).
27. D. C. LEE and R. CAMERON. J. Am. Chem. Soc. **93**, 4724 (1971).
28. W. WONG-NG and S. C. NYBURG. Can. J. Chem. In press.

Can. J. Chem. Downloaded from www.nrcresearchpress.com by 210.87.254.105 on 09/06/12
For personal use only.

Hydrolysis of trioxaadamantane ortho esters. II. Kinetic analysis and the nature of the rate-determining step

ROBERT A. MCCLELLAND AND PATRICK W. K. LAM

Department of Chemistry, University of Toronto, Scarborough Campus, Scarborough, Ont., Canada M1C 1A4

Received November 9, 1983

ROBERT A. MCCLELLAND and PATRICK W. K. LAM. Can. J. Chem. **62**: 1074 (1984).

A detailed kinetic study of the hydrolysis of a series of 3-aryl-2,4,10-trioxaadamantanes is reported. These ortho esters equilibrate with the ring-opened dialkoxycarbocation, in a very rapid process which could be studied using temperature-jump spectroscopy for aryl = 2,4-dimethylphenyl. Relaxation rate constants are of the order of 10^4 s^{-1}; these could be analyzed to provide the rate constants for both the ring opening and the ring closing. Product formation from this equilibrating mixture is much slower. In acid solutions (0.01 *M* H^+ − 50% H_2SO_4), first-order rate constants for product formation initially increase with increasing acidity, but a maximum is reached at 20−35% H_2SO_4 and the rate then falls. This behavior is explained by a counterbalancing of two factors. Increasing acidity increases the amount of the dialkoxycarbocation in the initial equilibrium, but, outside the pH region, it decreases the rate of hydrolysis of this cation through a medium effect. Rate constants over a range of pH have been measured for two trioxaadamantanes and for the cation DEt^+ derived by treatment of the ortho ester with triethyloxonium tetraafluoroborate. The latter models the cation formed in the ortho ester hydrolysis but it cannot ring close. Rate−pH profiles obtained in these systems are more complex than expected on the basis of rate-determining cation hydration. An interpretation is proposed with a change in rate-determining step between high pH and low pH. Cation hydration is rate determining at high pH but at low pH hemiorthoester decomposition becomes rate determining. Under these conditions the hemiorthoester equilibrates with both the dialkoxycarbocation and with the trioxaadamantane. The change in rate-determining step occurs because acid-catalyzed reversion of the hemiorthoester to dialkoxycarbocation is a faster process than acid-catalyzed hemiorthoester decomposition. This makes the latter rate-determining in acid solutions. Additional pathways available to the decomposition, however, make it the faster process at higher pH. A kinetic analysis furnishes all of the rate and equilibrium constants for the system, and provides support for the mechanistic interpretation. A comparison of these numbers with those obtained for the three stages in the hydrolysis of a simple monocyclic ortho ester underlines the novelty of the trioxaadamantane system.

ROBERT A. MCCLELLAND et PATRICK W. K. LAM. Can. J. Chem. **62**: 1074 (1984).

On rapporte une étude cinétique détaillée de l'hydrolyse d'une série d'aryl-3 trioxa-2,4,10 adamantanes. Ces orthoesters s'équilibrent par un processus très rapide avec le dialkoxycarbocation à cycle ouvert; cette réaction peut être étudiée grâce à la spectroscopie de saut de *T* lorsque l'unité aryle = diméthyl-2,4 phényle. Les constantes de vitesse de relaxation sont de l'ordre de 10^4 s^{-1}; on peut les analyser pour obtenir les constantes de vitesse d'ouverture et de fermeture de cycle. La formation des produits à partir du mélange à l'équilibre est beaucoup plus lente. Dans des solutions acides (0,01 *M* H^+ − 50% H_2SO_4), la constante de vitesse d'ordre un de la formation du produit augmente au départ avec l'acidité mais elle atteint un maximum à 20−35% de H_2SO_4; ensuite, la vitesse diminue. On explique ce comportement par l'effet opposé de deux facteurs. L'augmentation de l'acidité augmente la quantité de dialkoxycarbocation dans l'équilibre de départ, mais, hors de la région du pH, elle diminue la vitesse d'hydrolyse de ce cation via un effet de milieu. On a mesuré les constantes de vitesse pour un grand intervalle de pH pour deux trioxaadamantanes et pour le cation DEt^+ obtenu en faisant réagir l'orthoester avec le tétrafluoroborate de triéthyloxonium. Ce dernier sert de modèle pour le cation qui se forme lors de l'hydrolyse de l'orthoester mais il ne peut pas se refermer pour donner un cycle. Les profils de vitesse vs. pH obtenus das ces systèmes sont plus complexes que ceux auquels on pourrait s'attendre si l'on fait l'hypothèse que l'étape déterminante de la réaction est l'hydratation du cation. On propose une interprétation qui implique l'existence d'étapes déterminantes aux pH fort et faible. A pH élevé, l'hydratation du cation serait l'étape déterminante, mais à pH faible, la décomposition de l'hémiorthoester deviendrait l'étape déterminante. Dans ces conditions, l'hémiorthoester se met en équilibre à la fois avec le dialkoxycarbocation et avec le trioxaadamantane. Les changements dans l'étape déterminante se produisent parce que la reconversion acido-catalysée de l'hémiorthoester en dialkoxycarbocation est un processus plus rapide que la décomposition acido-catalysée de l'hémiorthoester. Ceci fait que ce dernier processus devient l'étape déterminante pour les solutions acides. Cependant, des voies additionnelles de décomposition qui sont disponibles font que ce processus est le plus rapide à pH élevé. Une analyse cinétique fournit toutes les vitesses et toutes les constantes d'équilibre pour le système et apporte des arguments pour l'interprétation du mécanisme. Une comparaison de ces nombres avec ceux obtenus pour ces trois étapes de l'hydrolyse d'un orthoester monocyclique simple souligne la nouveauté du système trioxaadamantane.

[Traduit par le journal]

In the preceding paper (1) we presented our evidence that the hydrolysis of trioxaadamantane ortho esters (T) occurs with reversible formation of the dialkoxycarbocation DH^+, and we provided a quantitative analysis of this equilibration (eq. [1] with R = H).

[1]

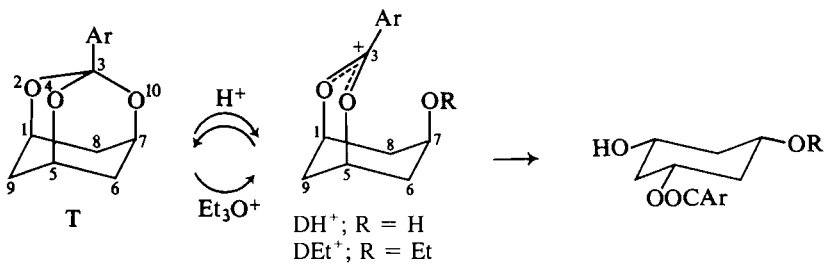

Can. J. Chem. Downloaded from www.nrcresearchpress.com by 210.87.254.5 on 09/06/12
For personal use only.

Can. J. Chem. Downloaded from www.nrcresearchpress.com by 210.87.254.5 on 09/06/12
For personal use only.

The trioxaadamantane system is highly unusual in this respect, in that with other ortho esters the dialkoxycarbocation-forming state is irreversible (in water solvent). Reversibility was in fact initially suggested by Lamaty, Moreau and co-workers, on the basis of observations made during kinetic studies (2, 3). These kinetics, however, referred to the overall hydrolysis, and we felt it important, in view of the unusual nature of this system, to see if the kinetics of the individual stages could be analyzed. In this paper we report such a study. Four separate areas of kinetic investigation can be defined: (a) a temperature-jump study of the cation − ortho ester equilibration; (b) a kinetic study in dilute and moderately concentrated H_2SO_4 solutions designed to analyze the effect of the shifting equilibrium between cation and ortho ester; (c) a kinetic study in aqueous solutions covering a range of pH of the cation DEt^+, prepared by treatment of the ortho ester with triethyloxonium tetrafluoroborate; and (d) a study at high temperatures of the ortho ester hydrolysis over a range of pH. The unusual slowness of the hydrolysis − one of the factors suggestive of reversible cation formation (2, 3) − has meant that previous studies have been limited to quite acidic solutions. In addition to the initial reversibility, we show here that there is a change in rate-determining step with changing pH, which is revealed only by studies over the more extended pH regions.

Experimental

Materials

3-(2,4-Dimethylphenyl)-2-4,10-trioxaadamantane was prepared in 30% yield from trimethyl 2,4-dimethylorthobenzoate as described in the previous paper (1), and had mp 130−132°C; ^{1}H nmr, δ: 7.53 (1H, d), 6.91 (2H, m), 4.50 (3H, m), 2.6−2.8 (3H, m), 2.76 (3H, s), 2.15 (3H, s), 1.65−1.85 (3H, m). *Anal.* calcd. for $C_{15}H_{18}O_3$: C 73.15, H 7.37; found: C 73.31, H 7.36. The trimethyl orthoester was prepared[1] in a two-step procedure involving the Friedl−Crafts reaction of aluminum trichloride and carbon tetrachloride with *m*-xylene, followed by substitution of the chlorines with sodium methoxide in methanol. The procedure here was essentially that employed for the preparation of trimethyl 2,4,6-trimethylorthobenzoate (4). Other trioxaadamantanes were described in the previous paper (1).

The cation DEt^+ with Ar = 4-$CH_3C_6H_4$ was prepared by treating 3-(4-methylphenyl)-2-4,10-trioxaadamantane (5 mmol) dissolved in dry CH_2Cl_2 (20 mL) with triethyloxonium fluoroborate (5 mmol). A precipitate forms over a short period of time, and this was filtered to give a hygroscopic white solid, ^{1}H nmr (96% D_2SO_4, external $(CH_3)_4Si$), δ: 8.05 (2H, d, ArH), 7.35 (2H, d, ArH), 5.70 (2H, wide singlet, H1, H5), 5.25 (1H, wide singlet, H7), 4.55 (2H, q, CH_2), 3.15 (2H, d, H6e, H8e), 2.2−2.7 (4H, m, H9e, H6a, H8a, H9a), 1.55 (3H, t, CH_3).

Kinetics

Rates of product formation from the trioxaadamantanes were obtained using a Unicam SP 1800 spectrophotometer thermostatted at 25.0 ± 0.1°C or 76.8 ± 0.2°C. In dilute acids (pH 7 to 10−20% H_2SO_4) the absorbance increase associated with the formation of the benzoate ester product was monitored (4-$CH_3C_6H_4$; 243 nm; C_6H_5, 225 nm; 4-ClC_6H_4, 245 nm; 3-ClC_6H_4, 253 nm; 4-$NO_2C_6H_4$, 267 nm; 2,4-$(CH_3)_2C_6H_3$, 250 nm). In more concentrated acids the absorbance decrease associated with the disappearance of the cation was monitored (4-$CH_3C_6H_4$, 283 nm; C_6H_5, 260 nm; 4-ClC_6H_4, 286 nm; 3-ClC_6H_4, 267 nm; 4-$NO_2C_6H_4$, 272 nm). First-order rate constants were evaluated as the slopes of plots in ln $(A_t - A_\infty)$ or ln $(A_\infty - A_t)$ versus time. Excellent linearity was observed in these plots. In a few cases it was verified that the rate constant was the same whether cation disappearance or product appearance was monitored. Rate constants were obtained in all cases as the average of two or three kinetic runs.

[1]R. A. McClelland and M. Ahmad. Unpublished.

First-order rate constants for the disappearance of the cation DEt^+ were obtained by following the disappearance of the cation at 283 nm. Reactions from pH 1 to pH 4 were carried out using the Unicam spectrophotometer by injecting 2.5 μL of a solution of the cation in CH_3CN into a thermostatted uv cell. Reactions at pH > 4 were carried out using a Durrum−Gibson stopped-flow spectrophotometer. In these experiments the cation solution in CH_3CN was added to a 0.01 *M* HCl solution which had been thermostatted in an external water bath. This solution was rapidly loaded into one syringe of the stopped-flow apparatus, where it was mixed with an appropriate buffer.

Temperature-jump experiments for the equilibrium reaction of 3-(2,4-dimethylphenyl)2-4,10-trioxaadamantane were performed on a Messanlagen Studiengesellschaft Gottingen T-jump spectrometer. A temperature jump of 3.1°C was applied to a microcell prethermostatted at 21.9°C. In order to minimize the extent of further hydrolysis of the equilibrating mixture, solutions were prepared immediately before use. Hydrolysis does occur, but that it is not a problem is demonstrated by the observation that the measured relaxation rate constants do not change with time, although the relaxation amplitude decreases. The chemical relaxation which occurs after the temperature rise produces an absorbance increase. This was displayed on the screen of a storage oscilloscope, and the photographed trace digitized to compute the relaxation rate constants. Good exponential decay curves were obtained. At least five determinations of relaxation time were made from each solution, and the results averaged.

Results and discussion

Equilibration

As mentioned previously (1), the equilibrium reaction of the trioxaadamantanes and the cations DH^+ is extremely rapid, and we turned to temperature-jump spectroscopy in an attempt to study its kinetics. Initial experiments were conducted on equilibrating solutions of 3-phenyl and 3-(4-methylphenyl)-trioxaadamantanes, but these failed to reveal a relaxation and were not further pursued. With the 2,4-dimethylphenyl system, however, a relaxation at the λ_{max} (280 nm) of the cation could be observed. Relaxation rate constants (τ^{-1}), were measured in 0.06 to 0.48 *M* $HClO_4$ with the ionic strength being kept constant at 0.5, and the following relationship observed (see Table S1[2] for raw data).

$$[2] \quad \tau^{-1}(s^{-1}) = (8.7 \pm 0.6) \times 10^3 + (8.5 \pm 0.3) \times 10^3\,[H^+]$$

The first number which will be defined as k_1^0 can be assigned to the acidity-independent ring closure of the cation, with the second number referring to the second-order rate constant for H^+-catalyzed ring opening of the ortho ester. These values lead to an equilibrium constant $K_R = [T][H^+]/[DH^+]$ calculated as

$$[3] \quad T + H^+ \underset{k_{-1}^0}{\overset{k_1^H}{\rightleftharpoons}} DH^+$$

as k_{-1}^0/k_1^H of 1.03. Spectroscopic determination of this constant, carried out as in the previous paper, gives a value of 1.05, in excellent agreement.

For comparison with other systems (see later) we wished to have some idea of the magnitudes of k_1^H and k_{-1}^0 for the parent 3-phenyl system. These can be estimated by assuming that the 2,4-dimethyl substituents exert the same effect here as in an acyclic system. Rate constants for acid-catalyzed dialkoxycarbocation formation from trimethyl 2,4-dimethylorthobenzoate and trimethyl orthobenzoate (eq. [4]) are 120 M^{-1} s^{-1} (see footnote 1) and 74 M^{-1} s^{-1} (5) respectively. There is little

[2]Supplementary material is available, at a nominal charge, from the Depository of Unpublished Data, CISTI, National Research Council of Canada, Ottawa, Ontario, Canada, K1A 0S2.

TABLE 1. Rate and equilibrium constant data for the hydrolysis of 3-aryl-2,4,10-trioxaadamantanes in dilute acid solutions (temperature 25°C)

Substituent	k_H(app), M^{-1} s^{-1}	pK_{DH^+}	k_2^0(app), s^{-1}
4-Me	4.0×10^{-4}	−0.77	2.4×10^{-3}
H	2.7×10^{-4}	−1.19	4.2×10^{-3}
4-Cl	2.0×10^{-4}	−2.00	2.0×10^{-2}
3-Cl	1.35×10^{-4}	−2.47	4.0×10^{-2}
4-NO_2	6.3×10^{-5}	−3.24	1.1×10^{-1}
Hammett ρ	−0.8	−2.7	+1.9

[4] $Arc(OMe)_3 + H^+ \rightarrow \overset{+}{Ar}C(OMe)_2$

difference here and we therefore estimate k_1^H for 3-phenyl-2,4,10-trioxaadamantane as 5×10^3 M^{-1} s^{-1}. A larger effect is observed for water addition to the dialkoxycarbocations (eq. [5]), $k(H_2O)$ being $10^{5.1}$ s^{-1} with Ar = phenyl (6) and $10^{3.8}$ with

[5] $\overset{+}{Ar}C(OMe)_2 + H_2O \rightarrow ArC(OH)(OMe)_2$

Ar = 2,4-dimethylphenyl[1]. These numbers are determined by extrapolation to water of rate constants actually measured in H_2SO_4 solutions (6). The slower rate in the 2,4-dimethyl case is undoubtedly associated with a steric inhibition to the nucleophilic addition. Assuming that a similar effect occurs in the trioxaadamantane case, we estimate k_{-1}^0 for 3-phenyl as 10^5. That these estimates are reliable is seen in the agreement between the calculated K_R (k_{-1}^0/k_1^H) of 20 and the spectroscopically observed value (1) of 16. These numbers also reveal why a relaxation could not be observed with the 3-phenyl system. They correspond to a maximum half-life for the relaxation of 7 μs and that is within the rise-time of our temperature-jump apparatus.

Hydrolysis kinetics in acid solutions

The overall hydrolysis in this system represents the formation of ester product from an equilibrating mixture of ortho ester and dioxanylium ion. In dilute acid solutions the relative concentration of the cation in the equilbrium is very small, and first-order rate constants obey the relationship of eq. [6] with values of k_H(app) listed in Table 1 (see Table S2 for raw data[2]).

[6] $k_{obsd} = k_H(app)[H^+]$

Lamaty, Moreau and co-workers (2, 3) conducted their kinetic studies under such conditions and observed the same relationship. This first-order dependency on hydronium ion concentration is of course typical of ortho ester hydrolysis. The values of k_H(app) are abnormally slow (2-phenyl-2-methoxy-1,3-dioxane, for example, has k_H equal to 3.0×10^4 M^{-1} s^{-1} (7) and this led to the original conclusion (2, 3) that the trioxaadamantane system is different. In terms of the mechanism,

[7] $T \underset{K_{DH^+}}{=} DH^+ \overset{k_2^0(app)}{\rightleftharpoons}$ product

the following relationship applies

[8] $$k_H(app) = \frac{k_2^0(app)}{K_{DH^+}}$$

where k_2^0(app) is a first-order rate constant representing the conversion of cation to product. Using values of K_{DH^+} determined spectroscopically in more concentrated acids (1), values

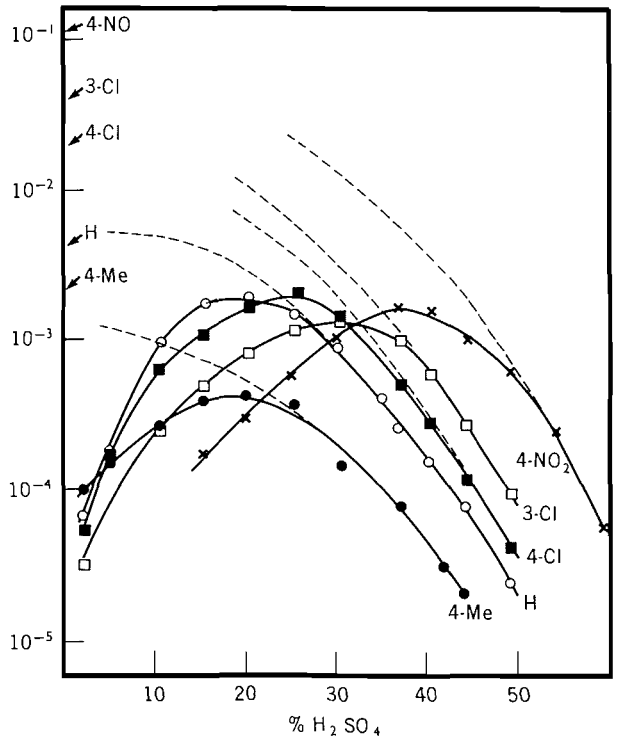

FIG. 1. First-order rate constants (s^{-1}, 25°C) for the hydrolysis of 3-aryl-2,4,10-trioxaadamantanes in sulfuric acid solutions. The dashed lines represent k_2(app) values calculated upon equilibrium correction. The arrows indicate values of k_2^0(app) calculated in water as $k_H(app)\cdot K_{DH^+}$ (Table 1).

of k_2^0(app) can be calculated and these are also listed in Table 1. It can be seen that the substituent effects on k_2^0(app) and K_{DH^+} are in opposing directions. Electron-withdrawing groups decrease the relative concentration of cation but accelerate its further hydrolysis. For the overall rate the former effect is more important.

In more concentrated acid solutions the equilibrium shifts towards the cation. Either the appearance of ester or the disappearance of the cation can be monitored, and within experimental error the same rate constant is obtained. A plot of these rate constants as a function of sulfuric acid concentration is shown in Fig. 1 (see Table S3 for data[2]); in each case the rate rises to a maximum at some intermediate acidity and then falls off in more concentrated acids. This maximum is much like that observed in the bimolecular acid hydrolysis of amides (8) and esters (9), and the explanation here is similar. Increasing acidity increases the relative concentrations of the cation, and thus tends to increase the rate. This is countered by a medium effect on the hydrolysis of the cation which tends to decrease the rate. The following relationship applies to the observed rates.

[9] $$k_{obs} = k_2(app)\left(\frac{[DH^+]}{[T] + [DH^+]}\right)$$

where k_2(app) replaces k_2^0(app) of eq. [7] because of the non-ideality of the reaction medium. The term in brackets represents the changing equilibrium position. This is equal to $h_T/(h_T + K_{DH^+})$ and can be calculated using the acidity function and dissociation constants determined in the previous paper. This allows for the calculation of values of k_2(app) and these are shown as the dashed lines in Fig. 1. (In more concentrated

Can. J. Chem. Downloaded from www.nrcresearchpress.com by 210.87.254.5 on 09/06/12
For personal use only.

Can. J. Chem. Downloaded from www.nrcresearchpress.com by 210.87.254.5 on 09/06/12
For personal use only.

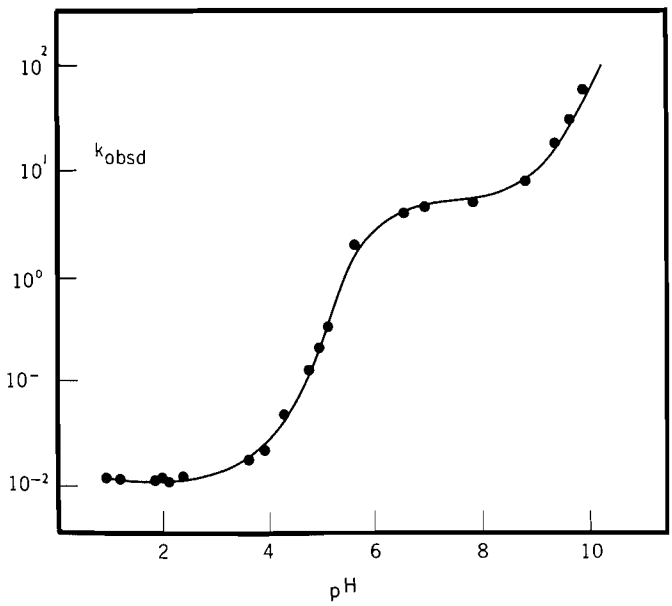

FIG. 2. First-order rate constants (s^{-1}, 25°C) for the hydrolysis of the cation DEt^+, Ar = 4-MeC_6H_4, as a function of pH.

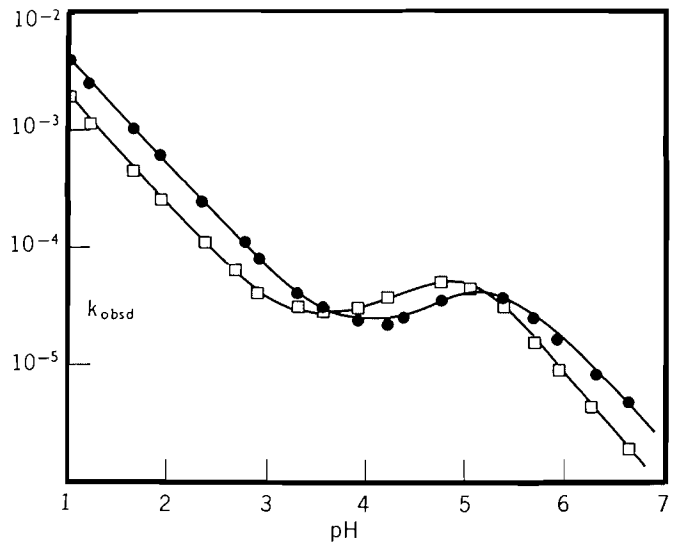

FIG. 3. First-order rate constants (s^{-1}, 76.8°C) for the hydrolysis of 3-aryl-2,4,10-trioxaadamantanes; (●) 4-MeC_6H_4, (◇) 4-ClC_6H_4.

acids where $[DH^+] \gg [T]$, $k_{obs} = k_2(app)$.) A series of parallel curves are produced, showing a monotonic decrease with increasing acidity. Also shown in Fig. 1 are values of $k_2^0(app)$ calculated from the dilute acid rate data as discussed previously, and referring to water alone. Within experimental error the $k_2(app)$ curves do extrapolate to these, as they should.

The simple interpretation of these kinetics is that $k_2(app)$ refers to the rate constant for hydration of the cation, and the decrease in $k_2(app)$ with increasing acidity is caused by a decrease in water activity combined with an activity-coefficient effect (6). The following data, however, indicate that this simple explanation cannot be correct.

Hydrolysis of the cation DEt^+

In the pH region the initial equilibrium favors trioxaadamantane and any addition of cation just results in ring closure. The consequence is that the hydrolysis kinetics for the cation cannot be studied directly. In order to overcome this problem, the cation DEt^+ (with Ar = 4-MeC_6H_4) was prepared as its borofluorate salt. This cation cannot ring close, and the kinetics of its hydrolysis were studied over a range of pH. First-order behavior was observed; rate constants are listed in Table S4[2] and depicted graphically in Fig. 2.

Trioxaadamantane hydrolysis over a range of pH

As will be discussed, the behavior of DEt^+ is not consistent with a simple rate-determining hydration, and we wondered if the ortho ester could be observed to exhibit similar behavior. In consequence, rate constants for two of the trioxaadamantanes were measured over a range of pH at 77°C. The higher temperature was employed in order to speed up the reaction sufficiently to enable the kinetics to be easily studied at the higher pH. Measurements were made under conditions for which eq. [6] had previously been applied; that is, with the initial equilibrium favoring trioxaadamantane. The kinetic data are given in Table S5[2]; rate–pH profiles are shown in Fig. 3. The behavior in acid solutions with pH < 3 does show the first-order dependency in H^+ concentration in accord with eq. [6], but as the pH is increased the profile becomes considerably more complex. In fact, there is a short region of pH where an inverse pH dependency is observed.

Kinetic analysis

Although their profiles are quite different, a common kinetic model explains the behavior of both the trioxaadamantanes and the cation DEt^+, the key feature being a change in rate-determining step between high pH and low pH. Equation [11] presents the appropriate scheme for the ortho ester.

[11]

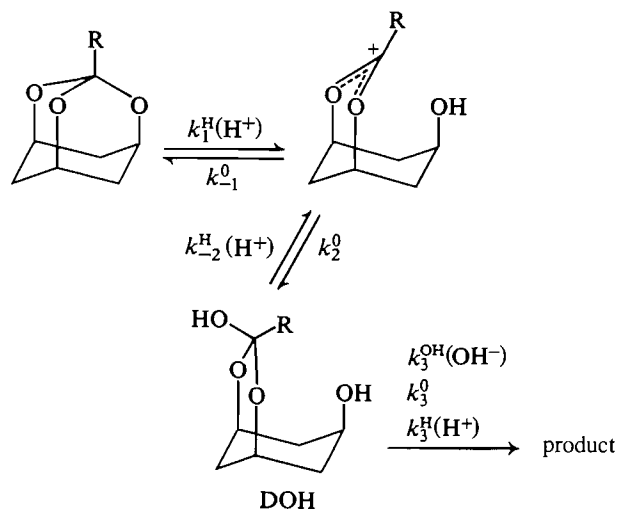

The rate and equilibrium behavior of the first stage have been discussed. Hydration of the dioxanylium ion occurs via simple water addition; the hemiorthoester DOH can return to cation in the microscopic reverse reaction which is H^+-catalyzed. The equilibrium constant K_R is defined as $[DOH][H^+]/[DH^+]$ and is equal to k_2^0/k_{-2}^H. We also define an equilibrium constant K_{13} as $[DOH]/[T] = K_R/K_{DH^+}$. Product is formed from the hemiorthoester via three pathways, with H^+ catalysis, OH^- catalysis, and water catalysis (a pH-independent process). The first stage is reversible under all conditions and is therefore never rate limiting. This fact is apparent from those experiments in which the cation is added to aqueous solutions and, regardless of pH, trioxaadamantane is generated. The requirement for such reversibility is $k_{-1}^0 \gg k_2^0$; that this condition is met will be

TABLE 2. Rate and equilibrium constant data for the hydrolysis of trioxaadamantanes (77°C) and the cation DEt^+

Constant	Trioxaadamantane T(4-MeC_6H_4)	Trioxaadamantane T(4-ClC_6H_4)	DEt^+
a	14	8.2	4.5
b	3.7×10^{-3}	2.4×10^{-3}	2.5×10^{-3}
c	1.1×10^{-6}	2.9×10^{-6}	4.2×10^{-7}
d	2.5×10^{3}	9.6×10^{3}	3×10^{4}
pK_{DH^+}	−0.77	−2.00	—
k_2^0, s^{-1}	86	8.2×10^{2}	4.5
k_{-2}^H, M^{-1} s^{-1}	2×10^{7}	5×10^{6}	2×10^{6}
pK_R	5.4	3.9	5.6
K_{13}	7×10^{7}	12×10^{-7}	—
k_3^{OH}, M^{-1} s^{-1}	5×10^{10}	5×10^{10}	5×10^{10}
k_3^0, s^{-1}	22	15	0.8
k_3^H, M^{-1} s^{-1}	7×10^{4}	1.2×10^{4}	5×10^{3}
k_2^{OH}, M^{-1} s^{-1}	—	—	5×10^{5}

shown presently. With the trioxaadamantane and cation in equilibrium, a stationary state assumption in hemiorthoester produces the following equation for the observed rate constant.

$$[12]\quad k_{obsd} = k_2^0\left(\frac{[H^+]}{K_{DH^+}}\right) \times \left\{\frac{\frac{k_3^H}{k_{-2}^H}[H^+] + \frac{k_3^0}{k_{-2}^H} + \frac{k_3^{OH}}{k_{-2}^H}[OH^-]}{\left(1 + \frac{k_3^H}{k_{-2}^H}[H^+] + \frac{k_3^0}{k_{-2}^H} + \frac{k_3^{OH}}{k_{-2}^H}[OH^-]\right.}\right\}$$

This has the form

$$[13]\quad k_{obsd} = a[H^+]\left\{\frac{b[H^+] + c + d[OH^-]}{(1+b)[H^+] + c + d[OH^-]}\right\}$$

with $a = k_2^0/K_{DH^+}$, $b = k_3^H/k_{-2}^H$, $c = k_3^0/k_{-2}^H$, and $d = k_3^{OH}/k_{-2}^H$. The profiles in Fig. 3 provide an excellent fit to this equation, giving the constants a–d listed in Table 2.

The change in rate-determining step is a consequence of k_{-2}^H being greater than k_3^H, as seen in the values of the constant b. This produces a situation in which, in acid solutions, the overall rate of the hemiorthoester decomposition stage is slower than the rate of reverse of the hydration stage. Not only are the trioxaadamantane and cation in equilibrium, but included as well is the hemiorthoester. It is the decomposition of this species which is rate determining. The other pathways available for this breakdown mean, however, that at some higher pH its rate becomes greater than the reverse of the second stage, which remains acid catalyzed. At this point cation hydration becomes rate limiting. Figure 4 is a schematic representation of the rate profile, idealizing the various sections by ignoring the regions where changeover from one behavior to another is occurring. The change in rate-determining step occurs near pH 5, at the intersection between C and D in the figure. In more acidic solutions, where hemiorthoester breakdown is rate limiting, the observed rate constant is given simply by $K_{13}(k_3^H[H^+] + k_3^0 + k_3^{OH}[OH^-])$, where K_{13} is the equilibrium constant relating trioxaadamantane and hemiorthoester. The profile in this region shows H^+ catalysis (A), water catalysis (B), and OH^- catalysis (C). As the pH is increased in region C, the third stage has become OH^- catalyzed while the reverse of the second

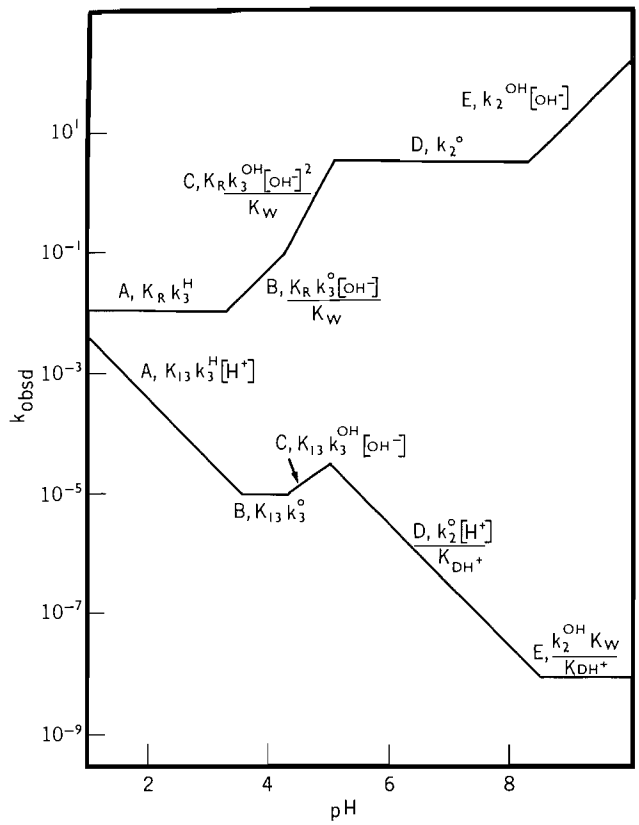

FIG. 4. Schematic representation of rate–pH profiles for the hydrolysis of trioxaadamantanes (bottom trace) and cations DEt^+ (top trace).

stage is still H^+ catalyzed, and an abrupt changeover in the relative magnitudes of the rates of these occurs. Hydration then becomes rate limiting and the observed rate constant in region D returns to an H^+ dependency, being equal to k_2^0 times $([H^+]/K_{DH^+})$, the bracketed term representing the cation–trioxaadamantane equilibrium.

In terms of the rate behavior in more concentrated acids discussed previously, the constant k_2^0 (app) in Table 1 is now seen to be equal to $K_R \cdot k_3^H$. The decrease in k_2 (app) which is seen in more concentrated acids is difficult to explain without going into a detailed analysis which is beyond the scope of this paper. In brief, it is related to a differential medium effect on the cation–hemiorthoester equilibrium position and the rate of acid-catalyzed breakdown of the latter, increasing sulfuric acid concentration shifting the equilibrium more towards the cation than it accelerates the rate.

The behavior exhibited by the trioxaadamantanes has a parallel with that of monocyclic ortho esters. Studies conducted over the past few years (7, 10–16) have shown that the exocyclic alkoxy group OR is lost in the dialkoxy carbocation-forming stage, with the key feature that k_3^H is usually signifi-

[14]

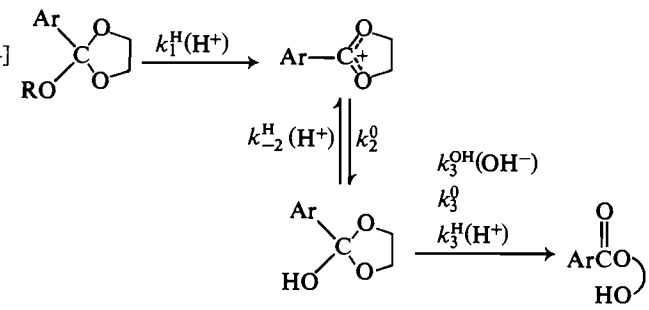

Can. J. Chem. Downloaded from www.nrcresearchpress.com by 210.87.254.5 on 09/06/12
For personal use only.

Can. J. Chem. Downloaded from www.nrcresearchpress.com by 210.87.254.5 on 09/06/12
For personal use only.

TABLE 3. Rate and equilibrium constant data for the hydrolysis of 3-phenyl-2,4,10-trioxaadamantane and 2-phenyl-2-methoxy-1,3-dioxane

Constant	Adamantane	Dioxane
k_1^H, M^{-1} s^{-1}	5×10^3	3×10^{4a}
k_{-1}^0, s^{-1}	10^5	—
pK_{DH^+}	−1.2	—
k_2^0, s^{-1}	10^1	10^{4c}
k_{-2}^H, M^{-1} s^{-1}	10^6	2×10^{4b}
pK_R	5	0.3^a
k_3^H, M^{-1} s^{-1}	3×10^3	3×10^{3a}
k_3^0, s^{-1}	1	1.0^a
k_3^{OH}, M^{-1} s^{-1}	10^{10}	10^{9d}

[a]Reference 7.
[b]Calculated as 0.8 k_1^H (see refs. 10, 15).
[c]$K_R \cdot k_{-2}^H$.
[d]R. A. McClelland and L. J. Santry, unpublished. 2-Phenyl-2-hydroxy-1,3-dioxalane has $k_3^{OH} = 5 \times 10^{10} M^{-1}$ s^{-1} (10).

cantly smaller than both k_1^H and k_{-2}^H. The latter two are in fact quite close in magnitude, since they represent similar processes, loss of an exocyclic OR and OH to form the same cyclic cation. The orgin of the effect is not completely understood. The significant factor appears (16) to be the requirement that a ring must open in the third stage, while the k_1^H and k_{-2}^H processes involve dissociation. It can be noted with the trioxaadamantanes that k_{-2}^H is again greater than k_3^H, and once again the exocyclic−endocyclic comparison applies.

With the monocyclic systems, the consequence of k_3^H being less than k_1^H and k_{-2}^H is that there is a change in slow step with changing pH. At high pH where hemiorthoester breakdown occurs by the other pathways, particularly that involving OH^- catalysis, the first stage is the slow stage. However, at low pH the third stage is rate limiting. In this case the ortho ester is converted to hemiorthoester more rapidly than the latter species goes on to product, so that the hemiorthoester actually accumulates as a transient intermediate. This is a different situation from that encountered with the trioxaadamantanes, where the change in slow step represents a change in the preferred mode of reaction of the hemiorthoester. With the trioxaadamantane, this species does not accumulate to any significant extent. For the monocyclic ortho esters, the appropriate kinetic analyses can furnish all of the rate constants of eq. [14], and these are listed in Table 3 for 2-phenyl-2-methoxy-1,3-dioxane, an appropriate analog of trioxaadamantane. A general feature exhibited by the monocyclic systems is the very large rate constants, usually near the diffusion limit, for the OH^- catalysis of the hemiorthoester breakdown. This has the consequence that this pathway becomes important in quite acidic solutions. As seen in Figs. 3 and 4, this is also observed with the hemiorthoester derived from the trioxaadamantane.

With the trioxaadamantanes the kinetic analysis can furnish k_2^0, since this is equal to $a \cdot K_{DH^+}$, but the other rate constants k_{-2}^H, k_3^H, k_3^0, and k_3^{OH} are provided only as ratios (see eq. [12]). To calculate these we have made the assumption that k_3^{OH} is a diffusion-limited rate constant and set it equal to $5 \times 10^{10} M^{-1}$ s^{-1}, the value found for 2-phenyl-2-hydroxyl-1,3-dioxalane (10). With this number in hand k_{-2}^H can be calculated as k_3^{OH}/d, and then k_3^H as $b \cdot k_{-2}^H$ and k_3^0 as $c \cdot k_{-2}^H$. The K_R value can also be calculated as k_2^0/k_{-2}^H and K_{13} as K_R/K_{DH^+}. Values of these constants are listed in Table 2.

With DEt^+ the kinetic analysis takes a similar form, except that now there is no equilibrium with the ortho ester, the starting point being the dioxanylium ion. Rate constants k_{obsd} are given by eq. [12], except that the term in $[H^+]/K_{DH^+}$ is not present. This means that the form of the equation, eq. [13], does not have the term in H^+ concentration before the bracket, so that the shape of the profile is quite different. The constant "a" is now equal to k_2^0, while b, c, and d have the same meaning as before. Values of these constants which provide the best fit to the experimental data are given in Table 2. Once again the assumption is made that $k_3^{OH} = 5 \times 10^{10} M^{-1}$ s^{-1}, to enable the calculation of the individual constants.

Some justification can be made for the numbers which arise, since the result is a pK_R value of 5.6 for DEt^+. Lower values of k_3^{OH} would mean lower values of k_{-2}^H and in consequence a smaller pK_R value. One can argue, however, that this pK_R is reasonable, or at the very least it cannot be smaller. The argument is based on the consideration that if pK_R were smaller, the kinetics associated with the disappearance of DEt^+ would not be simply first order; under some conditions biphasic kinetics should result. There should be one kinetic phase associated with the equilibration of the cation and the hemiorthoester, followed by a second phase as the equilibrating mixture is converted to product. For this to occur there must be a significant amount of hemiorthoester in the initial equilibrium, or $pH \geq pK_R$; otherwise the initial phase would be small or absent. It also requires conditions where the hemiorthoester decomposition is still rate limiting; that is, this decomposition must be slower than the equilibration. This latter requirement limits us to solutions with $pH < 5$. We did look for biphasic kinetics around this pH but were unable to observe any significant deviation from a simple first-order decay. We conclude therefore that we were not at a pH significantly above the pK_R, or, in other words, the value of pK_R of 5.6 calculated in the kinetic analysis is reasonable.

The top trace in Fig. 4 is a schematic representation of the rate profile for DEt^+. As with the trioxaadamantanes, the change in rate-determining step occurs near pH 5, and solutions more acidic than this have rate-determining hemiorthoester breakdown. In these solutions k_{obsd} is given by $(K_R/[H^+]) \times (k_3^H[H^+] + k_3^0 + k_3^{OH}[OH^-])$, the first bracketed term representing the equilibrium with the cation and the second bracketed term the three modes of hemiorthoester breakdown. In more basic solutions k_{obsd} is simply given by k_2^0, the rate constant for water addition. In basic solutions (pH > 8), a further dependency on OH^- is seen. This can be ascribed to a rate-limiting addition of hydroxide ion to the cation, with the symbolism k_2^{OH} for the second-order rate constant. It can be noted that a similar process will occur in basic solutions with the trioxaadamantane, that is, a rate-limiting addition of hydroxide ion to the dioxanylium ion in equilibrium with the ortho ester. The observed rate constant would be pH independent here (region E of the bottom trace in Fig. 4). Using the value of k_2^{OH} obtained with DEt^+, we calculate that the value of this pH-independent rate constant should be of the order to 10^{-8} s^{-1} to 10^{-10} s^{-1}, representing, in other words, a very slow process.

Comparison with other ortho esters

Table 3 compares rate and equilibrium constants for the three stages of the hydrolysis of a trioxaadamantane and a dioxane ortho ester, the numbers for the second and third stages of the former being based on DEt^+. There are several features of these data which can be commented upon.

Can. J. Chem. Downloaded from www.nrcresearchpress.com by 210.87.254.5 on 09/06/12
For personal use only.

(a) In its initial ring-opening reaction, the trioxaadamantane does not differ too greatly in its rate from that associated with the exocyclic cleavage in the first stage of the monocyclic system. The two systems, in fact, have quite similar orientations of the leaving group including the correct lone pair orientation for production of the dioxanylium ion.

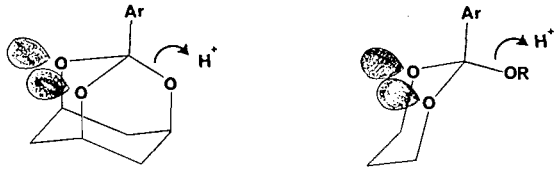

(b) The acceleration associated with the intramolecular nature of the reverse ring closure can be evaluated by comparing the constant k^0_{-1} for the trioxaadamantane with the rate constant k^0_2 for water addition to the dioxanylium ion generated in the dioxane system. Taking into account that the latter refers

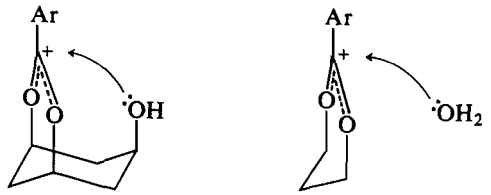

to water as solvent so that the comparison should actually be made with $k^0_2/55$, it is seen that the intramolecular reation is of the order of 10^3 faster. This, is, of course, one of the factors contributing to the reversibility of the ring opening.

(c) The other factor is that the rate constant k^0_2 for water addition to the dioxanylium cation in the trioxaadamantane system is unusually low, by a factor of about 10^3. (Compare here the two k^0_2 values.) That this is the case was suggested by Lamaty, Moreau and co-workers (3), although they were unable to estimate the magnitude of the effect. These authors presented a detailed explanation for the slowness of this reaction (3). The simple basis of their argument is that, for addition to occur with the correct lone pair orientation, one of the cyclohexane rings in the hemiorthoester must be placed in a boat configuration. This problem does not arise with a simple dioxanylium ion.

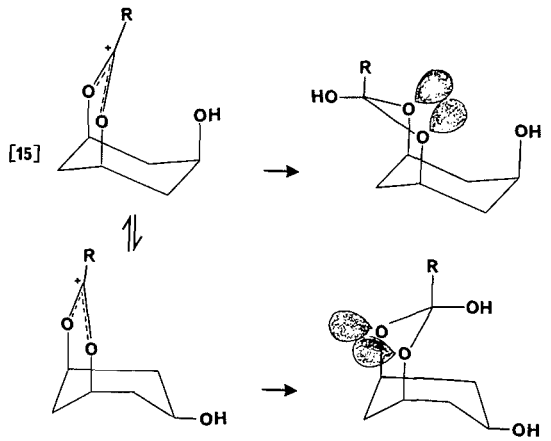

(d) The magnitude of this effect can be seen in thermodynamic terms in the pK_R values, which differ by approximately 5 log units. If this difference is entirely associated with the stability in the hemiorthoesters, then the hemiorthoester formed in the trioxaadamantane system is about 7–8 kcal/mol less stable than a simple 2-hydroxy-1,3-dioxane. That difference corresponds to the energy required for inversion of a chair to a boat cyclohexane.

(e) This same energy difference is also seen in K_{13}, the equilibrium constant relating trioxaadamantane and hemiorthoester. It can be argued that inherently there should be little difference in energy between an ortho ester and hemiorthoester, since both species have a tetrahedral carbon with three

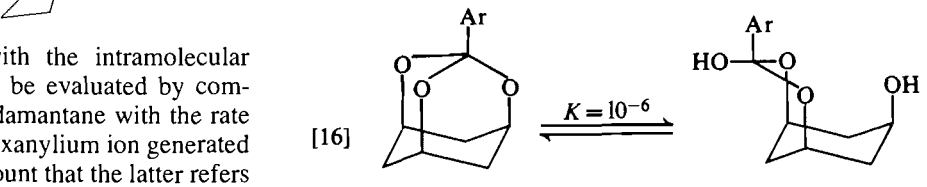

oxygen atoms attached. That assumption is in fact the basis of Guthrie's method for estimating free energies of hemiorthoester tetrahedral intermediates (17). The difference in the case involved here is once again related to the unusually high energy of the hemiorthoester.

Acknowledgement

Continued financial support of the Natural Sciences and Engineering Research Council of Canada is gratefully acknowledged.

1. R. A. McClelland and P. W. K. Lam. Can. J. Chem. **62**, 1068 (1984).
2. O. Bouab, G. Lamaty, and C. Moreau. J. Chem. Soc. Chem. Commun. 678 (1978).
3. O. Bouab, G. Lamaty, C. Moreau, O. Pomares, P. Deslongchamps, and L. Ruest. Can. J. Chem. **58**, 567 (1980).
4. R. A. McClelland and M. Ahmad. J. Am. Chem. Soc. **99**, 5356 (1977).
5. H. G. Bull, K. Koehler, T. C. Pletcher, J. J. Ortiz, and E. H. Cordes. J. Am. Chem. Soc. **93**, 3002 (1971).
6. R. A. McClelland and M. Ahmad. J. Am. Chem. Soc. **100**, 7031 (1978).
7. R. A. McClelland, S. Gedge, and J. Bohonek. J. Org. Chem. **46**, 886 (1981).
8. K. Yates and C. R. Smith. J. Am. Chem. Soc. **93**, 6578 (1971).
9. K. Yates and R. A. McClelland. J. Am. Chem. Soc. **89**, 2686 (1967); K. Yates. Acc. Chem. Res. **4**, 138 (1971).
10. M. Ahmad, R. G. Bergstrom, M. J. Cashen, Y. Chiang, A. J. Kresge, R. A. McClelland, and M. F. Powell. J. Am. Chem. Soc. **101**, 2669 (1979).
11. R. A. McClelland, M. Ahmad, J. Bohonek, and S. Gedge. Can. J. Chem. **57**, 1531 (1979).
12. R. A. McClelland and M. Alibhai. Can. J. Chem. **59**, 1169 (1981).
13. R. A. Burt, Y. Chiang, H. K. Hall, and A. J. Kresge. J. Am. Chem. Soc. **104**, 3687 (1982).
14. L. J. Santry and R. A. McClelland. J. Am. Chem. Soc. **105**, 3167 (1983).
15. R. A. McClelland and L. J. Santry. Acc. Chem. Res. In press.
16. Y. Chiang, A. J. Kresge, M. O. Lahti, and D. P. Weeks. J. Am. Chem. Soc. In press.
17. J. P. Guthrie. Acc. Chem. Res. **16**, 122 (1983).

Synthesis of des-*A*-*B*-secocholestanes[1]

WOJCIECH J. SZCZEPEK, JACEK W. MORZYCKI, ZBIGNIEW BOŃCZA-TOMASZEWSKI, MICHAŁ CHODYŃSKI AND WŁADYSŁAW J. RODEWALD
Department of Chemistry, University of Warsaw, Pasteura 1, 02093 Warszawa, Poland

Received August 2, 1983

WOJCIECH J. SZCZEPEK, JACEK W. MORZYCKI, ZBIGNIEW BOŃCZA-TOMASZEWSKI, MICHAŁ CHODYŃSKI, and WŁADYSŁAW J. RODEWALD. Can. J. Can. J. Chem. **62**, 1081 (1984).

Two independent synthetic routes to 10-oxo-5, 10-seco-des-*A*-cholestan-5-oic acid (**5**) are described. The route including the Baeyer–Villiger rearrangement of (10*R*)-des-*A*-cholestan-5-one (**2***a*), followed by hydrolysis of the lactone **3***a* obtained and oxidation of the C-10 hydroxyl group, seems to be superior to ozonolysis of the 5(10)-enol acetate **6** of des-*A*-ketone which resulted in the formation of 5,10-seco-des-*A*-19-norcholestan-5,10-dioic acid (**7**), in addition to the compound **5**. Product **7** and its 6-nor analog **12** have also been obtained by ruthenium tetroxide oxidation of the respective *A*-ring phenols **8**, **9**, and **11**.

WOJCIECH J. SZCZEPEK, JACEK W. MORZYCKI, ZBIGNIEW BOŃCZA-TOMASZEWSKI, MICHAŁ CHODYŃSKI et WŁADYSŁAW J. RODEWALD. Can. J. Can. J. Chem. **62**, 1081 (1984).

Nous avons décrit deux routes synthétiques indépendantes conduisant à l'acide 10-oxo-5,10-seco-des-*A*-cholestanique-5 (**5**). Il nous semble que la route via le réarrangement de Baeyer–Villiger de (10*R*)-des-*A*-cholestan-5-one (**2***a*), l'hydrolyse de lactone **3***a* obtenu et l'oxydation de groupe hydroxylique à C-10 est supérieur que l'autre qui consiste en l'ozonolyse de 5(10)-double liaison dans l'acetate **6** de la forme énolique de des-*A*-cétone. La dernière reaction donne en outre du composé **5** l'acide dicarboxylique **7**. Le produit **7** et son 6-nor analogue **12** ont été preparés aussi par l'oxydation des phenoles du noyau *A*, **8**, **9** et **11**, avec tetraoxyde de ruthenium.

Can. J. Chem. Downloaded from www.nrcresearchpress.com by 210.87.254.105 on 09/06/12
For personal use only.

During the last two decades a number of synthetic studies on steroids concerned heteroanalogs of these natural products. These investigations were continued for such a long period because medical tests of many synthetic compounds were very promising. The most interesting heteroanalogs from the point of view of their biological activity seemed to be compounds containing heteroatoms in place of quaternary carbon at ring junctions (i.e. 5, 10, 13 etc). However, such analogs are not readily available and very often their syntheses, although successfully accomplished in many cases (2, 3), are long, tedious, and inefficient. In contrast to these multistep methods, a different approach, consisting in the attachment of a suitable, high molecular weight fragment containing the heteroatom to the partially degraded steroid, could be envisaged. The same steroid component might then be used for the synthesis of many different heteroanalogs.

A few years ago we undertook some studies on an extensive degradation of steroids (1, 4). In the present contribution we describe our recent results in this field. Relatively short and efficient methods for the synthesis of keto-acid **5**, as well as diacids **7** and **12** have been elaborated. The application of these useful compounds in the synthesis of azasteroids will be demonstrated in a future publication.

The starting material was des-*A*-ketone **2** (5), obtained by the pyrolysis of the sodium salt **1***b* of *A*-seco-keto-acid (6) in the presence of a basic agent such as sodium phenylacetate or potassium acetate at about 300°C. The main reaction product, (10*R*)-des-*A*-ketone **2***a* (30–40% yield), was accompanied by a number of stereoisomers. The detailed analysis of neighbouring fractions from the chromatography of **2***a* and mother liquors after crystallization showed the presence of at least ten isomeric des-*A*-ketones with various configurations at the chiral centers. Only one of them, (10*S*)-des-*A*-ketone **2***b*, existed in a significant amount (5–8%) and was fully characterized. The cd (circular dichroism) spectra of **2***a* and **2***b* showed the negative Cotton effects, much more distinctive in the case of (10*R*)-des-*A*-ketone **2***a* and thus confirming its configuration at C-10. The equilibration experiment carried out under alkaline conditions proved the epimeric relationship between **2***a* and **2***b*.[2] The Baeyer–Villiger rearrangement of each des-*A*-cholestan-5-one (**2***a* or **2***b*) with *m*-chloroperbenzoic acid (MCPBA) afforded the corresponding des-*A*-lactone (**3***a* or **3***b*) in a very good yield (Scheme 1). The reactions proceeded with the retention of configuration at C-10. This was proved by the ^{1}H nmr spectra of **3***a* and **3***b* showing a broadened quartet for 10α-H in the case of (10*S*)-des-*A*-lactone **3***b* (a small coupling constant between the pseudo-equatorial 10α-H and axial 9α-H), whereas the β-proton at C-10 in the epimeric lactone **3***a* appeared as an unresolved (at 100 MHz) multiplet ($w/2$ = 19 Hz), suggesting a large diaxial coupling constant $J_{9\alpha,10\beta}$. Hydrolysis of the (10*R*)-5a-oxo-des-*A*-*B*-homo-5-oxacholestane (**3***a*) with methanolic–aqueous KOH provided the hydroxy-acid **4***a*. To prevent recyclization to the lactone, hydroxy-acid **4***a* was transformed into its methyl ester **4***b* before oxidation. The reaction of **4***b* with CPA (CrO_3, Py, HOAc, ref. 7) yielded keto-ester **5***b*. It should be emphasized that all transformations from **2** to **5** were very efficient and could be done in principle without any chromatography. However, an alternative, shorter method for the synthesis of compound **5** from des-*A*-ketone **2** seemed possible. It was reasonable to expect that oxidative cleavage of the double bond between C-5 and C-10 in an enol-ester of des-*A*-ketone **2** should provide the same keto-acid **5**. An ozonolysis of the known enol-acetate **6** (5) confirmed this supposition, though the reaction appeared to be less attractive from a synthetic point of view. The primary reaction products had an anhydride character (ir bands at 1760 and 1820 cm^{-1}) and were difficult to purify. The crude products were subjected to alkaline hydrolysis and then treated with diazomethane. The reaction resulted in the formation of two

[1] Part IV in our series on des-*A*- and des-*A*-*B*-secosteroids. For part III, see ref. 1.

[2] The isolation of **2***a* and **2***b* and their equilibration have been effected previously (private communication from Professor Peter Yates, University of Toronto).

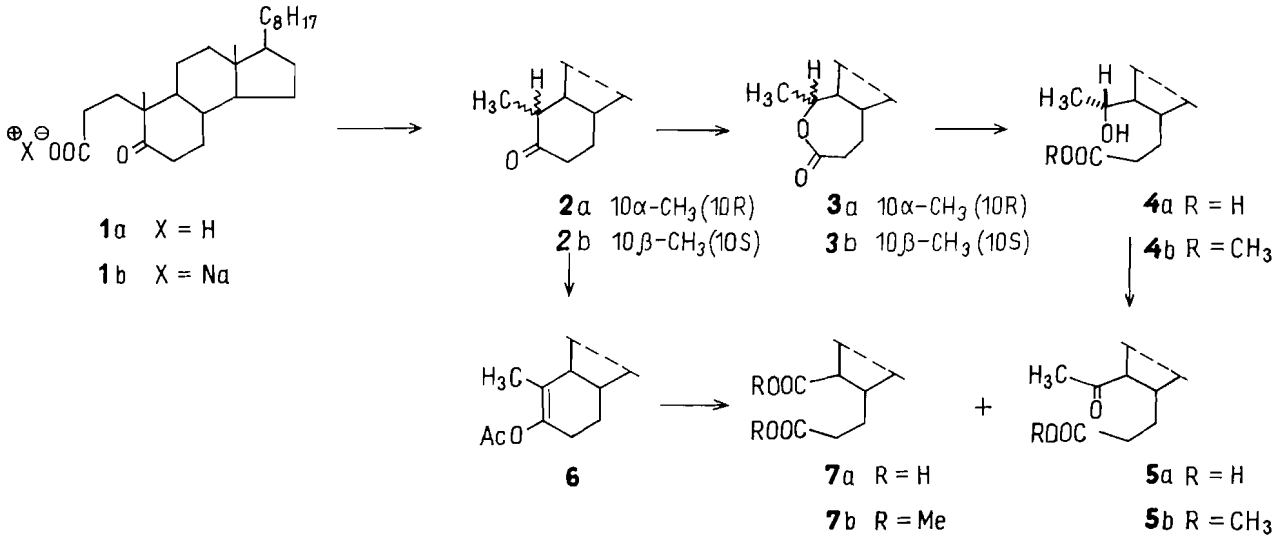

SCHEME 1

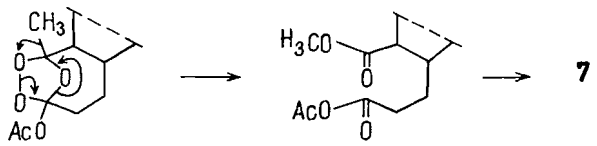

SCHEME 2

main products in almost equal amounts. The more polar product proved to be identical in all respects with a sample of the keto-ester **5***b* prepared as previously described. The second product of the ozonolysis was unexpectedly identified as diester **7***b*. To explain the formation of this product a migration of the methyl group with the pair of electrons from C-10 to an oxygen atom in an intermediary ozonide is proposed (Scheme 2). A similar course of reaction was observed during ozonolysis of α-pinene (8).

In searching for a better route to the diacid **7**, our attention has been drawn to the degradation of aromatic steroids by ruthenium tetroxide (9). 1-Hydroxy-4-methyl-1,3,5(10)-cholestatriene (**8**), obtained from 1,4-cholestadien-3-one by the known dienone–phenol rearrangement (10), when oxidized with RuO_4 afforded diacid **7***a* in 31% yield. The compound **7***a* and its dimethyl ester **7***b* were compared with the respective compounds obtained according to the method described above and proved to be identical.

In the oxidation by ruthenium tetroxide of phenol **8**, the degradation of ring *A* terminated at carbons 5 and 10 as expected. It was anticipated that the oxidation of the 6-oxo and *B*-nor derivatives **9** and **11** would yield the diacid **12**, having one carbon atom less than **7**, and therefore would be more convenient in the synthesis of steroid heteroanalogs. Indeed, 6-oxo-phenol **9** (11), when treated with RuO_4, underwent degradation to diacid **12** (Scheme 3). The same compound **12** was also obtained by oxidation of *B*-nor-phenol **11**, prepared from *B*-nor-1,4-cholestadien-3-one (**10**) (12).[3] The use of ruthenium

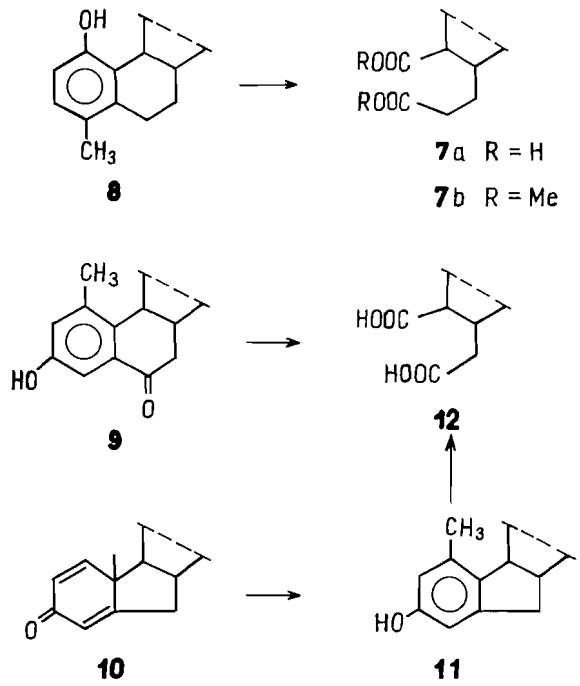

SCHEME 3

tetroxide for degradation of aromatic steroids to diacids was found to be superior to the ozonolysis of enol-acetate **6**.

Studies on the reconstruction of steroid systems from the des-*A*-*B*-seco derivatives described, with simultaneous introduction of the heteroatom, are under way.

Experimental

The melting points were determined on a Boetius micro melting point apparatus and are uncorrected. Optical rotations were measured on a Perkin–Elmer 241 polarimeter. The ir spectra were recorded on UR-20 and Unicam SP 1100 spectrophotometers. The ^1H nmr spectra were taken at 100 MHz (JEOL INM-4H-100) in $CDCl_3$ solutions with TMS as an internal standard. The cd spectra were measured on a Jasco ORD/UV-5 apparatus. Column chromatography was performed on silica gel (Kieselgel 60, 70–230 mesh, Merck) and on Alumina IB (Woelm). Thin layer chromatograms were developed on Silica Gel G

[3] It is noteworthy that 1-methyl-*B*-nor-phenol **11** is formed from *B*-nor-dienone **10** by a mechanism involving a simple methyl migration from C-10 to C-1, because a spiran intermediate, which is normally formed in such a rearrangement, would be highly strained (see ref. 13).

Can. J. Chem. Downloaded from www.nrcresearchpress.com by 210.87.254.105 on 09/06/12
For personal use only.

Can. J. Chem. Downloaded from www.nrcresearchpress.com by 210.87.254.105 on 09/06/12
For personal use only.

(Merck) and visualized with 50% sulfuric acid after heating. All solvents were dried and freshly distilled prior to use. The known 5-oxo-*A*-nor-3,5-secocholestan-3-oic acid (**1***a*) was prepared according to the procedure described in ref. 6.

Des-A-*cholestan-5-ones (2*a *and 2*b)

Variant (a)

To a solution of *A*-seco-keto-acid (**1***a*, 14.0 g) in methanol (100 mL) was added sodium hydroxide (1.5 g) dissolved in the same solvent (with a few drops of water). The methanol was evaporated and the solid residue was dried carefully under reduced pressure at 100°C. The above salt was melted with sodium phenylacetate (56 g) and heated under 15 Torr (1 Torr = 133.322 Pa) to remove easily volatile reaction products. The pyrolysis was contined at 300°C using an oil pump (0.04–0.10 Torr). Under these conditions all reaction products distilled off in the form of a colourless oil. The products were separated on Alumina IB. With a benzene–ether mixture (4:1), dibenzylketone (mp 34°C from hexane, lit. (14) mp 34.5°C) and ketone **2***a* were successively eluted. Compound **2***a* crystallized from hexane (3.5 g, 30% yield), mp 62–63°C (lit. (5) mp 62–63°C); $[\alpha]_D^{25}$ +12.4° (*c* 1.0); ν_{max} ($CHCl_3$): 1711 cm^{-1}; δ: 0.75 (s, 3H, 18-H), 1.00 (d, *J* = 7 Hz, 19-H); cd (hexane, *c* = 4.2 mg/mL): $[\theta]_{295}$ − 7143.

Variant (b)

A-seco-keto-acid (**1***a*, 10.1 g) in methanol was titrated with a methanolic solution of MeONa in the presence of phenolphthalein as an indicator. The solvent was removed and potassium acetate (15 g) was added. The pyrolysis was carried out in the same manner as described above. The crude reaction product was purified by silica gel column chromatography. The benzene elution afforded compound **2***a* in a pure state, yield 3.2 g (39%). Further elution with the same solvent gave (10*S*)-des-*A*-cholestan-5-one (**2***b*), yield 0.56 g (7%), mp 80–81°C (lit. (see footnote 2) mp 71–72°C); $[\alpha]_D^{26}$ +18.1° (*c* 1.0); ν_{max} ($CHCl_3$); 1706 cm^{-1}; δ: 0.75 (s, 3H, 18-H), 1.11 (d, *J* = 7 Hz, 19-H); cd (hexane, *c* = 13.1 mg/mL): $[\theta]_{300}$ − 2183. *Anal.* calcd. for $C_{23}H_{40}O$: C 83.1, H 12.1; found: C 83.0, H 12.2.

Equilibration experiment

A solution of (10*S*)-des-*A*-ketone **2***a* (15 mg) in methanol (10 mL) was treated with aqueous KOH (3 *N*, 1 mL) and refluxed for 30 min. The equilibrium mixture of **2***a* and **2***b* was obtained, as indicated by tlc.

*(10*R*)-5a-Oxo-des*-A-B-*homo-5-oxacholestane (3*a)

(10*R*)-Des-*A*-ketone **2***a* (3.2 g) and *m*-chloroperbenzoic acid (6.4 g) were dissolved in chloroform (100 mL) and allowed to stand for 3 days. The solvent was evaporated and the residue was treated with an ethereal solution of diazomethane. After removal of ether, the crude reaction product was absorbed on a silica gel column to separate the steroidal product from less polar aromatic esters. The rearrangement product, (10*R*)-des-*A*-lactone **3***a*, was eluted with a benzene–ether mixture (9:1) and crystallized from hexane. The compound **3***a* was obtained as colourless needles (2.2 g, 66%), mp 138–139°C; $[\alpha]_D^{25}$ +62.9° (*c* 1.0); ν_{max} ($CHCl_3$): 1729 and 1293 cm^{-1}; δ: 0.71 (s, 3H, 18-H), 1.31 (d, *J* = 7 Hz, 19-H), 4.40 (m, *w*/2 = 19 Hz, 1H, 10β-H). *Anal.* calcd. for $C_{23}H_{40}O_2$: C 79.3, H 11.6; found: C 79.2, H 11.4.

*(10*S*)-5a-Oxo-des*-A-B-*homo-5-oxacholestane (3*b)

(10*S*)-Des-*A*-ketone **2***b* (145 mg) and *m*-chloroperbenzoic acid (290 mg) were dissolved in chloroform (40 mL) and allowed to stand for 24 h. The reaction mixture was extracted twice with a saturated solution of sodium carbonate, washed with water, dried, and evaporated. The chromatography on a silica gel column afforded pure (10*S*)-des-*A*-lactone **3***b* (elution with benzene–ether mixture 9:1; yield 120 mg), mp 109–111°C (from hexane); $[\alpha]_D^{26}$ +28.7° (*c* 1.0); ν_{max} ($CHCl_3$): 1723 cm^{-1}; δ: 0.71 (s, 3H, 18-H), 1.42 (d, *J* = 7 Hz, 19-H), 4.58 (broadened q, *J* = 7 Hz, 1H, 10α-H). *Anal.* calcd. for $C_{23}H_{40}O_2$: C 79.3, H 11.6; found: C 79.1, H 11.6.

*10*R*-Hydroxy-5,10-seco-des*-A-*cholestan-5-oic acid (4*a) *and its methyl ester 4*b

A solution of (10*R*)-des-*A*-lactone **3***a* (1.4 g) in methanol (50 mL) was refluxed for 3 h with a 3% aqueous solution of potassium hydroxide (20 mL). After cooling, it was acidified with 2% hydrochloric acid (200 mL) and quickly extracted with chloroform. The extract was washed with water, dried (anhydrous Na_2SO_4), and evaporated. Crude hydroxy-acid **4***a* crystallized from hexane to yield 1.1 g of pure **4***a*, mp 114–117°C; ν_{max} ($CHCl_3$): 3400–2500 (COOH), 1720 cm^{-1}; δ: 0.69 (s, 3H, 18-H), 1.11 (d, *J* = 7 Hz, 19-H), 4.05 (m, 1H, 10-H), 7.40 (m, 2H, COOH and OH).

Methyl ester **4***b* of the hydroxy-acid was obtained by treating the free acid **4***a* with diazomethane in the usual manner as an amorphous solid, $[\alpha]_D^{25}$ +38.7° (*c* 1.2); ν_{max} ($CHCl_3$): 3612, 1737, 1265, and 1180 cm^{-1}; δ: 0.68 (s, 3H, 18-H), 1.12 (d, *J* = 7 Hz, 3H, 19-H), 3.68 (s, 3H, $COOCH_3$), 4.10 (m, 1H, 10-H). *Anal.* calcd. for $C_{24}H_{44}O_3$: C 75.7, H 11.7; found: C 75.6, H 11.6.

Methyl 10-oxo-5,10-seco-des-A-*cholestan-5-oate (5*b*) and 10-oxo-5,10-seco-des*-A-*cholestan-5-oic acid (5*a)

Chromium trioxide (2.0 g) was slowly added to the vigorously stirred solution of pyridine (3.2 g) in acetic acid (15 mL), maintaining the temperature at 15–20°C. After all CrO_3 had dissolved the reagent was diluted to a volume of 25 mL with acetic acid. Prepared in such a way, the 0.8 *M* solution of CPA was used for the oxidation.

Methyl ester **4***b* (0.8 g) dissolved in AcOH (1 mL) and frozen in the refrigerator was treated with 0.8 *M* CPA (9 mL). The reaction was stirred for 20 min at 20°C, then quenched by addition of water (150 mL). The reaction mixture was extracted 3 times with ether, the combined extracts were rinsed with sodium bicarbonate solution, water, dried over sodium sulfate, and evaporated. The crude material was essentially pure and slowly crystallized from methanol with a few drops of water to afford **5***b* (0.6 g), mp 29–32°C; $[\alpha]_D^{25}$ +36.2° (*c* 1.3); ν_{max} ($CHCl_3$): 1705 and 1730 cm^{-1}; δ: 0.76 (s, 3H, 18-H), 2.07 (s, 3H, $COCH_3$), 3.68 (s, 3H, $COOCH_3$). *Anal.* calcd. for $C_{24}H_{42}O_3$: C 76.1, H 11.2; found: C 76.4, H 11.0.

Hydrolysis of methyl ester **5***b* with methanolic–aqueous KOH carried out in the usual manner gave the free keto-acid **5***a* as a colourless oil; $[\alpha]_D^{26}$ +30.7° (*c* 1.0); ν_{max} ($CHCl_3$): 3450–2420 (COOH), 1716 (C=O) cm^{-1}; δ: 0.73 (s, 3H, 18-H), 2.09 (s, 3H, $COCH_3$), 11.14 (broad s, 1H, COOH).

Ozonolysis of 5-acetoxy-des-A-*5(10)-cholestene (6)*

Enolacetate **6** (1.5 g) was dissolved in tetrachloromethane (100 mL). An excess of ozone was passed through the solution, chilled in an ice-bath, until a blue colour appeared. The excess ozone was removed by a stream of nitrogen, the solvent carefully distilled off under reduced pressure, and the resulting ozonides were decomposed with zinc (dust) in acetic acid. The crude products obtained after the usual work-up of the reaction mixture, and containing the anhydrides, were subjected to KOH hydrolysis in methanolic–aqueous solution. The reaction mixture was diluted with water and extracted with benzene. The extract containing some neutral products was rejected. After acidification, the reaction mixture was extracted with chloroform. Acidic products obtained in such a way were treated with ethereal diazomethane right after isolation. The mixture of methyl esters was separated by silica gel column chromatography. With a benzene–ether (2.5%) mixture, the dimethyl ester of 5,10-seco-des-*A*-19-nor-cholestan-5,10-dioic acid (**7***b*) and the keto-ester **5***b* were eluted successively. Keto-ester **5***b* proved to be identical in all respects with the compound described above. Diester **7***b* did not show any tendency to crystallization; ν_{max} ($CHCl_3$): 1734, 1281, and 1173 cm^{-1}; δ: 0.78 (s, 3H, 18-H), 3.69 and 3.72 (2 × s, 2 × 3H, 2 × $COOCH_3$).

5,10-Seco-des-A-*norcholestan-5,10-dioic acid (7*a)

(a) Hydrolysis of diester **7***b* was carried out in the usual manner. The crude diacid **7***a* crystallized from ethyl acetate in an analytically pure state, mp 162.5–164.5°C; $[\alpha]_D^{25}$ +44.9° (*c* 1.1); ν_{max} (KBr): 3400–2400 (COOH) and 1714 cm^{-1}; δ: 0.77 (s, 3H, 18-H), 11.66 (s, 2H, 2 × COOH). *Anal.* calcd. for $C_{22}H_{38}O_4$: C 72.1, H 10.5; found: C 72.0, H 10.6.

(b) To a stirred solution of ruthenium tetroxide (from 0.4 g of

ruthenium dioxide, 100 mL of acetone, 3.0 g of sodium periodate, and 20 mL of water), 1.0 g of 1-hydroxy-4-methyl-1,3,5(10)-cholestatriene (**8**) was added. A solution of 10.0 g of sodium periodate in 50 mL of water and 50 mL of acetone was used to maintain the yellow color of the reaction. After 3 h of stirring at room temperature a few milliliters of 2-propanol were added to quench the reaction. The mixture was diluted with an equal amount of acetone and then filtered. Most of the acetone was removed *in vacuo*. The steroids were extracted with ether and the acid fraction was isolated in the usual way. Crystallization of the product from ethyl acetate afforded 0.298 g of diacid **7***a*, mp 162–164°C, which was identical in all respects with a sample prepared as previously described.

B-*Norcholesta-1,4-dien-3-one (**10**)*

A solution of *B*-norcholestenone (2 g) and DDQ (2,3-dichloro-5,6-dicyano-*p*-benzoquinone) (1.34 g) in dry dioxan (200 mL) was heated under reflux for 8 h. The solvent was distilled off and the residue was extracted with ether. The ethereal solution was washed with 5% aqueous NaOH and with water, and dried over sodium sulfate. Removal of the solvent under vacuum gave an oil which was chromatographed on alumina. A hexane–benzene (1:9) mixture eluted 1.2 g of dienone **10** which crystallized from methanol, mp 66–67°C; $[\alpha]_D^{25}$ −16° (*c* 1.2); ν_{max} ($CHCl_3$): 1660, 1638, and 1600 cm^{-1}; δ: 0.75 (s, 3H, 18-H), 1.22 (s, 3H, 19-H), 5.72 (s, 1H, 4-H), 6.08 (d, J = 10 Hz, 1H, 2-H), 7.01 (d, J = 10 Hz, 1H, 1-H). *Anal.* calcd. for $C_{26}H_{40}O$: C 84.7, H 10.9; found: C 84.6, H 10.7.

*3-Hydroxy-1-methyl-6,19-dinorcholesta-1,3,5(10)-triene (**11**)*

A solution of dienone **10** (0.6 g) in acetic anhydride (17 mL) was treated with concentrated sulfuric acid (0.3 g) and the reaction mixture was allowed to stand for 4 h. The mixture was poured into ice-water and the product was extracted with ether. The ethereal solution was washed with water and dried over sodium sulfate. Evaporation of the solvent gave a yellow foam. The crude product was hydrolyzed in methanol with 3 mL of 45% methanolic KOH solution for 4 h at reflux. After cooling, the solution was poured into ice-water and acidified with hydrochloric acid and then extracted with ether. The extract was dried over sodium sulfate. The solvent was evaporated and the yellow foam obtained (0.528 g) was chromatographed on a silica gel column. A hexane–benzene (1:9) mixture eluted 0.401 g of a crystalline phenol **11**, mp 129–131°C; $[\alpha]_D^{25}$ +17.4° (*c* 1.0); ν_{max} ($CHCl_3$): 3600, 1600, and 1480 cm^{-1}; δ: 0.65 (s, 3H, 18-H), 2.25 (s, 3H, 1-Me), 4.75 (s, 1H, OH), 6.30 (s, 1H, 4-H), 6.48 (s, 1H, 2-H). *Anal.* calcd. for $C_{26}H_{40}O$: C 84.7, H 10.9; found: C 84.5, H 10.7.

Des-A-*6,19-dinor-5,10-secocholestan-5,10-dioic acid (**12**)*

(a) 3-Hydroxy-1-methyl-1,3,5(10)-cholestatrien-6-one (**9**; 0.5 g) in acetone (30 mL) was added dropwise to a solution of ruthenium tetroxide (from 0.2 g of RuO_2, 25 mL of acetone, 1.5 g of sodium periodate, and 10 mL of water). The yellow colour of the reaction mixture was maintained by the addition of sodium periodate (4.8 g) in water (15 mL) and acetone (15 mL) during 15 h. The reaction was quenched with 2-propanol and the further work-up was identical to our previous experiment with RuO_4. The acid fraction (0.328 g) was crystallized from acetone to give diacid **12**, mp 189–191°C; $[\alpha]_D^{25}$ +32.2° (*c* 1.3); ν_{max} ($CHCl_3$): 3300–2600 (COOH) and 1715 cm^{-1}; δ: 0.69 (s, 3H, 18-H), 11.20 (s, 2H, 2 × COOH). *Anal.* calcd. for $C_{21}H_{36}O_4$: C 71.5, H 10.1; found: C 71.4, H 10.0.

(b) Phenol **11** (0.2 g) was oxidized as above with ruthenium tetroxide prepared from 0.08 g of RuO_2. The usual work-up of the reaction mixture afforded diacid **12** (0.098 g). Crystallization from acetone gave analytically pure **12**, mp 189–191°C, which was identical in all respects with a sample prepared as above.

Acknowledgments

Sincere thanks are extended to Mr. J. Babiński for excellent technical assistance, and to Miss L. Adamczyk and Mr. K. Zwierzyński for their skillful help in a number of experiments. We are very grateful to Dr. S. Zard (I.C.S.N.–C.N.R.S., Gif sur Yvette, France) for correcting the manuscript of this paper. The microanalyses and ir spectra were carried out by the Analytical and Spectral Services Laboratories of our Department to whom we are indebted. We also acknowledge the financial assistance of the Polish Academy of Sciences.

1. W. J. Rodewald and B. M. Jagodzińska. Pol. J. Chem. **54**, 709 (1980).
2. W. J. Rodewald and B. Achmatowicz. Tetrahedron, **27**, 5467 (1971).
3. W. J. Rodewald and J. W. Morzycki. Pol. J. Chem. **52**, 2107 (1978).
4. W. J. Rodewald and W. J. Szczepek. Rocz. Chem. **50**, 823 (1976).
5. M. P. Hartshorn and E. R. H. Jones. J. Chem. Soc. 1312 (1962).
6. W. J. Rodewald and J. Wicha. Rocz. Chem. **40**, 837 (1966).
7. K. E. Stensiö. Acta Chem. Scand. **25**, 1125 (1971).
8. F. Holloway, H. J. Anderson, and W. Rodin. Ind. Eng. Chem. **47**, 2111 (1955).
9. D. M. Piatak, G. Herbst, J. Wicha, and E. Caspi. J. Org. Chem. **34**, 116 (1969).
10. A. L. Wildsand and C. Djerassi. J. Am. Chem. Soc. **68**, 1712 (1946).
11. D. Burn, V. Petrow, and G. Weston. J. Chem. Soc. 29 (1962).
12. W. G. Dauben and G. I. Fonken. J. Am. Chem. Soc. **78**, 4736 (1956).
13. S. M. Bloom. J. Am. Chem. Soc. **81**, 4728 (1959).
14. A. McKenzie, E. M. Luis, and A. G. Mitchell. Ber. **65**, 798 (1932).

Can. J. Chem. Downloaded from www.nrcresearchpress.com by 210.87.254.105 on 09/06/12
For personal use only.

Oxidation of hydrocarbons. 12. Kinetics and mechanism of the oxidation of *trans*-cinnamic acid by ruthenate and perruthenate ions[1]

DONALD G. LEE[2] AND STUART HELLIWELL

Department of Chemistry, University of Regina, Regina, Sask., Canada S4S 0A2

Received May 30, 1983[3]

DONALD G. LEE and STUART HELLIWELL. Can. J. Chem. **62**, 1085 (1984).

Recent theoretical calculations by Rappé and Goddard have pointed to the importance of spectator oxo groups in stabilizing intermediates produced during the reduction of high-valent transition metal oxides; intermediates which contain triply-bonded metal oxo groups are predicted to be unusually stable. In an attempt to test these conclusions experimentally, the rates of oxidation of cinnamate ion by ruthenate and perruthenate ions have been studied. Since the most likely intermediate formed from perruthenate ion (but not ruthenate ion) would contain a stabilizing, triply-bonded spectator oxo group, it would be expected to react faster if the calculations are correct. In agreement with these predictions, it was found that the activation energy ($\Delta G^{\ddagger}$) for the ruthenate reaction was about 7 kcal/mol higher than for the corresponding perruthenate reaction.

DONALD G. LEE et STUART HELLIWELL. Can. J. Chem. **62**, 1085 (1984).

Les récents calculs théoriques de Rappé et Goddard ont mis en évidence l'importance des groupes oxo spectateurs dans la stabilisation des intermédiaires obtenus lors de la réduction d'oxydes de métaux de transition de valence élevée; d'après ces calculs, les intermédiaires qui contiennent les groupes oxo triplement liés au métal seront particulièrement stables. Dans le but de vérifier expérimentalement cette hypothèse, on a étudié les vitesses d'oxydation de l'ion cinnamate par les ions ruthénate et perruthénate. Puisque l'intermédiaire le plus communément formé à partir de l'ion perruthénate (mais non á partir de l'ion ruthénate) contiendrait le groupe spectateur oxo triplement lié, on pourrait s'attendre à ce qu'il soit plus réactif si les calculs sont corrects. En accord avec ces prévisions, on a trouvé que l'énergie d'activation ($\Delta G^{\ddagger}$) de la réaction du ruthénate est d'environ 7 kcal/mol plus élevée que celle de la réaction correspondante du perruthénate.

[Traduit par le journal]

Can. J. Chem. Downloaded from www.nrcresearchpress.com by 210.87.254.105 on 09/06/12
For personal use only.

Introduction

Transition metal oxides and oxyanions have been used extensively as oxidants in both inorganic and organic chemistry (1). The driving force in most such reactions is generally considered to be a lowering of the oxidation number of the oxidant, which may formally be considered as a flow of electrons into the *d* orbitals of the metal. Since many of the high-valent d^0, d^1, and d^2 oxidants are capable of accepting several electrons before reaching a stable oxidation state, these reactions usually proceed in several steps with the formation of a number of intermediates of greater or lesser stability. The reactions are consequently of interest from both a practical and a theoretical point of view.

Rappé and Goddard (2) have recently described results, obtained from a theoretical study, that are extremely useful for predicting which intermediates are most likely to be formed during the course of several of these reactions. By use of *ab initio* methods they found that the metal–oxo bonds present substantially influenced the stability of an intermediate. Metal–oxo groups which have triple bond character were found to impart greater stability to the intermediate than those metal–oxo groups which were doubly bonded.

The metal–oxo double bonds are formed by the overlap of a d_{z^2} orbital on the metal with a p_z orbital on oxygen to give a σ-bond (each element contributing one electron) and the parallel overlap of a d_{xz} orbital on the metal with a p_x orbital on the oxygen to give a π-bond. The metal–oxo triple bonds are formed, however, by the overlap of d_{xz} and d_{yz} orbitals on the metal with p_x and p_y orbitals on the oxygen to give two π-bonds along with a third bond formed by the overlap of a filled p_z orbital on the oxygen with an empty d_{z^2} on the metal. Since the triple bonds lend added stability to the structures under consideration, they would be formed whenever the appropriate orbitals were available. In order to identify these bonds in structural formulas, the convention of using two solid and one broken line was adopted; i.e., M≡O (2).

As an example of the importance of the nature of these spectator oxo groups, Rappé and Goddard pointed to the difference in the energy changes which take place as reactions [1] and [2] occurred. Reaction [1] is endothermic because it involves destruction of a metal–oxo triple bond, whereas reaction [2] is exothermic because it involves formation of a metal–oxo triple bond.

[1] 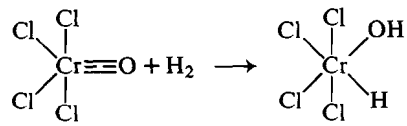

1

[2] 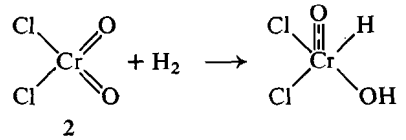

2

Spectator oxo groups with triple bonds can form only when two *d* orbitals are available for bonding to a single oxygen. In the case of chromyl chloride, **2**, a triple bond is not possible because use of both *d* orbitals for one bond would deprive the second oxygen of its π-bond. The bonding in chromyl chloride is thus analogous to the bonding in carbon dioxide, while the bonding in **1** is similar to that in carbon monoxide.

As a further example of the importance of this concept, Rappé and Goddard pointed to the difference in the reactions of chromyl chloride and permanganate ion with alkenes (2). Both oxides react with carbon–carbon double bonds to give the corresponding metallocyclooxetanes, **3** and **4** (3). However, **4** goes on to form the corresponding cyclic manganese(V) diester, **5** (and subsequently to yield diols (4) or cleavage prod-

[1] For part 11 see ref. 29.

[2] Author to whom correspondence may be addressed.

[3] Revision received January 10, 1984.

ucts (5)), while **3** does not (3, 6) because such a reaction would, presumably, cause disruption of the bonding of the spectator oxo group and thus be energetically unfavorable. In the case of **4**, on the other hand, formation of the cyclic diester is aided by the simultaneous formation of a triply-bonded spectator oxo group.

[3] 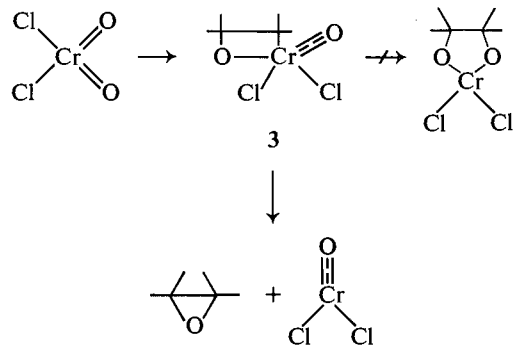

[4] 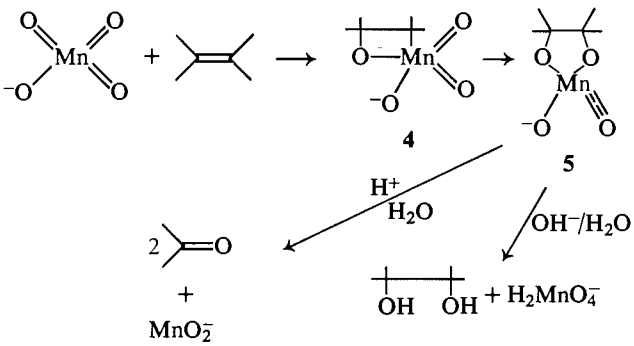

In an attempt to apply an independent experimental test to these theoretical conclusions, we have made a kinetic study of the oxidation of cinnamate ion by ruthenate (RuO_4^{2-}) and perruthenate (RuO_4^-) ions. Assuming that the metallocyclooxetane intermediates are formed in rapid equilibrium reactions, it is to be expected that perruthenate ion would react more readily with a carbon–carbon double bond to give an cyclic ruthenium(V) diester, **6**, as in eq. [5]. Such an intermediate would be stabilized by the spectator oxo group. However, a similar reaction would not occur as readily with ruthenate because formation of the corresponding cyclic ruthenium(IV) diester intermediate, **7**, could be achieved only by loss of the stability associated with the presence of a spectator oxo group in the metallocyclooxetane (eq. [6]).

[5] 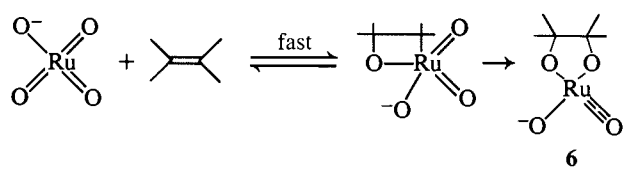

[6] 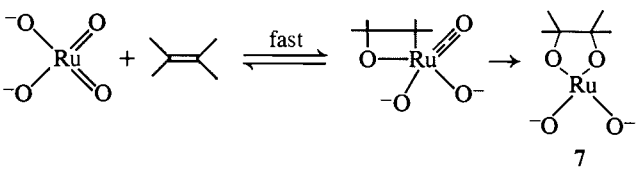

Since only cleavage products were obtained from the oxidation of either cinnamic or fumaric acids with both ruthenate and perruthenate, it appears likely that both reactions proceed

TABLE 1. Initial reaction rates for the oxidation of cinnamate ion by sodium ruthenate[a]

$[RuO_4]_i$ ($M \times 10^4$)	$Rate_i$ ($M\ s^{-1} \times 10^8$)[b]	$Rate_i/[RuO_4^{2-}]$ ($s^{-1} \times 10^5$)
3.60	1.97	5.47
2.93	1.68	5.73
2.28	1.20	5.26
1.63	0.807	4.95
1.17	0.594	5.08
0.719	0.387	5.38

[a]Temperature = 85°C; [NaOH] = 1.73 M; [cinnamate] = 4.44×10^{-3} M.
[b]$Rate_i = -(d[RuO_4^{2-}]/dt)_{initial}$.

TABLE 2. Dependence of initial ruthenate oxidation rates on cinnamate ion concentration[a]

[Cinnamate]($M \times 10^3$)	k_{obs} ($s^{-1} \times 10^5$)[b]	k_2 ($M^{-1}\ s^{-1} \times 10^2$)[c]
1.78	4.25	2.39
2.35	5.85	2.49
3.50	8.39	2.40
4.62	10.5	2.27
5.71	13.2	2.31

[a]Temperature = 85°C; [NaOH] = 0.967 M; $[RuO_4^{2-}] = 4.8 \times 10^{-4}$ M.
[b]k_{obs} = (initial rate)/$[RuO_4^{2-}]_i$.
[c]$k_2 = k_{obs}/[\text{cinnamate}]$.

by way of the cyclic diester intermediates depicted in eqs. [5] and [6]. When both of these reactions were studied under similar conditions (alkaline aqueous solutions) it was found that the rate of reaction of cinnamate ion with perruthenate ion is 5×10^5 times faster than the corresponding ruthenate reaction. This observation is therefore in agreement with the predictions made by Rappé and Goddard using *ab initio* theoretical methods (2). In the following paper we wish to describe our kinetic methods in greater detail and to show how the experimental and theoretical results can be combined to formulate mechanisms for these reactions.

Results and discussion

Ruthenate oxidations

Under conditions where the concentration of cinnamate ion was held in substantial excess, the initial reaction was found to be first order in both ruthenate (Table 1) and cinnamate ions (Table 2), but inversely dependent on hydroxide ion concentration (Fig. 1). The inverse dependence on base concentration could be associated with the fact that the reaction involves electron transfer between two anions; inclusion of a proton would presumably lead to a stabilization of the negatively charged transition state. Alternatively, the oxidation reaction could be preceded by a proton transfer in which the acid ruthenate ion, $HRuO_4^-$, was formed (eq. [7]) (7). Since it is known, for example, that the acid chromate ion, $HCrO_4^-$, is a more

[7] $RuO_4^{2-} + H^+ \rightleftharpoons HRuO_4^-$

vigorous oxidant than CrO_4^{2-}, it is not unlikely that a similar relationship would exist between $HRuO_4^-$ and RuO_4^{2-} (8).

The observed first-order dependence of the initial reaction on ruthenate concentration rules out the possibility that the reaction could involve a prior disproportionation of ruthenate into perruthenate (or ruthenium tetroxide) which would then act as

Can. J. Chem. Downloaded from www.nrcresearchpress.com by 210.87.254.105 on 09/06/12
For personal use only.

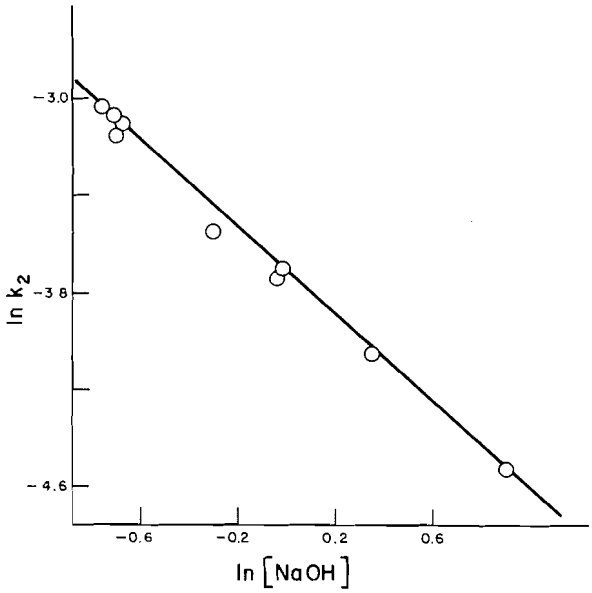

FIG. 1. Dependence of k_2 on base concentration; T = 85°C.

the actual oxidant (9). Occurrence of such a reaction would lead to a kinetic rate law that was initially second order in $[RuO_4^{2-}]$.

Work from several laboratories has indicated that reactions between high-valent transition metal oxides and alkenes proceed via organometallic intermediates which involve the formation of a π-bond between the carbon–carbon double bond and the metal (2, 3, 10). These π-complexes then rearrange to metallocyclooxetanes and eventually to cyclic diesters as in eq. [8]. In the case of ruthenate it is expected that formation of the metallocyclooxetane, **8**, would be quite rapid since it involves

[8]

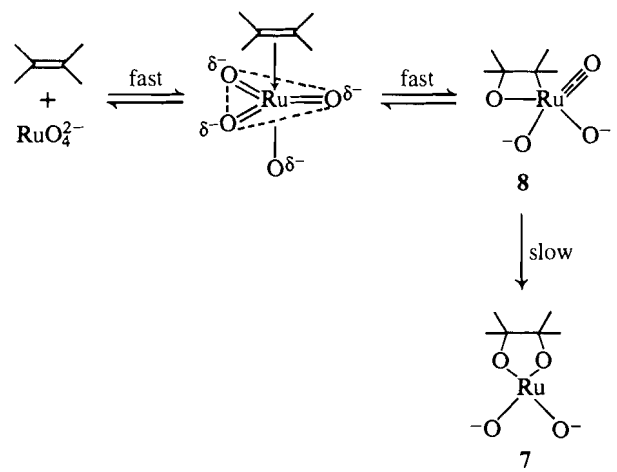

formation of a ruthenium(VI) compound with a triply-bonded spectator oxo (2). The slow step of the reaction sequence depicted in eq. [8] would therefore be the conversion of **8** into the cyclic ruthenium(IV) diester, **7**. Since this step results in a conversion of ruthenium from a d^2 to a d^4 state, it would be expected to be slower than the previous steps which involve no change in oxidation state.

The inverse secondary isotope effects that are observed when the olefinic hydrogens are sequentially replaced by deuterium (Table 3) establish that the α and β carbons have rehybridized from sp^2–p in the ground state to sp^3 in the transition state (11) and are consistent with the occurrence of the transition state

TABLE 3. Isotope effects on the initial reaction between cinnamate and ruthenate ions (reaction [9], Scheme 1)

Substrate[a]	k_2 (M^{-1} s^{-1} × 10^2)[b]	k_H/k_D
Cinnamate ion	5.94 ± 0.15	
Cinnamate-α-*d*	7.33 ± 0.09	0.81 ± 0.03
Cinnamate-β-*d*	7.02 ± 0.20	0.85 ± 0.04

[a][Substrate] = 1.21 × 10^{-3} M; [NaOH] = 0.532 M.
[b]Temperature = 85.0°C.

between structures **7** and **8**. The unfavorable entropy of activation (ΔS = −30.6 ± 1.3 eu) is also consistent with a highly structured transition state (12). The activation entropy for the reaction (Table 4) is, in fact, very similar to that for the oxidation of cinnamate ion by permanganate, which is known to proceed by way of a cyclic manganate(V) diester (13). The larger enthalpy of activation for the ruthenate reaction is probably a consequence of the fact that the cyclic diester, **5**, formed in the permanganate reaction (eq. [4]) is stabilized by the presence of a spectator oxo while the ruthenium(IV) diester, **7**, is not.

The first-order dependence of the rate of reaction on the concentration of ruthenate ion does not extend throughout the entire course of the reaction, as shown by the curvature in the plot of ln $[RuO_4^{2-}]$ vs. time (Fig. 2). This deviation from linearity is indicative of secondary reactions of the initially formed products. Although this could potentially lead to an unwieldly large number of possible reaction schemes, all but one reasonable possibility could be eliminated by the use of computer modeling. Employing a previously published program (14), we examined 28 possible reaction sequences by computing the rate constant for each step that is necessary to give the best fit between experimental and theoretical absorption values at various time intervals. Although several reaction schemes gave excellent fits for a particular set of conditions, only one sequence of reactions gave rate constants that were the same regardless of the initial reactant concentrations. This reaction sequence has been summarized in Scheme 1. The ability of this sequence to reproduce the experimental absorbance values is indicated by the data in Table 5.

The first step of this scheme is assumed to be a reaction between the unsaturated carboxylic acid and ruthenate to accommodate the previously described observation that the initial rate of reaction is first order in both RuO_4^{2-} and cinnamate ion. Since the first step was also observed to be inversely dependent on base concentration, it has been shown in Scheme 1 as being subject to acid catalysis. The value for k_2 could be determined directly from initial rate studies (Table 2); however, the magnitude of k_3 could not be exactly specified since any value large enough to maintain a steady-state concentration of the intermediate **7** was adequate. For the purpose of the computer simulation a rate constant of 80 M^{-1} s^{-1} was used. The values k_5 and k_6 were also assumed to be much larger than k_2 or k_4 and were arbitrarily set at 50 M^{-1} s^{-1}. Reactions [12] and [13] are the product-forming steps and in all likelihood refer to the oxidation of benzaldehyde and glyoxylate ion (which would be formed by the oxidative cleavage of the double bond) to give the corresponding carboxylic acids. Since such reactions were qualitatively found to be extremely fast under these conditions, the assumption that k_5 and k_6 would be large seems justified.

The structure of intermediate **9** is open to more speculation; however, at least one attractive possibility that is consistent

Can. J. Chem. Downloaded from www.nrcresearchpress.com by 210.87.254.105 on 09/06/12
For personal use only.

TABLE 4. Activation parameters for the reaction of cinnamate ion with MnO_4^-, RuO_4^-, and RuO_4^{2-}

Oxidant	Conditions	$\Delta H^{\ddagger}$ (kcal/mol)	$\Delta S^{\ddagger}$ (eu)	ΔG (kcal/mol)[a]	Temp. range
MnO_4^-	0.99 *M* $HClO_4$	4.2 ± 0.1	−30 ± 1	13.1 ± 0.4	12–41°C
MnO_4^-	0.50 *M* NaOH	4.7 ± 0.1	−29 ± 1	13.3 ± 0.4	0–40°C
RuO_4^-	0.39 *M* NaOH	5.0 ± 0.1	−32 ± 1	14.5 ± 0.4	7–45°C
RuO_4^{2-}	0.54 *M* NaOH	12.5 ± 0.5	−31 ± 2	21.7 ± 1.1	65–95°C

[a] $\Delta G^{\ddagger}$ calculated at 25°C.
[b] All plots of ln k/T vs. $1/T$ exhibited correlation coefficients of 0.998 or better for a minimum of 5 temperatures.

TABLE 5. Observed and calculated absorbances for the oxidation of cinnamate ion by sodium ruthenate

Time (5×10^2)	Absorbance (obs.)	Absorbance (calcd.)
0	0.803	0.803
1.83	0.778	0.775
5.09	0.726	0.728
8.17	0.686	0.687
12.4	0.633	0.637
16.8	0.587	0.590
21.2	0.545	0.549
25.8	0.507	0.510
32.0	0.464	0.464
39.4	0.417	0.417
49.8	0.365	0.364
61.2	0.322	0.320
75.4	0.282	0.282
93.0	0.244	0.256

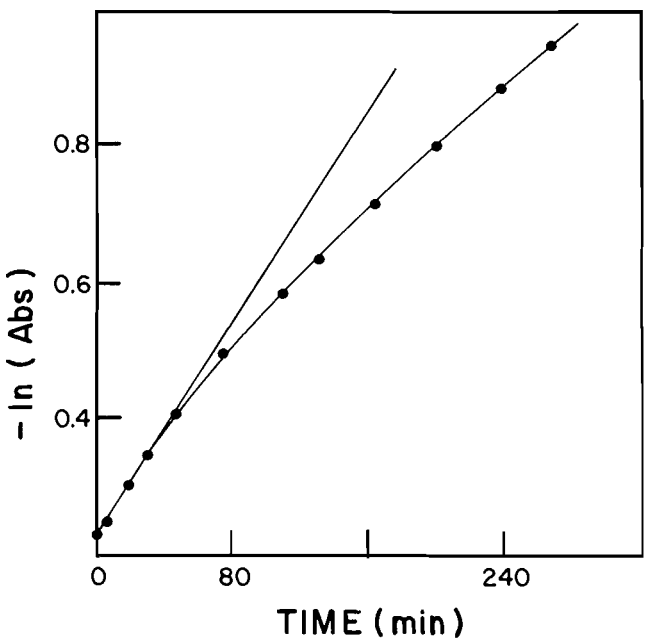

FIG. 2. Attempted first-order plot for the oxidation of cinnamate by ruthenate. $[RuO_4^{2-}] = 4.37 \times 10^{-4}$ *M*; [cinnamate] $= 5.71 \times 10^{-3}$ *M*; [NaOH] = 2.46 *M*; *T* = 85°C.

with all of the experimental evidence is available if **9** is assumed to be a cyclic ruthenate(VI) diester formed by the oxidation of **7**. Such a two-electron transfer reaction is consistent with the known properties of ruthenate under these conditions (15). Furthermore, it would not be unreasonable to observe a large rate constant for such a reaction; many similar electron

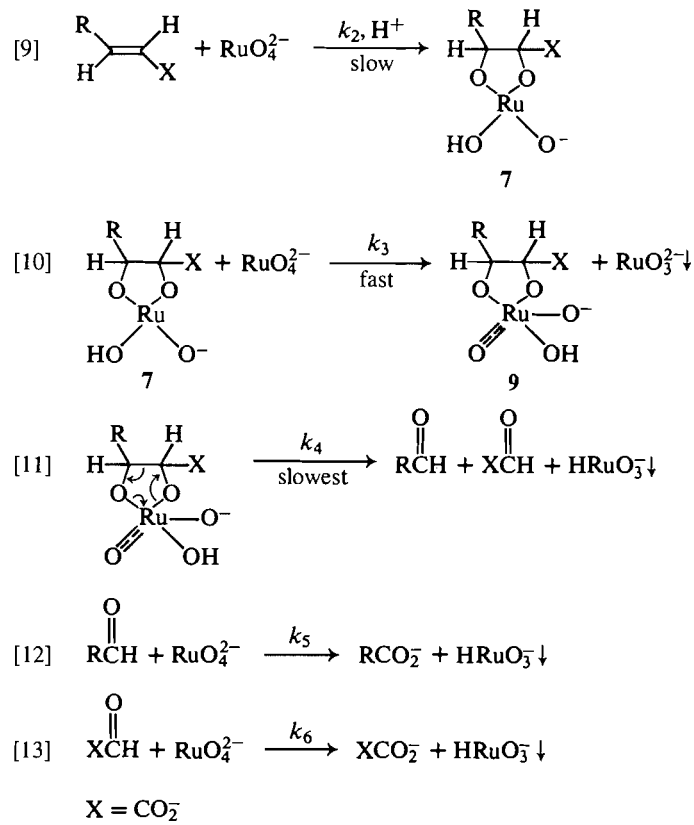

SCHEME 1

transfer processes between transition metal oxyanions are known to occur rapidly (16). Development of a triply-bonded spectator oxo group as the reaction progresses would also serve to increase its rate (2).

Intermediate **9** could undergo one of two possible reactions: (*i*) it could hydrolyze to give a diol, or (*ii*) it could undergo oxidative decomposition to give cleavage products. Since only compounds resulting from the cleavage of the carbon–carbon double bond could be found among the products of the reaction, it may be assumed that **9** decomposes as depicted in eq. [11].

Other evidence consistent with this suggestion includes the normal secondary kinetic isotope effects (Table 6) which are indicative of a rehybridization of the carbons from sp^3 to sp^2 as the reaction proceeds (11), and a favorable entropy of activation ($\Delta S^{\ddagger} = 7.7 \pm 2.1$ eu) as would be expected for a fragmentation reaction (12). A large enthalpy of activation (31.0 ± 0.7 kcal/mol) for this step is indicative of similar reactions in which σ-bonds are cleaved (12, 13). Finally, when the concentrations of the reactants and intermediates are calculated from the computer model for Scheme 1 and plotted against time it is

Can. J. Chem. Downloaded from www.nrcresearchpress.com by 210.87.254.105 on 09/06/12
For personal use only.

TABLE 6. Isotope effects on reaction [11] of Scheme 1

Substrate[a]	k_2 ($s^{-1} \times 10^5$)	k_H/k_D
Cinnamate ion	1.94 ± 0.01	
Cinnamate-α-*d*	1.37 ± 0.04	1.42 ± 0.05
Cinnamate-β-*d*	1.65 ± 0.07	1.18 ± 0.12

[a][Substrate] = 1.21×10^{-3} *M*; [NaOH] = 0.532 *M*.
[b]Temperature = 85.0°C.

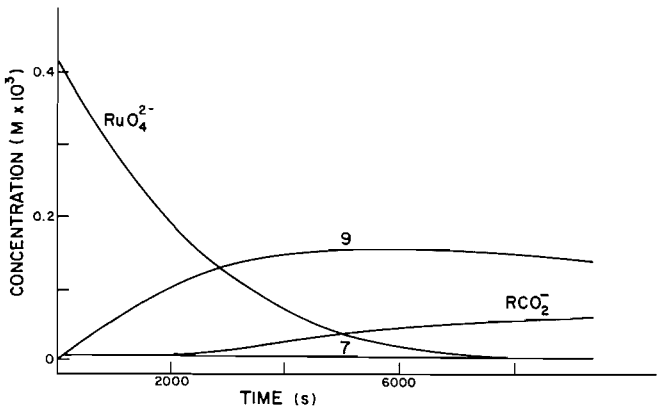

FIG. 3. Calculated concentrations of reactants, intermediates, and products for a reaction proceeding according to Scheme 1.

observed that **9** is the only intermediate which accumulates as the reaction proceeds (Fig. 3). Since this intermediate is in the same oxidation state as RuO_4^{2-}, it is not to be expected that its presence would produce detectable changes in the uv–vis spectrum as the reaction progresses (Fig. 4); oxyanions of a metal with the same oxidation state often have very similar spectra (17).

The rate law for the process summarized by the reactions in Scheme 1 may be derived by noting that reaction [10] does not result in a net change in oxidation state, the property which presumably controls the spectral changes that were used to monitor the rate of reaction. Therefore the experimental rate law would be given by eq. [14].

$$[14] \quad \frac{-d[Ru(VI)]}{dt} = \frac{k_2[RuO_4^{2-}][\text{ 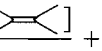 }]}{[OH^-]} + k_4[\mathbf{9}]$$

In the initial stages of the reaction, [**9**] will be vanishingly small; i.e., when $[RuO_4^{2-}] = [RuO_4^{2-}]_{initial}$, [**9**] = 0. Consequently, when initial reaction rates are considered, the last term in eq. [14] can be neglected and the rate law for the initial reaction is therefore first order in ruthenate, first order in cinnamate, and inversely dependent on base concentration. This is in accordance with the experimental observations (see Fig. 1 and Tables 1 and 2). As [**9**] increases, this approximation cannot be made and the rate expression becomes one obtained for consecutive reactions of mixed order (18). Such expressions are not amenable to treatment by classical methods and are best handled by numerical methods as has been done in this instance (18).

It may be noted, however, that the second term in eq. [14] will become dominant as the concentration of **9** increases (Fig. 3). When this happens one would expect the reaction to become second order in ruthenate since two moles of RuO_4^{2-} are consumed in the formation of **9**. As a consequence, deceptively

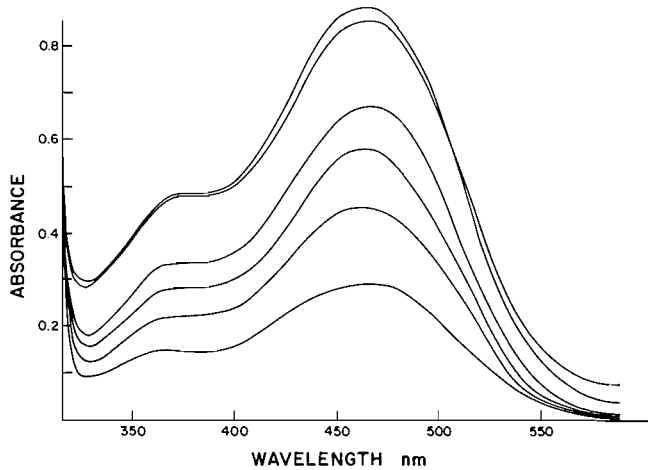

FIG. 4. Sequential scans as the oxidation of cinnamate by ruthenate proceeds. Spectra taken at 0, 196, 634, 1320, 2320, and 5380 s (top to bottom).

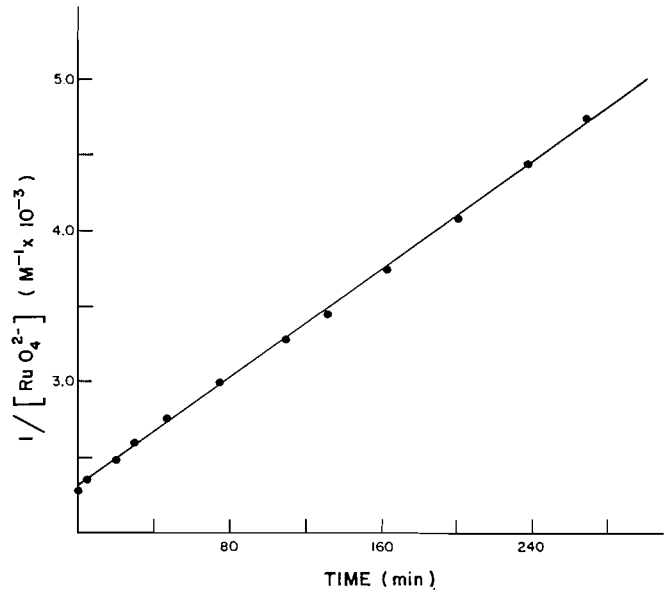

FIG. 5. Pseudo second-order plot for the oxidation of cinnamate by ruthenate. $[RuO_4^{2-}] = 4.37 \times 10^{-4}$ *M*; [cinnamate] = 5.71×10^{-3} *M*; [NaOH] = 2.46 *M*; *T* = 85°C.

good pseudo second-order plots are obtained when the oxidation of an excess of cinnamate is studied under non-initial rate conditions (Fig. 5).

Perruthenate oxidations

Because the reaction of perruthenate ion with cinnamate ion under alkaline conditions is so much faster than the corresponding reaction with ruthenate ions, it was not possible to study the two reactions at the same temperature or in exactly the same way. Whereas it was convenient to follow the rate of ruthenate oxidation at 85°C by use of conventional spectrophotometric methods, the rate of the perruthenate oxidations could only be followed at a lower temperature (21°C) and with the aid of a stopped-flow system.

The reaction was found to be first order in perruthenate (Fig. 6), first order in cinnamate ion (Fig. 7), and independent of base concentration (Table 7). As the reaction proceeded, the green perruthenate solution was rapidly changed into a bright orange solution that exhibited the same uv–vis absorption

Can. J. Chem. Downloaded from www.nrcresearchpress.com by 210.87.254.105 on 09/06/12
For personal use only.

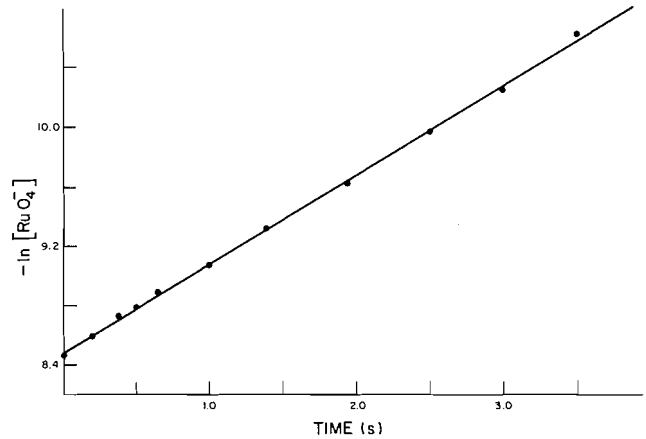

FIG. 6. Pseudo first-order plot for the oxidation of cinnamate by perruthenate. $[RuO_4^-] = 2.10 \times 10^{-4}$ *M*; [cinnamate] = 3.50×10^{-3} *M*; [NaOH] = 0.350 *M*; *T* = 21°C.

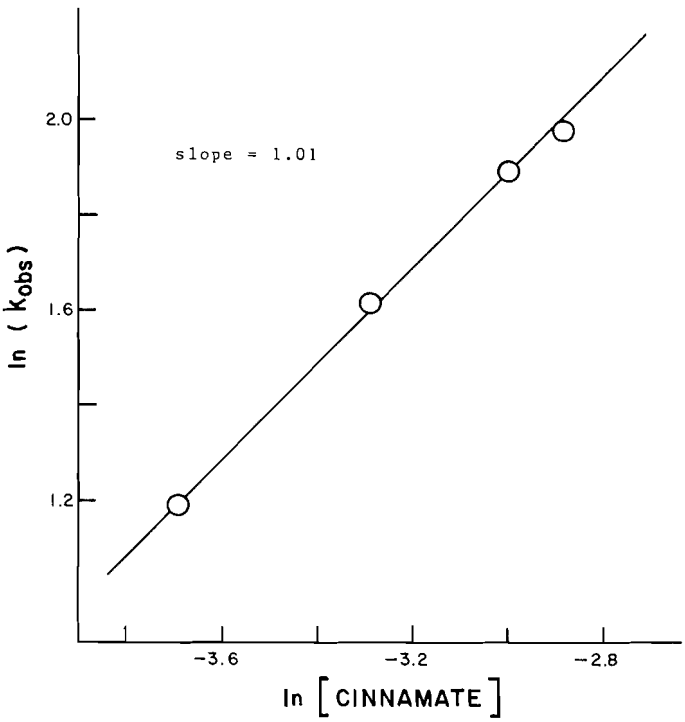

FIG. 7. Dependence of the rate of perruthenate oxidations on cinnamate concentration.

spectrum as ruthenate solutions. These solutions reacted more slowly to give ruthenium dioxide and benzoic acid.

The activation parameters for this reaction were found to be very similar to those observed for the corresponding reaction of permanganate with cinnamic acid (Table 4). Hence it appears as if the reaction likely involves an initial addition of the oxidant to the double bond, giving a ruthenium(V) cyclic diester, **10**, as in eq. [15]. However, since there was no indication of the formation of inorganic products other than RuO_4^{2-} the intermediate, **10**, must undergo a subsequent reaction leading to the formation of ruthenate. A likely possibility is that **10** could, in analogy with the corresponding cyclic manganese(V) diester, oxidatively decompose to give cleavage products and ruthenate(III) as in eq. [16]. The ruthenate(III) could then react with perruthenate to give ruthenate(VI) as in eq. [17].

TABLE 7. Effect of base concentration on the rate of oxidation of cinnamate ion by sodium perruthenate[a]

[NaOH] (*M*)	k (M^{-1} s^{-1})
0.040	190
0.080	199
0.140	196
0.200	191
0.280	179
0.350	177

[a][Substrate] = 3.50×10^{-2} *M*; temperature = 21.0°C; μ = 0.500 *M*.

TABLE 8. Isotope effects on the rate of oxidation of cinnamate ion by sodium perruthenate[a]

Substrate	[NaOH] (*M*)	k (M^{-1} s^{-1})
Cinnamate ion (1.75×10^{-3} *M*)	0.098	215 ± 6
Cinnamate-α-*d* (1.75×10^{-3} *M*)	0.098	222 ± 6
Cinnamate ion (3.40×10^{-2} *M*)	0.282	133 ± 2
Cinnamate-β-*d* (3.40×10^{-2} *M*)	0.282	138 ± 3

[a]Temperature = 21.0°C; μ = 0.500 *M*.

The lack of a substantial secondary deuterium isotope effect for this reaction sequence (Table 8) indicates that the carbon atoms are sp^2–p hybridized in the transition state. Consequently it appears as if the rate-determining step is likely oxidative decomposition of the cyclic ruthenium(V) diester as in eq. [16]. In this respect the mechanism is parallel to the one proposed above for RuO_4^{2-} oxidations, where decomposition of a similar cyclic diester was also found to be the slowest step in the reaction sequence.

[15] 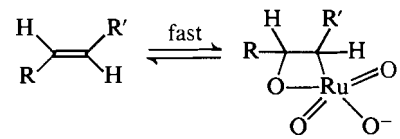

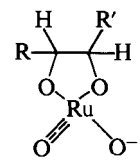

[16] 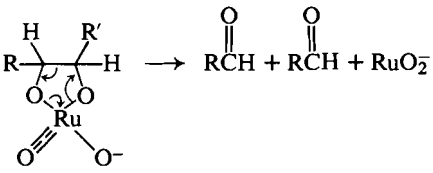

10

[17] $RuO_2^- + 3RuO_4^- + 4OH^- \longrightarrow 4RuO_4^{2-} + 2H_2O$

The difference in activation energies ($\Delta\Delta G^{\ddagger}$) for the oxidation of cinnamate by ruthenate and perruthenate is about 7 kcal/mol. From this it can be calculated that the rate of the

Can. J. Chem. Downloaded from www.nrcresearchpress.com by 210.87.254.105 on 09/06/12
For personal use only.

perruthenate reaction is about 5×10^5 times as fast as the corresponding ruthenate reaction at room temperature. Although part of this effect may be due to the higher reduction potential of perruthenate, a large portion must be attributed to a difference in the relative stabilities of the transition and ground states as described above. The fact that ruthenate, although a vigorous oxidant for alcohols, reacts very slowly with carbon–carbon double bonds has made it an excellent reagent for the oxidation of unsaturated alcohols (19). Several examples of its use for this purpose (20–22), as well as for the oxidation of certain saturated alcohols (23), have appeared in the recent literature.

Experimental

Sodium ruthenate (15, 24)

Ruthenium tetroxide (25) was first prepared by reaction of 5.0 g of hydrated ruthenium dioxide with 350 mL of commercial bleach (5.25% sodium hypochlorite). After stirring for approximately 10 min, the RuO_4 which had formed was extracted into carbon tetrachloride (5×75 mL) which in turn was washed with 3×100 mL distilled water to remove excess hypochlorite. An equal volume of 1.0 *M* NaOH was then added to the carbon tetrachloride solution and the heterogeneous mixture stirred for several hours (until the organic layer was colorless) and the deep orange basic ruthenate solution separated. Before being used in a kinetic experiment these solutions were heated at 75°C for several days. This ensures that all of the ruthenium is present in the +6 oxidation state and that the last traces of sodium hypochlorite have been removed. The purity and concentration of these solutions were then assayed using procedures described in the literature (24).

Sodium perruthenate (24, 26)

This reagent was also prepared from the reduction of ruthenium tetroxide. After the oxidation of hydrated ruthenium dioxide by bleach, as described above, a stream of air was used to carry the RuO_4 over into 0.3 *M* NaOH cooled at −3°C. The sodium perruthenate thus formed was allowed to stand at 0°C overnight to ensure complete reduction of ruthenium tetroxide to sodium perruthenate. Because of the instability of perruthenate solutions, these were made up as required.

Product studies

A solution of 4.5×10^{-2} *M* RuO_4^{2-} (170 mL of 1.0 *M* NaOH) was added to 0.30 g of cinnamic acid dissolved in 50 mL of 0.5 *M* NaOH. The reaction was allowed to proceed overnight at 60°C. The black ruthenium dioxide was filtered off and washed with warm distilled water. The basic solution was extracted with 3×75 mL portions of ether, saturated with sodium chloride, and acidified with dilute hydrochloric acid. The resulting solutions were extracted with 3×75 mL portions of ether. Evaporation of the ether after drying with anhydrous $MgSO_4$ left a white residue from the acid extract but nothing from the basic extract. Identification of the white residue indicated that it consisted of benzoic and some unreacted cinnamic acid. The yields based on unrecovered starting material were 99.0 and 99.5% benzoic acid for duplicate runs.

The oxidation of fumaric acid was carried out in a similar manner up to and including the filtering to remove ruthenium dioxide. After neutralizing the filtrate with hydrochloric acid, 10 mL of 10% $CaCl_2$ solution was added. This produced an immediate white precipitate of calcium oxalate. The solution was allowed to stand overnight at 70°C to ensure complete precipitation and coagulation of the calcium oxalate (27). The precipitate was then filtered through a sintered glass crucible, dried at 105°C, and weighed. Powder X-ray photographs taken of both this precipitate and a prepared sample of calcium oxalate were shown to be the same. Samples of the precipitate were then analyzed by dissolving a sample (about 0.2 g) in 20 mL of 1:8 H_2SO_4, diluting it with 70 mL of distilled water, heating to 80–90°C, and titrating with standard $KMnO_4$ solution (28). Yields of 88 and 95% oxalic acid were obtained for duplicate experiments.

When perruthenate ion reacted with cinnamic acid at 0°C, the deep yellow-green RuO_4^- color was instantly replaced by an intense orange color typical of ruthenate ion. The ruthenate color then was observed to disappear as ruthenium dioxide formation took place. Hence it was decided to attempt to quench the ruthenate formed with sodium arsenite in the following way. To 100 mL of 0.3 *M* NaOH (at 0°C) containing 0.40 g of cinnamic acid was added 175 mL of sodium perruthenate solution (0.025 *M*). Immediately following this addition, 125 mL of 0.1 *M* $NaAsO_2$ were added. However, due to the rapidity of the reactions, quenching was only partially successful and only a qualitative estimation of the products of the initial reaction could be made. Both benzaldehyde and benzoic acid were isolated after a work-up as described above. A more quantitative result was obtained when the reaction was allowed to go to completion without quenching. A 99% yield of benzoic acid was then obtained.

Kinetic studies

In the kinetic studies of the oxidation of cinnamic acid by both ruthenate and perruthenate, pseudo order techniques were used throughout; i.e. greater than a ten-times equivalent excess of substrate over oxidant was used. It was found unnecessary to maintain a constant ionic strength for the ruthenate oxidations because varying the ionic strength had little or no effect on the rate of reaction. However, since the rates of the perruthenate reactions were not independent of the ionic strength, it was maintained at a $\mu = 0.500$ *M* by use of sodium perchlorate for these reactions.

In the case of ruthenate oxidations, solutions of the desired base concentrations were made up (2-L batches) and stabilized at 75°C for 2 days. The reactions were then carried out in 125-mL ground glass-stoppered erlenmeyer flasks thermostated in an oil bath at 85°C. In a typical set of experiments, eight flasks, each containing 100 mL of ruthenate solution, were allowed to thermostat for 1 h before the desired amount of substrate was added to start the reaction. Aliquots were removed at appropriate intervals and then quenched by cooling in ice. Absorbance readings were made using a Perkin–Elmer 356 dual wavelength, double beam spectrophotometer. This instrument has the advantage that a reference beam compensates for any precipitate which may have formed during the reaction. The wavelengths used were 460 and 570 nm. Little absorption by ruthenate occurs at 570 nm, hence this wavelength was used as the reference beam. The absorbance readings were converted into ruthenate concentrations using a calibration curve based on ruthenate solutions of known concentrations.

In several experiments the aliquots were first cooled, then centrifuged to remove ruthenium dioxide and scanned from 300 to 600 nm in an attempt to detect possible intermediates. As the plots in Fig. 4 indicate, there was no evidence for the formation of long-lived intermediates. Time vs. absorbance plots obtained in this way were very similar to those obtained using the dual wavelength mode.

The reaction between perruthenate ion and cinnamate ion could be followed spectrophotometrically by monitoring the disappearance of perruthenate ion at 385 nm. Because of the rapid nature of the reaction, all experiments were performed using a Durrum Model D-110 stopped-flow spectrophotometer.

In a typical experiment, 0.5 mL of RuO_4 solution (ca. 0.05 *M*) was pipetted into a 125-mL erlenmeyer flask containing approximately 50 mL of a NaOH solution and a magnetic stirring bar. The flask was stoppered and the solution degassed by reducing the pressure to approximately 95 Torr and stirring. When all of the RuO_4 had been reduced to RuO_4^- (determined spectrophotometrically), one of the stopped-flow syringes was filled with this solution and the other with a solution of the substrate. Equal volumes of the two reactants were forced through the mixing jet and into the cuvette where the absorbance measurements were made. The resulting kinetic curve, traced on an oscilloscope, was then photographed. Determinations were usually carried out in triplicate.

In order to check for the formation of possible intermediates, kinetic curves were run at a number of different wavelengths and spectra synthesized as a function of time (Fig. 8). As may be seen from the

Can. J. Chem. Downloaded from www.nrcresearchpress.com by 210.87.254.105 on 09/06/12
For personal use only.

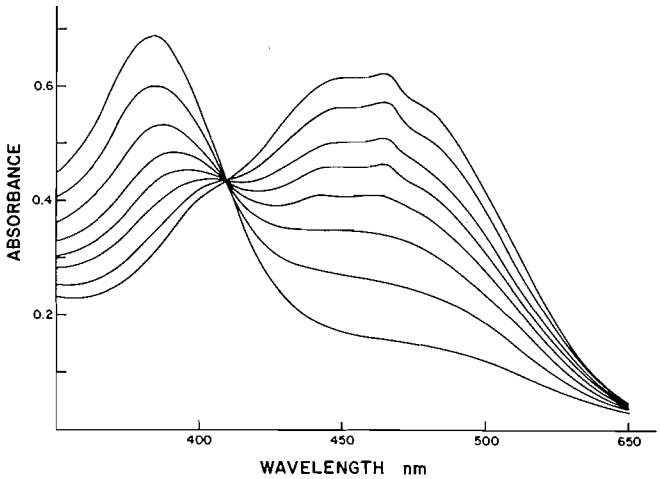

FIG. 8. Sequential scans as the oxidation of cinnamate by perruthenate proceeds. Spectra taken at 0.5-s intervals, top to bottom.

good isosbestic point, no intermediate could be detected, the spectra after 5 s having a close resemblance to that of ruthenate.

Acknowledgements

Financial assistance from the Natural Sciences and Engineering Research Council of Canada, the donors of the Petroleum Research Fund, administered by the American Chemical Society, and the Committee on Higher Education, Imperial Oil Limited is gratefully acknowledged.

1. R. STEWART. Oxidation mechanisms. Benjamin, New York. 1964; K. B. WIBERG. Oxidation in organic chemistry, Part A. Academic Press, New York. 1965; W. S. TRAHANOVSKY. Oxidation in organic chemistry, Parts B, C, and D. Academic Press, New York. 1973, 1978, and 1982; D. ARNDT. Manganese compounds as oxidizing agents in organic chemistry. Open Court, La Salle. 1981; D. G. LEE. The oxidation of organic compounds by permanganate ion and hexavalent chromium. Open Court, La Salle. 1981.
2. A. K. RAPPÉ and W. A. GODDARD III. J. Am. Chem. Soc. **104**, 448 (1982); **104**, 3287 (1982); A. K. RAPPÉ. Ph.D. Thesis, California Institute of Technology. 1980.
3. K. B. SHARPLESS, A. Y. TERANISHI, and J. E. BACKVALL. J. Am. Chem. Soc. **99**, 3120 (1977).
4. D. ARNDT. Manganese compounds as oxidizing agents in organic chemistry. Open Court, La Salle. 1981. pp. 207–212.
5. R. N. HASZELDINE. J. Chem. Soc. 4291 (1955); 4302 (1955); R. N. HASZELDINE and J. E. OSBORNE. J. Chem. Soc. 3880 (1955); R. N. HASZELDINE and K. LEEDHAM. J. Chem. Soc. 1548 (1953).
6. W. H. HARTFORD and M. DARRIN. Chem. Rev. **58**, 1 (1958); F. FREEMAN, P. J. CAMERON, and R. H. DUBOIS. J. Org. Chem. **33**, 3970 (1968); F. FREEMAN, P. D. MCCARTY, and N. J. YAMACHIKA. J. Am. Chem. Soc. **92**, 4621 (1970); K. B. SHARPLESS and A. Y. TERANISHI. J. Org. Chem. **38**, 185 (1973); F. W. BACHELOR and U. O. CHERIYAN. J. Chem. Soc. Chem. Commun. 195 (1973); Tetrahedron Lett. 3291 (1973); Can. J. Chem. **54**, 3383 (1976).
7. N. BAILEY, A. CARRINGTON, K. A. K. LOTT, and M. C. R. SYMONS. J. Chem. Soc. 290 (1960).
8. R. STEWART. *In* Oxidation in organic chemistry, Part A. *Edited by* K. B. Wiberg. Academic Press, New York. 1965. p. 35; F. H. WESTHEIMER and A. NOVICK. J. Chem. Phys. **11**, 506 (1943).
9. L. D. BURKE and J. F. HEALY. J. Chem. Soc. Dalton Trans. 1091 (1982).
10. D. G. LEE and N. A. NOURELDIN. J. Am. Chem. Soc. **105**, 3188 (1983).
11. A. STREITWIESER, R. H. JAGOW, R. C. FAHEY, and S. SUZUKI. J. Am. Chem. Soc. **80**, 2326 (1958); E. A. HALEVI. Prog. Phys. Org. Chem. **1**, 109 (1963); T. H. LOWRY and K. S. RICHARDSON. Mechanism and theory in organic chemistry. 2nd ed. Harper and Row, New York. 1981. pp. 210–212.
12. R. STEWART. The investigation of organic reactions. Prentice–Hall, Englewood Cliffs, N.J. 1966. p. 52; F. A. CAREY and R. J. SUNDBERG. Advanced organic chemistry, Part A. Plenum, New York. 1977. pp. 135–139.
13. F. FREEMAN, C. O. FUSELIER, C. R. ARMSTEAD, C. E. DALTON, P. A. DAVIDSON, E. M. KARCHESFSKI, D. E. KROCHMAN, M. N. JOHNSON, and N. J. JONES. J. Am. Chem. Soc. **103**, 1154 (1981); D. G. LEE and J. R. BROWNRIDGE. J. Am. Chem. Soc. **96**, 5517 (1974); K. B. WIBERG, C. J. DEUTSCH, and J. ROCEK. J. Am. Chem. Soc. **95**, 3034 (1973).
14. D. F. DETAR. J. Chem. Educ. **44**, 191 (1967).
15. D. G. LEE, U. A. SPITZER, J. CLELAND, and M. E. OLSON. Can. J. Chem. **54**, 2124 (1976).
16. J. HALPERN. Q. Rev. Chem. Soc. **15**, 207 (1961); F. BASOLO and R. G. PEARSON. Mechanisms in inorganic reactions. Wiley, London. 1958. Chapt. 7; K. L. BRIDGES, S. K. MUKHERJEE, and G. GORDON. Inorg. Chem. **11**, 2494 (1972); J. P. BIRK. J. Am. Chem. Soc. **91**, 3189 (1969); J. H. ESPENSON. J. Am. Chem. Soc. **92**, 1880 (1970).
17. D. G. LEE and R. STEWART. J. Am. Chem. Soc. **86**, 3051 (1964).
18. S. W. BENSON. The foundations of chemical kinetics. McGraw–Hill, New York. 1960. p. 33; K. J. LAIDLER. Chemical Kinetics. McGraw–Hill, New York. 1950. pp. 22–24.
19. M. SCHRODER and W. P. GRIFFITH. J. Chem. Soc. Chem. Commun. 58 (1979); D. G. LEE, D. T. HALL, and J. H. CLELAND. Can. J. Chem. **50**, 3741 (1972); D. G. LEE and J. R. BROWNRIDGE. Can. J. Chem. **51**, 2102 (1973).
20. E. J. COREY, R. L. DANHEISER, S. CHANDRASEKARAN, G. E. KECK, B. GOPALAN, S. D. LARSEN, P. SIRET, and J. L. GRAS. J. Am. Chem. Soc. **100**, 8034 (1978).
21. R. M. COATES, P. D. SENTER, and W. R. BAKER. J. Org. Chem. **47**, 3597 (1982).
22. A. I. DALTON, JR., H. J. DORAN, and R. D. H. MURRAY. U.S. Patent No. 4,225,694 (1980).
23. W. G. DAUBEN and A. F. CUNNINGHAM, JR. J. Org. Chem. **48**, 2842 (1983).
24. R. E. CONNICK and C. R. HURLEY. J. Am. Chem. Soc. **74**, 5012 (1952); G. NOWOGROCKI and G. TRIDOT. Bull. Soc. Chim. Fr. 684 (1965); D. L. BURKE and J. F. HEALY. J. Chem. Soc. Dalton Trans. 1091 (1982).
25. D. G. LEE and M. VAN DEN ENGH. *In* Oxidation in organic chemistry, Part B. *Edited by* W. S. Trahanovsky. Academic Press, New York. 1973. Chapt. 4.
26. A. CARRINGTON and M. C. R. SYMONS. J. Chem. Soc. 284 (1960).
27. I. M. KOLTHOFF and E. B. SANDELL. Textbook of quantitative inorganic analysis. 3rd ed. Macmillan, New York. 1952. p. 337.
28. D. A. SKOOG and D. M. WEST. Fundamentals of analytical chemistry. 2nd ed. Holt, Rinehart and Winston, New York. 1969. pp. 422–423.
29. D. G. LEE and K. C. BROWN. J. Am. Chem. Soc. **104**, 5076 (1982).

Can. J. Chem. Downloaded from www.nrcresearchpress.com by 210.87.254.105 on 09/06/12
For personal use only.

Anomalous 5-*endo-trig* reversals: general reactions of 7-oxabicyclo[2.2.1]heptenes and heptanes

B. A. KEAY, D. RAJAPAKSA, and R. RODRIGO[1]

Guelph–Waterloo Centre for Graduate Work in Chemistry, Department of Chemistry, University of Waterloo, Waterloo, Ont., Canada N2L 3G1

Received November 15, 1983

B. A. KEAY, D. RAJAPAKSA, and R. RODRIGO. Can. J. Chem. **62**, 1093 (1984).

Two general 5-*endo-trig* reversals of 7-oxabicyclo[2.2.1]heptanes and heptenes are described and discussed. The reverse-Michael reaction occurs with the aldehyde, ketone, ester, and nitrile derivatives while the reverse aldol reaction catalysed by acid is confined to the aldehydes and ketones. These properties of the title compounds are rationalized in terms of the geometric alignments of the bonding and antibonding orbitals of the bridging oxygen atom and its neighboring carbons. New isobenzofuran and cyclohexadiene syntheses form a part of the report.

B. A. KEAY, D. RAJAPAKSA et R. RODRIGO. Can. J. Chem. **62**, 1093 (1984).

On décrit et on discute de deux réactions générales 5-*endo-trig* inversées des oxa-7 bicyclo[2.2.1] heptanes et heptènes. La réaction inverse de Michael se produit dans le cas des dérivés de l'aldéhyde, de la cétone et du nitrile tandis que la réaction aldolique inverse se limite aux aldéhydes et aux cétones. On rationalise ces propriétés des composés mentionnés dans le titre en fonction des alignements des orbitales liantes et antiliantes de l'atome d'oxygène en position de pont et de ses atomes de carbone voisins. On rapporte également de nouvelles synthèses de l'isobenzofuranne et du cyclohexadiène.

[Traduit par le journal]

Can. J. Chem. Downloaded from www.nrcresearchpress.com by 210.87.254.105 on 09/06/12
For personal use only.

Early in our studies of the Diels–Alder reactions of isobenzofurans (1) we made the useful and intriguing discovery that adduct **1***a* was smoothly converted to the dihydronaphthalene **2***a* with methanolic sodium methoxide. The same reaction applied to the closely related adduct **3** was a key transformation in our recent synthesis (2) of (±) daunomycinone. An examination of the process with a variety of oxabicyclo adducts[2] was conducted and the results (Table 1, Entries 1, 3, 6, 8, 11, 13, 16, 18) confirmed the generality of the reaction. A reverse-Michael rationalization shown in Scheme 1 requires the development of some double bond character at a bridgehead and is also a 5-*endo-trig* reversal in violation of rules (3) formulated earlier and illustrated (4) with the furan **9**. No evidence could be obtained, however, to support any alternative mechanism; for example, no products of C(4)—O cleavage were ever observed, thus excluding the possibility of a simple nucleophilic displacement at C(1) and(or) C(4). Deuteration at C(2) took place with esters and nitriles (entries 5, 7, 10, 12, 15, and 17) and the deuterated products were *endo–exo* mixtures even when pure *endo* substrates (**1***c* and **1***d*, entries 5 and 7) were used. Oxabicyclo ketones and aldehydes could not be deuterated cleanly with methanolic methoxide because of the rapid formation of products under the conditions. After 1 h at 20°C with this reagent, **1***a* and **1***b*, for example, were converted to a 1:1 mixture of products (**2***a* and **2***b* respectively) and deuterated starting materials. The lower acidity of the esters and nitriles must be responsible for rapid reprotonation of their enolates in methanolic methoxide, permitting clean deuteration in these cases and revealing the existence of a kinetic barrier to the reverse-Michael fission of the C(1)—O bond. This behaviour is similar to the previously observed (4) deuteration of furan **9** and is interpreted similarly. Unlike the simple furan **9**, however, which was inert to all bases, these compounds do suffer a forbidden 5-*endo-trig* cleavage with the strong base LDA under aprotic conditions (entries 6, 8, 11, 13, 16, and 18). Base-catalysed aromatizations observed in entries 2, 4, and 9 and previously with sodium acetate in refluxing methanol (5) must also occur through an initial reverse-Michael cleavage followed by dehydration. Thus it is clear that the 7-oxabicyclo heptanes and heptenes are susceptible to a general 5-*endo-trig* reversal[3] in violation of Baldwin's rules and that this anomaly cannot be attributed to thermodynamic factors, i.e. release of strain resulting from the reaction.

Again, in the course of our studies on the synthesis of (±) daunomycinone, we obtained the surprising result that the hydrogenolysis of **3** in ethanol containing a few drops of perchloric acid produced not the expected tetralin but the phthalan **10** (95%). In attempting to understand the course of this unusual hydrogenolytic cleavage of the C(1)—C(2) bond, we subjected ketone **1***a* to perchloric acid – methanol treatment at room temperature for 5 min and obtained methoxy phthalan **11** (94%) whose structure was supported by spectroscopic data and by conversion to the Diels–Alder adduct **12** (72%) with dimethyl acetylene dicarboxylate. In the absence of methanol, similar acid treatment resulted in extensive decomposition, probably through the formation of isobenzofuran **13** which polymerizes. No aromatic product (**8***a*) could be detected. Evidently these ketones are extremely prone to reverse-aldol cleavage (Scheme 2) and the resulting oxonium ion is trapped as the alkoxy phthalan which may be isolated (**11**) or hydrogenolysed (**10**). In the absence of an alcohol, the hydroxy phthalan that might be formed instead is easily dehydrated to an unstable isobenzofuran **13**. We have previously observed that hydroxy phthalans (hemi-acetals) are much more unstable to acid than methoxy phthalans (acetals). In accordance with this rationale, we found that the stable isobenzofuran **14** provided a methyl vinyl ketone adduct **15**[4] that in turn produced a stable isobenzofuran **16** (95%) upon treatment with sulfuric acid, and the furanoid adduct **4***a* yielded furan **17** (78%) and acetophenone (13%). Aldehyde **1***b* behaved similarly but the re-

[1] Author to whom correspondence may be addressed.

[2] Prepared by Diels–Alder reaction of furans and isobenzofurans with the appropriate dienophiles and used as *endo–exo* mixtures.

[3] Some of our results have been recently confirmed; see ref. 6.

[4] Compound **14** was prepared in this laboratory (D. Rajapaksa and R. Rodrigo, unpublished work). Both **14** and **16** were characterized by mass, ^{1}H nmr and ir spectroscopy but could not be obtained pure enough for elemental analysis.

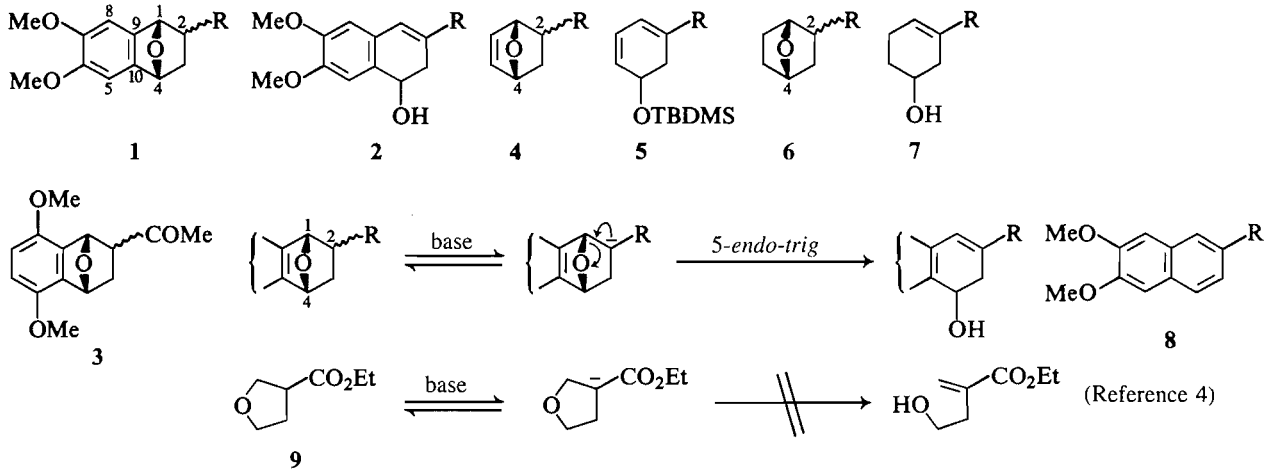

a (R = COMe) *b* (R = CHO) *c* (R = CO_2Me) *d* (R = CN)

SCHEME 1. Reverse-Michael reactions

TABLE 1. Reverse-Michael reactions

Entry	Bridged substrate*	Conditions: Base, solvent, temp (°C)	Product (isolated yield, %)
1.	**1***a*	NaOMe, MeOH, 20	**2***a* (90)
2.	**1***a*	NaOME, MeOH, 65	**8***a* (90)
3.	**1***b*	NaOMe, MeOH, 20	**2***b* (83)
4.	**1***b*	NaOMe, MeOH, 65	**8***b* (92)
5.	**1***c* (*endo* isomer)	NaOMe, MeOD, 20	2-Deuterio-**1***c* (95)*
6.	**1***c*	LDA, THF, 0	**2***c* (72)
7.	**1***d* (*endo* isomer)	NaOMe, MeOD, 65	2-Deuterio-**1***d* (95)*
8.	**1***d*	LDA, THF, −78	**2***d* (79)
9.	**4***a*	NaOMe, MeOH, 20	Acetophenone (90)
10.	**4***c*	NaOMe, MeOD, 20	2-Deuterio-**4***c* (95)*
11.	**4***c*	LDA, THF, 0	**5***c* (65)†
12.	**4***d*	NaOMe, MeOD, 65	2-Deuterio-**4***d* (95)*
13.	**4***d*	LDA, THF, −78	**5***d* (60)†
14.	**6***a*	NaOMe, MeOH, 20	**7***a* (60)
15.	**6***c*	NaOMe, MeOD, 20	2-Deuterio-**6***c* (95)*
16.	**6***c*	LDA, THF, 0	**7***c* (50)
17.	**6***d*	NaOMe, MeOD, 65	2-Deuterio-**6***d* (95)*
18.	**6***d*	LDA, THF, −78	**7***d* (65)

* *exo*–*endo* Mixtures unless otherwise specified.
† Isolated as TBDMS derivative after silylation.

sults were less clear-cut because of the formation and persistence of its dimethyl acetal (80%) under the same conditions. The existence of phthalan **18** (5%) and its dimethyl acetal (15%) was evident in the nmr spectrum of the reaction mixture. Ester and nitriles **1***c*, **1***d*, **4***c*, and **4***d* were indefinitely stable to the same conditions; **1***c* and **1***d* provided napthalenes **8***c* and **8***d* (50 and 69% respectively) after refluxing for 8 h, but **4***c* and **4***d* underwent extensive decomposition and no aromatic product was detected. Furan adducts are known to undergo reverse Diels–Alder reactions at moderate temperatures (7) and this might be responsible for the latter result. Similar ring disruptions of Diels–Alder adducts of both furan (8) and isobenzofuran (9) have been reported. The general reverse-aldol process described above is also a 5-*endo-trig* reversal in violation of Baldwin's rules. Like the reverse-Michael fission previously described, its occurrence cannot merely be a manifestation of strain release because it is difficult to see how **1***a* and **15**, for instance, can be converted into virtually non-aromatic isobenzofurans instead of aromatizing to stable naphthalenes, or how **1***b* can be content with forming an acetal instead of undergoing acid-catalysed aromatization to **8***b* (or the acetal thereof).

Other 5-*endo-trig* cyclizations have been reported (10) and those involving additions to immonium (11) and oxonium (12) double bonds rationalized on the basis of increased flexibility and decreased vectorial specificity, both consequences of the greater single bond character of these double bonds. Such explanations are clearly inapplicable to our reverse-Michael reactions, nor can any increase in carbonium ion character of the oxonium ion intermediate (Scheme 2) of our retro-aldol reactions provide enough flexibility for the reaction to occur in either direction.

X-ray crystallographic analyses (13) of the isobenzofuranoid adducts **1***a* and **1***c* established that the furanoid moiety (C(1)—C(2)—C(3)—C(4)—O) in each compound is rigidly held in two planes (C(1)—O—C(4) and C(1)—C(2)—

Can. J. Chem. Downloaded from www.nrcresearchpress.com by 210.87.254.105 on 09/06/12
For personal use only.

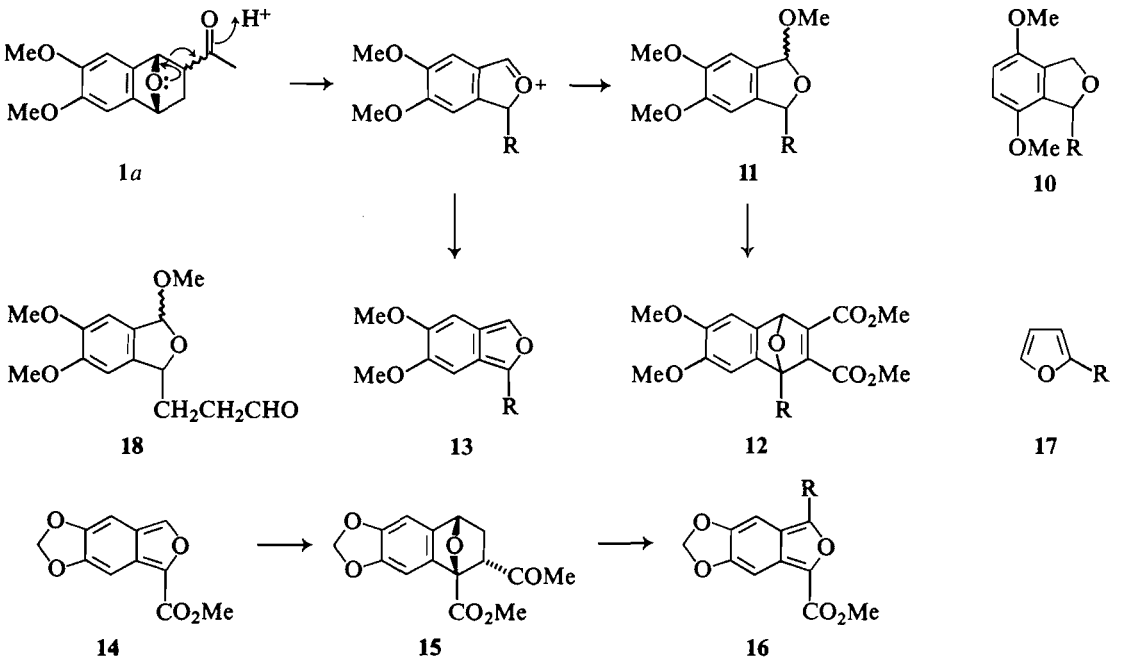

SCHEME 2. Retro-aldol reactions (R = $CH_2CH_2COCH_3$)

C(3)—C(4)) at 121.6° to each other. This geometry, quite unlike the simple furan **9**, is responsible in our opinion for the prevalence of the anomalous 5-*endo-trig* reversals. Enolate ions, formed in the reverse-Michael reaction, have a large coefficient (14) at C(2) in their HOMO and this orbital at C(2) is properly aligned in these systems (but not in the furan **9**) to interact with the relatively low-lying antibonding orbital of the C(1)—O bond (LUMO), weakening this bond and allowing the C(1)—C(2) π-bond to develop as the reaction proceeds (Fig. 1). Such a frontier orbital interaction decreases the kinetic barrier to the reverse-Michael reaction in the oxabicyclo systems. In the norbornyl radical of similar geometry, the well-known *exo*-specificity displayed in its reactions has been attributed (15) to interaction between the C—C bridge orbital and singly occupied *p* orbital at C(2).

The same molecular architecture accounts for the reverse-aldol process. One of the orbitals containing a non-bonded pair of electrons on the bridge oxygen atom is aligned antiperiplanar to the C(1)—C(2) bond. Interaction of this orbital (HOMO) with the antibonding orbital of the C(1)—C(2) bond (LUMO) results in weakening of the C(1)—C(2) bond and the growth of some π-bonding between C(1) and the oxygen (Fig. 2). Similar interactions in axial α-halogenotetrahydropyrans result in bond lengthening (C—X) and shortening (O—C) and have also been invoked to interpret the anomeric effect as a stabilizing influence (16). The presence of a protonated substituent at C(2) (aldehyde or ketone as in **1***a*, **4***a*, and **1***b*) provides a low energy pathway (retro-aldol) for bond breaking (C(1)—C(2)) and bond making (C(1)—O, π-bond) to take place, resulting in the formation of the cyclic oxonium ion. Esters and nitriles (**1***c*, **1***d*, **4***c*, and **4***d*) with their lower basicity are not known to undergo the acid-catalysed retro-aldol reaction and are therefore inert under the conditions. The behaviour of **4***a*, which prefers to form a furan **17** rather than aromatize to acetophenone by a 6:1 margin (78% **17**, 13% acetophenone) when exposed to acid, can thus be understood.

The synthetic potential of the reactions described herein must not be overlooked. We have used the reverse-Michael

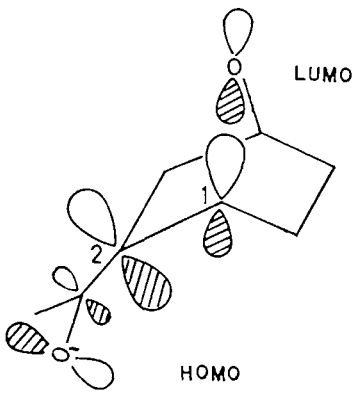

FIG. 1

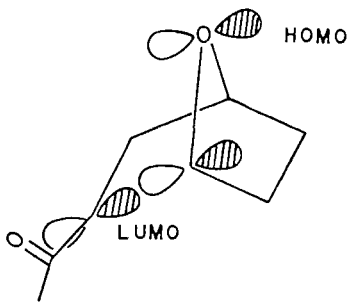

FIG. 2

reaction for short stereocontrolled syntheses (17) of some shikimic acids, and other applications to natural product synthesis are underway. The reverse-aldol reactions represent an unprecedented isobenzofuran → 1-substituted isobenzofuran conversion, which adds an extra element of versatility to our general isobenzofuran synthesis (1).

Experimental

General methods

Melting point determinations were made using a Buchi SMP-20

Can. J. Chem. Downloaded from www.nrcresearchpress.com by 210.87.254.105 on 09/06/12
For personal use only.

Can. J. Chem. Downloaded from www.nrcresearchpress.com by 210.87.254.105 on 09/06/12
For personal use only.

apparatus and are uncorrected. Infrared spectra were obtained on Beckman Model IR-10 or on Acculab 10 spectrophotometers. Nuclear magnetic resonance spectra were obtained on either Bruker WP-80 or Bruker WH-400 spectrophotometers. Samples were run in $CDCl_3$ solutions containing tetramethylsilane as an internal standard and chemical shifts (δ) and coupling constants (Hz) measured directly. Low and high resolution mass spectra were measured on a Varian VG Organic 7070F Mass Spectrometer. Flash column chromatography was performed using Merck 0.063–0.200 mm (70–230 mesh) Silica Gel 60 which was packed dry into glass columns. Combustion analyses were performed by Guelph Chemical Laboratories, Guelph, Ontario and(or) Canadian Microanalytical Service Ltd., Vancouver, British Columbia.

General procedure for deuteration of **1**c, **1**d, **4**c, **4**d, **6**c, *and* **6**d

The bicyclo adduct dissolved in methanol-d_1 was treated with sodium methoxide (3 equiv. freshly prepared from sodium and methanol-d_1) and the mixture stirred at the appropriate temperature (Table 1) for 2 h. D_2O was added and carbon dioxide bubbled through until the solution was neutral to pH paper. The methanol was removed under reduced pressure, the residue extracted into chloroform, and the solvent removed. The residual material was distilled or crystallized.

3-Acetyl-1,2-dihydro-1-hydroxy-6,7-dimethoxynaphthalene **2**a

The bicyclo ketone **1***a* (1 g), dissolved in methanol (15 mL), was treated with sodium methoxide (3 equiv. freshly prepared from sodium and methanol) and the mixture stirred at room temperature for 2 h. Water was added and carbon dioxide bubbled through until the solution was neutral to pH paper. The methanol was removed under reduced pressure, the residual material extracted with chloroform, and the extracts washed with water. Removal of the solvent and crystallization from dichloromethane gave **2***a* (90%), mp 158–162°C; ir ($CHCl_3$): 3400, 1650 cm^{-1}; ^1H nmr: 2.05 (d, 1H, $J_{1,OH}$ = 5.7 Hz; disappears with D_2O, —OH), 2.44 (s, 3H, —COMe), 2.6–3.2 (m, 2H, C(2)—*H*), 3.92, 3.95 (s, 3H each, 2 × OMe), 4.85 (dt, 1H, $J_{1,OH}$ = 5.7, $J_{1,2\alpha} = J_{1,2\beta}$ = 6.1 Hz, collapses to a triplet with D_2O, C(1)—H), 6.86, 7.04 (s, 1H each, 2 × Ar), 7.42 (broad s, 1H, vinyl-H); mass spectrum (intensity, assignment): 248 (8, M^+), 230 (76, $M^{\cdot+} - H_2O$), 215 (100, $M^{\cdot+} - H_2O - CH_3$). *Anal.* calcd. for $C_{14}H_{16}O_4$: C 67.73, H 6.50; found: C 67.38, H 6.47.

3-Formyl-1,2-dihydro-1-hydroxy-6,7-dimethoxynaphthalene **2**b

The bicyclo aldehyde **1***b* (1.5 g) was treated with sodium methoxide as described. Recrystallization from dichloromethane afforded **2***b* (83%), mp 132–134°C; ir ($CHCl_3$): 3400 (OH), 1660 (C=O) cm^{-1}; ^1H nmr: 2.4–2.9 (m, 3H, C(2)—H's and —OH), 3.9, 3.94 (s, 3H each, 2 × OMe), 4.86 (t, 1H, $J_{1,2}$ = 4.2 Hz, C(1)—H), 6.88, 7.06 (s, 1H each, 2 × Ar), 7.29 (broad s, 1H, vinyl-H), 9.61 (s, 1H, —CHO); mass spectrum (intensity, assignment): 234 (12, $M^{\cdot+}$), 216 (100, $M^{\cdot+} - H_2O$). *Anal.* calcd. for $C_{13}H_{14}O_4$: C 66.66, H 6.02; found: C 66.32, H 6.10.

2-Acetyl-6,7-dimethoxy naphthalene **8**a

The ketone **1***a* (1 g) was treated in the same manner as described for the preparation of **2***a* and the solution refluxed for 4 h. After neutralization and work-up as before, the residue was crystallized from methylene chloride (90%), mp 109–110°C; ir ($CHCl_3$): 1680 cm^{-1}; ^1H nmr: 2.69 (s, 3H), 4.03 (s, 6H), 7.15, 7.23 (s, 2 × 1H, H(5), H(8)), 7.71 (d, 1H, J = 8.5 Hz, H(4)), 7.92 (dd, 1H, J = 8.5 and 1.7 Hz, H(3)), 8.33 (d, 1H, J = 1.7 Hz, H(1)); mass spectrum: 230 ($M^{\cdot+}$), 215 ($M^{\cdot+}$ —CH_3). *Anal.* calcd. for $C_{14}H_{14}O_3$: C 73.03, H 6.13; found: C 73.25, H 6.20.

2-Formyl-6,7-dimethoxynaphthalene **8**b

The aldehyde **1***b* was treated as above and the product **8***b* crystallized from ether (92%), mp 86.5–88°C; ir ($CHCl_3$): 1695 (C=O) cm^{-1}; ^1H nmr: 4.04 (s, 6H), 7.18–7.26 (m, 2H), 7.8–8.19 (m, 3H), 10.10 (s, 1H, CHO); mass spectrum: 216 ($M^{\cdot+}$), 215 ($M^{\cdot+} - H$). *Anal.* calcd. for $C_{13}H_{12}O_3$: C 72.21, H 5.59; found: C 72.51, H 5.69.

3-Carbomethoxy-1,2-dihydro-1-hydroxy-6,7-dimethoxy naphthalene **2**c

Freshly prepared lithium diisopropylamide (1.1 equiv. in dry THF) was added to a solution of the ester **1***c* (0.1 g, 0.38 mmol) in dry THF (5 mL) at 0°C under nitrogen. Water (3 mL) was added after 10 min and the mixture poured into $CHCl_3$ (10 mL). After extraction with $CHCl_3$ (2 × 10 mL) the extracts were dried and the solvent removed to leave a solid which crystallized from ether (72%), mp 148–149°C; ir (KBr): 3450 (OH), 1720 (C=O) cm^{-1}; ^1H nmr: 1.81 (d, 1H, disappears with D_2O, —OH), 2.61–3.15 (m, 2H, C(2)—H's), 3.81, 3.89, 3.93 (s, 3H each, 2 × Ar—*OMe*, 1 × CO_2Me), 4.80 (q, 1H, collapses to a triplet with D_2O, J = 5.7 Hz, C(1)—H), 6.82, 7.01 (s, 1H each, Ar), 7.56 (broad s, 1H, vinyl-H); mass spectrum (intensity, assignment); 264 (18, $M^{\cdot+}$), 246 (100, $M^{\cdot+} - H_2O$). *Anal.* calcd. for $C_{14}H_{16}O_5$: C 63.63, H 6.10; found: C 63.36, H 6.04.

3-Cyano-1,2-dihydro-1-hydroxy-6,7-dimethoxy naphthalene **2**d

The cyanide **1***d* was treated with LDA as above at −78°C and the product **2***d* isolated and crystallized from dichloromethane (79%), mp 147–148°C; ir (KBr): 3480 (OH), 2200 (CN) cm^{-1}; ^1H nmr: 1.81 (d, 1H, disappears with D_2O, —OH), 2.73 (dd, 2H, J = 1.6 and 5.3 Hz, C(2)—H's), 3.90, 3.94 (s, 3H each, 2 × OMe), 4.82 (q, 1H, collapses to a triplet with D_2O, J = 5.3 Hz, C(1)—H), 6.75, 6.93 (s, 1H each, 2 × Ar), 7.19 (t, 1H, J = 1.6 Hz, vinyl-H); mass spectrum (intensity, assignment): 231 (1.5, $M^{\cdot+}$) 213 (100, $M^{\cdot+} - H_2O$). *Anal.* calcd. for $C_{13}H_{13}NO_3$: C 67.52, H 5.67, N 6.06; found: C 67.19, H 5.64, N 5.97.

*Acetophenone from 2-acetyl-7-oxabicyclo[2.2.1]hept-5-ene (***4**a)

Ketone **4***a* (0.25 g) in absolute methanol (3 mL) under nitrogen was treated with sodium methoxide as before and stirred at room temperature for 24 h. After work-up as before acetophenone (90%) was isolated and identified.

*1-*tert*-Butyldimethylsilyloxy-3-carbomethoxy-1,2-dihydrobenzene* **5**c

Freshly prepared LDA (1.2 equiv.) was added to a stirred solution of the ester **4***c* (4 g) in dry THF (25 mL) at 0°C under nitrogen. After 10 min, saturated aqueous ammonium chloride (10 mL) was added, THF removed, and the residue extracted into dichloromethane. The extract was dried (Na_2SO_4) and the solvent removed. The residue was treated with triethylamine (1.2 equiv.), dimethylamino pyridine (1 g), *tert*-butyldimethylsilylchloride (1.1 equiv.), and methylene chloride (100 mL) and stirred at room temperature for 12 h. The reaction mixture was filtered through a short column of silica gel using ethyl acetate – hexane (1 : 1) as the eluant. The solvents were removed and the residue distilled to provide **5***c* (65%), bp 86°C/0.05 Torr; ir (neat): 1712 (C=O); ^1H nmr: 0.04 (s, 6H, 2 × Me), 0.85 (s, 9H, *t*-Bu), 2.61 (dd, 1H, J = 9.0 and 1.7 Hz, —CH_2—), 3.73 (s, 3H, —CO_2Me), 4.48 (dt, 1H, J = 1.7 and 9.0 Hz, C*H*OR), 6.03 (m, 2H, vinyl-H's), 6.96 (m, 1H, vinyl-H); mass spectrum (intensity, assignment): 268 (4, $M^{\cdot+}$), 266 (7, $M^{\cdot+}$ − *t*-Bu). *Anal.* calcd. for $C_{14}H_{24}SiO_3$: C 62.64, H 9.01; found: C 62.55, H 8.89.

*1-*tert*-Butyldimethylsilyloxy-3-cyano-1,2-dihydrobenzene* **5**d

Freshly prepared LDA (1.2 equiv.) was added to a stirred solution of the cyanide **4***d* (3.68 g) in dry THF (25 mL) under nitrogen at −78°C. The reaction was processed as above and the product **5***d* (60%) obtained after distillation, bp 80°C/0.02 Torr; ir (neat): 2200 (CN) cm^{-1}; ^1H nmr: 0.07 (s, 6H, 2 × Me), 0.87 (s, 9H, *t*-Bu), 2.54 (dd, 2H, J = 1.7 and 8.0 Hz, —CH_2—), 4.40 (dt, 1H, J = 1.2 and 8.0 Hz, C*H*OR), 6.05 (m, 2H, vinyl-H's), 6.70 (m, 1H, vinyl-H); mass spectrum (intensity, assignment): 235 (3, $M^{\cdot+}$), 178 (100, $M^{\cdot+}$ − *t*-But). *Anal.* calcd. for $C_{13}H_{21}NOSi$: C 66.33, H 8.99, N 5.95; found: C 66.32, H 8.91, N 5.93.

1-Acetyl-5-hydroxy-cyclohexene **7**a

The ketone **6***a* (1 g) dissolved in dry methanol (5 mL) under nitrogen was treated with sodium methoxide and the reaction worked up as previously; ir (neat): 3400 (OH), 1655 (C=O); ^1H nmr: 1.5–2.8 (m, 6H, 3 × —CH_2—), 2.29 (s, 3H, —COMe), 3.10 (broad s, 1H, disappears with D_2O, —OH), 3.8–4.2 (m, 1H, —C*H*OH), 6.8–7.0

Can. J. Chem. Downloaded from www.nrcresearchpress.com by 210.87.254.105 on 09/06/12
For personal use only.

(m, 1H, vinyl-H); mass spectrum (intensity, assignment): 140 (45, $M^{+\cdot}$), 97 (100, $M^{+\cdot} - C_2H_3O$). *Anal.* calcd. for $C_8H_{12}O_2$: C 61.52, H 7.74; found: C 61.12, H 7.82.

1-Carbomethoxy-5-hydroxy-cyclohexene 7c

The ester **6***c* (1 g) in dry THF (30 mL) under nitrogen, was treated with LDA (1.1 equiv.) at 0°C. The reaction was processed as before to provide the oily product **7***c* which was distilled (50%) bulb-to-bulb; ir (neat): 3400 (OH), 1655 (C=O) cm^{-1}; ^1H nmr: 1.5–2.8 (m, 6H, 3 × —CH_2—), 2.29 (s, 3H, —COMe), 3.10 (broad s, 1H, disappears with D_2O, —OH), 3.8–4.2 (m, 1H, —C*H*OH), 6.8–7.0 (m, 1H, vinyl-H); mass spectrum (intensity, assignment): 140 (45, $M^{+\cdot}$), 97 (100, $M^{+\cdot} - C_2H_3O$). *Anal.* calcd. for $C_8H_{12}O_2$: C 61.52, H 7.74; found: C 61.12, H 7.82.

1-Cyano-5-hydroxy-cyclohexene 7d

The cyanide **6***d* (1 g) in dry THF (30 mL) under nitrogen was treated with LDA (1.1 equiv.) at −78°C. The reaction was processed as before to provide the oily product **7***d* which was distilled (65%) bulk-to-bulb; ir (neat): 3400 (OH), 2208 (CN) cm^{-1}; ^1H nmr: 1.5–2.8 (m, 6H, 3 × —CH_2—), 3.8–4.2 (m, 1H, C*H*OH), 6.55–6.8 (m, 1H, vinyl-H); mass spectrum (intensity, assignment): 123 (1, $M^{+\cdot}$), 105 (100, $M^{+\cdot} - H_2O$), 80 (100 $M^{+\cdot} - C_2H_3O$). *Anal.* calcd. for C_7H_9NO: C 68.27, H 7.37, N 11.37; found: C 68.30, H 7.48, N 11.11.

1,3-Dihydro-4,7-dimethoxy-1-(3-oxobutyl)isobenzofuran **10**

Ketone **4** (400 mg) was placed in ethanol (50 mL) containing 10% Pd/C (80 mg) and perchloric acid (25 drops). The mixture was hydrogenated at 40 psi for 8 h and filtered through Celite. Saturated bicarbonate was added (30 mL) and the ethanol removed *in vacuo*. The residue was extracted into chloroform (20 mL), dried, and the solvent removed to yield an oil (95%) which resisted crystallization; ir (neat): 1730 (C=O) cm^{-1}; ^1H nmr: 2.05 (s, 3H, COC*H*$_3$), 2.0–2.6 (m, 4H, CH_2—CH_2), 3.7 (s, 6H, 2 × OMe), 4.97 (m, 2H, CH_2—O), 5.3 (m, 1H, CH—O), 6.6 (s, 2H, ArH); ^{13}C nmr: 29.0 (t, *C*H$_2$—CH_2COMe), 29.95 (q, CO*C*H$_3$), 39.62 (t, —CH_2*C*H$_2$COMe), 55.79 (q, 2 × Ar—OMe), 71.7 (t, *C*H$_2$—O), 83.4 (d, *CH*—O), 110.3, 110.4 (d each, aromatic *C*—H), 129.4, 130.6 (s each, aromatic *C*—OMe), 208.9 (s, C=O); mass spectrum: 250 (8, $M^{+\cdot}$), 192 (91, $M^{+\cdot} - CH_3COCH_3$), 179 (100, $M^{+\cdot} - CH_2CH_2COCH_3$).

1,3-Dihydro-1,5,6-trimethoxy-3-(3-oxobutyl)isobenzofuran **11**

The ketone **1***a* (50 mg) in methanol (2 mL) was treated with perchloric acid (3 drops) at room temperature. The solution was neutralized with aqueous sodium bicarbonate after 5 min and extracted into ether (2 × 10 mL). The extracts were dried (Na_2SO_4) and the ether removed to leave an oil which was filtered through a column of silica gel with ethyl acetate – ligroin (1:1). The oil did not crystallize and ^1H nmr showed it to be a 1:1 mixture of diastereomers (94% total yield); ir (neat): 1705 (C=O) cm^{-1}; ^1H nmr (a 1:1 mixture of *cis* and *trans* diastereomers): 1.5–2.8 (m, 7H of each isomer, 2 × —CH_2— and COMe), 3.40, 3.50 (s, 3H each, phthalan-OMe of each isomer), 3.91 (s, 6H, 2 × ArOMe of each isomer), 5.0–5.5 (m, 1H of each isomer, C(3)—H), 6.01 (s, 1H, C(1)—H of *cis* isomer), 6.11 (d, 1H, C(1)—H of *trans* isomer), 6.71, 6.88 (s, 1H each of each isomer, Ar); mass spectrum (intensity, assignment): 280 (5, $M^{+\cdot}$), 248 (48, $M^{+\cdot}$ – MeOH), 222 (100, McLafferty rearrangement).

2,3-Dicarbomethoxy-1,4-epoxy-1,4-dihydro-6,7-dimethoxy-1-(3-oxobutyl)naphthalene **12**

The dihydroisobenzofuran **11** (240 mg) dissolved in dimethyl acetylene dicarboxylate (1.5 mL) and glacial acetic acid (0.1 mL) was heated on a steam bath for 1 h. The liquids were removed under high vacuum and residual thick oil crystallized from ether (72%), mp 83–84°C; ir (KBr): 1700 (C=O), 1720 (C=O); ^1H nmr: 2.16 (s, 3H, COMe), 2.68 (broad s, 4H, 2 × —CH_2), 3.77, 33.80 (s, 3H each, 2 × CO_2Me), 3.87 (s, 6H, 2 × ArOMe), 5.85 (s, 1H, bridge-H), 6.95, 7.04 (s, 1H each, Ar); mass spectrum (intensity, assignment): 390 (56, $M^{+\cdot}$), 248 (100, isobenzofuran). *Anal.* calcd. for $C_{20}H_{22}O_8$: C 61.53, H 5.68; found: C 61.39, H 5.72.

1-Carbomethoxy-3-(3-oxobutyl)-5,6-methylenedioxy isobenzofuran **16**

The adduct **15**[4] (100 mg) was heated under reflux in CH_2Cl_2 (20 mL) with concentrated H_2SO_4 (2 drops in 1 mL of MeOH) for 15 min. The reaction mixture was allowed to cool and washed with an aqueous solution of $NaHCO_3$ (10 mL). The aqueous layer was extracted again with CH_2Cl_2 (10 mL). The combined extracts were dried (Na_2SO_4) and the solvent removed. Addition of ether (5 mL) formed an amorphous powder, which was filtered off (95 mg, 95%); ir (KBr): 1690 (C=O), 1740 (C=O) cm^{-1}; ^1H nmr: 2.13 (s, 3H, $COCH_3$) 2.8–3.3 (m, A_2B_2 system —CH_2CH_2—) 3.9 (s, 3H, COOMe), 5.93 (s, 2H, OCH_2O), 6.65, 7.70 (s, 1H each, 2Ar); mass spectrum (intensity, assignment): 290 (67, $M^{+\cdot}$), 259 (22, $M^{+\cdot}$ – OMe) 247 ($M^{+\cdot}$ – COMe).

1-(3-Oxobutyl)furan **17**

Ketone **4***a* (1 g) was dissolved in methanol (2 mL) and treated with perchloric acid (2 drops) at room temperature. The mixture was stirred for 24 h, and saturated bicarbonate added to neutralize the acid. Removal of the methanol, followed by extraction into methylene chloride (2 × 25 mL), drying, and removal of the solvent afforded a 6:1 mixture of **17** and acetophenone. The mixture was separated on a silica gel column using ethyl acetate – ligroin (1:1) as solvent, yielding acetophenone (13%) and the furan **17** (ref. 18) (78%); ir (neat): 1710 (C=O) cm^{-1}; ^1H nmr: 2.21 (s, 3H, COMe), 2.7–3.0 (m, 4H, 2 CH_2's), 6.0, 6.35, 7.32 (broad s, 1H each, 3 furan H's); mass spectrum (intensity, assignment): 138 (3, $M^{+\cdot}$), 123 (100, $M^{+\cdot}$ – CH_3).

2-Carbomethoxy-6,7-dimethoxy naphthalene 8c

Ester **1***c* (0.5 g) was placed in methanol (5 mL), perchloric acid (3 drops) added, and the mixture refluxed for 8 h. It was cooled, neutralized with saturated sodium bicarbonate, the methanol removed, and the residue extracted with chloroform (2 × 10 mL). The extracts were dried and the solvent removed to leave a solid crystallized from chloroform to provide **8***c* (50%), mp 103–105°C; ^1H nmr: 3.95 (s, 3H, CO_2*Me*), 4.00 (s, 6H, 2 × OMe), 7.13, 7.2 (s, 1H each, Ar—H), 7.68 (d, 1H, J_{ortho} = 8.5 Hz, C(4)—H), 7.93 (dd, 1H, J_{ortho} = 8.5 Hz, J_{meta} = 1.4 Hz, C(3)—H), 8.44 (broad s, 1H, C(1)—H); mass spectrum: 246 (100, $M^{+\cdot}$), 215 (53, $M^{+\cdot}$ – OMe). *Anal.* calcd. for $C_{14}H_{14}O_4$: C 68.28, H 5.73; found: C 68.01, H 5.80.

2-Cyano-6,7-dimethoxy naphthalene 8d

Cyanide **1***d* (0.2 g) was treated in the same was as **1***c* and the product isolated similarly (69%), mp 116–118°C; ir (KBr): 2210 cm^{-1}; ^1H nmr: 4.05 (s, 6H, 2 × OMe), 7.15 (s, 2H, C(5)—H and C(8)—H), 7.47 (dd, 1H, J_{ortho} = 8.3 Hz, J_{meta} = 3.8 Hz, C(3)—H), 7.74 (d, 1H, J_{ortho} = 8.3 Hz, C(4)—H), 8.07 (broad s, 1H, C(1)—H); mass spectrum: 213 (100, $M^{+\cdot}$). *Anal.* calcd. for $C_{13}H_{11}NO_2$: C 73.22, H 5.20, N 6.57; found: C 73.34, H 5.12, N 6.38.

Acknowledgements

We thank the Natural Sciences and Engineering Research Council of Canada for financial support.

1. B. A. KEAY, D. K. W. LEE, and R. RODRIGO. Tetrahedron Lett. 3663 (1980); B. A. KEAY, H. P. PLAUMANN, D. RAJAPAKSA, and R. RODRIGO. Can. J. Chem. **61**, 1987 (1983).
2. B. A. KEAY and R. RODRIGO. Can. J. Chem. **61**, 637 (1983).
3. J. E. BALDWIN. J. Chem. Soc. Chem. Commun. 734 (1976).
4. J. E. BALDWIN, J. CUTTING, W. DUPONT, L. KRUSE, L. SILBERMAN, and R. C. THOMAS. J. Chem. Soc. Chem. Commun. 736 (1976); G. W. L. ELLIS, C. D. JOHNSON, and D. N. ROGERS. J. Am. Chem. Soc. **105**, 5090 (1983).
5. J. G. SMITH, S. S. WELANKIWAR, B. S. SHANTZ, E. H. LAI, and N. G. CHU. J. Org. Chem. **45**, 1817 (1980).
6. F. BRION. Tetrahedron Lett. 5299 (1982); A. J. GUILDFORD and R. W. TURNER. J. Chem. Soc. Chem. Commun. 466 (1983).
7. M. S. NEWMAN and V. LEE. J. Org. Chem. **42**, 1478 (1977), and references therein.

8. C. H. EUGSTER and P. BOSSHARD. Chimia, **15**, 528 (1961).
9. L. CONTRERAS, D. B. MACLEAN, R. FAGGIANI, and C. J. LOCK. Can. J. Chem. **59**, 1247 (1981); R. A. RUSSELL, D. E. MARSDEN, M. STERNS, and R. N. WARRENER. Aust. J. Chem. **34**, 1223 (1981).
10. B. GREGORY, E. BULLOCK, and T. S. CHEN. J. Chem. Soc. Chem. Commun. 1070 (1979); R. GRIGG, J. KEMP, J. MALONE, and A. TANGTHONGKUM. J. Chem. Soc. Chem. Commun. 648 (1980).
11. S. W. PELLETIER and N. V. MODY. *In* The alkaloids. Vol. 18. *Edited by* R. Rodrigo. Academic Press, New York. 1981. p. 149.
12. M. J. PERKINS, P. C. WONG, J. BARRETT, and G. DHALIWAL. J. Org. Chem. **46** 2196 (1981).
13. N. J. TAYLOR, B. A. KEAY, and R. RODRIGO. Can. J. Chem. **62**, 1099 (1984).
14. I. FLEMING. Frontier orbitals and organic chemical reactions. Wiley–Interscience, New York. 1976. pp. 43, 44.
15. K. FUKUI. Theory of orientation and stereoselection. Reactivity and structure concepts in organic chemistry. Vol. 2. Springer-Verlag, New York. 1975. p. 79; S. INAGAKI and K. FUKUI. Chem. Lett. 509 (1974).
16. C. ROMERS, C. ALTONA, H. R. BUYS, and E. HAVINGA. Top. Stereochem. **4**, 73 (1969); S. DAVID, O. EISENSTEIN, W. J. HEHRE, L. SALEM, and R. HOFFMAN. J. Am. Chem. Soc. **95**, 3806 (1973); I. FLEMING. Frontier orbitals and organic chemical reactions. Wiley–Interscience, New York. 1976. pp. 79, 80.
17. D. RAJAPAKSA, B. A. KEAY, and R. RODRIGO. Can. J. Chem. **62**, 826 (1984).
18. I. D. WEBB and G. T. BORCHEROT. J. Am. Chem. Soc. **73**, 752 (1951).

Can. J. Chem. Downloaded from www.nrcresearchpress.com by 210.87.254.105 on 09/06/12
For personal use only.

The crystal structures of 2-*endo*-acetyl and 2-*endo*-carbomethoxy-1,4-epoxy-6,7-dimethoxy-1,2,3,4-tetrahydronaphthalenes

N. J. TAYLOR, B. A. KEAY, AND R. RODRIGO

Department of Chemistry, Guelph–Waterloo Centre for Graduate Work in Chemistry, University of Waterloo, Waterloo, Ont., Canada N2L 3G1

Received November 15, 1983

N. J. TAYLOR, B. A. KEAY, and R. RODRIGO. Can. J. Chem. **62**, 1099 (1984).

Crystals of 2-*endo*-acetyl-1,4-epoxy-6,7-dimethoxy-1,2,3,4-tetrahydronaphthalene are orthorhombic, $a = 5.524(1)$, $b = 8.929(1)$, $c = 25.479(4)$ Å, $Z = 4$, space group $P2_12_12_1$; those of 2-*endo*-carbomethoxy-1,4-epoxy-6,7-dimethoxy-1,2,3,4-tetrahydronaphthalene are monoclinic, $a = 10.878(2)$, $b = 6.634(1)$, $c = 18.224(4)$ Å, $\beta = 92.76(2)°$, $Z = 4$, space group $P2_1/c$. Both structures were solved by direct methods and refined by full-matrix least-squares methods to final R values of 0.041 and 0.036 for 875 and 1327 reflections with $I \geq 3\sigma(I)$ respectively.

N. J. TAYLOR, B. A. KEAY et R. RODRIGO. Can. J. Chem. **62**, 1099 (1984).

Les cristaux de l'acétyl-2 *endo* époxy-1,4 diméthoxy-6,7 tétrahydro-1,2,3,4 naphtalène sont orthorhombiques, $a = 5{,}524(1)$, $b = 8{,}929(1)$, $c = 25{,}479(4)$ Å, $Z = 4$, groupe d'espace $P2_12_12_1$; ceux du carbométhoxy-2 *endo* époxy-1,4 diméthoxy-6,7 tétrahydro-1,2,3,4 naphtalène sont monocliniques, $a = 10{,}878(2)$, $b = 6{,}634(1)$, $c = 18{,}224(4)$ Å, $\beta = 92{,}76(2)°$, $Z = 4$ et groupe d'espace $P2_1/c$. Les deux structures ont été résolues par des méthodes directes et affinées par la méthode des moindres carrés (matrice entière) jusqu'à des valeurs finales respectives de R de 0,041 et 0,036 pour 875 et 1327 réflexions avec $I \geq 3\sigma(I)$.

[Traduit par le journal]

Introduction

In the preceding paper (1) we described two general 5-*endo-trig* reversals of 7-oxabicyclo[2.2.1] heptenes and heptanes. Our rationalization of these processes as reverse-Michael and reverse-aldol reactions in general violation of Baldwin's rules (2) relied heavily upon the geometry of two benzo derivatives determined by X-ray crystallography. Diels–Alder adducts of isobenzofurans have not been previously subjected to X-ray analysis with the exception (3) of one rather exotic adduct of 1,3-diphenylisobenzofuran. In this paper we report the results of our analyses of the *endo* isomers of **1***a* and **1***c*.

Experimental

Crystals of *endo* **1***a* and **1***c* were obtained as described previously (4).

2-endo-*Acetyl-1,4-epoxy-6,7-dimethoxy-1,2,3,4-tetrahydronaphthalene (**1**a)*

A crystal of dimensions 0.22 × 0.40 × 0.41 mm was mounted in a general orientation. Unit cell parameters were refined from the 2θ values of 15 general reflections ($20 < 2\theta < 30°$) measured with MoKα radiation ($\lambda = 0.71069$ Å). Crystal data at 21°C are:

$C_{14}H_{16}O_4$ fw = 248.48

Orthorhombic, $a = 5.524(1)$, $b = 8.929(1)$, $c = 25.479(4)$ Å, $V = 1256.7(3)$ Å^3, $Z = 4$, $\rho_c = 1.312$ g cm^{-3}, $F(000) = 528$, μ(MoKα) = 1.034 cm^{-1}. Systematically absent reflections; $h00$, $h = 2n + 1$; $0k0$, $k = 2n + 1$; $00l$, $l = 2n + 1$; space group $P2_12_12_1$ (D_2^4, No. 19).

Intensity data were measured with graphite-monochromated MoKα radiation on a Syntex $P2_1$ diffractometer using θ–2θ scans ($3.2 < 2\theta \leq 50.0°$) with a variable scan speed of 2.93–29.3° min^{-1} and a scan width of 1.0° below $K\alpha_1$ to 1.0° above $K\alpha_2$. Two standard reflections (120, 104) monitored after every 100 measurements fell by 4% during the data collection. These were used to scale the data to a common level. From a total of 1346 independent reflections measured, 875 (65.0%) with intensities $I \geq 3\sigma(I)$ were considered observed and used in the structure solution and refinement.

The structure was solved by direct methods (MULTAN 80), the positions of all non-hydrogen atoms being determined from an E-map. The structure was refined with anisotropic thermal parameters by full-matrix least-squares methods to an R of 0.079 ($R = \Sigma||F_o| - |F_c||/\Sigma|F_o|$). At this stage, all the hydrogen atoms were located from a difference Fourier synthesis and included in the refinement which converged at $R = 0.041$. In the final cycles of refinement an empirical weighting scheme of $w^{-1} = 2.11 - 0.012|F_o| + 0.0008|F_o|^2$ was utilized to give constant error throughout the various ranges of F_o magnitude and a weighted residual R_w of 0.044 ($R_w = (\Sigma w(|F_o| - |F_c|)^2/\Sigma w|F_o|^2)^{1/2}$). Scattering factors for non-hydrogen atoms were taken from ref. 5 and those for hydrogen from ref. 6. Programs used have been described elsewhere (7). On the final cycle of refinement, the mean and maximum parameter shifts were 0.05 and 0.21σ respectively. A final difference map was featureless with maximum residuals of 0.19 Å^{-3}. Final positional parameters are shown in Table 1. Anisotropic thermal parameters, carbon–hydrogen distances, and observed and calculated structure factors have been placed in the Depository of Unpublished Data.[1]

2-endo-*Carbomethoxy-1,4-epoxy-6,7-dimethoxy-1,2,3,4-tetrahydronaphthalene (**1**c)*

Experimental details are as above except where noted. Crystal dimensions were 0.32 × 0.33 × 0.42 mm. Crystal data are:

$C_{14}H_{16}O_5$ fw = 264.28

Monoclinic, $a = 10.878(2)$, $b = 6.634(1)$, $c = 18.224(4)$ Å, $\beta = 92.76(2)°$, $V = 1313.5(4)$ Å, $Z = 4$, $\rho_c = 1.336$ g cm^{-3}, $F(000) = 560$, μ(MoKα) = 1.095 cm^{-1}. Systematically absent reflections: $0k0$, $k = 2n + 1$; $h0l$, $l = 2n + 1$; space group $P2_1/c$ (C_{2h}^5, No.14).

During the data collection, the two standard reflections monitored (129, 500) showed only minor fluctuations (±2%). From a total of 2313 independent reflections measured ($3.2 < 2\theta \leq 50°$), 1327 (57.4%) with intensities $I \geq 3\sigma(I)$ were considered observed.

After direct methods solution, the structure was refined with anisotropic thermal parameters to an R of 0.090. Hydrogen atoms were located at this stage. The refinement converged at $R = 0.036$ with $R_w = 0.036$ ($w^{-1} = 2.39 - 0.032|F_o| + 0.0013|F_o|^2$). A final difference Fourier was featureless with maximum residuals of 0.18 eÅ^{-3}. Mean and maximum parameter shifts in the final refinement cycle were 0.09 and 0.33σ respectively. Final positional parameters are listed in Table 2. Anisotropic thermal parameters, carbon–hydrogen bond lengths, and observed and calculated structure factors have been placed in the Depository of Unpublished Data.[1]

[1] Structure factor tables, anisotropic thermal parameters (Table 5), and carbon–hydrogen distances (Table 6) are available, at a nominal charge, from the Depository of Unpublished Data, CISTI, National Research Council of Canada, Ottawa, Ont., Canada K1A 0S2.

Can. J. Chem. Downloaded from www.nrcresearchpress.com by 210.87.254.40 on 09/06/12
For personal use only.

Can. J. Chem. Downloaded from www.nrcresearchpress.com by 210.87.254.40 on 09/06/12
For personal use only.

TABLE 1. Final positional (fractional, × 10^4, hydrogen atoms, × 10^3) and isotropic thermal parameters (U × 10^3 Å) for the acetyl derivative **1***a*. $U_{eq} = {}^3\sqrt{U_{11}U_{22}U_{33}}$

Atom	*x*	*y*	*z*	U_{eq}/U_{iso}
O(1)	4818(6)	4338(4)	2118(1)	59
O(2)	1374(7)	4473(4)	−44(1)	56
O(3)	−1749(7)	6152(4)	426(1)	60
O(4)	−380(6)	821(4)	1640(1)	61
C(1)	4684(9)	3108(5)	1751(2)	47
C(2)	2963(9)	2009(5)	2054(2)	46
C(3)	1300(11)	3119(6)	2338(2)	51
C(4)	2241(9)	4617(6)	2143(2)	52
C(5)	−112(9)	5562(5)	1290(2)	45
C(6)	−166(9)	5426(5)	745(2)	45
C(7)	1531(9)	4502(5)	493(1)	42
C(8)	3144(9)	3662(5)	777(2)	42
C(9)	3213(8)	3822(5)	1316(2)	40
C(10)	1637(9)	4778(5)	1565(2)	42
C(11)	3400(13)	3876(8)	−315(2)	65
C(12)	−3407(12)	7152(6)	668(2)	63
C(13)	1784(9)	871(5)	1709(2)	47
C(14)	3395(15)	−234(10)	1445(3)	85
H(1)	633(9)	278(4)	164(1)	51(13)
H(2)	405(8)	152(5)	232(2)	54(14)
H(3A)	−54(8)	294(4)	224(1)	36(11)
H(3B)	143(10)	306(5)	272(2)	72(15)
H(4)	190(8)	542(5)	236(2)	50(13)
H(5)	−108(7)	612(4)	147(1)	33(11)
H(8)	407(7)	309(4)	62(1)	34(12)
H(11A)	323(10)	408(5)	−66(2)	70(15)
H(11B)	505(10)	440(5)	−18(2)	78(16)
H(11C)	341(9)	262(5)	−28(2)	57(14)
H(12A)	−469(12)	652(7)	92(2)	116(21)
H(12B)	−432(10)	762(5)	40(2)	73(16)
H(12C)	−241(10)	805(7)	82(2)	96(21)
H(14A)	485(12)	−16(7)	153(2)	111(25)
H(14B)	312(16)	−30(10)	116(3)	152(32)
H(14C)	289(17)	−122(10)	159(3)	195(39)

TABLE 2. Final positional (fractional, × 10^4, hydrogen atoms, × 10^3) and isotropic thermal parameters (U × 10^3 Å^2) for the carboxymethoxy derivative **1***c*. $U_{eq} = {}^3\sqrt{U_{11}U_{22}U_{33}}$

Atom	*x*	*y*	*z*	U_{eq}/U_{iso}
O(1)	8785(2)	2334(3)	2519(1)	84
O(2)	4612(1)	−1016(2)	776(1)	65
O(3)	3618(1)	1939(3)	1418(1)	69
O(4)	8063(2)	4798(4)	241(1)	122
O(5)	9026(2)	1846(4)	234(1)	93
C(1)	8744(2)	1615(5)	1772(1)	71
C(2)	9084(2)	3566(5)	1352(2)	74
C(3)	8496(3)	5203(5)	1821(2)	82
C(4)	7890(3)	3928(4)	2399(2)	76
C(5)	5573(2)	3104(4)	1968(1)	58
C(6)	4871(2)	1810(4)	1529(1)	53
C(7)	5415(2)	217(3)	1155(1)	51
C(8)	6682(2)	−16(4)	1185(1)	55
C(9)	7375(2)	1298(4)	1628(1)	56
C(10)	6834(2)	2797(4)	2023(1)	60
C(11)	5106(3)	−2759(4)	441(2)	67
C(12)	3034(3)	3694(5)	1677(2)	85
C(13)	8667(2)	3535(5)	552(2)	80
C(14)	8630(4)	1542(9)	−534(2)	117
H(1)	925(2)	43(4)	172(1)	67(7)
H(2)	997(2)	366(4)	135(1)	86(8)
H(3A)	790(2)	609(4)	150(1)	83(8)
H(3B)	910(2)	619(5)	209(1)	101(9)
H(4)	774(2)	464(4)	286(1)	72(8)
H(5)	524(2)	420(3)	222(1)	49(6)
H(8)	708(2)	−107(3)	90(1)	56(6)
H(11A)	439(2)	−350(4)	20(1)	75(7)
H(11B)	564(2)	−240(4)	5(1)	74(8)
H(11C)	553(2)	−373(4)	82(1)	83(8)
H(12A)	219(3)	359(5)	151(2)	113(11)
H(12B)	344(3)	499(5)	154(2)	111(11)
H(12C)	312(3)	361(5)	224(2)	152(13)
H(14A)	772(4)	175(6)	−60(2)	176(15)
H(14B)	897(4)	9(7)	−67(2)	184(15)
H(14C)	908(4)	252(7)	−76(2)	246(19)

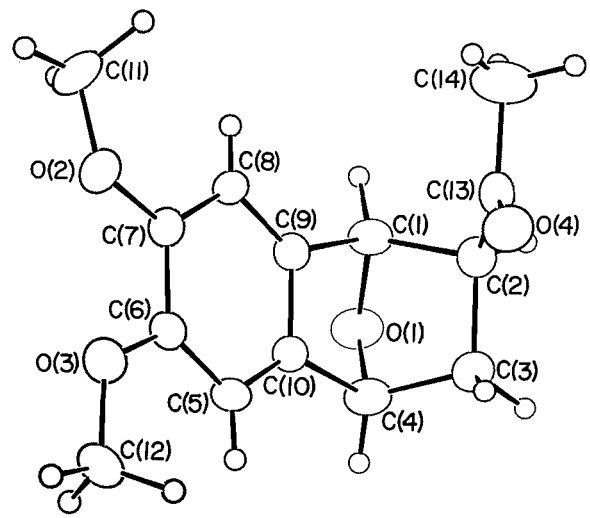

FIG. 1. ORTEP plot of **1***a*.

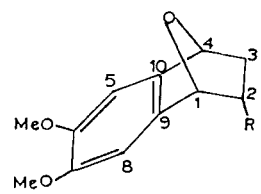

1

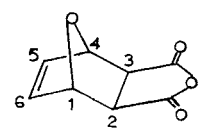

2

a (R = $COCH_3$)

c (R = CO_2CH_3)

Discussion

The molecular parameters determined for **1***a* and **1***c* are listed in Table 3 and an ORTEP plot of **1***a* is shown in Fig. 1. Most of the strain in these molecules resides in bond angle distortions; the angles at C(9) and C(10) in particular are severely distorted by C(1) and C(4) being pulled together (C(1) and C(4) are only 2.153(7) and 2.151(4) Å apart in **1***a* and **1***c* respectively) by the oxygen bridge. In general, the bond lengths and angles of the oxabicyclo moieties in **1***a* and **1***c* are comparable to those determined (8) for the furan – maleic anhydride adduct **2**. The only significant difference between the two systems is that the C(1)—O(1)—C(4) plane in **1***a* and **1***c* is tilted towards the benzene ring 7.4° more than the corresponding plane is tilted towards the 5,6-double bond in **2** (Table 4). Whether this discrepancy is a consequence of the

TABLE 3. Bond lengths (Å) and angles (°) for acetyl derivative **1***a* and carbomethoxy derivative **1***c*

Bond	Length		Bond	Length	
	1*a*	**1***c*		**1***a*	**1***c*
C(1)—O(1)	1.446(6)	1.441(3)	C(1)—C(2)	1.569(7)	1.557(4)
C(1)—C(9)	1.514(6)	1.514(3)	C(2)—C(3)	1.534(7)	1.540(4)
C(2)—C(13)	1.492(6)	1.506(4)	C(3)—C(4)	1.518(7)	1.526(4)
C(4)—O(1)	1.446(6)	1.446(3)	C(4)—C(10)	1.518(6)	1.508(4)
C(5)—C(6)	1.394(6)	1.379(3)	C(5)—C(10)	1.382(6)	1.386(3)
C(6)—O(3)	1.358(6)	1.372(3)	C(6)—C(7)	1.405(6)	1.404(3)
C(7)—O(2)	1.370(5)	1.360(3)	C(7)—C(8)	1.372(6)	1.386(3)
C(8)—C(9)	1.381(6)	1.386(3)	C(9)—C(10)	1.373(6)	1.377(3)
O(2)—C(11)	1.420(7)	1.425(3)	O(3)—C(12)	1.419(7)	1.418(4)
C(13)—O(4)	1.209(6)	1.191(4)	C(13)—O(5)	—	1.329(4)
C(13)—C(14)	1.490(10)	—	O(5)—C(14)	—	1.459(4)

Bond	Angle		Bond	Angle	
	1*a*	**1***c*		**1***a*	**1***c*
O(1)—C(1)—C(2)	100.8(2)	101.0(1)	O(1)—C(1)—C(9)	100.4(2)	101.2(1)
C(2)—C(1)—C(9)	107.3(2)	106.6(1)	C(1)—C(2)—C(3)	101.0(2)	101.5(1)
C(1)—C(2)—C(13)	113.6(2)	113.3(1)	C(3)—C(2)—C(13)	117.2(2)	115.6(1)
C(2)—C(3)—C(4)	102.1(2)	101.4(1)	O(1)—C(4)—C(3)	101.5(2)	101.5(1)
O(1)—C(4)—C(10)	101.0(2)	101.4(1)	C(3)—C(4)—C(10)	109.1(2)	107.9(1)
C(6)—C(5)—C(10)	118.3(2)	118.0(1)	C(5)—C(6)—C(7)	119.5(2)	121.1(1)
C(5)—C(6)—O(3)	124.6(2)	124.4(1)	C(7)—C(6)—O(3)	115.8(2)	114.5(1)
C(6)—C(7)—C(8)	120.8(2)	120.4(1)	C(6)—C(7)—O(2)	115.2(2)	115.1(1)
C(8)—C(7)—O(2)	123.9(2)	124.5(1)	C(7)—C(8)—C(9)	119.1(2)	117.7(1)
C(1)—C(9)—C(8)	134.3(2)	133.7(1)	C(1)—C(9)—C(10)	105.4(2)	104.5(1)
C(8)—C(9)—C(10)	120.3(2)	121.7(1)	C(4)—C(10)—C(5)	133.8(2)	133.6(1)
C(4)—C(10)—C(9)	104.4(2)	105.2(1)	C(5)—C(10)—C(9)	121.7(2)	120.9(1)
C(1)—O(1)—C(4)	96.2(2)	96.3(1)	C(7)—O(2)—C(11)	116.3(3)	117.3(1)
C(6)—O(3)—C(12)	117.1(3)	117.4(1)	C(2)—C(13)—O(4)	122.9(2)	125.8(1)
C(2)—C(13)—C(14)	117.1(3)	—	O(4)—C(13)—C(14)	120.0(3)	—
C(2)—C(13)—O(5)	—	110.7(1)	O(4)—C(13)—O(5)	—	123.5(1)
C(13)—O(5)—C(14)	—	117.2(2)			

TABLE 4. Least-squares planes
Equations of least-squares planes in the form $Ax + By + cz = D$
[Distances (Å) of the atoms from the planes]

Plane	Equation	Distances (Å)
Compound **1***a*		
Plane 1	$0.6738x + 0.7343y - 0.7642z = 3.4442$	[C(1) −0.002 C(4) 0.002 C(9) 0.004 C(10) −0.004]
Plane 2	$0.6236x + 0.0320y - 0.7811z = 5.1771$	[C(1) 0.009 C(2) −0.012 C(3) 0.013 C(4) −0.009]
Plane 3	$-0.0790x - 0.6437y + 0.7612z = 1.4050$	[C(1) 0 C(4) 0 O(1) 0]
Compound **1***c*		
Plane 1	$-0.0576x - 0.6166y + 0.7852z = 1.3365$	[C(1) −0.004 C(4) 0.004 C(9) 0.006 C(10) −0.006]
Plane 2	$0.8091x + 0.0728y + 0.5832z = 9.5192$	[C(1) 0.009 C(2) −0.012 C(3) 0.013 C(4) −0.009]
Plane 3	$0.7435x + 0.6344y \pm 0.2117z = 6.9524$	[C(1) 0 C(4) 0 O(1) 0]

	Dihedral angles (°)		
	(**1***a*)	(**1***c*)	(**2**)*
Planes 1–2	112.6	111.5	114.6
Planes 1–3	125.8	126.9	131.3
Planes 2–3	121.7	121.6	114.2

*Reference 8.

Can. J. Chem. Downloaded from www.nrcresearchpress.com by 210.87.254.40 on 09/06/12
For personal use only.

different configurations (*endo* in **1***a* and **1***c* and *exo* in **2**) of the adducts is open to question.

Acknowledgements

We thank the Natural Sciences and Engineering Research Council of Canada for their financial support.

1. B. A. KEAY, D. RAJAPAKSA, and R. RODRIGO. Can. J. Chem. **62**, 1093 (1984).
2. J. E. BALDWIN. J. Chem. Soc. Chem. Commun. 734 (1976); J. E. BALDWIN, J. CUTTING, W. DUPONT, L. KRUSE, L. SILBERMAN, and R. C. THOMAS. J. Chem. Soc. Chem. Commun. 736 (1976).
3. J. B. COULTAN, R. H. LEVIN, and J. CLARDY. J. Am. Chem. Soc. **98**, 6068 (1976).
4. B. A. KEAY, H. P. PLAUMANN, D. RAJAPAKSA, and R. RODRIGO. Can. J. Chem. **61**, 1987 (1983).
5. International tables for X-ray crystallography. Vol. IV. Kynoch Press, Birmingham, England. 1974.
6. R. F. STEWART, E. R. DAVIDSON, and W. T. SIMPSON. J. Chem. Phys. **42**, 3175 (1965).
7. A. J. CARTY, G. N. MOTT, N. J. TAYLOR, and J. E. YULE. J. Am. Chem. Soc. **100**, 3051 (1978).
8. S. BAGGIO, A. BARRIOLA, and P. K. DE PERAZZO. J. Chem. Soc. Perkin Trans. 2, 934 (1972).

Can. J. Chem. Downloaded from www.nrcresearchpress.com by 210.87.254.40 on 09/06/12
For personal use only.

Total synthesis of steroids. Part 2.[1] Preparation of C-10 methylated steroids. Regio- and stereocontrol in a diene addition to methyl Z-2-methyl-4-oxo-2-pentenoate

JAGABANDHU DAS, ROBERT A. DICKINSON, MASATOSHI KAKUSHIMA, GREGORY M. KINGSTON, GARY R. REID, YASUHIKO SATO, AND ZDENEK VALENTA

Department of Chemistry, University of New Brunswick, Bag Service #45222, Fredericton, N.B., Canada E3B 6E2

Received November 14, 1983

JAGABANDHU DAS, ROBERT A. DICKINSON, MASATOSHI KAKUSHIMA, GREGORY M. KINGSTON, GARY R. REID, YASUHIKO SATO, and ZDENEK VALENTA. Can. J. Chem. **62**, 1103 (1984).

A twelve-step total synthesis of 14-epi-androsta-4,9(11),15-triene-3,17-dione from methyl vinyl ketone, 2-methylcyclohexane-1,3-dione, acetylene, and methyl Z-2-methyl-4-oxo-2-pentenoate is described. Crucial steps include a stereo- and regio-selective diene addition, an efficient formation of ring D by C-acylation of an acetyl group, and a selective bromine substitution at C-15 in a 15,17-dione intermediate. The stereo- and regioselectivity of the diene addition is generalized for certain other bifunctional aliphatic dienophiles.

JAGABANDHU DAS, ROBERT A. DICKINSON, MASATOSHI KAKUSHIMA, GREGORY M. KINGSTON, GARY R. REID, YASUHIKO SATO et ZDENEK VALENTA. Can. J. Chem. **62**, 1103 (1984).

On décrit une synthèse totale en douze étapes de l'épi-14 androstatriène-4,9(11),15 dione-3,17 à partir de la méthylvinylcétone, de la méthyl-2 cyclohexanedione-1,3, de l'acétylène et du méthyl-2 oxo-4 pentène-2(Z) oate de méthyle. Les étapes clés comprennent une addition stéréo- et régiosélective de diène, une formation efficace du cycle D par une C-acylation d'un groupe acétyle et une substitution sélective par le brome en position 15 d'une dione-15,17 intermédiaire. On généralise à certains autres diènophiles aliphatiques bifonctionnels, la stéréo- et la régiosélectivité de l'addition de diène.

[Traduit par le journal]

Can. J. Chem. Downloaded from www.nrcresearchpress.com by 210.87.254.6 on 09/06/12
For personal use only.

The total synthesis of steroids (1) continues to provide useful ground for the testing of new synthetic strategies and methods (2). In particular, the establishment of the correct stereochemistry and the introduction of the desired functionality by an efficient, short route remains an interesting challenge.

We have previously reported (3) a successful elaboration of a "classical" synthetic scheme (4) represented in Fig. 1. Using 6-methoxy-1-vinyl-3,4-dihydronaphthalene as diene and 2,6-dimethyl-1,4-benzoquinone as dienophile, we have been able to complete the synthesis of *d,l*-estrone and of its 16,17-dehydro-17-acetyl derivative. Regiocontrol in the crucial diene addition was achieved by the use of boron trifluoride etherate, which reversed the reactivity of the dienophile (3, 5). The corresponding thermal addition was found to proceed exclusively in the undesired regio-sense.

We now wish to report, in detail, on the elaboration of this strategy to the synthetically more demanding C-10 methylated series.[2] Scheme 1 summarizes the approach in which diene trione monoacetal **13** was prepared from methyl vinyl ketone, 2-methylcyclohexane-1,3-dione, acetylene, and keto ester **10** in nine steps[3] and a 21% overall yield[4] based on dione **2**. The differentiation between the two keto groups in ring D of **13** to give enone **15** was then accomplished in two steps and a 68% yield. Scheme 2 shows the preparation of keto ester **10** (7) in two steps from pyruvic acid and acetone via pseudo acid **16** (8) in a 17% yield based on pyruvic acid.

All of the steps in the preparation of acetoxydienyl diene **9** and of dienophile **10** are precedented and will therefore be discussed only briefly. Triketone **3** (9–12) was obtained as a yellow oil in a Michael addition under mildly acidic reaction conditions. We have confirmed that the yield and purity of the product are significantly increased by using an aqueous medium and by omitting a basic catalyst (10, 11*b*) which is normally used in the standard preparations of **3** (12). Triketone **3** was then cyclized to enedione **4** with pyrrolidine in refluxing benzene (12, 13). Chiral Wieland–Miescher ketone **4** is accessible by an asymmetric synthesis via **3** using (*S*)-proline (9, 10). However, in the synthesis described here, racemic **4** was used and all compounds reported are therefore racemic. Treatment of **4** with lithium acetylide in liquid ammonia (13) gave the crystalline ethynyl carbinol **5** (13, 14), which on hydrogenation in pyridine with 5% palladium on barium sulfate (15) was selectively reduced to the crystalline allyl alcohol **6**.

The dehydration of **6** to **8** requires carefully chosen conditions, since the functionality of **6** is suitable for an undesirable acid-catalyzed reverse aldol reaction. The method of Bell *et al.* (16) proved excellent for the purpose. The intermediate allyl bromide **7** was prepared from **6** in a reaction with phosphorus tribromide in dimethylformamide and methylene chloride at −10°C and was then dehydrobrominated at 100°C after addition of 2 mol equivalents of lithium bromide and 3 mol equivalents of lithium carbonate to give **8** as a yellow oil of high purity. We have previously reported (17) that alcohol **6** can be converted to the corresponding carbamate on treatment with *p*-toluenesulfonyl isocyanate and that a subsequent vacuum distillation (18) leads to the desired diene **8**. The carbamate pyrolysis method has, in our hands, consistently given yields of 55–75% of dienes from **6** and other structurally related tertiary allyl alcohols. While it is thus satisfactory, it is clearly not as efficient as the bromine substitution–dehydrobromination sequence (16).

To complete the synthesis of the required acetoxydienyl di-

[1] For Part 1, see ref. 3.

[2] Part of this work has been reported previously in a preliminary form (6).

[3] The conversion **6** → **8** is considered to be one step since the intermediate allyl bromide **7** is dehydrobrominated to **8** without isolation (*vide infra*). The conversion **1** + **2** → **4** can be accomplished in one operation, but a two-step sequence is more efficient. Furthermore, the isolation of triketone **3** is preferred if a chiral synthesis is intended (9, 10). Similarly, the conversion **4** → **6** can in principle be done in one step using a vinyl Grignard reagent, but the use of acetylene is safer and more convenient.

[4] Yields in parentheses in Scheme 1 denote reactions in which the product was not purified by distillation, crystallization, or chromatography.

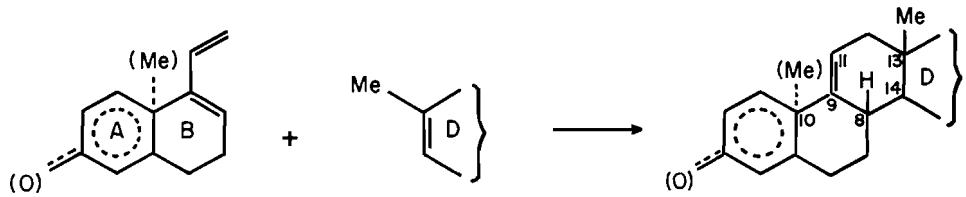

FIG. 1. General scheme for steroid synthesis.

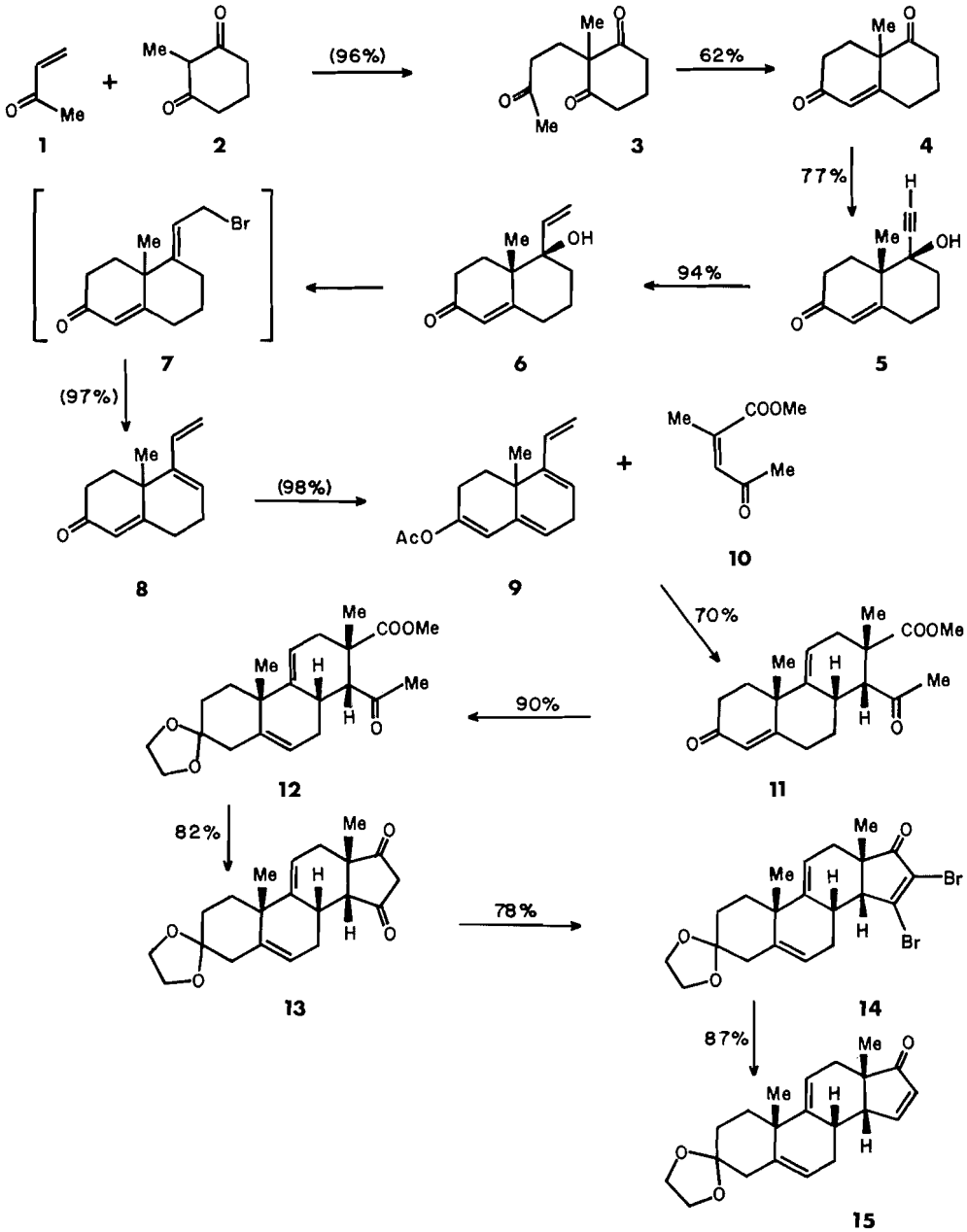

SCHEME 1

ene **9**, enone **8** was treated with anhydrous hydrogen bromide (prepared from 2 parts of 48% hydrobromic acid in 3 parts of acetic anhydride) in acetic anhydride at ambient temperature for 10 h. The resulting light green oil was homogeneous according to its ^{1}Hmr spectrum; since its color rapidly darkened to red on standing, however, it was used immediately after its preparation for the subsequent addition.

In order to prepare the required dienophile **10** (7), pyruvic acid was first condensed with acetone in the presence of 85% phosphoric acid to give the crystalline pseudo acid **16** (8). Treatment of **16** with methyl iodide and potassium carbonate in dry acetone then led to dienophile **10**. During isolation of **10**,

Can. J. Chem. Downloaded from www.nrcresearchpress.com by 210.87.254.6 on 09/06/12
For personal use only.

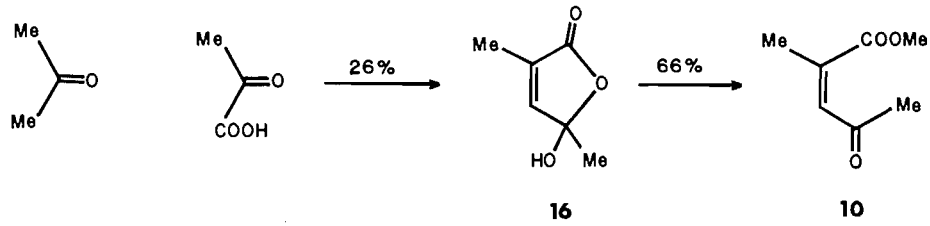

SCHEME 2

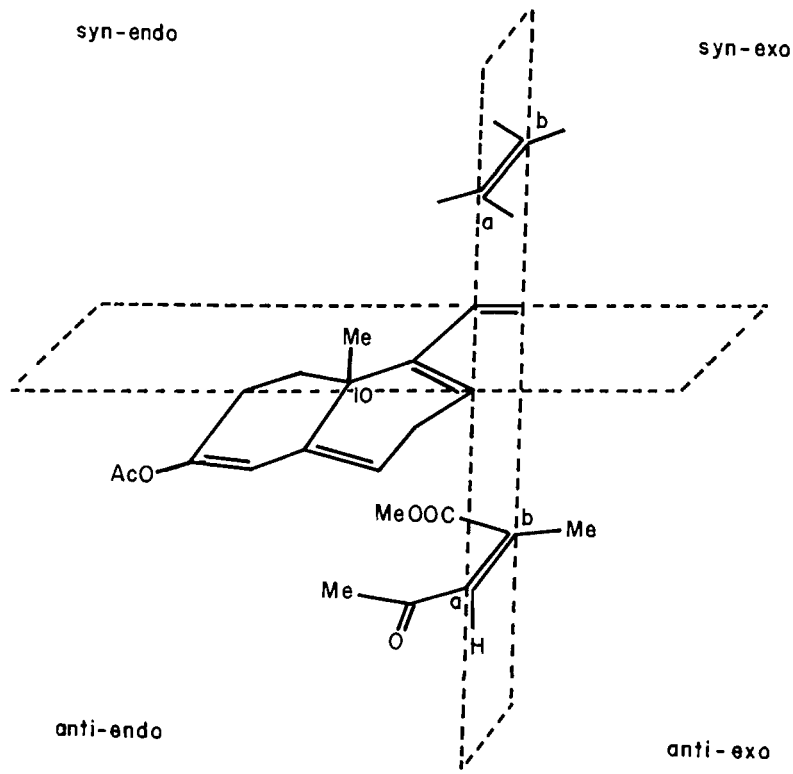

FIG. 2. Possible additions to **9**.

care had to be taken first to remove all potassium iodide formed, since it was found to catalyze the isomerization of **10** to the more stable *E*-isomer, particularly at elevated temperatures. Thus, although pure **10** was obtained in some vacuum distillations, purification by chromatography proved more reliable.

Catalyzed diene addition

The reaction of diene **9** with 2 mol equivalents of dienophile **10** in the presence of 1.5 mol equivalents of anhydrous tin tetrachloride[5] in methylene chloride at 0°C for 1 h gave crystalline adduct **11**, mp 155–156°C, in a conversion of 55% and a yield of 70% based on consumed **9**. The structure of **11** was established by X-ray diffraction. No other adduct could be found in a careful search of mother liquors and of chromatographic fractions. Both the starting diene and the product were isolated as enones (**8** and **11**, respectively), presumably because the corresponding enol acetates are slowly hydrolyzed in the presence of tin tetrachloride by traces of water during the reaction and this hydrolysis is completed during work-up.[6]

A complete regio- and stereoselectivity has thus been achieved in the addition **9** + **10**. The development of this control should now be discussed. As can be seen in Fig. 2, two mutually perpendicular planes intersecting at a straight line connecting the diene termini define four quadrants of space in which the dienophile substituents can be located during addition. Two of the quadrants contain space *syn* to the C-10 methyl group, the other two *anti* to this group. During the addition, a substituent in dienophile **10** (for example, the acetyl group) can then be oriented *endo* or *exo* relative to the diene π-system. This grouping can thus be located in any one of the four quadrants. Since, furthermore, this substituent can be situated at either terminus of the dienophile (a or b, Fig. 2), the two molecules (**9** + **10**) can in principle react via eight different transition states. The one shown in Fig. 2 by a complete drawing of the dienophile leads to the observed adduct **11**.

[5] Boron trifluoride etherate and aluminum chloride proved ineffective in this case.

[6] The 3-acetoxy-3,5-diene corresponding to **11**, mp 129–131°C, could be isolated in a 15–20% yield from a reaction run under scrupulously anhydrous conditions. It then hydrolyzed rapidly on mild acid treatment.

Can. J. Chem. Downloaded from www.nrcresearchpress.com by 210.87.254.6 on 09/06/12
For personal use only.

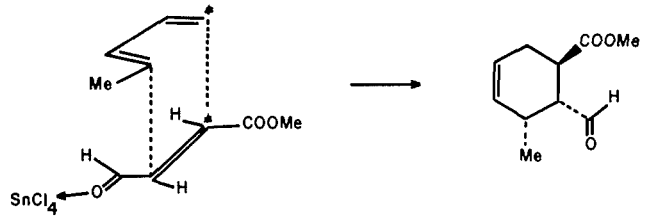

FIG. 3

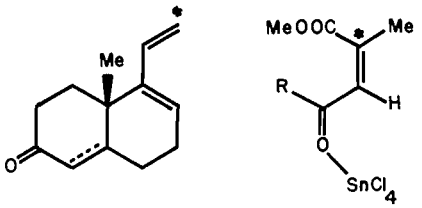

FIG. 4

Thus, three independent factors must be controlled: *syn–anti* and *endo–exo* stereochemistry and a–b (Fig. 2) regiochemistry. By studying many systems, we have found that complete regio- and *endo–exo* control can often be achieved with bifunctional dienophiles in which the two functions (at termini a and b) are both activating and in which one of these functions, the carbonyl group of an aldehyde or a ketone, complexes preferentially with a Lewis acid. The crucial finding is represented in Fig. 3. While the thermal addition of piperylene to methyl *E*-4-oxo-2-butenoate gives all four possible adducts, a catalyzed addition proceeds exclusively via that transition state in which the more nucleophilic terminus of piperylene (*) adds β to the formyl group and in which the formyl group is *endo* oriented (19). The simplest explanation for this finding is the postulate that the only reacting dienophile species is complexed at the formyl oxygen atom.

Since 1-vinylcyclohexene (5) and bicyclic dienes of the type indicated in Fig. 4[7] react exclusively in the same sense as piperylene in catalyzed additions,[8] it can be seen that the choice of the dienophile suitable for the construction of steroid rings C and D is clear. It must have an aldehyde, or possibly a ketone, at that dienophile terminus which will become C-14 in the steroid, and an ester group must be *cis* to it in order to establish the correct C-13 configuration (see Fig. 2). A ketone was chosen because it promised a more facile construction of ring D.

It remained to establish which diene(s) would add most efficiently from the side *anti* to the C-10 methyl group (Fig. 2). Clearly, an *anti* addition is required for the establishment of the correct configuration at C-8 and C-13 of the incipient steroid. Using 2,6-dimethyl-1,4-benzoquinone as a probe, we have found[7] that, in catalyzed additions, only acetoxydienyl diene **9** adds exclusively from the *anti* side. Enone **8** shows a slight preference for *syn* addition (17), while of the two ring A saturated ketones corresponding to **8**, the A,B-*trans* ketone adds preferentially *anti* (~2–4:1) and the A,B-*cis* ketone *syn* (~4–6:1). Thus, clearly, diene **9** possesses the A,B-ring geometry most suitable for an *anti* addition.

The exclusive *anti* addition to **9** may be due simply to the efficient flattening of the molecule which could then make the

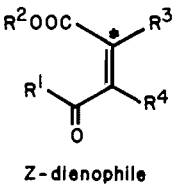

Z-dienophile

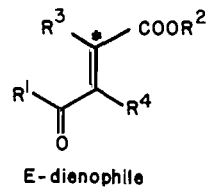

E-dienophile

FIG. 5

hindering effect of the quasi-axial C-10 methyl group the most pronounced. Inspection of models (Fig. 2) shows, however, that the bidentate catalyst could well complex not only with the carbonyl group of the dienophile, but also with the 5,6-double bond of the diene. Such a complexation is sterically only possible from the *anti* side. In this connection, it is interesting to note that the catalyzed addition to **9** is approximately one hundred times faster than a similar one to **8**.[9] The acceleration and stereoselection would both be well explained by a double complexation.

The principles discussed above can be used generally for synthetic planning, since the *endo–exo* as well as the regiopreference in additions of *Z*- and *E*-dienophiles of the type shown in Fig. 5 to suitable dienes in the presence of tin tetrachloride can now be predicted. In these dienophiles, R^1 can be an H-atom (17, 19) or an alkyl group (**10**) and R^3 can be an H-atom (19) or an alkyl group (17) as in **10**. Although we have not as yet studied cases in which R^3 is an H-atom and R^4 an alkyl group (Fig. 5), we are confident that such dienophiles will add well and will follow the rules established here. This confidence is based on the fact that, in certain cases, 2-alkyl-substituted enones undergo catalyzed diene additions, while the corresponding 3-alkyl-substituted enones do not.[10] For example, no catalyzed (or thermal) diene addition to 3-methyl-2-cyclohexenone has been reported, while catalyzed additions to 2-methyl-2-cyclohexenone are reasonably efficient (20). An alkyl substituent at the electrophilic terminus of the dienophile (asterisks in Fig. 5) can thus be expected to be more deactiviting[10] than one at the other terminus. It remains to establish experimentally whether R^3 and R^4 (Fig. 5) can be alkyl groups in the same dienophile.

Available evidence permits the above generalization only for bifunctional dienophiles in which an ester group competes with a ketone or an aldehyde for the catalyst. In all such cases, the complexing group (ketone or aldehyde) controls regiochemistry and *endo* stereochemistry. Clearly, it is of both theoretical and synthetic interest to establish whether comparable selectivities will be achievable using activating groups different from those indicated in Fig. 5. In an important study using a bifunctional dienophile, Danishefsky *et al.* (22) showed that, in thermal additions, the nitro group of *trans*-methyl β-nitroacrylate completely controls regiochemistry, but not *endo* stereochemistry. This result, which preparatively contributes to

[7] R. A. Dickinson and Y. Sato. Unpublished experiments in this department.

[8] Asterisk on diene terminus in Fig. 4 indicates the more nucleophilic center.

[9] The addition of ethyl *E*-2-methyl-4-oxo-2-butenoate to enone **8** under conditions comparable to those described here for the **9** + **10** addition required 4 days (17). This explains why no detectable quantity of a *syn*-adduct is formed in the **9** + **10** addition, although some dione **8** is formed by hydrolysis during the reaction, and **8** adds preferentially *syn*.

[10] In fact, to our knowledge, the only β-alkyl β-disubstituted dienophiles which have undergone a catalyzed diene addition are exceptionally reactive ones (low LUMO). Examples include **10** in this paper, ethyl *E*-2-methyl-4-oxo-2-butenoate (17), 2,6-dimethyl-1,4-benzoquinone (5), and a cross-conjugated cyclohexadienone described by Liotta *et al.* (21).

Can. J. Chem. Downloaded from www.nrcresearchpress.com by 210.87.254.6 on 09/06/12
For personal use only.

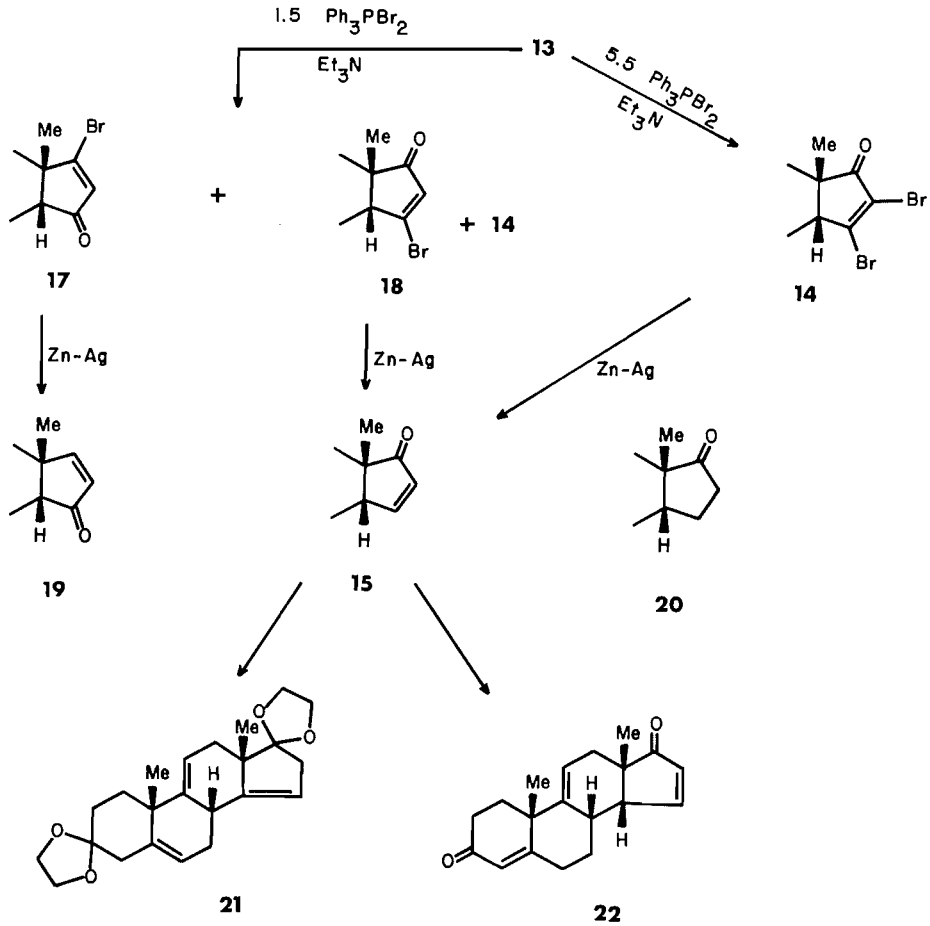

SCHEME 3

the synthesis of previously difficultly accessible cyclohexenes (22), gives a warning that, in general, regiocontrol and *endo* stereocontrol are two different, separable manifestations of the properties of a given activating substituent (23).

The third parameter, the *syn–anti* stereoselectivity (Fig. 2) in any particular addition, will of course depend on the exact nature of the diene and thus cannot be generalized.

Construction of ring D

The adduct **11** contains all C atoms required for the construction of ring D and the *cis*-arrangement of the ester and acetyl groups makes the required C-acylation a favourable process (24). In order to simplify the subsequent cyclization, **11** was first converted to acetal **12** on treatment with ethylene glycol and pyridinium tosylate (25) in boiling benzene or toluene. Mild acid hydrolysis of **12** gave pure adduct **11**, showing that no epimerization had occurred at the (steroid) C-14 position during the formation of **12**. Cyclization was then efficiently achieved by the treatment of acetal **12** with 6 mol equivalents of lithium bis(trimethylsilyl)amide (26) in tetrahydrofuran at 20°C for 2 h.[11] Dione **13** was isolated as a white powder, mp 195°C (dec.), showing the expected spectral properties, including a uv chromophore.

The dithiane derivative corresponding to **12** was also prepared from **11** in a 92% yield and cyclized in a similar manner in an 87% yield to the ring A dithiane corresponding to **13** (see Experimental). Work in the dithiane series was discontinued, however, because in contrast to the dioxalane series no useful ring D transformations could be effected. This lack of success included the method (27) which was found effective with **13** (see below).

It should be noted that the addition **9** + **10** followed by cyclization **12** → **13** is formally equivalent to the direct addition of **9** to 2-methyl-2-cyclopentene-1,4-dione. This latter addition was not attempted, since it was feared that enolization of the dione system on catalysis would diminish or destroy the reactivity of the dienophile or, at best, eliminate the required regioselectivity.[12]

The differentiation between the two keto groups in **13** proved a considerable challenge and its study produced a surprising result. While many methods, including the use of oxalyl chloride (28), failed to yield the desired β-halo enone (or at least a mixture of the two possible β-halo enones), the method developed by Piers and Nagakura (27) employing triphenylphosphine dibromide and triethyl amine in benzene was successful. Treatment of dione **13** with 1.5 mol equivalents of the reagent produced a mixture of bromo ketones **17** and **18** (Scheme 3) together with some dibromoketone **14** and starting material. In

[11] This method represents a significant improvement over our previous cyclization with sodium hydride in dimethylsulfoxide and toluene which gave **13** in a 41% yield (6). It can safely be assumed that the C,D-ring system in **13** is *cis*, not only for thermodynamic reasons, but also because we have evidence that an epimerization of the acetyl group in **12** prior to cyclization leads to an enol lactone via an O-acylation (6).

[12] NOTE ADDED IN PROOF: We have now found that 2-methyl-2-cyclopentene-1,4-dione does not add to **9** in the presence of tin tetrachloride or to piperylene in the presence of boron trifluoride etherate.

Can. J. Chem. Downloaded from www.nrcresearchpress.com by 210.87.254.6 on 09/06/12
For personal use only.

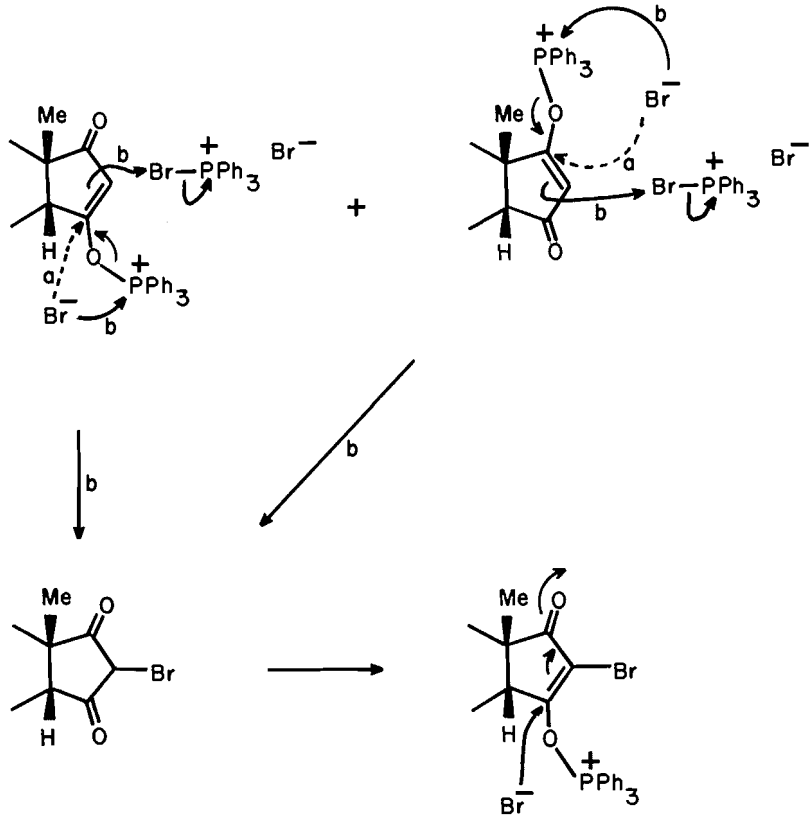

FIG. 6

contrast, treatment of **13** with 5.5 mol equivalents of the reagent gave **14** as the only product! Compounds **17** and **18** were found not to react further with triphenylphosphine dibromide!

Bromo enone **18** and dibromo enone **14** gave the desired enone **15** on reduction with a zinc–silver couple prepared by the method of Clark and Heathcock (28). A similar reduction of bromo enone **17** yielded enone **19**. The reduction of **14** with zinc in acetic acid gave ring D saturated ketone **20**.

The preparation of both possible ring D enones (**15** and **19**) facilitated structure assignments. In particular, the two enone protons were seen as clean doublets (J = 6 Hz) at δ 6.02 and 7.61, in the ^{1}Hmr spectrum of **19**, while the β-proton (C-15) showed as a double doublet (J = 5.9, 2 Hz) at δ 7.46 and the α-proton (C-16) as a double doublet (J = 5.9, 1.6 Hz) at δ 6.14 in the ^{1}Hmr spectrum of **15**. The structure of **15** was further confirmed by its conversion to the diacetal **21**. The accompanying shift of the ring D double bond to the 14,15-position as shown by the ^{1}Hmr spectrum of **21** is, of course, only compatible with a carbonyl group at C-17 in enone **15**. Finally, mild acid hydrolysis produced the dione **22**.

The remarkable action of triphenylphosphine dibromide (27), together with a very efficient zinc–silver couple reduction (28), has thus led to a facile, high yield differentiation between the two carbonyl groups in **13**. Concerning the puzzling events observed during the bromide–enol exchanges (Scheme 3), it can be speculated that subtle kinetic effects have led to an unusual – and very fortunate – result. Inspection of models of diketone **13** and of the two corresponding enols, as well as the consideration of the many abortive attempts to achieve efficient reactions at C-15 or at C-17 of **13**, indicate that both centers are sterically hindered. If the two probable first intermediates in the reaction sequence (27) are considered (Fig. 6), it can be seen that the bromide ion can, by path (a) indicated by dotted arrows in Fig. 6, add β to the carbonyl group and that a subsequent triphenylphosphine oxide elimination would then give the β-bromo enones (27). The relative amounts of the two resulting β-bromo enones **17** and **18** (Scheme 3) would thus be determined by the two velocities by which the first intermediates are formed. However, if the bromide ion attack (path (a)) is slow because of steric hindrance, then it is possible that, in the presence of a sufficient excess of triphenylphosphine dibromide, path (b) (or a nonconcerted equivalent) could be followed. This would then lead to a common bromo diketone intermediate. Since only one dibromo enone is formed (**14**), it must now be postulated that the bromo diketone reacts with the reagent exclusively at the C-15 position as indicated in Fig. 6.[13] The reason for this selectivity (as compared to the nonselectivity of the reaction with **13**) and for the complete absence of a 16-dibromo product is not clear.

In conclusion, a relatively short and efficient total synthesis of potentially useful steroid intermediates has been accomplished. While, to our knowledge, no naturally occurring steroids contain the 14-β-H atom present in **22**, the functionality present in **21** should permit, after a suitable differentiation of the functional groups, the introduction of the important 14-β-hydroxyl group (29). The 9,11-double-bond in **22** should

[13] The above is, however, not the only possible explanation. While it seems obligatory to postulate that the first intermediate bearing the —$OPPh_3$ grouping at C-17 is converted to the bromodiketone (Fig. 6) which can then be "recycled" to give **14**, it is possible that the first intermediate bearing the —$OPPh_3$ grouping at C-15 (Fig. 6) is brominated at C-16 without the loss of PPh_3. Subsequent addition of bromide ion to C-15, followed by elimination of triphenylphosphine oxide, would then give **14** directly. Again, however, it is not obvious why the two intermediates should have a different reactivity.

Can. J. Chem. Downloaded from www.nrcresearchpress.com by 210.87.254.6 on 09/06/12
For personal use only.

be suitable for the preparation of 11-oxygenated steroids (30), while steroids containing a 14-α-H atom should be accessible by catalytic hydrogenation of derivatives of **21** containing a 17-β substituent (31). Finally, chiral compounds are readily available, since the Wieland–Miescher ketone **4** can be prepared in either enantiomeric form using (*S*)- or (*R*)-proline (9, 10).

Experimental

Melting points were determined on a Kofler hot stage and are uncorrected. Ultraviolet (uv) spectra were recorded on a Beckman Model 25 spectrophotometer in ethanol solution. The wavelengths are reported in nanometers (nm) with ε values in parentheses. Infrared (ir) spectra were determined on both the Perkin–Elmer 727B and 598 infrared spectrophotometers in chloroform or carbon tetrachloride solution. Values are given in wave numbers (cm^{-1}) calibrated to the polystyrene band at 1601 cm^{-1}. Proton magnetic resonance (^{1}Hmr) spectra were recorded on a Varian T-60 spectrometer and high resolution ^{1}Hmr spectra were obtained on a Varian XL-200 spectrometer, both using deuterochloroform as solvent; chemical shift values are given in δ (ppm) scale relative to tetramethylsilane (TMS) used as internal reference. Low resolution mass spectra were measured on a Hitachi Perkin–Elmer RMU-6D mass spectrometer. High resolution mass spectra were measured by the Mass Spectrometry Laboratory, Department of Chemistry, University of Alberta, Edmonton, Alberta. Microanalyses were performed by Guelph Chemical Laboratories, Ltd., Guelph, Ontario. Chromatography was performed by flash chromatography (32) using silica gel 60 (230–400 mesh). Solutions were dried over anhydrous calcium chloride. The following abbreviations have been used: s, singlet; d, doublet; dd, double doublet; ddd, double doublet of doublets; q, quartet; b, broad; m, multiplet; dec., decomposition; ether, ethyl ether.

Enol acetylation of diene 8

To a solution of diene **8** (0.990 g, 5.26 mmol) in acetic anhydride (10 mL) at 0°C was added a solution of anhydrous HBr (20 drops) prepared from 48% HBr (4 mL) and acetic anhydride (6 mL). The solution was stirred at 20°C in an atmosphere of N_2 for 10 h and then diluted with a cold saturated solution of $NaHCO_3$ which was extracted with ether–hexanes (1:9). The extracts were washed successively with saturated $NaHCO_3$ solution and brine and then dried. Evaporation of the solvent *in vacuo* at 20°C yielded the acetoxydienyl diene **9** (1.19 g, 98%) as an unstable light green oil which was immediately used in the subsequent addition; ir ν_{max}: 1740, 1360, 1115, 900; ^{1}Hmr δ: 1.21 (3H, s, C(4a)—CH_3), 2.13 (3H, s, C(2)-ester), 2.81 (2H, m, C(7)—H(2)), 4.98 (1H, dd, *J* = 10 and 2 Hz, B proton), 5.31 (1H, dd, *J* = 17 and 2 Hz, A proton), 5.52 (1H, m, C(8)—H), 5.82 (2H, m, C(1)—H, C(6)—H), 6.40 (1H, ddd, *J* = 18, 10, and 1.5 Hz, X proton).

Methylation of pseudo acid 16. Dienophile 10

The known compound **10** (7) was prepared by our modified procedure. Pseudo acid **16** (10.0 g, 0.0780 mol) was taken up in dry acetone (300 mL, distilled from $KMnO_4$) and was stirred with anhydrous K_2CO_3 (37 g) at 20°C for 1 h. Methyl iodide (20 mL) was added and the reaction was stirred at 20°C for 18 h. The excess of K_2CO_3 was filtered and the mixture was diluted with dry pentane (500 mL) and filtered again to remove precipitated KI. The solvent was then evaporated *in vacuo* at 20°C and the residue was again diluted with pentane (50 mL) and more precipitated KI was removed by filtration. Concentration of the solution *in vacuo* at 20°C followed by chromatography using hexanes – ethyl acetate (9:1) as eluent gave **10** (7.35 g, 66%) as a yellow oil.

Catalyzed addition of 9 and 10

To a solution of **10** (1.50 g, 10.5 mmol) in CH_2Cl_2 (50 mL), freshly distilled from K_2CO_3, was added a 1 *M* solution of $SnCl_4$ in CH_2Cl_2 (75 mL, 7.5 mmol) at 0°C in an atmosphere of argon. To this solution was added a solution of enol acetate **9**, freshly prepared from diene **8** (0.990 g, 5.26 mmol) in CH_2Cl_2 (10 mL). The resulting wine red solution was stirred at 0°C for 1 h and then poured into a cold saturated solution of $NaHCO_3$ which was then thoroughly extracted with $CHCl_3$. The extracts were washed successively with saturated $NaHCO_3$ solution and H_2O and dried over anhydrous $MgSO_4$. The solvent was evaporated *in vacuo* and most of the adduct **11** was crystallized from ether while the residual product was chromatographed, eluting with hexanes – ethyl acetate (9:1), to give unreacted diene **8** (215 mg). Elution with hexanes – ethyl acetate (6:4) gave the desired adduct **11** which was crystallized from ether (950 mg, 55%, 70% based on consumed **8**), mp 155–156°C; ir ν_{max} (CCl_4): 1730, 1715, 1680; ^{1}Hmr (200 MHz) δ: 1.23 (3H, s, C—CH_3), 1.37 (3H, s, C—CH_3), 2.22 (3H, s, C(14)—$COCH_3$), 3.29 (1H, d, *J* = 7 Hz, C(14)—H), 3.69 (3H, s, C(13)—CO_2CH_3), 5.71 (2H, m, C(4)—H, C(11)—H); ms *m/e*: 330 (M^+). *Mol. Wt.* calcd. for $C_{20}H_{26}O_4$: 330.1831; found (high resolution ms): 330.1826. The structure of **11** was established by X-ray diffraction.

Acetalization of adduct 11

A mixture of dry benzene (35 mL), ethylene glycol (3.0 mL, 43 mmol), and pyridinium tosylate (PPTS) (25 mg, 0.10 mmol) was stirred at reflux in an argon atmosphere with a Dean–Stark distilling head connected. After water had been removed (ca. 40 mL of solvent replaced), the adduct **11** (200 mg, 0.605 mmol) was added and the reaction was heated at reflux under argon for 5.5 h. The cooled reaction mixture was diluted with ether and washed successively with saturated $NaHCO_3$ and brine solutions. The organic layer was dried and evaporated *in vacuo*. The residue was chromatographed, using hexanes – ethyl acetate (6:4) as eluent, to obtain unreacted adduct **11** (34 mg) and the product acetal **12** (169 mg, 75%, 90% based on recovered **11**) as colourless crystals, mp 155–157°C (hexanes/ether).

In a similar reaction, substituting toluene for benzene as solvent and refluxing under argon for 5 h, a yield of 88% of **12** was achieved with no unreacted adduct detected; ir ν_{max} (CCl_4): 1730, 1715, 1260, 1102; ^{1}Hmr δ: 1.21 (3H, s, C—CH_3), 1.23 (3H, s, C—CH_3), 2.23 (3H, s C(14)—$COCH_3$), 3.22 (1H, d, *J* = 7 Hz, C(14)—H), 3.67 (3H, s, C(13)—CO_2CH_3), 3.93 (4H, s, —OCH_2CH_2O—), 5.42 (1H, m, C—H vinylic), 5.65 (1H, m, C—H vinylic); ms *m/e*: 374 (M^+). *Mol. Wt.* calcd. for $C_{22}H_{30}O_5$: 374.2093; found (high resolution ms): 374.2099.

The dithiane derivative corresponding to **12** was prepared in the following manner. The adduct **11** (240 mg, 0.726 mmol) was suspended in anhydrous ether (10 mL) and stirred at 0°C in an argon atmosphere for 10 min. At this point an excess of 1,3-propanedithiol (0.12 mL, 1.2 mmol) was added, followed by the addition of a large excess of BF_3 etherate (5 mL). The adduct soon went into solution and the reaction was stirred at 20°C, under argon, for 5 h with five further additions of BF_3 etherate (5 × 2 mL) made throughout the reaction. The reaction mixture was carefully diluted with H_2O and extracted with ether. The organic layer was washed with a 5% $NaHCO_3$ solution until neutral, and with brine, dried, and evaporated *in vacuo*. The product dithiane was crystallized from ether (281 mg, 92%) as colourless crystals, mp 205–206°C; ir ν_{max}: 1727, 1716, 1260 (broad); ^{1}Hmr (200 MHz) δ: 1.20 (3H, s, C—CH_3), 1.22 (3H, s, C—CH_3), 2.22 (3H, s, C(14)—$COCH_3$), 3.21 (1H, d, *J* = 7 Hz, C(14)—H), 3.67 (3H, s, C(13)—CO_2CH_3), 5.41 (1H, s, (C(4)—H), 5.61 (1H, m, C(11)—H); ms *m/e*: 420 (M^+). *Mol. Wt.* calcd. for $C_{23}H_{32}S_2O_3$: 420.1793; found (high resolution ms): 420.1792.

Cyclization of acetal 12. Dione 13

To a solution of 1.60 *M* n-butyllithium in hexane (3.13 mL, 5.00 mmol) at −78°C in an atmosphere of argon was added 1,1,1,3,3,3-hexamethyldisilazane (1.05 mL, 5.00 mmol). The resulting white slurry was stirred at −78°C for 30 min, at which point dry THF (10 mL) was added and the solution was allowed to warm to ambient temperature. At this time a solution of acetal **12** (305 mg, 0.814 mmol) in THF (10 mL) was added over a period of 5 min. The reaction mixture was stirred under argon at 20°C for 2 h and was then diluted with ether and extracted with brine. The basic aqueous layer was then neutralized with a 10% oxalic acid solution and extracted thoroughly

Can. J. Chem. Downloaded from www.nrcresearchpress.com by 210.87.254.6 on 09/06/12
For personal use only.

Can. J. Chem. Downloaded from www.nrcresearchpress.com by 210.87.254.6 on 09/06/12
For personal use only.

with CH_2Cl_2. The organic layer was dried and evaporated *in vacuo*. Crystallization from ethyl acetate afforded **13** (228 mg, 82%) as a white powder, mp 195°C (dec.); uv λ_{max} (EtOH): 251 nm (variable) (13 680); (EtOH–OH^-): 262 nm (25 230); (EtOH–H^+): 247 nm (10 115); ir ν_{max}: 1722, 1590; ^{1}Hmr (200 MHz) δ: 1.22 (3H, s, C—CH_3), 1.23 (3H, s, C—CH_3), 3.95 (4H, m, —OCH_2CH_2O—), 4.53 (b, 1.5 H, C(16)—H(2)), 5.15 (0.5 H, s, C(16)—H vinylic), 5.40 (1H, m, C—H vinylic), 5.51 (1H, m, C—H vinylic); ms *m/e*: 342 (M^+). *Mol. Wt.* calcd. for $C_{21}H_{26}O_4$: 342.1831; found (high resolution ms): 342.1826.

As evidenced in the ^{1}Hmr data, the compound contains a mixture of D-ring dione and enone. In ethanol solution, as evidenced by the uv results, the compound is in equilibrium between the enol and enolate species.

The dithiane derivative corresponding to **13** was also prepared in a similar manner in an 87% yield, mp 181–183°C (ethyl acetate); uv λ_{max} (EtOH): 248–263 nm (variable); (EtOH–OH^-): 263.5 nm (30 260); (EtOH–H^+): 248 nm (22 610); ir ν_{max}: 1722, 1588 (broad); ^{1}Hmr δ: 1.24 (6H, broad s, C(10)—CH_3 and C(13)—CH_3), 2.95 (0.75 H, s, hydroxyl), 5.09 (0.5 H, s, C(16)—H(2)), 5.36 (0.75 H, s, C(16)—H vinylic), 5.47 (2H, m, C(4)—H, C(11)—H); ms *m/e*: 388 (M^+). *Anal.* calcd. for $C_{22}H_{28}S_2O_2$: C 68.00, H 7.26; found: C 67.99. H 7.32.

A D_2O exchange experiment resulted in the disappearance of the ^{1}Hmr signals at δ 2.95 and δ 5.09, representing the enol hydroxyl and the C-16 keto protons.

*Bromination of dione **13**. β-Bromo enones **17** and **18***

To an ice-cold solution of triphenylphosphine (85.0 mg, 0.324 mmol) in freshly distilled (from Na) benzene (10 mL), in an argon atmosphere, was added, dropwise, a 1 *M* solution of Br_2 in benzene (0.30 mL, 0.30 mmol). To the resulting white suspension of triphenylphosphine dibromide was added triethyl amine (0.050 mL, 0.36 mmol) and, finally, a suspension of diketone (70.0 mg, 0.204 mmol) in benzene (10 mL). The mixture was stirred under argon at 70°C for 16 h. The cooled reaction mixture was extracted with 5% NaOH solution and the aqueous layer was neutralized with 10% oxalic acid solution and extracted with CH_2Cl_2 to recover starting material (5 mg). The original organic layer was washed with H_2O and brine, dried, and evaporated *in vacuo*. The crude material was subjected to preparative thin-layer chromatography (1.0-mm silica gel 60 F_{254} plate), developing twice in hexanes – ethyl acetate (4:1). Two bands were collected and extracted with CH_2Cl_2–CH_3OH (10:1) to yield the dibromo ketone **14** (9 mg) and a mixture of bromo ketones **17** and **18** (16.5 mg, 21% based on recovered **13**) with the desired bromo enone **18** predominant (ratio 2:1). However, in two similar experiments the other bromo enone **17** was predominant by the same ratio. Crystallization from ether gave **18**, mp 113–116°C, exclusively; uv λ_{max}: 240 (11 990); ir ν_{max}: 2980, 1705, 1580; ^{1}Hmr (200 MHz) δ: 1.24 (3H, s, C—CH_3), 1.30 (3H, s, C—CH_3), 2.95 (2H, m, $W/2$ = 6 Hz, C—CH_2—), 3.95 (4H, m, —OCH_2CH_2O—), 5.37 (1H, m, C—H vinylic), 5.48 (1H, m, C—H vinylic), 6.40 (1H, s, C(16)—H); ms *m/e*: 404 (M^+), 406 (M^+ + 2). *Mol. Wt.* calcd. for $C_{21}H_{25}O_3Br$: 404.0987 (^{79}Br), 406.0967 (^{81}Br); found (high resolution ms): 404.0973 (^{79}Br) and 406.0986 (^{81}Br).

Bromo enone **17** was isolated as a crude oil from the mother liquors; ^{1}Hmr δ: 1.27 (6H, s, C(10)—CH_3 and C(13)—CH_3), 3.93 (4H, s, —OCH_2CH_2O—), 5.40 (2H, m, C(6)—H and C(11)—H), 6.30 (1H, s, C(16)—H).

The bromo enones **17** and **18** were further characterized by the reduction (see below) to their respective enones **19** and **15**. Bromo enone **18** and dibromo enone **14** both gave **15** upon reduction, while reduction of **17** gave enone **19**; ^{1}Hmr (200 MHz in methanol-d_4) δ: 1.23 (3H, s, C—CH_3), 1.24 (3H, s, C—CH_3), 3.88 (4H, m, —OCH_2CH_2O—), 5.36 (1H, m, C—H vinylic), 5.57 (1H, m, C—H vinylic), 6.02 (1H, d, C(16)—H), 7.61 (1H, d, C(17)—H). Finally, hydrolysis of the dioxalane protecting group gave the corresponding diene dione, mp 125—127°C, identical to the compound reported by us previously (6).

*Bromination of **13**. Dibromo enone **14***

To an ice-cold solution of triphenylphosphine (874 mg, 3.33 mmol) in freshly distilled (from Na) benzene (10 mL) in an atmosphere of argon was added, dropwise, a 1 *M* solution of Br_2 in benzene (3.30 mL, 3.30 mmol). To the resulting suspension was added triethylamine (0.460 mL, 3.30 mmol) and a suspension of diketone **13** (206 mg, 0.602 mmol) in benzene (10 mL). The mixture was refluxed under argon for 1 h, cooled, and filtered to remove excess triphenylphosphine dibromide. The filter cake was thoroughly washed with ether and the organic layer was washed with H_2O and brine, dried, and evaporated *in vacuo*. The crude product was chromatographed, eluting with hexanes – ethyl acetate (4:1), to yield the ring A deblocked derivative of **14** (4.5 mg) and dibromo enone **14** (225 mg, 78%) as colourless crystals, mp 164–166°C (ethyl acetate); uv λ_{max}: 257 nm (7915); ir ν_{max}: 2970, 1710, 1580, 1088; ^{1}Hmr (200 MHz) δ: 1.28 (3H, s, C—CH_3), 1.30 (3H, s, C—CH_3), 3.01 (2H, m, $W/2$ = 6 Hz, C—CH_2—), 3.94 (4H, m, —OCH_2CH_2O—), 5.34 (1H, m, C—H vinylic), 5.49 (1H, m, C—H vinylic); ms *m/e*: 482 (M^+), 484 (M^+ + 2), 486 (M^+ + 4). *Mol. Wt.* calcd. for $C_{21}H_{24}O_3Br_2$: 484.0071 (^{79}Br + ^{81}Br); found (high resolution ms): 484.0055.

The deblocked derivative of **14** was obtained as colourless crystals, mp 145–148°C (ethyl acetate); uv λ_{max}: 244 nm (22 980); ir ν_{max}: 2965, 1710, 1660, 1568; ^{1}Hmr (200 MHz) δ: 1.25 (3H, s, C—CH_3), 1.37 (3H, s, C—CH_3), 5.77 (2H, m, C(4)—H and C(11)—H); ms *m/e*: 438 (M^+), 440 (M^+ + 2), 442 (M^+ + 4). *Mol. Wt.* calcd. for $C_{19}H_{20}O_2Br_2$: 439.9809 (^{79}Br + ^{81}Br); found (high resolution ms): 439.9807.

*Reduction of dibromo enone **14**. Saturated ketone **20***

To the dibromo enone (49.0 mg, 0.101 mmol) in glacial acetic acid (10 mL) was added an excess of freshly acid washed (5% HCl) zinc dust and the mixture was stirred at 20°C, in an argon atmosphere, for 1 h. The mixture was filtered over Celite, diluted with ether, and washed with a saturated $NaHCO_3$ solution, until neutral, and with brine. The organic layer was dried and evaporated *in vacuo*. Crystallization from ether yielded the saturated ketone (31.0 mg, 93%) as colourless crystals, mp 181–182.5°C; ir ν_{max}: 2975, 1730, 1085; ^{1}Hmr (200 MHz) δ: 1.03 (3H, s, C—CH_3), 1.24 (3H, s, C—CH_3), 3.97 (4H, m, —OCH_2CH_2O—), 5.51 (2H, m, C(6)—H and C(11)—H); ms *m/e*: 328 (M^+). *Mol. Wt.* calcd. for $C_{21}H_{28}O_3$: 328.2038; found (high resolution ms): 328.2038.

*Reduction of dibromo enone **14**. Enone **15***

The dibromo enone (150 mg, 0.306 mmol) was refluxed in absolute methanol, under argon, for 16 h with a large excess of zinc–silver couple prepared from Zn dust (3.15 g) and silver acetate (100 mg) according to Heathcock's method (28). The cooled reaction mixture was filtered over Celite, evaporated *in vacuo*, and chromatographed, eluting with hexanes – ethyl acetate (5:1). Crystallization from ether yielded the enone (88.0 mg, 87%) as colourless crystals, mp 143–145°C; uv λ_{max}: 224 nm (8160); ir ν_{max}: 2965, 1695, 1082; ^{1}Hmr (200 MHz) δ: 1.13 (3H, s, C—CH_3), 1.15 (3H, s, C—CH_3), 2.84 (2H, m, $W/2$ = 6 Hz, C—CH_3), 3.91 (4H, m, —OCH_2CH_2O—), 5.55 (2H, m, C(6)—H and C(11)—H), 6.14 (1H, dd, J = 5.9 and 1.6 Hz, C(16)—H), 7.46 (1H, dd, J = 5.9 and 2.0 Hz, C(15)—H); ms *m/e*: 326 (M^+). *Mol. Wt.* calcd. for $C_{21}H_{26}O_3$: 326.1882; found (high resolution ms): 326.1878.

The structure of **15** was further confirmed by its conversion to the diacetal **21** by refluxing in toluene with a large excess of ethylene glycol and a catalytic amount of *p*-toluenesulfonic acid for 20 h. Crystallization from ethyl acetate gave diacetal **21**, mp 164–166°C; ^{1}Hmr (200 MHz) δ: 0.99 (3H, s, C—CH_3), 1.20 (3H, s, C—CH_3), 3.89 (4H, m, —OCH_2CH_2O—), 5.23 (1H, m, C(15)—H), 5.41 (1H, m, C—H vinylic), 5.49 (1H, m, C—H vinylic).

Mild acid hydrolysis (5% HCl/THF) of **15** yielded the dione **22** as colourless crystals, mp 137–138°C; uv λ_{max}: 232.5 nm (16 000); ir ν_{max}: 2960, 1702, 1665; ^{1}Hmr (200 MHz) δ: 1.08 (3H, s, C—CH_3), 1.28 (3H, s, C—CH_3), 5.62 (1H, m, C(11)—H), 5.68 (1H, s, C(4)—H), 6.19 (1H, dd, J = 5.9 and 1.6 Hz, C(16)—H), 7.42 (1H,

dd, J = 5.9 and 2 Hz, C(15)—H); ms m/e: 282 (M^+). *Mol. Wt.* calcd. for $C_{19}H_{22}O_2$: 282.1620; found (high resolution ms): 282.1626.

Acknowledgements

Financial support by the Natural Sciences and Engineering Research Council of Canada in the form of an operating grant, fellowships to R.A.D. and G.M.K., and a bursary to G.R.R. is gratefully acknowledged. The X-ray diffraction was performed by Dr. Peter S. White of this Department.

1. A. A. AKHREM and YU. A. TITOV. Total steroid synthesis. Am. ed. Plenum Press, New York, NY. 1970; K. NAKANISHI, T. GOTO, S. ITÔ, S. NATORI, and S. NOZOE (*Editors*). Natural product chemistry. Vol. 1. Academic Press, New York, NY. 1974; R. T. BLICKENSTAFF, A. C. GHOSH, and G. C. WOLF. Total synthesis of steroids. Academic Press, New York, NY. 1974; R. PAPPO. *In* The chemistry and biochemistry of steroids. Intra-Science Research Foundation, Santa Monica, CA. Research Reports Vol. 3, Nos. 1 and 2, 123 (1969); G. SAUCY and N. COHEN. MTP Int. Rev. Sci. Ser. One, **8**, 1 (1973); N. COHEN. Acc. Chem. Res. **9**, 412 (1976).
2. G. STORK and J. E. MCMURRY. J. Am. Chem. Soc. **89**, 5461 (1967); **89**, 5464 (1967); N. COHEN, B. L. BANNER, J. E. BLOUNT, M. TSAI, and G. SAUCY. J. Org. Chem. **38**, 3229 (1973); A. R. DANIEWSKI and M. KOCOR. J. Org. Chem. **40**, 3135 (1975); S. DANISHEFSKY and P. CAIN. J. Am. Chem. Soc. **98**, 4975 (1976); W. S. JOHNSON, S. ESCHER, and B. W. METCALF. J. Am. Chem. Soc. **98**, 1039 (1976); W. OPPOLZER, M. PETRZILKA, and K. BÄTTIG. Helv. Chim. Acta, **60**, 2964 (1977); R. L. FUNK and K. P. C. VOLLHARDT. J. Am. Chem. Soc. **99**, 5483 (1977); T. KAMETANI, H. NEMOTO, M. TSUBUKI, and M. NISHIUCHI. Tetrahedron Lett. 27 (1979); W. S. JOHNSON, L. R. HUGHES, and J. L. CARLSON. J. Am. Chem. Soc. **101**, 1281 (1979); A. R. DANIEWSKI, P. S. WHITE, and Z. VALENTA. Can. J. Chem. **57**, 1397 (1979); G. STORK and E. W. LOGUSH. J. Am. Chem. Soc. **102**, 1219 (1980); J. S. TEMPLE and J. SCHWARTZ. J. Am. Chem. Soc. **102**, 7381 (1980); J. TSUJI, Y. KOBAYASHI, and T. TAKAHASI. Tetrahedron Lett. 483 (1980); G. STORK, G. CLARK, and C. S. SHINER. J. Am. Chem. Soc. **103**, 4948 (1981); G. STORK and D. H. SHERMAN. J. Am. Chem. Soc. **104**, 3758 (1982); W. S. JOHNSON, D. BERNER, D. J. DUMAS, P. J. R. NEDERLOF, and J. WELCH. J. Am. Chem. Soc. **104**, 3508 (1982).
3. J. DAS, R. KUBELA, G. A. MACALPINE, Ž. STOJANAC, and Z. VALENTA. Can. J. Chem. **57**, 3308 (1979).
4. A. S. ONISHCHENKO. Diene synthesis. Translated by Israel Program for Scientific Translations, Jerusalem. Oldbourne Press, London. 1964, p. 423.
5. Ž. STOJANAC, R. A. DICKINSON, N. STOJANAC, R. J. WOZNOW, and Z. VALENTA. Can. J. Chem. **53**, 616 (1975).
6. M. KAKUSHIMA, J. DAS, G. R. REID, P. S. WHITE, and Z. VALENTA. Can. J. Chem. **57**, 3356 (1979).
7. N. L. WENDLER and H. L. SLATER. J. Org. Chem. **32**, 849 (1967).
8. E. BUCHTA and G. SATZINGER. Chem. Ber. **92**, 449 (1959); R. SCHEFFOLD and P. DUBS. Helv. Chim. Acta, **50**, 798 (1967).
9. W. Ger. Patent No. 2102623. Priority date Jan. 21, 1970; Z. G. HAJOS and D. R. PARRISH. J. Org. Chem. **39**, 1615 (1974); J. GUTZWILLER, P. BUCHSCHACHER, and A. FÜRST. Synthesis, 167 (1977).
10. W. Ger. Patent No. 2014757. Priority date March 20, 1970; U. EDER, G. SAUER, and R. WIECHERT. Angew. Chem. Int. Ed. Engl. **10**, 496 (1971).
11. (*a*) D. J. CRISPIN, A. E. VANSTONE, and J. S. WHITEHURST. J. Chem. Soc. C, 10 (1970); (*b*) Z. G. HAJOS and D. R. PARRISH. J. Org. Chem. **39**, 1612 (1974).
12. P. WIELAND and K. MIESCHER. Helv. Chim. Acta, **33**, 2215 (1950); S. RAMACHANDRAN and M. S. NEWMAN. *In* Organic synthesis. Vol. 41. *Edited by* J. D. Roberts. John Wiley and Sons, NY. 1961. p. 38; J. A. MARSHALL, D. E. SEITZ, W. R. SNYDER, and B. GOLDBERG. Synth. Commun. **4**, 79 (1974).
13. M. S. NEWMAN, S. RAMACHANDRAN, S. K. SANKARAPPA, and S. SWAMINATHAN. J. Org. Chem. **26**, 727 (1961).
14. I. N. NAZAROV and I. A. GURVICH. Zh. Obshch. Khim. **25**, 956 (1955).
15. S. SWAMINATHAN, J. P. JOHN, and S. RAMACHANDRAN. Tetrahedron Lett. 729 (1962); L. F. FIESER and M. FIESER. Reagents for organic synthesis. Vol. 1. John Wiley and Sons, NY. 1971, p. 566.
16. M. R. BELL, J. L. HERRMANN, JR., and V. AKULLIAN. U.S. Patent No. 4157349. June 5, 1979; J. RUPPERT, U. EDER, and R. WIECHERT. Chem. Ber. **106**, 3636 (1973).
17. M. KAKUSHIMA, L. ALLAIN, R. A. DICKINSON, P. S. WHITE, and Z. VALENTA. Can. J. Chem. **57**, 3354 (1979).
18. H. ULRICH and A. A. R. SAYIGH. Angew. Chem. Int. Ed. Engl. **5**, 704 (1966); L. C. ROACH and W. H. DALY. Chem. Commun. 606 (1970).
19. M. KAKUSHIMA, J. ESPINOSA, and Z. VALENTA. Can. J. Chem. **54**, 3304 (1976).
20. F. FRINGUELLI, F. PIZZO; A. TATICCHI, T. D. J. HALLS, and E. WENKERT. J. Org. Chem. **47**, 5056 (1982); J. DAS, M. KAKUSHIMA, Z. VALENTA, K. JANKOWSKI, and R. LUCE. Can. J. Chem. **62**, 411 (1984).
21. D. LIOTTA, M. SAINDANE, and C. BARNUM. J. Am. Chem. Soc. **103**, 3224 (1981).
22. S. DANISHEFSKY, M. P. PRISBYLLA, and S. HINER. J. Am. Chem. Soc. **100**, 2918 (1978).
23. M. KAKUSHIMA and D. G. SCOTT. Can. J. Chem. **57**, 1399 (1979).
24. J. E. BALDWIN. Chem. Commun. 734 (1976).
25. M. MIYASHITA, A. YOSHIKOSHI, and P. A. GRIECO. J. Org. Chem. **42**, 3772 (1977); R. STERZYCKI. Synthesis, 724 (1979).
26. U. WANNAGAT and H. NIEDERPRÜM. Chem. Ber. **94**, 1540 (1961); E. H. AMONOV-NEIZER, R. A. SHAW, D. L. SKOOLIN, and B. C. SMITH. J. Chem. Soc. 2997 (1965); S. C. WELCH, S. CHAYABUNJONGLERD, and A. S. C. RAO. J. Org. Chem. **45**, 4086 (1980).
27. E. PIERS and I. NAGAKURA. Synth. Commun. **5**, 193 (1975).
28. R. D. CLARK and C. H. HEATHCOCK. J. Org. Chem. **41**, 636 (1976).
29. CH. R. ENGEL and G. BACH. Steroids, **3**, 593 (1964); F. SONDHEIMER and R. L. WIFE. Tetrahedron Lett. 765 (1973); Y. KAMONO and G. R. PETTIT. J. Org. Chem. **38**, 2202 (1973); T. Y. R. TSAI, A. MINTA, and K. WIESNER. Heterocycles, **12**, 1397 (1979).
30. J. FRIED and E. F. SABO. J. Am. Chem. Soc. **75**, 2273 (1953); L. B. BARKLEY, M. W. TARRAR, W. S. KNOWLES, and H. RAFFELSON. J. Am. Chem. Soc. **76**, 5017 (1954); R. H. LENHARD and S. BERNSTEIN. J. Am. Chem. Soc. **77**, 6665 (1955); I. G. GUEST and B. A. MARPLES. J. Chem. Soc. C, 1468 (1971).
31. P. SPEISER and T. REICHSTEIN. Helv. Chim. Acta, **30**, 2143 (1947).
32. W. C. STILL, M. KAHN, and A. MITRA. J. Org. Chem. **43**, 2923 (1978).

Can. J. Chem. Downloaded from www.nrcresearchpress.com by 210.87.254.6 on 09/06/12
For personal use only.

Etude de la dissolution du bromure cuivreux formé sur le cuivre

ROBERT-LOUIS BROSSARD

Institut de recherche d'Hydro-Québec, C.P. 1000, 1800 Montée Ste-Julie, Varennes (Qué.), Canada J0L 2P0

Reçu le 19 octobre 1983

ROBERT-LOUIS BROSSARD. Can. J. Chem. **62**, 1112 (1984).

La dissolution du bromure cuivreux, formé par oxydation électrochimique du cuivre immergé en solution aqueuse de NaBr, a été étudiée. La concentration en NaBr a été variée de 0,1 *M* à 1,2 *M* alors que le pH était de 4. Le produit de corrosion accumulé sur l'électrode est constitué de cristaux de CuBr γ. La présence de ce composé contribue à l'enrichissement local de la solution en cuivre dissous près de l'électrode. Cet enrichissement se traduit par une tension d'électrode en circuit ouvert bien caractéristique. Elle est égale à environ −149 mV (ECS) sur une électrode en position stationnaire immergée dans une solution 0,2 *M* NaBr. La dissolution complète du CuBr coincide, pour sa part, à une chute rapide de la tension. Cette chute de tension a permis de définir le temps de transition τ à partir duquel la vitesse de dissolution du CuBr a été calculée. Par exemple, la vitesse de dissolution est de 0,074 ± 0,003 mA cm^{-2} en courant équivalent pour une électrode en position stationnaire en présence d'une solution 0,2 *M* NaBr non agitée. Elle est aussi constante jusqu'à la disparition complète du composé. Par ailleurs, l'utilisation de l'électrode à disque tournant a mis en évidence que la dissolution est entièrement dominée par la diffusion des ions en phase liquide. Les résultats expérimentaux sont compatibles avec la présence simultanée du $CuBr_2^-$ et du $CuBr_3^{2-}$ comme espèces diffusantes. Enfin, les courbes de polarisation potentiodynamiques montrent deux vagues d'oxydation. Une portion non négligeable du courant de dissolution, sinon la quasi-totalité, se traduit par la formation de CuBr sur l'électrode qui est le seul produit de corrosion présent.

ROBERT-LOUIS BROSSARD. Can. J. Chem. **62**, 1112 (1984).

The dissolution of cuprous bromide, formed by the electrochemical oxidation of copper immersed in aqueous NaBr, has been studied. NaBr concentration was varied between 0.1 and 1.2 *M* at pH 4. The corrosion product accumulating on the electrode is crystalline γ-CuBr. The presence of this material contributes to the local enrichment of dissolved copper close to the electrode. This enrichment leads to a characteristic electrode voltage in open circuit, which is about −149 mV (ECS) at a stationary electrode immersed in a solution of 0.2 *M* NaBr. The complete dissolution of CuBr coincides with a rapid fall in voltage which permits the definition of the transition time τ from which the speed of CuBr dissolution has been calculated. For example, the speed of dissolution is 0.074 ± 0.003 mA cm^{-2} in a current equivalent for a stationary electrode in the presence of a non-stirred solution of 0.2 *M* NaBr. This is constant until the complete disappearance of the CuBr. On the other hand, use of a rotating disc electrode demonstrates that the dissolution is entirely dominated by the diffusion of ions in the liquid phase. The experimental results are compatible with the simultaneous presence of $CuBr_2^-$ and $CuBr_3^{2-}$ as diffusing species. Finally, the potentiodynamic polarization curves show two oxidation waves. A non-negligible portion of the dissolution current, if not almost all, is associated with the formation of CuBr as the sole corrosion product on the electrode.

[Journal translation]

Can. J. Chem. Downloaded from www.nrcresearchpress.com by 210.87.254.42 on 09/06/12
For personal use only.

Introduction

La formation de bromure cuivreux sur le cuivre à l'abandon dans des solutions bromurées non désaérées a été observée (1 à 3). Dans les solutions désaérées de NaBr légèrement acides, le recouvrement de la surface par le CuBr γ coïncide avec la première vague d'oxydation observée sur les courbes *E* vs. *i* obtenues par balayage de la tension en mode linéaire (4). Cependant, la solubilité relative de ce composé dans les solutions qui contiennent des ions Br^- (5) contribue à le rendre plus ou moins stable en présence de ces solutions.

Le présent travail se propose d'approfondir l'étude de la dissolution du bromure cuivreux fraîchement formé durant l'oxydation du cuivre polarisé anodiquement. Les solutions contiennent entre 0,1 *M* et 1,2 *M* de NaBr.

Partie expérimentale

2.1 *La cellule et ses accessoires*

Les détails relatifs à la cellule et ses accessoires ainsi qu'aux électrodes de travail sont données dans un article précédent (6). L'électrode de cuivre se présentait sous la forme d'un fil de 0,064 cm de diamètre dont la surface était de ~0,4 cm^2, d'une plaque de 4 cm^2 ou d'un disque de 0,71 cm^2. Le fil et la plaque étaient en position verticale et immobile. Pour sa part, le disque était animé d'un mouvement de rotation et était en position horizontale.

2.2 *La préparation des essais*

Un barbottage d'azote de 6 h précédait l'immersion de l'électrode de cuivre dans la solution même si 0,5 h était suffisant. Les solutions contenaient entre 0,1 et 1,2 *M* de NaBr dissout. Un tampon à base de phtalate de potassium a été utilisé pour stabiliser le pH à 4.

La méthode employée par Shoesmith et Lee *et al.* (7, 8) a été retenue pour le polissage du cuivre; l'échantillon était poli mécaniquement par abrasion avec du papier au carbure de silicium pour se terminer par un polissage avec de l'alumine de 1 μm. L'échantillon était alors rinçé à l'alcool, à l'acétone puis à l'eau distillée avant son immersion.

2.3 *Les techniques expérimentales utilisées*

Les courbes tension–courant ont été obtenues en balayage linéaire de la tension. La vitesse de balayage généralement utilisé était de 12 mV s^{-1}. Un coulomètre servait à mesurer la quantité d'électricité qui traversait l'électrode durant l'oxydation et la réduction.

Par ailleurs, l'oxydation et la réduction ont été effectuées en l'absence de toute agitation sur une électrode de travail en position stationnaire. Le cas échéant, l'agitation était imposée par barbotage d'un gaz inerte ou par rotation de l'électrode durant les périodes en circuit ouvert seulement.

Enfin, l'approche expérimentale mise au point pour la mesure de la vitesse de dissolution du bromure cuivreux est décrite plus loin alors que les valeurs de la tension d'électrode sont données par rapport à l'électrode au calomel saturé, sauf indication contraire.

Résultats expérimentaux

3.1 *Apparition du bromure cuivreux*

Les enregistrements *E* vs. *i* reproduits à la figure 1 sont bien représentatifs du comportement de l'électrode de cuivre. La vitesse de balayage de la tension est de 12 mV s^{-1} alors que la solution non agitée contient 0,2 *M* de NaBr. Deux vagues d'oxydation et une vague de réduction bien définies sont obser-

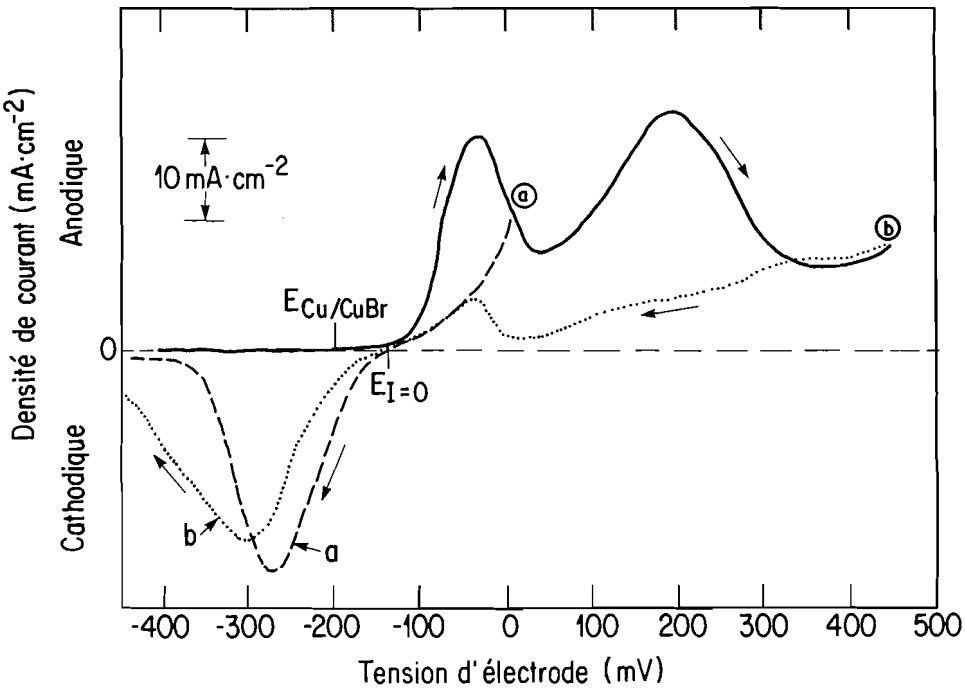

FIG. 1. Courbes de polarisation sur un fil de cuivre dans une solution 0,2 *M* NaBr. La solution est non agitée alors que dE/dt est égal à 12 mV s^{-1}. $E_{Cu/CuBr}$: tension réversible de la réaction Cu + Br^- = CuBr + é. $E_{I=0}$: tension à courant nul.

vées. Le sommet de la première vague d'oxydation a comme coordonnées −35 mV (E_{p1}) et 26 mA cm^{-2} (i_{p1}) alors que le sommet de la seconde coïncide avec +195 mV (E_{p2}) et 30 mA cm^{-2} (i_{p2}). Ainsi, les vagues d'oxydation sont anodiques par rapport à la tension réversible ($E_{Cu/CuBr}$) de la réaction:

[1] $Cu + Br^- = CuBr + e$

qui est donnée par (9, 10)

[2] $E_{Cu/CuBr} = -0{,}239 - 0{,}059 \log_{10} Br^-$

où $E_{Cu/CuBr}$ est en volt par rapport à l'électrode au calomel saturé.

Le CuBr γ fait son apparition sur la surface de l'électrode dans la région de la première vague d'oxydation (4).

Par ailleurs, le courant est légèrement plus élevé lors du balayage de retour entre ~340 mV et 450 mV. Ce comportement est attribué soit à l'oxydation partielle du bromure cuivreux, soit à sa redissolution partielle, soit à des variations dans sa morphologie ou les trois à la fois.

La vague cathodique, pour sa part, a un sommet qui est de 70 mV inférieur à la tension réversible $E_{Cu/CuBr}$. Dans l'exemple illustré à la figure 1, pour lequel la tension limite (E_L) est de 0 mV, les quantités d'électricité mises en jeu sont de 230 mC cm^{-2} du côté anodique (Q_{oxy}) et de 230 mC cm^{-2} du côté cathodique (Q_{red}). Il est alors raisonnable de penser que le CuBr, formé par oxydation anodique du cuivre, est complètement réduit. La réduction quasi complète de ce composé est confirmée par l'examen de la surface de l'électrode retirée après le retour du courant de réduction à une valeur négligeable.

Enfin, la vague de réduction devient visible sur les courbes *E* vs. *i* dès que E_L franchit le pied de la première vague d'oxydation (Fig. 2). Pour des valeurs croissantes de E_L, le profil de la vague de réduction demeure inchangé alors que Q_{red} tend à augmenter. On en déduit qu'il y a augmentation de la quantité de CuBr accumulé sur l'électode pour des valeurs croissantes de E_L.

3.2 *Passivation transitoire du cuivre*

Dans l'éventualité où le bromure cuivreux formé se dissout, dès le retour en circuit ouvert, il est envisageable qu'il y ait enrichissement local de la solution en cuivre dissous. Il est alors prévisible que la tension du cuivre traduise cet enrichissement local, si celui-ci est significatif.

La tension en circuit ouvert (E_{co}) du cuivre, en l'absence de précipité à sa surface, est représentée en fonction de la concentration en cuivre dissous à la fig. 3 alors que E_{co} du cuivre, en présence de précipité à sa surface, est donnée en fonction du temps à la fig. 4. E_{co} du cuivre en présence de précipité montre deux plateaux. Le premier plateau correspond à une tension voisine de −149 mV et est de 19 mV inférieur à la tension à courant nul ($E_{I=0}$) trouvée sur les courbes *E* vs. *i* (Fig. 2). La tension du premier plateau, −149 mV, coïncide avec une concentration en cuivre dissous de $0{,}53 \times 10^{-3}$ *M* d'après la figure 3 alors que la saturation en cuivre dissous est de $1{,}4 \times 10^{-3}$ *M*. Il est ainsi raisonnable de considérer qu'il y a enrichissement de la solution en cuivre dissous près de l'électrode lorsque celle-ci est recouverte de précipité.

Près du temps de transition τ, une chute rapide de la tension est observée et un deuxième plateau, compris entre −232 mV et −236 mV, est atteint. La tension du deuxième plateau dépend de la concentration en cuivre dissous au coeur de la solution. Quant au temps de transition τ, il est défini en suivant la même procédure que Shoesmith et Lee (8) pour l'étude de films d'oxydes du cuivre métastables.

L'examen de la surface au microscope à balayage a mis en évidence la disparition graduelle du produit de corrosion entre $t = 0$ et $t = \tau$ (Fig. 5a, 5b, 5c) alors que sa présence est marginale à partir de τ (Fig. 5d, 5e).

La dissolution du précipité doit aussi se traduire par un enrichissement de la solution en cuivre dissous jusqu'au temps de transition τ. La détermination de la concentration en cuivre

Can. J. Chem. Downloaded from www.nrcresearchpress.com by 210.87.254.42 on 09/06/12
For personal use only.

Can. J. Chem. Downloaded from www.nrcresearchpress.com by 210.87.254.42 on 09/06/12
For personal use only.

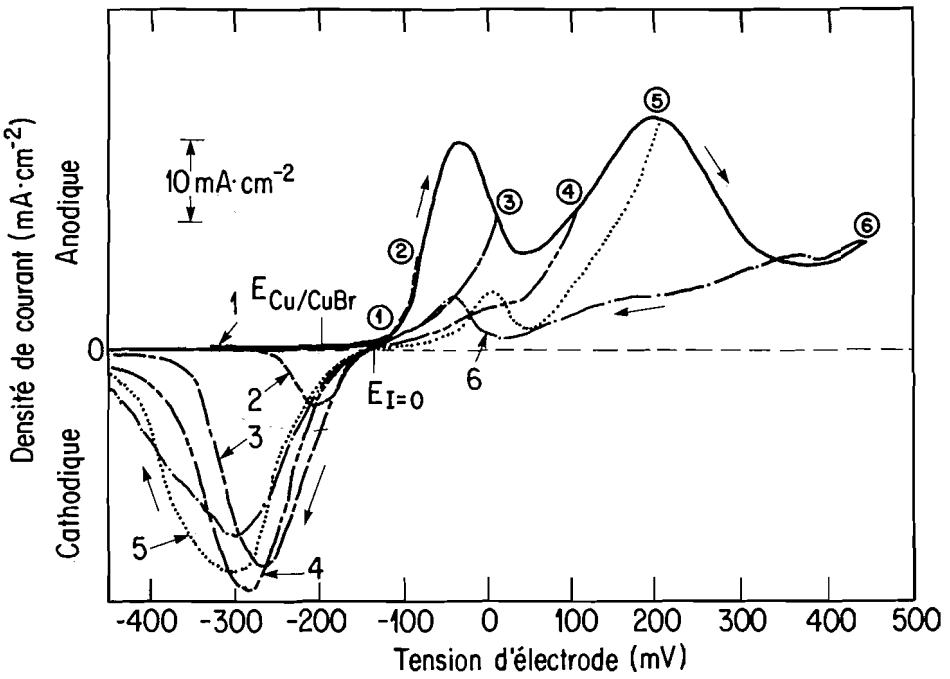

FIG. 2. Influence de la tension limite sur la vague de réduction. La solution est non agitée alors que l'électrode est un fil de cuivre. NaBr = 0,2 *M*, dE/dt = 12 mV s^{-1}.

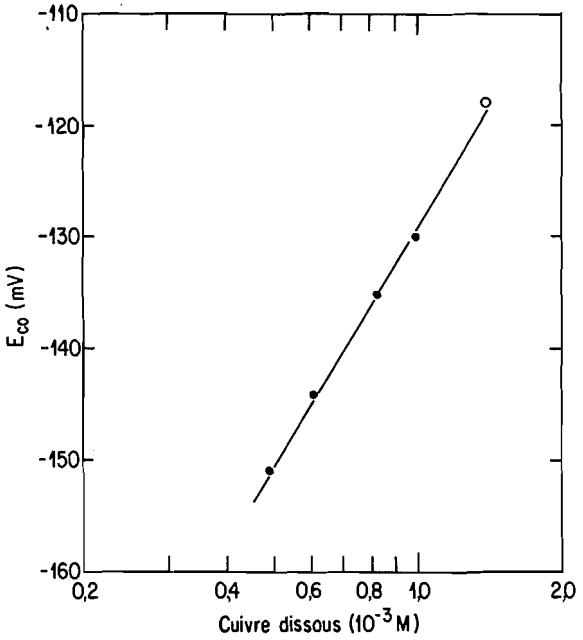

FIG. 3. Tension du cuivre en circuit ouvert en l'absence de précipité en fonction de la concentration en cuivre dissous. La solution est désaérée et non agitée alors que l'électrode est un fil de cuivre. NaBr = 0,2 *M*. E_{co}: tension de l'électrode en circuit ouvert. ○: correspond à la saturation en CuBr.

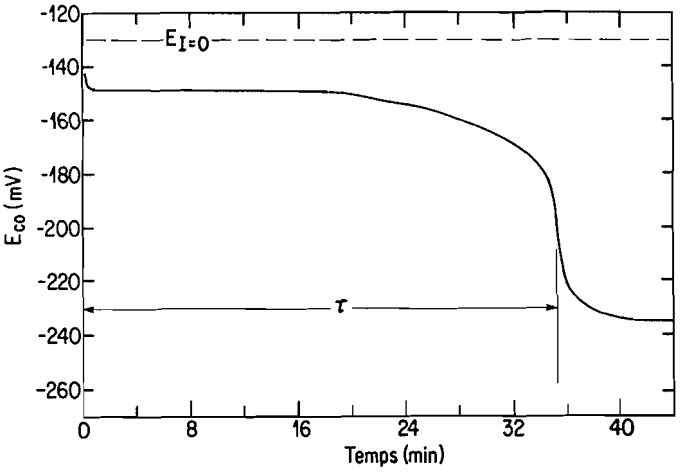

FIG. 4. Tension de l'électrode en circuit ouvert après la formation de CuBr. E_{co}: tension d'électrode en circuit ouvert. NaBr: 0,2 *M* solution non agitée. $E_{I=0}$: tension à courant nul obtenue sur les enregistrements potentiodynamiques (Fig. 2). Le fil de cuivre a été polarisé à la vitesse de 12 mV s^{-1}, depuis −450 mV jusqu'à 0 mV, pour être laissé à l'abandon dès 0 mV atteint.

a été obtenue à l'aide de la spectroscopie par absorption atomique entre $t = 0$ et $t = \tau$. Ce qui a permis de confirmer l'enrichissement de la solution en cuivre dissous entre $t = 0$ et $t = \tau$.

3.3 *Mesure de la quantité de bromure cuivreux présent sur le cuivre*

La surface de cuivre, complètement à nue au départ, subissait une oxydation électrochimique par enclenchement d'une tension de −300 mV suivi d'un balayage linéaire de la tension. La vitesse de balayage était de 12 mV s^{-1} alors que l'oxydation était arrêtée à 0 mV. Immédiatement après l'arrêt de l'oxydation, une tension de réduction constante et égale à −300 mV était imposée à l'électrode. Les charges électriques mises en jeu durant l'oxydation (Q_{oxy}) et la réduction (Q_{red})$_{t=0}$ étaient mesurées. Plus précisément, (Q_{red})$_{t=0}$ représente la quantité d'électricité obtenue par réduction complète du CuBr immédiatement après formation de ce composé.

La réduction du bromure cuivreux, réalisée dans ces conditions, est complétée après une demi-minute environ; le courant de réduction devient alors négligeable. La réduction complète de ce composé a été confirmée à partir de l'examen de la

Can. J. Chem. Downloaded from www.nrcresearchpress.com by 210.87.254.42 on 09/06/12
For personal use only.

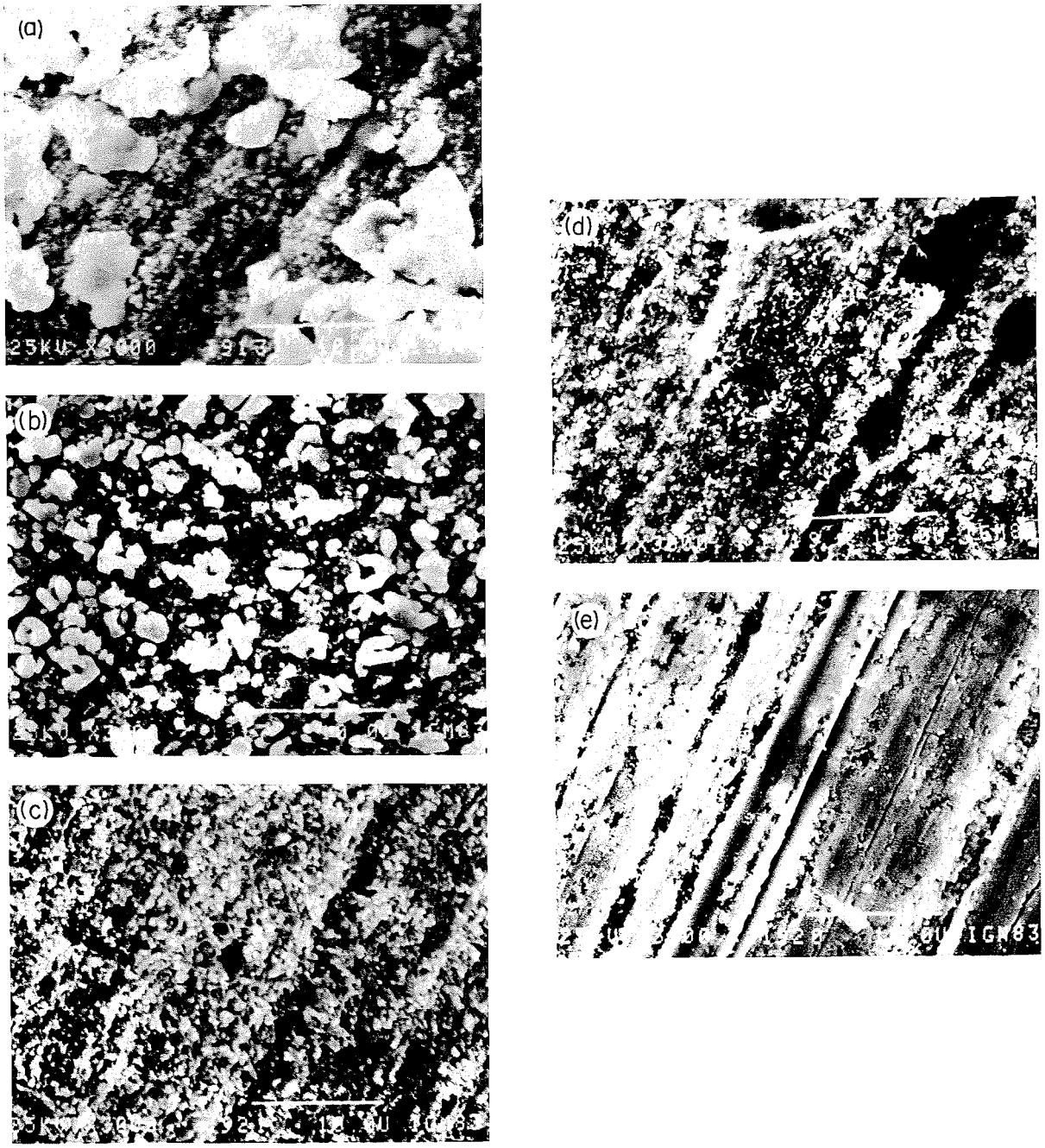

FIG. 5. Aspect de la surface de l'électrode durant la dissolution du CuBr. Les conditions d'oxydation sont celles de la fig. 4. NaBr = 0,2 *M*, solution non agitée. L'électrode est un fil de cuivre. Les durées en circuit ouvert sont: (a) 0,5 τ; (b) 0,88 τ; (c) 0,98 τ; (d) 1,01 τ; (e) 1,06 τ.

surface au microscope et de la mesure de la tension en circuit ouvert. Le comportement du bromure cuivreux soumis à une réduction rappelle celui du $Cu(OH)_2$ en solution alcaline (8).

Par ailleurs, la charge de réduction $(Q_{red})_{t=0}$ dépend de la charge en oxydation (Q_{oxy}) alors que le rapport $(Q_{red})_{t=0}/Q_{oxy}$ est constant lorsque les conditions d'oxydation sont identiques et ce, malgré les variations importantes de Q_{oxy} (Fig. 6) qui ont été observées. Dans l'exemple choisi ici, les charges Q_{oxy} et $(Q_{red})_{t=0}$ ont été mesurées pour plusieurs cycles successifs oxydation–réduction dans une solution non agitée de 0,2 *M* NaBr. Le rapport $(Q_{red})_{t=0}/Q_{oxy}$ demeure voisin de 0,98 alors que Q_{oxy} est compris entre 75,2 mC cm^{-2} et 137,8 mC cm^{-2}. Ce rapport tend à diminuer lorsque l'électrode est en position horizontale. La perte, qui correspond à la différence entre Q_{oxy} et $(Q_{red})_{t=0}$ est attribuée à la non précipitation du cuivre qui va en solution, à la dissolution partielle du précipité et, enfin, au fait que des cristaux de bromure cuivreux sont capables de n'être pas retenus à la surface de l'électrode.

La constance du rapport $(Q_{red})_{t=0}/Q_{oxy}$ permet de déduire la quantité de précipité présent en terme de charge $(Q_{red})_{t=0}$ à partir de la valeur de Q_{oxy}. Le rapport $(Q_{red})_{t=0}/Q_{oxy}$ varie un peu d'un échantillon à l'autre même si les conditions expérimentales sont les mêmes. Par conséquent, ce rapport a été déterminé pour chaque échantillon et la quantité de précipité présent sur le cuivre, dès le retour de l'électrode en circuit ouvert, a été calculée à partir de Q_{oxy}.

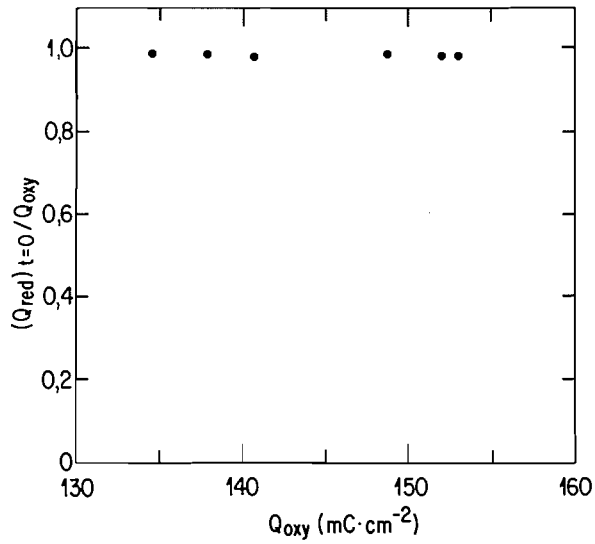

FIG. 6. Rapport $(Q_{red})_{t=0}/Q_{oxy}$ en fonction de Q_{oxy}. Q_{oxy}: quantité d'électricité mesurée durant l'oxydation. $(Q_{red})_{t=0}$: quantité d'électricité mesurée par réduction complète du CuBr immédiatement après oxydation. Condition d'oxydation: balayage en tension de −300 mV à 0 mV avec 12 mV s^{-1}. Condition de réduction: −300 mV durant 2 min. Solution 0,2 *M* NaBr, non agitée. L'électrode est un fil de cuivre.

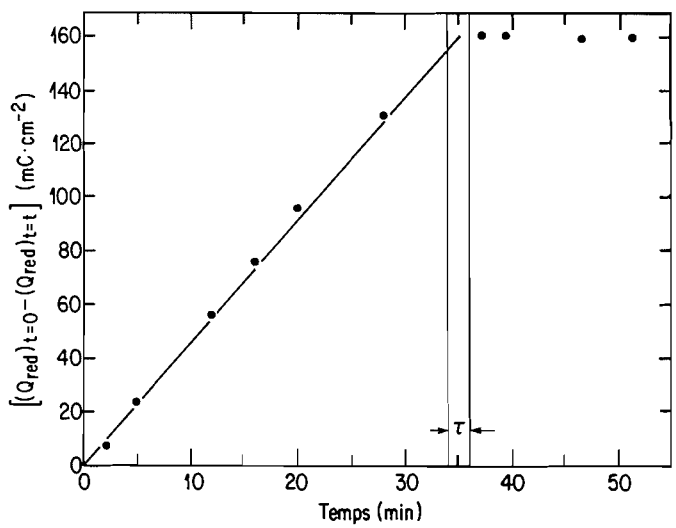

FIG. 7. Quantité de précipité qui passe en solution durant la période en circuit ouvert. $(Q_{red})_{t=t}$: quantité d'électricité obtenue par réduction du précipité après le temps *t*. $(Q_{red})_{t=0} - (Q_{red})_{t=t}$: quantité d'électricité équivalente en précipité qui va en solution durant le temps *t*. Les autres conditions expérimentales sont celles de la fig. 6.

3.4 *Vitesse de dissolution du bromure cuivreux sur une électrode immobile*

On a vue, d'une part, que la quantité de bromure cuivreux présent à la surface de l'échantillon est déterminable et que, d'autre part, la dissolution du CuBr en circuit ouvert s'achève complètement au temps de transition τ. De plus, il y a enrichissement de la solution en cuivre entre $t = 0$ et $t = \tau$.

La réduction du précipité après des durées variables de séjour en circuit ouvert (Fig. 7) a mis en évidence que la vitesse de dissolution (v) du CuBr est constante. La différence entre $(Q_{red})_{t=0}$ et $(Q_{red})_{t=t}$ est associée à la perte de bromure cuivreux durant le temps *t* où l'électrode est en circuit ouvert alors que

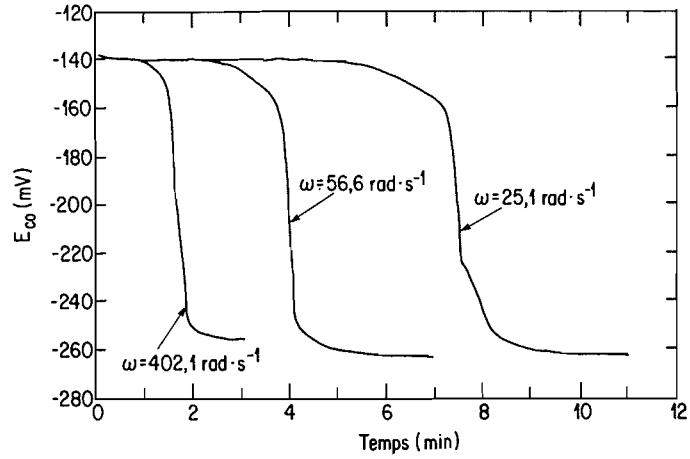

FIG. 8. Influence de la vitesse de rotation de l'électrode sur la tension en circuit ouvert. ω: vitesse de rotation. NaBr = 0,2 *M*. L'électrode est un disque qui tourne. Conditions d'oxydation: Balayage en tension de −300 mV à 0 mV avec 12 mV s^{-1}.

v est calculable à partir de la pente de la droite obtenue.

Pour une solution 0,2 *M* NaBr non agitée, *v* est de 0,077 mA cm^{-2}. De plus, l'ordonnée à l'origine de la relation $[(Q_{red})_{t=0} - (Q_{red})_{t=t}]$ en fonction du temps passe par zéro alors que la perte en CuBr cesse au temps τ où la dissolution de ce composé est complète.

La constance de *v* entre $t = 0$ et $t = \tau$ autorise donc le calcul de *v* à partir du rapport $(Q_{red})_{t=0}/\tau$. Cette approche a donné *v* égal à 0,071 mA cm^{-2} en courant équivalent pour 0,2 *M* NaBr (Fig. 4).

Enfin, la vitesse de dissolution est intimement liée à l'agitation de la solution réalisée à l'aide d'un barbottage d'un gaz inerte, par exemple. L'utilisation d'une électrode à disque tournant en cuivre a permis de fixer les conditions d'agitation et d'établir que la vitesse de dissolution est contrôlée par la diffusion en phase liquide.

3.5 *Vitesse de dissolution du CuBr sur une électrode tournante*

Les enregistrements de la tension en circuit ouvert en fonction du temps, reproduits à la figure 8, confirment que la vitesse de dissolution est étroitement liée à l'intensité de l'agitation. La valeur de *v*, calculée à partir de la variation transitoire de la tension en circuit ouvert, est donnée en fonction de la racine carrée de la vitesse de rotation de l'électrode (Fig. 9) pour ω compris entre 25 et 509 rad s^{-1} alors que la solution contient 0,2 *M* en NaBr dissous.

La linéarité de la relation *v* vs. $\omega^{1/2}$ avec une ordonnée à l'origine qui passe par zéro est la signature d'un processus de dissolution entièrement contrôlé par la diffusion dans la phase liquide (11).

Dans le cas de la figure 9, l'équation est:

[3] $\quad v = 0{,}074\ \omega^{1/2}$

où *v* est exprimé en mC cm^{-2} s^{-1} et ω en rad s^{-1}. La pente, 0,074, est en mC cm^{-2} s$^{-1/2}$.

3.6 *Influence de la concentration en ions bromures*

Pour une électrode immobile, on observe que l'allure des courbes E_{co} vs. temps est inchangée entre 0,08 *M* et 0,8 *M* en NaBr dissous (Fig. 10). Cependant, E_{co} se déplace vers des valeurs plus positives alors que le temps de transition augmente considérablement lorsque la concentration va de 0,8 *M* à 0,08 *M* en NaBr dissous.

Can. J. Chem. Downloaded from www.nrcresearchpress.com by 210.87.254.42 on 09/06/12
For personal use only.

Can. J. Chem. Downloaded from www.nrcresearchpress.com by 210.87.254.42 on 09/06/12
For personal use only.

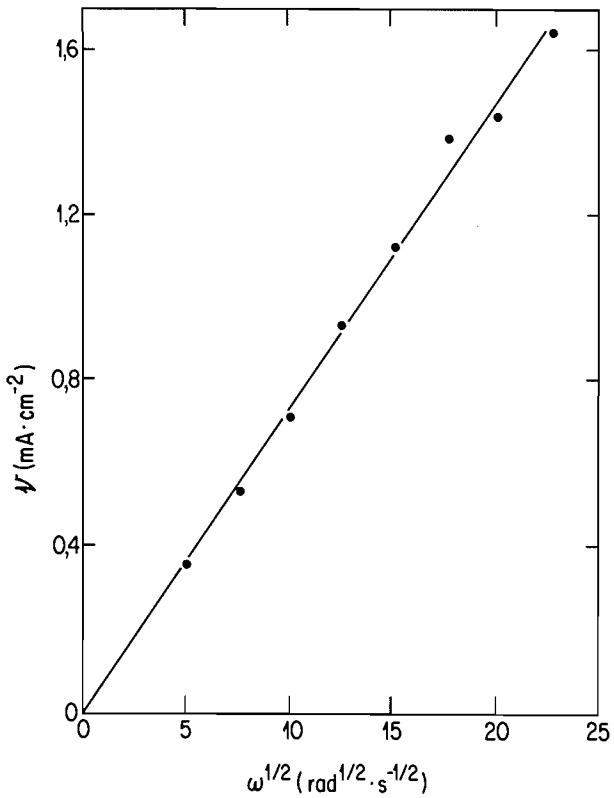

FIG. 9. Vitesse de dissolution en fonction de $\omega^{1/2}$ dans une solution 0,2 *M* NaBr. ν: vitesse de dissolution du CuBr en densité de courant équivalent. Les valeurs de ν sont déduites des courbes de la fig. 8 obtenues sur une électrode qui tourne.

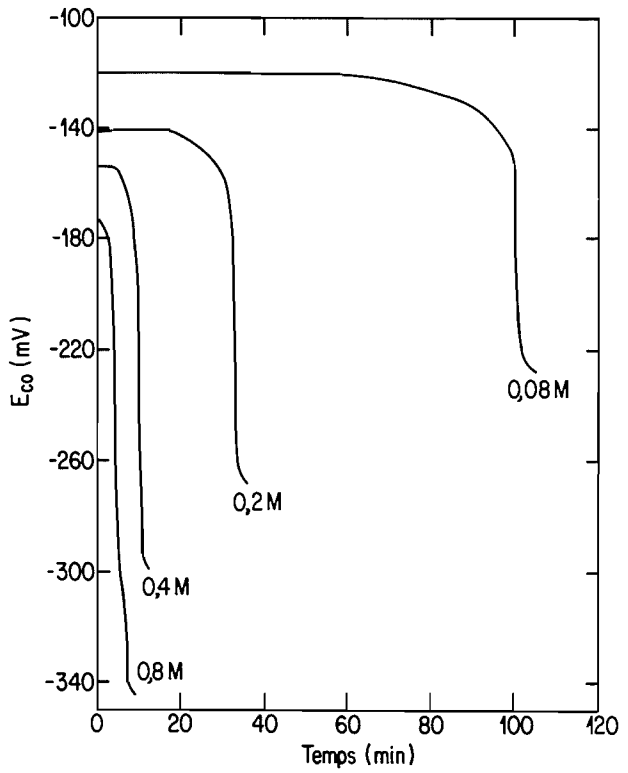

FIG. 10. Influence de la concentration en ions Br^- sur la tension en circuit ouvert. L'électrode est un fil de cuivre immobile et la solution est non agitée. Les échantillons ont été oxydés de telle sorte que $(Q_{red})_{t=0}$ soit de 130 ± 6 mC cm^{-2}.

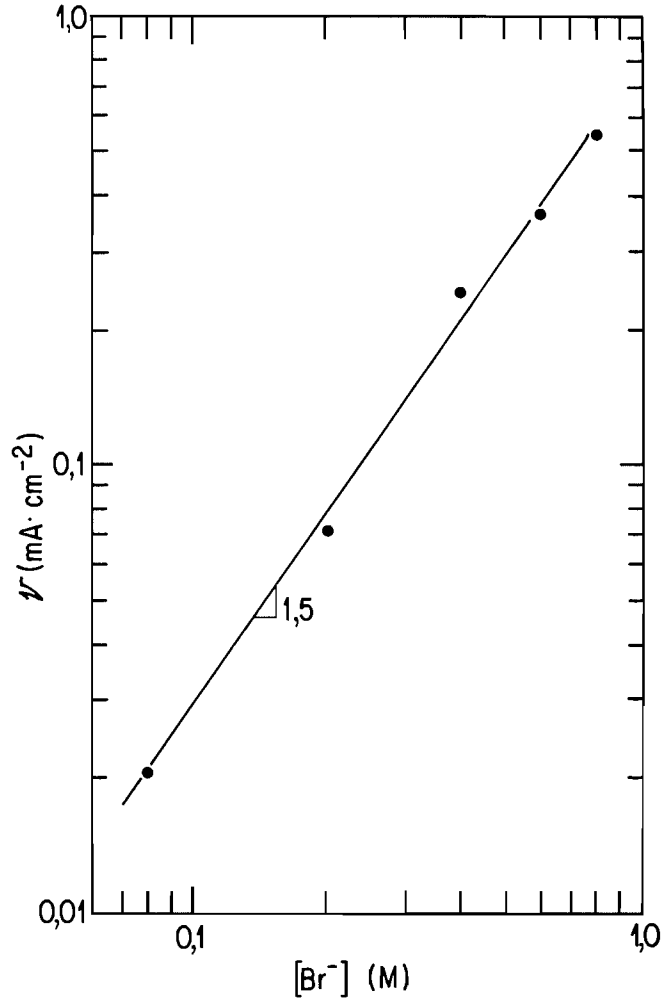

FIG. 11. Influence de la concentration en ions bromures sur la vitesse de dissolution du CuBr. Les valeurs de ν sont déduites des courbes E_{co} vs. temps de la fig. 10.

La valeur de ν, déterminée à partir des relations E_{co} vs. temps montrées à la figure 10, est donnée en fonction de la concentration en ions Br^- à la fig. 11. Ainsi, l'ordre de la réaction par rapport aux ions Br^- est de 1,5.

3.7 *Quantité de bromure cuivreux accumulée durant l'oxydation anodique du cuivre*

Rappelons que Q_{red}, qui correspond à la vague de réduction sur les courbes E vs. i (Fig. 2), tend à augmenter pour des valeurs croissantes de E_L. Pour leurs parts, les enregistrements E_{co} vs. temps, obtenus après oxydation électrochimique dans une solution 0,2 *M* NaBr sont reproduits à la figure 12 pour différentes valeurs de E_L. L'oxydation électrochimique a été réalisée dans les conditions expérimentales données à la fig. 2.

Les relations E_{co} vs. temps sont caractéristiques de la dissolution du bromure cuivreux dès que E_L est égal ou supérieur à −80 mV, environ. Par ailleurs, une augmentation considérable du temps de transition est observée avec un accroissement de E_L entre −80 mV et +450 mV. Les valeurs de τ sont données en fonction de E_L à la fig. 13 alors que les tensions E_{p1} et E_{p2} sont aussi indiquées. La quantité de CuBr a été déterminée en charge équivalente (Q_{CuBr}) à partir du produit de la vitesse de dissolution, qui est voisine de 0,071 mA cm^{-2} (Fig. 2), par le temps de transition.

La relation Q_{CuBr} vs. tension indique que l'accumulation du

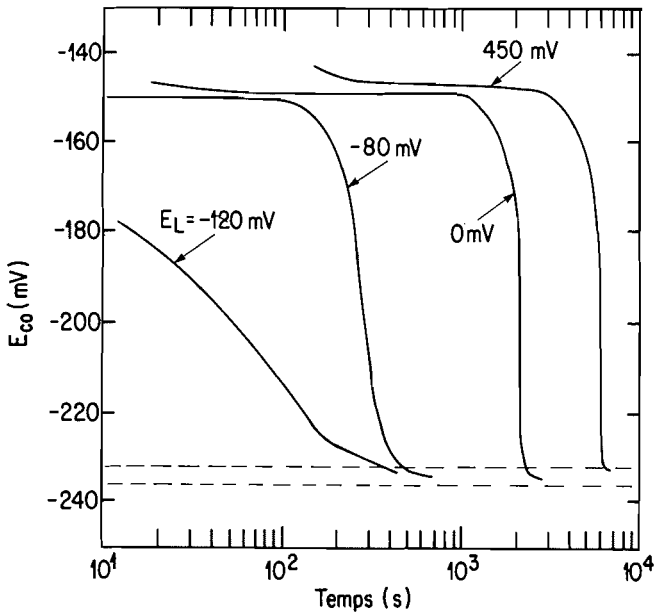

FIG. 12. Courbes E_{co} vs. temps pour différentes valeurs de la tension limite. Conditions de polarisation: Balayage en tension de −450 mV à la tension voulue (tension limite) à la vitesse de 12 mV s^{-1}. Solution: 0,2 *M* NaBr, non agitée. L'électrode est un fil de cuivre immobile.

produit de corrosion commence dans la partie ascendante de la première vague d'oxydation pour se poursuivre avec une tension croissante. Ainsi, Q_{CuBr} est de 95 mC cm^{-2} à E_{p1} comparée à 350 mC cm^{-2} à E_{p2} lorsque dE/dt est égal à 12 mV s^{-1} pour une solution 0,2 *M* NaBr.

Discussion

4.1 *Dissolution du bromure cuivreux*

La relation v vs. $\omega^{1/2}$ (Fig. 9) suggère que la diffusion d'une espèce ionique en solution est l'étape lente de la dissolution du bromure cuivreux (11). Par ailleurs, la formation d'intermédiaires comme le $CuBr_2^-$ (4) et le $CuBr_3^{2-}$ (5) est envisageable dans la gamme de concentration considérée dans le présent travail. Dans ce cas, les étapes les plus probables sont

[4] $\quad CuBr + XBr^- = (CuBr_{1+x}^{x-})_i$ étape rapide

qui est suivie de

[5] $\quad (CuBr_{1+x}^{x-})_i \rightarrow (CuBr_{1+x}^{x-})_s$ étape lente

les indices i et s indiquent la concentration à la surface de l'électrode et au sein de la solution, respectivement. La deuxième étape, qui est l'étape lente, correspond à la diffusion du $(CuBr_{1+x}^{x-})$ depuis la surface jusqu'au sein de la solution. La première étape, qui est une réaction globale, représente la formation du complexe $CuBr_2^-$ lorsque $X = 1$, du complexe $CuBr_3^{2-}$ lorsque $X = 2$ ou un mélange des deux espèces lorsque $1 < X < 2$.

L'étape lente est la diffusion des ions $(CuBr_{1+x}^{x-})_i$ et la vitesse de la réaction formée par les étapes [4] et [5] est donnée par la première loi de Fick, dont la forme simplifiée est:

$$[6] \quad v = XFD \frac{[(CuBr_{1+x}^{x-})_i - (CuBr_{1+x}^{x-})_s]}{\delta}$$

où v est la vitesse de la réaction en courant équivalent.

Lorsque $(CuBr_{1+x}^{x-})_i \gg (CuBr_{1+x}^{x-})_s$ la relation [6] devient:

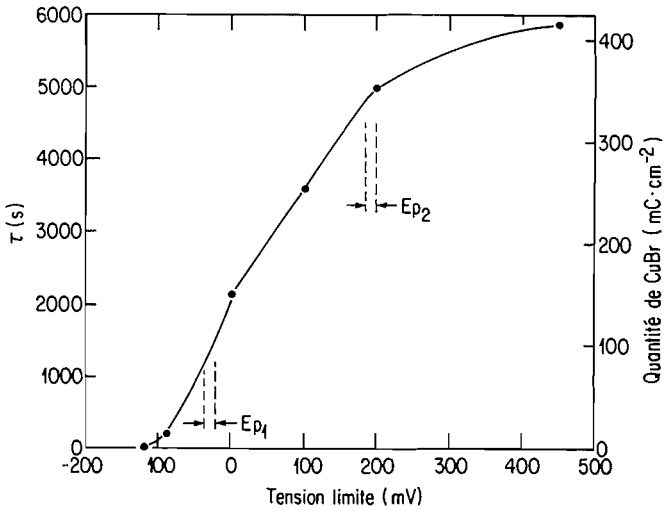

FIG. 13. Temps de transition et quantité de bromure cuivreux accumulé sur le fil de cuivre en fonction de la tension limite. Les conditions expérimentales sont celles de la fig. 12.

$$[7] \quad v = XFD \frac{(CuBr_{1+x}^{x-})_i}{\delta}$$

Pour sa part, l'utilisation de l'électrode à disque tournant permet d'écrire l'équation de Levich (11):

$$[8] \quad \delta = 1{,}61\, D_{CuBr_{1+x}^{x-}}^{1/3} \nu^{1/6} \omega^{-1/2}$$

La substitution de δ dans la relation [7] donne:

$$[9] \quad v = 0{,}62\, XF\nu^{-1/6} D_{CuBr_{1+x}^{x-}}^{2/3} \omega^{1/2} (CuBr_{1+x}^{x-})_i$$

où X, la charge de ou des espèces qui diffusent, est comprise entre 1 et 2; ν, la viscosité cinématique, est voisine de $0{,}96 \times 10^{-2}$ cm^2 s^{-1} (12); $D_{CuBr_{1+x}^{x-}}$ est le coefficient de diffusion de l'espèce $CuBr_2^-$, $CuBr_3^{2-}$ ou des deux espèces à la fois, selon la valeur de X; $(CuBr_{1+x}^{x-})_i$ est la concentration en cuivre à la surface de l'électrode alors que ω est la vitesse de rotation de l'électrode en radians par seconde.

Par ailleurs, la première étape, qui est l'étape rapide, permet d'envisager cette réaction dans un état voisin de l'équilibre, ce qui conduit à écrire:

$$[10] \quad K_e = \frac{(CuBr_{1+x}^{x-})_i}{(Br^-)^x}$$

où K_e est la constante d'équilibre de la réaction [4].

Les relations [9] et [10] permettent d'écrire:

$$[11] \quad v = 0{,}62\, XF\nu^{-1/6} D_{CuBr_{1+x}^{x-}}^{2/3} \omega^{1/2} K_e (Br^-)^x$$

D'après la figure 11, X est égal à 1,5. Pour sa part, le coefficient de diffusion est calculable à partir de l'expression [9] à la condition de connaître la relation expérimentale v vs. $\omega^{1/2}$ ainsi que la concentration en cuivre dissous au voisinage de l'électrode. Dans l'exemple montré à la fig. 8, E_{co} est égal à −140 mV durant la dissolution du CuBr, ce qui permet de déduire une concentration de $0{,}7 \times 10^{-3}$ *M* en cuivre dissous (Fig. 3). La valeur expérimentale de la pente $dv/d\omega^{1/2}$ est de 0,074 mC cm^{-2} $s^{-1/2}$ $rad^{-1/2}$ (Fig. 9). Ces valeurs conduisent à un coefficient de diffusion égal à $1{,}26 \times 10^{-5}$ cm^2 s^{-1}, ce qui est en harmonie avec la valeur de $1{,}4 \times 10^{-5}$ cm^2 s^{-1} trouvée précédemment (4).

Le fait que X soit égal à 1,5 (Fig. 11) tend à confirmer la formation concomittante des intermédiaires $CuBr_2^-$ et $CuBr_3^{2-}$

Can. J. Chem. Downloaded from www.nrcresearchpress.com by 210.87.254.42 on 09/06/12
For personal use only.

en quantités égales. Comme nous venons de le voir, la présence de ces intermédiaires comme espèces ioniques qui diffusent permet d'expliquer l'ensemble des résultats expérimentaux de façon cohérente.

Enfin, d'après la relation [10], la valeur de $(CuBr_{1+x}^{x-})_i$ est déterminée par l'équilibre de la réaction [4]. Il est alors prévisible que la vitesse de dissolution du bromure cuivreux soit indépendante de la quantité de CuBr présent sur le cuivre jusqu'à sa dissolution complète; ce qui est confirmé expérimentalement (Fig. 7).

4.2 *Accumulation du bromure cuivreux*

Les enregistrements E_{co} vs. temps (Fig. 12), obtenus après oxydation électrochimique pour différentes valeurs de E_L, suggèrent que le seul produit de corrosion qui s'accumule sur l'électrode est le bromure cuivreux dans la région de la première et de la deuxième vague d'oxydation.

Par ailleurs, le courant équivalent pour l'accumulation du CuBr sur l'électrode (dQ_{CuBr}/dt) est calculable à partir du produit de (dQ_{CuBr}/dE) (Fig. 13) par la vitesse de balayage imposée, dE/dt. Le courant équivalent ainsi trouvé est de 12,3 mA cm^{-2} entre 0 et 200 mV (Fig. 13). Pour sa part, le courant de dissolution est en moyenne de 18,7 mA cm^{-2} entre 0 mV et 200 mV (Fig. 1). On en déduit qu'une fraction non négligeable du courant de dissolution résulte en la formation de bromure cuivreux sur l'électrode dans la zone de la deuxième vague d'oxydation.

Conclusion

1. La présence de bromure cuivreux sur la surface du cuivre, suite à l'oxydation électrochimique de ce métal, contribue à l'enrichissement de la solution en cuivre dissous en contact avec l'électrode de cuivre. Cet enrichissement se traduit par une tension d'électrode bien caractéristique qui tombe dès la dissolution complète de ce composé.

2. La vitesse de dissolution du CuBr est constante jusque dans les instants qui précèdent sa dissolution complète.

3. La dissolution du bromure cuivreux est entièrement dominée par la diffusion d'une ou de plusieurs espèces ioniques qui se déplacent depuis l'électrode jusqu'au coeur de la solution. Les résultats expérimentaux s'expliquent entièrement à partir de la présence simultanée des espèces $CuBr_2^-$ et $CuBr_3^{2-}$ comme espèces ioniques qui diffusent.

4. Dans la région des vagues d'oxydation le seul produit de corrosion qui s'accumule sur l'électrode est le bromure cuivreux. La quantité d'électricité impliquée dans la région de la première vague se traduit presqu'entièrement par la formation de CuBr à la surface de cuivre alors que la formation de ce composé explique une part importante du courant de dissolution dans la région de la deuxième vague.

1. S. NAGESWAR et T. H. SETTY. Proc. Ind. Acad. Sci. Sect. A, **71**, 282 (1972).
2. J. FRANCO et N. K. PATEL. J. Inst. Chem. (India), **50**, 243 (1978).
3. J. FRANCO et N. K. PATEL. J. Electrochem. Soc. (India), **22**, 172 (1973).
4. L. BROSSARD. Can. J. Chem. **62**, 36 (1984).
5. K.-TH. WILKE. Krist. Tech. **3**, K53 (1968).
6. R. L. BROSSARD. Can. J. Chem. **60**, 616 (1982).
7. D. W. SHOESMITH, T. E. RUMMERY, D. OWEN et W. LEE. J. Electrochem. Soc. **123**, 790 (1976).
8. D. W. SHOESMITH et W. LEE. Electrochim. Acta, **22**, 1411 (1977).
9. W. LATIMER. Oxidation potentials. 2e éd. Prentice–Hall, New York. 1952.
10. C. E. WICKS et F. E. BLOCK. Bulletin 605, U.S. Bureau of Mines, Washington. p. 43.
11. V. G. LEVICH. Physicochemical hydrodynamics, Prentice–Hall, Englewood Cliffs, NJ. 1962.
12. R. PARSONS. Handbook of electrochemical constants. Butterworths Scientific Publ., London. 1959. p. 77.

Can. J. Chem. Downloaded from www.nrcresearchpress.com by 210.87.254.42 on 09/06/12
For personal use only.

Intermediates from ring-opening reactions. Reactions of 2-chloro-5-nitropyridine and 2-chloro-3-nitropyridine with deuteroxide ion in selected solvents

JOHN D. REINHEIMER, NICOLAS SOURBATIS, ROBERT L. LAVALLEE, DOUGLAS GOODWIN, AND GEORGE L. GOULD
Department of Chemistry, The College of Wooster, Wooster, OH 44691, U.S.A.

Received August 22, 1983

JOHN D. REINHEIMER, NICOLAS SOURBATIS, ROBERT L. LAVALLEE, DOUGLAS GOODWIN, and GEORGE L. GOULD. Can. J. Chem. **62**, 1120 (1984).

Open chain intermediates from the ring-opening reaction of aqueous sodium deuteroxide (2 mol) with 2-chloro-5-nitropyridine (1 mol) and 2-chloro-3-nitropyridine (1 mol) were isolated. These intermediates were purified, analyzed for elemental composition, and characterized by various spectrophotometric techniques. The intermediate formed from 2-chloro-5-nitropyridine and two equivalents of deuteroxide ion reacts with additional deuteroxide in D_2O in various polar solvents to reclose the pyridine ring. The kinetics of the ring closure reaction are reported and are supplemented with observations of salt and solvent effects upon the rate of closure. In addition, a mechanism for the ring closure is presented. The intermediate formed from 2-chloro-3-nitropyridine did not undergo a similar ring closure when reacted with additional deuteroxide, but instead formed various decomposition products. A reason for the failure of this ring closure is suggested.

JOHN D. REINHEIMER, NICOLAS SOURBATIS, ROBERT L. LAVALLEE, DOUGLAS GOODWIN et GEORGE L. GOULD. Can. J. Chem. **62**, 1120 (1984).

On a isolé des intermédiaires à chaîne ouverte formés lors de réactions d'ouverture de cycle, sous l'influence du deutéroxyde de sodium (2 mol), de la chloro-2 nitro-5 pyridine (1 mol) ou de la chloro-2 nitro-3 pyridine (1 mol). On a purifié ces intermédiaires, on en a fait l'analyse élémentaire et on les a caractérisés en faisant appel à diverses techniques spectrophotométriques. L'intermédiaire formé à partir de la chloro-2 nitro-5 pyridine et de deux équivalents d'ion deutéroxyde réagit avec le deutéroxyde dans du D_2O et dans divers solvants polaires pour reformer le cycle de la pyridine. On rapporte la cinétique de la réaction de fermeture de cycle et on fournit comme complément l'observation des effets du sel et du solvant sur la vitesse de fermeture de cycle. De plus, on propose un mécanisme pour cette réaction. L'intermédiaire formé à partir de la chloro-2 nitro-3 pyridine ne subit pas de fermeture de cycle lorsqu'on le fait réagir avec du deutéroxyde additionel; il se forme plutôt plusieurs produits de décomposition. On propose une explication pour l'absence de fermeture de cycle.

[Traduit par le journal]

Can. J. Chem. Downloaded from www.nrcresearchpress.com by 210.87.254.40 on 09/06/12
For personal use only.

Introduction

Nucleophilic attack on heterocyclic rings is well known (1–4). Subsequent reactions may yield ring-opened products (2–4) or the ring may open and close again (ANRORC mechanism) (1). Reinheimer *et al.* (5) found a ring-opening reaction with deuteroxide ion and 2-halo-5-nitropyridine in DMSO-d_6/D_2O solvent which yielded a stable intermediate *in situ*.

The intermediate was not isolated, but was characterized by its ^{13}C and ^1H nmr spectra. When additional NaOD in D_2O was added, the pyridine ring was again formed to yield the salt of 2-hydroxy-5-nitropyridine. We report further information on the isolation of this intermediate and on the cyclization reaction. A similar reaction of the isomer, 2-chloro-3-nitropyridine, with NaOD in D_2O yielded a stable intermediate. This material was also isolated as a solid, but its reaction with additional NaOD in D_2O did not result in cyclization. We report additional information on this reaction.

Experimental

All ^1H nmr spectra were taken on a Varian T-60 instrument with a probe temperature of 38°C. Carbon-13 nmr spectra were taken on a CFT-20 or JEOL FXQ 90 instrument at ambient temperatures. Infrared spectra were taken on a Perkin–Elmer 283B using Nujol mulls or KBr pellets. Raman spectra were obtained on a Beckman Raman spectrophotometer (model 700). All elemental analyses were done by Galbraith Laboratories Inc., Knoxville, Tennessee.

Preparation of the intermediates, 1 and 2

The open chain intermediates are polyfunctional sodium salts. Their water solubility and potential reactivity required the use of mild techniques to remove solvents and impurities. Charcoal treatment removed polymeric and colored impurities; the intermediate **1** was dissolved in acetone and passed through a silica gel column to remove salts; freeze-drying or rotary evaporation at room temperature was used to remove solvents.

1: Purified 2-chloro-5-nitropyridine (5) (Aldrich) (9.00 g) was dissolved in a solvent mixture of 85 mL of DMF, 50 mL of dioxane, and 40 mL of water at room temperature. Next, 40 mL of 2.79 *M* NaOH was added with stirring. Most of the solvent was quickly removed via rotary evaporation over gentle steam, and the mixture was filtered to remove insoluble materials. The filtrate was lyophylized and the solid was dissolved in water. This water solution was filtered through activated decolorizing carbon to yield a yellow solution which was subsequently lyophilized. The yellow solid was dissolved in acetone and passed through a 15 × 2.5 cm silica gel column (silica gel, 60–200 mesh Matheson, Coleman, and Bell) to remove salts. The eluent was placed on a rotary evaporator and concentrated to approximately 30 mL. The solution was then lyophilized to yield a light colored solid in a red oil. This material was dissolved in water and filtered through decolorizing carbon until a golden yellow solution was obtained. Again, this solution was lyophilized to yield a bright yellow solid. Filtration through charcoal and solvent evaporation were repeated until ^1H nmr showed no organic solvent impurities.

The ^{13}C and ^1H nmr spectra of the solid **1** were identical with those reported previously (5); mp 158–160°C (dec.). *Anal.* calcd. for $C_5H_3N_2O_3Na \cdot 1/2\ H_2O$: C 35.21, H 2.34, N 16.28; found: C 35.41, H 2.28, N 16.33.

2: 2-Chloro-3-nitropyridine (2.73 g) was placed in a round bottom flask with 30 mL of water. Sodium hydroxide, 15 mL of 2.33 *M*, was added to the stirred reaction mixture, which was kept at 55–60°C for 1 h. The dark colored reaction mixture was cooled, filtered, and lyophilized. It was then dissolved in water, filtered through decolorizing carbon, and recrystallized from H_2O/NaCl to give a yellow solid; ir ν_{max} (cm^{-1}) (Nujol): 2200 (C≡N), 1600 (HC=O); ^{13}C nmr (D_2O): 109.6, 116.7, 119.8, 146.2, 191.8; ^1H nmr (D_2O) δ: 9.3 (1H, d), 8.9 (1H, d), 5.1 (1H, pair of doublets). *Anal.* calcd. for $C_5H_3N_2O_3Na$: C 37.06, H 1.87, N 17.78; found: C 37.17, H 1.95, N 17.69.

Kinetics for the ring closure of 1 (prepared in situ*)*

A stock solution of 2-chloro-5-nitropyridine (0.408 *M*) was prepared in a solvent of composition ratio 9:1 (DMSO-d_6/D_2O) by

Can. J. Chem. Downloaded from www.nrcresearchpress.com by 210.87.254.40 on 09/06/12
For personal use only.

volume. The intermediate, **1**, was prepared by pipetting 0.500 mL of the stock solution and 0.100 mL of NaOD (4.08 *M*) into a 5-mm nmr tube. Then NaOD (4.08 *M*) and D_2O were pipetted into the nmr tube to give the desired deuteroxide concentration at constant solvent composition, namely, 0.45 mL of DMSO-d_6 + 0.25 mL of D_2O. The ^1H nmr integral trace of the aldehyde peak was observed vs. time. A plot of ln (integral trace) vs. time yielded a first-order plot and k_ψ. The second-order rate constant (k_2) was calculated from eq. [1], for the deuteroxide concentration did not change during a given kinetic run.

$$[1] \quad k_\psi = k_2[OD^-]$$

The data of Table 1 demonstrate that the reaction rate was also first order in deuteroxide ion.

Kinetic procedure with solid 1

The isolated intermediate **1** was weighed and dissolved in D_2O. This solution was diluted to volume with the appropriate solvent, DMSO-d_6, THF, dioxane, methanol, or acetone. A 0.500-mL aliquot was pipetted into a 5-mm nmr tube, and an aliquot of NaOD (4.08 *M*) solution was added. The reaction rate was observed and calculated in the manner given above.

Discussion

The reactions of 2-chloro-5-nitropyridine with deuteroxide ion in DMSO/D_2O solvent to yield ring-opened intermediates are given in eqs. [2] and [3]. Both **1** and **2** can be kept as stable products in solution, and they may also be isolated as analyzable solids.

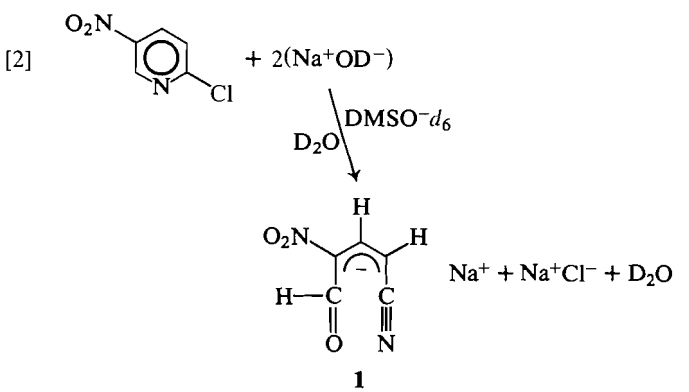

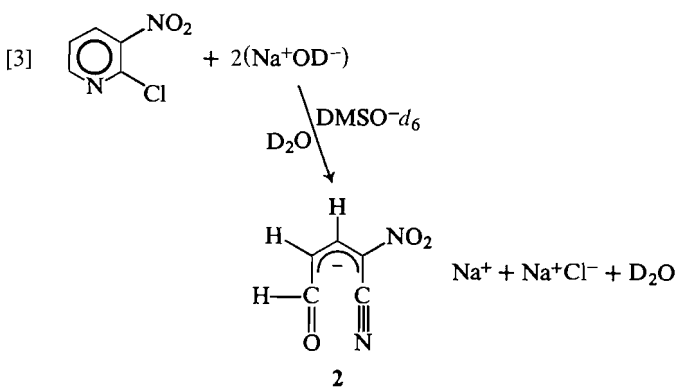

When **1** (prepared *in situ*) was treated with aqueous NaOD, it reacted to close the ring and form the Na^+ salt of 2-hydroxy-5-nitropyridine. The kinetics of this ring closure reaction showed that the reaction was first order in hydroxide ion and first order in 2-chloro-5-nitropyridine. If the rate-determining step of eq. [4] is **1** → **3**, then the rate equation would be eq. [5].

TABLE 1. Rate constants for the reaction of **1** with OD^- in DMSO-d_6/D_2O[a,c]

Compound **1** (mol/L)	$[OD^-]$ (mol/L)	$k_\psi \times 10^{-3}$ (s^{-1})[b]	$k_2 \times 10^{-3}$ (L/mols)
0.291[d]	0.145	0.324	2.23±0.2
0.291[d]	0.291	0.672	2.31±0.2
0.291[d]	0.582	1.34	2.30±0.2
0.31[e]	0.62	1.33	2.15±0.2
0.31[f]	0.62	0.90	1.45±0.2

[a]Temperature was 38°C.
[b]k_ψ was the average of 3 kinetic runs.
[c]Solvent composition was 0.45 mL DMSO-d_6 to 0.25 mL D_2O.
[d]Compound **1** prepared in solution.
[e]Solid **1** with NaCl (0.31 *M*).
[f]Solid **1** with no NaCl added.

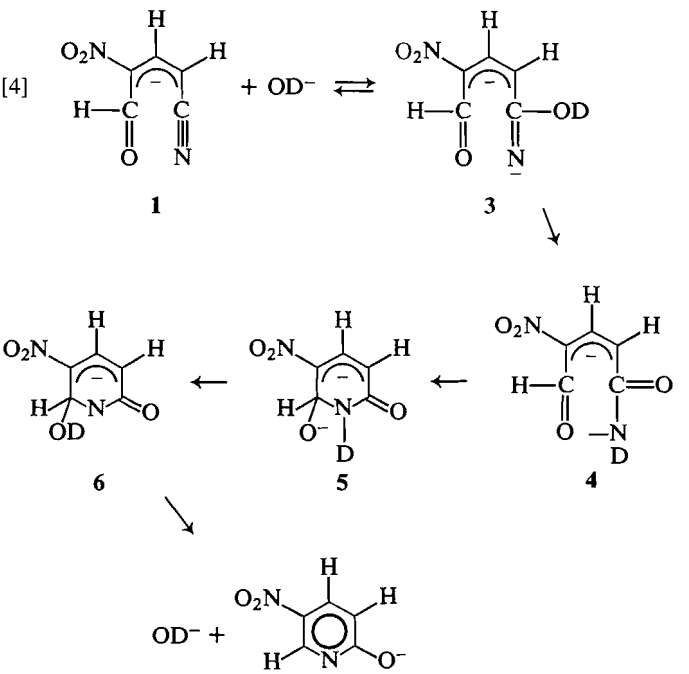

$$[5] \quad \frac{d\mathbf{1}}{dt} = k_2[OD^-][\mathbf{1}]$$

Since deuteroxide ion is regenerated, its concentration will be unchanged in a given experiment. Thus, eq. [6] holds true. In Table 1, the values k_ψ and k_2 are calculated from eq. [6]. A

$$[6] \quad \frac{-d\mathbf{1}}{dt} = k_\psi dt, \text{ where } k_\psi = k_2[OD^-]$$

second line of evidence that lends support to eq. [4] is the effect of salt on the reaction rate. In Table 1, the first 3 rows give k_ψ and k_2 for the intermediate which was prepared in solution containing equimolar NaCl (eq. [1]). In rows 4 and 5, the dissolved solid intermediate and the dissolved solid intermediate with added equimolar NaCl were the reagents. The added NaCl caused an increase in rate constant (k_2), from 1.45 to 2.15 × 10^{-3}, which was beyond experimental error. This positive salt effect may be attributed to the reaction of negative ion on a negative ion (6), deuteroxide ion on **1** as required by eq. [3]. The experimental rate constant for the solid **1** duplicated the rate constant for **1** prepared *in situ* only if the correct amount of by-product NaCl was added.

Can. J. Chem. Downloaded from www.nrcresearchpress.com by 210.87.254.40 on 09/06/12
For personal use only.

Why does changing $[Na^+Cl^-]$ have a large effect and changing $[Na^+OH^-]$ have little or no salt effect on k_2?. The data of Reinheimer and Hostetler (7) showed that rate constants for an aromatic nucleophilic substitution by hydroxide ion in dioxane/water show little change with increasing $[M^+OH^-]$, where $M^+ = Li^+$, Na^+, and K^+. However, when M^+ was tetrabutylammonium ion, the rate constants showed a very large salt effect with increasing concentration of ionic reagent. Applying this to the present system, the changing sodium deuteroxide concentration would have little effect on the rate constant. On the other hand, Na^+Cl^- does not form intimate ion pairs readily in aqueous solution, and will exert a considerable salt effect. We made no quantitative salt effect calculations, since Benson (6) has indicated that these quantitative theories are questionable in concentrated salt solutions.

The effect of cosolvents on the reaction rate constant of **1** and NaOD was also studied. Some D_2O was required to ensure solubility of the NaOD, and an inert organic solvent was needed to dissolve the reagent. Dioxane, tetrahydrofuran, dimethylsulfoxide, acetonitrile, acetone, and methanol were used as cosolvents. Acetonitrile and water tended to separate into layers, while acetone, **1**, and OD^- showed ^1H nmr lines that indicated a competing condensation reaction as well as ring closure. The remaining cosolvents, DMSO-d_6, dioxane, tetrahydrofuran, and methanol showed the same general trend, namely, that the reaction rate constant for ring closure increased with increasing water content, as seen in Table 2. This qualitative result is compatible with eq. [4], for the attack of a negative ion on a negative ion is favored by the more polar solvent (8). The hydrolysis of DMF in aqueous base provided a competing reaction. In the ring-closure reaction this hydrolysis caused complication, so that DMF was not a suitable solvent for ring closure. However, this hydrolysis could be used to advantage in the isolation of the ring-opened intermediate. The reaction of eq. [2] was very rapid, and the ring-closure reaction (eq. [4]) was much slower. DMF performed two functions, that of dissolving the organic reagent and that of preventing an excess of OD^-. The equation [6] indicates that the hydrolysis and substitution reactions have the requirement

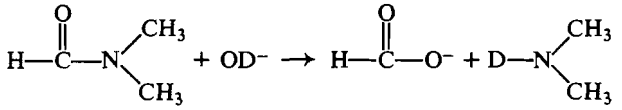

[6]

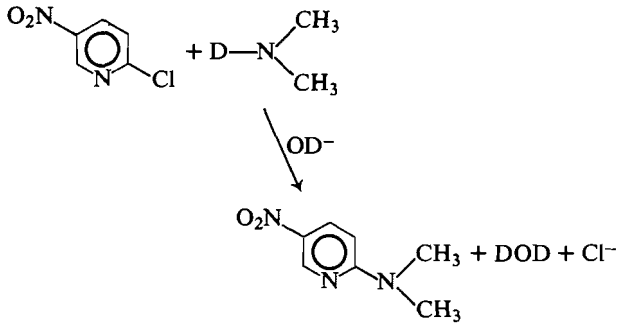

of 2 mol OD^- for 1 mol of 2-chloro-5-nitropyridine, so that there was no extra OD^- to initiate ring closure. Removal of the solvent, DMF, was easier than removal of DMSO and the yellow solid, 2-methylamino-5-nitropyridine, crystallized readily. The dimethylamino compound was removed from the ionic intermediate **1** by a methylene chloride extraction or by filtration, and identified by its known melting point and ^1H nmr spectrum.

TABLE 2. Solvent effects on the rate constant for the ring closure of **1**[a]

Solvent[b]	$k_2 \times 10^3$ (L/mol s)	No. of experiments
64% DMSO[c]	2.15	1
64% DMSO	1.50	2
50% DMSO	3.31	7
37% DMSO	10.20	2
100% D_2O	57.00	2
60% Dioxane	3.0	2
45% Dioxane	4.0	2
36% THF	6.9	2
55% Methanol	3.7	2

[a]Temperature was 38°C.
[b]The cosolvent was D_2O.
[c]An amount of NaCl equivalent to **1** was added.

The intermediate can be advantageously prepared and isolated from DMF, for the slower ring-closure reaction permits the hydrolysis reaction of DMF with hydroxide ion to dominate, thus preventing a local excess of hydroxide ion and the competing of the ring closure reaction.

The reaction of **2** with deuteroxide was quite different from **1**. The ^1H nmr spectrum of the reaction mixture gradually changed, not to the known spectrum of 2-hydroxy-3-nitropyridine, but to a singlet, $\delta = 8.3$. The change was slow in DMSO-d_6/D_2O solvent; a week was required to complete the reaction. The same singlet could be obtained in a few minutes by treating the aqueous solution with basic H_2O_2 at about 50°C. A solid was obtained by freeze-drying this reaction mixture. This showed a singlet in the ^{13}C nmr when noise decoupled, and a doublet when undecoupled. It was identified as sodium formate; this was confirmed by ^1H nmr comparisons with an authentic sample and by preparation of a *p*-bromophenacyl derivative. In a separate week-long experiment, the amount of sodium formate was measured by addition of sodium acetate to an nmr sample. The integral trace for this reaction mixture indicated that 1 mol of formate resulted from the H_2O_2 oxidation of **2**. The source of the formate was probably due to the base-induced cleavage of the aldehyde functional group, for the aldehyde hydrogen is not readily exchanged in basic solution. Other possible sources of formate seem to be less likely due to their formation in the solvent D_2O. The hydrolysis of CN^-, CNO^- would result in deuterated molecules which would not be observable in a ^1H nmr spectrum. In addition to the formate, another decomposition product identified from the reaction mixture with basic H_2O_2 was sodium isocyanate.[1] The iso-

[1]Treatment of **2** with basic H_2O_2 in water, a quick isolation of the yellow solid product by freeze-drying, immediately followed by a laser Raman spectrum, showed one line, 2180 cm^{-1} and some fluorescence. Three days later, this line has disappeared. This line did not correspond to ionic NaCN which absorbs at 2070–2090 cm^{-1} (9). Since the absorptions for formate are very weak in the Raman spectrum (10), we concluded that formate was not the cause of the line at 2180 cm^{-1}. We suspected sodium isocyanate and confirmed this by mixing a sample of KOCN and NaOH and lyophilizing. This sample showed two peaks, 2165 cm^{-1} and 2180 cm^{-1}. A ^1H nmr of this solid showed no peaks at $\delta = 8.3$. Our pure KOCN sample yielded one Raman peak at 2165 cm^{-1}. Therefore we feel that sodium isocyanate is a decomposition product of the reaction of **2** with basic H_2O_2, and in all probability a decomposition product of the reaction of **2** with hydroxide ion in DMSO-d_6.

cyanate was probably formed due to cleavage of the nitrile group of **2**. This is consistent with the mechanism presented in eq. [4] which shows the initial attack of deuteroxide ion on the nitrile group of **1**, except that in the case of the attack of **2**, the close proximity of the nitro group may lead to stabilization of the resulting carbanion if the DOCN leaves.

The drastic change in the course of the reaction of **1**, compared to **2**, with deuteroxide was surprising in view of the slight structural difference of **1** and **2**. The extensive resonance delocalization should tend towards planar structures, with the NO_2 group coplanar with the pentadienide moiety. The major difference, σ- vs. ρ-nitro group with respect to the C≡N or HC=O group, seems to be responsible for the changed reactivity. If the rate-determining step is attack on C≡N by deuteroxide for both **1** and **2**, the attack on **2** may be very slow, so that other reactions can compete.

A second possibility is that the deuteroxide ion attacks the C≡N group of **2**, but that cyclization cannot be completed because the H—C—N distance has been changed.

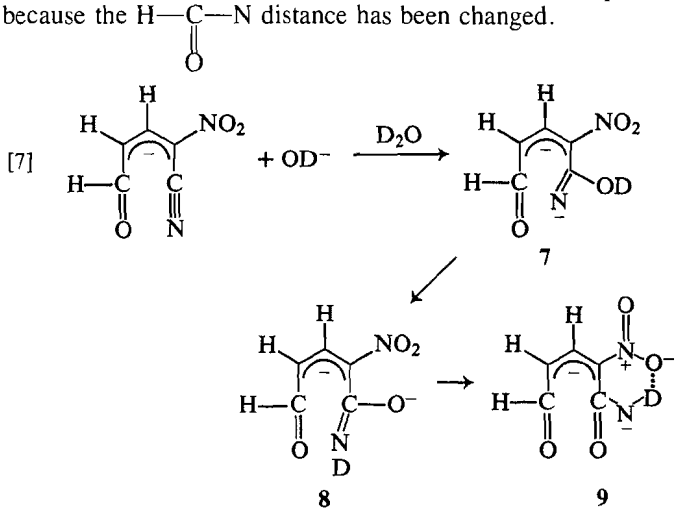

If **8** and **9** are the dominant conformers in solution, cyclization would not occur, for the aldehyde–nitrogen distance becomes larger. In **9**, H-bonding of the (HN--ONO) should enhance stability of **9**. In **8**, the repulsion of the *ortho* NO_2 and C=O would cause a slight rotation about the C—C bond between the carbon #2 (HN—C=O) and carbon #3 (C—NO_2). This rotation would result in a larger separation between N—H and the aldehyde group; this should effectively hinder cyclization. The electron-withdrawing effect of the *o*-nitro group may promote cleavage of the OCN^- moiety through stabilization of the resultant carbanion, thus permanently preventing cyclization. In either case, the specific effect of the NO_2 group may be responsible for blocking cyclization of **2**. If cyclization is very slow, other reactions of **2** become successful competitors.

Acknowledgements

Acknowledgement is made to the Donors of The Petroleum Research Fund, administered by the American Chemical Society, for partial support of this research. The authors also gratefully acknowledge support from the Research Corporation.

1. H. C. VAN DER PLAS. Acc. Chem. Res. **11**, 462 (1978).
2. D. M. SMITH. *In* Comprehensive organic chemistry. Vol. 4. *Edited by* Sir D. H. R. Barton and W. D. Ollis. Pergamon Press, Oxford. 1979. p. 50.
3. J. BECKER. Synthesis, 589 (1980).
4. J. CLARK. Lectures in heterocyclic chemistry. Vol. 3. J. Chem. Soc. 1976. pp. 179–192.
5. J. D. REINHEIMER, L. L. MAYLE, G. G. DOLNIKOWSKI, and J. T. GERIG. J. Org. Chem. **45**, 3097 (1980).
6. S. W. BENSON. The foundations of chemical kinetics. McGraw–Hill Book Co., Inc. New York. 1960. p. 127.
7. J. D. REINHEIMER and W. HOSTETLER. Ohio J. Sci. **64**, 275 (1964).
8. C. K. INGOLD. Structure and mechanism in organic chemistry. 2nd ed. Cornell Univ. Press, Ithaca, NY. 1969. p. 482ff.
9. D. KENDALL. Applied I.R. spectroscopy. Reinhold Publ. Co., New York. 1966. p. 501.
10. J. H. HIBBEN. Raman effect and its chemical applications. Reinhold Publ. Co., New York. 1939. p. 452ff.

Can. J. Chem. Downloaded from www.nrcresearchpress.com by 210.87.254.40 on 09/06/12
For personal use only.

The electron paramagnetic resonance spectrum of $S_3N_2^+$ [1]

SHIRLEY A. FAIRHURST[2] AND KEITH F. PRESTON
Division of Chemistry, National Research Council of Canada, Ottawa, Ont., Canada K1A 0R9

AND

LESLIE H. SUTCLIFFE
Department of Inorganic, Physical and Industrial Chemistry, Liverpool University, Liverpool L69 3BX, U.K.

Received December 6, 1983

SHIRLEY A. FAIRHURST, KEITH F. PRESTON, and LESLIE H. SUTCLIFFE. Can. J. Chem. **62**, 1124 (1984).

The epr spectrum of a persistent sulfur nitride radical cation, common to the oxidation of many sulfur–nitrogen compounds, has been obtained from materials highly enriched in both ^{15}N and ^{33}S. Analyses of solution and frozen spectra show that the carrier is planar $S_3N_2^+$ and that its ground state is $^2A_2$ in C_{2v} symmetry.

SHIRLEY A. FAIRHURST, KEITH F. PRESTON et LESLIE H. SUTCLIFFE. Can. J. Chem. **62**, 1124 (1984).

Un radical libre persistant, produit par l'oxydation de divers composés d'azote et de soufre, a été préparé à partir de matériaux enrichis en ^{15}N et ^{33}S. Les analyses de spectres RPE enregistrés en phase solide et liquide démontrent que le radical est $S_3N_2^+$, une molécule planaire à l'état fondamental $^2A_2$ avec symmetrie C_{2v}.

Can. J. Chem. Downloaded from www.nrcresearchpress.com by 210.87.254.42 on 09/06/12
For personal use only.

Introduction

A common product of the reaction of sulfuric acid with a number of cyclic sulfur–nitrogen compounds is a persistent free radical having an isotropic g-value of 2.011 and equal isotropic hyperfine interactions of 3.2 G with two ^{14}N ($I = 1$) nuclei (1–3). While there is a consensus of opinion regarding the presence of two spatially equivalent nitrogen atoms and a single positive charge in the carrier, its identity remains in doubt. Following measurements of the g- and ^{14}N-hyperfine interaction tensor components from a powder spectrum, McNeil, Murray, and Symons (2) rejected the original assignment (1) to SN_2^+ in favour of a symmetric (D_{2h}) radical cation $S_2N_2^+$ in which the semioccupied orbital (SOMO) consisted of roughly equal in-plane atomic p-orbital contributions from all four atoms. ^{33}S-labelling experiments (3), which demonstrated the presence of two equivalent spin-bearing sulfur atoms in the free radical, supported this assignment.

In more recent developments, Gillespie and co-workers (4, 5) showed that the same persistent isotropic spectrum arose upon dissolution of diamagnetic $S_6N_4^{2+}$ $(AsF_6^-)_2$ in methylene chloride; the carrier was also detected (6) in solid hexasulfur tetranitrogen dichloride, $S_6N_4Cl_2$, and in solutions of that compound in liquid SO_2. Crystallographic studies (4–6) of these $S_6N_4^{2+}$ salts indicate the presence of loosely bound pairs of $S_3N_2^+$ ions that have a cyclic, planar (C_{2v}) structure. Interestingly, the radical is also generated in high yield (7) during an unusual reaction between tetrahydrofuran and dithionitronium hexafluoroarsenate, S_2NAsF_6 (8).

In this article we report spectroscopic measurements made for liquid and frozen D_2SO_4 solutions of S_4N_4/S_4N_2 mixtures labelled with both ^{15}N ($I = 1/2$) and ^{33}S ($I = 3/2$). The spectra clearly show the presence of two equivalent nitrogens, two equivalent sulfurs and a third, unique sulfur in the free radical. Our data support the contention of Gillespie *et al.* (4, 5) that the spectrum is due to $S_3N_2^+$, a planar π-radical in which unpaired spin density is largely confined to p orbitals located on the nitrogen nuclei and the two equivalent sulfur nuclei.

[1]NRCC No. 23099.

[2]NRCC Research Associate 1981–1983. Present address: Department of Inorganic, Physical and Industrial Chemistry, Liverpool University, Liverpool L69 3BX, U.K.

Experimental

Free-radical spectra were generated by adding a 98% D_2SO_4 solution (>99.5 atom% D) to a small amount of a mixture of S_4N_4 and S_4N_2 contained in an evacuated 1 mm id epr tube. The sulfur nitride mixture enriched to 99 atom% in ^{15}N and to 59.2 atom% in ^{33}S was prepared according to the published procedure of Apter *et al.* (9). Deuterated sulfuric acid was employed to minimize interference from a secondary, proton-containing free radical reported by other workers (3). $^{15}NH_4Cl$ enriched to 99% in ^{15}N and used to prepare $^{15}NH_3$ was obtained from Prochem Ltd., Summit, NJ; elemental sulfur (59.2 atom% ^{33}S) was supplied by Oak Ridge National Laboratories, TN, and D_2SO_4 was obtained from the Aldrich Chemical Co., Milwaukee, WI.

Electron paramagnetic resonance spectra were recorded at 20°C and −196°C on a Varian E-12 spectrometer equipped with standard accessories for the measurement of microwave frequency and magnetic field intensity.

Results

The epr spectra observed at 20°C and −196°C for a D_2SO_4 solution of S_4N_4/S_4N_2 enriched to 99% in ^{15}N are shown in Figs. 1 and 2*a*, respectively. The liquid-phase spectrum (Fig. 1) is clearly due to equal hyperfine interactions (hfi = 4.5 G) of a single unpaired electron with two ^{15}N ($I = 1/2$) nuclei. At high gain, weak satellite absorptions were detectable outside the main spectrum. These were undoubtedly due to hyperfine interaction (8.8 G) with one or more ^{33}S nuclei ($I = 3/2$) present in natural abundance in the free radical. An experiment with sulfur nitride enriched to 59.2% in ^{33}S and to 99% in ^{15}N confirmed the participation of two equal ^{33}S isotropic hyperfine interactions of 8.8 G, and revealed the presence of a third sulfur having a 3 G isotropic hfi. The experimental and simulated liquid-phase spectra of the doubly enriched species are compared in Fig. 3. Resolution of the hyperfine structure in the experimental spectrum (Fig. 3*a*) deteriorates rapidly in the wings, an effect often encountered in ^{33}S spectra and attributable to anisotropy of the ^{33}S-hyperfine tensors (10).

Analysis of the powder spectrum of Fig. 2*a* in terms of colinear g- and ^{15}N-hyperfine tensors was straightforward, and the best simulated spectrum (11) is shown in Fig. 2*b*. The introduction of three additional ^{33}S-hyperfine interaction tensors and the mixture of ^{33}S-containing and ^{33}S-free radicals complicated the powder spectrum of the 59% ^{33}S, 99% ^{15}N sample considerably (Fig. 4). A complete analysis of this spec-

Can. J. Chem. Downloaded from www.nrcresearchpress.com by 210.87.254.42 on 09/06/12
For personal use only.

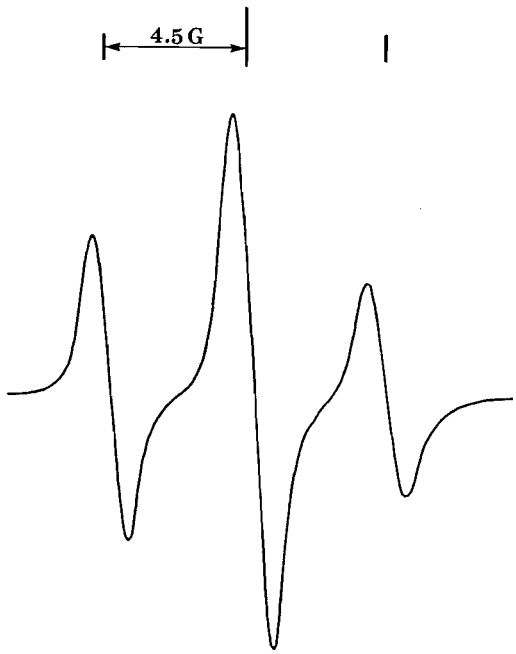

FIG. 1. First derivative epr spectrum at 20°C of D_2SO_4 solution of S_4N_4/S_4N_2 enriched to 99% in ^{15}N.

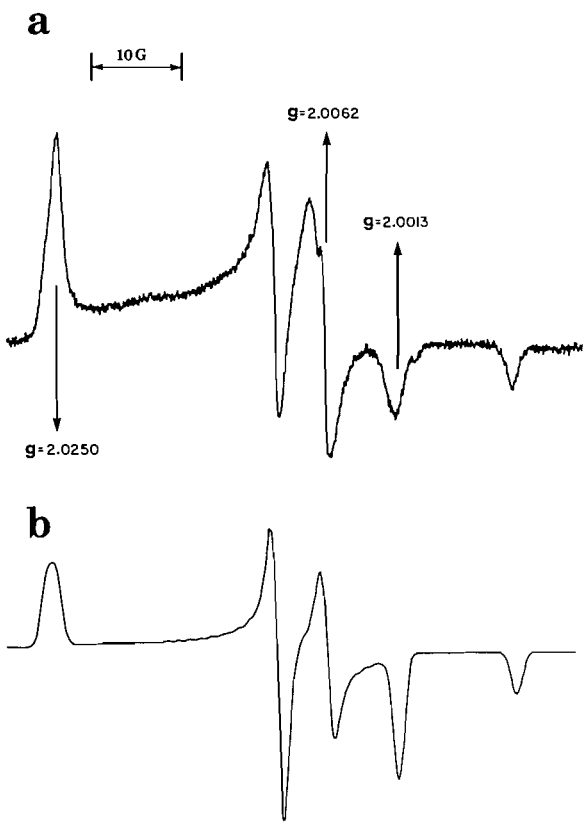

FIG. 2. (*a*) Experimental epr spectrum at −196°C of same sample used for Fig. 1. (*b*) Computer simulated powder spectrum using *g*- and ^{15}N-tensors of Table 1.

trum was not achieved. Tentative values for the components of the ^{33}S hfi tensors are given in Table 1 along with the *g*- and ^{15}N hfi tensors. We hope to achieve an exact analysis when elemental sulfur of higher enrichment in ^{33}S becomes available.

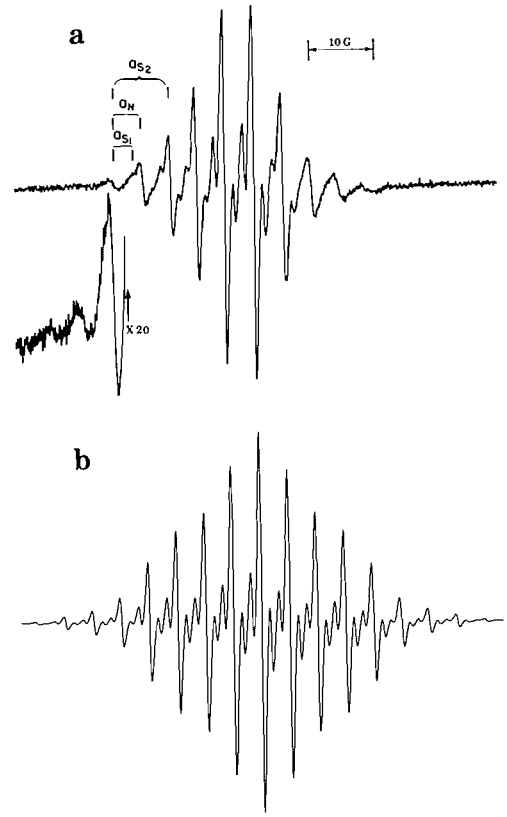

FIG. 3. Experimental (*a*) and simulated (*b*) epr spectra at 20°C of a D_2SO_4 solution of S_4N_4/S_4N_2 enriched to 99% in ^{15}N and to 59% in ^{33}S.

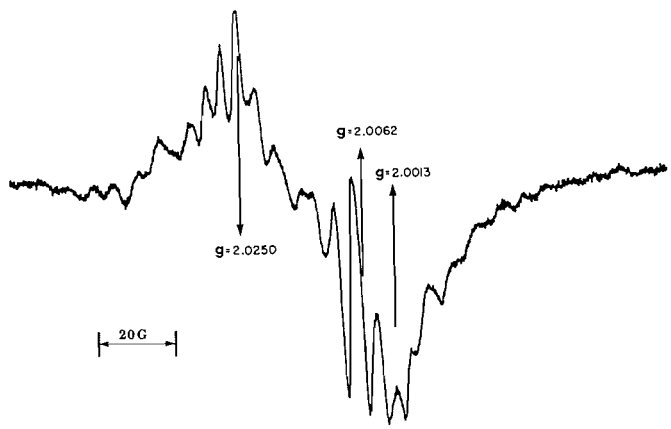

FIG. 4. Powder spectrum of the sample of Fig. 3 obtained at −196°C.

Discussion

Our solution spectra confirm the previous finding (1−3) that the free radical contains a pair of equivalent nitrogen nuclei and a pair of equivalent sulfur nuclei. In addition, we have demonstrated the presence of a unique sulfur nucleus which bears unpaired spin. Taken in conjunction with Gillespie's results (4, 5), these facts leave little doubt that the carrier of the spectrum is $S_3N_2^+$.

The powder spectra of Figs. 2 and 4 strongly suggest that all six tensors are colinear. Simulations of the spectrum of Fig. 2*a* showed that the direction of minimum g departed no more than 5° from the directions of maximum ^{15}N hfi. The situation is less

TABLE 1. g- and Hyperfine interaction tensors[a] for $S_3N_2^+$ in D_2SO_4

	g	$^{15}N(2)$	$^{33}S(2)$	$^{33}S(1)$
xx	2.0062	~1.0	~0	<1
yy	2.0013	13.0	22	8
zz	2.0250	~0	~5	<1
Average	2.0108	~5	~9	~3
Isotropic	2.0106	4.5	8.7	3.0
$\%s$		0.5(2.4)[b]	0.7(0.2)	0.2(−0.1)
$\%p_y$		15.3(51.8)	18.5(16.5)	7.0(−36.7)

[a]Values in Gauss.
[b]INDO I spin densities in parentheses.

clear for the ^{33}S hfis, but the spectrum of Fig. 4 certainly suggests that they are parallel to the other tensors. This inference and the exceedingly small atomic s-orbital unpaired spin (12) populations (Table 1) lead us to conclude that $S_3N_2^+$ is a π-radical in which unpaired spin density is confined to atomic p_y orbitals directed perpendicular to the molecular (xz) plane:

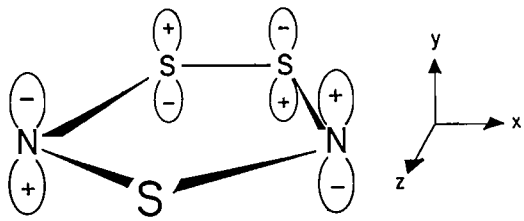

Extended Hückel MO calculations for a planar C_{2v} structure place the unpaired electron in an a_2 orbital to which the equivalent N($2p_y$) orbitals contribute 30% and the equivalent S($3p_y$) orbitals 70% spin density. The small spin densities detected in the unique sulfur $3p_y$ and in the atomic s orbitals are due to spin polarization. INDO I calculations for the lowest-energy planar configuration of $S_3N_2^+$ predict considerable negative spin density in the unique sulfur $3p_y$ orbital, but the computed unpaired spin densities are not in good agreement with experiment (Table 1).

Acknowledgments

L.H.S. wishes to express his thanks to the Director of the Divison of Chemistry, NRCC, for providing research facilities during the summer of 1983. The authors are indebted to Dr. J. R. Morton for stimulating and invaluable discussions.

1. D. CHAPMAN and A. G. MASSEY. Trans. Faraday Soc. **56**, 1426 (1960).
2. D. A. C. MCNEIL, M. MURRAY, and M. C. R. SYMONS. J. Chem. Soc. A, 1019 (1967).
3. S. A. LIPP, J. J. CHANG, and W. L. JOLLY. Inorg. Chem. **9**, 1970 (1970).
4. R. J. GILLESPIE, P. R. IRELAND, and J. E. VEKRIS. Can. J. Chem. **53**, 3147 (1975).
5. R. J. GILLESPIE, J. P. KENT, and J. F. SAWYER. Inorg. Chem. **20**, 3784 (1981).
6. R. W. H. SMALL, A. J. BANISTER, and Z. V. HAUPTMAN. J. Chem. Soc. Dalton. In press.
7. L. H. SUTCLIFFE. Unpublished results.
8. A. J. BANISTER, R. G. HEY, G. K. MACLEAN, and J. PASSMORE. Inorg. Chem. **21**, 1679 (1982).
9. S. APTER, M. CARRUTHERS, and L. H. SUTCLIFFE. Inorg. Chim. Acta, **31**, L445 (1978).
10. J. E. WERTZ and J. R. BOLTON. Electron spin resonance: elementary theory and practical applications. Chapt. 9, McGraw-Hill. 1972.
11. R. LEFEBVRE and J. MARUANI. J. Chem. Phys. **42**, 1480 (1965).
12. J. R. MORTON and K. F. PRESTON. J. Magn. Reson. **30**, 577 (1978).

Can. J. Chem. Downloaded from www.nrcresearchpress.com by 210.87.254.42 on 09/06/12
For personal use only.

Structural and spectroscopic studies of dipotassium 3,3,3′,3′-tetramethylcystinate trihydrate, $K_2[C_{10}H_{18}N_2O_4S_2]3H_2O$

ROMOLO FAGGIANI, HELEN ELAINE HOWARD-LOCK, COLIN JAMES LYNE LOCK, MARIA LURDES MARTINS, AND PHILIP STUART SMALLEY

Institute for Materials Research, McMaster University, Hamilton, Ont., Canada L8S 4M1

Received October 31, 1983

ROMOLO FAGGIANI, HELEN ELAINE HOWARD-LOCK, COLIN JAMES LYNE LOCK, MARIA LURDES MARTINS, and PHILIP STUART SMALLEY. Can. J. Chem. **62**, 1127 (1984).

The compound dipotassium 3,3,3′,3′-tetramethylcystinate trihydrate, $K_2[C_{10}H_{18}O_4N_2S_2]3H_2O$, has been prepared and characterized by single crystal X-ray diffraction. Crystals were monoclinic, $P2_1$, a = 6.160(1), b = 26.473(8), c = 6.193(1) Å, β = 113.94(1)°, with two formula units in the unit cell. Intensities were measured on a Syntex $P2_1$ diffractometer with use of MoKα radiation. The structure was solved by standard methods and refined to R_1 = 0.0469, R_2 = 0.0472 based on 2303 independent observed reflections. The C—S bonds (1.877(6), 1.891(6) Å) are longer than in many similar compounds although the S—S bond (2.040(2) Å) is not. The C—S—S—C torsional angle (108.7(3)°) is larger than normal in dithiol compounds. Other distances and angles are normal. Two types of potassium coordination are present, one a distorted octahedron, the other a distorted trigonal prism. In addition to the ionic interactions, hydrogen bonds involving the water molecules are important in stabilizing the structure.

ROMOLO FAGGIANI, HELEN ELAINE HOWARD-LOCK, COLIN JAMES LYNE LOCK, MARIA LURDES MARTINS et PHILIP STUART SMALLEY. Can. J. Chem. **62**, 1127 (1984).

On a préparé le trihydrate du tétraméthyl-3,3,3′,3′ cystinate de potassium, $K_2[C_{10}H_{18}O_4N_2S_2]3H_2O$ et on l'a caractérisé par diffraction de rayons-X sur un monocristal. Les cristaux sont monocliniques et appartiennent au groupe d'espace $P2_1$ avec a = 6,160(1), b = 26,473(8), c = 6,193(1) Å, β = 113,94(1)° avec deux unités par maille élémentaire. On a mesuré les intensités à l'aide d'un diffractomètre syntex $P2_1$ en utilisant une radiation MoKα. On a résolu la structure par des méthodes normales et on l'a affinée jusqu'à des valeurs de R_1 = 0,0469 et de R_2 = 0,0472 à partir de 2303 réflexions observées. Les liaisons C—S (1,877(6), 1,891(6) Å) sont plus longues que celles de plusieurs composés analogues bien que la liaison S—S ne le soit pas. L'angle de torsion C—S—S—C (108,7(3)°) est plus grand que ceux observés normalement dans les dithiols. Les autres distances et les autres angles sont normaux. Le potassium possède deux types de coordination, l'un est un octaèdre déformé tandis que l'autre est un prisme trigonal déformé. En plus des interactions ioniques, les liaisons hydrogènes impliquant les molécules d'eau sont importantes pour de la stabilité de la structure.

[Traduit par le journal]

Can. J. Chem. Downloaded from www.nrcresearchpress.com by 210.87.254.5 on 09/06/12
For personal use only.

Introduction

D-Penicillamine is used in the treatment of a large number of diseases (1), of which the best known is Wilson's disease (2). Surprisingly, for a compound so widely used as a drug, it has not been well characterized by physical chemical methods. We have been interested in the use of D-penicillamine as a treatment for rheumatoid arthritis (3) and as a ligand in preparing radiopharmaceuticals (4), and have made extensive physical chemical studies of the compound (5). Studies have shown that metabolites of D-penicillamine excreted in the urine include the disulphide containing compounds 3,3-dimethylcystine and 3,3,3′,3′-tetramethylcystine, which are formed by oxidation and exchange reactions (6, 7). The former metabolite is important in the D-penicillamine treatment of cystinuria since the mixed disulphide is much more soluble than cystine and is thus more readily excreted from the body (6, 7). We have obtained the potassium salt of the latter compound, 3,3,3′,3′-tetramethylcystine, accidentally. As part of our studies on D-penicillamine we attempted to isolate the D-penicillaminate anion. Instead we obtained the title compound which results from the aerial oxidation of the D-penicillaminate anion.

Experiments

Dipotassium 3,3,3′,3′-tetramethyl-D-cystinate trihydrate

D-(−)-Penicillamine (0.7920 g) was dissolved in 1.0 *M* aqueous KOH (5.30 mL), allowed to stand in air for 24 h, and then evaporated to dryness under vacuum. A white solid with very pale purple colour was obtained. The product was recrystallized by slow evaporation in air from H_2O. Large colourless crystals were obtained. The mp was 196°C, at which the crystals turned black and decomposed. A 5,5′-dithiobis(2-nitrobenzoic acid) test for sulphydryl groups was negative (8).

Spectral measurement

Solutions for nmr studies were prepared in D_2O and concentrations were about 100 mg (solid) mL^{-1} of solvent. External TMS was used as the reference. Proton nmr spectra were recorded on a Varian T60 Spectrometer.

Infrared spectra were recorded on both a Nicolet 7199FT-IR and a Perkin-Elmer Model 283 spectrophotometer. The samples were ground with KBr at a concentration of approximately 1% by weight and then pressed into pellets. To confirm that certain peaks were real and not manifestations of the pelleting procedure, the spectra of certain samples were also run in Nujol and again in hexachlorobutadiene. Spectra were calibrated with polystyrene. Raman spectra were excited by means of the 5145 Å radiation from a Spectra-Physics model 164-02 Argon ion laser and recorded on a Spex 14018 double monochromator. Solid samples were contained in glass melting point tubes, and solutions in nmr tubes. The spectrometer was calibrated regularly with a neon lamp; the wavelength readout scale was found not to change (±1 cm^{-1}). Vibrational spectra have been obtained for the following compounds: (*1*) dipotassium 3,3,3′,3′-tetramethyl-D-cystinate trihydrate, (*2*) D-(−)-penicillamine disulphide in H_2O, solutions at several pH values, and (*3*) D-(−)-penicillamine disulphide in D_2O solution.

Collection of the X-ray diffraction data

A plate-like single crystal was sealed in a Lindemann capillary for the X-ray studies. Precession photographs showed that the crystals of the disulphide were monoclinic. Unit cell parameters were obtained from least-squares fit of χ, φ, and 2θ for 15 reflections in the range 19.1° < 2θ < 31.8° measured on a Nicolet P3 diffractometer having graphite-monochromated MoKα_1 radiation (0.70926 Å at 22°C).

Can. J. Chem. Downloaded from www.nrcresearchpress.com by 210.87.254.5 on 09/06/12
For personal use only.

Crystal data are as follows:
$C_{10}H_{24}K_2N_2O_7S_2$ fw = 426.64
Space group $P2_1$ (No. 4), a = 6.160(1), b = 26.473(8), c = 6.193(1) Å, β = 113.94(1)°, V = 923.0(4) Å, Z = 2, ρ_c = 1.54 g cm^{-3}, ρ_o = 1.53(1) g cm^{-3}, linear absorption coefficient, μ = 7.03 cm^{-1}.

The crystal size is 0.23 × 0.30 × 0.37 mm, reflection measurements are on h, $\pm k$, $\pm l$ with systematic absence $0k0$ where $k = 2n + 1$. Standard reflections are 2 −1 −1 (0.032), 1 3 −2 (0.021) with esd in parentheses. Maximum 2θ = 45°, T = 22°C. Number of independent reflections, 2303; number of $I > 0$, 2224; number of variables in last cycle, 168; $R_1 = \Sigma||F_o| - |F_c||/\Sigma|F_o| = 0.0469$, $R_2 = \{\Sigma w(|F_o| - |F_c|)^2/\Sigma wF_o^2\}^{1/2} = 0.0472$. Final shift/error max. (ave.), 0.006(0.001); final difference, peak (location) 0.6 e Å^{-3} (0.32, −0.68, 0.39), valley (location), −0.5 e Å^{-3} (0.25, 0.30, 0.32), $w = (\sigma^2 + (0.03F_o)^2)^{-1}$. The density of the crystals was measured by flotation in a benzene–bromoform mixture. Intensities were also measured with use of the Nicolet P3 diffractometer and a coupled θ(crystal)–2θ(counter) scan. The methods of selection of scan rates and initial data treatment have been described (9, 10). Corrections were made for Lorentz polarization effects but not for absorption. This will make a maximum error in F_o of 1.0%.

Solution of the structure

The potassium and sulphur atoms were found from a three-dimensional Patterson map, and electron density difference syntheses revealed all other atoms.[1] Full-matrix least-squares refinement, minimizing $\Sigma w(|F_o| - |F_c|)^2$, was terminated when the maximum shift/error was less than 0.01. All non-hydrogen atoms were refined, the heavy atoms, K, S, and O and the carbon atoms attached to them being given anisotropic temperature factors. Although hydrogen atoms were located, no attempt was made to refine their positions. Throughout the refinement, scattering curves were taken from ref. 11 and anomalous dispersion corrections from ref. 12 were applied to the curves for K, S, O, N, C. The atomic positional parameters and isotropic temperature factors for non-hydrogen atoms are given in Table 1.[2]

Discussion

The isolation of the potassium salt of the 3,3,3′,3′-tetramethyl-D-cystinate anion, **A**, from a basic solution of D-penicillamine is not unexpected in light of the ease of oxidation of RS^- groups. The actual oxidation involved a transient purple species and we assume this was the radical **I**. Attempts to confirm the presence of the radical were unsuccessful. No esr signal could be obtained from solutions at room temperature, frozen solutions decolourized and no signal was obtained at 80 K.

The salt was isolated as the trihydrate and the structure of the anion is shown in Fig. 1. Bond lengths and angles are given in Table 2. The structure of the neutral disulphide has not been determined, although those of neutral *meso*-D-penicillamine disulphide, **B** (16), and of D-penicillamine disulphide, **C**, have been determined (17). We have compared our structure with these structures and also with those of the two forms of cystine (18–20), the protonated chloride and bromide salts of cystine (21–24), and *N*,*N*′-diglycyl-L-cystine (25). Most bond lengths and angles agree remarkably well with equivalent distances in the above compounds. The C—O distances in the carboxylate groups of **A** do not differ significantly (range 1.241(8) to 1.262(7) Å) like the values in the zwitterion cystine (range 1.21(2)–1.25(2) Å) and in contrast to the asymmetry in the protonated carboxylate group in the hydrochloride (C—OH 1.294(9), 1.307(8), 1.308(6) Å vs. C=O, 1.198(9), 1.182(10), 1.205(5) Å). Similarly the C—C—O angles are essentially equal (range 116.2(5)–118.4(5)°), like cystine (range 116(1)–118(1)°) and unlike the hydrohalides (C—C—OH, 112.1(5)–112.9(5)°) vs. C—C=O, 120.6(5)–122.7(3)°.

colourless purple

I

colourless

TABLE 1. Atomic positional parameters (× 10^4) and temperature factors (Å^2 × 10^3) for dipotassium 3,3,3′,3′-tetramethyl-D-cystinate trihydrate

Atom	x	y	z	U or U_{iso}[a]
C(1)	2975(11)	4455(2)	2896(11)	27(4)[a]
C(2)	2357(10)	3973(2)	3907(10)	26(1)
C(3)	4010(11)	3534(3)	4075(11)	31(4)[a]
C(4)	4096(12)	3435(3)	1693(13)	39(2)
C(5)	6498(13)	3568(3)	6073(13)	45(2)
S	2856(3)	2960(1)	5091(3)	34(1)[a]
N	2160(9)	4134(2)	6099(9)	32(1)
O(1)	5068(7)	4623(2)	3869(8)	27(3)[a]
O(2)	1366(7)	4663(2)	1161(8)	37(3)[a]
C(1′)	2271(11)	1259(3)	2517(11)	29(4)[a]
C(2′)	1316(10)	1738(3)	3233(11)	26(1)
C(3′)	484(11)	2130(2)	1195(11)	29(4)[a]
C(4′)	2386(12)	2213(3)	280(12)	40(2)
C(5′)	−1897(13)	2011(3)	−825(13)	43(2)
S′	−209(3)	2732(1)	2391(3)	34(1)[a]
N′	−463(10)	1583(2)	4099(10)	35(1)
O(1′)	824(8)	961(2)	1110(8)	33(3)[a]
O(2′)	4499(8)	1201(2)	3449(10)	47(4)[a]
K(1)	648(2)	0(0)	3388(2)	32(1)[a]
K(2)	6637(3)	635(1)	7626(3)	37(1)[a]
O(3)	6320(8)	410(2)	2100(10)	51(4)[a]
O(4)	1765(9)	736(2)	6985(8)	49(4)[a]
O(5)	6649(8)	4598(2)	10121(8)	40(3)[a]

[a] $U_{iso} = (1/3)(U_{11} + U_{22} + U_{33} + 2U_{13}\cos\beta)$.

[1] The space group chosen was $P2_1$. Space group $P2_1/m$ was not considered because it would have required both enantiomers to be present, and it seemed unlikely that under the mild conditions of preparation we would have racemized the D-penicillamine. The space group choice is justified by the successful solution of the structure.

[2] All calculations were carried out on CYBER 170/730 or CYBER 170/815 computers. Initial data treatment used the XRAY 76 package (13). The structure was solved with the SHELX package (14) and diagrams were prepared with the use of ORTEP-II (15). Tables of anisotropic temperature factors, hydrogen atom positional parameters, bond lengths and bond angles involving hydrogen, torsional angles and the moduli of F_o and F_c have been deposited and are available on request, at a nominal charge, from the Depository of Unpublished Data, CISTI, National Research Council of Canada, Ottawa, Ont., Canada K1A 0S2.

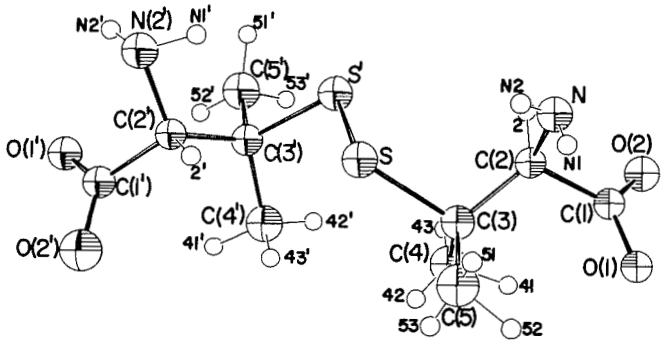

FIG. 1. The anion 3,3,3′,3′-tetramethyl-D-cystinate, showing the atom numbering. Hydrogen atoms are indicated by smaller script and affixes only.

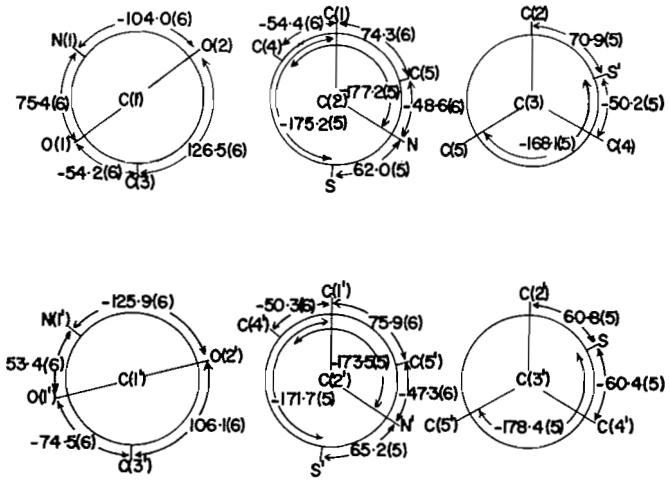

FIG. 2. Torsional angles in the 3,3,3′,3′-tetramethyl-D-cystinate anion.

One difference involves the C—S bonds. C—S bonds in thio-containing amino acids are typically 1.81–1.83 Å (26) but long bonds have been observed previously in disulphide containing amino acids (range 1.852(8) to 1.87(2) Å) (ref. 16 and references therein). However, the values observed for **A** are even larger (1.877(6), 1.891(6) Å). This is presumably because of the steric requirements of the methyl groups, since the S—S bond length (2.040(2) Å) agrees well with the others (range 2.032(4)–2.049(3) Å) (27). The C—S—S angles in **A** (108.3(2), 106.9(2)°) are very similar to the angles in **B** (107.9(3), 108.0(3)°), **C** (105.5(5), 105.5(5)°), cystine hydrochloride (104.0(4)°), and tetragonal cystine (104.1(5), 105.7(5)°) and only differ significantly from the exceptional hexagonal cystine (114.5(5)°).

The molecular anion, as with other symmetric disulphides (17), has roughly C_2 symmetry (see torsional angles in Fig. 2) and has a "right-handed" C—S—S—C conformation (20), like **C** (17) but unlike **B** (16). The C—S—S—C angle in **A**, like those in **B** (112.8(4)°) and **C** (119.4(4)°), is larger (108.7(3)°) than the normal range of 80–100° (16). Like Warner *et al.* (16), and in disagreement with Rosenfeld and Parthasarathy (17), we feel the large torsion angle is caused by repulsion between the methyl groups. Shortest H . . . H distances are H(42) . . . H(43), 2.6(1) Å, H(43) . . . H(42′), 2.6(1) Å comparable to those found by Rosenfeld and Parthasarathy (2.5–2.6(1) Å). We do not accept the argument that "the conformational difference . . . cannot be accounted for in terms of steric repulsion between the methyl groups, since . . . three shortest H . . . H . . . distances, 2.5–2.6(1) Å, are longer than the accepted . . . (Pauling) van der Waals distance of 2.4 Å" (17), since there is some ambiguity about the hydrogen van der Waals radius. Values of 1.2–1.45 Å have been used (28) and it has been argued that the latter value should be used in conformational problems of this type (29).

The carboxylate groups are antiperiplanar to the sulphur atoms, like **B** (16) and half of **C** (17) and unlike D-pencillamine (5). There are small deviations from the ideal staggered arrangements about the C(2)—C(3), C(2′)—C(3′) bonds (up to 16°) but such deviations are common and are caused by different repulsive interactions between the different sized groups.

One noteworthy feature of the conformations is the presence of very large N—C(2)—C(1)—O(1) (75.4(5)°) and N—C(2′)—C(1′)—O(1′) (53.4(6)°) torsional angles. These angles in other sulphur-containing amino acids (ref. 16 and references therein, ref. 5) are small, typically <15°, although in *meso*-penicillamine disulphide they are ~25°. In **A**, the conformation is clearly determined by interaction of the carboxylate groups

TABLE 2. Selected interatomic distances (Å) and angles (deg)

Bond	Distance	Bond	Distance
C(1)—C(2)	1.535(9)	C(1′)—C(2′)	1.541(9)
C(2)—C(3)	1.527(9)	C(2′)—C(3′)	1.552(9)
C(3)—C(4)	1.521(10)	C(3′)—C(4′)	1.511(10)
C(3)—C(5)	1.530(9)	C(3′)—C(5′)	1.524(9)
C(1)—O(1)	1.262(7)	C(1′)—O(1′)	1.241(8)
C(1)—O(2)	1.254(8)	C(1′)—O(2′)	1.261(7)
C(2)—N	1.474(8)	C(2′)—N′	1.460(8)
C(3)—S	1.891(6)	C(3′)—S′	1.877(6)
S—S′	2.040(2)	K(1)—O(1′)	2.933(5)
K(1)—O(2)[a]	2.727(5)	K(1)—O(3)[b]	2.683(5)
K(1)—N[c]	2.965(6)	K(1)—O(1)[d]	2.684(4)
K(1)—O(4)	2.827(5)	K(2)—O(2′)	2.812(6)
K(2)—O(1)[d]	2.887(5)	K(2)—O(4)	2.876(6)
K(2)—O(1′)[e]	2.746(4)	K(2)—O(2)[d]	2.817(6)
K(2)—O(3)	2.917(7)		

Atoms	Distance	Atoms	Distance
O(1′) . . . O(4)	2.901(8)	O(2) . . . O(5)	2.714(7)
O(1) . . . O(5)	2.895(8)	O(2′) . . . O(3)	2.663(8)
O(4) . . . N′	2.848(7)	O(5) . . . N	3.125(6)
O(5) . . . O(3)	2.796(7)		

Bonds	Angle	Bonds	Angle
O(1)—C(1)—O(2)	123.5(6)	O(1′)—C(1′)—O(2′)	125.6(6)
O(1)—C(1)—C(2)	118.2(5)	O(1′)—C(1′)—O(2′)	118.4(6)
O(2)—C(1)—C(2)	118.3(6)	O(2′)—C(1′)—C(2′)	116.2(5)
C(1)—C(2)—C(3)	113.1(6)	C(1′)—C(2′)—C(3′)	110.9(6)
C(1)—C(2)—N	105.2(5)	C(1′)—C(2′)—N′	107.8(6)
N—C(2)—C(3)	117.4(5)	N′—C(2′)—C(3′)	115.9(5)
C(2)—C(3)—C(4)	110.6(5)	C(2′)—C(3′)—C(4′)	110.6(5)
C(2)—C(3)—C(5)	115.7(6)	C(2′)—C(3′)—C(5′)	114.8(6)
C(2)—C(3)—S	107.8(5)	C(2′)—C(3′)—S′	107.5(5)
C(4)—C(3)—C(5)	112.1(7)	C(4′)—C(3′)—C(5′)	110.9(6)
C(4)—C(3)—S	110.4(5)	C(4′)—C(3′)—S′	111.1(5)
C(5)—C(3)—S	99.5(5)	C(5′)—C(3′)—S′	101.6(5)
C(3)—S—S′	108.3(2)	C(3′)—S′—S	106.9(2)

[a–e] Atoms are related to those in Table 2 by the transformations: *a*: $-x, y - 1/2, -z$; *b*: $x - 1, y, z$; *c*: $-x, y - 1/2, 1 - z$; *d*: $1 - x, y - 1/2, 1 - z$; *e*: $1 + x, y, 1 + z$.

Can. J. Chem. Downloaded from www.nrcresearchpress.com by 210.87.254.5 on 09/06/12
For personal use only.

TABLE 3. S . . . H and S′ . . . H non-bonded distances (Å)

Atoms	Distance	Atoms	Distance	Atoms	Distance
S . . . H(2′)	2.7(1)	S . . . H(51)	2.8(1)	S . . . H(43)	2.8(1)
S . . . H(42)	2.9(1)	S . . . H(N2)	2.9(1)	S . . . H(53)	2.9(1)
S . . . H(2)	3.0(1)	S . . . H(42′)[a]	3.0(1)	S′ . . . H(N1′)	2.5(1)
S′ . . . H(51′)	2.7(1)	S′ . . . H(2′)	2.7(1)	S′ . . . H(42′)	2.9(1)
S′ . . . H(53′)	2.9(1)	S′ . . . H(43)	3.0(1)	S′ . . . H(43′)	3.0(1)

[a]The atom is related to that in Table 1 by x, y, $1 + z$.

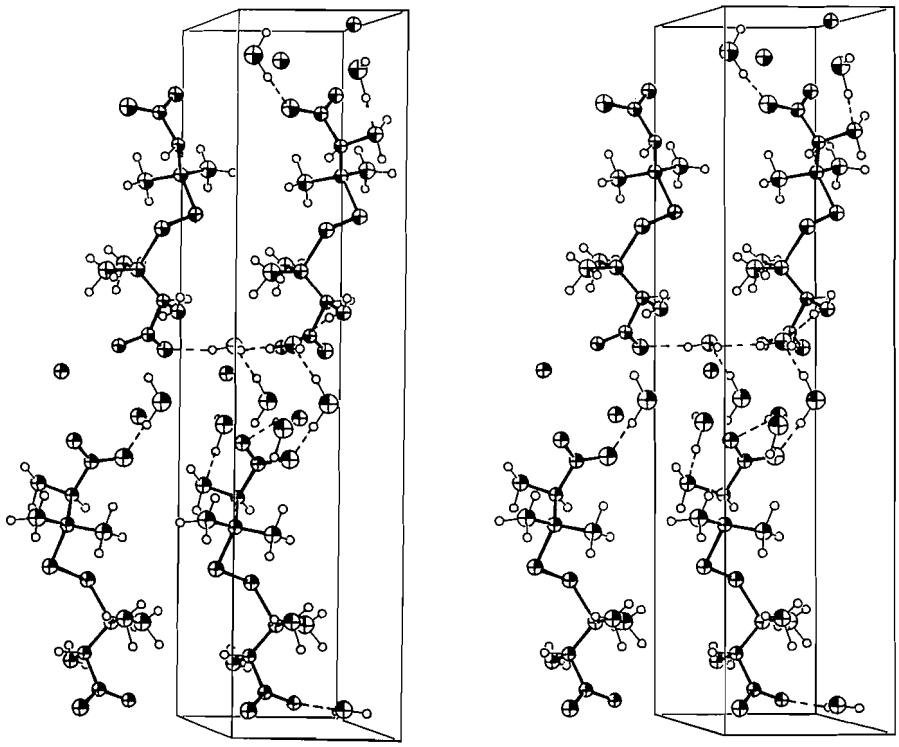

FIG. 3. The packing of dipotassium 3,3,3′,3′-tetramethyl-D-cystinate trihydrate within the unit cell. ***a*** and ***b*** are parallel to the bottom and side of the page respectively and the view is down ***c****.

with the pairs of methyl groups. The shortest O . . . H (methyl) distances are O(1) . . . H(52) 2.5(1) Å and O(1′) . . . H(52′) 2.7(1) Å which are both comparable to the van der Waals distance and any rotation of the carboxylate group to minimize the NCCO(1), O(1′) torsion angles will reduce these distances. It is noteworthy that where the repulsion is smaller (the longer O(1′) . . . H(52′) distance) the torsion angle is smaller. We have seen this effect of long-range non-bonded interactions determining the carboxylate conformation previously (30).

B has a number of S—H distances which are shorter than the van der Waals contact distance (3.05 Å) (17). We also find a number of such distances in **A** (Table 3). Two very short distances in **B** corresponded to internal NH . . . S hydrogen bonds and a similar interaction (S′ . . . H(N1′) 2.5(1) Å) is present in **A**. Otherwise, the distances are generally 0.3–0.1 Å shorter than the van der Waals distance. We find in **A** a somewhat similar distribution of hydrogen atoms to those in **B**; shorter S . . . H—C distances tend to occur in the S—S—C plane and longer distances tend to occur axial to the plane, but the distribution is not so clear-cut for **A**. Both the short H′(N1′) . . . S and long S . . . H(N2) (2.9(1) Å) hydrogen bonds are axial to the plane.

The coordination around the two potassium ions is different. Around K(1) there are six nearest neighbour atoms (O, N) forming a rough octahedron. There are also six atoms (O) around K(2), but these form a very distorted trigonal prism. The reason for the distortion is that two of the atoms are in the carboxylate group and thus are separated by only 2.2 Å. An alternative model for the coordination sphere is a square pyramid in which the apical position is filled by the two oxygen atoms of the carboxylate group.

The packing within the unit cell is shown in Fig. 3. The anions, which spiral up the ***b*** direction form layers parallel to ***ac*** and centred at $y = 1/4, 3/4$. These layers are held together by ionic bonds to potassium and hydrogen bonds to water molecules, which together form layers at roughly $y = 0, 1/2$. The hydrogen bonds, some of which are quite strong, are also important in providing bonding in the ***a*** and ***c*** directions, since the interactions between anions in the ***ac*** plane are only van der Waals. Thus O(1′) . . . O(4) . . . N′ hydrogen bonds anions related by the ***c*** translation. Water molecule, O(5), is very important since it acts as a link between translationally equivalent molecules in the ***b*** direction, through O(2′) . . . O(3) . . . O(5) . . . O(1) and also between equivalent molecules in the ***c*** (through O(7) . . . O(5) . . . N) and ***a*** (through O(1) . . . O(5) . . . O(2)) directions.

Can. J. Chem. Downloaded from www.nrcresearchpress.com by 210.87.254.5 on 09/06/12
For personal use only.

TABLE 4. Vibrational spectra of dipotassium 3,3,3′,3′-tetramethyl-D-cystinate trihydrate, wave numbers in cm^{-1}

Infrared[a]	Raman[b]	Assignments/ remarks[c]	Infrared[a]	Raman[b]	Assignments/ remarks[c]
3360(s, Δ = 300)		OH	1161(vw) }	1160(11) } × 2	rCH$_3$
3415(w)			1151(w) }	1150(5) }	
3380(w)	3378(7)		1113(s, shp)	1121(31) }	νCCN + ωNH$_2$
3357(w)	3356(8)	ν_aNH$_2$	1090(w)	1088(5) }	
3312(w)	3312(14)		988(s)	994(7)	νCC
3288(w)	3286(br, 6)	ν_sNH$_2$, νNH . . . O		980(sh, br)	ωNH$_2$
3160(s, Δ = 300)	3160(br, 2)	νOH . . . O		944(6)	ωNH$_2$
3000(w)	3000(23)		927(s, Δ = 25)	926(7, br)	rCH$_3$; in-phase
	2988(sh) }	ν_aCH$_3$	904(m)	902(33)	
2982(m)	2982(33) }		831(w) }	824(sh) }	rNH$_2$
2970(w)	2968(26) }	Several components	808(m) }	806(8) }	
2962(m)	2962(23) }		776(w) }	772(13) }	
2942(w)			768(w) }	764(10) }	
2926(w) }	2926(39) }	ν_sCH$_3$	748(m)	746(sh)	rCH$_3$
2912(w) }	2914(33) }				
2870(w)	2898(20)		719(w)		
	2870(sh) }	νCH	635(sh)		
	2860(12) }		615(ms, shp) Δ = 100	614(33)	ν_sC—S
	2750(3)	2 × 1375	602(ms)		ν_aC—S
	2704(3)	2 × 1352	558(vw, sh)		
2266(m, Δ = 150)		νN—H . . . O; hydrogen bonded	539(ms, shp)	540(100)	νS—S
			441(m, Δ = 18)	440(4)	
1666(sh, br)		δH—O—H; hydrogen bonded	404(m)	406(sh)	
1596(m) Δ = 40	1585(3, Δ = 30)	ν_aCO$_2$			
1560(m) } Δ = 60	1556(4) } Δ = 50	δNH$_2$; hydrogen bonded		394(6)	
1541(m) }	1536(4) }			380(11)	
1478(w)	1472(2)		366	362(8)	δCCO
1462(m, shp) } × 2	1458(7) }	δ_aCH$_3$	340(w)	342(6)	
1445(vw, sh) }	1450(5) }		324	326(9)	δCCS
	1438(6)			272(20)	δCSS
1411(s, Δ = 40)	1418(12)	ν_sCO$_2^-$		168(9)	
1381(m,shp)	1378(5)	δ_sCH$_3$, in-phase		142(24)	
1360(m) }	1356(7)			110(20)	
1347(m) }	1346(4)	δ_sCH$_3$, out-of-phase		90(26)	
1308(m) }	1306(6) }	τNH$_2$		70(6)	
1293(m) }	1290(6) }			62(28)	
1202(mw) }	1202(11) } × 2	νCN			
1108(mw) }	1188(4) }				

[a] Infrared notations: intensities, s = strong, m = medium, w = weak, br = broad, shp = sharp, sh = shoulder, v = very; Δ = full-width at half-maximum in cm^{-1}.

[b] Raman intensities, in parentheses, relative to the 540 cm^{-1} band, arbitrary intensity 100.

[c] Assignment notations: ν = stretching vibration; δ = deformation; s = symmetric; a = antisymmetric; τ = twist; r = rock; ω = wag.

The spectra and assignments for solid D-penicillamine disulphides are shown in Table 4. The spectra are very similar to those for D-penicillamine but show a general doubling of many of the bands. The νS—H and δS—H bands are absent, and the bands of the NH_3^+ group are replaced by those of the NH_2 group which show small shifts. The 700–500 cm^{-1} region is complicated by the fact that bands for the δCOOH, δCO_2^-, νC—S, and νS—S modes all occur in the same region. All these modes are fairly strong in the Raman spectra and should be good diagnostic bands if positively assigned. The fact that the band widths (in both Raman and infrared) differ is a help in the assignment; the CO_2^- and NH_2, NH_3^+ group bands are very broad, and the C—S and S—S bands very sharp.

In the lower frequency region new bands occur because of the disulphide bond: one νS—S and two νC—S are expected as well as a δCSS. These are assigned as shown in Table 4. The νS—S seems surprisingly high at first (very close to νC—S in D-penicillamine), but a search of related work suggests that 540 cm^{-1} is a reasonable value for νS—S in D-penicillamine disulphide (31, 32). Firstly, an examination of ranges of vibrational frequencies observed for νC—S and νS—S shows that these ranges do overlap, and νC—S in one compound can be lower than νS—S in another. For example, trithioacetone has νC—S at 513 cm^{-1}, diphenyl disulphide has νS—S at 542 cm^{-1}, as shown in Table 5. Secondly, work on sulphides and disulphides shows that νC—S decreases and νS—S increases with the number of CH_3 groups substituted adjacent to the sulphur atom. The addition of CH_3 groups may be expected to result in an increase in the C—S bond length, which was observed, with a consequent strengthening and shortening of the S—S bond, although this was not detected. Thus these two bands approach each other, and may even coincide. Table 5 shows that all the tertiary disulphides have an intense νS—S band near 540 cm^{-1}, as do di-*tert*-butyl and di-*tert*-pentyl disulphides. Diphenyl disulphide differs structurally from D-penicillamine disulphide (the phenyl ring substitution differs from tertiary alkyl substi-

Can. J. Chem. Downloaded from www.nrcresearchpress.com by 210.87.254.5 on 09/06/12
For personal use only.

TABLE 5. Comparison of wavenumbers (cm^{-1}) and distances (Å) for C—S and S—S bonds

Compound	S—S bonds		C—S bonds	
	ν, cm^{-1}	Å	ν, cm^{-1}	Å
Di-*tert*-butyl disulphide[a]	540 s		569 vs	
Di-*tert*-pentyl sulphide[a] (liquids)	541 s		560 vs	
Diphenyl disulphide[b] (solid)	542 vs	2.03	613 s	1.81,1.79
D-Penicillamine disulphide[c]	543 vs	2.049	614 s	1.866
2,2′-Biphenyl disulphide[b]	522 vs	2.05		1.757
SSC 98.2° (CS—SC) 69°				
Hexamethyl-*S*-trithiane[d]			513	
5-Thia-10,11-diazadispiro[3.1.3.2]undecane[d]			547	
6,7,13,14-Tetrathiadispiro[4.2.4.2]tetradecane[e]	541		541[f]	
7,8,15,16-Tetrathiadispiro[5.2.5.2]hexadecane[e]	547		547[f]	

[a] Reference 32.
[b] Reference 33.
[c] Reference 17.
[d] Reference 31, p. 223.
[e] Reference 31, p. 234.
[f] Apparent coincidence of νS—S and νC—S.

TABLE 6. ^{1}H nmr Measurements (δ in ppm from TMS)[a]

Functional group	δ in D_2O
pro R C(5)H_3	1.17
pro S C(4)H_3	1.27
C(2)H	3.17

[a] Solution ~0.1 *M*.

tution, in geometry and in amount of strain), but in the solid state is known to have conformations with low values (0–20°) of χSS—CC across its C—S bonds (in contrast with solutions). Since diphenyl disulphide has no COOH or CO_2^- group, there is no ambiguity about the assignment of the 542 cm^{-1} band to νS—S. Factors causing variations in frequency of νS—S bands of alkyl and cystine-related disulphides correlate with conformations of the CCSSCC moiety (7, 8).

The proton nmr of **A** is shown in Table 6. The assignment is made by comparison with penicillin (34). The presence of only two methyl signals and one CH signal suggests that the rough C_2 symmetry observed in the solid becomes exact, on average, in solution.

Acknowledgements

We thank the Natural Sciences and Engineering Research Council of Canada and McMaster University Science and Engineering Research Board for financial support of this work.

1. W. M. WEIGERT, H. OFFERMANNS, and P. SCHERBERICK. Angew. Chem. Internat. Ed. **14**, 330 (1975).
2. J. M. WALSHE. Am. J. Med. **2**, 487 (1956).
3. H. E. HOWARD-LOCK, W. F. KEAN, C. J. L. LOCK, A. MEWA, and P. S. SMALLEY. Seminars in Rheumatology. To be published.
4. K. J. FRANKLIN, H. E. HOWARD-LOCK, and C. J. L. LOCK. Inorg. Chem. **21**, 1941 (1982).
5. H. E. HOWARD-LOCK, C. J. L. LOCK, and P. S. SMALLEY. J. Cryst. Spectrosc. Res. **13**, 333 (1983).
6. D. R. LECAVALIER and J. C. CRAWHALL. J. Rheum. **8** (Supp. 7), 20 (1981).
7. F. PLANAS-BOHNE. J. Rheum. **8** (Supp. 7), 35 (1981).
8. G. L. ELLMAN. Archives Biochem. Biophys. **82**, 70 (1959).
9. B. LIPPERT, C. J. L. LOCK, B. ROSENBERG, and M. ZVAGULIS. Inorg. Chem. **16**, 1525 (1977).
10. R. P. HUGHES, N. KRISHNAMACHARI, C. J. L. LOCK, J. POWELL, and G. TURNER. Inorg. Chem. **16**, 314 (1977).
11. D. T. CROMER and J. T. WABER. *In* International tables for crystallography. Vol. IV. *Edited by* J. A. Ibers and W. C. Hamilton. Kynoch Press, Birmingham, England. Table 2.2B. pp. 99–101.
12. D. T. CROMER. *In* International tables for crystallography. Vol. IV. *Edited by* J. A. Ibers and W. C. Hamilton. Kynoch Press, Birmingham, England. Table 2.3.1. pp. 149, 150.
13. J. M. STEWART. The XRAY 76 System. Tech. Rep. TR-446, Computer Science Center, University of Maryland, College Park, MD. 1976.
14. G. M. SHELDRICK. SHELX, Programme for crystal structure determination. Cambridge University, England. 1976.
15. C. K. JOHNSON. ORTEP-II. Report ORNL-5138, Oak Ridge National Laboratory, TN. 1976.
16. L. G. WARNER, T. OTTERSEN, and K. SEFF. Acta Crystallogr. B**30**, 1077 (1974).
17. R. E. ROSENFELD and R. PARTHASARATHY. Acta Crystallogr. B**31**, 462 (1975).
18. B. M. OUGHTON and P. M. HARRISON. Acta Crystallogr. **10**, 479 (1957).
19. B. M. OUGHTON and P. M. HARRISON. Acta Crystallogr. **12**, 396 (1959).
20. M. O. CHANEY and L. K. STEINRAUF. Acta Crystallogr. B**30**, 711 (1974).
21. L. K. STEINRAUF, J. PETERSON, and L. H. JENSEN. J. Am. Chem. Soc. **83**, 4445 (1958).
22. S. C. GUPTA, A. SEQUEIRA, and R. CHIDAMBARAM. Acta Crystallogr. B**30**, 562 (1974).
23. D. D. JONES, I. BERNAL, M. N. FREY, and T. F. KOETZLE. Acta Crystallogr. B**30**, 1220 (1974).
24. J. PETERSON, L. K. STEINRAUF, and L. H. JENSEN. Acta Crystallogr. **13**, 104 (1960).
25. H. L. YAKEL and E. W. HUGHES. Acta Crystallogr. **7**, 291 (1954).
26. E. G. COX and G. A. JEFFREY. Proc. R. Soc. A**207**, 110 (1951).
27. T. OTTERSEN, L. G. WARNER and K. SEFF. Chem. Commun. 876 (1973).
28. J. E. HUHEEY. Inorganic chemistry, 2nd ed. Harper and Row, New York. 1978.
29. N. L. ALLMIGER, J. A. HIRSCH, M. A. MILLER, I. J. TYMINSKI, and F. A. VAN-CATLEDGE. J. Am. Chem. Soc. **90**, 1199 (1968).
30. A. CALVO, R. FAGGIANI, D. A. HARVEY, W. F. KEAN, H. E. HOWARD-LOCK, and C. J. L. LOCK. J. Cryst. Spectrosc. Res. **14**, 59 (1984).

Can. J. Chem. Downloaded from www.nrcresearchpress.com by 210.87.254.5 on 09/06/12
For personal use only.

31. S. K. FREEMAN. Applications of laser Raman spectroscopy. John Wiley and Sons, New York. 1974.
32. H. E. VAN WART and H. A. SCHERAGA. J. Phys. Chem. **80**, 1812 (1976).
33. H. E. VAN WART and H. A. SCHERAGA. J. Phys. Chem. **80**, 1823 (1976).
34. R. A. ARCHER, R. D. G. COOPER, P. V. DEMARCO, and L. F. JOHNSON. Chem. Commun. 1291 (1970).

Can. J. Chem. Downloaded from www.nrcresearchpress.com by 210.87.254.5 on 09/06/12
For personal use only.

Vibrational spectral studies of solutions at elevated temperatures and pressures. VI. Raman studies of perchloric acid

C. I. RATCLIFFE[1] AND D. E. IRISH

Guelph–Waterloo Centre for Graduate Work in Chemistry, Waterloo Campus, Department of Chemistry, University of Waterloo, Waterloo, Ont., Canada N2L 3G1

Received October 24, 1983

C. I. RATCLIFFE and D. E. IRISH. Can. J. Chem. **62**, 1134 (1984).

Raman spectra of perchloric acid in water have been measured for solutions spanning a wide concentration range and, for two specific concentrations, a wide range of temperatures. The acid is completely dissociated down to a water:acid mole ratio of about 1.8 at room temperature. At elevated temperatures it is still a very "strong" acid. As the concentration increases the apparent symmetry of the ClO_4^- ion decreases and a small amount of a new species assigned as associated $ClO_4^- \cdot (H_{aq})^+$ can be detected. The effects on the OH stretching bands of water, of temperature, ClO_4^-, and the excess acid protons are discussed.

C. I. RATCLIFFE et D. E. IRISH. Can. J. Chem. **62**, 1134 (1984).

On a mesuré les spectres Raman de l'acide perchlorique en solution aqueuse pour un large intervalle de concentrations et également, pour deux concentrations spécifiques, pour un large intervalle de températures. A la température ambiante, l'acide est complètement dissocié jusqu'à un rapport molaire eau:acid d'environ 1,8. A des températures plus élevées, l'acide demeure un acide très "fort". Lorsque la concentration augmente, la symétrie apparente de l'ion ClO_4^- diminue et on peut déceler la présence d'une faible quantité d'une nouvelle espèce identifiée comme étant l'ion associé $ClO_4^- \cdot (H_{aq})^+$. On discute des effets de la température, du ClO_4^- et des protons acides en excès sur les bandes d'élongation OH de l'eau.

[Traduit par le journal]

Can. J. Chem. Downloaded from www.nrcresearchpress.com by 210.87.254.105 on 09/06/12
For personal use only.

Introduction

As the temperature of water rises K_w increases (1, 2) and hydrolysis reactions are encountered more frequently in salt–water mixtures (3, 4). Such reactions can be controlled or prevented, of course, by controlling the acidity. At ambient temperatures perchloric acid is often used to control pH because the perchlorate ion does not complex with most cations and the acid is strong. (A recent determination suggests that there is no association above a water:acid mole ratio, $N = n_{H_2O}/n_{acid}$, of 1.8 (5).) Thus competing equilibria can frequently be neglected. When studying the properties of salts in water at elevated temperatures, it is important to know if these useful properties of perchloric acid are retained. Also, for the measurement of relative integrated Raman band intensities, an internal intensity standard is generally employed and at moderate temperatures the ν_1 line of the perchlorate ion is most frequently the preference for the reasons cited above. Thus, for our longer term goals, knowledge of the temperature dependence of the Raman spectra of aqueous solutions of perchloric acid is essential. It was also of interest to see if the much reduced dielectric constant of water at higher temperatures might promote formation of $HClO_4$. (Nitric and sulfuric acids show markedly enhanced association as the temperature increases.)

Swaddle *et al.* (6) have studied the kinetics of decomposition of 1.1–6.6 *m* aqueous perchloric acid in the range 295–332°C. (At 250°C very little, if any, decomposition occurs at these concentrations.) The reaction is autocatalytic and the overall stoichiometry is

$$4H^+ + 4ClO_4^- \rightarrow 2H_2O + 2Cl_2 + 7O_2$$

With two exceptions (7, 8), the Raman spectroscopy of perchloric acid solutions has received little attention in recent years. Most of the early studies (9–13) were attempts to determine the degree of dissociation α at various concentrations, using intensity measurements of the symmetric stretching mode ν_1 of the ClO_4^- ion. Studies were also made of the line broadening on increasing acid concentration; the broadening is thought to be due in part to rapid proton exchange and possibly from changes in solvent structure (14, 15). It will be seen later that the presence of a low frequency asymmetry in the lineshape of the ν_1 band may introduce a complication into the interpretation of the measurements of its intensity and line broadening, which was not recognised at the time. (Kreevoy and Mead (14) were the only ones to remark upon the asymmetry and it may be that the feature was obscured in most instances by the use of large slitwidths.)

There have been several ir and Raman studies of solid perchloric acid monohydrate (16–21) and dihydrate (22). Taylor and Vidale (18) obtained the Raman spectrum of a single crystal of the monohydrate and confirmed that its composition is $H_3O^+ \cdot ClO_4^-$. They also showed that the melt contains a significant proportion of molecular $HClO_4$. The ir of solid, liquid, and gaseous molecular $HClO_4$ and $DClO_4$, and the Raman of the solid and liquid have been studied by Karelin *et al.* (23, 24).

The most relevant works in the current context are as follows. (*a*) The Raman and ir study by Chernykh *et al.* (7). They showed that at higher concentrations the degeneracy of the ν_3 (F_2) mode of ClO_4^- is apparently lifted and ν_1 begins to appear in the ir (not allowed for T_d symmetry). Ion pairing of H_3O^+ and ClO_4^- was postulated. (*b*) The ir study of a large range of compositions ($N = 0 \rightarrow \infty$) by Leuchs and Zundel (5). They monitored the intensity of one of the bands of $HClO_4$ as N increased and found essentially complete dissociation at $N = 1.8$, in agreement with an nmr determination by Duerst (25). Apart from these measurements of α, Leuchs and Zundel were more concerned with the spectroscopy of the OH groups of $HClO_4$, H_2O, and $(H_{aq})^+$. The form of $(H_{aq})^+$ is of great interest, particularly with respect to the question of whether H_3O^+ and $H_5O_2^+$ exist as discrete entities in solution. (*c*) The Raman and ir study of glassy and liquid perchloric acid dihydrate by Thi *et al.* (8). This work, which appeared towards the end of the study being presented here, also included some spectra of the monohydrate and liquid $HClO_4$. They concluded that there is

[1] Present address: Chemistry Division, National Research Council of Canada, Ottawa, Ont., Canada K1A 0R6.

Can. J. Chem. Downloaded from www.nrcresearchpress.com by 210.87.254.105 on 09/06/12
For personal use only.

no $HClO_4$ or H_3O^+ in the $N = 2$ liquid or disordered states and that the acid proton is largely present as $H_5O_2^+$. They note that the lifting of the degeneracy of ν_3 of ClO_4^- implies some kind of interaction and assign shoulders on the low and high frequency sides of the ν_1 band to associated ionic and hydrogen bonded complex species respectively. (While this paper presents some very useful and interesting results we would question some of its conclusions.)

The effect of ClO_4^- on the vibrational bands of water is the subject of much ir and Raman literature (e.g. 26–35), because of the so-called structure-breaking effect; i.e. ClO_4^- produces an increase in the intensity of the high frequency end of the broad OH stretching band of water, implying an increase in the number of more weakly hydrogen bonded OH groups. In the case of the acid this is further complicated by the presence of $(H_{aq})^+$. So far the only spectroscopic work on the effects of ClO_4^- on the bands of water at high temperatures is the ir study of aqueous $NaClO_4$ by Valyashko *et al.* (36).

Experimental

Raman spectra were obtained using a digital drive, Jarrell-Ash 25-100 spectrometer (1 meter double Czerny-Turner monochromator), with an RCA 31034 photomultiplier and an SSR model 1105/1120 photon counting system. The 488.0 nm and 514.5 nm lines of a Spectra Physics Argon Ion Laser, model 165-03 were used for excitation. Instrument control and data collection were performed by means of a 32 K-byte PET Commodore computer.

The solutions were prepared using distilled water, 70–72% $HClO_4$ and 38% HCl (both J. T. Baker Analysed Reagents). The various concentrations were obtained volumetrically by diluting volumes of the stock acid solutions, and the acid concentrations were determined by titration. The densities of the solutions were measured in order to calculate mole ratios. Samples at lower acid concentrations were filtered through Millipore 0.6 μm polyvic filters before injection into the sample tubes. (The filters were attacked by acid at high concentrations.) To obtain spectra at ≈3°C and 25°C the samples were contained in sealed, thin-walled capillary tubes, which were held in a thermostatted copper block. The thick-walled, Pyrex glass capillary cells, high pressure system, and furnace, which have been described earlier (37), were used to obtain spectra of 5 *m* perchloric acid (N = 11.04) up to 300°C and of the 71% acid (N = 2.44) up to 200°C. (When an attempt was made to reach higher temperatures at this latter concentration, the generation of gas bubbles from decomposition of the acid was such that it became impossible to obtain a spectrum.)

The pressures of up to 11 MPa, used to maintain the liquid phase as the temperature was increased, are much too small to maintain a constant density. Consequently the concentration varies with temperature and for this reason the solutions are best characterised by their temperature-independent parameters – molality (mol kg^{-1} solvent) or mole ratio N. The mole ratio N will be used throughout this paper since it has more meaning on the molecular scale.

A sample of the solid perchloric acid monohydrate, under a small excess of concentrated acid (liquid) and sealed in a clear glass vial, was kindly supplied by the G. Frederick Smith Chemical Company. Spectra of the solid and molten monohydrate, and of the concentrated solution were obtained without opening the vial. (It was possible to melt a volume of the solid, *out of contact with the solution*, by resting the vial against the thermostatted copper block held at 60°C.) It is possible to obtain a good estimate of the mole ratio of the concentrated solution: since the solution is in equilibrium with solid monohydrate it should have a melting point at about room temperature (25–26°C). Using the freezing point curve of van Wyk (38) (and see also Brickwedde (39)), this corresponds to a composition of ≈79% $HClO_4$. (The melting point was actually checked by rapidly freezing the liquid, by dipping the vial in ice-water, and then observing the melting range, 22–33°C, though the bulk of the material melted in the range 24–28°C.) For this composition the mole ratio is therefore 1.5 ± 0.1, where the estimated error is rather pessimistic.

The explosive properties of highly concentrated $HClO_4$ and of perchlorates are well known and due care was exercised when handling the monohydrate and during the high temperature experiments.

Parallel ($I_\parallel$) and perpendicular ($I_\perp$) polarised spectra were obtained in many instances in order to observe the depolarisation ratio behaviour and to permit calculation of the isotropic spectra.

$$I_{iso} = I_\parallel - \frac{4}{3} I_\perp$$

$$I_{aniso} = \frac{4}{3} I_\perp$$

This proved to be very useful in clarifying and interpreting a number of features of the spectra.

Results and discussion

The results will be divided into two main sections, one concerning the bands of ClO_4^- and $HClO_4$ below 1400 cm^{-1} and the second concerning the O—H bands of the aqueous medium.

Section I. Vibrations of the ClO_4 unit

(a) Symmetry considerations

Before discussing the spectra it is useful to consider the effects of the possible perturbations on the symmetry of the ClO_4 unit and the corresponding spectroscopic activity of the modes. For equal extension or contraction of all 4Cl—O bonds the T_d symmetry is retained; extension or contraction of one Cl—O bond leads to C_{3v} symmetry; equal distortion of 2Cl—O bonds leads to C_{2v} symmetry; unequal distortion of 2Cl—O bonds leads to C_s symmetry; any other less symmetric distortion leads to C_1 symmetry. The correlation of the mode symmetries is presented in Table 1. Note that *any* distortion from T_d symmetry causes ν_1 and ν_2 to become ir allowed.

(b) Molecular $HClO_4$

At mole ratios down to about $N = 10$ the Raman spectrum of aqueous perchloric acid is essentially the same as that of perchlorate salts, with four well-defined bands which behave according to T_d symmetry. As the mole ratio decreases below $N = 10$, changes appear in the ν_1 and ν_3 region which become progressively more pronounced. Only at the very highest concentrations studied (N = 1.5 and 1) does an entirely *separate* set of bands due to $HClO_4$ begin to appear (see Fig. 1). There was no trace of molecular $HClO_4$ in the $N = 2.44$ solution at 25°C. This observation is in agreement with Zundel's (5) value of $N \leq 1.8$ for the appearance of $HClO_4$ in the ir spectrum. The $HClO_4$ Raman bands decrease in intensity by a factor of about ten relative to the ClO_4^- bands on going from N = 1 to 1.5; using Zundel's (5) value of $\alpha \approx 0.7$ for $N = 1$ a value of $\alpha \approx 0.96$ can be calculated for the $N = 1.5$ solution. This lends further weight to the original estimate of $N \approx 1.5$ for this solution, as this value for α falls at the correct point on Zundel's plot of α versus N.

The Raman spectrum of molecular $HClO_4$ in aqueous medium has not been reported previously, Table 2. It was found possible to subtract a ratio of the $N = 1.5$ spectrum from the $N = 1$ spectrum such that much of the ClO_4^- spectrum was removed. This subtraction enabled the determination of the frequencies of the weaker bands of $HClO_4$, specifically at 432 and 1220 cm^{-1}. The doublet at 578 and 585 cm^{-1} could readily be distinguished by using the isotropic and anisotropic spectra, since the band at 578 cm^{-1} is quite strongly polarised. This spectrum and the polarisation behaviour are consistent with a

TABLE 1. Possible normal modes and symmetries of ClO_4^-

	T_d	C_{3v}	C_{2v}	C_s	C_1
ν_1	A_1	A_1	A_1	A'	A
ν_2	E	E	$(A_1 + A_2)$	$(A' + A'')$	$2A$
ν_3, ν_4	F_2	$(A_1 + E)$	$(A_1 + B_1 + B_2)$	$(2A' + A'')$	$3A$
Infrared activity	F_2	All	$A_1B_1B_2$	All	All
Raman activity	← All modes →				

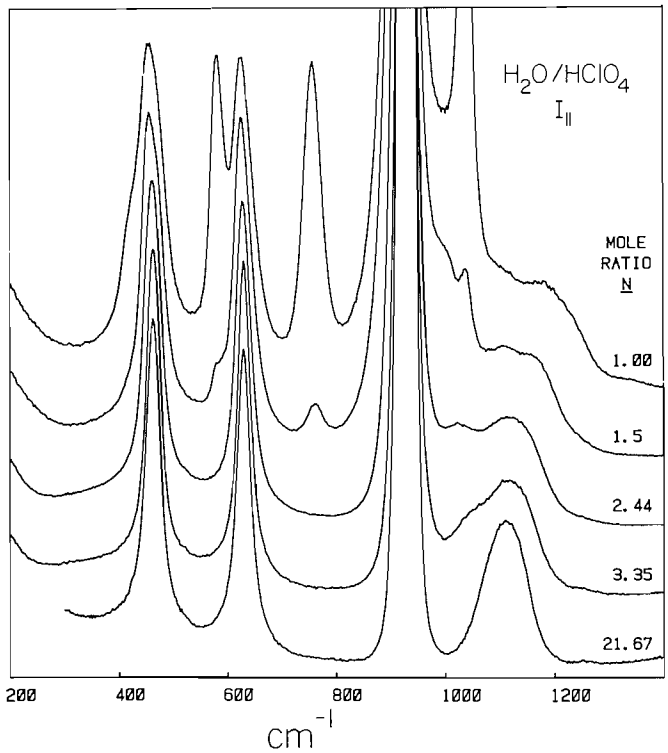

FIG. 1. Raman spectra ($I_{\parallel}$) of perchloric acid in the 200–1400 cm^{-1} region at the mole ratios indicated and 25°C.

very nearly C_{3v} character for the ClO_4 unit vibrations (similarly for pure liquid $HClO_4$ (23)); only when studied in detail in the gas phase does the true C_s character of $HClO_4$ become apparent (23).

In the aqueous mixture the stretching modes all shift to higher frequencies than the values reported for the pure liquid $HClO_4$ (23). The largest shift occurs for the Cl—O(H) stretching mode. It is likely that these shifts are due in part to different hydrogen bonding interactions: in pure $HClO_4$ the hydrogen bonding interaction has to be with other $HClO_4$ molecules, whereas in the aqueous mixtures the interaction is more likely to be with water or protonated water molecules.

In Fig. 1 it is clear that the spectra of ClO_4^- and $HClO_4$ are readily distinguishable. There can then be no doubt that the spectrum of the $N = 2.44$ solution at 200°C (Fig. 2) shows the presence of a very small amount of $HClO_4$. The bands at 757 and 1039 cm^{-1} are quite clear, although it should be noted that *some* of the apparent intensity increase in the 1039 cm^{-1} region is due to increased overlap of the ClO_4^- bands, which are broader at higher temperatures. It is also clear that the ν_2 and ν_4 bands of ClO_4^- show asymmetric broadenings to their low

TABLE 2. Raman bands (cm^{-1}) of molecular $HClO_4$ in the $N = 1$ mixture

$HClO_4$ $N = 1$	$HClO_4$ liquid (23)	Assignment
≈432	432	$\rho(ClO_3)$
578 p	577 p	$\delta_s(ClO_3)$
≈585	586	$\delta_{as}(ClO_3)$
757 p	742 p	ν(Cl—OH)
1039 p	1034 p	$\nu_s(ClO_3)$
1220	1209	$\nu_{as}(ClO_3)$

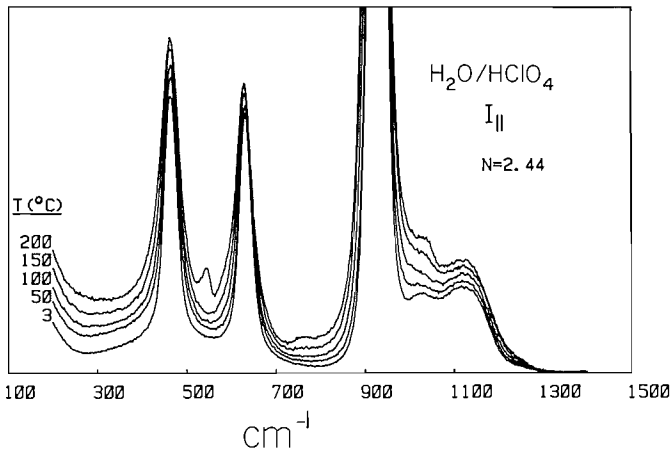

FIG. 2. Raman spectra ($I_{\parallel}$) of $N = 2.44$ perchloric acid in the 200–1400 cm^{-1} region, at the temperatures indicated.

frequency sides, due to the overlapping $HClO_4$ bands in these regions. It may be estimated, in the same manner as for the $N = 1.5$ solution earlier, that $\alpha \approx 0.99$ for this $N = 2.44$ solution at 200°C. (The amount of $HClO_4$ present can be estimated from the relative band intensities to be about 1/30th of that in the $N = 1$ solution.) The spectra of the $N = 11.04$ solution showed no trace of $HClO_4$ even at 300°C. This evidence indicates that perchloric acid is still a "strong" acid at such elevated temperatures.

Digressing slightly from the main theme, it should be mentioned here that the stretching modes of the dissolved decomposition products of perchloric acid, namely Cl_2 and O_2, could also be readily detected in the Raman spectra after periods at high temperature. The band due to Cl_2 at 542 cm^{-1} is visible in the 200°C spectrum of Fig. 2. The O_2 band was seen at ≈ 1549 cm^{-1}. These frequencies are somewhat lower than the gas phase values of 556 and 1554.7 cm^{-1} given by Herzberg (40).

(c) The ClO_4^- ion

With the exception of one feature the Raman spectra of solutions with $N > 10$ contain the characteristic four lines expected from a tetrahedral species (Table 3). But the ν_1 band has a very pronounced shoulder on its low frequency side. This band could have several origins and many experiments were performed to narrow down the possibilities, but a completely satisfactory explanation has not been found.

So far as we have been able to determine the shoulder appears in *all* spectra of aqueous solutions of ClO_4^- at all concentrations. It is strongly polarised, just as is the main ν_1 band. There is also evidence of its presence in spectra of ClO_4^- in organic solvents (this work and refs. 41 and 42), although overlapping solvent bands frequently mask the observation. For both aqueous perchloric acid and for $NaClO_4$ solutions the

Can. J. Chem. Downloaded from www.nrcresearchpress.com by 210.87.254.105 on 09/06/12
For personal use only.

TABLE 3. Frequencies of ClO_4^- at various mole ratios (values in cm^{-1})

Ratio (N)	>10‡	3.35	2.44	1.5	1.0 Melt ≈55°C	1.0 Solid
$\nu_2(E)$	462	462	462	457 +sh ≈475	457.5 +sh ≈480	457 +sh
$\nu_4(F_2)$	629	629	629	627 + asym.	626 + asym.	627 + asym.
	*−sh 927.7 p	*−sh 926.3 p	*−sh 924.5 p	*−sh 924.7 p	−sh p	−sh
$\nu_1(A_1)$	934.5 p	932.7 p +sh ≈1010 p	931.5 p +sh ≈1010 p	930.9 p +sh ≈1010 p	931 p +sh p	924
						995
		*1055	*1046	*1018	−sh	
$\nu_3(F_2)$	1113	*1112	*1110	*1111	1112	1110
		*1152	*1160	*1177	1170	1163
T_d	T_d	C_{3v} or lower symmetry			Lower than C_{3v}	C_s

* Values from bandfitting.

‡ For all concentrations with $N > 10$ the four frequencies were essentially constant within the accuracy of the experiment, although the bandwidths increased as N decreased.

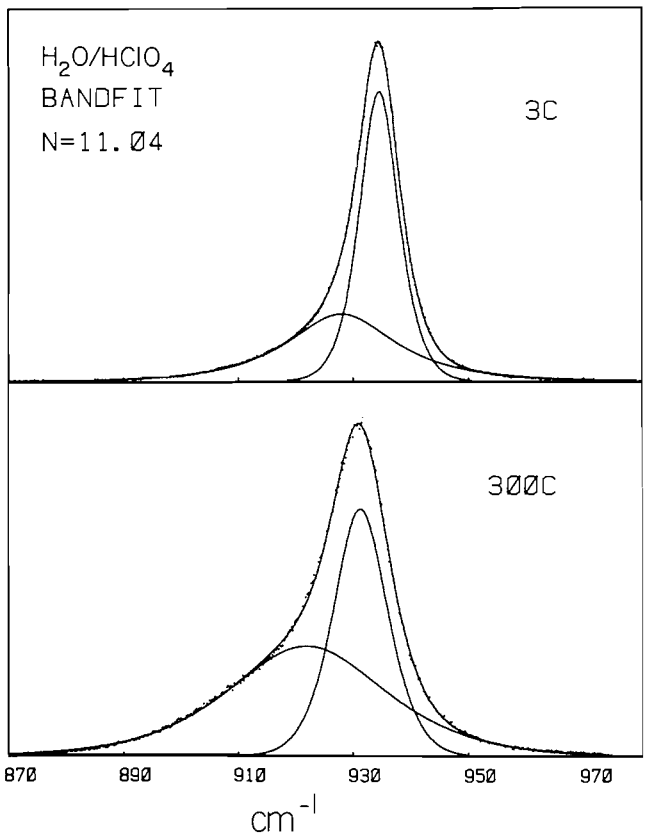

FIG. 3. The effect of temperature and results of bandfitting of the $\nu_1(ClO_4^-)$ band and its low frequency shoulder (N = 11.04).

intensity of the shoulder appears to increase relative to the main ν_1 band as either the concentration or the temperature (Fig. 3) is increased. However, these two effects are complicated by an overall broadening of the entire ν_1 band profile as concentration of acid is increased, attributed to proton transfer (14, 15), and as temperature is increased, in which case all bands of ClO_4^- broaden. Using the program BNDFT (43) good fits to the band profile were obtained with two symmetrical component bands (Fig. 3). These BNDFT results neglect a very much weaker and broader shoulder on the high frequency side of ν_1 which appears for the more concentrated solutions and which will be discussed later.

One explanation of the low frequency shoulder is that it is an enhanced $2\nu_2$ ($A_1 + E$) overtone in Fermi resonance with ν_1 (A_1) (*cf.* the spectrum of CCl_4 (44)). This correlates with the absence of a shoulder on the ν_1 band of SO_4^{2-} ion and IO_4^- ion; for these ions $2\nu_2$ is not sufficiently close in frequency to ν_1. The appearance of $2\nu_2$, sometimes as a distinct band (or bands if crystal field splittings are detected), has been established in spectra of molten perchlorate salts (45) and solids (this work and refs. 46–48).

Two facts are difficult to rationalize if Fermi resonance is invoked. The BNDFT results put the band due to the shoulder at a frequency of 928 cm^{-1}, *above* 2 × ν_2 (924 cm^{-1}) rather than below as expected, with a bandwidth of 22 cm^{-1}, which is *less* than that of ν_2 (26 cm^{-1}). (These values are for solutions at +3°C; at 300°C the frequencies are equal at 922 cm^{-1}.) Admittedly one might question the validity of bandfitting when Fermi resonance is involved. Also the large intensity increase of the shoulder with increase of temperature is not accounted for by Fermi resonance.

A second possibility is that the shoulder arises from a hot band (e.g. hot bands have been observed in the gas phase spectra of $FClO_3$ (49)). This raises the question of why this should occur for ClO_4^- and not for IO_4^- and SO_4^{2-}? Also the temperature dependence of the intensity does not follow the expected pattern: If the sideband is a hot band ν_1', then the intensity ratio of ν_1'/ν_1 should vary with temperature according to the Maxwell–Boltzmann populations of the excited state from which the ν_1' transition occurs and the ground state from which the ν_1 transition occurs; i.e.

$$\frac{I(\nu_1')}{I(\nu_1)} \alpha \exp(-\nu_E/kT)$$

where ν_E is the energy of the excited state relative to the ground state. Assuming that we are dealing with the first excited level of ν_2, a plot of ln $(I(\nu_1')/I(\nu_1))$ vs. $1/T$ should therefore be linear with a slope $-\nu_E/k$. The plot obtained using the intensities from BNDFT for the N = 11.04 sample at different temperatures is distinctly curved with tangential slopes which would give a range for ν_E of 160 to 580 cm^{-1} between 50 and 300°C. (Contrast this with ν_2 = 462 cm^{-1}.) Thus the hot band hypothesis is weakened.

A third possibility is that the shoulder arises from a new

Can. J. Chem. Downloaded from www.nrcresearchpress.com by 210.87.254.105 on 09/06/12
For personal use only.

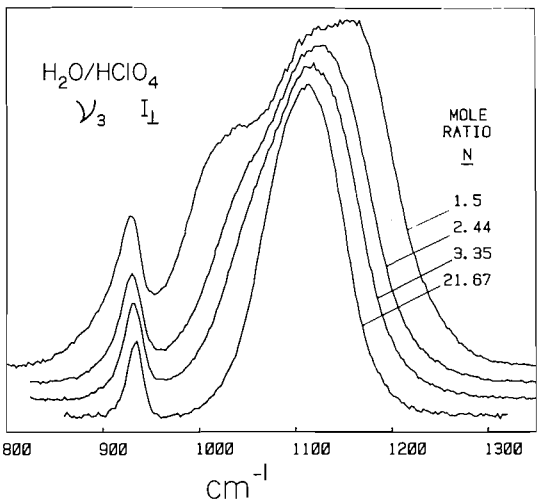

FIG. 4. Raman spectra ($I_\perp$) of the $\nu_3(ClO_4^-)$ band, at the mole ratios indicated and 25°C. A trace of $\nu_1(ClO_4^-)$ appears at ≈930 cm^{-1}.

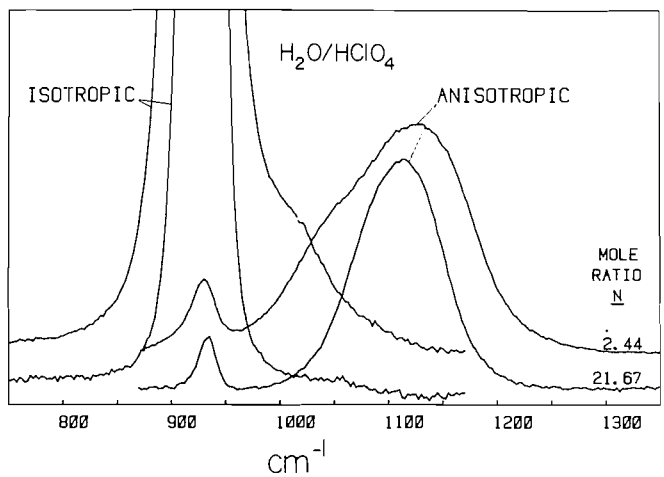

FIG. 5. Raman spectra (isotropic and anisotropic) of the ν_1 and $\nu_3(ClO_4^-)$ region at low and high mole ratios, showing the appearance of the isotropic, high frequency shoulder on ν_1.

species, *viz.* ClO_4^- bound to a cation. No other bands in the spectra give evidence of such a complex when $N > 10$. Furthermore, in cases where an interaction has been detected, for example Na^+ and $Li^+ClO_4^-$ solutions, ν_1 shows a broadening to the *high* frequency side as the concentration is raised (ref. 50 and this work).

The Fermi resonance explanation seems the most attractive of the various explanations, taken on its own. A fourth possibility is that a combination of all three effects contribute to the low frequency shoulder, dependent on the conditions.

We consider now the solutions of concentration $N = 10$ and lower. At these concentrations the Raman spectra are less in accord with a single ClO_4^- species of T_d symmetry. Infrared spectra may be more sensitive than Raman to the perturbation. Thus, although the two recent studies (5, 7) have not reported specific composition values, Zundel's results (5) suggest that the forbidden ν_1 line is detectable at concentrations as low as $N = 23$. Furthermore, as we shall see later, the Raman-active OH stretching bands of water are visibly affected in their high frequency range by perchloric acid at mole ratios as high as $N = 45$. This indicates strong solute–solvent interactions, which may be isotropic such that the symmetry of the ClO_4^- remains apparently T_d.

The lifting of T_d symmetry is indicated in the Raman by the ν_3 band which shows first an asymmetry and then a distinct shoulder on its low frequency side as N decreases below 10. ν_3 is considerably weaker than ν_1 and its appearance in the $I_\parallel$ polarised spectra is distorted by overlap with ν_1. Consequently we will refer mainly to the $I_\perp$ (or anisotropic) spectra, where ν_1 is largely removed (see Fig. 4). The two component appearance continues to $N = 2.44$ but for $N = 1.5$ there appears to be a third component on the high frequency side. Lifting of the degeneracy of ν_3 into two components implies C_{3v} symmetry. However, it is conceivable that a third band, implying even lower symmetry, is present all along but only becomes observable at $N < 2.44$. The bands of ν_2 and ν_4 do not show any discernible lifting of degeneracy until $N < 2.44$, when, like the ν_3 band, they develop an asymmetry to their high frequency sides. (Note that bands of molecular $HClO_4$ would appear at lower frequencies.) In theory, some of the components present when the degeneracies of ν_2, ν_3, and ν_4 are lifted should be polarised, and hence should appear in the isotropic spectra. There were traces of isotropic intensity in the regions of the high frequency shoulders of ν_2 and ν_4 and of the central component of ν_3 but we could not make a definitive assignment, considering the possible magnitude of errors involved in the baseline of the isotropic spectra. It is quite conceivable that the bands are only slightly polarised which, when combined with their weak intensity, makes them virtually invisible in the isotropic spectrum.

Inspection of the isotropic spectra shows that for the same conditions under which ν_3 develops its low frequency shoulder ν_1 develops a shoulder on its high frequency side. Its presence only becomes obvious in the isotropic spectra where it is not obscured by the overlapping anisotropic bands of ν_3 (Fig. 5). This new shoulder is very weak and broad (half width ≈80 cm^{-1}) when compared to ν_1 and its low frequency shoulder, but it clearly is a totally symmetric mode. It was also observed in the $N = 2$ liquid and glass spectra by Thi *et al.* (8). The shoulder also occurs in the spectra of deuterated solutions, and so the possibility that it could be a band of the protonated aqueous medium can be discarded, since a considerable shift would be expected.

Both this high frequency shoulder of ν_1 and the low frequency shoulder of ν_3 can be induced by increasing the acid concentration at constant ClO_4^- concentration (by addition of hydrochloric acid), though both the shoulders are less prominent than for the equivalent acid concentration of perchloric acid alone. These observations clearly show that the shoulders depend on both $[(H_{aq})^+]$ and $[ClO_4^-]$. Increasing temperature did not noticeably affect the shoulders in the $N = 2.44$ solution, apart from slight broadening. A summary of the frequencies of the bands and shoulders discussed above is given in Table 3.

As Thi *et al.* (8) point out, there are now four bands in the region above ν_1. There are no feasible overtone or hotband possibilities and so we will consider two possible origins for this situation, both of which involve the presence of a new ClO_4^- species. (*a*) The isotropic high frequency shoulder of ν_1 could be a polarised ν_3 component arising from a new, ClO_4^- species. Unfortunately this scheme means that there should also be strong ν_1, ν_2, and ν_4 bands arising from the new species (in addition to those of the original species): bands for which there is no positive evidence. Furthermore, it is odd that the isotropic component should be apparently totally polarised,

Can. J. Chem. Downloaded from www.nrcresearchpress.com by 210.87.254.105 on 09/06/12
For personal use only.

Can. J. Chem. Downloaded from www.nrcresearchpress.com by 210.87.254.105 on 09/06/12
For personal use only.

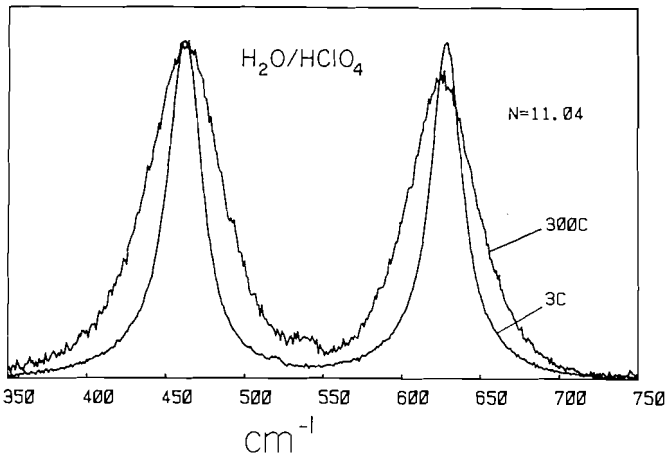

FIG. 6. Raman spectra of the ν_2 and ν_4 bands of perchloric acid (N = 11.04) at 3°C and 300°C.

TABLE 4. Peak frequencies and halfwidths (in parentheses) of ClO_4^- bands at extremes of temperature (values in cm^{-1})

	N = 11.04		N = 2.44	
	T = 3°C	T = 300°C	T = 3°C	T = 200°C
ν_2	462.0(25.5)	461.0(56.0)	462.0(38.0)	462.0(51.0)
ν_4	629.5(24.0)	625.0(51.0)	630.0(31.0)	628.0(43.0)
ν_1	934.5(9.3)	931.0(14.8)	931.5(18.0)	929.0(23.0)
ν_3	1111.0(98.0)	1106.0(118.0)	1127.0(145.0)	1127.0(160.0)

separated considerably from the other ν_3 components, and appear to show no significant shift as N is decreased, in contrast to the other new ν_3 components. (*b*) The second explanation is that the isotropic band is a symmetric stretching mode of a new, very dilute species, for which the ν_2, ν_3, and ν_4 modes (or their equivalents) are too weak to be seen. We visualise a species in which the aquated hydrogen ion is ion-paired to the perchlorate anion, analogous to the proton boundary structure II described by Zundel (5). This type of species was proposed by us before (51) to account for changes in the Raman spectrum of nitric acid. It is a consequence of proton transfer from the ionogen, $HClO_4$ in this case, to yield the ionised species $(H_{aq})^+ \cdot ClO_4^-$, which further dissociates to the respective solvated ions which disperse in the solvent as the water content is increased. This brings us close to the situation envisaged by Thi *et al.* (8) who concluded that the new species is an $H_5O_2^+$ ClO_4^- hydrogen-bonded complex in the N = 2 solution. We would prefer to write $(H_{aq})^+ \cdot ClO_4^-$, since we believe that there is insufficient evidence to be so specific. Probably the most essential feature of the complex is the *close* proximity of the positive charge of the excess acid proton to the ClO_4^- ion, which induces the hydrogen bonding.

Aside from these specific features, the overall effects of increasing temperature are a steady increase in width and a slight decrease in frequency. The spectra of the ν_2 and ν_4 bands at the extremes of temperature are shown in Fig. 6. Values of the *peak* frequencies and bandwidths of the four modes at the extremes of temperature are listed in Table 4. The asymmetries and the lifting of degeneracy are neglected in the data of Table 4.

Solid $H_3O^+ClO_4^-$

Included in Table 3 and shown in Fig. 7 are the bands in the

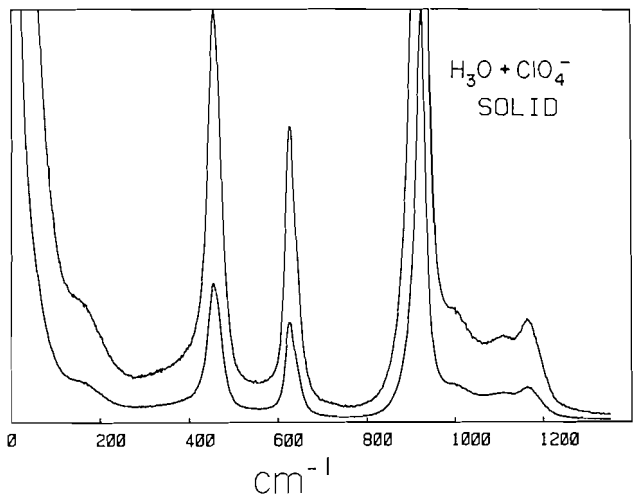

FIG. 7. Raman spectrum of solid $H_3O^+ClO_4^-$ below 1350 cm^{-1}, at 25°C.

ClO_4^- region of the room temperature phase of solid $H_3O^+ClO_4^-$ (at about 25°C). ν_2 and ν_4 show asymmetric broadening to their high frequency sides and there appear to be three components in the ν_3 region. In fact, the spectrum is remarkably similar to the spectra of the concentrated solutions with low values of N. However, the band observed at 995 cm^{-1} in the solid cannot be the equivalent of the isotropic shoulder at $\approx$1010 cm^{-1} in the liquid mixtures (assigned earlier to a new species), since it is quite clear from the crystal structure (52, 53) that there is only one kind of ClO_4^- ion. The structure also shows that the ClO_4^- ion has C_s site symmetry, and hence all degeneracy should be lifted (Table 5); further splittings due to the factor group correlations are not apparent and are therefore presumed to be small. Consequently one might readily assign the bands in the spectrum of the solid to those of a C_s perturbed ClO_4^- ion. However, the expected presence of the ν_2 band of H_3O^+ in the $\nu_3(ClO_4^-)$ region complicates the issue: Taylor and Vidale (18) originally assigned a peak at 1175 cm^{-1} to $\nu_2(H_3O^+)$ and the shoulder at 995 cm^{-1} to a librational mode of H_3O^+, whereas Thi *et al.* (8) assign the latter as $\nu_2(H_3O^+)$. Both of these interpretations seem not to have considered the lifting of the degeneracy of $\nu_3(ClO_4^-)$. Comparison of the new solid spectrum with that of the N = 1.5 liquid shows that the former has additional intensity at 1163 cm^{-1}, hinting that perhaps there are two bands superimposed: one a high frequency component of $\nu_3(ClO_4^-)$ and the other $\nu_2(H_3O^+)$. Obviously a Raman study of $D_3O^+ClO_4^-$ solid would be necessary to resolve this problem.

Another interesting feature of the solid's spectrum, from the point of view of earlier discussion, is the fact that the ν_1 band shows a strong low frequency asymmetry similar to that in the solution spectra. This cannot be due to a second species in this case, but $2\nu_2$ is a reasonable possibility.

The solid also shows a moderately-intense, broad shoulder at 160 cm^{-1} and another weaker one on the low frequency side of ν_2 in the 370–400 cm^{-1} region. These may be assigned to lattice modes (the higher frequency one is very likely a librational mode).

Section II. Vibrations of OH

The effects of increasing perchloric acid concentration on the OH stretching bands are illustrated in Fig. 8 for $N = \infty$ to 2.44 and in Fig. 9 for N = 2.44 to 1. Frequencies of the various

TABLE 5. Symmetry correlations for solid $H_3O^+ClO_4^-$ (room temperature phase)

Molecular point group T_d	Site group C_s	Factor group D_{2h}
A_1	A'	A_g
		B_{2g}
		B_{1u}
		B_{3u}
E	A''	B_{1g}
		B_{3g}
		A_u
F_2		B_{2u}

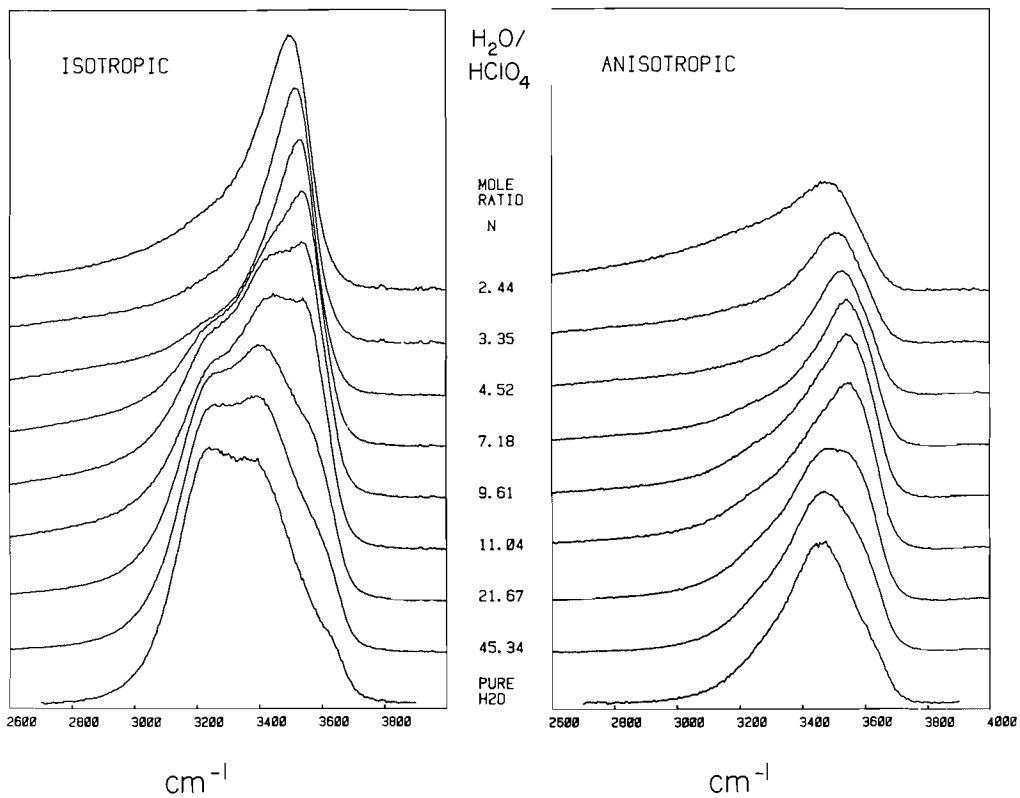

FIG. 8. Raman spectra (isotropic and anisotropic) of perchloric acid in the 2600–4000 cm^{-1} region, at the mole ratios indicated and 25°C (intensity has been normalised on the maximum of each isotropic spectrum).

features are given in Tables 6 and 7. In some cases we have also listed the "band edge", measured as the point of maximum slope on the high frequency side of the spectrum, which we introduced before (54) as an indication of the limiting high frequency for an OH oscillator which has minimum hydrogen bonding interactions.

At all mole ratios $N > 1.8$ the acid is dissociated and the constituents are ClO_4^- ions, H_2O, and $(H_{aq})^+$. $((H_{aq})^+$ is used here as a blanket term to cover all possible descriptions of the aquated acid proton.) The spectrum of pure water is quite complex (54), and the additional species present in solution, all interacting with each other, produce further complexity. Another complication is introduced when $HClO_4$ is present at $N < 1.8$. We suggest, by analogy with our interpretation of the spectrum of water (54), that for each species containing OH groups in perchloric acid solution (and indeed all acids), there exists a broad distribution of OH oscillator potentials, arising from the many different hydrogen bonding configurations which must be possible in the liquid state. These distributions and the various possibilities for intra- and inter-molecular correlation interactions which they present, cause a broadening and further complication of the OH stretching bands. All these

Can. J. Chem. Downloaded from www.nrcresearchpress.com by 210.87.254.105 on 09/06/12
For personal use only.

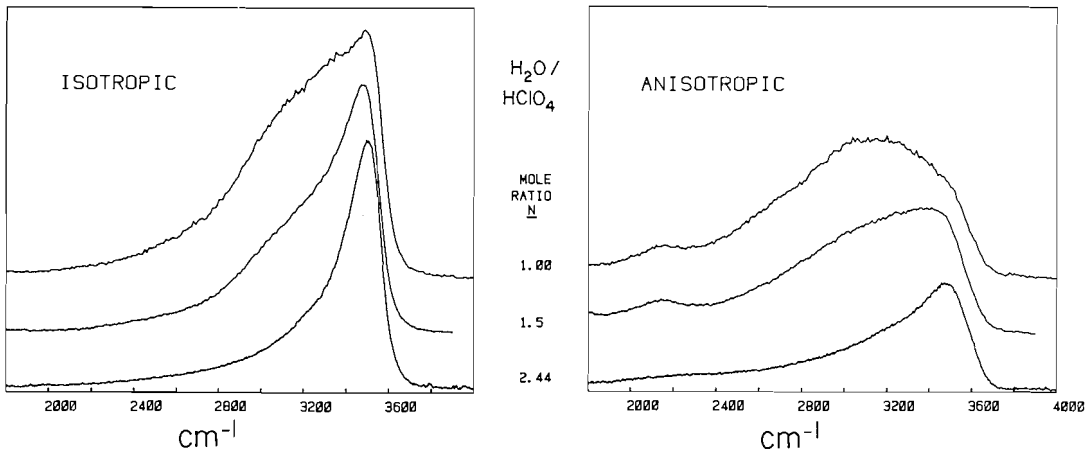

FIG. 9. Raman spectra (isotropic and anisotropic) of perchloric acid in the 1800–4000 cm^{-1} region at low mole ratios and 25°C (intensity has been normalised on the maximum of each isotropic spectrum).

TABLE 6. Features of the OH stretching bands of perchloric acid solutions as a function of mole ratio (values in cm^{-1})

Mole ratio N	Isotropic			Band edge	Anisotropic		Band edge
∞	3247	3353	≈3617	3657	3462	≈3590	(3660)
45.34	3245	3387	≈3572	3647	3467	≈3550	3647
21.67	≈3245	3402	≈3540	3640	3487	≈3540	3642
11.04	≈3245	3452	3527	3615	≈3485	3542	3637
9.61	3245	≈3480	3537	3607		3542	3635
7.18	3245		3537	3590		3542	3637
4.52	3245		3527	3580		3527	3635
3.35			3512	3570		3507	3620
2.44			3502	3562		3472	3587

* Figures with small underline indicate approximate positions of shoulders.

factors make it very difficult to interpret the spectra comprehensively, although one can attempt to produce a plausible qualitative picture.

(a) Effects of perchlorate ion

The first thing to notice in Fig. 8 is that even at $N = 45.34$ the band has changed from that of pure water. At high mole ratios where there is still a much greater number of H_2O molecules than excess acid protons, there is an overall shifting of intensity towards higher frequency as N decreases; intensity decreases in the 3250 cm^{-1} region and increases in the 3400–3600 cm^{-1} region. These effects are very similar to those observed for ClO_4^- salt solutions (26–35), and the shift of intensity is usually taken to imply that hydrogen bonding of the water surrounding the ClO_4^- ion is weakened (the so-called structure-breaking effect).

It is of interest to note that the spectra in the $N = \infty$ to 11.04 range do not consist of simple combinations of the spectrum of pure water and a spectrum of water interacting with ClO_4^- (i.e. a binary mixture), as it was *not* found possible to reproduce a spectrum at a particular value of N by adding together appropriate fractions of the spectrum of water and a spectrum at lower N.

As N decreases to 9.61 the upward shifting of intensity due to the structure-breaking effect produces a bandshape with a single sharp maximum at about 3535 cm^{-1}.

(b) Effects of the acid protons

The exact nature of the "$(H_{aq})^+$" present in acid solutions is a matter of some controversy. Giguère strongly argues that the proton is present only in H_3O^+ units, albeit hydrogen bonded to other H_2O molecules (55–57). On the other hand, Zundel strongly favours $H_5O_2^+$ groupings (provided there is enough water to form this) (5, 58, 59). He is then able to account for the intensity continuum to the low frequency side of the OH stretching mode, in terms of an easily polarisable hydrogen bond at the centre of the $H_5O_2^+$ unit. This intensity continuum is a characteristic of all acid solutions. We do not wish to go into all the arguments and counter-arguments at this point, but will emphasise a few things which are relevant in the current context.

TABLE 7. Frequencies (in cm^{-1}) of OH bands for $N < 2$

	$N = 1$	
$N = 1.5$	Melt	Solid
1602	1602	1575
≈2150	≈2180	≈2088
≈3100	≈3100	
≈3300	≈3300	3085
3465	3470	3255

The only situations in which the occurrence of distinct H_3O^+ and $H_5O_2^+$ ions has been satisfactorily established are in various solids (52, 53, 60–64) and in some non-aqueous solvent solutions (65, 66). Figure 10 shows the higher frequency bands of H_3O^+ in solid $H_3O^+ClO_4^-$ obtained in the present study.

Can. J. Chem. Downloaded from www.nrcresearchpress.com by 210.87.254.105 on 09/06/12
For personal use only.

TABLE 8. Ratios of species containing excess acid protons, in two limiting cases*

Mole ratio N $H_2O:HClO_4$	Degree of dissociation α	Maximum H_3O^+ No $H_5O_2^+$ $H_3O^+:H_2O$	Maximum $H_5O_2^+$, minimum H_3O^+ No H_2O $H_3O^+:H_5O_2^+$	Maximum $H_5O_2^+$, minimum H_3O^+ No H_3O^+ $H_5O_2^+:H_2O$
1.0	0.7	2.33 (3.5)	1.33 (0.8)	
1.5	≈1	2.0 (3.0)	1.0 (0.6)	
2.0	1	1.0 (1.5)	0 (0)	
2.5	1	0.67 (1.0)		2.0 (5.0)
5.0	1	0.25 (0.38)		0.33 (0.83)

* Figures in parentheses indicate the ratios of OH groups involved.

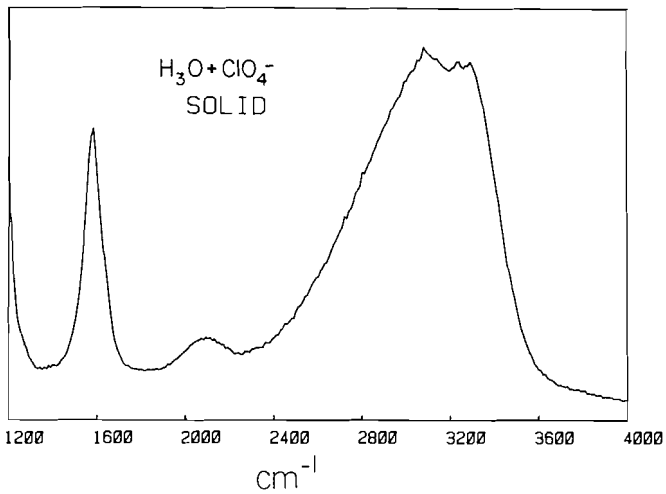

FIG. 10. Raman spectrum of solid $H_3O^+ClO_4^-$ from 1200 to 4000 cm^{-1}.

(These are essentially in agreement with Taylor and Vidale's spectrum (18).) One has only to look at the vibrational frequencies and assignments made for H_3O^+ in various solids (e.g. refs. 67, 68) to realise that the ion is not characterised by a fixed set of frequencies. Indeed the stretching mode frequencies depend very much on the degree of hydrogen bonding to the anions involved, ranging over 2468 to 3509 cm^{-1}. Moreover, it is clear from the structures of the solid higher hydrates of acids that H_3O^+ very readily hydrogen bonds to other H_2O molecules.

Evidence from the structures of the solid hydrates of perchloric acid (52, 53, 60–63), indicates strong hydrogen bonding of water molecules associated with the excess acid proton (i.e., in such units as $H_5O_2^+$, $H_3O^+ \cdot 2H_2O$, etc.), weaker hydrogen bonding interactions between water molecules on adjacent protonated units, and still weaker hydrogen bonding interaction to the ClO_4^- ions. One might expect, as is suggested by Zundel's work (5), that this hierarchy of hydrogen bonding strengths prevails in solution.

The intensity continuum mentioned above becomes clear (Figs, 8, 9) as N decreases below about 10. It increases steadily relative to the intensity at the high frequency end and is apparent in both isotropic and anisotropic spectra. At the same time the peak in the isotropic spectrum moves to lower frequency, which is probably a reflection of the stronger hydrogen bonding conditions introduced by the excess protons. (We also note a similar trend for the band edges, which decrease in frequency as N decreases, but over the whole range of N).

At $N = 1.5$ and 1 there is a dramatic broadening and increase of intensity on the low frequency side of the main peak, quite distinct from the intensity continuum. The OH stretching mode of molecular $HClO_4$ appears in the infrared as a broad band peaking in the region of 3340–3380 cm^{-1} (23). However, this probably accounts for only a small amount of the intensity of the shoulder, since even for the $N = 1$ liquid, where $\alpha = 0.7$, only about 1/10 of the total number of OH groups are present as $HClO_4$. Clearly most of the intensity of the shoulder must be due to an $(H_{aq})^+$ species, since at these very low mole ratios, all the water molecules must be radically affected by the excess protons.

TABLE 9. Main peaks of the OH stretching bands in solid perchloric acid hydrates (cm^{-1})

Hydrates	Band	
$H_3O^+ ClO_4^-$	3085	3255
$H_5O_2^+ ClO_4^-$ (8)	3224	3338
$H_7O_3^+ ClO_4^-$ (8)	3420	3590

It is useful to consider what species could be present. Table 8 lists the ratios of H_3O^+, $H_5O_2^+$, and H_2O which are possible in two limiting cases: (*i*) where there is a maximum amount of H_3O^+ and *no* $H_5O_2^+$ and (*ii*) where there is a maximum amount of $H_5O_2^+$. The ratios of the number of OH groups involved are also indicated in parentheses, since these are assumed to be more closely related to the observed intensities. It may be inferred from this that some H_3O^+ ions *must* be present for $N < 2$, but, if $H_5O_2^+$ is the preferred form, then H_3O^+ should disappear for $N \geq 2$. The intensity of the broad shoulder diminishes rapidly from $N = 1$ to $N = 2.44$; this suggests that it is due to H_3O^+ and that $H_5O_2^+$ does readily form at the expense of H_3O^+. However, since the shoulder can still be detected at $N = 2.44$, the equilibrium $H_2O + H_3O^+ \rightleftharpoons H_5O_2^+$ is not shifted completely to the right. (Although some might prefer to write $H_5O_2^+$ as $H_3O^+ \cdot H_2O$, this species does appear to have a distinctly different spectrum from that of H_3O^+.) Also note that the shoulder in the $N = 1$ and 1.5 spectra corresponds better with the position of the OH stretching bands of $H_3O^+ClO_4^-$ solid than to those of $H_5O_2^+ClO_4^-$ solid (see Table 9).

Another band which appears at the same time as the shoulder discussed above is the weak anisotropic peak at ≈2180 and ≈2150 cm^{-1} in the $N = 1$ and 1.5 spectra (see Fig. 9). A similar band appears in the spectrum of solid $H_3O^+ClO_4^-$, Fig. 10. The spectrum of the $N = 2$ liquid of Thi *et al.* (8) also shows this feature, but curiously it is absent or very much weaker in solid $H_5O_2^+ \cdot ClO_4^-$. This band too might therefore be associated with relatively discreet H_3O^+ units at low values of N. Its origin is likely a combination of a librational mode with the bending mode in the 1600 cm^{-1} region.

Can. J. Chem. Downloaded from www.nrcresearchpress.com by 210.87.254.105 on 09/06/12
For personal use only.

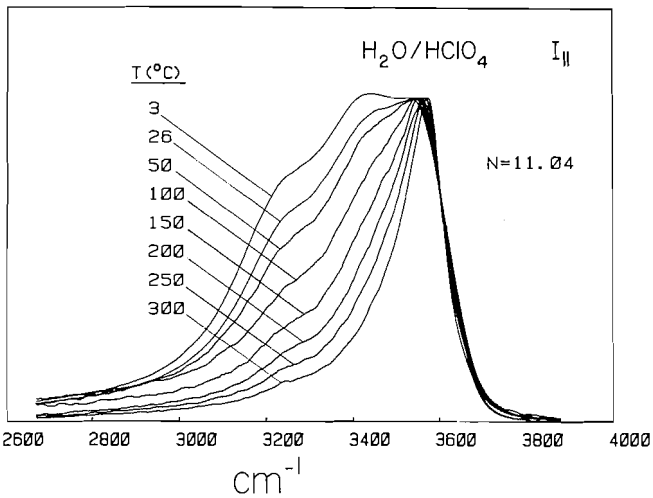

FIG. 11. Raman spectra ($I_{\parallel}$) of $N = 11.04$ perchloric acid in the 2700–3900 cm^{-1} region, at the temperatures indicated (intensity has been normalised on the high frequency maximum).

TABLE 10. Effect of temperature on the OH stretching bands of perchloric acid solution, $N = 2.44$ (values in cm^{-1})

	Isotropic		Anisotropic	
T(°C)	Peak	Band edge	Peak	Band edge
3	3492	3553	3470	3570
100	3517	3575	3482	3617
200	3545	3592	3528	3647

(c) The OH bending modes in the 1600 cm^{-1} region

The Raman spectra in this region show only one band at all values of N, ranging between 1602 cm^{-1} for the $N = 1$ liquid to 1638 cm^{-1} for pure water. This is in marked contrast to the infrared spectra (5, 7). These show a single band in the 1620–1645 cm^{-1} range at low concentration (high N), but as N decreases a new broader band grows in at 1700–1720 cm^{-1} and eventually dominates. Much interpretation has been based on these changes in the infrared (5, 7) and it may need to be reviewed in light of the Raman observations.

(d) Effects of temperature

Figure 11 shows the effect of increasing temperature on the $I_{\parallel}$ OH stretching bands of the $N = 11.04$ solution. At low temperatures the structure-breaking effect of ClO_4^- has already caused a large decrease in the number of the more strongly hydrogen-bonded OH groups, with a resultant increase of relative intensity at the high frequency end of the spectrum as compared to pure water. As the temperature increases the high frequency band edge remains at $\approx 3615 \pm 5$ cm^{-1} right up to 300°C, and all the changes involve a continuous reduction of intensity on the lower frequency side of the band. This observation is consistent with a steady shift in the distribution of hydrogen bond strengths of the water to the weaker end. The fixed position of the band edge is interesting since it once again suggests that this is the limiting high frequency for aqueous OH groups which have a minimum interaction with their surroundings. Another observation is that at 300°C there is very little difference between the spectra of pure water, for which the band edge of the isotropic spectrum is at 3607 cm^{-1}, and that of the $N = 11.04$ perchloric acid solution, though a close inspection reveals that the water spectrum is slightly broader.

The only other high temperature spectroscopic study of the effects of perchlorate in solution is the recent infrared work by Valyashko *et al.* (36) of the OD stretching mode of HDO in $NaClO_4$ solutions. Those spectra show a similar reduction of intensity on the low frequency side of the band.

In the case of the $N = 2.44$ solution versus temperature, the behaviour is somewhat different. At room temperature the main peak (in the isotropic spectrum) is already quite narrow, although there is also the weaker intensity continuum stretching to lower frequencies. However, the peak and band edge are shifted ≈ 40 cm^{-1} lower than for the $N = 11.04$ case. On heating, both the peak and the band edge frequencies increase, as indicated in Table 10. At this mole ratio, of course, one would expect a different behaviour, since the principal species is $(H_{aq})^+$, but even for this composition it is clear that increasing temperature causes an overall weakening of the hydrogen bonding.

Summary

In conclusion we summarise the main points of this work as follows:

(*1*) The Raman spectra of perchloric acid solutions are essentially in agreement with Zundel's infrared study (5) which indicated complete dissociation at water:acid mole ratios $N > 1.8$.

(*2*) The Raman spectrum of molecular $HClO_4$ in an aqueous medium has been reported for the first time.

(*3*) Perchloric acid remains a "strong" acid even at temperatures up to 300°C. However, the appearance of traces of molecular $HClO_4$ in concentrated acid solution at high temperatures shows that association does increase slightly, as might be expected.

(*4*) At $N > 10$ the Raman spectrum of ClO_4^- indicates essentially T_d symmetry. Investigations of the origin of the low frequency shoulder on the ν_1 band of ClO_4^- are still inconclusive.

(*5*) For $N < 10$ the degeneracy of the $\nu_3(ClO_4^-)$ mode lifted, indicating lower symmetry than T_d.

(*6*) The appearance of a new isotropic band on the high frequency side of $\nu_1(ClO_4^-)$ has been interpreted as indicative of a new species, presumed to be an associated ion-pair $(H_{aq})^+ \cdot ClO_4^-$.

(*7*) At low perchloric acid concentration (large N) the OH stretching bands reflect a "structure breaking" effect of the ClO_4^- ion, characteristic of perchlorate salt solutions.

(*8*) Effects on the ν_{OH} bands due to the excess acid protons become apparent at higher concentrations; the bands shift towards lower frequencies, indicating stronger hydrogen bonding conditions. Changes in the Raman spectra also suggest a rapid reduction in H_3O^+ as N increases from 1 to 2.

(*9*) The effect of increasing temperature on the ν_{OH} bands indicates a steady decrease in average hydrogen bonding strengths, just as in pure water.

Acknowledgement

This research was supported by grants from the Natural Sciences and Engineering Research Council of Canada.

1. W. L. MARSHALL and E. U. FRANCK. J. Phys. Chem. Ref. Data, **10**, 295 (1981).
2. G. OLOFSSON and L. G. HEPLER. J. Solution Chem. **4**, 127 (1975).
3. C. F. BAES, JR., and R. E. MESMER. Am. J. Sci. **281**, 935 (1981).

Can. J. Chem. Downloaded from www.nrcresearchpress.com by 210.87.254.105 on 09/06/12
For personal use only.

4. C. F. BAES, JR., and R. E. MESMER. The hydrolysis of cations. Wiley-Interscience, New York. 1976.
5. M. LEUCHS and G. ZUNDEL. J. Chem. Soc. Faraday II, **74**, 2256 (1978).
6. M. P. HENDERSON, V. I. MIASEK, and T. W. SWADDLE. Can. J. Chem. **49**, 317 (1971).
7. L. V. CHERNYKH, L. A. MYUND, N. E. RUMYANTSEVA, and D. N. GLEBOVSKII. Vestn. Leningr. Univ. Fiz. Khim. **4**, 56 (1979).
8. M. P. THI, M.-H. HERZOG-CANCE, A. POTIER, and J. POTIER. J. Raman Spectrosc. **12**, 238 (1982).
9. O. REDLICH, E. K. HOLT, and J. BIGELEISEN. J. Am. Chem. Soc. **66**, 13 (1944).
10. K. HEINZINGER and R. E. WESTON, JR. J. Chem. Phys. **42**, 272 (1965).
11. E. L. GASNER. Ph.D. Thesis, University of Chicago. 1965.
12. A. K. COVINGTON, M. J. TAIT, and W. F. K. WYNNE-JONES. Proc. R. Soc. A**286**, 235 (1965).
13. J. W. AKITT, A. K. COVINGTON, J. G. FREEMAN, and T. H. LILLEY. Trans. Faraday Soc. **65**, 2701 (1969).
14. M. M. KREEVOY and C. A. MEAD. Discuss. Faraday Soc. **39**, 166 (1965).
15. A. K. COVINGTON, M. J. TAIT, and LORD WYNNE-JONES. Discuss. Faraday Soc. **39**, 172 (1965).
16. J. T. MULLHAUPT and D. F. HORNIG. J. Chem. Phys. **24**, 169 (1956).
17. J. T. MULLHAUPT. Ph.D. Thesis, Brown University. 1958.
18. R. C. TAYLOR and G. L. VIDALE. J. Am. Chem. Soc. **79**, 5999 (1956).
19. R. SAVOIE and P. A. GIGUÈRE. J. Chem. Phys. **41**, 2698 (1964).
20. M. FOURNIER, G. MASCHERPA, D. ROUSSELET, and J. POTIER. Compt. Rend. Acad. Sc. Paris, **269**, 279 (1969).
21. M. FOURNIER and J. ROZIERE. Compt. Rend. Acad. Sc. Paris, **270**, 729 (1970).
22. A. C. PAVIA and P. A. GIGUÈRE. J. Chem. Phys. **52**, 3551 (1970).
23. A. I. KARELIN, Z. I. GRIGOROVICH, and V. YA. ROSOLOVSKII. Spectrochim. Acta, **31**A, 765 (1975).
24. A. I. KARELIN and Z. I. GRIGOROVICH. Spectrochim. Acta, **32**A, 851 (1976).
25. R. W. DUERST. J. Chem. Phys. **48**, 2275 (1968).
26. G. E. WALRAFEN. J. Chem. Phys. **52**, 4176 (1970).
27. G. BRINK and M. FALK. Can. J. Chem. **48**, 3019 (1970).
28. D. M. ADAMS, M. J. BLANDAMER, M. C. R. SYMONS, and D. WADDINGTON. Trans. Faraday Soc. **67**, 611 (1971).
29. L. J. BELLAMY, M. J. BLANDAMER, M. C. R. SYMONS, and D. WADDINGTON. Trans. Faraday Soc. **67**, 3435 (1971).
30. P. DRYJANSKI and Z. KĘCKI. J. Mol. Struct. **12**, 219 (1972).
31. M. C. R. SYMONS and D. WADDINGTON. J. Chem. Soc. Faraday II, **71**, 22 (1975).
32. T. J. V. FINDLAY and M. C. R. SYMONS. J. Chem. Soc. Faraday II, **72**, 820 (1976).
33. Z. KĘCKI. J. Mol. Struct. **45**, 23 (1978).
34. D. SCHIOBERG. Ber. Bunsenges. Phys. Chem. **85**, 513 (1981).
35. A. SOKOŁOWSKA and Z. KĘCKI. J. Mol. Struct. **101**, 113 (1983).
36. V. M. VALYASHKO, M. BUBACK, and E. U. FRANCK. Z. Naturforsch. **36**A, 1169 (1981).
37. D. E. IRISH, T. JARV, and C. I. RATCLIFFE. Appl. Spectrosc. **36**, 137 (1982).
38. H. J. VAN WYK. Z. Anorg. Allg. Chem. **48**, 1 (1906).
39. L. H. BRICKWEDDE. J. Res. N.B.S. **42**, 309 (1949).
40. G. HERZBERG. Molecular spectra and molecular structure. I. Spectra of diatomic molecules. Van Nostrand, New York. 1950.
41. D. W. JAMES and R. E. MAYES. Aust. J. Chem. **35**, 1775 (1982).
42. D. W. JAMES and R. E. MAYES. Aust. J. Chem. **35**, 1785 (1982).
43. T. JARV, J. T. BULMER, and D. E. IRISH. J. Phys. Chem. **81**, 649 (1977).
44. G. HERZBERG. Molecular spectra and molecular structure. II. Infrared and Raman spectra of polyatomic molecules. Van Nostrand, New York. 1945. p. 310.
45. M. H. BROOKER, A. S. QUIST, and G. E. BOYD. Chem. Phys. Lett. **9**, 242 (1971).
46. D. J. J. VAN RENSBURG and C. J. H. SCHULTE. J. Mol. Struct. **11**, 229 (1972).
47. G. J. ROSASCO. Unpublished results.
48. H. D. LUTZ, R. A. BECKER, W. ECKERS, B. G. HOLSCHER, and H. J. BERTHOLD. Spectrochim. Acta, **39**A, 7 (1983).
49. W. F. MURPHY, S. SUNDER, and H. KATZ. J. Raman Spectrosc. **7**, 76 (1978).
50. R. L. FROST, D. W. JAMES, R. APPLEBY, and R. E. MAYES. J. Phys. Chem. **86**, 3840 (1982).
51. D. E. IRISH and O. PUZIC. J. Solution Chem. **10**, 377 (1981).
52. F. S. LEE and G. B. CARPENTER. J. Phys. Chem. **63**, 279 (1959).
53. M. R. TRUTER. Acta Crystallogr. **14**, 318 (1961).
54. C. I. RATCLIFFE and D. E. IRISH. J. Phys. Chem. **86**, 4897 (1982).
55. P. A. GIGUÈRE. J. Chem. Ed. **56**, 571 (1979).
56. P. A. GIGUÈRE. J. Chem. Phys. **60**, 421 (1981).
57. P. A. GIGUÈRE and J. G. GUILLOT. J. Phys. Chem. **86**, 3231 (1982).
58. G. ZUNDEL. *In* The hydrogen bond. Vol. II. *Edited by* P. Schuster, G. Zundel, and C. Sandorfy. North-Holland Publishing Co., Amsterdam. 1976. Chapt. 15.
59. M. LEUCHS and G. ZUNDEL. Can. J. Chem. **58**, 311 (1980) and references therein.
60. C. E. NORDMAN. Acta Crystallogr. **15**, 18 (1962).
61. I. OLOVSSON. J. Chem. Phys. **49**, 1063 (1968).
62. J. ALMLÖF, J.-O. LUNDGREN, and I. OLOVSSON. Acta Crystallogr. B**27**, 898 (1971).
63. J. ALMLÖF. Acta Crystallogr. B**28**, 481 (1972).
64. J.-O. LUNDGREN and I. OLOVSSON. *In* The hydrogen bond. Vol. II. *Edited by* P. Schuster, G. Zundel, and C. Sandorfy. North-Holland Publishing Co., Amsterdam, 1976. Chapt. 10.
65. P. A. GIGUÈRE and C. MADEC. Chem. Phys. Lett. **37**, 569 (1976).
66. V. GOLD, J. L. GRANT, and K. P. MORRIS. J. Chem. Soc. Chem. Commun. 397 (1976).
67. J. M. WILLIAMS. *In* The hydrogen bond. Vol. II. *Edited by* P. Schuster, G. Zundel, and C. Sandorfy. North-Holland Publishing Co., Amsterdam. 1976. Chapt. 14 and references therein.
68. B. DESBAT and P. V. HUONG. Spectrochim. Acta, **31**A, 1109 (1975).

Can. J. Chem. Downloaded from www.nrcresearchpress.com by 210.87.254.105 on 09/06/12
For personal use only.

The electronic capacitor at a metal–electrolyte interface

G. A. MARTYNOV
Institute of Physical Chemistry of the USSR Academy of Sciences, Leninsky Prospect 31, Moscow 117312, USSR

AND

R. R. SALEM
D.I. Mendeleev Moscow Chemical and Technological Institute, Miusskaya square 9, Moscow 125047, USSR

Received February 9, 1983

G. A. MARTYNOV and R. R. SALEM. Can. J. Chem. **62**, 1145 (1984).

A model for the dense part of electrical double layer is proposed using the concept that conduction electrons penetrate into a solution to form an electronic capacitor on the metal surface. The potential drop between the metal and solution, the charge of the metal, its surface tension, and the electron work function for a metal–solution interface are calculated within the framework of the model, and the formulae derived are compared with experiment. It is shown that for a metal–vacuum interface of 38 metals in the left-hand subgroups of the Mendeleev table the discrepancy between the theoretical and experimental values of surface tension and work function does not exceed the experimental error (i.e. it is less than 10%); for six metals in the right-hand subgroups and especially for semimetals the theoretical error is two to three times higher. The density of free electrons in a metal determined in terms of the concepts of the model is shown to vary monotonously with the element number for all 54 metals with available experimental data.

A relationship, previously unknown, between surface tension and zero-charge potential is established, which enabled one to calculate the electronic capacitor charge for mercury (the theoretical value is 33 C/cm^2, and the experimental value is 36–38 C/cm^2). This paper also reports the calculated values of the integral capacity of a mercury electrode in water: the experimental value is 29 F/cm^2 (at the zero-charge point), and the theoretical value is 28 F/cm^2. The model predicts an increase of the capacity in the anodic region and a decrease in the cathodic region, in a good agreement with experiment. It should be stressed that although the theory includes only one fitting parameter, the density of free electrons in the metal, it correctly explains a wide range of phenomena.

G. A. MARTYNOV et R. R. SALEM. Can. J. Chem. **62**, 1145 (1984).

On propose un modèle pour la partie dense de la double couche électrique qui repose sur le concept que les électrons de conduction pénètrent dans une solution pour former une capacitance électronique à la surface métallique. A l'aide du modèle proposé, on a calculé la diminution du potentiel entre le métal et la solution, la charge du métal, sa tension de surface et la fonction de travail de l'électron pour une interface métal–solution; on compare les résultats expérimentaux avec les formules qui ont été dérivées. Pour 38 métaux des sous-groupes à gauche du tableau de Mendéleev dans le cas particulier d'une interface vide–métal, on montre, pour la tension de surface et pour la fonction de travail, que les différences entre les valeurs théorique et expérimentale ne dépassent pas les erreurs expérimentales (soit moins que 10%); pour six métaux des sous-groupes à droite du tableau et particulièrement pour les semimétaux, l'erreur théorique est deux à trois fois plus élevée. On démontre que la densité des électrons libres dans un métal, telle que déterminée en termes des concepts du modèle, varie d'une façon monotone avec le numéro de l'élément pour les 54 métaux pour lesquels des données expérimentales existent.

On a développé une nouvelle relation entre la tension de surface et le potentiel de charge zéro qui permet de calculer la capacité de charge électronique du mercure (alors que la théorie prévoit une valeur de 33 C/cm^2, la valeur expérimentale est de 36–38 C/cm^2). On rapporte aussi les valeurs de la capacité intégrale d'une électrode à mercure dans l'eau: la valeur expérimentale est 29 F/cm^2 (au point de charge zéro) alors que la valeur théorique est 28 F/cm^2. La théorie prévoit une augmentation de la capacité dans la région anodique et une diminution dans la région cathodique; les résultats expérimentaux sont en bon accord avec ces prédictions. Il est important de noter que même si la théorie n'implique que l'ajustement d'un seul paramètre, soit la densité des électrons libres dans le métal, elle permet d'expliquer correctement un grand nombre de phénomènes.

[Traduit par le journal]

Introduction

Most of the presently available experimental data on the dense part of electrical double layer (EDL) are analysed within the framework of the Stern molecular capacitor model. The procedure is as follows: first, we consider an experimental quantity, say, the capacity of a metal at the interface with a given solution, and then fit the parameters of the model so as to obtain the best agreement with experiment. The agreement thus obtained is, for the most part, quite satisfactory. However, if we attempt to describe a given relationship, for example, the variation of the capacity of a given metal in contact with different solvents by the molecular capacitor model, we see that the model fails (1). This topic will be considered at greater length in a future paper. Contradictions inherent in the Stern model have forced us to resort to an alternative model of the electronic double layer (1) suggested by Frenkel (2) and Rice (3) as early as in 1928. At that time the model had not attracted the attention of electrochemists, for the quantum theory of surface phenomena was only in the incipient stage and could contribute little to the understanding of the properties of the dense part of EDL. On the other hand, these properties were studied insufficiently, so that experimental data did not fit any particular model. Since the Stern model was the most simple and rested upon the already traditional and therefore more customary ideas of Helmholtz, it was given preference; and the ideas of Frenkel and Rice were fully forgotten for a long time. The situation has changed only in the last 3 or 4 years.

The contemporary state of the art in the problem is, briefly, that the existence of the electronic double layer at a metal–vacuum interface is commonly accepted. Furthermore, the electronic double layer seems to play a decisive role in the formation of surface properties of metals, and numerous papers are devoted to the theory of this effect (see, for instance, recent reviews (4–6)). The situation is, however, different for a

Can. J. Chem. Downloaded from www.nrcresearchpress.com by 210.87.254.105 on 09/06/12
For personal use only.

Can. J. Chem. Downloaded from www.nrcresearchpress.com by 210.87.254.105 on 09/06/12
For personal use only.

metal–solution interface. In electrochemistry, the concept of the electronic capacitor[1] is almost unknown. There are only a few papers where an attempt has been made to calculate the capacity of the dense part of EDL on the basis of this model (7–11) (see also related papers (12–14)).

The concept of the electronic capacitor has not been popular because the theory is rather complicated. The functional density method, on which the theory is based, always leads to a system of non-linear equations which can only be solved by a computer (4–6). Thus to extend the theory to the EDL at a metal–electrolyte interface, one should perform all calculations once more; success is not guaranteed, for it is not clear *a priori* how to incorporate the electrolyte solution into the equations. Comparison of the results thus obtained with experiments is also very complicated, as the parameters appearing in the equations are chosen "blindly". Furthermore, the equations should be solved repeatedly, unless an optimal set of the parameters is found to best describe the experimental data.

In such a situation, it is very important to develop a version of the theory that would give simple analytical expressions. This is, of course, possible only if the phenomenon is simplified to the extent that all secondary effects are neglected. Some information will inevitably be lost, but this will be more than compensated for by the simplicity of the formulae and by the ease of comparison of the results with experiment. This all should help in finding the range of phenomena where the model works and in judging optimal values of the parameters for constructing a more rigorous (and therefore more accurate) theory and should facilitate preliminary treatment of experimental results.

The first attempt at a "simplified" description of the electronic capacitor was made in ref. 1. In this paper we shall try to proceed further. As is shown below, the model developed in ref. 1 permits the description of almost all properties of the dense part of the EDL (surface tension, capacity, zero-charge potentials, etc.) for a very wide range of systems.

Mechanism of formation of the electronic capacitor

A metal may be considered, in the first approximation, as a potential well in which conduction electrons are free to move. When impinging the wall of such a potential well (the role of this wall is played by the interface between a metal and the surrounding medium, electrolyte), the electron density wave undergoes total internal reflection[2] according to laws similar in many respects to the laws of total reflection for light. This is not surprising, because the same principle, namely, the wave nature of matter, underlies both phenomena.

It has long been known that in the total reflection of light the incident wave penetrates into the surrounding medium at a distance of the order of the wavelength (15, 16). The same situation occurs when electrons are reflected from a metal–electrolyte interface.[3] As a result, a negatively charged electron cloud is formed outside the metal in the solution (the outer plate of the electronic capacitor). At the same time, in the inner part of the interface, inside the metal, a layer with a thickness of several angstroms is formed (the inner plate of the electronic capacitor) in which the positive charge of the metal ion core is not compensated, because a fraction of the electrons penetrates from the metal into the solution. It should be noted here that the electroneutrality of the system is by no means violated because the charges of both plates are equal (of course, this is valid only at the zero-charge point; at potentials different from the zero-charge potential the excess charge of the electrode is compensated by ions of the diffuse part of the electrical double layer (EDL)).

Whenever the electronic capacitor exists, a potential difference arises between the metal and the electrolyte bulk,[4] the metal being always charged positively. Since this potential difference is sufficiently high (usually 2–7 V, see below), it mainly determines the potential of the zero-charge point (ZCP) and the capacity of the dense part of EDL. Furthermore, the electrostatic energy stored in the electronic capacitor contributes significantly to the surface energy of the metal–electrolyte interface. At the same time, the electrostatic potential difference across the electronic capacitor does not affect the electrochemical potential of the electrons that form the capacitor, for this electrochemical potential is always equal to that of electrons in the metal bulk (recall that the former and latter electrons are in thermodynamic equilibrium).

The electronic capacitor at the surface of a metal owes its origin to the wave nature of matter, that is, to its fundamental quantum-mechanical properties (17). Therefore, the very fact of the existence of the electronic capacitor requires no additional evidence. The only point that may be discussed is a contribution of the electronic capacitor to some or other parameters of the dense part of EDL. Note in this connection that in the Stern–Grahame molecular capacitor model, now generally accepted, the effect of electrons on the properties of the dense part of EDL is completely disregarded.

Electron density distribution inside the electronic capacitor

Calculation of the surface properties of metals at the interface with vacuum shows that the model of non-interacting electrons in a square potential well describes quite satisfactorily the experimental data. On the contrary, a more accurate description of the electron subsystem with an allowance for many-particle and quantum effects and under complete self-consistency gives results which are in striking discrepancy with experiment (this discrepancy was partly relaxed when lattice discreteness was taken into account (6)). This implies that many-particle and quantum effects do not contribute significantly to the electron density distribution because for various reasons they almost completely cancel one another. Thus, there are two approaches to construct the theory of surface phenomena in metals at the interface with an electrolyte. First, one may attempt, using the simplified model, to achieve the best agreement with experiment. Second, one may repeatedly improve the initial model, which eventually will elucidate the reasons why the "second-order" effects are cancelled out and will explain the discrepancy (insignificant for the most part) between

[1] The term "electronic capacitor" was first introduced in ref. 1 to denote the electronic double layer.

[2] If the reflection were not total, the amplitude of the electron density wave in the surrounding medium would not vanish. This would mean that the electrons permanently leave the metal. This is, of course, in contradiction with the concept of thermodynamic equilibrium of a system.

[3] Since the concentration of electrons at the metal surface is very high, the concentration remains sufficiently high at a distance of several de Broglie wavelengths as well.

[4] This potential difference is an analog of the contact potential difference at the boundary between two metals. The analogy becomes even more convincing if we take into account that in both cases the effect is caused by the change in the electron density at the boundary between the two media.

Can. J. Chem. Downloaded from www.nrcresearchpress.com by 210.87.254.105 on 09/06/12
For personal use only.

the initial model and experiment (the origins of this discrepancy cannot, of course, be understood without improving the model).

We shall choose the first approach and confine ourselves to the simplest model of a metal (the "jelly" model) and the simplest description of this model as suggested by Smith (18).

The "jelly" model implies that the charge of the ion core is uniformly smeared over the entire bulk of the metal up to its boundary $z = 0$ where the charge vanishes jumpwise. The electrons, whose concentration inside the metal is ρ_m, are free to move against the background of this smeared positive charge. From the electroneutrality condition we immediately obtain $\rho_m = k_m n_m$ where n_m is the number of atoms of the metal core per unit volume, and k_m is the number of free electrons per atom.

While solving the problem of electron distribution near the metal surface by the Thomas–Fermi method, Smith derived a complicated non-linear equation for determining the electron density $\rho_e(z)$. He approximated the solution of this equation by the following expression:

$$[1^*] \quad z < 0,\ \rho_e(z) = \rho_m - \frac{1}{2}\rho_m e^{z/R};\ z > 0,\ \rho_e = \frac{1}{2}\rho_m e^{-z/R}$$

Here R is the variational parameter chosen to give the best approximation of the equation obtained (it is assumed in [1*] that the metal occupies the half-space $z < 0$ and the surrounding medium the half-space $z > 0$). Although these formulae are rather simple, they give quite satisfactory results, at least by an order of magnitude. Later on, Timashev (19) considered a more rigorous version of the Thomas–Fermi method and showed that at a large distance from the metal surface $z = 0$

$$[1^{**}] \quad z < 0,\ \rho_e(z) = \rho_m - \rho_m \frac{R_s}{R_s + R_m}\exp(z/R_m)$$

$$z > 0,\ \rho_e(z) = \rho_m \frac{R_m}{R_m + R_s}\exp(-z/R_s)$$

where $R_s = 8.33a_0$ ($a_0 = \hbar^2/me^2 = 0.529$ Å is the Bohr radius) and

$$[2] \quad R_m = \sqrt{\frac{\pi\hbar^2}{4me^2K_F}} = \sqrt{\frac{\pi a_0}{4K_F}}$$

is a characteristic distance at which the electric field inside a metal is screened (20) (R_m is an analog of the Debye radius R_D in an electrolyte). In [2], $\hbar$ is Planck's constant and $K_F = (3\pi^2\rho_m)^{1/3}$ is the Fermi wave vector; e is the charge of an electron and m is its mass.

We shall also describe the electron density distribution by formulae of the type [1*] and [1**], but instead of using various approximate equations for determining the distribution parameter, we shall try to find them from simple and obvious considerations.

The solution of the Schrödinger equation for the motion of a neutral particle of mass m in a potential well of a height W implies that outside the well (i.e. for $z > 0$) the electron density is (17)

$$[3] \quad z > 0,\ \rho_e^s(z) = \rho_0 \exp(-z/R_s)$$

where ρ_0 is the electron density at $z = 0$ and

$$[4] \quad R_s = \hbar/\sqrt{2mW}$$

The potential barrier W appearing in this expression is an independent parameter of the problem. Apparently, the value of this parameter determines the work done in the transfer of an electron from the "bulk" of the well (from point $z = -\infty$, to be exact) into the surrounding medium (point $z = +\infty$). Thus, W has the meaning of the work needed to transfer an electron from the metal to the surrounding medium (the electron work function).

Let us assume that inside the metal

$$[5] \quad z < 0,\ \rho_e^m(z) = \rho_m - (\rho_m - \rho_0)\exp(z/R_m) \times \frac{\cos(2K_Fz + \delta)}{\cos\delta}$$

where R_m is given by [2] and $\cos(2K_Fz + \delta)$ describes the so-called Friedel oscillations (of frequency $2K_F$ (21)) arising as a result of interference of the incident and reflected electron density waves (the constant δ allows for phase shift during the reflection).

The "test" functions ρ_e^s and ρ_e^m include two arbitrary parameters (ρ_0 and δ) which, in principle, can be determined by minimizing the energy function. This minimization leads, however, to very cumbersome expressions. Therefore, to find ρ_0 and δ, we shall use the conditions which are just as important as the conditions for minimum energy function. These conditions are (*i*) continuity of the electron density at $z = 0$

$$[6] \quad \rho_e^s(0) = \rho_e^m(0)$$

(*ii*) continuity of its first derivative

$$[7] \quad \frac{\partial\rho_e^s(0)}{\partial z} = \frac{\partial\rho_e^m(0)}{\partial z}$$

and (*iii*) conservation of the number of electrons

$$[8] \quad \int_{-\infty}^{0}[\rho_m - \rho_e^m(z)]\,dz = \int_0^{+\infty}\rho_e^s(z)\,dz$$

(evidently, this relation is valid only at the zero-charge point which is just considered here). Conditions [6] and [7] have appeared because $\rho_e(z)$ is determined by the electron wave function which, in turn, is a solution of the Schrödinger equation. And since the latter is a second-order differential equation, both its solution and the first derivative of the solution must be continuous. Formulae [3] and [5] are written in such a form that condition [6] is satisfied automatically. From [7] and [8] we find

$$[9] \quad \rho_0 = \frac{2\rho_m\beta}{\alpha^2 + (1+\beta)^2}$$

$$[10] \quad \operatorname{tg}\delta = \frac{1 + \alpha^2 - \beta^2}{\alpha(1 + \alpha^2 + \beta^2)}$$

where $\alpha = 2K_FR_m$, $\beta = R_m/R_s$.

In this manner we have determined all the constants appearing in [3] and [5].

Potential distribution inside the electronic capacitor

If $\rho_e(z)$ is known, one can find the charge density distribution in the electronic capacitor

$$[11] \quad z < 0,\ q_m(z) = e[\rho_m - \rho_e^m(z)] = e(\rho_m - \rho_0)\exp(z/R_m) \times \frac{\cos(2K_Fz + \delta)}{\cos\delta}$$

$$z > 0,\ q_s(z) = -e\rho_e^s(z) = -e\rho_0\exp(-z/R_s)$$

Can. J. Chem. Downloaded from www.nrcresearchpress.com by 210.87.254.105 on 09/06/12
For personal use only.

and then, using Poisson's equation,

$$z < 0,\ \psi_m''(z) = -\frac{4\pi}{\epsilon_m} q_m(z)$$

[12]

$$z > 0,\ \psi_s''(z) = -\frac{4\pi}{\epsilon_s} q_s(z)$$

calculate the potential distribution $\psi(z)$ inside the electronic capacitor (here ϵ_m and ϵ_s are the dielectric permittivities of the metal and solution, respectively).

Imposing ordinary electrostatic boundary conditions

$$z = -\infty,\ \psi_m = \psi_e^{m-s}$$

[13] $$z = 0,\ \begin{cases}\psi_m = \psi_s \\ \epsilon_m \psi_m' = \epsilon_s \psi_s'\end{cases}$$

$$z = +\infty,\ \psi_s = 0$$

on $\psi(z)$, we obtain after simple calculations

[14] $$z < 0,\ \psi_m(z) = \psi_e^{m-s} - \frac{4\pi e(\rho_m - \rho_0)R_m^2}{\epsilon_m \cos\delta} \exp(z/R_m) \times \left\{\frac{2\alpha}{(1+\alpha^2)^2}\sin(2K_F z + \delta) + \frac{(1-\alpha)^2}{(1+\alpha^2)^2}\cos(2K_F z + \delta)\right\}$$

[15] $$z > 0,\ \psi_s(z) = \frac{4\pi e \rho_0 R_s^2}{\epsilon_s} \exp(-z/R_s)$$

where the constant ψ_e^{m-s} is

[16] $$\psi_e^{m-s} = \frac{4\pi e \rho_m R_s^2}{\epsilon_s} \frac{2\beta}{\alpha^2 + (1+\beta)^2} \times \left\{1 + \frac{\epsilon_s \beta}{2\epsilon_m} \frac{3 - (\alpha^2 + \beta^2)}{1 + \alpha^2}\right\}$$

Calculation using this formula has shown that even for $\epsilon_s = 1$ the contribution of the second term in curly brackets does not exceed 3–5%. If this term is neglected, we obtain

[17] $$\psi_e^{m-s} = \frac{4\pi e \rho_m R_s^2}{\epsilon_s} \frac{2\beta}{\alpha^2 + (1+\beta)^2}$$

Since in real systems ϵ_s is much larger than unity, the error of [17] is even less than 3–5%. Since [17] is more than sufficient to satisfy our purpose, we shall use this formula below.

Surface tension

From the distribution of charge $q(z)$ and potential $\psi(z)$ (see [11], [14], and [15]) one can easily calculate the electrostatic component of surface tension

[18] $$\sigma_e \equiv \frac{1}{2}\int_{-\infty}^{+\infty} q(z)\,\psi(z)\,dz = \frac{1}{2} k Q_e^+ \psi_e^{m-s}$$

In this expression ψ_e^{m-s} is the total potential drop between the metal and solution (see [17]),

[19] $$Q_e^+ = \int_{-\infty}^{0} q_m(z)\,dz = e\rho_m R_s \frac{2\beta}{\alpha^2 + (1+\beta)^2}$$

is the charge of the positive plate of electronic capacitor (according to the electroneutrality condition [8], it is equal to the charge of the negative plate Q_e^-), and the constant k characterizes charge "blurring." Substituting $q(z)$ as [11] and $\psi(z)$ as [14] and [15] into integral [18], we find that k is almost exactly 0.5. We note that in real systems the surface tension has, besides a purely electrostatic component, the exchange–correlation component which contributes significantly to the final expression. The latter can effectively be taken into account by choosing the proper value of the constant k. Indeed, according to ref. 6, if the exchange–correlation interaction is allowed for, σ rises, as compared with the electrostatic case, from 51 to 102 erg/cm^2 for Cs, from 62 to 120 erg/cm^2 for Rb, from 71 to 142 erg/cm^2 for K, and from 114 to 228 erg/cm^2 for Na (these are taken from ref. 22, Table 2.6, p. 52). Thus, in all cases, the surface tension increases twice as compared with the values predicted by the "jelly" model. We shall take, therefore, $k = 1$ instead of $k = 0.5$. As is shown below, the formula

[20] $$\sigma = \frac{1}{2} Q_e^+ \psi_e^{m-s} = \frac{8\pi e^2 \rho_m^2 R_m^2 R_s}{\epsilon_s[\alpha^2 + (1+\beta)^2]^2}$$

gives quite satisfactory agreement with experiment in all cases.

It follows from [17] and [19] that the capacity of the electronic double layer is $K_e^{m-s} = Q_e^+/\psi_e^{m-s} = \epsilon_s/4\pi R_s$. Comparison of this expression with [20] shows that relations [17], [19], and [20] describe the electronic capacitor model in which the positive charge Q_e^+ is localized at the metal surface $z = 0$ (the inner plate of the capacitor) and the negative charge Q_e^- is localized at $z = R_s$ (the outer plate), the space between the plates being filled with a medium of dielectric permittivity ϵ_s.

Electron work function in vacuum

While calculating the surface tension of liquid metals for a metal–vacuum interface, we have found that the quantity $C = (1/\alpha)[\alpha^2 + (1+\beta)^2]$ remains practically constant (with an accuracy of not less than 5%) for all metals when particular values of W and ρ_m are substituted. The value of C (averaged over 50 metals) was estimated to be 3.14. Assuming therefore $C = \pi$ and solving the equation thus obtained for W, we get

$$W = (2e^2\alpha^2/a_0\pi)(\sqrt{\pi\alpha - \alpha^2} - 1)^2$$

Numerical calculations have also shown that for all 50 metals the value of $(\sqrt{\pi\alpha - \alpha^2} - 1)$ lies between 0.50 and 0.55. Therefore, we shall not make a significant error by putting $(\sqrt{\pi\alpha - \alpha^2} - 1) \simeq 1/2$, which gives

[21] $$W = \frac{e^2\alpha^2}{2\pi a_0} = \frac{e^2 K_F}{2\pi} = \frac{1.526}{\epsilon_s}\tilde{\rho}_m^{1/3}\ \text{eV}$$

where $\tilde{\rho}_m = \rho_m \times 10^{-22}$ cm^{-3}.

Substitution into [4] yields $R_s = \pi a_0/\alpha$. Since $\alpha^2 = \pi a_0 K_F = 1.108\tilde{\rho}_m^{1/3}$ and $R_m = \pi a_0/2\alpha$ (see [2]), $\beta = R_m/R_s = 0.5$ and the formula for surface tension takes the form

[22] $$\sigma = \frac{2e^2\rho_m\alpha^3}{3\pi[\alpha^2 + 2.25]^2} = \frac{465.9\,\tilde{\rho}_m^{3/2}}{[\tilde{\rho}_m^{1/3} + 2.031]^2}\left(\frac{\text{erg}}{\text{cm}^2}\right)$$

Correspondingly, from [18] and [19] we obtain

[23] $$\psi_e^{m-s} = \frac{4e\alpha^4}{3\pi^2 a_0[\alpha^2 + 2.25]} = \frac{4.075\,\tilde{\rho}_m^{2/3}}{[\tilde{\rho}_m^{1/3} + 2.031]}\ (\text{V})$$

[24] $$Q_e^+ = \frac{\pi a_0 e \rho_m}{\alpha[\alpha^2 + 2.25]} = \frac{22.82\,\tilde{\rho}_m^{5/6}}{\tilde{\rho}_m^{1/3} + 2.031}\left(\frac{\mu C}{\text{cm}^2}\right)$$

Thus, if the electron gas in a metal is ideal, all the parameters of the electronic capacitor are expressed in terms of the electron density in the metal bulk ρ_m and the dielectric permittivity of the surrounding medium ϵ_s.

Can. J. Chem. Downloaded from www.nrcresearchpress.com by 210.87.254.105 on 09/06/12
For personal use only.

TABLE 1. Comparison of k_m values from various sources

Metal	k_m Ref. 24	k_m Ref. 20	k_m Calcd. from eqs. [21] and [22]
Li	—	0.8	1.0
Na	0.9	1.14	1.25
K	1.15*	1.05	1.5
Rb	0.94*	1.08	1.5
Mg	1.2	1.7	2.0
Al	1.5	2.7	2.0
Cr	1.6	—	2.5
Cu	1.9	1.4	2.0
Ag	1.9	1.2	2.5
Cd	2.2*	—	2.0
Pt	2.2	—	3.5
Au	2.4	1.5	2.5

*According to ref. 25.

The liquid metal – vacuum interface

The formulae derived above become much simpler if the surrounding medium is vacuum, because in this case $\epsilon_s = 1$ and the only parameter of the system is the electron density $\rho_m = K_m (\rho/M) N_A$ (here $N_A = 6.023 \times 10^{23}$ mol^{-1} is Avogadro's number, M is the molecular weight of the metal, and ρ is its density in g/cm^3). In this relation the coefficient k_m is the number of free electrons per one metal atom. Unfortunately, we do not know this parameter; it can by no means be identified with the chemical valence of a given element (21, 22), for in the formation of a metallic bond between atoms, electrons may be adopted from inner shells (this adoption is usually called "hybridization" (23)). For example, in the case of alkali atoms in the crystalline state this effect gives rise to a 25–40% increase in the number of free electrons (as compared with the number of valence electrons) (23). For other metals estimates are difficult to make, since a given substance in different compounds has a different valence, and it is not known relative to which valence the hybridization factor is to be determined.

It seems that the constant k_m could be determined from electroconductivity, thermal conductivity, and other data, but the corresponding expressions always contain the effective electron mass, scattering cross section, and other parameters for which exact values are not now available (the situation is especially poor for liquid metals). We could, of course, determine k_m from Hall measurements (see first two lines of Table 1), but the Hall values are known for only a few metals, and for liquid metals the data are not available at all. Furthermore, comparison of the results of different authors (see Table 1) shows that the Hall k_m values suffer low accuracy. We have therefore calculated k_m from experimental values of σ and W, using formulae [21] and [22]. The last line of Table 1 shows that the values of k_m thus found agree with the Hall data within experimental error.

Table 2 lists the calculated results for liquid metals at the melting point T_m. For the sake of brevity, the table presents data for the 6th period of the Mendeleev table. The dependences of W, σ, and k_m on ρ_m for all metals are shown in Figs. 1–3 (54 metals altogether; experimental data are not available for the others). While choosing the values of k_m, we were guided by two requirements: first, k_m was chosen so that σ and W, as calculated by [21] and [22], would best agree with the experimental values σ_{exp} and W_{exp}; secondly, the values of k_m should vary smoothly both along the rows (periods) and columns (groups) of the Mendeleev table. The values of k_m thus obtained (see Fig. 1) were lower than the maximal valences for nearly all metals (except for the alkali metals), which seems to be quite reasonable. It can also be seen that along a period the values of k_m first rise to a certain maximum (the larger the period number, the higher the maximum) and then decrease.[5] We had to take $k_m = 3.0$, only for the lanthanides, Ce, Pr, Nd, and Gd, whereas for lanthanum $k_m = 3.5$. It seems that for these metals the true values of the density ρ at the melting point are lower than those listed in Table 2 (since the handbook (26) does not report these data, we took the values of ρ from ref. 27). Along a group (from top to bottom), the values of k_m either grow or remain constant (the latter being characteristic of semimetals and metals in the two neighbouring groups; see Fig. 1).

Consider first Table 2. It can easily be seen that for the first 11 metals the error in determining the work function $\delta_W = (W_{theor} - W_{exp})/W_{exp}$ and the error in determining the surface tension $\delta_\sigma = (\sigma_{theor} - \sigma_{exp})/\sigma_{exp}$ never exceed 10% (i.e. δ_W and δ_σ lie within the experimental error). Note that δ_W and δ_σ gradually increase with the element number, particularly in the case of δ_σ. For example, for Bi δ_W is as high as 58%, whereas δ_σ is much less and does not exceed, as a rule, 15% (only for mercury $\delta_\sigma = 34\%$). It is important, however, that the error in determining δ_σ is mainly determined by the inaccuracy of [21] for W. Indeed, if in the initial expression [20] the experimental value W_{exp} is substituted for W found by [21], we obtain, for mercury, $\sigma = 482$ erg/cm^2 which is only 3% less than $\sigma_{exp} = 497$ erg/cm^2. For platinum, a similar substitution reduces σ from 1985 to 1658 erg/cm^2, which is also much closer to σ_{exp} 1746 erg/cm^2 (the error = −5%). It seems that even when [21], the formula for the electron work function becomes invalid, [20], the formula for surface tension, still holds. This is probably due to the fact that [21] has an additional assumption that the electron gas is ideal, the assumption that was not used in the derivation of [20].

In the case of the metals in other periods, the scatter in δ_σ is much less than that in δ_W (see also Figs. 2 and 3). Only for 4 metals (Li, Ge, Zn, and Sb) $\delta_\sigma = 20-25\%$, for 8 metals (Be, Si, K, Ga, Ag, Pt, Mn, and Bi) $\delta_\sigma = 10-20\%$, and for the remaining 41 metals $\delta_\sigma < 10\%$. In other words, for the last group of metals the theoretical values and the experimental values agree to within experimental error. In Fig. 3 the scatter is much larger; only for 30 metals does the condition $\delta_W < 10\%$ hold true. It is remarkable, however, that the discrepancy observed is not of random character. The experimental values W_{exp} exceed the theoretical values for all the metals. This is, of course, true to within experimental accuracy (the highest positive value $\delta_W = 6.7\%$ is for hafnium, which can be attributed to a measurement error). In other words, there is no metal for which the maximal momentum p_e^{max} is less than the Fermi momentum $p_F = \hbar k_F$ (it should be stressed that failure to meet this condition spells disaster for the theory developed, since this would mean that every cell of the phase space contains more than two electrons, which, of course, contradicts Pauli's exclusion principle). Now for many metals $p_e^{max} > p_F$. Many of these metals belong to the right-hand subgroups (subgroups B) in the Mendeleev periodic table (in Fig. 1 these metals occupy five right-hand columns and in Fig. 3 they are ringed with a

[5] The other parameters, melting point, density (see Table 2), boiling point, etc., behave in a similar way.

TABLE 2. Calculated values of liquid metals at their melting point

Element No.	k_m Me	T_m (K)	ρ (g/cm^3)	$\rho_m\ 10^{-22}$ (cm^{-3})	W_{exp}† (eV)	W_{theor} (eV)	δ_W (%)	σ_{exp} (erg/cm^2)	σ_{theor} (erg/cm^2)	δ_σ (%)	$\left(-\frac{d\sigma}{dT}\right)_{exp}$ (erg/cm^2 K)	$\left(-\frac{d\sigma}{dT}\right)_{theor}$ (erg/cm^2 K)
55	$Cs^{1.5}$	28.6	1.85	1.27	1.81	1.65	−9.6	68.8	68.5	−0.5	0.05	0.02
56	$Ba^{2.5}$	727	3.32	3.64	2.30	3.34	1.7	277	254	8.2	0.07	0.06
57	$La^{3.5}$	930	5.96	9.04	3.20	3.18	−0.6	745	748	0.4	0.10	0.013
58	$Ce^{3.0}$	798	6.68	8.62	2.96	3.13	5.4	740	705	5.0	0.03	0.01
59	$Pr^{3.0}$	935	6.61	8.48	2.95	3.11	5.1	706	692	−2.0	0.08	0.01
60	$Nd^{3.0}$	1024	6.69	8.38	3.00	3.10	3.2	688	682	−0.9	0.05	0.02
64	$Gd^{3.0}$	1311	7.14	8.20	3.20	3.08	−4.0	670	666	−0.6	—	—
72	$Hf^{4.0}$	2220	12.0	16.2	3.60	3.86	6.7	1588	1460	−8.7	—	—
73	$Ta^{4.0}$	2996	15.0	22.5	4.10	4.30	4.7	2140	2111	−1.3	—	—
74	$W^{4.5}$	3395	16.7	24.7	4.55	4.44	−2.3	2316	2340	1.0	—	—
75	$Re^{4.5}$	3180	18.4	26.8	5.00	4.57	−9.4	2614	2561	−2.0	—	—
76	$Os^{4.5}$	3050*	20.1*	28.6	5.4(?)	4.67	−15.6	2500	2751	9.1	—	—
77	$Ir^{4.0}$	2454	20.0*	25.0	5.30	4.47	−18.5	2250	2321	3.0	—	—
78	$Pt^{3.5}$	1769	19.7	21.3	5.30	4.23	−25.3	1746	1985	12.0	0.31	0.08
79	$Au^{2.5}$	1063	17.2	13.1	4.20	3.60	−16.6	1139	1149	0.9	0.19	0.05
80	$Hg^{2.0}$	−38.9	13.7	8.2	4.52	3.08	−32	497	668	34	0.28	0.07
81	$Te^{2.0}$	302	11.2	6.6	3.67	2.86	−28	458	515	11.2	0.11	0.09
82	$Pb^{2.0}$	327	10.8	6.3	3.95	2.82	−40	455	491	7.2	0.08	0.04
83	$Bi^{2.0}$	272	10.1	5.8	4.35	2.74	−58	375	444	15.6	0.07	0.04

* The values of T_m, ρ, σ_{exp}, and $(d\sigma/dT)_{exp}$ without an asterisk are taken from ref. 26 and those with an asterisk from ref. 27 (in both cases recommended values were employed).

† The values W_{exp} are taken from refs. 28, 29 (recommended values).

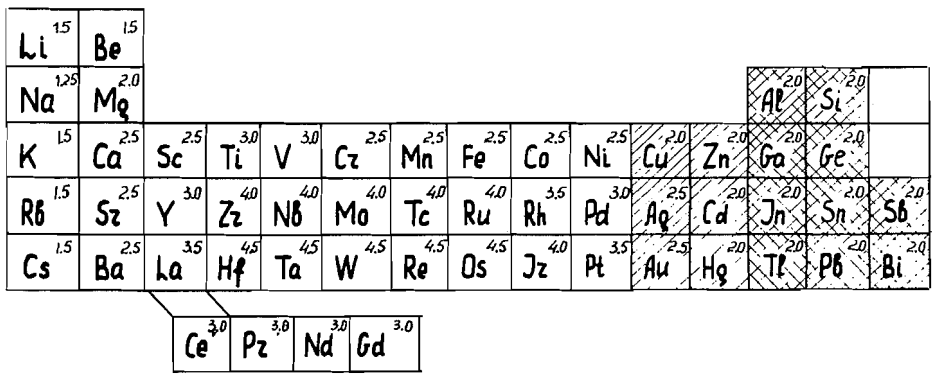

FIG. 1. The number of free electrons k_m per metal atom. The metals in the right-hand columns of the Mendeleev table (metals of subgroup B) are singly cross-hatched; semimetals are doubly cross-hatched.

dashed line). It is known that for at least some of these metals (viz., for mercury (30)) the Fermi surface is highly smeared; this precisely explains why $p_e^{max} > p_F$ for such metals.

Thus, for 30 out of 54 metals with available data, one can fit experimental values of σ and W by adjusting only one parameter, the number of free electrons k_m per atom. For the remaining 24 metals this is impossible, perhaps because the "imperfection" of the electron gas is not taken into account. The non-random character of the discrepancy is confirmed by the fact that the "abnormal" metals are grouped at the end of each period (particularly when they included all semimetals).

Differentiating expression [22] with respect to temperature T at $\epsilon_s = 1$, we obtain

$$[25]\quad \frac{d\sigma}{dT} = 388.5\ \tilde{\rho}_m^{3/2}\ \frac{3.655 + \tilde{\rho}_m^{1/3}}{(2.031 + \tilde{\rho}_m^{1/3})^3}\left[\frac{1}{k_m\rho}\frac{d(k_m\rho)}{dT}\right] \quad (\text{erg cm}^{-2}\ \text{K}^{-1})$$

Since the expression before the square brackets is always positive, the sign of $d\sigma/dT$ is determined by the sign of the derivative $d(k_m\rho)/dT$. And since in all the cases $d\rho/dT < 0$, $d\sigma/dT$ is also negative for k_m = constant, which is indeed the case. But numerical calculations by [25] under k_m = constant give values of $d\sigma/dT$ which are only 30–50% of the experimental values (see Table 2). We have to assume, therefore, that k_m also depends on temperature. Quantitative agreement with experiment may be obtained by putting

$$\frac{1}{k_m}\frac{dk_m}{dT} \simeq \frac{1}{\rho}\frac{d\rho}{dT}$$

Differentiating [21], the work function with respect to T, we find

$$[26]\quad \frac{1}{W}\frac{dW}{dT} = \frac{1}{3}\left[\frac{1}{k_m\rho}\frac{d(k_m\rho)}{dT}\right] \quad (\text{eV K}^{-1})$$

For most liquid metals $(1/\rho)\ (d\rho/dT)$ is of the order of 10^{-4}–10^{-5}, and for solid metals this quantity is about 10^{-5}–10^{-6}. Therefore, $(1/W)\ (dW/dT)$ is of the same order of magnitude, in excellent agreement with experiments (26, 31).

Can. J. Chem. Downloaded from www.nrcresearchpress.com by 210.87.254.105 on 09/06/12
For personal use only.

Can. J. Chem. Downloaded from www.nrcresearchpress.com by 210.87.254.105 on 09/06/12
For personal use only.

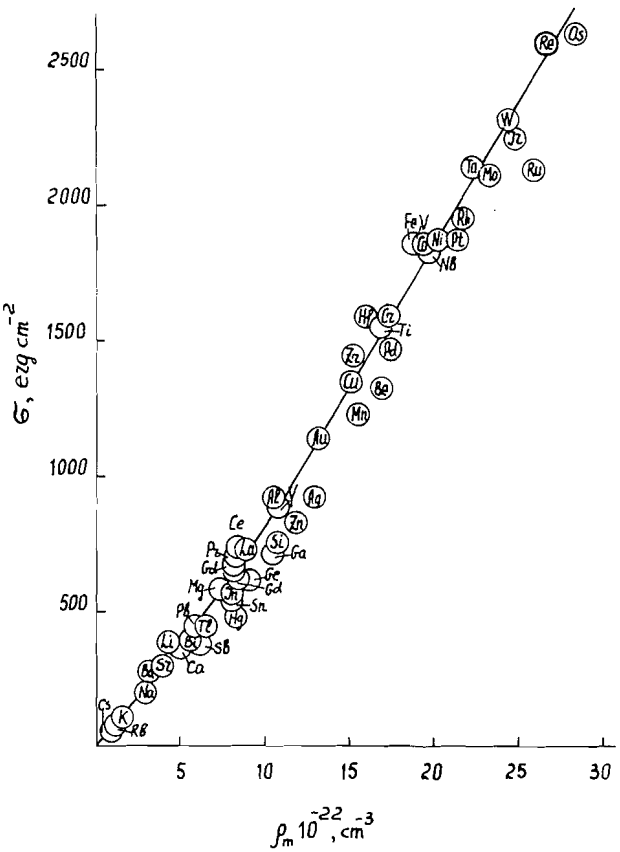

FIG. 2. The surface tension of liquid metals, σ, as a function of the electron density in the metal bulk, ρ_m. Experimental values of σ are taken from ref. 26.

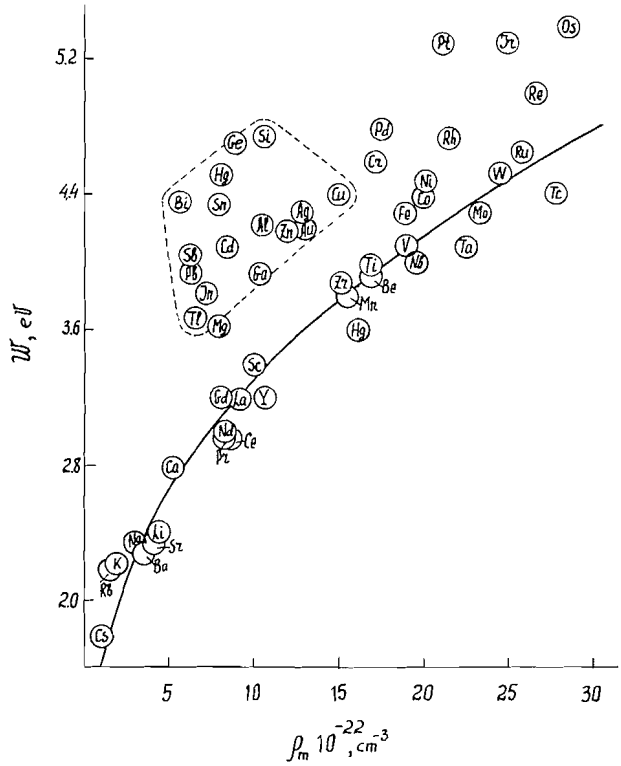

FIG. 3. The electron work function W as a function of the electron density in the metal bulk ρ_m. The metals of subgroup B are singly cross-hatched; semimetals are doubly cross-hatched. Experimental values of W are taken from ref. 28.

During melting, the density of a metal changes by several percent. It is a simple matter to calculate that in this case the change in the work function,

$$\Delta W \simeq \frac{W}{3}\frac{\Delta\rho}{\rho}$$

will be about 0.1 eV, which is also confirmed by experiments (for example, the experimental value of ΔW for copper is 0.13 eV (28)).

Since the derivation of the fundamental equations [20] and [21] does not require the metal to be in solid state or in liquid state, these formulae can be used for the calculation of σ and W both for liquid and solid metals. Furthermore, since the electron work function of a metal is practically the same in the liquid and the solid state, we may safely assume that the values of k_m obtained above for melts are very close to those for crystals. This opens promising potentials for quantitative calculations in the case of solid metals. It should be noted, however, that since the packing density of atoms on different crystal faces is different, the corresponding values of σ and W will also change.[6] This effect (which, of course, is absent in liquid metals) makes it possible to reconstruct, by the formulae derived above, the shape of the Fermi surface, using the values of W measured for different faces.

[6] When saying above that W does not change in going over from the liquid to solid state, we mean the value of W is averaged over all crystal faces. In an experiment, this averaging is attained by using polycrystalline samples.

Qualitative analysis of the properties of the electronic capacitor at the metal–electrolyte interface

Verification of the formulae derived above for the metal–vacuum interface has shown that they are quite reliable for developing a theory of the more complicated metal–electrolyte system. Now we turn to such a system, starting with the analysis of general properties of the dense part of EDL.

It was shown in refs. 32, 33 that for surface-inactive electrolytes the zero-charge potential (ZCP) and the behaviour of the integral capacity curves depend neither on the concentration of an electrolyte nor on its nature.

These facts can naturally be explained within the framework of the electronic capacitor model. Indeed, in dilute solutions there are thousands and even tens of thousands of solvent molecules per ion (for example, concentration 0.01 mol/dm^3 corresponds to 5000 water molecules per ion, and 0.001 mol/dm^3 to 50 000 water molecules per ion). Therefore, the electron work function for the metal – dilute solution interface at the ZCP practically does not differ from that for the metal – pure solvent interface. Hence in a dilute solution the properties of the electronic capacitor should not depend either on the concentration of dissolved ions or on their nature; this has been observed experimentally (but the situation may be quite different in very concentrated solutions).

The electrocapillary and charge curves, as well as the curves of the EDL dense part capacity versus the electrode potential, are always asymmetric about the zero-charge point; this fact is well known. The entropy of the EDL dense part is also asymmetric, its maximum being shifted to the negative potential range (relative to the ZCP) (34). Essentially, this asymmetry is observed for all electrodes and electrolytes.

Can. J. Chem. Downloaded from www.nrcresearchpress.com by 210.87.254.105 on 09/06/12
For personal use only.

The inequality between the anodic and cathodic potential regions is, in fact, predetermined by the properties of the electronic capacitor. Indeed, any metal at the boundary with any solvent is always charged positively because the double layer is formed as a result of the outflow of electrons from the metal. When applying an additional positive potential to the electrode, we further increase the potential drop that already exists. On the contrary, when applying a negative potential, we reduce the drop or even change its sign. Since the electric field in the electronic capacitor is 10^8 V/cm and higher, i.e. it is very strong, any change in the field must lead to a non-linear response of the medium. In this situation it is surprising that the asymmetry observed is not as large as expected.

Special attention should be drawn to specific adsorption. This adsorption, by definition, is determined by specific (i.e. nonelectrostatic) forces. But electrostatic forces are involved, because they prevent positive cations from (and, conversely, promote negative anions in) approaching very closely the surface of the positively charged metal. As a result, most inorganic anions are adsorbed well on an electrode, whereas most cations either are not adsorbed at all or are adsorbed poorly. This fact is a manifestation of the asymmetry mentioned above.

Thus, the most general porperties and governing laws of the structure of the EDL dense part are explained easily and naturally within the framework of the electronic capacitor model.

Surface tension of mercury at the zero-charge point

Consider a system of two solvents (say, H_2O and S) in contact with a mercury electrode (the solvents are not in contact with each other). Suppose that each solvent is kept (with the aid of auxiliary electrodes and batteries) at the zero-charge potential, which is, of course, different for H_2O and S. Since the sum of all potential drops in the circuit $Me/H_2O/Hg/S/H_2O/Me$ is equal to the applied potential difference $V_{Hg}^{H_2O-S}$, we have

$$[27]\quad \psi_e^{Hg-H_2O} - \psi_e^{Hg-S} + \Delta\psi_{lq}^{H_2O-S} = -V_{Hg}^{H_2O-S}$$

where $\Delta\psi_{lq}^{H_2O-S}$ is the liquid potential drop at the H_2O-S interface, ψ_e^{Hg-S} is the electronic potential drop at the electrode–solvent interface, and $V_{Hg}^{H_2O-S}$ is the voltage drop measured by a voltmeter with an infinitely high input resistence. Apparently, this relation can be rewritten in the form

$$[28]\quad \Delta\psi_{e(Hg)}^{H_2O-S} = \psi_e^{Hg-H_2O} - \psi_e^{Hg-S} = -[\Delta\psi_{lq}^{H_2O-S} + V_{Hg}^{H_2O-S}] = -\Delta\psi_{Hg}^{H_2O-S}$$

Calculations by formula [22] have shown that for all solvents at the boundary with mercury the charge Q_e^+ is approximately the same, ~0.33 C m^{-2}. Thus, multiplying the two sides of [28] by $0.5Q_e^+ = 0.165$ C m^{-2} and using $\sigma = 0.5Q\psi$, we obtain

$$[29]\quad \Delta\sigma_{Hg}^{H_2O-S} = \sigma^{Hg-H_2O} - \sigma^{Hg-S} = -\frac{1}{2}Q_e^+\,\Delta\psi_{Hg}^{H_2O-S}$$

The potential difference $V_{Hg}^{H_2O-S}$ can easily be determined in experiment with a high accuracy and the liquid potential drop $\Delta\psi_{lq}^{H_2O-S}$ can be estimated from simple model considerations (35) (unfortunately, the accuracy of such estimates is rather low), thereby making possible a comparison of [29] with experiment.

Figure 4 shows the values of $\Delta\sigma_{Hg}^{H_2O-S}$ and $\Delta\psi_{Hg}^{H_2O-S}$ for 51 different solvents. It can be seen that all these values are located rather closely to a straight line through the origin. Calculation of $0.5Q_e^+$ from the slope of this straight line gives 0.18

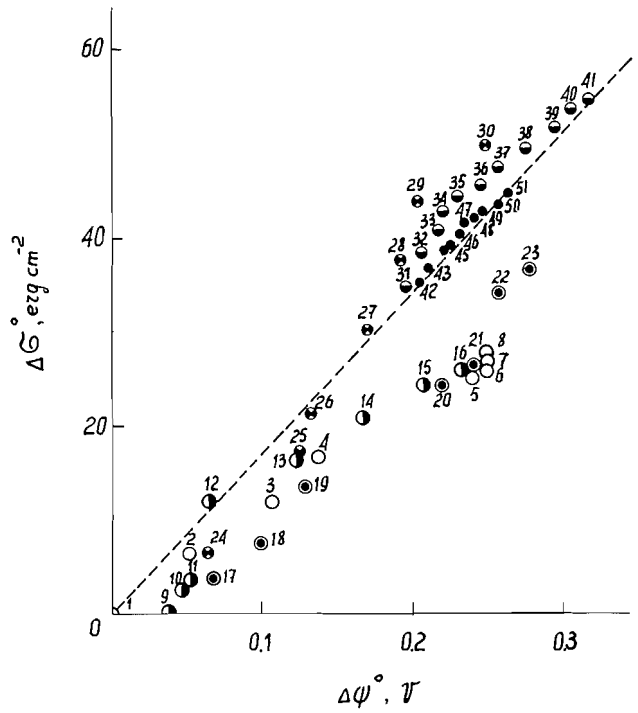

FIG. 4. The shift of the zero-charge potential $\Delta\psi_m^0 = \psi_m^0 - (\psi_m^0)_{H_2O}$ versus the change in surface tension $\Delta\sigma^0 = \sigma^0 - \sigma_{H_2O}^0$ for a mercury electrode at the interface with various solvents. Points *1–8*, saturated solution of NaCl in mixtures of water and ethanol (63); *9–16*, 0.1 *M* solution of HCCONa in mixtures of water and formic acid (64); *17–23*, 0.1 *M* LiCl in mixtures of water and acetone (46); *24–30*, 0.1 *M* LiCl in mixtures of water and diethylene glycol (50); *31–41*, 0.1 *M* LiCl in mixtures of formamide and dimethyl formamide (65); *42–51*, 0.1 *M* LiCl in mixtures of formamide and *N*-methyl formamide (66). The liquid potential drop was estimated from measurements in the following circuits: acetone–water Pt-$|H_2|HCl(H_2O)|KCl(H_2O)|HCl$(acetone + $H_2O)|H_2|$Pt; water – diethylene glycol Ag$|$AgCl$|$0.1 *N* LiCl$(H_2O)|KCl(H_2O)|$0.1 *N* LiCl(DEG + $H_2O)|$AgCl$|$Ag; formamide – dimethyl formamide Na(Hg)-$|NaCl_{sat}$(FA)$|NaCl_{sat}$(FA + DMF)$|$(Hg)Na (a similar circuit was used for studying the system formamide/*N*-methyl formamide).

C m^{-2}, which is very near the theoretical value 0.165 C m^{-2}. The scatter of experimental points may well be attributed to a low accuracy of determining the liquid potential drop.

Integral capacity of the electronic capacitor

By definition, the integral capacity of the electronic capacitor at the zero-charge point is $K_e^{m-s} = Q_e^+/\psi_e^{m-s}$. Substitution of ψ_e^{m-s} from [17] and Q_e^+ from [19] yields

$$[30]\quad K_e^{m-s} = \frac{Q_e^+}{\psi_e^{m-s}} = \frac{\epsilon_s}{4\pi R_s}$$

This formula includes the solvent dielectric permittivity which is to be determined. To find it, we note the time that the conduction electron stays outside the metal (i.e. in the solution) is $\sim 10^{-15}$ s.[7] This time is commensurable with the rotation period of optical electrons of solvent molecules, but is many orders less than the rotation period of the solvent molecule as a whole. Therefore, the solvent responds to an "exiting" electron only through the optical modes. In other words, $\epsilon_s = n_D^2$,

[7] The time of electron "escape" can be estimated by the relation $\tau = R_s/v_F$, where $v_F = P_F/m$ is the Fermi electron velocity.

Can. J. Chem. Downloaded from www.nrcresearchpress.com by 210.87.254.105 on 09/06/12
For personal use only.

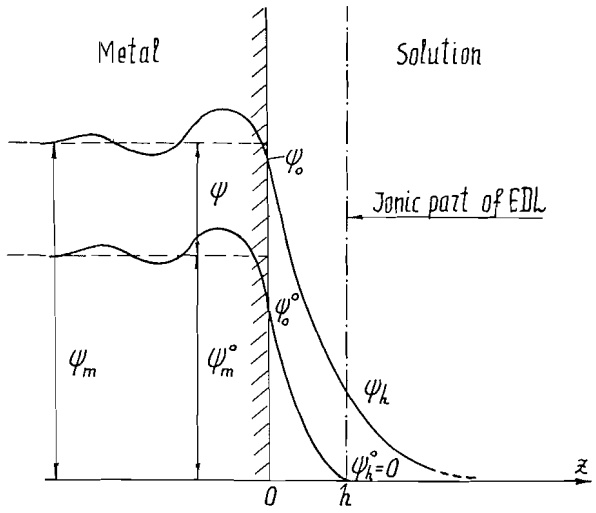

FIG. 5. Potential distribution in the electronic part of EDL for the electrode charge $Q_e \neq 0$.

where n_D is the refractive index. More accurate calculations for a point charge executing Brownian motion confirm this assumption (36).

If we use the tabular values of n_D and calculate K_e^{m-s} by formula [30], we see that it is several times less than the experimental value. However, this comes as no surprise as the measured capacity K_e and the capacity of the electronic capacitor K_e^{m-s} are different entities.

Let ψ_m^0 stand for the potential difference between the metal bulk and electrolyte bulk at the zero-charge point (see Fig. 5). Of course, this quantity cannot be measured directly in experiment; instead one usually measures the potential (at the zero-charge point) against a reference electrode. This potential, however, differs from ψ_m^0 only by a constant which is cancelled out in all further calculations. In what follows we shall use ψ_m^0, rather than the potential measured against a reference electrode.

Now let the charge Q_e be carried to the electrode. In this case its potential (measured against the electrolyte bulk) will be ψ_m, and the so-called total integral capacity of EDL takes the form

$$[31] \quad K_{m-s} = \frac{Q_e}{\psi_m - \psi_m^0}$$

To infer from this quantity the integral capacity of the density part of EDL, we note (see Fig. 5) that

$$[32] \quad \psi_m - \psi_m^0 = [(\psi_m - \psi_0) - (\psi_m^0 - \psi_0^0)] + [(\psi_0 - \psi_h) - (\psi_0^0 - \psi_h^0)] + (\psi_h - \psi_h^0)$$

We have seen above that for $Q_e = 0$, the potential difference $\psi_m^0 - \psi_0^0$ is very low. Since further consideration will be restricted to a potential region very near the zero-charge point, we shall assume, as before, $\psi_m \simeq \psi_0$. Thus,

$$[33] \quad \psi_m - \psi_m^0 = [(\psi_m - \psi_h) - (\psi_m^0 - \psi_h^0)] + (\psi_h - \psi_h^0)$$

Dividing this equality by Q_e and putting $K_e = Q_e/[(\psi_m - \psi_h) - (\psi_m^0 - \psi_h^0)]$ and $K_i = Q_e/(\psi_h - \psi_h^0)$,[8] we arrive at the familiar relation $K_{m-s}^{-1} = K_e^{-1} + K_i^{-1}$. Since $\psi_h^0 = 0$, we finally have

$$[34] \quad K_e = \frac{Q_e}{(\psi_m - \psi_h) - \psi_m^0}$$

[8] K_i is the integral capacity of the diffuse part of EDL.

Apparently, this formula differs significantly from [30]. To distinguish between these two quantities, we shall call K_e^{m-s} the capacity of the electronic capacitor and K_e the capacity of the dense part of EDL.

To calculate K_e, we shall employ the same electron density distribution $\rho_e(z)$ as for $Q_e = 0$

$$[35] \quad \rho_e(z) = \begin{cases} \rho_e^s(z) = \rho_0 \exp(-z/R_s), & z \geq 0 \\ \rho_e^m(z) = \rho_m - (\rho_m - \rho_0) \exp(z/R_m) \times \dfrac{\cos[\alpha(z/R_m) + \delta]}{\cos \delta}, & z \leq 0 \end{cases}$$

As before, the constants ρ_0 and δ of the distribution are found from the condition that the potential and its first derivative are continuous at $z = 0$ (see [6], [7]) and also from the condition that the number of particles is conserved, which in this case is written in the form,

$$[36] \quad \frac{Q_e}{e} = \int_0^\infty \rho_e^s(z)\, dz - \int_{-\infty}^0 [\rho_m - \rho_e^m(z)]\, dz$$

(the non-zero electrode charge Q_e is assumed to be neutralized by the charge of the diffuse part of EDL, Q_i). Substitution of [35] into [6], [7], and [36] yields

$$[37] \quad \rho_0 = \rho_m \frac{2\beta + (1 + \alpha^2)q}{\alpha^2 + (1 + \beta)^2}$$

$$[38] \quad \alpha \operatorname{tg} \delta = \frac{(1 + \alpha^2 - \beta^2) - (1 + \alpha^2)(1 + \beta)q}{(1 + \alpha^2 - \beta^2) - (1 + \alpha^2)q}$$

where the dimensionless charge is

$$[39] \quad q = Q_e/e\rho_m R_s$$

Defining the charge densities $q_m(z)$ and $q_s(z)$ by relations [11] and substituting them into Poisson's equation [12], we find the potential distribution

$$\psi_s(z) = \psi_h - \frac{4\pi Q_e}{\epsilon_s} z + \frac{4\pi e \rho_0 R_s^2}{\epsilon_s} \exp(-z/R_s), \quad z > 0$$

$$[40] \quad \psi_m(z) = \psi_m - \frac{4\pi e(\rho_m - \rho_0)R_m^2}{\epsilon_m \cos \delta} \exp(z/R_m) \times \left\{ \frac{2\alpha}{(1 + \alpha^2)^2} \sin\left[\alpha \frac{z}{R_m} + \delta\right] + \frac{1 - \alpha^2}{(1 + \alpha^2)^2} \cos\left[\alpha \frac{z}{R_m} + \delta\right] \right\}, \quad z < 0$$

The constant ψ_m appearing in this expression is determined from the condition that the potential is continuous at $z = 0$. Disregarding the potential drop inside the metal (i.e. the second term in the expression for $\psi_m(z)$, we obtain

$$[41] \quad \psi_m - \psi_h = \frac{4\pi e \rho_m R_s^2}{\epsilon_s} \frac{2\beta + (1 + \alpha^2)q}{\alpha^2 + (1 + \beta)^2}$$

In general, the work function $W = W_0 + e\psi$ where W_0 is the work function at the zero-charge point and $\psi = \psi_m - \psi_m^0 - \psi_h$. Thus,

$$[42] \quad R_s = R_{s0} \Big/ \sqrt{1 + \frac{e\psi}{W_0}}; \quad \beta = \beta_0 \sqrt{1 + \frac{e\psi}{W_0}}$$

On the other hand, since $\psi_h = 0$ at $Q_e = 0$,

$$\psi_m^0 = \frac{4\pi e \rho_m R_{s0}^2}{\epsilon_s} \frac{2\beta_0}{\alpha^2 + (1 + \beta_0)^2}$$

TABLE 3. Properties of some metal–solvent systems

Metal–solvent (electrolyte)	n_D^2 (ref. 37)	σ(erg/cm^2) (ref. 38)	W (eV)	K_c Theory	(F/cm^2) Exp.	$\Delta\psi_{Hg}^{H_2O-S}$ Theory	(V) Exp.
Hg–water (NaF)	1.78	425	2.61	29	29 (ref. 33)	0.52*	0.45*
Hg–acetonitrile ($LiClO_4$)	1.81	393	2.82	29	17–22 (ref. 40)	0.17	—
Hg–methanol (KF)	1.77	392	2.92	29	21 (ref. 41)	−0.29	0.05–0.17
Hg–formamide (KNO_3)	2.09	389	2.50	32	25 (ref. 44)	0.31	0.2
Hg–acetone (LiCl)	1.85	388	2.78	30	16 (ref. 46)	0.20	0.11–0.19
Hg–ethanol (KF)	1.85	387	2.78	30	20 (ref. 47)	0.20	0.15–0.25
Hg – ethylene glycol (KF)	2.05	381	2.49	31	20–43 (ref. 48)	0.27	—
Hg – dimethyl formamide ($NaClO_4$)	2.04	376	2.55	35	22 (ref. 49)	0.29	0.23–0.44
Hg – diethylene glycol (LiCl)	2.09	375	2.49	32	21 (ref. 50)	0.32	0.25
Hg – sulfolane (KPF_6)	2.19	373	2.37	33	21 (ref. 51)	0.34	—
Hg – dimethyl sulfoxide (KPF_6)	2.18	371	2.39	32	25–28 (ref. 52)	0.34	—
Hg–pyridine ($LiNO_3$)	2.28	363	2.33	33	20 (ref. 53)	0.4	—
Ga–water ($NaClO_4$)	1.78	647	2.35	31	135 (ref. 54)	0.08†	0.44–0.5

*This cell represents $\Delta\psi_{Me}^{V-H_2O} = \psi_e^{m-v} - \psi_e^{m-H_2O}$.

†This cell represents $\Delta\psi_{Q_e=0(H_2O)}^{Hg-Ga} = \psi_{e(Q_e=0)}^{Ga-H_2O} - \psi_{e(Q_e=0)}^{Hg-H_2O}$.

Subtracting this expression from [41] and taking into account [42], we find

$$[43]\quad \psi = \psi_m - \psi_m^0 - \psi_h = \frac{8\pi e\rho_m R_{s0} R_m}{\epsilon_s}\left(\frac{1}{Z} - \frac{1}{Z_0}\right) + \frac{4\pi R_{s0}}{\epsilon_s}\frac{1+\alpha^2}{Z} Q_c$$

where we have put, for brevity,

$$[44]\quad Z = \sqrt{1 + \frac{e\psi}{W_0}\left[\alpha^2 + \left(1 + \beta_0\sqrt{1 + \frac{e\psi}{W_0}}\right)^2\right]}$$

$$Z_0 = \alpha^2 + (1 + \beta_0)^2$$

Solving [43] for Q_c, dividing the two sides of the equality by ψ, and using $K_c = Q_c/\psi$, we obtain the final expression for the integral capacity of the electronic part of EDL

$$[45]\quad K_c = \frac{\epsilon_s}{4\pi R_{s0}}\frac{Z}{1+\alpha^2} + \frac{2e\rho_m R_m}{(1+\alpha^2)Z_0}\frac{Z - Z_0}{\psi}$$

At the zero-charge point, where $\psi = 0$ and $Z - Z_0 = 0$, this expression is reduced to

$$[46]\quad K_e^0 = \frac{\epsilon_s}{4\pi R_{s0}}\frac{Z_0}{1+\alpha^2} + \frac{e^2\rho_m R_m}{(1+\alpha^2)W_0}\left[1 + \frac{2\beta_0(1+\beta_0)}{Z_0}\right]$$

Note that the second term in [45] is always positive, since ψ and $Z - Z_0$ change sign simultaneously and $Z \geq Z_0$ for $\psi \geq 0$.

Interface between mercury and non-aqueous electrolyte solution

Expressions [45] and [46] for the capacity of the dense part of EDL include three parameters: ρ_m, ϵ_s, and W^{m-s}. Two of them, ρ_m and $\epsilon_s = n_D^2$, describe the bulk properties of a metal and solution; the third parameter, the electron work function W^{m-s} for a metal–solution interface, is determined by the interaction between the two media and is therefore different for different metal–solution couples. For liquid electrodes (mercury, gallium), W^{m-s} can be found from surface tension data. To this end, we modify formula [20] for σ. Substituting $\epsilon_s = n_D^2$ and taking into account that $R_s = \pi a_0/\alpha\gamma$, $\beta = 0.5\gamma$, where $\gamma^2 = W^{m-s}/W^{m-v}$, and the electron work function for a metal– vacuum interface $W^{m-v} = e^2\alpha^2/2\pi^2 a_0 = 1.256\,\tilde{\rho}_m^{1/3}$ eV (see [21]), we obtain

$$[47]\quad \sigma^{m-s} = \frac{2e^2\alpha^3\rho_m}{3\pi n_D^2\gamma[\alpha^2 + (1+\beta)^2]^2} = \frac{465.9\,\tilde{\rho}_m^{3/2}}{n_D^2\gamma[\tilde{\rho}_m^{1/3} + 0.902(1 + 0.5\gamma)^2]^2}\ \text{erg/cm}^2$$

Assuming n_D^2 and σ^{m-s} known from experiment and substituting $\tilde{\rho}_m = 8.13$ for mercury and 10.5 for gallium, we can find the only unknown quantity W^{m-s}. The results of such calculations for several solvents are listed in Table 3, which also presents the values of K_e^{theor} as calculated by formula [46] with W^{m-s} found from [47]. It can be seen that in most cases calculation results are rather close to experimental values K_e^{exp}. Only for the system Ga–H_2O does the difference $K_e^{exp} - K_e^{theor}$ significantly exceed the experimental error; in the other cases it is close to this error. Here we should point out two facts. First, the values of K_e^{exp} for a mercury – organic solvent interface were determined from the total capacity plots of the respective papers. Such a method of finding K_e suffers, of course, from low accuracy. It is not expected that the true values of K_e differ by more than several microfarads from the values listed in Table 3. Secondly, a large error for gallium seems to indicate that in this case the capacitor is formed via a special mechanism because the experimental value of K_e is unusually high for this metal. At the same time, mercury (as far as capacity is concerned) is a metal in which the capacitor is formed via the mechanism mentioned in the preceding section. Therefore, in the case of mercury all theoretical values of K_e are rather close to experimental ones.

Figure 6 shows the integral capacity K_e as a function of the electrode charge Q_e for the mercury–water system. The theoretical curve was calculated by formula [45] with the value $W^{Hg-H_2O} = 2.61$ eV found from surface tension data. The theory does not, of course, reflect all the features of experimental curves, especially for a large negative electrode charge. This is probably due to the fact that in the calculations we have not taken into account the dependence of the dielectric permittivity $\epsilon_s = n_D^2$ on the electric field in the outer plate of the electronic capacitor. Since this field can be as high as 10^8–10^9 V/cm, it can significantly affect n_D (interestingly, the discrepancy between theory and experiment is observed in the cathodic region where the field grows; in the anodic region the outer plate is "pulled" into the metal (see below) and the field decreases).

There is another way of experimentally verifying the theory

Can. J. Chem. Downloaded from www.nrcresearchpress.com by 210.87.254.105 on 09/06/12
For personal use only.

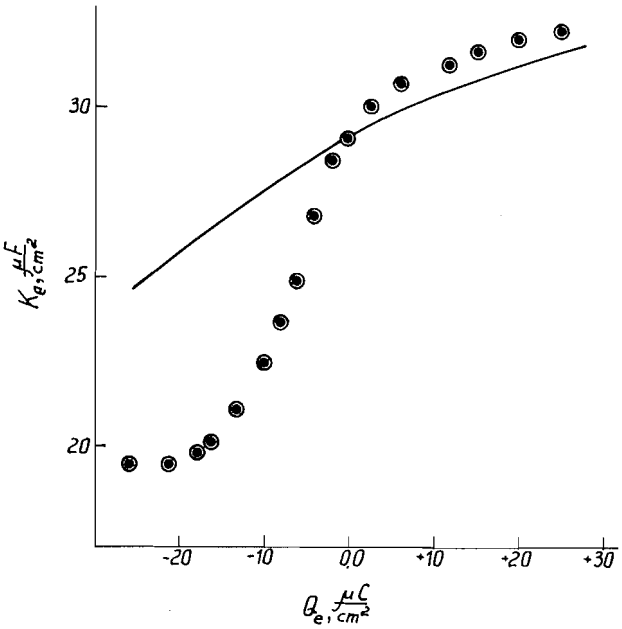

FIG. 6. Dependence of the integral capacity K_e on the electrode charge Q_e.

by the formulae derived above. Indeed, using formula [17], which by analogy with [47] can be written in the form

$$[48] \quad \psi_e^{m-s} = \frac{4e\alpha^4}{3\pi^2 a_0 n_D^2 \gamma[\alpha^2 + (1+\beta)^2]} = \frac{4.075\tilde{\rho}_m^{2/3}}{n_D^2\gamma[\tilde{\rho}_m^{1/3} + 0.902(1+0.5\gamma)^2]} \text{ (eV)}$$

we can calculate the difference of electrostatic potentials ψ_e^{m-s} between a metal and a solvent, and also between the same metal and water ($\psi_e^{m-H_2O}$). This permits calculation of the zero-charge points of mercury in a given solvent and in water $\Delta\psi_{Hg}^{H_2O-S} = \psi_e^{Hg-H_2O} - \psi_e^{Hg-S}$ (the left-hand side of formula [28]). On the other hand, the right-hand side of this formula can be calculated from experimental data. The corresponding results are listed in Table 3. It can be seen that the theory agrees satisfactorily with experiment (it should be noted here that the accuracy of estimating the right-hand side of [28] is very low because the exact values of the liquid potential drop are not presently available).

Metal–aqueous electrolyte solution interface

In the preceding section we have considered liquid electrodes, in which case surface tension data could be used for determining the electron work function. Such an approach is not applicable to crystalline electrodes, for in this case σ^{m-s} cannot be measured. It remains therefore to calculate W^{m-s} from the zero-charge potential. Consider, as in deriving relation [28], a closed electrical circuit which does not contain two solvents, but two metals in contact with the same solvent. Let one metal be platinum (a hydrogen electrode) and the other (Me) be chosen arbitrarily. We also assume that Me is kept at the zero-charge potential by a battery for which one terminal is connected to the hydrogen electrode and the other to the metal Me. Obviously, the sum of all potential drops in the circuit $Me/H_2O/Pt$ is equal to the applied voltage

$$\psi_e^{m-H_2O} + \psi_e^{H_2O-Pt} + \psi_e^{Pt-v} + \psi_e^{v-m} = -V^{Pt-m}$$

Since $\psi_e^{v-m} = -\psi_e^{m-v}$, etc., this expression can be rewritten in the form

$$[49] \quad \psi_e^{m-H_2O} = \psi_e^{m-v} + V^{m-Pt} - C$$

where the constant $C = \psi_e^{Pt-v} - \psi_e^{Pt-H_2O}$ characterizing the hydrogen electrode has the same value for all metals. It can be found from the data for liquid electrodes because in this case all the quantities appearing in [49] are known (see Table 3). Calculation yields $C = 0.31$ V for mercury and 0.38 V for gallium. Allowing for this discrepancy, we have taken the value $C = 0.34$, so that [49] is reduced to

$$[50] \quad \psi_e^{m-H_2O} = \psi_e^{m-v} + V^{m-Pt} - 0.34 \text{ (V)}$$

Since in this formula V^{m-Pt} can be determined experimentally and ψ_e^{m-v} can be calculated by [23], $\psi_e^{m-H_2O}$ is also known. Substituting the value thus obtained into the left-hand side of [48], we can easily find the work function W^{m-H_2O}. The corresponding values are listed in Table 4 which also presents the capacity at the zero-charge point K_e^0 as calculated using the values from ref. 46. It can be seen that for most metals the calculated values are rather close to the experimental ones. Only for four "anomalous" metals (In, Cd, Zn, and Ga) does the discrepancy significantly exceed the experimental error; for all the other metals it falls inside the accuracy limits.

Table 4 also lists the difference between surface tensions at the interface with vacuum and water, $\Delta\sigma$, as calculated by formulae [22] and [47]. The table shows that for almost all metals the theoretical values of $\Delta\sigma$ lie in the interval from 50 erg/cm^2 (mercury) to 165 erg/cm^2 (gallium). Only for four metals (Au, Cu, Rh, and Ir) the values of $\Delta\sigma$ do not fall into this interval. This is probably due to an error in measuring the zero-charge potential V^{Me-Pt}. Indeed, if we place the experimental values of V^{Me-Pt} in the corresponding cells of Mendeleev's table, we observe a distinct correlation. The only exceptions are Cu, Rh, and Au. (The situation is uncertain for Ir because it is located at the very end of the "filled" cells, so that the "correct" V^{Ir-Pt} value cannot be determined by interpolation.) Table 4 also lists $\psi_e^{m-H_2O}$, K_e^0, etc. calculated for these metals from the most probable values of V^{Me-Pt} obtained by interpolation. It can be seen that in this case $\Delta\sigma$ does not exhibit negative values.

To make a concluding remark, it can be seen from Table 2 and Figs. 2 and 3 that the theory developed in this paper is rather accurate only for metals in the left-hand subgroups of Mendeleev's table; for metals in the right-hand subgroups and especially for semi-metals theoretical errors increase significantly. However, for the metal–solution interface, comparison with experiment is performed only for metals in the right-hand subgroups and semi-metals because experimental data are now available only for these elements. The situation is also aggravated by the fact that most of these data are obtained in aqueous solutions, but water is known to be an anomalous solvent. It would be reasonable in this situation to deal with "normal" metals in the left-hand subgroups and with "normal" solvents without hydrogen bonds. Unfortunately, as we have already pointed out, such data are not available in the literature.

Electrocapillary curve

As was shown above, the surface tension of a metal at the zero-charge point, σ^0, is equal to the electrostatic energy of the electronic capacitor $1/2\, Q_e^+ \psi_e^{m-s}$. Therefore, the change in surface tension $\Delta\sigma = \sigma - \sigma^0$ caused by an external potential

Can. J. Chem. Downloaded from www.nrcresearchpress.com by 210.87.254.105 on 09/06/12
For personal use only.

TABLE 4. Some properties of $Me/H_2O/Pt$ systems

Me	$\tilde{\rho}_m$ (cm^{-3})	V^{m-Pt} (V)	ψ_e^{m-v} (V)	$\psi_e^{m-H_2O}$ (V)	W^{m-H_2O} (eV)	K_c^0 ($\mu F/cm^2$) Theory	K_c^0 ($\mu F/cm^2$) Exp.	$\Delta\sigma = \sigma^{m-v} - \sigma^{m-H_2O}$ (erg/cm^2)
Bi	5.64	−0.40	2.59	1.85	2.83	23	27 (ref. 56)	
Pb	6.60	−0.56	2.95	2.05	2.85	28	32 (ref. 55)	99
Tl	7.00	−0.71	3.24	2.19	2.79	28	24 (ref. 57)	130
Sn	7.24	−0.38	2.95	2.23	2.81	29	39 (ref. 55)	78
In	7.66	−0.63	3.38	2.41	2.65	29	80 (ref. 55)	120
		−0.71		2.33	2.80	28.8		136
Hg	8.13	−0.193	3.13	2.56	2.60	30	29 (ref. 33)	57
Cd	9.28	−0.68	3.70	2.68	2.80	29	52 (ref. 55)	142
Ga	10.5	−0.61	4.15	3.20	2.43	33	135 (ref. 55)	164
Zn	13.1	−0.64	4.67	3.69	2.46	31	100 (ref. 55)	144
Ag	14.6	−0.70	4.96	3.92	2.48	32	20–25	160
Au	14.8	+0.180	5.08	4.92	1.79	35	26–30 (ref. 59)	−80
		−0.36		4.38	2.14	32.9		+148
Cu	16.9	−0.05	5.42	5.03	1.97	35	29 (ref. 60)	−50
		−0.49		4.59	2.30	33.5		+106
Fe	21.3	−0.37	6.45	5.74	2.04	37	—	50
Co	22.5	−0.42	6.61	5.85	2.10	37	—	70
Ni	22.9	−0.37	6.59	5.88	2.15	38	—	70
Rh	25.4	+0.28	6.84	6.78	1.88	39	—	−220
		−0.28		6.22	2.17	38		+12
Ir	28.2	−0.06	6.86	−0.06	2.25	41	—	−130

difference should also be identified with change in the electronic capacitor electrostatic energy. It is known from electrostatics that the elementary work done during charging a capacitor is $dA = Q d\psi$, where Q is the capacitor charge. Since in our case an external energy source (battery) performs work *over* a system, $d\sigma = -dA = -Q_e d\psi = -K_e \psi d\psi$, where $K_e = Q_e/\psi$ is the electronic capacitor integral capacity defined by [45]. Expressing the latter as a power series in $e\psi/W_0$, we obtain

$$[51]\quad \Delta\sigma = -\int_0^{\psi}\left[K_c^0 + K_c^1\frac{e\psi}{W_0} + \ldots\right]\psi d\psi$$

$$= -\frac{1}{2}K_c^0\psi^2 - \frac{1}{3}K_c^1\frac{e\psi}{W_0}\psi^2 - \ldots = -\frac{1}{2}\chi K_c^0\psi^2$$

where the asymmetry coefficient

$$[52]\quad \chi = 1 + \frac{1}{6}\frac{K_c^1}{K_c^0}\frac{e\psi}{W_0} + \ldots$$

Here K_c^0 is given by relation [46] and

$$[53]\quad K_c^1 \simeq \frac{\epsilon_s}{8\pi R_s}\frac{\alpha^2 + (1+\beta_0)^2 + 2\beta_0(1+\beta_0)}{1+\alpha^2}$$

Since the asymmetry coefficient $\chi > 1$ in the anodic region ($\psi > 0$) and $\chi < 1$ in the cathodic region ($\psi < 0$), the electrocapillary curve should be steeper in the anodic region than in the cathodic region; this is indeed observed experimentally (see Fig. 7).

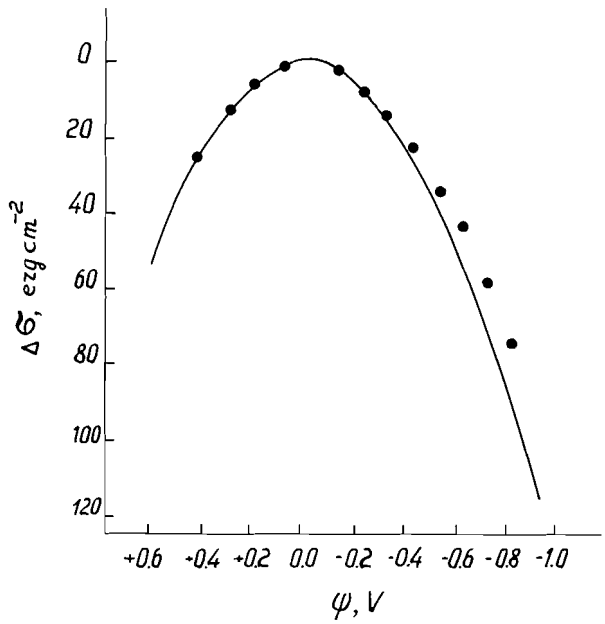

FIG. 7. Dependence of $\Delta\sigma$ on ψ for the system Hg – 1 N aqueous solution of H_2SO_4 + 0.1 N H_2SO_4 (68). Solid curve, theory; points, experiment.

The outer plate of an electronic capacitor

In conclusion, we should like to make several remarks which, in our opinion, could elucidate the physical picture of the phenomenon.

The electron density distribution in the outer plate of the electronic capacitor is described by a very simple formula $\rho_0(z) = \rho_0 \exp(-z/R_s)$ (see [3]). Since for all metals and solvents the value of R_s is very close to 1 Å, all electrons of the outer plate would seem to be localized also in a layer 1 Å thick. In practice, however, they penetrate into the solution to a depth about 10 times larger. Indeed, R_s does not determine the absolute thickness of the outer plate, but only that distance at which the electron density drops "e" times. For most metals, the electron density at the interface with a solution $\rho_0 \simeq 2 \times 10^{22}$ cm^{-3}, which amounts to the rather large value of 40 mol/dm^3. Therefore, at a distance $z = 5$ Å from the metal surface the electron density drops only to 0.8 mol/dm^3, and becomes equal to 0.01 mol/dm^3, i.e. really low, only at a distance of 10 Å. It is a simple matter to estimate that in a 10 Å boundary layer there are, on the average, 25 water molecules per electron. When we

Can. J. Chem. Downloaded from www.nrcresearchpress.com by 210.87.254.105 on 09/06/12
For personal use only.

Can. J. Chem. Downloaded from www.nrcresearchpress.com by 210.87.254.105 on 09/06/12
For personal use only.

go over to the far cathodic region the thickness of the outer plate of the electronic capacitor increases by ~20%, and in the far anodic region it decreases by ~10% (see above).

Variation of the electrode potential gives rise to a change not only in R_s but also in ρ_0. Simple estimates show that for the electrode charge $Q_e = 0.2-0.4$ C/m^2, ρ_0 vanishes, and the outer plate of the electronic capacitor disappears (electrons are completely "extracted" from the plate). On the contrary, similar estimates demonstrate that for $Q_e = -(0.2 - 0.3)$ C/m^2, the charge of the positive plate Q_e^+ vanishes.

An analysis of experimental data on the capacity of EDL at the ZCP shows that not only anions, but cations as well, can almost reach the metal surface. Since the radius of most inorganic ions is of the order of 1–2 Å, they can, apparently, penetrate quite easily into the outer plate of the electronic capacitor. This means that there is a transitional region separating the purely ionic part from the purely electronic part, the electrons and ions being present simultaneously inside this region. If the solution concentration is low and the Debye radius is much larger than the thickness of the transitional region, we may consider this region as an infinitely thin (as compared with the Debye radius) layer, characterized by an effective ψ_1-potential, and describe the ionic part of EDL located behind the transitional region (i.e. for $z > h$) by the Gouy–Chapman equations. But as the concentration increases, the situation changes, and a large part of the ionic double layer appears to lie inside the outer plate of the electronic capacitor even for $C \gtrsim 0.5$ mol/dm^3. If this is taken into account, the theory of the ionic part of EDL in concentrated solutions should be revised considerably.

Not only electrolyte ions, but solvent neutral molecules as well penetrate into the outer plate of the electronic capacitor where the electric field near the metal surface may be as high as 10^8-10^9 V/cm. Such a strong field can result not only in the deformation of solvent molecules (which may affect the catalytic activity of a given metal), but also in their decomposition into ions. For example, it was observed (61) that an almost dense monolayer of OH^- ions is formed on the surface of colloidal gold particles in water. In other work (62), this effect was interpreted as very strong (with an energy of about $20kT$ per molecule) adsorption of hydroxyl on the gold surface. It is very probable, however, that in this case we do not deal with ordinary adsorption, but with the decomposition of water molecules into H^+ and OH^- under the metal electric field.

Finally, while penetrating into water, metal electrons would seem to react immediately with it, thereby producing neutral hydrogen. Since the number of electrons in the outer plate of the electronic capacitor is very large, the reaction should proceed rather intensively. This is not the case, however. The reason is very simple; the energy of the electron in a hydrogen atom is much higher than the Fermi energy, so that such a reaction cannot take place. Thus, there is no contradiction in what has just been said.

Acknowledgement

We are indebted to Professor A. M. Brodsky for fruitful discussions.

1. G. A. MARTYNOV and R. R. SALEM. Electrical double layer at a metal – dilute electrolyte solution interface. Springer-Verlag, Berlin, Heidelberg, New York, Tokyo. 1983.
2. J. FRENKEL. Z. Phys. **51**, 232 (1928).
3. O. K. RICE. Phys. Rev. **31**, 1051 (1928).
4. A. BENNET. *In* New aspects in the study of the surface of solids. Mir, Moscow, 1977. (Russian translation.)
5. M. B. PARTENSKY. Usp. Fiz. Nauk, **128**, 69 (1979).
6. N. D. LANGE and W. KOHN. Phys. Rev. **1**, 12 (1970); **1**, 4555 (1970).
7. R. N. KUKLIN. Elektrokhimiya, **14**, 380 (1978).
8. R. R. SALEM. Zh. Fiz. Khim. **54**, 212 (1980).
9. S. TRASATTI. J. Electroanal. Chem. **91**, 293 (1978).
10. H. Y. KU and F. G. ULLMAN. J. Appl. Phys. **35**(2), 265 (1964).
11. V. A. KIRJANOV. Elektrokhimiya, **17**, 286 (1981).
12. J. GOODISMAN. Contemporary quantum chemistry. An introduction. Plenum, New York. 1977.
13. W. SCHMICKLER. J. Electroanal. Chem. **83**, 387 (1977); Ber. Bunsenges. Phys. Chem. **82**, 477 (1978).
14. J. P. BODIALI and J. GOODISMAN. J. Electroanal. Chem. **91**, 151 (1978).
15. M. BORN and E. WOLF. Principles of optics. Nauka, Moscow. 1970. (Russian translation.)
16. N. HARRICK. Internal reflection spectroscopy. Mir, Moscow. 1970. (Russian translation.)
17. L. D. LANDAU and E. M. LIFSHITS. Quantum mechanics. Moscow. 1969. (In Russian.)
18. J. R. SMITH. Phys. Rev. **181**, 522 (1969).
19. S. F. TIMASHEV. Elektrokhimiya, **15**, 730 (1979).
20. CH. KITTEL. Introduction to solid state physics. Nauka, Moscow. 1978. (Russian translation.)
21. MIRDEL. Electrophysics. Mir, Moscow. 1972. (Russian translation.)
22. V. F. UKHOV, R. M. KOBELEVA, G. V. DEDKOV, and A. I. TEMROKOV. Electron statistical theory of metals and ionic crystals. Nauka, Moscow. 1982. (In Russian.)
23. C. A. COULSON. Valence. Oxford University Press, London. 1961.
24. T. E. FEUCHTWANG, D. PAUDYAL, and W. PONG. Phys. Rev. B**26**, 4 (1982); B**26**, 1608 (1982).
25. F. J. BLATT. Physics of electronic conduction in solids. McGraw-Hill Book Company, New York. 1968.
26. V. I. NISHENKO and YA. I. FLOKA. A reference book on surface tension of liquid metals and alloys. Metallurgiya, Moscow. 1981. (In Russian.)
27. K. I. SMITTLES. Metals (a reference book). Metallurgiya, Moscow. 1980. (Russian translation.)
28. E. M. SAVITSKY, I. V. BUROV, G. V. PIROGOVA, and L. N. LITVIN. Electrical and emission properties of alloys. Nauka, Moscow. 1978. (In Russian.)
29. V. S. FOMENKO and I. A. PODCHERNYAEVA. Emission and adsorption properties of substances and materials. Atomizdat, Moscow. 1975. (In Russian.)
30. N. H. MARCH. *In* Physics of simple liquids. *Edited by* H. N. V. Temperley, Mir, Moscow. 1971. (Russian translation.)
31. V. K. SEMENCHENKO. Surface phenomena in metals and alloys. Mir, Moscow. 1975. (In Russian.)
32. D. C. GRAHAME. J. Am. Chem. Soc. **76**, 4819 (1954).
33. P. DELAHAY. Electrical double layer and kinetics of electrode processes. Mir, Moscow. 1967. (Russian translation.)
34. J. A. HARRISON, J. E. RENDLES, and D. J. SCHIFFRIN. J. Electroanal. Chem. **48**, 359 (1973).
35. E. A. GUGGENHEIM. J. Am. Chem. Soc. **52**, 1315 (1930).
36. P. N. SVIRKUNOV. Zh. Tekh. Fiz. **52**, 1526 (1982).
37. CH. RECHARD. Losungsmittel-Effekte in der organischen Chemie. Verlag Chemie, Berlin, 1969.
38. R. PAYNE. Adv. Electrochem. Electrochem. Eng. **7**, 1 (1970).
39. E. J. W. VERWEY. Recl. Trav. Chim. **61**, 564 (1942).
40. S. A. FATEEV. Candidate thesis, IELAN SSSR, 1971. (Institute of Electrochemistry of the USSR Academy of Sciences.)
41. D. C. GRAHAME. Z. Electrochem. **59**, 740 (1955).
42. B. B. DAMASKIN and R. I. KAGANOVICH. Elektrokhimiya, **13**, 293 (1977).
43. S. TRASATTI. Modern aspects of electrochemistry.Vol. 13.

Plenum Press, New York – London. 1979. p. 81.
44. R. PAYNE. J. Electroanal. Chem. **41**, 115 (1973).
45. R. R. SALEM. *In* Electrical double layer and adsorption on solid electrodes. Tartu, IV, 275 (1975). (In Russian.)
46. R. R. SALEM. Zh. Fiz. Khim. **49**, 2043 (1975).
47. S. MINC, M. JURKIEWIEZ, and J. JASTRZEBSKA. J. Electroanal. Chem. **10**, 473 (1965).
48. V. A. CHAGELASHVILI, J. I. JAPARIDZE, and B. B. DAMASKIN. Elektrokhimiya, **13**, 1300 (1977).
49. M. K. KAISHEVA, R. I. KAGANOVICH, and B. B. DAMASKIN. Elektrokhimiya, **9**, 1016 (1973).
50. R. R. SALEM and A. F. SHAROVARNIKOV. Elektrokhimiya, **9**, 1016 (1973).
51. J. LAWRENCE and R. PARSONS. Trans. Faraday Soc. **64**, 751 (1968).
52. R. PAYNE. J. Am. Chem. Soc. **89**, 489 (1967).
53. B. B. DAMASKIN, V. F. IVANOV, V. F. BALASHOVA, and V. F. KHONINA. Elektrokhimiya, **7**, 127 (1971).
54. A. N. FRUMKIN, N. B. GRIGORIEV, and I. A. BAGOTSKAYA. DAN SSSR, **157**, 957 (1964).
55. S. TRASATTI. J. Electroanal. Chem. **91**, 293 (1981).
56. A. N. FRUMKIN, M. P. PYARNOYA, N. B. GRIGORIEV, and U. V. PALM. Elektrokhimiya, **10**, 1130 (1974).
57. V. A. BULAVKA, N. B. GRIGORIEV, and YU. M. LOSHKAREV. *In* Electrical double layer and adsorption on solid electrodes, Tartu, IV, 48 (1975). (In Russian.)
58. A. G. ZELINSKY AND R. YU. BEK. Elektrokhimiya, **14**, 1825 (1978).
59. N. VAN NUONG and J. CLAVILIER. C. R. Acad. Sci. Paris, **272**, 1404 (1971).
60. L. YA. EGOROV and I. M. NOVOSEL'SKY. Elektrokhimiya, **6**, 521 (1970).
61. G. A. MARTYNOV, V. M. MULLER, G. L. KUZ'MINA, and I. P. BULATOVA. Kolloidn. Zh. **38**, 480 (1976).
62. G. A. MARTYNOV and G. L. KUZ'MINA. Kolloidn. Zh. **39**, 164 (1977).
63. R. S. MAIZLISH, A. P. TVERDOVSKY, and A. N. FRUMKIN. Zh. Fiz. Khim. **28**, 87 (1954).
64. J. LAWRENCE and R. PARSONS. Trans. Faraday Soc. **64**, 1655 (1968).
65. R. R. SALEM. Elektrokhimiya, **11**, 1097 (1975).
66. R. R. SALEM. *In* Electrical double layer and adsorption on solid electrodes, Tartu, IV, 275 (1975). (In Russian.)
67. B. CASE and R. PARSONS. Trans. Faraday Soc. **63**, 1224 (1966).
68. N. S. POLYANOVSKAYA and A. N. FRUMKIN. Elektrokhimiya, **1**, 538 (1965).

Can. J. Chem. Downloaded from www.nrcresearchpress.com by 210.87.254.105 on 09/06/12
For personal use only.

The synthesis of 3,3-dimethyltricyclo[6.3.0.0^{1,5}]undecan-4-one via β-enolate rearrangement.[1] A new approach to the pentalenene ring system

JEFFREY L. JURLINA,[2] HEMANT A. PATEL, AND J. B. STOTHERS
Department of Chemistry, University of Western Ontario, London, Ont., Canada N6A 5B7

Received December 21, 1983

JEFFREY L. JURLINA, HEMANT A. PATEL, and J. B. STOTHERS. Can. J. Chem. **62**, 1159 (1984).

The preparation of 3,3-dimethyltricyclo[6.3.0.0^{1,5}]undecan-4-one from 9,9-dimethyltricyclo[5.3.1.0^{1,5}]undecan-8-one by β-enolate rearrangement is described. The required [5.3.1.0^{1,5}]ketone was obtained in six steps from tricyclo[5.2.1.0^{1,5}]-dec-8-ene. This sequence provides a new entry into the tricyclo[6.3.0.0^{1,5}]undecane ring system which is characteristic of a number of recently encountered naturally occurring terpenes. The ^{13}C data for several of these tricyclic derivatives are presented.

JEFFREY L. JURLINA, HEMANT A. PATEL et J. B. STOTHERS. Can. J. Chem. **62**, 1159 (1984).

On décrit la préparation de la diméthyl-3,3 tricyclo[6.3.0.0^{1,5}]undécanone-4 via une transposition β-énolique de la diméthyl-9,9 tricyclo[5.3.1.0^{1,5}]undécanone-8. On a obtenu la cétone [5.3.1.0^{1,5}] requise en six étapes à partir du tricyclo[5.2.1.0^{1,5}]-décène-8. Cette série de réactions fournit une nouvelle voie d'accès au système tricyclo[6.3.0.0^{1,5}]undécane qui est caractéristique d'une certain nombre de terpènes naturels rencontrés récemment. On rapporte des données de rmn ^{13}C pour plusieurs de ces dérivés tricycliques.

[Traduit par le journal]

Over the past decade, several naturally occurring terpenes containing the tricyclo[6.3.0.0^{1,5}]undecane ring system have been described (1). Representative examples having this unusual bridged spirane moiety include pentalenene (**1**) (2), isocomene (**2**) (3), silphinene (**3**) (4), and structure **4**, incorrectly assigned to senoxydene (5). It has been established that **1** is the parent hydrocarbon of the pentalenolactone family of antibiotics (6). The discovery of these compounds has awakened interest in synthetic approaches to various members of the series and several total syntheses of **2** have been described (1),

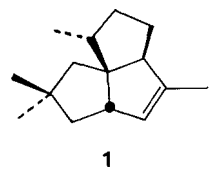

1

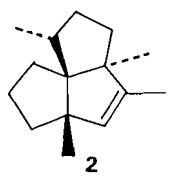

2

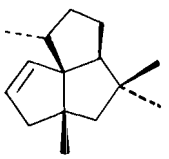

3

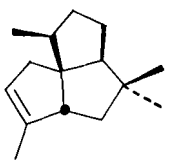

4

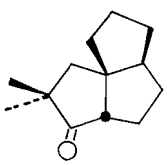

5

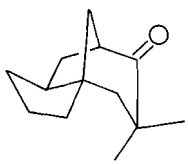

6

while two methods for each of **1** (2, 7) and **3** (7, 8) have been reported. It may be noted that before the discovery of these natural products the initial synthesis of this ring system was realized in the course of a study directed toward the isomeric [5.2.2.0^{1,6}] system (9). Our interest in the generation of interesting, less accessible polycyclic carbon skeletons by homoenolate rearrangement (10) led us to examine possible routes to the [6.3.0.0^{1,5}] system. We wish to report the preparation of 3,3-dimethyltricyclo[6.3.0.0^{1,5}]undecan-4-one (**5**) in good yield by homoenolization of 9,9-dimethyltricyclo[5.3.1.0^{1,5}]-undecan-8-one (**6**).

Ketone **6** was prepared from the known tricyclic olefin **7** (12) as outlined in Scheme 1, utilizing ring expansion via ketonization of a cyclopropoxide analog (11). Hydroboration of **7** with 9-BBN/THF furnished a 85:15 mixture of alcohols **8** and **9** which were separated by flash chromatography (13). Oxidation of **8** using Collins reagent (14) afforded **10** in 86% yield which, upon treatment with lithium diisopropylamide at −78°C followed by reaction with trimethylsilyl chloride and triethylamine, gave silyl enol ether **11** in 95% yield. Cyclopropanation of **11** using a zinc−silver couple and CH_2I_2 provided the tetracyclic ether **12**. On the basic of our earlier results for the homoketonization of polycyclic cyclopropoxides (10, 11), we anticipated that base-catalyzed cleavage of **12** at low temperature should favour ring expansion to the desired ketone **13**. In the event, treatment of **12** with NaOH−MeOH at 0°C afforded a single ketone lacking methyl absorption in both its ^{1}H and ^{13}Cmr spectra, consistent with expectations; precise mass measurement showed the molecular formula to be $C_{11}H_{16}O$. Treatment of **13** with $NaNH_2$−Et_2O−MeI (15) furnished the desired dimethylated analog **6**.

It can be mentioned that the ring expansion of **10** to **13** is exactly that required to improve the synthetic sequence leading to cedrol and cedrene described by Breitholle and Fallis (16). In fact these authors stated that a better synthesis would be realized if "the carbon bearing oxygen is locked in position in the starting ketone and final product", which is the case in the conversion of **10** → **13**. Although they noted that a closely related ring expansion using ferric chloride in the cleavage of the analog of **12** could be applicable, the required analog was not synthesized to investigate this possibility.

For the series **6**−**13**, ^{13}Cmr spectra were recorded to aid their characterization and these data are collected in Table 1. The assignments followed from the trends observed throughout the

[1]Part 109 in the series "^{13}Cmr studies"; for Part 108 see ref. 25.

[2]Present address: Department of Pharmacology, School of Medicine, University of Auckland, Auckland, New Zealand.

Can. J. Chem. Downloaded from www.nrcresearchpress.com by 210.87.254.105 on 09/06/12
For personal use only.

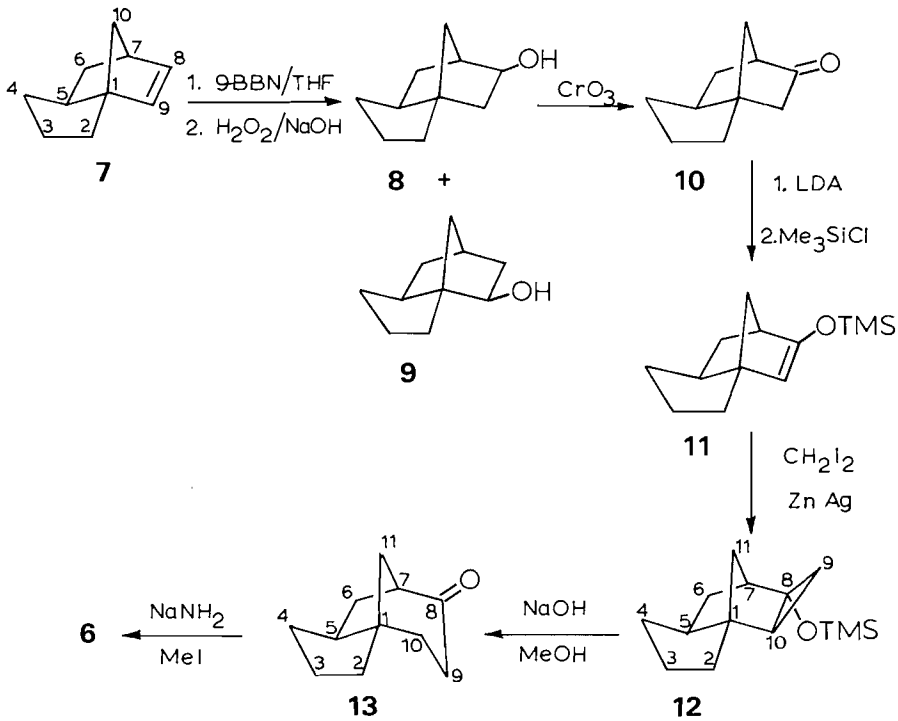

SCHEME 1

TABLE 1. ^{13}C shielding data[a] for **6**–**13**

Compound	C-1	C-2	C-3	C-4	C-5	C-6	C-7	C-8	C-9	C-10	C-11	Methyl
7	63.1	(27.0)	(26.8)	31.7	46.4	33.3	45.2	135.3	140.5	51.2		
8	56.2	28.2	26.5	33.1	47.1	34.2	47.7	75.6	45.9	37.1		
9	61.5	25.8	26.3	32.7	44.6	36.9	37.5	41.9	77.1	38.0		
10	55.7	28.9	26.4	33.0	46.3	33.1	54.1	218.9	49.2	40.7		
9,9-Me_2-**10**[b]	62.2	25.1	25.3	33.1	40.7	33.2	52.7	223.9	48.6	37.3		21.5 (*exo*) 18.4 (*endo*)
11	61.9	27.6	26.6	32.8	48.9	31.7	49.1	160.7	110.0	49.5		1.1
12	56.2	27.6	26.0	33.7	45.6	31.7	48.2	61.2	10.2	25.7	34.5	1.0
13[b]	52.4	36.1	26.7	35.1	46.4	36.6	54.1	214.6	35.7	37.3	41.4	
6	53.1	36.8	25.4	35.2	45.6	38.9	53.4	219.7	42.8	51.2	38.7	30.7 31.1

[a]In ppm from internal TMS in $CDCl_3$ solutions. Assignments for similar values in parentheses may be reversed.
[b]Assignments obtained from 2D INADEQUATE spectra.

series taking into account the expected effects of the substituents and by comparison with the results for **6** and the 9,9-dimethyl derivative of **10**, available from an earlier study (17), assignments for the latter having been unequivocally established from two-dimensional, double quantum coherence spectra, i.e. 2D-INADEQUATE experiments (18).

With **6** in hand, attention could be turned to its behavior under homoenolization conditions. By analogy with our earlier findings for the model [3.2.1] system (19), we could anticipate β-proton abstraction to occur at either, or both, C-6 and -11, potentially resulting in the formation of β-enolates **14** and **15**, respectively. Subsequent cleavage of these enolates via mode b (Scheme 2) will generate the rearranged ketones **16** and **5**, respectively. Treatment of **6** with *t*-BuO^-/*t*-BuOH at 185°C for extended reaction times gave, upon isolation with ether extraction, a neutral fraction in 80% yield, consisting of a 60:40 mixture of two ketones which were separable by flash chromatography. The minor component was found to be starting material **6**, which was recycled to produce more of the product mixture. The major product having the molecular formula $C_{13}H_{20}O$, as shown by precise mass measurement, is isomeric with **6** but contains a five-membered ring ketone according to its carbonyl absorption (1730 cm^{-1} ($CHCl_3$), δ_C 225.9), distinctly different from that for **6** (1692 cm^{-1}, 219.7). Thus, the product is **5**, arising by rearrangement after proton abstraction from C-6 in **6** to form **15** or an equivalent β-enolate. The ^{1}Hmr spectrum contained two methyl singlets, δ 1.045 and 1.105, two one-proton multiplets, δ 2.405 and 2.155, and complex absorptions, δ 1.24–1.95. As further proof of identity, $^1H/^2H$ exchange under mild conditions was examined. The rearranged ketone was stirred at room temperature in the presence of MeO^-/MeOD for 2.5 h and in the ^{1}Hmr spectrum of the recovered material **5**-d_1 (93% yield) the lowest field multiplet was missing, indicating essentially complete deuteration of the α-bridgehead. It may be noted that no exchange occurs in **6** under these conditions and none would be expected for **16**. Additional confirmation of this structural assignment was obtained from the ^{13}Cmr spectrum of a 1:1 mixture of **5** and **5**-d_1,

Can. J. Chem. Downloaded from www.nrcresearchpress.com by 210.87.254.105 on 09/06/12
For personal use only.

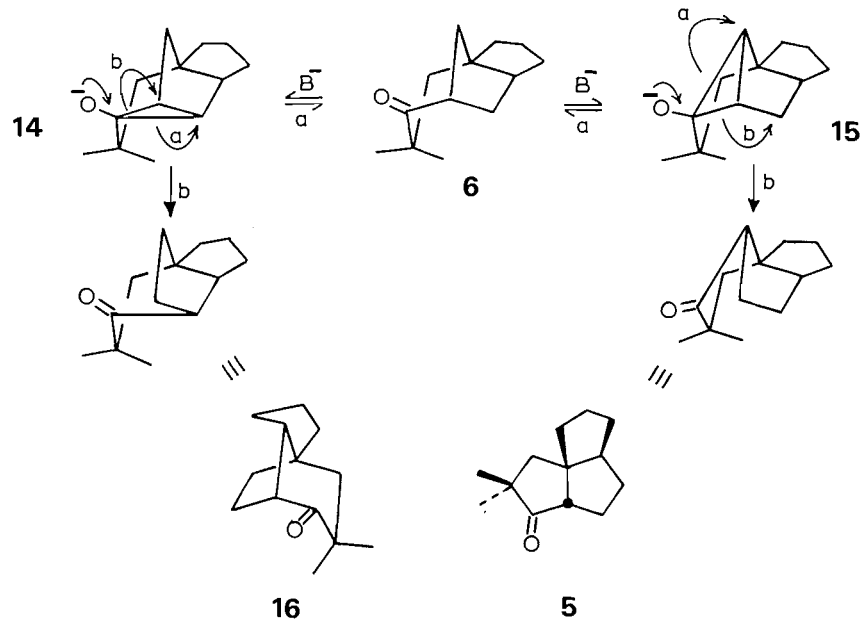

SCHEME 2

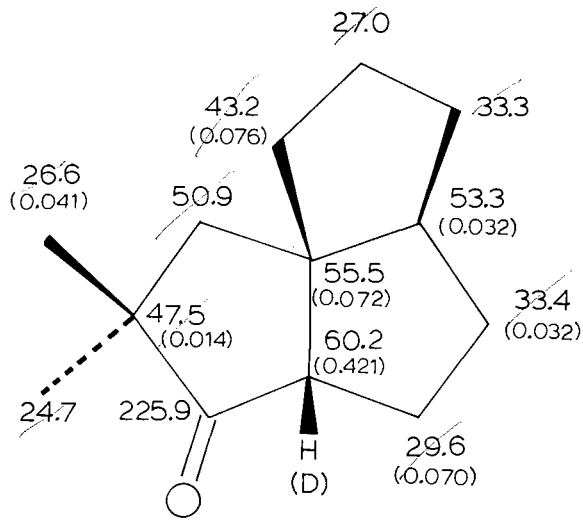

FIG. 1. ^{13}C shielding data for **5** and **5**-d_1 in $CDCl_3$ solution; values in parentheses are the ^2H-induced isotope shifts >0.012 ppm.

the data for which are shown in Fig. 1. Initially the assignments for **5** were made by comparisons with the data for some simpler [3.3.0] analogs (20) and were confirmed by the observed two- and three-bond, ^2H-induced isotope shifts for the **5**/**5**-d_1 mixture.

As expected, C-5 bearing deuterium appeared as a 1:1:1 triplet (J_{CD} = 20.2 Hz) with an α-isotope shift of 0.421 ppm. Of particular interest is the fact that the quaternary carbon at δ_C 55.5 and the methylene carbons at δ_C 29.6 and 43.2 exhibit isotope shifts of ~70 ppb (0.070 ppm), entirely consistent with expectations for structure **5**. The relatively large isotope shift exhibited by the second methylene carbon (δ 43.2), three bonds removed from the deuterium substituent, is indicative of a *syn*-periplanar orientation for these vicinal nuclei (17). The isotope shifted component is a poorly resolved triplet, J_{CD} ~ 0.7 Hz, confirming their vicinal relationship (17).

With structure **5** firmly established, we have shown that this synthetic sequence provides a new entry into the [6.3.0.$0^{1,5}$] ring system having the same stereochemistry as that of the naturally occurring species. The required configuration at C-1 and -8 is present from the outset and the stereochemistry of the rearrangement is constrained to give the correct configuration at the third chiral centre, C-5, because the alternative is too strained. The alternative would, in effect, be a substituted *trans* [3.3.0] system which is known to be disfavored by 6 kcal/mol in the parent bicyclo[3.3.0]octanes (21). Thus, an appropriately substituted analog of **6** could serve as the precursor for the generation of pentalenene (**1**) by β-enolate rearrangement. Studies directed toward this target, as well as others in the same family, are in progress and will be reported in due course.

Experimental

Melting points and boiling points are uncorrected. Thin layer chromatography (tlc) was done on Kiesel gel 60 F_{254} plates and flash chromatography (FC) columns were prepared as described in the literature (13). Tetrahydrofuran (THF) and ether were distilled from Na/benzophenone just before use. Pyridine, *tert*-butyl alcohol, diisopropylamine, and triethylamine were distilled from CaH_2 and stored over 4A molecular sieves. The following compounds were prepared by known methods and gave satisfactory physical and spectral data: pent-4-en-1-ol (22), pent-4-enylcyclopentadienes (12), and **7** (12).

Infrared spectra were recorded with a Beckman 4250 spectrophotometer. Mass spectra were obtained on a Varian MAT-311A system at 70 eV (direct inlet). Routine ^1Hmr spectra were recorded on a Varian T-60 instument, while data for pure samples were obtained with a Varian XL-200 spectrometer.The latter instrument was used to record the ^{13}C spectra (50.3 MHz) and comparison of the fully decoupled spectra with those obtained with either the APT (23) or INEPT (24) sequences served to identify the methyl, methylene, methine, and quaternary signals. The 2D INADEQUATE spectra (18) were obtained with the CCC2D pulse sequence of the XL software using a 2048 × 128 data point matrix transforming 2048 and 512 points respectively, with 2000 (**6**) and 2500 (9,9-Me_2-**10**) kHz sweep widths in both domains. The ^{13}C data are collected in Table 1. The spectrum for the mixture of **5**/**5**-d_1 was obtained using a **5** kHz sweep window, 16 K points, and a 64 K transform to provide digital resolution of 6 ppb (0.006 ppm). Isotope shifts > 12 ppb are presented, measured after resolution enhancement. The isotope shift for the carbonyl carbon was not examined.

Can. J. Chem. Downloaded from www.nrcresearchpress.com by 210.87.254.105 on 09/06/12
For personal use only.

Can. J. Chem. Downloaded from www.nrcresearchpress.com by 210.87.254.105 on 09/06/12
For personal use only.

exo-Tricyclo[5.2.1.0^{1,5}]decan-8-ol (8)

To a stirred solution of 9-BBN in THF (50 mL, 0.5 *M*) under nitrogen was added **7** (2.68 g, 0.02 mol) in THF (5 mL) at room temperature and the solution refluxed for 16 h. After cooling, the excess 9-BBN was slowly decomposed with cold water (2 mL) before the addition of 3 *M* aqueous NaOH (21 mL), followed by the *cautious* slow addition of H_2O_2 (21 mL, 30%) and MeOH (21 mL). After stirring at room temperature for 24 h, the reaction mixture was saturated with solid NaCl, whereupon the THF layer separated. After ether extraction (3 × 50 mL), the combined organic extracts were dried ($MgSO_4$) and the solvent evaporated under vacuum to give a thick oil (2.6 g, 90%) containing **8** and **9** in a 85:15 ratio. These isomeric alcohols were separated by FC (Et_2O – petroleum ether, 30:70) to furnish pure samples of each. Alcohol **8** (2.1 g): mp 47–49°C (lit. (12) mp 45–49°C); alcohol **9** (0.46 g): mp 35–36°C.

Tricyclo[5.2.1.0^{1,5}]decan-8-one (10)

To a stirred solution of Collins reagent prepared from CrO_3 (96.0 g, 0.06 mol), in pyridine (9.49 g) and methylene chloride (150 mL), was added, in one portion, alcohol **8** (1.52 g, 0.01 mol) in CH_2Cl_2 (5 mL) at room temperature and the stirring continued for 1 h. After decantation of the solvent, the tarry black residue was washed with CH_2Cl_2 (2 × 25 mL). The combined CH_2Cl_2 extracts were washed with aqueous NaOH (2 × 100 mL, 10%), aqueous HCl (100 mL, 10%), aqueous $NaHCO_3$ (100 mL, 10%), and water before drying over $MgSO_4$. After removal of the solvent, the residue was distilled to yield the colorless liquid **10** (1.3 g, 86%), bp 54°C/0.8 Torr; ir ($CHCl_3$): 1735 cm^{-1}.

8-Trimethylsilyloxytricyclo[5.2.1.0^{1,5}]dec-8-ene (11)

To a stirred solution of LDA (prepared from diisopropylamine (2.39 mL, 0.017 mol), THF (25 mL), *n*-BuLi (2.0 *M*, 7.5 mL) at −78°C, 20 min) under nitrogen was added a solution of **10** (1.5 g, 0.01 mol) in THF (3 mL) and the stirring was continued at −78°C for 35 min. The clear quenching solution (prepared by centrifugation of a mixture of trimethylsilyl chloride (2.54 mL) and Et_3N (0.55 mL) inTHF (10 mL) in a N_2-purged tube) was added and stirring continued at −78°C for an additional hour before the mixture was allowed to warm to room temperature over a period of 2 h. After 30 min at room temperature, the mixture was diluted with saturated $NaHCO_3$ solution (30 mL) and extracted with pentane (3 × 30 mL). The combined extracts were washed quickly with cold (0°C) HCl solution (35 mL, 2%), followed by $NaHCO_3$ (2 × 30 mL, 10%) and cold water before drying ($MgSO_4$). Removal of the solvent afforded **11** as a colorless liquid (2.1 g, 95%), bp 61°C/0.8 Torr; ir ($CHCl_3$): 1600 (C=C) cm^{-1}; ^{1}Hmr ($CDCl_3$) δ: 0.23 (s, 9H, Me_3Si), 1.40–2.2 (complex absorption, 11H), 2.60 (bs, 1H, H-7), 4.82 (s, 1H, H-9); *m/e* (relative intensity): 222 (M^+, 31), 207 (36), 168 (100), 107 (25), 76 (24), 74 (91). *Exact Mass* calcd. for $C_{13}H_{22}OSi$: 222.1440: found: 222.1434.

8-Trimethylsilyloxytetracyclo[5.3.1.0^{1,5}o^{8,10}]undecane (12)

Methylene iodide (0.9 mL, 8.5 mmol) was added to a mixture of Zn/Ag couple (0.975 g, 0.015 mol) in ether (3 mL) and this mixture was warmed until refluxing occurred without external heating. Upon cessation of reflux, Et_2O (10 mL) was added and the mixture stirred at room temperature for 1 h. Silyl enol ether **11** was then added and the reaction mixture was refluxed for 18 h. After cooling to 0°C, pyridine (1.38 mL) was slowly added with vigorous stirring. The resulting precipitate was removed by filtration and washed with Et_2O. After removal of solvent from the filtrate, the residue was taken up in pentane and the last traces of precipitate removed by further filtration. Evaporation of the solvent gave a colorless liquid **12** (0.76 g, 65%), bp 70–75°C/ 0.6 Torr; ^{1}Hmr ($CDCl_3$) δ: 0.17 (s, 9H, Me_3Si), 0.97 (bs, 2H, H-9), 1.1–2.0 (complex absorption, 12H), 2.40 (bs, 1h, H-7); *m/e* (relative intensity): 236 (M^+, 39), 221 (28), 179 (33), 147 (96), 107 (31), 80 (28), 75 (100), 73 (96). *Exact mass* calcd. for $C_{14}H_{24}OSi$: 236.1596; found: 236.1596.

Tricyclo[5.3.1.0^{1,5}]undecan-8-one (13)

To a stirred solution of **12** (0.76 g, 3.2 mmol) in MeOH (12 mL) was added aqueous NaOH (6 mL, 3 *M*) at 0°C and stirring continued for 2 h. Then the reaction mixture was left overnight in a refrigerator at 0°C. Water (6 mL) was added, the MeOH removed by evaporation, and the product extracted with CH_2Cl_2 (3 × 20 mL). The combined extracts were washed and then dried ($MgSO_4$). Removal of the solvent gave a yellow oil which was purified by FC (Et_2O – petroleum ether, 15:85) to furnish **13** (0.465 g, 88%), bp 58°C/0.2 Torr; ir ($CHCl_3$): 1705 cm^{-1}; ^{1}Hmr ($CDCl_3$) δ: 2.68 (t, J = 4 Hz, 1H, H-7), 1.2–2.5 (complex absorption, 15H); *m/e* (relative intensity): 164 (M^+, 44), 120 (61), 118 (24), 108 (30), 107 (100), 94 (24), 92 (25), 81 (36), 80 (64), 68 (32). *Exact Mass* calcd. for $C_{11}H_{16}O$: 164.1201; found: 164.1205.

9,9-Dimethytricyclo[5.3.1.0^{1,5}]undecan-8-one (6)

Ketone **13** (0.60 g, 3.7 mmol) in Et_2O (2 mL) was added to a vigorously stirred suspension of $NaNH_2$ (0.702 g, 0.018 mol) in Et_2O (25 mL) under nitrogen at room temperature and the mixture was stirred with gentle reflux for 3 h. After cooling, methyl iodide (1.37 mL, 0.022 mol) was added slowly and the mixture refluxed overnight, before the second addition of MeI (0.46 mL, 7.3 mmol). After refluxing for 3 h, the mixture was cooled and diluted with water (20 mL). The ether layer was separated and the aqueous phase extracted with Et_2O (3 × 25 mL). The combined extracts were dried ($MgSO_4$) and the product recovered by evaporation of the solvent. Distillation gave **6** as a colorless liquid (0.471 g, 67%), bp 62°C/0.2 Torr; ir ($CHCl_3$): 1692 cm^{-1}; ^{1}Hmr ($CDCl_3$) δ: 1.125 (s, 3H, Me), 1.170 (s, 3H, Me), 2.79 (dd, 1H, H-7), 1.30–2.25 (complex absorption, 13H); *m/e* (relative intensity): 192 (M^+, 100), 161 (27), 149 (77), 119 (43), 121 (59), 107 (62), 93 (35), 82 (61), 79 (83), 67 (35). *Exact Mass* calcd. for $C_{13}H_{20}O$: 192.1514; found: 192.1519.

3,3-Dimethyltricyclo[6.3.0.0^{1,5}]undecan-4-one (5)

A solution of **6** (0.192 g, 1 mmol) in *t*-BuO^-/*t*-BuOH (prepared from potassium metal (0.157 g) and *t*-BuOH (3.8 mL); H_2O content, 270 μg/mL) was prepared under nitrogen and quickly transferred to a predried, thick-walled glass tube (capacity ~42 mL). The solution was degassed and the tube sealed under vacuum (~0.1 Torr) before heating at 185°C for 480 h. After cooling, the reaction mixture was diluted with water (15 mL) and the neutral product was isolated by ether extraction (3 × 15 mL). Removal of ether furnished a yellow oil which was subjected to FC (Et_2O – petroleum ether, 5:95) to yield starting material **6** (0.059 g) and the new ketone **5** (0.095 g). The recovered **6** was recycled to give **5** (0.027 g) and **6** (0.015 g). Thus, the total yield of **5** was 0.122 g (69% based on recovered **6**) having the following properties: ir ($CHCl_3$): 1730 cm^{-1}; ^{1}Hmr ($CDCl_3$) δ: 1.045 (s, 3H, Me), 1.105 (s, 3H, Me), 2.155 (m, 1, H-8), 2.405 (dd, J ~ 6 Hz, 1H, H-5), 1.25–1.95 (complex absorption, 12H), *m/e* (relative intensity): 192 (M^+, 68), 135 (100), 108 (35), 107 (25), 80 (41). *Exact Mass* calcd. for $C_{13}H_{20}O$: 192.1514; found: 192.1519.

Preparation of 5-d$_1$

Ketone **5** (29 mg) was added to a stirred solution of MeO^-/MeOD (prepared from sodium (7 mg) and MeOD (0.5 mL)) at room temperature and the stirring was continued for 2.5 h. After the addition of D_2O (0.1 mL), Et_2O (15 mL) was added and the ethereal solution washed before drying over $MgSO_4$. Evaporation of the solvent afforded *5-d* (27 mg, 93%), the ^{1}Hmr spectrum of which contained no absorption below δ 2.25, indicative of essentially complete deuteration at C-5; ms: 4.5% d_0, 95.4% d_1 (total 0.954 D/molecule).

Acknowledgements

We are grateful for the financial assistance provided by the Natural Sciences and Engineering Research Council of Canada.

1. E. WENKERT and T. S. ARRHENIUS. J. Am. Chem. Soc. **105**, 2030 (1983), and references therein.
2. Y. OHFUNE, H. SHIRAHAMA, and T. MATSUMOTO. Tetrahedron Lett. 2869 (1976).
3. L. H. ZALKOW, R. N. HARRIS, D. VAN DERVEER, and J. A. BERTRAND. J. Chem. Soc. Chem. Commun. 456 (1977).

4. F. BOHLMANN and J. JAKUPOVIC. Phytochemistry, **19**, 259 (1980).
5. F. BOHLMANN and C. ZDERO. Phytochemistry, **18**, 1747 (1979); L. A. PAQUETTE, R. A. GALEMMO, and J. P. SPRINGER. J. Am. Chem. Soc. **105**, 6975 (1983).
6. D. E. CANE and A. M. TILLMAN. J. Am. Chem. Soc. **105**, 122 (1983).
7. G. D. ANNIS and L. A. PAQUETTE. J. Am. Chem. Soc. **104**, 4504 (1982).
8. T. TSUNODA, M. KODAMA, and S. ITO. Tetrahedron Lett. **24**, 83 (1983).
9. R. G. CARGILL and A. M. FOSTER. J. Org. Chem. **35**, 1971 (1970).
10. J. B. STOTHERS. Pure Appl. Chem. **53**, 1241 (1981); B. A. DAWSON, A. K. GHOSH, J. L. JURLINA, and J. B. STOTHERS. J. Chem. Soc. Chem. Commun. 204 (1983).
11. Y. HOYANO, V. PATEL, and J. B. STOTHERS. Can. J. Chem. **58**, 2730 (1980).
12. E. J. COREY and R. S. GLASS. J. Am. Chem. Soc. **89**, 2600 (1967).
13. W. C. STILL, M. KAHN, and A. MITRA. J. Org. Chem. **43**, 2923 (1978).
14. R. RATCLIFFE and R. RODEHORST. J. Org. Chem. **35**, 4000 (1970).
15. E. J. COREY, R. HARTMANN, and R. A. VATAKENCHERRY. J. Am. Chem. Soc. **84**, 2611 (1962).
16. E. G. BREITHOLLE and A. G. FALLIS. J. Org. Chem. **43**, 1964 (1978).
17. J. L. JURLINA and J. B. STOTHERS. J. Am. Chem. Soc. **104**, 4677 (1982).
18. A. BAX, R. FREEMAN, T. A. FRENKIEL, and M. H. LEVITT. J. Magn. Reson. **43**, 478 (1981).
19. A. L. JOHNSON, N. O. PETERSEN, M. B. RAMPERSAD, and J. B. STOTHERS. Can. J. Chem. **52**, 4143 (1974).
20. S. H. GROVER, D. H. MARR, J. B. STOTHERS, and C. T. TAN. Can. J. Chem. **53**, 1351 (1975).
21. E. ELIEL, N. A. ALLINGER, S. J. ANGYAL, and G. A. MORRISON. *In* Conformational analysis. Interscience, New York. 1965. p. 227.
22. L. A. BROOKS and H. R. SNYDER. Org. Synth. Coll. Vol. III, Wiley, New York. 1955. p. 698.
23. S. L. PATT and J. N. SHOOLERY. J. Magn. Reson. **46**, 535 (1982).
24. G. A. MORRIS and R. A. FREEMAN. J. Am. Chem. Soc. **107**, 760 (1979).
25. A. STOESSL and J. B. STOTHERS. Can. J. Chem. **62**, 549 (1984).

Can. J. Chem. Downloaded from www.nrcresearchpress.com by 210.87.254.105 on 09/06/12
For personal use only.

Substituent effects on benzyl radical hyperfine coupling constants. Part 2. The effect of sulphur substituents

DANIAL D. M. WAYNER AND DONALD R. ARNOLD[1]

Department of Chemistry, Dalhousie University, Halifax, N.S., Canada B3H 4J3

Received September 26, 1983

DANIAL D. M. WAYNER and DONALD R. ARNOLD. Can. J. Chem. **62**, 1164 (1984).

Several 4-substituted benzyl radicals of the general form $R(O_n)SC_6H_4CH_2\cdot$ (n = 0, 1, 2; R = Me, Ph, Tol, $COCH_3$, OCH_3) have been investigated by electron spin resonance (esr) spectroscopy. In general, the ability to delocalize spin density onto the substituent decreases as n increases. The effect of R on the spin density depends on the oxidation state of the sulphur. These trends are explained by considering the sulphur to be either a spin donor or a spin acceptor, depending on the oxidation state. The $\sigma^{\cdot}_{\alpha}$ values are determined.

DANIAL D. M. WAYNER et DONALD R. ARNOLD. Can. J. Chem. **62**, 1164 (1984).

Faisant appel à la résonance paramagnétique électronique (rpe), on a étudié plusieurs radicaux benzyles substitués en position 4, de structure générale $R(O_n)SC_6H_4CH_2\cdot$ (n = 0, 1, 2; R = Me, Ph, Tol, $COCH_3$, OCH_3). D'une façon générale, la facilité à délocaliser la densité de spin sur le substituant diminue avec une augmentation de n. L'effet de R sur la densité de spin dépend de l'état d'oxydation du soufre. On peut expliquer ces tendances en considérant le soufre comme étant soit un donneur de spin ou un accepteur de spin dépendant de son état d'oxydation. On a déterminé les valeurs $\sigma^{\cdot}_{\alpha}$.

[Traduit par le journal]

Introduction

Recently, we described the development of a series of substituent constants, sigma dot-alpha ($\sigma^{\cdot}_{\alpha}$), which were defined from the benzylic α-hydrogen hyperfine coupling constant (1) (eq. [1]).

$$[1] \quad \sigma^{\cdot}_{\alpha} = 1 - hfc_x/hfc_0$$

These substituent constants reflect the component of energy that may be attributed to spin delocalization in the substituted benzyl radical, relative to the unsubstituted radical. Other $\sigma^{\cdot}$ scales have been proposed (2). All of these were derived from relative rate data, and the radical substituent parameter was defined only after some assumption of the size of the polar contribution had been made. Furthermore, it was assumed that the measured effects were attributable only to changes in the nature of the transition state. This may be a valid assumption for ionic reactions, where the effects on the transition state relative to those on the starting material are large. Clearly, in free radical reactions this cannot be true (3).

The $\sigma^{\cdot}_{\alpha}$ scale offers major advantages over other $\sigma^{\cdot}$ scales. For example, the measured effects are free from polar factors in the transition state, and the substituent effects are attributable only to effects on the radical, not on the starting material.

The $\sigma^{\cdot}_{\alpha}$ scale has now been extended to include many other substituents (Table 1). Generally, it is found that *para* substituents decrease while *meta* substituents increase the α-hfc (there are exceptions to this generality). In this paper we describe the effect of sulphur-containing substituents on benzyl radical delocalization. The role of sulphur substituents in ionic reactions has been a subject of some controversy (4). Our results complement known ionic effects. Comparison of the free radical and ionic effects leads to an explanation of the trends observed.

Results

The benzyl radicals were generated in the esr (electron spin resonance) cavity by hydrogen atom abstraction from the corresponding toluenes or by bromine atom abstraction from the benzyl bromides. The observed hyperfine coupling constants are given in Table 2. In general, it is found that the order of delocalization of spin density by the substituents is: —SR > —S(O)R > —$S(O_2)$R (4*b*). The effect of R depends on the oxidation state of the sulphur.

TABLE 1. $\sigma^{\cdot}_{\alpha}$ Values

Substituent	$\sigma^{\cdot}_{\alpha}$	Substituent	$\sigma^{\cdot}_{\alpha}$
4-SMe	0.063	4-Cl	0.011
4-COMe	0.060	4-i-Pr	0.009
4-SPh	0.058	4-*t*-Bu	0.008
4-COPh	0.055	4-$S(O_2)$Me	0.005
4-COOMe	0.043	3-Me	0.002
4-CN	0.040	4-OCOPh	0.000
4-SCOMe	0.029	H	0.000
4-S(O)Ph	0.026	3-OMe	−0.001
4-OMe	0.018	3-OPh	−0.002
4-OPh	0.018	4-OCOMe	−0.005
4-S(O)Me	0.018	3-Cl	−0.007
4-$S(O_2)$Ph	0.018	3-F	−0.009
4-$SiMe_3$	0.017	4-CF_3	−0.009
4-S(O)OMe	0.016	4-F	−0.011
4-Me	0.015	3-COOMe	−0.014
4-$S(O_2)$OMe	0.013	3-CF_3	−0.017
4-Et	0.012	3-CN	−0.026

In the case of the sulphide, the 4-methylthio substituent delocalizes spin more effectively than the 4-tolylthio group.[2] This order is reversed for the corresponding sulphinyl and sulphonyl groups. Furthermore, the difference in a_{α} for the 4-methylthio- and the 4-tolylthiobenzyl, the 4-methylsulphinyl- and 4-tolylsulphinylbenzyl, and the 4-methylsulphonyl- and 4-tolylsulphonylbenzyl radicals increases as the oxidation state increases (these differences are −0.07 G, 0.12 G, and 0.22 G, respectively). Any explanation of the interaction of the sulphur-containing substituents with the benzyl radical must rationalize both the direction and magnitude of these trends.

[1]Author to whom correspondence may be addressed.

[2]The 4-tolyl derivatives are frequently more readily available than the phenyl derivatives. In the case of the 4-phenylsulphonylbenzyl radical, where the difference in a_{α} between the methyl and the phenyl derivatives is large, the difference between the phenyl and the tolyl derivatives is insignificant.

Can. J. Chem. Downloaded from www.nrcresearchpress.com by 210.87.254.105 on 09/06/12
For personal use only.

TABLE 2. Some benzyl radical hyperfine coupling constants[a]

Substituent		a_α	a_{ortho}	a_{meta}	a_x[b]
4-Methylthio	(—SMe)	15.23	5.08	1.73	0.90
4-Tolylthio	(—STol)	15.30	5.03	1.85	—
4-Acetylthiol	(—SC(O)Me)	15.77	5.03	1.81	—
4-Tolylsulphinyl	(—S(O)Tol)	15.83	5.10	1.80	—
4-Methoxy	(—OMe)[c]	15.95	5.02	1.60	0.75
4-Phenoxy	(—OPh)	15.95	5.11	1.70	—
4-Methylsulphinyl	(—S(O)Me)[c]	15.95	5.03	1.75	0.35
4-Phenylsulphonyl	(—$S(O_2)$Ph)	15.95	5.05	1.80	—
4-Tolylsulphonyl	(—$S(O_2)$Tol)	15.95	5.05	1.80	—
4-Methylsulphinate	(—S(O)OMe)	15.99	5.07	1.73	—
4-Methylsulphonate	(—$S(O_2)$OMe)[c]	16.04	5.03	1.71	—
4-Methylsulphonyl	(—$S(O_2)$Me)	16.17	5.09	1.78	1.05
—	(—H)[c]	16.25	5.10	1.70	6.13[d]
4-Acetyloxy	(—OC(O)Me)[c]	16.33	5.27	1.80	—

[a]Values are believed to be accurate to ± 0.03 G.
[b]Hydrogen of CH_3.
[c]Reference 1.
[d]*para*-Hydrogen.

Discussion

It is useful to review briefly the effects of sulphur-containing substituents in ionic reactions. The Hammett σ values for some sulphur-containing substituents are shown in Table 3 (6, 4*a*). The electron-withdrawing ability of the substituent increases as the oxidation state increases.

Sulphide may act as an electron-donating group (7) or an electron-withdrawing group (8), depending on the electron demand of the aryl or alkyl group to which it is bound. The ability of sulphide to act as both an acceptor or a donor has been explained by molecular orbital theory (9). The electron-donating ability of the 4-methylthio substituent is indicated by the σ^+ value (7) ($\sigma^+ = -0.60$). The stabilization of an adjacent carbanion by sulphur has been rationalized in terms of polarizability (9*c*) and hyperconjugation (9*a*).

Sulphinyl and sulphonyl groups are electron-withdrawing groups. The degree to which 3*d* orbitals are involved in the stabilization of adjacent carbanions has been a subject of controvesy (4*c*); however, there is convincing evidence that 3*d* orbitals can interact in the sulphone. Ramasamy *et al.* (10) found, from a study of angular correlation of positron annihilation radiation, that a well-marked increase in the region of *d*-orbital radial momentum is observed for arylalkyl sulphones. Such an increase was not found for sulphides. Work by Wolfe and co-workers (11) also has suggested that the role of *d* orbitals in α-sulphinyl and α-sulphonyl carbanions may be more important than previously believed.

The trends observed from the esr parameters of the substituted benzyl radicals are similar to those observed for the analogous methyl radicals (Tables 2 and 4).

Delocalization by —SR

The delocalization of a free radical by an adjacent sulphide group has been studied by esr spectroscopy (5, 12) and molecular orbital theory (13). The observed rotational barriers for XCH_2 radicals (where X = OMe, SMe) suggest that the π-bond formed for X = SMe is stronger than that for X= OMe. This result has been rationalized by Bernardi, Wolfe, and their co-workers (31) who suggest that the two-orbital three-electron interaction (Fig. 1b) is more important than the 3*d*-orbital effects (Fig. 1c). This greater stabilization by sulphur is thought to be a consequence of the lower lone pair ionization potential,

TABLE 3. Hammett σ constants for several sulphur-containing substituents

Substituent	σ	Reference
4-SMe	−0.047	6*a*
4-SPh	0.075	6*a*
4-S(O)Me	0.48	6*b*
4-S(O)Ph	0.47	6*a*
4-$S(O_2)$Me	0.72	6*a*
4-$S(O_2)$Ph	0.70	6*a*

TABLE 4. Hyperfine coupling constants for some substituted methyl radicals ($XCH_2\cdot$)[a]

X	a_α	a_γ
—SMe	16.5	3.6
—S(O)Me	20.0	—
—$S(O_2)$Me	22.3	2.1
—H	22.9	—

[a]Reference 5.

and hence the greater polarizability, of the sulphur relative to oxygen. The value of a_α for 4-methylthiobenzyl radical is less than that for 4-methoxybenzyl radical. A similar explanation may be offered to rationalize this effect.

The 4-tolylthiobenzyl radical has a slightly larger value of a_α than that value for the 4-methylthiobenzyl radical. While this difference is small (only 0.01 G outside experimental error), direct comparison of the experimental spectra shows the difference of 0.07 G is reproducible and real. Hudson and co-workers (12*a*), on the other hand, found that in the analogous methyl radicals the value of a_α for the phenylthiomethyl radical[2] was smaller than that for the methylthiomethyl radical. In the case of the benzyl radicals, the observed effect may be due to cross-conjugation in the 4-tolylthio derivative, which would decrease the polarizability (ionization potential) of the sulphur and, consequently, decrease the contribution of a valence bond structure such as Fig. 1b. Further support for this reasoning may be found. The value of a_α is larger in the 4-thiolacetylbenzyl radical than that in the 4-tolylthiobenzyl radical. The lone pair on sulphur will be conjugated more

Can. J. Chem. Downloaded from www.nrcresearchpress.com by 210.87.254.105 on 09/06/12
For personal use only.

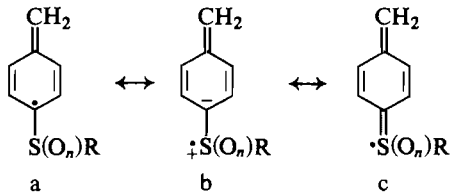

FIG. 1. The delocalization of a free radical by an adjacent sulphur substituent; (a) localized spin; (b) sulphur as a spin donor; (c) sulphur as a spin acceptor.

effectively to acetyl than to tolyl. Clearly, if conjugation through the sulphur were possible (Fig. 1c), the effect would be in the opposite direction (14).

It is found that a_α for 4-methoxybenzyl radical is the same as that for 4-phenoxybenzyl radical. On the other hand, the 4-acetoxybenzyl radical actually is less delocalizing relative to the unsubstituted radical.[3] The weakly conjugating phenyl group is not expected to have a great effect on the polarizability of the oxygen lone pairs. The strongly conjugating carbonyl group, on the other hand, will noticeably decrease the polarizability of the oxygen.

Delocalization by —S(O)R

It is evident from the values of a_α that the 4-methylsulphinyl group is less delocalizing than the 4-methylthio group (Table 2). This trend was also observed in the methyl radical series (5) (Table 4). The sulphinyl group is still able to participate in the two-orbital three-electron delocalization (Fig. 1b) since it has one lone pair of electrons. The delocalizing effect is less than it is for the corresponding sulphide, since the electronegative ligand will contract the orbital containing the lone pair (10). There is some spectroscopic evidence that the methylsulphinyl group is weakly donating; however, if the methylsulphinyl group is *para* to a strong donating group, it becomes a resonance acceptor (15).

In the delocalization of a benzyl radical by a sulphinyl group, is the sulphinyl group predominantly a spin donor or a spin acceptor? The value of a_x (the hyperfine coupling constant assigned to the substituent methyl group) is much less for the 4-methylsulphinylbenzyl radical than those values for either the 4-methylthiobenzyl radical or the 4-methylsulphonylbenzyl radicals. It has been suggested that the coupling to the methyl group in the methylthiomethyl radical is a result of hyperconjugative interactions with the spin on sulphur, while coupling in the methylsulphonylmethyl radical is a result of spin polarization (5). The hyperconjugative mechanism results in positive spin density, while spin polarization leads to negative spin density in the methyl group. In the case of the methylsulphinylmethyl radical, the smaller value for a_x reflects contributions from both of these mechanisms. This trend is also observed in the analogous benzyl radicals, so a similar explanation may be offered. However, since only the magnitude of the hyperfine coupling constant is known, it is impossible to determine from this evidence if the sulphinyl group is predominantly a spin donor or a spin acceptor.

[3]The decreased delocalization by a *para* substituent relative to the unsubstituted benzyl radical is observed only in those cases where the substituent is highly electronegative and a valence bond structure such as that in Fig. 1b is unfavourable (e.g. —F, —CF_3, —OCOMe). In these electron-poor benzyl radicals, the delocalization of spin density to the substituent is less effective than delocalization of spin density to hydrogen.

Replacement of the substituent methyl group with tolyl leads to a decrease in the benzylic hyperfine coupling constant. It is tempting to conclude from this evidence that the sulphinyl group is a spin acceptor, since the cross-conjugative effect found in the sulphide derivative is not observed. Replacement of the methyl group by tolyl can have two opposing effects. The first, which causes a decrease in delocalization of spin density, is cross-conjugation, which has already been discussed. The second effect, which leads to an increase in delocalization of spin density, may be a result of further stabilization of the MO which is accepting the spin (through conjugation). It is possible that the $3d$ orbitals on sulphur, which contract in the presence of the highly electronegative oxygen, contribute. We would suggest, therefore, that the sulphinyl group is a net spin donor.

Delocalization by —S(O_2)R

Since the sulphur in the 4-methylsulphonylbenzyl radical has no lone pairs, delocalization of a free radical is possible only with sulphur as a spin acceptor. Even though the $3d$ orbitals are contracted to a greater extent than those in the 4-methylsulphinylbenzyl radical, very little delocalization results (a_α is only 16.17 G). Under the most favourable conditions for $3d$-orbital interaction, extra delocalization, compared to the unsubstituted radical, amounts to an effect of only 0.08 G (compared to 1.02 G for the corresponding sulphide, where lone pair interactions dominate). The conclusion that the 4-methylsulphinyl group is a net spin donor, therefore, seems reasonable. The extra delocalization gained when the methyl group is replaced by tolyl (or phenyl) is almost twice as large as that found in the sulphinyl derivative. This serves to reinforce the idea that the tolyl group interacts to further stabilize the MO which is accepting the spin density, since through-conjugation with the more highly contracted $3d$ orbitals should be more effective.

Delocalization by —S(O)OMe and —S(O_2)OMe

While it is found that the 4-methylsulphinate group is less delocalizing than the 4-methylsulphinyl group, the corresponding 4-methylsulphonate group is more delocalizing than the 4-methylsulphonyl group. Again, these trends may be rationalized using the simple concepts outlined above. The 4-methylsulphinate group will be more delocalizing than the isomeric 4-methylsulphonyl group, since the former has a lone pair of electrons on the sulphur. The replacement of the methyl with methoxy (in the 4-methylsulphinyl group) will further contract the lone pair, decreasing the contribution of the structure shown in Fig. 1b.

The 4-methylsulphonate group is somewhat different. Since the sulphur has no lone pairs, the effect of the third oxygen is to further contract the $3d$ orbitals. Rather than becoming a less effective spin donor (as in the 4-methylsulphinate group), the 4-methylsulphonate group becomes a more effective spin acceptor.

It is more difficult to interpret the effects of the substituents on the observed esr parameters for the methyl radicals, since the substituents may induce changes in conformation at the radical centre. In addition, the possibility of through-space interactions cannot be precluded. One of the advantages of studying the esr parameters of the benzyl radicals is that the substituent undoubtedly will have a negligible effect on the conformation of the benzylic carbon. We would, therefore, not expect the a_α of the benzyl radicals to correlate with the a_α of the methyl radicals. However, there is a trend, at least, for the

Can. J. Chem. Downloaded from www.nrcresearchpress.com by 210.87.254.105 on 09/06/12
For personal use only.

four substituents in Table 4. There are also obvious differences.

The strong carbon–sulphur π-bond in the methylthiomethyl radical leads to restricted internal rotation at temperatures as high as −20°C (12*a*). There is no evidence for restricted internal rotation in the 4-methylthiobenzyl radical at −30°C (the two *meta* hydrogens still appear to be equivalent).

Sulphur-containing substituents, other than 4-methylthio, have seldom been used as substituents in the study of free radical reactions. As a result, it is difficult to assess how well the derived $\sigma^{\cdot}_{\alpha}$ values correlate with relative reactivity data. We predict, however, that, as in the past, the $\sigma^{\cdot}_{\alpha}$ values will prove to be useful in the Hammett or extended Hammett treatment of kinetic data.

Experimental

General information

The esr spectra were recorded on a Varian Associates E109B electron paramagnetic resonance spectrometer equipped with a liquid nitrogen variable temperature accessory. All spectra were recorded with the aid of the Nicolet 1170 signal averager. Typically, 16 spectra were averaged (2 min per spectrum). Coupling constants were measured directly from the oscilloscope and refined by computer simulation (24) using the IBM-PC. All spectra were reproducible within the experimental error. The estimated error of 0.03 G is the limit of resolution of the recording device used to plot the experimental spectra and the simulations. The ^{1}Hmr spectra were recorded on a Varian T-60 spectrometer and are reported in parts per million downfield from TMS. Infrared spectra were recorded on a Pye Unicam SP1000 infrared spectrometer and are reported in wave numbers. Melting points were recorded on a Sybron Corporation Thermodyne hotstage (uncorrected).

Materials

Di-*tert*-butyl peroxide (DTBP) and triethylsilane were obtained from Pfaltz and Bauer Inc. and were used without further purification. Hexamethylditin was obtained from Alpha Products and used without further purification. 4-Methoxyacetophenone (PMA) was obtained from Aldrich Chemical Company Inc. and was recrystallized twice from 95% ethanol prior to use. 4,4′-Dimethyldiphenylsulphoxide was also obtained from Aldrich and used without further purification. Chlorobenzene (J. T. Baker Chemicals Inc.) was stirred over concentrated sulphuric acid, washed successively with water, saturated sodium bicarbonate, and water, dried over anhydrous magnesium sulphate, and distilled through a Vigreux column.

Preparation of benzyl bromides

The method of Grice and Owen (16) was used for the conversion of substituted benzyl alcohols to the bromides. Typically, the benzyl alcohol (0.02 mol) was dissolved in benzene (100 mL). Hydrogen bromide gas was passed through the solution for 1 h or until the solution was saturated. The reactants were heated to reflux and the water which formed was removed via a Dean–Stark trap. The solution was then dried over anhydrous magnesium sulphate, filtered, and the solvent removed at reduced pressure. The bromide was then purified by sublimation.

4-(Methylthio)benzylbromide

The benzyl alcohol (3.0 g, 0.02 mol, Aldrich) was dissolved in benzene (100 mL). This solution was saturated with anhydrous hydrogen bromide (1 h) and the resulting solution refluxed for 1 h with a Dean–Stark trap. The solution was then dried over anhydrous magnesium sulphate, filtered, and the solvent was removed at reduced pressure. The bromide was purified by vacuum sublimation (40°C, 0.1 Torr) to give colourless crystals. The yield was 2.8 g, 65%; mp 43–44°C (lit. (16) mp 44°C); ^{1}Hmr ($CDCl_3$) δ: 7.21 (s, 4H), 4.43 (s, 2H), 2.45 (s, 3H).

4-(Bromomethyl)phenyl methylsulphone

4-(Methylthio)benzylalcohol (3.0 g, 0.02 mol) was dissolved in dichloromethane (100 mL). To this solution, at 0°C, 3-chloroperbenzoic acid (8.0 g, 0.045 mol) in dichloromethane (50 mL) was added dropwise over 30 min. The mixture was stirred for 18 h, filtered, washed successively with 5% sodium hydroxide and water, then dried over anhydrous magnesium sulphate. Evaporation of the solvent at reduced pressure gave 2.4 g of the benzyl alcohol (67%).

The benzyl alcohol (2.4 g, 0.013 mol) was dissolved in benzene (100 mL) and the solution was saturated with anhydrous hydrogen bromide. The resulting solution was refluxed under a Dean–Stark trap (2 h), dried with anhydrous magnesium sulphate, and the solvent evaporated at reduced pressure. The crude bromide was purified by sublimation (120°C, 0.1 Torr) to give colourless crystals. The yield was 2.0 g, 62%; mp 94–96°C (lit. (17) mp 95–95.8°C); ir ($CHCl_3$) cm^{-1}: 1155(s), 1322(s); ^{1}Hmr ($CDCl_3$) δ: 7.82 (m, 4H), 4.53 (s, 2H), 3.07 (s, 3H).

Preparation of substituted toluenes

The preparation of methyl-4-tolylsulphoxide and methyl-4-tolylsulphonate has been described previously (1).

4,4′-Dimethyldiphenylsulphide

4,4′-Dimethyldiphenylsulphoxide (5.0 g, 0.022 mol) was added to a stirred solution of cobalt(III) chloride hexahydrate (9.6 g, 0.040 mol) in ethanol (300 mL). The solution was cooled to 0°C. Sodium borohydride (7.6 g, 0.2 mol) was added over a 1-h period. The reduction proceeded as outlined by Chasar (18). Water was added, the mixture stirred for one further hour, and then the mixture was poured into water (500 mL). The solution was washed with diethyl ether (three 100-mL portions). The ethereal extracts were dried and the ether removed at reduced pressure, leaving an ethanolic solution from which the product crystallized. The yield was 4.0 g, 85%; mp 55–57°C (lit (19) mp 57.5°C); ^{1}Hmr ($CDCl_3$) δ: 7.17 (m, 8H), 2.30 (s, 6H).

4,4′-Dimethyldiphenylsulphone

4,4′-Dimethyldiphenylsulphoxide (5.0 g, 0.022 mol) in dichloromethane (100 mL) was allowed to sir at 0°C. 3-Chloroperbenzoic acid (4.2 g, 0.024 mol) was added over 1 h. The reaction mixture stirred for 18 h. Work-up consisted of washing the dichloromethane solution with water, 10% sodium bicarbonate solution, and finally with water. The dichloromethane was dried over anhydrous magnesium sulphate, filtered, and the solvent removed at reduced pressure. The product was recrystallized twice from chlorobenzene to give colourless platelets. The yield was 4.4 g, 81%; mp 157–158°C (lit (20) mp 158.1°C); ^{1}Hmr ($CDCl_3$) δ: 7.50 (m, 8H), 2.33 (s, 6H).

4-Methyldiphenylsulphone

4-Tolylsulphonylchloride (5.0 g, 0.03 mol) in benzene (50 mL) was added dropwise to a stirred solution of aluminum chloride (4.0 g, 0.03 mol) in benzene (100 mL) over 20 min. After the addition was complete, the mixture was slowly warmed to 60°C and stirred at that temperature until the evolution of hydrogen chloride has subsided (about 30 min). The mixture was then refluxed for an additional 1-h period after which it was carefully poured onto 200 g of crushed ice. This mixture was heated to break up the complex, the layers were separated, and the organic layer washed successively with 5% sodium bicarbonate and water. The solution was then dried over anhydrous magnesium sulphate and the solvent evaporated at reduced pressure. Recrystallization of the crude product from ethanol afforded colourless crystals. The yield was 4.8 g, 69%; mp 128–129°C (lit. (21) mp 129°C); ir ($CHCl_3$) cm^{-1}: 1161(s), 1320(s); ^{1}Hmr ($CDCl_3$) δ: 7.55 (m, 9H), 2.33 (s, 3H).

Methyl(4-tolylsulphinate)

The sulphinic ester was prepared by the method of Field and Locke (22). To a refluxing solution of ditolyldisulphide (3 g, 0.012 mol, Aldrich Chemical Company Inc.), chloroform (25 mL), and methanol (25 mL) in a 250-mL three-neck flask, lead tetraacetate (25 g) in chloroform (100 mL) was added dropwise over a 1-h period. The solution was allowed to reflux for an additional 24 h. Most of the solvent (100 mL) was distilled from the reaction flask, and water (20

Can. J. Chem. Downloaded from www.nrcresearchpress.com by 210.87.254.105 on 09/06/12
For personal use only.

Can. J. Chem. Downloaded from www.nrcresearchpress.com by 210.87.254.105 on 09/06/12
For personal use only.

mL) was added. The mixture was cooled, filtered through Celite, and washed with water until all traces of lead were removed (22). The solution was dried and the solvent was removed at reduced pressure. The yield was 3.8 g, 93%; ir (NaCl disk) cm^{-1}; 1080(s); ^{1}Hmr ($CDCl_3$) δ: 7.42 (m, 4H), 3.40 (s, 3H), 2.37 (s, 3H).

4-Tolylthioacetate

Acetylchloride (4.7 g, 0.06 mol) in benzene (50 mL) was added dropwise to a solution of 4-thiocresol (7.5 g, 0.06 mol) in benzene (100 mL) over 15 min. The solution was warmed to reflux for 1 h. The reaction mixture was cooled, washed three times with 10% sodium hydroxide and twice with water, and then dried over anhydrous magnesium sulphate. The solvent was removed at reduced pressure. The product was purified by distillation (85°C, 0.1 Torr (14)); ir (NaCl disk) cm^{-1}: 1712(s); ^{1}Hmr ($CDCl_3$) δ: 7.22 (bs, 4H), 2.33 (s, 6H).

4-Methyldiphenylether

This ether was prepared by the method of Bacon and Stewart (23). A mixture of 4-cresol (10.8 g, 0.1 mol), bromobenzene (7.85 g, 0.05 mol), and cuprous oxide (7.15 g, 0.05 mol) in 2,4,6-trimethylpyridine (25 mL) was refluxed for 48 h. The mixture was poured into 6 *M* HCl (200 mL) and extracted with ether (2 × 200 mL). The ether layer was then washed with 5% sodium hydroxide solution and water, and dried over anhydrous magnesium sulphate. The solvent was removed at reduced pressure and the product purified by distillation (104°C, 0.1 Torr). The yield was 5.0 g, 55%; ^{1}Hmr ($CDCl_3$) δ: 7.00 (m, 9H), 2.30 (s, 3H).

Electron spin resonance experiments

Toluenes

A static solution of DTBP (0.5 mL) and the toluene (100 mg) with PMA (45 mg) was irradiated in the esr spectrometer cavity using a filtered (methanol in a quartz tube) 1-kW Xe−Hg high pressure lamp. Temperatures ranged from 20°C to −60°C (depending on the solubility), with the majority of the samples examined at −20°C. All samples were purged with nitrogen for 5 min prior to irradiation.

Benzylbromides

Two methods were used to generate the benzyl radicals. In method 1, a static solution of DTBP (0.2 mL), triethylsilane (0.2 mL), and the bromide (50−100 mg), diluted if necessary with chlorobenzene, was purged with nitrogen and irradiated in the esr spectrometer cavity as described above. In method 2, a solution of the bromide (50−100 mg) in *tert*-butylbenzene or chlorobenzene was continuously purged while hexamethylditin (0.1 mL) was injected via the nitrogen purge tube. It was necessary to have a glass wool plug in the purge tube to filter the hexamethylditin. This solution was irradiated as described above. The use of chlorobenzene allowed cooling of the sample to temperatures as low as −20°C without precipitation of the hexamethylditin.

Control experiments

The linearity of the field was checked against the line of $[Cr(NH_3)_5Cl]Cl_2$ doped with 2% $[Co(NH_3)_5Cl]Cl_2$ (25). The accuracy of the field was checked against the coupling constants for Wursters blue perchlorate in ethanol (26). The esr spectra of the benzyl radical, the 3-cyanobenzyl radical, and the 4-fluorobenzyl radical all have been shown to be independent of solvent (up to 50% v/v chlorobenzene or carbon tetrachloride) and temperature (20°C to −60°C) (1). Similarly, the esr spectra of the 4-tolylthiobenzyl radical show no solvent effect (up to 50% v/v chlorobenzene) or temperature effect (20°C to −60°C). The spectra of the 4-methylthiobenzyl radical and the 4-methylsulphonylbenzyl radical show no temperature dependence between 0°C and −60°C. The insolubility of the bromides in DTBP precluded checking the esr spectra in this solvent. However, for each of the bromides, similar spectra were obtained using either chlorobenzene or dimethoxyethane as solvent.

Acknowledgements

This work was supported by a grant from the Natural Sciences and Engineering Research Council of Canada (including a scholarship to D.D.M.W.). The authors also acknowledge the contribution of Julian M. M. Dust.

1. (*a*) J. M. DUST and D. R. ARNOLD. J. Am. Chem. Soc. **105**, 1211 (1983); (*b*) J. Am. Chem. Soc. **105**, 6531 (1983).
2. (*a*) A. P. G. KIEBOOM. Tetrahedron, **28**, 1325 (1972); (*b*) R. ITO, T. MIGITA, N. MORIKAWA, and O. SIMAMURA. Tetrahedron, **21**, 955 (1965); (*c*) T. YAMAMOTO and T. OTSU. Chem. Ind. (London), 787 (1967); (*d*) H. SAKURAI, S. HAYISHI, and A. HOSOMI. Bull. Chem. Soc. Jpn. **44**, 1945 (1971); (*e*) T. H. FISHER and A. W. MEIERHOEFER. J. Org. Chem. **43**, 224 (1978); (*f*) W. J. LEIGH, D. R. ARNOLD, R. W. HUMPHREYS, and P. C. WONG. Can. J. Chem. **58**, 2537 (1980); (*g*) S. DINCTURK, R. A. JACKSON, H. TOWNSON, H. AGIRBAS, N. C. BILLINGHAM, and G. MARCH. J. Chem. Soc. Perkin Trans. 2, 1121 (1981).
3. A. M. DEP. NICHOLAS and D. R. ARNOLD. Can. J. Chem. In press.
4. (*a*) S. OAE. Organic chemistry of sulphur. Plenum Press, New York. 1977; (*b*) E. BLOCK. Reactions of organosulphur compounds. Academic Press, New York. 1978; (*c*) H. KWART and K. KING. d-Orbitals in the chemistry of silicon, phosphorus and sulphur. Springer Verlag, New York. 1977.
5. P. M. CARTON, B. C. GILBERT, H. A. H. LAUE, R. O. C. NORMAN, and R. C. SEALY. J. Chem. Soc. Perkin Trans. 2, 1246 (1975).
6. (*a*) H. H. SZMANT and G. SULD. J. Am. Chem. Soc. **78**, 3400 (1956); (*b*) F. G. BORDWELL and P. J. BOUTAN. J. Am. Chem. Soc. **79**, 717 (1957); (*c*) F. G. BORDWELL and P. J. BOUTAN. J. Am. Chem. Soc. **78**, 854 (1956); (*d*) F. G. BORDWELL and G. D. COOPER. J. Am. Chem. Soc. **74**, 1058 (1952).
7. H. C. BROWN and Y. OKAMOTO. J. Am. Chem. Soc. **80**, 4979 (1958).
8. S. OAE, M. YOSHIHARA, and W. TAGAKI. Bull Chem. Soc. Jpn. **40**, 951 (1967).
9. (*a*) N. D. EPIOTIS, R. L. YATES, S. BERNARDI, and S. WOLFE. J. Am. Chem. Soc. **98**, 5435 (1976); (*b*) S. WOLFE, A. RAUK, L. M. TEL, and I. G. CSIZMADIA. J. Chem. Soc. Chem. Commun. 96 (1970); (*c*) J. M. LEHN and G. WIPFF. J. Am. Chem. Soc. **98**, 7498 (1976); (*d*) F. BERNARDI, I. G. CSIZMADIA, H. B. SCHLEGEL, and S. WOLFE. Can. J. Chem. **63**, 1144 (1974).
10. S. RAMASAMY, V. M. KANAGASABAPATHY, and T. NAGARAJAN. Phys. Lett. A, **73**, 166 (1979).
11. D. J. MITCHELL, S. WOLFE, and H. B. SCHLEGEL. Can. J. Chem. **59**, 3280 (1981).
12. (*a*) I. BIDDLES, A. HUDSON, and J. T. WIPPEN. Tetrahedron, **28**, 867 (1972); (*b*) J. Q. ADAMS. J. Am. Chem. Soc. **92**, 4535 (1970); (*c*) P. J. KRUSIC and J. K. KOCHI. J. Am. Chem. Soc. **93**, 846 (1971).
13. F. BERNARDI, N. D. EPIOTIS, W. CHERRY, H. B. SCHLEGEL, M. H. WHANGBO, and S. WOLFE. J. Am. Chem. Soc. **98**, 469 (1976).
14. V. BALIAH and K. GANAPATHY. Trans. Faraday Soc. **59**, 1784 (1963).
15. N. C. CUTRESS, T. B. GRINDLEY, A. R. KATRITSKY, M. SHOME, and R. D. TOPSOM. J. Chem. Soc. Perkin Trans. 2, 268 (1974).
16. R. GRICE and L. N. OWEN. J. Chem. Soc. 1947 (1963).
17. Beilsteins Handbuch der Organischen Chemie. Vol. 6. Springer Verlag, New York. Supplement 4. pp. 2210, 1982.
18. D. W. CHASAR. J. Org. Chem. **36**, 613 (1971).
19. H. RHEINBOLDT and E. GIESBRECHT. J. Am. Chem. Soc. **69**, 2310 (1947).
20. H. RHEINBOLDT and E. GIESBRECHT. J. Am. Chem. Soc. **68**, 973 (1946).
21. H. R. HENZE and N. E. ARTMAN. J. Org. Chem. **22**, 1410 (1957).
22. H. E. BAUMGARTEN. Org. Synth. Coll. Vol. V. Wiley, New York. 1973. p. 723.
23. R. G. R. BACON and O. J. STEWART. J. Chem. Soc. 4953 (1965).
24. U. M. OEHLER and E. G. JANZEN. Can. J. Chem. **60**, 1542 (1982).
25. W. T. M. ANDRIESSEN. J. Magn. Reson. **23**, 339 (1976).
26. J. E. WERTZ and J. R. BOLTON. Electron spin resonance. McGraw−Hill, New York. 1972. Appendix.

Chemistry of shikimic acid derivatives. Synthesis of specifically labeled shikimic acid at C-3 or C-4[1]

LOLITA O. ZAMIR[2]

Université du Québec – Institut Armand-Frappier, Center for Bacteriology, 531 boulevard des Prairies, Laval-des-Rapides, Laval (Qué.), Canada H7N 4Z3

and

Center for Biochemical Research, State University of New York at Binghamton, Binghamton, NY 13901, U.S.A.

AND

CORINNE LUTHE

Université du Québec – Institut Armand-Frappier, Center for Bacteriology, 531 boulevard des Prairies, Laval-des-Rapides, Laval (Qué.), Canada H7N 4Z3

Received August 24, 1983

LOLITA O. ZAMIR and CORINNE LUTHE. Can. J. Chem. **62**, 1169 (1984).

Specifically labeled shikimic acids with tritium or deuterium at positions C-3 or C-4 were synthesized. Commercially available L-shikimic acid was converted to its 3- and 4-ketones, after suitable protection of the hydroxyl groups at C-4,C-5 and C-3,C-5. Reduction of the 3-keto- or 4-keto-shikimic acid derivatives with sodium borodeuteride and deprotection gave mostly 3-D-epi-shikimic acid or 4-D-shikimic acid. An internally assisted inversion of the 3-D-epi-shikimic acid derivative and deprotection gave 3-D-shikimic acid.

LOLITA O. ZAMIR et CORINNE LUTHE. Can. J. Chem. **62**, 1169 (1984).

Les acides shikimiques marqués spécifiquement avec du tritium ou deutérium aux positions C-3 et C-4 ont été synthétisés. Le procédé utilisé était de transformer l'acide L-shikimique de source commerciale en cétones C-3 et C-4 après avoir protégé les hydroxyles aux positions C-4,C-5 et C-3,C-5. La réduction des dérivés cétoniques C-3 et C-4 des acides shikimiques par le borohydrure de sodium deutéré suivie de l'élimination des groupements protecteurs donna en majorité les composés 3-D-epi et 4-D- de l'acide shikimique. Une inversion du composé 3-D-epi de l'acide shikimique accompagnée du retrait des groupements protecteurs donna l'acide 3-D-shikimique.

Can. J. Chem. Downloaded from www.nrcresearchpress.com by 210.87.254.6 on 09/06/12
For personal use only.

Introduction

Shikimic acid is a key precursor for an enormous number of aromatic compounds, e.g. aromatic amino acids, vitamins, and a host of secondary metabolites. Shikimic acid is the ideal precursor for tracer type studies because it is generally permeable to cells and is chemically stable. In our laboratory, we will investigate the biochemical intermediates to aromatic amino acids, and in particular, the arogenate (2–5) and spiro-arogenate (6, 7) segments. Synthesis of labeled shikimic acid with deuterium or tritium at C-3 and C-4 is the first step in achieving this objective.

An enzymatic preparation of shikimic acid-6*R*-6T and -6*S*-6T (8) and shikimic acid-2-D (9) has previously been reported. Recently, Christopherson and Morrison (10) prepared 3-^{3}H-shikimic acid, however, as an undefined mixture of both 3-^{3}H-shikimate and 3-^{3}H-epi-shikimate. In this article we describe the synthesis of specifically labeled shikimic acid with deuterium or tritium at position C-3 or C-4. An unexpected observation was made: an intermediary ketone rearranged during purification by flash chromatography.

Results and discussion

The detailed synthetic steps in the preparation of C-3 and C-4 labeled shikimic acids are outlined in Fig. 1.

Synthesis of 3-D- or 3-T-shikimic acid

Our approach consisted of protecting the hydroxyl groups at C-4 and C-5 and generating the 3-keto species. The deuterium or tritium label was introduced by reduction with sodium borodeuteride or tritiated sodium borohydride, respectively. An internally assisted inversion followed by deprotection should then yield 3-D- or 3-T-shikimic acid.

Shikimic acid **1** was esterified (11) in the usual manner, with diazomethane, to afford methyl shikimate **2** (12) which was readily transformed into its corresponding 3,4-orthoformate **3**, without any concurrent reaction at the C-5 alcohol. Protection of the latter as its *tert*-butyldimethylsilyl ether (**4**) (13), followed by an acid hydrolysis of the orthoester moiety, gave diol **12**. The allylic alcohol was selectively oxidized using pyridinium dichromate (14) to afford α,β-unsaturated ketone **10**, which then underwent acetylation in the usual manner (15) to generate acetate **11**. Unfortunately, the reduction of the latter by $NaBH_4$ (or its labeled analogues) yielded predominantly the thermodynamically more stable β-alcohol (β/α = 90:10). In order to re-establish the correct α-stereochemistry of the hydroxyl group at C-3, alcohol **15** was transformed into its allylic mesylate **17**; solvolysis of this acetoxy-mesylate in methanol containing 1.1 equivalents of potassium acetate (16) at 70°C readily afforded orthoacetate **6** with the desired α-stereochemistry at C-3. Flash chromatography (17) of the crude product **6**, followed by acid hydrolysis and re-acetylation, gave diacetate **13** in 25% yield based on ketone **11**. Its 200 MHz ^{1}H nmr spectrum (Fig. 2) was identical to that of an authentic sample of **13**. Furthermore, both mass spectral and 200 MHz ^{1}H nmr data of deuterated diacetate **13** indicated a quantitative incorporation of the label at C-3. Desilylation with tetra-*n*-butylammonium fluoride afforded the desired deprotected alcohol as a mixture of acetates in 83% yield, after flash chromatography. The deacetylation–demethylation sequence was effected by alkaline hydrolysis in methanol–water. The shikimic acid thus obtained (after *in situ* tetra-silylation) was pure

[1]Presented in part as a communication (see ref. 1).

[2]Correspondence to: Lolita O. Zamir, Université du Québec – Institut Armand-Frappier, Center for Bacteriology, 531 boulevard des Prairies, Laval (Qué.), Canada H7N 4Z3.

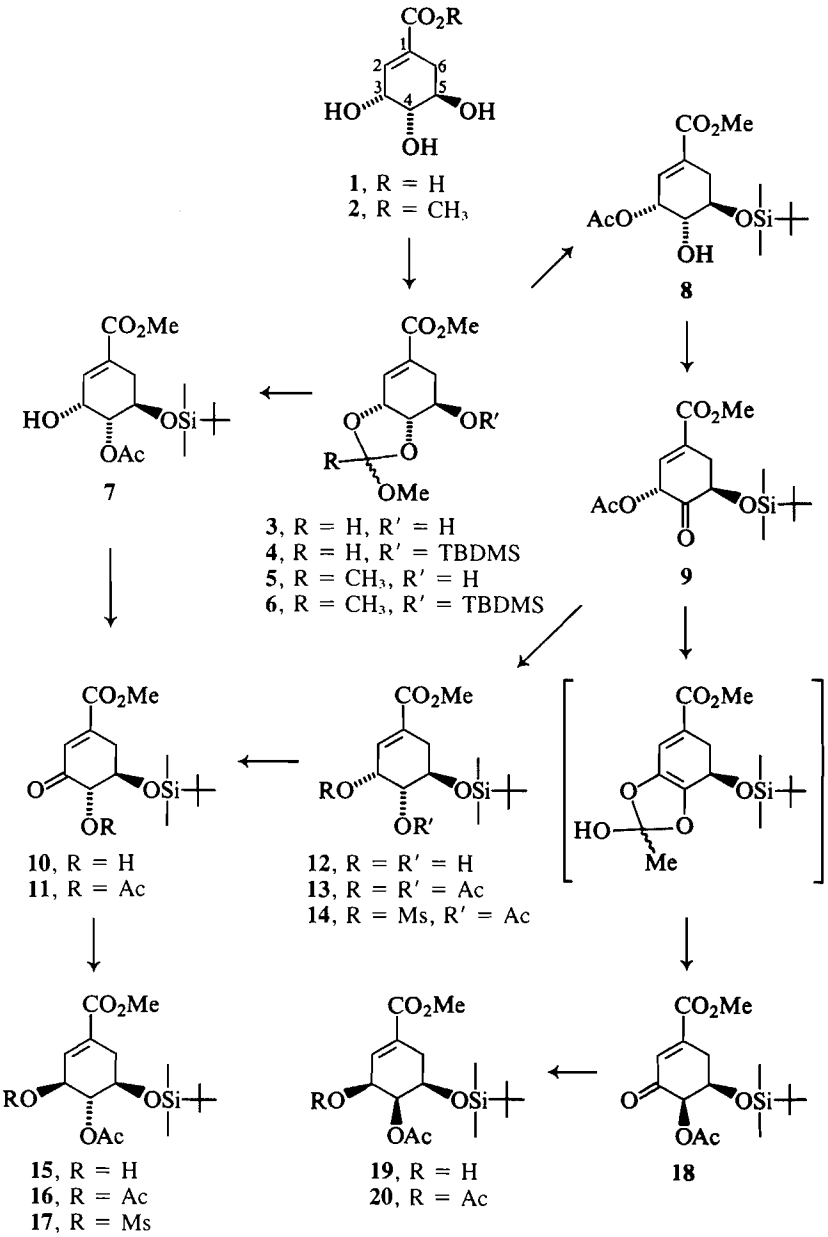

FIG. 1. Synthetic intermediates to specifically labeled shikimic acid at positions C-3 and C-4.

(98%) by gas chromatography, and had an identical mass spectrum to that of an authentic tetra-trimethylsilylated sample. In the case of the labeled shikimic acid derivative, there was no mass spectral evidence for any deuterium loss to have occurred during the final deblocking sequence (Fig. 3).

Synthesis of 4-D- or 4-T-shikimic acid

An oxidation–reduction sequence on the 4-alcohol enables the introduction of deuterium or the tracer tritium at the C-4 position. The protecting groups at C-3 and C-5 were found to be critical in determining the ease of oxidation of the C-4 alcohol. A feasible approach utilized the alcohol **8** having an acetate on C-3 and a *tert*-butyldimethylsilyl group on the C-5 hydroxyl. The 5-hydroxyl function of 3,4-orthoacetate **5** was protected as its *tert*-butyldimethylsilyl ether; the orthoacetate moiety was then hydrolyzed, yielding two monoacetates **7** and **8**, each possessing a free, oxidizable C-4 or C-3 hydroxyl group.

Since these two alcohols displayed very similar mobility on thin-layer chromatography, their separation was most easily effected by selectively oxidizing the allylic one using pyridinium dichromate, prior to chromatography. This allylic oxidation gave ketone **11**, identical to **11** obtained previously.

Alcohol **8** was found to be rather resistant towards most oxidizing reagents. It was finally transformed into its corresponding ketone **9**, albeit in low yield, by reaction with Jones reagent for 5 h. It was very unstable and any attempted purification of crude 4-ketone **9**, by flash chromatography, resulted in its almost complete conversion to α,β-unsaturated ketone **18**, a product thought to arise via enolization, followed by acyl migration and kinetic protonation. Its structure was confirmed by ^{1}H nmr decoupling experiments on both ketones **11** and **18**. Borohydride reduction of this undesired ketone gave predominantly the thermodynamically more stable β-alcohol **19**, which was characterized as its acetate **20**.

Hence, crude ketone **9** (which contained ketone **11**) was

Can. J. Chem. Downloaded from www.nrcresearchpress.com by 210.87.254.6 on 09/06/12
For personal use only.

Can. J. Chem. Downloaded from www.nrcresearchpress.com by 210.87.254.6 on 09/06/12
For personal use only.

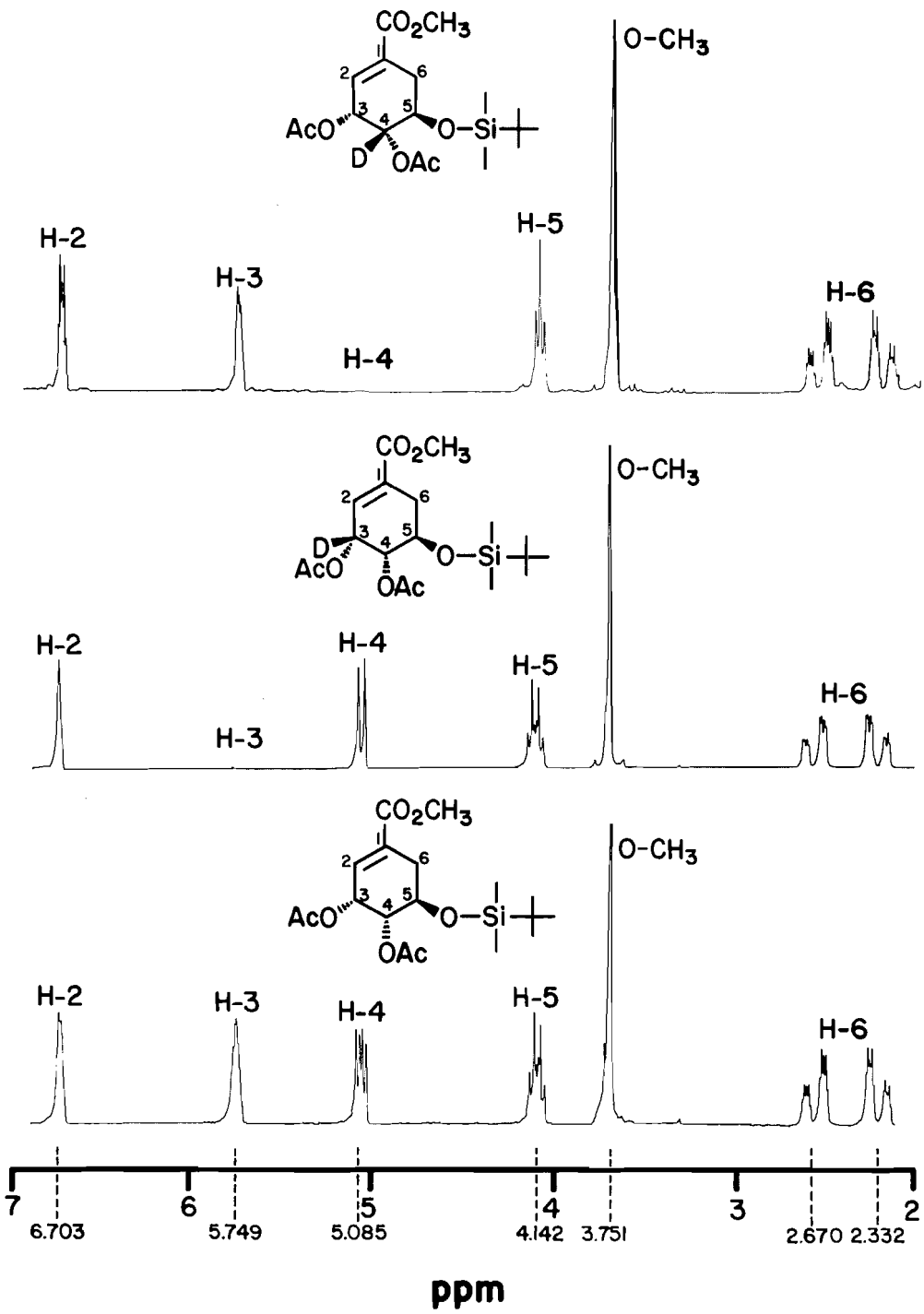

FIG. 2. Analysis of specifically labeled shikimic acid derivative at C-3 and C-4 by proton nmr. The 200 MHz ^{1}H nmr spectrum of unlabeled shikimic acid derivative (**13**) in $CDCl_3$ is shown on the bottom scale. The spectrum shown in the middle represents this derivative labeled with deuterium at C-3. The upper spectrum shows **13** labeled at C-4 with deuterium.

immediately reduced with $NaBH_4$ (or its labeled analogues), seemingly stereospecifically, to give alcohol **8**. The purification of alcohol **8** by flash chromatography was facilitated by a prior pyridinium dichromate oxidation of the allylic alcohols; the purified product **8** (obtained in 12% yield based on starting material, unlabeled **8**) was then acetylated in the conventional manner, thereby rendering it less water soluble, as well as eminently distinguishable from other shikimate isomers by ^{1}H nmr characterization. Mass spectral and 200 MHz ^{1}H nmr data of deuterated diacetate **13** indicated 100% incorporation of the label at C-4 (average of 4 runs) (Figs. 2, 3). Total deprotection, as described earlier for the C-3 labeled series, gave authentic shikimic acid. There was no mass spectral evidence (Fig. 3) of any deuterium loss having occurred in the final deprotection sequence.

Experimental

Mass spectra (ms) were obtained on a HP 5984 or LKB-9000 mass spectrometer, at 70 eV. Infrared (ir) spectra were obtained on a Perkin–Elmer 297 spectrophotometer. Proton magnetic resonance

Can. J. Chem. Downloaded from www.nrcresearchpress.com by 210.87.254.6 on 09/06/12
For personal use only.

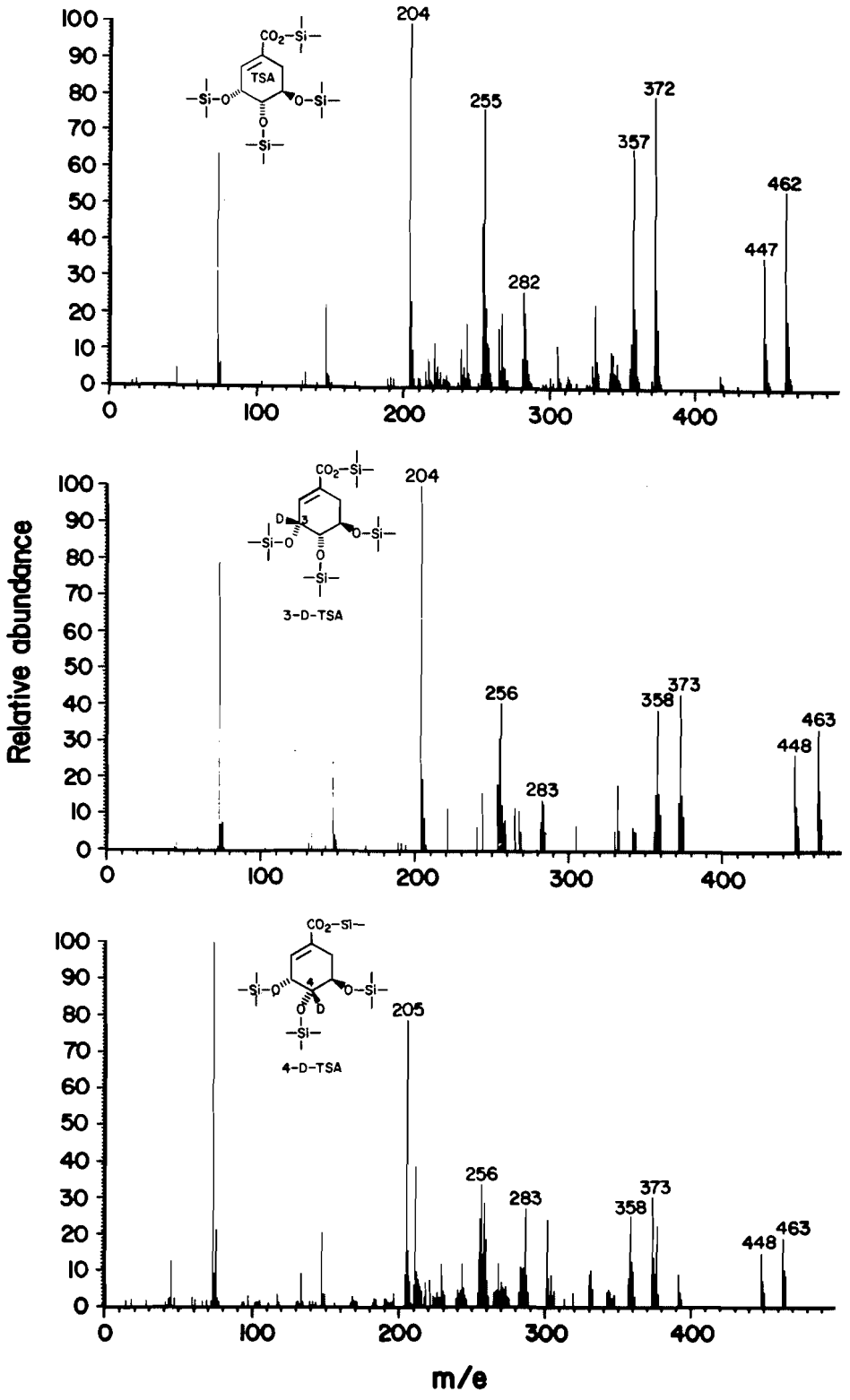

FIG. 3. Analysis by mass spectrometry of shikimic acids specifically labeled at positions C-3 and C-4. The trimethylsilyl derivatives were analysed. The upper mass spectrum shows unlabeled trimethyl silylated shikimic acid. The middle mass spectrum represents trimethyl silylated shikimic acid labeled at C-3. The bottom mass spectrum was obtained from trimethyl silylated shikimic acid labeled at C-4. (Abbreviation: TSA = trimethyl silylated derivative of shikimic acid.)

(^{1}H nmr) spectra were recorded on Varian T-60, T-60A, and XL-200 spectrophotometers. Ultraviolet (uv) spectra were taken on a Perkin–Elmer 559A instrument. Chemical shifts for 60 MHz spectra were measured using either tetramethylsilane as an internal standard or, in the case of compounds containing a TBDMS group, the methyl groups of the latter were set as the standard. Analytical thin-layer chromatography (tlc) was carried out using Merck Silica Gel 60 F_{254} aluminium backed plates. All column chromatography was performed using the "flash chromatography" technique described by Still *et al.* (17) using 32–63 μm (400–230 mesh) silica gel.

Can. J. Chem. Downloaded from www.nrcresearchpress.com by 210.87.254.6 on 09/06/12
For personal use only.

Methyl shikimate 2

To a methanolic solution (90 mL) of shikimic acid **1** (2.00 g, 11.48 mmol) was added ethereal diazomethane until the solution remained yellow. The reaction mixture was maintained at room temperature for 15 min and then the solvents were removed at reduced pressure to afford the desired methyl shikimate **2** (2.32 g) in quantitative yield (99%); mp 115–116°C (lit. (18) mp 113–114°C); ms *m/e* (of trimethylsilylated sample): 389 ($M^+ - CH_3$), 373 ($M^+ - OMe$), 314 ($M^+ - Me_3SiOH$), 299 ($M^+ - Me_3SiOH - CH_3$), 204 ($Me_3SiOCH{=}CHOSiMe_3^+$, 100%).

Orthoformates 3 and 4

To a suspension of methyl shikimate **2** (1.14 g, 6.06 mmol) in methylene chloride (20 mL) under a nitrogen atmosphere was added first trimethyl orthoformate (1.5 mL, 15 mmol), then *p*-toluenesulfonic acid (81 mg, 0.42 mmol). After all the starting material was dissolved (1 h), the reaction mixture was cooled at 5°C and excess solid Na_2CO_3 was added. The product was then extracted with ethyl acetate (2 × 400 mL, prewashed with Na_2CO_3); the ethyl acetate extracts were washed with aqueous Na_2CO_3 (5 × 50 mL), water (3 × 50 mL), and dried over $MgSO_4$. Removal of the solvents under reduced pressure gave orthoformate **3** (1.4 g) in quantitative yield (99%). To its solution in dry dimethylformamide (8 mL) under a nitrogen atmosphere, at 5°C, were added *tert*-butyldimethylsilyl chloride (1.01 g, 6.70 mmol) and imidazole (912 mg, 13.4 mmol); the reaction mixture was stirred at room temperature for 1 h. It was then extracted with ether (2 × 300 mL); the ether extracts were washed with aqueous $NaHCO_3$ (2 × 80 mL), H_2O (4 × 50 mL), and dried over $MgSO_4$. Evaporation of the solvents gave orthoformate **4** (2 g) as an oil in 95% yield; ^1H nmr ($CDCl_3$) δ: 0.00 (s, 3H, $SiCH_3$), 0.03 (s, 3H, $SiCH_3$), 0.82 (s, 9H, $SiCMe_3$), 2.1–2.5 (m, 2H, C(6)H), 3.17 (s, 0.6H, OCH_3), 3.27 (s, 2.4H, OCH_3), 3.67 (s, 3H, CO_2CH_3), 3.7–4.3 (m, 2H, C(4)H, C(5)H), 4.6–4.9 (m, 1H, C(3)H, 5.60 (s, 0.8H, $HC(OR)_3$), 5.63 (s, 0.2H, $HC(OR)_3$), 6.6–6.8 (m, 1H, C(2)H).

Diol 12

A solution ($MeOH/H_2O/HCl$ = 100 : 1 : 0.1 (10 mL)) of orthoester **4** (2.0 g, 5.8 mmol) was stirred at room temperature for approximately 20 min (no starting material by tlc); aqueous $NaHCO_3$ (1 mL) and excess solid $NaHCO_3$ were then added to effect a complete hydrolysis of the intermediate formates. The reaction mixture was then extracted with ethyl acetate (2 × 350 mL); the ethyl acetate extracts were washed with water (3 × 100 mL, 3 × 50 mL) until the washings remained neutral, dried over $MgSO_4$, and evaporated to give diol **12** as an oil in 65% yield; ^1H nmr ($CDCl_3$) δ: 0.00 (s, 6H, $SiMe_2$), 0.78 (s, 9H, $SiCMe_3$), 2.1–2.6 (m, 2H, C(6)H), 3.2–4.5 (m, 5H, C(3)H, C(4)H, C(5)H, 2OH), 3.63 (s, 3H, CO_2CH_3), 6.5–6.8 (m, 1H, C(2)H).

Ketones 10 and 11

To diol **12** (1.09 g, 3.61 mmol) in dry dimethylformamide (10 mL) at 15°C under a nitrogen atmosphere was added pyridinium dichromate (1.76 g, 4.68 mmol). After 5 min the cold bath was removed and the reaction mixture was stirred at room temperature for 0.5 h. The product was then extracted with ethyl acetate (2 × 400 mL); the ethyl acetate extracts were washed with water (2 × 100 mL, 3 × 50 mL) till the washings remained neutral, dried over $MgSO_4$, and evaporated to give ketone **10** as an oil in 65% yield (low yield due to water solubility of ketone); ir (film) ν_{max}: 1685 (C=C—C=O), 1720 (CO_2Me), 3500 (OH) cm^{-1}; ^1H nmr ($CDCl_3$) δ: 0.00 (s, 6H, $SiMe_2$), 0.78 (s, 9H, $SiCMe_3$), 2.4–3.0 (m, 2H, C(6)H, 3.2–4.3 (m, 3H C(4)H, C(5)H, OH), 3.72 (s, 3H, CO_2CH_3), 6.5–6.8 (m, 1H, C(2)H). Ketone **10** was acetylated in the usual manner (acetic anhydride, *N,N*-dimethylaminopyridine in anhydrous ether) to yield quantitatively ketone **11** as an oil; ir (film) ν_{max}: 1700 (C=C—C=O), 1725 (CO_2CH_3), 1750 ($OCOCH_3$) cm^{-1}; uv λ_{max} (EtOH): 233 nm (ε = 69 000); ^1H nmr ($CDCl_3$, 200 MHz) δ: 0.057 (s, 3H, $SiCH_3$), 0.085 (s, 3H, $SiCH_3$), 0.862 (s, 9H, $SiCMe_3$), 2.175 (s, 3H, $COCH_3$), 2.544–3.133 (ABq, 2H, J_{6ax} = 2.622, ddd, $J_{6ax,6eq}$ = 18.6 Hz, $J_{5,6ax}$ = 9.5 Hz, $J_{2,6ax}$ = 3.1 Hz, J_{6eq} = 3.073, dd, $J_{6ax,6eq}$ = 18.6 Hz, $J_{5,6eq}$ = 5.5 Hz, C(6)H), 3.833 (s, 3H, CO_2CH_3), 4.085–4.215 (ddd, 1H, $J_{5,6eq}$ = 5.5 Hz, $J_{5,6ax}$ = 9.6 Hz, $J_{4,5}$ = 11.0 Hz, C(5)H), 5.303 (d, 1H, $J_{4,5}$ = 11 Hz, C(4)H), 6.797 (d, 1H, $J_{2,6ax}$ = 3.1 Hz, C(2)H); ms *m/e*: 285 ($M^+ - CMe_3$), 243 ($M^+ - CMe_3$ —CH_2=C=O), 225 ($M^+ - CMe_3$ —AcOH).

Alcohols 15 and 16

To ketone **11** (684 mg, 2 mmol) in ethanol (10 mL) at 5°C was added sodium borohydride (76 mg, 2 mmol) all at once; the reduction reaction was complete instantaneously. The product was extracted with ether (2 × 600 mL); the ether extracts were washed with pH 4 buffer (4 × 100 mL), water (4 × 100 mL), dried over $MgSO_4$, and evaporated under reduced pressure to give epimeric alcohols **7** and **15** (α/β = 1:9) in 65% yield after flash chromatography (petroleum ether – ethyl acetate = 7:1). The mixture of alcohols **7** and **15** was acetylated in the usual manner to give their corresponding oily acetates **13** and **16**, for spectral identification.

For the introduction of tritium at the 3-position, the above experimental procedure was identical in all respects except that: (1) the reaction was performed on 1 mmol of ketone; (2) 100 mCi of tritiated $NaBH_4$ (5–20 Ci/mmol) (Amersham Searle Corp.) (in 3 mL ethanol) was added to ketone **11** (in 3 mL EtOH); after 10 min, cold sodium borohyride (1 molar equiv.) was added.

Alcohol 15: ^1H nmr ($CDCl_3$) δ: 0.00 (s, 6H, $SiMe_2$), 0.82 (s, 9H, $SiCMe_3$), 2.02 (s, 3H, $COCH_3$), 2.2–2.6 (m, 2H, C(6)H), 3.2–3.5 (m, 1H, OH), 3.69 (s, 3H, CO_2CH_3), 3.8–4.3 (m, 2H, C(3)H, C(5)H), 4.7–5.0 (m, 1H, C(4)H, 6.6–6.8 (m, 1H, C(2)H).

Acetate 16: ^1H nmr (200 MHz, $CDCl_3$) δ: 0.038 (s, 3H, $SiCH_3$), 0.066 (s, 3H, $SiCH_3$), 0.843 (s, 9H, $SiCMe_3$), 2.039 (s, 6H, $2COCH_3$), 2.269–2.827 (bABq, 2H, C(6)H), 3.741 (s, 3H, CO_2CH_3), 3.850–3.973 (ddd, 1H, $J_{5,6eq}$ = 5.8 Hz, $J_{4,5}$ = $J_{5,6ax}$ = 9.5 Hz, C(5)H), 5.070–5.158 (dd, 1H, $J_{3,4}$ = 7.8 Hz, $J_{4,5}$ = 9.8 Hz, C(4)H), 5.490–5.567 (m, 1H, C(3)H), 6.570–6.595 (dd, 1H, $J_{2,3}$ = $J_{2,6}$ = 2.4 Hz).

Mesylates 14 and 17

To a mixture of epimeric alcohols **7** and **15** (433 mg, 1.27 mmol) in dry methylene chloride (10 mL) at 5°C under a nitrogen atmosphere was added first triethylamine (1.05 mL, 7.53 mmol), then methanesulfonyl chloride (0.30 mL, 3.88 mmol); the reaction was over immediately and the product extracted with ether (2 × 175 mL). The ether extracts were washed with cold dilute aqueous HCl (2 × 25 mL), cold aqueous $NaHCO_3$ (3 × 25 mL), H_2O (4 × 25 mL), and dried over $MgSO_4$. Evaporation of the solvents under reduced pressure gave oily allylic mesylates **14** and **17** (531 mg) in quantitative yield (99%). The latter were submitted immediately to the inversion reaction.

Diacetate 13 from mesylate 17

A solution of crude allylic mesylates **17** and **14** (536 mg, 1.27 mmol) and potassium acetate (161 mg, 1.64 mmol), in dry methanol (8 mL) under a nitrogen atmosphere, was stirred at 70°C for 1.5 h. The reaction mixture was cooled to room temperature and excess solid Na_2CO_3 added; the product was then extracted with ether (2 × 175 mL, prewashed with Na_2CO_3); the ether extracts were washed with aqueous Na_2CO_3 (1 × 120 mL, 4 × 60 mL), water (4 × 30 mL), and dried over $MgSO_4$. Evaporation of the solvents followed by flash chromatography (petroleum ether/ethyl acetate/triethylamine = 120:8:0.2) gave orthoester **6** (contaminated with small amounts of hydrolysis products **7** and **8**, which were produced during chromatography) in 30% yield (based on ketone **11**). Its ^1H nmr spectrum was identical to that of authentic orthoester **6**. Hydrolysis, followed by acetylation, as for orthoester **6**, gave diacetate **13** as an oil, which had a 200 MHz ^1H nmr spectrum identical to that of authentic diacetate **13**.

Shikimic acid from silylated diacetate 13

To diacetate **13** (200 mg, 0.52 mmol) in dry tetrahydrofuran (5 mL) at 5°C under a nitrogen atmosphere was added tetra-*n*-butylammonium fluoride (0.7 mmol). After 0.5 h, water (50 mL) was added and the reaction mixture was extracted with ethyl acetate (2 × 600 mL); the ethyl acetate extracts were washed with water (6 × 60 mL), dried over $MgSO_4$, and evaporated to give the desired desilylated alcohol (some

Can. J. Chem. Downloaded from www.nrcresearchpress.com by 210.87.254.6 on 09/06/12
For personal use only.

acetate migration seemed to have occurred since the product was indicated as two spots of similar R_f on tlc) in 80% yield after flash chromatography (petroleum ether − ethyl acetate = 8:7).

To the desilylated product obtained (117 mg, 0.43 mmol) in MeOH (3 mL) at 5°C was added $NaOH/H_2O$ (86 mg/0.9 mL); after 0.5 h, the reaction mixture was brought to room temperature and stirred for 2 h; it was then neutralized at 15°C with acidic resin (AM − 120 H^+); evaporation of the solvents gave shikimic acid **1** in 90% yield with a mass spectrum identical to that of an authentic sample; ms *m/e* (of trimethylsilylated sample): 462 (M^+), 447 ($M^+ - CH_3$), 372 ($M^+ - Me_3SiOH$), 357 ($M^+ - Me_3SiOH - CH_3$), 282 ($M^+ - 2\ Me_3SiOH$), 204 ($Me_3SiOCH{=}CHOSiMe_3^+$, 100%).

Orthoacetate 5

To a suspension of methyl shikimate **2** (2.24 g, 11.92 mmol) in methylene chloride (90 mL), under a nitrogen atmosphere at room temperature, was added first trimethyl orthoacetate (3.50 mL, 27.85 mmol), then *p*-toluenesulfonic acid (113 mg). After all the starting material was dissolved (1 h), the reaction mixture was cooled (5°C) and excess solid Na_2CO_3 was added. The product was then extracted with ethyl acetate (2 × 600 mL, prewashed with Na_2CO_3); the ethyl acetate extracts were washed with aqueous Na_2CO_3 (5 × 50 mL), water (3 × 50 mL), and dried over $MgSO_4$. Removal of the solvents under reduced pressure gave orthoacetate **5** as an oil in 90% yield; ir (film) ν_{max}: 1715 (CO_2CH_3), 3470 (OH) cm^{-1}; ^1H nmr (CCl_4) δ: 1.35 (s, 3H, CH_3), 2.1−2.6 (m, 2H, C(6)H), 3.02 (s, 0.75H, OCH_3), 3.15 (s, 2.25H, OCH_3), 3.2−4.3 (m, 3H, C(4)H, C(5)H, OH), 3.65 (s, 3H, CO_2CH_3), 4.5−4.9 (m, 1H, C(3)H), 6.6−6.8 (m, 1H, C(2)H).

Orthoacetate 6

To a solution of alcohol **5** (2.8 g, 11.5 mmol) in dry dimethylformamide (10 mL) under a nitrogen atmosphere were added *tert*-butyldimethylsilyl chloride (2.1 g, 13.8 mmol) and imidazole (3.9 g, 57.3 mmol). After 1 h at 45°C, the reaction mixture was extracted with ether (2 × 500 mL); the ether extracts were washed with water (3 × 100 mL, 4 × 60 mL), dried over $MgSO_4$, and evaporated to yield silylated orthoester **6** as an oil in quantitative yield; ^1H nmr (CCl_4) δ: 0.0 (s, 6H, $SiMe_2$), 0.78 (s, 9H, $SiCMe_3$), 1.34 (s, 3H, CH_3), 2.1−2.5 (m, 2H, C(6)H), 3.00 (s, 0.75H, OCH_3), 3.13 (s, 2.25H, OCH_3), 3.65 (s, 3H, CO_2CH_3), 3.7−4.3 (m, 2H, C(4)H, C(5)H), 4.4−4.9 (m, 1H, C(3)H), 6.6×6.9 (m, 1H, C(2)H).

Alcohols 7 and 8

A solution ($MeOH/H_2O/AcOH$ = 90 mL:30 mL:3.0 mL) of orthoester **6** (3.93 g, 11.0 mmol) was stirred at room temperature for 1 h; after this time, 600 mL of toluene were added and the solvents were removed under reduced pressure. This procedure was repeated a total of three times to give a mixture of alcohols **7** and **8**. These were used without prior separation in the subsequent oxidation step. A sample of 3-alcohol **7** was obtained as an oil by flash chromatography (petroleum ether − ethyl acetate = 4:1) for spectral identification; ir (film) ν_{max}: 1720 (CO_2CH_3), 1745 ($OCOCH_3$), 3470 (OH) cm^{-1}; ^1H nmr ($CDCl_3$, 200 MHz) δ: 0.057 (s, 3H, $SiCH_3$), 0.075 (s, 3H, $SiCH_3$), 0.837 (s, 9H, $SiCMe_3$), 2.01−2.07 (bs, 1H, OH), 2.072 (s, 3H, $COCH_3$), 2.218−2.609 (bABq, 2H, C(6)H), 3.747 (s, 3H, CO_2CH_3), 4.176−4.252 (ddd, 1H, $J_{5,4}$ = 6.5 Hz, $J_{5,6ax} = J_{5,6eq}$ = 4.5 Hz, C(5)H), 4.574−4.642 (bs, 1H, C(3)H), 4.929−4.982 (dd, 1H, $J_{4,5}$ = 6.5 Hz, $J_{3,4}$ = 4.2 Hz, C(4)H), 6.781−6.805 (m, 1H, C(2)H); ms *m/e*: 329 ($M^+ - CH_3$), 313 ($M^+ - OCH_3$), 287 ($M^+ - CMe_3$), 284 (M^+ − AcOH), 269 (M^+ − AcOH − CH_3), 227 ($M^+ - CMe_3$ − AcOH), 195 ($M^+ - H_2O - Me_3CSiMe_2O$).

Diacetate 13

To a mixture of alcohols **7** and **8** (172 mg, 0.50 mmol) in anhydrous ether (10 mL) were added *N,N*-dimethylaminopyridine (12 mg, 0.10 mmol), then acetic anhydride (0.14 mL, 1.5 mmol). After 1 h, the reaction mixture was extracted with ether (2 × 175 mL); the ether extracts were washed with H_2O (5 × 20 mL), dried over $MgSO_4$, and evaporated to give oily diacetate **13** in quantitative yield; ir (film)ν_{max}: 1720 (CO_2Me), 1750 (OAc) cm^{-1}; ^1H nmr (200 MHz, $CDCl_3$) δ: 0.066 (s, 3H, $SiCH_3$), 0.085 (s, 3H, $SiCH_3$), 0.853 (s, 9H, $SiCMe_3$), 2.018 (s, 3H, $COCH_3$), 2.047 (s, 3H, $COCH_3$), 2.210−2.716 (bABq, 2H, C(6)H), 3.751 s, 3H, CO_2CH_3), 4.101−4.182 (ddd, 1H, $J_{5,6ax}$ = $J_{5,6eq}$ = 4.6 Hz, $J_{4,5}$ = 7.0 Hz, C(5)H), 5.057−5.112 (dd, 1H, $J_{3,4}$ = 3.9 Hz, $J_{4,5}$ = 7.0 Hz, C(4)H), 5.723−5.776 (m, 1H, C(3)H), 6.681−6.713 (m, 1H, C(2)H); ms *m/e*: 329 ($M^+ - CMe_3$), 269 ($M^+ - CMe_3$ − AcOH), 227 ($M^+ - CMe_3$ − AcOH − $CH_2{=}C{=}O$), 195 (M^+ − AcOH − Me_3CSiMe_2O).

Ketone 11 and alcohol 8

To a mixture of alcohols **7** and **8** (3.58 g, 10.4 mmol) in dry dimethylformamide (10 mL) under a nitrogen atmosphere was added pyridinium dichromate (4.0 g, 10.6 mmol). The reaction mixture was stirred at 45°C for 1 h; following the addition of 110 mL water, the product was extracted with ether (2 × 600 mL); the ether extracts were washed with H_2O (3 × 100 mL, 4 × 70 mL), dried over $MgSO_4$, and the solvent removed under reduced pressure to yield a mixture of 3-ketone **11** and 4-alcohol **8**. These were separated by flash chromatography (petroleum ether − ethyl acetate = 7:1), to give 1.5 g of **11** and 1.45 g of **8** as oils, slightly contaminated with some unoxidized 3-alcohol **7** (traces of **7** on tlc plates).

3-Ketone 11: had the same spectral properties described earlier (identical ir, uv, and ^1H nmr spectra).

4-Alcohol 8: ir (film)ν_{max}: 1720 (CO_2CH_3), 1735 ($OCOCH_3$), 3500 (OH) cm^{-1}; ^1H nmr ($CDCl_3$) δ: 0.00 (s, 6H, $SiMe_2$), 0.80 (s, 9H, $SiCMe_3$), 2.00 (s, 3H, $COCH_3$)0, 2.2−2.6 (m, 3H, C(6)H, OH), 3.61 (s, 3H, CO_2CH_3), 3.6−4.2 (m, 2H, C(4)H, C(5)H), 5.4−5.6 (m, 1H, C(3)H), 6.4−6.7 (m, 1H, C(2)H); ms *m/e*: 287 ($M^+ - CMe_3$), 269 (M^+ − AcOH − CH_3), 227 ($M^+ - CMe_3$ − AcOH), 195 ($M^+ - H_2O$ − Me_3CSiMe_2O).

Oxidation and reduction of alcohol 8

To alcohol **8** (447 mg, 1.3 mmol) in acetone (10 mL) at room temperature was added Jones reagent (11) (0.35 mL); additional Jones reagent was then added after the following total time intervals: 1 h/0.2 mL; 2.5 h/0.1 mL. After 5 h, the reaction mixture was extracted with ether (2 × 600 mL); the ether extracts were washed with H_2O (5 × 100 mL, 4 × 70 mL), dried over $MgSO_4$, and evaporated to give a mixture of 3-ketone **11** and 4-ketone **9**, as well as a small amount of 3-ketone **18**. This mixture was immediately submitted to borohydride reduction.

To the mixture of ketones obtained above (290 mg, 0.85 mmol) in EtOH (7 mL) at 5°C was added sodium borohydride (32 mg, 0.85 mmol); the reduction reaction proceeded instantaneously and after 10 min the reaction mixture was poured into cold dilute aqueous HCl (80 mL). The product was immediately extracted with ether (2 × 600 mL); the ether extracts were washed with cold dilute aqueous HCl (1 × 100 mL), water (5 × 60 mL), dried over $MgSO_4$, and evaporated under reduced pressure to give a mixture of alcohols **8**, **15**, and **19**. In order to facilitate the separation of these alcohols, the allylic ones were oxidized to their respective ketones using pyridinium dichromate.

A complete oxidation of the allylic alcohols necessitated two successive oxidations with pyridinium dichromate. To a mixture of alcohols **8**, **15**, and **19** (250 mg, 0.73 mmol) in dry dimethylformamide (4 mL) under a nitrogen atmosphere was added pyridinium dichromate (250 mg, 0.67 mmol). The reaction mixture was stirred at 45°C for 1 h; it was then extracted with ether (2 × 500 mL); the ether extracts were washed with H_2O (8 × 50 mL), dried over $MgSO_4$, and evaporated. The crude residue was then oxidized once again, by the same procedure, to give a complete oxidation of the allylic alcohols **15** and **19** to the corresponding 3-ketones **11** and **18**. These were separated from **8** by flash chromatography (petroleum ether − ethyl acetate 4:1). The alcohol **8** isolated was obtained in 12% overall yield.

In order to prepare the derivative with deuterium at the 4-position sodium borodeuteride was used. For the introduction of tritium at the 4-position, the above experimental procedure was identical in all respects except that: (1) total reaction time for the Jones oxidation was kept to 3.5 h; (2) 200 mCi of the tritiated sodium borohydride (5−20 mCi/mmol) (Amersham Searle Corp.) (in 4 mL EtOH) was added to the mixture of ketones (in 4 mL EtOH) over a 10-min period; after 15 min (total reaction time from the beginning of addition), the tritiated

$NaBH_4$ (1 molar equiv.) was added.

Attempts to purify 4-ketone **9** by flash chromatography resulted in its almost complete conversion to 3-ketone **18**. It was reduced with sodium borohydride in the usual manner to liquid alcohol **19**, which was characterized as its oily diacetate **20**.

3-Ketone 18: ir (film) ν_{max}: 1710 (C=C—C=O), 1725 (CO_2Me), 1750 ($OCOCH_3$) cm^{-1}; uv λ_{max} (EtOH): 233 nm (ϵ = 57 000); ^1H nmr (200 MHz, $CDCl_3$) δ: 0.018 (s, 3H, $SiCH_3$), 0.039 (s, 3H, $SiCH_3$), 0.790 (s, 9H, $SiCMe_3$), 2.185 (s, 3H, $COCH_3$), 2.741–2.983 (ABq, $H_{6'}$ = 2.926, ddd, 1H, $J_{2,6'}$ = 0.8 Hz, $J_{5,6'}$ = 2.9 Hz, $J_{6'6''}$ = 19.1 Hz, $H_{6''}$ = 2.803, ddd, 1H, $J_{5,6''}$ = $J_{2,6''}$ = 2.8 Hz, $J_{6',6''}$ = 19.1 Hz, C(6)H), 3.825 (s, 3H, CO_2CH_3), 4.458–4.500 (ddd, 1H, $J_{4,5}$ = 2.4 Hz, $J_{5,6'}$ = $J_{5,6''}$ = 3.0 Hz, C(5)H), 5.375 (d, 1H, $J_{4,5}$ = 2.3 Hz, C(4)H), 6.792–6.809 (dd, 1H, $J_{2,6'}$ = 0.8 Hz, $J_{2,6''}$ = 2.6 Hz, C(2)H); ms *m/e*: 285 (M^+ – CMe_3), 243 (M^+ – CMe_3 – CH_2=C=O), 225 (M^+ – CMe_3 – AcOH).

Alcohol 19: ir (film) ν_{max}: 1725 (CO_2Me), 1735 ($OCOCH_3$), 3450 (OH) cm^{-1}; ^1H nmr ($CDCl_3$) δ: 0.00 (s, 6H, $SiMe_2$), 0.76 (s, 9H, $SiCMe_3$), 2.01 (s, 3H, $COCH_3$), 2.3–2.6 (m, 2H, C(6)H), 3.63 (s, 3H, CO_2CH_3), 4.0–4.3 (m, 2H, C(4)H, C(5)H), 4.7–4.8 (m, 1H, C(3)H), 6.7–6.9 (m, 1H, C(2)H; ms *m/e*: 287 (M^+ – CMe_3), 269 (M^+ – CMe_3 – H_2O), 245 (M^+ – CMe_3 – CH_2=C=O), 227 (M^+ – CMe_3 – AcOH), 195 (M^+ – H_2O – Me_3CSiMe_2O).

Diacetate 20: ir (film) ν_{max}: 1720 (CO_2Me), 1745 (OAc) cm^{-1}; ^1H nmr (200 MHz, $CDCl_3$) δ: 0.042 (s, 3H, $SiCH_3$), 0.052 (s, 3H, $SiCH_3$), 0.833 (s, 9H, $SiCMe_3$), 2.025 (s, 3H, $COCH_3$), 2.049 (s, 3H, $COCH_3$), 2.447–2.571 (bABq, 2H, C(6)H), 3.750 (s, 3H, CO_2CH_3), 3.935–4.022 (ddd, 1H, $J_{4,5}$ = 1.8 Hz, $J_{5,6ax}$ = 9.4 Hz, $J_{5,6eq}$ = 6.2 Hz, C(5)H), 5.370–5.397 (dd, 1H, $J_{4,5}$ = 1.6 Hz, $J_{3,4}$ = 3.6 Hz, C(4)H), 5.573–5.611 (m, 1H, C(3)H), 6.563–6.593 (m, 1H, C(2)H); ms *m/e*: 329 (M^+ – CMe_3), 269 (M^+ – CMe_3 – AcOH), 227 (M^+ – CMe_3 – AcOH – CH_2=C=O), 195 (M^+ – AcOH – Me_3CSiMe_2O).

^1H nuclear magnetic resonance and mass spectrometric data of 3- and 4-deuterated shikimic acid derivatives

C-4-Deuterated diacetate 13: ^1H nmr (200 MHz, $CDCl_3$) δ: 0.057 (s, 3H, $SiCH_3$), 0.075 (s, 3H, $SiCH_3$), 0.844 (s, 9H, $SiCMe_3$), 2.007 (s, 3H, $COCH_3$), 2.036 (s, 3H, $COCH_3$), 2.248–2.715 (bABq, 2H, C(6)H), 3.740 (s, 3H, CO_2CH_3), 4.094–4.176 (ddd, 1H, $J_{4,5}$ = 7.0 Hz, $J_{5,6ax}$ = $J_{5,6eq}$ = 4.7 Hz, C(5)H), 5.048–5.084 (d, 1H, $J_{4,5}$ = 7.1 Hz, C(4)H), 6.681–6.690 (bs, 1H, C(2)H); ms *m/e*: 330 (M^+ – CMe_3), 270 (M^+ – CMe_3 – AcOH), 228 (M^+ – CMe_3 – AcOH – CH_2=C=O).

C-3-Deuterated shikimic acid: ms *m/e* (of trimethylsilylated sample): 463 (M^+), 448 (M^+ – CH_3), 373 (M^+ – Me_3SiOH), 358 (M^+ – Me_3SiOH – CH_3), 283 (M^+ – 2 Me_3SiOH), 204 (Me_3SiOCH=$CHOSiMe_3^+$, 100%).

C-4-Deuterated alcohol 8: ^1H nmr (200 MHz, $CDCl_3$) δ: 0.100 (s, 3H, $SiCH_3$), 0.110 (s, 3H, $SiCH_3$), 0.888 (s, 9H, $SiCMe_3$), 2.129 (s, 3H, $COCH_3$), 2.155–2.803 (bABq, 2H, C(6)H), 2.243 (bs, 1H, OH), 3.758 (s, 3H, CO_2CH_3), 4.078–4.128 (dd, 1H, $J_{5,6}$ = 5.0 Hz, C(5)H), 5.649–5.666 (bs, 1H, C(3)H), 6.718–6.753 (m, 1H, C(2)H); ms *m/e*: 288 (M^+ – CMe_3), 270 (M^+ – AcOH – CH_3), 288 (M^+ – CMe_3 – AcOH).

C-4-deuterated shikimic acid: ms *m/e* (of trimethylsilylated sample): 463 (M^+), 448 (M^+ – CH_3), 373 (M^+ – Me_3SiOH), 358 (M^+ – Me_3SiOH – CH_3), 283 (M^+ – 2 Me_3SiOH), 205 (Me_3SiOCH=$CDOSiMe_3^+$).

C-4-Deuterated diacetate 13: ^1H nmr (200 MHz, $CDCl_3$) δ: 0.062 (s, 3H, $SiCH_3$), 0.082 (s, 3H, $SiCH_3$), 0.850 (s, 9H, $SiCMe_3$), 2.015 (s, 3H, $COCH_3$), 2.044 (s, 3H, $COCH_3$), 2.252–2.723 (bABq, 2H, C(6)H), 3.748 (s, 3H, CO_2CH_3), 4.113–4.159 (dd, 1H, $J_{5,6}$ = 4.6 Hz, C(5)H), 5.735–5.751 (bs, 1H, C(3)H), 6.676–6.712 (m, 1H, C(2)H); ms *m/e*: 330 (M^+ – CMe_3), 270 (M^+ – CMe_3 – AcOH), 228 (M^+ – CMe_3 – AcOH – CH_2=C=O).

Acknowledgements

We thank Dr. George Just for valuable discussions throughout the proceedings of this work; Dr. Orval Mamer and Ms. Jane Montgomery, The Biomedical Mass Spectrometry Unit, McGill University, for the mass spectra; Dr. Françoise Sauriol, McGill University, for the 200 MHz ^1H nmr spectra; and Dr. Cong-Danh Nguyen, in our laboratory, for improving the isotopic purity of 4-^2H-shikimic acid. Financial support from N.I.H. (to Lolita Zamir) and a post-doctoral fellowship from Université du Québec, Institut Armand-Frappier (to Corinne Luthe) are gratefully acknowledged.

1. L. O. ZAMIR and C. LUTHE. Tetrahedron Lett. 4409 (1983).
2. S. L. STENMARK, D. L. PIERSON, G. I. GLOVER, and R. A. JENSEN. Nature (London) **247**, 290 (1974).
3. L. O. ZAMIR, R. A. JENSEN, B. H. ARISON, A. W. DOUGLAS, and J. R. BOWEN. J. Am. Chem. Soc. **102**, 4499 (1980).
4. L. O. ZAMIR, E. D. JUNG, and R. D. TIBERIO. Bioorg. Chem. **11**, 32 (1982).
5. G. S. BYNG, J. F. KANE, and R. A. JENSEN. Crit. Rev. Microbiol. **9**, 227 (1983).
6. L. O. ZAMIR, R. TIBERIO, E. JUNG, and R. A. JENSEN. J. Biol. Chem. **258**, 6848 (1983).
7. L. O. ZAMIR, E. JUNG, and R. A. JENSEN. J. BIOL. CHEM. **258**, 6492 (1983).
8. D. K. ONDERKA and H. G. FLOSS. J. Am. Chem. Soc. **91**, 5894 (1969)
9. B. W. SMITH, M. I. TURNER, and E. HASLAM. Chem. Commun. 842 (1970).
10. R. I. CHRISTOPHERSON and J. F. MORRISON. Arch. Biochem. Biophys. **220**, 444 (1983).
11. L. F. FIESER and M. FIESER. Reagents for organic synthesis. Vol. 1. John Wiley & Sons, New York. 1968. pp. 142–192.
12. H. O. L. FISHER and G. DANGSCHAT. Helv. Chim. Acta, **17**, 1200 (1934).
13. E. J. COREY, and A. VENKATESWARLU. J. Am. Chem. Soc. **94**, 6190 (1972).
14. E. J. COREY and G. SCHMIDT. Tetrahedron Lett. 399 (1979).
15. G. HÖFLE, W. STEGLICH, and H. VORBRÜGGEN. Angew. Chem. Int. Ed. Engl. **17**, 569 (1978).
16. G. JUST and C. LUTHE. Can. J. Chem. **58**, 2286 (1980).
17. W. C. STILL, M. KAHN, and A. MITRA. J. Org. Chem. **43**, 2923 (1978).
18. J. I. G. CADOGAN, R. A. RAPHAEL, and C. W. REES. *In* Heilbron's Dictionary of Organic Compounds. Vol. 5. 5th ed. Chapman and Hall, New York. 1982. p. 4998.

Can. J. Chem. Downloaded from www.nrcresearchpress.com by 210.87.254.6 on 09/06/12
For personal use only.

Syntheses of some pyrimidine N-oxides

MISA V. JOVANOVIC
Department of Chemistry, Southern Methodist University, Dallas, Texas 75275, U.S.A.

Received April 26, 1983[1]

MISA V. JOVANOVIC. Can. J. Chem. **62**, 1176 (1984).

Various monosubstituted pyrimidines and methylpyrimidines were N-oxidized with a number of different peracids. In general, they are more susceptible to side reactions accompanying N-oxidation (i.e., decomposition, annular carbon oxidation, ring opening) than other π-deficient diazine and triazine analogs. Unsymmetrical pyrimidines, which can potentially yield two isomeric products, were N-oxidized preferentially at the site *para* to strong electron-donating substituents. Weaker ring-activating groups, such as methyl, are mainly *ortho* directing and only aid in the N-oxidation of pyrimidine nuclei having *ortho*/*para*-directing substituents.

MISA V. JOVANOVIC. Can. J. Chem. **62**, 1176 (1984).

On a oxydé l'azote de diverses pyrimidines et méthylpyrimidines monosubstituées en faisant appel à un certain nombre de peracides. Par rapport aux analogues déficients en électrons comme les diazines et les triazines, les pyrimidines sont en général plus susceptibles de subir les réactions secondaires (comme la décomposition, l'oxydation des carbones du cycle et l'ouverture du cycle) qui accompagnent les réactions d'oxydation de l'azote. Les pyrimidines non symétriques, qui peuvent éventuellement conduire à deux produits isomères, s'oxydent préférentiellement en position *para* des substituants fortement électrodonneurs. La présence sur le cycle de groupes moins activants, comme le méthyle, provoque une oxydation préférentielle en position *ortho*; ces groupes n'aident à l'oxydation de l'azote des noyaux pyrimidines que s'ils portent des substituants orientant vers les positions *ortho* et *para*.

[Traduit par le journal]

Can. J. Chem. Downloaded from www.nrcresearchpress.com by 210.87.254.40 on 09/06/12
For personal use only.

As part of an extensive study of the halogenation of diazine N-oxides (1, 2), it became necessary to prepare a number of pyrimidine N-oxides. A literature search soon revealed a paucity of these compounds, with major emphasis being placed on the syntheses of polysubstituted pyrimidine N-oxides (3). Among the known monosubstituted compounds are the various monomethyl (4, 5), the 2-methoxy- and 4-methoxypyrimidine N-oxides (6, 7), and a number of 5-substituted derivatives recently prepared by Kobayashi *et al.* (8) and by us (9). The synthesis of pyrimidine 1,3-dioxide via a cyclization reaction has also recently been described (10).

It is well known that pyrimidines yield their corresponding N-oxides in poor yields (3). We have observed earlier that for the 1,2,4-triazine series, 6-aza analogs of pyrimidines, N-oxidation is generally readily accomplished at room temperature (11, 12). Thus, N-oxidation of some pyrimidines was attempted under similarly mild conditions.

Results and discussion

Since 2-methoxypyrimidine 1-oxide, **1**, has been described in the literature without the presentation of experimental details (6), we elected to examine its preparation first. When 2-methoxypyrimidine, **2**, was treated with peracetic acid in acetic acid solution, at room temperature, *three* isomeric products were isolated. The major component of this mixture was the expected N-oxide, **1**, obtained in 18% yield. 1-Methoxy-2-oxo-1,2-dihydropyrimidine, **3**, and 5-hydroxy-2-methoxypyrimidine, **4**, were also isolated. Structural proofs of these compounds rest on their elemental analyses, mass spectral fragmentation patterns, and ^{1}H nmr spectra (see Table 2 and Experimental). The formation of the methoxy derivative, **3**, follows a known pattern in the pyridine series (3) and probably results from an alkylation/dealkylation rearrangement of compound **1**. The isolation of the hydroxy derivative, **4**, is akin to the formation of 5-hydroxy-6-phenylpyrimidine 1-oxide from 4-phenylpyrimidine 1,3-dioxide, upon treatment with acetic anhydride (13).

The N-oxidation of a number of 2-substituted (**2**, **5**–**10**), 2-substituted-4-methyl- (**11**–**13**), 4-substituted (**14**–**20**), and 4-substituted-6-methyl- (**21**–**24**) pyrimidines, under the reaction conditions listed in Table 1, showed that peracetic acid generally gives the desired N-oxides in higher yields than *m*-chloroperbenzoic acid (MCPBA).

Among the 2-substituted pyrimidines (**5**–**10**), 2-aminopyrimidine, **7**, was readily N-oxidized under the reaction conditions given in Table 1. This reactivity decreases with the 2-monomethylamino derivative, **8**, and disappears altogether with 2-dimethylamino-, **9**, and 2-acetamido-, **10**, substituents. Similarly, the 2-chloro compound, **5**, is not reactive enough, while the moderately activating 2-methyl derivative, **6**, is, and yielded the desired 2-methylpyrimidine 1-oxide, **29**.

As expected, the presence of two electron-donating groups (**11**–**13**, **21**–**24**) increases the reactivity of the pyrimidine ring towards N-oxidation, and higher yields of N-oxides were obtained. For the 2-substituted-4-methylpyrimidines and for the 4-substituted-6-methylpyrimidines, the formation of two isomeric mono-N-oxides was possible. In the first instance, N-oxidation of 2-substituted-4-methylpyrimidines (**11**–**13**)

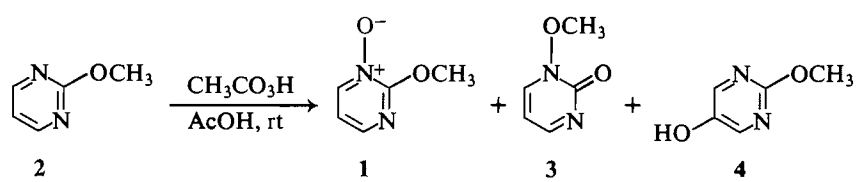

[1]Revision received October 27, 1983.

Can. J. Chem. Downloaded from www.nrcresearchpress.com by 210.87.254.40 on 09/06/12
For personal use only.

TABLE 1. N-Oxidation of pyrimidines

Substituent (No.)	Peroxyacid employed (time (h); temp. (°C))	N-oxide formed (% yield, compound no.)
2-Cl (**5**)	CF_3CO_3H (1–9; 60)	No reaction
	CH_3CO_3H (2–48; 60)	
2-CH_3 (**6**)	*m*CPBA (24; 25)	1-(5%, **29**)
	CH_3CO_3H (3–6; 60)	1-(30%, **29**)[a]
2-NH_2 (**7**)	*m*CPBA (4; 60)[b]	1-(40%, **30**)
2-$NHCH_3$ (**8**)	*m*CPBA (4; 60)	1-(5%, **31**)
	CH_3CO_3H (3–5; 60)	1-(30%, **31**)
2-$N(CH_3)_2$ (**9**)	*m*CPBA (5.5; 60)	No reaction
2-$NHCOCH_3$ (**10**)	*m*CPBA (4–48; 60)[b]	No reaction
2-OCH_3 (**2**)	CH_3CO_3H (7–14; 60)	1-(18%, **1**)
2-NH_2, 4-CH_3 (**11**)	*m*CPBA (4; 60)[b]	1-(7%, **32**)
		3-(46%, **33**)
2-$NHCH_3$, 4-CH_3 (**12**)	*m*CPBA (4–6; 60)	3-(38%, **34**)
		1-(0%)
2,4-Di-CH_3 (**13**)	CH_3CO_3H	1-(38%, **35**)
	Na_2WO_4 (48; 60)	3-(20%, **36**)[c]
4-NH_2 (**14**)	*m*CPBA (4; 60)[b]	1-(25%, **42**)
		3-(trace, **43**)
4-$NHCH_3$ (**15**)	*m*CPBA (4; 60)	1-(5%, **44**)
		3-(none)
	CH_3CO_3H (3; 60)	1-(11%, **44**)
		3-(none)
4-$N(CH_3)_2$ (**16**)	CH_3CO_3H (3; 60)	1-(10%, **45**)
4-$NHCOCH_3$ (**17**)	CH_3CO_3H (5.5, 60)[b]	No reaction
4-N-morpholino (**18**)	CH_3CO_3H (3–5, 60)	No reaction
4-CH_3 (**19**)	*m*CPBA (24; 25)	1-(21%, **46**)[c]
		3-(23%, **47**)
	CH_3CO_3H (?, 65)	1-(3 parts, **46**)[d]
		3-(1 part, **47**)
4-OCH_3 (**20**)	CH_3CO_3H (3–6; 60)	1-(29%, **48**)
4-NH_2, 6-CH_3 (**21**)	*m*CPBA (7; 60)[b]	1-(36%, **38**)[e]
		3-(0%)
4-$NHCH_3$, 6-CH_3 (**22**)	*m*CPBA (4; 60)	1-(33%, **39**)
		3-(0%)
4,6-Di-CH_3 (**23**)	*m*CPBA (24; 25)	1-(or 3 equivalent) (75%, **40**)[c]
4-OCH_3, 6-CH_3 (**24**)	CH_3CO_3H (6; 60)	1-(70%, **41**)[f]
		3-(0%)

[a]Data from ref. 4.
[b]*m*CPBA = *m*-chloroperbenzoic acid in CH_3CN.
[c]Data from ref. 15.
[d]No percentage yields are given in ref. 4.
[e]Isolated previously from KNH_2/NH_3 reaction with 4-chloro-6-methylpyrimidine 1-oxide.
[f]Made previously by nucleophilic substituion on 4-phenoxy-6-methylpyrimidine 1-oxide.

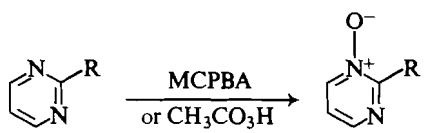

5 R = Cl	No reaction
6 R = CH_3	**29** R = CH_3
7 R = NH_2	**30** R = NH_2
8 R = $NHCH_3$	**31** R = $NHCH_3$
9 R = $N(CH_3)_2$	No reaction
10 R = $NHCOCH_3$	No reaction

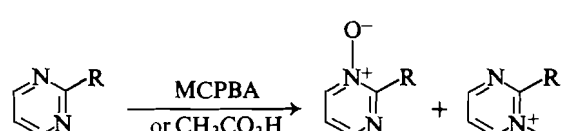

11 R = NH_2	**32** R = NH_2	**33** R = NH_2
12 R = $NHCH_3$	—	**34** R = $NHCH_3$
13 R = CH_3	**35** R = CH_3	**36** R = CH_3

furnished mainly the 3-oxides, the N-oxides *ortho* to both substituents. Thus, the apparently *more* sterically hindered nitrogen was oxidized, This behaviour is not a sterically controlled one, but reflects the *ortho*-activating effect of the methyl group reinforcing the *ortho*-activating effect of the 2-substituent.

However, 2-phenyl-4-methylpyrimidine, **25**, afforded the 1-oxide, **37**, only (14). In this case, it seems that the size of the R group was the limiting factor for the formation of the 3-oxide.

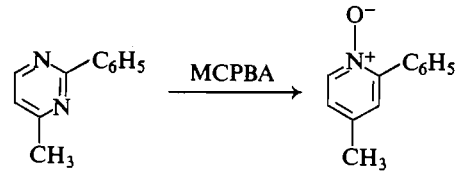

25 37

In the series of 4-methyl-6-substituted pyrimidines (**21**–**24**), the 1-oxides were formed exclusively. The nitrogen which is *ortho* to the methyl group and *para* to the substituent was oxidized. Thus, in those instances where the substituent R can have either an *ortho*- or a *para*-directing influence, the latter appears to be the controlling factor.

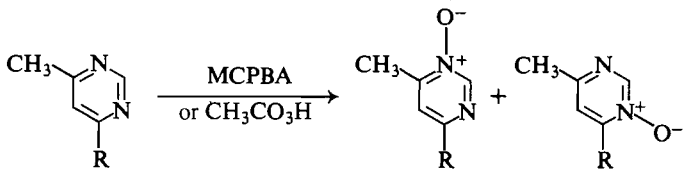

21 R = NH_2	**38** R = NH_2	—
22 R = $NHCH_3$	**39** R = $NHCH_3$	—
23 R = CH_3	**40** R = CH_3	**40**[2]
24 R = OCH_3	**41** R = OCH_3	—

The formation of two isomeric mono-N-oxides was also possible with 4-substituted pyrimidines (**14**–**20**). Among the groups examined, only when R = CH_3, **19**, are both isomers obtained in significant amounts. With 4-aminopyrimidine, **14**, the N-oxidation was also achieved *ortho* to the amino group and 4-aminopyrimidine 3-oxide, **43**, was detected and isolated in small quantity (see Table 1). However, neither 4-acetamidopyrimidine, **17**, nor the 4-morpholino derivative, **18**, were N-oxidized under these conditions. No reasonable rationale for this behavior can be offered at this time.

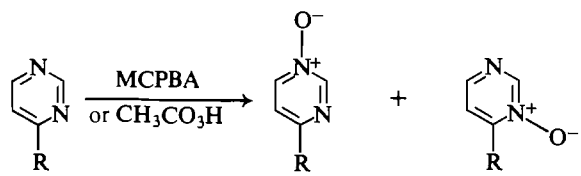

14 R = NH_2	**42** R = NH_2	**43** R = NH_2
15 R = $NHCH_3$	**44** R = $NHCH_3$	—
16 R = $N(CH_3)_2$	**45** R = $N(CH_3)_2$	—
17 R = $NHCOCH_3$	—	—
18 R = NC_4H_8O	—	—
19 R = CH_3	**46** R = CH_3	**47** R = CH_3
20 R = OCH_3	**48** R = OCH_3	—

We had observed that with 3-substituted-1,2,4-triazines, the 2-oxides were formed when the substituent was a tautomerizable amino group, while the 1-oxides were obtained with other substituents (12). This selectivity clearly does *not* carry over into the pyrimidine ring system, where only a trace of the analogous 3-oxide, **43**, was obtained when 4-aminopyrimidine, **14**, was oxidized.

Proton nuclear magnetic resonance effects

We have already described the proton chemical shift changes which occur in various 1,2,4-triazines upon oxidation of either N-1 or N-2 (12). In the few known pyrimidine N-oxides, N-1 oxidation caused shielding of H-2, H-4, and H-6 by 0.3, 0.3, and 0.5 ppm, respectively (12). The chemical shift of the proton *meta* to the N-oxide function (H-5) was not affected by N-oxidation. This information was used in a general sense to establish the sites of N-oxidation in this study, where ambiguous (see Table 2). A compilation of all of the now known pyrimidine N-oxides (in $CDCl_3$) affords the following data (δ (ppm) N-oxide − δ (ppm) non-oxide):

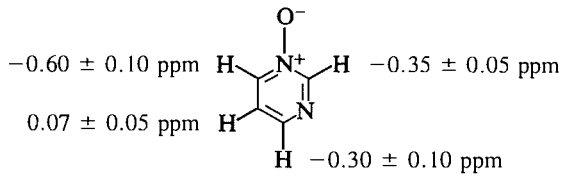

Thus, the major proton shielding effect upon N-oxidation of pyrimidines is at H-6 (0.6 ppm), while H-2 and H-4 are similarly shielded (0.3 and 0.35 ppm). Only a negligible deshielding effect occurs at H-5. The difference can well be explained by considering the resonance contributing forms **26**, **27**, and **28** to the ground state of the pyrimidine N-oxides.

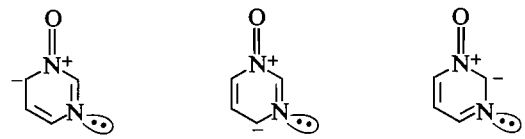

26 **27** **28**

Canonical forms **27** and **28** are expected to be less stable than **26** because of the lone-pair repulsion between the nitrogen lone pair of electrons and the charge on C-2 and C-4, respectively. This repulsion does not exist in structure **26**. Thus, it contributes more substantially to the ground state of pyrimidine N-oxides. This, in turn, is reflected by the greater shielding of H-6, as compared to H-2 and H-4.

Experimental

General procedure A

In a typical experiment, 3.40 mmol of 85% *m*-chloroperbenzoic acid dissolved in 60 mL of reagent grade acetonitrile was added dropwise (10 min) to 26.0 mmol of the appropriate pyrimidine in 120 mL of acetonitrile. The reaction mixture was heated at 60–65°C for the time indicated (Table 1). The reaction mixture was then evaporated *in vacuo*, and the residue was sublimed (monosubstituted aminopyrimidine N-oxides) or dissolved in an excess of saturated aqueous Na_2CO_3 solution, and was extracted with methylene chloride (3 × 100 mL portions). The combined extracts were dried over anhydrous K_2CO_3, filtered, and evaporated under reduced pressure to yield the N-oxide.

General procedure B

The N-oxidations with peracetic acid were carried out as described in the literature (14).

N-Oxidation of 2-methoxypyrimidine (2)

To a solution of 3.0 g (27.3 mmol) of 2-methoxypyrimidine (**2**) dissolved in 10 mL of glacial acetic acid was added 5 mL of 34% hydrogen peroxide and the solution was warmed on a water bath at 60–65°C for 7 h. The acetic acid was removed by distillation under reduced pressure (70 Torr). The temperature did not exceed 35°C. The greenish-yellow oily residue was basified with an excess of 20%

[2]The two "isomers" are identical owing to the symmetry of **23**.

Can. J. Chem. Downloaded from www.nrcresearchpress.com by 210.87.254.40 on 09/06/12
For personal use only.

TABLE 2. Nuclear magnetic resonance spectral data of some pyrimidines and their N-oxides

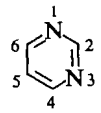

Substituents	Compound[a] (mp °C)[b]	Chemical shifts (δ (ppm))[c,d] H-2	H-4	H-5	H-6	Substituent(s)	Coupling constants (Hz) $J_{4,5}$	$J_{5,6}$	$J_{4,6}$	$J_{2,5}$	$J_{2,4}$	$J_{2,6}$
2-NH_2*	**7**	—	8.57	6.68	8.57	NH_2: 6.97	4.5	4.5	—	—	—	—
2-NH_2, 1-oxide*	**30** (186–188)	—	8.79	7.12	8.27	NH_2: 8.07	5.0	6.0	2.0	—	—	—
2-$NHCH_3$	**8**		8.41	6.63	8.41	$NHCH_3$: 3.11 NH: 5.80	5.0	5.0	—	—	—	—
2-$NHCH_3$, 1-oxide	**31** (124–126)	—	8.29	6.59	7.99	$NHCH_3$: 3.12 NH: 7.40	5.0	6.5	2.0	—	—	—
2-OCH_3	**2**	—	8.58	6.98	8.58	OCH_3: 4.05	4.5	4.5	—	—	—	—
2-OCH_3, 1-oxide	**1** (100–101)	—	8.55	7.00	8.01	OCH_3: 4.22	5.0	6.0	1.7	—	—	—
2-NH_2, 4-CH_3	**11**	—	—	6.46	8.11	CH_3: 2.33	—	6.0	—	—	—	—
2-NH_2, 4-CH_3, 1-oxide*	**32** (233–235)	—	—	6.95	8.59	CH_3: 2.62 NH_2: 7.84	5.0	—	—	—	—	—
2-$NHCH_3$, 4-CH_3	**12**	—	—	6.40	8.15	$NHCH_3$: 2.98 NH: 5.88	—	4.5	—	—	—	—
2-$NHCH_3$, 4-CH_3, 1-oxide	**34** (169–171)	—	—	6.54	7.84	CH_3: 2.51 $NHCH_3$: 3.13 NH: 7.50	5.0	—	—	—	—	—
4-NH_2*	**14**	9.12	—	7.26	8.60	NH_2: 8.12	—	5.8	1.3	—	—	0.4
4-NH_2, 1-oxide*[e]	**42** (196–197)	8.65	—	7.64	7.25	NH_2: 8.40	—	8.0	—	—	—	2.5
4-$NHCH_3$	**15**	8.55	—	6.38	8.16	$NHCH_3$: 2.93 NH: 7.35	—	6.0	1.4	—	—	0.4
4-$NHCH_3$, 1-oxide	**44** (137.5–139)	8.10	—	6.53	7.42	$NHCH_3$: 3.08	—	6.0	—	—	—	2.0
4-$N(CH_3)_2$	**16**	8.55	—	6.41	8.18	$N(CH_3)_2$: 3.05	—	6.0	1.4	—	—	0.4
4-$N(CH_3)_2$, 1-oxide	**45** (52–54) (0.05 Torr)	8.08	—	6.57	7.38	$N(CH_3)_2$: 3.14	—	6.0	—	—	—	2.0
4-OCH_3	**20**	8.83	—	6.76	8.46	OCH_3: 4.00	—	6.0	1.0	—	—	0.5
4-OCH_3, 1-oxide	**48** (132–134)	8.75	—	6.97	8.33	OCH_3: 4.03	—	6.0	—	—	—	2.0
4-NH_2, 6-CH_3**	**21**	8.40	—	6.25	—	CH_3: 2.44	—	—	1.0	—	—	—
4-NH_2, 6-CH_3, 1-oxide**	**38** (232–234)	8.05	—	6.55	—	CH_3: 2.40	—	—	—	—	—	—
4-$NHCH_3$, 6-CH_3**	**22**	8.47	—	6.33	—	$NHCH_3$: 3.30 CH_3: 2.56	—	—	1.0	—	—	—
4-$NHCH_3$, 6-CH_3, 1-oxide**	**39** (146–147.5)	8.00	—	6.53	—	CH_3: 2.44	—	—	—	—	—	—
4-OCH_3, 6-CH_3	**24**	8.65	—	6.62	—	OCH_3: 3.92 CH_3: 2.47	—	—	1.0	—	—	—
4-OCH_3, 6-CH_3, 1-oxide	**41** (135–136)	8.48	—	6.80	—	OCH_3: 4.09	—	—	—	—	—	—

[a]For all compounds elemental analyses were within ±0.3 percent of the calculated values.
[b]Melting points were taken on a Thomas–Hoover melting point apparatus.
[c]The nmr spectra of starred compounds are in DMSO-d_6, double-starred are in CH_3OD, the remaining compounds are in $CDCl_3$.
[d]Downfield from TMS.
[e]The size of the coupling constant (8 Hz), as well as the chemical shifts, suggest that this compound exists in DMSO, at least to some extent, in the imino form.

aqueous K_2CO_3 solution. The mixture was then extracted with chloroform (5 × 30 mL), the combined chloroform extracts were dried over anhydrous K_2CO_3, and the solvent was evaporated *in vacuo*, leaving 1.5 g (43.6%) of white prisms. These crystals contained impurities (starting material and compounds **3** and **4**) in addition to the desired oxide (**1**). The product was dissolved in a mixture of 5 mL CH_2Cl_2/2.5 mL dry methanol and was passed through a short 25-mL column of neutral alumina (grade III). The first fraction which was eluted with CH_2Cl_2 was compound **1**, the second fraction contained compound **2**. Elution with 95% ethylacetate/5% methanol gave substances **3** and **4**, which were further separated by thick-layer chromatography with the same eluent.

As the reaction time was increased to 14–18 h at 60°C (or one week at room temperature), almost all of the starting material was converted to compounds **3** and **4** at the expense of the N-oxide **1**.

1. M. V. JOVANOVIC and W. W. PAUDLER. J. Org. Chem. **48**, 1064 (1983).
2. M. V. JOVANOVIC and W. W. PAUDLER. J. Org. Chem. Submitted.
3. A. R. KATRITZKY and J. M. LAGOWSKI. Chemistry of the heterocyclic N-oxides. Academic Press, London. 1971.
4. R. H. WILEY and S. C. SLAYMAKER. J. Am. Chem. Soc. **79**, 2233 (1957).
5. M. OGATA, H. WATANABE, K. TORI, and H. KANO. Tetrahedron Lett. **19** (1964).
6. F. BELLAMY, P. MARTZ, and T. STREITH. Tetrahedron Lett. **19**, 3189 (1974).
7. H. YAMANAKA. Chem. Pharm. Bull. (Tokyo) **7**, 297 (1959).
8. Y. KOBAYASHI, I. KUMADAKI, and H. SATO. Chem. Pharm. Bull. (Tokyo) **17**, 1045 (1969).
9. S. A. KRUEGER and W. W. PAUDLER. J. Org. Chem. **37**, 4188 (1972).
10. A. Y. TIHONOV and L. B. VOLODARSKY. Khim. Geterotsikl. Soedin. 259 (1977).
11. W. W. PAUDLER and T. K. CHEN. J. Org. Chem. **36**, 787 (1971).

Can. J. Chem. Downloaded from www.nrcresearchpress.com by 210.87.254.40 on 09/06/12
For personal use only.

12. R. J. RADEL, B. T. KEEN, C. WONG, and W. W. PAUDLER. J. Org. Chem. **42**, 546 (1977).
13. W. F. SEDOVA and V. P. MAMEV. Khim. Geterotsikl. Soedin. 827 (1979).
14. T. KATO, H. YAMANAKA, and T. SHIBATA. Yakugaku Zasshi, **87**, 1096 (1967).
15. S. A. HUMPHREY. Ph.D. Thesis, Ohio University (1971).

Can. J. Chem. Downloaded from www.nrcresearchpress.com by 210.87.254.40 on 09/06/12
For personal use only.

^{33}S and ^{17}O nuclear magnetic resonance study of liquid sulfur dioxide

RODERICK E. WASYLISHEN[1], J. BRUCE MACDONALD, AND JAN O. FRIEDRICH
Department of Chemistry, Dalhousie University, Halifax, N.S., Canada B3H 4J3

Received November 25, 1983

RODERICK E. WASYLISHEN, J. BRUCE MACDONALD, and JAN O. FRIEDRICH. Can. J. Chem. **62**, 1181 (1984).

The sulfur-33 chemical shift and ^{33}S and ^{17}O nmr relaxation data are reported for liquid sulfur dioxide. The ^{33}S nucleus in SO_2 is highly deshielded, 375 ± 2 ppm to high frequency of the sulfate anion. The rotational correlation time of SO_2 at 294 K, 0.3 ps, is only about twice that calculated using an inertial model. The temperature dependence of the ^{33}S and ^{17}O nmr relaxation data can be described by an average activation energy of 6.3 ± 0.6 kJ mol^{-1}. The effective rotational correlation time derived from ^{33}S nmr line widths is used to calculate the ^{17}O quadrupolar coupling constant, e^2qQ/h = 6.6 ± 0.7 MHz, in SO_2.

RODERICK E. WASYLISHEN, J. BRUCE MACDONALD et JAN O. FRIEDRICH. Can. J. Chem. **62**, 1181 (1984).

On rapporte les déplacements chimiques du soufre-33 et les données de relaxation rmn du ^{33}S et du ^{17}O pour le bioxyde de soufre liquide. Le noyau de ^{33}S du SO_2 est fortement déblindé; par rapport à l'ion sulfate, il apparaît à une fréquence 375 ± 2 ppm plus élevée. Le temps de corrélation rotationelle du SO_2 à 294 K, 0,3 ps, est seulement le double de celui calculé en utilisant un modèle inertiel. On peut décrire l'effet de la température sur les données de relaxation en rmn du ^{33}S et du ^{17}O par une énergie d'activation moyenne de 6,3 ± 0,6 kJ mol^{-1}. On a utilisé le temps de corrélation rotationelle effectif déduit de la largeur des raies en rmn du ^{33}S pour calculer la constante de couplage quandrupolaire du ^{17}O, e^2qQ/h = 6,6 ± 0,7 MHz, dans du SO_2.

[Traduit par le journal]

Introduction

Although oxygen-17 chemical shifts have been previously reported for sulfur dioxide (1, 2), there appear to be no ^{33}S or ^{17}O nmr relaxation data on this simple molecule. Furthermore, we have been unable to find any information in the literature regarding the rotational dynamics of SO_2 in the liquid phase (−10.1 to −75.5°C at atmospheric pressure (3)). Here we wish to report the ^{33}S nmr chemical shift of liquid SO_2 and the temperature dependence of the ^{33}S and ^{17}O nmr relaxation rates.

Theory

Both ^{33}S and ^{17}O are quadrupolar nuclei with rather large quadrupole moments, $I = 3/2$ ($Q = -0.055 \times 10^{-28}$ m^2) and $I = 5/2$ ($Q = -0.026 \times 10^{-28}$ m^2), respectively (2*b*, 4). These properties combined with the low natural abundances of ^{33}S and ^{17}O, 0.76% and 0.037% respectively, have to some extent impeded nmr studies of these isotopes. For quadrupolar nuclei, interactions between the nuclear quadrupole moment and the surrounding electric field gradient, for example, provide an extremely efficient mechanism for nuclear relaxation (5). Under conditions of extreme narrowing ($2\pi\nu\tau_c \ll 1$)

$$[1]\quad \frac{1}{T_1} = \frac{1}{T_2} = \pi\nu_{1/2} = \frac{3\pi^2}{10}\,\frac{2I+3}{I^2(2I-1)}\left(1+\frac{\eta^2}{3}\right) \times (e^2q_{zz}Q/h)^2\tau_c$$

where ν is the Larmor precession frequeny in Hz, τ_c is the effective rotational correlation time (6), $\nu_{1/2}$ is the line width at half maximum height, $e^2q_{zz}Q/h$ is the quadrupolar coupling constant, and η is an asymmetry parameter, $(q_{yy} - q_{xx})/q_{zz}$. For SO_2 the ^{33}S nuclear quadrupolar coupling constant and asymmetry parameter have been measured by Bird and Townes (7) using microwave spectroscopy, $(e^2q_{zz}Q/h)$ = 25.71 ± 0.03 MHz and η = 0.87. The corresponding ^{17}O values have not been reported; however, from the results of the present study we are able to provide an estimate of the ^{17}O quadrupole coupling constant.

[1]Author to whom all correspondence should be directed.

Experimental

All nmr measurements were carried out on a Nicolet 360 NB (B_0 = 8.48 T) using a broad-band variable temperature 10-mm probe. Sulfur-33 line widths were measured at 27.727 MHz using $\pi/2$ pulses (45 μs). The ^{33}S line width of a 4 *m* $(NH_4)_2SO_4$ solution was less than or equal to 5.5 Hz, and we believe that the contribution of magnet field inhomogeneity to the observed line widths was less than 5 Hz at all temperatures. Acquisition times of 0.2 s were used at all temperatures; typically, 5000 scans were used in acquiring each spectrum.

Oxygen-17 spin-lattice relaxation times were carried out at 48.974 MHz using the inversion recovery pulse sequence which uses compensating pulses (8). The $\pi/2$ pulse width was 38 μs. Typically, 16 scans were required for $S/N > 200$. T_1 was calculated using a non-linear three-parameter least-squares fitting procedure available on the Nicolet software.

A special homemade nmr tube was designed and used to minimize diffusion between the gas and liquid phases (9).

Results

(a) *Chemical shifts*

At 294 K the ^{33}S nmr resonance of SO_2 (Fig. 1) is 375 ± 2 ppm to high frequency of the $^{33}SO_4^{2-}$ resonance of 4 *m* $(NH_4)_2SO_4$ solution, or 707 ppm to high frequency of CS_2. This extends the known range of ^{33}S chemical shifts by approximately 340 ppm (10); previously, the least shielded ^{33}S resonance was that of K_2MoS_4 (11). It is of interest to point out that the central ^{7}O nucleus of ozone is also highly deshielded, 1032 ppm, with respect to H_2O (2*b*, 12).

(b) *Rotational correlation times from ^{33}S nuclear magnetic resonance line widths*

Observed ^{33}S nmr line widths as a function of temperature are given in Table 1. From a plot of ln $\nu_{1/2}$ vs. $10^3/T$, Fig. 2, an activation energy of 6.9 ± 0.4 kJ mol^{-1} is evaluated. Such a value is typical of a non-associated liquid (13). By substitution of the ^{33}S quadrupole coupling constant into eq. [1], and the equation describing the straight line of Fig. 2, we obtain the expression (eq. [2]) below which describes the temperature dependence of the rotational correlation time, τ_c.

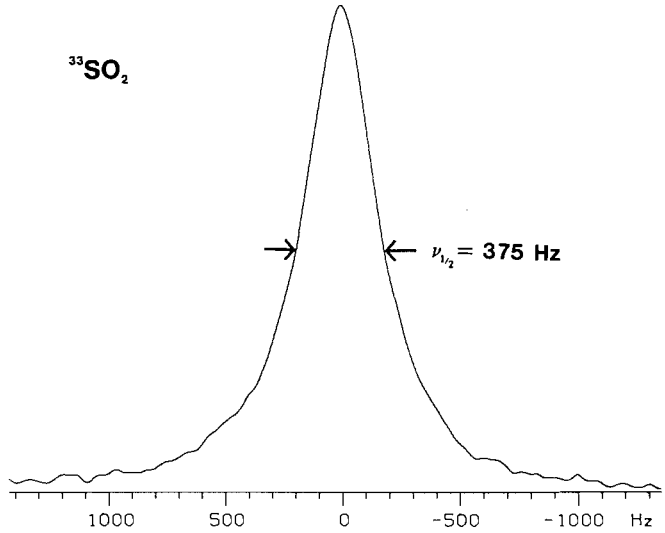

FIG. 1. 27.727 MHz sulfur-33 nmr spectrum of liquid SO_2 (at saturation pressure) at 294 K.

$$[2]\quad \tau_c = 1.791 \times 10^{-14} \exp(833/T)$$

The error bars in Fig. 2 correspond to an estimated error of ±5%. Although this is probably a realistic value at 20°C, ±10% may be more appropriate at the lower temperatures where it is difficult to measure accurate line widths because of acoustic ringing (14). At 202 K the value of T_2^*, $(\pi\nu_{1/2})^{-1}$, is approximately 271 μs, only about six times longer than the $\pi/2$ pulse width of our spectrometer; therefore we expect some lineshape distortions at these lower temperatures.

At the highest temperature studied, 294 K, the effective rotation correlation time calculated using eq. [2] is 0.30 ps. It is of interest to compare this characteristic time with that calculated by an inertial model (6). Sulphur dioxide (**I**) may crudely be approximated as a prolate spheroid since $I_1 = 9.5 \times 10^{-46}$ kg m^2, $I_2 = 8.1 \times 10^{-46}$ kg m^2, and $I_3 = 1.4 \times 10^{-46}$ kg m^2 (7). For a prolate spheroid

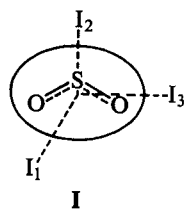

I

($I_1 = I_2 > I_3$) we have previously shown (15):

$$[3]\quad \tau_{FR} = (3)^{-1/2}\left(\frac{I_1 I_3}{2\pi kT(I_1 - I_3)}\right)^{1/2} \ln\left[\frac{1 + \left(\frac{I_1 - I_3}{I_1}\right)^{1/2}}{1 - \left(\frac{I_1 - I_3}{I_1}\right)^{1/2}}\right]$$

Substitution of $I_1 = I_2 = 8.8 \times 10^{-49}$ kg m^2 and $I_3 = 1.4 \times 10^{-46}$ kg m^2 into eq. [3] gives $\tau_{FR} = 0.15$ ps. The implication is that the rotational motion of sulfur dioxide cannot be described as small step diffusion since $\chi \simeq 2$(6, 16).

$$[4]\quad \chi = \left(\frac{3\pi}{2}\right)^{1/2} \tau_2 \left(\frac{KT}{I}\right)^{1/2}$$

For small step diffusion $\chi \gg 1$ (6, 16). At 202 K $\tau_c = 1.1 \pm 0.1$ ps, $\tau_{FR} = 0.18$ ps, and $\chi \simeq 7$, suggesting that rotations may be regarded as approaching small step diffusion.

TABLE 1. Temperature dependence of ^{33}S nuclear magnetic resonance line widths and ^{17}O T_1 values in liquid sulfur dioxide

^{33}S nmr data		^{17}O nmr data	
Temperature	$\nu_{1/2}$(±5%)	Temperature	T_1(±5%)
294 K	315 Hz	294 K	0.0789 s
274	410	273	0.0602
270	420	257	0.0528
257	450	243	0.0450
238	615	228	0.0381
223	735	213	0.0329
215	860	202	0.0255
206	1130		
202	1175		

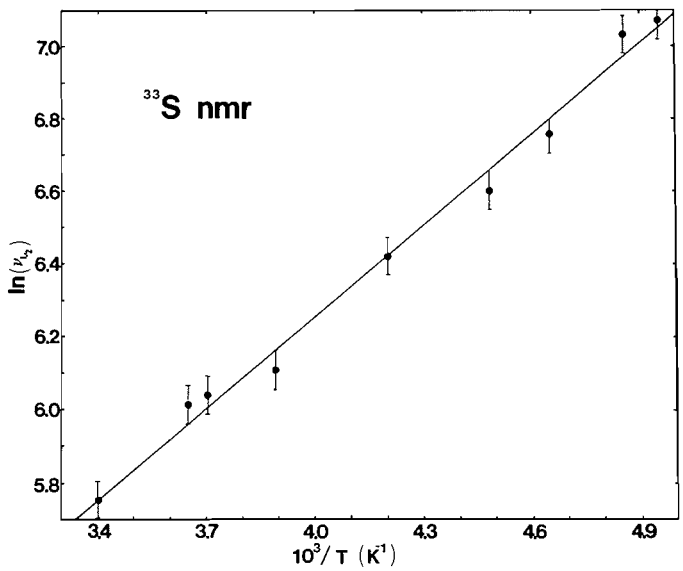

FIG. 2. Plot of ln $\nu_{1/2}$ vs. $10^3/T$ for liquid SO_2. $\nu_{1/2}$ is the ^{33}S nmr line width measured at half maximum height.

At the lower temperatures we have attempted to test the hydrodynamic model of Hu and Zwanzig (6, 17) under the slip boundary condition. Under these conditions, motion about the symmetry axis (labelled 3 in **I**) is relatively free while rotations about the 1 and 2 axes are more hindered because neighbouring molecules must be displaced. Anisotropic rotations of SO_2 have been inferred from vibrational spectroscopy (18). Using standard procedures (6, 15–17) we calculate $\tau_{slip} \simeq 2$ ps at 202 K, which is almost twice the observed correlation time. This agreement is satisfactory in view of our assumptions regarding the geometry of SO_2 (prolate spheroid, $a = b = 1.9$ Å and $c = 2.7$ Å); also it is probably not meaningful to use a hydrodynamic model for a molecule which is probably not undergoing small step rotational diffusion.

(c) *^{17}O nuclear magnetic resonance spin-lattice relaxation times and the quadrupole coupling constant*

The ^{17}O nmr line widths of liquid SO_2 are relatively sharp, less than 15 Hz, at all temperatures and allow accurate measurements of the spin-lattice relaxation time, T_1 (Table 1). An Arrhenius plot of ln T_1^{-1} vs. $10^3/T$ gives a straight line, Fig. 3, of slope 5.7 ± 0.5 kJ mol^{-1}.

Assuming the same effective rotational correlation time for ^{17}O and ^{33}S nuclear spin relaxation, and that the ^{17}O asymmetry parameter is small, substitution into eq. [1] gives an effective

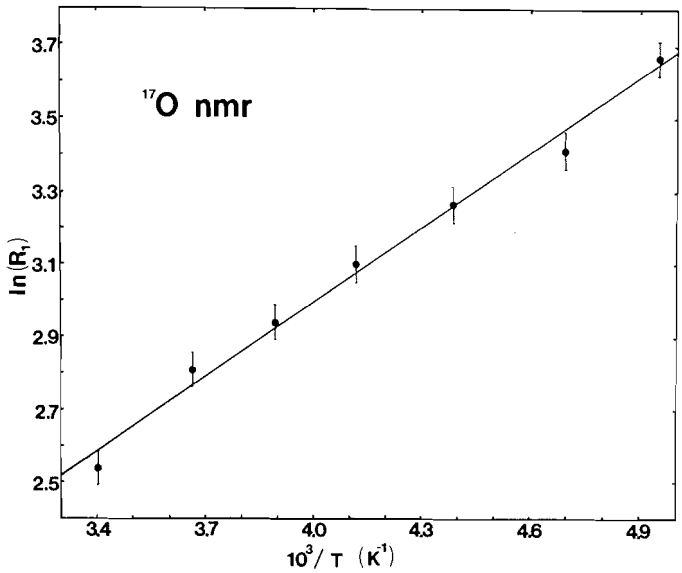

FIG. 3. Plot of ln R_1 vs. $10^3/T$ for liquid SO_2. R_1 is the rate of the ^{17}O spin lattice relaxation.

^{17}O quadrupole coupling constant, e^2qQ/h, of 6.64 MHz. We believe the error in this value is less than ±10%. The oxygen-17 quadrupole coupling constant in SO_2 has not been previously reported; however, Poplett (19) has reported a value 7.340 ± 0.005 MHz for the S=O fragments of solid sulfuric acid. The asymmetry parameter was only 0.06 ± 0.05; therefore our assumption that η is small in SO_2 appears justified.

Acknowledgements

We wish to thank NSERC for an operating grant and a major installation grant to purchase the Nicolet 360 nmr spectrometer.

1. H. E. WEAVER, B. M. TOLBERT, and R. C. LAFORCE. J. Chem. Phys. **23**, 1956 (1955).
2. (*a*) B. N. FIGGIS, R. G. KIDD, and R. S. NYHOLM. Proc. R. Soc. London Ser. A, **269**, 469 (1962); (*b*) J.-P. KINTZINGER. NMR: Basic Princ. Prog. **17**, 1 (1981).
3. (*a*) R. A. ZINGARO. *In* Nonaqueous solvents. D. C. Health and Company, Lexington, Massachusetts. 1968. p. 47. (*b*) T. C. WADDINGTON. Non-aqueous solvents. Thomas Nelson and Sons Ltd., London. 1969. p. 40.
4. S. BÜTTGENBACH, M. HERSCHEL, G. MEISEL, E. SCHRÖDL, W. WITTE, and W. J. CHILDS. Z. Physik, **266**, 271 (1974).
5. A. ABRAGAM. The principles of nuclear magnetism. Oxford University Press, London. 1961.
6. R. T. BOERÉ and R. G. KIDD. *In* Annual reports on NMR spectroscopy. Vol. 13. *Edited by* G. A. Webb. Academic Press, New York. 1981.
7. G. R. BIRD and C. H. TOWNES. Phys. Rev. **94**, 1203 (1954).
8. R. FREEMAN, S. P. KEMPSELL, and M. H. LEVITT. J. Magn. Reson. **38**, 453 (1980).
9. T. C. FARRAR and E. D. BECKER. Pulse and Fourier transform NMR. Academic Press, New York. 1971. p. 43.
10. (*a*) C. MCFARLANE and W. MCFARLANE. *In* Nmr and the periodic table. *Edited by* R. K. Harris and B. E. Mann. Academic Press, New York. 1978. Section 12B, pp. 401–402; (*b*) F. W. WEHRLI. *In* Annual reports on NMR spectroscopy. Vol. 9. *Edited by* G. A. Webb. Academic Press, New York. 1979. p. 126.
11. P. KRONACK, O. LUTZ, and A. NOLLE. Z. Naturforsch. Teil A, **35**, 226 (1980).
12. I. J. SOLOMON, J. N. KEITH, A. J. KACMAREK, and J. K. RANEY. J. Am. Chem. Soc. **90**, 5408 (1968).
13. D. A. WRIGHT, D. E. AXELSON, and G. C. LEVY. *In* Topics in Carbon-13 NMR spectroscopy. Vol. 3 *Edited by* G. C. Levy. John Wiley and Sons, New York. 1978. p. 103.
14. E. FUKUSHIMA and S. B. W. ROEDER. Experimental pulse NMR – a nuts and bolts approach. Addison–Wesley Publishing Company, Inc., Reading, Massachusetts, USA. 1981.
15. R. E. WASYLISHEN, B. A. PETTITT, and W. DANCHURA. Can. J. Chem. **55**, 3602 (1977).
16. R. E. WASYLISHEN and B. A. PETTITT, Can. J. Chem. **55**, 2564 (1977).
17. C.-M. HU and R. ZWANZIG. J. Chem. Phys. **60**, 4354 (1974).
18. (*a*) J. JACOB, J. LECLERC, and J. VINCENT-GEISSE. J. Chim. Phys. Physicochim. Biol. **66**, 970 (1969); (*b*) C. R. Acad. Sci. Paris, Ser. B, **256**, 976 (1967).
19. I. J. F. POPLETT. J. Magn. Reson. **44**, 488 (1981).

Attempts to develop new synthetic entries into the tricyclo[3.3.0.0^{3,7}]octane skeleton

PELAYO CAMPS[1]

Departamento de Química Orgánica, Facultad de Ciencias Químicas de San Sebastián, Universidad del País Vasco, Alza, Guipuzcoa, Spain

AND

MARTA FIGUEREDO

Departamento de Química Orgánica, Facultad de Ciencias, Universidad Autónoma de Barcelona, Bellaterra, Barcelona, Spain

Received August 18, 1983

PELAYO CAMPS and MARTA FIGUEREDO. Can. J. Chem. **62**, 1184 (1984).

The attempts to synthesize dimethyl tricyclo[3.3.0.0^{3,7}]octane-1,5-dicarboxylate, **1**, and some related compounds by formation of a C3—C7 bond from appropriate bicyclo[3.3.0]octane derivatives, either through intramolecular C—H carbene insertion or by ketone-to-cyclopentanol photocyclization, are described. Two alternative syntheses for the key precursor, dimethyl *cis*-3-oxobicyclo[3.3.0]octane-1,5-dicarboxylate, **2**, are included. Also, the formation of dimethyl 3-hydroxytricyclo[3.3.0.0^{3,7}]octane-1,5-dicarboxylate, **24**, by reduction of dimethyl *cis*-3,7,dioxobicyclo[3.3.0]octane-1,5-dicarboxylate, **9**, under Clemensen-like reaction conditions is reported.

PELAYO CAMPS et MARTA FIGUEREDO. Can. J. Chem. **62**, 1184 (1984).

On décrit des essais de synthèse du tricyclo[3.3.0.0^{3,7}]octane dicarboxylate-1,5 de méthyle (**1**) et de quelques composés apparentés qui impliquent la formation d'une liaison C3—C7 à partir des dérivés bicyclo[3.3.0]octane appropriés soit via une insertion intramoléculaire du C—H d'un carbène soit par la photocyclisation d'une cétone en cyclopentanol. On inclut deux modes de synthèse du précurseur fondamental, l'oxo-3 bicyclo[3.3.0]octane dicarboxylate-1,5 de méthyle-*cis* (**2**). On rapporte également la synthèse de l'hydroxy-3 tricyclo[3.3.0.0^{3,7}]octanedicarboxylate-1,5 de méthyle (**24**) par réduction du dioxo-3,7 bicyclo[3.3.0]octane dicarboxylate de méthyle-*cis* (**9**) dans des conditions semblables à celles d'une réaction de Clemensen.

[Traduit par le journal]

The synthesis and chemistry of tricyclo[3.3.0.0^{3,7}]octane derivatives have been matters of continuous interest (1) since the first compound possessing this carbon skeleton was synthesized in 1964 (1*a*). The greatest interest comes from the special behaviour of many of these derivatives that are prone to rearrange (Fig. 1) because of the great strain energy (1*q*, *u*) of this tricyclic skeleton, which might be viewed as a norbornane with a methylene bridge connecting the 2 and 5 positions. Some aspects that have also received attention are the symmetry (1*b*, *p*, *s*, *x*), pharmacology (1*e*), and microbiological reactions (1*v*, *y*) of some of these derivatives.

All of the syntheses of tricyclo[3.3.0.0^{3,7}]octane derivatives that can be found in the literature have been schematically collected in Fig. 2. Only the third procedure has been applied to different substrates and it seems to be a quite general method. Although only one example corresponding to the fourth procedure has been described, this transformation could also be of wide applicability. The rest of the syntheses can not, in principle, be considered as general methods, but as special cases. In particular, in the last one, the tricyclic compound was formed by an anomalous reaction during the attempted pinacol reduction of the starting diketone, and although the same type of reaction has been also observed (2) in related compounds with the [*m*.3.3]propellane skeleton, it was not observed with *cis*-bicyclo[3.3.0]octane-3,7-dione itself.

The strain energy of the tricyclo[3.3.0.0^{3,7}]octane skeleton is clearly shown by the cationic transformations experienced by many of its derivatives (1*c*, *f*, *g*, *k*, *o*, *r*, *w*), and also by the easy conversion of 3,7-dimethyltricyclo[3.3.0.0^{3,7}]octan-1-ol into *cis*-1,5-dimethylbicyclo[3.3.0]octan-3-one (1*j*) and tricyclo[3.3.0.0^{3,7}]octan-2-one into norbornane-2-carboxylic acid (1*d*), by reaction with potassium *tert*-butoxide in *tert*-butyl alcohol. Accordingly, the described syntheses of compounds containing this carbon skeleton generally imply irreversible reactions in the key step.

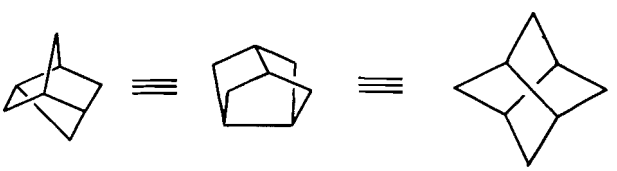

FIG. 1

As part of our interest in the synthesis of polyquinanes we have studied possible synthetic approaches to dimethyl tricyclo[3.3.0.0^{3,7}]octane-1,5-dicarboxylate, **1**. Since the application of the only general method described for the synthesis of diester **1** (third procedure of Fig. 2) would require the use of a not easily accessible starting material, and the rest of the described methods (see Fig. 2) are not general, we considered it more interesting to attempt the synthesis of **1** by developing a new approach to its tricyclic skeleton.

The key step in our synthesis would be the intramolecular insertion of a carbene into the appropriate C—H bond, as shown in Fig. 3. Since the reaction is irreversible, the success of the synthesis would be dependent on the relative rate of this insertion compared with other possible carbene transformations, such as C2(4)—H or C6(8)—H insertions, that would give rise to an alkene or a cyclobutane derivative respectively.

Many examples of intramolecular C—H insertions of carbenes of synthetic interest can be found in the literature (3). Great variations in yields, due to small structural modifications, are often observed. However, among the many fac-

[1] Author to whom correspondence may be addressed. Present address: Departamento de Química Orgánica, Facultad de Farmacia, Universidad de Valencia, Valencia, Spain.

Can. J. Chem. Downloaded from www.nrcresearchpress.com by 210.87.254.105 on 09/06/12
For personal use only.

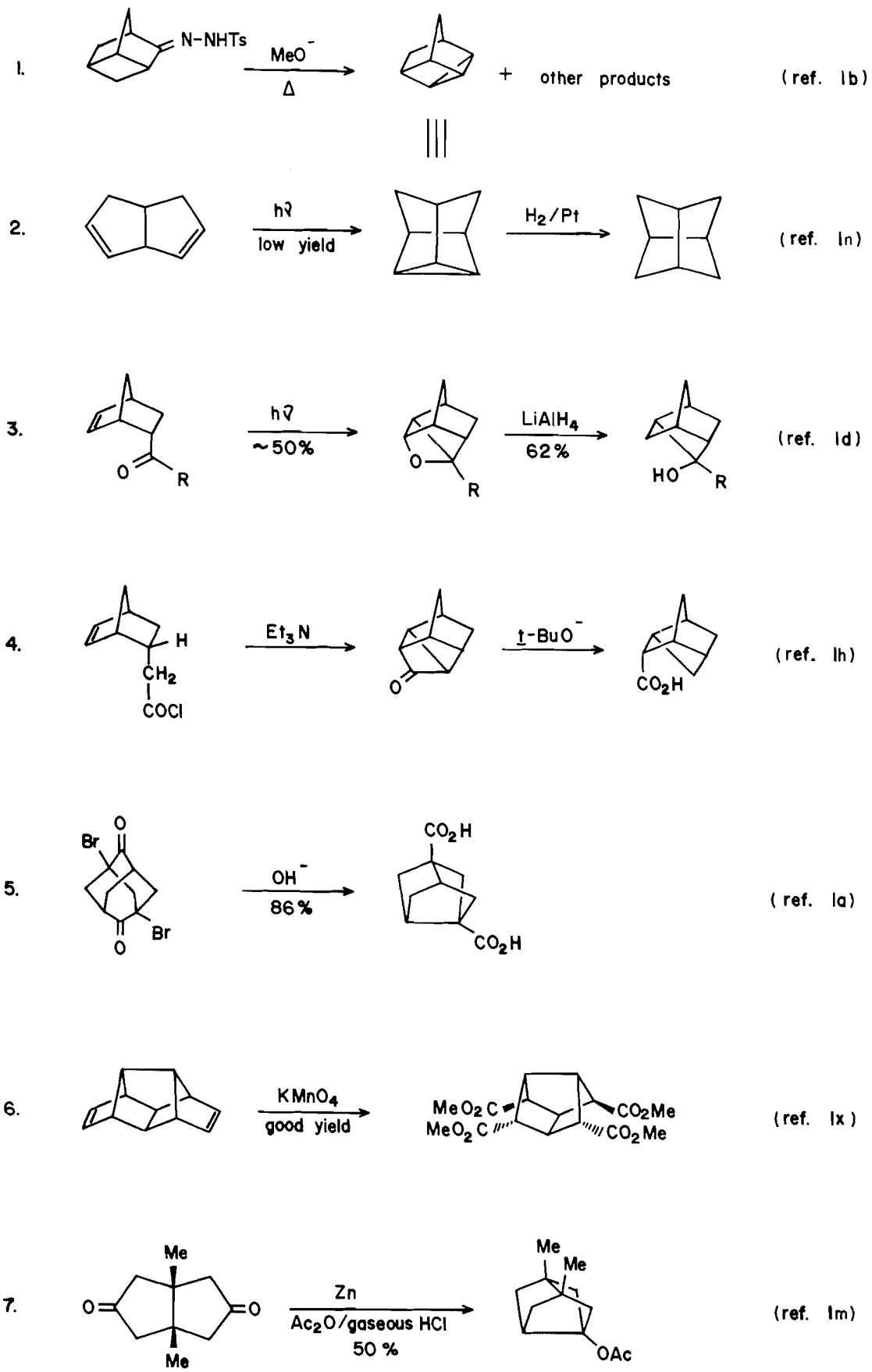

FIG. 2

Can. J. Chem. Downloaded from www.nrcresearchpress.com by 210.87.254.105 on 09/06/12
For personal use only.

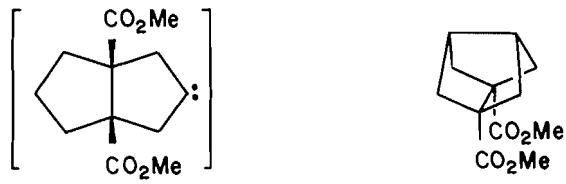

1

FIG. 3

tors that control the intramolecular insertion of a carbene into a particular C—H bond, the appropriate distance between the divalent carbon atom and the C—H bond in which insertion should take place is of major importance. Taking dimethyl *cis*-3-oxobicyclo[3.3.0]octane-1,5-dicarboxylate, **2**, as a model for the intermediate carbene, the distance between C3 and C7 in the required conformation of **2** to form the C3—C7 bond was calculated (4) to be only ca. 0.3 Å greater than the corresponding distance in compounds in which the insertion does take place in good yields, such as bicyclo[3.3.1]nonan-3-one (3*b*), **3**, and tricyclo[5.2.1.$0^{2,6}$]decan-10-one (3*c*), **4** (Fig. 4). Moreover, a population of 35.5% for that conformation of ketodiester **2** was calculated (4). Also, the fact that *cis*-1,5-dimethylbicyclo[3.3.0]octane-3,7-dione gives, on reduction, a tricyclo[3.3.0.$0^{3,7}$]octane derivative (1*j*) (Fig. 2) shows that the distance between C3 and C7 in some *cis*-1,5-disubstituted bicyclo[3.3.0]octane derivatives is short enough for bond formation.

To generate the intermediate carbene shown in Fig. 3, we prepared ketodiester **2** by two independent routes. The first one, outlined in Fig. 5, makes use of the synthesis of *cis*-1,5-disubstituted bicyclo[3.3.0]octane-3,7-diones (see Fig. 6) developed by Weiss and co-workers (5), and widely used by other authors (6), to synthesize dimethyl *cis*-3,7-dioxobicyclo[3.3.0]octane-1,5-dicarboxylate, **9**, whose conversion into ketodiester **2** requires only the reduction of one of its ketonic functions.

In our case, the required 1,2-dicarbonyl compound was dimethyl 2,3-dioxobutanedioate, **6**, a compound that can be prepared by reaction of disodium dihydroxytartrate, **5**, with anhydrous methanol saturated with gaseous hydrogen chloride (7), in approximately 50% yield of distilled product. To obviate the tedious purification of **6**, we carried out the Weiss reaction with crude **6** as described in the Experimental, isolating a solid that was characterized as hexamethyl *cis*-3,7-dioxobicyclo[3.3.0]-octane-1,2,4,5,6,8-hexacarboxylate, **8** (13.9% yield from **5**), through its spectroscopic and analytical data and its high yield conversion into dimethyl *cis*-3,7-dioxobicyclo[3.3.0]octane-1,5-dicarboxylate, **9**. The 60 MHz ^{1}H nmr spectrum of compound **8** in $CDCl_3$ shows that it exists as a complex mixture of tautomers.

The conversion of compound **8** into dioxodiester **9** was carried out by the method of Krapcho and Lovey (8), by heating a solution of the compound in DMSO containing small amounts of NaCl and water. When hydrolysis and decarboxylation of compound **8** were carried out by refluxing it with aqueous HCl, partial hydrolysis of the methoxycarbonyl groups at C1 and C5 was also observed. The ^{1}H nmr spectrum of compound **9** is very simple, consisting of an AB system for the methylene protons (δ 3.20 and 2.42, J = 18 Hz) apart from the methoxyl absorption.

Since the mother liquors from the crystallization of compound **8** still contained this compound (tlc), we subjected the crude extract of the reaction of compounds **6** and **7** to the Krapcho conditions of decarbomethoxylation (8), isolating **9** in 12% overall yield from salt **5**. Reaction of compound **9** with one equivalent of ethanedithiol catalyzed by boron trifluoride etherate in ethyl acetate yielded a mixture of starting compound **9**, dimethyl *cis*-3,3-ethylenedithio-7-oxobicyclo[3.3.0]octane-1,5-dicarboxylate, **10**, and dimethyl *cis*-3,3,7,7-bisethylenedithiobicyclo[3.3.0]octane-1,5-dicarboxylate, **11**, in the approximate ratio 8:6:1, which was separated by column chromatography. Reaction of compound **10** with Raney Ni in ethanol gave a crude product whose ir spectrum showed that reduction of the ketone function had also taken place. This crude product, after oxidation with Jones reagent, gave dimethyl *cis*-3-oxobicyclo[3.3.0]octane-1,5-dicarboxylate, **2**. Although the yield of compound **10** was acceptable if **9** was recovered, the experimental difficulties of this transformation encouraged us to develop an alternative synthesis through the sequence shown in Fig. 7.

The starting material for this sequence was *cis*-bicyclo-[4.3.0]non-3-ene-1,6-dicarboxylic acid, **13** (9, 10). Reaction of diacid **13** with an excess of an ethereal solution of diazomethane gave, quantitatively, dimethyl *cis*-bicyclo[4.3.0]non-3-ene-1,6-dicarboxylate, **14**.

Potassium permanganate oxidation of diester **14** under phase transfer catalysis conditions (11) gave *meso*-1,2-bismethoxycarbonylcyclopentane-1,2-diacetic acid, **15**, in 75% yield, which on reaction with excess of ethereal diazomethane gave dimethyl *meso*-1,2-bismethoxycarbonylcyclopentane-1,2-diacetate, **16**. Trimethyl *cis*-3-oxobicyclo[3.3.0]octane-1,2,5-tricarboxylate, **17**, was obtained in 91% yield by Dieckmann cyclization of tetraester **16**. Decarbomethoxylation of ketotriester **17** using the Krapcho conditions (8) led to ketodiester **2** in 92% yield. The sequence depicted in Fig. 7 can be easily carried out on a fairly large scale and is thus the method of choice to prepare ketodiester **2**.

Some attempts to convert diacid **15** directly into ketodiester **2** by pyrolysis in the presence of catalytic amounts of barium hydroxide led only to the formation of 3-oxatricyclo-[3.3.3.$0^{1,5}$]undecane-2,4,7-trione, **18**, in 82% yield (Fig. 8). Acid hydrolysis of **2** gave the corresponding *cis*-3-oxobicylo[3.3.0]octane-1,5-dicarboxylic acid, **19**, which was dehydrated using a catalytic amount of concentrated sulfuric acid to give ketoanhydride **18**.

Compound **18** was also obtained, although in lower yield, from anhydride **12**. Potassium permanganate oxidation of compound **12** under phase transfer conditions (11) gave *cis*-2,4-dioxo-3-oxabicyclo[3.3.0]octane-1,5-diacetic acid, **20**, in only 33% yield. Compound **20**, however, was transformed into ketoanhydride **18**, in 84% yield, by pyrolysis in the presence of a catalytic amount of barium hydroxide.

In order to carry out the transformation depicted in Fig. 3, we chose the Bamford–Stevens procedure (3*a*). Ketodiester **2** was transformed into the corresponding tosylhydrazone, **21**, in 84% yield, by reaction with tosylhydrazide in glacial acetic acid at room temperature. Thermal decomposition of its sodium salt **22** (200°C/1 Torr) gave, as the major reaction product (72% isolated yield), dimethyl *cis*-bicyclo[3.3.0]oct-2-ene-1,5-dicarboxylate, **23**. None of the minor products formed in this reaction was the desired diester **1** (glc/ms). Lower yields of compound **23** were obtained by thermal decomposition of salt **22** prepared from tosylhydrazone **21** and less than a molar equivalent of sodium methoxide in anhydrous methanol, or by

Can. J. Chem. Downloaded from www.nrcresearchpress.com by 210.87.254.105 on 09/06/12
For personal use only.

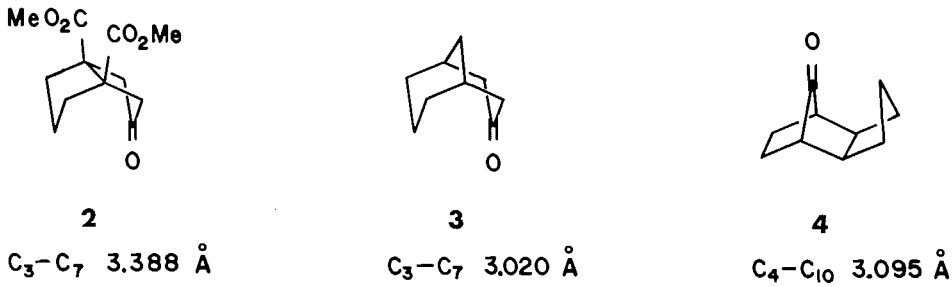

FIG. 4

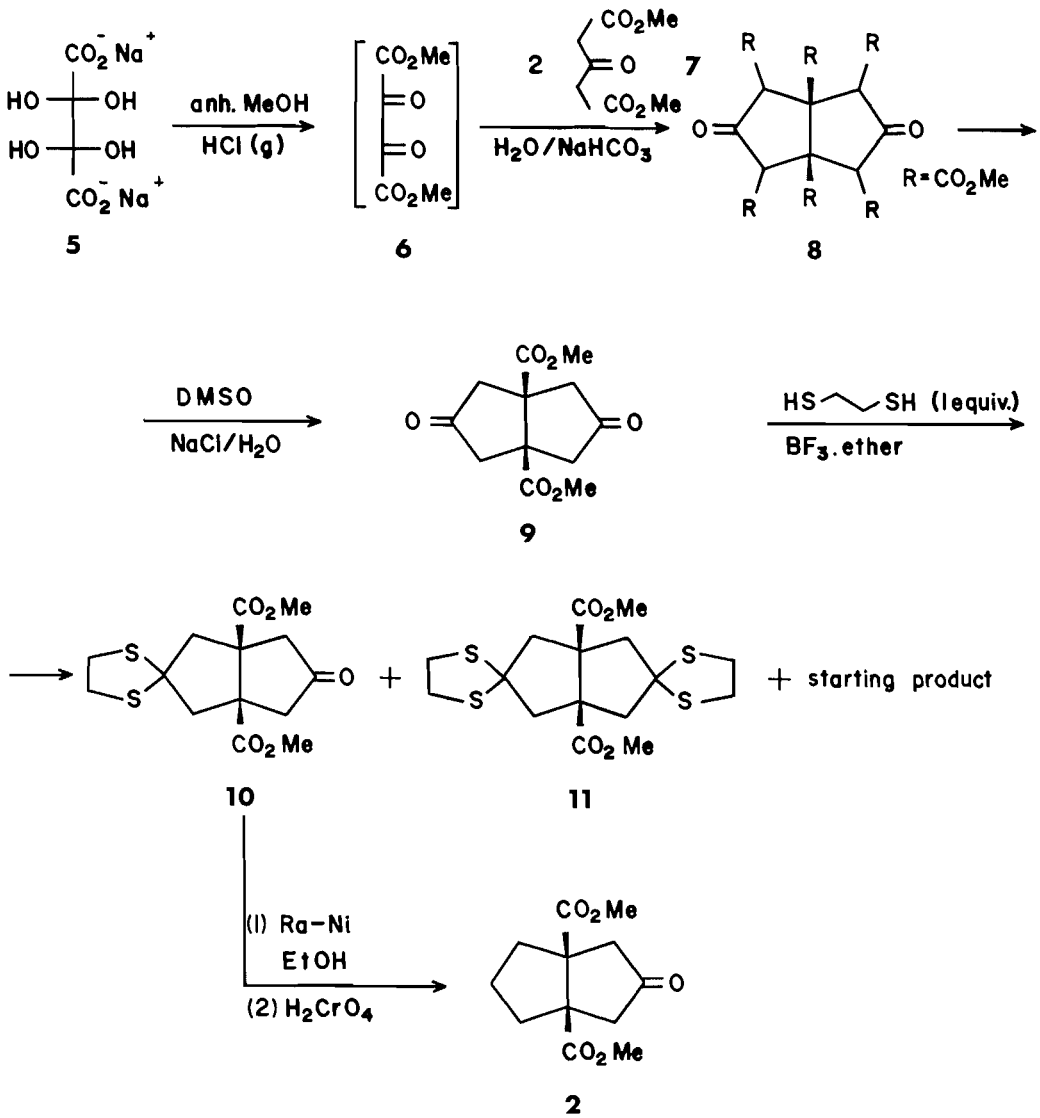

FIG. 5

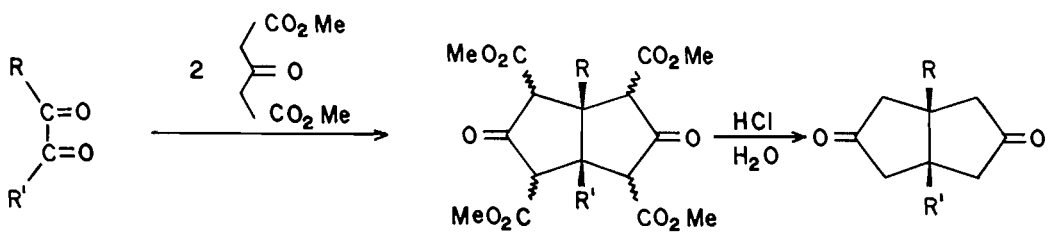

FIG. 6

Can. J. Chem. Downloaded from www.nrcresearchpress.com by 210.87.254.105 on 09/06/12
For personal use only.

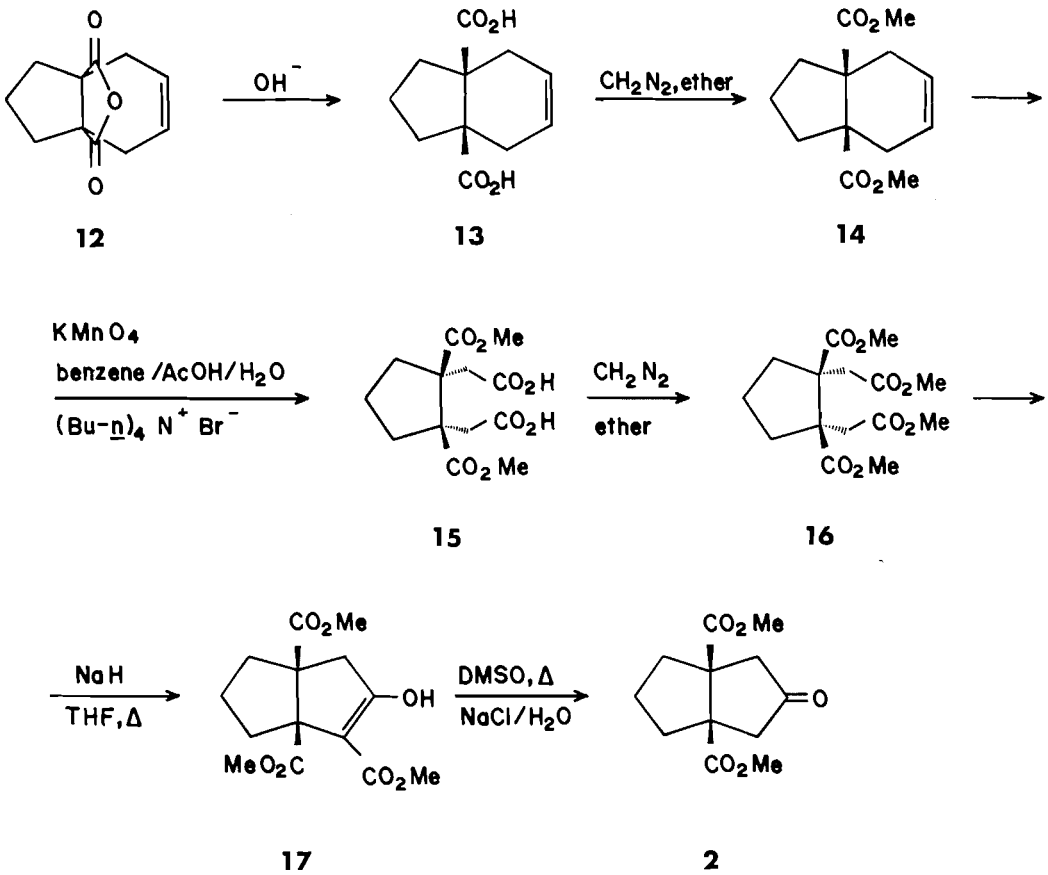

FIG. 7

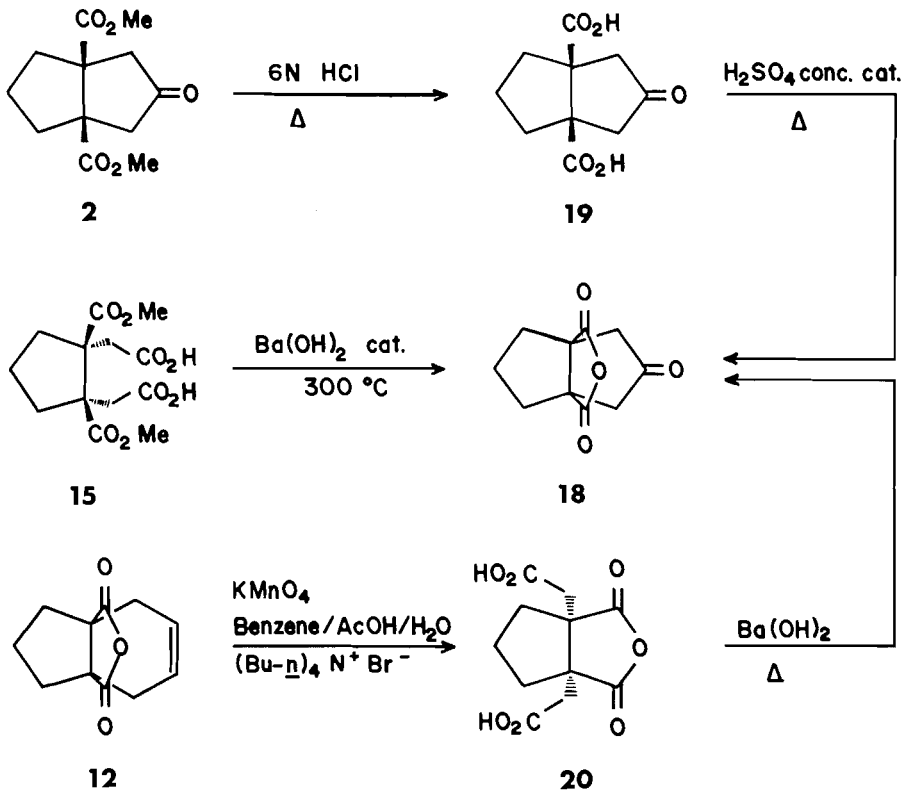

FIG. 8

Can. J. Chem. Downloaded from www.nrcresearchpress.com by 210.87.254.105 on 09/06/12
For personal use only.

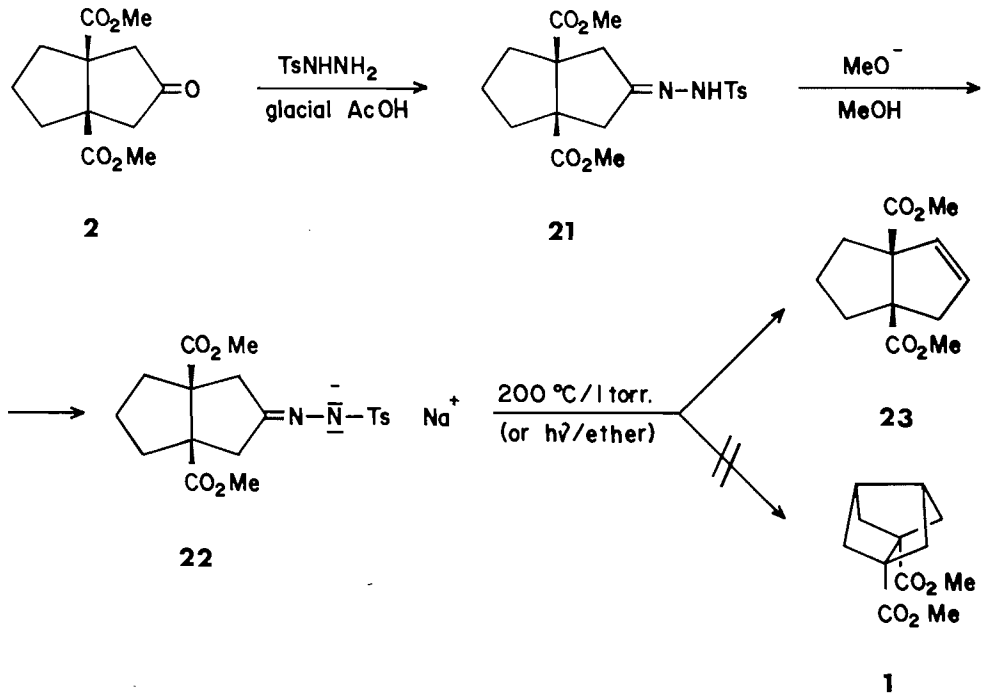

FIG. 9

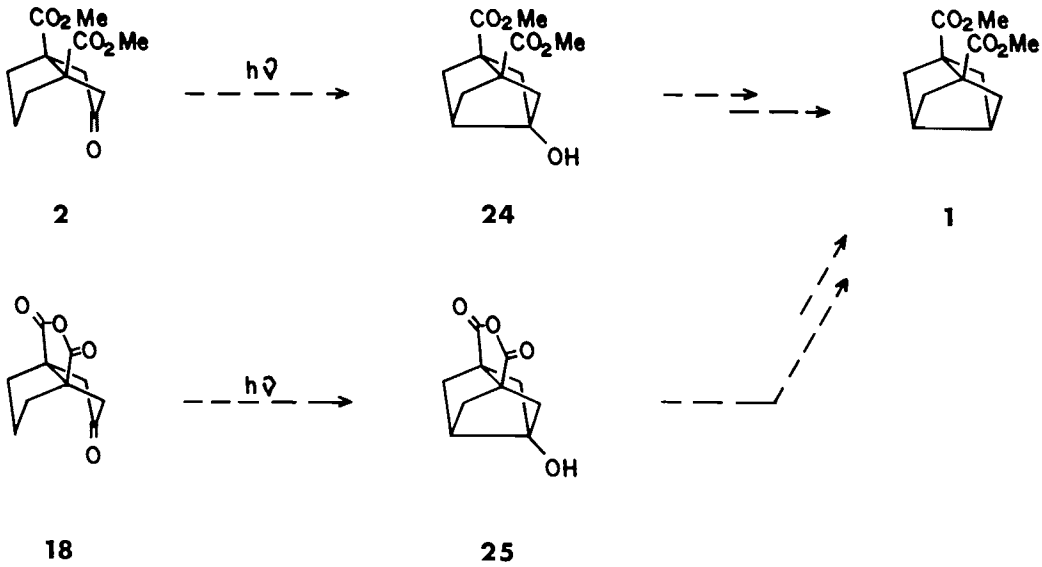

FIG. 10

photochemical decomposition of salt **22** suspended in ether or DME (Fig. 9).

Another approach to the tricyclo[3.3.0.0^{3,7}]octane skeleton, capable of being used to synthesize diester **1**, would be that shown in Fig. 10. It is known that photolysis of ketones can give cyclobutanol derivatives (12) by intramolecular abstraction of a hydrogen atom from the γ-position and combination of the resulting carbon radicals. In special cases, where hydrogen abstraction from the γ-position is difficult or not possible, abstraction from the δ-position can take place with formation of cyclopentanols (13).

Irradiation of ketodiester **2** under the conditions described by Paquette and co-workers (13) (benzene – *tert*-butyl alcohol or *tert*-butyl alcohol, Pyrex filter) left the starting material unchanged. Using a quartz filter, small amounts of compounds of molecular weights that could correspond to the addition of water, methanol, ethanol, propanol, and butanol were detected (glc/ms), the major product being in all cases the starting compound **2**. No formation of dimethyl 3-hydroxytricyclo-[3.3.0.0^{3,7}]octane-1,5-dicarboxylate, **24**, was ever observed. In a similar manner, irradiation of ketoanhydride **18** did not give the desired alcohol **25**. In this case, after irradiating for three days, most of the starting material was consumed, and formation of compounds whose molecular weights (glc/ms) could correspond to the addition of water and methanol was also observed.

Compound **24** could be prepared, although in only 5.4% yield, by reduction of dioxodiester **9** under the conditions (Zn/Ac_2O/gaseous HCl) used by Borden and Ravindranathan (1*j*) to reduce *cis*-1,5-dimethylbicyclo[3.3.0]octane-3,7-dione

Can. J. Chem. Downloaded from www.nrcresearchpress.com by 210.87.254.105 on 09/06/12
For personal use only.

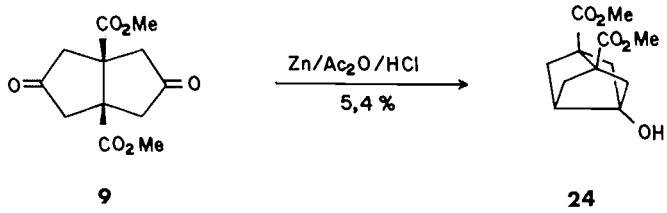

FIG. 11

to 3,7-dimethyltricyclo[3.3.0.0^{3,7}]oct-1-yl acetate. The spectroscopic data of this compound (ir, ^{1}H nmr ^{13}C nmr, ms) and elemental analysis are all concordant with its structure. However, the low yield of this reaction did not make it attractive for the synthesis of diester **1** (Fig. 11).

The low yield conversion of dioxodiester **9** into the hydroxydiester **24**, as compared with similar transformations (1*j*, 2), the failure of the synthesis of diester **1** by intramolecular C—H carbene insertion with formation of a C3—C7 bond from an appropriate bicyclo[3.3.0]octane precursor, and the fruitless attempts to transform bicyclo[3.3.0]octan-3-one derivatives photochemically into the corresponding tricyclo[3.3.0.0^{3,7}]-octan-1-ols, must be the consequence of a too long C3 . . . . C7 distance in the required conformation of the studied bicyclo[3.3.0]octane derivatives to form a C3—C7 bond. Probably the presence of larger substituents at C1 and C5 in the bicyclo[3.3.0]octane precursor and the connection of such substituents to form propellane derivatives make the C3 and C7 atoms closer and favour the formation of the C3—C7 bond as is the case for *cis*-1,5-dimethylbicyclo[3.3.0]octane-3,7-dione (1*j*), [6.3.3]propellane-10,13-dione (2), and [10.3.3]propellane-14,17-dione (2).

Work is in progress to synthesize diester **1** by using the method shown in the second procedure of Fig. 2.

Experimental

Infrared spectra were recorded on a Perkin–Elmer spectrometer model Infracord 720. The ^{1}H nmr spectra were taken at 60 MHz on a Perkin–Elmer R-12A spectrometer, while 80 MHz ^{1}H and 20 MHz ^{13}C nmr spectra were recorded on a Bruker model WP80SY spectrometer. Chemical shifts are given in ppm relative to internal TMS (δ scale). Mass spectra were recorded on Hewlett–Packard spectrometers model 5930A or 5985B, using the electron impact and chemical ionization techniques, always at 70 eV. Microanalyses were carried out at the Analytical Section of the "Instituto de Química Bio-orgánica" of Barcelona (C.S.I.C.) or at the Facultad de Ciencias, Universidad Autónoma de Barcelona. The glc analyses were performed with a Hewlett–Packard, model 5830A, or a Perkin–Elmer, model Sigma-1, chromatograph. Medium pressure 125- or 400-W mercury lamps were used in the photochemical reactions. Melting points were determined on a Kofler hot-stage and are uncorrected. Calculations were carried out at the Computing Center of Hokkaido University, Sapporo, Japan, on a HITAC M-200H system.

Dimethyl cis-*3,7-dioxobicyclo[3.3.0]octane-1,5-dicarboxylate, 9*

A mixture of 100 g (0.44 mol) of disodium dihydroxytartrate, **5**, and 400 mL anhydrous methanol was saturated with hydrogen chloride at 0°C (7), and allowed to stand in the refrigerator (5°C) for five days. The precipitated sodium chloride was filtered and thoroughly washed with anhydrous methanol. The filtrate was concentrated at reduced pressure, keeping the temperature below 40°C, to give 97.37 g of crude dimethyl 2,3-dioxobutanedioate, **6**, as a yellow viscous product that contains some hydrochloric acid.

Part of this product (35.26 g) was placed in a flask fitted with a magnetic stirrer, and 400 mL saturated aqueous $NaHCO_3$ solution (0.33 equiv. of base) plus 5.0 g solid $NaHCO_3$ to compensate the base consumed in neutralizing the acid present in the crude **6** (70 mL of the $NaHCO_3$ solution) were added. To this solution, 55.86 g (0.32 mol) of dimethyl 3-oxoglutarate, was added and the mixture stirred at room temperature for 7 days. The solution was acidified with 6 *N* HCl and extracted with $CHCl_3$ (5 × 150 mL). The extracts were washed with water and dried over anhydrous Na_2SO_4. Evaporation of the solvent gave 59.40 g of a complex mixture that was subjected as such to the Krapcho (8) decarbomethoxylation conditions.

A mixture of the whole crude product obtained before, 100 mL DMSO, 26.5 mL (1.47 mol) water, and 7.2 g (0.12 mol) NaCl was heated at 130–140°C for 4 h. After cooling at room temperature, 150 mL water was added and the mixture extracted with chloroform (3 × 100 mL + 4 × 50 mL). The extracts were washed with saturated aqueous $NaHCO_3$ solution (4 × 50 mL) and water (3 × 50 mL), and dried over anhydrous Na_2SO_4. Evaporation of the solvent gave 17.83 g of crude product which was distilled at reduced pressure. The fraction collected at 160–170°C/0.5 Torr (11.85 g) gave, on crystallization from methanol, 7.63 g of pure ketodiester **9**, sublimed at 125°C/15 Torr, mp 97–98°C (18% overall yield from salt **5**; in other runs the yield was in the range of 12%); ir ($CHCl_3$) ν: 1750 (s) cm^{-1}; ^{1}H nmr (60 MHz, $CDCl_3$) δ: 3.71 (s, 6H), 3.36 and 3.06 (d, *J* = 18 Hz, 4H), 2.56 and 2.26 (d, *J* = 18 Hz, 4H); ^{13}C nmr ($CDCl_3$) δ: 47.0 (t), 52.9 (c), 56.2 (s), 172.8 (s), 210.0 (s); ms: 254 (M$^+$, 35), 226(10), 223(26), 222(9), 194(27), 162(24), 135(29), 127(100), 99(33). *Anal.* calcd. for $C_{12}H_{14}O_6$: C 56.69, H 5.55; found: C 56.59, H 5.57.

Isolation of hexamethyl cis-*3,7-dioxobicyclo[3.3.0]octane-1,2,4,5,6,8-hexacarboxylate, 8*

From a reaction like that described before, starting from 2.0 g of salt **5**, the crude product of the reaction with dimethyl 3-oxoglutarate, **7** (4.38 g), after several crystallizations from ethanol, gave 780 mg of **8** (13.9% yield from **5**), mp 161–163°C; ir (KBr) ν: 3050 (w), 1760 (s), 1740 (s), 1675 (s) cm^{-1}; ^{1}H nmr (80 MHz, $CDCl_3$) δ: 10.52 (broad), 4.93–3.54 (complex absorption); ms: 486 (M$^+$, 3), 455(3), 454(8), 426(16), 394(50), 363(27), 335(75), 303(63), 271(52), 263(33), 244(39), 213(39), 59(100). *Anal.* calcd. for $C_{20}H_{22}O_{14}$: C 49.39, H 4.56; found: C 49.39, H 4.70.

Reaction of ketodiester 9 with ethanedithiol

A mixture of 2.203 g (8.67 mmol) of diketodiester **9** in 50 mL ethyl acetate, 812 mg (8.62 mmol) ethanedithiol, and 2.2 mL boron trifluoride etherate was allowed to stand at room temperature for 16 h. After adding 15 mL water, the organic phase was separated and washed with aqueous $NaHCO_3$ (2 × 10 mL) and water (3 × 10 mL), and dried over anhydrous Na_2SO_4. Evaporation of the solvent yielded 2.411 g of a mixture that was separated by low pressure column chromatography (14), using 50 g silica gel (230–400 mesh) and a mixture of hexanes – ethyl acetate as eluent, into three fractions: 1.130 g starting material; 995 mg monothioketal, **10** (71.4% yield if **9** was recovered), and 200 mg bisthioketal, **11** (11.4% yield if **9** was recovered).

Physical and spectroscopic data of dimethyl cis-*3,3-ethylenedithio-7-oxobicyclo[3.3.0]octane-1,5-dicarboxylate, 10*

Melting point 115–117°C (ethanol); ir (KBr) ν: 1740 (s), 1720 (s) cm^{-1}; ^{1}H nmr (80 MHz, $CDCl_3$) δ: 3.71 (s, 6H), 3.43 and 3.24 (d, *J* = 15.2 Hz, 2H), 3.33 (m, 4H), 3.13 and 2.90 (d, *J* = 18.4 Hz, 2H), 2.75 and 2.52 (d, *J* = 18.4 Hz, 2H), 2.68 and 2.49 (d, *J* = 15.2 Hz, 2H); ^{13}C nmr ($CDCl_3$) δ: 39.8, 40.8, 47.6, 52.4, 55.0, 60.1, 66.9, 173.8, 212.3; ms: 330 (M$^+$, 49), 299(12), 271(36), 266(11), 211(43), 199(100), 183(54), 123(42), 91(49), 69(42), 59(83). *Anal.* calcd. for $C_{14}H_{18}S_2O_5$: C 50.89, H 5.49, S 19.41; found: C 51.25, H 5.50, S 19.02.

Physical and spectroscopic data of dimethyl cis-*3,3,7,7-bisethylenedithiobicyclo[3.3.0]octane-1,5-dicarboxylate, 11*

Melting point 92–94°C (ethanol); ir (KBr) ν: 1720 (s) cm^{-1}; ^{1}H nmr (80 MHz, $CDCl_3$) δ: 3.70 (s, 6H), 3.31 (m, 8H), 3.24 and 3.05 (d, *J* = 15.2 Hz, 4H), 2.88 and 2.69 (d, *J* = 15.2 Hz, 4H); ^{13}C nmr ($CDCl_3$) δ: 39.8, 40.6, 52.0, 55.0, 64.4, 67.3, 174.1; ms: 406 (M$^+$, 7), 375(2), 346(5) 167(27), 149(57), 81(63), 69(100). *Anal.* calcd. for

Can. J. Chem. Downloaded from www.nrcresearchpress.com by 210.87.254.105 on 09/06/12
For personal use only.

Can. J. Chem. Downloaded from www.nrcresearchpress.com by 210.87.254.105 on 09/06/12
For personal use only.

$C_{16}H_{22}S_4O_4$: C 47.26, H 5.45, S 31.45; found: C 47.38, H 5:44, S 31.62.

Dimethyl cis-*3-oxobicyclo[3.3.0]octane-1,5-dicarboxylate,* **2**

A mixture of 750 mg (2.27 mmol) of monothioketal **10**, 7.5 g Raney Ni, and 20 mL ethanol was heated under reflux for 8 h. The mixture was filtered through a 2-cm pad of silica gel and the residue thoroughly washed with hot ethanol. Evaporation of the solvent gave a crude product that showed hydroxyl absorption in its infrared spectrum. This crude product was dissolved in 20 mL acetone and treated with 1.5 mL of Jones reagent. After stirring for 16 h at room temperature, the acetone was evaporated, the residue was diluted with 5 mL water, neutralized with saturated aqueous $NaHCO_3$ solution, and extracted with chloroform (5 × 5 mL). The organic extracts were washed with water and dried over anhydrous Na_2SO_4. Evaporation of the solvent gave a crude product which, chromatographed through 50 g silica gel (230–400 mesh) (14) using hexanes – ethyl acetate as eluent, gave 302 mg of ketodiester **2** (55.4% yield), bp 150°C(oven)/0.9 Torr; ir ($CHCl_3$) ν: 1740 (s) cm^{-1}; ^1H nmr (80 MHz, $CDCl_3$) δ: 3.69 (s, 6H), 3.14 and 2.91 (d, J = 19 Hz, 2H), 2.63–1.67 (complex absorption, 2.48 and 2.23 (d, J = 19 Hz), total 8H); ^{13}C nmr ($CDCl_3$) δ: 23.1, 36.6, 48.4, 52.3, 60.1, 174.9, 213.3; ms: 240 (M^+, 7), 212(15), 209(13), 152(31), 121(43), 93(100), 91(46), 79(54), 77(50), 59(44), 39(45). *Anal.* calcd. for $C_{12}H_{16}O_5$: C 59.99, H 6.71; found: C 60.17, H 6.72.

Physical and spectroscopic data of cis-*bicyclo[4.3.0]non-3-ene-1,6-dicarboxylic acid,* **13**

Melting point 143–144°C (water) (lit. (11) mp 154°C); ir (KBr) ν: 3600–2200 (s), 1690 (s) cm^{-1}; ^1H nmr (acetone-d_6) δ: 9.0 (broad, 2H), 5.7 (m, 2H), 2.9–1.5 (complex absorption, 10H); ^{13}C nmr (acetone-d_6) δ: 19.4, 32.9, 35.9, 52.5, 124.3, 177.9; ms: 192 ($M^+ - H_2O$, 5), 164(35), 119(96), 91(100), 79(19), 77(26); ms (chemical ionization, isobutane): 211 ($M^+ + 1$) and 193 ($M^+ - H_2O + 1$). *Anal.* calcd. for $C_{11}H_{14}O_4$: C 62.85, H 6.71; found: C 62.78, H 6.71.

Dimethyl cis-*bicyclo[4.3.0]non-3-ene-1,6-dicarboxylate,* **14**

A freshly distilled solution of diazomethane in ether was slowly added to 16.49 g (78.5 mmol) of diacid **13** until no nitrogen evolution was observed. Evaporation of the solvent gave a product that, distilled at 145°C/0.15 Torr, gave 19.01 g of diester **14** (quantitative yield); ir (film) ν: 3050 (w), 1735 (s) cm^{-1}; ^1H nmr (60 MHz, $CDCl_3$) δ: 5.8–5.6 (complex absorption, 2H), 3.65 (s, 6H), 2.8–1.6 (complex absorption, 10H); ^{13}C nmr ($CDCl_3$) δ: 18.8 (m), 31.8 (t), 34.7 (t), 51.6 (c), 52.3 (s), 123.3 (d), 176.3 (s); ms: 206 (M^+ – MeOH, 9), 178(30), 119(100), 118(41), 91(82); ms (chemical ionization, isobutane): 239 ($M^+ + 1$) and 207 (M^+ – MeOH + 1). *Anal.* calcd. for $C_{13}H_{18}O_4$: C 65.53, H 7.61; found: C 65.28, H 7.69.

meso-*1,2-Bismethoxycarbonylcyclopentane-1,2-diacetic acid,* **15**

To a cold solution (ice bath) of 5.3 g (33.54 mmol) of $KMnO_4$ in 50 mL water, a solution of 2.35 g (9.87 mmol) of diester **14** and 34 mg (0.11 mmol) tetra-*n*-butylammonium bromide in 33 mL acetic acid, and 165 mL benzene were added, and the mixture was stirred at room temperature for 16 h. The reaction mixture was cooled and treated with 5.83 g Na_2SO_3 followed by 12 mL 6 *N* HCl. The organic phase was separated and the aqueous one extracted with 50 mL benzene. Working up the benzene extracts, a residue of 277 mg, which did not contain starting material or diacid **15**, was obtained. Afterwards, the aqueous phase was extracted with ether (5 × 50 mL), and the ether extracts were washed with water (2 × 20 mL) and dried over anhydrous Na_2SO_4. Evaporation of the solvent gave 2.22 g of diacid **15** (75% yield), mp 177–179°C (ether); ir (KBr) ν: 3600–2400 (m), 1740 (s), 1700 (s) cm^{-1}; ^1H nmr (60 MHz, D_2O/NaOH) δ: 3.67 (s, 6H), 3.18 and 2.90 (d, J = 16.8 Hz, 2H), 2.58–1.49 (complex absorption, 2.41 and 2.13 (d, J = 16.8 Hz), total 8H); ^{13}C nmr (D_2O + dioxane) δ: 20.6 (m), 32.4 (m), 38.3 (t), 53.6 (c), 58.4 (s), 175.8(s), 177.0 (s); ms: 271 (M^+ – MeO, 7), 253(9), 243(9), 239(14), 229(44), 224(21), 211(14), 196(17), 183(23), 165(62), 151(45), 137(70), 91(79), 79(66), 77(57), 59(100); ms (chemical ionization, isobutane): 303 ($M^+ + 1$) and 271 (M^+ – MeOH + 1). *Anal.* calcd. for $C_{13}H_{18}O_8$: C 51.66, H 6.00; found: C 51.80, H 6.03.

Dimethyl meso-*1,2-bismethoxycarbonylcyclopentane-1,2-diacetate,* **16**

A freshly distilled solution of diazomethane in ether was slowly added to 12.7 g (42.05 mmol) of diacid **15** until no nitrogen evolution was observed. Evaporation of the solvent gave a crude product that, crystallized from methanol, yielded 12.72 g of tetraester **16** (92% yield), mp 95–97°C; ir (KBr) ν: 1720 (s) cm^{-1}; ^1H nmr (60 MHz, $CDCl_3$) δ: 3.64 (s, 12H), 3.33 and 3.07 (d, J = 16 Hz, 2H), 2.82–1.47 (complex absorption, 2.44 and 2.18 (d, J = 16 Hz), total 8H); ^{13}C nmr ($CDCl_3$) δ: 20.5, 32.0, 37.9, 51.6, 52.1, 57.6, 171.3, 173.3; ms: 299 (M^+ – MeO, 36), 257(47), 238(32), 225(43), 213(22), 197(39), 179(100), 165(40), 151(66), 91(48), 79(31), 77(33), 59(52); ms (chemical ionization, isobutane): 331 ($M^+ + 1$) and 299 (M^+ – MeOH + 1). *Anal.* calcd. for $C_{15}H_{22}O_8$: C 54.54, H 6.71; found: C 54.33, H 6.48.

Trimethyl cis-*3-oxobicyclo[3.3.0]octane-1,2,5-tricarboxylate,* **17**

A solution of 11 g (33.3 mmol) tetraester **16** in 100 mL anhydrous THF was slowly added to a cold suspension (ice bath) of approximately 2 g (83.3 mmol) of NaH (from 4 g of 50% dispersion of NaH in mineral oil, by washing with anhydrous THF) in 100 mL anhydrous THF. When the addition was finished, the mixture was heated under reflux for 3 h. The cold mixture was neutralized with 6 *N* HCl and made slightly acidic with 0.1 *N* HCl. The organic phase was separated and the aqueous one extracted with $CHCl_3$ (2 × 50 mL + 2 × 25 mL). The $CHCl_3$ extracts and the organic phase were mixed, washed with water (2 × 10 mL), and dried over anhydrous Na_2SO_4. Evaporation of the solvent gave 10.83 g of crude product. Distillation of 1.094 g of this crude product gave 918 mg of **17** (91% yield), bp 130°C (oven)/0.15 Torr; ir (film) ν: 3600–3200 (m), 1740 (s), 1660 (s), 1620 (s) cm^{-1}; ^1H nmr (80 MHz, $CDCl_3$) δ: 10.68 (broad, 1H), 3.81–3.39 (complex absorption, 3.74 (s), 3.66 (s), 3.61 (s), 9H), 2.71–1.54 (complex absorption, 2.48 (d, J = 18.2 Hz), total 8H); ^{13}C nmr ($CDCl_3$) (corresponding to the major enol form) δ: 24.8, 34.4, 40.9, 42.9, 51.3, 52.0, 52.3, 59.4, 66.9, 103.0, 169.0, 174.9, 175.6; ms: 298 (M^+, 2), 266(3), 238(22), 206(33), 179(63), 147(58), 119(100), 117(81), 91(75), 59(33). *Anal.* calcd. for $C_{14}H_{18}O_7$: C 56.37, H 6.08; found: C 56.46, H 5.95.

Ketodiester 2 from ketotriester 17

A mixture of 1.0 g (3.36 mmol) of ketotriester **17**, 212 mg (3.62 mmol) NaCl, 186 mg (10.3 mmol) water, and 2 mL DMSO was heated at 140°C for 2 h. To the cold mixture, 10 mL water was added and the solution extracted with $CHCl_3$ (5 × 10 mL). The chloroform extracts were washed with water and dried over anhydrous Na_2SO_4. Evaporation of the solvent gave a crude product which on distillation yielded 741 mg of pure ketodiester **2** (92% yield), bp 125°C (oven) /0.6 Torr.

cis-*3-Oxobicyclo[3.3.0]octane-1,5-dicarboxylic acid,* **19**

A mixture of 480 mg (2.0 mmol) of ketodiester **2** and 1.5 mL 6 *N* HCl was heated under reflux for 18 h. Evaporation of the volatile products gave a residue that, dried at reduced pressure over anhydrous KOH, gave 410 mg of ketodiacid **19** (97% yield), mp 165–182°C (dec.) (ether–benzene); ir (KBr) ν: 3650–2500 (m), 1735 (s), 1690 (s) cm^{-1}; ^1H nmr (80 MHz, acetone-d_6) δ: 10.33–9.87 (broad), 3.08–1.67 (complex absorption, 3.06 and 2.83 (d, J = 18.3 Hz), 2.55 and 2.32 (d, J = 18.3 Hz)); ^{13}C nmr (acetone-d_6) δ: 23.4, 37.1, 49.1, 60.5, 176.5, 213.7; ms: 212 (M^+, 5) 194(51), 166(38), 152(62), 138(25), 121(55), 94(67), 93(91), 79(98), 77(68), 60(72), 45(76), 39(100). *Anal.* calcd. for $C_{10}H_{12}O_5$: C 56.60, H 5.70; found: C 56.82, H 5.74.

3-Oxatricyclo[3.3.3.0^{1,5}]undecane-2,4,7-trione, **18**

In a 10-mL flask, 100 mg (0.47 mmol) of ketodiacid **19** and a trace of concentrated sulfuric acid were placed. The flask was connected to a rotary microdistillation apparatus and heated at 160°C/15 Torr. The distillate (84 mg) was sublimed at 75°C/0.2 Torr to give 78 mg of pure **18** (86% yield), mp 184–186°C; ir (KBr) ν: 1840 (m), 1780 (s), 1745

Can. J. Chem. Downloaded from www.nrcresearchpress.com by 210.87.254.105 on 09/06/12
For personal use only.

(s) cm^{-1}; ^1H nmr (80 MHz, acetone-d_6) δ: 3.20 and 2.95 (d, J = 19.5 Hz, 2H), 2.72 and 2.47 (d, J = 19.5 Hz, 2H), 2.68–1.50 (complex absorption, 6H); ^{13}C nmr (DMSO-d_6) δ: 25.8, 39.2, 46.2, 58.5, 175.9, 212.8; ms: 194 (M^+, 8), 122(24), 94(100), 79(81). *Anal.* calcd. for $C_{10}H_{10}O_4$: C 61.85, H 5.19; found: C 61.55, H 5.20.

cis-2,4-Dioxo-3-oxabicyclo[3.3.0]octane-1,2-diacetic acid, ***20***

To a cold solution (ice bath) of 538 mg (3.4 mmol) $KMnO_4$ in 5 mL water, a mixture of 192 mg (1.0 mmol) anhydride **12** and 3 mg (0.009 mmol) tetra-*n*-butylammonium bromide in 3.5 mL acetic acid and 16.5 mL benzene was added, and the mixture was stirred at room temperature for 1 h (at that time the $KMnO_4$ colour had disappeared). The mixture was treated with 600 mg (4.76 mmol) Na_2SO_3 followed by 1.2 mL 6 *N* HCl. The organic phase was separated and the aqueous one extracted with benzene (2 × 5 mL). Afterwards, the aqueous phase was extracted with ether (6 × 10 mL). The ether extracts were washed with water (2 × 2 mL) and dried over anhydrous Na_2SO_4. Evaporation of the solvent gave 84 mg of diacid **20** (33% yield), mp 173–176°C (ether–pentane). Evaporation of the aqueous phase and extraction of the solid residue with acetone did not give more diacid **20**. Infrared (KBr) ν: 3600–2450 (m), 1840 (w), 1770 (s), 1700 (s) cm^{-1}; ^1H nmr (80 MHz, acetone-d_6) δ: 10.24–8.88 (broad, 2H), 3.28 and 3.05 (d, J = 18.5 Hz, 2H), 3.03 and 2.80 (d, J = 18.5 Hz, 2H), 2.65–1.00 (complex absorption, 6H); ^{13}C nmr (acetone-d_6) δ: 23.5, 37.0, 39.9, 56.2, 173.1, 177.2; ms: 194(20), 184(6), 166(25), 152(23), 138(100), 94(67), 93(80), 91(35), 79(83), 77(45), 45(31), 39(31); ms (chemical ionization, isobutane): 257 (M^+ + 1). *Anal.* calcd. for $C_{11}H_{12}O_7$: C 51.57, H 4.72; found: C 51.38, H 4.75.

Ketoanhydride ***18*** *from diacid* ***20***

A finely ground mixture of 80 mg (0.31 mmol) diacid **20** and 5 mg (0.03 mmol) anhydrous $Ba(OH)_2$ was placed in a 10-mL flask that was connected to a rotary microdistillation apparatus and heated at 185°C/0.5 Torr. The distilled product (60 mg) was sublimed at 160°C/15 Torr to give 51 mg of pure **18** (84% yield).

Ketoanhydride ***18*** *from diacid* ***15***

A finely ground mixture of 400 mg (1.32 mmol) diacid **15** and 10 mg (0.06 mmol) anhydrous $Ba(OH)_2$ was placed in a 25-mL flask that was connected to a distillation apparatus. The flask was immersed in a melted metal bath at 300°C for 5 min. The solid condensed in the neck of the flask was taken up and, crystallized from benzene–hexane, gave 210 mg of **18** (82% yield).

Dimethyl cis-*3-(p-toluenesulfonylhydrazono)bicyclo[3.3.0]octane-1,5-dicarboxylate,* ***21***

A solution of 1.0 g (4.2 mmol) of ketodiester **2** and 1.55 g (8.32 mmol) tosylhydrazide in 40 mL glacial acetic acid was allowed to stand at room temperature for 15 h. Water was added until turbidity appeared, and the mixture was left in the refrigerator (0°C) for 24 h. The precipitated solid was filtered and dried in vacuum over anhydrous KOH, giving rise to 1.44 g tosylhydrazone **21** (84% yield), mp 128–130°C; ir (KBr) ν: 3230 (m), 1730 (s), 1660 (m), 1175 (s), 1095 (s) cm^{-1}; ^1H nmr (60 MHz, $CDCl_3$) δ: 8.1–7.1 (complex absorption, 7.92 and 7.78 (d, J = 8 Hz), 7.37 and 7.23 (d, J = 8 Hz), total 5H), 3.6 (broad singlet, 6H), 3.4–1.5 (complex absorption, 2.42 (s), total 13H); ms: 408 (M^+, 3), 377(10), 349(5), 253(29), 221(31), 193(90), 165(67), 133(48), 105(86), 91(100), 79(33), 77(35), 65(46). *Anal.* calcd. for $C_{19}H_{24}N_2SO_6$: C 55.87, H 5.92, N 6.86, S 7.85; found: C 55.90, H 6.08, N 6.90, S 7.96.

Pyrolysis of the sodium salt of ***21****,* ***22****. Dimethyl* cis-*bicyclo[3.3.0]-oct-2-ene-1,5-dicarboxylate,* ***23***

A mixture of 408 mg (1.0 mmol) tosylhydrazone **21**, 70 mg (1.3 mmol) anhydrous sodium methoxide, and 10 mL anhydrous methanol was heated under reflux for 2 h. The solvent was eliminated at reduced pressure at room temperature and the residue dried at 0.5 Torr for 16 h. The flask containing the salt of the tosylhydrazone **21** was connected to a rotary microdistillation apparatus and heated at 200°C/1 Torr. It distilled 161 mg of alkene **23** (72% yield), sublimed at 80°C/15 Torr, mp 68–70°C (methanol–benzene); ir ($CHCl_3$) ν: 3050 (m), 1730 (s) cm^{-1}; ^1H nmr (80 MHz, $CDCl_3$) δ: 5.79 (dt, J = 5.7 Hz, J' = 2.3 Hz, 1H), 5.48 (dt, J = 5.7 Hz, J' = 2.3 Hz, 1H), 3.65 (s, 3H), 3.63 (s, 3H), 3.20 (dt, J = 17.3 Hz, J' = 2.3 Hz, 1H), 2.52–1.30 (complex absorption, 7H); ^{13}C nmr ($CDCl_3$) δ: 24.3, 36.2, 40.5, 45.1, 51.7, 62.2, 71.1, 131.2, 132.8, 174.9, 176.1; ms: 224 (M^+, 0.2), 192(32), 165(31), 164(100), 105(67). *Anal.* calcd. for $C_{12}H_{16}O_4$: C 64.27, H 7.19; found: C 63.94, H 7.21.

Photochemical decomposition of the sodium salt of ***21***

A suspension of the salt **22**, obtained as described before from 100 mg tosylhydrazone **21**, in 40 mL ether was placed in a Pyrex photoreactor and deoxygenated by bubbling argon. The reactor was stoppered and the mixture irradiated with a 125-W lamp for 17 h. The suspension was filtered and the solvent evaporated from the filtrate to give 82 mg of a complex mixture (glc/ms), which on column chromatography gave 13 mg of alkene **23** (23% yield) as the only identifiable product. None of the other products formed in this reaction could be characterized as diester **1** (glc/ms).

Dimethyl 3-hydroxytricyclo[3.3.0.0^{3,7}]octane-1,5-dicarboxylate, ***24***

Forty milliliters acetic anhydride were saturated with anhydrous hydrogen chloride at −5°C, and then 936 mg (3.69 mmol) of diketodiester **9** were added. Activated zinc (15) was added in small portions, keeping the temperature of the reaction mixture below −10°C, until no more was consumed (15 g). The mixture was stirred at −5°C for 2 h and filtered, washing the residue with cold acetic anhydride. The filtrate was poured into 200 mL methanol at −70°C and allowed to stand for 16 h. The volatile products were evaporated, the residue was dissolved in 50 mL CH_2Cl_2 and washed with water (2 × 50 mL), 10% aqueous $NaHCO_3$ solution (2 × 50 mL), water (50 mL), and dried over anhydrous Na_2SO_4. Evaporation of the solvent gave 639 mg of crude product consisting mainly of starting material. Acidification of the aqueous phase and extraction with CH_2Cl_2 gave, after the usual work-up, 169 mg of a mixture of starting material and a new compound (46% relative area by glc). By column chromatography of this mixture (6 g silica gel, hexanes–$CHCl_3$ as eluent), 48 mg of hydroxydiester **24** was obtained (5.4% yield), bp 135–140°C (oven)/0.2 Torr. On standing, it crystallized, mp 73–76°C; ir (film) ν: 3700–3100 (m), 3020 (m), 1730 (s) cm^{-1}; ^1H nmr (80 MHz, $CDCl_3$) δ: 3.67 (s, 6H), 3.06–2.76 (broad, 1H), 2.38–1.72 (complex absorption, 9H); ^{13}C nmr ($CDCl_3$) δ: 44.9, 49.3, 51.7, 54.7, 55.9, 81.6, 172.5; ms: 209 (M^+ − MeOH, 20), 180(31), 140(100), 121(40), 108(79), 93(51), 91(72), 81(55), 77(69), 59(86); ms (chemical ionization, isobutane): 241 (M^+ + 1) and 209 (M^+ − MeOH + 1). *Anal.* calcd. for $C_{12}H_{16}O_5$: C 59.99, H 6.71; found: C 59.83, H 6.93.

Attempts to photocyclize ketodiester ***2*** *to hydroxydiester* ***24***

(a) *Pyrex filter*

A solution of 85 mg (0.35 mmol) ketodiester **2** in 25 mL benzene – *tert*-butyl alcohol (4:1) was placed in a pyrex photoreactor and nitrogen was bubbled through it for 1 h. The reactor was stoppered and the solution was irradiated with a 125-W lamp for 20 h. Evaporation of the solvent gave a residue which, when analyzed by glc, was shown to be the starting material. Similar results were obtained by carrying out the reaction in *tert*-butyl alcohol as solvent.

(b) *Quartz filter*

A solution of 75 mg (0.31 mmol) ketodiester **2** in 2 mL benzene – *tert*-butyl alcohol (5:1) was placed in a quartz tube. After bubbling in nitrogen for 1 h, the tube was stoppered and the solution was irradiated with a 400-W lamp, using a quartz refrigeration system, for 16 h. Evaporation of the solvent gave a crude product which when analyzed by glc/ms, was shown to contain mainly the starting material and minor amounts of other components with molecular weights of 258, 272, 286, 300, and 314. None of them correspond to the hydroxydiester **24**.

Attempt to photocyclize ketoanhydride ***18*** *to hydroxyanhydride* ***25***

A solution of 23 mg (0.12 mmol) ketoanhydride **18** in 2 mL of a mixture of benzene – *tert*-butyl alcohol (4:1) was placed in a quartz tube. After deoxygenating and irradiating the solution for 3 days with

a 400-W lamp, using a quartz refrigeration system, the solvent was evaporated and the residue analyzed by glc/ms. The major component of the residue had a molecular weight of 212, corresponding to the addition of water. Also, minor amounts of starting material and compounds with molecular weights of 226 and 210 were detected. None of them correspond to the expected **25**.

Acknowledgements

A fellowship from "Ministerio de Educación y Ciencia" to M. Figueredo is gratefully acknowledged. We are indebted to Dr. C. Jaime for carrying out the molecular mechanics calculations and to Prof. E. Ōsawa from the Department of Chemistry, Faculty of Science, Hokkaido University, Sapporo, Japan, for facilities to carry out such calculations. We gratefully thank Dr. F. Sánchez-Ferrando (Universidad Autónoma de Barcelona) for recording the 20 MHz ^{13}C and 80 MHz ^{1}H nmr spectra, Dr. A. Virgili and P. de March (Universidad Autónoma de Barcelona) for running the ms spectra, M. Guerra (Instituto de Química Bio-orgánica, C.S.I.C., Barcelona) for the elemental analyses, and A. Gil de Gómez (Facultad de Química de San Sebastián, Universidad del País Vasco) for carrying out the pyrolysis of compound **15.**

1. (*a*) O. W. WEBSTER and L. H. SOMMER. J. Org. Chem. **29**, 3103 (1964); (*b*) P. K. FREEMAN, V. N. MALLIKARJUNA RAO, and G. E. BIGAM. Chem. Commun. 511 (1965); (*c*) B. R. VOGT, S. R. SUTER, and J. R. E. HOOVER. Tetrahedron Lett. 1609 (1968); (*d*) R. R. SAUERS, W. SCHINSKI, and M. M. MASON. Tetrahedron Lett. 79 (1969); (*e*) J. R. E. HOOVER. U.S. Patent No. 3,496,228 (1967); (*f*) P. K. FREEMAN, R. B. KINNEL, and T. D. TIMOTHY. Tetrahedron Lett. 1059 (1970); (*g*) R. R. SAUERS and B. R. SICKLES. Tetrahedron Lett. 1067 (1970); (*h*) R. R. SAUERS and K. W. KELLY. J. Org. Chem. **35**, 3286 (1970); (*i*) W. T. BORDEN, U. VARMA, M. CABELL, and T. RAVINDRANATHAN. J. Am. Chem. Soc. **93**, 3800 (1971); (*j*) W. T. BORDEN and T. RAVINDRANATHAN. J. Org. Chem. **36**, 4125 (1971); (*k*) R. R. SAUERS, K. W. KELLY, and B. R. SICKLES. J. Org. Chem. **37**, 537 (1972); (*l*) R. R. SAUERS, W. SCHINSKI, M. M. MASON, E. M. O'HARA, and B. BYRNE. J. Org. Chem. **38**, 642 (1973); (*m*) I. K. MOISEEV, P. G. BELYAEV, T. A. MRATKHUZINA, N. P. TKACHERA, and S. S. NOVIKOV. Izv. Akad. Nauk SSSR, Ser. Khim. 54 (1973); (*n*) P. K. FREEMAN, T. D. TIMOTHY, and V. N. MALLIKARJUNA RAO. J. Org. Chem. **38**, 3823 (1973); (*o*) R. R. SAUERS and E. M. O'HARA. J. Am. Chem. Soc. **96**, 2510 (1974); (*p*) M. NAKAZAKI, K. NAEMURA, and Y. KONDO. J. Org. Chem. **41**, 1229 (1976); (*q*) L. CARBALLEIRA, J. CASADO, and M. A. RIOS. An. Quim. **73**, 3 (1977); (*r*) E. N. PETERS. Tetrahedron Lett. 751 (1977); (*s*) M. NAKAZAKI, K. NAEMURA, and N. ARASHIBA. J. Org. Chem. **43**, 888 (1978); (*t*) M. R. SMITH and J. M. HARRIS. J. Org. Chem. **43**, 3588 (1978); (*u*) J. GASTEIGER and O. DAMMER. Tetrahedron, **34**, 2939 (1978); (*v*) M. NAKAZAKI, H. CHIKAMATSU, K. NAEMURA, M. NISHINO, H. MURAKAMI, and M. ASAO. J. Org. Chem. **44**, 4588 (1979); (*w*) R. R. SAUERS, C. A. WESTON, and B. I. DENTZ. J. Org. Chem. **45**, 2813 (1980); (*x*) H. PARK and L. A. PAQUETTE. J. Org. Chem. **45**, 5378 (1980); (*y*) M. NAKAZAKI, H. CHIKAMATSU, K. NAEMURA, T. SUZUKI, M. IWASAKI, Y. SASAKI, and T. FUJII. J. Org. Chem. **46**, 2726 (1981); (*z*) M. NAKAZAKI, K. NAEMURA, H. HARADA, and H. NARUTAKI. J. Org. Chem. **47**, 3470 (1982).
2. S. YANG and J. M. COOK. J. Org. Chem. **41**, 1903 (1976).
3. (*a*) R. H. SHAPIRO. Organic reactions. Vol. 23. John Wiley and Sons, Inc., New York. 1976. p. 405; (*b*) M. R. VEGAR and R. J. WELLS. Tetrahedron Lett. **10**, 2565 (1969); (*c*) J. R. NEFF and J. E. NORDLANDER. J. Org. Chem. **41**, 2590 (1976).
4. C. JAIME AND E. ŌSAWA. Tetrahedron. **39**, 2769 (1983).
5. (*a*) U. WEISS and J. M. EDWARDS. Tetrahedron Lett. 4885 (1968); (*b*) J. OEHLDRICH, J. M. COOK, and U. WEISS. Tetrahedron Lett. 4549 (1976); (*c*) S. YANG-LAN, M. MUELLER-JOHNSON, J. OEHLDRICH, D. WICHMAN, J. M. COOK, and U. WEISS. J. Org. Chem. **41**, 4053 (1976); (*d*) R. MITSCHKA, U. WEISS, and J. M. COOK. J. Am. Chem. Soc. **100**, 3973 (1978); (*e*) A. GAWISH, R. MITSCHKA, U. WEISS, and J. M. COOK. Tetrahedron Lett. **22**, 211 (1981); (*f*) K. AVASTHI, M. N. DESHPANDE, WEN-CHING HAN, J. M. COOK, and U. WEISS. Tetrahedron Lett. **22**, 3475 (1981); (*g*) W. C. HAN, K. TAKAHASHI, J. M. COOK, U. WEISS, and J. V. SILVERTON. J. Am. Chem. Soc. **104**, 318 (1982); (*h*) R. MITSCHKA, J. OEHLDRICH, K. TAKAHASHI, J. M. COOK, U. WEISS, and J. V. SILVERTON. Tetrahedron, **37**, 4521 (1982).
6. (*a*) S. YANG and J. M. COOK. J. Org. Chem. **41**, 1903 (1976); (*b*) R. W. WEBER and J. M. COOK. Can. J. Chem. **56**, 189 (1978); (*c*) W. G. DAUBEN and D. M. WALKER. J. Org. Chem. **46**, 1103 (1981); (*d*) S. H. BERTZ, G. RIHS, and R. B. WOODWARD. Tetrahedron, **38**, 63 (1982).
7. N. DENH and E. CERATH. Bull. Soc. Chim. Fr. 589 (1976).
8. A. P. KRAPCHO and A. J. LOVEY. Tetrahedron Lett. **14**, 957 (1973).
9. R. E. WESIGARD, JR., R. K. RUSSELL, and L. A. PAQUETTE. J. Am. Chem. Soc. **96**, 7474 (1974).
10. R. D. HAMORTH, B. G. HUTLEY, R. G. LEACH, and G. RODGERS. J. Chem. Soc. 2720 (1962).
11. A. P. KRAPCHO, J. R. LARSON, and J. M. ELDRIDGE. J. Org. Chem. **42**, 3749 (1977).
12. D. C. NECKERS. Mechanistic organic photochemistry. Reinhold Publishing Corporation, New York. 1967. p. 177.
13. R. J. TERNANSKY, D. W. BALOGH, and L. A. PAQUETTE. J. Am. Chem. Soc. **104**, 4503 (1982).
14. W. C. STILL, M. KHAN, and A. MITRA. J. Org. Chem. **43**, 2923 (1978).
15. L. F. FIESER and M. FIESER. Reagents for organic synthesis. Vol. 2. John Wiley and Sons, Inc., New York. 1969. p. 461.

Can. J. Chem. Downloaded from www.nrcresearchpress.com by 210.87.254.105 on 09/06/12
For personal use only.

Six pyrimidonium salts: determination of their crystal structures and studies of their prototropic behaviour in solution[1]

THOMAS W. S. LEE, STEVEN J. RETTIG, ROSS STEWART,[2] AND JAMES TROTTER[2]
Department of Chemistry, University of British Columbia, 2036 Main Mall, Vancouver, B.C., Canada V6T 1Y6

Received October 19, 1983

THOMAS W. S. LEE, STEVEN J. RETTIG, ROSS STEWART, and JAMES TROTTER. Can. J. Chem. **62**, 1194 (1984).

Six methyl-substituted 2-pyrimidonium chloride salts have been prepared and the rates of hydrogen exchange of their reactive methyl groups (at the 4- and 6-positions) have been determined in DCl/D_2O solution. Adjacent methyl groups, whether on nitrogen or carbon, activate the exchanging centres, whereas more distant methyl groups have a deactivating effect. The molecular geometry of the salts has been determined by X-ray crystallography with the view to determining whether the presence of strain in the pyrimidonium ring can account for the activating effect of adjacent methyl. The most reactive compound, the 1,5,6-trimethylpyrimidonium chloride, has a geometry that is consistent with high reactivity, viz. a non-planar ring and short H . . . H intermethyl distance. However, the 1,4,5,6-tetramethyl compound, which also is non-planar and has an extremely short 5–6 intermethyl distance (1.99 Å), is not highly reactive; that is, the heightened strain is unable to overcome the deactivating inductive effect of the additional methyl group. We conclude that deviations from ring planarity and short intermethyl distances are insufficient to account for the activation produced by adjacent methyl though they appear to be contributing factors to this effect.

THOMAS W. S. LEE, STEVEN J. RETTIG, ROSS STEWART et JAMES TROTTER. Can. J. Chem. **62**, 1194 (1984).

On a préparé six chlorures de pyrimidonium-2 portant des substituants méthyles et on a déterminé les vitesses d'échange d'hydrogène, catalysées par une solution de DCl/D_2O, de leurs groupes méthyles réactifs (en positions 4 et 6). Les groupes méthyles adjacents qu'ils soient sur l'azote ou sur le carbone activent les centres d'échange tandis que les groupes méthyles plus éloignés ont un effet désactivant. On a déterminé la géométrie moléculaire des sels par cristallographie de rayons-X dans le but de déterminer si la présence de contrainte dans le cycle pyrimidonium peut intervenir dans l'effet activant des groupes méthyles adjacents. Le composé le plus réactif, le chlorure de triméthyl-1,5,6 pyrimidonium a une géométrie qui justifie sa grande réactivité soit l'existence d'un cycle qui n'est pas plan et le fait que les distances H . . . H interméthyliques sont courtes. Dans le cas du composé tétraméthyl-1,4,5,6, le cycle n'est pas plan et la distance entre les méthyles-5,6 est très courte (1.99 Å); malgré ces caractéristiques, ce composé n'est pas très réactif et ceci implique que l'encombrement accru n'est pas suffisant pour contrebalancer l'effet inductif désactivant du groupe méthyle additionnel. Nous concluons que le manque de planéité dans les cycles et le fait que les distances entre les méthyles sont courtes ne sont pas des conditions suffisantes pour expliquer l'activation provoquée par la présence d'un groupe méthyle adjacent même s'il semble qu'ils sont des facteurs qui contribuent à cet effet.

[Traduit par le journal]

Introduction

Methyl groups at the 4- and 6-positions in 2-pyrimidones, **1**, and their protonated or alkylated derivates, **2** (Y = H or alkyl), are activated sites that exchange their protons with those of the solvent (1, 2). They are two of several heterocyclic systems that show unusual effects of neighbouring alkyl substitution (3–9). In brief, introduction of an alkyl group (usually methyl) at a position that is adjacent to the reactive methyl group has an activating effect on proton loss, whereas one introduced at a more distant location has a deactivating effect.

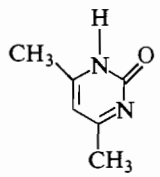

1

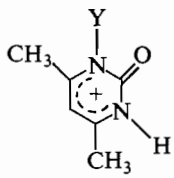

2

The deactivating effect of next-but-one methyl, which is commonly of the order of 20 or more, is in the expected direction, although its magnitude is perhaps surprising. Proton exchange involves loss of a proton (eq. [1]) from the active site and the electronic effect of alkyl should stabilize the reactant and decrease the rate.

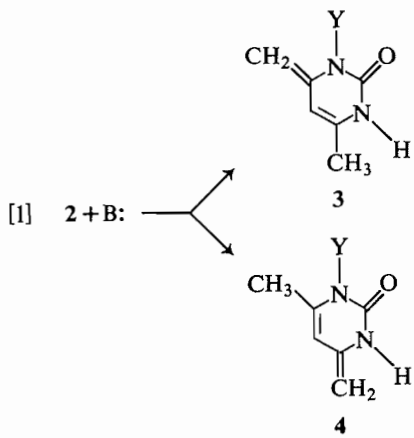

[1] **2** + B:

3

4

We have considered a number of possibilities (1, 2) for the rate increase produced by an adjacent methyl group. These include the attractive notion that steric strain caused by the interaction of adjacent methyl groups is relieved upon proton loss as the substrate, which is highly resonance stabilized, is converted to the intermediates **3** or **4**, which can adopt a non-planar arrangement without undue loss of stabilization.

In the present work the rates of exchange of activated methyl groups (4- or 6-position) of six pyrimidonium ions have been measured in 0.106 molar DCl in D_2O. This medium was chosen so as to allow both protonated and alkylated species to be studied under identical conditions. The molecular geometry of these cations was then determined by means of an X-ray crys-

[1] This paper is dedicated to Professor Jack Dunitz on the occasion of his 60th birthday, 29 March 1983.

[2] To whom correspondence should be addressed.

Can. J. Chem. Downloaded from www.nrcresearchpress.com by 210.87.254.105 on 09/06/12
For personal use only.

Can. J. Chem. Downloaded from www.nrcresearchpress.com by 210.87.254.105 on 09/06/12
For personal use only.

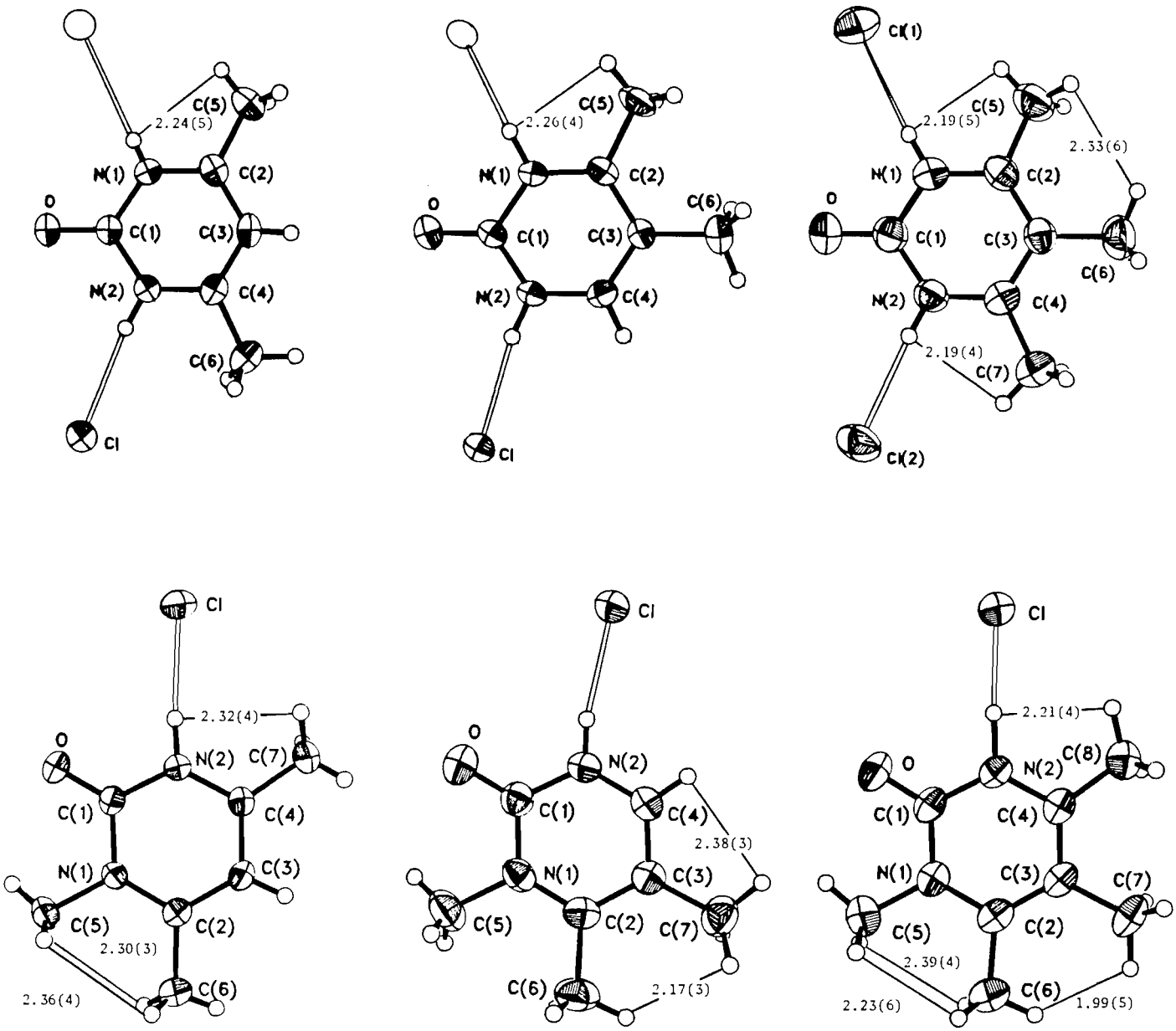

FIG. 1. Views of the molecules **5**, **6**, **7** (top) and **8**, **9**, **10** (bottom).

tallographic study of their chloride salts. The results described herein reveal the presence of significant strain in some of the more reactive species, though this strain falls far short of providing a full explanation of the rate effects that have been observed.

Results

Crystal structures of the 2-pyrimidone hydrochlorides ***5–10***

The results are shown in Tables 1–6. Each of the structures consists of 2-pyrimidonium cations and chloride anions, the packing being dominated by N—H . . . Cl hydrogen bonding (see Table 6). The structures of **5–7** (wherein each cation possesses two NH protons) contain infinite chains of alternating cations and anions linked by N—H . . . Cl hydrogen bonds. In **5** this arrangement is planar, all non-hydrogen atoms residing on a crystallographic mirror plane, while in **6** the chain spirals about the twofold screw-axis. The chains in **7** contain two crystallographically independent Cl^- anions, each of which resides on a crystallographic twofold axis perpendicular to the direction of propagation; thus adjacent cations are related by a twofold rotation about an axis containing the symmetrically bridging chloride anion. The structures of **8–10**, *N*-methylated derivatives of **5–7**, respectively, consist of strongly N—H . . . Cl hydrogen-bonded ion-pairs (Fig. 1) separated from one another by van der Waals distances. The mean N . . . Cl and H . . . Cl distances of 3.03 and 2.08 Å in **8–10** are shorter than the corresponding distances of 3.14 and 2.30 Å in **5–7**, consistent with the fact that each chloride ion is involved in only one hydrogen bond in the compounds **8–10** while those in **5–7** are each involved in two. These N—H . . . Cl hydrogen bonds are all relatively strong, the average N . . . Cl and H . . . Cl distances compiled for a number of such interactions being 3.23 and 2.4 Å, respectively (10, 11).

The most notable structural feature exhibited by this series of compounds is the steric interaction between the methyl substituents. This steric strain arises primarily from intramolecular

Can. J. Chem. Downloaded from www.nrcresearchpress.com by 210.87.254.105 on 09/06/12
For personal use only.

TABLE 1. Crystallographic data for 2-pyrimidone hydrochlorides

Parameter	Value[a]					
	5	**6**	**7**	**8**	**9**	**10**
Formula	$C_6H_9ClN_2O$	$C_6H_9ClN_2O$	$C_7H_{11}ClN_2O$	$C_7H_{11}ClN_2O$	$C_7H_{11}ClN_2O$	$C_8H_{13}ClN_2O$
fw	160.60	160.60	174.63	174.63	174.63	188.66
Crystal system	Orthorhombic	Monoclinic	Orthorhombic	Monoclinic	Monoclinic	Orthorhombic
a	14.2523(7)	6.7175(8)	11.4592(7)	6.8243(4)	10.4250(7)	6.2619(4)
b	6.6674(4)	15.8743(8)	14.5931(10)	7.2882(2)	8.3646(4)	9.7646(5)
c (Å)	8.0192(5)	7.3013(9)	10.5894(7)	16.7938(10)	10.2352(7)	15.6205(11)
β (deg)	90	102.038(6)	90	96.709(3)	107.190(3)	90
V (Å^3)	762.03(7)	761.5(1)	1770.8(2)	829.55(8)	852.65(9)	955.1(1)
Z	4	4	8	4	4	4
ρ_c (g/cm^3)	1.400	1.401	1.310	1.398	1.360	1.312
F(000)	336	336	736	368	368	400
Space group	*Pnma*	$P2_1/c$	*Pbcn*	$P2_1/n$[b]	$P2_1/c$	$P2_12_12_1$
Crystal dimensions (mm)	0.16 × 0.35 × 0.52	0.09 × 0.20 × 0.40	0.22 × 0.22 × 0.50	0.15 × 0.45 × 0.55	0.20 × 0.40 × 0.45	0.08 × 0.27 × 0.32
μ(Mo-K$_\alpha$) cm^{-1}	4.3	4.3	3.8	4.0	3.9	3.8
Integration points	96	64	76	80	98	96
Transmission factors	0.857–0.908	0.915–0.960	0.913–0.933	0.908–0.956	0.849–0.938	0.899–0.976
Data collected	*h*, *k*, *l*	*h*, *k*, ±*l*	*h*, *k*, *l*	*h*, *k*, ±*l*	*h*, *k*, ±*l*	*h*, *k*, *l*
2θ (max)°	65	65	65	60	60	60
Unique reflections	1468	2737	3175	2413	2479	1615
Observed reflections	807	1375	1103	1627	1603	941
R	0.043	0.031	0.033	0.033	0.031	0.026[c]
R_w	0.046	0.039	0.031	0.045	0.040	0.025
R (all data)	0.092	0.096	0.148	0.063	0.062	0.070
Error	2.073	1.785	0.745	1.940	1.676	0.493

[a]4,6-Dimethyl-2-pyrimidone hydrochloride, **5**; 5,6-dimethyl-2-pyrimidone hydrochloride, **6**; 4,5,6-trimethyl-2-pyrimidone hydrochloride, **7**; 1,4,6-trimethyl-2-pyrimidone hydrochloride, **8**; 1,5,6-trimethyl-2-pyrimidone hydrochloride, **9**; 1,4,5,6-tetramethyl-2-pyrimidone hydrochloride, **10**.

[b]Non-standard setting of $P2_1/c$, equivalent positions: ± (x, y, z; $\frac{1}{2} - x$, $\frac{1}{2} + y$, $\frac{1}{2} - z$).

[c]Residuals slightly higher for the mirror image which was refined in parallel.

TABLE 2. Final positional (fractional × 10^4, Cl × 10^5, H × 10^3) and isotropic thermal parameters ($U \times 10^3$ Å^2) with estimated standard deviations in parentheses

Atom	x	y	z	U_{eq}/U_{iso}	Atom	x	y	z	U_{eq}/U_{iso}
		5					**6**		
Cl	−14680(4)	25000	49205(7)	43	Cl	−13236(6)	37755(3)	−14270(6)	43
O	825.3(14)	2500	1779(2)	64	O	3606(2)	2098.0(8)	210(2)	57
N(1)	2185(2)	2500	3265(3)	38	N(1)	6194(2)	2856.4(9)	1968(2)	35
N(2)	757(2)	2500	4610(2)	36	N(2)	3153(2)	3500.8(9)	701(2)	38
C(1)	1223(2)	2500	3105(3)	40	C(1)	4249(3)	2762.4(11)	899(3)	38
C(2)	2649(2)	2500	4706(3)	39	C(2)	7026(2)	3578.1(10)	2691(2)	33
C(3)	2144(2)	2500	6168(3)	41	C(3)	5844(3)	4312.5(10)	2469(2)	35
C(4)	1187(2)	2500	6098(3)	38	C(4)	3902(3)	4235.1(10)	1455(3)	37
C(5)	3687(2)	2500	4674(5)	62	C(5)	9173(3)	3562(2)	3697(4)	50
C(6)	569(3)	2500	7591(4)	57	C(6)	6670(4)	5134.8(13)	3320(3)	53
H(N1)	248(2)	250	259(4)	39(8)	H(N1)	701(4)	239.0(14)	214(3)	54(6)
H(N2)	14(2)	250	460(3)	43(8)	H(N2)	185(4)	352.5(12)	4(3)	42(5)
H(3)	239(2)	250	711(4)	41(7)	H(4)	302(3)	467.4(12)	133(3)	42(5)
H(5a)	392(3)	250	369(6)	105(15)	H(5a)	997(4)	397(2)	315(4)	64(7)
H(5b)	393(2)	115(5)	515(3)	77(8)	H(5b)	914(5)	368(2)	484(5)	91(10)
H(6a)	91(3)	250	864(6)	94(13)	H(5c)	991(5)	308(2)	345(4)	101(10)
H(6b)	15(2)	135(4)	756(3)	102(9)	H(6a)	787(4)	527.9(14)	278(3)	57(6)
					H(6b)	568(4)	558(2)	312(3)	66(7)
					H(6c)	714(4)	509.9(14)	472(4)	67(7)
		7					**8**		
Cl(1)	50000	11957(6)	25000	61	Cl	43199(6)	−20255(6)	67909(2)	41
Cl(2)	50000	51567(7)	75000	64	O	2097(2)	−1793(2)	4611.3(8)	44
O	5552(2)	3145(2)	5045(2)	68	N(1)	1540(2)	1120(2)	4122.2(7)	28
N(1)	3894(2)	2840(2)	3925(2)	47	N(2)	2945(2)	601(2)	5438.7(7)	30
N(2)	3941(2)	4044(2)	5322(2)	44	C(1)	2193(2)	−151(2)	4718.9(8)	29
C(1)	4548(3)	3329(2)	4785(3)	48	C(2)	1659(2)	2951(2)	4248.1(8)	30
C(2)	2787(2)	3037(2)	3595(2)	44	C(3)	2444(3)	3622(2)	4990.2(10)	33
C(3)	2219(2)	3764(2)	4159(2)	44	C(4)	3094(2)	2413(2)	5594.3(9)	29
C(4)	2840(3)	4278(2)	5026(3)	44	C(5)	801(3)	362(3)	3330.1(10)	37
C(5)	2271(4)	2439(3)	2602(4)	65	C(6)	921(3)	4199(3)	3576.4(12)	43
C(6)	961(3)	3989(3)	3881(4)	65	C(7)	3930(3)	2970(3)	6412.3(10)	42
C(7)	2354(4)	5098(3)	5673(4)	64	H(N)	332(3)	−24(3)	582.6(11)	45(5)
H(N1)	423(2)	240(2)	354(3)	49(9)	H(3)	258(3)	480(3)	511.8(11)	37(5)
H(N2)	432(3)	440(2)	584(3)	77(11)	H(5a)	−46(3)	75(3)	318.1(12)	55(6)
H(5a)	277(4)	204(3)	231(4)	116(16)	H(5b)	78(3)	−77(4)	335.2(12)	43(6)
H(5b)	151(4)	214(3)	283(4)	129(16)	H(5c)	170(4)	76(4)	299.3(14)	68(7)
H(5c)	195(4)	276(3)	198(4)	130(19)	H(6a)	104(3)	528(4)	372.7(14)	56(7)
H(6a)	87(3)	459(3)	338(4)	120(15)	H(6b)	−40(3)	388(3)	335.0(14)	63(7)
H(6b)	60(4)	348(3)	349(4)	135(18)	H(6c)	154(3)	398(4)	313.7(14)	59(7)
H(6c)	52(5)	399(3)	465(5)	174(25)	H(7a)	410(4)	408(5)	647(2)	70(8)
H(7a)	289(3)	537(3)	617(4)	107(16)	H(7b)	473(5)	211(5)	664(2)	102(11)
H(7b)	210(4)	546(3)	515(4)	107(17)	H(7c)	303(5)	273(5)	673(2)	118(12)
H(7c)	168(4)	493(3)	625(4)	146(19)					
		9					**10**		
Cl	30980(3)	62131(5)	32442(3)	48	Cl	74051(15)	58026(8)	34762(4)	51
O	479.1(11)	6736.9(14)	5427.4(12)	58	O	8063(3)	3080(2)	5199.2(14)	55
N(1)	1297.1(10)	5402.0(13)	7465.5(11)	39	N(1)	5478(4)	3096(2)	6239.0(13)	39
N(2)	2493.2(12)	5488.1(13)	5878.5(12)	41	N(2)	5408(4)	4646(2)	5110.6(15)	40
C(1)	1361.3(13)	5947(2)	6190.9(14)	41	C(1)	6439(5)	3560(3)	5491(2)	40
C(2)	2296.1(13)	4581(2)	8345.0(13)	39	C(2)	3620(4)	3625(3)	6548(2)	38
C(3)	3426.1(13)	4127.7(15)	7973.2(14)	40	C(3)	2638(5)	4720(3)	6137(2)	39
C(4)	3478.8(13)	4638.0(15)	6711.5(14)	39	C(4)	3565(4)	5201(3)	5394(2)	38
C(5)	78(2)	5874(3)	7813(2)	61	C(5)	6528(6)	1920(4)	6651(2)	52
C(6)	2171(2)	4204(3)	9730(2)	60	C(6)	2746(7)	2964(4)	7334(2)	54
C(7)	4546(2)	3125(2)	8868(2)	58	C(7)	614(6)	5372(4)	6456(3)	55
H(N)	261(2)	585(2)	511(2)	52(4)	C(8)	2658(7)	6330(3)	4860(2)	52
H(4)	417(2)	436(2)	638(2)	47(4)	H(N)	614(5)	501(3)	451(2)	80(11)
H(5a)	−36(2)	497(3)	814(2)	88(7)	H(5a)	693(6)	213(3)	725(2)	65(11)
H(5b)	−55(4)	617(3)	704(4)	124(11)	H(5b)	552(7)	107(5)	664(3)	137(18)
H(5c)	20(3)	668(3)	839(3)	99(8)	H(5c)	783(6)	173(4)	638(2)	81(13)

Can. J. Chem. Downloaded from www.nrcresearchpress.com by 210.87.254.105 on 09/06/12
For personal use only.

TABLE 2. (*Concluded*)

Atom	*x*	*y*	*z*	U_{eq}/U_{iso}	Atom	*x*	*y*	*z*	U_{eq}/U_{iso}
H(6a)	213(3)	522(3)	1016(3)	108(9)	H(6a)	264(7)	197(4)	726(2)	71(10)
H(6b)	153(3)	364(3)	974(2)	78(7)	H(6b)	365(6)	305(4)	780(2)	68(12)
H(6c)	297(3)	364(3)	1031(3)	96(8)	H(6c)	146(6)	339(4)	749(2)	67(12)
H(7a)	428(2)	199(3)	895(2)	75(6)	H(7a)	92(7)	629(4)	663(3)	112(16)
H(7b)	533(2)	312(3)	850(2)	75(6)	H(7b)	−45(8)	534(5)	607(3)	111(18)
H(7c)	491(2)	363(2)	993(3)	83(7)	H(7c)	−9(9)	496(5)	696(3)	156(23)
					H(8a)	266(6)	712(3)	522(2)	59(9)
					H(8b)	348(5)	646(3)	430(2)	62(11)
					H(8c)	134(7)	611(4)	468(3)	94(15)

TABLE 3. Bond lengths with estimated standard deviations in parentheses[a]

	Bond length					
Atoms	**5**	**6**	**7**	**8**	**9**	**10**
C(1)—O	1.208(3)	1.213(2)	1.217(3)	1.214(2)	1.215(2)	1.213(3)
C(1)—N(1)	1.383(3)	1.388(2)	1.384(4)	1.403(2)	1.409(2)	1.396(3)
C(1)—N(2)	1.384(3)	1.381(2)	1.384(4)	1.375(2)	1.372(2)	1.381(4)
N(1)—C(2)	1.340(3)	1.341(2)	1.353(3)	1.358(2)	1.353(2)	1.366(3)
C(2)—C(3)	1.383(3)	1.408(2)	1.389(4)	1.391(2)	1.400(2)	1.395(4)
C(3)—C(4)	1.372(4)	1.371(2)	1.390(4)	1.381(2)	1.383(2)	1.386(4)
C(4)—N(2)	1.350(3)	1.347(2)	1.350(3)	1.354(2)	1.337(2)	1.355(3)
N(1)—Me/H	0.69(3)	0.92(2)	0.85(3)	1.477(2)	1.477(2)	1.476(4)
C(2)—Me	1.484(4)	1.481(2)	1.493(4)	1.494(2)	1.500(2)	1.495(4)
C(3)—Me/H	0.83(3)	1.506(2)	1.512(4)	0.89(2)	1.512(2)	1.508(4)
C(4)—Me/H	1.490(4)	0.91(2)	1.491(4)	1.484(2)	0.92(2)	1.498(4)
N(2)—H	0.88(3)	0.91(2)	0.87(3)	0.91(2)	0.88(2)	1.10(3)

[a] All distances in Å; bonds not involving hydrogen have been corrected for libration in which case the quoted esd is that derived from the least-squares analysis for the uncorrected bond distance.

TABLE 4. Bond angles with estimated standard deviations in parentheses

	Bond angle (deg)					
Atoms	**5**	**6**	**7**	**8**	**9**	**10**
O—C(1)—N(1)	123.4(2)	122.9(2)	123.4(3)	122.71(13)	122.79(13)	123.7(3)
O—C(1)—N(2)	123.1(2)	124.24(15)	123.6(3)	122.31(14)	123.08(13)	122.1(3)
N(1)—C(1)—N(2)	113.5(2)	112.91(15)	113.0(3)	114.97(13)	114.12(11)	114.2(2)
C(1)—N(1)—C(2)	125.1(2)	125.76(14)	125.0(3)	122.23(12)	123.22(11)	123.0(2)
C(1)—N(1)—(Me/H)	122(3)	117.4(13)	117(2)	116.44(14)	114.82(13)	115.3(3)
C(2)—N(1)—(Me/H)	113(3)	116.7(13)	118(2)	121.27(13)	121.88(13)	121.5(3)
C(1)—N(2)—C(4)	124.0(2)	123.42(14)	124.8(3)	125.06(13)	123.86(12)	124.7(3)
C(1)—N(2)—H(N2)	118(2)	121.9(12)	118(2)	114.1(13)	117.8(12)	115(2)
C(4)—N(2)—H(N2)	118(2)	114.7(12)	117(2)	120.8(14)	118.2(12)	120(2)
N(1)—C(2)—C(3)	118.6(2)	119.24(14)	119.7(2)	119.89(13)	120.36(12)	120.4(3)
N(1)—C(2)—Me	118.8(2)	117.85(15)	115.7(3)	118.38(14)	118.31(14)	116.2(3)
C(3)—C(2)—Me	122.6(2)	122.9(2)	124.6(3)	121.73(15)	121.32(14)	123.4(3)
C(2)—C(3)—C(4)	119.2(2)	116.25(14)	117.4(2)	119.59(14)	116.32(12)	117.7(3)
C(2)—C(3)—(Me/H)	124(2)	121.6(2)	122.3(3)	125.3(12)	123.41(13)	123.0(3)
C(4)—C(3)—(Me/H)	117(2)	122.1(2)	120.3(3)	115.1(12)	120.27(13)	119.3(3)
N(2)—C(4)—C(3)	119.5(2)	122.34(15)	120.0(2)	118.26(14)	121.97(12)	119.9(3)
N(2)—C(4)—(Me/H)	116.5(2)	116.4(12)	116.7(3)	117.41(14)	116.4(11)	116.0(3)
C(3)—C(4)—(Me/H)	124.0(2)	121.1(12)	123.3(3)	124.32(14)	121.5(11)	124.1(3)

van der Waals contacts between hydrogen atoms (shown in Fig. 1) and is relieved by a combination of exocyclic bond angle deformations and deviations of the six-membered rings from planarity. These small (<0.02 Å) but significant deviations from planarity are observed only when two adjacent ring carbon atoms are substituted (**6**, **7**, **9**, and **10**). Thus in **5** (in which there are no adjacent methyl-substituted ring atoms) the ring is planar. The potential steric interaction between the C(2)—methyl groups (common to all six molecules; crystallographic numbering scheme) and the N(1)—methyl substituent in **8**–**10** appears to be relieved primarily by deformation of the exocyclic angles about N(1) (C(5)—N(1)—C(2) = 121.3–121.9°, C(5)—N(1)—C(1) = 114.8–116.4° in **8**–**10**). The six-membered ring of **8** is thus also planar while those in

Can. J. Chem. Downloaded from www.nrcresearchpress.com by 210.87.254.105 on 09/06/12
For personal use only.

TABLE 5. Intraannular torsion angles

Atoms	Intraannular torsion angle					
	5[a]	6	7	8	9	10
N(2)—C(1)—N(1)—C(2)	0.0	−2.9(2)	1.8(4)	0.5(2)	3.8(2)	3.0(3)
C(1)—N(1)—C(2)—C(3)	0.0	3.7(3)	−1.7(4)	−0.2(2)	−4.7(2)	−3.0(4)
N(1)—C(2)—C(3)—C(4)	0.0	−2.0(2)	1.8(4)	−0.1(2)	3.3(2)	2.6(4)
C(2)—C(3)—C(4)—N(2)	0.0	−0.2(3)	−2.2(4)	0.2(2)	−1.4(2)	−2.6(4)
C(3)—C(4)—N(2)—C(1)	0.0	1.0(3)	2.6(4)	0.1(2)	0.8(2)	3.1(4)
C(4)—N(2)—C(1)—N(1)	0.0	0.4(2)	−2.3(4)	−0.4(2)	−1.9(2)	−3.1(4)

[a]Crystallographic mirror symmetry.

TABLE 6. Geometry of N—H . . . Cl hydrogen bonds

Atoms	Geometry					
	5	6	7[a]	8	9	10
N(2)—H . . . Cl			Cl(2)			
N . . . Cl (Å)	3.181(2)	3.114(1)	3.071(2)	3.034(1)	3.007(1)	3.059(2)
H . . . Cl (Å)	2.30(3)	2.22(2)	2.21(3)	2.13(2)	2.14(2)	1.96(3)
N—H . . . Cl (deg)	173(2)	172(2)	166(3)	175(2)	167(2)	175(3)
N(1)—H . . . Cl (Cl at)	$\frac{1}{2} + x, y, \frac{1}{2} - z$	$1 + x, \frac{1}{2} - y, \frac{1}{2} + z$	Cl(1)	—	—	—
N . . . Cl (Å)	3.195(2)	3.170(2)	3.106(3)	—	—	—
H . . . Cl (Å)	2.51(3)	2.30(2)	2.25(3)	—	—	—
N—H . . . Cl (deg)	179(3)	159(2)	176(3)	—	—	—
H . . . Cl . . . H (deg)	120.4(9)	113.8(7)	77.4(13), 120.3(15)	—	—	—

[a]This structure contains two independent Cl atoms, each lying on a crystallographic twofold axis.

6 and **9** adopt irregular conformations approximating flattened N(1)—envelopes, and those in **7** and **10** have flattened chair conformations.

The six cations contain essentially localized C=O double bonds (mean C—O = 1.213(3) Å) and the slightly shortened C(1)—N bonds (mean C(1)—N = 1.387 Å) indicate a bond order of approximately 1.15. Bond lengths in the N—C(2)—C(3)—C(4)—N portions of the rings (mean N—C = 1.350 and mean C—C = 1.381 Å) are similar to those in pyridine, indicating full delocalization of the two double bonds formally present in this portion of the ring. The symmetrically substituted compounds **5** and **7** show the expected twofold symmetry, while the remaining structures show clearly the substituent-induced deviations from twofold symmetry (see Tables 3 and 4). The N—Me distances in **8**–**10** are virtually identical, mean N—C = 1.477(1) Å. The C(3)—Me bonds are significantly longer than the (C(2)/C(4))—Me bonds (means of 1.510(3) and 1.491(6) Å, respectively).

Reaction rates and their relation to ionic structure

The rate constants for the exchange of the hydrogen atoms of the 4- and 6-methyl groups are shown in Table 7 together with five geometrical factors that seem to be the most relevant with respect to the question of strain. These are (*a*) the presence of short intermethyl distances (less than 2.40 Å), (*b*) the sum of the torsional angles given in Table 5 (in order to have a measure of the rings' overall deviation from planarity), (*c*) the torsional angles C(1)—N(1)—C(2)—C(3), (*d*) the torsional angles N(1)—C(2)—C(3)—C(4), and (*e*) the torsional angles C(2)—C(3)—C(4)—N(2). (These particular torsional angles were chosen because they include all the ring atoms to which methyl groups are attached and would be the most likely to show deviations due to crowding.)

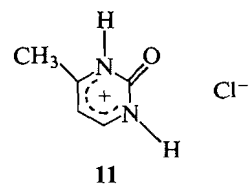

11

In order to facilitate comparison of the two kinds of data in Table 7, the rate data have been corrected for symmetry and normalized with respect to compound **11**, which contains no methyl groups other than that undergoing exchange.

Compound **5** is the only one of the six ions that has a completely planar ring. Its low reactivity compared to **11**, which we can assume is also planar, is the result of the electronic effect of the methyl groups on each other. The isomer **6** is some 30 times as reactive as **5** and its torsional angles show it to deviate significantly from planarity, although it does not suffer from intermethyl crowding. The trimethyl species **7** has a comparable degree of non-planarity to that of **6** (torsional angle sum slightly greater, average of the relevant angles slightly less) and, moreover, has a short intermethyl distance. However, this compound has a very low reactivity, due presumably to the electronic effect of the additional methyl group overwhelming any strain that is associated with its presence.

Compound **8** is interesting in that it has an almost planar ring and yet a moderately high reactivity for the 6-methyl group and a very low reactivity for the 4-methyl group. With respect to the 6-methyl group the adjacent *N*-methyl group is activating and the more distant 4-methyl group deactivating, the latter effect being slightly the greater.

Species **9** is an isomer of **7** and **8** and is by far the most reactive of the compounds studied. It does deviate from planar-

Can. J. Chem. Downloaded from www.nrcresearchpress.com by 210.87.254.105 on 09/06/12
For personal use only.

TABLE 7. Rate and structural data for **5**–**10**

Compound		Exchange rate 10^5 s^{-1}, 30°C normalized[a]		Intermethyl distance	Sum of torsional angles[b]	Relevant torsional angles[d] ω_1	ω_2	ω_3
5	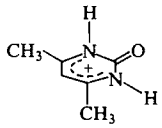 Cl⁻	0.68	0.047	—	0	0	0	0
6	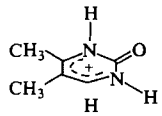 Cl⁻	10.6	1.5	Normal	10.2	3.7	2.0	0.2
7	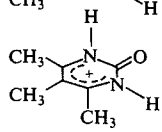 Cl⁻	0.56	0.038	Short	12.4	1.7	1.8	2.2
8	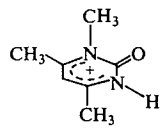 Cl⁻	2.2 (6)[c] 0.21 (4)	0.30 0.029	Short	1.6	0.2	0.1	0.2
9	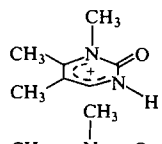 Cl⁻	42.8	5.9	Short	15.9	4.7	3.3	1.4
10	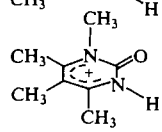 Cl⁻	4.1 (6)[c] 0.16 (4)	0.56 0.022	Very short	17.4	3.0	2.6	2.6

[a] Corrected for symmetry (**5** and **7**) and normalized with respect to compound **11** ($k = 7.3 \times 10^{-5}$ s^{-1}).
[b] From Table 5.
[c] Position 6 is adjacent to the *N*-methyl group.
[d] ω_1 = C(1)—N(1)—C(2)—C(3), ω_2 = N(1)—C(2)—C(3)—C(4), ω_3 = C(2)—C(3)—C(4)—N(2).

ity more than its isomers and does have a shorter intermethyl distance than either of them.

Species **10** shows a comparable degree of deviation from planarity to that of **9** and in addition has one short and one very short intermethyl distance. Its two active methyl groups, however, have reactivities that are little different from those in compound **8**, a species with an almost planar ring. We have also prepared the fully methylated iodide salt **12** and find that its reactivity is low (little different from that of **7**). Unfortunately, we have been unable to prepare the chloride salt of this compound for X-ray analysis.

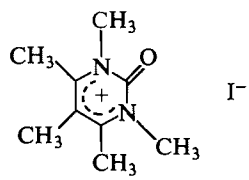

12

A number of conclusions might be drawn from the above results, depending on which species one chooses to compare. The high reactivity of **6** compared to **5** could be ascribed to loss of planarity in the ring, though not to any crowding of the methyl groups. The high reactivity of **8** (6-methyl) with respect to **5** could possibly be ascribed to a slightly short intermethyl distance but not to a loss of ring planarity. The very high reactivity of **9** might be ascribed to the existence of both a non-planar ring and a short intermethyl distance (2.17 Å). The lower reactivity of **10**, however, shows that an extremely short intermethyl distance (1.99 Å) is not sufficient to overcome the electronic effect of methyl.

Elements of strain are clearly present in some of the more reactive pyrimidonium ions, with the strain being sometimes manifested in a deviation from ring planarity and sometimes in a short intermethyl distance. A large degree of strain, however, is not sufficient to cause high reactivity (compound **10**), nor is a fairly low degree of strain incompatible with high reactivity (compound **9**).

We conclude that the presence of methyl groups on adjacent carbon atoms can destabilize species such as pyrimidonium ion as a result of steric compression or deviations from ring planarity but that these effects seem insufficiently large or consistent to account satisfactorily for the rate reversal that accompanies the relocation of a methyl group from a position that is next-but-one to one that is immediately adjacent to a reactive methyl site. We are presently exploring the effect of size and polarizability of the attacking base in these and other systems to see if a reverse steric effect is present here as well.

Experimental

Materials

All compounds used for kinetic studies and X-ray crystallographic measurement were purified by several recrystallizations in methanol–ethanol.

4,6-Dimethyl-2-pyrimidone hydrochloride (**5**), 5,6-dimethyl-2-

Can. J. Chem. Downloaded from www.nrcresearchpress.com by 210.87.254.105 on 09/06/12
For personal use only.

Can. J. Chem. Downloaded from www.nrcresearchpress.com by 210.87.254.105 on 09/06/12
For personal use only.

pyrimidone hydrochloride (**6**), 1,4,6-trimethyl-2-pyrimidone hydrochloride (**8**), 1,5,6-trimethyl-2-pyrimidone hydrochloride (**9**), and 1,4,5,6-tetramethyl-2-pyrimidone hydrochloride (**10**) were prepared by treating the respective pyrimidone with dilute hydrochloric acid solution followed by recrystallization. The procedures for preparing these pyrimidones and 1,3,4,5,6-pentamethyl-2-pyrimidone hydroiodide, **12**, were reported in refs. 1 and 12.

4,5,6-Trimethyl-2-pyrimidone hydrochloride, **7**, was obtained by neutralizing 4,5,6-trimethyl-2-pyrimidone with dilute hydrochloric acid solution followed by recrystallization. The pyrimidone was prepared by treating urea with 3-methyl-2,4-pentandione in concentrated hydrochloric acid solution, essentially by the method of Hale (12). Recrystallization of the crude product from ethanol – ethyl acetate gave 4,5,6-trimethyl-2-pyrimidone: mp 248°C; ^{1}H nmr ($CDCl_3$) δ 2.04 (s, 3H), 2.40 (s, 6H). *Anal.* calcd. for $C_7H_{10}ON_2$: C 60.85, H 7.30, N 20.27; found: C 60.88, H 7.14, N 20.35.

6-Methyl-2-pyrimidone hydrochloride, **11**, was prepared by treating urea (0.06 mol) with 1,1-dimethoxy-3-butanone (0.06 mol) in a mixture of ethanol (10 mL) and hydrochloric acid (10 *N*, 10 mL). Within 1 h, the mixture yielded yellow crystals which were recrystallized to give 77% yield of **11**: mp 236°C (decomp.); ^{1}H nmr (D_2O) δ 2.70 (s, 3H), 6.98 (d, 1H), 8.64 (d, 1H). *Anal.* calcd. for $C_5H_7N_2OCl$: C 40.97, H 4.81, N 19.11, Cl 24.19; found: C 40.97, H 4.88, N 18.94, Cl 24.00.

Kinetics

The exchange experiments of methyl protons in **5**–**12** were conducted in DCl/D_2O solution at 30°C using a T-60 nmr spectrometer, essentially as previously described (1).

X-ray crystallographic analyses of the 2-pyrimidone hydrochlorides ***5–10***

Crystallographic data are presented in Table 1. In each case crystals were mounted in general orientations on an Enraf-Nonius CAD4-F diffractometer. Unit-cell parameters were refined by least-squares on 2 sin θ/λ values for 25 high-order reflections (2θ = 35–55°) measured at 22°C with Mo-Kα_1 radiation (λ = 0.70930 Å).

Intensities were measured with graphite-monochromated Mo-Kα radiation (λ = 0.71073 Å). An ω–2θ scan at ~1–10.06° min^{-1} over a range of (s_w + 0.35 tan θ) degrees in ω (extended by 25% on both sides for background measurement, with s_w = 0.60, 0.60, 0.60, 0.70, 0.55, and 0.57 for **5**–**10** respectively). The intensities of three check reflections, measured every hour throughout each data collection, showed only small random fluctuations in each case. The data were processed[3] and corrected for absorption using the Gaussian integration method (13, 14). In each case those reflections which had intensities greater than 3σ(I) above background, where $\sigma^2(I) = S + 2B + (0.04(S - B))^2$ with S = scan count and B = normalized background count, were employed in the solution and refinement of the structures.

The structures were solved by direct methods, the coordinates of all non-hydrogen atoms being determined from E-maps and those of the hydrogen atoms from subsequent difference syntheses. The non-hydrogen atoms were refined with anisotropic thermal parameters and the hydrogen atoms with isotropic thermal parameters. The scattering factors of ref. 15 were used for the non-hydrogen atoms and those of ref. 16 for the hydrogen atoms. Corrections for anomalous scattering (17) were applied for Cl atoms. The weighting scheme, $w = 1/\sigma^2(F)$ where $\sigma^2(F)$ is derived from the previously defined $\sigma^2(I)$ gave uniform average values of $w(|F_o| - |F_c|)^2$ over ranges of both $|F_o|$ and sin θ/λ and was employed in the final stages of each refinement. The function minimized was $\Sigma w(|F_o| - |F_c|)^2$, $R = \Sigma||F_o| - |F_c||/\Sigma|F_o|$, and $R_w = (\Sigma w(|F_o| - |F_c|)^2/\Sigma w|F_o|^2)^{1/2}$. Parameter shifts on the final cycles of refinement did not exceed 0.25 σ and final difference maps were essentially featureless. The final positional and thermal parameters appear in Tables 2 and 8,[4] respectively. Measured and calculated structure factors have been placed in the Depository of Unpublished Data.[4]

In the case of **5**, the systematic absences allow space groups *Pnma* or $Pn2_1a$; the former was indicated by the E-statistics and the structure was solved and successfully refined in the centrosymmetric space group. However, the thermal parameters (Table 8) indicate possible small displacements from exact mirror symmetry; the rms vibrations normal to ***b*** are in the range 0.17–0.24 Å, and parallel to ***b*** are 0.21–0.35 Å, with the larger values being for O, C(5), and C(6). These vibrations are not exceptionally large, and the greater values parallel to ***b*** may well be a real thermal effect. Refinement in $Pn2_1a$ seems neither profitable nor desirable, since the possible small displacements involved scarcely justify the introduction of additional parameters. The molecule does appear to be virtually planar.

The thermal motion in each of the structures (Fig. 1) has been analyzed in terms of the rigid-body modes of translation, libration, and screw-motion (18). The rms errors in the U_{ij} (derived from the least-squares analyses) are 0.0015, 0.0008, 0.0010, 0.0007, 0.0007, and 0.0015 Å^2 for **5**–**10**, respectively. Analysis of the cations gave physically reasonable rigid-body parameters and rms ΔU_{ij} values of 0.0020, 0.0014, 0.0017, 0.0014, 0.0010, and 0.0014 Å^2 for **5**–**10**, respectively. The appropriate bond lengths have been corrected for libration (18, 19), using shape parameters q^2 of 0.08 for all atoms involved. Corrected bond lengths appear in Table 3; corrected angles do not differ by more than 1σ from the uncorrected values in Table 4. Intra-annular torsion angles defining the conformations of the six-membered rings are given in Table 5 and details of the N—H . . . Cl hydrogen bonding in Table 6. Uncorrected bond lengths, bond lengths and angles involving hydrogen, and a complete listing of torsion angles (Tables 9–12) have been deposited.[4]

1. R. STEWART and T. W. S. LEE. J. Org. Chem. **47**, 2075 (1982).
2. R. SRINIVASAN, S. J. GUMBLEY, and R. STEWART. Tetrahedron, **35**, 1257 (1979).
3. R. STEWART, S. J. GUMBLEY, and R. SRINIVASAN. J. Am. Chem. Soc. **102**, 6188 (1980).
4. R. STEWART, R. SRINIVASAN, and S. J. GUMBLEY. Can. J. Chem. **59**, 2755 (1981).
5. R. STEWART, S. J. GUMBLEY, and R. SRINIVASAN. Tetrahedron, **35**, 2783 (1979).
6. E. PIQUENARD and P. DIZABO. Can. J. Chem. **59**, 1270 (1981).
7. S. A. KREUGER and W. P. PAUDLER. J. Org. Chem. **37**, 4188 (1972).
8. G. P. GISBY, S. E. ROYALL, and P. G. SAMMES. J. Chem. Soc. Perkin Trans. I, 169 (1982).
9. C. K. BRADSHER, T. G. WALLIS, I. J. WESTERNMAN, and H. A. PORTER. J. Am. Chem. Soc. **99**, 2588 (1977).
10. W. C. HAMILTON and J. A. IBERS. Hydrogen bonding in solids. W. A. Benjamin, New York. 1968.
11. G. C. PIMENTEL and A. L. MCCLELLAN. Ann. Rev. Phys. Chem. **22**, 347 (1971).
12. W. J. HALE. J. Am. Chem. Soc. **36**, 104 (1914).
13. P. COPPENS, L. LEISEROWITZ, and D. RABINOVICH. Acta Crystallogr. **18**, 1035 (1965).
14. W. R. BUSING and H. A. LEVY. Acta Crystallogr. **22**, 457 (1967).
15. D. T. CROMER and J. B. MANN. Acta Crystallogr. Sect. A, **24**, 321 (1968).

[3] The computer programs used include locally written programs for data processing and locally modified versions of the following: MULTAN 80, multisolution program by P. Main, S. J. Fiske, S. E. Hull, L. Lessinger, G. Germain, J. P. Declercq, and M. M. Woolfson; ORFLS, full-matrix least-squares, and ORFFE, function and errors, by W. R. Busing, K. O. Martin, and H. A. Levy; FORDAP, Patterson and Fourier syntheses, by A. Zalkin; and ORTEP II, illustrations, by C. K. Johnson.

[4] The structure factor tables, Table 8 (anisotropic thermal parameters), and other materials mentioned in the text are available, at a nominal charge, from the Depository of Unpublished Data, CISTI, National Research Council of Canada, Ottawa, Ont., Canada K1A 0S2.

16. R. F. STEWART, E. R. DAVIDSON, and W. T. SIMPSON. J. Chem. Phys. **42**, 3175 (1965).
17. D. T. CROMER and D. LIBERMAN. J. Chem. Phys. **53**, 1891 (1970).
18. V. SCHOMAKER and K. N. TRUEBLOOD. Acta Crystallogr. Sect. B, **24**, 63 (1968).
19. D. W. J. CRUICKSHANK. Acta Crystallogr. **9**, 747 (1956); **9**, 754 (1956); **14**, 896 (1961).

Can. J. Chem. Downloaded from www.nrcresearchpress.com by 210.87.254.105 on 09/06/12
For personal use only.

The reaction of methyl radicals with neopentane in flow photolysis at 607–823 K

HIROSHI FURUE, KIM C. MANTHORNE, AND PHILIP D. PACEY
Department of Chemistry, Dalhousie University, Halifax, N.S., Canada B3H 4J3

Received October 12, 1983

HIROSHI FURUE, KIM C. MANTHORNE, and PHILIP D. PACEY. Can. J. Chem. **62**, 1203 (1984).

Acetone was photolyzed in the presence of a large excess of neopentane in a flow system at total pressures between 7 and 150 Torr and at 607–823 K. For reactions

[1] $CH_3 + C(CH_3)_4 \rightarrow CH_4 + (CH_3)_3CCH_2$

and

[2] $2CH_3 \rightarrow C_2H_6$

the quotient of rate coefficients, k_1^2/k_2, was calculated from CH_4 and C_2H_6 yields and was extrapolated to the high pressure limit, $k_1^2/k_{2,\infty}$. Taking $k_{2,\infty}$ as 2.2×10^{10} L mol^{-1} s^{1}, Arrhenius parameters for reaction [1] were found to be: $\log_{10} A$ (L mol^{-1} s^{-1}) = 10.0 ± 0.1, E_A = 62 (±2) kJ mol^{-1}. In combination with data from the literature for the temperature range 365–953 K, the Arrhenius plot for $k_1/k_{2,\infty}^{1/2}$ was strongly curved, with a heat capacity of activation of 71 ± 4 J K^{-1} mol^{-1}.

HIROSHI FURUE, KIM C. MANTHORNE et PHILIP D. PACEY. Can. J. Chem. **62**, 1203 (1984).

On a photolysé l'acétone en présence d'un grand excès de néopentane dans un système à écoulement opérant sous des pressions de 7 à 150 Torr et à des températures variant entre 607 et 823 K.

Utilisant les rendements en CH_4 et en C_2H_6, on a calculé le rapport des coefficients de vitesse k_1^2/k_2 et on l'a extrapolé

[1] $CH_3 + C(CH_3)_4 \rightarrow CH_4 + (CH_3)_3CCH_2$

et

[2] $2CH_3 \rightarrow C_2H_6$

jusqu'à la pression limite supérieure, $k_1^2/k_{2,\infty}$. Si on fixe que $k_{2,\infty}$ est égal à $2,2 \times 10^{10}$ L mol^{-1} s^{1}, on a trouvé que les paramètres d'Arrhénius pour la réaction [1] sont: $\log A$ (L mol^{-1} s^{-1}) = 10,0 ± 0,1 et E_A = 62 (±2) kJ mol^{-1}. En combinant ces données avec celles répertoriées dans la littérature pour l'intervalle de température allant de 365 à 953 K, la courbe d'Arrhénius pour $k_1/k_{2,\infty}^{1/2}$ est fortement incurvée avec une capacité calorifique d'activation de 71 ± 4 J K^{-1} mol^{-1}.

[Traduit par le journal]

Can. J. Chem. Downloaded from www.nrcresearchpress.com by 210.87.254.42 on 09/06/12
For personal use only.

Introduction

Hydrogen abstraction by methyl radicals has been studied well at temperatures above 700 K by pyrolysis of hydrocarbons and at temperatures below 600 K by photolysis of acetone, azomethane, and dimethyl mercury in hydrocarbons (1). These studies revealed significant differences in activation energies (for neopentane, 67 kJ mol^{-1} at high temperatures compared to 42–50 kJ mol^{-1} at low temperatures), suggesting that the Arrhenius plots for the reactions are curved. In the present study, data are obtained from 600 to 800 K, where experimental data are scarce, by photochemically generating methyl radicals in a flow reactor. The use of a flow reactor makes photolysis experiments possible at higher temperatures than with conventional, static reactors.

Neopentane, $C(CH_3)_4$, was chosen for this study because only primary hydrogens are transferred. A small amount of acetone (1.0–6.3 mol%) was added to generate the methyl radicals photochemically. The most important sources of CH_4 and C_2H_6 in the system are likely to be the following (2, 3):

[1] $CH_3 + C(CH_3)_4 \rightarrow CH_4 + (CH_3)_3CCH_2$

[2] $2CH_3 \rightarrow C_2H_6$

[3] $CH_3 + (CH_3)_2CO \rightarrow CH_4 + CH_2COCH_3$

Writing down the expressions for the steady-state rates of formation of CH_4 and C_2H_6, and combining these so as to eliminate the concentration of CH_3 and rearranging, one obtains:

$$[4] \quad \frac{k_1^2}{k_2} = \frac{[CH_4]^2}{[C(CH_3)_4]^2[C_2H_6]t\{1 + k_3[(CH_3)_2CO]/(k_1[C(CH_3)_4])\}^2}$$

To use this equation to determine k_1^2/k_2, it is necessary to know the ratio k_3/k_1 and the initial concentrations of neopentane and acetone and it is necessary to measure the concentrations of CH_4 and C_2H_6 formed after photolysis times, t.

A pressure dependence of this quotient is expected, as k_2 is known to depend on pressure. This dependence may be displayed as a function of inverse pressure on a Lindemann–Hinshelwood plot (4). The intercept of such a plot should be approximately equal to the high pressure limiting quotient, $k_1^2/k_{2,\infty}$.

Experimental

A description of most parts of the apparatus has been given elsewhere (4, 5). A quartz flow reactor tube of 11 mm id, having parallel quartz windows at both ends, was heated by 45 cm long nichrome-wound resistive furnace. A thermocouple was placed in a 4 mm od quartz tube beside the reactor, and was moved along the reactor to obtain a temperature profile. During an experiment it was positioned at the midpoint to enable the correction of any drift of temperature.

At one end of the reactor was placed an optical train composed of a 100 W high pressure Hg lamp (Osram HBO 100 w/2), an iris, a mirror, a collimating lens, and a Pyrex filter. The reagent bulbs and tubing were painted black to prevent premature photolysis. The light intensity within the reactor was tested with a thermistor and was found

Can. J. Chem. Downloaded from www.nrcresearchpress.com by 210.87.254.42 on 09/06/12
For personal use only.

to vary by only 5% from end to end of the reactor and was not found to vary perpendicular to the reactor axis.

Neopentane (Matheson, 99.87%) was degassed at nitrogen-boiling and toluene-melting temperatures. Acetone (A. C. S.) was fractionally distilled, and the middle fraction was degassed at the nitrogen-boiling temperature. Mixtures of acetone in neopentane were prepared and equilibrated overnight before use. The reagent mixture was routinely checked for any impurity from acetone decomposition in the storage containers. Product concentrations were analyzed in a gas chromatograph with a 1 m silica gel column at 50°C.

Results

The reactor extended about 7 cm outside the furnace at both ends. To determine whether reaction could occur in these regions, an experiment was performed with full light intensity but with the furnace off. No formation of CH_4 or C_2H_6 was observed.

Temperature gradients occurred at both ends of the furnace and it was necessary to learn what weight should be given to these regions. Experiments were performed at full light intensity with about 100 Torr of neopentane containing 2.5% acetone at 659, 707, and 770 K. Activation energies were found to be 50 kJ mol^{-1} for C_2H_6 and 85 kJ mol^{-1} for formation of CH_4. Consequently, the various regions of the reactor were weighted by the factor, exp $[-64\ kJ\ mol^{-1}/(RT)]$, using a preliminary estimate of the mean activation energy, in a computer program described elsewhere (6). The experimental temperature profile was interpreted with the aid of this program to determine the average reaction temperature and the effective furnace length. In typical experiments, it was found that 90% of the reaction occurred within 10 K of the average reaction temperature. At 823 K, it was found that the activation energy increased because of thermal initiation and an activation energy of 284 kJ mol^{-1} was used in the above program.

Residence times and reactant conversions had little effect on the quotient in eq. [4]. In experiments[1] at 8 Torr and 608 K and with 12 residence times from 0.9 to 18 s, no significant effect was found. Only at 823 K, where the conversion reached its maximum value of 8×10^{-3}, was a significant effect found. At this temperature the quotient was extrapolated to time $t = 0$ to eliminate the effect of secondary reactions. At all other temperatures, the values of the quotient at different residence times were simply averaged.

The light intensity was varied by restricting the light beam with iris apertures of areas 0.10 and 0.23 cm^2 and by leaving the light beam unrestricted. At 609 K and 7 Torr, the rate of formation of C_2H_6 varied by a factor of 4.7 but the quotient in eq. [4] stayed constant within 6%.

Variation of the total pressure in the range from 7 to 150 Torr while other parameters remained fixed did affect the kinetics. The rate of formation of C_2H_6 increased with increasing pressure. The quotient in eq. [4] decreased slightly at high pressure, as seen in the form of a Lindemann–Hinshelwood plot in Fig. 1 for experiments at 608 K. Here k_3/k_1 was calculated from the recommended Arrhenius parameters of ref. 1. The straight line was determined by least squares. For this and other temperatures, the intercepts, $k_1^2/k_{2,\infty}$, were found to have uncertainties between 4% and 10%. Two experimental pressures, close to 30 and 90 Torr, were used at the other temperatures. The values

[1]Tables of data are available, at a nominal charge, from the Depository of Unpublished Data, National Science Library, National Research Council of Canada, Ottawa, Ont., Canada K1A 0S2.

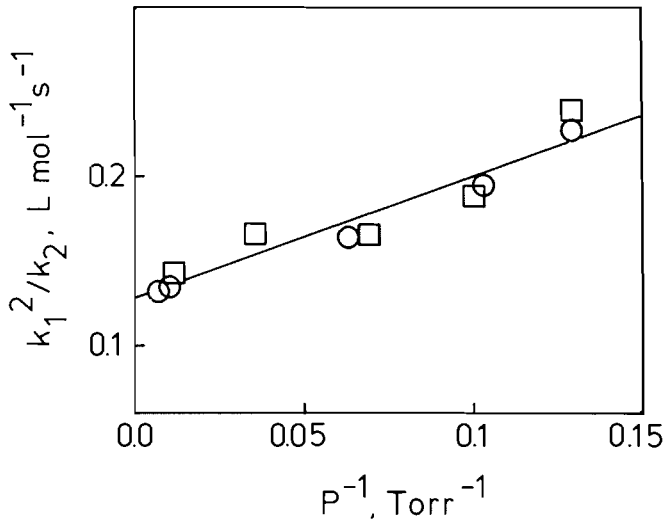

FIG. 1. Lindemann–Hinshelwood plot of the quotient, k_1^2/k_2, calculated from eq. [4], at varying reactant pressures at 608 K; ○, 0.010 mole fraction $(CH_3)_2CO$; □, 0.063 mole fraction $(CH_3)_2CO$; —, least-squares straight line.

of $P_{1/2}$, the ratios of slopes to intercepts of such plots, were 6 ± 1 Torr at 608 K, 7 ± 2 Torr at 659 K, 7 ± 3 Torr at 707 K, 10 ± 2 Torr at 770 K, and 15 ± 3 Torr at 823 K. Here and elsewhere quoted uncertainties are standard deviations.

The mole fraction of acetone in the reagent mixture was varied from 0.010 to 0.063. Values of the quotient $k_1^2/k_{2,\infty}$, calculated from experiments with different mole fractions of acetone, are shown in Fig. 1 to be in good agreement.

The square roots of intercepts of Lindemann–Hinshelwood plots from this work are shown in the form of an Arrhenius plot in Fig. 2, together with data from the literature. Arrhenius parameters for reaction [1], calculated assuming $\log_{10} k_{2,\infty}/L\ mol^{-1}\ s^{-1} = 10.34$ (1, 13), are listed in Table 1. Except for the results of ref. 12, for which the temperature range was narrow, the Arrhenius parameters generally increase with increasing temperature.

Discussion

Any first-order surface termination reaction would be most competitive with reaction [2] in conditions with small radical concentrations (i.e., small intensity and $[(CH_3)_2CO]$). Concentrations of photochemically hot radicals would be most competitive with those of thermal radicals in conditions with short chain lengths (i.e., large intensity and acetone mole fraction). The quotient k_1^2/k_2 was found to be independent of intensity and of acetone mole fraction, indicating that surface terminations and hot radical reactions were unimportant. Furthermore, extrapolation, as in Fig. 1, to the high pressure limit, where chain lengths were long and radical concentrations large, should have eliminated any effect of such processes.

The ratio k_3/k_1 in eq. [4] was extrapolated from low temperature data (1), supposing that any Arrhenius plot curvature is equal for the two reactions. Because of the small acetone mole fractions, if the Arrhenius plot for reaction [3] were straight, the calculated value of k_1 would be affected by 2% or less.

Furimsky and Laidler (7) showed that the concentrations of CH_3 and $(CH_3)_3CCH_2$ radicals were similar to each other at 608 K in the mercury-photosensitized decomposition of neopentane. The $(CH_3)_3CCH_2$ radical, whose relative concen-

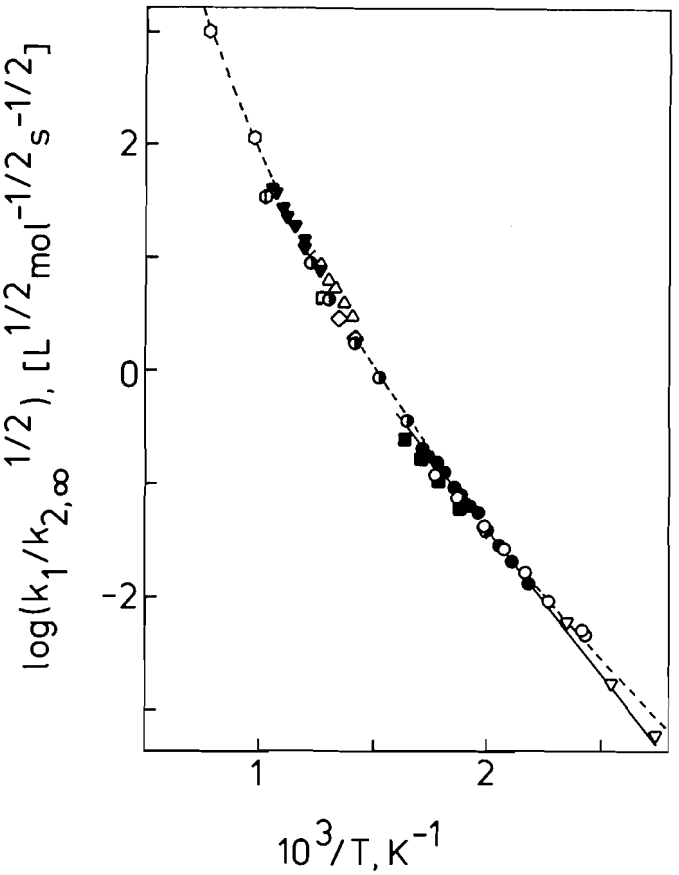

FIG. 2. Arrhenius plot for the quotient $k_1/k_{2,\infty}^{1/2}$, after ref. 1: ○, ref. 2; ●, ref. 3; ▼, ref. 4; ■, ref. 7; ▽, ref. 8; △, ref. 9; □, ref. 10; ⊙, ref. 11; ◇, ref. 12; ×, ref. 13; ⊛, ref. 14; ◑, this work; —, preferred Arrhenius line, ref. 1; - - -, least-squares fit to eq. [5].

tration decreased with increasing temperature, was shown not to interfere with the calculation of k_1^2/k_2 (7). The CH_3CO radical was formed in the photodecomposition step in the present work (15). From Arrhenius parameters in the literature (1, 16), it was calculated that CH_3 was five or more orders of magnitude greater in concentration than CH_3CO. We conclude that CH_3CO and $(CH_3)_3CCH_2$ did not interfere with the calculation of k_1^2/k_2 in the present work.

The method of extrapolation in Fig. 1 may introduce uncertainty into the high pressure value, $k_1^2/k_{2,\infty}$. Forst has shown that this method is justified by theory if the pressures are sufficiently high (17). Experimental values of k_2 as a function of pressure at 823 K are available (13). When values of k_1^2/k_2 at 823 K from the present work were multiplied by values of $k_2/k_{2,\infty}$ from ref. 13, the value of $k_1^2/k_{2,\infty}$ was only 4% less than the value obtained from an analogue of Fig. 1. We conclude that the Lindemann–Hinshelwood extrapolations gave reliable intercepts under the present conditions.

The intercepts agreed well with results in the literature. The following is a list of differences between values of $\log_{10} k_1/k_{2,\infty}^{1/2}$ from this work and those at the same temperatures from data or Arrhenius parameters in the literature: 608 K, +0.09 (7), +0.05(3); 707 K, −0.06 (12); 823 K, −0.10 (4), −0.07 (13).

The data in Fig. 2 and Table 1 confirm an earlier suggestion (4) that the Arrhenius plot for reaction [1] is a curve. Such curves are sometimes (18–20) interpreted by means of the equation

TABLE 1. Arrhenius parameters for reaction [1]

T (K)	Reference	$\log_{10} A$ (L mol^{-1} s^{-1})	E_A (kJ mol^{-1})
365–495	8	8.9±0.1	49±1
411–565	2	8.1±0.1	42±1
458–582	3	8.92±0.04	49.4±0.4
503–608	7	8.7	48
607–823	This work	10.0±0.1	62±2
703–743	12	8.7	43
713–823	9	10.8	72
793–953	4	10.5±0.1	67±2
1030–1300	11	11.8	90

$$[5] \quad k = BT^{C/R} \exp(-D/RT)$$

where C is LaMer's heat capacity of activation (21, 22) and B, C, and D are usually taken as independent of temperature. The logarithmic form of eq. [5] was fitted by non-linear least squares to the photochemical results in Fig. 2 and to the pyrolytic results of refs. 4, 12, and 13. The points in Fig. 2 were given equal weight, corresponding to an assumption that all were subject to similar fractional uncertainties (20); $k_{2,\infty}$ was again given the value of refs. 1 and 13. The parameters were found to be $C = 71 \pm 4$ J K^{-1} mol^{-1}, $D = 14 \pm 3$ kJ mol^{-1} and $\log_{10} B$ (L^{-1} mol^{-1} s^{-1} K$^{-8.5}$) $= 17.8 \pm 1.6$. The resulting dashed curve on Fig. 2 fitted the data within a standard deviation of 0.05 log units.

By differentiating the logarithmic form of eq. [5], one obtains the following expressions for the Arrhenius parameters:

$$[6] \quad E_A = D + CT$$

$$[7] \quad \log_{10} A = \log_{10} Be^{C/R} + (C/R) \log_{10} T$$

Fitting these expressions to the parameters in Table 1, C was found to be 61 ± 12 J K^{-1} mol^{-1} from the activation energies and 65 ± 14 J K^{-1} mol^{-1} from the pre-exponential factors. The three values of C agreed within their uncertainties. To argue that the Arrhenius plot is linear ($C = 0$), it would be necessary to reject all results above 608 K or else to reject all photochemical results.

Sources of the curvature were suggested in ref. 4. If the weak bending modes in the activated complex behave as hindered internal rotations, they could contribute 20 to 30 J K^{-1} mol^{-1} (22). The possibility of enhanced reaction from an excited state is difficult to evaluate (23). Tunnelling can contribute 100 J K^{-1} mol^{-1} or more to C, especially for reactions with high activation barriers (21). We note that certain hydrogen atom transfer reactions of Cl and OH, for which smaller values of C (15 to 50 J K^{-1} mol^{-1}) have been observed (18–20), have lower activation barriers than reaction [1]. Tunnelling calculations on this reaction are recommended.

In conclusion, it has been demonstrated that flow photolysis can extend the range of photolysis temperatures by more than 200 K and can link the previously discordant pyrolytic and photolytic data for reaction [1].

Acknowledgement

The authors wish to thank the Natural Sciences and Engineering Research Council of Canada for grants in support of this research.

Can. J. Chem. Downloaded from www.nrcresearchpress.com by 210.87.254.42 on 09/06/12
For personal use only.

1. J. A. KERR and M. J. PARSONAGE. Evaluated kinetic data on gas phase hydrogen transfer reactions of methyl radicals. Butterworths, London. 1976.
2. A. F. TROTMAN-DICKENSON, J. R. BIRCHARD, and E. W. R. STEACIE. J. Chem. Phys. **19**, 163 (1951).
3. J. A. KERR and D. TIMLIN. J. Chem. Soc. A, 1241 (1969).
4. P. D. PACEY. Can. J. Chem. **51**, 2415 (1973).
5. P. D. PACEY. Chem. Phys. Lett. **23**, 394 (1973).
6. P. D. PACEY and J. H. PURNELL. J. Chem. Soc. Faraday Trans. I, **68**, 1462 (1972).
7. E. FURIMSKY and K. J. LAIDLER. Can. J. Chem. **50**, 1123 (1972).
8. R. E. BERKLEY, I. SAFARIK, H. E. GUNNING, and O. P. STRAUSZ. J. Phys. Chem. **77**, 1734 (1973).
9. M. P. HALSTEAD, R. S. KONAR, D. A. LEATHARD, R. M. MARSHALL, and J. H. PURNELL. Proc. R. Soc. A**310**, 525 (1969).
10. G. M. CÔME, F. BARONNET, G. SCACCHI, R. MARTIN, and M. NICLAUSE. C. R. Acad. Sci. Paris, Ser. C, **267**, 1192 (1968).
11. J. N. BRADLEY and K. O. WEST. J. Chem. Soc. Faraday Trans. I, **72**, 8 (1976).
12. P. M. MARQUAIRE and G. M. CÔME. React. Kinet. Catal. Lett. **9**, 171 (1978).
13. P. D. PACEY and J. H. WIMALASENA. J. Phys. Chem. **84**, 2221 (1980).
14. G. L. PRATT and D. ROGERS. J. Chem. Soc. Faraday Trans. I, **77**, 2751 (1981).
15. H. ADACHI, N. BASCO, and D. G. L. JAMES. Int. J. Chem. Kinet. **13**, 1251 (1981).
16. S. W. BENSON and H. E. O'NEAL. Kinetic data on gas phase unimolecular reactions. National Bureau of Standards, Washington, D.C. 1970.
17. W. FORST. J. Phys. Chem. **76**, 342 (1972).
18. W. C. GARDINER, W. G. MALLARD, and J. H. OWEN. J. Chem. Phys. **60**, 2290 (1974).
19. J. H. LEE, J. V. MICHAEL, W. A. PAYNE, and L. J. STIEF. J. Chem. Phys. **66**, 2690 (1977).
20. R. J. CVETANOVIC, D. L. SINGLETON, and G. PARASKEVOPOULOS. J. Phys. Chem. **83**, 50 (1979).
21. P. D. PACEY. J. Chem. Phys. **71**, 2966 (1979).
22. P. D. PACEY. J. Chem. Phys. **77**, 3540 (1982).
23. R. ZELLNER. J. Phys. Chem. **83**, 18 (1979).

Can. J. Chem. Downloaded from www.nrcresearchpress.com by 210.87.254.42 on 09/06/12
For personal use only.

The synthesis of derivatives of lactosamine and cellobiosamine to serve as probes in studies of the combining site of the monoclonal anti-I Ma antibody

TING C. WONG[1] AND RAYMOND U. LEMIEUX

Department of Chemistry, University of Alberta, Edmonton, Alta., Canada T6G 2G2

Received November 24, 1983

TING C. WONG and RAYMOND U. LEMIEUX. Can. J. Chem. **62**, 1207 (1984).

Syntheses are reported for a variety of structures used in a continuation of our studies of the combining site of the monoclonal anti-I Ma antibody. These structures include the *N*-acetyl, *N*-formyl, and *N*-pivalyl derivatives of methyl β-D-lactosaminide, the ethyl, propyl, isopropyl, and isobutyl β-glycosides of *N*-acetyllactosamine and the βDGal(1→4)βDGlcNAc(1→6)-, βDGal(1→4)βDGlcNH$_2$(1→6)-, βDGal(1→4)βDGlcNCOCF$_3$(1→6)-, and βDGlc(1→4)βDGlcNAc(1→6)-derivatives of 1,2;3,4-di-*O*-isopropylidene-α-D-galactopyranose. Also, preparations of 6-deoxy-βDGal(1→4)βDGlcNAc(1→6)α,βDGal and βDGlcNAc(1→6)βDGal(1→4)βDGlcNAcOCH$_3$ are described.

TING C. WONG et RAYMOND U. LEMIEUX. Can. J. Chem. **62**, 1207 (1984).

On rapporte les synthèses de diverses structures utilisées dans la suite d'études relatives au site de combinaison de l'anticorps monoclonal anti-I Ma. Ces structures comprennent les dérivés *N*-acétyle, *N*-formyle et *N*-pivalyle du β-D-lactosaminide de méthyle, les β-glycosides d'éthyle, de propyle, d'isopropyle et d'isobutyle de la *N*-acétyllactosamine et les dérivés βDGal(1→4)βDGlcNAc(1→6)-, βDGal(1→4)βDGlcNH$_2$(1→6)-, βDGal(1→4)βDGlcNCOCF$_3$(1→6)-, et βDGlc(1→4)-βDGlcNAc(1→6)- du di-*O*-isopropylidène-1,2;3,4-α-D-galactopyrannose. On décrit également les préparations du déoxy-6β-βDGal(1→4)βDGlcNAc(1→6)α,βDGal et βDGlcNAc(1→6)βDGal(1→4)βDGlcNAcOCH$_3$

[Traduit par le journal]

Can. J. Chem. Downloaded from www.nrcresearchpress.com by 210.87.254.42 on 09/06/12
For personal use only.

Introduction

In a previous communication (1), we reported the synthesis of the βDGal(1→4)βDGlcNAc(1→6) derivative of 1,2;3,4-di-*O*-isopropylidene-α-D-galactopyranose (**2**). Evidence had accumulated that only atoms about the C-6 group of the reducing

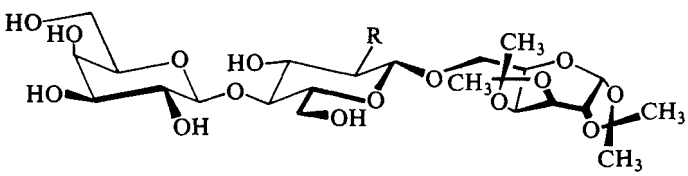

1, R = NH_2; **2**, R = NHAc; **3**, R = $NHCOCF_3$

DGal unit of the trisaccharide βDGal(1→4)βDGlcNAc(1→6)-DGal (2, 3) are involved in binding of this unit with the monoclonal anti-I Ma antibody. Evidence was later presented (4) that the binding involves a surface which extends from the C-6 grouping over the acetamido group of the βDGlcNAc unit to near the C-6″ methylene group of the terminal βDGal unit and which appears compatible for interfacing with a basically non-polar cleft at the surface of the protein.

Since the conformer which is accepted by the combining site places the reducing DGal unit in an orientation where it is not extensively bound and, therefore, largely remaining in the aqueous phase (4), it was to be expected that the di-*O*-isopropylidene derivative **2** would be a good inhibitor unless important steric interactions were encountered between the isopropylidene groups and protein structure other than that involved with the combining site. Indeed, compound **2** proved to be an excellent inhibitor, about 0.76 times that of the trisaccharide itself (5). For this reason and in light of other evidence for only marginal involvement of the reducing DGal unit (2–4), it was decided to test simple alkyl glycosides of *N*-acetyl-β-lactosamine (i.e., βDGal(1→4)βDGlcNAc—OR). Since these, in fact, proved to be superior inhibitors of the binding of the monoclonal anti-I Ma antibody with the OG protein (5), the more convenient examination of modifications of the simple methyl glycoside (**14**) of *N*-acetyl-β-lactosamine was adopted. The purpose of this communication is to report the synthetic efforts in this regard.

Discussion of results

Previously (1), the amine (**1**) formed on hydrazinolysis of the phthalimido derivative of **1** was directly *N*-acetylated to form **2**. The amine (**1**) has now been isolated and converted to the *N*-trifluoroacetyl derivative (**3**). It then became recognized (5) that βDGal(1→4)βDGlcNAcOCH$_3$ (**14**) was 2.8 times superior, as an inhibitor of the anti-I Ma antibody, to the trisaccharide βDGal(1→4)βDGlcNAc(1→6)α,βDGal. Consequently, structural modifications to further examine the engagement of the acetamido group employed the simple methyl glycosides **7** and **8**, which contain *N*-formyl and *N*-pivalyl groups, respectively. In order to prepare these compounds, the acetylated azidobromide (**4**) was synthesized from hexa-*O*-acetyl-D-lactal (6) for conversion by Koenigs–Knorr reaction with methanol to form **5** which was deacetylated to methyl 2-azido-2-deoxy-β-D-lactoside (**6**). Reduction of the azide provided the amine

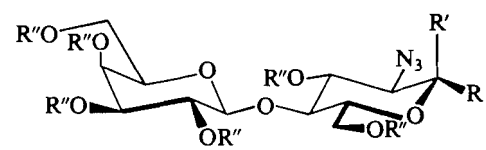

4, R = H, R′ = Br, R″ = Ac
5, R = OCH_3, R′ = H, R″ = Ac
6, R = OCH_3, R′ = H, R″ = H

which was converted to both its *N*-formyl (**7**) and *N*-pivalyl (**8**) derivatives.

The methyl (**14**), ethyl (**15**), propyl (**16**), and isobutyl (**18**) β-glycosides of *N*-acetyllactosamine were conveniently prepared from the hexa-*O*-acetyl-2-deoxy-2-phthalimido-α,β-D-lactosyl chloride (7) in the usual manner (1, 8).

In order to examine the possible engagement of the

[1] Taken from a thesis presented in partial fulfillment of the Ph.D. degree, 1983.

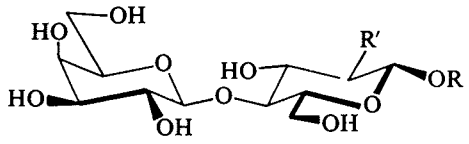

7, R = CH_3, R′ = NHCHO
8, R = CH_3, R′ = $NHCOC(CH_3)_3$
14, R = CH_3, R′ = NHAc
15, R = CH_2CH_3, R′ = NHAc
16, R = $CH_2CH_2CH_3$, R′ = NHAc
17, R = $CH(CH_3)_2$, R′ = NHAc
18, R = $CH_2CH(CH_3)_2$, R′ = NHAc

6″-hydroxyl group of βDGal(1→4)βDGlcNAc(1→6)α,βDGal in the binding with anti-I Ma, the 6″-deoxy derivative (**28**) was prepared starting from the 4′,6′-*O*-benzylidene derivative (**20**) of benzyl 2-deoxy-2-phthalimido-β-D-lactopyranoside (**19**).

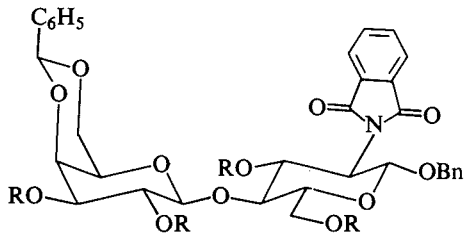

20, R = H
21, R = Ac

Acetylation to **21** followed by acid hydrolysis of the benzylidene group then provided the 4′,6′-diol (**22**) which could be preferentially mesylated at the 6′-position and the product acetylated to form **23**. As expected (9), replacement of the mesyloxy group was difficult but treatment with potassium iodide in dimethylformamide for 72 h at 80°C provided the 6′-iodide (**24**) in 32% yield. Reduction of the iodide with tri-*n*-butyl tin hydride in the presence of 2,2′-azobisisobutyronitrile (10) was utilized to prepare the acetylated 6′-deoxy compound **25** in 50% yield.

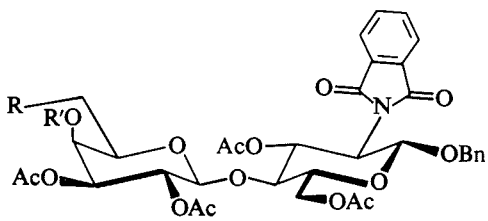

22, R = OH, R′ = H
23, R = OSO_2CH_3, R′ = Ac
24, R = I, R′ = Ac
25, R = H, R′ = Ac

The 6′-deoxy compound (**25**) was then converted to the phthalimidobromide **26** in the usual manner (7) and used for the preparation of the 6″-deoxy-βDGal(1→4)βDGlcNAc(1→6)-α,β-D-galactose (**28**) following well established procedures (11).

In order to gain evidence on the possible involvement of the 4″-hydroxyl group of the terminal βDGal unit in the binding of the trisaccharide derivative **2** with the anti-I Ma antibody, it was decided to synthesize its 4″-epimer (**39**). This was accomplished in a manner very similar to that used to prepare **2** (1). The crude product (**29**) from the azidonitration (6) of hexa-*O*-

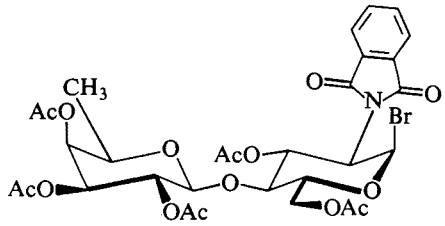

26

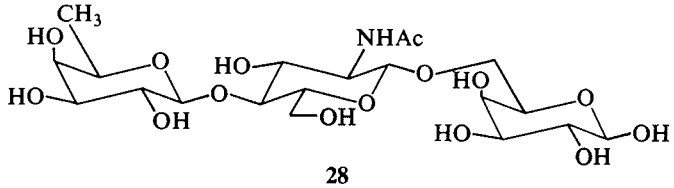

28

acetyl-D-cellobial was treated with *N*,*N*-dimethylbromoforminium bromide (Vilsmeier reagent) (11) to convert any 1-acetamido-2-azido-1,2-dideoxy derivative (**6**) to the acetylated 2-azidoglycosyl bromide (**30**) and then directly with lithium bromide to convert the 2-azido-1-nitrates to form the major amount of the bromide (**30**) (12). The yield of the crystalline product was 32% from the hexa-*O*-acetyl-D-cellobial. The acetylated azidobromide (**30**) was then converted to the acetylated

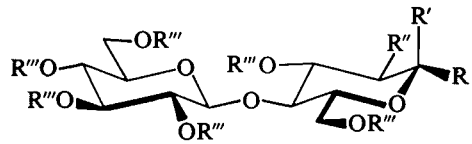

30, R = H, R′ = Br, R″ = N_3, R‴ = Ac
31, R = OBn, R′ = H, R″ = N_3, R‴ = Ac
32, R = OBn, R′ = H, R″ = N_3, R‴ = H
33, R = OBn, R′ = H, R″ = NH_2, R‴ = H
34, R = OBn, R′ = H, R″ = NPhth, R‴ = Ac
35, R = OH, R′ = H, R″ = NPhth, R‴ = Ac
36, R = Cl, R′ = H, R″ = NPhth, R‴ = Ac
37, R = (*O*→6)-1,2;3,4-diisopropylidene-αDGal, R′ = H, R″ = NPhth, R‴ = Ac
38, R = (*O*→6)-1,2;3,4-diisopropylidene-αDGal, R′ = H, R″ = NH_2, R‴ = H
39, R = (*O*→6)-1,2;3,4-diisopropylidene-αDGal, R′ = H, R″ = NHAc, R‴ = H

benzyl β-D-glycoside **31** which crystallized in 66% yield. Deacetylation to **32**, followed by reduction of the azide group with hydrogen sulfide, then provided benzyl 2-amino-2-deoxy-β-D-cellobioside (**33**) which was converted by way of **34** and **35**

41

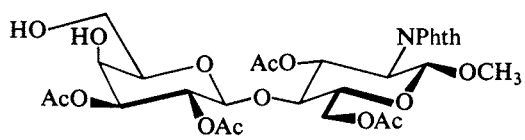

42

Can. J. Chem. Downloaded from www.nrcresearchpress.com by 210.87.254.42 on 09/06/12
For personal use only.

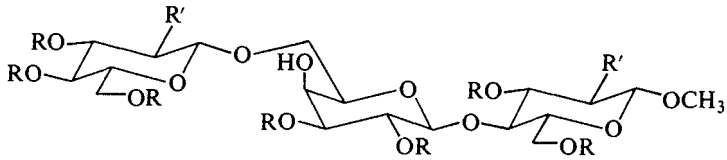

43, R = Ac, R′ = NPhth
44, R = H, R′ = NHAc

to the hexa-*O*-acetyl-2-deoxy-2-phthalimido-α,β-cellobiosyl-chloride (**36**) in the usual manner (11). Condensation of **36** with 1,2;3,4-di-*O*-isopropylidene-α-D-galactopyranose using *sym*-collidine – silver trifluoromethanesulfonate as promoter (8) provided the desired product (**37**) in 65% yield after recrystallization. Deblocking of **37** to form the amine **38** and *N*-acetylation provided the desired compound **39**.

Since core structure oligosaccharides of human blood group determinants are known to occur as branched structures which contain βDGlcNAc units at both the 3- and 6-positions of a βDGal unit, the βDGlcNAc(1→6) derivative (**44**) of methyl *N*-acetyl-β-lactosaminide (**14**) was prepared. The 4′,6′-*O*-benzylidene derivative of **9** was prepared and acetylated to form **41**. Acid hydrolysis provided the diol **42** which was glycosylated using tri-*O*-acetyl-2-deoxy-2-phthalimido-β-D-glucopyranosyl bromide under standard conditions (8). A 50% yield of the desired product (**43**) was obtained, which by deblocking and *N*-acetylation in the usual manner provided the desired βDGlcNAc(1→6)βDGal(1→4)βDGlcNAcOCH$_3$ (**44**) in 81% yield.

Experimental

General methods

Thin layer chromatograms (tlc) were performed on precoated silica gel 60-F254 plates (E. Merck, Darmstadt) and visualized by quenching of fluorescence and (or) by charring after spraying with 5% sulfuric acid in ethanol. For column chromatography, silica gel 60 (0.063–0.20 mm) (Fluka AG Chemische Fabrik, CH-9470, Buchs SG) was used for elution under atmospheric pressure and, for medium pressure (flash) chromatography, silica gel 60 (0.040–0.063 mm) (E. Merck, Darmstadt) was used. For high pressure liquid reverse phase chromatography (hplc), a C18 column (5 μm, 8-mm id) (Waters Associates, Milford, MA 01757) was used. For gel filtration, Sephadex LH-20 (Pharmacia Fine Chemicals AB, Uppsala, Sweden) and Bio-Gel P-2 (200–400 mesh) (Bio-Rad Laboratories, Richmond, CA) were used. Membrane dialysis was performed under medium pressure UM05 Diaflo membrane (Amico, Lexington, MA 02173). Dowex 1-X8(OH^-) resin was obtained from J. T. Baker Chemical Co., Phillipsburg, NJ, and Amberlite IR-120(H^+) resin was obtained from Mallinckrodt, Inc., Paris, KY.

In organic solvents (usually $CDCl_3$), the ^1H and ^{13}C chemical shifts (δ, in ppm) are relative either to internal 1% tetramethylsilane (δ = 0) or to chloroform with δ = 7.27. When deuterium oxide was the solvent, the reference was the HOD signal set at 4.80 ppm for ^1H nmr and the external dioxane signal set at 66.88 ppm for ^{13}C nmr.

1,2;3,4-Di-O-isopropylidene-6-O-[2-amino-2-deoxy-4-O-(β-D-galactopyranosyl)-β-D-glucopyranosyl]-α-D-galactopyranose (1)

A solution of 1,2;3,4-di-*O*-isopropylidene-6-*O*-[3,6-di-*O*-acetyl-4-*O*-(tetra-*O*-acetyl-β-D-galactopyranosyl)-2-deoxy-2-phthalimido-β-D-glucopyranosyl]-α-D-galactopyranose (1) (0.357 g, 0.37 mmol) and 85% hydrazine hydrate (0.12 g, 2.39 mmol) in ethanol (3 mL) was refluxed for 2 h. The white solid obtained after solvent removal was applied directly to a Sephadex LH-20 column and eluted with ethanol–water (1:1). Solvent removal from the main fraction gave a white solid (0.17 g, 0.29 mmol, 78%); ^1H nmr δ: 5.73 (d, 1H, H-1, $J_{1,2}$ = 5.0 Hz), 4.61 (dd, 1H, H-2, $J_{2,3}$ = 2.0 Hz), 4.48 (2d, 2H, H-1′ and H-1″ overlapping, J = 7.6 Hz and 7.6 Hz), 4.16 (m, 2H, H-4 and H-5), 3.05 (dd, 1H, H-2′), 1.60, 1.51, 1.43, 1.42 (4s, 12H, 2 OOC(CH$_3$)$_2$), 4.75, 4.05–3.53 (dd and m, 14H, remaining protons).

1,2;3,4-Di-O-isopropylidene-6-O-[2-acetamido-2-deoxy-4-O-(β-D-galactopyranosyl)-β-D-glucopyranosyl]-α-D-galactopyranose (2)

Compound **1** (30 mg, 0.05 mmol) was taken up in methanol–water (1:1, 2 mL) containing acetic anhydride (0.4 mL) and left at room temperature for about 5 h. The oil obtained after solvent removal was applied to a Sephadex LH-20 column and eluted with ethanol–water (1:1). Solvent removal and freeze-drying of the main fraction gave a white solid (26 mg, 0.042 mmol, 82%); ^1H nmr δ: 5.66 (d, 1H, H-1, $J_{1,2}$ = 5.0 Hz), 4.58 (d, 1H, H-1′, $J_{1',2'}$ = 7.6 Hz), 4.56 (dd, 1H, H-2, $J_{2,3}$ = 2.0 Hz), 4.50 (d, 1H, H-1″, $J_{1'',2''}$ = 7.6 Hz), 4.42 (bd, 1H, H-4), 2.05 (s, 3H, NHAc methyl), 1.60, 1.51, 1.43, 1.42 (4s, 12H, OOC(CH$_3$)$_2$), 4.11–3.53 (m, 16H, remaining protons).

Removal of the isopropylidene groups provided the previously reported (1) trisaccharide, βDGal(1→4)βDGlcNAc(1→6)α,βDGal.

1,2;3,4-Di-O-isopropylidene-6-O-[2-deoxy-2-trifluoroacetamido-4-O-(β-D-galactopyranosyl)-β-D-glucopyranosyl]-α-D-galactopyranose (3)

A solution of compound **1** (30 mg, 0.051 mmol) and *S*-ethyl trifluorothioacetate (13) (90 mg, 0.634 mmol) in methanol (2 mL) was kept at room temperature for 2 days. The oil obtained after solvent removal was applied to a silica gel column and eluted with methanol. The white solid obtained after solvent removal of the first fraction was filtered through a Sephadex LH-20 column in ethanol–water (1:1). Solvent removal and freeze-drying of the main fraction gave a white solid (20 mg, 0.029 mmol, 57%); ^1H nmr δ: 5.66 (d, 1H, H-1, $J_{1,2}$ = 5.0 Hz), 4.73 (d, 1H, H-1′, $J_{1',2'}$ = 7.6 Hz), 4.55 (dd, 1H, H-2, $J_{2,3}$ = 2.0 Hz), 4.50 (d, 1H, H-1″, $J_{1'',2''}$ = 7.6 Hz), 4.41 (dd, 1H, H-4), 1.60, 1.50, 1.42 (3s, 12H, OOC(CH$_3$)$_2$), 4.08–3.54 (m, 16H, remaining protons).

Methyl 3,6-di-O-acetyl-2-azido-2-deoxy-4-O-(tetra-O-acetyl-β-D-galactopyranosyl)-β-D-glucopyranoside (5)

A solution of 3,6-di-*O*-acetyl-2-azido-2-deoxy-4-*O*-(tetra-*O*-acetyl-β-D-galactopyranosyl)-α-D-glucopyranosyl bromide (**4**) (6) (1.0 g, 1.46 mmol), mp 154–155°C, $[\alpha]_D^{23}$ +86.2° (*c* 1.0, chloroform) in dry nitromethane (4 mL) was added dropwise to a stirred mixture of methanol (15 mL), silver carbonate (1.80 g, 6.54 mmol), and Drierite (2.0 g) cooled to −15°C. After stirring at −15°C for 24 h, the solids were removed and the filtrate was worked up in the usual manner. The oily product was applied to a column of silica gel and the chromatogram was developed with ethyl acetate – hexane (3:2). The main fraction left an oil which, on addition of diethyl ether, precipitated a solid (602 mg, 0.95 mmol, 65%), mp 75–77°C; $[\alpha]_D^{23}$ +1.40° (*c* 1.0, chloroform); ^1H nmr ($CDCl_3$) δ: 5.36 (bd, 1H, H-4, $J_{3,4}$ = 2.8 Hz), 5.10 (dd, 1H, H-2′, $J_{1',2'}$ = 7.5 Hz, $J_{2',3'}$ = 10.0 Hz), 5.00 (dd, 1H, H-3, $J_{2,3}$ = 9.5 Hz, $J_{3,4}$ = 8.9 Hz), 4.95 (dd, 1H, H-3′, $J_{3',4'}$ = 3.2 Hz), 4.49 (dd, 1H, H-6a, $J_{5,6a}$ = 1.6 Hz, $J_{6a,6b}$ = 11.0 Hz), 4.45 (d, 1H, H-1′), 4.27 (d, 1H, H-1). 4.21–4.05 (m, 3H, H-6′a, H-6′b, and H-6b overlapping), 3.88 (bt, 1H, H-5′), 3.72 (dd, 1H, H-4, $J_{4,5}$ = 8.9 Hz), 3.57 (s, 3H, OCH$_3$, signal for H-5 underneath the OCH$_3$signal), 3.38 (dd, 1H, H-2), 2.21–1.98 (6s, 18H, OCOCH$_3$).

Methyl 2-azido-2-deoxy-4-O-(β-D-galactopyranosyl)-β-D-glucopyranoside (6)

The acetate (**5**) (500 mg, 0.78 mmol) was dissolved in 0.02 *N*

Can. J. Chem. Downloaded from www.nrcresearchpress.com by 210.87.254.42 on 09/06/12
For personal use only.

Can. J. Chem. Downloaded from www.nrcresearchpress.com by 210.87.254.42 on 09/06/12
For personal use only.

sodium methoxide – methanol (10 mL) and left at room temperature for 1 h. The solution was neutralized with IR-resin 120(H^+). Evaporation left a colorless solid (285 mg, 0.75 mmol, 96%), mp 227.5–229.5°C; $[\alpha]_D^{24}$ 0° (*c* 0.3, water); ^{1}H nmr (D_2O) δ: 4.50 (d, 1H, H-1′, $J_{1',2'}$ = 8.0 Hz), 4.46 (d, 1H, H-1, $J_{1,2}$ = 8.0 Hz), 4.00 (dd, 1H, H-6a, $J_{5,6a}$ = 2.2 Hz, $J_{6a,6b}$ = 12.0 Hz), 3.94 (bd, 1H, H-4′, $J_{3',4'}$ = 3.0 Hz), 3.61 (s, 3H, OCH_3), 3.55 (dd, 1H, H-2′, $J_{2',3'}$ = 9.5 Hz), 3.35 (dd, 1H, H-2, $J_{2,3}$ = 9.0 Hz), 3.86–3.45 (m, 8H, remaining protons).

*Methyl 2-formamido-2-deoxy-4-*O*-(β-*D*-galactopyranosyl)-β-*D*-glucopyranoside (7)*

A suspension of the azido compound (**6**) (40 mg, 0.11 mmol) in methanol (12 mL) was hydrogenated at atmospheric pressure and room temperature for 4 h using 5% palladium on charcoal (40 mg). The catalyst was removed and the combined filtrates were concentrated to about 5 mL and cooled to 0°C. Formyl acetate (14) (2 mL) was added. Solvent removal left a white solid which was applied to a column of Sephadex LH-20. Elution with ethanol–water (1:1) produced a main fraction as a white solid (32 mg, 0.083 mmol, 75%); ^{1}H nmr (D_2O) δ: 8.23 (s, 0.7H, *Z* formyl proton (15)), 8.02 (s, 0.3H, *E* formyl proton (15)), 4.56 (d, 0.7H, *Z* H-1, $J_{1,2}$ = 7.5 Hz), 4.53 (d, 0.3H, *E* H-1, $J_{1,2}$ = 7.5 Hz), 4.51 (d, 1H, H-1′, $J_{1',2'}$ = 7.5 Hz). The remainder of the signals were in general agreement with expectation and required a high state of purity. However, a very slight trace of a signal for an acetyl group was present.

*Methyl 2-pivalamido-2-deoxy-4-*O*-(β-*D*-galactopyranosyl)-β-*D*-glucopyranoside (8)*

The azido compound (**6**) (20 mg, 0.055 mmol) was hydrogenated in methanol as was described above for the preparation of compound **7** and the solution (1 mL) was added dropwise to a solution of dicyclohexylcarbodiimide (150 mg) and pivalic acid (50 mg) in methanol (9 mL) cooled to 0°C. After stirring at room temperature overnight, the precipitate was removed and the filtrate was evaporated to dryness. The residue was extracted with ethanol–water (1:1, 1.5 mL) and the extract was applied to a column of Sephadex LH-20 which was eluted with ethanol–water (1:1). The main fraction provided a colorless solid (17 mg, 0.038 mmol, 70%); ^{1}H nmr (D_2O) δ: 4.53 (m, 1H, H-1, $J_{1,2}$ = 8.0 Hz), 4.49 (d, 1H, H-1′, $J_{1',2'}$ = 7.5 Hz). The remainder of the spectrum to higher field was essentially the same as that for the *N*-acetyl and *N*-formyl compounds (**14** and **7**) except for the signal for the pivaloyl group at 1.20 ppm (s, 9H).

*Alkyl 3,6-di-*O*-acetyl-4-*O*-(tetra-*O*-acetyl-β-*D*-galactopyranosyl)-2-deoxy-2-phthalimido-β-*D*-glucopyranosides (9–13)*

3,6-Di-*O*-acetyl-4-*O*-(tetra-*O*-acetyl-β-D-galactopyranosyl)-2-deoxy-2-phthalimido-α,β-D-glucopyranosyl bromide (7) (mp 104–111°C; $[\alpha]_D^{25}$ +35.7° (*c* 1.0, chloroform), 0.293 g, 0.37 mmol) in dry nitromethane (2 mL) was added to a solution of the dry alcohol (1 mL), *sym*-collidine (50 μL), and silver triflate (0.114 g, 0.44 mmol) in dry nitromethane (5 mL) cooled to −15°C. The mixture was stirred at −15°C for 1 h. The reaction mixture was diluted with chloroform (10 mL) and the solid was removed by filtration. The filtrate was washed with saturated sodium thiosulfate solution (10 mL), cold water (10 mL), and saturated sodium bicarbonate solution (3 × 10 mL). The solvent removal after drying with sodium sulfate left a white solid. In each case the yields were in the range 70–80% after recrystallization from ethyl acetate – hexane. The ^{1}H nmr spectra were in general accord with expectation.

Methyl glycoside (9): mp 227.5–229.5°C; $[\alpha]_D^{24}$ + 19.8° (*c* 0.4, chloroform); ^{1}H nmr δ: 5.75 (dd, 1H H-3, $J_{2,3}$ = 10.5 Hz, $J_{3,4}$ = 8.0 Hz), 5.28 (d, 1H, H-1, $J_{1,2}$ = 8.0 Hz), 4.52 (d, 1H, H-1′, $J_{1',2'}$ = 8.0 Hz). *Anal.* calcd. for $C_{33}H_{39}O_{18}N$: C 53.74, H 5.33, N 1.90; found: C 53.23, H 5.34, N 1.94.

Ethyl glycoside (10): mp 249–250°C; $[\alpha]_D^{24}$ + 11.4° (*c* 0.4, chloroform); ^{1}H nmr δ: 5.74 (dd, 1H, H-3, $J_{2,3}$ = 10.5 Hz, $J_{3,4}$ = 8.0 Hz), 5.36 (dd, 1H, H-1, $J_{1,2}$ = 8.0 Hz), 4.52 (d, 1H, H-1′, $J_{1',2'}$ = 8.0 Hz). *Anal.* calcd. for $C_{34}H_{41}O_{18}N$: C 54.33, H 5.30, N 1.95; found: C 54.14, H 5.58, N 1.83.

n-Propyl glycoside (11): mp 227–229°C; $[\alpha]_D$ +13.5° (*c* 0.4, chloroform); ^{1}H nmr δ: 5.73 (dd, 1H, H-3, $J_{2,3}$ = 10.5 Hz, $J_{3,4}$ = 8.0 Hz), 5.32 (d, 1H, H-1, $J_{1,2}$ = 8.0 Hz), 4.52 (d, 1H, H-1, $J_{1',2'}$ = 8.0 Hz). *Anal.* calcd. for $C_{35}H_{43}O_{18}N$: C 54.90, H 5.66, N 1.83; found: C 55.02, H 5.65, N 1.85.

Isopropyl glycoside (12): mp 255.5–258.5°C; $[\alpha]_D^{24}$ +3.6° (*c* 0.4, chloroform); ^{1}H nmr δ: 5.72 (dd, 1H, H-3, $J_{2,3}$ = 10.5 Hz, $J_{3,4}$ = 8.0 Hz), 5.42 (d, 1H, H-1, $J_{1,2}$ = 8.0 Hz), 4.52 (d, 1H, H-1′, $J_{1',2'}$ = 8.0 Hz). *Anal.* calcd. for $C_{35}H_{43}O_{18}N$: C 54.90, H 5.66, N 1.83; found: C 54.56, H 5.65, N 1.81.

Isobutyl glycoside (13): mp 199–203°C; $[\alpha]_D^{24}$ +15.0° (*c* 0.4, chloroform); ^{1}H nmr δ: 5.75 (dd, 1H, H-3, $J_{2,3}$ = 10.5 Hz, $J_{3,4}$ = 8.0 Hz), 5.32 (d, 1H, H-1, $J_{1,2}$ = 8.0 Hz), 4.52 (d, 1H, H-1′, $J_{1',2'}$ = 8.0 Hz). *Anal.* calcd. for $C_{36}H_{45}O_{18}N$: C 55.46, H 5.82, N 1.80; found: C 56.19, H 5.91, N 1.83.

*Alkyl 2-acetamido-2-deoxy-4-*O*-(β-*D*-galactopyranosyl)-β-*D*-glucopyranosides (14–18)*

Compounds **9** to **13** were deacetylated using 0.025 *M* sodium methoxide in methanol. In each case, the solution was acidified with Amberlite IR-120(H^+) and taken to dryness. The residue was dissolved in pyridine and the solution kept at 115°C for 10 h prior to being taken to dryness. This residue was then treated with hydrazine in ethanol and the product *N*-acetylated in the usual manner. The ^{1}H nmr spectra were in general agreement with expectation and the assignments of the signals for the anomeric hydrogens were by spin-decoupling experiments.

Methyl glycoside (14): mp 283–285.5°C; $[\alpha]_D^{24}$ −26.7° (*c* 0.25, water); ^{1}H nmr δ: 4.52 (2d, 2H, H-1, H-1′ overlapping, *J* = 8.0 Hz and 8.0 Hz).

Ethyl glycoside (15): mp 274–275°C; $[\alpha]_D^{24}$ −24.0° (*c* 0.9, water); ^{1}H nmr δ: 4.59 (d, 1H, H-1, $J_{1,2}$ = 8.0 Hz), 4.50 (d, 1H, H-1′, $J_{1',2'}$ = 8.0 Hz).

Propyl glycoside (16): mp 276.5–278°C; $[\alpha]_D^{24}$ −20.7° (*c* 0.35, water); ^{1}H nmr δ: 4.55 (d, 1H, H-1, $J_{1,2}$ = 8.0 Hz), 4.50 (d, 1H, $J_{1',2'}$ = 8.0 Hz).

Isopropyl glycoside (17): mp 264–266°C; $[\alpha]_D^{24}$ −16.7° (*c* 0.25, water); ^{1}H nmr δ: 4.68 (d, 1H, H-1, $J_{1,2}$ = 8.0 Hz), 4.54 (d, 1H, H-1′, $J_{1',2'}$ = 8.0 Hz).

Isobutyl glycoside (18): mp 282.5–284.5°C; $[\alpha]_D^{24}$ −23.5° (*c* 0.25, water); ^{1}H nmr δ: 4.58 (d, 1H, H-1, $J_{1,2}$ = 8.0 Hz), 4.52 (d, 1H, H-1′, $J_{1,2}$ = 8.0 Hz).

*Benzyl 4-*O*-(β-*D*-galactopyranosyl)-2-deoxy-2-phthalimido-β-*D*-glucopyranoside (19)*

Benzyl 3,6-di-*O*-acetyl-4-*O*-(tetra-*O*-acetyl-β-D-galactopyranosyl)-2-deoxy-2-phthalimido-β-glucopyranoside (7) (0.5 g, 0.62 mmol) was treated with 0.2 *N* sodium methoxide in methanol (150 mL) for 5 min at room temperature. The solution was then neutralized with Amberlite IR-120(H^+), the resin immediately removed, and the filtrate taken to dryness. The residue (0.39 g) was dissolved in dry pyridine (10 mL) for heating at 110°C for 10 h. Solvent removal left a crystalline residue (0.28 g, 82%), mp 254–257°C, $[\alpha]_D$ −44.8° (*c* 0.17, methanol), which appeared homogeneous (tlc) and which was used directly for the preparation of **20**.

*Benzyl 4-*O*-(4,6-*O*-benzylidene-β-*D*-galactopyranosyl)-2-deoxy-2-phthalimido-β-*D*-glucopyranoside (20)*

Compound **19** (0.80 g, 1.42 mmol), α,α-dimethoxytoluene (0.43 g, 2.84 mmol), and *p*-toluenesulfonic acid monohydrate (11 mg) in dry acetonitrile (15 mL) were stirred at room temperature for 7 h. After neutralization with triethylamine, the solvent was removed to leave an oil which was applied to a column of silica gel and eluted with ethyl acetate – methanol (9:1). Solvent removal of the main fraction left a solid (0.78 g) which was redissolved in methanol (5 mL). Diethyl ether was added to turbidity and on storage crystals were deposited (0.54 g, 0.83 mmol, 58%); mp 206–207°C; $[\alpha]_D^{24}$ −72.4° (*c* 1.1, chloroform); ^{1}H nmr (CD_3OD) δ: 7.81 (s, 4H, phthalimido), 7.61–7.25 (m, 5H, benzylidene aromatic), 7.10 (s, 5H, benzyl aromatic), 5.60 (s, 1H, benzylidene methine), 5.20 (d, 1H, H-1); ^{13}C nmr

Can. J. Chem. Downloaded from www.nrcresearchpress.com by 210.87.254.42 on 09/06/12
For personal use only.

δ: 105.5 (C-1′), 101.5 (benzylidene methine), 98.6, 82.0, 77.3, 76.9, 73.8, 71.9, 80.0, 70.3, 69.5, 67.8 (C-6′), 61.7 (C-6), 57.9. *Anal.* calcd. for $C_{34}H_{35}O_{12}N$: C 62.86, H 5.43, N 2.16; found: C 62.22, H 5.28, N 2.14.

*Benzyl 3,6-di-*O*-acetyl-4-*O*-(2,3-di-*O*-acetyl-4-6-*O*-benzylidene-*β*-*D*-galactopyranosyl)-2-deoxy-2-phthalimido-*β*-*D*-glucopyranoside (21)*

Compound **20** (0.62 g, 0.96 mmol) was dissolved in acetic anhydride – pyridine (1:2) and heated at 80°C for 3 h. Solvent removal left a yellowish foam which was decolorized by passing through a short column of silica gel and eluted with ethyl acetate. Removal of the solvent gave a solid which was recrystallized from ethanol. The yield of this pure product was 81%, mp 210–212°C. The ^{1}H nmr spectrum was consistent with the structural assignment. *Anal.* calcd. for $C_{42}H_{43}O_{16}N$: C 61.69, H 5.30, N 1.71; found: C 61.35, H 5.32, N 1.24.

*Benzyl 3,6-di-*O*-acetyl-4-*O*-(2,3,4-tri-*O*-acetyl-6-deoxy-6-iodo-α-*D*-galactopyranosyl)-2-deoxy-2-phthalimido-α-*D*-glucopyranoside (24)*

The benzylidene compound (**21**) (0.47 g, 0.58 mmol) was treated with 80% aqueous acetic acid at 80°C for 3 h. Solvent removal left a foam which was applied to a silica gel column and eluted with ethyl acetate – hexane (4:1). Solvent removal of the main fraction left a solid, in 82% yield, with an ^{1}H nmr spectrum that was consistent with the structural assignment for the desired diol (**22**).

Methanesulfonyl chloride (60 mg, 0.52 mmol) was added in two batches (15-min interval) to a solution of the diol (**22**) (0.3 g, 0.41 mmol) in dry pyridine (2 mL) cooled to −20°C. The reaction mixture was kept at −20°C for 12 h. A few drops of water were added and the solution was allowed to warm to room temperature. Solvent removal left an oil which was applied to a silica gel column and eluted with ethyl acetate – hexane (4:1). The main fraction contained an oil (**23**) (0.18 g) which was treated with potassium iodide (0.5 g) in *N,N*-dimethylformamide (2 mL) at 80°C for 72 h. The reaction mixture was diluted with chloroform (10 mL) and washed with cold water (3 × 10 mL) before drying over sodium sulfate. The residue, after solvent removal, was applied to a column of silica gel and the chromatogram was developed with ethyl acetate – hexane (3:2). The main fraction contained an amorphous solid (0.12 g, 0.13 mmol, 32%) which appeared pure (tlc); ^{1}H nmr δ: 7.83–7.69 (m, 4H, phthalimido), 7.12 (s, 5H, benzyl aromatic), 5.80 (dd, 1H, H-3, $J_{2,3}$ = 10.5 Hz, $J_{3,4}$ = 8.2 Hz), 5.55 (dd, 1H, H-4′, $J_{3',4'}$ = 3.4 Hz, $J_{4',5'}$ = 1.0 Hz), 5.36 (d, 1H, H-1, $J_{1,2}$ = 8.5 Hz), 5.11 (dd, 1H, H-2′, $J_{1',2'}$ = 7.5 Hz, $J_{2',3'}$ = 10.5 Hz), 4.97 (dd, 1H, H-3′), 4.82 (d, 1H, benzyl CH_AH_B, $J_{A,B}$ = 12.0 Hz), 4.58 (dd, 1H, H-6a, $J_{6a,5}$ = 2.0 Hz), 4.55 (d, 1H, H-1′), 4.53 (d, 1H, benzyl-CH_AH_B), 4.28 (d, 1H, H-2), 4.17 (dd, 1H, H-6b, $J_{6b,5}$ = 4.5 Hz), 3.94 (dd, 1H, H-4, $J_{4,5}$ = 10.0 Hz), 3.86 (m, 1H, H-5), 3.76 (m, 1H, H-5′), 3.10 (m, 2H, H-6′a and b), 2.16–1.91 (5s, 15H, 5 $OCOCH_3$). *Anal.* calcd. for $C_{37}H_{41}O_{16}NI$: I 14.42; found: I 14.53.

*Benzyl 3,6-di-*O*-acetyl-4-*O*-(2,3,4-tri-*O*-acetyl-6-deoxy-*β*-*D*-galactopyranosyl)-2-deoxy-2-phthalimido-*β*-*D*-glucopyranoside (25)*

A mixture of the iodo compound (**24**) (0.11 g, 0.12 mmol), tri-*n*-butyl tin hydride (0.14 g, 0.48 mmol), and 2,2′-azobisisobutyronitrile (5 mg) in toluene was heated at 55°C for 20 h. Solvent removal left an oil which was applied to a column of silica gel and the chromatogram was developed with ethyl acetate – hexane (1:1). Removal of solvent from the second fraction gave an oil (48 mg, 0.05 mmol, 50%); ^{1}H nmr δ: 7.86–7.70 (m, 4H, phthalimido), 7.16 (s, 5H, benzyl aromatic), 5.76 (dd, 1H, H-3, $J_{2,3}$ = 10.5 Hz, $J_{3,4}$ = 7.0 Hz), 5.41 (d, 1H, H-1, $J_{1,2}$ = 7.2 Hz), 5.22 (dd, 1H, H-4′, $J_{3',4'}$ = 3.5 Hz, $J_{4',5'}$ = 1.0 Hz), 5.14 (dd, 1H, H-2′, $J_{1',2'}$ = 7.5 Hz, $J_{2',3'}$ = 10.0 Hz), 4.98 (dd, 1H, H-3′), 4.84 (d, 1H, benzyl CH_AH_B, J_{AB} = 12.0 Hz), 4.58 (dd, 1H, H-6a, $J_{6a,5}$ = 1.5 Hz), 4.56 (d, 1H, benzyl CH_AH_B), 4.55 (d, 1H, H-1′), 4.26 (dd, 1H, H-2), 4.17 (dd, 1H, H-6b, $J_{6b,5}$ = 3.5 Hz), 3.88 (dd, 1H, H-4), 3.80 (dd, 1H, H-5), 3.74 (dd, 1H, H-5′, $J_{5',(C'6)H3}$ = 7.0 Hz), 2.15–1.89 (5s, 15H, 5 $OCOCH_3$), 1.26 (d, 3H, (C6′)H3).

*1,2;3,4-Di-*O*-isopropylidene-6-*O*-[3,6-di-*O*-acetyl-4-*O*-(2,3,4-tri-*O*-acetyl-6-deoxy-*β*-*D*-galactopyranosyl)-2-deoxy-2-phthalimido-*β*-*D*-glucopyranosyl]-α-*D*-galactopyranose (27)*

3,6-Di-*O*-4-*O*-(2,3,4-tri-*O*-acetyl-6-deoxy-β-D-galactopyranosyl)-2-deoxy-2-phthalimido-β-D-glucopyranosyl bromide (**26**) (27 mg, 0.037 mmol) was prepared from **25** by the same procedure as was described (7) for the preparation of the corresponding derivative of lactosamine as the glycosyl chloride, except that *N,N*-dimethylbromoforminium bromide (11) was used as the halogenating reagent. The bromide (**26**) was condensed with 1,2;3,4-di-*O*-isopropylidene-α-D-galactopyranose in the same manner as was previously described (1) for the preparation of the acetylated form of **2**. The yield was 18 mg (54%) of an oil after chromatography; ^{1}H nmr δ: 7.92–7.68 (m, 4H, phthalimido), 5.81 (dd, 1H, H-3′, $J_{2',3'}$ = 10.5 Hz, $J_{3',4'}$ = 8.0 Hz), 5.46 (d, 1H, H-1′, $J_{1',2'}$ = 8.5 Hz), 5.20 (dd, 1H, H-4″, $J_{3'',4''}$ = 3.5 Hz, $J_{4'',5''}$ = 1.0 Hz), 5.13 (d, 1H, H-1, $J_{1,2}$ = 5.2 Hz), 5.09 (dd, 1H, H-2″, $J_{1'',2''}$ = 7.5 Hz, $J_{2'',3''}$ = 10.5 Hz), 4.96 (dd, 1H, H-3″), 4.53 (dd, 1H, H-6′a), 4.51 (d, 1H, H-1″), 4.40 (dd, 1H, H-3, $J_{2,3}$ = 2.5 Hz, $J_{3,4}$ = 8.0 Hz), 4.22 (dd, 1H, H-2′), 4.15 (dd, 1H, H-6′b), 4.11 (dd, 1H, H-2), 4.00 (dd, 1H, H-4, $J_{4,5}$ = 1.5 Hz), 3.88 (dd, 1H, H-4′), 3.83 (m, 1H, H-5′), 3.74 (m, 1H, H-5″), 3.66 (m, 1H, H-5), 2.16–1.90 (5s, 15H, acetyl methyl), 1.40, 1.22, 1.03, 1.02 (4s, 12H, 2 $OCO(CH_3)_2$), 1.16 (d, 3H, (C6″)H_3, $J_{5'',(C6'')H3}$ = 7.0 Hz).

*6-*O*-[2-Acetamido-2-deoxy-4-*O*-(6-deoxy-*β*-*D*-galactopyranosyl)-*β*-*D*-glucopyranosyl]-*D*-galactopyranose (28)*

Hydrazinolysis of **27** and then *N*-acetylation was carried out by procedures as described for the preparation of compound **1**. Removal of isopropylidene groups by acid hydrolysis, following the procedures described for the preparation of compound **4**, afforded a white solid (4 mg) which was purified by chromatography on a column of Sephadex LH-20; ^{1}H nmr δ: 5.28 (d, 0.35H, H-1α, $J_{1\alpha,2\alpha}$ = 3.5 Hz), 4.63 (d, 0.65H, H-1α, $J_{1\alpha,2\alpha}$ = 8.0 Hz), 4.58 (d, 1H, H-1′, $J_{1',2'}$ = 7.8 Hz), 4.46 (d, 1H, H-1″, $J_{1'',2''}$ = 7.5 Hz), 2.08 (s, 3H, $NCOCH_3$), 1.27 (d, 3H, ($C_{6''}$)$H_{3'}$, $J_{(C6'')H3',5''}$ = 7.0 Hz).

*Crude 3,6-di-*O*-acetyl-2-azido-2-deoxy-4-*O*-(tetra-*O*-acetyl-*β*-*D*-glucopyranosyl)-α,β-*D*-glucopyranosyl nitrate (29)*

Hexa-*O*-acetyl-cellobial (16) (mp 129.5–133°C; $[\alpha]_D^{25}$ −24.5° (*c* 1.1, chlroform)) (45 g, 1.08 mol) in acetonitrile (315 mL) was added to a mixture of sodium azide (8.0 g, 0.124 mol) and ceric ammonium nitrate (135 g, 0.3 mol) cooled to −15°C (6). The resulting suspension was vigorously stirred with cooling for 8 h. The solid was removed by filtration and washed with toluene (700 mL) and the combined filtrate and washings were poured on ice (~500 g). The organic layer was separated and washed with cold water (3 × 500 mL) before drying over sodium sulfate. Solvent removal by evaporation *in vacuo* at 45°C left a solid foam (45 g).

*3,6-Di-*O*-acetyl-2-azido-2-deoxy-4-*O*-(tetra-*O*-acetyl-*β*-*D*-glucopyranosyl)-α-*D*-glucopyranosyl bromide (30)*

N,N-dimethylbromoforminium bromide (13.3 g, 0.061 mol) was added to a solution of the crude product **29** (40 g) in dichloromethane (12) (60 mL). The mixture was stirred at room temperature for 3 h to result in a clear red solution before lithium bromide (50 g, 0.57 mol) was added (12). The suspension was stirred for 7 h. The mixture was then diluted with dichloromethane (60 mL) and the supernatant was decanted onto ice (500 g). The organic layer was separated and washed with saturated sodium bicarbonate solution (4 × 200 mL) and water (200 mL) before drying with anhydrous sodium sulfate. Solvent removal by evaporation left a foam which was redissolved in the minimum amount of ethyl acetate. On cooling, the solution deposited a solid (15.6 g, 0.0228 mol, 32% from hexa-*O*-acetyl-cellobial), mp 136.5–138°C. Recrystallization from ethyl acetate and n-hexane provided the analytical sample, mp 140–141°C; $[\alpha]_D^{24}$ 79.7° (*c* 1.3, chloroform); FTIR ($CHCl_3$Cast) max: 2114 (N_3); ^{1}H nmr δ: 6.35 (d, 1H, H-1, $J_{1,2}$ = 3.8 Hz), 5.45 (dd, 1H, H-3, $J_{2,3}$ = 10.1 Hz, $J_{3,4}$ = 8.4

Can. J. Chem. Downloaded from www.nrcresearchpress.com by 210.87.254.42 on 09/06/12
For personal use only.

Hz), 5.14 (dd, 1H, H-3', $J_{2',3'}$ = 9.0 Hz, $J_{3',4'}$ = 9.0 Hz), 5.06 (dd, 1H, H-4', $J_{4',5'}$ = 9.0 Hz), 4.91 (dd, 1H, H-2', $J_{1',2'}$ = 7.8 Hz), 4.51 (d, 1H, H-1'), 4.49 (dd, 1H, H-6a), 4.38 (dd, 1H, H-6'a, $J_{6'a,6'b}$ = 12.5 Hz), $J_{6'a,5'}$ = 4.5 Hz), 4.20 (m, 1H, H-5), 4.15 (dd, 1H, H-6b, $J_{6b,5}$ = 4.0 Hz), 4.03 (dd, 1H, H-6'b, $J_{6'b,5'}$ = 2.5 Hz), 3.81 (dd, 1H, H-4, $J_{4,5}$ = 9.0 Hz), 3.66 (dd and m, 2H, H-2 and H-5' overlapping), 2.10–1.94 (6s, 17H, 6 $OCOCH_3$). *Anal.* calcd. for $C_{24}H_{32}O_{15}N_3Br$: C 42.24, H 4.73, N 6.16, Br 11.76; found: C 41.93, H 4.64, N 6.01, Br 11.89.

*Benzyl 3,6-di-*O*-acetyl-2-azido-2-deoxy-4-*O*-(tetra-*O*-acetyl-*β*-D-glucopyranosyl)-*β*-D-glucopyranoside (31)*

A solution of the azidobromide (**30**) (9.75 g, 14.3 mmol) in nitromethane (20 mL) was added in small portions to a stirred mixture of benzyl alcohol (6 mL), silver carbonate (15 g, 54.5 mmol), and Drierite (15 g), which was cooled to −25°C. After stirring at −25°C for 2 h, the solids were removed by filtration and washed with dichloromethane (20 mL). Solvent removal left a syrup which was applied to a column of silica gel and the chromatogram was developed with ethyl acetate – hexane (5:6). Solvent removal of the second fraction gave an oil which crystallized on addition of diethyl ether (6.68 g, 9.4 mmol, 66%), mp 155–158°C; $[\alpha]_D^{24}$ −16.4° (*c* 2.0, chloroform); ^{1}H nmr ($CDCl_3$) δ: 7.32 (s, 5H, benzyl aromatic protons), 4.88 and 4.66 (2d, 2H, benzyl CH_2), 4.47 (d, 1H, H-1', $J_{1',2'}$ = 8.0 Hz), 4.38 (d, 1H, H-1, $J_{1,2}$ = 8.0 Hz), 3.44 (dd, 1H, H-2, $J_{2,3}$ = 10.5 Hz), 2.14–1.96 (4s, 12H, 4 $OCOCH_3$). *Anal.* calcd. for $C_{31}H_{39}O_{16}N_3$: C 52.47, H 5.54, N 5.92; found: C 52.27, H 5.61, N 6.02.

*Benzyl 2-azido-2-deoxy-4-*O*-(β-D-glucopyranosyl)-β-D-glucopyranoside (32)*

Compound **31** (4.0 g, 5.64 mmol) was deacetylated in 0.01 *N* sodium methoxide – methanol (75 mL) and the product isolated in the usual manner. The substance crystallized from methanol (2.37 g, 5.19 mmol, 92%), mp 195–198°C; $[\alpha]_D^{24}$ −7.4° (*c* 0.4, methanol). *Anal.* calcd. for $C_{19}H_{27}O_{10}N_3$: C 49.89, H 5.95, N 9.19; found: C 49.69, H 5.99, N 9.24.

*Benzyl 2-amino-2-deoxy-4-*O*-(β-D-glucopyranosyl)-β-D-glucopyranoside (33)*

A slow stream of hydrogen sulfide was bubbled through an ice-cold solution of the azide (**32**) (2.0 g, 4.38 mmol) in pyridine (25 mL) and triethylamine (15 mL) for 2.5 h. The solution was evaporated to dryness and the residue was extracted with methanol–water (1:1). The extract was filtered through a bed of diatomaceous earth and solvent removal left a dark-colored solid (1.96 g). The solid was taken up in water and clarified by centrifugation. Freeze-drying of the supernatant left a yellowish white solid (1.58 g, 3.67 mmol, 84%); $[\alpha]_D^{25}$ −28.2° (*c* 0.6, water); ^{1}H nmr (D_2O) δ: 7.46 (s, 5H, benzyl aromatic), 4.54–4.50 (2d, 2H, H-1 and H-1' overlapping, *J* = 8.0 Hz and 7.5 Hz), 2.72 (dd, 1H, H-2, $J_{1,2}$ = 8.0 Hz, $J_{2,3}$ = 9.5 Hz).

*Benzyl 3,6-di-*O*-acetyl-4-*O*-(tetra-*O*-acetyl-*β*-D-glucopyranosyl)-2-deoxy-2-phthalimido-*β*-D-glucopyranoside (34)*

Phthalic anhydride (97 mg, 0.65 mmol) was added to a solution of the amine (**33**) (0.489 g, 1.13 mmol) in pyridine (4 mL). The solution was heated to 60°C for 20 min. Triethylamine (0.1 g, 0.99 mmol) and more phthalic anhydride (97 mg, 0.65 mmol) were added and the solution was evaporated to dryness. The residue was taken up in pyridine – acetic anhydride (2:1, 3 mL) and heated at 80°C for 3 h. Solvent removal left a dark solid foam which was applied to a column of silica gel and the chromatogram was developed with ethyl acetate – hexane (1:1). Solvent removal of the main fraction left an oil which was dissolved in diethyl ether for decolorization with charcoal. The resultant solution, on storage in an open flask for 2 days, deposited crystals (0.55 g, 0.69 mmol, 60%), mp 138–140°C; $[\alpha]_D^{24}$ −22.6° (*c* 0.95, chloroform); ^{1}H nmr ($CDCl_3$) δ: 7.80–7.68 (m, 4H, phthalimido), 7.12–7.04 (m, 5H, benzyl aromatic), 5.72 (dd, 1H, H-3, $J_{2,3}$ = 10.0 Hz, $J_{3,4}$ = 8.0 Hz), 5.35 (d, 1H, H-1, $J_{1,2}$ = 8.4 Hz), 5.14 (dd, 1H, H-3', $J_{2',3'}$ = 9.0 Hz, $J_{3',4'}$ = 9.0 Hz), 4.92 (dd, 1H, H-2', $J_{1',2'}$ = 7.6 Hz), 4.81 (d, 1H, benzyl CH_AH_B, J_{AB} = 12.0 Hz), 4.58 (dd, 1H, H-6a), 4.56 (d, 1H, H-1'), 4.51 (d, 1H, benzyl CH_AH_B), 4.33 (dd, 1H, H-6'a, $J_{6'a,6'b}$ = 12.5 Hz, $J_{6'a,5}$ = 5.0 Hz), 4.26 (dd, 1H, H-2), 4.16 (dd, 1H, H-6b, $J_{6a,6b}$ = 12 Hz, $J_{6b,5}$ = 5.0 Hz), 4.02 (dd, 1H, H-6'b, $J_{6'b,5'}$ = 2.0 Hz), 3.87 (dd, 1H, H-4, $J_{4,5}$ = 8.0 Hz), 3.78 (m, 1H, H-5), 3.64 (m, 1H, H-5'). *Anal.* calcd. for $C_{32}H_{37}NO_{18}$: C 57.56, H 5.33, N 1.73; found: C 57.03, H 5.33, N 1.69.

*3,6-Di-*O*-acetyl-4-*O*-(tetra-*O*-acetyl-β-D-glucopyranosyl)-2-deoxy-2-phthalimido-α,β,-glucopyranosyl chloride (36)*

Compound **34** was hydrogenated in ethanol – ethyl acetate (1:1) at 50 psi (1 psi = 6.89 kPa) and room temperature using 5% palladium on charcoal as catalyst for 20 h. The yield of **35** was quantitative; ^{1}H nmr ($CDCl_3$) δ: 7.90–7.70 (m, 4H, phthalimido), 6.00 (dd, 0.2H, H-3α), 5.76 (dd, 0.8H, H-3β), 5.64 (d, 0.8H, H-1β), 5.34 (d, 0.2H, H-1α), 2.21–1.82 (6s, 18H, 6 $OCOCH_3$).

A solution of *N,N*-dimethylchloroforminium chloride (95 mg, 0.74 mmol), the alcohol (**35**) (0.13 g, 0.18 mmol), and *sym*-collidine (0.1 g, 0.82 mmol) in dichloromethane (2 mL) was stirred at room temperature for 1 h. The reaction mixture was diluted with chloroform (10 mL) and washed successively with cold water (10 mL) and saturated sodium bicarbonate solution (3 × 10 mL). Drying with sodium sulfate and solvent removal left a solid (0.122 g, 0.16 mmol, 89%); ^{1}H nmr δ: 7.82–7.66 (m, 4H, phthalimido), 6.48 (dd, 0.2H, H-3α), 6.12 (d, 0.8H, H-1α, $J_{1\alpha,2\alpha}$ = 9.0 Hz), 6.08 (d, 0.2H, H-1α, $J_{1\alpha,2\alpha}$ = 3.6 Hz), 5.66 (dd, 0.8H, H-3β), 2.12–1.82 (6s, 18H, 6 $OCOCH_3$).

*1,2;3,4-Di-*O*-isopropylidene-6-*O*-[3,6-di-*O*-acetyl-4-*O*-(tetra-*O*-acetyl-β-D-glucopyranosyl)-2-deoxy-2-phthalimido-β-D-glucopyranosyl]-α-D-galactopyranose (37)*

The chloride (**36**) (0.1 g, 0.13 mmol) in nitromethane (0.5 mL) was added to a solution of 1,2;3,4-di-*O*-isopropylidene-α-D-galactopyranose (33 mg, 0.13 mmol), *sym*-collidine (16 mg, 0.13 mmol), and silver triflate (33 mg, 0.13 mmol) in dry nitromethane (1:5 mL) cooled to −20°C. The mixture was stirred for 3 h and then worked up in the usual manner. The yield was 65% after recrystallization from chloroform – diethyl ether, mp 235–237°C; $[\alpha]_D^{23}$ −20.7° (*c* 0.4, chloroform); ^{1}H nmr δ: 7.90–7.66 (m, 4H, phthalimido), 5.78 (dd, 1H, H-3', $J_{2',3'}$ = 10.8 Hz, $J_{3,4}$ = 8.0 Hz), 5.45 (d, 1H, H-1', $J_{1',2'}$ = 9.0 Hz), 5.12 (d, 1H, H-1, $J_{1,2}$ = 5.0 Hz, overlapped), 4.58 (d, 1H, H-1'', $J_{1'',2''}$ = 8.0 Hz, overlapped), 2.17–1.88 (6s, 18H, 6 $OCOCH_3$), 1.40, 1.24, 1.04 (3s, 12H, 2 $OOC(CH_3)_2$). *Anal.* calcd. for $C_{44}H_{55}NO_{23}$: C 54.71, H 5.74, N 1.45; found: C 55.67, H 5.96, N 1.45.

*1,2;3,4-Di-*O*-isopropylidene-6-*O*-[2-acetamido-2-deoxy-4-*O*-(β-D-glucopyranosyl)-β-D-glucopyranosyl]-α-D-galactopyranose (39)*

Hydrazinolysis of **37** to **38** followed by *N*-acetylation as described for the preparation of **1** gave a product which was applied to a column of Sephadex LH-20 and the chromatogram was developed with ethanol–water (1:1). On solvent removal, the main fraction left a white solid (10.6 mg, 0.017 mmol, 71%); ^{1}H nmr δ: 5.64 (d, 1H, H-1, $J_{1,2}$ = 5.0 Hz), 4.55 (m, 3H, H-1', H-1'', H-2 overlapping), 4.40 (dd, 1H, H-4), 2.10 (s, 3H, NHAc methyl), 1.61–1.42 (4s, 12H, 2 $OOC(CH_3)_2$).

*Methyl 3,6-di-*O*-acetyl-4-*O*-(2,3-di-*O*-acetyl-β-D-galactopyranosyl)-2-deoxy-2-phthalimido-β-D-glucopyranoside (42)*

Deacetylation of **9** as reported for the preparation of **19** provided methyl 4-*O*-(β-D-galactopyranosyl)-2-deoxy-2-phthalimido-β-D-glucopyranoside (**40**) as an amorphous solid in quantitative yield. This product was then converted to the acetylated 4',6'-*O*-benzylidene derivative **41** using the procedure described for the conversion of **19** to **21**. This product was hydrolyzed to the diol **42**, under the conditions used to convert **21** to **22**, and obtained as a syrup, in 48% yield from compound **40**, which appeared pure (tlc and ^{1}H nmr); ^{1}H nmr δ: 7.90–7.75 (m, 4H, phthalimido), 5.35 (d, 1H, H-1, $J_{1,2}$ = 8.0 Hz), 5.34 (dd, 1H, H-2', $J_{1',2'}$ = 8.0 Hz, $J_{2',3'}$ = 10.0 Hz), 4.95 (dd, 1H, H-3', $J_{3',4'}$ = 2.4 Hz), 3.74 (bm, 1H, H-5'), 3.50 (s, 3H, OCH_3), 2.22, 2.16, 2.15, 2.02 (4s, 12H, 4 $OCOCH_3$).

*Methyl 3,6-di-O-acetyl-4-O-[2,3-di-O-acetyl-6-O-(3,4,6-tri-O-acetyl-2-deoxy-2-phthalimido-β-D-glucopyranosyl)-β-D-galactopyranosyl]-2-deoxy-2-phthalimido-β-D-glucopyranoside (**43**)*

3,4,6-Tri-*O*-acetyl-2-deoxy-2-phthalimido-β-D-glucopyranosyl bromide (8) (74 mg, 0.15 mmol) in nitromethane (2 mL) was added to a solution of the diol (**42**) (48 mg, 0.074 mmol), *sym*-collidine (9.0 mg, 0.074 mmol), and silver triflate (19 mg, 0.074 mmol) in dry nitromethane (0.5 mL) cooled to −15°C. The mixture was allowed to warm to room temperature and stirred overnight. The solids were removed by filtration and the solution was diluted with chloroform (5 mL) before washing with sodium thiosulfate solution (5 mL), cold water (5 mL), and sodium bicarbonate solution (2 × 5 mL). Solvent removal, after drying over anhydrous sodium sulfate, left a solid foam which was applied to a column of silica gel and the chromatogram was developed with ethyl acetate – hexane (1:1). Solvent removal of the second fraction left a pure white solid (40 mg, 0.037 mmol, 50%); ^{1}H nmr δ: 7.90–7.70 (m, 8H, phthalimido), 5.82–5.65 (2dd, 2H, H-3 and H-3″), 5.50–5.30 (dd, 2H, H-1 and H-1″), 5.25–3.72 (m, 17H, remaining protons), 3.46 (s, 3H, OCH_3), 2.20, 2.12, 2.10, 1.92, 1.86 (5s, 21H, 7 $OCOCH_3$).

*Methyl 4-O-[6-O-(2-acetamido-2-deoxy-β-D-glucopyranosyl)-β-D-galactopyranosyl]-2-acetamido-2-deoxy-β-D-glucopyranoside (**44**)*

Hydrazinolysis of **43** followed by *N*-acetylation as described for the preparation of **1** provided a solid which was dissolved in water and applied to a Biogel P-2 column. Elution with water–ethanol (9:1) resulted in the isolation of a main fraction which, on evaporation, left a solid (16 mg, 0.027 mmol, 81%); ^{1}H nmr δ: 4.65 (d, 1H, H-1′, $J_{1',2'}$ = 8.0 Hz), 4.50 (2d, 2H, H-1 and H-1″, $J_{1,2} = J_{1'',2''}$ = 7.5 Hz), 3.55 (s, 3H, OCH_3), 2.12, 2.11 (2s, 6H, 2 $NCOCH_3$), 4.05–3.42 (m, 18H); ^{13}C nmr δ: 174.7, 174.6 (2 N*C*OCH_3), 103.2, 102.0, and 101.2 (C-1, C-1′, C-1″), 79.3, 76.0, 74.9, 73.9, 72.7, 72.6, 71.0, 70.1, 68.7, 68.4, 60.09 and 60.2, 57.2 (OCH_3), 55.7, 55.1, 22.5, 22.4. Both the nmr spectra required a high state of purity.

Acknowledgements

This research was supported by a grant (A0172 to R.U.L.) from the Natural Sciences and Engineering Research Council of Canada and studentships to T.W. from the Alberta Heritage Foundation for Medical Research. The nmr and microanalyses were provided by the Spectral and Analytical Service Laboratories of this department.

1. R. U. LEMIEUX, S. Z. ABBAS, and B. Y. CHUNG. Can. J. Chem. **60**, 68 (1982).
2. T. FEIZI, E. A. KABAT, G. VICARI, B. ANDERSON, and W. L. MARSH. J. Immunol. **106**, 1578 (1971).
3. T. FEIZI, R. A. CHILDS, K. WATANABE, and S. HAKOMORI. J. Exp. Med. **149**, 975 (1979).
4. E. A. KABAT, J. LIAO, M. H. BURZYNSKA, T. C. WONG, H. THØGERSEN, and R. U. LEMIEUX. Mol. Immunol. **18**, 873 (1981).
5. R. U. LEMIEUX, T. C. WONG, J. LIAO, and E. A. KABAT. Mol. Immunol. Submitted.
6. R. U. LEMIEUX and R. M. RATCLIFFE. Can. J. Chem. **57**, 1244 (1979).
7. R. U. LEMIEUX, S. Z. ABBAS, M. H. BURZYNSKA, and R. M. RATCLIFFE. Can. J. Chem. **60**, 63 (1982).
8. R. U. LEMIEUX, T. TAKEDA, and B. Y. CHUNG. Am. Chem. Soc. Symp. Series, **39**, 90 (1976).
9. A. C. RICHARDSON. Carbohydr. Res. **10**, 395 (1969).
10. H. G. KUIRILA and L. W. MENOPACE. J. Org. Chem. **28**, 2165 (1963).
11. R. U. LEMIEUX, S. Z. ABBAS, and B. Y. CHUNG. Can. J. Chem. **60**, 58 (1982).
12. S. SABESAN and R. U. LEMIEUX. Can. J. Chem. **62**, 644 (1984).
13. R. L. WHISTLER and A. K. M. ANISUZZAMAN. *In* Methods in carbohydrate chemistry. Vol. 8. *Edited by* R. L. Whistler and J. N. BeMiller. Academic Press, New York. 1980. p. 297.
14. W. M. ZU RECKENDORF and E. BISCHOF. Chem. Ber. **105**, 2546 (1972).
15. M. F. CZARNIECKI and E. R. THORNTON. J. Am. Chem. Soc. **99**, 8273 (1977).
16. W. N. HAWORTH, E. L. HIRST, H. R. STREIGHT, H. A. THOMAS, and I. J. WEBB. J. Chem. Soc. 2639 (1930).

Can. J. Chem. Downloaded from www.nrcresearchpress.com by 210.87.254.42 on 09/06/12
For personal use only.

The application of double-quantum and spin echo nuclear magnetic resonance spectroscopy to the assignment of ^{1}H chemical shifts of RNA oligomers

DONALD W. HUGHES[1] AND THOMAS NEILSON
Department of Biochemistry, McMaster University, Hamilton, Ont., Canada L8N 3Z5

AND

JAN M. CODDINGTON[2] AND RUSSELL A. BELL[1]
Department of Chemistry, McMaster University, Hamilton, Ont., Canada L8S 4M1

Received November 10, 1983

DONALD W. HUGHES, THOMAS NEILSON, JAN M. CODDINGTON, and RUSSELL A. BELL. Can. J. Chem. **62**, 1214 (1984).

Specific assignment of the non-exchangeable base and ribose anomeric protons is difficult for oligoribonucleotides with a high pyrimidine content. Problems arise from the narrow range of pyrimidine H-6 chemical shifts and the overlap of pyrimidine H-5 resonances with the ribose anomeric proton signals. To solve these problems two multiple pulse methods were used which depend on the scalar coupling between H-6 and H-5. The first method was double-quantum nmr which established the connectivity between specific pyrimidine H-6 and H-5 resonances. A refocussing pulse was added to the end of the double-quantum pulse sequence to improve the identification of several H-6 and H-5 connectivities in a single experiment. The second procedure involved homonuclear decoupled spin echo nmr to remove H-5 signals selectively from the ribose anomeric proton region. These techniques are illustrated by the assignment of the spectra of the oligoribonucleotides UpUpC, UpUpU, GpCpUpC, and UpApGpCpUpU.

DONALD W. HUGHES, THOMAS NEILSON, JAN M. CODDINGTON et RUSSELL A. BELL. Can. J. Chem. **62**, 1214 (1984).

Pour les oligoribonucléotides ayant une forte teneur en pyrimidine, il est difficile de faire des attributions spécifiques pour les protons non échangeables de la base et les protons anomères du ribose. Les problèmes proviennent du domaine étroit des déplacements chimiques du H-6 de la pyrimidine et du recouvrement des résonances des H-5 de la pyrimidine avec les signaux des protons anomères du ribose. Pour solutionner ces problèmes, on a utilisé deux méthodes à pulsation multiple qui dépendent du couplage scalaire entre H-6 et H-5. La première méthode est celle de la rmn à double quantum qui établit la relation entre les résonances spécifiques du H-6 et du H-5 de la pyrimidine. On a ajouté une nouvelle pulsation focalisante à la fin de la séquence de pulsation à double quantum pour améliorer l'identification des différentes fonctions du H-6 et du H-5 dans une expérience unique. La deuxième méthode fait intervenir la rmn à écho de spin avec découplage homonucléaire pour éliminer sélectivement les signaux du H-5 de la région du proton anomère du ribose. On illustre ces techniques par l'identification des spectres des oligoribonucléotides UpUpC, UpUpU, GpCpUpC et UpApGpCpUpU.

[Traduit par le journal]

Can. J. Chem. Downloaded from www.nrcresearchpress.com by 210.87.254.105 on 09/06/12
For personal use only.

Introduction

The ability of nmr spectroscopy to provide information about the solution structure and stability of RNA single strands and double helices depends on the accurate assignment of individual proton resonances. In short oligomers with a heterogeneous base composition, assignment of the non-exchangeable base and ribose anomeric protons at high temperature ($\geq$ 70°C to minimize base stacking and base pairing interactions) can be achieved by a combination of incremental analysis (1, 2) and empirically derived chemical shift parameters (3, 4). As the pyrimidine content of an oligomer increases, the above procedures can become ambiguous when attempting to identify the H-6 and H-5 AX doublets and the anomeric (H-1′) proton resonance of a specific pyrimidine base (Fig. 1). Problems arise from the narrow range of pyrimidine H-6 chemical shifts and the overlap of the H-5 resonance with the ribose H-1′ protons. The situation is further complicated since many of the nmr studies of oligoribonucleotides involve monitoring chemical shift changes as a function of temperature (5, 6), which may result in more severe overlap of pyrimidine resonances. This type of experiment tends to make two-dimensional nmr techniques impractical when the amount of spectrometer time for data acquisition and processing is limited.

In this paper we report on the application of two multiple pulse sequences that can help in analyzing spectra of oligoribonucleotides containing pyrimidine bases. These methods, which depend on the scalar coupling between H-6 and H-5, are double-quantum nmr, which established the connectivity between specific pyrimidine H-6 and H-5 resonances, and homonuclear decoupled spin echo nmr, which removed H-5 signals selectively from the ribose H-1′ region.

The double-quantum nmr experiment uses the DOUBTFUL pulse sequence:

$$90^\circ_x - \tau - 180^\circ_y - \tau - 90^\circ_x - \Delta - 90^\circ_\phi - \mathrm{ACQ}_0$$

developed by Hore *et al.* (7, 8) and is a variation of the INADEQUATE technique (9). Double-quantum coherence is generated by the application of two 90°_x pulses in the $90^\circ_x - \tau - 180^\circ_y - \tau - 90^\circ_x$ portion of the pulse sequence (10–12). The insertion of the 180°_y pulse removes the effects of chemical shift and field inhomogeneity on the magnetization. The coherence is allowed to evolve during the variable delay Δ, after which it is converted into observable transverse magnetization by a 90°_ϕ pulse of variable phase. The 90°_ϕ pulse and receiver undergo 32-step phase cycling to remove any remaining single-quantum coherence (9). A spin echo pulse has been included at the end of the pulse sequence to refocus the AX transitions.

$$90^\circ_x - \tau - 180^\circ_y - \tau - 90^\circ_x - \Delta - 90^\circ_\phi - \tau - 180^\circ_x - \tau - \mathrm{ACQ}_0$$

This modification improves the visualization of the AX connectivities.

---

[1] Authors to whom correspondence should be addressed.

[2] Present address: Department of Chemistry, University of California, San Diego, La Jolla, California 92023, U.S.A.

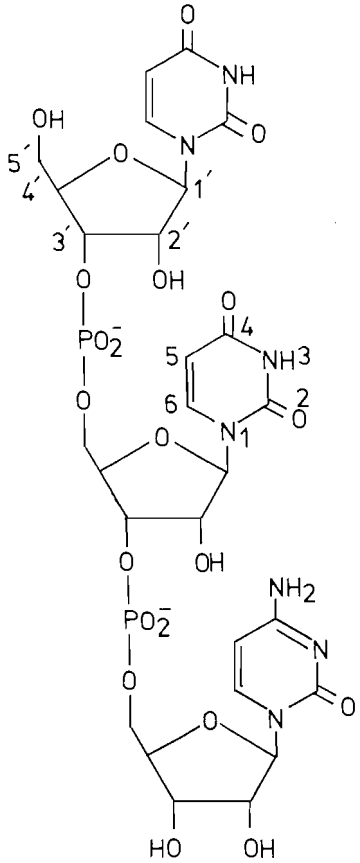

FIG. 1. The structure and numbering of the triribonucleotide diphosphate UpUpC.

The selective nature of the double-quantum experiment results from an amplitude modulation of the double-quantum coherence during the evolution period which is carried over to the observed magnetization. The intensity (I_{DQ}) of the double-quantum coherence for a defined coupling constant J and delay times τ and Δ is given by (7, 10, 12):

$$[1] \quad I_{DQ} = \sin(2\pi J\tau)\cos(\omega_1\Delta)$$

The values of ω_1 represent the relative separation of the sum of the Larmor frequencies for the coupled nuclei ($\Omega_A + \Omega_X$) and the transmitter frequency ω:

$$[2] \quad \omega_1 = (\Omega_A + \Omega_X) - 2\omega$$

When $\omega_1 = 0$ (the transmitter placed at the average frequency of the A and X spins), the double-quantum coherence reaches its optimum intensity at $\tau = 1/4J$ and does not experience any modulation. For non-zero values of ω_1, the observed magnetization displays a modulation whose rate is dependent on ω_1. If a series of spectra is acquired with different values of Δ and added together, only those transitions from coupled spins with a double-quantum frequency identical to the transmitter frequency will be observed, while all other signals will be cancelled. In practice, AX systems with double-quantum frequencies close to the one being excited may produce signals which are out of phase and of reduced intensity. This observation can be used to identify several AX connectivities in a single experiment.

Elimination of the pyrimidine H-5 resonances from the spectrum was achieved by a spin echo method originally proposed by Campbell *et al.* (13) for the measurement of coupling constants. It was later shown by Rabenstein and Nakashima (14) to be an effective procedure for selective removal of unwanted signals. The technique uses the Hahn spin echo (15) pulse sequence

$$90° - \tau - 180° - \tau - \text{echo}$$

with homonuclear decoupling during signal acquisition. Irradiation of the pyrimidine H-6 produces a singlet for H-5 whose intensity is modulated since the spins are coupled during the formation of the echo. This modulation results in the singlet being nulled at $\tau = 1/4J$ (13, 14) and produces a spectrum containing only partially modulated doublets for the anomeric protons. The phase of the H-1′ signals was corrected by displaying the spectrum in the absolute value mode.

The oligoribonucleotides[3] UpUpC, UpUpU, GpCpUpC, and UpApGpCpUpU were examined to demonstrate the use of these procedures in analyzing the spectra of oligomers containing overlapped pyrimidine base and ribose anomeric proton resonances.

Experimental procedures

The oligoribonucleotides used in this study were chemically synthesized by a phosphotriester method (16–18).

The single pulse ^{1}H nmr spectra were recorded at 250.13 MHz on a Bruker WM-250 spectrometer over a sweep width of 1.9 kHz in 32K data points (acquisition time: 8.618 s). Suppression of the HDO resonance was achieved by irradiation for 1.0 s prior to acquisition. Sample temperature was maintained at 70.5 ± 1.0°C by a Bruker BVT-1000 variable temperature unit and the temperature checked by thermocouple measurement. Spectra were accumulated in 80–128 scans and resolution enhanced by Gaussian multiplication.

Double-quantum spectra were acquired in 16K (acquisition time: 4.096 s) using the DOUBTFUL pulse sequence:

$$90°_x - \tau - 180°_y - \tau - 90°_x - \Delta - 90°_\phi - \text{ACQ}_\theta$$

or the modified pulse sequence for refocussing transitions:

$$90°_x - \tau - 180°_y - \tau - 90°_x - \Delta - 90°_\phi - \tau - 180°_x - \tau - \text{ACQ}_\theta$$

The 90° pulse length was 7.0 μs. The value of τ was set to $1/4J$ which for the uridine H-6 and H-5 doublets ($^3J_{5,6} = 8.1$ Hz) was 0.031 s. The variable delay Δ was initially 0.005 s and was incremented 19 times in steps of 0.002 s to a final value of 0.043 s. Each Δ value was accumulated in 32 scans to match the 32-phase cycling sequence of the final $90°_\phi$ detection pulse and the receiver. All the FID's were successively added to a total of 640 scans for each spectrum. The transmitter frequency was positioned either at the double-quantum frequency of the coupled spins (average of the AX-frequencies) or offset a specified distance (see Results and discussion). A delay of 0.5 s was used between pulse sequences.

Spin echo spectra were acquired in 32K using the pulse sequence, $90° - \tau - 180° - \tau - \text{echo}$, with $\tau = 1/4J = 0.031$ s. This value of τ resulted in the uridine H-6 and H-5 doublets appearing 90° out of phase in the absence of spin decoupling. The homonuclear decoupler was gated to provide solvent suppression during the relaxation delay (1.0 s) and to irradiate the pyrimidine H-6 resonances during acquisition. Spectra were accumulated in 200 scans. The free induction decays were processed using Gaussian multiplication for resolution enhancement and the spectra were phased using the absolute value mode.

Samples were lyophilized twice from D_2O and then dissolved in

[3] Abbreviations used: Ribosyl 5′-UpUpC-3′. Oligoribonucleotides are written in the normal 5′→3′ sequence, and the bases are numbered from the 5′ end: $^{\text{UpUpC}}_{1\,2\,3}$.

Can. J. Chem. Downloaded from www.nrcresearchpress.com by 210.87.254.105 on 09/06/12
For personal use only.

Can. J. Chem. Downloaded from www.nrcresearchpress.com by 210.87.254.105 on 09/06/12
For personal use only.

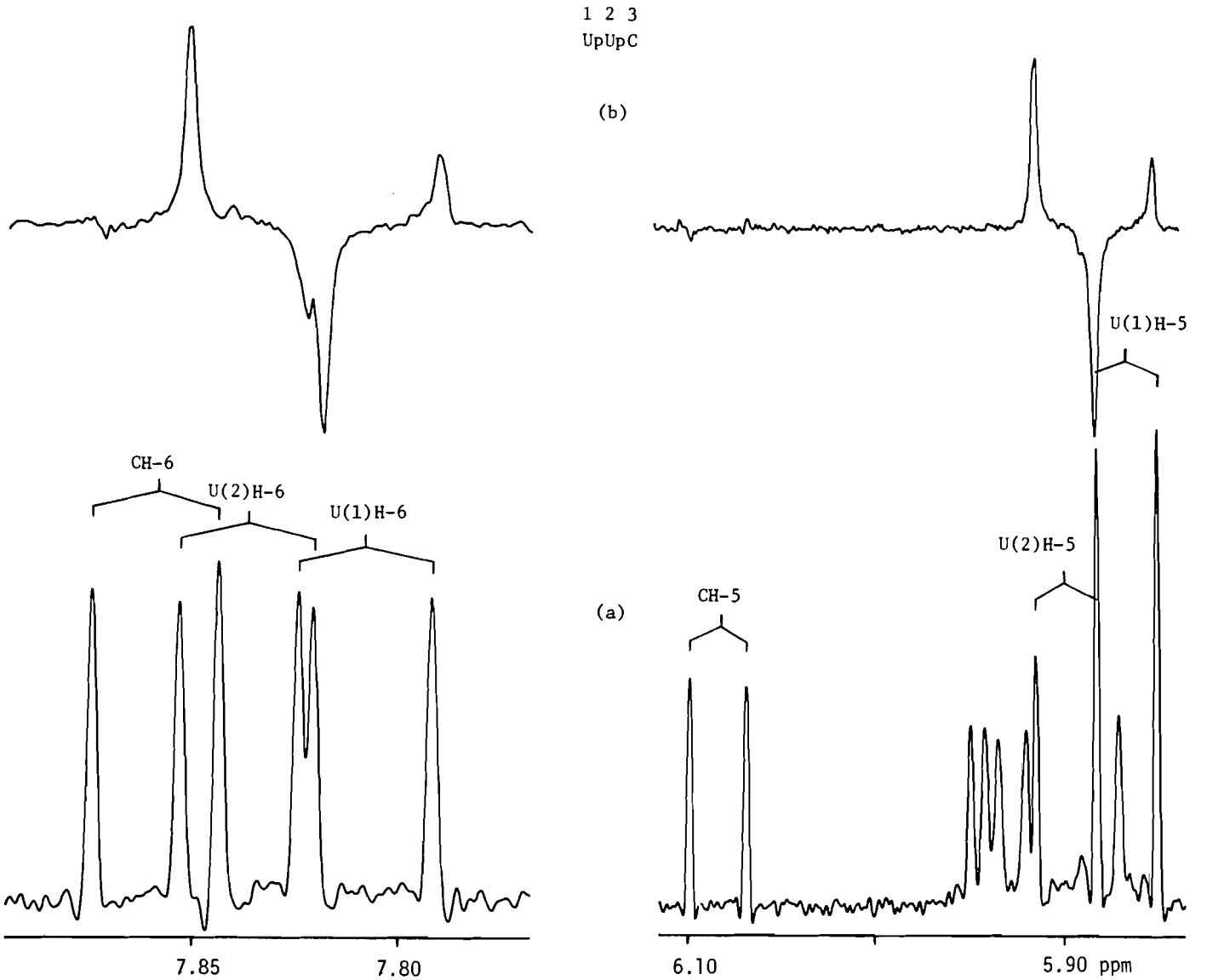

FIG. 2. (a) 250 MHz ^{1}H nmr of UpUpC displaying resolution enhanced spectrum of the pyrimidine base and ribose anomeric protons at 70.5°C. (b) Double-quantum spectrum recorded using the DOUBTFUL pulse sequence with the transmitter at the double-quantum frequency of U(2)H-6 and H-5 protons. The free induction decay was processed without the use of any weighting functions.

100% D_2O (Aldrich) which contained 0.01 *M* sodium phosphate buffer (pD 7.0) and 1.0 *M* sodium chloride. The sample concentrations ranged from 0.06–0.015 *M*. Chemical shifts are reported in ppm relative to DSS (sodium 4,4-dimethyl-4-silapentan-1-sulfonate) using *tert*-butyl alchohol-OD (1.231 ppm) as internal reference.

Results and discussion

Double-quantum and spin echo pulse methods were initially used on the triribonucleotides, UpUpC (Fig. 1) and UpUpU. These short oligomers were chosen since their spectra clearly illustrate how the multiple pulse techniques can solve the typical problems encountered when studying pyrimidine-containing sequences. UpUpC was the first sequence to be analyzed because its 70.5°C ^{1}H spectrum (Fig. 2a) was sufficiently resolved to allow a number of preliminary assignments to be made. The cytidine H-6 (7.859 ppm) and H-5 (6.084 ppm) doublets were readily distinguished from the corresponding uridine resonances (Table 1) by both the magnitude of the coupling constant $^3J_{5,6}$ (cytidine: 7.6 Hz; uridine: 8.1 Hz) and the lower field chemical shift usually observed for CH-5 signals relative to UH-5 protons. Centered around the 5.90 ppm region were the two partially overlapped uridine H-5 resonances and the three doublets from the ribose anomeric protons. A complete analysis required the determination of which uridine H-6 and H-5 protons were coupled, resolving and assigning the ribose H-1′ signals, and finally assigning the uridine resonances to a specific nucleotide in the sequence.

When the double-quantum pulse sequence was used to establish the connectivity of several pyrimidine H-6 and H-5 protons, the transmitter was positioned within or near the region of double-quantum frequencies defined by the lowest and highest field pairs of H-6 and H-5 resonances. In the case of UpUpC, the lowest field pair of uridine H-6 (7.837 ppm) and H-5 (5.931 ppm) protons were assumed to be coupled and the transmitter was placed at their double-quantum frequency. The spectrum shown in Fig. 2b resulted from the application of the DOUBTFUL pulse sequence without a refocussing pulse. The specifically excited AX transitions appeared with maximum intensity

Can. J. Chem. Downloaded from www.nrcresearchpress.com by 210.87.254.105 on 09/06/12
For personal use only.

TABLE 1. ^{1}H chemical shifts and coupling constants for the pyrimidine triribonucleotides at 70.5°C

	^{1}H Chemical shifts	
Proton	1 2 3 UpUpC	1 2 3 UpUpU
U(1)H-6	7.808	7.808
U(2)H-6	7.837	7.831
C(3)H-6	7.859	
U(3)H-6		7.820
U(1)H-5	5.867	5.881
U(2)H-5	5.899	5.911
C(3)H-5	6.084	
U(3)H-5		5.907
U(1)H-1′	5.861	5.868
U(2)H-1′	5.931	5.941
C(3)H-1′	5.942	
U(3)H-1′		5.914
Proton	$^3J_{1'2'}$	
U(1)H-1′	5.0	5.2
U(2)H-1′	5.5	5.4
C(3)H-1′	3.7	
U(3)H-1′		4.5

and the characteristic up/down pattern (9). This spectrum demonstrates the advantage of the double-quantum experiment over techniques such as spin decoupling, since the coupled protons are clearly shown without the complication of overlapping resonances. The experiment confirmed the assumption of a coupling between the lowest field pair of uridine H-6 and H-5 protons.

With the completion of the analysis of the base protons, it was then possible to examine the ribose anomeric protons. From Fig. 3a it was apparent that the highest field H-1′ doublet was overlapped with a uridine H-5 signal. The H-5 resonances were removed from the spectrum by the application of the homonuclear decoupled spin echo method. The experiment was designed to eliminate signals from pyrimidines which caused the most severe overlap problems. In the case of UpUpC the decoupler was positioned between the U(1) and U(2)H-6 doublets and sufficient decoupler power applied to irradiate both H-6 protons. The resulting spectrum (Fig. 3b) permitted easier identification of the H-1′ doublets. The H-1′ protons were assigned to specific bases by selective irradiation of the H-1′ protons with low levels of decoupling power to remove the five-bond coupling between H-1′ and H-5 ($^5J_{1',5}$ = 0.3–0.5 Hz) (19, 20).

Assigning the proton signals to a particular base in the UpUpC sequence was achieved by considering that the 5′ terminal uridine does not have a 5′ phosphate which would deshield the H-6 and H-5 protons. The resonances at 7.808, 5.867, and 5.861 ppm were therefore assigned to the U(1)H-6, H-5, and H-1′ protons, respectively. The remaining chemical shift assignments are summarized in Table 1. This analysis was in agreement with recently published data on UpUpC, obtained at 500 MHz (21).

The spectrum of UpUpU (Fig. 4a) was difficult to interpret since all the bases were identical and the weak ring current shielding properties of the uridine base (22, 23) resulted in the H-6 resonances being separated by only 0.02–0.01 ppm.

TABLE 2. ^{1}H chemical shifts and coupling constants for the oligoribonucleotides GpCpUpC and UpApGpCpUpU at 70.5°C

Proton	^{1}H Shift for 1 2 3 4 GpCpUpC	Proton	^{1}H Shift for 1 2 3 4 5 6 UpApGpCpUpU
GH-8	7.960	U(1)H-6	7.680
C(2)H-6	7.778	AH-8	8.305
UH-6	7.776	AH-2	8.171
C(4)H-6	7.828	GH-8	7.908
		CH-6	7.732
C(2)H-5	5.888	U(5)H-6	7.773
UH-5	5.836	U(6)H-6	7.797
C(3)H-5	6.064		
		U(1)H-5	5.798
GH-1′	5.863	CH-5	5.850
C(2)H-1′	5.909	U(5)H-5	5.834
UH-1′	5.882	U(6)H-5	5.881
C(4)H-1′	5.925		
		U(1)H-1′	5.753
		AH-1′	5.994
		GH-1′	5.786
		CH-1′	5.885
		U(5)H-1′	5.897
		U(6)H-1′	5.895
Proton	$^3J_{1'2'}$	Proton	$^3J_{1'2'}$
GH-1′	5.0	U(1)H-1′	4.7
C(2)H-1′	4.7	AH-1′	4.7
UH-1′	5.0	GH-1′	5.1
C(4)H-1′	4.0	CH-1′	4.4
		U(5)H-1′	4.3
		U(6)H-1′	5.4

Chemical shifts of the H-5 signals were estimated by locating pairs of transitions which were separated by 8.1 Hz. The remaining transitions were tentatively assigned to H-1′ protons.

Following the procedure discussed in the previous section for the selection of the transmitter frequency, it was found that assuming the two lowest field uridine H-6 doublets at 7.831 and 7.820 ppm were coupled to the overlapped H-5 signals centered near 5.91–5.90 ppm resulted in similar double-quantum frequencies. These pairs of AX systems could be differentiated by either increasing the number of Δ values or exploiting the dependence of signal intensity on the value of ω_1 in the cosine term of eq. [1] (7, 8). Using the latter approach, the transmitter was positioned 3.0 Hz (i.e. ω_1 = 6.0 Hz) to low field of the double-quantum frequency of the H-6 and H-5 protons at 7.831 and 5.911 ppm, respectively. It was expected that the intensities of the three pairs of H-6/H-5 doublets would decrease with increasing separation of the transmitter and double-quantum frequencies. The double-quantum spectrum (Fig. 4b) was recorded with a refocussing pulse at the end of the pulse sequence. The transitions of the lowest field H-6 at 7.831 ppm were of higher intensity than those centered at 7.820 ppm. Although the overlapped H-5 protons near 5.910 ppm were insufficiently resolved to show any intensity differences, the intensity pattern of the H-6 transitions can only arise from the 7.831 ppm H-6 being coupled to the H-5 at 5.911 ppm (Table 1). The presence of the refocussing pulse clearly displayed the connectivity between the uridine doublets at 7.808 and 5.881 ppm, since these transitions were inverted and had lower intensities. These differences in signal phase and intensity illustrated how the position of the transmitter frequency

Can. J. Chem. Downloaded from www.nrcresearchpress.com by 210.87.254.105 on 09/06/12
For personal use only.

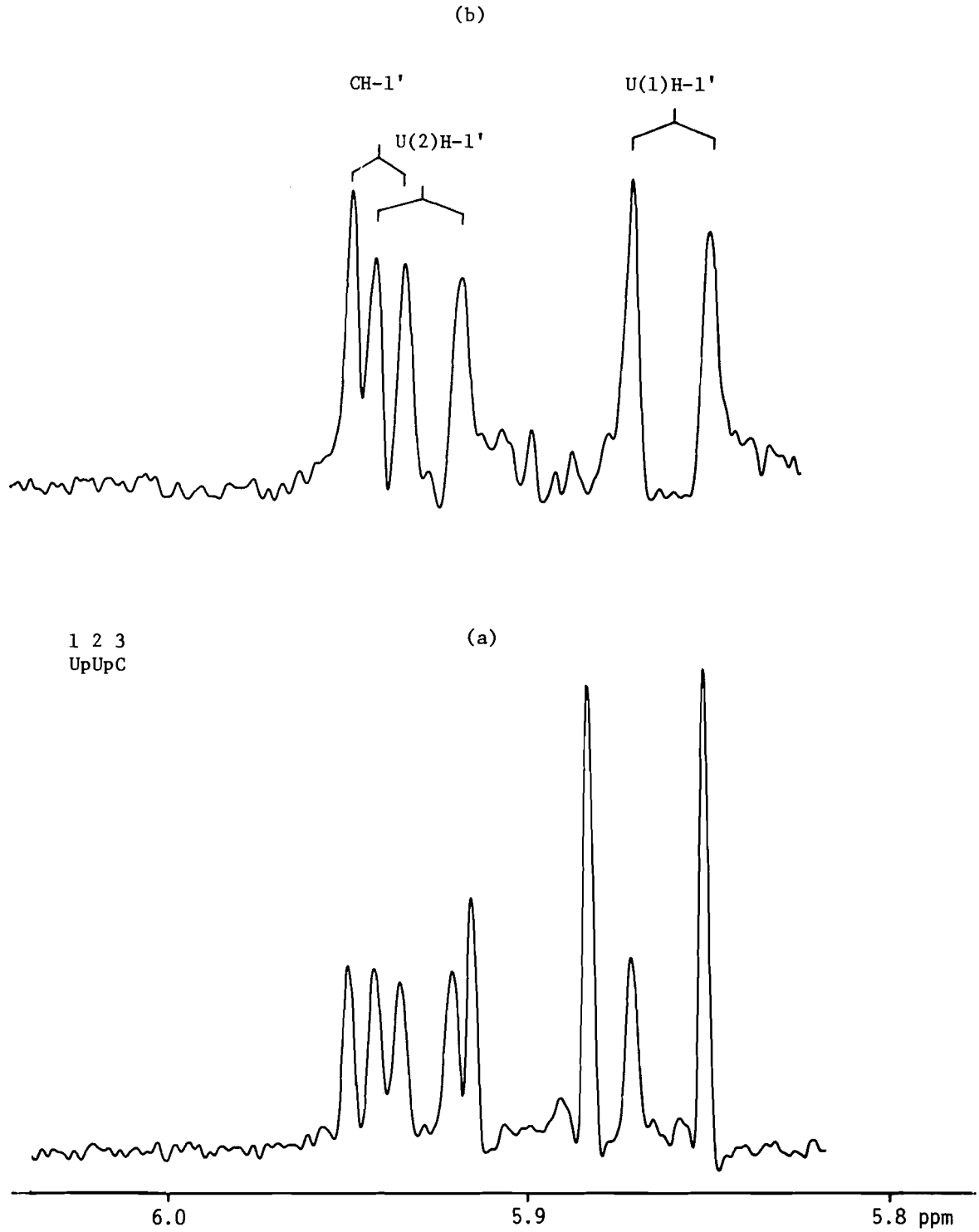

FIG. 3. (a) Expansion of Fig. 2a showing the ribose anomeric and U(2) and U(3)H-5 protons of UpUpC at 70.5°C. (b) Spin echo spectrum of the ribose anomeric protons obtained with irradiation of the U(2) and U(3)H-6 protons. This spectrum was resolution enhanced and phase corrected by displaying the spectrum in the absolute value mode.

can be manipulated to improve the information content of the double-quantum spectrum.

In the region containing the anomeric proton signals of UpUpU only one H-1′ doublet at 5.868 ppm could be identified. Resolution of the H-1′ resonances by the spin echo method took advantage of the overlap of the H-6 doublets since they could all be irradiated simultaneously. From the spin echo spectrum (not shown) it was possible to identify all the H-1′ signals, particularly the doublets at 5.941 and 5.914 ppm which were almost completely obscured by the H-5 signals.

Assignment of the base chemical shifts to specific uridine residues (Table 1) followed the reasoning used for UpUpC with the highest field H-6 and H-5 being assigned to the 5′ terminal position. The H-6 and H-5 chemical shifts for U(1) and U(2) were expected to be similar for both UpUpC and UpUpU, since a pyrimidine at the 3′ terminal should have relatively little

Can. J. Chem. Downloaded from www.nrcresearchpress.com by 210.87.254.105 on 09/06/12
For personal use only.

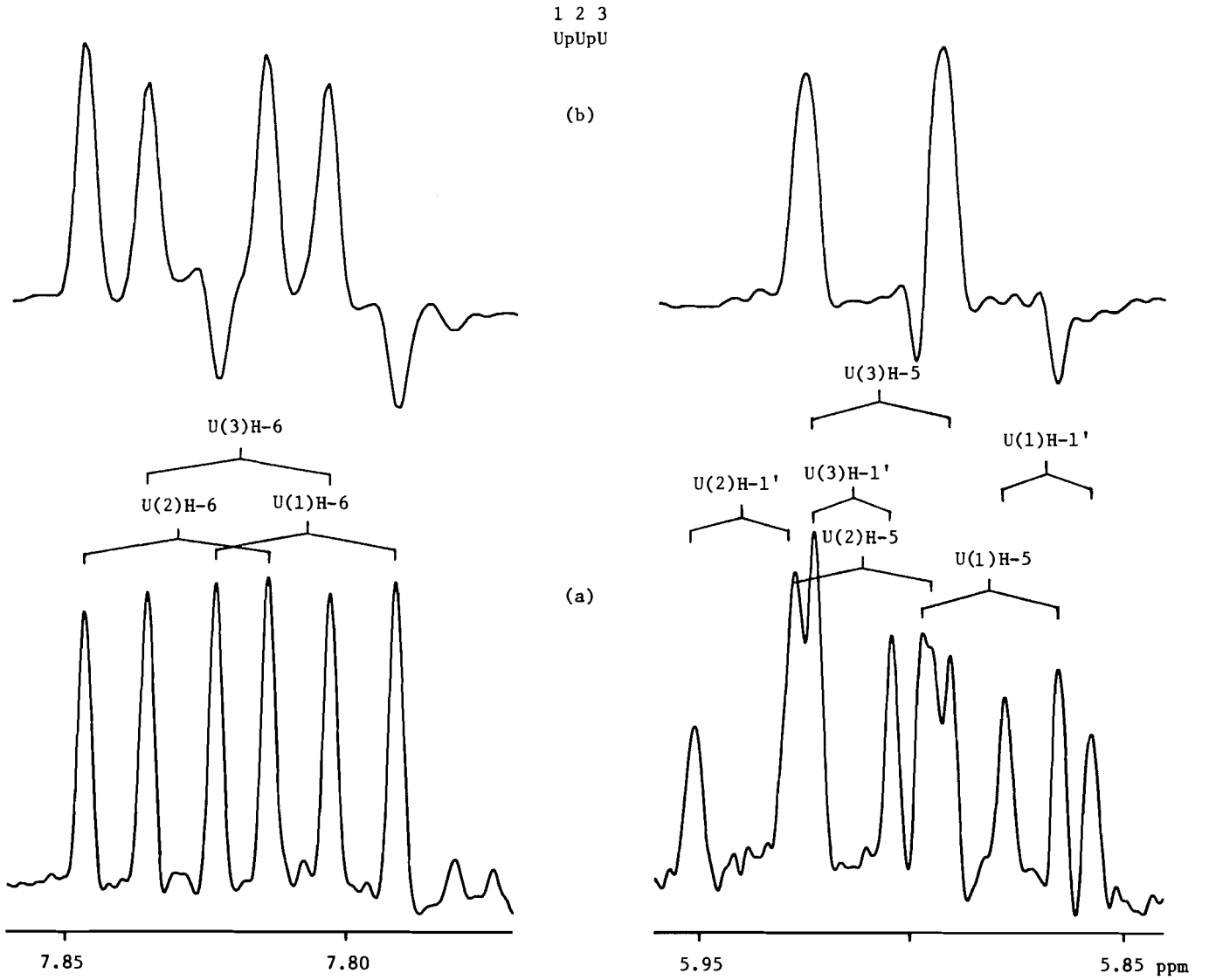

FIG. 4. (a) 250 MHz ^{1}H nmr spectrum of UpUpU at 70.5°C. (b) Resolution enhanced double-quantum spectrum obtained with a refocussing pulse at the end of the DOUBTFUL pulse sequence.

shielding effect on neighbouring bases in a weakly stacked UpUpPy (Py = pyrimidine) sequence at high temperatures (22, 23). The H-1′ resonances were only tentatively assigned by comparison with data from UpUpC and UpU. Definitive connectivities between H-5 and H-1′ protons could not be obtained from low power decoupling experiments because of the overlap of these resonances.

Another example of the use of negative or out-of-phase signals in determining pyrimidine H-6/H-5 connectivity was provided by the spectra of GpCpUpC (Figs. 5a and 5b). This oligomer was first reported in a 90 MHz ^{1}H nmr study of duplex formation by two non-self-complementary tetraribonucleotides (24). The improved resolution at 250 MHz enabled analysis of the H-1′ and H-5 resonances and correction of chemical shift assignments (Table 2). The doublets at 7.77 ppm result from the overlap of the UH-6 and C(2)H-6 resonances. Differentiation of the two cytidine H-6 doublets was based on the shielding effect of the neighbouring guanosine on the C(2) base protons (22, 23). The doublet at 6.024 ppm was assigned to C(4)H-5, while the C(2)H-5 signal was overlapped with H-1′ resonances between 5.87 and 5.94 ppm. The UH-5 doublet was observed at 5.836 ppm.

Confirmation of this analysis was obtained via the double-quantum experiment by setting the transmitter frequency on the double-quantum frequency of the UH-6/H-5 spin system. Using the ω_1 values for each cytidine in the cosine term of eq. [1], it was possible to calculate, by summation of the intensities for all values of Δ used in the experiment, that the C(2)H-6/H-5 doublets would have a significant negative intensity relative to those of C(4). The calculated intensities were verified by the negative C(2)H-5 doublet and the absence of any observable signals for the C(4)H-6 and H-5 at the signal-to-noise level of the spectrum in Fig. 5b. Overlap of the C(2)H-6 transitions with the more intense and positive UH-6 transitions resulted in cancellation of the C(2)H-6 doublet.

The H-1′ resonances were resolved by recording a spin echo spectrum (not shown) with irradiation of the U and C(2)H-6 protons. Removal of the U and C(2)H-5 resonances revealed H-1′ doublets at 5.882 and 5.863 ppm (U and GH-1′, respectively). The H-1′ chemical shifts in Table 2 were assigned by comparison with constituent di- and trinucleotides in the GpCpUpC sequence and use of previously observed shielding

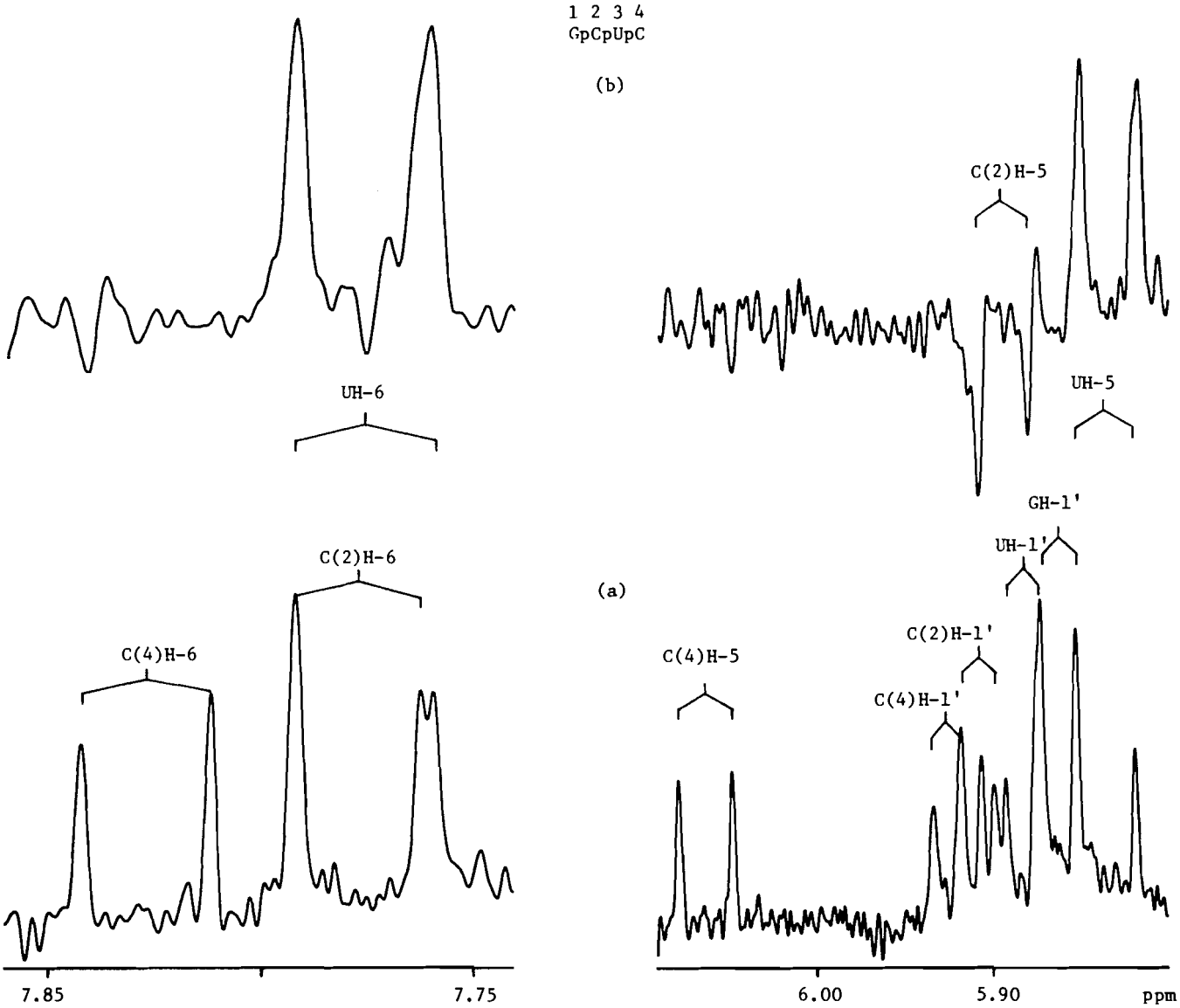

FIG. 5. (a) 250 MHz ^{1}H nmr spectrum of GpCpUpC at 70.5°C. (b) Double-quantum spectrum obtained with the transmitter at the double-quantum frequency of the uridine H-6/H-5 spin system.

trends (22, 23).

The final oligomer examined was the hexaribonucleotide, UpApGpCpUpU. This oligomer is currently being investigated since the bases at positions 2–5 have the potential of forming a self-complementary duplex with opposing unpaired uridines at each end of the duplex. It was therefore necessary to distinguish the H-6 and H-5 resonances of the terminal uridines 1 and 6 from each other and from those of the uridine at position 5. From the 70.5°C spectrum, the purine base protons and adenosine H-1′ could be readily assigned (Table 2). The pyrimidine H-6 resonances (Fig. 6a) were well resolved, which permitted the assignment of the doublet at 7.732 ppm to the CH-6. The region between 5.75 and 5.90 ppm was difficult to interpret since it contained doublets from four pyrimidine H-5 protons and five ribose anomeric protons. Doublets centered at 5.798 and 5.881 ppm were tentatively assigned as UH-5 signals since the peak separation corresponded to the $^3J_{5,6}$ values of 8.1 Hz. The CH-5 and the third UH-5, which had to be located between 5.85 and 5.90 ppm, could not be clearly identified because of overlap with three H-1′ signals.

As a result of the complexity of the H-5 and H-1′ region, two double-quantum spectra were required to assign the four pyrimidine H-6 and H-5 connectivities. In the first experiment the highest field pair of H-6 (7.680 ppm) and H-5 (5.799 ppm) doublets were assumed to arise from U(1) since this assignment agreed with the previous results for 5′ terminal pyrimidines (Table 1). The U(1) protons should also experience the ring current shielding effect of the 3′ adenosine (22, 23). The double-quantum spectrum verified the above assumption; however, no other transitions were observed. The second double-quantum experiment was performed with the transmitter at the double-quantum frequency of the UH-6 and H-5 doublets at 7.773 and 5.834 ppm, respectively. This transmitter position was chosen due to its proximity to the double-quantum frequencies of the cytidine and the third uridine. Signals from these bases could be connected using the relationship of signal intensity and phase with the separation of double-quantum and transmitter frequencies. In Fig. 6b the high intensity and positive signals at 7.773 and 5.834 ppm confirmed the coupling of these uridine protons. The CH-6 at 7.732 ppm and CH-5 at

Can. J. Chem. Downloaded from www.nrcresearchpress.com by 210.87.254.105 on 09/06/12
For personal use only.

Can. J. Chem. Downloaded from www.nrcresearchpress.com by 210.87.254.105 on 09/06/12
For personal use only.

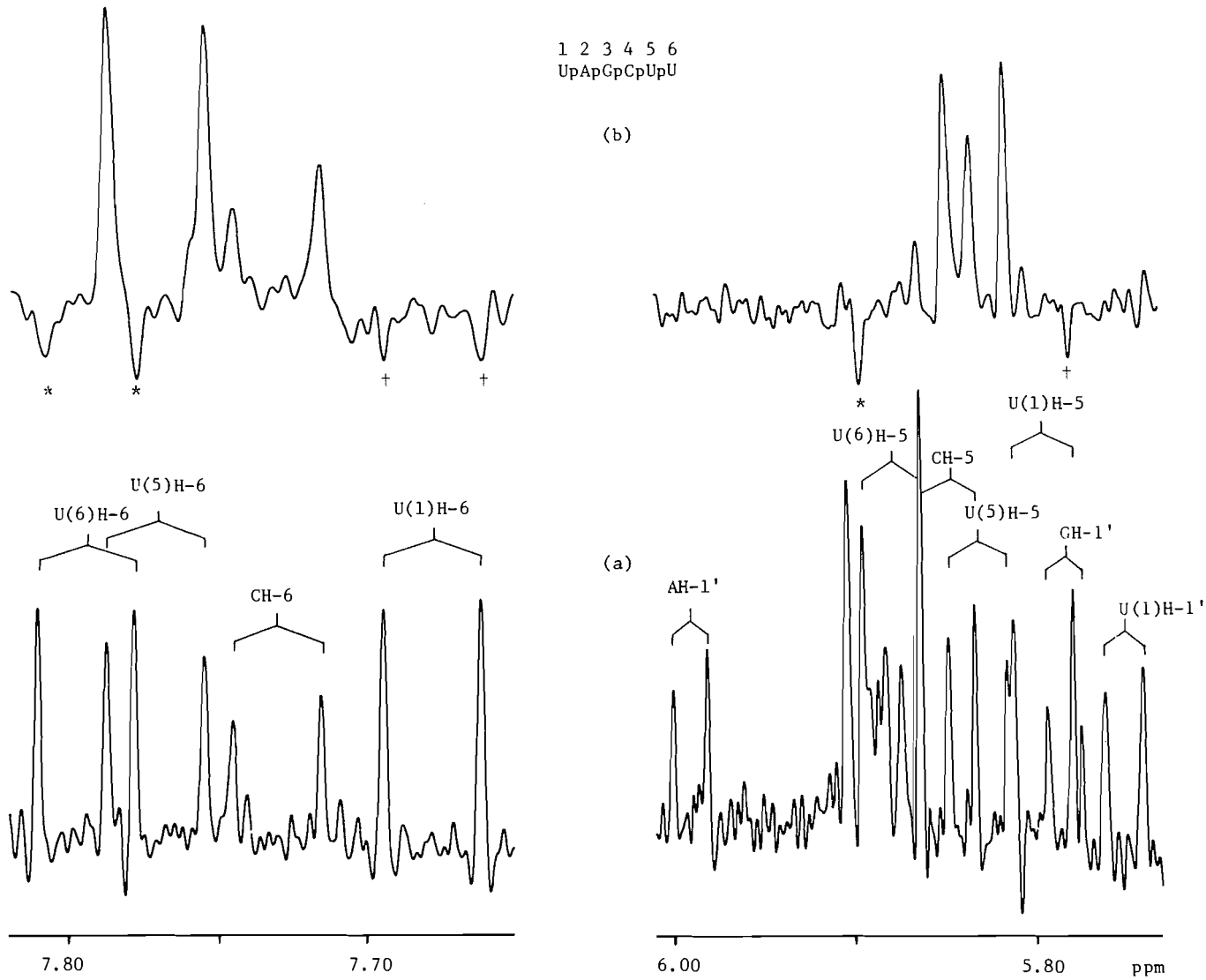

FIG. 6. (a) 250 MHz ^{1}H nmr spectrum (resolution enhanced) of UpApGpCpUpU at 70.5°C. (b) Resolution enhanced double-quantum spectrum showing in-phase transitions for the pyrimidine base protons of U(5) and C and inverted signals for U(6) (*) and U(1) (†).

5.850 ppm were observed as positive signals with lower intensity. The inverted and low intensity transitions marked by the asterisks indicated the connectivity of the UH-6 at 7.797 ppm and the UH-5 at 5.881 ppm. The upfield transition of this UH-5 was cancelled due to overlap with the positive CH-5 transition. Also visible were inverted, low intensity peaks from the U(1)H-6 and H-5 (indicated by the symbol †).

Assignment of the U(5) and U(6) base protons (Table 2) relied on the next-nearest-neighbour shielding effect of G(3) (22, 23) on the chemical shifts of the U(5)H-6 and H-5 protons. These assignments also follow from comparison with data on ApGpCpU (25). With the exception of AH-1′, chemical shift assignments for the remaining ribose anomeric protons were tentative, particularly for the three overlapping anomeric doublets near 5.89 ppm.

Conclusions

The multiple pulse methods presented here offer a superior alternative to spin decoupling when dealing with spectra of RNA sequences containing several pyrimidines. The removal of overlapping signals by the spin echo pulse sequence in combination with homonuclear spin decoupling improved the precision of both the chemical shifts and the coupling constants, $^3J_{1',2'}$, of the ribose anomeric protons. This technique is also applicable to other first order multiplets (14). Double-quantum experiments provided a high degree of specificity not present with spin decoupling when identifying the connectivities of overlapped AX systems. Addition of the refocussing pulse improved the observation of in-phase or inverted signals and permitted the determination of several connectivities in a single experiment. Selectivity in the double-quantum experiment was achieved by using the relationship in eq. [1] between signal intensity and phase and the difference in transmitter and double-quantum frequencies.

Acknowledgements

We thank Dr. Dirk Alkema for synthesizing the compounds used in this study. The authors acknowledge financial support from the National Cancer Institute of Canada and the Natural Sciences and Engineering Research Council of Canada.

1. P. N. BORER, L. S. KAN, and P. O. P. TS'O. Biochemistry, **14**, 4847 (1975).
2. P. O. P. TS'O, J. L. ALDERFER, P. N. BORER, and L. S. KAN. *In*

Structure and conformation of nucleic acids and protein – nucleic acid interactions. *Edited by* M. Sundaralingam and S. T. Rao. University Park Press, Baltimore, MD. 1975. pp. 193–206.
3. P. A. HADER, D. ALKEMA, R. A. BELL, and T. NEILSON. J. Chem. Soc. Chem. Commun. 10 (1982).
4. R. A. BELL, D. ALKEMA, J. M. CODDINGTON, P. A. HADER, D. W. HUGHES, and T. NEILSON. Nucleic Acids Res. **11**, 1143 (1983).
5. D. ALKEMA, P. A. HADER, R. A. BELL, and T. NEILSON. Biochemistry, **21**, 2109 (1982).
6. M. PETERSHEIM and D. H. TURNER. Biochemistry, **22**, 269 (1983).
7. P. J. HORE, E. R. P. ZUIDERWEG, K. NICOLAY, K. DIJKSTRA, and R. KAPTEIN. J. Am. Chem. Soc. **104**, 4286 (1982).
8. P. J. HORE, R. M. SCHEEK, A. VOLBEDA, R. KAPTEIN, and J. H. VAN BOOM. J. Magn. Reson. **50**, 328 (1982).
9. A. BAX, R. FREEMAN, and S. P. KEMPSELL. J. Am. Chem. Soc. **102**, 4849 (1980).
10. W. P. AUE, E. BARTHOLDI, and R. R. ERNST. J. Chem. Phys. **64**, 2229 (1976).
11. A. WOKAUN and R. R. ERNST. Chem. Phys. Lett. **52**, 407 (1977).
12. G. BODENHAUSEN. Prog. Nucl. Magn. Reson. Spectrosc. **14**, 137 (1981).
13. I. D. CAMPBELL, C. M. DOBSON, R. G. RATCLIFFE, and R. J. P. WILLIAMS. J. Magn. Reson. **31**, 341 (1978).
14. D. L. RABENSTEIN and T. T. NAKASHIMA. Anal. Chem. **51**, 1465A (1979).
15. E. L. HAHN. Phys. Rev. **80**, 580 (1950).
16. T. NEILSON and E. S. WERSTIUK. J. Am. Chem. Soc. **96**, 2295 (1974).
17. T. E. ENGLAND and T. NEILSON. Can. J. Chem. **54**, 1714 (1976).
18. E. S. WERSTIUK and T. NEILSON. Can. J. Chem. **54**, 2689 (1976).
19. F. E. HRUSKA. Can. J. Chem. **49**, 2111 (1971).
20. T. SCHLEICH, T. R. LUSEBRINK, B. P. CROSS, and N. P. JOHNSON. Nucleic Acids Res. **2**, 459 (1975).
21. A. M. GRONENBORN, B. J. KIMBER, G. M. CLORE, and L. W. MCLAUGHLIN. Nucleic Acids Res. **11**, 5691 (1983).
22. J. R. EVERETT, D. W. HUGHES, R. A. BELL, D. ALKEMA, T. NEILSON, and P. J. ROMANIUK. Biopolymers, **19**, 557 (1980).
23. R. A. BELL, J. R. EVERETT, D. W. HUGHES, D. ALKEMA, P. A. HADER, T. NEILSON, and P. J. ROMANIUK. Biopolymers, **20**, 1383 (1981).
24. D. W. HUGHES, R. A. BELL, T. E. ENGLAND, and T. NEILSON. Can. J. Chem. **56**, 2243 (1978).
25. T. NEILSON, P. J. ROMANIUK, D. ALKEMA, D. W. HUGHES, J. R. EVERETT, and R. A. BELL. Nucleic Acids Res., Symposium Series No. 7, 293 (1980).

Can. J. Chem. Downloaded from www.nrcresearchpress.com by 210.87.254.105 on 09/06/12
For personal use only.

Glycosides from *Muscari comosum*. 5.[1] Structure of muscaroside B[2]

M. ADINOLFI, G. BARONE, R. LANZETTA, G. LAONIGRO, L. MANGONI, AND M. PARRILLI[3]
Istituto di Chimica Organica e Biologica della Università di Napoli, Via Mezzocannone 16, 80134 Napoli, Italy

Received October 26, 1983

M. ADINOLFI, G. BARONE, R. LANZETTA, G. LAONIGRO, L. MANGONI, and M. PARRILLI. Can. J. Chem. **62**, 1223 (1984).

A further component of the glycoside mixture extracted from the bulbs of *Muscari comosum* has been completely characterized by chemical degradative study and spectral investigation. This glycoside, **2**, termed muscaroside B, possesses an α-L-arabinofuranosyl(1→2)-α-L-arabinopyranosyl(1→3)[α-L-rhamnopyranosyl(1→2)]-β-D-glucopyranosyl(1→2)-α-L-arabinopyranosyl(1→6)-β-D-glucopyranosyl chain linked at the 3-position of eucosterol.

M. ADINOLFI, G. BARONE, R. LANZETTA, G. LAONIGRO, L. MANGONI et M. PARRILLI. Can. J. Chem. **62**, 1223 (1984).

Faisant appel à des études spectrales et à des dégradations chimiques, on a complètement caractérisé un nouveau composé du mélange glycosidique extrait des bulbes du *Muscari comosum*. Ce glycoside, **2**, que l'on appelle muscaroside B, possède une chaîne α-L-arabinofuranosyl(1→2)-α-L-arabinopyranosyl(1→3)[α-L-rhamnopyranosyl(1→2)]-β-D-glucopyranosyl-(1→2)-α-L-arabinopyranosyl(1→6)-β-D-glucopyranosyl qui est liée à la position 3 de l'eucostérol.

[Traduit par le journal]

Can. J. Chem. Downloaded from www.nrcresearchpress.com by 210.87.254.40 on 09/06/12
For personal use only.

Continuing our study on glycosides (1–4) of bulbs of *Muscari comosum* Mill. (Liliaceae), from which we extracted muscaroside A, **1**, we report now the structural elucidation of muscaroside B, **2**, which possesses an α-L-arabinofuranosyl-

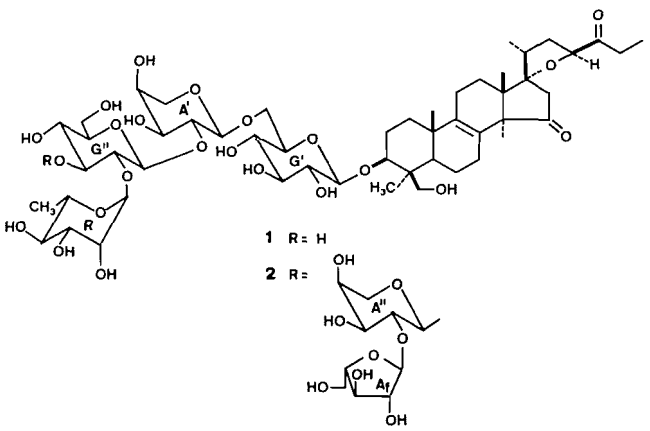

(1→2)-α-L-arabinopyranosyl(1→3)[α-L-rhamnopyranosyl(1→2)]-β-D-glucopyranosyl(1→2)-α-L-arabinopyranosyl(1→6)-β-D-glucopyranosyl chain as its sugar moiety linked at the 3-carbon of eucosterol.

Muscaroside B was isolated from column (silica gel) chromatography followed by hplc (high performance liquid chromatography) (C-18 reverse phase column) of the crude glycoside mixture extracted from bulbs. It was shown to be homogeneous by spectroscopy (^{1}H nmr and ^{13}C nmr), levorotatory ($[\alpha]_D^{CH_3OH}$ −32°) and melting at 202–206°C upon recrystallization from ethanol. Chemical analysis gave $C_{62}H_{98}O_{31}$, according to the pseudomolecular ion peaks (MNa^+ 1361 *m/e*, MK^+ 1377 *m/e*) in the FAB mass spectrum.

On enzymatic hydrolysis it yielded eucosterol as the aglycone, identified by comparison (tlc, mp, ^{1}H nmr, ms) to an authentic sample, while acid hydrolysis (7% H_2SO_4), which caused decomposition of the aglycone (3), allowed rhamnose, glucose, and arabinose to be identified as the monosaccharide units of the sugar chain by tlc, hplc, and ^{1}H nmr analysis of the water-soluble fraction of the hydrolysate through comparison with the behaviour of equilibrated authentic samples of the monosaccharides. The ^{1}H nmr spectroscopy and hplc also allowed us to establish the 1:2:3 molar ratio of rhamnose, glucose, and arabinose, through integration of the anomeric proton signals in DMSO-d_6 and calculation of the peak areas, respectively. Isolation of the three pure monosaccharides by hplc and determination of their rotation established the D-configuration of glucose and L-configuration of rhamnose and of arabinose. The configuration of arabinose was confirmed by the positive response of a D-galactose dehydrogenase test (5, 6).

Permethylation (DMF/NaI/MeI) of muscaroside B followed by acid hydrolysis (2 *N* HCl/dioxane) yielded, after silica gel column and thin layer chromatography, pure 2,3,4-tri-*O*-methyl-L-rhamnopyranose, 2,3,5-tri-*O*-methyl-L-arabinofuranose, 2,3,4-tri-*O*-methyl-D-glucopyranose, 3,4-di-*O*-methyl-L-arabinopyranose, and 4,6-di-*O*-methyl-D-glucopyranose. All, except the latter, were identified by comparison (tlc, ^{1}H nmr) to authentic samples. The structure of the last product was established by inspection of the ^{1}H nmr spectrum of the triacetate (Ac_2O/pyridine), where the signals of the 1-H (δ 6.28, $J_{1,2}$ = 3.7 Hz), the 2-H (δ 5.01, dd, $J_{1,2}$ = 3.7 Hz, $J_{2,3}$ = 10.0 Hz), and the 3-H (δ 5.43, t, $J_{2,3}$ = 10.0 Hz, $J_{3,4}$ = 10.0 Hz) protons bonded to the positions involved in the interglycosidic linkages were much more clearly distinguished than in the non-acetylated compound.

The above data show that muscaroside B possesses a branched sugar chain, with nodal D-glucopyranose having the branches at its 2- and 3-positions, and with L-rhamnopyranose and L-arabinofuranose as the terminal units. The inner units should be D-glucopyranose, linked at the 6-position, and two L-arabinopyranose units, both linked at the 2-position. The presence of two L-arabinopyranose units was also confirmed when the mixture of 3,4-di-*O*-methyl-L-arabinopyranose and 2,3,4-tri-*O*-methyl-D-glucopyranose was isolated by hplc from the crude permethylation–hydrolysis product and ^{1}H nmr integration established a 2:1 ratio between the anomeric protons of the components.

Having thus established the interglycosidic linkages and the sugar ring size in muscaroside B, the β-configuration at the anomeric centres of both glucose units and the α-configuration at each of the other four were suggested by consideration of the

[1] Part 4: ref. 4 (relevant structures, missing in ref. 4, appear as an erratum in this issue, p. 1228.

[2] Preliminary communication: XIV Convegno Nazionale della Divisione di Chimica Organica della Società Chimica Italiana, Santa Margherita Ligure, Italia. 1983.

[3] Author to whom correspondence should be addressed.

TABLE 1. Calculated and observed contribution of the sugar chain to the $[M]_D$ of muscaroside B, **2**

Chain	$[M]_D$
Methyl α-D-glucopyranoside	+309°[a]
Methyl β-D-glucopyranoside	−66°[a]
Methyl α-L-arabinopyranoside	+17°[a]
Methyl β-L-arabinopyranoside	+245°[a]
Methyl α-L-rhamnopyranoside	−111°[a]
Methyl β-L-rhamnopyranoside	+170°[a]
Methyl α-L-arabinofuranoside	−205°[b]
Methyl β-L-arabinofuranoside	−77°[b]
α-L-rha*p* + α-L-ara*f* + α-L-ara*p* + β-D-glu*p* + α-L-ara*p* + β-D-glu*p*	−414°[c]
$[M]_{D_{muscaroside\ B}} - [M]_{D_{eucosterol}}$	−508°

[a] Reference 25.
[b] Reference 26.
[c] All other possible combinations give much more positive values.

molecular rotation values in the light of Klyne's rule (7) (Table 1).

The ^{13}C and ^{1}H nmr spectra agreed with all above conclusions and also indicated the attachment position of the sugar chain to the aglycone moiety.

Of the six signals due to the anomeric protons in the ^{1}H nmr spectrum of muscaroside B (see Experimental), the one at δ 6.05 (d, J = 1.5 Hz) was assigned to the anomeric proton of the α-arabinofuranose unit, since it was correlated by heteronuclear selective decoupling to the signal of the A_f-1 carbon at δ 109.99. The signal at δ 5.98 (d, J = 1.8 Hz) was assigned to the anomeric proton of the α-rhamnopyranose unit (8, 9). The signal at δ 4.98 (d, J = 7.7 Hz) may be safely attributed to the anomeric proton of the β-glucopyranose unit linked at the 6-position, because of the coupling constant value (10); in addition, selective decoupling correlated this signal to that of the carbon G′-1 at δ 106.20. Finally, the signal at δ 5.21 (d, J = 7.2 Hz) was attributed to the β-anomeric proton of the G″ unit on the basis of the coupling constant value (10) and the remaining signals at δ 5.29 (d, J = 4.4 Hz) and δ 5.18 (d, J = 6.1 Hz) to the 1-H protons of the two arabinopyranose units. The different $J_{1,2}$ values of the two latter signals may be thought to reflect a difference in the proportion between the two possible conformations $^{4}C_1$ and $^{1}C_4$ (11); the same suggestion was provided by consideration of the ^{13}C-shifts of the carbons of A′ and A″ units (see below). The nmr data do not allow us to draw any conclusion about the configuration of the anomeric centres of the arabinopyranose units. However, application of Klyne's rule safely indicates α-configuration for both centres since the two alternative combinations (obtained by supposing the presence of one or two β-arabinopyranose units in the sugar chain) imply contributions (−186° or +42°, respectively) to the $[M]_D$ of **2** much further from the observed value (−508°).

In the ^{13}C spectrum (Table 2) the signals were assigned by comparison to those of muscaroside A and of appropriate reference compounds. Assignment was facilitated by measuring the chemical shift changes (Table 2, DIS column) in pyridine-d_5 obtained by replacing the hydroxyl protons with deuterium atoms; these allow easy distinction between the carbons which are involved in interglycosidic linkages and those which are not (these latter are shifted to a greater extent). The deuterium-induced isotope shifts (12) have been used only once in the case of a trisaccharide-chain saponin in pyridine for assignment purposes (13).

The glycosylation shift (+8.8) observed for the C-3 of the aglycone moiety revealed (14–17) that the sugar chain is linked at this carbon. Deshielding of G′-6 and of G″-2 and G″-3 and shielding of G′-5 and of G″-4 confirmed the above established interglycosidic linkages involving the glucose units; furthermore, the small value (+1.4) of the glycosylation shift of G″-2 indicated (18) that the nodal glucose unit carries the rhamnopyranose unit directly linked at this position. The unchanged chemical shifts of the carbons of the arabinofuranose and rhamnopyranose units, as compared to those of the corresponding methylglycosides and, for the latter, to the analogue unit in muscaroside A, agreed with their terminal location. In addition, the R-3 and R-5 shift values (δ 72.90 and δ 70.24, respectively) agreed with the α-configuration of the pertinent anomeric centre (the values given for methyl β-rhamnopyranoside are δ 75.3 and δ 73.4, respectively) (8). As for the lines of the two arabinopyranose units, a set of values was tentatively attributed (see Table 2) to the A′ unit, owing to their close similarity to the corresponding values of muscaroside A; with this assumption, the better agreement of the shifts of A″-4 and A″-5, with respect to A′-4 and A′-5, with the values given for methyl α-arabinopyranoside could indicate (11) that the A″ unit possesses the $^{1}C_4$ conformation to a greater extent, according to the suggestion above drawn from consideration of the $J_{1,2}$ values.

The lines of G′-1, R-1, and A_f-1 were correlated to the corresponding anomeric protons by heteronuclear selective decoupling experiments; the J^{1}_{C-H} values of G′-1 and R-1 (159 and 169 Hz, respectively) (19) and the chemical shift of A_f-1 (δ 109.99) (20) agreed with the configuration at the pertinent anomeric centres. Because of the close chemical shifts of the anomeric protons of G″, A′, and A″ units, no clearly interpretable result came from selective decoupling experiments involving these protons and carbons G″-1, A′-1, and A″-1, respectively, whose resonance values therefore remained interchangeable.

As for the sequence of the monosaccharide units in the sugar chain of muscaroside B, a significant Overhauser effect measured for the signal at δ 4.98 of the anomeric proton of the β-D-glucopyranose unit, linked at its 6-position, upon irradiation of the 30-H_3 protons, clearly indicated that this glucose unit is directly attached to the aglycone moiety.

The above data led to only three possible sugar sequences, **3**–**5**, for muscaroside B. Definitive evidence in favour of sequence **3** (≡formula **2**) was obtained by mass spectrometry. As described in detail elsewhere (21), application of FAB technique allowed us to observe a fragmentation pattern in which the consecutive losses of one arabinose, one arabinose, one rhamnose, and one glucose residue were seen. This safely established that one branch of the chain consisted of two, and only two, arabinopyranose units.

ara*f*-ara*p*-glu*p*-ara*p*-glu*p*-aglycone **3**
|
rha*p*

ara*f*-glu*p*-ara*p*-ara*p*-glu*p*-aglycone **4**
|
rha*p*

ara*f*-ara*p*-ara*p*-glu*p*-glu*p*-aglycone **5**
|
rha*p*

Can. J. Chem. Downloaded from www.nrcresearchpress.com by 210.87.254.40 on 09/06/12
For personal use only.

TABLE 2. ^{13}C nuclear magnetic resonance shifts of muscaroside B, **2**, muscaroside A, **1**, and reference substances (glycosylation shift, $J^{1}_{C\text{-}1,\,1\text{-}H}$)[a]

Carbon	Reference substances[b,c]	Muscaroside A (sugar moiety)[c,d]	Muscaroside B[c]	Carbon	Reference substances[b,c]	Muscaroside B[c]
			DIS[e]			
G′-1	A 105.4	106.1 (*158*)	106.20 0.06 (*159*)	1	E 35.9	35.63
G′-2	74.8	75.4	75.35 0.14	2	29.0	27.34
G′-3	78.1	78.2	78.23 0.17	3	80.0	88.85 (+8.8)
G′-4	71.4	71.5	71.82 0.15	4	43.2	44.35
G′-5	78.1	75.2 (−2.6)	75.62 0.04 (−2.5)	5	51.3	51.25
G′-6	62.5	68.7 (+6.2)	68.76 0.05 (+6.3)	6	18.9	18.73
				7	27.3	27.34
A′-1	B 105.9	101.2 (−4.7, *166*)	101.45[f] 0.02	8	133.1	132.83
A′-2	72.2	79.3 (+7.1)	79.40 0.02 (+7.2)	9	136.4	136.18
A′-3	74.4	72.3 (−2.1)	72.33 0.14 (−2.1)	10	37.7	37.19
A′-4	69.1	66.5	67.05 0.17	11	20.9	20.76
A′-5	66.6	64.2	63.24 0.05	12	23.3	23.14
				13	47.6	47.65
G″-1	A 105.4	103.1 (−2.3, *154*)	102.78[f] 0.01	14	58.0	57.98
G″-2	74.8	78.3 (+3.5)	76.17 0.06 (+1.4)	15	215.2	215.10
G″-3	78.1	77.7 (−0.4)	87.27 0.08 (+9.2)	16	52.0	51.91
G″-4	71.4	71.5	68.90 0.10 (−2.5)	17	91.3	91.22
G″-5	78.1	78.3	77.69 0.02	18	20.4	20.44
G″-6	62.5	62.7	61.79 0.10	19	20.0	19.37
				20	43.4	43.33
R-1	C 102.4	102.0 (*171*)	102.45 0.03 (*169*)	21	17.2	17.13
R-2	71.9	72.7	71.88 0.13	22	36.9	36.87
R-3	72.5	72.7	72.90 0.14	23	81.9	81.80
R-4	73.6	74.3	73.93 0.12	24	211.9	211.31
R-5	69.4	69.5	70.24 0.03	25	32.4	32.29
R-6	18.4	18.7	18.73 0.01	26	7.6	7.61
				30	23.4	23.14
A″-1	B 105.9		102.64[f] 0.01	31	64.4	63.11
A″-2	72.2		77.76 0.01 (+5.6)	32	24.1	24.14
A″-3	74.4		72.46 0.16 (−1.9)			
A″-4	69.1		68.06 0.16			
A″-5	66.6		65.67 0.07			
A_f-1	D 110.4		109.99 0.06 (*177*)			
A_f-2	83.0		81.80 0.17			
A_f-3	78.5		78.67 0.16			
A_f-4	85.5		85.27 0.02			
A_f-5	62.7		62.52 0.12			

[a] Assignment of signals with very close chemical shifts may be interchanged.
[b] Reference substances: A, methyl β-D-glucopyranoside (27); B, methyl α-L-arabinopyranoside (27); C, methyl α-L-rhamnopyranoside (27); D, methyl α-L-arabinofuranoside (13); E, eucosterol (4).
[c] Measured in pyridine-d_5.
[d] Reference 4.
[e] Differential isotopic shift (28).
[f] Interchangeable values.

Experimental[4]

Melting points were determined with a Kofler block. Rotations were determined on a Perkin–Elmer 141 polarimeter. The hplc was performed with a Varian 5020 instrument using a differential refractometer Waters R 401 as the detector. The tlc was carried out on precoated silica gel layers (0.25 mm, Merck F_{254}). Silica gel 0.05–0.20 (Merck) was used for column chromatography. Sugars and methylated sugars were detected with aniline phthalate or *p*-anisaldehyde, glycoside and aglycone with chromium oxide/sulphuric acid. The ^1H (270 MHz) and ^{13}C nmr (67.88 MHz) spectra were taken on a Fourier transform Bruker instrument WH270 (TMS as internal reference) with an Aspect 2000 computer with 48K memory (32K data). Nuclear Overhauser enhancement effects were obtained in the difference mode as reported in ref. 2. Mass spectra were recorded with a Kratos 902 instrument.

Reference methylated sugars

2,3,4-Tri-*O*-methyl-L-rhamnopyranose, 2,3,4-tri-*O*-methyl-D-glucopyranose, and 3,4-di-*O*-methyl-L-arabinopyranose were prepared as in ref. 4.

2,3,5-Tri-*O*-methyl-L-arabinopyranose was prepared by permethylation (NaH/DMF/MeI) (4) of methyl L-arabinopyranoside (obtained as in ref. 22) followed by acid hydrolysis (1:1 2 *N* HCl/dioxane, 4 h, reflux); ^1H nmr ($CDCl_3$) δ: 5.35 (bs, anomeric proton of α-anomer (23)), 5.31 (d, J = 4.0 Hz, anomeric proton of β-anomer (23)); methoxyl protons appeared at δ 3.48 (3H, s), 3.44 (3H, s), 3.43 (3H, s), 3.42 (6H, s), and 3.40 (3H, s).

Isolation of muscaroside B

Fraction b (ref. 4; 2 g) was three successive times subjected to

[4] With the assistance of Italo Giudicianni.

Can. J. Chem. Downloaded from www.nrcresearchpress.com by 210.87.254.40 on 09/06/12
For personal use only.

Can. J. Chem. Downloaded from www.nrcresearchpress.com by 210.87.254.40 on 09/06/12
For personal use only.

semipreparative hplc (Lichrosorb RP-18 (7 μm), 70:30 methanol–water, 5 mL min^{-1}, 75 mg in 1 mL of 70:30 methanol–water), and further purified by recrystallization from ethanol to give muscaroside B, **2** (320 mg); mp 202–206°C; $[\alpha]_D$ −32° (*c* 1, methanol); FAB ms *m/e*: 1361 (MNa^+), 1372 (MK^+). Elemental analysis: C 55.5, H 7.3% ($C_{62}H_{98}O_{31}$ requires C 55.6, H 7.4%). The ^{13}C nmr data are given in Table 2. For the deuterium-induced isotope shift experiment, a sample of **2** (80 mg) was dissolved in pyridine-d_5 (2 mL) and the ^{13}C nmr spectrum was measured (30°C); then the sample was evaporated, dissolved in warm deuterium oxide (1 mL), and freeze-dried; this procedure was repeated three times and then the ^{13}C spectrum was taken (30°C) in pyridine-d_5 (2 mL). The ^1H nmr data, δ: 0.93 and 0.95 (3H, s each, 18-H_3 and 19-H_3), 1.03 (3H, t, $J_{25,26}$ = 7.3 Hz, 26-H_3), 1.05 (3H, d, $J_{20,21}$ = 6.6 Hz, 21-H_3), 1.55 (3H, s, 30-H_3), 1.70 (3H, s, 32-H_3), 1.75 (3H, d, $J_{5,6}$ = 6.1 Hz, R-6-H_3), 2.46 (2H, q, $J_{25,26}$ = 7.3 Hz, 25-H_2), 2.38 and 3.06 (2H, ABq, J_{AB} = 19.0 Hz, 16-H_2), 4.98 (1H, d, $J_{1,2}$ = 7.7 Hz, G′-1-H), 5.18 (1H, d, $J_{1,2}$ = 6.1 Hz, A′-1-H or A″-1-H), 5.21 (1H, d, $J_{1,2}$ = 7.2 Hz, G″-1-H), 5.29 (1H, d, $J_{1,2}$ = 4.4 Hz, A″-1-H or A′-1-H), 5.98 (1H, d, $J_{1,2}$ = 1.8 Hz, R-1-H), 6.05 (1H, d, $J_{1,2}$ = 1.5 Hz, A_f-1-H).

Enzymatic hydrolysis of muscaroside B

Muscaroside B (33 mg) was subjected to enzymatic hydrolysis with digestive juice of *Helix pomatia* by the procedure described in ref. 4. Work-up gave eucosterol (5 mg), identical (mp, tlc, ^1H nmr, and ms) to an authentic sample (3, 24).

Acid hydrolysis of muscaroside B

Acid hydrolysis of muscaroside B, analysis (tlc, hplc, and ^1H nmr) of the resulting monose mixture, separation by hplc of the individual monose components, rotation determination of these latter, and the D-galactose dehydrogenase test for L-arabinose were performed as for muscaroside A (4).

Permethylation of muscaroside B

Muscaroside B (80 mg) was permethylated with MeI/DMF/NaH as described for muscaroside A (4).

Acid hydrolysis of permethylated muscaroside B

Permethylated muscaroside B (80 mg) was hydrolyzed with 1:1 2 *N* HCl/dioxane (10 mL) by refluxing for 6 h. The cooled mixture was neutralized with solid Na_2CO_3 and evaporated. The residue was extracted with chloroform and the chloroform extract was evaporated. The residue (80 mg) was chromatographed on a column of silica gel (12 g). Elution with chloroform containing increasing percentages of ethyl acetate yielded pure 2,3,4-tri-*O*-methyl-L-rhamnopyranose (10 mg), 2,3,5-tri-*O*-methyl-L-arabinofuranose (9 mg), 2,3,4-tri-*O*-methyl-D-glucopyranose (11 mg), 3,4-di-*O*-methyl-L-arabinopyranose (17 mg), and 4,6-di-*O*-methyl-D-glucopyranose (10 mg). All except the latter were identified (tlc, 1:9 methanol–chloroform; ^1H nmr: see above and ref. 4) by comparison with authentic samples.

The 4,6-di-*O*-methyl-D-glucopyranose sample obtained was converted into the triacetate by acetylation with acetic anhydride in dry pyridine (room temperature, 12 h). Usual work-up gave 4,6-di-*O*-methyl-1,2,3-tri-*O*-acetyl-D-glucopyranose (mainly α-anomer); ^1H nmr ($CDCl_3$), δ: 2.00, 2.10 and 2.14 (3H, s each, 3 × CH_3COO—), 3.42 and 3.47 (3H, s each, 2 × CH_3O—), 5.01 (1H, t, $J_{1,2}$ = 3.7 Hz, $J_{2,3}$ = 10.0 Hz, 2-H), 5.43 (1H, t, $J_{2,3}$ = 10.0 Hz, $J_{3,4}$ = 10.0 Hz, 3-H), 6.28 (1H, d, $J_{1,2}$ = 3.7 Hz, 1-H).

The hplc of a sample of the crude permethylation–hydrolysis product (Lichrosorb NH_2 (10 μm) column, 95:5 acetonitrile–water, 5 mL min^{-1}) allowed isolation of the mixture of 3,4-di-*O*-methyl-L-arabinopyranose and 2,3,4-tri-*O*-methyl-D-glucopyranose; a 2:1 ratio between the two components was established by ^1H nmr integration of the anomeric proton signals of the former (δ 4.62 and δ 5.29, α- and β-anomer, respectively) and of the latter (δ 5.32 and δ 4.61, α- and β-anomer, respectively) (4).

Acknowledgments

This investigation was supported by MPI (Ministero della Pubblica Istruzione) and by CNR (Consiglio Nazionale delle Ricerche). The nmr spectra were performed at the Centro di Metodologie Chimico-Fisiche della Università di Napoli.

1. M. PARRILLI, M. ADINOLFI, and L. MANGONI. Gazz. Chim. Ital. **109**, 611 (1979).
2. M. PARRILLI, R. LANZETTA, M. ADINOLFI, and L. MANGONI. Tetrahedron, **36** 3591 (1980).
3. M. PARRILLI, R. LANZETTA, V. DOVINOLA, M. ADINOLFI, and L. MANGONI. Can. J. Chem. **59**, 2261 (1981).
4. M. ADINOLFI, G. BARONE, R. LANZETTA, G. LAONIGRO, L. MANGONI, and M. PARRILLI. Can. J. Chem. **61**, 2633 (1983).
5. O. OLSEN, K. W. RASMUSSEN, and H. SORENSEN. Phytochemistry, **20**, 1857 (1981).
6. E. O. BLACHNITZKY, F. WENGENMAYER, and G. KURZ. Eur. J. Biochem. **47**, 235 (1974).
7. W. KLYNE. Biochem. J. **47**, 4 (1950).
8. R. KASAI, J. OKIHARA, K. ASAKAWA, I. MITZUTANI, and O. TANAKA. Tetrahedron, **35**, 1427 (1979).
9. T. KONOSHIMA, H. FUKUSHIMA, H. INUI, K. SATO, and T. SAWADA. Phytochemistry, **20**, 139 (1981).
10. T. D. INCH. Nuclear magnetic spectroscopy in the study of carbohydrates and related compounds. *In* Annual reports on NMR spectroscopy. Vol. 5A. *Edited by* E. F. Money. Academic Press, London, 1972. p. 305, and references therein.
11. H. ISHII, I. KITAGAWA, K. MATSUSHITA, K. SHIRAKAWA, K. TORI, T. TOZYO, M. YOSHIKAWA, and Y. YOSHIMURA. Tetrahedron Lett. 1529 (1981).
12. K. BOCK and H. TØGERSEN. Nuclear magnetic resonance in the study of mono- and oligosaccharides. *In* Annual reports on nmr spectroscopy. Vol. 13. *Edited by* E. F. Money. Academic Press, London. 1982. p. 1.
13. R. ENCARNATION, L. KENNE, G. SAMUELSSON, and F. SANDBERG. Phytochemistry, **20**, 1939 (1981).
14. K. YAMASAKY, H. KOHDA, T. KOBAYASHI, R. KASAI, and O. TANAKA. Tetrahedron Lett. 1005 (1976).
15. R. KASAI, M. SUZUO, J. T. ARAKAWA, and O. TANAKA. Tetrahedron Lett. 175 (1977).
16. K. TORI, Y. YOSHIMURA, S. SEO, K. SAKURAWI, Y. TOMITA, and H. ISHII. Tetrahedron Lett. 4163 (1976); 4167 (1967).
17. K. TORI, S. SEO, Y. YOSHIMURA, H. ARITA, and Y. TOMITA. Tetrahedron Lett. 179 (1977).
18. S. B. MAHATO, N. P. SAHU, A. N. GANGULY, R. KASAI, and O. TANAKA. Phytochemistry, **19**, 2017 (1980).
19. K. BOCK and C. PEDERSEN. J. Chem. Soc. Perkin Trans. 2, 293 (1974).
20. M. P. WILLIAMSON and D. H. WILLIAMS. Tetrahedron Lett. 4187 (1980).
21. M. ADINOLFI, L. MANGONI, G. MARINO, M. PARRILLI, and R. SELF. Biochem. Mass Spectrom. In press.
22. P. A. MIED and Y. C. LEE. Anal. Biochem. **49**, 534 (1972).
23. J. D. STEVENS and H. G. FLETCHER, JR. J. Org. Chem. **33**, 1799 (1968).
24. R. ZIEGLER and C. TAMM. Helv. Chim. Acta, **59**, 1967 (1976).
25. H. OTSUKA, T. AKIYAMA, K. KAWAI, S. SHIBATA, O. INONE, and Y. OGIHARA. Phytochemistry, **17**, 1349 (1978).
26. K. P. TIWARI and M. MASOOD. Phytochemistry, **19**, 1244 (1980).
27. S. SEO, Y. TOMITA, K. TORI, and Y. TOSHIMUA. J. Am. Chem. Soc. **100**, 3331 (1978).
28. P. E. PFEFFER, K. M. VALENTINE, and F. W. PARRISH. J. Am. Chem. Soc. **101**, 1265 (1979).

ADDITIONS AND CORRECTIONS/AJOUTS ET CORRECTIONS

Can. J. Chem. Downloaded from www.nrcresearchpress.com by 210.87.254.105 on 09/06/12
For personal use only.

Vol. 60, 1982

J. P. Wignacourt, G. Mairesse, P. Barbier, A. Lorriaux-Rubbens, and F. Wallart. Existence and characterization of double salts in indium trihalide – potassium halide – water systems at 21°C (halide = Cl, Br).

Page 1747. From a single-crystal structure analysis, the data (X-ray, Raman) given to be characteristic of compound **D** in Fig. 3, p. 1749, have been proven to be those of a new salt: $KInBr_4$ (1). The formulation $K_3In_2Br_9$ was previously proposed from the results of the "wet rest" method, the chemical analysis, and the X-ray powder pattern of the samples.

Furthermore, a synthetic melt $3KBr - 2InBr_3$ had the same powder pattern as the "**D**" compound without any evidence of excess KBr. A new investigation in this area of this very complicated solubility diagram is needed to clear the existence of $K_3In_2Br_9$.

$KInBr_4$, the first compound in which a tetrahedral InX_4^- anion is associated to an alkaline cation, has been obtained by isothermal evaporation (21°C) of a solution containing 80.2 g $InBr_3$ and 2.5 g KBr in 100 g of solution.

1. J. P. WIGNACOURT, F. ABRAHAM, and G. MAIRESSE. Acta Crystallogr. In press.

Vol. 61, 1983

M. Sunitha Kumari and Etalo A. Secco. I. Order–disorder transitions and solid state reaction kinetics in $Na_2SO_4-K_2SO_4$ system.

Page 594. In our literature search on this system (1) the phase diagrams reported by Perrier and Bellanca (2) and by Eysel (3) escaped our notice. Although there is general agreement between our phase diagram and their diagrams on the major features, these latter authors include a number of unconfirmed solid–solid lines enclosing various solid phase areas which were not detected in our study. It is also to be noted that the phase transition temperatures in the earlier reported diagrams are in agreement with our temperatures for the same features recorded on the cool mode of DTA; otherwise our temperatures are usually higher.

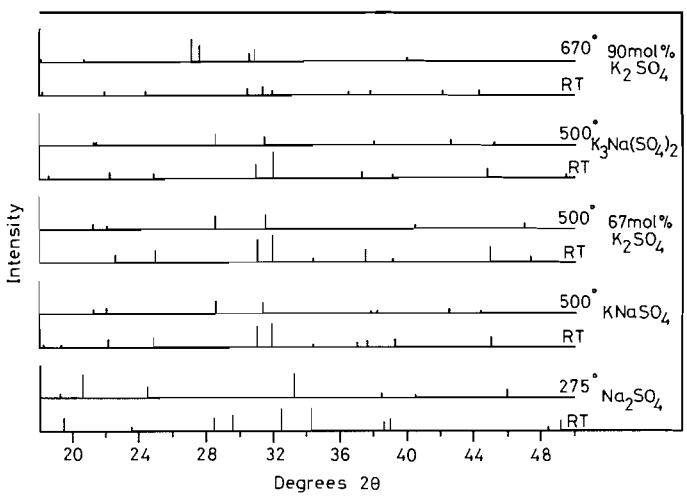

FIG. 1. X-ray diffraction peaks for $Na_2SO_4-K_2SO_4$ system at room temperature and high temperature.

Also reported (1) are X-ray diffraction data for $KNaSO_4$ and $K_3Na(SO_4)_2$ at 25°C and 500°C. Given in Fig. 1 are the redetermined X-ray diffraction pattern for $K_3Na(SO_4)_2$ at 500°C along with X-ray diffraction patterns for additional compositions in the $Na_2SO_4-K_2SO_4$ system. The RT (room-temperature) and high-temperature patterns of $K_3Na(SO_4)_2$ and intermediate compositions resemble very much the patterns of $KNaSO_4$, hence its structure. The earlier high-temperature X-ray diffraction data on $K_3Na(SO_4)_2$ might be explained on the basis that while the sample holder indicated 500°C the $K_3Na(SO_4)_2$ sample was below its transition temperature, thus exhibiting only lattice expansion.

1. M. S. KUMARI and E. A. SECCO. Can. J. Chem. **61**, 594 (1983).
2. C. PERRIER and A. BELLANCA. Period. Mineral. Rome, **11**, 169 (1940).
3. W. EYSEL. Am. Mineral. **58**[7–8], 736 (1973).

Osvald Knop, T. Stanley Cameron, Margaret Ann James, and Michael Falk. Alkylammonium hexachlorostannates(IV), $(R_nNH_{4-n})_2SnCl_6$: crystal structure, infrared spectrum, and hydrogen bonding.

Page 1620. Right-hand column: line 10 of text, *read* $*(n\text{-}Bu_3NH)_2SnCl_6$ (3BHS) *instead of* $*(n\text{-}BuNH_3)_2SnCl_6$ (1BHS).

Page 1623. Right-hand column: line 2 of text, *read* Fig. 3, bottom, *instead of* Fig. 3, top; line 4 of text, *read* Fig. 3, top, *instead of* Fig. 3, bottom; line 9 from bottom, *read* . . . and again in $P2_1/m$ with the nitrogens and the adjacent carbons having the same coordinates as in the $P2_1/m$ refinement but with the other C atoms in a twofold disorder with respect to reflection . . . *instead of* . . . and again in . . . . . to reflection . . .

Page 1625. Caption of Fig. 3, *reverse* top *and* bottom.

Page 1626. Footnote 4, *read* ~3.36 Å *instead of* ~5.36 Å.

Page 1629. Right-hand column: line 14 from bottom, *read* 293 K *instead of* 10 K.

Page 1631. Right-hand column: line 8 from bottom, *read* N···Cl *instead of* N···C.

Page 1634. Left-hand column: line 3 of text, *read* Fig. 19*B* *instead of* Fig. 18*B*; line 11 from bottom, *read* above *instead of* below. Right-hand column: line 24 from top, *read* 3150 *instead of* 3220.

Page 1635. Right-hand column: line 3, *read* 3PHS and 3BHS *instead of* 2PHS and 2BHS.

Page 1642. Right-hand column: line 6 of text, *read* 2RHS *instead of* 2MHS.

M. Adinolfi, G. Barone, R. Lanzetta, G. Laonigro, L. Mangoni, and M. Parrilli. Glycosides from *Muscari comosum*. 4. Structure of muscaroside A.

Page 2633. The structures of compounds **1**–**5** were inadvertently omitted from the original article and are published here.

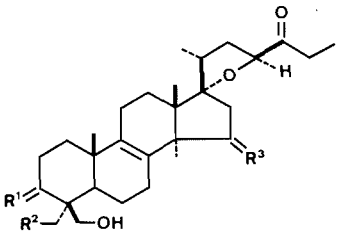

	R^1	R^2	R^3
1		H	O
2	O	H	O
3		OH	H, H
4	O	OH	H, H

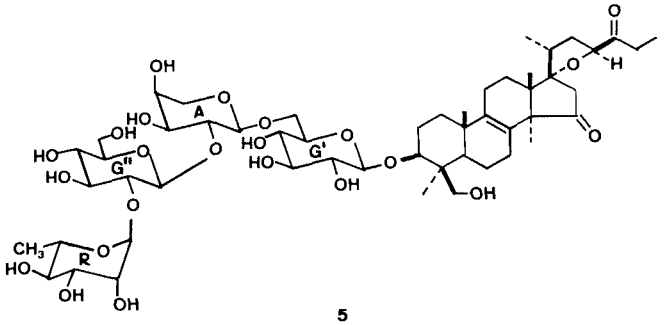

5

Can. J. Chem. Downloaded from www.nrcresearchpress.com by 210.87.254.105 on 09/06/12
For personal use only.

Characterization of a clathrate hydrate of nitrogen trifluoride[1]

D. W. DAVIDSON, S. K. GARG, C. I. RATCLIFFE, J. S. TSE, and S. R. GOUGH
Division of Chemistry, National Research Council of Canada, Ottawa, Ont., Canada K1A 0R9

Received November 9, 1983

D. W. DAVIDSON, S. K. GARG, C. I. RATCLIFFE, J. S. TSE, and S. R. GOUGH. Can. J. Chem. **62**, 1229 (1984).

NF_3 is found to form a type I clathrate hydrate with a $Pm3n$ cubic unit cell dimension of 11.91 Å at 110 K and a dissociation pressure of 16.5 atm at 0°C. Dielectric studies below 100 K give, for reorientation of the NF_3 dipole in the structure I cages, an average activation energy of 0.79 kcal mol^{-1}. Well-resolved absorption peaks arising from NF_3 incorporated in small and large cages of the structure II hydrate formed with SF_6 give activation energies of 1.05 and 0.29 kcal mol^{-1}, respectively. ^{19}F nmr lineshapes show in addition the presence of faster reorientation about the NF_3 symmetry axis which is not completely removed even at 1.6 K. The pronounced effect of molecular oxygen impurity on the nmr linewidths at high magnetic fields and very low temperatures is discussed.

D. W. DAVIDSON, S. K. GARG, C. I. RATCLIFFE, J. S. TSE et S. R. GOUGH. Can. J. Chem. **62**, 1229 (1984).

On a trouvé que le NF_3 forme un hydrate de clathrate de type I avec une dimension de maille élémentaire cubique $Pm3n$ de 11,91 Å, à 110 K, et une pression de dissociation de 16,5 atm à 0°C. Les études diélectriques réalisées en-dessous de 100 K sur la réorientation du dipôle NF_3 dans les cages de la structure I, donnent une énergie d'activation moyenne de 0,79 kcal/mol. Les pics d'absorption bien résolus, provenant du NF_3 incorporé dans les petites et les grandes cages de la structure de l'hydrate II formé avec le SF_6, donnent respectivement des énergies d'activation de 1,05 et de 0,29 kcal/mol. La forme des pics en rmn du ^{19}F révèle de plus la présence d'une réorientation plus rapide autour de l'axe de symétrie du NF_3 qui n'est pas complètement éliminée même à 1,6 K. On discute de l'effet prononcé de l'impureté de l'oxygène moléculaire sur la largeur des pics en rmn à haut champ et à très basse température.

[Traduit par le journal]

That nitrogen trifluoride should form a clathrate hydrate is evident from its molecular size and chemical inertness toward water, as was pointed out long ago by von Stackelberg (1). No attempt to form NF_3 hydrate, however, has hitherto been recorded. We report here the identification of a structure I clathrate hydrate of NF_3 and the results of dielectric and ^{19}F nmr studies of reorientation of NF_3 molecules encaged in the structure I lattice as well as in structure II double hydrates formed with tetrahydrofuran, *p*-dioxane, and sulphur hexafluoride.

Experimental methods

NF_3 hydrate samples were prepared by condensing NF_3 (Air Products and Chemicals Inc.) at low temperatures into a pressure vessel containing degassed H_2O or D_2O ice and several stainless steel rods and allowing NF_3 and water to react at the temperatures and (final) pressures given in Table 1. During the reaction period the pressure vessel was rolled so as to subject the solid sample to continuous grinding. Hydrate formation was monitored by the fall in gas pressure, which was normally complete in 24 h.

Tetrahydrofuran (THF), *p*-dioxane (*p*D), and SF_6 individually form hydrates of structure II. Double hydrates of NF_3 with THF and *p*D were prepared by subjecting mixtures which contained 17 mol of D_2O per mole of structure II hydrate-former to the NF_3 pressures shown in Table 1. The SF_6–NF_3 double hydrate was formed from H_2O ice and a gas mixture containing about 44 mol% SF_6. Again reaction was promoted by rolling and grinding.

The NF_3 hydrate dissociation pressure was determined as the constant value to which the pressure rose after each of a series of substantial pressure reductions (2).

X-ray powder diffraction photographs were taken at ~110 K with a flat-plate camera using MoKα radiation and Zr filtering (3).

Sample disks for dielectric study were formed by pressing hydrate powder in a pre-cooled die at 1 kbar pressure. The sample was mounted in a three-terminal cell contained in an Andonian Liquid Helium Cryostat. Measurements were made (4) between 0.1 Hz and 10 MHz at temperatures down to 2 K. The complex permittivities measured were less than the true hydrate permittivities because of the presence of rough surfaces and internal voids related to low sample plasticity at the low temperatures necessary to prevent hydrate decomposition during pressing. The kinetic information given by the frequency and temperature dependence of the complex permittivity is, however, not appreciably affected by these factors.

^{19}F nmr derivative spectra of powder samples were recorded at 56 or 8 MHz with low-level marginal oscillators and 83 Hz amplitude modulation. Normally a number of signal sweeps were accumulated and averaged in a Digital RT11/23 computer programmed for second moment and other calculations. The nmr probe was contained in an Andonian cryostat with the tail-piece positioned between the pole pieces of a Bruker electromagnet. In both the nmr and dielectric studies temperature was controlled and measured by carbon and germanium thermometers below 80 K and by copper–constantan thermocouples at higher temperatures.

The presence of a substantial quantity of molecular oxygen was indicated by the ^{19}F nmr lineshapes observed at very low temperatures. Subsequent gas chromatographic analysis gave 0.71 ± 0.02 mol% O_2 and 0.42 ± 0.02 mol% N_2 as the principal impurities in the NF_3 employed.

Results

Hydrate dissociation pressures

Figure 1 illustrates the sequence of pressure changes following periodic release of NF_3 gas from a pressure vessel containing NF_3 hydrate at 0°C. This method of determining the hydrate dissociation pressure (2) is straightforward but deserves some comment, since it appears that it may be incorrectly applied. Under isothermal conditions the constant pressure reached at 0°C corresponds to the three-phase equilibrium between hydrate, liquid water, and gas. Gas released is made up by decomposition of the necessary amount of hydrate. The small rise of pressure after gas release which occurs at pressures well above the three-phase equilibrium pressure and at pressures too low for hydrate to be present arises from increase in temperature as the gas recovers from the instantaneous cooling produced by pressure reduction.

The dissociation pressure of NF_3 hydrate is 16.5 ± 0.2 atm at 0°C and 3.7 ± 0.2 atm at −40°C. This hydrate is therefore more stable than the hydrates of CH_4 and CF_4 whose dis-

[1]NRCC No. 23098.

TABLE 1. Preparation of NF_3 clathrate hydrate samples

Structure	Host	Second guest	T (°C)	NF_3 pressure (atm)	Measurement
I	H_2O	—	−25	23	X-ray diffraction
	H_2O	—	−25	35	Decomposition P
	H_2O	—	−40	9	Decomposition P
	D_2O	—	−25	14	NMR, dielectric
II	D_2O	THF	0	9.6	NMR, dielectric
	D_2O	*p*D	−40	10.0	Dielectric
	D_2O	*p*D	−30	4.8	NMR, dielectric
	H_2O	SF_6	−25	3.3(NF_3), 2.6(SF_6)	Dielectric

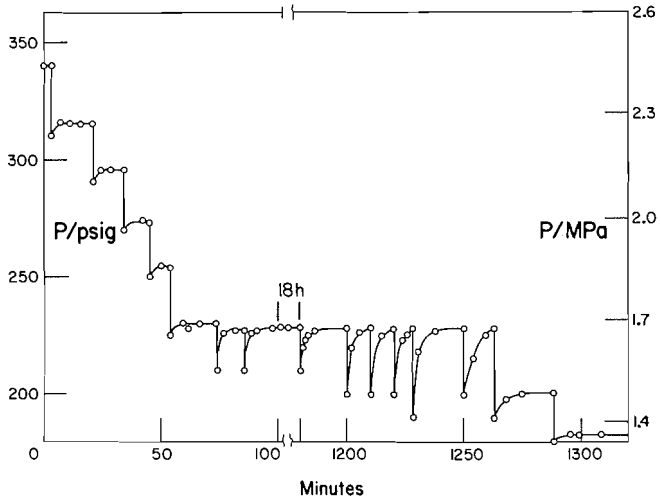

FIG. 1. Pressure changes following pressure reductions over NF_3 hydrate at 0°C.

sociation pressures at 0°C are, respectively, 26.0 (5) and 41.5 atm (6).

Unit cell parameter

The X-ray powder diffraction pattern of the NF_3 hydrate specimen examined was that of a structure I hydrate (space group $Pm3n$), with no lines attributable to ice. Indexing of the 11 most intense lines gave for the unit cell parameter $a = 11.91 \pm 0.02$ Å at 110 K. Values reported by Bertie *et al.* (7–9) for other structure I hydrates at a similar temperature are xenon 11.84 Å, ethylene oxide 11.89 Å, trimethylene oxide 11.95 Å, and cyclopropane 11.98 Å.

Dielectric behaviour

Dielectric dispersion and absorption curves measured below 100 K in NF_3 deuteriohydrate are shown for a number of frequencies in Fig. 2. This low-temperature absorption arises from the relatively weakly hindered reorientation of encaged NF_3 molecules. The absorption is weak because of the small dipole moment of 0.234 D (10) and broad (see Cole–Cole plots of Fig. 3) because of a wide distribution of reorientational relaxation rates. It includes broad, overlapping contributions from NF_3 molecules in both the 14- and 12-hedral cages. In an attempt to resolve these contributions, the low-temperature dielectric behaviour of a number of NF_3-containing structure II double hydrates was examined, with the expectation that NF_3 would almost exclusively occupy only the otherwise empty 12-hedral cages of structure II.

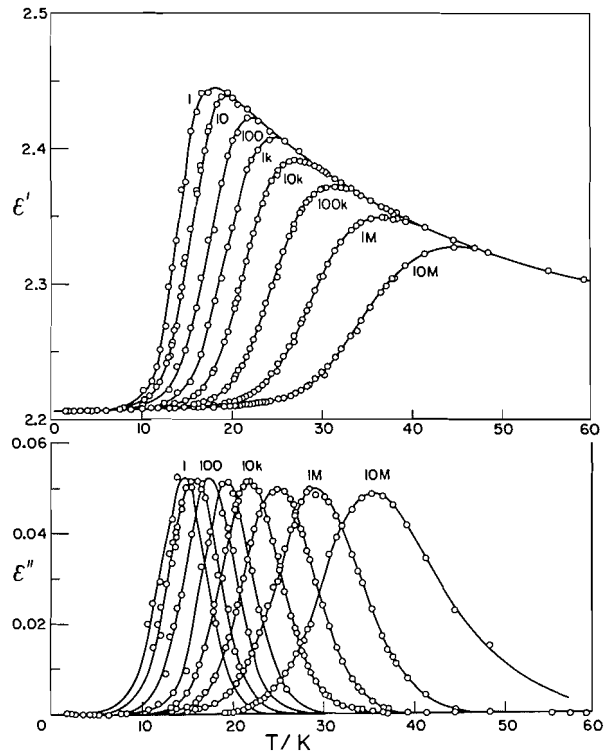

FIG. 2. Low temperature permittivity and loss curves of NF_3–D_2O hydrate. Numbers denote frequencies in Hz.

The absorption seen in THF–NF_3–D_2O hydrate was indistinguishable in its frequency- and temperature-dependence from that shown by THF–H_2O hydrate itself (11); the NF_3 absorption underlay the broad, two-orders-of-magnitude stronger absorption by THF (dipole moment = 1.63 D) for which maximum ϵ'' at 10 kHz occurs at 24 K.

The first-*p*-dioxane double hydrate sample, prepared at high NF_3 pressure (Table 1), proved to contain considerable structure I NF_3 hydrate. The second *p*D–NF_3–D_2O sample was entirely structure II. Its absorption (Fig. 4) apparently consisted of overlapping contributions from *p*D in the 16-hedra and NF_3 in the 12-hedra, together with a distinct region of relatively small absorption below 10 K. As previously reported (12), although the stable chair form of *p*D has no permanent dipole moment, the presence of two large opposed exocentric dipoles in the molecule results in a polarization of the water molecules of the cage which depends on the orientation of the dioxane molecule; the effect is comparable to the presence of a permanent dipole moment of about 0.2 D. Figure 4 shows the

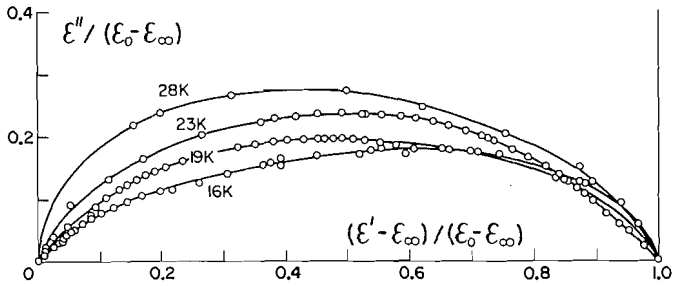

FIG. 3. Normalized Cole–Cole plots of NF_3-D_2O hydrate.

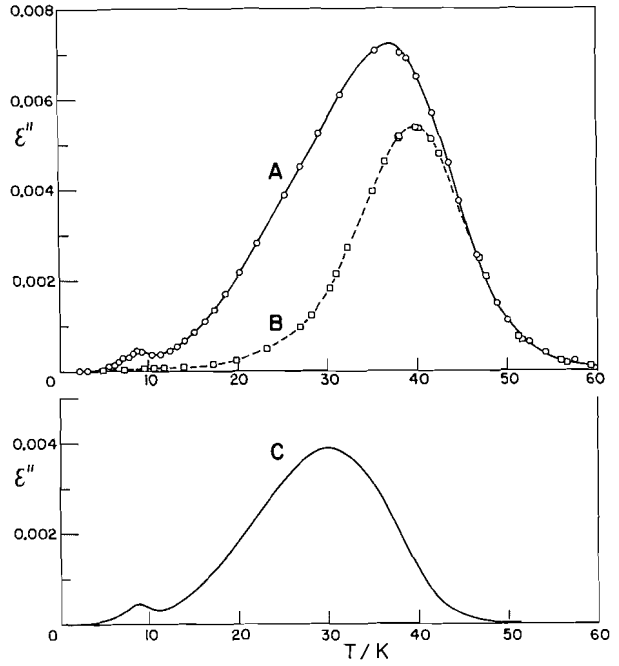

FIG. 4. Dielectric absorption at 10 kHz in *p*-dioxane–NF_3-D_2O hydrate (*A*) and in $pD-H_2O$ hydrate (*B*). Curve *C* is obtained by subtraction of *B* from *A*.

effect of subtracting dielectric absorption previously measured for *p*D hydrate itself (12). Gas chromatographic analysis having shown negligible amounts of impurity in the *p*D employed, the weak absorption below 10 K was assigned to a small population of NF_3 in the 16-hedral cages.

Figure 5 shows the absorption in the double hydrate of SF_6, a molecule which does not give rise to detectable dielectric absorption. Here the two well-resolved absorption regions may be unequivocally assigned to reorientation of NF_3 molecules in the 12- and 16-hedral cages.

Wide-line ^{19}F nmr

The lineshapes of NF_3-D_2O hydrate at a number of temperatures are shown in Fig. 6 and the temperature dependence of the second moment of the linewidth in Fig. 7. The spectra were recorded at 56 MHz (rather than 8 MHz) to take advantage of the greater signal-to-noise ratio realizable at this frequency. The large anisotropy of the magnetic shielding tensor of the fluorine nuclei in NF_3 (13) makes the 56 MHz lineshapes very asymmetric at low temperatures.

The pronounced changes in lineshape which occur below 10 K indicate the presence of a low temperature (i.e. fast) motion which is not dielectrically active in NF_3 hydrate and

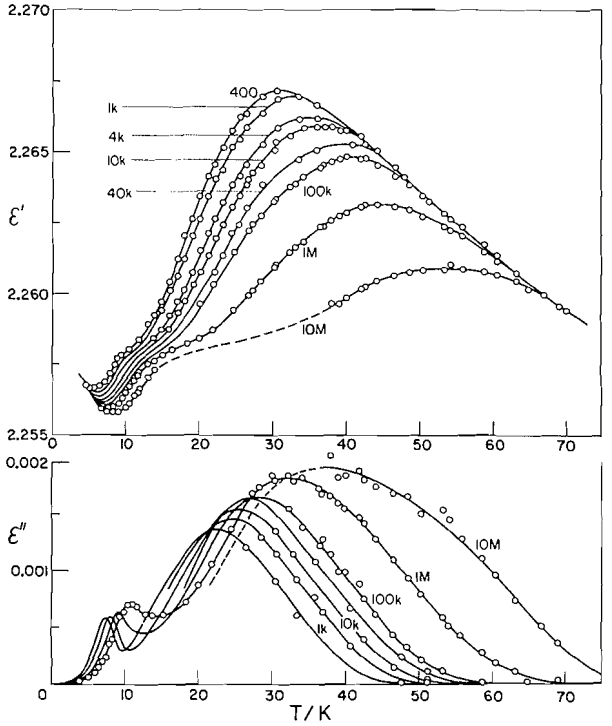

FIG. 5. Permittivity and loss curves of $SF_6-NF_3-H_2O$ hydrate. Many experimental points have been omitted for clarity.

which therefore must arise from reorientation of NF_3 about its symmetry axis. Even at 1.6 K the lineshape (Fig. 6) has a narrow central component which appears to be due to the persistence of three-fold rotation on the part of a small number of NF_3 molecules. The line narrowing which occurs (mainly) between 15 and 30 K correlates well with the dielectric absorption and arises from more general reorientation processes of the NF_3 molecule.

Figures 8 and 9 show low temperature lineshapes of NF_3 encaged in D_2O hydrates of THF (56 MHz) and *p*D (8 MHz). These suggest that there is less persistence at very low temperature of axial rotation of NF_3 molecules in the 12-hedral structure II cages than for molecules primarily in the 14-hedra of structure I.

At 8 MHz the asymmetry of the lineshape is relatively small. The 1.64 K spectrum (Fig. 9*A*) is very nearly that of rigid NF_3 molecules while the 4.26 K spectrum (*B*) includes a substantial contribution from molecules undergoing axial reorientation. Thus the latter may be satisfactorily represented by superposition of the rigid-lattice lineshape calculated (14) from the geometry (15) and shielding tensor (13) of NF_3 with Gaussian broadening (β = 0.8 G) (*C*) and the lineshape calculated (16) for a symmetric three spin-1/2 system rotating about its symmetry axis, with negligible chemical shift anisotropy and β = 0.7 G (*D*). The fields at zero-crossing of the two contributions are slightly shifted with respect to one another.

Discussion

Second moments

Table 2 gives second moments of the ^{19}F linewidth of NF_3 in D_2O hydrates of structures I and II, as calculated from the structures and chemical shielding tensors, for various modes of motion of NF_3 in the rigid hydrate lattice. The shielding tensor σ_{11} = 260, σ_{22} = −60, and σ_3 = −200 ppm with respective

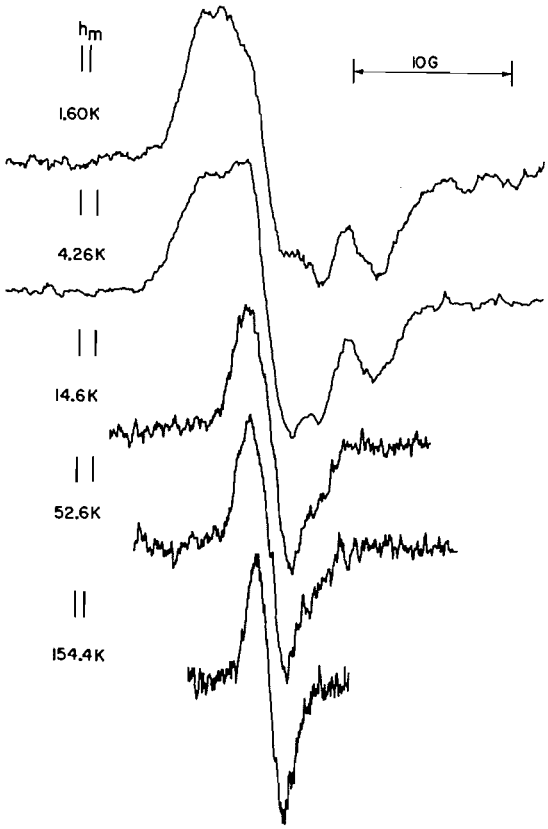

FIG. 6 ^{19}F nmr lineshapes of NF_3-D_2O hydrate at 56 MHz.

components along the NF bond, perpendicular to the plane of symmetry containing NF, and in the plane of symmetry and perpendicular to NF (13), becomes, in the presence of rotation about the three-fold axis, the axially symmetric tensor $\sigma_\parallel = -112$, $\sigma_\perp = 56$ ppm. The tabulated second moments are based on 60% occupancy by NF_3 of the small cages of both structures, 97% occupancy by NF_3 of the large cages of structure I, and 100% occupancy of the large structure II cages by THF or pD. The results are not very sensitive to these assumptions.

There is satisfactory agreement between the calculated rigid-lattice second moments of 56 MHz and those approached at the lowest temperatures of measurement only when the broadening effect of molecular oxygen impurity (17) is taken into account. This effect is treated in the Appendix. However, the second moment of the NF_3-pD-D_2O hydrate at 1.64 K (*cf.* Fig. 9*A*) is 6.9 G^2 at 8 MHz, a frequency low enough that neither oxygen nor chemical shift anisotropy contribute appreciably. The difference between this value and the calculated value of 7.7 G^2 (Table 2) may be largely the result of rotational oscillations of NF_3 (18).

For NF_3 hydrate itself the contribution of O_2 to the second moment at 56 MHz is no more than about 3 G^2 at 1.7 K and above 6 K the fall of second moment (Fig. 7) is mainly the result of increasing rotational mobility of NF_3. The lineshapes show overlap between the contributions of molecules which are still rigid and of molecules undergoing three-fold rotation up to 16 K, and thereafter show overlap between contributions from three-fold rotation and more general reorientational processes. As in other structure I hydrates of guest molecules of less than cubic symmetry (19), reorientation of the guest molecules is not isotropic even at the highest temperature of measurement:

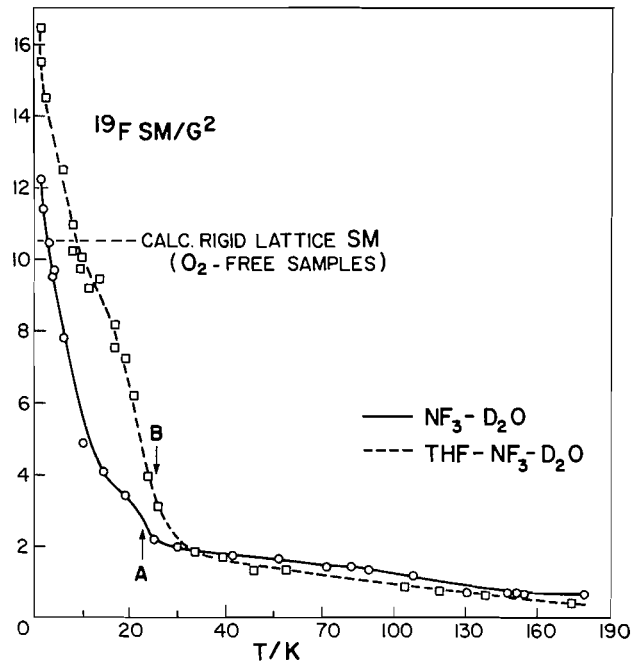

FIG. 7. Second moments of ^{19}F lines of NF_3-D_2O and $THF-NF_3-D_2O$ hydrates at 56 MHz. Temperature scale changes at 50 K. Arrows mark temperatures of maximum 10 kHz dielectric loss in (*A*) NF_3-D_2O and (*B*) $SF_6-NF_3-H_2O$ hydrates.

the second moment at 181 K (0.67 G^2) is more than twice the isotropic value (Table 2). Reorientation takes place between generally inequivalent preferred sites which are anisotropically distributed, especially in the 14-hedral cages. Thus, high-temperature second moments are smaller for NF_3 in the 12-hedra of the THF and pD double D_2O hydrates (~0.47 G^2 at 174 K and 56 MHz and ~0.37 G^2 at 155 K and 8 MHz, respectively).

The reorientational processes

Plots of the frequencies of dielectric measurement versus the reciprocal of the temperature at which maximum dielectric loss occurs are given in Fig. 10. Activation energies E_A obtained from the slopes are shown in Table 3. It is emphasized that these are average values and that NF_3 molecules exhibit a wide distribution of dipolar reorientation rates even within cages of the same size. In the structure I hydrate NF_3 molecules in the 14- and 12-hedra make overlapping contributions to ϵ''. The major contribution to the aggregate activation energy of 0.79 kcal/mol is from molecules in the larger cages which contain perhaps 85% of the NF_3 molecules (see below).

Separate dielectric absorption peaks from the same kind of molecule in different sized cages of a hydrate have hitherto not been observed. The broadness of the absorption arising from molecules within a particular type of cage, particularly within the least spherical 14-hedra, in general precludes such resolution in structure I. However, the case of NF_3 shows that the environments within the structure II 12- and 16-hedral cages are sufficiently different as to give rise to well-separated absorption regions. Since, however, simple type II hydrates are formed by molecules which are too large to fit into 12-hedra, one can expect to observe relaxation of molecules of the same kind in the two kinds of cage only in double hydrates which contain species small enough to occupy the small cages. In such cases the Langmuir constants of the large molecules (e.g.,

TABLE 2. Calculated second moments (G^2) of ^{19}F lines of NF_3 in D_2O hydrates

Contribution	Structure I			Structure II		
	Rigid NF_3	C_3 rotation	Isotropic rotation	Rigid NF_3	C_3 rotation	Isotropic rotation
Intra NF_3						
^{19}F	6.84	1.71	0	6.84	1.71	0
^{14}N	0.34	0.07	0	0.34	0.07	0
Inter NF_3	0.20	0.16	0.13	0.10	0.09	0.075
D_2O	0.22	0.17	0.11	0.26	0.19	0.12
Shielding anisotropy*	2.90 (0.06)	0.49 (0.01)	0	2.90 (0.06)	0.49 (0.01)	0
THF or pD	—	—	—	0.10	0.08	0.064
Total	10.5 (7.7)	2.60 (2.12)	0.24	10.5 (7.7)	2.63 (2.15)	0.26

*Evaluated at 56 MHz, with 8 MHz contribution in parentheses.

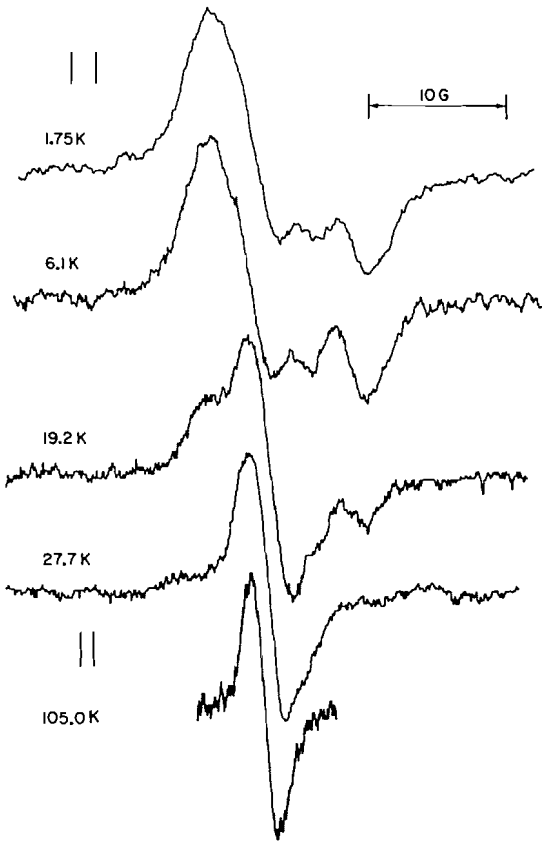

FIG. 8. ^{19}F lineshapes of THF–NF_3–D_2O hydrate at 56 MHz.

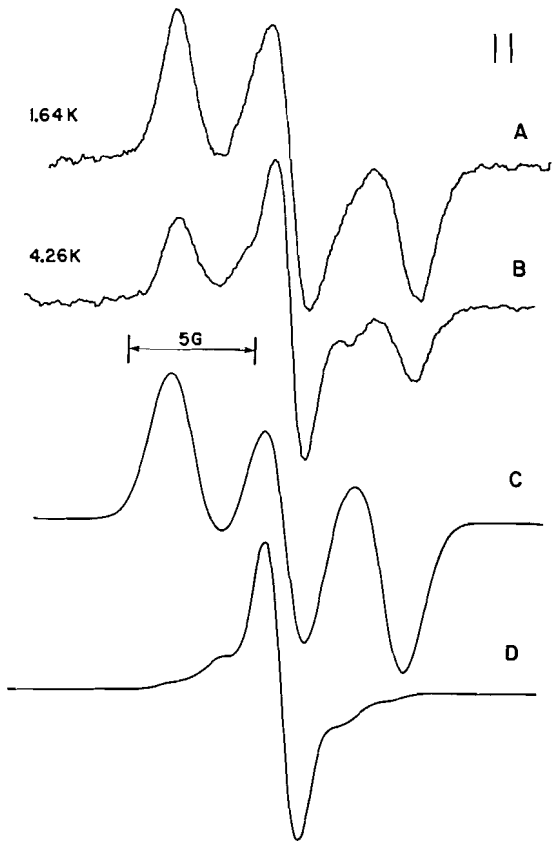

FIG. 9. Low temperature ^{19}F lineshapes of p-dioxane–NF_3–D_2O hydrate at 8 MHz (A, B) and calculated lineshapes for rigid NF_3 molecules (C) and molecules rotating about their three-fold axis (D).

THF, pD, SF_6) for occupancy of the 16-hedra are much larger than for the small molecules (e.g., NF_3). We estimate from the measured permittivities that no more than about 5% of the 16-hedra are occupied by NF_3 under the conditions of preparation of the pD and SF_6 double hydrates.

Figure 10 shows that the reorientation of NF_3 molecules is appreciably slower in the double hydrate of pD than in the double hydrate of SF_6. p-Dioxane is one of the largest molecules (van der Waals diameter 7.2 Å), and SF_6 one of the smallest (5.85 Å), to form a hydrate of structure II. The lattice parameter of pD hydrate (17.28 ± 0.04 Å at 125 K (12)) is consistently larger, on average by 1%, than the comparable values for seven other structure II hydrates (3, 20). It appears that the unit cell of pD hydrate is not uniformly expanded relative to other hydrates but that expansion of the 16-hedral cages to accommodate pD molecules is accompanied by contraction or distortion of other cages so as to make reorientation of NF_3 more difficult.

Reorientation of NF_3 about its symmetry axis is more rapid than reorientation about other axes. In structure I the activation energy for three-fold rotation may be roughly estimated from the temperature $T_{1/2}$ at which the change in second moment due to this rotation has reached its mid-point (21). For $T_{1/2}$ = 7.0

TABLE 3. Dielectric absorption by encaged NF_3

Hydrate	Type	Polyhedra occupied	T (K) of maximum ϵ'' at 10 kHz	E_A (kcal mol^{-1})
NF_3-D_2O	I	14(~85%) 12	22.2 K	0.79
$pD-NF_3-D_2O$	II	12 16	30.0 9.2	1.31 0.37
$SF_6-NF_3-H_2O$	II	12 16	25.4 7.9	1.05 0.29

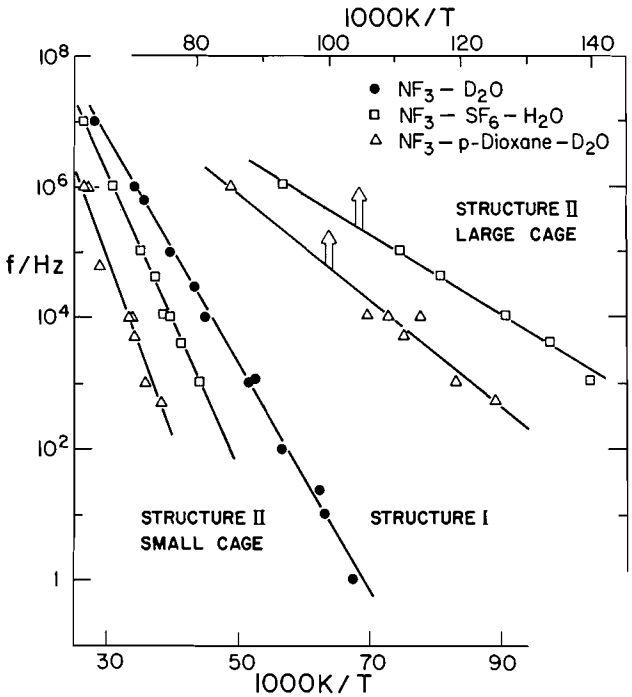

FIG. 10. Arrhenius plots for dielectric absorption by encaged NF_3.

K, one finds an activation energy (~0.23 kcal/mol) about one-third as large as for the dielectrically-active reorientation (Table 3).

Examples of other guest molecules which reorient more rapidly about the symmetry axis than about other axes are known. For the structure II hydrates of CF_3I and cyclobutanone, for example, this is clearly shown by comparison of dielectric relaxation and nmr spin–lattice relaxation times (22). In these cases the moments of inertia are substantially less about the polar symmetry axis than about other axes. For NF_3, however, the moment of inertia is almost twice as great about the symmetry axis as about axes perpendicular to this direction. The N atom of NF_3 appears to be preferentially held to the cage wall by attractive forces to the water molecules. The pyramidal NF_3 molecule best fits the cage contour in this configuration which seems also to be favoured by electrostatic attraction between the NF_3 dipole and the water dipoles.

Cage occupancy

NF_3 hydrate is a structure I hydrate in which the degree of occupancy of the small cages is substantially smaller than of the large cages. The nearly equal ($\theta_S \approx \theta_L$) and nearly complete occupancy of the two kinds of cage by such small molecules as CH_4 and H_2S is not typical of the great majority of the 40 molecules which are known to form structure I hydrates. Although reliable compositions are few (23), the recent studies of Cady (24) show the expected fall of θ_S (measured under hydrate – liquid water – gas equilibrium conditions) with increasing size of the guest molecule. For Xe, SO_2, and CH_3Cl, molecules with maximum van der Waals diameters of 4.60, 5.27, and 5.55 Å, Cady estimates θ_S = 0.65, 0.26, and 0.05, respectively, at 0°C. The low value for Xe has confirmed the results of ^{129}Xe nmr studies (25). There is evidence that CF_4 (diameter 5.35 Å) occupies very few of the small cages (26, 27).

Even though NF_3 hydrate samples in the present study were prepared at higher pressures than correspond to three-phase equilibrium, the consumption of NF_3 (maximum diameter = 5.16 Å) was consistently less than necessary for high cage occupancy. Our results suggest that θ_S is 0.5 to 0.6 for the equilibrium structure I hydrate at 0°C and that this hydrate contains 6.5 to 6.7 water molecules per molecule of NF_3.

1. M. VON STACKELBERG. Naturwissenschaften, **36**, 327 (1949).
2. G. TAMMANN and G. J. R. KRIGE. Z. Anorg. Allgem. Chem. **146**, 179 (1925).
3. D. F. SARGENT and L. D. CALVERT. J. Phys. Chem. **70**, 2689 (1966).
4. S. R. GOUGH. J. Phys. E: Sci. Instrum. **15**, 530 (1982).
5. S. L. MILLER. Nature and occurrence of clathrate hydrates, in natural gases in marine sediments. *Edited by* I. R. Kaplan. Plenum Press, New York. 1974. p. 151.
6. S. L. MILLER, E. I. EGER and C. LUNDGREEN. Nature, **221**, 468 (1969).
7. J. E. BERTIE and S. M. JACOBS. J. Chem. Phys. **77**, 3230 (1982).
8. J. E. BERTIE, F. E. BATES, and D. K. HENDRICKSEN. Can. J. Chem. **53**, 71 (1975).
9. J. E. BERTIE and S. M. JACOBS. Can. J. Chem. **55**, 1777 (1977).
10. S. N. GHOSH, R. TRAMBARULO, and W. GORDY. J. Chem. Phys. **21**, 308 (1953).
11. S. R. GOUGH, R. E. HAWKINS, B. MORRIS, and D. W. DAVIDSON. J. Phys. Chem. **77**, 2969 (1973).
12. S. R. GOUGH, J. A. RIPMEESTER, and D. W. DAVIDSON. Can. J. Chem. **53**, 2215 (1975).
13. A. B. HARRIS, E. HUNT, and H. MEYER. J. Chem. Phys. **18**, 159 (1950).
14. S. K. GARG, J. A. RIPMEESTER, and D. W. DAVIDSON. J. Chem. Phys. **77**, 2847 (1982).
15. M. OTAKE, C. MATSUMUYA, and Y. MORINO. J. Mol. Spectrosc. **28**, 316 (1968).
16. E. R. ANDREW and R. BERSOHN. J. Chem. Phys. **18**, 159 (1950).
17. J. A. RIPMEESTER, S. K. GARG, and D. W. DAVIDSON. J. Magn. Reson. **38**, 537 (1980).
18. S. K. GARG, J. A. RIPMEESTER, and D. W. DAVIDSON. J. Magn. Reson. **35**, 145 (1979).
19. D. W. DAVIDSON and J. A. RIPMEESTER. J. Glaciology, **21**, 33 (1978).
20. J. E. BERTIE and S. M. JACOBS. J. Chem. Phys. **69**, 4105 (1978).
21. D. W. DAVIDSON, S. K. GARG, S. R. GOUGH, R. E. HAWKINS, and J. A. RIPMEESTER. Can. J. Chem. **55**, 3641 (1977).

22. D. W. DAVIDSON and J. A. RIPMEESTER. *In* Inclusion compounds Vol. II. *Edited by* J. L. Atwood, J. E. D. Davies, and D. D. MacNicol. Academic Press, London. 1984.
23. D. W. DAVIDSON. *In* Water: a comprehensive treatise. Vol. 2. *Edited by* F. Franks. Plenum Press, New York. 1973. p. 115.
24. G. H. CADY. J. Phys. Chem. To be published.
25. J. A. RIPMEESTER and D. W. DAVIDSON. J. Mol. Struct. **75**, 67 (1981).
26. S. L. MILLER. Private communication.
27. J. S. TSE and D. W. DAVIDSON. Proc. 4th Can. Permafrost Conf. National Reasearch Council of Canada, 1982. p. 329.

Appendix

Effect of oxygen on low-temperature nuclear magnetic resonance lineshapes

It is well known that the solubility of air in clathrate hydrates is extraordinarily large because of the ability of nitrogen and oxygen to occupy the cages (23). This is particularly true of simple structure II hydrates in which the small cages are otherwise unoccupied. The pronounced effects of oxygen on spin–lattice relaxation times and the effect of relatively large concentrations of oxygen on the proton lineshapes and second moments of THF deuteriohydrate have previously been treated (17). The effects of small concentrations of oxygen are qualitatively different, however, and we consider these here in the context of the ^{19}F lineshape of enclathrated NF_3.

The assumption that encaged molecular oxygen makes a gas-like contribution to the magnetic susceptibility leads (17) to a local magnetic field H_{par} in the direction of the applied field H_0

$$H_{par} = \frac{1.660}{T} \cdot \frac{3\cos^2\theta - 1}{r^3} H_0$$

where r is the distance from the O_2 molecule in Å and θ the angle between r and H_0. The resulting paramagnetic contribution to the second moment of a magnetic nucleus at a distance r from an O_2 molecule in a polycrystalline sample is

$$SM_{par} = \frac{2.204 H_0^2}{T^2 r^6}$$

Since cages are located at discrete distances r_i from one another,

$$SM_{par} = \Sigma n_i S_i(r_i)$$

where $S_i(r_i)$ is the second moment due to an O_2 molecule located in the ith set of cages and n_i is the number of O_2 molecules in that set.

For the structure II THF–NF_3 double hydrate we assume that NF_3 and O_2 occupy only the small cages, the large cages being occupied by THF. The contribution to the ^{19}F second moment at 1.75 K and 56 MHz (H_0 = 14000 G) from an O_2 molecule in one of the six nearest neighbour small cages at r_1 = 6.08 Å is S_1 = 2790 G^2; similarly, O_2 in one of the 12 second neighbour cages at r_2 = 10.53 Å contributes S_2 = 103 G^2.

The lineshape at low temperatures is completely dominated by nearest neighbour oxygen molecules *if these are present in sufficient abundance*, as was the case for THF hydrate prepared under 3 atm of oxygen (17). However, for small amounts of oxygen (say a degree of cage occupancy by oxygen of $\theta \leqslant 0.01$) the resonances of only a few NF_3 molecules will be broadened by the fields of first and second neighbour O_2 molecules to give at very low temperatures broad weak signals which are buried in noise.

To estimate the observable effect of more distant oxygen molecules, we assume these to be continuously distributed and take

$$SM_{par} = \frac{2.204 H_0^2}{T^2} \int_{r_0}^{\infty} \frac{4\pi r^2 \rho \, dr}{r^6}$$

where ρ is the probability of an oxygen molecule occurring in 1 $Å^3$. Since the cubic unit cell of 17.2 Å size contains 16 small cages, $\rho = 0.0031\theta$, where θ is the chance that an oxygen molecule occupies any one cage, and

$$SM_{par} = \frac{0.0286\theta H_0^2}{T^2 r_0^3}$$

Here r_0 is the minimum separation at which O_2 gives an observable contribution to the lineshape. Somewhat arbitrarily, we take r_0 = 12 Å and find for the same H_0 and T as before that

$$SM_{par} = 1060\theta$$

A value of θ may be estimated from

$$\theta = \frac{K(O_2)P(O_2)}{1 + K(O_2)P(O_2) + K(NF_3)P(NF_3)}$$

where the K's are the Langmuir constants and the P's the partial pressures of the gases in equilibrium with the hydrate under the conditions of formation. In the absence of information about $K(NF_3)$ we take $K(NF_3) = K(O_2) = 0.16$ atm^{-1} (17) for the small cages of THF hydrate at 0°C. The minimum hydrate oxygen content anticipated from the 0.7 mol% oxygen impurity found by analysis is $\theta = 0.0043$, whence SM_{par} = 4.6 G^2 at 1.75 K for the hydrate formed under 10 atm of NF_3 at 0°C. Maximum oxygen content of the hydrate corresponds to trapping of oxygen from air during the original formation of THF hydrate and its ineffectual removal by freeze pumping. At most, $P(O_2) = (0.20 + 0.07)$ atm in that case, $\theta = 0.017$ and SM_{par} = 18 G^2.

The excess second moment of some 6 G^2 measured for THF–NF_3 hydrate at 56 MHz and 1.75 K (Fig. 7) and its rapid fall with increasing temperature may reasonably be ascribed to the effect of O_2 present at a concentration of $\theta \approx 0.006$ or 0.08% by weight.

At considerably higher temperatures the effects of first and second neighbour O_2 molecules become observable. Thus at 20 K, S_1 and S_2 are 21 and 0.7 G^2 respectively and for $\theta \approx 0.006$ these can contribute some 0.8 G^2 to the second moment, while now the contribution from more remote O_2 molecules becomes less than 0.05 G^2.

For NF_3 hydrate itself the effect of O_2 on the second moment of the sample studied (Fig. 7) was about one-third as great as for the THF–NF_3 hydrate sample.

The structure of merosinigrin confirmed

JOHN F. RICHARDSON AND M. H. BENN
Chemistry Department, The University, Calgary, Alta., Canada T2N 1N4

Received December 20, 1983

JOHN F. RICHARDSON and M. H. BENN. Can. J. Chem. **62**, 1236 (1984).

An X-ray crystallographic study of merosinigrin confirmed the structure as 1,2-*S*,*O*-(1*R*,2*S*-1-cyano-2-methyl-1,2-ethanediyl)-1-thio-β-D-glucopyranose. The compound crystallizes in the space group *P*1 with a = 6.699(1), b = 9.347(1), c = 5.328(2) Å, α = 103.56(2), β = 109.14(3), γ = 86.71(1)°, and Z = 1. The structure was refined by full-matrix least-squares techniques to a final agreement value of R = 0.031. Merosinigrin provides what appears to be the first example of the anomeric effect in a thiane (1,4-oxathiane) system with cyano as the polar substituent.

JOHN F. RICHARDSON et M. H. BENN. Can. J. Chem. **62**, 1236 (1984).

Une étude cristallographique par diffraction des rayons-X a permis de confirmer que la structure de la mérosinigrine est celle du 1,2-*S*,*O*-(cyano-1 méthyl-2 éthanediyl-1*R*,2*S*) thio-1β-D-glucopyrannose. Le composé cristallise dans le groupe d'espace *P*1 avec a = 6,699(1), b = 9,347(1), c = 5,328(2) Å, α = 103,56(2), β = 109,14(3), γ = 86,71(1)° et Z = 1. On a affiné la structure par les techniques des moindres carrés (matrice complète) jusqu'à une valeur de R = 0,031. Il semble que la mérosinigrine offre le premier exemple d'un effet anomère dans un thiane (oxathiane-1,4) portant un groupe cyano comme substituant polaire.

[Traduit par le journal]

Can. J. Chem. Downloaded from www.nrcresearchpress.com by 210.87.254.105 on 09/06/12
For personal use only.

In a communication published in this journal a few years ago (1), structure **1** was proposed for merosinigrin, a product of the reaction of methanolic potassium methoxide with potassium allylglucosinolate (sinigrin) (2).

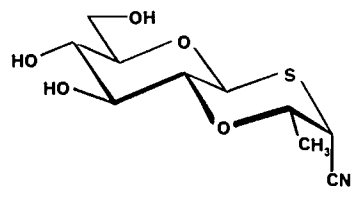

1

This structure was largely deduced from evidence provided by ir, and ^{1}H and ^{13}C nmr spectroscopy. While this rapidly established the gross features of the bicyclic system[1] and the stereochemistry of the glucopyranose ring, the positioning of the methyl and cyano substituents rested upon nOe (nuclear Overhauser effect) measurements. Crucial was the observation that irradiation of the H(2) proton produced a 17% enhancement of the signal due to H(3),[2] while no such effect was observed upon irradiation of the methyl protons (1).

It seemed worthwhile to check the validity of these nmr analyses, so we recently subjected merosinigrin to an X-ray crystallographic analysis. The results of this study, which we now report, fully confirmed **1** as the structure merosinigrin.

Experimental

Merosinigrin was prepared from sinigrin (U.S. Biochemical Corp.) according to the literature procedure (2) and was obtained in ca. 5% yield, mp 192–194°C. The ir spectrum (KBr disc) of this material was superimposable upon that of our previous preparation (1).

[1]Prof. P. Laur of the RWTH-Aachen reached a similar conclusion. (Personal communication from Prof. Laur.)

[2]The numbering which we use here follows the crystallographic notation as set out in Fig. 1; in the numbering system which we employed before (1), these were designated H-2 and H-9 respectively.

Structure determination

Crystal data

$C_{10}H_{15}NO_5S$ fw = 261.30

Space group *P*1, a = 6.6991(1), b = 9.347(1), c = 5.328(2) Å, α = 103.56(2), β = 109.14(3), γ = 86.71(1)°, V = 306.3(5) Å^3, Z = 1, ρ_c = 1.417 g cm^{-3} (21°C; MoKα, λ = 0.71069 Å, graphite monochromator) and μ(MoKα) = 2.74 cm^{-1}.

A crystal of approximate dimensions 0.5 × 0.5 × 0.4 mm^3 was mounted on an Enraf–Nonius CAD4F diffractometer. Intensity data were collected at room temperature using the ω–2θ scan technique with a scan range of 1.5 (0.70 + 0.347 tan θ). The intensity was calculated as $I = [P - 2(B1 + B2)]\,Q$, where P is the central 64 steps of a 96-step scan, $B1$ and $B2$ are the background counts, and Q is the scan rate. The standard deviation of the intensity, $\sigma(I) = [P + 4(B1 + B2)]^{1/2}\,Q$. Three standard reflections measured every 2500 s of X-ray exposure time showed no decomposition of the crystal had occurred during the data acquisition period. A total of 1796 unique reflections were measured for the octants $+h$, $\pm k$, $\pm l$ to a maximum θ = 25°, of which 1401 were considered observed ($F_o > 3\sigma(F_o)$). The data were corrected for background, Lorentz, and polarization effects, but an absorption correction was not considered necessary.

The coordinates of the SC(1)C(2)O(1) fragment were determined by direct methods (MULTAN 78) (3). Structure factor and difference Fourier calculations revealed the positions of the remaining non-hydrogen atoms. The structure was refined by full-matrix least-squares techniques based on F, minimizing the function $\Sigma w(|F_o| - |F_c|)^2$, where w was set to 1.0. All computations were performed using the XRAY 76 system of programs (4) implemented on a Honeywell computer with a Multics operating system. Scattering factors for non-hydrogen atoms were those of Cromer and Mann (5) and those for H were taken from ref. 6. Anomalous dispersion corrections were included for non-hydrogen atoms (7). Hydrogen atoms were readily located from a difference Fourier map and included in the model in these positions with isotropic thermal parameters set to 1.1 times the U_{equiv} of the atom to which they are bonded. Hydrogen parameters were not refined. The model converged for 1401 reflections and 151 variables with the agreement factors $R = \Sigma(||F_o| - |F_c||)/\Sigma|F_o| = 0.031$ and $R_w = [\Sigma w(|F_o| - |F_c|)^2/\Sigma w|F_o|^2]^{1/2} = 0.032$. In the final cycle, the maximum shift/error was 0.01, the goodness of fit value was 5.4, and the largest peak of residual electron density was 0.30 e Å^{-3} and is of no chemical significance. The absolute stereochemistry of the molecule is uniquely determined by the known chirality of the D-glucopyranose ring.

TABLE 2. Final positional parameters and isotropic temperature factors for Ru(OEP)(PPh_3)Br·solvate. Coordinates are multiplied by 10^5 for Ru and Br, and by 10^4 for all other atoms

Atom	x	y	z	B_{iso}	Atom	x	y	z	B_{iso}
Ru	38414(11)	56138(9)	23871(5)	2.29(7)[a]	C(42)	3030(13)	6423(10)	1384(6)	2.6(4)
Br	55644(15)	56015(13)	25449(7)	3.47(10)[a]	C(43)	2969(13)	7260(11)	1131(6)	2.7(4)
P	1479(4)	5645(4)	2176(2)	3.2(3)[a]	C(44)	3151(14)	7880(11)	1498(7)	3.4(4)
N(1)	3856(10)	6535(8)	2924(5)	2.7(3)	C(45)	3316(13)	7447(10)	1956(6)	2.4(4)
N(2)	3818(9)	4669(7)	2916(4)	1.8(3)	C(43A)	2748(15)	7382(12)	596(7)	4.1(5)
N(3)	3191(10)	4686(8)	1861(5)	2.4(3)	C(43B)	1517(18)	7301(14)	220(8)	6.4(6)
N(4)	3219(10)	6548(8)	1856(5)	2.5(3)	C(44A)	3133(14)	8861(11)	1438(6)	3.0(4)
C(11)	3569(12)	7846(9)	2412(6)	1.3(3)	C(44B)	2050(14)	9279(13)	1423(6)	4.0(4)
C(12)	3790(13)	7433(10)	2846(6)	2.2(4)	C(51)	756(13)	6639(11)	1837(6)	3.1(4)
C(13)	4125(13)	7867(11)	3323(6)	2.6(4)	C(52)	495(16)	6730(14)	1336(8)	5.5(5)
C(14)	4388(13)	7237(11)	3671(6)	2.7(4)	C(53)	−133(20)	7549(15)	1097(9)	7.7(7)
C(15)	4245(13)	6404(10)	3432(6)	2.4(4)	C(54)	−340(16)	8121(14)	1383(8)	5.3(5)
C(13A)	4107(15)	8832(12)	3385(7)	3.8(4)	C(55)	50(17)	8021(15)	1869(8)	6.5(6)
C(13B)	2892(16)	9174(13)	3223(7)	5.2(5)	C(56)	610(17)	7312(13)	2102(8)	5.7(5)
C(14A)	4744(15)	7334(12)	4213(7)	3.8(4)	C(61)	681(14)	4704(11)	1809(6)	3.2(4)
C(14B)	3794(17)	7215(14)	4395(8)	6.1(6)	C(62)	818(16)	3959(12)	2065(7)	5.0(5)
C(21)	4438(12)	5583(12)	3654(5)	2.5(3)	C(63)	199(17)	3175(15)	1812(8)	6.6(6)
C(22)	4206(13)	4797(10)	3421(6)	2.6(4)	C(64)	−471(17)	3240(15)	1332(8)	6.2(6)
C(23)	4365(14)	3955(11)	3674(6)	3.2(4)	C(65)	−658(22)	3971(17)	1071(10)	9.7(8)
C(24)	4081(13)	3348(11)	3310(6)	2.8(4)	C(66)	10(20)	4714(16)	1335(9)	8.3(7)
C(25)	3791(14)	3761(11)	2823(7)	3.2(4)	C(71)	942(12)	5621(13)	2650(6)	3.0(4)
C(23A)	4652(15)	3824(12)	4215(7)	4.3(5)	C(72)	−223(15)	5540(14)	2520(7)	4.9(5)
C(23B)	3669(19)	3939(15)	4367(9)	7.1(6)	C(73)	−674(15)	5486(13)	2870(7)	4.6(5)
C(24A)	4054(16)	2357(12)	3359(7)	4.6(5)	C(74)	−11(14)	5585(13)	3334(6)	3.9(4)
C(24B)	2798(16)	1974(14)	3135(8)	5.9(6)	C(75)	1125(15)	5667(15)	3491(7)	5.4(5)
C(31)	3535(14)	3475(10)	2373(6)	2.9(4)	C(76)	1585(14)	5705(13)	3137(7)	4.6(4)
C(32)	3254(13)	3792(10)	1919(6)	2.3(4)	C(101)[b]	1997(47)	1210(37)	84(21)	12.3(18)
C(33)	3037(12)	3362(10)	1468(6)	2.3(4)	C(102)[b]	2411(36)	500(33)	269(16)	10.2(13)
C(34)	2819(13)	3988(10)	1105(6)	2.6(4)	C(103)	1364(36)	86(27)	−63(16)	20.4(17)
C(35)	2976(14)	4814(11)	1360(6)	3.3(4)	C(104)	495(38)	285(33)	54(20)	22.3(19)
C(33A)	3007(14)	2390(11)	1392(7)	3.7(4)	C(105)[b]	2031(45)	−332(36)	−87(21)	8.7(16)
C(33B)	1907(16)	1970(13)	1309(8)	5.4(5)	C(111)	3062(30)	1013(23)	4378(14)	16.2(13)
C(34A)	2516(15)	3899(12)	564(7)	4.4(5)	C(112)	4220(35)	797(28)	4554(15)	20.2(16)
C(34B)	1244(19)	4004(15)	248(9)	7.3(7)	C(113)	4477(32)	−64(32)	4960(19)	19.0(17)
C(41)	2872(12)	5624(12)	1148(5)	2.5(3)					

[a] For atoms with anisotropic temperature factors, $B = 8\pi^2 (U_{11} + U_{22} + U_{33})/3$.
[b] Atom with occupancy less than 1.0. Occupancies: C(101), 0.55; C(102), 0.60; C(105), 0.45.

Can. J. Chem. Downloaded from www.nrcresearchpress.com by 210.87.254.105 on 09/06/12
For personal use only.

priate halogen anaerobically, or the hydrogen halide in the presence of air. The latter process occurs via an acid-promoted O_2 oxidation of Ru(II) according to the reactions shown in eq. [1] (5):

$$[1]\quad Ru^{II} + O_2 \rightleftharpoons Ru^{III} + O_2^- \xrightarrow{H^+} HO_2\cdot \rightarrow \tfrac{1}{2}O_2 + \tfrac{1}{2}H_2O_2$$

The O_2 reaction with the Ru(II) complexes is thermodynamically unfavourable but the superoxide product, that has been detected by esr (5), is stabilized as the protonated form, prior to disproportionation to oxygen and hydrogen peroxide. Phosphine oxide is generated as a by-product in the HX/O_2 reactions, presumably via peroxide oxidation of the phosphine. The net stoichiometry is given in eq. [2], although this was not established quantitatively.

$$[2]\quad 2\,Ru^{II}L_2 + O_2 + 2\,HX \rightarrow 2\,Ru^{III}LX + L + LO + H_2O \qquad (L = PPh_3)$$

The formation of Ru(OEP)(EtOH)(OEt) by reaction of O_2 with Ru(OEP)$(EtOH)_2$ (23) probably utilizes the proton of ethanol for the superoxide generation. Access to the $[Ru(OEP)(PPh_3)_2]^+$ cation is obtained by oxidation of Ru(OEP)$(PPh_3)_2$ using $Et_3O^+PF_6^-$.

Bromine or O_2/HX oxidation of Ru(OEP)$(P^nBu_3)_2$ leads to isolation of the ionic species $[Ru(OEP)(P^nBu_3)_2]^+$ as the Br^- or Br_3^- salt. The formation of the bis(phosphine) cationic species as opposed to the bromo(phosphine) species with PPh_3 could result from the stronger basicity and(or) lower cone-angle of the butylphosphine (24, 25). Chlorine oxidation of Ru(OEP)$(P^nBu_3)_2$, which is not described in the experimental section, almost certainly yields $[Ru(OEP)(P^nBu_3)_2]Cl$ as judged by an initial uv/visible spectrum that is identical to that of the bromide salt; a good sample for microanalysis was not obtained, however, because of quite rapid degradation in the solid state to Ru(OEP)$(P^nBu_3)Cl$. This intramolecular ligand exchange process has been described in some detail for the corresponding bromide system (8).

The Ru(OEP)$(P^nBu_3)X$ complexes (X = Br, Cl) are best prepared by halogen oxidation of Ru(OEP)$(CO)P^nBu_3$, formed *in situ* from Ru(OEP)(CO)EtOH. The noted green intermediate in the Br_2 reaction is likely to be a porphyrin cation radical species, either $Ru^{II}(OEP)^{+\cdot}(CO)Br$, which is known to react with 1 equiv. of P^nBu_3 to give Ru(OEP)$(P^nBu_3)Br$ (8), or more

Can. J. Chem. Downloaded from www.nrcresearchpress.com by 210.87.254.105 on 09/06/12
For personal use only.

TABLE 1. Positional ($\times 10^4$) and equivalent isotropic thermal parameters ($\times 10^3$) for merosinigrin

Atom	x/a	y/b	z/c	$U_{equiv.}$*
S†	5953	9732	8783	35
C(1)	8078(6)	11101(4)	9853(7)	31
C(2)	10244(6)	10417(4)	10798(7)	37
O(1)	10616(4)	9362(2)	8591(5)	34
C(3)	9275(5)	8103(4)	7669(7)	28
C(4)	10006(5)	7016(3)	5541(6)	23
C(5)	8473(5)	5693(3)	4256(7)	27
C(6)	6202(5)	6188(3)	3254(7)	26
O(2)	5689(3)	7194(3)	5444(5)	28
C(7)	6987(5)	8477(3)	6368(7)	25
C(8)	7882(6)	11832(4)	7634(7)	37
N	7717(7)	12347(4)	5864(7)	57
C(9)	12005(7)	11552(5)	11882(10)	59
O(3)	12050(3)	6509(3)	6775(5)	30
O(4)	8875(4)	4758(3)	1996(6)	50
C(10)	4649(5)	4908(4)	2241(7)	34
O(5)	2539(3)	5337(3)	1166(5)	39

*$U_{equiv} = 1/3\Sigma U_{ii}$.
†Coordinates set to define the origin.

TABLE 2. Bond lengths (Å) and angles (deg) for merosinigrin

Bond	Distance	Bond	Distance
S—C(1)	1.823(4)	C(3)—C(7)	1.519(4)
S—C(7)	1.815(3)	C(4)—C(5)	1.529(4)
C(1)—C(2)	1.528(5)	C(4)—O(3)	1.418(3)
C(1)—C(8)	1.466(6)	C(5)—C(6)	1.521(4)
C(8)—N	1.127(6)	C(5)—O(4)	1.406(4)
C(2)—O(1)	1.427(4)	C(6)—O(2)	1.440(4)
C(2)—C(9)	1.504(6)	C(6)—C(10)	1.509(5)
O(1)—C(3)	1.412(4)	C(10)—O(5)	1.414(4)
C(3)—C(4)	1.524(5)	O(2)—C(7)	1.414(4)

Atoms	Angle	Atoms	Angle
C(7)—S—C(1)	94.9(2)	C(3)—C(4)—O(3)	110.2(2)
S—C(1)—C(2)	111.4(2)	C(5)—C(4)—O(3)	108.7(2)
S—C(1)—C(8)	109.7(2)	C(4)—C(5)—O(4)	112.6(3)
C(2)—C(1)—C(8)	111.9(4)	C(4)—C(5)—C(6)	111.0(2)
C(1)—C(8)—N	177.5(3)	C(6)—C(5)—O(4)	106.8(2)
C(1)—C(2)—O(1)	110.6(3)	C(5)—C(6)—O(2)	110.2(2)
C(1)—C(2)—C(9)	112.0(3)	C(5)—C(6)—C(10)	111.8(3)
O(1)—C(2)—C(9)	107.6(4)	O(2)—C(6)—C(10)	107.3(3)
C(2)—O(1)—C(3)	113.5(3)	C(6)—C(10)—O(5)	112.6(3)
O(1)—C(3)—C(4)	107.5(3)	C(6)—O(2)—C(7)	110.5(3)
O(1)—C(3)—C(7)	111.6(3)	O(2)—C(7)—C(3)	110.2(3)
C(7)—C(3)—C(4)	108.9(2)	O(2)—C(7)—S	105.8(2)
C(3)—C(4)—C(5)	109.8(3)	S—C(7)—C(3)	112.1(2)

Discussion

Atomic coordinates and $U_{equivalent}$ values for non-hydrogen atoms are given in Table 1 and bond lengths and angles are summarized in Table 2.[3] A perspective view of the molecule is given in Fig. 1. The crystal structure is found to have extensive intermolecular hydrogen bonding interactions. In particular

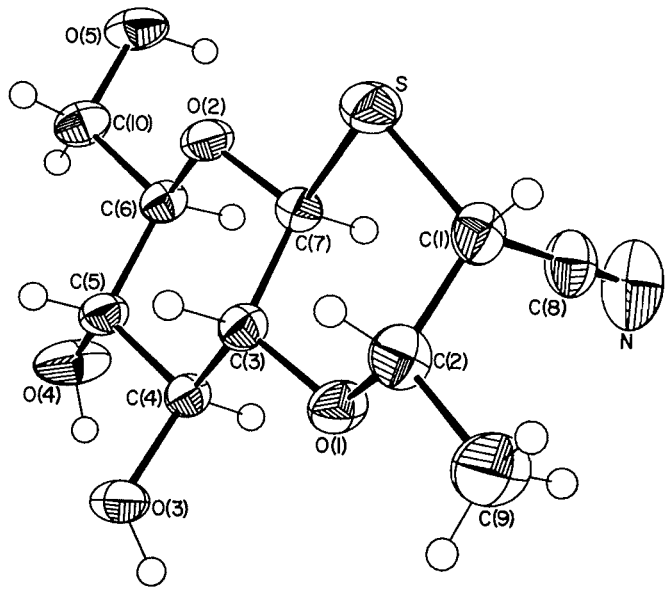

FIG. 1. ORTEP perspective drawing of merosinigrin showing the atomic numbering scheme. Thermal ellipsoids are drawn at the 50% probability level and H atoms are included as spheres of radius 0.1 Å. H atoms are labelled according to the atom to which they are bonded; thus H(1) is bonded to C(1), etc.

three such bonds are found: O(3)—H(3)O . . . O(2) (at 1 + x, y, z), O(3) . . . O(2) = 2.810(4) Å, and H(3)O . . . O(2) = 2.03 Å; O(4)—H(4)O . . . O(5) (at 1 + x, y, z), O(4) . . . O(5) = 2.736(4) Å, and H(4)O . . . O(5) = 1.90 Å; O(5)—H(5)O . . . O(3) (at 1 − x, y, 1 − z), O(5) . . . O(3) = 2.728(4) Å, and H(5)O . . . O(3) = 1..83 Å.

The molecular structure consists of two fused 6-membered rings, each in a chair conformation. The chirality at C(1) and C(2) is *R* and *S*, respectively, relative to the known chirality of the β-D-glucopyranose ring. The cyano function adopts an axial disposition and, as there was evidence for C—H exchange at C(1) without epimerization (1), we conclude that this orientation is thermodynamically preferred and constitutes an example of the anomeric effect. So far as we are aware, merosinigrin provides the first illustration of this effect in a cyanothiane system, although it is well established for a variety of thianes carrying other polar substituents (8).

Acknowledgements

Financial support of this work was provided by NSERC, and we also wish to thank Dr. K. A. Kerr for providing access to the diffractometer.

1. M. BENN. Can. J. Chem. **58**, 1892 (1980).
2. W. SCHNEIDER and F. WREDE. Ber. **47**, 2225 (1914).
3. P. MAIN, S. E. HULL, L. LESSINGER, G. GERMAIN, J-P. DECLERCQ, and M. M. WOOLFSON. MULTAN78. University of York, York, England. 1978.
4. J. M. STEWART (*Editor*). Technical Report TR-446. Computer Science Centre, University of Maryland. 1976.
5. D. T. CROMER and J. B. MANN. Acta Crystallogr. Sect. A, **24**, 321 (1968).
6. R. F. STEWART, E. DAVIDSON, and W. SIMPSON. J. Chem. Phys. **42**, 3175 (1968).
7. International tables for X-ray crystallography. Kynoch Press, Birmingham, England. 1974.
8. A. J. KIRBY. The anomeric effect and related stereoelectronic effects at oxygen. Springer Verlag, New York. 1983. pp. 23–25, and references therein.

[3]A complete set of structure factor listings, anisotropic thermal parameters, and hydrogen atom parameters are available at a nominal charge, upon request from the Depository of Unpublished Data, CISTI, National Research Council of Canada, Ottawa, Ontario, Canada K1A 0S2.

Preparation and characterization of some ruthenium(III) porphyrins, including the crystal structure of bromo(octaethylporphinato)(triphenylphosphine)ruthenium(III)

BRIAN R. JAMES,[1] DAVID DOLPHIN,[1] AND T. W. LEUNG
Department of Chemistry, University of British Columbia, Vancouver, B.C., Canada V6T 1Y6

AND

FREDERICK W. B. EINSTEIN[1] AND ANTHONY C. WILLIS
Department of Chemistry, Simon Fraser University, Burnaby, B.C., Canada V5A 1S6

Received November 28, 1983

BRIAN R. JAMES, DAVID DOLPHIN, T. W. LEUNG, FREDERICK W. B. EINSTEIN, and ANTHONY C. WILLIS. Can. J. Chem. **62**, 1238 (1984).

Some ruthenium(III) complexes Ru(porp)(L)X and [Ru(porp)L_2]X, (porp = dianion of octaethylporphyrin (OEP) or tetraphenylporphyrin (TPP); L = PPh_3, P"Bu_3; X = Br, Cl) have been prepared from the precursor complexes Ru(porp)L_2 or Ru(porp)(CO)L using as oxidant the halogens, or air in the presence of the hydrogen halides. The X = PF_6 salts can be made using $Et_3O^+PF_6^-$ as oxidant. Ruthenium(II) porphyrin π-cation radical intermediates have sometimes been detected. The X-ray crystal structure of Ru(OEP)(PPh_3)Br, the first reported for a ruthenium(III) porphyrin, reveals that metal is displaced 0.049 Å from the plane of the pyrrole N atoms towards the phosphine. The Ru(OEP)(py)Br and [Ru(OEP)(py)CH_3CN]PF_6 complexes have been synthesized from Ru(OEP)(CO)py. The ruthenium(III) complexes are low-spin as shown by magnetic and esr data. Optical and ^1H nmr data, the latter showing large paramagnetic shifts, are also presented.

BRIAN R. JAMES, DAVID DOLPHIN, T. W. LEUNG, FREDERICK W. B. EINSTEIN et ANTHONY C. WILLIS. Can. J. Chem. **62**, 1238 (1984).

On a préparé quelques complexes du ruthénium(III), soit le Ru(porp)(L)X et le [Ru(porp)L_2]X, (porp = le dianion de l'octaéthylporphyrine (OEP) ou de la tétraphénylporphyrine (TPP); L = PPh_3, p"Bu_3; X = Br, Cl), à partir des complexes précurseurs Ru(porp)L_2 ou Ru(porp)(CO)L et en utilisant comme oxydants soit les halogènes soit l'air en présence d'halogénures d'hydrogène. On peut préparer les sels du type X = PF_6 en utilisant le $Et_3O^+PF_6^-$ comme oxydant. On a quelquefois décelé des radicaux cations ruthénium(II) porphyrines comme intermédiaires. La structure cristalline du Ru(OEP)(PPh_3)Br, la première structure rapportée pour un complexe de ruthénium(III) prophyrine, révèle que la phosphine attire le métal qui est déplacé de 0,049 Å par rapport aux atomes d'azote du plan du pyrrole. On a synthétisé les complexes de Ru(OEP)(py)Br et de [Ru(OEP)(py)CH_3CN]PF_6 à partir du Ru(OEP)(CO)py. Le spin des complexes de ruthénium(III) est faible comme le révèlent les données magnétiques et de la rpe. On présente également les données optiques ainsi que de la rmn du ^1H qui montrent de grands déplacements paramagnétiques.

[Traduit par le journal]

Introduction

Interest in the chemistry of ruthenium porphyrin systems continues to grow. Certain ruthenium(II) complexes in solution show reactivity towards small gas molecules such as O_2, CO, and N_2 (1–3), and have been shown to have catalytic activity in oxidation and decarbonylation reactions (4, 5). Ruthenium(III) systems can catalytically utilize iodosylbenzene as an oxidant for saturated and unsaturated hydrocarbons, and isolated oxo-ruthenium(IV) porphyrin cation radical intermediates appear to be good models for the active enzymatic species utilized during cytochrome P450 oxidations (6, 7).

Our continuing developments in the synthetic area of ruthenium porphyrin chemistry (8, 9) are reported in this paper, which describes the synthesis and characterization of some neutral and ionic ruthenium(III) complexes, including the X-ray structure of Ru(OEP)(PPh_3)Br,[2] which has been used as a precursor for oxo-ruthenium(IV) species (7).

Experimental

The materials, methods, and instrumentation used have been largely described in earlier papers (8, 9). The complexes Ru(OEP)(CO)EtOH (8), Ru(TPP)(CO)EtOH (10), Ru(OEP)(CO)py (11), and Ru(porp)L_2: porp = OEP, TPP; L = PPh_3, P"Bu_3 (8, 9), were synthesized according to the literature procedures. No special precautions were taken generally to exclude trace water, although the CH_2Cl_2 was distilled from calcium hydride (8).

Conductivity measurements were performed in CH_3NO_2 solution. Evans' method (12) was used to determine the magnetic susceptibility of Ru(TPP)(PPh_3)Br (in CH_2Cl_2); other susceptibilities were measured on a Faraday balance (13). Diamagnetic corrections for the porphyrin were taken from the literature (14, 15), and otherwise calculated using Pascal's constants (16, 17). The ^1H nmr spectra were recorded on a Varian XL-100 operating in the FT-mode. The esr spectra were recorded in frozen toluene at 77 K on a Varian E-3.

Preparation of complexes

The yields obtained in the synthetic procedures described below, which were carried out under Ar unless noted otherwise, were usually in the 60–80% range. The uv/visible spectra of the isolated complexes are given in Table 1.

Bromo(octaethylporphinato)(triphenylphosphine)ruthenium(III)

To 500 mg of Ru(OEP)(PPh_3)$_2$ (0.43 mmol) dissolved in 75 mL of CH_2Cl_2 was added dropwise 10 mL of Br_2 (0.2 g, 1.2 mmol) in CH_2Cl_2. After stirring the solution for 1 h, the solvent was removed and the residue redissolved in 3 mL CH_2Cl_2 prior to chromatography on silica gel (1 cm × 10 cm, 5% H_2O). A red band was eluted with CH_2Cl_2/MeOH (1:1 v/v) to yield a solid, which was redissolved in 5 mL of CH_2Cl_2 and reprecipitated as purple-red crystals by addition of 30 mL hexane. A non-eluted green band remained on the top of the column.

An alternative synthetic procedure is to use, instead of the Br_2 solu-

[1] Authors to whom correspondence should be addressed: synthetic and spectroscopic aspects (B.R.J., D.D.), crystallography (F.W.B.E.).

[2] Ligand abbreviations used: porp = dianion of octaethylporphyrin (OEP), tetraphenylporphyrin (TPP), or mesoporphyrin IX (MpIX); py = pyridine, im = imidazole.

Can. J. Chem. Downloaded from www.nrcresearchpress.com by 210.87.254.42 on 09/06/12
For personal use only.

Can. J. Chem. Downloaded from www.nrcresearchpress.com by 210.87.254.42 on 09/06/12
For personal use only.

TABLE 1. Optical spectral data for some ruthenium(III) porphyrin complexes in CH_2Cl_2 solution

Complex	λ_{max} (nm) (log ϵ)
Ru(OEP)(PPh_3)Br	510(4.05), 405(4.86), 360sh(4.50)
Ru(OEP)(PPh_3)Cl	510(3.97), 403(4.90)
$[Ru(OEP)(PPh_3)_2]^+PF_6^-$	520br(4.15), 393(4.98)
$[Ru(OEP)(PPh_3)_2]^+PF_6^-$ [a]	520(4.08), 410(4.80), 370sh(4.60)
Ru(TPP)(PPh_3)Br	525(4.03), 413(5.10), 345(4.47)
$[Ru(OEP)(P''Bu_3)_2]^+Br^-$ [b]	515(4.00), 412(4.69), 363(4.76)
Ru(OEP)($P''Bu_3$)Br [b]	510(4.00), 408(4.92), 360(4.67)
Ru(OEP)($P''Bu_3$)Cl	510(3.97), 403(4.90)
Ru(OEP)(py)Br	535sh(4.10), 506(4.15), 397(4.95)
$[Ru(OEP)(py)CH_3CN]^+PF_6^-$	525br(4.12), 395(4.86)

[a] Spectrum obtained in the presence of excess PPh_3.
[b] The data agree well with our earlier work (8).

tion, a saturated CH_2Cl_2 solution of HBr and carry out the reaction in air; the work-up procedure is unchanged. Electron spin resonance $g_\perp$ = 2.28, $g_\parallel$ = 1.98; μ = 2.0 BM; nmr[3] δ_{TMS} ($CDCl_3$): +2.7 (3H, *p*-H), +0.5 (24H, CH_3), −8.8 (8H, CH_2), −9.9 (4H, meso-H), −14.6 (12H, *o*- and *m*-H), −18.5 (8H, CH_2); ms *m/e*: 896 (100), Ru(OEP)PPh_3^+; 715, 713 (20), Ru(OEP)Br^+; 634 (100), Ru(OEP)$^+$. *Anal.* calcd. for $C_{54}H_{59}N_4BrPRu$: C 66.45, H 6.09, N 5.74, P 3.17; found: C 65.81, H 6.49, N 5.49, P 2.98.

Crystals for X-ray work were obtained by slowly evaporating a 1:1 CH_2Cl_2/hexane solution over a few days, and contained a solvent hexane molecule.

Chloro(octaethylporphinato)(triphenylphosphine)ruthenium(III)

The complex was prepared by the procedure described above for the bromo analogue except that saturated solutions of Cl_2 or HCl were used; esr $g_\perp$ = 2.30, $g_\parallel$ = 1.98; μ = 2.1 BM; nmr[3] δ_{TMS} ($CDCl_3$): +2.4 (3H, *p*-H), +0.5 (24H, CH_3), −8.9 (8H, CH_2), −9.9 (4H, meso-H), −14.6 (12H, *o*- and *m*-H), −18.3 (8H, CH_2); ms *m/e*: 896 (100), Ru(OEP)PPh_3^+; 634 (90) Ru(OEP)$^+$; 448 (80), Ru(OEP)-$(PPh_3)^{2+}$. *Anal.* calcd. for $C_{54}H_{59}N_4ClPRu$: C 69.62, H 6.38, N 6.01, P 3.32; found: C 69.40, H 6.91, N 5.51, P 3.17.

(Octaethylporphinato)bis(triphenylphosphine)ruthenium(III) hexafluorophosphate

To 300 mg of Ru(OEP)(PPh_3)$_2$ (0.26 mmol) dissolved in 50 mL of CH_2Cl_2 was added 0.1 g $Et_3O^+PF_6^-$ (0.40 mmol) together with a few drops of H_2O. After stirring for 30 min, the solution was evaporated and the resulting residue redissolved in 10 mL CH_2Cl_2. Addition of 50 mL of hexane allowed for crystallization of the product. Infrared $\nu(PF_6)$: 560, 840 cm^{-1}; Λ = 135 mho cm^2 mol^{-1}. *Anal.* calcd. for $C_{74}H_{72}N_4P_3F_6Ru$: C 66.35, H 5.72, N 4.30; found: C 65.53, H 5.76, N 4.20.

Bromo(tetraphenylporphinato)(triphenylphosphine)ruthenium(III)

This complex was prepared from Ru(TPP)(PPh_3)$_2$ by the Br_2 or HBr procedure described above for the OEP analogue; μ = 1.9 BM; ms *m/e*: 1056 (1), Ru(TPP)(PPh_3)Br^+; 976 (100), Ru(TPP)(PPh_3)$^+$; 795, 793 (15), Ru(TPP)Br^+; 714(60), Ru(TPP)$^+$. *Anal.* calcd. for $C_{62}H_{43}N_4PBrRu\cdot\frac{1}{2}CH_2Cl_2$: C 68.34, H 4.04, N 5.10; found: C 68.21, H 3.96, N 5.25.

*(Octaethylporphinato)bis(tri-*n*-butylphosphine)ruthenium(III) tribromide (or bromide)*

To 500 mg of Ru(OEP)($P''Bu_3$)$_2$ (0.48 mmol) dissolved in 75 mL hexane was added dropwise 5 mL of Br_2 (0.2 g, 1.2 mmol) in hexane. The microcrystalline product that separated was filtered, washed with pentane, and dried *in vacuo*. Electron spin resonance $g_\perp$ = 2.34, $g_\parallel$ = 1.98; Λ = 110 mho cm^2 mol^{-1}. *Anal.* calcd. for $C_{60}H_{98}N_4P_2Br_3Ru$: C 56.38, H 7.72, N 4.38, Br 18.77; found: C 55.86, H 7.72, N 4.46, Br 18.7. A saturated solution of HBr in hexane could be used aerobically in lieu of the Br_2 solution, in which case the complex was isolated as the bromide salt, [Ru(OEP)($P''Bu_3$)$_2$]Br, that has been prepared previously from the bis(phosphine) precursor using CH_2Cl_2 solutions of Br_2 (8).

*Bromo(octaethylporphinato)(tri-*n*-butylphosphine)ruthenium(III)*

This complex may be synthesized via Br_2 oxidation of the isolated Ru(OEP)(CO)$P''Bu_3$ complex as described earlier (8), or via the same precursor formed *in situ* as described here.

To 500 mg of Ru(OEP)(CO)EtOH (0.71 mmol) dissolved in 30 mL CH_2Cl_2 was added dropwise a solution of $P''Bu_3$ (0.5 mL phosphine in 20 mL CH_2Cl_2), until the Soret absorption indicated complete formation of Ru(OEP)(CO)$P''Bu_3$ (the 393-nm band of the ethanol precursor is replaced by one at 408 nm). A solution of Br_2 (0.1 g, 0.6 mmol in 10 mL CH_2Cl_2) was then added dropwise. The reaction solution turned green initially but soon became red. After 15 min of stirring, the solvent was removed to give a residue that was redissolved in 5 mL of CH_2Cl_2; addition of 25 mL hexane deposited crystals of the product in quantitative yield. Electron spin resonance $g_\perp$ = 2.31, $g_\parallel$ = 1.98; μ = 2.3 BM; Λ = 4.0 mho cm^2 mol^{-1}; ms *m/e*: 916 (20), Ru(OEP)($P''Bu_3$)Br^+; 836 (100), Ru(OEP)($P''Bu_3$)$^+$; 715, 713 (5), Ru(OEP)Br^+; 634 (30), Ru(OEP)$^+$. *Anal.* calcd. for $C_{48}H_{71}N_4BrPRu$: C 62.93, H 7.81, N 6.12; found: C 62.33, H 7.91, N 6.30.

*Chloro(octaethylporphinato)(tri-*n*-butylphosphine)ruthenium(III)*

This complex was prepared in quantitative yield by the *in situ* method described above for the bromo analogue, but using for the oxidation a saturated solution of Cl_2 in CH_2Cl_2. Mass spectra *m/e*: 870 (10), Ru(OEP)($P''Bu_3$)Cl^+; 836 (100), Ru(OEP)($P''Bu_3$)$^+$; 634 (20), Ru(OEP)$^+$. *Anal.* calcd. for $C_{48}H_{71}N_4ClPRu\cdot\frac{1}{2}CH_2Cl_2$: C 63.73, H 7.95, N 6.13; found: C 64.46, H 8.09, N 5.84.

Bromo(octaethylporphinato)(pyridine)ruthenium(III)

A solution of the Ru(OEP)(CO)py complex (500 mg, 0.67 mmol in 10 mL CH_3CN and 200 mL toluene) was irradiated in a Hanovia apparatus for 4 h (a medium pressure 450-W mercury vapour bulb); the optical spectrum then showed complete absence of the carbonyl-pyridine species (18) and new absorption maxima at 530, 497, and 406 nm attributable to Ru(OEP)(py)(CH_3CN) (11). Solvent was removed under vacuum, and the resulting solid was dissolved in 25 mL CH_3CN and oxidized by adding dropwise 5 mL of CH_3CN containing 0.1 g Br_2 (0.6 mmol). After stirring for 30 min, the solution was evaporated to dryness and the resulting solid redissolved in 5 mL of CH_2Cl_2 prior to addition of 30 mL of hexane. The product crystallized out. Mass spectra *m/e*: 715, 713 (20), Ru(OEP)Br^+; 634 (100), Ru(OEP)$^+$. *Anal.* calcd. for $C_{41}H_{49}N_5BrRu$: C 62.11, H 6.23, N 8.83; found: C 61.68, H 5.94, N 8.60.

Acetonitrile(octaethylporphinato)(pyridine)ruthenium(III) hexafluorophosphate

To 200 mg of Ru(OEP)(py)Br (0.25 mmol) dissolved in 30 mL of CH_3CN was added 0.1 g $AgPF_6$ (0.40 mmol) as a suspension in 5 mL CH_3CN. After stirring for 15 min, the solution was evaporated to dryness, and 3 mL of CH_2Cl_2 was then added to the residue. After filtering off the AgBr, 15 mL hexane was added to the filtrate in order to effect crystallization of the product. μ = 2.3 BM; Λ = 120 mho cm^2 mol^{-1}; ir: $\nu(PF_6)$: 560, 840 cm^{-1}; ν(CN) not observed. *Anal.* calcd. for $C_{43}H_{52}N_2F_6PRu$: C 57.45, H 5.83, N 9.35; found: C 57.13, H 5.72, N 8.69.

X-Ray crystallographic analysis

Crystals of Ru(OEP)(PPh_3)Br·solvate were obtained as very thin needles. A section 0.104 × 0.678 × 0.054 mm was cut from one of the thickest needles and mounted on a glass fibre with its longest dimension approximately parallel to the fibre axis. X-ray photographs (CuKα radiation) revealed Laue $2/m$ symmetry and systematic extinctions $0k0$: $k = 2n + 1$, $h0l$: $l = 2n + 1$, uniquely determining the space group as $P2_1/c$.

The crystal was transferred to a Picker FACS-I four-circle auto-

[3] The paramagnetic convention is used; signals downfield from Me_4Si are referred to as negative and those upfield as positive.

Can. J. Chem. Downloaded from www.nrcresearchpress.com by 210.87.254.42 on 09/06/12
For personal use only.

mated diffractometer employing graphite-crystal monochromatized MoKα radiation. Accurate cell dimensions were obtained by a least-squares analysis of the setting angles of 18 reflections ($16.5° < 2\theta < 21.9°$), widely separated in reciprocal space, which were accurately centered on the detector.

Crystal data:

$C_{54}H_{59}N_4BrPRu(C_6H_{14})$ fw = 1062.26

Monoclinic, $P2_1/c$, $a = 13.037(3)$, $b = 15.372(3)$, $c = 29.577(7)$ Å, $\beta = 115.19(2)°$, $V = 5363.7$ Å^3, $Z = 4$, $D_o = 1.32$, $D_c = 1.315$ g cm^{-3}, μ(MoKα) = 10.9 cm^{-1}, λ(MoKα$_1$) = 0.7093 Å.

The intensities of unique set of data (*hkl* and $\bar{h}kl$) were collected for $3° \leq 2\theta \leq 40°$ using a $\theta-2\theta$ scan running at 2° min^{-1}. The scan width was 1.6° plus a correction for $\alpha_1-\alpha_2$ dispersion. Stationary-crystal stationary-detector background counts were taken for 0.25 × scan time on each side of every scan to determine the intensity and the associated standard deviation.[4] A total of 5042 reflections were measured of which 2536, with $I > 2.3\ \sigma(I)$, were regarded as observed and used in structure solution and refinement. Two standards were measured after every 80 reflections. They showed a 6% decrease in intensity over the length of data collection, so data were scaled accordingly. ψ-scans of two axial reflections showed only small variations in intensity as the crystal was rotated. This had been anticipated as the crystal cross-section was small and μ was also small. Consequently, no absorption correction was applied to the data.

The structure was solved by heavy-atom methods and refined by block-diagonal least-squares. The coordinates of the Ru and Br atoms were determined from a Patterson synthesis. Successive refinement and difference Fourier syntheses led to the location of all atoms of the OEP and PPh_3 groups. Those H atoms which could be located geometrically were included in subsequent refinement at their calculated positions, but their parameters were not refined.[5] Refinement with anisotropic temperature factors for Ru, Br, and P (others isotropic) converged to $R = 0.10$.[6] A difference map at this stage revealed eight peaks which were not attached to the Ru(OEP)(PPh_3)Br molecule. These were assigned as C atoms and included in refinement with variable occupancies: some gave reduced occupancies, others retained values of about 1.0. The occupancies of these atoms were then fixed at appropriate values for subsequent refinement. Their identities could not be unambiguously determined but, taking into account which solvents were used in the preparation and recrystallization, reasonable assignments can be made. Five of them, along with their inversion images, constitute a ten-numbered "molecule" with terminal members having occupancies of about 0.5. We believe that this arises from disordered packing of *n*-hexane molecules in this region of the unit cell which, on average, gives an inversion centre at (0,0,0). The remaining unidentified atoms are connected to their symmetry-related images to produce a six-membered chain which, once again, is thought to be *n*-hexane, though some of the bond lengths and angles do not fit this model very well. Poor packing of solvate molecules within the unit cells of porphyrins is not unusual (19, 20). All features in a difference map were <0.9(1) eÅ^{-3}, the five largest being near the Ru and Br atoms. There was little evidence that introducing anisotropic temperature factors for the C and N atoms would substantially improve the agreement, so refinement was terminated at this stage. Final $R = 0.076$, $R_w = 0.077$ for 292 variables. Shift-to-error ratios in the final cycle of least-squares ≤ 0.04.

Refinement was by block-diagonal least-squares, minimizing the function $\Sigma w(|F_o| - |F_c|)^2$, where $w = [(\sigma(F))^2 + 0.0004\ F^2]^{-1}$. Neutral-atom scattering factors with anomalous dispersion corrections (21) were used throughout. Computer programs (22) were run on a PDP-8e computer.

Final positional and thermal parameters are listed in Table 2. Anisotropic thermal parameters for Ru, Br and P, H atom coordinates, selected least-squares planes, and structure factor listings have been deposited.[7] Figure 1 shows the numbering scheme of the porphyrin atoms and the averaged geometry assuming that the halves of all of the pyrrole rings are equivalent.[8]

Bond lengths and angles are given in Table 3. Figure 2 shows the molecular structure of the complex, and Fig. 3 shows a stereoscopic packing drawing.

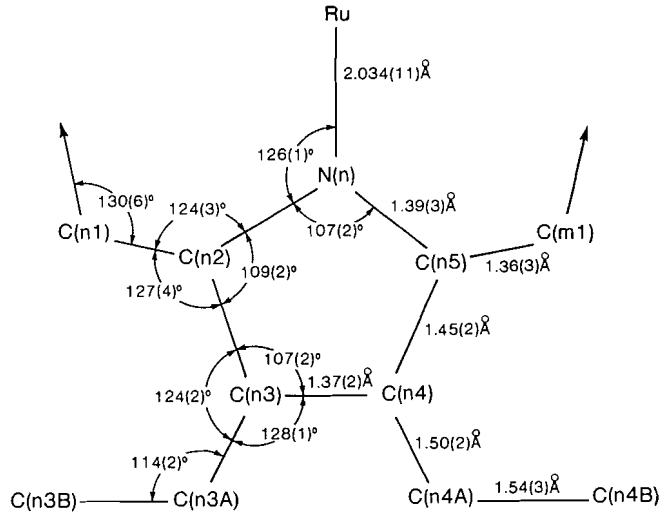

FIG. 1. Atom-labelling scheme for the pyrrole rings and averaged geometry.

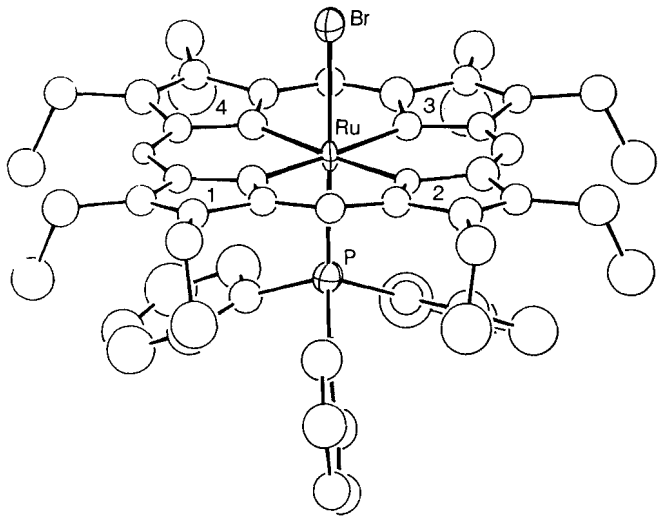

FIG. 2. Molecular structure of Ru(OEP)(PPh_3)Br showing numbering of pyrrole rings. Thermal ellipsoids enclose 50% probability levels. Hydrogen atoms have been deleted for clarity.

Results and discussion

Syntheses and characterization of the complexes

The ruthenium(III) complexes Ru(porp)(PPh_3)X (porp = OEP, TPP; X = Br, Cl) are readily synthesized by oxidation of the ruthenium(II) precursors Ru(porp)(PPh_3)$_2$ using the appro-

[4] $I = S - 2(B_1 + B_2)$; $\sigma(I) = (S + 4(B_1 + B_2))^{1/2}$ where S = count during scan, B = background count.

[5] H isotropic temperature factors were derived from those of the C atoms to which they were attached.

[6] $R = \Sigma||F_o| - |F_c||/\Sigma|F_o|$; $R_w = (\Sigma_w(|F_o| - |F_c|)^2/\Sigma_w|F_o|^2)^{1/2}$.

[7] Complete set of data can be obtained, at a nominal charge, from the Depository of Unpublished Data, CISTI, National Research Council of Canada, Ottawa, Ontario, Canada K1A 0S2.

[8] The esd's are derived from the formula $S = (\Sigma_m(X_m - \bar{X})^2/(m - 1))^{1/2}$.

TABLE 3. Interatomic distances (Å) and angles (°)

a. Coordination sphere

Bond	Length (Å)	Bond	Angle (°)
Ru—Br	2.552(2)	Br—Ru—P	175.9(1)
Ru—P	2.412(5)	Br—Ru—N(1)	88.8(4)
Ru—N(1)	2.025(13)	Br—Ru—N(2)	89.4(3)
Ru—N(2)	2.040(11)	Br—Ru—N(3)	88.4(3)
Ru—N(3)	2.025(12)	Br—Ru—N(4)	87.9(3)
Ru—N(4)	2.047(13)	P—Ru—N(1)	93.6(4)
		P—Ru—N(2)	93.9(3)
		P—Ru—N(3)	89.3(4)
		P—Ru—N(4)	88.8(4)
		N(1)—Ru—N(2)	89.7(5)
		N(1)—Ru—N(3)	177.1(5)
		N(1)—Ru—N(4)	91.0(5)
		N(2)—Ru—N(3)	89.8(5)
		N(2)—Ru—N(4)	177.2(5)
		N(3)—Ru—N(4)	89.3(5)

b. Phosphine

Bond	Length (Å)	Bond	Length (Å)	Bond	Length (Å)
P—C(51)	1.85(2)	P—C(61)	1.84(2)	P—C(71)	1.81(2)
C(51)—C(52)	1.38(3)	C(61)—C(62)	1.34(3)	C(71)—C(72)	1.41(2)
C(52)—C(53)	1.51(3)	C(62)—C(63)	1.47(3)	C(72)—C(73)	1.39(2)
C(53)—C(54)	1.33(3)	C(63)—C(64)	1.32(3)	C(73)—C(74)	1.28(2)
C(54)—C(55)	1.31(3)	C(64)—C(65)	1.33(3)	C(74)—C(75)	1.36(2)
C(55)—C(56)	1.33(3)	C(65)—C(66)	1.45(4)	C(75)—C(76)	1.41(2)
C(56)—C(51)	1.36(3)	C(66)—C(61)	1.30(3)	C(76)—C(71)	1.33(2)
Bond	**Angle (°)**	**Bond**	**Angle (°)**	**Bond**	**Angle (°)**
Ru—P—C(51)	113.7(5)	Ru—P—C(61)	114.5(6)	Ru—P—C(71)	122.1(5)
C(51)—P—C(61)	107.4(8)	C(51)—P—C(71)	99.3(8)	C(61)—P—C(71)	97.6(8)
P—C(51)—C(52)	120.2(14)	P—C(61)—C(62)	115.5(14)	P—C(71)—C(72)	121.3(12)
P—C(51)—C(56)	118.6(14)	P—C(61)—C(66)	125.4(15)	P—C(71)—C(76)	124.3(12)
C(56)—C(51)—C(52)	121(2)	C(66)—C(61)—C(62)	119(2)	C(76)—C(71)—C(72)	114(1)
C(51)—C(52)—C(53)	115(2)	C(61)—C(62)—C(63)	120(2)	C(71)—C(72)—C(73)	123(2)
C(52)—C(53)—C(54)	118(2)	C(62)—C(63)—C(64)	117(2)	C(72)—C(73)—C(74)	119(2)
C(53)—C(54)—C(55)	122(2)	C(63)—C(64)—C(65)	124(2)	C(73)—C(74)—C(75)	121(2)
C(54)—C(55)—C(56)	122(2)	C(64)—C(65)—C(66)	116(2)	C(74)—C(75)—C(76)	120(2)
C(55)—C(56)—C(51)	120(2)	C(65)—C(66)—C(61)	123(2)	C(75)—C(76)—C(71)	122(2)

c. Porphyrin

	Lengths (Å) for different *n*, *m*, *p*			
Bond	1,2,4	2,3,1	3,4,2	4,1,3
C(n1)—C(n2)	1.35(2)	1.36(2)	1.33(2)	1.38(2)
C(n5)—C(m1)	1.39(2)	1.30(2)	1.37(2)	1.39(2)
N(n)—C(n2)	1.40(2)	1.37(2)	1.38(2)	1.32(2)
N(n)—C(n5)	1.38(2)	1.42(2)	1.40(2)	1.41(2)
C(n2)—C(n3)	1.45(2)	1.47(2)	1.41(2)	1.47(2)
C(n5)—C(n4)	1.44(2)	1.47(2)	1.45(2)	1.44(2)
C(n3)—C(n4)	1.35(2)	1.35(2)	1.38(2)	1.39(2)
C(n3)—C(n3A)	1.50(2)	1.49(3)	1.51(2)	1.49(2)
C(n4)—C(n4A)	1.48(2)	1.53(3)	1.48(2)	1.52(2)
C(n3A)—C(n3B)	1.54(3)	1.54(3)	1.49(3)	1.52(3)
C(n4A)—C(n4B)	1.56(3)	1.59(3)	1.53(3)	1.53(2)
	Angles (°) for different *n*, *m*, *p*			
Bond	**1,2,4**	**2,3,1**	**3,4,2**	**4,1,3**
C(p5)—C(n1)—C(n2)	125.6(14)	127.4(14)	138.7(16)	127.6(14)
C(n1)—C(n2)—N(n)	126.6(14)	125.4(14)	117.9(14)	125.6(15)
C(m1)—C(n5)—N(n)	123.7(14)	120.2(15)	123.1(15)	127.0(14)

Can. J. Chem. Downloaded from www.nrcresearchpress.com by 210.87.254.42 on 09/06/12
For personal use only.

TABLE 3. (*Concluded*)

C(n1)—C(n2)—C(n3)	124.3(14)	125.0(15)	130.3(15)	123.7(14)
C(m1)—C(n5)—C(n4)	128.0(15)	134.7(16)	126.4(15)	126.1(14)
N(n)—C(n2)—C(n3)	108.8(13)	109.6(13)	111.8(14)	110.7(14)
N(n)—C(n5)—C(n4)	108.4(13)	105.1(14)	110.4(14)	106.9(13)
C(n2)—N(n)—C(n5)	107.0(13)	108.6(12)	104.2(12)	109.0(13)
C(n2)—N(n)—Ru	125.7(10)	126.3(10)	128.5(10)	127.1(11)
C(n5)—N(n)—Ru	127.2(10)	124.9(10)	127.1(10)	123.8(10)
C(n2)—C(n3)—C(n4)	106.6(14)	105.7(14)	107.7(14)	104.4(14)
C(n5)—C(n4)—C(n3)	109.2(14)	110.6(15)	105.7(14)	109.1(15)
C(n2)—C(n3)—C(n3A)	124.2(15)	125.7(15)	126.0(14)	126.3(15)
C(n5)—C(n4)—C(n4A)	122.7(15)	121.1(15)	123.9(15)	123.8(15)
C(n4)—C(n3)—C(n3A)	129.2(15)	128.3(16)	126.3(15)	129.4(15)
C(n3)—C(n4)—C(n4A)	128.2(15)	128.3(16)	130.5(15)	127.1(15)
C(n3)—C(n3A)—C(n3B)	111.6(15)	116.0(16)	114.5(15)	115.7(15)
C(n4)—C(n4A)—C(n4B)	115.8(15)	112.9(15)	111.8(15)	112.8(14)

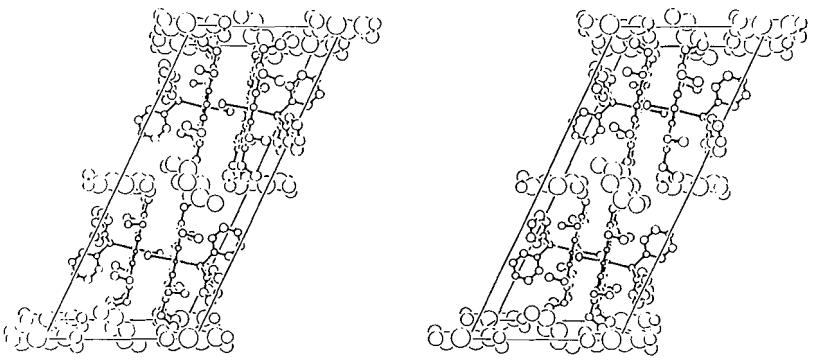

FIG. 3. Stereoscopic view of the unit cell showing crystal packing. The origin is located at the top left-hand corner with *a* across, *b* out of the page, and *c* obliquely down.

Can. J. Chem. Downloaded from www.nrcresearchpress.com by 210.87.254.42 on 09/06/12
For personal use only.

likely $[Ru^{II}(OEP)^{+\bullet}(CO)P^nBu_3]^+$. Loss of carbon monoxide from such Ru(II) cation radical species appears to trigger the intramolecular electron transfer (IMET) to generate Ru(III) (8, 26); subsequent coordination of phosphine or bromide would generate the bromo(phosphine) product. The O_2 oxidation of $Ru(MpIX)Im_2$ to give $[Ru(MpIX)Im_2]^+$ has been shown earlier to occur via an outer-sphere process, and initial electron transfer to the dioxygen from the porphyrin periphery to give a Ru(II) porphyrin cation radical species was suggested (27); the excess imidazole present in the solution presumably acts as a proton source (see above).

Br_2 oxidation of Ru(OEP)(CO)py does not generate cation radical species (26), and thus formation of Ru(OEP)(py)Br requires a photochemical decarbonylation procedure prior to the oxidation step. The bromide can be removed using silver salts in CH_3CN to generate the corresponding cationic complex containing the coordinated nitrile.

Attempts to oxidize $Ru(TPP)(P^nBu_3)_2$ with X_2 or O_2/HX resulted in the formation of impure green compounds: the colour, coupled with a quite sharp esr signal at $g = 2.00$, strongly suggests the present of cation radical species containing the $[Ru^{II}(TPP)^{+\bullet}]$ moiety (8). The reason for the contrasting behaviour of the $Ru(TPP)(PPh_3)_2$ complex, which yields Ru(TPP)(PPh$_3$)X (see above), is not immediately clear but, if the oxidations proceed via an outer-sphere mechanism, then plausible intermediates are $[Ru^{II}(TPP)^{+\bullet}(PR_3)_2]^+X^-$ species, and whether subsequent IMET occurs must depend at least partly on the nature of the axial ligands. A more basic phosphine would be expected to stabilize Ru(III) relative to Ru(II) (8, 28) and thus a key feature may be the entrance of X^- into the coordination sphere of the metal with displacement of a phosphine; this would be easier with the PPh_3 system, on both electronic and steric grounds. The successful generation of $[Ru(OEP)(P^nBu_3)_2]^+$ from $Ru(OEP)(P^nBu_3)_2$ may result from the stronger basicity of OEP compared to TPP (29). The Br_2 oxidation of $Ru(TPP)(CO)P^nBu_3$, formed *in situ* from the ethanol adduct, gave an unidentified green compound, that again suggests that the $[Ru^{II}(porp)^{+\bullet} \rightarrow Ru^{III}(porp)]$ process occurs less readily with TPP systems.

The six-coordinate ruthenium(III) products have magnetic susceptibilities in the range of 1.9–2.3 BM, confirming the expected one unpaired electron in low-spin d^5 systems. The frozen solution esr spectra (Fig. 4) show a broad signal centred at about $g = 2.3$ and a weaker but sharper signal at $g = 1.98$; these are typical of low-spin d^5 Ru(III) complexes in tetragonally-distorted octahedral structures (5, 30) and are assigned to $g_\perp$ and $g_\parallel$, respectively. The ^1H nmr signals noted in the experimental section for the Ru(OEP)(PPh$_3$)X complexes (X = Br, Cl) were generally broad and coupling constants were not obtained; the assignments are based on the relative intensities and those reported for the porphyrin ring with the paramagnetic $[Ru(OEP)]_2$ complex (31). The two different axial ligands induce an anisochrony of the methylene protons within OEP, and the large chemical shift difference between the diastereotopic protons (~10 ppm) originates from differential π-spin density transfer from the porphyrin system to each of the protons (31). The porphyrin meso protons appear as a relatively sharp singlet, little shifted from that in six-coordinate diamagnetic $Ru^{II}(OEP)$ complexes (9, 32). Proton nmr signals for the other Ru(III) complexes were too broad and weak to

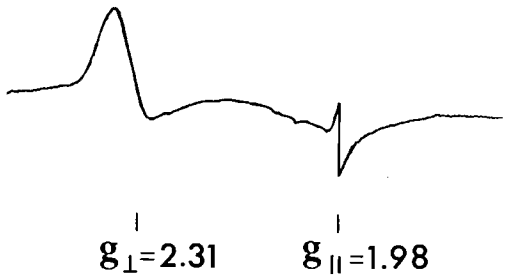

FIG. 4. Frozen solution esr spectrum of Ru(OEP)(P"Bu_3)Br in toluene at 77 K.

analyze satisfactorily.

The optical spectra (Table 1) show in each case a single absorption maximum in the 500–550 nm region, and two more intense maxima of comparable magnitude in the 360–415 nm Soret region. The log ϵ values of the Soret bands are in the 4.5–5.0 range, and are at least 0.3 lower than that of the major Soret band of six-coordinate ruthenium(II) porphyrin complexes; this coupled with the two-peak maxima of the latter makes it simple to distinguish qualitatively the presence of the two oxidation states. Figure 5 of ref. 8 shows spectra of the $[Ru(OEP)(P"Bu_3)_2]^+$ and $Ru(OEP)(P"Bu_3)_2$ species and these are representative of all the six-coordinate complexes. The spectrum of the $[Ru(OEP)(PPh_3)_2]^+$ cation changes on the addition of excess phosphine, implying dissociation of a phosphine ligand (26); that recorded in the presence of excess phosphine is attributed to the six-coordinate complex, and agrees with one measured earlier on a species formed *in situ* by adding excess PPh_3 to $[Ru^{II}(OEP)^{+\bullet}(CO)]^+$ (8).

Structure description of Ru(OEP)(PPh_3)Br·solvate

This is the first time that the structure of a Ru(III) porphyrin has been reported.[9] The Ru atom is approximately octahedrally coordinated by the four pyrrole N atoms of the porphyrin, the P atom of the PPh_3 group, and the Br atom, and is displaced 0.049(1) Å from the plane of the pyrrole N atoms in the direction of the P atom.

The Ru—N distances range from 2.025 (12) to 2.047 (13) Å. In general, Ru(III) is expected to show shorter bond lengths than Ru(II) (34) on account of contraction of electron density with increasing charge. However, comparison of high or low-spin six-coordinate Fe^{II} and Fe^{III} species shows that the magnitude of the effect is reduced in porphyrin complexes (35). Ru—N (equatorial) bond lengths in Ru(II) porphyrins have been reported for $Ru(OEP)(PPh_3)_2$ (ranging from 2.044(3) to 2.057(3) Å) (9), $Ru(OEP)py_2$ (from 2.032(6) to 2.050(5) Å) (36), Ru(TPP)(CO)py (from 2.036(6) to 2.058(6) Å) (37), Ru(TPP)(CO)EtOH (2.048(5) and 2.051(5) Å) (10), and $Ru(TPP)(Ph_2PCH_2PPh_2)_2$ (2.038(8) and 2.045(8) Å) (19). Numerically, the average of the Ru—N bonds in the present structure is shorter than for the Ru(II) complexes, but the esd's are too large to call the difference statistically significant. The porphyrin core shows a small degree of doming (N(n) atoms average 0.07 Å displacement from the porphyrin least-squares plane; C(n1), C(n2), C(n3) average −0.01 Å; C(n3), C(n4) average −0.04 Å; where P is on the positive side of the plane) with the terminal C atoms of the ethyl groups directed in a ++, ++, ++, ++ manner (38) towards the phosphine. The Ru atom is displaced 0.127(2) Å from the porphyrin least-squares plane and 0.049(2) Å from the N_4 plane. The average geometry of the pyrrole rings is shown in Fig. 1 and, within its precision, is in agreement with values previously reported for OEP metalloporphyrins (9, 38, 39).

The Ru—P distance of 2.412(5) Å is at the high end of the range of 2.2–2.4 Å normally found for Ru—P bonds (9, 19, 40). A close contact between phenyl group C(71)—C(76) and part of the porphyrin (C(21) . . . H(76) = 2.44 Å) causes the P atom to be deflected away from this side of the molecule, so that angles P—Ru—N (3 and 4) are less than 90° even though the Ru atom is on the same side of the N_4 plane as the P atom. This contact also causes angle Ru—P—C(71) to be considerably larger than those to C(51) and C(61), and for C(21) to be pushed out of the plane of the porphyrin.

The Ru—Br bond is 2.552(2) Å, which is typical for terminal bromines coordinated at ruthenium (41).

Concluding remarks

Some procedures have been established for the synthesis of ruthenium(III) porphyrin complexes from ruthenium(II) precursors. The oxidations can be effected using Br_2 or Cl_2, or the corresponding hydrogen halides in the presence of air, or the $Et_3O^+PF_6^-$ salt if non halide-containing complexes are required. The primary synthetic routes into ruthenium porphyrin chemistry generally involve Ru(porp)(CO)L (L = EtOH) precursors. If L = a tertiary phosphine, the oxidations to Ru(III) occur with concomitant loss of CO via intermediate porphyrin π-cation radical species; with L = py, a photodecarbonylation is required prior to the oxidation step in order to effect good conversion to Ru(III) products. In general, OEP systems react cleanly, giving high yields of red/purple Ru(III) complexes, while TPP products are often contaminated with green cation radical species.

The first structure of a ruthenium(III) porphyrin complex, $Ru(OEP)(PPh_3)Br$, is reported, and such species generally are important as precursors to models for heme proteins (especially cytochrome P450).

Acknowledgements

This work was supported by grants from the Natural Sciences and Engineering Research Council of Canada, and the United States Institutes of Health (AM 17989). We thank also Dr. R. C. Thompson for assistance with the magnetic susceptibility measurements, and Johnson, Matthey Ltd. for the loan of ruthenium.

1. N. P. FARRELL, D. DOLPHIN, and B. R. JAMES. J. Am. Chem. Soc. **100**, 324 (1978).
2. B. R. JAMES, A. W. ADDISON, M. CAIRNS, D. DOLPHIN, N. P. FARRELL, D. R. PAULSON, and S. WALKER. *In* Fundamental research in homogeneous catalysis. Vol. 3. *Edited by* M. Tsutsui. Plenum Press, New York. 1979. p. 751.
3. L. F. BARRINGER, D. P. RILLEMA, and J. H. HAM. J. Inorg. Biochem. In press.
4. G. DOMAZETIS, B. R. JAMES, B. TARPEY, and D. DOLPHIN. Am. Chem. Soc. Symp. Series, No. 152, 243 (1981).
5. B. R. JAMES, S. R. MIKKELSEN, T. W. LEUNG, G. M. WILLIAMS, and R. WONG. Inorg. Chim. Acta, **85**, 209 (1984).
6. D. DOLPHIN, B. R. JAMES, and T. LEUNG. Inorg. Chim. Acta, **79** (B7), 25 (1983).
7. T. LEUNG, B. R. JAMES, and D. DOLPHIN. Inorg. Chim. Acta, **79** (B7), 180 (1983).

[9] The structures of Ru(OEP)(EtOH)(OEt), and the Ru(OEP)-(PPh_3)Br complex described here, have been presented at a conference (23, 33).

Can. J. Chem. Downloaded from www.nrcresearchpress.com by 210.87.254.42 on 09/06/12
For personal use only.

Can. J. Chem. Downloaded from www.nrcresearchpress.com by 210.87.254.42 on 09/06/12
For personal use only.

8. M. BARLEY, J. Y. BECKER, G. DOMAZETIS, D. DOLPHIN, and B. R. JAMES. Can. J. Chem. **61**, 2389 (1983).
9. S. ARIEL, D. DOLPHIN, G. DOMAZETIS, B. R. JAMES, T. W. LEUNG, S. J. RETTIG, J. TROTTER, and G. M. WILLIAMS. Can. J. Chem. **62**, 755 (1984).
10. J. J. BONNET, S. S. EATON, G. R. EATON, R. H. HOLM, and J. A. IBERS. J. Am. Chem. Soc. **95**, 2141 (1973).
11. G. M. BROWN, F. R. HOPF, J. A. FERGUSON, T. J. MEYER, and D. G. WHITTEN. J. Am. Chem. Soc. **95**, 5939 (1973).
12. D. F. EVANS. J. Chem. Soc. 2003 (1959).
13. F. G. HERRING, B. LANDA, R. C. THOMPSON, and C. F. SCHWERDTFEGER. J. Chem. Soc. (A) 528 (1971).
14. W. R. SCHEIDT, D. K. GEIGER, and K. J. HALLER. J. Am. Chem. Soc. **104**, 495 (1982).
15. B. C. CHOW and I. A. COHEN. Bioinorg. Chem. **1**, 57 1971).
16. W. L. JOLLY. The synthesis and characterization of inorganic compounds. Prentice–Hall Inc., Englewood, New Jersey. 1970.
17. R. S. DRAGO. Physical methods in chemistry. W. B. Saunders, Philadelphia. 1977.
18. A. ANTIPAS, J. W. BUCHLER, M. GOUTERMAN, and P. D. SMITH. J. Am. Chem. Soc. **100**, 3015 (1978).
19. R. G. BALL, G. DOMAZETIS, D. DOLPHIN, B. R. JAMES, and J. TROTTER. Inorg. Chem. **20**, 1556 (1981).
20. W. R. SCHEIDT, Y. J. LEE, D. K. GEIGER, K. TAYLOR, and K. HATANO. J. Am. Chem. Soc. **104**, 3367 (1982).
21. International tables for X-ray crystallography. Vol. IV. Kynoch Press, Birmingham, England. 1974.
22. A. C. LARSON and E. J. GABE. Computing in crystallography. Delft University Press, Delft, Holland. 1978.
23. J. P. COLLMAN and P. J. BROTHERS. 185th ACS National meeting. Seattle, Washington. 1983. Abstract INOR 21.
24. T. ALLMAN and R. G. GOEL. Can. J. Chem. **60**, 716 (1982).
25. C. A. TOLMAN. J. Am. Chem. Soc. **92**, 2953 (1970); **92**, 2956 (1970).
26. M. H. BARLEY. Ph.D. thesis, University of British Columbia. 1983.
27. D. R. PAULSON, A. W. ADDISON, D. DOLPHIN, and B. R. JAMES. J. Biol. Chem. **254**, 7002 (1979).
28. D. DOLPHIN, B. R. JAMES, A. J. MURRAY, and J. R. THORNBACK. Can. J. Chem. **58**, 1125 (1980), and references therein.
29. B. R. JAMES. *In* The porphyrins. Vol. V. *Edited by* D. Dolphin. Academic Press, New York. 1978. p. 205.
30. O. K. MEDHI and U. AGARWALA. Inorg. Chem. **19**, 1381 (1980).
31. J. P. COLLMAN, C. E. BARNES, T. J. COLLINS, P. J. BROTHERS, J. GALLUCCI, and J. A. IBERS. J. Am. Chem. Soc. **103**, 7030 (1981).
32. G. DOMAZETIS, B. R. JAMES, and D. DOLPHIN. Inorg. Chim. Acta, **54**, L47 (1981).
33. M. H. BARLEY, T. W. LEUNG, D. DOLPHIN, and B. R. JAMES. 185th ACS National meeting. Seattle, Washington. 1983. Abstract INOR 73.
34. M. E. GRESS, C. CREUTZ, and C. O. QUICKSALL. Inorg. Chem. **20**, 1522 (1981).
35. (*a*) C. A. REED, T. MASHIKO, W. R. SCHEIDT, K. SPARTALIAN, and G. LANG. J. Am. Chem. Soc. **102**, 2302 (1980); (*b*) W. R. SCHIEDT and C. A. REED. Chem. Rev. **81**, 543 (1981).
36. F. R. HOPF, T. P. O'BRIEN, W. R. SCHEIDT, and D. G. WHITTEN. J. Am. Chem. Soc. **97**, 277 (1975).
37. R. G. LITTLE and J. A. IBERS. J. Am. Chem. Soc. **95**, 8583 (1973).
38. F. W. B. EINSTEIN and A. C. WILLIS. Inorg. Chem. **17**, 3040 (1978).
39. (*a*) J. L. HOARD. *In* Porphyrins and metalloporphyrins. *Edited by* K. M. Smith. Elsevier, Amsterdam. 1975. Chapt. 8; (*b*) W. R. SCHEIDT. *In* The porphyrins. Vol. III. *Edited by* D. Dolphin. Academic Press, New York. 1978. Chapt. 10.
40. (*a*) I. D. BROWN, M. C. BROWN, and F. C. HAWTHORNE (*Editors*). Bond index to the determinations of inorganic crystal structures. Institute for Materials Research, McMaster University, Hamilton. 1969–1981; (*b*) L. A. WILKES, J. H. NELSON, J. P. MITCHENER, M. W. BABICH, W. C. RILEY, B. J. HELLAND, R. A. JACOBSON, M. Y. CHENG, K. SEFF, and L. B. MCCUSKER. Inorg. Chem. **21**, 1376 (1982), and references therein.
41. (*a*) K. BRODERSEN, H. K. BREITBACK, and G. THIELE. Z. Anorg. Allg. Chem. **357**, 162 (1968); (*b*) S. MERLINO and G. MONTAGNOLI. Acta Crystallogr. Sect. B, **24**, 424 (1968); (*c*) M. G. B. DREW, D. A. RICE, and C. W. TIMEWELL. Inorg. Nucl. Chem. Lett. **7**, 59 (1971); (*d*) M. A. BENNETT, G. B. ROBINSON, I. B. TOMKINS, and P. O. WHIMP. J. Organometal. Chem. **32**, C19 (1971); (*e*) J. E. FERGUSSON, C. T. PAGE, and W. T. ROBINSON. Inorg. Chem. **15**, 2270 (1976).

Orientation et dynamique moléculaire de sondes paramagnétiques en phase lamellaire dibutylephosphate de sodium/eau

C. CHACHATY

Département de Physico-Chimie, Centre d'Etudes Nucléaires de Saclay, 91191 Gif-sur-Yvette Cedex, France

Reçu le 24 mai 1983[1]

C. CHACHATY. Can. J. Chem. **62**, 1246 (1984).

Les solutions aqueuses de dibutylephosphate de sodium (NaDBP) en concentrations de 3 à 4 mol L^{-1} forment, entre 280 et 340 K, une phase cristalline liquide lamellaire. On étudie par rpe l'orientation et la dynamique moléculaire dans cette phase, de sondes paramagnétiques telles que l'ion vanadyle et les radicaux nitroxydes, tempoamine, tempone et tempobutanamide.

L'ion VO^{2+} forme, avec le groupe phosphate, un complexe dont l'axe magnétique z est orienté en moyenne selon la normale au plan lamellaire. La mobilité moléculaire à l'interface entre les couches d'eau et de DBP^- est donnée par le temps de corrélation de nutation de l'axe z que l'on déduit de la largeur totale du spectre par la relation empirique $\tau_R = a[1 - (A_\parallel/A_{ZZ})]^b$. Les paramètres $a = 2{,}95 \times 10^{-11}$ s et $b = -1{,}42$ sont déterminés par des mesures en fonction de la viscosité, des largeurs de raies et de l'anisotropie du couplage hyperfin de VO^{2+}

La tempoamine et la tempone se localisent dans les domaines polaires de la mésophase avec une réorientation rapide autour de la direction N—O orientée en moyenne selon le directeur de la phase lamellaire. L'anisotropie de réorientation de ces radicaux est attribuable selon les cas à la formation de liaisions hydrogène avec les groupes phosphates ou les molécules d'eau interstitielles. On établit quelques corrélations entre la rpe de ces sondes paramagnétiques et la rmn de ^2H et ^{31}P des molécules de substrat.

C. CHACHATY. Can. J. Chem. **62**, 1246 (1984).

Aqueous solutions of sodium dibutylphosphate (NaDBP) give rise to lamellar liquid crystalline phase between 280 and 340 K for NaDBP concentrations ranging from 3 to 4 mol L^{-1}. The orientation and dynamic behaviour of several paramagnetic probes such as the vanadyl ion, tempoamine, tempone and tempobutanamide dissolved in this phase have been investigated by esr.

The vanadyl ion binds to the phosphate group, forming a complex, the z magnetic axis of which is on the average perpendicular to the lamellar plane. The molecular mobility at the H_2O/DBP^- interface is given by the reorientation correlation time of the z axis, which is derived from the total width of the spectrum, using the empirical relation $\tau_R = a[1 - (A_\parallel/A_{ZZ})]^b$. The parameters $a = 2.95 \times 10^{-11}$ s and $b = -1.42$ are obtained from the viscosity dependence of the esr line widths and of the anisotropic hyperfine couplings.

The tempone and tempoamine are localized in the polar domains of the mesophase, reorienting rapidly about the N—O direction which is, on the average, parallel to the director of the lamellar plane. The anisotropic motion of these radicals is assigned to hydrogen bonding which occurs, according to the cases, with water molecules or phosphate groups. Some correlations are established between the esr of spin probes and ^2H and ^{31}P nmr experiments on substrate molecules.

Can. J. Chem. Downloaded from www.nrcresearchpress.com by 210.87.254.40 on 09/06/12
For personal use only.

I. Introduction

L'étude par résonance magnétique de solutions aqueuses micellaires de dibutylephosphate de sodium (NaDBP) nous a conduits à mettre récemment en évidence la formation de cristaux liquides lyotropes pour des concentrations élevées en NaDBP (1). L'évolution avec la température et la concentration en NDBP de l'anisotropie de déplacement chimique de ^{31}P ou du couplage quadrupolaire de deutérium de l'eau, ainsi que l'observation au microscope polarisant, ont permis de délimiter le domaine d'existence d'une phase lamellaire (Fig. 1). Cette phase, caractérisée par diffraction de rayons X, consiste en une alternance de doubles couches hydrocarbonées et de domaines polaires contenant les groupes phosphates et l'eau interstitielle, d'épaisseurs respectives $8{,}5 < D_1 < 9{,}8$ et $9{,}2 > D_2 > 7{,}1$ selon la teneur en eau (Fig. 2).

Nous nous sommes proposés d'étudier par résonance magnétique nucléaire (rmn) et par résonance paramagnétique électronique (rpe) l'orientation et la dynamique des molécules de substrat ou de sondes paramagnétiques dissoutes dans ce milieu. Nous nous limiterons ici aux principaux résultats de l'étude par rpe, ceux de la rmn, dont l'interprétation est en cours, ayant fait l'objet d'une publication préliminaire (2).

Les sondes paramagnétiques intervenant dans ce travail ont été choisies en fonction de leurs dimensions moléculaires, inférieures ou comparables à celles de NaDBP et de leur aptitude à s'associer à des degrés divers avec les molécules de substrat. Ainsi l'ion vanadyle forme un complexe de coordination avec l'anion DBP^- alors que les nitroxydes mentionnés au Tableau 1 sont susceptibles soit de s'incorporer dans la couche hydrocarbonée (tempobutanamide), soit de former des liaisons hydrogène avec les constituants polaires de la mésophase (tempone et tempoamine). Les radicaux nitroxydes et à un moindre degré l'ion VO^{2+} sont souvent utilisés pour l'étude par rpe de cristaux liquides thermotropes ou de membranes phospholipidiques (3). Il n'existe par contre que peu d'exemples d'études analogues sur des mésophases lyotropes formées à partir de petites molécules amphiphiles où, comme dans le cas présent, on tente d'établir des corrélations entre la réorientation de ces sondes mesurée par rpe et celle des molécules de substrat déduites d'expériences de résonance et de relaxation nucléaires.

II. Conditions expérimentales

L'acide dibutyle phosphorique (OSI, France) a été purifié par dissolution dans l'eau alcaline pour éliminer le tributylephosphate insoluble dans ce milieu. L'acide dibutylephosphorique était séparé de l'acide monophosphorique par acidification de la solution aqueuse et extraction au tétrachlorure de carbone, suivie d'une distillation sous pression réduite pour éliminer le solvant. La pureté de l'acide dibutylephosphorique, supérieure à 98% était contrôlée par rmn de ^1H, ^{13}C et ^{31}P.

La phase cristalline liquide était formée soit par addition progressive d'une solution concentrée $NaOH/H_2O$ à l'acide di-

[1] Revision reçue le 11 janvier 1984.

Can. J. Chem. Downloaded from www.nrcresearchpress.com by 210.87.254.40 on 09/06/12
For personal use only.

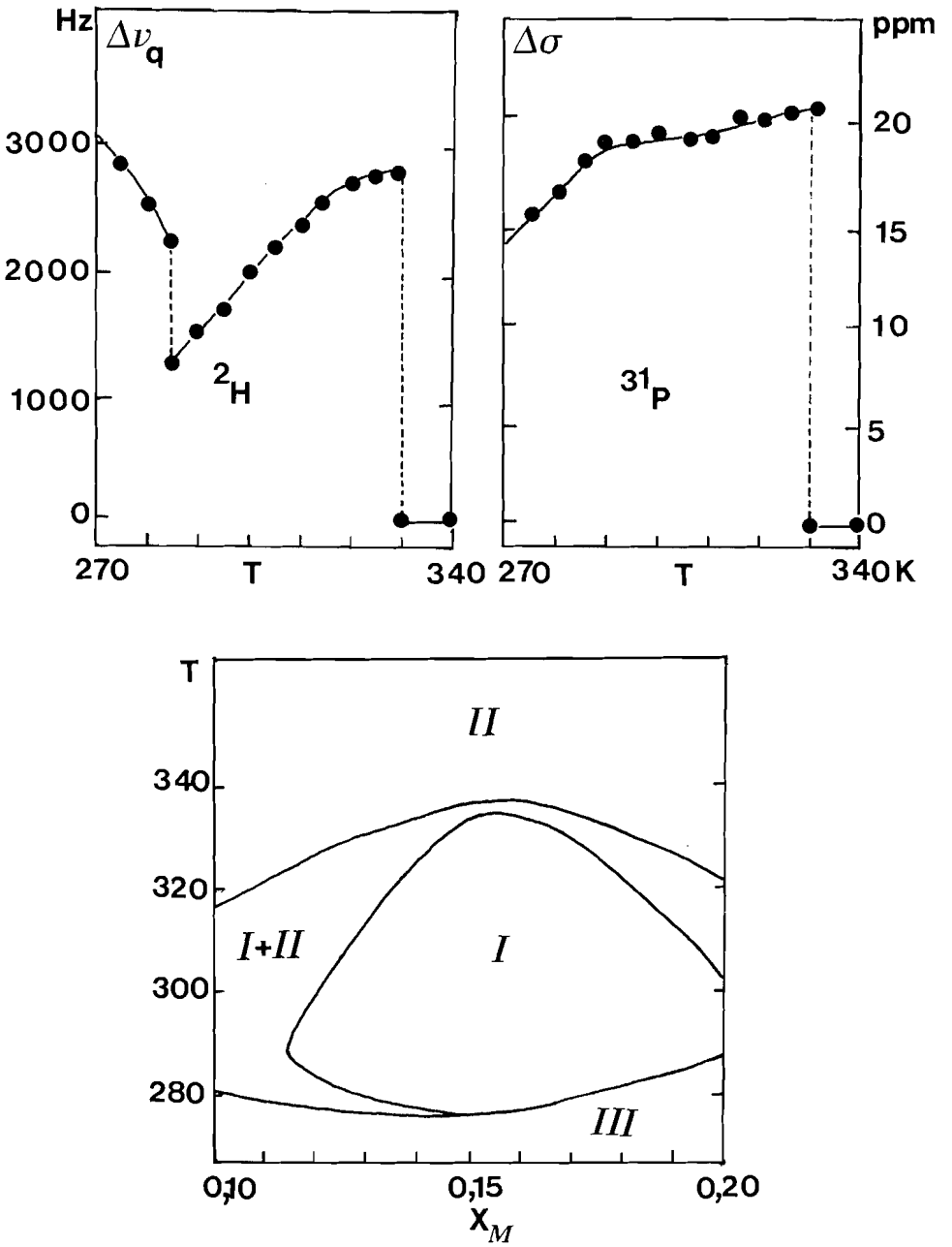

FIG. 1. Variation avec la température de l'écart quadrupolaire de ^{2}H et de l'anisotropie de déplacement chimique $\Delta\sigma = |\sigma_\parallel - \sigma_\perp|$ de ^{31}P dans le système NaDBP/H_2O pour une fraction molaire X_M = 0,165 de NaDBP. Diagrammes de phases: I, phase lamellaire; II, liquide isotrope; III, gel ou solide hétérogène (coagel).

butylephosphorique, soit par dissolution de NaDBP dans H_2O. La solution visqueuse était homogénéisée par chauffage à 50–60°C pendant plusieurs heures. Les radicaux 2,2,6,6-tétraméthyl-4-pipéridinone-1-oxyl (tempone) et 4-amino-2,2,6,6-tétraméthylpipéridine-1-oxyl (tempoamine) ainsi que le sulfate de vanadyle proviennent d'Aldrich Chemical. La tempobutanamide a été synthétisée par action du chlorure d'acide correspondant sur la 2,2,6,6-tétraméthylpipéridine-1-oxyl-4-ol et purifiée par chromatographie.

Les expériences de rpe ont été effectuées sur un spectromètre Varian E9 à une fréquence de 9,15 GHz et avec une modulation de 100 KHz. L'échantillon était placé dans un système à température variable V 257. Dans la plupart des expériences nous avons utilisé une cellule rectangulaire de section interne 3,5 × 0,5 mm (Wilmad WG 808) que l'on orientait par rapport au champ magnétique.

Le champ magnétique étant calibré à l'aide d'un magnétomètre Varian F8, les facteurs g étaient mesurés par rapport à une référence externe de DPPH (système Varian Fieldial Mark II) dont le g effectif, compte tenu de sa position par rapport à la cavité, est de 2,00375 ± 0,00005.

III. Paramètres d'ordre et largeurs des raies

Paramètres d'ordre

L'orientation moléculaire par rapport au directeur de la mésophase est définie par les paramètres d'ordre S_{ii} qui ont pour expression (4, 5):

$$[1] \quad S_{ii} = \frac{1}{2}\langle 3\cos^2\theta'_i(t) - 1\rangle$$

$\theta'_i(t)$ étant l'angle dépendant du temps entre un axe i du système de référence moléculaire et le directeur de la mésophase. Le système de référence choisi étant celui des axes principaux

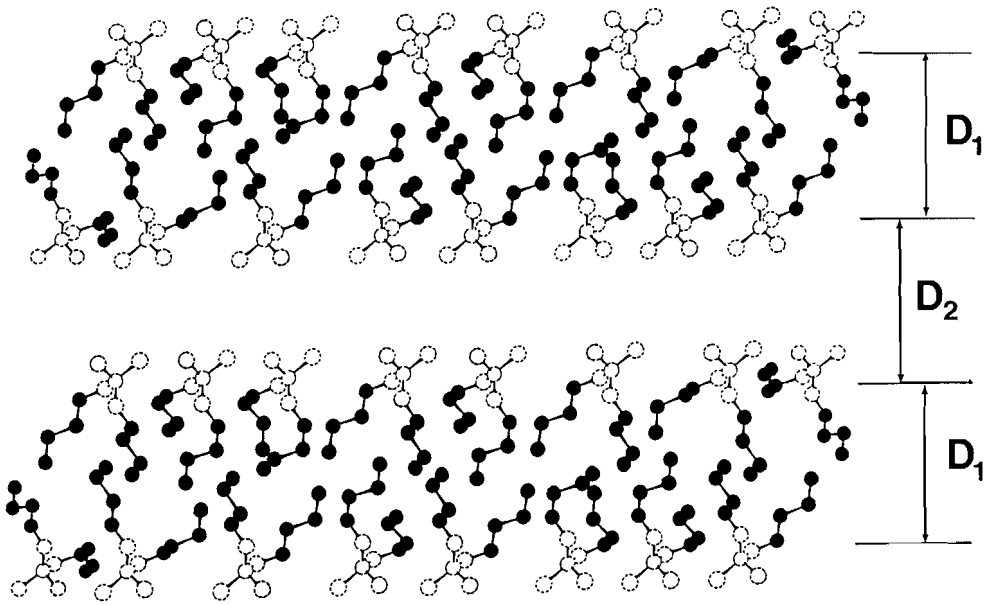

FIG. 2. Délimitation des domaines polaires (D_2) et non polaires (D_1) de la phase lamellaire NaDBP/H_2O.

TABLEAU 1. Valeurs principales des tenseurs **A** et **g**

	A_{zz} (G)	A_{xx} A_{yy}	A_0	g_{zz}	$g_{xx} \approx g_{yy}$	g_0
VO^{2+} ($Z\|\|$ V—O)	204 ± 2	78 ± 2	120 ± 2	1,932 ± 0,003	1,987 ± 0,003	1,969 ± 0,003

Nitroxydes

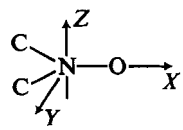

		A_{zz}	$A_{xx} \approx A_{yy}$	A_0*	g_{zz}	g_{xx}	g_{yy}	g_0*
Tempone	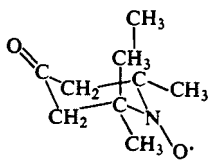	34 ± 0,2	5,35 ± 0,2	14,9 ± 0,05	2,0026 ± 0,0002	2,0094 ± 0,0003	2,0062 ± 0,0003	2,0061 ± 0,0001
Tempoamine	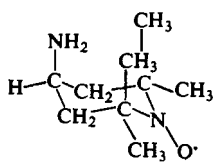	35 ± 0,2	6,4 ± 0,2	15,93 ± 0,5	2,0026 ± 0,0002	2,0098 ± 0,0003	2,0062 ± 0,0003	2,0062 ± 0,0001
Tempobutanamide	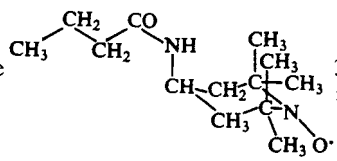	34,6 ± 0,2	6,475 ± 0,2	15,85 ± 0,05	2,0024 ± 0,0002	2,0092 ± 0,0003	2,0066 ± 0,0003	2,00607 ± 0,0001

*Mesuré en phase isotrope.

x, y et z, communes aux tenseurs de couplage hyperfin **A** et au tenseur **g**, désignés tous deux par **T**, la réorientation moléculaire autour du directeur nous donne (4, 5):

$$[2] \quad T_{\|} - T_{\perp} = S_{11}T_{xx} + S_{22}T_{yy} + S_{33}T_{zz}$$

Pour les radicaux nitroxydes, l'axe z coïncide avec celui de l'orbitale de l'électron non apparié, centrée sur l'azote et l'axe x est aligné à quelques degrés près selon la liaison N—O (6). Dans le cas de l'ion VO^{2+} l'axe z est orienté selon la liaison V—O et les axes x et y sont pratiquement équivalents. Les valeurs principales de ces tenseurs, indiquées dans le tableau 1, ont été déterminées par simulation des spectres de rpe en ma-

Can. J. Chem. Downloaded from www.nrcresearchpress.com by 210.87.254.40 on 09/06/12
For personal use only.

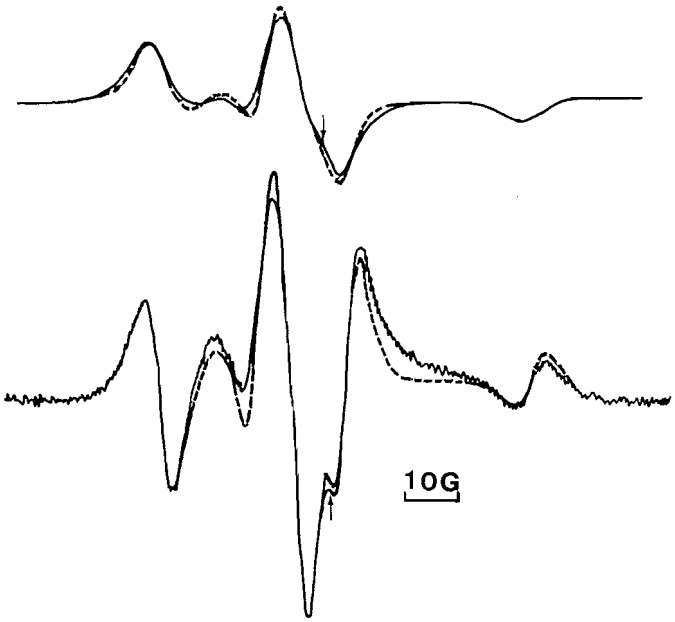

FIG. 3. Détermination des valeurs principales des tenseurs **A** et **g** du radical tempobutanamide par simulation des dérivées première et seconde du spectre rpe en milieu rigide; (—) spectres expérimentaux; (- - -) spectres calculés avec les paramètres du Tableau 1. Les flèches verticales correspondent à $g = 2{,}00375$.

trice rigide NaDBP/H_2O à $T < 120$ K. Alors que les tenseurs **A** de ces sondes paramagnétiques et le tenseur **g** de VO^{2+} peuvent être considérés comme axiaux autour de z, le tenseur **g** des nitroxydes dévie notablement de la symétrie axiale.

Dans nos conditions expérimentales, la résolution limitée de la dérivée première d'absorption des spectres de nitroxydes en milieu rigide ne donne que g_{zz} et $\frac{1}{2}(g_{xx} + g_{yy})$. La position des singularités de la dérivée seconde dépend par contre beaucoup plus fortement de l'asymétrie du tenseur **g**, définie par $\Delta g = (g_{xx} - g_{yy})/(g_{zz} - g_0)$ avec $g_0 = \frac{1}{3}(g_{xx} + g_{yy} + g_{zz})$. Nous avons donc déterminé les valeurs principales de **g** à partir de la dérivée seconde des spectres de rpe en vérifiant cette mesure par simulation des spectres (Fig. 3). Les valeurs de Δg obtenues sont respectivement de $-0{,}75$, $-0{,}92$ et -1 pour la tempobutylamide, la tempone et la tempoamine, en bon accord avec les valeurs que l'on calcule d'après les données de la littérature (voir par ex. les références 7, 8).

La mesure des paramètres d'ordre a été effectuée à partir de la position des singularités associées aux valeurs principales des tenseurs **A** et **g** en écrivant la relation [2] sous la forme:

$$[3] \quad \frac{T_{\parallel} - T_{\perp}}{T_{zz} - \frac{1}{2}(T_{xx} + T_{yy})} = S_{33} + \frac{1}{2}\frac{(T_{xx} - T_{yy})(S_{11} - S_{22})}{T_{zz} - \frac{1}{2}(T_{xx} + T_{yy})}$$

Comme $A_{xx} \cong A_{yy}$, S_{33} est donné directement par mesure de l'écart hyperfin alors que S_{11} et S_{22} sont obtenus à partir de l'anisotropie de **g**. Cette mesure n'est valable que si la réorientation moléculaire est rapide par rapport à $\Delta A/h$ et à $\Delta g \beta B_0/h$ (9), ΔA et Δg représentant l'anisotropie des tenseurs **A** et **g** et B_0 le champ magnétique directeur.

Largeurs de raies

Dans le domaine des movements rapides spécifié plus haut, les largeurs de raies liées au temps de relaxation électronique T_2, permettent de déterminer les temps de corrélation de réorientation moléculaires par une expression de la forme (10):

$$[4] \quad T_2^{-1} = \gamma_0 \Delta B(m_I) = a + bm_I + cm_I^2$$

$\gamma_0 = g_0 \beta/\hbar$ est le rapport gyromagnétique de l'électron, m_I le nombre quantique nucléaire et $\Delta B(m_I)$ la demi-largeur de raie à mi-hauteur d'une lorentzienne (élargissement homogène).

Pour un couplage hyperfin exprimé en gauss, les constantes a, b et c ont pour expressions (10):

$$[5] \quad a = \frac{1}{6} B_0^2 \hbar^2 \beta_e^2 \sum_{K=-2}^{2} (-1)^K F_g^{(K)} F_g^{(-K)} G_1^{(K)}(\omega) + \frac{1}{12} I(I+1) \gamma_e^2 \sum_{K=-2}^{2} (-1)^K F_A^{(K)} F_A^{(-K)} G_2^{(K)}(\omega)$$

$$b = \frac{1}{6} B_0 \hbar^{-1} \beta_e \sum_{K=-2}^{2} [(-1)^K (F_A^{(K)} F_g^{(-K)} + F_A^{(-K)} F_g^{(K)})] G_1^{(K)}(\omega)$$

$$c = \frac{1}{6} \gamma_e^2 \sum_{K=-2}^{2} (-1)^K F_A^{(K)} F_A^{(-K)} \left[G_1^{(K)}(\omega) - \frac{1}{2} G_2^{(K)}(\omega) \right]$$

$G_1^{(K)}(\omega)$ et $G_2^{(K)}(\omega)$ sont des combinaisons linéaires des densités spectrales $J(\omega)$ qui seront explicitées plus loin

$$[6] \quad \begin{aligned} G_1^{(K)}(\omega) &= 4J_0^{(K)}(0) + 3J_1^{(K)}(\omega_S) \\ G_2^{(K)}(\omega) &= J_0^{(K)}(\omega_S) + 3J_1^{(K)}(\omega_A) + 6J_2^{(K)}(\omega_S) \end{aligned}$$

avec $\omega_S = \gamma_0 B_0$, $\omega_A \cong \gamma_0 A_0$, A_0 étant la constante de couplage hyperfin de contact.

$F_T^{(K)}$ avec $K = 0, \pm 1, \pm 2$ désigne l'une des composantes des tenseurs **A** ou **g** en base sphérique:

$$[7] \quad \begin{aligned} F_T^{(0)} &= \sqrt{\frac{2}{3}} \left(T_{zz} - \frac{1}{2}(T_{xx} + T_{yy}) \right) \\ F_T^{(\pm 1)} &= 0 \\ F_T^{(\pm 2)} &= \frac{1}{2}(T_{xx} - T_{yy}) \end{aligned}$$

Dans le cas d'une réorientation autour d'un axe moléculaire Δ_M, ces composantes deviennent:

$$[8] \quad F'^{(K')} = \sum_{K=-2}^{2} D_{K'K}^{(2)}(0, \beta, \gamma) F^{(K)}$$

$D_{K'K}^{(2)}$ désignant la matrice de Wigner d'ordre 2.

Les densités spectrales de la relation [6] sont de la forme (11, 12):

$$[9] \quad J_M^K(\omega, \Theta) = J' + J'' P_2(\cos\Theta) + J''' P_4(\cos\Theta)$$

$P_2(\cos\Theta)$ et $P_4(\cos\Theta)$ désignent les polynômes de Legendre d'ordre 2 et 4, θ étant l'angle entre B_0 et Δ_L (Fig. 4). J', J'' et J''' sont des combinaisons linéaires des densités spectrales correspondant à $\Theta = 0$, et qui ont pour expression générale (11, 13):

$$[10] \quad J_M^K(\omega, 0) = \bar{d}_{KM}^2 \frac{\tau_K}{1 + \omega^2 \tau_K^2}$$

avec K ou $M = 0, \pm 1, \pm 2$.

Les temps de corrélation τ_0, τ_1, τ_2 sont liés aux coefficients de diffusion rotationnelle $D_{\parallel}$ et $D_{\perp}$, par la relation (14, 15):

$$[11] \quad \tau_K^{-1} = C[6D_{\perp} + (D_{\parallel} - D_{\perp})K^2]$$

où C est un coefficient dépendant du modèle de mouvement (diffusion Brownienne ou réorientation par sauts). Ceci nous donne:

Can. J. Chem. Downloaded from www.nrcresearchpress.com by 210.87.254.40 on 09/06/12
For personal use only.

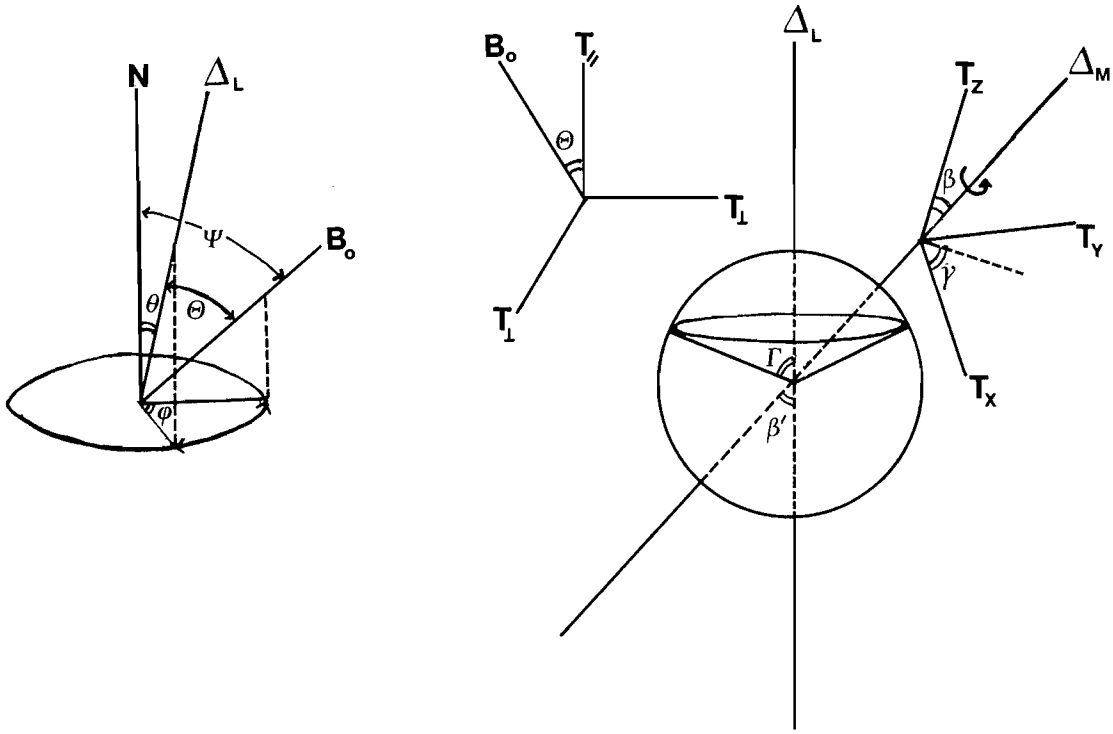

FIG. 4. Définition des angles et des axes. *N*: axe de référence de l'échantillon, généralement normal au plan de la cellule rectangulaire ou au plan moyen de la phase lamellaire orientée; Δ_L: directeur local; Δ_M: axe de rotation moléculaire préférential; **T**: tenseurs **A** ou **g**. Ces tenseurs sont moyennés par réorientation autour de Δ_M et Δ_L.

$$[12]\quad \tau_1 = \frac{6\tau_0}{5 + (D_\parallel/D_\perp)}, \qquad \tau_2 = \frac{6\tau_0}{2 + 4(D_\parallel/D_\perp)}$$

τ_0, que l'on désignera également par τ_R correspond au mouvement de nutation de l'axe moléculaire Δ_M autour du directeur Δ_L. Dans la relation [10] $\bar{d}^2_{KM}$ est le carré moyen d'un élément de la matrice de rotation entre les axes moléculaires et un système de référence fixe. L'expression de $\bar{d}^2_{KM}$ en fonction des paramètres d'ordre P_2 (cos β') = $\frac{1}{2}\langle 3\cos^2\beta' - 1\rangle$ et $\bar{P}_4$ (cos β') = $\frac{1}{8}\langle 35\cos^4\beta' - 30\cos^2\beta' + 3\rangle$ est donné dans les références 11 ou 13, pour un modèle de réorientation par sauts, β' étant l'angle dépendant du temps entre Δ_M et Δ_L (Fig. 4). $\bar{P}_2$ (cos β') est donné par l'écart hyperfin des raies de résonance:

$$[13]\quad \frac{A_\parallel - A_\perp}{A_{zz} - \frac{1}{2}(A_{xx} + A_{yy})} = \frac{1}{2}\bar{P}_2(\cos\beta')[3\cos^2\beta - 1] = S_{33}$$

où β désigne l'angle entre Δ_M et l'axe z du tenseur de couplage hyperfin.

La relation entre $\bar{P}_2$ (cos β') et $\bar{P}_4$ (cos β') dépend du modèle de réorientation proposé. Dans le cas présent $\bar{P}_4$ (cos β') a été déduit de $\bar{P}_2$ (cos β') mesuré expérimentalement en admettant que l'axe moléculaire Δ_M effectue un mouvement aléatoire de nutation à l'intérieur d'un cône centré sur Δ_L (Fig. 4) (16) ou que ce mouvement dépend d'un potentiel de la forme $U(\beta')/kT = -\lambda\sin^2\beta'$ (17). Une étude en cours sur la dépendance angulaire de la relaxation de ^{31}P dans le système NaDBP/H_2O montre que ce second modèle rend le mieux compte des résultats expérimentaux, de sorte que nous l'avons également adopté pour le calcul des largeurs de raies des radicaux nitroxydes.

Du fait de la distribution statique d'orientation des directeurs Δ_L des domaines formant la phase cristalline liquide, il est généralement nécessaire de confirmer la détermination des paramètres d'ordre S_{ii} et des largeurs de raies par simulation des spectres de rpe. Dans ce but nous avons écrit un programme APL qui permet de calculer ces spectres en fonction des paramètres cités plus haut, pour une forme de raie gaussienne ou lorentzienne selon que l'on se trouve dans les conditions de mouvements lents (VO^{2+}) ou rapides (nitroxydes). Pour une forme de raie lorentzienne par exemple, la dérivée première d'absorption a pour expression (18)

$$[14]\quad F(B) = -\frac{2}{\pi}\sum_{m_I=-1}^{+1}\int_0^{2\pi}\int_0^{\pi} \times \frac{G(\phi)\,G(\theta)\,P(\theta,\phi)\,\Delta B(B - B_R)\sin\theta\,d\phi\,d\theta}{(\Delta B^2 + (B - B_R)^2)^2}$$

B est le champ magnétique variable, ΔB la demi-largeur de raie à mi-hauteur, θ l'angle entre le directeur local Δ_L et l'axe référence N, ϕ l'angle entre la projection de B_0 sur un plan perpendiculaire à N et la projection de Δ_L sur ce plan (Fig. 4). B_R et $P(\theta,\phi)$ désignent respectivement le champ magnétique de résonance et la probabilité de transition. $G(\theta)$ et $G(\phi)$ représentent les fonctions de distribution statique du directeur Δ_L centrées sur θ_0 ou ϕ_0, assimilées à une gaussienne (16):

$$[15]\quad G(u) = \frac{1}{\Delta u_m\sqrt{2\pi}}\exp\left[-\frac{1}{2}\left(\frac{u - u_0}{\Delta u_m}\right)^2\right]$$

Pour une orientation donnée de Δ_L, qui est l'axe de symétrie des tenseurs **A** et **g** moyennés par la réorientation moléculaire autour du directeur, le champ magnétique de résonance B_R a pour expression (18):

$$[16]\quad B_R = \frac{h\nu_0/\beta - [(A_\parallel g_\parallel)^2\cos^2\Theta + (A_\perp^2 g_\perp^2)\sin^2\Theta]^{1/2} m_I}{(g_\parallel^2\cos^2\Theta + g_\perp^2\sin^2\Theta)^{1/2}} + B'_R$$

Can. J. Chem. Downloaded from www.nrcresearchpress.com by 210.87.254.40 on 09/06/12
For personal use only.

avec Θ = arc cos (cos θ cos ψ + sin θ cos ϕ sin ψ), ν_0 étant la fréquence du spectromètre et B'_R le terme du second ordre dont on trouvera l'expression dans la réf. 18.

Le temps de calcul des spectres a été considérablement réduit en replaçant l'intégration sur θ et ϕ de l'équation [14] par une simple intégration sur Θ (Fig. 4):

$$[17]\quad F(B) = -\frac{2}{\pi}\sum_{m_I=-1}^{+1}\int_0^{\pi/2}\frac{G(\Theta)P(\Theta)\Delta B(B-B_R)}{(\Delta B^2-(B-B_R)^2)^2}\,d\Theta$$

$P(\Theta)$ est la probabilité de transition (19):

$$[18]\quad P(\Theta) = \frac{1}{2}g_\perp^2\left\{1+\frac{g_\parallel^2}{g_\parallel^2\cos^2\Theta+g_\perp^2\sin^2\Theta}\right\}$$

$G(\Theta)$ est la distribution de probabilités de l'angle Θ calculée numériquement à partir de l'expression:

$$[19]\quad G(\Theta) = \mathcal{N}\frac{G(\phi)G(\theta)\sin\theta\,\Delta\Theta}{\Theta(\theta+\Delta\theta,\phi+\Delta\phi)-\Theta(\theta,\phi)}$$

$\Delta\Theta$, $\Delta\theta$ et $\Delta\phi$ étant des pas angulaires constants et $\mathcal{N}$ un facteur de normalisation. Le nombre de points d'intégration sur Θ est réduit par troncature de $G(\Theta)$ et cette fonction peut être utilisée dans des calculs successifs.

La dépendance angulaire de ΔH intervient dans les relations [14] et [17]. Elle est soit ajustée empiriquement sous la forme:

$$[20]\quad \Delta B = (\Delta B_\parallel^2\cos^2\Theta + \Delta B_\perp^2\sin^2\Theta)^{1/2}$$

soit calculée en fonction des paramètres d'ordre et des temps de corrélation τ_K. Dans ce second cas, on tient compte de l'élargissement inhomogène par une largeur de raie additionnelle:

$$[21]\quad \Delta B' = \Delta B_1 + \Delta B_2\cos^2\Theta$$

ΔB_1 et ΔB_2 sont des paramètres ajustables qui correspondent respectivement aux parties scalaire et dipolaire du couplage hyperfin non résolu des protons. Pour une orientation donnée, la largeur pic à pic de la dérivée d'une raie d'absorption dans l'approximation d'une forme lorentzienne est donc:

$$[22]\quad \Delta B_{pp} = \frac{2}{\sqrt{3}}[(\gamma_0 T_2)^{-1} + \Delta B')]$$

T_2 étant calculé à partir des relations [4]–[12].

Dans le cas des nitroxydes étudiés ici, le second terme de la relation [21] est négligeable étant donné le faible couplage dipolaire des protons, moyenné à zéro par la réorientation moléculaire rapide. La simulation des spectres nous a donné les valeurs optimales $\Delta B' = 0{,}3 \pm 0{,}05$ G pour la tempone et $\Delta B' = 0{,}9 \pm 0{,}1$ G pour la tempoamine et la tempobutanamide. Ces valeurs sont voisines de la demi-largeur à mi-hauteur:

$$[23]\quad \sigma = 0{,}59\left(\sum_i n_i a_{H_i}^2\right)^{1/2}$$

de l'enveloppe de la structure hyperfine des protons assimilés à une gaussienne. Les constantes de couplage hyperfin a_H des protons de la tempone (20) et de la tempoamine (21) donnent en effet respectivement $\Delta B' \cong \sigma = 0{,}225$ G et 0,83 G.

Pour certaines simulations, la contribution de la structure hyperfine non résolue a été introduite par convolution gaussienne des spectres. Cette procédure ne donne pas de différences notables avec l'utilisation de la relation [22].

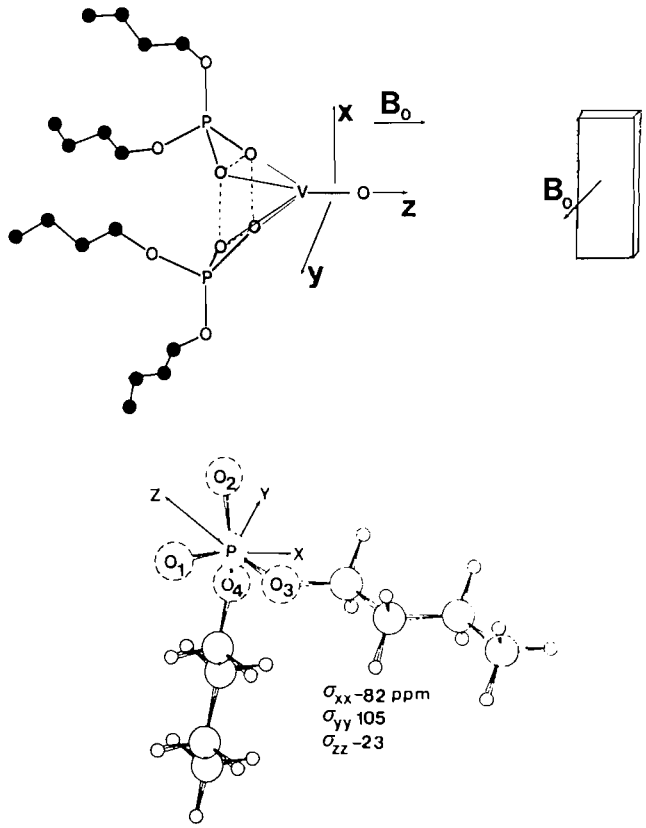

FIG. 5. Orientation des axes principaux des tenseurs **A** et **g** de VO^{2+} pour $\psi = 0$, $\theta_0 = 0$, x et y étant équivalents. Tenseur de déplacement chimique σ de ^{31}P.

IV. Résultats et discussion

Ion vanadyle

L'étude par rmn de la complexation de VO^{2+} par DBP^- en milieu micellaire indique la formation d'un complexe bidentate avec deux molécules de monomère (1) représenté sur la figure 5. Dans la phase lamellaire ce complexe donnera une orientation moyenne de l'axe V—O perpendiculaire aux doubles couches de DBP^-. Le spectre rpe de VO^{2+} apportera donc des informations sur la distribution d'orientation du directeur et la mobilité moléculaire à l'interface DBP^-/H_2O.

Les amplitudes des singularités du spectre de VO^{2+} correspondant aux orientations de l'axe de symétrie et du plan principal des tenseurs **g** et **A** parallèles à B_0, varient par rotation de la cellule rectangulaire. On observe que les singularités parallèles, correspondant à $T_\parallel$, ont une amplitude maximale ou minimale selon que B_0 est perpendiculaire ou parallèle au plan de la cellule, alors que les singularités perpendiculaires varient en sens inverse (Fig. 6). Cette dépendance angulaire indique que les doubles couches de la phase lamellaire s'orientent préférentiellement dans le plan de la cellule. On observe parfois un comportement inverse, qui correspond à une orientation aléatoire de Δ_L dans le plan de la cellule. L'apparition de l'un ou l'autre type d'orientation depend d'une manière critique du traitement thermique de l'échantillon. La transition entre la phase lamellaire et la phase III par refroidissement à $T < 280$ K entraîne la disparition de l'effet d'orientation, que l'on retrouve par recuit prolongé de l'échantillon entre 300 et 330 K.

De la symétrie quasi-axiale et de l'orientation des tenseurs magnétiques de VO^{2+}, il résulte que la relaxation électronique de cet ion ne dépend au premier ordre que du seul temps de

Can. J. Chem. Downloaded from www.nrcresearchpress.com by 210.87.254.40 on 09/06/12
For personal use only.

Can. J. Chem. Downloaded from www.nrcresearchpress.com by 210.87.254.40 on 09/06/12
For personal use only.

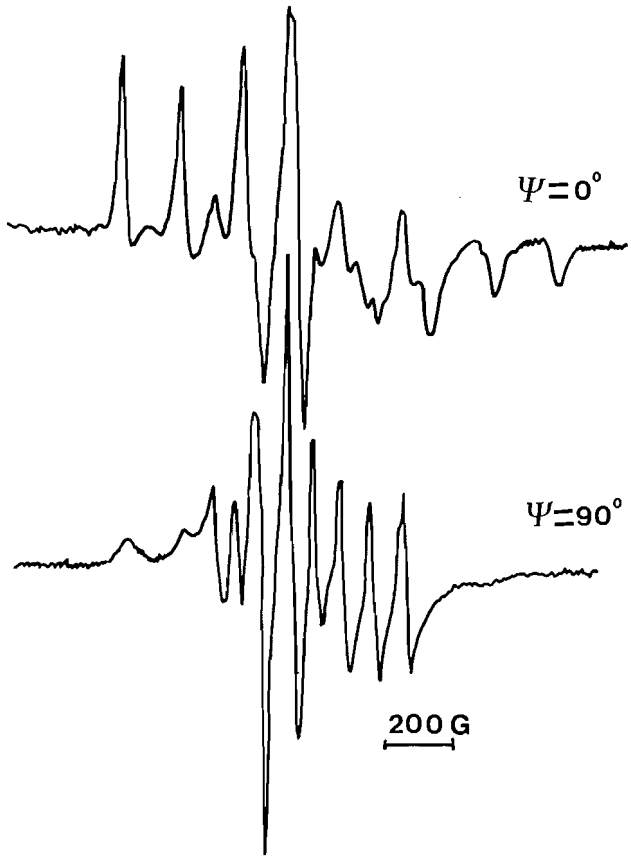

FIG. 6. Spectres de l'ions VO^{2+} en phase lamellaire NaDBP/H_2O, $X_M = 0{,}13$ pour les orientations perpendiculaires ($\psi = 0°$) et parallèle ($\psi = 90°$) de la cellule par rapport à B_0. Ces spectres indiquent que l'axe V—O s'oriente préférentiellement selon la normale au plan de la cellule ($\theta_0 = 0$).

corrélation $\tau_R = \tau_0$ de nutation de l'axe V—O autour du directeur local Δ_L de la phase lamellaire. La rpe de VO^{2+} en solutions de viscosité variable (1) indique que la détermination de τ_R par des mesures de largeurs de raies (éq. [4]) ne s'applique que pour $\tau_R < 3 \times 10^{-10}$ s, étant donné la grandeur de l'anisotropie du couplage hyperfin ($A_\parallel - A_\perp \simeq 3{,}5 \times 10^8$ Hz). La comparaison des spectres de VO^{2+} dans la mésophase NaDBP/H_2O avec des systèmes analogues (22) ou des spectres théoriques (23, 24) montre que l'échelle de temps des mouvements de réorientation se situe entre 10^{-8} et 10^{-9} s.

Dans ces conditions, la largeur totale $\Delta A = 7\,A_\parallel$ du spectre de VO^{2+}, mesurée entre les pics extrêmes sur un échantillon polyorienté, dépend du temps de corrélation τ_R (23) et donne un paramètre d'ordre $0{,}7 < S^*_{33} < 1$ supérieur au paramètre d'ordre $S_{33} = \bar{P}_2$ (cos β′) donnant l'orientation moyenne de V—O autour de Δ_L. La distinction entre S_{33} et S^*_{33}, que McConnell désigne respectivement par "ensemble-average order parameter" et "frequency-amplitude order parameter" est discutée dans la réf. 9. L'anisotropie de déplacement chimique du phosphore donne $S_{33} \simeq 0{,}5$ à 0,65 selon la fraction molaire de NaDBP; on peut admettre des valeurs assez proches de celles-ci pour l'ion VO^{2+} lié aux groupes phosphates.

En milieu isotrope, τ_R peut être évalué par la relation empirique (14, 23):

$$[24] \quad \tau_R = \alpha\,(1 - S)^\beta$$

valable pour $0{,}8 < S = A_\parallel/A_{ZZ} < 1$, α et β étant des constantes

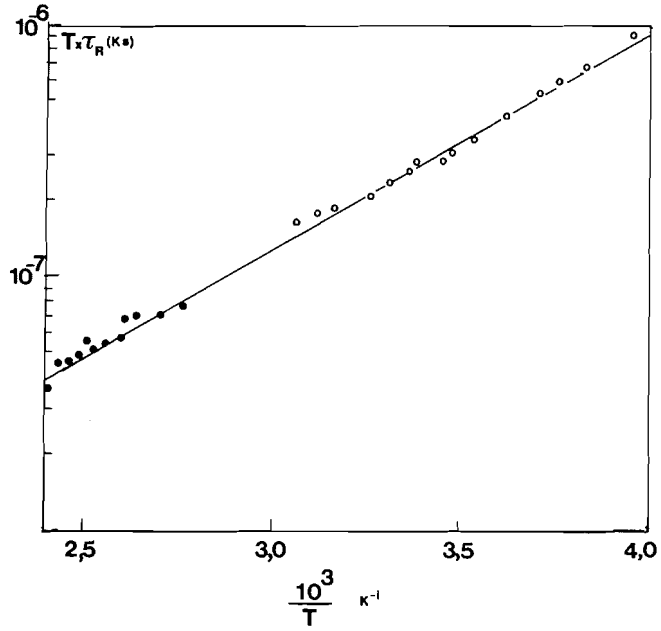

FIG. 7. Détermination des paramètres α et β de la relation $\tau_R = \alpha\,(1 - A_\parallel/A_{ZZ})^\beta$ à partir du spectre rpe de $VO(AA)_2$ dans l'acide dibutylphosphorique. (●) $T \times \tau_R$ est donné par la dépendance des largeurs de raies en fonction de m_I, pour $\tau_R < 3 \times 10^{-10}$ s (relation [4]). (○) $T \times \tau_R$ est calculé à partir des rapports $A_\parallel/A_{ZZ}$ pour $\alpha = 2{,}95 \times 10^{-11}$ s et $\beta = -1{,}42$.

dépendant du modèle de réorientation (14). L'application de cette relation à un milieu anisotrope a été effectué par Polnaszek *et al.* (25) dans le cas de radicaux nitroxydes, en tenant compte de la contribution, dans un certain domaine, de la décroissance de S_{33} avec la température. Dans le cas présent, on ne note pas de discontinuité dans la variation de S entre 280 et 350 K malgré les transitions de phase III → I et I → II (Fig. 1), cette dernière annulant S_{33}. On peut donc admettre que la décroissance de S avec la température ne dépend que de τ_R. Des valeurs de α et β ont été données par Bruno *et al.* (23) pour un modèle de diffusion Brownienne, en fonction de la largeur de raie résiduelle $\Delta B'$ ($\alpha = 1{,}02 \times 10^{-11}$ s, $\beta = -1{,}97$ et $\alpha = 1{,}38 \times 10^{-11}$ s, $\beta = -1{,}84$ pour $\Delta B' = 1$ G ou 7,5 G). Il nous a paru préférable de déterminer ces deux paramètres en mesurant la variation avec la température de S pour l'acétylacétonate de vanadyle ($VO(AA)_2$) dans l'acide dibutylephosphorique (HDBP).

La relation de Stokes–Einstein, avec une viscosité variant exponentiellement avec $1/T$ (voir par exemple, la réf. 26), nous donne:

$$[25] \quad \tau_R = \frac{V}{kT}\,\eta_0 \exp\left(\frac{E}{kT}\right)$$

où V est le volume moléculaire et η la viscosité du solvant. A des températures supérieures à 360 K pour lesquelles $\tau_R < 3 \times 10^{-10}$ s, ce temps de corrélation est obtenu par la dépendance des largeurs de raies avec m_I (éq. [4]). Ayant vérifié que log ($\tau_R \times T$) varie linéairement avec $1/T$, avec une énergie d'activation de $3{,}9 \pm 0{,}2$ kcal mol^{-1}, l'extrapolation de cette fonction dans le domaine des mouvements lents ($128 < T < 320$ K) permet de calculer τ_R. En mesurant le rapport S dans ce domaine, on obtient $\alpha = (2{,}95 \pm 0{,}03) \times 10^{-11}$ s et $\beta = -1{,}42 \pm 0{,}02$, par les moindres carrés (Fig. 7).

La variation de τ_R avec la température pour des fractions molaires de NaDBP $X_M = 0{,}13$ et $X_M = 0{,}165$ est donnée par

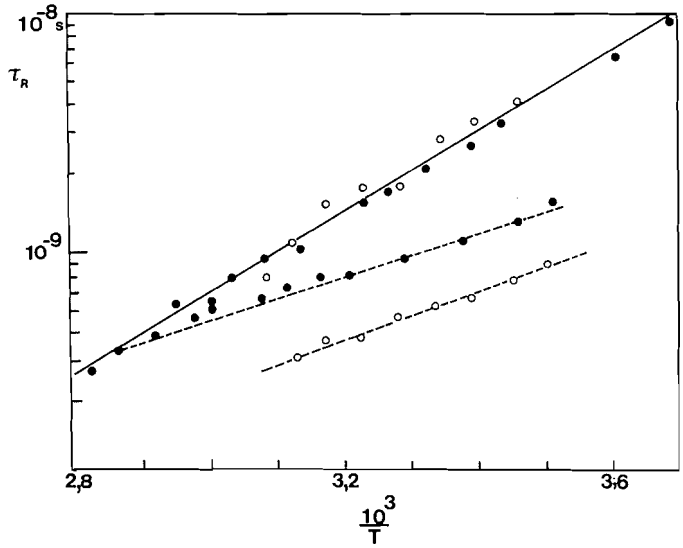

FIG. 8. Temps de corrélation de nutation de l'axe z des tenseurs **A** et **g** de VO^{2+} et du tenseur σ de ^{31}P autour du directeur Δ_L perpendiculaire à la phase lamellaire, déterminés par la largeur totale du spectre de VO^{2+} (●) ou par relaxation longitudinale de ^{31}P (○). (—) X_M = 0,165; (- - -) X_M = 0,13.

la figure 8. Le temps de corrélation τ_R déterminé par la rpe de VO^{2+} a été comparé à celui fourni par la relaxation nucléaire longitudinale de ^{31}P, qui donne la mobilité des groupes phosphate à l'interface entre les domaines polaires et non polaires de la mésophase, les axes z des tenseurs magnétiques de VO^{2+} et du tenseur de déplacement chimique de ^{31}P étant orientés perpendiculairement au plan lamellaire. La relaxation de ^{31}P comporte une contribution de l'anisotropie de déplacement chimique (ADC) et de l'interaction dipolaire avec les protons voisins (DIP), qui ont pour expressions respectives:

$$[26] \quad (T_1^{-1})_{ADC} = \omega_p^2 \sum_{K=-2}^{2} F^{(K)} F^{(-K)} J_{1K}(\omega_p)$$

avec:

$$[27] \quad F_\sigma^{(0)} = \sqrt{\frac{2}{3}}\left[\sigma_{zz} - \frac{1}{2}(\sigma_{xx} + \sigma_{yy})\right]$$

$$F_\sigma^{(\pm 1)} = 0$$

$$F_\sigma^{(\pm 2)} = \frac{1}{2}(\sigma_{xx} - \sigma_{yy})$$

σ_{ii} étant les valeurs principales du tenseur de déplacement chimique de ^{31}P données dans la figure 5, et:

$$[28] \quad (T_1^{-1})_{DIP} = \frac{1}{3} \sum_{K=-2}^{2} F_D^{(K)} F_D^{(-K)} [J_{0K}(\omega_H - \omega_p) + 3J_{1K}(\omega_p) + 6J_{2K}(\omega_H + \omega_p)]$$

avec:

$$[29] \quad F_D^{(0)} = \sqrt{\frac{3}{2}}\gamma_p \gamma_H \hbar\, r_{PH}^{-3}, \qquad F_D^{(\pm 1)} = F_D^{(\pm 2)} = 0$$

r_{PH} étant la distance effective proton–phosphore évaluée à 2,3 Å d'après la relaxation de ^{31}P en milieu micellaire (1). Les densités spectrales sont données par les relations [9] et [10]. On remarque sur la figure 8 que pour la plus forte de ces concentrations, qui correspond à peu près à la rigidité maximum de la phase lamellaire, ces deux méthodes sont en accord et nous donnent $\tau_R = (2,4 \pm 0,2) \times 10^{-9} \exp[4200\,(1/T - 1/300)]$ s soit $E_0 = 8,3 \pm 0,3$ kcal mol^{-1}. τ_R se situe donc dans une échelle de temps de 10^{-9} à 3×10^{-9} s, comparable à celle observée par rpe de VO^{2+} (22) ou de radicaux nitroxydes (4) dans d'autres mésophases lyotropes, qui correspondrait à un mouvement moléculaire coopératif entraînant une déformation de l'interface entre les domaines polaires et non polaires (22) et donc à une fluctuation d'orientation du directeur de la phase lamellaire.

A plus faible concentration en NaDBP (X_M = 0,13), la relaxation nucléaire de ^{31}P et la rpe de VO^{2+} donnent respectivement $\tau_R = (5,5 + 0,5) \times 10^{-10} \exp[2500\,(1/T - 1/300)]$ s et $(1,0 \pm 0,1) \times 10^{-9} \exp[2200\,(1/T - 1/300)]$ s soient $E_0 = 5,0 \pm 0,3$ kcal mol^{-1} et $E_0 = 4,3 \pm 0,3$ kcal mol^{-1}. Cette différence d'un facteur deux entre ces déterminations de τ_R est interprétable par un accroissement de la liberté de réorientation avec la teneur en eau. En effet, la réorientation moléculaire autour de l'axe z intervient dans la relaxation de ^{31}P mais non dans le spectre rpe de l'ion VO^{2+} dont les tenseurs magnétiques sont axiaux selon cette direction. Ce point doit être vérifié par une étude en cours sur l'effet de la concentration sur la relaxation de ^{31}P et la largeur totale du spectre rpe du complexe VO^{2+}/NaDBP dans tout le domaine d'existence de la phase lamellaire.

Radicaux nitroxydes

En phase lamellaire NaDBP/H_2O, les constantes de couplage des radicaux nitroxydes sont de 14,9, 15,9 et 15,85 G respectivement pour la tempone, la tempoamine et la tempobutanamide. Pour ces mêmes radicaux a_N est de 13 G en milieu apolaire et de 16 G (tempone) ou de 17 G (tempoamine) en solution aqueuse. Le groupe nitroxyle de ces sondes paramagnétiques est donc localisé dans les domaines polaires de la mésophase.

L'anisotropie du couplage hyperfin de l'azote qui, en phase lamellaire, croît dans l'ordre tempobutanamide, tempone, tempoamine, ainsi que l'anisotropie de **g** permettent de déterminer les paramètres d'ordre S_{ii}. Cette mesure, généralement effectuée en cellule rectangulaire, est réalisée en orientant la cellule parallèlement puis perpendiculairement au champ magnétique et vérifiée par simulation des spectres selon ces deux orientations.

La tempobutanamide possède une chaîne de longueur comparable à celle du dibutylephosphate et susceptible de s'incorporer dans des doubles couches hydrocarbonées de la phase lamellaire. Son spectre présente une faible variation d'écart hyperfin et un déplacement de la raie centrale par rotation de l'échantillon entre les angles $\psi = 0°$ et $\psi = 90°$ qui nous donnent $A_\parallel - A_\perp = 1,4 \pm 0,2$ G, $g_\parallel - g_\perp = -3,14 \times 10^{-4}$ et donc $S_{33} = 5 \times 10^{-2}$, $S_{22} = -1,2 \times 10^{-2}$ et $S_{11} = -3,8 \times 10^{-2}$, sans variation notable avec la température. La simulation des spectres de la tempobutanamide (Fig. 9) indique une réorientation quasi-isotrope. Etant donné la faible anisotropie du couplage hyperfin, les temps de corrélation τ_R dont la variation avec la température est donnée dans la figure 10, ont été déterminés à partir des largeurs de raies mesurées directement sur les spectres comme en phase isotrope. Le comportement de la tempobutanamide, très voisin de celui que l'on observe en phase liquide isotrope, suggère une forte perturbation de l'ordre local de la mésophase, ce qui nous a conduit à étudier plus en détail d'orientation et la dynamique de la tempoamine et de la tempone dont les dimensions sont inférieures à celles des molécules de NaDBP.

Can. J. Chem. Downloaded from www.nrcresearchpress.com by 210.87.254.40 on 09/06/12
For personal use only.

Can. J. Chem. Downloaded from www.nrcresearchpress.com by 210.87.254.40 on 09/06/12
For personal use only.

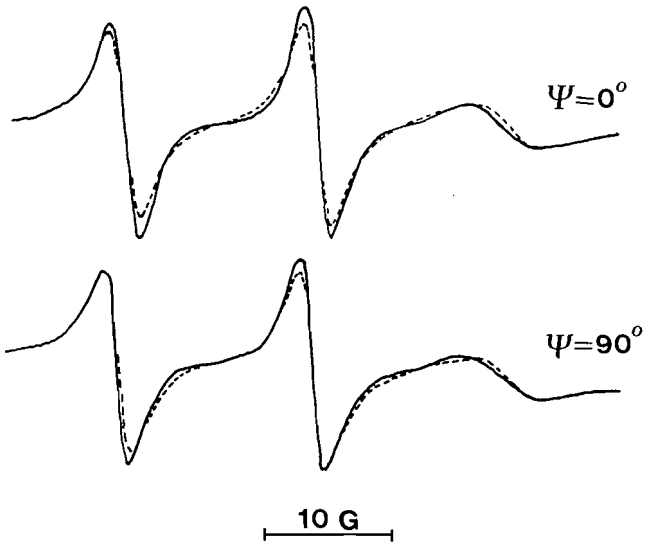

FIG. 9. Tempobutanamide en phase lamellaire (T = 300 K, X_M = 0,13). Les spectres en pointillés sont simulés avec les paramètres: S_{11} = −0,0125, S_{22} = −0,0385, S_{33} = 0,051, τ_R = 1,5 × 10^{-9} s, $\Delta B'$ = 0,8 G.

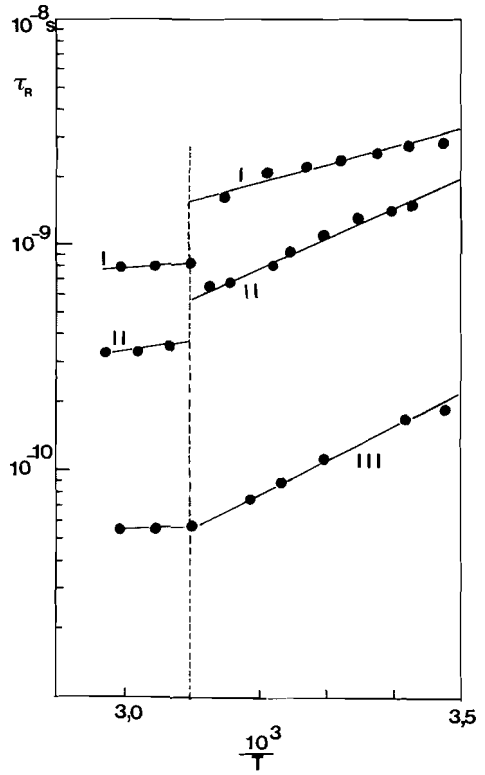

FIG. 10. Dépendance avec la température de $\tau_0 = \tau_R$: (I) tempoamine, (II) tempobutanamide, (III) tempone en solution dans NaDBP/H_2O, X_M = 0,13. Le trait pointillé correspond à la transition entre les phases lamellaire et isotrope. Les facteurs préexponentiels et les énergies d'activation sont donnés dans le Tableau 2.

Les spectres de la tempoamine polyorientée ou partiellement orientée (Fig. 11) ont été enregistrés immédiatement après la transition III → I (280 K) puis après recuit de l'échantillon jusqu'à 320 K, quelques degrés au-dessus de la transition I → II (~325 K). Les spectres correspondant aux orientations ψ = 0° et ψ = 90° de la cellule rectangulaire montrent que la tempo-

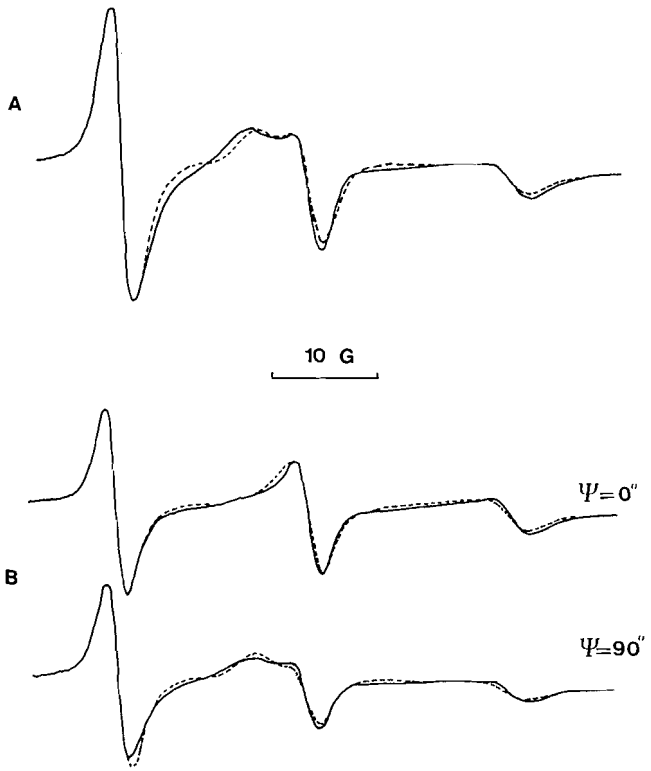

FIG. 11. Spectres de la tempoamine en phase lamellaire X_M = 0,13 à 290 K, avant réchauffement à la transition lamellaire → isotrope. A: Orientation aléatoire des radicaux; B: radicaux partiellement orientés dans le plan de la cellule rectangulaire ($\Delta\theta_m$ = 40°, θ_0 = 90°). (—) Spectres expérimentaux; (- - -) spectres calculés avec: τ_0 = 2,5 × 10^{-9} s; τ_2 = 5 × 10^{-10} s; S_{11} = 0,73; S_{22} = −0,46; S_{33} = −0,27. L'élargissement inhomogène est introduit par convolution gaussienne du spectre avec $\Delta B'$ = 0,8 G.

amine se réoriente préférentiellement autour de l'axe N—O• ($A_\parallel$ = 10,7 G, $A_\perp$ = 18,4 G, $g_\parallel$ = 2,0085, $g_\perp$ = 2,005) et que le directeur Δ_L est orienté en moyenne parallèlement au plan de la cellule. La simulation de ces spectres indique en outre que la distribution angulaire statique de Δ_L peut être représentée par une gaussienne de largeur 40° centrée sur θ_0 = 90°.

Après réchauffement de l'échantillon au-delà de la transition entre la phase lamellaire et la phase isotrope, puis refroidissement lent dans le champ magnétique, on observe un alignement de l'axe N—O de la tempoamine selon l'axe de l'échantillon. La rotation de l'échantillon autour de cet axe n'entraîne qu'une faible différence entre les spectres enregistrés selon les orientations ψ = 0 et ψ = 90°, dont on peut rendre compte par une distribution étroite d'orientation de Δ_L autour des angles ϕ_0 = 90° et θ_0 = 90° (Fig. 12). Ce comportement que l'on observe également par rmn de ^2H et ^{31}P (2) correspond à une orientation de Δ_L perpendiculaire au champ magnétique.

Pour une orientation perpendiculaire de la cellule par rapport à B_0 (ψ = 0), le spectre rpe de la tempoamine est pratiquement symétrique par rapport à la ligne de base (Fig. 12). L'ecart hyperfin de ce spectre et le facteur g de la raie centrale qui varient de 18,3 G à 18,1 G et de 2,0053 à 2,0051 entre 295 K et 325 K (Tableau 2) donnent les valeurs moyennes de paramètres d'ordre S_{11} = 0,6, S_{22} = −0,35, S_{33} = −0,25.

Dans l'hypothèse d'une réorientation axiale, S_{33} est donné par la relation [13]. On montre facilement que les autres paramètres d'ordre peuvent s'écrire:

TABLEAU 2. Paramètres d'ordre et temps de corrélation de réorientation des radicaux nitroxydes en phase lamellaire NaDPB/H_2O (X_M = 0,13)

		T (K)				
	Paramètre	288	294	303	313	322
Tempoamine	S_{11}	0,608	0,606	0,603	0,603	0,597
	S_{22}	−0,352	−0,355	−0,357	−0,357	−0,362
	S_{33}	−0,256	−0,251	−0,246	−0,246	−0,235
		T (K)				
		288	293	303	308	313
Tempone	S_{11}	0,1396	0,1385	0,1403	0,1474	0,1514
	S_{22}	−0,1083	−0,1005	−0,0985	−0,1034	−0,1054
	S_{33}	−0,0314	−0,038	−0,0425	−0,044	−0,046
Tempobutanamide		$290 < T < 325$ K				
		$S_{11} = -0{,}038$	$S_{22} = -0{,}012$	$S_{33} = 0{,}05$		

Temps de corrélation: $\tau_R = (\tau_R)_{300} \exp\left[\frac{E}{R}\left(\frac{1}{T} - \frac{1}{300}\right)\right]$

Tempoamine: $(\tau_R)_{300} = 2{,}35 \times 10^{-9}$ s, $E = 3{,}75$ kcal mol^{-1}

T(K)	288	292	296	301	306	316
$D_\parallel/D_\perp$	6	8	9	10	11	9

Tempone: $(\tau_R)_{300} = 1{,}1 \times 10^{-10}$ s, $E = 5{,}9$ kcal mol^{-1}, $\frac{D_\parallel}{D_\perp} = 2{,}5 \pm 0{,}5$

Tempobutanamide: $(\tau_R)_{300} = 1{,}15 \times 10^{-9}$ s, $E = 5{,}6$ kcal mol^{-1}, $\frac{D_\parallel}{D_\perp} = 1$

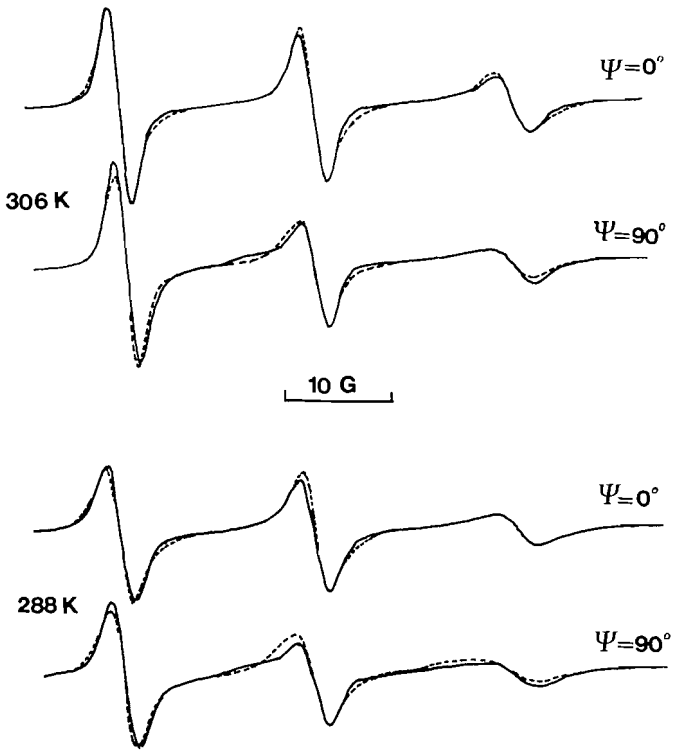

FIG. 12. Spectres de la tempoamine orientée par refroidissement de l'échantillon dans le champ magnétique, à partir de la phase isotrope (X_M = 0,13). (—) Spectres expérimentaux; (- - -) spectres calculés à partir des paramètres du Tableau 2. Le spectre correspondant à ψ = 90° est calculé pour une distribution gaussienne d'orientations de Δ_L avec $\Delta\theta_m$ = 10°, θ_0 = 90°, $\Delta\phi_m$ = 25°, ϕ_0 = 90° (éq. [15]). La distribution des angles ϕ n'a pas d'influence sur les spectres correspondant à ψ = 0° alors que la distribution des angles θ contribue à l'élargissement inhomogène des raies.

$$S_{11} = \frac{1}{2}\bar{P}_2(\cos\beta')\,[3\sin^2\beta\cos^2\gamma - 1] \quad [30]$$

$$S_{22} = \frac{1}{2}\bar{P}_2(\cos\beta')\,[3\sin^2\beta\sin^2\gamma - 1]$$

où γ désigne l'angle azimuthal de Δ_M dans le système d'axes moléculaires x, y, z (Fig. 4), ici égal à zéro, étant donné la symétrie du radical tempoamine. L'angle β entre Δ_M et l'axe z des tenseurs **A** et **g** est alors donné par la relation:

$$[31]\quad \beta = \arccos\left[\frac{1}{\sqrt{3}}\left(\frac{\rho+3}{\rho+1}\right)^{1/2}\right]$$

que l'on déduit des équations [13] et [30] en prenant $\rho = (S_{11} - S_{22})/S_{33}$. On obtient ainsi $\beta \simeq 72°$ soit une déviation de 18° entre les axes x et Δ_M, avec $\bar{P}_2(\cos\beta') \simeq 0{,}7$. Il est peu probable qu'une telle déviation corresponde à la réalité, d'une part parce que la rpe et la cristallographie des nitroxydes étudiés ici indiquent que l'angle entre l'axe x et l'axe de moindre inertie (direction N—O') ne dépasse pas 10° (6), d'autre part parce que le meilleur accord entre les largeurs de raies calculées et observées est realisée pour β = 90° et $\bar{P}_2(\cos\beta') = 0{,}6$. Il n'est pas exclu que la différence entre cette valeur effective de l'angle β et celle donnée par la relation [31] résulte de ce que le tenseur de diffusion moleculaire n'est pas parfaitement axial, comme nous l'avons admis en prenant pour simplifier les calculs de largeurs de raies, $D_\parallel = D_{xx}$, $D_\perp = \frac{1}{2}(D_{yy} + D_{zz})$.

La dynamique de réorientation de la tempoamine a été déterminée à partir des largeurs de raies mesurées sur les spectres symétriques obtenus pour l'orientation ψ = 0 de l'échantillon par rapport au champ magnétique (Fig. 12). Pour cela on a utilisé un programme qui recherche par la méthode des moindres carrés le meilleur accord entre les largeurs de raies et celles calculées à partir des relations [4]–[13] en prenant comme

Can. J. Chem. Downloaded from www.nrcresearchpress.com by 210.87.254.40 on 09/06/12
For personal use only.

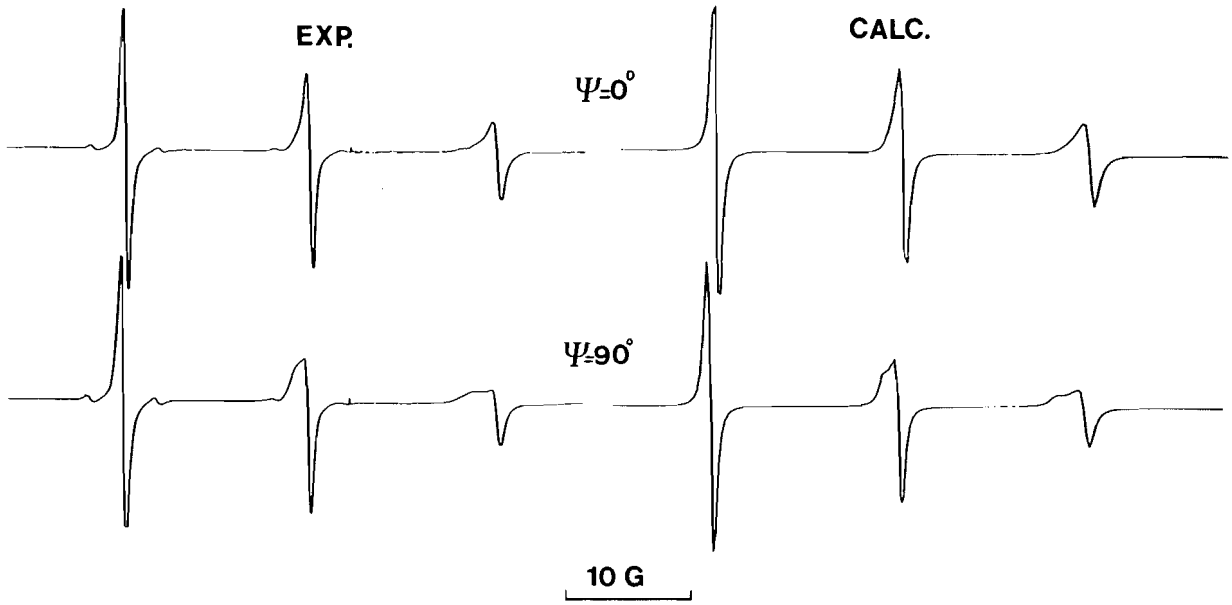

FIG. 13. Spectres de la tempone à 300 K (X_M = 0,13). Les paramètres utilisés pour la simulation de ces spectres sont donnés dans le Tableau 2, avec une distribution gaussienne d'orientations de Δ_L de largeur $\Delta\theta_m$ = 25° autour de θ_0 = 90° et une largeur inhomogène de raie de 0,3 G.

paramètres ajustables τ_0, τ_2 et donc $D_\parallel/D_\perp$, ainsi que la largeur inhomogène de raie $\Delta B'$ (eq. [22] que l'on trouve comprise entre 0,8 et 1 G. La validité de cette méthode a été vérifiée par simulation des spectres, pour une forme Lorentzienne de raie (Fig. 12). Dans tout le domaine de température étudié, on observe que $\tau_2 \ll \tau_0$, ce qui indique une réorientation rapide autour de l'axe Δ_M. Le rapport $D_\parallel/D_\perp$ varie de 5 à 11 entre 295 K et 325 K (phase lamellaire) et diminue à 3 en milieu isotrope. Que l'on envisage une réorientation par sauts ou une diffusion brownienne, ce rapport est beaucoup plus élevé que celui auquel on peut s'attendre d'après les dimensions moléculaires de la tempoamine, comparables à celles de la tempone que nous verrons plus loin. L'association par liaison hydrogène de la tempoamine avec les groupes phosphates du NaDBP est suggérée par la valeur quasi équivalente du paramètre $\bar{P}_2$ (cos β′) que l'on obtient par rpe (Tableau 2) et par rmn du phosphore. On note également sur la figure 10 que τ_R est du même ordre de grandeur que le temps de corrélation du mouvement de nutation de l'axe z du groupe phosphate (Fig. 8) avec $E_0 \simeq 3.75$ kcal mol^{-1} pour la tempoamine et $E_0 \simeq 4.3$ kcal mol^{-1} pour ce groupe.

Des expériences similaires ont été effectuées sur la tempone dissoute en phase lamellaire. Les spectres obtenus pour les orientations $\psi = 0$ et $\psi = 90°$ de la cellule rectangulaire (Fig. 13) ont été interprétés comme pour la tempoamine par une orientation de N—O en moyenne parallèle au plan de la cellule avec une distribution angulaire de largeur ~25° autour de θ_0 = 90°. Les positions des singularités du spectre correspondant à $\psi = 90°$ donnent en moyenne $S_{11} = 0,14$, $S_{22} = -0,10$ et $S_{33} = -0,04$. Les relations [13] et [31] nous donnent $\beta = 67°$ et $\bar{P}_2$ (cos β′) ≅ 0,15, cependant ici encore les amplitudes relatives et les largeurs de raies calculées concordent mieux avec l'expérience pour $\beta = 90°$.

La dynamique de réorientation de la tempone en phase lamellaire a été étudiée en déterminant τ_0 et $D_\parallel/D_\perp$ par comparaison des amplitudes relatives de raies I_0/I_{+1} et I_{-1}/I_{+1} du spectre expérimental obtenu pour $\psi = 0$, avec celles calculées en fonction de ces deux paramètres, pour une distribution gaussienne d'orientations de Δ_L de largeur 25° autour de $\theta_0 = 90°$. En phase lamellaire, le rapport $D_\parallel/D_\perp = 2,5 \pm 0,5$ est nettement supérieur à la valeur de 1,36 calculée à partir des dimensions moléculaires de la tempone $d_{x'}$ = 4,2 Å selon la direction N—O, $d_{z'}$ = 2,7 Å dans le plan de symétrie moléculaire et $d_{y'}$ = 3 Å (7). En phase isotrope on obtient par contre $D_\parallel/D_\perp \simeq 1$ avec $\tau_0 \cong \tau_2 = 6 \times 10^{-11}$ s à 330 K. En phase lamellaire $\tau_0 = \tau_R$ est inférieur d'un facteur 10 environ à celui de la tempoamine (Fig. 10) et comparable à celui des molécules d'eau interstitielles mesuré par relaxation de ^{2}H et ^{17}O ($8 \times 10^{-11} < \tau_R < 2,5 \times 10^{-10}$ pour $320 > T > 300$ K) (2). On note également que les paramètres d'ordre S_{ii} augmentent en valeur absolue avec la température. Ce phénomène, pour lequel nous n'avons pas trouvé jusqu'à présent d'interprétation satisfaisante, est également observé pour le deutérium (Fig. 1) et l'oxygène 17 de l'eau (2). Ces deux faits nous suggèrent que l'anisotropie de réorientation de la tempone en phase lamellaire résulte de la formation de liaisons hydrogènes entre les molécules d'eau et les oxygènes des groupes nitroxyle et carbonyl qui définissent l'orientation de l'axe de rotation moléculaire Δ_M.

V. Conclusion

Ce travail, mené en parallèle avec des expériences de résonance nucléaire, constitue une première partie d'une étude sur la dynamique et l'orientation moléculaire dans les phases cristallines liquides provenant de solutions aqueuses concentrées d'alkylphosphates.

Le spectre rpe de l'ion vanadyle, lié au groupe phosphate, permet de mesurer, en complément de la relaxation de ^{31}P, la mobilité moléculaire à l'interface des domaines polaire et non polaire de la mésophase.

La tempobutanamide effectue un mouvement de réorientation quasi-isotrope avec un paramètre d'ordre moléculaire $\bar{P}_2$ (cos β′) ≅ 0 en raison soit de rotations internes multiples, soit d'une désorganisation du réseau bidimensionnel de la mésophase due à la dimension de ces sondes, comparable à celles de dibutylphosphate.

La tempone et la tempoamine sont localisées dans les couches polaires de la mésophase et se réorientent préféren-

Can. J. Chem. Downloaded from www.nrcresearchpress.com by 210.87.254.40 on 09/06/12
For personal use only.

tiellement autour de la liaison N—O dont l'orientation moyenne est parallèle au directeur de la phase lamellaire. Bien que ces deux sondes aient des dimensions moléculaires comparables, les temps de corrélation de réorientation et le paramètre d'ordre $\bar{P}_2$ (cos β') sont beaucoup plus importants pour la tempoamine que pour la tempone. Il est probable que la tempoamine forme à la fois des liaisons hydrogène avec l'eau et avec les oxygènes d'un groupe phosphate alors que la tempone ne se lie qu'aux molécules d'eau. Ces interactions paraissent seules susceptibles d'expliquer la forte anisotropie de réorientation de ces deux radicaux nitroxydes en phase lamellaire.

1. S. BELAID et C. CHACHATY. J. Colloid Interface Sci. **86**, 277 (1982).
2. C. CHACHATY et J. P. QUAEGEBEUR. J. Phys. Chem. **87**, 4341 (1983).
3. L. J. BERLINER (*Editeur*). Spin labelling, theory and applications. Vol. I et II. Academic Press, New York. 1976 et 1979.
4. H. SCHINDLER et J. SEELIG. J. Chem. Phys. **59**, 1841 (1973).
5. J. SEELIG. *Dans* Spin labelling, theory and applications. Vol. I. *Edité par* L. J. Berliner. Academic Press, New York. 1976. Chap. 10.
6. J. LAJCZEROWITZ-BONNETEAU. *Dans* Spin labelling, theory and applications. Vol. I. *Edité par* L. J. Berliner. Academic Press, New York. 1976. Chap. 6.
7. J. S. HWANG, R. P. MASON, L. P. HWANG et J. H. FREED. J. Phys. Chem. **79**, 489 (1975).
8. E. MEIROVITCH. J. Phys. Chem. **87**, 845 (1983).
9. H. M. MCCONNELL. *Dans* Spin labelling, theory and applications. Vol. I. *Edité par* L. J. Berliner. Academic Press, New York. 1976. Chap. 13.
10. P. L. NORDIO. *Dans* Spin labelling, theory and applications. Vol. I. *Edité par* L. J. Berliner. Academic Press, New York. 1976. Chap. 2.
11. J. H. FREED. J. Chem. Phys. **66**, 4183 (1977).
12. G. R. LUCKHURST et C. ZANNONI. Proc. R. Soc. Lond. Ser. A, **353**, 87 (1977).
13. C. ZANNONI, G. F. PEDULLI, L. MASOTTI et A. SPISINI. J. Magn. Reson. **43**, 143 (1981).
14. J. H. FREED. *Dans* Spin labelling, theory and applications. Vol. I. *Edité par* L. J. Berliner. Academic Press, New York. 1976. Chap. 3.
15. W. J. LIN et J. H. FREED. J. Phys. Chem. **83**, 379 (1979).
16. O. H. GRIFFITHS et P. C. JOST. *Dans* Spin labelling, theory and applications. Vol. I. *Edité par* L. J. Berliner. Academic Press, New York. 1976. Chap. 12.
17. G. R. LUCKHURST, M. SETAKA et C. ZANNONI. Mol. Phys. **28**, 49 (1974).
18. W. GORDY. Theory and applications of electron spin resonance. John Wiley, New York. 1980. Chapt. 5.
19. B. BLEANEY. Proc. Phys. Soc. **75**, 621 (1960).
20. R. W. KREILICK. J. Chem. Phys. **46**, 4260 (1967).
21. J. LABSKY, J. PILAR et J. LOVY. J. Magn. Reson. **35**, 515 (1980).
22. R. F. CAMPBELL et M. W. HANNA. J. Phys. Chem. **30**, 1892 (1976).
23. G. V. BRUNO, M. P. EASTMAN et J. K. HARRING. J. Phys. Chem. **81**, 111 (1977).
24. R. F. CAMPBELL et J. H. FREED. J. Phys. Chem. **84**, 2666 (1980).
25. C. F. POLNASZEK, D. MARSH et I. C. P. SMITH. J. Magn. Reson. **43**, 54 (1981).
26. G. M. BARROW. Physical chemistry. McGraw Hill, New York. 1973. pp. 535–536.

Can. J. Chem. Downloaded from www.nrcresearchpress.com by 210.87.254.40 on 09/06/12
For personal use only.

Quadrupolar interactions in amines as determined by ^{1}H nuclear magnetic resonance: mono- and dimethylamines[1]

JAMES D. HALLIDAY, PATRICK E. BINDNER, and SHAHSULTAN PADAMSHI

Physical Chemistry Branch, Atomic Energy of Canada Limited, Research Company, Chalk River Nuclear Laboratories, Chalk River, Ont., Canada K0J 1J0

Received December 13, 1983

JAMES D. HALLIDAY, PATRICK E. BINDNER, and SHAHSULTAN PADAMSHI. Can. J. Chem. **62**, 1258 (1984).

Nitrogen-14 quadrupole interactions have been observed in the nonexchanging amino proton ^{1}H nmr spectra of rigorously purified liquid mono- and dimethylamines over the temperature range −82°C to +81°C. The proton lineshapes have been analyzed to yield ^{14}N spin-lifetimes (τ) as a function of temperature. Activation energies and correlation times for molecular reorientation in the liquids have been calculated from these data and the results compared with those from ^{14}N nmr measurements.

JAMES D. HALLIDAY, PATRICK E. BINDNER et SHAHSULTAN PADAMSHI. Can. J. Chem. **62**, 1258 (1984).

L'examen des spectres rmn du ^{1}H de mono- et de diméthylamines liquides rigoureusement purifiées, à des températures allant de −82°C à +81°C, a permis d'observer les interactions quadrupolaires de l'azote-14 avec les protons aminés qui ne peuvent pas s'échanger. On a analysé la forme des raies des protons afin d'obtenir les temps de vie des spin du ^{14}N en fonction de la température. Utilisant ces données, on a calculé les énergies d'activation et les temps de corrélation des réorientations moléculaires dans les liquides et on a comparé les résultats avec ceux obtenus à partir d'autres mesures de rmn du ^{14}N.

[Traduit par le journal]

Introduction

Analysis of the proton lineshapes (1, 2) for molecules in which the proton is spin-coupled to a ^{14}N nucleus represents an alternate way of obtaining data on ^{14}N quadrupole interactions in the liquid phase. The temperature dependence of the ^{14}N spin-lifetimes (τ) leads to activation energies and correlation times for molecular dynamical processes (3) in the liquids. Comparison of data from both ^{1}H and ^{14}N nmr spectra of the methyl substituted ammonias had not been possible previously because of loss of ^{14}N—H spin coupling owing to rapid amino proton exchange, even in distilled samples (4). We have succeeded in obtaining anhydrous, amino proton exchange free methylamine (5) and dimethylamine and have analyzed the temperature dependence of the amino proton line shapes. A comparison is made between these data and the ^{14}N nmr studies by Atkins, Loewenstein, and co-workers (6, 7).

Experimental

Anhydrous dimethylamine (Eastman) was prepared by a technique similar to that previously reported for the preparation of anhydrous methylamine (5). A glass apparatus (Fig. 1), which allowed keeping the solution under vacuum at all times, contained 8 Wilmad 528 (5-mm) nmr tubes and 2 reservoirs A, B. After evacuation of the system a saturated solution of cesium dimethylamide in dimethylamine under vacuum was added and the vessel was sealed with a J. Young Co. Ltd. valve, C. The very reactive cesium dimethylamide solution was allowed to contact the walls of the apparatus for 24 h to remove any traces of adventitious water. Hydrogen gas was pumped off after freezing the solution with liquid nitrogen and, upon thawing, the amide solution was poured into reservoir A, the amine cryodistilled back into B using liquid nitrogen, and the vessel rinsed with this distillate. This procedure for washing all of the amide solution into A was repeated 15 times or until no amide uv absorbance was detected in the attached optical cells. A sample was then distilled into an nmr tube and sealed off. Repeated rinsings followed until there was no difference in the amino and methyl group proton nmr spectra in successive nmr tube samples.

Anhydrous trimethylamine was also prepared in an attempt to measure quadrupole effects through H—C—^{14}N coupling. Since there are no amino protons to exchange, purification was simplified. The amine was allowed to contact a potassium mirror in a glass flask with a J. Young Co. Ltd. valve for at least 24 h to remove any residual water. It was then cryodistilled into a 5-mm nmr tube and sealed off.

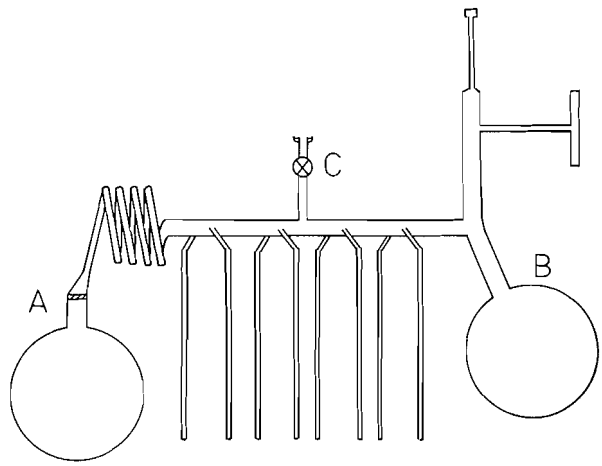

FIG. 1. Schematic of apparatus used for the preparation of anhydrous dimethylamine nmr samples.

The nmr spectra (^{1}H) were obtained with a Bruker HX90 spectrometer (90 MHz, 2.114 T) equipped with a Bruker B-ST100/700 variable temperature controller (±0.5°C) and Nicolet 1174 signal averager.

Results

The data presented in this paper for ^{14}N spin-lifetimes in dimethylamine, methylamine, and ammonia have been obtained from current research ($(CH_3)_2NH$), previous research (CH_3NH_2 (5)), and the literature (NH_3 (8)). The previously obtained ^{14}N spin-lifetime data for ammonia (8) and methylamine (5) were originally used to allow calculation of the base-catalyzed exchange kinetics in the $NH_3/\bar{N}H_2$ and $CH_3NH_2/CH_3\bar{N}H$ systems. The ^{14}N spin-lifetimes' relevance to the determination of ^{14}N quadrupolar parameters was not addressed in these papers.

For the anhydrous dimethylamine case a typical amino pro-

[1]AECL No. 8299.

Can. J. Chem. Downloaded from www.nrcresearchpress.com by 210.87.254.40 on 09/06/12
For personal use only.

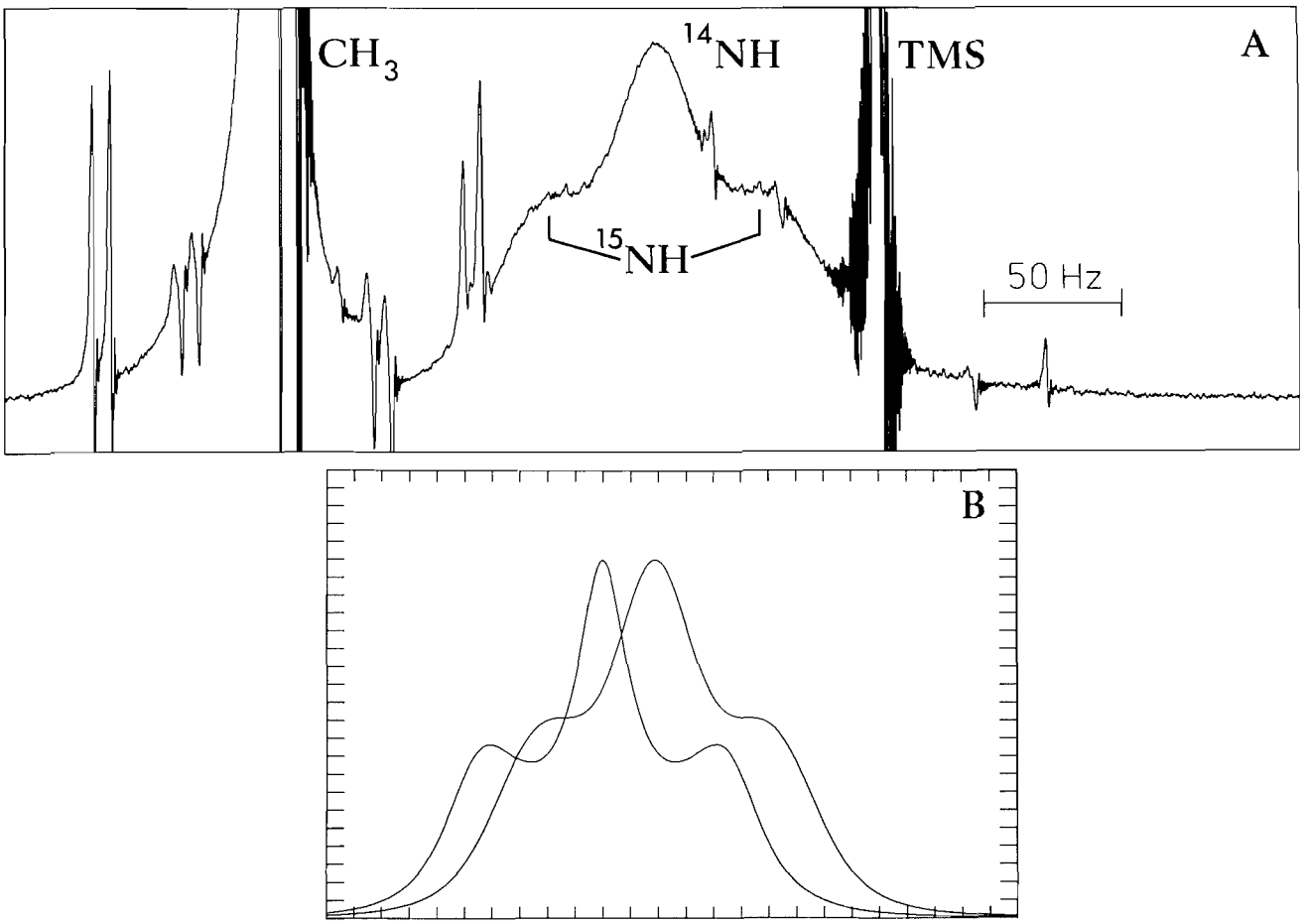

FIG. 2. A. Amino proton spectrum of anhydrous dimethylamine at 58.4°C. The calculated spectra (B) show both the uncoupled spectrum and the effects of spin-coupling with the methyl protons (J = 6.3$_4$ Hz). This latter spectrum is offset to the right for clarity.

TABLE 1. ^{14}N—H and H—^{14}N—C—H Coupling constants

Compound	$J_{^{14}NH}$ (Hz)	$J_{H^{14}NCH}$ (Hz)
Ammonia[a]	43.8	—
Methylamine	46.7	7.04
Dimethylamine	49.2	6.34

[a]Reference 8.

ton nmr spectrum is shown in Fig. 2, along with the simulated spectrum calculated using the procedure of Sack (1) and Pople (2), described below. These amino resonances are broader than those measured for methylamine (5), indicating an increased asymmetry in the electric field gradient at the ^{14}N nucleus with increased methyl group substitution on the nitrogen nucleus. Since amino proton exchange has been suppressed by the purification technique (the methyl groups show sharp multiplets through coupling with the non-exchanging amino proton(s)), the lineshape observed is due solely to coupling with both the ^{14}N nucleus and the protons on the methyl groups. This coupling is included in the theoretical calculation of the spectra.

Lineshape simulation for a proton spin-coupled to a ^{14}N nucleus

The amino proton nmr spectra were analyzed for ^{14}N spin-lifetimes using a lineshape function developed by Sack (1) and Pople (2) and modified with a linewidth parameter by Kintzinger *et al.* (9).

The lineshape is given by eq. [1]

$$[1]\quad I(\nu) \propto R(\mathbf{W}\cdot\mathbf{A}^{-1}\cdot\mathbf{1})$$

where R denotes "real part of", $\mathbf{W}$ is a vector containing the probabilities of the spin states in the ^{14}N, and $\mathbf{A}$ is a lineshape matrix given by eq. [2]

$$[2]\quad \mathbf{A} = \begin{bmatrix} \beta_1 & \frac{1}{\tau} & \frac{2}{\tau} \\ \frac{1}{\tau} & \beta_2 & \frac{1}{\tau} \\ \frac{2}{\tau} & \frac{1}{\tau} & \beta_3 \end{bmatrix}$$

The diagonal elements of $\mathbf{A}$ are defined by eqs. [3]–[5]

$$[3]\quad \beta_1 = i2\pi(\nu_0 - \nu + J_{^{14}NH}) - 3/\tau - 1/T_2$$

$$[4]\quad \beta_2 = i2\pi(\nu_0 - \nu) - 2/\tau - 1/T_2$$

$$[5]\quad \beta_3 = i2\pi(\nu_0 - \nu - J_{^{14}NH}) - 3/\tau - 1/T_2$$

where τ is the ^{14}N spin-lifetime, $1/T_2$ is the linewidth parameter, and $\mathbf{1}$ is the unit matrix.

The following procedure was used to simulate the amino proton spectra for dimethylamine.

1. The H^{14}NCH coupling constant was determined by comparison of the experimental methyl spectrum of this tightly coupled system with simulated spectra calculated with the Quantum Chemistry Program Exchange (QCPE) computer program DNMR3 (10).

2. The ^{14}N—H coupling constant was determined through

Can. J. Chem. Downloaded from www.nrcresearchpress.com by 210.87.254.40 on 09/06/12
For personal use only.

Can. J. Chem. Downloaded from www.nrcresearchpress.com by 210.87.254.40 on 09/06/12
For personal use only.

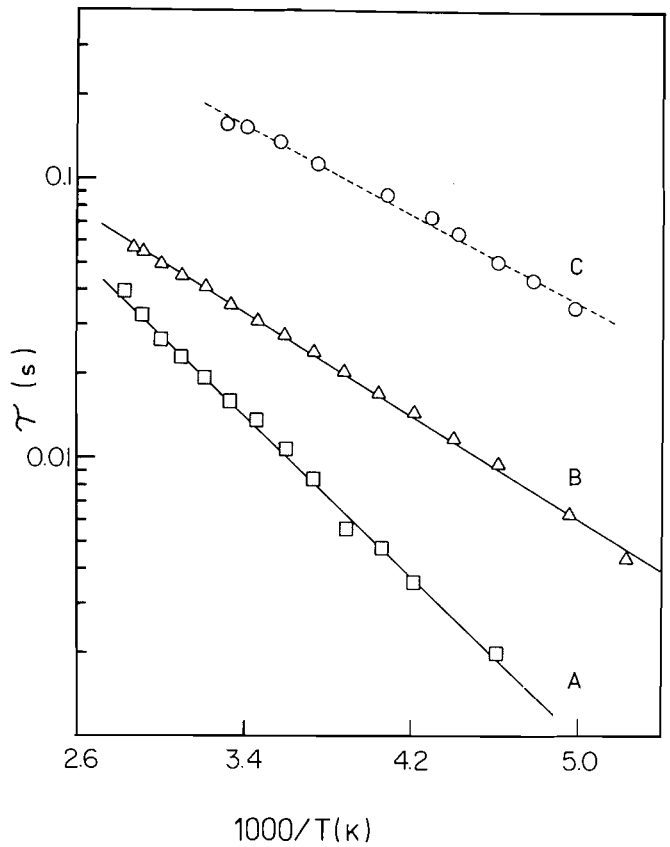

FIG. 3. Natural logarithm of ^{14}N spin-lifetimes, τ(s) vs. reciprocal absolute temperature for: A, dimethylamine; B, methylamine (5); and C, ammonia (8).

TABLE 2. Calculated correlation times τ_q and τ_c at 25°C and the required parameters for their determination

Parameter	Ammonia	Methylamine	Dimethylamine
χ (MHz)[a]	3.161	3.986	4.650
b[a]	0.0	0.186	0.169
^{14}N T_1 (s)	0.03251	0.00701	0.00308
η (N·s·m^{-2})[b]	1.33×10^{-4}	2.14×10^{-4}	1.86×10^{-4}
A (cm)[b]	2.024×10^{-8}	2.403×10^{-8}	2.730×10^{-8}
τ_q(s)	2.08×10^{-13}	6.00×10^{-13}	10.05×10^{-13}
τ_c(s)	1.12×10^{-12}	3.02×10^{-12}	3.85×10^{-12}

[a]Reference 15.
[b]Reference 16.

the experimentally observable ^{15}N—H coupling constant. For dimethylamine the ^{15}NH natural abundance (0.37%) spectrum is visible as a small septet on either side of the broad ^{14}N—H line (Fig. 2A). The magnitudes of the ^{14}NH and ^{15}NH coupling constants are theoretically related through the gyromagnetic ratios for the two nuclei, so that

$$J_{^{14}NH} = -\frac{\gamma_{^{14}N}}{\gamma_{^{15}N}} \cdot J_{^{15}NH}$$

The coupling constants are given in Table 1.

3. The QCPE computer program LAOCN-4A (11) was used to simulate the amino proton spectra in the absence of quadrupolar effects.

4. The above coupling constants and the Sack (1) equation were used to expand each spectral line in step 3, then the envelope of all the lines was obtained by summation for comparison with the experimental spectra.

The calculated spin-lifetimes, τ, are shown in Fig. 3 as a function of temperature. Our previous data for methylamine (5) and the data of Swift *et al.* for ammonia (8) are also included to show the complete series.

An attempt was also made to observe ^{14}N quadrupole effects in trimethylamine through changes in the methyl resonance ^1H spectra. However, as with methylamine and dimethylamine, no vicinal coupling could be measured. This H—C—^{14}N coupling ($J_{HC^{14}N} \leq 0.5$ Hz) has only been measured in very symmetrical compounds ($(CH_3)_4\overset{+}{N}$) where the electric field gradient at the nitrogen nucleus is zero by symmetry or very weak (12).

Discussion

Molecular dynamical parameters that may be derived from the ^{14}N spin-lifetimes shown in Fig. 3 are the molecular reorientation correlation time for isotropic tumbling (τ_q) and the activation energy for molecular reorientation.

1. *Correlation times, τ_q*

The ^{14}N spin-lifetimes are directly related to ^{14}N spin-lattice relaxation times, T_1, by $T_1 = \tau/5$ (13). The correlation time τ_q may be calculated from eq. [6]

$$[6] \quad 1/T_1 = \frac{3}{8}\left(1 + \frac{b^2}{3}\right)(e^2qQ/\hbar)^2\tau_q$$

where $e^2qQ/h = \chi$, the quadrupole coupling constant (MHz) and b is the asymmetry parameter of the electric field gradient. The calculated τ_q (25°C) are given in Table 2, with literature values for χ and b (15) and the ^{14}N T_1 (25°C) determined from the ^{14}N spin-lifetimes measured. The ammonia value of 2.08×10^{-13} s is in good agreement with data from Atkins *et al.* (6) who found τ_q for NH_3 of 1.8×10^{-13} s and τ_q for ND_3 of 2.3×10^{-13} s from ^{14}N data. We may compare these experimentally determined τ_q with a simple theoretical value, τ_c, based on the assumption of a liquid composed of hard spheres with radius A and viscosity η.

$$[7] \quad \tau_c = 4\Pi\eta A^3/kT \qquad \text{(ref. 14)}$$

A may be estimated from the molar volume, V_m (3), assuming hexagonal closepacked spheres: $A = (0.74\ V_m/(4\pi N_0/3))^{1/3}$ where N_0 is Avogadro's number. The values of τ_c (25°C), η, and A are also given in Table 2.

Our data for τ_q are significantly shorter than the values of τ_c estimated from a simple hard sphere model. Similar disagreements have also been noted in other studies (3) with the hard sphere model giving consistently longer estimates of τ_c than experimental values.

2. *Activation energies*

The Arrhenius activation energies for molecular reorientation in ammonia, methylamine, and dimethylamine may be obtained from the slope of the temperature dependence of the ^{14}N spin-lifetimes (τ) in a ln τ vs. $1/T$ plot (Fig. 3). The activation energies calculated from the ^1H nmr data are given in Table 3, along with data obtained from the literature for ^{14}N nmr relaxation time measurements.

The two methods agree within the experimental error limits for ammonia and dimethylamine but the activation energy of methylamine from the ^1H data is less than that reported from the ^{14}N data (8.8 kJ mol^{-1} vs. 11.6 kJ mol^{-1}). It is unlikely that this can be attributed to any residual amino proton exchange in the system because the amino proton coupling to the methyl group

TABLE 3. Comparison of E_a from ^1H and ^{14}N nuclear magnetic resonance measurements

Compound	E_a (^1H) (kJ mol^{-1})	E_a (^{14}N) (kJ mol^{-1})
NH_3	7.59±0.23	7.87±0.21[a]
ND_3	—	7.87±0.25[a]
CH_3NH_2	8.82±0.10	—
CH_3ND_2	—	11.63±0.59[b]
$(CH_3)_2NH$	13.82±0.25	—
$(CH_3)_2ND$	—	13.39±0.42[b]
$(CH_3)_3N$	—	5.02±0.17[b]

[a]Reference 6.
[b]Reference 7.

protons was well resolved even at the highest temperature. Calculation of the ^{14}N spin lifetimes from the ^{14}N data (7) shows that at 60°C the value is comparable to that obtained from the ^1H spectra but at −73°C the value is lower.

The accounts for the higher activation energy from the ^{14}N data. Thus any interaction with the protons that would increase with decreasing temperature might be the source of this difference. Increased molecular association through hydrogen bonding in the methylamine at reduced temperatures fulfills the requirements stated and it is conceivable that this could influence the ^1H nmr spectra such that it would lead to slightly differing values for the calculated τ.

In conclusion, we have shown that ^1H nmr measurements on protons spin-coupled to ^{14}N in carefully purified simple aliphatic amines can provide data on the quadrupolar interactions within the molecules that are in reasonable agreement with ^{14}N nmr studies (6, 7). Slight differences may be accounted for through hydrogen bonding effects.

Acknowledgements

The authors would like to thank Dr. J. H. Rolston for helpful discussions.

1. R. A. SACK. Mol. Phys. **1**, 163 (1958).
2. J. POPLE. Mol. Phys. **1**, 168 (1958).
3. W. B. MONIZ and H. S. GUTOWSKY. J. Chem. Phys. **38**, 1155 (1963).
4. (*a*) L. PAOLILLO and E. D. BECKER. J. Mag. Reson. **3**, 200 (1970); (*b*) K. P. SHRESTHA and K. L. HENOLD. J. Am. Chem Soc. **95**, 6699 (1973).
5. J. D. HALLIDAY and P. E. BINDNER. J. Phys. Chem. **83**, 1829 (1979).
6. P. W. ATKINS, A. LOEWENSTEIN, and Y. MARGALIT. Mol. Phys. **17**, 329 (1969).
7. A. LOEWENSTEIN and R. WAIMAN. Mol. Phys. **25**, 49 (1973).
8. T. J. SWIFT, S. B. MARKS, and W. G. SAYRE. J. Chem. Phys. **44**, 2797 (1966).
9. J. P. KINTZINGER, J. M. LEHN, and R. L. WILLIAMS. Mol. Phys. **17**, 135 (1969).
10. Quantum Chemistry Program Exchange, D. A. Kleier and G. Binsch. Program No. 165, DNMR3.
11. Quantum Chemistry Program Exchange, Jean A. Musso. Program No. 232, LAOCN-4A.
12. J. M. LEHN and J. P. KINTZINGER. Nitrogen-14 nuclear quadrupole effects. *In* Nitrogen NMR. *Edited by* M. Witanowski and G. A. Webb. Plenum Press, New York. 1973. Chapt. 3. p. 143.
13. A. ABRAGAM. The principles of nuclear magnetism. Oxford University Press, Oxford, England. 1961.
14. N. BLOEMBERGEN, E. M. PURCELL, and R. V. POUND. Phys. Rev. **73**, 679 (1948).
15. E. A. C. LUCKEN. Nuclear quadrupole coupling constants. Academic Press, New York. 1969. p. 221.
16. The Matheson unabridged gas data book. Matheson Gas Products, 1974.

Can. J. Chem. Downloaded from www.nrcresearchpress.com by 210.87.254.40 on 09/06/12
For personal use only.

Analytic results for finite systems of ringed flory polymers

JOHN L. SPOUGE

Theoretical Division, University of California, Los Alamos National Laboratory, Los Alamos, NM 87545 USA

Received August 29, 1983

JOHN L. SPOUGE. Can. J. Chem. **62**, 1262 (1984).

We examine Flory's RA_f model of polymerization for a finite closed system of N monomers. Monomers have f functional groups of type A. Random stepwise reaction between A's, regardless of ring formation, bonds the monomers together.

We give exact statistics for the resulting polymer distribution and verify the results of the Falk and Thomas computer simulation. As $N \rightarrow \infty$, Flory's modification of the Stockmayer distribution gives the distribution of finite polymers, and cyclization is confined to the gel.

Similar results hold for Flory's A_gRB_{f-g} model.

JOHN L. SPOUGE. Can. J. Chem. **62**, 1262 (1984).

Nous examinons le modèle de polymérisation RA_f de Flory pour un système formé de N monomères. Les monomères ont f groupes fonctionnels de type A. Une réaction aléatoire par étapes entre des groupes A, sans égard à la formation de cycles, relie ensemble les monomères.

Nous donnons des statistiques exactes relatives à la distribution du polymère qui en résulte et nous vérifions les résultats de la simulation par ordinateur de Falk et de Thomas. Lorsque $N \rightarrow \infty$, la modification apportée par Flory à la distribution de Stockmayer permet de déterminer la distribution des polymères finis et la cyclisation est confinée au gel.

On obtient des résultats analogues avec le modèle A_gRB_{f-g} de Flory.

[Traduit par le journal]

Introduction

Flory's RA_f model (1) serves as a paradigm of chemical polymerization. In this model, each monomeric unit has f functional groups of type A. Stepwise reaction between A's bonds the units together, forming polymers.

Let α be the proportion of A's which have reacted at a given time. Assuming that the A's react independently with probability α, and that *intramolecular reaction does not occur*, Flory (2) showed that an infinite polymer (gel) formed only for $f \geqq 3$ and that gelation took place at

$$[1] \quad \alpha_c = (f - 1)^{-1}$$

If the initial monomers have concentration 1, Stockmayer (3) showed that when the extent of reaction is α, the n-mer concentration is

$$[2] \quad x_n = \frac{w_n}{n!} \frac{\alpha^{n-1}(1 - \alpha)^{fn-2n+2}}{f^{n-1}}$$

where

$$[3] \quad w_n = \frac{f^n(fn - n)!}{(fn - 2n + 2)!}$$

is the number of ways of constructing one polymer from n units under classical statistics (i.e., all A's, though chemically identical, are distinguishable). Exclusion of intramolecular reaction ensures that only branched-chain polymers form.

Although Stockmayer's derivation indicated that eq. [2] was valid only for $\alpha < \alpha_c$, Flory (4) held that eq. [2] was valid for all α. Flory himself (ref. 4, p. 192) says: "in deducing these distribution equations it was merely necessary to assume, or rather to make the approximation, that no intramoleclular reactions occur *within finite species*" (italics his).

Whiteway *et al.* (5) challenged the restriction of intramolecular reaction to the gel as logically inconsistent, sparking a debate (6–8) which was settled by the Falk and Thomas (9) computer simulation.

In their "Rings Allowed Model", Falk and Thomas took a finite, closed system of N monomers. They paired the fN functional groups stepwise at random while keeping track of polymer sizes n and bond numbers b (i.e., $b = n - 1$ for ringless polymers). As $N \rightarrow \infty$, they found that the limiting distribution of finite polymers approached eq. [2] for all α; asymptotically, rings did not occur for $\alpha < \alpha_c$ and were "limited to infinite polymers" for $\alpha > \alpha_c$, thereby vindicating Flory's assumptions. Donoghue (10) also confirmed Flory's gel predictions by simulation.

In their "Rings Forbidden Model", Falk and Thomas performed a similar simulation but excluded intramolecular reactions and derived results consistent with Stockmayer's formulas. Ziff and Stell (11) later confirmed analytically that in the Stockmayer model, the gel reacts neither with the sol nor itself; whereas in Flory's model, it reacts with both.

Donoghue and Gibbs (12–14) gave asymptotics for the Stockmayer model; this paper gives asymptotics for the Flory Model, which is the "Rings Allowed Model" of Falk and Thomas. Our results confirm the conclusions drawn by Falk and Thomas.

Polymer distribution and cyclization

Consider a closed system of N RA_f monomers in which B bonds join $2B$ of the fN functional groups. If the functional groups are distinguishable, there are

$$[4] \quad \Omega_{NB} = \frac{(fN)!}{(fN - 2B)!\, 2^B B!}$$

ways this can occur. Equation [4], first given by Harris (15), is proved as follows. Label the A's $1, 2, \ldots, fN$ and choose $2B$ of them. Permute the chosen A's $(2B!)$ and bond the A's in the 1st, 3rd, 5th, ... positions to the A's following them. This overestimates Ω_{NB} by a factor of $2^B B!$ since order within bonded pairs is immaterial (2^B), as is the order of the bonded pairs themselves $(B!)$.

The proportion of reacted A's is

$$[5] \quad \alpha = \frac{2B}{fN}$$

Let m_{nb} be the number of n-mers containing b bonds, and let $\Omega_{NB}(m_{nb})$ be the number of realizations of the system which

Can. J. Chem. Downloaded from www.nrcresearchpress.com by 210.87.254.40 on 09/06/12
For personal use only.

Can. J. Chem. Downloaded from www.nrcresearchpress.com by 210.87.254.40 on 09/06/12
For personal use only.

produce m_{nb} b-bonded n-mers. Clearly

$$[6] \quad \Omega_{NB} = \sum_{(m_{nb})} \Omega_{NB}(m_{nb})$$

the sum being over $m_{nb} = 0, 1, 2, \ldots$.

The expected number of b-bonded n-mers, averaged over the Ω_{NB} system states, is

$$[7] \quad E_{NB}(m_{nb}) = \frac{\Sigma m_{nb}\Omega_{NB}(m_{nb})}{\Omega_{NB}}$$

(We abbreviate E_{NB} to E in future and sums are over $m_{nb} = 0, 1, 2 \ldots$ unless otherwise stated.)

But

$$[8] \quad \sum m_{nb}\Omega_{NB}(m_{nb}) = \frac{N!}{(N-n)!n!} w_{nb}\Omega_{N-n,B-b}$$

where w_{nb} is the number of ways of bonding n units into a b-bonded n-mer. (w_n of eq. [3] is now $w_{n,n-1}$.)

Proof: The number of ways of bonding the system to produce m_{nb} b-bonded n-mers ($\Omega(m_{nb})$) and then painting one of the m_{nb} b-bonded n-mers black (m_{nb}) is equal to the number of ways of painting n of the initial N units black, combining them into a black b-bonded n-mer (w_{nb}) and then forming $B - b$ bonds among the remaining $N - n$ units. In each case the system has a total of N units, B bonds, and one black b-bonded n-mer.

The expected concentration of b-bonded n-mers in the system, normalized so that the initial monomeric concentration is 1, is

$$[9] \quad x_{nb} = \frac{E(m_{nb})}{N}$$

Although we have no closed form of w_{nb} except when $b = n - 1$ ($w_{n,n-1}$ is the w_n of eq. [3]), eqs. [4] [7], [8], and [9] yield an exact expression for x_{nb}. Repeated use of the inequality $1 \geqq (1 - a)(1 - b) \geqq 1 - (a + b)$ yields

$$[10] \quad \frac{K!}{(K-k)!} = K^k\left(1 - \frac{1}{K}\right)\left(1 - \frac{2}{K}\right)\ldots\left(1 - \frac{k-1}{K}\right)$$
$$= K^k\left[1 + O\left(\frac{k^2}{K}\right)\right]$$

Hence,

$$[11] \quad x_{nb} = \frac{w_{nb}}{n!}\frac{\alpha^b(1-\alpha)^{fn-2b}}{f^b} N^{(n-1)-b}\left[1 + O\left(\frac{n^2}{N}\right)\right]$$

When $b = n - 1$ (ringless polymer), eq. [11] is in asymptotic agreement with eq. [2]. There are no ringed polymers ($b > n - 1$) of finite size in the limit as $N \to \infty$.

Analogously to eq. [8], we may prove

$$[12] \quad \sum m_{nb}(m_{nb} - 1)\Omega_{NB}(m_{nb}) = \frac{N!}{(N-2n)!n!n!} \times w_{nb}^2\Omega_{N-2n,B-2b}$$

by blackening two b-bonded n-mers in the system. Following the logic of eqs. [7]–[11], we find

$$[13] \quad \mathrm{var}\left(\frac{m_{nb}}{N}\right) = \frac{E^2(m_{nb}) - E^2(m_{nb})}{N^2} = O\left(\frac{n^2}{N}\right)$$

so that the concentration of b-bonded n-mers is asymptotically the same for almost all realizations of the system.

Falk and Thomas also examined the system cyclization

$$[14] \quad C = \frac{B - \sum_{(nb)}(n-1)m_{nb}}{N}$$

which gives the number of bonds per unit in excess of those required for ringless polymers. ((nb) denotes a sum over $n = 1, 2, 3, \ldots$, and $b = n - 1, n, n + 1, \ldots$.)

Units are conserved,

$$[15] \quad N = \sum_{(nb)} nm_{nb}$$

so the expected cyclization is

$$[16] \quad \bar{C} = E(C) = \frac{f\alpha}{2} - 1 + \sum_{(nb)} x_{nb}$$

If the last term is asymptotically equal to the total concentration of polymers in the Flory model, then use of eq. [13] of Ziff and Stell (11) gives

$$[17] \quad \bar{C} = \begin{cases} 0 & \alpha < \alpha_c \\ \dfrac{f\alpha}{2} - 1 + \dfrac{1}{2}[f(1-\alpha)\zeta^{f-1} - (f-2)\zeta^f] & \alpha > \alpha_c \end{cases}$$

where ζ is the only positive root of

$$[18] \quad \zeta + \zeta^2 + \cdots + \zeta^{f-2} = \frac{1-\alpha}{\alpha}$$

Equations [17] and [18] agree with the Falk and Thomas simulation. Proof rests on verification of the hypothesis following eq. [16].

Equations [9] and [15] show

$$[19] \quad \sum_{(nb)} nx_{nb} = 1 \qquad x_{nb} \geqq 0$$

and we note that

$$[20] \quad w_{nb} \leqq w_{n,b-1}(fn)^2 \leqq \cdots \leqq w_{n,n-1}(fn)^{2[b-(n-1)]}$$

since the number of ways of building a b-bonded n-mer is less than the number of ways of building a $(b - 1)$-bonded n-mer and then bonding two more groups together. Inequality [20], though unnecessarily weak, is all we require.

Let $0 < \epsilon < \frac{1}{2}$ and let (n_ϵ) denote a sum over all $n \leqq N^{1/2-\epsilon}$. Then we can bound the total concentration of ringed polymers of size $\leqq N^{1/2-\epsilon}$:

$$[21] \quad \sum_{(n_\epsilon)}\sum_{b \geqq n} x_{nb} \leqq \sum_{(n_\epsilon)} x_{n,n-1}\sum_{b \geqq n} O\left(\frac{n^2}{N}\right)^{b-(n-1)}$$
$$\leqq \sum_{(n_\epsilon)} x_{n,n-1}O(n)O\left(\frac{n^2}{N}\right) \leqq O(N^{-2\epsilon})$$

Note eqs. [11] and [20]. The inner sum has $O(n)$ terms, since an n-mer has at most $\frac{1}{2}fn$ bonds. Equation [19] completes the proof.

If $\sim(n_\epsilon)$ denotes a sum over all $n > N^{1/2-\epsilon}$, then

$$[22] \quad \sum_{\sim(n_\epsilon)}\sum_{b \geqq n-1} x_{nb} \leqq N^{-1/2+\epsilon}\sum_{\sim(n_\epsilon)}\sum_{b \geqq n-1} nx_{nb} \leqq N^{-1/2+\epsilon}$$

If $\epsilon = 1/6$, then eqs. [11], [21], and [22] show the total polymer concentration deviates from the Flory value by $O(N^{-1/3})$, thereby proving eq. [17] (except when the error term from eq. [11], $O(\Sigma n^2 x_{nb})$, diverges for the Flory distribution at $\alpha = \alpha_c$).

Using the novel techniques of Whittle (16), section 6, a tortuous derivation which I omit yields

$$[23] \quad \sum_{(nb)} n^2 x_{nb} \sim N(1 - \zeta^f)^2 \qquad \alpha > \alpha_c$$

where ζ is given by eq. [18]. This result is consistent with a "gel" containing $N(1 - \zeta^f)$ units as predicted by the Flory model.

The A_gRB_{f-g} model

This model, also introduced by Flory (1), is like the RA_f model except that monomers have g A groups and $f - g$ B groups. Only A—B bonds form. Spouge (17) gives the principal results for the model.

As before, random stepwise reaction between A's and B's produces B bonds between N units. If α is the proportion of reacted A groups and β the proportion of reacted B groups, then

$$[24] \quad r = \frac{B}{N} = g\alpha = (f - g)\beta$$

The number of ways of forming B bonds between N monomers is

$$[25] \quad \Omega_{NB} = \frac{(gN)!}{(gN - B)!} \frac{[(f - g)N]!}{[(f - g)N - B]!} \frac{1}{B!}$$

The logic of eqs. [6] – [11] gives

$$[26] \quad x_{nb} = \frac{w_{nb}}{n!} \frac{(1 - \alpha)^{gn-b}(1 - \beta)^{(f-g)n-b} r^b}{g^b(f - g)^b} \times N^{(n-1)-b}\left[1 + O\left(\frac{n^2}{N}\right)\right]$$

where w_{nb} is the number of ways of building a b-bonded n-mer from A_gRB_{f-g} units. This agrees with previous results.

Further results for the A_gRB_{f-g} model are similar to those for the RA_f model.

Discussion

This paper shows that Flory's exclusion of the intramolecular reaction in finite polymers, but not in the gel, is logically consistent. If intramolecular reaction is not specifically favored, it is negligible except in the gel because any sol molecule contains an infinitesimal proportion of the functional groups available for reaction. This fact, long known and now proven, has spurred the development of models which specifically incorporate intramolecular reaction (18, 19).

Donoghue's (14) analysis of gel statistics in the Stockmayer model is more precise than is presently possible for the Flory model. Mathematical techniques for handling the divergent generating functions introduced by rings are few and require exploration. Whittle (16) gives some techniques for handling such functions. The Flory RA_f model is the special case $H(x) = (1 + x)^f$ of his paper as been shown by Spouge (20).

Acknowledgements

This work was supported by a Fellowship from the Medical Research Council of Canada. Revisions were supported by the U.S. Department of Energy.

1. P. J. FLORY. Principles of polymer chemistry. Cornell University Press, Ithaca, New York. 1953. Chapt. 9.
2. P. J. FLORY. J. Am. Chem. Soc. **63**, 3082 (1941); **63**, 3091 (1941); **63**, 3096 (1941).
3. W. H. STOCKMAYER. J. Chem. Phys. **11**, 45 (1943).
4. P. J. FLORY. Chem. Rev. **38**, 137 (1946).
5. S. G. WHITEWAY, I. B. SMITH, and C. R. MASSON. Can. J. Chem. **48**, 33 (1970).
6. C. R. MASSON, I. B. SMITH, and S. G. WHITEWAY. Nature, **234**, 97 (1971).
7. R. F. T. STEPTO. Can. J. Chem. **52**, 1188 (1974).
8. C. R. MASSON and S. G. WHITEWAY. Can. J. Chem. **52**, 1190 (1974).
9. M. FALK and R. E. THOMAS. Can. J. Chem. **52**, 3285 (1974).
10. E. DONOGHUE. Macromolecules, **15**, 1634 (1982).
11. R. M. ZIFF and G. STELL. J. Chem. Phys. **73**, 3492 (1980).
12. E. DONOGHUE and J. H. GIBBS. J. Chem. Phys. **70**, 2346 (1979).
13. E. DONOGHUE and J. H. GIBBS. J. Poly. Sci. Poly. Symp. **63**, 131 (1978).
14. E. DONOGHUE. J. Chem. Phys. **77**, 4236 (1982).
15. F. E. HARRIS. J. Chem. Phys. **23**, 1518 (1955).
16. P. WHITTLE. Adv. Appl. Prob. **12**, 94 (1980).
17. J. L. SPOUGE. Macromolecules, **16**, 831 (1983).
18. M. GORDON and G. R. SCANTLEBURY. J. Chem. Soc. B, **1** (1966).
19. W. B. TEMPLE. Macromol. Chem. **160**, 277 (1972).
20. J. L. SPOUGE. Proceedings of the conference on random graphs, Poznan, North Holland, 1983. To be published.

Can. J. Chem. Downloaded from www.nrcresearchpress.com by 210.87.254.40 on 09/06/12
For personal use only.

Effects of solvent structure on electron reactivity and radiolysis yields: 2-propanol/water mixed solvents[1]

JOANNA CYGLER[2] AND GORDON R. FREEMAN
Department of Chemistry, University of Alberta, Edmonton, Alta., Canada T6G 2G2

Received August 23, 1984

JOANNA CYGLER and GORDON R. FREEMAN. Can. J. Chem. **62**, 1265 (1984).

Reaction of solvated electrons with nitrobenzene, N, is nearly diffusion controlled in both pure solvents; $k_N \sim 10^{10}$ dm^3/mol s. The value of k_N is approximately proportional to the inverse viscosity η^{-1} in the pure solvents, and in the mixed solvents at different temperatures. However, on going from zero to 74 mol% water at the same temperature k_N is independent of the 40% increase of η. Electron diffusion in the mixed solvents is not a simple function of fluidity.

Reaction with the inefficient scavengers tryptophane ($k_S \sim 10^9$ dm^3/mol s) and phenol ($k_S \sim 10^7$–10^8 dm^3/mol s) correlates inversely with the electron optical absorption energy. The latter is related to the trap depth in the solvent; electrons in deeper traps have less tendency to react with molecules of low electron affinity.

Addition of 3 mol% 2-PrOH to water at 296 K increases the value of $G\epsilon_{max}$ by 16%, although the value in pure 2-PrOH is three-fold smaller than that in pure water. The increase is attributed to an increase in the free ion yield, caused by an increase in the product of the electron thermalization range and the microscopic dielectric constant of the fluid between the ion and electron, averaged over the time that they exist as a correlated pair. Addition of a small amount of alcohol to water increases the orderliness of the water structure.

JOANNA CYGLER et GORDON R. FREEMAN. Can. J. Chem. **62**, 1265 (1984).

La réaction des électrons solvatés avec le nitrobenzène, N, est une réaction qui est à toutes fins pratiques contrôlée par la diffusion dans les deux solvants à l'état pur; $k_N \sim 10^{10}$ dm^3/mol s. La valeur de k_N est approximativement proportionnelle à l'inverse de la viscosité η^{-1} dans les solvants purs et dans les solvants mixtes à différentes températures. Cependant, si on opère à une température constante et que l'on fait varier la quantité d'eau de zéro jusqu'à 74 mol% d'eau, la valeur de k_N ne varie pas malgré une augmentation de 40% de la valeur de η. La diffusion des électrons dans les solvants mixtes n'est pas une fonction simple de la fluidité.

La réaction avec des pièges inefficaces comme le tryptophane ($k \sim 10^9$ dm^3/mol s) et le phénol ($k \sim 10^7$–10^8 dm^3/mol s) est en corrélation inverse avec l'énergie d'absorption optique de l'électron. Cette énergie est reliée à la profondeur du piège dans le solvant; les électrons localisés dans les pièges les plus profonds ont moins tendance à réagir avec les molécules qui ont une petite affinité électronique.

L'addition de 3 mol% de PrOH-2 à l'eau à 296 K augmente la valeur de $G\epsilon_{max}$ de 16% bien que la valeur dans le PrOH à l'état pur soit 3 fois plus faible que dans l'eau pure. On attribue l'augmentation à une augmentation du rendement en ion libre provoquée par une augmentation du produit du domaine de la thermalisation de l'électron et de la constante diélectrique microscopique du fluide entre l'ion et l'électron pondéré par rapport au temps où ils existent sous forme de paire d'ions. L'addition de petites quantités d'alcool à l'eau augmente l'ordre de la structure de l'eau.

[Traduit par le journal]

Can. J. Chem. Downloaded from www.nrcresearchpress.com by 210.87.254.6 on 09/06/12
For personal use only.

Introduction

Solutions of hydroxy-compounds in water show many interesting abnormalities and for that reason have been the subject of intensive studies in many fields. Especially interesting are monohydric alcohol–water mixtures, because they deviate greatly from ideal behaviour.

In spite of many studies of various properties of alcohol–water mixtures, for example excess thermodynamic functions (1–9), viscosities (1–3, 10–13), acoustics (13), and dielectric relaxation (1, 14, 15), the nature and structure of these systems is little understood. The peculiar behaviour can be qualitatively attributed to the polar/non-polar bifunctional nature of alcohol molecules, which, depending on the composition of the mixture, can enhance or diminish the amount of orderliness in the intermolecular structure of the liquid.

In this laboratory, various aspects of electron behaviour in hydroxylic solvents have been studied (16–24). Recently (22, 23) it was found that the optical absorption spectra of solvated electrons in alcohol–water mixtures display a strong composition dependence, which was attributed to changes in solvent structure. One might therefore expect to find changes in electron reaction rate constants. The aim of the present work was to determine the reactivity of solvated electrons with different types of scavengers in 2-propanol/water mixtures of various composition.

Experimental

Materials

Spectral grade (99+%) 2-propanol, nitrobenzene (99%), L-tryptophane (99%), and phenol (99+%) were obtained from Aldrich Co. Reagent grade sodium borohydride was obtained from Fisher Scientific Co.

The 2-propanol (2-PrOH) was stored over freshly activated (200°C) molecular sieves 4A for one week and then fractionally distilled. Sodium borohydride (2 g/L) and a new portion of freshly activated molecular sieves were added to the distillation flask. The distillate was carefully protected from moisture by a tube filled with molecular sieves and silica gel. The distillation was performed under UHP argon (Liquid Carbonic Co.) atmosphere. The middle 50% of the alcohol was collected and stored under UHP argon in a flask equipped with a syphon system. Argon pressure was used to transfer alcohol from the storage flask without contaminating the rest of it with air.

The purity of 2-PrOH treated in the above way was checked by uv spectrophotometry. The spectrum was completely structureless at wavelengths down to 220 nm. The water content as measured by the Karl-Fischer method (25) was 0.2 mol%.

The water was always freshly, triply distilled from acidic dichromate, basic permanganate, and no added reagent, under nitrogen

[1] Financially assisted by the Natural Sciences and Engineering Research Council of Canada.

[2] On leave from the Institute of Radiation Chemistry, Technical University of Łódź, Poland.

(Commercial grade, Liquid Carbonic Co.) atmosphere. Nitrobenzene was purified by simple distillation and stored under UHP argon.

Phenol and tryptophane were used as received.

Techniques

Mixtures of 2-PrOH and water were prepared by volume measurement. Stock solutions of scavengers were prepared in volumetric flasks. Nitrobenzene was injected by a microliter syringe. Tryptophane and phenol solutions were prepared by weight. The actual solutions for measurements, made from properly diluted stock solutions, were poured into Spectrosil cells (10 mm optical path) and bubbled with UHP argon at ~15 cm^3/min through long stainless steel needles for ~45 min before sealing the cells (17).

The concentration of scavenger was determined after bubbling, by spectrophotometric measurements at 258 nm (nitrobenzene), 273 nm (phenol), or 281 nm (tryptophane). Solutions of phenol and sometimes of tryptophane had to be diluted in order to measure their concentrations. In such cases the concentration measurements were performed after the pulse radiolysis experiments were completed.

The methods of irradiation, dosimetry, and optical measurements were similar to those described earlier (19, 26). The 100 ns pulses of 1.9 MeV electrons delivered a dose of 2–3 × 10^{16} eV/g. The temperature was controlled to within ±0.5°C. The optical measurements were performed at the absorption maximum of the solvated electron band at each temperature, on the basis of the results obtained by Leu (22, 23).

Results and discussion

A. Yields of solvated electrons

The values of $G\epsilon_{max}$ were measured at the end of the pulse for various compositions of 2-PrOH/H_2O mixture in the absence of scavenger, at 296 K. The results are shown in Fig. 1. Since the decay of e^-_s under the conditions of our experiments was first order, all electrons observed were free-ion solvated electrons. The densities of solutions used in $G\epsilon_{max}$ calculations were taken from Roux and co-workers (8).

The value of $G\epsilon_{max}$ in pure water agrees to within 2% with those reported earlier (23, 27). For pure 2-PrOH, using ϵ_{max} = 1.3 × 10^4 M^{-1} cm^{-1} (28) we obtain $G(e^-_s)$ = 1.2; this agrees with the value 1.2 ± 0.2 obtained from scavenging studies (16).

In the mixtures with low alcohol content, $G\epsilon_{max}$ is very sensitive to composition. Small addition of alcohol to water causes quite a dramatic increase of $G\epsilon_{max}$ values. The value reaches a sharp maximum for ~3 mol% of 2-PrOH. With further increase of the alcohol content the $G\epsilon_{max}$ values decrease. Similar dependence of $G\epsilon_{max}$ on the composition of water alcohol mixtures has been observed by Leu and Jha (23*b*) in methanol, ethanol, and 1-propanol. The initial increase of $G\epsilon_{max}$ values correlates with a small increase of the energy of the peak of the e^-_s spectrum, $E_{\epsilon max}$, for small amounts of alcohol in water (22). The maximum in the plot of $G\epsilon_{max}$ against mixture composition is the most pronounced for 1-PrOH, and so is the increase of $E_{\epsilon max}$. This behaviour can be discussed in terms of solvent structure changes. There are experimental evidences that the addition of a small amount of monohydric alcohol changes the structure of liquid water. No complete model of water structure yet exists. A group of oversimplified models, each able to explain certain properties of water, known under the common name of "mixture models" (29–31), are generally used. Some of them assume that liquid water consists of two different types of species: hydrogen bonded molecules which form 3-dimensional clusters, similar to those proposed for ice V, and free non-bonded molecules. Interstitial models, which are a special class of mixture models, assume that non-bonded water molecules occupy cavities between bonded clusters (30, 31).

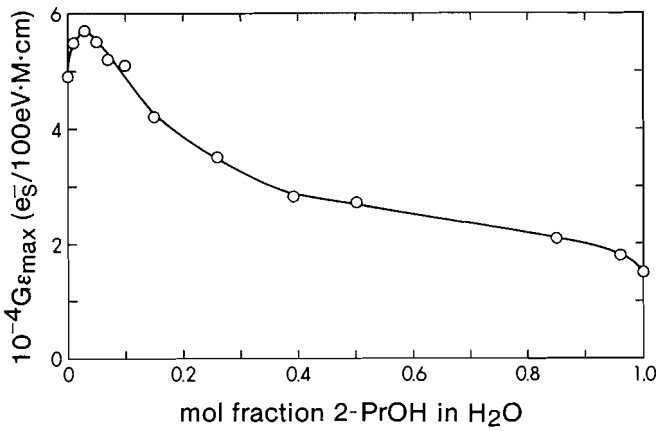

FIG. 1. Composition dependence of $G\epsilon_{max}$ for free-ion solvated electrons in 2-PrOH/H_2O mixtures, at the end of a 100 ns pulse, 296 K.

In contrast to pure water, monohydric alcohols do not form a 3-dimensional structure. They form linear polymers which exist in equilibrium with non-bonded molecules (1). The association of alcohols tends to decrease with increasing molecular weight and in the sequence primary, secondary, tertiary. Addition of a small amount of alcohol to water leads at first to enhancement of water structure. This is confirmed by such experimental facts as the composition dependence of thermodynamic functions of mixing (1, 2, 4, 6), partial molar volumes and expansibilities (5, 7–9, 32), structural contribution to the temperature of maximum density (TMD) of alcohol–water mixtures (33, 34), mutual diffusion coefficients (35–37), and sound absorption and velocity (13).

Excess entropy of mixing is negative and decreases rapidly for small alcohol concentrations in water, reaching a minimum around 20 mol% of alcohol (1, 2).

Partial molar volumes display a sharp minimum and partial molar expansibilities a maximum in the low concentration range (2–7 mol%) of alcohol (5, 7–9, 32).

There is a maximum for the structural contribution to the temperature of maximum density in aqueous solutions of alcohols between 2 and 4 mol% of alcohol (33, 34).

Especially interesting is the behaviour of viscosity, η, and related parameters for aqueous alcohol solutions. Addition of a small amount of alcohol to water rapidly increases the viscosity of the mixture, which reaches a maximum around 20 mol% of alcohol (1–3, 10, 11, 13) (Fig. 2). The derivative curve $\Delta\eta/\Delta x_2$, where x_2 is the mole fraction of alcohol, has a sharp maximum for a few mol% of ethanol in water (2, 3). This behaviour is believed to be typical for the structure stabilization processes. Also, as was shown by Ueberreiter (32), the so-called structure temperatures of mixtures of water with various alcohols have a maximum in the range of 0–20 mol% of alcohol. In a similar concentration range the mutual diffusion coefficients have a minimum in alcohol–water solutions (35–37). All the above facts can be qualitatively explained on the basis of the Samoilov interstitial model (30), as formulated by Franks (31) (who introduced such terms as hydrophobic and hydrophilic solvation), indicating stabilization of the water structure. Alcohol molecules fill the cavities between ice-like clusters, stabilizing their structure. The power of stabilization increases with the size of the hydrophobic alkyl group. This is

Can. J. Chem. Downloaded from www.nrcresearchpress.com by 210.87.254.6 on 09/06/12
For personal use only.

Can. J. Chem. Downloaded from www.nrcresearchpress.com by 210.87.254.6 on 09/06/12
For personal use only.

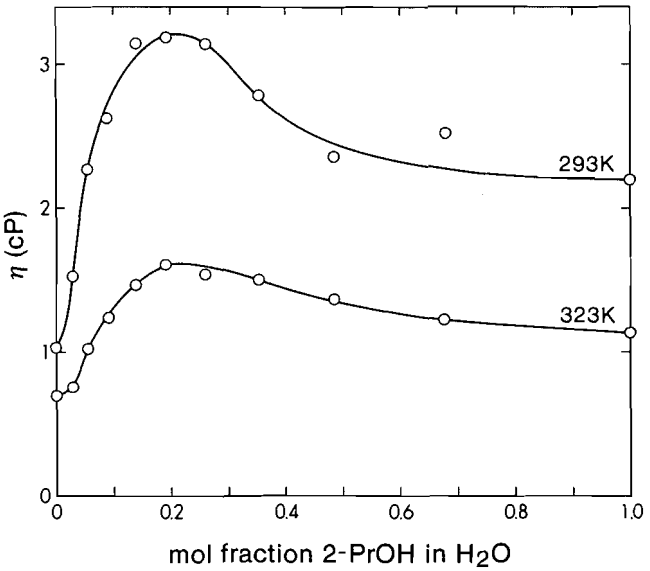

FIG. 2. Composition dependence of shear viscosity in 2-PrOH/H_2O mixtures. Data from ref. 13.

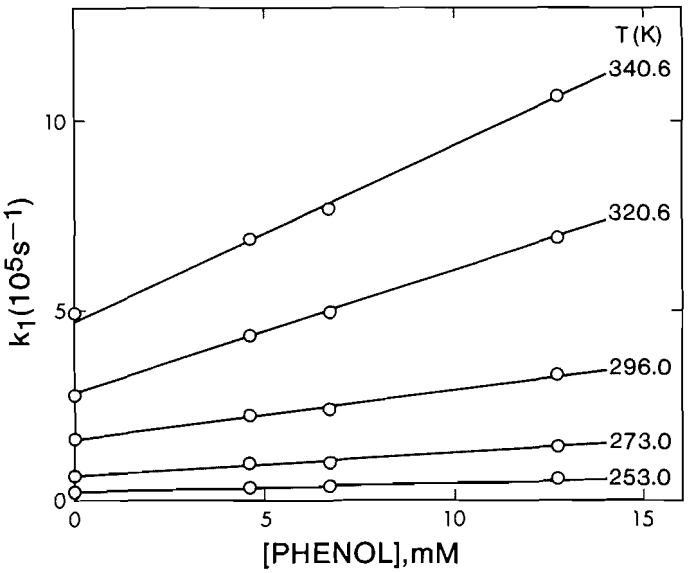

FIG. 3. First order rate constants, k_1, of the reaction of solvated electrons with phenol in 61 mol% H_2O/2-PrOH at various temperatures.

confirmed by the facts that the longer the alkyl group of the alcohol, the higher is the structure temperature (32), and at the same time the minimum of the mutual diffusion coefficient curve is shifted towards smaller alcohol concentrations (37). Further increase of alcohol content decreases the structure temperature, which finally reaches zero, and increases the mutual diffusion coefficient. Water–alcohol mixtures become normal, "free" liquids ($T_0 = 0$) sooner when the alkyl group is the smaller. The mutual diffusion coefficient after passing through a minimum increases with further increase of alcohol concentration faster when the alkyl group is the shorter. Thus the structure-making power of an alcohol increases with the size of its hydrophobic group.

The behaviour of $G\epsilon_{max}$ values of solvated electrons as a function of 2-PrOH content in the mixture (Fig. 1) follows a pattern similar to those discussed above. It is assumed that the addition of 3 mol% of alcohol to water would negligibly alter the value of ϵ_{max}, so the increase in the structuredness of the fluid apparently increases the free ion yield. A larger free ion yield implies a larger value of the product of the distance between the geminate electron and ion, and the dielectric constant of the fluid between them. This can be accomplished in two ways which are not mutually exclusive: *1*, the increased order in the structure might increase the thermalization range of the electron (23*b*); *2*, the new structure might contain more favorably oriented electron-localization sites that result in a higher time-averaged dielectric constant between the electron and its geminate cation during their lifetime as a correlated pair.

It has been suggested that the increase of $G(e^-_s)$ upon addition of 1 *M* (2 mol%) of an alcohol to water is due to the inhibition of the spur reaction [1] by [2] (38–41).

[1] $[e^-_s + \dot{O}H \rightarrow OH^-_s]$

[2] $[\dot{O}H + RCH_2OH \rightarrow H_2O + R\dot{C}HOH]$

However, the assumption that reaction [3] does not occur is unwarranted (see discussion in ref. 23*b*).

[3] $[e^-_s + R\dot{C}HOH \rightarrow RCHOH^-_s]$

Furthermore, the rate of decay of e^-_s in water containing alcohol would be lower than that in pure water because of the much greater viscosity of the former, with consequently lower diffusion coefficients (23*b*).

B. Reaction rates of e^-_s with scavengers in 2-PrOH/H_2O

For the kinetics studies the following mol% H_2O were chosen: 100, 99, 74, 61, 15, 8, 0.

Second order rate constants k_2 of solvated electrons with three scavengers of different reactivities were measured at temperatures between the freezing point of the mixture and 360 K. The scavengers were nitrobenzene ($k^{298}_{2,H_2O} \approx 10^{10}$ dm^3/mol s), tryptophane ($k^{298}_{2,H_2O} \approx 10^8$ dm^3/mol s), and phenol ($k^{298}_{2,H_2O} \approx 10^7$ dm^3/mol s). First order decay constants, k_1, of e^-_s were measured for several different concentrations of each scavenger at a given temperature. The second order rate constant k_2 was obtained from the slope of the plot of k_1 against the scavenger concentration.

Typical plots of k_1 are shown in Fig. 3.

The Arrhenius plot of k_2 values obtained from the data in Fig. 3 is presented in Fig. 4. The parameters of the Arrhenius equation $k_2 = A_2 \exp(-E_2/kT)$ are listed in Table 1. The table also contains values of k_2 at 298 K. The k_2 values in pure water and 2-PrOH are in satisfactory agreement with the data reported earlier (20, 21, 42, 43).

The reaction of nitrobenzene with e^-_s is two times faster in pure water than in 2-PrOH, which correlates inversely with the viscosities of these solvents (13). This reaction is nearly diffusion controlled (18). Figure 5 shows the plot of k_2 against η in the mixtures at two temperatures. The value of k_2 changes approximately as $\eta^{-1.0}$ over a four-fold range in the unmixed solvents and in a given mixed solvent as a function of temperature. However, on going from zero to 74 mol% water at 298 K, k_N is nearly independent of the 1.4-fold increase of η. There is therefore a large difference between the temperature and composition effects, even for the nearly diffusion-controlled reaction. It was reported earlier that in a series of normal aliphatic alcohols (21) and glycols (24) at 298 K the rate constant for nitrobenzene reacting with e^-_s follows the relation $k_2 \propto \eta^{-0.6}$. Neither water nor 2-PrOH fitted this correlation. The

TABLE 1. Solvated electron reaction rate parameters

	Nitrobenzene[e]				Tryptophane[f]				Phenol[g]			
mol% H_2O	k_2[a,b]	E_2[c]	log A_2[a]	$\Delta S_2^{\ddagger}$[d]	k_2[a,b]	E_2[c]	log A_2[a]	$\Delta S_2^{\ddagger}$[d]	k_2[a,b]	E_2[c]	log A_2[a]	$\Delta S_2^{\ddagger}$[d]
0	1.3×10^{10}	16	13.0	4					2.0×10^{8}	20	11.8	−18
8					1.5×10^{9}	23	13.2	7	4.9×10^{7}	16	10.4	−45
15	1.3×10^{10}	19	13.4	12	1.5×10^{9}	24	13.4	11	2.8×10^{7}	15	10.1	−51
61	1.2×10^{10}	23	14.0	23	5.6×10^{8}	22	12.6	−3	1.4×10^{7}	22	11.0	−34
74	1.3×10^{10}	21	13.8	20	4.0×10^{8}	22	12.5	−5	1.7×10^{7}	21	11.0	−34
99	2.6×10^{10}	17	13.4	11	3.4×10^{8}	20	12.0	−15	2.9×10^{7}	18	10.6	−42
100	2.5×10^{10}	18	13.6	15	3.2×10^{8}	21	12.3	−10	2.5×10^{7}	20	10.9	−36

[a] k_2 and A_2 units dm^3/mol s.
[b] 298 K.
[c] kJ/mol.
[d] J/mol K.
[e] Concentration range of nitrobenzene $(1-8) \times 10^{-5}$ M.
[f] Concentration range of tryptophane $(1-15) \times 10^{-4}$ M. Due to its poor solubility in 2-PrOH it was impossible to prepare solutions of smaller H_2O content than 8 mol%.
[g] Concentration range of phenol $(1-13) \times 10^{-3}$ M. Values at 0, 15, 61, and 100% water are averages of two sets.

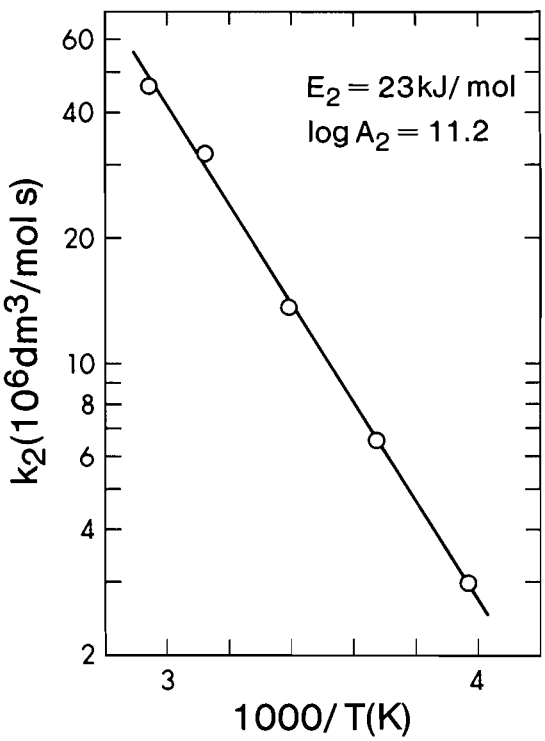

FIG. 4. Arrhenius plot of k_2 values obtained from slopes in Fig. 2.

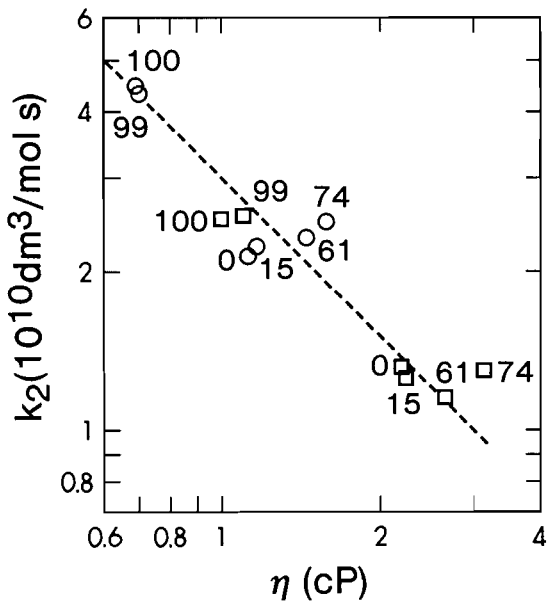

FIG. 5. Viscosity dependence of rate constant k_2 of the reaction of solvated electrons with nitrobenzene. □, 293 K; ○, 323 K. Numbers indicate mol% water; ---, slope = −1.0.

results indicate a complex dependence of e^-_s diffusion coefficient upon solvent structure; its independent measurement is in order.

The rate constants of e^-_s reacting with tryptophane and phenol are smaller than those with nitrobenzene by one and two orders of magnitude, respectively. For tryptophane the rate constant increases with the increase of alcohol concentration in the mixture, regardless of the complex changes in viscosity shown in Fig. 2. The value of k_2 is 4.7 times greater in 92 mol% 2-PrOH than in pure water, while $(\eta_{92\%}/\eta_{H_2O})^{-1} = 0.46$. This is in agreement with the previous reports of Afanassiev and Freeman (20, 21). They proposed that for less efficient scavengers the reaction rate is determined by the e^-_s trap depth rather than the viscosity. The deeper the trap, the more difficult it is for an electron to jump up to a scavenger molecule, which results in a lower rate constant k_2. The energy E_r half way up the red side of the e^-_s optical absorption band was chosen as the measure of trap depth. The energy E_r is connected with $E_{\epsilon max}$ at the maximum of the absorption band, by the relation

$$[1] \quad E_r = E_{\epsilon max} - W_r$$

where W_r is the portion of the width at half height that is on the red side of $E_{\epsilon max}$ (26).

Phenol is the least efficient of these e^-_s scavengers. The value of its k_2 is an order of magnitude greater in pure 2-PrOH than in water. In the water-rich mixtures the value of k_2 for phenol is highest for 1 mol% 2-PrOH. This is the region of rapid increases in η, $d\eta/dx$, and $G\epsilon_{max}$. As discussed in the previous paragraph, in this concentration range of alcohol there are structure-making effects. They apparently assist the capture of the electron by the aromatic molecule. This conclusion is supported by the smaller value of the activation energy (Table 1).

In alcohol-rich solutions, an increase of 2-PrOH concen-

Can. J. Chem. Downloaded from www.nrcresearchpress.com by 210.87.254.6 on 09/06/12
For personal use only.

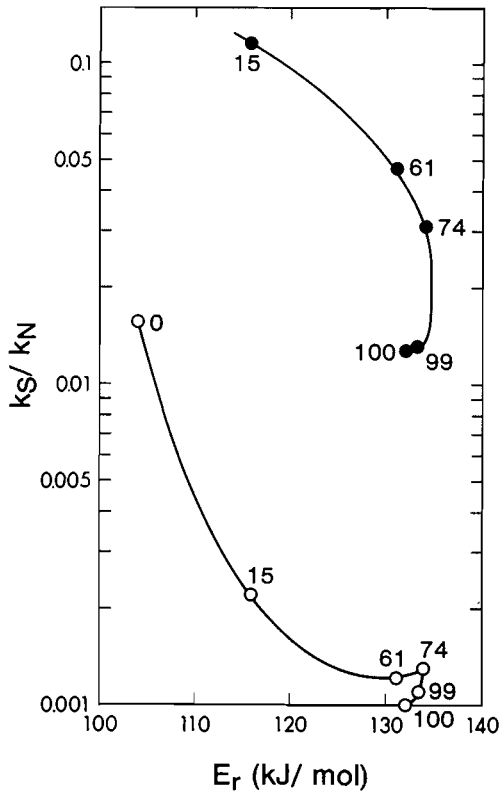

FIG. 6. Effect of electron solvation energy, represented by E_r, on the normalized rate constant of electron reaction with scavenger S, represented by k_S/k_N, at 298 K. The rate constant k_N for nitrobenzene is used to normalize the others for diffusion effects. S: tryptophane ●, phenol ○. Numbers indicate mol% water.

tration is followed by an increase of k_2 for phenol, up to the value 2.0×10^8 dm^3/mol s in pure 2-PrOH. The activation energy and entropy have minima at between 15 and 8 mol% water. The minima cannot be explained on the basis of changes in E_r, which decreases monotonically in this concentration range (22, 23). However, between 0 and 10 mol% of water in 2-PrOH there is a sharp decrease of W_b, the portion of the width at half height on the blue side of $E_{\epsilon max}$ (22). The quantity $E_b = E_{\epsilon max} + W_b$ has a minimum at 10 mol% water (22, 23). This is a characteristic feature for 2-PrOH/H_2O solutions and was not found in mixtures of primary or tertiary alcohols with water. In the secondary alcohol 2-PrOH, the high energy side of the band is relatively broad and is rapidly reduced in width by the addition of a small amount of water. This is probably attributable to changes in the electron solvation sites.

The peculiar solvent effects on the electron reaction efficiencies with tryptophane and phenol are illustrated by normalizing the latter to the nearly diffusion-controlled rate with nitrobenzene. The ratio k_S/k_N is plotted against E_r in Fig. 6; N is nitrobenzene and S is the other scavenger. There is a general decrease of k_S/k_N with increasing E_r as found in other systems. However, the interpretation of the shapes in the water-rich solutions awaits further investigation.

1. F. FRANKS and D. J. G. IVES. Q. Rev. **20**, 1 (1966).
2. F. FRANKS (*Editor*). Physico-chemical processes in mixed aqueous solvents. Elsevier, New York. 1967.
3. R. L. KAY, G. P. CUNNINGHAM and D. F. EVANS. *In* Hydrogen-bonded solvent systems. *Edited by* A. K. Covington and P. Jones. Taylor and Francis, London. 1965. pp. 249–260.
4. D. M. ALEXANDER and D. J. T. HILL. Aust. J. Chem. **22**, 347 (1969).
5. G. C. BENSON and O. KIYOHARA. J. Solution Chem. **9**, 791 (1980).
6. G. C. BENSON, P. J. D'ARCY, and O. KIYOHARA. J. Solution Chem. **9**, 931 (1980).
7. F. FRANKS and H. T. SMITH. Trans. Faraday Soc. **64**, 2962 (1968).
8. G. ROUX, D. ROBERTS, G. PERRON, and J. E. DESNOYERS. J. Solution Chem. **9**, 629 (1980).
9. H. HØILAND. J. Solution Chem. **9**, 857 (1980).
10. W. WEBER. Rheol. Acta, **14**, 1012 (1975).
11. A. D'APRANO, I. D. DONATO, E. CAPONETTI, and V. AGRIGENTO. J. Solution Chem. **8**, 793 (1979).
12. M. YUSZ, G. P. METHUR, and R. A. STAGER. J. Chem. Eng. Data, **22**, 32 (1977).
13. M. AKRAMOVA, O. SH. SHOKIROV, and T. NURITDINOV. Dokl. Akad. Nauk. Tadzhikskoy SSR, **XIX**, 27 (1976).
14. G. AEKERLOEF. J. Am. Chem. Soc. **59**, 4125 (1932).
15. J. SJOEBLOM. Finn. Chem. Lett. 245 (1979).
16. K. N. JHA and G. R. FREEMAN. J. Chem. Phys. **51**, 2846 (1969).
17. K. N. JHA, G. L. BOLTON, and G. R. FREEMAN. J. Phys. Chem. **76**, 3876 (1972).
18. G. L. BOLTON and G. R. FREEMAN. J. Am. Chem. Soc. **98**, 6825 (1976).
19. K. OKAZAKI and G. R. FREEMAN. Can. J. Chem. **56**, 2313 (1978).
20. A. M. AFANASSIEV, K. OKAZAKI, and G. R. FREEMAN. Can. J. Chem. **57**, 839 (1979).
21. A. M. AFANASSIEV, K. OKAZAKI, and G. R. FREEMAN. J. Phys. Chem. **83**, 1244 (1979).
22. A. D. LEU, K. N. JHA, and G. R. FREEMAN. Can. J. Chem. **60**, 2342 (1982).
23. (*a*) A. D. LEU. Ph.D. thesis, University of Alberta. 1980; (*b*) A. D. LEU, K. N. JHA, and G. R. FREEMAN. Can. J. Chem. **61**, 1115 (1983).
24. K. M. IDRISS-ALI and G. R. FREEMAN. Radiat. Phys. Chem. **23**, 89 (1984).
25. A. J. VOGEL. Quantitative inorganic analysis. 3rd ed. Longmans, London. 1968. p. 944.
26. F. J. JOU and G. R. FREEMAN. (*a*) Can. J. Chem. **54**, 693 (1976); (*b*) J. Phys. Chem. **81**, 909 (1977); (*c*) J. Phys. Chem. **83**, 261 (1979).
27. E. J. HART and M. ANBAR. The hydrated electron. Wiley–Interscience, New York. 1970.
28. G. E. HALL and G. A. KENNEY-WALLACE. Chem. Phys. **32**, 313 (1978).
29. G. NEMETHY and H. A. SCHERAGA. J. Chem. Phys. (*a*) **36**, 3382 (1969); (*b*) **41**, 680 (1964).
30. O. YA. SAMOILOV. Structure of aqueous electrolyte solutions and the hydration of ions. Consultants Bureau, New York. 1965.
31. F. FRANKS. *In* Hydrogen-bonded solvent systems. *Edited by* A. K. Covington and P. Jones. Taylor and Francis, London. 1968. pp. 31–47.
32. K. UEBERREITER. Macromol. Chem. Rapid Commun. **1**, 139 (1980).
33. D. D. MACDONALD, A. MACLEAN, and J. B. HYNE. J. Solution Chem. **8**, 97 (1979).
34. F. FRANKS and B. WATSON. Trans. Faraday Soc. **63**, 329 (1967).
35. B. R. HAMMOND and R. H. STOKES. Trans. Faraday Soc. **49**, 890 (1956).
36. K. C. PRATT and W. A. WAKEHAM. Proc. R. Soc. London, A**336**, 393 (1975).
37. A. B. PORAY-KOSHIC, O. P. YAKOREV, A. M. SAZONOV, and G. A. SHMUYLOVICH. Izv. Vys. Ucheb. Zaved. Khim. I, Khim. Tekh. **24**, 1230 (1981).
38. E. M. FIELDEN and E. J. HART. Radiat. Res. **32**, 564 (1967).
39. G. V. BUXTON. Proc. R. Soc. London, A**328**, 9 (1972).

Can. J. Chem. Downloaded from www.nrcresearchpress.com by 210.87.254.6 on 09/06/12
For personal use only.

40. C. D. JONAH, E. J. HART, and M. S. MATHESON. J. Phys. Chem. **77**, 1838 (1973).
41. C. D. JONAH, M. S. MATHESON, J. R. MILLER, and E. J. HART. J. Phys. Chem. **80**, 1267 (1976).
42. E. J. LAND and M. EBERT. Trans. Faraday Soc. **63**, 1181 (1967).
43. R. C. ARMSTRONG and A. J. SWALLOW. Rad. Res. **40**, 563 (1969).

Can. J. Chem. Downloaded from www.nrcresearchpress.com by 210.87.254.6 on 09/06/12
For personal use only.

The crystal and molecular structure of *endo*-7-hydroxy-2,4-dioxa-3-oxobicyclo[3.3.1]nonane

WINNIE WONG-NG[1] AND STANLEY C. NYBURG

Department of Chemistry, University of Toronto, Toronto, Ont., Canada M5S 1A1

Received September 16, 1983

WINNIE WONG-NG and STANLEY C. NYBURG. Can. J. Chem. **62**, 1271 (1984).

The crystal and molecular structure of the title compound are described. Crystals are orthorhombic, space group $Pna2_1$, a = 10.977(3), b = 6.489(2), c = 9.811(2) Å, Z = four molecules per cell. Atom C(4), to which the hydroxyl group is attached, appears to have been moved outwards (away from hydroxyl). This resembles similar movements in *chair–chair* bicyclo[3.3.1]nonanes where intramolecular repulsion is thought to be responsible. In the present molecule, however, the more likely cause is the presence of an intermolecular hydrogen bond.

WINNIE WONG-NG et STANLEY C. NYBURG. Can. J. Chem. **62**, 1271 (1984).

On décrit les structures cristalline et moléculaire du composé mentionné dans le titre. Les cristaux sont orthorhombiques, groupe d'espace $Pna2_1$, a = 10,977(3), b = 6,489(2), c = 9,811(2) Å, Z = 4 molécules par unité. L'atome C(4), auquel le groupe hydroxyle est attaché, semble être déplacé vers l'extérieur (s'éloigne de l'hydroxyle). Ceci ressemble à des déplacements semblables dans les bicyclo[3.3.1]nonanes *chaise–chaise* où l'on croit que la répulsion intramoléculaire en est responsable. Dans la présente molécule, il semble toutefois que ce déplacement soit dû à la présence d'une liaison hydrogène intramoléculaire.

[Traduit par le journal]

Introduction

It is known that 2,4,10-trioxaadamantanes, **1**, hydrolyse much more slowly than the corresponding acyclic *ortho*-esters **2** (1, 2). It is thought that hydrolysis of **1** is governed by a rate-determining decomposition of the intermediate oxocarbonium ion, **3**, which is known to be formed very quickly

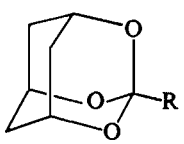

1

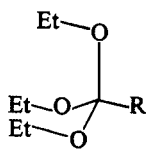

2

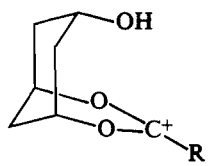

3

when sulfuric acid is added to the ester (3). The carbonate corresponding to **1** (i.e. with R = oxygen) has recently been prepared and is also slow to hydrolyse. An analog **4** of the putative intermediate has also been prepared and, since its molecular structure is of some interest, its crystal structure is the subject of this paper.

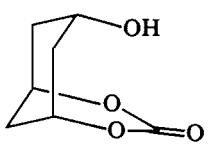

4

Experimental

Crystals of the title compound were colorless and in the form of triangular plates. One such crystal, 0.32 × 0.11 mm thick, was used for X-ray analysis mounted normal to the goniometer axis.

After preliminary photographic examination, intensity data were collected on an automated Picker four-circle diffractometer using Ni-filtered CuKα radiation and pulse height discrimination. Data were collected in θ–2θ scan mode at 2° min^{-1} with a scan width of 2°. A standard reflection remeasured every 40 reflections showed the crystal to be stable.

A total of 701 reflections was recorded in the range sin θ ≤ 0.89. Of these, 110 had (scan − Σb) < $2\sigma(I)$ and were considered insignificant on the basis $\sigma(I)$ = (scan + Σb)$^{1/2}$ where Σb is the total background count. Unit cell dimensions were obtained by least squares from the θ, φ, and χ settings of 12 reflections. Systematic absences were $0kl$ for $k + l$ odd, $h0l$ for h odd. Crystal data are as follows:

$C_7H_{10}O_4$ fw = 158.16

Orthorhombic, $Pna2_1$ or $Pnam$ (former confirmed by structure analysis); a = 10.977(3), b = 6.489(2), c = 9.811(2) Å, V = 698.8(3) Å^3. D_c (for Z = 4), 1.50 Mg m^{-3}; 22°C; λ(CuKα) = 1.5418 Å; μ(CuKα) = 10.7 cm^{-1}.

Structure solution and refinement

The structure was solved using MULTAN 80 (4). E statistics indicated an acentric structure, i.e. space group $Pna2_1$ rather than $Pnam$. Ten phase sets were generated for the 230 reflections with $E > 1$. The phase set with the highest combined figure of merit gave a stereochemically feasible structure. Full-matrix anisotropic least-squares refinement was carried out on the non-hydrogen atoms using XFLS3 (5). All hydrogen atoms were revealed on the ΔF map on which the largest spurious peak was 0.25 e Å^{-3}. Except for H(O1) whose position was taken from the map, all hydrogen atoms had d_{C-H} set to 1.0 Å and were kept in fixed calculated positions. They were given the same anisotropic temperature factors as the atoms to which they were attached. The scattering factors used were those of Cromer and Mann (6), without correction for anomalous dispersion. No absorption corrections were applied. $\sigma(F_o)$ was taken as $[\{\sigma(I)/Lp\}^2 + 0.02F_o^4]^{1/2}/2F_o$ where Lp is the Lorentz-polarization factor. Isotropic extinction corrections were applied according to Coppens and Hamilton (7), ($\bar{T}$ = 0.04 cm, G_{iso}^0 = 0.185). The penultimate value of R fell from 0.056 to 0.044. Tables of anisotropic temperature factors and phased F values have been deposited.

Fractional atomic co-ordinates are given in Table 1. Table 2(*a*) lists bond lengths and intermolecular distances and Table 2(*b*) the bond angles. Table 3 gives the least-squares planes. An ORTEP (8) plot of the molecule giving the atomic numbering scheme is shown in Fig. 1. Figure 2 shows the packing of the molecules within one unit cell.

[1] Present address: JCPDS-International Center for Diffraction Data, 1601 Park Lane, Swarthmore, PA 19806, U.S.A.

Can. J. Chem. Downloaded from www.nrcresearchpress.com by 210.87.254.105 on 09/06/12
For personal use only.

Can. J. Chem. Downloaded from www.nrcresearchpress.com by 210.87.254.105 on 09/06/12
For personal use only.

TABLE 1. Fractional atomic co-ordinates × 10^4 (with esd's in parentheses) for non-hydrogen atoms; × 10^3 for hydrogen atoms

Atom	*x*	*y*	*z*
O(1)	3989(3)	530(6)	5927*
O(2)	1833(3)	2092(5)	7469(6)
O(3)	768(3)	1024(7)	5713(6)
O(4)	1674(3)	−1362(6)	6932(6)
C(1)	2208(5)	−433(9)	9222(8)
C(2)	2438(5)	−1927(8)	8101(8)
C(3)	3780(5)	−2069(7)	7646(8)
C(4)	4306(4)	40(7)	7310(6)
C(5)	3939(4)	1766(8)	8300(8)
C(6)	2599(5)	1641(8)	8670(8)
C(7)	1401(5)	551(9)	6668(7)
H(O1)	435	165	550
H(C1A)	133	−40	948
H(C1B)	270	−81	1005
H(C2)	216	−332	842
H(C3A)	384	−296	682
H(C3B)	428	−271	840
H(C4)	522	−7	732
H(C5A)	411	311	784
H(C5B)	446	164	913
H(C6)	244	269	938

* Fixed arbitrarily.

Discussion

In *chair–chair* bicyclo[3.3.1]nonanes, **5**, the existence of a repulsive strain between rings can be inferred from the distances of atoms A, A′, and F from the mean planes BCDE and B′C′DE, respectively. In the absence of strain it is assumed that these distances would be about 0.73 Å. Thus, in a derivative with CH_3 at D and CH_2R at E, X-ray structure analysis (9) shows that A and A′ lie 0.51 and 0.45 Å from their appropriate mean planes whereas F lies 0.71 and 0.72 Å from them. This implies a repulsive strain between the rings. Similar effects are found in other *chair–chair* bicyclo[3.3.1]nonanes (10, 11[2]). The repulsive strain in all three molecules is caused, presumably, not only by interactions between the carbon atoms at

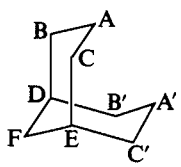

5

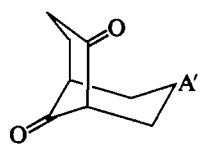

6

A and A′ (unstrained distance ca. 2.52 Å, that usually found ca. 3.05 Å) but also by the opposing methylene hydrogen atoms which are close together (ca. 2.05 Å) in these molecules. Further evidence of this type can be adduced from the crystal structure analysis of a *chair–boat* bicyclo[3.3.1]nonane, **6** (12). This structure would be expected to be free from intramolecular strain and indeed, the carbon atom at A′ is found to be 0.70 Å from its appropriate plane as would be expected in an unstrained molecule.

[2] The extensively substituted molecule of ref. 11 is erroneously said to have the *boat–boat* conformation. It is actually *chair–chair* and we calculate the displacements of the atoms from their appropriate planes as: A, 0.56; A′, 0.50; and F, 0.65 and 0.74 Å.

TABLE 2

(*a*) Atomic distances

(*i*) Bond lengths

Bond	Length
O(1)—C(4)	1.436(6)
O(2)—C(6)	1.477(9)
O(2)—C(7)	1.357(8)
O(3)—C(7)	1.206(8)
O(4)—C(2)	1.466(9)
O(4)—C(7)	1.304(7)
C(1)—C(2)	1.48(1)
C(1)—C(6)	1.519(8)
C(2)—C(3)	1.542(8)
C(3)—C(4)	1.522(7)
C(4)—C(5)	1.536(8)
C(5)—C(6)	1.518(7)

(*ii*) Intramolecular distances

Atoms	Distance
O(1)...C(7)	2.932(6)
O(1)...O(2)	2.985(6)
O(1)...O(4)	2.989(6)
C(4)...C(7)	3.268(6)
O(1)...O(3)	3.556(5)

(*iii*) Intermolecular distances

Atoms	Distance
O(1)...O(3)	2.976(6)
H(O1)...O(3)	2.178(4)

(*b*) Bond angles (deg)

Bonds	Angle
C(6)—O(2)—C(7)	121.0(5)
C(2)—O(4)—C(7)	121.7(5)
C(2)—C(1)—C(6)	105.4(5)
O(4)—C(2)—C(1)	108.7(5)
O(4)—C(2)—C(3)	109.6(5)
C(1)—C(2)—C(3)	114.5(5)
C(2)—C(3)—C(4)	111.8(5)
O(1)—C(4)—C(3)	108.2(4)
O(1)—C(4)—C(5)	111.9(4)
C(3)—C(4)—C(5)	114.8(5)
C(4)—C(5)—C(6)	111.5(5)
O(2)—C(6)—C(1)	107.5(5)
O(2)—C(6)—C(5)	110.5(5)
C(1)—C(6)—C(5)	114.0(5)
O(2)—C(7)—O(3)	117.6(5)
O(2)—C(7)—O(4)	120.4(5)
O(3)—C(7)—O(4)	122.0(6)

The geometry of the molecule studied here would, at first sight, seem to imply the presence of the same kind of repulsive intermolecular interaction as shown by *chair–chair* bicyclo[3.3.1]nonanes. The atom at position A, C(4), is only 0.514(6) Å from the mean plane of C(2), C(3), C(5), and C(6) whereas C(1) is 0.729(7) Å from this plane (Table 3, plane *1*). Atom O(1) is about equidistant from O(2), O(4), and O(7) at 2.99, 2.99, and 2.93 Å, respectively, but there is no indication of a repulsive interaction here. If the C(2), O(4), C(7), O(2), C(6) system be considered in two halves hinged about O(2)...O(4) (Table 3, planes *2* and *3*), there is a small angle

TABLE 3. Best least-squares planes, $AX + BY + CZ = D$ where X, Y, Z are real orthogonal coordinates (in Å)

Atoms defining the best least-squares plane	Plane coefficients Displacements of atoms from plane (Å)
Plane *1* C(2)C(3)C(5)C(6)	$A = -0.255(5)$, $B = 0.252(4)$, $C = -0.933(8)$, $D = -8.407(4)$ C(1), −0.729(7); C(2), −0.009(8); C(3), 0.007(7); C(4), 0.514(6); C(5), −0.008(7); C(6), 0.009(7)
Plane *2* O(2)O(3)O(4)C(7)	$A = 0.811(6)$, $B = 0.073(3)$, $C = -0.579(5)$, $D = -2.518(2)$ O(2), 0.000(5); O(3), 0.001(5); O(4), 0.000(5); C(7), −0.002(6)
Plane *3* C(2)O(4)O(2)C(6)	$A = 0.818(7)$, $B = 0.072(3)$, $C = -0.570(7)$, $D = -2.438(3)$ C(2), 0.003(7); O(4), −0.002(5); O(2), 0.002(5); C(6), −0.003(6)

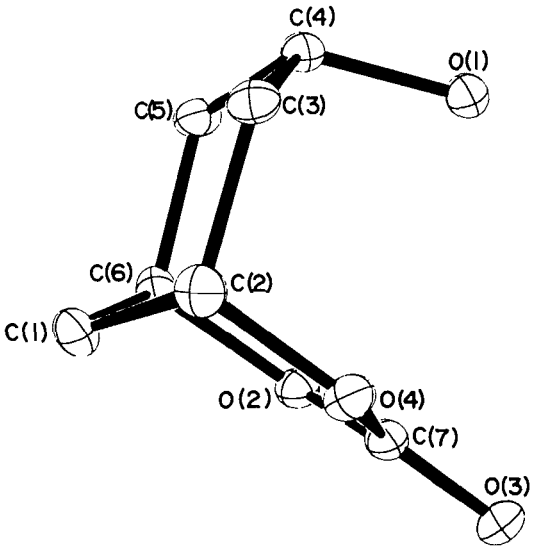

FIG. 1. ORTEP plot of molecule showing atom numbering scheme and 50% probability ellipsoids.

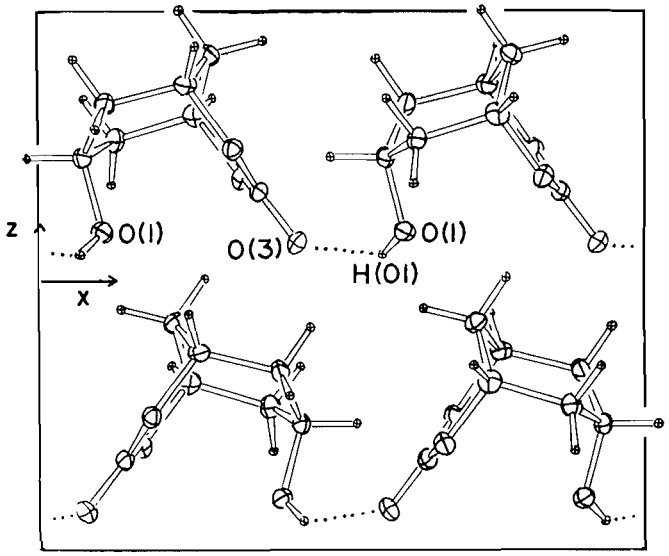

FIG. 2. Content of one unit cell in *y*-projection.

between the planes, 0.7(4)°. This is too small to be significant but, in any case, is such as to bring O(3) slightly closer to, rather than slightly further from, O(1). Thus repulsive intramolecular interaction of the type postulated for *chair–chair* bicyclo[3.3.1]nonanes seems to be absent although it should be recognised that the 2,4-dioxa-3-oxo system is probably very resistant to out-of-plane deformation.

A possible alternative reason for O(1) being further from O(3) than might have been expected is the presence of a O(1)—H(O1)...O(3) intermolecular hydrogen bond (Fig. 2) with O(1)—H(O1), 0.93 Å, H(O1)...O(3), 2.178(4) Å and the O(1)—H(O1)...O(3) angle, 119.8°. Such a bond could cause a movement of O(1) away from O(3) of the same molecule.

Successful refinement shows the crystal to belong to space group $Pna2_1$ and not to *Pnam*. Commonly this choice arises because the true structure is a slightly distorted version of a possible *Pnam* structure. This is not the case here, however. If the structure were *Pnam* the four molecules per cell would need to have either mirror planes or centers of symmetry. The molecules have, in fact, pseudo mirror planes but these planes are not oriented even approximately as required by *Pnam*. This can be seen in Fig. 2, where, if the structure were *Pnam* there would be mirror planes of symmetry at $z = 1/4, 3/4$.

The non-hydrogen atoms of the molecule show significant departures from m (C_s) symmetry. In particular, bonds O(2)—C(7) and O(4)—C(7) are 1.357(8) and 1.304 Å, respectively. Differences in chemically equivalent interbond angles are also present: O(2)—C(7)—O(3), 117.6°, O(4)—C(7)—O(3), 111.9°, O(1)—C(4)—C(3), 108.2°. Hydrogen bonded atom H(O1) lies 0.62 Å from the mean midplane of the molecule. It is difficult to see, however, how a hydrogen bond could be the cause of such marked asymmetry in C—O bond lengths and in O—C—O interbond angles.

Acknowledgements

We are grateful to Professor R. A. McClelland for supplying the crystals and to the Natural Sciences and Engineering Research Council of Canada for financial assistance.

1. O. BOUAB, G. LAMATY, and C. MOREAU. J. Chem. Soc. Chem. Commun. 678 (1978).
2. O. BOUAB, G. LAMATY, C. MOREAU, O. POMARES, P. DESLONGCHAMPS, and L. RUEST. Can. J. Chem. **58**, 567 (1980).
3. W. K. LAM and R. A. MCCLELLAND. J. Chem. Soc. Chem.

Can. J. Chem. Downloaded from www.nrcresearchpress.com by 210.87.254.105 on 09/06/12
For personal use only.

Commun. 883 (1980).
4. G. GERMAIN, P. MAIN, and M. M. WOOLFSON. Unpublished program.
5. W. R. BUSING, K. O. MARTIN, and H. A. LEVY. ORXFLS3, an extensively modified version of ORFLS. Report ORNL-TM-305, Oak Ridge National Laboratory, TN. 1962.
6. D. T. CROMER and J. B. MANN. Acta Crystallogr. A**24**, 321 (1968).
7. P. COPPENS and W. C. HAMILTON. Acta Crystallogr. A**26**, 71 (1970).
8. C. K. JOHNSON. ORTEP, Report ORNL-3794, Oak Ridge National Laboratory, TN. 1965.
9. W. A. C. BROWN, J. MARTIN, and G. A. SIM. J. Chem. Soc. 1844 (1965).
10. N. C. WEBB and M. R. BECKER. J. Chem. Soc. (B), 1317 (1967).
11. G. D. ANDREETTI, G. BOCELLI, and P. SGARABOTTO. Cryst. Struct. Commun. **2**, 495 (1973).
12. P. W. HICKMOTT, P. J. COX, and G. A. SIM. J. Chem. Soc. Perkin I, 2544 (1974).

Can. J. Chem. Downloaded from www.nrcresearchpress.com by 210.87.254.105 on 09/06/12
For personal use only.

Surface photochemistry: the amide Photo-Fries rearrangement[1]

MAGDY M. ABDEL-MALIK AND PAUL DE MAYO

Photochemistry Unit, Department of Chemistry, The University of Western Ontario, London, Ont., Canada N6A 5B7

Received December 2, 1983

MAGDY M. ABDEL-MALIK and PAUL DE MAYO. Can. J. Chem. **62**, 1275 (1984).

The Photo-Fries rearrangement of eight anilides on the surface of dry silica gel has been examined. The rearrangement occurs quite cleanly, giving somewhat more of the *para* isomer than that obtained in methanolic solution. A test for intermolecularity on the silica gel surface showed that, as in solution, the radical pair intermediates do not separate. This contrasts with the behaviour of a previously reported dibenzyl ketone derivative.

MAGDY M. ABDEL-MALIK et PAUL DE MAYO. Can. J. Chem. **62**, 1275 (1984).

On a étudié la transposition de photo-Fries de huit anilides, à la surface de gel de silica sec. La transposition se produit d'une façon assez propre; dans ce cas, il se forme plus d'isomère *para* qu'en solution méthanolique. La détermination de l'intermolécularité à la surface du gel de silica a démontré que, comme en solution, la paire de radicaux intermédiaires ne se sépare pas. Ceci est en opposition avec le comportement rapporté antérieurement pour un dérivé de la dibenzylcétone.

[Traduit par le journal]

Can. J. Chem. Downloaded from www.nrcresearchpress.com by 210.87.254.6 on 09/06/12
For personal use only.

Introduction

Several years ago Anderson and Reese (1) observed that catechol monoacetate in ethanolic solution rearranged upon irradiation. Since then the reaction has been studied at length (2) and interest in this, the Photo-Fries rearrangement, continues. The mechanism established is that of Kobsa (3): homolysis to give a radical pair which recombines efficiently in the solvent cage (cf. *inter alia* ref. 4). The scope of the reaction has been greatly extended (5) and now encompasses amides (6–9).

Some time ago the possibility that a silica gel surface might act as a restraining agent on radical pairs generated thereon was examined. The concept was tested on the Photo-Fries rearrangement of esters (10) and found to be successful and led to the further study of excited species on silica gel surfaces (11, 12).

The reasons for studying the possibility of carrying out the amide Photo-Fries on dry silica gel were two-fold. Firstly, the quantum yield of the rearrangement, especially in polar solvents, was low (6*b*, 8). This was interpreted as an indication of rapid radical recombination in the solvent cage without significant molecular movement. The homolysis was attributed (6*b*) to predissociation (Scheme 1). Since at that time it had been reported (13) that radicals derived from azoisobutyronitrile photolysis were anchored on the surface of a silica gel slurry via the nitrogen, it seemed possible that such bonding might delay recombination and allow the radicals to rotate. However, these earlier findings have since been shown to be in error (11*b*). Secondly, it was hoped that the proportion of *ortho* to *para* reaction (Scheme 1) might be usefully altered by adsorption. During the completion of this work the use of β-cyclodextrin, to achieve the same end, was reported (9).

Results and discussions

The photolyses of compounds **1***a*–**1***h* was examined. Their physical properties are recorded in Table 1 (Experimental section), the results being presented in Table 2. The reproducibility may be assessed by the results for **1***a*. Also contained in Table 2 are the results of photolyses in methanolic solution, a solvent approximating silica gel in polarity (14).

The experiments performed on silica gel appeared cleaner than those in solution and though the conversions were lower,

[1]Publication No. 316 from the Photochemistry Unit, Department of Chemistry, The University of Western Ontario.

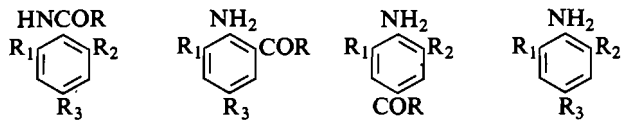

1 **2** **3** **4**

a, $R_1 = R_2 = R_3 = H$; R = Me
b, $R_1 = R = Me$; $R_2 = R_3 = H$
c, $R_1 = R_2 = H$; $R = R_3 = Me$
d, $R_1 = R_2 = R = Me$; $R_3 = H$
e, $R_1 = R_2 = R_3 = H$; R = Ph
f, $R_1 = Me$; $R_2 = R_3 = H$; R = Ph
g, $R_1 = R_2 = H$; $R_3 = Me$; R = Ph
h, $R_1 = R_2 = Me$; $R_3 = H$; R = Ph
i, $R_1 = R_2 = H$; $R_3 = Cl$; R = Et

SCHEME 1

TABLE 1. Properties of starting material and products

	Melting point[a] (°C)	δ N*H*	δ CO*CH*$_3$	δ Ar*CH*$_3$	Reference
1*a*	113–114(115)		2.18		18
2*a*	Oil (oil)	6.24	2.58		7
3*a*	107–109(106)	4.06	2.52		7
1*b*	109–110(110)		2.26	2.18	18
2*b*	53– 54 (55)	6.4	2.60	2.18	19
3*b*	107–108(110)	4.06	2.32	2.20	20
1*c*	143–144(146)		2.30	2.14	18
2*c*	43– 44 (41)	6.06	2.48	2.26	21
1*d*	176–178(177)		2.22	1.52	18
3*d*	108–109	4.04	2.32	2.22	
1*e*	162–163(163)				16
2*e*	105–106(105)	6.04			7
3*e*	121–122(123)	4.17			7
1*f*	143–145(145)			2.36	18
2*f*	52– 53 (52)	6.20		2.22	22
3*f*	110–111(111)	4.12		2.20	17
1*g*	157–158(158)			2.36	18
2*g*	58– 59 (62)	5.90		2.18	17
1*h*	167–168(168)			2.24	18
3*h*	140–141 (86)	4.04		2.20	23
1*i*	142 (141)	(CH$_2$) 2.38	(CH$_3$) 1.24	24	
2*i*	76– 78 (80)	6.26	(CH$_2$) 2.96	(CH$_3$) 1.22	25

[a]Literature values in parentheses.

TABLE 2. Yield of Photo-Fries rearrangement products

Amide	System[f]	Yield 1[b] Conversion 1[a]	2	3	4[c]	2/3 (o/p)
Ia	A	73	30	22	7	1.4
		64	57	36	8	1.6
			(20)[d]	(25)[d]	(18)[d]	
	B	63	37	33	6	1.1
		70	23	21	5	1.1
Ib	A	47	24	28	15	0.9
	B	40	30	46	9	0.7
Ic	A	51	53	—	20	
	B	47	71	—	13	
Id	A	7	—	32	10	
	B	8	—	58	18	
Ie	A	87	36	18	—	2.0
			(14)[d]	(12)[d]	(Trace)[d]	1.1
	B	27	48	45	—	1.1
If	A	71	15	15	—	1.0
	B	32	32	49	—	0.7
Ig	A	75	19	—	—	—
	B	8[e]	73	—	—	—
Ih	A	60	—	12	—	—
	B	30	—	27	—	—

[a]Based on the recovered material.
[b]Based on material consumed.
[c]±5%.
[d]In ethanol.
[e]Different silica gel sample used.
[f]A, methanol solution; B, dry silica gel.

the yields based on unrecovered material were somewhat higher. There was also a decrease in aniline formation and other unidentified by-products, presumably, in part, because of the lack of a good hydrogen donor to reduce the radicals. Surprisingly, considering that these results suggest restraint on the movement on the radical pair, the reactions on silica gel vis-a-vis those in solution favoured the formation of the *para*-substituted ketone. This is particularly noteworthy in the case of benzanilide (**1***e*) where the *o/p* ratio changes by a factor of two. Other examples tended in the same direction, but were not so marked. We consider that the gel surface may permit more time for rotation, as compared with recombination times, or, less likely, the time to diffuse away, than does the solvent. However, in view of the large changes in behaviour recorded in solution accompanying polarity change in the solvent attribution of such changes to an adsorption phenomenon can only be tentative.

The Photo-Fries rearrangement has been shown to be "intramolecular" for amides in solution (6*d*, 7). We have demonstrated that the same situation holds for the surface reaction. Irradiation on the dry gel surface of a mixture of **1***c* and **1***i* did not reveal the formation of any products (cross-products) of intermolecular reaction: the only ketones produced were **2***c* and **2***i*. This is in contrast to the photolysis on silica gel of the dibenzyl ketone **5** (11) which gave the dibenzyls from both intra- and intermolecular combination.

This dichotomy in behaviour is to be attributed to the very probable photolysis of the amide via the singlet and that of the ketone via the triplet (15). The amide photolysis resembles

5

more that of the ester **6** (11*a*), the multiplicity of whose fission is not known. Related compounds have, however, been shown by Givens (16) to photolyse via the singlet. The "intramolecular" nature of the rearrangement on the silica gel may be construed as evidence in favour of a singlet reaction under these conditions. The singlet process has been well-established in solution by Shizuka and his collaborators (6*b*).

6

Experimental

Melting points are uncorrected and were measured on a Reichert hot stage; nmr spectra were obtained on a Varian XL-100 MHz; mass spectra on a MAT 311A. A Varian model 3700 gas chromatograph connected to a Hewlett-Packard 3390A integrator was used for gc analysis. In all cases the injector and flame ionization detector were set at 220°C. Two columns were used for analysis: column A was 10% OV 101 Chromosorb W; column B was carbowax 20M on chromosorb W (HP; 80–100 mesh).

Materials

Merck silica gel 60, 230–400 mesh was used in the flash chromatography. All the starting materials were prepared as described in the literature and recrystallized until there was no further improvement in

Can. J. Chem. Downloaded from www.nrcresearchpress.com by 210.87.254.6 on 09/06/12
For personal use only.

Can. J. Chem. Downloaded from www.nrcresearchpress.com by 210.87.254.6 on 09/06/12
For personal use only.

the melting point (see Table 2). The irradiation products reported in Table 2 were isolated from preparative scale experiments in solution and the flash chromatography technique was used in the separation process. The isolated compounds were sublimed and then crystallized. Chromatography was unsuccessful for the isolation of 3,5-dimethyl-4-aminobenzophenone (**3***h*). The latter compound was synthesized from 2,6-dimethylbenzanilide, benzoyl chloride, and anhydrous zinc chloride for 24 h at 220–240°C (17). The structure of this compound followed from spectral data and precise mass (*m/e*, 225.11527; calcd. 225.11535). The nmr data, mp (Table 2) and precise mass (*m/e* 211.09959; calcd. 211.09970) found for **2***f* were in accord with the structure of 3-methyl-2-aminobenzophenone. 3,5-Dimethyl-4-aminoacetophenone (**3***d*) had *m/e* (%) 163 (M^+ $C_9H_{13}ON$(45)) 148 (100 M − CH_3) and 120 (38 M − —CO—CH_3) (precise mass *m/e* 163.0999, calcd. 163.0997).

Irradiations

General procedure

A Rayonet reactor equipped with 254.7 nm lamps was used for photolysis of solutions and for silica gel experiments.

(A) Photolysis of solutions: The methanolic solutions of the esters were contained in quartz tubes which were degassed by purging with dry nitrogen for 15–20 min. A quartz immersion well was used as a cooling system to keep the temperature 18–20°C in the irradiation (24 h) of acetanilide derivatives (3.0×10^{-2} *M*). Air circulation was used to control the temperature at 20–25°C in the irradiation (48 h) of benzanilide derivatives (1.0×10^{-2} *M*).

(B) Photolysis of samples of silica gel: The Rayonet reactor was placed on its side and the sample cell was rotated in the centre of the reactor using a rotary evaporator motor and was air cooled to keep the internal temperature in the range of 20–25°C. The samples were irradiated for the same length of time as the solutions. The concentrations for the acetanilide group were 9.97×10^{-5} mol/g and for the benzanilide group were 5.46×10^{-5} mol/g.

Preparation of silica gel samples

For silica gel sample preparation the apparatus illustrated in Fig. 1 was used. The cell itself was of quartz joined by a graded seal to Pyrex. The silica gel (5 g) was placed in the cell. With stopcocks A and C open to the pump and B and D closed the gel was heated at 200°C (1 mm Hg) overnight. After cooling C was closed, the sample placed in F, and the system reevacuated; C was then opened and the sample transferred. The same procedure was used to distil dry methylene chloride via B into the cell. The amount of methylene dichloride was enough to cover the gel: the slurry was sonicated for 10 min. The receiver attached to B was then cooled and the solvent distilled from the cell. Finally, with B closed and A opened to the pump, the gel was degassed at 1 mm Hg (133.32 Pascals) for ~5 h. The system was then disconnected from the vacuum, the cell cooled in liquid nitrogen, and the flame sealed at E.

Sample analysis

The silica gel was extracted with methanol, the methanol removed by distillation, and the residue containing some silica gel extracted with chloroform to constant weight. The acetanilide group products were analysed by nmr using about 4-methoxybenzophenone as a calibrating compound and using the acetyl signals as probes. Anilines were estimated by glc analysis after prior quantitative sublimation: the same calibrating compound was used. *o*-Toluidine was analyzed on column A as was 2,6-dimethylaniline. Column B was used for aniline and *p*-toluidine.

In all the benzanilide analyses column A was used with tetracosane as reference (temperature 80–220°C).

Mixed experiment

(a) Silica gel: 66 mg of an equimolecular mixture of *p*-methylacetaniline and *p*-chloropropionylanilide were adsorbed onto 5 g silica gel as previously described, and irradiated in the usual way. The analysis showed the presence of two new peaks. Isolation by chromatography gave unreacted starting materials together with 5-methyl-2-aminoacetophenone and 5-chloro-2-aminopropiophenone. Authentic samples were prepared by separate irradiation in methanol. Traces of *p*-toluidine and *p*-chloroaniline were observed. The conversions of *p*-methylacetanilide and *p*-chloropropionylanilide were 35 and 47%, respectively.

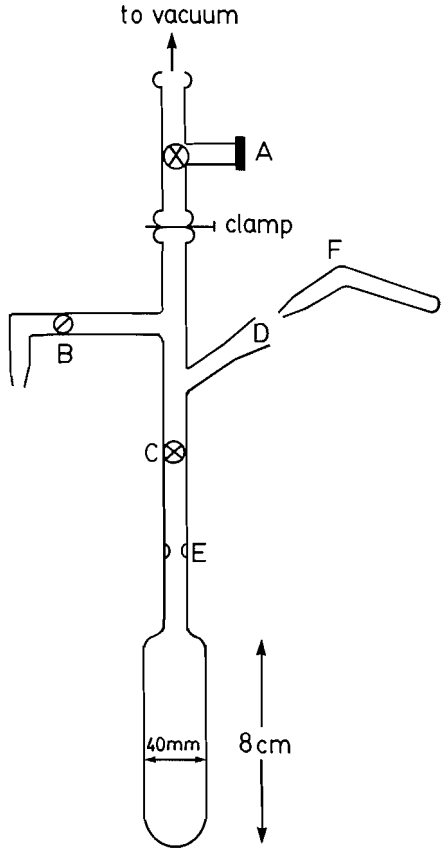

FIG. 1. Apparatus for the preparation of silica gel samples (see text).

(b) Methanol solution: a similar mixture of amides dissolved in 25 mL methanol was irradiated. Up to ~50% conversion glc analysis showed the presence of the same four components as found on silica gel.

1. J. C. ANDERSON and C. B. REESE. Proc. Chem. Soc. 217 (1960).
2. D. BELLUS and P. HRDLOVIC. Chem. Rev. **67**, 599 (1967); D. BELLUS. Adv. Photochem. **8**, 109 (1971); V. I. STENBERG. Org. Photochem. **1**, 127 (1967).
3. H. KOBSA. J. Org. Chem. **27**, 2293 (1962).
4. J. W. MEYER and G. S. HAMMOND. J. Am. Chem. Soc. **94**, 2219 (1972); R. A. FINNEGAN and D. KNUTSON. J. Am. Chem. Soc. **89**, 1970 (1967).
5. J. MARTENS and K. PRAEFKE. J. Organomet. Chem. **198**, 321 (1980).
6. (*a*) M. FISCHER. Chem. Ber. **102**, 342 (1969); Tetrahedron Lett. 4295 (1968); 2281 (1969); (*b*) H. SHIZUKA. Bull. Chem. Soc. Jpn. **42**, 52 (1969); **42**, 57 (1969); H. SHIZUKA and I. TANAKA. Bull. Chem. Soc. Jpn. **41**, 2343 (1968); S. ISHIDA, Y. HASHIDA, H. SHIZUKA, and K. MATSUI. Bull. Chem. Soc. Jpn. **52**, 1135 (1979); (*c*) J. STUMPE, A. MELHORN, and K. SCHWETLICK. J. Photochem. **8**, 1 (1978); (*d*) M. Z. A. BADR, M. M. ALY, and F. F. ABDEL-LATIF. J. Org. Chem. **44**, 3244 (1979); H. J. HAGEMAN. Rec. Trav. Chim. **91**, 1447 (1972).
7. D. ELAD. Tetrahedron Lett. 873 (1963); D. ELAD, D. V. RAO, and V. I. STENBERG. J. Org. Chem. **30**, 3252 (1965).
8. (*a*) V. AVILA, H. E. GSPONER, and C. M. PREVITALI. Rev. Latinoamer. Quim. **11**, 145 (1980) (Chem. Abstr. **94**, 78036*b* (1981)); (*b*) J. J. COSA, H. MENEZ, and C. M. PREVITALI. Ann.

Assoc. Quim. Argentina, **70**, 1 (1982) (Chem. Abstr. **96**, 190534*e* (1982)).
9. R. CHENEVERT and R. PLANTE. Can. J. Chem. **61**, 1092 (1983).
10. D. AVNIR, P. DE MAYO, and I. ONO. J. Chem. Soc. Chem. Commun. 1109 (1978).
11. (*a*) D. AVNIR, L. J. JOHNSTON, P. DE MAYO, and S. K. WONG. J. Chem. Soc. Chem. Commun. 958 (1981); (*b*) L. J. JOHNSTON, P. DE MAYO, and S. K. WONG. J. Org. Chem. In press; Can. J. Chem. In press.
12. R. K. BAUER, R. BORENSTEIN, P. DE MAYO, K. OKADA, M. RAFALSKA, W. R. WARE, and K. C. WU. J. Am. Chem. Soc. 104, 4635 (1982); P. DE MAYO, A. NAKAMURA, P. W. K. TSANG, and S. K. WONG. J. Am. Chem. Soc. **104**, 6824 (1982).
13. P. A. LEERMAKERS, L. D. WEIS, and H. T. THOMAS. J. Am. Chem. Soc. **87**, 4403 (1965).
14. P. A. LEERMAKERS, H. T. THOMAS, L. D. WEIS, and F. C. JAMES. J. Am. Chem. Soc. **88**, 5075 (1966).
15. P. S. ENGEL. J. Am. Chem. Soc. **92**, 6074 (1970).
16. B. MATUSZEWSKI, R. S. GIVENS, and C. NEYWICK. J. Am. Chem. Soc. **95**, 595 (1973).
17. J. F. J. DIPPY and V. MOSS. J. Chem. Soc. 2205 (1952).
18. Dictionary of organic compounds. 5th ed. Chapman and Hall, N.Y. 1982.
19. J. R. KENEFORD, J. S. MORLEY, and J. C. E. SIMPSON. J. Chem. Soc. 1702 (1948).
20. T. SATO. Bull. Soc. Chim. Jpn. **32**, 1130 (1959).
21. D. OCKENDEN and K. SCHOFIELD. J. Chem. Soc. 612 (1953).
22. E. REEDER and L. H. STERNBACH. U.S.P. 3, 239, 564 (Chem. Abstr. **64**, 19498*a* (1966)).
23. D. ARTINI, A. BUTTINONI, E. DRADI, W. LOGEMANN, V. MANDELLI, P. MELLONI, R. TOMMASINI, G. TOSOLINI, and G. VITA. Arzneim Forsch **21**, 30 (1971) (Chem. Abstr. **74**, 86060 *g* (1971)).
24. F. D. CHATTAWAY. J. Chem. Soc. **81**, 637 (1902).
25. J. F. KENEFORD and J. C. E. SIMPSON. J. Chem. Soc. 354 (1948).

Can. J. Chem. Downloaded from www.nrcresearchpress.com by 210.87.254.6 on 09/06/12
For personal use only.

Surface photochemistry: the effect of surface modification on the photophysics of naphthalene and pyrene adsorbed on silica gel[1]

RICHARD K. BAUER, PAUL DE MAYO, LALGUDI V. NATARAJAN, AND WILLIAM R. WARE
Photochemistry Unit, Department of Chemistry, The University of Western Ontario, London, Ont., Canada N6A 5B7

Received December 5, 1983

RICHARD K. BAUER, PAUL DE MAYO, LALGUDI V. NATARAJAN, and WILLIAM R. WARE. Can. J. Chem. **62**, 1279 (1984).

The influence of heat treatment and of added coadsorbates on the surface photophysics of pyrene and naphthalene adsorbed on silica gel is reported. When the silica gel surface is partially dehydroxylated, the distribution of pyrene or naphthalene is inhomogeneous, as indicated by multiexponential fluorescence decay and broad emission spectra. Addition of polar coadsorbates renders the surface more homogeneous with singlet lifetimes approaching solution values. The pretreatment and addition of coadsorbates, in the case of pyrene, also influence the relative importance of dynamic excimer formation vis-a-vis ground state association.

RICHARD K. BAUER, PAUL DE MAYO, LALGUDI V. NATARAJAN et WILLIAM R. WARE. Can. J. Chem. **62**, 1279 (1984).

On a examiné l'influence, sur la photophysique du pyrène et du naphtalène adsorbé sur du gel de silice, des substances coadsorbées ainsi que celle du traitement de la surface par la chaleur. Lorsque la surface du gel de silice est partiellement déshydroxylée, la distribution du pyrène ou du naphtalène n'est pas homogène comme l'indiquent la désintégration de fluorescence multiexponentielle et le spectre d'émission qui est élargi. L'addition de produits de coadsorption polaires rend la surface plus homogène avec des temps de vie du singulet qui s'approchent des valeurs observées en solution. Le traitement préalable et l'addition de produits de coadsorption, dans le cas du pyrène, influencent également l'importance relative de la formation de l'excimère dynamique par rapport à l'association dans l'état fondamental.

[Traduit par le journal]

Can. J. Chem. Downloaded from www.nrcresearchpress.com by 210.87.254.6 on 09/06/12
For personal use only.

Introduction

In recent years there has been considerable interest in the photophysics and photochemistry of molecules adsorbed on oxide surfaces such as alumina and silica gel. The purpose of these investigations has been two-fold: to observe how the surface interactions may modify the behaviour of the excited molecules, and to use photochemistry as a tool to probe the substrate surface. Amongst the techniques employed that of fluorescent spectroscopy has so far been used most intensively both on silica gel (1–5), alumina (6–13), and porous glass (14).

The surface of silica gel consists of siloxane bridges between atoms of tetracovalent silicon. The terminal oxygen functions — the silanols — have been shown by infrared studies to be geminal, vicinal, or isolated (15–23). These functions, in an amorphous framework, serve to render the silica gel surface inhomogeneous. The binding of molecules with π-systems or with lone pair electrons is largely by hydrogen bonding to the silanols or to physically adsorbed water molecules. As a consequence of the varied silanol environment the emission of aromatic hydrocarbons adsorbed on "active" surfaces is characterized by broader emission and excitation spectra, and also by a multi-exponential decay of usually shorter mean decay time. This is in contrast to that observed in solution where the spectra are well resolved and the lifetimes are much higher.

Since heat treatment of silica gel modifies the number and nature of the surface silanols, it is to be expected that the fluorescence behaviour will also be changed. Heat treatment of silica gel first induces loss of the physically adsorbed water molecules and, subsequently, dehydroxylation of the silanol groups. The number of hydroxyl groups on the silica gel surface depends strongly on the temperature of pretreatment of the samples studied (15–24). Measurements performed by Fripiat and Uytterhoeven (21), amongst others, indicate that the amount of free water rapidly decreases with increasing temperature and, for temperatures higher than about 250°C, it is reduced to nil. The number of silanol groups decreases more slowly; starting at ~6 OH/100 Å^2, it is reduced to ~2 OH/100 Å^2 at 500°C and to ~1 OH/100 Å^2 at 800°C. Up to 450°C the dehydroxylation process can be reversed by exposing the silica gel to water vapour, for higher temperatures this process is slow. If the heating is taken to ~700°C, or higher, only isolated OH groups remain on the surface (21, 23). Fripiat and Uytterhoeven's (21) findings have been recently supported by nmr studies (24) in which, additionally, the proportion of geminal-hydroxyl sites to single hydroxyl sites, previously the subject of much debate, was determined. In the temperature range 500–700°C, the surface concentration of geminal-hydroxyl sites remains roughly constant, but the ability to regenerate silanols by exposure to water vapour decreases suddenly. Therefore, heating the surface of SiO_2 to temperatures higher than 500°C followed by rehydration changes the proportion of isolated to geminal-hydroxyl sites. At higher temperatures (700–900°C), all geminal and vicinal OH groups are removed from the surface and only siloxane and isolated silanols remain.

Heat treatment of silica gel, with and without subsequent partial or complete hydration, thus offered the possiblity of surface modification, with attendant increase in homogeneity; a process that promised to be revealed by emission studies. We report here the results of such studies both of dehydrated silica gel and of silica subsequently modified by the addition of water and various alcohols.

Experimental section

Materials

Silica gel (Merck 60, 35–75 mesh) was used as adsorbent. Pyrene (Aldrich, 99+%) was purified by recrystallization from ethanol and vacuum sublimation. Naphthalene was zone refined. Cyclohexane (Fisher Scientific) spectroanalysed grade contained 56 μg/mL water (Karl Fischer). Cyclohexane passed through fresh silica gel column contained 26 μg/mL water. The water content was lowered to 2 μg/mL by distillation over P_2O_5 and storage on molecular sieves (4 Å). For most of the experiments, cyclohexane dried with a silica gel column was used. Methanol and 1-decanol were spectroanalyzed grades. The silica gel surface area (560 m^2/g) was determined by the

[1] Publication 315 from the Photochemistry Unit.

method of Hoffman *et al.* (25). Monolayer coverages for naphthalene and pyrene were taken very roughly as 100 mg/g silica gel.

Photophysical studies

1. Preparation of samples: The different methods of silica gel treatment for the sample preparation are summarized as follows: (*a*) heating in vacuum at 800°C for 4 h, undried cyclohexane was used for dissolving the hydrocarbon; (*b*) heating in air at 800°C for 4 h, undried cyclohexane was used for dissolving the hydrocarbon; (*c*) heating in vacuum at 700°C for 4 h, undried cyclohexane was used for dissolving the hydrocarbon; (*d*) heating in vacuum at 700°C for 4 h; (*e*) heating in vacuum at 600°C for 4 h; (*f*) heating in air at 600°C for 4 h; (*g*) heating in the presence of dry O_2 at 600°C for 4 h; (*h*) heating in the presence of dry N_2 at 600°C for 4 h; (*i*) heating in vacuum at 600°C for 4 h followed by exposure to air for 1 h; and (*j*) heating in vacuum at 500°C for 4 h.

In general, the silica gel (2 g) was heated in vacuum for 4 h at the desired temperature and then cooled down to room temperature in vacuum. This heating period was selected because Sindorf and Maciel (24) reported that under such conditions 90% dehydration occurred. The deaerated (freeze–thaw method) naphthalene or pyrene solution (2 mL/g SiO_2) was then added to the cooled silica gel (20°C) in vacuum. The cyclohexane was then evaporated and the remaining adsorbate-covered silica gel evacuated to 2E-5 Torr for 30 min. For most of the experiments a measured volume of deaerated water, methanol, hexanol, or decanol was then transferred, in vacuum, on to the silica gel. If necessary, heating of the apparatus with a hot air gun to about 70°C was employed. After transfer of the additive, pumping was terminated. During the transfer, the silica gel was shaken to ensure an even distribution of the additive. The amount of water introduced in the cyclohexane (dried on a silica gel column) was about 50 μg/g SiO_2, equal to 2.8×10^{-6} mol/g SiO_2, a quantity much less than the lowest amount of water deliberately added. After preparation of the sample of pyrene or naphthalene on silica gel it was transferred to a quartz cuvette (1 mm) in vacuum, sealed, and tumbled 1 h to achieve an even distribution of adsorbed molecules (3).

2. Fluorescence decay measurements: Fluorescence decay was measured with a Photochemical Research Associates (PRA) System 3000 Nanosecond Spectrofluorometer. Detailed description of the experimental techniques is given elsewhere (1–4). The decays were not single exponential, and it was necessary to use a two component decay with four parameters, according to eq. [1] (26, 27).

$$[1] \quad I_F(t) = A_1[\exp(-\lambda_1 t)] + A_2[\exp(-\lambda_2 t)]$$

The average lifetime was calculated from eq. [2].

$$[2] \quad \bar{\tau} = \frac{A_1\tau_1^2 + A_2\tau_2^2}{A_1\tau_1 + A_2\tau_2}$$

The average decay times τ are reproducible to within ±5% for multiple samples of the same experiment.

Relative quantum yields were calculated from eqs. [3] and [4]

$$[3] \quad \phi_1 = A_1\tau_1/(A_1\tau_1 + A_2\tau_2)$$

$$[4] \quad \phi_2 = A_2\tau_2/(A_1\tau_1 + A_2\tau_2)$$

For example, the percentage of the short decay component (τ_2) was calculated as $\phi_2 \times 100$.

The steady state emission and excitation spectra were measured on a Perkin-Elmer 650-40 computer-controlled fluorescence spectrophotometer (1–4).

Results

Influence of surface preparation on the photophysics of naphthalene

For naphthalene adsorbed on silica gel the pretreatment consisted in the gel's being heated at different temperatures in different gases or in vacuum. The highest temperature used was 800°C. In Fig. 1 are presented emission spectra, obtained with

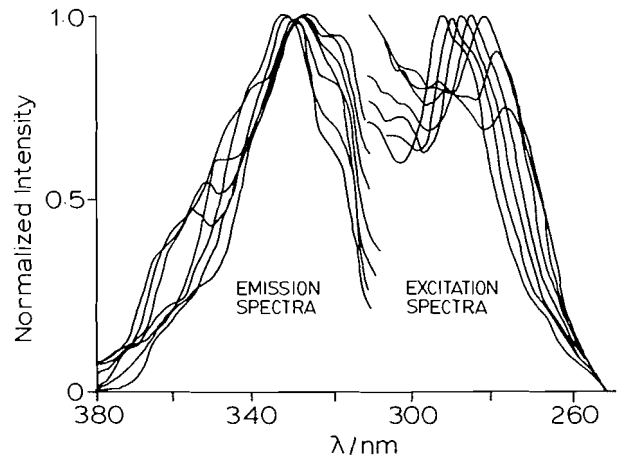

FIG. 1. Excitation and emission spectra of naphthalene adsorbed on silica gel. The silica gel was heated in vacuum for 4 h at 800°C (Preparation (*a*)). Naphthalene coverage was 0.2 mg/g SiO_2. As the excitation was varied from 270 to 300 nm, emission varied from 332 to 350 nm.

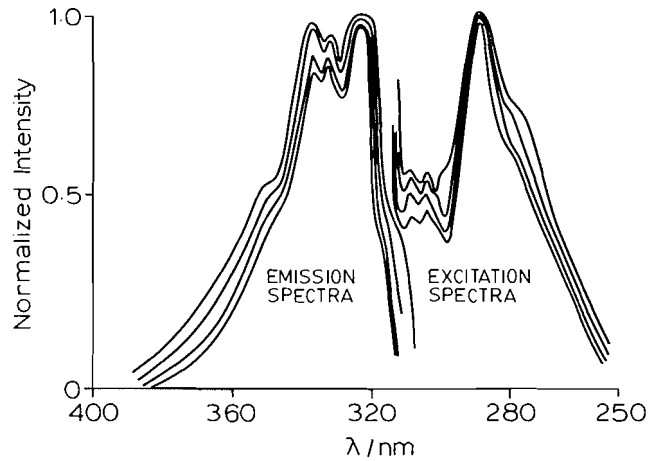

FIG. 2. Excitation and emission spectra of naphthalene adsorbed on silica gel with different emission and excitation wavelengths. The silica gel was heated for 4 h in open air at 800°C (Preparation (*b*)). Napthalene coverage was 0.2 mg/g SiO_2. Excitation varied from 270 to 300 nm, emission varied from 332 to 350 nm.

different excitation wavelengths, together with excitation spectra, monitored at different emission wavelengths, of naphthalene adsorbed on SiO_2 pretreated at 800°C. The sets of different spectra must arise because the heat treatment has rendered the surface very inhomogeneous and the naphthalene molecules find themselves in many different environments. There is a systematic shift of the excitation spectra with emission wavelength. The observed increase of the excitation spectral intensity above 300 nm is to be attributed to strong scattering. The decay of the emission is strongly nonexponential with a highly shortened mean decay time of only 6.67 ns and a 67% (ϕ_2) contribution from the short component.

These characteristics of the surface changed if the sample was heated at the same temperature but exposed to air (Fig. 2). Although these spectra also show some dependence on excitation or viewing wavelengths, they indicate a much more homogeneous surface. The decay approaches more closely a single exponential. The observed mean decay time was 49.1 ns with only 12.8% contribution from the shorter component (Fig.

Can. J. Chem. Downloaded from www.nrcresearchpress.com by 210.87.254.6 on 09/06/12
For personal use only.

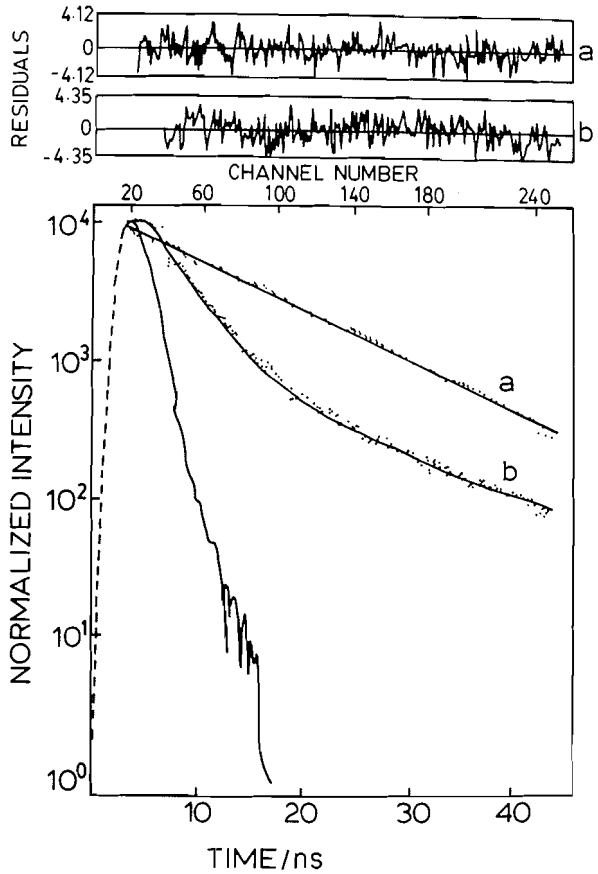

FIG. 3. The decay of naphthalene fluorescence. Emission wavelength is 333 nm: (*a*) silica gel was heated in open air for 4 h at 800°C (Preparation (*b*)); (*b*) silica gel was heated in vacuum for 4 h at 800°C (Preparation (*a*)).

3). Lowering the temperature in the sample preparation to 700°C and 600°C with exposure to air results in differences between the emission spectra with different excitation wavelengths becoming almost negligible. For the sample heated to 600°C, the decay approaches a single exponential with only 8.5% contribution from the shorter component.

The vibronic structure of the naphthalene fluorescence also depended on whether the SiO_2 was heated in vacuum or in air. In vacuum the fine structure of the adsorbed naphthalene fluorescence almost disappeared (Fig. 4*a*). The ratio of the intensity of the first maximum to the intensity of the first minimum, I/I_{min} indicated in Fig. 4 may serve as a measure of the vibronic structure.

To determine why heating in air improved the homogeneity of the silica gel surface a series of samples was prepared for which the silica gel was heated to 600°C in vacuum, in dried oxygen, in dried nitrogen, and in dried air. The emission spectra of these samples were very similar and showed low vibronic resolution and pronounced non-exponentiality of the decay with low mean decay time of 40 ns. If the sample was heated in vacuum, cooled, and then exposed to the open air for 1 h, the vibronic resolution increased and the decay time lengthened to 45 ns.

These observations suggested that the spectral behaviour of adsorbed naphthalene depends on the amount of water adsorbed during exposure to air. To verify this, a set of samples was prepared for which the silica gel was heated to 700°C in vacuum and, prior to naphthalene adsorption, a measured

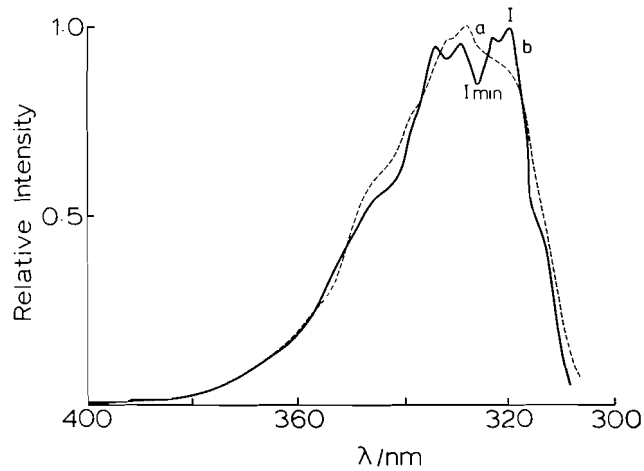

FIG. 4. Emission spectra of naphthalene: (*a*) silica gel heated to 700°C in vacuum for 4 h (Preparation (*c*)); (*b*) silica gel heated at 700°C in vacuum for 4 h (Preparation (*c*)). Water, 5.5×10^{-4} mol/g SiO_2, was added. The excitation wavelength was 285 nm.

amount of water was added. The deaerated water was transferred in vacuum from an additional side arm in the closed vacuum system. The amount of water added ranged from 2.8×10^{-5} to 1.14×10^{-3} mol/g SiO_2. As can be seen (Fig. 4*b*), the addition of water strongly influenced the SiO_2 surface. The most pronounced vibronic structure is present in the sample with 5.5×10^{-4} mol/g SiO_2 of water added. The longest decay time of 50 ns ($\bar{\tau}$) and the smallest contribution from the short decay component (8.5%) were observed for a sample with 2.8×10^{-4} mol/g SiO_2 of water.

Effect of surface modification on the photophysics of pyrene

Since pyrene has been suggested as an indicator of the polarity of its environment in solution (28, 29), measurements of the influence of water on the silica gel surface were made with adsorbed pyrene. As observed with naphthalene, the mean decay time increased with increasing amounts of water and the decay itself approached a single exponential with the contribution from the short component dropping from 45% for the dry sample (700°C) to 8% for the sample with 4.2×10^{-4} mol/g of added water. The data are summarised in Table 1. It can be seen that the higher the temperature, the shorter the mean lifetime of the pyrene and the more pronounced the effect of adding water on the decay time. The emission spectra of pyrene adsorbed on silica gel with different amounts of water added are shown in Fig. 5. The vibronic structure depends very strongly on the water content which causes an increase in the second band as well as the intensity ratio I_0/I_2. It is particularly striking that if the water content is 4.2×10^{-4} mol/g SiO_2, the decay time changes from 66.6 ns to 312 for a heating treatment of 700°C. The emission spectral area as well as the intensity ratio I_0/I_2 are most affected by the addition of water after the highest temperature heat treatment.

The question arose whether the behaviour of water was unique in this respect or whether other polar molecules would similarly influence the silica gel surface. Methanol was selected as a possible candidate, and the results are presented in Table 2. The amount of methanol adsorbed was varied from 3.75×10^{-5} mol/g SiO_2 to 7.5×10^{-4} mol/g SiO_2 for low pyrene concentrations. The influence of MeOH on the emission spectrum and the decay time is more pronounced (Table 2) than that of water. For instance, the decay time for one sample with

Can. J. Chem. Downloaded from www.nrcresearchpress.com by 210.87.254.6 on 09/06/12
For personal use only.

TABLE 1. Effect of addition of water on pyrene adsorbed on silica gel

Amount of H_2O added (mol/g SiO_2)	Decay times τ_1	τ_2	τ	% 2nd component	I_0/I_2	Relative area[g]
0[a,b]	191	34	168	15	1.80	0.59
2.8×10^{-5}[a,b]	241	74	221	12	1.68	0.75
1.4×10^{-4}[a,b]	263	111	249	9.5	1.60	0.91
4.2×10^{-4}[a,b]	258	86	250	5	1.60	1.00
0[b,c]	120	21	85	35	1.78	0.34
2.8×10^{-5}[b,c]	254	72	221	18	1.78	0.75
1.4×10^{-4}[b,c]	308	122	291	9	1.46	0.96
4.2×10^{-4}[b,c]	308	133	293	9	1.44	1.00
1.4×10^{-3}[b,c]	302	116	294	4	1.44	1.10
0[b,d]	104	21	66	45	1.72	0.29
2.8×10^{-5}[b,d]	217	45.9	200	11	1.76	0.72
1.4×10^{-4}[b,d]	283	101	242	23	1.62	0.95
4.2×10^{-4}[b,d]	329	122	312	8	1.35	1.00
0[e,f]	186	32	151	23	—	0.48
1.9×10^{-5}[d,e]	225	36	201	13	—	0.77
1.4×10^{-4}[d,e]	304	91	275	14	—	0.92
4.2×10^{-4}[d,e]	323	111	300	11	—	1.00

[a] Silica gel preparation is as (*j*) in the Experimental section.
[b] Pyrene coverage is 0.05 mg/g SiO_2.
[c] Silica gel preparation is as (*e*) in the Experimental section.
[d] Silica gel preparation is as (*d*) in the Experimental section.
[e] Pyrene coverage is 0.5 mg/g SiO_2.
[f] The experimental conditions are as (*c*) in the Experimental section.
[g] Area ratio is calculated from integrated area of the emission spectrum from 360 to 460 nm.

methanol coadsorbed becomes as long as 383 ns with only 2.8% intensity contributed by the short component. This is to be compared with the decay time of pyrene in MeOH and in cyclohexane which are 370 and 430 ns, respectively. The I_0/I_2 ratio also is reduced from 1.75 to 1.14. This is to be compared with the value of 1.35 (29) for MeOH solution.

n-Decanol was also used as a coadsorbate. At the same molar concentration the binding from hydrogen bonding would be expected to be similar to that of methanol, but the hydrophobic tail might interact with, and perhaps cover, the hydrophobic siloxane functions, thus reducing pyrene–siloxane interactions. There might also be steric interference with the approach of pyrene to non-bonded silanols. In the event, *n*-decanol resolved the emission spectrum and increased the decay time more efficiently than MeOH or water at the same concentration (Fig. 6 and Table 3). The intensity ratios I_0/I_2 also changed more rapidly.

In the experiments described so far, the pyrene coverage was ~0.05%. We have previously reported for higher coverages (~1%) the observation of excimer-like emission (1, 3, 4) from pyrene. It has been shown that, with other treatments of the surface and with glycerol or decanol additives, there was evidence for both ground state association and dynamic excimer formation. We, therefore, increased the pyrene coverage in the present experiments under more controlled conditions to observe the effect of surface modification by adding water, methanol, hexanol, and decanol. As seen in Fig. 7, and Tables 1, 2, and 3, with increasing water or MeOH there is an increase of excimer-like emission. This is also seen in the ratio I_{470}/I_{392} where I_{470} refers to the excimer intensity. Thus methanol produces a more significant effect on excimer intensity than does water. The excitation spectra (MeOH at 1.2×10^{-3} mol/g SiO_2) corresponding to excimer emission and monomer emission are different. That corresponding to the 470 nm emission is red-shifted as compared to that at 393 nm (Fig. 8), suggesting the occurrence of ground state bimolecular association. On the other hand, at the same concentration of *n*-decanol the two excitation spectra are almost identical (Fig. 9). Further, the *n*-decanol curve for excimer emission has a pre-exponential term A_2 which is *negative*, with values of A_2 and A_1 which are numerically almost equal (Table 3). For methanol the values of A_2 and A_1 are both positive. In the former situation, therefore, kinetic excimer formation is dominant whereas ground state association predominates in the latter (4, 30).

To confirm that there was a relationship between the contribution of the hydrophobic moiety, i.e., the carbon chain, and dynamic excimer formation, an intermediate length alcohol, *n*-hexanol, was investigated (1.10×10^{-3} mol/g SiO_2) at ~1% pyrene coverage, a large excimer growth was seen and $A_2/A_1 = -0.65$, indicative of dynamic excimer formation. The excitation spectra for 470 nm emission and 393 nm emission,

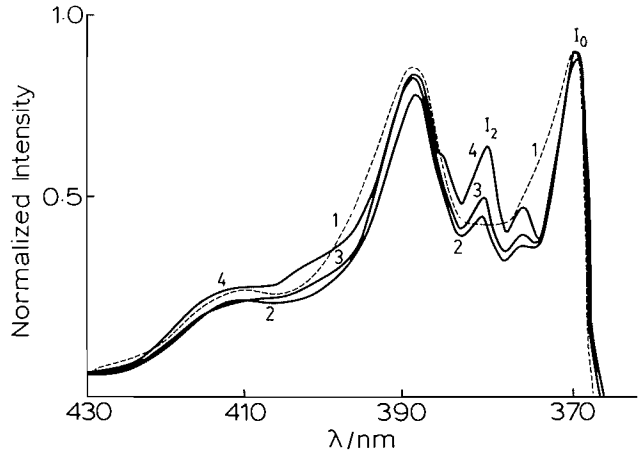

FIG. 5. Effect of addition of water on the emission spectra of pyrene coverage is 0.05 mg/g SiO_2. Silica gel was heated in vacuum to 700°C for 4 h (Preparation (*d*)). Varying amounts of water were added in a closed system. (*1*), 0; (*2*), 4.2×10^{-5} mol/g SiO_2; (*3*), 1.4×10^{-4} mol/g SiO_2; (*4*), 4.2×10^{-4} mol/g SiO_2. The excitation wavelength was 332 nm.

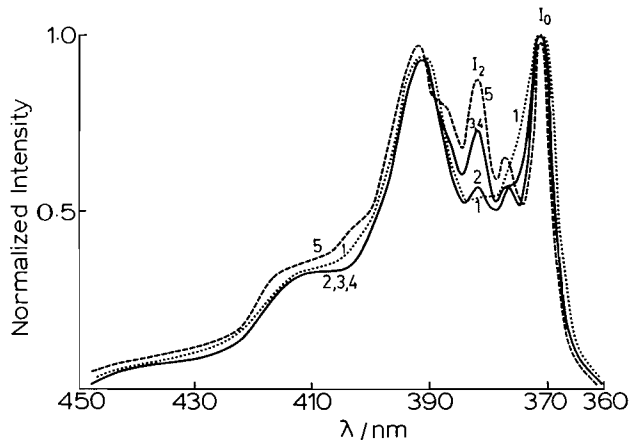

FIG. 6. Effect of 1-decanol addition on the emission spectra of pyrene adsorbed on silica gel. Silica gel heated in vacuum to 700°C for 4 h (Preparation (*d*)). (*1*), 0; (*2*), 1×10^{-5}; (*3*), 5×10^{-5}; (*4*), 6.5×10^{-5}; (*5*), 1.1×10^{-4}. Decanol concentrations were in mol/g SiO_2. Pyrene coverage is 0.05 mg/g. The excitation wavelength was 332 nm.

Can. J. Chem. Downloaded from www.nrcresearchpress.com by 210.87.254.6 on 09/06/12
For personal use only.

TABLE 2. Effect of methanol addition on pyrene adsorbed on silica gel[a]

Methanol (mol/g SiO_2)	Decay times: Monomer emission τ_1	τ_2	τ	% 2nd component	Excimer emission[d] A_1	τ_1	A_2	τ_2	I_0/I_2	Excimer ratio[e] I_{470}/I_{392}
0[b]	98	20	65	45					1.75	
3.75×10^{-5}[b]	183	29	150	21.4					1.65	
7.50×10^{-5}[b]	290	78	256	15.6					1.48	
1.25×10^{-4}[b]	358	109	344	5.5					1.21	
3.75×10^{-4}[b]	370	87	360	3.25					1.17	
5.0×10^{-4}[b]	401	125	389	4.5					1.14	
7.5×10^{-4}[b]	390	81	383	2.8					1.14	
0[c]		30	163	22	0.06	77	0.08	15	1.40	0.21
3.75×10^{-5}[c]	278	58	250	12.7	0.35	68	0.15	4.54	1.19	0.33
5.0×10^{-4}[c]	369	65	366	4	0.35	64	0.22	3.33	1.10	0.46
1.2×10^{-3}[c]	353	33	349	1.52	0.17	68	0.18	7.14	1.10	0.57

[a] Preparation of silica gel is as (*d*) in the Experimental section.
[b] Pyrene coverage is 0.05 mg/g SiO_2.
[c] Pyrene coverage is 1 mg/g SiO_2.
[d] No excimer emission was observed for the low pyrene coverage.
[e] Excimer intensity is accounted for by the ratio of the intensity of the excimer-like emission at 470 nm to the emission at 392 nm.

TABLE 3. Effect of 1-decanol addition on pyrene adsorbed on silica gel[a]

1-Decanol (mol/g SiO_2)	Decay times: Monomer emission τ_1	τ_2	τ	% 2nd component	Excimer emission[d] A_1	τ_1	A_2	τ_2	I_0/I_2	Excimer ratio[e] I_{470}/I_{392}
0[b]	98	20	65	45					1.75	
1.0×10^{-5}[b]	131	21	120	25					1.65	
5.0×10^{-5}[b]	301	45	290	6.5					1.20	
6.5×10^{-5}[b]	340	53	320	4					1.22	
1.1×10^{-4}[b]	367	67	360	2					1.14	
0[c]	200	30	163	22	0.06	77	0.09	16	1.40	0.21
1.3×10^{-4}[c]	357	75	343	5.5	0.12	103	0.38	3.2	~1	0.32
1.3×10^{-3}[c]	271	88	240	11	0.48	155	−0.37	45	0.84	0.37

[a] Preparation of silica gel is as (*d*) in the Experimental section.
[b] Pyrene coverage is 0.05 mg/g SiO_2.
[c] Pyrene coverage is 1 mg/g SiO_2.
[d] No excimer emission was observed for the low pyrene coverage.
[e] Excimer intensity is accounted for by the ratio of the intensity of the excimer-like emission at 470 nm to the emission at 392 nm.

though not identical, were more similar than those observed for methanol (Fig. 10). Ground state association is also indicated. As with pyrene at low coverage, the additives resolve the emission spectra and also increase the monomer decay times (Tables 2, 3). Similarly, for the higher coverage of pyrene with increasing additives the monomer decay approaches a single exponential with a low contribution from the short-lived component.

Discussion

The experimental fluorescence decay data have been analyzed in terms of a four-parameter model, i.e., a two component decay. While direct comparison with this same model for solution excimer behavior appears to provide insight into the behavior of pyrene on silica gel, it must be understood that no exact physical significance is intended to be associated with the derived parameters. A six-parameter model would not seem appropriate and this type of system is too complex to permit the sort of analysis that might lead to quantitative interpretation of the parameters of the double experimental model employed here. This model has therefore been used to systematize the experimental data and form the basis of the discussion of the behavior of pyrene on the surface.

The experimental results with naphthalene and pyrene show that heating of the silica gel in vacuum to 500–700°C causes the adsorbed hydrocarbons to have broad and structureless fluorescence spectra with low quantum efficiency and substantially non-exponential decay. The addition of coadsorbed polar molecules such as water, methanol, hexanol, or decanol on the surface results in an increase in quantum efficiency, higher resolution of vibronic structure, and a large increase in decay time which approaches a single exponential. Furthermore, with increasing amounts of additives, the ratio of the vibronic bands, I_0/I_2, decreases. If this behaviour can indeed be compared with

Can. J. Chem. Downloaded from www.nrcresearchpress.com by 210.87.254.6 on 09/06/12
For personal use only.

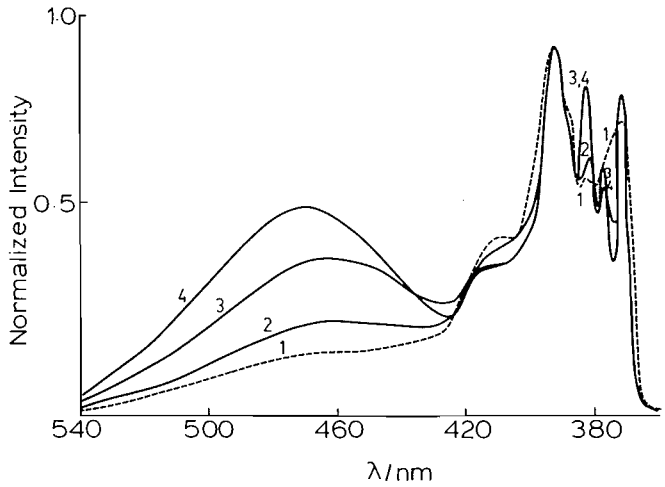

FIG. 7. Effect of methanol addition on the excimer-like emission of pyrene adsorbed on silica gel heated in vacuum at 700°C (Preparation (*d*)). Pyrene coverage is 1 mg/g SiO_2. The excitation wavelength was 347 nm. (*1*), 0 MeOH; (*2*), 3.75×10^{-5}; (*3*), 5×10^{-4}; (*4*), 1.3×10^{-3}, methanol concentrations are in mol/g SiO_2.

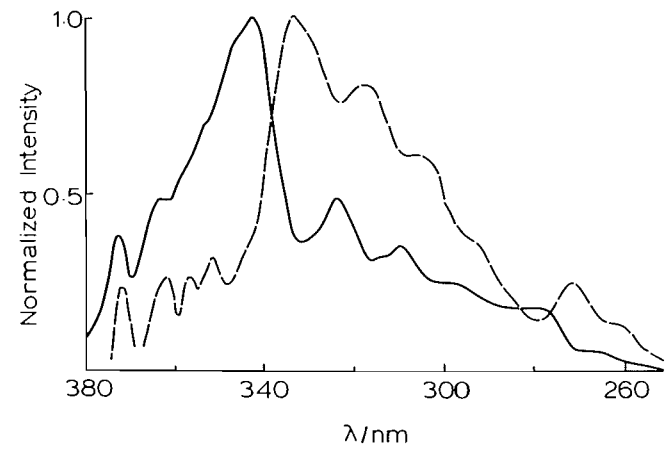

FIG. 8. Excitation spectra of emission of pyrene adsorbed on silica gel heated in vacuum at 700°C (Preparation (*d*)) and 1.3×10^{-3} mol/g SiO_2 of methanol added. Pyrene coverage was 1 mg/g SiO_2. Emission 470 nm (—), emission 393 nm (- - -).

that observed in solution (28, 29), it indicates a change in the polarity of the surface.

It is well established, theoretically (31) and experimentally (32–34), that the binding of adsorbed molecules, including aromatic hydrocarbons, takes place by hydrogen bonding to the silanol functions. Furthermore, of the various environments in which the silanol function may find itself, it is what is isolated, freely vibrating, and not hydrogen bonded to another silanol or to water, that is the most effective in binding (35–37). In the present instance, because of the dimension of the adsorbed naphthalene and pyrene, even when the dehydration of the surface is taken to about ~2 silanols/100 Å^2 (21), there must be more than one hydrogen bond per molecule. Because of the relatively small number of binding sites, their strength, and their nonuniform distribution there are, apparently two consequences.

First, the various molecules will be in a variety of local environments. The consequences are that there will be a family of similar, but not identical, emitting species, resulting in a complex decay, here expressed as the sum of two exponential.

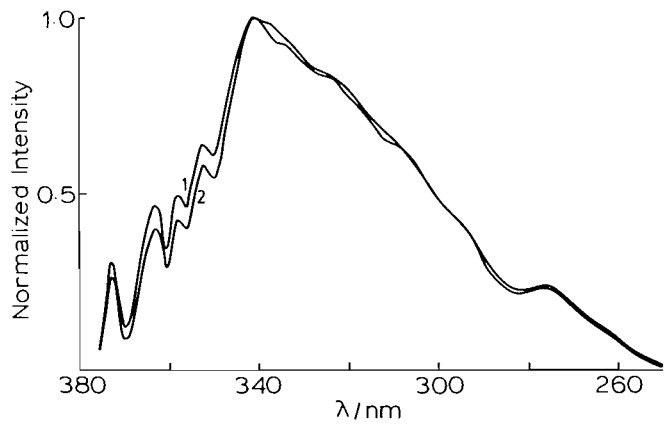

FIG. 9. Excitation spectra of pyrene adsorbed on silica gel. Silica gel heated in vacuum to 700°C (Preparation (*d*)) and 1.3×10^{-3} mol/g SiO_2 of 1-decanol added. Pyrene coverage is 1 mg/g SiO_2. (*1*), Emission at 470 nm; (*2*) emission at 393 nm.

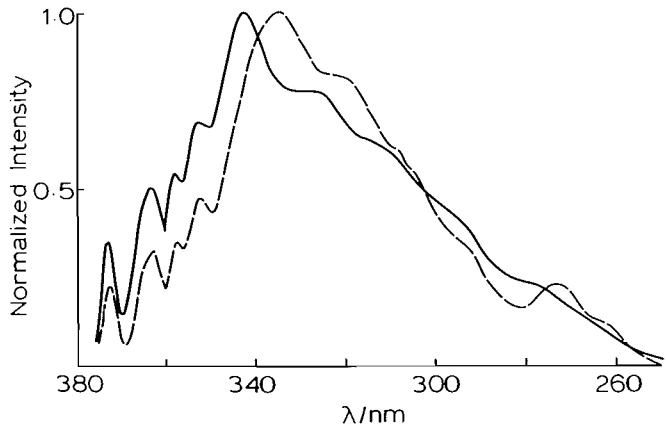

FIG. 10. Excitation spectra of emission of pyrene adsorbed on silica gel. Silica gel heated to 700°C in vacuum (Preparation (*d*)). 1-Hexanol, 1.3×10^{-3} mol/g SiO_2, was added. Pyrene coverage was 1 mg/g SiO_2; — emission 470 nm, - - - emission 393 nm.

Their emission spectra will likewise not be identical. A second consequence is that the low coverage and sparsely, isolated silanol population render hydrocarbon motion limited and the proximity of two pyrene molecules less likely; dynamic excimer formation is not observed. At higher pyrene concentration (1), with comparatively few sites available, the chances of static ground state association becomes higher and the existence of such complexes has been reported (1).

The remaining silanol functions make for a polar local environment, more so, perhaps, than when dissipated by hydrogen bonding to adjacent silanols or water. This polarity could, according to recent work (28, 29), be reflected in the I_0/I_2 ratio of the peak in the pyrene emission spectrum. Indeed, the ratio is found to be in the range 1.7–1.8. Since the I_0/I_2 ratio of pyrene in water is reported to be 1.85 (38), this might be interpreted as an argument for a high polarity in the immediate vicinity of the pyrene molecule. However, it is not immediately clear why the addition of water should *decrease* the ratio to ~1.44 when water itself is more polar than the isolated silanol. The striking increase of resolution of vibrational structure of the emission spectra and the increase of decay times for the increasing amounts of water added must be rationalized by an interaction of water with the surface. Water not only binds to the isolated silanol groups through hydrogen bonding but also

Can. J. Chem. Downloaded from www.nrcresearchpress.com by 210.87.254.6 on 09/06/12
For personal use only.

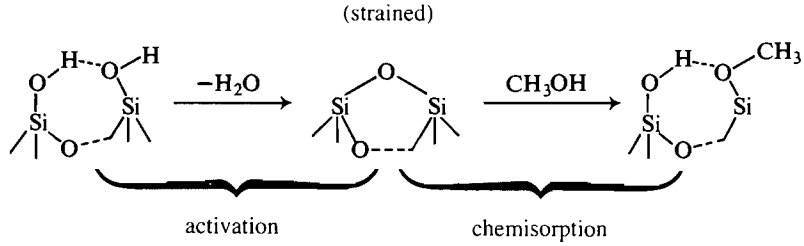

SCHEME 1

hydrolyses strained siloxane bonds formed by heating, thereby increasing the number of vicinal hydroxyl groups. Probably the first effect precedes the second, since rehydration is slow with drastically dehydrated silica gel and since the water has little to which it can anchor because the siloxane bonds are known to be hydrophobic (35). Iler (39) and others (40) have suggested that the rate-limiting step may instead involve the association of molecular water with uncondensed silanol functions. We are presently unable to decide the extent to which both contribute; in either case, the strongly interactive isolated silanol is removed (24) and this may be responsible for the I_0/I_2 decrease. Alternatively, the suggested use (29) of I_0/I_2 may not extend to silica gel surfaces: protonic solvents also are aberrant on this "Py scale" which appears to be insensitive to hydrogen bonding (29).

For the same molar concentration per gram of SiO_2, methanol as the coadsorbing additive is more efficient than water in resolving the vibrational structure of pyrene emission and also increasing the decay time. This decay times, as high as 383 ns with only ~2% contribution from the short decay component, were observed for methanol concentrations of 7.5×10^{-4} mol/g SiO_2. This value compares with that of 370 ns observed in methanol and 430 ns in cyclohexane. The surface is now much more homogeneous than that obtained by the addition of water, and approximates a two-dimensional system as described by Dacey (41).

As in the case of water, it has been shown, by infrared studies (22) of methanol adsorption on silica gel activated by heating between 200–950°C, that the formation of two species occurs on the surface. The first is methanol, hydrogen bonded to isolated silanol groups (physical adsorption), and the other involves the formation of Si—O—CH_3 bonds (chemisorbed methanol). The latter is a consequence of reaction with strained, easily-breakable siloxane linkages, as shown in Scheme 1. Evidence of interaction of CH_3OH with siloxane groups is provided by the observation that methanol adsorption increases with increase of preheat treatment of silica gel. Both surface methylation and the physical adsorption through hydrogen bonding renders the surface more uniform, in a polar sense, to pyrene and, in fact, the environment of the pyrene could approximate that of methanolic solution as hydration with water approximates aqueous solution.

On a molar basis 1-decanol is even more effective in inducing spectral resolution in pyrene than is methanol or water, presumably in part because of its greater cross-section. Here, in addition, adsorption can probably occur to the siloxanes without perturbing the silanols, as has been reported for octadecanol (42).

Excimer formation

Excimer-like emission has already been reported at higher pyrene coverages (1, 4). With increasing amounts of additives the excimer-like intensity at 470 nm increased. With methanol (1.3×10^{-3} mol/g) ground state bimolecular association was indicated by the difference in excitation spectra (4) at 393 nm (monomer) and at 470 nm (dimer). The excimer-like emission is to be attributed to the excitation of preformed pairs of pyrene molecules. The absence of any negative pre-exponential term A_2 (30) (Table 2) also implies the absence of predominant dynamic excimer formation which in turn would indicate that the mobility of pyrene is restricted. On the other hand, for 1-decanol predominant dynamic excimer formation is indicated by the negative value of A_2 (Table 3) and the value of ratio of A_2/A_1 (−0.85). Also the excitation spectra for 393 nm and 470 nm emission are now almost identical (Fig. 9). The presence of the 1-decanol has not only rendered the environment of the pyrene molecules more uniform but has increased the diffusion rate. 1-Hexanol also resolves the monomer emission and evidence is seen of some dynamic excimer formation ($A_2/A_1 = -0.65$). The excitation spectra at 393 nm and 470 nm were not quite as similar as with 1-decanol: it is concluded that both ground state association and dynamic excimer formation are important in this case.

Presumably the surface now resembles that of an alkylated silica gel, approaching what may be achieved by silylation. On such a surface a hydrocarbon will be more generally but more weakly bound, and hence have a lower activation energy for motion: diffusion will thus be facilitated.

In an earlier publication, we reported that 1-adamantanol as a coadsorber behaved differently from 1-decanol (4). The emission spectrum of pyrene in the presence of 1-adamantanol was diffuse and the decay was multiexponential with a short mean decay time. No dynamic excimer formation was observed. The area of cross-section is, however, roughly equal to that of 1-hexanol which, as described, behaves differently. This difference must be attributed to the different shapes of these two molecules. 1-Hexanol should be able to interact with all isolated silanols, but 1-adamantanol may not; it should be recollected that ca. 99% of the silica gel surface is on the *inside* of the granules. Furthermore, the rigidity of the adamantanol framework and its hydrophobicity may render many of the isolated silanols inaccessible if a consequence of bonding would entail close interaction of the cycloalkyl residue with a second silanol; an interaction that would be avoided by the flexible 1-hexanol by coiling. Finally, it may well be that the hydroxyl function may be too hindered to react chemically with strained siloxanes, as do at least water and methanol, i.e., chemisorption may be impossible.

Conclusions

When the silica gel is dry, the distribution of pyrene or naphthalene is inhomogeneous and the surface yields a broader emission spectrum and multiexponential decay; the polarity of the surface also is high. When the dried surface is saturated with polar additives, the surface becomes homogeneous, as

Can. J. Chem. Downloaded from www.nrcresearchpress.com by 210.87.254.6 on 09/06/12
For personal use only.

seen by the highly resolved emission spectra and the near single exponential decay. The singlet lifetime of pyrene approaches that observed in solution. In this context the behaviour of the surface may be best described as approaching that of a two-dimensional gas or liquid (41). The effectiveness of the additive alcohol in rendering the "surface" more homogeneous increases with chain length and presumably signals interaction with the siloxane framework (42).

Acknowledgments

Acknowledgment is made by P. de M. to the donors of the Petroleum Research Fund, administered by the American Chemical Society, for partial support of this work, and to the Natural Sciences and Engineering Research Council of Canada for additional support. W.R.W. acknowledges support from the Natural Sciences and Engineering Research Council of Canada for support of this work.

1. K. HARA, P. DE MAYO, W. R. WARE, A. C. WEEDON, G. S. K. WONG, and K. C. WU. Chem. Phys. Lett. **69**, 105 (1980).
2. R. K. BAUER, P. DE MAYO, W. R. WARE, and K. C. WU. J. Phys. Chem. **86**, 3781 (1982).
3. R. K. BAUER, R. BORENSTEIN, P. DE MAYO, K. OKADA, M. RAFALSKA, W. R. WARE, and K. C. WU. J. Am. Chem. Soc. **104**, 4635 (1982).
4. R. K. BAUER, P. DE MAYO, K. OKADA, W. R. WARE, and K. C. WU. J. Phys. Chem. **87**, 460 (1983).
5. C. FRANCIS, J. LIN, and A. SINGER. Chem. Phys. Lett. **94**, 162 (1983).
6. G. BECK and J. K. THOMAS. Chem. Phys. Lett. **94**, 553 (1983).
7. H. ISHIDA, H. TAKAHASHI, and H. TSUBOMURA. Bull. Chem. Soc. Jpn. **43**, 3130 (1970).
8. H. ISHIDA, H. TAKAHASHI, and H. TSUBOMURA. J. Am. Chem. Soc. **92**, 275 (1970).
9. H. ISHIDA and H. TSUBOMURA. J. Photochem. **2**, 285 (1973/74).
10. D. OELKRUG, M. PLAUSCHINAT, and R. W. KESSLER. J. Lumin. **18/19**, 434 (1979).
11. D. OELKRUG, M. RADJAIPOUR, and H. ERBSE. Z. Phys. Chem. Frankfurt am Main, **88**, 23 (1974).
12. D. OELKRUG, H. ERBSE, and M. PLAUSCHINAT. Z. Phys. Chem. Frankfurt am Main, **96**, 283 (1975).
13. D. OELKRUG, G. SCHREM, and I. ANDRA. Z. Phys. Chem. Frankfurt am Main, **106**, 197 (1977).
14. N. NAKASHIMA and D. PHILLIPS. Chem. Phys. Lett. **97**, 337 (1983).
15. F. H. VAN CAUWELAERT, P. A. JACOBS, and J. B. UYTTERHOEVEN. J. Phys. Chem. **76**, 1434 (1973).
16. J. A. HOCKEY. Chem. Ind. London, 57 (1965).
17. S. KONDO, M. MUROYA, and K. FUJI. Bull. Chem. Soc. Jpn. **47**, 553 (1974).
18. A. J. VAN ROOSMALEN and J. C. MOL. J. Phys. Chem. **82**, 2748 (1978).
19. I. TSUCHLYA. J. Phys. Chem. **86**, 4107 (1982).
20. S. KONDO, K. TOMOI, and C. PAK. Bull. Chem. Soc. Jpn. **52**, 2046 (1979).
21. J. J. FRIPIAT and J. UYTTERHOEVEN. J. Phys. Chem. **66**, 800, (1962).
22. E. BORELLO, A. ZECCHINA, and C. MORTERRA. J. Phys. Chem. **71**, 2938 (1967); **71**, 2945 (1967).
23. A. V. KISELEV and V. I. LYGIN. Infrared spectra of surface compounds. John Wiley and Sons, New York. 1975. Chapts. 4–7.
24. D. W. SINDORF and G. E. MACIEL. J. Am. Chem. Soc. **105**, 1487 (1983).
25. R. L. HOFFMANN, D. G. MCCONNELL, G. R. LIST, and C. D. EVANS. Science, **157**, 590 (1967).
26. C. LEWIS, W. R. WARE, L. DUEMENY, and T. L. NEMZEK. Rev. Sci. Instrum. **44**, 107 (1973).
27. W. R. WARE, J. C. ANDRE, and D. V. O'CONNOR. J. Phys. Chem. **83**, 1333 (1979).
28. K. KALYANASUNDARAM and J. K. THOMAS. J. Am. Chem. Soc. **99**, 2039 (1977).
29. D. C. DONG and M. A. WINNIK. Photochem. Photobiol. **35**, 17 (1982).
30. J. B. BIRKS. Photophysics of aromatic molecules. Wiley-Interscience, New York. 1970. Chapts. 4, 7.
31. P. HOBZA, J. SAUER, C. MORGENEYER, J. HURYCH, and R. ZAHRADNIK. J. Phys. Chem. **85**, 4061 (1981); R. S. MULLIKEN. J. Am. Chem. Soc. **74**, 811 (1952).
32. W. POHLE. J. Chem. Soc. Faraday Trans. I, **78**, 2101 (1982).
33. M. BASILA. J. Chem. Phys. **35**, 1151 (1961).
34. L. R. SNYDER. J. Phys. Chem. **67**, 2622 (1963).
35. G. A. GALKIN, A. V. KISELEV, and V. I. LYGIN. Trans. Faraday Soc. **60**, 431 (1964); K. G. KRASILNIKOV, Y. F. KISELEV, and E. A. SYSOEV. Akad. Nauk. SSSR Dokl. **116**, 990 (1957); A. V. VOLKOV, A. V. KISELEV, and V. I. LYGIN. Zh. Fiz. Khim. **48**, 1214 (1974).
36. M. L. HAIR and W. HERTL. J. Phys. Chem. **73**, 4269 (1969).
37. C. CLARK-MONKS and B. ELLIS. J. Colloid. Interface Sci. **44**, 37 (1973).
38. Y. TAKEHIKO, M. HOSHINO, and M. IMAMURA. J. Phys. Chem. **86**, 4426 (1982).
39. R. K. ILER. The chemistry of silica, solubility, polymerization and surface properties and biochemistry. Wiley, New York. 1979.
40. G. J. YOUNG. J. Colloid. Sci. **13**, 67 (1958); G. J. YOUNG and T. P. BURSH. J. Colloid. Sci. **15**, 361 (1960).
41. J. R. DACEY. Ind. Eng. Chem. **57**, 26 (1965).
42. M. J. D. LOW and P. L. LEE. J. Colloid. Interface Sci. **45**, 148 (1973).

Can. J. Chem. Downloaded from www.nrcresearchpress.com by 210.87.254.6 on 09/06/12
For personal use only.

Interactions de l'ion Ag^+ avec la glutarimide

JOHANNE PERRON ET ANDRÉ L. BEAUCHAMP[1]

Département de Chimie, Université de Montréal, C.P. 6210, Succ. A, Montréal (Qué.), Canada H3C 3V1

Reçu le 1 décembre 1983

JOHANNE PERRON et ANDRÉ L. BEAUCHAMP. Can. J. Chem. **62**, 1287 (1984).

Le composé 1:1 de l'ion Ag^+ avec la glutarimide a été étudié par diffraction des rayons X, par spectroscopie infrarouge et par rmn ^1H et ^{13}C. Les cristaux sont monoclinques, $C2/c$, a = 13,497(3) Å, b = 9,503(2) Å, c = 9,600(4) Å, β = 92,30(3)°, Z = 4 molecules par maille. La structure a été affinée au moyen de 1086 réflexions MoK$\bar{\alpha}$ d'intensité significative jusqu'à un facteur R de 0,027. La moitié des atomes d'argent est linéairement coordonnée aux atomes d'azote de deux coordinats glutarimides déprotonés, tandis que l'autre moitié est entourée d'un tétraèdre déformé de quatre oxygènes carbonyles appartenant à deux ensembles $[Glu-Ag-Glu]^-$ adjacents. Les groupes $[Glu-Ag-Glu]^-$ réunis par l'atome Ag à coordination tétraédrique forment des chaînes infinies selon l'axe c. La complexation produit plusieurs changements dans le spectre infrarouge de la glutarimide. Ils peuvent être reliés à la disparition du vibrateur N—H et à la modification des indices de liaison dans la portion —C(O)—N—C(O)— du coordinat. Les spectres rmn montrent que la glutarimide coordonnée conserve un miroir lorsque le composé d'argent est dissous dans DMSO. Ceci laisse supposer que les atomes Ag liés à l'oxygène sont largement dissociés en solution, ce qui laisse les ions linéaires $[Glu-Ag-Glu]^-$ comme espèce complexe prédominante.

JOHANNE PERRON and ANDRÉ L. BEAUCHAMP. Can. J. Chem. **62**, 1287 (1984).

The 1:1 complex formed between Ag^+ ions and glutarimide was investigated by X-ray diffraction, infrared spectroscopy, and ^1H and ^{13}C nmr. The crystals are monoclinic, $C2/c$, a = 13.497(3) Å, b = 9.503(2) Å, c = 9.600(4) Å, β = 92.30(3)°, Z = 4 molecules per cell. The structure was refined on 1086 nonzero MoK$\bar{\alpha}$ reflections to R = 0.027. One half of the Ag atoms are linearly coordinated to the N atoms of two deprotonated glutarimide ligands, whereas the other half are surrounded by an approximate tetrahedron of four carbonyl oxygens belonging to two adjacent $[Glu-Ag-Glu]^-$ units. The $[Glu-Ag-Glu]^-$ groups are joined by tetrahedrally coordinated Ag atoms into infinite chains along the c axis. Complexation introduces a number of changes in the infrared spectrum of glutarimide. They can be related to the disappearance of the N—H vibrator and the change of bond orders in the —C(O)—N—C(O)— portion of the ligand. The nmr spectra show that coordinated glutarimide retains a mirror plane when the Ag complex is dissolved in DMSO. This suggests that the O-bonded Ag atoms dissociate to a large extent in solution, leaving the linear $[Glu-Ag-Glu]^-$ ions as the major glutarimide complex species.

Introduction

Dans le but de préciser la nature des interactions de l'ion Ag^+ avec les acides nucléiques (1), les réactions de cet ion avec différents composés modèles ont été etudiées dans notre laboratoire. Nous avons montré que l'uridine (**1**) forme avec l'ion

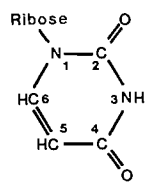

1

Ag^+ en milieu aqueux des espèces de stoechiométries 2:1 et 2:2. Toutefois, la structure de ces espèces n'a pu être déterminée sur des échantillons solides à cause de leur grande solubilité et de l'instabilité de leurs solutions saturées. Avec la méthyl-1 thymine (HMT, **2**), un composé de formule

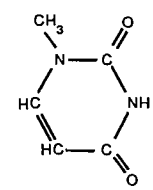

2

$Ag[Ag(MT)_2]$ a été préparé (2). La moitié des atomes d'argent dans ce composé est linéairement reliée à l'atome N(3) déprotoné de la thymine pour créer des motifs $[MT-Ag-MT]^-$, alors que l'autre moitié est entourée d'un tétraèdre déformé constitué de fonctions carbonyles appartenant à deux ensembles $[MT-Ag-MT]^-$ voisins dans le cristal. Des solides de type $M'[MT-Ag-MT]$ (où $M' = Na^+, K^+$) ont été obtenus, mais sous une forme qui ne se prête pas à un travail cristallographique (3). Nous nous sommes donc tournés vers les imides cycliques, qui renferment un ensemble —C(O)—N(H)—C(O)— semblable à celui de l'uracile et de la thymine. L'étude du système Ag^+–succinimide (**3**) par plusieurs méthodes a effectivement montré l'existence de deux sortes d'ions Ag^+ (4, 5) comme pour les dérivés de l'uracile. Le présent article décrit les résultats obtenus avec la glutarimide (HGlu, **4**), qui possède un cycle à six atomes la rapprochant de l'uracile et la thymine.

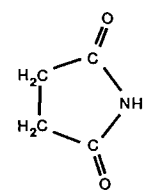

3

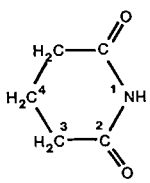

4

[1] Auteur à qui adresser toute correspondance.

Can. J. Chem. Downloaded from www.nrcresearchpress.com by 210.87.254.6 on 09/06/12
For personal use only.

Can. J. Chem. Downloaded from www.nrcresearchpress.com by 210.87.254.6 on 09/06/12
For personal use only.

Partie expérimentale

Instruments et réactifs

Les spectres infrarouges ont été obtenus à l'aide d'un spectrophotomètre Beckman 4250 au moyen de pastilles de KBr ou d'émulsions dans le Nujol ou l'hexachlorobutadiène. La précision des nombres d'onde est de ± 5 cm^{-1} entre 4000 et 2000 cm^{-1} et ± 3 cm^{-1} entre 2000 et 500 cm^{-1}.

Les spectres rmn ont été enregistrés au moyen d'un appareil Bruker modèle WH-90 pour les spectres ^{1}H et modèle WH-80 (en opérant à 20,11 MHz) pour les spectres ^{13}C. Le solvant utilisé pour les deux noyaux était le DMSO-d_6 Silanor (Merck, Sharp et Dohme Canada) d'une pureté isotopique de 99,5% et contenant 1% de tétraméthylsilane comme référence interne.

La glutarimide (Aldrich Chemicals) a été utilisée sans autre purification.

Préparation du composés Ag–glutarimide

Ce composé est connu depuis longtemps (6). Nous l'avons préparé sous forme de fines aiguilles à partir d'un mélange de glutarimide, de $AgNO_3$ et de NaOH selon des rapports 1:1:1. Les cristaux utilisés pour les études aux rayons X ont été obtenus lors de tentatives de préparation de $Li[Ag(Glu)_2]$ et $Na[Ag(Glu)_2]$, qui n'ont pas pu être isolés. A une solution de 0,70 g (6 mmol) de glutarimide et 0,43 g (2,5 mmol) de $AgNO_3$ dans 20 mL d'eau à la température ambiante, on ajoute goutte à goutte une solution de 5 mmol d'hydroxyde (0,22 g, $LiOH.H_2O$ ou 0,20 g NaOH). Après addition de la moitié de l'hydroxyde, un précipité blanc apparaît, puis se redissout lorsqu'on poursuit l'addition. Par évaporation à l'abri de la lumière, on isole des cristaux incolores prismatiques de composition AgGlu.

Données cristallographiques

$C_{10}H_{12}Ag_2N_2O_4$ m = 439,95

Monoclinique, $C2/c$, a = 13,497(3), b = 9,503(2), c = 9,600(4) Å, β = 92,30(3)°, V = 1230,3 Å^3, Z = 4, D_o = 2,32(2) g cm^{-3}, D_c = 2,374 g cm^{-3}, λ(MoK$\bar{\alpha}$) = 0,71069 Å (monochromateur de graphite), T = 298(3) K, dimensions du cristal: 0,066 mm × 0,081 mm × 0,188 mm, μ(MoKα) = 31,6 cm^{-1}, transmission = 0,71–0,82.

Mesures d'intensité et résolution de la structure

Les groupes spatiaux Cc et $C2/c$ sont compatibles avec les extinctions systématiques. La structure a été interprétée selon le groupe centrosymétrique $C2/c$ et ce choix a été ultérieurement confirmé par le succès de l'affinement. La détermination précise des constantes réticulaires et les mesures d'intensités ont été faites au moyen d'un diffractomètre Enraf–Nonius CAD4, selon la méthode décrite antérieurement (7). Un ensemble de 1086 taches hkl et $hk\bar{l}$ dans une sphère limitée par $2\theta \leq 50°$ a été mesuré et 750 d'entre elles ($I > 3\sigma(I)$), corrigées pour l'absorption, ont été retenues pour la résolution.

La structure a été résolue par la méthode de l'atome lourd et affinée par moindres carrés sur $|F_o|$ en inversant la totalité de matrice. Les positions atomiques ont été affinées pour tous les atomes, y compris ceux d'hydrogène. Les facteurs d'agitation thermique affinés étaient isotropes pour l'hydrogène, anisotropes pour les autres atomes. Le fond continu sur la carte de Fourier différence finale était inférieur à $\pm 0,28$ e/Å^3. Les facteurs d'accord sont R = 0,027 et R_w = 0,033.

Les coordonnées atomiques sont réunies au tableau 1. Les facteurs d'agitation thermique et le tableau des facteurs de structure sont déposés en archive.[2]

TABLEAU 1. Coordonnées atomiques (× 10^4, Ag × 10^5, H × 10^3)

Atome	X	Y	Z
Ag(1)	50000	50000	50000
Ag(2)	50000	67023(8)	25000
O(1)	3693(3)	4946(4)	2347(4)
O(2)	4477(4)	1812(4)	5745(4)
N(1)	4151(4)	3392(5)	4027(5)
C(1)	3658(4)	3732(6)	2803(6)
C(2)	3071(5)	2630(8)	2001(7)
C(3)	3494(5)	1180(7)	2225(6)
C(4)	3606(5)	891(7)	3763(7)
C(5)	4109(5)	2072(6)	4567(6)
H(21)	298(6)	292(8)	115(8)
H(22)	237(5)	275(7)	234(7)
H(31)	408(5)	104(7)	188(7)
H(32)	315(4)	37(5)	171(5)
H(41)	397(5)	4(7)	393(7)
H(42)	298(5)	84(6)	396(6)

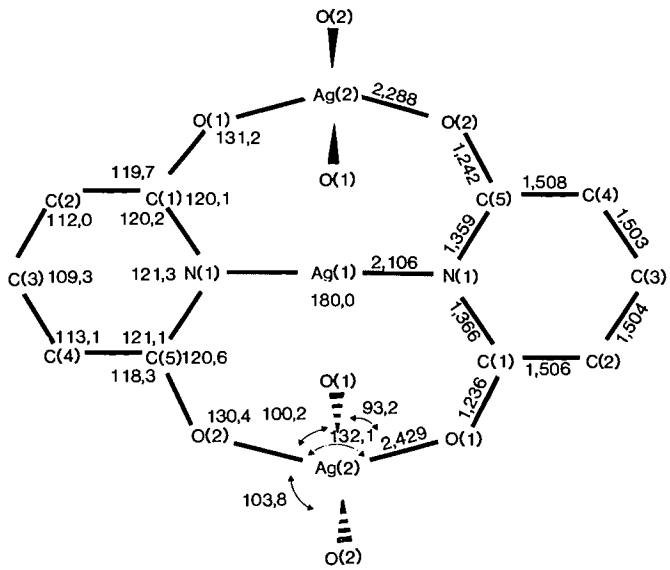

FIG. 1. Schéma du motif moléculaire avec les distances interatomiques et les angles de liaisons. Les atomes d'hydrogène ne sont pas représentés. Les écarts-types sont: 0,004–0,005 Å, Ag—O(N); 0,007–0,009 Å, autres; 0,2°, angles autour de Ag; 0,4–0,5°, autres. L'angle N—Ag—N est rigoureusement égal à 180° par symétrie.

Résultats et discussion

Description de la structure

Les trois sites potentiels de coordination, soit O(1), O(2) et N(1), sont pleinement utilisés (Fig. 1). Le composé contient deux atomes d'argent non équivalents. L'atome Ag(1) occupe un centre de symétrie cristallographique. Il se trouve donc linéairement coordonné (180° par symétrie) à l'atome d'azote de deux molécules de glutarimide déprotonée. La longueur des liens Ag(1)—N(1) (2,106(5) Å) est légèrement supérieure à celles de composés analogues avec la méthylthymine (2,081(4) Å) (2) et de la succinimide (2,079(5) Å) (4). Les deux coordinats de l'ensemble [Glu–Ag–Glu]$^-$ sont à peu près coplanaires, de sorte que chacun des côtés de cet ensemble peut jouer le rôle de chélatant grâce à une paire de groupes carbonyles. De fait, chaque ensemble [Glu–Ag–Glu]$^-$ est lié à deux atomes Ag(2) distincts dans le cristal. Réciproquement, chaque atome Ag(2) est entouré de deux paires d'oxygènes carbonyles appartenant à deux ensembles [Glu–Ag–Glu]$^-$, qui lui assurent un environnement à peu près tétraédrique (Fig. 1). Les distances Ag(2)—O (2,429(4) et 2,288(4) Å) sont un peu plus courtes que celles obtenues avec la méthylthymine (2,512(4) et 2,333(4) Å). L'écart entre les distances Ag(2)—O(1) et

[2] Les facteurs de structure, les facteurs d'agitation thermique, les calculs de plans moyens, ainsi que les distances et angles impliquant les atomes d'hydrogène peuvent être obtenus en s'adressant au Dépôt de Données Non-publiées, ICIST, Conseil National de Recherches du Canada, Ottawa, Ont., Canada K1A 0S2.

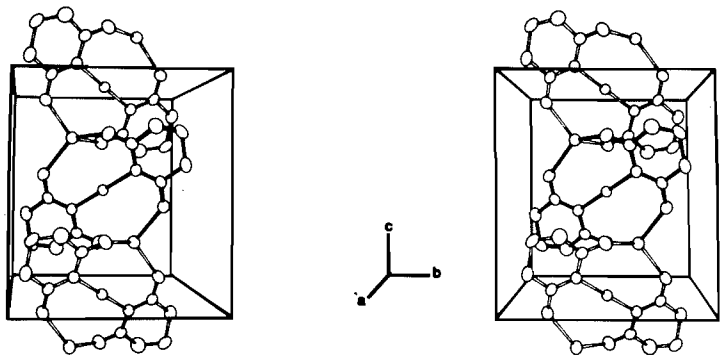

FIG. 2. Vue stéréo de l'enchaînement moléculaire le long de l'axe *c*. Le motif en traits pleins correspond à celui de la figure 1.

Ag(2)—O(2) semble lié essentiellement à des conditions de rangement moléculaire, puisque O(1) et O(2) sont chimiquement équivalents.

Les liaisons C—N (moy. 1,363, σ = 0,007 Å) sont plus courtes et les liaisons C=O (moy. 1,239, σ = 0,007 Å) sont plus longues que dans la glutarimide même (moy. 1,382 et 1,215 Å, σ = 0,003 Å, respectivement) (8). Ces variations sont en accord avec une contribution accrue des formes limites **5***b* et **5***c* dans l'anion (**5**). La coordination de l'argent aux

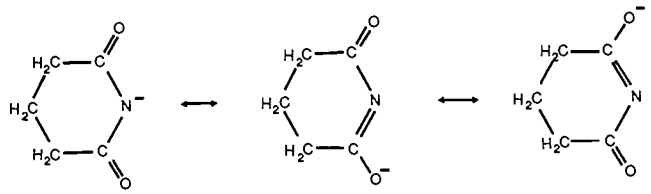

5a 5b 5c

5

atomes d'oxygène favorise encore davantage ces formes limites, tandis que la coordination sur l'azote tend à en diminuer l'importance, bien qu'à un degré moindre que ne le ferait l'hydrogène dans la glutarimide neutre. La distribution électronique dans l'anion de glutarimide complexé est donc intermédiaire entre celle de l'anion libre et celle de la forme neutre protonée. Ces changements se répercutent également sur les angles de liaisons: l'angle C(1)—N(1)—C(5) diminue de 5,6° et les angles N(1)—C—C voisins augmentent de ~3,5° par rapport à ceux de la glutarimide (8). Un effet analogue a été noté pour la succinimide (4) et se rencontre couramment pour les purines (9). Notons que ces changements angulaires dans le cycle ne provoquent pas de changement notable des angles N—C—O et que seuls les angles C—C—O sont modifiés.

La glutarimide conserve dans le complexe la conformation observée pour la molécule neutre (8). Les atomes N(1), C(1), C(2), C(4) et C(5) définissent un ensemble à peu près plan. Les écarts des atomes à ce plan sont significatifs (6,5σ), mais assez faibles ($\leq$0,040(6) Å). Le groupe méthylène C(3), le plus éloigné de l'azote, se trouve à 0,633(6) Å de ce plan et confère à la glutarimide une conformation "enveloppe". L'oxygène carbonyle O(1) n'est qu'à 0,034(4) Å de ce plan, tandis que O(2) s'en écarte davantage (0,168(5) Å), dans la direction de l'argent auquel il est lié.

L'empilement moléculaire est représenté à la figure 2. Le cristal est constitué d'ensembles $[Glu-Ag-Glu]^-$ linéaires et à peu près plans, reliés entre eux par des atomes Ag(2) de manière à constituer des colonnes infinies orientées selon l'arête *c* de la maille. De telles colonnes traversent la face *ab* au centre et à chacun des coins. Entre les colonnes, il n'existe que des contacts de van der Waals normaux.

Spectroscopie infrarouge

Les spectres infrarouges de la glutarimide en solution dans le chloroforme et l'acétonitrile ont été discutés par Thompson *et al.* (10). L'influence de la concentration sur les régions spectrales ν(N—H) et ν(C=O) a permis de conclure à un équilibre entre le monomère et un dimère lié par ponts hydrogène dans ces solvants. Le spectre rapporté au tableau 2 a été obtenu sur le solide. De manière générale, il diffère peu de celui des solutions, et les régions ν(N—H) et ν(C=O) sont semblables à celles de la forme associée en solution. Ceci est attribuable au fait que les vibrateurs N—H et C=O se trouvent dans des conditions analogues dans le solide et dans le dimère en solution. En effet, les molécules de glutarimide dans le cristal sont associées en rubans au moyen de liaisons N—H . . . O impliquant l'une des fonctions carbonyles et laissant l'autre libre (8). Les attributions proposées au tableau 2 ont été faites par comparaison avec les résultats de Thompson *et al.* (10).

Comme le complexe d'argent renferme la forme anionique de la glutarimide, les bandes dues au lien N—H doivent disparaître du spectre. C'est bien le cas de la bande ν(NH) dédoublée à 3195 et 3095 cm^{-1}. L'absorption résiduelle à 3150 cm^{-1} est probablement due à une harmonique de la vibration ν(C=O) observée à 1582 cm^{-1}, puisque ce même mode apparaissant à 1665 cm^{-1} dans la glutarimide semble également produire une harmonique à 3375 cm^{-1}. La bande large située à 835 cm^{-1} est attribuée à la déformation N—H hors-plan, par comparaison avec la position et la forme de la bande analogue de la succinimide à 823 cm^{-1} (4, 11). Dans le complexe Ag–glutarimide, il ne reste dans cette région que deux absorptions faibles à 853 et 869 cm^{-1}, que Thompson *et al.* (10) attribuent à des mouvements ν(CC) et δ(CCH). Quant à la déformation N—H dans le plan, elle semble se coupler à d'autres mouvements, pour contribuer aux bandes situées vers 1330 et 1055 cm^{-1}. La région 1330 cm^{-1} est trop compliquée pour qu'on puisse clairement identifier des changements dans le composé d'argent, mais le déplacement de la bande à 1061 cm^{-1} vers 969 cm^{-1} semble relié à la déprotonation du coordinat dans le complexe.

Les résultats cristallographiques indiquent que la redistribution des électrons dans le coordinat complexé entraîne une diminution de l'indice de la liaison C=O et une augmentation de celui de la liaison C—N. Le spectre infrarouge appuie cette conclusion. Les modes carbonyles se déplacent depuis 1720 et 1670 cm^{-1}, vers 1625 et 1580 cm^{-1}, respectivement, lors de la complexation. L'accroissement de l'indice de liaison C—N se

Can. J. Chem. Downloaded from www.nrcresearchpress.com by 210.87.254.6 on 09/06/12
For personal use only.

Can. J. Chem. Downloaded from www.nrcresearchpress.com by 210.87.254.6 on 09/06/12
For personal use only.

TABLEAU 2. Spectres infrarouges de la glutarimide et de son complexe d'argent

	HGlu	$Ag[AgGlu_2]$
$2\nu_s$(C=O)	3375 tf	3150 tf
A′ ν(NH)	3195 F	—
	3095 F	—
A′,A″ ν(CH)	2975 m	2995 m
	2915 m	2960 m
	2855 f, ép	2900 f
	2835 f	2870 f
	1825 f	
A″ ν(C=O)	1730 F	1628 F
	1715 F	
A′ ν(C=O)	1671 F	1587 F
		1575 ép
	1556 f	1555 f
	1536 f	1537 f
A′,A″ $\delta(CH_2)$ + δ(CCH)	1475 m	1472 f
A′,A″ $\delta(CH_2)$ + δ(CCH)	1430 F	1448 M
	1416 F	1424 M
A′ δ(CCH) + $\delta(CH_2)$	1372 F	1380 F
A″ δ(CCH) + $\delta(CH_2)$	1359 F	1365 F
A′ w(NH) + γ(C=O)	1342 F	1347 F
A″ γ(NH) + δ(CCH)	1331 F	1329 F
A′ ν(C—N) + δ(CCH)	1277 F	1303 M
A″ ν(C—N) + γ(NH)	1260 F	—
A′,A″ δ(CCH)	1186 F	1189 F
A″ δ(CCH)	1151 F	1145 F
A′ δ(CCH) + w(NH)	1061 F	969 M
A″ γ(C=O) + δ(CCH)	927 M	929 M
A′ δ(CCH) + ν(CC)		869 tf
A′ ν(CC) + δ(CCH)		853 tf
A″ γ(NH)	840 M, large	—
A″ ν(C—C) + ν(CN)	763 M	778 M
A′ δ(CCH) + ν(C—C)	673 M	682 M
A″ δ(CCH) + γ(C=O)	613 M	626 M
A′ ν(C—N) + ν(CC)	552 F	575 f
A″ δ(CCN) + w(C=O)	445 F	

répercute sur le doublet 1277/1260 cm^{-1}, qui donne une bande à 1303 cm^{-1}. Un déplacement semblable sur la bande située à 1193 cm^{-1} dans la succinimide a été proposé comme un indice de déprotonation de l'imide (4). Certains autres déplacements sont également notés; par exemple, les bandes à 763 et 673 cm^{-1} passent respectivement à 778 cm^{-1} et 682 cm^{-1} dans le composé d'argent.

Spectroscopie de résonance magnétique nucléaire ^1H et ^{13}C

Les spectres de la glutarimide et de son complexe d'argent ont été étudiés dans le DMSO-d_6. Les pics du spectre ^{13}C ont été attribués par Hasan (12). Le spectre ^1H est interprété au moyen de la multiplicité et l'intégration des pics. Les valeurs des déplacements chimiques sont données au tableau 3. L'ensemble des modifications observées lors de la complexation est semblable à ceux qu'on retrouve pour les complexes de la phtalimide et la succinimide (4).

Dans le spectre ^1H, on retrouve à champ faible (10,58 ppm) la résonance du proton N—H qui disparaît comme prévu lors de la complexation. Les deux spectres (coordinat et complexe) présentent un triplet correspondant aux quatre protons en α du carbonyle. Un multiplet plus blindé, intégrant pour deux protons, est dû aux protons en β du carbonyle. Le triplet à 2,45 ppm et le multiplet à 1,83 ppm de HGlu apparaissent à 2,36 et 1,77 ppm respectivement dans le complexe. Ce blindage est relié à l'accroissement de densité électronique introduit dans le cycle par la substitution du proton par l'argent moins électro-attracteur.

Dans le spectre ^{13}C, le signal C=O apparaît à champ très faible (173,75 ppm) pour le ligand et à champ plus bas pour le complexe (181,14 ppm, $\Delta\delta = +7{,}39$ ppm). Ce déplacement également relié à la poussée des électrons vers le cycle, résulte de la hausse de polarité du lien C=O lors de la complexation (4, 13). Les carbones en α et en β des carbonyles subissent également un blindage, mais à un degré moindre ($\Delta\delta = +0{,}74$ ppm et $\Delta\delta = +1{,}91$ ppm respectivement).

Discussion

La structure cristalline du complexe de la glutarimide et celle du composé analogue de la méthyl-1 thymine présentent plusieurs points communs. Dans les deux cas, la moitié des atomes d'argent est linéairement reliée aux atomes d'azote de deux coordinats déprotonés, tandis que l'autre moitié est entourée de deux paires de fonctions carbonyles provenant de deux ensembles $[L-Ag-L]^-$ différents. Cette ressemblance tient au fait que le segment —C(O)—N—C(O)— adopte la même répartition spatiale dans les deux cas. En effet, si l'on excepte le groupe méthylène en position 4, la glutarimide possède comme la thymine un cycle à peu près plan et ce cyle possède six atomes. Il s'ensuit que la séparation O . . . O est la même des deux côtés de l'ensemble $[L-Ag-L]^-$ (Fig. 1) et que cette séparation est juste suffisante pour donner une interaction bidentate chélatante avec un autre atome d'argent. Cette géométrie particulière permet de construire des chaînes infinies très stables, dans lesquelles chaque ensemble $[L-Ag-L]^-$ interagit des deux côtés avec des atomes Ag(2) et chaque atome Ag(2) interagit avec deux anions complexes. Par contre, pour un cycle à 5 atomes comme celui de la succinimide, les angles internes plus petits placeraient les groupes carbonyles à une distance plus grande l'un de l'autre dans l'espèce linéaire $[Suc-Ag-Suc]^-$. Pour donner une interaction bidentate avec un premier atome d'argent, une paire de carbonyles doit se rapprocher l'un de l'autre (**6**), ce qui rend impossible une

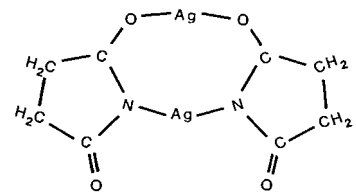

6

seconde interaction bidentate chélatante par l'autre paire de groupes carbonyles du même anion complexe, comme nous l'avons précédemment observé (4). La conformité particulière pour le cas des cycles à six atomes semble donc conduire à une stabilisation accrue des solides $Ag[AgL_2]$, qui par leur plus faible solubilité empêchent d'obtenir des sels comme $Li[AgL_2]$ et $Na[AgL_2]$, qui sont isolables avec la succinimide (4).

Les chaînes infinies présentes dans le cristal doivent se rompre pour permettre au composé d'entrer en solution dans le DMSO. Les spectres rmn ^1H et ^{13}C montrent que le miroir passant par l'azote et le groupe méthylène en position 4 de la glutarimide est conservé dans le complexe présent en solution. A cause de la stabilité du lien Ag—N indiquée par la courte distance interatomique et l'obtention d'ensembles linéaires N—Ag—N dans les composés de ce genre (2, 4), il est fort

TABLEAU 3. Spectres de résonance magnétique nucléaire ^1H et ^{13}C de la glutarimide et du complexe d'argent

	^1H			^{13}C		
	NH	$(CH_2)(\alpha)$	$(CH_2)(\beta)$	C=O	C(α)	C(β)
HGlu	10,58	2,45	1,83	173,75	31,35	17,56
$Ag[AgGlu_2]$		2,36	1,77	181,14	32,09	19,47

probable que l'ion linéaire $[Glu-Ag-Glu]^-$ persiste en solution. Une interaction additionnelle avec d'autres ions Ag^+, qui ne pourrait se faire qu'avec une seule paire de groupes carbonyles à la fois, serait incompatible avec l'équivalence des deux moitiés du coordinat indiquée par la rmn, à moins que cet atome d'argent s'échange rapidement d'une paire de carbonyles à l'autre. Une explication également plausible serait une

$$Ag[AgGlu_2] \xrightarrow{DMSO} [Ag(DMSO)_n]^+ + [AgGlu_2]^-$$

dissociation du complexe dans le DMSO, pour donner une cation Ag^+ solvaté par DMSO et l'anion $[Glu-Ag-Glu]^-$ aperçu dans le solide.

Remerciements

Nous remercions M. J. Olivier pour l'acquisition des données de diffraction des rayons X, J. Lessard qui a bien voulu nous transmettre une copie de la référence 5 avant publication, ainsi que le Conseil National de Recherches en Sciences Naturelles et en Génie du Canada pour son support financier.

1. G. L. EICHHORN. Inorganic biochemistry. Elsevier, Amsterdam. 1973. chap. 34; S. K. ARYA et J. T. YANG. Biopolymers, **14**, 1847 (1975); M. DAUNE, C. A. DEKKER et H. K. SCHACHMAN. Biopolymers, **4**, 51 (1966); G. L. EICHHORN, J. J. BUTZOW, P. CLARK et E. TARIEN. Biopolymers, **5**, 283 (1967); R. H. JENSEN. Ph.D. Thesis, California Institute of Technology, 1965; F. KLOTZ. Doctorate Dissertation. *Resumé par* M. Daune. Met. Ions Biol. Syst. **4**, 1 (1974).
2. F. GUAY et A. L. BEAUCHAMP. J. Am. Chem. Soc. **101**, 6260 (1979).
3. F. GUAY. Thèse de Doctorat, Université de Montréal. 1983.
4. J. PERRON et A. L. BEAUCHAMP. Inorg. Chem. Sous presse.
5. J. Y. HUOT, D. SERVE et J. LESSARD. Can. J. Chem. **61**, 1890 (1983).
6. Beilstein Handbuch fur Organischen Chemie. Vol. XXI. 1935. p. 382.
7. F. BÉLANGER-GARIÉPY et A. L. BEAUCHAMP. J. Am. Chem. Soc. **102**, 3461 (1980).
8. C. S. PETERSEN. Acta Chem. Scand. **25**, 379 (1971).
9. R. TAYLOR et O. KENNARD. J. Am. Chem. Soc. **104**, 3209 (1982).
10. J. W. THOMSPON, JR., G. E. LEROI et A. I. POPOV. Spectrochim. Acta Part A, **31**, 1553 (1975).
11. T. WOLDBAEK, P. KLAEBOE et D. H. CHRISTENSEN. Acta Chem. Scand. Ser. A, **30**, 531 (1976).
12. M. U. HASAN. Org. Magn. Reson. **14**, 447 (1980).
13. V. GALLASSO, G. PELLIZER, H. LEBAIL et G. C. PAPPALARDO. Org. Magn. Reson. **8**, 457 (1976).

Can. J. Chem. Downloaded from www.nrcresearchpress.com by 210.87.254.6 on 09/06/12
For personal use only.

Effect of substituents in the formation of diacetanilides[1]

NAGARAJ R. AYYANGAR AND KUMAR V. SRINIVASAN
National Chemical Laboratory, Pune 411 008, India

Received October 18, 1983

NAGARAJ R. AYYANGAR and KUMAR V. SRINIVASAN. Can. J. Chem. **62**, 1292 (1984).

A number of diacetanilides, including some which have not been reported so far, have been synthesized from the corresponding monoacetyl derivatives and characterized by spectral and elemental analyses. A tlc/fid method for the quantitative estimation of the relative amounts of mono- and diacetyl derivatives has been standardized. Linear correlation of the extent of diacetylation with Hammett σ-values of substituents and basicity constants of monoacetyl derivatives has been established. A plausible mechanism for the diacetylation reaction based on experimental observations has been suggested. An explanation for the anomalous behaviour of acetanilides containing electron-withdrawing substituents in the *ortho* position has been put forth.

NAGARAJ R. AYYANGAR et KUMAR V. SRINIVASAN. Can. J. Chem. **62**, 1292 (1984).

Utilisant les dérivés monoacétylés correspondants comme produits de départ, on a synthétisé un certain nombre de diacétanilides (dont quelques-uns qui n'avaient pas été rapportés jusqu'à maintenant) qui ont été caractérisés par des analyses spectrales et élémentaires. On a standardisé une méthode ccm/fid permettant d'évaluer quantitativement les proportions relatives de dérivés mono- et diacétylés. On a établi des corrélations linéaires entre les pourcentages de diacétylation et, d'une part, les valeurs de Hammett des substituants et, d'autre part, avec les constantes de basicité des dérivés monoacétylés. On suggère une mécanisme plausible pour la réaction de diacétylation qui tient compte des observations expérimentales. On propose aussi une explication pour le comportement anormal des acétanilides portant des substitutants électroaffinitaires en positions *ortho*.

[Traduit par le journal]

Can. J. Chem. Downloaded from www.nrcresearchpress.com by 210.87.254.5 on 09/06/12
For personal use only.

Introduction

N,N-Diacetylamines play a key role as intermediates in acetyl transfer reactions in biochemical synthesis (1–5). Some of the diacetylamines have insecticidal (6, 7), flea-repellant (8), anti-ulcer and anti-secretory (9, 10), flame proofing (11), and immunostimulant and immunoregulatory (12) properties. Conformational (13, 14), thermodynamic (15), and mass spectrometric (16) studies of the diacetylamines have been reported. The methods of preparation of the diacetylamines involve the reaction of amines with acetylating agents such as acetyl chloride, acetic anhydride, and ketene and enol esters in presence of catalysts such as pyridine, sulphuric acid, and sodium acetate (17–22). An improved method for diacetylation of primary amines by acetic anhydride uses cupric acetate and magnesium as catalyst (5). The latter removes acetic acid from the reaction by forming insoluble magnesium acetate. It was observed that the presence of a positive or negative substituent in the *ortho* position to an amino group of a primary arylamine facilitated the formation of diacetyl derivative (18, 19) at the expense of monoacetyl derivative. If the primary arylamines with chloro, bromo, or nitro substituents in the *ortho* position are acetylated under monoacetylation conditions the formation of monoacetyl derivative has been retarded. This has been atrributed to the *ortho* effect which reduces the basicity of the nitrogen atom, the driving force for the monoacetylation reaction (23).

The diacetyl compounds thus have recently been attracting considerable interest. The detailed course of the diacetylation reaction is discussed in the present communication. Acetylation of aromatic amines results in the initial formation of monoacetanilides which undergo further acetylation to diacetanilides. Monoacetyl derivatives of anilines with suitable substituents in the *ortho*, *meta*, and *para* positions have been used as starting materials in our study.

[1]NCL Communication No. 3292.

Results

Diacetylation of the corresponding monoacetyl derivatives was carried out under identical conditions using an excess of acetic anhydride. The relative amounts of the mono- and diacetyl derivatives in the reaction mixtures were estimated by thin-layer chromatographic (tlc) procedure with flame ionization detection (fid) of the eluted fractions. Acetic anhydride and acetic acid present in the reaction mixture did not intefere in the estimations. Under our experimental conditions, the reaction was not reversible. Further confirmation of the irreversibility of the reaction was obtained by refluxing diacetanilide with 10% molar excess of Analytical Reagent (AR) grade glacial acetic acid for 4.0 h. The tlc/fid analysis indicated no formation of monoacetyl derivative. Material balance for the formation of diacetanilides from the corresponding monoacetyl derivatives could be established within ±1%.

The basicity constants (pK_{BH^+}) of the monoacetyl derivatives, Hammett σ-values (24) of substituents, yield of diacetyl derivatives, and R_f values are recorded in Table 1. We found that the extent of formation of diacetanilides had a linear correlation with Hammett σ-values of substituents (Fig. 1) and pK_{BH^+} of the monoacetanilides (Fig. 2). For the *p*-nitro substituent, σ^- and not the σ value was found to give a better correlation (Fig. 1).

Discussion

Since the acetylation reaction is electrophilic in nature, it is important to consider the basicities of the monacetanilides used. Substituted acetanilides are very weak bases (Table 1). They lack adequate spectral differences in their acid and base forms and have insufficient solubility for potentiometric titrations. The experimental determination of their basicity constants is difficult. As such, the available literature on experimental pK_{BH^+} values of acetanolides is scarce. The pK_{BH^+} values of most of the acetanilides used in the present study (Table 1) are experimental values reported in the literature (25,

TABLE 1. A comparison of basicity constants of monoacetanilides **1** (25, 26), Hammett σ-values (24) of substituents, yield of diacetanilides **2**, and R_f values of **1** and **2** (tlc/fid)

Compound no.	Substituted acetanilides **1**	$-pK_{BH^+}$	Σσ	% Yield of diacetanilides **2**	R_f	
					1	**2**
1	—	1.59	0.00	86.70	0.42	0.62
2	4-Br	1.91	0.22	79.80	0.33	0.60
3	4-Cl	1.88	0.24	75.30	0.32	0.63
4	3-Cl	2.05	0.37	70.87	0.43	0.63
5	2-Cl	1.35	0.67	99.80	0.53	0.67
6	2,6-DiCl	—	—	100.00	0.47	0.68
7	2,4,6-TriCl	—	—	100.00	0.54	0.75
8	4-NO_2	2.59	1.27*	35.25	0.28	0.64
9	3-NO_2	2.46	0.71	55.90	0.32	0.53
10	2-NO_2	—	—	100.00	0.33	0.58
11	4-CH_3	1.27	−0.14	88.82	0.35	0.61
12	3-CH_3	1.67	−0.06	86.66	0.40	0.64
13	2-CH_3	1.63	0.10	80.88	0.43	0.62
14	2,6-DiCH_3	—	—	100.00	0.33	0.60
15	2-CH_3,5-NO_2	2.71†	—	91.50	0.32	0.59
16	4-CH_3,3-NO_2	2.38†	0.57	66.00	0.33	0.57
17	4-OCH_3	1.21	−0.28	94.18	0.33	0.63
18	2-OCH_3,5-NO_2	2.54†	0.71	61.00	0.50	0.60
19	2,6-DiC_2H_5	—	—	98.50	0.43	0.64

*σ^- and not σ-value was employed for the 4-nitro substituent.
†Values predicted from the regression equation (27): $pK_{BH^+} = -1.55 - 1.39\ \Sigma\sigma$.

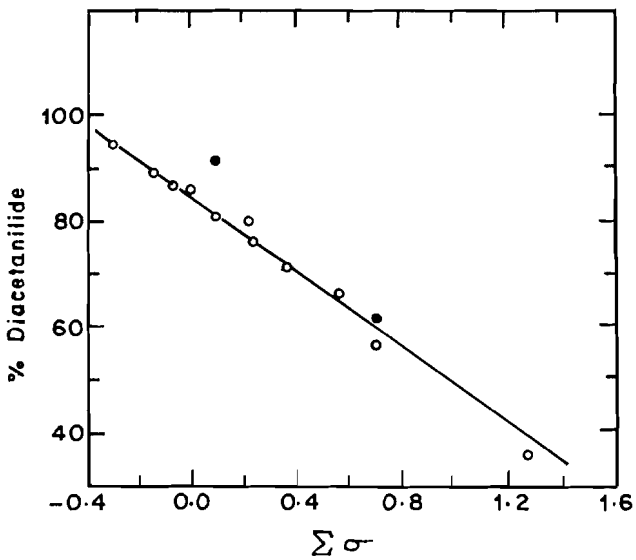

FIG. 1. The effect of Hammett σ-values of substituents on % yield of diacetanilide; ○: *meta*- and *para*-substituted; ●: *ortho*-substituted diacetanilide.

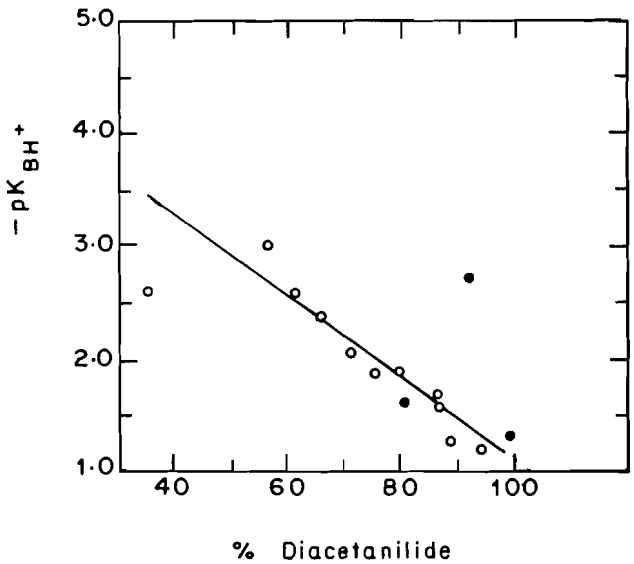

FIG. 2. Variation of % diacetanilide formation with pK_{BH^+} of acetanilide; ○: *meta* and *para*-substituted; ●: *ortho*-substituted acetanilide.

26). For compounds **15**, **16**, and **18** the interim pK_{BH^+} values have been predicted from the regression equation (27) derived from linear correlation of pK_{BH^+} values with Hammett σ-values of substituents. Acetanilides can become either O- or N-protonated in acid media. The known evidence is strongly in favour of predominant O-protonation on the basis of (a) uv spectral changes observed on protonation of the acetanilides (b) the greater electronegativity of the oxygen atom, and (c) resonance stabilization of the O-protonated species by the unshared electron pair on the nitrogen atom (26). Recently, the data obtained from the study of nitrogen proton resonances of primary amides were shown to be consistent with the assumption of N-protonation as the major pathway for proton exchange for primary amides (28).

Our experimental evidence is in favour of higher basicity for the oxygen as compared to the nitrogen, as is clear from the following discussion. A plausible mechanism for the formation of diacetanilides from the monoacetyl derivatives is shown in Scheme 1. While suggesting the mechanism, the following experimental observations have been taken into account, viz.: (a) the *ortho* substituents in acetanilides have facilitated the diacetyl derivative formation, particularly for *ortho* disubstituted acetanilides where quantitative conversions to the diacetanilides have been observed, irrespective of whether the *ortho* substituents are electron withdrawing or electron repelling (Table 1); (b) linear correlations such as those indi-

Can. J. Chem. Downloaded from www.nrcresearchpress.com by 210.87.254.5 on 09/06/12
For personal use only.

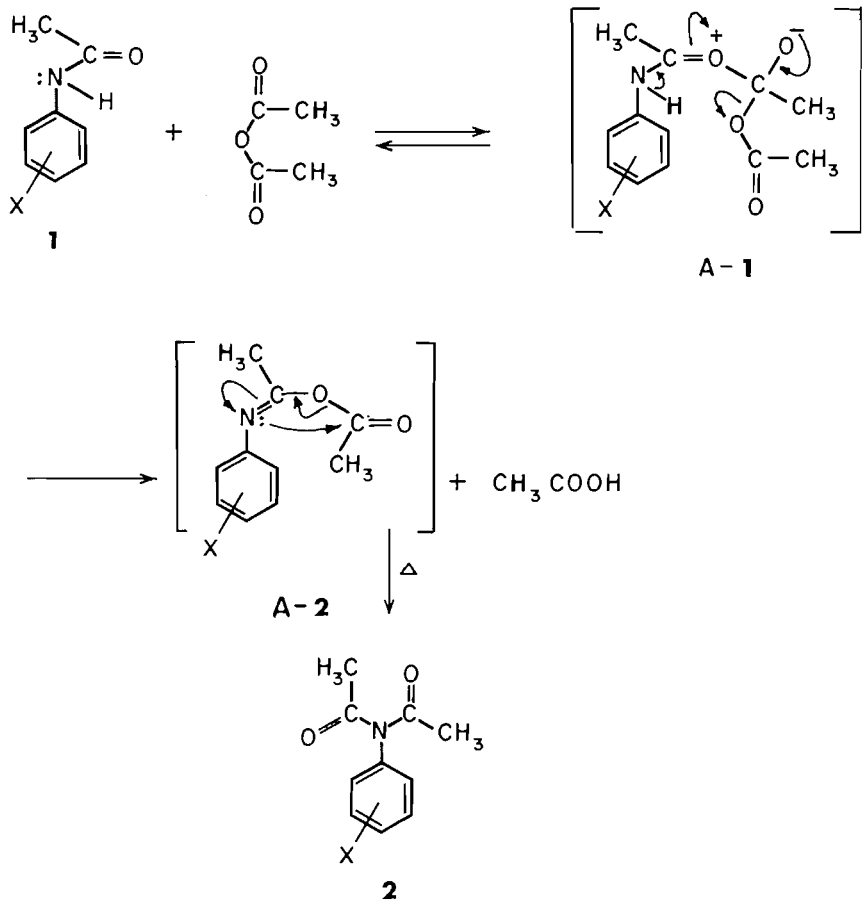

SCHEME 1

cated in Figs. 1 and 2. Hence the initial electrophilic reaction of the carbonyl carbonium ion of acetic anhydride is on the more basic carbonyl oxygen of the acetanilide to form the intermediate complex A-1. The positive charge on the oxygen is then stabilized by the electron drift from the nitrogen atom, forming the intermediate A-2 with the liberation of acetic acid. The formation of the diacetyl derivative then takes place via the acid catalysed rearrangement of the intermediate A-2 at the high temperature of the reaction. Attack on amide nitrogen would not be favoured, since such substituents decrease the basicity of the amide nitrogen either by intramolecular hydrogen bonding or, where this is disrupted by solvent effects, by their strong electron-withdrawing inductive effects. This would result in a lower yield of diacetyl derivative, which is contrary to the experimental results obtained (Table 1). It is apparent that the extent of diacetanilide formation would be governed by the electron density of the nitrogen atom in the intermediate A-2. In analysing the effect of substituents, the comparisons have been made with the unsubstituted acetanilide. The deviations in % yields of substituted diacetanilides from that of the unsubstituted diacetanilide are recorded in Table 2.

Effect of substituents at the meta *and* para *positions*

The substituents at the *meta* and *para* positions would enhance or decrease the basicity of nitrogen by the inductive, hyperconjugation, and resonance effects. The conformational studies of the monoacetanilides (29, 30) as well as our experimental results (Table 2) are in agreement with the above considerations. It may be noted that the *meta* isomer forms a relatively lesser amount of the diacetyl derivative than the *para* isomer, since only the inductive effect comes into play with the *meta* substituent.

TABLE 2. Deviation of % yield of substituted diacetanilides from unsubstituted diacetanilide

Compound no.	Substituent	Deviation* %
2	4-Br	−6.9
3	4-Cl	−11.4
4	3-Cl	−15.9
8	4-NO_2	−51.5
9	3-NO_2	−30.8
11	4-CH_3	+2.1
12	3-CH_3	−0.04
13	2-CH_3	−5.8
15	2-CH_3,5-NO_2	+4.8
16	4-CH_3,3-NO_2	−20.7
17	4-OCH_3	+7.5
18	2-OCH_3,5-NO_2	−25.7

*negative: decrease in yield; positive: increase in yield.

Effect of substituents at the ortho *position*

Due to steric considerations, the —C=N linkage in the intermediate A-2 is no longer in the same plane as the π-electron cloud of the benzene ring for any significant resonance interaction. Hence it is the inductive and steric effects which would predominantly determine the extent of diacetylation. Thus the actual amount of diacetanilide formed by acet-*o*-toluidide is less than that of acetanilide, due to steric hin-

Can. J. Chem. Downloaded from www.nrcresearchpress.com by 210.87.254.5 on 09/06/12
For personal use only.

Can. J. Chem. Downloaded from www.nrcresearchpress.com by 210.87.254.5 on 09/06/12
For personal use only.

drance (Table 2). However, the presence of alkyl groups at both *ortho* positions has increased the basicity of nitrogen to such an extent that quantitative conversions to the diacetanilides were observed (Table 1). The presence of a nitro group in the *para* position to the methyl group in compound 15 enhances the electron-donating ability of the methyl group, which results in increased diacetanilide formation (Table 2). The surprisingly lowered yield of diacetyl derivative exhibited by 2-methoxy-5-nitro acetanilide suggests that the steric *ortho* effect has taken a secondary place and the major contribution seems to have come from the inductive effect of the *meta* nitro substituent (Fig. 1). Substituents such as nitro and chloro groups exert their electron-withdrawing inductive effects via σ-bonds, localizing the π-electrons of the —C=N linkage on the nitrogen which is no longer in conjugation with the benzene ring. The enhanced nitrogen basicity in such cases has resulted in nearly quantitative conversions to the diacetyl derivatives.

In conclusion, the formation of a monoacetyl derivative may proceed via an arylamine acetate intermediate complex, decomposing to the monoacetyl derivative and acetic acid. The stability of the complex is governed by the substituents present. The diacetylation, which is a subsequent acetylation of the monoacetyl derivative, must involve the more basic amide oxygen as the initial reaction site, forming the amidine intermediate, which rearranges to the diacetanilide. The experimental results, as discussed above, strongly favour O-protonation concepts for acetamides and related substances in acid medium. Furthermore, the tlc/fid method of estimation, described above, serves as a useful quality control test for some commercially important acetyl derivatives such as acetanilide, paracetamol, and phenacetin, which are important drug intermediates. It is quite apparent that the formation of a diacetanilide during the manufacturing process which employs acetylation as a major unit process cannot be overlooked.

Experimental

Melting points were recorded in capillary tubes. Infrared spectra were recorded on a Perkin–Elmer 221 spectrophotometer, proton nmr spectra on a Varian T-60 spectrometer using TMS as internal standard, mass spectra were recorded on a CEC-21-110-B mass spectrometer, and tlc/fid estimations were carried out on an Iatroscan Th-10 tlc/fid analyser (Newman-Howells Assoc. Ltd., U.K.) connected to a two-pen flat-bed type strip chart recorder VP-6621A (National, Japan).

Preparation of monoacetyl derivatives

A mixture of the aniline (100 mmol), pyridine (100 mmol), and acetic anhydride (110 mmol) was stirred and heated in a boiling water bath for 2 h. The monoacetyl derivatives were isolated by drowning in water, filtered, washed well with water, and purified by several recrystallizations, using dilute ethanol as solvent. The acetanilides (**1**) prepared (melting points in parentheses) are as follows. 4-bromo (168°C); 4-chloro (178°C); 3-chloro (72°C); 2-chloro (87°C); 2,6-dichloro (190°C); 2,4,6-trichloro (207°C); 4-nitro (207°C); 3-nitro (155°C); 2-nitro (94°C); 4-methyl (148°C); 3-methyl (65°C); 2-methyl (110°C); 2,6-dimethyl (178°C); 2-methyl,5-nitro (152°C); 4-methyl,3-nitro (144°C); 4-methoxy (132°C); 2-methoxy-5-nitro (178°C); 2,6-diethyl (136°C). Commercial acetanilide was recrystallized twice from boiling water (mp 113°C).

Preparation of diacetyl derivatives

A mixture of the monoacetyl derivative (70 mmol) and acetic anhydride (40 mL) was refluxed for 4 h. Excess acetic anhydride and acetic acid formed in the reaction were removed by distillation at 95°C under reduced pressure. The following work-up procedures were adopted depending upon whether the residue after removal of the solvents is a solid or liquid at room temperature.

(a) *Diacetyl derivative (solid)*

The residual solid is boiled with petroleum ether (bp 40–60°C) (100 mL) for a few minutes and filtered hot. The filtrate is concentrated to 70 mL and allowed to cool. The sparingly soluble monoacetyl derivative crystallized out, and was filtered off. Further concentration of the filtrate yielded the diacetyl derivative in its pure form. The procedure was repeated if traces of the monoacetyl derivative still remained, as judged by tlc.

(b) *Diacetyl derivative (liquid)*

The residual oily liquid was subjected to fractional distillation under reduced pressure when the diacetyl derivatives distilled out as colourless liquids.

The following known diacetanilides were synthesized (their spectral and elemental analysis are in agreement with their constitutions; their purities checked by tlc/fid): (**1**) diacetanilide, mp 36°C (lit. (5) mp 36°C); (**2**) 4-bromo-, mp 74°C (lit. (18) mp 74.5°C); (**3**) 4-chloro, mp 65°C (lit (5) mp 65°C); (**5**) 2-chloro, bp 136°C/5 Torr (lit. (31) bp 136°C/5 Torr); (**7**) 2,4,6-trichloro, mp 81°C (lit. (32) mp 81–82°C); (**8**) 4-nitro, mp 135°C (lit (33) mp 135°C); (**10**) 2-nitro, mp 94°C (lit. (34) mp 94°C); (**11**) 4-methyl, mp 45°C (lit. (34) mp 45°C); (**12**) 3-methyl, bp 165°C/16 Torr (lit. (35) bp 164–168°C/16 Torr); (**13**) 2-methyl, bp 152°C/20 Torr (lit. (19) bp 153°C/20 Torr); (**15**) 2-methyl,5-nitro, mp 81°C (lit. (36) mp 81–83°C); (**16**) 4-methyl,3-nitro, mp 77°C (lit. (37) mp 77–78°C); and (**17**) 4-methoxy, mp 60°C (lit. (35) mp 60°C).

The following new diacetyl derivatives, so far not reported in literature, have been synthesized.

(**4**) 3-Chloro, bp 151–152°C/5 Torr; ir (Nujol): 1720 (C=O), 1585, 1470, 1410, 1360, 1285, 1200, 1090, 1070, 950, and 920 cm^{-1}; ^1H nmr (CCl_4) δ: 2.2 (s, 6H, $COCH_3$) and 6.9–7.6 (m, 4H, Ar-H); ms *m/e*: 211 (M^+), 213, 172, 171, 170 ($M^+ + 1 - CH_2{=}C{=}O$), 169, 129, 128, 127 (base) ($M^+ + 2 - 2$ ($CH_2{=}C{=}O$)), 111, and 99. *Anal.* calcd. for $C_{10}H_{10}ClNO_2$: C 56.7, H 4.7, N 6.6, Cl 16.7; found: C 56.5, H 4.4, N 6.6, Cl 16.5.

(**6**) 2,6-Dichloro, mp 63–64°C; ir (Nujol): 1720 (C=O), 1570, 1450, 1350, 1290, 1235, 1040, 1020, and 950 cm^{-1}; ^1H nmr (CCl_4) δ: 2.3 (s, 6H, $COCH_3$) and 7.1–7.5 (m, 4H, Ar-H); ms *m/e*: 246 (M^+), 244, 205 ($M^+ + 1 - CH_2{=}C{=}O$), 203, 186, 168, 165, 162, 161 (base,) 147, 145, and 135. *Anal.* calcd. for $C_{10}H_9Cl_2NO_2$: C 48.8, H 3.7, N 5.7, Cl 28.8; found: C 49.2, H 3.9, N 6.1, Cl 28.8.

(**9**) 3-Nitro, mp 64°C; ir (Nujol): 1740, 1710, 1540, 1470, 1380, 1360, 1250, 1170, 1095, 1038, and 950 cm^{-1}; ^1H nmr (CCl_4) δ: 2.6 (s, 6H, $COCH_3$) and 7.5–8.4 (m, 4H, Ar-H); ms *m/e*: 222 (M^+), 182, 181 ($M^+ + 1 - CH_2{=}C{=}O$), 180, 165, 164, 163, 139, 138 ($M^+ + 2 - 2$ ($CH_2{=}C{=}O$)) (base), 133, 108, and 92. *Anal.* calcd. for $C_{10}H_{10}N_2O_4$: C 54.0, H 4.5, N 12.6; found: C 53.8, H 4.9, N 12.8.

(**14**) 2,6-Dimethyl, bp 111–112°C/5 Torr; ir (Nujol): 1715 (C=O), 1600, 1475, 1360, 1275, 1180, 1160, 1010, and 942 cm^{-1}; ^1H nmr (CCl_4) δ: 2.1 (s, 6H, CH_3), 2.2 (s, 6H, $COCH_3$), and 7.2 (s, 3H, Ar-H); ms *m/e*: 205 (M^+), 204 (base), 164 ($M^+ + 1 - CH_2{=}C{=}O$), 163, 121 ($M^+ - 2$ ($CH_2{=}C{=}O$)), 120, 106, and 91. *Anal.* calcd. for $C_{12}H_{15}NO_2$: C 70.6, H 7.3, N 6.8; found: C 70.9, H 7.3, N 7.0.

(**18**) 2-Methoxy,5-nitro, mp 109–110°C; ir (Nujol): 1710 (C=O) 1590, 1530, 1495, 1370, 1250, 1210, 1100, 1035, and 970 cm^{-1}; ^1H nmr (CCl_4) δ: 2.2 (s, 6H, $COCH_3$), 2.9 (s, 3H, OCH_3), and 7.0 (s, 3H, Ar-H); ms *m/e*: 252 (M^+), 211 ($M^+ + 1 - CH_2{=}C{=}O$), 210 (base), 169 ($M^+ + 1 - 2$ ($CH_2{=}C{=}O$)), 168, 167, 153, 151, 150, 138, 122, 121, and 91. *Anal.* calcd. for $C_{11}H_{12}N_2O_5$: C 52.3, H 4.8, N 11.1; found: C 52.0, H 4.9, N 11.5.

(**19**) 2,6-Diethyl, mp 47–48°C; ir (Nujol): 1708 (C=O), 1455, 1365, 1280, 1247, 1190, 1018, and 950 cm^{-1}; ^1H nmr (CCl_4) δ: 1.2 (t, 6H, CH_3), 2.2 (s, 6H, $COCH_3$), 2.4 (q, 4H, CH_2), and 7.3 (s, 3H, Ar-H); ms *m/e*: 233 (M^+), 190 ($M^+ - 1 - CH_2{=}C{=}O$), 189 (base), 188, 175, 173, 148 ($M^+ - 1 - 2$ ($CH_2{=}C{=}O$)), 147, 133, 131, 120, 117, and 91. *Anal.* calcd. for $C_{14}H_{19}NO_2$: C 72.1, H 8.1, N 6.5; found: C 72.3, H 8.2, N 6.5.

Diacetylation experiments

The nineteen mono-, di-, and trisubstituted monoacetyl derivatives were diacetylated in cylindrical tubes (6.5 cm × 2.5 cm id,) fitted with reflux condensers and calcium chloride guard tubes through ground glass joints, with an excess of acetic anhydride, at reflux temperature, in a single oil bath, under identical conditions. The oil bath was heated on a hot plate and the heating rate was controlled by a dimmerstat. To 7 mmol of the monoacetyl derivative in each tube was added 4 mL of acetic anhydride. The reaction was carried out under reflux for 4 h. The tubes were cooled to ambient temperature and the contents were diluted to 25 mL with acetone (AR) in standard volumetric flasks.

Thin-layer chromatographic flame ionization detection estimations

The relative amounts of the mono- and diacetyl derivatives in the reaction mixtures were determined by a tlc/fid instrument making use of a thin-layer chromatographic (tlc) procedure with flame ionization detection (fid) of the eluted fractions.

Standard solutions

Approximately 180-200 mg of the pure mono- and diacetyl derivatives were accurately weighed, dissolved, and diluted to 10 mL with acetone (AR) in standard volumetric flasks.

Solvents

A mixture of AR grade chloroform and acetone, in the proportion of 94:6 by volume, was used for development.

Procedure

The samples (diluted reaction mixtures) were spotted in volumes of 1 μL each with a fine microliter syringe on the Chromarods. The Chromarod is a silica rod 0.9 mm in diameter and 150 mm long, having a sintered uniform coating of active adsorbent mixed with glass powder with a mean thickness of 75 μm. The spotted rods were dried at 40°C for 15 min in a thermostatically controlled oven. The rods were then eluted with chloroform–acetone (94:6) in the development tank, over a distance of 10 cm. After the development, the rods were dried in the thermostatically controlled oven at 40°C to dry off the solvents. Quantitative detection of the separated components was obtained by passing the Chromarods through the flame ionizaton detector of the instrument and the chromatograms were recorded. Standard solutions of the pure mono- and diacetyl derivatives were spotted and eluted under identical conditions. The response factors were calculated from the areas under the recorded peaks, which are directly proportional to the concentrations of the corresponding components on the rod from which the estimations were done. The areas were directly read off the chart by measuring the height of the appropriate step on the integral trace. Each estimation was a mean of at least four consecutive spottings and elutions.

1. S. A. BERNHARD, A. BERGER, J. H. CARTER, E. KATCHALSKI, M. SELA, and Y. SHALITIN. J. Am. Chem. Soc. **84**, 2421 (1962).
2. T. WIELAND, H. LAND, and D. LIBSCH. Justus Liebigs Ann. Chem. **597**, 227 (1955).
3. L. A. COHEN and B. WITCOP. Angew. Chem. **73**, 264 (1961).
4. M. T. BEHME and E. H. CORDES. J. Org. Chem. **29**, 1255 (1964).
5. H. J. MEYER, C. NOLDE, I. THOMSEN, and S. D. LAWESSON. Bull. Soc. Chim. Belg. **87**, 621 (1978).
6. German Patent No. 2, 654, 090; June 23, 1977.
7. S. African Patent No. 78, 02, 648; May 11, 1979.
8. V. M. GAVRYUSHINA, Y. A. NAUMOV, L. K. ADELFINSKAYA, V. P. DREMOVA, and S. N. SMIRNOVA. Khim. Sredstva Zashch. Rast. **5**, 82 (1975).
9. D. M. BEATIE, R. CROSSLEY, and D. G. HILL. Eur. J. Med. Chem. Chim. Ther. **14**, 105 (1979).
10. British Patent No. 1, 532, 239; Nov. 15, 1978.
11. Japanese Patent No. 77, 25, 117; Feb. 24, 1977.
12. U. S. Patent No. 4, 216, 160; Aug. 5, 1980.
13. G. TETU, J. C. DUPLAN, N. PELLISSIER, and E. LAURENT. J. Chem. Res. (S), **3**, 98 (1978).
14. A.-N. VERESHCHAGIN. Izv. Akad. Nauk SSSR Ser. Khim. **4**, 787 (1981).
15. J. WADSO. Acta Chim. Scand. **19**, 1079 (1965).
16. C. NOLDE, S. O. LAWESSON, J. H. BOWIE, and R. G. COOKS. Tetrahedron, **24**, 1051 (1968).
17. P. KAY. Chem. Ber. **26**, 2951 (1893).
18. F. ULFERS and A. VON JANSON. Chem. Ber. **27**, 93 (1894).
19. J. J. SUDBOROUGH. J. Chem. Soc. **86**, 533 (1901).
20. A. ONO. Chem. Ind. (London), 130 (1982).
21. E. S. ROTHMAN, S. SEROTA, and D. SWERN. J. Org. Chem. **29**, 646 (1964).
22. R. P. MARIELLA and K. H. BROWN. J. Org. Chem. **36**, 735 (1971).
23. S. TAKAHASHI. Oita Daigaku Gakugeigakubu Kenkyu Kiyo, Shizenkagaku, **9**, 96 (1960).
24. D. D. PERRIN, B. DEMPSEY, and E. P. SERJEANT. pK_a prediction for organic acids and bases. Chapman and Hall, London. 1981.
25. D. W. JOHNSON and H. E. SHERWOOD. Aust. J. Chem. **25**, 81 (1972).
26. J. C. GIFFNEY and C. J. O'CONNOR. J. Chem. Soc. Perkin Trans. 2, **7**, 706 (1975).
27. N. R. AYYANGAR and K. V. SRINIVASAN. J. Chromatogr. **267**, 399 (1983).
28. A. G. REDFIELD and S. WAELDER. J. Am. Chem. Soc. **101**, 6151 (1979).
29. R. F. C. BROWN, L. RADOM, S. STERNHILL, and I. D. RAE. Can. J. Chem. **46**, 2577 (1968).
30. I. D. RAE. Can. J. Chem. **46**, 2589 (1968).
31. S. A. ABBAS and N. J. HICKINBOTTOM. J. Chem. Soc. (C), 1305 (1966).
32. F. D. CHATTAWAY and H. IRWING. J. Chem Soc. 142 (1933).
33. P. GRAMMATICAKIS. Bull. Soc. Chim. Fr. **6**, 1956 (1960).
34. P. GRAMMATICAKIS. Bull. Soc. Chim. Fr. 158 (1950).
35. R. A. ABRAMOVITCH. J. Chem. Soc. 1413 (1957).
36. J. J. BROWN and R. K. BROWN. Can. J. Chem. **33**, 1819 (1955).
37. T. GLINSUKON, E. K. WEISBERGER, T. BENJAMIN, and P. P. ROLLER. J. Chem. Eng. Data, **20**, 208 (1975).

Can. J. Chem. Downloaded from www.nrcresearchpress.com by 210.87.254.5 on 09/06/12
For personal use only.

Comments: Electron paramagnetic resonance characterization and conformation of daunorubicin semiquinone intermediate implicated in anthracycline metabolism, cardiotoxicity, and anticancer action

TULSI MUKHERJEE[1]
Chemistry Division, Bhabha Atomic Research Centre, Bombay 400 085, India

AND

NICHOLAS J. F. DODD
Paterson Laboratories, Christie Hospital and Holt Radium Institute, Manchester M2O 9BX, England

Received October 11, 1983
(Ref.: Can. J. Chem. **59**, 3212 (1981))

Can. J. Chem. Downloaded from www.nrcresearchpress.com by 210.87.254.42 on 09/06/12
For personal use only.

Lown and Chen have used a stock solution of concentration 8×10^{-2} *M* for both the quinones. Although daunorubicin hydrochloride is soluble in water, it is somewhat difficult to solubilize it to the extent of 8×10^{-2} *M*. In the case of quinizarin, an equivalent solubility in water is impossible. In the course of our pulse radiolysis (work to be published) and epr studies (1) on quinizarin, we have used the chemical from Aldrich (as have the above authors) as well as from Sigma. A triply recrystallized sample of quinizarin showed a solubility in water of a few micromoles per litre only. The compound is more soluble in hot water, but precipitates again on cooling. It has a rather low solubility even in alcohol and aqueous micellar solutions of different detergents (cetyl trimethyl ammonium bromide, CTAB; triton X-100, TX 100, and sodium lauryl sulphate, SLS), in which similar compounds like juglone, naphthazarin, etc. are found to be much more soluble. For this reason, we had to use a solvent system comprising 5 *M* isopropanol and 1 *M* acetone. Even then the maximum solubility attained was just better than 10^{-4} *M*. A 2-sulphonate derivative of quinizarin was also synthesized to overcome this solubility problem. We could obtain a solubility of ca. 10^{-3} *M* in water. It therefore appears that the authors might have used some isomeric form of quinizarin, which is more soluble in water and which may give rise to a radical equivalent to that obtained from quinizarin on reduction. A few examples of such indirect radical formation methods have been given by Russell and Neugebauer (2). The ir, nmr, and ms analyses of the quinizarin sample used by Lown and Chen will be welcome. Our sample proved to be genuine quinizarin on these analyses.

Lown and Chen report that they recorded their spectra with "free access to atmospheric oxygen". In the course of our pulse radiolysis work (3) involving adriamycin and related compounds and our epr work involving the same compounds, we found that the corresponding semiquinones are very susceptible to the presence of a trace quantity of oxygen. We could not observe an epr signal on irradiation of aerated quinone solutions. The signals in deaerated systems disappeared instantly on opening the epr tubes to air. We can explain this from consideration of the one-electron reduction potential (E_7^1) of the couples, e.g. adriamycin/adriamycin semiquinone (3) and $O_2/O_2^{\cdot -}$ (4), viz., −328 mV and −155 mV respectively, at pH 7. The reaction [1] was seen to go to virtual completion to the right with rate constants of 3.5×10^8 M^{-1} s^{-1} (k_f) and 4.1×10^5 M^{-1} s^{-1} (k_b) respectively.

$$[1] \quad {}^{+}HAdH_2^{\cdot -} + O_2 \underset{k_b}{\overset{k_f}{\rightleftharpoons}} {}^{+}HAdH_2 + O_2^{\cdot -}$$

Following Kalyanaraman *et al.* (5), the half-life of the daunorubicin radicals in aerated solutions can be estimated as ca. <7.5 μs only. Surprisingly, Rao *et al.* (6) have themselves stated, "In contrast, the reduced form of daunorubicin is air sensitive and solutions of it are completely reoxidized extremely rapidly".

The corresponding E_7^1 value for the quinizarin system is around −270 mV in the mixed solvent system used and the reaction [1] goes to the right for this system as well as for quinizarin 2-sulphonate in water. All these semiquinones thus spontaneously reduce O_2 to $O_2^{\cdot -}$ at pH 7.4 and it is, therefore, highly unlikely that they can be observed in epr under the condition of "free access to atmospheric oxygen". At atmospheric pressure and 25°C, there will be ca. 2.65×10^{-4} *M* O_2 present in the system, sufficient to drive reaction [1] to the right. On the other hand, a few quinones having an E_7^1 value close to that of the $O_2/O_2^{\cdot -}$ system (4), such as naphthazarin (E_7^1 = −109 mV (7)) and juglone ($E_7^1 \approx -95$ mV, unpublished data), can be reduced to the corresponding semiquinone by excess reductant in the presence of a trace quantity of oxygen, due to establishment of equilibrium of the type of [1]. This equilibrium is totally shifted to the right in the case of daunorubicin, adriamycin, and quinizarin.

The statement about past work as given by Lown and Chen (their refs. 7, 18, and 19) is slightly erroneous. While an epr spectrum in aqueous solution has been attributed to the daunorubicin semiquinone (8–10), a somewhat different spectrum in 50% aqueous DMSO has been attributed to the daunorubicinone semiquinone (10). The epr spectrum was obtained in aqueous solution by Sinha and Chignell (9) using borohydride as reductant, but in the absence of oxygen, and adding the reductant in 5 small installments over a period of 25 min. We obtained well-resolved epr spectra for most of the semiquinones we studied (1). The semiquinones were generated by different techniques like pulsed irradiation with electrons of an aqueous deaerated solution at appropriate pH and containing excess formate (3, 7), photolysis in the presence of isopropanol, and photolysis in aqueous micellar solutions of CTAB, TX 100, and SLS. We failed, however, to obtain any well-resolved epr signal from adriamycin in aqueous solution, either by any of the above three methods or by borohydride reduction, even at the highest sensitivity of our epr spectrometer (Varian model E9). We obtained a well-resolved electrolytically generated epr signal in DMSO or DMF. In aqueous solution, the epr spectra of other semiquinones including quinizarin(1) and adriamycinone were well resolved. Reduction with borohydride was complicated. A very weak unresolved epr signal was obtained from adriamycin. The uv–visible absorption spectrum of a solution containing

[1] Author to whom correspondence may be addressed.

adriamycin and excess borohydride showed that the spectrum changed with time and not to that of the semiquinone. Kalyanaraman *et al.* (5) also showed a progressive change in the epr spectrum of daunorubicin semiquinone. Since daunorubicin and adriamycin have essentially comparable chemical structure as far as epr is concerned and both have different structural sites in the molecule capable of undergoing reduction, it is quite likely that these two quinones undergo borohydride reduction of a more complex nature.

The spectra shown by Lown and Chen (Figs. 2 and 3) are not very different from our spectra of adriamycin semiquinone in DMSO and quinizarin semiquinone in water (1), respectively. Exact comparison is, however, difficult. The chemical structures of the radicals shown in these figures appear to be incorrect; since the pK_a values of the semiquinone radicals are 2.9 (adriamycin and daunorubicin) (3) and 3.3 (quinizarin), the form of the semiquinones at pH 7.4 will be almost exclusively zwitterionic for the former (3) and anionic for the latter. Also, the strong intramolecular hydrogen bonding in the semiquinone has not been taken into consideration at all. Such H-bonding causes the second —OH to ionize at a pH nearly 11 units higher than that for the first —OH (3, 7). The zwitterionic or anionic structure and the strong intramolecular H-bonding naturally affect the electron density at different positions, and consequently affect the epr spectrum. This raises a further question regarding the authenticity of a computer simulation. It should also be pointed out that any quantitative theoretical analysis is impossible unless these structural features are taken into consideration. The one-electron LCAO–MO calculations shown by Lown and Chen are also bound to be only approximate, and not quantitative as claimed, due to the same reasons.

The statement by Lown and Chen that no deuterium effect was observed for quinizarin semiquinone is questionable. The splitting definitely changes in D_2O for quinizarin and similar hydroxyquinones (1, 11, 12). Adams *et al.* (13) and Vincow and Fraenkel (14) (ref. 23 in Lown's paper) do not support Lown and Chen, since neither paper gives spectra and their reported splittings are different from those given by Lown and Chen.

Lastly, we believe that reduction with excess borohydride does not result in the pure semiquinone alone, but that further reduction takes place, leading probably to other products and to the rupture of the O–sugar ring, thus forming daunorubicinone and adriamycinone semiquinones, responsible for the well-resolved epr spectra hitherto reported in the borohydride reduction of these compounds. This hypothesis was supported earlier by Kalyanaraman *et al.* (5) and, further, by the fact that we obtained a well-resolved spectrum in an aqueous solution of adriamycinone, but not from adriamycin or daunorubicin. This point obviously merits further work in future.

1. N. J. F. DODD and T. MUKHERJEE. Biochem. Pharmacol. **33**, 379 (1984).
2. G. A. RUSSELL and F. A. NEUGEBAUER. Org. Magn. Reson. **1**, 125 (1969).
3. E. J. LAND, T. MUKHERJEE, A. J. SWALLOW, and J. M. BRUCE. Arch. Biochem. Biophys. **225**, 116 (1983).
4. D. MEISEL and G. CZAPSKI. J. Phys. Chem. **79**, 1503 (1975).
5. B. KALYANARAMAN, E. PEREZ-RAYES, and R. F. MASON. Biochem. Biophys. Acta, **630**, 119 (1980).
6. G. M. RAO, J. W. LOWN, and J. A. PLAMBECK. J. Electrochem. Soc. **125**, 540 (1978).
7. E. J. LAND, T. MUKHERJEE, A. J. SWALLOW, and J. M. BRUCE. J. Chem. Soc. Faraday Trans. 1, **79**, 391 (1983).
8. S. SATO, M. IWAIZUMI, K. HANDA, and Y. TAMURA. Gann, **68**, 603 (1977).
9. B. K. SINHA and C. F. CHIGNELL. Chem. Biol. Interact. **28**, 301 (1979).
10. B. K. SINHA. Chem. Biol. Interact. **30**, 67 (1980).
11. J. A. PEDERSEN and R. H. THOMSON. J. Magn. Reson. **43**, 373 (1981).
12. J. GENDELL, W. R. MILLER, JR., and G. K. FRAENKEL. J. Am. Chem. Soc. **91**, 4369 (1969).
13. M. ADAMS, M. S. BLOIS, and R. H. SANDS. J. Chem. Phys. **28**, 774 (1958).
14. G. VINCOW and G. K. FRAENKEL. J. Chem. Phys. **34**, 1333 (1961).

Can. J. Chem. Downloaded from www.nrcresearchpress.com by 210.87.254.42 on 09/06/12
For personal use only.

Reply to comments: Electron paramagnetic resonance characterization and conformation of daunorubicin semiquinone intermediate implicated in anthracycline metabolism, cardiotoxicity, and anticancer action

J. W. LOWN
Department of Chemistry, University of Alberta, Edmonton, Alta., Canada T6G 2G2

Received November 25, 1983

Can. J. Chem. Downloaded from www.nrcresearchpress.com by 210.87.254.40 on 09/06/12
For personal use only.

Because of the widespread clinical utility of the anthracyclines in the treatment of human malignancies (1–3) and because of the severe limitations imposed on their use by the cardiotoxicity they display (5, 6), recent work in this area has focused on their mechanism of action and on the molecular origin of the cardiotoxicity. Recent evidence links the latter effect to the in vivo redox behaviour of the anthracyclines in leading, *inter alia*, to lipid peroxidation in cardiac tissue (6–8). An analysis of the structural features in the anthracyclines which control their in vivo redox activity has permitted a twentyfold reduction in cardiotoxicity with no sacrifice in antileukemic efficacy (9). As a result of these investigations, there has been considerable interest in the detection and characterization of the free radicals to which these drugs give rise, including the corresponding semiquinones which are obligatory intermediates in the generation of reactive oxygen species.

While it is much more convenient experimentally to generate, stabilize, and study these semiquinones under nonphysiological conditions as Mukherjee suggests, e.g. by pulse radiolysis or generation in DMSO or isopropyl alcohol and acetone or photolysis in micellar suspensions of CTAB, TX100, or SLS or by electrolysis, these conditions do not relate to the in vivo situation (2–4, 6). For this reason and as described in our paper (10), we were at pains to generate and study anthracycline semiquinones under conditions that more closely correspond to physiological (e.g. in which epr signals are evident from cell cultures treated with anthracyclines (6, 11)). An additional reason for selecting aqueous conditions over an organic solvent was the evident sensitivity of the hyperfine couplings of the semiquinone to medium effects (12). Therefore it was considered that any attempt to deduce stereochemical information from the epr spectrum of the semiquinone (of interest because of its suggested role as a site-specific radical (6)) should deal with the unperturbed species. Therefore we employed dilute aqueous solutions at pH 7.2 in the presence of mild reducing agents. As anticipated, this use of aqueous conditions necessarily required considerable sacrifice in stability of the radicals and made their detection by epr extremely difficult, for example, because of the dielectric loss. The epr spectrum of the daunorubicin semiquinone was in fact obtained, although with considerable difficulty, since, as in the corresponding generation by NADPH–hepatic microsomal system by Sato *et al.* (11), the weak epr signals appeared only after the dissolved oxygen was consumed. Our experimental conditions were therefore very similar to those reported by Kalyanaraman *et al.* (13) for the generation of daunomycinone semiquinone in aqueous solution using borohydride as reductant. Mukherjee is evidently unable to repeat their experiment. In contrast, his statement "On the other hand quinones . . . can be reduced to the corresponding semiquinone by excess of reductant without rigorous exclusion of air" is in fact in accord with the conditions we employed. The extended discussion in the Comment to prove that semiquinones react with oxygen merely emphasizes the obvious. Moreover, we do not claim that "stoichiometric one-electron reduction" is taking place. Since our experiments were not designed to quantify the amounts of radical species or measure rates of reactions, the concentrations of the dilute aqueous solutions were selected so as to give detectable epr spectra. The quinizarin used was pure by spectroscopic criteria using ir, ^{1}H nmr, and ms and gave rise to an epr spectrum closely similar to that reported by Vincow and Fraenkel (14) and others (15) produced by mild reduction in aqueous solutions.

The fact that our aqueous solution conditions give rise to the epr spectrum of daunorubicin semiquinone has been supported recently by Kleyer and Koch (16), who generated it by mild reduction at ca. 10^{-4} *M* and state "The (epr) signal was assigned to the semiquinone of daunomycin based upon the *g*-value and splitting constants which are similar to those determined by Lown and co-workers in aqueous medium. The signal is significantly different from that observed for semiquinone **9** (7-deoxydaunomycinone) in methanol". This is contrary to Mukherjee's speculation on the identity of these species. The fact that the semiquinone of the parent antibiotic may be generated cleanly by these mild reducing conditions, albeit in low concentration, is also confirmed by Kleyer and Koch (16) in that "No additional paramagnetic species were observed". These authors also provide evidence that daunorubicin semiquinone does not eliminate the sugar moiety, contrary to Mukherjee's contention.

We have already dealt with the question of the form of the semiquinones in aqueous solution as it relates to the pK_a values of the phenolic OH groups (p. 3214 of paper) (10). We point out that the pK_a values of the phenolic OH groups anticipated to be in the region of 3 to 4 will result in the semiquinones being in anionic forms (and this implies a zwitterionic form for daunorubicin semiquinone). The good match of the experimental epr spectrum and the computer simulation shown in our Fig. 3 and reported independently by Vincow and Fraenkel (14) is in accord with the view that hyperfine coupling from the exchangeable OH protons is negligible or disappears in the line width, in contrast to the situation when DMSO is used as a solvent (12).

Finally, other workers have documented evidence that treatment of daunorubicin with borohydride does not effect glycosidic cleavage (17), contrary to Mukherjee's speculations.

1. F. ARCAMONE. *In* Topics in antibiotic chemistry. *Edited by* P. Sammes. Wiley, New York. 1975. pp. 101–128.
2. F. ZUNINO, R. A. GAMBETTA, A. DI MARCO, and A. ZACCARA. Biochim. Biophys. Acta, **277**, 489 (1972).
3. A. DI MARCO, F. ZUNINO, R. SILVESTRINI, C. GAMBRUCCHI, and R. A. GAMBETTA. Biochem. Pharmacol. **20**, 1323 (1971).
4. G. BONNADONNA and S. MONFARDINI. Lancet, **1**, 837 (1964).
5. B. SMITH. Br. Heart J. **31**, 607 (1969).
6. N. R. BACHUR, S. L. GORDON, and M. V. GEE. Mol. Pharmacol. **13**, 901 (1977).
7. J. H. DOROSHOW, G. Y. LOCKER, and C. E. MYERS. J. Clin. Invest. **65**, 128 (1980).

8. T. GOODMAN and P. HOCHSTEIN. Biochem. Biophys. Commun. **77**, 797 (1977).
9. J. W. LOWN, H. H. CHEN, J. A. PLAMBECK, and E. M. ACTON. Biochem. Pharmacol. **31**, 575 (1982).
10. J. W. LOWN and H. H. CHEN. Can. J. Chem. **59**, 3212 (1981).
11. S. SATO, M. IWAIZUMI, K. HANDA, and V. TAMURA. Gann, **68**, 603 (1977).
12. R. B. SINHA. Chem. Biol. Interact. **30**, 67 (1980).
13. B. KALYANANAMAN, E. PERES-RAYES, and R. F. MASON. Biochim. Biophys. Acta, **630**, 119 (1980).
14. G. VINCOW and G. K. FRANKEL. J. Chem. Phys. **34**, 1333 (1961).
15. M. ADAMS, M. S. BLOIS, and R. H. SANDS. J. Chem. Phys. **28**, 774 (1958).
16. D. L. KLEYER and T. H. KOCH. J. Am. Chem. Soc. **105**, 2504 (1983).
17. J. JOLLES and G. PONSINET. Ger. Patent No. 2,202,690 (July 27, 1972); Chem. Abstr. **77**, 164320 (1972).

Can. J. Chem. Downloaded from www.nrcresearchpress.com by 210.87.254.40 on 09/06/12
For personal use only.

Kinetic and thermodynamic control of pseudobase formation from C-3 substituted 1-methylquinolinium cations

JOHN W. BUNTING AND NORMAN P. FITZGERALD
Department of Chemistry, University of Toronto, Toronto, Ont., Canada M5S 1A1

Received November 3, 1983

JOHN W. BUNTING and NORMAN P. FITZGERALD. Can. J. Chem. **62**, 1301 (1984).

The kinetic and thermodynamic control of pseudobase formation from 3-W-1-methylquinolinium cations has been studied for a variety of substituents (W). Spectral data indicate that, in both aqueous and methanolic solution, the C-2 pseudobases predominate at equilibrium for W = H and Br, while the C-4 pseudobases are the thermodynamically preferred species for W = $CONH_2$, CO_2CH_3, CN, and NO_2. Stopped-flow studies indicate that in all cases the C-2 pseudobases are the kinetically-controlled products upon basification of the aqueous solutions of these cations. Equilibrium constants (pK_{R+}) have been measured for pseudobase formation at both C-2 and C-4 for each W in all cases where they are experimentally accessible. Substituent effects upon pK^2_{R+} correlate with σ_m for W, while pK^4_{R+} depends upon σ_p^-. These substituent effects allow the prediction of pK^2_{R+} = 15.4 and pK^4_{R+} = 17.4 for the 1-methylquinolinium cation. Rates of C-2 to C-4 pseudobase equilibration have been measured in all cases where the latter species is thermodynamically more stable. These kinetic data allow the evaluation of rate constants for C-4 pseudobase equilibration with each cation. In all cases except W = CN, C-2 pseudobase formation is complete within the mixing time of the stopped-flow instrument.

JOHN W. BUNTING et NORMAN P. FITZGERALD. Can. J. Chem. **62**, 1301 (1984).

On a étudié le contrôle cinétique et thermodynamique de la formation de pseudobases à partir de cations W-3 méthyl-1 quinolinium portant plusieurs substituants W. Les données spectrales indiquent que, tant en solution aqueuse que méthanolique, les pseudobases en C-2 prédominent à l'équilibre lorsque W = H ou Br alors que les pseudobases en C-4 sont les espèces thermodynamiquement préférées lorsque W = $CONH_2$, CO_2CH_3, CN et NO_2. Des études par flux stoppé indiquent que, dans tous les cas, les pseudobases en C-2 sont les produits de contrôle cinétique lorsque les solutions aqueuses de ces cations sont rendues basiques. On a mesuré les constantes d'équilibre (pK_{R+}) pour la formation de pseudobases tant en C-2 qu'en C-4 pour tous les substituants W dans tous les cas où ceci était expérimentalement possible. On a pu établir une corrélation entre les effets des substituants sur les pK^2_{R+} et les σ_m des W; les valeurs de pK^4_{R+} dépendent de σ_p^-. Ces effets de substituants permettent de prédire des valeurs de pK^2_{R+} = 15,4 et pK^4_{R+} = 17,4 pour le cation méthyl-1 quinolinium.

Dans tous les cas où les dernières sont les espèces thermodynamiquement les plus stables, on a mesuré les vitesses d'équilibration des pseudobases C-2 en C-4. Ces données cinétiques permettent d'évaluer les constantes de vitesse pour l'équilibration de chaque pseudobase C-4 avec son cation. Dans tous les cas, excepté lorsque W = CN, la formation de la pseudobase en C-2 est complète en dedans du temps de mélange dans l'appareil à flux stoppé.

[Traduit par le journal]

Can. J. Chem. Downloaded from www.nrcresearchpress.com by 210.87.254.105 on 09/06/12
For personal use only.

Quinolinium cations are well known to be susceptible to nucleophilic addition at either C-2 or C-4 to give 1,2-dihydro- and 1,4-dihydro-quinolines, respectively (1–4). Thus, whereas cyanide ion addition to the 1-methylquinolinium cation occurs at C-4 to give **1** (5, 6), the Reissert compound **2** is isolated from mixtures of quinoline and benzoyl chloride in the presence of cyanide ion and is presumably formed by addition of cyanide ion at C-2 of the 1-benzoylquinolinium cation (7). For neither **1** nor **2** is it clear whether these are the products of kinetic or thermodynamic control.

Methoxide ion addition to the 1-methylquinolinium cation in methanol gives the C-2 adduct (**3**: R = CH_3) (8). By analogy to this latter observation, it is generally assumed that pseudobase formation in aqueous solution would give the C-2 adduct

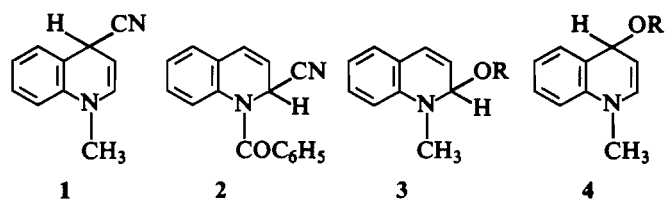

1 **2** **3** **4**

(**3**: R = H) as the thermodynamically most stable pseudobase rather than the isomeric C-4 adduct (**4**: R = H). This assumption is supported by the observation that 2-quinolones are obtained upon oxidation of quinolinium cations in aqueous base (9), although the possibility that this latter observation reflects a kinetic preference in oxidations of the C-2 and C-4 pseudobases rather than the relative thermodynamic stabilities of these pseudobases has never been satisfactorily addressed.

In a kinetic study (10) of hydroxide ion addition to the 1-methyl-3-nitroquinolinium cation (**5**: W = NO_2), it was found that whereas the C-2 pseudobase (**6**: W = NO_2) is the kinetically controlled product, the thermodynamically more stable pseudobase is the C-4 hydroxide adduct (**7**: W = NO_2). If the above assumption that the thermodynamically preferred

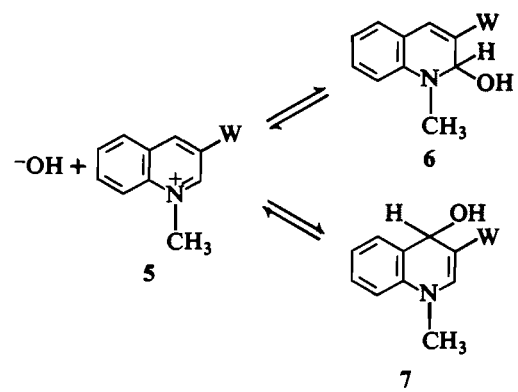

5 **6** **7**

pseudobase of the 1-methylquinolinium cation is **3**: R = H is correct, it is then required that the presence of the 3-nitro substituent in this ring system should have a pronounced effect upon the relative thermodynamic stabilities of the 1,2-dihydro- and 1,4-dihydro-quinoline isomers. This in turn raises the question of whether the nitro group is unique in this regard, and

Can. J. Chem. Downloaded from www.nrcresearchpress.com by 210.87.254.105 on 09/06/12
For personal use only.

also whether different pseudobases are obtained in kinetically and thermodynamically controlled additions of hydroxide ion (and also in other nucleophilic additions) to other C-3 substituted quinolinium cations. Analogous studies on nucleophilic addition to pyridinium cations have been reported; in this system the preferred products of kinetic and thermodynamic control seem to be quite dependent on both the substituents on the pyridinium ring and also the nature of the attacking nucleophile (11).

We now wish to report a detailed kinetic and equilibrium study of pseudobase formation for a variety of C-3 substituted 1-methylquinolinium cations (**5**) in aqueous solution. It becomes clear that the influence of the nitro substituent upon kinetic and thermodynamic control of pseudobase formation is typical of all C-3 substituents that are electron-withdrawing via a resonance effect ("σ_p^- substituents"). However, linear free energy relationships allow a prediction that the C-2 pseudobase of the 1-methylquinolinium cation is both the kinetically and thermodynamically preferred species.

Experimental

3-Bromoquinoline, 3-quinolinecarbonitrile, and 3-quinolinecarboxylic acid were commercial products (Aldrich Chemical Co.).

3-Quinolinecarboxamide

3-Quinolinecarbonitrile (5.6 g) and Amberlite IRA 400 ion exchange resin (10 g) were refluxed in a mixture of water (35 mL) and acetonitrile (20 mL) for 2 h. After cooling and filtration, the solvent was removed on the rotary evaporator and the amide product was recrystallized from water; mp 190–192°C (lit. (12) mp 193–194°C).

Methyl 3-quinolinecarboxylate

An anhydrous methanolic solution (50 mL) of 3-quinolinecarboxylic acid (1 g) was saturated with dry hydrogen chloride, and kept for 72 h. After neutralization with sodium carbonate, the solid sodium chloride was filtered off and the solvent was removed on the rotary evaporator. The ester product was recrystallized from hexane in 45% yield; mp 70–72°C (lit. (13) mp 73–74°C).

1-Methylquinolinium salts

The appropriate 3-W-quinoline was either stirred with excess methyl bromide in acetone in a Fisher pressure bottle or refluxed with methyl iodide in ethanol. After several recrystallizations from ethanol, these salts were characterized by ^{1}Hmr spectroscopy in D_2O and halide ion titration by the Vollhard method.

Determination of pK_{R+}

Equilibrium pK^E_{R+} values were determined spectrophotometrically by the general method of Albert and Serjeant (14) in aqueous buffers of ionic strength 0.1 at 25°C on the Varian Cary 210 spectrophotometer. Buffer solutions were prepared by addition of hydrochloric acid to aqueous solutions of either K_2HPO_4, $(HOCH_2)_3CNH_2$, $Na_2B_4O_7$ or Na_2CO_3, or from standard solutions of KOH adjusted to ionic strength 0.1 with KCl.

pK_{R+} values of unstable species were similarly measured from instantaneous absorbances after mixing neutral aqueous solutions of the quinolinium cations with appropriate buffers on the Durrum–Gibson stopped-flow spectrophotometer. Reported pK_{R+} values are averages of at least eight different values obtained from solutions buffered in the range pH = $pK_{R+} \pm 1$.

Kinetic studies

All kinetic data were obtained by mixing neutral aqueous solutions of the quinolinium cations with appropriate buffers to give final ionic strength 0.1 in the stopped-flow spectrophotometer at 25°C. Absorbance vs. time curves at an appropriate wavelength were digitized (118 data points), and the data were collected and fitted to first-order rate equations with the Tekronix 4051 minicomputer. Individual rate constants for pseudobase formation (k_f) and decomposition (k_d) were evaluated from the observed pseudo-first-order rate constants for cation–pseudobase equilibration by the standard algebraic methods described previously (10, 15).

TABLE 1. Electronic absorption spectra of 1,2-dihydro- and 1,4-dihydroquinolines[a]

	λ_{max} (nm)			
W	OH[b]	OCH_3[b]	**8**	**9**
H		335(8)	345(8)	303(16)
Br	333	335	344(18)	318(18)
$CONH_2$	314	316		344(18)
CO_2CH_3	315[c]	310	422[d]	346(18)
CN	304	300	410(19)	333(17)
NO_2	401(10)		510(20)	420(20)

[a] Parenthetical numerals indicate appropriate literature references; unreferenced data are from the current work.
[b] Longest wavelength absorption maximum of the thermodynamically more stable pseudobase in water or methanol.
[c] Approximate value due to rapid ester hydrolysis in aqueous base (see text).
[d] For the ethyl ester (19).

Results

The 3-W-1-methylquinolinium cations **5**: W = Br, $CONH_2$, CO_2CH_3, CN, and NO_2 all display reversible pH-dependent electronic absorption spectra in aqueous solution. The C-3 unsubstituted cation displays a pH-independent electronic absorption spectrum, indicating that within the accessible pH range (pH < 14) there is no significant pseudobase formation. In very basic aqueous solutions this latter cation is known to undergo an irreversible disproportionation reaction (9).

Hydroxide ion attack may occur at either the C-2 or C-4 position of the cations **5** to give the pseudobases **6** or **7** respectively. The longest wavelength absorption maximum in the spectrum of the pseudobase derived from each **5** is indicated in Table 1 along with analogous data for the corresponding methoxide adducts in methanol and the corresponding 3-W-1-methyl-1,2-dihydroquinolines (**8**) and 3-W-1-methyl-1,4-dihydroquinolines (**9**). In all cases the 1,2-dihydroquinoline derivatives (**8**) absorb at significantly longer wavelengths than their 1,4-dihydroquinoline isomers (**9**). None of the pseudobases derived from **5**: W = $CONH_2$, CO_2CH_3, or CN show absorption maxima in the vicinity of 400 nm, as appear in the spectra of the corresponding 1,2-dihydroquinolines (**8**),

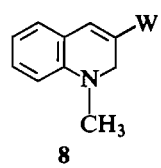

8

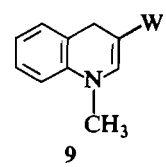

9

and this effectively rules out the C-2 adducts (**6**) as being the predominant pseudobase species in these cases. In fact, these pseudobases, like the methoxide adducts, absorb at approximately 30 nm shorter wavelength than do the corresponding 1,4-dihydroquinoline derivatives (**9**).

The 3-bromo derivative is the only case in Table 1 for which the C-2 adduct (**6**) can reasonably be proposed as the predominant aqueous pseudobase species. It should be noted that in all cases the absorption maxima for the hydroxide adducts in water are very similar to those for the methoxide adducts in meth-

Can. J. Chem. Downloaded from www.nrcresearchpress.com by 210.87.254.105 on 09/06/12
For personal use only.

TABLE 2. Proton magnetic resonance spectra of the trideuteriomethoxide adducts of 3-W-1-methylquinolinium cations[a]

W	δ (ppm)
H[b]	3.12 (3H, s), 5.66 (1H, d), 5.70 (1H, d),[c] 6.6–7.3 (5H, m)
Br	3.16 (3H, s), 5.62 (1H, s),[c] 6.6–7.3 (5H, m)
$CONH_2$	3.50 (3H, s), 5.86 (1H, s), 7.0–7.8 (5H, m)
CO_2CH_3	3.34 (3H, s),[d] 3.50 (3H, s), 5.70 (1H, s), 7.0–7.8 (5H, m)
CN	3.52 (3H, s), 5.50 (1H, s), 7.1–7.8 (5H, m)

[a]In 0.1 *M* $NaOCD_3$ in CD_3OD relative to tetramethylsilane as internal reference.
[b]From ref. 8.
[c]Slowly exchanges with solvent deuterium without any other spectral change.
[d]OCH_3 signal slowly exchanges with OCD_3.

anolic solution. The methoxide adduct of the parent 1-methylquinolinium cation has been conclusively shown (8) to be **3**: R = CH_3, and the close similarity of the spectral data for W = H and Br in Table 1 confirms the 1,2-dihydroquinoline character for the pseudobase derived from **5**: W = Br.

The above structural interpretations of pseudobase structure are further supported by the ^{1}Hmr spectral data for the trideuteriomethoxide adducts of **5** (Table 2). The H(2)—H(3) coupling constant was of particular importance in the unambiguous assignment (8) of the spectrum of the trideuteriomethoxide adduct of **5**: W = H to the C-2 adduct (**3**: R = CD_3). Analogous coupling constant data are not applicable to the C-3 substituted species of the current study; however, all spectra in Table 2 can be assigned by reference to the known **3**: R = CD_3 and suitable related spectra in the literature. The spectrum of the trideuteriomethoxide adduct of **5**: W = Br is almost identical to that of **3**: R = CD_3, lacking only the signal for H(3) at δ 5.66 ppm. In particular, the signal for H(2) slowly disappears due to base-catalyzed exchange of this proton with solvent deuterium, as is also observed for **3**: R = CD_3, and the chemical shifts for the N-methyl protons differ by only 0.04 ppm for W = H and Br. Thus the identity of the trideuteriomethoxide adduct of **5**: W = Br as the C-2 adduct seems secure.

The chemical shifts of the N-methyl protons for W = $CONH_2$, CO_2CH_3, and CN in Table 2 all lie 0.4 ppm downfield of the N-methyl protons for W = H and Br. This observation is particularly significant, because it is firmly established (21) that, independent of the nature of W, the chemical shifts of the N-methyl protons of the 1,4-dihydroquinolines **9** are uniformly 0.3–0.4 ppm downfield of the corresponding signals in the 1,2-dihydroquinolines **8**. Thus this shift implies that the trideuteriomethoxide adducts of **5**: W = $CONH_2$, CO_2CH_3, and CN are the C-4 adducts rather than the C-2 adducts as deduced above for W = H and Br. The remainder of the chemical shift data in Table 2 are not sufficiently distinctive to allow further interpretation. However, this assignment seems secure in the light of the data in Table 1 and the identification of the isomeric C-2 and C-4 hydroxide adducts in the stopped-flow experiments discussed below.

All spectral data for hydroxide and methoxide adducts discussed above refer to stable species that are present in equilibrated basic solutions of the cations **5**. However, rapid mixing of neutral aqueous solutions of these cations with aqueous base in the stopped-flow spectrophotometer allows the observation of an intermediate which is rapidly converted to the stable pseudobase species of Table 1. Since the exact details of the spectral observations on the stopped-flow time scale differ in detail for each W, it is preferable to now discuss each C-3 substituted 1-methylquinolinium cation individually.

5: W = NO_2

In an earlier investigation (10), the C-2 adduct (**6**: W = NO_2; pK^2_{R+} = 9.16) was shown to be formed in times less than the mixing time in the stopped-flow spectrophotometer; however, this species rapidly rearranges to **7**: W = NO_2 as the thermodynamically more stable product (pK^4_{R+} = 6.82). In more basic aqueous solutions, this pseudobase undergoes a deprotonation to generate the corresponding alkoxide ion (**10**) with pK_{RO^-} = 13.0 (8).

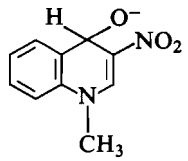

10

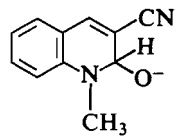

11

5: W = CN

The pH dependence of the electronic absorption spectrum of this cation indicates the presence of two different acid–base equilibria in aqueous solutions. In dilute base, the species having λ_{max} = 304 nm in Table 1, and identified above as the C-4 pseudobase **7**: W = CN, is in equilibrium with **5**: W = CN, and pK^E_{R+} = 9.02 ± 0.06 has been evaluated. This species in turn is in equilibrium in more basic solutions (pK_a = 13.40 ± 0.05) with a conjugate base having λ_{max} = 388 nm. This bathochromic shift of 84 nm between dilute and concentrated base is far greater than can be rationalized in terms of simple alkoxide ion formation upon deprotonation of **7**: W = CN, and suggests that this pK_a = 13.40 is associated with an extensive electronic reorganization within the molecule. In view of the similarity of the spectrum of this conjugate base to that of the 1,2-dihydroquinolines in Table 1, we suggest that the alkoxide ion (**11**) of the C-2 pseudobase **6**: W = CN is the thermodynamically most stable species in the vicinity of pH 14.

When neutral aqueous solutions of the cation **5**: W = CN are mixed with basic buffer solutions in the stopped-flow spectrophotometer, the absorbance changes at constant wavelength indicate the occurrence of two rapid reactions. This phenomenon is illustrated in Fig. 1 for pH 10.16 at 420 nm, which is a wavelength at which neither **5** nor the equilibrium pseudobase species (**7**) significantly absorbs. The initial rapid reaction generates a species which absorbs relatively strongly at this wavelength, but this species subsequently decomposes in a slower reaction to give the observed equilibrium species. Since we do not have access to a scanning stopped-flow instrument, we have not determined the complete spectrum of this intermediate species; however, repetitive runs at several wavelengths indicate λ_{max} in the vicinity of 400 nm. This observation is consistent with this intermediate being a 3-cyano-1,2-dihydroquinoline derivative (Table 1), and suggests that the C-2 pseudobase (**6**: W = CN) is the kinetically controlled species in these solutions, while the C-4 pseudobase (**7**: W = CN) is the thermodynamically more stable product. This result is exactly analogous to that previously reported for the corresponding 3-nitroquinoline derivative (10). The pH dependence of the maximum absorbance at 420 nm was found to be consistent with a pK_a value of 10.10 ± 0.04, and we assign this as the pK^2_{R+} value for formation of the C-2 pseudobase of **5**: W = CN.

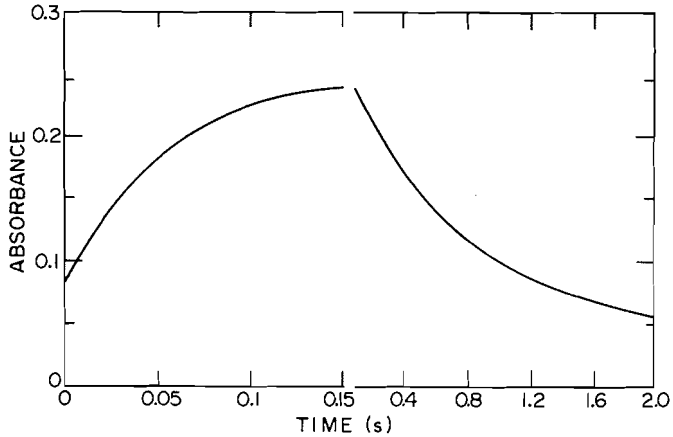

FIG. 1. Time dependence of the absorbance at 420 nm upon mixing a neutral aqueous solution of the 3-cyano-1-methylquinolinium cation with aqueous buffer of pH 10.16.

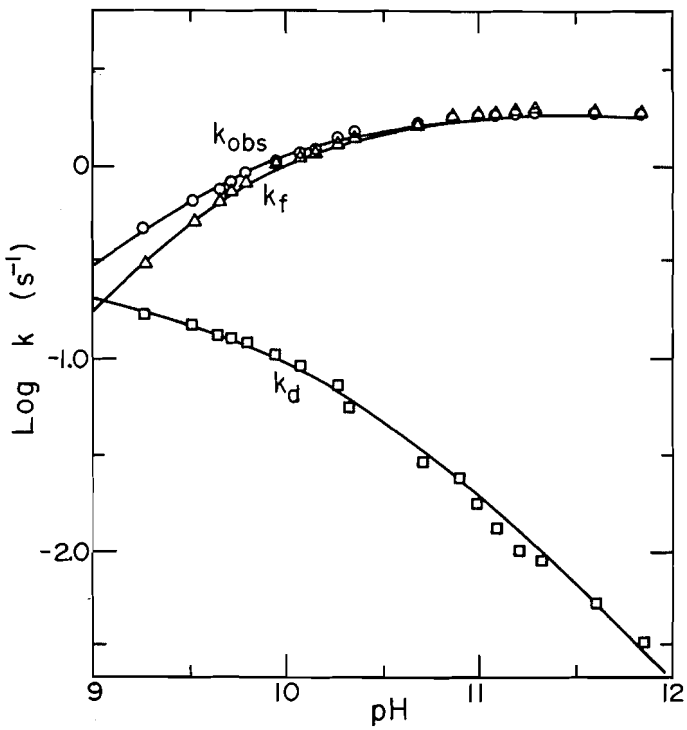

FIG. 2. The pH dependence of k_{obs}, k_f, and k_d for the equilibration of the C-2 and C-4 pseudobases of the 3-cyano-1-methylquinolinium cation.

Both the fast and slow reactions in Fig. 1 proved to be kinetically first order in the quinolinium cation. For the fast reaction, pseudo-first-order rate constants (k_{fast}) were evaluated at a number of pH values in the range pH 10–11. At pH < 10 the absorbance change becomes too small to allow accurate evaluation of these rate constants, while for pH > 11 this reaction becomes too rapid to allow investigation by the stopped-flow technique. These rate constants represent the rate of equilibration of **5** and **6**, and may be used to evaluate the individual forward (k_f for formation of **6**) and reverse (k_d for reversion of **6** to **5**) rate constants in the usual way (15). In this pH range, k_f proved to be linear in [$^-$OH], allowing the second-order rate constant for hydroxide ion attack at C-2 of **5**: W = CN to be evaluated as 7.8 (±0.7) × 10^5 M^{-1} s^{-1}, while k_d = 98 ± 8 s^{-1} was pH independent.

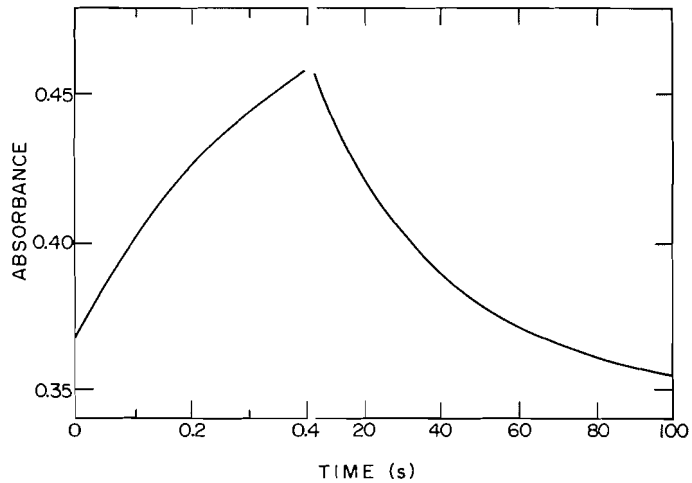

FIG. 3. Time dependence of the absorbance at 315 nm upon mixing a neutral aqueous solution of the 3-methoxycarbonyl-1-methylquinolinium cation with aqueous buffer of pH 10.96.

The pseudo-first-order rate constant (k_{obs}) for the slower reaction involving a decrease in absorbance at 420 nm was evaluated over the range pH 9–12. This pH dependence is displayed in Fig. 2. The individual rate constants for formation (k_f) and decomposition (k_d) of the C-4 pseudobase (**7**) can be calculated from k_{obs} as previously described (10) for the 3-nitroquinolinium cation. The pH profiles for k_f and k_d are also included in Fig. 2, and allow the evaluation of k^4_{OH} = 1.55 (±0.07) × 10^4 M^{-1} s^{-1} for hydroxide ion attack at C-4 of **5**: W = CN and k_2 = 0.16 ± 0.1 s^{-1} for the microscopic reverse of this process.

The greater thermodynamic stability displayed by the C-4 pseudobase over its C-2 isomer for W = CN is consistent with the recent observation of Roberts *et al.* (21) that 3-cyano-1,4-dihydro-1-methylquinoline (**9**: W = CN) has significantly greater thermodynamic stability than its 1,2-dihydro isomer (**8**: W = CN).

5: *W = CO_2CH_3*

This methyl ester is rapidly hydrolyzed in aqueous base and consequently the equilibrium of this quinolinium cation with its pseudobase is not maintained. When neutral aqueous solutions of **5**: W = CO_2CH_3 are mixed with basic buffer solutions (pH > 11.5), a species absorbing in the vicinity of 400 nm is formed within the mixing time of the stopped-flow instrument. Thus in this case the increase in absorbance due to the formation of the C-2 adduct is much faster than that observed for **5**: W = CN (Fig. 1). The pH dependence of the initial absorbance at 420 nm immediately after mixing allows the evaluation of pK^2_{R+} = 12.39 ± 0.03 for C-2 pseudobase formation from this cation.

The subsequent decrease in absorbance at 420 nm consists of a fast phase and a slower phase. This phenomenon is more obvious if this reaction is observed at 315 nm, in which case the fast reaction produces an increase in absorbance while the slower reaction results in a decrease in absorbance (Fig. 3). The pH dependence of the maximum absorbance attained at 315 nm is consistent with a pK_a = 11.25 ± 0.06, and we assign this as the pK^E_{R+} value for formation of the equilibrium pseudobase (predominantly **7**) from **5**: W = CO_2CH_3. This increase in absorbance at 315 nm is kinetically first order in quinolinium cation. Pseudo-first-order rate constants (k_{obs}) were evaluated over the range pH 11–13. The pH dependence of k_{obs} is similar

Can. J. Chem. Downloaded from www.nrcresearchpress.com by 210.87.254.105 on 09/06/12
For personal use only.

TABLE 3. Equilibrium and rate constants for pseudobase formation from 3-W-1-methylquinolinium cations[a]

		5 ⇌ 7			5 ⇌ 6			[7][d]
W	pK^E_{R+}	pK^4_{R+}[b]	k^4_{OH}[c]	k_2[c]	pK^2_{R+}	k^2_{OH}[c]	k_2[c]	[6]
H	>14	17.4	2[e]		15.4[f]	1000[g]		0.01
Br	12.34	15.1[e]			12.34			2×10^{-3}
$CONH_2$	12.09	12.18	450	5.5	12.83			4.3
CO_2CH_3	11.25	11.28	1040	1.9	12.39			28
CN	9.02	9.06	1.6×10^4	0.16	10.10	7.7×10^5	98	26
NO_2[h]	6.82	6.82	1.3×10^5	0.007	9.16			180

[a] All data for aqueous solution, ionic strength 0.1, at 25°C.
[b] From eq. [5].
[c] Units: k^2_{OH}, k^4_{OH} (M^{-1} s^{-1}); k_2 (s^{-1}).
[d] Equilibrium ratio of **7** and **6** from eq. [6].
[e] From eq. [8].
[f] From eq. [4].
[g] From eq. [9].
[h] Data from ref. 10.

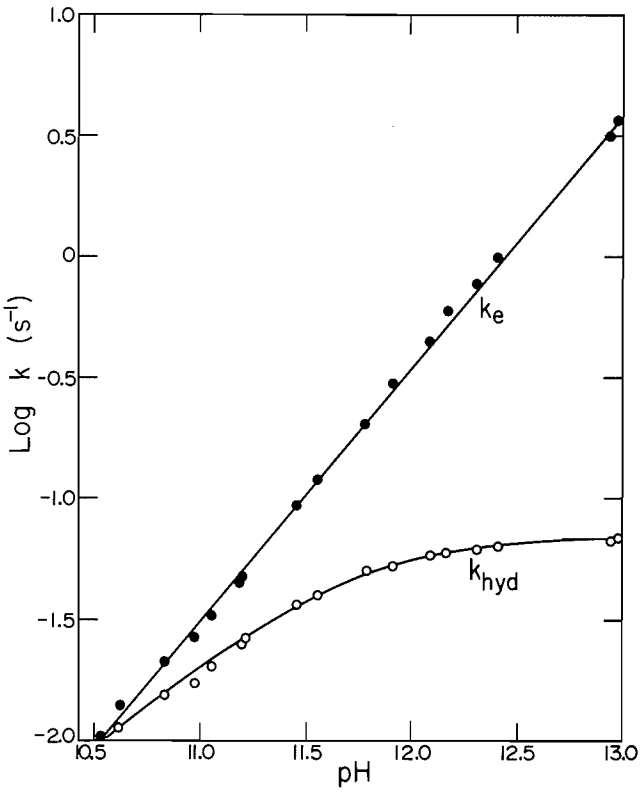

FIG. 4. The pH dependence of k_{hyd} and k_e for **5**: W = CO_2CH_3.

to that shown in Fig. 2, and after separation of k_f and k_d, k^4_{OH} = 1.04 (±0.08) × 10^3 M^{-1} s^{-1} for hydroxide ion attack at C-4 of **5**: W = CO_2CH_3 and k_2 = 1.9 ± 0.1 s^{-1} for pseudobase decomposition to the cation were evaluated.

The slow reaction seen in Fig. 3 is also kinetically first order in total quinoline species present. The pseudo-first-order rate constant (k_{hyd}) for this process was determined over the range pH 10.5–12.5 and is displayed in Fig. 4. As discussed below, we believe this reaction to be the hydrolysis of the methyl ester.

5: W = $CONH_2$

pK^E_{R+} = 12.09 ± 0.03 was calculated for the equilibrated pseudobase species from the pH dependence of the absorbance at 315 nm of basic aqueous solutions of this cation. Further very slow spectral changes were noted to occur in basic solutions containing equilibrated mixtures of the cation and pseudobase; however, this phenomenon was not investigated further.

A species absorbing in the vicinity of 400 nm is formed in basic solutions within the mixing time of the stopped-flow instrument. We assign this as the C-2 pseudobase, and have measured pK^2_{R+} = 12.83 ± 0.03 from the pH dependence of this initial absorbance. This absorbance decreases in a reaction that is kinetically first order in quinolinium cation. Pseudo-first-order rate constants were evaluated over the region pH 12.4–13.5, and allow the calculation of k^4_{OH} = 450 ± 10 M^{-1} s^{-1} and k_2 = 5.5 ± 0.2 s^{-1} for C-4 pseudobase formation and decomposition respectively.

5: W = Br

From equilibrated aqueous solutions of this cation, pK^E_{R+} = 12.34 ± 0.02 was obtained, and is assigned to C-2 pseudobase formation as discussed above. Cation–pseudobase equilibration at every pH is complete within the mixing time of the stopped-flow spectrophotometer, and no transitory species absorbing in the vicinity of 400 nm is apparent.

Discussion

All rate and equilibrium constants obtained for cation–pseudobase equilibration for the quinolinium cations **5** are collected in Table 3. In all cases hydroxide ion attack at C-2 to give **6** is much faster than attack at C-4, and for all W except cyano this C-2 attack is too rapid to allow measurement by stopped-flow methods. This much faster rate of attack at C-2 than at C-4 ensures that the pK_{R+} value measured for the transitory species present immediately upon mixing is a pure pK_{R+} for C-2 pseudobase formation. For all W except bromo this kinetically controlled C-2 pseudobase species is subsequently converted into its thermodynamically more stable C-4 isomer, and in each of these cases the equilibrium pK_{R+} (pK^E_{R+}) is lower than that of the kinetic product. In general, we may define this equilibrium pK_{R+} by:

$$[1] \quad K^E_{R+} = \frac{[H^+]([\mathbf{6}] + [\mathbf{7}])}{[\mathbf{5}]}$$

$$[2] \quad = \frac{[H^+][\mathbf{6}](1 + [\mathbf{7}]/[\mathbf{6}])}{[\mathbf{5}]} = K^2_{R+}(1 + [\mathbf{7}]/[\mathbf{6}])$$

$$[3] \quad = \frac{[H^+][\mathbf{7}](1 + [\mathbf{6}]/[\mathbf{7}])}{[\mathbf{5}]} = K^4_{R+}(1 + [\mathbf{6}]/[\mathbf{7}])$$

Can. J. Chem. Downloaded from www.nrcresearchpress.com by 210.87.254.105 on 09/06/12
For personal use only.

Can. J. Chem. Downloaded from www.nrcresearchpress.com by 210.87.254.105 on 09/06/12
For personal use only.

Thus the equilibrium ratio of pseudobases ([**7**]/[**6**]) can be evaluated from eq. [2] for W = $CONH_2$, CO_2CH_3, CN, and NO_2, and is included in Table 3. Provided this ratio is much larger than 1, pK^E_{R+} will be equal to pK^4_{R+}; if this is not the case, this ratio can be used to calculate pK^4_{R+} from eq. [3]. Of these four substituents, only in the case of W = $CONH_2$ is this ratio small enough to cause a significant difference between pK^E_{R+} and pK^4_{R+} (Table 3).

The substituent dependences of pK^2_{R+}, pK^4_{R+}, and k^4_{OH} in Table 3 have been considered in terms of various forms of the Hammett σ constants. For pK^2_{R+}, by far the best fit is obtained by making use of *meta* substituent constants (eq. [4]); attempted fits using σ_p (corr. coeff. = 0.948) or σ_p^- (corr. coeff. = 0.860) are much less statistically significant.

$$[4] \quad pK^2_{R+} = -8.9\ (\pm 0.1)\ \sigma_m + 15.4\ (\pm 0.4) \qquad \text{(corr. coeff. = 0.985)}$$

This dependence of pK^2_{R+} upon σ_m suggests that the electronic interactions of C-3 substituents with the positively charged nitrogen atom are the predominant influences in determining the substituent dependence of pK^2_{R+}.

For pK^4_{R+}, the best fit is with σ_p^- (eq. [5]), rather than σ_p (corr. coeff. = 0.990) or σ_m (corr. coeff. = 0.993).

$$[5] \quad pK^4_{R+} = -8.4\ (\pm 0.3)\ \sigma_p^- + 17.4\ (\pm 0.3) \qquad \text{(corr. coeff. = 0.999)}$$

This correlation with σ_p^- can be rationalized in terms of the importance of resonance contributors such as **12** in the stabilization of the enamine unit of these C-4 pseudobases. A close correlation of pK_{R+} with σ_p^- was also found (22) for pseudobase formation from C-4 substituted isoquinolinium cations in which analogous resonance stabilization of the enamine moiety is present (e.g. **13**). Interestingly, the ρ = −8.8 ± 0.4 for pK_{R+} in these latter C-4 substituted isoquinolinium cations is identical within experimental error to ρ = −8.4 ± 0.3 for pK^4_{R+} for these C-3 substituted quinolinium cations.

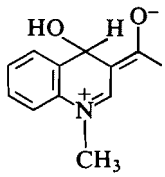

12

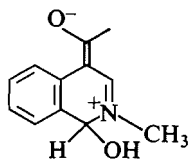

13

Equation [4] allows the prediction of pK^2_{R+} = 15.4 ± 0.4 for the parent 1-methylquinolinium cation, which is somewhat smaller than the value of 16.5 previously predicted (8) from substituent effects upon pK_{R+} for ring substituted 1-cyanoquinolinium cations (23). Equation [5] indicates that pK^4_{R+} for this ion is 17.4 ± 0.3, and so it seems clear that the C-2 pseudobase of the 1-methylquinolinium cation has significantly greater thermodynamic stability than the isomeric C-4 pseudobase. Similarly, eq. [5] predicts the C-4 pseudobase of the 3-bromo derivative to be less stable than the experimentally observed C-2 isomer. These quantitative correlations of substituent effects are entirely consistent with the assigned thermodynamic stabilities made above for various W substituents in **6** and **7** on the basis of spectral considerations.

Equations [4] and [5] allow the prediction of the relative thermodynamic stabilities for any **5** for which the appropriate substituent constants are available. It is clear that, in general, substituents which are strongly electron withdrawing by resonance (σ_p^- substituents) favour formation of the C-4 pseudobase, while weakly electron-withdrawing or electron-releasing substituents will favour the preferential formation of the C-2 pseudobase. Combination of eqs. [2]–[5] gives eq. [6] which allows the prediction of the equilibrium ratio of the C-4 and C-2 pseudobases of **5** for any W for which the appropriate substituent constants are available.

$$[6] \quad \log ([\mathbf{7}]/[\mathbf{6}]) = -8.9\ \sigma_m + 8.4\ \sigma_p^- - 2.0$$

The substituent dependence of k^4_{OH} for hydroxide ion attack at C-4 may be correlated with either σ_m, σ_p, or σ_p^- as shown by eqs. [7], [7*a*], and [7*b*].

$$[7] \quad \log k^4_{OH} = 5.5\ (\pm 0.3)\ \sigma_m + 1.2\ (\pm 0.1) \qquad \text{(corr. coeff. = 0.998)}$$

$$[7a] \quad \log k^4_{OH} = 3.9\ (\pm 0.2)\ \sigma_p^- + 0.2\ (\pm 0.2) \qquad \text{(corr. coeff. = 0.997)}$$

$$[7b] \quad \log k^4_{OH} = 5.8\ (\pm 0.4)\ \sigma_p + 0.5\ (\pm 0.2) \qquad \text{(corr. coeff. = 0.996)}$$

The marginally better correlation with σ_m (eq. [7]) and the lack of a clear preference for σ_p^- indicates that, as expected, resonance stabilization involving W is less important in the transition state for hydroxide ion attack at C-4 than it is in the product (**7**) itself. Combination of eqs. [5] and [7*a*] gives eq. [8].

$$[8] \quad \log k^4_{OH} = -0.46\ pK^4_{R+} + 8.3$$

Equation [8] may be compared with eq. [9] deduced previously (24) for C-2 pseudobase formation from a variety of substituted quinolinium cations.

$$[9] \quad \log k^2_{OH} = -0.45\ pK^2_{R+} + 10.0$$

Application of eq. [9] to C-2 pseudobase formation from **5**: W = CN, predicts $k^2_{OH} = 3 \times 10^5\ M^{-1}\ s^{-1}$, which is in reasonable agreement with the experimental value in Table 3 for this reaction. The application of eq. [9] in this case suggests that, in general, steric effects from C-3 substituents are far less important than electronic effects, a result which is also confirmed by the reasonable correlations obtained in eqs. [4]–[7] where steric effects are ignored. Equations [8] and [9] may also be used to predict second-order rate constants of $1000\ M^{-1}\ s^{-1}$ and $2\ M^{-1}\ s^{-1}$ for hydroxide ion attack at C-2 and C-4, respectively, in the parent 1-methylquinolinium cation.

The similar slopes of the linear relationships in eqs. [8] and [9] are consistent with the general observation that Bronsted values for such reactions are usually close to 0.5 (25, 26). These relationships also indicate that, for a quinolinium cation having C-2 and C-4 pseudobases of equal thermodynamic stabilities, the rate of hydroxide ion attack at C-2 will be 50-fold greater than at C-4. This factor of 50 represents the difference in intrinsic reactivities (27) of hydroxide ion at C-2 and C-4 of quinolinium cations. An alternative interpretation of eqs. [8] and [9] suggests that k^4_{OH} will only be greater than k^2_{OH} when pK^4_{R+} is more than 3.8 units smaller than pK^2_{R+}. This pK_{R+} is not approached for any case in Table 3 and, consequently, in all cases the C-2 pseudobase is the kinetically controlled species, even in those cases in which the C-4 pseudobase is of greater thermodynamic stability.

Pseudobase formation by the 10-methylacridinium cation (eq. [10]) is formally analogous to pseudobase formation at C-4 of these 1-methylquinolinium cations. It is therefore of interest

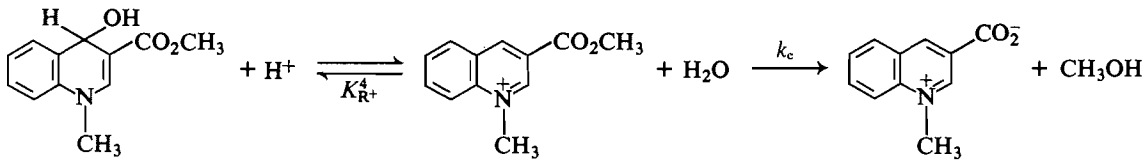

14

SCHEME 1

to test the applicability of eq. [8] to this case. For the 10-methylacridinium cation, $pK_{R+} = 10.01$ (15), and in this case eq. [8] predicts $k_{OH} = 5000\ M^{-1}\ s^{-1}$, which is almost exactly tenfold greater than the experimentally observed value of $550\ M^{-1}\ s^{-1}$ (15).

[10] 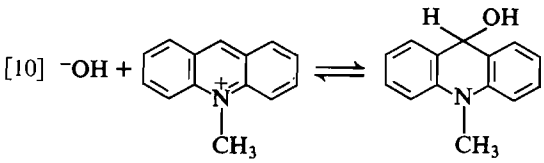

The slow reaction displayed in Fig. 3 can be rationalized as being ester hydrolysis. Since ester hydrolysis in the cation **5**: W = CO_2CH_3 should be much faster than in either of the corresponding pseudobases **6** or **7**, we formulate this hydrolysis as in Scheme 1, which starts from the thermodynamically more stable C-4 pseudobase.

Using this scheme,

$$d[\mathbf{14}]/dt = k_{hyd}([\mathbf{6}] + [\mathbf{5}])$$
$$= k_{hyd}(1 + K^4_{R+}/[H^+])[\mathbf{5}]$$
$$= k_c[\mathbf{5}]$$

Thus,

[11] $$k_c = k_{hyd}(1 + K^4_{R+}/[H^+])$$

Values of k_c calculated in this way from the experimentally determined k_{hyd} are included in Fig. 4, and indicate that log k_c is linear in pH, and of slope 1. This is consistent with k_c representing the base-catalyzed hydrolysis of **5**: W = CO_2CH_3, with the second-order rate constant of $39 \pm 2\ M^{-1}\ s^{-1}$ for this process. This value is in reasonable agreement with $58\ M^{-1}\ s^{-1}$ for the second-order rate constant for the base-catalyzed hydrolysis of the analogous ester **15** derived from nicotinic acid (28), and lends further credence to this analysis.

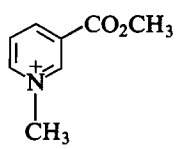

15

Acknowledgement

We appreciate the continued support of this work by the Natural Sciences and Engineering Research Council of Canada.

1. R. BRAMLEY and M. D. JOHNSON. J. Chem. Soc. 1372 (1965).
2. M. H. PALMER. The structure and reactions of heterocyclic compounds. Edward Arnold Ltd., London. 1967. p. 130.
3. C. K. INGOLD. Structure and mechanism in organic chemistry. 2nd ed. G. Bell and Sons Ltd., London. 1969. p. 839.
4. G. T. PILYUGIN and B. M. GUTSULYAK. Russ. Chem. Rev. **32**, 167 (1963).
5. A. KAUFMANN and A. ALBERTINI. Chem. Ber. **42**, 3776 (1909).
6. A. D. AINLEY and H. KING. Proc. R. Soc. B, **125**, 60 (1938).
7. A. REISSERT. Chem. Ber. **38**, 1603 (1905).
8. J. W. BUNTING and W. G. MEATHREL. Can. J. Chem. **50**, 917 (1972).
9. H. DECKER. Chem. Ber. **25**, 442 (1892); **25**, 3326 (1892).
10. J. W. BUNTING and W. G. MEATHREL. Can. J. Chem. **52**, 303 (1974).
11. S. W. H. DAMJI and C. A. FYFE. J. Org. Chem. **44**, 1757 (1979); **44**, 1761 (1979).
12. S. SHINKAI, H. HAMADA, Y. KUSANO, and O. MANABE. J. Chem. Soc. Perkin Trans. 2, 699 (1979).
13. F. C. UHLE and W. A. JACOBS. J. Org. Chem. **10**, 76 (1945).
14. A. ALBERT and E. P. SERJEANT. Ionization constants of acids and bases. Methuen, London. 1962.
15. J. W. BUNTING and W. G. MEATHREL. Can. J. Chem. **51**, 1965 (1973).
16. J. W. BUNTING and W. G. MEATHREL. Tetrahedron Lett. 133 (1971).
17. M. FERLES and O. KOCIAN. Collect. Czech. Chem. Commun. **44**, 2238 (1979).
18. N. P. FITZGERALD. M.Sc. Thesis, University of Toronto, 1983.
19. Y. KIKUGAWA, M. KURAMOTO, I. SAITO, and S. YAMADA. Chem. Pharm. Bull. **21**, 1914 (1973).
20. T. SEVERIN, D. BATZ, and H. LERCHE. Chem. Ber. **101**, 2731 (1968).
21. R. M. G. ROBERTS, D. OSTOVIC, and M. M. KREEVOY. J. Org. Chem. **48**, 2053 (1983).
22. J. W. BUNTING, V. S. F. CHEW, and S. SINDHUATMADJA. Can. J. Chem. **59**, 3195 (1981).
23. C. J. COOKSEY and M. D. JOHNSON. J. Chem. Soc. B, 1191 (1968).
24. J. W. BUNTING and D. J. NORRIS. J. Am. Chem. Soc. **99**, 1189 (1977).
25. W. J. ALBERY. Ann. Rev. Phys. Chem. **31**, 227 (1980).
26. J. HINE. J. Am. Chem. Soc. **93**, 3701 (1971).
27. C. F. BERNASCONI. Pure Appl. Chem. **54**, 2335 (1982).
28. J. A. ZOLTEWICZ and L. W. DEADY. J. Org. Chem. **37**, 501 (1972).

Can. J. Chem. Downloaded from www.nrcresearchpress.com by 210.87.254.105 on 09/06/12
For personal use only.

Deshielding γ−*gauche* effects in ^{13}C magnetic resonance: a comparison of the conformational behaviour of the acetyl group in cyclohexane and 5-substituted-1,3-dioxane systems

G. W. BUCHANAN, S. H. PREUSSER, and V. L. WEBB

Ottawa−Carleton Institute for Research and Graduate Studies in Chemistry, Dept. of Chemistry, Carleton University, Ottawa, Ont., Canada K1S 5B6

Received December 23, 1983

G. W. BUCHANAN, S. H. PREUSSER, and V. L. WEBB. Can. J. Chem. **62**, 1308 (1984).

Low temperature (173 K) ^{13}C spectra of acetylcyclohexane, 1-acetyl-1-methylcyclohexane, and 5-acetyl-5-methyl-1,3-dioxane are reported. Data permit the first direct measurement of $-\Delta G^0$ for the acetyl group bonded to cyclohexane. The value obtained, 1.02 ± 0.05 kcal/mol in $CS_2-CD_2Cl_2$ solution, is considerably lower than that determined by equilibration methods. Factors contributing to observed axial−equatorial carbonyl carbon chemical shift differences for substituted cyclohexanes and 1,3-dioxanes are discussed.

G. W. BUCHANAN, S. H. PREUSSER et V. L. WEBB. Can. J. Chem. **62**, 1308 (1984).

Opérant à basse température (173 K), on a examiné les spectres rmn du ^{13}C de l'acétylcyclohexane, de l'acétyl-1 méthyl-1 cyclohexane et de l'acétyl-5 méthyl-5 dioxanne-1,3. Les données ont permis de faire la première mesure directe du $-\Delta G^0$ du groupe acétyle lié à un cyclohexane. La valeur obtenue, 1,02 ± 0,05 kcal/mol pour une solution dans le $CS_2-CD_2Cl_2$, est considérablement plus faible que celle déterminée par des méthodes d'équilibration. On discute des facteurs contribuant aux différences de déplacements chimiques des carbones des carbonyles axiaux et équatoriaux observées dans les cyclohexanes et dioxannes-1,3 substitués.

[Traduit par le journal]

Can. J. Chem. Downloaded from www.nrcresearchpress.com by 210.87.254.105 on 09/06/12
For personal use only.

Introduction

Carbon-13 nmr spectroscopy is now a well-established technique in stereochemical analysis (1). In particular, γ-effects (below) have been utilized,

the best known cases being the upfield or shielding γ−*gauche* interactions (1).

Furthermore, the γ-*anti* effect is now well documented and it is clear that one must consider the electronegativity of the atoms (2, 3) involved as well as the degree of substitution (4) on the terminal carbon in assessing the influence of γ−*anti* groups on ^{13}C chemical shifts.

Recently (5) we reported an example in which the axial formyl carbon of cyclohexane carboxaldehyde (A) was *deshielded* relative to its equatorial counterpart in (E) by ca. 1 ppm. This is the first example of a *deshielding* γ−*gauche*

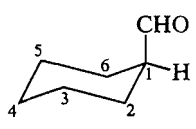

(A)

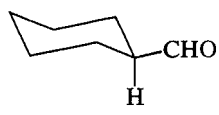

(E)

effect in a ring system lacking heteroatoms. It was rationalized via the known fact that in the preferred conformation of (A) the formyl proton does not sterically interfere with the *syn*-axial protons on C-3 and C-5 since the C=O tends to eclipse the C_1-C_6 or C_1-C_2 bond.

For heterocyclic systems such as 1,3-dioxanes (6) it is known that an axial 5-CH_3 group, for example, is deshielded relative to its equatorial counterparts, a result attributed to the removal of the *syn*-axial hydrogens from the γ positions (below).

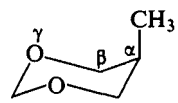

In an attempt to explore the scope and origin of deshielded axial carbonyl carbons we present a comparison of γ−*gauche* effects in some substituted cyclohexane and 1,3-dioxane molecules. ^{13}C spectra of acetylcyclohexane, 1-acetyl-1-methylcyclohexane, and 5-acetyl-5-methyl-1,3-dioxane, recorded at temperatures where ring immersion is slow on the nmr timescale, are reported.

The influence of solvent on chemical shifts and conformational equilibria has been explored and the data permit the first nmr determination of $-\Delta G^0$ for the acetyl group bonded to cyclohexane.

Results and discussion

(a) *Acetylcyclohexanes*

^{13}C chemical shifts for acetylcyclohexane **1** at 293 K in two solvent media and for individual conformers **1***A* and **1***B* at 173 K are presented in Table 1. Resonance assignments at 293 K were made on the basis of off-resonance ^1H decoupling, APT (7) experiments, and well-established trends of acyl group substitution (8). Distinction between resonances for C-3,5 and C-4 was made on the basis of relative intensity measurements in the nOe suppressed spectrum. The present assignments are consistent with earlier data of Pehk and Lippmaa (9) for **1** in Et_2O solution, except for interchange of C-4 and C-3,5 assignments.

At 173 K, in $CS_2-CD_2Cl_2$ solvent, three new resonances, attributed to **1***A*, appear which were not present at 293 or 203 K, each having relative intensity of ca. 5% of the intensity of corresponding carbons for **1***B*. From intensity data, the equilibrium constant for the process below was determined to be 19.4.

TABLE 1. ^{13}C chemical shifts of acetylcyclohexane conformers ($\delta_c \pm 0.01$)

Compound	Solvent	C-1	C-2,6	C-3,5	C-4	C=O	CH_3
1†	$CD_2Cl_2-CS_2$	51.30	28.75	26.10	26.41	209.58	27.50
1A*	$CD_2Cl_2-CS_2$	n.o.‡	27.14	25.30	n.o.	210.52	n.o.
1B*	$CD_2Cl_2-CS_2$	51.05	28.49	26.11	26.22	210.90	28.03
1†	C_7D_8	51.19	28.75	26.01	26.37	209.23	27.41
1A*	C_7D_8	n.o.	n.o.	n.o.	n.o.	209.09	n.o.
1B*	C_7D_8	50.75	28.44	25.98	26.18	209.92	27.72

*At 173.0 ± 2.0 K.
†At 293.0 ± 2.0 K.
‡Abbreviation: n.o. ≡ not observable.

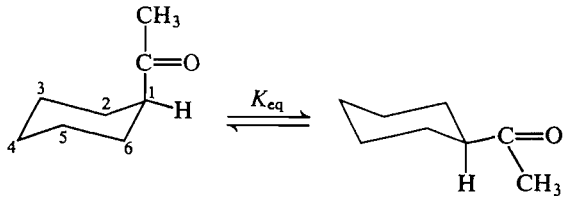

1A ***1B***

Using $-\Delta G^0 = RT \ln K_{eq}$, this translates into a value of 1.02 ± 0.05 kcal/mol for the conformational free energy of the acetyl group. This is, to our knowledge, the first nmr determination of this parameter. Previous results from equilibration measurements (10) yielded a value of 1.52 ± 0.02 kcal/mol for $-\Delta G^0_{COCH_3}$, so that it is clear that the direct determination yields a considerably lower effective "size" for the acetyl group than do equilibration data obtained for MeOH solutions. The acetyl group is, however, somewhat "larger" than the formyl group for which, in these laboratories, both ^{13}C and ^1H nmr (5, 11) give $-\Delta G^0$ values of ca. 0.84 kcal/mol. Another estimate for $-\Delta G^0_{C-H}$ in CD_2Cl_2 solution is 0.96 kcal/mol (12), also from low temperature ^{13}C nmr.

It is interesting to note that the carbonyl carbon of ***1A*** is *shielded* relative to ***1B*** by ca. 0.5 ppm. This is in contrast to results for formylcyclohexane in which the axial carbonyl was deshielded relative to its equatorial counterpart (5).

It was argued (5) that the known high preference for a conformation in which the C=O bond eclipses the $C_1 \cdots C_6$ (or $C_1 \cdots C_2$) bond was responsible for the deshielded axial formyl carbon resonance. In the axial acetyl case, however, such a conformation (below) would be considerably less favoured, due to the presence of an additional *gauche* interaction between the acetyl methyl and C_2 or C_6 of the ring.

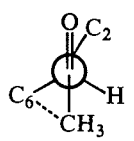

Unfortunately this argument canot be extended further since at present there are no experimental data available regarding preferred conformations about the $C_1-\overset{O}{\overset{\|}{C}}$ bond of axial acetyl functions bonded to cyclohexane.

For the toluene-d_8 solution of **1**, the axial carbonyl is again shielded relative to its equatorial counterpart, in this instance by 0.83 ppm. The equilibrium ***1A*** ⇌ ***1B*** appears to be more biased toward ***1B*** in this solvent, giving $-\Delta G^0 = 1.21 \pm 0.05$ kcal/mol as the conformational free energy of the acetyl function.

The upfield "γ" shift in the axial conformer is also apparent in the C-3,5 resonance for ***1A***, which is at $\delta_c = 25.30$ vs. 26.11 for C-3,5 of ***1B***, in $CD_2Cl_2-CS_2$ solvent. Using our shift of 27.27 ppm for cyclohexane at 173 K in $CD_2Cl_2-CS_2$, one can obtain the following α,β, and γ shift parameters for acetyl group substitution:

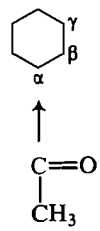

$\alpha_{eq} = +23.78$, $\beta_{ax} = -0.13$, $\beta_{eq} = +1.22$, $\gamma_{ax} = -1.97$, and $\gamma_{eq} = -1.16$.

Since the conformational equilibrium ***1A*** ⇌ ***1B*** is highly biased, we have included in this work a study of a less biased model compound which will allow one to augment the data re $-\Delta G^0$ for the acetyl group, and the apparent solvent dependence of this parameter. To this end, 1-acetyl-1-methylcyclohexane **2** was prepared and examined by ^{13}C nmr at 173 K. Results are given in Table 2 for the equilibrium ***2A*** ⇌ ***2B*** shown below.

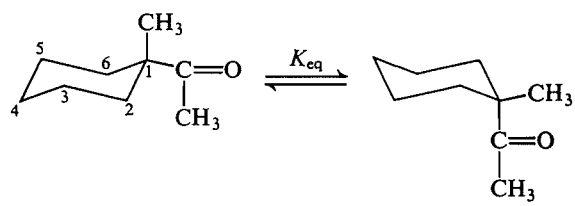

2A ***2B***

Spectral assignments in the CH_3 region at 173 K were greatly aided by the *J*-modulated spin echo or APT (7) method, since methyl resonances are negative while CH_2's are positive under the conditions used (*vide infra*).

It is known that the axial CH_3 group of methylcyclohexane is shielded by ca. 6 ppm relative to its equatorial counterpart (13, 14). An even greater difference is noted for conformer ***2A*** where the $*CH_3-C_1$ resonance appears 9.19 ppm upfield of that present in the more abundant conformer ***2B***, in $CD_2Cl_2-CS_2$ solution. In toluene-d_8 solution the difference is somewhat smaller (7.74 ppm).

Also, in accord with results for ***1A*** and ***1B***, the axial carbonyl function of ***2B*** is again shielded by ca. 0.5 ppm relative

Can. J. Chem. Downloaded from www.nrcresearchpress.com by 210.87.254.105 on 09/06/12
For personal use only.

TABLE 2. ^{13}C chemical shifts of 1-acetyl-1-methylcyclohexane conformers ($\delta_c \pm 0.01$)

Compound	Solvent	C-1	C-2,6	C-3,5	C-4	C=O	*CH_3—C(=O)	*CH_3—C_1
2†	CD_2Cl_2–CS_2	48.47	35.05	23.38	26.29	213.03	24.75	25.04
2*A**	CD_2Cl_2–CS_2	47.17	32.79	21.71	n.o.‡	214.85	n.o.	18.91
2*B**	CD_2Cl_2–CS_2	48.96	35.36	23.96	26.03	214.26	25.49	28.10
2†	C_7D_8	48.25	35.03	23.36	26.25	210.87	24.26	25.01
2*A**	C_7D_8	46.77	32.57	19.75	n.o.	212.18	n.o.	19.93
2*B**	C_7D_8	48.56	35.16	23.84	25.89	211.61	24.69	27.67

*At 173.0 ± 2.0 K.
†At 293.0 ± 2.0 K.
‡n.o. ≡ not observable.

TABLE 3. ^{13}C chemical shifts for 5-acetyl-5-methyl-1,3-dioxane conformers ($\delta_c \pm 0.01$)

Compound	Solvent	C-2	C-4,6	C-5	C=O	*CH_3—C(=O)	*CH_3—C_5
3†	CD_2Cl_2–CS_2	93.91	72.96	47.35	210.34	26.09	17.55
3*A**	CD_2Cl_2–CS_2	n.o.‡	71.03	46.24	209.50	25.74	18.03
3*B**	CD_2Cl_2–CS_2	93.59	72.51	47.53	210.41	26.36	16.89
3†	C_7D_8	93.91	72.90	47.22	209.08	26.01	17.40
3*A**	C_7D_8	n.o.	n.o.	46.07	210.38	25.82	18.31
3*B**	C_7D_8	93.66	72.55	47.27	209.98	26.38	16.72

*At 173.0 ± 2.0 K.
†At 293.0 ± 2.0 K.
‡n.o. ≡ not observable.

to its counterpart in an equatorial acetyl moiety in **2***A* for both solvent media.

From relative intensities determined in the nOe suppressed spectra, the average value of K_{eq} for the process **2***A* ⇌ **2***B* is 6.9 in CD_2Cl_2–CS_2 solvent and 5.6 in toluene-d_8. Using the currently accepted (14) value of 1.75 ± 0.06 kcal/mol for $-\Delta G^0_{CH_3}$, and assuming additivity, one obtains values of 1.09 ± 0.05 and 1.16 ± 0.05 kcal/mol for $-\Delta G^0_{CCH_3}$ (=O) in CS_2–CD_2Cl_2 and toluene-d_8 solutions respectively. These results are within 0.1 kcal/mol of those determined directly from **1***A* ⇌ **1***B*, indicating that the assumption of additivity of conformational free energies of 1,1-disubstituted cyclohexanes is valid to at least the first approximation for the present materials. In past work there are reports of successful application of additivity assumptions (15) as well as cases where significant deviations from additivity have arisen (16) in 1,1-disubstituted compounds.

(b) *5-Acetyl-5-methyl-1,3-dioxane* **3**

^{13}C chemical shifts for **3** at 293 K in two solvent media and for individual conformers **3***A* and **3***B* at 173 K are listed in Table 3. Room temperature shifts are in accord with those recently reported for **3** in $CDCl_3$ solution (17).

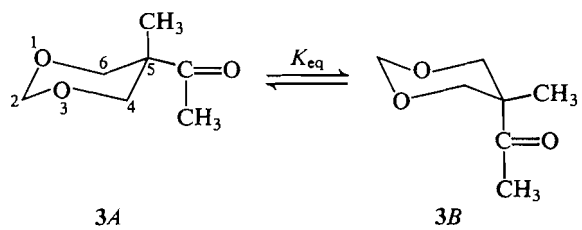

3*A* **3***B*

From previous low temperature ^1H work (17), K_{eq} for the above process was determined to be 8.1 in CS_2 solution at 183 K. ^{13}C spectra at 173 K (nOe suppressed) yield, from relative intensity data, K_{eq} values of 8.3 and 8.9 for CD_2Cl_2–CS_2 and C_7D_8 solutions respectively.

It is of interest to compare the *CH_3—C_5 and the carbonyl shifts of **3***A* and **3***B* with those of **2***A* and **2***B*, since there are no *syn*-axial hydrogens in **3** relative to an axial C-5 substituent. In **3***A* and **3***B*, the axial CH_3 becomes *deshielded* relative to its equatorial counterpart by 1.14 ppm in CD_2Cl_2–CS_2 solution and by 1.59 ppm in C_7D_8. This is in contrast to the highly shielded axial CH_3 observed in **2***A* vs. **2***B*. The present difference in CH_3 shifts in 1,3-dioxanes is very similar to that reported earlier (6) for methyl groups of 2-tert-butyl-5,5-dimethyl-1,3-dioxane (below), in CS_2 solution.

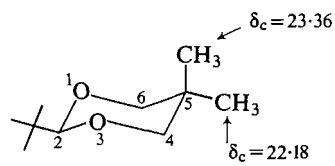

Regarding the carbonyl resonances, the *axial* carbonyl in **3***B* is deshielded by 0.91 ppm relative to its equatorial counterpart in **3***A* for the CD_2Cl_2–CS_2 solution. This appears to reflect the general trend of deshielded axial carbons when potentially *syn*-axial hydrogens are removed from the γ–*gauche* positions.

In the aromatic solvent toluene-d_8, however, this effect is reversed. The axial carbonyl resonance of **3***B* is now *shielded* by 0.40 ppm relative to its equatorial counterpart in **3***A*. This presumably reflects the existence of subtle intermolecular ring current effects of the aromatic solvent on the solute in the preferred collision complex. Thus it is clear that influences of aromatic solvent–solute complex geometry can reverse "normal" stereochemical substituent effects in carbonyl-

Can. J. Chem. Downloaded from www.nrcresearchpress.com by 210.87.254.105 on 09/06/12
For personal use only.

containing solute molecules.

To conclude, we have demonstrated that the conformational free energy of the acetyl group bonded to cyclohexane as determined directly by ^{13}C nmr is substantially lower than that previously determined by equilibration measurements (10). Also the deshielding γ–*gauche* effect on carbonyl carbon resonances appears to be dependent upon several factors, including the conformation about the ring – carbonyl carbon bond and the presence or absence of an aromatic solvent, at least in 1,3-dioxanes.

Experimental

(a) *Materials*

Acetylcyclohexane was obtained from Fluka A. G. and distilled before use. Synthesis of 5-acetyl-5-methyl-1,3-dioxane was performed according to procedures described in the literature (18, 19). Preparation of 1-acetyl-1-methylcyclohexane also followed published methods (20).

(b) *Spectra*

The ^{13}C nmr spectra were obtained at 50.3 MHz using a Varian XL-200 spectrometer. Sample concentrations were 1.0 *M* in 1:1 CD_2Cl_2–CS_2 or in C_7D_8 containing 5% TMS in 10-mm o.d. tubes. For the nOe suppressed spectra, the ^1H decoupler was gated off during the delay between observed pulses. Other conditions were as follows: sweep width = 12 000 Hz, number of data points = 32 000, acquisition time = 1.3 s, pulse width = 7.0 μs (45°), and repetition rate = 3.0 s. Typically, 1000 accumulations were required for the 173 K spectra. For the *J*-modulated spin echo (APT) (7) experiments, D2 was set at 7.0×10^{-3} s.

Acknowledgements

We are grateful to the Natural Sciences and Engineering Research Council of Canada for continued financial support. Also we thank Mr. K. Bourque for his expert technical assistance.

1. N. K. WILSON and J. B. STOTHERS. Top. Stereochem. **8**, 1 (1973).
2. E. L. ELIEL, W. F. BAILEY, L. D. KOPP, R. L. WILLER, D. M. GRANT, R. BERTRAND, K. A. CHRISTIANSEN, D. K. DALLING, M. W. DUCH, E. WENKERT, F. M. SCHELL, and D. W. COCHRAN. J. Am. Chem. Soc. **97**, 322 (1975).
3. W. KITCHING, M. MARRIOT, W. ADCOCK, and D. DODDRELL. J. Org. Chem. **41**, 671 (1976).
4. W. A. AYER, L. M. BROWNE, S. FUNG, and J. B. STOTHERS. Can. J. Chem. **54**, 3272 (1976).
5. G. W. BUCHANAN. Can. J. Chem. **60**, 2908 (1982).
6. A. J. JONES, E. L. ELIEL, D. M. GRANT, M. C. KNOEBER, and W. F. BAILEY. J. Am. Chem. Soc. **93**, 4772 (1971).
7. S. L. PATT and J. N. SHOOLERY. J. Magn. Reson. **46**, 535 (1982).
8. F. W. WEHRLI and T. WIRTHLIN. Interpretation of carbon-13 NMR spectra. Heyden and Son Ltd., London. 1976. p. 37.
9. T. PEHK and E. LIPPMAA. Org. Magn. Reson. **3**, 679 (1971).
10. E. L. ELIEL and M. C. REESE. J. Am. Chem. Soc. **90**, 1560 (1968).
11. G. W. BUCHANAN and A. R. MCCARVILLE. Can. J. Chem. **50**, 1965 (1972).
12. E. L. ELIEL and K. M. PIETRUSIEWICZ. Polish J. Chem. **55**, 1265 (1981).
13. F. A. L. ANET, C. H. BRADLEY, and G. W. BUCHANAN. J. Am. Chem. Soc. **93**, 258 (1971).
14. H. BOOTH and J. R. EVERETT. J. Chem. Soc. Chem. Commun. 278 (1976).
15. J. J. UEBEL and H. W. GOODWIN. J. Org. Chem. **33**, 3317 (1968).
16. N. L. ALLINGER and C. D. LIANG. J. Org. Chem. **33**, 3319 (1968).
17. A. DENIS, M. DELMAS, A. GASET, and J.-P. GORRICHON. Can. J. Chem. **60**, 1962 (1982).
18. J.-P. GORRICHON, A. GASET, and M. DELMAS. Synthesis, 219 (1979).
19. M. DELMAS, A. DENIS, J. P. GORRICHON, and A. GASET. Synth. Commun. **10**, 517 (1980).
20. T. SAKAI, T. KATAYAMA, and A. TAKEDA. J. Org. Chem. **46**, 2924 (1981).

Can. J. Chem. Downloaded from www.nrcresearchpress.com by 210.87.254.105 on 09/06/12
For personal use only.

Nuclear magnetic resonance studies of the acid–base chemistry of amino acids and peptides. IV. Mixed disulfides of cysteine, penicillamine, and glutathione

YVON THERIAULT, BRUCE V. CHEESMAN, ALAN P. ARNOLD, AND DALLAS L. RABENSTEIN[1]
Department of Chemistry, University of Alberta, Edmonton, Alta., Canada T6G 2G2

Received December 13, 1983

YVON THERIAULT, BRUCE V. CHEESMAN, ALAN P. ARNOLD, and DALLAS L. RABENSTEIN. Can. J. Chem. **62**, 1312 (1984).

The acid–base chemistry of the ammonium groups of penicillamine–glutathione mixed disulfide and cysteine–glutathione mixed disulfide has been characterized by ^{13}C nmr and that for the ammonium groups of penicillamine–cysteine mixed disulfide by ^{1}H nmr. The mixed disulfides were formed by thiol/disulfide exchange. Chemical shift titration data were obtained simultaneously for the mixed disulfides, the thiols, and the symmetrical disulfides in the mixture. Since the fractional titration of individual ammonium groups can be obtained directly from chemical shift data, it was not necessary to isolate the mixed disulfides. The chemical shift data indicate that the two ammonium groups of each of the mixed disulfides are titrated over the same pH range, with the acidity of the ammonium group of the penicillamine and cysteine parts of the penicillamine–glutathione and cysteine–glutathione mixed disulfides 4.4 and 3.9 times as acidic as those of the glutathione part. In the penicillamine–cysteine mixed disulfide, the penicillamine ammonium group is 1.7 times as acidic as that of the cysteine part. Macroscopic and microscopic acid dissociation constants are reported for each of the mixed disulfides. The advantages of nmr as a method for characterizing the acid–base chemistry of mixed disulfides are discussed.

YVON THERIAULT, BRUCE V. CHEESMAN, ALAN P. ARNOLD et DALLAS L. RABENSTEIN. Can. J. Chem. **62**, 1312 (1984).

On a caractérisé la chimie acide–base des groupes ammonium des disulfures mixtes pénicillamine–glutathion et cystéine–glutathion en faisant appel à la rmn du ^{13}C et celle des groupes ammonium du disulfure mixte pénicillamine–cystéine par la rmn du ^{1}H. Les disulfures mixtes ont été obtenus via un échange thiol/disulfure. On a obtenu simultanément les données de titrage du déplacement chimique pour les disulfures mixtes, les thiols et les disulfures symétriques du mélange. Il n'est pas nécessaire d'isoler les disulfures mixtes puisqu'on peut obtenir directement le titrage fractionnel des groupes ammonium individuels à partir des données de déplacement chimique. Ces données indiquent que les deux groupes ammonium de chaque disulfure sont titrés dans le même domaine de pH. Les acidités des groupes ammonium des portions pénicillamine et cystéine des disulfures mixtes pénicillamine–glutathion et cystéine–glutathion sont respectivement 4,4 et 3,9 fois plus élevées que celle de la partie glutathion. Dans le disulfure mixte pénicillamine–cystéine l'acidité du groupe ammonium de la pénicillamine est de 1,7 fois plus élevée que celle de la cystéine. On rapporte les constantes macroscopique et microscopique de dissociation acide pour chaque disulfure mixte. On discute des avantages de la rmn en tant que méthode de caractérisation de la chimie acide–base des disulfures mixtes.

[Traduit par le journal]

Can. J. Chem. Downloaded from www.nrcresearchpress.com by 210.87.254.40 on 09/06/12
For personal use only.

Introduction

Thiols are oxidized by disulfides in two steps:

[1] $RSH + R'SSR' \rightleftarrows RSSR' + R'SH$

[2] $RSH + RSSR' \rightleftarrows RSSR + R'SH$

Oxidation of RSH to RSSR occurs via the stable mixed disulfide RSSR'. Oxidation of thiols by disulfides is important in the biological chemistry of thiols (1, 2), and numerous mixed disulfides have been identified in biological systems, including cysteine–homocysteine mixed disulfide in human plasma (3–5), cysteine–penicillamine mixed disulfide in human urine (6), cysteine–glutathione mixed disulfide in liver homogenate (7) and calf lens (8), and glutathione – coenzyme A mixed disulfide in rat (9) and bovine (10) liver.

Although the acid–base chemistry of many thiols and disulfides has been characterized, there are no reports on the acid–base chemistry of mixed disulfides. Their acid–base chemistry is of interest because the kinetics and equilibria of the thiol/disulfide exchange reactions described by eqs. [1] and [2] depend on the protonation states of the species involved. As part of a study of the kinetics and equilibria of thiol/disulfide exchange reactions of biological molecules, we have characterized the acid–base chemistry of penicillamine–glutathione mixed disulfide (PSSG, **1**), cysteine–glutathione mixed disulfide (CSSG, **2**), and penicillamine–cysteine mixed disulfide (PSSC, **3**).

[1] Author to whom correspondence should be addressed.

The acid–base chemistry of **1**–**3** was characterized by using the pH dependence of the chemical shifts of selected resonances in their ^{1}H or ^{13}C nuclear magnetic resonance (nmr) spectra. Since chemical shifts give directly the fractional protonation of the various acidic groups (11), it is not necessary that the solution being titrated contain pure mixed disulfide. Nuclear magnetic resonance spectra were obtained for **1**–**3** in mixtures prepared by reacting the appropriate thiols and disulfides. In this way, chemical shift titration data were obtained simultaneously for the thiols and symmetrical disulfides as well as for the mixed disulfides.

Experimental

D-Penicillamine, glutathione, glutathione disulfide, and D,L-cysteine were obtained from Sigma Chemical Co., D,L-cystine from ICN Pharmaceuticals, and D-penicillamine disulfide from Aldrich Chemical Co. The thiols and disulfides were used as received.

The pH measurements were made at 25°C with a Fisher Accumet pH meter equipped with a standard glass electrode and a fiber-tipped, saturated calomel reference electrode. The pH meter was calibrated with standard solutions having nominal pH values of 4.00, 7.00, and 10.00 at 25°C. The exact pH value of each standard solution was established, and periodically checked, by comparison with freshly prepared NBS pH standard solutions.

The ^{1}H nmr spectra were measured at 200 MHz and 25°C on a Bruker WH-200 nmr spectrometer operating in the pulse/Fourier transform mode. All nmr spectra were obtained on aqueous solutions. To avoid the dynamic range problem, the water resonance was reduced in intensity by saturation with a decoupler pulse applied at the water resonance frequency for 2 s prior to the observation pulse (12).

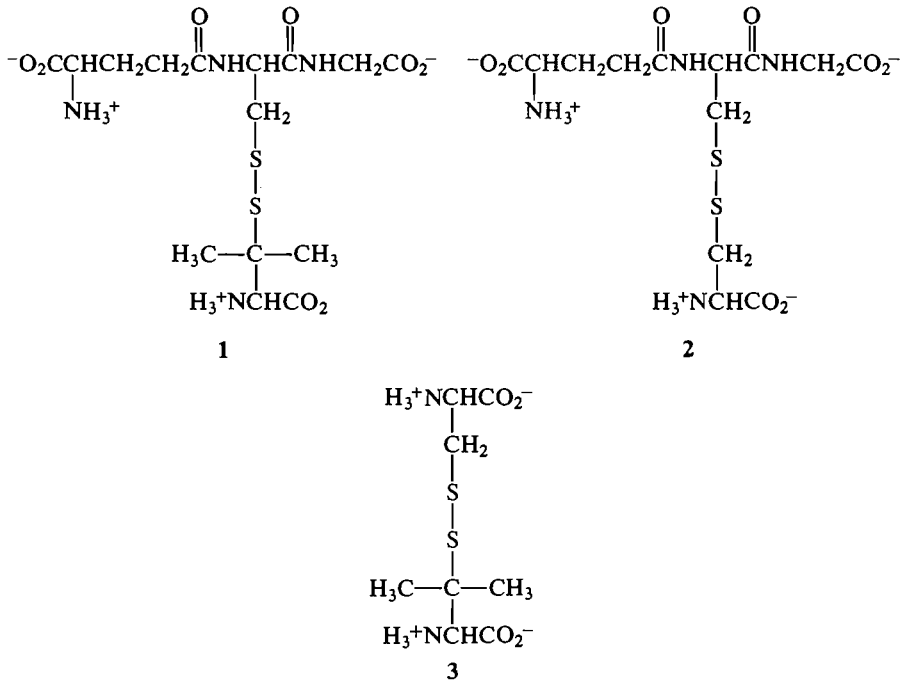

1

2

3

Can. J. Chem. Downloaded from www.nrcresearchpress.com by 210.87.254.40 on 09/06/12
For personal use only.

The spectrometer was run in the unlocked mode since the magnet shows no detectable drift over the time required to obtain a spectrum. The ^1H chemical shifts were measured relative to the methyl resonance of *tert*-butanol (TBA), which was added to the solution at a concentration of ~0.01 *M*. The chemical shifts are reported relative to the methyl resonance of sodium 2,2-dimethyl-2-silapentane-5-sulfonate (DSS); the resonance for TBA is 1.2397 ppm to high frequency from that of DSS.

The ^{13}C nmr spectra were measured at 90.56 MHz on a Bruker WM-360 nmr spectrometer operating in the pulse/Fourier transform mode. For ^{13}C measurements on **1**, the solvent was doubly distilled H_2O; for ^{13}C measurements on **2**, the solvent was a mixture of 10% D_2O/90% H_2O. The sample temperature was maintained at 25°C by collecting free induction decays under conditions of inverse gated decoupling (nOe suppressed) to minimize heating of the sample and by blowing chilled air over the sample tube in the probe. The ^{13}C chemical shifts were measured relative to internal dioxane, but are reported relative to tetramethylsilane (TMS). The resonance for dioxane is at 67.40 ppm to high frequency from TMS.

Solutions were prepared in water which had been purified by distilling it twice and then passing it through a Barnstead D8902 Ultrapure mixed bed ion-exchange resin. KCl (0.4 *M*) was added for ionic strength control. The solvent mixture was deoxygenated by bubbling with argon or nitrogen before the addition of thiol to minimize oxidation by dissolved oxygen. The appropriate thiol/disulfide pair was then added and allowed to react according to eqs. [1] and [2] to form the desired mixed disulfide. The thiol was added in four portions, the pH adjusted to near 8, and the solution allowed to react for 13 to 24 h after each addition. The solution was bubbled with oxygen between additions to oxidize the thiols to disulfides. This procedure resulted in more mixed disulfide than is present at equilibrium in a solution prepared from the same total amounts of thiol and disulfide. The total concentrations of penicillamine (PSH) and glutathione disulfide (GSSG) added in the preparation of PSSG were 0.20 *M* and 0.078 *M* respectively. In the preparation of CSSG, the total added concentrations were 0.21 *M* and 0.078 *M* for cysteine (Cys) and GSSG. For PSSC, the added concentrations of PSH and CSSC were 0.03 *M* and 0.09 *M*. Insoluble CSSC was removed by filtration from solutions of CSSG and PSSC.[2]

Samples for nmr measurement were prepared by adjusting the pH of the final solutions to the low pH end of the pH range of interest with concentrated acid, and then withdrawing samples at closely spaced pH intervals as the pH was increased by the addition of concentrated base.

Acid dissociation constants were evaluated from the chemical shift data as mixed activity–concentration constants (activity of hydrogen ion[3] – concentration of acid and its conjugate base). The weighted nonlinear least-squares curve fitting program KINET (14) was used to evaluate the macroscopic acid dissociation constants from the chemical shift data.

Results

Penicillamine–glutathione mixed disulfide

Spectrum C in Fig. 1 is the ^{13}C nmr spectrum of the solution prepared by reacting PSH with GSSG.[4] Also shown in Fig. 1 are ^{13}C spectra for PSH, PSSP, GSH, and GSSG at the same pH. Resonance 0 is for dioxane; resonances 1–4 are for the C_α, C_β, CH_3, and CH_3 carbons respectively of PSH; resonances 5–8 are for the same carbons of PSSP; resonances 19–24 are for the Cys-C_α, Glu-C_α, Gly-C_α, Glu-C_γ, Glu-C_β, and Cys-C_β carbons of GSH; and resonances 25–30 are for the Glu-C_α, Cys-C_α, Gly-C_α, Cys-C_β, Glu-C_γ, and Glu-C_β carbons of GSSG. The extra resonances (9–18) in spectrum C are for PSSG. Resonances 9–12, 14, and 16 were assigned to specific carbons of PSSG on the basis of their chemical shifts and the changes in their chemical shifts when the ammonium groups were titrated. The resonances at 55.18, 44.29, 32.39, and 27.12 ppm were assigned to the Glu-C_α, Gly-C_α, Glu-C_γ, and Glu-C_β carbons, respectively, of all three species (GSH, GSSG, and PSSG) on the basis of (*i*) the chemical shifts observed for GSH and GSSG alone, (*ii*) the expected similarity of the chemical shifts of these carbons in all three species, since they are far removed from the thiol or disulfide groups, and (*iii*) the intensities of the resonances.

To characterize the acid–base chemistry of the ammonium groups of PSSG, ^{13}C spectra were measured as a function of pH over the pH range 4–12 for the solution used to obtain spec-

[2] CSSC has a solubility of 2.8×10^{-4} *M* at pH 6.95 and 25°C (13).

[3] Activity of hydrogen ion as approximated by $10^{-(\text{pH meter reading})}$.

[4] The carbonyl region is not shown in Fig. 1.

Can. J. Chem. Downloaded from www.nrcresearchpress.com by 210.87.254.40 on 09/06/12
For personal use only.

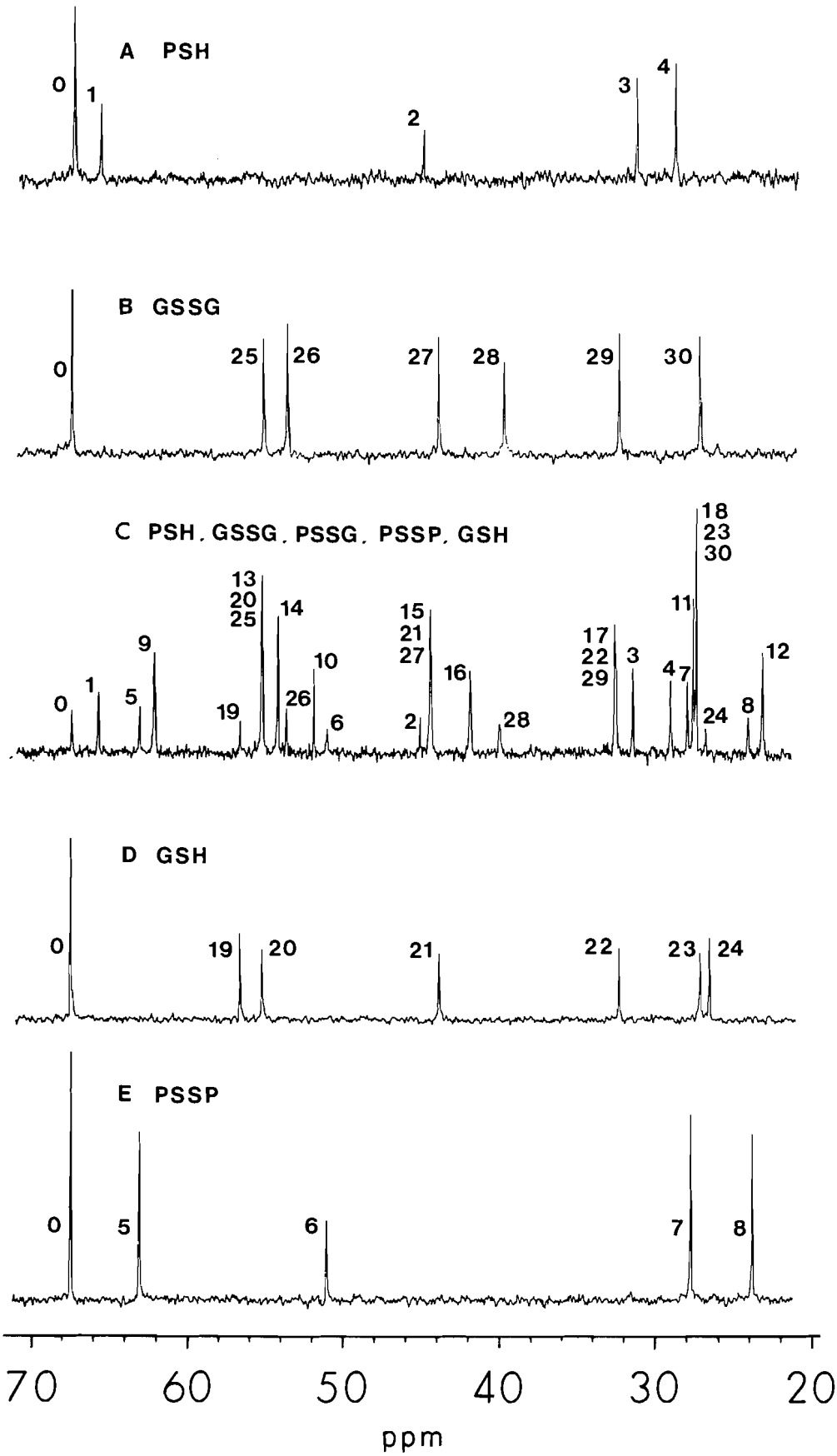

FIG. 1. The ^{13}C nmr spectra of (A) 0.1 *M* PSH, (B) 0.1 *M* GSSG, (C) 0.064 *M* PSH, 0.019 *M* PSSP, 0.101 *M* PSSG, 0.022 *M* GSH, and 0.014 *M* GSSG, (D) 0.1 *M* GSH, and (E) 0.1 *M* PSSP. Each solution contained 0.03 *M* dioxane. Solutions A, B, D, and E were at pH 4.0; solution C was at pH 4.52.

Can. J. Chem. Downloaded from www.nrcresearchpress.com by 210.87.254.40 on 09/06/12
For personal use only.

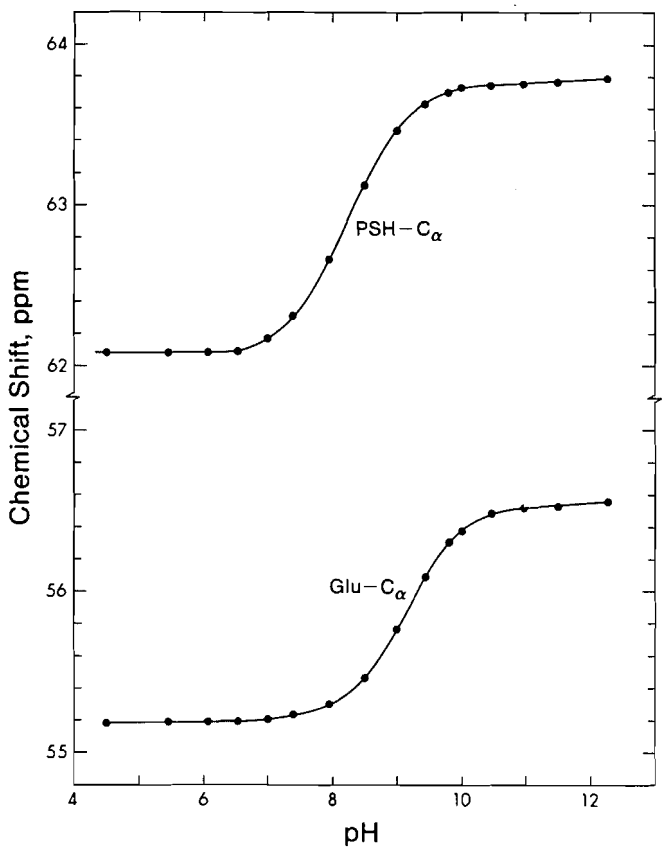

FIG. 2. pH dependence of the chemical shifts of the penicillamine and glutamyl α carbons of PSSG.

trum C. Chemical shift titration data for the PSH-C_α and Glu-C_α carbons of PSSG are presented in Fig. 2. Because there are 11 bonds separating the PSH-C_α carbon from the glutamyl ammonium group in PSSG, changes in the chemical shift of the PSH-C_α resonance can be assumed to be due only to changes in the protonation state of the penicillamine ammonium group (15). Likewise, changes in the chemical shift of the resonance for the Glu-C_α carbon can be assumed to be due only to changes in the protonation rate of the glutamyl ammonium group. Thus, the chemical shift data in Fig. 2 indicate that the two ammonium groups of PSSG are titrated over the same pH range, as described by the titration scheme for PSSG in Fig. 3.

At low pH, PSSG has 5 titratable protons. As the pH is increased, the three carboxylic acid groups are titrated first; K_1–K_3 are the macroscopic acid dissociation constants for their titration. Then, over the pH range studied in this work, the two ammonium groups are titrated; k_{1234}, k_{1235}, k_{12345}, and k_{12354} are the microscopic constants for their dissociation. The specific species to which a given microconstant refers is indicated by its subscript; the last number in the subscript denotes the group dissociating in that step, while the preceding numbers denote groups titrated in preceding steps. The three carboxylic acid groups are labelled 1–3, and the PSH and Glu ammonium groups are labelled 4 and 5 respectively. The microconstants for the ammonium groups are related to the macroconstants K_4 and K_5:

$$[3] \quad K_4 = k_{1234} + k_{1235}$$

$$[4] \quad K_5 = \frac{k_{12345}k_{12354}}{k_{12345} + k_{12354}}$$

Both the macroconstants and the microconstants for the ammonium groups were evaluated from the chemical shift data in Fig. 2. First, the macroconstants were evaluated by the procedure described previously (11). In this procedure, the fractional titration of each of the two ammonium groups is calculated from the chemical shift data using eq. [5].

$$[5] \quad f_d = \frac{\delta_{obs} - \delta_p}{\delta_d - \delta_p}$$

where f_d is the fractional deprotonation, δ_{obs} the observed chemical shift at the particular pH, and δ_p and δ_d the chemical shifts at low and high pH where the ammonium groups are completely protonated and deprotonated, respectively. The fractional deprotonation curves for groups 4 and 5 are shown in Fig. 4. The average number of titratable ammonium protons per molecule, $\bar{p}$, is then calculated as a function of pH from the fractional titration data.

$$[6] \quad \bar{p} = 2 - f_{4,d} - f_{5,d}$$

where $f_{4,d}$ and $f_{5,d}$ represent the fractional deprotonation of groups 4 and 5. The $\bar{p}$ values vs. pH data are also shown in Fig. 4.

In terms of the protonated species in the macroscopic titration sequence, $\bar{p}$ is given by

$$[7] \quad \bar{p} = \frac{2[H_2A] + [HA]}{[H_2A] + [HA] + [A]}$$

which leads to

$$[8] \quad \bar{p} = \frac{2a_H^2 + K_4a_H}{a_H^2 + a_HK_4 + K_4K_5}$$

Values were obtained for K_4 and K_5 by curve fitting the $\bar{p}$ vs. pH data in Fig. 4 to eq. [8]. The results are given in Table 1. The solid curve through the $\bar{p}$ vs. pH data in Fig. 4 is the theoretical curve predicted by eq. [8] for the values listed in Table 1 for K_4 and K_5.

Microconstants were calculated from the macroconstants by calculating with eq. [9] the ratio of the concentrations of species **2** and **3** (Fig. 3), which is equal to the ratios k_{1234}/k_{1235} and k_{12354}/k_{12345}

$$[9] \quad \frac{[\mathbf{2}]}{[\mathbf{3}]} = \frac{f_{4,d} - \alpha_2}{f_{5,d} - \alpha_2}$$

where α_2 is the fractional concentration of species **4**. α_2 was calculated from the macroconstants using eq. [10].

$$[10] \quad \alpha_2 = \frac{K_4K_5}{a_H^2 + a_HK_4 + K_4K_5}$$

The average value obtained for the ratio from data at 8 pH values is 4.38 with a standard deviation of 0.53. The microconstants listed in Table 1 for PSSG were calculated from this ratio and the macroconstants using eqs. [3] and [4].

Macroconstants for the ammonium and thiol groups of GSH and PSH and the two ammonium groups of GSSG and PSSP were also calculated from ^{13}C chemical shift data obtained simultaneously with that for PSSG. The results are given in Table 1. Microconstants for GSSG and PSSP were calculated directly from the macroconstants since the two ammonium groups in each molecule are identical. The microconstants listed for the ammonium groups of PSH and GSH were taken from the literature.

TABLE 1. Macroscopic and microscopic acid dissociation constants for thiols, symmetrical disulfides, and mixed disulfides[a,b,c]

Molecule	Acid group	Acid dissociation constant	pK	Molecule	Acid group	Acid dissociation constant	pK
Penicillamine–glutathione mixed disulfide	$NH_3^+ + NH_3^+$	K_4[d]	8.13 ± 0.02	Glutathione	$NH_3^+ + SH$	K_3	8.67 ± 0.03
	$NH_3^+ + NH_3^+$	K_5[d]	9.24 ± 0.01		$NH_3^+ + SH$	K_4	9.44 ± 0.03
	NH_3^+ (PS)[e]	k_{1234}[f]	8.22 ± 0.06		NH_3^+	k_{124}[h]	9.14[h]
	NH_3^+ (GS)[e]	k_{1235}[f]	8.66 ± 0.06	Penicillamine	$NH_3^+ + SH$	K_2	8.04 ± 0.04
	NH_3^+ (GS)	k_{12345}[f]	9.15 ± 0.06		$NH_3^+ + SH$	K_3	10.64 ± 0.03
	NH_3^+ (PS)	k_{12354}[f]	8.51 ± 0.06		NH_3^+	k_{12}[i]	8.7[j]
Cysteine–glutathione mixed disulfide	$NH_3^+ + NH_3^+$	K_4	8.55 ± 0.02	Cysteine	NH_3^+	k_{12}[i]	8.86[k]
	$NH_3^+ + NH_3^+$	K_5	9.30 ± 0.02	Glutathione disulfide	$NH_3^+ + NH_3^+$	K_5	8.73 ± 0.05
	NH_3^+ (CS)[e]	k_{1234}[f]	8.61 ± 0.04		$NH_3^+ + NH_3^+$	K_6	9.49 ± 0.04
	NH_3^+ (GS)	k_{1235}[f]	9.19 ± 0.04		NH_3^+	k_{12345}[l]	9.03 ± 0.05
	NH_3^+ (GS)	k_{12345}[f]	9.23 ± 0.04		NH_3^+	k_{123456}[l]	9.19 ± 0.04
	NH_3^+ (CS)	k_{12354}[f]	8.65 ± 0.04	Penicillamine disulfide	$NH_3^+ + NH_3^+$	K_3	7.76 ± 0.02
Penicillamine–cysteine mixed disulfide	$NH_3^+ + NH_3^+$	K_3	8.04 ± 0.01		$NH_3^+ + NH_3^+$	K_4	8.71 ± 0.02
	$NH_3^+ + NH_3^+$	K_4	8.93 ± 0.01		NH_3^+	k_{123}[m]	8.06 ± 0.02
	NH_3^+ (PS)[e]	k_{123}[g]	8.24 ± 0.02		NH_3^+	k_{1234}[m]	8.41 ± 0.02
	NH_3^+ (CS)	k_{124}[g]	8.47 ± 0.02	Cysteine disulfide (cystine)	$NH_3^+ + NH_3^+$	K_3	7.95[n]
	NH_3^+ (CS)	k_{1234}[g]	8.73 ± 0.02		$NH_3^+ + NH_3^+$	K_4	8.95[n]
	NH_3^+ (PS)	k_{1243}[g]	8.50 + 0.02		NH_3^+	k_{123}[m]	8.25
					NH_3^+	k_{1234}[m]	8.65

[a] 25°C, 0.4 M KCl.
[b] Literature values were recalculated to an ionic strength of 0.4 M using the Davies equation (ref. 24).
[c] This work, unless indicated otherwise. The uncertainties given for the macroconstants are the linear estimates of the standard deviations of the best fit values from the nonlinear least-squares calculations (14). The uncertainties given for the microconstants for PSSG, CSSG, and PSSC were estimated from the relative standard deviations of the macroconstants and the ratios ([**2**]/[**3**], eq. [9]) used to calculate the microconstants.
[d] Composite macroscopic constants due to simultaneous dissociation of the two NH_3^+ groups over the same pH region. See Fig. 3.
[e] PS, GS, and CS refer to the penicillamine, glutathione, and cysteine parts of the mixed disulfides PSSG, CSSG, and PSSC.
[f] Microscopic constants as defined in Fig. 3.
[g] The ammonium group of the PS part of PSSC is labelled 3 and that of the CS part as 4.
[h] The microscopic constant of the ammonium group of the diprotonated (NH_3^+, SH) form of GSH. Reference 19.
[i] The microscopic constant for the ammonium group of the diprotonated (NH_3^+, SH) form of PSH or CSH.
[j] Reference 21.
[k] Reference 22.
[l] Because of symmetry, $k_{12345} = k_{12346}$ and $k_{123456} = k_{123465}$.
[m] Because of symmetry, $k_{123} = k_{124}$ and $k_{1234} = k_{1243}$.
[n] Reference 23.

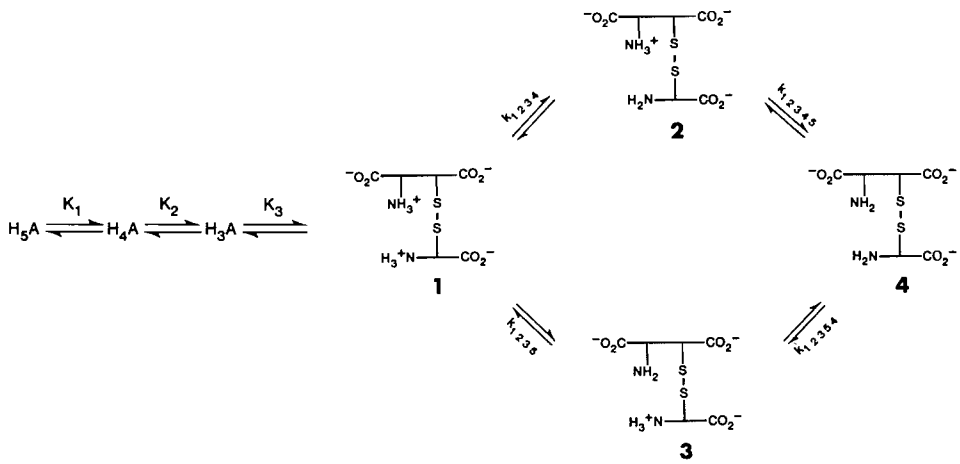

FIG. 3. The microscopic acid dissociation scheme for the ammonium groups of PSSG and CSSG.

Cysteine–glutathione mixed disulfide

The ^{13}C nmr spectra were obtained as a function of pH for the final solution of CSSG prepared by reacting CSH with GSSG. Macroscopic and microscopic constants for the two ammonium groups of CSSG were evaluated from the pH dependence of the chemical shifts of the resonances for the Glu-C_α and Cys-C_α (CS part) carbons using the procedures described above. The results are given in Table 1. The fractional titration and $\bar{p}$ data are presented in Fig. 5. The value obtained for the ratio [**2**]/[**3**] (eq. [9]) from data at 9 pH values was 3.89 ± 0.31.

Can. J. Chem. Downloaded from www.nrcresearchpress.com by 210.87.254.40 on 09/06/12
For personal use only.

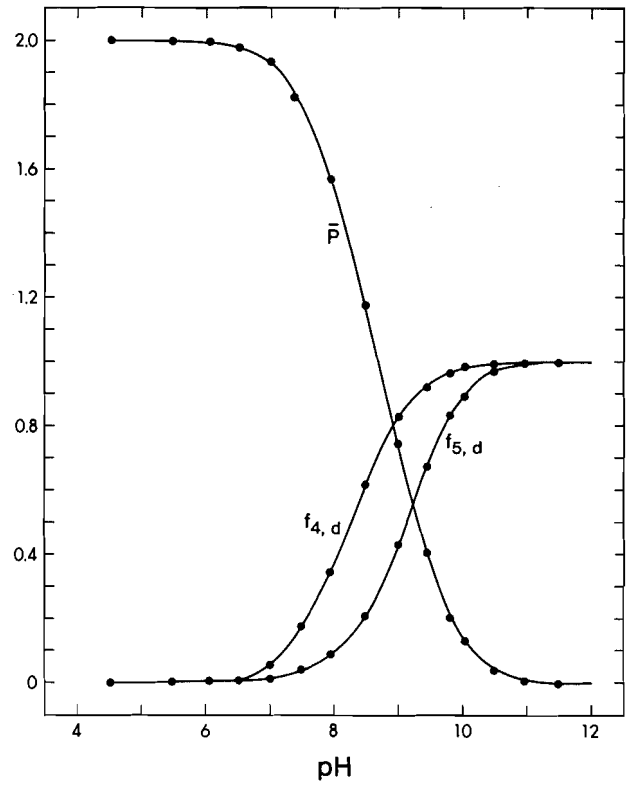

FIG. 4. The pH dependence of the fractional titration of the penicillamine ($f_{4,d}$) and glutamyl ($f_{5,d}$) ammonium groups of PSSG and the average number of ammonium protons per molecule ($\bar{p}$). The smooth curve through the $\bar{p}$ data is the theoretical curve predicted by the macroconstants in Table 1.

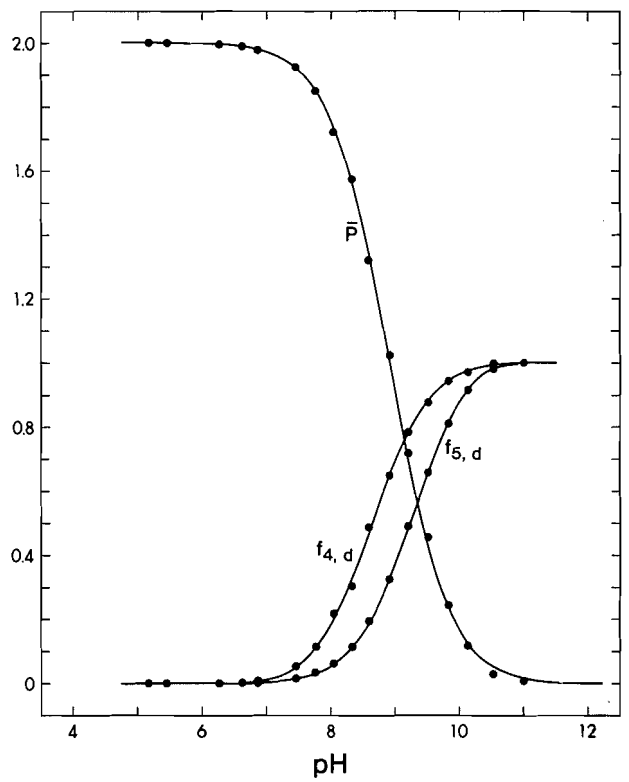

FIG. 5. The pH dependence of the fractional titration of the cysteine ($f_{4,d}$) and glutamyl ($f_{5,d}$) ammonium groups of CSSG and the average number of ammonium groups per molecule ($\bar{p}$). The smooth curve through the $\bar{p}$ data is the theoretical curve predicted by the macroconstants in Table 1.

Penicillamine–cysteine mixed disulfide

The acid–base chemistry of the two ammonium groups of PSSC was characterized using the pH dependence of the chemical shifts of the resonances for the C_α protons of the PSH and Cys parts of the molecule. Although the resonance for the C_α proton of the Cys part is in the same region as that for CSH and CSSC, there was no interference because CSH had been oxidized and CSSC is relatively insoluble. Since the C_α proton of the PSH part of PSSC is seven bonds removed from the ammonium group of the Cys part, changes in its chemical shift over the pH range 4–12 are assumed to be due only to titration of the PSH ammonium group. Likewise, changes in the chemical shift of the C_α proton of the Cys part are assumed to be due to titration of its ammonium group.

Fractional titration of each of the 2 ammonium groups was calculated as a function of pH from the chemical shift data. The ammonium groups of the PSH and Cys parts are labelled 3 and 4 respectively. $\bar{p}$ was then calculated as a function of pH. The fractional titration and $\bar{p}$ data are shown as a function of pH in Fig. 6. K_3 and K_4 were obtained from the $\bar{p}$ vs. pH data over the pH range 4–12, and microscopic constants were calculated from the macroconstants as described above. The results are listed in Table 1. The value obtained for the ratio [**2**]/[**3**] (eq. [9]) from data at 21 pH values was 1.70 ± 0.05.

Discussion

The nmr chemical shift data for PSSG, CSSG, and PSSC indicate that the two ammonium groups in each mixed disulfide are similar in acidity. Thus, the monoprotonated form of each molecule exists as a mixture of two protonation isomers. For PSSG, the ratio of the isomers, [**2**]/[**3**], is 4.4. For CSSG, the ratio is 3.9. For PSSC, the ratio of the concentration of the PSH protonated species to that of the Cys protonated species is 1.7. This ratio is independent of pH, as indicated by the species distribution diagram for PSSG in Fig. 7.

The ammonium groups of the PSH and Cys parts of PSSG and CSSG, respectively, are more acidic than are the ammonium groups of the GSH part. This is as would be predicted by the relative acidities of the ammonium groups of PSSP, CSSC, and GSSG (Table 1). However, even though the two ammonium groups in PSSG and in CSSG are separated by twelve bonds, their acidity does depend on the actual molecule and thus it is not possible to predict their acidities from acid dissociation constants for related molecules. For example, pk_{1234} = 8.22 for PSSG while pk_{123} = 8.06 for PSSP and pk_{123} = 8.24 for PSSC. For Cys, pk_{1234} = 8.61 for CSSG while pk_{123} = 8.25 for CSSC and pk_{124} = 8.47 for PSSC. Further evidence for interaction of the two ammonium groups in a given molecule is provided by the large differences between the two microconstants for a particular group. For example, if the two ammonium groups dissociate independently of each other, successive macroconstants will differ by a factor of 4 and the two microconstants for a particular ammonium group will be equal. The dependence of the acidity of one ammonium group on the protonation state of the other ammonium group is approximately the same for PSSP, GSSG, PSSC, and PSSG ($\Delta pk \sim$ 0.3–0.4), and zero within experimental error for CSSG.

One trend suggested by the results in Table 1 is that oxidation increases the acidity of ammonium groups close to the sulfur. For example, pk_{12} is 8.7 for PSH whereas pk_{123} is 8.06

Can. J. Chem. Downloaded from www.nrcresearchpress.com by 210.87.254.40 on 09/06/12
For personal use only.

Can. J. Chem. Downloaded from www.nrcresearchpress.com by 210.87.254.40 on 09/06/12
For personal use only.

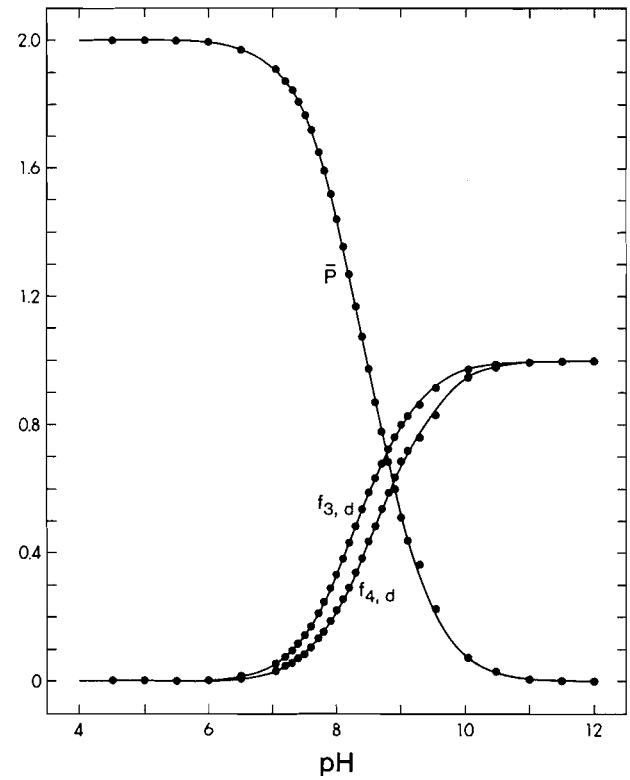

FIG. 6. The pH dependence of the fractional titration of the penicillamine ($f_{3,d}$) and cysteine ($f_{4,d}$) ammonium groups of PSSC and the average number of ammonium groups per molecule ($\bar{p}$). The smooth curve through the $\bar{p}$ data is the theoretical curve predicted by the macroconstants in Table 1.

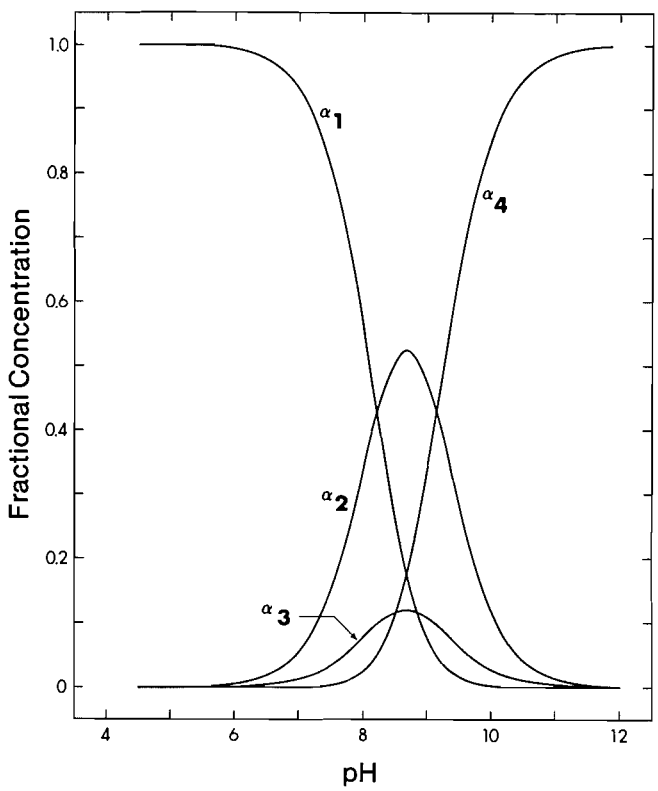

FIG. 7. pH dependence of the distribution of PSSG among its various ammonium protonated forms. α represents the fractional concentration of the species indicated by the subscript. The species are identified in Fig. 3.

for PSSP, pk_{1234} is 8.22 for PSSG, and pk_{123} is 8.24 for PSSC. Similarly, pk_{12} for Cys is 8.86, while pk_{123} is 8.14 for CSSC, pk_{1234} is 8.65 for CSSG, and pk_{123} is 8.24 for PSSC. In contrast, changes in the acidity of the ammonium group of GSH upon oxidation of the more distant thiol group are much less and show no apparent trend.

There are no values available for comparison with those reported in Table 1 for PSSG, CSSG, and PSSC. However, the values reported for PSSP, GSSG, GSH, and PSH agree well with literature values (16–20). The absence of literature values for the mixed disulfides may be due to the fact that methods generally used to measure acid dissociation constants require pure compounds. However, this is not a requirement for the nmr method since the ratio of protonated to deprotonated forms is obtained directly from chemical shift data. Thus, the nmr method is ideally suited to the characterization of the acid–base chemistry of mixed disulfides; the mixed disulfides can be formed from the appropriate thiols and disulfides by thiol/disulfide exchange, and their acid–base chemistry characterized using chemical shift data obtained from nmr measurements on the resulting mixture. Another advantage of the nmr method is that it provides information about both the macroscopic and the microscopic acid–base chemistry.

Acknowledgements

This research was supported by the Natural Sciences and Engineering Research Council of Canada, the Alberta Heritage Foundation for Medical Research, and the University of Alberta. Financial support of Y.T. by an AHFMR Studentship and of A.P.A. by an AHFMR Fellowship is gratefully acknowledged.

1. P. C. JOCELYN. Biochemistry of the SH group. Academic Press, London. 1972. p. 121.
2. Y. M. TORCHINSKY. Sulfur in proteins. Pergamon Press, New York. 1981. p. 57.
3. J. A. SCHNEIDER, K. H. BRADLEY, and J. E. SEEGMILLER. J. Lab. Clin. Med. **71**, 122 (1968).
4. G. W. FRIMPTER. J. Biol. Chem. **236**, PC51 (1961).
5. G. W. FRIMPTER. J. Clin. Invest. **42**, 1956 (1963).
6. L. ELDJARN and L. HAMBRAEUS. Scand. J. Clin. Lab. Invest. **16**, 153 (1964).
7. W. J. P. NEISH and A. RYLETT. Biochem. Pharmacol. **12**, 913 (1963).
8. D. H. CALAM and S. G. WALEY. Biochem. J. **93**, 526 (1964).
9. R. N. ONDARZA. Biochim. Biophys. Acta, **107**, 112 (1965).
10. S. H. CHANG and D. R. WILKEN. J. Biol. Chem. **240**, 3136 (1965).
11. D. L. RABENSTEIN and T. L. SAYER. Anal. Chem. **48**, 1141 (1976).
12. J. P. JESSON, P. MEAKIN, and G. KNEISSEL. J. Am. Chem. Soc. **95**, 618 (1973).
13. I. M. KOLTHOFF, W. STRICKS, and R. C. KAPOOR. J. Am. Chem. Soc. **77**, 4733 (1955).
14. J. L. DYE and V. A. NICELY. J. Chem. Educ. **48**, 443 (1971).
15. D. L. RABENSTEIN and T. L. SAYER. J. Magn. Reson. **24**, 27 (1976).
16. D. D. PERRIN and R. P. AGARWAL. *In* Metal ions in biological systems. Vol. 2. *Edited by* H. Sigel. Marcel Dekker, Inc., New York. 1973. p. 167.
17. D. L. RABENSTEIN, R. GUEVREMONT, and C. A. EVANS. *In* Metal Ions in Biological Systems. Vol. 9. *Edited by* H. Sigel. Marcel Dekker, Inc., New York. 1979. p. 103.
18. D. D. PERRIN and I. G. SAYCE. J. Chem. Soc. (A), 53 (1968).

19. D. L. RABENSTEIN. J. Am. Chem. Soc. **95**, 2797 (1973).
20. R. B. MARTIN and J. T. EDSALL. Bull. Soc. Chim. Biol. **40**, 1763 (1958).
21. E. W. WILSON and R. B. MARTIN. Arch. Biochim. Biophys. **142**, 445 (1971).
22. E. COATES, C. G. MARSDEN, and B. RIGG. Trans. Faraday Soc. **65**, 3032 (1969).
23. J. P. CASEY and R. B. MARTIN. J. Am. Chem. Soc. **94**, 6141 (1972).
24. C. W. DAVIES. J. Chem. Soc. 2093 (1938).

Can. J. Chem. Downloaded from www.nrcresearchpress.com by 210.87.254.40 on 09/06/12
For personal use only.

Aromatic sulphonates and the hydrolysis of 2-(*p*-nitrophenoxy)tetrahydropyran

STELLA O'LEARY

Pulp and Paper Research Institute of Canada, 570 St. John's Boulevard, Pointe Claire, P.Q., Canada H9R 3J9

Received May 10, 1983[1]

STELLA O'LEARY. Can. J. Chem. **62**, 1320 (1984).

The rate of hydrolyis of 2-(*p*-nitrophenoxy)tetrahydropyran was measured in a variety of buffers in water at 30°C. At low ionic strength (μ = 0.05), 3,6-disulphonaphthoxyacetic acid catalysed the reaction. The second-order rate constant was 20 times faster than predicted from pK_a. At high ionic strength ($\mu \doteq 0.5$), plots of k_{obs} vs. total buffer concentration for both 3,6-disulphonaphthoxyacetic acid and 6,8-disulphonaphthyoxyacetic acid go through a maximum. Polyacrylic acid catalysed the reaction. The results are discussed in terms of aggregation and salt effects.

STELLA O'LEARY. Can. J. Chem. **62**, 1320 (1984).

Opérant à 30°C et dans une variété de tampons, on a mesuré les vitesses d'hydrolyse du (*p*-nitrophénoxy)-2 tétrahydropyranne. A des forces ioniques faibles (μ = 0,05), l'acide disulfo-3,6 naphtoxyacétique catalyse la réaction. La constante de vitesse du second ordre est 20 fois plus rapide que la vitesse prédite en se basant sur le pK_a. A des forces ioniques plus élevées (μ = 0,5), les courbes des k_{obs} vs. les concentrations totales de tampon passent par un maximum tant pour l'acide disulfo-3,6 naphtoxyacétique que pour l'acide disulfo-6,8 naphtoxyacétique. L'acide polyacrylique catalyse la réaction. On discute des résultats en termes d'aggrégats et d'effets de sel.

[Traduit par le journal]

Introduction

In addition to the hydronium ion catalysis normally observed in acetal hydrolysis the hydrolysis of 2-(*p*-nitrophenoxy)-tetrahydropyran (PNPTHP) in water and mixtures of dioxane–water is characterized by general acid catalysis and a pH-independent unimolecular decomposition above pH 4 (1, 2).

This observation has been attributed by Fife to two factors: (1) the decrease in basicity relative to other acetals, due to the electron-withdrawing nature of the *p*-nitrophenoxy group, and (2) a carbonium ion which is not especially destabilized compared with, for example, one derived from a sugar.

p-Nitrophenylglycosides are not subject to general acid catalysis because the electron-withdrawing effect of the hydroxyl groups on the glycone destabilizes the carbonium ion sufficiently to cause the C—O bond cleavage to remain rate determining (3–5).

In the catalysis of glycoside hydrolysis by enzymes, such as lysozyme, the cellulases, and amylases, it is probable – and for lysozyme, at least, there is strong supporting evidence – that the reaction is also general acid catalysed (6, 7). This poses the question of which features of enzyme structure are responsible.

In the case of lysozome, an important factor appears to be stabilization of the incipient carbonium ion by a neighbouring carboxylate anion (6–8). A second factor, strain in the substrate ground state caused by binding to the enzyme, may also be important (9, 10). In the amylase case, it is becoming obvious from X-ray crystallographic data that substrate strain must be a significant feature of catalysis (11). There are no data at present on the three-dimensional structure or active-site geometry of a cellulase.

The ultimate goal of the present work is to find a catalyst for the hydrolysis of cellulose which would be functional at higher pH than concentrated mineral acids. To this end, model studies of glycoside hydrolysis were initiated and this report contains the first results of this work. PNPTHP was chosen as a model substrate as it is closely related in structure to the phenyl glycosides but is much easier to hydrolyse because it lacks the electron-withdrawing hydroxyl groups on the pyran ring. Its hydrolysis is subject to general acid catalysis, as is enzyme-catalysed hydrolysis of glycosides.

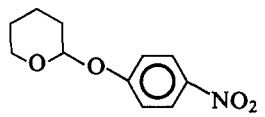

PNPTHP

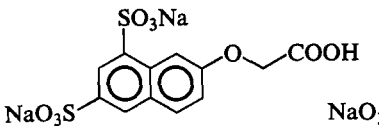

6,8-SNOA

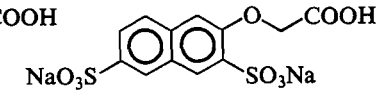

3,6-SNOA

The sulphonaphthoxyacetic acids (6,8-SNOA and 3,6-SNOA) were chosen as catalysts because they bear a structural resemblance to the direct dyes which bind to cellulose, they are water soluble, and they have a carboxylic acid group which will be protonated at a higher pH than the sulphonate anions, thus enabling the molecules to act as general acid catalysts. It was hoped that the sulphonate anions at positions 8 and 3 respectively might be suitably positioned to offer some electrostatic stabilization of the incipient carbonium ions. Examination of CPK space-filling models shows that the necessary contacts are possible.

Experimental

Substrate and catalysts

PNPTHP was prepared by the method of Fife and Jao (1). The oil obtained on evaporation of solvent gave pale yellow crystals after column chromatography.

6,8-Disulphonaphthoxyacetic acid (6,8-SNOA) and 3,6-disulphonaphthoxyacetic acid (3,6-SNOA) were prepared as follows: the appropriate naphthol disulphonic acid, di-salt (Eastman Kodak Co.), was recrystallized twice from hot water with charcoal treatment. One equivalent of purified naphthol and two equivalents of monochloroacetic acid were refluxed together in 10% NaOH for 1.25 h. The solution was allowed to cool, then acidified, and the product collected by filtration. This material was then recrystallized from hot water. In both cases the di-sodium salt was obtained (rather than the tri-acid form), because titration with NaOH took just one equivalent of base.

[1]Revision received December 21, 1983.

Can. J. Chem. Downloaded from www.nrcresearchpress.com by 210.87.254.40 on 09/06/12
For personal use only.

Can. J. Chem. Downloaded from www.nrcresearchpress.com by 210.87.254.40 on 09/06/12
For personal use only.

6,8-SNOA: white crystals; nmr (DMSO): 4.8 (s, 2H), 7.1–8.5 (complex, 5H). *Anal.* calc. for $C_{12}H_8O_9S_2Na_2 \cdot 4\ H_2O$: C 30.13, H 3.37, S 13.40; found: C 29.58, H 3.19, S 13.48.

3,6-SNOA: white solid; nmr (D_2O): 5.1 (s, 2H), 7.2–8.8 (complex, 5H). *Anal.* calc. for $C_{12}H_8O_9S_2Na_2 \cdot 1\ H_2O$: C 33.96, H 2.37, S 15.11; found: C 34.41, H 2.21, S 14.43.

Polyacrylic acid (PAA) (Aldrich Chemical Company) was obtained as a 65% solution in water, average mol wt. 2000, and used without further purification. Naphthoxyacetic acid (NOA) (Aldrich Chemical Company) was recrystallized twice from hot acetone to give sparkling white crystals. Phenoxyacetic acid (POA) (Anachemia Chemicals Ltd.) was used without further purification.

Kinetics

Rates of hydrolysis were measured spectrophotometrically by following the increase in absorbance due to *p*-nitrophenol release in a Gilford Model 250 spectrophotometer equipped with a Gilford 6050 chart recorder. The temperature was maintained at 30.0 ± 0.1°C by a Haake Model FE constant temperature circulator. The wavelengths used were 330 nm for acetic acid buffer, 340 nm for formic, chloroacetic, and polyacrylic acid buffers, and 355 nm for NOA, POA, 6,8-SNOA, and 3,6-SNOA buffers.

Buffers were prepared in distilled, deionized water. Where indicated, constant ionic strength was maintained by addition of NaCl. The NOA, 6,8-SNOA, and 3,6-SNOA buffers were sensitive to light and were stored, wrapped in foil, in the refrigerator.

Reaction was initiated by adding 10 μL of substrate ($3.2 \times 10^{-2}\ M$ in CH_3CN) to 3 mL of buffer solution, by means of a 10-μL Hamilton microsyringe. The cuvette was then capped and inverted several times. Infinity points were taken after ten half-lives. Reactions were plotted (log (O.D. − O.D.$_\infty$) vs. *t*) for three half-lives and good first-order kinetics were obtained. Most rate constants are the average of at least three runs, with a mean deviation of 5%. The pH of each solution was measured after reaction was complete. Deviations were never more than 0.03 from the original value.

pH

Buffers were prepared, pH measurements made, and potentiometric titrations carried out on a Radiometer Titrator TT2 or an Orion Research Model 601A/ digital Ionalyser pH metre, standardized with aqueous buffers (Fisher Scientific Company).

Results

Common buffers

The rate of hydrolysis of PNPTHP in water at 30°C, μ = 0.5 was measured in acetic, formic, chloroacetic, polyacrylic, NOA, 6,8-SNOA, and 3,6-SNOA buffers. Acetic, formic, and chloroacetic acids acted as general acid catalysts, i.e. the rate increased linearly with total buffer concentration and the slope of the line was inversely dependent on pH (Fig. 1). The second-order rate constants are given in Table 1 and are essentially the same as those observed by Armas *et al.* (13). A Bronsted plot of these data is linear with a slope of −0.43. Some experiments at low salt (μ = 0.05) were also done with acetic and formic acids at pH 3.7 and 2.8 respectively. The formic acid results are identical to those obtained at μ = 0.5. The rate constants for acetic acid at μ = 0.05 are slightly faster.

Polyacrylic acid (PAA)

The polyacrylic acid had an average chain length of 28. An average pK_a was estimated from potentiometric titration to be 5.8. A plot of k_{obs} vs. total buffer concentration at pH 4.7 shows a clear departure from second-order kinetics with a plateau reached at 0.5 *M* buffer (Fig. 2).

Sulphonaphthoxyacetic acid (SNOA)

The pK_a of both sulphonaphthoxyacetic acids was determined by potentiometric titration to be 3.4. Plots of k_{obs} vs. total buffer concentration are also non-linear for these compounds at high ionic strength but here the rate goes through a maximum (Fig. 3). The rates were measured at two different values of pH. The rates of hydrolysis were greater at low pH and the maxima were more pronounced. The rate of hydrolysis was also measured in SNOA buffers ($1 \times 10^{-3}\ M$) in 50% (v/v) dioxane–water at 50°C, μ = 0.5. The rate was much slower than in water, but essentially the same for both compounds ($5.0 \times 10^{-5}\ s^{-1}$).

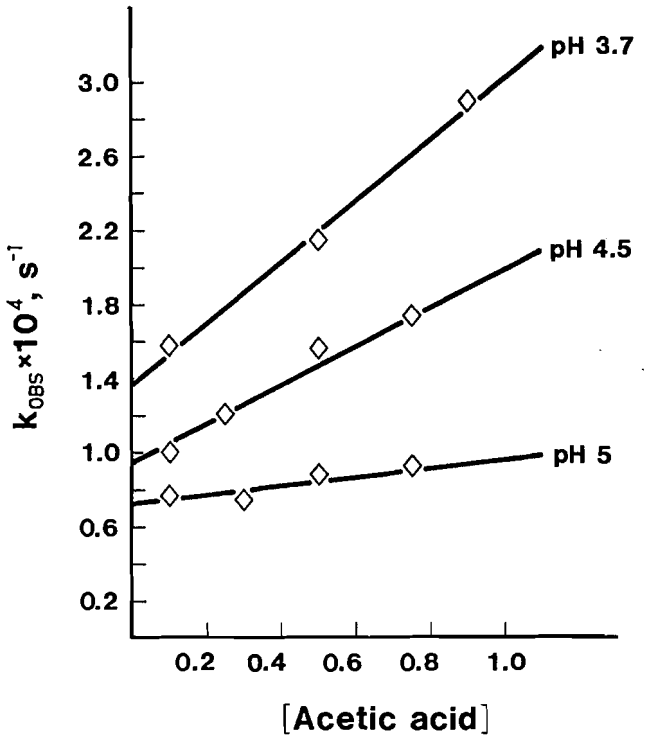

FIG. 1. $k_{obs} \times 10^4\ s^{-1}$ vs. total acetic acid concentration (*M*) at various pH values. *T* = 30 ± 0.1°C, μ = 0.5, [PNPTHP] = $1.0 \times 10^{-4}\ M$.

TABLE 1. Second-order rate constants for general acid catalysis of 2-PNPTHP hydrolysis at 30°C in water, μ = 0.5

Acid	$k_2 \times 10^4$ (L mol^{-1} s^{-1})	pK_a
Acetic	2.0	4.75
Formic	3.5	3.75
Chloroacetic	15.3	2.85

To determine the effect of ionic strength on this reaction, 3,6-SNOA-catalysed hydrolysis was carried out at pH 2.8, both in the absence of added salt and at μ = 0.05 and at pH 3.1, μ = 0.05. Under these low-salt conditions, the rate increased linearly with buffer concentration: the slopes were 2.01×10^{-2} and 1.58×10^{-2} L mol^{-1} s^{-1} respectively (Fig. 4) at pH 2.8, and 1.06×10^{-2} L mol^{-1} s^{-1} at pH 3.1.

Naphthoxyacetic acid (NOA)

Hydrolysis rates with naphthoxyacetic acid were measured in 10% EtOH–water owing to the sparing solubility of this compound in water (Fig. 3). The pK_a in this solvent was determined by potentiometric titration to be 3.7.

Phenoxyacetic acid (POA)

The rate of hydrolysis of PNPTHP at 30°C, μ = 0.05 in

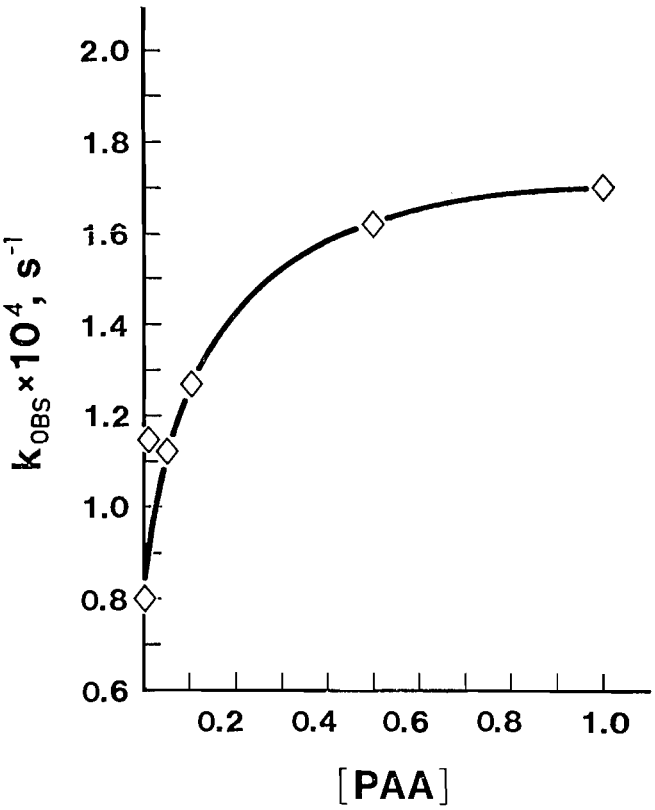

FIG. 2. $k_{obs} \times 10^4\ s^{-1}$ vs. total polyacrylic acid concentration (M). pH = 4.7, T = 30 ± 0.1°C, μ = 0.5, [PNPTHP] = 1×10^{-4} M.

aqueous phenoxyacetic acid was determined at four different values of pH around the pK_a, which is 3.1 for this compound. The second-order rate constant was determined to be 2.33×10^{-3} L mol^{-1} s^{-1} (Fig. 6).

Background hydrolysis

The rate of hydrolysis in water at 30°C, μ = 0.5 was obtained over the pH range 2.8 to 5 by extrapolation to zero buffer concentration of plots of observed rate constants versus buffer concentration (Fig. 5). In accordance with the observations at 50°C of Fife and Brod (2), the rate is strongly dependent on pH below pH 4 and becomes less so in less acidic solutions. The background rates at μ = 0.05 were determined in a similar manner. The values for μ = 0.5 are all slightly higher than for μ = 0.05.

Discussion

It is obvious from the results in Figs. 3 and 4 that ionic strength is important in the hydrolysis of PNPTHP in aromatic sulphonaphthoxyacetic acid buffers. It appears that the aromatic sulphonates are aggregating in the high salt solutions, where the presence of large amounts of sodium ions can stabilize the close proximity of sulphonate anions. At low ionic strength, the tendency of large aromatic compounds to aggregate in aqueous solution is offset by the negative electrostatic interactions of the anions. It is of course well known that high salt concentrations generally lower the rate of micellar-catalysed reactions and also the critical micelle concentration of surfactants (12).

The hydrolysis of PNPTHP in micellar solutions has been studied previously in the pH range 1–3 with no added salt (13). The second-order rate constant for reaction with H^+ was measured and found to be very sensitive to surfactant structure (all the surfactants were long-chain alkyl sulphonates). The second-order rate constants went through a maximum.

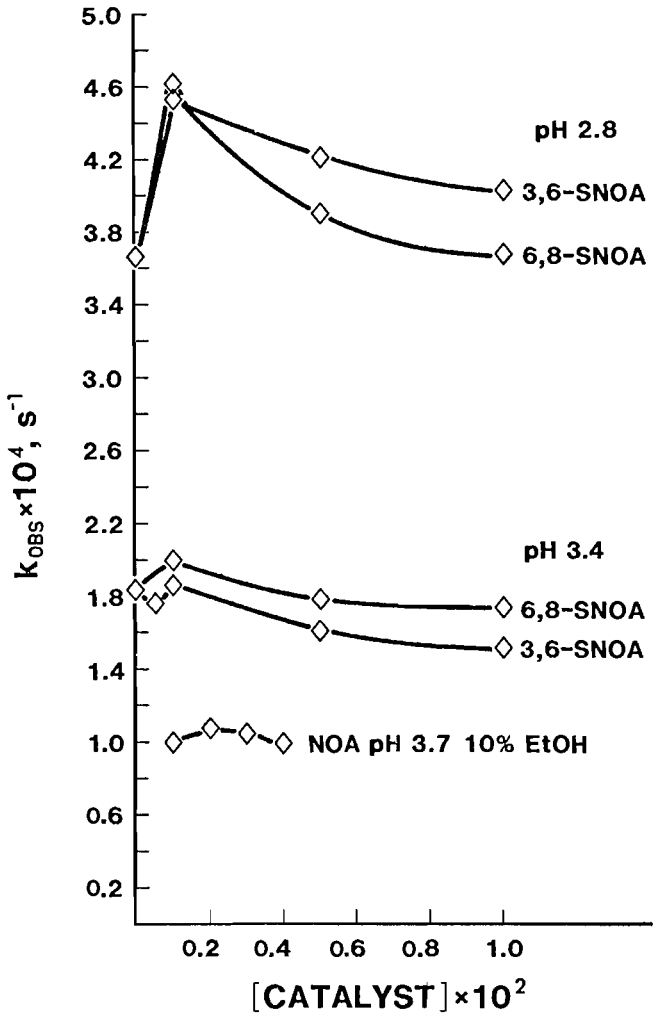

FIG. 3. $k_{obs} \times 10^4\ s^{-1}$ vs. total catalyst concentration $\times 10^2$ (M) for 3,6-SNOA, 6,8-SNOA, and NOA. T = 30 ± 0.1°C, μ = 0.5, [PNPTHP] = 1×10^{-4} M.

The rates of hydrolysis of *p*-nitrobenzaldehyde dialkyl acetals in long-chain sulphonic acid micelles with no added salt have also been measured (14). In this case the second-order rate constants reach a plateau once all the substrate has been bound to the micelle. In both these cases reaction is catalysed in the presence of anionic micelles.

In the case of the aromatic sulphonate 3,6-SNOA, the reaction is second order at μ = 0.05 and also with no added salt. The second-order rate constants are 1.58×10^{-2} and 2.01×10^{-2} L mol^{-1} s^{-1} respectively. This means that the 3,6-SNOA-catalysed reaction is 23 times faster than predicted by its pK_a (8.33×10^{-4} L mol^{-1} s^{-1}) (Fig. 6). There are two factors which are probably contributing to this enhanced catalytic effect: (1) stabilization of the incipient carbonium ion by the sulphonate anion at position 3 of the naphthyl ring, and (2) hydrophobic binding between catalyst and substrate. Examination of CPK space-filling models shows possible contacts between the naphthyl ring of the catalyst and either the pyran or phenyl rings of the substrate, while maintaining good contact between the sulphonate anion and the incipient carbonium ion (Fig. 7). Estimating the relative magnitude of the two effects is

Can. J. Chem. Downloaded from www.nrcresearchpress.com by 210.87.254.40 on 09/06/12
For personal use only.

Can. J. Chem. Downloaded from www.nrcresearchpress.com by 210.87.254.40 on 09/06/12
For personal use only.

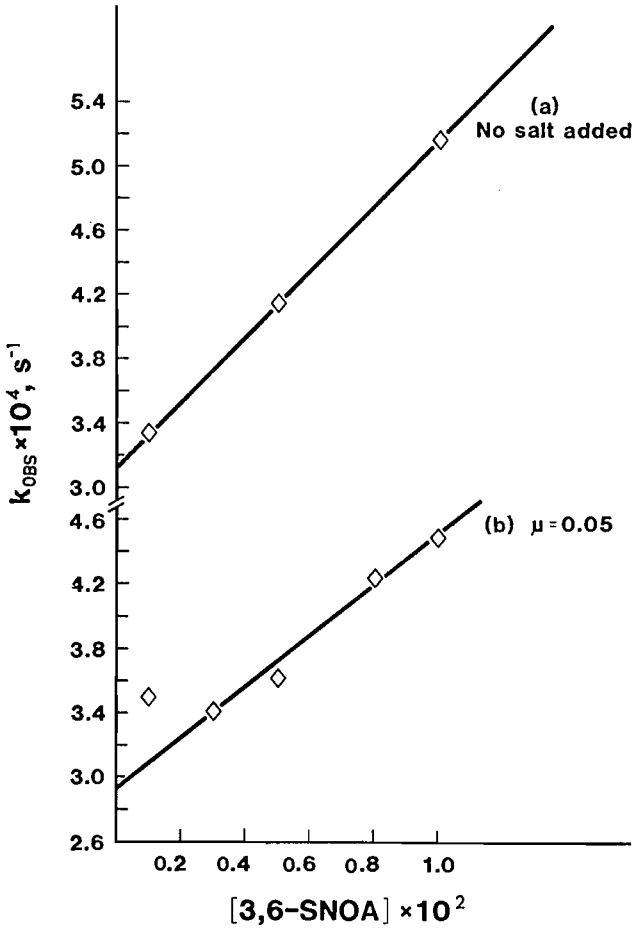

FIG. 4. $k_{obs} \times 10^4$ s^{-1} vs. total 3,6-SNOA concentration $\times 10^2$ (M). pH = 2.8, T = 30.0 ± 0.1°C, [PNPTHP] = 1×10^{-4} M. (a) No added salt, (b) μ = 0.05.

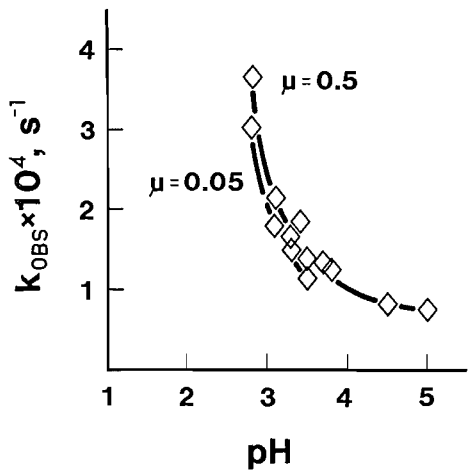

FIG. 5. $k_{obs} \times 10^4$ s^{-1} vs. pH for background hydrolysis of PNPTHP (1×10^{-4} M). T = 30 ± 0.1°C, μ = 0.5 and 0.05.

rather tricky: hydrophobic effects alone might be responsible for a rate enhancement of about ten-fold (15) while a 1:1 electrostatic effect could give a fifteen-fold enhancement (16). The results reported in the present work are of the same order of magnitude. Moreover, they apparently represent true second-order kinetics as opposed to micellar reaction.

To factor out the relative contributions of hydrophobic and

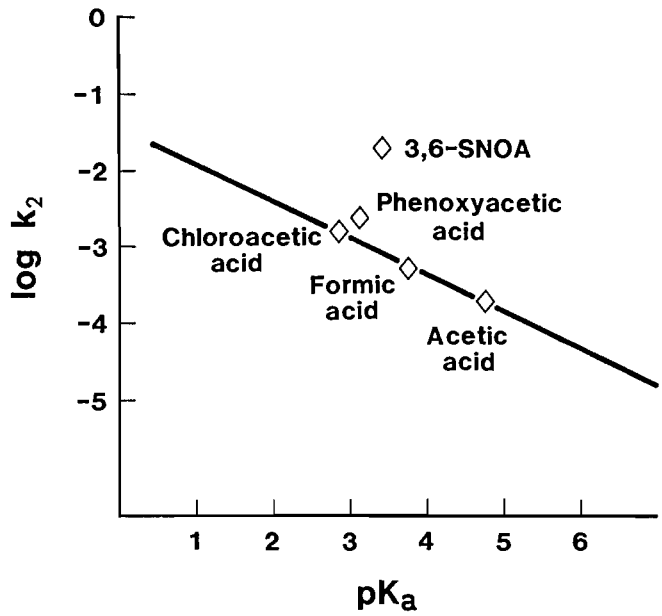

FIG. 6. Bronsted plot (log k_2 vs. pK_a) for chloracetic, formic, acetic, and phenoxyacetic acids and 3,6-SNOA.

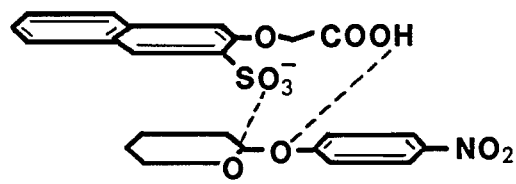

FIG. 7. Possible hydrophobic contact between naphthyl ring of catalyst and pyran ring of substrate. Dashed lines indicate possible contact between sulphonate anion and incipient oxocarbonium ion, and between carboxylic acid group and oxygen atom of leaving group.

electrostatic effects, suitable control experiments must be done. It is not possible to compare the sulphonaphthoxyacetic acids directly with naphthoxyacetic acid over the same range of concentration because of the very sparing solubility of the latter compound in water or in 10% ethanol water (4×10^{-3} M seems to be the upper limit on solubility in 10% ethanol–water.) A truer comparison would probably be with 6-sulpho-2-naphthoxyacetic acid or phenoxyacetic acid. Both compounds would be more water soluble and examination of CPK models shows that the carboxylic and sulphonate groups of the former cannot interact simultaneously with PNPTHP.

The rates of hydrolysis in phenoxyacetic acid buffers were measured at μ = 0.05, T = 30°C, at several different total buffer concentrations and pH values. The true second-order rate constant was determined to be 2.33×10^{-3} L mol^{-1} s^{-1}. This is twice the value expected from the Bronsted plot for a simple carboxylic acid of pK_a 3.1. The enhancement is probably small enough to be attributable to experimental error but is also consistent with the sort of enhancement which might be expected for hydrophobic binding involving only one phenyl group (16).

If the twofold enhancement is really due to hydrophobic binding, then there remains a 10-fold enhancement to be explained by electrostatic stabilization of the incipient carbonium ion by the catalyst sulphonate anion. This is of the same order of magnitude as that observed by Guthrie and Ueda in an ester hydrolysis where the negatively-charged ester was electro-

statically bound to the positively-charged catalyst (16).

If the twofold rate enhancement observed for phenoxyacetic acid is indeed due to experimental error, then the full 23-fold enhancement should be attributable to electrostatic stabilization. It seems fair to say that a ten-to-twenty-fold rate enhancement due to intermolecular electrostatic stabilization has been observed in this system.

This compares not unfavourably with Fife's observation of a 100-fold enhancement due to electrostatic stabilization in acetal hydrolysis in an intramolecular system (8), the phthalaldehydic acid system.

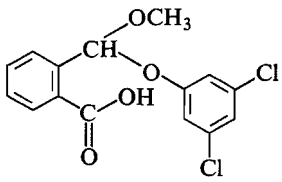

Phthalaldehydic acid methyl 3,5-dichlorophenyl acetal

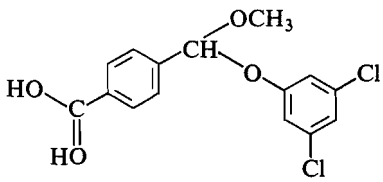

Terephthalaldehydic acid methyl 3,5-dichlorophenyl acetal

Fife has observed (8) that anion stabilization of a developing carbonium ion should be capable of generating significant rate enhancements, but only in reactions where there is a relatively large amount of C—O bond breaking in the transition state. This is the case for the phthalaldehydic acid acetal (8) and is also the case for PNPTHP (1). The present observation of electrostatic stabilization of acetal hydrolysis in PNPTHP seems to bear out the theory. It is also the first example of electrostatic stabilization of acetal hydrolysis where the reaction has been shown to be truly second order.

The basis for comparison used here is the Bronsted plot, which actually represents hydrolysis at $\mu = 0.5$, while the 3,6-SNOA values were measured at $\mu = 0.05$. Some experiments were done with formic and acetic acids at $\mu = 0.05$ and the results are very similar to the $\mu = 0.5$ values. If there is a strong effect of ionic strength upon the simple carboxylic acid-catalysed reaction, one would expect it to be in the direction of increasing reaction rates with increasing salt concentration. Therefore, the value of 8.33×10^{-4} L mol^{-1} s^{-1}, for a simple carboxylic acid of pK_a 3.4, probably represents an upper limit. The background hydrolysis rates at $\mu = 0.05$ are all slightly lower than the corresponding rates at $\mu = 0.5$ (Fig. 5).

The polyacrylic acid has a catalytic effect on the rate of hydrolysis, which reaches a plateau at 0.5 *M*. This probably indicates the formation of micelles or aggregates. The pH was such that the polyacrylic acid was essentially protonated and the concentrations at the upper end of the range were very high (1 *M*).

Acknowledgements

The financial support of the National Research Council of Canada in the form of an Industrial Post-doctoral Fellowship to the author under the Industrial Research Assistance Program, is gratefully acknowledged. The author also wishes to thank Professor J. Peter Guthrie, of the University of Western Ontario, for critical discussion of the manuscript.

1. T. H. FIFE and L. K. JAO. J. Am. Chem. Soc. **90**, 4081 (1969).
2. T. H. FIFE and L. H. BROD. J. Am. Chem. Soc. **92**, 1681 (1970).
3. D. PISZKIEWICZ and T. C. BRUICE. J. Am. Chem. Soc. **89**, 6237 (1967).
4. D. PISZKIEWICZ and T. C. BRUICE. J. Am. Chem. Soc. **90**, 2156 (1968).
5. D. PISZKIEWICZ and T. C. BRUICE. J. Am. Chem. Soc. **90**, 5844 (1968).
6. D. C. PHILLIPS. Sci. Am. **215**, 78 (1969).
7. J. A. RUPLEY and V. GATES. Proc. Natl. Acad. Sci. U.S.A. **57**, 496 (1967).
8. T. H. FIFE and T. G. PRZYSTAS. J. Am. Chem. Soc. **99**, 6693 (1977).
9. A. WARSHEL and M. LEVITT. J. Mol. Biol. **103**, 227 (1976).
10. J. A. KELLY, A. R. SIELECKI, B. D. SYKES, M. N. J. JAMES, and D. C. PHILLIPS. Nature, **282**, 875 (1979).
11. F. PAYAN, R. HASER, M. PIERROT, M. FREY, J. P. ASTIER, B. ABADIE, E. DUEE, and G. BUISSON. Acta Crystallogr. Sect. B, **36**, 416 (1980).
12. E. H. CORDES and R. B. DUNLAP. Acc. Chem. Res. Sect. B, **2**, 329 (1969).
13. A. ARMAS, H. CLEMENTE, J. CORONEL, F. CREAZZOLA, A. CUENCA, J. FRANCIS, A. MALPICA, D. QUINTERO, R. ROMERO, J. SALAZAR, N. SANCHEZ, R. VON BERGEN, J. BAUMRUCKER, M. CALZADILLA, and E. H. CORDES. J. Org. Chem. **37**, 875 (1972).
14. C. A. BUNTON, L. S. ROMSTED, and G. SAVELLI. J. Am. Chem. Soc. **101**, 1253 (1979).
15. J. P. GUTHRIE and S. O'LEARY. Can. J. Chem. **53**, 2150 (1975).
16. J. P. GUTHRIE and Y. UEDA. Can. J. Chem. **54**, 2745 (1976).

Can. J. Chem. Downloaded from www.nrcresearchpress.com by 210.87.254.40 on 09/06/12
For personal use only.

Radical addition, decomposition, and isomerization reactions in the pyrolysis of ethane and ethylene

ALLAN L. MACKENZIE,[1] PHILIP D. PACEY,[2] AND JAYANTHA H. WIMALASENA[3]
Department of Chemistry, Dalhousie University, Halifax, N.S., Canada B3H 4J3

ALLAN L. MACKENZIE, PHILIP D. PACEY, and JAYANTHA H. WIMALASENA. Can. J. Chem. **62**, 1325 (1984).

Pure C_2H_6, pure C_2H_4, and a mixture of these have been pyrolyzed at 892 to 905 K and 23 to 250 Torr in a flow reactor system. Rates of formation of CH_4, C_3H_6, and 1-C_4H_8 were consistent with a mechanism involving the following radical addition, decomposition, and isomerization reactions:

[A] $C_2H_5 + C_2H_4 \rightleftharpoons 1\text{-}C_4H_9 \rightarrow 1\text{-}C_4H_8 + H$

[B] $C_2H_5 + C_2H_4 \rightleftharpoons 1\text{-}C_4H_9 \rightarrow 2\text{-}C_4H_9 \rightarrow C_3H_6 + CH_3$

[C] $CH_3 + C_2H_4 \rightleftharpoons 1\text{-}C_3H_7 \rightarrow C_3H_6 + H$

In pure C_2H_6 pyrolysis, some CH_4 and C_3H_6 also appeared to be formed by the decomposition of the product, n-C_4H_{10}. It was found that $k_A = 5.2\ (\pm 0.6) \times 10^4$ L mol^{-1} s^{-1} at 902 K and $k_B = 2.3\ (\pm 0.2) \times 10^4$ L mol^{-1} s^{-1} at 898 K. Arrhenius parameters for k_A were calculated from data in the literature. Process [C] was measured relative to the abstraction.

[15] $CH_3 + C_2H_4 \rightarrow CH_4 + C_2H_3$

It was found that $k_C/k_{15} = 1.7\ (\pm 0.7)$ at 896 K.

ALLAN L. MACKENZIE, PHILIP D. PACEY et JAYANTHA H. WIMALASENA. Can. J. Chem. **62**, 1325 (1984).

Utilisant un appareil à écoulement et opérant à des températures allant de 892 à 905 K et à des pressions allant de 23 à 250 Torr, on a effectué la pyrolyse du C_2H_6 et du C_2H_4 à l'état pur ainsi que d'un mélange de ces deux composés. Les vitesses de formation du CH_4, du C_3H_6 et du C_4H_8 sont en accord avec un mécanisme qui implique une addition radicalaire et des réactions de décomposition et d'isomérisation

[A] $C_2H_5 + C_2H_4 \rightleftharpoons 1\text{-}C_4H_9 \rightarrow 1\text{-}C_4H_8 + H$

[B] $C_2H_5 + C_2H_4 \rightleftharpoons 1\text{-}C_4H_9 \rightarrow 2\text{-}C_4H_9 \rightarrow C_3H_6 + CH_3$

[C] $CH_3 + C_2H_4 \rightleftharpoons 1\text{-}C_3H_7 \rightarrow C_3H_6 + H$

Lors de la pyrolyse du C_2H_6 à l'état pur, il semble aussi se former du CH_4 et du C_3H_6 par décomposition du produit, le n-C_4H_{10}. On a trouvé que $k_A = 5{,}2\ (\pm 0{,}6) \times 10^4$ L mol^{-1} s^{-1} à 902 K et $k_B = 2{,}3\ (\pm 0{,}2) \times 10^4$ L mol^{-1} s^{-1} à 898 K. On a calculé les paramètres d'Arrhénius pour le k_A à partir de données trouvés dans la littérature. On a mesuré la vitesse de la réaction C par rapport à celle de l'abstraction

[15] $CH_3 + C_2H_4 \rightarrow CH_4 + C_2H_3$

On a trouvé que $k_c/k_{15} = 1{,}7\ (\pm 0{,}7)$ à 896 K.

[Traduit par le journal]

Introduction

Most laboratory studies of alkane pyrolysis have focussed on the early, primary reactions. In industrial pyrolysis, in contrast, conversions are large, and reactions of the product olefins become important (1, 2). The subject of this article is the addition of methyl and ethyl radicals to ethylene, and the subsequent decomposition and isomerization reactions of the adduct radicals. Conversions have been kept small to avoid complications, but the results should be valid at greater conversions.

The major primary reactions in the pyrolysis of ethane are as follows (3–5):

[1] $C_2H_6 \rightarrow 2CH_3$

[2] $CH_3 + C_2H_6 \rightarrow CH_4 + C_2H_5$

[3] $C_2H_5 \rightarrow C_2H_4 + H$

[4] $H + C_2H_6 \rightarrow H_2 + C_2H_5$

[5a] $2C_2H_5 \rightarrow C_4H_{10}$

[5b] $2C_2H_5 \rightarrow C_2H_4 + C_2H_6$

Lin and Back (4) showed that the ethylene produced may participate in the following sequence:

[6,−6] $C_2H_5 + C_2H_4 \rightleftharpoons 1\text{-}C_4H_9$

[7] $1\text{-}C_4H_9 \rightarrow 1\text{-}C_4H_8 + H$

These may be considered as a combined process:

[A] $C_2H_5 + C_2H_4 \rightarrow 1\text{-}C_4H_8 + H$

The rate of reaction [3] is much greater than that of reaction [5b]. Making the steady-state assumption, the concentrations of products as a function of time may be obtained as Taylor series. The leading terms in some of these are

$$[C_2H_4] = k_3[C_2H_5]_0 t + \ldots$$

$$[C_4H_{10}] = k_{5a}[C_2H_5]_0^2 t + \ldots$$

$$[1\text{-}C_4H_8] = (1/2)\, k_A k_3 [C_2H_5]_0^2 t^2 + \ldots$$

Hence the subscript 0 indicates a radical concentration after the steady state is established, but before secondary reactions sig-

[1]Present address: Diagnostic Chemicals Ltd., Charlottetown, P.E.I., Canada.

[2]To whom all correspondence should be addressed.

[3]Present address: Department of Chemistry, University of Sri Jayewardenepura, Nugegoda, Sri Lanka.

Can. J. Chem. Downloaded from www.nrcresearchpress.com by 210.87.254.6 on 09/06/12
For personal use only.

nificantly affect this concentration. These three equations may be combined to give

$$[8] \qquad k_A k_{5a}^{-1/2} = 2[1\text{-}C_4H_8][C_2H_4]^{-1}[C_4H_{10}]^{-1/2}t^{-1/2} + \ldots$$

In the copyrolysis of ethane and ethylene, the leading term for $[C_2H_4]$ becomes the initial concentration and a similar procedure leads to the following equation:

$$[9] \qquad k_A k_{5a}^{-1/2} = [1\text{-}C_4H_8][C_2H_4]^{-1}[C_4H_{10}]^{-1/2}t^{-1/2} + \ldots$$

The copyrolysis may also be used to study the process

$$[B] \qquad C_2H_5 + C_2H_4 \rightarrow C_3H_6 + CH_3$$

This is believed (4, 5) to consist of reactions [6] and [−6], followed by

$$[10] \qquad 1\text{-}C_4H_9 \rightarrow 2\text{-}C_4H_9$$

$$[11] \qquad 2\text{-}C_4H_9 \rightarrow C_3H_6 + CH_3$$

Steady-state treatment leads to

$$[12] \qquad k_B k_{5a}^{-1/2} = [C_3H_6][C_2H_4]^{-1}[C_4H_{10}]^{-1/2}t^{-1/2} + \ldots$$

In the pyrolysis of pure ethylene, it would be difficult to use reaction [5*a*] as a reference, as butane yields are very small (6−8). An alternative is

$$[12] \qquad C_2H_5 + C_2H_4 \rightarrow C_2H_6 + C_2H_3$$

which is the major source of ethane in this system. A similar procedure leads to

$$[14] \qquad k_A k_{13}^{-1} = [1\text{-}C_4H_8][C_2H_6]^{-1}$$

In ethylene pyrolysis, methyl radicals formed by process [B] may react as follows (5, 6):

$$[15] \qquad CH_3 + C_2H_4 \rightarrow CH_4 + C_2H_3$$

$$[16,-16] \qquad CH_3 + C_2H_4 \rightleftharpoons 1\text{-}C_3H_7$$

$$[17] \qquad 1\text{-}C_3H_7 \rightarrow C_3H_6 + H$$

The latter two reactions may be considered as the process:

$$[C] \qquad CH_3 + C_2H_4 \rightarrow C_3H_6 + H$$

The following relationships are predicted to apply:

$$[18] \qquad k_B k_{13}^{-1} = (1/2)([CH_4] + [C_3H_6])[C_2H_6]^{-1}$$

$$[19] \qquad k_B k_{15}(k_{15} + k_C)^{-1}k_{13}^{-1} = [CH_4][C_2H_6]^{-1}$$

The present article describes experimental tests of equations [8], [9], [12], [14], [18], and [19].

Experimental

The flow system and the purification of reagents have been described elsewhere (8, 9). A 1 m, 10% NaOH on alumina (100/120 mesh) column, operated at 296 K, was used for gas chromatographic analysis of CH_4, C_2H_6, and C_3H_6 from C_2H_4 pyrolysis. A 0.75 m silica gel (100/120 mesh, acid washed) column at 323 K was used for analysis of CH_4, C_2H_6, and C_4H_8 from C_2H_4 pyrolysis. The other analyses were performed with a 4.75 m, 10% squalane on Chromosorb P (NAW 100/120 mesh) column at 273 K.

Results

Experiments[4] have been performed at reactor temperatures from 892 to 905 K and with residence times from 0.3 to 51 s and conversions of 8% or less.

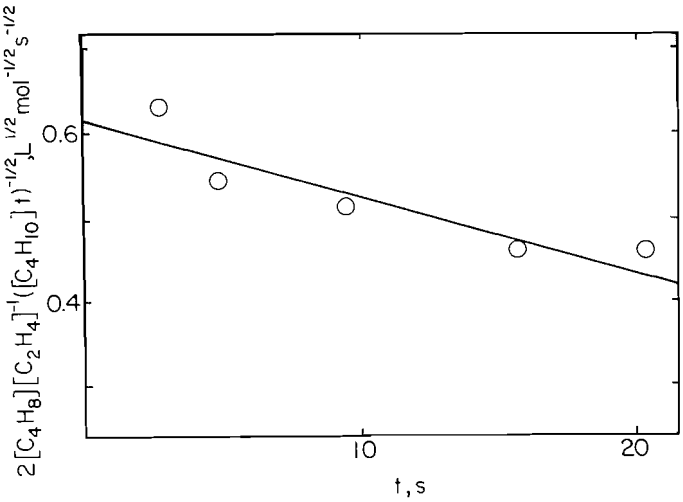

FIG. 1. The quotient of produet yields in eq. [8], as a function of reactor residence time for experiments at 200 Torr and 902 K in an 8 mm internal diameter reactor: ○, experimental points; —, least-squares straight line.

TABLE 1. Results from the pyrolysis of pure C_2H_6

P (Torr)	T (K)	$k_A \times 10^{-4}$ (L mol^{-1} s^{-1})
60	902	5.6
70	902	4.7
90	902	5.6
100	902	4.6
148	905	5.5
200	902	5.8
250	903	4.4
Average	902	5.2±0.6*
Order		−0.03±0.09

*Here and elsewhere, quoted uncertainties are standard deviations.

Pure ethane

Yields of C_2H_4, 1-C_4H_8, and *n*-C_4H_{10} have been measured in the pyrolysis of pure ethane and the quotient of yields appearing in eq. [8] has been calculated. Results of experiments at 902 K and 200 Torr are shown in Fig. 1. It can be seen that the quotient declines slightly with increasing residence time because of higher terms in eq. [8]. The value of $k_A k_{5a}^{-1/2}$ has been taken as the intercept. From $k_{5a} = 9 \times 10^9$ L mol^{-1} s^{-1}, determined in related experiments (9, 10), values of k_A have been calculated from intercepts at this and other pressures. The results are listed in Table 1.

Ethane−ethylene mixtures

Mixtures of 75 mol% C_2H_6 with 25% C_2H_4 have been pyrolyzed at two pressures. Yields of C_3H_6, 1-C_4H_8, and C_4H_{10} have been measured. The right-hand sides of eqs. [9] and [12] have been calculated and extrapolated to find the intercepts, $k_A k_{5a}^{-1/2}$ and $k_B k_{5a}^{-1/2}$, as in Fig. 1. The resulting values of k_A and k_B are listed in Table 2.

Pure ethylene

Pure C_2H_4 has been pyrolyzed. Various combinations of CH_4, C_2H_6, C_3H_6, and 1-C_4H_8 yields were measured with the different chromatographic columns. The quotients of product

[4]Tables of data are available, at a nominal charge, from the Depository of Unpublished Data, National Research Council of Canada, Ottawa, Ont., Canada K1A 0S2.

Can. J. Chem. Downloaded from www.nrcresearchpress.com by 210.87.254.6 on 09/06/12
For personal use only.

TABLE 2. Results of the pyrolysis of 75% C_2H_6 and 25% C_2H_4 at 902 K

P (Torr)	$k_A \times 10^{-4}$ (L mol^{-1} s^{-1})	$k_B \times 10^{-4}$ (L mol^{-1} s^{-1})
60	5.6	2.50
90	5.9	2.55
Average	5.8	2.53

TABLE 3. Results of the pyrolysis of pure C_2H_4

P (Torr)	T (K)	$k_A \times 10^4$ (L mol^{-1} s^{-1})	$k_B \times 10^{-4}$ (L mol^{-1} s^{-1})	$\frac{k_B k_{15}}{(k_{15} + k_C)k_{13}}$
23	894		2.20	0.10
35	895			0.07
35	900	4.5		0.10
42	895		2.21	0.14
47	892			0.13
53	899		2.14	0.08
58	896	4.7		0.10
61	892			0.08
73	897			0.11
78	893			0.07
130	898		2.23	0.14
Average	896	4.6	2.20±0.04	0.10±0.03
Order			0.01±0.02	0.10±0.18

yields in eqs. [14], [18], and [19] were found to be independent of reaction time, within experimental uncertainty. For this reason the quotients were not extrapolated to initial values; instead, simple averages were taken. The value of k_{13} was taken as 8×10^4 L mol^{-1} s^{-1}, from related experiments (8). Values of k_A, k_B, and the quotient in eq. [19] are listed in Table 3.

Discussion

The rate parameters in the tables are independent of pressure, within experimental uncertainty. The parameters are also independent of the feedstock, especially when the variations in temperature are taken into account. These facts confirm that the mechanisms assumed are reasonable and that the chosen literature values of k_{5a} and k_{13} (8–10) are consistent.

Process [A]

Lin and Back (4) have measured the rate of formation of C_4H_8 in C_2H_6 pyrolysis at 824 to 893 K. If eq. [8] is applied to their data, one finds $\log_{10} k_A$ (L mol^{-1} s^{-1}) = 8.1(±0.5) − 57 (±8) kJ mol^{-1}/2.3RT. At 900 K, this gives $k_A = 6.4 \times 10^4$ L mol^{-1} s^{-1}, in satisfactory agreement with the average of the present results, 5.2(±0.6) × 10^4 L mol^{-1} s^{-1}.

The ratio $[C_4H_8]/[C_2H_6]$ has been measured in C_2H_4 pyrolysis at much lower temperatures and was found to increase with pressure (6, 7). The following expressions may be calculated from the data at 773 K (6) and 787 K (7), respectively: $[C_4H_8]/[C_2H_6]$ = 0.75(±0.11) + 3.8(±0.4) × 10^{-3} Torr^{-1} P or 0.57 (±0.17) + 2.4(±0.9) × 10^{-3} Torr^{-1} P. The pressure-dependent term appears to be caused by an alternative source of C_4H_8, a source for which there is an extra C_2H_4 molecule in the critical complex. This source could involve the transfer of H from C_4H_9 to C_2H_4, as suggested in ref. 11, or the isomerization of 1-C_6H_{13} and subsequent decomposition of 3-C_6H_{13}, as suggested in ref. 6. These processes are expected to have lower activation energies than process [A] and would make a negligible contribution under the conditions of the present work. The pressure-independent terms above, 0.75 and 0.57, are similar to the value from the present work, 0.58, indicating that process [A] and reaction [13] must have activation energies which differ by 12 kJ mol^{-1} or less.

If reaction [6] is assumed to be at or near equilibrium, then $k_A = K_6 k_7$, where K_6 is the equilibrium constant. Calculating K_6 from thermochemistry (12), one finds $\log_{10} k_7$ (s^{-1}) = 13.4(±0.5) − 149(±8) kJ mol^{-1}/2.3RT and at 900 K, $k_7 = 5.4 \times 10^4$ s^{-1}. This is almost two orders of magnitude less than the predicted value of k_{-6} (12), confirming the validity of the equilibrium assumption just used. The Arrhenius parameters are similar to values of 13.8 and 159 kJ mol^{-1} recommended in ref. 12 for the related reaction, [17].

Process [B]

Arrhenius parameters for process [B] have previously been reported from studies of the pyrolysis of pure C_2H_6 (4, 5). These parameters lead to values of k_B at 900 K about twice as great as the values in Tables 2 and 3. In the present work, it has been confirmed that C_3H_6 yields from pure C_2H_6 pyrolysis are greater than predicted using the values of k_B in Tables 2 and 3. It has also been found that the chordal rate of formation of butane, $[C_4H_{10}]/t$, declines with time at about the same rate as $[C_3H_6]/t$ increases. Propylene is a major product of the chain decomposition of butane. This suggests that much of the C_3H_6 formed from pure C_2H_6 at these temperatures comes from the decomposition of C_4H_{10}, as well as from process [B]. Equations [12] and [18], used to calculate the values in Tables 2 and 3, depend on initial rates, and would not be affected by decomposition of C_4H_{10} formed.

At lower temperatures, the main source of C_3H_6 in pure and mixed C_2H_6 and C_2H_4 is believed (3, 4, 6, 13, 14) to be the process consisting of reactions [6], [−6], and

[20] 1-C_4H_9 + C_2H_4 → 1-C_6H_{13}

[21] 1-C_6H_{13} → 2-C_6H_{13}

[22] 2-C_6H_{13} → C_3H_6 + C_3H_7

This sequence will be referred to as process [D]. In the pyrolysis of ethylene at 773 and 803 K (6, 15), the ratio $([C_3H_6] + [CH_4])[C_2H_6]^{-1}$ was found to be proportional to $[C_2H_4]$ within experimental uncertainty. In Table 3, this ratio is found to be independent of $[C_2H_4]$ at 896 K. Such behavior suggests that process [D] is dominant at the lower temperatures and process [B] at the upper temperature. Lin and Back (4) estimated experimentally that the difference in activation energies for these processes is about 155 kJ mol^{-1}. This difference is sufficient to explain the observed change in the dependence on $[C_2H_4]$ between 773 and 896 K.

The average value of k_B from the tables is 2.3(±0.2) × 10^4 L mol^{-1} s^{-1}. The ratio of the rate of isomerization [10] to decomposition [7] of the 1-butyl radical is found to be 0.44(±0.06). This may be compared with a value of 0.2 (±0.1) for deuterated ethyl radicals (16).

Reaction [15] and process [C]

The values in the final column in Table 3 are more scattered than the others because of the difficulty in measuring the small CH_4 peaks. Taking k_B/k_{13} from the present work, one finds $k_C/k_{15} = 1.7$ (±0.7). This may be compared with the analogous ratio for the ethyl radical, $k_A/k_{13} = 0.58$ (± 0.01). For methyl, the addition–decomposition process is favoured over abstraction; the reverse is true for ethyl. The CH_3 addition reaction, [16], is about 14 kJ mol^{-1} more exothermic than the C_2H_5

Can. J. Chem. Downloaded from www.nrcresearchpress.com by 210.87.254.6 on 09/06/12
For personal use only.

addition, [6] (12). Since these reactions are believed to be in equilibrium and the subsequent decompositions should have similar rates, all of this exothermicity difference should be reflected in the rates. Reaction [15] is also more exothermic than reaction [13], but only part of this difference should be reflected in the activation energies of the forward reactions, part in the activation energies of the reverse processes.

Acknowledgements

The authors thank the Natural Sciences and Engineering Research Council of Canada for a grant in support of this research. J.H.W. thanks the Dorothy J. Killam Trust for the award of a scholarship.

1. J. N. BRADLEY. *In* Frontiers of free radical chemistry. *Edited by* W. A. Pryor. Academic Press, New York. 1980. p. 73.
2. J. H. PURNELL. *In* Frontiers of free radical chemistry. *Edited by* W. A. Pryor. Academic Press, New York. 1980. p. 93.
3. C. P. QUINN. Trans. Faraday Soc. **59**, 2543 (1963).
4. M. C. LIN and M. H. BACK. Can. J. Chem. **44**, 2369 (1966).
5. P. D. PACEY and J. H. PURNELL. Ind. Eng. Chem. Fundam. **11**, 233 (1972).
6. M. H. BACK and R. MARTIN. Int. J. Chem. Kinet. **11**, 774 (1979).
7. D. DELLISTE, C. RICHARD, and R. MARTIN. J. Chim. Phys. **78**, 655 (1981).
8. A. L. MACKENZIE, P. D. PACEY, and J. H. WIMALASENA. Can. J. Chem. **61**, 2033 (1983).
9. P. D. PACEY and J. H. WIMALASENA. Chem. Phys. Lett. **76**, 433 (1980).
10. P. D. PACEY and J. H. WIMALASENA. Can. J. Chem. **62**, 293 (1984).
11. M. L. BOYD, T. M. WU, and M. H. BACK. Can. J. Chem. **46**, 2415 (1968).
12. S. W. BENSON and H. E. O'NEAL. Kinetic data on gas phase unimolecular reactions. NSRDS-NBS 21. 1970.
13. M. P. HALSTEAD and C. P. QUINN. Trans. Faraday Soc. **64**, 103 (1968).
14. F. BILLAUD, F. BARONNET, and M. NICLAUSE. J. Chim. Phys. **77**, 357 (1980).
15. G. AYRANCI and M. H. BACK. Int. J. Chem. Kinet. **15**, 83 (1983).
16. A. S. GORDON, D. C. TARDY, and R. IRETON. J. Phys. Chem. **80**, 1400 (1976).

Can. J. Chem. Downloaded from www.nrcresearchpress.com by 210.87.254.6 on 09/06/12
For personal use only.

Theoretical study on dinitrogen complexes. Relation between facility of protonation and difference of electronic structures of d^6 and d^8 complexes

KENZI HORI[1] AND TOKIO YAMABE[2]

Department of Hydrocarbon Chemistry, Faculty of Engineering, Kyoto University, Sakyo-ku, Kyoto, Japan 606

Received June 30, 1983[3]

KENZI HORI and TOKIO YAMABE. Can. J. Chem. **62**, 1329 (1984).

Electronic structures of different *d* configurations have been studied in relation to the facility of protonation to dinitrogen ligand in Cr(0) and Co(I) complexes. The d^6 Cr complex has much better MO's for protonation than the d^8 Co complex. This difference largely affects the protonation energies and the reduction of nitrogen molecule in these complexes.

KENZI HORI et TOKIO YAMABE. Can. J. Chem. **62**, 1329 (1984).

On a étudié les structures électroniques de différentes configurations *d* en relation avec la facilité de protonation du ligand diazoté de complexes Cr(0) et Co(I). Le complexe d^6 du Cr possède des OM beaucoup plus propices à la protonation que celles du complexe d^8 du Co. Cette différence affecte grandement les énergies de protonation et la réduction de la molécule d'azote dans ces complexes.

[Traduit par le journal]

Can. J. Chem. Downloaded from www.nrcresearchpress.com by 210.87.254.42 on 09/06/12
For personal use only.

Introduction

Reduction of molecular dinitrogen by transition metal complexes has been a major goal since the first dinitrogen complex $Ru(NH_3)_5(N_2)^{2+}$, was synthesized (1). Subsequently, many dinitrogen complexes have been synthesized with a wide range of transition metals (2). For Mo and W complexes, the dinitrogen ligand can be reduced to NH_3(3). It is known that two Mo atoms are included at the active site of nitrogenase. Therefore, Mo with d^6 configuration is considered a key factor for the reduction of the dinitrogen ligand.

In order to reduce the dinitrogen ligand, it is necessary to form protonated species. Neither these compounds nor reduction products have ever been obtained from mononuclear complexes without Mo and W being the central metal. On the other hand, both protonated species and reduction products were obtained by treating d^6 Mo(0) and W(0) complexes in solution with HCl or H_2SO_4 as acids (4). The reduction of the dinitrogen ligand requires the existence of a d^6 metal. Therefore, one of the most important themes of dinitrogen complex chemistry is to answer the question, "Why Mo or W?".

Electrophilic attack of a proton on dinitrogen complexes involves both the highest occupied molecular orbital (HOMO) and a lone pair orbital of the N_2 ligand, (n_N), and they control the position and/or direction in forming the N—H bond. In d^6 complexes, these electronic features will be considerably different from those in d^8 or d^{10} systems. It is important to compare these properties in d^6 nitrogen complexes with those in different *d*-configurations.

In this paper, electronic structures of a d^6 Cr complex, $Cr(PH_3)_4(N_2)$ and a d^8 complex, $CoH(PH_3)_3(N_2)$, are examined and the relation between the *d*-configuration and the facility of protonation is investigated using *ab initio* MO calculations.

Method of calculations

The MO calculations were carried out with the GAUSSIAN-76 program (5). The basic sets of Cr and Co, given by Roos *et al.* (6), are contracted to [5*s*2*p*2*d*], and *p*-type orbitals of 1G are added to the basis set (7). The basis sets used for the central metals seem rather small, but even such small basis sets may be acceptable for describing such qualitative features as orbital patterns. For the ligands, STO-3G minimal basis sets internal to the program were adopted. The geometries of the Cr and Co complexes are shown as structures **1** and **2**. They have C_4 and C_{3v} symmetries, respectively (8).

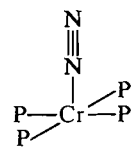

1

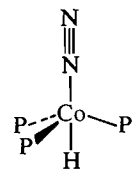

2

A five-coordinated Cr complex is adopted for the model of Mo or W analogues because of the simplicity of calculations. Since the orbital nature may be different between complexes with and without the sixth dinitrogen ligand, $Cr(PH_3)_4(N_2)_2$ with the optimized Cr—N and N—N bond lengths were also calculated and examined. The geometries of the M—N_2 moiety were optimized as functions of the M—N and N—N bond lengths by energy minimization (8); this is because they are unknown in the Cr complex. Moreover, natures of the moiety probably have more influence on protonation process since protons electrophilically attack on the dinitrogen ligand. On the other hand, other parts of dinitrogen complexes do not participate in the reduction of dinitrogen ligands. Therefore, Cr—P(2.53 Å), Co—P (2.18 Å), and Co—H (1.60 Å) lengths are fixed in all calculations.[4]

Results and discussion

Co—N and N—N bond lengths in $CoH(PPh_3)_3(N_2)$ observed by Davis *et al.* (9) are 1.829 and 1.123 Å, respectively. The optimized values of these lengths are 2.061 and 1.134 Å, respectively. While the calculated N—N length is very close to the observed value, the calculated Co—N length is slightly larger than the observed value. The small basis sets used here may cause a slight overestimation of the M—N bond length.

[1]Present address: Department of Chemistry, Faculty of Liberal Arts, Yamaguchi University, Yamaguchi, Japan 753.

[2]To whom all correspondence should be addressed.

[3]Revision received January 16, 1984.

[4]As the Cr—P bond length in dinitrogen complexes has never been reported, it is determined by referring M—P lengths in Mo or W analogues. The symmetries of complexes are taken from the crystallographic analysis of Co complex and W or Mo analogues.

Can. J. Chem. Downloaded from www.nrcresearchpress.com by 210.87.254.42 on 09/06/12
For personal use only.

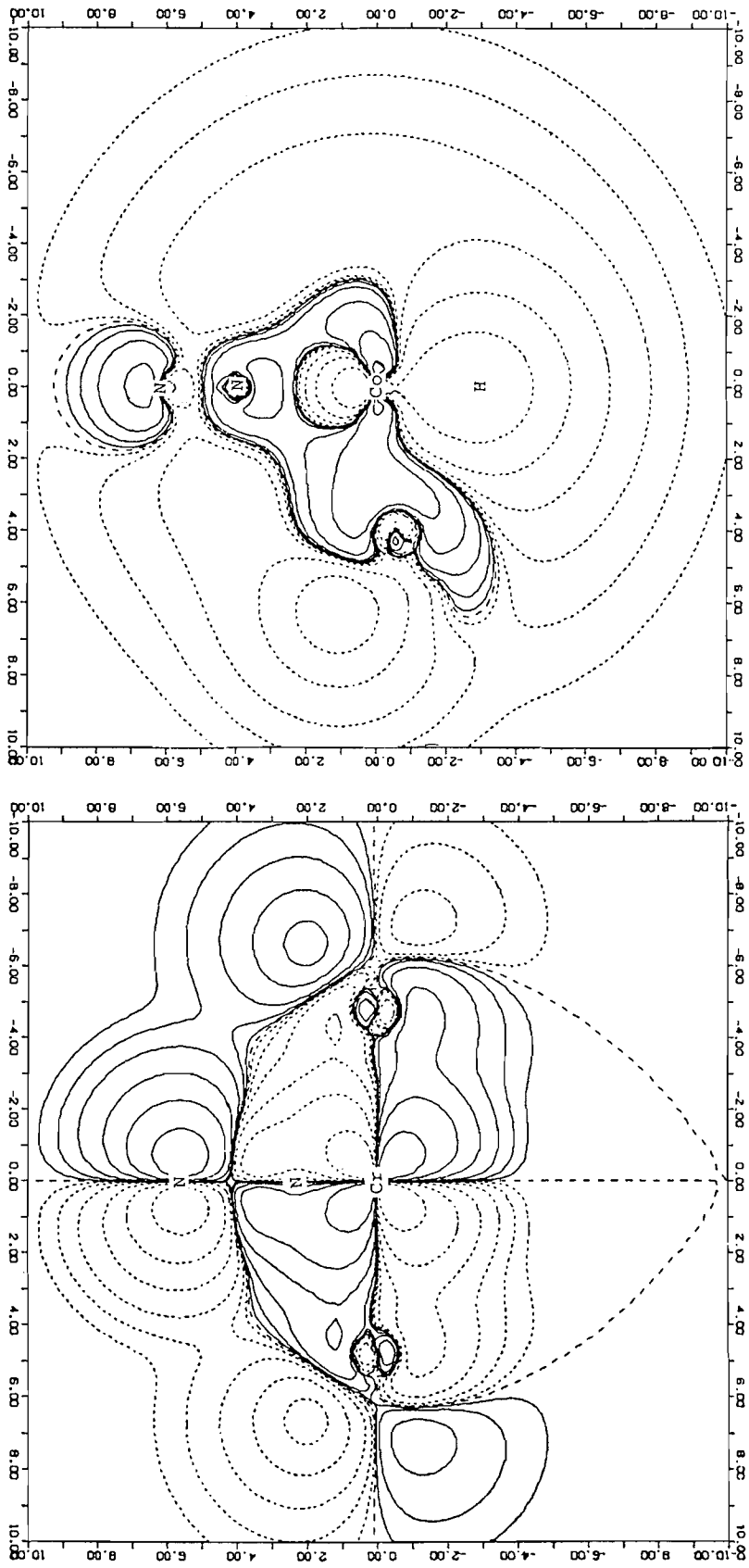

$Cr(PH_3)_4(N_2)$ (a)

$Co(PH_3)_3H(N_2)$ (b)

FIG. 1. Molecular orbitals of dinitrogen complexes: (*a*) and (*b*) are HOMO's of Cr and Co complexes, respectively; (*c*) and (*d*) are n_N's of them, respectively.

Can. J. Chem. Downloaded from www.nrcresearchpress.com by 210.87.254.42 on 09/06/12
For personal use only.

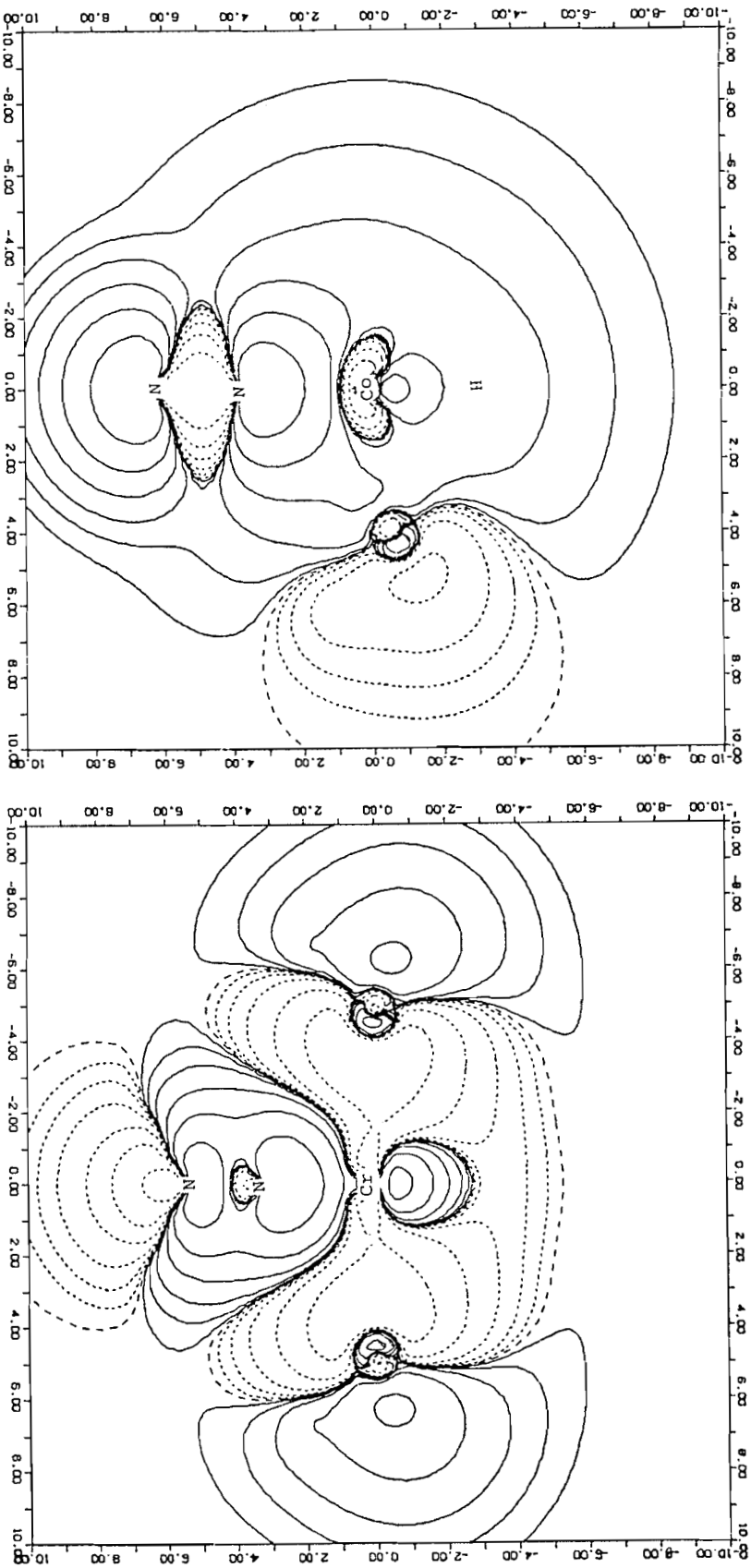

$Cr(PH_3)_4(N_2)$ (c) $Co(PH_3)_3H(N_2)$ (d)

FIG. 1. (*Concluded*)

Can. J. Chem. Downloaded from www.nrcresearchpress.com by 210.87.254.42 on 09/06/12
For personal use only.

Those in the Cr complexes are calculated to be 1.774 and 1.162 Å, respectively.

As mentioned above, MO's involved in protonation will be largely different in d^6 and d^8 complexes. HOMO and n_N of dinitrogen complexes are closely related to the MO's and are represented in Fig. 1. The HOMO of Cr complex is d_π (Fig. 1*a*) with a large p_x coefficient of the terminal nitrogen atom (N_T) while that of Co is the MO which has a large contribution of a hydride ligand as shown in Fig. 1*b*. Orbital energies are −0.033 and −0.159 au, respectively. While the Co complex has a d_π orbital similar to that of the Cr complex, it is mainly constructed from the d_{xz} orbital of Co plus a small contribution from the p_x orbital of N_T. The lone-pair nature in n_N of the Co complex is larger than that of Cr as is illustrated in Fig. 1*c* and 1*d*. However, the first orbital is much lower than the second one, and the orbital energies of Co and Cr complexes are calculated to be −0.569 and −0.378 au, respectively. It means that the d^6 Cr complex has an electronic structure for protonation more preferable than that of the d^8 Co complex. In other words, the Cr complex has a stronger Lewis basicity, the ability to donate its own electron density, than that of the Co complex. These electronic features strongly influence the magnitude of the protonation energies.

At this point, it is necessary to compare the MO properties in the five- and six-coordinated Cr complexes. The calculated results show that $Cr(PH_4)_4(N_2)_2$ also has d_π and n_N orbitals similar to those of the coordinatively unsaturated model. The orbital energies of the former are calculated to be −0.064 and −0.447 au, respectively. They are lower by 0.031 and 0.009 au, respectively, in comparison with those calculated for the five-coordinated complex. However, they are still higher than the corresponding MO's of the Co complex (−0.159 and −0.569 au) for HOMO and n_N, respectively. Therefore, it is possible to compare their qualitative nature in dinitrogen complexes by using the simple model adopted here.

Protonation energies were calculated on the assumption that the geometry of the metal moieties, $CoH(PH_3)_3(N_2)$ and $Cr(PH_3)_4(N_2)$, are taken to be the same as those of their parent complexes. In the Co complex, the NNH angle and the N—H length are 180.0° and 1.05 Å, respectively. In Cr complex they are 120.0° and 1.05 Å, respectively. In order to estimate protonation energies more correctly, 4-31G basis sets were adopted for the N_2 moieties. The energies for Co and Cr complexes are calculated to be 300.5 and 147.2 kcal/mol. This trend is consistent with that expected by the difference of MO's calculated. The protonation energy for the Co complex is similar to that calculated for a nitrogen molecule (123.0 kcal/mol) although N_2H^+ has not been observed in the usual solvents. On the other hand, the protonation energy of the Cr complex is larger than that of NH_3 (225.4 kcal/mol), which forms NH_4^+ in aqueous solution. The protonated species have been regarded as intermediates on the way of reduction. The existence of these compounds in solution requires larger protonation energy than the solvent. It is therefore necessary to gain a protonation energy as large as that calculated for the Cr complex to form stable intermediates.

It has never been reported that the nitrogen molecule in $Ru(NH_3)_5(N_2)^{2+}$ is reduced to NH_3 or N_2H_4 although the complex has the same d^6 configuration as Cr(0) and Mo(0) complexes. The energy levels of d electrons in the divalent Ru complex is much lower than those in the latter, and therefore the Ru complex has poorer Lewis basicity than the latter. The strong Lewis basicity with the Cr complex largely influences the reduction of the dinitrogen ligand.

On the other hand, it is known that dinitrogen ligand in Mo and W complexes can be reduced to NH_3 and N_2H_2 while in other d^8 or d^{10} complexes these reduction products have never been obtained. These experimental results are also attributed to the difference in Lewis basicity originating from their electronic structures of the latter complexes. Although the central metal as model adopted here is different from those in Mo and W complexes, these metals all have d^6 electron configuration. Therefore the characteristic MO feature in the d^6 complexes largely affects the possibility of the reduction of the nitrogen molecule in transition metal complexes.

Acknowledgements

Permission to use FACOM M-200 Computer at the Data Processing Center of Kyoto University is gratefully acknowledged. The authors also thank the Computer Center, Institute for Molecular Science, for the use of HITAC M200H Computer. The work was carried out by a grant-in-aid from the Ministry of Education.

1. A. D. ALLEN and C. V. SENOFF. Chem. Commun. 621 (1965).
2. M. M. T. KHAN and A. E. MARTELL. Homogeneous catalysis by metal complexes". Vol. 1. Academic Press, New York. 1974.
3. J. CHATT and R. L. RICHARDS. Chem. Commun. 1010 (1972).
4. J. CHATT, A. L. PEARMAN, and R. L. RICHARDS. Nature, London, **253**, 39 (1975); T. TAKAHASHI, Y. MIZOBE, M. SATO, M. HARAKAWA, Y. UCHIDA, and M. HIDAI. J. Am. Chem. Soc. **102**, 7461 (1980).
5. J. S. BINKLEY, P. C. HARIHARAN, R. SEEGER, J. A. POPLE, and M. D. NEWTON. Quantum Chemistry Program Exchange No. 368.
6. B. ROOS, A. VEILLARD, and G. BIGOT. Theor. Chim. Acta, **20**, 1 (1971).
7. J. R. JENSEN and R. F. FESKE. Theor. Chim. Acta, **48**, 241 (1978).
8. T. YAMABE, K. HORI, and K. FUKUI. Inorg. Chem. **21**, 2046 (1982).
9. B. R. DAVIS, N. C. PANE, and J. A. IBERS. Inorg. Chem. **8**, 2719 (1969).

Alkyne isomerization reagents: mixed alkali metal amides[1]

SUZANNE R. ABRAMS

Plant Biotechnology Institute, National Research Council of Canada, Saskatoon, Sask., Canada S7N 0W9

Received January 4, 1984

SUZANNE R. ABRAMS. Can. J. Chem. **62**, 1333 (1984).

Addition of sodium and potassium alkoxides, particularly potassium *tert*-butoxide, to the lithium salts of either 1,2-diaminoethane or 1,3-diaminopropane afford alkyne isomerization reagents that effect triple bond migration to the end of a methylene chain under milder conditions and in higher yield than do previously reported reagents.

SUZANNE R. ABRAMS. Can. J. Chem. **62**, 1333 (1984).

L'addition d'alcoolates de sodium ou de potassium, particulièrement le *tert*-butylate de potassium, à des sels de lithium de diamino-1,2 éthane ou de diamino-1,3 propane fournit des réactifs permettant d'effectuer l'isomérisation de la triple liaison d'alcynes vers l'extrémité de la chaîne méthylène en utilisant des conditions expérimentales beaucoup plus douces et avec de meilleurs rendements que ceux rapportés antérieurement avec d'autres réactifs.

[Traduit par le journal]

Can. J. Chem. Downloaded from www.nrcresearchpress.com by 210.87.254.5 on 09/06/12
For personal use only.

In connection with other studies of triple bond migration in long chain compounds, we required an alkyne isomerization reagent (1, 2) that could be prepared free of impurities. It was suspected that side reactions were taking place during preparation of the reagent, the sodium salt of 1,3-diaminopropane, from sodium hydride and 1,3-diaminopropane, as the reaction produced a brown solution. We now report the preparation and use of a new, cleaner reagent which causes triple bonds to be isomerized to the terminus of a long chain rapidly and under mild conditions. This system is much more amenable to larger scale preparations of terminal alkynes and alkynols.

Lithium metal reacts with 1,3-diaminopropane to give a white suspension of the alkali metal amide in the colourless diamine (3, 4). Reaction of sodium or potassium hydride with 1,3-diaminopropane affords brown reaction mixtures. While the last two are very effective isomerization reagents, rearrangements with the lithium amide proceed slowly. We anticipated that addition of sodium or potassium salts to the preformed lithium reagent might effect exchange of the cation and afford a clean, colourless, potent isomerization reagent.

To study the progress of rearrangement reactions we employed a model system we have used previously (3), the isomerization of 2- to 9-decyn-1-ol with n-decanol as internal standard. Figure 1 shows the rate of formation of the terminal isomer using $LiNH(CH_2)_3NH_2$ alone (6.5 equivalents of reagent 2.0 *M* in 1,3-diaminopropane at 70°C). In an hour 9-decyn-1-ol comprises 91% of the total decyn-1-ol mixture, but the yield based upon the internal standard is only 52%. Addition of one equivalent of potassium carbonate to the preformed lithium reagent, which did not appear to dissolve in the medium, or of potassium chloride, which did dissolve, gave no change in the rate or in the yield. When one equivalent of potassium *tert*-butoxide was employed, a yellow reagent was obtained that gave marked improvement in the rate of the reaction (99% 9-decyn-1-ol in 15 min) and a yield of 65%. Isomerization of 2-decyn-1-ol with potassium *tert*-butoxide alone in 1,3-diaminopropane gave no terminal isomer. Increasing the ratio of potassium *tert*-butoxide to 2-decyn-1-ol to 4:1 and decreasing the temperature of the reaction to ambient led to a pale lemon-yellow reagent that gave vastly improved results (Fig. 2).

A variety of other potassium and sodium alkoxides were tested using the conditions optimized with potassium *tert*-butoxide. Table 1 summarizes the results obtained. It is interesting to observe that in the sodium series, the methoxide derived reagent is superior to the ethoxide and the isopropoxide, while in the potassium series *tert*-butoxide gives the best results. This apparent reversal in reactivity is most likely due to the greater solubility of potassium *tert*-butoxide in the diamine.

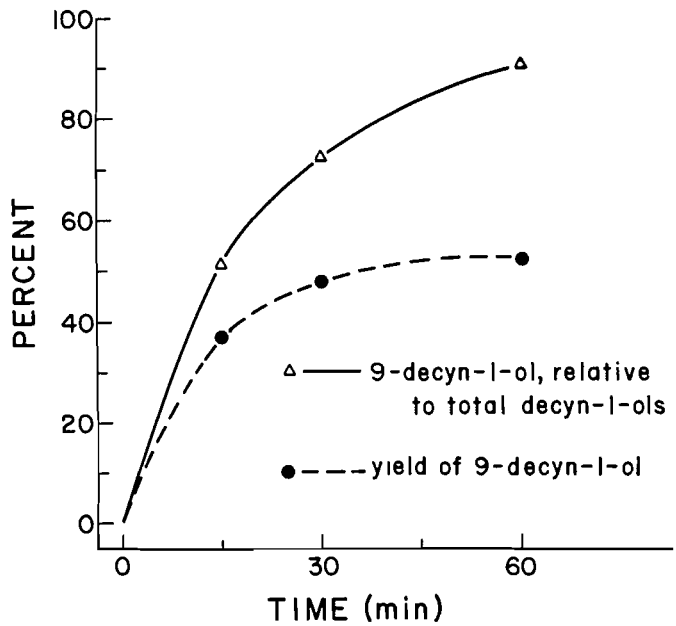

FIG. 1. Isomerization of 2- to 9-decyn-1-ol (1.0 equivalent) using $LiNH(CH_2)_3NH_2$ (6.5 equivalents), 2.0 *M* in 1,3-diaminopropane, at 70°C

Addition of potassium *tert*-butoxide to the colourless lithium salt of 1,2-diaminoethane resulted in rapid development of an intense purple colour which faded after about 5 min affording a brown solution. Wotiz *et al.* (5) have observed similar coloration in the reaction of strong bases with vicinal diamines. They postulated the intermediacy of pyrazine type radical species. Although by-products are obviously being formed in the current case, the reagent produced is very effective, affording 99% 9-decyn-1-ol in 93% yield in 15 min at room temperature, using the same ratios of alkoxide, diamine, and substrate.

The new mixed systems are particularly useful for preparative purposes. Both 1,2-diaminoethane and 1,3-diaminopropane work well. Reactions may be scaled up easily and the

[1]NRCC No. 22965.

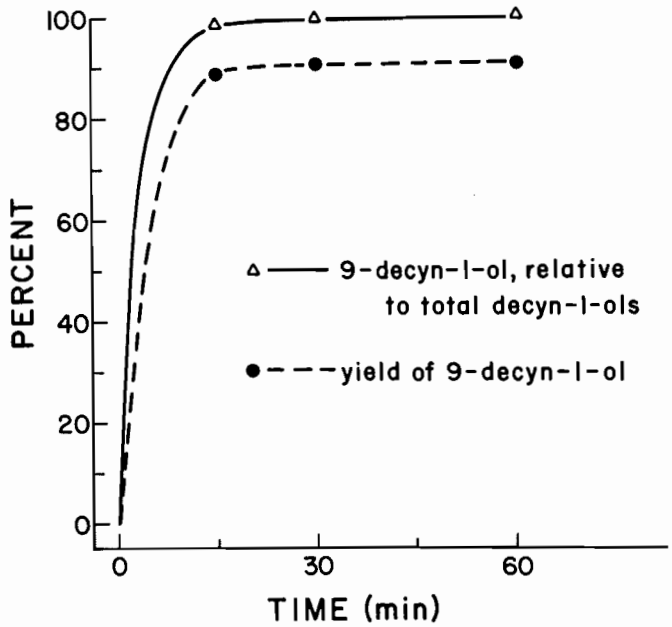

FIG. 2. Isomerization of 2- to 9-decyn-1-ol (1.0 equivalent) using $LiNH(CH_2)_3NH_2$ (6.5 equivalents), 2.0 *M* in 1,3-diaminopropane, with added potassium *tert*-butoxide (4.0 equivalents) at 20°C.

TABLE 1. Isomerization of 2- to 9-decyn-1-ol using reagents prepared from $LiNH(CH_2)_3NH_2$ and added salts[a]

Salt added	9-Decyn-1-ol: % of all decyn-1-ols[b]	9-Decyn-1-ol: Yield (%)[b,c]	Reagent colour, remarks
$NaOCH_3$	62	49	Pale yellow
$NaOC_2H_5$	36	25	Dark brown
$NaOCH(CH_3)_2$	28	23	Brown
KOH	6	5	Pale yellow KOH poorly soluble, reaction mixture viscous
$KOCH_3$	92	67	Pale yellow $KOCH_3$ poorly soluble, reaction mixture viscous
KOC_2H_5	99	85	Red brown
$KOC(CH_3)_3$	99	89	Pale yellow

[a]6.5 Equivalents of $LiNH(CH_2)_3NH_2$, 4 equivalents of added salt, 1.0 equivalent of 2-decyn-1-ol, 0.1 equivalent n-decanol, at room temperature.
[b]After 15 min reaction.
[c]Based upon glc results using internal standard.

reagents are relatively inexpensive. Crude products are entirely free of mineral oil, which is advantageous in the synthesis of hydrocarbons. Table 2 summarizes results obtained for acetylene isomerizations of a variety of substrates, and both diamines. Yields are of pure products. Reaction conditions required to effect complete isomerization of the triple bond along a 24-carbon chain have been reduced from overnight at 80°C with a yield of 47% (2) to 2 h at room temperature with a yield of chromatographed 23-tetracosyn-1-ol of 82%. An isomerization reaction of 7-tetracosyn-1-ol to 23-tetracosyn-1-ol is described in full.

TABLE 2. Isomerization of alkynes and alkynols with lithium alkyl amides and added potassium *tert*-butoxide[a]

Starting material	Product	Reaction conditions/time (h)	Yield (%)
2-Decyn-1-ol	9-Decyn-1-ol	1,3-Diaminopropane 0.5	76
2-Decyn-1-ol	9-Decyn-1-ol	1,2-Diaminoethane 0.5	72
7-Tetradecyne	1-Tetradecyne	1,3-Diaminopropane 0.25	86
7-Tetradecyne	1-Tetradecyne	1,2-Diaminoethane 0.25	87
7-Tetracosyn-1-ol	23-Tetracosyn-1-ol	1,3-Diaminopropane 2.0	82
7-Hexadecyn-1-ol	15-Hexadecyn-1-ol	1,3-Diaminopropane 1.0	65
2-Nonyn-1-ol	8-Nonyn-1-ol	1,3-Diaminopropane 0.5	86

[a]Using 6.5 equivalents $LiNH(CH_2)_3NH_2$, 4.0 equivalents KO*t*Bu, 1.0 equivalent substrate, room temperature.

Experimental

Decyn-1-ol/decanol mixtures were analyzed as described previously (6). Proton nmr spectra were obtained on a Varian EM 390 spectrometer, with deuterochloroform as solvent and internal tetramethylsilane as reference. Melting points are uncorrected.

23-Tetracosyn-1-ol

Under a slight positive pressure of dry nitrogen, 1,3-diaminopropane (10.0 mL, previously distilled from BaO and stored over 4 Å sieves) was added to lithium (140 mg, 20 mmol, washed free of mineral oil with hexane). The mixture was heated and stirred at 70°C for approximately 2 h until the blue colour had discharged, and a milky white suspension of the lithium salt was obtained. The mixture was cooled to room temperature and potassium *tert*-butoxide (1.3 g, 12 mmol) was added all at once, affording a pale yellow solution. After stirring for 15 min addition of 7-tetracosyn-1-ol (2) (1.05 g, 3.0 mmol) in one portion resulted in the reaction mixture turning orange with suspended white solid. Stirring was continued for a further 2.0 h and the mixture poured into water. The product was extracted with $CHCl_3$ (4×). The combined organic phases were washed successively with water, and dilute HCl and NaCl solution, the dried over Na_2SO_4. The solution was filtered and the solvent evaporated to yield 1.0 g white solid. The product was chromatographed over silicic acid (100 g), eluting with 50% ether/50% hexane, to give 23-tetracosyn-1-ol (860 mg, 82%), mp (CH_3OH) 76–77°C (lit. (2) mp 77–78°C); ^1H nmr: 3.65 (t, J = 6 Hz, 2H), 2.20 (m, 4H), 1.90 (t, J = 2.5 Hz, 1H), and 1.2–1.9 (m, 4H).

Acknowledgements

The expert technical assistance of Angela C. Shaw is gratefully acknowledged. The 2- to 8-nonyn-1-ol isomerization was carried out by Darwin Reed.

1. C. A. BROWN and A. YAMASHITA. J. Am. Chem. Soc. **97**, 891 (1975); J. Chem. Soc. Chem. Commun. 959 (1976).
2. S. R. MACAULAY. J. Org. Chem. **45**, 734 (1980).
3. S. R. ABRAMS. Can. J. Chem. **61**, 1073 (1983).
4. L. REGGEL, S. FRIEDMAN, and I. WENDER. J. Org. Chem. **23**, 1136 (1958).
5. J. H. WOTIZ, R. D. KLEOPFER, P. M. BARELSKI, C. C. HINKLEY, and D. F. KOSTER. J. Org. Chem. **37**, 1758 (1972).
6. S. R. MACAULAY. Can. J. Chem. **58**, 2567 (1980).

Can. J. Chem. Downloaded from www.nrcresearchpress.com by 210.87.254.5 on 09/06/12
For personal use only.

Further studies on the synthesis of symmetrical anhydrides and 2,4-disubstituted-5(4*H*)-oxazolones from *N*-alkoxycarbonylamino acids using soluble carbodiimide

ALENKA PAQUET,[1] FRANCIS M. F. CHEN, AND N. LEO BENOITON

Department of Biochemistry, University of Ottawa Health Sciences, Ottawa, Ont., Canada K1H 8M5

Received November 28, 1983

ALENKA PAQUET, FRANCIS M. F. CHEN, and N. LEO BENOITON. Can. J. Chem. **62**, 1335 (1984).

Pure symmetrical anhydrides of *N*-alkoxycarbonyl (ROCO)-valine, for R = ethyl, *tert*-butyl, trichloroethyl, *p*-nitrobenzyl, *p*-methoxybenzyl, and 9-fluorenylmethyl, and *N*-ethoxycarbonylaminoisobutyric acid have been prepared using 0.5 equivalents of *N*-ethyl-*N'*-(3-dimethylaminopropyl)carbodiimide hydrochloride in dichloromethane followed by removal of side-products by washing with aqueous solutions. When an excess of carbodiimide was used, 2-alkoxy-5(4*H*)-oxazolone was also generated, except when R = trichloroethyl. High yields of pure 5(4*H*)-oxazolone were obtained when R = ethyl. The 2-(9-fluorenylmethyloxy)-5(4*H*)-oxazolone gradually underwent a β-elimination during manipulation or storage.

ALENKA PAQUET, FRANCIS M. F. CHEN et N. LEO BENOITON. Can. J. Chem. **62**, 1335 (1984).

On a préparé les anhydrides symétriques purs de la *N*-alkoxycarbonyl (ROCO)-valine (où R = éthyl, *tert*-butyl, trichloroéthyl, *p*-nitrobenzyl, *p*-méthoxybenzyl et fluorènyl-9 méthyl) et de l'acide *N*-éthoxycarbonyl aminoisobutyrique en utilisant 0.5 équivalents de chlorhydrate de *N*-éthyl, *N'*-(diméthylamino-3 propyl)carbodiimide dans le dichlorométhane et en enlevant ensuite les produits secondaires par lavage avec des solutions aqueuses. Lorsqu'on utilise un excès de carbodiimide, il y a aussi formation de l'alkoxy-2 (4*H*)-oxazolone-5 (sauf lorsque R = trichloroéthyl). On a obtenu de bons rendements de la (4*H*)-oxazolone-5 lorsque R = éthyl. La (fluorènyl-9 méthyloxy)-2 (4*H*)-oxazolone-5 subit lentement une élimination au cours des manipulations ou de l'entreposage.

[Traduit par le journal]

The solid phase method of peptide synthesis according to Merrifield (1) involves the carbodiimide-mediated reaction of an *N*-alkoxycarbonylamino acid (**1**) with the amino group of a polymer-supported peptide chain. The activated intermediates undergoing aminolysis are the *O*-acylisourea (**2**) which is formed initially, the symmetrical anhydride (**3**) produced by the reaction of **2** with **1**, and in some cases the 2-alkoxy-5(4*H*)-oxazolone (**4**) generated by cyclization of **2**(2) or the reaction of carbodiimide with **3**(3) (see refs. 4 and 5 for reviews). In the modified version, the symmetrical anyhrides are preformed by reaction of **1** with 0.5 equiv. of dicyclohexylcarbodiimide and used without isolation after removal of the dialkylurea by filtration (see ref. 4).

Purified anhydrides **3** ($R^1 = (CH_3)_3C$) are available from the acid salt and phosgene (6). Their use to eliminate side-reactions has been recommended (7). Our realization that $(Boc\text{-}Val)_2O$[2] was resistant to aqueous washes (8) led us to develop a simple procedure for preparing anhydrides **3** using a soluble carbodiimide. Reaction of **1** with 0.5 equiv. of EDC in dichloromethane followed by washing the solution with aqueous acid and sodium hydrogen carbonate gave excellent yields of **3** ($R^1 = (CH_3)_3C$ and $C_6H_5CH_2$) except for derivatives of valine and isoleucine (9). It transpired that in the latter cases a second neutral product, the 2-alkoxy-5(4*H*)-oxazolone (**4**), was also formed, in 20% yield (2). Further study revealed that by increasing the amount of EDC to 1.5 equiv., more 5(4*H*)-oxazolone than anhydride was produced by the reaction. Pure compounds **4***a* were obtained from the mother liquors after

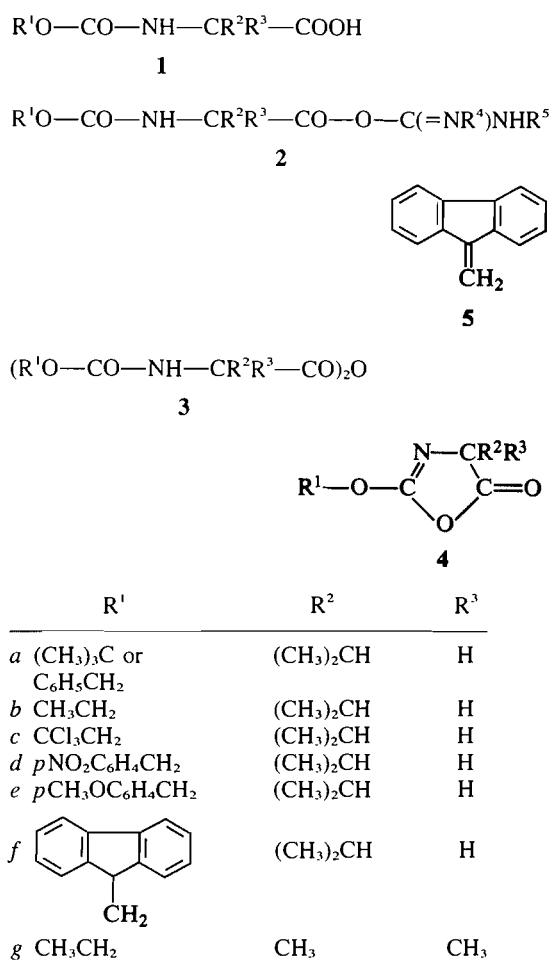

	R^1	R^2	R^3
a	$(CH_3)_3C$ or $C_6H_5CH_2$	$(CH_3)_2CH$	H
b	CH_3CH_2	$(CH_3)_2CH$	H
c	CCl_3CH_2	$(CH_3)_2CH$	H
d	$pNO_2C_6H_4CH_2$	$(CH_3)_2CH$	H
e	$pCH_3OC_6H_4CH_2$	$(CH_3)_2CH$	H
f		$(CH_3)_2CH$	H
g	CH_3CH_2	CH_3	CH_3

[1]On sabbatical leave, 1981–1982. Permanent address: Food Research Institute, Canada Department of Agriculture, Ottawa, Ont., Canada K1A 0C6.

[2]*Abbreviations*: Aib, aminoisobutyric acid; Boc, *tert*-butoxycarbonyl; Eoc, ethoxycarbonyl; Fmc, 9-fluorenylmethlyoxycarbonyl; Mbc, *p*-methoxybenzyloxycarbonyl; Nbc, *p*-nitrobenzyloxycarbonyl; Tec, 2,2,2-trichloroethoxycarbonyl; EDC, *N*-ethyl-*N'*-(3-dimethylaminopropyl)carbodiimide hydrochloride. The abbreviations for the alkoxycarbonyl groups have been selected for consistency with the rationale that the first two letters signify the substituted alkyl group and the c represents the oxycarbonyl moiety. This allows for subsequent use of the same two letters in the abbreviated representation of the corresponding alcohols and chloroformates.

Can. J. Chem. Downloaded from www.nrcresearchpress.com by 210.87.254.42 on 09/06/12
For personal use only.

TABLE 1. Properties of symmetrical anhydrides **2**

Anhydride	Yield (%)	Melting point[a] (°C)	$[\alpha]_D^{24}$[b]	(*c*)	Molecular formula	Analysis: Calcd./found C	H	N
(Eoc-Val)$_2$O, *b*	80	105–106	+27°	(1.0)	$C_{16}H_{28}N_2O_7$	53.32	7.83	7.77
						53.29	7.88	7.67
(Tec-Val)$_2$O, *c*	87	144–145	+11.3°	(1.5)	$C_{12}H_{22}Cl_6N_2O_7$	33.94	3.92	4.93
						33.97	3.69	5.05
(Nbc-Val)$_2$O, *d*	79	123–124	+22.7°	(0.7)	$C_{26}H_{30}N_4O_{11}$	54.35	5.26	9.74
						53.78	5.44	9.48
(Mbc-Val)$_2$O, *e*	68	110–111	+17.6°	(3.1)	$C_{28}H_{36}N_2O_9$	61.75	6.66	5.14
						61.93	6.94	5.24
(Fmc-Val)$_2$O, *f*	85	173–174[c]	+2.8°	(1.0)	$C_{40}H_{40}N_2O_7$			
(Eoc-Aib)$_2$O, *g*	68	99–100	—		$C_{14}H_{24}N_2O_7$	50.59	7.78	8.42
						50.24	7.65	8.94

[a]*d* crystallized during evaporation of solvent, *c*, *f* were crystallized from CH_2Cl_2 – light petroleum, *e* was crystallized from CH_2Cl_2–hexane, and *b*, *g* were crystallized by addition of Et_2O.
[b]Chloroform.
[c]Literature (10) mp 173–174°C.

precipitation of the anhydrides using light petroleum (2). Our discovery of the implication of these novel 2-alkoxy-5(4*H*)-oxazolones in some carbodiimide-mediated reactions has prompted us to examine the general applicability of the method used for their preparation. Implicit in this study was the assessment of the method of preparing the corresponding symmetrical anhydrides. The results are described in this communication.

Valine bearing various urethane-type protectors was reacted with 0.5 equiv of EDC in dichloromethane. Removal of the water-soluble components by a mild aqueous acid and alkali wash provided the pure symmetrical anhydrides of *N*-ethoxycarbonyl-, *N*-trichloroethoxycarbonyl-, *N*-*p*-nitrobenzyloxycarbonyl-, and *N*-9-fluorenylmethyloxycarbonyl-L-valine in 79–87% yields (Table 1). A lower yield (68%), paralleling the lower yields previously obtained for the *tert*-butoxycarbonyl and benzyloxycarbonyl derivatives (9), was obtained for the *p*-methoxybenzyloxycarbonyl derivative. This poorer synthetic efficiency was due to the formation of the 5(4*H*)-oxazolone (**4***e*) as second product, and some release of the alkoxy group yielding *p*-methoxybenzyloxy alcohol. Generation of the alcohol implies concomitant formation of the *N*-carboxyanhydride which would have been destroyed by the aqueous washes. Formation of the 5(4*H*)-oxazolone (**4***g*), which was readily removed by precipitation of the anhydride with ether, also accounted for the lower yield (68%) in the preparation of *N*-ethoxycarbonylaminoisobutyric anhydride (**3***g*) (Table 1). The success with the derivatives of valine and aminoisobutyric acid in this work, combined with the previous work where unhindered residues gave high yields of **3** for R^1 = $(CH_3)_3C$ and $C_6H_5CH_2$(9), demonstrates that this method of preparing symmetrical anydrides is of general applicability. Since the original report (9), it has been used by others to prepare anhydrides of 9-fluorenylmethyloxycarbonylamino acids (10). The analogous reaction of *N*-acylamino acids and protected peptide acids with EDC gives the 2,4-dialkyl-5(4*H*)-oxazolone instead of the anhydride (11, 12, 5). Isolated anhydrides have been used in solid phase synthesis (10) and for synthesis in solution in aqueous dimethylformamide (13).

Reaction of acids **1***b–g* with 1.5 equiv. of EDC followed by removal of water-soluble components by an acid and alkali wash gave a mixture of anhydrides **3** and 5(4*H*)-oxazolones **4** in all cases except for Tec-Val-OH (**1***c*). The presence of the 5(4*H*)-oxazolone in the mixtures, as well as the proportions of the two products, could be established by ^{1}H nmr spectroscopy by virtue of the two characteristic differences previously identified between **3***a* and **4***a*, namely, the upfield shift in δ of the methyleneoxy protons of **4** relative to **3**, and the change in character of the C^α proton. In valine derivatives in particular where R^2 = $(CH_3)_2CH$, the C^α (R^3) proton multiplet in **1** or **3** becomes a sharp doublet in **4** due to removal of the —NH proton. These differences in nmr spectra are tabulated in Table 2. An additional feature of the spectra is the change in the two side-chain methyl group doublets in **3***a–f* which coalesce into a triplet in the corresponding cyclic structures **4***a–f*.

TABLE 2. Nuclear magnetic resonance data on the differences between anhydrides **3** and 5(4*H*)-oxazolones **4**[a]

		3	**4**	>CH[b] in **4**
a $(CH_3)_3CO$—	s	1.46	1.60	4.13
a $C_6H_5CH_2O$—	s	5.06	5.40[c]	4.20
b CH_3CH_2O—	t[d]	4.18	4.41	4.13
b CH_3CH_2O—	t[d]	1.26	1.41	
d $pNO_2C_6H_4CH_2O$—	s	5.20	5.46	4.18
e $pCH_3OC_6H_4CH_2O$—	s	5.00	5.20	
f >$CHCH_2O$—	m	4.40	4.50	4.08
g CH_3CH_2O—	t	4.13	4.43	
g CH_3CH_2O—	q	1.23	1.43	
g $(H_3C—)_2$	s	1.56	1.44	

[a]δ in ppm relative to $(CH_3)_4Si$ in $CDCl_3$.
[b]Sharp doublet, J = 4 Hz.
[c]Changes to 5.30 in a 1:1 mixture of **3** and **4**.
[d]J = 7 Hz.

The complete absence (<1%) of oxazolone in the neutral product obtained from Tec-Val-OH was confirmed by reacting it with methylamine. Equimolar amounts of Tec-Val-NHCH$_3$ and Tec-Val-OH were generated, indicating that it was exclusively the anhydride. Aminolysis of an oxazolone produces no acid (<1%) from this reaction (5, 12). Its presence in a mixture makes the amide-to-acid ratio >1.

Among the substrates examined, the ethoxycarbonyl derivatives responded uniquely to the presence of excess EDC. The amount of anhydride formed was greatly diminished (8% yield), and eight times as much oxazolone was produced. Complete removal of the anhydride by precipitation with light petro-

Can. J. Chem. Downloaded from www.nrcresearchpress.com by 210.87.254.42 on 09/06/12
For personal use only.

Can. J. Chem. Downloaded from www.nrcresearchpress.com by 210.87.254.42 on 09/06/12
For personal use only.

leum allowed subsequent recovery of the 2-ethoxy-5(4*H*)-oxazolones **4***b* and **4***g* from the mother liquors in 62–68% yield. These were stable at −5°C at least for several days.

On the other hand, excess EDC had only a minor effect on the generation of anhydride from Mbc-Val-OH. Most of it (74% yield) could be removed by precipitation with light petroleum. 5(4*H*)-Oxazolone was present in the mother liquor, but its manipulation resulted in partial decomposition as evidenced by the liberation of *p*-methoxybenzyl alcohol.

An excess of EDC produced roughly equal amounts of anhydride and 5(4*H*)-oxazolone from the remaining substrates, Nbc-Val-OH and Fmc-Val-OH. Neither oxazolone could be purified by precipitating out the anhydride with light petroleum. Pure stable 2-*p*-nitrobenzyloxy-5(4*H*)-oxazolone **4***d* was finally obtained, albeit in low yield, by extraction into the hexane. The oxazolone from Fmc-Val-OH was destroyed by aqueous sodium hydrogen carbonate, producing 9-fluorenylmethyl alcohol. Most of the compound survived contact with water, and oxazolone **4***f*, free of anhydride, was obtained by extraction of an aqueous suspension of the mixture with light petroleum. It contained ≈15% of dibenzofulvene (**5**), and gradually decomposed on standing or in solution in deuterochloroform, producing more of the fulvene but no alcohol. The dibenzofulvene results from a β-elimination, the usual mechanism implicated in Fmc–NH cleavage (14) and is attributed to an auto-catalyzed β-elimination, namely the action of the basic secondary nitrogen atom of one molecule of 5(4*H*)-oxazolone on a second molecule. The instability exhibited by **4***f*, the oxazolone from Fmc-Val-OH, contrasts with the relative stability of the oxazolone from Boc-Val-OH (2).

In this and the previous work (2), only Tec-Val-OH amongst the N-alkoxycarbonylamino acids **1** failed to give rise to the 2-alkoxy-5(4*H*)-oxazolone in the presence of EDC. The reaction is therefore a general one for this type of derivative, except for those containing an unusually strong electron-withdrawing alkoxy group. It also pertains to derivatives of residues which are not β-methyl substituted (e.g. Ala, Leu) (2), though considerably less 5(4*H*)-oxazolone was present in the final reaction mixtures. In line with accepted notions on carbodiimide reactions, the immediate precursor of the oxazolone is considered to be the *O*-acylisourea (**2**) (ref. 2; see also ref. 5). Some oxazolone may arise from attack of the carbodiimide on the anhydride (3), but this is a slow reaction, and indications are that this can be at best a minor source for the oxazolone. The first and only other source identified for compounds **4** is the action of triethylamine on the acids **1** previously treated with chloride-forming reagents (15, 16). Examples have been restricted to a few benzyloxycarbonylamino acid derivatives.

Experimental

General

EDC (17) was purchased from Sigma Chemical Co. St. Louis. Light petroleum refers to the 30–60°C fraction, from Baker (Canlab). Magnesium sulfate was used for drying solutions. Solvents were removed at room temperature using a rotary evaporator. Melting points were taken by the capillary method and are uncorrected. Optical rotations were measured with a Perkin–Elmer model 141 polarimeter using a 1-dm tube. Proton nmr spectra were recorded with a Varian T60 spectrometer. Chemical shifts are given in ppm relative to tetramethylsilane as internal standard for solutions in deuterochloroform. Elemental analyses were carried out by Mr. G. Morris of the Microanalytical Services of Agriculture Canada. Tec-Val-OH and Fmc-Val-OH were prepared using the corresponding succinimidyl carbonates (18). Mbc-Val-OH was obtained using the acyl azide (19).

N-Ethoxycarbonylamino acids

These were prepared using ethyl chloroformate according to the method used to prepare *N*-benzyloxycarbonylphenylalanine (20). Eoc-Val-OH(**1***b*), 90% yield, $[\alpha]_D^{24}$ −0.1° (*c* 1.0 ethanol). *Anal.* calcd. for $C_8H_{15}NO_4$: C 50.78, H 7.99, N 7.34; found: C 50.66, H 8.00, N 7.42. Eoc-Aib-OH (**1***g*), 48% yield, mp 81–83°C. *Anal.* calcd. for $C_7H_{13}NO_4$: C 47.99, H 7.48, N 7.99; found: C 47.72, H 7.24, N 8.03.

p-*Nitrobenzyloxycarbonyl-L-valine* (**1**d)

This compound was obtained in 71% yield using the chloroformate (21) and in 88% yield using the succinimidyl carbonate (18), mp 75–76°C $[\alpha]_D^{24}$ +4.8° (*c* 2.0 ethanol). *Anal.* calcd. for $C_{13}H_{16}N_2O_6$: C 52.70, H 5.44, N 9.45; found: C 52.76, H 5.85, N 9.03.

Symmetrical anhydrides (3)

These were prepared according to a published procedure (9) except that the solvent was not replaced by ethyl acetate (5) for work-up. A solution of the acid (**1**) (1mmol) and soluble carbodiimide EDC (0.5 mmol) in dichloromethane (20 mL) was stirred at 23°C for 2 h. The solution was washed successively with cold aqueous citric acid, sodium chloride, sodium bicarbonate, and sodium chloride, dried, and the solvent was removed by evaporation at 0°C. Physical data of the products appear in Tables 1 and 2. Only the *p*-methoxycarbonyl derivative **3***e* was difficult to crystallize. The crude product contained (nmr) 10–15% of 5(4*H*)-oxazolone **4***e* and some *p*-methoxybenzyl alcohol. The nmr spectra of anhydrides **3** were identical with those of the parent acids **1** except in the acid proton region (see Table 2).

2,4-Disubstituted-5(4H)-oxazolones (**4**)

These were prepared as described previously using an excess of EDC (2) but without the addition of $Et_3N \cdot HCl$. A solution of protected acid **1** (2 mmol) in CH_2Cl_2(20 mL) was added dropwise over 20 min to a stirred solution of EDC (3 mmol) in CH_2Cl_2(100 mL). After 30 min, the mixture was washed with cold 10% aqueous citric acid (20 mL), saturated aqueous $NaHCO_3$ (20 mL), and water (20 mL), and dried. The solvent was removed, light petroleum was added, and the mixture was left at −5°C. Products were isolated as described below. Pertinent nmr data appear in Table 2.

(S)-*2-Ethoxy-4-isopropyl-5(4*H*)-oxazolone* (**4**b)

Eoc-Val-OH (3 mmol) was reacted with EDC and the mixture was manipulated as described above. The mixture was filtered after 3 h of cooling to give 43.4 mg (8% yield) of $(Eoc\text{-}Val)_2O$. Evaporation of the mother liquor gave **4***b* as an oil (0.32 g; 62% yield), $[\alpha]_D^{24}$ − 51.1° (*c* 1.0, $CHCl_3$). *Anal.* calcd. for $C_8H_{13}NO_3$: C 56.12, H 7.65, N 8.17; found: C 55.77, H 7.59, N 8.38.

*Attempted preparation of 2-trichloroethoxy-5-isopropyl-5(4*H*)-oxazolone* (**4**c)

Tec-Val-OH (**1***c*) (2 mmol) was reacted with EDC and the mixture was manipulated as described above. Filtration after 5 h of cooling gave 0.38 g (66.6% yield) of $(Tec\text{-}Val)_2O$. Evaporation of the mother liquor gave a residue whose nmr spectrum corresponded to that of the anhydride. In a second experiment the product, after removal of the CH_2Cl_2, was mixed with an excess of CH_3NH_2 in anhydrous ether. The mixture was filtered to give $Tec\text{-}Val\text{-}O^- \cdot {}^+NH_3CH_3$. The mother liquor was evaporated to give Tec-Val-$NHCH_3$, mp 128–129°C, $[\alpha]_D^{25}$ −11.7° (*c* 0.67, $CHCl_3$). *Anal.* calcd. for $C_9H_{15}Cl_3N_2O_3$: C 35.37, H 4.94, N 9.16; found: C 35.27, H 5.16, N 9.04. The molar ratio of methylamine salt to methylamide was 1.03. This demonstrates that the mixture had not contained a significant amount of 5(4*H*)-oxazolone (see ref. 5).

(S)-*2-p-Nitrobenzyloxy-4-isopropyl-5(4*H*)-oxazolone* (**4**d)

Nbc-Val-OH (**1***d*) (2 mmol) was reacted with EDC and the mixture was manipulated as described above. The residue after removal of the CH_2Cl_2 contained anhydride and 5(4*H*)-oxazolone in a 1:1 ratio. Separation by light petroleum extraction was inefficient. Pure **4***d* was obtained in low yield by extraction into hexane and evaporation of the solvent. *Anal.* calcd. for $C_{13}H_{14}N_2O_5$: C 56.11, H 5.07; found: C 56.03, H 5.28.

Attempted preparation of 2-p-*methoxybenzyloxy-4-isopropyl-5(4*H*)-oxazolone (4e)*

Mbc-Val-OH (**1***e*) (5.19 mmol) was reacted with EDC and the mixture was manipulated as described above. Filtration after 5 h of cooling gave 0.40 g (74%) of (Mbc-Val)$_2$O. The filtrate contained some 5(4*H*)-oxazolone (**4***e*) but it could not be purified without some decomposition, with the concomitant liberation of *p*-methoxybenzyl alcohol.

(S)-*2-(9-Fluorenylmethyloxy)-4-isopropyl-5(4*H*)-oxazolone (4f)*

Fmc-Val-OH (**1***f*) (2 mmol) was reacted with EDC as described above. After 30 min, the solvent was removed and the residue was partitioned between cold light petroleum and water. The mixture was separated and the organic phase was washed twice with water. The solution was dried, and the solvent was removed to give 0.36 g (≈50%) of **4***f*; nmr δ: 4.08 (d, C^{α}—H), containing 15% of dibenzofulvene, nmr δ: 6.0 (s, H_2C=). The 5(4*H*)-oxazolone is completely decomposed after standing 16 h at 23°C, and is rapidly destroyed by aqueous $NaHCO_3$. A solution in $CDCl_3$ at 23°C decreased in concentration by 15% in 24 h, with the concomitant formation of dibenzofulvene. Variation of the synthetic reaction conditions had no significant effect on the outcome of the reaction.

*2-Ethoxy-4,4-dimethyl-5-(4*H*)-oxazolone (4g)*

Eoc-Aib-OH (1 mmol) was reacted with EDC as described above. Cooling the residue under light petroleum gave solid anhydride (0.08 mmol), followed by 0.10 g (68%) of **4***g*, semi-solid, after evaporation of the solvent. *Anal.* calcd. for $C_7H_{11}NO_3$: C 53.49, H 7.05, N 8.90; found: C 53.70, H 7.15, N 8.94.

1. R. B. MERRIFIELD. J. Am. Chem. Soc. **85**, 2149 (1963).
2. N. L. BENOITON and F. M. F. CHEN. Can. J. Chem. **59**, 384 (1981).
3. N. L. BENOITON and F. M. F. CHEN. J. Chem. Soc. Chem. Commun. 2225 (1982).
4. G. BARANY and R. B. MERRIFIELD. *In* The peptides. Vol. 2. *Edited by* E. Gross and J. Meienhofer. Academic Press, New York. 1979. p. 1.
5. N. L. BENOITON. *In* The peptides. Vol. 5. *Edited by* E. Gross and J. Meienhofer. Academic Press, New York. 1983. p. 217.
6. T. WIELAND, F. FLOR, and C. BIRR. Justus Liebigs Ann. Chem. 1595 (1973).
7. J. REBEK and D. FEITLER. J. Am. Chem. Soc. **96**, 1606 (1974).
8. F. M. F. CHEN and N. L. BENOITON. Can. J. Biochem. **56**, 38 (1978).
9. F. M. F. CHEN, K. KURODA, and N. L. BENOITON. Synthesis, 928 (1978); 232 (1979).
10. F. P. HEIMER, C. D. CHANG, T. LAMBROS, and J. MEIENHOFER. Int. J. Peptide Protein Res. **18**, 237 (1981).
11. F. M. F. CHEN, K. KURODA, and N. L. BENOITON. Synthesis, 230 (1979).
12. N. L. BENOITON and F. M. F. CHEN. *In* Peptides 1982. Proc. 17th Eur. Peptide Symp. *Edited by* K. Blaha and P. Malon. Walter de Gruyter, Berlin. 1983. p. 167.
13. N. L. BENOITON and F. M. F. CHEN. FEBS Lett. **125**, 104 (1981).
14. L. A. CARPINO and G. Y. HAN. J. Am. Chem. Soc. **92**, 5748 (1970).
15. M. MIYOSHI. Bull. Chem. Soc. Jpn. **46**, 212 (1973).
16. J. H. JONES and M. J. WITTY. J. Chem. Soc. Perkin Trans. **1**, 3203 (1979).
17. J. C. SHEEHAN, P. A. CRUIKSHANK, and G. L. BOSHART. J. Org. Chem. **26**, 2525 (1961).
18. A. PAQUET. Can. J. Chem. **60**, 976 (1982).
19. F. WEYGAND and E. NINTZ. Z. Naturforsch. Teil B, **20**, 429 (1965).
20. W. GRASSMANN and E. WÜNSCH. Chem. Ber. **91**, 462 (1958).
21. D. T. GISH and F. H. CARPENTER. J. Am. Chem. Soc. **75**, 950 (1953).

Can. J. Chem. Downloaded from www.nrcresearchpress.com by 210.87.254.42 on 09/06/12
For personal use only.

Transient spectroscopy and kinetics of the reactions of mesocyclic diamines with *tert*-butoxyl and with ketone triplets. Effects of ring conformation[1]

J. C. SCAIANO[2] AND LAURA C. STEWART
Division of Chemistry, National Research Council of Canada, Ottawa, Ont., Canada K1A 0R6

AND

P. LIVANT[2] AND A. W. MAJORS
Chemistry Department, Auburn University, Auburn, AL 36849, U.S.A.

Received November 9, 1983

J. C. SCAIANO, LAURA C. STEWART, P. LIVANT, and A. W. MAJORS. Can. J. Chem. **62**, 1339 (1984).

Absolute rate constants for the reactions of *tert*-butoxyl and triplet benzophenone, with a series of di-*tert*-amines have been obtained via laser flash photolysis. These diamines have in common the feature that the nitrogen centers are in the backbone of an aliphatic eight-membered ring at positions 1 and 5. A modest rate enhancement is observed, particularly for **1** in its H-abstraction reaction with *tert*-butoxyl, which may be explained by the operation of a stereoelectronic effect. From the absorption maxima of the radical cations of these diamines (produced quenching acetophenone triplets), information concerning the conformations of the eight-membered rings may be inferred. It is concluded that these radical-cations are stabilized by relatively strong through-space bonding interactions between the two nitrogen centers.

J. C. SCAIANO, LAURA C. STEWART, P. LIVANT et A. W. MAJORS. Can. J. Chem. **62**, 1339 (1984).

Faisant appel à la photolyse flash au laser, on a obtenu les constantes de vitesse absolues des réactions du *tert*-butoxyle et du triplet de la benzophénone avec diverses amines di-tertiaires. Toutes ces diamines sont caractérisées par le fait que les centres azotés sont situés en positions 1 et 5 d'un cycle aliphatique à huit chaînons. En particulier lors de la réaction d'abstraction d'hydrogène du composé **1** par le *tert*-butoxyle, on observe une légère augmentation de la vitesse de réaction que l'on peut expliquer par un effet stéréoélectronique. On peut déduire des informations relatives aux conformations des cycles à huit chaînons à partir des absorptions maximales des cations radicaux de ces diamines (produits par le piégeage des triplets de l'acétophénone). On en conclut que ces cations radicaux sont stabilisés par des interactions de liaison à travers l'espace qui sont relativement fortes et qui impliquent les deux azotes.

[Traduit par le journal]

Can. J. Chem. Downloaded from www.nrcresearchpress.com by 210.87.254.42 on 09/06/12
For personal use only.

Introduction

The study of medium-ring (so-called mesocyclic) systems has provided chemists with a number of surprising results. In particular, heteroatom-substituted eight-membered rings are peculiar. 1,5-Dithiacyclooctane shows appreciable S−S interaction as evidenced by a splitting of 0.43 eV in its photoelectron (PE) spectrum (1). 1,4-Dithiacycloheptane, 1,5-dithiacyclononane, and 1,6-dithiacyclodecane each shows negligible S−S interaction (<0.1 eV), indicating that in the eight-membered case the conformation has the two sulfurs in close proximity. Also, electrochemical oxidation of these same bis-sulfides (2) occurs in the range 0.34−0.75 V (1,5-dithiacyclooctane is the most easily oxidized) as compared with normal sulfides 0.66−1.32 V. These oxidation potentials reflect the properties of the radical cations: that is, S----$S^{+}\cdot$ interaction is greatest in the 1,5-dithiacyclooctane radical cation. Other aspects of the peculiar eight-membered ring have been reviewed by Anet (3).

Bicyclic mesocycle-containing systems are also fascinating. The 3,7-diheteroatom bicyclo[3.3.1] skeleton may be thought of as a 1,5-diheteroatom cyclooctane with the addition of a one-carbon bridge across 3, 7. Here the commonly encountered chair−chair conformation (with respect to the bicyclic skeleton) is actually an example of the rare boat−boat form of an eight-membered ring. Recent PES study of 3,7-dimethyl-3,7-diazabicyclo[3.3.1]nonane (4) **1** showed that in the gas-phase the compound adopted the chair−chair form, probably with some flattening of the wings. We have examined the reactions of **1**−**3** with alkoxy radicals and ketone triplets, leading to the corresponding α-aminoalkyl radicals or radical cations.

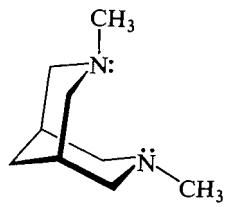

1

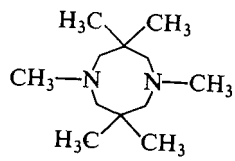

2

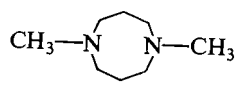

3

Since the conformation of **1** is known with fair certainty, the behaviour of **1** serves to model a system in which transannular interaction in the ground state is large. The behaviour of **2** and **3** may then be compared to **1**, as well as with representative monoamines. A comparison of kinetic and spectroscopic parameters determined using laser photolysis techniques allows the evaluation of the importance of geometry on the behaviour of these substrates and the resulting radical-cations.

Particularly relevant to our study is the recent report by Lewis *et al.* (5) of cooperative effects in the exciplex interactions of stilbenes with mono and diamines; in the case of the former, exciplex quenching can be achieved by increasing concentration of amines. In the case of diamines the effects are strongly dependent upon conformational factors, in particular, the ability of the two nitrogen centers to approach enough for a considerable interaction to develop. Steric effects have been shown to play an important role. Grellman and Suckow had

[1]NRCC No. 23070.
[2]To whom correspondence should be addressed.

Can. J. Chem. Downloaded from www.nrcresearchpress.com by 210.87.254.42 on 09/06/12
For personal use only.

also observed an example of exciplex quenching by amines (6).

In a recent study of proton affinities and ionization energies of bicyclic amines and diamines, Alder *et al.* (7) have shown that the stabilization of the diamine radical-cations by interaction with the second nitrogen center can exceed 11 kcal/mol.

Experimental

Compounds were either commercial samples or were prepared by literature procedures or slight modifications thereof, viz. **1**, **2**, and **3** (8). Purity was checked by gas chromatography.

Laser flash photolysis experiments were performed using a Molectron UV-24 nitrogen laser (337.1 nm, ~8 ns, up to 10 mJ/pulse) for excitation. A Tektronix R-7912 transient digitizer initially captures the signals, which are then transferred to a PDP-11/23 computer that also controls the experiment and provides suitable processing, storage and hardcopy facilities. Further details can be found elsewhere (9).

Results

Hydrogen abstraction by tert-*butoxyl*

Photodecomposition of di-*tert*-butyl peroxide in the presence of amines in a 1:2 (v/v) mixture of benzene and peroxide leads to hydrogen abstraction from the amine by *tert*-butoxyl, reactions [1] and [2].

$$[1]\quad Bu'OOBu' \xrightarrow{h\nu} 2Bu'O\cdot$$

$$[2]\quad Bu'O\cdot + RCH_2NR_2' \xrightarrow{k_A} Bu'OH + \dot{R}CHNR_2'$$

It has been established that the transient absorption signals from radicals of the type $\dot{R}CHNR_2'$ are, while detectable, relatively weak and not convenient for kinetic studies of this type (10–12). We have preferred to use a "probe technique", that we have described earlier (13), and used widely for *tert*-butoxyl (11, 13–16) and other radicals (17). Briefly, a second substrate, capable of generating strong, easily detectable signals is added to the system, so as to make the monitoring of the kinetic signals straightforward. It is well established that diphenylmethanol is a very convenient choice (13–16); reaction with *tert*-butoxyl yields the easily detectable diphenylhydroxymethyl radical:

$$[3]\quad Bu'O\cdot + Ph_2CHOH \xrightarrow{k_p} Bu'OH + Ph_2\dot{C}OH$$

The experimental pseudo-first order rate constant, associated with the build-up of the signal due to $Ph_2\dot{C}OH$ is given by:

$$[4]\quad k_{exp} = k_d + k_p[Ph_2CHOH] + k_A[Amine]$$

where k_d represents all first, or pseudo-first, order modes of *tert*-butoxyl decay (such as β-scission or abstraction from the solvent). At constant diphenylmethanol eq. [4] reduces to eq. [5].

$$[5]\quad k_{exp} = k_0 + k_A[Amine]$$

Diphenylmethanol was typically kept constant at around 0.1 *M*, while the amine concentrations were changed. Figure 1 shows a representative plot used to determine k_A. Values for k_A are listed in Table 1.

The absorption spectra of the α-aminoalkyl radicals derived from **1**, **2**, and **3** can be detected during flash photolysis. Figure 2 shows the spectra for the radicals from **1** and **2**. They are nearly identical, and they strongly resemble the spectrum of $\cdot CH_2N(CH_3)_2$ (10, 11). The spectrum of the α-aminoalkyl radical derived from **1** decays with clean second-order kinetics when monitored at 370 nm, having a decay constant:

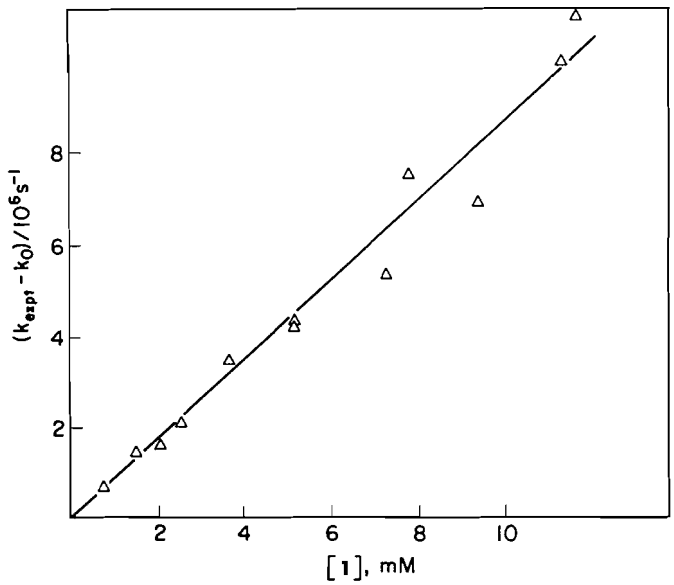

FIG. 1. Determination of k_A for **1** according to eq. [5], using 0.1 *M* diphenylmethanol as a probe.

TABLE 1. Kinetic parameters at 300 K[a]

Substrate	k_A ($Bu'O\cdot$)[b]	k_q[c]
Triethylamine	1.8×10^8	4.1×10^9
DABCO[d]	2.8×10^7	3.1×10^9
1	8.7×10^8	5.9×10^9
2	5.9×10^8	5.4×10^9
3	6.1×10^8	6.3×10^9

[a]All values in units of M^{-1} s^{-1}.
[b]1:2 benzene:di-*tert*-butyl peroxide solvent.
[c]For benzophenone in benzene.
[d]1,4-Diazabicyclo[2.2.2]octane.

$$2k_t/\epsilon = 1.25 \times 10^6 \text{ cm s}^{-1}$$

which compares well with the corresponding value for $\cdot CH_2N(CH_3)_2$. Here ε is the extinction coefficient for the corresponding α-aminoalkyl radical at the monitoring wavelength.

Quenching of benzophenone triplets

The quenching of benzophenone triplets by amines **1**–**3** was examined in benzene at 300 K. The signals were monitored at 540 nm where both benzophenone triplet and the ketyl radical derived from it absorb. The absorbance of the latter is weaker than the former at this wavelength. In the presence of amine, a fast decay (quenching of triplet by H-abstraction from amine) followed by a slow decay (subsequent reactions of the radicals produced in the quenching step) is observed. The ratio of optical density after and before triplet decay is a measure of the yield of ketyl radical. Using triethylamine as an actinometer (18), it can be estimated that at least 80% of the quenching takes place via formation of ketyl radicals (i.e. by H-abstraction from the amine), reactions [6] and [7].

$$[6]\quad Ph_2CO \xrightarrow{h\nu} {}^{1}Ph_2CO^* \xrightarrow{ISC} {}^{3}Ph_2CO^*$$

$$[7]\quad {}^{3}Ph_2CO^* + RCH_2NR_2' \rightarrow Ph_2\dot{C}OH + \dot{R}CHNR_2'$$

The slope of plots of the reciprocal triplet lifetime (τ_T^{-1}) vs. amine concentrations is the quenching rate constant, k_q; these are listed in Table 1.

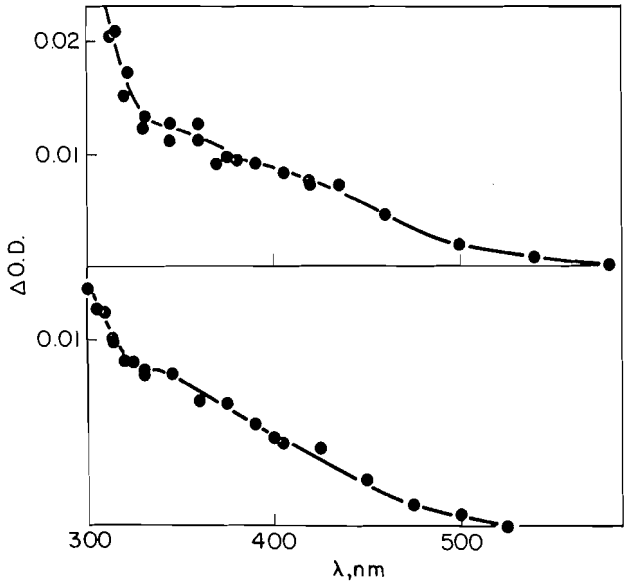

FIG. 2. Spectra of the α-aminoalkyl radicals produced by reaction of *tert*-butoxyl with **1** (top) and **2** (bottom).

Hydrogen abstraction from **1**–**3** by benzophenone triplet is roughly an order of magnitude faster than these abstractions by *tert*-butoxyl. We note that while the products of reaction in benzene reflect hydrogen abstraction, the process may involve charge transfer interactions and, indeed, the radical ions may be the expected products in polar media.

Quenching of acetophenone triplets

In polar solvents, in this case acetonitrile:water 4:1 (v/v), excited acetophenone undergoes single-electron transfer with an amine to give the acetophenone radical-anion and the amine radical-cation, both of which can be observed on the time scale of the present experiments.

[8] $PhCOCH_3 \xrightarrow{h\nu} \rightarrow PhCOCH_3^*$

[9] $PhCOCH_3^* + R_3N \xrightarrow{k_q} [PhCOCH_3]^{-\cdot} + R_3N^{+\cdot}$

For $R_3N = Et_3N$ we observe a transient maximum at ~445 nm, which we assign to the ketone radical-anion. The signals due to the amine radical-cation are expected to be very weak in this spectral region and easily monitored only in the uv region. To our initial surprise, we found that when the substrate was any of the mesocyclic diamines used in this work there were strong, readily observable signals in the visible region, in addition to those expected from the ketone radical-anion (*vide supra*). The new signals can be deconvoluted by subtracting those of the ketone radical-anion and show maxima in the 480–590 nm region, depending on the substrate (**1**–**3**). These signals are not due to the ketyl radical, $PhC(OH)CH_3$, which is known to absorb at 415 nm (19) and whose spectrum was also recorded in our laboratory by photoreduction of acetophenone by 1-phenylethanol. The new signals in the 480–590 nm region are attributed to the corresponding diamine radical-cations.

After investing considerable effort into deconvoluting the signals mentioned above, we discovered that a rather simple experimental trick allowed the straightforward separation of the spectra. The introduction of a trace of oxygen (≤1% O_2 in the gas phase above the solution) into the diamine–acetophenone system leads to rapid reaction of the acetophenone radical-anion with oxygen, leaving an unadulterated spectrum of the diamine radical-cation. The spectra obtained using the O_2-injection method are shown in Fig. 3 and the absorption maxima are recorded in Table 2. Triethylamine radical cation exhibits an absorption maximum at λ ≤ 350 nm under these conditions. The cyclic diamines show an extremely large shift to longer wavelengths.

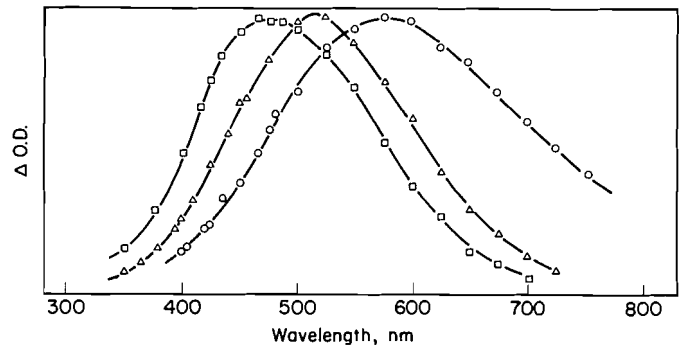

FIG. 3. Transient spectra of the radical cations from **1** (△), **2** (○), and **3** (□) produced by reaction of acetophenone triplets in 1:4 water–acetonitrile using the oxygen injection technique (see text).

TABLE 2. Spectroscopic data for the various diamines examined

Amines	λ_{max}, nm[a]	IP_1, eV	IP_2, eV	Δ_{NN}, eV
1	520	7.84	8.35	0.51
2	584	7.35	8.05	0.70
3	480	8.02	8.02	≤0.2

[a]Transient absorption of radical cation in 1:4 water:acetonitrile at 300 K.

Discussion

Kinetics

Our kinetic results have been summarized in Table 1. The very low value for 1,4-diazabicyclo[2.2.2]octane (DABCO) has been explained in terms of a stereoelectronic effect (11). The value for triethylamine was chosen as a point of reference because essentially free rotation about the C—N bonds would average the stereoelectronic effect in this case. Rate constants for hydrogen abstraction from **1**, **2**, and **3** are all substantially higher than for triethylamine. To some extent this difference must reflect an increase in the reaction path degeneracy (i.e. two amine centers rather than one); however, the value of k_A is in all cases over twice that for the monoamine, generally displaying a modest rate enhancement. The effect is more marked for **1**, and suggests that one of the two non-equivalent hydrogens of each —CH_2— is held (at least part of the time) in a conformation favorable to H-abstraction. From molecular mechanics calculations (*vide infra*) we find the dihedral angles shown below (Newman projection down an N—CH_2 bond of **1**).

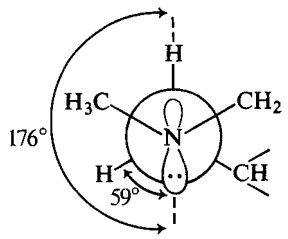

Can. J. Chem. Downloaded from www.nrcresearchpress.com by 210.87.254.42 on 09/06/12
For personal use only.

Can. J. Chem. Downloaded from www.nrcresearchpress.com by 210.87.254.42 on 09/06/12
For personal use only.

The anti hydrogen is the likely candidate for abstraction, since the developing *p*-orbital would be in a good position to overlap with the nitrogen lone pair. The anti hydrogen would not be as effective in this regard as a hydrogen which eclipses the lone pair. Because of this, and because six of the fourteen α-hydrogens of **1** are N—CH_3 hydrogens for which no stereoelectronic effect is to be expected, the rate enhancement is modest.

The effect observed in the case of benzophenone triplets is very small; in fact, smaller than the increase in reaction path degeneracy. This is hardly surprising since these processes approach diffusion control, and for a diffusion controlled process one would not expect to observe any effect (i.e., the "chemistry" no longer determines the kinetic behaviour).

Spectroscopy

The spectra in Fig. 3 are the first reported that unequivocally show that radical-cations from diamines with suitable geometry involve considerable interaction between the two nitrogen centers.

In a study relevant to the discussion presented herein Halpern (20) attributed a shift in the fluorescence maximum from 282 nm for trimethylamine to 365 nm for *N,N,N′,N′*-tetramethyl-1,3-propanediamine to internal excimer formation in the diamine case.

More recently, Lewis *et al.* (5) studied the quenching of stilbene singlet by mono- and diamines. Their results led them to conclude that the positive charge on the nitrogen in these exciplex-mediated reactions could be stabilized by a second nitrogen center in inter- or intramolecular interactions which effectively amount to a through-space (and perhaps relatively loose) three electron bond. In the present case, the molecular orbitals formed by symmetric (n_+) and antisymmetric (n_-) combination of the nitrogen "lone pair" orbitals will be split to an extent dependent on the strength of the nitrogen−nitrogen interaction (which we will call Δ_{NN}). Presumably, in the radical cation the n_+ is doubly occupied and the n_- is singly occupied, to a first approximation. The stronger the nitrogen−nitrogen interaction is, the higher in energy the n_- orbital moves, and the lower in energy and longer in wavelength the excitation process from the n_- HOMO becomes.

Thus the absorption spectrum of the radical cation provides information about Δ_{NN} and about the proximity of the two nitrogens, if it is assumed Δ_{NN} is a through-space interaction, and that the observed visible absorption band corresponds to excitation of the n_- electron to the LUMO.[3]

From the results in Table 2, $\mathbf{2}\cdot^+$ has the two nitrogens in closest proximity, in $\mathbf{1}\cdot^+$ they are less intimate, and in $\mathbf{3}\cdot^+$ the N—N distance is largest. All three exhibit *some* N−N interaction since on formation of the radical cation the electron is donated to ketone triplet from an antibonding (n_-) orbital, leaving a N—N "bond" of bond order 0.5 where no bond existed before.

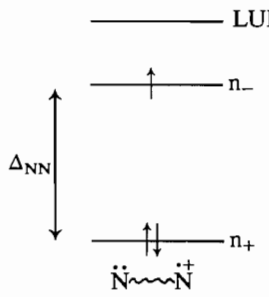

It is not surprising that $\mathbf{1}\cdot^+$ would manifest a significant nitrogen−nitrogen interaction, since the proximity of the heteroatoms is fairly rigidly fixed by the bicyclic skeleton. It is surprising, however, that the (presumably) more flexible monocyclic systems would manifest a significant nitrogen−nitrogen interaction. To rationalize these results, molecular mechanics calculations (21) were performed which were designed to probe whether the change in geometry from two pyramidal nitrogens to one pyramidal and one trigonal nitrogen *in itself* engenders a shortening of the N—N distance. That is, disregarding partial bond formation and charge−dipole interactions, does the alteration of one nitrogen from pyramidal to flat have the effect of drawing the two nitrogens together? Suffice it to say that molecular mechanics calculations showed a plethora of ring conformations energetically accessible to **2** and **3** and their respective radical cations, and the details of these calculations as well as a variable temperature nmr study of **2** will be reported shortly. In the context of the present discussion it is fair to conclude that in **1**−**3** the loss of a single electron (*a*) leads to a reduction in strain energy (3.5−7.5 kcal/mol) and (*b*) has almost no effect on the N—N distance (contraction by only 1% at most). Therefore, the two nitrogens are not thrown together upon ionization by the steric demands of the ring. They may or may not be thrown together by formation of a partial bond ("3-electron σ-bond" (7)) between them. Assuming for the moment no dramatic change in geometry upon loss of a single electron, one may infer something about the geometry of the radical cations (and hence about their λ_{max} values) from any technique which sheds light on the geometry of the parent diamines.

As mentioned in the Introduction, Δ_{NN} is available for **1** from examination of the doublet separation of the lone pair ionization band in the photoelectron spectrum, viz. Δ_{NN} = 0.51 eV (4). We have obtained the photoelectron spectrum of **2** and **3** and we find Δ_{NN} = 0.70 eV and Δ_{NN} = ≤0.2 eV (one band), respectively. These results are consistent with an ordering of N—N interactions as **2** > **1** >**3**, which is exactly the ordering of λ_{max} for the radical cations. Therefore, either the N−N interaction in the radical cation is dictated by the steric demands of the ring, and the λ_{max} values *should* mirror the Δ_{NN}'s found from photoelectron spectroscopy of the parent amines, or the N−N interaction in the radical cation is dictated mainly by the three-electron σ-bond between nitrogens and the agreement with PES results on the parent diamines is fortuitous. Probably both effects are at work. At any rate, the discovery of a nonrigid system showing such remarkable cooperative effects in *both* the ground state and the radical cation is of interest.

Acknowledgements

Parts of this research were supported by an Auburn University Intramural Grant-in-Aid (No. 80-168). P.L. acknowledges partial support by the donors of the Petroleum Research Fund, administered by the American Chemical Society. We also wish to thank Professor S. D. Worley for obtaining the photoelectron spectra, Professor F. D. Lewis for valuable discussions and a preprint of ref. 5, and Mr. S. E. Sugamori for technical assistance.

[3]In fact the same trends would be expected of higher energy bands as well.

1. W. N. SETZER, B. R. COLEMAN, G. S. WILSON, and R. S. GLASS. Tetrahedron, **37**, 2743 (1981).

2. G. S. WILSON, D. D. SWANSON, J. Y. KLUG, R. S. GLASS, M. D. RYAN, and W. K. MUSKER. J. Am. Chem. Soc. **101**, 1040 (1979).
3. F. A. L. ANET. Topics Curr. Chem. **45**, 159 (1974).
4. P. LIVANT, K. A. ROBERTS, M. D. EGGERS, and S. D. WORLEY. Tetrahedron, **37**, 1853 (1981).
5. W. HUB, S. SCHNEIDER, F. DÖRR, J. D. OXMAN, and F. D. LEWIS. J. Phys. Chem. **87**, 4351 (1983).
6. K. J. GRELLMAN and O. SUCKOW. Chem. Phys. Lett. **32**, 250 (1975).
7. R. W. ALDER, R. J. ARROWSMITH, A. CASSON, R. B. SESSIONS, E. HEILBRONNER, B. KOVAC, H. HUBER, and M. TAAGEPERA. J. Am. Chem. Soc. **103**, 6137 (1981).
8. J. E. DOUGLASS and T. B. RATLIFF. J. Org. Chem. **33**, 355 (1968); M. W. WILLIAMS. J. Org. Chem. **33**, 3946 (1968); J. HERNANDEZ-MORA and N. CORDERO-ANTUNANO. Carib. J. Sci. **14**, 77 (1974).
9. J. C. SCAIANO. J. Am. Chem. Soc. **102**, 7747 (1980).
10. J. C. SCAIANO. J. Phys. Chem. **85**, 2851 (1981).
11. S. GRILLER, J. A. HOWARD, P. R. MARRIOTT, and J. C. SCAIANO. J. Am. Chem. Soc. **103**, 619 (1981).
12. P. R. MARRIOTT, A. L. CASTELHANO, and D. GRILLER. Can. J. Chem. **60**, 274 (1982).
13. H. PAUL, R. D. SMALL, JR., and J. C. SCAIANO. J. Am. Chem. Soc. **100**, 4520 (1978).
14. M. V. ENCINAS and J. C. SCAIANO. J. Am. Chem. Soc. **103**, 6393 (1981).
15. P. C. WONG, D. GRILLER, and J. C. SCAIANO. J. Am. Chem. Soc. **104**, 5106 (1982).
16. R. D. SMALL, JR., J. C. SCAIANO, and L. K. PATTERSON. Photochem. Photobiol. **29**, 49 (1979).
17. C. CHATGIALOGLU, K. U. INGOLD, and J. C. SCAIANO. J. Am. Chem. Soc. **104**, 5119 (1982); **104**, 5123 (1982); **105**, 3292 (1983); J. C. SCAIANO and L. C. STEWART. J. Am. Chem. Soc. **105**, 3609 (1983).
18. S. INBAR, H. LINSCHITZ, and S. G. COHEN. J. Am. Chem. Soc. **102**, 1419 (1980).
19. H. LUTZ, E. BREHERET, and L. LINDQVIST. J. Phys. Chem. **77**, 1758 (1973).
20. A. M. HALPERN and P. O. CHAN. J. Am. Chem. Soc. **97**, 2971 (1975).
21. N. L. ALLINGER and Y. H. YUH. "MM2", Quantum Chemistry Program Exchange, Program No. 395.

Can. J. Chem. Downloaded from www.nrcresearchpress.com by 210.87.254.42 on 09/06/12
For personal use only.

Rhenium carbonyl derivatives incorporating the bidentate chelating pyrazolyl gallate ligands, $[Me_2Ga(N_2C_3HR_2)_2]^-$ and $[Me_2Ga(N_2C_3HR_2)(OH)]^-$ (where R = H or Me)

BRENDA M. LOUIE AND ALAN STORR

Department of Chemistry, University of British Columbia, Vancouver, B.C., Canada V6T 1Y6

Received November 8, 1983

BRENDA M. LOUIE and ALAN STORR. Can. J. Chem. **62**, 1344 (1984).

The reaction of the symmetrical bidentate chelating pyrazolyl gallate ligands $[Me_2Ga(N_2C_3HR_2)_2]^-$ (where R = H or Me) with the rhenium dimer molecule $[Re(CO)_4Cl]_2$ are described. In addition, the novel unsymmetrical bidentate chelating pyrazolyl gallate ligands $[Me_2Ga(N_2C_3HR_2)(OH)]^-$ are introduced and their reactivities towards the $[Re(CO)_4Cl]_2$ molecule detailed. Substitution reactions of the tetracarbonyl rhenium species produced by the above reactions are described, and possible conformations for the various complexes are suggested on the basis of ^1H nmr and ir results.

BRENDA M. LOUIE et ALAN STORR. Can. J. Chem. **62**, 1344 (1984).

On décrit la réaction de ligands chélatants bidentates symétriques, les gallates de pyrazolyle $[Me_2Ga(N_2C_3HR_2)_2]^-$ (où R = H ou Me), avec la molécule dimère de rhénium $[Re(CO)_4Cl]_2$. De plus, on introduit de nouveaux ligands chélatants bidentates qui ne sont pas symétriques, les gallates de pyrazolyle $[Me_2Ga(N_2C_3HR_2)(OH)]^-$, et on détaille leurs réactivités vis-à-vis la molécule de $[Re(CO)_4Cl]_2$. On décrit les réactions de substitution des espèces rhénium tétracarbonyle produites par les réactions décrites ci-dessus et, en se basant sur des spectres ir et de rmn du ^1H, on suggère des conformations possibles pour les divers complexes.

[Traduit par le journal]

Can. J. Chem. Downloaded from www.nrcresearchpress.com by 210.87.254.42 on 09/06/12
For personal use only.

Introduction

The syntheses of the bidentate chelating ligands $[Me_2Ga(N_2C_3HR_2)_2]^-$ (where R = H or Me), and their complexation to divalent transition metal ions have been detailed previously (1–4). In addition, a number of allylic Ni and Pd complexes containing these ligands have also been reported (5). Recently Mn, Mo, and W carbonyl derivatives incorporating the ligand where R = H have been described (6). The present account details the reactions of $[Re(CO)_4Cl]_2$ with the above symmetrical ligands. The syntheses of the novel unsymmetrical ligands $[Me_2Ga(N_2C_3HR_2)(OH)]^-$ (where R = H or Me) and their reactivity towards the above Re dimer are also described.

Experimental

Starting materials

Air-sensitive materials were handled in a glove box under an atmosphere of oxygen-free dry nitrogen or in a nitrogen-blanketed apparatus. Tetrahydrofuran (THF) was dried by refluxing over sodium/benzophenone and stored in the dry box following distillation. Benzene and methylene chloride were treated in a similar manner after refluxing over molten potassium and P_2O_5 respectively. Pyrazole (Aldrich) and PPh_3 (MCB) were used as supplied. $[Re(CO)_4Cl]_2$ was prepared from $Re_2(CO)_{10}$ (Strem) and Cl_2 (Matheson) as described in the literature (7). The symmetric bidentate gallium ligands $Na^+[Me_2Ga(N_2C_3HR_2)]^-$ (R = H or Me) were prepared as described previously (4) and used as THF solutions. $[Me_2Ga(OH)]_4$ was prepared from Me_3Ga(4) by a literature method (8). Analytical and ir data for the complexes described below are given in Table 1. ^1H nmr data are given in Table 2.

Preparation of $[Me_2Ga(N_2C_3H_3)_2]Re(CO)_4$

To a solution of $[Re(CO)_4Cl]_2$ (1.000 g, 1.498 mmol) dissolved in 50 mL THF two molar equivalents of $Na^+[Me_2Ga(N_2C_3H_3)_2]^-$ in 25 mL of the same solvent were added and the resultant mixture was stirred overnight. The THF was then removed *in vacuo* and the remaining off-white residue extracted with benzene and filtered. Evaporation of benzene resulted in a sticky, air-sensitive pale yellow solid. Residual solvents were removed by drying this solid at ~45°C *in vacuo* for several days. Yield ~60–70%.

Preparation of $[Me_2Ga(N_2C_3HR_2)_2]Re(CO)_3X$ [R = H or Me; X = PPh_3 or $N_2C_3H_4$]

For these reactions the $[Me_2Ga(N_2C_3HR_2)_2]Re(CO)_4$ (R = H or Me) complexes were not isolated but were prepared in THF solution as described above. Assuming a 100% yield, one molar equivalent of X dissolved in 25 mL THF was added and the resultant solution stirred for 12 h. The solvent was subsequently removed *in vacuo* and the remaining residue extracted with benzene and filtered. The complexes where R = H were air-stable white powders or colourless prisms. Yields ~90–100%. When R = Me the products could only be solidified after extended drying *in vacuo*. Impurities of X, $[Me_2Ga(N_2C_5H_7)]_2$ and $Re_2(CO)_{10}$ were sublimed out of these reaction mixtures. Although the products were moderately air stable as solids they quickly decomposed in solution on exposure to air. Yields ~30–35%.

Preparation of the ligands $Na^+[Me_2Ga(N_2C_3HR_2)(OH)]^-$ (R = H or Me)

In a typical preparation $[Me_2Ga(OH)]_4$ (0.905 g, 1.938 mmol) and $Na^+(N_2C_3H_3)^-$ (0.698 g, 7.755 mmol), both dissolved in 30 mL THF, were combined and the mixture stirred overnight. The clear, colourless solution was diluted with THF to 250.0 mL in a volumetric flask and aliquots were withdrawn for use in the following reactions.

Preparation of $[Me_2Ga(N_2C_3HR_2)(OH)]Re(CO)_3X$ (R = H or Me; X = CO or PPh_3)

These complexes were prepared using a similar procedure to that described above for the analogous compounds containing the $[Me_2Ga(N_2C_3H_3)_2]^-$ ligand. When X = CO, the hydroxo products were extracted with CH_2Cl_2, due to insolubility in benzene. The compounds were isolated as air-sensitive, off-white powders. Yields ~50–60%.

Spectra and analysis

Mass spectra were recorded on a Varian MAT CH4 mass spectrometer operating at 70 eV. Infrared spectra were recorded on a Perkin Elmer 598 spectrometer and ^1H nmr spectra were obtained on either a Bruker WP-80 or a Varian XL-100 spectrometer using FT techniques. Elemental analyses were performed by Mr. P. Borda of the U.B.C. Microanalytical Laboratory.

Results and discussion

The dimethylbis(1-pyrazolyl)gallate ligand, $[Me_2Ga(N_2C_3H_3)_2]^-$, reacted with $[Re(CO)_4Cl]_2$ to form an unstable tetracarbonyl complex with the gallate ligand occupying *cis* positions in the octahedral molecule. The monomeric nature of the product was confirmed by mass spectral analysis. A weak parent ion signal due to the ion $[Me_2Ga(N_2C_3H_3)_2]Re(CO)_4^+$ (=

TABLE 1. Analytical and ir data for

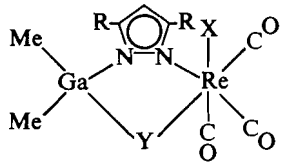

X	Y	R	Calculated (%) C	H	N	Found (%) C	H	N	ν_{CO}(cm^{-1}) cyclohexane (Nujol)	ν_{NH} (cm^{-1}) (Nujol)	ν_{OH} (cm^{-1}) (Nujol)
CO	$N_2C_3HR_2$	H	27.9	2.4	10.3*	28.5	2.9	11.0	2028, 1933, 1919, 1905 (2028, 1911 br)†		
PPh_3	$N_2C_3HR_2$	H	45.4	3.5	7.3	45.2	3.7	7.2	2031, 1937, 1908 (2022, 1900 br)		
$N_2C_3H_4$	$N_2C_3HR_2$	H	29.4	2.8	14.7	29.3	2.8	14.5	2030, 1926, 1912 (2022, 1915 br)	3378	
PPh_3	$N_2C_3HR_2$	Me	48.2	4.3	6.8	47.3	4.1	6.0	2021, 1911, 1899 (2021, 1924 br, 1901 br)		
$N_2C_3H_4$	$N_2C_3HR_2$	Me	34.4	3.8	13.4	33.7	3.7	13.2	2024, 1920 br, 1902 br (2020, 1916 br, 1900 br)	3375	
CO	OH	H	22.4	2.1	5.8	22.4	2.2	6.0	2037, 1930, 1920, 1912 (2010 br, 1870 br)		3570
PPh_3	OH	H	43.6	3.5	3.9	43.2	3.3	3.3	2030, 1934, 1899 (2025, 1932 br, 1895 br)		3600
CO	OH	Me	27.3	3.0	5.3‡	27.8	3.4	5.9	2030, 1917, 1904 (2000 br, 1875 br)		3580
PPh_3	OH	Me	45.2	3.9	3.8	45.6	3.7	3.2	2028, 1932, 1894 (2028, 1930 br, 1892 br)		3595

*Calculated with 0.15 THF.
†br = broad.
‡Calculated with 0.25 THF.

TABLE 2. ^1H nmr data for

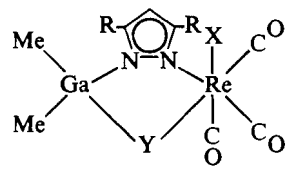

X	Y	R	τ (ppm)* —$GaMe_2$	R	^4H	X	NH	OH
CO	$N_2C_3HR_2$	H	10.02s, 10.04s	2.10d, 2.53d	3.83t			
PPh_3	$N_2C_3HR_2$	H	9.87s, 9.89s	2.60d, 2.69d	4.27t	2.88m, 3.07m		
$N_2C_3H_4$	$N_2C_3HR_2$	H	9.07s, 9.94s	2.56dd, 2.65dd	4.05t	3.10m, 4.33m, 4.71m	1.81br	
PPh_3	$N_2C_3HR_2$	Me	10.06s, 10.10s	8.03s, 8.37s	4.30s	2.69m, 3.01m		
$N_2C_3H_4$	$N_2C_3HR_2$	Me		See discussion				
CO	OH	H		Not soluble				
PPh_3	OH	H	10.11s, 10.60s	(Under PPh_3)	4.11t			10.29s
CO†	OH	Me	10.39s	7.14s, 7.68s	4.00s			9.53s
PPh_3	OH	Me	10.07s, 10.60s	7.98s, 8.15s	4.42s			10.29s

*Measured in C_6D_6 ($\tau_{C_6H_6}$ = 2.84 ppm), s = singlet, d = doublet, t = triplet, dd = doublet of doublets, m = multiplet, br = broad.
†Measured in d^6-acetone ($\tau_{acetone}$ = 7.89 ppm).

P^+) was observed with a relative intensity of ~2.5% of the most intense signal which corresponded to the ion, P − CO − Me^+. Intense signals were also observed for ions resulting from the successive loss of four CO groups from either the P^+ or P − Me^+ ions. In addition to the expected signals arising from the tetracarbonyl species the mass spectrum also contained weak signals due to ions arising from the complex [MeGa$(N_2C_3H_3)_3$]$Re(CO)_3$. The appearance of this minor product was not entirely unexpected as similar results have been observed in analogous systems. Thus, when the dihydrobis(1-pyrazolyl)-borate ligand, $[H_2B(N_2C_3H_3)_2]^-$, was reacted with the pentacarbonyls, $M(CO)_5Br$ (where M = Mn or Re), at room temperature no tetracarbonyl complex formed. Instead the compounds $[H_2B(N_2C_3H_3)_2]M(CO)_3(N_2C_3H_4)$ were isolated in low yields

Can. J. Chem. Downloaded from www.nrcresearchpress.com by 210.87.254.42 on 09/06/12
For personal use only.

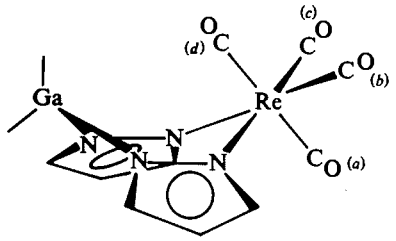

FIG. 1. Proposed conformation of the tetracarbonyl complex $[Me_2Ga(N_2C_3H_3)_2]Re(CO)_4$.

together with the corresponding decacarbonyl, $M_2(CO)_{10}$. Furthermore, when the above Mn borate complex was refluxed in THF for 24 h an internal condensation reaction took place, resulting in the compound $[HB(N_2C_3H_3)_3]Mn(CO)_3$ (9). In addition when the gallate ligand, $[Me_2Ga(N_2C_3H_3)_2]^-$, was stirred with $Mn(CO)_5Br$ in THF, with no added pyrazole present, the complex $[Me_2Ga(N_2C_3H_3)_2]Mn(CO)_3(N_2C_3H_4)$ was isolated in low yield (6). Again, in this reaction, no evidence of the expected tetracarbonyl species was observed.

The introduction of methyl groups at the 3- and 5-positions of the pyrazolyl rings of the gallate ligand led to a rhenium tetracarbonyl complex of much lower stability. In fact, although spectral evidence for the desired complex was observed, attempts at isolating a pure sample of $[Me_2Ga(N_2C_5H_7)_2]Re(CO)_4$ were unsuccessful. Repeated contamination of the product with the known stable dimer $[Me_2Ga(N_2C_5H_7)]_2$ (3) indicate that the complex was disproportionating.

It is well known that transition metal complexes containing the bis(1-pyrazolyl)gallate or -borate ligands generally adopt a boat conformation for the central M—(N—N)$_2$—M′, (where M = transition metal, M′ = B or Ga) six-membered ring. This situation is dictated by a combination of steric and electronic factors (3, 10). Such a conformation in the complex $[Me_2Ga(N_2C_3H_3)_2]Re(CO)_4$ places the two gallium methyl groups in inequivalent environments (Fig. 1) and leads to two singlets for the $GaMe_2$ group in the ^1H nmr spectrum of the compound (Table 2). On reaction of the tetracarbonyl complexes $[Me_2Ga(N_2C_3HR_2)_2]Re(CO)_4$ (R = H or Me), with PPh_3 or pyrazole, $N_2C_3H_4$, monosubstituted tricarbonyl products were formed. The ^1H nmr spectra (Table 2) of the products from these reactions clearly indicated that the position of substitution must be at position (*a*) or (*d*) of Fig. 1 since the two bridging pyrazolyl groups gave only one set of signals. The solution ir spectra of these tricarbonyl products (Table 1) each contained three strong bands in the carbonyl stretching region, a pattern indicative of facial coordination of the three CO groups (11) and strongly supportive of substitution at either position (*a*) or (*d*) in the original syntheses. This pattern of substitution would also be predicted on *trans*-effect arguments — the CO group *trans* to another CO group would be expected to be more labile than one opposite to a pyrazolyl group. A recent X-ray structure determination of the complex $[Me_2Ga(N_2C_3H_3)_2]Mn(CO)_3(N_2C_3H_4)$ shows definitively this type of arrangement, with the pyrazole ligand occupying the (*a*) position in the molecule (6). Molecular models indicate that this would be the sterically favored position of substitution since bulky substituents in the (*d*) position may clash with the pseudo axial methyl group on the gallium atom.

The ^1H nmr spectrum of the complex $[Me_2Ga(N_2C_3H_3)_2]Re(CO)_3(N_2C_3H_4)$ is shown in Fig. 2*a* and an expanded view of

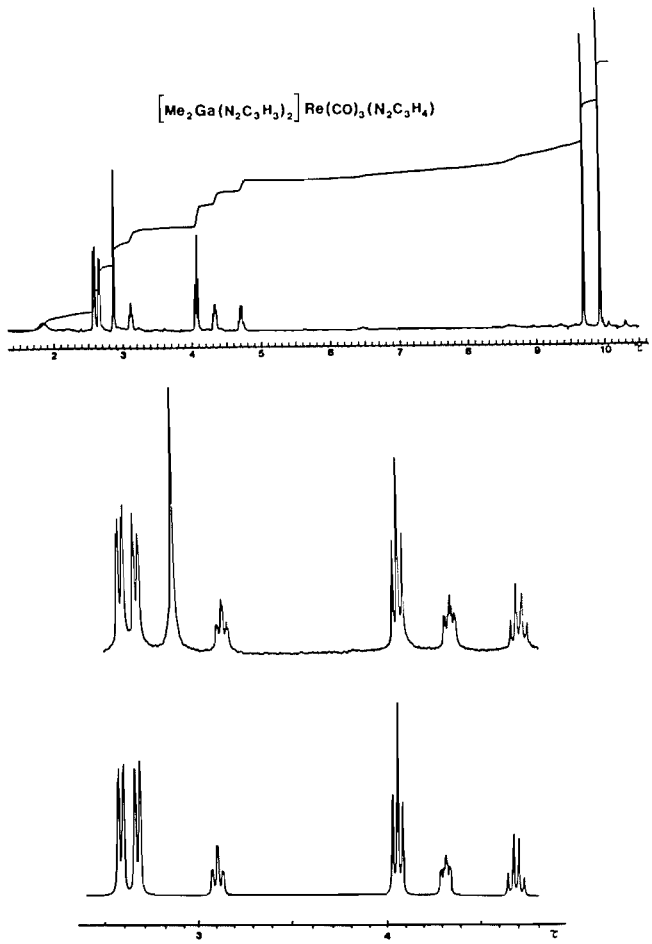

FIG. 2. (top) Room temperature 100 MHz ^1H nmr of $[Me_2Ga(N_2C_3H_3)_2]Re(CO)_3N_2C_3H_4$ in C_6D_6 solution. (middle) Expanded pyrazolyl proton region of above spectrum. (bottom) Computer simulated spectrum of pyrazolyl proton region of spectrum (top) using coupling constants given in Table 3.

the "pyrazolyl proton" region of the spectrum is shown in Fig. 2*b*. The latter clearly shows small cross-ring couplings in addition to the normal J_{HCCH} couplings usually observed in the ^1H nmr spectra of pyrazolyl complexes. A computer-simulated spectrum (Fig. 2*c*) based on the parameters given in Table 3 fits very closely to the experimental spectrum.

The complexes $[Me_2Ga(N_2C_3HR_2)_2]Re(CO)_3X$ (where R = Me; X = PPh_3 or $N_2C_3H_4$) were less stable than the corresponding complexes where R = H, and could only be isolated in low yields. Steric effects could be an important factor contributing to this observed instability, especially with the bulky PPh_3 ligand. The reaction of $[Me_2Ga(N_2C_5H_7)_2]Re(CO)_4$ with $N_2C_3H_4$ resulted in a solid which analyzed correctly for the expected product $[Me_2Ga(N_2C_5H_7)_2]Re(CO)_3(N_2C_3H_4)$. The mass spectrum showed a parent ion signal and a pattern of signals predictable from the expected fragmentation of the molecular ion. In addition, ir data indicated a facially coordinated tricarbonyl complex although the two lower frequency bands were broader than normal and the 1902 cm^{-1} vibration displayed a shoulder at 1908 cm^{-1}. The ^1H nmr spectrum of the complex was not easily interpretable, containing many more signals than expected. Thus the product should display two Ga—Me signals and one NH signal. However, the $GaMe_2$ region of the room temperature spectrum showed four sharp signals at 9.11, 9.18, 9.64, and 9.73 τ. In addition two NH

Can. J. Chem. Downloaded from www.nrcresearchpress.com by 210.87.254.42 on 09/06/12
For personal use only.

TABLE 3. ^{1}H nmr data for

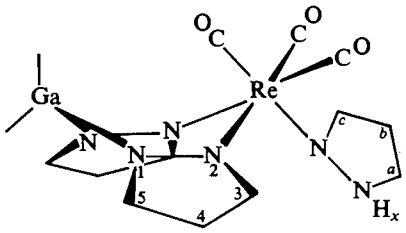

Proton	Chemical shift (τ)*	Coupling constants (Hz)
H_3	2.56	J_{34}=2.1, J_{35}=0.5
H_4	4.05	J_{43}=J_{45}=2.1
H_5	2.65	J_{53}=0.5, J_{54}=2.1
H_a	4.33	J_{ab}=2.4, J_{ac}=0.6, J_{ax}=1.5
H_b	4.71	J_{ba}=2.4, J_{bc}=J_{bx}=2.3
H_c	3.10	J_{ca}=0.6, J_{cb}=J_{cx}=2.3
H_x	(1.81)†	

*Measured in C_6D_6 solution at room temperature ($\tau_{C_6H_6}$ = 2.84 ppm).
†Not included in Fig. 3.

signals at 1.53 and 2.14 τ and complicated patterns in the pz—^{4}H and pz—Me regions of the spectrum were observed. The main signals could be assigned to the following molecular arrangements:

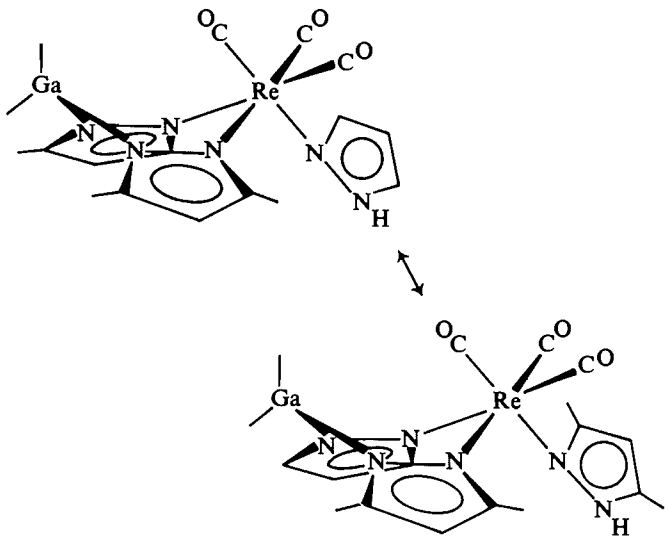

To explain the ^{1}H nmr and ir results it is proposed that the complex $[Me_2Ga(N_2C_5H_7)_2]Re(CO)_3(N_2C_3H_4)$ is fluxional in solution and that the fluxional process leads to an exchange between the terminal "pyrazole" and the bridging "pyrazolyl" rings. A possible mechanism for the proposed exchange is illustrated below:

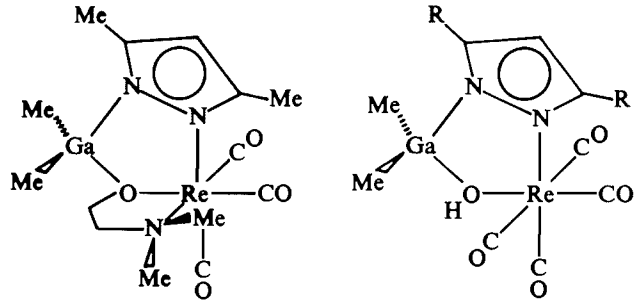

(*a*) (*b*)

FIG. 3. (*a*) Conformation of five-membered [—Ga(—N—N—)-Re—O—] ring in the complex $[Me_2Ga(N_2C_5H_7)(OCH_2CH_2NMe_2)]$-$Re(CO)_3$. (*b*) Proposed conformation of five-membered [—Ga-(—N—N—)Re—O—] rings in the complexes $[Me_2Ga(N_2C_3HR_2)$-$(OH)]Re(CO)_4$.

In this scheme the terminal pyrazole group is shown in the (*d*) position of Fig. 1, an arrangement which may be preferred for this ligand or could arise via a simple Ga—$(N—N)_2$—Re boat flip if this group started out in the (*a*) position. A hydrogen switch then alternates the pyrazole and 3,5-dimethyl pyrazole groups as the terminal ligand. A similar mechanism has been proposed previously to explain the solution behaviour of the anionic species $\{[Me_2Ga(N_2C_3H_3)_2]_2M(CO)_3(N_2C_3H_4)\}^-$, (where M = Mo or W). Thus the ^{1}H nmr spectra of these two species displayed but one set of signals for both the terminal pyrazole and bridging pyrazolyl groups (6). Additional support for the proposed mechanism of the fluxional process comes with the formation of the complex $[MeGa(N_2C_5H_7)_2(N_2C_3H_3)]$-$Re(CO)_3$ upon heating a C_6D_6 solution of the compound $[Me_2Ga(N_2C_5H_7)_2]Re(CO)_3(N_2C_3H_4)$ at ~70°C. In the fluxional process described it can be seen that the "mobile" hydrogen is brought within close range of a methyl group on the gallium atom, making a methane elimination reaction feasible (cf. ref. 9).

The novel unsymmetrical bidentate chelating gallate ligands $[Me_2Ga(N_2C_3HR_2)(OH)]^-$ (where R = H or Me) have been prepared via bridge cleavage reactions of the weakly associated tetrameric $(Me_2GaOH)_4$ molecule (12) with the appropriate sodium pyrazolide. The ligands reacted with the dimer $[Re-(CO)_4Cl]_2$ to give the tetracarbonyl species $[Me_2Ga(N_2C_3HR_2)$-$(OH)]Re(CO)_4$. Both complexes, like the tetracarbonyls described above, have one CO group which is very labile and easily replaced by a PPh_3 ligand.

The geometry of the five-membered ring formed by the ligand at the Re centre is of interest. An X-ray structure of the complex $[Me_2Ga(N_2C_5H_7)(OCH_2CH_2NMe_2)]Re(CO)_3$ (13) shows a facial coordination of the tridentate gallate ligand but more importantly a near planarity for the [—Ga—(N—N)—Re—O—] five-membered ring (Fig. 3*a*). It seems likely that the present bidentate ligand could be coordinated in a similar manner (Fig. 3*b*). Such a planar geometry, of course,

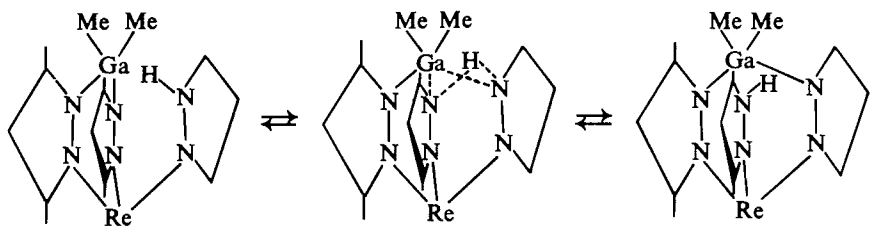

Can. J. Chem. Downloaded from www.nrcresearchpress.com by 210.87.254.42 on 09/06/12
For personal use only.

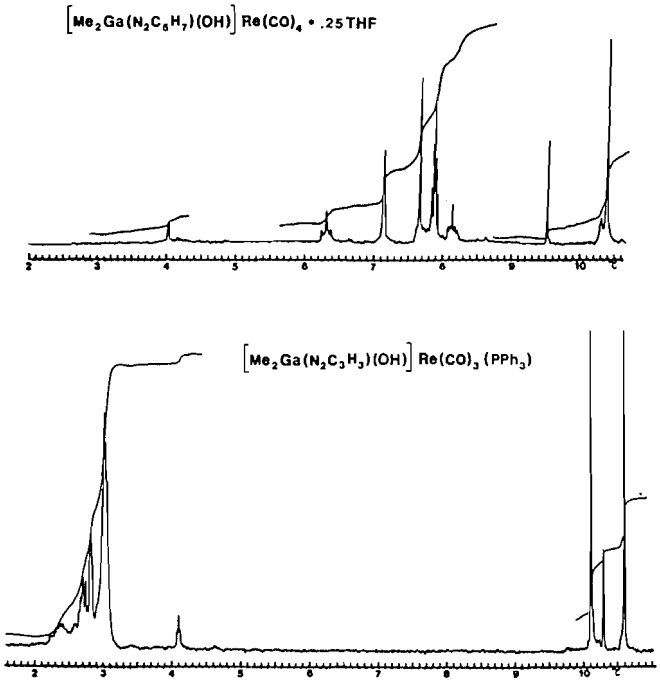

FIG. 4. Room temperature 100 MHz ^{1}H nmr of (top) $[Me_2Ga(N_2C_5H_7)(OH)]Re(CO)_4 \cdot 0.25THF$ in d_6-acetone, (bottom) $[Me_2Ga(N_2C_3H_3)(OH)]Re(CO)_3(PPh_3)$ in C_6D_6.

makes the two methyl groups on the gallium atom structurally equivalent, and this is consistent with the singlet observed for the $GaMe_2$ protons in the ^{1}H nmr spectrum of the complex $[Me_2Ga(N_2C_5H_7)(OH)]Re(CO)_4$ (Fig. 4*a*). Substitution of a PPh_3 group for a CO group leads to non-equivalence of the two Ga—Me groups (Fig. 4*b*) and consequently must be occurring at a position mutually *cis* to both donor atoms of the chelating gallate ligand. Facial coordination of the three remaining CO groups is also indicated by the three strong ν_{CO} stretching vibrations in the ir spectra (11) of the substituted products.

The mass spectra of the complexes $[Me_2Ga(N_2C_3HR_2)(OH)]Re(CO)_3(PPh_3)$ displayed predictable sets of signals. When R = H the monomer parent ion, P^+, signal was observed, with the most intense signal arising from the $P - CO^+$ ion. When R = Me no parent ion signal was observed but major signals attributable to the ions $P - Me^+$ (10%), $P - CO^+$ (20%), and $P - Me - PPh_3^+$ (100%) dominated the spectrum.

The present $[Me_2Ga(N_2C_3HR_2)(OH)]^-$ bidentate ligands have only one related system in the literature and that is the tridentate ligand $[MeGa(N_2C_5H_7)_2(OH)]^-$ which appeared serendipitously in some products from reactions involving the symmetrical tridentate ligand $[MeGa(N_2C_5H_7)_3]^-$ (14).

Our investigations are expanding to include other related unsymmetric bidentate ligands with the oxygen donor functionality of the present systems being replaced by —SR or $—PR_2$ groupings.

Acknowledgement

We thank the Natural Sciences and Engineering Research Council of Canada for financial support.

1. D. F. RENDLE, A. STORR, and J. TROTTER. J. Chem. Soc. Dalton Trans. 176 (1975).
2. F. G. HERRING, D. J. PATMORE, and A. STORR. J. Chem. Soc. Dalton Trans. 711 (1975).
3. D. J. PATMORE, D. F. RENDLE, A. STORR, and J. TROTTER. J. Chem. Soc. Dalton Trans. 718 (1975).
4. K. R. BREAKELL, D. J. PATMORE, and A. STORR. J. Chem. Soc. Dalton Trans. 749 (1975).
5. K. S. CHONG, S. J. RETTIG, A. STORR, and J. TROTTER. Can. J. Chem. **59**, 996 (1981).
6. S. E. ANSLOW, K. S. CHONG, S. J. RETTIG, A. STORR, and J. TROTTER. Can. J. Chem. **59**, 3123 (1981).
7. G. DOLCETTI and J. R. NORTON. Inorg. Synth. **16**, 35 (1976).
8. M. J. SPRAGUE, G. E. GLASS, and R. S. TOBIAS. Inorg. Synth. **12**, 67 (1970).
9. A. BOND and M. GREEN. J. Chem. Soc. A, 682 (1971).
10. S. TROFIMENKO. Acc. Chem. Res. **4**, 17 (1971).
11. D. M. ADAMS. Metal–ligand and related vibrations. Edward Arnold Ltd., London. 1967. Chapt. 3.
12. G. S. SMITH and J. L. HOARD. J. Am. Chem. Soc. **81**, 3907 (1959).
13. B. M. LOUIE, S. J. RETTIG, A. STORR, and J. TROTTER. Unpublished results.
14. K. R. BREAKELL, S. J. RETTIG, A. STORR, and J. TROTTER. Can. J. Chem. **57**, 139 (1979).

Can. J. Chem. Downloaded from www.nrcresearchpress.com by 210.87.254.42 on 09/06/12
For personal use only.

Theory of ^{13}C and ^{1}H paramagnetic shifts in uranocene. Does it indicate *f* orbital covalency?

BRUCE R. MCGARVEY
Department of Chemistry, University of Windsor, Windsor, Ont., Canada N9B 3P4

Received October 6, 1983

BRUCE R. MCGARVEY. Can. J. Chem. **62**, 1349 (1984).

The paramagnetic shift resulting from *f* orbital covalency for lanthanide fluorides has been successfully treated theoretically in earlier studies. This theoretical method has been modified to calculate the paramagnetic shift for ^{13}C and ^{1}H in uranocenes. It is shown that the very large anisotropy in the magnetic moment makes the treatments in the literature incorrect. The so-called "contact shift" in ^{13}C is in reality three terms: (*1*) a dipolar contribution from spin in the carbon p_z orbital, (*2*) a dipolar contribution from spin in the nearest neighbor carbon p_z orbitals, and (*3*) an induced Fermi contact term. Contribution (*1*) is the largest. For ^{1}H there are contributions from the direct dipolar interaction of spin in the nearest carbon p_z orbital and the induced Fermi contact term. Both terms are nearly equal in magnitude. The theory, however, predicts a much smaller magnitude and the incorrect sign for the shift as measured experimentally. The measured shift must, therefore, result from a polarization mechanism in which exchange interactions between the *f* electrons and electrons in filled orbitals cause spin delocalization into the ligand σ orbitals. It is argued that this polarization mechanism operates primarily through the overlap of the outer 6*s* and 6*p* orbitals of the uranium atom with the σ orbitals of the ligand making the observed nmr shifts insensitive to the nature of the bonding between the ligand and the uranium atom. We conclude, therefore, that the question of how much *f* orbitals are involved in covalent bonds between uranium and the ligands in uranocene cannot be answered by measuring the paramagnetic shift in ^{13}C or ^{1}H.

BRUCE R. MCGARVEY. Can. J. Chem. **62**, 1349 (1984).

Dans des études antérieures, on avait traité d'un point de vue théorique et avec succès des déplacements paramagnétiques résultant de la covalence de l'orbitale *f* des fluorures de lanthanides. On a modifié cette méthode théorique pour calculer les déplacements paramagnétiques du ^{13}C et du ^{1}H dans des uranocènes. On montre que, dû à la très grande anisotropie du moment magnétique, tous les traitements rapportés dans la littérature sont incorrects. Tout ce qu'on appelle "déplacement de contact" en rmn du ^{13}C recouvre en réalité trois termes: (*1*) une contribution dipolaire du spin dans l'orbitale p_z du carbone, (*2*) une contribution dipolaire de la part du spin dans les orbitales p_z du carbone voisin le plus près et (*3*) un terme de contact de Fermi induit. La contribution (*1*) est la plus importante. Dans le cas du ^{1}H, on observe des contributions provenant d'une interaction dipolaire directe du spin dans l'orbitale p_z du carbone le plus près ainsi que le terme de contact de Fermi induit. L'importance de chacun de ces deux termes est à peu près du même ordre de grandeur. La théorie, cependant, prédit un ordre de grandeur beaucoup plus faible et un signe incorrect pour le déplacement tel qu'il est mesuré expérimentalement. Les déplacements mesurés doivent, dans ce cas, provenir d'un mécanisme de polarisation dans lequel les interactions d'échange entre les électrons *f* et les électrons des orbitales saturées provoquent une délocalisation de spin vers les orbitales du ligand. On prétend que ce mécanisme de polarisation opère principalement par l'intermédiaire du recouvrement des orbitales périphériques 6*s* et 6*p* de l'atome d'uranium avec les orbitales du ligand rendant ainsi les déplacements chimiques observés en rmn insensibles à la nature de la liaison entre le ligand et l'atome d'uranium. Nous concluons alors que la réponse à la question relative à l'importance de la participation des orbitales *f* dans la liaison covalente entre l'uranium et les ligands dans l'uranocène ne peut être obtenue par une mesure du déplacement paramagnétique du ^{13}C ou du ^{1}H.

[Traduit par le journal]

Introduction

In earlier studies (1) we have developed a model for calculating the paramagnetic shift arising from a covalent interaction between *f* orbitals of a rare earth ion and the *s* and *p* orbitals of the ligand atom. This model was successfully applied in a series of studies of ^{19}F nmr in lanthanide fluoride solids (2–9). These studies revealed that the covalent interaction was large enough to dominate the paramagnetic shift for lanthanides in the second half of the series. The shift in the first half appeared to be dominated by the spin polarization mechanism of Watson and Freeman (10). No comparable analysis of shifts in actinide complexes appears to have been done.

A large number of organometallic actinide compounds have been made and their nmr spectra studied in solution. Much of this nmr work has been reviewed by Fischer (11) and by Luke and Streitweser (12). In those cases in which the pseudo-contact shift could be reliably estimated, it was found that when the pseudo-contact shift was subtracted from the experimental shift that a sizeable shift, which has generally been called the contact shift, remained. The existence of this contact shift has been cited as evidence of covalency between the actinide and the ligand but it is rarely clearly stated which orbitals of the actinide are involved, although it seems to be generally assumed that the π orbitals of the ligands are where the transferred spin resides. The sign of the shifts, however, suggests that the shifts are determined mainly by the polarization transfer mechanism which involves the σ electrons of the ligand rather than the π electrons.

Our earlier studies on the lanthanides have shown that when the orbital momentum and spin–orbit interaction are not quenched by the crystal field (as is the case in the lanthanides and actinides), then unpaired electrons in *p* orbitals on the ligand atoms can make as great or greater a contribution to the isotropic shift as the *s* electrons do through the Fermi contact shift. The sign of this contribution depends on the nature of the ground and excited states of the complex in question. Thus the treatment of the shift as just a contact shift, using equations that were derived for the transition metal complexes, is very suspect.

We have decided that it would be of some interest to extend our theory to the actinide complexes to see what sort of shifts are predicted when the spin is transferred to the ligand through *f* orbital covalency. We have chosen to study the uranocene molecule, $U(C_8H_8)_2$. The high symmetry of this molecule

Can. J. Chem. Downloaded from www.nrcresearchpress.com by 210.87.254.6 on 09/06/12
For personal use only.

Can. J. Chem. Downloaded from www.nrcresearchpress.com by 210.87.254.6 on 09/06/12
For personal use only.

makes it a good candidate for theoretical study and the extensive number of nmr studies of it and its derivatives gives us something with which to compare our calculations.

What is the ground state of uranocene?

U(IV) has an f^2 configuration with the lowest state being $^3H_4$. The point symmetry group of $U(C_8H_8)_2$ is either D_{8h} or D_{8d} and since it will make no difference in the calculations we will assume the former for convenience. The eight-fold symmetry results in a crystal field with no spherical harmonics with $M > 0$ and, therefore, the $^3H_4$ state is split by the crystal field into five states which are:

$$|J,M_J\rangle = |4,\pm4\rangle;\ |4,\pm3\rangle;\ |4,\pm2\rangle;\ |4,\pm1\rangle;\ |4,0\rangle$$

There is no agreement in the literature as to which of these five states is the ground state. The $|4,\pm4\rangle$, $|4,\pm3\rangle$, and $|4,0\rangle$ states have all been suggested as the ground state in uranocene.

Karracker (13) predicted $|4,\pm4\rangle$ ground state based on theoretical considerations. This was confirmed by Hayes and Edelstein (14) in their analysis of the magnetic susceptibility of powders of uranocene, neptunocene, and plutonocene. Amberger *et al.* (15) fitted their susceptibility data to a model in which the ground state was $|4,0\rangle$ with the $|4,\pm1\rangle$ state only 17 cm^{-1} above it. Dallinger *et al.* (16) found with Raman studies that the first excited state was at 466 cm^{-1} and differed from the ground state by $\Delta M_J = \pm1$. They proposed a ground state of $|4,\pm4\rangle$ with the first excited state being $|4,\pm3\rangle$ by fitting the theoretical susceptibility against the experimental susceptibility versus temperature plot. They obtained a slightly poorer fit when the two states were reversed.

Fischer (11) has estimated $(\mu_\parallel^2 - \mu_\perp^2)$ to be 8.8 Bohr magnetons from pseudo-contact shift studies and claims this requires a $|4,\pm3\rangle$ ground state with the first excited state being $|4,\pm2\rangle$. Luke and Streitweiser (12) have also estimated the pseudo-contact shift and obtain a value of $(\mu_\parallel^2 - \mu_\perp^2) = 12.5$ Bohr magnetons which we estimate would best fit a ground state of $|4,\pm3\rangle$ with the first excited state being $|4,\pm4\rangle$. Hayes and Edelstein (14) also predicted a $|4,\pm3\rangle$ ground state on the basis of Wolfsberg–Helmholtz MO computations.

The present evidence suggests three possibilities: $|4,\pm4\rangle$ is ground state with $|4,\pm3\rangle$ at 466 cm^{-1} or $|4,\pm3\rangle$ is ground state with either $|4,\pm4\rangle$ or $|4,\pm2\rangle$ at 466 cm^{-1}. We will do our calculations for all three possibilities.

Molecular orbitals of $U(C_8H_8)_2$

For D_{8h} the MO's for the p_z orbitals of COT (cyclooctatetraene) will be given using the numbering system for individual carbon atoms as shown below.

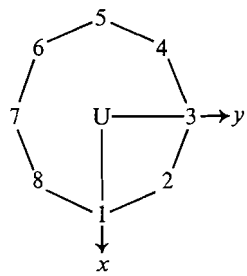

The lower ring has atom number 9 under 1, 10 under 2, etc. Since the f orbitals belong to the A_{2u}, E_{1u}, E_{2u}, and E_{3u} irreducible representations, we give in eq. [1] only the π MO's belonging to those representations.

$$\phi(A_{2u}) = \frac{1}{4}[p_z^1 + p_z^2 + p_z^3 + p_z^4 + p_z^5 + p_z^6 + p_z^7 + p_z^8 + p_z^9 + p_z^{10} + p_z^{11} + p_z^{12} + p_z^{13} + p_z^{14} + p_z^{15} + p_z^{16}]$$

$$\phi(E_{1u})[x(5z^2 - r^2)] = \frac{1}{4}[\sqrt{2}p_z^1 + p_z^2 - p_z^4 - \sqrt{2}p_z^5 - p_z^6 + p_z^8 - \sqrt{2}p_z^9 - p_z^{10} + p_z^{12} + \sqrt{2}p_z^{13} + p_z^{14} - p_z^{16}]$$

$$\phi(E_{1u})[y(5z^2 - r^2)] = \frac{1}{4}[p_z^2 + \sqrt{2}p_z^3 + p_z^4 - p_z^6 - \sqrt{2}p_z^7 - p_z^8 - p_z^{10} - \sqrt{2}p_z^{11} - p_z^{12} + p_z^{14} + \sqrt{2}p_z^{15} + p_z^{16}]$$

[1]
$$\phi(E_{2u})[z(x^2 - y^2)] = \frac{1}{\sqrt{8}}[p_z^1 - p_z^3 + p_z^5 - p_z^7 + p_z^9 - p_z^{11} + p_z^{13} - p_z^{15}]$$

$$\phi(E_{2u})[zxy] = \frac{1}{\sqrt{8}}[p_z^2 - p_z^4 + p_z^6 - p_z^8 + p_z^{10} - p_z^{12} + p_z^{14} - p_z^{16}]$$

$$\phi(E_{3u})[x(x^2 - 3y^2)] = \frac{1}{4}[\sqrt{2}p_z^1 - p_z^2 + p_z^4 - \sqrt{2}p_z^5 + p_z^6 - p_z^8 - \sqrt{2}p_z^9 + p_z^{10} - p_z^{12} + \sqrt{2}p_z^{13} - p_z^{14} + p_z^{16}]$$

$$\phi(E_{3u})[y(3x^2 - y^2)] = \frac{1}{4}[p_z^2 - \sqrt{2}p_z^3 + p_z^4 - p_z^6 + \sqrt{2}p_z^7 - p_z^8 - p_z^{10} + \sqrt{2}p_z^{11} - p_z^{12} + p_z^{14} - \sqrt{2}p_z^{15} + p_z^{16}]$$

The appropriate atomic orbitals for the $|4,4\rangle$, $|4,3\rangle$, and $|4,2\rangle$ states of the f^2 configuration are given in eq. [2] below.

$$|4,4\rangle = \frac{1}{\sqrt{5\cdot6\cdot11}}\{3\sqrt{3}(f_3^+f_1^- + f_3^-f_1^+) - 3\sqrt{30}f_3^-f_2^- - \sqrt{2}f_2^+f_1^+ - 2f_3^+f_0^+\}$$

[2]
$$|4,3\rangle = \frac{1}{4\sqrt{3\cdot5\cdot11}}\{-24\sqrt{3}f_3^-f_1^- + 8\sqrt{2}(f_2^-f_1^+ + f_2^+f_1^-) + 16(f_3^+f_0^- + f_3^-f_0^+) - 4\sqrt{6}f_2^+f_0^+ - 4\sqrt{3}f_3^+f_{-1}^+\}$$

$$|4,2\rangle = \frac{1}{\sqrt{5\cdot6\cdot7\cdot11}}\{-14\sqrt{2}f_2^-f_1^- - 28f_3^-f_0^- + 7\sqrt{6}(f_2^+f_0^- + f_2^-f_0^+) + 7\sqrt{3}(f_3^+f_{-1}^- + f_3^-f_{-1}^+) - 2\sqrt{15}f_1^+f_0^+ - 9\sqrt{2}f_2^+f_{-1}^+ - \sqrt{30}f_3^+f_{-2}^+\}$$

The f orbitals are combinations of real functions that match the above π orbitals in symmetry. We therefore combine the π orbitals in an analogous fashion to give the complex functions listed in eq. [3] below.

$$[3]\quad \begin{array}{ll} f_0 = |z(5z^2 - 3r^2)\rangle & \phi_0 = \phi(A_{2u}) \\ f_{\pm1} = \frac{1}{\sqrt{2}}[\mp|x(5z^2 - r^2)\rangle - i|y(5z^2 - r^2)\rangle] & \phi_{\pm1} = \frac{1}{\sqrt{2}}\{\mp\phi(E_{1u})[x(5z^2 - r^2)] - i\phi(E_{1u})[y(5z^2 - r^2)]\} \\ f_{\pm2} = \frac{1}{\sqrt{2}}[|z(x^2 - y^2)\rangle \pm i|xyz\rangle] & \phi_{\pm2} = \frac{1}{\sqrt{2}}\{\phi(E_{2u})[z(x^2 - y^2)] \pm i\phi(E_{2u})[xyz]\} \\ f_{\pm3} = \frac{1}{\sqrt{2}}[\mp|x(x^2 - 3y^2)\rangle - i|y(3x^2 - y^2)\rangle] & \phi_{\pm3} = \frac{1}{\sqrt{2}}\{\mp\phi(E_{3u})[x(x^2 - 3y^2)] - i\phi(E_{3u})[y(3x^2 - y^2)]\} \end{array}$$

We now combine the metal f orbital and the π ligand orbitals to get the complex MO's listed in eq. [4].

$$[4]\quad \begin{array}{l} F_0 = N_0 f_0 - b_0\phi_0 \\ F_{\pm1} = N_1 f_{\pm1} - b_1\phi_{\pm1} \\ F_{\pm2} = N_2 f_{\pm2} - b_2\phi_{\pm2} \\ F_{\pm3} = N_3 f_{\pm3} - b_3\phi_{\pm3} \end{array}$$

We now replace the f orbitals in eq. [2] with the F functions of eq. [4]. It is these functions that will be used to calculate the contribution of covalent bonding between f orbitals and the π orbitals of COT to the paramagnetic shift. In practice we will calculate the shift for atom 1 and will need to worry only about the p_z^1, p_z^2, and p_z^8 terms in the above MO's.

Calculation of paramagnetic shift for ^{13}C

The calculation of the paramagnetic shift is a straightforward but tedious procedure using the theory of Kurland and McGarvey (17). If there is only one excited state to include in the calculation, the equation for the shift takes on the following form:

$$\left(\frac{\Delta H}{H}\right)_{i=(x,y,z)} = \frac{1}{qkT}\left[\langle 4,3|\mu_i|4,3\rangle\langle 4,3|\frac{A_{Ni}}{g_N\mu_N}|4,3\rangle + \langle 4,4|\mu_i|4,4\rangle\langle 4,4|\frac{A_{Ni}}{g_N\mu_N}|4,4\rangle\, e^{-\Delta/kT} + \frac{kT}{\Delta} \times (1 - e^{-\Delta/kT})\langle 4,4|\mu_i|4,3\rangle\langle 4,3|\frac{A_{Ni}}{g_N\mu_N}|4,4\rangle\right]$$

$$[5]\quad q = 2(1 + e^{-\Delta/kT})$$

$$\mu_i = -g_J\mu_e J_i$$

$$\frac{A_{Ni}}{g_N\mu_N} = \frac{8}{3}\pi g_e\mu_e \sum_j \delta(r_j)(s_i)_j + g_e\mu_e \sum_j [(3s_j\cdot r_j)(r_i)_j - r_j^2(s_i)_j]r_j^{-5} + 2\mu_e \sum_i r_j^{-3}(l_i)_j$$

where we have assumed the ground state to be $|4,\pm3\rangle$ and the excited state to be $|4,\pm4\rangle$, Δ is the energy difference between the two states, and the other symbols have their usual meanings. To obtain the result when $|4,\pm4\rangle$ is the ground state and $|4,\pm3\rangle$ the excited state, we simply make Δ negative in value and to obtain the shift when the excited state is $|4,\pm2\rangle$, we simply replace $|4,\pm4\rangle$ by $|4,\pm2\rangle$ in the above equation.

The matrix elements of eq. [5] are given in the Appendix along with the steps needed in their computation. The calculation was done for carbon nucleus 1 and contributions from unpaired spin on neighboring atoms 2 and 8 have been included. The A_{2p} term comes from p_z^1 and the R^{-3} term comes from p_z^2 and p_z^8. The Fermi contact term Q has contributions from all three atoms and is estimated by standard methods (18).

Using the matrix elements in the Appendix and eq. [5], the shift is calculated for the x, y, and z principal directions and the results are given in eq. [6]. Please note that the shift for both x and y must be calculated because the local symmetry around the carbon nucleus is not axial, even though the molecule itself has axial symmetry. The equations given in eq. [6] are for the case when the ground state is $|4,\pm3\rangle$ and the nearest excited state is $|4,\pm4\rangle$.

$$\left(\frac{\Delta H}{H}\right)_z = \frac{\mu_e}{3300kT(1 + e^{-\Delta/kT})}\left[\frac{A_{2p}}{g_N\mu_N} - \frac{g_e\mu_e}{R^3} + \frac{Q}{2g_N\mu_N}\right]\{9[35b_3^2 - 2b_2^2 + 35b_1^2 - 2b_0^2] + 4[133b_3^2 + 134b_2^2 - b_1^2 - 2b_0^2]e^{-\Delta/kT}\}$$

$$[6]\quad \left(\frac{\Delta H}{H}\right)_{x,y} = \frac{\mu_e(1 - e^{-\Delta/kT})}{6600\Delta(1 + e^{-\Delta/kT})}\left\{\left[-\frac{A_{2p}}{g_N\mu_N} + C_{x,y}\frac{g_e\mu_e}{R^3} + \frac{Q}{g_N\mu_N}\right][62b_3^2 + 4b_2^2 + 58b_1^2 + 8b_0^2] + D_{x,y}\left[-\frac{A_{2p}}{g_N\mu_N} + \frac{Q}{g_N\mu_N}\right] \times [9b_1^2 - 12\sqrt{30}b_2b_0 + 12\sqrt{15}b_3b_1]\right\} \qquad C_x = -1.1213;\ C_y = 3.1213;\ D_x = -1;\ D_y = +1$$

The average value for the shift is given in eq. [7].

$$[7]\quad \left(\frac{\Delta H}{H}\right)_{ave} = \frac{\mu_e}{1100kT(1 + e^{-\Delta/kT})}\left\{\left[\frac{A_{2p}}{g_N\mu_N} + \frac{Q}{2g_N\mu_N} - \frac{g_e\mu_e}{R^3}\right][(35b_3^2 - 2b_2^2 + 35b_1^2 - 2b_0^2) + \frac{4}{9}e^{-\Delta/kT}(133b_3^2 + 134b_2^2 - b_1^2 - 2b_0^2)] + \frac{1}{9}\left[-\frac{A_{2p}}{g_N\mu_N} + \frac{Q}{g_N\mu_N} + \frac{g_e\mu_e}{R^3}\right]\left(\frac{kT}{\Delta}\right)(1 - e^{-\Delta/kT})(62b_3^2 + 4b_2^2 + 58b_1^2 + 8b_0^2)\right\}$$

The corresponding equation when the excited state is $|4,\pm2\rangle$ is as follows:

Can. J. Chem. Downloaded from www.nrcresearchpress.com by 210.87.254.6 on 09/06/12
For personal use only.

$$[8]\quad \left(\frac{\Delta H}{H}\right)_{ave} = \frac{\mu_e}{1100kT(1 + e^{-\Delta/kT})}\left\{\left[\frac{A_{2p}}{g_N\mu_N} + \frac{Q}{2g_N\mu_N} - \frac{g_e\mu_e}{R^3}\right][(35b_3^2 - 2b_2^2 + 35b_1^2 - 2b_0^2) + \frac{1}{63}e^{-\Delta/kT}(377b_3^2 + 100b_2^2 + 85b_1^2 + 362b_0^2)] + \frac{7}{9}\left[-\frac{A_{2p}}{g_N\mu_N} + \frac{Q}{g_N\mu_N} + \frac{g_e\mu_e}{R^3}\right]\left(\frac{kT}{\Delta}\right)(1 - e^{-\Delta/kT})(19b_3^2 + 14b_2^2 + 11b_1^2 + 22b_0^2)\right\}$$

Please note that because the orbital momentum and spin–orbit coupling are not quenched, the dipolar terms of A_{2p} and R^{-3} are not averaged out and therefore make a major contribution to what many people refer to as the "contact shift".

Calculation of paramagnetic shift for ^{1}H

The ^{1}H shift resulting from spin in the p_z orbital of the neighboring carbon atom is readily calculated from the present equations. We simply drop out the A_{2p} and R^{-3} terms and replace $Q/g_N\mu_N$ by $(Q/g_N\mu_N - g_e\mu_eR^{-3})$ in the z shift equation, by $(Q/g_N\mu_N + 2g_e\mu_eR^{-3})$ in the x term, and by $(Q/g_N\mu_N - g_e\mu_eR^{-3})$ in the y term. The Q now is the appropriate hyperfine term for ^{1}H in aromatic radicals and the R^{-3} term is the dipolar contribution from the spin in the carbon p_z orbital which does not average out to zero when the angular momentum is not quenched. The resulting shift equation for the case of a $|4,\pm3\rangle$ ground state with the first excited state of $|4,\pm4\rangle$ is as follows:

$$[9]\quad \left(\frac{\Delta H}{H}\right)_{ave} = \frac{\mu_e}{2200kT(1 + e^{-\Delta/kT})}\left\{\left[\frac{Q}{g_N\mu_N} - \frac{g_e\mu_e}{R^3}\right][(35b_3^2 - 2b_2^2 + 35b_1^2 - 2b_0^2) + \frac{4}{9}e^{-\Delta/kT}(133b_3^2 + 134b_2^2 - b_1^2 - 2b_0^2) + \frac{1}{9}\left[\frac{2Q}{g_N\mu_N} + \frac{g_e\mu_e}{R^3}\right]\left(\frac{kT}{\Delta}\right)(1 - e^{-\Delta/kT})(62b_3^2 + 4b_2^2 + 58b_1^2 + 8b_0^2) - \left[\frac{g_e\mu_e}{R^3}\right]\left(\frac{kT}{\Delta}\right)(1 - e^{-\Delta/kT})(3b_1^2 - 4\sqrt{30}b_2b_0 - 4\sqrt{15}b_3b_1)\right\}$$

and for the excited state of $|4,\pm2\rangle$ the equation becomes

$$[10]\quad \left(\frac{\Delta H}{H}\right)_{ave} = \frac{\mu_e}{2200kT(1 + e^{-\Delta/kT})}\left\{\left[\frac{Q}{g_N\mu_N} - \frac{g_e\mu_e}{R^3}\right][35b_3^2 - 2b_2^2 + 35b_1^2 - 2b_0^2) + \frac{1}{63}e^{-\Delta/kT}(377b_3^2 + 100b_2^2 + 85b_1^2 + 362b_0^2)] + \frac{7}{9}\left[\frac{2Q}{g_N\mu_N} + \frac{g_e\mu_e}{R^3}\right]\left(\frac{kT}{\Delta}\right)(1 - e^{-\Delta/kT})(19b_3^2 + 14b_2^2 + 11b_1^2 + 22b_0^2) + \frac{2}{9}\left[\frac{g_e\mu_e}{R^3}\right]\left(\frac{kT}{\Delta}\right) \times (1 - e^{-\Delta/kT})(81b_1^2 + 4\sqrt{30}b_2b_0 - 4\sqrt{15}b_1b_3)\right\}$$

Comparison with experiment

We can now attempt to calculate numerical values to compare with experimental values. The following values were used for the parameters in the equations:

$A_{2p}(^{13}C) = 90.8$ MHz

$Q(^{13}C) = 21.83$ MHz

$g_e\mu_eg_N\mu_NR^{-3}(^{13}C) = 7.39$ MHz

$Q(^1H) = -75.6$ MHz

$g_e\mu_eg_N\mu_NR^{-3}(^1H) = 78.97$ MHz

To obtain estimates of the magnitude and sign of the shifts predicted by these equations, we need to make assumptions concerning the values of the four b parameters. One reasonable assumption would be to assume that only the topmost filled π orbital in the COT ion would be involved in covalent bonding with the f orbitals. This would assume that $b_0 = b_1 = b_3 = 0$, since the E_{2u} is the topmost filled level. Another possible assumption is to make all π orbitals equally involved in bonding, which would assume that $b = b_0 = b_1 = b_2 = b_3$. The results of making these two assumptions for three different arrangements of states are given in Table 1.

The values in Table 1 should be compared to what most experimentalists have called the contact shift, that is, the isotropic shift from which the pseudo-contact shift has been subtracted. Fischer (11) reports the following values for these shifts:

$(\Delta H/H)_{con}(^{13}C) = -140.8$ ppm

$(\Delta H/H)_{con}(^1H) = 38.1$ ppm

Luke and Streitweiser (12) report for ^{1}H a value of 34.2 ppm. A comparison of the experimental values with the table entries quickly reveals that the theory will not account for the experimental results, since it would require in most cases that b^2 or b_2^2 be negative or, in one case where the signs agree, it would require an unreasonably large value of b_2^2. We must therefore conclude that the major contribution to the contact shift in uranocene comes from spin transfer mechanisms other than the one investigated here.

It must not be concluded from the above arguments that f orbital covalency is unimportant in uranocene, because in the most likely cases examined, that is for a $|4,\pm3\rangle$ ground state with only b_2 different from zero, the predicted contribution to the shift is quite small for reasonable values of b_2^2 and would be difficult to detect. Thus we have shown the existence of a sizeable contact shift in uranocene and its derivatives is not an indication of covalency, at least in the f orbitals, and any changes in the shift do not necessarily indicate changes in covalency.

Polarization mechanism of spin transfer

The polarization mechanism of spin transfer is more difficult to handle in a theoretical or semi-theoretical manner. In principle, exchange interactions between the unpaired spins in the f orbitals induce a small uncoupling (or polarization) of paired spins in filled orbitals of the system. This is in general small,

Can. J. Chem. Downloaded from www.nrcresearchpress.com by 210.87.254.6 on 09/06/12
For personal use only.

TABLE 1. Paramagnetic shifts (ppm)

Ground state	$\|4,\pm3\rangle$	$\|4,\pm3\rangle$	$\|4,\pm4\rangle$
Excited state	$\|4,\pm4\rangle$	$\|4,\pm2\rangle$	$\|4,\pm3\rangle$
	$b_0 = b_1 = b_3 = 0$		
$(\Delta H/H)_{ave}(^{13}C)$	$67.5b_2^2$	$-74.3b_2^2$	$964.8b_2^2$
$(\Delta H/H)_{ave}(^{1}H)$	$-16.7b_2^2$	$-0.68b_2^2$	$-198.1b_2^2$
	$b = b_0 = b_1 = b_2 = b_3$		
$(\Delta H/H)_{ave}(^{13}C)$	$1210b^2$	$971.7b^2$	$2078b^2$
$(\Delta H/H)_{ave}(^{1}H)$	$-245.3b^2$	$-270.8b^2$	$-1282b^2$

but if the filled orbital involves an *s* orbital of the atom in question, the Fermi contact term will be large enough to produce a measureable effect. Quite a few filled orbitals could make a contribution to this effect and this makes interpretation of such shifts very difficult.

A simple model was used to interpret and predict the polarization component of the nmr shift in lanthanide fluorides (2–9) which can be applied to uranocene. This will at least allow us to compare the magnitude of the effect between the lanthanides and the actinides. In this model, it was assumed that the matrix elements of A_{Ni} were proportional to the matrix elements of S_i. That is

$$[11]\quad \langle 4M|A_{Nz}|4M\rangle = K_{\parallel}\langle 4M|S_z|4M\rangle$$
$$\langle 4M|A_{Nx}|4M\rangle = K_{\perp}\langle 4M|S_x|4M\rangle$$

Using this formalism and assuming a ground state of $|4,\pm3\rangle$ and first excited state of $|4,\pm4\rangle$, we obtain for the average shift

$$[12]\quad (\Delta H/H)_{ave} = -[g_J(g_J - 1)\mu_e/3kTg_N\mu_N(1 + e^{-\Delta/kT})] \times [(9 + 4e^{-\Delta/kT})K_{\parallel} + 14(1 - e^{-\Delta/kT})(kT/\Delta)K_{\perp}]$$

If we assume $K_{\parallel} = K_{\perp} = K$ and if we assume that the entire ^{13}C shift in uranocene is due to the polarization mechanism, we calculate a K value of -0.899 MHz from eq. [12]. This is, surprisingly, close to the value estimated by Edelstein *et al.* (19) who assumed a $|4,\pm4\rangle$ ground state with no contributing excited states. $K_{ave} = -1.82$ MHz for ^{19}F—Gd^{3+} and -2.23 MHz for ^{19}F—Eu^{2+}. Since K is a hyperfine constant and is proportional to g_N, we must scale these numbers by the ratio of g_N's before comparing them. $K = -0.899$ MHz would become -3.36 MHz for a ^{19}F nucleus. Thus the polarization of spin in the carbon atom adjacent to the U^{4+} is only slightly larger than that of the fluorine ion adjacent to Gd^{3+} or Eu^{2+}.

Can we determine which filled orbitals in the molecule make the major contributions to spin transfer by polarization? Streitweiser *et al.* (20) have proposed that it is the filled bonding orbitals which involve *f* and *d* orbitals of uranium combined with π orbitals of the COT anion. We consider this to be unlikely for two reasons. First, these orbitals will have only a small admixture of the *f* and *d* orbitals so that the exchange integrals with the *f* electrons will be small (and therefore the spin polarization will be small) and this coupled with the fact that these MO's do not have any direct admixture of carbon *s* orbitals makes it highly unlikely that polarization of these orbitals can account for the measured nmr shift. The magnitude of K estimated earlier would require a polarization of the spin of better than 10% in the π orbitals if this were the only source of the nmr shift. Second, these orbitals would contribute only by a double polarization which would yield a shift of opposite sign to that observed. A more likely source is the polarization of the outer 6*s* and 6*p* electrons in the uranium. Overlap of these electrons with the σ bonding electrons of the COT anion will result in a renormalization of the two sets of orbitals which will (10), in turn, result in a polarization of the 2*s* and 2*p* orbitals of the carbon atom. If this is the case, we would expect the nmr shift to be related more to overlap of the outer electrons in the metal and ligand atoms (which is a function of the bond distance) than to the nature of the bonding interactions. If this is the case, we would expect the nmr shift of ^{13}C to be similar for any carbon attached directly to the uranium atom. This appears to be borne out in the limited data available on ^{13}C shifts.

In eq. [12], K is divided by g_N so that we can infer from the fact that the magnitude of the ^{1}H shift in uranocene is less than one third that of the ^{13}C shift that the polarization of the spin near the ^{1}H nucleus is less than one third of that near the ^{13}C nucleus. This is reasonable since the polarization must be transmitted through the C—H bond which also causes the reversal in sign of the polarization. Again we would expect the ^{1}H shift to be influenced only slightly by bonding changes, if the spin polarization is transmitted primarily by overlap between the outer electrons of the uranium and carbon atoms. It has been commented on several times (11, 12) that the "contact" shift in $(C_5H_5)_3UX$ compounds varies only slightly with X. Further, the "contact" shift in $U(C_8H_8)_2$ is not much different than that observed in $U(C_5H_5)_4$.

Conclusions

There are several conclusions to be drawn from this work. The theoretical approach used in the work has been successfully applied to the lanthanide system, where it showed that covalency involving the *f* orbitals played a major role in determining the paramagnetic shift for the ions in the second half of the series. Thus we have every expectation that the present calculations should give a good estimate of the sign and magnitude of the shift from *f* orbital covalency in uranocene. The failure of the calculations to explain the sign and magnitude of the observed shifts must, therefore, indicate that either there is little covalency or (more likely) the ground state is $|4,\pm3\rangle$ with covalency involving primarily the E_{2u} π MO of COT, since this was shown to lead to very small paramagnetic shifts.

The paramagnetic shift must be determined mostly by the polarization mechanism of spin transfer. It appears that this mechanism operates mainly through the overlap of the outer 6*s* and 6*p* orbitals of uranium with the σ bonding orbitals of the carbon atom. Therefore, the nmr shift in these complexes is not very sensitive to the nature of the bonding between the ligand and the uranium atom.

Another important, but less obvious, conclusion is the importance of terms other than the Fermi contact term in determining the sign and magnitude of the isotropic shift in actinide complexes. The A_{2p} term was larger than the Q term in the ^{13}C

Can. J. Chem. Downloaded from www.nrcresearchpress.com by 210.87.254.6 on 09/06/12
For personal use only.

computations and the R^{-3} term was just as large as the Q term in the ^1H case. Thus these calculations point out that it is unreasonable to characterize the isotropic shift as a contact shift in the actinide systems and even more unreasonable to consider the shift as a measure of the esr Q parameter for unpaired electrons in the π system.

Acknowledgement

This work was supported by an operating grant from the Natural Sciences and Engineering Research Council of Canada.

Appendix

Calculation of the $\langle 4M|\mu_i|4M'\rangle$ matrix elements in eq. [5] is straightforward. We take $g_J = 4/5$ and $J_i = L_i + S_i$. If we further assume that only the central orbital part of the MO contributes to L_i, we obtain the matrix elements

$$\langle 44|\mu_z|44\rangle = -(4\mu_e/165)[123N_3^2 + 68N_2^2 + 7N_1^2 - 66] \approx -(16/5)\mu_e$$

$$\langle 43|\mu_z|43\rangle = -(\mu_e/15)[39N_3^2 + 4N_2^2 + 11N_1^2 - 18] \approx -(12/5)\mu_e$$

$$\langle 42|\mu_z|42\rangle = -(2\mu_e/1155)[831N_3^2 + 556N_2^2 - N_1^2 - 462] \approx -(8/5)\mu_e$$

[A1] $$\langle 44|\mu_x|43\rangle = -(\sqrt{2}\mu_e/55)[7N_3N_2 + 45N_2N_1 + 14N_1N_0 - 22] \approx -(4\sqrt{2}/5)\mu_e$$

$$\langle 44|\mu_y|43\rangle = -i\langle 44|\mu_x|43\rangle$$

$$\langle 43|\mu_x|42\rangle = -(\mu_e/55\sqrt{14})[149N_3N_2 + 15N_2N_1 + 298N_1N_0 - 154] \approx -(2\sqrt{14}/5)\mu_e$$

$$\langle 43|\mu_y|42\rangle = -i\langle 43|\mu_x|42\rangle$$

The final values in the above equations are obtained by assuming $N_3 = N_2 = N_1 = N_0 \approx 1$, which should be a reasonable assumption for f orbitals.

The calculation of the $\langle 4M|A_{Ni}/g_N\mu_N|4M'\rangle$ matrix elements is more laborious. We first consider the A_{Nz} terms. Since these terms are centered on the ligand nucleus, we consider only the ϕ_m terms in the MO's. Since these have only p_z orbitals, we can ignore the orbital momentum part of A_{Nz} in eq. [5]. In fact, the only portion of the A_{Nz} operator that makes a contribution is the s_z terms, so that we write

[A2] $$A_z's_z = \sum_j [(8/3)\pi g_e\mu_e\delta(r_j) + g_e\mu_e(3\cos^2\theta_j - 1)r_j^{-3}]s_{zj}$$

The $\langle 4M|A_{Nz}/g_N\mu_N|4M'\rangle$ matrix elements then take the general form

[A3] $$\langle 4M|A_{Nz}/g_N\mu_N|4M'\rangle = A(MM')\sum_{m=0}^{3} a(MM'm)b_m^2 \times \langle\phi_m|A_z'|\phi_m\rangle$$

where the coefficients for appropriate MM' values are as follows:

MM'	$A(MM')$	$a(MM'0)$	$a(MM'1)$	$a(MM'2)$	$a(MM'3)$
44	1/330	2	1	−134	−133
33	1/110	2	−35	2	−35
22	1/2310	−362	−85	−100	−377

It is quickly established that all the $\langle\phi_m|A_z'|\phi_m\rangle$ are identical, so that calculation of one will suffice. Since our nucleus of interest is carbon nucleus 1, we assume only it and its nearest neighbours, nuclei 2 and 8, will make a contribution. Thus we can write

[A4] $$\langle\phi_m|A_z'|\phi_m\rangle \approx 16^{-1}[\langle p_z^1|A_z'|p_z^1\rangle + \langle p_z^2|A_z'|p_z^2\rangle + \langle p_z^8|A_z'|p_z^8\rangle]$$

The dipolar (second term in eq. [A2]) term in A_z' gives contributions from all three nuclei. For nucleus 1 we obtain

[A5] $$\langle p_z^1|A_z'|p_z^1\rangle = (4/5)g_e\mu_e\langle r^{-3}\rangle = 2A_{2p}/g_N\mu_N$$

For nuclei 2 and 8 we use the point dipole form of A_z', which is $g_e\mu_e(3\cos^2\Omega - 1)R^{-3}$. R is the distance between nucleus 1 and nucleus 2 or 8 and Ω is the angle between this direction vector and the z axis. Since $\Omega = 90°$, we get

[A6] $$\langle p_z^2|A_z'|p_z^2\rangle = \langle p_z^8|A_z'|p_z^8\rangle = -g_e\mu_eR^{-3}$$

The Fermi contact term (first term in eq. [A2]) would give zero for the MO's in eq. [1]. However, we know from free radical studies of such aromatic rings that polarization of filled bonding σ orbitals produces a hyperfine interaction proportional to the density of spin in the p_z orbital on the nucleus in question plus the density in the nearest neighbours. Since the hyperfine interaction of a spin in ϕ_m is calculated for the z direction by $\langle\phi_m|A_z'|\phi_m\rangle$ and the fraction of spin on any nucleus is 16^{-1} for each ϕ_m orbital, we can write for eq. [A4] the following:

[A7] $$\langle\phi_m|A_z'|\phi_m\rangle = [2A_{2p} - 2g_e\mu_eg_N\mu_NR^{-3} + Q]/16g_N\mu_N$$

where $Q/16$ is the Fermi contact part of the hyperfine interaction constant for a free radical with unpaired spin in a ϕ_m orbital. Q can be estimated by procedures given in ref. 18.

A similar procedure is adopted for the $A_{Nx}/g_N\mu_N$ and $A_{Ny}/g_N\mu_N$ terms. The general form for the matrix elements is

[A8] $$\langle 4M|A_{Nx,y}/g_N\mu_N|4M'\rangle = (+1, -i)B(MM') \times \sum_{m=0}^{3} b(MM'm)b_m^2\langle\phi_m|A_{x,y}'|\phi_m\rangle + (+1, +i)C(MM') \times \langle\phi_1|A_{x,y}'|\phi_{-1}\rangle[c(MM'1)b_1^2 + c(MM'2)b_2b_0 + c(MM'3)b_3b_1]$$

the coefficients in eq. [A8] are as follows:

MM'	$B(MM')$	$b(MM'0)$	$b(MM'1)$	$b(MM'2)$	$b(MM'3)$
43	$\sqrt{2}/330$	−4	−29	−2	−21
32	$\sqrt{14}/660$	22	11	14	19

	$C(MM')$	$c(MM'1)$	$c(MM'2)$	$c(MM'3)$
43	$1/110\sqrt{2}$	3	$-4\sqrt{30}$	$4\sqrt{15}$
32	$1/2640\sqrt{14}$	−81	$-4\sqrt{30}$	$-4\sqrt{15}$

Can. J. Chem. Downloaded from www.nrcresearchpress.com by 210.87.254.6 on 09/06/12
For personal use only.

In an analogous fashion to that used for the $A_{N_z}/g_N\mu_N$ terms we find

[A9] $$\langle\phi_m|A_x'|\phi_m\rangle = [-A_{2p} - 1.1213 g_e\mu_e g_N\mu_N R^{-3} + Q]/16 g_N\mu_N$$

[A10] $$\langle\phi_m|A_y'|\phi_m\rangle = [-A_{2p} + 3.1213 g_e\mu_e g_N\mu_N R^{-3} + Q]/16 g_N\mu_N$$

The cross terms are:

[A11] $$\langle\phi_1|A_{x,y}'|\phi_{-1}\rangle = [A_{2p} - Q]/16 g_N\mu_N$$

These cross terms disappear when we compute the average nmr shift.

1. B. R. McGARVEY. J. Chem. Phys. **65**, 955 (1976); **65**, 962 (1976).
2. M. R. MUSTAFA, B. R. McGARVEY, and E. BANKS. J. Magn. Reson. **25**, 341 (1977).
3. A. REUVENI and B. R. McGARVEY. J. Magn. Reson. **29**, 21 (1978).
4. R. J. BOOTH, M. R. MUSTAFA, and B. R. McGARVEY. Phys. Rev. B**17**, 4150 (1978).
5. A. REUVENI and B. R. McGARVEY. J. Magn. Reson. **34**, 181 (1979).
6. B. R. McGARVEY. J. Chem. Phys. **70**, 4971 (1979).
7. A. REUVENI and B. R. McGARVEY. J. Magn. Reson. **36**, 7 (1979).
8. R. J. BOOTH and B. R. McGARVEY. Phys. Rev. B**21**, 1627 (1980).
9. L. C. STUBBS and B. R. McGARVEY. J. Magn. Reson. **50**, 249 (1982).
10. R. E. WATSON and A. J. FREEMAN. Phys. Rev. **156**, 251 (1967).
11. R. D. FISCHER. *In* Organometallics of the *f*-elements. *Edited by* T. D. Marks and R. D. Fischer. D. Reidell Pub. Co., Boston, MA. 1979. p. 337.
12. W. D. LUKE and A. STREITWEISER, JR. *In* Lanthanide and actinide chemistry and spectroscopy. Am. Chem. Soc. Symp. Ser. 131. *Edited by* N. M. Edelstein. Am. Chem. Soc. Washington, D.C. 1970. p. 93.
13. D. G. KARRACKER. Inorg. Chem. **12**, 1105 (1973).
14. R. G. HAYES and N. EDELSTEIN. J. Am. Chem. Soc. **94**, 8688 (1972).
15. H. D. AMBERGER, R. D. FISCHER, and B. KANELLAKOPULUS. Theoret. Chim. Acta, **37**, 105 (1975).
16. R. F. DALLINGER, P. STEIN, and T. G. SPIRO. J. Am. Chem. Soc. **100**, 7865 (1978).
17. R. J. KURLAND and B. R. McGARVEY. J. Magn. Reson. **2**, 286 (1970).
18. J. E. WERTZ and J. R. BOLTON. Electron spin resonance elementary theory and practical applications. McGraw-Hill, Inc. New York. 1972.
19. N. EDELSTEIN, G. N. LA MAR, F. MARES, and A. STREITWEISER, JR. Chem. Phys. Lett. **8**, 399 (1971).
20. A. STREITWEISER, JR., D. DEMPF, G. N. LA MAR, D. G. KARRAKER, and N. EDELSTEIN. J. Am. Chem. Soc. **93**, 7343 (1971).

Can. J. Chem. Downloaded from www.nrcresearchpress.com by 210.87.254.6 on 09/06/12
For personal use only.

Simple lower and upper bounds for isomerization energies

PAUL G. MEZEY
Department of Chemistry, University of Saskatchewan, Saskatoon, Sask., Canada S7N 0W0

Received August 30, 1983

PAUL G. MEZEY. Can. J. Chem. **62**, 1356 (1984).

Lower and upper bounds for the energies of various isomers can be obtained by a simple inspection of the nuclear charges. The bounds are quantum-mechanically rigorous, and are strictly applicable only to specific nuclear geometries and require only back-of-the-envelope type calculations.

PAUL G. MEZEY. Can. J. Chem. **62**, 1356 (1984).

On peut évaluer facilement les limites inférieures et supérieures des énergies de divers isomères en se basant sur une inspection simple des charges nucléaires. Les limites sont rigoureuses sur la base de la mécanique quantique, elles peuvent s'appliquer d'une façon stricte uniquement pour des géométries nucléaires spécifiques et peuvent être déterminées par des calculs simples pouvant se faire sur le dos d'une enveloppe.

[Traduit par le journal]

Can. J. Chem. Downloaded from www.nrcresearchpress.com by 210.87.254.6 on 09/06/12
For personal use only.

Most chemists believe that even approximate quantum chemical calculations of isomerization energies of molecules require time-consuming computations with complex computer programs. Yet, rigorous (although rather loose) upper and lower bounds of some isomerization energies can be obained by simple back-of-an-envelope type calculations, if energy values for some other isomers and/or for some other isoelectronic species are known.

Consider a general molecule M of w nuclei of nuclear charges $z_1, z_2, \ldots z_w$, and of arbitrary geometry. Let us assume that an isomeric molecule, ISOM, can be obtained from M by a permutation of the nuclei otherwise having the same geometry, implying in general that at least one of the isomers has a distorted geometry, as compared to its equilibrium nuclear arrangement. Consider a third molecule, that is isoelectronic with M and ISOM, and contains the same total number of protons, i.e. the sum of nuclear charges is the same. We shall consider first the simplest case and take this third molecule as a single atom, UA (united atom), containing all the protons of M.

Let us assume that all these molecules are in their electronic ground states, or all of them are in the lowest state of a given electronic manifold (e.g. lowest triplet or lowest doublet state, etc.). Then, M, ISOM, and UA fulfill the conditions for a corollary (1) of a quantum chemical theorem on the abstract nuclear charge space (2) and we can write that

$$[1] \quad (1 - \alpha)E_e\,(\mathrm{UA}) + \alpha E_e(\mathrm{M}) \leq E_e\,(\mathrm{ISOM})$$

Here E_e stands for the electronic energy of the given electronic state, and number α fulfills the following constraints:

$$[2] \quad 0 \leq \alpha \leq 1$$

$$[3] \quad \alpha z_i(\mathrm{M}) \leq z_i\,(\mathrm{ISOM}) \qquad i = 1, 2, \ldots, w$$

(The theorem states that all open sets of the level set topology set up by the electronic energy functional on an abstract nuclear charge space are convex. The proof and some related results are given elsewhere (1–5).) For example, α can be chosen as the minimum ratio of nuclear charge pairs:

$$[4] \quad \alpha = \min_i \{z_i\,(\mathrm{ISOM})/z_i(\mathrm{M})\}$$

Let us interchange now the roles of the two isomers M and ISOM, then we obtain

$$[5] \quad (1 - \alpha')\,E_e(\mathrm{UA}) + \alpha' E_e(\mathrm{ISOM}) \leq E_e(\mathrm{M})$$

with

$$[6] \quad \alpha' = \min_i \{z_i(\mathrm{M})/z_i(\mathrm{ISOM})\}$$

where α' is not in general the same as α. However, if only two nuclei are interchanged in the isomerization, then necessarily $\alpha = \alpha'$ for the minimum ratios.

Combining inequalities [1] and [5] we obtain

$$[7] \quad (1 - \alpha)E_e(\mathrm{UA}) + \alpha E_e(\mathrm{M}) \leq E_e(\mathrm{ISOM}) \leq (1/\alpha')E_e(\mathrm{M}) + (1 - 1/\alpha')E_e(\mathrm{UA})$$

That is, we have obtained both an upper and a lower bound for the electronic energy of isomer ISOM. If energy values for molecule M and for the single atom UA are available, then all that is needed for the evaluation of upper and lower energy bounds for isomer ISOM is a trivial calculation of α and α'. The above is a rigorous quantum chemical result within the non-relativistic Born–Oppenheimer approximation. It is also valid for less accurate electronic energies, e.g. it is valid at the Hartree–Fock limit, or for energies obtained in any finite basis set calculations, if the *same* finite basis set is used for all the species to which the theorem is applied.

Although the result is rigorous and always valid, the actual lower and upper bounds are in general very loose bounds (however, significant improvements are possible, *vide infra*). Apart from their extreme simplicity, they have little practical value in their above form, although they are of some theoretical interest in setting energy bounds for extensive domains of multidimensional potential energy surfaces. In practice their use is suggested only for very rough guidelines or for a quick test to guard against gross errors in more elaborate quantum chemical calculations, which may easily require a million times more numerical operations. It should also be pointed out that total energy changes are generally accompanied by much larger (often by several orders of magnitude larger) changes in the electronic energy. Hence, bounds which would appear very loose for total energies can be quite consistent with the scale of electronic energy variations.

It is of some interest that the relation is valid for any distorted geometry, even for the extreme case of dissociated fragments, as long as the *same* distortion is applied to both isomers.

The looseness of the above energy bounds stems from the involvement of the united atom UA in the relation, since

E_c(UA) is much below the energies of the isomers. Even if the coefficient $(1 - \alpha)$ of E_c(UA) is a small number (the smallest with the largest α value permitted by relation [3]), the $(1 - \alpha)E_c$(UA) term renders the bounds loose. On the other hand, the relations are the simplest to apply if UA is involved, and numerical values for E_c(UA) are readily available.

Much tighter and more useful energy bounds can be obtained if the set of molecules involved does not include UA. The same general relation of ref. 1 can be applied to M, ISOM, and a sequence of isoelectronic and isoprotonic molecules $M_1, \ldots, M_{n-1}$ of the same geometry, if for a sequence of numbers $\alpha_1, \ldots, \alpha_{n-1}, \alpha_n$ the following conditions apply:

[8] $\alpha_j \geq 0$

$j = 1, \ldots, n$

[9] $\sum_{j=1}^{n} \alpha_j = 1$

[10] $\sum_{j=1}^{n} \alpha_j z_i(M_j) = z_i(\text{ISOM})$

for every $i = 1, \ldots, w$

where the M_n = M notation is used. Then from the general result of ref. 1 the following inequality is obtained for isomers M, ISOM, and molecules M_j:

[11] $\alpha_1 E_c(M_1) + \ldots + \alpha_{n-1} E_c(M_{n-1}) + \alpha_n E_c(M) \leq E_c$ (ISOM)

The above relation gives much tighter energy bounds. Although its use is somewhat less convenient than relations [3] and [7], involving well known E_c(UA) values, nevertheless, suitable $E_c(M_j)$ values are often available. Relation [11] is the simplest if $n = 2$, i.e. if only one molecule, in addition to isomer M, is involved on the left hand side.

In the following we shall show examples for the application of relations [3], [7], as well as [11].

To illustrate the application of inequalities [7] take, for example, the ground electronic states of isomers HOCN and HNCO at a common geometry. Their nuclear charges are (1, 8, 6, 7) and (1, 7, 6, 8), respectively, with a sum of 22, hence UA = Ti, titanium. Following a simple inspection of these nuclear charges we can conclude that

[12] $\alpha = \alpha' = 7/8$

fulfills conditions [4] and [6]. Substitution into inequality [7] gives

[13] $(1/8)E_c(\text{Ti}) + (7/8)E_c(\text{HOCN}) \leq E_c(\text{HNCO}) \leq (8/7)E_c(\text{HOCN}) - (1/7)E_c(\text{Ti})$

that is, lower and upper bounds are obtained for the electronic energy of isomer HNCO. We may test relation [13] against the available numerical data. Considering the Hartree–Fock limits throughout, the value reported (6) for titanium is $E_{HF}(\text{Ti}) = -848.406$ atomic units (au), whereas on the basis of *ab initio* studies (7), values close to the Hartree–Fock limits for the *electronic energies* of HOCN and HNCO can be estimated as −225.127 au and −226.406 au, respectively. Substitution into relation [13] gives

$$-303.037 \text{ au} \leq -226.406 \text{ au} \leq -136.087 \text{ au}$$

that is, both bounds are valid with very wide margins. Whereas the actual numbers may change if the molecular geometries are distorted, inequalities [13] give valid bounds for isomer HNCO for any *distorted geometry*, as long as the same distortion is applied to both HOCN and HNCO, e.g., the same relation [13] is applicable to dissociated fragment pairs HO + CN and HN + CO, or to corresponding points along dissociation pathways.

In order to illustrate the application of relation [11] and to obtain tighter bounds for the above isomers, consider molecule M_1 = fluoroacethylene, HCCF. Choosing $\alpha_1 = \alpha_2 = 0.5$, for isomers HOCN (= M_2 = M) and HNCO (= ISOM), relations [8] and [9] are evidently valid, as well as all four relations of type [10]:

[14] $0.5 \times 1 + 0.5 \times 1 = 1$

[15] $0.5 \times 6 + 0.5 \times 8 = 7$

[16] $0.5 \times 6 + 0.5 \times 6 = 6$

[17] $0.5 \times 9 + 0.5 \times 7 = 8$

Consequently, for *any* common geometry the relation

[18] $0.5\ E_c(\text{HCCF}) + 0.5\ E_c(\text{HOCN}) \leq E_c(\text{HNCO})$

is necessarily valid, if all these species are in the lowest electronic state of a given type. For a typical nuclear arrangement the obtained energy bound is about two orders of magnitude tighter than that calculated using relation [1].

One important feature of the loose [7] and, especially, of the tighter [11] bounds is the fact that they can be applied easily to very large molecular systems, for which even semiempirical quantum chemical calculations are impractical or impossible. Such applications to large zeolite cluster models will be reported shortly (8).

The general results [1], [7], and [11] are given for the electronic energies. If total energies are of interest, then the corresponding total energy relations can be obtained by adding the respective nuclear repulsion terms E_n to the electronic energies E_c, $E_t = E_c + E_n$. Knowing the nuclear charges, E_n can be calculated by elementary application of Coulomb's law.

Acknowledgement

This work has been supported by a grant from the Natural Sciences and Engineering Research Council of Canada.

1. P. G. MEZEY. Theor. Chim. Acta, **59**, 321 (1981).
2. P. G. MEZEY. Int. J. Quant. Chem. **22**, 101 (1982).
3. P. G. MEZEY. Mol. Phys. **47**, 121 (1982).
4. P. G. MEZEY. J. Chem. Phys. **78**, 6182 (1983).
5. P. G. MEZEY. *In* Chemical applications of topology and graph theory. *Edited by* R. B. King. Elsevier, Amsterdam. 1983. pp. 75–98.
6. E. CLEMENTI and C. ROETTI. At. Data Nucl. Data Tables, **14**, 177 (1974).
7. D. POPPINGER, L. RADOM, and J. A. POPLE. J. Am. Chem. Soc. **99**, 7806 (1977).
8. P. G. MEZEY. *In* Catalytic materials: relationship between structure and reactivity. *Edited by* E. Derouane. Am. Chem. Soc. Symp. Ser. **248**, 145 (1984).

Can. J. Chem. Downloaded from www.nrcresearchpress.com by 210.87.254.6 on 09/06/12
For personal use only.

Ortho-diquaternary aromatic compounds. V. Chirality and structure in hindered benzenes and napthalenes[1]

L. Ross C. Barclay

Department of Chemistry, Mount Allison University, Sackville, N.B., Canada E0A 3C0

AND

Sydney Brownstein,[2] Eric J. Gabe, and F. L. Lee

Division of Chemistry, National Research Council of Canada, Ottawa, Ont., Canada K1A 0R9

Received July 19, 1983[3]

L. Ross C. Barclay, Sydney Brownstein, Eric J. Gabe, and F. L. Lee. Can. J. Chem. **62**, 1358 (1984).

Ortho-disubstituted aromatics with bulky substituents are distorted so that the substituents are above and below the approximate plane of the aromatic system. This introduces chirality which was observed by proton resonance spectroscopy with and without the use of a chiral shift reagent. The more nearly planar naphthalene systems invert their chiral configurations more rapidly. Crystals of 1,2-benzenediacetic acid, α,α,α′,α′-tetramethyldimethyl ester are monoclinic, space group $A2/a$ with a = 10.665(3), b = 8.467(2), c = 17.198(4) Å and β = 105.94(2)°. The torsion angle between the 1,2 substituents is 12.1°. Crystals of 2,3-naphthalene diacetic acid, α,α,α′,α′-tetramethyldimethyl ester are also monoclinic, space group $P2_1/c$ with a = 9.0992(14), b = 18.849(3), c = 11.319(2) Å and β = 113.88(1)°. The analogous torsion angle in this case is 8.9°.

L. Ross C. Barclay, Sydney Brownstein, Eric J. Gabe et F. L. Lee. Can. J. Chem. **62**, 1358 (1984).

Les composés aromatiques portant deux substituants encombrants dans les positions *ortho* sont déformés d'une façon telle que les substituants sont situés au-dessus et au-dessous du plan approximatif du système aromatique. Ceci introduit une chiralité que l'on a observé par rmn du proton, avec ou sans utilisation d'un réactif chiral de déplacement. Les systèmes naphtaléniques, qui sont plus proches de la planéité, intervertissent leurs configurations chirales plus rapidement. Les cristaux de l'ester diméthylique de l'acide benzène bis(diméthylacétique)-1,2 sont monocliniques et appartiennent au groupe d'espace $A2/a$ avec a = 10,665(3), b = 8,467(2), c = 17,198(4) Å et β = 105,94(2)°. L'angle de torsion entre les substituants 1 et 2 est de 12,1°. Les cristaux de l'ester diméthylique de l'acide naphtalène bis(diméthylacétique)-2,3 sont également monocliniques et appartiennent au groupe d'espace $P2_1/c$ avec a = 9,0992(14), b = 18,849(3), c = 11,319(2) Å et β = 113,88(1)°. Dans ce cas, l'angle de torsion est de 8,9°.

[Traduit par le journal]

Introduction

Ortho-disubstituted aromatics which have bulky substituents are likely to experience severe steric strain. For *ortho* di-*t*-butylbenzene the strain energy has been found to be 22.3 ± 0.5 kcal/mol (1). The steric strain in 1,2,4,5-tetra-*t*-butylbenzene is relieved by angular distortions of up to 10° in the benzene ring and by stretching of the exocyclic bonds, from a normal value of 1.53 Å (2) to 1.57 Å, but without sacrificing the planarity of the benzene ring nor of the carbon atoms attached directly to it (3). Similarly in 1,3,6,8-tetra-*t*-butylnaphthalene the aromatic carbon – quaternary carbon bond length is stretched from 1.53 Å for the non-hindered *t*-butyl group to 1.56 Å for the hindered one (4).

If an aromatic ring has two *ortho*-substituents which are bent above and below its plane the molecule is potentially chiral. An example is the stereo pair stick diagram of 1,2-benzenediacetic acid, α,α,α′,α′-tetramethyldimethyl ester (**2**), which is reproduced in Fig. 3. This chirality would be lost if there were rapid exchange of the position of the above-plane and below-plane groups via a planar intermediate. Such exchange most probably accounts for earlier unsuccessful attempts to chemically resolve α,α,α′,α′-tetramethyl-1,2-benzene diacetic acid (5). The barrier to flipping between equivalent non-planar states of 1,8-di-*t*-butylnaphthalene was found to be 24 kcal/mol (6).

It is well known that the protons of a methylene group adjacent to a chiral centre display magnetic non-equivalence (7). It has also been frequently observed that the resonance signals of chiral molecules can be split into those of their *d* and *l* diastereomers on complexing with chiral shift reagents (8). This study attempts to determine if there are some *ortho* substituted benzenes and naphthalenes where the substituents are bent out of the plane of the aromatic ring and also the rate of averaging via a planar intermediate. High resolution proton resonance spectroscopy and single crystal X-ray diffraction techniques have been employed to study the problem, in both solution and the solid state.

Experimental

β,β′-Dihydroxy-*o*-di-*t*-butylbenzene (**1**), 1,2-benzenediacetic acid, α,α,α′,α′-tetramethyldimethyl ester (**2**), β,β′-dihydroxy-2,3-di-*t*-butylnaphthalene (**3**) and 2,3-naphthalenediacetic acid α,α,α′,α′-tetramethyldimethyl ester (**4**) were available from previous studies (5, 9). Proton resonance spectra were obtained in the Fourier Transform mode at an operating frequency of 100 MHz on a hybrid Varian XL-100 Nicolet 1010 apparatus.

X-ray intensity data for the compounds **2** and **4** were measured on a Picker 4-circle automatic diffractometer using graphite monochromatised MoKα radiation with θ/2θ scan methods and line profile analysis (10). The unit cell constants were obtained by least-squares refinement of the setting angles of reflections with 2θ > 40° and 45°, respectively, (λ(MoKα$_1$) = 0.70932 Å). The relevant experimental details are given in Table 1. The intensities were corrected for Lorentz and polarization effects, using measured values for direct beam polarization (11). Absorption corrections were not considered to be justified because the effects are small.

Both structures were solved by the application of MULTAN (12). After several cycles of refinement with isotropic temperature factors, the hydrogen atoms were located in a difference map. The structures were refined further by full-matrix least-squares with anisotropic tem-

[1] NRCC No. 23185.

[2] To whom all correspondence should be addressed.

[3] Revision received February 3, 1984.

Can. J. Chem. Downloaded from www.nrcresearchpress.com by 210.87.254.105 on 09/06/12
For personal use only.

TABLE 1. X-ray experimental details

Compound	**2**	**4**
Molecular formula	$C_{16}H_{22}O_4$	$C_{20}H_{24}O_4$
Space group	$A2/a$	$P2_1/c$
a (Å)	10.665(3)	9.0992(14)
b (Å)	8.467(2)	18.849(3)
c (Å)	17.198(4)	11.319(2)
β (deg)	105.94(2)	113.88(1)
Z	4	4
$D_{calcd.}$ (Mg m^{-3})	1.236	1.229
Radiation	MoKα(0.71069 Å)	MoKα(0.71069 Å)
μ(mm^{-1})	0.094	0.079
Reflections measured	3006	4648
Unique reflections	2184	3132
No. with $I_{net} > 2\sigma(I_{net})$	1244	1691
Agreement ($\Sigma\Delta I/\Sigma I$)	0.017	0.013
Final R_1 ($\Sigma\|F_o - F_c\|/\Sigma\|F_o\|$)	0.051	0.048
(with weak reflections)	0.100	0.108
Final R_2 ($\Sigma_w(F_o - F_c)^2/\Sigma_w F_o^2$)	0.036	0.024
(with weak reflections)	0.036	0.025

TABLE 2. Atomic parameters X, Y, Z, and B_{eq} for **2**, esd's refer to the last digit printed

Atom	x	y	z	B_{eq}[a]
C1	0.19995(19)	0.0751(3)	0.46278(11)	2.55(10)
C5	0.2054(3)	−0.2141(3)	0.46280(15)	4.30(15)
C6	0.16048(24)	−0.0715(3)	0.42810(15)	3.67(13)
C7	0.12518(22)	0.2204(3)	0.41769(13)	2.89(11)
C8	0.0849(3)	0.3373(3)	0.47456(16)	3.67(13)
C9	−0.0045(3)	0.1726(4)	0.35506(19)	4.61(15)
C10	0.19808(24)	0.3076(3)	0.36529(13)	3.23(12)
C11	0.3412(4)	0.2803(5)	0.28224(21)	5.03(18)
O1	0.18465(18)	0.44542(20)	0.34856(9)	4.73(10)
O2	0.27159(16)	0.20982(19)	0.33531(9)	3.80(8)
H51	0.1734(20)	−0.309(3)	0.4332(12)	4.5(6)
H61	0.0923(19)	−0.071(3)	0.3788(12)	4.3(6)
H81	0.0410(23)	0.281(3)	0.5104(15)	5.9(7)
H82	0.1586(19)	0.3997(23)	0.5083(13)	4.1(6)
H83	0.0192(21)	0.415(3)	0.4409(12)	5.4(6)
H91	−0.0512(22)	0.268(3)	0.3291(13)	4.7(6)
H92	−0.0590(22)	0.111(3)	0.3806(13)	5.0(7)
H93	0.0153(21)	0.109(3)	0.3066(14)	5.8(7)
H111	0.431(3)	0.352(4)	0.3147(17)	11.6(11)
H112	0.291(3)	0.350(3)	0.2469(16)	7.5(9)
H113	0.363(3)	0.196(4)	0.2508(21)	11.6(13)

[a] B_{eq} is the arithmetic mean of the principal axes of the thermal ellipsoid.

perature factors for the non-hydrogen atoms. Counting statistics weights were used throughout ($w = 1/\sigma^2(F_o)$). Intensity statistics on **2** clearly indicated the space group $A2/a$. Subsequent refinement in Aa and $A2/a$ confirmed this. The final R values are given in Table 1. Scattering factors for neutral atoms were taken from International tables for X-ray crystallography (1974). The final positional and equivalent isotropic temperature factors are given in Tables 2 and 3. Tables of thermal parameters and structure factors are deposited as supplementary material.[4] All calculations were performed using the NRC PDP8-E system of programs (13), adapted for a VAX11/780 computer.

[4] Complete set of data is available, at a nominal charge, from the Depository of Unpublished Data, CISTI, National Research Council of Canada, Ottawa, Ont., Canada K1A 0S2.

Results and discussion

Proton magnetic resonance studies

The spectrum of **1** in $CDCl_3$ at room temperature shows two sharp lines of equal intensity for the methylene hydrogens. These are considerably broadened and only partially resolved at 55°C, with the spectral changes normally found in a two-site exchange situation. The chemical shift values are listed in Table 4. This non-equivalence, which is partly averaged at higher temperature, may be due to the chiral nature of the molecules because of displacement of the substituents above and below the plane of the aromatic ring or may arise from the presence of a dimer in the solution. With the addition of a chiral shift reagent, europium tris[3-(heptafluoropropylhydroxymethylene)-*d*-camphorato], ($Eu(hfc)_3$), the methylene signals are broadened and shifted but the non-equivalence remains at 0°C. It is no longer observable at room temperature. The effect of a shift reagent suggests that the non-equivalence is not due to dimer formation. The dimer, if present, would be dissociated by the shift reagent and non-equivalence would never be observed. A potential problem in ascribing the two lines to magnetic non-equivalence due to an adjacent chiral centre is the lack of observed proton–proton spin-coupling.

If the observed non-equivalence is due to dimer formation it should be accentuated in a less polar solvent than $CDCl_3$. Therefore the studies were repeated in CS_2 and the results are also listed in Table 4. Separate lines from the CH_2 protons were not observed with or without $Eu(hfc)_3$ in CS_2 solution. It is therefore likely that dimer formation is not the cause of the observed non-equivalence in $CDCl_3$ solution. The changes in chemical shift and their temperature dependence suggest that aggregation may possibly be occurring in CS_2.

It is reasonable to suppose that a correspondingly substituted naphthalene would have similar aggregation in solution as **1**. It is also possible that the ease of distortion of the aromatic ring, and hence the barrier to rapid inversion about the plane of the aromatic ring, may be different for the benzene and naphthalene analogues. The same proton resonance measurements were also made on **3** and the results included in Table 4. Only at 0°C in $CDCl_3$ and with $Eu(hfc)_3$ is splitting observed. The results in Tables 4 and 5, which frequently show splitting of the methyl signals for the benzene derivatives, but rarely for the naphthalene derivatives, are interpreted in terms of averaging

Can. J. Chem. Downloaded from www.nrcresearchpress.com by 210.87.254.105 on 09/06/12
For personal use only.

Can. J. Chem. Downloaded from www.nrcresearchpress.com by 210.87.254.105 on 09/06/12
For personal use only.

TABLE 3. Atomic parameters X, Y, Z, and B_{eq} for **4**, esd's refer to the last digit printed

Atom	x	y	z	B_{eq}[a]
C1	0.7265(4)	0.06638(18)	0.5063(3)	3.47(18)
C2	0.8110(3)	0.08973(15)	0.6315(3)	2.86(16)
C3	0.7542(3)	0.15422(16)	0.66881(25)	2.92(16)
C4	0.6151(4)	0.18429(18)	0.5792(3)	3.45(18)
C5	0.5284(3)	0.15864(17)	0.4515(3)	3.18(17)
C6	0.3858(4)	0.19301(18)	0.3630(3)	4.20(19)
C7	0.3158(4)	0.16669(23)	0.2402(3)	4.97(22)
C8	0.3770(4)	0.10760(22)	0.2003(3)	4.99(22)
C9	0.5112(4)	0.07298(18)	0.2831(3)	4.32(20)
C10	0.5875(3)	0.09897(16)	0.4127(3)	3.27(17)
C11	0.9534(3)	0.04248(15)	0.7190(3)	2.86(16)
C12	0.9504(5)	−0.03274(20)	0.6613(3)	4.03(21)
C13	0.9514(5)	0.02871(22)	0.8522(3)	3.71(21)
C14	1.1179(4)	0.07067(17)	0.7346(3)	3.44(18)
C15	1.2662(5)	0.1336(3)	0.6375(5)	5.0(3)
C16	0.8384(3)	0.19564(16)	0.7996(3)	3.16(17)
C17	1.0189(5)	0.20701(23)	0.8366(4)	4.25(22)
C18	0.7672(5)	0.27108(22)	0.7946(4)	4.76(25)
C19	0.8103(4)	0.16197(16)	0.9127(3)	3.52(18)
C20	0.6259(6)	0.0999(4)	0.9744(5)	5.5(3)
O1	1.24125(23)	0.05832(12)	0.82706(19)	5.55(13)
O2	1.11233(24)	0.10745(11)	0.63142(18)	3.91(12)
O3	0.90282(23)	0.16699(11)	1.02446(17)	5.04(13)
O4	0.66675(23)	0.13026(11)	0.87343(17)	4.12(12)
H11	0.763(3)	0.0261(11)	0.4778(20)	1.4(6)
H41	0.572(3)	0.2259(11)	0.6006(20)	1.9(6)
H61	0.3449(22)	0.2494(10)	0.3956(17)	1.1(5)
H71	0.218(3)	0.1874(13)	0.1813(23)	4.8(8)
H81	0.325(3)	0.0884(12)	0.1133(21)	3.7(7)
H91	0.5409(21)	0.0233(9)	0.2392(16)	0.5(5)
H121	1.036(3)	−0.0628(12)	0.7226(20)	2.9(6)
H122	0.839(3)	−0.0585(14)	0.6416(23)	5.2(8)
H123	0.964(3)	−0.0320(14)	0.5801(22)	4.7(8)
H131	0.999(3)	0.0698(13)	0.9124(22)	4.0(8)
H132	1.017(3)	−0.0128(13)	0.8879(22)	4.4(8)
H133	0.836(3)	0.0173(14)	0.8428(24)	5.5(9)
H151	1.340(4)	0.0959(16)	0.650(3)	7.9(13)
H152	1.233(4)	0.1608(17)	0.557(3)	9.7(14)
H153	1.314(4)	0.1679(18)	0.716(3)	11.3(14)
H171	1.091(3)	0.1633(14)	0.8744(23)	5.2(9)
H172	1.033(3)	0.2259(15)	0.765(3)	5.3(10)
H173	1.065(3)	0.2429(15)	0.912(3)	6.7(9)
H181	0.640(3)	0.2692(14)	0.776(3)	5.7(9)
H182	0.834(3)	0.2943(13)	0.8823(22)	4.4(8)
H183	0.783(3)	0.2991(14)	0.7334(24)	5.1(9)
H201	0.692(4)	0.0619(20)	1.015(4)	12.6(17)
H202	0.516(4)	0.0771(18)	0.931(3)	12.2(14)
H203	0.628(6)	0.1343(22)	1.023(4)	10.1(23)

[a] B_{eq} is the arithmetic mean of the principal axes of the thermal ellipsoid.

of the magnetic non-equivalence being easier for the naphthalene than the corresponding benzene compound. It has been established that line broadening from shift reagents at low temperatures precludes their use for accurate kinetic studies below about 40°C (14). Therefore only qualitative conclusions can be presented.

Since the data on the —CH_2OH compounds are slightly equivocal a similar series of measurements were made on compounds **2** and **4** where the substituent is —$COOCH_3$. The binding of this group to the shift reagent should be weaker than for the CH_2OH group and there should be little tendency for

TABLE 4. Chemical shifts of **1** and **3** as a function of solvent, temperature, and shift reagent

Compound	Solvent	T (°C)	δCH_3	δCH_2
1	$CDCl_3$	0	1.553	3.851; 3.915
1	$CDCl_3$	25	1.552	3.845; 3.909
1	$CDCl_3$	45	1.637	3.930; 3.987
1	$CDCl_3$	55	1.636	3.926; 3.984
1	$CDCl_3$ + Eu(hfc)$_3$	0	2.521	6.184; 6.233
1	$CDCl_3$ + Eu(hfc)$_3$	25	2.488	5.78
1	CS_2	0	1.452	3.69
1	CS_2	25	1.452	3.690
1	CS_2 + Eu(hfc)$_3$	0	3.856	—
1	CS_2 + Eu(hfc)$_3$	25	2.488	6.249
3	$CDCl_3$	0	1.614	3.93
3	$CDCl_3$	25	1.635	3.959
3	$CDCl_3$ + Eu(hfc)$_3$	0	1.841	4.468; 4.524
3	$CDCl_3$ + Eu(hfc)$_3$	25	1.846	4.455
3	CS_2	0	1.311	3.368
3	CS_2	25	1.542	3.775
3	CS_2 + Eu(hfc)$_3$	0	2.787	4.027
3	CS_2 + Eu(hfc)$_3$	25	2.984	3.499

TABLE 5. Chemical shifts of **2** and **4** as a function of temperature and shift reagent

Compound	Solvent	T (°C)	$\delta(CH_3)_2$	δOCH_3
2	CS_2	−20	1.487	3.492
2	CS_2	0	1.493	3.498
2	CS_2	25	1.503	3.505
2	CS_2 + Eu(hfc)$_3$	−20	2.897; 2.922	4.377[a]
2	CS_2 + Eu(hfc)$_3$	0	2.757; 2.778	4.332[a]
2	CS_2 + Eu(hfc)$_3$	25	2.557	4.243
4	CS_2	−20	1.600	3.479
4	CS_2	0	1.606	3.488
4	CS_2	25	1.617	3.502
4	CS_2 + Eu(hfc)$_3$	−20	2.213	3.918
4	CS_2 + Eu(hfc)$_3$	0	2.230	3.929
4	CS_2 + Eu(hfc)$_3$	25	2.228	3.933

[a] There is evidence from a DISPA plot (15) that these are two unresolved lines.

dimerization in solution. The results are listed in Table 5. There is no evidence for non-equivalence of the methyl groups in **2** or **4** in the absence of shift reagent. When Eu(hfc)$_3$ is added to the solutions a splitting of the methyl groups at low temperature is observed with **2** but not with **4**.

From all of these observations we may conclude that all the compounds studied are chiral in solution. This lack of symmetry is removed by motional averaging which has a lower energy barrier in the case of the naphthalene compounds than the benzene compounds.

X-ray crystal structure studies

Bond lengths and angles for compounds **2** and **4** are shown in Figs. 1 and 2, respectively. It should be noted that the thermal parameters of H11, H41, H61, and H91 are exceptionally small. This may be an artifact of the refinement but we

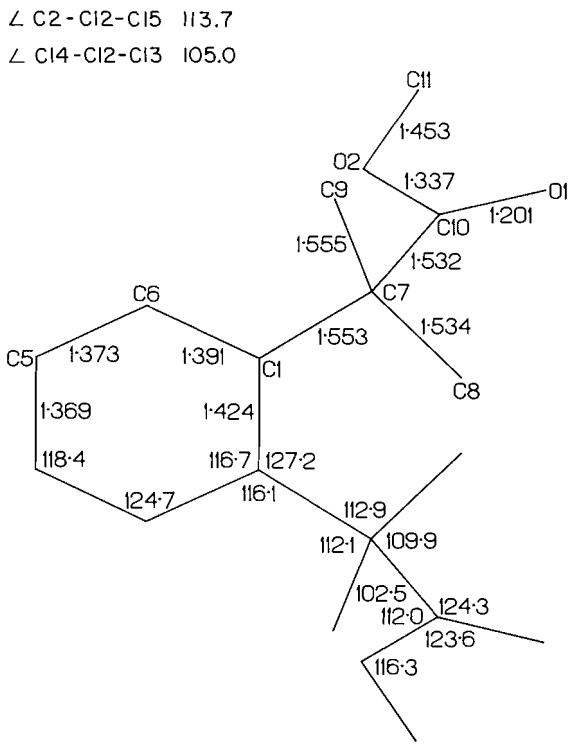

FIG. 1. Bond lengths and angles for **2**.

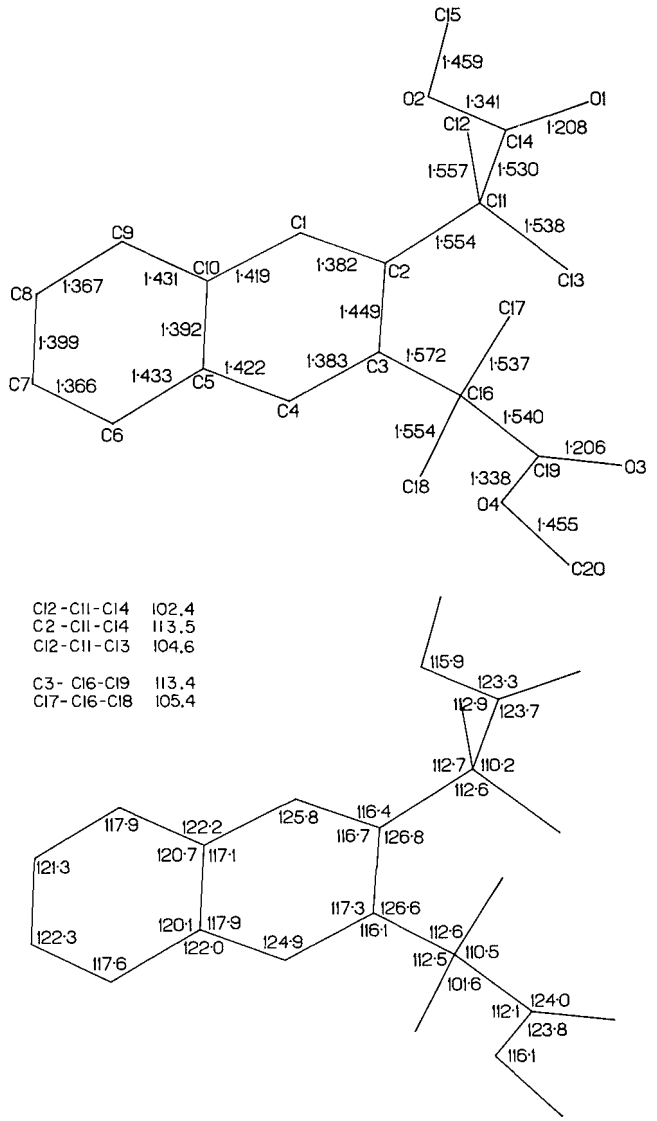

FIG. 2. Bond lengths and angles for **4**.

can offer no satisfactory explanation. Lists of structure factors and anisotropic thermal parameters are also lodged with the Depository of Unpublished Data.[4]

The molecule of **2** uses a crystallographic two-fold axis, but as this is a symmetry operator of the first kind it is still possible for the molecule to possess "handedness" (chirality). In fact the molecules of **2** and **4** both show such handedness because of the out-of-plane distortions of the $—(CH_3)_2COOCH_3$ group. In **2** this distortion produces a 12.1° torsion angle between the two substituents on atoms C_1 and C_2, and in **4** the torsion angle is 8.9°. It should be emphasized that because the space groups of **2** and **4** are both centrosymmetric, left- and right-handed molecules exist in both crystals. The chirality of **2** is clearly illustrated by the stereo pair representation of Fig. 3.

The benzene ring of **2** is distorted so that atoms C_1 and C_2 are −0.032 and +0.032 Å from the plane and C_5 and C_4 are +0.019 and −0.019 Å out-of-plane. The substituents atoms C_7 and C_{12} are −0.203 and +0.203 Å, respectively from the plane. There is less distortion of the unsubstituted aromatic ring of **4** (C_5 to C_{10}) than for the benzene ring of **2** with C_5, C_8, and C_9 0.013, 0.004, and 0.001 Å above the plane and C_6, C_7, and C_{10} 0.008, 0.001, and 0.010 Å below the plane. The substituted aromatic ring of **4** is also very nearly planar with C_3 and C_{10} at +0.024 and +0.020 Å, respectively, and C_1, C_2, C_4, and C_5 at −0.003, −0.019, −0.008, and −0.015 Å. However, there is a dihedral angle of 2.83° between the planes of the two rings. The substituent atoms C_{11} and C_{16} of **4** are at −0.132 and +0.161 Å from the plane of the substituted benzene ring. Therefore, one may say that there are greater deviations from planarity in **2** than in **4**. The lengths of the exocyclic carbon–carbon bonds are similar in both **2** and **4** and also similar to those found for other hindered *t*-butyl substituted aromatic compounds (3, 4). The aromatic carbon–carbon bonds of the ring atoms attached to the bulky substituents, C1—C2 in **2**, and C2—C3 in **4**, are also significantly lengthened.

Since the bulk of the *ortho*-substituents is the same for the benzene and napthalene compounds but the structures of the napthalene compounds were found to be more nearly planar, it follows that there is a greater steric strain energy in the naphthalene series. We can assume that the steric strain for the substituent groups to pass each other in the transition state for moving from above to below the plane of the aromatic ring is the same for the benzene and naphthalene compounds since the relevant bond lengths and angles for the two are similar. This implies that the difference in energy between the ground state and the planar transition state for exchange of substituent positions relative to the aromatic ring will be less for the naphthalene compounds than the corresponding benzene compounds. Such a result is in fact inferred from the proton resonance observations. Therefore the structural results obtained for the solids are consistent with the proton magnetic resonance results in solution.

Can. J. Chem. Downloaded from www.nrcresearchpress.com by 210.87.254.105 on 09/06/12
For personal use only.

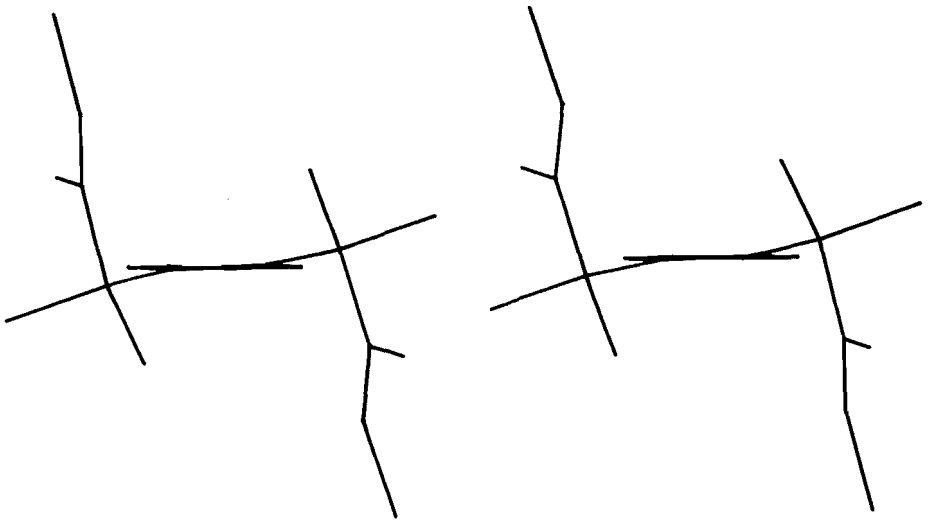

FIG. 3. A stereo pair presentation for **2** viewed along the plane of the benzene ring.

Acknowledgement

L.R.C.B. wishes to thank the Natural Sciences and Engineering Research Council of Canada for financial support.

1. E. M. ARNETT, J. C. SANDA, J. M. BOLLINGER, and M. BARBER. J. Amer. Chem. Soc. **89**, 5389 (1967).
2. F. A. KEIDEL and S. H. BAUER. J. Chem. Phys. **25**, 1218 (1956).
3. C. H. STAM. Acta Crystallogr. **B28**, 2715 (1972).
4. J. HANDAL, J. G. WHITE, R. W. FRANCK, Y. H. YUH, and N. L. ALLINGER. J. Am. Chem. Soc. **99**, 3345 (1977).
5. L. R. C. BARCLAY, C. E. MILLIGAN, and N. D. HALL. Can. J. Chem. **40**, 1664 (1962).
6. J. E. A. ANDERSON, R. W. FRANCK, and W. L. MANDELLA. J. Am. Chem. Soc. **94**, 4608 (1972).
7. P. M. NAIR and J. D. ROBERTS. J. Am. Chem. Soc. **79**, 4565 (1957).
8. M. HOLK and A. MANNSCHRECK. Org. Magn. Reson. **12**, 28 (1979).
9. L. R. C. BARCLAY, G. R. NIXON, H. M. FOOTE, and S. L. BARCLAY. Can. J. Chem. **47**, 4313 (1969).
10. D. F. GRANT and E. J. GABE. J. Appl. Cryst. **11**, 114 (1978).
11. Y. LE PAGE, E. J. GABE, and L. D. CALVERT. J. Appl. Cryst. **12**, 25 (1979).
12. G. GERMAIN, P. MAIN, and M. M. WOOLFSON. Acta Crystallogr. **A27**, 368 (1971).
13. A. C. LARSON and E. J. GABE. Computing in crystallography. *Edited by* H. Schenk, R. Olthof-Hazekamp, H. van Koningsveld, and G. C. Bassi. Delft Univ. Press. 1978. p. 81.
14. H. N. CHENG and H. S. GUTOWSKY. J. Phys. Chem. **84**, 1049 (1980).
15. A. G. MARSHALL and D. C. ROE. Anal. Chem. **50**, 756 (1978).

Can. J. Chem. Downloaded from www.nrcresearchpress.com by 210.87.254.105 on 09/06/12
For personal use only.

Structural studies of organoboron compounds. XX.[1] (Salicylaldoximato-*O*,*N*)diphenylboron

WOLFGANG KLIEGEL

Institut für Pharmazeutische Chemie, der Technischen Universität Braunschweig, 3300 Braunschweig, Beethovenstraße 55, Bundesrepublik Deutschland

AND

STEVEN J. RETTIG AND JAMES TROTTER

Department of Chemistry, University of British Columbia, 2036 Main Mall, Vancouver, B.C., Canada V6T 1Y6

Received November 9, 1983

WOLFGANG KLIEGEL, STEVEN J. RETTIG, and JAMES TROTTER. Can. J. Chem. **62**, 1363 (1984).

Crystals of (salicylaldoximato-*O*,*N*)diphenylboron are triclinic, a = 10.125(2), b = 10.797(1), c = 14.760(2) Å, α = 89.05(1), β = 86.98(1), γ = 83.18(1)°, Z = 4, space group $P\bar{1}$. The structure was solved by direct methods and was refined by full-matrix least-squares procedures to R = 0.040 and R_w = 0.048 for 4145 reflections with $I \geq 3\sigma(I)$. The structure consists of two crystallographically independent, but essentially identical, molecules linked by strong O—H···O hydrogen bonds to form continuous spirals along the a axis. The Ph_2B moiety is chelated by the phenolic oxygen and oxime nitrogen atoms of the ligand resulting in the formation of a non-planar six-membered chelate ring. Important libration-corrected mean bond lengths are O—B = 1.516(1), N—B = 1.609(2), and C—B = 1.613(2) Å.

WOLFGANG KLIEGEL, STEVEN J. RETTIG et JAMES TROTTER. Can. J. Chem. **62**, 1363 (1984).

Les cristaux de (salicylaldoximato-*O*,*N*)diphénylbore sont tricliniques; a = 10,125(2), b = 10,797(1), c = 14,760(2) Å, α = 89,05(1), β = 86,98(1), γ = 83,18(1)°, Z = 4, groupe d'espace $P\bar{1}$. On a résolu la structure par des méthodes directes et on l'a affinée par la méthode des moindres carrés (matrice entière) jusqu'à des valeurs de R = 0,040 et de R_w = 0,048 pour 4145 réflexions avec $I \geq 3\sigma(I)$. La structure consiste en deux molécules qui sont cristallographiquement indépendantes, mais essentiellement identiques, et qui sont liées par de fortes liaisons hydrogènes O—H···O formant ainsi une spirale continue le long de l'axe a. L'unité Ph_2B est chélatée par l'oxygène phénolique et par l'azote de l'oxime du ligand; il en résulte la formation d'un chélate cyclique à six chaînons qui n'est pas plan. Les longueurs de liaison importantes, corrigées pour la libration, sont: O—B = 1,516(1), N—B = 1,609(2) et C—B = 1,613(2) Å.

[Traduit par le journal]

Introduction

Spectroscopic data and chemical behavior of different boron chelates of salicylaldoxime support the assumption that they contain six-membered heterocyclic rings with intramolecular N→B coordination (1). This structure was already suggested for the diphenylboron chelate **4** by Umland and Schleyerbach (2) who first reported the synthesis of this compound from salicylaldoxime (**1**) and diphenylborinic acid anhydride. The chelate structure **4** would derive from the (*E*)-form of salicylaldoxime (**1**), which has been verified by X-ray crystallographic analysis (3) and which is also represented in several metal chelates of salicylaldoxime (4–8). Nevertheless, the seven-membered isomeric chelate structure **5**, which could result from a configurational change of (*E*)-salicylaldoxime to the (*Z*)-isomer under the influence of the Lewis-acid borinic acid reagent during the synthesis, could not be excluded unambiguously by chemical or spectroscopic means (1). Moreover, the seven-membered ring system of **5** has been verified in various boron chelates of salicylaldehydnitrones **7** (9).

An X-ray crystallographic study was undertaken to decide between the two structures **4** with N→B coordination and **5** with O→B coordination. To avoid thermal stress which can cause the transformation of the diphenylboron chelate into the pentacyclic dimer **6** of a monophenylboron derivative of salicylaldoxime (1, 10), the compound was recrystallized from methanol/acetonitrile or methanol/water under mild conditions.

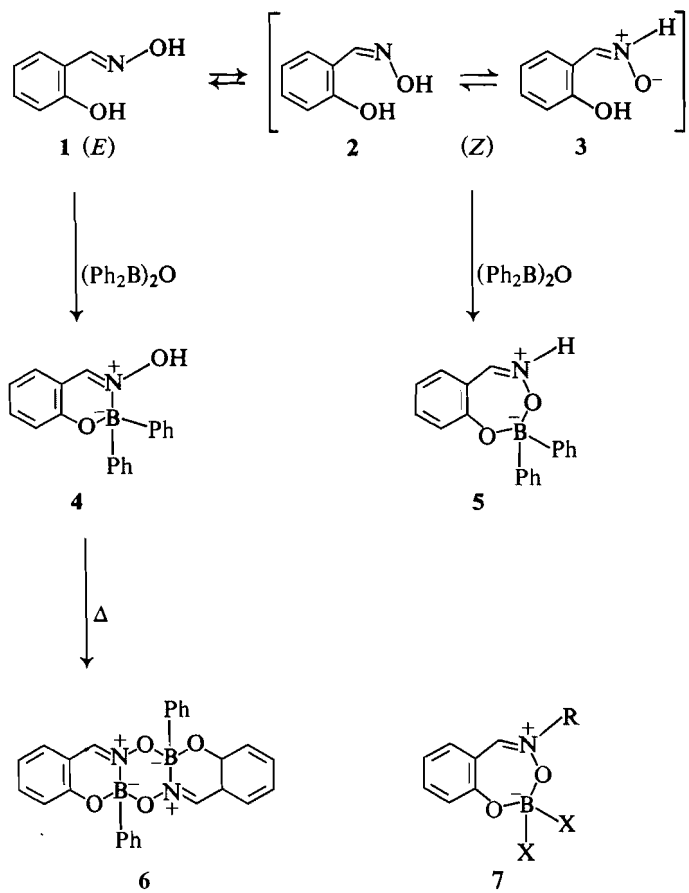

[1]For Part XIX, see ref. 23.

Can. J. Chem. Downloaded from www.nrcresearchpress.com by 210.87.254.42 on 09/06/12
For personal use only.

TABLE 1. Final positional (fractional × 10^5, H × 10^4) and isotropic thermal parameters (U × 10^3 Å^2) with estimated standard deviations in parentheses

Atom	x	y	z	U_{eq}*/U_{iso}	Atom	x	y	z	U_{eq}*/U_{iso}
O(1)	75148(11)	34759(10)	20767(7)	43	C(14′)	26097(16)	33962(14)	42736(10)	40
O(2)	109719(11)	19859(11)	15284(9)	52	C(15′)	13227(20)	32473(19)	45457(13)	60
N	98439(12)	28632(12)	15793(8)	40	C(16′)	7688(25)	36265(23)	53913(16)	75
C(1)	76233(16)	46280(15)	17332(10)	41	C(17′)	14921(27)	41634(21)	59877(15)	72
C(2)	88599(17)	49263(15)	13686(11)	45	C(18′)	27664(29)	43254(29)	57413(16)	93
C(3)	89761(23)	61457(18)	10591(14)	59	C(19′)	33187(24)	39468(26)	48998(15)	81
C(4)	78930(25)	70373(20)	11035(15)	70	B′	32125(18)	29522(17)	32855(12)	39
C(5)	66862(24)	67334(19)	14769(14)	63	H(O2)	11437(26)	2026(22)	2071(18)	105(8)
C(6)	65406(19)	55424(17)	17920(12)	50	H(3)	9811(21)	6314(18)	817(14)	69(6)
C(7)	99934(17)	39938(16)	13695(11)	45	H(4)	7994(22)	7852(21)	919(15)	88(7)
C(8)	85190(15)	13534(15)	25793(10)	41	H(5)	5922(22)	7362(19)	1531(14)	75(6)
C(9)	84148(19)	983(17)	24665(14)	55	H(6)	5692(20)	5322(17)	2078(13)	61(5)
C(10)	84405(22)	−7311(21)	32016(16)	68	H(7)	10882(20)	4238(16)	1226(12)	58(5)
C(11)	85910(20)	−3061(25)	40599(15)	72	H(9)	8317(19)	−236(18)	1858(14)	68(6)
C(12)	87178(19)	9206(24)	41891(13)	63	H(10)	8422(21)	−1595(21)	3082(14)	75(7)
C(13)	86757(16)	17493(19)	34598(11)	49	H(11)	8545(23)	−900(21)	4570(16)	92(7)
C(14)	79730(15)	18272(14)	8213(10)	38	H(12)	8877(23)	1244(20)	4805(16)	88(7)
C(15)	66266(18)	17093(19)	7493(13)	55	H(13)	8720(16)	2618(16)	3577(11)	46(5)
C(16)	61468(23)	12250(21)	−133(15)	67	H(15)	6061(21)	1986(18)	1262(14)	70(6)
C(17)	70068(24)	8268(20)	−7272(15)	66	H(16)	5247(26)	1186(21)	−43(16)	92(8)
C(18)	83354(22)	9248(18)	−6796(13)	60	H(17)	6678(21)	457(19)	−1239(15)	77(6)
C(19)	88125(18)	14219(16)	855(11)	47	H(18)	9012(23)	627(20)	−1195(16)	90(7)
B	84343(17)	23456(17)	17525(12)	38	H(19)	9773(20)	1487(17)	107(13)	60(5)
O(1′)	25917(11)	18421(10)	29632(7)	42	H(O2′)	6221(24)	3203(21)	2932(16)	86(7)
O(2′)	56381(12)	33108(12)	34270(9)	56	H(3′)	5606(23)	−1042(19)	4039(14)	74(6)
N′	47474(13)	24257(13)	33812(9)	42	H(4′)	4036(22)	−2579(22)	4000(15)	87(7)
C(1′)	29781(16)	6734(14)	32688(10)	40	H(5′)	1894(20)	−2047(18)	3525(13)	66(6)
C(2′)	42715(17)	3535(16)	35620(12)	50	H(6′)	1261(20)	34(17)	3031(12)	60(6)
C(3′)	46701(23)	−8807(19)	38304(16)	70	H(7′)	6073(19)	1071(16)	3679(12)	53(5)
C(4′)	38095(25)	−17566(20)	38135(17)	74	H(9′)	2293(21)	5500(19)	3233(15)	76(6)
C(5′)	25308(23)	−14288(18)	35212(13)	61	H(10′)	2232(25)	6960(23)	1990(16)	97(8)
C(6′)	21121(19)	−2305(16)	32477(11)	47	H(11′)	2980(21)	6297(20)	526(16)	81(6)
C(7′)	51750(18)	12859(18)	35462(12)	51	H(12′)	3827(21)	4137(19)	299(15)	76(6)
C(8′)	31142(16)	39738(15)	24777(10)	42	H(13′)	3900(17)	2754(17)	1474(11)	50(5)
C(9′)	26242(23)	52147(17)	26082(13)	61	H(15′)	803(23)	2858(21)	4145(16)	88(7)
C(10′)	25692(27)	60701(21)	18903(15)	74	H(16′)	−140(29)	3533(23)	5548(18)	111(9)
C(11′)	30220(22)	57042(21)	10341(14)	65	H(17′)	1134(22)	4476(20)	6571(16)	82(7)
C(12′)	35121(19)	44880(20)	8836(13)	56	H(18′)	3320(32)	4770(27)	6143(22)	139(11)
C(13′)	35471(16)	36303(18)	15992(11)	47	H(19′)	4229(28)	4089(23)	4753(17)	103(8)

*U_{eq} = (1/3) trace U_{diag}.

Experimental

(Salicylaldoximato-O,N)diphenylboron (3-hydroxy-2,2-diphenyl-1-oxa-3-azonia-2-borata-1,2-dihydronaphthalene) (4)

The compound was synthesized from salicylaldoxime and oxybis(diphenylborane) by the literature method (2). Melting point 157°C; lit. (2) 157°C. Crystals suitable for X-ray analysis were obtained by slow evaporation of a methanol/water solution. A crystal bounded by the six faces (followed by their distances in mm from a common origin): ±(0 1 1), 0.163, ±(0 1 −1), 0.256, ±(1 0 0), 0.313 was mounted in a general orientation. Unit-cell parameters were refined by least-squares on 2 sin θ/λ values for 25 reflections (2θ = 40−45°) measured on a diffractometer with Mo-Kα Radiation (λ(Kα$_1$) = 0.70930, λ(Kα$_2$) = 0.71359 Å). Crystal data at 22°C are:

$C_{19}H_{16}BNO_2$ fw = 301.15

Triclinic, a = 10.125(2), b = 10.797(1), c = 14.760(2) Å, α = 89.05(1), β = 86.98(1), γ = 83.18(1)°, V = 1599.8(4) Å^3, Z = 4, ρ_c = 1.250 gcm^{-3}, F(000) = 632, μ(Mo-Kα) = 0.75 cm^{-1}. Absent reflections: none, space group $P\bar{1}$ (C_i^1, No. 2, reduced cell) from structure analysis.

Intensities were measured with graphite-monochromated Mo-Kα radiation on an Enraf-Nonius CAD4-F diffractometer. An ω−2θ scan at 1.44−10.06° min^{-1} over a range of (0.65 + 0.35 tan θ) deg in ω (extended by 25% on both sides for background measurement) was employed. Data were measured to 2θ = 55°. The intensities of three check reflections, measured every 3600 s throughout the data collection, remained constant to within 2.5%. Of the 7310 independent reflections measured and processed,[2] 4145 (57%) had intensities greater than 3σ(I) above background where $\sigma^2(I) = S + 2B + (0.04(S - B))^2$ with S = scan count and B = normalized background count.

The structure was solved by direct methods in the centrosymmetric space group $P\bar{1}$ (strongly indicated by the E-statistics), the coordinates of all non-hydrogen atoms being determined from an E-map. After full-matrix least-squares refinement of the non-hydrogen atoms with anisotropic thermal parameters to R = 0.080, a difference map gave

[2]The computer programs used include locally written programs for data processing and locally modified versions of the following: MULTAN 80, multisolution program by P. Main, S. J. Fiske, S. E. Hull, L. Lessinger, G. Germain, J. P. Declercq, and M. M. Woolfson; ORFLS, full-matrix least-squares, and ORFFE, function and errors, by W. R. Busing, K. O. Martin and H. A. Levy; FORDAP, Patterson and Fourier syntheses, by A. Zalkin; ORTEP II, illustrations, by C. K. Johnson.

Can. J. Chem. Downloaded from www.nrcresearchpress.com by 210.87.254.42 on 09/06/12
For personal use only.

Can. J. Chem. Downloaded from www.nrcresearchpress.com by 210.87.254.42 on 09/06/12
For personal use only.

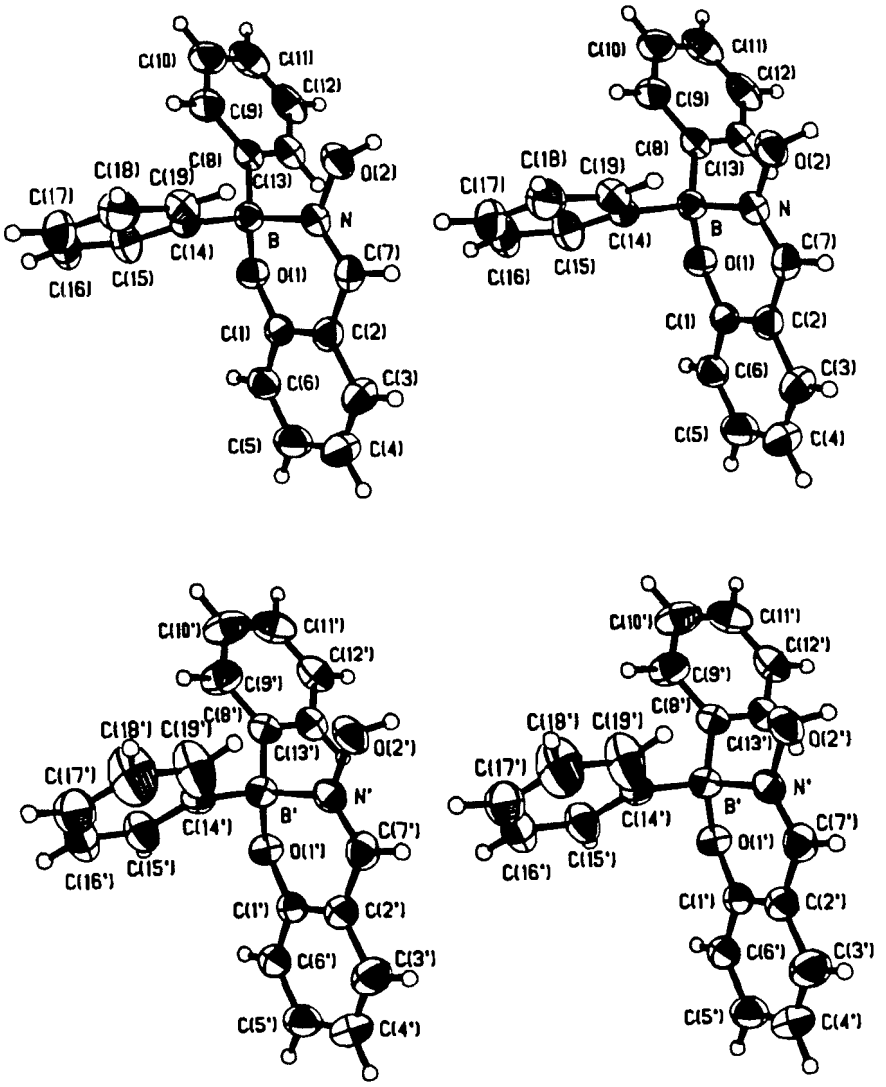

FIG. 1. Stereoscopic views of two independent (salicylaldoximato-*O*,*N*)diphenylboron molecules. 50% probability thermal ellipsoids are shown for the non-hydrogen atoms. Hydrogen atoms have been assigned artificially small thermal parameters for the sake of clarity.

the positions of all hydrogen atoms which were refined with isotropic thermal parameters in subsequent least-squares cycles. The scattering factors of ref. 11 were used for non-hydrogen atoms and those of ref. 12 for hydrogen atoms. The weighting scheme, $w = 1/\sigma^2(F)$ where $\sigma^2(F)$ is derived from the previously defined $\sigma^2(I)$, gave uniform average values of $w(|F_o| - |F_c|)^2$ over ranges of both $|F_o|$ and $\sin\theta/\lambda$ and was employed in the final stages of refinement. Unobserved reflections were not included in the refinement. Convergence was reached at $R = 0.040$ and $R_w = 0.048$ for 4145 reflections with $I \geq 3\sigma(I)$. For all 7310 reflections $R = 0.088$. The function minimized was $\Sigma w(|F_o| - |F_c|)^2$, $R = \Sigma||F_o| - |F_c||/\Sigma|F_o|$ and $R_w = (\Sigma w(|F_o| - |F_c|)^2/\Sigma w|F_o|^2)^{1/2}$.

On the final cycle of refinement the mean and maximum parameter shifts corresponded to 0.05 and 0.68σ, respectively. The maximum parameter shift was associated with the *y* coordinate of H(18′). The mean error in an observation of unit weight was 1.851. A final difference map was essentially featureless, residual densities ranging from -0.24 to $+0.157$ e Å^{-3}. The final positional and thermal parameters appear in Tables 1 and 5,[3] respectively. Measured and calculated structure factors have been placed in the Depository of Unpublished Data.[3]

The ellipsoids of thermal motion for the non-hydrogen atoms are shown in Fig. 1. The thermal motion has been analysed in terms of the rigid-body modes of translation, libration, and screw motion (13). The rms standard error in the temperature factors σU_{ij} (derived from the least-squares analysis) is 0.0010 Å^2. Analyses of the two independent molecules indicated significant independent motion of the phenyl rings. The 7-atom BPh and 11-atom groups consisting of the fused-ring system plus O(2) were separately analysed (rms ΔU_{ij} = 0.0014–0.0025 Å^2). The appropriate bond distances have been corrected for libration (13, 14), using shape parameters q^2 of 0.08 for all atoms involved. Corrected bond lengths appear in Table 2 along with the uncorrected values; corrected bond angles do not differ by more than 1σ from the uncorrected values given in Table 3. Intra-annular torsion angles defining the conformations of the six-membered chelate rings are listed in Table 4. Bond lengths and angles involving hydrogen and a complete listing of torsion angles (Tables 6–8) are included as supplementary material. Corrected bond lengths (esd's taken as equal to those associated with the uncorrected values) are employed in the discussion.[4]

[3]The structure factor table, Table 5 (anisotropic thermal parameters) and other material mentioned in the text are available, at a nominal charge, from the Depository of Unpublished Data, CISTI, National Research Council of Canada, Ottawa, Ont., Canada K1A 0S2.

[4]All bond lengths referred to in the discussion except those for compound **8** have been corrected for libration.

TABLE 2. Bond lengths (Å) with estimated standard deviations in parentheses

Bond	Length		Bond	Length	
	Uncorr.	Corr.		Uncorr.	Corr.
O(1)—C(1)	1.350(2)	1.355	O(1′)—C(1′)	1.353(2)	1.359
O(1)—B	1.513(2)	1.516	O(1′)—B′	1.512(2)	1.516
O(2)—N	1.394(2)	1.397	O(2′)—N′	1.394(2)	1.397
N —C(7)	1.279(2)	1.283	N′ —C(7′)	1.279(2)	1.285
N —B	1.600(2)	1.607	N′ —B′	1.603(2)	1.611
C(1)—C(2)	1.407(2)	1.414	C(1′)—C(2′)	1.403(2)	1.411
C(1)—C(6)	1.386(2)	1.389	C(1′)—C(6′)	1.389(2)	1.392
C(2)—C(3)	1.403(2)	1.407	C(2′)—C(3′)	1.403(3)	1.408
C(2)—C(7)	1.434(2)	1.438	C(2′)—C(7′)	1.438(3)	1.441
C(3)—C(4)	1.370(3)	1.373	C(3′)—C(4′)	1.361(3)	1.364
C(4)—C(5)	1.387(3)	1.392	C(4′)—C(5′)	1.390(3)	1.397
C(5)—C(6)	1.382(3)	1.387	C(5′)—C(6′)	1.374(3)	1.379
C(8)—C(9)	1.385(2)	1.393	C(8′)—C(9′)	1.385(2)	1.396
C(8)—C(13)	1.398(2)	1.405	C(8′)—C(13′)	1.389(2)	1.397
C(8)—B	1.609(2)	1.614	C(8′)—B′	1.610(2)	1.613
C(9)—C(10)	1.395(3)	1.399	C(9′)—C(10′)	1.393(3)	1.397
C(10)—C(11)	1.376(3)	1.384	C(10′)—C(11′)	1.370(3)	1.378
C(11)—C(12)	1.363(3)	1.371	C(11′)—C(12′)	1.365(3)	1.376
C(12)—C(13)	1.387(3)	1.392	C(12′)—C(13′)	1.392(2)	1.396
C(14)—C(15)	1.394(2)	1.403	C(14′)—C(15′)	1.370(2)	1.391
C(14)—C(19)	1.387(2)	1.397	C(14′)—C(19′)	1.383(3)	1.401
C(14)—B	1.605(2)	1.609	C(14′)—B′	1.609(2)	1.614
C(15)—C(16)	1.383(3)	1.388	C(15′)—C(16′)	1.389(3)	1.394
C(16)—C(17)	1.372(3)	1.382	C(16′)—C(17′)	1.354(3)	1.372
C(17)—C(18)	1.367(3)	1.376	C(17′)—C(18′)	1.353(4)	1.373
C(18)—C(19)	1.391(3)	1.396	C(18′)—C(19′)	1.383(3)	1.388

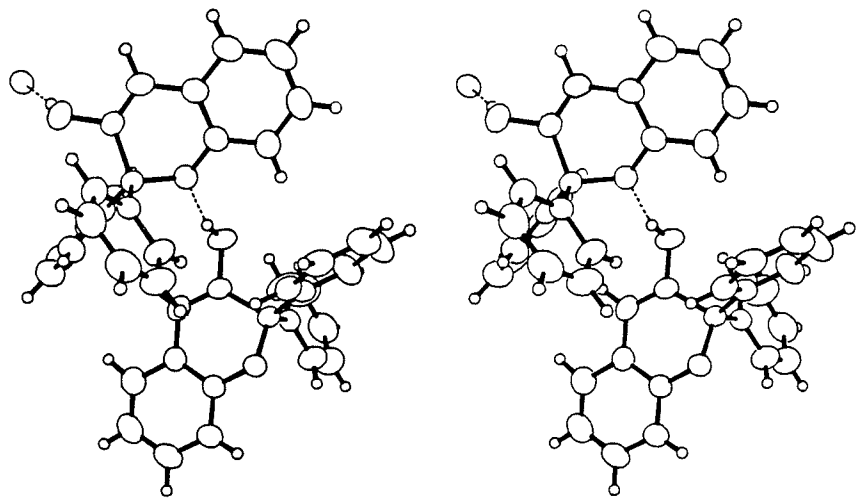

FIG. 2. Stereoscopic view of the asymmetric unit showing the spatial relationship between the two independent molecules. Hydrogen bonds are represented by broken lines.

Results and discussion

The X-ray analysis confirms the six-membered chelate structure **4** containing an intramolecular N→B interaction. The structure is thus consistent with that found earlier for **6** (10), to which **4** is transformed upon heating.

The crystal structure of **4** consists of discrete molecules linked by strong O—H···O hydrogen bonds (O(2)—H(O2)···O(1′) ($1 + x, y, z$), O···O = 2.737(3), H···O = 1.80(3) Å, O—H···O = 167(2)°; O(2′)—H(O2′)···O(1), O···O = 2.699(2), H···O = 1.82(2) Å, O—H···O = 161(2)°) to form continuous spirals along the *a* axis. The two crystallographically independent molecules are related to one another by a pseudo-twofold screw axis along *a*; coordinates of unprimed atoms are approximately given by the operation ($1/2 + x, 1/2 - y, 1/2 - z$) on the coordinates of the corresponding primed atoms. The spatial disposition of the two molecules and the intermolecular H-bonding are shown in Fig. 2. There are short C—H···O contacts between chains (C(18′)—H(18′)···O(2′) ($1 - x, 1 - y, 1 - z$), C···O = 3.453(2), H···O = 2.54(3) Å, C—H···O = 152(2)°). There are also a pair of close intermolecular H···H contacts between phenyl rings on adjacent molecules along the chain (H(13)···H(15′) ($1 + x, y, z$) = 2.35(3) and H(13′)···H(15) = 2.25(3) Å).

The two independent molecules of the asymmetric unit have

Can. J. Chem. Downloaded from www.nrcresearchpress.com by 210.87.254.42 on 09/06/12
For personal use only.

Can. J. Chem. Downloaded from www.nrcresearchpress.com by 210.87.254.42 on 09/06/12
For personal use only.

TABLE 3. Bond angles (deg) with estimated standard deviations in parentheses

Bonds	Angle (deg)	Bonds	Angle (deg)
C(1)—O(1)—B	121.90(12)	C(1′)—O(1′)—B′	121.41(12)
O(2)—N —C(7)	117.66(13)	O(2′)—N′ —C(7′)	117.96(14)
O(2)—N —B	117.13(12)	O(2′)—N′ —B′	116.50(13)
C(7)—N —B	124.56(13)	C(7′)—N′ —B′	124.75(14)
O(1)—C(1)—C(2)	120.00(14)	O(1′)—C(1′)—C(2′)	120.35(14)
O(1)—C(1)—C(6)	120.10(15)	O(1′)—C(1′)—C(6′)	119.74(15)
C(2)—C(1)—C(6)	119.8(2)	C(2′)—C(1′)—C(6′)	119.8(2)
C(1)—C(2)—C(3)	119.4(2)	C(1′)—C(2′)—C(3′)	119.2(2)
C(1)—C(2)—C(7)	119.14(15)	C(1′)—C(2′)—C(7′)	119.26(15)
C(3)—C(2)—C(7)	121.3(2)	C(3′)—C(2′)—C(7′)	121.5(2)
C(2)—C(3)—C(4)	120.4(2)	C(2′)—C(3′)—C(4′)	120.4(2)
C(3)—C(4)—C(5)	119.5(2)	C(3′)—C(4′)—C(5′)	119.8(2)
C(4)—C(5)—C(6)	121.5(2)	C(4′)—C(5′)—C(6′)	121.2(2)
C(1)—C(6)—C(5)	119.4(2)	C(1′)—C(6′)—C(5′)	119.5(2)
N —C(7)—C(2)	120.15(15)	N′ —C(7′)—C(2′)	119.8(2)
C(9)—C(8)—C(13)	117.1(2)	C(9′)—C(8′)—C(13′)	116.7(2)
C(9)—C(8)—B	122.80(15)	C(9′)—C(8′)—B′	123.29(15)
C(13)—C(8)—B	120.08(15)	C(13′)—C(8′)—B′	120.01(15)
C(8)—C(9)—C(10)	121.5(2)	C(8′)—C(9′)—C(10′)	121.4(2)
C(9)—C(10)—C(11)	119.7(2)	C(9′)—C(10′)—C(11′)	120.5(2)
C(10)—C(11)—C(12)	120.0(2)	C(10′)—C(11′)—C(12′)	119.6(2)
C(11)—C(12)—C(13)	120.3(2)	C(11′)—C(12′)—C(13′)	119.9(2)
C(8)—C(13)—C(12)	121.4(2)	C(8′)—C(13′)—C(12′)	122.0(2)
C(15)—C(14)—C(19)	116.2(2)	C(15′)—C(14′)—C(19′)	115.4(2)
C(15)—C(14)—B	118.20(14)	C(15′)—C(14′)—B′	120.76(15)
C(19)—C(14)—B	125.53(14)	C(19′)—C(14′)—B′	123.9(2)
C(14)—C(15)—C(16)	122.2(2)	C(14′)—C(15′)—C(16′)	122.2(2)
C(15)—C(16)—C(17)	120.1(2)	C(15′)—C(16′)—C(17′)	120.8(2)
C(16)—C(17)—C(18)	119.4(2)	C(16′)—C(17′)—C(18′)	118.5(2)
C(17)—C(18)—C(19)	120.4(2)	C(17′)—C(18′)—C(19′)	120.7(2)
C(14)—C(19)—C(18)	121.8(2)	C(14′)—C(19′)—C(18′)	122.4(2)
O(1)—B —N	103.77(12)	O(1′)—B′ —N′	103.92(12)
O(1)—B —C(8)	107.06(12)	O(1′)—B′ —C(8′)	106.79(12)
O(1)—B —C(14)	111.46(13)	O(1′)—B′ —C(14′)	111.69(13)
N —B —C(8)	109.45(12)	N′ —B′ —C(8′)	108.64(13)
N —B —C(14)	109.60(12)	N′ —B′ —C(14′)	107.68(12)
C(8)—B —C(14)	114.89(13)	C(8′)—B′ —C(14′)	117.28(13)

TABLE 4. Intra-annular torsion angles (deg) with standard deviations in parentheses

Atoms	Values (deg)		
	4	**4′**	**9***
B —O(1)—C(1)—C(2)	−26.8(2)	−27.4(2)	−30.3
O(1)—C(1)—C(2)—C(7)	−0.1(2)	0.9(2)	−4.6
C(1)—C(2)—C(7)—N	9.8(2)	9.1(3)	13.6
B —N —C(7)—C(2)	6.7(2)	6.7(3)	11.4
C(7)—N —B —O(1)	−27.6(2)	−27.5(2)	−39.5
C(1)—O(1)—B —N	37.0(2)	37.0(2)	49.0

*Signs opposite to those quoted in ref. 15 for direct comparison.

nearly identical structures (Fig. 1). In each molecule there is a short intramolecular C—H···O contact (C(19)—H(19)···O(2), C···O = 3.246(2) and 3.137(3), H···O = 2.57(2) and 2.46(3) Å, C—H···O = 125(1) and 127(2)°). Corresponding bond lengths and angles in the two molecules are presented side-by-side in Tables 2 and 3 for ease of comparison. Mean[5] bond lengths will be employed in subsequent discussion.

[5]Here and elsewhere in this report mean values refer to weighted means with rms deviations from the mean in parentheses.

The significantly non-planar C_3BNO chelate rings have conformations which may be described as either B-envelopes or half-chairs with B and O atoms displaced in opposite directions from the approximate plane formed by the four other ring atoms, very similar to those in **6** (10), **9** (15), and in the related molecule (salicylaldehydato)diphenylboron (16). The chelate ring in the *N*-aryl derivative **9**, however, deviates more from planarity than those in **4** as indicated by the torsion angles compared in Table 4. In the square-planar metal complexes bis(salicylaldoximato)M(II) (where M = Ni (4, 5), Cu (6), and Pd (7)), the chelate rings were found to be nearly planar although a conformation similar to that found here was reported for the compound bis(5-chlorosalicylaldoximato)copper(II) (8). The six independent aromatic rings are either planar within experimental error or nearly so, the maximum deviation of any atom from the respective C_6 mean plane being 0.0090(23) Å for C(4).

Bond lengths in **4** are very similar to the values reported for the free ligand **1** itself (3), the "chelated" proton in **1** being replaced by the diphenylborenium cation in **4**. The N—B distance of 1.609(2) Å is similar to the longer of two N(sp^2)—B bonds in **6** (1.602(2) Å) and that in the related Schiff-base complex **8** (17) (uncorrected value of 1.601(4) Å), but is significantly shorter than the distance of 1.638(5) Å in the *N*-aryl

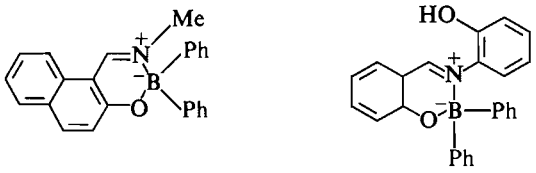

8 9

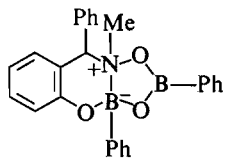

10

derivative **9** (15). The O—B distance in **4** (1.516(1) Å) is significantly longer than the distance between the phenolic oxygen and boron in **6** (mean 1.481(7) Å) or in the tricyclic compound **10** (18) (1.445(2) Å), slightly longer than in **8** (1.506(3) Å, uncorrected), or in (salicylaldehydato)diphenylboron (1.500(4) Å) (16). An even longer bond of this type has been observed in the Ph_2B chelate **9** (O—B = 1.524(5) Å). The C=N and N—O bonds of the oxime moiety in **4** are essentially the same as those in the free oxime **1** and are similar to values reported for various oximes and derivatives thereof (19–21). The geometry of the B-substituted phenyl rings is as expected (22) and the mean B—C distance of 1.613(2) Å is normal.

Acknowledgments

We thank the Natural Sciences and Engineering Research Council of Canada for financial support and the University of British Columbia Computing Centre for assistance.

1. W. KLIEGEL and D. NANNINGA. Monatsh. Chem. **114**, 465 (1983).
2. F. UMLAND and C. SCHLEYERBACH. Angew. Chem. **77**, 426 (1965).
3. C. E. PFLUGER and R. L. HARLOW. Acta Crystallogr. Sect. B, **29**, 2608 (1973).
4. L. L. MERRITT, C. GUARE, and A. E. LESSOR. Acta Crystallogr. **9**, 253 (1956).
5. R. C. SRIVASTAVA, E. C. LINGAFELTER, and P. C. JAIN. Acta Crystallogr. **22**, 922 (1967).
6. M. A. JARSKI and E. C. LINGAFELTER. Acta Crystallogr. **17**, 1109 (1964).
7. C. E. PFLUGER and R. L. HARLOW. Acta Crystallogr. Sect. B, **26**, 1631 (1970).
8. P. L. ORIOLI, E. C. LINGAFELTER, and B. W. BROWN. Acta Crystallogr. **17**, 1113 (1964).
9. W. KLIEGEL and D. NANNINGA. J. Organomet. Chem. **243**, 373 (1983).
10. S. J. RETTIG and J. TROTTER. Can. J. Chem. **61**, 206 (1983).
11. D. T. CROMER and J. B. MANN. Acta Crystallogr. Sect. A, **24**, 321 (1968).
12. R. F. STEWART, E. R. DAVIDSON, and W. T. SIMPSON. J. Chem. Phys. **42**, 3175 (1965).
13. V. SCHOMAKER and K. N. TRUEBLOOD. Acta Crystallogr. Sect. B, **24**, 63 (1968).
14. D. W. J. CRUICKSHANK. Acta Crystallogr. **9**, 747 (1956); **9**, 754 (1956); **14**, 896 (1961).
15. R. ALLMANN, E. HOHAUS, and S. OLEJNIK. Z. Naturforsch. **37b**, 1450 (1982).
16. S. J. RETTIG and J. TROTTER. Can. J. Chem. **54**, 1168 (1976).
17. O. E. KOMPAN, N. G. FURMANOVA, YU. T. STRUCHKOV, L. M. SITKINA, V. A. BREN', and V. I. MINKIN. Zh. Strukt. Khim. **21**(2), 90 (1980); J. Struct. Chem. **21**, 195 (1980).
18. W. KLIEGEL, D. NANNINGA, S. J. RETTIG and J. TROTTER. Can. J. Chem. **62**, 845 (1984).
19. W. KLIEGEL, D. NANNINGA, S. J. RETTIG, and J. TROTTER. Can. J. Chem. **61**, 2329 (1983).
20. F. BACHECHI and L. ZAMBONELLI. Acta Crystallogr. Sect. B, **28**, 2489 (1972).
21. S. J. RETTIG and J. TROTTER. Can. J. Chem. **53**, 765 (1975).
22. A. DOMENICANO, A. VACIAGO, and C. A. COULSON. Acta Crystallogr. Sect. B, **31**, 221 (1975); **31**, 1630 (1975).
23. W. KLIEGEL, S. J. RETTIG, and J. TROTTER. Can. J. Chem. **62**, 515 (1984).

Can. J. Chem. Downloaded from www.nrcresearchpress.com by 210.87.254.42 on 09/06/12
For personal use only.

Fluorescence characteristic and molecular interaction in the excited state of 1,2,3,4-tetrahydroquinoline

KAKALI CHATTERJEE, SANTANU LAHA, SANKAR CHAKRAVORTI, TAPAN GANGULY, AND SUKHENDU B. BANERJEE[1]

Optics Department, Indian Association for the Cultivation of Science, Jadavpur, Calcutta-700032, India

Received August 17, 1983

KAKALI CHATTERJEE, SANTANU LAHA, SANKAR CHAKRAVORTI, TAPAN GANGULY, and SUKHENDU B. BANERJEE. Can. J. Chem. **62**, 1369 (1984).

Fluorescence spectra of 1,2,3,4-tetrahydroquinoline (THQ) in binary and ternary mixtures in nonpolar and hydrogen bonding solvents at different temperatures are investigated. A probable case of partial protonation of THQ at 300 K due to hydrogen bonding in the excited state with ethanol is reported. At 77 K, there is no significant hydrogen bonding interaction between these molecules. Interaction between the n-orbital of triethylamine (TEA) and the π-electron system of excited THQ results in the formation of a CT-type complex which causes slow quenching of the fluorescence of THQ at 300 K. This quenching is not observed at 77 K because restriction of molecular orientation at 77 K prevents the formation of such complex. In pyridine, the fluorescence is strongly quenched both at room temperature and at 77 K. This has been attributed to π-electronic delocalization interaction between the fluorescer THQ and the nonfluorescing quencher pyridine. Possibility of conformational change is suggested. Rate constants associated with suitable reaction scheme for depletion of excited state are estimated. It is indicated that the quenching of fluorescence may be largely diffusion controlled.

KAKALI CHATTERJEE, SANTANU LAHA, SANKAR CHAKRAVORTI, TAPAN GANGULY et SUKHENDU B. BANERJEE. Can. J. Chem. **62**, 1369 (1984).

Les spectres de fluorescence de la tétrahydroquinone-1,2,3,4 (THQ) ont été examinés à différentes températures et dans des mélanges binaires et tertiaires de solvants non-polaires et de solvants exerçant des biens hydrogène. On remarque que le THQ dans son état excité subit une liaison hydrogène avec l'éthanol ce qui vraisemblablement provoque la protonation partielle du THQ à 300 K. Par contre on ne retrouve aucun lien hydrogène entre ces deux même substances à 77 K. A 300 K, l'intéraction entre l'orbitale n de la triéthylamine (TEA) et les π électrons du THQ excité provoque la formation d'un complexe de transfert de charge qui entraîne une extinction de la fluorescence du THQ. Cet effet n'est cependant pas observé à 77 K ce qui s'explique par la restriction imposée sur l'orientation moléculaire qui empêche la formation d'un tel complexe. Dans la pyridine, la fluorescence est fortement diminuée aussi bien à la température ambiante qu'à 77 K. On attribue cet effet a l'interaction des systèmes d'électrons délocalisés présents; on soupçonne de plus un changement de conformation. Les vitesses de réaction pour la dépopulation des états excités été mesurées. En conclusion, il semble que l'extinction de la fluorescence soit largement controlée par diffusion.

[Traduit par le journal]

Introduction

Effect of solvent–solute interaction, including hydrogen-bonding, on the fluorescence and phosphorescence spectra of molecules in solution has been extensively studied (1–14). Specifically hydrogen bonding interactions bring about many changes in the spectra such as spectral shift, intensification of spectra, as well as quenching of fluorescence in specific solvents. Hydrogen bonding abilities of molecules are usually different in the ground and excited electronic states. A number of organic molecules form stronger hydrogen bonds in the excited states (7, 12). A few extreme cases of strong hydrogen bonding in the excited state leading to protonation (15) or deprotonation (16) of molecules in donor or acceptor solvent, as the case may be, are known. As regards the phenomenon of fluorescence quenching due to hydrogen bonding, possible reaction schemes providing routes for nonradiative energy loss have been described (17–23), but a clear interpretation of the phenomenon is lacking.

Hydrogen bonding in 1,2,3,4-tetrahydroquinoline (THQ) molecule, a bicyclic secondary amine, in the ground state was studied by ultraviolet and infrared absorption spectroscopy (24). In this molecule, the N—H group is in the alicyclic-like ring 2 (Fig. 1(*a*)) and according to Booth (25), the molecule is a mixture of rapidly inverting half-chair structure with equal proportions of axial and equatorial conformations. It was suggested (24) that intermolecular hydrogen bond with dioxane brought about conformational change favourable for large participation of nitrogen lone pair in the π-electronic system of the benzene-like ring. The purpose of this work was to study hydrogen bonding properties of THQ in the excited state. Probable reaction schemes for depletion of excited state and changes in the position and intensity of fluorescence bands of the molecule due to hydrogen bonding reactions in different solvents at 300 and 77 K are described in this paper.

Experimental

Pure 1,2,3,4-tetrahydroquinoline (THQ) supplied by Fluka, Switzerland was used after distillation under reduced pressure. Solvents cyclohexane (CH), methylcyclohexane (MCH), dioxane, and ethanol (EtOH) were of spectroscopic grade and solvents triethyl amine (TEA), pyridine, and acetonitrile, obtained from E. Merck, were repeatedly distilled under vacuum before use and were tested for the absence of any fluorescence. At room temperature, CH or MCH was the "inert" solvent while at 77 K, MCH was used to obtain a glassy matrix. The fluorescence and excitation spectra were recorded with a Perkin-Elmer model MPF 44A fluorescence spectrophotometer provided with corrected spectra unit and the absorption spectra with a Shimadzu UV-VIS spectrophotometer model 210A. The fluorescence quantum yield of THQ in CH was measured from the corrected area under fluorescence curve relative to that of phenanthrene (26) in identical condition and the fluorescence life time τ was determined therefrom (27).

Results and discussion

In a previous paper (24) it was reported that spectral changes characteristic of H-bonding in the ground state such as change in N—H stretching frequency, red-shift and intensification of absorption bands, were observed in the ir and uv absorption

[1]To whom all correspondence should be addressed.

Can. J. Chem. Downloaded from www.nrcresearchpress.com by 210.87.254.42 on 09/06/12
For personal use only.

TABLE 1. Equilibrium constants in the ground (K_g), in the excited (K_e) state, and frequency shifts ($\delta\nu$) of THQ in different solvents

Solvents	K_g (L M^{-1})	K_e (L M^{-1})	α	$\delta\nu_{excit}$ (300 K) (cm^{-1})	$\delta\nu_{fluor}$ (300 K) (cm^{-1})	$\delta\nu_{excit}$ (77 K) (cm^{-1})	$\delta\nu_{fluor}$ (77 K) (cm^{-1})
Dioxane	3.7	14.7	1.0	−125	−474	−293	−268
EtOH	4.0	26.6	2.2	−175	−1468	−366	−334
(Acetonitrile)*	—	—	—	—	(−203)*	—	—

*See text.

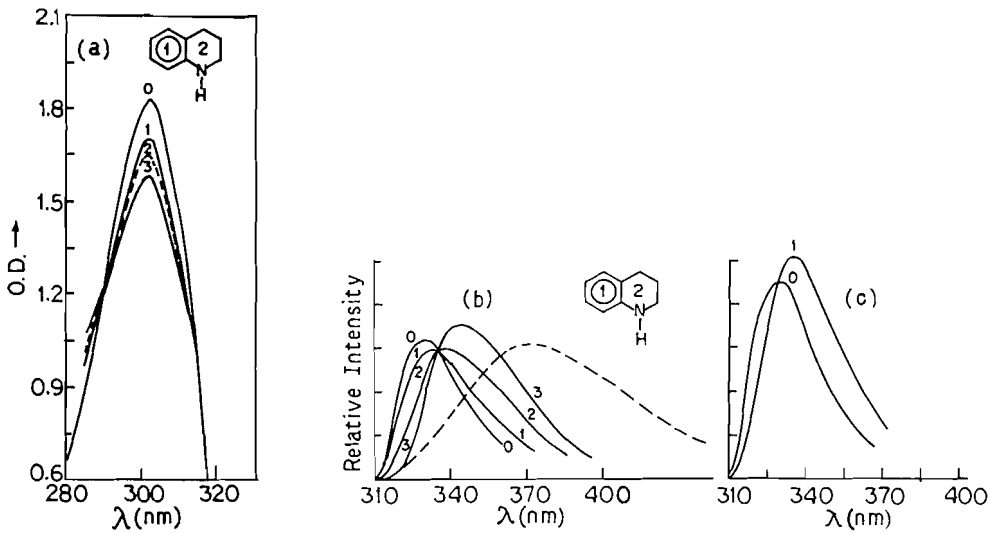

FIG. 1. (*a*) Ultraviolet absorption curves for THQ (2.6×10^{-4} *M* L^{-1} in CH) at 300 K. Concentration (*M* L^{-1}) of EtOH in *0*, 0; *1*, 0.017; *2*, 0.69; *3*, 0.86. (*b*) Fluorescence spectra of THQ (2.64×10^{-4} *M* L^{-1} in CH) at 300 K (excitation wavelength = 290 nm). Concentration (*M* L^{-1}) of EtOH in *0*, 0; *1*, 0.023; *2*, 0.69; *3*, 0.83. Dotted curve: spectrum of protonated tetrahydroquinolium ion in aqueous acid solution. (*c*) Fluorescence spectra of THQ (2.64×10^{-4} *M* L^{-1} in CH) at 300 K (excitation wavelength = 290 nm). Concentration (*M* L^{-1}) of acetonitrile in *0*, 0; *1*, 0.80.

spectra of THQ in CH solution in the presence of dioxane. In this work it is found that hydrogen bonding between excited THQ and dioxane is stronger as is evident from larger fluorescence spectral shift compared to shift of excitation spectrum due to hydrogen bonding (Table 1). When EtOH is used in place of dioxane a small red shift and a small change in intensity of ultraviolet absorption bands are observed as the concentration of EtOH is increased in steps (Fig. 1(*a*)). The infrared spectrum does not provide any conclusive evidence of formation of hydrogen bond between THQ in the ground state and EtOH. Therefore it is not possible to assess the contribution of such bond in effecting the changes of the absorption spectra relative to other factors like dispersion or electrostatic forces, especially when it is remembered that secondary amines are weak H-bonding agents. It is interesting to find that the fluorescence spectrum of THQ in CH or in MCH is strongly influenced by the presence of EtOH and a very large shift of about 1468 cm^{-1} of the fluorescence band occurs (Table 1). One tempting possible interpretation is that THQ forms strong hydrogen bond with EtOH in the excited state, though only weak bond, if any, is formed in the ground state of THQ. To test if hydrogen bonding is in any way responsible for the fluorescence spectral shift, the fluorescence spectrum was recorded when EtOH was replaced by acetonitrile, a non-hydrogen bonding solvent having a higher dielectric constant ($\epsilon \sim 38$) than EtOH ($\epsilon \sim 25$). It can be seen from Fig. 1(*c*) and Table 1 that only a small red shift of 203 cm^{-1} is produced with acetonitrile. This possibly gives indirect support to the supposition that the large red shift of the fluorescence band in EtOH−THQ−CH system is to be ascribed to strong hydrogen bonding between excited THQ and EtOH. The strong hydrogen bond is indicative of the amine acting as a proton acceptor (28) to EtOH. It seems, however, that the red shift is too large to be accounted for by simple H-bonding. Protonated tetrahydroquinolium ion in aqueous acid solution emits fluorescence near 26 946 cm^{-1} (Fig. 1(*b*)) which is shifted towards red from the fluorescence of "free" THQ by about 3425 cm^{-1}. The corresponding band in EtOH—CH or EtOH—MCH is at 28 803 cm^{-1} showing a red shift of 1468 cm^{-1}. It may be speculated that though an actual protolytic reaction should be disregarded in ethanol, the strong H-bonding of the excited THQ molecule with EtOH, which acts as a proton donor, may lead to partial protonation of THQ, to which the large red shift may be attributed. These results refer to measurement of fluorescence spectra at 300 K. Interestingly, there is no such remarkably large red shift of the fluorescence band of THQ in EtOH—MCH glass matrix at 77 K. The red shift is only about 366 cm^{-1}, comparable with the excitation red shift of about 334 cm^{-1} (Table 1), showing that at 77 K, there is no significant hydrogen bonding interaction between EtOH and THQ in the excited state, in contrast to what was observed at 300 K. The same is true for THQ in dioxane and MCH at 77 K. It may thus be generally concluded that in the viscous media at the low temperature, there is no increase in H-bond strength between

Can. J. Chem. Downloaded from www.nrcresearchpress.com by 210.87.254.42 on 09/06/12
For personal use only.

Can. J. Chem. Downloaded from www.nrcresearchpress.com by 210.87.254.42 on 09/06/12
For personal use only.

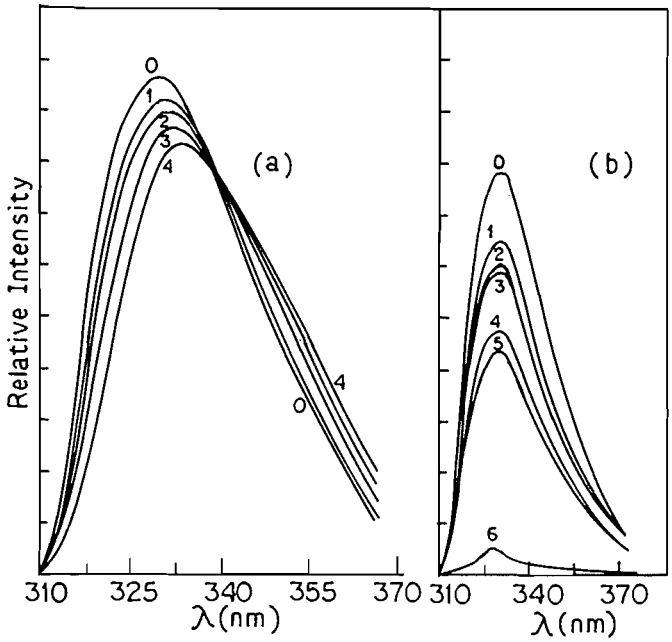

FIG. 2. (*a*) Fluorescence spectra of THQ (2.60×10^{-4} *M* L^{-1} in CH) at 300 K (excitation wavelength = 290 nm). Concentration (*M* L^{-1}) of TEA in *0*, 0; *1*, 0.05; *2*, 0.089; *3*, 0.22; *4*, 0.45. (*b*) Fluorescence spectra of THQ (5.2×10^{-4} *M* L^{-1} in CH) at 300 K (excitation wavelength is 290 nm). Concentration (*M* L^{-1}) of pyridine in *0*, 0; *1*, 3.75×10^{-4}; *2*, 1.25×10^{-3}; *3*, 3.6×10^{-3}; *4*, 7.25×10^{-3}; *5*, 1.25×10^{-2}; *6*, 9×10^{-1}.

excited THQ and hydrogen bonding solvents EtOH and dioxane behaving either as proton donor or acceptor relative to the bond strength in the ground state.

The ground state equilibrium constant, K_g, calculated from absorption measurement is given in Table 1. From the changes of the fluorescence spectra of THQ at 300 K in dioxane or EtOH in CH solution, the equilibrium constant, K_e, in the first excited singlet state is calculated utilising the frequently used equation (15),

$$[1] \quad \frac{1 - f_0/f}{Q} = -K_e + K_e\alpha(f_0/f)$$

where f_0 and f represent relative fluorescence intensities of THQ in CH without and with the H-bonding solvent whose concentration is Q, respectively, and α is the ratio of the fluorescence yield of H-bonded and free THQ molecules. Equation [1] holds under the condition that the extinction coefficients of free and H-bonded THQ molecules are equal at the wavelength of an exciting light. For the THQ–EtOH–CH system the excitation wavelength chosen is 290 nm, which corresponds to the isosbestic point in the absorption curves of this system reproduced in Fig. 1(*a*). Fluorescence intensities f_0 and f's are measured at 346 nm which corresponds to wavelength of the fluorescence spectrum due to hydrogen bonded THQ in EtOH (Fig. 1(*b*)). In the case of the THQ–dioxane–CH system, the excitation wavelength is chosen at 310 nm near which difference between the extinction coefficients (ϵ) of free and bonded species is very small (24).

A linear plot is obtained by taking $(1 - f_0/f)/[Q]$ as ordinate and (f_0/f) as abscissa. From the intercept and slope of the graph α and K_e are calculated. The calculated values are included in Table 1, from which it is seen that K_e values are larger than K_g values.

More pronounced changes in fluorescence are produced by TEA and particularly by pyridine, when they are used as H-bonding solvents. In TEA, at 300 K, the fluorescence intensity falls off very slowly and the band shifts towards longer wavelength (Fig. 2(*a*)) as the concentration of TEA is increased in steps in the binary mixture of THQ in CH. In the case of pyridine, however, the fluorescence intensity falls off more rapidly (Fig. 2(*b*)) without any appreciable shift of the fluorescence bands. It is to be noted that in the concentration range in which the changes in the fluorescence spectrum are produced by TEA or pyridine, no noticeable change in the absorption spectrum is observed with the same solvents. In other words, the changes in the fluorescence spectrum of THQ in CH by H-bonding interaction with TEA or pyridine arise at much lower concentration of these solvents than that producing any changes of consequence in the absorption spectra. Fluorescence quenching by hydrogen bonding interaction of THQ with pyridine, which has conjugate π-electron system, may occur due to CT interaction between the π-electron systems of the fluorescer THQ and proton acceptor pyridine (1–4, 6, 17, 29). It is also possible that when THQ enters into H-bonding with pyridine there is a change of conformation of the molecule, favourable for π-electron delocalization via the H-bond between the fluorescer THQ and the non-fluorescing pyridine. The quenching by TEA may be ascribed to the interaction between n-orbital of TEA and π-electron system of excited THQ molecule (13, 30).

The following reaction scheme describing the situation may be examined:

$$\mathrm{DH} + \mathrm{A} \underset{K_g}{\rightleftharpoons} \mathrm{DH} \cdots\cdots \mathrm{A}$$

$$\mathrm{DH} \rightarrow \mathrm{DH}^*$$

$$\mathrm{DH}^* + \mathrm{A} \underset{K_2}{\overset{K_1}{\rightleftharpoons}} (\mathrm{D}^{\delta+}\text{—}\mathrm{H} \cdots\cdots \mathrm{A}^{\delta-})^*$$

$$K_f \quad K_i \qquad K_{f'} \quad K_{i'}$$

$$\mathrm{DH} + h\nu_f \quad \mathrm{DH} \qquad \mathrm{DH} + h\nu_{f'} \quad \mathrm{DH}$$

where

$$\tau = 1/(K_i + K_f), \qquad \tau' = 1/(K_{i'} + K_{f'})$$

K_1 = bimolecular rate constant of H-bonding reaction, K_2 = unimolecular rate constant of dissociation of H-bond, $K_{f'}$ = rate constant associated with possible transfer of electronic excitation to nonfluorescent acceptor A.

When no H-bonded complex worth noting is formed in the ground state, Mataga *et al.* (6) used for calculating the rate constants K_1 and K_2, the equations

$$[2] \quad \frac{f/f_0 - 1}{[Q]} = \frac{\alpha\tau K_1}{1 + K_2\tau'} - \frac{\tau K_1}{1 + K_2\tau'}(f/f_0)$$

and

$$[3] \quad f_0/f = 1 + K_1\tau[Q]$$

where τ is the fluorescence decay time in the absence of a quencher. Equation [3] is nothing but the simple Stern–Volmer equation valid for notable quenching and is applicable in the case of pyridine. Equation [2] may be used for the quencher TEA in which no notable quenching takes place. By plotting f_0/f versus quencher pyridine concentration, τK_1 is estimated from the slope of the curve and from the measured

Can. J. Chem. Downloaded from www.nrcresearchpress.com by 210.87.254.42 on 09/06/12
For personal use only.

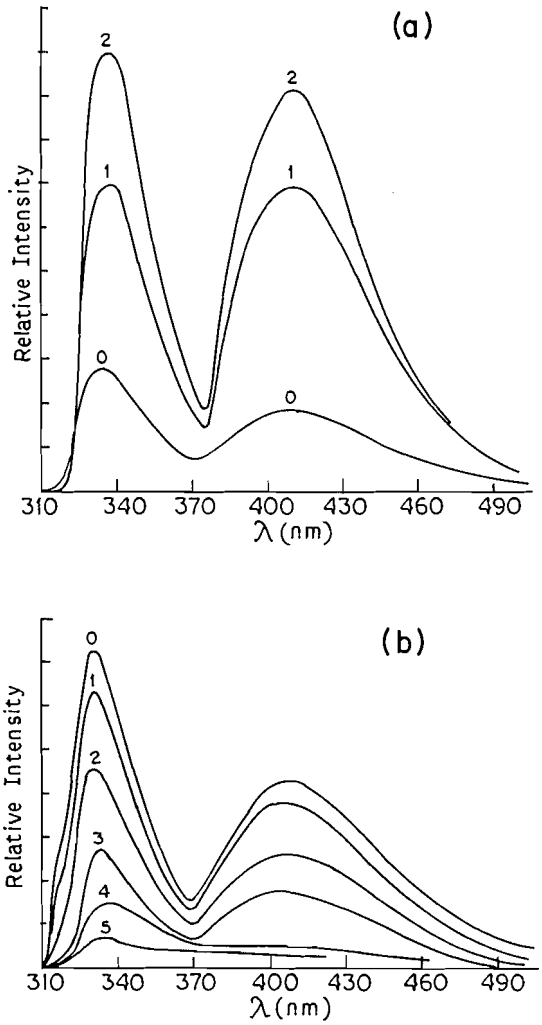

FIG. 3. (*a*) Fluorescence spectra of THQ (5.2×10^{-4} *M* L^{-1} in MCH) at 77 K (excitation wavelength is 290 nm). Concentration (*M* L^{-1}) of TEA in *0*, 0; *1*, 4.2×10^{-2}; *2*, 1.4×10^{-1}. (*b*) Fluorescence spectra of THQ (5.2×10^{-4} *M* L^{-1} in MCH) at 77 K (excitation wavelength is 290 nm). *0*, $C_{Pyridine} = 0$, *1*, $C_{Pyridine} = 3.75 \times 10^{-4}$ *M* L^{-1}, *2*, $C_{Pyridine} = 1.25 \times 10^{-3}$ *M* L^{-1}, *3*, $C_{Pyridine} = 3.6 \times 10^{-3}$ *M* L^{-1}, *4*, $C_{Pyridine} = 7.25 \times 10^{-3}$ *M* L^{-1}, *5*, $C_{Pyridine} = 1.25 \times 10^{-2}$ *M* L^{-1}.

value of $\tau = 2.37 \times 10^{-8}$ s. K_1 has been evaluated for the system THQ–pyridine–CH to be 0.3×10^{10} which is comparable with the diffusion-controlled rate constant, $K_d = 8RT/3000\eta = 0.6 \times 10^{10}$, indicating that the quenching of fluorescence of the THQ–CH system by pyridine is largely diffusion controlled.

Going back to the reaction scheme shown above it can be said that in the case of TEA, both $K_{f'}$ and $K_{i'}$ have competitive role even at high concentration of TEA whereas in the case of pyridine where remarkable quenching occurs without significant shift, $K_{i'}$ dominates over $K_{f'}$. In other words, at 300 K the excited hydrogen-bonded complex is rather stable in the case of TEA whereas in the case of pyridine immediate nonradiative degradation of electronic excitation energy takes place.

At 77 K, intensity of fluorescence due to THQ in TEA–MCH does not diminish. It is possible that in the rigid matrix at the low temperature, molecular orientation during the lifetime of the excited molecule which may be necessary for formation of CT-complex according to previous authors (13, 31), is restricted. Actually at 77 K, the emitted fluorescence is intensified as the concentration of TEA is increased (Fig. 3(*a*)). At the present stage, it is difficult to offer any definite interpretation of this observation. In pyridine–MCH, on the other hand, the fluorescence as well as the phosphorescence of THQ is strongly quenched even at 77 K (Fig. 3(*b*)). This indicates that the process of nonradiative transfer of energy to the nonfluorescing pyridine molecule through π-electronic delocalization via hydrogen bond between THQ and pyridine is efficiently operative at the low temperature.

1. N. MATAGA, Y. KAIFU, and M. KOIZUMI. Nature, **175**, 731 (1955).
2. N. MATAGA, Y. KAIFU, and M. KOIZUMI. Bull. Chem. Soc. Jpn. **29**, 115 (1956).
3. N. MATAGA and S. TSUNO. Bull. Chem. Soc. Jpn. **30**, 368 (1957); **30**, 711 (1957).
4. N. MATAGA. Bull. Chem. Soc. Jpn. **31**, 481 (1958).
5. T. KUBOTA and H. MIYAZAKI. J. Chem. Soc. Jpn. **79**, 916 (1958).
6. N. MATAGA, Y. TORIHASHI, and Y. KAIFU. Z. Physik. Chem. N.F. **34**, 379 (1962).
7. S. SUZUKI and H. BABA. J. Chem. Phys. **38**, 349 (1963).
8. H. BABA, L. GOODMAN, and P. C. VALENTI. J. Am. Chem. Soc. **88**, 5410 (1966).
9. I. YAMAZAKI, H. TAKEDA, and H. BABA. Bull. Chem. Soc. Jpn. **53**, 541 (1980).
10. T. TAMAKI. Bull. Chem. Soc. Jpn. **53**, 577 (1980).
11. H. INOUE, Y. HIROSHIMA, and K. TOMIYAMA. Bull. Chem. Soc. Jpn. **54**, 2209 (1981).
12. S. LAHA, S. CHAKRAVORTI, T. GANGULY, and S. B. BANERJEE. Chem. Phys. Lett. **85**, 350 (1982).
13. K. CHATTERJEE, S. LAHA, S. CHAKRAVORTI, T. GANGULY, and S. B. BANERJEE. Chem. Phys. Lett. **100**, 88 (1983).
14. K. E. AL-ANI and M. AL-SABTI. J. Phys. Chem. **87**, 446 (1983).
15. M. NAKAMIZO. Spectrochim. Acta, **22**, 2039 (1966).
16. N. MATAGA and Y. KAIFU. Mol. Phys. **7**, 137 (1963).
17. N. MATAGA and T. KUBOTA. Molecular interactions and electronic spectra. Marcel Dekker Inc., New York. 1970. p. 346.
18. R. B. CUNDALL and M. W. JONES. Photochemistry. Vol. 11. The Royal Society of Chemistry, Burlington House, London. 1981. p. 124.
19. G. G. ALOISI, F. MASETTI, and U. MAZZUCATO. Chem. Phys. Lett. **29**, 502 (1974).
20. D. REHM and A. WELLER. Israel J. Chem. **8**, 259 (1970).
21. D. REHM and A. WELLER. Z. Physik. Chem. N. F. **69**, 183 (1970).
22. J. B. BIRKS. Photophysics of aromatic molecules. Wiley Interscience, New York. 1970.
23. A. WELLER. Progress in reaction kinetics. Vol I. *Edited by* G. Porter. Pergamon, London. 1961. p. 187.
24. T. GANGULY and S. B. BANERJEE. Can. J. Chem. **60**, 741 (1982).
25. H. BOOTH. J. Chem. Soc. 1841 (1964).
26. W. R. DAWSON and M. W. WINDSOR. J. Phys. Chem. **72**, 3251 (1968).
27. J. BENDIG, M. SIEGMUND, and S. HELM. Adv. Mol. Relax. Int. Proc. **14**, 121 (1979).
28. H. N. ROSENBURG and E. EIMUTIS. Spectrochim. Acta, **22**, 1751 (1966).
29. N. IKEDA, T. OKADA, and N. MATAGA. Bull. Chem. Soc. Jpn. **54**, 1025 (1981).
30. H. LEONHARDT and A. WELLER. Z. Physik Chem. N.F. **29**, 277 (1961).
31. N. MATAGA and T. KUBOTA. Molecular interactions and electronic spectra. Marcel Dekker Inc., New York. 1970. p. 444.

The gas phase reactivity of chloronium ions by high pressure mass spectroscopy

JOHN A. STONE, WILLIAM M. SPLINTER, AND DENA E. SPLINTER
Chemistry Department, Queen's University, Kingston, Ont., Canada K7L 3N6

Received November 1, 1983

JOHN A. STONE, WILLIAM M. SPLINTER, and DENA E. SPLINTER. Can. J. Chem. **62**, 1373 (1984).

The reactions of $CH_3ClCH_3^+$ (**I**) and $CH_3ClCH_2Cl^+$ (**II**) with a range of bases have been studied in a high pressure ion source. Reactant ion monitoring has been used to obtain the relative reactivities. Transfer of CH_3^+ from **I** and CH_2Cl^+ from **II** are the only reactions observed with N- and O-containing bases. Following addition of CH_2Cl^+ from **II**, the lower alkyl aromatics (ArH) yield either $ArHCH_2Cl^+$ or the benzyl ions $ArCH_2^+$ and $ArCHCl^+$ while CH_3^+ transfer leads only to $ArHCH_3^+$. The reactivities of the alkyl aromatics increase with increasing exothermicity (benzene → mesitylene) and there is an increasingly negative temperature coefficient of reactivity in the same order.

JOHN A. STONE, WILLIAM M. SPLINTER et DENA E. SPLINTER. Can. J. Chem. **62**, 1373 (1984).

On a étudié les réactions du $CH_3ClCH_3^+$ (**I**) et du $CH_3ClCH_2Cl^+$ (**II**) avec un certain nombre de bases dans une source d'ions à haute pression. On a utilisé la technique de l'enregistrement de l'ion qui réagit pour obtenir les réactivités relatives. Les seules réactions observées avec les bases contenant de l'azote ou de l'oxygène sont celles du transfert de CH_3^+ à partir de **I** et de CH_2Cl^+ à partir du composé **II**. Après l'addition de CH_2Cl^+ à partir du composé **II**, les dérivés aromatiques alkylés inférieurs (ArH) conduisent soit au $ArHCH_2Cl^+$ ou aux ions benzyliques $ArCH_2^+$ et $ArCHCl^+$; par ailleurs, le transfert de CH_3^+ conduit uniquement à l'ion $ArHCH_3^+$. La réactivité des composés aromatiques alkylés augmente avec l'exothermicité (benzène → mésityléne) et le coefficient de température évolue vers des valeurs de plus en plus négatives lorsqu'on procède dans le même ordre.

[Traduit par le journal]

Introduction

Dialkylchloronium ions are good and selective alkylating agents in the liquid and gaseous phases (1–4). For example, $CH_3ClCH_3^+$ transfers a methyl cation to alkyl aromatics (ArR) in the gas phase with a reaction efficiency which increases with increasing exothermicity of reaction [1]

[1] $CH_3ClCH_3^+ + ArR \rightarrow CH_3Cl + ArRCH_3^+$

We used the technique of Reactant Ion Monitoring (RIM) (2, 5) to determine the relative rates of these reactions in the high pressure ion source of a mass spectrometer and found the relative reactivity of ArR to increase in the order toluene < xylenes < mesitylene. Neither benzene nor fluorobenzene was observed to react but in a subsequent publication Sen Sharma and Kebarle (3) showed that benzene does indeed react, but very slowly ($k \sim 10^{-12}$ cm^3 molecule^{-1} s^{-1} at 298 K).

In our RIM study $CH_3ClCH_3^+$ was generated by argon resonance photoionization of CH_3Cl in an approximately 50/50 He/CH_3Cl mixture at about 1 Torr total pressure.

[2] $CH_3Cl \xrightarrow{h\nu} CH_3Cl^+ + e$

[3] $CH_3Cl^+ + CH_3Cl \rightarrow CH_3ClH^+ + CH_2Cl$

[4] $CH_3ClH^+ + CH_3Cl \rightarrow CH_3ClCH_3^+ + HCl$

The advantage of this photoionization is that no fragmentation of the molecular ion occurs and therefore only one reactant ion is present but a big disadvantage is that the ion intensity is small and consequently the signal-to-noise ratio is poor. The photoionization study was also limited to ambient temperature since the ion current from the field free high pressure ion source employed decreased significantly with increasing temperature. Increased ion current is obtainable using electron impact ionization but at the expense of having more than one reagent ion. We report on the use of such ionization in this paper.

The electron impact initiated ion chemistry of methyl chloride is well documented (6–9). CH_3Cl^+, CH_2Cl^+, and CH_3^+ are the major primary ions and these in CH_3Cl at 1 Torr lead to only two ions of significance at long times viz the two chloronium ions $CH_3ClCH_3^+$ and $CH_3ClCH_2Cl^+$. The former ion arises from CH_3Cl^+ by reactions [3] and [4]. CH_2Cl^+ was found to be unreactive towards CH_3Cl in low pressure experiments (6–8) but $CH_3ClCH_2Cl^+$ was observed at pressures of CH_3Cl greater than 0.4 Torr and it was suggested that it was formed in the following sequence (9).

[5] $CH_3^+ + CH_3Cl \rightarrow CH_2Cl^+ + CH_4$

[6*a*] $CH_2Cl^+ + CH_3Cl \rightarrow CH_3ClH^+ + CHCl$

[6*b*] $\xrightarrow{M} CH_3ClCH_2Cl^+$

Our objective in this work was to confirm and extend our studies of the CH_3^+ transfer reactions of $CH_3ClCH_3^+$ with aromatics and also to study reactions with N- and O-containing bases. We have also studied CH_2Cl^+ transfer from $CH_3ClCH_2Cl^+$ to the same series of bases. Pulsed electron beam, high pressure mass spectrometry (10, 11) has been used to observe the temporal sequences of ion molecule reactions in some of these systems.

Experimental

The field free ion source and the quadrupole ion detection system have been described (2, 11). RIM experiments were carried out in the manner which has been described in detail (2, 5) and will therefore only be briefly described.

CH_3Cl from a reservoir at atmospheric pressure and the helium carrier gas eluting from a gas chromatograph are mixed prior to entry into the ion source which operates at pressures from 0.5 to 1.2 mm Hg. The CH_3Cl/He pressure ratio is usually in the range 0.1 to 1, 500 eV electrons provide continuous ionization and the signal due to the ion of interest, $CH_3ClCH_3^+$ or $CH_3ClCH_2Cl^+$, is continuously monitored. The steady signal is decreased when a reactive compound elutes from the chromatograph, the decrease in signal providing a measure of its reactivity. The monitored ion current and the chromatograph flame ionization detector trace are displayed on a two pen strip chart recorder running at 5 in. min^{-1}. The monitored ion current appears like an inverted gc trace (2). The relative reactivity R_A/R_B of two compounds, A and B, with a given reactant ion is (5)

$$\frac{R_A}{R_B} = \frac{\ln\left(1 - \frac{\Delta I_A}{I^0}\right)}{\ln\left(1 - \frac{\Delta I_B}{I^0}\right)} \frac{W_{(1/2)B} C_B}{W_{(1/2)A} C_A}$$

where I^0 is the ion current in the absence of reactive eluent, ΔI_A and ΔI_B are the measured maximum decreases in I^0 when A and B are eluting, $W_{1/2}$ is the (inverted) peak width at half height and C_A and C_B are the concentrations of A and B in the sample injected into the chromatograph. The latter concentrations are checked by the gc flame ionization detector (FID).

The increased signal-to-noise ratios obtained with the electron impact source enable decreases in ion signal of less than 5% to be measured with good precision (±5%). The majority of the signal is nullified by a bucking potential and the residue is amplified using the range switch of the strip chart recorder. The gc and ms "peaks" were gaussian and of the same width but the heights varied with sensitivity to FID and RIM.

All samples injected into the isothermally operated gas chromatograph contained up to four compounds of interest, each at a concentration of about 0.15 *M* in a suitable solvent, either *n*-hexane or dodecane. A 0.1 to 0.5 μL injection was used and the split at the column exit was such that about 5% of the eluent entered the ion source. The temperature range over which the ion source could be operated was from 75°C (determined by the heating effect of the electron emitting filament) to 230°C (obtained by the use of cartridge heaters embedded in the source block).

The kinetics of some of the systems were observed qualitatively by pulsing the electron beam using a blocking pulse on the beam defining plate (10). Samples of the required composition were made up in a heated oven and bled slowly into the ion source. Normalized ion currents were obtained as functions of time in the usual manner. Because it was necessary to cover a fairly wide mass range, a satisfactory determination of mass discrimination in the whole system could not be made and only order of magnitude estimates of rate constants are given.

Results and discussion

Relative reaction rates were obtained under ion source conditions where $CH_3ClCH_3^+$ and $CH_3ClCH_2Cl^+$ were the only ions of significance in the spectrum in the absence of chromatographic eluent. Initial ionization of CH_3Cl in the CH_3Cl/He mixture was either by direct electron impact, which yields mainly CH_3Cl^+ with lesser amounts of CH_3^+ and CH_2Cl^+, or by charge transfer from He^+. The latter reaction is ~300 kcal mol^{-1} exothermic and will lead to more fragmentation. The yields of $CH_3ClCH_3^+$ and $CH_3ClCH_2Cl^+$ were in the ratio of 2:1. No solvation of these ions by CH_3Cl was observed.

Products of the reactions of $CH_3ClCH_3^+$ and $CH_3ClCH_2Cl^+$

The ionic products formed by the reactions of $CH_3ClCH_3^+$ and $CH_3ClCH_2Cl^+$ with neutral, M, were identified by averaging repetitive mass spectral scans taken as M eluted from the gas chromatograph. The concentration of M was adjusted so that only the halonium ions reacted and not their precursors. The appearance of MH^+ was taken to signify reaction with precursor CH_3ClH^+ although, as described later, MH^+ can arise from other sources. The products were identified under conditions such that they constituted no more than 5% of total ionization. The mass spectral patterns of these product ions were not exactly reproducible (±10%) under these conditions but the absence of a product ion, i.e. less than 0.1% total ionization, could be determined. The results are summarized in Table 1.

Only four product ions are of significance. These have formulae represented by MCH_3^+, MCH^+, MCH_2Cl^+, and $MCCl^+$. $CH_3ClCH_3^+$ yields the arenium ion (**I**) with aromatics by transfer of CH_3^+ (reaction [1]) (2, 3) and $CH_3ClCH_2Cl^+$ could presumably transfer CH_3^+ or CH_2Cl^+ to yield either **I** or **II**

TABLE 1. Product ion yields from the reactions of $CH_3ClCH_3^+$ and $CH_3ClCH_2Cl^+$ with neutrals M, yields are expressed as % of total products (351 K)

M	Yield			
	MCH^+	MCH_3^+	MCl^+	MCH_2Cl^+
Benzene	28	4	17	52
Toluene	13	21	9	57
o-Xylene	<2	30	0	68
p-Xylene	0[a]	40	<3	57
m-Xylene	0	38	0	62
Mesitylene	0	75	0	25
Ethylbenzene	15	23	0	62
Nitrobenzene	<5	56	<5	34
Pyridine	0	83	0	17
Ethylpyridine	0	72	0	28
Chlorobenzene	0	78	0	22
Methoxytoluene	0	44	0	56
Cyclohexanone	0	66	0	33
Dihydropyran	0	86	0	14
Tetrahydrofuran	0	79	0	21
N-Methylpyrrole	0	90	0	10

[a] A value of 0 means not detectable.

[7a] $CH_3ClCH_2Cl^+ + M \longrightarrow CH_3Cl + MCH_2Cl^+$

[7b] $\longrightarrow CH_2Cl_2 + MCH_3^+$

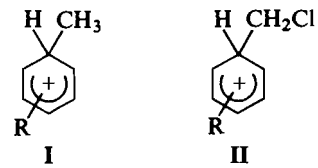

I **II**

Sen Sharma and Kebarle (3, 12) have shown that in an asymmetrical dialkyl chloronium ion, RClR′, the more weakly bonded alkyl group is the one yielding the more stable cation. Theoretical studies are in agreement (13). For example, with CH_3ClR, the dissociation energy for removal of R^+, $D(CH_3Cl—R^+)$, decreases in the order $CH_3^+ > C_2H_5^+ > i\text{-}C_3H_7^+ > t\text{-}C_4H_9^+$. We therefore expect CH_2Cl^+ to be much more weakly bound than CH_3^+ in $CH_3ClCH_2Cl^+$ and that reaction [7*a*] will predominate over [7*b*]. The relative yields of MCH_3^+ and MCH_2Cl^+ are consistent with this assumption although it cannot be proved by RIM studies.

The modes of formation of MCH^+ and of $MCCl^+$ were investigated further by substituting CH_4 for He as buffer gas. In $CH_4/CH_3Cl/C_6H_6$ (20/1/0.01), essentially no $CH_3ClCH_2Cl^+$ was formed and neither $C_7H_7^+$ $(MCH)^+$ nor $C_7H_6Cl^+$ $(MCCl^+)$ were observed. MCH^+, in addition to $MCCl^+$, therefore arises only from $CH_3ClCH_2Cl^+$. With perdeuterated benzene, MCH^+ and $MCCl^+$ became $C_7D_5H_2^+$ and $C_7D_5HCl^+$, respectively. With toluene-d_8 the ions were $C_8D_7H_2^+$ and $C_8D_7HCl^+$. Therefore, arenium ion (**II**) can either be collisionally stabilized to yield MCH_2Cl^+ or lose H_2 or HCl forming $MCCl^+$ and MCH^+, respectively. These are both benzyl ions since in their formation one H is lost from the aromatic ring, for example, following the addition of CH_2Cl^+ to C_6D_6 [8*a*] or [8*b*] may occur.

[8a] 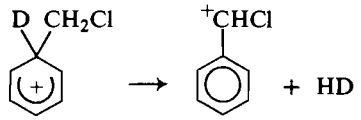

[8b] 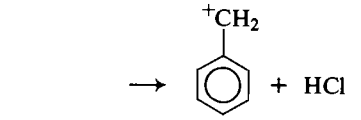

Further confirmation that $C_7H_7^+$ in $C_6H_6/He/CH_3Cl$ is the benzyl cation was furnished by the observation of an ion at m/e 169 which shifted to m/e = 180 when C_6D_6 was used. The intensity of the ion decreased with increase of temperature. Following the work of Ausloos (14) and Sen Sharma and Kebarle (15) we suggest that this ion results from the reaction of the benzyl cation with benzene.

[9] 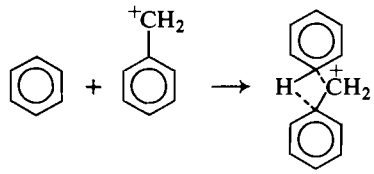

Icr studies have shown that following the addition of both CH_2Cl^+ (16) and CH_2F^+ (17) to benzene at low pressure ($<10^{-3}$ Torr), there is exclusive loss of HCl or HF and no stabilized $C_7H_8Cl^+$ or $C_7H_8F^+$ is observed. This can be attributed to the high exothermicity of reactions [10] and [11].

[10] $CH_2F^+ + C_6H_6 \rightarrow [C_7H_8F^+] \rightarrow C_6H_5CH_2^+ + HF$
$\Delta H^\circ = -71$ kcal mol^{-1}

[11] $CH_2Cl^+ + C_6H_6 \rightarrow [C_7H_8Cl^+] \rightarrow C_6H_5CH_2^+ + HCl$
$\Delta H^\circ = -56$ kcal mol^{-1}

Speranza and Pepe (4) do observe both $C_6H_5CH_2F$ and $C_6H_5CH_2Cl$ as neutral products ascribed to the removal of protons from the collisionally stabilized arenium ions produced in γ-irradiated $CH_3X/C_6H_6/NH_3$ (X = F, Cl) gaseous mixtures at pressures ranging from 100 to 760 Torr. The present results show that CH_3Cl^+ ions will not be present as suggested at the high CH_3Cl concentrations used but rather the reacting ions will be $CH_3ClCH_2Cl^+$. Reaction [7a] is less exothermic than reaction [11] by the $CH_3Cl-CH_2Cl^+$ binding energy. Collisional stabilization is still required for the appearance of $C_6H_5CH_2Cl$ but the energy to be removed is now decreased by ~30 kcal mol^{-1} (see later).

With the exception of $C_6H_5NO_2$ there is no H_2 or HCl loss from **II** for the N and O bases for which addition will occur at the heteroatom. As noted previously (2), addition to $C_6H_5NO_2$ must be mainly at O since the molecule does not fit the previously determined correlation for aromatics of increasing reactivity with decreasing ionization potential. This location has been confirmed as we find no D^+ transfer to added $(CH_3)_3N$ as would occur if arenium ions **I** or **II** were formed. For example D^+ transfer was observed with mesitylene-d_{12}.

For compounds in Table 1 the loss of H_2 and HCl from **II** is significant only from the lower alkyl aromatics, benzene, toluene, and ethylbenzene, and the importance of these losses decreases with increasing length of the alkyl chain. This demonstrates the increased stabilization of the positive charge in the arenium ion with increased polarizability of the alkyl group.

The xylenes and mesitylene show essentially no H_2 or HCl loss in keeping with the high stability of arenium ions with more than one methyl substituent (18). It is also to be noted that the relative ion yield from the addition of CH_2Cl^+ ($(MCH_2Cl^+ + MCH^+)/MCH_3^+$) decreases as the number of methyl substituents increases. The preponderance of MCH_3^+ with mesitylene is as for the N and O bases.

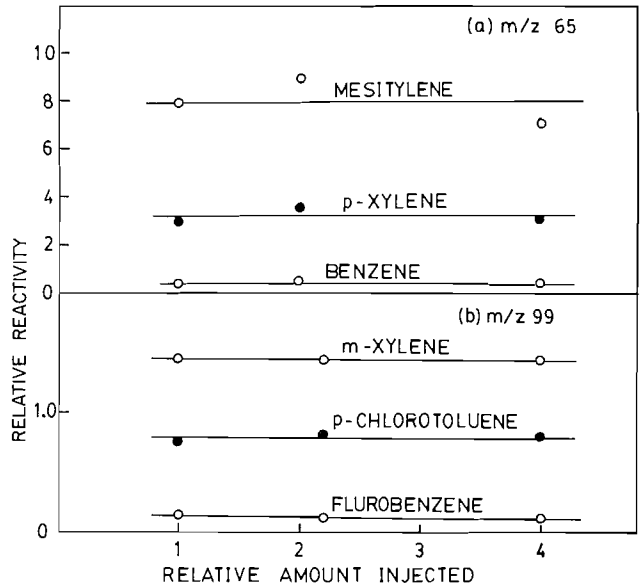

FIG. 1. Relative reactivities (toluene = 1.0) of neutrals towards (*a*) $CH_3ClCH_3^+$ (*m/z* 65) and (*b*) $CH_3ClCH_2Cl^+$ (*m/z* 99). Volumes injected into chromatograph were 0.1 to 0.4 μL dodecane containing neutrals at approximately 0.15 *M*.

If relative product yields are taken as indicative of reaction rates, and with the knowledge that $CH_3ClCH_3^+$ predominates by a factor of two in the ion source plasma, it can be seen that the rate of reaction of $CH_3ClCH_3^+$ with the N and O bases is greater than that of $CH_3ClCH_2Cl^+$ while the reverse is true for the lower alkyl aromatics. For the latter compounds there is a trend towards greater relative reactivity of $CH_3ClCH_3^+$ as the number of alkyl substituents increases.

Relative rates of reaction by RIM

For RIM to succeed in giving reliable relative rate data the amount of reactive neutral M must be sufficient to give a measurable decrease in ion signal (ΔI) but not excessive so that precursors of the monitored ion also react. The latter condition is presumed to be shown when new product ions appear and/or when the relative rate of reaction changes with increasing concentration of M. Figure 1 shows that the relative rates of reaction do not change when the concentration of M is changed by a factor of five for neutrals of widely differing reactivities. $\Delta I/I^\circ$ is less than 4% at the high end of the concentration range employed.

The relative reactivities of a series of nucleophiles with both $CH_3ClCH_3^+$ and $CH_3ClCH_2Cl^+$ are shown in Table 2, all values being given with reference to reactivity towards toluene. It was apparent from the concentrations of M required to give the same relative decrease $\Delta I/I_0$ for each of the two monitored ions that $CH_3ClCH_2Cl^+$ reacts considerably faster with the less reactive compounds than does $CH_3ClCH_3^+$. Table 2 also shows that there is a much larger range of reactivity with $CH_3ClCH_3^+$ than with $CH_3ClCH_2Cl^+$, a factor of 100 vs. a factor of 20. However, the order of reactivities is essentially identical, fluorobenzene being the least reactive and cyclohexanone, nitrobenzene, and 2-chloropyridine being the most reactive. In fact,

TABLE 2. The relative reactivities of neutrals with $CH_3ClCH_3^+$ (m/z 65) and $CH_3ClCH_2Cl^+$ (m/z 99) (351 K)

Neutral	m/e 65	m/e 99
Fluorobenzene	0.19 (0.0)[a]	0.14
Benzene	0.34 (0.0)[a] (0.11)[b]	0.49
Chlorobenzene	0.48	0.37
p-Fluorotoluene	0.56	0.49
m-Fluorotoluene	0.73	0.53
Bromobenzene	0.93	1.1
p-Chlorotoluene	0.88	0.80
m-Chlorotoluene	1.1	0.93
Toluene	1.00	1.00
Ethylbenzene	1.9 (1.7)[a]	1.3
Butylbenzene	2.7 (1.7)[b]	1.8
o-Xylene	3.2 (6.1)[a]	1.5
p-Xylene	3.3	1.4
m-Xylene	4.1	1.4
Mesitylene	8.4 (13.1)[a]	1.8
Methoxybenzene	4.7	1.8
2-Methoxytoluene	9.1	2.0
Nitrobenzene	15.0 (21)[a]	2.9
3,4-Dihydropyran	1.6	0.33
Tetrahydrofuran	10.3	—[c]
Cyclohexanone	18.7	2.1
Pyridine	8.7	1.2
2-Chloropyridine	15.1	2.5
N-Methylpyrrole	11.2	1.9
Aniline	10.8 (13.8)[a]	1.9
Triethylamine	7.6	1.3
Cyclohexene	0.69	0.40

[a] Reference 2.
[b] Reference 3.
[c] Not determined.

with the exception of dihydropyran, all the N- and O-containing bases are much more reactive with both ions than are all the alkylbenzenes except mesitylene. A similar observation has been made by Sen Sharma and Kebarle (3) for the reaction of $CH_3ClCH_3^+$ with a much more limited range of compounds. The significantly higher reactivity of 2-chloropyridine compared with the more basic pyridine suggests that electrophilic attack on this compound may be occurring at Cl as well as at N.

The alkyl aromatics show a wide range of reactivity with both halonium ions. The order of increasing reactivity is the same as we found previously for $CH_3ClCH_3^+$ with a much more limited set of compounds (2). The relative reactivities do not compare too well, however, with these previous values (Table 2) and neither does the value of 0.11 for benzene (calculated using Fig. 10 of ref. 3) compare well with the value of 0.34 found in this study. The range of reactivities of the alkyl aromatics in this study is less than that in ref. 2. The results for benzene in Table 2 are not consistent with the product yields in Table 1 which show little reactivity with $CH_3ClCH_3^+$ when judged by the yield of $C_6H_6CH_3^+$. This will be discussed later.

We noted previously (2) that the reactivity of M towards $CH_3ClCH_3^+$ increases with decreasing ionization potential and hence with increasing proton affinity (P.A.). P.A. is in general directly proportional to methyl cation affinity (MCA) for similar compounds (13) and so the rates of reaction of these aromatics increase with increasing MCA. This is also the direction of increasing exothermicity of reaction [1] (Table 3). There is insufficient information available to calculate the exothermicity of CH_2Cl^+ transfer (reaction [7*a*]) but as a rough estimate all reaction exothermicities will be increased compared with those for $CH_3ClCH_3^+$ by the difference in binding energies to CH_3Cl of the group transferred, i.e., $D(CH_3Cl—CH_3^+) - D(CH_3Cl—CH_2Cl^+)$ which is ~30 kcal mol^{-1}.

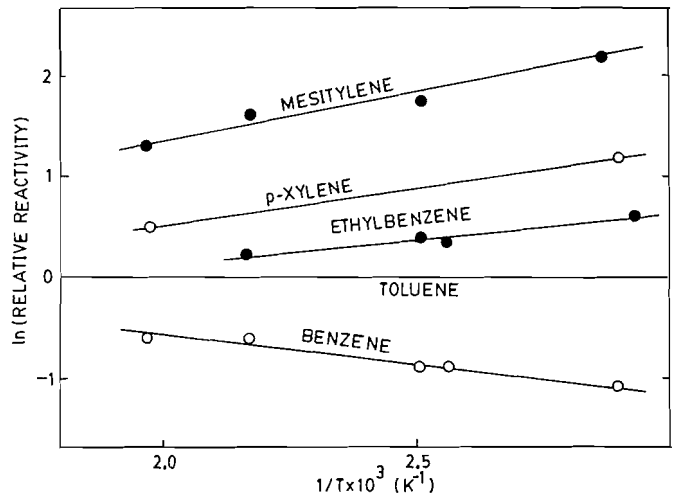

FIG. 2. Relative reactivities of neutrals towards $CH_3ClCH_3^+$ as functions of temperature.

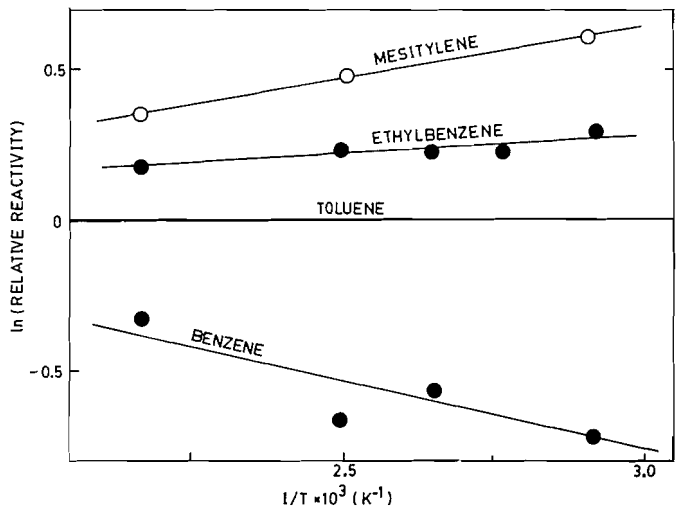

FIG. 3. Relative reactivities of neutrals towards $CH_3ClCH_2Cl^+$ as functions of temperature.

All the reactions are very exothermic but the large variation in reaction rates shows that for the slower reactions the collisional efficiency ($k_{reaction}/k_{collision}$) must be low.

The effect of temperature on relative reactivities

Although RIM has been employed to obtain data on numerous reagent ions there is no record of it having been used to measure relative reactivities at other than a fixed temperature. A problem arises since only relative reactivities are measured and if all reactant neutrals have the same temperature coefficient for reaction with the monitored ion then the relative reactivities will be independent of temperature.

Each of the alkyl aromatics examined showed a change of relative reactivity towards both halonium ions as the temperature was changed over the range 70–230°C (Figs. 2 and 3). No significance can be placed on the fact that benzene shows a temperature dependence of the opposite sign to the other

TABLE 3. The thermochemistry of the reaction $CH_3ClCH_3^+ + B \rightarrow BCH_3^+ + CH_3Cl$[a, b]

B	$\Delta H_f^0(B)$	$PA(BCH_3)$[c]	$\Delta H_f^0(BCH_3^+)$[d]	$\Delta H_f^0(BCH_3—H)$[e]	$\Delta H^0_{reaction}$[f]
Benzene	19.8	187.4	190.3	12.0	−25
Toluene	12.0	194.6	175.4	4.3	−32
o-Xylene	4.6	197.0	165.4	−3.3	−34
m-Xylene	4.1	200.6	161.8	−3.3	−38
p-Xylene	4.3	195.8	166.4	−3.3	−33
Mesitylene	−3.8	206.6	142.1	−17	−49

[a] All units in kcal mol^{-1}.
[b] BCH_3^+ is an *ipso* protonated species.
[c] Values from ref. 21. All values corrected to $PA(NH_3) = 207.5$ kcal mol^{-1}.
[d] Estimated using data for stabilization by CH_3 groups of a proton on a benzene ring (22).
[e] The enthalpy of formation of BCH_3 less the *ipso* H atom.
[f] The enthalpy of reaction.

aromatics since all rates are relative to those of toluene whose reactivity is arbitrarily assigned a zero temperature coefficient. The result is, however, consistent with the finding of Sen Sharma and Kebarle (3) that the rate constant for the reaction of benzene with $CH_3ClCH_3^+$ has a positive temperature coefficient whereas the analogous reactions involving toluene and isopropyl benzene have negative coefficients. It is gratifying that RIM can demonstrate temperature dependences of reaction rates, albeit only in favourable cases.

The increasingly negative temperature dependence of relative reactivity of the alkyl aromatics with increasing exothermicity of reaction has not been noted before. There is no obvious explanation for this observation which we are investigating further.

Pulsed electron beam studies

RIM provides a measure of the relative reactivity of M towards the long lived ions in the ion source plasma but it can give no absolute rate constants, nor can it show the sequence of ions in a reaction. Such information is provided by pulsed electron beam, high pressure mass spectrometry. Due to the unknown mass discrimination in the instrument used, the reaction sequence is obtainable but only rough estimates of reaction rate constants can be made.

The results for pure CH_3Cl alone with no M present are shown in Fig. 4. Only the two chloronium ions are of significance during the time of observation and at long times $CH_3ClCH_3^+$ is dominant. A first order decay of $CH_3ClCH_2Cl^+$ therefore leads to $CH_3ClCH_3^+$, presumably with CH_2Cl_2 as the neutral product. The rate constant for this displacement reaction is $\sim 10^{-13}$ molecule cm^{-3} s^{-1}.

[12] $CH_3Cl + CH_3ClCH_2Cl^+ \rightarrow CH_3ClCH_3^+ + CH_2Cl_2$

An estimate of the enthalpy of formation of $CH_3ClCH_2Cl^+$ can be obtained if it is assumed that for this reaction $\Delta G^0 \approx \Delta H^0$, i.e., $\Delta S^0 = 0$. This approximation should be reasonable given the similar nature of CH_3Cl and CH_2Cl_2. For reaction [12] to be observed $\Delta H^0 \leq 0$ and using the dissociation energy $D(CH_3Cl—CH_3^+) = +64$ kcal mol^{-1} (13), $\Delta H_f^0(CH_3ClCH_3^+) = +175.9$ kcal mol^{-1}, $\Delta H_f^0(CH_3ClCH_2Cl^+) \leq +173$ kcal mol^{-1} and $D(CH_3Cl—CH_2Cl^+) \leq +36$ kcal mol^{-1}. This latter value is far less than $D(CH_3Cl—CH_3^+) = 64$ kcal mol^{-1} and closer to $D(CH_3Cl—C_2H_5^+) = 31$ kcal mol^{-1} (12). The switching reaction [12] will have an effect on the RIM experimental results. Since for the less reactive compounds, $CH_3ClCH_2Cl^+$ reacts faster than $CH_3ClCH_3^+$ then even when reaction with the latter is very slow as for example with benzene, a faster reaction with $CH_3ClCH_2Cl^+$ can lead to an enhanced reduction in

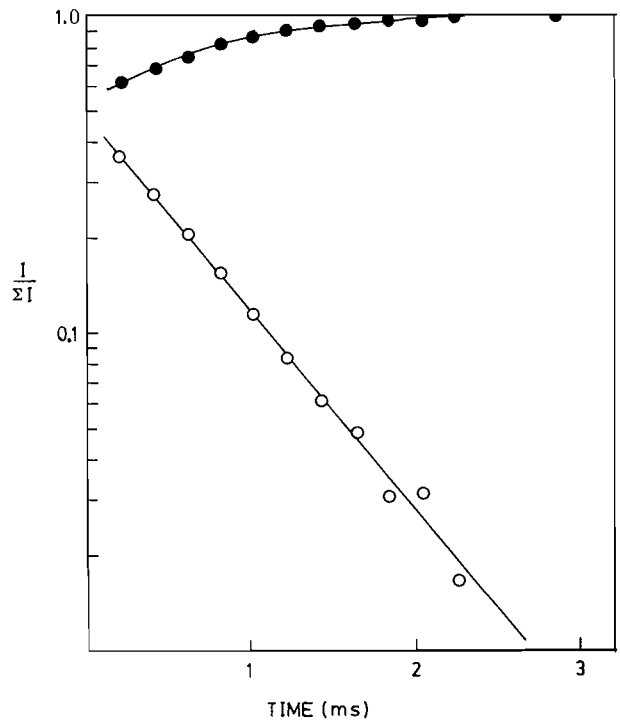

FIG. 4. The temporal variations of normalized ion yields in pure CH_3Cl at 0.90 Torr and 444 K. ●, $CH_3ClCH_3^+$, ○, $CH_3ClCH_2Cl^+$. The rate constant for the disappearance of $CH_3ClCH_2Cl^+$ is approximately 10^{-13} cm^3 $molecule^{-1}$ s^{-1}.

the monitored $CH_3ClCH_3^+$ ion. The errors in the RIM relative rates are expected to be the greatest for the least reactive compounds and become proportionately smaller for the more reactive ones when less neutral is required for a measurable decrease in monitored ion current. This explains why the rate of reaction relative to toluene for $CH_3ClCH_3^+$ obtained by RIM is higher for benzene than we found previously (2) and than was found by Sen Sharma and Kebarle (3). It is disturbing, however, that the relative rates of reaction did not show a variation with the amount of material added (Figs. 2 and 3) which should signal a problem due to a slow disappearance of one of the monitored ions. It is to be noted that this complication does not affect the validity of the RIM results for $CH_3ClCH_2Cl^+$.

Figure 5 shows the strictly pseudo first order decays of $CH_3ClCH_3^+$ and $CH_3ClCH_2Cl^+$ in the presence of mesitylene and confirms the qualitative RIM observation of the greater reactivity of the former ion. It is noted that the maximum yields

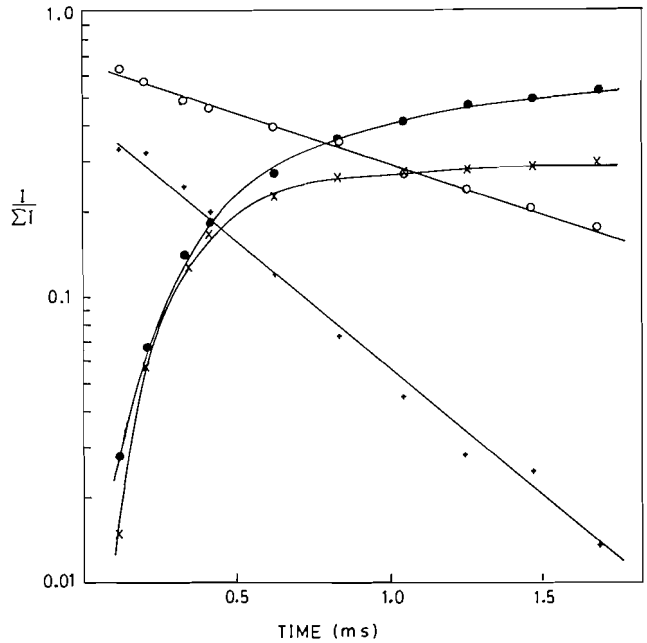

FIG. 5. The temporal variations of normalized ion yields. He, 0.59 Torr; CH_3Cl, 0.25 Torr; mesitylene, 1.6×10^{-4} Torr; 443 K. ○, $CH_3ClCH_3^+$; +, $CH_3ClCH_2Cl^+$; ●, mesitylene·CH_3^+; ×, mesitylene·CH_2Cl^+. The first order rate constants are: $CH_3ClCH_3^+$, approximately 2×10^{-10} cm^3 molecule^{-1} s^{-1}; $CH_3ClCH_2Cl^+$, approximately 5×10^{-10} cm^3 molecule^{-1} s^{-1}.

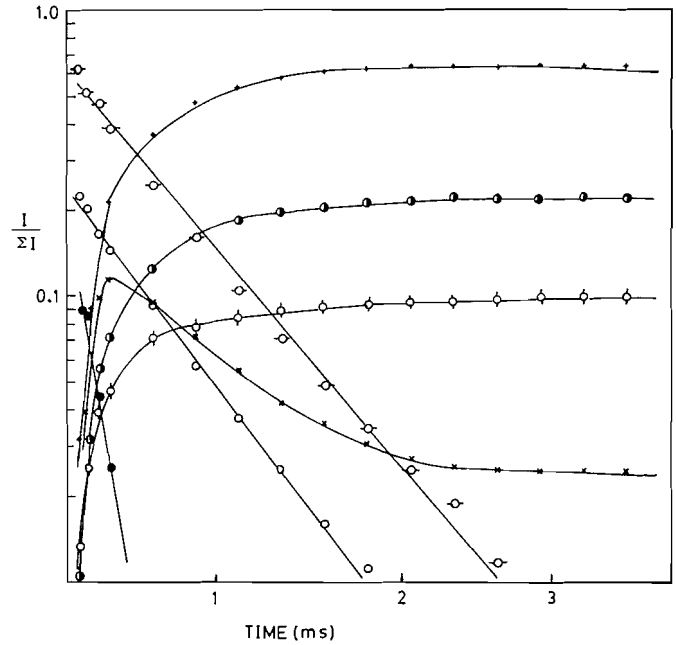

FIG. 6. The temporal variations of normalized ion yields. CH_4, 0.58 Torr; CH_3Cl, 0.48 Torr; *o*-xylene, 5×10^{-4} Torr; 449 K. —○—, $CH_3ClCH_3^+$; ○, $CH_3ClC_2H_5^+$; ●, $CH_3ClCH_2Cl^+$; +, *o*-xylene·CH_3^+; ◑, *o*-xylene·$C_2H_5^+$; ×, *o*-xylene·CH_2Cl^+; ○, *o*-xylene·H^+. The first order rate constants are: $CH_3ClCH_3^+$, approximately 1×10^{-10} cm^3 molecule^{-1} s^{-1}; $CH_3ClC_2H_5^+$, approximately 1.2×10^{-10} cm^3 molecule^{-1} s^{-1}; $CH_3ClCH_2Cl^+$, approximately 7×10^{-10} cm^3 molecule^{-1} s^{-1}.

of the adducts $C_9H_{12}CH_3^+$ and $C_9H_{12}CH_2Cl^+$ are very close to the initial yields of the respective halonium ion precursors. In this system reaction [12] is of little consequence because of the high reactivity of the mesitylene.

When CH_4 rather than He was used as a buffer gas, three halonium ions were formed, viz. $CH_3ClCH_3^+$, $CH_3ClCH_2Cl^+$, and $CH_3ClC_2H_5^+$. Their decays were always pseudo first order and their rates of reaction with the lower alkylbenzenes increase in the order $CH_3ClCH_3^+ < CH_3ClC_2H_5^+ < CH_3ClCH_2Cl^+$. The example of *o*-xylene is shown in Fig. 6. All the reaction products result from the displacement of CH_3Cl by the *o*-xylene.

[13] $CH_3ClR^+ + C_8H_{10} \rightarrow CH_3Cl + C_8H_{10}R^+$

The more weakly bonded $CH_3ClC_2H_5^+$ reacts a little more rapidly than $CH_3ClCH_3^+$ and we may assume that since $CH_3ClCH_2Cl^+$ reacts even more rapidly that the binding energy $D(CH_3Cl—CH_2Cl^+)$ is probably less than $D(CH_3Cl—C_2H_5^+)$ = 31 kcal mol^{-1} (12).

With the more reactive mesitylene (Fig. 7) $CH_3ClCH_3^+$ actually reacts more rapidly than does $CH_3ClC_2H_5^+$ and entropy rather than energy factors must now be important in the transition state. Protonated *o*-xylene and mesitylene (MH^+) are formed at long reaction times (Figs. 6 and 7) and obviously do not arise from the reaction of M with the early but unobserved ion CH_3ClH^+. The major precursor ion of MH^+ in both systems is MCH_2Cl^+ although with mesitylene both MCH_3^+ and $MC_2H_5^+$ also contribute as shown by the slow decline of their relative yields at long reaction times. The proton transfer reaction in the mesitylene system is shown in reaction [14], it being assumed that the initially formed *ipso*-substituted ions rearrange rapidly by H^+ migration.

[14]

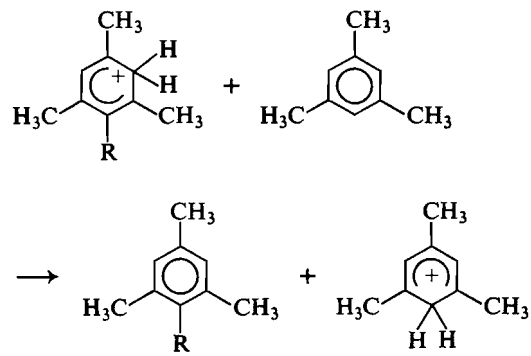

The relative rates of reaction [14] increase with R in the order $C_2H_5 < CH_3 \ll CH_2Cl^+$, which is as expected since it is the reverse of the order of the stabilizing effect of R on a protonated benzene ring. The proton affinities of both 1,3,4,5-tetramethylbenzene and 1,3,5-trimethyl-4-ethylbenzene will be greater than that of mesitylene, so that for R = CH_3 or C_2H_5 reaction [13] is slightly endothermic and the rate of reaction should be low (19), as is observed. The much more rapid reaction for R = CH_2Cl shows the destabilization caused by the inductive effect of a Cl substituent on CH_3 and for this group reaction [14] may be thermoneutral or even slightly exothermic.

Conclusions

The ion–molecule chemistry initiated by dialkylchloronium ions has many interesting facets. The very wide range of reactivities with aromatic compounds is unusual, as is the negative temperature coefficient of reactivity for a bimolecular displacement reaction. The products of the alkylation reaction depend

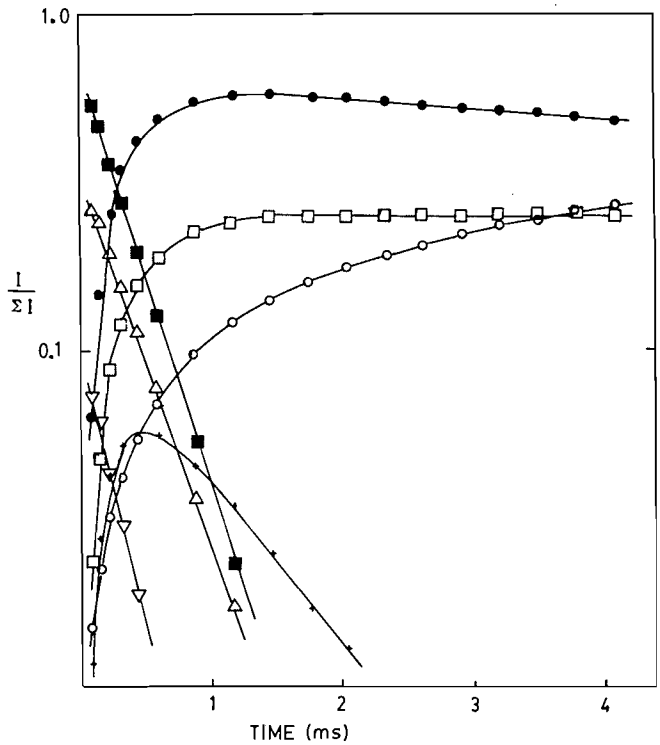

FIG. 7. The temporal variations of normalized ion yields. CH_4, 0.60 Torr; CH_3Cl, 0.20 Torr; mesitylene, 1.6×10^{-4} Torr; 345 K. ■, $CH_3ClCH_3^+$; △, $CH_3ClC_2H_5^+$; ▽, $CH_3ClCH_2Cl^+$; ●, mesitylene·CH_3^+; □, mesitylene·$C_2H_5^+$; +, mesitylene·CH_2Cl^+; ○, mesitylene·H^+. The first order rate constants are: $CH_3ClCH_3^+$, approximately 7×10^{-10} cm^3 molecule^{-1} s^{-1}; $CH_3ClC_2H_5^+$, approximately 5×10^{-1} cm^3 molecule^{-1} s^{-1}; $CH_3ClCH_2Cl^+$, approximately 1×10^{-9} cm^3 molecule^{-1} s^{-1}.

not only on the exothermicity of the reaction but also on the stabilization of the initially formed adduct ion afforded by substituents in the aromatic ring. The qualities of the halonium ions as alkylating agents are due to the moderating influence of CH_3Cl on the alkyl cation. The alkylmethyl halonium ions may be regarded as alkyl ions solvated by CH_3Cl. This solvation lowers the reactivity of the bare ion (20) and decreases the exothermicity of the alkylation reaction. Alkylation may then proceed with less likelihood of decomposition of the ion–neutral adduct.

Reactant ion monitoring has been shown to be a useful technique for obtaining the relative reactivities of neutrals with ions but it is obvious that the reaction sequences for all ions in the ion source plasma should be determined to ensure that the chosen reactant ions are in fact unreactive except towards these neutrals. This is not an easy task at the best of times but for slow reactions it is impossible to accomplish without time resolution as in pulsed high pressure mass spectrometry and ion cyclotron resonance spectrometry or spatial resolution as in the flowing afterglow. RIM can provide useful information on relative reaction rates and we have demonstrated that under certain conditions, one can observe the effects of temperature on reaction rates. In our estimation the technique is well suited to survey type experiments when many compounds can be quickly screened for reaction with a single ion. The best values for relative reaction rates will be obtained for fast reactions as has been well demonstrated (5).

Acknowledgement

The authors thank the Natural Sciences and Engineering Research Council of Canada and Queen's University for financial assistance.

1. G. A. OLAH. Halonium ions. Wiley Interscience, New York. 1975.
2. J. A. STONE, M. S. LIN, and J. VARAH. Can. J. Chem. **59**, 2412 (1981).
3. D. K. SEN SHARMA and P. KEBARLE. J. Am. Chem. Soc. **104**, 19 (1982).
4. M. SPERANZA and N. PEPE. J. Chem. Soc. Perkin Trans. 2, 1179 (1979).
5. F. HATCH and M. S. B. MUNSON. J. Phys. Chem. **82**, 2362 (1978).
6. N. A. MCASKILL. Aust. J. Chem. **22**, 2275 (1969).
7. J. L. BEAUCHAMP, D. HOLTZ, S. D. WOODGATE, and S. L. PATT. J. Am. Chem. Soc. **94**, 2398 (1972).
8. A. A. HEROD, A. G. HARRISON, and N. A. MCASKILL. Can. J. Chem. **49**, 2217 (1971).
9. Z. LUCZYNSKI, W. MALICKI, and H. WINCEL. Int. J. Mass Spectrom. Ion Phys. **15**, 321 (1974).
10. D. K. BOHME, J. A. STONE, R. S. MASON, R. S. STRADLING, and K. R. JENNINGS. Int. J. Mass Spectrom. Ion Phys. **37**, 283 (1981).
11. J. A. STONE, D. E. SPLINTER, and S. Y. KONG. Can. J. Chem. **60**, 910 (1982).
12. D. K. SEN SHARMA and P. KEBARLE. J. Am. Chem. Soc. **100**, 5828 (1978).
13. S. P. MCMANUS. J. Org. Chem. **47**, 3070 (1982).
14. P. AUSLOOS, J.-A. A. JACKSON, and S. G. LIAS. Int. J. Mass Spectrom. Ion Phys. **33**, 269 (1980).
15. D. K. SEN SHARMA and P. KEBARLE. Can. J. Chem. **59**, 1592 (1981).
16. S. A. BENEZRA, M. K. HOFFMAN, and M. M. BURSEY. J. Am. Chem. Soc. **92**, 7501 (1970).
17. J. BEAUCHAMP. *In* Interactions between ions and molecules. *Edited by* P. Ausloos. Plenum Press, New York. 1974. p. 413.
18. M. KILPATRICK and F. E. LUBORSKY. J. Am. Chem. Soc. **75**, 577 (1953).
19. D. K. BOHME, G. I. MACKAY, and H. I. SCHIFF. J. Chem. Phys. **73**, 4976 (1980).
20. D. K. BOHME, A. B. RAKSHIT, and G. I. MACKAY. J. Am. Chem. Soc. **104**, 1100 (1982).
21. D. H. AUE and M. T. BOWERS. *In* Gas phase ion chemistry. Vol 2. *Edited by* M. T. Bowers. Academic Press. 1979.
22. J. L. DEVLIN, J. F. WOLF, R. W. TAFT, and W. J. HEHRE. J. Am. Chem. Soc. **98**, 1990 (1976).

Laser-induced chemical reactions in ethanol by multiphoton absorption

SERGIO ROBERTO DE ANDRADE LEITE,[1] PAULO CELSO ISOLANI, AND JOSÉ MANUEL RIVEROS[2]
Instituto de Química, Universidade de São Paulo, Caixa Postal 20.780, São Paulo, Brazil

Received May 16, 1983[3]

SERGIO ROBERTO DE ANDRADE LEITE, PAULO CELSO ISOLANI, and JOSÉ MANUEL RIVEROS. Can. J. Chem. **62**, 1380 (1984).

The chemical reactions initiated by multiphoton absorption in gaseous ethanol were studied in the pressure range of 0.1 to 10 Torr under irradiation of a focused TEA CO_2 laser. The predominant reaction is a unimolecular elimination: $C_2H_5OH \rightarrow C_2H_4 + H_2O$, which is particularly important at low pressures and lower laser intensities. This process has not been previously identified in pyrolysis studies. At higher pressures and higher laser intensities, H_2, CO, and CH_4 also become important reaction products which are claimed to originate from a higher energy channel. Several arguments are provided to show that the increasing yield of CO and CH_4 at higher levels of excitation of the ethanol molecule are not consistent with a radical mechanism.

SERGIO ROBERTO DE ANDRADE LEITE, PAULO CELSO ISOLANI et JOSÉ MANUEL RIVEROS. Can. J. Chem. **62**, 1380 (1984).

Opérant à des pressions allant de 0,1 à 10 Torr et à l'aide d'une irradiation provenant d'un laser focalisé TEA à CO_2, on a étudié les réactions chimiques initiées par des absorptions multiphotons dans l'éthanol gazeux. La réaction principale consiste en une élimination unimoléculaire: $C_2H_5OH \rightarrow C_2H_4 + H_2O$, qui est particulièrement importante à de faibles pressions et à de faibles intensités du laser. On n'avait pas identifié ce processus antérieurement lors d'études de pyrolyse. Lorsqu'on utilise de plus fortes pressions et un laser à plus haute puissance, la formation de H_2, CO et CH_4, comme produits de la réaction, devient importante et l'on croit que ces produits sont formés par le biais d'une voie impliquant un niveau d'énergie plus élevé. On apporte plusieurs arguments pour montrer que les augmentations de rendement en CO et en CH_4, lorsqu'on opère à des niveaux d'excitation de la molécule d'éthanol qui sont plus élevés, ne sont pas en accord avec un mécanisme radicalaire.

[Traduit par le journal]

Can. J. Chem. Downloaded from www.nrcresearchpress.com by 210.87.254.6 on 09/06/12
For personal use only.

Introduction

Chemical reactions initiated by multiphoton excitation in the infrared region have generated a great deal of interest in recent years (1–3). At low pressures, where the excitation occurs under collision-free conditions, the resulting processes can be adequately described as unimolecular reactions for which statistical rate theories may be applied (4–7). Considerable development has also been achieved in the different theoretical aspects of vibrational multiphoton excitation. While many questions are still at large, the approach advanced by Quack (8–11) provides a valuable framework towards the understanding of the basic role of the different variables in the collisionless experiment.

Reactions induced by multiphoton excitation at higher pressures, and in the collision regime, are not always subject to simple interpretations. Much effort has been dedicated to distinguish between true laser-induced processes and conventional pyrolysis (12). In some cases, experiments under these conditions can be used to an advantage as an interesting methodology for bimolecular chemical reactions in the gas phase (13–16).

The present interest in the basic aspects of the gas phase chemistry of ethanol, a promising fuel and chemical feedstock, has led us to investigate the behavior of ethanol under multiphoton excitation from a CO_2 laser. Furthermore, ethanol represents an interesting case because several primary processes may be envisioned as a result of ir multiphoton absorption,

[1] $C_2H_5OH + nh\nu \rightarrow C_2H_4 + H_2O$

[2] $\rightarrow CH_3CHO + H_2$

[3] $\rightarrow H_2CO + CH_4$

[4] $\rightarrow \cdot CH_3 + \cdot CH_2OH$

Other bond fission channels could also be considered in principle, although of higher endothermicity.

[5] $C_2H_5OH \rightarrow \cdot C_2H_5 + \cdot OH$ $\quad \Delta H^0 = 92$ kcal mol^{-1}

[6] $\rightarrow C_2H_5O\cdot + \cdot H$ $\quad \Delta H^0 = 104$ kcal mol^{-1}

[7] $\rightarrow CH_3\dot{C}HOH + \cdot H$ $\quad \Delta H^0 \approx 90$ kcal mol^{-1}

There are no pertinent data on the activation energies for the first three processes in the absence of a catalyst. For reaction [4], it can be safely assumed that $E_a \sim 82$ kcal mol^{-1}, the estimated carbon–carbon bond energy.[4] The pyrolysis of ethanol at temperatures around 600°C and in the pressure range of 50 to 350 Torr has been claimed to be a homogeneous free-radical reaction initiated by process [4] (18). The main products in the early stages of the reaction are H_2 (53%), CO (11%), CH_4 (16%), and CH_3CHO (20%). At 300 Torr, addition of 1 Torr of NO results in a ten-fold inhibition, lending support to a free-radical mechanism. Later studies (19) also conclude that H_2 and CH_3CHO are the main products at these temperatures although the initiation process is proposed to be dissociation of a carbon–hydrogen bond (20).

The chemistry of ethanol under multiphoton excitation from a pulsed HF laser has been previously investigated (21). A distinct variation of product yield has been observed as a function of pressure in the range of 0.04 to 43.6 Torr. At 1 Torr, the quantum yield for C_2H_4 is an order of magnitude larger than that of C_2H_6, and two orders of magnitude larger than that of CH_4. At 40 Torr, the quantum yield of C_2H_4 is nine times larger than that of C_2H_6, but only three times larger than that of CH_4. While process [1] is apparently the main channel at low pressure, processes [1], [2], and [4] are claimed to be involved at higher pressures. Another related study revealed that ethanol pumped by a CO_2 laser at pressures of 1 Torr or less, in the presence of 2-propanol and HBr, decomposes unimolecularly

[1]Present address: Instituto de Química, Universidade Estadual Paulista Julio de Mesquita, Araraquara, São Paulo, Brazil.

[2]To whom all correspondence should be addressed.

[3]Revision received January 9, 1984.

[4]Estimated ΔH^0_{298} ($\cdot CH_2OH$) = -8 kcal mol^{-1}, from group equivalent values (17).

Can. J. Chem. Downloaded from www.nrcresearchpress.com by 210.87.254.6 on 09/06/12
For personal use only.

by process [1] in a non-thermal reaction (22). A very brief and recent report (23) establishes C_2H_4 and H_2 as the main products at 1 Torr, and claims formation of CH_4 via a non-radical mechanism, namely process [3].

Ethanol displays a wide absorption band in the 9.6 μm region involving three fundamental modes: 1089 cm^{-1} (C—O asym stretch), 1062 cm^{-1} (CH_3 rocking), and 1033 cm^{-1} (CH_3 rocking) (24, 25). Considerable overlap among these bands, even at low pressures, allows for pumping by many lines of the CO_2 laser.

The present study reports the chemistry resulting from multiphoton excitation of ethanol in the 9.6 μm region and in the pressure range of 0.1 to 10 Torr. The product distribution suggests a multiplicity of mechanisms related apparently to differences in the final level of excitation of the C_2H_5OH molecule. Process [1] is shown to be the most important reaction under these conditions, unlike the pyrolytic studies which reveal ethylene in minor quantities.

Experimental section

Irradiations were carried out with a multimode line tunable TEA CO_2 laser (Tachisto, Model 215G). Typical operating conditions resulted in pulses made up of a 50 ns spike (FWHM), containing about 65% of the energy, and a 1 μs tail.[5] Laser energies were monitored with a Coherent Radiation pyroelectric detector.

Samples were handled in a grease-free glass vacuum line. The irradiation cells were made of glass, 22 cm in length and 2 cm inside diameter, and provided with NaCl windows. The laser beam was focused by a 25 cm focal length CdTe lens onto a spot located 15 cm behind the entrance window. No reaction was observed with an unfocused beam. There was no luminescence visible to the naked eye at the windows, at the walls, or at the focal point for neat ethanol with the described geometry at pressures as high as 15 Torr. The pressure inside the cell was continuously monitored by a capacitance manometer (MKS Baratron) attached directly to the system.

Irradiated samples were analyzed qualitatively by ir spectroscopy. Quantitative yields were determined by gas phase chromatography using thermal conductivity detection. The sensitivity of the detector was calibrated with known quantities of the appropriate compound. Analysis was usually carried out after 100 to 200 pulses, corresponding typically to less than 15% decomposition of ethanol. Product yields obtained as average values of samples irradiated under similar experimental conditions displayed a reproducibility better than 10%. The deviations were likely due to fluctuations in laser power and in the number of hot spots.

While several laser lines were tested for efficiency in promoting reactions in ethanol, the most thorough experiments were performed with the P(20) line at 1046.85 cm^{-1}. The nature and relative abundance of products originating from irradiation with the P(20), and the R(20) line at 1078.58 cm^{-1}, showed no significant differences. The system failed to yield any reaction when pumped with the P(20) line of the 10.6 μm band at 944.21 cm^{-1}.

Results

The net efficiency of ethanol decomposition under infrared multiphoton excitation was initially established by measuring the pressure increase as a function of the number of pulses. The behavior of neat ethanol in the 0.5 to 10 Torr pressure range is displayed in Fig. 1. These experiments were run under low product conversion conditions to avoid sizable contribution from chemical reactions of the products themselves. The data are reported as the normalized pressure increment per pulse,

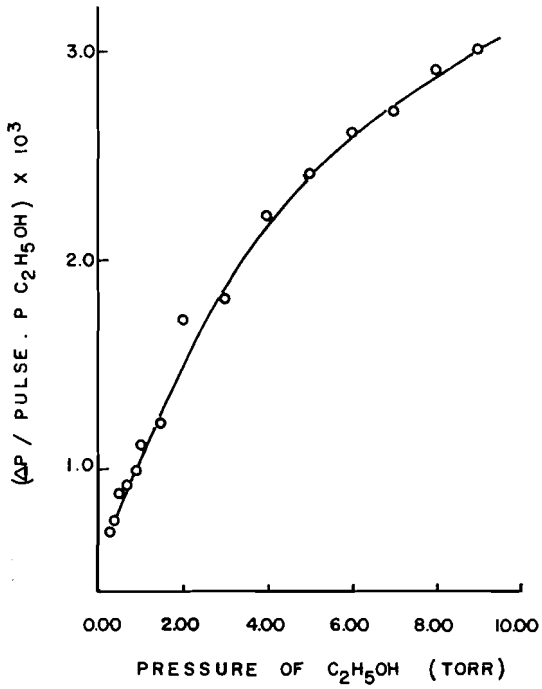

FIG. 1. Total normalized yield of ethanol decomposition, measured as the pressure increment per laser pulse, as a function of ethanol pressure. Laser energy = 1 J.

and were obtained from the number of pulses required to increase the initial pressure by 10%. Below 0.5 Torr, there is a marked increase in efficiency which has not been investigated in detail.

Analysis of the products revealed detectable quantities of H_2, C_2H_4, CO, CH_4, C_2H_2, and C_2H_6. Acetaldehyde was observed only in trace quantities by gc. No attempt was made to measure the amount of water vapor produced in these processes.

Figure 2 shows the normalized yield for different products as a function of pressure after 200 laser shots at 1 J of energy. It is noticeable that the rise in yield per pulse plotted in Fig. 1 can be correlated with the increasing production of CH_4 and CO as a function of pressure. On the other hand, while the amount of C_2H_4 decreases slowly in the pressure range, the sum of C_2H_4 plus C_2H_2 (presumably formed from hot ethylene) remains essentially constant in this interval. A single measurement carried out at 6 Torr reveals that the yield of H_2, at this pressure, is 6% less than C_2H_4.

Dilution of ethanol with argon as a buffer gas also resulted initially in a sizable enhancement of the yield per pulse as a function of buffer gas pressure. The data shown in Fig. 3. were again obtained by following the behavior of the total pressure of the system during the number of laser shots necessary to produce a 10% variation in the initial pressure of C_2H_5OH. Analysis of the products by gc showed that the rising net efficiency of decomposition was due to more efficient formation of CH_4 and CO.

The possible participation of free-radical mechanisms in the laser-initiated decomposition of ethanol was probed with known scavenging agents. The net yield per laser pulse of ethanol in the presence of NO was plotted in Fig. 4, for the case where the partial pressure of C_2H_5OH was maintained at 1 Torr. The laser energy was kept at 1 J, and the procedure adopted was similar to the previous cases. At 10 Torr of total pressure, an equimolar mixture of C_2H_5OH and NO after 200 laser shots

[5]The pulse shapes were measured with a photon drag detector at the M.I.T. Regional Laser Center.

Can. J. Chem. Downloaded from www.nrcresearchpress.com by 210.87.254.6 on 09/06/12
For personal use only.

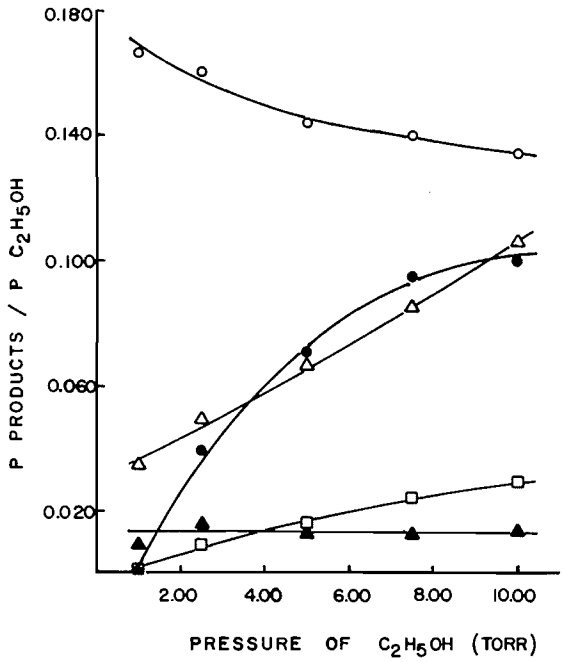

FIG. 2. Individual normalized product yields after 200 laser shots as a function of ethanol pressure. ○, Ethylene; ●, methane; □, acetylene; ▲, ethane; △, carbon monoxide. Laser energy = 1 J.

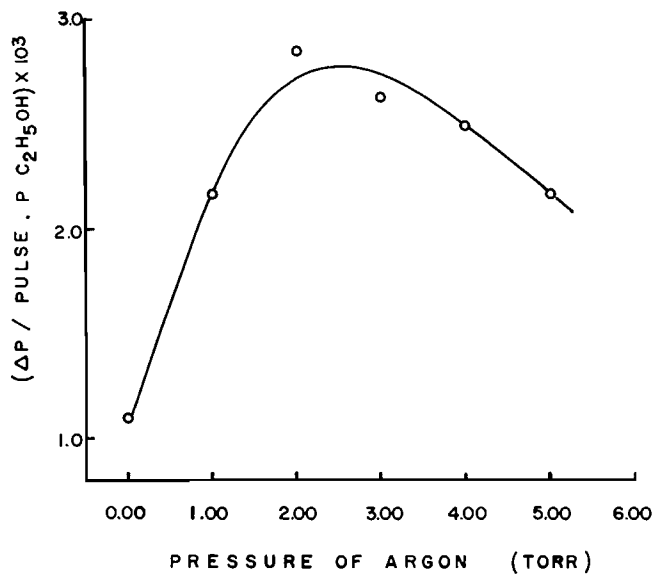

FIG. 3. Total normalized yield of ethanol decomposition (pressure increment per laser pulse) at 2 Torr of C_2H_5OH as a function of argon pressure. Laser energy = 1 J.

produces about 20% less ethylene than neat C_2H_5OH. The effect on CH_4, CO, and C_2H_6 was even less pronounced. Even at high NO-to-C_2H_5OH ratios, the overall inhibition remained small and products like HCN were not detected by ir or gc. Experiments carried out in the presence of propylene displayed no significant inhibition.

Irradiation of C_2H_5OH in the presence of O_2 gave rise to pale blue luminescence in the focal region which became weak after the initial 50 to 100 pulses. Quantitative product yields after 250 pulses showed no significant variations except for the formation of small quantities of CO_2.

The use of shorter laser pulse widths, obtained by reducing

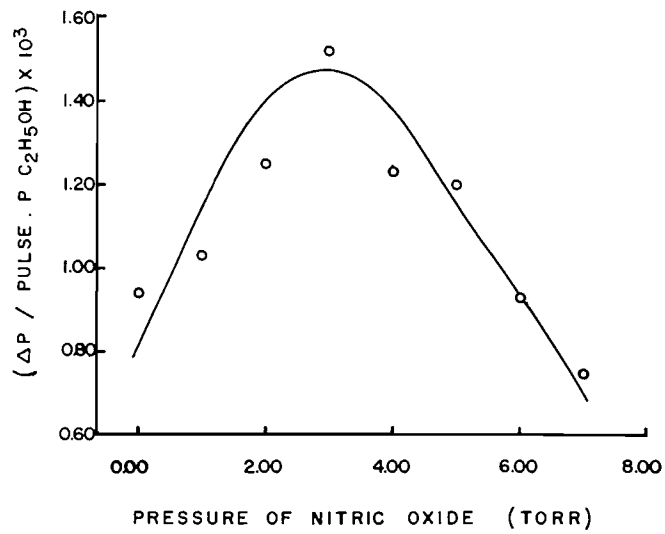

FIG. 4. Total normalized yield of ethanol decomposition (pressure increment per laser pulse) at 1 Torr of C_2H_5OH as a function of NO pressure. Laser energy = 1 J.

the nitrogen in the flow mixture of the laser, and at constant laser energy, enhances significantly the ease of ethanol decomposition per laser shot. Table 1 shows that this enhancement is due again to significant changes in the product distribution which favors CH_4 and CO at the higher laser intensities.

The relative product distribution is also affected by variation of the laser energy between 0.4 and 1.2 J. Relevant data for neat ethanol at 10 Torr appears in Table 2. These experiments are of somewhat more complex interpretation because both, intensity and fluence, are varying in each case. Nevertheless, it is clear that CH_4 and CO become increasingly important at higher fluences and higher intensities, while the ratio (C_2H_4/C_2H_6) remains essentially unchanged.

The kinetics of the decomposition of ethanol, as followed by the ir absorption spectrum of ethanol, shows that the decomposition processes are first order with respect to ethanol approximately during the first 50 pulses.

Finally, the absorption processes in ethanol under the experimental conditions have been found to obey a Beer–Lambert relationship in the pressure range and even above 20 Torr. Because of the focused geometry, it is not possible to obtain a meaningful absorption coefficient from these measurements.

Discussion

Chemical reactions induced by multiphoton excitation under focused conditions, and in the pressure range where this study was carried out, usually involve more than one mechanism because of the large fluence at the focal point. Thus, high local heating, energy pooling, and radical–radical processes may become important in these situations.

The dramatic change in product distribution observed in ethanol under multiphoton excitation over a relatively narrow pressure range (Fig. 2) suggests that several mechanisms are intervening in the overall chemistry. Furthermore, there are strong indications that the final level of excitation of ethanol in these processes are both pressure and intensity dependent. Several systems have been previously investigated in which reaction channels of different activation energies and frequency factors can be shown to compete under MPE conditions (26, 27). Such experiments have been advocated as sensitive probes

TABLE 1. Product yields (in Torr) as a function of laser pulse width after 200 shots, laser energy = 0.5 J, pressure of C_2H_5OH = 5 Torr

	Yield				
Pulse*	CO	CH_4	C_2H_4	C_2H_2	C_2H_6
Long (~1.7 μs)	0.075	0.053	0.334	0.005	0.043
Short (~1.2 μs)	0.145	0.096	0.353	0.017	0.052

*The actual pulse width is uncertain in these experiments because the response time of the pre-amplifier used for the measurements is not better than 300 ns.

TABLE 2. Product yields (in Torr) as a function of laser energy after 200 shots; pressure of C_2H_5OH = 10 Torr

	Yield				
Energy (J)	CO	CH_4	C_2H_4	C_2H_2	C_2H_6
0.4	0.235	0.200	0.420	0.029	0.039
0.7	0.660	0.665	1.02	0.142	0.080
1.0	1.05	1.05	1.36	0.253	0.130

of internal energy and its distribution within the molecule. A precise interpretation of the different reaction channels in ethanol is, however, obscured by the fact that the primary dissociation processes have not been characterized kinetically.

Ethylene is clearly the dominant product at the lower pressures and lower laser intensities for ethanol. This fact strongly argues in favor of process [1] as the lowest energy pathway even though no quantitative measurements have been carried out for the other reaction product, namely, H_2O. This observation is similar to that reported for ethanol at low pressures pumped by either an HF or CO_2 laser (21, 23), but distinct from the low temperature pyrolysis (18).

Reaction [1], which has not been identified as a unimolecular decomposition in thermal experiments, can be viewed as a four-center elimination of H_2O. This mechanism is analogous to HX elimination in alkyl halides and in $(CH_3)_3COH$ (28). A careful comparison with the available data for these systems allows us to place an estimate of 65 kcal mol^{-1} for the activation energy of reaction [1] and a frequency factor in the range of 10^{13} s^{-1}.

The appearance of acetylene among our products is common to many multiphoton experiments under focused geometry, and characteristic of high local temperature. Thus, the formation of C_2H_2 can be rationalized in terms of decomposition of "hot" ethylene molecules, or by further laser pumping of ethylene itself (29).

The presence of other products clearly establishes that reaction [1] is not the only channel. In particular, the relative amounts of CO and CH_4 do not follow a well-defined stoichiometry at the lower pressures. The growth of CO and CH_4 as a function of pressure (as well as that of C_2H_2) must be associated with either higher energy processes, or as a result of thermal chemistry. The fact that this effect is noticeable not only in neat ethanol, but in varying degrees in mixtures with Ar, NO, and O_2 indicates that a general energy transfer mechanism must be responsible for this behavior. Rotational hole filling due to collisions during the laser pulse can be an effective mechanism that allows for more efficient pumping through the discrete ladder (30, 31), and may be more important in a given pressure range than V−V or V−T deactivating collisions of highly excited species. A second possibility which could explain the increase of the "thermal" products, CH_4 and CO, as a function of pressure is the achievement of a common temperature among the different degrees of freedom.

The fact that CO and CH_4 are also favored at higher laser intensities (shorter pulses) supports our contention that these products originate from a higher energy pathway than reaction [1]. Pulse-duration effects have been demonstrated for a number of systems (32, 33) and illustrate that the ultimate energy content of the molecule can be dictated by peak power as a consequence of competition in the continuum between optical pumping and dissociation. This is particularly true in cases of high fluences typical of focused experiments.

The above considerations enable us to conclude that rotational hole filling, higher intensity and fluence are all responsible for a higher final excitation level of the ethanol molecule.

The actual mechanism by which CO and CH_4 are formed is a matter of some conjecture. The observation that CO and CH_4 result apparently from a higher energy channel could be interpreted as the result of free radical reactions initiated by a bond scission process like [4]. This step may be expected to have a high A factor (~10^{16} s^{-1}) and a high activation energy (~82 kcal mol^{-1}) and could account for its increasing participation in the overall mechanism at a final higher energy content of the excited C_2H_5OH. The presence of free radicals can be inferred from the appearance of ethane among the products, and the detection of the CH species (34). Yet, three experimental observations cast some doubts as to whether process [4] can be solely responsible for the increasing yield of CH_4 and CO at higher pressures: (*i*) the lack of any significant inhibition by NO; (*ii*) the small product changes observed when ethanol is pumped in mixtures with O_2; and (*iii*) the fact that the amount of C_2H_6 remains essentially constant in the pressure range where CH_4 and CO grow rapidly, and with increasing fluence and intensity.

It is thus apparent that either process, [2] or [3], or both, are also likely to be involved in the formation of CH_4, CO, and H_2. The fact that only trace quantities of CH_3CHO are detected, and no CH_2O could be interpreted as indicative of thermal decomposition of either aldehyde within the same laser pulse, or by intense local heating, or by large internal energy deposition in the product leading to facile decomposition. The pyrolysis of acetaldehyde is in itself a free-radical process initiated by the step

$$CH_3CHO^* \rightarrow \cdot CH_3 + \cdot CHO$$

which demands 79 kcal mol^{-1} of activation energy (35). Direct pumping of CH_3CHO,[6] or destruction by the laser pulse (36) are nevertheless very inefficient processes. On the other hand, a large fraction of the exit barrier energy has been shown to be converted into internal energy in four-center type elimination reactions (5). The other possibility is to consider process [3] followed by thermal decomposition of H_2CO

$$C_2H_5OH \rightarrow CH_4 + CH_2O$$

$$CH_2O^* \rightarrow CO + H_2$$

a mechanism reminiscent of that proposed in the multiphoton excitation of CH_3OH (37). A comparison of activation energies and A factors is not straightforward in these cases to account for

[6] J. M. Riveros and O. Santini Filho. Unpublished results.

Can. J. Chem. Downloaded from www.nrcresearchpress.com by 210.87.254.6 on 09/06/12
For personal use only.

pronounced changes in mechanisms.

We believe that our present data cannot unequivocally distinguish between the several possibilities advocated for the higher energy channel. Yet, the results clearly establish some distinct differences with high pressure thermal chemistry. Thus, in our pressure range, process [1] can be identified as a true laser-induced process.

Our present work reinforces the idea that ethanol is indeed a case which displays a rich chemistry under vibrational MPE. It is also our belief that these results warrant further exploration, both on the conventional pyrolysis and on the primary dissociation processes of ethanol.

Acknowledgements

The authors would like to thank FAPESP and CNPq for equipment support, and a graduate research fellowship from FAPESP (SRAL). The technical assistance of Mr. Geraldo Ayrosa is also gratefully acknowledged.

1. W. C. DANEN and J. C. JANG. *In* Laser-induced chemical processes. *Edited by* J. I. Steinfeld. Plenum Press, New York. 1981.
2. P. A. SCHULZ, AA. S. SUDBØ, D. J. KRAJNOVICH, H. S. KWOK, Y. R. SHEN, and Y. T. LEE. Ann. Rev. Phys. Chem. **30**, 379 (1979).
3. V. S. LETOKHOV. Phys. Today, **33**, 34 (1980).
4. E. R. GRANT, P. A. SCHULZ, AA. S. SUDBØ, Y. R. SHEN, and Y. T. LEE. Phys. Rev. Lett. **40**, 115 (1978).
5. AA. S. SUDBØ, P. A. SCHULZ, Y. R. SHEN, and Y. T. LEE. J. Chem. Phys. **69**, 2312 (1978).
6. AA. S. SUDBØ, P. A. SCHULZ, E. R. GRANT, Y. R. SHEN, and Y. T. LEE. J. Chem. Phys. **70**, 912 (1979).
7. P. A. SCHULZ, AA. S. SUDBØ, E. R. GRANT, Y. R. SHEN, and Y. T. LEE. J. Chem. Phys. **72**, 4985 (1980).
8. M. QUACK. J. Chem. Phys. **69**, 1282 (1978).
9. M. QUACK. Ber. Bunsenges. Phys. Chem. **83**, 757 (1979).
10. M. QUACK. J. Chem. Phys. **83**, 1287 (1979).
11. M. QUACK. J. Chem. Phys. **85**, 318 (1981).
12. W. C. DANEN, W. D. MUNSLOW, and D. W. SETSER. J. Am. Chem. Soc. **99**, 6961 (1977).
13. B. L. EARL and A. M. RONN. Chem. Phys. Lett. **41**, 29 (1976).
14. S. T. LIN and A. M. RONN. J. Chem. Phys. **49**, 255 (1977).
15. I. R. SLAGLE and D. GUTMAN. J. Am. Chem. Soc. **103**, 149 (1981).
16. E. WÜRZBERG, A. J. GRIMLEY, and P. L. HOUSTON. Chem. Phys. Lett. **57**, 373 (1978).
17. J. L. FRANKLIN. J. Chem. Phys. **21**, 2029 (1953).
18. J. A. BARNARD and H. W. D. HUGHES. Trans. Faraday Soc. **56**, 55 (1960).
19. B. C. CAPELIN, G. INGRAM, and J. KOKOLIS. Microchem. J. **19**, 229 (1974).
20. G. INGRAM and S. M. H. RIZVI. Microchem. J. **19**, 253 (1974).
21. L. SELWYN, R. A. BACK, and C. WILLIS. Chem. Phys. **32**, 323 (1978).
22. W. C. DANEN. J. Am. Chem. Soc. **101**, 1187 (1979).
23. A. GANDINI and R. A. BACK. J. Photochem. **18**, 241 (1982).
24. J. P. PERCHARD and M. L. JOSIEN. J. Chim. Phys. **65**, 1834 (1968).
25. A. J. BARNES and H. E. HALLAM. Trans. Faraday Soc. **66**, 1932 (1970).
26. R. N. ROSENFELD, J. I. BRAUMAN, J. R. BARKER, and D. M. GOLDEN. J. Am. Chem. Soc. **99**, 8069 (1977).
27. P. A. HACKETT, C. WILLIS, M. DROUIN, and E. WEINBERG. J. Phys. Chem. **84**, 1573 (1980).
28. P. J. ROBINSON and K. A. HOLBROOK. Unimolecular reactions. Wiley-Interscience, New York. 1972.
29. J. H. HALL, JR., M. L. LESIECKI, and W. A. GUILLORY. J. Chem. Phys. **68**, 2247 (1978).
30. C. R. QUICK, JR., and C. WITTIG. J. Chem. Phys. **69**, 4201 (1978).
31. J. STONE, E. THIELE, M. F. GOODMAN, J. C. STEPHENSON, and D. S. KING. J. Chem. Phys. **73**, 2259 (1980).
32. D. M. BRENNER. Chem. Phys. Lett. **57**, 357 (1978); D. M. BRENNER. J. Phys. Chem. **86**, 41 (1982).
33. J. S. MCKILLOP, R. J. GORDON, and R. N. ZARE. J. Chem. Phys. **77**, 2895 (1982).
34. I. V. MESSING, J. V. FILSETH, C. M. SADOWSKI, and T. CARRINGTON. J. Chem. Phys. **74**, 3874 (1981).
35. S. W. BENSON. J. Chem. Phys. **40**, 105 (1964).
36. J. KRAMER. J. Phys. Chem. **86**, 26 (1982).
37. S. E. BIALKOWSKI and W. A. GUILLORY. J. Chem. Phys. **67**, 2061 (1977).

Can. J. Chem. Downloaded from www.nrcresearchpress.com by 210.87.254.6 on 09/06/12
For personal use only.

Nuclear magnetic resonance studies. XL.[1] Tricyclooctanone rearrangement, [3.2.1.0]→[3.3.0.0], via γ-enolization and a ^{2}Hmr study of H/D exchange in tricyclic ketones

A. K. CHENG,[2] ASHIM K. GHOSH,[3] AND J. B. STOTHERS

Department of Chemistry, University of Western Ontario, London, Ont., Canada N6A 5B7

Received January 12, 1984

A. K. CHENG, ASHIM K. GHOSH, and J. B. STOTHERS. Can. J. Chem. **62**, 1385 (1984).

The effect of strongly basic conditions (*t*-BuO$^-$/*t*-BuOH/185°C) on the *exo* and *endo* isomers of 7,7-dimethyltricyclo[3.2.1.0^{2,4}]octan-6-one has been examined. While the *exo* isomer is stable, the *endo* isomer readily rearranges to 4,4-dimethyltricyclo[3.3.0.0^{2,8}]octan-3-one (**6**) which subsequently undergoes reduction of the three-membered ring. The initial transformation is one of very few examples of γ-enolate rearrangement. Experiments in *tert*-butyl alcohol-O-d_1 were carried out to establish the several sites of deuterium incorporation in the initial ketones and in **6** using ^{2}Hmr. These results reveal the stereochemistry of γ-enolate formation and cleavage as well as the stereoselectivities and relative rates of the exchange processes.

A. K. CHENG, ASHIM K. GHOSH et J. B. STOTHERS. Can. J. Chem. **62**, 1385 (1984).

On a étudié l'effet de conditions fortement basiques (*t*-BuO$^-$/*t*-BuOH/185°C) sur les isomères *exo* et *endo* de la diméthyl-7,7 tricyclo[3.2.1.0^{2,4}] octanone-6. Alors que l'isomère *exo* est stable, l'isomère *endo* se transpose facilement en diméthyl-4,4 tricyclo[3.3.0.0^{2,8}] octanone-3 (**6**) qui subit une réduction subséquente pour donner un cycle à trois chaînons. La transformation initiale correspond à un des rares exemples de transposition d'un énolate γ. On a effectué des expériences dans l'alcool *tert*-butylique O-d_1 afin de pouvoir déterminer, grâce à la rmn du ^{2}H, quels sont les divers sites d'incorporation du deutérium dans le produit (**6**) et dans les cétones initiales. Ces résultats permettent de déterminer la stéréochimie de la formation et du clivage de l'énolate γ ainsi que les stéréosélectivités et les vitesses relatives des processus d'échanges.

[Traduit par le journal]

Introduction

Following the original discovery that, under strongly basic conditions, a ketonic carbonyl group can activate proton abstraction from carbons more than one bond removed (1), many examples involving both acyclic and polycyclic monoketones have been described (2). Most of these cases concern β-enolization, i.e., proton abstraction from β-carbons. Very few examples of γ-enolization have been encountered and, heretofore, only one has been found to lead to skeletal rearrangement, namely, the isomerization of half-cage ketone **1** to **2** (3). The formation of γ-enolates has been inferred from the observation of H/D exchange at C-8, the *syn*-methyl carbon, of camphor (4), at C-6 and -7 in 3,3-dimethylbicyclo[3.3.0]octan-2-one (5), and at the *endo*-6-methyl carbon of 3,3,6,6-tetramethyl[2.2.1]heptan-2-one (6). The conversion of *sym*-tetramethyldiphenylacetone to 2-isopropyl benzoic acid (7) can be viewed formally as rearrangement through a γ-enolate, but specific activation of proton abstraction from the phenyl ring by the carbonyl group seems unlikely and the process cannot be taken as a true example of γ-enolization within the usual frame of reference. For each of the systems exhibiting γ-enolization the γ-carbon is either held relatively close to the carbonyl carbon by skeletal restraints as in **1** or may closely approach the carbonyl group in certain conformations.

The observations of β- and γ-enolization in a variety of systems stirred interest in the reverse process, the protonation of the homoenolic species or homoketonization. Such studies not only provide supporting evidence for the existence of proposed intermediates but also give information on the stereochemistry of the process. One of the early studies of β-enolate ketonization involved the treatment of 1-acetoxynortricyclene

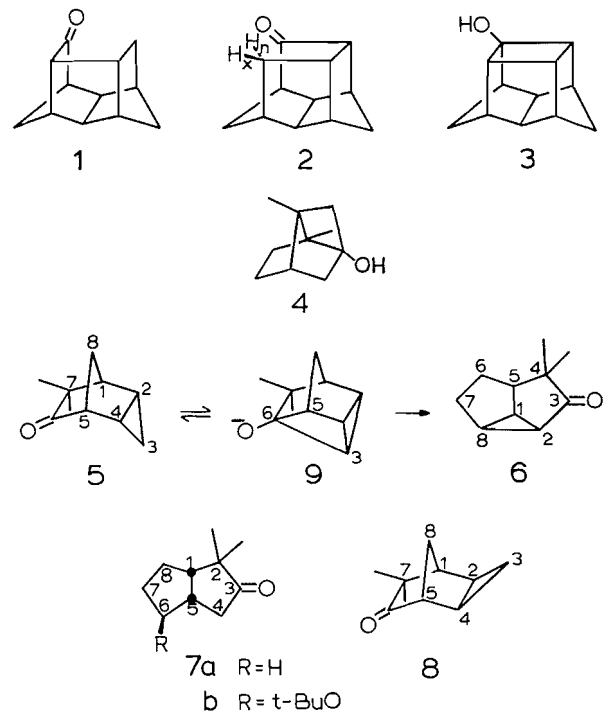

with various bases in deuterated media (8). In all cases, *exo*-6-deuterionorcamphor was the major product (>95%), showing that inversion of configuration is strongly favored. Subsequently, examinations of several other β-enolates have demonstrated that β-enolate cleavages tend to be highly stereoselective, generally proceeding with inversion although a number of highly strained polycyclic systems exhibit retention of configuration (2). Homoketonization of several γ-enolates has also received attention. An early example was the finding that base-catalyzed homoketonization of the bird-cage alcohol **3** gave the same mixture of **1** and **2** as that obtained by the treatment of **1** in strong base (3); thus, the alkoxide of **3** is

[1] For Part XXXIX see ref. 23; for Part XXXVIII see ref. 24.

[2] Present address: Dept. 357, Beckman Instruments, Brea, California 92621, U.S.A.

[3] Present address: Dept. of Chemistry, Washington University, St. Louis, Missouri 63130, U.S.A.

Can. J. Chem. Downloaded from www.nrcresearchpress.com by 210.87.254.105 on 09/06/12
For personal use only.

undoubtedly the γ-enolate formed from **1**. Furthermore, homoketonization of **3** in *t*-BuO^-/*t*-BuOD gave **2**-d_x having H_n largely replaced with deuterium while only traces replaced H_x (9). These data established that the cleavage of **3** proceeded with 95 ± 3% retention of configuration. Examinations of several other substituted cyclobutanols have also revealed high stereoselectivities favoring retention (2). Strong evidence to support the formation of a cyclic γ-enolate in camphor, as had been proposed to account for H/D exchange at the *syn*-methyl carbon (4), has been provided by the preparation of **4**, homoketonization of which, in a deuterated medium, gave 8-deuteriocamphor exclusively (10).

Our interest in remote enolization has led to the examination of other ketones which appear to be potentially capable of rearrangement through γ-enolates. A study of the 7,7-dimethyltricyclo[3.2.1.$0^{2,4}$]octan-6-ones has revealed a new example of such rearrangement. Although the *exo* isomer is stable under the usual reaction conditions (*t*-BuO^-/*t*-BuOH, 185°C), the *endo* isomer **5** is smoothly transformed to 4,4-dimethyltricyclo[3.3.0.$0^{2,8}$]octan-3-one (**6**). Experiments in *tert*-butyl alcohol-O-d_1 showed that all three compounds undergo multiple site H/D exchange. From ^{2}Hmr spectra, the location and stereochemistry of the exchange processes were established. In this paper we wish to describe the results of these experiments, a preliminary report of which has appeared (11).

Results and discussion

Homoenolization experiments

Following our usual procedures (12), the *endo*-tricyclic ketone **5** (13) was dissolved in anhydrous *t*-BuO^-/*t*-BuOH (1.27 *M*) to furnish a solution 0.26 *M* in **5**. Aliquots of this solution were transferred to glass tubes under nitrogen, sealed under vacuum, and heated to 185°C for varying periods of time. The neutral product (>80% yields) from each tube was isolated by pentane extraction and analyzed by gas–liquid chromatography (glc). Over the course of 100 h, glc revealed the smooth disappearance of starting material **5** and the appearance of three new components. The major new component **6** in the earlier samples was found to reach a maximum concentration (~60%) in ca. 50 h but its relative concentration decreased progressively thereafter. The amounts of the second and third new components **7***a* and *b* increased smoothly with increasing reaction time such that the ratio of these three materials was ca. 2:2:1 after 100 h. The distribution of components in the neutral fraction as a function of time is given in Table 1A. Three minor components constituting <5% of the product in the longest runs were not investigated. Samples of **6**, **7***a*, and **7***b* were readily obtained by preparative glc and each gave rise to strong carbonyl absorption in the infrared, showing these to be ketones.

Ketone **6** (1713 cm^{-1}, $CHCl_3$) exhibited a ^{1}Hmr spectrum having prominent methyl singlets (δ, $CDCl_3$) at 0.85 and 1.10 with the following multiplets: 2.66 (bq, 1H), 2.43 (bt, 1H), 1.35 (m, 1H), and complex absorption 1.6–2.1 (5H). Its ^{13}Cmr spectrum contained ten signals (δ_c, $CDCl_3$): CH_3, 17.0, 28.7; CH_2, 25.2, 35.6; CH, 30.8, 34.0, 36.0, 50.4; C, 51.3; and C=O, 219.5. A precise mass measurement showed the molecular formula to be $C_{10}H_{14}O$ which in conjunction with the nmr data is consistent with the tricyclic structure **6**. Since the parent ketone had been described (14), a sample was prepared following the literature procedure and dimethylated using the $NaNH_2/CH_3I$ method (15). The resulting product was identical to **6**, thereby confirming the assigned structure.

TABLE 1. Composition[a] of the neutral product obtained under homoenolization conditions (*t*-BuO^-/*t*-BuOH at 185°C)

Time (h)	**5**	**6**	**7***a*	**7***b*	Other
A. From **5**					
6	67	20	13	—	—
13	45	36	18	Trace	—
30	19	50	22	8	<1
47	8	58	24	9	1
63	~2.5	57	29	10	~1.5
76	—	48	33	16	3
95	—	40	38	17	<5
B. From **6**					
64	—	60	22	18	
120	—	22	48	30	
160	—	11	54	35	

[a]Determined as % of the total by glc using a 6% FFAP column.

The second ketonic product **7***a* (1730 cm^{-1}, $CHCl_3$) was found to have the molecular formula $C_{10}H_{16}O$ by precise mass measurement. Its proton spectrum also contained two methyl singlets (1.03, 1.08) with multiplets centred at 2.70 (2H), 2.25 (1H), 2.04 (1H), and complex absorption 0.9–1.9 (6H). The ^{13}C spectrum consisted of ten signals (δ_c, $CDCl_3$): CH_3, 19.8, 26.9; CH_2, 25.8, 28.6, 32.8, 43.1; CH, 35.1, 54.2; C, 49.4; and C=O, 223.6. These data suggested the bicyclic structure **7***a*. This conclusion was confirmed by reduction of **6** with potassium in alcohol followed by oxidation of the resulting alcohols which furnished the identical ketone.

The third ketonic product has a molecular formula of $C_{14}H_{24}O_2$, by precise mass measurement. In addition to its strong carbonyl absorption at 1740 cm^{-1} in the infrared, there was strong absorption at 1130 cm^{-1} indicative of an ethereal oxygen–carbon stretching mode. The proton spectrum contained three methyl singlets at δ 1.00, 1.05, and 1.20 in the ratio 1:1:3, a multiplet (3.80, 1H), and complex absorption, 1.30–3.30 (8H). Its ^{13}C spectrum had twelve signals: CH_3, 19.2, 26.5, 28.6 (rel. int. 1:1:3); CH_2, 27.1, 36.0, 40.7; CH, 44.0, 52.3, 80.2; —C— 49.4, 73.4; and C=O, 222.8. On the basis of these data, structure **7***b* was assigned to this ketone.

To establish that **7***a* and *b* are generated from **6**, samples of the latter, prepared as described above, were subjected to the usual homoenolization conditions. It was found that **6** was slowly converted to a mixture of **7***a* and *b* as anticipated; Table 1B includes the neutral product composition as a function of time.

Under the reaction conditions employed for the rearrangement of **5**, the isomeric *exo*-tricyclooctanone **8** was found to be stable (>80% recovery) with no evidence for the formation of rearranged products in the neutral fraction by glc analysis even after >110 h at 185°C.

With the structure of **6** confirmed by independent synthesis, the transformation of **5** → **6** must involve proton abstraction from C-3 leading to the intermediate γ-enolate **9** (or its equivalent), which could then suffer cleavage of the original C-5,-6 bond to generate **6** or return to starting material. From the experiments with **6** alone there was no evidence for the formation of **5**, indicating that the cleavage **9** → **6** is irreversible. From the H/D exchange studies described later, this conclusion was confirmed.

The conversion of **6** → **7** requires a reducing agent but we have been unable to detect an oxidized product. With lithium

Can. J. Chem. Downloaded from www.nrcresearchpress.com by 210.87.254.105 on 09/06/12
For personal use only.

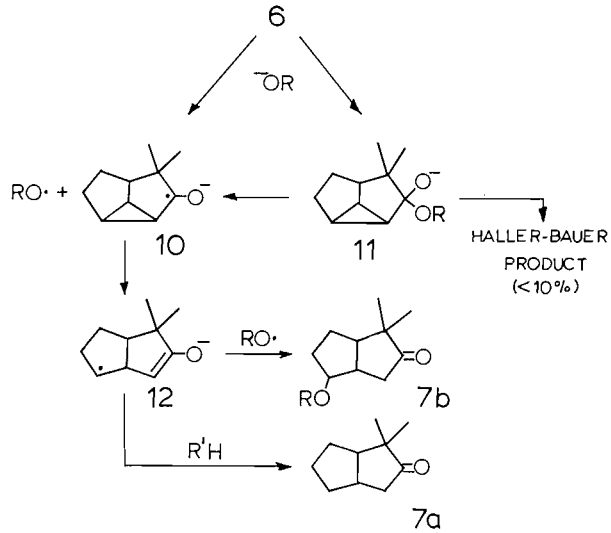

SCHEME 1

aluminium hydride, **6** was reduced in high yield to a 3:2 mixture of the corresponding epimeric alcohols in which the three-membered ring is intact. This was established by oxidation of the alcohol mixture with $K_2Cr_2O_7/H_2SO_4$ in ether to furnish **6** in high yield. As noted above, **6** is readily reduced with potassium metal in *tert*-butyl alcohol to a 2:1 mixture of bicyclic alcohols which upon oxidation gave **7***a* in high yield. Treatment of **6** with *t*-BuO^-/*t*-BuOH at reflux gave no reaction even after 135 h. Thus, the formation of **7***b* by a Michael addition of *t*-BuO^- to **6** seems unlikely. We suggest that the transformation of **6** to **7** occurs by electron transfer from the *tert*-butoxide anion, either directly to form **10** or by homolysis of the addition product **11** formed by reaction of *t*-BuO^- at the carbonyl group of **6** (see Scheme 1). Haller–Bauer cleavage of **11** to form an ester almost undoubtedly occurs, but this cannot be a major pathway since the acid fraction from the homoenolization of **5** constitutes less than 10% of the total product after the longest reaction times. The acidic product was not characterized in this work. Ketyl **10** can open to form **12** which subsequently gains a hydrogen atom from solvent to give **7***a* or reacts with *tert*-butoxide radical, formed in the direct generation of **10** from **6**, to furnish **7***b*. Evidence of electron transfer from *t*-BuO^- has been reported by other workers (16).

H/D Exchange experiments

To determine the regio- and stereoselectivity of proton abstraction in **5** under the strongly basic conditions, its homoenolization was examined in a deuterated medium. After treatment of **5** in *t*-BuO^-/*t*-BuOD at 185°C, samples of **5**-d_x and **6**-d_x were isolated by preparative glc and their ^{2}Hmr spectra were recorded. For **5**-d_x from a 6-h run the spectrum contained four signals, as illustrated in Fig. 1B, the assignments for which were obtained by comparison with the ^{1}Hmr spectrum (Fig. 1A). In the latter, prominent singlets at 0.985 and 1.103 arise from the two methyl groups and these were correlated with the methyl ^{13}C signals at 25.4 and 19.5 ppm (13), respectively, by selective decoupling; thus, it follows that the higher field signal (0.985) arises from the *exo*-methyl group since the less shielded carbon is *exo* (13). The lowest field multiplet at 2.67 was readily ascribed to the bridgehead H-5 while the pattern at 2.18–2.40 (3H) could be attributed to H-1 and the 8-methylene protons. The latter give rise to an AB pattern, J_{AB} = 9.5 Hz, further split by additional smaller coupling interactions; the higher field portion, δ 2.22, is coupled to H-5, J = 1.2 Hz, and to H-1, at 2.35, with J = 2.2 Hz and could be assigned to the *anti*-8 proton. Double irradiation at 2.67 (H-5) revealed $J_{5,anti\text{-}8}$ and reduced the multiplet at 1.83 to a doublet of triplets (J = 3.3, 8.5 Hz), thereby identifying the H-4 absorption, $J_{4,5}$ = 4.5 Hz. An analogous change in the multiplet at 1.57 occurred upon double irradiation at 2.35; thus, H-2 absorbs at 1.57. Since the 3-methylene absorption was obscured by the strong methyl signals, shift reagent studies were required to complete the spectral analysis.

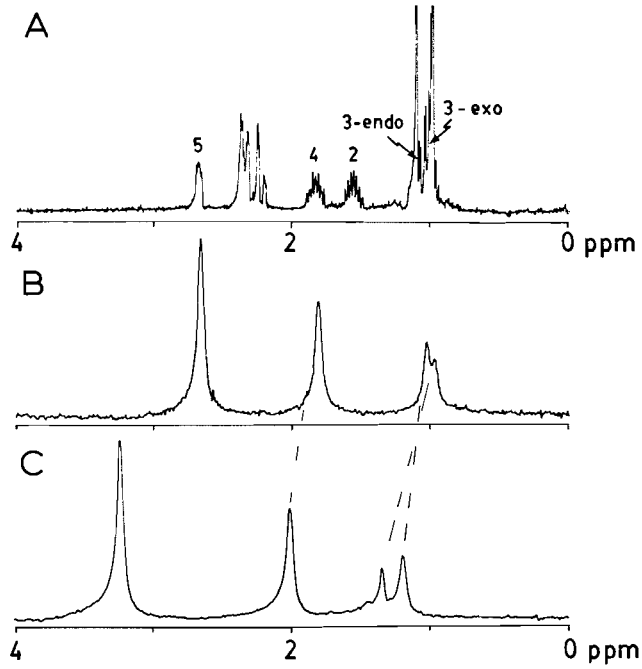

FIG. 1. Nuclear magnetic resonance spectra of **5**. (A) 200 MHz ^{1}H spectrum of **5** in $CDCl_3$; (B) 30.7 MHz ^{2}H spectrum of **5**-d_x in $CHCl_3$; (C) ^{2}H spectrum of **5**-d_x in $CHCl_3$ containing 0.06 equiv. of Eu(fod)$_3$.

Upon the addition of Eu(fod)$_3$, the lowest field signal exhibited the largest shift as expected for the α-bridgehead proton. The shift difference, ν_{AB}, for the 8-methylene protons doubled in the presence of 0.07 equiv. of Eu(fod)$_3$ confirming that the higher field portion of the "AB" system is due to the *anti*-8 proton. In the high field region of the spectrum, the methyl signals shifted smoothly to lower field revealing an eight-line pattern attributable to the *exo*-3 proton. Double irradiation of the *syn*-8 proton absorption reduced this pattern to an apparent quartet by eliminating a splitting of 2.2 Hz which must be the long range coupling interaction between the *exo*-3 and *syn*-8 protons. A five-line multiplet was barely discernible in the high field region and was ascribed to the *endo*-3 proton but the pattern was partially obscured by the lower field methyl signal. Consequently, the spectrum was also examined after the addition of Pr(fod)$_3$, in which case the two multiplets for the 3-protons were clearly resolved. All of the assignments for the individual multiplets were confirmed by the appropriate decoupling experiments and the ^{2}Hmr spectrum could now be interpreted. The four signals (Fig. 1B) establish that exchange occurred at C-5, C-4, the *exo*-methyl, and the *exo*-3 positions. The latter assignments were confirmed by examination of the effect of added Eu(fod)$_3$ (Fig. 1C). Mass spectrometric analysis of this sample showed it to contain 1.83 atoms ^{2}H per molecule and integration of the ^{2}H spectrum (Fig. 1C) indicated the deuterium distribution to be 0.28 (*exo*-3-^{2}H), 0.55 (4-^{2}H), 0.82

Can. J. Chem. Downloaded from www.nrcresearchpress.com by 210.87.254.105 on 09/06/12
For personal use only.

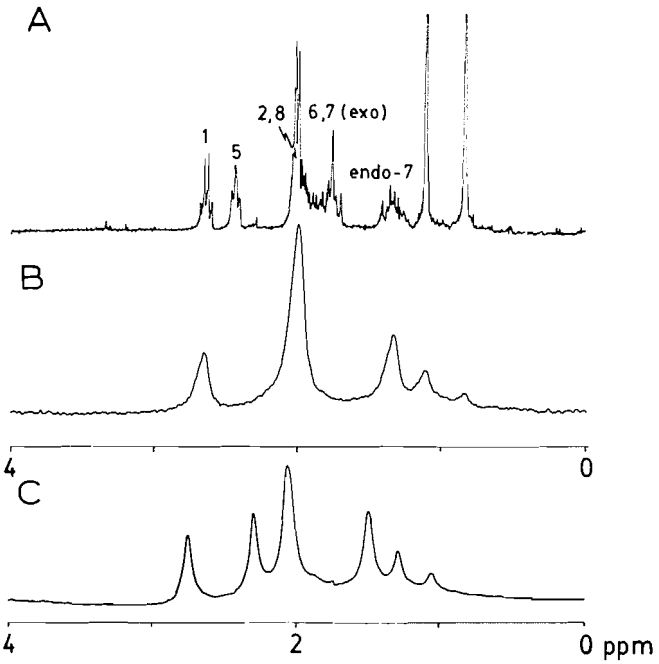

FIG. 2. Nuclear magnetic resonance spectra of **6**. (A) ^{1}H spectrum (200 MHz) of **6** in $CDCl_3$; (B) 30.7 MHz ^{2}H spectrum of **6**-d_x (in $CHCl_3$) generated from **5** after 18 h in *t*-BuO^-/*t*-BuOD at 185°C; (C) ^{2}H spectrum of **6**-d_x in $CHCl_3$ containing 0.05 equiv. of $Eu(fod)_3$.

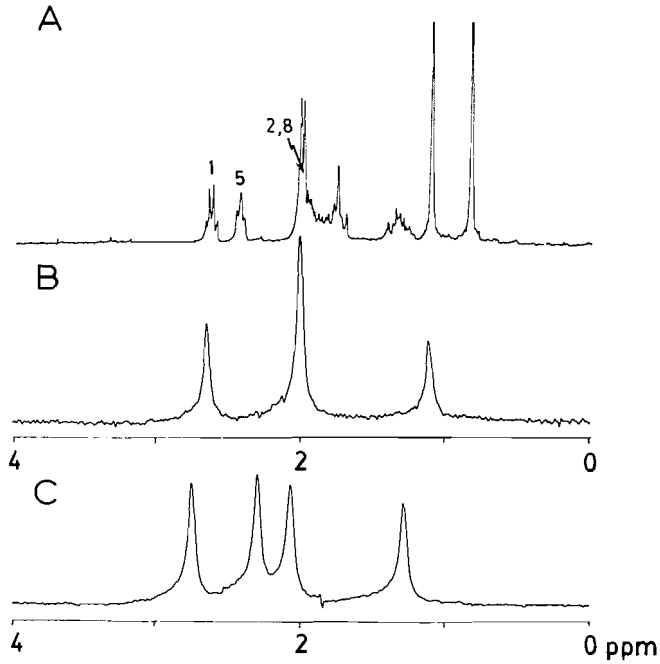

FIG. 3. Nuclear magnetic resonance spectra of **6**. (A) 200 MHz ^{1}H spectrum of **6** in $CDCl_3$; (B) 30.7 MHz ^{2}H spectrum of **6**-d_x (in $CHCl_3$) after 31 h in *t*-BuO^-/*t*-BuOD at 185°C; (C) ^{2}H spectrum of **6**-d_x in $CHCl_3$ containing 0.05 equiv. of $Eu(fod)_3$.

(5-^{2}H), and 0.18 (*exo*-Me) atoms ^{2}H.

The rearrangement product **6**-d_x isolated from a 18-h reaction exhibited the ^{2}Hmr spectrum illustrated in Fig. 2B; the ^{1}H spectrum of **6** is shown in Fig. 2A. Of the two methyl singlets in the latter spectrum, that at δ 1.10 was correlated with the less shielded of the two ^{13}C methyl signals (δ_c, 28.7) by selective decoupling; thus these signals were assigned to the *exo*-methyl group and those at δ 0.85 and δ_c 17.0 to the *endo*-methyl. The broadened "quartet", a doublet of triplets with longer range couplings, at δ 2.66 could be assigned to H-1, and the broadened "triplet" at δ 2.43 to H-5. The multiplet at δ 1.35 was assigned to the *endo*-7-H on the basis of its higher shielding relative to the other skeletal protons, attributable to its orientation with respect to the carbonyl group, i.e. lying above the plane of the carbonyl bond in the shielding cone. The complex absorption in the region 1.7–2.1 integrated for five protons, accounting for the remaining skeletal protons. Upon the addition of increasing amounts of $Eu(fod)_3$, a doublet of doublets was shifted out of this pattern and exhibited the greatest sensitivity to added shift reagent (1.5 ppm/0.2 equiv. of $Eu(fod)_3$), thereby identifying it as the H-2 absorption. With 0.06 equiv. of $Eu(fod)_3$ the H-1 absorption was shifted to δ 2.81, the H-5 pattern to 2.60, the *endo*-7 multiple to 1.63, and the H-2 multiplet to 2.43. Spin-decoupling experiments confirmed these assignments from the following results. Irradiation at δ 1.63 had little effect on the three low field multiplets, while irradiation at 2.43 (H-2) eliminated a 5-Hz coupling in the 2.81 (H-1) pattern with little effect on the 2.60 multiplet. Decoupling at δ 2.60 (H-5) collapsed the 2.81 (H-1) pattern to a triplet, while decoupling at 2.81 changed the absorptions at 2.60 (H-5) and 2.43 (H-2) to doublets. Finally, irradiation at δ 2.15 produced a doublet at 2.43 (H-2) and a triplet at 2.81 (H-1) without affecting the 2.60 (H-5) pattern, thus H-8 absorbs at 2.15.

From Fig. 2B it is apparent that **6**-d_x contains deuterium at several sites including the 1-, *endo*-7-, and both methyl positions. In the presence of shift reagent a clear signal emerged from the large band at δ 2.0 (Fig. 2B) whose sensitivity to added $Eu(fod)_3$ identified it as a 2-deuteron; with 0.05 equiv. of $Eu(fod)_3$ the resulting shift dispersion is shown in Fig. 3C. Unfortunately, additional shift reagent failed to resolve the largest peak although it was consistently broader than the other signals. It was tentatively concluded that this is the absorption of two nearly equivalent ^{2}H nuclei. Mass spectrometric analysis showed this sample to contain 3.55 atoms ^{2}H/molecule. Integration of the ^{2}H spectrum indicated the distribution to be 0.25 and 0.09 atoms ^{2}H at the *exo*- and *endo*-methyl sites, respectively, 0.45 at C-1, and 0.69 at the *endo*-7- and 2-positions, while the absorption at 2.1 ppm represented 1.38 atoms ^{2}H, confirming that deuterium is at two nearly equivalent sites which are presumably the 8- and *exo*-7-positions.

Deuterium incorporation in **6** results from exchange in **5** before conversion to **6** *and* from exchange after its formation. To examine the latter processes separately, samples of **6** were treated with *t*-BuO^-/*t*-BuOD at 185°C. The ^{2}H spectra of the recovered **6**-d_x samples differed significantly from those for **6**-d_x generated from **5** described above, as illustrated in Fig. 3B for a sample isolated after 31 h at 185°C in deuterated base. Upon the addition of 0.05 equiv. of $Eu(fod)_3$ the absorption initially at 2.0 ppm was clearly resolved into two components, δ 2.30 and 2.08, assignable to deuterium at C-2 and -8, respectively. This sample contained 2.71 atoms ^{2}H/molecule by mass spectrometric analysis and the distribution was found to be 0.59, 0.75, 0.78, and 0.59 atoms ^{2}H at C-1, -2, -8, and the *exo*-methyl site, respectively. There was no detectable deuterium at the *endo*-methyl site even with the somewhat longer reaction time which was chosen to test for such exchange.

With these results one can now consider the various exchange processes in these compounds. For **5**, exchange proceeds at four sites, with that at C-4 and -5 presumably activated

Can. J. Chem. Downloaded from www.nrcresearchpress.com by 210.87.254.105 on 09/06/12
For personal use only.

Can. J. Chem. Downloaded from www.nrcresearchpress.com by 210.87.254.105 on 09/06/12
For personal use only.

by the inductive effect of the carbonyl group. Preferential exchange at the *exo*-methyl group has been observed in several polycyclic systems (2) and evidence supporting the intermediacy of a cyclopropoxide in this process has been presented for a number of bicyclic ketones (17). Exchange at C-3 is stereospecific with deuterium only in the *exo* orientation. This is indicative of the reversible formation of **9**, opening with *inversion* to return to **5**. Since all other γ-homoketonizations for which the stereochemistry has been examined proceed with *retention* of configuration, the cleavage of **9** → **5** with inversion is the first such example. The rearrangement of the deuterated **5** to **6** will produce **6**-d_x bearing deuterium at C-2, -7 and -8, and the *endo*-methyl carbon, because the relative orientation of the methyl group is reversed upon conversion of **5** → **6**. Since bridgehead exchange occurs at C-5 in **5** before rearrangement and this carbon picks up deuterium upon the opening of **9** → **6**, both the *exo* and *endo*-7 sites in **6** will be partially deuterated regardless of the stereochemistry of the ring opening; thus we have no information on the stereoselectivity of the cleavage. For **6**-d_x obtained directly from **6** only four ^{2}H signals were apparent after 31 h (Fig. 3C). No deuterium was found at the *endo*-methyl or at C-7! The absence of ^{2}H at C-7 established that the cleavage of **9** → **6** is unidirectional. Since only hydrogens bonded to the *exo*-methyl and cyclopropyl carbons undergo exchange, **6** does not undergo γ-enolization. For **6**-d_x generated from **5** in the deuterated medium (Figs. 2B, C) the signals for ^{2}H at C-7 and the *endo*-methyl group must arise from exchange *before* the formation of **6** while those for ^{2}H at C-1 and the *exo*-methyl group represent exchange *after* its formation. Thus, **6** exhibits the usual preferential *exo*-methyl exchange.

Although **8**, the *exo* isomer of **5**, was found to be stable under the conditions for rearrangement of **5**, this does not preclude the occurrence of H/D exchange. Consequently samples of **8** were treated with *t*-BuO$^-$/*t*-BuOD at 185°C for various times. After 18 h, samples were found to contain 2.27 atoms ^{2}H/molecule by mass spectrometry and ^{2}Hmr revealed five sites of exchange for which the ^{2}H distribution was determined by integration. The ^{2}Hmr signals and ^{2}H content were as follows: δ 2.58 (0.83), 1.37 (0.13), 1.05 (0.05), 0.92 (0.83), and 0.43 (0.43). The ^{1}Hmr spectrum of **8** exhibited methyl singlets at δ 1.055 and 1.160 which, by correlation with the ^{13}C spectrum, could be assigned to the *exo*- and *endo*-methyl hydrogens, respectively. Thus, **8** undergoes slow exchange preferentially at the *exo*-methyl site, as expected. In addition, the ^{1}H spectrum contained broadened singlets at δ 2.185 and 2.575, assignable to the bridgehead protons at C-1 and -5, respectively, broadened doublets at 1.210 and 1.375 (the C-8 protons), a "quartet" at 0.43 (one of the 3-protons), with multiplets centred at 1.30 (1H) and 0.95 (2H). From these data, it was deduced that exchange occurred at C-3, -5, -8, and the *exo*-methyl, as well as at one other site.

Confirmation that deuterium was present at C-3, -4, and -5 was provided by examination of the ^{13}C spectrum of this sample, which could be compared with the spectrum of **8** described previously (13). In the spectrum of **8**-d_x, strong singlets were apparent for C-1 (δ 44.0), C-7 (48.3), and the methyl carbons (20.9 and 23.9) while all other absorptions exhibited the typical effects of deuterium substitution at sites adjacent to the individual carbons. It can be noted that the deuterium content at the *exo*-methyl and C-8 sites was too low to be clearly detectable in the spectrum of this 17-mg sample. The strongly attenuated singlet for C-8 at δ 22.0 was accompanied by a prominent singlet 0.095 ppm towards higher field, constituting good evidence for ^{2}H at C-5 since two-bond ^{2}H isotope effects on ^{13}C shieldings are typically 0.1 ppm (18). The expected singlet at δ 13.4 for C-2 was also strongly attenuated and accompanied by two signals at 0.115 and 0.205 ppm higher field, indicative of one *and* two β-deuterons, thereby revealing ^{2}H uptake at C-3 and -4. The absorption pattern for C-3 was more complex. In addition to the expected weak singlet at δ 5.3 and an isotope-shifted component at 0.115 ppm higher field, there were two 1:1:1 triplets, each with J_{CD} = 24 Hz, the centres of which were separated by 0.115 ppm; the central peak of the less shielded triplet was 0.285 ppm upfield from the δ 5.3 signal for C-3. The isotope-shifted singlet indicates the presence of ^{2}H at C-4 while the triplets arise from those molecules bearing deuterium on C-3, with and without ^{2}H at C-4. While the integrated intensities of these patterns for C-2, -3, and -8 were comparable to those for C-1 and -7, the intensity of the absorption for C-4 was decreased by ca. 80%, providing additional evidence for ^{2}H exchange at this site. For those species bearing a 4-deuteron, the C-4 absorption will be a triplet and these signals will be relatively weak because of the substantially reduced Overhauser effect. Furthermore, additional deuterium at C-3 and/or C-5 will exert isotope effects. Consequently it was not surprising that the triplet patterns were not discernible in this spectrum. The absorption consisted of the expected signal at δ 9.8 together with isotope-shifted components at 0.100 and 0.185 ppm higher field, indicative of ^{2}H at C-3 and -5. Finally, C-5 gave rise to a two-line pattern whose total intensity was comparable to that for C-4; the expected singlet at δ 48.9 was accompanied by a signal at 0.105 ppm higher field, consistent with ^{2}H uptake at C-4 and -8.

While the foregoing data established that ^{2}H exchange occurred at C-3, -4, -5, -8, and the *exo*-methyl sites in **8**-d_x, additional information was required to determine the stereochemistry of exchange at the methylene groups (C-3 and -8). To this end, the effect of shift reagent on the ^{1}H spectrum of **8** was examined. In the presence of 0.54 equiv. of Eu(fod)$_3$, multiplets for each of the eight skeletal protons were separately resolved, permitting complete assignments. The broadened singlets initially at δ 2.185 and 2.575 shifted 1.45 and 3.73 ppm downfield, confirming their assignments to H-1 and -5, respectively. The 8-methylene protons initially absorbing at δ 1.210 and 1.375 as broadened doublets, $J \sim 12$ Hz, shifted 1.55 and 2.35 ppm, thereby identifying these patterns as the *anti* and *syn* signals, respectively. A pair of multiplets, appearing as ill-defined triplets, was clearly resolved in the shifted spectrum; these patterns initially near δ 0.95 and 1.30 exhibited similar shifts of ca. 1.8 ppm and could be assigned to H-4 and -2. The two remaining multiplets, the 1:3:3:1 "quartet" at δ 0.43 and a 1:2:2:2:1 "quintet", initially partially obscured near 0.95, were found to shift 0.78 and 1.05 ppm, respectively; these arise from the 3-protons. Since the "quartet" was least sensitive to added shift reagent, it was assigned to H-3 *cis* to the vicinal cyclopropyl methine protons, H-2 and -4. The four-line pattern, with spacings of 6.6 Hz, is that expected for a proton with comparable coupling to three nonequivalent neighbors. The quintet with spacings of 3.3 Hz can arise from a proton coupled to three neighbors for which one coupling constant is twice as large as the other two; thus, the spacings indicate that J = 6.6 and 3.3 Hz. Since it is well known that $J_{cis} > J_{trans}$ for vicinal coupling in cyclopropyl rings (19), the observed quartet and quintet patterns for the 3-protons *cis* and *trans*, respectively, to H-2 and -4 confirm the assignments. Additional

Can. J. Chem. Downloaded from www.nrcresearchpress.com by 210.87.254.105 on 09/06/12
For personal use only.

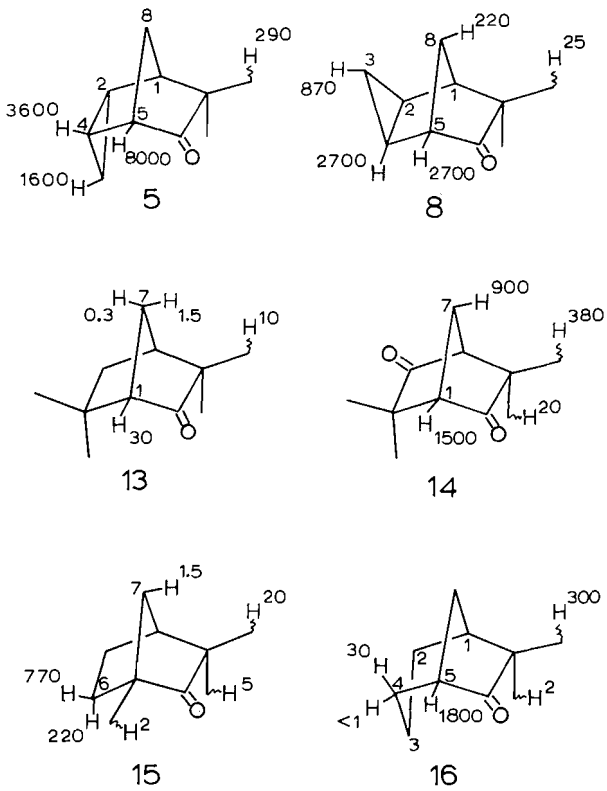

FIG. 4. Deuterium exchange rates ($k \times 10^8\ s^{-1}$) at the various sites in **5**, **8**, and **13**–**16** by β- and γ-enolization at 185°C in *t*-BuO^-/*t*-BuOD.

confirmation of all of these assignments was obtained from a series of spin decoupling experiments. Thus, deuterium exchange at the 3- and 8-methylene sites in **8** is highly stereoselective with observable ^2H found only at the *cis* and *syn* orientations, respectively.

Approximate first-order rate constants for exchange at the various sites in **5** and **8** were extracted from the deuterium incorporation data and these are given in Fig. 4 together with published data for the closely related systems **13** (6), **14** (6), **15** (12), and **16** (20). In our earlier study (12) of fenchone (**15**) exchange at C-7 was not detected but, in a more recent examination, Werstiuk *et al.* (6) found that slow exchange indeed occurs with a distinct preference for the *syn* over the *anti* site even though it would appear that the *anti* hydrogen is the less hindered. However, the rate of *syn* exchange was found to be the same as that in **13** for which the *syn*- and *anti*-7 hydrogens are in similar steric environments but exhibit a *syn*/*anti* preference of 5:1. Much faster exchange at C-7 was found for diketone **14**, apparently attributable to an activating effect of the second carbonyl group (21). On the other hand, only *syn* exchange occurs at C-8 in **8** and at a rate >100 times that for both **13** and **15**, while the same process in **5**, if it occurs, must proceed at a rate comparable to that for **13** and **15**, since no deuterium was observed at C-8 in **5** which rearranges with a rate constant of ca. $2 \times 10^{-5}\ s^{-1}$. While the stereospecificity of the exchange at C-8 in **8** could be attributed to steric hindrance, the increased reactivity for the process is difficult to explain. There is also a marked increase in reactivity for exchange at the 5-bridgehead carbon in both **5** and **8** relative to **13**; both **5** and **8** undergo exchange at C-5 at rates greater than those exhibited by **14** and **16** at the corresponding bridgeheads. It appears that the inductive effect of the carbonyl group in **5** and **8** is enhanced, thereby increasing the acidity of the hydrogens at both C-4 and -5. While it is well known that cyclopropyl hydrogens are more acidic than their alicyclic counterparts, the lack of exchange at C-2 in each of these systems shows that the carbonyl group exerts a significant effect. Furthermore, the rate of exchange at C-4 in both **5** and **8** is distinctly faster than that at C-3, although the latter presumably bears the more acidic hydrogen. The stereospecificity at C-3 can be ascribed to steric factors since the hydrogen exhibiting exchange is much less hindered in each case. Finally it may be noted that, while methyl exchange occurs with the usual *exo*-preference, the rates for **5** and **8** differ by a factor of 10, with that for **5** comparable to the rate found for the [3.2.1] analog **16**. Clearly, rather subtle factors govern the reactivity of exchange in these compounds and additional data are required before definitive interpretations can be put forward.

In the case of **6**, deuterium exchange at the *exo*-methyl carbon appears to proceed with $k \sim 1.2 \times 10^{-6}\ s^{-1}$ at 185°C, which is comparable to the rate of methyl exchange in 2,2,5,5-tetramethylcyclopentanone (20). Exchange of the skeletal hydrogens, however, is too fast at 185°C to give meaningful rate data and, consequently, a series of runs was carried out at 170°C to obtain the following rate constants: 45, 20, and 10 $\times 10^{-6}\ s^{-1}$ for the 1-, 2-, and 8- positions, respectively. These exchange rates are considerably greater than those found for the systems in Fig. 4 because the inductive effect of the α-carbonyl group can be expected to enhance the acidity of these cyclopropyl hydrogens.

At the present time, examination of some closely related systems is in progress, not only as an extension of our search for rearrangements proceeding via γ-enolization but also to investigate similar exchange processes in other polycyclic systems containing three-membered rings, as an aid to the understanding of the enhanced reactivities found for ketones **5** and **8**.

Experimental

General

The preparations of **5** and **8** have been described (13) and the general procedures for the rearrangement and exchange experiments, reported previously (12), were followed. To a solution of the base, prepared *in situ* by dissolving potassium metal in dry *tert*-butyl alcohol under a nitrogen atmosphere, was added the ketone to give a solution containing ketone – *t*-BuO^-/*t*-BuOH in a molar ratio of 1:4:40. Aliquots were placed in glass tubes which were sealed after degassing and heated at an appropriate temperature for various times. For the exchange experiments, *tert*-butyl alcohol-O-d_1 (99% deuterated and <0.005 *M* in water) was used. After cooling, the ketonic products were isolated by pentane extraction and the product mixtures analyzed by gas–liquid chromatography (glc). Preparative glc using either a 6% FFAP or 10% Carbowax on Chromosorb W column were employed to isolate samples of each ketone.

Nuclear magnetic resonance spectra:

The ^1H, ^2H, and ^{13}Cmr spectra were recorded using a Varian XL-200 spectrometer in the Fourier transform mode utilizing, for ^1H and ^{13}C, the ^2H signal of the $CDCl_3$ solvent as a lock; the ^2H spectra were obtained in $CHCl_3$ solution without lock since the field drift is negligible over the few hours required to obtain satisfactory S:N levels. The effect of Eu(fod)$_3$, as shift reagent, was utilized to increase the shift dispersion in both the ^1H and ^2H spectra to permit unambiguous assignments for specific nuclei; ^1H assignments, confirmed through a series of spin decoupling experiments, gave definitive ^2H assignments since ^1H and ^2H shieldings are essentially identical. Integration of the dispersed ^2H spectra indicated the extent of ^2H incorporation at the various sites undergoing exchange, while the total ^2H content was

Can. J. Chem. Downloaded from www.nrcresearchpress.com by 210.87.254.105 on 09/06/12
For personal use only.

determined by mass spectrometry with a Varian MAT-311A instrument.

4,4-Dimethyltricyclo[3.3.0.0^{2,8}]octan-3-one (6)

Tricyclo[3.3.0.0^{2,8}]octan-3-one was prepared from 2-cyclopenten-1-acetyl chloride in 83% yield using the sequence described by Monti *et al.* (14), and exhibited the same ir (ν_{max} (film): 1720 cm^{-1}) and ^{1}Hmr spectra as those reported. Its ^{13}Cmr spectrum contained the following signals: δ_c ($CDCl_3$): 219.4 (C=O), 24.7, 41.0, 47.0 ($3CH_2$'s), 30.7, 36.3, 37.6 and 38.9 (4CH's). Dimethylation using sodamide and methyl iodide (15) furnished **6** in 65% yield, isolated by preparative glc (FFAP); ir ($CHCl_3$): 1713 cm^{-1}; ^{1}Hmr (described in text); ^{13}Cmr ($CDCl_3$), δ_c: 219.5 (C=O), 51.3 (C-4), 50.4 (C-5), 25.2 (C-6), 35.6 (C-7), 33.9 (C-8), 30.8 (C-2), 36.0 (C-1), 28.7 (*exo*-Me), and 17.0 (*endo*-Me). *Exact Mass* calcd. for $C_{10}H_{14}O$: 150.1044; found: 150.1044.

Reduction of 6

(a) A solution of **6** (200 mg) in ether (5 mL) was added dropwise to a refluxing suspension of lithium aluminium hydride (27 mg) in ether (20 mL) under a nitrogen atmosphere and the mixture refluxed for 3 h. After cooling and the dropwise addition of water (20 mL), the product was isolated by ether extraction to afford a mixture of two alcohols (175 mg, 86% yield) in a ratio of ca. 3:2; ^{1}Hmr ($CDCl_3$) δ: 4.07 (d, $J \sim 5.5$ Hz, 1H), 3.50 (bs, 1H), 0.86 (S, 3H, Me), 0.98 (s, 3H, Me); ^{13}Cmr ($CDCl_3$) δ_c (major component): 78.5 (CHOH), 52.2 (quat C), 53.6, 30.1, 30.0, 26.0 (CH's), 33.0, 24.1 (CH_2's), 21.6, 22.9 (CH_3's); minor component: 83.2 (CHOH), 49.6 (quat C), 54.3, 33.3, 33.2, 32.0 (CH's), 30.7, 25.6 (CH_2's), 19.2, 27.7 (CH_3's). Oxidation of this mixture (125 mg) with sodium dichromate/H_2SO_4 in ether according to Brown *et al.* (22) gave a single ketonic product (100 mg, 80% yield) which was identical in all respects with **6**.

(b) Ketone **6** (250 mg) was dissolved in *tert*-butyl alcohol (20 mL) and the solution heated to reflux. Metallic potassium (1 g) was added to the solution and refluxing was continued until the potassium completely dissolved. After the addition of water (50 mL), the product was extracted with pentane (3 × 20 mL) and the combined extracts washed thoroughly with water (8 × 20 mL) before drying over anhydrous $MgSO_4$. Evaporation of the solvent gave a clear oil (140 mg, 55% yield) which was shown by ^{1}H and ^{13}Cmr to be a 2:1 mixture of two alcohols; ^{1}Hmr ($CDCl_3$) δ: 3.79 (dd, $J \sim 7$, 9.5 Hz), 3.71 (dd, $J \sim 6$, 6.5 Hz), 0.97 (s, CH_3), 0.955 (s, CH_3), 0.89 (s, $2CH_3$'s); ^{13}Cmr ($CDCl_3$) δ_c (major component): 8.30 (CHOH), 43.5 (quat C), 53.1, 39.5 (CH's), 39.8, 34.7, 28.2, 28.0 (CH_2's), 29.0, 18.0 (CH_3's); minor component: 79.1 (CHOH), 43.0 (quat C), 53.3, 37.0 (CH's), 39.6, 35.5, 29.3, 27.6 (CH_2's), 22.7, 22.5 (CH_3's). Oxidation of this mixture of alcohols (80 mg) gave a single ketonic product identical with the second ketone produced by rearrangement of **5** and characterized as 2,2-dimethyl-*cis*-bicyclo[3.3.0]octan-3-one (**7***a*) on the basis of the following data: ir ($CHCl_3$): 1730 cm^{-1}; ^{1}Hmr (described in the text); ^{13}Cmr ($CDCl_3$) δ_c: 223.6 (C=O), 54.3 (C-1), 49.4 (C-2), 43.1 (C-4), 35.2 (C-5), 32.9 (C-6), 25.8 (C-7), 28.6 (C-8), 26.9 (*exo*-Me), and 19.9 (*endo*-Me); *m/e* (relative intensity): 152 (28), 110 (63), 95 (35), 82 (54), 81 (75), 79 (35), 69 (35), 67 (100), 54 (48). *Exact Mass* calcd. for $C_{10}H_{16}O$: 152.1206; found: 152.1200.

2,2-Dimethyl-exo-*6*-tert-*butoxy*-cis-*bicyclo[3.3.0]octan-3-one* (7b)

The third ketonic component from the rearrangement of **5** was assigned structure **7***b* on the basis of the following data: ir ($CHCl_3$): 1130, 1740 cm^{-1}; ^{1}Hmr ($CDCl_3$) δ: 1.00 (s, 3H, CH_3), 1.05 (s, 3H, CH_3), 1.20 (s, 9H, CH_3), 3.80 (m, 1H, —CHO—), 1.30–3.0 (complex absorption, 8H); ^{13}Cmr ($CDCl_3$) δ_c: 222.8 (C=O), 52.3 (C-1), 49.4 (C-2), 40.7 (C-4), 44.0 (C-5), 80.2 (C-6), 36.0 (C-7), 27.1 (C-8), 26.5 (*exo*-Me), 19.2 (*endo*-Me), 28.6 and 73.4 (Me and quat C of *tert*-butyl). *Exact Mass* calcd. for $C_{14}H_{24}O_2$: 224.1764; found: 224.1770.

Acknowledgements

We wish to thank the Natural Sciences and Engineering Research Council of Canada for financial support of this work. We are grateful for the technical assistance provided by Mary Ellen Sturgeon and Valerie Richardson and for valuable discussions with D. H. Hunter, D. D. Tanner, and E. W. Warnhoff.

1. A. NICKON and J. L. LAMBERT. J. Am. Chem. Soc. **84**, 4604 (1962); **88**, 1905 (1966).
2. (*a*) D. H. HUNTER, J. B. STOTHERS, and E. W. WARNHOFF. *In* Rearrangements in ground and excited states. Vol. 1. *Edited by* P. de Mayo. Academic Press, New York. 1980. pp. 410–437; (*b*) N. H. WERSTIUK. Tetrahedron, **39**, 205 (1983).
3. R. HOWE and S. WINSTEIN. J. Am. Chem. Soc. **87**, 915 (1965); T. FUKUNAGA. J. Am. Chem. Soc. **87**, 917 (1965); T. FUKUNAGA and R. A. CLEMENT. J. Org. Chem. **42**, 270 (1977).
4. A. NICKON, J. L. LAMBERT, J. E. OLIVER, D. F. COVEY, and J. MORGAN. J. Am. Chem. Soc. **98**, 2593 (1976).
5. A. L. JOHNSON, N. O. PETERSEN, M. B. RAMPERSAD, and J. B. STOTHERS. Can. J. Chem. **52**, 4143 (1974).
6. N. H. WERSTIUK, S. YEROUSHALMI, and G. TIMMINS. Can. J. Chem. **61**, 1945 (1983).
7. R. A. DYLLICK-BRENZINGER and J. B. STOTHERS. J. Chem. Soc. Chem. Commun. 108 (1979).
8. A. NICKON, J. H. HAMMONS, J. L. LAMBERT, and R. O. WILLIAMS. J. Am. Chem. Soc. **85**, 3713 (1963).
9. A. B. CROW and W. T. BORDEN. Tetrahedron Lett. 1967 (1976).
10. W. A. DADSON and T. MONEY. Can. J. Chem. **58**, 2524 (1980).
11. A. K. CHENG, A. K. GHOSH, I. SHEEPY, and J. B. STOTHERS. Can. J. Chem. **59**, 3379 (1981).
12. A. L. JOHNSON, J. B. STOTHERS, and C. T. TAN. Can. J. Chem. **53**, 212 (1975).
13. A. K. CHENG and J. B. STOTHERS. Org. Magn. Reson. **9**, 355 (1977).
14. S. A. MONTI, D. J. BUCHECK, and J. C. SHEPARD. J. Org. Chem. **34**, 3080 (1969).
15. E. J. COREY, R. HARTMANN, and R. A. VATAKANCHERRY. J. Am. Chem. Soc. **84**, 2611 (1962).
16. K. A. BILEVITCH, N. N. PUBNOV, and O. Y. OKHLOBYSTIN. Tetrahedron Lett. 3465 (1968); E. C. ASHBY, A. B. GOEL, and J. N. ARGYROPOULOS. Tetrahedron Lett. **23**, 2273 (1982).
17. V. PATEL and J. B. STOTHERS. Can. J. Chem. **58**, 2728 (1980).
18. J. L. JURLINA and J. B. STOTHERS. J. Am. Chem. Soc. **104**, 4677 (1982), and references therein.
19. L. M. JACKMAN and S. STERNHELL. Applications of nuclear magnetic resonance spectroscopy in organic chemistry. Pergamon Press Ltd., Oxford. 1969. p. 286.
20. A. K. CHENG, J. B. STOTHERS, and C. T. TAN. Can. J. Chem. **55**, 447 (1977).
21. N. H. WERSTIUK. Can. J. Chem. **52**, 2211 (1975).
22. H. C. BROWN, C. P. GARG, and K.-T. LIU. J. Org. Chem. **36**, 397 (1971).
23. A. STOESSL and J. B. STOTHERS. Can. J. Chem. **61**, 378 (1983).
24. A. DOUX-GAYAT, G. DEFAGO, H. KERN, A. STOESSL, and J. B. STOTHERS. J. Chem. Soc. Chem. Commun. 157 (1983).

Condensation of cyclic and acyclic imines with phthalide anions. Synthesis of protoberberines and substituted 3,4-dihydro-2-methyl-1(2*H*)-isoquinolones[1]

RICHARD MARSDEN AND DAVID B. MACLEAN[2]
Department of Chemistry, McMaster University, Hamilton, Ont., Canada L8S 4M1

Received February 1, 1984

RICHARD MARSDEN and DAVID B. MACLEAN. Can. J. Chem. **62**, 1392 (1984).

3,4-Dihydroisoquinolines react with anions derived from phthalides and 3-methylphthalides in tetrahydrofuran yielding 13-hydroxy-8-oxotetrahydroprotoberberines and 13-hydroxy-13-methyl-8-oxotetrahydroprotoberberines, respectively. Only one of two possible diastereomers is formed. The lactams may be reduced to the corresponding protoberberines with lithium aluminium hydride. The reaction of the acyclic imine, 3,4-dimethoxybenzylideneméthylamine, with anions derived from phthalide, 3-phenylphthalide, and 5,6-dimethoxyphthalide, has been investigated. In all cases separable mixtures of diastereomeric substituted 3,4-dihydro-1(2*H*)-isoquinolones were formed.

RICHARD MARSDEN et DAVID B. MACLEAN. Can. J. Chem. **62**, 1392 (1984).

Les dihydro-3,4 isoquinoléines, dans le tétrahydrofuranne, réagissent avec les anions provenant des phthalides et des méthyl-3 phthalides pour conduire respectivement aux hydroxy-13 oxo-8 tétrahydroprotoberbérines et aux hydroxy-13 méthyl-13 oxo-8 tétrahydroprotoberbérines. Il ne se forme qu'un seul des deux diastéréoisomères. On peut réduire les lactames en protoberbérines correspondantes en faisant appel à l'hydrure double de lithium et d'aluminium. On a étudié la réaction de l'imine acyclique, diméthoxy-3,4 benzylidèneméthylamine, avec les anions provenant du phthalide, du phènyl-3 phthalide et du diméthoxy-5,6 phthalide. Dans tous les cas, il se forme des mélanges, que l'on peut séparer, des diastéréoisomères des dihydro-3,4 (2*H*)-isoquinolones-1 substituées.

[Traduit par le journal]

The reaction of imines with phthalide anions derived from phthalides and lithium diisopropylamide (LDA) was reported in a preliminary communication in 1980 by Dodsworth *et al.* (1). A more complete account of their work leading to the formation of various diarylisoquinolones has recently appeared (2). In the interim we reported our initial studies on the reaction of phthalide anions with 3,4-dihydroisoquinolines, a reaction that leads in one step to the protoberberine ring system (3). Here we give a full account of our initial work, and its extension to the synthesis of 13-methylprotoberberines. We also report the preparation of several 2-methyl-3-phenyl-4-hydroxy-3,4-dihydro-1(2*H*)-isoquinolones and a pair of 2-methyl-3,4-diphenyl-4-hydroxy-3,4-dihydro-1(2*H*)-isoquinolones.

Dodsworth *et al.* (2) showed that the anions of phthalide (**1***a*) and 5,6-dimethoxyphthalide (**1***b*) react with a variety of diaryl imines **2** to form 3,4-dihydro-1(2*H*)-isoquinolones substituted at C-2 and C-3 by the aryl groups present in imine **2** and at C-4 by an OH group. (The generation of two new chiral centres leads to the formation of racemic diastereomers as shown in Scheme 1.) This reaction very likely proceeds by initial attack of phthalide anion at the carbon atom of the carbon–nitrogen double bond with transfer of charge to nitrogen. The negatively charged nitrogen then attacks the phthalide carbonyl carbon to form a tetrahedral intermediate which opens to form the isoquinolone. Dodsworth *et al.* found that the formation of the *cis* isomer **3** was favored over the *trans* **4** in a ratio of ca. 2:1, and that the isomers may be differentiated on the basis of their coupling constants in their ^{1}H nmr spectra. The *cis* isomer **3** shows J = 6.0–6.6 Hz and the *trans* isomer **4**, J = 2.0–2.2 Hz, with the coupling constants reflecting a dihedral angle of ca. 55° in the *cis* isomer and ca. 90° in the *trans* isomer. Examination of Dreiding models showed that these dihedral angles are reasonable in minimizing steric interactions. Cushman *et al.* (4) had observed coupling constants of the same order for a related group of *cis*- and *trans*-3,4-disubstituted-

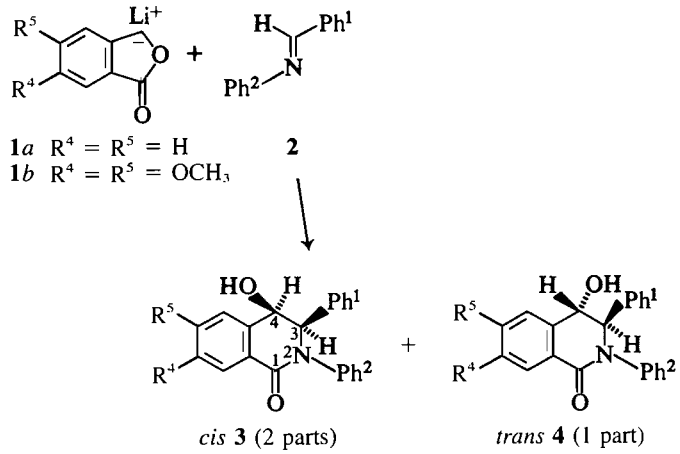

SCHEME 1

3,4-dihydro-1(2*H*)-isoquinolones. Elimination reactions carried out on the mesylates of **3** and **4** supported the stereochemical assignment.

We have found that 3,4-dihydroisoquinolines **5** (cyclic imines) react readily with phthalide anions **1**, to form 13-hydroxy-8-oxotetrahydroprotoberberines **6** in a single step, as shown in Scheme 2. Three such compounds have been prepared in yields ranging from 60–68%. The lactams underwent reduction with $LiAlH_4$ in THF to the corresponding 13-hydroxytetrahydroprotoberberines **7** in yields of 75–85%. Only one of the two possible racemic diastereomers has been isolated in the condensation so that the reaction is highly stereoselective in contrast to the reaction with acyclic imines (1, 2). Compounds **6***b* (5), **7***b* (5, 6), and **7***c* (epiophiocarpine) (6–10) are described in the literature; the physical properties recorded for these compounds correspond to those of the substances prepared here. In particular, the ^{1}H and ^{13}C nmr spectra of **7***c* and the ^{1}H nmr spectrum of **7***b* are in accord with our observations. The coupling constants between the hydrogens at C-13 and C-14 in the bases **7** are in keeping with a *trans* relationship between them; for **7***a*, $J_{13,14}$ = 8.4 Hz, for **7***b*, $J_{13,14}$ = 8.1 Hz,

[1] A preliminary account of part of this work has appeared (3).
[2] Author to whom correspondence may be addressed.

Can. J. Chem. Downloaded from www.nrcresearchpress.com by 210.87.254.105 on 09/06/12
For personal use only.

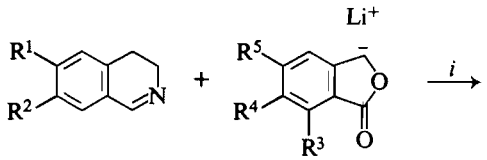

5a $R^1 = R^2 = OCH_3$
5b $R^1 + R^2 = OCH_2O$

1a $R^3 = R^4 = R^5 = H$
1b $R^4 = R^5 = OCH_3$; $R^3 = H$
1c $R^5 = H$; $R^3 = R^4 = OCH_3$

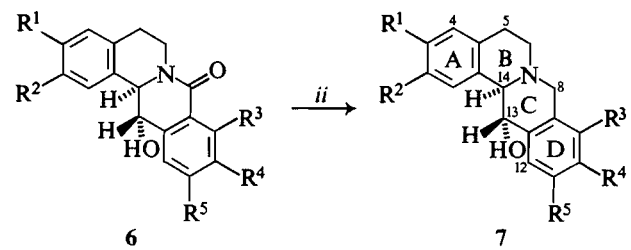

6 **7**

6a and **7a** $R^1 = R^2 = OCH_3$; $R^3 = R^4 = R^5 = H$
6b and **7b** $R^1 = R^2 = R^4 = R^5 = OCH_3$; $R^3 = H$
6c and **7c** $R^1 + R^2 = OCH_2O$; $R^3 = R^4 = OCH_3$; $R^5 = H$

i, THF, −40°C
ii, $LiAlH_4$, THF

SCHEME 2

and for **7c**, $J_{13,14} = 8.4$ Hz. The same configuration may be assigned to **6a**, **6b**, and **6c** since one would not expect hydride reduction to alter the relative configuration of the two relevant hydrogens. The hydrogens at C-13 and C-14 in the lactams **6** had very similar chemical shifts and it was not possible to draw conclusions about their stereochemistry from their ^1H nmr spectra. However, in the 13-acetyl derivative of **6c** the signals for H-13 and H-14 are well separated, appearing, respectively, at δ 5.81 and δ 4.68 with $J = 10.1$ Hz, in accord with a *trans* configuration of the two hydrogen atoms.

Only two 13-hydroxyprotoberberines have been found in nature, namely ophiocarpine (**11**) and 13-hydroxystylopine (**12**), which has the same configuration as ophiocarpine. The compounds prepared here are diastereomeric with the naturally occurring compounds. The conversion of 13-hydroxyprotoberberines to tetrahydroprotoberberines has been reported previously (6, 11, 13) so that this synthesis provides another and convenient route to this class of alkaloids. Other synthetic approaches to this group of alkaloids may be found in several reviews (11, 14–16).

This method of synthesis has now been applied to the preparation of 13-methyltetrahydroprotoberberines. For this purpose 3-methylphthalide **8a** and 6,7-methylenedioxy-3-methylphthalide **8b** were investigated as starting materials in place of the phthalides examined previously. The former was prepared according to the method of Bray *et al.* (17) and the latter by an adaptation of the method developed by Hung *et al.* (18) for the conversion of benzyl alcohols to phthalides as illustrated in Scheme 3. Both 3-methylphthalides, **8a** and **8b**, formed anions with LDA and reacted readily with 6,7-dimethoxy-3,4-dihydroisoquinoline **5a** to form the expected adducts **9a** and **9b**. Again the reaction was stereoselective and led to the formation of only one of the two possible diastereomers as shown in Scheme 4. The assignment of stereochemistry to **10**, the hydride reduction product of **9b**,

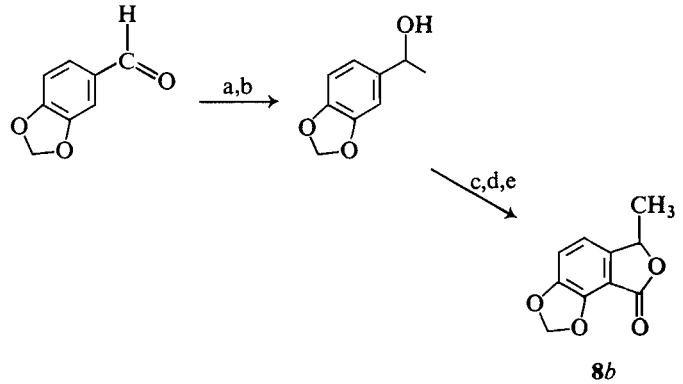

8b

a, CH_3MgI; b, NH_4Cl; c, BuLi (2.2 equiv.); d, CO_2; e, HCl (aq.)

SCHEME 3

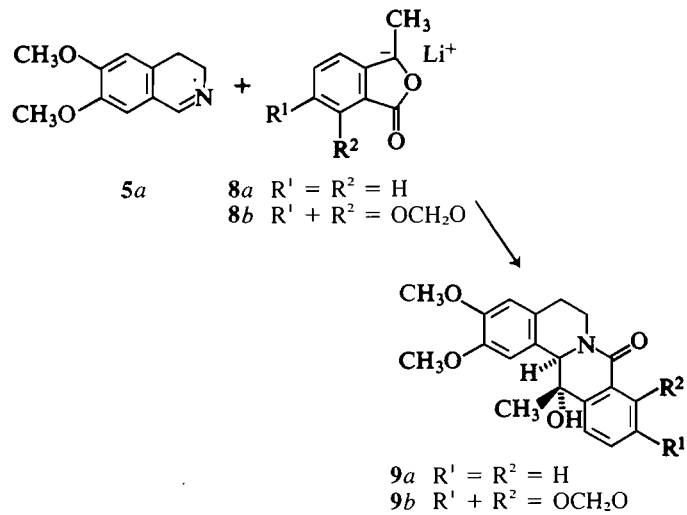

5a **8a** $R^1 = R^2 = H$
8b $R^1 + R^2 = OCH_2O$

9a $R^1 = R^2 = H$
9b $R^1 + R^2 = OCH_2O$

SCHEME 4

and by implication to **9a** and **9b**, is based on ^1H nmr studies and on analogy to the nmr spectra of 13-hydroxy- and 13-methyltetrahydroprotoberberines. The signal at H-1 in ophiocarpine appears at δ 6.77 and in epiophiocarpine **7c** at δ 7.39. The signal of H-1 in **10** appears at δ 7.47, indicating that this proton is deshielded just as in the case of epiophiocarpine and that the OH group is pseudoequatorial. A comparison of the C-methyl signal of **10** with those of 13-methyltetrahydroprotoberberines (19) is also revealing. Thus the methyl group of cavidine, in which the C-methyl is pseudoaxial in ring C, resonates at δ 0.98 while in the epimeric compound, thalictrifoline (Scheme 5), the C-methyl group resonates at δ 1.48. In **10** the C-methyl group resonates at δ 1.23, suggesting that it is pseudoaxial. It would be expected to be deshielded relative to cavidine because of the geminal OH group. Further support for this stereochemistry comes from comparison of the C-methyl signals of **9b** and **10**. In the lactam **9b** the C-methyl group resonates at δ 1.10, above that of **10**, presumably because it lies in the shielding cone of the carbonyl group.

Dehydration of **9b** with *p*-toluenesulfonic acid yielded **11**, a compound previously prepared by Ninomiya *et al.* (20). The physical properties of **11** corresponded closely with those reported by the earlier workers and there can be no doubt about their identity even though a direct comparison was not made. Ninomiya *et al.* have reported the reduction of **11** to

Can. J. Chem. Downloaded from www.nrcresearchpress.com by 210.87.254.105 on 09/06/12
For personal use only.

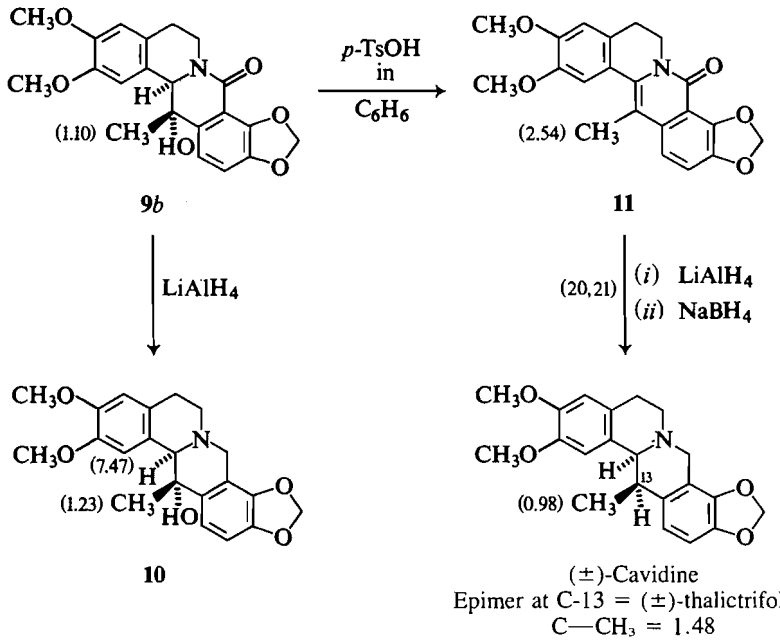

9b 11

10

(±)-Cavidine
Epimer at C-13 = (±)-thalictrifoline
C—CH_3 = 1.48

SCHEME 5

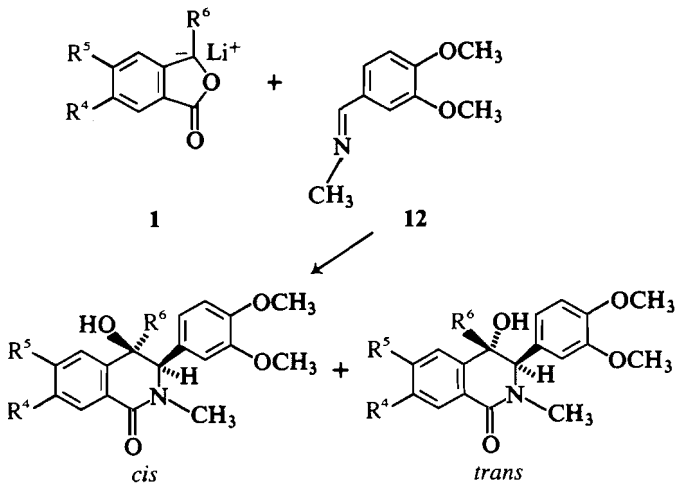

1 12

13, $R^4 = R^5 = OCH_3$; $R^6 = H$ — **14**, $R^4 = R^5 = OCH_3$; $R^6 = H$
16, $R^4 = R^5 = R^6 = H$ — **17**, $R^4 = R^5 = R^6 = H$
18, $R^4 = R^5 = H$; $R^6 = C_6H_5$ — **19**, $R^4 = R^5 = H$; $R^6 = C_6H_5$

SCHEME 6

(±)-cavidine (20) and have quoted another source (21), not available to us, that (±)-cavidine may be converted to (±)-thalictrifoline (epimeric with cavidine at C-13). The reactions are outlined in Scheme 5. The reaction of 3-methylphthalide anions with 3,4-dihydroisoquinolines therefore provides a new route to the diastereomeric 13-methyltetrahydroprotoberberines.

We next investigated the reaction of 3,4-dimethoxybenzylidenemethylamine **12** with lithium phthalide **1***a* ($R^1 = R^2 = R^3 = H$) and lithium 5,6-dimethoxyphthalide **1***b* ($R^1 = R^2 = OCH_3$; $R^3 = H$) to determine whether imines derived from methylamine would be suitable substrates in this reaction (Scheme 6). We found in the reaction of **1***b* with **12** that the *cis* **13** and *trans* **14** isomer were formed but that the overall yield of 40% was less than with the cyclic imine. The *cis* isomer was isolated as an amorphous solid but yielded a crystalline acetate **15**. Both **13** and **14** gave typical ^1H nmr spectra as described by Dodsworth *et al.* (2) and it was on this basis that the stereochemical assignments were made. Somewhat improved yields were obtained when anhydrous $ZnCl_2$ was added to the solution of lithium anion before addition of the imine; the combined yield of *cis* and *trans* isomers was 50%. Apparently exchange of Li for Zn reduced the basicity of the anion so that addition competed more effectively with proton abstraction. In a second experiment using Li phthalide **1***a* and $ZnCl_2$ both isomers were again formed in a combined yield of 57% and in a ratio of *cis*/*trans* ≈ 2:1, as in the first experiment with $ZnCl_2$. The *cis* isomer is designated **16**, the *trans* isomer, **17**.

Finally we examined the feasibility of preparing 3,4-diphenylisoquinolones by using 3-phenylphthalide **1***d* ($R^4 = R^5 = H$; $R^6 = C_6H_5$) as starting material. The reaction with 3,4-dimethoxybenzylidenemethylamine proceeded normally, yielding a mixture of the *R**,*R** **18** (57%) and *R**,*S** **19** (9%) isomers that correspond, respectively, to the *cis* and *trans* isomers examined earlier with phenyl replacing H at C-4. The stereochemical assignments are not secure in the case of **18** and **19**, being based on the chemical shift of only one signal in the nmr, namely, the hydrogen at C-3. In all the isoquinolones examined in this study, the signal for H-3 in the *cis* isomer resonated at lower field than the corresponding proton in the *trans* isomer. For **18** and **19**[3] the values are 4.64 in **18** (*cis* *R**,*R**) and 4.53 in **19** (*trans*, *R**,*S**). The isomer formed in higher yield and the less polar isomer (based on tlc) in all cases has been the *cis* isomer and the assignment of stereochemistry to **18** and **19** conforms with this pattern.

Further support for the stereochemical assignment comes from an examination of the ^{13}C nmr spectra of **13**, **14**, **16**, **17**, **18**, and **19** recorded in Table 1. The signals for C-3 and C-4 in the *cis* isomers **13** and **16**, whose stereochemistry is evident from their ^1H nmr spectra, are shielded by 2–3 ppm relative to

[3] *cis*-Isomer refers to the situation where the hydrogen at C-3 is *cis* to the phenyl at C-4, and *trans* isomer to the situation where H-3 and the phenyl at C-4 are *trans*.

Can. J. Chem. Downloaded from www.nrcresearchpress.com by 210.87.254.105 on 09/06/12
For personal use only.

TABLE 1. ^{13}C chemical shifts of the isoquinolones*

Compound	C-1	N—CH_3	C-3 and C-4
13	164.3	34.2	67.41, 67.74
14	163.9	34.7	70.6, 72.0
16	164.3	34.4	67.3, 68.2
17	164.0	34.7	70.3, 72.1
18	164.2	34.5	74.5, 75.2
19	163.8	34.8	76.2, 76.7

* Other unassigned signals, except for O—CH_3 which all absorbed in the region 56.2± 0.4, are listed below for each compound.

13: ArCH, 107.1, 110.4, 111.4, 111.8, 121.2; ArC, 120.0, 126.3, 133.0, 148.7, 149.2, 149.5, 152.7. **14**: ArCH, 109.9, 110.0, 110.7, 111.5, 118.7; ArC, 121.1, 129.5, 130.5, 148.9, 149.4, 149.6, 152.4. **16**: ArCH, 111.4 (2), 121.3, 124.2, 127.7, 128.2, 132.6; ArC, 126.1 (2), 139.2, 149.4, 149.7. **17**: ArCH, 109.9, 111.7, 118.4, 123.9, 128.0, 128.8, 129.3, 132.5. **18**:† ArCH, 111.5, 121.9, 125.7, 126.3, 127.5, 128.2, 128.6, 129.1, 133.1; ArC, 127.1, 141.3, 145.0, 149.5, 149.9. **19**:† ArCH, 110.8, 127.2, 127.7, 128.0, 128.6, 129.1, 132.3; ArC, 128.5, 129.5, 139.9, 140.7, 148.4, 148.9.

† Several overlapping signals.

(a) Acyclic, *E*-imine (b) Acyclic or cyclic, *Z*-imine

FIG. 1. Proposed orientation of the reactants leading to the *cis* isomer (a), and *trans* isomer (b).

their respective *trans* isomers **14** and **17**. The same is true for the pair **18** and **19**; the C-3 and C-4 signals are shielded by ca. 1.5 ppm in **18** relative to **19**. A small but consistent shielding of the N—CH_3 signal in the three *cis* isomers is observed, whereas the opposite effect is found for the carbonyl carbon. All the data are consistent with **18** having the *R*,R** and **19** the *R*,S** relative configuration.

It is apparent that the reaction with acyclic imines is not nearly as stereoselective as the reaction with the cyclic imines. Moreover, the *cis* isomer is favored in the acyclic series by a factor of 2:1 whereas the *trans* isomer would appear to be the sole reaction product in the case of the cyclic imines studied. The explanation advanced by Dodsworth *et al.* (2) to account for the preferred formation of *cis* isomers in the acyclic series will not serve for the cyclic systems; an alternative explanation is offered below.

Acyclic imines exist almost exclusively in the *E* configuration (22, 23) while the cyclic imines studied here can exist only in a *Z* configuration. Isomerism is possible in the acyclic system in the presence of a nucleophile and some *Z* isomer may be present in the reaction system and react as such. The explanation of Dodsworth *et al.* that the favored transition state is one in which the phenyl group of the imine places itself remote from the phthalide phenyl is a satisfactory explanation for the stereochemical preference found for the *cis* isomer for reaction with acyclic imines. However, it fails for the cyclic imines studied because they give solely *trans* products.

A model that reconciles the behaviour of acyclic and cyclic systems is illustrated in Fig. 1. The essential feature of the model is that the lone pair of the nitrogen atom and the two oxygen atoms of the phthalide ring become coordinated with lithium. The fourth ligand may be the C-atom at C-3 of another lithium phthalide or a solvent molecule. Such a model would require that acyclic imines react in the *E* configuration and orient themselves with respect to the phthalide as in Fig. 1(a) to form the *cis* isomers, and react in the *Z* configuration as in Fig. 1(b) to form the *trans* isomers. Cyclic imines are constrained by their structures to the *Z* configuration. Experiments to test this proposal will be undertaken.

Experimental

Apparatus, materials, and methods

Unless otherwise stated, the ^1H nmr spectra were continuous wave, run at 90 MHz on a Varian EM 390 spectrometer. The samples were dissolved in $CDCl_3$ using tetramethylsilane (TMS) as the internal standard. Chemical shifts, quoted as δ values, were measured in relation to TMS. The symbols s, singlet, d, doublet, t, triplet, q, quartet, and m, multiplet are used in reporting spectra. The Fourier transform spectra were run on either a Bruker WP80 (80 MHz) or WM250 (250 MHz) spectrometer. The ^{13}C nmr spectra were run at 62.9 MHz on a Brucker WM250 FT spectrometer at 22.7°C, or at 20.115 MHz on a Bruker WP80.

Mass spectra were recorded on a V.G. Micromass 7070 F mass spectrometer at 70 eV. Infrared spectra were recorded on a Perkin–Elmer 283 spectrometer in $CHCl_3$ solution. Melting points were determined using a Gallenkamp apparatus and are uncorrected. The microanalyses were performed by the Guelph Chemical Laboratories Ltd., Guelph, Ontario.

Thin layer chromatography (tlc) was performed using Polygram Sil G/UV_{254} plates. Flash column chromatography (24) was employed using Kieselgel 60 (230–400 mesh).

All reactions involving lithiation steps were carried out in flame-dried apparatus under a blanket of argon, using septa and syringes for transfer of reagents. Diisopropylamine was refluxed over calcium hydride and distilled onto molecular sieves (4 Å). THF was dried by distillation from Na/benzophenone under a nitrogen atmosphere just prior to use. Anhydrous $ZnCl_2$ was obtained by heating a sample above its melting point for 5 min, cooling under vacuum, and storage under vacuum. Other solid reagents were stored over P_2O_5 under vacuum.

The following compounds were prepared by standard methods and gave satisfactory physical data: meconin (18), *m*-meconin (25), 3-phenylphthalide (26), and 6,7-dimethoxy-3,4-dihydroisoquinoline (27).

Preparation of 6,7-methylenedioxy-3,4-dihydroisoquinoline

(a) *3,4-Methylenedioxy-β-nitrostyrene*

To a solution of piperonal (15 g, 0.1 mol) in glacial acetic acid (150 mL) were added nitromethane (10.2 g, 0.17 mol) and ammonium acetate (20 g), and the mixture heated on a steam bath for 6 h. The resulting dark red solution was poured onto crushed ice (350 g) and allowed to stand for 2 h. The yellow precipitate was filtered, washed with water, and crystallized from ethanol as yellow needles (15.3 g, 79.3%), mp 159–160°C (lit. (28, 29) mp 161°C); ^1H nmr δ: 6.10 (2H, s, —OCH_2O—), 6.91 (1H, d, J = 8.0 Hz, ArC-5H), 7.04 (1H, d, J = 2.0 Hz, ArC-2H), 7.13 (1H, dd, J = 8.0 Hz and 2.0 Hz, ArC-6H), 7.51 (1H, d, J = 13.5 Hz, vinyl-H), 7.99 (1H, d, J = 13.5 Hz, vinyl-H).

(b) *Homopiperonylamine*

A solution of 3,4-methylenedioxy-β-nitrostyrene (9.6 g, 50 mmol) in dry THF (200 mL) was added dropwise to a stirred slurry of $LiAlH_4$ (6 g, 150 mmol) in refluxing THF (300 mL) over a period of 3 h, and refluxing continued for another 5 h. The mixture was cooled in an ice bath and excess $LiAlH_4$ decomposed by careful addition of water (6 mL), 15% NaOH (6 mL), and water (18 mL), in that order. Ether (500 mL) was added and the inorganic material removed by filtration. Evaporation of the filtrate to dryness gave a brown oil which was distilled under vacuum to give a colourless oil (5.9 g, 72%), bp 75–80°C/0.05 Torr (1 Torr = 133.32 Pa), hydrochloride mp

Can. J. Chem. Downloaded from www.nrcresearchpress.com by 210.87.254.105 on 09/06/12
For personal use only.

Can. J. Chem. Downloaded from www.nrcresearchpress.com by 210.87.254.105 on 09/06/12
For personal use only.

206–207°C (lit. (30) mp 208–210°C); ^{1}H nmr δ: 1.15 (2H, broad s, exchanges with D_2O, —NH_2), 2.55–3.05 (4H, m, —CH_2CH_2—), 5.90 (2H, s, —OCH_2O—), 6.5–6.8 (3H, m, Ar-H).

(c) *Homopiperonyl formamide*

Homopiperonylamine (5.8 g, 35 mmol) and formic acid (2.4 g of a 90% aqueous solution, 47 mmol) were heated under reflux for 20 h. Bulb-to-bulb distillation at 0.13 Torr gave a fraction at 150–170°C (air bath temperature) which solidified on cooling (5.9 g, 87%). Crystallization from ether–acetone gave white crystals, mp 59–61°C (lit. (31) mp 60–62°C); ^{1}H nmr δ: 2.6–2.9 (2H, m, benzylic), 3.3–3.7 (2H, m, CH_2N—), 5.91 (2H, s, —OCH_2O—), 6.5–6.9 (3H, m, Ar-H), 8.19 (1H, broad s, CHO).

(d) *6,7-Methylenedioxy-3,4-dihydroisoquinoline (norhydrastinine)*

This compound was prepared from homopiperonyl formamide according to the method of Slemon *et al.* (31) in 42% yield.

3-Methylphthalide ***8****a*

Prepared according to the procedure of Bray *et al.* (17) in 70% yield, this compound exhibited a red coloration which persisted after two distillations. Its ^{1}H nmr spectrum, however, contained no extraneous peaks, and the material was used in subsequent steps without further purification; ir ($CHCl_3$) ν_{max}: 1760 cm^{-1} (γ-lactone); ^{1}H nmr δ: 1.65 (3H, d, J = 7.0 Hz, —CH_3), 5.58 (1H, q, J = 7.0 Hz, benzylic), 7.4–8.1 (4H, m, aromatic).

α-Methyl-3,4-methylenedioxybenzyl alcohol

A solution of piperonal (10.5 g, 70 mmol) in dry ether (100 mL) was added dropwise over 1 h to a solution of CH_3MgI (77 mmol, made from 1.9 g Mg and 10.95 g CH_3I) in dry ether (100 mL) at room temperature. After stirring a further 2 h the mixture was quenched in an ice-cold solution of NH_4Cl. Standard extraction procedure using ether gave a pale yellow oil (10.3 g, 88.6%) which was used without further purification; ^{1}H nmr δ: 1.42 (3H, d, J = 7.0 Hz, —CH_3), 2.20 (1H, broad s, exchanges with D_2O, —OH), 4.78 (1H, q, J = 7.0 Hz, benzylic), 5.90 (2H, s, —OCH_2O—), 6.78 (2H, broad s, aromatic), 6.89 (1H, broad s, aromatic).

3-Methyl-6,7-methylenedioxyphthalide ***8****b*

The method described here utilizes the demonstrated synthesis of phthalides from benzyl alcohols by Hung *et al.* (18). α-Methyl-3,4-methylenedioxybenzyl alcohol (2.49 g, 15 mmol) was dissolved in dry THF (75 mL) under argon at room temperature and treated dropwise with n-BuLi (20 mL of a 1.65 *M* solution in hexane, 33 mmol, 2.2 equiv.) over 15 min, cooling if necessary to maintain ambient temperature. The turbid, dark orange solution was stirred another 45 min and treated with gaseous CO_2 for 1 h, and subsequently with HCl (85 mL of a 10% solution). After stirring for 0.5 h, the upper organic layer was separated and kept. The lower aqueous layer was extracted with CH_2Cl_2, the extract combined with the aforementioned organic layer, dried (Na_2SO_4), and evaporated, yielding a yellow solid. Flash chromatography (silica, eluting with CH_2Cl_2–hexane, 80:20) gave a solid which crystallized from methanol as white needles (1.11 g, 38.5%), mp 143–145°C; ir ($CHCl_3$) ν_{max}: 1765 cm^{-1} (γ-lactone); ^{1}H nmr δ: 1.59 (3H, d, J = 6.0 Hz, —CH_3), 5.48 (1H, q, J = 6.0 Hz, benzylic), 6.16 (2H, s, —OCH_2O—), 6.83 and 7.08 (2H, ABq, J = 8.0 Hz, aromatic). *Mol. Wt.* calcd. for $C_{10}H_8O_4$: 192.042; found (hrms): 192.042.

3,4-Dimethoxybenzylidenemethylamine ***12***

Methylamine (12.1 g of a 15.4% w/w solution in benzene (32), equivalent to 1.86 g CH_3NH_2, 60 mmol) was added to a solution of 3,4-dimethoxybenzaldehyde (6.64 g, 40 mmol) in benzene and the whole heated under reflux in a Dean–Stark apparatus (a balloon was attached to the condensor to minimize loss of CH_3NH_2) for 3 h. A further portion of methylamine solution (4 g, 20 mmol) was added to the cooled mixture and refluxing continued for 2 h. This was repeated, after which a test sample examined by ^{1}H nmr showed quantitative conversion to the imine. The solution was evaporated to dryness to give a cream colored solid in quantitative yield; ^{1}H nmr δ: 3.50 (3H, d, J = 2.0 Hz, —NCH_3), 3.90 (3H, s, —OCH_3), 3.93 (3H, s, —OCH_3), 6.88 (1H, d, J = 8.0 Hz, Ar-5H), 7.15 (1H, dd, J = 8.0 Hz and 2.0 Hz, Ar-6H), 7.42 (1H, d, J = 2.0 Hz, Ar-2H), 8.21 (1H, m, CH=N).

General procedure for reaction of phthalides ***1****a*, ***1****b, and* ***1****c with dihydroisoquinolines* ***5***

A solution of the appropriate phthalide in dry THF (ca. 2 mL per mmol) was added dropwise to a solution of lithium diisopropylamide (LDA, 1.1 equiv.) at −70°C (LDA was prepared by addition of a solution of 1.65 *M* nBuLi in n-hexane to an equivalent amount of diisopropylamine in dry THF at −10°C (ca. 5 mL per mmol)). The yellow or orange anion thus prepared was stirred for 15 min, the temperature raised to −40°C, and the solution treated with a solution of the dihydroisoquinoline in dry THF (2 mL per mmol). After stirring for 1 h at −40°C, the mixture was allowed to warm to room temperature and stirred overnight. The THF was then evaporated, water added, and the contents extracted with chloroform, dried (Na_2SO_4), and evaporated to dryness to give the crude products.

trans-*13-Hydroxy-2,3-dimethoxy-8-oxotetrahydroprotoberberine* ***6****a*

Generation of the anion from phthalide (***1****a*, 0.2 g, 1.5 mmol) gave a suspension at −70°C, which dissolved to give a clear orange solution at −40°C. Addition of 6,7-dimethoxy-3,4-dihydroisoquinoline (0.287 g, 1.5 mmol) and work-up gave a yellow foam. Flash chromatography (silica, eluting with $CHCl_3$ + 1.5% MeOH) gave ***6****a* as a creamy crystalline powder (295 mg, 60.5%), mp 180–181°C (EtOH – pet. ether 30–60°C); ir ($CHCl_3$) ν_{max}: 1645 cm^{-1}; ^{1}H nmr (250 MHz) δ: 2.7–3.0 (3H, m, C-5 H's and C-6 H, ax.), 3.86 (3H, s, —OCH_3), 3.88 (3H, s, —OCH_3), 4.6–4.7 (2H, distorted s, C-13 and C-14 H's), 4.9–5.0 (1H, m, C-6 H, eq.), 6.72 (1H, s, C-4 H), 6.98 (1H, s, C-1 H), 7.43 (1H, t, J = 7.7 Hz, C-10 or C-11 H), 7.57 (1H, t, J = 7.7 Hz, C-11 or C-10 H), 7.68 (1H, d, J = 7.7 Hz, C-12 H), 8.06 (1H, d, J = 7.7 Hz, C-9 H); C-9, C-10, C-11, and C-12 H signals also show *meta* coupling (ca. 1Hz); ^{13}C nmr δ: 30.6 (C-5), 39.8 (C-6), 56.5, 56.6 (OMe), 62.0 (C-14), 72.1 (C-13), 112.4, 112.7, 124.2, 128.4, 128.7, 132.7 (ArCH); 124.9, 128.0, 129.4, 141.5, 147.9, 148.9 (ArC), 164.6 (C=O). ms, m/z (%): 325 (8) M$^+$, 192 (100), 134 (10). *Anal.* calcd. for $C_{19}H_{19}NO_4$: C 70.15, H 5.85, N 4.31%; found: C 70.26, H 5.68, N 4.47%.

trans-*13-Hydroxy-2,3-dimethoxytetrahydroprotoberberine* ***7****a*

A solution of lactam ***6****a* (65 mg, 0.2 mmol) in dry THF (20 mL) was added to a slurry of $LiAlH_4$ (150 mg, 4 mmol) in dry THF (30 mL) under argon, and the whole heated under reflux for 8 h. Water (1 mL) was carefully added to the cooled mixture, which was then filtered and the filtrand washed with $CHCl_3$. The filtrate was dried (Na_2SO_4) and evaporated to dryness to give ***7****a* as a pale yellow solid (46 mg, 74%), mp 162–164°C (from CH_2Cl_2 – pet. ether 30–60°C); ir ($CHCl_3$) ν_{max}: 2850–2750 cm^{-1} (Bohlmann bands); ^{1}H nmr (250 MHz) δ: 2.65–2.8 (2H, m, C-5 H's), 3.0–3.22 (2H, m, C-6 H's), 3.55 (1H, d, J = 8.4 Hz, C-14 H), 3.90 (2H, s, C-8 H's), 3.91 (6H, s, 2 × —OCH_3), 4.78 (1H, d, J = 8.4 Hz, C-13 H), 6.65 (1H, s, C-4 H), 7.11 (1H, d, J = 7.0 Hz, C-9 H), 7.2–7.35 (2H, m, C-10 and C-11 H's), 7.57 (2H, broad s, C-1 and C-12 H's), ms, m/z (%): 311 (4) M$^+$, 192 (100), 120 (22). *Mol. Wt.* calcd. for $C_{19}H_{21}NO_3$: 311.150; found (hrms): 311.152.

trans-*13-Hydroxy-2,3,10,11-tetramethoxy-8-oxotetrahydroprotoberberine* ***6****b*

Addition of 6,7-dimethoxy-3,4-dihydroisoquinoline (0.57 g, 3 mmol) to the yellow-orange anion of *m*-meconin (0.582 g, 3 mmol) and work-up gave a yellow oil. Flash chromatography (silica, applying the oil to the column in EtOAc–CH_2Cl_2, 1:1, then eluting with EtOAc) yielded ***6****b* as a white powder (0.79 g, 68.4%), mp 208–210°C (EtOH – pet. ether 30–60°C) (lit. (5) mp 210–212°C); ir ($CHCl_3$) ν_{max}: 1640 cm^{-1}; ^{1}H nmr (250 MHz) δ: 2.7–3.0 (3H, m, C-5 H's and C-6 H, ax.), 3.87 (3H, s, —OCH_3), 3.88 (3H, s, —OCH_3), 3.94 (3H, s, —OCH_3), 3.97 (3H, s, —OCH_3), 4.5–4.7 (2H, m, C-13 and C-14 H's), 4.85–4.95 (1H, m, C-6 H, eq.), 6.73 (1H, s, C-4 H), 6.98 (1H, s, C-1 H), 7.17 (1H, s, C-12 H), 7.58 (1H, s, C-9 H); ms, m/z (%): 385 (3) M$^+$, 194 (8), 192 (100); ^{13}C nmr δ: 30.2 (C-5), 39.4

Can. J. Chem. Downloaded from www.nrcresearchpress.com by 210.87.254.105 on 09/06/12
For personal use only.

(C-6), 56.0, 56.2 (4 × OCH_3), 62.0 (C-14), 71.6 (C-13), 106.7, 110.8, 111.9, 112.0 (ArCH), 120.2, 124.7, 129.1, 135.1, 147.4, 148.4, 148.8, 152.7 (ArC), 164.3 (C-8).

trans-*13-Hydroxy-2,3,10,11-tetramethoxytetrahydroprotoberberine* **7**b

Reduction of lactam **6***b* (62 mg, 0.16 mmol) with $LiAlH_4$ (120 mg, 3.2 mmol) by the method previously described gave **7***b* as a pale yellow solid (39 mg, 65.3%), mp 157–159°C (CH_2Cl_2 – pet. ether 30–60°C) (lit. (6) mp 158–160°C, (5) mp 197–199°C); ir ($CHCl_3$) ν_{max}: 2850–2750 cm^{-1} (Bohlmann bands); ^1H nmr (250 MHz) δ: 2.65–2.8 (2H, m, C-5 H's), 3.0–3.2 (2H, m, C-6 H's), 3.51 (1H, d, J = 8.1 Hz, C-14 H), 3.82 (2H, s, C-8 H's), 3.90 (12H, s, 4 × —OCH_3), 4.74 (1H, d, J = 8.1 Hz, C-13 H), 6.59 (1H, s, C-9 or C-4 H), 6.65 (1H, s, C-4 or C-9 H), 7.08 (1H, s, C-12 H), 7.58 (1H, s, C-1 H); ms, m/z (%): 371 (1) M^+, 192 (100), 180 (38).

trans-*13-Hydroxy-2,3-methylenedioxy-9,10-dimethoxy-8-oxotetrahydroprotoberberine* **6**c

Addition of 6,7-methylenedioxy-3,4-dihydroisoquinoline (0.245 g, 1.4 mmol) to the golden yellow anion of meconin (0.272 g, 1.4 mmol) and work-up gave a yellow foam. Treatment with EtOAc afforded **6***c* as a white powder (165 mg, 32%). The mother liquor was subjected to flash chromatography (silica, eluting with ethyl acetate) yielding an additional sample of **6***c* (170 mg, 33%), mp 205–206°C (EtOAc); ir ($CHCl_3$): ν_{max} 1650 cm^{-1}; ^1H nmr (250 MHz) δ: 2.7–2.85 (3H, m, C-5 H's and C-6 H, ax.), 3.89 (3H, s, —OCH_3), 3.99 (3H, s, —OCH_3), 4.4–4.5 (2H, m, C-13 and C-14 H's), 5.0–5.1 (1H, m, C-6 H, eq.), 5.93–5.95 (2H, m, —OCH_2O—), 6.70 (1H, s, C-4 H), 6.82 (1H, s, C-1 H), 7.07 (1H, d, J = 8.4 Hz, C-11 H), 7.35 (1H, d, J = 8.4 Hz, C-12 H); ^{13}C nmr δ: 31.0 (C-5), 38.7 (C-6), 56.5 (OCH_3), 61.8 (OCH_3), 62.2 (C-14), 71.9 (C-13), 101.4 (OCH_2O), 109.2 (2), 115.9, 119.2 (ArCH), 122.0, 125.2, 130.8, 134.2, 146.4, 147.4, 150.1, 153.8 (ArC), 162.0 (C-8); ms, m/z (%): 369 (1) M^+, 194 (9), 176 (100). *Anal.* calcd. for $C_{20}H_{19}NO_6$: C 65.04, H 5.15, N 3.79%; found: C 65.13, H 5.05, N 3.86%. Treatment of **6***c* with acetic anhydride and pyridine under reflux for 90 min gave the 13-acetoxy derivative, mp 165–167°C (EtOAc – pet. ether, 30–60°C); ir ($CHCl_3$) ν_{max}: 1760, 1735 (sh), 1650 cm^{-1}; ^1H nmr (250 MHz) δ: 2.14 (3H, s, $OCOCH_3$), 2.7–3.0 (3H, m, C-5 H's and C-6 H ax.), 3.89 (3H, s, OCH_3), 4.01 (3H, s, OCH_3), 4.68 (1H, d, J = 10.1 Hz, C-14 H), 4.95–5.10 (1H, m, C-6 H eq.), 5.81 (1H, d, J = 10.1 Hz, C-13 H), 5.93 (2H, s, OCH_2O), 6.66 (2H, s, C-1 and C-4 H's), 6.89 (1H, d, J = 8.4 Hz, C-11 H), 7.03 (1H, d, J = 8.4 Hz, C-12 H).

trans-*13-Hydroxy-2,3-methylenedioxy-9,10-dimethoxytetrahydroprotoberberine ((±)-epiophiocarpine* **7**c)

Reduction of lactam **6***c* (111 mg, 0.3 mmol) with $LiAlH_4$ (230 mg, 6 mmol) as before furnished **7***c* as a pale yellow powder (90 mg, 85%), mp 177–179°C (EtOAc) (lit. (7) mp 178–179°C, (8) mp 181–183°C), showing ir, ^1H nmr, ^{13}C nmr, ms, and tlc behaviour in agreement with literature data and with an authentic sample.

*(13*S**,14*R**)-13-Hydroxy-13-methyl-2,3-dimethoxy-8-oxotetrahydroprotoberberine* **9**a

Addition of 6,7-dimethoxy-3,4-dihydroisoquinoline (0.382 g, 2 mmol) to the orange anion of 3-methylphthalide (0.296 g, 2 mmol) and work-up gave a white solid. Crystallization from $CHCl_3$ gave **9***a* as a white powder (0.4 g, 59%). An additional sample (90 mg, 13%) was obtained by recrystallizing the evaporated mother liquor from EtOH, and a final sample (100 mg, 15%) was obtained by flash chromatography of the second mother liquor (silica, applying the sample onto the column in warm $CHCl_3$, and eluting with $CHCl_3$ + 2.5% MeOH) to give a total yield of 0.59 g, 87%, mp 226–228°C; ir ($CHCl_3$) ν_{max}: 1640 cm^{-1}; ^1H nmr (250 MHz) δ: 1.13 (3H, s, —CH_3), 2.7–3.0 (3H, m, C-5 H's and C-6 H, ax.), 3.86 (3H, s, —OCH_3), 3.90 (3H, s, —OCH_3), 4.92 (1H, s, C-14 H), 4.95–5.05 (1H, m, C-6 H, eq.), 6.73 (1H, s, C-4 H), 7.03 (1H, s, C-1 H), 7.41 (1H, t, J = 7.7 Hz, C-10 or C-11 H), 7.56 (1H, t, J = 7.7 Hz, C-11 or C-10 H), 7.69 (1H, d, J = 7.7 Hz, C-12 H), 8.08 (1H, d, J = 7.7 Hz, C-9 H); C-10, C-11, C-12, and C-13 signals also show *meta* coupling (ca. 1 Hz); ^{13}C nmr δ: 23.9 (C—CH_3), 29.8 (C-5), 39.3 (C-6), 56.2, 56.4 (OCH_3), 64.2 (C-14), 74.4 (C-13), 112.1, 112.4, 123.2, 128.1, 128.7, 132.7 (ArCH), 123.2, 127.1, 130.6, 146.1, 147.7, 148.8 (ArC), 164.3 (C-8); ms, m/z (%): 339 (3) M^+, 192 (100), 148 (10). *Anal.* calcd. for $C_{20}H_{21}NO_4$: C 70.80, H 6.19, N 4.13%: found: C 70.41, H 6.43, N 4.09%.

*(13*S**,14*R**)-13-Hydroxy-13-methyl-2,3-dimethoxy-9,10-methylenedioxy-8-oxotetrahydroprotoberberine* **9**b

Addition of 6,7-dimethoxy-3,4-dihydroisoquinoline (0.573 g, 3 mmol) to the orange anion of 3-methyl-6,7-methylenedioxyphthalide (0.576 g, 3 mmol) and work-up gave a yellow foam. Flash chromatography (silica, eluting with $CHCl_3$ + 2.5% MeOH) yielded **9***b* as a white powder (920 mg, 80%), mp 281–284°C (dec.) (EtOH): ir ($CHCl_3$) ν_{max}: 1645 cm^{-1}; ^1H nmr (250 MHz) δ: 1.10 (3H, s, —CH_3), 2.65–2.9 (3H, m, C-5 H's and C-6 H, ax.), 3.86 (3H, s, —OCH_3), 3.90 (3H, s, —OCH_3), 4.83 (1H, s, C-14 H), 4.95–5.05 (1H, m, C-6 H, eq.), 6.07 and 6.18 (2H, 2 × d, J = 1.2 Hz, nonequivalent —OCH_2O—), 6.72 (1H, s, C-4 H), 6.94 (1H, d, J = 8.1 Hz, C-11 H), 6.99 (1H, s, C-1 H), 7.15 (1H, d, J = 8.1 Hz, C-12 H); ^{13}C nmr δ: 24.0 (C—CH_3), 29.6 (C-5), 38.6 (C-6), 56.2, 56.3 (2 × OCH_3), 64.2 (C-14), 74.4 (C-13), 102.6 (OCH_2O), 111.4, 111.9, 112.3, 116.1 (ArCH), 123.0, 130.5, 139.4, 147.5, 148.0, 148.6 (ArC), 162.0 (C-8); ms, m/z (%): 383 (4) M^+, 192 (100). *Anal.* calcd. for $C_{21}H_{21}NO_6$: C 65.80, H 5.48, N 3.66%; found: C 65.66, H 5.64, N 3.72%.

*(13*S**,14*R**)-13-Hydroxy-13-methyl-2,3-dimethoxy-9,10-methylenedioxytetrahydroprotoberberine* ***10***

Reduction of lactam **9***b* (100 mg, 0.27 mmol) with $LiAlH_4$ (205 mg, 5.4 mmol) gave **10** as white blocks with a faint pink tinge (76 mg, 78.9%), mp 162–164°C with darkening (EtOH); ir ($CHCl_3$) ν_{max}: 2840–2750 cm^{-1} (Bohlmann bands); ^1H nmr (250 MHz) δ: 1.23 (3H, s, —CH_3), 2.5–2.7 (2H, m, C-5 H's), 3.0–3.15 (2H, m, C-6 H's), 3.65 (1H, d, J = 15.2 Hz, C-8 H), 3.69 (1H, s, C-14 H), 3.85 (3H, s, —OCH_3), 3.87 (3H, s, —OCH_3), 4.0 (1H, d, J = 15.2 Hz, C-8 H), 5.94 and 5.97 (2H, 2 × d, J = 1.3 Hz, nonequivalent —OCH_2O—), 6.60 (1H, s, C-4 H), 6.77 (1H, d, J = 8.2 Hz, C-11 H), 7.11 (1H, d, J = 8.2 Hz, C-12 H), 7.47 (1H, s, C-1 H); ms, m/z (%): 369 (1) M^+, 351 (2), 192 (100), 178 (6), 163 (25). *Anal.* calcd. for $C_{21}H_{23}NO_5$: C 68.29, H 6.23, N 3.79%; found: C 68.55, H 6.21, N 3.69%.

13,14-Didehydro-2,3-dimethoxy-13-methyl-9,10-methylenedioxyberbine-8-one ***11***

Lactam **9***b* (65 mg) in benzene was heated under reflux in a Dean–Stark apparatus for 3 h with *p*-toluenesulfonic acid (20 mg). Evaporation of the benzene gave a yellow solid which was crystallized twice from EtOH, yielding a white powder (48 mg, 77.5%) which adopted a greenish tinge on standing, mp 250–252°C (lit. (20) mp 243–245°C); ir ($CHCl_3$) ν_{max}: 1640 cm^{-1}; ^1H nmr δ: 2.54 (3H, s, —CH_3), 2.83 (2H, t, J = 6.0 Hz, C-5 H's), 3.92 (3H, s, —OCH_3), 3.95 (3H, s, —OCH_3), 4.19 (2H, t, J = 6.0 Hz, C-6 H's), 6.21 (2H, s, —OCH_2O—), 6.79 (1H, s, C-4 H), 7.10 (1H, s, C-1 H), 7.22 (2H, s, (collapsed AB quartet), C-11 and C-12 H's).

cis- *And* trans-*6,7-dimethoxy-3-(3,4-dimethoxyphenyl)-4-hydroxy-2-methyl-3,4-dihydro-1(2*H*)-isoquinolones* ***13*** *and* ***14***

(a) *without* $ZnCl_2$

Addition of a solution of 3,4-dimethoxybenzylidenemethylamine **12** (0.269 g, 1.5 mmol) in dry THF to the anion of *m*-meconin (0.291 g, 1.5 mmol) and work-up, in the manner described earlier, gave a yellow foam. Flash chromatography (silica, eluting with $CHCl_3$ + 1% MeOH) gave the following two components: (*i*) *cis* isomer **13** (169 mg, 30.2%), amorphous solid, R_f 0.25 (silica, EtOAc); ir ($CHCl_3$) ν_{max}: 1640 cm^{-1}; ^1H nmr δ: 3.07 (3H, s, —NCH_3), 3.67 (3H, s, —OCH_3), 3.80 (3H, s, —OCH_3), 3.87 (3H, s, —OCH_3), 3.93 (3H, s, —OCH_3), 4.65 (1H, d, J = 6.0 Hz, C-3 H), 5.3–5.6 (1H, m (on addition of D_2O sharpens to a doublet, J = 6.0 Hz), C-4 H), 6.5–6.85 (3H, m, protons of the 3-phenyl substituent), 7.0 (1H, s, C-5 H), 7.70

Can. J. Chem. Downloaded from www.nrcresearchpress.com by 210.87.254.105 on 09/06/12
For personal use only.

(1H, s, C-8 H); ms, *m/z* (%): 373 (14) M^+, 194 (14), 180 (100).

The acetate **15** was prepared by dissolution of **13** (52 mg, 0.14 mmol) in pyridine (2 mL), addition of acetic anhydride (1 mL), and stirring for 7 days. Evaporation to dryness followed by flash chromatography (silica, eluting with EtOAc) afforded **15** as a glass which crystallized from EtOH (41 mg, 71%), mp 187–189°C; ir ($CHCl_3$) ν_{max}: 1750 and 1645 cm^{-1}; ^1H nmr δ: 2.09 (3H, s, —$OCOCH_3$), 3.04 (3H, s, —NCH_3), 3.69 (3H, s, —OCH_3), 3.83 (3H, s, —OCH_3), 3.88 (3H, s, —OCH_3), 3.97 (3H, s, —OCH_3), 4.87 (1H, d, J = 6 Hz, C-3 H), 6.31 (1H, d, J = 6 Hz, C-4 H), 6.45–6.85 (4H, m, C-5 H and aromatic protons of C-3 phenyl substituent), 7.72 (1H, s, C-8 H); ms, *m/z* (%): 415 (12) M^+, 355 (46), 194 (100). *Anal.* calcd. for $C_{22}H_{25}NO_7$: C 63.61, H 6.02, N 3.37%; found: C 63.69, H 6.10, N 3.27%. (*ii*) *trans* Isomer **14** (55 mg, 9.8%), mp 201–203°C (EtOH); R_f 0.15 (silica, EtOAc); ir ($CHCl_3$ ν_{max}: 1635 cm^{-1}; ^1H nmr δ: 3.0 (3H, s, —NCH_3), 3.73 (3H, s, —OCH_3), 3.80 (3H, s, —OCH_3), 3.87 (6H, s, 2 × OCH_3), 4.60 (1H, broad s (on addition of D_2O sharpens to a doublet, J = 2 Hz), C-3 H), 4.80 (1H, broad s (on addition of D_2O sharpens to a doublet, J = 2 Hz), C-4 H), 6.45–6.85 (4H, m, C-5 H and protons of the 3-phenyl substituent), 7.42 (1H, s, C-8 H); ms, *m/z* (%): 373 (18.5) M^+, 194 (8.5), 180 (100). *Anal.* calcd. for $C_{20}H_{23}NO_6$: C 64.34, H 6.17, N 3.75%; found: C 64.59, H 6.26, N 3.64%.

(b) *With $ZnCl_2$*

The anion of *m*-meconin was generated in the normal manner, and added to anhydrous $ZnCl_2$ (2 equiv.). The mixture was warmed to −10°C and stirred until homogeneity was achieved. After cooling to −40°C, the imine was added as previously. Subsequent work-up and chromatography gave the *cis* isomer **13** in 35% yield and the *trans* isomer **14** in 16% yield.

cis- *And* trans-*3-(3,4-dimethoxyphenyl)-4-hydroxy-2-methyl-3,4-dihydro-1(2H)-isoquinolones **16** and **17***

The anion of phthalide (0.536, 4 mmol) was generated, treated with $ZnCl_2$ (2 equiv.), and the imine (0.716 g, 4 mmol) added, all by the procedure previously described. Work-up and flash chromatography (silica, eluting with $CHCl_3$ + 1.5% MeOH) gave the following two components: (*i*) *cis* isomer **16** (490 mg, 39.1%), mp 132–133°C (EtOH–Et_2O); R_f 0.33 (silica, EtOAc); ir ($CHCl_3$) ν_{max}: 1640 cm^{-1}; ^1H nmr δ: 3.08 (3H, s, —NCH_3), 3.57 (3H, s, —OCH_3), 3.75 (3H, s, —OCH_3), 4.66 (1H, d, J = 6.0 Hz, C-3 H), 5.47 (1H, broad s (on addition of D_2O sharpens to a doublet, J = 6.0 Hz), C-4 H), 6.4–6.75 (3H, m, protons of the 3-phenyl substituent), 7.3–7.6 (3H, m, C-5, C-6, and C-7 H's), 8.0–8.2 (1H, m, C-8 H); ms, *m/z* (%): 313 (43) M^+, 180 (100), 134 (42). *Anal.* calcd. for $C_{18}H_{19}NO_4$: C 69.01, H 6.07, N 4.47%; found: C 68.81, H 5.84, N 4.67%. (*ii*) *trans* Isomer **17** (230 mg, 18.4%), mp 145–146°C (EtOAc – pet. ether, 80–100°C); R_f 0.25 (silica, EtOAc); ir ($CHCl_3$) ν_{max}: 1640 cm^{-1}; ^1H nmr (250 MHz) δ: 2.94 (3H, s, —NCH_3), 3.67 (3H, s, —OCH_3), 3.78 (3H, s, —OCH_3), 4.41 (1H, broad s (on addition of D_2O sharpens to a doublet, J = 1.7 Hz), C-3 H), 4.67 (1H, broad s (on addition of D_2O sharpens to a doublet, J = 1.7 Hz), C-4 H), 6.45–6.52 (2H, m, C-2 and C-6 H's of the 3-phenyl substituent), 6.67 (1H, d, J = 8.1 Hz, C-5 of the 3-phenyl substituent), 7.2–7.45 (3H, m, C-5, C-6, and C-7 H's), 7.97 (1H, m, C-8 H); ms, *m/z* (%): 313 (27) M^+, 180 (100), 134 (13). *Anal.* calcd. for $C_{18}H_{19}NO_4$: C 69.01, H 6.07, N 4.47%; found: C 68.92, H 6.12, N 4.51%.

(R,R*)- And (R*,S*)-3-(3,4-dimethoxyphenyl)-4-hydroxy-4-phenyl-2-methyl-3,4-dihydro-1(2H)-isoquinolones **18** and **19***

The blood-red anion of 3-phenylphthalide (0.525 g, 2.5 mmol), generated using LDA, was added to anhydrous $ZnCl_2$ (2 equiv.), and treated with 3,4-dimethoxybenzylidenemethylamine (0.448 g, 2.5 mmol), all in the normal manner. Subsequent work-up and flash chromatography (silica, eluting with $CHCl_3$) gave the following two components: (*i*) (*3R*, 4R**) isomer **18** (555 mg, 57.1%), mp 167–169°C (EtOH); R_f 0.45 (silica, EtOAc); ir ($CHCl_3$) ν_{max}: 1645 cm^{-1}; ^1H nmr (80 MHz) δ: 2.87 (3H, s, —NCH_3), 3.62 (3H, s, —OCH_3), 3.82 (3H, s, —OCH_3), 4.64 (1H, s, C-3 H), 6.53 (1H, broad s, C-2 H of 3-phenyl substituent), 6.76 (2H, broad s, C-5 and C-6 H's of 3-phenyl substituent), 7.30 (5 H, s, C-4 phenyl group), 7.1–7.75 (3H, m, C-5, C-6, and C-7 H's), 8.1–8.4 (1H, m, C-8 H); ms, *m/z* (%): 389 (3) M^+, 210 (21) 180 (100). *Anal.* calcd. for $C_{24}H_{23}NO_4$: C 74.04, H 5.91, N 3.60%; found: C 73.81, H 6.01, N 3.55%. (*ii*) (*3S*,4R**)-Isomer **19** (85 mg, 8.7%), mp 210–212°C (EtOH – pet. ether 80–100°C); R_f 0.42 (silica, EtOAc); ir ($CHCl_3$ ν_{max}: 1635 cm^{-1}; ^1H nmr (250 MHz) δ: 3.01 (3H, s, —NCH_3), 3.36 (3H, s, —OCH_3), 3.74 (3H, s, —OCH_3), 4.53 (1H, s, C-3 H), 5.6–5.95 (1H, broad hump, aromatic), 6.05–6.4 (1H, broad hump, aromatic), 6.50 (1H, d, J = 8.3 Hz, aromatic), 7.05–7.3 (5 H, m, aromatic), 7.35–7.45 (3H, m, aromatic), 8.15–8.25 (1H, m, C-8 H); ms, *m/z* (%): 389 (3) M^+, 210 (20), 180 (100). *Anal.* calcd. for $C_{24}H_{23}NO_4$: C 74.04, H 5.91, N 3.60%; found: C 73.87, H 5.90, N 3.59%.

Acknowledgements

We thank the Natural Sciences and Engineering Research Council of Canada for financial support of this work. We also thank B. Sayer and I. Thompson for recording many of the nmr spectra and F. Ramelan for the mass spectra.

1. D. J. DODSWORTH, M. P. CALCAGNO, E. U. EHRMANN, and P. G. SAMMES. Tetrahedron Lett. **21**, 5075 (1980).
2. D. J. DODSWORTH, M. P. CALCAGNO, E. U. EHRMANN, A. M. QUESEDA, O. NUNEZ S., and P. G. SAMMES. J. Chem. Soc. Perkin Trans. 1, 1453 (1983).
3. R. MARSDEN and D. B. MACLEAN. Tetrahedron Lett. **24**, 2063 (1983).
4. M. CUSHMAN, J. GENTRY, and F. W. DEKOW. J. Org. Chem. **42**, 1111 (1977).
5. M. SHAMMA and V. ST. GEORGIEV. Tetrahedron, **32**, 211 (1976).
6. T. KAMETANI, H. MATSUMOTO, Y. SATOH, H. NEMOTO, and K. FUKUMOTO. J. Chem. Soc. Perkin Trans. 1, 376 (1977).
7. I. W. ELLIOT, JR. J. Heterocycl. Chem. **4**, 639 (1967).
8. M. HANAOKA, C. MUKAI, and Y. ARATA. Heterocycles, **6**, 895 (1977).
9. Y. KONDO, H. INOUE, and J. IMAI. Heterocycles, **6**, 953 (1977).
10. K. IWASA, M. SUGIURA, and N. TAKAO. J. Org. Chem. **47**, 4275 (1982).
11. P. W. JEFFS. *In* The alkaloids. Vol. 9. *Edited by* R. H. F. Manske. Academic Press, New York. 1967. p. 41.
12. P. W. JEFFS and J. D. SCHARVER. J. Org. Chem. **40**, 644 (1975).
13. A. R. BATTERSBY and H. SPENCER. J. Chem. Soc. 1087 (1965).
14. M. SHAMMA. The isoquinoline alkaloids. Academic Press, New York. 1972. Chapt. 16.
15. M. SHAMMA and J. L. MONIOT. Isoquinoline alkaloids research: 1972–1977. Plenum Press, New York. 1978. Chapt. 19.
16. T. KAMETANI, M. IHARA, and T. HONDA. Heterocycles, **4**, 483 (1976).
17. N. F. BRAY, R. L. BAUMGARTEN, and E. EDELSON. J. Chem. Eng. Data, **22**, 359 (1977).
18. T. V. HUNG, B. A. MOONEY, R. H. PRAGER, and J. M. TIPPETT. Aust. J. Chem. **34**, 383 (1981).
19. C. K. YU, D. B. MACLEAN, R. G. A. RODRIGO, and R. H. F. MANSKE. Can. J. Chem. **48**, 3673 (1970).
20. I. NINOMIYA, T. NAITO, and H. TAKASUGI. J. Chem. Soc. Perkin Trans. I, 1791 (1975).
21. H. TAGUCHI and I. IMASEKI. Yakugaku Zasshi, **84**, 955 (1964); Chem. Abstr. **62**, 4067 (1965).
22. G. W. BUCHANAN and B. A. DAWSON. Org. Magn. Reson. **13**, 293 (1980).
23. D. PITEA, G. FAVINI, and G. CAPIETTI. J. Chem. Soc. Perkin Trans. 2, 2038 (1977).
24. W. C. STILL, M. KAHN, and A. MITRA. J. Org. Chem. **43**, 2923 (1978).
25. G. A. EDWARDS, W. H. PERKIN, JR., and F. W. STOYLE. J. Chem. Soc. **127**, 195 (1925).
26. F. ULLMAN. Ann. **291**, 23 (1896).

27. W. M. WHALLEY and M. MEADOW. J. Chem. Soc. 1067 (1953).
28. W. J. GENSLER and C. M. SAMOUR. J. Am. Chem. Soc. **73**, 5555 (1951).
29. B. NALLIAH. Ph.D. Thesis, University of Waterloo, Waterloo, Ont. May 1974.
30. M. ERNE and F. RAMIREZ. Helv. Chim. Acta, **33**, 912 (1950).
31. C. E. SLEMON, L. C. HELLWIG, J.-P. RUDER, E. W. HOSKINS, and D. B. MACLEAN. Can. J. Chem. **59**, 3055 (1981).
32. R. B. MOFFETT. *In* Organic Syntheses Coll. Vol. IV. *Edited by* N. Rabjohn. John Wiley and Sons, New York. 1963. p. 605.

Can. J. Chem. Downloaded from www.nrcresearchpress.com by 210.87.254.105 on 09/06/12
For personal use only.

COMMUNICATIONS

Synthetic approaches to β-lactam antibiotics: a stereocontrolled synthesis of *trans* 3-(*S*)-amino-4-(*S*)-ethyl-2-oxo-1-azetidine[1]

STEPHEN HANESSIAN AND SOUMYA P. SAHOO
Department of Chemistry, Université de Montréal, Montréal, P.Q., Canada H3C 3V1

Received January 30, 1984

STEPHEN HANESSIAN and SOUMYA P. SAHOO. Can. J. Chem. **62**, 1400 (1984).

A synthesis of the title compound, an immediate precursor of the biologically active 4-ethyl monobactam, from 2-amino-2-deoxy-D-glucose is described. The strategy allows for the synthesis of a variety of β-substituted α-amino acids, which are otherwise difficultly accessible.

STEPHEN HANESSIAN et SOUMYA P. SAHOO. Can. J. Chem. **62**, 1400 (1984).

La synthèse d'un précurseur de l'antibiotique 4-ethyl monobactame, à partir du 2-amino-2-deoxy-D-glucose est décrite. La stratégie suivie permet la synthèse d'un nombre d'acide α-aminés contenant un substituant sur la position β, et qui sont difficilement accessibles par d'autres voies.

Can. J. Chem. Downloaded from www.nrcresearchpress.com by 210.87.254.5 on 09/06/12
For personal use only.

Since the discovery of the monobactams, a family of monocyclic β-lactam antibiotics produced by various gram-negative bacteria (1), extensive studies have been devoted to the synthesis of the parent structure **1** (2) as well as its analogs (3). These intense efforts have been rewarded by the emergence of aztreonam, a *trans* 3-(*S*)-amino-4-(*S*)-methyl-2-oxo-1-azetidinesulfonic acid substituted with a heterocyclic moiety at N-3, as a clinical candidate. Related structures with a *cis*-substitution pattern are also known (4). A noteworthy feature

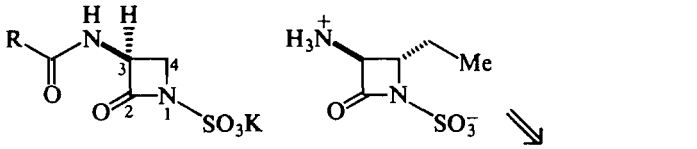

1 **2**

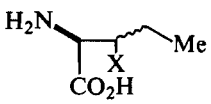

3, X = OH
4, X = NH_2

of the 4-substituted monobactams is their higher intrinsic antibacterial activity and resistance to β-lactamases as manifested, for example, by the N-acyl derivative of a racemic structure corresponding to expression **2** (3). Since the structures of the naturally-occurring monobactams do not lend themselves to chemical modification at the C-4 position, recourse has been made to totally synthetic and semi-synthetic routes in order to probe into aspects of structure–activity relationships (3, 5). As with any synthetic program with a biological objective, the quest for enantiomerically pure targets becomes a matter of concern.

Compared to the structurally more impressive bicyclic β-lactam antibiotics, the synthesis of the monobactams as exemplified by the optically pure title compound may appear to present a trivial exercise (for some recent syntheses of 4-substituted azetidinones, see for example ref. 6). Indeed, a simple retrosynthetic analysis of the target reveals logical progeny from a 2-amino-3 hydroxy pentanoic acid (L-ethylserine) **3**, or a 2,3-diaminopentanoic acid **4** as potential chirons (7). These, however, are not readily available amino acids in optically pure form, hence the reason why the title compound was prepared and tested as a racemic mixture (3, 5). The prospects of azetidinone formation in the β-hydroxy-α-amino acid series must be dealt with with some caution because of the propensity for elimination, racemization, and intramolecular reactions (see for example, ref. 8). We have recently found an expedient solution to this problem in the facile 3-step transformation of N-[(benzyloxy)carbonyl]-L-serine *p*-methoxyphenylamide into 3-(*S*)-1-amino-2-oxo-1-azetidine, the parent monobactam structure corresponding to **1** (9).

In this paper, we describe a general synthetic protocol for the stereocontrolled access to optically active 2-amino-3-hydroxy acids with a specific application to the total synthesis of the title monobactam precursor **2**. The strategy utilizes 2-amino-2-deoxy-D-glucose as a chiral template in which, quite fortuitously, the sense of chirality of the amine-bearing carbon atom is convergent with C-3 in the target. Stereocontrolled attack by an ethyl Grignard on the aldehyde function of **6** which is readily available from **5** (10) was expected to occur in an anticipated sense to give a high preponderance of the desired material (Scheme 1). Adjustment of functionality and manipulation of expendable appendages would thus lead to the intended target. These chemical events were experimentally realized.

Acetonation of **5** gave the crystalline diacetonide derivative (98%), mp 54–56°C; $[\alpha]_D$ − 28.2° ($CHCl_3$). Conversion to the aldehyde **6** followed by treatment with methylmagnesium chloride led to a nearly quantitative yield of a 4:1 mixture of isomers **7** and **8** which were readily separated by preparative hplc.[2,3] Hydrolysis of the acetal functions in the major isomer **7** (syrup, $[\alpha]_D$ 0 ± 1° ($CHCl_3$), MH^+ 410), followed by oxidative cleavage (11) gave N-Cbz L-threonine **11**, characterized as the crystalline *p*-methoxybenzamide derivative **12**, mp 165–167°C; $[\alpha]_D$ −63.2° ($CHCl_3$), identical with an authentic sample. Thus, nucleophilic attack on the aldehyde took place

[1] Reported in part at the Symposium on Stereocontrolled Elaboration of Organic Molecules, San Miniato, Italy, Sept. 12–16, 1983.

[2] Waters Prep. 500 chromatograph using 20% ethyl acetate in hexanes as eluent.

[3] New compounds reported in this paper were adequately characterized by spectroscopic (nmr, 90, 400 MHz; mass) and analytical data.

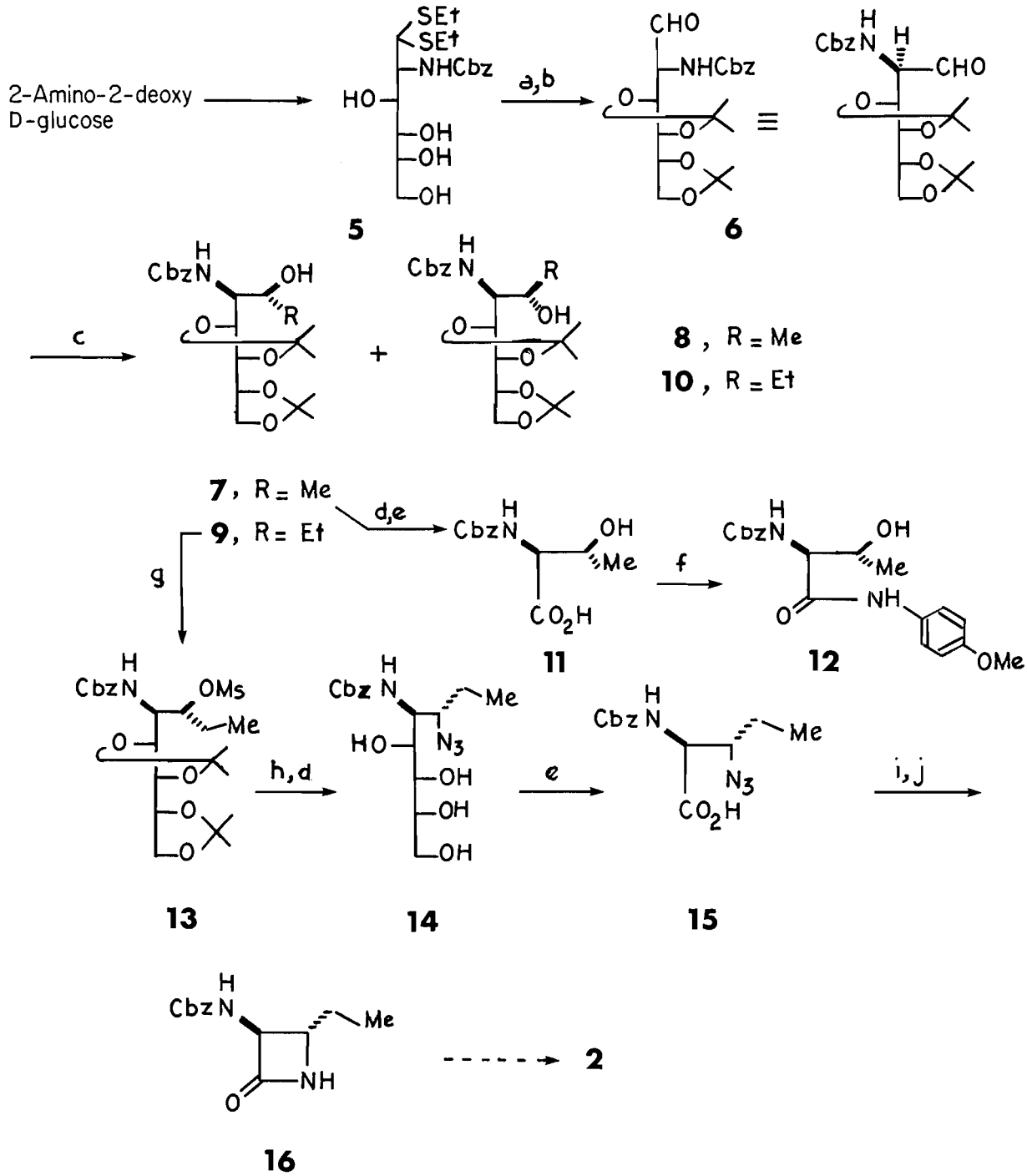

SCHEME 1. Abbreviations: a. acetone, camphorsulfonic acid, dimethoxypropane, 3 h (98%); b. aq. acetone, $HgCl_2$, HgO, 2 h, 83%; c. MeMgCl or EtMgBr, THF, 0°C, then r.t., 3–4 h, ~quant.; d. 80% aq. AcOH, 60°C, 18 h, ~quant.; e. $NaIO_4$–$KMnO_4$, aq. acetone, 18 h, (60%); f. *p*-anisidine, ethyl(diethylaminopropyl) carbodiimide hydrochloride, 2–3 h; g. MsCl, Et_3N, CH_2Cl_2, 0°C, then r.t., ~quant.; h. $n\text{-}Bu_4NN_3$, toluene, 80°C, 18 h, 80%; i. Ra-Ni, MeOH, 15 min; j. Ph_3P, dipyridyldisulfide (1.1 equiv. each, MeCN, reflux 18 h, 1 mmol of amine/180 mL solvent); 50% (2 steps).

in the anticipated manner, and it was expected that bulkier Grignard reagents would increase the stereoselectivity even more. Thus, treatment of **6** with ethylmagnesium bromide gave a 9:1 mixture of isomers **9** and **10**, in almost quantitative yield, which were easily separated by flash column chromatography. The major component **9**, $[\alpha]_D$ +9.2° ($CHCl_3$), MH^+ 424, was mesylated to **13** (syrup, ~quant.) and the potential amino group was introduced by an inversion process to give the azide **14** as a syrup (80%); $[\alpha]_D$ +2° ($CHCl_3$). Oxidative cleavage then gave the β-azido acid **15** (syrup, 60%)[4] which was reduced and subjected to a variety of ring closure procedures.[5] We

[4] The corresponding methyl ester showed $[\alpha]_D$ +22.2° ($CHCl_3$); MH^+ 307.

[5] A variety of methods, including various carbodiimide-related cyclizations, led to decomposition or unidentified products. Methods for azetidinone formation of 3,4-disubstituted systems, from the corresponding β-amino acids, are not widely known, see ref. 9.

Can. J. Chem. Downloaded from www.nrcresearchpress.com by 210.87.254.5 on 09/06/12
For personal use only.

found a minor modification of the Ohno method (12) to be the most effective, particularly at higher dilutions than originally reported. With this proviso, it was possible to obtain the target β-lactam **16** in 50% yield (2 steps), $[\alpha]_D$ −34.3° (MeOH); ir ($CHCl_3$): 1770 cm^{-1} (β-lactam); 1750 cm^{-1} (Cbz); ^1H nmr (400 MHz, $CDCl_3$), ppm: 4.37, H-3 (dd, $J_{3,4}$ = 1.8 Hz; $J_{3,NH}$ = 8.25 Hz); 3.5, H-4 (ddd, $J_{4,3}$ = 1.8 Hz, $J_{4,4''}$ = 6.5 Hz, $J_{4,4''}$ = 6.7 Hz); etc; MH^+ 249. Compound **16** (racemic form) has been previously transformed into the corresponding N-sulfonic acid and the latter further elaborated into biologically active N-acyl derivatives (3, 5).

The presently described route to optically active β-hydroxy amino acids can nicely converge with the Squibb process (2, 5) or related ones (8) which rely on a Mitsunobu reaction (13) in the β-lactam ring-forming step. Our methodology also provides access to rare amino acids. For example, reaction of **6** with phenylmagnesium bromide gave the corresponding carbinol as the preponderant, if not exclusive, product having the expected stereochemistry. Oxidative degradation would lead to 2-(*R*)-amino-3-(*R*)-hydroxyphenyl propionic acid (phenylserine) which is commercially available in racemic form (for some recent reviews on the asymmetric synthesis of amino acids, see ref. 14).

Finally, it should be noted that even though the C-4—C-6 segment of the original amino sugar is sacrificed en route to the target β-lactam, its inherent functional and stereochemical features have served their intended useful purpose, firstly, to provide the chiral framework that secured the high degree of stereoselection in the Grignard reaction and, secondly, to act as a latent carboxyl group of the target amino acid. In view of the very low cost of this amino sugar and the obvious advantages of the strategy, the planned "burning off" of essentially half the original molecule may be tolerable.

Acknowledgments

We wish to acknowledge generous financial support from NSERCC and Le Ministère de l'éducation du Québec, as well as from Sandoz (Vienna). We also thank Dr. P. M. Tan for high resolution nmr spectra and Mr. M. Evans for mass spectra.

1. R. B. SYKES, C. M. CIMARUSTI, D. P. BONNER, K. BUSH, D. M. FLOYD, N. H. GEOROGOPAPADAKOU, W. KOSTER, W. C. LIU, W. L. PARKER, P. A. PRINCIPE, M. L. RATHUM, W. A. SLUSARCHYK, W. H. TREJO, and J. S. WELL. Nature, **291**, 489 (1981); A. IMADA, K. KITANO, K. KINTAKA, M. MUROI, and M. ASAI. Nature, **289**, 590 (1981); see also C. M. CIMARUSTI and R. B. SYKES. Chem. Br. 302 (1983).
2. W. L. PARKER, W. H. KOSTER, C. M. CIMARUSTI, D. M. FLOYD, W. LIU, and M. L. RATHUM. J. Antibiot. **35**, 189 (1982); W. L. PARKER and M. L. RATHUM. J. Antibiot. **35**, 300 (1982); C. M. CIMARUSTI, H. E. APPLEGATE, H. W. CHANG, D. M. FLOYD, W. H. KOSTER, W. A. SLUSARCHYK, and M. G. YOUNG. J. Org. Chem. **47**, 179 (1982); D. M. FLOYD, A. W. FRITZ, and C. M. CIMARUSTI. J. Org. Chem. **47**, 176 (1982).
3. C. M. CIMARUSTI, D. P. BONNER, H. BREVER, H. W. CHANG, A. W. FRITZ, D. M. FLOYD, T. P. KISSICK, W. H. ROSTER, D. KRONENTHAL, F. MASSA, R. H. MUELLER, J. PLUSCEC, W. A. SLUSARCHYK, R. B. SYKES, M. TAYLOR, and E. R. WEAVER. Tetrahedron, **39**, 2577 (1983).
4. S. KISHIMOTO, M. SENDAI, S. HASHIGUCHI, M. TOMIMOTO, Y. SATOH, T. MATSUO, M. KONDO, and M. OCHIAI. J. Antibiot. **36**, 1421 (1983); C. C. WEI, J. TENGI, and M. WEIGELE. 25th Interscience Conference on Antimicrobial Agents and Chemotherapy, Las Vegas, Nevada, Oct. 24, 1983, Abstract 324.
5. R. B. SYKES, W. L. PARKER, C. M. CIMARUSTI, W. H. KOSTER, W. A. SLUSARCHYK, A. W. FRITZ, and D. M. FLOYD. U.K. Patent No. 2,071,650. 1981.
6. G. GEORG and T. DURST. J. Org. Chem. **48**, 2092 (1983); H. MATSUNAGA, T. SAKAMAK, H. NAGAOKA, and Y. YAMADA. Tetrahedron Lett. **24**, 3009 (1983); A. J. BILOSKI, R. D. WOOD, and B. G. GANEM. J. Am. Chem. Soc. **104**, 3233 (1982); and references cited therein, see also ref. 3.
7. S. HANESSIAN. *In* The total synthesis of natural products: the 'chiron' approach. *Edited by* J. E. Baldwin. Pergamon Press, Oxford, England. 1983.
8. M. J. MILLER, P. G. MATTINGIY, M. A. MORRISON, and J. F. KERWIN, JR. J. Am. Chem. Soc. **102**, 7026 (1980); A. K. BOSE, D. P. SAHU, and M. S. MANHAS. J. Org. Chem. **46**, 1229 (1981); C. A. TOWNSEND and L. T. NGUYEN. J. Am. Chem. Soc. **103**, 4582 (1981).
9. S. HANESSIAN, C. COUTURE, and H. WYSS. To be published.
10. M. W. WHITEHOUSE, P. W. KENT, and C. A. PASTERNAK. J. Chem. Soc. 2315 (1954).
11. R. U. LEMIEUX and E. VON RUDOLFF. Can. J. Chem. **33**, 1701 (1955); **33**, 1710 (1955).
12. S. KOBAYASHI, T. IIMORI, T. IZAWA, and M. OHNO. J. Am. Chem. Soc. **103**, 2406 (1981).
13. M. WADA and O. MITSUNOBU. Tetrahedron Lett. 1279 (1972); O. MITSUNOBU. Synthesis, 1 (1981).
14. K. WEINGES and B. STEMMLE. Recent. Dev. Chem. Nat. Carbon Compd. **7**, 89 (1976); K. DRAUZ, A. KLEEMAN, and J. MARTENS. Angew. Chem. Int. Ed. Engl. **21**, 584 (1982); J. W. APSIMON and R. P. SEGUIN. Tetrahedron, **35**, 2797 (1979); I. WAGNER and H. MUSSO. Angew. Chem. Int. Ed. Engl. **22**, 816 (1983).

Can. J. Chem. Downloaded from www.nrcresearchpress.com by 210.87.254.5 on 09/06/12
For personal use only.

A stereoselective synthesis of digitoxin. On cardioactive steroids. XIII[1]

THOMAS Y. R. TSAI, HAOLUN JIN, AND KAREL WIESNER[2]

Natural Products Research Centre, University of New Brunswick, Fredericton, N. B., Canada E3B 6E2

Received February 15, 1984

THOMAS Y. R. TSAI, HAOLUN JIN, and KAREL WIESNER. Can. J. Chem. **62**, 1403 (1984).

The first highly stereoselective synthesis of digitoxin is described. The furyl derivative of digitoxigenin was coupled with one unit of digitoxose using our previously described acid catalyzed method. For the second and third glycosylation a new method involving ethyl thioglycosides and 1,3-participation by a *p*-methoxy benzoate group was developed. As the final step after deprotection of the triglycoside, the 17-furyl group in the steroid aglycone was converted to a butenolide by our oxidative method.

THOMAS Y. R. TSAI, HAOLUN JIN et KAREL WIESNER. Can. J. Chem. **62**, 1403 (1984).

On décrit la première synthèse très stéréosélective de la digitoxine. On a couplé le dérivé furyle de la digitoxigénine avec une unité de digitoxose en faisant appel à la méthode acido-catalysée que nous avons décrite antérieurement. Afin de réaliser les deuxième et troisième glycosylations, on a développé une nouvelle méthode impliquant les thioglycosides d'éthyle et une participation-1,3 d'un groupement *p*-méthoxy benzoate. Dans la dernière étape, qui suit la déprotection du triglycoside, on utilise notre méthode oxydative pour transformer, en buténolide, le groupement furyle en position 17 de l'aglycone stéroidique.

[Traduit par le journal]

Can. J. Chem. Downloaded from www.nrcresearchpress.com by 210.87.254.105 on 09/06/12
For personal use only.

Digitoxin (**16**), first in the form of crude Digitalis extracts, later as a pure crystalline glycoside, has been used in medicine for 200 years. Even today, in spite of the deadly toxicity of natural Digitalis glycosides, these compounds belong among the ten most prescribed drugs. Our interest in the total synthesis of digitoxin started when it became desirable to attach the natural digitoxin glycosidic side chain to our totally synthetic relatively nontoxic cardenolide and bufadienolide analogues in order to prolong their duration of action and modify some other of their pharmacologic parameters.

The reaon why digitoxin, in spite of its importance, resisted previous attempts at total synthesis was the nonexistence of a highly stereoselective β-glycosylation method for 2-deoxy sugars in general and digitoxose in particular. We have partly remedied this situation in a previous communication of this series (2) in which we have shown that a 1,3-participation of a urethane group can control the stereochemistry of the acid catalyzed glycosylation of a digitoxose derivative.[3]

The starting material for the present synthesis was the protected glycoside **6** (mp 151−153°C; $[\alpha]_D$ −7.68; ^{1}Hmr ($CDCl_3$) δ: 8.03, 6.98 (d, J = 10 Hz, 2H each, 4 aromatic H), 7.34, 7.23, 6.49 (br s, 1H each, furan), 5.56 (br s, 1H, 3′-H), 4.93 (d, J = 10 Hz, 1H, 1′-H), 4.08 (br s, 1H, 3-H), 3.90 (s, 3H, —OCH_3), 1.35 (d, J = 6 Hz, 3H, 6′-CH_3), 0.92 (s, 3H, 19-CH_3), 0.71 (s, 3H, 18-CH_3)) which we have prepared by the previously described stereoselective method (2) followed by a simple modification of the protecting groups as portrayed in the formulae **1**−**6**.

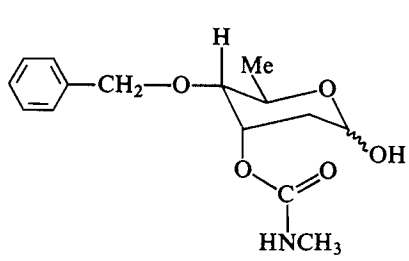

1

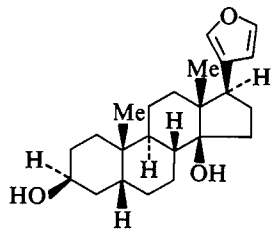

2

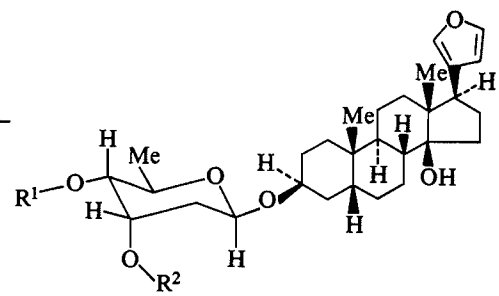

3 R^1 = Bzl, R^2 = $CONHCH_3$

4 R^1 = Bzl, R^2 = H, mp = 166.5−168°C; $[\alpha]_D$ = +6.22

5 R^1 = Bzl, R^2 = —CO— 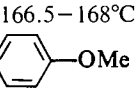 —OMe

6 R^1 = H, R^2 = —CO— 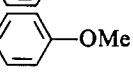 —OMe

3 → **4** $LiAlH_4$/THF reflux; **4** → **5** *p*-methoxybenzoyl chloride/pyridine; **5** → **6** Pd/C, H_2

[1]For Part XII, see ref. 1.

[2]Author to whom correspondence should be addressed.

[3]In ref. 2 we have neglected to quote the preparation of digitoxigenin β-digitoxoside in a yield of 35%, β/α stereoselectivity 1.4:1 (cf. ref. 3). We thank the authors for drawing our attention to their paper.

Can. J. Chem. Downloaded from www.nrcresearchpress.com by 210.87.254.105 on 09/06/12
For personal use only.

It soon became clear that it is not possible to continue the synthesis by the same method. With glycosidic bonds present, both in starting material and product, cleavage predominated over glycosylation and the higher glycosides were obtained only in traces. In order to deal with the second and third stage of the synthesis, we have prepared by simple acid catalyzed glycosylation (anhydrous CH_2Cl_2 *p*-toluenesulfonic acid) the ethyl α-thioglycosides **7** and **8** and the corresponding β-glycosides (4(*a*)).[4] Treatment of **6** in CH_2Cl_2 at 20°C for 40 h with 4 mol of the α-thioglycoside **7**, 4 mol of $HgCl_2$, and

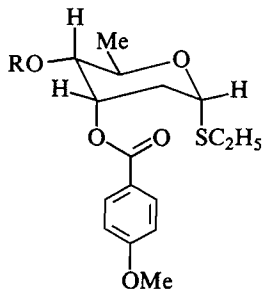

7 R = O_2N—C(=O)—, mp = 94–95°C; $[\alpha]_D$ = +214.12

8 R = MeO—C(=O)—, mp = 104–105°C; $[\alpha]_D$ = +266.51

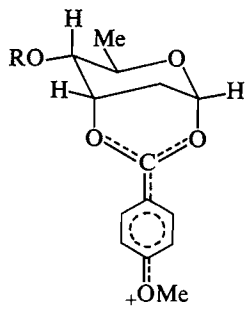

9

an excess of $CdCO_3$ yielded the oily product **10** besides starting material. Compound **10** was obtained in a yield of 60% on the basis of starting material not recovered (^{1}Hmr ($CDCl_3$) δ: 8.19, 8.03, 7.96, 6.99 (m, 12H in all, 12 aromatic H), 7.34, 7.22, 6.48 (br s, 1H each, furan), 5.76, 5.68 (br s, 1H each, 3′- and 3″-H), 5.06 (d, J = 10 Hz, 1H, 1″-H), 4.86 (m, $W_{1/2}$ = 20 Hz, 2H, 1′- and 4″-H), 4.05 (br s, 1H, 3-H), 3.92, 3.90 (s, 3H each, OCH_3 × 2), 3.52 (dd, J = 4, 10 Hz, 1H, 4′-H), 1.35, 1.16 (d, J = 6 Hz, 3H each, 6′- and 6″-CH_3), 0.91 (s, 3H, 19-CH_3), 0.70 (s, 3H, 18-CH_3)). A trace of a product containing an α-glycosidic linkage was found in some runs and separated. The use of the corresponding β-thioglycoside gave the identical result. For this reason the more easily available α-glycosides **7** and **8** were employed throughout the synthesis. We believe that the species **9** plays a part in the glycosylation reaction. In none of the systems tried have we observed a displacement of the thioglycosidic bond without participation and with inversion of configuration as described by Ferrier *et al.* (5). Ammonolysis of **10** in methanol yielded 90% of an equilibrium mixture of **11** and **12** in a ratio 3.5:1. Compound

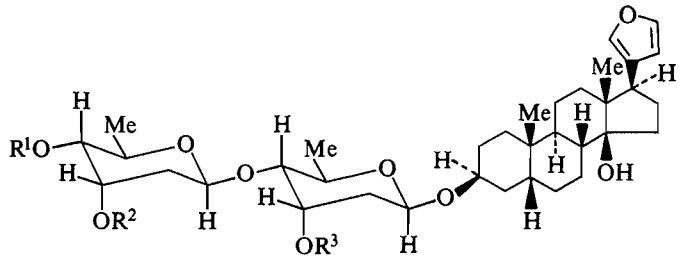

10 R^1 = O_2N—C(=O)—, R^2 = R^3 = MeO—C(=O)—

11 R^1 = H, R^2 = R^3 = MeO—C(=O)—

12 R^2 = H, R^1 = R^3 = MeO—C(=O)—

13 R^1 = R^2 = R^3 = H

12 could be reequilibrated to yield the same product in the identical ratio. Both products **11** and **12** remained oily. (**11**: ^{1}Hmr ($CDCl_3$) δ: 8.03, 6.98 (m, 4H each, aromatic H), 5.64, 5.45 (br s, 1H each, 3′- and 3″-H), 4.88 (m, $W_{1/2}$ = 20 Hz, 2H, 1′- and 1″-H), 4.03 (br s, 1H, 3-H), 3.90, 3.89 (s, 3H each, OCH_3 × 2), 3.47 (m, 2H, 4′- and 4″-H); **12**: ^{1}Hmr ($CDCl_3$) δ: 8.02, 6.96 (m, 4H each, aromatic H), 5.63 (br s, 1H, 3′-H), 5.00, 4.85 (d, J = 10 Hz, 1H each, 1′- and 1″-H), 4.68 (dd, J = 4, 10 Hz, 1H, 4″-H), 4.29 (br s, 1H, 3″-H), 3.89, 3.87 (s, 3H each, OCH_3 × 2), 3.47 (dd, J = 4, 10 Hz, 1H, 4′-H).) Reduction of compound **11** with $LiAlH_4$ yielded **13** ($[\alpha]_D$ +4.15; mp 185–187°C; ^{1}Hmr ($CDCl_3$) δ: 7.33, 7.23, 6.49 (br s, 1H each, furan), 4.91 (m, $W_{1/2}$ = 20 Hz, 2H, 1′- and 1″-H), 4.27, 4.15, 4.05 (br s, 1H each, 3-, 3′-, and 3″-H), 3.28 (m, $W_{1/2}$ = 20 Hz, 2H, 4′- and 4″-H), 1.29, 1.23 (d, J = 6 Hz, 3H each, 6′- and 6″-CH_3), 0.91 (s, 3H, 19-CH_3), 0.69 (s, 3H, 18-CH_3)) identical with a product obtained by partial hydrolysis (two-phase system *p*-toluenesulfonic acid in H_2O/CH_2Cl_2) of the naturally derived compound **15** (2).

Coupling of the protected glycoside **11** with the thioglycoside **8** under identical conditions as in the step **6** → **10** yielded 58% of the protected glycoside **14** identical with the same derivative obtained by treatment of naturally derived **15** (2) with *p*-methoxybenzoylchloride and pyridine ($[\alpha]_D$ +112.92; mp 159–161°C; ^{1}Hmr ($CDCl_3$) **20** δ: 8.05, 7.98, 7.80, 6.98, 6.81 (m, 16H in all, aromatic H), 7.33, 7.22, 6.48 (br s, 1H each, furan), 5.67, 5.59 (br s, 2H and 1H, 3′-, 3″-, and 3‴-H), 4.96, 4.82 (d, J = 10 Hz, and m, $W_{1/2}$ = 20 Hz, 4H in all, 1′-, 1″-, 1‴-, and 4‴-H), 3.90, 3.89, 3.81 (s, 12H in all, OCH_3 × 4), 3.41 (m, 2H, 4′- and 4″-H), 1.26, 1.21, 1.14 (d, J = 6 Hz, 3H each, 6′-, 6″-, and 6‴-CH_3), 0.90 (s, 3H, 19-CH_3), 0.70 (s, 3H, 18-CH_3)). No product containing an α-glycosidic linkage was found. Finally, $LiAlH_4$ reduction of **14** gave 87% of compound **15**, identical by mixture mp and all spectral and chromatographic criteria with the same material described in our previous communication (2). The oxidative conversion of the furyl derivative **15** to either digitoxin (**16**) or isodigitoxin (**17**)[5] can be found in the same publication (2).

It remains to be mentioned that (for reasons which we shall discuss in a full publication) the thioglycoside method is only mildly stereoselective when used in the first step of the syn-

[4]For the preparation of ethyl thioglycosides by glycosylation with a Lewis acid, see ref. 4 (*b*).

[5]We have now found that **17** (mp 149–150°C) contains ether of crystallization. After vigorous drying at elevated temperature *in vacuo*, **17** melts at 214–216°C.

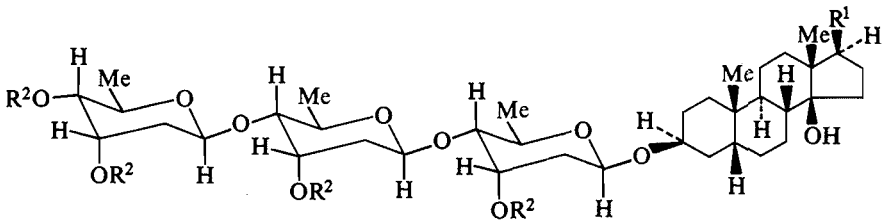

14 $R^2 = MeO-C_6H_4-CO-$, $R^1 =$

15 $R^2 = H$, $R^1 =$

16 $R^2 = H$, $R^1 =$

17 $R^2 = H$, $R^1 =$

thesis and consequently we have preferred to prepare compound **6** by our acid catalyzed method (2).

Acknowledgements

We wish to thank the Natural Sciences and Engineering Research Council of Canada, the New Brunswick Heart Foundation, and Advance Biofactures Corporation, New York, for the support of these studies.

1. K. WIESNER, T. Y. R. TSAI, A. SEN, R. KUMAR, and M. TSUBUKI. Helv. Chim. Acta, **66**, 2632 (1983).
2. H. JIN, T. Y. R. TSAI, and K. WIESNER. Can. J. Chem. **61**, 2442 (1983).
3. J. BOIVIN, C. MONNERET, and M. PAIS. Tetrahedron Lett. No. 13, 1111 (1978).
4. (*a*) H. JIN. Ph.D. Thesis, University of New Brunswick, 1984 (in preparation); (*b*) R. U. LEMIEUX. Can. J. Chem. **24**, 1079 (1951).
5. R. J. FERRIER, R. W. HAY, and N. VENTHAVIYASAR. Carbohydr. Res. **27**, 55 (1973).

Can. J. Chem. Downloaded from www.nrcresearchpress.com by 210.87.254.105 on 09/06/12
For personal use only.

The chemistry of thujone. X.[1] Thujone as a chiral synthon for the preparation of sesquiterpenes. Synthesis of (+)-α-eudesmol and (−)-α-selinene

JAMES P. KUTNEY AND ASHOK K. SINGH

Department of Chemistry, University of British Columbia, 2036 Main Mall, University Campus, Vancouver, B.C., Canada V6T 1Y6

Received January 25, 1984

JAMES P. KUTNEY and ASHOK K. SINGH. Can. J. Chem. **62**, 1407 (1984).

Efficient synthetic routes to the chiral sesquiterpenes (+)-α-eudesmol (**7**) and (−)-α-selinene (**9**) from a thujone-derived intermediate (**2**) are described.

JAMES P. KUTNEY et ASHOK K. SINGH. Can. J. Chem. **62**, 1407 (1984).

On décrit des méthodes efficaces de synthèse des sesquiterpènes chiraux (+)-α-eudesmol (**7**) et (−)-α-selinène (**9**) à partir de l'intermédiaire (**2**) dérivé de la thujone.

[Traduit par le journal]

In a recent series of papers (2–4) we have described the preparation of the natural chiral sesquiterpenes (+)-β-cyperone (2), (+)-carissone (3), and β-elemol (4) of the eudesmane series by appropriate transformations of the chiral synthon thujone (**1**)[2] as the starting material.

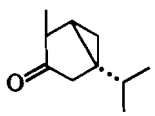

1

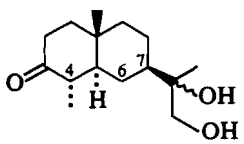

2

In these studies the thujone derived keto-diols (general structure **2**) became important intermediates, as for example, in the syntheses of β-elemol (4) and (+)-carissone (3). On the basis of these successful conversions it was possible to assign the absolute configuration in **2** at the chiral centres C-7, C-5, and C-10, as shown, thereby allowing these intermediates to be utilized in further syntheses of naturally occurring sesquiterpenes. In this publication we wish to describe a highly stereoselective synthesis of (+)-α-eudesmol (**7**) and (−)-α-selinene (**9**), proceeding through the intermediate **2**.

The synthetic route to (+)-α-eudesmol (**7**) is outlined in Scheme 1 and our experiments with respect to this study are discussed first.

The mixture of known ketodiols **2**, prepared as previously described (4), was converted quantitatively into an inseparable mixture of isomeric tosylhydrazones **3** by treatment with tosylhydrazine and BF_3 in benzene. Since the subsequent steps in the synthesis eliminate the chirality at C-11, separation into the pure isomers was not essential at this time.

The hydrazones **3** were then converted to the corresponding isomeric hydroxyalkenes **4** and **5** using the Bamford–Stevens procedure (for a review of this reaction, see ref. 5). The major components were readily separated by chromatography over silver nitrate impregnated silica gel and it was thus shown that **4** constitutes 70% of the original mixture while **5** is present in 30%.

Treatment of **4** with tosylchloride in pyridine afforded **6**, which was readily reduced by LAH in ether to (+)-α-eudesmol (**7**). The latter compound proved to be identical in every respect with the natural (+)-α-eudesmol (6) (see Experimental).

On the other hand, oxidation of **4** with $NaIO_4$ in aqueous methanol provided the chiral ketone **8** (Scheme 2) in 79% yield. This intermediate could be considered for the synthesis of (−)-α-selinene (**9**) as summarized in Scheme 2.

In our initial studies with **8** we proceeded to react the latter under normal Wittig reaction conditions, that is, methyl triphenylphosphonium bromide, sodium hydride, and dimethyl sulfoxide (7). Unfortunately the conversion of **8** to **9**, under

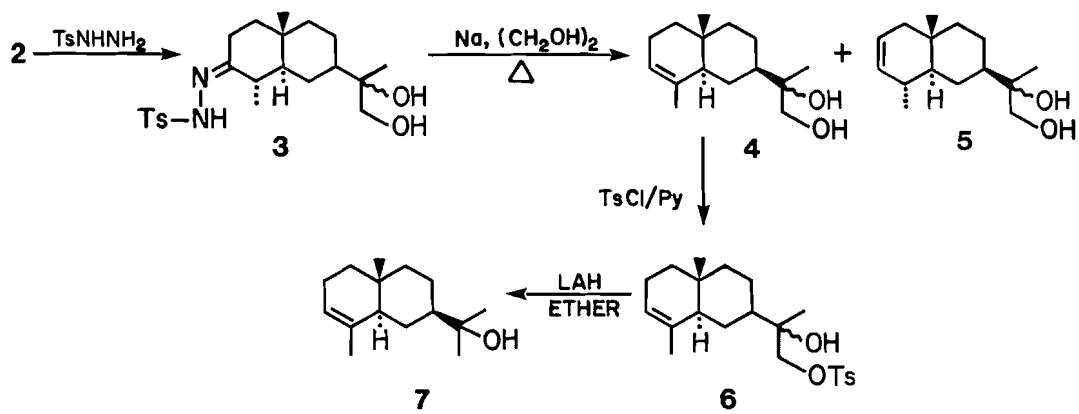

SCHEME 1

[1] For part IX, see ref. 1.

[2] Thujone is the major component (ca. 80%) of the steam distillate from the slash (waste) of Western red cedar.

Can. J. Chem. Downloaded from www.nrcresearchpress.com by 210.87.254.105 on 09/06/12
For personal use only.

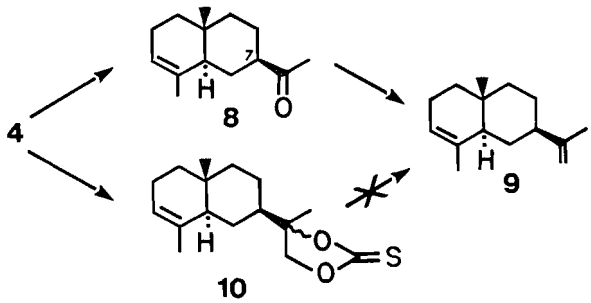

SCHEME 2

these conditions, proceeded in only 3% yield. We then turned to the use of a crystalline form of the Wittig reagent as developed by Schlosser and Schaub (8). To our delight a marked improvement was achieved and a 69% yield of **9** was realized.

It is interesting to consider the possibility of epimerization at the chiral centre C-7 in **8** during the basic conditions employed in the Wittig reaction, thereby altering the stereochemistry at this position in the resultant product **9**. Firstly it must be noted that the absolute stereochemistry at C-7, as shown in **8**, is established from our earlier studies relating to the synthesis of (+)-carissone and from nmr spectroscopy (nine-line resonance, tt, $J_{aa} = 12$; $J_{ae} = 4$ Hz centered at 2.40 ppm for the axial C-7 proton). When **8** was treated under the conditions utilized in the Wittig olefination process ($NaNH_2$ in THF, room temperature, 40 min) the starting material was recovered. It is therefore clear that the stereochemical assignment as illustrated for (−)-α-selinene (**9**) is secure.

Finally the alternative pathway 4 → 10 → 9 as outlined in Scheme 2 was also considered. However, although the thiocarbonate **10** could be prepared, its conversion to **9** met with failure and this sequence was therefore abandoned.

In conclusion, it is clear that thujone can indeed serve as an efficient chiral synthon for these types of sesquiterpenes. In a subsequent publication we will demonstrate the further utility of this compound in an efficient synthesis of optically active sesquiterpene lactones.

Experimental

Melting points were determined on a Reichert hot stage apparatus and are uncorrected. Ultraviolet spectra were recorded on a Cary 15 spectrophotometer in methanol solution. Infrared spectra were measured on a Perkin–Elmer 710 spectrophotometer using chloroform as solvent. The ^{1}Hmr spectra were recorded on Bruker WH-400, Bruker WP-80, Varian XL-100, or Nicolet–Oxford H-270 instruments. Deuteriochloroform was used as the solvent with TMS as internal standard. Low resolution mass spectra were determined on either an AEI-MS-902 or an Atlas CH-4B spectrometer. High resolution mass measurements were made on an AEI-MS-50 spectrometer. Optical rotations were recorded on a Perkin–Elmer 141 polarimeter using a cell with a path length of 10 cm. Microanalyses were performed by Mr. P. Borda, Microanalytical Laboratory, University of British Columbia. Column chromatography utilized Merck silica gel 60 (70–230 mesh). Preparative and thin layer chromatography utilized Merck silica gel GF_{254}. Petroleum ether refers to the fraction with boiling range 30–60°C.

Hydrazones 3

To a solution of hydroxyketone **2** (369 mg) and *p*-toluene sulfonyl hydrazide (271 mg) in benzene (50 mL) was added a drop of boron trifluoride etherate. The solution was stirred under argon at ambient temperature for 4 h. The resulting mixture was evaporated under reduced pressure, diluted with water (10 mL), extracted with THF–ether (100 mL, 1:1 v/v), and dried ($MgSO_4$). The solvent was removed under reduced pressure giving hydrazones **3** (598 mg, 98%), which were crystallized from ether–THF – pet. ether; mp 98–100°C; ir ν_{max}: 3488, 1600, 1378, 1173 cm^{-1}; uv λ_{max}: 225 (ε 13 288), 274 (988) nm; ^{1}Hmr δ: 0.89 (3H, s), 0.93 (1H, m), 0.99, 1.00 (3H, s, two sets), 1.03, 1.13 (3H, d, J = 6 Hz, two sets), 1.16–1.36 (2H, m), 1.38–1.75 (5H, m, including 1.48 (1H, bs, D_2O exchangeable)), 1.78–2.38 (6H, m, including 2.07 (1H, bs, D_2O exchangeable)), 2.43, 2.44 (3H, s, two sets), 2.56 (1H, m), 3.44 (1H, m), 3.58 (1H, m), 3.75 (1H, bs), 7.30, 7.36 (2H, d, J = 8 Hz, two sets), 7.80, 7.85 (2H, d, J = 8 Hz, two sets); ms *m/e*: 422 (M^+), 391, 278, 266. High resolution molecular weight determination, calcd. for $C_{22}H_{34}N_2O_4S$: 422.2239; found: 422.2248. *Anal.* calcd. for $C_{22}H_{34}N_2O_4S$: C 62.56, H 8.06, N 6.63; found: 62.29, H 7.96, N 6.30.

Diols 4 and 5

The tosyl hydrazones **3** (545 mg) in ethylene glycol (22 mL) containing dissolved sodium metal (568 mg) were heated at 155–165°C in an oil bath for 30 min under argon. The mixture was cooled, diluted with 20 mL water, and extracted with methylene chloride (2 × 100 mL). The organic extracts were dried ($MgSO_4$), concentrated, and the residue was chromatographed on silica gel impregnated with silver nitrate. Elution with petroleum ether – ethyl acetate (1:1 v/v) provided diols **4** (117.8 mg, 38%) and **5** (50.5 mg, 17%) as viscous oils. The physical properties of **4** are as follows: ir ν_{max} (neat): 3338 cm^{-1}; ^{1}Hmr δ: 0.78 (3H, s), 0.96 (1H, m), 1.14, 1.16 (3H, s, two sets), 1.17–1.58 (8H, m, including 1.58 (1H, bs, D_2O exchangeable)), 1.60, 1.63 (3H, s, two sets), 1.73 (1H, m), 1.84–1.92 (2H, m, including 1.90 (1H, bs, D_2O exchangeable)), 1.97 (1H, m), 2.09 (1H, m), 3.43, 3.45 (1H, d, J = 12 Hz, two sets), 3.58, 3.61 (1H, d, J = 12 Hz, two sets), 5.32 (1H, bs); ms *m/e*: 238 (M^+), 220, 205, 207, 189, 163. High resolution molecular weight determination, calcd. for $C_{15}H_{26}O_2$: 238.1923; found: 238.1938. *Anal.* calcd. for $C_{15}H_{26}O_2$: C 75.63, H 10.92; found: C 75.38, H 10.91. And for **5**, ir ν_{max} (neat): 3373 cm^{-1}; ^{1}Hmr δ: 0.83 (3H, s), 0.88 (1H, m), 0.97, 0.99 (3H, d, J = 6 Hz, two sets), 1.13, 1.14 (3H, s, two sets), 1.15–1.42 (2H, m), 1.45–1.60 (4H, m, including 1.55 (1H, s, D_2O exchangeable)), 1.64 (1H, dt, J = 12, 6 Hz), 1.68–1.85 (4H, m, including 1.83 (1H, bs, D_2O exchangeable)), 1.88 (1H, dt, J = 12, 6 Hz), 3.44, 3.45 (1H, d, J = 12 Hz, two sets), 3.57, 3.60 (1H, d, J = 12 Hz, two sets), 5.43 (1H, m), 5.54 (1H, m); ms *m/e*: 238 (M^+), 220, 207, 189. High resolution molecular weight determination, calcd. for $C_{15}H_{26}O_2$: 238.1933; found: 238.1923. *Anal.* calcd. for $C_{15}H_{26}O_2$: C 75.63, H 10.92; found: C 75.39, H 11.17.

Tosylates 6

To a well-stirred solution of diols **4** (45 mg) in 2 mL of pyridine was added, portion-wise, *p*-toluenesulphonyl chloride (108 mg). After 40 h at ambient temperature, the mixture was diluted with water (5 mL) and thoroughly extracted with ether (2 × 50 mL). The combined extracts were washed with water and saturated brine and dried ($MgSO_4$). The crude residue, after evaporation of the solvent *in vacuo*, was chromatographed on silica gel (40 g). Elution with ether – petroleum ether (3:7 v/v) afforded tosylates **6** (63.4 mg, 86%) as a viscous oil; ir ν_{max} (neat): 3512, 1598, 1453, 1353, 1183 cm^{-1}; uv λ_{max}: 222 (ε 12 418), 250 (2 179), 272 (871) nm; ^{1}Hmr δ: 0.74 (3H, s), 0.95 (1H, m), 1.12, 1.15 (3H, s, two sets), 1.24–1.53 (7H, m), 1.55, 1.58 (3H, s, two sets), 1.66 (1H, m), 1.79 (1H, s, D_2O exchangeable), 1.84 (1H, m), 1.95 (1H, m), 2.08 (1H, m), 2.46 (3H, s), 3.90, 3.91 (1H, d, J = 10 Hz, two sets), 3.97, 4.01 (1H, d, J = 10 Hz, two sets), 5.31 (1H, bs), 7.36 (2H, d, J = 8 Hz), 7.81 (2H, d, J = 8 Hz); ms *m/e*: 392 (M^+), 374, 359, 229, 220. High resolution molecular weight determination, calcd. for $C_{22}H_{32}O_4S$: 392.2021; found: 392.2013. *Anal.* calcd. for $C_{22}H_{32}O_4S$: C 67.35, H 8.16; found: C 66.95, H 8.41.

(+)-α-Eudesmol 7

A solution of tosylates **6** (100 mg) in ether (5 mL) was added to a stirred suspension of lithium aluminium hydride (50 mg) in dry ether (10 mL) and the mixture refluxed for 2 h. The cooled mixture was

Can. J. Chem. Downloaded from www.nrcresearchpress.com by 210.87.254.105 on 09/06/12
For personal use only.

decomposed with ice water, extracted with ether, and dried ($MgSO_4$). The solvent was distilled under reduced pressure to give an oil which solidified on standing. Recrystallization from petroleum ether afforded (+)-α-eudesmol **7** (49.5 mg, 86%); mp 74–75°C; $[\alpha]_D$ +28.6° (*c* 1.05, $CHCl_3$) (lit. (6) mp 74–75°C, $[\alpha]_D$ +28.5° (*c* 1.2, $CHCl_3$)); ir ν_{max}: 3575 cm^{-1}; ^{1}Hmr δ: 0.78 (3H, s), 0.98 (1H, m), 1.04–1.20 (2H, m), 1.21 (3H, s), 1.22 (3H, s), 1.26–1.51 (6H, m), 1.53 (1H, bs, D_2O exchangeable), 1.63 (3H, s), 1.88 (1H, dd, J = 10, 2Hz), 1.96 (1H, m), 2.10 (1H, m), 5.33 (1H, bs); ms *m/e*: 222 (M^+), 204, 189. High resolution molecular weight determination, calcd. for $C_{15}H_{26}O$: 222.1984; found: 222.1974. *Anal.* calcd. for $C_{15}H_{26}O$: C 81.08, H 11.71; found: C 81.16, H 11.56.

Ketone 8

To a solution of diols **7** (80 mg) in methanol (3.5 mL) and water (0.7 mL) was added $NaIO_4$ (233 mg). The resulting mixture was stirred at room temperature for 30 min. After the successive addition of a saturated solution of NaCl (7 mL) and sodium thiosulphate (7 mL), the product was extracted with ether–THF (100 mL, 1:1 v/v) and dried over $MgSO_4$. Solvent was removed and the residue chromatographed on silica gel (15 g), then eluted with ether – petroleum ether (0.3:9.7, v/v) to give as an oil **8** (55 mg, 79%); $[\alpha]_D$ −19.1° (*c* 0.44, $CHCl_3$); ir ν_{max} (neat): 1708 cm^{-1}; ^{1}Hmr δ: 0.81 (3H, s), 1.17–1.38 (4H, m), 1.52 (1H, dt, J = 12, 4 Hz), 1.63 (3H, s), 1.64–1.78 (2H, m), 1.88–1.96 (2H, m), 2.00 (1H, m), 2.09 (1H, m), 2.17 (3H, s), 2.40 (1H, tt, J = 12, 4 Hz, 9 lines), 5.35 (1H, bs); ms *m/e*: 206 (M^+), 191, 163. High resolution molecular weight determination, calcd. for $C_{14}H_{22}O$: 206.1671; found: 206.1662. *Anal.* calcd. for $C_{14}H_{22}O$: C 81.55, H 10.68; found: C 81.47, H 10.79.

(−)-α-Selinene 9

Ketone **8** (30 mg) in THF (2 mL) was added to a mixture of methyl triphenylphosphonium bromide (1 g) and THF (8 mL) which had been stirred for 40 min at room temperature. After the mixture had been stirred for an additional 40 min, the excess of reagent decomposes with cold water. The reaction mixture was extracted with petroleum ether and dried over $MgSO_4$. Evaporation of the solvent and purification by preparative layer chromatography with petroleum ether gave pure **9** as an oil, yield 20.6 mg (69%): $[\alpha]_D$ −12.9° (*c* 0.21, $CHCl_3$) (lit. (9) $[\alpha]_D$ −14.5° ($CHCl_3$, 1%)); ir ν_{max} (neat): 1641, 1440, 1375, 890 cm^{-1}; ^{1}Hmr δ: 0.81 (3H, s), 1.12–1.27 (2H, m), 1.30–1.38 (2H, m), 1.46 (1H, dt, J = 12, 4 Hz), 1.51–1.59 (2H, m), 1.61 (3H, s), 1.75 (3H, s), 1.78 (1H, m), 1.88–2.01 (3H, m), 2.10 (1H, m), 4.69 (1H, s), 4.72 (1H, s), 5.81 (1H, bs); ms *m/e*: 204 (M^+), 189, 175. High resolution molecular weight determination, calcd. for $C_{15}H_{24}$: 204.1878; found: 204.1878. *Anal.* calcd. for $C_{15}H_{24}$: C 88.24, H 11.76; found: C 88.25, H 11.88.

Acknowledgements

Financial aid from the Natural Sciences and Engineering Research Council of Canada is gratefully acknowledged. The authors would also like to thank Mr. Alan Moss and Associates for generous samples of cedar leaf oil. We are grateful to Dr. Lewis S. L. Choi for helpful discussions and assistance.

1. J. P. KUTNEY, P. GRICE, K. PIOTROWSKA, S. J. RETTIG, J. SZYKULA, J. TROTTER, and L. V. CHU. Helv. Chim. Acta, **66**, 1820 (1983).
2. J. P. KUTNEY, J. BALSEVICH, and P. GRICE. Can. J. Chem. **58**, 2641 (1980).
3. J. P. KUTNEY and A. K. SINGH. Can. J. Chem. **60**, 1842 (1982).
4. J. P. KUTNEY and A. K. SINGH. Can. J. Chem. **61**, 1111 (1983).
5. R. H. SHAPIRO. Org. React. **23**, 205 (1976); R. M. ADLINGTON and A. G. M. BARRETT. Acc. Chem. Res. **16**, 55 (1983).
6. D. C. HUMBER, A. R. PINDER, and R. A. WILLIAMS. J. Org. Chem. **32**, 2335 (1967), and earlier papers cited therein.
7. E. J. COREY and J. M. CHAYKOVSKY. J. Org. Chem. **28**, 1128 (1963).
8. M. SCHLOSSER and B. SCHAUB. Chimia, **36**, 396 (1982).
9. B. MAURER and A. GRIEDER. Helv. Chim. Acta, **60**, 2177 (1977), and references cited therein.

Can. J. Chem. Downloaded from www.nrcresearchpress.com by 210.87.254.105 on 09/06/12
For personal use only.

Comparison of conformational information obtained by nuclear magnetic resonance and X-ray spectroscopies for 3-substituted thiazolidine-2-thiones

OLIVIER NUZZO, MARCEL PIERROT, AND ANDRÉ BALDY

Service de Cristallochimie, Faculté des Sciences et Techniques, Centre de Saint Jérôme, 13397 – Marseille Cedex 13, France

AND

MICHEL CHANON[1] AND FRANÇOISE CHANON

G.A.M.A. – Faculté des Sciences et Techniques, Centre de Saint Jérôme, 13397 – Marseille Cedex 13, France

Received July 27, 1983[2]

OLIVIER NUZZO, MARCEL PIERROT, ANDRÉ BALDY, MICHEL CHANON, and FRANÇOISE CHANON. Can. J. Chem. **62**, 1410 (1984).

X-ray crystallographic determinations of 3-phenyl- and 3-cyclohexyl-thiazolidine-2-thiones are reported as a method for finding the origin of the discrepancy between ^{13}C and *R*-(Lambert) methods of determining the puckering in the ring. It is found that in the solid state, the puckering angles are 23.2° and 7.5° for the 3-phenyl and 3-cyclohexyl derivatives, respectively. The comparison of intramolecular and intermolecular distances for both compounds strongly suggests that these values are a fair representation of what is going on in solution. Therefore it is deduced that the puckering angle in these systems is probably better obtained by the ^{13}C nmr shift approach than by the *R*-Lambert method (in agreement with the most recent Lambert results). Both thiazolidine-2-thiones display a common property – S(1)C(2)S(2)N(3) lie in the same plane. N substitution is, however, different; all of the atoms of either the N-phenyl or of the N-cyclohexyl substituent are not in the S(1)C(2)S(2)N(3) plane. Only the C(6) atom of the N-cyclohexyl group is in the plane and the C(6) atom of the N-phenyl moiety is 0.12 Å out of this plane.

OLIVIER NUZZO, MARCEL PIERROT, ANDRÉ BALDY, MICHEL CHANON et FRANÇOISE CHANON. Can. J. Chem. **62**, 1410 (1984).

On rapporte les données cristallographiques pour la phényl-3 et la cyclohexyl-3 thiazolidinethiones-2 afin de trouver l'origine de la divergence des résultats quant au plissement du cycle apportés par la méthode du *R* de Lambert et la méthode de l'effet γ en rmn ^{13}C. On trouve qu'à l'état solide les angles de torsion de la liaison C—C sont 23,2° et 7,5° respectivement pour les dérivés phényl-3 et cyclohexyl-3. La comparaison des distances intra et intermoléculaires pour ces deux dérivés suggère fortement que les valeurs précédentes donnent une bonne approximation de l'état en solution. On en conclut que l'angle de torsion dans ces systèmes se rapproche plus de celui déduit par l'approche rmn ^{13}C que celui donné par la méthode du *R* (en accord avec les résultats les plus récents de Lambert). Les deux thiazolidinethiones-2 ont une propriété commune: S(1)C(2)S(2)N(3) sont dans le même plan. La localisation de la liaison N-substituant est cependant différente: seul l'atome C(6) du groupe N-cyclohexyl est dans le plan tandis que l'atome C(6) du groupe N-phényl est hors du plan (0, 12 Å).

Introduction

The aim of this paper is to obtain further information concerning the conformational modifications of the 1,3-thiazolidine-2-thione ring which we studied previously (1*a*, 1*b*) by ^1H and ^{13}C nmr. Kubiak and Glowink (2*a*) recently reported on the X-ray analysis of tetrakis(1,3-thiazolidine-2-thione)palladium(II) dichloride 1,3-thiazolidine-2-thione (1:2), while Raper and Oughtred (2*b*) gave the crystal structure of 1,3-thiazolidine-2-thione. In the present paper we will deal with the comparison of results from nmr and X-ray crystallography of N-substituted thiazolidine-2-thiones:

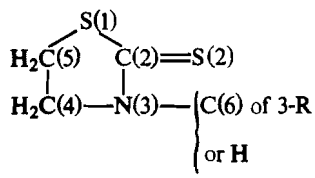

Spectroscopic studies suggested that in the solution: (1) the S(1)C(2)S(2)N(3) (C(6) or H) fragment for compounds with 3-R = H, Me, Et, iPr, *t*Bu is planar (3); (2) the five-membered ring is puckered, with a C(4)C(5) torsional angle φ whose value was evaluated. The application of Lambert's *R*-value equation (4) to differently substituted alkylthiazolidine-2-thiones provides an average value of 40°, whereas an upper limit of 25° is deduced from ^{13}C-γ effects in *cis*-4,5-dimethylthiazolidine-2-thione (1*a*); (3) the set of stable conformations was described by the equilibrium (1*a*):

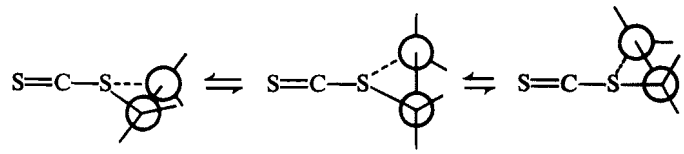

C(5) out-of-plane envelope | C(4)C(5) out-of-plane half-chair | C(4) out-of-plane envelope

We showed that transannular interactions are negligible for this system; vicinal constraints and van der Waals requirements of the substituents control this conformational equilibrium.

To gain a deeper insight into the origin of the discrepancy in torsional angles obtained by the two approaches we report here on the X-ray crystallographic results of 3-phenylthiazolidine-2-thione (**1**) and 3-cyclohexylthiazolidine-2-thione (**2**).

Experimental

The compounds were prepared as previously reported (5) and crystals were obtained by slow evaporation at room temperature of benzene–cyclohexane solutions.

Space group and cell parameters were obtained from preliminary X-ray photographs. Crystals were mounted on a CAD-4 Enraf–Nonius diffractometer equipped with a graphite monochromator [MoK_α λ = 0.7107 Å]. Unit cell parameters were refined by least squares on 2 sin θ/λ values for 25 reflections. Intensities were

[1] Author to whom correspondence may be addressed.

[2] Revision received January 23, 1984.

Can. J. Chem. Downloaded from www.nrcresearchpress.com by 210.87.254.6 on 09/06/12
For personal use only.

Can. J. Chem. Downloaded from www.nrcresearchpress.com by 210.87.254.6 on 09/06/12
For personal use only.

TABLE 1. 3-Phenylthiazolidine-2-thione positional parameters and their estimated standard deviations

Atoms	x	y	z	B_{eq} (Å^2)*
S(1)	0.24626(7)	0.41767(7)	−0.1378(1)	4.52(1)
S(2)	0.23807(6)	0.14890(6)	0.000	4.17(1)
C(2)	0.2879(2)	0.2992(2)	0.0114(3)	3.01(4)
N(3)	0.3611(2)	0.3466(2)	0.1271(3)	2.97(3)
C(4)	0.4043(2)	0.4782(2)	0.0942(4)	3.99(5)
C(5)	0.3221(3)	0.5446(3)	−0.0239(5)	4.91(6)
C(6)	0.4177(2)	0.2695(2)	0.2559(3)	2.88(4)
C(7)	0.3927(2)	0.2893(3)	0.4297(4)	3.64(5)
C(8)	0.4515(3)	0.2190(3)	0.5556(4)	4.65(6)
C(9)	0.5331(2)	0.1301(3)	0.5042(5)	4.67(5)
C(10)	0.5564(2)	0.1114(3)	0.3299(4)	4.48(6)
C(11)	0.4989(2)	0.1810(2)	0.2041(4)	3.65(5)
H1C(4)	0.400(3)	0.512(3)	0.210(4)	5*
H2C(4)	0.490(3)	0.465(3)	0.012(5)	5*
H1C(5)	0.358(3)	0.616(3)	−0.109(5)	5*
H2C(5)	0.259(3)	0.585(3)	0.071(4)	5*
HC(7)	0.327(3)	0.343(3)	0.465(5)	5*
HC(8)	0.444(3)	0.237(3)	0.676(5)	5*
HC(9)	0.583(3)	0.085(3)	0.610(5)	5*
HC(10)	0.630(3)	0.045(3)	0.284(5)	5*
HC(11)	0.520(3)	0.174(3)	0.071(5)	5*

* Anisotropically refined atoms are given in the form of the isotropic equivalent thermal parameter B_{eq} defined as: $4/3\,[a^2B(1,1) + b^2B(2,2) + c^2B(3,3) + ab\cos\gamma\,B(1,2) + ac\cos\beta\,B(1,3) + bc\cos\alpha\,B(2,3)]$ where a, b, c, α, β, and γ are the cell parameters. B factors for the hydrogen atoms were all set equal to 5 and were not refined.

TABLE 2. 3-Cyclohexyl thiazolidine-2-thione positional parameters and their estimated standard deviations

Atoms	x	y	z	B_{eq} (Å^2)*
S(1)	0.3805(2)	0.0857(2)	0.18723(8)	6.50(3)
S(2)	0.4951(2)	0.1735(1)	0.32153(9)	6.83(3)
C(2)	0.4013(5)	0.0753(5)	0.2782(3)	4.70(1)
N(3)	0.3335(4)	−0.0169(3)	0.3059(2)	4.69(8)
C(4)	0.2531(7)	−0.0870(5)	0.2565(3)	7.50(1)
C(5)	0.2773(6)	−0.0471(5)	0.1834(3)	6.50(1)
C(6)	0.3332(5)	−0.0464(4)	0.3825(2)	4.70(1)
C(7)	0.1991(5)	−0.0383(4)	0.4142(2)	5.30(1)
C(9)	0.2040(5)	−0.0640(5)	0.4936(3)	6.20(1)
C(9)	0.2659(6)	−0.1870(5)	0.5087(3)	6.20(1)
C(10)	0.3980(6)	−0.1972(5)	0.4747(3)	6.50(1)
C(11)	0.3952(5)	−0.1706(5)	0.3959(3)	5.70(1)
H1C(4)	0.274(3)	−0.171(2)	0.262(1)	5*
H2C(4)	0.159(2)	−0.076(2)	0.270(1)	5*
H1C(5)	0.327(3)	−0.108(2)	0.158(1)	5*
H2C(5)	0.200(3)	−0.032(2)	0.155(1)	5*
H1C(6)	0.390(3)	0.011(2)	0.408(1)	5*
H1C(7)	0.138(3)	0.092(3)	0.395(1)	5*
H2C(7)	0.156(3)	0.043(2)	0.402(1)	5*
H1C(8)	0.108(2)	−0.055(2)	0.516(1)	5*
H2C(8)	0.260(3)	−0.003(3)	0.516(1)	5*
H1C(9)	0.210(3)	−0.245(3)	0.490(1)	5*
H2C(9)	0.275(3)	−0.202(2)	0.559(1)	5*
H1C(10)	0.436(2)	−0.269(2)	0.486(1)	5*
H2C(10)	0.458(3)	−0.133(2)	0.498(1)	5*
H1C(11)	0.342(3)	−0.235(3)	0.374(1)	5*
H2C(11)	0.480(3)	−0.175(3)	0.374(1)	5*

* See Table 1 (footnote).

measured using an $\omega-2\theta$ scan of 0.91° to 10.06° min^{-1} over a range of (1.0 + 0.35 tan θ) degrees in ω. The intensities of three check reflections measured every 5000 s throughout the data collection remained constant to within 2%. Crystal data at 20°C are:

3-Phenylthiazolidine-2-thione (1)

$C_9H_9S_2N$ fw: 195.2

Orthorhombic, a = 11.777 (3); b = 10.346 (3); c = 7.668 (2) Å; V = 934 Å^3; Z = 4; ρ_{obs} = 1.40 (2); ρ_{calc} = 1.39; $F(000)$ = 408; μ = 0.5 cm^{-1}. Space group: $Pna2_1$; 2071 reflections ($2\theta_{max}$ = 60°) measured on a crystal ca 0.4 × 0.4 × 0.5 mm; 1571 symmetry-related reflections were averaged (agreement factor on I = 0.01) and finally 1268 with $I > 3\sigma(I)$ were kept for structure determination.

3-Cyclohexylthiazolidine-2-thione (2)

$C_9H_{15}S_2N$ fw: 201.2

Orthorhombic, a = 10.276 (5); b = 10.916 (5); c = 18.81 (1) Å; V = 2110 Å^3; Z = 8; ρ_{obs} = 1.27 (3); ρ_{calc} = 1.27; $F(000)$ = 864; μ = 0.5 cm^{-1}. Space group: $Pbca$; crystal size: 0.4 × 0.25 × 1.0 mm; 1721 reflections measured ($2\theta_{max}$ = 50°) from which 1144 independent reflections with $I > 3\sigma(I)$ were kept for structure determination.

Determination of the structures

All computations were performed on a PDP 11/44 using the SDP software package (6). After data reduction, an absorption correction (7) was made for the N-cyclohexyl compound (**2**) in view of the anisotropic shape of the crystal. The structures were solved by direct methods (MULTAN (8)). After full matrix refinement of all non-hydrogen atoms with anisotropic thermal parameters, difference Fourier maps gave the positions of the hydrogen atoms. Subsequent least-squares cycles including the refinement of the positional parameters for the hydrogen atoms were performed and the refinements converged with R = 0.027 for 3-phenylthiazolidine-2-thione and with R = 0.042 for 3-cyclohexylthiazolidine-2-thione. ($R = \Sigma(\|F_o| - |F_c\|)/\Sigma|F_o|$ where F_o and F_c are the observed and calculated structure factor amplitudes. The function minimized in all least-squares calculations was $\Sigma w(|F_o| - |F_c|)^2$ where w = 1 for all reflections with $I > 3\sigma(I)$. Final positional and thermal parameters are presented in Tables 1 and 2.[3]

Discussion

Compound 1

This set of crystallographic data (Fig. 1a) shows that the thiazolidine-2-thione ring in **1** displays a twist form, with C(4) and C(5), respectively, displaced from the S(1)C(2)S(2)N(3) plane by 0.193 Å and −0.176 Å. The C(4)—C(5) torsional angle ϕ is 23.2°, in agreement with the value provided by the ^{13}C nmr study, in contrast with the information provided by the R-approach (1*a*).

The S(2)—C(6) intramolecular distance (3.14 Å, Fig. 1a) is shorter than the 3.44 Å limiting value given by R.F. Bryan *et al.* (9). So, steric interactions between thione sulfur S(2) and the phenyl ring control the ring conformation. Steric strain is relieved in two ways. First, the phenyl ring is rotated 80.7° with respect to the plane through S(1)C(2)N(3)S(2) (Figs. 2a and 3a). A value of 58° had been estimated for the rings of the more conjugated 1-phenyl-4-Δ-imidazoline-2-thione (10). Second, C(6) is 0.127 Å out of the mean plane of the five-membered ring (Fig. 2b). It appears that the phenyl ring, in such a conformation, does not induce any specific torsion in the C-4—C(5) fragment. Therefore the measured torsional angle ϕ

[3] Copies of the structure factor tables, thermal parameters, intermolecular distances, and least-squares planes tables, are available, at a nominal charge, from the Depository of Unpublished Data, CISTI, National Research Council of Canada, Ottawa, Ont., Canada K1A 0S2.

Can. J. Chem. Downloaded from www.nrcresearchpress.com by 210.87.254.6 on 09/06/12
For personal use only.

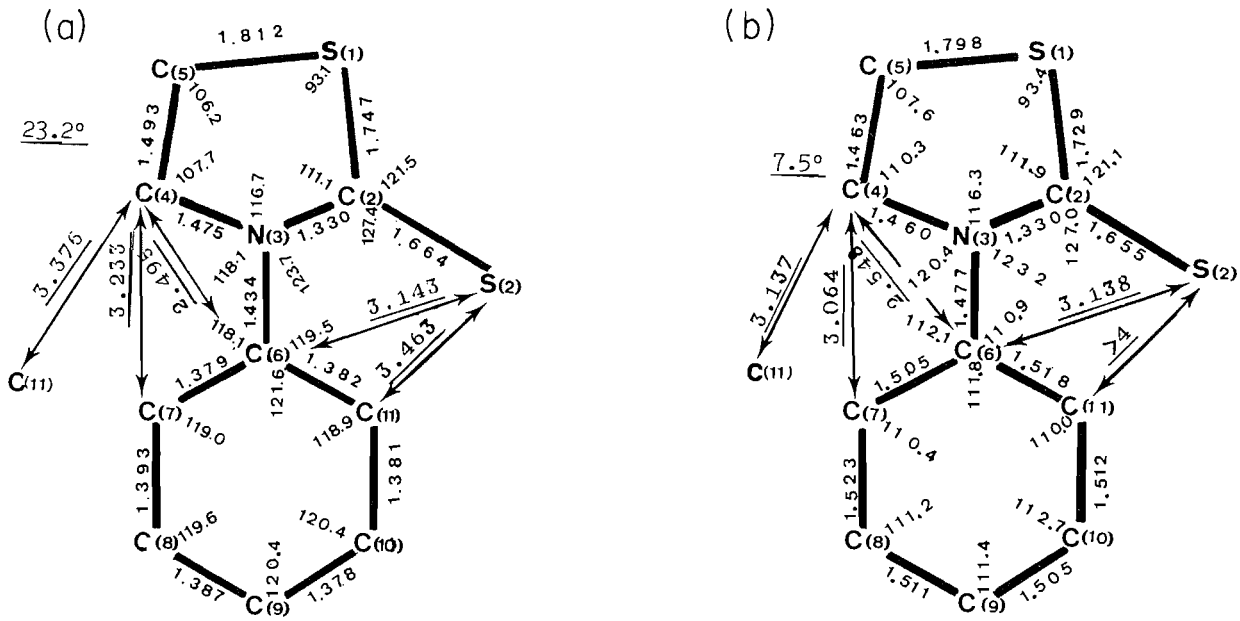

FIG. 1. Bond lengths (Å), intramolecular distances (Å), angles (°), and torsional angles, ϕ (°); (a) 3-phenylthiazolidine-2-thione (**1**); (b) 3-cyclohexylthiazolidine-2-thione (**2**).

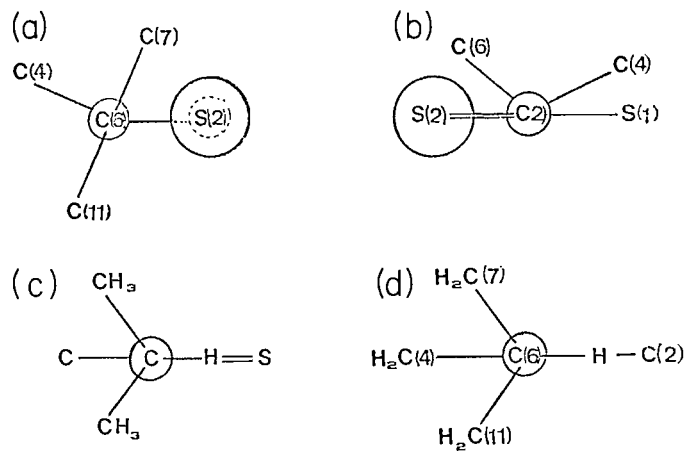

FIG. 2. Newman projections; (a) 3-phenylthiazolidine-2-thione (**1**), projection along C(6)—N(3); (b) 3-phenylthiazolidine-2-thione (**1**), projection along C(2)—N(3); (c) 3-isopropyl-4-Δ-thiazoline-2-thione, projection along $(CH_3)_2HC$—N bond (13); (d) 3-cyclohexylthiazolidine-2-thione (**2**), projection along C(6)—N(3).

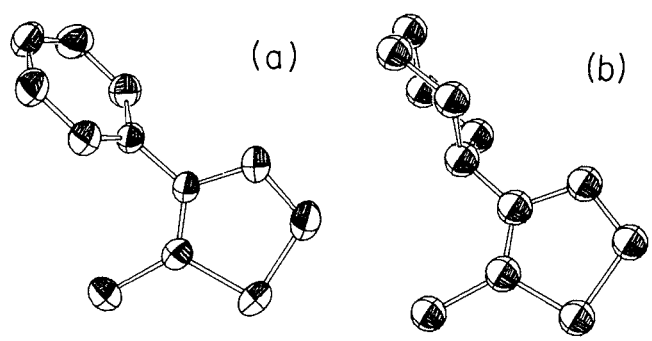

FIG. 3. View of the molecules; thermal ellipsoids are drawn at 50% probability level; (a) 3-phenylthiazolidine-2-thione (**1**); (b) 3-cyclohexylthiazolidine-2-thione (**2**).

(23.2°) is probably a good approximation to the one expected for an N-unsubstituted ring. This contrasts with the case of:

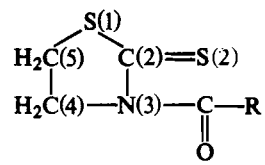

3 R = *p*-bromophenyl (9)
4 R = $(CH_2)_4$—C—thiazolidine-2-thione (11)
O

Presumably because of potential lone-pair repulsions between S(2) and O, the observed conformation has these two atoms *trans* to each other. Then the C═O group induces a distorsion around the C(4)—C(5) bond because of the van der Waals repulsions with the C(4)H_2 fragment (ϕ_3 = 33° for **3**; ϕ_4 = 34.3° for **4**).

Compound 2

The crystallographic data (Fig. 1b) show that the five-membered ring is nearly planar. C(4) and C(5) distances from the S(1)C(2)S(2)N(3)C(6) plane are respectively −0.059 Å and +0.057 Å. The conformation is a very flat C(4)C(5) out-of-plane half-chair with a C(4)—C(5) torsional angle ϕ of 7.5°. The geometries of the **1** and **2** five-membered rings are in sharp contrast (Fig. 1). This set of values suggests that C(4) and C(5) gain partial sp^2 character when passing from 3-R = phenyl to 3-R = cyclohexyl, as observed in the 2-phenyliminothiazolidine ring (12). The cyclohexyl ring is a perfect chair conformation (Figs. 1b and 3b) with the C(6) and C(9) atoms out of the six-membered ring mean plane [VI][4] respectively by −0.664 Å and +0.640 Å; C(6) is in the best plane of the thiazolidine-2-thione ring [V].[4] The two rings [V] and [VI] are

[4] [VI] is the C(7)C(8)C(10)C(11) plane; [V] is the S(1)C(2)S(2)N(3) plane.

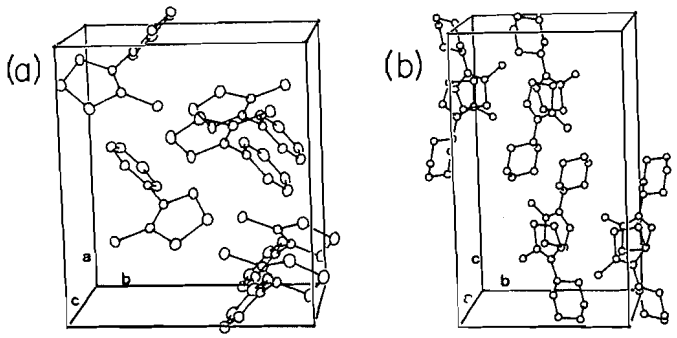

FIG. 4. View of the packing arrangement. (a) Viewed along *c* (**1**); (b) viewed along *a* (**2**).

nearly perpendicular: 91.8° (Figs. 1b and 3b) with the cyclohexyl ring being displaced towards C(4). A similar kind of preferential conformation has been found for 3-isopropyl-4-methyl-4-Δthiazoline-2-thione (13) and for 1-isopropyl-4-Δ-imidazoline-2-thione (10) (Fig. 2c).

Therefore, in **2**, no important steric interactions between the [VI] ring and S(2) exist, so S(6) can stay in plane [V]; the S(2)—C(6) distance is 3.138 Å, similar to case **1**, 3.143 Å. But van der Waals strain between $C(7)H_2$, $C(11)H_2$, and $C(4)H_2$ (Fig. 2d) prevents C(4) from moving away from the C(6)N(3)C(2) plane; thus the five-membered ring displays a far smaller torsional angle. In this case, too, steric hindrance between the thione sulfur S(2) and the substituent ring controls the conformation.

The intermolecular distances (depository material) are more numerous and shorter in **1** than in **2**, but none are less than the sums of the van der Waals radii given by N.L. Allinger (14). Then it seems that the "packing effect" is less pronounced in the 3-cyclohexylthiazolidine-2-thione case than in the 3-phenyl one. By comparison, the intramolecular distances are smaller (Figs. 1), so we can conclude that ring conformation is controlled mainly by intramolecular steric effects.

Crystal cohesion in **1** arises from overlap of the phenyl ring with the thione sulfur (Fig. 4a), and in **2** it lies in inverse superposition of two five-membered rings while six-membered chair rings fit together with other molecules (Fig. 4b).

Conclusions

It appears that the thiazolidine-2-thione ring is very flexible and can easily adopt different conformations. This can be explained by intramolecular steric effects between the N-substituent and the thione sulfur. As indicated by J. B. Lambert (4*d*), the torsional angle is overestimated by a considerable amount using the *R*-value method for a five-membered ring. Further work is in progress, aiming at delineating systematically the issue of solid state versus solution conformational data of this heterocyclic, conformationally-mobile system (15, 16).

1. (*a*) F. CHANON, M. RAJZMANN, M. CHANON, J. METZGER, and G. POUZARD. Can. J. Chem. **58**, 599 (1980); (*b*) F. CHANON, M. RAJZMANN, M. CHANON, J. METZGER, G. POUZARD, and T. DRAKENBERG. Can. J. Chem. **58**, 604 (1980).
2. (*a*) M. KUBIAK and T. GLOWINK. Acta Crystallogr. Sect. B, **38**, 2031 (1982). (*b*) E. S. RAPER and R. E. OUGHTRED. Inorg. Chim. Acta Lett. **77**, L89 (1983).
3. F. CHANON. Thèse Sciences, Marseille, France (1977).
4. (*a*) J. B. LAMBERT. J. Am. Chem. Soc. **89**, 1836 (1967); (*b*) Acc. Chem. Res. **4**, 87 (1971); (*c*) B. FUCHS. *In* Topics in stereochemistry. Vol. 10. *Edited by* E. L. Eliel and N. L. Allinger. Interscience, New York. 1978. pp. 1–94; (*d*) J. B. LAMBERT, J. J. PAPAY, E. STEDMAN-MAGYAR, and M. K. NEUBERG. J. Am. Chem. Soc. **95**, 4458 (1973); (*e*) J. B. LAMBERT. Org. Magn. Reson. **17**, 265 (1981); (*f*) J. ELGUERO and J. DE MENDOZA. Heterocycl. Chem. **3**, 111 (1982); (*g*) Heterocycl. Chem. **3**, 151 (1982).
5. R. A. BAFFORD, F. CHANON, M. CHANON, and J. METZGER. Bull. Soc. Chim. Fr. **3**, 971 (1973).
6. B. A. FRENZ. *In* Computing in crystallography. *Edited by* H. Schenk, R. Olthofhazekamp, H. Van Koninosueld, and G. Bassi. Delft Univ. Press. 1978 pp. 64–71.
7. P. COPPENS and M. EIBSCHUTZ. Acta. Crystallogr. **19**, 524 (1965).
8. P. MAIN, M. M. WOOLFSON, and G. GERMAIN. MULTAN, a system of computer program for the automatic solution of a crystal structure from X-ray diffraction data. University of York, England and Louvain, Belgium. 1977.
9. R. F. BRYAN, P. HARTLEY, S. PECKLER, E. FUJITA, Y. NAGAO, and K. SENO. Acta Crystallogr Sect. B, **36**, 1709 (1980).
10. D. BOUIN-ROUBAUD, J. KISTER, M. RAJZMANN, and L. BOUSCASSE. Can. J. Chem. **59**, 2883 (1981).
11. E. FUJITA, Y. NAGAO, K. SENO, S. TAKAO, T. MIYASAKA, M. KUNURA, and W. H. WATSON. J. Chem. Soc. Perkin Trans. 1, 915 (1979).
12. D. PETROVIC, B. RIBAR, G. ARGAY, A. KALMAN, and W. NOWACKI. Acta Crystallogr. Sect. B, **33**, 106 (1977).
13. C. ROUSSEL, A. LIDERY, M. CHANON, J. METZGER, and J. SANDSTROM. J. Am. Chem. Soc. **98**, 2847 (1976).
14. N. L. ALLINGER. Adv. Phys. Org. Chem. **13**, 1 (1976).
15. (*a*) F. G. RIDDEL. Q. Rev. Chem. Soc. **21**, 364 (1967); (*b*) Nucl. Magn. Reson. **9**, 222 (1980); (*c*) Nucl. Magn. Reson. **10**, 222 (1981).
16. N. W. THOMAS, S. RAMDAS, and J. M. THOMAS. Mol. Cryst. Liq. Cryst. **93**, 157 (1983).

Can. J. Chem. Downloaded from www.nrcresearchpress.com by 210.87.254.6 on 09/06/12
For personal use only.

The ultraviolet absorption spectrum of oxalic acid vapor[1]

R. A. BACK

Division of Chemistry, National Research Council of Canada, 100 Sussex Drive, Ottawa, Ont., Canada K1A 0R6

Received July 7, 1983[2]

R. A. BACK. Can. J. Chem. **62**, 1414 (1984).

The ultraviolet absorption spectrum of oxalic acid vapor has been studied for the first time. Low-resolution spectra show a moderately weak (ϵ_{max} = 25 M^{-1} cm^{-1} at 277 nm) banded absorption system beginning at about 310 nm and extending to 250 nm where a stronger absorption begins. Medium-resolution spectra show a complex vibrational fine-structure at wavelengths above about 287 nm, with many sharp line-like R-branch heads, each corresponding to a different vibrational transition. A vibrational analysis was completed for $^{12}C_2O_4H_2$, $^{12}C_2O_4D_2$, and $^{13}C_2O_4H_2$, and electronic origins were estimated to be at 31903.2, 31970.2, and 31949.4 cm^{-1}, respectively (about 313 nm). Strong features were assigned to progressions in ν_2' and ν_3', the C=O and C—O stretching vibrations, with prominent sequences in ν_{10}, the C—C torsional vibration, running to the blue, implying that $\nu_{10}' > \nu_{10}''$.

This absorption system has been assigned to the first excited singlet state, designated $\tilde{A}$, corresponding to a $\pi^* \leftarrow n_+$, $^1A_u \leftarrow {}^1A_g$ transition of planar *trans*-oxalic acid. High-resolution spectra of several bands show rotational fine-structure, and a partial analysis was carried out on the 2_0^1 and $2_0^1 10_1^1$ bands of $^{12}C_2O_4H_2$, based on apparently-simple diverging P-branches.

R. A. BACK. Can. J. Chem. **62**, 1414 (1984).

On a étudié pour la première fois le spectre d'absorption ultraviolet de la vapeur d'acide oxalique. Les spectres à basse résolution montrent la présence d'un système de bandes d'absorption (ϵ_{max} = 25 M^{-1} cm^{-1} à 277 nm) qui sont modérément faibles, qui commencent à 310 nm et qui s'étendent jusqu'à 250 nm alors que commencent une absorption plus forte. Les spectres à moyenne résolution montrent une structure fine vibrationnelle complexe à des longueurs d'onde commençant à environ 287 nm, avec plusieurs têtes de branche R, qui donne l'apparance de raies étraites, chacune correspondant à une transition vibrationnelle différente. On a effectué une analyse vibrationnelle pour les composés suivants: $^{12}C_2O_4H_2$, $^{12}C_2O_4D_2$, $^{13}C_2O_4H_2$ et on a évalué que leurs origines électroniques sont respectivement à 31903,2, 31970,2 et 31949,4 cm^{-1} (environ 313 nm). On a attribué les fortes caractéristiques aux progressions dans ν_2' et ν_3', les vibrations d'élongations de C=O et de C—O, avec des bandes fortes dans ν_{10}, la vibration de torsion C—C, allant jusqu'au bleu et impliquant que $\nu_{10}' > \nu_{10}''$.

On a attribué ce système d'absorption au premier état singulet excité que l'on désigne par $\tilde{A}$ et qui correspond à une transition $\pi^* \leftarrow n_+$, $^1A_u \leftarrow {}^1A_g$ de l'acide oxalique *trans* qui est planaire. Les spectres à haute résolution de plusieurs bandes montrent une structure fine rotationnelle et on a effectué une analyse partielle des bandes 2_0^1 et $2_0^1 10_1^1$ du $^{12}C_2O_4H_2$ qui est basée sur les branches P divergentes apparemment simples.

[Traduit par le journal]

Introduction

Oxalic acid in solution shows a weak absorption beginning about 300 nm with a maximum around 260 nm, which has been attributed to a $\pi^* \leftarrow n_+$ transition, the lowest excited singlet state (1). A phosphorescence excitation spectrum in the same region, measured in frozen EPA solution at 77 K, showed broad vibrational features which were thought to be a progression in a carbonyl stretching mode (1).

No corresponding vapor-phase spectrum of oxalic acid has been reported, probably because of its low volatility and ease of thermal decomposition. Oxalic acid is of interest through its close structural similarity to glyoxal and biacetyl, both of which have been the subjects of intense spectroscopic, photophysical, and photochemical investigation. The present study was undertaken in conjunction with photochemical experiments in this laboratory (2).

Experimental

Oxalic acid vapor and White-cell mirror surfaces proved to be mutually destructive at the temperatures required, and all spectra finally reported were obtained using a single-pass quartz cell about 4 m long and 25 mm in diameter, heated to 130 to 140°C. Oxalic acid vapor was supplied from a sidearm containing the solid anhydrous acid held at a somewhat lower temperature, giving vapor pressures of 1 to 3 Torr. Oxalic acid decomposes appreciably at these temperatures, so the vapor was pumped away and replenished frequently to avoid loss and accumulation of products. Some absorption bands of formic acid, a major decomposition product, were observed below 250 nm. All the other reported products, H_2O, CO, CO_2, and H_2, are transparent above 200 nm.

Anhydrous oxalic acid of 99% purity was obtained from Aldrich. Oxalic acid-d_2 and mixtures of oxalic acid-h_2, -*hd*, and -d_2 were obtained by mixing with D_2O or appropriate H_2O-D_2O mixtures and then removing water by prolonged pumping at room temperature. Oxalic acid-*c*-13 with 90 atom% *c*-13 was purchased from Merck, Sharp and Dohme of Canada Ltd.

Low-resolution spectra were obtained with a Heath modular double-beam spectrophotometer modified to take 4 m absorption cells. Medium-resolution spectra were photographed using an Eagle 6.6 m spectrograph with a grating with 600 lines/mm used in the 2nd order, to give a dispersion of 1.2 Å/mm. High-resolution spectra were obtained with an Ebert 7.3 m spectrograph, with a grating of 300 lines/mm, in the 20th order, for a dispersion of about 0.096 Å/mm.

Results

The low-resolution spectrum in Fig. 1 shows a moderately weak absorption, typical of a $\pi^* \leftarrow n_+$ transition, beginning about 310 nm, with ϵ_{max} of about 25 M^{-1} cm^{-1} at 277 nm, and broad vibrational features. There is some indication of vibrational fine structure at long wavelengths, confirmed in the medium resolution spectra in Fig. 2, and at still higher resolution (Fig. 3) rotational fine structure is evident. A much stronger absorption begins at about 252 nm, with sharp vibrational features superimposed (Fig. 1) which are due to formic acid.

[1]NRCC No. 23152.

[2]Revision received February 28, 1984.

Can. J. Chem. Downloaded from www.nrcresearchpress.com by 210.87.254.6 on 09/06/12
For personal use only.

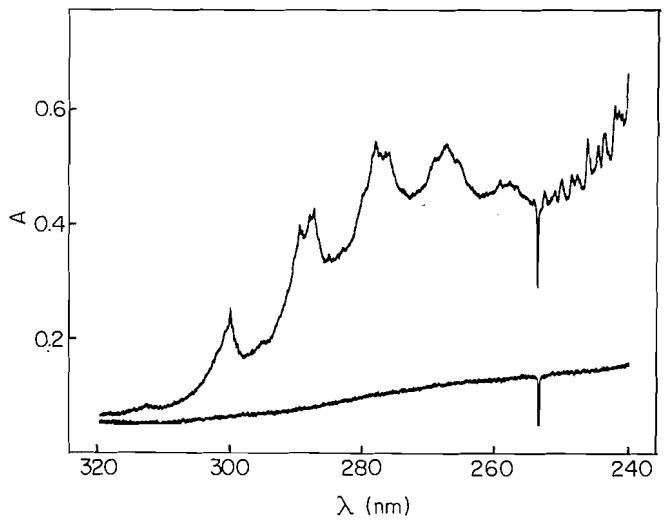

FIG. 1. Low-resolution spectrum of oxalic acid vapor.

Discussion

Before analysing the observed spectra, the molecular structure of oxalic acid must be considered. Electron diffraction studies (3, 4) showed a planar carbon–oxygen skeleton for the oxalic acid monomer, and four structures are possible:

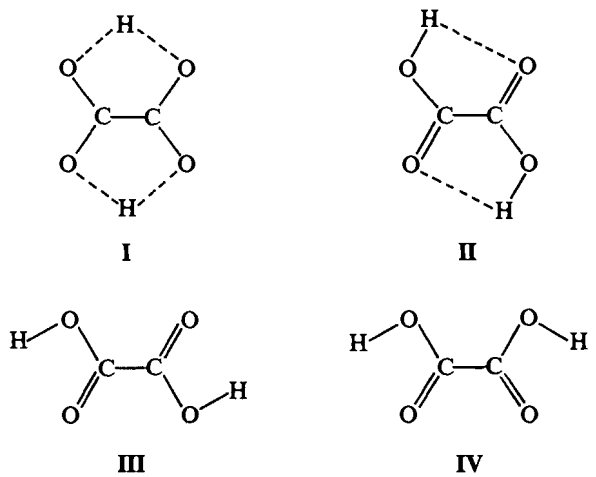

Structures **I** and **II** have strong internal hydrogen bonding, with **I** being a resonance hybrid of the two possible forms of **II**. Electron diffraction showed two distinctly different C—O bond lengths, with the carbonyl groups in a *trans* configuration (3, 4), apparently ruling out structures **I** and **IV**, and this is supported by infrared and Raman observations of reasonably normal O—H and C=O stretching frequencies (4–7). Shibata and Kimura (3) also argued that the skeletal planarity implied the hydrogen bonded structure **II**, and the same "chelated" structure was supported by Pava and Stafford (5) on the basis of O—H, O—D, and C=O stretching frequencies observed in the vapor-phase infrared spectrum of oxalic acid and oxalic acid-d_2. Glyoxal, however, has a planar structure without the benefit of chelation (8), and similar forces to those that hinder rotation about the C—C bond in glyoxal should be operative in oxalic acid. The infrared evidence for chelation has also been criticized by Stace and Oralratmanee (7), who concluded that no clear decision could be made between structures **II** and **III**. Formic acid monomer has been shown (9) to be planar, with *cis*

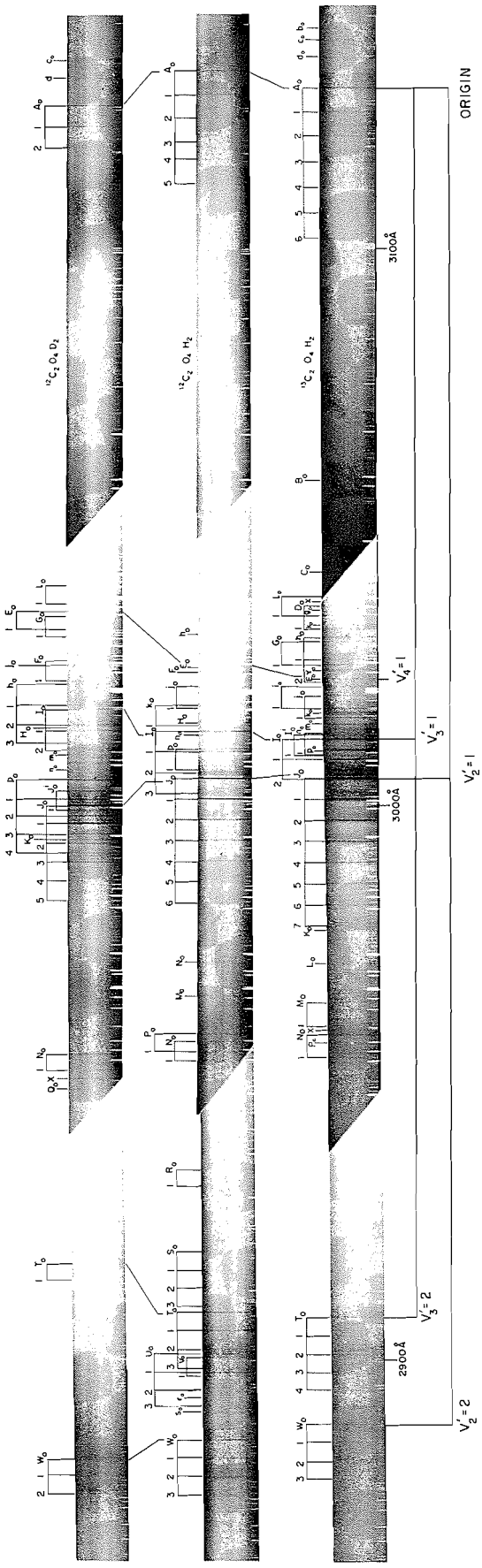

FIG. 2. Medium-resolution spectra of $^{12}C_2O_4D_2$, $^{12}C_2O_4H_2$, and $^{13}C_2O_4H_2$. Sharp features marked are R-branch heads; see text and Tables 3–5 for vibrational assignments.

Can. J. Chem. Downloaded from www.nrcresearchpress.com by 210.87.254.6 on 09/06/12
For personal use only.

Can. J. Chem. Downloaded from www.nrcresearchpress.com by 210.87.254.6 on 09/06/12
For personal use only.

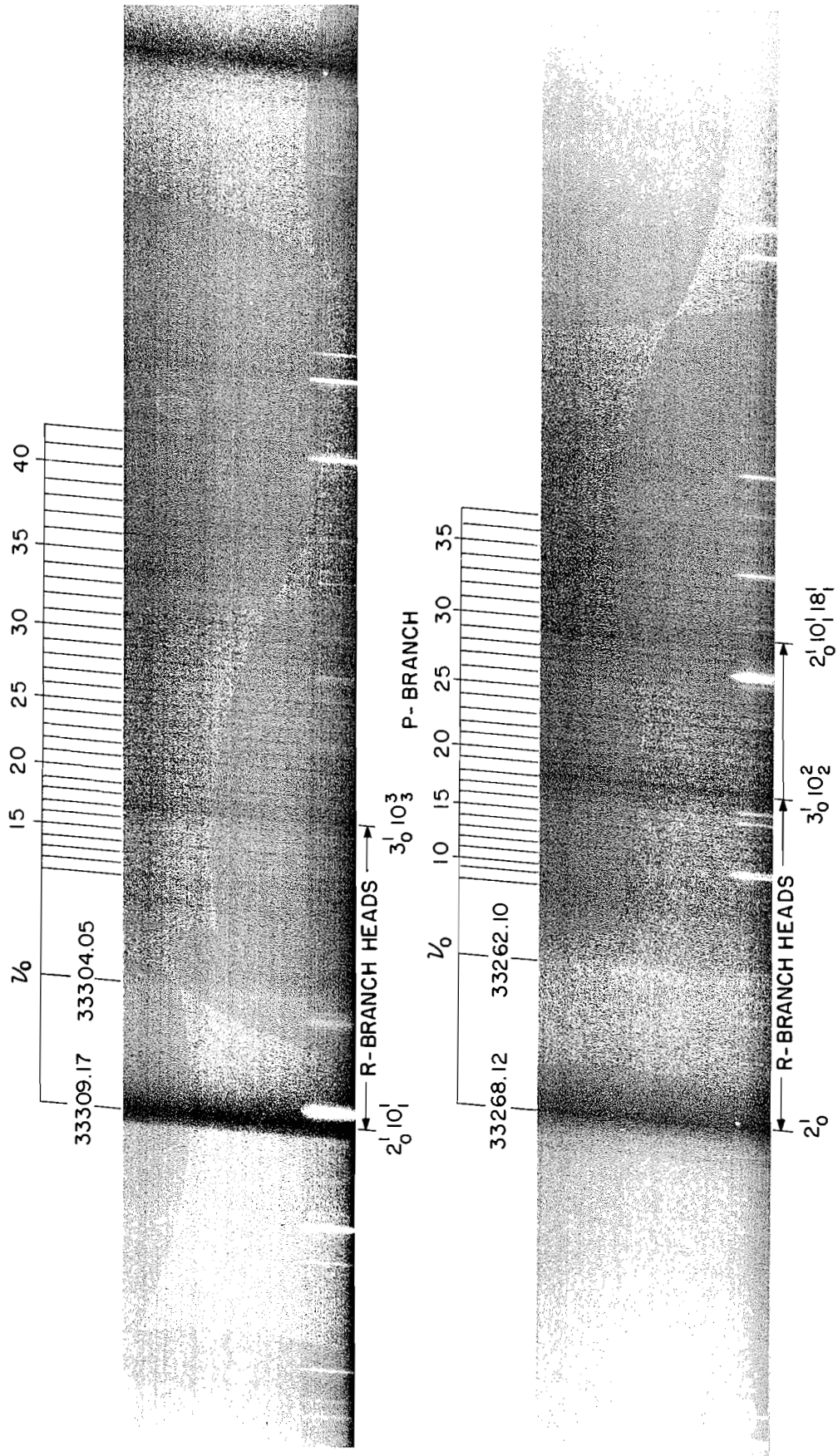

FIG. 3. High-resolution spectra of the 2_0^1 and $2_0^1 10_1^1$ bands of $^{12}C_2O_4H_2$.

TABLE 1. Fundamental vibrations of planar *trans*-oxalic acid*

Vibration	Species	Approximate description	Ground-state frequency (cm^{-1})
ν_1	A_g	O—H stretching	3472–3490 (calculated) (7)
ν_2	A_g	C=O stretching	1800 (Raman)
ν_3	A_g	C—O stretching	1423 (Raman)
ν_4	A_g	C—O—H bending	1195 (Raman)
ν_5	A_g	C—C stretching	815 (Raman)
ν_6	A_g	O=C—O rocking	625 (calculated) (7)
ν_7	A_g	O=C—O bending	405 (Raman)
ν_8	A_u	O—H wagging	800 (cf. glyoxal, ν_6) (8)
ν_9	A_u	O=C—O wagging	460 (?) (infrared)
ν_{10}	A_u	C—C torsion	89 (present work)
ν_{11}	B_g	O—H wagging	1050 (cf. glyoxal, ν_8) (8)
ν_{12}	B_g	O=C—O wagging	620 (?) (infrared)
ν_{13}	B_u	O—H stretching	3470 (infrared)
ν_{14}	B_u	C=O stretching	1812 (infrared)
ν_{15}	B_u	C—O stretching	1325 (infrared)
ν_{16}	B_u	C—O—H bending	1275 (infrared)
ν_{17}	B_u	O=C—O bending	660 (infrared)
ν_{18}	B_u	O=C—O rocking	306 (calculated) (7) 287 (present work)

*Infrared and Raman data taken from ref. 7.

TABLE 2. Main progressions from low-resolution spectra (Fig. 1)

Band maxima for $C_2O_4H_2$			Band maxima for $C_2O_4D_2$		
λ (nm)	ν (cm^{-1})	Difference	λ (nm)	ν (cm^{-1})	Difference
300.2	33311		300.2	33311	
		1387			1387
288.2	34698		288.2	34698	
		1364			1429
277.3	36062		276.8	36127	
		1405			1340
266.9	37467		266.9	37467	
		1353			1323
257.6	38820		257.8	38790	
		Ave. 1377			*Ave. 1370*

and *trans* isomers and a barrier to rotation around the C—O single bond of 10–15 kcal/mol and a corresponding torsional vibration frequency of 640 cm^{-1}. The *cis* isomer is the more stable one, and by analogy structure **III** should perhaps be more stable than **II** unless the latter is sufficiently stabilized by hydrogen bonding. The planarity of formic acid suggests that the hydrogen atoms of oxalic acid should also lie in the plane of the C—O skeleton. With regard to structure **IV**, both *cis* and *trans* isomers of glyoxal are known to exist, with the *trans* form much more abundant (10). In the following analysis, an initial working assumption will be made that structure **II** is responsible for the observed spectra.

Vibrational analysis

The frequencies of the 18 fundamental vibrational modes of the ground state of the planar *trans* isomer of oxalic acid listed in Table 1, are not all well established.. Some frequencies shown are from infrared and Raman spectra, while others are estimated, and assignments have been aided by comparison with known frequencies of *trans*-glyoxal and formic acid. The numbering and the assignments shown are appropriate to both structures **II** and **III** if the effects of hydrogen bonding are minimal; for structure **II** with strong hydrogen bonds, the numbering and descriptions of several of the vibrations would be altered (7).

The low-resolution spectra of both $C_2O_4H_2$ and $C_2O_4D_2$ (Fig. 1) show obvious strong progressions of bands with average frequency intervals of 1377 and 1370 cm^{-1}, respectively (Table 2). There appears to be a second, weaker progression in the same frequency lying about 500 cm^{-1} to the blue. By analogy with glyoxal and other $\pi^* \leftarrow n$ spectra, it is reasonable to assign these progressions to excitation of the symmetric carbonyl stretching mode, ν_2', in the upper state, with the weaker progression probably corresponding to excitation of one quantum of an in-plane vibration such as ν_5' or ν_6'. The medium-resolution photographic spectra in Fig. 2, however, reveal a much more complex vibrational structure in these apparently simple bands. The bands centred around 300 nm, corresponding to the first strong band in Fig. 1, are the strongest features of these spectra. Much weaker bands lying to the red around 313 nm in all three isotopic species also show fine structure; the next strong bands to the blue, around 290 nm, show some structure but are becoming diffuse, while all spectra at shorter wavelengths are completely diffuse.

Prominent in each spectrum in Fig. 2 are many sharp line-like features. From high-resolution spectra it will be seen later that these are composite R-branch heads, and each corresponds to a different vibronic transition. Frequencies of these branch-heads are listed in Tables 3–5, together with vibrational assignments. Capital letters are used to designate those features in Fig. 2 corresponding to the electronic origin band and to bands involving excitation of the symmetric vibrational modes, ν_2' to ν_7'. Small-case letters designate bands involving the low-frequency modes, ν_{10} and ν_{18} (mostly hot bands). Numerical subscripts indicate members of ν_{10} sequence bands, while a few unassigned features are labelled X. In the following vibrational analysis, it is convenient to use these easily measured sharp features to calculate frequency differences, rather than using true band origins which can only be determined accurately for a few bands with resolved rotational structure. In the latter, the band origins lie typically 5 or 6 wave numbers to the red of the

Can. J. Chem. Downloaded from www.nrcresearchpress.com by 210.87.254.6 on 09/06/12
For personal use only.

Can. J. Chem. Downloaded from www.nrcresearchpress.com by 210.87.254.6 on 09/06/12
For personal use only.

TABLE 3. Sharp features in medium-resolution spectrum of oxalic acid (Fig. 2) (all frequencies in cm^{-1} *in vacuo*)

Symbol	ν	ν_{10} sequence intervals	Vibrational assignment	Comments
A_0	31909.246		Origin	
		43.61		
A_1	31952.859		10_1^1	
		43.41		
A_2	31996.27		10_2^2	
		44.60		
A_3	32040.87		10_3^3	
		30.50		Small interval $A_4 - A_3$
A_4	32071.37		10_4^4	
		45.87		
A_5	32117.24		10_5^5	
h_0	32980.48		$2_0^1 18_1^0$	$\nu''_{18} = 287$
E_0	33043.461		4_0^1	$\nu'_4 = 1134$
F_0	33054.046		$5_0^1 6_0^1$	$\nu'_5 + \nu'_6 = 1145$
j_0	33084.492		$3_0^1 10_1^0$	$\nu''_{10} = 89$
		43.94		
k_0	33120.250		$3_0^1 18_1^1$	$(\nu''_{18} - \nu'_{18}) = 53$
j_1	33128.43		$3_0^1 10_2^1$	
		35.81		
H_0	33152.372		5_0^2	$2\nu'_5 = 1243$
k_1	33156.062		$3_0^1 10_1^1 18_1^1$	
I_0	33173.290		3_0^1	$\nu'_3 = 1264$
		40.57		
n_0	33180.736		$2_0^1 10_1^0$	$\nu''_{10} = 87$
p_0	33208.431		$2_0^1 18_1^1$	$(\nu''_{18} - \nu'_{18}) = 60$
		42.44		
I_1	33213.862		$3_0^1 10_1^1$	
		41.31		
p_1	33250.87		$2_0^1 10_1^1 18_1^1$	
I_2	33255.170		$3_0^1 10_2^2$	
		41.71		
J_0	33267.849		2_0^1	$\nu'_2 = 1359$
		41.09		
I_3	33296.876		$3_0^1 10_3^3$	
J_1	33308.934		$2_0^1 10_1^1$	
		41.44		
J_2	33350.369		$2_0^1 10_2^2$	
		41.84		
J_3	33392.210		$2_0^1 10_3^3$	
		42.11		
J_4	33434.317		$2_0^1 10_4^4$	
		42.65		
J_5	33476.965		$2_0^1 10_5^5$	
		42.81		
J_6	33519.775		$2_0^1 10_6^6$	

Symbol	ν	ν_{10} sequence intervals	Vibrational assignment	Comments
L_0	33638.236		$2_0^1 7_0^1$	$\nu'_7 = 370$
M_0	33712.17		$3_0^1 6_0^1$	$\nu'_6 = 539$
P_0	33789.309		$3_0^1 5_0^1$	$\nu'_5 = 616$
		37.37		
N_0	33806.452		$2_0^1 6_0^1$	$\nu'_6 = 538$
		39.16		
P_1	33826.678		$3_0^1 5_0^1 10_1^1$	
N_1	33845.605		$2_0^1 6_0^1 10_1^1$	
R_0	34072.518		$3_0^1 6_0^1 7_0^1$	$\nu'_7 = R_0 - M_0 = 361$
		34.48		
R_1	34107.000		$3_0^1 6_0^1 7_0^1 10_1^1$	
S_0	34244.62		$3_0^1 6_0^2$	$\nu'_6 = S_0 - M_0 = 533$
		40.46		
S_1	34285.08		$3_0^1 6_0^2 10_1^1$	
		37.28		
S_2	34322.357		$3_0^1 6_0^2 10_2^2$	
		37.66		
S_3	34360.02		$3_0^1 6_0^2 10_3^3$	
T_0	34375.232		3_0^2	$\nu'_3 = T_0 - I_0 = 1202$
		39.49		
T_1	34414.717		$3_0^2 10_1^1$	
		40.81		
T_2	34455.528		$3_0^2 10_2^2$	
U_0	34465.601		$2_0^1 3_0^1$	$\nu'_3 = U_0 - J_0 = 1198$
		41.35		
V_0	34471.542		$2_0^1 5_0^2$	$\nu'_5 = 602$
		39.86		
T_3	34496.87		$3_0^2 10_3^3$	
		40.91		
U_1	34505.456		$2_0^1 3_0^1 10_1^1$	
V_1	34512.45		$2_0^1 5_0^2 10_1^1$	
		40.89		
U_2	34546.346		$2_0^1 3_0^1 10_2^2$	
r_0	34561.76		$2_0^2 10_1^0$	$\nu''_{10} = 90$
		31.66		
U_3	34578.01		$2_0^1 3_0^1 10_3^3$	
s_0	34592.366		$2_0^2 18_1^1$	$(\nu''_{18} - \nu'_{18}) = 60$
W_0	34652.472		2_0^2	$\nu'_2 = W_0 - J_0 = 1385$
		40.59		
W_1	34693.066		$2_0^2 10_1^1$	
		40.22		
W_2	34733.288		$2_0^2 10_2^2$	
		39.76		
W_3	34773.05		$2_0^2 10_3^3$	

Can. J. Chem. Downloaded from www.nrcresearchpress.com by 210.87.254.6 on 09/06/12
For personal use only.

TABLE 4. Sharp features in medium-resolution spectrum of oxalic acid-d_2 (Fig. 2) (all frequencies in cm^{-1} *in vacuo*)

Symbol	ν	ν_{10} sequence intervals	Vibrational assignment	Comments	Symbol	ν	ν_{10} sequence intervals	Vibrational assignment	Comments
c_0	31891.97		10^0_1	$\nu''_{10} = 84$	p_0	33273.252		$2^1_0 18^1_1$	$(\nu''_{18} - \nu'_{18}) = 52$
							39.00		
d_0	31924.32		18^1_1	$(\nu''_{18} - \nu'_{18}) = 52$	J_0-*iso*	33295.944		2^1_0 (hd)	$^{12}C_2O_4HD$ feature
A_0	31976.185		Origin		p_1	33312.251		$2^1_0 10^1_1 18^1_1$	
		38.67					38.35		
A_1	32014.855		10^1_1		J_0	33325.366		2^1_0	$\nu'_2 = 1349$
		39.41					33.20		
A_2	32054.265		10^2_2		J_1-*iso*	33334.296		$2^1_0 10^1_1$ (hd)	$^{12}C_2O_4HD$ feature
							35.84		
e_0	32889.15		$3^1_0 18^0_1$	$\nu''_{18} = 243$	p_2	33345.454		$2^1_0 10^2_2 18^1_1$	
		35.67					36.91		
e_1	32924.82		$3^1_0 10^1_1 18^0_1$		J_1	33361.203		$2^1_0 10^1_1$	
E_0	32939.412		4^1_0	$\nu'_4 = 963$	p_3	33382.366		$2^1_0 10^3_3 18^1_1$	
							40.25		
G_0	32953.541	34.65	6^2_0	$\nu'_6 = 489$	K_0	33393.715		$3^1_0 7^1_0$	$\nu'_7 = 262$; seems low
							38.74		
E_1	32974.061	33.76	$4^1_0 10^1_1$		J_2	33401.448		$2^1_0 10^2_2$	
G_1	32987.302		$6^2_0 10^1_1$		p_4	33421.109		$2^1_0 10^4_4 18^1_1$	
							37.79		
F_0	33037.38		$5^1_0 6^1_0$	$\nu'_6 = F_0 - A_0 - 578 = 483$	J_3	33439.237		$2^1_0 10^3_3$	
							38.20		
j_0	33045.88	38.61	$3^1_0 10^0_1$	$\nu''_{10} = 86$	J_4	33477.436		$2^1_0 10^4_4$	
							38.18		
F_1	33075.989		$5^1_0 6^1_0 10^1_1$		J_5	33515.611		$2^1_0 10^5_5$	
h_0	33082.757		$2^1_0 18^0_1$	$\nu''_{18} = 242$	N_0	33831.319		$2^1_0 6^1_0$	$\nu'_6 = 506$
		40.86					32.56		
h_1	33123.623		$2^1_0 10^1_1 18^0_1$		N_1	33863.883		$2^1_0 6^1_0 10^1_1$	
I_0	33132.260	40.13	3^1_0	$\nu'_3 = 1156$	X	33881.880			
h_2	33163.745		$2^1_0 10^2_2 18^0_1$		Q_0	33903.627		$2^1_0 5^1_0$	$\nu'_5 = 578$
		42.11							
H_0	33166.473		5^2_0	$\nu'_5 = 595$	T_0	34273.195		3^2_0	$\nu'_3 = T_0 - I_0 = 1141$
							36.09		
I_1	33174.370	37.71	$3^1_0 10^1_1$		T_1	34309.285		$3^2_0 10^1_1$	
h_3	33201.457	39.14	$2^1_0 10^3_3 18^0_1$		W_0	34694.269		2^2_0	$\nu'_2 = W_0 - J_0 = 1369$
							39.47		
I_2	33213.509		$3^1_0 10^2_2$		W_1	34733.743		$2^2_0 10^1_1$	
							38.16		
m_0	33223.644		$2^1_0 18^2_2$	$(\nu''_{18} - \nu'_{18}) = p_0 - m_0 = 49$	W_2	34771.899		$2^2_0 10^2_2$	
n_0	33252.690		$2^1_0 10^0_1$	$\nu''_{10} = 72$					

TABLE 5. Sharp features in medium-resolution spectrum of oxalic acid-$^{13}C_2$ (Fig. 2) (all frequencies in cm^{-1} *in vacuo*)

Symbol	ν	ν_{10} sequence intervals	Vibrational assignment	Comments
a_0	31676.647		18_1^0	$\nu''_{18} = 278$
		39.57		
a_1	31716.22		$10_1^1 18_1^0$	
b_0	31847.85		18_2^2	$(\nu''_{18} - \nu'_{18}) = d_0 - b_0 = 53$
c_0	31866.62		10_1^0	$\nu''_{10} = 88$
d_0	31900.69		18_1^1	$(\nu''_{18} - \nu'_{18}) = 55$
A_0	31955.429		Origin	
		43.10		
A_1	31998.531		10_1^1	
		44.14		
A_2	32042.669		10_2^2	
		47.84		
A_3	32090.510		10_3^3	
		46.45		
A_4	32136.96		10_4^4	
		46.74		
A_5	32183.70		10_5^5	
		47.79		
A_6	32231.49		10_6^6	
B_0	32688.917		7_0^2	$\nu'_7 = 367$
C_0	32864.466		$6_0^1 7_0^1$	$\nu'_6 = C_0 - A_0 - 370 = 539$
e_0	32908.214		$3_0^1 18_1^1$	$\nu''_{18} = 282$
X	32920.907			
D_0	32927.828	39.46	$5_0^1 7_0^1$	$\nu'_5 = D_0 - A_0 - 370 = 583$
g_0	32933.53		$2_0^1 18_2^1$	$(\nu''_{18} - \nu'_{18}) = h_0 - g_0 = 56$
e_1	32947.671		$3_0^1 10_1^1 18_1^0$	
		45.49		
f_0	32962.62		$7_0^3 10_1^0$	$\nu''_{10} = 91$
D_1	32973.317		$5_0^1 7_0^1 10_1^1$	
h_0	32989.653		$2_0^1 18_1^0$	$\nu''_{18} = 279$
G_0	32998.621	43.30	6_0^2	$\nu''_6 = 522$
h_1	33032.953	45.25	$2_0^1 10_1^1 18_1^0$	
G_1	33043.870		$6_0^2 10_1^1$	
Y_0	33053.579	46.29	7_0^3	$\nu'_7 = Y_0 - B_0 = 365$
E_0	33071.427		4_0^1	$\nu'_4 = 1116$
h_2	33079.245		$2_0^1 10_2^2 18_1^0$	

Can. J. Chem. Downloaded from www.nrcresearchpress.com by 210.87.254.6 on 09/06/12
For personal use only.

TABLE 5. (*Continued*)

Symbol	ν	ν_{10} sequence intervals	Vibrational assignment	Comments
i_0	33085.097		$3_0^1 18_2^2$	$(\nu''_{18} - \nu'_{18}) = k_0 - i_0 = 53$
j_0	33104.212	44.13	$3_0^1 10_1^0$	$\nu''_{10} = 86$
i_1	33129.226		$3_0^1 10_1^1 18_2^2$	
k_0	33137.619	43.91	$3_0^1 18_1^1$	$(\nu''_{18} - \nu'_{18}) = 52$
j_1	33148.121		$3_0^1 10_2^1$	
m_0	33160.413		$2_0^1 18_2^2$	$(\nu''_{18} - \nu'_{18}) = p_0 - m_0 = 51$
n_0	33178.013		$2_0^1 10_1^0$	$\nu''_{10} = 91$
I_0-*iso*	33181.934		$3_0^1(^{12}C-^{13}C)$	$^{12}C^{13}CO_4H_2$ feature
I_0	33190.309	41.31	3_0^1	$\nu'_3 = 1235$
p_0	33211.475	40.76	$2_0^1 18_1^1$	$(\nu''_{18} - \nu'_{18}) = 58$
n_1	33219.321	40.75	$2_0^1 10_2^1$	
I_1-*iso*	33222.689		$3_0^1 10_1^1(^{12}C-^{13}C)$	$^{12}C^{13}CO_4H_2$ feature
I_1	33230.883		$3_0^1 10_1^1$	
J_0	33269.165	40.87	2_0^1	$\nu'_2 = 1314$
I_2	33271.749	41.09	$3_0^1 10_2^2$	
J_1	33310.250	42.72	$2_0^1 10_1^1$	
J_2	33352.969	41.75	$2_0^1 10_2^2$	
J_3	33394.723	42.45	$2_0^1 10_3^3$	
J_4	33437.170	42.59	$2_0^1 10_4^4$	
J_5	33479.763	43.26	$2_0^1 10_5^5$	
J_6	33523.021	42.91	$2_0^1 10_6^6$	
J_7	33565.928		$2_0^1 10_7^7$	
K_0	33573.73		$3_0^1 7_0^1$	$\nu'_7 = 384$
L_0	33640.739		$2_0^1 7_0^1$	$\nu'_7 = 372$
M_0	33721.736	43.08	$2_0^1 6_0^1$	$\nu'_6 = 532$
M_1	33764.819		$2_0^1 6_0^1 10_1^1$	
X	33783.481			

Can. J. Chem. Downloaded from www.nrcresearchpress.com by 210.87.254.6 on 09/06/12
For personal use only.

TABLE 5. (*Concluded*)

Symbol	ν	ν_{10} sequence intervals	Vibrational assignment	Comments
N_0	33789.126		$3_0^1 6_0^1$	$\nu_6' = 520$
		47.99		
P_0	33805.601		$2_0^1 5_0^1$	$\nu_5' = 616$
N_1	33837.124		$3_0^1 6_0^1 10_1^1$	
T_0	34383.500		3_0^2	$\nu_3' = T_0 - I_0 = 1193$
		39.99		
T_1	34423.487		$3_0^2 10_1^1$	
U_0	34456.541	40.11	$2_0^1 3_0^1$	$\nu_3' = U_0 - J_0 = 1187$
T_2	34463.593		$3_0^2 10_2^2$	
		39.56		
T_3	34503.15		$3_0^2 10_3^3$	
		39.55		
T_4	34542.702		$3_0^2 10_4^4$	
W_0	34615.371		2_0^2	$\nu_2' = W_0 - J_0 = 1346$
		45.24		
W_1	34660.613		$2_0^2 10_1^1$	
		40.02		
W_2	34700.63		$2_0^2 10_2^2$	
		34.74		
W_3	34735.37		$2_0^2 10_3^3$	

R-branch heads, and little error should be introduced by using the latter to estimate frequency differences.

The electronic origin

Location of the band corresponding to the electronic origin of the present band system requires some discussion. An obvious choice at first glance is the strong feature marked J_0 in Fig. 2, close to the first strong maximum in the low-resolution spectra (Fig. 1). This raises a problem, however, in assigning the much weaker system of bands, labelled A, around 313 nm. The intensity of the latter seems about right for a ν_2' hot band, but the observed frequency difference of 1359 cm^{-1} for $J_0 - A_0$ for $^{12}C_2O_4H_2$ is much too low for ν_2'', and is in fact more appropriate for ν_2', the excited-state frequency. A ν_3'' hot band is perhaps a possibility, as this vibration also appears to be active in the transition, but again the frequency difference is appreciably below the Raman frequency of 1423 cm^{-1} reported for ν_3''. Another possibility is that the bands at 313 nm are due to weak absorption by the *cis* isomer of oxalic acid, present in low concentration; in the analogous glyoxal spectrum, weak absorption by the *cis* isomer appears 1467 cm^{-1} to the red of that of *trans*-glyoxal (10). A telling argument against this possibility is the general similarity of the *A* and *J* bands (Fig. 2) and more particularly the sequence-band intervals (Tables 3–5) which are very similar. By contrast, in glyoxal, intervals in the corresponding sequences in the torsional vibration differ by a factor of two in the *cis* and *trans* isomers (10). Finally, the observed isotope shifts offer the most convincing evidence in the identification of the electronic origin. Deuterium isotope shifts of +58 and +67 cm^{-1} for J_0 and A_0, respectively are both compatible with expected zero-point energy differences. The carbon-13 isotope shift of only +1.32 cm^{-1} for J_0 is, however, much too small, while the shift of 46 cm^{-1} for A_0 appears reasonable. The analogous isotope shift in *trans*-glyoxal (8) is +14 cm^{-1}, but oxalic acid has considerably more vibrational modes involving the carbon atoms which change frequency in the transition. All things considered, it must be concluded that the band, A_0, despite its relative weakness, corresponds to the electronic origin of the present system. It will be seen that subsequent detailed analysis of the spectrum supports this conclusion. It is also assumed in the analysis that all the bands observed are due to the *trans* isomer of oxalic acid.

Noting again that the frequencies shown in Tables 3–5 are for R-branch head maxima, and assuming that for the A_0 bands these lie the same distance to the blue of the band origin as in J_0 for $^{12}C_2O_4H_2$ (see below, Table 10), the true electronic origins for $^{12}C_2O_4H_2$. $^{12}C_2O_4D_2$, and $^{13}C_2O_4H_2$ are estimated to be at 31903.2, 31970.2, and 31949.4 cm^{-1}, respectively. The chief uncertainty in these values lies in the assumed separation of the R-head maxima from the origins; the A_0 bands themselves were too weak to photograph in high resolution.

Sequence bands and hot bands involving ν_{10}, the C—C torsional vibration

Many of the features listed in Tables 3–5 can be grouped into obvious regular sequences, running with decreasing intensity to the blue, with intervals between members of 40–45 cm^{-1} in $^{12}C_2O_4H_2$, and $^{13}C_2O_4H_2$ and 35–40 cm^{-1} in $^{12}C_2O_4D_2$. There seems little doubt that these sequence bands can be assigned to transitions from thermally populated levels of ν_{10}'', the torsional vibration around the C—C bond. Microdensitometer measurements indicate a decrease of between 20 and 40% between adjacent members, which from the Boltzmann factor corresponds to an energy difference of between 60 and 150 cm^{-1}, assuming constant transition probability. From Table 1 it is clear that ν_{10}'' is the only vibrational mode at all likely to have such a low frequency. The $\pi^* \leftarrow n_+$ spectrum of glyoxal shows similar sequence bands involving the corresponding C—C torsion vibration (8), lending support to the present assignment. As in glyoxal, the sequences de-

Can. J. Chem. Downloaded from www.nrcresearchpress.com by 210.87.254.6 on 09/06/12
For personal use only.

crease in intensity towards the blue, implying that $\nu'_{10} > \nu''_{10}$. Intervals between sequence members are listed in Tables 3–5, and show considerable variation, both within single sequences and between sequences. Several sequences are very regular (J_0 to J_6 in $^{12}C_2O_4H_2$, for example) while others are less so; the A-sequence in $^{12}C_2O_4H_2$ shows a very small interval between A_3 and A_4, while the J-sequence in $^{12}C_2O_4D_2$ has a large interval between J_1 and J_2.

In addition to the $\Delta V_{10} = 0$ sequence bands, a few weak bands have been assigned to simple hot bands corresponding to ($V'_{10} = 0$, $V'_{10} = 1$) transitions. The features labelled C_0 in $^{13}C_2O_4H_2$ and $^{12}C_2O_4D_2$ lie 89 and 84 cm^{-1} to the red of the origin band. These values for ν''_{10} can be combined with sequence interval values of about 43 and 39 cm^{-1} (from $A_1 - A_0$) to give values of 132 and 123 cm^{-1}, respectively, for ν'_{10}. Stronger hot bands, j_0 and n_0, were observed with all three isotopic species to the red of the strong features I_0 and J_0, giving values of ν''_{10} close to those from c_0 (above), with the ^{12}C and ^{13}C isotopic species almost the same, as expected for a torsional vibration about the C—C axis. Several other ν''_{10} hot bands, f_0, j_1, n_1, and r_0 were assigned in one or the other of the isotopic oxalic acids.

Hot bands and sequences involving ν_{18}, the asymmetric O=C—O rocking mode

A single weak feature in the $^{13}C_2O_4H_2$ spectrum lying 279 cm^{-1} to the red of the origin band, A_0, has been assigned to a simple hot band of ν''_{18}, for which a Raman frequency of 306 cm^{-1} has been reported (7) for $^{12}C_2O_4H_2$. Similar bands were found lying to the red of strong features such as I_0 and J_0 in all three spectra, and have also been assigned to ν''_{18} hot bands, listed in Table 6. Also evident in all three spectra are a few short sequences with intervals between 50 and 60 cm^{-1}, usually with one or two members, occasionally three, and these we have attributed to $\Delta V_{18} = 0$ sequences, also listed in Table 6. These sequences run with decreasing intensity to the red, indicating, as might be expected that $\nu''_{18} > \nu'_{18}$. Taking values of ν''_{18} of 287, 279, and 243 cm^{-1} for $^{12}C_2O_4H_2$, $^{13}C_2O_4H_2$, and $^{12}C_2O_4D_2$, respectively, and values for the corresponding ν_{18} sequence intervals (Table 6) of 55, 54, and 51 cm^{-1}, values of ν'_{18} = 232, 225, and 192 cm^{-1} can be estimated for the three isotopic species.

Excitation of the symmetric vibrations, ν'_2 to ν'_7

In Fig. 4 is an energy-level plot and vibrational assignments for the three isotopic oxalic acids showing the sharp features from Fig. 2 which remain when all hot bands and sequence bands involving ν_{10} and ν_{18} are removed. The strongest feature, J_0, is assigned to the carbonyl stretching vibration, $V'_2 = 1$, with W_0 corresponding to the second member of the progression. The low-resolution spectrum in Fig. 1 indicates that the progression continues to at least $V'_2 = 5$, with perhaps maximum intensity at $V'_2 = 3$, but no sharp features are evident beyond W_0, $V'_2 = 2$. ν'_2 exhibits a slight negative anharmonicity in all three isotopic species.

The next strongest features in the spectrum, I_0 and T_0, are assigned to a progression in ν'_3, and again it is evident from the low-resolution spectrum that these progressions continue to shorter wavelengths; in fact the broad maxima at low resolution are composites of ν'_2 and ν'_3, overlaid and broadened by the complex sequences and hot bands discussed above, rather far from simple carbonyl stretching progressions.

Bands labelled E_0 in all three spectra are assigned to excitation of one quantum of ν'_4. A number of rather weak bands are assigned to excitations of ν'_5, ν'_6, and ν'_7; these are mostly combination bands, especially combinations with the strong ν'_2 and ν'_3 bands, J_0 and I_0. In Table 7 are listed all the vibrational frequencies derived from the present spectrum. Several features may be noted. Values of ν'_2 are markedly reduced from the ground-state value (1800), as usually found in $\pi^* \leftarrow$ n transitions of carbonyl compounds; less usual is the slight negative anharmonicity in ν'_2. The torsional frequency, ν_{10}, as noted earlier, is increased in the excited state, as in glyoxal (8), but both the frequency and the change in frequency are less than in the latter, probably reflecting the repulsion between the oxygen atoms in planar oxalic acid not present in *trans*-glyoxal. The value of ν'_5, approximately described as a C—C stretching vibration, is *decreased* in the excited state, despite the increase in ν'_{10} and the probable decrease in the C—C bond length (see below). The explanation is probably that ν_5 is very far from a pure C—C stretching vibration, so that any increase in the C—C force constant is more than outweighed by decreases in the other force constants involved. Glyoxal shows a similar decrease in the "C—C stretching" vibration in the excited state (8). The isotope effects in Table 7 are compatible with the approximate descriptions of the vibrations, noting again that several of these, notably ν_4 to ν_7, are probably very mixed in character (7). An exception is the value of ν'_7 for $^{12}C_2O_4D_2$, which is much too low for any normal isotope effect, although there seems no alternative assignment for the feature K_0 in Fig. 2 on which it is based.

Rotational analysis

High-resolution spectra of a number of the bands showed rotational fine structure. This was most clearly evident in the bands labelled J_0 and J_1 in the medium-resolution spectrum of $^{12}C_2O_4H_2$ (Fig. 2) which we have assigned to 2^1_0 and $2^1_0 10^1_1$ vibronic transitions respectively; the high-resolution spectra are shown in Fig. 3. Each band shows sharp features in what appears to be a diverging P-branch, a band origin marked by a sharp onset of absorption, and what appears to be a very strong R-branch head which corresponds to one of the sharp features noted in the medium-resolution spectra. Two much weaker R-branch heads, assigned to $3^1_0 10^3_3$ and $3^1_0 10^4_4$ vibronic transitions, can also be distinguished.

There have been two electron-diffraction determinations of the structure of oxalic acid in the gas phase, both of which favored structure **II**, as discussed earlier (3, 4). Using the structural parameters from the more recent work of Nahlovska *et al.* (4), (r(C—C) = 1.548 Å, r(C=O) = 1.208 Å, r(C—O) = 1.339 Å, r(O—H) = 1.056 Å, ∠C—C=O = 123.1°, ∠O=C—O = 125.0°, and ∠C—O—H = 104.4°) moments of inertia and rotational constants were calculated for structure **II** (Table 8). Stace and Oralratmanee (7) have argued that structure **III** cannot be ruled out, so rotational parameters were also calculated for structrure **III**, assuming the same bond lengths and angles, but with the O—H bonds rotated through 180°, and are shown in parentheses in Table 8. In both structures, the molecule is a strongly asymmetric top, with the c-axis, the axis of symmetry, perpendicular to the molecular plane, and closer to a prolate rather than an oblate symmetric top (κ negative).

Excited-state rotational constants were also calculated, using two models, and are shown in Table 9. In model 1, the C=O bond length was increased to 1.258 Å and the C—C bond length decreased to 1.480 Å, the same percentage changes observed in the first excited singlet state of glyoxal (8). Other

Can. J. Chem. Downloaded from www.nrcresearchpress.com by 210.87.254.6 on 09/06/12
For personal use only.

TABLE 6. ν_{18} sequences and hot bands (cm^{-1} *in vacuo*)

Compound	Band symbol	Vibrational assignment	$\nu''_{18} - \nu'_{18}$	ν''_{18}
$^{12}C_2O_4H_2$	I_0	3_0^1	53.04	
	k_0	$3_0^1 18_1^1$		
	h_0	$2_0^1 18_1^0$		287
	J_0	2_0^1	59.42	
	p_0	$2_0^1 18_1^1$		
	W_0	2_0^2	60.01	
	s_0	$2_0^2 18_1^1$		
$^{12}C_2O_4D_2$	A_0	Origin	51.87	
	d_0	18_1^1		
	I_0	3_0^1		243
	e_0	$3_0^1 18_1^0$		
	h_0	$2_0^1 18_1^0$		242
	J_0	2_0^1	52.11	
	p_0	$2_0^1 18_1^1$	49.61	
	m_0	$2_0^1 18_2^2$		
$^{13}C_2O_4H_2$	a_0	18_1^0		278
	A_0	Origin	54.74	
	d_0	18_1^1	52.84	
	b_0	18_2^2		
	h_0	$2_0^1 18_1^0$	56.12	
	g_0	$2_0^1 18_2^1$		
	e_0	$3_0^1 18_1^0$		282
	I_0	3_0^1	52.69	
	k_0	$3_0^1 18_1^1$	52.52	
	i_0	$3_0^1 18_2^2$		
	h_0	$2_0^1 18_1^0$		279
	J_0	2_0^1	57.69	
	p_0	$2_0^1 18_1^1$	51.07	
	m_0	$2_0^1 18_2^2$		

bond lengths and angles, which changed little in glyoxal, were left unchanged. In model 2, the C—C bond length was reduced by only half as much, to 1.514 Å, and a small increase was made in the C—O bond length to 1.346 Å, the same percentage change as in the C—H bond in glyoxal. Other bond lengths and angles were the same as in model 1. The smaller decreases in the C—C bond length is to take into account increased repulsion between the carbonyl and hydroxyl oxygen atoms in oxalic acid, relative to glyoxal, which is borne out by the longer C—C bond in the ground state (1.548 vs. 1.51 Å in

Can. J. Chem. Downloaded from www.nrcresearchpress.com by 210.87.254.6 on 09/06/12
For personal use only.

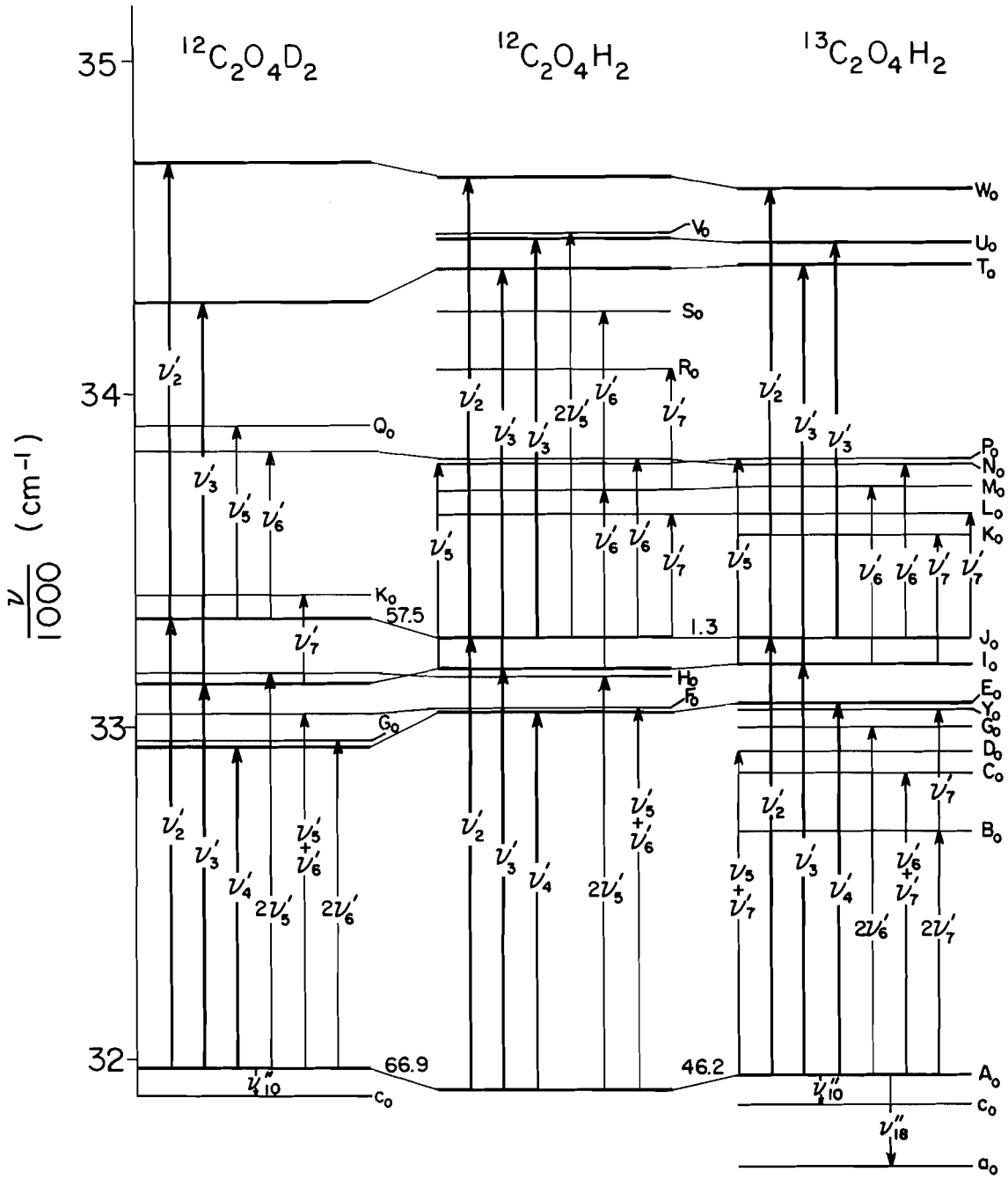

FIG. 4. Vibrational energy levels of the $\tilde{A}$ state of oxalic acid, oxalic acid-d_2, and oxalic acid-$^{13}C_2$, based on the R-branch heads in Fig. 2. For simplicity, sequence bands and other hot bands involving ν_{10} and ν_{18} have been omitted except those to the red of the origin.

glyoxal), by the lower torsional frequency in the ground state (89 vs. 127 cm^{-1} in glyoxal), and by the much smaller increase in the torsional frequency in the first excited state (89 to 132 vs. 127 to 232 cm^{-1} in glyoxal). The molecule in both models of the excited state, for both structures, remains a strongly asymmetric top, with structure **III** definitely closer to prolate; structure **II** is almost midway between prolate and oblate, with κ close to zero (Table 8).

Both planar structures **II** and **III** belong to point-group C_{2h}, and the first excited singlet state, π^*-n_+, is expected to correspond to a $^1A_u - ^1A_g$ transition (1). The two bands in Fig. 3, 2_0^1 and $2_0^1 10_1^1$, will be $^1A_u - ^1A_g$ and $^1A_g - ^1A_u$ vibronic transitions, respectively, with the transition moment parallel to the *c*-axis, perpendicular to the plane of the molecule (11).

Analysis of the rotational structure in Fig. 2 presents some difficulty. Standing out most clearly are the sharp features in the "P-branches" for "*J*" between about 10 and 40, which show an apparently simple regular structure, and the strong "R-branch" heads. Positions of these features were measured from a photographic print to an accuracy of ± 0.02 cm^{-1} and are listed in Tables 10 and 11. Regular rotational features can arise in the spectra of strongly asymmetric tops in a variety of ways (11, 12). In particular, Hollas (12) has discussed the "low-*K*, high-*J*" approximation in which a *prolate* asymmetric top behaves like an *oblate* symmetric top, with the regular features in the spectrum corresponding to coincident band

Can. J. Chem. Downloaded from www.nrcresearchpress.com by 210.87.254.6 on 09/06/12
For personal use only.

TABLE 7. Vibrational frequencies obtained from medium-resolution spectra (fundamental frequencies are underlined; all frequencies in cm^{-1} *in vacuo*)

Assignment	Frequency		
	$^{12}C_2O_4D_2$	$^{12}C_2O_4H_2$	$^{13}C_2O_4H_2$
		Upper state	
ν_2'	1349 ($J_0 - A_0$) 1369 ($W_0 - J_0$)	1359 ($J_0 - A_0$) 1385 ($W_0 - J_0$)	1314 ($J_0 - A_0$) 1346 ($W_0 - J_0$)
ν_3'	1156 ($I_0 - A_0$) 1141 ($T_0 - I_0$)	1264 ($I_0 - A_0$) 1202 ($T_0 - I_0$)	1235 ($I_0 - A_0$) 1193 ($T_0 - I_0$) 1187 ($U_0 - J_0$)
ν_4'	963 ($E_0 - A_0$)	1134 ($E_0 - A_0$)	1116 ($E_0 - A_0$)
ν_5'	578 ($Q_0 - J_0$) 595 $\frac{1}{2}$($H_0 - A_0$)	616 ($P_0 - I_0$) 622 $\frac{1}{2}$($H_0 - A_0$) 602 $\frac{1}{2}$($V_0 - J_0$)	616 ($P_0 - I_0$) 583 ($D_0 - A_0 - 370$)
ν_6'	506 ($N_0 - J_0$) 489 $\frac{1}{2}$($G_0 - A_0$) 483 ($F_0 - A_0 - 578$)	538 ($N_0 - J_0$) 539 ($M_0 - I_0$) 533 ($S_0 - M_0$) 529 ($F_0 - A_0 - 616$)	520 ($N_0 - J_0$) 532 ($M_0 - I_0$) 539 ($C_0 - A_0 - 370$) 522 $\frac{1}{2}$($G_0 - A_0$)
ν_7'	262 ($K_0 - I_0$)	370 ($L_0 - J_0$) 361 ($R_0 - M_0$)	372 ($L_0 - J_0$) 384 ($K_0 - I_0$) 365 ($Y_0 - B_0$) 367 $\frac{1}{2}$($B_0 - A_0$)
ν_{10}'	123 (see text)	132 (see text)	132 (see text)
ν_{18}'	192 (see text)	232 (see text)	225 (see text)
		Ground state	
ν_{10}''	84 ($A_0 - c_0$) 72 ($J_0 - n_0$)	89 ($I_0 - j_0$) 87 ($J_0 - n_0$) 90 ($W_0 - r_0$)	88 ($A_0 - c_0$) 91 ($Y_0 - f_0$) 86 ($I_0 - j_0$) 91 ($J_0 - n_0$)
ν_{18}''	243 ($I_0 - e_0$) 242 ($J_0 - h_0$)	287 ($J_0 - h_0$)	278 ($A_0 - a_0$) 282 ($I_0 - e_0$) 279 ($J_0 - h_0$)

TABLE 8. Calculated rotational constants for oxalic acid for structure **II***

Parameter	Ground state	Excited state 1	Δ	Excited state 2	Δ
A	0.1908 (0.2029)	0.1838 (0.1947)	−0.0070 (−0.0082)	0.1829 (0.1936)	−0.0079 (−0.0093)
B	0.1272 (0.1174)	0.1318 (0.1216)	+0.0046 (+0.0042)	0.1280 (0.1182)	+0.0008 (+0.0008)
C	0.0763 (0.0744)	0.0768 (0.0749)	+0.0005 (+0.0005)	0.0753 (0.0734)	−0.0010 (−0.0010)
$\frac{1}{2}(A + B)$	0.1590 (0.1602)	0.1578 (0.1582)	−0.0012 (−0.0020)	0.1555 (0.1559)	−0.0035 (−0.0043)
$\frac{1}{2}(B + C)$	0.1018 (0.0959)	0.1043 (0.0983)	+0.0025 (+0.0024)	0.1017 (0.098)	−0.0001 (−0.0001)
κ	−0.1109 (−0.3307)	+0.0280 (−0.2204)		−0.0204 (−0.2546)	
θ	7.5° (9.0°)	4.5° (6.5°)		4.6° (7.0°)	

*Rotational constants are in cm^{-1}, values in parentheses are for structure **III**; $\Delta = A' - A''$, etc.; κ = asymmetry parameter $(2B\text{-}A\text{-}C)/(A\text{-}C)$; θ = angle between C—C bond and principal axis "*a*".

heads rather than simple rotational lines. If the present spectrum of oxalic acid is treated this way, with the transition moment perpendicular to the plane of the molecule, parallel to the *c*-axis, a type-*C* band is expected for an $A_u - A_g$ transition, and the quadratic coefficient for a regular diverging series of features should equal ΔC. The facts, however, do not support this interpretation of the spectrum. The band contour is that of an *A*-type band; the quadratic coefficient is much larger than

Can. J. Chem. Downloaded from www.nrcresearchpress.com by 210.87.254.6 on 09/06/12
For personal use only.

TABLE 9. Mean rotational constants for oblate nearly-symmetric top approximation* (cm^{-1})

Constant	From 2_0^1 band	From $2_0^1 10_1^1$ band	Calculated (from Table 8) Excited state 1	Excited state 2
$\tilde{B}''$	0.1625	0.1618	0.1590 (0.1602)	0.1590 (0.1602)
$\tilde{B}'$	0.1586	0.1573	0.1578 (0.1582)	0.1555 (0.1559)
$\tilde{B}'' - \tilde{B}'$	0.0039	0.0045	0.0012 (0.0020)	0.0035 (0.0043)

*Calculated values are for structure **II**, with values for structure **III** in parentheses.

TABLE 10. Frequencies of P-branch lines of 2_0^1 band

J	ν_J (cm^{-1} *in vacuo*)	J	ν_J (cm^{-1} *in vacuo*)
11	33258.06	27	33250.57
12	33257.72	28	33250.04
13	33257.22	29	33249.54
14	33256.86	30	33248.96
15	33256.39	31	33248.41
16	33256.03	32	33247.88
17	33255.58	33	33247.27
18	33255.11	34	33246.72
19	33254.62	35	33246.17
20	33254.16	36	33245.56
21	33253.67	37	33245.01
22	33253.20		
23	33252.70	*Other features*	
24	33252.17	Origin ν_0	33262.10
25	33251.62	R-head (max.)	33268.12
26	33251.11	R-head (edge)	33268.75

TABLE 11. Frequencies of P-branch lines of $2_0^1 10_1^1$ band

J	ν_J (cm^{-1} *in vacuo*)	J	ν_J (cm^{-1} *in vacuo*)
11	33300.01	30	33290.38
12	33299.55	31	33289.79
13	33299.14	32	33289.11
14	33298.71	33	33288.60
15	33298.22	34	33288.01
16	33297.76	35	33287.34
17	33297.30	36	33286.66
18	33296.83	37	33285.99
19	33296.34	38	33285.31
20	33295.83	39	33284.63
21	33295.31	40	33283.96
22	33294.85	41	33283.28
23	33294.28	42	33282.61
24	33293.76		
25	33293.25	*Other features*	
26	33292.66	Origin ν_0	33304.05
27	33292.10	R-head (max.)	33309.17
28	33291.52	R-head (edge)	33309.63
29	33290.95		

reasonably might be expected for ΔC, and there is no alternation in intensity as might be expected from the presence of two hydrogen atoms in the molecule (cf. Fig. 6.111, p. 426 of ref. 12).

Curiously, if the data in Tables 10 and 11 are analysed as if they correspond to simple P-branches of parallel (type-*A*) bands of an *oblate* nearly-symmetric top, reasonable rotational constants are obtained. Frequencies of such a P-branch should be given approximately by the equation

$$[1]\quad \nu(J,K) = \nu_0 - J(\tilde{B}'' + \tilde{B}') - J^2(\tilde{B}'' - \tilde{B}') - K^2(C'' - C') + K^2(\tilde{B}'' - \tilde{B}')$$

in which $\tilde{B} = \frac{1}{2}(A + B)$.

In Fig. 5 are shown plots of $(\nu_0 - \nu)/J$ against J, which from eq. [1], neglecting the K^2 terms for low K and high J, should give straight lines, with intercepts of $\tilde{B}'' + \tilde{B}'$ and slopes of $\tilde{B}'' - \tilde{B}'$, and values of $\tilde{B}''$ and $\tilde{B}'$ obtained this way are shown in Table 9. These plots were also used to fix the J-numbering since an increase or decrease in the numbering by one led to pronounced curvature in both plots. Similarly, it can be shown that the R-branch head will occur at $J = (3\tilde{B}' - \tilde{B}'')/2(\tilde{B}'' - \tilde{B}')$. Using the values of $\tilde{B}'$ and $\tilde{B}''$ obtained from the P-branch data, the positions of the R-branch heads are calculated to be at $\nu - \nu_0 = 6.91$ and 6.13 cm^{-1} for

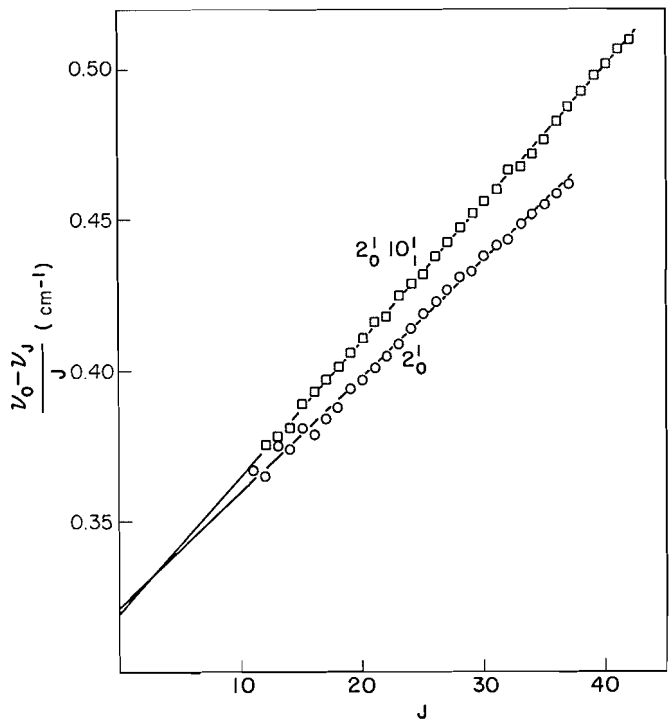

FIG. 5. Plots of $(\nu_0 - \nu_J)/J$ vs. J for the P-branches of the 2_0^1 and $2_0^1 10_1^1$ bands of $^{12}C_2O_4H_2$, used to obtain estimates of $\tilde{B}''$ and $\tilde{B}'$.

Can. J. Chem. Downloaded from www.nrcresearchpress.com by 210.87.254.6 on 09/06/12
For personal use only.

the 2_0^1 and $2_0^1 10_t^1$ bands respectively, which may be compared with measurements from the spectra of 6.65 and 5.58 (Fig. 3). The calculated positions of the R-branch heads are extremely sensitive to the value taken for ν_0, and the agreement with the observed positions, which are also not sharply defined, is probably as good as can be expected.

In Table 9, mean rotational parameters from the foregoing analysis are compared with calculated values taken from Table 8. The agreement with the absolute values of $\tilde{B}$ is reasonable for both excited-state models, but the measured $\Delta\tilde{B}$ values are compatible only with model 2, in which the C—C bond length was decreased half as much as in glyoxal (discussed earlier). Uncertainties in the analysis and the calculations preclude any choice between structures **II** and **III**. There is a real and appreciable difference in $\Delta\tilde{B}$ between the two bands in Fig. 3, which is in fact reflected throughout the medium resolution spectrum (Fig. 2) in which the R-head of the first sequence band is always noticeably sharper than the sequence origin. The larger $\Delta\tilde{B}$ in the sequence bands presumably reflects inertial defects associated with the out-of-plane torsional motion.

It is not clear why such a simple rotational analysis should apparently be applicable to the sharp features in Fig. 3. One possibility is that they correspond to a single ($K_a'' = 0$, $K_a' = 0$) sub-band of a parallel transition, and that all other sub-bands for $K_a' > 0$ are weakened and broadened by predissociation, as is observed, for example, in the $\tilde{B}-\tilde{X}$ system of diimide (13). There is certainly diffuse absorption underlying the sharp features in Fig. 3, and weak diffuse Q-branches are also evident as expected for $K_a' > 0$ (cf. Fig. 110, p. 262, ref. 11); diffuse absorption could also contribute to the strong R-branch heads. The molecule should certainly be predissociated in the excited state, with yields of photolysis close to unity throughout the whole absorption system, independent of pressure, and fluorescence extremely weak (2).

It is also not clear why the sharp features in Fig. 3 should resemble a type-*A* rather than a type-*C* band, as shown by the lack of a strong Q-branch and the fit of the data to $\tilde{B} = \frac{1}{2}(A + B)$ and not to $\tilde{B} = \frac{1}{2}(B + C)$ (Tables 8 and 9). Proper understanding of this rotational structure must await measurement of a band less overlapped by sequence bands and diffuse absorption, perhaps the (0,0) band at reduced temperatures, to which contour analysis could be applied. The low vapour pressure and weak absorption makes this experimentally difficult.

Acknowledgements

I am grateful to Mr. M. Barnett and Mr. J. M. Parsons for assistance in photographing and measuring the spectra, and to Dr. D. A. Ramsay for helpful discussions. I am also grateful to one of the referees for pointing out several errors, and problems in the original rotational analysis.

1. H. J. MARIA and S. P. MCGLYNN. J. Mol. Spectrosc. **42**, 177, 296 (1972).
2. R. A. BACK and S. YAMAMOTO. J. Phys. Chem. To be published.
3. S. SHIBATA and M. KIMURA. Bull. Chem. Soc. Jpn. **27**, 485 (1954).
4. Z. NAHLOVSKA, B. NAHLOVSKY, and T. G. STRAND. Acta Chem. Scand. **24**, 2617 (1970).
5. B. M. PAVA and F. E. STAFFORD. J. Phys. Chem. **72**, 4628 (1968).
6. S. J. CYVIN and I. ALFHEIM. Acta Chem. Scand. **24**, 2648 (1970).
7. B. C. STACE and C. ORALRATMANEE. J. Mol. Struct. **18**, 339 (1973).
8. F. W. BIRSS, D. B. BRAUND, A. R. H. COLE, R. ENGELMAN, JR., A. A. GREEN, S. M. JAPAR, R. NANES, B. J. ORR, D. A. RAMSAY, and H. SZYSZKA. Can. J. Phys. **55**, 390 (1977) and references therein.
9. I. C. HISATSUNE and J. HEICKLEN. Can. J. Spectrosc. **18**, 135 (1973).
10. R. Y. DONG and D. A. RAMSAY. Can. J. Phys. **51**, 1491 (1973); D. A. RAMSAY and C. ZAULI. Acta Phys. Acad. Sci. Hung. **35**, 79 (1974).
11. G. HERZBERG. Electronic spectra of polyatomic molecules. Van Nostrand Reinhold, New York. 1966.
12. J. M. HOLLAS. High resolution spectroscopy. Butterworths, London. 1982.
13. P. S. NEUDORFL, R. A. BACK, and A. E. DOUGLAS. Can. J. Chem. **59**, 506 (1981).

Can. J. Chem. Downloaded from www.nrcresearchpress.com by 210.87.254.6 on 09/06/12
For personal use only.

An FT-ir study of *cis*- and *trans*-dichlorodiammineplatinum(II) bound to inosine-5′-monophosphate

H. A. TAJMIR-RIAHI AND T. THEOPHANIDES

Département de Chimie, Université de Montréal, Montreal (Qué.), Canada H3C 3V1

Received November 2, 1983

H. A. TAJMIR-RIAHI and T. THEOPHANIDES. Can. J. Chem. **62**, 1429 (1984).

Inosine-5′-monophosphate disodium salt (5′-IMPNa$_2$) reacts with *cis*-dichlorodiammineplatinum(II) (*cis*-DDP) and its *trans*-isomer (*trans*-DDP) to give complexes of the type *cis*- and *trans*-Pt(NH$_3$)$_2$(IMPNa$_2$)$_n$Cl$_2$.xH$_2$O, n = 1 or 2 and Pt(IMPNa$_2$)$_n$Cl$_2$.xH$_2$O, where n = 1, 2, or 3 and x = 0–6. In the 1:2 platinum complexes the nucleotide binds only to the N$_7$-atom of the purine ring system, while in the 1:1 metal complexes there is indication for Pt–carbonyl interaction (bridging or chelation) in addition to the N$_7$-bonding at neutral pH values with *cis*-DDP.

Solution FT-ir studies (H$_2$O and D$_2$O) showed that the 1:1 species formed with *cis*-DDP at neutral pH's behaved differently from those with *trans*-DDP. The carbonyl stretching vibration of the free base at 1685 cm^{-1} (H$_2$O) and 1670 cm^{-1} (D$_2$O) exhibited marked spectral changes in intensity, shifting, and shape upon complexation, whereas the reaction with the *trans*-isomer produced only slight perturbations in the above region.

H. A. TAJMIR-RIAHI et T. THEOPHANIDES. Can. J. Chem. **62**, 1429 (1984).

Le sel de l'inosine-5′-monophosphate (5′-IMPNa$_2$) réagit avec le *cis*-dichlorodiammineplatine(II), (*cis*-DDP) et son isomère-*trans* (*trans*-DDP) et forme des complexes de type *cis*- et *trans*-Pt(NH$_3$)$_2$(IMPNa$_2$)$_n$Cl$_2$.xH$_2$O et Pt(IMPNa$_2$)$_n$-Cl$_2$.xH$_2$O, où n = 1, 2 ou 3 et x = 0–6. Dans ces complexes 1:2, le nucléotide est fixé au platine par l'azote N$_7$ de l'anneau purique, tandis que dans les complexes 1:1 avec le *cis*-DDP et à pH neutre le nucléotide est fixé au platine par l'azote N$_7$ et le carbonyle C$_6$=O (liaison pontée ou chelatée).

Des études spectroscopiques ir-TF en solution (H$_2$O et D$_2$O) montrent que l'espèce 1:1 formée avec le *cis*-DDP à pH neutre se comporte différemment du complexe formé avec le *trans*-DDP. La fréquence de valence de la liaison carbonyle de la base libre à 1685 cm^{-1}(H$_2$O) et à 1670 cm^{-1} (D$_2$O) montre des modifications importantes en intensité, déplacement, et forme de la bande, lorsque il se forme le complex *cis*-DDP, au contraire l'isomère *trans* ne produit que de très faibles perturbations à cette bande.

[Traduit par le journal]

Introduction

Since the discovery of the antitumor activity of *cis*-DDP and other related platinum compounds (1), which seem to bind DNA in tumor cells (2), several attempts have been made (2–7) to explain the mechanism of action of *cis*-DDP *in vitro* and *in vivo*. The N$_7$-bonding of mononucleotides (GMP, IMP, and AMP) to the *cis*-DDP and other metals has been reported both in solid state and in solutions (8). However, the possibility of a direct metal–carbonyl interaction, in addition to N$_7$-bonding, has been the subject of a long controversy (8, 9). It has been suggested (2) that the effectiveness of the platinum antitumor agent is based on the interaction of the drug with the guanine bases at N$_7$ in the GC pairs (7, 10, 11) in nucleic acids and also on the interaction with the O$_6$ of the carbonyl group of guanine (12, 13). Such an interaction could lead to deprotonation of N$_1$ of the guanine residue and eventually lead to a mispairing of guanine with thymine and finally cause the cell death (2, 13*c*). Several attempts have been made (12–14) to demonstrate the direct metal–carbonyl coordination in addition to the N$_7$-bonding; however, no crystallographic evidence could be obtained. Recently, the structural analysis of a series of platinum blue compounds containing DNA components (uracil and thymine derivatives) showed (15–17) direct metal–carbonyl bonding as well as Pt–nitrogen interaction (bridging). Bau *et al.* have recently analysed (18) the crystal structure of Cu$_4$(5′-IMPH$_{-1}$)$_2$(*o*-phen)$_4$(H$_2$O)$_4^{2+}$ in which two of the Cu(II) cations show N$_7$—O$_6$ bonding (bridging) while the two other Cu(II) ions show N$_1$- and phosphate bonding.

More recent spectroscopic studies (19, 20) showed that platinum(II) could interact with a guanosine residue and lead to the formation of a direct metal–carbonyl bonding, if the reaction was performed under basic conditions (pH = 9–10). These studies are concerned with the tautomeric conversion of a keto-imine (A) to an enol-imine (B) form, in acidic and basic solutions, respectively. On the basis of the above observations it was concluded that the deprotonation of the B form at basic pH values in the presence of platinum or other metal cations could lead to the formation of a negatively charged oxygen atom at O_6^- which would give a chelated metal–nucleobase compound linked to the metal via the N$_7$-atom and the carbonyl oxygen atom of the guanine residue at O$_6$. Most recently, it has been shown theoretically (21) that if a monomer complex in 1:1 ratio is formed between Pt(NH$_3$)$_2$Cl$_2$ and a guanine residue of DNA, the most stable bonds formed would be those of N$_7$—Pt—O$_6$ chelation.

The marked similarities of 5′-IMP coordination chemistry to that of guanosine-5′-monophosphate (5′-GMP), prompted us to study the interaction between 5′-IMPNa$_2$ and *cis*- and *trans*-DDP at neutral pH's. The present solution infrared study shows that there is a metal–carbonyl interaction in the case of 1:1 complexes in addition to the Pt—N$_7$ bond only with the *cis*-DDP and not with the *trans*-DDP.

In the present work the different behaviour of *cis*- and *trans*-interaction towards 5′-IMPNa$_2$ in solution and in several solid isolated platinum(II)–nucleotide complexes is described. Furthermore, a correlation between the spectral changes and the coordination sites used by the mononucleotide, with possible assignments of the ir vibrational frequencies is given. The

Can. J. Chem. Downloaded from www.nrcresearchpress.com by 210.87.254.5 on 09/06/12
For personal use only.

structure of 5′-IMPNa$_2$ with the numbering of the atoms is illustrated below.

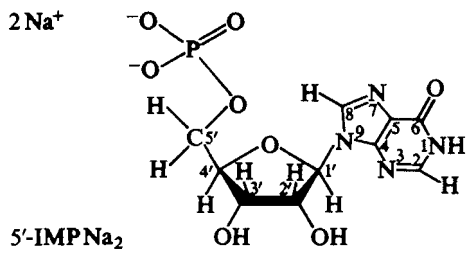

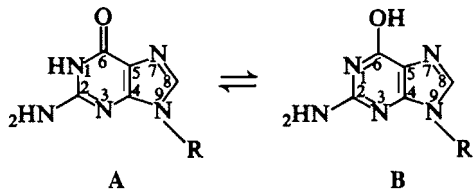

Experimental

Materials

5′-IMP in acid and sodium salt forms were purchased from Sigma Chemical Company. D_2O (99.8) was from Cambridge Isotope Laboratories. K_2PtCl_4 was from Johnson Matthey Chemicals, and it was converted to *cis*- and *trans*-DDP by published methods (22, 23) and purified as reported (24). All the other chemicals were reagent grade and used as supplied.

Preparation of the stock solutions

Solutions of the platinum compounds were prepared by mixing the *cis*- and *trans*-DDP with an IMPNa$_2$ solution in H_2O or D_2O to give a 1 : 1 ratio (0.05 mol) and were kept in the dark with constant shaking for a period of 8 days. The pH (pD) of the solutions was adjusted to 7.0 ± 0.2 with 0.1 *N* NaOH (NaOD) or $HClO_4$ ($DClO_4$). The solution pH values were measured every day before and after recording the spectra with a Fisher Accumet Model 630 pH meter, and for D_2O solutions the meter reading was corrected as described in the literature (25).

Synthesis of the platinum compounds

The Pt(II) compounds with 5′-IMPNa$_2$ were prepared by the addition of stoichiometric amounts of K_2PtCl_4 or *cis*- and *trans*-DDP to the solution of the mononucleotide in 200 mL water, in the presence of appropriate amounts of NaCl at room temperature and at pH = 7. The solutions were kept in the dark for one week and then the amount of water was reduced to 50 mL under low pressure at 50°C. Ethanol (50 mL) was then used to precipitate the compound. This was washed with ethanol several times, then dried over $CaCl_2$ and analyzed to show a composition of $[Pt(IMPNa_2)_n]Cl_2.xH_2O$, where n = 1, 2, or 3 and x = 4−6. The *cis*- or *trans*-DDP give compounds of the formula $[Pt(NH_3)_2(IMPNa_2)_n]Cl_2.xH_2O$, where n = 1 or 2 and x = 0−2. The compounds and hygroscopic, soluble in water or acidic solutions, but not in common organic solvents. They show high values of molar conductivity Λ_M (400−80 Ω^{-1} cm^2 mol^{-1}) at 25°C in water solutions. This is mainly due to the presence of Na^+ ions (26) associated with the 5′-IMPNa$_2$, preventing us to draw a conclusion on the ionic nature of these compounds. The analytical data are given in Table 1.

FT-ir spectra

Infrared spectra have been recorded on a DIGILAB FTS-15C/D Fourier Transform Infrared Interferometer equipped with a wide range HgCdTe detector (Infrared Associates, New Brunswick, NJ), a KBr Beam Splitter and a Globar source.

A sealed BaF_2 cell (International Crystal Laboratories) with a nominal path length of 0.0124 cm was used (for solutions) and the instrument was purged with nitrogen.

Normally 500 to 1000 interferograms of 2048 points were recorded with an optical velocity of 1.2 cm s^{-1} and a maximum optical retardation of 0.25 cm, co-added and Fourier transformed with four levels of zero filling for a spectral resolution of 4 cm^{-1}.

The interferograms of the D_2O solutions were apodized with a triangular function while water liquid and vapor was subtracted from the absorbance spectra of the aqueous solutions, then the resulting spectrum was smoothed using a Lorentzian function $F(X) = 1/1 + X^2/CVF^2$ where X is the distance of the point being weighted (in points) from the current point and CVF is the convolution factor, "CVF = 1" approximately. This is a common procedure which affects, however the resolution by a factor of 2, which corresponds to an effective resolution of 8.

Conductance measurements

The molar conductivities of the Pt−IMP compounds were measured on a conductoscope, E365B Metrohm.

Elemental analysis

The Pt(II) content has been determined by atomic absorption. C, H, and N were analysed by Schwarzkopf Microanalytical Laboratory (USA). The halide was determined as silver halide.

Results and discussion

Interaction of cis- *and* trans-*$Pt(NH_3)_2Cl_2$ and 5′-IMPNa$_2$ in solution*

Figure 1 shows the recorded FT-ir spectra of the *cis*- and *trans*-DDP with 5′-IMPNa$_2$ for the 1 : 1 ratio in H_2O at 27°C and pH = 7, after 1 day, 5 days, and 8 days. Figure 2 shows the corresponding reactions in D_2O solutions under similar conditions. The strong and broad absorption band at 1685 cm^{-1} in water solutions related mainly to the C_6=O stretching vibration (27, 28) of the free 5′-IMPNa$_2$, exhibited considerable intensity changes (shifting and splitting) between day *1* and day *5* and finally shifted to a lower frequency near 1635 cm^{-1} between days *5* and *8* upon *cis*-DDP complexation. For the *trans* isomer a small shift of that band towards higher frequencies ($\Delta\bar{\nu}$ = 5 cm^{-1}) was observed (Fig. 1). Similar trends were observed for the C_6=O stretching vibration at 1670 cm^{-1} in D_2O solutions upon interaction with *cis*- and *trans*-DDP. The shifting of the carbonyl stretching vibration towards a lower frequency ($\Delta\bar{\nu}$ = 50 cm^{-1}) with the *cis*-DDP, and that there was no change upon reaction with the *trans*-DDP is clearly a positive indication of an interaction of the *cis*-DDP with the carbonyl group (bridging or chelation). It is worth noting that the solid state complexes isolated from the above aqueous solutions after standing for a period of *8* days by precipitation with ethanol showed similar spectral changes in the carbonyl stretching region (Fig. 3). The carbonyl stretching frequency of 5′-IMPNa$_2$ at 1675 cm^{-1} shifted to a lower frequency at 1622 cm^{-1} in the spectrum of the structurally known (18) $[Cu_4(IMP_{-H})_2(o\text{-phen})_4(H_2O)_4^{2+}]^{2+}$, where a bridging Cu—$N_7O_6$—Cu has been observed. This carbonyl band shifted towards a higher frequency at 1680 cm^{-1} in the spectrum of the known (29) $[Cu(IMP)(dpa)(H_2O)]_2$ compound, where there is no Cu−purine interaction, the copper being linked only to the phosphates. The infrared study of the structurally known $[Cu(IMP).H_2O]_n$ (30) showed that the carbonyl stretching vibration of the free nucleotide at about 1680 cm^{-1} appeared at 1690 cm^{-1} upon base metalation and this is characteristic of an uncomplexed carbonyl group, metal-bonding is through the N_7- and the phosphate oxygen atoms here. A similar trend was found in the ir spectra of the structurally characterized (12, 31) $[cis\text{-}Pt(NH_3)_2(IMP)_2]^{2+}$, where the Pt-bonding is through the

Can. J. Chem. Downloaded from www.nrcresearchpress.com by 210.87.254.5 on 09/06/12
For personal use only.

TABLE 1. Analytical data for platinum(II)–IMP complexes

Compounds		% Pt	% C	% H	% N	% Cl
$K[Pt(IMP)Cl_3]4H_2O$	Found	23.90	15.36	2.38	7.40	12.95
	Calcd.	24.20	14.90	2.48	6.95	13.22
$[Pt(IMP)_2Cl_2]6H_2O$		16.90	21.31	2.77	9.87	6.10
		17.13	21.35	2.84	9.96	6.31
$[Pt(IMP)_3Cl]Cl6H_2O$		12.25	22.38	3.00	10.71	4.35
		12.55	23.18	3.09	10.81	4.57
cis-$[Pt(NH_3)_2(IMP)]Cl_22H_2O$		26.50	15.97	3.04	12.07	9.45
		26.74	16.46	3.01	11.52	9.73
cis-$[Pt(NH_3)_2(IMP)_2]Cl_2C_2H_5OH$		17.45	23.20	3.51	12.36	6.00
		17.22	23.32	3.18	13.43	6.27
trans-$[Pt(NH_3)_2(IMP)Cl]Cl$		27.90	17.94	3.57	12.62	10.10
		28.13	17.32	2.60	12.12	10.25
trans-$Pt(NH_3)_2(IMP)_2]Cl_2C_2H_5OH$		17.50	23.78	3.37	12.97	5.95
		17.22	23.32	3.18	13.36	6.27

TABLE 2. Carbonyl stretching frequencies of 5′-$IMPNa_2$ in different coordination environments

Compound[a]	C_6=O stretching frequency (cm^{-1})	Binding sites	References
Solid state			
5′-$IMPNa_2$	1675	—	18
$Cu_4(IMP)_2(o\text{-phen})_4(H_2O)_4^{2+}$	1622	N_7—O_6	18
$Cu(IMP)(dpa)(H_2O)_2$	1680	Phosphate	29
$[Cu(IMP)H_2O]_n$	1690	N_7- and phosphate	30
cis-$Pt(NH_3)_2(IMP)_2^{2+}$	1690	N_7-atom	12 and this work
Solutions (H_2O)			
5′-$IMPNa_2$	1685	—	This work
cis-$Pt(NH_3)_2(IMP)Cl_2$	1635	Possible N_7—O_6	This work
trans-$Pt(NH_3)_2(IMP)Cl_2$	1690	N_7-only	This work
Solutions (D_2O)			
5′-$IMPNa_2$	1670	—	This work
cis-$Pt(NH_3)_2(IMP)Cl_2$	1680, 1630	Possible N_7—O_6	This work
trans-$Pt(NH_3)_2(IMP)Cl_2$	1680	N_7-only	This work

[a]*o*-phen: *o*-phenananthroline.
dpa: dipyridylamine.

N_7-atom in both purine rings. The spectral changes occurred for the carbonyl group of the 5′-$IMPNa_2$ in different coordination environments are given in Table 2. Recently, Lippert *et al.* have reported (15) an X-ray structural and infrared analysis of several metal–methylthyminato complexes of *cis*-DDP and Ag^+ that showed direct metal–carbonyl bonding. It was shown that the C=O stretching vibration of the free nucleobase at 1660 cm^{-1} exhibited shifting towards lower frequencies upon direct Pt(II) or Ag–carbonyl interaction, whereas when the carbonyl did not interact with the metal there was no considerable perturbation of this vibrational frequency (15). Similar behaviour was observed in an infrared study (32) of a series of methylthymine compounds with CH_3Hg^+ and Ag^+ cations. The direct coordination of the Ag – carbonyl oxygen atom caused splitting and shifting of the C=O stretching vibration of the free base to a lower frequency in the Ag–methylthymine compound, while N_3-coordination of the CH_3Hg^+ moiety did not alter the position of the carbonyl absorption band considerably. It has been also suggested (19) that deprotonation of N_1^- of the guanine nucleobase moiety under basic conditions in the presence of the $Pt(en)^{2+}$ cation could lead to the formation of N_7—Pt—O_6 chelation. The N_7—Pt—O_6 interaction was also proposed (33) in the guanosine reaction with $PtenCl_2$ from nmr spectra of the $[Pt(en)(Guo)]^{2+}$ complexes. It is interesting to note that the solution studies of *cis*- and *trans*-DDP with 5′-$GMPNa_2$ at neutral conditions showed similar shifting and splitting of the C_6=O stretching frequency from 1690 cm^{-1} to about 1600 cm^{-1} upon *cis*-complexation, whereas the *trans*-DDP interaction produced no alteration in this frequency (34).

The distinct spectral similarities in the carbonyl region of the [*cis*-$Pt(NH_3)_2(IMP)]Cl_2$ and that of the structurally known $[Cu_4(IMP)_2(o\text{-phen})_4(H_2O)_4^{2+}]$ (Table 2) are indicative of a bridging platinum–IMP compound via the oxygen atom of the carbonyl group and the N_7-atom of the imidazol ring with a possible dimer formula, $[Pt_2(IMP)_2(NH_3)_4(H_2O)]^{2+}$. This is under investigation in our laboratory and attempts are being made to obtain single crystals of this material for X-ray analysis. The spectral similarities of the [*trans*-$Pt(NH_3)_2(IMP)_2]Cl_2$ to that of the structurally known (12, 31) N_7-bonded [*cis*-$Pt(NH_3)_2(IMP)_2]^{2+}$ compound (see Table 2) indicate that only N_7-bonding with platinum exists in the *trans*-IMP compound.

The absorption bands at about 1595, 1560, and 1535 cm^{-1} in the spectrum of the free base assigned to the skeletal vibrations (27, 28) of the ring system showed marked intensity changes upon *cis*-interaction (Fig. 1), whereas with the *trans*-isomer only the imidazole band at 1535 cm^{-1} exhibited changes indi-

Can. J. Chem. Downloaded from www.nrcresearchpress.com by 210.87.254.5 on 09/06/12
For personal use only.

Can. J. Chem. Downloaded from www.nrcresearchpress.com by 210.87.254.5 on 09/06/12
For personal use only.

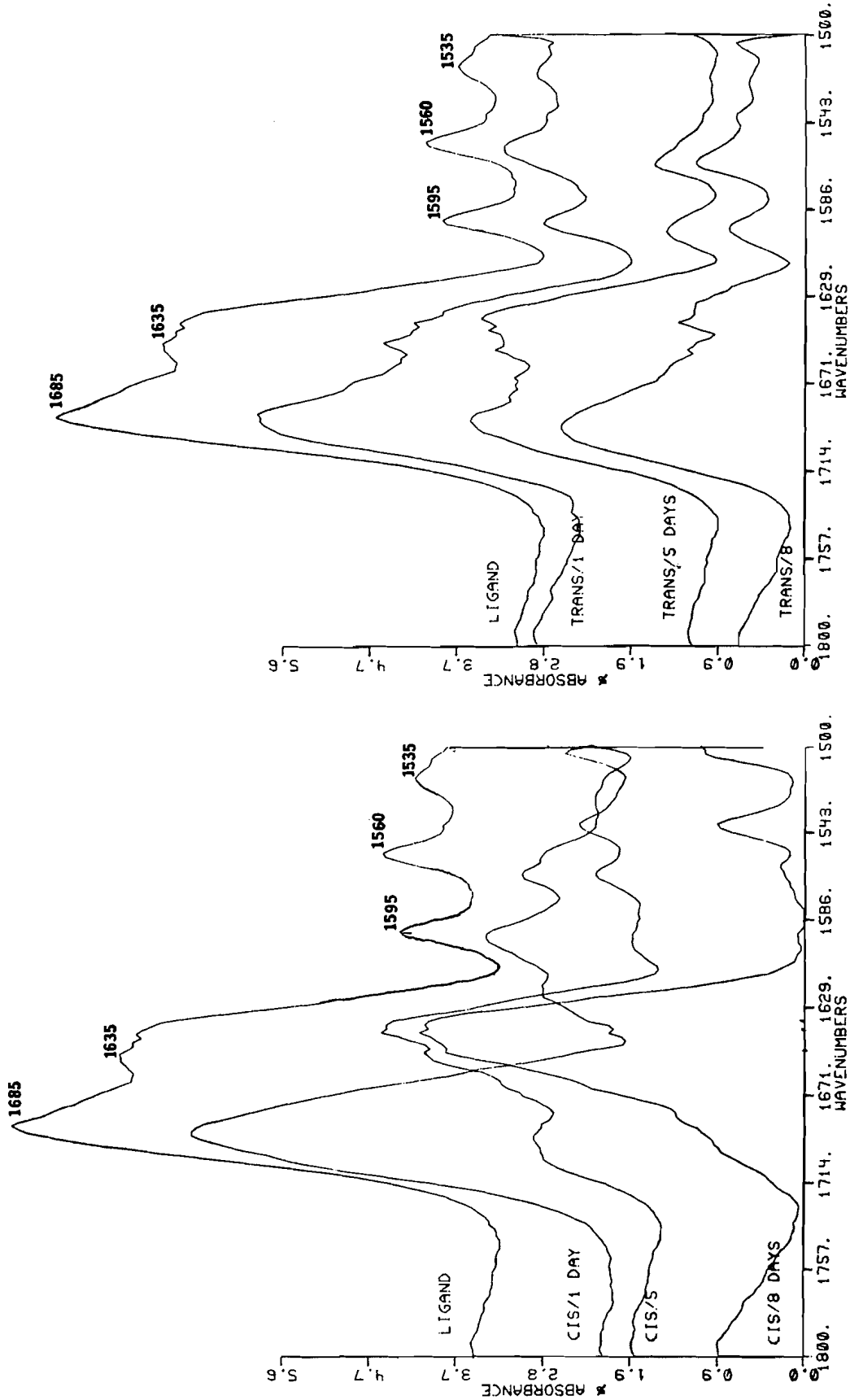

FIG. 1. FT-ir spectra of 5′-IMPNa$_2$ and its interaction in aqueous solution with *cis*- and *trans*-Pt(NH$_3$)$_2$Cl$_2$ at pH = 7 in the ratio of 1 : 1 (0.05 mol).

Can. J. Chem. Downloaded from www.nrcresearchpress.com by 210.87.254.5 on 09/06/12
For personal use only.

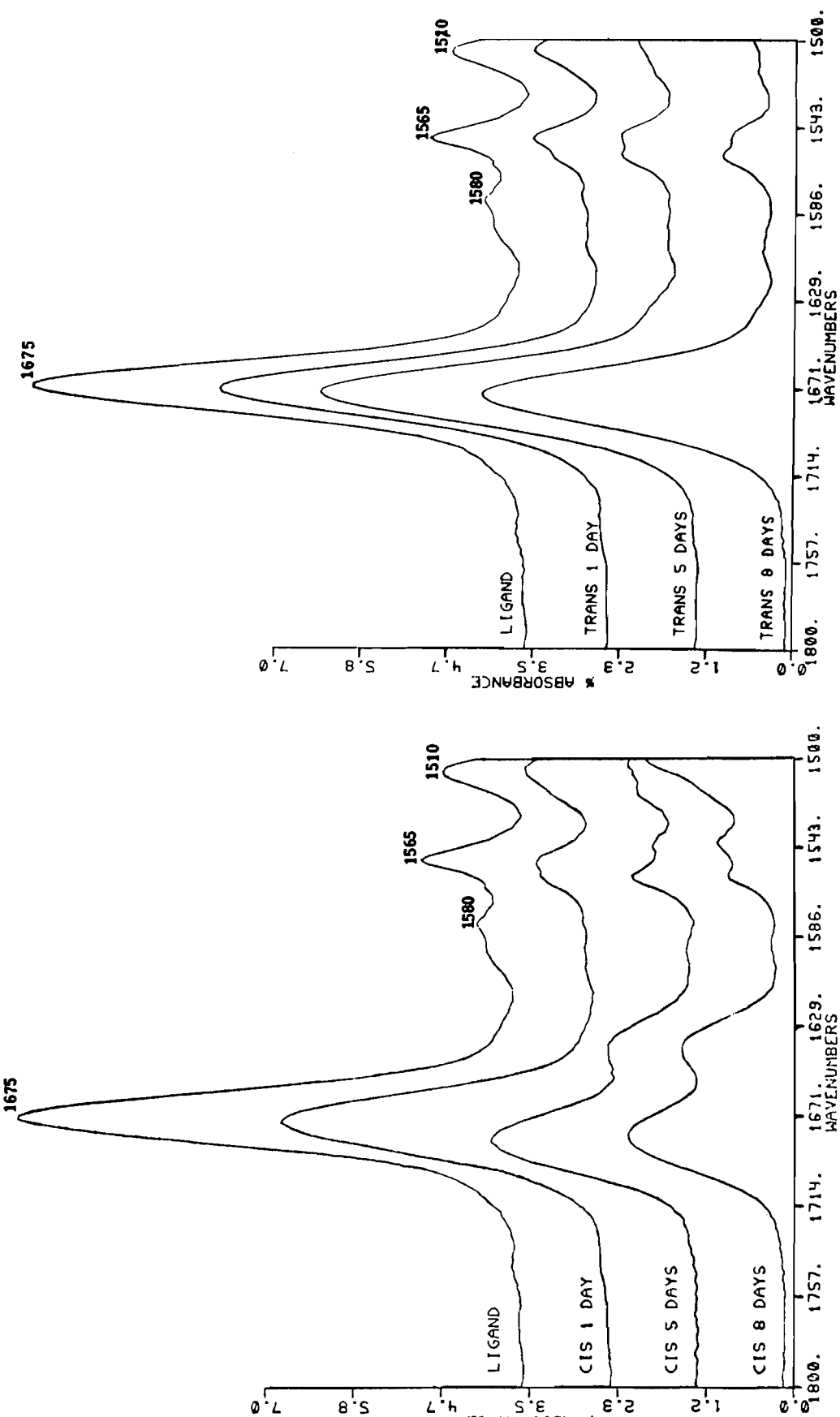

FIG. 2. FT-ir spectra of 5′-IMPNa$_2$ and its interaction in D_2O solution with *cis*- and *trans*-Pt$(NH_3)_2Cl_2$ at pD = 7 in the ratio of 1:1 (0.05 mol).

Can. J. Chem. Downloaded from www.nrcresearchpress.com by 210.87.254.5 on 09/06/12
For personal use only.

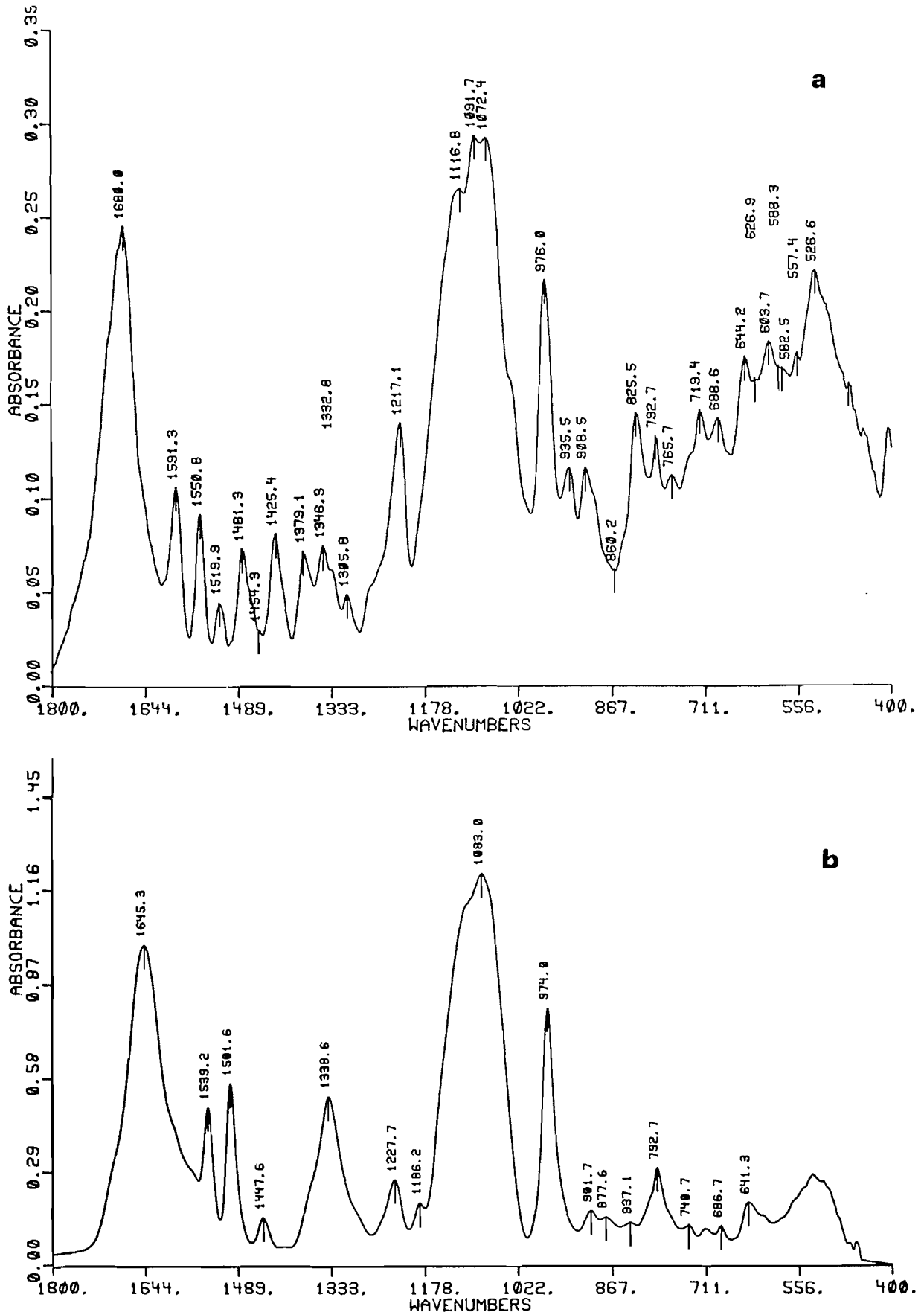

FIG. 3. FT-ir spectra of the free 5′-IMPNa$_2$ and its 1:1 platinum complexes obtained from neutral solutions: (*a*) 5′-IMPNa$_2$ and (*b*) *cis*-Pt(NH$_3$)$_2$(IMP)Cl$_2$.2H$_2$O.

Can. J. Chem. Downloaded from www.nrcresearchpress.com by 210.87.254.5 on 09/06/12
For personal use only.

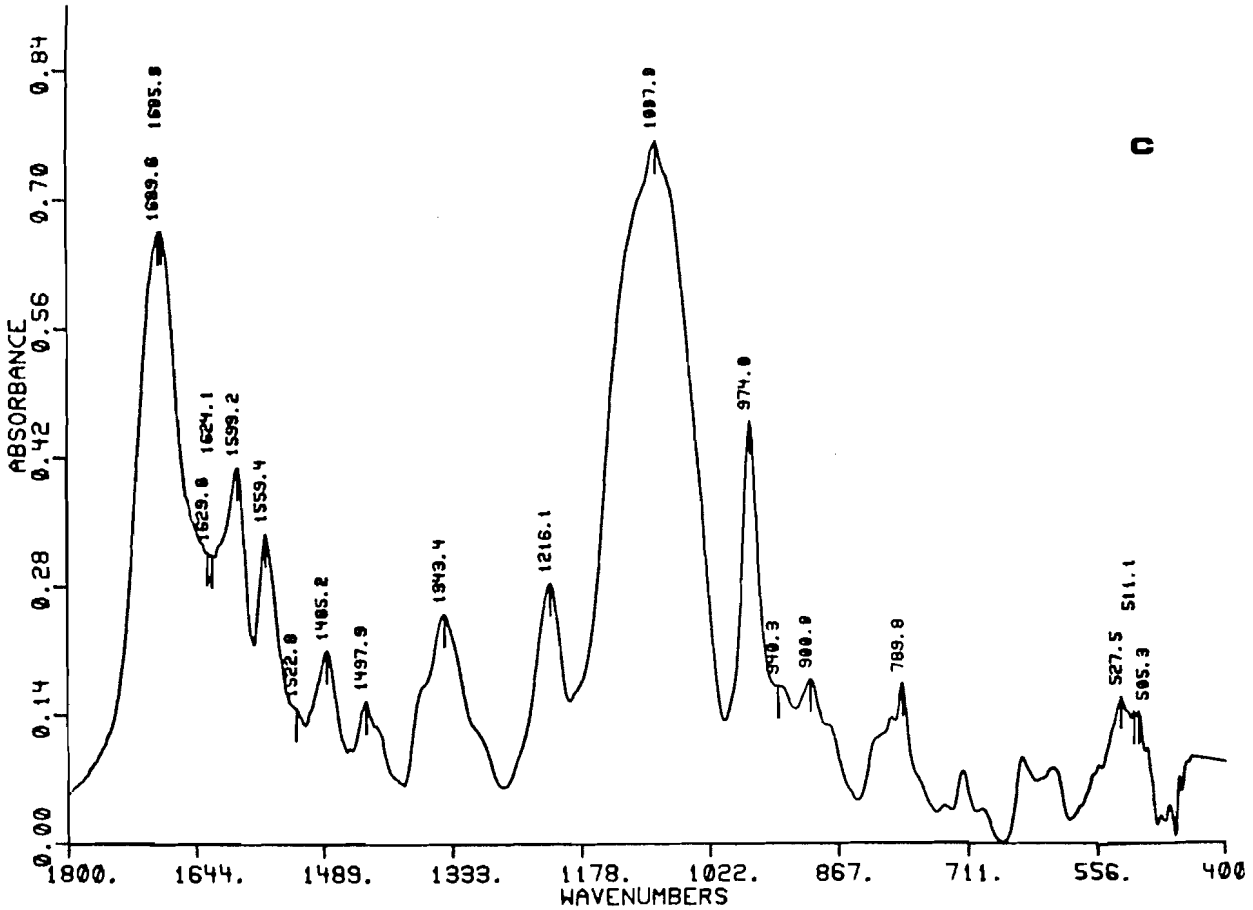

FIG. 3 (*Concluded*). FT-ir spectra of the free 5′-IMPNa$_2$ and its platinum complexes obtained from neutral solutions: (*c*) *trans*-Pt(NH$_3$)$_2$(IMP)Cl$_2$.

cating an N_7-bonding (Fig. 1). Since the C_6=O and the C=C stretching vibrations of the ring system are strongly coupled, it seems that upon carbonyl coordination the double bond stretching region is strongly affected as a consequence of uncoupling and delocalization of the π electrons in the heterocyclic ring and the exocyclic C_6=O group.

Solid-state platinum–IMP complexes

Structural analysis of $[Pt(NH_3)_2(IMPNa_2)_2]^{2+}$ shows (12, 31) that the Pt(II) ion is bonded to the N_7-atoms of both purine rings and to two NH_3 groups in a square plane arrangement. Furthermore, the coordination polyhedron around each Na^+ ion is completed by the sugar OH groups and water molecules. The carbonyl and the phosphate groups are hydrogen bonded to metal-coordinated H_2O molecules. In this work the FT-ir spectra of 5′-IMPNa$_2$ and its defined platinum compounds have been recorded and compared with that of the structurally known $[Pt(NH_3)_2(IMP)_2]^{2+}$. This comparison has allowed the observation of the characteristic features of each structural type of compound obtained here and the establishment of a correlation between the spectral changes and the binding sites used by the 5′-IMPNa$_2$ molecule. The results obtained are discussed for the two different regions, namely, 3700–2700 cm^{-1} and 1800–400 cm^{-1}. In the region 3700–2700 cm^{-1} the asymmetric and symmetric stretching vibration (27, 28) of NH, OH, H_2O, CH, and CH_2 groups of the free base are observed and showed no appreciable changes upon metalation. The rearrangement of the strong hydrogen bonding network of the free nucleotide (36) in the crystal structure of the platinum compound (12, 31) caused small shifts of the bands to higher frequencies. The main features of the spectra of the solid compounds with possible assignment are given in Table 3.

Drastic spectral changes occurred in the 1800–400 cm^{-1} region of the spectra upon complexation. A strong and broad absorption band at 1680 cm^{-1} of the free 5′-IMPNa$_2$ molecule, mainly related (27, 28) to the C_6=O stretching frequency, showed considerable intensity changes and shifted towards lower frequencies in the spectra of the 1:1 *cis*-$[Pt(NH_3)_2(IMP)]Cl_2$ and K[P(IMP)Cl$_3$] complexes (Figs. 3, 4 and Table 3). The shift of the carbonyl stretching frequency to lower frequencies ($\Delta\bar{\nu}$ = −35 cm^{-1}) in the spectra of these compounds is indicative of metal–carbonyl interaction. Similar observations have been made by Bau *et al.* (18) in the spectra of $[Cu_4(IMP)_2(o\text{-phen})_4(H_2O)_4]^{2+}$, where the Cu(II) ion binds to N_7 and O_6 of two IMP molecules (Table 2). On the other hand, the carbonyl stretching vibration of the free ligand at 1680 cm^{-1} shifted towards higher frequencies at about 1690 cm^{-1} in the spectra of all the other platinum–IMP complexes studied here (Figs. 3, 4, and Table 3). Similar high shifts have been observed for the structurally analysed (12, 31) *cis*-$[Pt(NH_3)_2(IMP)_2]^{2+}$ compound, where the platinum coordination takes place only through the N_7-atom of the imidazol ring (Table 2).

Three other absorption bands with medium intensities at about 1590, 1550, and 1520 cm^{-1} assignable mainly to the skeletal C_4—N_3, C_4—C_5, and C_4—N_9 stretching vibrations,

Can. J. Chem. Downloaded from www.nrcresearchpress.com by 210.87.254.5 on 09/06/12
For personal use only.

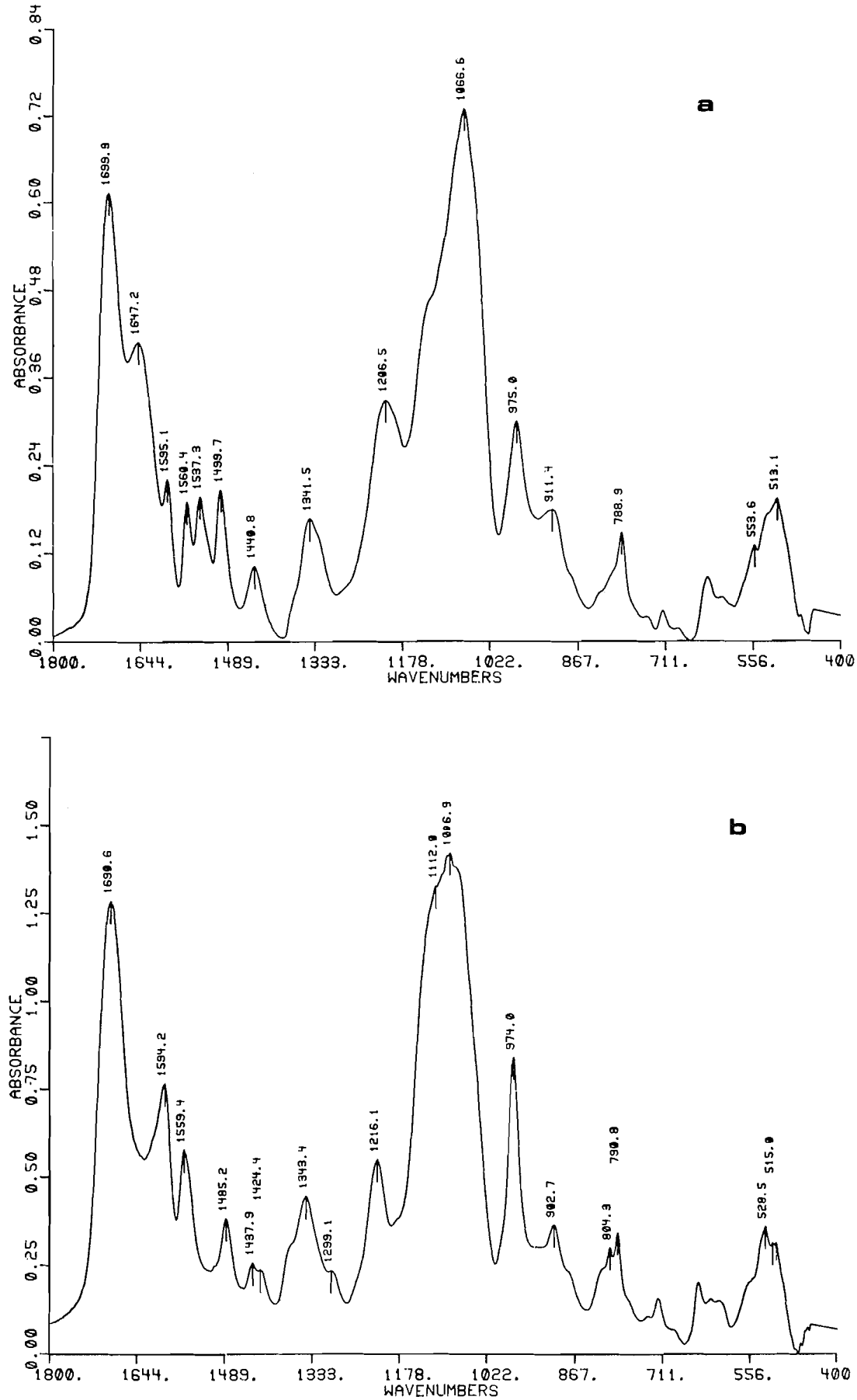

FIG. 4. FT-ir spectra of platinum–IMP complexes in the solid state: (*a*) $K[Pt(IMP)Cl_3].4H_2O$ and (*b*) $Pt(IMP)_2Cl_2.6H_2O$.

Can. J. Chem. Downloaded from www.nrcresearchpress.com by 210.87.254.5 on 09/06/12
For personal use only.

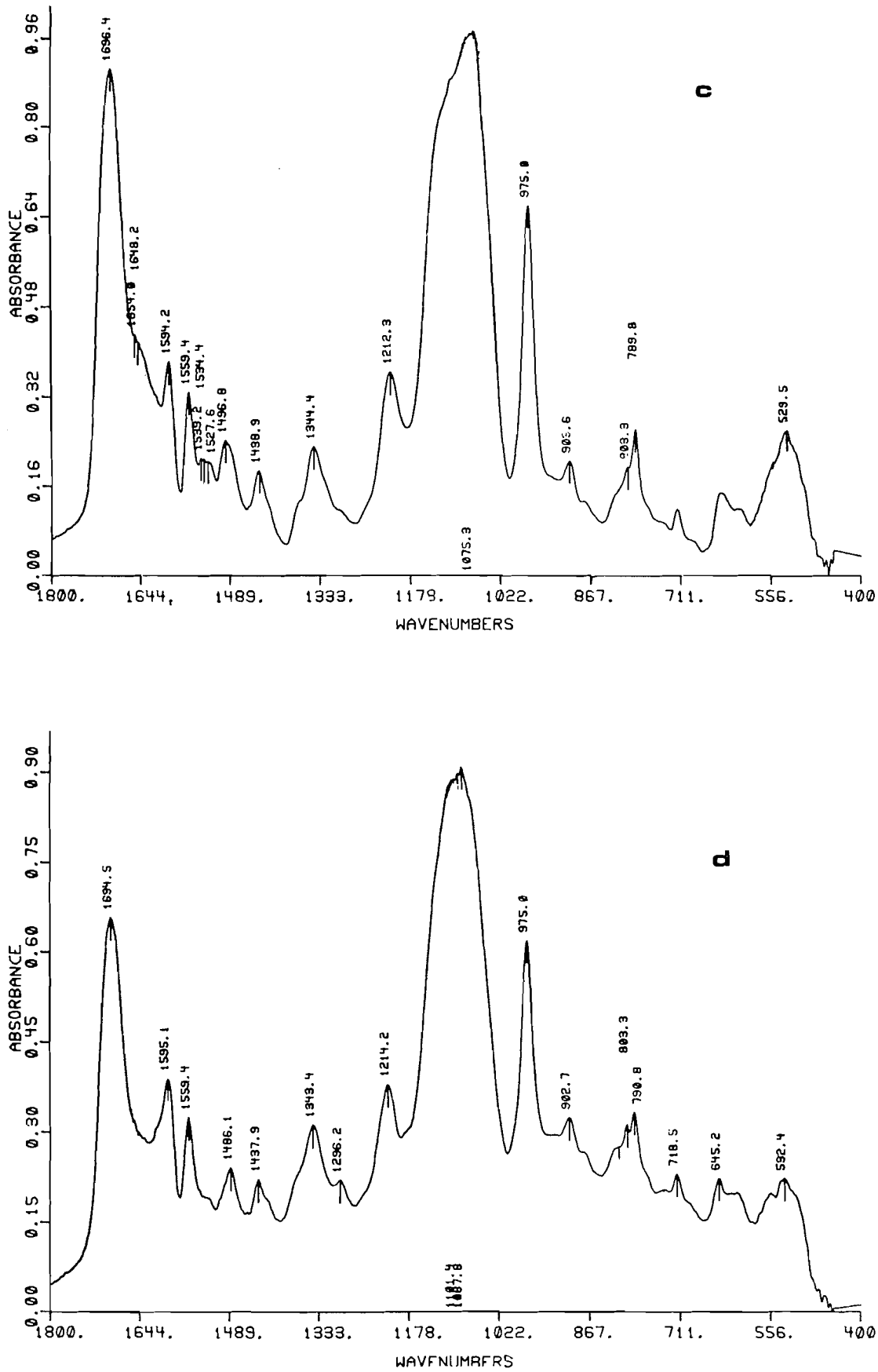

FIG. 4 (*Concluded*). FT-ir spectra of platinum-IMP complexes in the solid state: (*c*) *cis*-$Pt(NH_3)_2(IMP)_2Cl_2.C_2H_5OH$ and (*d*) *trans*-$Pt(NH_3)_2(IMP)_2Cl_2.C_2H_5OH$.

Can. J. Chem. Downloaded from www.nrcresearchpress.com by 210.87.254.5 on 09/06/12
For personal use only.

TABLE 3. FT-ir absorption bands (cm^{-1}) of the free 5′-IMPNa$_2$ and its platinum(II) compounds with possible assignment in the region 4000–400 cm^{-1}

5′-IMPNa$_2$	K[Pt(IMP)Cl$_3$].4H$_2$O	[Pt(IMP)$_2$Cl$_2$].6H$_2$O	[Pt(IMP)$_3$Cl]Cl.6H$_2$O	*cis*-[Pt(NH$_3$)$_2$(IMP)]Cl$_2$.2H$_2$O	*cis*-[Pt(NH$_3$)$_2$-(IMP)$_2$]Cl$_2$C$_2$H$_5$OH	*trans*-[Pt(NH$_3$)$_2$-(IMP)Cl]Cl	*trans*-[Pt(NH$_3$)$_2$-(IMP)$_2$]Cl$_2$.C$_2$H$_5$OH	Possible assignments (27, 28, 35, 37, 41, 42, 45)
3427 bs	3460 s	3750 b	3460 b	3440 b	3450 b	3440 b	3460 bs	ν_{NH}
3302 bs	3340 s	3320 s	3330 s	3320 b	3310 bs	3315 bs	3260 bs	ν_{OH}
3082 s	3130 s	3120 s	3115 m	3100 m	3110 s	3120 s	3142 s	ν_{C_8-H}
3047 s	3060 s	3050 m	3040 m	3050 m	3055 m	3060 m	3050 m	ν_{NH}
2950 m	2950 m	2960 m	2955 m	2960 m	2960 m	2955 m	2960 m	ν_{CH_2}
2870 m	2860 m	2880 m	2870 m	2875 m	2885 m	2875 m	2880 m	ν_{CH}
1680 bs	1700 bs 1647 s	1696 bs	1695 vs	1645 vs	1695 vs	1690 vs	1691 bs	$\nu_{C_6=O} + \nu_{C_6=C_5}$
1591 m	1595 m	1595 m	1595 sh	1595 sh	1595 s	1597 vs	1594 s	$\delta_{NH} + \nu_{C_4-N_3}$
1551 m	1560 m	1559 m	—	—	1559 s	1560 s	1559 s	$\nu_{C_4-C_5} - \delta_{N_1-H} + \nu_{C_6-N_1}$
1520 w	1537 m	1534 w	1540 m	1540 m	1530 vw	1532 sh	—	$\nu_{C_4-N_9} + \nu_{C_5-N_7}$
1480 m	1500 s	1497 m	1502 s	1502 s	1486 m	1486 m	1485 m	$\nu_{C_8-H} + \nu_{N_7-C_8}$
1425 m	1440 m	1439 m	1440 m	1448 w	1438 m	1440 w	1438 m	$\delta_{CH_2} + \delta_{CH}$
1379 m	1360 sh	1362 sh	1305 sh	1360 sh	1365 sh	1360 sh	1365 sh	$\nu_{C_8-N_9} + \nu_{N_7-C_8} + \delta_{N_1H}$
1346 m	1342 s	1344 m	—	1339 s	1341 s	1341 s	1343 s	
1333 sh	1330 sh	1331 sh	—	—	—	—	—	$\nu_{C_5-N_7}$
1306 w	—	—	—	1300 sh	1298 sh	1298 sh	1299 sh	
1260 vw	—	1250 vw	1255 vw	1228 m	—	—	—	$\delta_{C_8-H} + \nu_{N_7-C_8}$
1217 s	1207 s	1212 s	1212 s	1186 vw	1214 s	1221 s	1116 s	
1117 s	1130 sh	1120 sh	1125 sh	1120 sh	1118 sh	1120 s	1112 sh	ν_{C-O} of sugar
1092 vs	—	—	—	—	—	—	—	$\nu_{PO_3^{2-}}$ deg.
1072 s	1067 bs	1070 bs	1071 bs	1083 bs	1088 bs	1087 bs	1087 bs	
1040 sh	—	—	—	—	—	—	—	ν_{C-O} of sugar
976 vs	976 s	975 vs	975 vs	974 s	975 vs	973 vs	974 s	$\nu_{PO_3^{2-}}$ symmetric
936 m	912 m	—	915 vw	—	—	—	—	Ribose–phosphate stretching
909 m	900 sh	904 w	900 vw	902 vw	903 m	901 m	902 w	
825 s	820 sh	805 sh	820 vw	837 vw	830 sh	803 sh	805 sh	Ribose–phosphate stretching
793 s	789 m	790 m	790 m	793 m	791 m	790 m	791 m	Ribose–phosphate stretching
760 m	750 sh	750 sh	—	750 sh	750 sh	752 sh	740 sh	Ribose–phosphate stretching
719 s	720 w	720 w	715 w	519 w	720 w	719 w	718 w	
688 m	692 vw	692 vw	690 sh	690 sh	692 vw	691 sh	692 sh	Ring breathing mode
644 m	650 m	650 m	640 m	645 w	650 w	646 w	650 m	Ring deformation
558 m	600 sh	600 sh	602 sh	600 vw	610 vw	600 vw	610 w	NH out-of-plane def.
527 s	556 sh	550 sh	—	550 w	555 w	550 sh	550 sh	PO_3^{2-} symmetric def.
500 sh	529 s	529 s	526 s	523 m	530 m	525 m	528 s	Skeletal def.
540 sh	—	—	—	—	—	—	515 sh	
480 vw	440 sh	440 vw	430 vw	445 sh	440 vw	430 vw	420 vw	PO_3^{2-} deg. def.

b, broad; s, strong; v, very; m, medium; ν, stretching and δ, bending.

Can. J. Chem. Downloaded from www.nrcresearchpress.com by 210.87.254.5 on 09/06/12
For personal use only.

respectively (27, 28), exhibited major intensity changes upon metal complex formation (Figs. 3, 4, and Table 3). The changes observed in these vibrational frequencies are mainly due to the N_7- and/or O_6 bonding, where both coordination sites (N_7- and O_6) are involved. The perturbation of the above vibrations is much stronger (Figs. 1–3) in the case of *cis*-$[Pt(NH_3)_2(IMP)]Cl_2$ and $K[Pt(IMP)Cl_3]$ than in the other complexes.

The absorption band with medium intensity at 1480 cm^{-1} mainly related to the C_8—N_7 stretching and C_8—H bending vibrations (35) shifted to a higher frequency in the spectra of the complexes. The shift of this band ($\Delta\bar{\nu}$ = 5–20 cm^{-1}) towards higher frequencies is consistent with the C=N^+ frequency. Since it has been found (38) that the C=N^+ groups have in general higher frequencies than the parent C=N groups, therefore, it seems that metalation (39) or protonation (40) of the C=N group slightly increases this vibrational frequency.

The other absorption bands at about 1380, 1346, 1333, 1260, and 1217 cm^{-1} have been attributed mainly to the purine ring vibrational frequencies (27, 41). They showed marked spectral changes (intensity changes and shifting) upon N_7-metalation (Table 3). These absorption bands are assigned to the N_7—C_8, C_8—N_9, C_5—N_7 stretchings and C_8—H bending vibrations. An absorption band with medium intensity at 688 cm^{-1} assigned to the ring breathing mode (27) appeared at a higher frequency in the spectra of the complexes (Table 3). Similar behaviour was observed for this absorption frequency in a series of N_7-metalated 5′-GMP complexes and is characteristic of N_7-bonding (35).

Phosphate vibrational frequencies

The vibrational frequencies of mononucleotides together with their metal-complexes have been discussed earlier (35). The ir spectra of 5′-$IMPNa_2$ show five absorption bands in the region 1100–400 cm^{-1} assignable to the phosphate group PO_3^{2-} vibrational frequencies (42): 1072 cm^{-1} (broad and strong) assigned to the PO_3^{2-} degenerate stretching; 976 cm^{-1} (strong) assigned to PO_3^{2-} symmetric stretching; 825 cm^{-1} (medium intensity) assigned to the ribose–phosphate stretching, and two other absorption bands at about 525–550 and 420–480 cm^{-1} assigned to the symmetric and degenerate deformation modes of the PO_3^{2-} group, respectively (Table 3).

The two absorption bands at 1072 and 976 cm^{-1} are sensitive to a direct metal–phosphate coordination. The FT-ir spectra of the structurally known (30, 43) $[Cu(IMP).H_2O]_n$ and $[Zn(IMP).H_2O]_n$ containing direct metal–phosphate bonding, showed shifting and splitting of these two bands, whereas the infrared spectra of the corresponding Co(II) and Ni(II) complexes (35) containing an indirect metal–phosphate interaction, through coordinated water molecules (44) exhibited no considerable changes in these vibrational frequencies.

The infrared spectra of all platinum complexes studied here showed no changes in the bands at 1072 and 976 cm^{-1} (Figs. 3, 4, and Table 3), indicating no direct metal–phosphate coordination for these Pt–IMP complexes.

Sugar vibrational frequencies

The sugar vibrational frequencies appeared as broad and strong bands at about 3600–2700 cm^{-1} (27, 42), the ribose ring also contains several sharp and fine absorption bands, in the region 1400–400 cm^{-1} that are mainly overlapped by the strong and broad absorption bands of the phosphate group and that of the base bands. The band at 1117 cm^{-1} assigned to the C—O stretching of the ribose ring (42) showed no major changes in the spectra of the platinum complexes (Table 3) which indicates no direct metal–sugar interaction. The other absorption bands at about 900–700 cm^{-1} assigned to the ribose–phosphate stretching vibrations (45) exhibited some intensity changes and shifting (Table 3) upon ligand metalation. The slight changes observed may be due to the conformational changes around the ribose–phosphate bond (46, 47) or to conformational changes of the sugar ring due to the direct or indirect metal–phosphate interaction.

Conclusion

Based on the comparison of spectroscopic changes from structurally known *cis*-$[Pt(NH_3)_2(IMP)_2]^{2+}$ and other Cu–IMP derivatives and the platinum compounds synthesized here, the following concluding remarks can be made: (*a*) The interaction between *cis*-DDP and 5′-$IMPNa_2$ in aqueous solutions leads to the formation of N_7–O_6 complexes with most probably N_7–O_6 bridging. The *trans*-isomer interaction gave complexes with an N_7–metal linkage only. (*b*) The other platinum–IMP complexes isolated as solids in this work show N_7-bonding. Only the 1:1 *cis*-$[Pt(NH_3)_2(IMP)]Cl_2$ and $K[Pt(IMP)Cl_3]$ complexes have shown N_7—O_6 bonding (bridging or chelation) as is concluded from ir spectral analysis. (*c*) No direct metal–phosphate complexes both in solution or in the solid state were obtained in this study.

Acknowledgments

We wish to acknowledge the financial support of Natural Sciences and Engineering Research Council of Canada and the gift of platinum salts from Johnson Matthey Chemicals Ltd.

1. B. ROSENBERG, L. VANCAMP, J. E. TROSKO, and V. H. MANSOUR. Nature, London, **222**, 385 (1969).
2. B. ROSENBERG. Biochimie, **60**, 859 (1978) and references therein.
3. L. G. MARZILLI. Prog. Inorg. Chem. **23**, 255 (1977).
4. G. Y. CHU, S. MANSY, R. S. E. DUNCAN, and R. S. TOBIAS. J. Am. Chem. Soc. **100**, 593 (1978); **100**, 607 (1978).
5. A. J. P. ALIX, L. BERNARD, M. MANFAIT, P. K. GANGULI, and T. THEOPHANIDES. Inorg. Chim. Acta, **55**, 147 (1981).
6. D. P. STROMMAN and W. L. PETICOLAS. Biopolymers, **21**, 969 (1982).
7. P. K. GANGULI and T. THEOPHANIDES. Eur. J. Biochem. **101**, 377 (1979); Inorg. Chim. Acta, **55**, L43 (1981).
8. T. G. SPIRO (*Editor*). Nucleic acid – metal ion interaction. Wiley, New York. 1980. pp. 33, 181.
9. A. W. PRESTOYKO, S. T. CROOK, and S. K. CARTER. *cis*-Platinum. Academic Press, New York. 1980. p. 22.
10. J. P. JANGOWSKI, J. P. MACQUET, and J. L. BUTOUR. Biochimie, **60**, 901 (1978).
11. P. J. STONE, A. D. KELMAN, and F. M. SINEX. Nature, London, **251**, 736 (1974).
12. D. M. L. GOODGAME, I. JEEVES, F. L. PHILLIPS, and A. C. SKAPSKI. Biochim. Biophys. Acta, **378**, 153 (1975).
13. J. P. MACQUET and T. THEOPHANIDES. (*a*) Biopolymers, **14**, 781 (1975); (*b*) Bioinorg. Chem. **5**, 59 (1975); (*c*) Biochim. Biophys. Acta, **402**, 166 (1975).
14. J. DEHAND and J. JORDANOV. J. Chem. Soc. Chem. Commun. 598 (1976).
15. B. LIPPERT and D. NEUGEBAUER. Inorg. Chim. Acta, **46**, L11 (1980); **46**, 171 (1980); **78**, 161 (1983).
16. B. LIPPERT and D. NEUGEBAUER. Inorg. Chim. Acta, **67**, 151 (1982); Inorg. Chem. **21**, 451 (1982); J. Am. Chem. Soc. **104**, 6599 (1982).
17. C. G. LOCK, H. J. PERESIE, B. ROSENBERG, and G. TURNER.

J. Am. Soc. **100**, 3371 (1978); Inorg. Chem. **20**, 804 (1981).
18. R. W. GELLERT, B. E. FISCHER, and R. BAU. J. Am. Chem. Soc. **102**, 7812 (1980).
19. A. PASINI and R. MENA. Inorg. Chim. Acta, **56**, L17 (1981).
20. L. G. MARZILLI, B. DE CASTRO, and C. SOLORZANO. J. Am. Chem. Soc. **104**, 461 (1982).
21. T. P. CARSEY and E. A. BOUDREAUX. Chem.-Biol. Interact. **30**, 189 (1980).
22. S. C. DHARA. Indian J. Chem. **8**, 193 (1970).
23. G. B. KAUFFMAN and D. O. COWAN. Inorg. Synth. **7**, 239 (1963).
24. G. RAUDASCHL, B. LIPPERT, and J. D. HOESCHELE. Inorg. Chim. Acta, **78**, L43 (1983).
25. P. K. GLASCOE and F. H. LONG. J. Phys. Chem. **64**, 188 (1960).
26. R. G. BHATTACHARYYA and L. BHADURI. J. Inorg. Nucl. Chem. **40**, 733 (1978).
27. R. C. LORD and G. J. THOMAS. Spectrochim. Acta, **23**A, 2551 (1967).
28. M. TSUBOI, S. TOKAHOSHI, and I. HORADA. Physicochemical properties of nucleic acid. Vol. 2. *Edited by* J. Duchense. Academic Press, New York. 1973.
29. R. W. GELLERT, B. E. FISCHER, and R. BAU. Biochem. Biophys. Res. Commun. **88**, 1443 (1979).
30. K. AOKI. J. Chem. Commun. 600 (1977).
31. T. J. KISTENMACHER, C. C. CHIANG, P. CHALILPOYIL, and L. MARZILLI. J. Am. Chem. Soc. **101**, 1143 (1979).
32. F. GUAY, A. L. BEAUCHAMP, C. GILBERT, and R. SAVOIE. Can. J. Spectrosc. **28**, 13 (1983).
33. N. HADJILIADIS and T. THEOPHANIDES. Inorg. Chim. Acta, **16**, 77 (1976).
34. W. L. PETICOLAS, J. KUFFMAN, H. A. TAJMIR-RIAHI, and T. THEOPHANIDES. To be published.
35. H. A. TAJMIR-RIAHI and T. THEOPHANIDES. Can. J. Chem. **61**, 1813 (1983).
36. N. NAGASHIMA and Y. IITAKA. Acta Crystallogr. B**24**, 1136 (1968); B**30**, 320 (1974); S. T. RAO and M. SUNDARALINGAM. J. Am. Chem. Soc. **91**, 1210 (1969).
37. S. MANSY and W. L. PETICOLAS. Biochemistry, **15**, 2650 (1976).
38. C. SANDORFY. The chemistry of the carbon–nitrogen double bond. *Edited by* S. Patai. John Wiley, New York. 1970. p. 42.
39. F. A. HART, M. UL-HUQUE, and C. N. GAUGHLAN. Chem. Commun. 1240 (1970); J. Inorg. Nucl. Chem. **31**, 145 (1969).
40. J. I. BULLOCK, M. F. C. LADD, D. C. POVEY, and H.A. TAJMIR-RIAHI. Acta Crystallogr. B**35**, 2013 (1979).
41. L. CHINSKY, P. Y. TURPIN, M. DUQUESNE, and J. BRAHMS. Biopolymers, **17**, 1347 (1978).
42. M. TSUBOI. Infrared and Raman spectroscopy in basic principles in nucleic acid chemistry. Vol. 1. Academic Press. 1974. p. 399; Adv. Chem. Phys. **7**, 435 (1964).
43. P. DE MEESTER, D. M. L. GOODGAME, T. J. JONSE, and A. C. SKAPSKI. Biochim. Biophys. Acta, **353**, 392 (1974).
44. K. AOKI. Bull. Chem. Soc. Jpn. **48**, 1260 (1975).
45. M. J. LANE and G. J. THOMAS, JR. Biochemistry, **18**, 3839 (1979).
46. G. MAKRIGIANNIS, P. PAPAGIANNAKOPOULOS, and T. THEOPHANIDES. Inorg. Chim. Acta, **46**, 263 (1980).
47. T. THEOPHANIDES (*Editor*). Infrared and Raman spectroscopy of biological molecules. Reidel Publishing Company, Dordrecht, Holland. 1979. pp. 205–223.

Can. J. Chem. Downloaded from www.nrcresearchpress.com by 210.87.254.5 on 09/06/12
For personal use only.

The retroaldol reaction of cinnamaldehyde

J. PETER GUTHRIE,[1] KEVIN J. COOPER, JOHN COSSAR, BRIAN A. DAWSON, AND KATHLEEN F. TAYLOR
Department of Chemistry, University of Western Ontario, London, Ont., Canada N6A 5B7

Received November 15, 1983

J. PETER GUTHRIE, KEVIN J. COOPER, JOHN COSSAR, BRIAN A. DAWSON, and KATHLEEN F. TAYLOR. Can. J. Chem. **62**, 1441 (1984).

Rate and equilibrium constants have been measured for the hydration and retroaldol reactions of cinnamaldehyde. The equilibrium constant for the 1,4-addition of water to cinnamaldehyde is 4.42×10^{-3}. The rate constants for hydroxide catalyzed reaction, extrapolated to zero hydroxide concentration (to correct for the addition of hydroxide to the aldol carbonyl), are: $k_{12}^0 = 2.20 \times 10^{-3} M^{-1} s^{-1}$; $k_{21}^0 = 0.456 M^{-1} s^{-1}$; and $k_{23}^0 = 9.08 \times 10^{-2} M^{-1} s^{-1}$. The rate of the formation reaction was measured by adding small amounts of acetaldehyde to alkaline solutions of benzaldehyde: $k_{32}^0 = 0.63 M^{-1} s^{-1}$ and $K_{overall} = 1480 M^{-1}$. The course of the synthetically useful reaction of acetaldehyde with benzaldehyde is discussed in the light of these results.

J. PETER GUTHRIE, KEVIN J. COOPER, JOHN COSSAR, BRIAN A. DAWSON et KATHLEEN F. TAYLOR. Can. J. Chem. **62**,1441 (1984).

On a mesuré les constantes de vitesse et d'équilibre des réactions d'hydratation et rétroaldolique du cinnamaldéhyde. La constante d'équilibre de l'addition-1,4 de l'eau sur le cinnamaldéhyde est de $4,42 \times 10^{-3}$. Les constantes de vitesse pour la réaction catalysée par l'hydroxyde, extrapolées à une concentration d'hydroxyde égale à zéro (pour corriger l'addition de l'hydroxyde sur le carbonyle de l'aldol), sont de $k_{12}^0 = 2,02 \times 10^{-3} M^{-1} s^{-1}$; $k_{21}^0 = 0,456 M^{-1} s^{-1}$; et $k_{23}^0 = 9,08 \times 10^{-2} M^{-1} s^{-1}$. On a mesuré la vitesse de la réaction de formation en ajoutant de petites quantités d'acétaldéhyde à des solutions alcalines de benzaldéhyde: $k_{32}^0 = 0,63 M^{-1} s^{-1}$ and $K_{global} = 1480 M^{-1}$. A la lumière de ces résultats, on discute du déroulement de la réaction de l'acétaldéhyde avec le benzaldéhyde qui présente de l'intéret comme réaction de synthèse.
[Traduit par le journal]

Can. J. Chem. Downloaded from www.nrcresearchpress.com by 210.87.254.105 on 09/06/12
For personal use only.

Introduction

We have reported a study (1) of the equilibrium constants for aldol condensation reactions. Since we consider it important to have a reliable set of rate and equilibrium constants for a set of simple aldol reactions and need such data for an examination of rate–equilibrium correlations for the aldol reaction, we have undertaken the investigation of the kinetics of various aldol reactions, studying them in the reverse sense to avoid the difficulties of side reactions which plague the kinetics of aldol reactions in the forward sense. The case of cinnamaldehyde is of interest because it is cited as a textbook example of thermodynamic control in the aldol reaction (2), yet has not been studied kinetically. Meyers and Durandatta (3) have reported a method for preparing the aldol corresponding to cinnamaldehyde, i.e. 3-hydroxy-3-phenylpropanal. This compound proved essential to the investigation, because the equilibrium constant for dehydration to cinnamaldehyde is quite large and cannot be measured directly by studying the hydration of cinnamaldehyde, yet must be known to sort out the kinetics.

Results and discussion

The retroaldol reaction of cinnamaldehyde can be followed spectrophotometrically; when cinnamaldehyde, as a solution in acetonitrile, is injected into aqueous sodium hydroxide solution there is a smooth disappearance of the absorbance at 285 nm, which follows a simple first-order rate law; see Fig. 1. Thus one can see no sign of the two stages which are believed to be essential for this reaction; eq. [1]

$$[1]\quad \mathrm{Ph{-}CH{=}CH{-}CHO} \underset{k_{21}}{\overset{k_{12}}{\rightleftharpoons}} \mathrm{Ph{-}CHOH{-}CH_2{-}CHO}$$

$$\mathrm{Ph{-}CHOH{-}CH_2{-}CHO} \underset{k_{32}}{\overset{k_{23}}{\rightleftharpoons}} \mathrm{Ph{-}CHO + CH_3{-}CHO}$$

The two phases of the reaction are quite apparent when the aldol, 3-phenyl-3-hydroxy-2-butanal, is injected into aqueous sodium hydroxide solution; the absorbance at 285 nm first rises and then, about 1000 times more slowly, falls again; see Fig. 2. The rate of the slow fall in absorbance is essentially identical

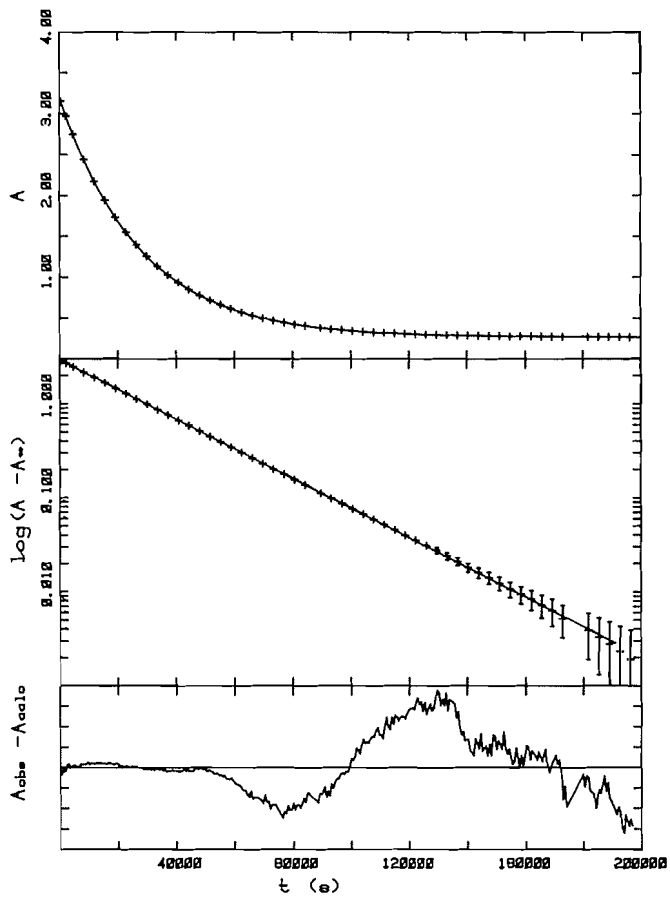

FIG. 1. Absorbance vs. time for the reaction of $7.82 \times 10^{-5} M$ cinnamaldehyde in 0.1 *N* NaOH. Followed at 285 nm, using 10-cm cells.

[1] Author to whom correspondence may be addressed.

Can. J. Chem. Downloaded from www.nrcresearchpress.com by 210.87.254.105 on 09/06/12
For personal use only.

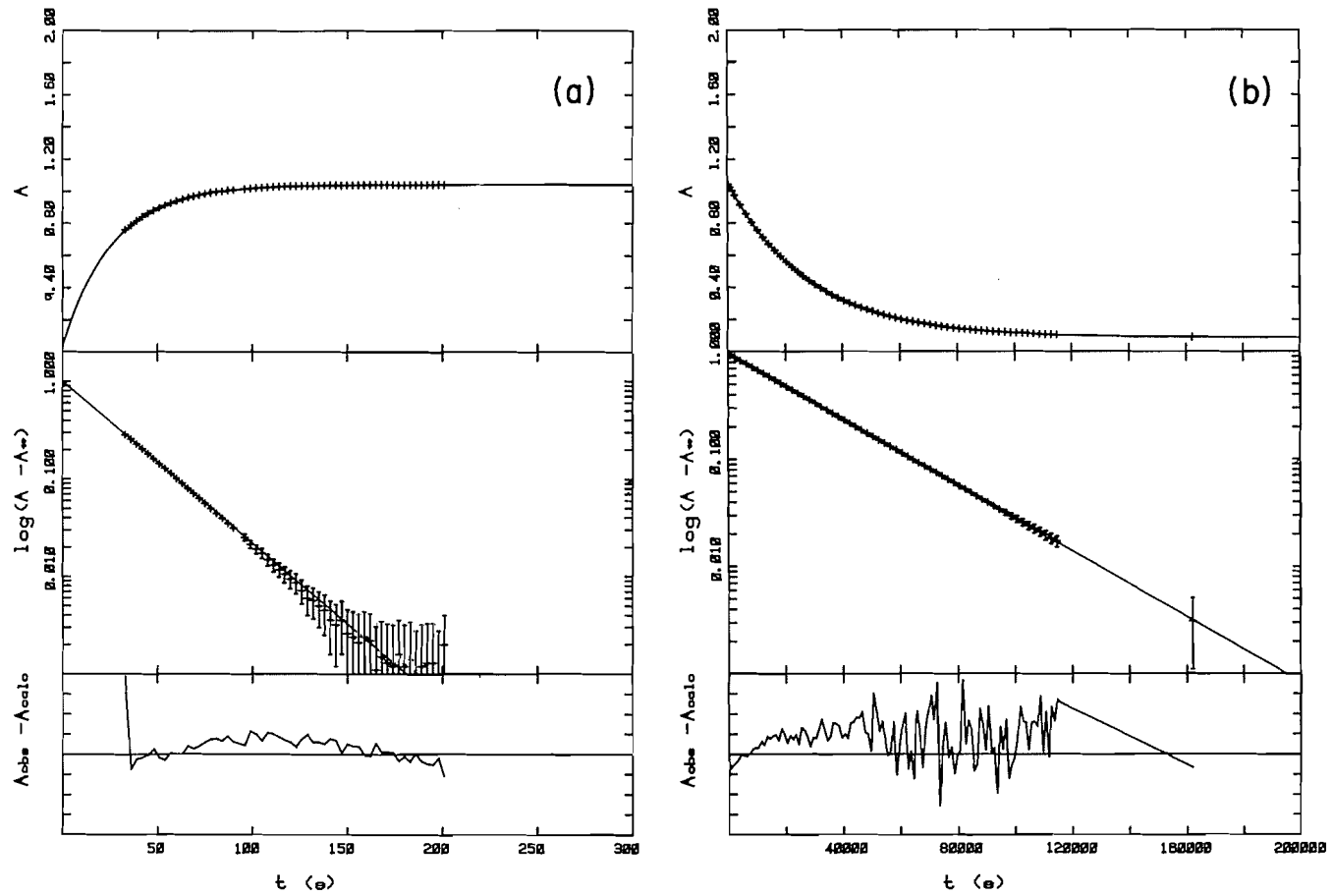

FIG. 2. Absorbance vs. time for the reaction of 5.33×10^{-6} *M* 3-hydroxy-3-phenylpropanal in 0.1 *N* NaOH. (a) Initial phase, appearance of cinnamaldehyde. (b) Final phase, disappearance of cinnamaldehyde. Followed at 285 nm, using 10-cm cells.

to the rate of disappearance of the absorbance of cinnamaldehyde when the latter is used to initiate reaction. Analysis of the two-phase kinetic data permits evaluation of the rate constants. For the system of interest, where a low concentration of aldol product undergoes retroaldol cleavage, the rate of the second-order aldol formation process, described by k_{32}, is negligible. A rigorous solution of the kinetics equations is possible following the procedure described in Moore and Pearson (4), but to an excellent approximation the two stages of the reaction can be treated independently. For the fast reaction,

$$A = A_\infty + \alpha \exp(-\lambda_2 t)$$

and for the slow reaction,

$$A = A_\infty + \beta \exp(-\lambda_3 t)$$

where: $-\alpha \cong C_2^0 k_{21} \epsilon_1/\lambda_2$; $\beta \cong C_1^0 \epsilon_1$ starting from cinnamaldehyde; $\beta \cong C_2^0 k_{21} \epsilon_1/\lambda_2$ starting from the aldol; $\lambda_2 \cong k_{21} + k_{23}$; $\lambda_3 \cong k_{12}/(1 + k_{21}/k_{23})$; ϵ_1 = extinction coefficient for cinnamaldehyde; and C_i^0 = initial concentration of cinnamaldehyde ($i = 1$) or aldol ($i = 2$). Then:

$$k_{21} = |\alpha|\lambda_2/C_2^0\epsilon_1$$

$$k_{23} = \lambda_2 - k_{21}$$

$$k_{12} = \lambda_3(1 + k_{21}/k_{23})$$

Table 1 shows the results of applying this analysis to the experimental data for cinnamaldehyde and the corresponding aldol. The individual rate constants show the expected first-order dependence upon the hydroxide concentration, but there is clearly a decrease in k'_{21} and k'_{23}[2] as the hydroxide concentration increases; see Fig. 3. This phenomenon has been observed for crotonaldehyde, and is attributed to ionization of the carbonyl hydrate, or equivalently to addition of hydroxide to the aldehyde carbonyl, leading to a lower concentration of the kinetically significant form of the aldol. Since both k'_{21} and k'_{23} respond to hydroxide concentration in the same way, it is best to fit $\lambda_2/[OH^-]$ to the equation:

$$[3] \quad \lambda_2/[OH^-] = (\lambda_2^0/[OH^-])/(1 + a[OH^-])$$

Similar equations apply to k'_{21} and k'_{23}, but propagation of errors leads to greater scatter, and the effect is close to the limits of detection for k'_{23}. We calculated values for k_{21}^0 and k_{23}^0 from the individual values of k'_{21} and k'_{23}, and then averaged them. Table 2 shows the second-order rate constants for the individual steps evaluated in this work, extrapolated to zero hydroxide concentration.

The value of a which we obtained was 4.66 ± 1.17; it is easily shown that $a = K_a/K_w\,(1 + 1/K_{hydration})$. The hydration constant may be estimated, using the linear free energy

[2] We use the following notation for rate constants: k_{ij} are the rate constants obtained from the analysis described at a given value of $[OH^-]$; $k'_{ij} = k_{ij}/[OH^-]$ are the apparent second-order (third-order for k_{32}) rate constants; and k_{ij}^0 are the second- or third-order rate constants corrected for hydrate ionization to zero hydroxide ion concentration. All rate constants refer to species at covalent hydration equilibrium.

TABLE 1. Kinetic results for cinnamaldehyde[a]

(a) Reactions starting with cinnamaldehyde

[NaOH]	β	$10^5 \times \lambda_3$	$10^4 \times k_{12}$
0.1[b]	0.400 ± 0.001	3.45 ± 0.02	1.87 ± 0.15
0.06[b]	0.389 ± 0.001	2.32 ± 0.02	1.26 ± 0.10
0.03[b]	0.382 ± 0.001	1.05 ± 0.005	0.568 ± 0.045
0.1[c]	1.55 ± 0.004	4.15 ± 0.03	2.25 ± 0.18
0.03[c]	1.38 ± 0.003	1.10 ± 0.01	0.595 ± 0.047
0.01[c]	1.26 ± 0.005	0.395 ± 0.005	0.214 ± 0.017
0.1[d]	2.931 ± 0.0003	3.63 ± 0.001	1.96 ± 0.16
0.1[d]	2.943 ± 0.0092	3.61 ± 0.04	1.97 ± 0.16
0.1[e,f]	0.963 ± 0.0001	3.52 ± 0.001	1.69 ± 0.44

(b) Reactions starting with 3-hydroxy-3-phenylpropanal

[NaOH]	α	$10^2 \times \lambda_2$	$10^2 \times k_{21}$	$10^2 \times k_{23}$
0.098[e]	0.978 ± 0.0042	3.688 ± 0.011	2.90 ± 0.20	0.771 ± 0.207
0.046[e]	1.00 ± 0.0008	2.33 ± 0.002	1.92 ± 0.13	0.417 ± 0.134
0.0096[g]	0.215 ± 0.001	0.480 ± 0.003	0.422 ± 0.029	0.0578 ± 0.029
0.0096[h]	2.08 ± 0.0029	0.496 ± 0.002	0.423 ± 0.029	0.0731 ± 0.029
0.0046[e]	1.02 ± 0.0038	0.269 ± 0.004	0.224 ± 0.016	0.0451 ± 0.016

(c) Reactions starting with acetaldehyde plus benzaldehyde

[NaOH]	10^4[PhCHO]	10^5[CH_3CHO]	α	$10^5 k_{obs}$
0.104	3.12	2.9	0.250	5.39 ± 0.009
0.101	9.04	8.9	1.036	7.65 ± 0.012
0.101	30.3	28.0	3.74[i]	15.63 ± 0.058

[a] In aqueous solution at 25°C, μ = 0.1 *M* (KCl); all pseudo first-order rate constants are in s^{-1}.
[b] 1.70×10^{-5} *M* cinnamaldehyde, 1-cm cells.
[c] 7.82×10^{-5} *M* cinnamaldehyde, 1-cm cells.
[d] 1.34×10^{-5} *M* cinnamaldehyde, 10-cm cells.
[e] 5.33×10^{-6} *M* 3-hydroxy-3-phenylpropanal, 10-cm cells.
[f] Second phase of a reaction starting with 3-hydroxy-3-phenylpropanal.
[g] 1.07×10^{-6} *M* 3-hydroxy-3-phenylpropanal, 10-cm cells.
[h] 1.07×10^{-5} *M* 3-hydroxy-3-phenylpropanal, 10-cm cells.
[i] Followed at 310 nm.

relation[3] of Greenzaid *et al.* (5) as 3.52 ± 1.4 (error based on the errors reported by Greenzaid *et al.* for their parameters). This calculation required a σ* value for Ph—CH(OH)—CH_2, which we estimate as σ* ($PhCH_2CH_2$) + σ* ($HOCH_2CH_2$) − σ* (CH_3CH_2), using values of σ* from Perrin *et al.* (3), and estimating σ* ($HOCH_2CH_2$) as 0.4σ* ($HOCH_2$) (3). K_a for the hydrate can be calculated (7) as 13.16. These values lead to a predicted value of $a = 5.4$, in excellent agreement with the value which was obtained.

In order to determine the overall equilibrium constant for cinnamaldehyde formation we measured kinetics of the reaction of benzaldehyde and acetaldehyde in aqueous alkali. It is necessary to use excess benzaldehyde and low, limiting quantities of acetaldehyde in order to keep the acetaldehyde concentration low enough to preclude formation of crotonaldehyde. This condition can be satisfied because of the very favorable overall equilibrium constant for the condensation of acetaldehyde with benzaldehyde. Kinetics were carried out with 0.1 *N* NaOH and varying concentrations of benzaldehyde. In each case the acetaldehyde was ca. 1/10 the benzaldehyde concentration, low enough to ensure pseudo first-order kinetics, high enough to give a useful absorbance change superimposed on the background absorption of benzaldehyde. Although the background absorbance was small enough for the two lower concentrations of benzaldehyde to permit the reaction to be followed at 285 nm, for the highest concentration of benzaldehyde, 3.03×10^{-3} *M*, it was necessary to follow the reaction at 310 nm. A solution of benzaldehyde in 0.1 *N* NaOH showed no absorbance change over times comparable to those for the kinetics runs.

The observed rate of reaction is the rate of approach to equilibrium and includes both forward and reverse reaction, as is shown in eq. [2]

$$[2] \quad k_{obs} = k_{rev} + k_{fwd}\,[PhCHO]$$

Figure 4 shows that the points measured starting with cinnamaldehyde fall at the intercept of a line fitting the runs for approach to equilibrium, as they must by our interpretation. The best line through the points is $k_{obs} = (3.58 \pm 0.03) \times 10^{-5} + (0.0452 \pm 0.00402)$[PhCHO], corresponding to an overall apparent equilibrium constant of 1263 ± 113 M^{-1}.

The rate constant in the forward direction can be expressed in terms of the rate constants of eq. [1] as $k_{fwd} = k_{32}k_{21}/(k_{21} + k_{23})$. Using values of k^0_{23} and k^0_{21} from Table 2 we obtain $k'_{32} = 0.56 \pm 0.05\ M^{-2}\ s^{-1}$.

As we discussed above for the reverse reactions, we must consider the effect of hydroxide addition to the starting materials for the condensation, in order to extract the true third-order rate constants for the hydroxide catalyzed reaction at zero hy-

[3] For RR'C=O + $H_2O \rightleftharpoons$ RR'C(OH)$_2$, $\log K_{hydration} = 1.70\Sigma\sigma^* + 2.03\Delta - 2.81$, where Δ = number of aldehydic protons and $K_{hydration}$ is dimensionless, i.e. activity of water = 1 (5).

Can. J. Chem. Downloaded from www.nrcresearchpress.com by 210.87.254.105 on 09/06/12
For personal use only.

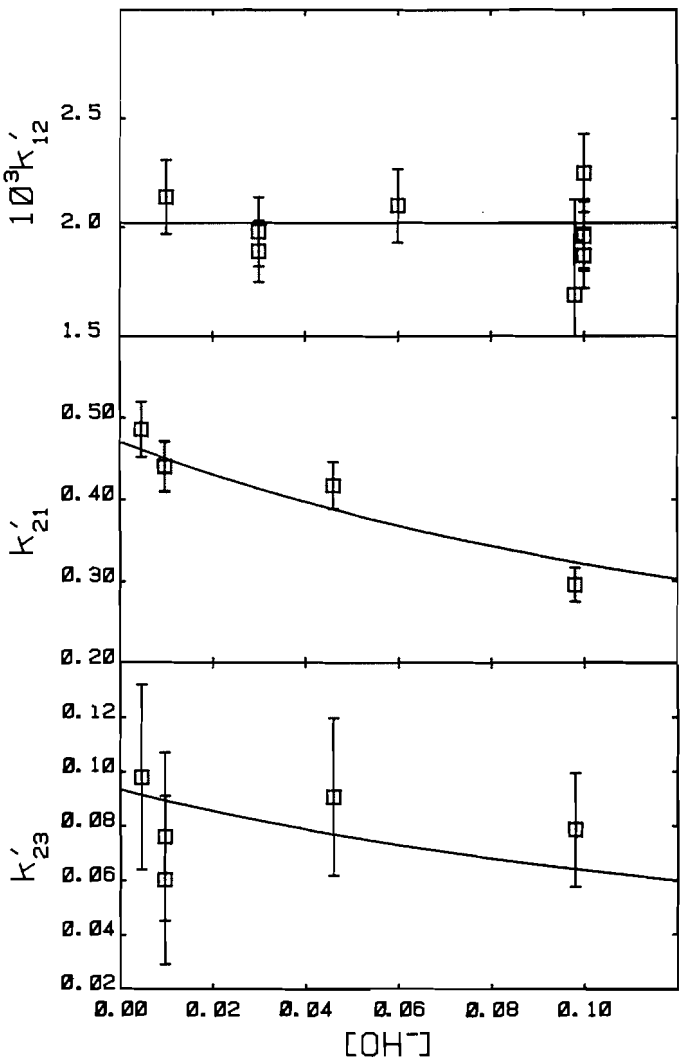

FIG. 3. Dependence of apparent second-order rate constants upon $[OH^-]$. Lines for k'_{21} and k'_{23} calculated using equations of the form of [3] with $a = 4.66$. The line for k'_{12} represents the weighted average value.

droxide concentration. It may be shown that the correction takes the form:

$$k'_{fwd} = k^0_{fwd}/(1 + b[OH^-])\,(1 + c[OH^-])$$

where b and c are analogous to a, defined above for the ketol, but refer to acetaldehyde and benzaldehyde respectively. From the literature values for the pK_a of acetaldehyde hydrate (13.48, ref. 8) and for the hydration constant for acetaldehyde (1.06, ref. 9) we can calculate that b is 1.48; from the equilibrium constant for addition of hydroxide to benzaldehyde (0.18, ref. 10) and the knowledge that hydration is negligible (10), we can calculate that c is 0.18. For 0.1 N NaOH these values lead to a net correction of $k'_{fwd} = k^0_{fwd}/1.17$. Thus $k^0_{32} = 0.65 \pm 0.06$. A similar correction must be made to $K_{overall}$, leading to $K^0_{overall} = 1480 \pm 133\ M^{-1}$.

We have previously reported equilibrium constants for the aldol condensation leading to cinnamaldehyde, and for the dehydration step (1). For the dehydration, our value, based on thermodynamic calculations using disproportionation reactions, was 424 ($\Delta G^0 = -3.59 \pm 1.63$); from the kinetics measured in this work the equilibrium constant is 226 ± 17 ($\Delta G^0 = -3.21 \pm 0.04$), in satisfactory agreement. For the

TABLE 2. Rate constants at zero hydroxide concentration for the retro-aldol reaction of cinnamaldehyde[a]

Rate constant	Value
$10^3 \times k^0_{12}$ [b]	2.02 ± 0.13
k^0_{21} [b]	0.456 ± 0.018
$10^2 \times k^0_{23}$ [b]	9.08 ± 2.26
k^0_{32} [c]	0.63 ± 0.06

[a] In aqueous solution at 25°C, μ = 0.1 M (KCl); average values for rate constants.

[b] Second-order rate constant for hydroxide catalyzed reaction, $M^{-1}\ s^{-1}$.

[c] Third-order rate constant for hydroxide catalyzed reaction, $M^{-2}\ s^{-1}$.

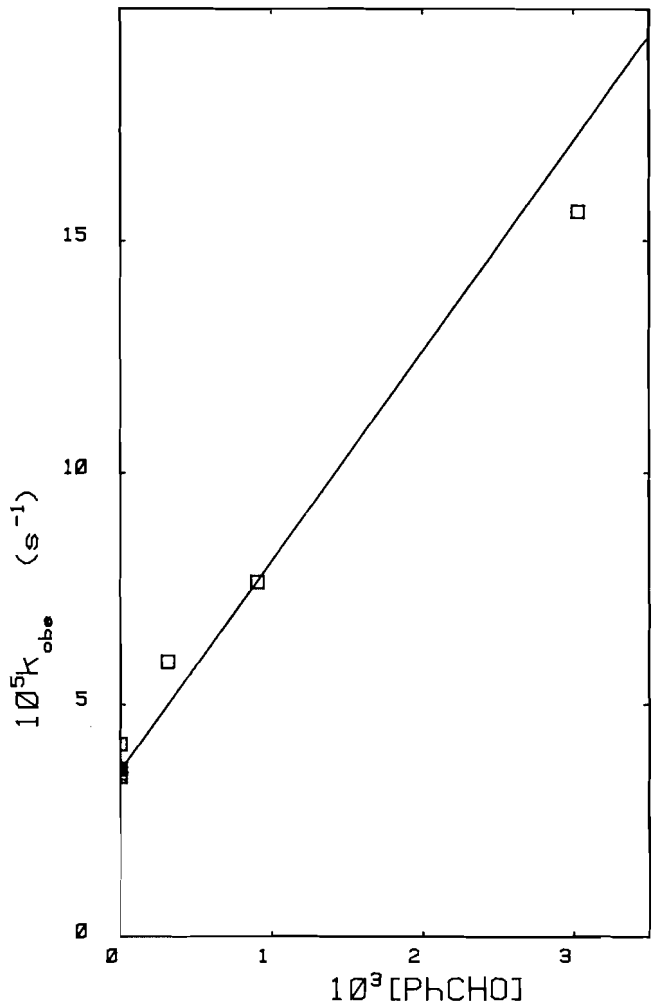

FIG. 4. Dependence of rate constants for approach to equilibrium for reactions starting with acetaldehyde plus benzaldehyde upon $[benzaldehyde]_0$. The points at $[benzaldehyde]_0 = 0.0$ represent reactions starting with cinnamaldehyde. The line is fitted by weighted least squares.

aldol addition step, our value, based on thermodynamic calculations using disproportionation reactions, was 39 ($\Delta G^0 = -2.18 \pm 1.00$). From the kinetics measured in this work the equilibrium constant is 6.5 ± 0.8 ($\Delta G^0 = -1.11 \pm 0.07$), in not so satisfactory agreement. The discrepancy is just equal to the combined uncertainties. Thus our use of disproportionation

Can. J. Chem. Downloaded from www.nrcresearchpress.com by 210.87.254.105 on 09/06/12
For personal use only.

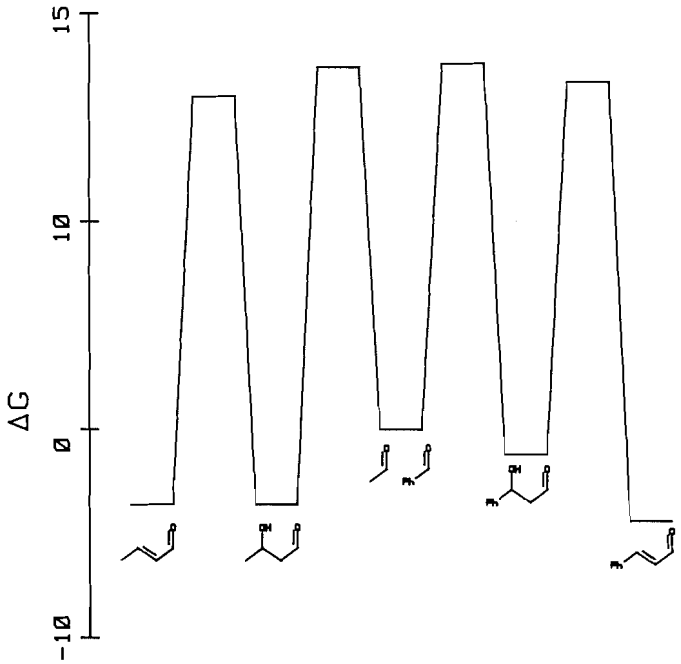

FIG. 5. Reaction coordinate diagram for the system starting with acetaldehyde plus benzaldehyde. Free energies of activation were calculated from the rate constants in Table 2 and ref. 11.

reactions to estimate thermochemical quantities gives useful approximate values.

It is instructive to draw a reaction coordinate diagram for the condensation of acetaldehyde with benzaldehyde, now that the rate constants are available from this and earlier work (11). Figure 5 shows such a diagram, and makes it clear that 3-hydroxybutanal and 2-butenal will indeed accumulate in the early stages of a reaction, but will be replaced by the more slowly formed but more stable cinnamaldehyde at long times. This picture is of course oversimplified, in that it ignores the possible further aldol reactions of 3-hydroxybutanal and 2-butenal which would be expected to be competitive with the simple condensations.

In terms of this simple picture, we can calculate that for initial concentrations of [acetaldehyde] = [benzaldehyde] = 0.01 *M*, the final concentration of cinnamaldehyde will be 0.00684 *M*, with 0.00085 *M* each of 3-hydroxybutanal and crotonaldehyde, so that the yield is 68% and r = [cinnamaldehyde]/([acetaldol] + [crotonaldehyde]) = 4.03. The predicted yield of cinnamaldehyde and the predicted value of r both increase at higher concentrations: 84%, $r = 7$ at 0.1 *M* reactants; 90%, $r = 9$ at 1 *M* reactants. This is likely to prove illusory because of the increasing rate of polymerization to be expected at higher concentrations of acetaldehyde; polymerization was neglected in these simple calculations, as were the effects of solubility.

Experimental

Materials

Cinnamaldehyde was redistilled in vacuum before use.

3-Hydroxy-3-phenylpropanal

This was prepared following the procedure reported by Meyers *et al.* (3); their procedure, involving reaction of the lithium salt of 2-methyl-2-thiazoline with benzaldehyde, led to a product with the nmr spectrum expected (3) for 2-(2-hydroxy-2-phenylethyl)-2-thiazoline, as did the aluminum amalgam reduction of this material to give 2-(2-hydroxy-2-phenylethyl)-1,3-thiazolidine. When mercuric ion catalyzed hydrolysis was attempted we did not obtain a material with the nmr spectrum reported (3), but rather an oil, which gave a solid on addition of n-pentane to an ether solution. The solid was recrystallized from $CHCl_3$; mp 115–117°C (dec.). The 2,4-dinitrophenylhydrazone of this solid was prepared and recrystallized from ethanol/ethyl acetate; mp 250–251°C (lit. (12) mp for cinnamaldehyde 2,4-DNP 252°C). A solution of 2-(2-hydroxy-2-phenylethyl)-1,3-thiazolidine, (0.5 g) in acetonitrile (ca. 15 mL) was added over 5 min to a solution of $HgCl_2$ in 80% acetonitrile–water (10 mL) at 0°C. After stirring 10 min, water (15 mL) was added, and the white precipitate filtered off. The filtrate was extracted using 1:1 ether–pentane (4 × 25 mL), the extracts were dried (Na_2SO_4), and the solvent evaporated to leave a pale yellow oil (0.25 g). The nmr spectra ($CDCl_3$) of this oil were consistent with 3-hydroxy-3-phenylpropanal; ^1H, δ: 9.6 (t, 1H), 7.2 (s, 5H), 5.1 (t, 1H), 3.4 (s, 1H), 2.7 (d of t, 2H); ^{13}C, δ: 202.0 (CHO), 142.8, 128.6, 127.8, 125.6 (Ph), 68.9, 52.1 (CH(OH), CH_2).

The sample was dissolved in a few milliliters of ether, and an equal volume of petroleum ether was added. The bright yellow precipitate was filtered off, and the clear, essentially colorless solution was cooled with Dry Ice; fluffy white crystals formed and were filtered off, but melted below 0°C on warming. This material was used for kinetics.

Methods

The procedure for kinetics was as previously described (13, 14). The reactions were followed at 285 nm, except for the formation experiment at highest benzaldehyde concentration. For this experiment the adsorption due to benzaldehyde at 285 nm was too high to permit the reaction to be followed, so it was followed at 310 nm.

The final solutions from retroaldol kinetics experiments had absorbances appropriate to the anticipated products. This will be illustrated for the 7th entry in Table 1. The initial and final absorbances (based on the least-squares parameters) were 3.20 and 0.267 respectively. The corresponding apparent extinction coefficients were 2.4×10^4 and 2.0×10^3. The extinction coefficient for cinnamaldehyde at 285 nm is 2.3×10^4 (12); that for benzaldehyde at 285 nm is 1.5×10^3, (this work). From the overall equilibrium constant of 1480 M^{-1} we can calculate that 2.65×10^{-7} *M* cinnamaldehyde would be present at equilibrium, along with 1.31×10^{-5} *M* benzaldehyde (and 1.31×10^{-5} *M* acetone, which would make a negligible contribution to the absorbance). The calculated apparent extinction coefficient is 1.96×10^3. The agreement is satisfactory, confirming that the reactions are well behaved.

1. J. P. GUTHRIE. Can. J. Chem. **56**, 962 (1978).
2. C. D. GUTSCHE and D. J. PASTO. Fundamentals of organic chemistry. Prentice-Hall, Englewood Cliffs, New Jersey. 1975. p. 925.
3. A. L. MEYERS, J. L. DURANDATTA, and R. MUNAVU. J. Org. Chem. **40**, 2025 (1975).
4. J. W. MOORE and R. G. PEARSON. Kinetics and mechanism. 3rd ed. Wiley, New York. 1981. p. 296.
5. P. GREENZAID, Z. LUZ, and D. SAMUEL. J. Am. Chem. Soc. **89**, 749 (1967).
6. D. D. PERRIN, B. DEMPSEY, and E. P. SERJEANT. pK_a Prediction for organic acids and bases. Chapman and Hall, London. 1981.
7. J. HINE and G. F. KOSER. J. Org. Chem. **36**, 1348 (1971).
8. R. P. BELL and P. T. MCTIGUE. J. Chem. Soc. 2983 (1960).
9. J. L. KURZ. J. Am. Chem. Soc. **89**, 3524 (1967).
10. P. GREENZAID. J. Org. Chem. **38**, 3164 (1973).
11. J. P. GUTHRIE. Can. J. Chem. **52**, 2037 (1974).
12. I. HEILBRON. Dictionary of organic compounds. *Edited by* A. H. Cook, H. M. Bunbury, and D. H. Hey. Eyre and Spottiswoode, London. 1965.
13. J. P. GUTHRIE. Can. J. Chem. **59**, 45 (1981).
14. J. P. GUTHRIE and B. A. DAWSON. Can. J. Chem. **61**, 171 (1983).
15. O. H. WHEELER and L. A. KAPLAN (*Editors*). Organic electronic spectral data. Vol. 3. Wiley, New York. 1966.

Can. J. Chem. Downloaded from www.nrcresearchpress.com by 210.87.254.105 on 09/06/12
For personal use only.

ipso Nitration. XXIV.[1] Nitration of 2-methylphenols. Formation and rearrangement of 6-methyl-6-nitrocyclohexa-2,4-dienones

GORDON G. CROSS, ALFRED FISCHER, GEORGE N. HENDERSON, AND TREVOR A. SMYTH
Department of Chemistry, University of Victoria, Victoria, B.C., Canada V8W 2Y2

Received January 17, 1984

GORDON G. CROSS, ALFRED FISCHER, GEORGE N. HENDERSON, and TREVOR A. SMYTH. Can. J. Chem. **62**, 1446 (1984).

Nitration of *o*-cresol and some mono-, di-, and trimethyl derivatives in acetic anhydride at −60°C gives 6-methyl-6-nitrocyclohexa-2,4-dienones. The dienones are more labile than the isomeric 4-methyl-4-nitrocyclohexa-2,5-dienones and, if the 2-position of the dienone is not blocked, undergo regiospecific rearrangement to 6-nitro-*o*-cresols. 2,3,6-Trimethyl- and 2,3,5,6-tetramethylphenol also give a 2,5-dienone with nitro attached to a secondary carbon.

GORDON G. CROSS, ALFRED FISCHER, GEORGE N. HENDERSON et TREVOR A. SMYTH. Can. J. Chem. **62**, 1446 (1984).

La nitration, dans l'anhydride acétique et à −60°C, de l'*ortho*-crésol et de quelques-uns de ses dérivés mono-, di- et tri-méthylés conduit à des méthyl-6 nitro-6 cyclohexadiène-2,4 ones. Ces dièmones sont plus labiles que les méthyl-4 nitro-4 cyclohexadiène-2,5 ones isomères et, si la position 2 de la dièmone n'est pas bloquée, elles subissent une transposition régiospécifique conduisant aux nitro-6 *o*-crésols. Les triméthyl-2,3,6 et tétraméthyl-2,3,5,6 phénols conduisent aussi à des diène-2,5 ones dans lesquelles le groupe nitro est attaché à un carbone secondaire.

[Traduit par le journal]

Can. J. Chem. Downloaded from www.nrcresearchpress.com by 210.87.254.5 on 09/06/12
For personal use only.

Introduction

Nitration of 2,4,6 trisubstituted phenols often gives nitrodienones (2, 3). Normally the 2,5-dienone is formed, although formation of a 2,4-dienone has been reported (4). Nitration of *p*-methylphenyl acetate gives 4-methyl-4-nitrocyclohexa-2,5-dienone, and other 4-alkylphenyl acetates give the corresponding dienones (5–7). *p*-Cresol behaves similarly. In this report we describe the formation of 6-methyl-6-nitrocyclohexa-2,4-dienones by nitration of *o*-cresol and some of its derivatives.[2]

Results and discussion

Nitration of *o*-cresol (**1***a*) with nitric acid in acetic anhydride at temperatures from −40°C to −78°C gave a mixture of dienone **2***a*, 6-nitro-*o*-cresol (**4***a*), and 4-nitro-*o*-cresol (**5***a*) (Scheme 1). The amount of dienone obtained increased with decrease in temperature. At −78°C the ratio of the products **2***a*/**4***b*/**5***b* was 67:19:14, at −60°C 62:22:16, and at −50°C 56:23:21. *o*-Cresol was also nitrated in [$^2H_6$]acetic anhydride, so that the ^1H nmr spectrum of the methyl region could be determined. Dideuterio-*o*-cresol **1***b* was nitrated to form the corresponding dienone **2***b*. Dienone **2***a* isomerized slowly ($t_{1/2}$ ≈ 7 h) in the reaction mixture at −40°C and survived for only a few minutes when the temperature was raised to −20°C. 6-Nitro-*o*-cresol (**4***a*) was formed, regiospecifically. Addition of the reaction mixture at −60°C to fourteen times its volume of ether at −60°C, followed by careful addition of excess ice-cold 30% aqueous ammonia to the resulting solution and further work-up at low temperature (< −20°C), gave a mixture of **2***a* and nitrocresols. Pure dienone **2***a* can be obtained by passing an ethereal solution of the dienone and nitrophenols through a column of alumina at −78°C.[3] The isolated dienone also isomerized regiospecifically to **4***a*. When the reaction mixture was quenched at −60°C and work-up was carried out at 0°C a mixture of the nitrophenols **4***a* (85%) and **5***a* (15%) was obtained, but no dienone. Under these conditions the dienone isomerized to **4***a* during the work-up process.

Identification of the dienones, all of which were labile and some, including **2***a*, at temperatures as low as −40°C, was by ^1H nmr spectroscopy. The ^{13}C nmr spectra were also obtained for several of the compounds and these confirmed the structural assignments. Dienone **2***a* had ^1H nmr peaks in acetic anhydride at δ 6.17 (d, 1), 6.6 (m, 2), 7.31 (8 lines, 1) ppm. These were assigned as follows. The spectrum of the deuterated dienone **2***b* showed that peaks at δ 7.31 and 6.60 ppm arise from the 3- and 5-protons. The peak at δ 6.17 ppm in the spectrum of **2***a*, which exhibits a simple 10-Hz coupling, must be the 2H, since the 4-H would exhibit strong couplings to the two adjacent protons, and the 4-H, together with the 3-H, must be responsible for the complex absorption at δ 6.6 ppm. Confirmation of the correctness of these assignments was provided by the close correspondence of the computer simulated spectrum to the observed spectrum. The methyl protons in **2***a* were observed in [$^2H_6$]acetic anhydride at δ 1.74 ppm and, for the isolated dienone dissoved in [^2H]chloroform, at δ 1.84 ppm. These absorptions are above the range of aromatic methyl protons and are characteristic of methyl *ipso* to nitro. In the ^{13}C nmr spectra of **2***a* the tetrahedral and carbonyl carbon atoms have characteristic absorptions at δ 91.3 and 192.5 ppm respectively.

Nitration of 2,3-dimethylphenol (**1***c*) in acetic anhydride at −60°C gave 5,6-dimethyl-6-nitrocyclohexa-2,4-dienone (**2***c*) (52%) and the 4-nitro- and 6-nitrophenols **5***c* (24%) and **4***c* (24%), respectively. The dienone decomposed when the temperature of the reaction mixture was raised, although some was still present after 25 min at 0°C indicating that dienone **2***c* is more stable than **2***a*. Regioselective formation of the 6-nitrophenol **4***c* was indicated by the fact that, after neutralization of excess nitric acid with triethylamine and warming the reaction mixture to ambient temperature, this isomer constituted 75% of the product **4***c* and **5***c* although in the nitration mixture **4***c* and **5***c* were originally present in equal amount.

Nitration of 2,4-dimethylphenol (**1***d*) in acetic anhydride at −60°C gave two dienones in approximately equal amounts. Since both dienones exhibited the 10-Hz coupling characteristic of vicinal vinyl protons they were assigned as 4,6-dimethyl-6-nitrocyclohexa-2,4-dienone (**2***d*) and 2,4-dimethyl-6-nitrocyclohexa-2,5-dienone (**3***d*). The third possible isomer, 2,4-dimethyl-6-nitrocyclohexa-2,4-dienone, does not have vicinal vinyl protons. After 60 min at −60°C all of the substrate had been nitrated and the ratio of the products **2***d*/**3***d*/**4***d* was

[1] For part XXIII, see ref. 1.
[2] Some of this work has been reported in preliminary form in ref. 8.
[3] S. Sankararaman. Unpublished work.

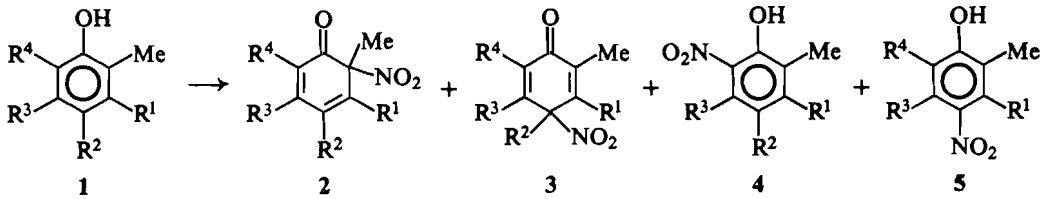

1 **2** **3** **4** **5**

a $R^1 = R^2 = R^3 = R^4 = H$		*g* $R^1 = R^3 = Me$	$R^2 = R^4 = H$	
b $R^1 = R^3 = H$	$R^2 = R^4 = D$	*h* $R^1 = R^4 = Me$	$R^2 = R^3 = H$	
c $R^1 = Me$	$R^2 = R^3 = R^4 = H$	*i* $R^1 = R^2 = H$	$R^3 = R^4 = Me$	
d $R^1 = R^3 = R^4 = H$	$R^2 = Me$	*j* $R^1 = R^3 = H$	$R^2 = R^4 = Me$	
e $R^1 = R^2 = R^4 = H$	$R^3 = Me$	*k* $R^1 = R^3 = R^4 = Me$	$R^2 = H$	
f $R^1 = R^2 = R^3 = H$	$R^4 = Me$			

SCHEME 1

38:44:18. Dienone **2***d* disappeared after 20 min at −40°C. Dienone **3***d* survived to 0°C. The assignments are in accord with the observation that 2,5-dienones are more stable than 2,4-dienones. The peaks of 2,4-dimethyl-6-nitrophenol (**4***d*) increased as the dienones disappeared and **4***d* was the only species observed when the reaction mixture, after 90 min at −60°C, was treated with triethylamine (to remove excess nitric acid) before warming to ambient temperature. When the reaction mixture was warmed without destroying the excess nitric acid, the 2,4-dimethyl-6-nitrophenol was further nitrated to 2,4-dimethyl-4,6-dinitrocyclohexa-2,5-dienone or 4,6-dimethyl-2,6-dinitrocyclohexa-2,4-dienone (^{1}H nmr δ 7.07(s) and 7.82(s) ppm).

Nitration of 2,5-dimethylphenol in acetic anhydride at −40°C gave variable results. In some experiments yields of the dienone **2***e* were in excess of 90% but in others only 60% **2***e* was obtained together with **4***e* and **5***e*. At −20°C the dienone slowly isomerized, regioselectively, to the 6-nitrophenol **4***e*. Neutralization of excess nitric acid with trimethylamine followed by warming to ambient temperature gave a mixture of **4***e* (66%) and **5***e* (34%). Careful quenching of the reaction mixture at −65°C and work-up at low temperature gave a product which, when extracted into [^{2}H]chloroform, was **2***e* (80%) and **4***e* (20%) (the 4-nitrophenol **5***e* is rather insoluble in chloroform). When this solution was warmed to ambient temperature, the dienone isomerized to the 6-nitrophenol **4***e*.

Nitration of 2,6-dimethylphenol in acetic anhydride at −60°C gave 2,6-dimethyl-6-nitrocyclohexa-2,4-dienone (**2***f*) and 2,6-dimethyl-4-nitrophenol (**5***f*). Much of the nitrophenol precipitated and was filtered off at −78°C. The filtrate contained a mixture of **2***f* (80%) and **5***f* (20%). When the temperature was raised to −20°C the nitrophenol began to disappear and was replaced by a species with a broad singlet at δ 7.74 ppm, assigned as 2,6-dimethyl-4,6-dinitrocyclohexa-2,4-dienone. At 0°C no nitrophenol remained. At ambient temperature both dienones disappeared and were replaced by a species assigned as 2-methyl-4-nitro-6-nitromethylphenol. Careful neutralization of the reaction mixture at −65°C with aqueous ammonia and work-up at low temperature gave, after dissolution of the product in [^{2}H]chloroform at −60°C, a solution of dienone **2***f*. The nitrophenol was insoluble in chloroform at this temperature. The dienone isomerized to the nitrophenol **5***f* on warming this solution to ambient temperature. When the reaction mixture was worked up by pouring the solution into a mixture of ether and aqueous ammonia at 0°C, a mixture of **5***f* (66%) and 2,6-dimethyl-*p*-benzoquinone (34%) was obtained.

Nitration of 2,3,5-trimethylphenol at −60°C gave, after 17 min, the dienone **2***g* (77%) and the nitrophenols **4***g* and **5***g* (23%). After 35 min at −60°C the peaks of the nitrophenols had disappeared, presumably as a result of crystallization, as yellow crystals had formed. On warming to 0°C a broad singlet appeared at δ 6.42 ppm, assigned as either 2,6-dinitro-3,5,6-trimethylcyclohexa-2,4-dienone or its 4,6-dinitro isomer. Careful neutralization of the reaction mixture with aqueous ammonia at −65°C and work-up at low temperature gave a mixture of the dienone **2***g* (70%) and the nitrophenols **4***g* (8%) and **5***g* (22%). The dienone rapidly isomerized regiospecifically to **4***g* at ambient temperature, and over 24 h at −20°C, in [^{2}H]chloroform. When the reaction mixture was worked up by pouring into a mixture of ether and ammonia at −60°C and the mixture then warmed to 0°C, a mixture of **2***g* (15%), **4***g* (57%), and **5***g* (28%) was obtained.

Nitration of 2,3,6-trimethylphenol in acetic anhydride at −60°C gave three intermediate dienones. The species which had broad singlets at δ 5.85 and 6.90 ppm and which isomerized quantitatively to **5***h* is assigned the 2,5-dienone structure **3***h* on the basis of the nmr spectrum (the highest field proton is attached to the tetrahedral carbon) and the relative stability (dienones with nitro attached to a secondary carbon are not expected to be stable because of the facile tautomerization to the nitrophenol). The dienone with the broadened doublets at δ 6.24 and 7.05 ppm (J = 7 Hz) is assigned as **2***h* and that which had a singlet with fine splitting at 6.44 ppm is assigned as **2***i*. These assignments follow from the observation that in the ^{1}H nmr spectra of 2,4-dienones the 3-H is at lowest field and the 4-H and 5-H absorb at similar positions at higher field. Furthermore, the 7-Hz coupling identifies the **2***h* structure. The **2***i* structure would exhibit a 10-Hz coupling. The initial ratio of **3***h*/**2***h*/**2***i* at −60°C was 30:32:38. When the temperature was raised to −40°C, **3***h* disappeared over 45 min and an equal amount of **5***h* was formed. The dienones **2***h* and **2***i* survived for 30 min when the reaction mixture was warmed to ambient temperature. Neutralization of excess nitric acid by the addition of triethylamine to the reaction mixture at −60°C, followed by warming to ambient temperature, gave the nitrophenol **5***h* as the sole product. Careful neutralization of the reaction mixture at −60°C with aqueous ammonia and work-up at low temperature gave a 60:40 mixture of **2***h* and **2***i* which was dissolved in [^{2}H]chloroform–[^{2}H$_3$]acetonitrile. The dienones isomerized to the nitrophenol **5***h* at ambient temperature and some 2,3,5-trimethylbenzoquinone was also formed in the nmr sample.

Nitration of 2,4,6-trimethylphenol in acetic anhydride at

Can. J. Chem. Downloaded from www.nrcresearchpress.com by 210.87.254.5 on 09/06/12
For personal use only.

Can. J. Chem. Downloaded from www.nrcresearchpress.com by 210.87.254.5 on 09/06/12
For personal use only.

−60°C gave a mixture of the 2,4- and 2,5-dienones **2***i* and **3***j*. Both dienones survived when the reaction mixture was warmed to ambient temperature but **2***j* isomerized to **3***j* over 30 min at that temperature. Careful quenching and work-up of the reaction mixture at low temperature gave a mixture of the two dienones. In [$^2H_6$]acetone at ambient temperature **2***j* isomerized to **3***j* over 2 h and **3***j* isomerized to 2,6-dimethyl-4-nitromethylphenol over 3 days. The isomerization of **3***j* to 2,6-dimethyl-4-nitromethylphenol has been reported previously (9). Pure **3***j* was obtained by crystallization of the crude dienone from ether.

Nitration of 2,3,5,6-tetramethylphenol (**1***k*) in acetic anhydride at −60°C gave two dienones. A species (22%) which exhibited a broad singlet at δ 5.77 ppm and which disappeared when the temperature was raised to −40°C is assigned as **3***k*. The species (78%) which exhibited a broad singlet at δ 6.20 ppm and which survived until the temperature was raised to ambient temperature is assigned as **2***k*.

Prior to the present work the only 2,4-dienone that had been obtained by nitration of phenol was 2,6-di-*tert*-butyl-4-chloro-6-nitrocyclohexa-2,4-dienone from nitration of 2,6-di-*tert*-butyl-4-chlorophenol (4). Ershov and Zlobina also studied the nitration of 2,4,6-trialkylphenols, but obtained only the 2,5-dienones (10). Earlier the corresponding 2,5-dienones had been obtained on nitration of 2,6-di-*tert*-butyl-4-methylphenol (11) and 2,4,6-tri-*tert*-butylphenol (12). Ershov *et al.* also studied the nitration of 2,6-dialkylphenols, but did not observe the formation of dienones (13). However, they deduced from kinetics studies that a transient intermediate was formed in the nitration of a 2,6-dialkylphenol and they assigned this intermediate the 2,5-dienone structure (14). Our results show that formation of the 2,4-dienone occurs readily and extensively in even the simplest substituted phenol (*o*-cresol) and that mesitol, which is known to form a 2,5-dienone (10), also forms a previously undetected 2,4-dienone. The *ortho*-methyl substituent appears to exert a directing effect to the *ipso* position, and particularly so in comparison with unsubstituted positions. *ipso* Nitration occurs to an extent of more than 60% in *o*-cresol, whereas nitration at the unsubstituted 6 position is around 20% and at the 4 position even less. Nitration of phenol and, presumably, the methylphenols is complicated by nitrous acid catalysis which affects the isomer distribution. If nitration via nitrosation is important under our conditions (which would likely require concentrations of nitrous acid $> 10^{-3}$ mol dm^{-3} (15)) it must exhibit a preference for *ipso* attack. The *para* position is more reactive when it is itself substituted – a *para*-methyl group directs to its own *ipso* position – as indicated by the fact that the 2,5-dienone is formed to about the same extent as the 2,4-dienone when 2,4-dimethylphenol is nitrated. Formation of the 2,4-dienones at a rate competitive with 2,5-dienones reflects transition state control. The 2,5-dienone is thermodynamically more stable than the 2,4-dienone, as is shown by the fact that in the case of the dienones from mesitol the 2,4-dienone isomerizes to the 2,5-dienone. The 2,4-dienones are more labile than the 2,5-dienones: the dienone from *p*-cresol survives at ambient temperature, whereas that from *o*-cresol starts to rearomatize at −40°C. In the cases of those 2,4-dienones which have an unsubstituted 2 position, the rearomatization process is regioselective with the nitro group migrating to the 2 position and not the 4 position: the 6-nitrophenol is formed. It was proposed previously that the oxygen function played a role in this process, forming a phenyl nitrate intermediate (8, 16). However, more recently we have observed examples of 1,5 sigmatropic migration of the nitro group in 6-nitrocyclohexa-2,4-dienes (17) and it seems likely that a similar process could be operative in the case of the 2,4-dienones.

Nitration of 2,3,6-trimethylphenol and of 2,3,5,6-tetramethylphenol gave in each case a transient dienone, assigned as the 2,5-dienone, in addition to the expected 2,4-dienones. These 2,5-dienones have the nitro group attached to a secondary carbon and result from addition of the nitronium ion at an unsubstituted nuclear position. They are more labile than the dienones formed by addition of the nitronium ion *ipso* to a methyl group, because of the extremely facile prototropic tautomerization to the nitrophenol. Such a dienone is a likely intermediate in the nitration of a phenol at an unsubstituted position since, in the precursor hydroxynitrocyclohexadienyl cation, deprotonation at oxygen, to give the dienone, should be more rapid than deprotonation at carbon, to give the nitrophenol. However, for most such dienones the reverse protonation at the carbonyl oxygen and eventual deprotonation at carbon is sufficiently rapid for the dienone not to be detectable. In the cases of the dienones **3***h* and **3***k* it is likely that steric hindrance slows up the prototropic processes to an extent such that the dienone lifetime moves into the observable range.

Experimental

The ^{1}H nmr spectra at 90 and 250 MHz were determined using Perkin–Elmer R32 and Bruker WM250 spectrometers, respectively. The latter instrument was also used for ^{13}C nmr determination at 62.9 MHz. Mass spectra were obtained on a Hitachi Perkin–Elmer RMU7 spectrometer. Combined gas chromatography and mass spectrometry was carried out on a Finnigan 3300 system. Gas chromatography was carried out on a Varian 3700 gas chromatograph using a 25-m fused silica SE30 capillary column. *o*-Cresol, 2,3-dimethylphenol, 2,4-dimethylphenol, 2,3,5-trimethylphenol, 2,3,6-trimethylphenol, 2,4,6-trimethylphenol, 2,6-dimethyl-4-nitrophenol, and 2-methyl-4-nitroaniline were from Aldrich. 2,3,4,6-Tetramethylphenol was from Tokyo Kasei. 2,6-Dimethylphenol was from Eastman Kodak. 2,5-Dimethyl-4-nitroaniline was from Pfaltz and Bauer Inc.

4,6-[$^2H_2$]-*o*-Cresol was prepared by adding with stirring PBr_3 (4 cm^3) and *o*-cresol (5.4 g) to D_2O (50 g) under an argon atmosphere (18). The mixture was heated under reflux for 4 h, cooled, and extracted with ether (4 × 50 cm^3). The combined ethereal extract was washed with water, aqueous sodium bicarbonate, and water, dried ($MgSO_4$), and distilled. The 4,6-[$^2H_2$]-*o*-cresol (4.34 g) had bp 190–191°C, ^{1}H nmr ($CDCl_3$) δ: 2.19 (s, 3, C*H*$_3$), 5.41 (s, 1, O*H*), 7.02 (s, 1, 3-*H*), 7.07 (s, 1, 5-H) ppm.

4-Nitro-*o*-cresol (**5***a*) was prepared by diazotization of 2-methyl-4-nitroaniline followed by hydrolysis in boiling aqueous sulfuric acid, following the procedure for *m*-nitrophenol (19). The product was crystallized from methylene chloride – pentane, sublimed (60–100°C, 35 Pa), and the sublimate decolorized with charcoal and recrystallized from methylene chloride to give **5***a*, mp 97–98°C (lit. (20) mp 94.6–95°C); ^{1}H nmr ($CDCl_3$/$(CD_3)_2CO$) δ: 2.27 (s, 3, C*H*$_3$), 6.92 (d, 1, $J_{5,6}$ = 8 Hz, 6-*H*), 7.95 (dd, 1, $J_{5,6}$ = 8 Hz, $J_{3,5}$ = 3 Hz, 5-*H*), 8.02 (d, 1, $J_{3,5}$ = 3 Hz, 3-*H*) ppm; ^{13}C nmr ($CDCl_3$) δ$_c$: 15.8 (*C*H$_3$), 115.0 (*C*-6), 123.8 (*C*-5), 125.6 (*C*-2), 127.0 (*C*-3), 141.0 (*C*-4), 160.4 (*C*-1) ppm; ms (70 eV) *m*/*e* (relative intensity): 153.043 (100, M_r $^{12}C_7{}^1H_7{}^{14}N^{16}O_3$: 153.043), 137 (10), 123 (23), 107 (14), 95 (15), 81 (10), 79 (16), 78 (11), 77 (52).

2,5-Dimethyl-4-nitrophenol (**5***e*) was prepared by diazotization of 2,5-dimethyl-4-nitroaniline followed by hydrolysis of the diazonium salt (19). After recrystallization from ethanol–water **5***e* had mp 124–125°C (lit. (21) mp 117–119°C); ^{1}H nmr ($CDCl_3$/$(CD_3)_2CO$) δ: 2.23 (s, 3, 2-C*H*$_3$), 2.52 (s, 3, 5-C*H*$_3$), 6.73 (s, 1, 6-*H*), 7.92 (s, 1, 3-*H*), 8.25 (br, s, 1, O*H*) ppm; ^{13}C nmr ($CDCl_3$) δ$_c$: 15.2 (2-*C*H$_3$), 21.2 (5-*C*H$_3$), 118.3 (*C*-6), 123.0 (*C*-2), 128.5 (*C*-3), 135.0 (*C*-5),

Can. J. Chem. Downloaded from www.nrcresearchpress.com by 210.87.254.5 on 09/06/12
For personal use only.

141.4 (*C*-4), 158.5 (*C*-1); ms (70 eV) *m/e* (relative intensity): 168 (12), 167.061 (97, M_r $^{12}C_8{}^1H_9{}^{14}N^{16}O_3$: 167.058), 151 (18), 150 (100), 122 (22), 120 (12), 95 (18), 94 (15), 91 (37), 78 (10), 77 (53).

Nitration of o-*cresols*

A solution of nitric acid (15 mmol) in acetic anhydride (4.3 cm^3) at −60°C was added with stirring to a solution of the phenol (5 mmol) in acetic anhydride (9.9 cm^3) at −60°C. A sample of the reaction mixture was transferred to a nmr tube using a precooled pipette stored under argon and the progress of the reaction monitored at −60°C for 60 min and then at 20°C temperature intervals. After 1–2 h the remaining nitric acid in the bulk reaction mixture was neutralized by the addition of excess triethylamine (25 mmol) previously cooled to −60°C and the solution subsequently warmed to ambient temperature. The nitrodienones isomerized to nitrocresols on this treatment and the mononitrocresol(s) were then characterized by ^{1}H nmr. Alternatively, the reaction mixture was poured into a mixture of 30% aqueous ammonia (30 cm^3) and ether (50 cm^3) at −60°C. The resulting mixture was warmed to 0°C, the ether layer separated, the aqueous layer extracted with ether (3 × 50 cm^3), and the combined ethereal extracts washed with brine, dried, and the ether evaporated to yield the mononitrocresol(s).

In order to obtain the ^{13}C nmr spectrum of the nitrodienone it was necessary to remove the acetic anhydride without decomposing the dienone. A mixture of the nitrodienone and nitrocresol(s) was prepared in acetic anhydride at −60°C as described above, but on twice the scale. The solution was poured into ether (400 cm^3) at −60°C and ice-cold 30% aqueous ammonia was added to the stirred solution, a little at a time, so that the temperature did not rise above −60°C. The ethereal layer was decanted off and rapidly washed with brine (2 × 400 cm^3) at −20°C. The ether solution was dried ($MgSO_4$) at −78°C and the ether evaporated at −40°C. The solid residue was swirled with $CDCl_3$ (3 cm^3) at −60°C and the ^{1}H and ^{13}C nmr spectra of the solution determined at that temperature. Finally the solution was warmed to ambient temperature so that the product of isomerization of the nitrodienone could be determined. 4-Methyl-4-nitrocyclohexa-2,5-dienones were more stable than the 2,4-dienones and could be worked up at 0°C.

Prior to the development of the technique for isolation of the dienones, some of the nitration reactions were studied in [$^2H_6$]acetic anhydride in order to determine the ^{1}H nmr shifts of the dienone methyls.

Characterization of nitration products

o-*Cresol* (*1*a)

6-Methyl-6-nitrocyclohexa-2,4-dienone (**2***a*) had ^{1}H nmr (Ac_2O, $(CD_3CO)_2O$) δ: 1.74 (s, 3, CH_3) 6.17 (d, 1, 2-*H*), 6.58 (4-*H*), 6.60 (5-*H*), 7.31 (8 lines, 1, 3-*H*) ppm, $J_{2,3}$ = 9.9, $J_{3,4}$ = 6.7, $J_{3,5}$ = 0.8, $J_{4,5}$ = 9.8 Hz; ($CDCl_3$) δ: 1.84 (s, 3), 6.26 (d, 1, *J* = 10 Hz), 6.54 (2), 7.27 (1) ppm; ^{13}C nmr ($CDCl_3$) δ_c: 23.1 (CH_3), 91.3 (*C*-6), 124.2 and 124.8 (*C*-4 and *C*-2), 136.5 (*C*-5), 142.5 (*C*-3), 192.5 (*C*-1) ppm. 6-Nitro-*o*-cresol (**4***a*) was isolated from the residue obtained on work-up of the nitration mixture. Sublimation (55°C, 1.3 kPa), followed by recrystallization from ether–pentane, gave **4***a*, mp 69–70°C (lit. (22) mp 70°C); ^{1}H nmr ($CDCl_3$) δ: 2.30 (s, 3, CH_3), 6.85 (t, 1, $J_{3,4}$ = 8 Hz, $J_{4,5}$ = 8 Hz, 4-*H*), 7.44 (d, 1, $J_{3,4}$ = 8 Hz, 3-*H*), 7.95 (d, 1, $J_{4,5}$ = 8 Hz, 5-*H*) ppm; ^{13}C nmr ($CDCl_3$) δ_c: 15.7 (CH_3), 119.2 and 122.6 (*C*-4 and *C*-5), 129.5 (*C*-2), 133.4 (*C*-6), 138.1 (*C*-3), 153.7 (*C*-1) ppm; ms (70 eV) *m/e* (relative intensity): 153.042 (100, M_r $^{12}C_7{}^1H_7{}^{14}N^{16}O_3$: 153.043), 137 (24), 123 (33), 111 (26), 109 (28), 107 (24), 105 (22), 97 (41), 95 (40), 91 (26), 85 (22), 83 (34), 82 (20), 81 (38), 79 (27), 77 (65). The minor isomer **5***a* was characterized by comparison of the ^{1}H nmr peaks attributed to the isomer in the mixture with those of the authentic compound.

*4,6-Dideuterio-*o*-cresol* (*1*b)

2,4-Dideuterio-6-methyl-6-nitrocyclohexa-2,4-dienone (**2***b*) had ^{1}H nmr (Ac_2O) δ: 6.60 (s, 5-*H*), 7.30 (s, 3-*H*) ppm; 4-deuterio-6-nitro-*o*-cresol (**4***b*) had δ: 7.54 (s, 3-*H*) and 7.95 (s, 5-*H*) ppm and 6-deuterio-4-nitro-*o*-cresol (**5***b*) had δ: 7.98 (s, 5-*H*), 8.02 (s, 3-*H*) ppm.

2,3-Dimethylphenol (*1*c)

5,6-Dimethyl-6-nitrocyclohexa-2,4-dienone (**2***c*) had ^{1}H nmr (Ac_2O) δ: 6.09 (d, 1, 2-*H*), 6.33 (br d, 1, 4-*H*), 7.26 (dd, 1, 3-*H*) ppm, $J_{2,3}$ = 10.0, $J_{3,4}$ = 6.2, $J_{4,5\text{-}CH_3}$ = 1.1 Hz. 2,3-Dimethyl-6-nitrophenol (**4***c*) and 2,3-dimethyl-4-nitrophenol were isolated from the residue obtained on work-up of the nitration mixture. Sublimation (50°C, 7 Pa), followed by recrystallization of the sublimate from ethanol–water, gave **4***c*, mp 48–49°C (lit. (23) mp 48.5–49°C); ^{1}H nmr ($CDCl_3$) δ: 2.20 (s, 3, 2-CH_3), 2.30 (s, 3, 3-CH_3), 6.75 (d, 1, $J_{4,5}$ = 9 Hz, 4-*H*), and 7.83 (d, 1, $J_{4,5}$ = 9 Hz, 5-*H*) ppm; ^{13}C nmr ($CDCl_3$) δ_c: 11.3 (2-CH_3), 20.5 (3-CH_3), 121.2 and 121.4 (*C*-4 and *C*-5), 126.8 (*C*-2), 131.5 (*C*-6), 147.5 (*C*-3), 153.2 (*C*-1) ppm; ms (70 eV) *m/e* (relative intensity): 167.061 (100, M_r $^{12}C_8{}^1H_9{}^{14}N^{16}O_3$: 167.058), 150 (18), 121 (18), 120 (10), 92 (11), 91 (33), 77 (26). The material which did not sublimate was triturated with ether, the ether solution was washed with brine, the ether was evaporated, and the residue was crystallized from ether–pentane. Recrystallization from ethanol–water gave **5***c*, mp 126–127°C (lit. (24) mp 123–125°C); ^{1}H nmr ($CDCl_3$/$(CD_3)_2CO$) δ: 2.20 (s, 3, 2-CH_3), 2.40 (s, 3, 3-CH_3), 6.79 (d, 1, $J_{5,6}$ = 9 Hz, 6-*H*), 7.65 (d, 1, $J_{5,6}$ = 9 Hz, 5-*H*) ppm; ^{13}C nmr ($CDCl_3$) δ_c: 12.0 (2-CH_3), 16.1 (3-CH_3), 112.5 (*C*-6), 123.9 (*C*-5), 124.9 (*C*-2), 134.3 (*C*-3), 144.3 (*C*-4), 157.2 (*C*-1) ppm; ms (70 eV) *m/e* (relative intensity): 167.057 (100, M_r $^{12}C_8{}^1H_9{}^{14}N^{16}O_3$: 167.058), 150 (99), 122 (14), 120 (10), 104 (14), 95 (19), 94 (22), 91 (40), 79 (10), 78 (12), 77 (60).

2,4-Dimethylphenol (*1*d)

4,6-Dimethyl-6-nitrocyclohexa-2,4-dienone (**2***d*) had ^{1}H nmr (Ac_2O) δ: 6.16 (d, 1, 2-*H*), 6.25 (br s, 1, 5-*H*), 7.19 (d, 1, 3-*H*) ppm, $J_{2,3}$ = 10 Hz, $J_{2,5}$ = 0.5 Hz, $J_{3,5}$ = 1 Hz, $J_{5,4\text{-}CH_3}$ = 1.5 Hz. 2,4-Dimethyl-4-nitrocyclohexa-2,5-dienone (**3***d*) had δ: 6.37 (d, 1, 6-*H*), 6.96 (br, 1, 3-*H*), 7.18 (dd, 1, 5-*H*), $J_{3,2\text{-}CH_3}$ = 1.4 Hz, $J_{3,5}$ = 3.2 Hz, $J_{5,6}$ = 10 Hz. 2,4-Dimethyl-6-nitrophenol (**4***d*) had ^{1}H nmr (Ac_2O) δ: 7.35 (s, 3-*H*), 7.70 (s, 5-*H*) ppm. Work-up of the nitration mixture after quenching at −60°C gave a brown oil. Crystallization from ethanol–water gave yellow-brown crystals, mp 68–70°C. This material was dissolved in hot pentane, then filtered, which removed the brown colour as a gummy material. The filtrate was evaporated and the residue crystallized from ethanol–water to give **4***d*, mp 70–71°C (lit. (25) mp 72°C); ^{1}H nmr ($CDCl_3$) δ: 2.26 (s, 6, 2-CH_3 and 4-CH_3), 7.26 (s, 1, 3-*H*), 7.73 (s, 1, 5-*H*) ppm; ^{13}C nmr ($CDCl_3$) δ_c: 15.6 (2-CH_3), 20.2 (4-CH_3), 121.8 (*C*-5), 128.9 and 129.0 (*C*-2 and *C*-4), 133.1 (*C*-6), 139.4 (*C*-3), 151.7 (*C*-1) ppm; ms (70 eV) *m/e* (relative intensity); 167.057 (99 M_r $^{12}C_8{}^1H_9{}^{14}N^{16}O_3$: 167.058), 137 (10), 121 (10), 119 (10), 111 (12), 109 (13), 97 (17), 95 (18), 93 (12), 91 (30), 86 (100), 85 (12), 83 (15), 81 (18), 77 (24).

2,5-Dimethylphenol (*1*e)

3,6-Dimethyl-6-nitrocyclohexa-2,4-dienone (**2***e*) had ^{1}H nmr (Ac_2O, $(CD_3CO)_2O$) δ: 1.71 (s, 6-CH_3), 6.01 (s, 1, 2-H), 6.46 (d, 1, 4-*H*), 6.61 (d, 1, 5-*H*) ppm, $J_{4,5}$ = 9.7 Hz (the 3-CH_3 peak is obscured by peak(s) of other components); ($CDCl_3$) δ: 1.80 (s, 3, 6-CH_3), 2.20 (s, 3, 3-CH_3), 6.09 (s, 1, 2-*H*), 6.45 (s, 2, 4-*H* and 5-*H*) ppm; ^{13}C nmr ($CDCl_3$) δ_c: 23.1 (6-CH_3), 23.6 (3-CH_3), 90.1 (*C*-6), 121.8 (*C*-2), 128.0 (*C*-4), 135.3 (*C*-5), 156.1 (*C*-3), 191.9 (*C*-1) ppm. 2,5-Dimethyl-6-nitrophenol (**4***e*) was obtained when the $CDCl_3$ solution of dienone **2***e* was warmed to ambient temperature. Recrystallization of the residue from ethanol–water gave **4***e*, mp 34°C (lit. (26) mp 34–34.5°C); ^{1}H nmr ($CDCl_3$) δ: 2.23 (s, 3, 2-CH_3), 2.51 (s, 3, 5-CH_3), 6.69 (d, 1, $J_{3,4}$ = 8 Hz, 4-*H*), 7.22 (d, 1, $J_{3,4}$ = 8 Hz, 3-*H*), and 10.60 (s, 1, O*H*) ppm; ^{13}C nmr ($CDCl_3$) δ_c: 15.7 (2-CH_3), 22.2 (5-CH_3), 122.9 (*C*-4), 126.6 (*C*-2), 133.8 (*C*-5), 134.9 (*C*-6), 135.9 (*C*-3), 153.6 (*C*-1) ppm; ms (70 eV) *m/e* (relative intensity): 168 (10), 167.063 (94, M_r $^{13}C_8{}^1H_9{}^{14}N^{16}O_3$: 167.058), 150 (42), 120 (43), 106 (11), 97 (12), 95 (27), 94 (11), 93 (13), 92 (28), 91 (45), 83 (13), 81 (12), 78 (11), 77 (36). The presence of the minor isomer **5***e* in the product from nitration was demonstrated by comparison of

Can. J. Chem. Downloaded from www.nrcresearchpress.com by 210.87.254.5 on 09/06/12
For personal use only.

the ^{1}H nmr and glc retention time with those of an authentic sample of **5***e*.

*2,6-Dimethylphenol (**1**f)*

2,6-Dimethyl-6-nitrocyclohexa-2,4-dienone (**2***f*) had ^{1}H nmr (Ac_2O) δ: 6.47 (apparent d, 2, 4-*H* and 5-*H*), 7.09 (m, 1, 3-H) ppm, $J_{3,4}$ = 6, $J_{3,5}$ = 1, $J_{3,2\text{-}CH_3}$ = 1.5, $J_{4,5}$ = 10 Hz; ($CDCl_3$) δ: 1.82 (s, 3, (6-CH_3), 2.00 (s, 3, 2-CH_3), 6.37 and 6.50 (m, 2, 4-*H* and 5-*H*), 7.04 (br d, 1, 3-*H*) ppm; ^{13}C nmr ($CDCl_3$) δ_c: 15.8 (2-CH_3), 23.2 (6-CH_3), 91.3 (*C*-6), 124.7 (*C*-4), 133.0 (*C*-2), 134.1 (*C*-5), 138.9 (*C*-3), 193.4 (*C*-1) ppm. On warming the $CDCl_3$ solution of the dienone to ambient temperature, 2,6-dimethyl-4-nitrophenol (**5***f*) was formed. Crystallization from ethanol–water gave **5***f*, mp 172–174°C (lit. (27) mp 170.5–170.6°C); ^{1}H nmr ($CDCl_3$/$(CD_3)_2CO$) δ: 2.30 (s, 6, 2- and 6-CH_3), 7.87 (s, 2, 3- and 5-*H*) ppm; ^{13}C nmr ($CDCl_3$) δ_c: 15.9 (2- and 6-CH_3), 123.8 (*C*-2 and *C*-6), 124.5 (*C*-3 and *C*-5), 140.9 (*C*-4), 157.9 (*C*-1) ppm; ms (70 eV) *m/e* (relative intensity): 167.059 (100, M_r $^{12}C_8{}^1H_9{}^{14}N^{16}O_3$: 167.058), 137 (19), 91 (41), and 77 (56). The identity was confirmed by comparison of the glc retention time with that of an authentic sample. 2,6-Dimethyl-*p*-benzoquinone, obtained with **5***f* when the nitration mixture was quenched with ammonia and worked up, had ^{1}H nmr ($CDCl_3$) δ: 1.96 (s, 6) and 6.50 (s, 2) ppm and identical retention time on glc with that of the authentic quinone.

*2,3,5-Trimethylphenol (**1**g)*

3,5,6-Trimethyl-6-nitrocyclohexa-2,4-dienone (**2***g*) had ^{1}H nmr (Ac_2O) δ: 5.97 (s, 1, 2-*H*), 6.26 (s, 1, 4-*H*) ppm; ($CDCl_3$) δ: 1.78 (s, 3, 6-CH_3), 1.94 (s, 3, 5-CH_3), 2.15 (s, 3, 3-CH_3), 5.98 (br s, 1, 2-*H*), 6.18 (br s, 1, 4-*H*) ppm; ^{13}C nmr ($CDCl_3$) δ_c: 18.0 (5-CH_3), 23.1 (6-CH_3), 23.8 (3-CH_3), 94.5 (*C*-6), 119.1 (*C*-2), 125.2 (*C*-4), 145.0 (*C*-5), 158.1 (*C*-3), 194.4 (*C*-1) ppm. Crystallization from ether–pentane of the mixture of nitrophenols **4***g* (74%) and **5***g* (26%), obtained on work-up of the nitration mixture after all of the dienone **2***g* had isomerized, gave **4***g*, mp 80–81°C (lit. (28) mp 78–79°C); ^{1}H nmr ($CDCl_3$) δ: 2.16 (s, 3, 2-CH_3), 2.24 (s, 3, 3-CH_3), 2.50 (s, 3, 5-CH_3), 6.60 (s, 1, 4-*H*) ppm; ^{13}C nmr ($CDCl_3$) δ_c: 11.7 (2-CH_3), 20.5 (3-CH_3), 22.4 (5-CH_3), 124.5 (*C*-2), 125.2 (*C*-4), 133.2 (*C*-5 and *C*-6), 145.4 (*C*-3), 153.9 (*C*-1) ppm; ms (70 eV) *m/e* (relative intensity): 181.073 (100 M_r $^{12}C_9{}^1H_{11}{}^{14}N^{16}O_3$: 181.074), 164 (61), 163 (14), 134 (23), 106 (13), 91 (21), 77 (11); ms (methane C.I.) 182 (*M* + 1), 210 (*M* + 29), 222 (*M* + 41). The minor product **5***g* was not isolated. It had ^{1}H nmr (in a mixture with **4***g*) δ: 2.14 (s), 6.49 (s) ppm. It could be separated from **4***g* by gas chromatography, and a methane C.I. mass spectrum was obtained which showed peaks at *m/e* 182 (*M* + 1) and 210 (*M* + 29).

*2,3,6-Trimethylphenol (**1**h)*

2,3,6-Trimethyl-4-nitrocyclohexa-2,5-dienone (**3***h*) had ^{1}H nmr (Ac_2O) δ: 5.85 (br s, 1, 4-*H*), 6.90 (br s, 1, 5-*H*) ppm; 2,3,6-trimethyl-6-nitrocyclohexa-2,4-dienone (**2***i*) had ^{1}H nmr (Ac_2O) δ: 6.44 (s, 4-*H* and 5-*H*) ppm; ($CDCl_3$–CD_3CN) δ: 1.73 (s, 3, 6-CH_3), 1.89 (s, 3, 2-CH_3), 2.13 (s, 3, 3-CH_3), 6.37 (s, 2, 4-*H* and 5-*H*) ppm; ^{13}C nmr ($CDCl_3$–CD_3CN) δ_c: 11.0 (2-CH_3), 21.2 (3-CH_3), 23.2 (6-CH_3), 90.7 (*C*-6), 128.5 or 129.8 (*C*-2), 129.8 (*C*-4), 132.6 (*C*-5), 150.0 (*C*-3), 192.5 (*C*-1) ppm; 2,5,6-trimethyl-6-nitrocyclohexa-2,4-dienone (**2***h*) had ^{1}H nmr (Ac_2O) δ: 6.24 (br d, 4-*H*), 7.05 (br d, 3-*H*) ppm, $J_{3,4}$ = 6.9 Hz; ($CDCl_3$–CD_3CN) δ: 1.73 (s, 3, 6-CH_3), 1.89 (s, 6, 2-CH_3 and 5-CH_3), 6.19 (br d, 1, 4-*H*), 6.98 (br d, 1, 3-*H*) ppm, $J_{3,4}$ = 6.9 Hz; ^{13}C nmr ($CDCl_3$–CD_3CN) δ_c: 15.4 (2-CH_3), 17.9 (5-CH_3), 23.3 (6-CH_3), 96.0 (*C*-6), 121.5 (*C*-4), 129.8 or 128.5 (*C*-2), 140.5 (*C*-3), 143.5 (*C*-5), 195.4 (*C*-1) ppm. The ^{13}C nmr peaks of the mixture of dienones were assigned on the basis of the relative amounts of the isomers present, the peak heights, the splitting pattern in a gated experiment, and the calculated shifts based on the methyl substituent effects in the other dienones. 2,3,6-Trimethyl-4-nitrophenol (**5***h*) was formed when the solution of dienones **2***h* and **2***i* in $CDCl_3$–CD_3CN was warmed to ambient temperature. After recrystallization from methylene chloride **5***h* had mp 97–98°C; ^{1}H nmr ($CDCl_3$) δ: 2.35 (s, 3, 2- or 6-CH_3), 2.38 (s, 3, 6- or 2-CH_3), 2.53 (s, 3, 3-CH_3), 5.56 (br s, 1, O*H*), 7.70 (s, 1, 5-*H*) ppm; ^{13}C nmr ($CDCl_3$) δ_c: 12.3 (2-CH_3), 15.6 and 16.0 (3-CH_3 and 6-CH_3) 120.7 (*C*-6), 123.7 (*C*-2), 124.6 (*C*-5), 131.5 (*C*-3), 143.9 (*C*-4), 155.6 (*C*-1); ms (70 eV) *m/e* (relative intensity): 181.074 (61, M_r $^{12}C_9{}^1H_{11}{}^{14}N^{16}O_3$: 181.074), 165 (12), 164 (76), 136 (23), 134 (10), 122 (10), 115 (10), 109 (32), 108 (25), 107 (17), 105 (18), 95 (12), 94 (15), 93 (20), 92 (17), 91 (100), 81 (26), 79 (46), 78 (14), 77 (50). Some 2,3,5-trimethyl-*p*-benzoquinone (δ: 1.96 (s, 6), 2.04 (s, 3), 6.55 (s, 1) ppm) was formed in one sample on exposure to air.

*2,4,6-Trimethylphenol (**1**j)*

2,4,6-Trimethyl-6-nitrocyclohexa-2,4-dienone (**2***j*) had ^{1}H nmr (Ac_2O) δ: 6.12 (br s, 5-*H*), 6.94 (br s, 3-*H*) ppm; ($(CD_3)_2CO$) δ: 1.68 (s, 3, 6-CH_3), 1.89 (s, 3, CH_3), 1.97 (s, 3, CH_3), 6.16 (br s, 1, 5-*H*), 6.97 (br s, 1, 3-*H*) ppm; 2,4,6-trimethyl-4-nitrocyclohexa-2,5-dienone (**3***j*) had ^{1}H nmr (Ac_2O) δ: 6.94 (s) ppm; ($(CD_3)_2CO$) δ: 1.89 (s, 9), 6.97 (s, 2) ppm; ($CDCl_3$) δ: 1.86 (s, 3, 4-CH_3), 1.94 (s, 6, 2-CH_3 and 6-CH_3), 6.84 (s, 2, 3-*H* and 5-*H*) ppm; ^{13}C nmr ($CDCl_3$) δ_c: 16.2 (2-CH_3 and 6-CH_3), 26.1 (4-CH_3), 84.7 (*C*-4), 137.1 (*C*-2 and *C*-6), 138.2 (*C*-3 and *C*-5), 185.3 (*C*-1) ppm. 2,6-Dimethyl-4--nitromethylphenol obtained on isomerization of dienone **3***j* had ir (film): 3480 (OH), 1558 (NO_2) cm^{-1}; ^{1}H nmr ($CDCl_3$) δ: 2.19 (s, 6, 2- and 6-CH_3), 5.24 (s, 2, CH_2NO_2), 7.01 (s, 2, 3- and 5-*H*) ppm; ^{13}C nmr ($CDCl_3$) δ_c: 15.8 (2-CH_3 and 6-CH_3), 79.8 (CH_2–NO_2), 121.4 (*C*-4), 124.1 (*C*-2 and *C*-6), 130.4 (*C*-3 and *C*-5), 153.8 (*C*-1) ppm.

1. A. FISCHER and G. N. HENDERSON. Can. J. Chem. **59**, 2314 (1981).
2. V. V. ERSHOV, A. A. VOLOD'KIN, and G. N. BOGDANOV. Russ. Chem. Rev. **32**, 75 (1963).
3. A. J. WARING. Adv. Alicyclic Chem. **1**, 172 (1966).
4. V. V. ERSHOV and G. A. ZLOBINA. Izv. Akad. Nauk SSSR Ser. Khim. 2235 (1963).
5. D. J. BLACKSTOCK, M. P. HARTSHORN, A. J. LEWIS, K. E. RICHARDS, J. VAUGHAN, and G. J. WRIGHT. J. Chem. Soc. B, 1212 (1971).
6. A. H. CLEMENS, M. P. HARTSHORN, K. E. RICHARDS, and G. J. WRIGHT. Aust. J. Chem. **30**, 113 (1977).
7. C. E. BARNES, K. S. FELDMAN, M. W. JOHNSON, H. W. LEE, and P. C. MYHRE. J. Org. Chem. **44**, 3925 (1979).
8. A. FISCHER and G. N. HENDERSON. Tetrahedron Lett. 4661 (1980).
9. P. HELSBY and J. H. RIDD. J. Chem. Soc. Perkin Trans. 2, 311 (1983).
10. V. V. ERSHOV and G. A. ZLOBINA. Izv. Akad. Nauk SSSR Ser. Khim. 1667 (1963).
11. F. BELL and R. D. WILSON. J. Chem. Soc. 2340 (1956).
12. C. D. COOK and R. C. WOODWORTH. J. Am. Chem. Soc. **75**, 6242 (1953).
13. V. V. ERSHOV, G. A. ZLOBINA, and G. A. NIKIFOROV. Izv. Akad. Nauk SSSR Ser. Khim. 1877 (1963).
14. G. A. ZLOBINA and V. V. ERSHOV. Izv. Akad. Nauk SSSR Ser. Khim. 189 (1966).
15. K. SCHOFIELD. Aromatic nitration. Cambridge University Press, Cambridge. 1980. p. 241.
16. R. G. COOMBES, J. G. GOLDING, and P. HADJIGEORGIOU. J. Chem. Soc. Perkin Trans. 2, 1451 (1979).
17. G. S. BAPAT, A. FISCHER, G. N. HENDERSON, and S. RAYMAHASAY. J. Chem. Soc. Chem. Commun. 119 (1983).
18. A. A. BOTHNER-BY and E. MOSER. J. Am. Chem. Soc. **90**, 2347 (1968).
19. H. GILLMAN and A. H. BLATT. Org. Synth., Coll. Vol. I. 2nd ed. 1941.
20. Beilsteins Handbuch der organischen Chemie, Vol. 6, p. 366.
21. H. E. ALBERT and W. C. SEARS. J. Am. Chem. Soc. **76**, 4979 (1954).
22. M. J. ASTLE and W. P. CROPPER. J. Am. Chem. Soc. **65**, 2395 (1943).

23. A. HOLLER, C. HUGGETT, and F. A. RATHMANN. J. Am. Chem. Soc. **72**, 2034 (1950).
24. W. CARRUTHERS and A. DOUGLAS. J. Chem. Soc. 2813 (1959).
25. D. S. TARBELL. J. Org. Chem. **7**, 251 (1942).
26. A. C. HOLLER and R. V. HUCH. Anal. Chem. **21**, 1385 (1949).
27. G. W. WHELAND, R. M. BROWNELL, and E. C. MAYO. J. Am. Chem. Soc. **70**, 2492 (1948).
28. Beilsteins Handbuch der organischen Chemie. 2nd Supplement. Vol. 6. p. 483.

Can. J. Chem. Downloaded from www.nrcresearchpress.com by 210.87.254.5 on 09/06/12
For personal use only.

Comparison of methods for determination of boron in heavy water moderator

L. W. GREEN,[1] E. C. DAVEY, J. GULENS, T. H. LONGHURST, AND J. P. MISLAN
Chalk River Nuclear Laboratories, Atomic Energy of Canada Limited Research Company, Chalk River, Ont., Canada K0J 1J0

Received December 14, 1983

L. W. GREEN, E. C. DAVEY, J. GULENS, T. H. LONGHURST, and J. P. MISLAN. Can. J. Chem. **62**, 1452 (1984).

Five analysis methods were compared for the determination of boron in heavy water moderator: isotope dilution mass spectrometry, spectrophotometry, neutron activation, inductively coupled plasma – atomic emission spectrometry, and ion selective electrode potentiometry. Ten samples were analysed by each method; the results showed close agreement between all of the methods. Only mass spectrometry achieved the required precision (<1% rsd) for samples taken during initial reactor operation, but all of the methods achieved sufficient precision (<10% rsd) for samples taken during normal operation. For samples for which the ^{10}B concentration must be determined, only mass spectrometry and neutron activation are applicable.

L. W. GREEN, E. C. DAVEY, J. GULENS, T. H. LONGHURST et J. P. MISLAN. Can. J. Chem. **62**, 1452 (1984).

On a comparé cinq méthodes d'analyse pour la détermination du bore dans des modérateurs à l'eau lourde: la spectrométrie de masse par dilution isotopique, la spectrophotométrie, l'activation neutronique, la spectrométrie d'émission atomique par plasmas induits par radiofréquence et la potentiométrie à l'aide d'électrodes spécifiques à certains ions. On a analysé dix échantillons par chacune des méthodes. Seule la spectrométrie de masse a permis d'obtenir la précision requise (coefficient de variation plus petit que 1%) pour des échantillons prélevés au cours de l'opération initiale du réacteur, mais toutes les méthodes donnent une précision suffisante (coefficient de variation plus petit que 10%) pour des échantillons obtenus durant le cours normal des opérations. Si on doit déterminer les concentrations en ^{10}B dans les échantillons, seules la spectrométrie de masse et l'activation neutronique peuvent être utilisées.

[Traduit par le journal]

Can. J. Chem. Downloaded from www.nrcresearchpress.com by 210.87.254.42 on 09/06/12
For personal use only.

Introduction

Boron, in the form of boric acid, is added to the heavy water moderator of CANDU™ power reactors to compensate for excess reactivity that exists during initial operation conditions and to serve as a readily removable reactivity shim during long term operation (1). It is also used during reactor commissioning to calibrate the reactivity worth of control devices such as the liquid zone control system, mechanical control absorbers, and adjuster rod adsorbers. The mass 10 isotope of boron is well suited for these purposes because its thermal neutron capture cross section is large (3.81×10^{-21} cm^2) and varies linearly with the inverse of neutron velocity over a wide velocity range.

For calibration of the reactivity devices and for many of the reactivity assessments during normal operation, an uncertainty of less than 1 part in 1000 in the neutron balance (uncertainty ≤1 mk) is required. This corresponds to a precision of ±0.03 μg/g (2 s) for ^{10}B or, in the case of isotopically natural boron, ±0.12 μg/g for total boron. The ^{10}B concentration is ~1.5 μg/g during initial operation and decreases to ~0.15 μg/g during normal operation, thus relative uncertainties of ≤2% (2 s) for the initial operation samples and of ≤20% for the normal operation samples are required for an analysis method. A method that can detect the ^{10}B isotope is preferable, but since frequently the boron isotopic composition is known or can be inferred, determination of total boron concentration is sufficient.

Currently at the generating stations, spectrophotometric methods (2, 3) are used for total boron determinations and a neutron activation method (1*a*) is used for ^{10}B determinations. Additionally, samples are periodically analysed by isotope dilution mass spectrometry (IDMS), to verify both the boron isotopic composition and total concentration.

Stewart (8) has reviewed the status of moderator boron analysis up to 1977, but since then some newer methods have been applied. The purpose of this work was to assess the accuracy, precision, and suitability of both old and new methods for the determination of boron in heavy water moderator. Five methods were investigated: spectrophotometry (chromotropic acid), neutron activation (NA), IDMS, inductively coupled plasma atomic emission spectroscopy (ICP-AES), and ion selective electrode (ISE) potentiometry (fluoroborate electrode). Ten moderator samples were distributed to each participant and each sample was analysed in duplicate or triplicate.

[1] To whom all correspondence should be addressed.

Experimental

Sampling

Five samples of heavy water moderator were obtained at the sampling stations of each of the Wolsung and Point Lepreau nuclear generating plants during their Phase B commissioning periods. Samples were collected and stored in leakproof polyethylene bottles (CANLAB series B7504) that had been rinsed with moderator prior to sample collection. Spectrophotometric and, for the Wolsung samples, neutron activation analyses were completed at the generating stations. For the other methods, samples were sent to the Chalk River Nuclear Laboratories, subdivided, and distributed to the various participants. The above described CANLAB bottles were used for sample subdivision; these were leached in 1 *M* Na_2CO_3, rinsed with deionized water and dried before use. Contact of the samples with glassware was avoided.

Methods

Isotope dilution mass spectrometry

The National Bureau of Standards (NBS) recommended procedure for mass spectrometry of boron was used (4). Accurately weighed aliquots of sample (~5 g) and spike (NBS SRM 952 solution) were mixed with sodium carbonate solution, evaporated to dryness under nitrogen flow at ~35°C, dissolved and mixed in 0.5 mL of deionized water, re-evaporated to dryness, and dissolved in 30 μL of deionized water. Approximately 5 μL of this solution was deposited and dried on a tantalum centre filament. The $Na_2BO_2^+$ ions were measured at masses 88 and 89. The NBS boron standard SRM 951 (10/11 atomic ratio = 0.2473) was used to standardize this and all other methods.

Special care was taken to avoid boron contamination. Solutions were stored and handled in plastic containers that had been leached overnight in 1 *M* Na_2CO_3 solution and rinsed with deionized water. High purity Aristar (BDH Chemicals Ltd., Poole, Eng.) sodium carbonate was used in sample preparation; sufficient Na_2CO_3 was added

TABLE 1. Determined concentrations and isotopic composition of boron in heavy water moderator

Sample	Concentration of boron (μg total B/g D_2O)					10/11 atomic ratio
	IDMS	Spec.	NA	ICP-AES	ISE	IDMS
W1	8.42	8.6	7.9	8.2	8.3	0.2455
W2	8.60	9.1	7.6	8.6	8.5	0.2465
W3	7.59	9.4	8.0	7.5	7.6	0.2465
W4	10.02	9.6	10.4	9.9	9.8	0.2469
W5	8.65	9.4	8.0	8.2	8.3	0.2465
PL1	7.97	7.9	7.7	8.2	7.9	0.2465
PL2	5.65	5.6	5.5	5.7	5.3	0.2443
PL3	8.22	8.2	8.4	8.5	8.2	0.2472
PL4	10.05	9.8	10.5	10.4	10.4	0.2467
PL5	6.02	5.9	5.5	6.4	6.3	0.2437
rsd (ls)	0.5%	10%	6%	2%	5%	0.25%
t^a		1.12	1.21	0.63	0.78	

"IDMS values used as "true" values. Tabulated t-value for 95% confidence and 9° of freedom is 2.26.

to each sample to yield an approximately equimolar sodium and boron content. Deionized light water was used for all dissolutions and dilutions.

Spectrophotometry

The chromotropic acid procedure described by Kuemmel and Mellon (2) was used. Absorbance measurements were recorded on a Perkin-Elmer Coleman 55 spectrophotometer at 360 nm. Samples were closely bracketed by standards to avoid calibration errors due to non-linearity. A disodium chromotropate stock solution was prepared fresh each week and stored in the dark to avoid photodecomposition. Furthermore, once samples were mixed with reagents exposure to light was minimized.

Neutron activation

The Boron-10 Analyser and methodology described by Davey (1*a*) were used. Samples and standards were diluted with light water to the 0.1 to 0.5 μg/g ^{10}B range, and evaporated on aluminum planchets in five successive 0.2 mL quantities in an oven at 95°C. For the Point Lepreau samples, the planchets were roughened by sandblasting to achieve satisfactory surface wetting; this was not necessary for the Wolsung planchets. The planchets were exposed to a thermal neutron flux of 1×10^9 neutrons m^{-2} s^{-1} derived from a heavy water moderated ^{252}Cf source, and the 1.47 MeV α particles from the ^{10}B (n, α) ^7Li reaction were simultaneously counted. The mass spectrometrically determined isotopic composition was used to compute the total [B] from the determined [^{10}B].

Inductively coupled plasma atomic emission spectroscopy

The procedure was similar to that reported for a D.C. argon plasma spectrometer (5). Samples were directly aspirated into the plasma and boron I emission was monitored at 249.68 nm. The plasma emission spectrometer consisted of a Jobin-Yvon 38P Spectrometer, a Plasmatherm 2.5 kW, 27.12 MHz source and a hybrid nebulizer torch consisting of an Instruments SA concentric nebulizer, a Perkin-Elmer spray chamber, and a Plasmatherm quartz torch. Typical instrumental conditions were: incident power, 1.3 kW; reflected power, 5 W; coolant flow-rate, 13 L min^{-1}; auxiliary flow rate, 1.4 L min^{-1}; and sample uptake, 0.9 mL min^{-1}. For calibration, standards were prepared in reactor grade 99.7% D_2O. Resolution was insufficient to separate the emission lines of the two boron isotopes.

Ion selective electrode potentiometry

Boric acid was converted to the fluoroborate anion and analysed by the method described by Gulens and Leeson (6). Due to the limited volume of sample available for analysis, the samples were diluted ten-fold with 94.5% D_2O prior to the conversion step. The fluoroborate sensing module was stored between use in a heavy water solution containing 5 μg B/g as BF_4^-.

Results and discussion

Preliminary results showed that significant biases were obtained with the neutron activation method for the Point Lepreau measurements when the planchets were not roughened and with the ICP-AES method when the deuterium concentration of the heavy water used for preparation of standards did not match that of the samples. For example, the neutron activation results for the Point Lepreau samples were ~40% low when unroughened planchets were used; this was likely due to poor surface wetting and loss of H_3BO_3 during the drying step. The ICP-AES results for all the samples were 10% low when standards were prepared in 94.8% D_2O; reactor grade deuterium content is 99.8%. These low results were attributed to a viscosity effect.

The final results of the interlaboratory comparison are listed in Table 1. The estimated precision of each method is included; relative standard deviations were determined from six or more replicate analyses on typical samples. As expected, the IDMS method demonstrated much higher precision than the others. Because of its higher precision and proven reliability over many years, the IDMS method was chosen as a reference method against which the others were compared; the mean IDMS values for each sample were used as the population mean or "true" values in t-tests (7).

The results in Table 1 show consistent good agreement between each method and the reference method, and the given t-test values indicate that there were not any systematic differences in the methods. There is one large deviant, the spectrophotometric result for sample W3.

Of the methods investigated, only IDMS achieved the high level of precision required for reactivity assessment during initial reactor operation, but all of the methods were suitable for reactivity assessment during normal operation. The ICP-AES method proved to be the most convenient method; it was ~3 times faster than the others and had minimal operational difficulties. The results in Table 1 show that the precision and accuracy of this method were better than those of the others, except for IDMS. The IDMS and NA methods have the advantage of capability of ^{10}B determination; the spectrophotometric and potentiometric methods have the advantages of low cost and portability.

Can. J. Chem. Downloaded from www.nrcresearchpress.com by 210.87.254.42 on 09/06/12
For personal use only.

Acknowledgments

We thank C. MacNeil (Pt. Lepreau N.G.S.) and D. Burt (AECL Eng. Co.) for the station data and N. L. Elliot, P. L. J. Faught, R. T. Faught, and P. K. Leeson for technical assistance.

1. (*a*) E. C. DAVEY. Atomic Energy of Canada Limited Report AECL-7718, 1982; (*b*) A. A. PASANEN. Fundamentals of CANDU reactor nuclear design. Report TDAI-244, Atomic Energy of Canada Limited Engineering Company, Sheridan Park Research Community, Mississauga, Ont., Canada L5K 1B2. 1980.
2. D. F. KUEMMEL and M. G. MELLON. Anal. Chem. **29**, 378 (1957).
3. R. H. TUXWORTH, R. J. SPEEDY, and R. MATSUMOTO. Atomic Energy of Canada Limited Report AECL-3137, 1968.
4. E. J. CATANZARO, C. E. CHAMPION, E. L. GARNER, G. MARINENKO, K. J. SAPPENFIELD, and W. R. SHIELDS. Natl. Bur. Stand. Spec. Publ. 260-17, 1970.
5. J. W. BALL, J. M. THOMPSON, and A. E. JENNE. Anal. Chim. Acta, **98**, 67 (1978).
6. J. GULENS and P. K. LEESON. Anal. Chem. **52**, 2235 (1980).
7. H. A. LAITINEN and W. E. HARRIS. Chemical analysis. 2nd ed. McGraw-Hill, New York. 1975. Chapt. 26.
8. R. B. STEWART. Analytical chemistry for boron in heavy water moderator — a review of AECL development. Report WNRE-348. Atomic Energy of Canada Limited Research Company. 1977.

Can. J. Chem. Downloaded from www.nrcresearchpress.com by 210.87.254.42 on 09/06/12
For personal use only.

Skeletal isomerization of cyclohexene on Al_2O_3 and $AlPO_4-Al_2O_3$ catalysts

J. M. CAMPELO, A. GARCIA, J. M. GUTIERREZ, D. LUNA, AND J. M. MARINAS
Department of Organic Chemistry, Faculty of Sciences, Cordoba University, Cordoba-5, Spain

Received October 31, 1983

J. M. CAMPELO, A. GARCIA, J. M. GUTIERREZ, D. LUNA, and J. M. MARINAS. Can. J. Chem. **62**, 1455 (1984).

Cyclohexene skeletal isomerization, in a microcatalytic pulse reactor, was investigated using Al_2O_3 and $AlPO_4-Al_2O_3$ as catalysts. Apparent rate constants and apparent activation energies were calculated according to the kinetic model of Bassett–Habgood. Selectivity studies concluded that 1-MCP and 3-MCP were competitive products with a first-order kinetics. The rate constants as well as the selectivity at 1-MCP increase with an increase in the number and strength of stronger acid sites, measured by means of the irreversible adsorption of aniline in cyclohexane, at 298 K, using a spectrophotometric method. The parallel reaction pathway, proposed for $AlPO_4$ catalysts, agrees with both the observed rates and selectivities using Al_2O_3 and $AlPO_4-Al_2O_3$ catalysts.

J. M. CAMPELO, A. GARCIA, J. M. GUTIERREZ, D. LUNA et J. M. MARINAS. Can. J. Chem. **62**, 1455 (1984).

Utilisant le Al_2O_3 et le $AlPO_4-Al_2O_3$ comme catalyseurs, on a étudié l'isomérisation du squelette du cyclohexène dans un réacteur microanalytique pulsé. On a calculé les constantes apparentes de vitesse et les énergies apparentes d'activation en utilisant le modèle cinétique de Bassett et Habgood. Des études de sélectivité ont permis de conclure que les 1-MCP et 3-MCP sont des produits compétitifs avec une cinétique du premier ordre. Les constantes de vitesse ainsi que la sélectivité en faveur du 1-MCP augmentent avec une augmentation du nombre de sites acides et de l'acidité de ces sites tels que mesurés grâce à l'adsorbtion irréversible de l'aniline dans le cyclohexane, à 298 K, en faisant appel à une méthode spectrophotométrique. Le modèle réactionnel parallèle, proposé pour les catalyseurs de $AlPO_4$, correspond aussi bien aux vitesses qu'aux sélectivités observées lors de l'utilisation des catalyseurs Al_2O_3 et $AlPO_4-Al_2O_3$.

[Traduit par le journal]

Can. J. Chem. Downloaded from www.nrcresearchpress.com by 210.87.254.105 on 09/06/12
For personal use only.

Introduction

In a previous study, we have shown that the precipitation agent of the $AlPO_4$ catalysts exerts a strong effect on the acid properties as well as on the catalytic activity for the skeletal isomerization of cyclohexene (1). Thus, the $AlPO_4$ obtained by precipitation with propylene oxide has the greatest number of acid sites of high strength, when titrated vs. aniline, exhibiting the highest isomerization activity and selectivity to 1-methylcyclopentene, which, together with 3-methylcyclopentene, are the isomerization products. These products are obtained by parallel reactions according to a carbocationic mechanism with rearrangement of intermediates.

The present paper deals with the study of surface acidity and catalytic activity in the cyclohexene skeletal isomerization on $AlPO_4-Al_2O_3$ catalysts obtained by precipitation with ethylene or propylene oxide. This study also includes the Al_2O_3 catalyst that constitutes the $AlPO_4-Al_2O_3$ systems.

As in a previous work, the cyclohexene skeletal isomerization has been carried out in a microcatalytic pulse reactor according to the Bassett–Habgood model (2) developed for first-order processes where the surface reaction is the rate-determining step.

Experimental

Catalysts

The Al_2O_3 (AL) was obtained by precipitation with aqueous ammonia from an aqueous solution of aluminum nitrate.

The $AlPO_4-Al_2O_3$ (75:25 wt.%) systems were obtained by adding aluminum hydroxide, obtained as in the AL case, in a reaction medium where the precipitation of $AlPO_4$, from $AlCl_3.6H_2O$ and H_3PO_4 (85 wt.%) aqueous solutions, has been initiated by addition of ethylene (BA) or propylene (BPA) oxide. The total precipitation of $AlPO_4$ is then carried out by addition of ammonium hydroxide solution. The pH value at the precipitation "end-point" was 6.1 in both cases.

The three samples received the same thermal treatment, namely, drying at 393 K for 24 h and calcination at 923 K for 3 h in a muffle furnace.

The detailed description of the syntheses has been described previously (3, 4).

Physico-chemical properties

The physico-chemical properties of the catalysts have already been researched. Thus, the surface area was determined by the BET method (5) and the porosity detection was carried out by means of the Lecloux method (6) using n_3 due to the monolayer value. Pore size analysis was made using the "corrected modelless" method for mesopores (7).

The surface acidity was determined by titration with cyclohexylamine, pyridine, and aniline from cyclohexane solutions (spectroscopic grade, Merck) at 298 K using a spectrophotometric method previously described (1, 8, 9).

Apparatus and procedure

The CH isomerization was carried out in a microcatalytic pulse reactor according to a method described elsewhere (1). However, in this work we have maintained a constant catalyst loading of 150 mg ($\leq$0.7 mm), except for the BA sample that exhibits the highest activity.

CH was obtained from Merck and was used after purifying it by a column of alumina previously calcined at 573 K for 3 h.

The reaction products are analyzed by glc as previously reported (1), using a 3-m stainless steel column of 2-mm diameter, filled with 5% squalane on Chromosorb G AW-DMCS 80/100.

Results and discussion

Textural and surface acid properties

The adsorption isotherm is type II of Brunauer's classification for $AlPO_4-Al_2O_3$ catalysts, while it is type IV for Al_2O_3, and pronounced hysteresis loops are shown for the three samples. By application of the "corrected modelless" method for mesopore analysis, the cylindrical model could fit the criteria of corrected analysis. The textural properties thus obtained, surface area, pore volume, and main pore radius, are presented in Table 1.

[1]All correspondence concerning this paper should be addressed to: Prof. Dr. J. M. Campelo Pérez, Departamento de Química Orgánica, Facultad de Ciencias, Universidad de Córdoba, Avda. Medina Azahara s/n° Córdoba-5 (España).

TABLE 1. Textural properties and surface acidity of $AlPO_4-Al_2O_3$ and Al_2O_3 catalysts

Catalysts	S ($m^2\ g^{-1}$)	V ($mL\ g^{-1}$)	r (nm)	CY (pK_a = 10.6) $x_m \cdot 10^6$	CY (pK_a = 10.6) $b \cdot 10^{-4}$	PY (pK_a = 5.3) $x_m \cdot 10^6$	PY (pK_a = 5.3) $b \cdot 10^{-4}$	AN (pK_a = 4.6) $x_m \cdot 10^6$	AN (pK_a = 4.6) $b \cdot 10^{-4}$
AL	151	0.31	2.0	172	5.7	77	8.6	6	15.1
BA	263	0.53	3.0	620	5.1	300	12.4	60	194.1
BPA	237	0.70	2.5	684	5.7	385	11.4	35	29.3

As regards the surface acid properties, the chemical interaction adsorbate–surface can be accomplished by applying the linear transformed Langmuir adsorption isotherm [1]

$$[1]\quad C/x = 1/bx_m + C/x_m$$

as in the $AlPO_4$ case.

The monolayer coverage, x_m, which corresponds to the theoretical amount of base adsorbed by 1.0 g of solid systems if all sites are covered, must be assumed as a measure of the acid sites corresponding to specific pK_a of the base.

Since the linearization of the Langmuir isotherm assumes uniformity of sites, besides x_m, we can also use the b constant which depends on the interaction strength of the base with the acid site, i.e. the site strength. These b values displayed a greater experimental error since they are obtained from the intercept at the origin.

Thus the reproducibility of the titration method has been checked experimentally and the measurements were repeated 2–3 times. The relative error was about 6% for x_m values, while the b values were reproducible to within about 15%.

The surface distribution of x_m and b values is presented in Table 1. As can be seen, the irreversible adsorption of the base, x_m, agrees with its specific pK_a; thus, the sequence obtained in all cases is CY > PY > AN. Therefore, the difference between the x_m values for CY and the other bases (PY or AN) is a measure of the number of weaker acid sites.

The $AlPO_4-Al_2O_3$ system obtained by precipitation with propylene oxide (BPA) shows the highest number of acid sites with respect to CY and PY, while the number of strong acid sites are lower than the BA sample. On the other hand, the alumina AL only exhibits acidity vs. CY and PY with a very low number of acid sites.

With respect to the strength of acid sites measured by the constant b, the BA sample is the one which shows the highest value, ahead of PY and AN, especially in the latter case.

Thus, from a general point of view, the present results show that the precipitation agent of the $AlPO_4-Al_2O_3$ system exerts an influence on the number and strength of acid sites, as in the $AlPO_4$ catalysts, the system obtained with ethylene oxide being the one which possesses the highest strength of acid sites.

Catalytic activity

As in the previous study of the CH skeletal isomerization on $AlPO_4$ catalysts, the reaction rate is free from transport influences, and the isomerization was maintained at low conversion levels (<8%). Also, 1-MCP and 3-MCP are the only isomerization products detected due to the short contact time of the reaction. For sample AL, only 1-MCP was obtained.

The isomerization activity, expressed by the total conversion to 1- and 3-MCP, is adjusted to the Bassett–Habgood equation [2] (2), as can be seen in Fig. 1.

$$[2]\quad \ln (1/1 - X) = RT \cdot kK\ (W/Q)$$

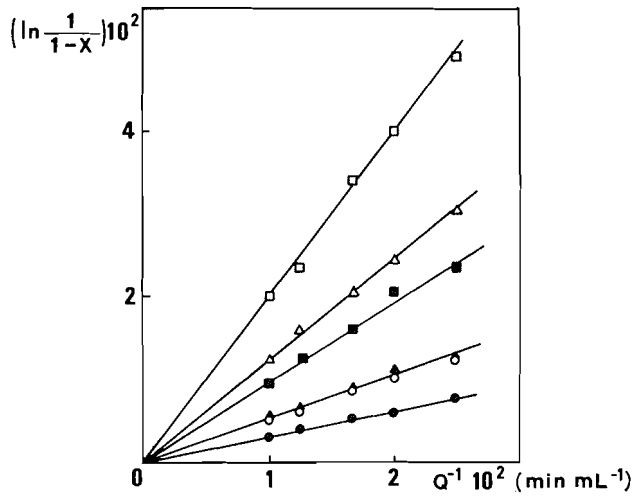

FIG. 1. Test of first-order rate law for cyclohexene isomerization. BA 151 mg (○) 573 K; (△) 623 K; (□) 673 K. BPA 149 mg (●) 573 K; (▲) 623 K; (■) 673 K.

TABLE 2. Apparent rate constant and apparent activation energies for CH isomerization on Al_2O_3 and $AlPO_4-Al_2O_3$

Catalyst	T (K)	$kK \times 10^6$ (mol $atm^{-1}\ g^{-1}\ s^{-1}$)	E_a (kJ mol^{-1})
A	573	0.22±0.02	
	623	0.26±0.02	21.2±1.9
	673	0.37±0.03	
BA	573	1.20±0.08	
	623	2.67±0.19	44.3±4.0
	673	4.06±0.28	
BPA	573	0.73±0.05	
	623	0.94±0.07	36.2±3.3
	673	1.96±0.14	

Thus, the skeletal isomerization of CH is a first-order kinetic process, the rate of surface reaction being the rate-determining step.

The apparent rate constants, kK, at a fixed temperature, from the plots ln $(1/1 - X)$ vs. $1/Q$, and the apparent activation energy, E_a, from ln [ln $(1/1 - X)$] vs. $1/T$, were obtained in each case and are collected in Table 2.

As can be seen from the data in Table 2, the catalytic activity of alumina AL is very low as corresponds to the small number and strength of its acid sites. On the other hand, the BA catalyst exhibits higher activity than the BPA sample, as a consequence of its larger number of stronger acid sites.

Taking into account the previous results (1), the sites responsible for the CH skeletal isomerization seem to be those

Can. J. Chem. Downloaded from www.nrcresearchpress.com by 210.87.254.105 on 09/06/12
For personal use only.

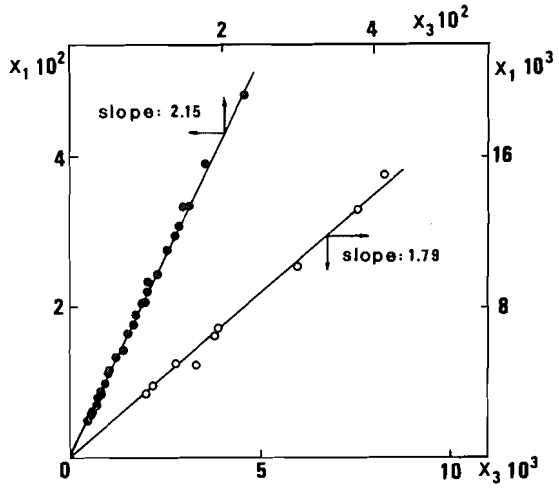

FIG. 2. Selectivity factors: X_1 vs. X_3 on BA (●) and BPA (○) catalysts. (Data at every temperature.)

titrated vs. AN through the x_m and b values working simultaneously.

On the other hand, the concentration of 1-MCP was always higher than 3-MCP for BA and BPA samples, and these isomerization products are competitors, with a first-order kinetics, since the application of the Wheeler criterion (10) on the kinetic selectivity factor, σ, leads to a straight line, as can be seen in Fig. 2 where the plots of X_1 vs. X_3 appear.

[3] $\sigma = K_1/K_3 = X_1/X_3$

A least-squares regression analysis and a "t-test" of significance, performed on the regression coefficients, show the accuracy of fit of the data, in all experimental conditions, in the straight lines of Fig. 2.

As Fig. 2 contains points at the three temperatures, the apparent activation energies for 1- and 3-MCP formation are identical for each catalyst. Besides, the selectivity to 1-MCP for the BA sample is larger than for the BPA sample, as corresponds to its higher acid strength (high values of x_m and b vs. AN).

Thus, as in the previous study on the CH skeletal isomerization for $AlPO_4$ catalysts, the different σ values for each catalyst are due to different A_1/A_3 ratios, since for each catalyst the formation of 1- and 3-MCP has identical apparent activation energies. So, both isomerization products are obtained by a carbocationic mechanism (11–14) with a rearrangement of intermediates, across parallel reactions, as has been shown previously (1).

For an AL sample, the 1,3-hydride shift that changes the tertiary carbenium ion I into a secondary ion (IV) is not as easy as corresponds to its low surface acidity. So, the 3-MCP formation on an AL catalyst is difficult and thus is not observed in the present experimental conditions.

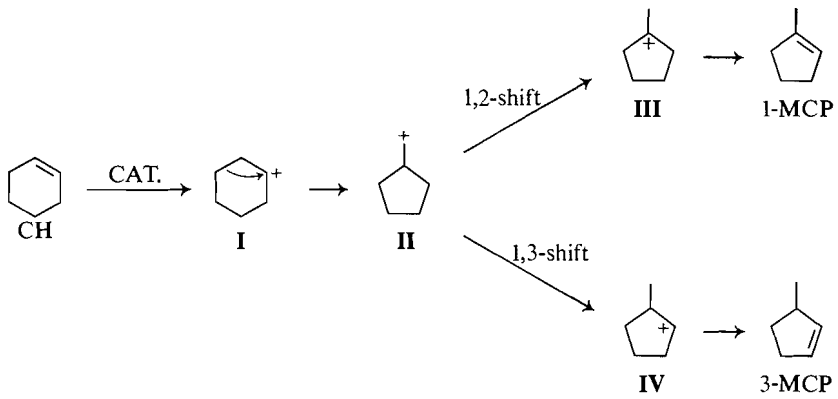

Conclusions

The present results, together with those previously obtained (1), show that the stronger acid sites are necessary for the CH skeletal isomerization to 1- and 3-MCP on $AlPO_4$, Al_2O_3, and $AlPO_4$–Al_2O_3 catalysts, and that the apparent rate constant, kK, and the selectivity at 1-MCP increase with an increase in the number (x_m) and strength (b) of stronger acid sites (vs. AN), both acting simultaneously.

The previously proposed mechanism, through intermediates with a more or less developed carbocationic character, agrees with these experimental results.

Acknowledgements

This work has been possible thanks to a grant from the Comisión Asesora de Investigación Científica y Técnica (CAICYT), project No. 0249/81.

1. J. M. CAMPELO, A. GARCIA, J. M. GUTIERREZ, D. LUNA, and J. M. MARINAS. Can. J. Chem. **61**, 2567 (1983).
2. D. BASSETT and H. W. HABGOOD. J. Phys. Chem. **64**, 769 (1960).
3. J. M. CAMPELO, J. M. MARINAS, and R. PEREZ-OSSORIO. Proc. 5th Symp. Iberoamerican Catal. Lisbon, 1976. Vol. 1, p. 84.
4. J. M. CAMPELO and J. M. MARINAS. Afinidad, **38**, 398 (1981).
5. S. BRUNAUER, P. H. EMMETT, and E. TELLER. J. Am. Chem. Soc. **77**, 5860 (1930).
6. A. LECLOUX and J. P. PIRARD. J. Colloid Interface Sci. **70**, 265 (1979).
7. S. BRUNAUER, R. SH. MIKHAIL, and E. BODOR. J. Colloid Interface Sci. **24**, 541 (1967).
8. J. M. MARINAS, C. JIMENEZ, J. M. CAMPELO, M. A. ARAMENDIA, V. BORAU, and D. LUNA. Proc. 7th Symp. Iberoamerican Catal. La Plata, 1980. p. 79.
9. J. M. CAMPELO, A. GARCIA, D. LUNA, and J. M. MARINAS. Afinidad **39**, 61 (1982).
10. A. WHEELER. Adv. Catal. **3**, 250 (1951).
11. D. A. BEST and W. WOJCIECHOWSKI. J. Catal. **47**, 343 (1977).
12. G. SAITO, K. SATO, and N. ABE. Bull. Chem. Soc. Jpn. **36**, 1064 (1978).

Can. J. Chem. Downloaded from www.nrcresearchpress.com by 210.87.254.105 on 09/06/12
For personal use only.

13. V. KRISHNASAMY and P. RATNASAMY. J. Indian Chem. Soc. **49**, 839 (1982).
14. B. OZIMEK and B. RADOMYSKI. React. Kinet. Catal. Lett. **21**, 315 (1982).

Nomenclature

A: preexponential factor of Arrhenius equation
AN: aniline (λ_{max}: 232 nm)
b: Langmuir's constant (L mol^{-1})
C: concentration of titrating agent in solution, at equilibrium with the adsorbate on the surface acid sites (mol L^{-1})
CH: cyclohexene
CY: cyclohexylamine (λ_{max}: 225 nm)
E_a: apparent activation energy (kJ mol^{-1})
k: rate constant of the surface process (s^{-1})
K: adsorption constant of the CH on the catalyst (mol atm^{-1} g^{-1})
MCP: methylcyclopentene
PY: pyridine (λ_{max}: 252 nm)
Q: flow rate of the carrier gas (mL s^{-1})
r: main pore radius (nm)
S: surface area (BET method, m^2 g^{-1})
T: reaction temperature (K)
V: pore volume (mL g^{-1})
W: catalyst weight (mg)
x: amount of titrating agent adsorbed on the acid sites (mol g^{-1})
x_m: monolayer coverage; the theoretical amount of titrating agent that may be chemically adsorbed by 1.0 g of solid system (mol g^{-1})
X: molar fractionary conversion
σ: kinetic selectivity factor
λ: wavelength of the maximum absorption (nm)
Subscripts: 1: 1-MCP; 3: 3-MCP

Can. J. Chem. Downloaded from www.nrcresearchpress.com by 210.87.254.105 on 09/06/12
For personal use only.

Effects of solvents on a model of rhodopsin consisting of a conjugated imine and substituted acetic acids

MARTINE BISSONNETTE, HOA LE THANH, AND DANIEL VOCELLE[1]

Département de chimie, Université du Québec à Montréal, Montréal (Qué.), Canada H3C 3P8

Received December 22, 1983

MARTINE BISSONNETTE, HOA LE THANH, and DANIEL VOCELLE. Can. J. Chem. **62**, 1459 (1984).

A model system of rhodopsin consisting of a dienylidene Schiff base and different halogeno acids has been studied in two solvents, chloroform and methanol, by uv and 400-MHz nmr spectroscopies. The uv results indicate that in chloroform, a nonpolar solvent, monohalogenoacetic acids can protonate the Schiff base only partially, while nmr data show that the aldimine hydrogen is slightly affected by acids and that the acidic proton is moving rapidly between the donor and the acceptor. In methanol, data indicate a leveling effect. In relation with rhodopsin, our results imply that, depending on the environment surrounding the chromophore, the state of protonation of the Schiff base could be strongly affected. Finally, our model shows experimental evidence that Nakanishi's external point charge could be operating in visual pigments.

MARTINE BISSONNETTE, HOA LE THANH et DANIEL VOCELLE. Can. J. Chem. **62**, 1459 (1984).

Un modèle de la rhodopsine comprenant une base de Schiff diénylidène et différents acides halogénés a été étudié dans le chloroforme et le méthanol par les spectroscopies ultraviolette et résonance magnétique nucléaire (400 MHz). Les résultats dans l'uv indiquent que dans un solvant non polaire comme le chloroforme, les acides acétiques monohalogénés peuvent protoner la base de Schiff que partiellement tandis que la rmn montre que l'hydrogène de l'aldimine n'est que peu affecté par la présence d'acides et que le proton acide se déplace rapidement entre le donneur et l'accepteur. Dans le méthanol, les données indiquent la présence d'un effet équalisateur dû au solvant. Extrapolés à la rhodopsine, nos résultats impliquent que l'état de protonation du chromophore peut être affecté grandement par le milieu environnant la base de Schiff. Finalement, notre modèle présente quelques données expérimentales tendant à montrer l'existence d'une charge externe près du chromophore telle que préconisée par Nakanishi.

Introduction

The electronic spectrum of rhodopsin, the visual pigment responsible for vision, is of fundamental importance in the study of the molecular mechanism of vision (1). Bovine rhodopsin absorbs at 500 nm while the hydrochloride salt of retinylidene butylamine absorbs at 440 in methanol (2). The 60-nm difference between rhodopsin and the model has been termed the "opsin shift" by Nakanishi *et al.* (3) and it represents the red shift of the chromophore due to the effects of the protein environment. This opsin shift has been ascribed by Nakanishi to an external point charge located near the 11-*cis* double bond of retinal. This widely accepted theory is presented in Fig. 1.

More recently, Mordechai and Nakanishi (4) have devised a polyene iminium system where the effect of a carboxylate anion in close proximity to the polyenic group could be evaluated. Again, the external point charges were shown to be contributors to the spectroscopic characteristics of the model system. Other factors were shown to be important also: the distance between the minimum nitrogen and the counteranion (an effect already described by Blatz and co-workers (5)) and solvent polarity.

In a recent note (6), we have proposed a model where (1) the protonating species was a carboxylic acid; (2) the presence of polar groups (halogen, cyano, etc.) could serve as an external point charge; (3) solvent effects could also be measured. *trans-trans*-2,4-Heptadienylidene *tert*-butyl amine (**1**) was used as a model of retinal since, according to Nakanishi *et al.* (3), this fragment of the chromophore is where the interactions occur. Figure 2 shows our model, which should be compared to Nakanishi's external point charge model.

In that note it was said that in chloroform certain acids like trifluoroacetic acid (TFA), propiolic acid, and cyanoacetic acid (CAA) in a 1:1 molar ratio with **1** gave ultraviolet (uv) spectra which indicated the presence of an equilibrium between a protonated and an unprotonated imine. Proton magnetic resonance data indicated that this was not so simple. In fact, it was not possible to relate the deshielding of the hydrogens located on the double bonds with the percentage of protonation evaluated by the uv method. It was concluded that more data were necessary in order to understand completely the behavior of the Schiff base in the presence of acids.

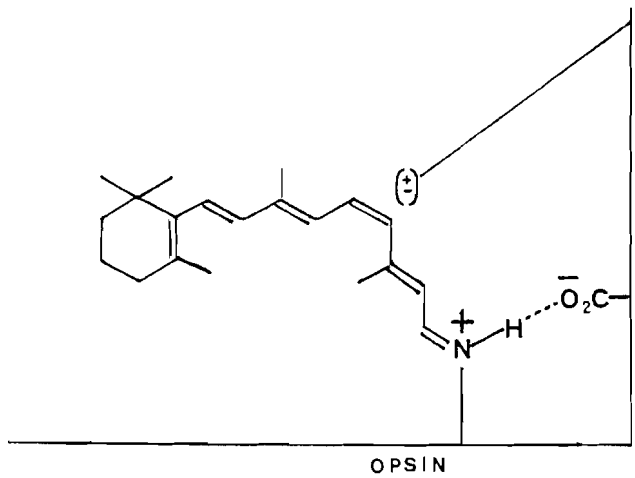

FIG. 1. Nakanishi's external point charge model of rhodopsin.

In the present paper, we are presenting results obtained by the use of five more acids, by varying the ratio of acids toward imine **1** and by extending our study not only in chloroform but also in methanol.

Materials and methods

Synthesis of *trans-trans*-2,4-heptadienylidene *tert*-butylamine (**1**) was made according to the procedure of Kosower and Sorensen (7). This imine is rather unstable to oxygen, light, and heat so that a freshly distilled sample is required. Proton magnetic resonance (^{1}H nmr) was used to check its purity. All acids and solvents were thoroughly dried,

[1] Author to whom all correspondence should be addressed.

Can. J. Chem. Downloaded from www.nrcresearchpress.com by 210.87.254.42 on 09/06/12
For personal use only.

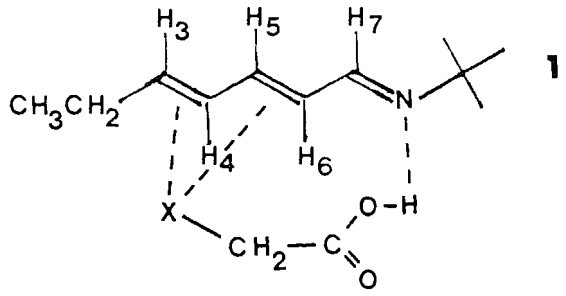

1

FIG. 2. Our model of rhodopsin: 2,4-*trans*-*trans*-heptadienylidene *tert*-butylamine (**1**) interacting with a substituted acetic acid.

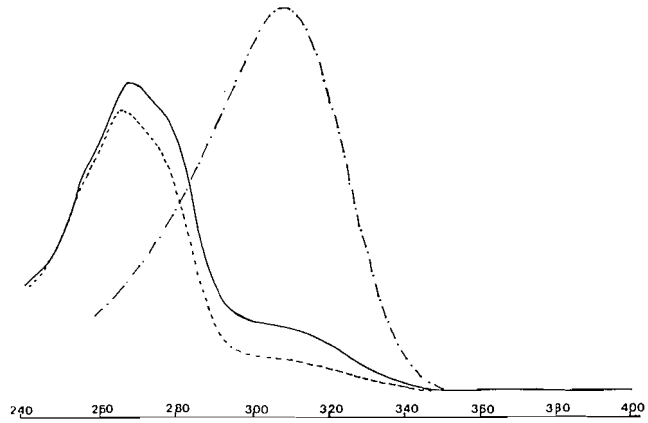

FIG. 3. Ultraviolet spectra of **1** in $CHCl_3$ in a 1:1 molar concentration with (- - -) CH_2ICO_2H; (–) CH_2FCO_2H; (–○–) $CHCl_2CO_2H$.

since protonated Schiff bases are readily hydrolysed. Chloroform was passed on a column of basic alumina in order to remove traces of hydrogen chloride. Under such conditions, spectra of **1** in $CHCl_3$ did not show any significant band in the 300-nm region. Special attention was given to prevent hydrolysis, which was kept minimal. Solutions were prepared in 10^{-4} *M* concentrations for uv studies and 10^{-2} *M* concentrations for nmr. The uv spectra were recorded on a Cary 17 and the nmr studies were done on a Bruker WH 400/DS (400 MHz) spectrometer.

Results

(a) *Ultraviolet studies*

In $CHCl_3$

Ultraviolet spectra of the Schiff base **1** mixed with different halogenated acetic acids in chloroform are shown in Figs. 3, 4, and 5.

Figures 3 to 5 indicate that monohalogenoacetic acids, in a 1:1 molar ratio with the Schiff base **1**, give spectra composed of two bands: one at 267 nm, the other at 310 nm. The 267-nm band represents the unperturbed imine band, while the 310-nm band is due to the protonated imine (6). This new band represents approximately 20% protonation. Since in high excess of the acid, the 310-nm band only is present, it is possible to measure the molar adsorptivity ϵ of the protonated imine in such conditions; thus, the Schiff base **1** in the presence of excess monochloroacetic acid has an ϵ of around 26 000 L mol^{-1} cm^{-1} at 310 nm. By measuring the ϵ at that wavelength it is possible to evaluate the proportion of the 310-nm band; it represents about 22% for the mixture of **1** with monochloroacetic acid and 17% for **1** with monobromacetic acid. Table 1 gives the percentage of protonation of **1** with a series of acids.

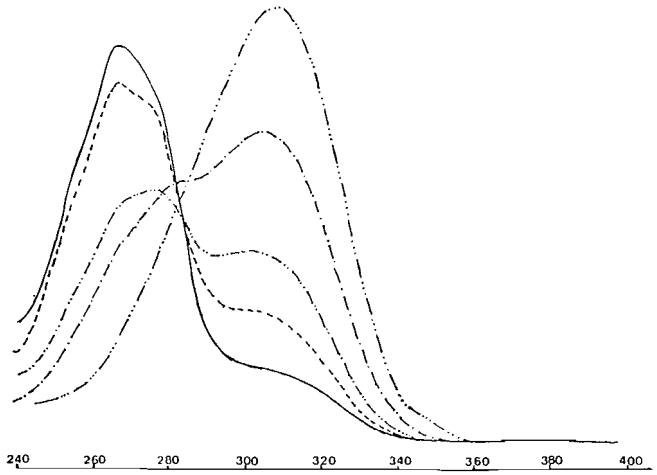

FIG. 4. Ultraviolet spectra of **1** in $CHCl_3$ with varying concentrations of CH_2ClCO_2H: (–) 1:1 (- - -) 1:2; (–···–) 1:4; (–·–) 1:10; (–···–) 1:50 molar ratio.

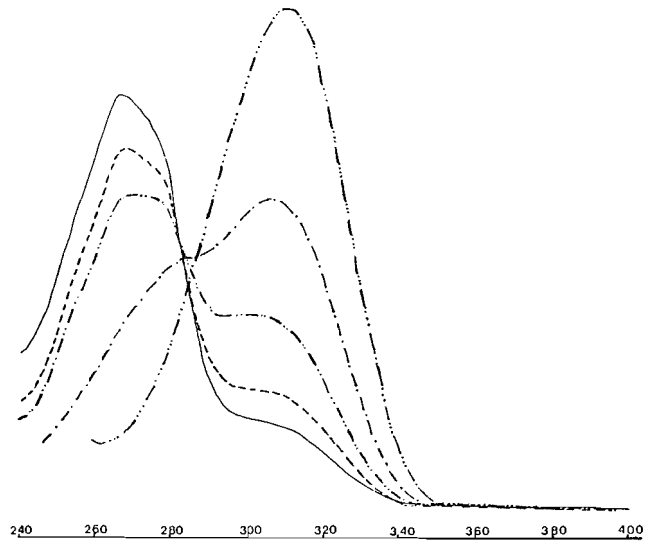

FIG. 5. Ultraviolet spectra of **1** in $CHCl_3$ with varying concentrations of CH_2BrCO_2H: (–) 1:1 (- - -) 1:2; (–···–) 1:4; (–·–) 1:10; (–···–) 1:50 molar ratio.

All the acids which gave a two-band system were mixed with the Schiff base **1** in high excess (1:100). In all cases except propionic acid, only the band at 310 nm resulted, the 267-nm band being completely absent. With propionic acid which afforded no protonation (the 310-nm band being barely present) in a 1:1 molar ratio, no red shift could be observed when a high excess of acid was used. In contrast, 3-nitropropanoic acid, with a pK_a in water of 3.7, was able to completely shift the 267-nm band to 310 nm when a high excess was used.

The effects toward the imine of varying the concentrations of the acids were studied particularly for both monochloro and monobromoacetic acids (Figs. 4 and 5). These spectra show that by increasing the amount of the acid compared to the Schiff base the 310-nm band increases while the 267-nm band decreases. The shape of the 267-nm band is also altered in the process; a growing shoulder appears around 280 nm. It could be due to the presence of the increasing 310-nm band, since the spectrum of unprotonated **1** shows a large and asymmetric band with a shoulder in that region. Other interpretations are possible, such as the presence of some Rydberg bands superimposed

Can. J. Chem. Downloaded from www.nrcresearchpress.com by 210.87.254.42 on 09/06/12
For personal use only.

Can. J. Chem. Downloaded from www.nrcresearchpress.com by 210.87.254.42 on 09/06/12
For personal use only.

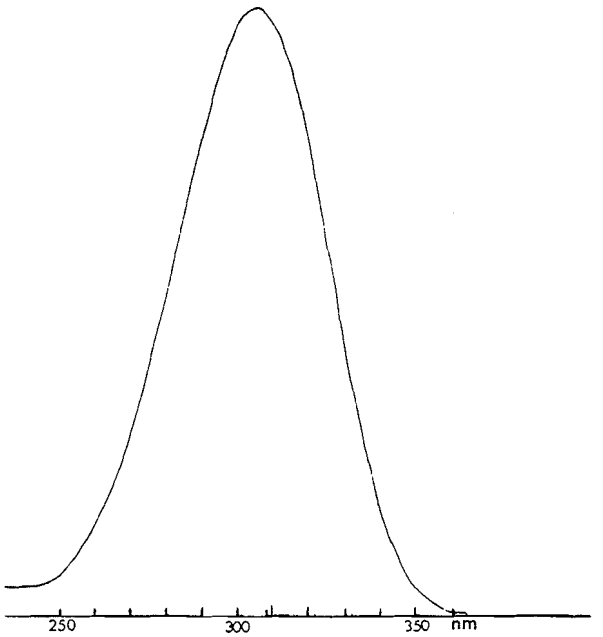

FIG. 6. Ultraviolet spectrum of **1** in CH_3OH in a 1:1 molar concentration with trichloroacetic acid.

TABLE 1. Percentage of protonation as measured by the ε of the 310-nm band in $CHCl_3$

System studied	%
1/CH_2FCO_2H	18
1/CH_2ClCO_2H	22
1/CH_2BrCO_2H	17
1/CH_2ICO_2H	6
1/$CHCl_2CO_2H$	100
1/CCl_3CO_2H	100
1/CF_3CO_2H	51
1/$HC{\equiv}CCO_2H$	48
1/$NCCH_2CO_2H$	50
1/$O_2NCH_2CO_2CO_2H$	5

TABLE 2. Chemical shifts of H_3 to H_7 of **1** with halogenoacetic acids in $CDCl_3$

System studied*	H_7	H_6	H_5	H_4	H_3
1/CH_2FCO_2H	7.84	6.90	7.05	6.37	6.38
1/CH_2ClCO_2H	7.90	6.85	7.17	6.44	6.44
1/CH_2BrCO_2H	7.82	6.85	6.90	6.33	6.33
1/CH_2ICO_2H	7.81	6.79	6.92	6.35	6.27
1/$CHCl_2CO_2H$	7.93	6.90	7.20	6.39	6.47
1/CCl_3CO_2H†	7.97	6.94	7.19	6.35	6.44
1/CCl_3CO_2H‡	8.04	6.67	7.35	6.47	6.59
1†	7.87	6.26	6.57	6.18	5.95

*In a 1:1 molar ratio.
†From ref. 6.
‡In a 1:10 molar ratio.

on the $\pi^* \leftarrow \pi$ band (8), but the spectra do not allow a clear interpretation.

In CH_3OH

All five halogenated acetic acids were studied in methanol with the series of acids, TCA, TFA, CAA, 3-nitropropionic acid, and propionic acid. The spectrum of **1** with TCA in a 1:1 molar ratio is shown in Fig. 6.

TABLE 3. Deshielding values of H_3 to H_7 due to the presence of carboxylic acids in $CDCl_3$

System studied	H_7	H_6	H_5	H_4	H_3
1/CH_2FCO_2H	−0.03	0.64	0.48	0.19	0.43
1/CH_2ClCO_2H	0.03	0.59	0.60	0.26	0.49
1/CH_2BrCO_2H	−0.05	0.59	0.33	0.15	0.38
1/CH_2ICO_2H	−0.06	0.53	0.35	0.17	0.32
1/$CHCl_2CO_2H$	0.06	0.64	0.63	0.19	0.52
1/CCl_3CO_2H	0.10	0.68	0.62	0.17	0.49

Only one band is present with a max at 307 nm. All the other acids give superimposable spectra to the one of Fig. 6.

(b) *Nuclear magnetic resonance (nmr) studies*

In $CDCl_3$

The same acids mixed with **1** were studied in $CDCl_3$ by using a 400-MHz instrument. Figure 7(a) shows the actual spectrum of the heptadienylidene Schiff base while Fig. 7(b) shows the spectrum of **1** mixed with TCA in equimolar concentration. Identification of each set of peaks was possible by using a double resonance technique.

Table 2 presents the data for each ethylenic hydrogen of **1** taken at its peak center.

Table 3 shows the deshielding effect caused by the carboxylic acids on all of these hydrogens.

The numbers represent the difference in ppm between the value for a hydrogen of **1** in $CDCl_3$ compared with the value of that same hydrogen when an acid is present. It is important to note that H_7 is a doublet even in the presence of the carboxylic acids. This is unexpected, since protonation of the nitrogen of the imine of **1** should give four peaks of equal intensities (a double doublet), proton exchange with $CDCl_3$ not being possible. In contrast, HCl gives such a quartet. Using TCA in varying concentrations with the Schiff base **1**, it was found that for a molar ratio of 1:3 the desired quartet appeared (Fig. 8).

No correlation was found between the deshielding values of the ethylenic hydrogens (Table 3) and the pK_a of the acids measured in water (since the pK_as are not known in chloroform). Also, no correlation was found between the percentages of protonation as measured by uv and the deshielding values of Table 3.

In CD_3OD

Table 4 presents the results of the same study as previously described, but this time in deuterated methanol.

From Table 4 it is possible to note a slight variation in the chemical shifts of the ethylenic hydrogens. The contrast between these results in CD_3OD and those in $CDCl_3$ (Table 2) is striking; however, it was expected in the light of the uv results obtained.

Discussion

From comparing the results presented above in chloroform and in methanol one conclusion can readily be drawn: there is a leveling effect occurring in methanol. Blatz and co-workers (5) have previously proposed such an effect in their uv study of *N*-retinylidene *n*-butylamine (NRBA) in the presence of very strong acids like HCl, H_2SO_4, etc.. Since they could not observe any variation in the λ_{max} of NRBA with different acids, they invoked solvation of protonated NRBA by methanol. They called this non-variation of the λ_{max} in methanol the leveling

Can. J. Chem. Downloaded from www.nrcresearchpress.com by 210.87.254.42 on 09/06/12
For personal use only.

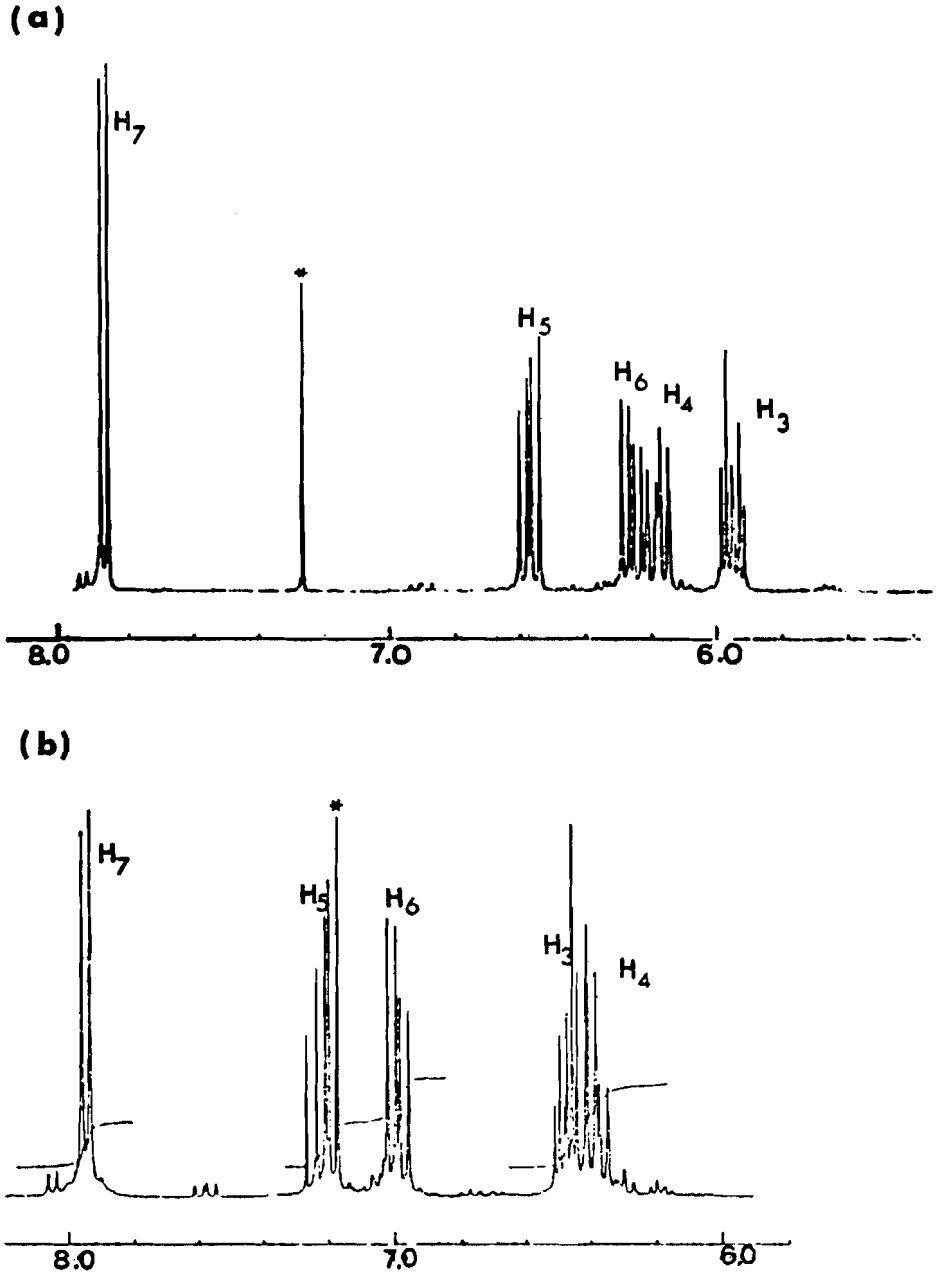

FIG. 7. 400-MHz ^{1}H nmr in $CDCl_3$ (a) of 2,4-*trans*-*trans*-heptadienylidene *tert*-butylamine (**1**) showing the ethylenic protons H_3 to H_7 and (b) of a mixture of **1** with trichloroacetic acid in a 1:1 molar ratio.

effect of methanol. The same kinds of results were obtained in our study in methanol. Both uv and nmr data show no variation, whatever the acids used. Comparing H_6 values obtained in $CDCl_3$ and in CD_3OD, it is possible to note a strong deshielding value in $CDCl_3$ but only a small one in CD_3OD. This could be explained by the fact that, in $CDCl_3$, the carbonyl group of the counteranion affects H_6, while in CD_3OD only a small effect is expected since the solvent replaces the counteranion. The similarity of the results in deuterated methanol and the small deshielding effect on H_6, combined with the nonvariation of the uv spectra, support the hypothesis that a leveling effect is operating in methanol.

It is interesting also to note that H_3 and H_5 are strongly deshielded by acids both in $CDCl_3$ and in CD_3OD, the deshielding being bigger in CD_3OD than in $CDCl_3$. This represents the effect of protonation of the Schiff base by the different acids through resonance.

A most important aspect of our study of **1** by ^{1}H nmr is the impact of the acids on H_7 (that is —C*H*=N—). In deuterated chloroform H_7 is only slightly shifted by the presence of acids (less than 0.1 ppm), while in CD_3OD the deshielding reaches nearly 0.5 ppm. This effect on H_7 through the use of different solvents might explain the controversy surrounding the ^{13}C nmr results of rhodopsin (9). Since nmr data for H_7 reflect the fundamental state of the imine bond, there must exist a relation between nmr characteristics of the imine proton (RC*H*=N—) and the ^{13}C of the carbon bearing the imine linkage (R*C*H=N—). Our results indicate that in a nonpolar solvent the aldimine proton (H_7) is very slightly affected by acids, while in a more polar solvent the effect is much greater. The ^{13}C nmr should indicate the same thing for the aldimine carbon. Extended to rhodopsin, our reasoning means that, depending

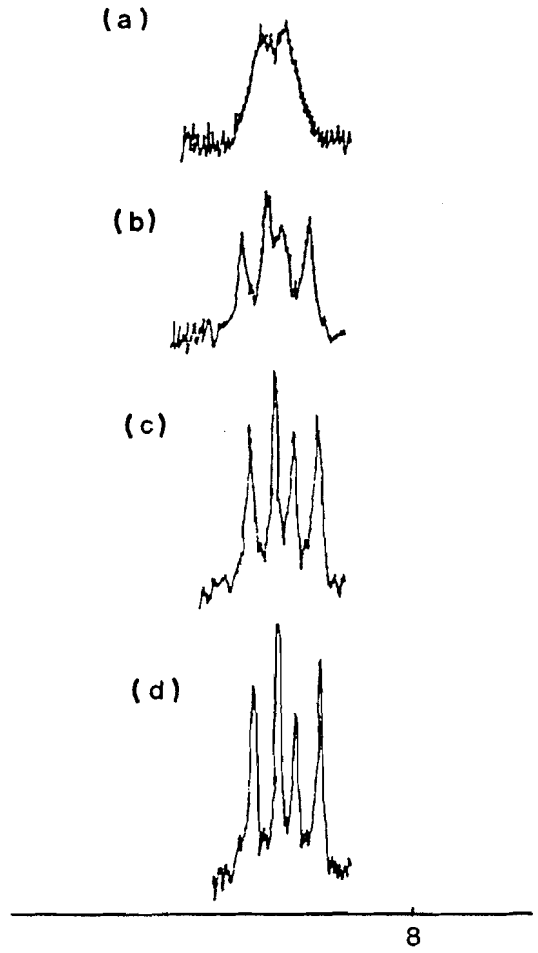

FIG. 8. ^1H nuclear magnetic resonance of **1** with trichloroacetic acid in $CDCl_3$. (a) 1:2; (b) 1:3; (c) 1:4; (d) 1:5 molar ratio. Exceptionally, these spectra were obtained on a Varian EM360L.

on the milieu in which rhodopsin is studied, ^{13}C nmr could indicate protonation or no protonation. Especially important is the use of detergents in extraction of visual pigments: depending on their characteristics, different answers could be obtained. Thus, the nature of detergents has been judged crucial in *in vitro* regeneration of visual pigments (10), and photoconversion of bathorhodopsin to rhodopsin and isorhodopsin is strongly influenced by detergents (11). If no effect of detergents on the state of protonation of rhodopsin has been seen as yet, such an effect has been invoked by Lam and Packer (12) for bacteriorhodopsin.

In chloroform (or $CDCl_3$), uv and nmr data are particularly interesting. Only HCl, TCA, and dichloroacetic acid (DAA) are able to completely shift the 267-nm band to 310 nm. It will be noted that λ_{max} for all three acids is the same; this is somewhat surprising since Blatz (5) noted a variation in the λ_{max} of NRBA in the presence of strong acids in nonpolar solvents. With all the other acids, only a partial shift occurred. For these acids, it is possible to explain the results by establishing the following equilibrium, eq. [1]:

[1] $$RCH{=}N{-}R' + R''CO_2H \rightleftharpoons \left[RCH{=}\overset{+}{N}(H){-}R'\right]\bar{O}_2CR''$$

For the monohalogeno acids, the mixture observed by uv

TABLE 4. Chemical shifts of H_3 to H_7 of **1** with halogenoacetic acids in CD_3OD

System studied*	H_7	H_6	H_5	H_4	H_3
1/CH_2FCO_2H	8.61	6.50	7.66	6.61	6.77
1/CH_2ClCO_2H	8.58	6.61	7.62	6.61	6.74
1/CH_2BrCO_2H	8.58	6.62	7.62	6.62	6.74
1/CH_2ICO_2H	8.57	6.61	7.61	6.61	6.73
1/$CHCl_2CO_2H$	8.62	6.60	7.68	6.61	6.78
1/CCl_3CO_2H	8.62	6.63	7.68	6.63	6.78
1/CF_3CO_2H	8.64	6.64	7.68	6.64	6.77
1/$HC{\equiv}CCO_2H$	8.62	6.65	7.68	6.62	6.78
1/$NCCH_2CO_2H$	8.56	6.62	7.58	6.62	6.72
1/$O_2NCH_2CH_2CO_2H$	8.53	6.62	7.57	6.62	6.71
1	8.05	6.33	6.85	6.33	6.17

* In a 1:1 molar ratio.

consists of approximately 80% of the imine (λ_{max} 267) and 20% of the salt (λ_{max} 310). In the presence of a large concentration of acids the equilibrium is shifted to the right as expected. Accordingly, the percentage of the salt increases with the proportion of acid so that at a ratio of 1:50 the imine has completely disappeared. As was said before, there is no correlation between the percentage of the salt and the pK_a of the acid measured in water (6). Considering that in chloroform carboxylic acids are very weak acids and that their difference in acidity could be considered negligible, it is possible to rationalize our results by invoking the ability of the polar groups (Cl, Br, I, F) to stabilize one of the resonance forms of the protonated Schiff base, eq. [2].

[2] $$C_2H_5CH{=}CH{-}\overset{+}{C}H{-}CH{=}CH{-}N(H){-}R \quad X{-}CH_2{-}COO^- \longleftrightarrow C_2H_5\overset{+}{C}H{-}CH{=}CH{-}CH{=}CH{-}N(H){-}R \quad X{-}CH_2{-}\bar{C}OO$$

That this could be true is seen by looking at the nmr results. Table 3 shows a pronounced deshielding on H_5 and H_3. It is worth mentioning that propionic acid (no polar group present) has a slight effect on H_3 and H_5 while 3-nitropropanoic acid induces a strong deshielding (6). With halogens, chlorine has the greatest stabilizing effect (especially di- and trichloro). This interpretation of our results is consistent with the external point charge advocated by Nakanishi.

Finally, the fact that H_7 in $CDCl_3$ appears as a doublet in the nmr spectra must be fully discussed. It has been shown (Fig. 8) that, by varying the concentration of TCA, a quartet could be obtained like the one seen for HCl. A quartet is expected for a system such as $=C(H){-}C(H){=}N{-}$. Since, with TCA and DAA, the uv spectra show full protonation, to observe such a quartet is to be expected. As Fig. 7(b) shows, a doublet is present when equimolar concentrations are used. From these results it must be concluded that, in $CDCl_3$, the proton is wandering between the acceptor and the donor, eq. [3].

Can. J. Chem. Downloaded from www.nrcresearchpress.com by 210.87.254.42 on 09/06/12
For personal use only.

[3] 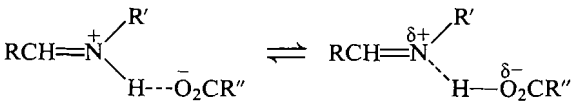

When high concentrations of acid are used, the proton resides a longer time with the nitrogen and a quartet ensues. In a 1:1 molar ratio, the proton is moving rapidly between the nitrogen and the oxygen of the carboxylate anion so that it is as though it were not there; a doublet is the result. This means that protonation and hydrogen bridging (13) become undistinguisable. When extrapolated to rhodopsin, our interpretation of our results means that not only the solvents or detergents are important, but that the spectroscopic techniques used could lead to conflicting conclusions.

Acknowledgments

The authors are grateful to the Laboratoire régional de RMN à haut champ (Mr. Phan Viet Minh Tan) of the University of Montreal for gathering all the 400-MHz nmr spectra. We owe many thanks also to Professor Camille Sandorfy of the University of Montreal for helpful discussions and, finally, to the National Research Council for financial support through grant A0943.

1. A. KROPF and R. HUBBARD. Ann. N.Y. Acad. Sci. **74**, 266 (1958).
2. (*a*) M. OTTOLENGHI. Adv. Photochem. **12**, 97 (1980); (*b*) R. R. BIRGE. Ann. Rev. Biophys. Bioeng. **10**, 315 (1981); (*c*) B. HONIG. Curr. Top. Membr. Transp. **16**, 371 (1982).
3. K. NAKANISHI, V. BALOGH-NAIR, M. ARNABOLDI, K. TSUJIMOTO, and B. HONIG. J. Am. Chem. Soc. **102**, 7945 (1980).
4. S. MORDECHAI and K. NAKANISHI. J. Am. Chem. Soc. **105**, 4033 (1983).
5. (*a*) P. E. BLATZ and J. H. MOHLER. Biochemistry, **14**, 2304 (1975); (*b*) P. E. BLATZ and P. A. LIEBMAN. Exp. Eye Res. **17**, 573 (1973); (*c*) P. E. BLATZ and J. H. MOHLER. Biochemistry **11**, 2340 (1972); (*d*) P. E. BLATZ, J. H. MOHLER, and H. V. NAVANGUL. Biochemistry, **11**, 848 (1972); (*e*) J. O. ERICKSON and P. E. BLATZ. Vision Res. **8**, 1367 (1968).
6. M. BISSONNETTE and D. VOCELLE. Spectros. Int. J. **2**, 120 (1983).
7. E. H. KOSOWER and T. S. SORENSEN. J. Org. Chem. **25**, 692 (1963).
8. D. VOCELLE, A. DARGELOS, R. POTTIER, and C. SANDORFY. J. Chem. Phys. **66**, 2860 (1977).
9. (*a*) J. SHRIVER, G. MATEESCU, R. FAGER, D. TORCHIA, and E. W. ABRAHAMSON. Nature (London) **270**, 271 (1977); (*b*) M. ARNABOLDI, G. MOTTO, K. TSUJIMOTO, V. BALOGH-NAIR, and K. NAKANISHI. J. Am. Chem. Soc. **101**, 7082 (1979); (*c*) G. D. MATEESCU, D. D. MUCCIO, W. G. COPAN, and E. W. ABRAHAMSON. J. Photochem. **17**, 63 (1981); (*d*) J. SHRIVER, G. D. MATEESCU, and E. W. ABRAHAMSON. Methods Enzymol. **81**, 698 (1982); (*e*) G. S. HARBISON, J. HERZFELD, and R. G. GRIFFIN. Biochemistry, **22**, 1 (1983).
10. V. BALOGH-NAIR and K. NAKANISHI. *In* New comprehensive biochemistry. Vol. 3. *Edited by* Tamm. Elsevier Biomedical Press, New York. 1982. pp. 292–296.
11. (*a*) N. SASAKI, F. TOKUNAGA, and T. YOSHIZAWA. FEBS Lett. **114**, 1 (1980); (*b*) Photochem. Photobiol. **32**, 433 (1980).
12. E. LAM and L. PACKER. Arch. Biochem. Biophys. **221**, 557 (1983).
13. (*a*) K. PETERS, M. L. APPLEBURY, and P. M. RENTZEPIS. Proc. Natl. Acad. Sci. U.S.A. **74**, 3119 (1977); (*b*) P. DUPUIS, F. I. HAROSI, J. M. LECLERCQ, C. SANDORFY, and D. VOCELLE. Acta Phys. Acad. Sci. Hung. **51**, 223 (1981).

Can. J. Chem. Downloaded from www.nrcresearchpress.com by 210.87.254.42 on 09/06/12
For personal use only.

Marcus theory and the existence or non-existence of transition states in gas phase deprotonation of carbon acids

SAUL WOLFE
Department of Chemistry, Queen's University, Kingston, Ont., Canada K7L 3N6

Received October 19, 1983

SAUL WOLFE. Can. J. Chem. **62**, 1465 (1984).

At the 3-21G (3-21G*) computational level, the intrinsic barriers associated with proton transfer between XCH_2^- and CH_3X have been found to be essentially constant (ca. 10 kcal/mol) for X = H, F, SH, Cl. According to the Marcus rate-equilibrium treatment of proton transfer reactions, this result means that transition states should not exist for gas phase reactions $HO^- + CH_3X \rightleftarrows H_2O + XCH_2^-$, when the energy change exceeds 20 kcal/mol. This prediction has been confirmed for two cases (X = H, F) in which the energy change is less than 20 kcal/mol, and two cases (X = SH, Cl) in which the energy change is greater than 20 kcal/mol.

SAUL WOLFE. Can. J. Chem. **62**, 1465 (1984).

Faisant appel à des calculs au niveau 3-21G (3-21G*), on a trouvé que les barrières intrinsèques associées au transfert de proton entre le XCH_2^- et le CH_3X sont essentiellement constantes (soit environ 10 kcal/mol) pour X = H, F, SH, Cl. D'après le traitement vitesse-équilibre fait par Marcus des réactions de transfert de proton, ce résultat signifie qu'il ne devrait pas y avoir d'états de transition pour les réactions en phase gazeuse du $HO^- + CH_3X \rightleftarrows H_2O + XCH_2^-$, lorsque la variation d'énergie dépasse 20 kcal/mol. Cette prédiction est confirmée dans deux cas (X = H, F) pour lesquels les variations d'énergie sont inférieures à 20 kcal/mol et dans deux cas (C = SH, Cl) dans lesquels la variation d'énergie est supérieure à 20 kcal/mol.
[Traduit par le journal]

There is an extensive literature on rate-equilibrium relationships associated with electron transfer, atom transfer, proton transfer, and alkyl transfer reactions of the type A—B + C → A + B—C (1). To account for deviations from Brönsted behaviour that are observed when A and C are allowed to vary greatly, a number of equations have been derived that relate $\Delta E^{\ddagger}$, the energy barrier of the reaction, not only to ΔE, the overall energy change, but also to $\Delta E_0^{\ddagger}$, an intrinsic kinetic quantity. Most commonly, $\Delta E_0^{\ddagger}$ has been taken as the average of the barriers associated with the identity reactions A—B + A → A + B—A and C—B + C → C + B—C. Although the mathematical forms of these equations differ, and different physical models have been employed to obtain them, Murdoch has shown (2) that they can be generalized to [1], where g_1 and g_2 are functions that govern the relative importance of the kinetic and thermodynamic contributions to the overall barrier.

$$[1] \quad \Delta E^{\ddagger} = \Delta E(1 + g_1) + \tfrac{1}{2}\Delta E_0^{\ddagger}(1 - g_2)$$

A particularly successful variant of eq. [1] is the Marcus eq. [2] (3), in which $g_1 = \Delta E/4\Delta E_0^{\ddagger}$, and $g_2 = (\Delta E/4\Delta E_0^{\ddagger})^2$. The derivation of eq. [2] assumes a single stationary point between the reactants (A—B + C) and the products (A + B—C), which can be either an energy maximum (transition state) or an energy minimum (stable intermediate) (4).

$$[2] \quad \Delta E^{\ddagger} = \Delta E_0^{\ddagger} + \tfrac{1}{2}\Delta E + (\Delta E)^2/16\Delta E_0^{\ddagger}$$

Gas phase transfer reactions create problems for the application of the Marcus treatment, because the reaction coordinate may contain additional stationary points. In particular, for alkyl transfer reactions (B = alkyl), both experiment (5) and theory (6) suggest that, when C is an anion, reactant (A—B···C) and product (A···B—C) ion–molecule complexes are present. In Fig. 1, which illustrates such behaviour, eq. [2] refers only to the central portion, from A—B···C to A···B—C, and its application requires the characterization of all three stationary points. This is a difficult experimental problem when many combinations of A and C are to be studied. A computational

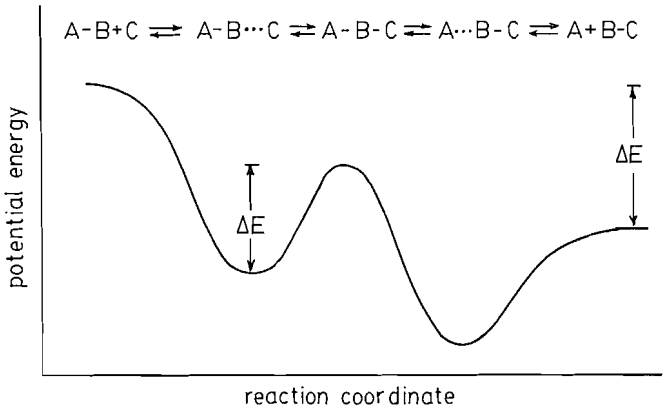

FIG. 1. Typical gas phase reaction coordinate for an exothermic gas phase transfer reaction AB + C → A + BC when C is an anion.

test of eq. [2] is also feasible, and has recently been performed, for the S_N2 reaction, for twenty combinations of A and C. Excellent agreement with the Marcus equation was observed (7).

A useful consequence of the applicability of the Marcus treatment is that this treatment predicts no stationary points to exist between reactants and products when $|\Delta E| \geq 4\Delta E_0^{\ddagger}$. This condition appears to apply also to gas phase reactions; for example, at the 4-31G computational level, the reaction $F^- + CH_3Cl \rightarrow FCH_3 + Cl^-$ proceeds with $\Delta E = -59.2$ kcal/mol, and $\Delta E_0^{\ddagger}$ is 8.6 kcal/mol. No transition state should, therefore, exist for this reaction at this computational level, and none could be found (8).

This result is relevant to a problem of interest in this laboratory, viz., the kinetic acidities of the diastereotopic methyl protons of compounds CH_3X (X = sulfide, sulfoxide, sulfone, and sulfonium) in reaction [3] (9). At the 3-21G* level (10), the calculated $-\Delta E$ for these reactions range from 23.4 kcal/mol

$$[3] \quad HO^- + CH_3X \rightarrow H_2O + {}^-CH_2X$$

for X = sulfide to 181.1 kcal/mol for X = sulfonium. For

Can. J. Chem. Downloaded from www.nrcresearchpress.com by 210.87.254.5 on 09/06/12
For personal use only.

transition states to exist in these reactions, $\Delta E_0^{\ddagger}$ would have to exceed 5.85 kcal/mol in the case of X = sulfide and 45.28 kcal/mol in the case of X = sulfonium. The processes that define $\Delta E_0^{\ddagger}$ in these cases are summarized by eqs. [4] and [5], where $\Delta E_0^{\ddagger} = \frac{1}{2}(\Delta E_{OO}^{\ddagger} + \Delta E_{CC}^{\ddagger})$, and the intrinsic barriers $\Delta E_{OO}^{\ddagger} = E_2 - E_1$ and $\Delta E_{CC}^{\ddagger} = E_4 - E_3$.

[4] $HO^- + HOH \rightleftarrows [HO\cdots HOH]^- \rightleftarrows [HO{-}H{-}OH]^- \rightleftarrows [HOH\cdots OH]^- \rightleftarrows HOH + OH^-$
1 **2** **1**

[5] $XCH_2^- + CH_3X \rightleftarrows [XCH_2\cdots HCH_2X]^- \rightleftarrows [XCH_2{-}H{-}CH_2X]^- \rightleftarrows [XCH_2H\cdots CH_2X]^- \rightleftarrows XCH_3 + CH_2X^-$
3 **4** **3**

There has been recent interest in the magnitude of $\Delta E_{OO}^{\ddagger}$, in connection with studies of anionic hydrogen bonds (11). With full geometry optimization of **1** and **2**, the barrier is calculated to be 0.21, 1.03, and 0.77 kcal/mol, at the 4-31G, 6-31G*, and 6-31G** levels, respectively. As will be seen below, no barrier is found at the 3-21G* level.[1] This means that the deprotonation reaction $HO^- + CH_3X$ (X = sulfide) will have no transition state if $\Delta E_{CC}^{\ddagger}$ (X = SR) < 11.7 kcal/mol (i.e., $-\Delta E/2$); the deprotonation reaction $HO^- + CH_3X$ (X = sulfonium) will have no transition state if $\Delta E_{CC}^{\ddagger}$ (X = $^+SR_2$) < 90.6 kcal/mol. Since the strategy to be adopted for a computational investigation of reaction [3] for various X would depend upon the presence or absence of transition states in such reactions, the magnitudes of the previously unknown $\Delta E_{CC}^{\ddagger}$, and the manner in which these depend on X had to be established.

The purposes of the present work are, therefore, as follows: (*1*) to calculate $\Delta E_{CC}^{\ddagger}$ at the 3-21G* level for the series X = H, F, SH, Cl; (*2*) where the magnitudes of $\Delta E_{CC}^{\ddagger}$ and ΔE for reaction [3] indicate that a transition state should exist, to find this transition state and the reactant and product ion–molecule complexes; (*3*) where no transition state is predicted to exist, to check that no transition state can be found. All computations were performed on a Perkin–Elmer 3251 computer, using GAUSSIAN 80 (13), with full optimization of the structures.

Results and discussion

Tables 1 and 2 list, respectively, the total energies and selected geometrical parameters of the species required for the application of the Marcus treatment. The various ΔE of interest, based on the data of Table 1, are summarized in Table 3. These are as follows: ΔE_{st}, the stabilizing effect of X upon XCH_2^-, from the isodesmic reaction [6], ΔE_w and ΔE_b (see Fig. 2), $\Delta E_{CC}^{\ddagger}$, $\Delta E_0^{\ddagger}$, $4\Delta E_0^{\ddagger}$, and ΔE for reaction [3].

[6] $CH_3^- + XCH_3 \rightarrow CH_4 + XCH_2^-$

Comparison of neutral (XCH_3) and anionic (XCH_2^-) structures

Computations on XCH_3 and XCH_2^- systems have been performed recently by Pross *et al.* (14) and by Schleyer (15). The trends observed in those comprehensive studies are reproduced in the present, more limited, work. Although, based on Schleyer's calculations with a triply split valence basis set (15), ΔE_{st} is overestimated at the 3-21G* level, it is clear that each of X = F, SH, Cl stabilizes XCH_2^- relative to X = H.

The stabilization associated with X = SH is of a different nature than that associated with X = F, Cl, since the C—X bond length of XCH_2^- is significantly shorter for X = SH, and is significantly longer for X = F, Cl, than the C—X bond length of CH_3X. In the spirit of the discussion in refs. 14 and 15, the HOMO of $HSCH_2^-$ is stabilized by the $n_C - \sigma_{SH}^*$ orbital interaction, a π-accepting (hyperconjugative) mechanism. This mechanism is not available in FCH_2^- and $ClCH_2^-$, which are stabilized by σ-electron withdrawal. The HOMO's of these latter anions are dominated by the $n_C - n_X$ destabilizing orbital interaction; this destabilization is relieved by an increase in the C—X bond length, and a decrease in the energy of n_C, which corresponds to greater pyramidalization of the carbanion. In the case of $ClCH_2^-$, the increase in the C—Cl bond length (0.41 Å), and the increased pyramidalization ($\angle HCCl$ = 91.7°, compared to $\angle HCS$ = 112.0° in $HSCH_2^-$) are so large that this anion should be regarded as a carbene solvated by Cl^-. A similar conclusion has been reached concerning the antiperiplanar conformation of $^-CH_2{-}SH_2^+$ (16).

Effect of X upon ΔE_w, ΔE_b, and $\Delta E_{CC}^{\ddagger}$

All of the **3** and **4** species were constrained to the staggered (antiperiplanar) conformations shown in Table 2. This choice was checked for X = H: the eclipsed structures **5** and **6** are

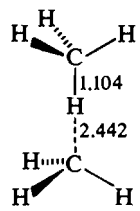

5

$E = -79.231664$

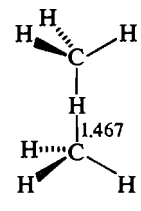

6

$E = -79.216153$

marginally less stable than the staggered structures, and the calculated $\Delta E_{CC}^{\ddagger}$ (9.73 kcal/mol) is 0.09 kcal/mol higher (17).

The most significant finding is that the intrinsic barriers $\Delta E_{CC}^{\ddagger}$ do not appear to depend on X. This results from a cancellation of the energetic effects of X upon the ion–molecule complexes **3** and the transition structures **4**; both species are stabilized to the same extent by X ≠ H. In the general reaction $XCH_2^- + HCH_2X \rightleftarrows$ **3** or **4**, an increase in the stability of XCH_2^- must lead to a *decrease* in the reactivity of this anion towards the proton donor, which is counter-balanced by an *increase* in the reactivity of XCH_3 towards the proton acceptor.

Consequences of the relationship between ΔE and $4\Delta E_0^{\ddagger}$

From the last two columns of Table 3, and the Marcus condition for the existence or non-existence of a transition state, it follows that reactions [7] and [8] should have transition states, but [9] and [10] should not.

[7] $HO^- + CH_4 \rightarrow H_2O + CH_3^-$

[1]The 3-21G (12) and 3-21G* basis sets are the same for atoms of the first row. In the 3-21G* basis set, a set of six *d*-type functions is added to second row atoms.

Can. J. Chem. Downloaded from www.nrcresearchpress.com by 210.87.254.5 on 09/06/12
For personal use only.

Can. J. Chem. Downloaded from www.nrcresearchpress.com by 210.87.254.5 on 09/06/12
For personal use only.

TABLE 1. Calculated total energies

Species	Energy (au)[a]
HO^-	−74.86863
CH_3^-	−39.23940
$HSCH_2^-$	−434.95724
$ClCH_2^-$	−496.13058
FCH_2^-	−137.57674
H_2O	−75.58596
CH_4	−39.97688
CH_3SH	−435.63727
CH_3Cl	−496.79500
CH_3F	−138.28189
1	−150.54104
2	−150.54104
3 (X = H)	−79.23167
(X = F)	−275.88397
(X = Cl)	−992.94738
(X = SH)	−870.61401
4 (X = H)	−79.21630
(X = F)	−275.86449
(X = Cl)	−992.93046
(X = SH)	−870.59978

[a]1 au = 627.5 kcal/mol.

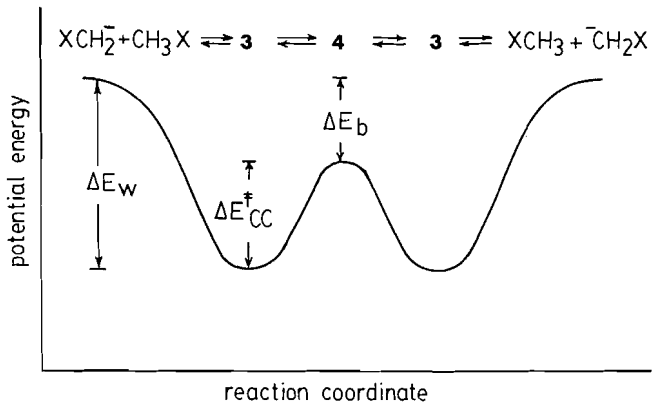

FIG. 2. Reaction coordinate associated with the intrinsic barrier $\Delta E^{\ddagger}_{CC}$, and definitions of the quantities ΔE_w and ΔE_b.

[8] $HO^- + FCH_3 \rightarrow H_2O + FCH_2^-$

[9] $HO^- + HSCH_3 \rightarrow H_2O + HSCH_2^-$

[10] $HO^- + ClCH_3 \rightarrow H_2O + ClCH_2^-$

The attack of HO^- upon the antiperiplanar methyl proton of CH_3SH was examined, but the search for a transition structure was terminated when this search had reached **7**, i.e., H_2O + $^-CH_2SH$, separated by 4 Å. Clearly reaction [9] proceeds directly to product, with no transition state, as predicted by the Marcus treatment. An analogous structure (**8**) was obtained for reaction [10].

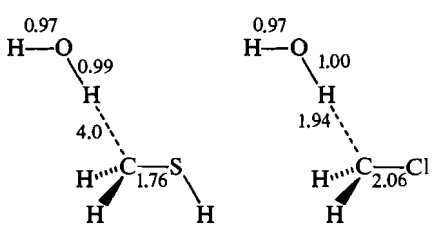

7 8

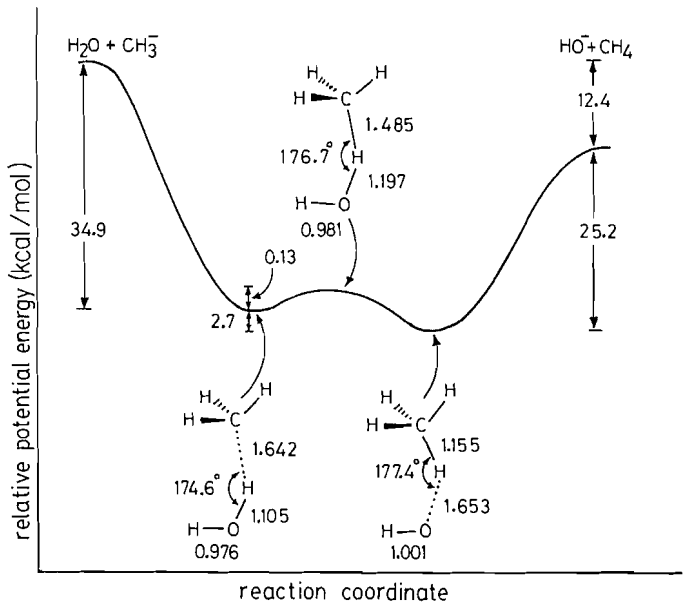

FIG. 3. Calculated gas phase reaction coordinate for the exothermic reaction $H_2O + CH_3^- \rightarrow HO^- + CH_4$, and the relative energies and structures of the stationary points on this reaction coordinate.

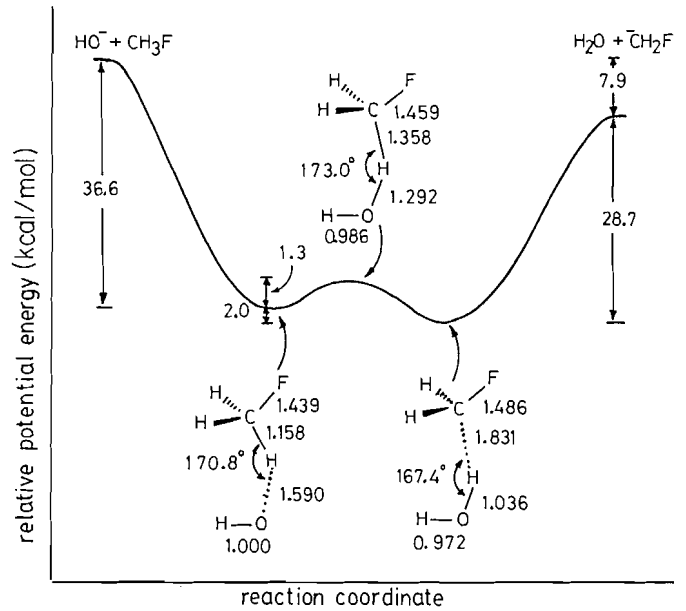

FIG. 4. Calculated gas phase reaction coordinate for the exothermic reaction $HO^- + CH_3F \rightarrow H_2O + {}^-CH_2F$, and the relative energies and structures of the stationary points on this reaction coordinate.

On the other hand, as summarized in Figs. 3 and 4, reactant and product ion−molecule complexes and transition structures do exist for reactions [7] and [8]. It will be noted that the applicability of the Marcus treatment does not depend on the direction of the reaction, since [7] is endothermic, while [8] is exothermic.

When stationary points are found for a series of related reactions, the Bell−Evans−Polanyi−Leffler−Hammond effect states (18) that *the more exothermic the reaction, the more closely the transition structure resembles the higher energy*

TABLE 2. Selected bond lengths (Å) for XCH_2^-, XCH_3, **3**, and **4**

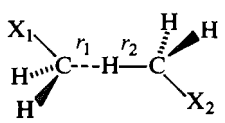

3

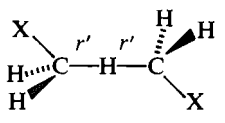

4

Species	r_{CX}	r_1	r_2	r_{CX_1}	r_{CX_2}	r'	r_{CX}
XCH_2^-							
X = H	1.121						
X = F	1.522						
X = HS	1.772						
X = Cl	2.222						
XCH_3							
X = H	1.083						
X = F	1.404						
X = HS	1.823						
X = Cl	1.806						
3							
X = H		2.442	1.104	1.114	1.088		
X = F		2.298	1.094	1.501	1.425		
X = HS		2.247	1.106	1.787	1.826		
X = Cl		2.176	1.096	2.133	1.849		
4							
X = H						1.467	1.099
X = F						1.458	1.464
X = HS						1.444	1.815
X = Cl						1.423	1.935

reactants. The data just presented for reactions [7] and [8] allow a first test of this principle for gas phase proton transfer from carbon acids. Since [7] is more exothermic (in the exothermic direction) than [8], it is expected that the transition structure of [7] should resemble its higher energy reactant $[HO—H\cdots CH_3]^-$ more than the transition structure of [8] resembles its higher energy reactant $[HO\cdots H—CH_2F]^-$. An examination of the change in the HO—H bond lengths between the reactants and the transition structures for the two reactions reveals that, in [7], this bond lengthens by 8.4%, but in [8] this bond shortens by 18.8%. A more comprehensive study of the relationship between the geometries of the stationary points and the energetics of proton transfer from carbon acids is in progress.

Summary and conclusions

The concept of a reaction coordinate is an essential feature of the transition state theory of chemical reactions. If the reaction coordinate is defined as the minimum energy reaction path from reactants to products, it is clear that the reaction coordinate constitutes only a small region of a more complex energy hypersurface. The topologies of such hypersurfaces have been the subject of much recent work (19), and the many problems associated with the computational characterization of their "critical" (20) or stationary points have been pointed out (21). It is, therefore, useful to know prior to a computational search that the supposed structure of interest actually exists. That the existence or non-existence of transition structures can be predicted in advance is a facet of the Marcus approach that does not appear to have been exploited previously. As seen in the present work, the reliability of this aspect of Marcus theory will greatly facilitate future theoretical investigations of reaction coordinates and rate-equilibrium relationships.

TABLE 3. Energy changes associated with reactions [3], [5], and [6][a]

X	ΔE_{st}[b]	ΔE_w[c]	ΔE_b[c]	$\Delta E^{\ddagger}_{CC}$	$\Delta E^{\ddagger}_0$	$4\Delta E^{\ddagger}_0$	ΔE[d]
H	0	−9.66	0.02	9.64	4.82	19.28	12.64
F	−20.3	−15.90	−3.68	12.22	6.11	24.44	−7.64
SH	−36.0	−12.24	−3.31	8.93	4.47	17.86	−23.41
Cl	−45.8	−13.68	−3.06	10.62	5.31	21.24	−33.20

[a]In kcal/mol.
[b]Refers to reaction [6].
[c]See Fig. 2.
[d]Refers to reaction [3].

Acknowledgements

This research has been supported by the Natural Sciences and Engineering Research Council of Canada (NSERCC). The author thanks NSERCC and Queen's University for funds to purchase the Perkin–Elmer 3251 computer employed for the computations, and Professor S. Scheiner for a helpful discussion on the subject of intrinsic barriers.

1. Faraday Discussions of the Chemical Society. No. 74. Electron and proton transfer. 1982.
2. J. R. MURDOCH. J. Am. Chem. Soc. **105**, 2159 (1983).
3. R. A. MARCUS. J. Chem. Phys. **24**, 966 (1956).
4. D. E. MAGNOLI and J. R. MURDOCH. J. Am. Chem. Soc. **103**, 7465 (1981).
5. W. E. FARNETH and J. I. BRAUMAN. J. Am. Chem. Soc. **98**, 7891 (1976); W. N. OLMSTEAD and J. I. BRAUMAN. J. Am. Chem.

Can. J. Chem. Downloaded from www.nrcresearchpress.com by 210.87.254.5 on 09/06/12
For personal use only.

Soc. **99**, 4219 (1977).
6. H. B. SCHLEGEL, K. MISLOW, F. BERNARDI, and A. BOTTONI. Theoret. Chim. Acta, **44**, 245 (1977).
7. S. WOLFE, D. J. MITCHELL, and H. B. SCHLEGEL. J. Am. Chem. Soc. **103**, 7694 (1981).
8. D. J. MITCHELL. Ph.D. Thesis. Queen's University. Kingston, Ont. 1981.
9. S. WOLFE, A. STOLOW, and L. A. LAJOHN. Can. J. Chem. **62**, 1470 (1984).
10. W. J. PIETRO, M. M. FRANCL, W. J. HEHRE, D. J. DEFREES, J. A. POPLE, and J. S. BINKLEY. J. Am. Chem. Soc. **104**, 5039 (1982).
11. S. SCHEINER, M. M. SZCZESNIAK, and L. D. BIGHAM. Int. J. Quant. Chem. **23**, 739 (1983); C. M. ROHLFING, L. C. ALLEN, C. M. COOK, and H. B. SCHLEGEL. J. Chem. Phys. **78**, 2498 (1983).
12. J. S. BINKLEY, J. A. POPLE, and W. J. HEHRE. J. Am. Chem. Soc. **102**, 939 (1980).
13. J. S. BINKLEY, R. A. WHITESIDE, R. KRISHNAN, R. SEEGER, D. J. DEFREES, H. B. SCHLEGEL, S. TOPIOL, L. R. KAHN, and J. A. POPLE. QCPE, **13**, 406 (1981).
14. A. PROSS, D. J. DEFREES, B. A. LEVI, S. K. POLLACK, L. RADOM, and W. J. HEHRE. J. Org. Chem. **46**, 1693 (1981).
15. G. W. SPITZNAGEL, T. CLARK, J. CHANDRASEKHAR, and P. VON R. SCHLEYER. J. Comp. Chem. **3**, 363 (1982).
16. D. J. MITCHELL, S. WOLFE, and H. B. SCHLEGEL. Can. J. Chem. **59**, 3280 (1981).
17. R. HOFFMANN, C. C. LEVIN, and R. A. MOSS. J. Am. Chem. Soc. **95**, 629 (1973).
18. S. WOLFE, D. MITCHELL, and H. B. SCHLEGEL. J. Am. Chem. Soc. **103**, 7692 (1981).
19. P. G. MEZEY. Theoret. Chim. Acta, **62**, 133 (1982) and references therein; J. SIMONS, P. JØRGENSEN, H. TAYLOR, and J. OZMENT. J. Phys. Chem. **87**, 2745 (1983).
20. M. R. PETERSON. Ph.D. Thesis. University of Toronto. 1981.
21. K. MÜLLER. Angew. Chem. Intl. Ed. Engl. **19**, 1 (1980).

Can. J. Chem. Downloaded from www.nrcresearchpress.com by 210.87.254.5 on 09/06/12
For personal use only.

Stereoelectronic effects and the kinetic acidities of diastereotopic hydrogens

SAUL WOLFE, ALBERT STOLOW, AND LAWRENCE A. LAJOHN
Department of Chemistry, Queen's University, Kingston, Ont., Canada K7L 3N6

Received October 19, 1983

SAUL WOLFE, ALBERT STOLOW, and LAWRENCE A. LAJOHN. Can. J. Chem. **62**, 1470 (1984).

A general qualitative treatment is proposed which accounts for the relative reactivities of diastereotopic hydrogens adjacent to a heteroatom in proton transfer, hydride transfer, and hydrogen atom transfer reactions. This treatment focuses on the structures of the reactive intermediates formed in such reactions, which can be predicted or understood in terms of qualitative molecular orbital arguments, and on the manner in which these intermediates will undergo readdition of H^+, H^-, or $H\cdot$. The procedure has been tested, for the specific case of proton transfer reactions, by a direct computational approach to the energy differences between diastereomeric transition states of reactions $HO^- + CH_3X \rightarrow H_2O + {}^-CH_2X$ (X = sulfide, sulfoxide, sulfone, sulfonium). The computations support the qualitative treatment, and are in all cases in near quantitative agreement with the extensive experimental data concerning the diastereotopic selectivities exhibited in these systems.

SAUL WOLFE, ALBERT STOLOW et LAWRENCE A. LAJOHN. Can. J. Chem. **62**, 1470 (1984).

On propose une méthode qualitative générale qui tient compte des réactivités relatives des hydrogènes diastéréotopiques adjacents à un hétéroatome lors de réactions de transfert de protons, d'hydrures ou d'atomes d'hydrogène. Cette méthode met l'accent à la fois sur la structure des intermédiaires réactifs formés au cours de telles réactions, qui peuvent être prévus ou compris en termes d'arguments qualitatifs d'orbitales moléculaires, et sur la façon dont ces intermédiaires peuvent subir une nouvelle addition de H^+, H^- ou $H\cdot$. On a vérifié cette méthode, dans le cas spécifique de réactions de transfert de proton, par une technique de calculs directs des différences d'énergie entre les états de transition diastéréoisomères des réactions: $HO^- + CH_3X \rightarrow H_2O + {}^-CH_2X$ (X = sulfure, sulfoxyde, sulfone, sulfonium). Les calculs sont en accord avec l'approche qualitative et, dans tous les cas, ils sont aussi en accord quasi-quantitatif avec les données expérimentales extensives relatives aux sélectivités diastéréotopiques observées dans ces systèmes.

[Traduit par le journal]

Can. J. Chem. Downloaded from www.nrcresearchpress.com by 210.87.254.6 on 09/06/12
For personal use only.

Introduction

Heterotopic selectivity in a reversible non-enzymatic reaction was first recorded experimentally by Rauk *et al.* in 1965 (ref. 1, see ref. 2 for a recent discussion of terminology), with the observation that the diastereotopic methylene protons of benzyl methyl sulfoxide have different kinetic acidities. In 0.25 *M* NaOD–D_2O at 15°C, the ratio of the rate constants for hydrogen-deuterium exchange of these protons is 16.7. This observation was quickly confirmed (3), and extended to the hydrogen exchange behaviour of other sulfoxides (4), sulfones (5), and sulfonium salts (6), and to demonstrations that α-lithiated dithianes (7), sulfoxides (8), and sulfonium salts (9) are generated and/or quenched with significant selectivity.

Although diastereotopic selectivity in reversible and irreversible proton transfer reactions of sulfur-containing species is thus well established experimentally, a completely satisfactory analysis of the phenomenon has been difficult to achieve, because the magnitude and, in some cases, even the direction of the effect can be changed by a change in the experimental conditions. For example, the magnitude and direction of the selectivity in the hydrogen–deuterium exchange of sulfoxides depend upon the solvent (3*b*, 4*i*); and the magnitude and direction of the selectivity in the formation and quenching of α-lithiosulfoxides depend upon the presence, absence, and nature of added lithium salts (8*j*, *k*).

Selectivity in carbon–hydrogen bond breaking processes is not restricted to proton transfer reactions, or to sulfur-containing systems; hydride (10) and hydrogen atom transfer reactions (11) of diastereotopic hydrogens also exhibit selectivity.

One of the objectives of the present work is to suggest a qualitative treatment that can be applied generally to the prediction of the relative reactivities of diastereotopic hydrogens when solvation and related factors can be ignored. A second objective is to check these qualitative predictions quantitatively for proton transfer reactions by direct calculation of the energies of diastereomeric transition states associated with proton abstraction adjacent to sulfide, sulfoxide, sulfone, and sulfonium moieties. A third objective is to provide detailed comparisons between theory and experiment, where such comparisons can be justified.

A qualitative treatment of diastereotopic selectivity

The methyl hydrogens of methanol are diastereotopic. In the staggered conformation **1**, one of these hydrogens (H_a) is antiperiplanar to the O—H bond, and the other two (H_g) are *gauche*. The diastereotopic relationship between H_a and H_g is reflected in certain ground state properties of the molecule: C—H_g is ca. 0.006 Å longer than C—H_a (12), and the C—H_g stretching force constant is lower by ca. 0.1 mdyn/Å (13). On the basis of this difference in stretching force constants it has been calculated, by two quite different procedures (14, 15), that D(C—H_g), the bond dissociation energy of C—H_g, is 5 kcal/mol lower than D(C—H_a) (95 versus 100 kcal/mol). The lower of these numbers corresponds to the experimental D(C—H) of methanol.

How do these differences in the properties of the diastereotopic hydrogens translate into differences in reactivity? As shown in Scheme 1, removal of $H\cdot$, H^-, and H^+ from the carbon atom of methanol leads, respectively, to $HOCH_2\cdot$, $HOCH_2^+$, and $HOCH_2^-$. The structures of these reactive intermediates are known (16–18), and are shown in **2**–**4**. In each case, the factors responsible for the adoption of these structures are also known: for example, the structure of **2** can be understood in terms of the pyramidalizing effect of a heteroatom on an adjacent radical centre (19), coupled with the stabilization resulting from a two-orbital three-electron interaction (20); an α-heteroatom-stabilized carbocation adopts a planar structure such as **3** in order to maximize charge transfer from the higher energy non-bonding orbital on the heteroatom to the unoccu-

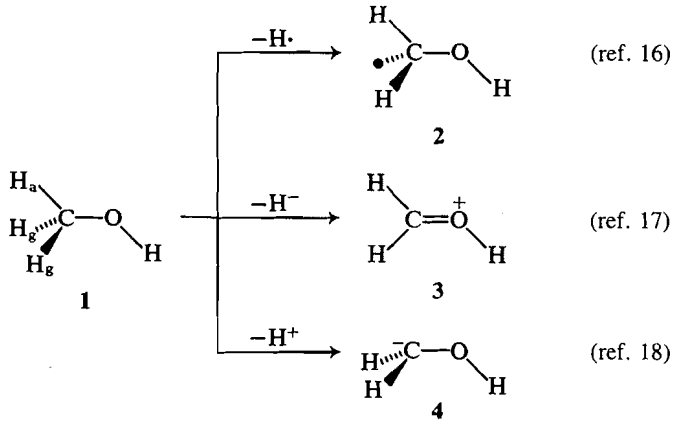

SCHEME 1

pied acceptor orbital at the cationic centre (17); and an α-heteroatom-stabilized carbanion adopts a conformation (e.g., **4**) that maximizes charge transfer from the non-bonding orbital on carbon to a σ* or π* orbital of the activating moiety (21).

Inspection of the radical **2** suggests that it is formed from **1** by the loss of H_g, i.e., H_g of **1** is more reactive than H_a. Since this is the result expected on the basis of the difference in bond dissociation energies, there appears to be a relationship between the structure of the reactive intermediate **2** and the radical reactivities of the diastereotopic hydrogens of methanol. Two assumptions are necessary to support such a relationship, viz., (*i*) the transition state for the process **1** → **2** must be product-like; (*ii*) the readdition of hydrogen to a non-planar centre must proceed with retention of configuration, the microscopic reverse of the abstraction process.

Rapid progress in the development of gradient optimization techniques (22, 23) is beginning to lead to theoretical studies aimed at the direct computation of the geometries and energies of transition structures. A recent application of such procedures to the S_N2 reaction (24) led to striking support for the principle (25) that *the transition state resembles the product in an endothermic reaction*. Since the reactions depicted in Scheme 1 are strongly endothermic, it follows that their transition states resemble the species **2**–**4**, in accord with assumption (*i*). Assumption (*ii*) is related to the arguments by Fraser *et al.* (4*i*), Fava and co-workers (6*c*), and King and du Manoir (8*h*) that stereoselectivity can be observed in hydrogen exchange reactions only if the more reactive of two diastereotopic hydrogens is removed and replaced with retention of configuration.

The direction of addition of H^- to **3** is well-known (26): addition will proceed, with an O—C—H^- angle of ca. 110°, from the plane perpendicular to the plane of the cation. Clearly, the H^- that adds to **3** becomes H_g of methanol. This allows the prediction that hydride abstraction from **1** will exhibit a kinetic preference for C—H_g.

In the case of the addition of H^+ to the non-planar carbanion **4**, this proton will become H_a. Consequently, proton abstraction from **1** should exhibit a kinetic preference for C—H_a.

If the skeleton of methanol is incorporated into that of tetrahydropyran (**5**), it is seen that H_g of **1** corresponds to the axial

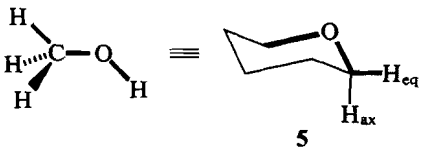

5

hydrogen adjacent to oxygen, and H_a of **1** corresponds to the equatorial hydrogen. It follows that hydrogen and hydride abstraction adjacent to oxygen will exhibit a kinetic preference for an axial site, but proton abstraction will exhibit a kinetic preference for an equatorial site. All three of these predictions are in accord with the available experimental data on radical (11), hydride (10), and proton (27) abstraction adjacent to oxygen.

The argument just presented has focused solely on the stereoelectronic effect of the heteroatom, and has ignored the possibly countervailing influences of the solvent, the nature of the abstracting agent, and the remainder of the substrate molecule. For example, axial approach of the abstracting species would be deterred by 1,3-diaxial interactions that are absent in an equatorial approach. This effect is seen in reactions of trityl cation (28): although tetrahydrofuran and diethyl ether undergo hydride abstraction readily, the corresponding reaction with tetrahydropyran is too slow to measure.

In addition, although the argument has focused for simplicity on stereoelectronic effects and the reactivities of diastereotopic hydrogens adjacent to ether oxygen, the approach is general and should be applicable to any system for which the structures of the reactive intermediates are known or can be predicted. An example of such a system is the series of carbanions resulting from the reaction $HO^- + CH_3X \rightarrow H_2O + {}^-CH_2X$ (X = SR, SOR, SO_2R, SR_2^+). Since the structures of these carbanions are known and understood (29, 30), it should be possible to predict the relative kinetic acidities of diastereotopic hydrogens adjacent to each of these sulfur-containing moieties. As will be seen, these predictions are in every case consistent with experiment. This comparison is discussed below, in conjunction with a more rigorous theoretical analysis of the problem that is based on a computational treatment of the diastereomeric transition states associated with the above series of reactions.

A quantitative treatment of diastereotopic selectivity

A number of conceptual and technical problems had first to be overcome, viz.:

(*1*) To what kind of experimental information can computations be compared, as a test of the validity of these computations? The extensive research on H/D exchange of the diastereotopic methylene protons of benzyl methyl sulfoxide (1, 3*b*) suggests the nature of the required comparison. The selectivities observed in this reaction, and in the exchange of conformationally constrained sulfoxides (4*c*, *e*, *i*) are strongly solvent dependent because of effects associated with ion-pairing and internal return. However, in an important study, Fraser has shown (31) that these complicating effects are unimportant in water solvent. This result implies that kinetic data for water solvent do reflect the difference in the kinetic acidities of diastereotopic protons. Therefore, theoretically computed selectivities could reasonably be compared to experimental selectivities determined in water. Where such data were not available, but trends in water and methanol had been found to be the same, data from the latter solvent were employed for the comparison;

(*2*) What choice of R represents the best compromise between meaningful results and computational practicality? Based on the recent study of ${}^-CH_2X$ (X = SH, SMe, SHO, SOMe, SO_2H, SO_2Me, $^+SH_2$, $^+SMe_2$) (29, 30), systems with R = H and R = Me exhibit the same trends in their structures and proton affinities. Therefore, R = H was selected for the present study. The 3-21G* basis set (32) was employed, since this basis set has been found (29, 30) to reproduce accurately

Can. J. Chem. Downloaded from www.nrcresearchpress.com by 210.87.254.6 on 09/06/12
For personal use only.

Can. J. Chem. Downloaded from www.nrcresearchpress.com by 210.87.254.6 on 09/06/12
For personal use only.

the structural effects in these sulfur-containing systems;

(*3*) With R = H, how can a transition structure for proton abstraction from carbon be described, to the exclusion of transition structures for other competing processes? For example, the reaction $HO^- + CH_3SH_2^+$ may proceed by proton abstraction from carbon (to yield the ylide CH_2SH_2), by proton abstraction from sulfur (to yield CH_3SH), or by S_N2 displacement on carbon (to yield CH_3OH). Only the first of these processes was of interest but, with R = H, deprotonation at sulfur is energetically preferred.

After extensive experimentation, the following protocol was adopted. As exemplified in **6***a*, HO^- was allowed to approach H_a, the hydrogen of $CH_3SH_2^+$ that is antiperiplanar to the sulfur lone pair, along the extension of the C—H_a bond ($\angle$C—H_a—O = 180°), and the S—C—H_a bond angle and H_a—C—S—H dihedral angle were held to their values in $CH_3SH_2^+$. For the deprotonation of H_g, HO^- approached along the extension of the C—H_g bond, with the S—C—H_g and H_g—C—S—H angles maintained as in $CH_3SH_2^+$ (**6***b*);

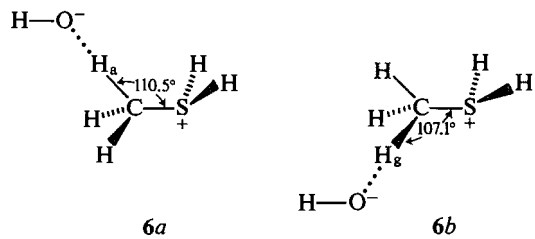

6*a* **6***b*

(*4*) Do these calculated reactions have transition states? This question can be posed as a result of insights gained from the application of the Marcus rate-equilibrium treatment (33) to gas phase proton transfer reactions (34). As discussed in detail elsewhere (34), it was clear at the outset that, in the gas phase, all of the reactions $HO^- + CH_3X$ (X = sulfide, sulfoxide, sulfone, sulfonium) would proceed directly to product. It was, therefore, necessary to assume that the reaction surface differs in the regions of H_a and H_g, and the dynamics of the attack of HO^- upon these hydrogens was followed, from a distance of 3 Å to a distance of 1.5 Å. All geometrical parameters of the resulting supermolecule were optimized at each distance, with the exception of those noted above. As will be seen, this procedure led to acceptable results.

After the present work was essentially complete, somewhat analogous theoretical treatments of the ene reaction of singlet oxygen (35) and the deprotonation of acetaldehyde (36) were reported.

The calculations were performed with the programme GAUSSIAN 80 (37), using the 3-21G* basis set. With the exceptions noted, all geometrical parameters were optimized in every case, using the appropriate gradient procedure.

Results and discussion

$HO^- + CH_3SH_2^+ \rightarrow H_2O + CH_2SH_2$

The structures of the reactant and product are shown in **7** and **8** (30). The reaction leads to a 0.2 Å decrease in the C—S bond length, and the carbon centre of the ylide **8** is planar, with the HCH plane bisecting the HSH plane. The non-bonding orbital on the ylide carbon is perpendicular to the HCH plane. The postulate that the reverse reaction **8** → **7** proceeds by proton transfer to the carbon non-bonding orbital of **8** leads to the prediction that this proton becomes H_g of the reactant, i.e., H_g of **7** has the higher kinetic acidity.

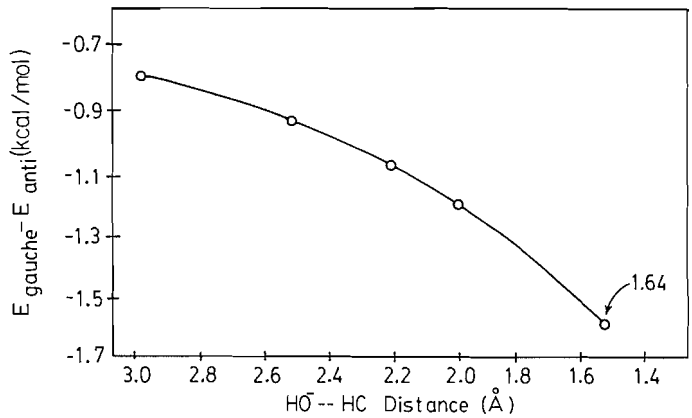

FIG. 1. A plot showing the difference in the energies of **6***b* and **6***a* as the HO⁻---HC distance is decreased from 3 Å to 1.5 Å.

The structures corresponding to attack of HO^- upon C—H_g and C—H_a are shown in **9** and **10**, for an HO . . . H distance of 1.5 Å. At this distance, the C—S bond length of **9** is 0.045 Å shorter than that of the reactant; in addition, C—H_g has lengthened from 1.079 to 1.252 Å, and the other two methyl hydrogens now form an HCH angle of 113°, an increase from the tetrahedral angles in **7**. On the other hand, in **10**, the C—S bond length is unchanged from that of **7**, although C—H_a has lengthened from 1.077 to 1.233 Å. The total energy of **9** is lower, by 1.64 kcal/mol, and, as seen in Fig. 1, the energy

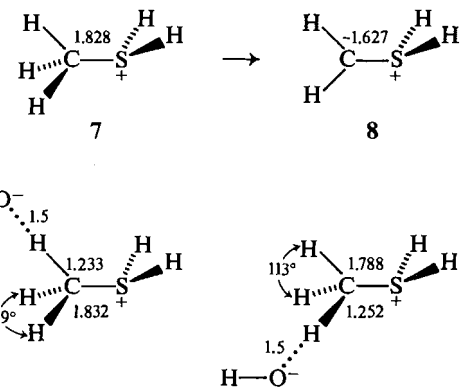

E = −511.04198 (1.64 kcal/mol) E = −511.04460 (0.0)

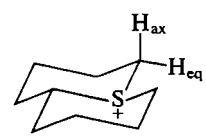

11

difference between the diastereomeric structures increases progressively to this value of 1.64 kcal/mol as the HO . . . H distance is decreased from 3.0 to 1.5 Å. Based on the equation $k_g/k_a = \exp(1640/RT)$, the selectivity is calculated to be k_g/k_a = 12 at 60°C, or one order of magnitude.

The relevant experimental data are those of Fava, for the conformationally constrained compound **11**, in NaOD–D_2O at 60°C (38). The equatorial (H_{eq}) and axial (H_{ax}) protons of this compound correspond, respectively, to H_g and H_a of **7**. The experimental result is k_{eq}/k_{ax} = 35, and is consistent with (*i*) a one order of magnitude greater kinetic acidity of k_{eq}; (*ii*) some reduction of k_{ax} associated with interactions between OD^- and

the 1,3-diaxial hydrogens of the sulfur-containing ring; (*iii*) selective reprotonation of a planar ylide (9*c*) from the equatorial direction.

Based on this first comparison, the theoretical approach to the problem appears to be adequate, and the notion that stereoselectivity in the deprotonation step can be predicted from a knowledge of the structure of the product is supported.

$HO^- + CH_3SHO \rightarrow H_2O + {}^-CH_2SHO$

Structures **12** and **13** are Newman projections of the reactant and the product (30). The bond lengths are, in **12**, C—S = 1.794 Å, S—O = 1.490 Å; in **13**, C—S = 1.675 Å, S—O = 1.523 Å. Proceeding as above, HO^- was positioned 1.5 Å from the extensions of C—H_1, C—H_2, and C—H_3, and the geometries and energies of the resulting diastereomeric species were calculated. The resulting relative energies (kcal/mol) and bond lengths (Å) are, for attack on H_1, 0.0; C—S = 1.760, S—O = 1.511; for attack on H_2, 7.3; C—S = 1.766, S—O = 1.504; for attack on H_3, 9.2; C—S = 1.783, S—O = 1.502. The calculated relative reactivities at 30°C are $H_1:H_2:H_3 = 4.3 \times 10^6:23:1$. At 84.5°C, the calculated relative reactivities are $H_1:H_2:H_3 = 4.5 \times 10^5:15:1$, or $k_1 \gg k_2 > k_3$.

The relevant experimental data are those of Katritzky, for sulfoxides **14** and **15**, in methanol at 84.5° (4*e*), and those of Fraser, for sulfoxide **16**, in methanol at 30° (4*i*). The latter workers have recalculated Katritzky's rate constants, and these corrected values are employed here. Katritzky has provided some data for the exchange of **14** and **15** in water solvent at 90°; although these are not extensive, they indicate that the same ordering of relative reactivities is observed in water and in methanol.

As seen in **12**, the dihedral angles in the model sulfoxide of the present work are not ethane-like, because the angles at sulfur are not tetrahedral. The calculated relative reactivities are, therefore, not precisely comparable to those of the experimental systems whose dihedral angles are not known with certainty, but it is clear that the calculations predict highest reactivity for a hydrogen opposite the sulfinyl oxygen, and lowest reactivity for a hydrogen that lies near the axis of the sulfur lone pair.

Because of the rigidity of **16**, the dihedral angles reported for it from measurements on Dreiding models are probably more certain; these are reproduced in **17** and **18**. Of the four hydrogens H_1'—H_4' shown in these two structures, H_1' is opposite the sulfinyl oxygen, but closer to the axis of the sulfur lone pair than is H_1 of **12**; H_2' corresponds to H_2 of **12**, but is closer to the sulfinyl oxygen; H_3' corresponds very closely to H_3 of **12**; H_4' has no counterpart in **12**.

The experimental relative reactivities are $H_1':H_2':H_3':H_4' = 250:6.7:1.0:0.03$ at 30°C, or $k_1' \gg k_2' > k_3'$. The theoretical results are in agreement with this trend. If the difference in the dihedral angles of **12** and **16** is taken into account, the agreement improves: the least reactive hydrogens of **16** are H_3' and H_4', whose C—H bonds lie closest to the axis of the sulfur lone pair. The ratio $H_2'/H_4' = 200$, for hydrogens that otherwise lie in the same region of the molecule, also reflects the substantial retardation associated with increased eclipsing of a C—H bond with the axis of the sulfur lone pair. Since an analogous effect is seen when H_1' is compared to H_1, the experimental relative reactivity of H_1' could be lower than that calculated for H_1 by a factor of at least 10^2, as has been found.

Turning to Katritzky's data for compounds **14** and **15**, the relative reactivities in methanol solvent at 84.5°, as recalculated by Fraser, are $H_1':H_2':H_3' = 10:2:1$, or $k_1' > k_2' > k_3'$. The differences are much smaller than those observed for the rigid sulfoxide **16**, but the trend remains in agreement with that given by the theoretical calculations.

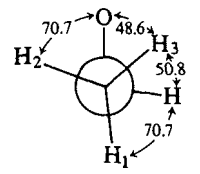

12

$\angle SCH_1 = 109.35°$
$\angle SCH_2 = 108.75°$
$\angle SCH_3 = 110.40°$

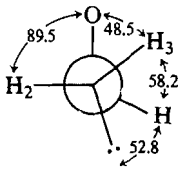

13

$E = -584.96103$ (0.0 kcal/mol)
$E = -584.94944$ (7.3)
$E = -584.94644$ (9.2)

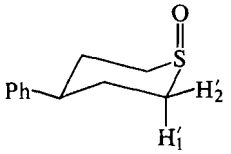

14

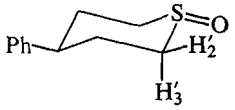

15

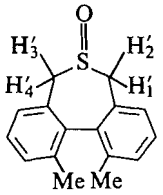

16

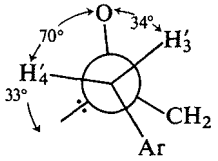

17

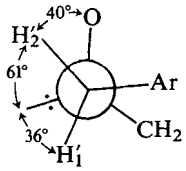

18

In the model reaction **12** → **13**, only one sulfinylcarbanion is formed. Attempts to optimize fully the structures of the carbanions corresponding to removal of H_2 and H_3 of **12** resulted in rotation to **13**. This kind of conformational change cannot occur in the cyclic structures **14**–**16**, and the formation of three carbanions can be envisaged with these cyclic structures. To simulate the effect of such conformational constraint in the deprotonation of **12**, H_1, H_2, and H_3 were removed, and the C—S and S—O bond lengths of the resulting anions were optimized, but C—S rotation was not permitted to occur. Relative to the stable structure **13**, the resulting energies were **12** − H_1, 6.6; **12** − H_2, 16.5; **12** − H_3, 17.2 kcal/mol.

It is clear that there is a one-to-one relationship between diastereotopic selectivity in the deprotonation of a sulfoxide and the relative stability of the resulting carbanion. In terms of the principal thesis of the present work, the notion that stereoselectivity in the deprotonation step can be predicted from a knowledge of the structure of the product is again supported.

Finally, it should be noted that allowing for the slight differences in dihedral angles already discussed, Fraser's interpretation (4*i*) of the origin of the diastereotopic selectivity in the exchange of benzyl methyl sulfoxide in water is strongly supported by the present calculations.

$HO^- + CH_3SHO_2 \rightarrow H_2O + {}^-CH_2SHO_2$

The structures of the reactant and product are shown in **19**

Can. J. Chem. Downloaded from www.nrcresearchpress.com by 210.87.254.6 on 09/06/12
For personal use only.

and **20** (30). Deprotonation leads to a 0.136 Å shortening of the C—S bond, and the carbon centre of the anion **20** is planar. The non-bonding orbital on this carbon atom lies in the same plane as the S—H bond. Inspection of **20** leads to the prediction that H_a of **19** has the higher kinetic acidity.

The structures corresponding to attack of HO^- upon H_a and H_g of **19** are shown in **21** and **22**, for an HO . . . H distance of 1.5 Å; **21** is lower in energy by 0.265 kcal/mol. The calculated selectivity is $k_a/k_g = 1.5$ between 30–80°C.

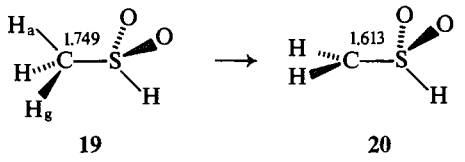

19 **20**

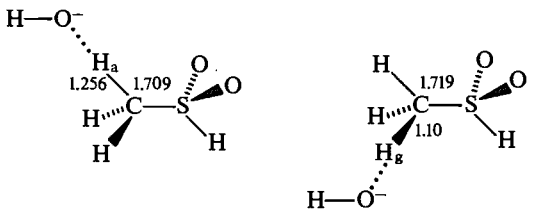

21 **22**

$\angle SCH_a = 108.3°$ $\angle SCH_g = 110.1°$
$E = -659.41185$ (0.0) $E = -659.41143$ (0.265)

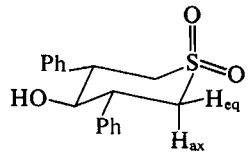

23

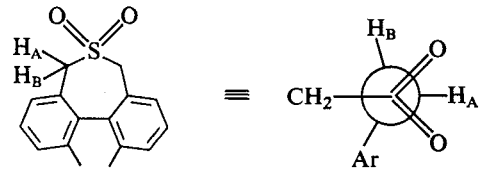

24

The experimental data are again from Katritzky (5*b*), for compound **23** at 36°C, and Fraser (5*a*), for compound **24** at 80°C. In **23**, H_{eq} corresponds to H_a of **19**; in **24**, H_A corresponds to H_a of **19**. The experimental selectivities are $k_{eq}/k_{ax} = 1.6$ for **23**, and $k_A/k_B = 3$ for **24**. Although the agreement between theory and experiment seems remarkable in this case, this must be fortuitous. In the case of sulfone **23** the medium for the exchange was DMSO–D_2O–OD^-; for **24** the medium was *t*BuOD–PhO^-. Ion-pairing effects can be expected to be important in such media, rendering the significance of the comparison between experimental and theoretical selectivities suspect.

Nevertheless, the calculations support the prediction, based on the structure of the α-sulfonylcarbanion, that diastereotopic selectivity in the deprotonation of **19** favors H_a.

$$HO^- + CH_3SH \rightarrow H_2O + {}^-CH_2SH$$

The structures of the reactant and product are shown in **25** and **26** (29). The anion **26** has a non-planar configuration at carbon, and the non-bonding orbital on carbon lies in the S—H plane. Inspection of this structure allows the prediction that H_a of **25** has the higher kinetic acidity.

The structures corresponding to attack of HO^- upon H_a and H_g of **25** are shown in **27** and **28**, for an HO . . . H distance of

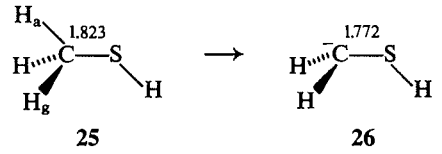

25 **26**

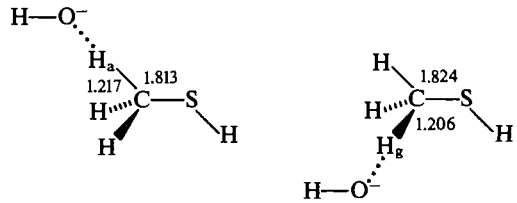

27 **28**

$\angle SCH_a = 106.8°$ $\angle SCH_g = 111.3°$
$E = -510.56730$ (0.0) $E = -510.56554$ (1.11)

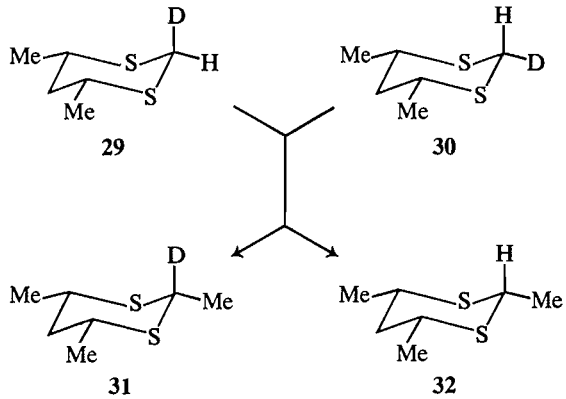

29 **30**

31 **32**

1.5 Å; **27** is lower in energy by 1.11 kcal/mol. The calculated selectivity is $k_a/k_g = 9.1$ at −20°C.

Experimental work on hydrogen exchange in thianes has not been reported. Hydrogen–tritium exchange in 1,3-dithianes has been studied (39), but the experiments were conducted in *t*-butanol solvent, and the relative reactivities of the diastereotopic C2 protons were not determined explicitly. The most relevant experimental data appear to be those of Eliel (7), for the reaction of the diastereomeric anancomeric dithianes **29** and **30**, in the temperature range −20 to −25°C with, successively, butyllithium and methyl iodide in tetrahydrofuran solvent. These reactions lead to a mixture of **31** and **32**. Because of the nature of these experiments, application of the Curtin equations (40) to the mass spectral information leads directly to k_e/k_a, the ratio of the kinetic acidities towards butyllithium. This was found to be 8.6, compared to the theoretical value of 9.1 for the stereoelectronic effect of one sulfur atom.

Summary and conclusions

The present work has demonstrated two connections: a quantitative connection between theoretical diastereotopic selectivities based on a transition state approach to the problem, and selectivities observed experimentally for a variety of sulfur-containing systems; and a qualitative connection between these theoretical selectivities and the structures of the reactive intermediates.

The latter connection may be of particular interest to experimentalists, because qualitative molecular orbital arguments that deal with the structures of reactive intermediates such as **2**–**4** and the reactive intermediates of the present work are well developed (41), and are becoming more common as the concepts of charge transfer and stabilizing orbital interactions become more familiar.

Can. J. Chem. Downloaded from www.nrcresearchpress.com by 210.87.254.6 on 09/06/12
For personal use only.

Can. J. Chem. Downloaded from www.nrcresearchpress.com by 210.87.254.6 on 09/06/12
For personal use only.

Acknowledgements

This work has been supported by grants from the Natural Sciences and Engineering Research Council of Canada, and the Sandoz Forschungsinstitut, Vienna. Grateful acknowledgement is also made to Queen's University for generous allocation of computer time.

1. A. RAUK, E. BUNCEL, R. Y. MOIR, and S. WOLFE. J. Am. Chem. Soc. **87**, 5498 (1965).
2. E. L. ELIEL. Top. Curr. Chem. **105**, 1 (1982).
3. (*a*) J. E. BALDWIN, R. E. HACKLER, and R. M. SCOTT. Chem. Commun. 1415 (1969); (*b*) T. DURST, R. R. FRASER, M. R. MCCLORY, R. B. SWINGLE, R. VIAU, and Y. Y. WIGFIELD. Can. J. Chem. **48**, 2148 (1970).
4. (*a*) E. BULLOCK, J. M. W. SCOTT, and P. D. GOLDING. Chem. Commun. 168 (1968); (*b*) M. NISHIO. Chem. Commun. 562 (1968); (*c*) R. R. FRASER, GURUDATA, R. N. RENAUD, C. REYES-ZAMORA, and R. B. SWINGLE. Can. J. Chem. **47**, 2767 (1969); (*d*) M. CINQUINI, S. COLONNA, U. FOLLI, and F. MONTANARI. Bull. Sci. Fac. Chim. Ind. Bologna, **27**, 203 (1969); (*e*) B. J. HUTCHINSON, K. K. ANDERSEN, and A. R. KATRITZKY. J. Am. Chem. Soc. **91**, 3839 (1969); (*f*) R. R. FRASER and F. J. SCHUBER. Chem. Commun. 397 (1969); (*g*) R. R. FRASER and F. J. SCHUBER. Can. J. Chem. **48**, 633 (1970); (*h*) R. LETT, S. BORY, B. MOREAU, and A. MARQUET. Tetrahedron Lett. 3255 (1971); (*i*) R. R. FRASER, F. J. SCHUBER, and Y. Y. WIGFIELD. J. Am. Chem. Soc. **94**, 8795 (1972); (*j*) M. B. D'AMORE and J. I. BRAUMAN. Chem. Commun. 398 (1973).
5. (*a*) R. R. FRASER and F. J. SCHUBER. Chem. Commun. 1474 (1969); (*b*) M. D. BROWN, M. J. COOK, B. J. HUTCHINSON, and A. R. KATRITZKY. Tetrahedron, **27**, 593 (1971).
6. (*a*) G. BARBARELLA, A. GARBESI, and A. FAVA. Helv. Chim. Acta, **54**, 371 (1971); (*b*) O. HOFER and E. L. ELIEL. J. Am. Chem. Soc. **95**, 8045 (1973); (*c*) G. BARBARELLA, A. GARBESI, A. BOICELLI, and A. FAVA. J. Am. Chem. Soc. **95**, 8051 (1973); (*d*) G. BARBARELLA, A. GARBESI, and A. FAVA. J. Am. Chem. Soc. **97**, 5883 (1975); (*e*) G. D. ANDREETTI, F. BERNARDI, A. BOTTONI, and A. FAVA. J. Am. Chem. Soc. **104**, 2176 (1982).
7. (*a*) A. A. HARTMANN and E. L. ELIEL. J. Am. Chem. Soc. **93**, 2572 (1971); (*b*) E. L. ELIEL, A. ABATJOGLOU, and A. A. HARTMANN. J. Am. Chem. Soc. **94**, 4786 (1972).
8. (*a*) T. DURST. J. Am. Chem. Soc. **91**, 1034 (1969); (*b*) T. DURST. Tetrahedron Lett. 4171 (1971); (*c*) T. DURST, R. VIAU, R. VAN DEN ELZEN, and C. H. NGUYEN. Chem. Commun. 1334 (1971); (*d*) T. DURST, R. VIAU, and M. R. MCCLORY. J. Am. Chem. Soc. **93**, 3077 (1971); (*e*) M. NISHIO. Tetrahedron Lett. 4839 (1972); (*f*) K. NISHIHATA and M. NISHIO. J. Chem. Soc. Perkin II, 1730 (1972); (*g*) R. VIAU and T. DURST. J. Am. Chem. Soc. **95**, 1346 (1973); (*h*) J. F. KING and J. R. DU MANOIR. Can. J. Chem. **51**, 4082 (1973); (*i*) S. BORY and A. MARQUET. Tetrahedron Lett. 4155 (1973); (*j*) J. F. BIELLMANN and J. J. VICENS. Tetrahedron Lett. 2915 (1974); (*k*) T. DURST and M. MOLIN. Tetrahedron Lett. 63 (1975); (*l*) G. CHASSAING, R. LETT, and A. MARQUET. Tetrahedron Lett. 471 (1978); (*m*) G. SOLLADIE, R. ZIMMERMANN, and R. BARTSCH. Tetrahedron Lett. **24**, 755 (1983).
9. (*a*) D. M. ROUSH, E. M. PRICE, L. K. TEMPLETON, D. H. TEMPLETON, and C. H. HEATHCOCK. J. Am. Chem. Soc. **101**, 2971 (1979); (*b*) S. L. GRAHAM and C. H. HEATHCOCK. Tetrahedron Lett. **21**, 3865 (1980); (*c*) G. BARBARELLA, P. DEMBECH, and A. GARBESI. Tetrahedron Lett. **23**, 763 (1982).
10. S. J. ANGYAL and K. JAMES. Aust. J. Chem. **23**, 1209 (1970); A. S. PERLIN. Can. J. Chem. **49**, 1972 (1971).
11. V. MALATESTA and K. U. INGOLD. J. Am. Chem. Soc. **103**, 609 (1981); A. L. J. BECKWITH and C. J. EASTON. J. Am. Chem. Soc. **103**, 615 (1981); D. GRILLER, J. A. HOWARD, P. R. MARRIOTT, and J. C. SCAIANO. J. Am. Chem. Soc. **103**, 619 (1981).
12. J. S. BINKLEY, J. A. POPLE, and W. J. HEHRE. J. Am. Chem. Soc. **102**, 939 (1980).
13. P. J. KRUEGER, J. JAN, and H. WIESER. J. Mol. Struct. **5**, 375 (1970); A. SERRALLACH, R. MEYER, and HS. H. GÜNTHARD. J. Mol. Spectrosc. **52**, 94 (1974).
14. F. BERNARDI, H. B. SCHLEGEL, and S. WOLFE. J. Mol. Struct. **35**, 149 (1976).
15. D. C. MCKEAN. Chem. Soc. Rev. **7**, 399 (1978).
16. G. CIRELLI, T.-K. HA, R. MEYER, and HS. H. GÜNTHARD. Chem. Phys. **72**, 15 (1982); S. SAEBE, L. RADOM, and H. F. SCHAEFER III. J. Chem. Phys. **78**, 845 (1983).
17. Y. APELOIG, P. V. R. SCHLEYER, and J. A. POPLE. J. Am. Chem. Soc. **99**, 1291 (1977); T. CLARK and P. V. R. SCHLEYER. Tetrahedron Lett. 4641 (1979).
18. A. PROSS, D. J. DEFREES, B. A. LEVI, S. K. POLLACK, L. RADOM, and W. J. HEHRE. J. Org. Chem. **46**, 1693 (1981); G. W. SPITZNAGEL, T. CLARK, J. CHANDRASEKHAR, and P. V. R. SCHLEYER. J. Comp. Chem. **3**, 363 (1982).
19. V. MALATESTA, R. D. MCKELVEY, B. W. BABCOCK, and K. U. INGOLD. J. Org. Chem. **44**, 1872 (1979); A. R. GREGORY and V. MALATESTA. J. Org. Chem. **45**, 122 (1980).
20. R. F. HUDSON. Angew. Chem. Int. Ed. Engl. **12**, 36 (1973).
21. N. D. EPIOTIS, R. L. YATES, F. BERNARDI, and S. WOLFE. J. Am. Chem. Soc. **98**, 5435 (1976).
22. P. PULAY. *In* Applications of electronic structure theory. *Edited by* H. F. Schaefer III. Plenum Press, New York. 1977.
23. H. B. SCHLEGEL. Ph.D. Thesis. Queen's University. 1975; H. B. SCHLEGEL. J. Comp. Chem. **3**, 214 (1982).
24. S. WOLFE, D. J. MITCHELL, and H. B. SCHLEGEL. J. Am. Chem. Soc. **103**, 7692 (1981).
25. M. G. EVANS and M. POLANYI. Trans Faraday Soc. **31**, 875 (1935); R. P. BELL. Proc. R. Soc. Ser. A. **154**, 414 (1936); J. E. LEFFLER. Science, **117**, 340 (1953); G. S. HAMMOND. J. Am. Chem. Soc. **77**, 334 (1955).
26. (*a*) H. B. BÜRGI, J. D. DUNITZ, J. M. LEHN, and G. WIPFF. Tetrahedron, **30**, 1653 (1974); H. B. BÜRGI and J. D. DUNITZ. Acc. Chem. Res. **16**, 153 (1983); (*b*) H. B. BÜRGI, J. M. LEHN, and G. WIPFF. J. Am. Chem. Soc. **96**, 1956 (1974).
27. A. I. MEYERS, A. L. CAMPBELL, A. G. ABATJOGLOU, and E. L. ELIEL. Tetrahedron Lett. 4159 (1979).
28. S. SLOMKOWSKI and S. PENCZEK. Chem. Commun. 1347 (1970); S. PENCZEK, P. KUBISA, and K. MATYJASZEWSKI. Adv. Polymer Sci. **37**, 1 (1980).
29. S. WOLFE, L. A. LAJOHN, F. BERNARDI, A. MANGINI, and G. TONACHINI. Tetrahedron Lett. **24**, 3789 (1983).
30. S. WOLFE, A. STOLOW, and L. A. LAJOHN. Tetrahedron Lett. **24**, 4071 (1983).
31. R. R. FRASER and L. K. NG. J. Am. Chem. Soc. **98**, 4334 (1976).
32. W. J. PIETRO, M. M. FRANCL, W. J. HEHRE, D. J. DEFREES, J. A. POPLE, and J. S. BINKLEY. J. Am. Chem. Soc. **104**, 5039 (1982).
33. Faraday Discussions of the Chemical Society. No. 74. Electron and proton transfer. 1982.
34. S. WOLFE. Can. J. Chem. **62**, 1465 (1984).
35. K. YAMAGUCHI, T. FUENO, I. SAITO, T. MATSUURA, and K. N. HOUK. Tetrahedron Lett. **22**, 749 (1981).
36. H. A. RACHID, C. LARRIEU, M. CHAILLET and J. ELGUERO. Tetrahedron, **39**, 1307 (1983).
37. J. S. BINKLEY, R. A. WHITESIDE, R. KRISHNAN, R. SEEGER, D. J. DEFREES, H. B. SCHLEGEL, S. TOPIOL, L. R. KAHN, and J. A. POPLE. Q.C.P.E. **13**, 406 (1981).
38. G. BARBARELLA, P. DEMBECH, A. GARBESI, F. BERNARDI, A. BOTTONI, and A. FAVA. J. Am. Chem. Soc. **100**, 200 (1978).
39. S. OAE, W. TAGAKI, and A. OHNO. Tetrahedron, **20**, 427 (1964).
40. D. Y. CURTIN and D. B. KELLOM. J. Am. Chem. Soc. **75**, 6011 (1953).
41. S. WOLFE, M.-H. WHANGBO, and D. J. MITCHELL. Carbohydrate Res. **69**, 1 (1979); M.-H. WHANGBO and S. WOLFE. Isr. J. Chem. **20**, 36 (1980).

Comment: Infrared absorption and resonance Raman scattering of photochromic triphenylformazans

HUBERT LANGBEIN AND ULRICH-WALTER GRUMMT
Sektion Chemie, Friedrich-Schiller-Universität Jena, 6900 Jena (G.D.R.)

(Ref. Can. J. Chem. **61**, 809 (1983))
Received February 9, 1984

In a very interesting paper by Lewis and Sandorfy (1), the existence of four isomers **A**, **B**, **C**, **D** of unsubstituted triphenylformazan (2–4) was called in question because only two of them, **A** and **D**, could be detected by means of vibrational spectroscopy.

It is obvious from our kinetic data obtained from flash photolysis (3) that the lifetime of **B** is too short as to allow detection by a nontime-resolved spectroscopic method. At room temperature the concentration of **B** is negligibly small in any photostationary state.

The experimental conditions used by Lewis and Sandorfy when preparing the yellow nonchelate form **D** also exclude the presence of appreciable concentrations of **C** in the photostationary states because of the following reasons. The effective wavelength applied for generating **D** for the ir-measurements was 546 nm (medium pressure mercury arc in combination with a 475 nm cut-off filter). This wavelength generates a photostationary state $\mathbf{D} \underset{h\nu}{\overset{h\nu}{\rightleftarrows}} \mathbf{C}$ which is nearly quantitatively shifted to the left side since $\epsilon_\lambda^{\mathbf{D}} < \epsilon_\lambda^{\mathbf{C}}$ for $\lambda > 470$ nm (2) and $\Phi_{\mathbf{C}\rightarrow\mathbf{D}} > \Phi_{\mathbf{D}\rightarrow\mathbf{C}}$. The same applies for continuous irradiation with the laser line $\lambda' = 488$ nm which was used for recording the resonance Raman spectra. We calculate a conversion ratio of $C_{\mathbf{C}}/C_{\mathbf{D}} < 0.1$ in the photostationary state for that wavelength. Furthermore, because CCl_4 upon irradiation is highly prone to trace contamination by hydrochloric acid and the thermal transformations of the formazan isomers are known to be extremely sensitive to acid catalysis, this photostationary state is expected to be even farther shifted to the left due to a reduced lifetime of **C** in CCl_4.

Thus the experimental results presented by Lewis and Sandorfy do not contradict our findings, particularly they do not allow one to doubt the existence of four isomers for which unequivocal evidence has been given under different experimental conditions.

1. J. W. LEWIS and C. SANDORFY. Can. J. Chem. **61**, 809 (1983).
2. H. LANGBEIN. J. Prakt. Chem. **321**, 655 (1979).
3. U.-W. GRUMMT and H. LANGBEIN. J. Photochem. **15**, 329 (1981).
4. R. KUHN and H. M. WEITZ. Chem. Ber. **86**, 1189 (1953).

Can. J. Chem. Downloaded from www.nrcresearchpress.com by 210.87.254.6 on 09/06/12
For personal use only.

Some investigations of the chemistry of tellurium chloride pentafluoride, its reaction with caesium fluoride, and the preparation of *cis* and *trans* methoxytellurium(VI) chloride tetrafluoride, $(CH_3O)TeClF_4$

LAWRENCE J. LAWLOR AND JACK PASSMORE[1]

Department of Chemistry, University of New Brunswick, Fredericton, N.B., Canada E3B 6E2

Received October 19, 1983

LAWRENCE J. LAWLOR and JACK PASSMORE. Can. J. Chem. **62**, 1477 (1984).

The reaction of $TeClF_5$ with CH_3OH, and CH_3OSiMe_3, leads to a mixture of *cis*- and *trans*-$(CH_3O)TeClF_4$ in a ratio of 1:6, as well as some unidentified Te(IV) product. The vibrational spectrum of the 1:6 mixture of *cis*- and *trans*-$(CH_3O)TeClF_4$ was accounted for on the basis of the predominant pseudo-C_{4v} *trans* isomer. $TeClF_5$ is unreactive towards anhydrous HF, SbF_5, $AlCl_3$, SO_2, F_2, and ClF at room temperature. Over the temperature range 70−250°C it thermally decomposes to TeF_6, TeF_4, and Cl_2. It slowly reacts with CsF to form $CsTeF_5$, TeF_6, Cl_2, and small amounts of ClF, and with $HNMe_2$ it is also reduced to form $TeF_4 \cdot HNMe_2$.

LAWRENCE J. LAWLOR et JACK PASSMORE. Can. J. Chem. **62**, 1477 (1984).

La réaction du $TeClF_5$ avec le CH_3OH et le CH_3OSiMe_3 conduit à un mélange de $(CH_3O)TeClF_4$ *cis* et *trans* dans un rapport de 1:6 en plus de quelques produits de Te(IV) non identifiés. On a expliqué le spectre de vibration du mélange en se basant sur la présence prédominante de l'isomère *trans* de symétrie pseudo C_{4v}. Le $TeClF_5$ est inerte vis-à-vis du HF, du SbF_5, du $AlCl_3$, du SO_2, du F_2 et du ClF anhydres, à la température ambiante. Dans l'intervalle de température allant de 70 à 250°C, il se décompose thermiquement en TeF_6, TeF_4 et Cl_2. Il réagit lentement avec le CsF pour former le $CsTeF_5$, le Cl_2 et de petites quantités de ClF. Le $HNMe_2$ le réduit également avec formation de $TeF_4 \cdot HNMe_2$.

[Traduit par le journal]

Can. J. Chem. Downloaded from www.nrcresearchpress.com by 210.87.254.42 on 09/06/12
For personal use only.

Introduction

Tellurium chloride pentafluoride was first prepared in low yield by the reaction of elemental fluorine with tellurium tetrachloride (1). Large amounts of tellurium hexafluoride and chlorine were also produced from which the product was not separated. Nevertheless, $TeClF_5$ was reported to be reduced by olefins and phosphorus trifluoride (1). A convenient high yield synthesis of pure tellurium chloride pentafluoride has been developed in this laboratory (2, 3), making an exploration of its chemistry possible.

It is well known that sulphur hexafluoride is extremely inert chemically, especially towards nucleophiles, and that its low reactivity is mainly due to kinetic rather than thermodynamic factors (4). Sulphur chloride pentafluoride, on the other hand, has an extensive chemistry (4−10). The reactivity of the hexafluorides of group six increase as the group is descended, and tellurium hexafluoride can directly form a variety of substituted derivatives (11−14). It also forms compounds in which the coordination number of tellurium appears to have increased to 7 or 8. For example, it reacts with NMe_3 to form $2NMe_3 \cdot TeF_6$ (15) and with caesium and rubidium fluorides to form the corresponding salts of TeF_7^- and TeF_8^{2-} (16). It was therefore envisaged that tellurium chloride pentafluoride would be more reactive than either tellurium hexafluoride or sulphur chloride pentafluoride. Reactions of tellurium chloride pentafluoride with a variety of reagents are reported below. In the course of these investigations, *cis*- and *trans*-$(MeO)TeClF_4$ were prepared and characterised (17). Very recently Seppelt and coworker have reported some photochemical reactions of tellurium chloride pentafluoride in which the chlorine atom has been replaced by some other groups (18, 19).

Experimental

Except when stated, apparatus, reagents, and techniques are the same as those previously described (2, 20, 21).

Volatile reactive fluorides were manipulated in a Monel vacuum line and reactive solids in a Vacuum Atmospheres Dri-Box equipped with a Dri-Train. Infrared spectra of gaseous materials were obtained by using a stainless steel cell equipped with AgCl windows. F.E.P. reaction vessels (volume ca. 10 mL) were constructed from $\frac{1}{2}$ in od tubing and connected to the metal vacuum line via a Whitey 1KS4 valve and stainless steel $\frac{1}{4}$ in. Swagelok fitting. High pressure reactions were carried out in Monel vessels (volume ca. 50 mL) or a Parr bomb (volume ca. 45 mL). Pyrex vessels (volume ca. 30 mL) equipped with 1KS4 Whitey valves were also used as reaction vessels.

^{19}F nmr chemical shifts are quoted relative to CCl_3F with positive chemical shifts corresponding to high shielding. ^1H nmr chemical shifts are relative to Me_4Si. Raman spectra were obtained by the 5145 Å exciting line of a 2W Argon Ion Spectra Physics Laser. The slit width was 4 cm^{-1}. $CH_3OTeClF_4$ samples, for which Raman spectra were obtained, were contained in sealed thin walled F.E.P. tubing.

Mass spectra were obtained using a Varian V-5900 I.C.R. spectrometer operating at 70 eV. Quantitative elemental analyses were performed by Alfred Bernhardt Mikroanalytisches Laboratorium, West Germany or Butterworth Laboratories Ltd., Great Britain.

The purity of starting materials was routinely established by X-ray powder photography or infrared or Raman spectroscopy. Literature methods were used to prepare $TeClF_5$ (2, 3), $CsTeF_5$ (22), and TeF_4 (23, 24). Me_3SiCl (Petrarch) and C_6F_6 were used without further purification. Me_3SiOMe (ICN-K and K Pharmaceuticals) and anhydrous methanol were stored over molecular sieve (3 Å) before use. Dimethyl amine (Matheson) was dried by repeated distillation from molecular sieves (3 Å) over which it was stored. CsF (Ozark-Mahoning) was heated at 150°C *in vacuo* for 12 h, then ground prior to reaction. SbF_5 (Ozark-Mahoning) was purified by vacuum distillation at room temperature. Anhydrous HF (Matheson) was dried over K_2NiF_6. Fluorine was stored over NaF. SO_2 (Matheson) was evacuated at −196°C to remove oxygen and dried over CaH_2 before use.

Thermal stability of $TeClF_5$

$TeClF_5$ (0.90 g) was heated in a well fluorinated Monel Parr bomb at 70°C for 20 days. The product (0.90 g) was $TeClF_5$ containing a trace of TeF_6 (ir) which was reheated at 110°C for 2 months. The product (0.90 g) contained $TeClF_5$, TeF_6, and a trace of SiF_4 (ir). The mixture was heated at 180°C for 20 days and the products (0.86 g) identified (ir) as $TeClF_5$, TeF_6, traces of SiF_4, and the presence of

[1]To whom all correspondence should be addressed.

TABLE 1. Some reactions and attempted reactions of $TeClF_5$

Reaction[a]	Conditions and comments	Products
1. $TeClF_5$ (2.05) F_2 (9.21)	Monel vessel (50 mL) 10 days, rt	$TeClF_5$ + trace TeF_6 (ir)[b]
$TeClF_5$ (5.81) F_2 (23.2)	Parr bomb (45 mL) 3 days, 165°C	$TeClF_5$:TeF_6 ratio ca. 1:5 (^{19}F nmr)
2. $TeClF_5$ (2.62) ClF (6.61)	Monel vessel 14 days, rt	$TeClF_5$ trace TeF_6 (ir)
3. $TeClF_5$ (1.60) Anhydrous HF (24.0)	Well passivated F.E.P. vessel (10 mL) 2 phases present	$TeClF_5$, HF (^{19}F nmr)
4. $TeClF_5$ (2.18) SO_2 (3.88)	Pyrex vessel (30 mL) $TeClF_5$ dissolves in SO_2	$TeClF_5$, SO_2 traces SiF_4 (ir)
5. $TeClF_5$ (3.91) $AlCl_3$ (4.27)	Pyrex vessel (*a*) overnight rt, (*b*) overnight 45°C	Volatiles, $TeClF_5$, (*a*) trace SiF_4 (ir), (*b*) as above
6. $TeClF_5$ (4.03) SbF_5 (4.66)	Pyrex vessel equipped with a Rotoflo valve and a side arm containing a capillary. $TeClF_5$ dissolved in SbF_5	SbF_5, $TeClF_5$ (Raman of material poured into capillary side arm)
7. $TeClF_5$ (5.22) Solid KOH (5.54)	F.E.P. vessel. Reaction with bubbling left 7 days	Volatiles (0.3 g) TeF_6, $TeClF_5$, Cl_2 (ir, Raman) Solid (1.32 g) white powder, $KTeF_5$ + lines in the Raman spectrum at 750, 689, and 670 cm^{-1}
8. $TeClF_5$ (6.62) Me_3SiCl (6.27)	Pyrex vessel (*a*) Warmed to rt giving a milky white solution (*b*) Rt for 2 days, quantity of white solid increased with time, liquid became yellow	(*a*) Volatiles contained Me_3SiF and $TeClF_5$ (ir) (*b*) Volatiles (1.90 g) Me_3SiF, $TeClF_5$ and SiF_4 (ir, Raman). Solid (0.43 g) $TeCl_4$ (Raman, X-ray powder diffraction photography)
9. $TeClF_5$ (2.81) Me_4Si (3.09)	F.E.P. vessel (*a*) Overnight rt (*b*) 8 h, ca. 75°C	(*a*) $TeClF_5$, Me_4Si (ir) (*b*) $TeClF_5$, Me_4Si (ir, ^{19}F nmr)
10. TeF_6 (8.53) Me_3SiCl (13.4)	Pyrex vessel 8 h, 75°C	TeF_6, Me_3SiCl (ir, ^{19}F nmr)
11. $TeClF_5$ (2.28) H_2 (11.16)	Quartz vessel uv radiation (*a*) 4 h, sides of vessel covered with a white solid (*b*) Overnight	(*a*) Volatiles contain SiF_4, $TeClF_5$ + trace TeF_6 (*b*) Volatiles SiF_4. Solid. Unidentified broad peaks in Raman spectrum at 680, 500, 435, and 280 cm^{-1}

[a]Amounts of reactant are given in mmoles in parentheses.
[b]Method of identification, in the table and elsewhere in the text, is given in parentheses.

chlorine was implied by its physical properties. In another experiment, $TeClF_5$ was heated at 250°C in a Monel vessel overnight giving TeF_6, $TeClF_5$, and solid TeF_4 (ir).

Attempted reactions of $TeClF_5$ with F_2, ClF, HF, SO_2, $AlCl_3$, SbF_5, solid KOH, Me_3SiCl, Me_4Si, and H_2 under uv radiation are listed in Table 1.

Reaction of $TeClF_5$ with CsF

In a typical reaction $TeClF_5$ (8.53 mmol) was condensed onto CsF (4.11 mmol) in a glass vessel and the mixture stirred at rt. After 15 days the volatile products contained $TeClF_5$, TeF_6, and SiF_4 (ir) and the physical properties of the mixture suggested the presence of chlorine. After 30 days the volatile products (1.3584 g), TeF_6, $TeClF_5$, SiF_4, and Cl_2 (ir, Raman, and ^{19}F nmr) were removed, leaving a solid (1.4065 g) which was shown to contain $CsTeF_5$ (Raman) and CsF (X-ray powder photography). The volatile reaction products were held at −78°C and a portion of these products condensed onto sulphur dioxide. The presence of SO_2ClF (ir) in this material infers the presence of ClF in the volatile product of the reaction of CsF and $TeClF_5$. A number of similar reactions carried out under different conditions are given in Table 2.

Reaction of $CsTeF_5$ with ClF

Chlorine monofluoride (7.52 mmol) was condensed onto $CsTeF_5$ (5.85 mmol) in a Monel vessel and left at rt for 3 days. The volatiles (0.5083 g) contained TeF_6, Cl_2, and a trace of $TeClF_5$ (ir, Raman, ^{19}F nmr). The Raman spectrum of the solid product (1.80 g) showed it to contain $CsTeF_5$ (25) and $CsClF_2$ (26).

Reaction of $TeClF_5$ with dimethyl amine ($HNMe_2$)

In a typical reaction SO_2 (5.03 mmol) was condensed onto $TeClF_5$ (5.91 mmol) in a F.E.P. vessel. $HNMe_2$ (5.56 mmol) was added in two aliquots. After each addition the reaction vessel was held at −22°C, 0°C and rt for 30, 15, and 15 min, respectively. A white solid was observed at −22°C and at 0°C, but the product changed to a clear liquid on warming to rt. The final product consisted of a clear layer of viscous material below a slightly yellow non-viscous liquid. The more volatile phase contained SO_2ClF and Cl_2 (ir, Raman, ^{19}F nmr). The viscous product was identified as $TeF_4 \cdot HNMe_2$ by comparing its infrared spectrum to that of $TeF_4 \cdot HNMe_2$ prepared by the reaction of TeF_4 with $HNMe_2$. The ^{19}F nmr spectrum of the product in SO_2 consisted of one intense peak at 42.4 ppm (40.8 ppm for $TeF_4 \cdot HNMe_2$ in acetonitrile prepared from TeF_4). A peak attributable to a ^{125}Te—F coupling was not observed. Table 3 lists other similar reactions.

Reactions of $TeClF_5$ with CH_3OH

$TeClF_5$ (9.4 mmol) and CH_3OH (8.44 mmol) were consecutively condensed on Na_2CO_3 (3.9 mmol) in an F.E.P. vessel and held at 0°C and rt for 10 h and 3 days, respectively. Two volatile components were condensed out of the reaction mixture. A more volatile yellow

Can. J. Chem. Downloaded from www.nrcresearchpress.com by 210.87.254.42 on 09/06/12
For personal use only.

TABLE 2. Reactions of CsF with $TeClF_5$

Reactant	Conditions	Products[a]
1. $TeClF_5$ (12.81 mmol) CsF (3.40 mmol)	90°C, 25 days	CsF/$CsTeF_5$ (1.1233 g), TeF_6, $TeClF_5$, Cl_2, SiF_4 (2.6729 g)
2. $TeClF_5$ (15.54 mmol) CsF (3.33 mmol)	80–90°C in C_6F_6 15 days	CsF/$CsTeF_5$ (1.2747 g), TeF_6, $TeClF_5$, Cl_2
3. $TeClF_5$ (6.19 mmol) CsF (3.82 mmol)	55°C,[b] 20 days	CsF/$CsTeF_5$ (1.64 g), TeF_6, $TeClF_5$, Cl_2 (0.44 g)

[a]The individual components of the volatile material have not been separated.
[b]Here an F.E.P. reaction vessel was used.

TABLE 3. Reactions of $TeClF_5$ with $HNMe_2$

Reactants	Products[a]
1. $TeClF_5$ (6.00 mmol) $HNMe_2$ (6.33 mmol)	$TeF_4 \cdot HNMe_2$[b] (1.5554 g) Cl_2, $HNMe_2$ (0.2320 g)
2. $TeClF_5$ (3.72 mmol) $HNMe_2$ (2.99 mmol)	$TeF_4 \cdot HNMe_2$ (0.84 g) $TeClF_5$, Cl_2, TeF_6 (trace) (0.33 g)

[a]The individual components of the volatile material have not been separated.
[b]Infrared spectrum in cm^{-1} of liquid $TeF_4 \cdot HNMe_2$, 3220 vs, br; 2980 w; 2805 w, br; 2425 w; 1600 m; 1465 s; 1410 m; 1250 w, br; 1168 m, br; 1080 sh; 1050 w; 1016 s; 818 s; 728 w; 690 w; 621 s; 480 vs, br.

TABLE 4. Reactions of $TeClF_5$ with Me_3SiOMe

Reactants	Products[a]
1. $TeClF_5$ (4.95 mmol) Me_3SiOMe (5.00 mmol) CCl_3F (5.48 mmol)	$CH_3OTeClF_4$ (0.70 mmol) $TeClF_5$, Me_3SiF, CCl_3F (2.342 g) Involatile liquid (0.3424 g)[b]
2. $TeClF_5$ (3.67 mmol) Me_3SiOMe (3.15 mmol)	$CH_3OTeClF_4$ (1.70 mmol) $TeClF_5$, Me_3SiF (0.6228 g) Involatile liquid (0.1597 g)

[a]The individual components of the volatile material have not been separated.
[b]^{19}F nmr consisted of broad peaks at δCCl_3F + 38 ppm, with no $^{125}Te-F$ coupling. Raman showed broad peaks at 2969, 2856, 682, 652, and 529 cm^{-1}.

TABLE 5. Mass spectrum of $CH_3OTeClF_4$[a,b]

272, $CH_3OTeClF_4^+$ (9); 253, $CH_3OTeClF_3^+$ (10); 237, $CH_3OTeF_4^+$ (28); 212, ? (32); 199, $CH_3OTeF_2^+$ (100); 187, TeF_3^+ (80); 168, TeF_2^+ (29); 165, $TeCl^+$ (41); 130, Te^+ (9)

[a]Isotopes ^{122}Te, ^{123}Te, ^{124}Te, ^{125}Te, ^{126}Te, and ^{128}Te were also observed in the correct ratios, *m/e* numbers quoted are for ^{130}Te and ^{35}Cl.
[b]Numbers in parentheses represent the relative intensity of the ion.

liquid (0.59 g) contained SiF_4, $TeClF_5$, and TeF_6 (ir). A less volatile clear liquid (0.56 g) was identified as a mixture of *cis*- and *trans*-$(CH_3O)TeClF_4$ (ir, Raman, ^{19}F nmr). The weight of remaining solid was 1.47 g greater than that of Na_2CO_3 reactant.

Reaction of $TeClF_5$ with Me_3SiOCH_3

Me_3SiOMe (4.76 mmol) was condensed onto $TeClF_5$ (4.99 mmol) in an F.E.P. vessel in three aliquots. After each addition the mixture was held at 0°C for 20 min with stirring. A white solid formed and disappeared on warming to rt for 0.5 h prior to the addition of the next aliquot. The product volatile at −78°C (0.6431 g) contained $TeClF_5$ and Me_3SiF (ir). The remaining volatile liquid contained $CH_3OTeClF_5$ and a trace of Me_3SiF (ir). The trace of Me_3SiF was removed by subjecting the mixture, held at −45°C, to a dynamic vacuum for 10 min. The $CH_3OTeClF_4$ (4.20 mmol) was condensed out of the vessel, leaving a trace of a clear involatile liquid. The results of some similar reactions are given in Table 4.

Anal. calcd. for $CH_3OTeClF_4$: Te 47.08, F 28.04, Cl 13.08, C 4.43, H 1.11; found: Te 46.67, F 27.71, Cl 12.91, C 4.71, H 1.35. The mass spectrum of $CH_3OTeClF_4$ is given in Table 5.

Results and discussion

Preparation of cis- *and* trans-*$CH_3OTeClF_4$*

cis- and *trans*-$(CH_3O)TeClF_4$ were prepared by the reaction of $TeClF_5$ with CH_3OH in the presence of Na_2CO_3, and with $MeOSiMe_3$ at room temperature according to reactions [10] and [11].

[10] $TeClF_5 + CH_3OH \rightarrow CH_3OTeClF_4 + HF$

[11] $TeClF_5 + CH_3OSiMe_3 \rightarrow CH_3OTeClF_4 + Me_3SiF$

The hydrogen fluoride generated in reaction [10] was neutralised by the Na_2CO_3 present. In both reactions some uncharacterised Te(IV) containing involatile liquid was also produced that had peaks in the Raman spectrum in the methyl stretching region (3000–2800 cm^{-1}) and in the TeF, TeO stretching region (700–500 cm^{-1}). The nature of the oxidised product was not established.

The reaction of TeF_6 and methyl alcohol in the presence of NaF led to CH_3OTeF_5, and with Na_2CO_3 to predominately *cis*-$(CH_3O)_2TeF_4$ (14). As far as we are aware there are no reports of reactions of methyl alcohol with $SClF_5$.

Characterisation of cis- *and* trans-*$CH_3OTeClF_4$*

The elemental analyses and mass spectrum (Table 5) were consistent with the formation of $CH_3OTeClF_4$. The proton and fluorine nmr data are listed in Table 6 with the fluorine chemical shifts estimated by the method of Dean and Evans (27) with adjustable parameters determined from the reported chemical shifts of $TeClF_5$ (1) and CH_3OTeF_5 (14). The spectrum of *cis*-$CH_3OTeClF_4$ was simulated by the computer program LAME (28). The crude values of the coupling constants together with the line positions were given as input to the program which refined the values to give a good fit in very few iterations. The ratio of *cis*-to-*trans* isomer was estimated to be ca. 1:6. Consistently the ratio of *cis*-to-*trans* $HOTeClF_4$ given on hydrolysis of $TeClF_5$ was 1:4 (17). In addition the reaction of $SClF_5$ with R_2NSiMe_3 (R = CH_3) led to only *trans*-R_2NSClF_4 (9). Random replacement of fluorine atoms would lead to a three-fold predominance of the *cis* isomer. It is possible that the *trans* isomer is the thermodynamically favoured product. A tellurium chlorofluoride of the type *trans*-$RTeClF_4$ (R = C_2F_5 (29–31)) has been prepared, but as far as we are aware this is the first report of a *cis*-chlorofluoride of composition $RTeClF_4$.

Can. J. Chem. Downloaded from www.nrcresearchpress.com by 210.87.254.42 on 09/06/12
For personal use only.

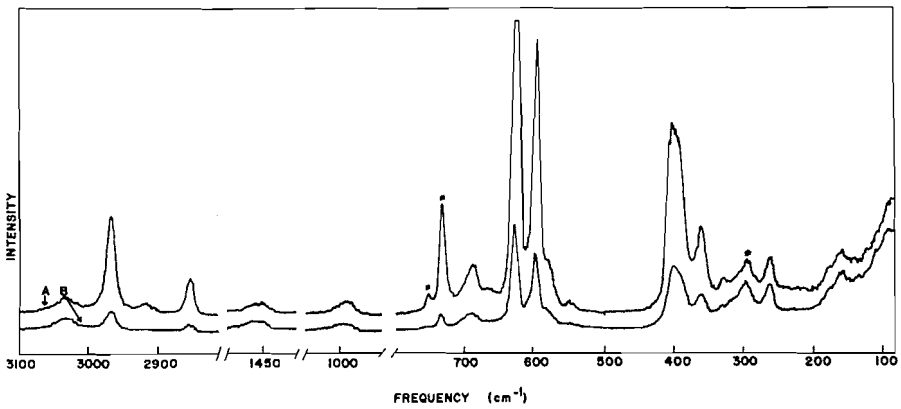

FIG. 1. Raman spectrum of $CH_3OTeClF_4$. *A*, incident polarisation parallel; *B*, incident polarisation perpendicular (*F.E.P. peaks).

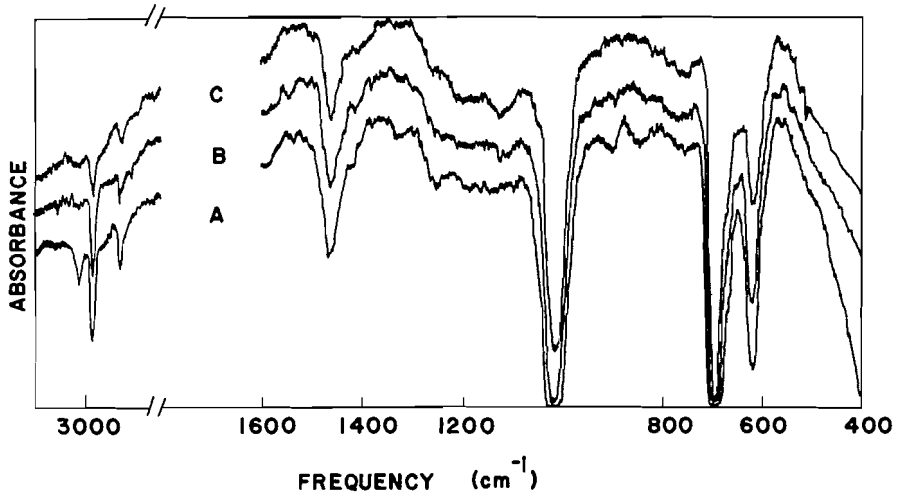

FIG. 2. Infrared spectrum of gaseous $CH_3OTeFClF_4$ at *A*, 25; *B*, 10; and *C*, 5 mm pressure in a 10 cm stainless steel gas cell with AgCl windows.

TABLE 6. Nuclear magnetic resonance data for $CH_3OTeClF_4$[a]

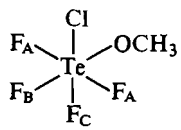

1

trans-$CH_3OTeClF_4$	*cis*-$CH_3OTeClF_4$ (**1**)	
8.9 (9.7)	19.2 (9.7)	F_A
	−4.3 (−2.8)	F_B (*trans* to — OCH_3)
	54.3 (48.4)	F_C (*trans* to —Cl)
	160	J_{AB}
	170	J_{BC}
	145	J_{AC}
3.8		H
2		J_{HF}
150		$J_{^{125}Te-^{1}H}$
3619		$J_{^{125}Te-^{19}F}$

[a]Numbers in parentheses are estimated chemical shifts by method of Dean and Evans. Coupling constants are reported in Hz, estimated uncertainty ±5 Hz. Chemical shifts are quoted in ppm relative to CCl_3F, with increase in positive shifts with increase in shielding. ^1H nmr chemical shifts are reported with respect to $(CH_3)_4Si$.

TABLE 7. Vibrational spectrum of $CH_3OTeClF_4$[a]

Infrared (gas)[b]		Raman (liquid)			
$(cm)^{-1}$	I	(cm^{-1})	I	Pol.	Tentative assignment
3021	w	3030	(5)	dp	ν_{asym} CH_3
2970	m	2964	(25)	p	ν_{sym} CH_3
2858	w	2852	(8)	p	
1462	m	1450	(3)	p	ν_{sym} ν_{asym} CH_3
1012	vvs	992	(4)	p	C—O
693	vs	692	(6)	p	ν_{asym} TeF_4
		670			
619	vs	629	(100)	p	ν_{sym} TeF_4
595	sh	599	(33)	p	Te—O
		583	(1)	p	TeF_4 out-of-phase
		398	(74)	p	Te—Cl
		364	(25)	p	TeF_4 out-of-plane
		331	(1)	p	ν_{sym} TeF_4 in plane or $\delta(OTeF_4)$
		262	(7)	dp	ν_{asym} TeF_4 in plane
		158	(7)	dp	$\delta(ClTeF_4)$

[a]See Figs. 1 and 2 for the infrared and the Raman spectra.
[b]s = strong, m = medium, w = weak, sh = shoulder, v = very.

Vibrational spectra of trans-$CH_3OTeClF_4$

The vibration spectrum of $CH_3OTeClF_4$ is given in Figs. 1 and 2 and the frequencies are listed in Table 7 with tentative assignments made on the basis of C_{4v} *trans*-$CH_3OTeClF_4$. The major features of the spectrum can be accounted for in this way, although it is known that ca. 15% is in fact the *cis* isomer. Presumably the weaker spectrum of the *cis* isomer has absorp-

Can. J. Chem. Downloaded from www.nrcresearchpress.com by 210.87.254.42 on 09/06/12
For personal use only.

TABLE 8. Comparison of TeF, TeO, and TeCl stretching frequencies of $AgOTeF_5$, $CH_3OTeClF_4$, *trans*-$C_2F_5TeClF_4$, and $TeClF_5$[a]

Assignment in C_{4v} point group	$AgOTeF_5$		$CH_3OTeClF_4$		$C_2F_5TeClF_4$		$TeClF_5$	
	Infrared	Raman	Infrared	Raman	Infrared	Raman	Infrared	Raman
a_1		588						
$\nu_1\nu$(TeF′) or	585	580	—	—	—	—	711	708
ν(TeX, X = O, C)	—	—	595	599	—	219	—	—
$\nu_2\nu_{sym}(TeF_4)$	650	650	619	629	612	606	662	659
$\nu_3\delta_{sym}(TeF_4)$ out-of-plane	—	—	—	364	—	306	317	312
$\nu_4\nu$(TeCl) or	—	—	—	398	—	414 407	410.5 404	413 407
ν(TeO)	863 850	861 852	—	—	—	—	—	—
b_1								
$\nu_5\nu_{sym}$ (TeF_4) out-of-phase	—	664	—	583	—	569	—	651
$\nu_6\delta_{asym}(TeF_4)$ out-of-plane	—	—	—	—	—	—	—	—
b_2								
$\nu_7\delta_{sym}(TeF_4)$ in-plane	—	—	—	—	—	274	—	302
e								
$\nu_8\nu_{asym}(TeF_4)$	637	—	693	692	682	683	726	726
$\nu_9\delta(F^tTeF_4)$ or	330	327	—	—	—	—	324.5	327
$\delta(XTeF_4$, X = O, C)	—	—	—	331(?)	—	—	—	—
$\nu_{10}\delta_{asym}(TeF_4)$ in-plane	280	282	—	262	—	251	259	259
$\nu_{11}\delta(ClTeF_4)$	—	—	—	158	—	133	—	167
$\delta(XTeF_4$, X = O, C)	345	347	—	—	—	—	—	—

[a]Frequencies are in cm^{-1}.

tions at similar frequencies to that of the *trans* isomer, and these are hidden under the *trans* isomer peaks. The vibrations of the CH_3 group have been assigned by comparison with CH_3X (X = Br, Cl, F, I, OH) (32–34). The intense infrared band at 1012 cm^{-1} has been assigned to the CO stretching frequency by comparison with CH_3OH (33). The rest of the spectrum was assigned by comparison with the spectrum of $TeClF_5$ (35), $OTeF_5^-$ (36), and *trans*-$C_2F_5TeClF_4$ (29–31) (Table 8). It is assumed that *trans*-$CH_3OTeClF_4$ has C_{4v} symmetry. Two Raman bands at 692 and 583 cm^{-1} are e and b_2 modes, respectively, but are found to be polarised. This implies that the pseudo-C_{4v} symmetry in *trans*-$CH_3OTeClF_4$ is reduced by the presence of the bent $TeOCH_3$ entity.

General thermal and chemical stability of $TeClF_5$

Tellurium chloride pentafluoride appears to be stable indefinitely at room temperature. Over the temperature range 70–250°C it thermally decomposes to TeF_6, TeF_4, and Cl_2. Sulphur chloride pentafluoride is reported (5) to decompose at 400°C to SF_6, SF_4, and Cl_2.

Tellurium chloride pentafluoride like TeF_6 and $SClF_5$ does not react at room temperature with the strong acid, anhydrous hydrogen fluoride, or the strong Lewis acids antimony pentafluoride and aluminium trichloride. It is also unreactive towards the strong oxidising agents chlorine monofluoride and fluorine under ambient conditions. At 165°C TeF_6 was formed in the reaction of fluorine and $TeClF_5$. It does not react with the potential reducing agents sulphur dioxide or elemental mercury (2) at room temperature; however, it is reduced by PF_3 and olefins (1). In photochemical reactions of $SClF_5$ with olefins, addition of Cl and SF_5 occurs across the double bond (7, 8). There is no reaction of $TeClF_5$ with hydrogen, but under uv radiation reduction occurs. Not surprisingly, no evidence was obtained for Te_2F_{10} (c.f. S_2F_{10} (5)). Tellurium chloride pentafluoride is slowly hydrolysed by water at room temperature, leading to the formation of *cis*- and *trans*-$HOTeClF_4$ (c.f. *cis*- and *trans*-$(CH_3O)TeClF_5$ below), other $(HO)_xTeClF_{5-x}$ (17) species, $(HO)_xTeF_{6-x}$ ($m = 1 \rightarrow 4$) (11, 13, 37), and some tellurium(IV)-containing product (17, 28). Tellurium hexafluoride is also slowly hydrolysed under similar conditions (11), but no reaction occurs with sulphur chloride pentafluoride.

Reactions of $TeClF_5$ with CsF, KOH, and $HNMe_2$

Caesium fluoride reacts slowly at room temperature with $TeClF_5$. The products $CsTeF_5$, TeF_6, and Cl_2 were identified, and the presence of ClF was inferred as a product, as the gaseous products reacted with SO_2 to form SO_2ClF. In an attempt to establish a possible route for this reaction, $CsTeF_5$ was reacted with ClF leading to $CsClF_2$, TeF_6, and Cl_2.

The inhomogeneous reaction of $TeClF_5$ with solid KOH led to products that included $KTeF_5$, TeF_6, and Cl_2. Reduction to a tellurium(IV) product was also observed in the reaction of $TeClF_5$ and $HNMe_2$ which proceeded essentially quantitatively according to eq. [9].

[9] $TeClF_5 + HNMe_2 \rightarrow TeF_4 \cdot HNMe_2 + \text{"ClF"}$

The chlorine monofluoride was not observed directly, but in a reaction in which sulphur dioxide was present, SO_2ClF was detected. The analogous reaction of NMe_3 and TeF_6 led to the

Can. J. Chem. Downloaded from www.nrcresearchpress.com by 210.87.254.42 on 09/06/12
For personal use only.

stable $2NMe_3 \cdot TeF_6$ (15). Some reduction of tellurium(VI) to tellurium(IV) was also observed in the reactions of $TeClF_5$ with H_2O (17), MeOH, and $MeOSiMe_3$.

Reaction of $TeClF_5$ and TeF_6 with Me_3SiCl

Tellurium chloride pentafluoride reacts at room temperature with Me_3SiCl to form $TeCl_4$, Cl_2, Me_3SiF. Presumably $TeCl_2F_4$ is formed initially, which itself, or the decomposition product TeF_4, reacts preferentially with Me_3SiCl leading to the observed products. Tellurium hexafluoride did not react with Me_3SiCl under similar conditions. This implies that reactions of $TeClF_5$ of this sort involve the positive chlorine of $TeClF_5$. An analogous reaction of $SClF_5$ led to SCl_2, Cl_2, and $(CH_3)_3SiF$ (38).

Acknowledgments

We wish to thank Dr. T. B. McMahon for the mass spectrum of $CH_3OTeClF_4$, E. K. Richardson and Dr. R. Kaiser for the ^{19}F nmr spectra, and the Natural Sciences and Engineering Research Council of Canada for financial support and for a scholarship (L.J.L.).

1. G. W. FRASER, R. D. PEACOCK, and P. M. WATKINS. Chem. Commun. 1257 (1968).
2. C. LAU and J. PASSMORE. Inorg. Chem. **13**, 2278 (1974).
3. M. P. MURCHIE and J. PASSMORE. Inorg. Synth. In press.
4. F. A. COTTON and G. WILKINSON. Advanced inorganic chemistry. 4th ed. Wiley, New York. 1980. p. 521.
5. M. SCHMIDT, W. SIEBERT, and K. W. BAGNELL. *In* Comprehensive inorganic chemistry. Vol. 2. Pergamon Press, New York. 1973. pp. 795, 935; H. L. ROBERTS. Q. Rev. **15**, 30 (1961) and references therein.
6. B. COHEN and A. G. MACDIARMID. J. Chem. Soc. A, 1780 (1966).
7. R. D. DRESDNER and T. R. HOOPER. *In* Fluorine chemistry reviews. Vol. 4. Marcel Dekker, New York. 1969. p. 1.
8. F. SEEL. *In* Sulfur in organic and inorganic chemistry. Vol. 2. Marcel Dekker, New York. 1972. p. 201.
9. T. KITAZUME and J. M. SHREEVE. J. Am. Chem. Soc. **99**, 3690 (1977).
10. G. KLEEMAN and K. SEPPELT. Angew. Chem. Int. Ed. **17**, 516 (1978).
11. U. ELGAD and H. SELIG. Inorg. Chem. **14**, 140 (1975).
12. K. SEPPELT. Inorg. Chem. **12**, 2837 (1973); G. W. FRASER, R. D. PEACOCK, and P. M. WATKINS. J. Chem. Soc. A, 1125 (1971).
13. W. TÖTSCH and F. SLADKY. J. Chem. Soc. Chem. Commun. 927 (1980).
14. G. W. FRASER and J. B. MILLAR. J. Chem. Soc. Dalton Trans. 2029 (1974).
15. E. L. MEUTTERTIES and W. D. PHILLIPS. J. Am. Chem. Soc. **79**, 2975 (1957).
16. H. SELIG, S. SARIG, and S. ABRAMOWITZ. Inorg. Chem. **13**, 1508 (1974).
17. L. LAWLOR. Ph.D. Thesis. University of New Brunswick, Fredericton. 1980.
18. J. S. THRASHER and K. SEPPELT. Abstract I-31, 8th European Symposium on Fluorine Chemistry, August 21–26, 1983, Jerusalem, Israel.
19. J. S. THRASHER and K. SEPPELT. Angew. Chem. In press.
20. C. LAU and J. PASSMORE. J. Fluorine Chem. **7**, 261 (1976).
21. L. LAWLOR and J. PASSMORE. Inorg. Chem. **18**, 2921 (1979).
22. N. N. GREENWOOD, A. C. SARMA, and B. P. STRAUGHAN. J. Chem. Soc. A, 1446 (1966).
23. D. LENTZ, H. PRITZKOW, and K. SEPPELT. Inorg. Chem. **17**, 1926 (1978).
24. K. SEPPELT. Inorg. Synth. **20**, 33 (1980).
25. J. C. JUMAS, M. MAURIN, and E. PHILIPPOT. J. Fluorine Chem. **10**, 219 (1977).
26. K. O. CHRISTE, W. SAWODNY, and J. P. GUERTIN. Inorg. Chem. **6**, 1159 (1967).
27. P. A. W. DEAN and D. F. EVANS. J. Chem. Soc. A, 1154 (1968).
28. C. W. HAIGH. Dept. of Chem., University College, Swansea, Great Britain.
29. C. D. DESJARDINS, C. LAU, and J. PASSMORE. Inorg. Nucl. Chem. Lett. **10**, 151 (1974).
30. C. LAU. Ph.D. Thesis, University of New Brunswick. 1975.
31. C. LAU, J. PASSMORE, E. K. RICHARDSON, T. K. WHIDDEN, and P. S. WHITE. To be published.
32. J. ALDOUS and I. M. MILLS. Spectrochim. Acta, **18**, 1073 (1962).
33. R. G. LEE, R. H. HUNT, and E. K. PLYLER. J. Mol. Spectrosc. **57**, 138 (1975).
34. S. D. ROSS. Inorganic infrared and Raman spectra. McGraw Hill, London. 1972.
35. W. V. F. BROOKS, M. ESHAQUE, C. LAU, and J. PASSMORE. Can. J. Chem., **54**, 817 (1976).
36. E. MAYER and F. SLADKY. Inorg. Chem. **14**, 589 (1975).
37. W. TÖTSCH, P. PERINGER, and F. SLADKY. J. Chem. Soc. Chem. Commun. 841 (1981).
38. R. C. KUMAR and J. M. SHREEVE. Z. Naturforsch, **36B**, 1407 (1981).

Can. J. Chem. Downloaded from www.nrcresearchpress.com by 210.87.254.42 on 09/06/12
For personal use only.

Oxidation of 1-butene by nitrous oxide over manganese(III) and related transition metal oxides

ROBERT A. ROSS[1] AND CRAIG FAIRBRIDGE[2]

Department of Chemistry, Lakehead University, Thunder Bay, Ont., Canada P7B 5E1

Received October 13, 1983

ROBERT A. ROSS and CRAIG FAIRBRIDGE. Can. J. Chem. **62**, 1483 (1984).

The oxidation of 1-butene by nitrous oxide over manganese(III) oxide was studied in a continuous flow system from 573 to 673 K. Kinetic parameters were derived from the exponential relationship: $r = ka\,P_{N_2O}^{0.5}P_{C_4H_8}^{0.4}$ over reactant partial pressure ranges, $0.30 < P_{N_2O} < 2.60$ kPa and $0.43 < P_{C_4H_8} < 8.27$ kPa. The reaction mechanism proposed involves a complex sequence of steps which include surface radical reactions. On the basis of a comparison of specific reaction rates, the catalytic activity series for the reaction over a number of transition metal oxides was: $CuO > Fe_2O_3 > NiO > Mn_2O_3 > Cr_2O_3 > TiO_2 > Sc_2O_3 > SnO > ZnO > V_2O_5 > Al_2O_3$.

ROBERT A. ROSS et CRAIG FAIRBRIDGE. Can. J. Chem. **62**, 1483 (1984).

On a étudié l'oxydation du butène-1 par l'oxyde de manganèse(III) dans un système à écoulement continu entre 573 et 673 K. On a déduit les paramètres cinétiques à partir de la relation exponentielle: $r = ka\,P_{N_2O}^{0.5}P_{C_4H_8}^{0.4}$ à des pressions partielles des réactifs allant de $0{,}30 < P_{N_2O} < 2{,}60$ kPa et de $0{,}43 < P_{C_4H_8} < 8{,}27$ kPa. Le mécanisme réactionnel proposé fait intervenir une suite complexe d'étapes qui comprend des réactions radicalaires de surface. En se basant sur une comparaison de vitesses spécifiques de réactions, on a pu établir la série suivante pour les activités catalytiques d'un grand nombre d'oxydes de métaux de transition vis-à-vis de la réaction: $CuO > Fe_2O_3 > NiO > Mn_2O_3 > Cr_2O_3 > TiO_2 > Sc_2O_3 > SnO > ZnO > V_2O_5 > Al_2O_3$.

[Traduit par le journal]

Can. J. Chem. Downloaded from www.nrcresearchpress.com by 210.87.254.5 on 09/06/12
For personal use only.

Introduction

The catalytic performance of manganese oxides in several redox reactions involving hydrocarbons with oxygen or nitrogen oxides has been reported recently. The work has included the oxidation of ethane by nitric oxide over unsupported manganese(III) oxide (1) and the oxidation of 1-butene and ethane by oxygen over manganese(III) oxide supported on carbon fibres (2). The results of these experiments pointed to complex surface mechanisms with rate-controlling steps most probably associated with the interactions of species within the adsorbed layer.

In the present investigation an attempt has been made to evaluate the kinetics of the catalysis of 1-butene by nitrous oxide over manganese(III) oxide. Measurements of reaction rates were supplemented by structural analysis. A general comparison of the catalytic activities in the reaction of metal oxides of the first transition series has also been carried out.

Experimental

A Hewlett-Packard Research Chromatograph Model 5754 B was used for in-line product analysis from the glass flow system and quartz reactor (3) with high-purity helium as a carrier gas and columns packed with Poropak Q, 120–300 mesh. A Beckman NO/NO_x analyzer, Model 951, was placed in series with the gas chromatograph.

Experimental reaction rates were recorded at steady catalyst activity and at less than 15% hydrocarbon conversions. Effects of space velocity, catalyst mass, and particle size were evaluated in the usual way (4) to determine conditions which minimized heat and mass transfer effects. As a result, kinetic measurements were conducted on manganese(III) oxide with a total gas flow rate of 350 mL min^{-1} (NTP) on 1 g catalyst samples having <37 μm maximum diameter and surface area 15.5 $m^2\,g^{-1}$.

Catalysts were examined by low-temperature gas adsorption (krypton, BET, 77 K, $\sigma = 19.5$ Å^2), X-ray and chemical analysis. Infrared spectra were recorded on a Beckman IR-12 spectrophotometer using 0.5 wt% KBr pellets. The catalyst surfaces were examined by scanning electron microscopy, Cambridge Stereoscan 600, and X-ray photoelectron spectroscopy, Vacuum Generator ESCA-3.

α-Manganese(III) oxide was prepared and analyzed as previously described (1, 5). Scandium(III) oxide (99.9% pure), zinc(II) oxide (99.99%), chromium(III) oxide (99%), iron(III) oxide (99.99%), vanadium (V) oxide (99.9%), and tin(II) oxide (99.99%) were obtained from Alfa Inorganics Limited. Copper(II) oxide (99%) and nickel(II) oxide (99.99%) were obtained from BDH Chemicals Limited. Aluminum(III) oxide (99.9%) and titanium(IV) oxide (99%) were purchased from Baker Chemical Company. All oxides were heated in air at 773 K for 10 h and stored in desiccators prior to activation in the experiments.

Carbon dioxide, 99.5%, nitrogen, 99.99%, and helium, 99.99%, were obtained from Canadian Liquid Air Limited, and nitrous oxide, 99.9%, from Liquid Carbonic Limited.

Results

Reaction rate measurements on manganese(III) oxide

The rate of the catalytic reaction, measured as the rate of nitrogen or carbon dioxide production, decreased slightly for the first hour of reaction at 673 K and remained constant thereafter for a minimum of 24 h. The conversion of 1-butene at this temperature amounted to 15% with only nitrogen, carbon dioxide, and water as the products of reaction.

Rate-order measurements based on the rates of nitrogen, r_1, and carbon dioxide, r_2, production were determined when the systems had achieved a steady state after pretreatment with 2.66 kPa nitrous oxide and 2.66 kPa 1-butene for 3 h at 623 K.

With the partial pressure of the hydrocarbon maintained at 3.05 kPa, the effects of from 0.30 to 4.93 kPa nitrous oxide on the experimental rates were observed, Fig. 1. The rate order with respect to nitrous oxide was 0.5 for partial pressures <2.60 kPa. At higher pressures, the rate of reaction increased with increasing nitrous oxide partial pressure.

The partial pressure of 1-butene was altered from 0.43 to 8.27 kPa while nitrous oxide partial pressure was held constant at 2.49 kPa. The rate order was 0.4 with respect to 1-butene, Fig. 1. The partial pressures of nitrous oxide and 1-butene were

[1] Present address: Alcan International Limited, Kingston Laboratories, P.O. Box 8400, Kingston, Ont., Canada K7L 4Z4.

[2] Present address: Department of Energy, Mines and Resources, 555 Booth Street, Ottawa, Ont., Canada K7L 0G1.

Can. J. Chem. Downloaded from www.nrcresearchpress.com by 210.87.254.5 on 09/06/12
For personal use only.

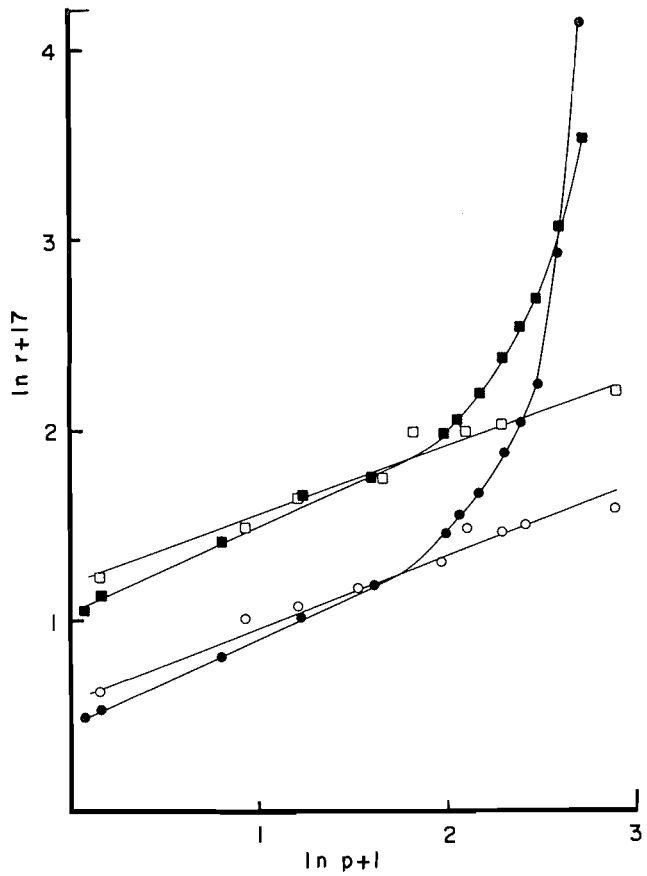

FIG. 1. Effects of component partial pressures on the N_2O/C_4H_8 reaction over Mn_2O_3; $P_{C_4H_8}$, □, r_1, ○, r_2; P_{N_2O}, ■, r_1, ●, r_2.

TABLE 1. Reaction rate constants for the oxidation of 1-butene by nitrous oxide over manganese(III) oxide

Temperature (K)	$k_1 \times 10^{-5}$ (nitrogen)	$k_2 \times 10^{-5}$ (carbon dioxide)
673	46.7	35.5
663	35.4	24.6
653	28.8	18.1
643	21.4	12.6
633	14.2	8.46
623	8.90	5.70
613	6.76	3.92
603	4.60	2.60
593	3.08	1.71
583	1.97	1.11
573	1.30	0.711

maintained at 2.48 and 2.58 kPa, respectively, and that of carbon dioxide was adjusted from 0.62 to 8.33 kPa. This had no effect on the rate r_1, and the reaction was zero order with respect to CO_2. Variations in the partial pressure of water vapour from 0.09 to 2.10 kPa with nitrous oxide (2.48 kPa) and 1-butene (2.58 kPa) partial pressure held constant had no effect on the rate.

Based on these results, the rate of reaction was expressed by:

$$[1] \quad r_1 = k_1 P_{N_2O}^{0.5} P_{C_4H_8}^{0.4}$$

and

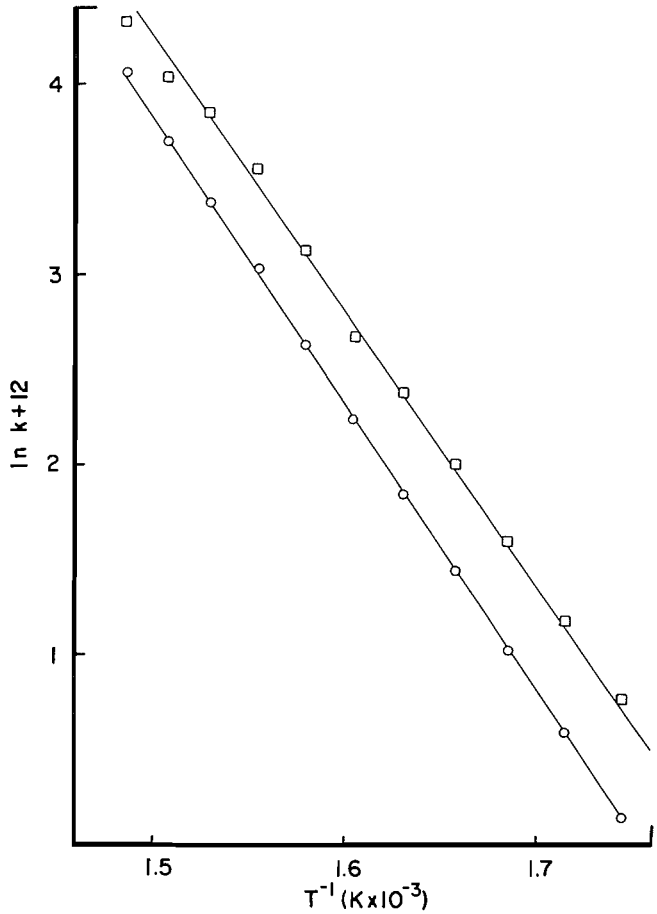

FIG. 2. Arrhenius plots for the N_2O/C_4H_8 reaction over Mn_2O_3; □, k_1, ○, k_2.

$$[2] \quad r_2 = k_2 P_{N_2O}^{0.5} P_{C_4H_8}^{0.4}$$

where $0.30 < P_{N_2O} < 2.60$ kPa.

The effects of temperature on catalyst activity were determined after the oxide had been conditioned in 2.23 kPa nitrous oxide and 2.78 kPa 1-butene at 673 K for 3 h. Reaction rate constants were calculated at 10 K intervals from 673 to 573 K, Table 1, using the integrated form of eqs. [1] and [2]. When plotted in the Arrhenius fashion, these data gave apparent activation energies of 117 ± 4 and 126 ± 4 kJ mol^{-1} and pre-exponential factors 6.09×10^5 and 1.94 $mol^{0.1}$ $L^{-0.1}$ m^{-2} s^{-1} for the nitrogen and carbon dioxide rates, respectively, Fig. 2.

Effects of reaction conditions on catalyst properties

The catalyst surface area was 15.5 m^2 g^{-1} after reaction in all cases. Chemical analysis gave 69.0 wt% manganese (theory 69.59%) and X-ray diffraction showed only *d*-spacings corresponding to γ-Mn_2O_3 — 2.48, 2.74, 3.08, 1.54, 1.56, 1.81, and 2.06 Å.

The infrared spectrum of the catalysts after reaction resembled those observed previously for catalysts in the N_2O/C_2H_6 and O_2/C_2H_6 reactions (6) with bands at 615, 490, 425, and 350 cm^{-1}. Under the scanning electron microscope the used catalyst particles showed somewhat round edges with a high degree of surface roughness similar to the reported condition of manganese(III) oxide prior to catalysis (7).

X-ray photoelectron spectra were corrected for charging by reference to the C(1*s*) line at 285.0 eV. The Mn, $2p_{3/2}$, spec-

TABLE 2. Catalyst activity measurements for the N_2O/C_4H_8 reaction at 673 K

Catalyst	Surface area ($m^2\ g^{-1}$)	Experimental rates (mol $m^{-2}\ s^{-1}$) r_1	r_2
CuO	4.1	6.82×10^{-6}	3.28×10^{-6}
Fe_2O_3	6.0	1.58×10^{-6}	9.10×10^{-7}
NiO	2.5	6.72×10^{-7}	3.19×10^{-7}
Mn_2O_3	15.5	2.20×10^{-7}	9.74×10^{-8}
Cr_2O_3	3.1	4.85×10^{-8}	—
TiO_2	9.0	2.48×10^{-8}	—
Sc_2O_3	2.3	1.41×10^{-8}	—
SnO	9.0	1.36×10^{-8}	—
ZnO	11.7	1.04×10^{-8}	—
V_2O_5	6.1	8.77×10^{-9}	—
Al_2O_3	2.8	7.68×10^{-9}	—

trum gave a binding energy of 642.0 eV in all used samples, while for unreacted manganese(III) oxide the value was 640.7 eV. The O(1*s*), binding energy was 528.7 eV before reaction; after reaction two binding energy values of 530.0 and 533.0 eV were observed. No N(1*s*) spectra were observed.

Related oxides

A number of metal oxides — Sc_2O_3, TiO_2, V_2O_5, Cr_2O_3, Mn_2O_3, Fe_2O_3, Al_2O_3, NiO, CuO, ZnO, and SnO — were evaluated as possible catalysts for the nitrous oxide/1-butene reaction. The catalytic reaction generally produced nitrogen, carbon dioxide, and water in measureable quantities at temperatures >623 K.

The catalytic activity of each oxide was assessed by determining the rates of nitrogen and carbon dioxide formation at 673 K. As in previous studies, 1 g catalyst samples were used and the total gas flow rate was 350 mL min^{-1}. The catalysts were pretreated with nitrous oxide and 1-butene, both at 2.66 kPa partial pressure for 12 h at 673 K. Each reactant was passed separately over the catalyst to ensure that no reaction occurred until both were present.

Surface areas were determined after reaction and are presented in Table 2 along with the experimental rate data.

Discussion

Various relationships based on Langmuir–Hinshelwood kinetics (8, 9) were tested for the N_2O/C_4H_8 reaction over manganese(III) oxide on the basis of statistical criteria (10, 11). The equation which gave the best correlation for all of the rate order data was adopted. It is not possible to uniquely determine the mechanism of a reaction from such an equation but a mechanism which has a theoretical basis and is consistent with the form of the expression can be postulated.

The relationship was:

$$[2]\quad r = \frac{kaP_{N_2O}^{0.5}bP_{C_4H_8}^{0.5}}{(1 + aP_{N_2O}^{0.5} + bP_{C_4H_8}^{0.5})^2} \times (P_{N_2O}P_{C_4H_8})$$

As shown in Fig. 3, plots of $P^{0.5}$ versus $(P^{1.5}/r)^{0.5}$ were linear. The form of the equation suggests that an irreversible bimolecular reaction occurs between adsorbed reactants where each species is adsorbed on two surface sites (12). Further steps will involve the interaction of nitrous oxide and 1-butene, as indicated by the $(P_{N_2O}P_{C_4H_8})$ term, suggesting a complex overall surface process.

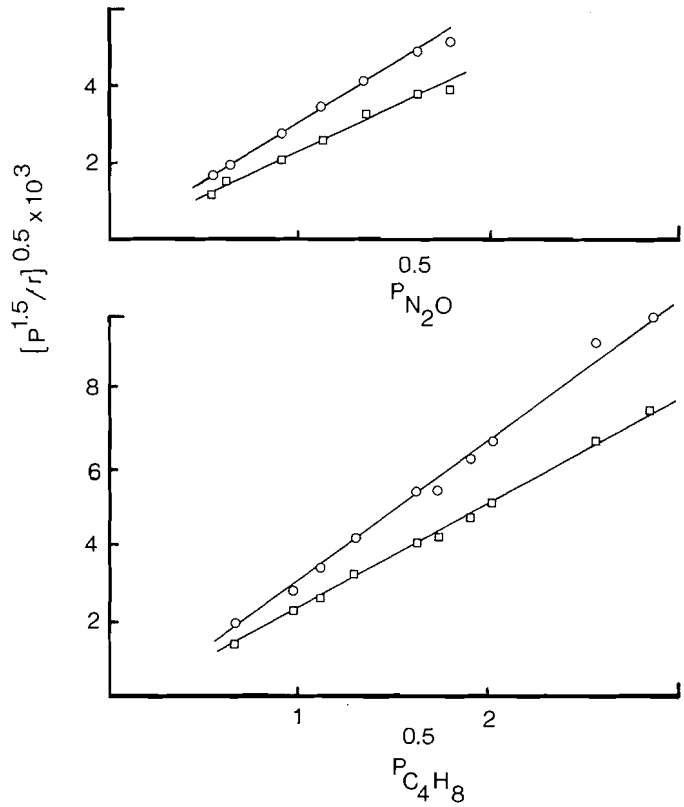

FIG. 3. Reduced plots of the Langmuir–Hinshelwood expression (2) for the N_2O/C_4H_8 reaction at 628 K over Mn_2O_3; □, r_1, ○, r_2.

$$[3]\quad C_4H_8(g) \leftrightarrow C_4H_{8(ads)}$$

$$[4]\quad N_2O + [O] + C_4H_{8(ads)} \rightarrow C_4H_{7(ads)} + [OOH] + N_2$$

$$[5]\quad C_4H_8 + S + [OOH] \rightarrow C_4H_{7(ads)} + [O] + H_2O$$

S is a surface site and [O] and [OOH] are, respectively, surface oxygen and hydroperoxide species. Further reactions are represented by:

$$[6]\quad 2C_4H_{7(ads)} + 23N_2O \rightarrow 8CO_2 + 7H_2O + 23N_2$$

The apparent activation energy was very close to that found for the nitrous oxide/ethane reaction on a similar catalyst (6).

The deviation from 0.5 order in nitrous oxide at partial pressures above 2.60 kPa indicates that the rate of reaction increases with P_{N_2O}. In these conditions, the conversion of N_2O becomes greater than 15% and heat and mass transfer effects become important. A pseudo steady state condition may be achieved with respect to 1-butene adsorption. The rate limiting step becomes eq. [6] with adsorption and reaction of N_2O subject to transport limitations.

The initial step in the oxidation of 1-butene over bismuth molybdate was also believed to involve C—H bond rupture as in eq. [4] (13, 14) while the decomposition of nitrous oxide over similar manganese oxide catalysts gave activation energies of 118 (15) and 146 (10) kJ mol^{-1}. The formation of peroxides from nitrous oxide as proposed in eq. [4] has been noted (15). Equation [6] summarizes a complex series of steps which may include surface radical reactions (17).

X-ray photoelectron spectroscopy indicated that two surface oxygen species were present from the evidence of two O(1*s*) binding energy values. The lower value was close to that expected for chemisorbed oxygen in metal oxides and the higher value was characteristic of that associated with the presence of

Can. J. Chem. Downloaded from www.nrcresearchpress.com by 210.87.254.5 on 09/06/12
For personal use only.

molecular oxygen species (18). In the complete oxidation of hydrocarbons, oxygen is activated and adsorbed on the catalyst surface as O^- and O_2^- species (18, 19) which lead to the formation of epoxy or peroxy intermediates.

A catalytic activity series for this redox reaction over the transition metal oxides may be proposed on the basis of a comparison of reaction rates, thus giving an overall sequence of reactivity in decreasing order:

$$CuO > Fe_2O_3 > NiO > Mn_2O_3 > Cr_2O_3 > TiO_2 > Sc_2O_3 > SnO > ZnO > V_2O_5 > Al_2O_3$$

Close examination of Table 2 reveals that the difference in r_1 between titanium (IV) oxide and aluminum(III) oxide is of the same order of magnitude as that between each of the first five oxides in the series. Together with the low value of r_1 and the fact that r_2 could not be measured for these oxides, this suggests that the position of the last six members of the series are not as unequivocally determined as the first five.

The series is similar to those generally observed for catalytic oxidation reactions (20, 21), with the exception of the position of iron(III) oxide. It resembles those found for the nitric oxide/carbon dioxide reaction (22), the nitrous oxide/carbon dioxide reaction (23), and the decomposition of nitric (24) and nitrous (25) oxides.

Possible relationships between the rate of the reaction at 673 K and various properties of the oxides were examined.

Heats of oxygen desorption, q, have been related to catalytic activity for a number of reactions over transition metal oxides and reasonable correlations have been found between q and the activation energy of oxygen isotopic exchange (26) and the metal/oxygen bond energy in oxidation reactions (20, 21). The following expected activity series on these bases would be:

$$Co_3O_4 > CuO > NiO > MnO_2 > Cr_2O_3 > Fe_2O_3 > V_2O_5 > ZnO > TiO_2$$

Oxygen desorption was thought to occur in the rate-limiting step of the decomposition of nitric (27) and nitrous oxides (25). The heat of desorption was influenced by the oxide stoichiometry (26) where q usually increased with the removal of surface oxygen, except for chromium(III) and iron(III) oxides.

However, it has been shown that surface oxygen does not occupy a continuous distribution of states on the oxide, but rather that mobile oxygen may be present on discrete surface states (28). Quantitative correlations between catalytic activity and oxygen mobility imply a knowledge of the oxygen states involved, and these may change with surface location, temperature, time, and reagent concentrations. A shift to higher states might therefore cause large distortions of the general activity series.

No clear correlation was discernible between the catalytic reaction rate and the metal/oxygen bond length or the charge/radius ratio with respect to the cation (29).

Plots of ln A against the apparent activation energy for the present and previous data (1, 2, 6) showed a linear trend in which a change in value of one of the Arrhenius parameters for the reaction was offset by a corresponding change in the other. A number of theoretical models have been proposed to explain this compensation effect, and these have been summarized recently (30).

If the present data are converted to the units used by Galwey (30), then

$$[7] \quad \log A = B = eE$$

and e becomes 0.1042. A value very close to that found in the oxidation reactions of propene and acetylene over various oxides (30). This observation suggests that the general form of the rate-limiting step is similar in these related reactions.

1. R. A. Ross and C. Fairbridge. Can. J. Chem. **59**, 2232 (1981).
2. C. Fairbridge, J. R. MacCallum, and R. A. Ross. Can. J. Chem. **60**, 2749 (1982).
3. D. V. Fikis, W. J. Murphy, and R. A. Ross. Can. J. Chem. **56**, 2530 (1978).
4. C. N. Satterfield. Mass transfer in heterogeneous catalysis. MIT Press. 1970.
5. E. F. McCaffrey, D. G. Klissurski, and R. A. Ross. J. Catal. **26**, 380 (1972).
6. C. Fairbridge and R. A. Ross. Can. J. Chem. **60**, 893 (1982).
7. C. Fairbridge. Ph.D. Thesis, The University of St. Andrews, St. Andrews, Fife, Scotland. 1981.
8. K. H. Yang and O. A. Hougen. Chem. Eng. Prog. **46**, 146 (1950).
9. O. A. Hougen and K. M. Watson. Chemical process principles. Part III. Wiley, New York. 1966.
10. S. W. Weller. Chemical reaction engineering reviews. *Edited by* H. M. Hulbert. Am. Chem. Soc., Washington, DC. 1975.
11. R. W. Maatman. Adv. Catal. **29**, 97 (1980).
12. P. H. Emmett. (*Editor*). Catalysis. Vol. V, Reinhold, New York. 1954.
13. Ph. A. Batist, B. C. Lippens, and G. C. A. Schuit. J. Catal. **5**, 55 (1966).
14. Ph. A. Batist, C. J. Kaptijns, B. C. Lippens, and G. C. A. Schuit. J. Catal. **7**, 33 (1967).
15. A. Cimino and V. Indovina. J. Catal. **17**, 54 (1970).
16. L. Rheaume and G. Parravano. J. Phys. Chem. **63**, 264 (1959).
17. M. W. Roberts. Adv. Catal. **29**, 55 (1980).
18. J. Haber. Pure Appl. Chem. **50**, 923 (1978).
19. J. Haber and M. Witko. Acc. Chem. Res. **14**, 1 (1981).
20. G. K. Boreskov. Kinet. Katal. **14**, 2 (1973).
21. G. K. Boreskov. Dokl. Akad. Nauk SSR, **213**, 926 (1973).
22. T. G. Alkhazov, G. Z. Gasan-Zade, and M. Yu. Sultanov. Kinet. Katal. **17**, 699 (1976).
23. B. W. Krupay and R. A. Ross. Can. J. Chem. **57**, 713 (1979).
24. J. Amirnazmi, J. E. Benson, and M. Boudart. J. Catal. **30**, 55 (1973).
25. E. R. S. Winter. J. Catal. **19**, 32 (1970).
26. A. K. Boreskov, V. V. Popovskii, and V. A. Sazanov. Kinet. Katal. **9**, 307 (1968).
27. E. R. S. Winter. J. Catal. **22**, 158 (1971).
28. B. Halpern and J. E. Germain. J. Catal. **37**, 49 (1975).
29. E. F. McCaffrey, D. G. Klissurski, and R. A. Ross. Paper No. 3, Proc. Fifth Intern. Cong. Catal. *Edited by* J. W. Hightower. North Holland, Amsterdam. 1973.
30. A. K. Galwey. Adv. Catal. **26**, 247 (1977).

Can. J. Chem. Downloaded from www.nrcresearchpress.com by 210.87.254.5 on 09/06/12
For personal use only.

Quenching of the singlet and triplet state of benzene in condensed phase

H. A. KHWAJA, G. P. SEMELUK, AND I. UNGER

Department of Chemistry, University of New Brunswick, Fredericton, N.B., Canada E3B 6E2

Received October 5, 1983

H. A. KHWAJA, G. P. SEMELUK, and I. UNGER. Can. J. Chem. **62**, 1487 (1984).

Quenching of the fluorescence of benzene by halocarbons in methanol, ethanol, acetonitrile, and cyclohexane has been investigated. It proceeds via a reversible exciplex intermediate formed between excited singlet benzene and ground state halocarbon. Quenching is controlled by the polarity of the medium. Excited singlet benzene interacts with acetonitrile solvent and a longer wavelength emission due to this complex is observed.

The effect of CCl_4, CH_3CN, $CHCl_3$, and CH_3CCl_3 on the triplet and singlet excited states of benzene in a methylcyclohexane–isopentane mixture at 77 K has been examined. Carbon tetrachloride and acetonitrile are far more effective quenchers than either $CHCl_3$ or CH_3CCl_3. In the case of the latter pair enhanced intersystem crossover competes with complex formation.

H. A. KHWAJA, G. P. SEMELUK et I. UNGER. Can. J. Chem. **62**, 1487 (1984).

On a étudié le piégeage de la fluorescence du benzène par les halocarbones dans le méthanol, l'éthanol, l'acétronitrile et le cyclohexane. Il se produit via un exciplex intermédiaire réversible qui se forme entre le benzène singulet excité et l'état fondamental de l'halocarbone. Le piégeage est controlé par la polarité du milieu. Le benzène à l'état singulet excité interagit avec l'acétonitrile et on observe que la longueur d'onde de l'émission est plus élevée à cause de ce complexe.

On a étudié l'effet du CCl_4, du CH_3CN, du $CHCl_3$ et du CH_3CCl_3 sur les états triplet et singulet excités du benzène dans un mélange de méthylcyclohexane/isopentane à 77 K. Le tétrachlorure de carbone et l'acétonitrile sont des pièges beaucoup plus efficaces que le $CHCl_3$ ou le CH_3CCl_3. Dans le cas de cette dernière paire, une augmentation dans les échanges entre systèmes est en compétition avec la formation de complexe.

[Traduit par le journal]

Introduction

Exciplex formation between excited singlet or triplet state species and ground state partners of a different chemical nature has been demonstrated to be a key pathway in fluorescence and phosphorescence quenching (1–3). Some exciplexes exhibit fluorescence which is characterized by a red-shift with respect to the uncomplexed excited monomeric state, a lack of vibronic structure, and different decay characteristics. Nonemissive exciplexes have also been shown to exist (2–6). In such cases, indirect evidence is obtained for the intermediacy of exciplexes. Typical examples are the quenching of aromatic hydrocarbons and carbonyl excited states by aromatic compounds (7), olefins (8), and amines (9). In most of these systems the interposition of exciplexes is supported by a dependence of the quenching rate constant on both the ionization potential of the donor and the electron affinity or the reduction potential of the acceptor.

Since exciplexes possess total or partial charge-transfer nature, the rate of these processes should increase when the dielectric constant and the polarizability of the solvent increase (10–12), and this dependence should reflect the degree of charge transfer. A number of experimental (13, 14) and theoretical studies (15, 16) have confirmed this view. The decrease in exciplex emission in polar solvents appears to be due to ionic dissociation of the exciplex to free solvated radical ions (17).

Halocarbons, and CCl_4 in particular, have been shown to be efficient fluorescence quenchers for a number of molecules (18–21). It has also been shown that polar solvents increase this quenching (22, 23). In a previous publication we reported on the fluorescence quenching of benzene vapour by a number of halocarbons (6). We report here on the effect of solvent polarity on this reaction in liquid phase and on the rates of quenching by CCl_4, CH_3CN, $CHCl_3$, and CH_3CCl_3 in solid phase.

Experimental

Materials

Benzene (spectrograde 99.9%) was obtained from Fischer Scientific Company and was used without any further purification. CCl_4 and CH_2Cl_2 were GC spectrophotometric quality obtained from the J. T. Baker Chemical Company. CH_3CCl_3 (analytical reagent grade 99.5) was obtained from BDH Chemicals Ltd. These halogenated methanes were further purified by gas–liquid chromatography using a Hewlett-Packard Model 7620 A chromatograph attached to a 579 A collecting unit, with He as the carrier gas; detection was by flame ionization. The chromatographic procedure gave a purity of >99.9% for each of the materials. $CFCl_3$ was commercially available from Matheson Company (>99%) and was used as received.

The sources of the solvents were as follows: hexane, Sigma Chemical Company; ethanol, Consolidated Alcohols Ltd.; methanol and acetonitrile, BDH Chemicals Ltd.; methyl cyclohexane and isopentane, Matheson, Coleman and Bell. The solvents were used as received. Blank runs were made with solvent alone which showed no fluorescence emission at the maximum sensitivity of the instrument, in the spectral region of interest.

Apparatus and procedures

Absorption spectra were obtained with a Perkin-Elmer 402 spectrophotometer. Fluorescence spectra were recorded with a modified Aminco-Bowman spectrophotofluorometer (SPF). Most details of the apparatus and data collection and processing have been given previously (6, 24).

All quenching experiments were carried out in deoxygenated solution at room temperature with λ_{ex} = 254 nm. Samples were degassed prior to use by the freeze–pump–thaw method with a minimum of three cycles at better than 5×10^{-6} Torr. Sample cells (1 cm × 1 cm) were made of quartz and had a side arm made of Pyrex tubing to facilitate the freeze–pump–thaw procedure.

Preparation of samples involved adding an aliquot of stock solution of benzene to each sample along with the required quantity of quencher and diluting to volume with solvent. The benzene concentration used was chosen such that it would be approximately 20% absorbing in a 1 cm cell at 254 nm; a 2×10^{-3} *M* solution was found to be satisfactory. The quencher concentrations were in the 2×10^{-3} *M* to 8×10^{-3} *M* range. At λ_{ex} 254 nm and the concentrations used in this study, CCl_4 has an extinction coefficient of $\simeq$0.14 L mol^{-1} cm^{-1}. Thus absorption due to C_6H_6 is $\simeq$200 times greater than that due to CCl_4 and k_q's should not be negligibly affected by absorption of the latter.

Fluorescence yields are based on that of C_6H_6 being 0.06, 0.04, and

Can. J. Chem. Downloaded from www.nrcresearchpress.com by 210.87.254.5 on 09/06/12
For personal use only.

0.029 in hexane, ethanol, and methanol, respectively, at λ_{ex} = 254 nm (25).

The solid phase studies were carried out in a 1:1 methylcyclohexane, isopentane mixture at 77 K. The cells were 2 mm cylindrical quartz tubes; these were placed in a quartz microdewar flask whose bottom was in the shape of a finger transparent to uv light. Dry warm N_2 was circulated around the Dewar to prevent condensation on the outside of the Dewar and to reduce ice formation within the liquid nitrogen in the Dewar. An Aminco-Kiers rotating shutter operating at a chopping rate of 50 Hz was used to isolate and record phosphorescence spectra. All solutions were outgassed several times and hermetically selaed *in vacuo* prior to usage. The benzene concentration was 2×10^{-3} *M* while quencher concentrations ranged from 0 to 0.5 *M*.

Results and discussion

Liquid phase

The effect of CCl_4, CH_3CCl_3, and CH_2Cl_2, and $CFCl_3$ on the fluorescence intensities of solutions of C_6H_6 in hexane was examined. In each case quenching obeys a Stern–Volmer relationship. Figure 1 shows plots of Φ_f^0/Φ_f versus the concentration of quencher, where Φ_f^0 and Φ_f refer to fluorescence yields of C_6H_6 in the absence and presence of quencher, respectively. The least-squares fit of the data to a straight line was obtained in all cases by excluding the Stern–Volmer intercept (0,1) from the calculation as a more stringent test of how closely the best fit line extrapolates to an intercept of 1. The effect of CCl_4 on the excited singlet state of C_6H_6 was also examined in CH_3CN, C_2H_5OH, and CH_3OH. The results in C_2H_5OH and CH_3OH are summarized in Fig. 2. Bimolecular quenching rate constants, k_q, were derived from the slope of Stern–Volmer plots and the singlet fluorescence lifetimes τ of C_6H_6. Values for τ were obtained from the literature, for conditions similar to those used in this study. The data are given in Table 1.

Halocarbons efficiently quench C_6H_6 fluorescence in hexane with k_q's ranging from 3.4×10^8 L mol^{-1} s^{-1} for the C_6H_6–$CFCl_3$ system to 6.7×10^9 L mol^{-1} s^{-1} for the C_6H_6–CCl_4 pair. Quenching is more efficient by about two orders of magnitude in aromatic–halocarbon systems than in aliphatic ketone – halocarbon systems (18).

In the absence of a distinct exciplex emission quenching cannot automatically be ascribed to the formation of a charge transfer complex. Other quenching mechanisms need to be ruled out and typical exciplex behaviour such as a linear dependence of ln k_q vs. EA (electron affinity of acceptor) or ID_D (ionization potential of donor) must be established (28). In the present instance, singlet–singlet energy transfer between C_6H_6 and halocarbons can be ruled out since the fluorescence spectrum of C_6H_6 does not overlap with the absorption spectrum of any of the halocarbons. Quenching due to the enhancement of nonradiative processes is unlikely. No evidence was observed for photochemical reaction subsequent to excitation nor was there any evidence for ground state complex formation, the absorption spectrum of C_6H_6 remaining unchanged on addition of each of the halocarbons.

There is a reasonably good linear correlation between ln k_q and EA (see Fig. 3). This, coupled with gas phase studies on the same systems (6) and improbability of other quenching paths, supports a charge-transfer complex as being responsible for the quenching of the C_6H_6 fluorescence. Finally, k_q is sensitive to solvent polarity which is typical of charge transfer exciplexes (29). A slope of 3.3 eV^{-1} is obtained from Fig. 3, a value similar to that obtained by us (6, 30) for the quenching of singlet aromatics by chloromethanes in the vapour phase. The magnitude of the gradient is much less than $1/RT \simeq 39$ eV^{-1}, the value expected for a full electron transfer from excited aromatic to quencher.

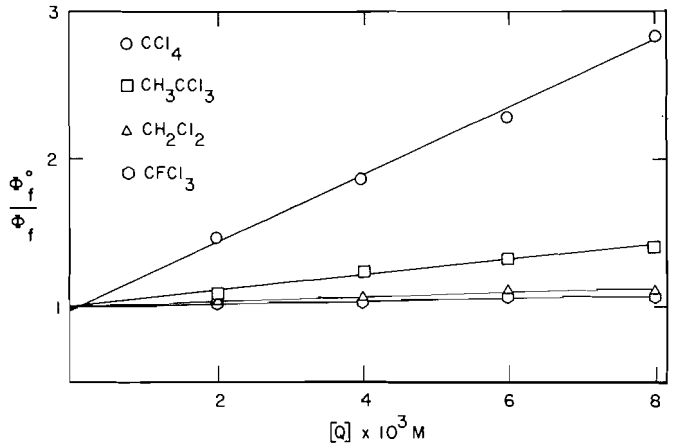

FIG. 1. Stern–Volmer plots for the quenching of benzene fluorescence by CCl_4, CH_3CCl_3, CH_2Cl_2, and $CFCl_3$ in hexane solution ($[C_6H_6] = 2 \times 10^{-3}$ *M*, λ_{ex} = 254 nm, *T* = 298 K).

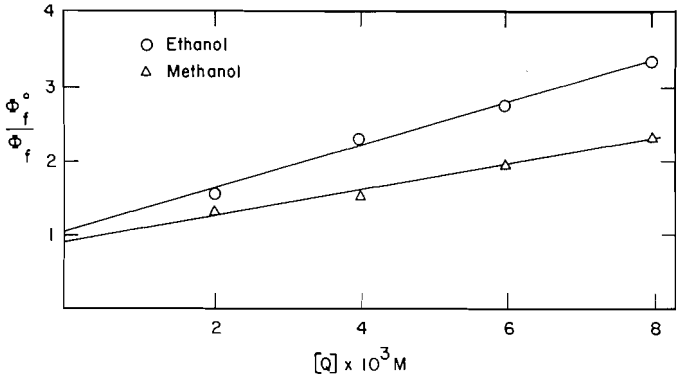

FIG. 2. Stern–Volmer plots for the quenching of benzene fluorescence by CCl_4 in ethanol and methanol solutions ($[C_6H_6] = 2 \times 10^{-3}$ *M*, λ_{ex} = 254 nm, *T* = 298 K).

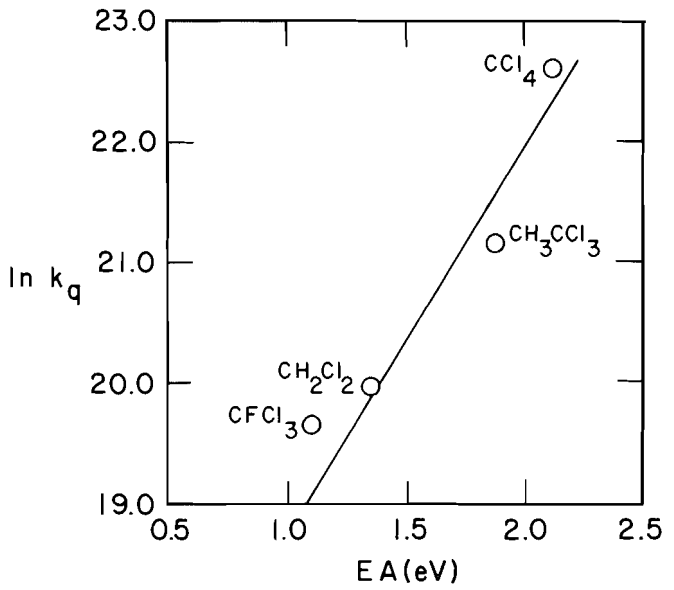

FIG. 3. Plot of ln k_q vs. EA for benzene singlet quenching by CCl_4, CH_3CCl_3, CH_2Cl_2, and $CFCl_3$ in hexane solution.

Can. J. Chem. Downloaded from www.nrcresearchpress.com by 210.87.254.5 on 09/06/12
For personal use only.

TABLE 1. Solution phase singlet state quenching of benzene by halocarbons (λ_{ex} = 254 nm, T = 298 K)

Quencher	Solvent	Dielectric constant	Viscosity[a] (cP)	Slope (L mol^{-1}) % st. dev.	τ (ns)	$k_q \times 10^{-9}$ (L mol^{-1} s^{-1})
CCl_4	Hexane	1.88	0.31	225.8 5.2	33.6[b]	6.72
CH_3CCl_3	Hexane	1.88	0.31	52.6 8.1	33.6[b]	1.57
CH_2Cl_2	Hexane	1.88	0.31	15.8 5.8	33.6[b]	0.47
$CFCl_3$	Hexane	1.88	0.31	11.5 4.9	33.6[b]	0.34
CCl_4	Ethanol	24.6	1.08	288.8 5.5	28[c]	10.31
CCl_4	Methanol	32.7	0.55	171.9 9.8	20[c]	8.60

[a]Reference 26.
[b]Reference 27.
[c]Reference 25.

Solvent viscosity has been postulated to have an effect on the rate of formation and dissociation of exciplexes (31). Though not extensive, our study indicates that solvent viscosity does not play an important role in exciplex formation in the C_6H_6–halocarbon systems. On the other hand, solvent polarity clearly does enhance quenching and a mechanism consistent with the results is given below as reactions [1] to [6]

[1] $D + h\nu \xrightarrow{I_a} {}^1D^*$

[2] ${}^1D^* \xrightarrow{k_1} D + h\nu_f$

[3] ${}^1D^* \xrightarrow{k_2} D$ or ${}^3D^*$

[4] ${}^1D^* + Q \underset{k_4}{\overset{k_3}{\rightleftharpoons}} {}^1(D\cdots Q)^*$

[5] ${}^1(D\cdots Q)^* \xrightarrow{k_5} D + Q$

[6] ${}^1(D\cdots Q)^* \xrightarrow{k_6} D^{\cdot+} + Q^{\cdot-}$

where D and Q are the ground state benzene and halocarbon molecules, respectively, an asterisk indicates the electronically excited state, and the prefixed superscript is the multiplicity of the electronic state.

Employing the usual steady-state treatment we obtain eq. [7].

[7] $\Phi_f^0/\Phi_f = 1 + K_{sv}[Q]$

The Stern–Volmer constant K_{sv} is given by eq. [8].

[8] $K_{sv} = k_q\tau$

The lifetime of the excited singlet benzene, τ, is $(k_1 + k_2)^{-1}$ and the measured quenching rate constant, k_q, is given by eq. [9].

[9] $k_q = \left[\dfrac{k_3(k_5 + k_6)}{k_4 + k_5 + k_6}\right]$

In nonpolar solvents k_6 is zero; in polar solvents it has a non-zero value which increases with increasing dielectric constant of the solvent. As k_6 increases, the numerator in eq. [9] increases more rapidly than the denominator; thus k_q would be expected to increase with increasing solvent polarity which is consistent with experimental observation.

Studies in CH_3CN solvent showed that a complex is formed between it and excited singlet C_6H_6. In addition to the normal fluorescence band of C_6H_6 centered around 276 nm, two new structureless bands were observed with maxima at ~355 and 405 nm. These data do not warrant any further conclusions at this time.

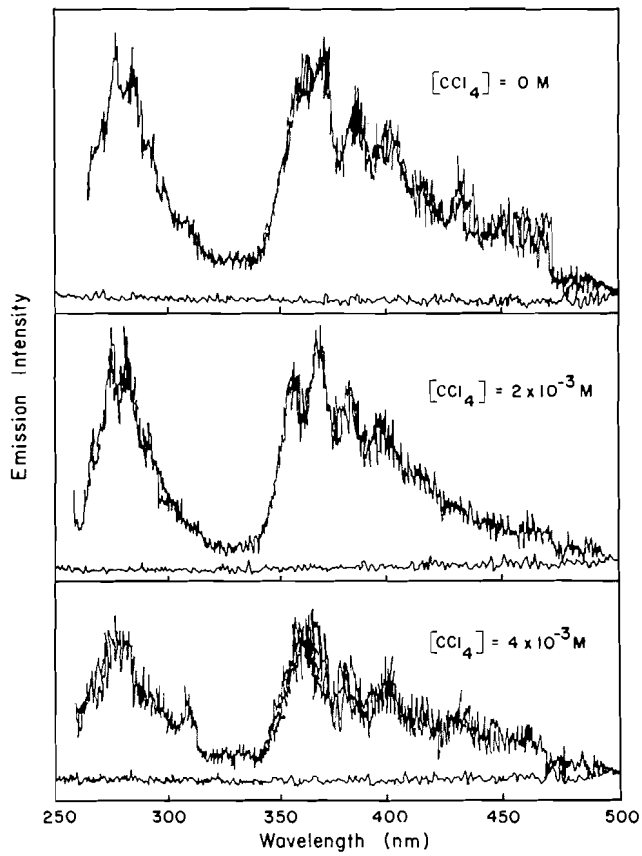

FIG. 4. Fluorescence and phosphorescence emission spectra of benzene perturbed by CCl_4 in MCH/ISPT at 77 K ($[C_6H_6] = 2 \times 10^{-3}$ M, λ_{ex} = 254 nm).

Solid phase

Quenching of C_6H_6 fluorescence and phosphorescence in solid phase by CCl_4, CH_3CN, $CHCl_3$, and CH_3CCl_3 is depicted in Figs. 4 to 7. Our experimental setup for solid phase studies

Can. J. Chem. Downloaded from www.nrcresearchpress.com by 210.87.254.5 on 09/06/12
For personal use only.

Can. J. Chem. Downloaded from www.nrcresearchpress.com by 210.87.254.5 on 09/06/12
For personal use only.

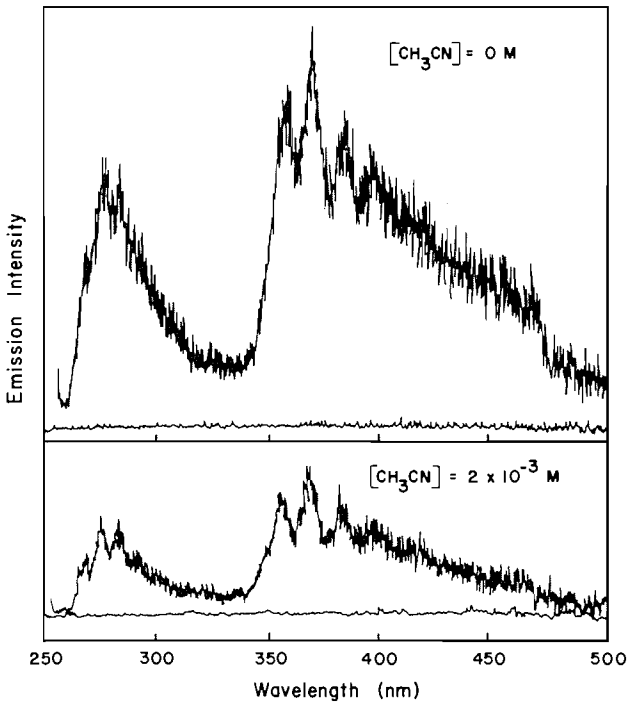

FIG. 5. Fluorescence and phosphorescence emission spectra of benzene perturbed by CH_3CN in 3 MP at 77 K ($[C_6H_6] = 2 \times 10^{-3}$ M, $\lambda_{ex} = 254$ nm).

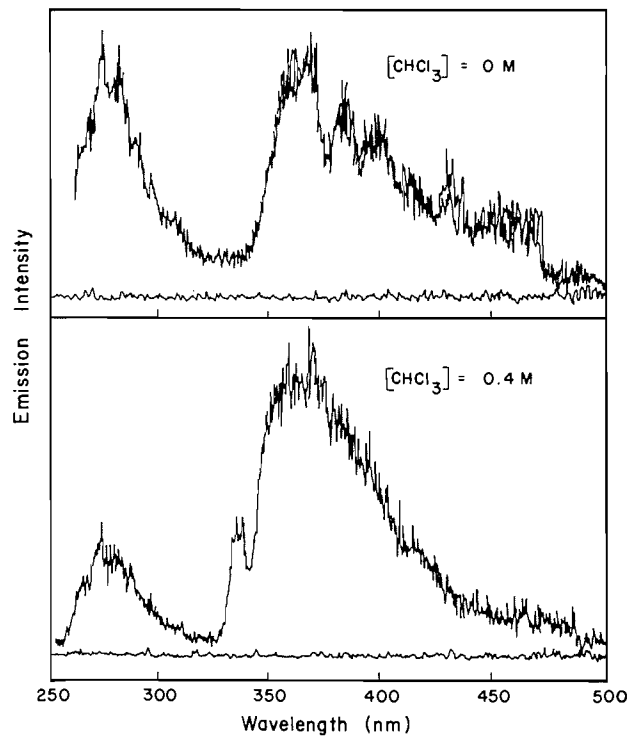

FIG. 6. Fluorescence and phosphorescence emission spectra of benzene perturbed by $CHCl_3$ in MCH/ISPT at 77 K ($[C_6H_6] = 2 \times 10^{-3}$ M, $\lambda_{ex} = 254$ nm).

did not allow for the determination of amount of light absorbed; consequently, we were not able to determine quantum yields. However, care was taken to ensure that the amount of light absorbed would be approximately the same for each of the glassy matrix solutions. Thus, Figs. 4–7 are expected to present a reasonable comparison picture of the effect of these quenchers since the same experimental setup when used for vapour and liquid phase studies showed very little variation in absorbed light intensity from run to run.

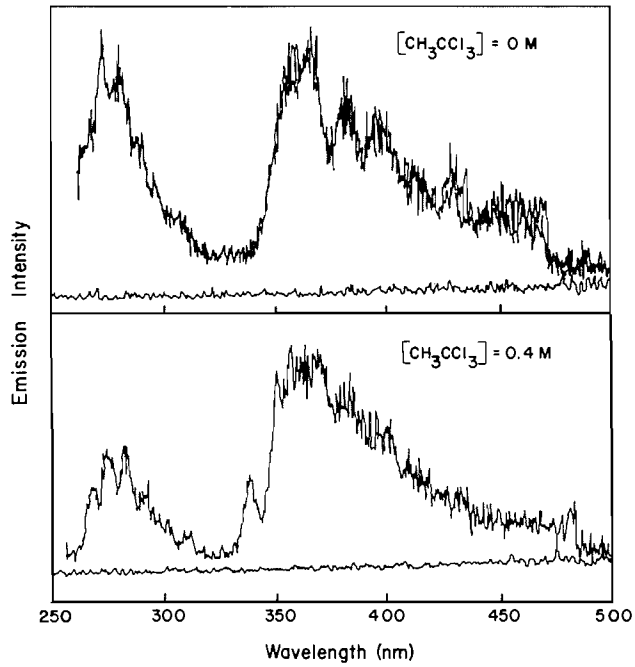

FIG. 7. Fluorescence and phosphorescence emission spectra of benzene perturbed by CH_3CCl_3 in MCH/ISPT at 77 K ($[C_6H_6] = 2 \times 10^{-3}$ M, $\lambda_{ex} = 254$ nm).

Inspection of Figs. 4 and 5 shows that CCl_4 and CH_3CN are comparable and efficient quenchers of the emission of C_6H_6 excited at 254 nm. The phosphorescence emission is quenched to the same extent as the fluorescence and this indicates that CCl_4 and CH_3CN have little effect on the triplet state of C_6H_6 with the decrease in its production being due to a decrease in singlet state population. Inspection of Figs. 6 and 7 shows that $CHCl_3$ and CH_3CCl_3 are also comparable quenchers but far less effective than CCl_4 and CH_3CN. It takes 4×10^{-1} M of $CHCl_3$ or CH_3CCl_3 to give approximately the same amount of fluorescence quenching as that produced by 4×10^{-4} M CCl_4. At these high concentrations of $CHCl_3$ and CH_3CCl_3 the enhanced intersystem crossover apparently competes with fluorescence quenching and a relative increase in phosphorescence is observed (see Figs. 6 and 7). Clearly, halocarbons can promote two reactions viz., reactions [10] and [11].

$$[10] \quad {}^1D^* + Q \xrightarrow{k_{10}} (D\cdots Q)^*$$

$$[11] \quad {}^1D^* + Q \xrightarrow{k_{11}} {}^3D^* + Q$$

For CCl_4 (and probably CH_3CN) $k_{10} \gg k_{11}$ whereas for $CHCl_3$ and CH_3CCl_3, k_{10} must be of the same order of magnitude as k_{11}.

Acknowledgement

The authors are grateful to the Natural Sciences and Engineering Research Council of Canada for financial support of this work.

1. A. WELLER. The exciplexes. *Edited by* M. S. Gordon and W. R. Wale. Academic Press, New York, NY. 1975. p. 23.

2. D. A. LABIANCA, G. N. TAYLOR, and G. S. HAMMOND. J. Am. Chem. Soc. **94**, 3693 (1972).
3. L. S. BUMGARNER, M. D. SCHUH, and M. P. THOMAS. J. Phys. Chem. **86**, 4029 (1982).
4. H. MORRISON and G. PANDEY. Chem. Phys. Lett. **96**, 126 (1983).
5. K. MIZUNO, C. PAC, and H. SAKURAI. J. Am. Chem. Soc. **96**, 2993 (1974).
6. H. A. KHWAJA, G. P. SEMELUK, and I. UNGER. Can. J. Chem. **60**, 1767 (1982) and references therein.
7. R. O. LOUTFY and R. W. YIP. Can. J. Chem. **51**, 1881 (1973).
8. G. JONES, M. SOUTHANOM, and S. H. CHIANG. J. Photochem. **12**, 267 (1980).
9. M. V. ENCINAS and J. C. SCAIANO. J. Am. Chem. Soc. **101**, 7740 (1979).
10. H. LEONHARDT and A. WELLER. Ber. Bunsenges. Phys. Chem. **67**, 791 (1963).
11. A. A. GORMAN, C. T. PAREKH, M. A. J. RODGERS, and P. G. SMITH. J. Photochem. **9**, 11 (1978).
12. J. SCHROEDER and F. WILKINSON. J. Chem. Soc. Faraday Trans. II, **75**, 896 (1979).
13. K. E. AL-ANI and M. AL-SABTI. J. Phys. Chem. **87**, 446 (1983).
14. Y. WANG, M. C. CRAWFORD, and K. B. EISENTHAL. J. Am. Chem. Soc. **104**, 5874 (1982).
15. A. WELLER. Pure Appl. Chem. **54**, 1885 (1982).
16. E. GAWEDA, MANDZIUK, and J. PROCHAROW. Adv. Mol. Relax. Inter. Processes, **23**, 45 (1982).
17. D. REHM and A. WELLER. Isr. J. Chem. **8**, 259 (1970).
18. R. O. LOUTFY and A. C. SOMERSALL. Can. J. Chem. **54**, 760 (1976).
19. G. E. JOHNSON. J. Phys. Chem. **84**, 2940 (1980).
20. T. IWASAKI, T. SAWADA, M. OKUYAMA, and H. KAMADA. J. Phys. Chem. **82**, 371 (1978).
21. T. TAKAHASHI, K. KIKUCHI, and H. KOKUBUN. J. Photochem. **14**, 67 (1980).
22. A. AHMAD and G. DUROCHER. Photochem. Photobiol. **34**, 573 (1981).
23. N. SELVARAFAN, M. M. PANICKER, S. VAIDYANATHAN, and V. RAMAKRISHNAN. Ind. J. Chem. **18**, 23 (1979).
24. A. B. ADDISON, G. P. SEMELUK, and I. UNGER. J. Lumin. **15**, 323 (1977).
25. R. B. CUNDALL and L. C. PEREIRA. J. Chem. Soc. Faraday Trans. II, **68**, 1152 (1972).
26. S. L. MUROV. Handbook of photochemistry. M. Dekker, Inc., NY. 1973.
27. P. M. FROEHLICH and H. A. MORRISON. J. Phys. Chem. **76**, 3566 (1972).
28. J. KLEIN, V. PLAZANET, and G. LAUSTRIAT. J. Chim. Phys. Physicochim. **67**, 302 (1970).
29. B. D. GHOSH and R. BASU. J. Phys. Chem. **84**, 1887 (1980).
30. H. A. KHWAJA, G. P. SEMELUK, and I. UNGER. Can. J. Chem. In press.
31. N. C. YANG, S. B. NEOH, T. NAITO, L. K. NG, D. A. CHERNOFF, and D. B. MCDONALD. J. Am. Chem. Soc. **102**, 2806 (1980).

Can. J. Chem. Downloaded from www.nrcresearchpress.com by 210.87.254.5 on 09/06/12
For personal use only.

Photoréactivité des complexes nitriles – cuivre (I) et (II). II. Système cyanure d'allyle – cuivre (I) et (II)

MICHÈLE BOLTE ET JACQUES LEMAIRE

Laboratoire de Photochimie, E.R.A. N° 929, Université de Clermont II, B.P. 45, 63170 Aubière, France

Reçu le 6 décembre, 1982[1]

MICHÈLE BOLTE et JACQUES LEMAIRE. Can. J. Chem. **62**, 1492 (1984).

La complexation du cuivre(I) avec le cyanure d'allyle se fait par transfert de charge entre le métal et le groupement nitrile. Elle induit la transformation du cyanure d'allyle en crotonitrile (isomère α,β insaturé). Le cuivre(II) se fixe également sur l'azote du nitrile par un transfert de charge —C≡N → Cu^{II}. La photoréactivité des complexes avec le cuivre(II) montre que le ligand complexé se comporte comme un nitrile α,β insaturé.

MICHÈLE BOLTE and JACQUES LEMAIRE. Can. J. Chem. **62**, 1492 (1984).

Through complexation with copper I, the allyl cyanide ligand has been shown to be converted in the dark into *cis* + *trans* crotonitrile. The photoreactivity of allyl cyanide – copper II complexes provides evidence that the ligand behaves like an α,β unsaturated nitrile. In both cases, the copper atom is bonded with the nitrogen atom of the allyl cyanide by charge transfer from the ligand to the metal (LMCT).

Can. J. Chem. Downloaded from www.nrcresearchpress.com by 210.87.254.105 on 09/06/12
For personal use only.

La photoréactivité des complexes de cuivre(I) et (II) a connu un développement important durant ces dernières années. Notamment, l'aptitude du cuivre I à se fixer sur les doubles liaisons éthyléniques a permis la synthèse photochimique de nombreux dérivés cyclobutaniques (1, 2). L'emploi de CuCl comme catalyseur a été décrit pour la dimérisation de molécules à cycle tendu telles que le norbornène ou le bicyclopentadiène (1). L'utilisation du triflate de cuivre CF_3SO_3Cu a permis l'obtention de dérivés cyclobutaniques à partir de composés à double liaison extracyclique (3):

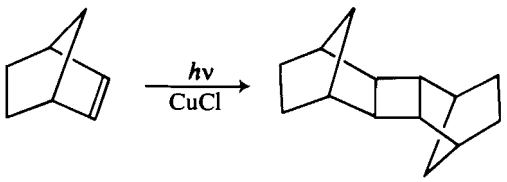

(ref. 1)

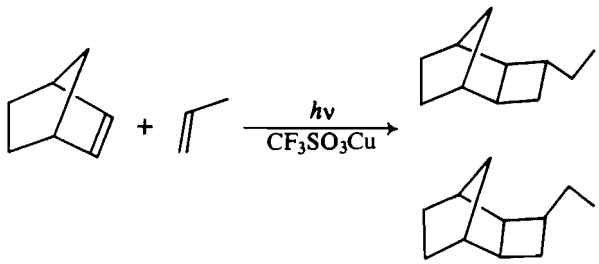

(ref. 3)

Par ailleurs, la photo-isomérisation du norbornadiène en quadricyclane, catalysée par un sel de cuivre I est un système envisagé pour la récupération de l'énergie solaire (4).

En ce qui concerne le cuivre(II), de nombreux systèmes contenant des protéines complexes ou des macrocycles polyazotés ont été étudiés (5, 6). Gagné *et al.* ont décrit un

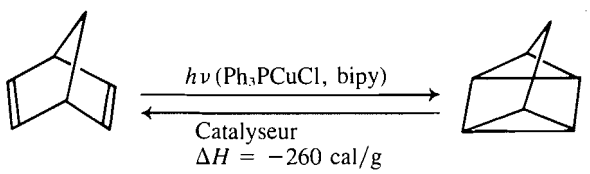

(ref. 4)

complexe Cu^{II} – macrocycle tétraazoté qui peut fixer photochimiquement un cinquième ligand sur le cuivre (CO, CH_3CN ou la 1-méthyl imidazole) (7).

Dans un précédent mémoire, nous avons décrit la photoréactivité des complexes du cuivre(I) et (II) avec différents nitriles saturés ou α,β insaturés (8). La position en α,β de la double liaison dans les complexes cuivre–nitrile insaturés semble être un facteur déterminant de la photoréactivité de ces complexes. Ainsi, nous avons pu établir que la délocalisation existant dans le ligand facilite le transfert de charge —C≡N → Cu du ligand vers le cuivre:

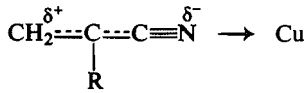

R = H ou CH_3

Dans le cas du cuivre(I), cette délocalisation favorise la formation des complexes dans lequels le métal est lié à la double liaison ou au groupement nitrile; l'association avec la double liaison reste cependant minoritaire.

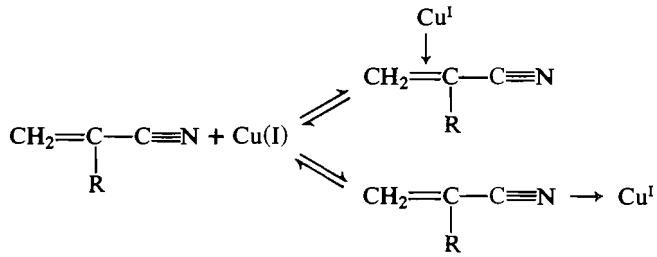

R = H ou CH_3

Les photoréactivités associées à ces deux types de complexation sont différentes. La complexation du cuivre sur la double liaison induit sélectivement la photodimérisation cyclobutanique du ligand. La complexation avec le groupement nitrile augmente le rendement quantique d'isomérisation *trans*→*cis*: ainsi le crotonitrile CH_3—CH=CH—C≡N pour lequel les valeurs des rendements quantiques d'isomérisation $\phi^0_{t\to c}$ et $\phi^0_{c\to t}$ sont multipliées par un facteur trois lors de l'irradiation en présence de CuCl (9). Il en est de même pour le cinnamonitrile C_6H_5—CH=CH—C≡N dont le rendement $\phi^0_{t\to c}$ augmente de 0,28 (sans CuCl) à 0,42 (avec CuCl) (10). De plus, dans les deux cas, l'isomérisation de nitrile est assistée par le complexe

[1]Revision reçue le 14 février, 1984.

Can. J. Chem. Downloaded from www.nrcresearchpress.com by 210.87.254.105 on 09/06/12
For personal use only.

TABLEAU 1. Spectre Raman

Région	Cyanure d'allyle	CuCl dans le cyanure d'allyle
1350–1700 cm^{-1}	1410 m	1410 m
	1420 mf	1420 mf
	1620 f	1620 f
	1624 f	1624 f
	1629 f	1629 f
	1647 TF	1647 TF
2000–2500 cm^{-1}	2222 f	2222 f
	2227 f	2227 f
	2251 F (large)	2251 F (large) ν(C≡nitrile)
	2264 ep.	2264 ep.
		2279 mf ν(C≡N complexé)

R—CH=CH—C≡N—Cu^{I} (effet catalytique du cuivre(I)).

L'étude des systèmes nitriles–cuivre(II) a montré que la présence d'une double liaison conjuguée avec le groupement nitrile augmente aussi le rendement quantique de réduction du cuivre(II) (8).

Il apparaissait donc que la position de la double liaison en α,β du groupement nitrile était un facteur déterminant de la photoréactivité des complexes nitriles–cuivre. Afin de vérifier cette conclusion, nous avons entrepris l'étude de système cuivre – nitrile β,γ insaturé, soit:

CH_2=CH—CH_2—C≡N, CuCl
et CH_2=CH—CH_2—C≡N, $CuCl_2$

Résultats expérimentaux

Dans les systèmes étudiés, le nitrile sert de ligand avec le cuivre et de solvant pour le complexe formé. Les spectres d'absorption que nous décrivons correspondent aux transitions supplémentaires inhérentes à la formation d'un complexe entre le métal et le ligand.

(a) Système CH_2=CH—CH_2—C≡N, CuCl

CuCl est très soluble dans le cyanure d'allyle, on peut obtenir des solutions de concentration en CuCl égale à 0,5 *M*. Lorsqu'on dissout du chlorure cuivreux dans le nitrile, on note une augmentation importante de densité optique entre 250 et 320 nm sans qu'il soit possible de déterminer un maximum d'absorption.

Le spectre Raman de ces solutions permet de mettre en évidence un transition supplémentaire à 2279 cm^{-1} (Tableau 1). On ne note, par ailleurs, aucune autre modification du spectre.

Nous observons à l'obscurité, la transposition lente du cyanure d'allyle en son isomère α,β insaturé, le crotonitrile:

$$CH_2{=}CH{-}CH_2{-}C{\equiv}N \xrightarrow[\theta = 20°C]{\Delta,\ CuCl} \underset{\substack{(cis\ +\ trans)\\ 50\%\quad 50\%}}{CH_3{-}CH{=}CH{-}C{\equiv}N}$$

Cette réaction d'ordre apparent 1 se fait avec une constante de vitesse $k = 5{,}7 \times 10^{-5}$ mn^{-1} calculée sur l'apparition des crotonitriles. La transposition en crotonitrile est catalysée par CuCl; l'emploi d'une solution, par exemple de concentration égale à 0,1 *M* en CuCl permet de transformer 20% du cyanure d'allyle pris à l'état pur, soit 2,4 mol.

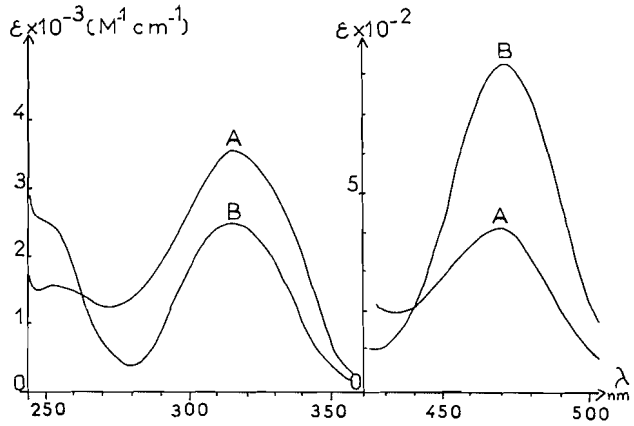

FIG. 1. Spectres d'absorption de $CuCl_2$ dans le cyanure d'allyle.

TABLEAU 2. Spectres d'absorption de $CuCl_2$ dans le cyanure d'allyle

A $c > 10^{-3}$ *M*		B $c < 5 \times 10^{-4}$ *M*	
λ_{max} (nm)	ϵ_{max} (M^{-1} cm^{-1})	λ_{max} (nm)	ϵ_{max} (M^{-1} cm^{-1})
256	1550	250	2700
312	3450	315	2650
468	410	470	815

Nous n'avons pas observé d'accélération du phénomène par excitation photochimique à 254 nm.

(b) *Systèmes CH_2=CH—CH_2—C≡N—$CuCl_2$*

$CuCl_2$ est relativement peu soluble dans le cyanure d'allyle. La concentration en sel de cuivre est généralement comprise entre 5×10^{-3} *M* et 2×10^{-4} *M*. Dans ces conditions, on obtient des spectres d'absorption comportant deux transitions en uv et une dans le visible (Fig. 1). Selon la concentration en $CuCl_2$, on observe deux spectres différents correspondant à des complexes que nous désignerons par "A" et "B"; le complexe "A" apparaît à des concentrations en $CuCl_2$ supérieures à 10^{-3} *M*; le complexe "B" est observé quand la concentration en $CuCl_2$ devient inférieure à 5×10^{-4} *M*. La dilution d'une solution contenant le complexe "A" entraîne l'apparition rapide du complexe "B". Les solutions concentrées évoluent dans le temps: on observe une modification spectrale lente conduisant au spectre obtenu en solution diluée. Cependant, on peut conserver le complexe "A" quelques jours sans modification notable de son spectre d'absorption. Le tableau 2 regroupe les caractéristiques spectrales des spectres d'absorption observés dans les différents domaines de concentration de $CuCl_2$.

L'addition de LiCl (Cl/Cu ~ 3) à la solution concentrée de $CuCl_2$ dans le cyanure d'allyle entraîne une modification du spectre d'absorption et notamment une très forte augmentation de la transition à 468 nm ($\epsilon_{max} = 1200\,M^{-1}\,cm^{-1}$). Une addition supplémentaire de LiCl (Cl/Cu ~ 8) ne modifie que très légèrement le spectre, on voit apparaître un épaulement à environ 405 nm (Fig. 2).

Nous avons irradié le complexe "A" en lumière monochromatique de longueur d'onde 254, 313 et 491,6 nm correspondant à chacune des transitions du complexe. Quelle que soit la longueur d'onde utilisée, on observe le même phénomène en deux étapes: la transformation de "A" en "B" durant laquelle le faisceau des courbes correspondantes présente deux points isobestiques à 263 et 440 nm (Fig. 3); puis la disparition de la

TABLEAU 3. Rendements quantiques de transformation A→B et de disparition

$CuCl_2$ dans	λ_{irr} = 253,7 nm		λ_{irr} = 296* ou 313** nm		λ_{irr} = 491,6 nm	
	$\phi^0_{A\to B}$	ϕ^0_{disp}	$\phi^0_{A\to B}$	ϕ^0_{disp}	$\phi^0_{A\to B}$	ϕ^0_{disp}
$CH_2{=}CH{-}CH_2{-}C{\equiv}N$	0,57	0,17	0,96**	0,27**	0,68	0,26
$CH_3C{\equiv}N$[a]	0,20	0,02	0,20*	0,02	0,08	0,08
$CH_2{=}CH{-}C{\equiv}N$[a]	0,38	0,15	0,77*	0,18*	0,35	0,17
$CH_2{=}C(CH_3){-}C{\equiv}N$[a]	0,19	0,10	0,47*	0,17*	1,0	0,34
$CH_3{-}CH{=}CH{-}C{\equiv}N$ (*cis*)[a]				0,25**		0,50

[a]Notre précédent travail (8).

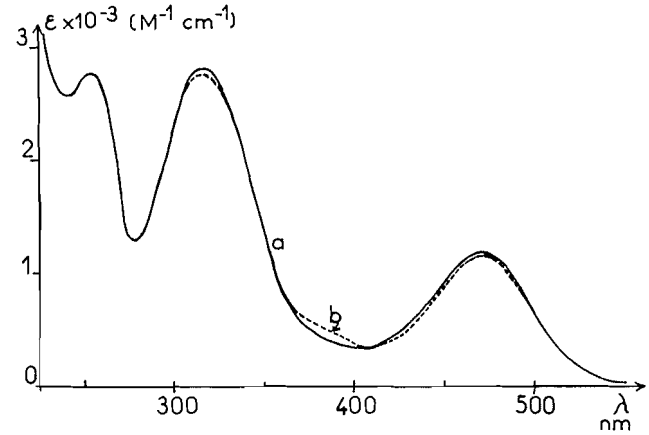

FIG. 2. Spectre d'absorption de $CuCl_2$ dans le cyanure d'allyle en présence d'un excès d'ions Cl^-: (a) Cl/Cu = 4; (b) Cl/Cu = 10.

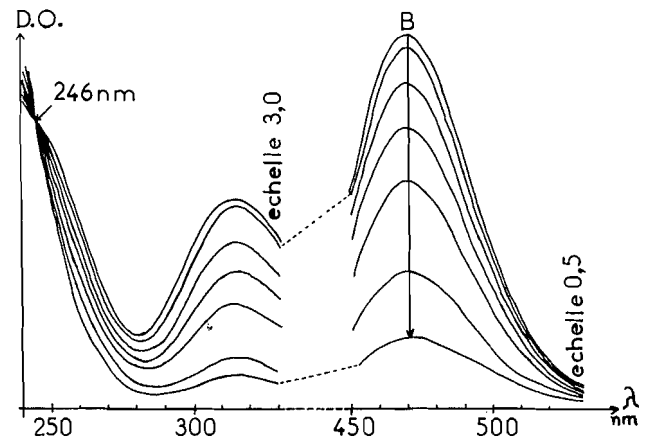

FIG. 4. Photoréduction du complexe cyanure d'allyle − $CuCl_2$ (B) à λ_{irr} = 313 ou 491,6 nm.

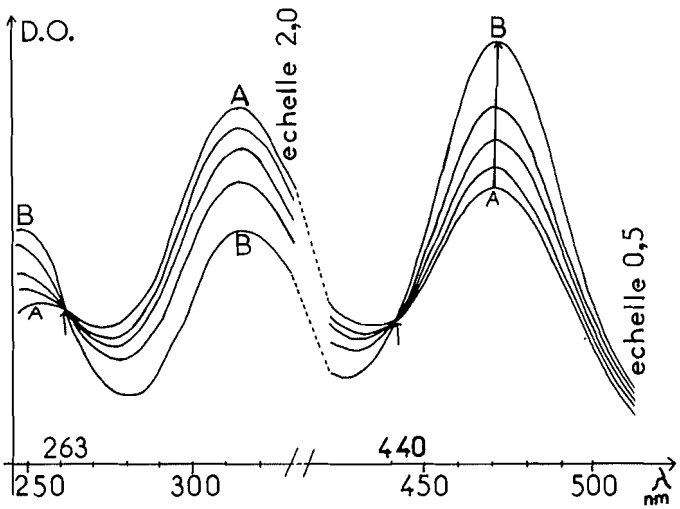

FIG. 3. Evolution photochimique d'une solution de complexe cyanure d'allyle − $CuCl_2$ (A).

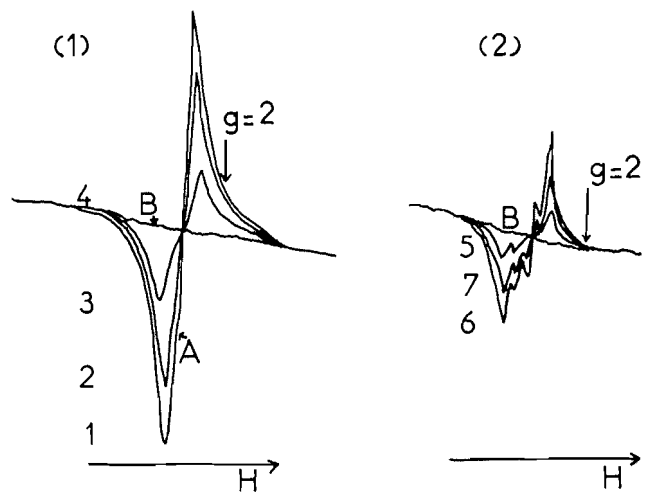

FIG. 5. Spectres rpe de solutions du $CuCl_2$ dans le cyanure d'allyle: Evolution du signal en fonction du temps d'irradiation: (1) tranformation A → B; (2) disparition de B.

transition dans le visible. En suivant cette réaction, on note la présence d'un point isobestique à 246 nm (λ_{irr} = 313 ou 491,6 nm) (Fig. 4). Les transitions à 250 et 315 nm disparaissent egalement.

Les rendements quantiques de transformation A → B et de disparition de B sont rassemblés dans le tableau 3. Ces derniers ont été calculés à partir du complexe "B" pur (solution diluée). Dans tous les cas, les rendements quantiques ont été mesurés par spectroscopie uv sur la modification spectrale de la transition dans le visible.

En rpe, le complexe "A" est caractérisé par un signal symétrique à g = 2,136 (Fig. 5); l'addition de LiCl n'entraîne pas l'apparition d'un nouveau signal. Lorsque la solution (complexe "A") évolue thermiquement ou photochimiquement, on observe la disparition progressive du signal. Le complexe "B" qui correspond à une absorption maximum dans le visible ne

Can. J. Chem. Downloaded from www.nrcresearchpress.com by 210.87.254.105 on 09/06/12
For personal use only.

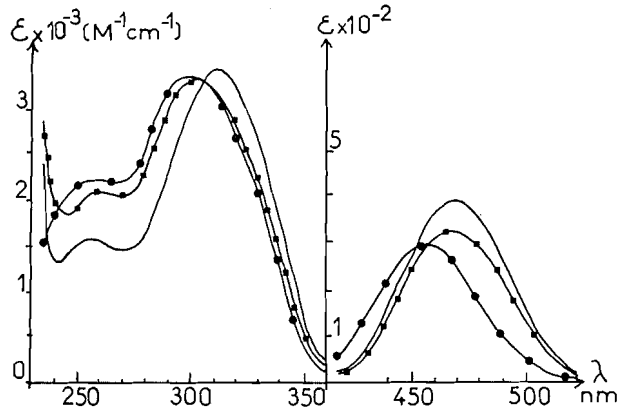

FIG. 6. Complexes nitrile–$CuCl_2$ (A) avec CH_3CN (-●-●-), CH_2=CH—CN (-■-■-) et CH_2=CH—CH_2—CN (———).

présente aucun signal en rpe. Par irradiation de ce complexe, il apparaît de nouveau un signal à quatre raies qui disparaît en fin de photoréaction. Cette étude a été également réalisée avec le système $CuCl_2$–CH_3CN pour lequel nous obtenons des résultats tout à fait analogues.

Discussion

A. *Système cyanure d'allyle – cuivre(I)*

L'étude en spectroscopie Raman montre que le cuivre(I) se fixe uniquement sur le groupement nitrile. En effet, dans un précédent mémoire (11), il a été établi que l'augmentation de fréquence du mode ν(C≡N) correspond à une complexation du cuivre(I) avec le ligand, de type —C≡N → Cu(I).

La complexation avec la double liaison observée avec les nitriles α,β insaturés est donc directement liée à la conjugaison présente dans la molécule et à l'appauvrissement en électrons qui en résulte:

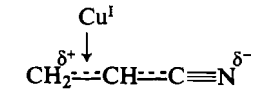

La transposition du cyanure d'allyle en crotonitrile à l'obscurité, est analogue à celle décrite par Mialhe et Vessière (12) pour les composés allyliques en présence d'une base:

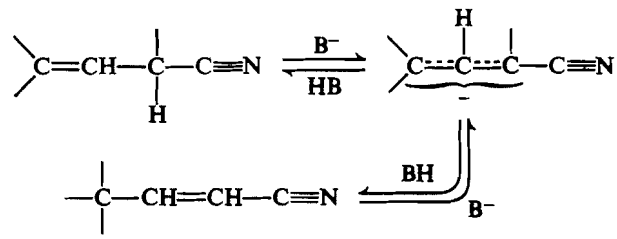

B = diéthylamine

Dans notre cas, en l'absence de base, l'hydrogène placé en α du groupement nitrile est rendu plus labile par la complexation avec le cuivre, ce qui favorise la migration de la double liaison:

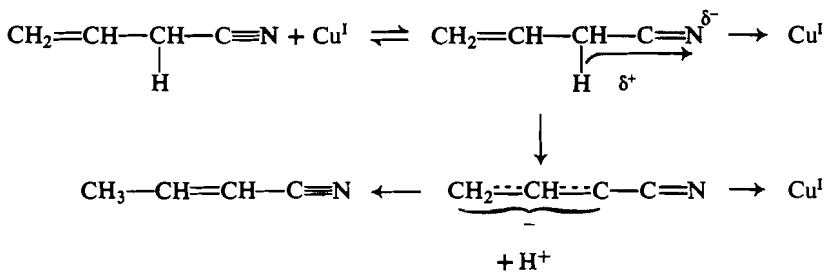

La stéréochimie du carbanion formé ne favorise aucun isomère en particulier, les crotonitriles *cis* et *trans* se forment en quantités équivalentes. Il n'apparaît aucune modification notable de ce processus par excitation photochimique.

L'étude photochimique des systèmes crotonitrile (*cis* ou *trans*) – Cu^I (9) a montré que le phénomène majoritaire est la désactivation par isomérisation *trans* ⇌ *cis* du ligand. L'état photostationnaire obtenu contient les deux isomères en égales proportions. Par ailleurs, la photodimérisation cyclobutanique observée avec le complexe crotonitrile *cis* – Cu^I est un phénomène extrêmement minoritaire qu'il est donc impossible de mettre en évidence à partir du cyanure d'allyle.

B. *Systèmes cyanure d'allyle – cuivre(II)*

Comme le montre la figure 6, les spectres d'absorption des complexes "A" et "B" sont analogues à ceux obtenus avec un ligand saturé (acétonitrile); la fixation du métal se fait exclusivement sur l'azote du groupement nitrile (8) (caractère de donneur σ de ce groupement).

L'absorption à 470 nm dans le visible est caractéristique d'un complexe tétracoordoné du cuivre(II) (13). Sykora *et al.* indiquent effectivement que la mise en solution de $CuCl_2$ ($c_{CuCl_2} \sim 10^{-3}$ *M*) dans l'acétonitrile correspond à l'apparition de différents complexes $CuCl(CH_3CN)_3^+$ (17%), $CuCl_3(CH_3CN)^-$ (26%) et $CuCl_2(CH_3CN)_2$ (52%) Cu^{2+} (4%). Ils indiquent également la présence d'un signal rpe qui disparaît par irradiation. L'addition d'ions Cl^- à cette solution entraîne la formation de $CuCl_3^-$ (96% pour un rapport $Cu^{2+}/Cl^- = 1/3$) puis celle de $CuCl_4^{2-}$ (λ_{max} = 404 nm) obtenu presque pur pour un rapport $Cu^{2+}/Cl^- = 1/8$.

La mise en solution de $CuCl_2$ dans le cyanure d'allyle provoque en proportions vraisemblablement différentes, la formation des complexes mentionnées ci-dessus. L'addition d'ions Cl^- à cette solution favorise la formation de $CuCl_3^-$; par contre, une addition supplémentaire d'ions Cl^- ne permet l'obtention de $CuCl_4^{2-}$ qu'en très faible quantité (épaulement à 404 nm).

Le signal symétrique observé en rpe à g = 2,136 pour une solution concentrée du $CuCl_2$ dans le cyanure d'allyle avec et sans LiCl est attribué au complexe $CuCl_3RCN^-$. La disparition de ce signal provisoire thermiquement ou photochimiquement correspond à la transformation A → B mise en évidence par spectroscopie d'absorption. L'absence de signal rpe pour le complexe "B" alors que l'absorption dans le visible est maximum indique la présence de cuivre(II) fortement solvaté par les

Can. J. Chem. Downloaded from www.nrcresearchpress.com by 210.87.254.105 on 09/06/12
For personal use only.

Can. J. Chem. Downloaded from www.nrcresearchpress.com by 210.87.254.105 on 09/06/12
For personal use only.

molécules de nitriles. Par ailleurs, la réapparition d'un signal rpe différent du précédent, observée en poursuivant l'irradiation, montre que le complexe "B" est effectivement un complexe de cuivre(II). L'hypothèse d'une structure dimère pourrait expliquer la disparition du signal rpe soit par liaison directe métal–métal, soit par super-échange par l'intermédiaire du ligand. Cependant cette hypothèse est en contradiction avec l'obtention du complexe "B" par dilution et son existence dans un domaine de concentration inférieure à 5×10^{-4} *M*. Le cuivre(II) se trouve donc fortement solvaté par les molécules de nitriles et il y a couplage entre les électrons du cuivre(II) paramagnétique et les électrons du ligand. Ce même phénomène a été observé avec les complexes chrome(III) – acides aminés pour lesquels l'addition en quantités croissantes d'acide aminé à une solution aqueuse de chrome(III) entraîne la disparition progressive du signal rpe (14).

L'ensemble de ces résultats nous conduit à décrire le complexe "B" présent en solution diluée comme une entité neutre tétracoordonnée autour du cuivre:

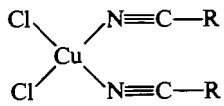

Le complexe "A" est, comme nous l'avons déjà indiqué, un mélange instable de différentes espèces dont $CuCl^+$, $CuCl_3^-$ et $CuCl_2$. Par dilution, activation thermique ou photochimique, on observe la transformation de ces différents complexes en une seule entité, le complexe neutre solvaté "B".

Par excitation dans chacune des trois bandes de transfert de charge du complexe "B", on observe la destruction du complexe (réapparition du signal du cuivre(II) en rpe) et photoréduction du cuivre(II) en cuivre(I).

En ce qui concerne la cinétique de photoréduction, les valeurs des rendements quantiques (Tableau 3) sont élevées, de l'ordre de celles obtenues avec les nitriles α,β insaturés; elles sont bien supérieures à celles observées avec l'acétonitrile. Elles ne varient que relativement peu avec la longueur d'onde d'excitation.

Cette similitude de comportement avec les nitriles α,β insaturés, indique que le cyanure d'allyle complexé avec le cuivre possède à l'état excité une conjugaison importante qui favorise le transfert de charge du ligand vers le cuivre(II) et donc la réduction du Cu^{II} en Cu^{I}. Cependant, en l'état actuel de nos connaissances, il n'est pas possible de préciser si le cyanure d'allyle complexé se comporte déjà à l'état fondamental comme un ligand α,β insaturé. Nous n'avons pas observé, à l'obscurité, de transposition en crotonitrile induite par le cuivre(II). Il convient toutefois de noter que les concentrations de cuivre(II) mises en jeu sont nettement inférieures à celles observées pour le cuivre(I) et que la mise en évidence d'une telle transposition peut s'avérer plus difficile. Il s'est avéré également impossible d'identifier les photoproduits d'oxydation du cyanure d'allyle.

Conclusion

Les résultats obtenus pour le système cyanure d'allyle – Cu^{I} montrent que, lorsque la double liaison n'est pas conjuguée avec le groupement nitrile, on n'observe pas de complexation du cuivre(I) sur la double liaison. La seule complexation mise en évidence est une liaison par transfert de charge entre le groupement nitrile et le cuivre, quelle que soit la valence du cuivre, (I) ou (II).

Avec le cuivre(I), cette complexation favorise la migration de la double liaison et entraîne la transposition du cyanure d'allyle en son isomère α,β insaturé, le crotonitrile (*cis* et *trans*). La liaison $—C\equiv N \rightarrow Cu^{II}$ observée avec le cuivre divalent induit une photoréactivité analogue à celle d'un complexe $CuCl_2$ – nitrile α,β insaturé.

Partie expérimentale

Le cyanure d'allyle (Merck) est distillé afin d'éliminer les impuretés qu'il contient. Ainsi distillé, il ne peut être conservé que quelques semaines à l'obscurité. Le liquide se teinte ensuite progressivement en jaune et l'impureté qu'il contient empêche toute complexation avec le cuivre.

Les spectres d'absorption uv–visible ont été enregistrés sur un appareil Cary 118CX. les crotonitriles *cis* et *trans* ont été analysés par chromatographie en phase gazeuse sur un appareil Carlo Erba Fractovap 2101 équipé d'une colonne Carbowax 20M. Les mélanges réactionnels sont mis en solution dans l'acétonitrile et analysés sur une colonne dont la température est fixée à 100°C.

Les spectres Raman ont été faits sur un spectromètre Jobin Yvon, modèle Ramanor HG 28 équipé de deux réseaux holographiques concaves. La raie d'excitation 514,5 nm est celle d'un laser à argon ionisé Spectraphysics Modèle 164.

Les spectres de rpe ont été faits sur un appareil ER 200D Brucker. Les solutions dégazées à l'argon, sont placées dans des cellules plates (épaisseur 0,1 mm). Les conditions de travail sont les suivantes: fréquence 9,52 MHz, modulation de champ 400 kHz, modulation d'amplitude 4 G, puissance 56 mW.

La manipulation de sels et complexes de cuivre(I) est faite uniquement en boîte à gants sous atmosphère d'azote sec. Les solutions de $CuCl_2$ sont préparées à l'air mais elles sont dégazées puis irradiées sous vide. Les dégazages sont faits par des cycles de congélation–décongélation dans l'azote liquide (trois cycles).

Les irradiations à 254 nm des solutions de CuCl dans le nitrile ont été faites dans un réacteur en quartz cylindrique entouré de six tubes à vapeur de mercure basse pression ($I_0 \simeq 3 \times 10^{16}$ photons/cm^3 s). Les actinométries sont faites avec l'oxalate d'uranyle. Les irradiations à 313 nm et 491,6 nm sont faites en faisceau parallèle avec une lampe à vapeur de mercure moyenne pression équipée d'un monochromateur Bausch et Lomb "haute intensité". Les solutions de $CuCl_2$ sont irradiées dans des cellules cylindriques de 1 cm de rayon et de 1 cm ou 1 mm de longueur. Les actinométries sont faites avec le ferrioxalate de potassium (0,006 *M* ou 0,15 *M*).

1. D. J. TRECKER, R. S. FOOTE, J. P. HENRY et J. E. MCKEON. J. Am. Chem. Soc. **88**, 3021 (1966).
2. R. G. SALOMON et J. K. KOCHI. J. Am. Chem. Soc. **96**, 1137 (1974).
3. R. G. SALOMON et A. SINHA. Tetrahedron Lett. **16**, 1367 (1978).
4. K. MARUYAMA, K. TARDA, Y. NARUTA et Y. YAMAMOTO. Chem. Lett. 1259 (1980).
5. U. SAKAGUCHI et A. W. ADDISON. J. Chem. Soc. Dalton Trans. 600 (1979).
6. P. G. GRAHAM et D. C. WEATHERBURN. Aust. J. Chem. **34**, 291 (1981).
7. R. R. GAGNE, J. L. ALLISON, R. J. GALL et C. A. KOYAL. J. Am. Chem. Soc. **99**, 7170 (1977).
8. M. BOLTE et J. LEMAIRE. Nouveau J. Chim. **4**, 461 (1980).
9. M. BOLTE et M. MASSAUX. Inorg. Chim. Acta, **52**, 191 (1981).
10. M. BOLTE, M. MASSAUX et J. ZAREMBOVITCH. Inorg. Chim. Acta. À paraître.
11. J. ZAREMBOVITCH et M. MASSAUX. Inorg. Chim. Acta, **52**, 183 (1981).
12. Y. MIALHE et R. VESSIÈRE. Bull. Soc. Chim. Fr. 4181 (1968).
13. J. SYKORA, E. HORVATH et J. GAZO. Z. Anorg. Allg. Chem. **442**, 245 (1978).
14. B. ROBERT. Thèse de Docteur-Ingénieur n° 2, 10 février 1984, Université de Clermont-Ferrand II, France.

Discreteness-of-charge effects in electrode kinetics. III. The electroreduction of aquopentamminochromium(III) cation in the presence of specifically adsorbed iodide anions

W. RONALD FAWCETT[1] AND KVETA MARKUŠOVÁ[2]

Guelph–Waterloo Centre for Graduate Work in Chemistry (Guelph Campus), Department of Chemistry, University of Guelph, Guelph, Ont., Canada N1G 2W1

Received December 5, 1983

W. RONALD FAWCETT and KVETA MARKUŠOVÁ. Can. J. Chem. **62**, 1497 (1984).

The kinetics of electroreduction of the aquopentamminochromium(III) cation have been studied at a Hg electrode in acidified aqueous solutions of NaI + $NaClO_4$ with an ionic strength of 0.25 *M*. The rate of reaction increased with increase in iodide concentration due to the accelerating effect of this anion when it is adsorbed on the electrode. Analysis of the double layer effect indicates that the rate acceleration is greater than that predicted by the Frumkin theory chiefly because the reaction site is closer to the electrode than to the outer Helmholtz plane.

W. RONALD FAWCETT et KVETA MARKUŠOVÁ. Can. J. Chem. **62**, 1497 (1984).

Opérant dans des solutions aqueuses acidifiées de NaI + $NaClO_4$ et à une force ionique de 0,25 *M*, on a étudié la cinétique de l'électroréduction du cation aquopentamminochrome(III) à une électrode de Hg. Dû à l'effet accélérant de l'iodure lorsqu'il est adsorbé sur l'électrode, la vitesse de la réaction augmente avec une augmentation de la concentration en iodure. L'analyse de l'effet de double couche indique que l'augmentation de la vitesse est plus grande que celle que l'on pourrait prédire en se basant sur la théorie de Frumkin; ceci est principalement dû au fait que le site réactionnel est plus près de l'électrode que le plan extérieur de Helmholtz.

[Traduit par le journal]

Can. J. Chem. Downloaded from www.nrcresearchpress.com by 210.87.254.40 on 09/06/12
For personal use only.

Introduction

In a previous paper of this series (1), double layer effects on the electroreduction of hexamminocobalt(III) cation were examined in mixed electrolyte solutions of constant ionic strength containing nitrate and fluoride anions. Analysis of these effects proved to be rather complex for two reasons. Firstly, the reaction occurs at potentials close to the point of zero charge (p.z.c.) where the ionic composition of the double layer changes most rapidly. Secondly, the reactant has some tendency to ion pair especially with the F^- anion so that it is possible that the average charge on the reactant changes with composition of the base electrolyte. Analysis of double layer effects on the reduction of Cr(III) ions is expected to be somewhat simpler since these species are reduced at more negative potentials at which the predominant ions in the double layer are cations in the absence of anionic adsorption. The double layer effect is then classified as Type I (2) and is the simplest possible from the point of view that attractive ion–ion interactions in the vicinity of the reaction site can be neglected.

The reactant chosen for the present study, namely, $Cr(NH_3)_5OH_2^{3+}$ was investigated previously by Anson *et al.* (3), and Weaver and Satterberg (4) in solutions of high ionic strength. These authors found that the experimental transfer coefficients for reduction of this cation and hexamminochromium(III) were significantly greater than that for the reduction of hexaquochromium(III). In addition, the increase in the logarithm of the rate of reduction at constant potential due to the adsorption of a fixed amount of iodide anion at the electrode was at least twice as large in the case of the ammino-complex. In discussing these results, it was suggested (4) that the reaction site for the ammino-complex is closer to the electrode than that for the aquo-complex. As a result, changes in the potential at the reaction site due to anion adsorption have a much larger effect on the reaction rate.

The purpose of the present study was to examine the effect of adsorbed iodide ion on the reduction of $Cr(NH_3)_5OH_2^{3+}$ in more detail with quantitative estimation of the change in the potential drop across the diffuse layer, ϕ^d. Due to the fact that deficiencies in the Gouy–Chapman theory used to calculate ϕ^d are expected to become more important as the ionic strength increases, the experiments reported here were carried out at a lower ionic strength.

Experimental

The kinetic data were obtained by d.c. polarography using a dropping mercury electrode with a flow rate of 0.26 mg s^{-1} and droptime of 2 s. The depolarizer obtained from Dr. R. J. Balahura was purified by recrystallization; the chromium content was confirmed analytically and the nature of the ligands spectroscopically. At a concentration of 0.5 m*M*, the polarographic waves exhibited a maximum which became more pronounced as the concentration of iodide in the solution increased. In order to eliminate polarographic maxima, the depolarizer concentration was kept low (0.133 m*M*) and higher iodide concentrations avoided. The solutions were kept at a low pH to prevent hydrolysis of the depolarizer by maintaining a $HClO_4$ concentration of 0.01 *M*. The diffusion coefficient of $Cr(NH_3)_5OH_2^{3+}$ in solutions with an ionic strengh of 0.25 *M* was 6.72×10^{-6} cm s^{-1}. The salts used as base electrolytes, namely, $NaClO_4$ and NaI were purified and dried according to procedures described earlier (5, 6). The concentration of $NaClO_4$ + NaI was 0.24 *M*. The rate constant was calculated from the ratio of the observed current to its diffusion limited value using Koutecký's theory including correction for electrode sphericity (7). The reference electrode was a calomel system with a 4.16 *M* NaCl solution, and the counter electrode a Pt cylinder. All experiments were carried out at 25°C.

The potential drop across the diffuse layer, ϕ^d was estimated with consideration of the contribution of the reactant and product to the ionic strength as described earlier (1). The double layer data used were those obtained earlier for the system xM NaI + $(0.25 - x)M$ NaF (6). Accordingly, it was assumed that the ClO_4^- anion is not adsorbed in the potential region where kinetic data were obtained, and that its role in the double layer is the same as that of the F^- anion.

[1]Present address: Department of Chemistry, University of California at Davis, Davis, CA 95616, U.S.A.

[2]On leave from Šafárik University, Košice, Czechoslovakia.

Can. J. Chem. Downloaded from www.nrcresearchpress.com by 210.87.254.40 on 09/06/12
For personal use only.

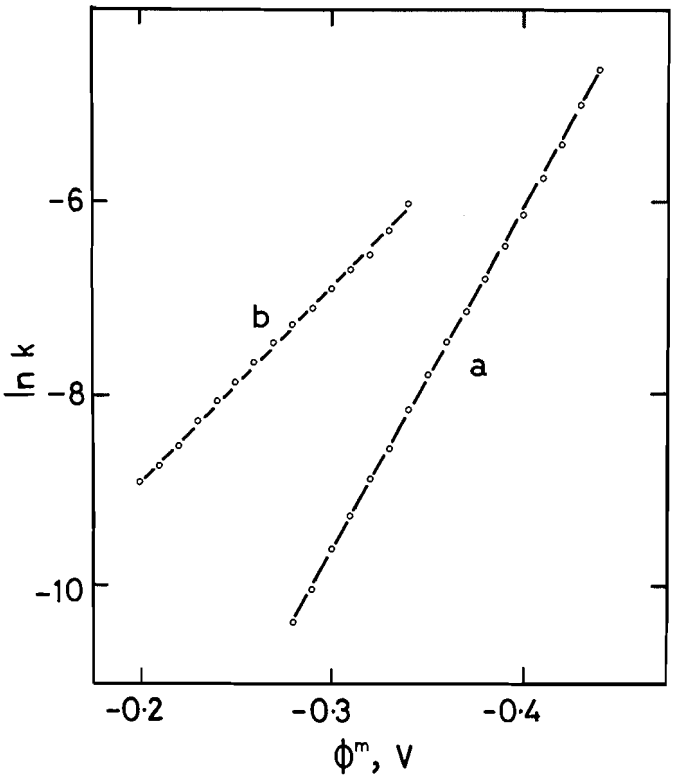

FIG. 1. Plots of the logarithm of the rate constant for reduction of $Cr(NH_3)_5H_2O^{3+}$ at mercury against electrode potential on the rational scale in solutions of (*a*) 0.24 *M* $NaClO_4$ + 0.01 *M* $HClO_4$ and (*b*) 0.04 *M* NaI + 0.20 *M* $NaClO_4$ + 0.01 *M* $HClO_4$.

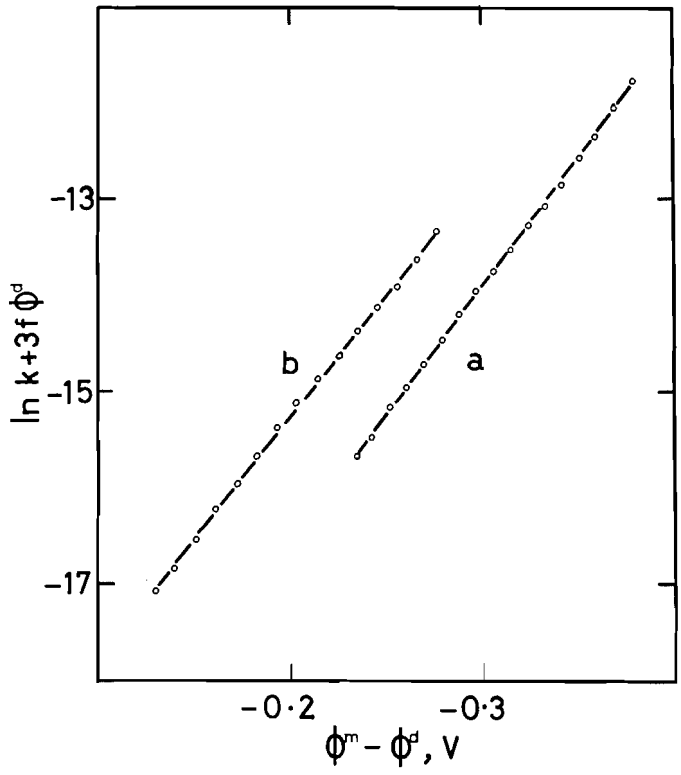

FIG. 2. Plots of the logarithm of the corrected rate constant, ln k + $3f\phi^d$ for reduction of $Cr(NH_3)_5H_2O^{3+}$ at mercury against the potential drop across the inner layer, $\phi^m - \phi^d$ in solutions of (*a*) 0.24 *M* $NaClO_4$ + 0.01 *M* $HClO_4$ and (*b*) 0.04 *M* NaI + 0.20 *M* $NaClO_4$ + 0.01 *M* $HClO_4$.

Results

Kinetic data were obtained in six different electrolyte solutions of composition xM NaI + $(0.24 - x)M$ $NaClO_4$ + 0.01 *M* $HClO_4$ where x = 0, 0.0063, 0.01, 0.016, 0.025, and 0.04 *M*. Data obtained in solutions where x = 0 and 0.04 *M* are shown in Fig. 1. As expected, the rate constant increases with increase in I^- concentration at constant electrode potential. The acceleration is attributed to the shift in the potential drop across the diffuse layer in the negative direction with increase in the extent of I^- ion adsorption, and the corresponding increase in the rate of reduction of the positively charged reactant. The experimental transfer coefficient α_{ex} obtained in the electrolyte with no I^- anion (x = 0) was 0.91. This value can be compared with values of 0.72 obtained by Anson *et al.* (3) in 1 *M* $NaClO_4$ + 0.01 *M* $HClO_4$, and 0.73 obtained by Weaver and Satterberg (4) in the same electrolyte. Since the double layer effect is reduced with increase in ionic strength, its influence on α_{ex} is smaller in the data obtained earlier (3, 4). If one corrects for the double layer effect assuming that the reaction site is on the outer Helmholtz plane (o.H.p.), then one can obtain the apparent transfer coefficient α_a, which is given by

$$[1] \quad \alpha_a = \frac{\alpha_{ex} - z(d\phi^d/d\phi^m)}{1 - (d\phi^d/d\phi^m)}$$

where z is the charge on the reactant, and $d\phi^d/d\phi^m$, the change in ϕ^d with electrode potential, ϕ^m. For the present base electrolyte, ignoring possible specific adsorption of ClO_4^- anion, $d\phi^d/d\phi^m$ = 0.098. It follows that α_a = 0.68 when z is assumed to be 3. Weaver and Satterberg (4) estimated that $d\phi^d/d\phi^m$ is in the range 0.055 to 0.085 in 1 *M* $NaClO_4$ but apparently did not consider the influence of the highly charged reactant and product on ϕ^d and $d\phi^d/d\phi^m$. Choosing the lower limit (0.055), the value of α_a estimated from their data is 0.59. Both values are greater than the result expected for a reaction occurring on the o.H.p., namely, 0.5, and support the conclusion reached earlier that the reaction site for the ammino-complexes of Cr(III) and Co(III) is in the inner layer (3, 4, 8). In the absence of discreteness-of-charge effects, attractive ion–ion interactions and surface coverage effects, the true or intrinsic transfer coefficient α can be calculated from the apparent value using the equation

$$[2] \quad \alpha = (\alpha_a - \lambda z)/(1 - \lambda)$$

where λ is a dimensionless fraction determined by the distance between the reaction plane (r.p.) and o.H.p., and the dielectric permittivity of the medium between these planes. If it is assumed that α is 0.5, then λ equals 0.072, indicating that the potential at the reaction site is 7.2% more negative than the average potential on the o.H.p. It follows that a very small shift in the potential at the reaction site has a large effect on the rate of reaction and apparent transfer coefficient in the case of highly charged reactants.

Corrected Tafel plots (c.T.p.) for the present data are shown in Fig. 2 for the case that the charge on the reactant is assumed to be 3+. Neglecting discreteness-of-charge effects, the corrected rate of reaction is given by

$$[3] \quad \ln k + zf\phi^d = \ln k_0 - \alpha_a f(\phi^m - \phi^d)$$

where k is the rate constant for the reduction reaction, and k_0, its value when both ϕ^m and ϕ^d are zero, that is, at the p.z.c. in an electrolyte which does not specifically adsorb. It is clear

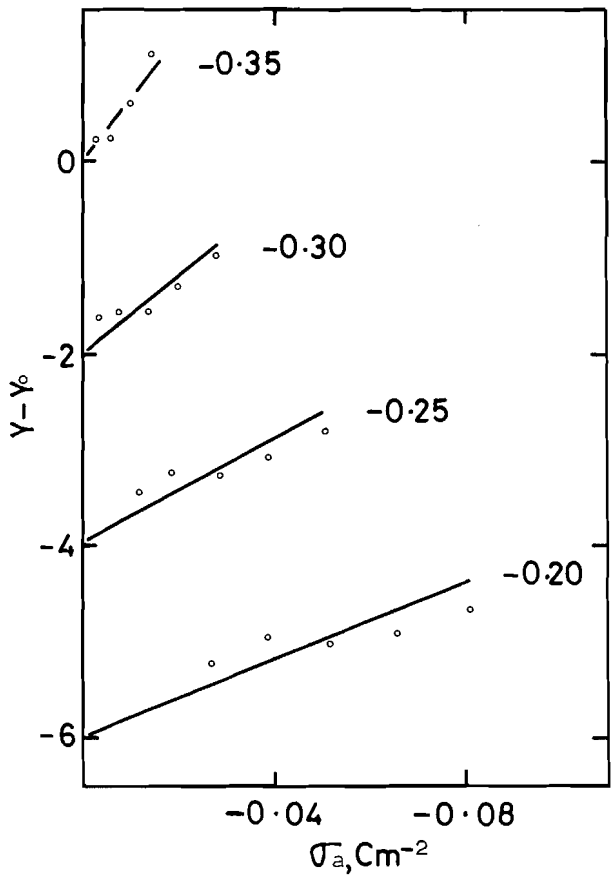

FIG. 3. Plots of the logarithm of the corrected rate constant, $y = \ln k + 3f\phi^d$ for reduction of $Cr(NH_3)_5OH_2^{3+}$ at mercury in mixed $NaClO_4$–NaI solution with respect to that in $NaClO_4$, y_0 against adsorbed charged density due to iodide anions, σ_a for constant potential drop across the inner layer, $\phi^m - \phi^d$. The value of $\phi^m - \phi^d$ in volts is indicated adjacent to each curve. The ordinate scale is correct for the data at −0.35 V whereas the data at −0.30, −0.25, and −0.20 V have been shifted down by 2, 4, and 6 units, respectively.

from the c.T.p. that the classical theory is not able to account for the accelerating effect of the adsorbed I^- anions, the corrected rate constant being higher in the system 0.04 *M* NaI + 0.20 *M* $NaClO_4$ with respect to the value in 0.24 *M* $NaClO_4$ by a factor of 4. As expected, the value of the apparent transfer coefficient calculated from the slope of the c.T.p. obtained in the absence of I^- ion is the same (0.68) as that found on the basis of eq. [1]. Values of α_a for data obtained in the presence of I^- ion are somewhat lower (~0.58), suggesting that the classical analysis is not valid for these systems. If one assumes that ion pairs are involved in the electrode reaction, as was done earlier in analyzing data for the reduction of $Co(NH_3)_6^{3+}$, and sets $z = 2$ in the c.T.p., then the separation between the c.T.p. for the systems considered in Figs. 1 and 2 would be significantly larger. This fact is an indirect support for the assumption that ion pairs are not involved in the present electrode reaction, and that the charge should be set equal to 3+ in constructing the c.T.p. It should be noted that the classical technique for determining z (9, 10) using kinetic data obtained in solutions of varying composition cannot be applied to the present system since the Frumkin equation (eq. [3]) does not correctly describe the double layer effect. Furthermore, an alternate method (11) which makes use of data obtained at a fixed electrolyte composition, for instance, 0.24 *M* $NaClO_4$ in the present case, is also not applicable because ϕ^d is approximately a linear function of ϕ^m in the potential range of interest.

The change in the corrected rate constant, $y = \ln k + zf\phi^d$ with adsorbed I^- anion charge density at constant $\phi^m - \phi^d$ is illustrated in Fig. 3 from which it is apparent that the extent by which a fixed amount of adsorbed I^- anion influences y is a function of $\phi^m - \phi^d$. At the most negative potentials the influence is greatest, and it decreases steadily as $\phi^m - \phi^d$ becomes more positive. A similar trend was found for the effect of adsorbed I^- on the corrected rate of reduction of tetrathionate anion (12). In assessing the variation in y with adsorbed charge density, σ_a it should be remembered that according to the Frumkin model of double layer effects, y should be independent of solution composition, and therefore, σ_a, when the effect of the latter is considered in estimating ϕ^d. It is clear that the Frumkin model is not able to describe the present results, and in fact, only accounts for ~50% of the variation in ln k with solution composition illustrated in Fig. 1.

The variation in y with σ_a may be attributed to the dependence of the local potential at the reaction site on the extent of iodide adsorption, and attractive ion–ion interactions between the reacting cation and the adsorbed anions. On the basis of the theory presented earlier (2), the change in y with respect to its value in the absence of adsorbed anions, y_0 is given by

$$[4] \quad y - y_0 = \frac{(\alpha - z)f(1 - \lambda)(1 - g)}{K_2}\sigma_a - \frac{a_{\neq}\sigma_a}{RT}$$

where g is a dimensionless parameter related to the degree that repulsive interactions between adsorbent anions are screened by their electrostatic environment, K_2, the integral capacity of the region between the inner Helmholtz plane (i.H.p.) and the o.H.p., and $a_{\neq}$, the parameter accounting for interaction between the reacting cation and adsorbed anions in the activated state. According to the exclusion disc model for discreteness-of-charge effects (13), the parameter g is close to unity. When it is exactly one, the local potential ψ^r is given by (2)

$$[5] \quad \psi^r = \phi^d + \lambda(\phi^m - \phi^d)$$

that is, by the same expression that applies in the absence of specific adsorption. This means that the change in the local potential in the inner layer with position is independent of the value of σ_a provided that the local dielectric permittivity and thus λ are also independent of σ_a. When $g = 1$, the contribution of the first term on the r.h.s. of eq. [4] is zero. In most cases, g is not exactly one, and in the case of iodide adsorption for the conditions of the present experiment, it is less than one (6, 12). In fact, since $(\alpha - z)$ is negative, the first term leads to an increase in the corrected rate of reaction with increase in the extent of iodide adsorption. The second term, which accounts for attractive interactions between the reacting cation and adsorbed anions, also depends on σ_a and is positive. This implies that the interaction parameter $a_{\neq}$ is positive. On the basis of models developed to estimate $a_{\neq}$ (14, 15), this parameter changes with the dielectric properties of the medium in the vicinity of the reaction site, and therefore, is expected to change with electrode potential.

In order to assess the relative contributions of the two effects discussed above, the parameters characterizing iodide adsorption at Hg from the NaI–NaF system are required. On the basis of the data obtained earlier (6), $K_2 = 0.662$ Fm^{-2} and $g = 0.86$ at $\phi^m - \phi^d = -0.2$ V. From the value of α_a for the present system (0.68), $(\alpha - z)(1 - \lambda)$ is equal to −2.32. It follows that $(\alpha - z)f(1 - \lambda)(1 - g)/K_2$ is equal to −19.1 m^2

Can. J. Chem. Downloaded from www.nrcresearchpress.com by 210.87.254.40 on 09/06/12
For personal use only.

C^{-1} at −0.2 V. As $\phi^m - \phi^d$ is made more negative, both the capacity K_2 and the parameter g decrease somewhat. As a result $(\alpha - z)f(1 - \lambda)(1 - g)/K_2$ increases. From the plots in Fig. 3, $dy/d\sigma_a$ varies from -20 m^2 C^{-1} at −0.20 V to -50 m^2 C^{-1} at −0.35 V. These results indicate that the observed variation in the corrected rate of reaction with σ_a can be attributed entirely to the discreteness-of-charge effect; in other words, the role of possible attractive interactions between the adsorbed anions and the reacting cation expressed through the term $a_{\neq}\sigma_a/RT$ is quite negligible.

Discussion

In agreement with results obtained earlier in solutions of higher ionic strength (3, 4), the present data show clearly that the effect of adsorbed iodide on the kinetics of reduction of $Cr(NH_3)_5OH_2^{3+}$ is considerably greater than that predicted by the Gouy–Chapman model. Furthermore, as discussed in the earlier work (3, 4), this observation can be attributed chiefly to the fact that the reaction site for this complex ion is in the inner layer, presumably between the i.H.p. and o.H.p. Thus, as the potential at the reaction site becomes more negative, the rate of reduction of this highly charged cationic reactant is significantly accelerated. In the context of the analysis of the double effect used here, it is interesting to estimate the extent to which discreteness-of-charge effects are important in determining the magnitude of the observed acceleration. On the basis of the model presented earlier (2), the difference between the local potential at the reaction site ψ^r and the average potential on the o.H.p., ϕ^d is given by

$$[6] \quad \psi^r - \phi^d = \lambda(\phi^m - \phi^d) + \frac{(1 - \lambda)(1 - g)\sigma_a}{K_2}$$

When λ is defined as K_i/K_{rd} where K_i is the integral capacity of the inner layer and K_{rd}, the integral capacity of the region between the r.p. and the o.H.p., the above expression is valid for any reaction site in the inner layer. The extent to which specific adsorption modifies this potential difference at constant potential drop across the inner layer is given by

$$[7] \quad \Psi_d = \left[\frac{\partial(\psi^r - \phi^d)}{\partial\sigma_a}\right]_{\phi^m - \phi^d} = \frac{(1 - \lambda)(1 - g)}{K_2}$$

Using the double layer parameters for the NaI–NaF system and assuming $\lambda = 0.1$, this coefficient is equal to 0.19 m^2 F^{-1} at $\phi^m - \phi^d = -0.2$ V, and 0.29 m^2 F^{-1} at $\phi^m - \phi^d = -0.3$ V. Thus, it increases with change in $\phi^m - \phi^d$ in the negative direction, and as a result, the observed change in the corrected rate constant also increases (Fig. 3). When the reaction site is closer to the electrode, λ is larger, and Ψ_d decreases, reflecting the fact that the screening of attractive interactions between the reactant and the adsorbed anions becomes more effective the closer the reaction site is to the electrode. It is also interesting to note that if g is greater than unity, as is true in the case of nitrate adsorption (16), Ψ_d is negative, and one should observe that the corrected rate of reaction y decreases with increase in σ_a at constant $\phi^m - \phi^d$. Under these circumstances, the local potential is somewhat more positive than the value given by eq. [5], and deceleration of the reduction of a cation would be observed with increase in adsorbed anionic charge density. If the discreteness-of-charge effect is ignored, then the difference between the average potential on the r.p., ϕ^r and that on the o.H.p. for reaction sites between the i.H.p. and o.H.p. is given by (2)

$$[8] \quad \phi^r - \phi^d = \lambda(\phi^m - \phi^d) + \frac{\lambda\sigma_a}{K_1}$$

where K_1 is the integral capacity of the region between the electrode and the i.H.p. The extent to which specific adsorption modifies this potential difference is given by

$$[9] \quad \Psi_a = \left[\frac{\partial(\phi^r - \phi^d)}{\partial\sigma_a}\right]_{\phi^m - \phi^d} = \frac{\lambda}{K_1}$$

Assuming $\lambda = 0.1$, Ψ_a is equal to 0.24 m^2 F^{-1} at $\phi^m - \phi^d = -0.2$ V, and 0.25 m^2 F^{-1} at −0.3 V. First of all, it is immediately apparent that the coefficients Ψ_a and Ψ_d are approximately equal at the most positive value of $\phi^m - \phi^d$, and that they are of the same order of magnitude for the chosen value of λ. This result is not surprising considering the fact that the discreteness-of-charge effect is not expected to play an important role when λ is small and the reaction site is close to the o.H.p. On the other hand, Ψ_a changes negligibly with $\phi^m - \phi^d$ so that one could not account for the observed variations in $dy/d\sigma_a$ (Fig. 3) on the basis of a model which ignored discreteness-of-charge. Furthermore, as the reaction site is moved closer to the electrode, Ψ_a increases whereas Ψ_d decreases. In addition, for a given reaction site in the inner layer, one should always observe acceleration of the reduction of a cation independent of the nature of the adsorbed anion. In conclusion, although the present data do not provide unequivocal evidence for the importance of discreteness-of-charge effects, they can be rationalized in all details on the basis of the discreteness-of-charge model.

Because of the relative simplicity of the double layer effect for the present system, it was possible to conclude that attractive interaction between the reactant and adsorbed anions do not constitute an important contribution to the observed acceleration of the reaction rate in the presence of iodide ions. This result is expected when shielding of the reactant from the adsorbed anions is strong, as predicted by the theory of discreteness-of-charge effects (2, 13–15). Furthermore, $Cr(NH_3)_5OH_2^{3+}$ has been shown by Anson (3) and Weaver (4) to be an outer sphere reactant (17), that is, a reactant which does not interact strongly with the electrode. It follows that the reaction site for $Cr(NH_3)_5OH_2^{3+}$ is expected to be further away from the electrode than the i.H.p., and on the basis of the evidence presented above, between the i.H.p. and o.H.p.

There has been considerable discussion in the literature (8, 18, 19) relating to the question of whether kinetic data can be used to demonstrate failure of the Gouy–Chapman–Stern model of the potential distribution in the double layer. There is no doubt that the diffuse layer model is seriously defective in solutions involving multivalent ions (20, 21). Calculations by Henderson and Blum (22) suggest that $d\phi^d/d\phi^m$ is somewhat less than the value predicted by Gouy–Chapman theory in 1–1 electrolytes when more realistic models are used for the diffuse layer. In this case, the estimate of α_a made above is low. It follows that one cannot use defects in the Gouy–Chapman model to argue that the reaction site is on the o.H.p. Furthermore, it should be kept in mind that the Gouy–Chapman model was used to obtain the adsorbed charge densities (6) employed in the analysis of the present kinetic data. In this sense, any systematic error in the values of σ_a will also be present in the kinetic analysis. If the increase in y with σ_a reported in Fig. 3 is attributed to an error in ϕ^d, then $|\phi^d|$ is underestimated by 10 mV for a change in y by one logarithmic unit. Given that $d\phi^d/d\sigma_a = 0.28$ m^2 F^{-1}, the corresponding

Can. J. Chem. Downloaded from www.nrcresearchpress.com by 210.87.254.40 on 09/06/12
For personal use only.

error in the estimate of σ_a would be 0.036 C m^{-2}. It is difficult to imagine that σ_a would be in error by this amount especially considering the facts that the data were obtained at constant ionic strength, and that values of σ_a are being used for constant $\phi^m - \phi^d$. Thus, it is concluded that a better model of the diffuse layer would change the kinetic parameters but would not change qualitatively the conclusions made above regarding the nature of the double layer effect.

In conclusion, it would be interesting to examine the double layer effect for the present reactant or a related species in the presence of an adsorbed anion such as nitrate for which the screening parameter g is greater than one. Such an experiment would provide unequivocal evidence of the discreteness-of-charge effect. Experiments with this goal in mind are currently in progress.

Acknowledgement

The financial support of the Natural Sciences and Engineering Research Council of Canada is gratefully acknowledged.

1. W. R. FAWCETT and K. MARKUŠOVÁ. Can. J. Chem. **61**, 2821 (1983).
2. W. R. FAWCETT. Can. J. Chem. **59**, 1844 (1981).
3. F. C. ANSON, M. G. FINN, and A. YAMADA. Inorg. Chem. **16**, 2124 (1977).
4. M. J. WEAVER and T. L. SATTERBERG. J. Phys. Chem. **81**, 1772 (1977).
5. B. G. CHAUHAN, W. R. FAWCETT, and A. LASIA. J. Phys. Chem. **81**, 1476 (1977).
6. W. R. FAWCETT and T. A. MCCARRICK. J. Electrochem. Soc. **123**, 1325 (1976).
7. J. KOUTECKÝ and J. ČIŽEK. Coll. Czech. Chem. Commun. **21**, 836 (1956).
8. T. L. SATTERBERG and M. J. WEAVER. J. Phys. Chem. **82**, 1784 (1978).
9. A. N. FRUMKIN, O. A. PETRII, and N. V. NIKOLAEVA-FEDOROVICH. Electrochim. Acta, **8**, 177 (1963).
10. L. GIERST. Trans. Symposium on Electrode Processes. *Edited by* E. Yeager. Wiley, New York. 1960. pp. 109–138.
11. W. R. FAWCETT, J. E. KENT, and Y. C. KUOLEE. J. Electroanal Chem. **20**, 357 (1969).
12. W. R. FAWCETT and K. MARKUŠOVÁ. Can. J. Chem. **60**, 2038 (1982).
13. K. ROBINSON and S. LEVINE. J. Electroanal. Chem. **47**, 395 (1973).
14. W. R. FAWCETT and S. LEVINE. J. Electroanal. Chem. **65**, 505 (1975).
15. R. GUIDELLI. J. Electroanal. Chem. **74**, 347 (1976).
16. W. R. FAWCETT and J. B. SELLAN. Can. J. Chem. **55**, 3871 (1977).
17. M. J. WEAVER and F. C. ANSON. Inorg. Chem. **15**, 1871 (1976).
18. M. J. WEAVER and F. C. ANSON. J. Electroanal. Chem. **65**, 711 (1975).
19. F. C. ANSON and B. A. PARKINSON. J. Electroanal. Chem. **85**, 317 (1977).
20. M. LOZADA-CASSOU, R. SAAVEDRA-BARRERA, and D. HENDERSON. J. Chem. Phys. **77**, 5150 (1982).
21. M. LOZADA-CASSOU and D. HENDERSON. J. Phys. Chem. **87**, 2821 (1983).
22. D. HENDERSON and L. BLUM. Can. J. Chem. **59**, 1906 (1981).

Can. J. Chem. Downloaded from www.nrcresearchpress.com by 210.87.254.40 on 09/06/12
For personal use only.

Ab initio SCF + CI calculation of rotational energy barriers in CH_2—X—CH_2 species

F. VOLATRON

Laboratoire de Chimie Théorique (CNRS-UA 506), Bâtiment 490, Université de Paris-Sud, 91405 Orsay Cédex — France

Received October 19, 1983

F. VOLATRON. Can. J. Chem. **62**, 1502 (1984).

The rotational energy barriers in CH_2—X—CH_2 species (X = NH, O, CH_2) are calculated by means of *ab initio* SCF + CI calculations. With the most sophisticated CI calculations, they are found to be equal to 36.1, 20.6, and 1.1 kcal/mol for X = NH, O, and CH_2, respectively. These values are briefly discussed with respect to the valence bond analysis of the wave function.

F. VOLATRON. Can. J. Chem. **62**, 1502 (1984).

Faisant appel à des calculs *ab initio* en champ autocohérent + CI, on a calculé les barrières d'énergie rotationnelle dans les espèces CH_2—X—CH_2 (X = NH, O, CH_2). Avec les calculs CI les plus sophistiqués, on trouve qu'elles sont égales à 36,1, 20,6 et 1,1 kcal/mol respectivement pour X = NH, O et CH_2. On discute brièvement de ces valeurs par rapport à l'analyse des liaisons de valence des fonctions d'ondes.

[Traduit par le journal]

Introduction

1,3-Dipoles of CH_2—X—CH_2 type (X = NH, O) are generated by ring opening of a three-membered ring (see ref. 1 for X = NH, ref. 2 for X = O). They are intermediates along the reaction path for the *cis–trans* isomerization reaction (3) (Scheme 1) and can be trapped by a dipolarophile (a = b) to give a five-membered cycloadduct (1, 2) (Scheme 2).

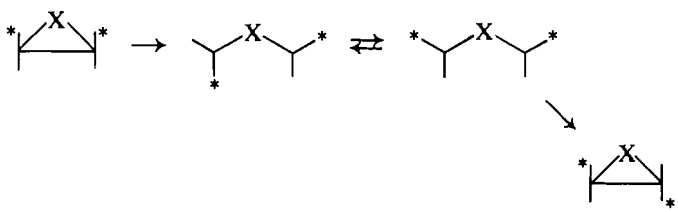

SCHEME 1. Reaction pathway for *cis–trans* isomerization of three-membered rings.

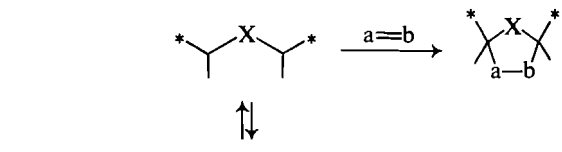

SCHEME 2. Formation of cycloadduct by trapping 1,3-dipole intermediate.

In the latter, if cycloaddition with a = b is fast relative to isomerization process, the stereochemistry of the cycloadduct reveals the initial opening mode of the three-membered ring (see ref. 4(*a*) for X = NH, ref. 4(*b*) for X = O). In both kinds of experiments, the rotation in the planar CH_2—X—CH_2 species is a crucial factor for mechanism analysis: (*i*) in the *cis–trans* isomerization, this step controls the formation of the reaction product; (*ii*) in reactions involving a dipolarophile, the rapid *cis–trans* isomerization of planar intermediate can lead to a loss of stereoselectivity in the final cycloadduct. Such a loss of stereoselectivity has been already observed in the case of substituted oxiranes (5) (X = O) and it could result from a rather low rotational energy barrier in the intermediate carbonyl ylide species (6).

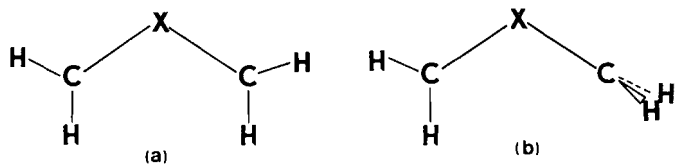

FIG. 1. Geometrical definition of EE and EF structures.

The aim of this paper is the study of barriers of rotation in such species (CH_2—X—CH_2 with X = O and X = NH) by means of *ab initio* calculations. In order to understand the role of increasing electronegativity of the central X atom, we also studied the extreme case in which X = CH_2, corresponding to the trimethylene diradical.

Two structures have been studied for each species: the edge-to-edge (EE) structure in which both CH_2 groups lie in the ∠CXC plane (Fig. 1*a*) and the edge-to-face (EF) structure in which a CH_2 group is orthogonal to that plane (Fig. 1*b*). The rotational energy barrier is assumed to be the energy difference between EE and EF structures.

Method of calculation

As shown in a previous paper (7*a*, for theoretical calculations on the photochemical properties of such intermediates, see ref. 7*b*), a proper description of both EE and EF structures needs an open shell SCF calculation followed, at least, by a (3 × 3) configuration interaction (CI) involving the three singlet configurations built from the two frontier molecular orbitals. These structures have been optimized at the STO3G (8) + (3 × 3) CI level with the GAUSSIAN 70 (9) program using the Nesbet (10) restricted hamiltonian for open shell systems. Then these optimized structures have been recomputed at the 4-31G (11) + extended CI level with the MONSTERGAUSS (12) program using the Davidson's (13) triplet open shell hamiltonian which ensures a more rapid convergence of the CI procedure. For extended CI calculations, we used the CIPSI (14) algorithm whose main features are the following: from SCF calculation, a few number of determinants are selected (*S*-space), the diagonalization of the associated hamiltonian matrix leading to the zeroth order wave function and energy. All the determinants built by single and double excitation from the determinants belonging to the *S*-space are treated by a second order perturbation leading to the calculation of the perturbation coefficient. If this coefficient is

Can. J. Chem. Downloaded from www.nrcresearchpress.com by 210.87.254.42 on 09/06/12
For personal use only.

Can. J. Chem. Downloaded from www.nrcresearchpress.com by 210.87.254.42 on 09/06/12
For personal use only.

greater than an arbitrarily fixed threshold (τ), the corresponding determinant is included in the *S*-space. This iterative procedure is completed when all the perturbation coefficients are lower than the threshold. This process allows (*i*) a rigourous selection of the determinants belonging to the zeroth order multideterminantal wave function and (*ii*) to calculate by perturbation the contribution of other excited configurations to the correlation energy. We performed these CI calculations at three distinct levels: (*1*) *S* is limited to the determinants built from the frontier orbitals. Then diagonalization in *S*-space is equivalent to the (3 × 3) CI. This type of calculation will be referred as S_{min}; (*2*) the threshold (τ) is fixed at 0.03; and (*3*) the threshold (τ) is fixed at 0.02.

For each calculation, we report the variational diagonalization energy in the *S*-space, the total energy including perturbational contributions, and the norm (*N*) of perturbational correction of the variational zeroth order wave function.

Results

(A) Wave function analysis

(1) EF structure

The geometrical parameters for the three EF structures are depicted in Fig. 2.

• *Calculation with* S_{min}

For X = CH_2 and X = O, the optimized structures are symmetrical with respect to the ∠CXC plane. The two frontier orbitals — non-bonding *n* orbital carried by C_3 and π^*_{cx} orbital (7) — are orthogonal and the zeroth order wave function of the singlet ground state is described by the $^1n\pi^*$ configuration.

For X = NH, the situation is more complicated since geometrical optimization leads to an out-of-plane motion of the central hydrogen atom (H_N) which destroys the symmetry plane. Therefore, the zeroth order wave function of the singlet ground state is a mixing of the three singlet configurations built on the frontier orbitals:

$$\psi^0 = 0.760^1n\pi^* + 0.384\pi^{*2} - 0.525n^2$$

• *Extension of* S*-space*

The extension of the *S*-space has been performed as described above. We found no determinant with coefficient greater than 0.03. This shows that the configurations involved in the limited (3 × 3) CI are by far the most important for the description of EF structure. When lowering the threshold to 0.02, the *S* dimension grows to 7, 8 , and 10 for X = NH, O, and CH_2, respectively. The zeroth order wave function is only slightly perturbed by the new determinants (mainly representing correlation effects in the terminal methylene groups):

$$\psi^0_{NH} = 0.758^1n\pi^* + 0.383\pi^{*2} - 0.527n^2 + \ldots$$

$$\psi^0_{O} = 0.998^1n\pi^* + \ldots$$

$$\psi^0_{CH_2} = 0.998^1n\pi^* + \ldots$$

The accuracy of this zeroth order wave function can be tested by calculating the norm (*N*) of perturbation correction (Table 1). The values reported in Table 1 show that the norm of the perturbation correction is almost independent of the *S*-space dimension, thus confirming that the zeroth order wave function corresponding to S_{min} is already a rather good approximation of the total wave function.

(2) EE structure

Geometrical parameters for optimized EE structures are depicted in Fig. 3. Note that, for X = NH, the H_N atom lies in the CNC plane in order to allow an allyl-like resonance stabilization in the π system.

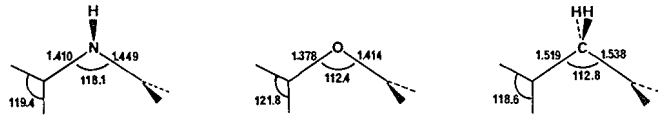

FIG. 2. Geometrical parameters for the three EF structures. The CH_2 groups are assumed trigonal. Out-of-plane bending of central hydrogen atom in CH_2—NH—CH_2 is 38.3°.

TABLE 1. Norm of perturbation correction (*N*) depending on the *S*-space dimension (EF structures)

	N		
X	S_{min}	τ = 0.03	τ = 0.02
NH	0.105	0.105	0.104
O	0.104	0.104	0.103
CH_2	0.098	0.098	0.098

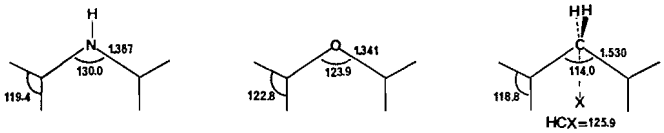

FIG. 3. Geometrical parameters for the three EE structures. The CH_2 groups are assumed trigonal.

• *Calculation with* S_{min}

Simple Hückel calculations on the π system of planar CH_2—X—CH_2 species show that an increasing electronegativity of the central group (X = NH, O, CH_2) leads to a reduction of the energy gap between the frontier molecular orbitals π_2 and π_3. Therefore, the energy gap between the ground configuration $[\pi_2^2]$ and the first doubly excited configuration $[\pi_3^2]$ being smaller, the mixing of these configurations should increase. This tendency is confirmed by the expression of the zeroth order wave functions:

$$\psi^0_{NH} = 0.914\pi_2^2 - 0.404\pi_3^2$$

$$\psi^0_{O} = 0.872\pi_2^2 - 0.489\pi_3^2$$

$$\psi^0_{CH_2} = 0.731\pi_2^2 - 0.683\pi_3^2$$

In the latter, one can note that the coefficients of π_2^2 and π_3^2 are almost equal because trimethylene species is almost a "pure" diradical with a singlet ground state wave function approximately given by (15):

$$\psi^0 = \frac{1}{\sqrt{2}}(\pi_2^2 - \pi_3^2)$$

• *Extension of* S*-space*

Consider first the EE structure for X = CH_2. As we have just seen, this structure can be mainly described by the diradical structure:

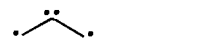

One electron is localized on each terminal carbon and a pair of electrons in the central π_{CH_2} orbital. The predominance of this valence bond structure can be interpreted by recognizing the

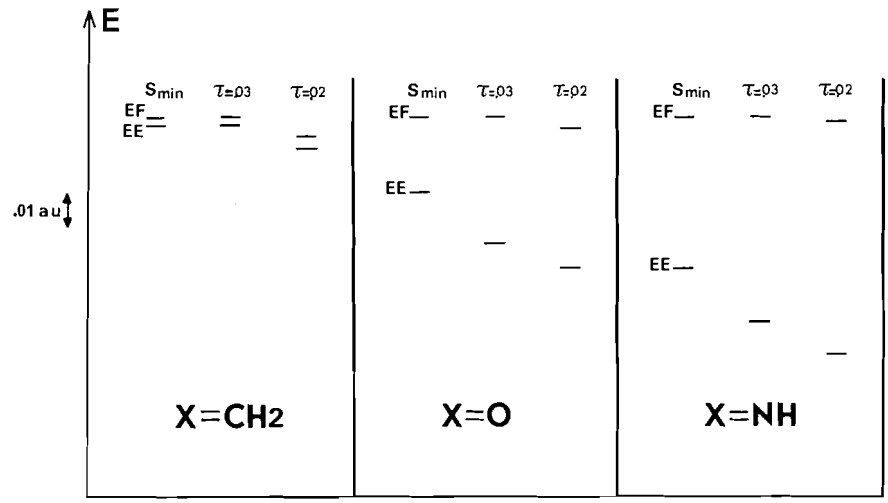

FIG. 4. Evolution of EE and EF energies with increasing S-space size. In each case, the energy of EF structure, calculated at the S_{min} CI level, is arbitrarily taken as origin. The absolute energies are −132.7780, −152.5644, and −116.8610 au for X = NH, O and CH_2, respectively.

large energy difference between the $2p$ and the π_{CH_2} orbitals.

In this description, the two unpaired electrons are rather well correlated by a CI limited to the S_{min} space. In other words, this electronic correlation problem is almost identical to a two electrons problem in which a (3 × 3) CI gives the proper correlation energy. Then, extension of the CI is only useful for correlating the two electrons localized in the π_{CH_2} orbital. Indeed, only eight determinants are needed in the S-space when the threshold is fixed to 0.02.

On the contrary, when X = NH, the central lone pair interacts more strongly with the carbon $2p$ orbitals and new valence bond structures contribute to the description of the ground state (16):

These structures represent the classical zwitterionic forms:

Now, an important part of the wave function localizes two electrons in the same $2p$ orbital of terminal carbon. So CI expansion is useful not only to correlate the two electrons in the central lone pair, but also to correlate the electron pair localized in the $2p$ orbital of terminal atoms. This is illustrated by an increase of S-space to 26 determinants when the threshold is 0.02. For X = O, we get an intermediate dimension of 20 determinants for S. In Table 2 are reported the norm of perturbation correction N computed for each type of calculation.

The results illustrate our preceeding discussion: for X = CH_2, the high diradical character ensures a rather good description even at a limited S-space dimension (N = 0.096). The increase of the CI size does not improve noticeably the accuracy of the wave function. On the contrary, for X = NH, the limited CI gives a more approximate wave function (N = 0.118), a result which can be notably improved (N = 0.104) by an increase of the S-space dimension. An intermediate result is found for X = O since the diradical character of carbonyl ylide is intermediate between those of azomethine ylide (X = NH) and trimethylene (X = CH_2) (17).

TABLE 2. Norm of perturbation correction (N) depending on the S-space dimension (EE structures)

	N		
X	S_{min}	τ = 0.03	τ = 0.02
NH	0.118	0.108	0.104
O	0.115	0.107	0.103
CH_2	0.096	0.096	0.095

TABLE 3. Calculated rotational barriers at various level of CI (perturbative terms are not taken into account)

	Barrier (kcal/mol)		
X	S_{min}	τ = 0.03	τ = 0.02
NH	24.9	33.8	38.3
O	12.7	20.7	23.3
CH_2	1.4	1.4	2.0

(B) Rotational energy barriers

(1) Variational zeroth order energy

In the preceeding section, it has been shown that EF structures are rather well described at the SCF + S_{min} CI level while EE structures are more sensitive to CI extension. As a consequence, an increase of the rotational barrier with the CI size is expected. Furthermore, the rotational energy barrier increase should be more and more important going from X = CH_2 to X = O and X = NH. Both these tendencies are confirmed by calculation of zeroth order energies with various sizes of S-space (Fig. 4). The computed energy barriers are reported in Table 3.

Although the results given by a limited CI (S_{min}) leads to an energy barrier order in agreement with that computed with more extended CI calculations, they are not very good from a quantitative point of view, since these values are at least 50% lower than the most sophisticated ones. Note that the increase of the barrier with the size of the CI has been already reported by Yamaguchi (18) on study of methylene peroxide CH_2OO.

Can. J. Chem. Downloaded from www.nrcresearchpress.com by 210.87.254.42 on 09/06/12
For personal use only.

TABLE 4. Rotational barriers taking into account the perturbation terms in correlation energy

X	Barrier (kcal/mol) S_{min}	$\tau = 0.03$	$\tau = 0.02$
NH	36.7	35.2	36.1
O	22.7	21.2	20.6
CH_2	1.0	1.0	1.1

(2) Influence of perturbation terms

In Table 4 are reported the rotational barriers taking into account the part of correlation energy computed by perturbation treatment.

First, one can note a small dependence of the computed rotational barrier with the various size of *S*-space, the maximum variation being 10%. Furthermore, the computed barriers are close to those found using the zeroth order energies at our highest level of CI.

Discussion

The calculated values are not directly comparable to experimental data only available for highly substituted species: for the (*exo,exo*)-1-cyano, 1,3-diphenylcarbonyl ylide HΦC—O—CΦCN, the rotational barrier is found in the range of 12−16 kcal/mol, and for the (*exo,exo*)-1,3-dimethyldicarboxylate

(N_4-methoxyphenyl) azomethine ylide (CHR—N—CHR with R = —$COOCH_3$) this barrier is 22.0 kcal/mol (1*c*). Computed energy barriers are systematically higher than the experimental ones. Note, however, that the ratio between theoretical (unsubstituted molecules) and experimental (substituted molecules) values is nearly 1.5 both for X = O (carbonyl ylide) and X = NH (azomethine ylide).

This trend shows the strong connection between rotational energy barrier and diradical character of the CH_2—X—CH_2 intermediate: as the weight of the diradical structure increase, the rotational energy barrier decreases. It can be related to the weakening of the π bonding between X and C, arising from the decreasing participation in the wave function of VB structures such as:

Going from X = NH to X = O and X = CH_2, the allyl-like resonance in the four π electron system decreases, making it easier to rotate around C—X bond.

Finally, our results show that calculations which include the perturbation terms lead to rather stable values for the energy barrier (Table 4) whatever the extension of *S*-space from S_{min}.

Acknowledgment

Dr. Y. Jean is gratefully acknowledged for suggesting this study and many fruitful discussions.

1. (*a*) R. HUISGEN, W. SCHEER, and H. MÄDER. Angew. Chem. Int. Ed. **8**, 602 (1969); **8**, 604 (1969); (*b*) R. HUISGEN and H. MÄDER. J. Am. Chem. Soc. **93**, 1777 (1971); (*c*) H. HERMANN, R. HUISGEN, and H. MÄDER. J. Am. Chem. Soc. **93**, 1779 (1971).
2. R. HUISGEN. Angew. Chem. Int. Ed. **16**, 572 (1977).
3. R. J. CRAWFORD and H. H. J. MCDONALD. Can. J. Chem. **50**, 428 (1972).
4. (*a*) R. HUISGEN, W. SCHEER, and H. HUBER. J. Am. Chem. Soc. **89**, 1753 (1967); (*b*) H. HAMBERGER and R. HUISGEN. Chem. Commun. 1190 (1971).
5. (*a*) A. DAHMEN, H. HAMBERGER, R. HUISGEN, and V. MARKOWSKI. Chem. Commun. 1191 (1971); (*b*) V. MARKOWSKI and R. HUISGEN. Chem. Commun. 439 (1977); (*c*) R. HUISGEN and V. MARKOWSKI. Chem. Commun. 440 (1977).
6. F. VOLATRON, NGUYEN TRONG ANH, and Y. JEAN. J. Am. Chem. Soc. **105**, 2359 (1983).
7. (*a*) Y. JEAN and F. VOLATRON. Chem. Phys. Lett. **83**, 91 (1981); (*b*) B. BIGOT, A. SEVIN, and A. DEVAQUET. J. Am. Chem. Soc. **101**, 1095 (1979); O. P. STRAUSZ, R. K. GOSAVI, G. R. DE MARÉ, M. R. PETERSON, and I. G. CSIZMADIA. Chem. Phys. Lett. **70**, 31 (1980); G. R. DE MARÉ, M. R. PETERSON, I. G. CSIZMADIA, and O. P. STRAUSZ. J. Comp. Chem. **1**, 141 (1980); M. R. PETERSON and G. R. DE MARÉ. J. Mol. Struct. **88**, 1 (1982).
8. W. J. HEHRE, R. F. STEWART, and J. A. POPLE. J. Chem. Phys. **51**, 2567 (1969).
9. W. J. HEHRE, W. A. LATHAN, R. DITCHFIELD, M. D. NEWTON, and J. A. POPLE. Program n° 236, Q.C.P.E. Indiana University, Bloomington, IN.
10. R. K. NESBET. Rev. Mod. Phys. **35**, 552 (1963).
11. R. DITCHFIELD, W. J. HEHRE, and J. A. POPLE. J. Chem. Phys. **54**, 724 (1971).
12. M. PETERSON and R. POIRIER. Department of Chemistry, University of Toronto, Toronto, Ont.
13. E. R. DAVIDSON. Chem. Phys. Lett. **21**, 565 (1973).
14. B. HURON, J. P. MALRIEU, and P. RANCUREL. J. Chem. Phys. **58**, 5745 (1973).
15. L. SALEM and C. ROWLAND. Angew. Chem. Int. Ed. **11**, 92 (1972).
16. P. C. HIBERTY and C. LEFORESTIER. J. Am. Chem. Soc. **100**, 2012 (1978); P. C. HIBERTY and G. OHANESSIAN. J. Am. Chem. Soc. **104**, 66 (1982).
17. E. F. HAYES and A. K. Q. SIU. J. Am. Chem. Soc. **93**, 2090 (1973).
18. K. YAMAGUCHI, S. YABUSHITA, T. FUENO, S. KATO, K. MOROKUMA, and S. IWATA. Chem. Phys. Lett. **71**, 563 (1980).

Can. J. Chem. Downloaded from www.nrcresearchpress.com by 210.87.254.42 on 09/06/12
For personal use only.

Examination of the molecular properties of D-fructose and L-sorbose by *ab initio* LCAO-MO calculations

WALTER A. SZAREK, SIRKKA-LIISA KORPPI-TOMMOLA, OLIVIER R. MARTIN, AND VEDENE H. SMITH, JR.
Carbohydrate Research Institute and Department of Chemistry, Queen's University, Kingston, Ont., Canada K7L 3N6

Received September 29, 1983

WALTER A. SZAREK, SIRKKA-LIISA KORPPI-TOMMOLA, OLIVIER R. MARTIN, and VEDENE H. SMITH, JR. Can. J. Chem. **62**, 1506 (1984).

Ab initio SCF LCAO-MO calculations at the STO-3G level have been performed on β-D-fructopyranose (**1**) and α-L-sorbopyranose (**2**) using crystallographic data as the geometrical input. Molecular properties of **1** and **2** are discussed in terms of orbital energies, total energy. ionization potentials, Mulliken population analysis, and electrostatic potentials, with a particular emphasis on the possible consequences of these features as regards the sweet taste of these two ketoses. No correlation was found, for example, with the electrostatic, point-charge distribution since the calculated hydrogen-bonding abilities would lead to the prediction of **2** being sweeter than **1**. On the other hand, non-bonded overlap populations between oxygen and hydroxyl-hydrogen atoms reveal the presence of intramolecular interactions, which may have a determinant influence on the taste of these molecules and which could explain why D-fructose is much sweeter than its epimer at C-5, namely, L-sorbose.

WALTER A. SZAREK, SIRKKA-LIISA KORPPI-TOMMOLA, OLIVIER R. MARTIN et VEDENE H. SMITH, JR. Can. J. Chem. **62**, 1506 (1984).

Des calculs *ab initio* d'orbitales moléculaires (SFC LCAO) ont été réalisés au niveau STO-3G pour le β-D-fructopyranose (**1**) et l'α-L-sorbopyranose (**2**) en utilisant les dimensions cristallographiques comme données géométriques. Les propriétés moléculaires des composés **1** et **2** telles que les énergies orbitalaires, l'énergie totale, les potentiels d'ionisation, l'analyse des populations de Mulliken, et les potentiels électrostatiques, sont discutées en mettant l'accent sur les conséquences possibles de ces caractéristiques sur la douceur de ces deux céto-sucres. Par exemple il n'existe pas de relation avec la distribution de charges électriques ponctuelles: prises comme mesure de l'aptitude à former des liaisons hydrogène, elles prédiraient en effet que **2** est plus doux que **1**. En revanche, les populations de recouvrement non-liant entre atomes d'oxygène et d'hydrogène de groupe hydroxyle révèlent la présence d'interactions intramoléculaires qui pourraient avoir une influence déterminante sur la saveur de ces composés, et expliquer pourquoi le D-fructose est beaucoup plus doux que son épimère en C-5, le L-sorbose.

Can. J. Chem. Downloaded from www.nrcresearchpress.com by 210.87.254.40 on 09/06/12
For personal use only.

Introduction

As part of a study (1) of molecular properties of D-fructose and L-sorbose, having as the ultimate goal the determination of some effects responsible for the high sweet taste of D-fructose and for the surprizing difference of sweetness between these two ketoses, *ab initio* quantum mechanical calculations on β-D-fructopyranose (**1**) and α-L-sorbopyranose (**2**) have been performed, and we report and discuss, in this article, the results of these investigations in terms of orbital energies, ionization potentials, Mulliken population analysis, and electrostatic potentials.

Very few studies have been reported in which *ab initio* calculations have been used to investigate structural features of an entire sugar molecule. In the course of their studies on the properties of the components of nucleic acids, Berthod and Pullman (2) performed *ab initio* computations on ribose using Clementi's minimal basis set (3) of Gaussian functions and crystallographic data as the geometrical input. The two anomers of D-glucopyranose as well as a disaccharide (β-maltose) have been studied by means of *ab initio* calculations at the minimal basis-set level by Rasmussen and co-workers (4); the molecular geometry used had been optimized by a purely classical method previously developed by them (empirical force-field method) (5).

Method

Owing to the large size (24 atoms, 96 electrons), on the scale of *ab initio* calculations, of D-fructose and L-sorbose, our study has been limited to only one conformer of each ketose in its pyranoid form. The conformers chosen are those found by neutron diffraction to be the preferred ones in the crystalline state: β-D-fructopyranose (**1**) in the $^2C_5$ (D) conformation with the CH_2OH group adopting a *gauche/gauche* orientation (6), and α-L-sorbopyranose (**2**) in the $^2C_5$ (L) conformation with the CH_2OH group in a *gauche/trans* disposition (7). The precise geometrical input was taken from crystallographic data (6–8). The torsion angles for α-L-sorbopyranose, which have not been reported, were evaluated using a BASIC computer program designed to calculate interatomic distances and bond angles as well as torsion angles from fractional atomic coordinates (9) (Table 1). Furthermore, the neutron diffraction study of **2** (7) revealed a very short (0.917 Å) bond length for the O-1—H bond, a result attributed to the increased thermal motion of the disordered CH_2OH group (0.625 *gauche/trans*, 0.375 *gauche/gauche* orientation). Because this artificially shortened bond length would affect the results of the Mulliken population analysis (10), the standard bond length (0.96 Å) was, therefore, adopted for the O-1—H bond of **2**.

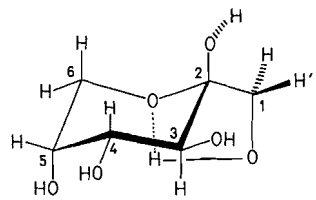

1

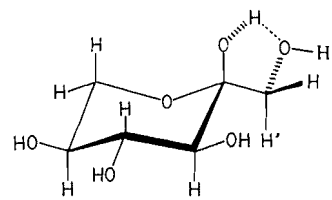

2

The STO-3G minimal basis set (11) was used and the *ab initio* SCF-LCAO computations were peformed by means of the Gaussian 76 system of programs (12).

Results and discussion

Orbital energies

In order of increasing energy, the first six orbitals (from

TABLE 1. Torsion angles for **2**[a]

Ring torsion angles		Exocyclic torsion angles (degrees)			
Bonds	Angle	Bonds	Angle	Bonds	Angle
$O_6—C_2—C_3—C_4$	−55.33	$C_6—O_6—C_2—C_1$	174.7	$O_2—C_2—C_1—H$	75.5
$C_2—C_3—C_4—C_5$	52.82	$O_6—C_2—C_1—O_1$	78.0	$O_2—C_2—C_1—H'$	−163.1
$C_3—C_4—C_5—C_6$	−51.52	$C_4—C_3—C_2—O_2$	65.3	$O_2—C_2—C_3—H$	−176.7
		$C_5—C_4—C_3—O_3$	174.7	$H—C_3—C_4—H$	175.8
		$C_2—C_3—C_4—O_4$	−174.4	$H—C_4—C_5—H$	−171.9
		$C_3—C_4—C_5—O_5$	−171.5	$H—C_5—C_6—H$	173.6
				$H—C_5—C_6—H$	53.7
		$H'—C_1—O_1—H$	2.4		
		$C_1—C_2—O_2—H$	56.8		
		$H—C_3—O_3—H$	14.8		
		$H—C_4—O_4—H$	7.0		
		$H—C_5—O_5—H$	−36.9		

[a]Calculated from fractional atomic coordinates of **2** (7); $H' = H_{pro\text{-}R}$.

−20.260 to −20.242 hartrees for **1**, −20.263 to −20.231 hartrees for **2**) of the 48 occupied molecular orbitals of each of **1** and **2** are almost pure 1*s* atomic orbitals of the oxygen atoms (contribution ~99.4%). The second set of six orbitals (−11.149 to −11.091 hartrees for **1**, −11.150 to −11.094 hartrees for **2**) is comprised of almost pure 1*s* atomic orbitals of carbon. The energy levels of the core orbitals are represented schematically in Fig. 1. The lowest-lying O(1*s*) orbital in **1** belongs to O-3 whereas in **2** it belongs to O-6; Rasmussen's calculations (4) on hexopyranoses have revealed that the lowest-lying O(1*s*) orbital is that of the ring oxygen and, in this respect, β-D-fructopyranose (**1**) seems to be an exception. In both **1** and **2**, the lowest-lying C(1*s*) orbital, which is the C(1*s*) orbital having the largest bonding energy, belongs to the anomeric carbon, C-2. The binding-energy difference ("chemical shift") between the binding-energy of the C-2 (1*s*) orbitals and the average of the other C(1*s*) orbitals is almost the same in **1** (1.35 eV) as in **2** (1.37 eV).

The following group of six orbitals, which are preponderantly constituted by 2*s* atomic orbitals of oxygen, extends in energy from −1.357 to −1.26 hartrees, and the final main group of 30 orbitals from −1.011 to −0.311 hartree for **1**, and from −1.004 to −0.306 hartree for **2**. Inspection of the Mulliken overlap population matrix reveals that the highest-occupied molecular orbital (HOMO) of both **1** and **2** has primary contributions from the lone pairs of the hydroxyl group at C-3 and of the ring oxygen atom (see Table 2). The energy of the lowest-unoccupied molecular orbital (LUMO) is 0.470 hartree for **1** and 0.480 hartree for **2**.

As shown in Table 2, the ionization potentials, calculated according to Koopmans' theorem (13) (vertical potentials), are ~8.4 eV for **1** and **2**. The only experimental values available for correlation are those measured for D-ribose (14); these values are somewhat larger than those calculated for **1** and **2**. However, it has been shown (15) that small basis sets, such as STO-3G, seem to underestimate the orbital energies and a correction of 1.85 eV is needed to match the results of larger basis-set calculations, and experimental values. If such a correction is applied to the orbital energies of **1** and **2**, the energies of the first and second HOMO (Table 2) fall in the same range as those observed for D-ribose.

Total energies and dipole moments

The total energy calculated for β-D-fructopyranose is −674.417 hartrees and for α-L-sorbopyranose −674.428 hartrees. The energy difference between the two molecules is 0.011 hartree (6.9 kcal/mol), α-L-sorbopyranose being the more stable. Thus, these *ab initio* values give an energy difference of the right sign. However, as determined from the conformational free energies (2.30 kcal/mol for the all-equatorial *sorbo* isomer, 2.85 kcal/mol for the *fructo* isomer) (16), the energy difference between the two ketoses which are epimeric at C-5 is expected to be of the order of 0.5 kcal/mol, a value equivalent to the energy contribution of a 1,3-*syn*-diaxial interaction present in β-D-fructopyranose. In view of the fact that *ab initio* energy differences constitute only a small fraction of the total energies, the qualitative agreement is noteworthy.

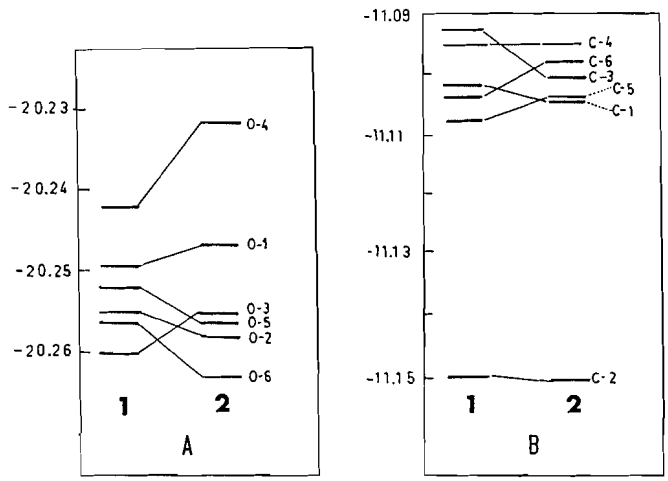

FIG. 1. Core energies (hartree) of **1** and **2**. (*A*) Almost pure O(1*s*) orbitals; (*B*) almost pure *C*(1*s*) orbitals.

The dipole moments have been calculated to be 2.03 and 3.03 debye units for **1** and **2**, respectively.

Mulliken population analysis

The net atomic charges (Q) derived by Mulliken population analysis for **1** and **2** are listed in Table 3.

As expected (4), the atoms can be separated into classes according to the elements to which they are bonded. Thus, the anomeric carbon atom carries the most positive charge, the methylene carbon atoms (C-1 and C-6) are almost neutral, and the methine carbon atoms bear an average charge of +0.059 e in **1** and +0.067 e in **2**. Correlation of the Q_C values with the experimental ^{13}C chemical shifts of **1** and **2** (Table 4) revealed

Can. J. Chem. Downloaded from www.nrcresearchpress.com by 210.87.254.40 on 09/06/12
For personal use only.

TABLE 2. Description of the HOMO's of **1** and **2** and ionization potentials

	Molecular orbital	Eigenvalue (hartree)	Ionization potential (eV)[a]	MO coefficients
1	ϵ_{48}	−0.311	8.46	−0.389 (O-3, $2p_y$) −0.358 (O-6, $2p_y$)
	ϵ_{47}	−0.327	8.90	−0.495 (O-6, $2p_x$) 0.395 (O-5, $2p_z$) 0.314 (O-3, $2p_z$) −0.302 (O-6, $2p_y$)
2	ϵ_{48}	−0.306	8.33	0.487 (O-3, $2p_x$) −0.424 (O-6, $2p_x$)
	ϵ_{47}	−0.322	8.76	−0.438 (O-4, $2p_z$) 0.430 (O-5, $2p_x$) −0.426 (O-6, $2p_x$)

[a]1 hartree = 27.210 eV.

a linear relationship; linear regression analysis of the data gave the following expression (correlation coefficient $r = 0.9917$):

[1] $Q_C = 0.0070\delta(^{13}C) - 0.4386$

This result is consistent with the statement (19) that *ab initio* STO-3G Mulliken charges can be used to calculate ^{13}C chemical shifts or vice versa, the linear relationship between these parameters being valid, however, only in sets of similar molecules. Equation [1] suggests a downfield shift with increasing positive character of carbon, a trend exhibited by situations in which both $2s$ and $2p$ populations vary, whereas typical sp^3 carbons follow the inverse trend (see ref. 19). Interestingly, the 1,3-*syn*-diaxial interaction between HO-5 and H-3, which is responsible for the upfield shift of C-3 in **1** with respect to the chemical shift of C-3 in **2**, is clearly reproduced by the present *ab initio* calculations: the C-3—H bond of **1** is polarized, as shown by the comparison of the atomic charges on C-3 (0.049 e) and H (C-3) (0.081 e) in **1** with the corresponding charges in **2** (0.066 and 0.050 e, respectively) in which the interaction is absent. This through-space interaction is also revealed by the Mulliken overlap population, $\zeta_{O\text{-}5,H(C\text{-}3)}$ (156.7 au for **1**, 0.0 for **2**).

Equation [1] was used to estimate the net atomic charges Q_C in 5-deoxy-β-D-*threo*-hexulopyranose (18), a close analog of **1** and **2** and a compound having great significance in a study of the sweetness of these sugars. The results are reported in Table 4. The change of charge density at C-5 on deoxygenation is 0.266 e toward a negative charge; this effect is slightly larger than that occasioned by deoxygenation at C-2 (β-D-arabinopyranose → 2-deoxy-β-D-*erythro*-pentopyranose) (0.158 e) as determined from CNDO/2 charges (20).

Using the net atomic charges at the oxygen and hydrogen atoms as a measure of their basicity and acidity, respectively, the following, decreasing sequence of acidities of the hydrogen atoms can be derived from the data in Table 3:

(**1**): H(O-4) > H(O-1) > H(O-3) = H(O-5) > H(O-2)

(**2**): H(O-4) > H(O-2) > H(O-1) > H(O-5) > H(O-3)

The basicities of the oxygen atoms decrease in the following order:

(**1**): O-4 > O-2 > O-5 > O-1 > O-3 > O-6

(**2**): O-4 > O-1 > O-2 > O-5 > O-3 > O-6

Thus, in both **1** and **2**, the hydroxyl group at C-4 seems to exhibit the highest values. In order to establish if this feature is merely a result of the short covalent-bond length of the O-4—H bond (0.948 Å in **1**, 0.941 Å in **2**), *ab initio* MO calculations at the STO-3G level using the Gaussian 80 system of programs (21) were performed on the same molecular conformations of **1** and **2** but with the standard bond length (0.96 Å) for all of the O—H bonds. The results are listed also in Table 3. The modified order of basicities of the oxygen atoms is the following:

(**1**): O-2 > O-4 > O-5 > O-1 > O-3 > O-6

(**2**): O-1 > O-4 > O-2 > O-5 > O-3 > O-6

The acidities of the hydroxyl groups are in the following sequence:

(**1**): H(O-1) > H(O-4) > H(O-3) = H(O-5) > H(O-2)

(**2**): H(O-2) > H(O-4) > H(O-1) > H(O-3) > H(O-5)

Thus, the hydroxyl group at C-4 retains its strong acidic and basic nature. However, the strongest hydrogen-bond donor in **1** is now the HO-1 group and the strongest hydrogen-bond acceptor the anomeric hydroxyl group; the weak acidity of the latter, usually considered to be the most acidic hydroxyl group in carbohydrate molecules, is noteworthy. In **2** the normal order is restored with the HO-2 group being the strongest hydrogen-bond donor and the HO-1 group the strongest hydrogen-bond acceptor. These results are in sharp contrast with the hydrogen-bonding abilities determined from the infrared and Raman spectra of **1** and **2** (22). In particular, the HO-4 group was shown to be involved in the weakest hydrogen bonds in crystalline **1** and **2**, and the HO-2 group to participate in the strongest hydrogen bonds in **1**. These discrepancies are attributable at least partly to the completely different conditions under which these properties were determined; the present theoretical calculations were performed on isolated molecules and took into consideration only intramolecular interactions, whereas intermolecular hydrogen bondings are the most important in the solid state.

According to Shallenberger's theory (23), sweet taste is thought to occur through hydrogen bonding between a topologically well-defined AH,B site on the sweet molecule and a complementary B,AH site on the receptor of the tongue, and the intensity of the sweetness response depends on the strength of such bonding. The principal saporous unit of β-D-fructopyranose has been assigned (24) to the HO-2 (AH) and HO-1 (B) groups. On the basis of the relative hydrogen bonding abilities of HO-1 and 2 of **1** and **2**, our theoretical investigations would lead to the prediction that L-sorbose is sweeter than D-fructose. This result is in obvious disagreement with the actual taste experience (sweetness ratio **1**/**2**: 64 (25), 115 (26)), and shows that the sweetness of D-fructose is not related primarily to the electronic point-charge distribution in the molecule.

In the present study, Mulliken population analysis was used to gain some theoretical information on the existence of intramolecular hydrogen bonding in **1** and **2**. The non-bonded overlap populations between oxygen and hydroxyl-hydrogen atoms, $\zeta_{O,H}$ (see Table 5), thus reveal that the only intramolecular interaction in **1** is a hydrogen bond between the ring oxygen (O-6) and the HO-1 proton (see structures **1** and **2**); this interaction has been shown by neutron diffraction analysis (6) to be present in the crystalline state. The absence of a hydrogen

Can. J. Chem. Downloaded from www.nrcresearchpress.com by 210.87.254.40 on 09/06/12
For personal use only.

TABLE 3. Net atomic charges in units of elementary charge

	Charge			Charge			
Atom	1	2	Atom	1	2	1[a]	2[a]
C-1	−0.006	−0.003	O-1	−0.311	−0.330	−0.317	−0.328
C-2	0.244	0.249	O-2	−0.322	−0.319	−0.331	−0.323
C-3	0.049	0.066	O-3	−0.301	−0.302	−0.303	−0.307
C-4	0.066	0.074	O-4	−0.331	−0.333	−0.325	−0.324
C-5	0.063	0.062	O-5	−0.317	−0.311	−0.318	−0.312
C-6	−0.001	−0.003	O-6	−0.288	−0.282	−0.289	−0.312
H(C-1)	0.067	0.061	H(O-1)	0.202	0.199	0.207	0.199
H′(C-1)	0.072	0.069	H(O-2)	0.186	0.209	0.194	0.213
H(C-3)	0.081	0.050	H(O-3)	0.196	0.189	0.198	0.195
H(C-4)	0.049	0.064	H(O-4)	0.210	0.210	0.205	0.202
H(C-5)	0.054	0.052	H(O-5)	0.196	0.192	0.198	0.192
H(C-6)	0.084	0.070					
H′(C-6)	0.069	0.067					

[a]Charges calculated for the OH groups using the standard (0.96 Å) OH bond length.

TABLE 4. ^{13}C-Chemical shifts (δ)[a] and calculated net charges (Q_C)[b] for **1**, **2**, and 5-deoxy-D-*threo*-hexulose (**3**)

	1		2		3	
Carbon	δ[c]	Q_C	δ[c]	Q_C	δ[d]	Q_C[e]
1	64.7	−0.006	64.5	−0.003	64.8	0.013
2	99.1	0.244	98.5	0.249	99.3	0.253
3	68.4	0.049	71.4	0.066	73.3	0.072
4	70.5	0.066	74.8	0.074	69.4	0.045
5	70.0	0.063	70.3	0.062	33.9	−0.202
6	64.1	−0.001	62.7	−0.003	59.8	−0.022

[a]In ppm downfield from tetramethylsilane, in deuterium oxide.
[b]In units of elementary charge.
[c]Data taken from ref. 17.
[d]Data taken from ref. 18.
[e]Calculated from eq. [1].

TABLE 5. Some non-bonded overlap populations $\zeta_{O,H}$[a] between oxygens and hydroxyl hydrogens in **1** and **2** and corresponding distances (Å)

	1		2	
Groups	r(O . . . H)	$\zeta_{O,H}(\times 10^4)$	r(O . . . H)	$\zeta_{O,H}(\times 10^4)$
O-6 . . . HO-1	2.460	13.45	3.315	−0.23
O-6 . . . HO-2	2.560	3.00	2.579	1.17
O-6 . . . HO-5	3.742	0.0	4.052	0.0
O-1 . . . HO-2	3.903	0.0	2.453	17.0
O-1 . . . HO-3	3.333	0.23	4.209	0.0
O-2 . . . HO-1	3.947	0.0	3.633	0.34
O-3 . . . HO-1	4.284	0.0	4.863	0.0
O-3 . . . HO-4	2.852	0.89	3.605	−0.19
O-4 . . . HO-3	3.423	−0.29	3.234	−0.40
O-4 . . . HO-5	2.873	2.61	3.703	−0.26
O-5 . . . HO-4	3.950	−0.10	3.222	0.0

[a]Data from Gaussian 80 calculations using the stardard OH bond length.

bond between the axial HO-5 group and O-6, once invoked (27) to be responsible for the high sweet taste of D-fructose and later shown (18) to be irrelevant by studies on "5-deoxyfructose" (5-deoxy-D-*threo*-hexulose), is noteworthy. In **2**, the main hydrogen bond occurs between O-1 and the anomeric hydroxyl proton (HO-2). As anticipated, the overlap populations are much smaller than those involved in covalent bonding (for example, $\zeta_{O\text{-}1,H} = 0.262$ in **1**).

As the Raman spectroscopic studies (28) of aqueous solutions of D-fructose as well as the recent study (29) of Bock and Lemieux on the molecular conformation of sucrose in dimethylsulfoxide appear to indicate, intramolecular hydrogen bonds present in the crystalline state of a sugar exist also in solution; these interactions might have a profound influence on the taste of **1** and **2**. Thus, the rotation of the hydroxymethyl group in **1** is inhibited by the O-6 . . . H(O-1) hydrogen bond, and the anomeric hydroxyl as well as O-1 are free to interact with the sweet taste receptor. On the other hand, the corresponding sites are internally hydrogen bonded in **2**, with HO-2 acting as a hydrogen donor; this interaction might prevent efficient binding of **2** with the receptor and might be one of the reasons why L-sorbose is much less sweet than D-fructose.

Molecular electrostatic potentials

The molecular electrostatic potentials around the oxygen atoms of **1** and **2** were calculated from the present STO-3G wave functions (from Gaussian 76 calculations) by the method of Peeters and Sana (30); maps of the potentials around O-1 and O-2 of **1** and **2** are shown in Fig. 2. Noteworthy is the crowded potential around O-1 of **2**, a feature attributable to the existence of a hydrogen bond between this atom and H(O-2). In the case of **1**, however, the map shows the regular isopotential contours around the O-1 nucleus. The calculated potentials (Table 6) are generally stronger in **2** than in **1**, and the order of minima follows the following sequence:

(**1**): O-4 > O-2 > O-3 > O-1 > O-5 > O-6

(**2**): O-4 > O-3 > O-2 > O-1 > O-5 > O-6

This order would correspond to an order of reactivity of the oxygen atoms toward an electrophilic reagent, and, for example, the O-4 atom would be predicted to be the most attractive site for protonation in both molecules. However, a lack of experimental data prevents any correlation with the actual reactivities of the hydroxyl groups of the keto-hexopyranoses.

Conclusion

The work described in this article represents the first attempt

Can. J. Chem. Downloaded from www.nrcresearchpress.com by 210.87.254.40 on 09/06/12
For personal use only.

Can. J. Chem. Downloaded from www.nrcresearchpress.com by 210.87.254.40 on 09/06/12
For personal use only.

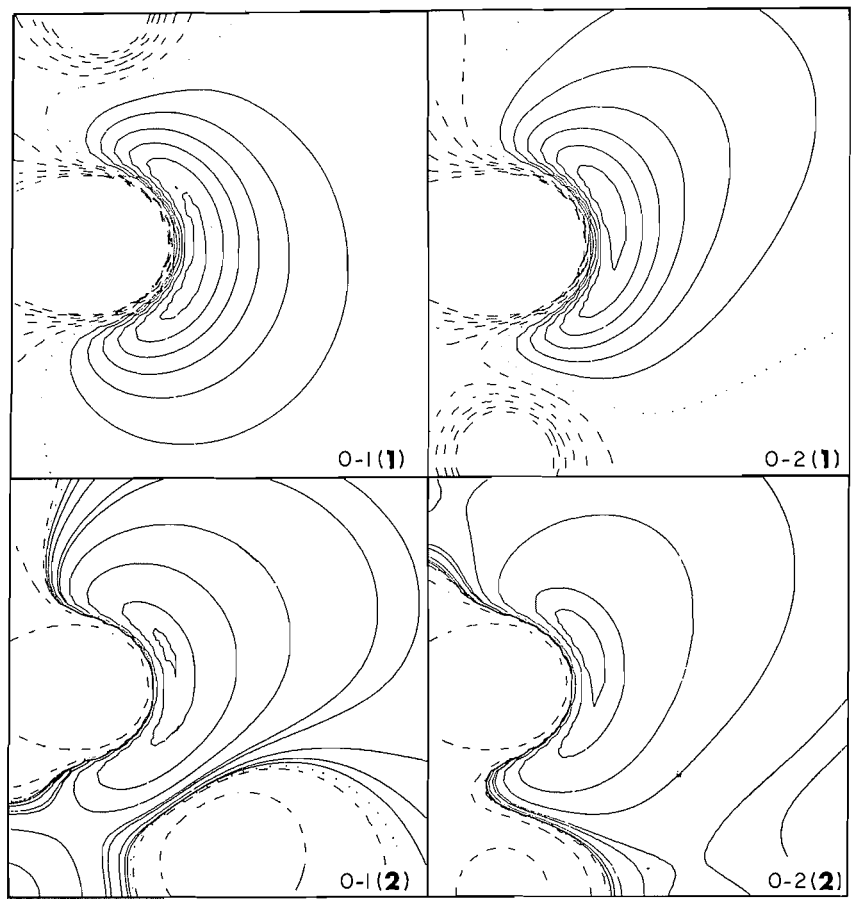

FIG. 2. Molecular electrostatic potentials around O-1 and O-2 of **1** and **2**. The potentials are constructed in the planes bisecting the C-1, O-1, H(O-1) angle for O-1, and the C-2, O-2, H(O-2) angle for O-2.

TABLE 6. Minima of the molecular electrostatic potentials[a] around the oxygen atoms of **1** and **2**

Compound	O-1	O-2	O-3	O-4	O-5	O-6
1	−63.8	−65.9	−65.5	−68.5	−63.5	−50.2
2	−64.3	−69.3	−70.2	−72.4	−62.8	−53.0

[a] $V(r)_{min}$ values in kcal/mol.

to correlate results of quantum mechanical calculations on carbohydrate molecules with their sweetness. The *ab initio* study of β-D-fructopyranose (**1**) and its epimer at C-5, α-L-sorbopyranose (**2**), does not reveal any prominent difference in the electronic properties of the atoms presumed to be involved in their saporous unit, which might be related to the high sweet taste of **1** and the markedly lower sweetness of **2**. However, Mulliken population analysis suggests some intramolecular interactions, such as hydrogen bonding between HO-1 and O-6 in **1**, and between HO-2 and O-1 in **2**, which might play an important role as regards the taste of these molecules.

Interestingly, the HO-4 function seems to be the most reactive of the secondary hydroxyl groups of **1** and **2**, a finding, the experimental confirmation of which, would be a worthy undertaking.

Acknowledgements

The authors are grateful to the Natural Sciences and Engineering Research Council of Canada for its support of this work in the form of grants (to W.A.S. and V.H.S.), and to the Neste O. Y. Foundation and Emil Aaltonen Foundation of Finland for financial assistance (to S.-L. K.-T.). They also wish to acknowledge the valuable assistance of Dr. D. J. Mitchell and Mr. L. LaJohn in connection with the calculations on the sugar molecules.

1. S.-L. KORPPI-TOMMOLA. Ph.D. Thesis, Queen's University. Kingston, Ont. 1982.
2. H. BERTHOD and A. PULLMAN. Theor. Chim. Acta, **47**, 59 (1978).
3. E. CLEMENTI, J. M. ANDRÉ, M.-C. ANDRÉ, D. CLINT, and D. HAHN. Acta Phys. Acad. Sci. Hung. **27**, 493 (1969).
4. S. MELBERG, K. RASMUSSEN, R. SCORDAMAGLIA, and C. TOSI. Carbohydr. Res. **76**, 23 (1979).
5. K. KILDEBY, S. MELBERG, and K. RASMUSSEN. Acta Chem. Scand. Ser. A, A**31**, 1 (1977); S. MELBERG and K. RASMUSSEN. Acta. Chem. Scand. Ser. A, A**32**, 187 (1978).
6. S. TAKAGI and G. A. JEFFREY. Acta Crystallogr. Sect. B, B**33**, 3510 (1977).
7. S. NORDENSON, S. TAKAGI, and G. A. JEFFREY. Acta Crystallogr. Sect. B, B**35**, 1005 (1979).
8. J. A. KANTERS, G. ROELOFSEN, B. P. ALBLAS, and I. MEINDERS. Acta Crystallogr. Sect. B, B**33**, 665 (1977).
9. J. D. DUNITZ. X-Ray analysis and the structure of organic molecules. Cornell University Press, Ithaca and London. 1979. Appendix I.
10. R. S. MULLIKEN. J. Chem. Phys. **23**, 1833 (1955); **23**, 1841 (1955); **23**, 2338 (1955); **23**, 2343 (1955).
11. W. J. HEHRE, R. F. STEWART, and J. A. POPLE. J. Chem. Phys. **51**, 2657 (1969).
12. J. S. BINKLEY, R. A. WHITESIDE, P. C. HARIHARAN, R. SEEGER,

J. POPLE, W. J. HEHRE, and M. D. NEWTON. QCPE, **11**, 368 (1978).
13. T. KOOPMANS. Physica, **1**, 104 (1933).
14. J. S. KWIATKOWSKI and B. PULLMAN. Int. J. Quantum Chem. **15**, 499 (1979).
15. H. E. POPKIE, W. S. KOSKI, and J. KAUFMAN. J. Am. Chem. Soc. **98**, 1342 (1976).
16. J. F. STODDART. Stereochemistry of carbohydrates. Wiley-Interscience, New York. 1971. p. 90.
17 S. J. ANGYAL and G. S. BETHELL. Aust. J. Chem. **29**, 1249 (1976).
18. O. R. MARTIN, S.-L. KORPPI-TOMMOLA, and W. A. SZAREK. Can. J. Chem. **60**, 1857 (1982).
19. S. FLISZÁR, G. CARDINAL, and M.-T. BÉRALDIN. J. Am. Chem. Soc. **104**, 5287 (1983).
20. Y. A. ZHDANOV, V. I. MINKIN, R. M. MINJAEV, I. I. ZACHAROV, and Y. E. ALEXEEV. Carbohydr. Res. **29**, 405 (1973).
21. J. S. BINKLEY, R. A. WHITESIDE, R. KRISHNAN, R. SEEGER, D. J. DEFREES, H. B. SCHLEGEL, S. TOPIOL, L. R. KHAN, and J. A. POPLE. QCPE, **13**, 406 (1981).
22. W. A. SZAREK, S.-L. KORPPI-TOMMOLA, H. F. SHURVELL, V. H. SMITH, JR., and O. R. MARTIN. Can. J. Chem. **62**, 1512 (1984).
23. R. S. SHALLENBERGER. J. Food Sci. **28**, 584 (1963); New Sci. **407**, 569 (1964); R. S. SHALLENBERGER and T. E. ACREE. Nature, **216**, 480 (1967); J. Agric. Food Chem. **17**, 701 (1963).
24. R. S. SHALLENBERGER. Pure Appl. Chem. **50**, 1409 (1978); Zuckerindustrie, **104**, 121 (1979).
25. Y. TSUZUKE and J. YAMAZAKI. Biochem. Z. **323**, 525 (1953).
26. R. S. SHALLENBERGER. *In* Sweetness and sweeteners. *Edited by* G. G. Birch, L. T. Green, and C. B. Coulson. Applied Science Publishers, London. 1972. p. 42.
27. M. G. LINDLEY and G. G. BIRCH. J. Sci. Food Agric. **26**, 117 (1975); G. G. BIRCH. CRC Critical Rev. Food Sci. Nutr. **8**, 54 (1976).
28. M. MATHLOUTHI, C. LUU, A. M. MEFFROY-BIGET, and D. V. LUU. Carbohydr. Res. **81**, 213 (1980).
29. K. BOCK and R. U. LEMIEUX. Carbohydr. Res. **100**, 63 (1982).
30. D. PEETERS and M. SANA. QCPE, **11**, 360 (1978).

Can. J. Chem. Downloaded from www.nrcresearchpress.com by 210.87.254.40 on 09/06/12
For personal use only.

A Raman and infrared study of crystalline D-fructose, L-sorbose, and related carbohydrates. Hydrogen bonding and sweetness

WALTER A. SZAREK, SIRKKA-LIISA KORPPI-TOMMOLA, HERBERT F. SHURVELL, VEDENE H. SMITH, JR., AND OLIVIER R. MARTIN

Department of Chemistry, Queen's University, Kingston, Ont., Canada K7L 3N6

Received October 21, 1983

WALTER A. SZAREK, SIRKKA-LIISA KORPPI-TOMMOLA, HERBERT F. SHURVELL, VEDENE H. SMITH, JR., and OLIVIER R. MARTIN. Can. J. Chem. **62**, 1512 (1984).

Raman and infrared spectra of polycrystalline samples of four structurally related sugars, namely D-fructose, L-sorbose, 5-deoxy-D-*threo*-hexulose (5-deoxy-D-fructose), and D-arabinose are reported. Three regions of the spectrum have been studied: the OH stretching region 3650–3100 cm^{-1}, the CH stretching region 3000–2800 cm^{-1}, and the "fingerprint" region 1600–200 cm^{-1}. Raman spectra in the region 200–10 cm^{-1} have also been recorded. Bands in the OH stretching region have been correlated with the O—H . . . O distances obtained from recent neutron diffraction studies. The results are discussed in relation to hydrogen bonding and relative sweetness of these sugars.

Detailed assignments are given for the bands in the CH stretching region, and it is shown that the spectra are very sensitive to small structural changes in the molecule. Spectra are presented for the "fingerprint" region and some characteristic "group" frequencies are noted for ketohexoses and aldopentoses.

WALTER A. SZAREK, SIRKKA-LIISA KORPPI-TOMMOLA, HERBERT F. SHURVELL, VEDENE H. SMITH, JR. et OLIVIER R. MARTIN. Can. J. Chem. **62**, 1512 (1984).

Nous rapportons les spectres Raman et infrarouge d'échantillons polycristallins de quatre sucres de structure apparentée, le D-fructose, le L-sorbose, le désoxy-5-D-*threo*-hexulose et le D-arabinose. Trois régions du spectre ont été étudiées: la région du stretching OH, 3650–3100 cm^{-1}, la région du stretching CH, 3000–2800 cm^{-1}, et la région du "fingerprint", 1600–200 cm^{-1}. Les spectres Raman ont également été enregistrés dans la région 200–10 cm^{-1}. Les bandes dans la région du stretching OH ont été mises en corrélation avec les distances O—H . . . O tirées d'études récentes par diffraction de neutrons. Les résultats sont discutés en rapport avec les liaisons hydrogène et la douceur relative de ces sucres.

Nous donnons les attributions détaillées des bandes de la région du stretching CH, et montrons que les spectres sont très sensibles à des changements de structure mineurs dans la molécule. La région du "fingerprint" des spectres est représentée et quelques fréquences caractéristiques de "groupes" sont relevées pour les cétohexoses et les aldopentoses.

Can. J. Chem. Downloaded from www.nrcresearchpress.com by 210.87.254.105 on 09/06/12
For personal use only.

Introduction

The objective of the present work was to study the relationship between the vibrational spectra and the structures of four sugars, namely D-fructose, L-sorbose, 5-deoxy-D-*threo*-hexulose (5-deoxy-D-fructose), and D-arabinose, in order to evaluate some aspects of the current theories of the origin of sweetness of sugars.

D-Fructose (**I**) is a well-known member of the family of ketoses. It occurs widely in nature and is known to be the sweetest of the naturally occurring sugars. Shallenberger's hypothesis (1) of sweetness suggests that it is induced by the existence of a suitable AH,B system, where A and B are each electronegative atoms in a particular geometric disposition and H is an acidic proton. According to this model, a molecule exhibits sweet taste by hydrogen bonding with the complementary AH,B system on the receptor site.

The only isomer of D-fructose isolated so far in crystalline form is β-D-fructopyranose. It has been suggested (2) that the unit giving rise to sweetness is the anomeric hydroxyl group (the AH moiety) and O-1 (the B moiety); this proposal is supported by the lower degree of sweetness of β-D-arabinopyranose (**IV**) and of 2,6-anhydro-D-mannitol, two structural analogs of β-D-fructopyranose (**I**) which lack the hydroxymethyl and the 2-hydroxyl group, respectively. Surprizingly, the epimer at C-5 of **I**, namely α-L-sorbopyranose (**II**), which contains the same AH,B unit, was found (3) to exhibit a markedly lower sweetness than **I** (sweetness order: **I** > **IV** > **II**), a result which suggested that the hydroxyl group at C-5 in these molecules might play an important role in their sweetness. However, this possibility was found (4) not to be the case in our separate study involving 5-deoxy-D-*threo*-hexulose

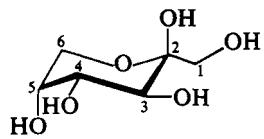

D-Fructose
(**I**)

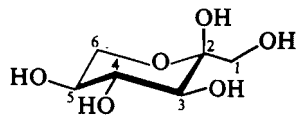

L-Sorbose
(**II**)

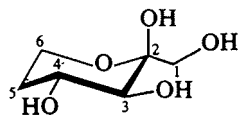

5-Deoxy-D-*threo*-hexulose
(**III**)

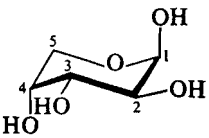

D-Arabinose
(**IV**)

(**III**). Compound **III** was shown to be nearly as sweet as β-D-fructopyranose.

It has been suggested (3) that differences in intensity of sweetness amongst sugars can be attributed to differences in the nature of the hydrogen bonding of the molecules. Information on hydrogen bonding can be obtained from the positions and widths of OH stretching bands in the vibrational spectra. These bands have been studied, therefore, in the infrared and Raman spectra of D-fructose, L-sorbose, 5-deoxy-D-*threo*-hexulose, and D-arabinose. Recently, O—H . . . O distances in **I**, **II**, and **IV** have been obtained from neutron diffraction studies (5–9), and the existence of possible correlations between the OH stretching frequencies and the O—H . . . O distances in these molecules has been examined.

Two other regions of the vibrational spectra should provide

Can. J. Chem. Downloaded from www.nrcresearchpress.com by 210.87.254.105 on 09/06/12
For personal use only.

structural information on sugar molecules. The CH stretching modes of the various methylene and methine groups in the molecules are expected to give bands between 3000 and 2800 cm^{-1}, and the "fingerprint" region between 1600 and 300 cm^{-1} often contains characteristic group frequencies. These two regions of the spectra of **I–IV** have been examined also in the present work.

Raman spectra of aqueous solutions of D-fructose have been reported recently (10–12). Several publications have reported (13–23) infrared spectra of various monosaccharides, and a complete normal coordinate calculation has been performed for α- and β-D-glucose (24, 25). However, the relationship between the frequencies of stretching modes of hydrogen-bonded OH groups and the O—H . . . O distances has not been studied previously for D-fructose, L-sorbose, and D-arabinose. Also, we are not aware of any detailed assignments of bands in the CH stretching region of these molecules.

Experimental

Commercial samples of D-fructose, L-sorbose, and D-arabinose were recrystallized from water–methanol. The sample of 5-deoxy-β-D-*threo*-hexulose was synthesized in this laboratory previously (4).

Infrared spectra were recorded on Perkin-Elmer models 598 and 180 spectrophotometers. The spectra were recorded from KBr pellets. Frequencies in the region 4000–3100 cm^{-1} are believed to be correct to within ±10 cm^{-1} in those cases where the bands are very broad. Wavenumbers of the sharp bands in the region 4000–2800 cm^{-1} are believed to be correct to within ±2 cm^{-1}.

Room-temperature Raman spectra were recorded on a Jarrell-Ash 25-305 spectrophotometer. To obtain Raman spectra at reduced temperatures the powdered polycrystalline samples were tamped into a small hole in a copper finger attached to a liquid nitrogen-cooled low-temperature cell; these spectra were recorded using a Jarrell-Ash 25-100 monochromator and a photon counting system. The spectra were excited by the 514.5 nm line of Spectra-Physics model 164 argon ion lasers operating at powers between 200 and 600 mW. The instruments were calibrated using atomic emission lines from neon lamps; wavenumbers reported are believed to be accurate to within ±5 cm^{-1} above 3100 cm^{-1}, and ±1 cm^{-1} in the regions from 3100 cm^{-1} to 2700 cm^{-1} and from 1600 cm^{-1} to 10 cm^{-1}.

Results and discussion

The molecules **I–IV** are structurally close analogs, which exist preponderantly in the $^2C_5$ (or $^1C_4$) conformation. The Raman and infrared spectra were obtained from these molecules in their crystalline state. The crystallographic parameters were obtained for **I** and **II** from neutron diffraction studies (5, 6), and for **IV** from an X-ray investigation (7) performed on β-DL-arabinopyranose and from neutron diffraction studies (8, 9) performed on β-L-arabinopyranose. The X-ray study (7) revealed that both *arabino* enantiomers adopt the same hydrogen-bond structure in the crystal lattice.

Figure 1 shows Raman and infrared spectra in the OH stretching region of **I–IV**. The Raman bands are all very weak in this region, but serve to confirm the positions of many features of the strong infrared bands. Figure 2 shows the Raman and infrared spectra in the CH stretching region. In this case the Raman lines are strong and sharp. Figure 3 shows the "fingerprint" and the very low frequency region (1600–10 cm^{-1}) of the Raman spectra of **I–IV**. The three regions of the vibrational spectra are discussed separately.

The OH stretching region

β-D-*Fructopyranose (I)*

The hydrogen-bond structure of **I**, with the bonds being

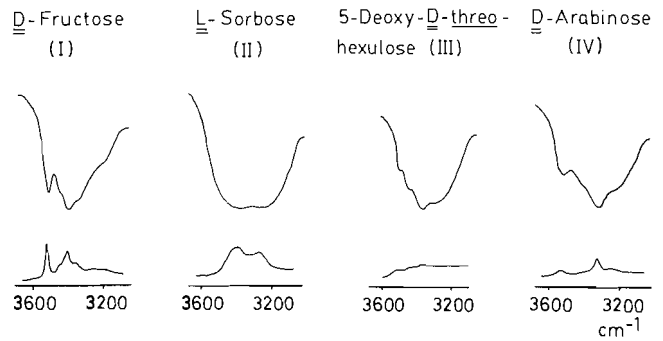

FIG. 1. Raman (lower trace) and infrared (upper trace) spectra in the OH stretching region of **I–IV** recorded at room temperature.

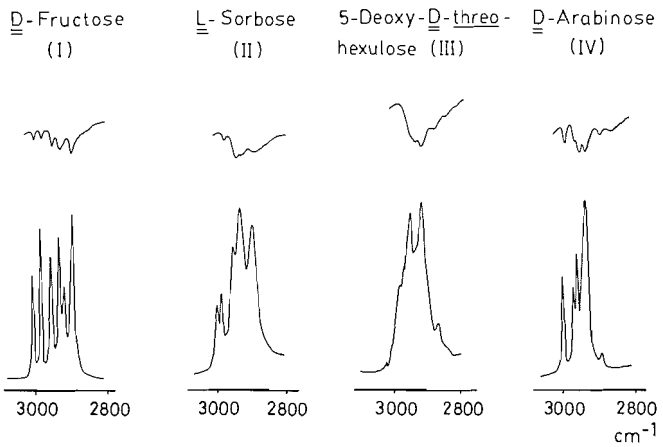

FIG. 2. Raman (lower trace) and infrared (upper trace) spectra in the CH stretching region of **I–IV** recorded at room temperature.

classified according to Jeffrey and Takagi's (26) statistical analysis, as well as the assignments of the OH stretching frequencies, are reported in Table 1. As shown by the crystallographic analysis of **I** (5), the anomeric HO-2 group is bound in an infinite chain with a very short hydrogen bond of length 1.750 Å, a value which indicates strong hydrogen bonding. The HO-1 and HO-3 groups act both as donors and acceptors in the infinite-chain structure, their hydrogen-bond lengths being, however, longer (1.965 and 1.977 Å, respectively) than that of HO-2; in addition, each of these hydroxyl groups participates in an asymmetric, bifurcated hydrogen-bond system (26) involving the ring oxygen atom, a type of interaction which has been shown (27) to be energetically comparable to, or even more favorable (by 1–2 kcal/mol) than, a normal, linear hydrogen bond. The HO-5 group is part of the infinite-chain structure and, being both a donor and an acceptor, forms strong hydrogen bonds. However, these bonds are not as strong as those formed by HO-2 (on the basis of hydrogen-bond lengths), or by HO-1 and HO-3, which are involved in bifurcated bonding. Finally, the HO-4 group belongs to the class of finite-chain, donor-type only, hydroxyls, which were shown (26) to form weaker hydrogen bonds.

On the basis of these evaluations, the following decreasing order of strengths of the hydrogen bonds formed by the hydroxyl groups in **I** can be proposed.

HO-2 > HO-1 > HO-3 > HO-5 > HO-4

Frequencies in the Raman and infrared spectra have been

TABLE 1. The hydrogen bond structure[a] and ν(OH) frequencies of **I**, **II**, and **IV**

Compound	Bond	Type[b]	O—H (Å)	H . . . O (Å)	ν(OH)[c] (cm^{-1}) Raman	ν(OH)[c] (cm^{-1}) Infrared
I	O-2—H . . . O-1	I, DA	0.979	1.750	3190	3190
	O-1—H . . . O-3	I, DA	0.972	1.965	3305	—
	O-3—H . . . O-5	I, DA	0.964	1.977	3365	3350
	O-5—H . . . O-2	I, DA	0.963	1.869	3395	3415
	O-4—H . . . O-2	F, D	0.948	2.065	3500	3525
II	O-3—H . . . O-4	F, DA	0.974	1.746	3180	3230
	O-2—H . . . O-5	I, DA	0.969	1.882	3272	
	O-5—H . . . O-2	I, DA	0.962	1.953		
	O-1A—H . . . O-3	F, D	0.917	1.867	3360	3380
	O-1B—H . . . O-3	F, D	0.932	2.151		
	O-4—H . . . O-6	F, DA	0.941	1.932	3420	
IV	O-2—H . . . O-3	I, DA	0.979	1.735	3230	3230
	O-3—H . . . O-2	I, DA	0.975	1.801	3320	3345
	O-1—H . . . O-5	S, D	0.952	1.820	3400	—
	O-4—H . . . O-2	S, D	0.920	2.201	3535	3545

[a] From refs. 5–9.
[b] I = infinite chain, F = finite chain, DA = donor-acceptor, S = single link, D = donor only.
[c] From Raman spectra recorded at 77 K and ir spectra recorded at room temperature.

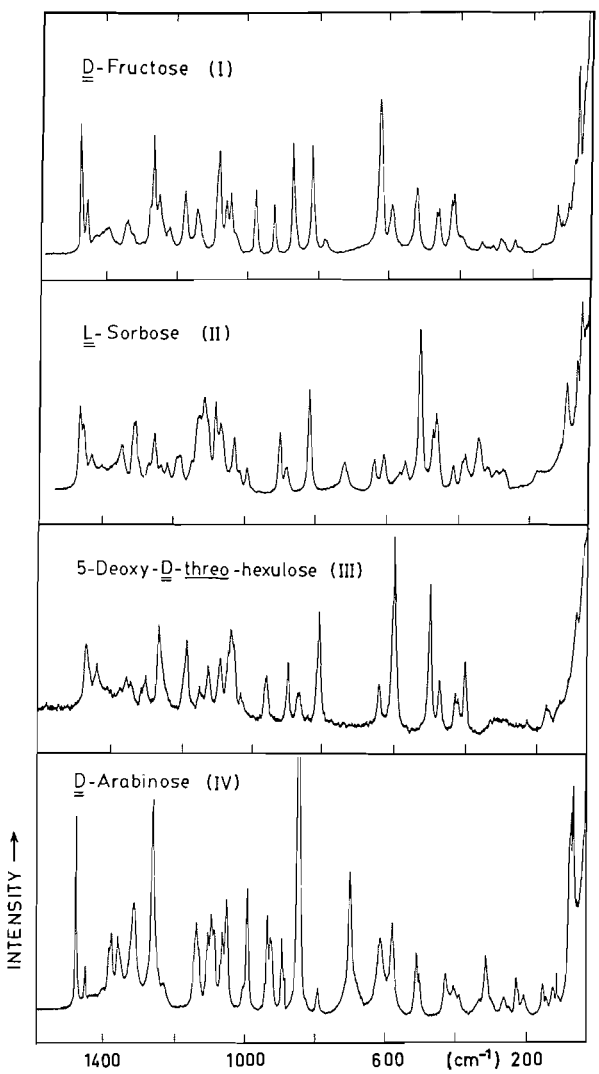

FIG. 3. Partial Raman spectra of **I**–**IV**.

assigned on the basis of the tenet that the strongest hydrogen bonding gives rise to the lowest frequency OH stretching mode. The Raman frequencies of Table 1 were obtained from spectra recorded at 77 K. Bands are often sharper and better resolved at low temperature; in the present case the broad band observed at 3415 cm^{-1} in the room-temperature spectrum of **I** (see Fig. 1) is observed as a triplet having maxima at 3395, 3365, and 3305 cm^{-1} in the low-temperature spectrum. These bands are all shifted to lower frequencies at 77 K. This shift is a characteristic feature of hydrogen-bonded hydroxyl groups (18–21).

According to the order of hydrogen-bonding strengths of the hydroxyl groups, the four bands observed in the low-temperature Raman spectrum of **I** are assigned as follows: the sharp band at 3500 cm^{-1} (3525 cm^{-1} at room temperature) to the weakly bound O-4—H, the band at 3395 cm^{-1} (3415 cm^{-1} at room temperature) to O-5—H, and the bands at 3365 cm^{-1} and at 3305 cm^{-1} to O-3—H and O-1—H, respectively, both being involved in bifurcated bonding. It is proposed that the low-frequency infrared shoulder at 3190 cm^{-1} arises from the ν(OH) mode of the strongly hydrogen-bonded HO-2 group.

α-L-*Sorbopyranose (II)*

The classification of the hydroxyl groups in **II** is presented in Table 1, together with the assignments of the OH stretching bands.

According to crystallographic data (6), the HO-2 and HO-5 groups of **II** form an infinite-chain system of hydrogen bonding and are thus strongly bonded, with distances of 1.882 Å (O-2—H . . . O-5) and 1.953 Å (O-5—H . . . O-2). The rather long distance between O-5—H and O-2 is attributable to the fact that O-5—H is participating also in a weak interaction with O-3 (2.582 Å); the hydrogen-bonding pattern of HO-5 is an example of an asymmetric, bifurcated interaction (26) with distances being close to the average experimental values (1.95 and 2.50 Å). The HO-3 group is involved in a complex hydrogen-bond structure; in addition to having a very short (1.746 Å) and strong bond to O-4, this group serves also as a double acceptor of the O-1—H and O-5—H hydroxyls. The HO-1 in both of the possible conformers of the hydroxymethyl

Can. J. Chem. Downloaded from www.nrcresearchpress.com by 210.87.254.105 on 09/06/12
For personal use only.

TABLE 2. Correlation of the ν(OH) frequencies of **I**, **II**, and **IV** with the O—H and H . . . O bond lengths

Compound	ν(OH) (cm^{-1})	O—H (Å)	H . . . O (Å)	Comments
I	(3170)[a]	0.979	1.750	Long O—H
II	3180	0.974	1.746	short H . . . O
IV	(3210)[a]	0.979	1.735	distances
II	3272	0.969	1.882	
II	3272	0.962	1.953[c]	Intermediate
IV	(3300)[a]	0.974	1.801	O—H and
I	3305	0.972	1.965[c]	H . . . O
II	3360	0.917[b]	1.867	distances
II	3360	0.932[b]	2.151[c]	
I	3365	0.964	1.977[c]	
I	3395	0.963	1.964	
IV	(3380)[a]	0.952	1.820	
II	3420	0.941	1.932	Short O—H
I	3500	0.948	2.065	long H . . . O
IV	3535	0.920	2.201	distances

[a] Low-temperature frequency estimated from observed, room-temperature Raman frequency.
[b] Shortened because of increased thermal motion (5).
[c] Lengthened because of the bifurcated bond (27).

group is at the origin of a finite-chain structure. In the *gauche/trans* conformer (62.5%), the O-1A—H hydroxyl acts as a donor only with a medium-strong bond to O-3 of length 1.867 Å. In the *gauche/gauche* conformer, the O-1B—H group forms a symmetrical, bifurcated hydrogen bond with O-3 and O-4 in which the H . . . O distances (2.151 Å to O-3, 2.209 Å to O-4) are very close to the optimal value of 2.2 Å (26). As in the case of the asymmetric type, this type of bonding was found (27) to be at least as stable as a normal, linear bond. Thus, the hydrogen-bonding ability of the HO-1 group can be considered to be independent of the conformation of the hydroxymethyl group. The HO-4 group can be classified in the group of the finite-chain, medium strongly bonding hydroxyls.

The above discussion suggests the following order of hydrogen-bonding capacity of the hydroxyl groups in **II**.

HO-3 > HO-2 > HO-5 > HO-1 > HO-4

In the room-temperature Raman and infrared spectra of **II** (see Fig. 1), broad bands having two maxima at 3410 cm^{-1} and 3260 cm^{-1} are observed. At 77 K the Raman spectrum shows four distinct bands having frequencies 3420, 3360, 3272, and 3180 cm^{-1}. The following assignments are suggested for these frequencies. The band at 3180 cm^{-1} arises from the O-3—H mode. The absorption at 3272 cm^{-1} is attributable to both O-2—H and O-5—H modes. The band at 3360 cm^{-1} is attributable to the O-1—H mode and that at 3420 cm^{-1} to the stretching mode of the HO-4 group.

5-Deoxy-β-D-threo-*hexulopyranose (III)*

Because no crystallographic data are available for this molecule, its O—H stretching frequencies are discussed in relation to the assignments made for **I**, **II**, and **IV**.

The room temperature Raman spectrum of **III** (see Fig. 1) showed very weak features, and no frequencies could be obtained. In contrast, four bands were observed in the room temperature infrared spectrum; these are a medium–strong shoulder at 3500 cm^{-1}, a shoulder at 3440 cm^{-1}, a band at 3360 cm^{-1}, which is the strongest feature of the spectrum, and a broad band centered at 3250 cm^{-1}. On the basis of the data of Table 2, two of the four hydroxyl groups of **III** would be expected to exhibit very short O—H bond lengths and to form hydrogen bonds of long distances. Moreover, these hydroxyls are probably of the donor-type only, and are linked to the finite-chain system or form a single link. The bands at 3500 cm^{-1} and 3440 cm^{-1} are attributed to these two hydroxyls. The band at 3360 cm^{-1} suggests the presence of a hydroxyl group which is medium-strongly bonded in a hydrogen-bonding network and which has an O—H bond of average length; this hydroxyl may be part of the infinite-chain structure and would belong to the class of donor–acceptor hydroxyls. Finally, **III** exhibits a strongly bonded hydroxyl similar to O-2—H in **I**, O-3—H in **II**, and O-2—H in **IV** (for detailed parameters, see Table 1); the band at 3250 cm^{-1} is attributed to this hydroxyl.

β-D-*Arabinopyranose (IV)*

This molecule has only four distinct hydrogen bonds and exhibits no secondary interaction such as the bifurcated bonding observed in the crystal structures of **I** and **II**. Therefore, its OH stretching region should be particularly amenable to analysis using the relationship between the OH stretching frequencies and the hydrogen-bond strengths. Table 1 lists the hydroxyl groups of **IV** in increasing order of hydrogen-bond lengths.

The room-temperature spectra in the OH stretching region of D-arabinose are shown in Fig. 1. The observed bands were assigned according to the hydrogen-bond lengths of the OH groups as follows: the band at 3230 cm^{-1} to the most strongly bonded hydroxyl, O-2—H, the band at 3320 cm^{-1} to O-3—H, the band at 3400 cm^{-1} to the anomeric hydroxyl, and the high frequency band at 3535 cm^{-1} to the weakly bound O-4—H. These assignments are included in Table 1.

Correlation of the ν(OH) frequencies with crystallographic data

Table 2 lists the ν(OH) frequencies observed in the low-temperature Raman spectra of **I** and **II**, and the low-temperature Raman frequencies for **IV** estimated from observed room-temperature frequencies. The corresponding O—H and H . . . O bond lengths are included in this table. It should be noted that low-temperature frequencies are approximately 20 cm^{-1} lower than those obtained from room-temperature spectra. Inspection of bond lengths and frequencies reveals two regions in which the observed frequencies clearly show an inverse correlation with the O—H bond lengths and a direct correlation with the H . . . O bond lengths.

In the region below 3250 cm^{-1} appear the bands of those hydroxyls which clearly have longer than average O—H bond lengths (0.968 Å in carbohydrates, see ref. 8) and a very short hydrogen-bond length (average value for **I**, **II**, and **IV**, 1.745 Å). In the region above 3400 cm^{-1} are the bands of those hydroxyls having O—H distances considerably shorter than the average, and having very long H . . . O bond lengths (~2.0 Å). In the middle-frequency region, 3400–3250 cm^{-1}, there is a wider distribution of the values for both the covalent- and hydrogen-bond lengths.

Correlation of OH stretching modes with sweetness

In previous studies (3, 28) a high-frequency band, which appears in the infrared spectra of some sugar molecules, has been empirically correlated to their sweetness. This band was observed in the present study at 3525 cm^{-1} for **I**, at 3535 cm^{-1} for **IV**, and at 3500 cm^{-1} for **III**. The frequencies were obtained from the room-temperature Raman spectra. The corresponding band was not observed for **II**. In the case of **I**, the

Can. J. Chem. Downloaded from www.nrcresearchpress.com by 210.87.254.105 on 09/06/12
For personal use only.

TABLE 3. The CH stretching frequencies (cm^{-1})[a, b] of crystalline **I**, **II**, and **IV**

I		II		IV		
Raman	Infrared	Raman	Infrared	Raman	Infrared	Assignment[c]
3014 s	3014 vw	3006 m	—	—	—	$\nu_a(CH_2)$ of C-1
2987 s	2990 vw	2988 m	2988 vw	3000 s	2998 w	$\nu_a(CH_2)$ of C-6 (5)
2962 s	2958 w	2961 s	2954 w	2961 sh	—	ν(CH) of C-4 (3)
2956 m	—	2948 m, br	—	2957 s	2956 w	ν(CH) of C-5 (4)
2936 s	2935 w	2935 s, br	2938 w, br	2938 vs	2938 w	$\nu_s(CH_2)$ of C-6 (5)
2918 m	—	2917 m, br	—	2930 sh	2932 sh	ν(CH) of C-3 (2)
2895 s	2900 w	2899 s, br	2900 w, br	—	—	$\nu_s(CH_2)$ of C-1

[a] v = very, s = strong, m = medium, w = weak, br = broad, sh = shoulder.
[b] Raman spectra recorded at 77 K, infrared spectra recorded at room temperature.
[c] Numbers in parentheses refer to the carbon atoms of **IV**.

TABLE 4. The CH stretching frequencies (cm^{-1})[a] of **III**

Raman	Infrared	Assignment
2979 sh	—	$\nu_a(CH_2)$
2969 sh	2955 sh	$\nu_a(CH_2)$
2950 s	2940 s	$\nu_s(CH_2)$ of C-5 and C-6
2930 m	—	ν(CH)
2914 s	2920 s	$\nu_s(CH_2)$ of CH_2OH
2890 w	2898 w	Combination or overtone

[a] See footnotes of Table 3.

band was assigned to stretching of the weakly bonded HO-4 group, and, in **IV**, to HO-4 (which corresponds to HO-5 in a ketohexose). In the case of **II**, the HO-4 group was also found to be the most weakly bonded hydroxyl, but its band appeared at a lower frequency, namely, 3420 cm^{-1}. The HO-4 group of ketohexoses has not been correlated with the sweetness of these sugars, and it is suggested that the high-frequency band is merely a result of the molecular parameters, such as O—H bond lengths and hydrogen-bond structure, that a particular molecule exhibits.

Since the interaction with the receptor site occurs presumably through hydrogen bonding, those hydroxyls which are strong hydrogen-bond donors and which have their ν(OH) bands at low frequencies might be expected to be of particular relevance. In **I**, such a hydroxyl is the anomeric HO-2 group, which has been identified as the proton-donor moiety of the AH,B saporous unit, while in **II**, such a hydroxyl is the HO-3 hydroxyl. The stretching frequencies of these two hydroxyls are at 3200 cm^{-1} and below. The anomeric hydroxyl of **II** thus would appear to exhibit a weaker hydrogen-bonding capacity than does the anomeric hydroxyl of **I**, a feature which may be of significance in the fact that **II** is considerably less sweet than **I**.

The CH stretching region

The room-temperature Raman and infrared spectra of **I**–**IV** in the region 3100–2800 cm^{-1} are shown in Fig. 2.

Compounds **I** and **II** both have seven fundamental CH stretching modes, while **IV** has six, and **III** eight. However, because of the inherent width of some lines and the consequent overlap, not all of these CH stretching fundamentals are observed in the spectra recorded at room temperature. In contrast, in the low-temperature Raman spectra, seven lines are observed for each of **I** and **II** and six for **IV**. The observed frequencies and assignments are listed in Table 3 for these three molecules. Assignments for **III** are given in Table 4 and are discussed separately. It should be mentioned that some of the weaker bands in the spectra in the CH stretching region might possibly be due to overtones or combinations of CH_2 deformation modes in Fermi resonance with CH stretching modes.

There are some striking differences in the spectra of **III** compared to those of the other three molecules. Firstly, the high-frequency bands at ~3000 cm^{-1}, which are present in the spectra of the latter compounds, are not observed in the spectra of **III**. Secondly, the CH stretching bands of **III** seem to be broader and more overlapped than those of the other three sugars. Therefore, it was decided to compare the CH stretching frequencies of **I**, **II**, and **IV**, and, on the basis of proposed assignments, to analyze then the CH stretching fundamentals of **III**.

The major difference in the spectra of **I** and **II** compared to that of **IV** is that the two bands at 3014 cm^{-1} and 2895 cm^{-1} in **I**, and at 3006 cm^{-1} and 2899 cm^{-1} in **II**, are not present in the spectrum of **IV**. This feature is attributable to the difference in the molecular structure at the anomeric centre: **I** and **II** each have a hydroxymethyl group at the anomeric carbon, whereas in **IV**, this group is replaced by a hydrogen atom. Thus, it appears that the two bands arise from the two CH stretching modes of the hydroxymethyl group. The band at 3014 cm^{-1} in **I** (3006 cm^{-1} in **II**) is assigned to the antisymmetric $\nu_a(CH_2)$ mode, and the band at 2895 cm^{-1} in **I** (2899 cm^{-1} in **II**) to the symmetric $\nu_s(CH_2)$ mode. In the case of ethanol, the antisymmetric and symmetric CH_2 stretching modes of the hydroxymethyl group are observed at 2953 cm^{-1} and at 2900 cm^{-1}, respectively (29).

The three molecules **I**, **II**, and **IV** each have a ring-methylene group in a similar molecular environment. Thus, it is expected that the bands of the two CH stretching modes arising from this group should appear at approximately the same frequencies. Each of these compounds exhibits a high-frequency band having medium-strong intensity. The frequencies of these bands are the following: 2987 cm^{-1} for **I**, 2988 cm^{-1} for **II**, and 3000 cm^{-1} for **IV**. On the basis of the present assignment of the $\nu_a(CH_2)$ mode of the hydroxymethyl group, each of these bands is identified as an antisymmetric CH_2 stretching mode of the ring-methylene group. The corresponding symmetric $\nu_s(CH_2)$ modes are observed at 2936 cm^{-1} for **I**, 2935 cm^{-1} for **II**, and 2938 cm^{-1} for **IV**. The frequencies of these ring-methylene stretching modes are higher than those observed for related compounds, namely, 1,4-dioxane (30) and simple tetrahydropyran derivatives (31). Also, the present as-

Can. J. Chem. Downloaded from www.nrcresearchpress.com by 210.87.254.105 on 09/06/12
For personal use only.

Can. J. Chem. Downloaded from www.nrcresearchpress.com by 210.87.254.105 on 09/06/12
For personal use only.

signment is not in agreement with that of Mathlouthi and Luu (10), who assigned a band at 2988 cm^{-1} to the ν(CH) mode of a methine group and bands at 2946 and 2908 cm^{-1} to $\nu_a(CH_2)$ and $\nu_s(CH_2)$, respectively. However, it is felt that the present assignment is reasonable on the basis of the total assignment of the CH stretching modes of the three molecules.

A medium-strong band which appears at 2967 cm^{-1} in the spectrum of **IV** is not present in the spectra of **I** and **II**. This band is identified as the anomeric ν(CH) mode. As noted above, in the cases of **I** and **II**, the anomeric CH group is replaced by the hydroxymethyl group.

There are three more bands to identify, namely, those arising from the stretching vibrations of the methine groups, at C-3, C-4, and C-5 in **I** and **II**, or at C-2, C-3, and C-4 in **IV**. Compounds **I** and **IV** each have two axial hydrogen atoms and one equatorial hydrogen atom at these respective positions, whereas compound **II** has the hydrogens at C-3, C-4, and C-5 in the axial orientation. The Raman bands which arise from these methine groups are believed to be the following: in **I**, 2962 cm^{-1} (medium-strong), 2956 cm^{-1} (sharp shoulder), and 2918 cm^{-1} (medium-strong); in **IV**, 2961 cm^{-1} (shoulder), 2957 cm^{-1} (medium-strong), and 2930 cm^{-1} (weak shoulder on the intense band at 2938 cm^{-1}); in **II**, 2961 cm^{-1} (medium-strong), 2948 cm^{-1} and 2917 cm^{-1} (shoulders on the intense band at 2936 cm^{-1}). Assignments of these bands have been made on the basis of the similarities or differences in molecular environment.

The relative intensities of these three methine fundamentals appear to be comparable in magnitude from molecule to molecule, except in the case of the bands of **IV** at 2961 cm^{-1} and 2957 cm^{-1}, the intensity ratio of which is opposite to that of the corresponding bands of **I** or **II**; the relative intensities may be disturbed by possible combination bands or overtones in this region.

The above results indicate that the spectra are very sensitive, even to small structural changes. Thus, the shift in the frequency of the $\nu_a(CH_2)$ band of the hydroxymethyl group in **I** (3014 cm^{-1}) and in **II** (3006 cm^{-1}) may be attributable to the difference in conformation of this group. In **I**, the group adopts a *gauche/gauche* conformation (5), whereas in **II**, it is predominantly in a *gauche/trans* conformation (6). The other structural difference between these two molecules is the configuration at C-5; the band of the C-5—H group of **I** was observed at a higher frequency than that of the corresponding group of **II**. Analogous behavior has been observed for the NH stretching vibrations of piperidine (32).

5-Deoxy-D-threo-*hexulose (**III**)*

This deoxy sugar contains three methylene groups. A total of six bands should arise from these groups; in addition, two bands from the ring-methine stretching modes should be observed. The room-temperature Raman spectrum reveals that the CH stretching fundamentals are situated in a very narrow spectral region, a feature which causes an overlap of the bands. The frequency region 3000–2700 cm^{-1} is dominated by two intense bands, namely, those at 2950 cm^{-1} and 2914 cm^{-1}. By analogy with the assignments for **I**, **II**, and **IV**, these two bands are assigned to the symmetric $\nu(CH_2)$ stretching modes of **III**. The two symmetric vibrations of the ring-methylene groups are assumed to coincide and to give rise to the band at 2950 cm^{-1}, and the band at 2914 cm^{-1} is assigned to $\nu_s(CH_2)$ of the hydroxymethyl group. The corresponding frequencies for **I** are 2938 and 2900 cm^{-1}, respectively.

TABLE 5. Raman frequencies (cm^{-1})[a, b, c, d] of **I**–**IV** in the region between 1500 and 50 cm^{-1}

I	II	III	IV
1470 s	1466 s	1468 s	1474 s
1455 m	1454 m	—	1449 w
1430 w	1430 m	1438 m	1375 m
1340 w	1350 w	1357 w	1356 m
—	1310 m	1302 w	1309 m
1263 s	1256 s	1265 s	1259 s
1175 m	1187 m	1186 s	—
1143 m	1113 s, d	1126 m	1146 m
1079 s	1082 s	1092 m	1093 m, t
1060 m	1069 s	1064 s	1065 m
1047 m	1029 m	1052 sh	1051 m
977 m	995 w	964 m	992 m
925 m	900 s	901 s	932 m, d
871 s	884 m	869 m	896 m
—	—	—	841 vs
817 s	817 s	813 s	—
626 w	637 m	646 m	—
594 m	612 m	609 vs	613 m
524 m	552 m	—	578 m
—	509 s	501 s	509 m
465 m, d	468 m, d	473 m	—
423 m, d	418 w	430 w	428 m
—	345 m	403 m	313 m
287 m	271 m	—	263 w
250 m	—	229 w	228 m
234 sh	—	—	206 w
175 vw	179 w	173 m	152 m
—	—	—	143 sh
132 m	—	136 vw	126 w
101 w	95 s	—	115 w
74 vs	67 s	87 m	76 vs
—	53 s	—	67 vs

[a] v = very, s = strong, m = medium, w = weak, sh = shoulder.
[b] d = doublet, t = triplet.
[c] Some assignments are given in the Results and discussion section.
[d] Frequencies below 300 cm^{-1} are accurate to within ±4 cm^{-1}.

The high-frequency shoulders at 2979 and 2969 cm^{-1} on the Raman band at 2950 cm^{-1} are assigned to the antisymmetric CH_2 stretching modes. Again, the ring-methylene modes are assumed to be degenerate and to give rise to a single band at 2979 cm^{-1}; $\nu_a(CH_2)$ of the hydroxymethyl group is observed at 2969 cm^{-1}.

Finally, the band at 2930 cm^{-1} is attributed to the stretching fundamental of C-3—H or C-4—H. The other methine fundamental may be overlapped by the intense $\nu_s(CH_2)$ bands. The assignments are summarized in Table 4.

Frequencies below 1600 cm^{-1}

It has been shown (24, 25) that most of the normal modes of vibrations of carbohydrate molecules in this region are highly coupled and hence very difficult to identify. Consequently, the following discussion of the Raman frequencies of **I**–**IV** is concerned only with the bands which are common to all of these molecules and with the intense bands which can be regarded as being characteristic for ketohexoses or for aldopentoses. The Raman frequencies of these four molecules are given in Table 5 and the spectra shown in Fig. 3.

Can. J. Chem. Downloaded from www.nrcresearchpress.com by 210.87.254.105 on 09/06/12
For personal use only.

Each of the four molecules exhibits the characteristic CH_2 deformation band (24, 25, 33–35) in the 1475–1450 cm^{-1} region. In the case of **I**, **II**, or **IV**, two bands are observed in this region, whereas **III** shows only one intense band at 1468 cm^{-1}. The band at ~1260 cm^{-1} is common to the spectra of all four molecules. In the case of an aqueous solution of D-fructose (10), the corresponding band has been assigned to the CH_2 twisting mode, and, in the cases of crystalline D-glucose and related molecules, the band has been identified as a highly coupled mode of the hydroxymethyl group (24, 25, 36).

A sharp, intense band is observed at 1175 cm^{-1} in the spectrum of **I** and at 1186 cm^{-1} in that of **III**. In the spectrum of **II** the corresponding band appears as a doublet having frequencies 1192 cm^{-1} and 1187 cm^{-1}, and in the spectrum of **IV**, which has no hydroxymethyl group, the band is absent. It is proposed that this band is associated with C—O stretching and H—C—O bending modes of the hydroxymethyl group, and that the two conformations of the hydroxymethyl group in **II** give rise to two separate bands.

Another type of absorption, which appears in the spectra of the three ketohexoses but is not observed in the spectrum of the aldopentose, is observed as an intense band at 817 cm^{-1} in the spectra of **I** and **II**, and at 813 cm^{-1} in the spectrum of **III**. It seems reasonable to attribute this absorption also to a vibration of the hydroxymethyl group. The absorption probably involves CC and CO stretching modes, which usually give rise to bands in this region (37, 38).

The spectrum of **IV** exhibits a very intense band at 841 cm^{-1}; this type of absorption was not observed in the spectra of the three ketohexoses. This absorption is characteristic of all aldose sugars which contain an equatorial hydrogen at the anomeric carbon atom (24, 39, 40).

In the region below 800 cm^{-1} both the frequency and the intensity patterns appear to be characteristic of each individual molecule; thus, the bands corresponding to a common vibrational mode are difficult to identify. For example, the strongest band in this region in the case of **I** is found at 626 cm^{-1}, whereas in the cases of **II**–**IV**, the strongest bands are observed at 509 cm^{-1}, 609 cm^{-1}, and 698 cm^{-1}, respectively.

Several weak bands are observed in the region between 300 and 100 cm^{-1} in the Raman spectra of all four molecules. These may be associated with low-frequency ring-deformation modes such as ring twisting and puckering. The strong Raman bands below 100 cm^{-1} are probably associated with lattice modes of the crystals.

Acknowledgement

The authors are grateful to the Natural Sciences and Engineering Research Council of Canada for its support of this work.

1. R. S. SHALLENBERGER and T. E. ACREE. Nature, **216**, 480 (1967).
2. R. S. SHALLENBERGER. Pure Appl. Chem. **50**, 1409 (1978); Zuckerindustrie, **104**, 121 (1979).
3. G. G. BIRCH. CRC Critical Rev. Food Sci. Nutr. **8**, 54 (1976).
4. O. R. MARTIN, S.-L. KORPPI-TOMMOLA, and W. A. SZAREK. Can. J. Chem. **60**, 1857 (1982).
5. S. TAKAGI and G. A. JEFFREY. Acta Crystallogr. Sect. B, B**33**, 3510 (1977).
6. S. NORDENSON, S. TAKAGI, and G. A. JEFFREY. Acta Crystallogr. Sect. B, B**35**, 1005 (1979).
7. S. H. KIM and G. A. JEFFREY. Acta Crystallogr. **22**, 537 (1967).
8. S. TAKAGI and G. A. JEFFREY. Acta Crystallogr. Sect. B, B**33**, 3033 (1977).
9. G. A. JEFFREY, A. ROBBINS, R. K. MCMULLAN, and S. TAKAGI. Acta Crystallogr. Sect. B, B**36**, 373 (1980).
10. M. MATHLOUTHI and D. V. LUU. Carbohydr. Res. **78**, 225 (1980).
11. M. MATHLOUTHI, C. LUU, A.-M. MEFFROY-BIGET, and D. V. LUU. Carbohydr. Res. **81**, 213 (1980).
12. T. W. BARRETT. Spectrochim. Acta, **37**A, 233 (1981).
13. A. J. MITCHELL and H. G. HIGGINS. Tetrahedron, **21**, 1109 (1965).
14. H. SPEDDING. J. Chem. Soc. 3617 (1961).
15. A. B. FOSTER, R. HARRISON, J. LEHMAN, and J. M. WEBBER. J. Chem. Soc. 4471 (1963).
16. H. S. AARON. Top. Stereochem. **11**, 1 (1979).
17. G. A. JEFFREY. Carbohydr. Res. **28**, 233 (1973).
18. R. G. ZHBANKOV. J. Polym. Sci., Part C, **16**, 4629 (1965).
19. A. J. MITCHELL. Carbohydr. Res. **5**, 229 (1967).
20. A. J. MITCHELL. Aust. J. Chem. **21**, 1257 (1968).
21. A. J. MITCHELL. Aust. J. Chem. **21**, 2451 (1968).
22. G. A. KOGAN, V. M. TUL'CHINSKY, M. L. SHULMAN, S. E. ZURABYAN, and A. YA. KHORLIN. Carbohydr. Res. **26**, 191 (1973).
23. J. UMEMURA, G. I. BIRNBAUM, D. R. BUNDLE, W. F. MURPHY, H. J. BERNSTEIN, and H. H. MANTSCH. Can. J. Chem. **57**, 2640 (1979).
24. P. D. VASKO, J. BLACKWELL, and J. L. KOENIG. Carbohydr. Res. **23**, 407 (1972).
25. J. J. CAEL, J. L. KOENIG, and J. BLACKWELL. Carbohydr. Res. **32**, 79 (1974).
26. G. A. JEFFREY and S. TAKAGI. Acc. Chem. Res. **11**, 264 (1978).
27. M. D. NEWTON, G. A. JEFFREY, and S. TAKAGI. J. Am. Chem. Soc. **101**, 1997 (1979).
28. R. S. SHALLENBERGER. J. Food Sci. **28**, 584 (1963).
29. A. J. BARNES and H. E. HALLAM. Trans. Faraday Soc. **66**, 1932 (1970).
30. R. G. SNYDER and G. ZERBI. Spectrochim. Acta, **23**A, 391 (1967).
31. R. H. MARCHESSAULT. Pure Appl. Chem. **5**, 107 (1962).
32. P. J. KRUEGER and J. JAN. Can. J. Chem. **48**, 3236 (1970).
33. I. NAKAGAWA. Nippon Kagaku Zasshi, **77**, 68 (1956).
34. C. Y. LIANG and R. H. MARCHESSAULT. J. Polym. Sci. **39**, 269 (1959).
35. J. BLACKWELL, P. D. VASKO, and J. L. KOENIG. J. Appl. Phys. **41**, 4375 (1970).
36. P. D. VASKO, J. BLACKWELL, and J. L. KOENIG. Carbohydr. Res. **19**, 297 (1971).
37. W. SAWODNY, K. NIEDENZY, and J. W. DAWSON. Spectrochim. Acta, **23**A, 799 (1967).
38. K. NAKADA. Spectrochim. Acta, **18**, 745 (1962).
39. S. A. BARKER, E. J. BOURNE, M. STACEY, and D. H. WHIFFEN. J. Chem. Soc. 171 (1954).
40. S. A. BARKER, E. J. BOURNE, R. STEPHENS, and D. H. WHIFFEN. J. Chem. Soc. 3408 (1954).

Structural elucidation of the capsular polysaccharide of *Neisseria meningitidis* group H[1]

FRANCIS MICHON, RENÉ ROY, AND HAROLD J. JENNINGS
Division of Biological Sciences, National Research Council of Canada, Ottawa, Ont., Canada K1A 0R6

AND

FRASER E. ASHTON
Bureau of Microbiology, The Laboratory Center for Disease Control, Ottawa, Ont., Canada K1A 0L2

Received December 13, 1983

FRANCIS MICHON, RENÉ ROY, HAROLD J. JENNINGS, and FRASER E. ASHTON. Can. J. Chem. **62**, 1519 (1984).

The capsular polysaccharide from newly isolated *Neisseria meningitidis* group H elaborates a structurally unique polysaccharide which is the group specific antigen. The polysaccharide contains D-galactose, glycerol, and phosphate in the molar ratio of 1:1:1 and is composed of the following basic repeating unit:

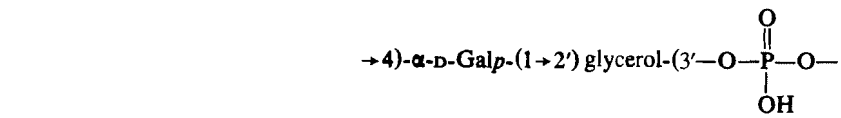

The polysaccharide contains *O*-acetyl groups, in the molar ratio of 0.8:1.0 with D-galactose, which are essential to the formation of the major group specific determinant based on serological experiments described. Although all the *O*-acetyl groups are located on D-galactopyranosyl residues, the substitution pattern is complex, 60% of the residues being substituted at *O*-3 and 20% at *O*-2.

FRANCIS MICHON, RENÉ ROY, HAROLD J. JENNINGS et FRASER E. ASHTON. Can. J. Chem. **62**, 1519 (1984).

Le polysaccharide capsulaire recémment isolé de la bactérie *Neisseria meningitidis* Groupe H possède une structure unique qui est de plus l'antigène spécifique du groupe. Le polysaccharide contient des residus de D-galactose, glycérol et phosphate sous un rapport de 1:1:1 et il est constitué de l'unité répétitive de base suivante:

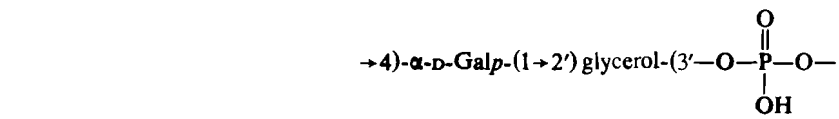

Le polysaccharide contient des groupes *O*-acétyles, dans un rapport molaire de 0,8:1,0 avec le D-galactose, qui sont essentiels pour l'expression de l'immunospécificité du groupe, résultats basés sur les expériences sérologiques décrites. Bien que tous les groupes *O*-acetylés soient localisés sur les résidus D-galactopyrannosyles, le schéma de substitution est complexe: 60% des residus sont substitués en *O*-3 et 20% en *O*-2.

[Traduit par le journal]

Introduction

Neisseria meningitidis is a Gram-negative organism that has been classified serologically (1, 2) into groups A, B, C, D, 29E, W135, X, Y, Z, and newly isolated group L (3). Except for group D, each group produces a unique, capsular polysaccharide that is the antigen responsible for group specificity (1–3). The structures of all these capsular polysaccharides have been determined (2, 4). In 1981 Ding *et al.* (5) described three new serogroups, isolated in China, and designated them groups H, I, and K. As a continuation of our structural studies on the meningococcal polysaccharides we now report the structure of the group H polysaccharide. Preliminary serological studies and the identification of galactose, glycerol, and phosphate as components of the H polysaccharide have recently been reported.[2]

Experimental

Materials

The *Neisseria meningitidis* strain 1890 (H) was obtained from Dr. Shao-qing Ding, National Institute for the Control of Pharmaceutical and Biological Products, Beijing, China and was grown in a chemically defined medium (NCDM) (6). The capsular polysaccharide was isolated and purified as previously described (6), using an initial Cetavlon precipitation to obtain the crude polysaccharide. It had $[\alpha]_D$ +119° (*c*, 0.33 in water). D,L-α-Glycerophosphate was obtained from Sigma Chemical Co., St. Louis, MO, and crystalline floridoside was obtained from Dr. J. S. Craigie, National Research Council Canada, Atlantic Research Laboratory, Halifax, N.S. and was isolated from the common red alga *Chondus crispus*.

Analytical methods

Phosphorus was determined by the method of Chen *et al.* (7). Solutions were concentrated below 50°C under diminished pressure in a rotary evaporator. Periodate oxidation of the de-*O*-acetylated H polysaccharide (10 mg) was performed using 0.05 *M* sodium metaperiodate (10 mL) and the oxidation was allowed to continue for 72 h at room temperature in the dark.

Instrumental methods

Optical rotations were determined on a Perkin–Elmer 243 instrument with 1-dm semi-micro cells at 23 ± 1°C.

Gas–liquid chromatography (gc) was performed on a Hewlett–Packard 5710A instrument equipped with a flame ionization detector and a model 3380A electronic integrator. Glass columns (2 mm × 180 mm) were used with the following packings and programs: (A) 3% SP2340 on 80–100 mesh Supelcoport, from 180°C (delay 2 min) to 240°C at 4°C/min; (B) 3% OV17 on 80–100 mesh Chromosorb W,

[1]NRCC No. 23257.

[2]R. H. Tiesjema *et al.* Presented at the 5th International Conference on Cerebrospinal Meningitis, March 1983, Marseille, France.

Can. J. Chem. Downloaded from www.nrcresearchpress.com by 210.87.254.42 on 09/06/12
For personal use only.

from 180°C (delay 2 min) to 270°C at 6°C/min. Combined gas–liquid chromatography – mass spectrometry (gc–ms) was carried out on a Hewlett–Packard 5985B instrument using the above columns and an ionization potential of 70 eV. Chemical ionization (CI) spectra were obtained using methane as the vector gas.

The ^{13}C nmr spectra were recorded in 10-mm tubes at 25°C on a Varian CFT 20 instrument operating at 20 MHz in the Fourier transform mode with complete proton decoupling. Chemical shifts are reported in parts per million (ppm) downfield from external tetramethylsilane, and the ^{2}H resonance of deuterium oxide was used as the field-frequency lock signal. Polysaccharides and oligosaccharides were examined as solutions in deuterium oxide (30–100 mg/mL).

The ^{1}H nmr spectra were recorded at 80°C with a Varian 400-MHz spectrometer (Regional High Resolution N.M.R. Laboratory, University of Montreal, Quebec) in the pulsed Fourier transform mode. The polysaccharides (3–5 mg) were twice lyophilized from 99.7% D_2O and examined in 99.96% D_2O solution. The apparent first order coupling constants (Hz) were measured directly, and the chemical shifts (δ) are expressed relative to external sodium 2,2-dimethyl-2-silapentane-5-sulfonate. The HOD signal was removed from the spectra by saturation and some of the protons were assigned by selective homonuclear irradiation.

Glycose analysis

Complete acid hydrolyses of the polysaccharides and oligosaccharides were carried out with either 2 *M* trifluoroacetic acid for 8 h at 100°C, or 0.5 *M* trifluoroacetic acid for 16 h at 100°C. The component sugars were detected as their alditol acetates (8) by gc–ms analysis using column A.

Dephosphorylation of the H polysaccharide

The polysaccharide (15 mg) was dissolved in 48% hydrofluoric acid (1 mL) and left for 72 h at 5°C in a Teflon flask. The hydrofluoric acid was then neutralized using Dowex-1 (OH^-) ion-exchange resin (60 mL). The products of dephosphorylation were purified by passage through a Sephadex G-50 column (1.5 cm × 90 cm) using a 0.02 *M* pyridinium acetate buffer (pH 5.4) as eluant and a Waters R403 differential refractometer for monitoring the components.

De-O-acetylation of the H polysaccharide

Complete de-*O*-acetylation of the H polysaccharide was carried out at 25°C for 16 h using either 0.1 *M* sodium hydroxide or 0.02 *M* ammonium hydroxide. The solutions were neutralized with acetic acid (1 *M*) and the de-*O*-acetylated polysaccharide was purified by passage of the neutralized solution through a Sephadex G50 gel-filtration column; it had $[\alpha]_D$ +115° (*c*, 0.29 in water). Partial de-*O*-acetylation was achieved by absorbing the H polysaccharide onto Dowex-1 (OH^-) anion-exchange resin for 1 h and then eluting it from the resin using 0.6 *M* sodium chloride solution. The partially de-*O*-acetylated polysaccharide was obtained by lyophilization of the dialysed sodium chloride eluate.

Methylation analysis

The de-*O*-acetylated H polysaccharide and its oligosaccharide component were methylated with methyl iodide in the presence of methyl sulfinyl anion according to the method of Hakomori (9). The methylated products were recovered by passage of the reaction mixtures through a column of Sephadex LH20 column (30 cm × 1 cm) using chloroform as eluant. The eluted products were detected on thin layer chromatography plates by 10% sulfuric acid in ethanol. The permethylated products were hydrolysed using 0.5 *M* trifluroacetic acid for 16 h at 100°C and the methylated sugars were reduced with sodium borohydride, acetylated with pyridine – acetic anhydride (1:1 v/v) for 1 h at 100°C, and analysed by gc–ms (10) using column B. The permethylated oligosaccharide component of the H polysaccharide was also analysed directly by the above procedure.

Immunodiffusion

Double radial immunodiffusion was performed in 1.0% agarose gels in PBS containing 2% polyethylene glycol (mol. wt. 6000) at 25°C.

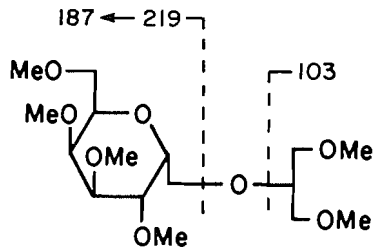

FIG. 1. Methylated oligosaccharide obtained from the H polysaccharide with some primary fragments.

Antisera to the H polysaccharide

Antisera to the H polysaccharide were prepared by injecting whole group H organisms in rabbits as previously described (11).

Quantitative microprecipitin experiments

Quantitative microprecipitin experiments were carried out by the method of Kabat and Mayer (12) using 0.1 mL of antiserum (diluted 5 times in PBS at pH 7.0) and 0.1 mL of antigen solution containing from 5 to 100 μg of polysaccharide. Precipitates were dissolved in 0.1 mL of 0.1 *M* sodium hydroxide and the protein content was determined by the method of Lowry *et al.* (13).

Results and discussion

Isolation and characterization of 2′-O-α-D-galactopyranosylglycerol

Dephosphorylation of the H polysaccharide using 48% aqueous hydrogen fluoride yielded only one chromatographically pure disaccharide component. Hydrolysis of the disaccharide yielded D-galactose and glycerol as determined by gc–ms, the D-configuration being assigned to the galactose residue by virtue of the high positive rotation of the original disaccharide.

Methylation of the disaccharide and subsequent gc–ms analysis of the permethylated compound gave a fragmentation pattern in its mass spectrum consistent with pure 2′-*O*-2,3,4,6-tetra-*O*-methyl-α-D-galactopyranosyl-1′,3′-di-*O*-methylglycerol (Fig. 1). The following fragments are listed using the terminology of Kochetkov and Chizov (14). Primary ions (of the A series) characteristic of the terminal non-reducing hexosyl residue were *m/e* 219 (aA_1), 187 (aA_2), and 155 (aA_3); those of the glycerol moiety were *m/e* 103 (bA_1) and 163 (abJ_1). Expected secondary ions also appeared at *m/e* 101, 88, 71, 59, and 45. The gc–ms analysis in the chemical ionization (CI) mode also gave fragments consistent with the structure. A base peak at *m/e* 187, peaks at 219 (44), peak $(M + H)^+$ at 339, *M* at 338, and $(M - H)^+$ at 337, together with other ions generated by the subsequent loss of methanol from $(M + H)^+$ at *m/e* 305, 273, and 241 (14). The abJ_1 ion at *m/e* 163 was also a dominant feature (11.7%) in the CI spectrum. Hydrolysis of the permethylated compound yielded 2,3,4,6-tetra-*O*-methyl-D-galactopyranose and 1,3-di-*O*-methylglycerol, as indicated by gc–ms, which is also consistent with the above structure.

The ^{13}C nmr spectrum of the disaccharide is also consistent with the above structural evidence and the chemical shifts and assignments of the nine carbon signals are listed in Table 1. The fact that three free hydroxymethyl signals (at 61.6, 62.3, and 62.6 ppm) appear in the spectrum indicates that both hydroxymethyl groups of the glycerol moiety must be unsubstituted, thus implying that linkage occurs at C-2′ (79.9 ppm). Except for the highly characteristic galactopyranosyl anomeric signal (C-1) at 99.3 ppm, most of the other carbons of the galactopyranosyl residue can be readily assigned by

Can. J. Chem. Downloaded from www.nrcresearchpress.com by 210.87.254.42 on 09/06/12
For personal use only.

TABLE 1. Carbon-13 chemical shifts of polysaccharides and component saccharides[a]

Polysaccharide and component saccharides	Galactopyranosyl residue								Glycerol residue		
	C-1	C-2	C-3	C-4	C-5	C-6	CH_3 ($COCH_3$)	C=O ($COCH_3$)	C-1′	C-2′	C-3′
H. Polysaccharide											
3-*O*-Acetyl residue	99.2	67.1	72.7(—)[b,d]	73.2(5.4)[c]	71.8(—)[b,d]	62.0	21.9	174.9	62.4	78.5(5.5)[c]	65.6(—)[b,d]
2-*O*-Acetyl residue	96.6	73.0	67.8(—)[b,d]	75.6(—)[c]	71.8(—)[b,c]	62.0	21.6	174.7	62.4	78.5(5.5)[c]	65.6(—)[b,d]
De-*O*-acetylated H polysaccharide	99.3	69.6	70.0(—)[b,d]	75.8(6.0)[c]	71.9(3.4)[b]	62.0	—	—	62.5	78.3(7.7)[c]	65.8(5.1)[b]
α-D-Gal*p*(1→2′)glycerol	99.3	69.7	70.5[e]	70.6[e]	72.3	61.6[f]	—	—	62.3[f]	80.0	62.6[f]
D,L-α-Glycerophosphate	—	—	—		—	—			63.5	72.4(6.5)[c]	66.0(4.9)[b]

[a]In parts per million from external tetramethylsilane.
[b]^2J ($^{31}P—^{13}C$).
[c]^3J ($^{31}P—^{13}C$)
[d]Note resolved.
[e,f]Tentative assignments.

comparison with previous assignments made on α-D-galactopyranose (15). One minor deviation from the above coincidence of signals was that the C-5 signal of the disaccharide was displayed downfield by 0.9 ppm compared to the C-5 signal of α-D-galactopyranose (15). This displacement can be attributed to the nature of the aglycone as no similar displacement occurs in the C-5 signal of methyl α-D-galactopyranoside (15). Assignments for the 2′-*O*-α-D-galactopyranosylglycerol differ from those assigned by Norton *et al.* (16) who reversed the assignments of C-2 and C-3.

The above evidence indicated that the disaccharide was 2′-*O*-α-D-galactopyranosylglycerol (floridoside) which has been isolated crystalline from the *Rhodophyceae* (17). Crystallization of our preparation of the disaccharide was induced in ethanol by seeding the solution with authentic crystalline floridoside. The crystals had $[\alpha]_D$ +159° (*c*, 0.38 in H_2O) (lit. (17) $[\alpha]_D$ +162° (*c*, 1.0 in H_2O)) and mp 129.5°−130.5°C undepressed on admixture with authentic floridoside.

Structure of the H polysaccharide

Chemical analyses indicate that the H polysaccharide contains phosphate in a molar ratio of 1:1 with D-galactose. Therefore the simple nine resonance ^{13}C nmr spectrum of the de-*O*-acetylated H polysaccharide (Fig. 2) is only consistent with it having a repeating unit of 2′-*O*-α-D-galactopyranosylglycerol-phosphate. To complete the structure of the H polysaccharide it was necessary to assign the position of the phosphate diester linkages joining the disaccharide repeating units and the *O*-acetyl substituents. The presence of *O*-acetyl substituents in the native H polysaccharide was indicated by characteristic methyl (—$COCH_3$) signals at 21.6 and 21.9 ppm (18, 19) in its ^{13}C nmr spectrum (Table 1).

Because the glycerol residue of the disaccharide repeating unit is linked at C-2′, the phosphate diester must be linked to one of its remaining two primary hydroxymethyl groups. This is consistent with the ^{13}C nmr spectrum of the de-*O*-acetylated H polysaccharide which exhibits two signals with chemical shifts characteristic of free primary hydromethyl groups (18, 19), which at 62.0 and 62.4 ppm could be assigned to C-6 and C-1′ respectively. The ^{13}C chemical shifts of the native and de-*O*-acetylated H polysaccharide are listed in Table 1 together with $^{13}C—^{31}P$ coupling constants. The signal at 65.8 ppm can be assigned to the phosphate-linked hydroxymethyl group at C-3′ by virtue of its characteristic chemical shift (18, 19) and the fact that it is a doublet due to two-bond $^{13}C—^{31}P$ coupling, $^2J_{C\text{-}3',P}$ = 5.1 Hz.

The linkage of the phosphate diester to the galactopyranosyl residue must be assigned to C-4 from an analysis of the ^{13}C nmr spectrum of the de-*O*-acetylated H polysaccharide. Neither the C-1 nor C-2 signals of the galactopyranosyl residue of the H polysaccharide are significantly displaced in comparison with the signals of C-1 and C-2 in the disaccharide repeating unit (Table 1), thus indicating the lack of a substituent at C-2 (α effect) or C-3 (β effect) (18, 19). This analysis is entirely consistent with the results of the Smith degradation of the de-*O*-acetylated H polysaccharide. The periodate oxidized polysaccharide was reduced with sodium borohydride, dephosphorylated with aqueous hydrogen fluoride, and hydrolysed with 2 *M* trifluoroacetic acid for 6 h at 100°C. This analysis yielded glycerol, threitol, and galactitol in the ratio of 0.8:1.0:1.0 as determined by gc−ms analysis. The presence of threitol confirms that C-4 is indeed the site of the phosphate diester linkage, as it could only be formed from C-6, C-5, C-4, and C-3 of the α-D-galactopyranosyl residue. The detection of equimolar amounts of threitol and galactitol indicates that only half the α-D-galactopyranosyl residues of the de-*O*-acetylated H polysaccharide were oxidized despite using an excess of oxidant over a protracted period of time. One possible explanation is that the stability of some of the galactopyranosyl residues could be due to hydrogen bonding between the phosphate anion and their 3-OH groups. The stability of apparently periodate-sensitive sugar residues in other charged polysaccharides has also been attributed to a similar type of hydrogen bonding (20). The low estimation of glycerol in the foregoing analysis can be attributed to the volatility of glycerol triacetate in the evaporation procedures used. Thus the de-*O*-acetylated H polysaccharide can be represented by the repeating unit depicted in Fig. 2.

To complete the structure of the native H polysaccharide it was now necessary to locate its *O*-acetyl substituents. That all the *O*-acetyl groups were situated on the galactopyranosyl residues could be ascertained from the fact that C-1′ of the glycerol residue was shown to be unsubstituted by ^{13}C nmr. The C-1′ signal had an identical chemical shift in the ^{13}C nmr spectra of both the native and de-*O*-acetylated H polysaccharides. The detection of two methyl (—$COCH_3$) signals in the ^{13}C nmr spectrum of the H polysaccharide (Fig. 3) and the complexity of the spectrum in comparison with that of the

Can. J. Chem. Downloaded from www.nrcresearchpress.com by 210.87.254.42 on 09/06/12
For personal use only.

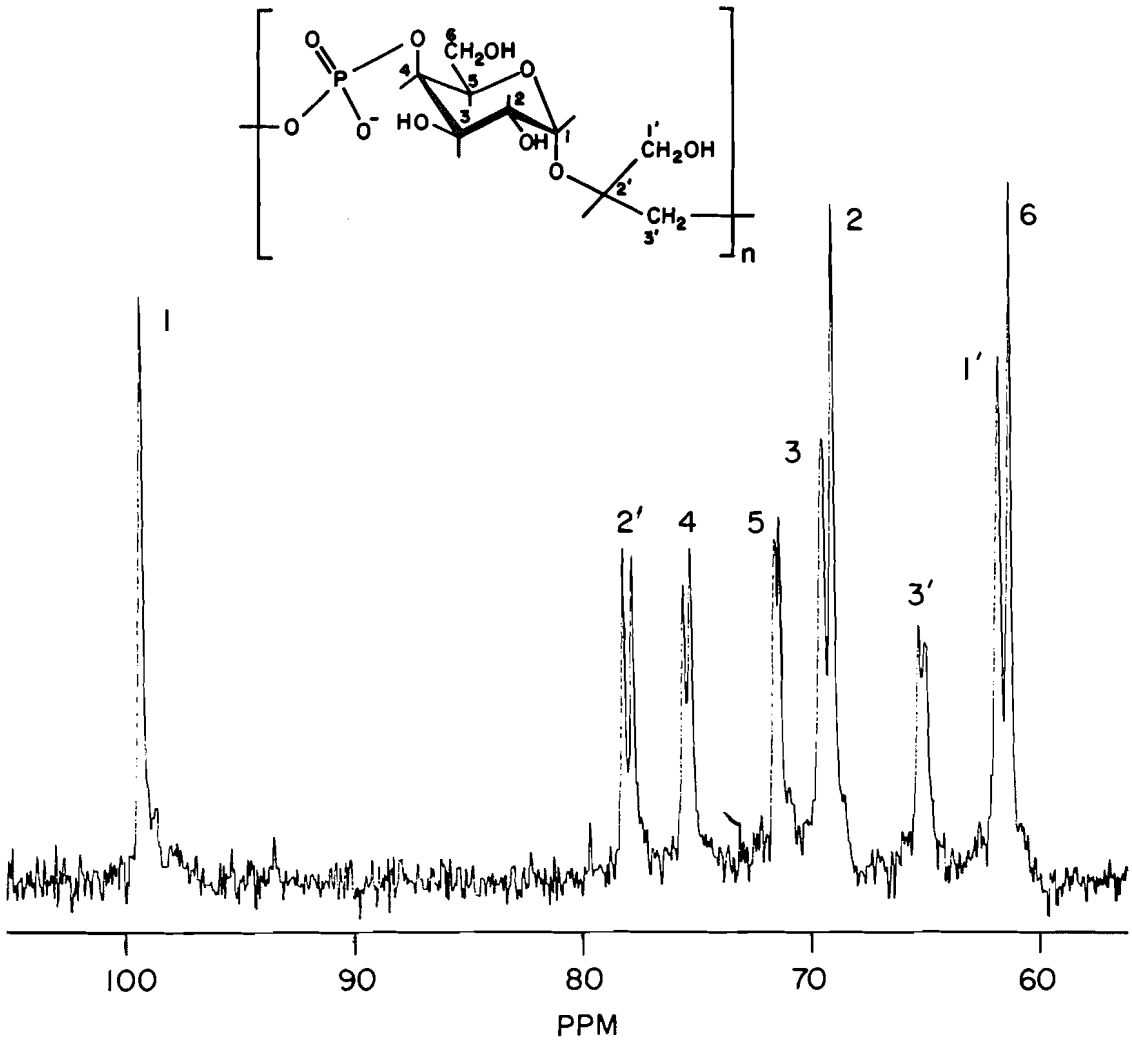

FIG. 2. Fourier-transformed ^{13}C nmr spectra of the de-*O*-acetylated H polysaccharide taken with an acquisition time of 0.5 s, spectral width 4 kHz, and 132 000 free induction decays. Inset: the repeating unit of the de-*O*-acetylated H polysaccharide.

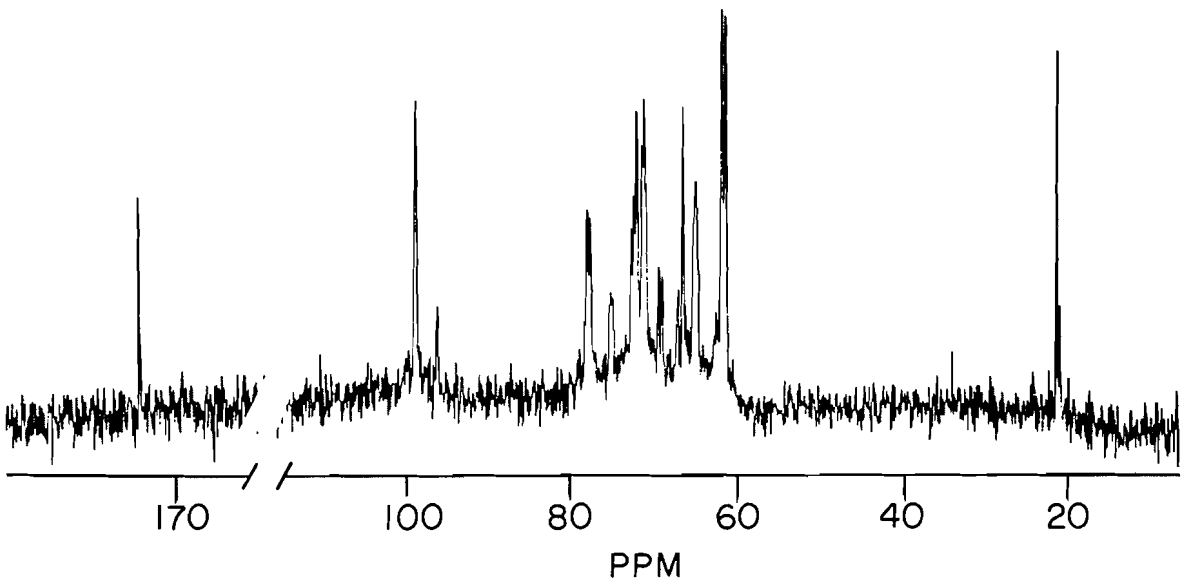

FIG. 3. Fourier-transformed ^{13}C nmr spectra of the H polysaccharide taken with an acquisition time of 0.5 s, spectral width 4 kHz, and 300 000 free induction decays.

Can. J. Chem. Downloaded from www.nrcresearchpress.com by 210.87.254.42 on 09/06/12
For personal use only.

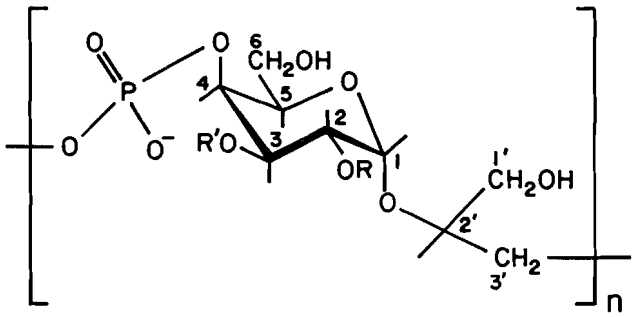

1 R = R′ = H

2 R = H, R′ = $COCH_3$

3 R = $COCH_3$, R′ = H

FIG. 4. The three different β-D-galactopyranosyl residues present in the H polysaccharide.

TABLE 2. Chemical shifts[a] and coupling constants of galactopyranosyl signals in the ^1H nmr spectra of H polysaccharide

Proton	Native H		De-*O*-acetylated H	
	Chemical shift (δ)	Coupling constant (Hz)	Chemical shift (δ)	Coupling constant (Hz)
H-1	5.19(d)	3.8	5.19(d)	3.8
	5.25(d)	3.2	—	—
	5.32(d)	2.7	—	—
H-2	5.01(dd)	3.5, 10.4	—	—
H-3	5.08(dd)	2.2, 6.8	—	—
H-4	4.66(dd)	2.5, 8.8	—	—
	4.63(dd)	nr nr		
	4.55(dd)	nr nr	4.55(dd)	2.7, 8.9
CH_3 ($COCH_3$)	2.20(s)	—	—	—
	2.17(s)	—	—	—

[a]Expressed relative to external sodium 2,2-dimethyl-2-silapentane-5-sulfonate (DSS); d, doublet; dd, doublet of doublets; s, singlet; nr, not resolved.

de-*O*-acetylated H polysaccharide is only consistent with a complex *O*-acetyl substitution pattern. In addition to signals that can be assigned to unsubstituted galactopyranosyl residues, other signals can be assigned on the assumption that other galactopyranosyl residues are substituted with *O*-acetyl groups either at *O*-2 or *O*-3 (Table 1).

This complex substitution pattern, shown in Fig. 4, was readily resolved using high resolution 400-MHz ^1H nmr spectroscopy. The assignments of some signals pertinent to this analysis are listed in Table 2 together with their chemical shifts and coupling constants. The ^1H nmr spectrum of the H polysaccharide exhibits three anomeric doublets at δ 5.19, 5.25, and 5.32 in the ratio of 1:1:3, representative of unsubstituted galactopyranosyl residues, galactopyranosyl residues substituted at *O*-2, and galactopyranosyl residues substituted at *O*-3, respectively. Thus only 80% of the galactopyranosyl residues are substituted with *O*-acetyl groups, which is also consistent with the intensity ratio of anomeric (1H) and *O*-acetyl (3H) protons in the ^1H nmr spectrum being 1:2.5. Two doublet of doublets at δ 5.08 and 5.01 in the intensity ratio of 2:1 can be assigned to H_3 and H_2 of the galactopyranosyl residues substituted at *O*-3 and *O*-2, respectively, by *O*-acetyl groups. The

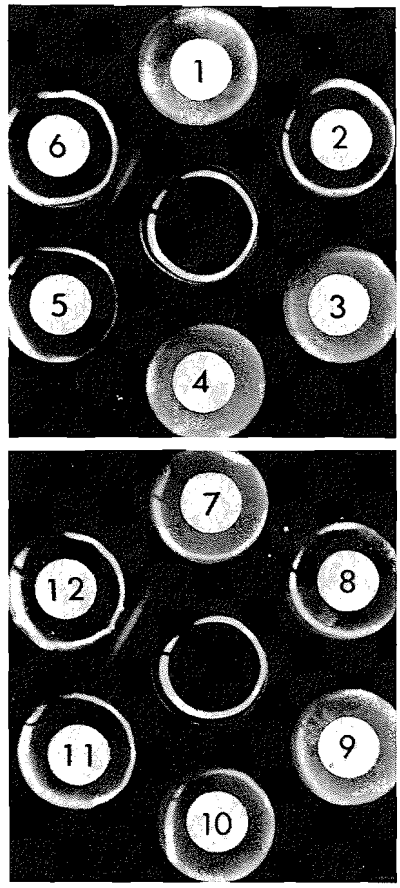

FIG. 5. Double diffusion in agar of meningococcal grouping sera gainst purified capsular polysaccharide of *N. meningitidis* group of H. Central wells contain the H polysaccharide; peripheral wells 6 and 12 contain anti-group H serum; remaining wells (1 to 5 and 7−11) contain A, B, C, X, Y, Z, 29E, W135, I, and K grouping sera respectively.

aforementioned assignment is also corroborated by an analysis of the complex H-4 signal in the ^1H nmr of the H polysaccharide. The signal is composed of three doublet of doublets at δ 4.66, 4.63, and 4.55 in an intensity ratio of 3:1:1 and an overall intensity ratio of 1:1 with the anomeric protons. The doublet of doublets at δ 4.55 is present in the ^1H nmr of the de-*O*-acetylated H polysaccharide (Table 2) and can therefore be assigned to H-4 of the unsubstituted galactopyranosyl residues, while the doublet of doublets at δ 4.63 can be assigned, by virtue of its intensity, to galactopyranosyl residues substituted by *O*-acetyl groups at *O*-2, and the doublet of doublets at δ 4.66 to the same residues substituted at *O*-3. The above assignment is also compatible with the presence of two methyl signals at δ 2.17 and 2.20 in the intensity ratio of 3.1:1.0, which can be attributed to the two *O*-acetyl groups of the differently substituted galactopyranosyl residues.

Using ^1H nmr spectroscopy, the distribution of *O*-acetyl groups in the partially de-*O*-acetylated H polysaccharide could also be determined. From the intensities of the anomeric proton signals mentioned previously (Table 2) one could deduce that 65% of the galactopyranosyl residues are unsubstituted, 25% are substituted by *O*-acetyl at *O*-3, and 10% are substituted by *O*-acetyl at *O*-2.

The H polysaccharide was demonstrated to be group specific in immunodiffusion experiments shown in Fig. 5. In these experiments the H polysaccharide gave a precipitin line only

Can. J. Chem. Downloaded from www.nrcresearchpress.com by 210.87.254.42 on 09/06/12
For personal use only.

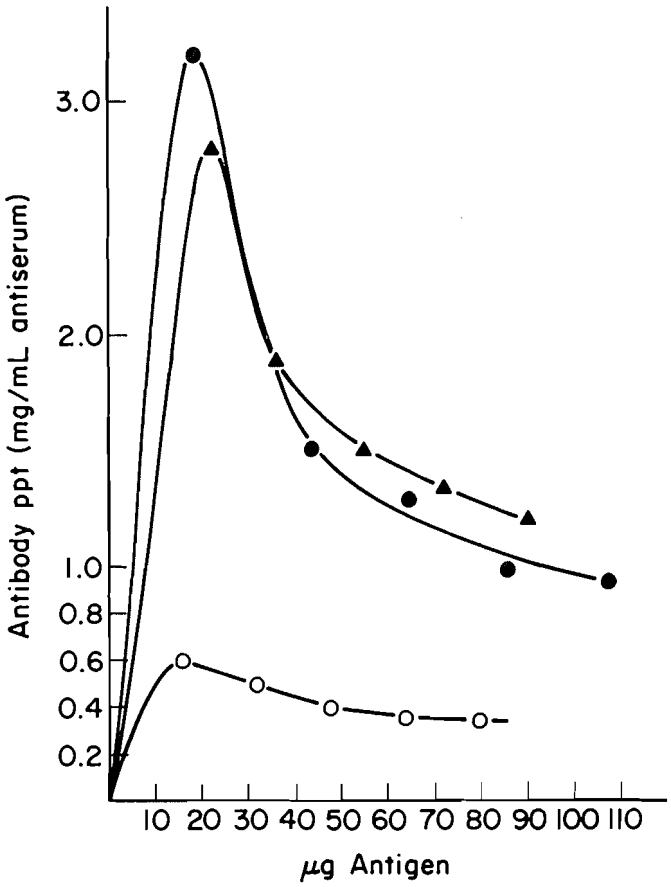

FIG. 6. Quantitative precipitin curves of the H polysaccharide ●—●, the partially de-*O*-acetylated H polysaccharide ▲—▲, and the de-*O*-acetylated H polysaccharide ○—○.

with an antiserum made to its homologous organisms and not to the antisera raised to all the other known meningococcal serogroups.

Quantitative serological experiments using the native and modified H polysaccharide with the aforementioned group H specific antiserum are shown in Fig. 6. These experiments demonstrate that some of the *O*-acetyl groups are essential to the formation of the group-specific determinant. While the native H polysaccharide precipitated 3.2 mg of antibody from 1 mL of antiserum, the de-*O*-acetylated H polysaccharide precipitated less than one fifth of this amount. It is interesting to note that removal of more than half of the *O*-acetyl substituents from the H polysaccharide barely affected its ability to precipitate the maximum amount of antibody. Because only 10% of galactopyranosyl residues substituted at *O*-2 remain in this partially de-*O*-acetylated H polysaccharide, it is perhaps indicative of the more populous 3-*O*-acetyl group being immunodominant.

Acknowledgements

The authors wish to thank Dr. J. S. Craigie for the authentic crystalline floridoside and Fred Cooper for recording the mass spectra.

1. E. C. GOTSCHLICH, T. Y. LUI, and M. S. ARTENSTEIN. J. Exp. Med. **129**, 1349 (1969).
2. H. J. JENNINGS. Adv. Carbohydr. Chem. Biochem. **41**, 155 (1983).
3. F. E. ASHTON, A. RYAN, B. DIENA, and H. J. JENNINGS. J. Clin. Microbiol. **17**, 722 (1983).
4. H. J. JENNINGS, C. W. LUGOWKI, F. E. ASHTON, and J. A. RYAN. Carbohydr. Res. **112**, 105 (1983).
5. S.-Q. DING, R.-B. YE, and H.-C. ZHANG. J. Biol. Standard **9**, 307 (1981).
6. D. R. BUNDLE, H. J. JENNINGS, and C. P. KENNY. J. Biol. Chem. **249**, 4797 (1974).
7. P. S. CHEN, J. V. TORIBA, and H. WARNER. Anal. Chem. **28**, 1756 (1956).
8. J. S. SAWARDEKER, J. H. SLONEKER, and A. R. JEANES. Anal. Chem. **37**, 1602 (1965).
9. S. HAKOMORI. J. Biochem. (Tokyo) 205 (1964).
10. B. LINDBERG. Methods Enzymol. **28B**, 178 (1972).
11. F. E. ASHTON, A. RYAN, B. B. DIENA, and C. E. FRASCH. Can. J. Microbiol. **25**, 784 (1979).
12. E. A. KABAT and M. M. MAYER. *In* Experimental immunochemistry. Thomas, Springfield, IL. 1961. p. 241.
13. O. H. LOWRY, N. J. ROSEBROUGH, A. L. FARR, and R. J. RANDALL. J. Biol. Chem. **193**, 265 (1951).
14. N. K. KOCHETKOV and O. S. CHIZOV. Adv. Carbohydr. Chem. Biochem. **21**, 39 (1966).
15. A. S. PERLIN, B. CASU, and H. J. KOCH. Can. J. Chem. **48**, 2596 (1970).
16. R. S. NORTON, M. A. MACKAY, and L. J. BOROWITZKA. Biochem. J. **202**, 699 (1982).
17. J. S. CRAIGIE, J. MCLACHLAN, and R. D. TOCHER. Can. J. Bot. **46**, 605 (1968).
18. H. J. JENNINGS and I. C. P. SMITH. Methods Enzymol. **50**, 39 (1978).
19. H. J. JENNINGS and I. C. P. SMITH. Methods Carbohydr. Chem. **8**, 87 (1980).
20. J. E. SCOTT and M. J. TIGWELL. Biochem. J. **173**, 103 (1978).

Can. J. Chem. Downloaded from www.nrcresearchpress.com by 210.87.254.42 on 09/06/12
For personal use only.

Multiphoton absorption and decomposition studies of cyclobutanone close to the collisionless regime[1]

R. A. BACK

Division of Chemistry, National Research Council of Canada, Ottawa, Ont., Canada K1A 0R6

AND

D. K. EVANS AND H. M. ADAMS

Atomic Energy of Canada Research Company, Chalk River Nuclear Laboratories, Chalk River, Ont., Canada K0J 1J0

Received January 23, 1984

R. A. BACK, D. K. EVANS, and H. M. ADAMS. Can. J. Chem. **62**, 1525 (1984).

Studies of the multiphoton absorption (MPA) and decomposition (MPD) of cyclobutanone have been extended to short pulses (10 and 40 ns fwhm) and low pressures (0.01 − 1.3 kPa) spanning conditions from essentially no gas kinetic collisions during the laser pulse to a collisional regime. MPA results are modelled by a rotational hole-filling model with a system relaxation time of 0.07 (kPa ns)$^{-1}$ and no dependence on laser intensity is observed. By contrast, decomposition appears to be more efficient using a 10 ns pulse than one of 40 ns. Results are reported for both major and minor products and a mechanism for MPD consistent with these results is discussed.

R. A. BACK, D. K. EVANS et H. M. ADAMS. Can. J. Chem. **62**, 1525 (1984).

On a étendu les études d'absorption et de décomposition multiphoton (AMP et DMP) de la cyclobutanone de façon à inclure de courtes pulsations (10 et 40 ns fwhm) et de faibles pressions (0,01 − 1,3 kPa) et à couvrir des conditions allant esentiellement de l'absence de collisions cinétiques en phase gazeuse pendant l'impulsion du laser jusqu'à un régime impliquant des collisions. On représent les résultats de l'AMP par un modèle rotationel de remplissage de cavité avec un temps de relaxation du système de 0,07 (kPa ns)$^{-1}$ et on n'a observé aucune relation avec l'intensité du laser. La décomposition au contraire semble être plus efficace lorqu'on utilise une impulsion de 10 ns au lieu de 40 ns. On rapporte les résultats relatifs aux produits principaux et secondaires et on discute d'un mécanisme de la DMP qui est en accord avec les résultats.

[Traduit par le journal]

Introduction

The multiphoton absorption and decomposition in cyclobutanone have been studied in several laboratories (1−5). This work has been done with conventional CO_2 lasers with relatively long pulses (≥ 1 μs) and mostly at fairly high pressures, up to several kPa, and therefore in the "collisional" regime, where both absorption and decomposition may be strongly modified by collisions. Cyclobutanone is interesting because it decomposes fairly easily, exhibiting two clean unimolecular decomposition paths,

[1] cyclobutanone → C_2H_4 + H_2CCO

[2] cyclopropane + CO

with relative rates and activation energies well defined from thermal reaction studies (6). Other higher-energy channels, less well defined, yield propylene, acetylene, and other hydrocarbons. Measurement of product ratios from these several channels should yield information about the energy of molecules decomposing in the multiphoton process.

The present paper describes the extension of the studies of multiphoton absorption and decomposition in cyclobutanone into the collision-free regime, using the Chalk River variable pulse CO_2 laser and the single pulse photoacoustic absorption technique developed at CRNL. Using 10 and 40 ns fwhm pulses, we have made absorption measurements with an average of between 0.3 and 4.5 gas-kinetic collisions per molecule during the pulse, and decomposition experiments with between 0.01 to 4.5 collisions per molecule during the pulse (7). Measurements under these conditions should clarify the role of collisions both in absorption and decomposition.

Experimental

All irradiations were performed using the prototype variable pulse CO_2 laser system built by Lumonics Inc. (8).

The laser was tuned to the 9P(20) line at 1046.9 cm^{-1} with temporally smooth pulses of 10 or 40 ns fwhm. The energy contrast ratio was kept to at least 10 by use of saturable absorbers. Pulse energy to the samples was varied by use of calibrated CaF_2 absorbers.

The multiphoton absorption measurements were made using the single-pulse photoacoustic technique (9). A typical photoacoustic measurement involves recording pulse energy and microphone voltage for about 1000 laser pulses. Calibration factors to convert microphone voltage to absorbed energy were determined by a conventional transmission experiment at relatively low fluences (0.01 − 0.1 J/cm^2) using an arrangement similar to that of ref. 10 with the absorption cross-section corrected for the radial profile of the beam and for attenuation along the cell (10). The temporal dependence of absorption was measured by using two photon drag detectors and comparing the pulse shape of a 40 ns pulse before and after passage through a 46 cm cell containing 1.333 kPa of cyclobutanone. Calibration measurements were made at cyclobutanone pressures of 0.333, 0.667, 1.000, and 1.333 kPa using the 10 ns pulse and photoacoustic measurements were made at these pressures for both 10 and 40 ns pulses, corresponding to an average of 0.3 to 4.5 collisions during the pulse (7).

Multiphoton decomposition experiments were performed in Pyrex cells 46 cm long, 2.5 cm in diameter and fitted with greaseless valves and NaCl windows mounted at 7° to the cell axis to prevent back reflections causing self-oscillation of the amplifier section of the laser system. BaF_2 lenses of 50 or 100 cm focal length were used. Fluences are given by the laser pulse energy divided by the area of the beam waist. For the 1.6, 2.2, and 3.5 J/cm^2 studies the 100 cm lens was used; however, at higher fluences the short pulse damaged the cell windows, so fluence dependence studies were done using a 50 cm focal length lens. Cyclobutanone pressures from 0.013 − 1.333 kPa were used in the decomposition studies.

Products were analysed with a gas chromatograph using a phenyl isocyanate column and flame ionization detection. Relative yields are more precise than the absolute determinations.

[1]AECL No. 8473, NRCC No. 23252.

Can. J. Chem. Downloaded from www.nrcresearchpress.com by 210.87.254.105 on 09/06/12
For personal use only.

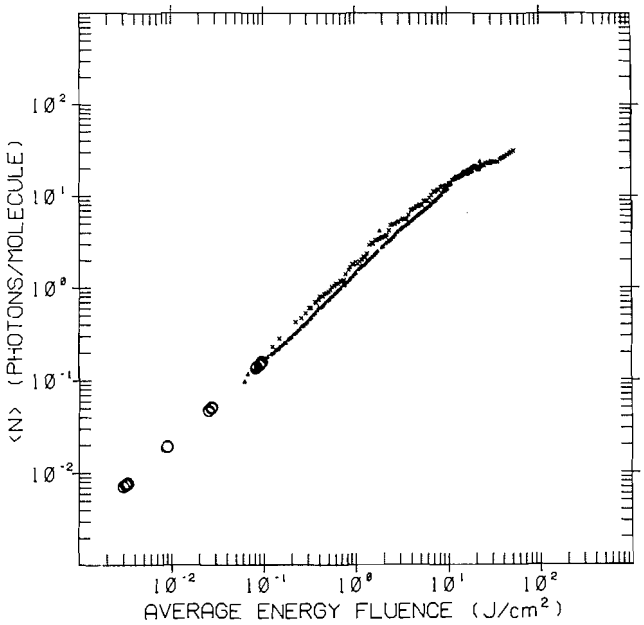

FIG. 1. The intensity dependence of multiphoton absorption by cyclobutanone. Calibration results (○) for 1.333 kPa and a 10 ns fwhm pulse and calibrated photoacoustic results for 1.333 kPa, 10 ns (△) and 0.333 kPa, 40 ns (×) are shown. At the same pressure times pulse width there is no intensity dependence observed.

Results and discussion

Multiphoton absorption

The multiphoton absorptions measured in these experiments show very little dependence on laser fluence or intensity. This can be seen in Fig. 1 where the calibrated values of $\langle n \rangle$, the average number of photons absorbed per molecule, are plotted in log−log form against fluence for a 10 ns pulse at 1.333 kPa and a 40 ns pulse at 0.333 kPa pressure of cyclobutanone.

Also shown in Fig. 1 (○) are the values of $\langle n \rangle$ determined by the transmission experiment. The photoacoustic measurements are calibrated by ensuring that there is an overlap of the $\langle n \rangle$ values from calibration and microphone measurements. (In Fig. 1, each of the points in each cluster of calibration results is an average of 100 laser pulses for a total of 2000 pulses to obtain a calibration factor for each pressure.)

The product of pulse width and pressure is constant in these two experiments, so there is the same number of collisions during the pulse. Although the laser intensity is four times higher in the shorter pulse, the differences in the two plots are within the uncertainty of the photoacoustic measurement. The slopes are close to unity except at high fluence, implying cross-sections independent of fluence. Table 1 summarizes measurements of $\langle n \rangle$ and cross-sections obtained from such measurements. The photoacoustic data used to compare with calibration results were restricted to fluences ≤ 2 J/cm^2 because at higher fluences the assumptions inherent in the photoacoustic measurement no longer hold. In particular, as decomposition becomes appreciable, energy is lost (the reaction is endothermic), so that the rise in temperature, and hence the rise in pressure measured by the microphone, is reduced. This probably explains why the lines in Fig. 1 curve downward at high fluence.

In Fig. 2 we have plotted $\langle n \rangle$ at fluences of 0.5 and 1.0 J/cm^2 against the product of pressure and pulse width, which is proportional to the number of collisions during the pulse. The curves drawn are calculated on the assumption that rotational relaxation by collisions is responsible for the rise in $\langle n \rangle$ with increasing values (pressure × pulse width, $p\tau$). If only a fraction of the molecules is initially in an appropriate rotational state to absorb radiation, and this is replenished by a first-order process, the system can be described by the equation

$$\frac{\langle n \rangle(p\tau) - \langle n \rangle_\infty}{\langle n \rangle_0 - \langle n \rangle_\infty} = \exp\,[-kp\tau]$$

where $\langle n \rangle_0$ and $\langle n \rangle_\infty$ are low-pressure and high-pressure limits respectively, p is pressure and τ is the fwhm of the pulse. The data at each of the two fluences can be fitted with a common value of $k = 0.07$ (kPa ns)$^{-1}$ for the two curves (11). This is a composite rate constant corresponding to the several collisions required to bring a molecule into a resonant rotational level, and is not directly comparable with the value of 0.225 in the same units reported by Starov *et al.* (3) for a single relaxing collision. The ratio of these values, 3.2, should in fact correspond to the average number of collisions required to bring all the molecules into resonance with the laser radiation. The ratio $\langle n \rangle_0/\langle n \rangle_\infty$ had a value of 0.25 at both fluences, which may be interpreted as the fraction of molecules initially capable of absorbing laser radiation, and may be compared with a value of 0.3 chosen by Starov *et al.* (3) to fit their model to their observations.

In another study of cyclobutanone, Harrison and co-workers (2) measured a value of $\langle n \rangle$ of 3 or 4 at a fluence of 0.67 J/cm^2 at a laser frequency of 1073 cm^{-1}, *independent* of pressure from 0.04 to 2.7 kPa. The pulse length from their conventional CO_2 laser was not clearly reported, but was probably long enough to place their measurements, even at the lowest pressure, in the plateau region of Fig. 2. Thus there is no conflict between our results and theirs when the pulse length as well as pressure is considered.

Finally, our photon drag measurements showed that absorption was uniform throughout the 40 ns pulse at 1.333 kPa, the lowest pressure permitting quantitative measurement; at 0.667 kPa, the absorption also appeared uniform within the accuracy of the observations. Thus no net depletion of absorbing species could be observed during the pulse.

Multiphoton decomposition

Decomposition products were those observed previously; ethylene was the major product measured, with cyclopropane

TABLE 1. The least squares fits of the number of photons per molecule ($\langle n \rangle$) and cross section (σ) to laser fluence (E)* for the form $\log \langle n \rangle = a + b \log E$ and $\log \sigma = c + d \log E$

Pressure (kPa)	Pulse width (ns)	a	b	c	d
0.333	40	0.263	0.998	−19.119	−0.0023
0.667	40	0.251	0.948	−19.153	−0.0523
1.000	40	0.321	0.914	−19.099	−0.0862
1.333	40	0.323	0.871	−19.119	−0.129
0.333	10	−0.0217	0.928	−19.435	−0.0723
0.667	10	0.0377	1.016	−19.336	0.0166
1.000	10	0.135	1.010	−19.242	0.0099
1.333	10	0.184	0.981	−19.206	−0.0191

*Only measurements for $E \leq 2$ J/cm^2 were used. The reason for this restriction is discussed in the text.

Can. J. Chem. Downloaded from www.nrcresearchpress.com by 210.87.254.105 on 09/06/12
For personal use only.

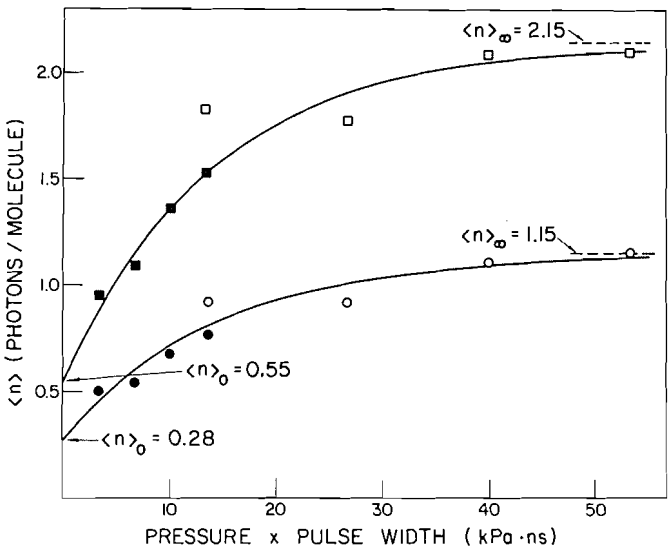

FIG. 2. The pressure dependence of multiphoton absorption by cyclobutanone at fixed laser fluences (○, ● — 0.5 J/cm^2 and □, ■ — 1.0 J/cm^2, filled symbols for 10 ns pulses, open for 40 ns pulses). The curves are a first order relaxation model which is discussed in the text.

between 3 and 7% of the ethylene and propylene between 1 and 60% of the cyclopropane. At higher fluences, significant yields of methane, ethane, acetylene, and traces of other C_3 and C_4 hydrocarbons were observed. Ketene and CO, which presumably were formed in conjunction with ethylene and cyclopropane in reactions [1] and [2], were not measured. In Fig. 3 is shown a log−log plot of P, the probability of decomposition per pulse for a molecule in the central cylindrical portion of the irradiation zone (12), as a function of the fluence at the centre (corrected for attenuation) for pressures of cyclobutanone of 0.333 and 1.333 kPa, pulse length of 10 and 40 ns fwhm, and using both the 50 and 100 cm focal length lenses. It was assumed in calculating P that the observed decomposition occurred entirely in the central reaction zone. Each experiment consisted of a sequence of between 50 and 1000 pulses with the laser operating at 2 Hz. The extent of decomposition in an experiment (based on the total cell contents, not just the gas in the beam) varied from less than 1% to about 40%, and a first-order correction for the depletion of the cyclobutanone during the experiment was applied in calculating P. The corrected values showed no significant variation with percent decomposition. Values of P for 1.333 kPa were consistently higher than those at 0.333 kPa, but within the experimental scatter, there does not appear to be a dependence of P on the pulse width or the focal length of the lens. At fluences greater than about 5 J/cm^2, values of P exceed unity, clearly implying that extensive decomposition was occurring outside the central cylindrical zone.

A series of experiments was done at three incident fluences, similar to those used in earlier studies (1−4) (about 1.7, 2.3, and 3.6 J/cm^2) using pulse lengths of both 10 and 40 ns and four pressures of cyclobutanone. The products measured, product ratios, percent of sample decomposed, and P are given in Table 2. For all pressures with the 40 ns pulse, P was proportional to (fluence)$^{2.8}$. About the same dependence was found for the 10 ns pulse at a pressure of 1.333 kPa cyclobutanone; however, with decreasing pressure the fluence dependence became stronger.

From these experiments, we have interpolated the values of

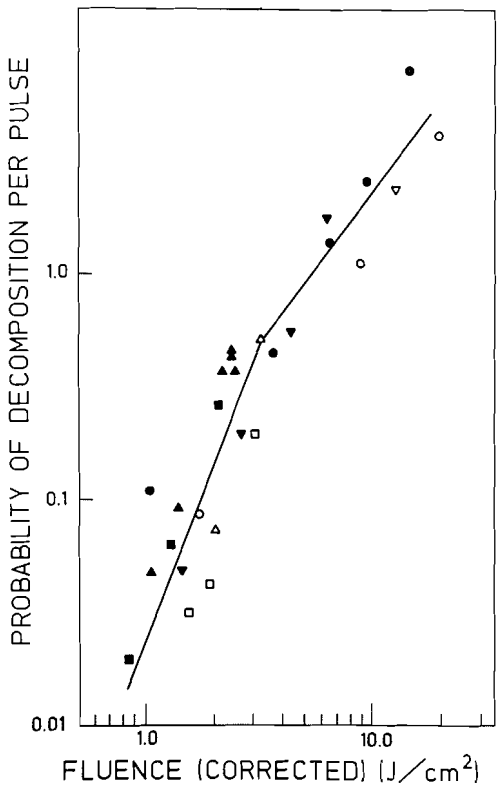

FIG. 3. Probability of decomposition in the central cylindrical region vs. laser fluence for two focal lengths and pressures. □, ■ — 40 ns, 100 cm focal length; ○, ● — 40 ns, 50 cm focal length; △, ▲ — 10 ns, 100 cm focal length; ▽, ▼ — 10 ns, 50 cm focal length; filled symbols — 1.333 kPa, open symbols — 0.333 kPa.

P for a fluence of 2 J/cm^2 for each pulse width and pressure and these are plotted in Fig. 4 against $p\tau$ in log−log form. The decomposition will be enhanced with increasing $p\tau$ as additional molecules become resonant with the laser radiation. If the decomposition process were unmodified by collision, the increase in P with increasing $p\tau$ should be no more than linearly proportional to the increase in absorption (Fig. 2) but, in fact, the increase evident in Fig. 4 is much larger than this. Furthermore, plotting P against $p\tau$ fails to bring the data for the two pulse widths into coincidence as it did for the absorption measurements (Fig. 2), with the values of P for the 10 ns pulse lying about a factor of 5 too high to give a single continuous curve. Since the MPA experiments (see Fig. 1) show that the energy absorbed is nearly the same for the two pulse widths, it appears that at this fluence this energy is used much more efficiently when delivered in a shorter time.

In Fig. 5, values of the two product ratios C_3H_6/C_2H_4 and propylene/C_3H_6 (where C_3H_6 = cyclopropane plus propylene) are plotted against corrected central fluence for a number of pressures using 10 ns pulses. At higher fluences, and higher conversions, the C_3H_6/C_2H_4 ratio was found to increase with increasing conversion. Product ratios obtained at 15% or less conversion were found to be independent of conversion and only such experimental results are plotted in Fig. 5. A similar plot for the 40 ns results shows that the product ratios lie about 10% below those for the shorter pulse. The experimental scatter is such that this difference is not definitely established; however, ratios from previous experiments with a conventional long-pulse CO_2 laser were appreciably lower again, continuing the trend to lower ratios with increasing pulse length. The

Can. J. Chem. Downloaded from www.nrcresearchpress.com by 210.87.254.105 on 09/06/12
For personal use only.

TABLE 2. Summary of results of the multiphoton decomposition experiments, corrections as described in the text are made to obtain the points plotted in the figures

Initial pressure of cyclobutanone (kPa)	Number of pulses	Fluence (J/cm^2)	C_2H_4 (Pa)	Δ (Pa)	C_3H_6 (Pa)	CH_4/C_2H_4	C_2H_6/C_2H_4	C_2H_2/C_2H_4	Percent decomposition	P
					(*a*) 10 ns fwhm pulses					
1.333	500	9.96	126.8	5.9	2.7	0.0107	0.00866	0.0508	10.15	1.76
0.333	500	13.5	42.1	1.7	1.1	0.0126	0.0194	0.0991	13.5	2.38
0.333	1000	2.15	42.0	2.2	0.22				13.3	0.0733
0.667	500	2.43	60.7	3.3	0.55				9.68	0.105
1.000	500	2.41	95.9	5.2	0.81				10.19	0.110
1.333	500	2.20	108.5	5.8	0.60				8.62	0.0927
1.167	500	2.26	89.2	4.6	0.62				8.09	0.0857
0.833	500	2.20	72.9	3.9	0.73				9.31	0.100
0.167	1000	2.11	33.6	1.5	0.45				21.3	0.123
0.500	1000	2.22	111.9	6.2	1.8	0.000384	0.000787		24.0	0.141
0.333	1000	3.43	127.9	6.3	3.8	0.00446	0.00888	0.0223	41.4	0.514
0.667	500	3.46	176.1	8.6	4.5	0.00606	0.00901	0.0272	28.4	0.343
1.000	500	3.43	246.5	12.8	5.9	0.00573	0.00676	0.0233	26.5	0.317
1.333	500	3.49	373.7	18.7	10.7	0.00656	0.00599	0.0188	30.2	0.370
0.167	500	3.26	42.8	2.1	1.1	0.00383	0.00748	0.0174	27.6	0.332
0.500	200	3.46	64.7	3.0	1.5	0.00518	0.0115	0.0309	13.8	0.382
0.833	200	3.51	110.4	5.1	2.5	0.00868	0.0101	0.327	14.2	0.394
1.167	200	3.42	163.3	7.7	3.7	0.00659	0.00452	0.0241	15.0	0.418
1.333	1	3.3	0.98						0.08	0.404
1.333	300	3.93	240.8	12.3	5.3	0.00559	0.00482	0.0191	19.4	0.370
1.333	120	3.80	125.2	6.1	2.9	0.00806	0.00715	0.0252	10.1	0.456
1.333	50	3.78	52.3	2.4	0.95	0.0111	0.00617	0.0296	4.17	0.438
0.267	500	1.76	13.9	0.56	0.07				5.44	0.0575
0.533	500	1.61	26.0	1.25	0.14				5.14	0.0542
0.800	500	1.57	30.1	1.60	0.15				3.99	0.0419
1.067	500	1.62	37.7	1.8	0.23				3.73	0.0391
1.333	500	1.67	58.3	2.8	0.19				4.59	0.0483
0.067	500	1.70	0.86	0.032	0.008				1.35	0.014
0.013	500	1.77	0.46	0.028	0.005				3.69	0.0388
0.067	1000	2.38	18.9	0.83	0.36	0.000682	0.000759		30.2	0.187
0.013	1000	2.44	1.67	0.058	0.016				13.0	0.0726
0.067	300	3.54	12.5	0.48	0.35	0.00306	0.00541	0.0112	20.1	0.392
0.013	300	3.63	1.33	0.042	0.022				10.5	0.190
1.333	100	2.31*	0.741	0.033	0.0029				0.06	0.048
1.333	100	4.19*	2.97	0.14	0.058	0.00166	0.00324	0.0261	0.24	0.196
1.333	100	6.95*	8.25	0.35	0.21	0.0108	0.0102	0.0493	0.66	0.545
					(*b*) 40 ns fwhm pulses					
1.333	500	30.0*	547.7	20.3	8.4	0.0123	0.00895	0.0957	43.23	9.30
1.333	50	22.0*	58.9	2.2	0.90	0.00986	0.00505	0.0568	4.64	7.80
0.333	50	22.1*	7.73	0.23	0.11	0.00984	0.0106	0.0748	2.43	4.05
1.333	50	14.8*	19.6	0.74	0.32	0.00865	0.00544	0.0364	1.55	2.57
1.333	100	10.4*	20.8	0.87	0.45	0.00633	0.00558	0.0244	1.66	1.37
0.333	100	10.1	4.3	0.13	0.068	0.00467	0.00695	0.0290	1.34	1.11
1.333	200	6.09	13.4	0.59	0.16	0.000651	0.000968	0.00117	1.06	0.438
1.333	500	1.91	7.5	0.38	0.033				0.67	0.109
0.333	500	1.99	1.7	0.055	0.004				0.535	0.0874
0.333	500	1.79	9.7	0.28	0.010				2.99	0.0312
0.667	500	1.66	22.3	0.83	0.038				3.46	0.0363
1.000	500	1.67	30.7	1.18	0.049				3.20	0.0335
1.333	500	1.59	24.4	0.84	0.011				1.89	0.0196
0.333	200	2.19	5.2	0.16	0.005				1.62	0.042
0.667	200	2.25	19.3	0.78	0.091				3.03	0.079
1.000	200	2.17	24.1	0.96	0.085				2.52	0.0658
1.333	200	2.20	31.1	1.3	0.077				2.43	0.0632
0.333	100	3.49	11.9	0.40	0.079				3.71	0.194
0.667	100	3.51	34.0	1.40	0.37	0.000314	0.000965	0.00125	5.37	0.284
1.000	100	3.55	49.5	2.1	0.52	0.000499	0.000585	0.000887	5.21	0.275
1.333	100	3.61	62.3	2.9	0.57	0.000360	0.000426	0.000246	4.93	0.260

*Experiment done using 50 cm focal length lens. For all others a 100 cm focal length lens was used.

Can. J. Chem. Downloaded from www.nrcresearchpress.com by 210.87.254.105 on 09/06/12
For personal use only.

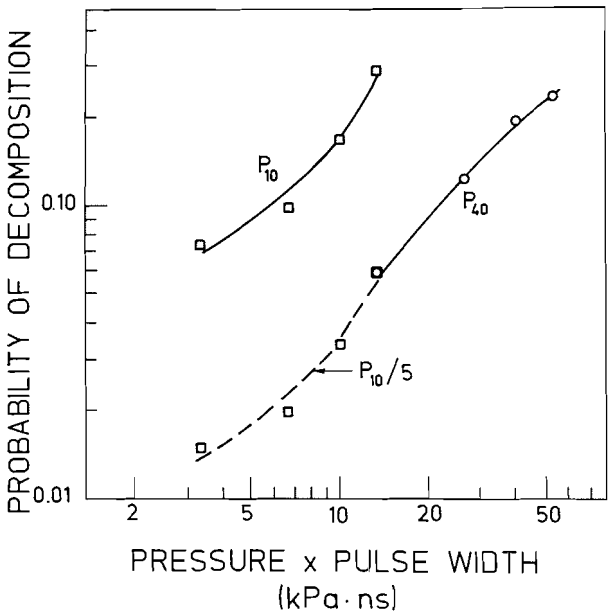

FIG. 4. Probability of decomposition in the cylindrical region, P, vs. pressure times pulse width at 2 J/cm^2. □ — 10 ns pulse, ○ — 40 ns pulse. The dotted line is the results for 10 ns divided by five.

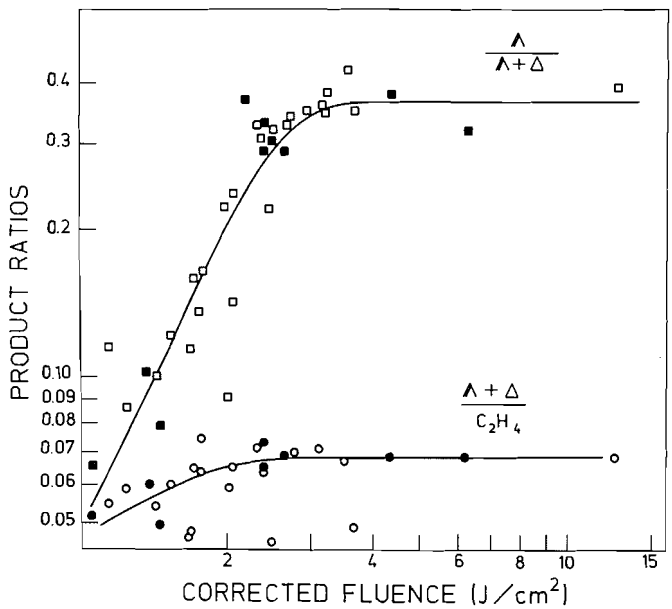

FIG. 5. The ratio of C_3H_6 (total) to C_2H_4 (○, ●) and of propylene to total C_3H_6 (□, ■) vs. fluence corrected for absorption losses at a variety of pressures.

product ratios have little dependence on fluence in the present experiments, with no variation above 3 J/cm^2. This behaviour probably reflects extensive decomposition outside the central focal zone at high fluence, the same effect that caused P to rise above unity in Fig. 3, with consequent reduction in the effective average fluence for the decomposition. With the 10 ns pulse there is no significant variation in the product ratios with pressure; however, with the 40 ns pulse, the product ratios decrease as pressure decreases below about 0.67 kPa.

The propylene/C_3H_6 ratio for irradiation with a 40 ns pulse shows a greater fluence dependence at low fluence than the C_3H_6/C_2H_4 ratio but like the latter it levels out at high fluence,

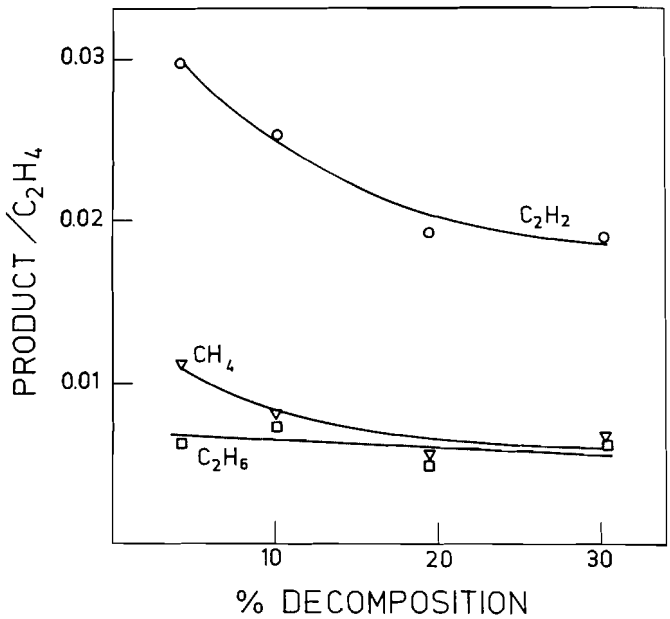

FIG. 6. The ratios of each of C_2H_2, CH_4, and C_2H_6 to C_2H_4 as a function of sample conversion at 1.333 kPa using a 10 ns pulse focussed to 2.30 ± 0.15 J/cm^2 (corrected) with a 100 cm focal length lens.

probably for the same reason.

Acetylene, methane, and ethane have been reported before as minor products but were not measured systematically. They became measurable in the present experiments only at fluences above 2 J/cm^2. All three are products of the thermal (13) and infrared laser-induced (14) decomposition of ethylene, which suggests that they might be of secondary origin in the present system. Figure 6 shows the dependence of those products, relative to ethylene, on conversion for a typical series of experiments and it is clear that the accumulation of ethylene (or other products) with increasing number of pulses does not enhance the relative yields of C_2H_2, CH_4, or C_2H_6 which in fact appear to decline at higher conversions. The possibility remains that they are derived from secondary decomposition of ethylene within a single pulse, since in the reaction zone, conversion after a single pulse was about 40% in these experiments. The C_2H_2/C_2H_4 at all pressures tends to be higher for the 10 ns pulse than for the 40 ns pulse. This suggests that the more efficient conversion of energy to reaction with the shorter pulse noted earlier might correspond to the absorbed energy having a different distribution such that a larger fraction are excited to higher levels. These would decompose more efficiently and at higher energies, thus favouring high energy channels. These arguments are only valid if the C_2H_2 is a primary photochemical product. A similar trend was observed for CH_4 and C_2H_6 but there was larger scatter in the results.

The mechanism of multiphoton decomposition

The present results offer somewhat conflicting evidence about the mechanism of decomposition. The higher probability of decomposition in the shorter pulse after allowing for differences in absorption (Fig. 4) implies a competition between pumping by the laser radiation and collisional deactivation at least during the 40 ns pulse, with decomposition occurring during or shortly after the pulse. For such a decomposition, however, P should decrease with increasing pressure as the absorbed energy is shared among more molecules, whereas in

Can. J. Chem. Downloaded from www.nrcresearchpress.com by 210.87.254.105 on 09/06/12
For personal use only.

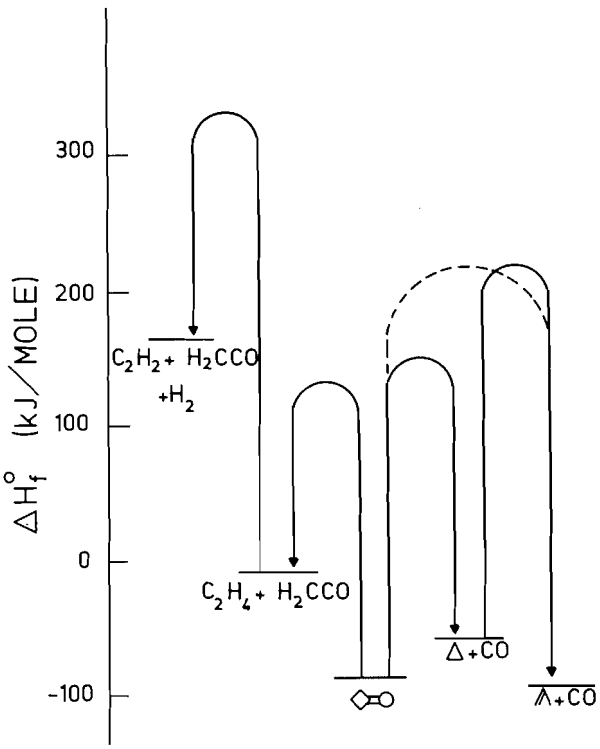

FIG. 7. The energy relations in cyclobutanone decomposition based on heats of formation from Benson and O'Neal (18).

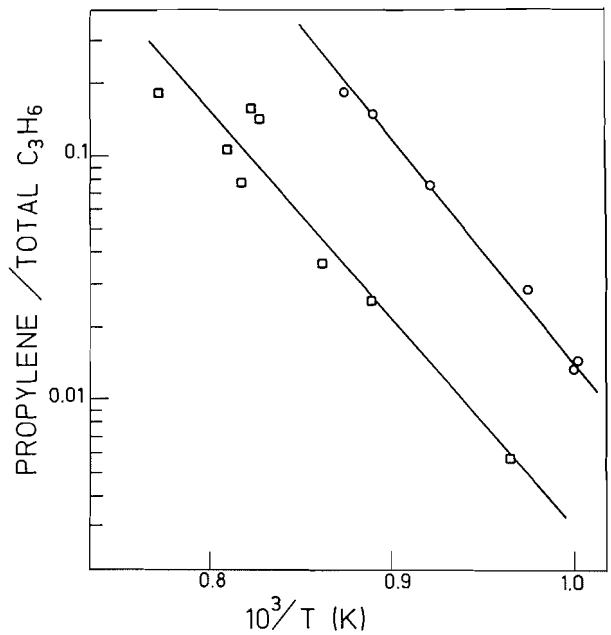

FIG. 8. The fraction of propylene to total C_3H_6 vs. a temperature derived from the two main channel ratios. For 0.333 kPa the slope of the line leads to $E_a \approx 175$ kJ/mol and for 1.333 kPa, $E_a \approx 160$ kJ/mol. Results for 0.667 and 1.000 kPa give lines with similar slopes.

fact an increase in P was observed. These observations may be reconciled if the decomposition were a sum of two processes; the first a fast, almost collision-free decomposition in which collisions deactivate excited molecules, reducing P, and the second a slower decomposition of the collisionally equilibrated hot gas remaining after the pulse. Probability of decomposition in the first process will decrease as pressure increases and intensity may affect channel ratios, while that for the second, P increases with increasing pressure as has often been observed with longer pulses (15–17) and will depend only on fluence. This dual mechanism is rather similar to that suggested in a previous study of cyclobutanone at lower pressures (4). The C_3H_6/C_2H_4 and propylene/total C_3H_6 ratios appear to reflect a similar behaviour, as they are somewhat higher with the shorter pulse, but do not decline with increasing pressure. Unfortunately, uncertainties in the true reaction volume and the effective fluence, caused by attenuation effects and reaction occurring outside the central focal zone, as discussed earlier, prevent any quantitative test of the suggested mechanism.

It has been suggested that in the thermal decomposition of cyclobutanone, propylene comes from the isomerization of vibrationally excited cyclopropane formed in reaction [2] and not from secondary decomposition of thermalized cyclopropane. Previous multiphoton decomposition studies and the present results support this conclusion. The energies of the several decomposition processes are shown in Fig. 7 using information from Benson and O'Neal (18). In Fig. 8, we have plotted, in Arrhenius form, the fraction of total C_3H_6 converted to propylene for the 40 ns results. The temperature in these plots has been calculated from the observed relative rates of reactions [1] and [2] using the equation

$$[3] \quad R_1/R_2 = (3.60/2.34) \exp [6000/RT]$$

Equation [3] should give a measure of the effective temperature of the decomposing cyclobutanone molecules if they are internally relaxed after excitation so that a unimolecular thermal decomposition description is appropriate. The plot in Fig. 8 yields an "activation energy" of about 165 kJ/mol. A similar calculation using the 10 ns results (which are more scattered) gives an "activation energy" of about 130 kJ/mol. If all the energy in the transition state (Fig. 7) were available to the cyclopropane produced in the primary decomposition, one would expect to require an additional energy of about 60 kJ/mol to form propylene. If none were available, 274 kJ/mol would be needed to form propylene from cyclopropane in the hot gas following the laser pulse. The observed intermediate value suggests that some energy is carried over from the first step but not the maximum available.

The minor products, C_2H_2, C_2H_6, and CH_4 probably come from H-atom cracking reactions in the hot gas following the pulse, similar to those in the high-temperature decomposition of ethylene.

1. M. H. BACK and R. A. BACK. Can. J. Chem. **57**, 1511 (1979).
2. R. G. HARRISON, H. L. HAWKINS, R. M. LEO, and P. JOHN. Chem. Phys. Lett. **70**, 555 (1980).
3. V. STAROV, N. SELAMOGLU, and C. STEEL. J. Phys. Chem. **85**, 320 (1982).
4. R. A. BACK. Can. J. Chem. **60**, 2542 (1982).
5. S. KODA, Y. OHNUMA, T. OHKAWA, and S. TSUCHIYA. Bull. Chem. Soc. Jpn. **53**, 3447 (1980).
6. A. T. BLADES. Can. J. Chem. **47**, 615 (1969); T. H. MCGEE and A. SCHLEIFER. J. Phys. Chem. **76**, 963 (1972); **77**, 1317 (1973); A. T. BLADES and S. SANDHU. J. Phys. Chem. **77**, 1316 (1973).
7. R. J. CAMPBELL and E. W. SCHLAG. J. Am. Chem. Soc. **89**, 5130 (1967).
8. A. W. PASTERNAK, D. J. JAMES, J. A. NILSON, D. K. EVANS, R. D. MCALPINE, H. M. ADAMS, and E. B. SELKIRK. App. Opt. **20**, 3849 (1981).

Can. J. Chem. Downloaded from www.nrcresearchpress.com by 210.87.254.105 on 09/06/12
For personal use only.

9. S. L. CHIN, D. K. EVANS, R. D. MCALPINE, and W. N. SELANDER. App. Opt. **21**, 65 (1982).
10. D. K. EVANS, R. D. MCALPINE, and H. M. ADAMS. J. Chem. Phys. **77**, 3551 (1982).
11. R. D. MCALPINE, D. K. EVANS, and H. M. ADAMS. J. Chem. Phys. **78**, 5990 (1983).
12. R. S. HALLSWORTH and N. R. ISENOR. Chem. Phys. Lett. **22**, 283 (1973).
13. M. L. BOYD, T.-M. WU, and M. H. BACK. Can. J. Chem. **46**, 2415 (1968).
14. N. C. PETERSON, R. G. MANNING, and W. BRAUN. J. Res. Natl. Bur. Stand. **83**, 117 (1978).
15. D. K. EVANS, R. D. MCALPINE, and F. K. MCCLUSKY. Chem. Phys. **32**, 81 (1978).
16. R. D. MCALPINE, D. K. EVANS, and F. K. MCCLUSKY. Chem. Phys. **39**, 263 (1979).
17. D. K. EVANS, R. D. MCALPINE, and F. K. MCCLUSKY. Chem. Phys. Lett. **65**, 226 (1979).
18. S. W. BENSON and H. E. O'NEAL. Kinetic data on gas phase unimolecular reactions. NSRDS-NBS21, Washington. 1970.

Can. J. Chem. Downloaded from www.nrcresearchpress.com by 210.87.254.105 on 09/06/12
For personal use only.

Stereocontrolled routes to *cis*-hydroxyamino sugars. Part VI. A synthesis of garosamine[1]

HENRY W. PAULS[2,3] AND BERT FRASER-REID[3]

Department of Chemistry, University of Waterloo, Waterloo, Ont., Canada N2L 3G1

Received October 14, 1983

HENRY W. PAULS and BERT FRASER-REID. Can. J. Chem. **62**, 1532 (1984).

The exocyclic olefin, **5**, obtained from the known epoxy uloside, methyl 2,3-anhydro-β-D-*erythro*-pentopyranosid-4-ulose, **3**, reacts with ammonia or methylamine to give the 3-amino-3-deoxy or 3-methylamino-3-deoxy derivatives respectively. The benzamide, **8***c*, obtained from the former, reacts with iodonium ion to give an oxazoline in which the *cis* relationship between the tertiary alcohol and the 3-amino group of garosamine is secured. Deiodination is followed by a one-pot *N*-methylation and reduction. A hydrolysis gives methyl α-L-garosamimide **2**. In a second route, the urethane, **16***c*, reacts with iodonium ion to give an oxazolidone **17***a*. This reaction establishes the *cis*-hydroxyamino moiety and circumvents the *N*-methylation/reduction steps. Deiodination followed by deprotection yields methyl α-L-garosaminide **2**. Both routes require eight steps from **3** with overall yields of 14% and 11%, respectively.

HENRY W. PAULS et BERT FRASER-REID. Can. J. Chem. **62**, 1532 (1984).

L'oléfine exocyclique, **5**, qui est obtenue de l'époxy uloside connu, anhydro-2,3 β-D-*érythro*-pentopyrannoside ulose-4 de méthyle, **3**, réagit avec l'ammoniac ou la méthylamine pour donner, suivant le cas, soit le dérivé amino-3 déoxy-3 ou méthylamino-3 déoxy-3. Le benzamide **8***c*, obtenu à partir du premier de ces dérivés, réagit avec l'ion iodonium pour donner une oxazoline dans laquelle on a fixé, entre l'alcool tertiaire et le groupe amino-3, la relation *cis* qui existe dans la garosamine. Après l'élimination de l'iode, on effectue, dans le même ballon, une *N*-méthylation suivie d'une réduction. Une hydrolyse conduit à la α-L-garosamimide de méthyle, **2**. Dans une deuxième voie de synthèse, on fait réagir l'uréthane **16***c* avec l'ion iodonium pour obtenir une oxazolidone **17***a*. Cette réaction permet d'établir la relation *cis* de la portion amino-alcool et évite les étapes de *N*-méthylation/réduction. L'élimination de l'iode, suivie d'une déprotection, conduit au produit **2**. Chacune des voies requiert huit étapes à partir du produit **3** et leurs rendements respectifs sont de 14% et 11%.

[Traduit par le journal]

Introduction

The *C*-gentamycins are the principle components of an antibiotic complex produced by *Micromonospora purpurea* NRRL 2953 and *Micromonospora echinospora* NRRL 2985 under anaerobic conditions (1). Widespread clinical use has established them as major broad-spectrum antibiotics, and the advent of semi-synthetic methods has raised the possibility of obtaining novel, more potent modifications (2). A common, essential subunit of all three is the amino sugar garosamine, **1**, which occurs also in a number of other potent aminocyclitol antibiotics, sisomycin (3), G-52 (4), and XK-62-2 (5). Accordingly, a reliable synthetic route to **1** has been of interest for some time, and was the reason for our entry into the area of amino sugar synthesis (6–10).[4]

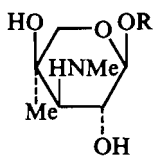

1 R = H
2 R = Me

Two structural features, the tertiary alcohol and the *cis*-hydroxyamino moiety, had posed challenges for earlier syn-

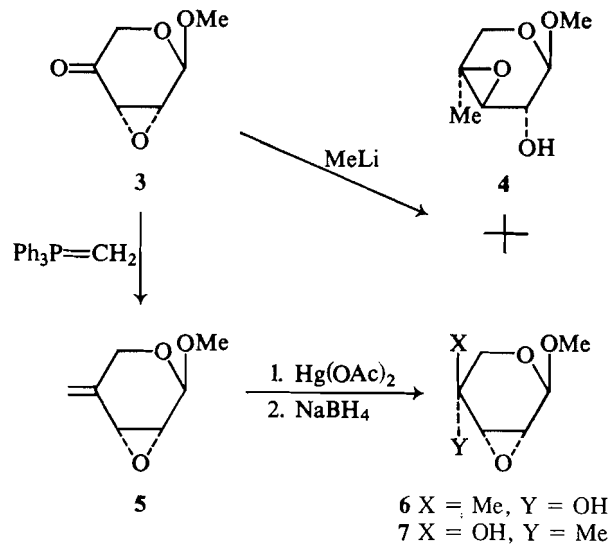

SCHEME 1

thesis of garosamine (11, 12). The first of these by zu Reckendorf and Bishop (11), served to establish the correct structure of **1**; but major problems were encountered which caused low yields. The synthesis of the Schering group led by Wright (12) employed a clever solution to the problematic tertiary alcohol. However, this did not constitute a general solution to *cis*-hydroxyamino features.

From these publications (11, 12) it is apparent that the tertiary alcohol is a major obstacle, and some early exploratory investigations in our group convinced us that there would be no easy solutions. Thus the known epoxy uloside **3** seemed to be a plausible intermediate. Paulsen and Eberstein had shown that methyllithium addition to **3** gave virtually equal amounts of **4** and **6** (13). We decided to examine the hydration of the exo-

[1]Part I is the preliminary account of this work, ref. 6. Part II is the preliminary account of the accompanying paper, ref. 7. Part III, see ref. 8; Part IV, see ref. 9; Part V, see ref. 10.

[2]Holder of NSERC Postgraduate Scholarship, 1981–1982.

[3]Present address: Gross Chemical Laboratory, Duke University, Durham, NC 27706, U.S.A. Correspondence may be addressed to B.F-R.

[4]This study was part of a project supported by a PRAI grant to B.F-R. and Bristol Laboratories, Candiac, Quebec 1975–1977.

Can. J. Chem. Downloaded from www.nrcresearchpress.com by 210.87.254.105 on 09/06/12
For personal use only.

Can. J. Chem. Downloaded from www.nrcresearchpress.com by 210.87.254.105 on 09/06/12
For personal use only.

cyclic olefin **5**, which could be obtained cleanly by a Wittig reaction of **3**. However, the yield of **5** was variable because of the high volatility of the material. We had hoped that, in keeping with our studies on frontalin (14), hydration of the double bond would lead to the desired lyxoside **7**. Unfortunately, the single product obtained from oxymercuration–demercuration of **5** proved to be the riboside **6**.

With regard to the second problem, the *cis*-hydroxyamino moiety, we were interested in developing a general methodology for this structural feature. Winstein *et al.* had achieved the halolactonization of simple allylic amides to afford oxazolines (5). Application of this methodology to **8***b* would not only establish the *cis*-hydroxyamino component, but would simultaneously secure the troublesome tetiary hydroxyl group. In this and the accompanying manuscript (16) we give full details of some of our results.

Results and discussion

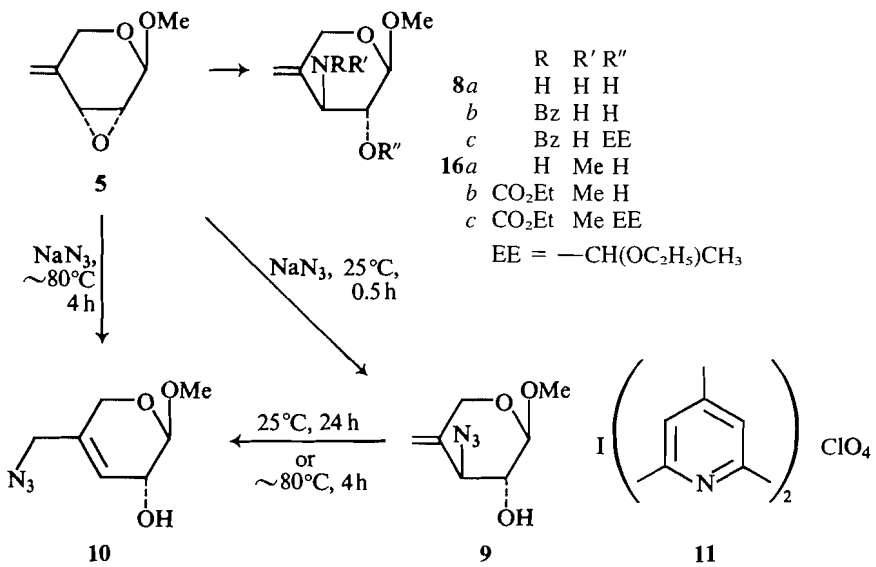

	R	R′	R″
8*a*	H	H	H
b	Bz	H	H
c	Bz	H	EE
16*a*	H	Me	H
b	CO_2Et	Me	H
c	CO_2Et	Me	EE

EE = —$CH(OC_2H_5)CH_3$

SCHEME 2

Route I

The appropriate precursor would be the amine **8***a*, obtainable by S_N2 attack at the allylic position of **5**. Azidolysis was examined initially, and some pertinent data relating to this are summarized in Scheme 2. At low temperatures, a clean S_N2 reaction occurred at the allylic site, C-3, to give the azido alcohol **9**, there being only traces of the S_N2' product **10**, barely detectable by tlc. With refluxing aqueous ethanol, compound **10** was the sole product after 4 h. The latter could be obtained alternatively by heating **9** in ethanol, or by allowing **9** to stand at room temperature for 24 h.

The sigmatropic rearrangement to the thermodynamically more stable **10** detracted from **9** as an intermediate and hence ammonolysis was examined. The best procedure was to saturate an ice-cold ethanol solution of the epoxide **5**, contained in a pressure vessel, with the amine, seal and place the vessel in an oil bath, and gradually raise the temperature to 80°C. Under these conditions, the primary amine **8***a* was obtained in 97% yield.

The benzamide **8***b* was prepared, but in contrast to Winstein's case (5), no reaction could be induced with *N*-bromosuccinimide. Typical iodolactonization conditions (I_2/KI/H_2O/THF) were also unsuccessful.

Iodonium dicollidine perchlorate (17) **11** was adopted, since in our experience this salt is a reliable source of iodonium ions (18). Indeed, treatment of the benzamides **8***b* or **8***c* with the salt in chloroform (Scheme 3) yielded the iodo-oxazolines **12***a* or **12***b* respectively, which were smoothly deiodinated by treatment with tri-n-butyltin hydride to **13***a* and **13***b* respectively.

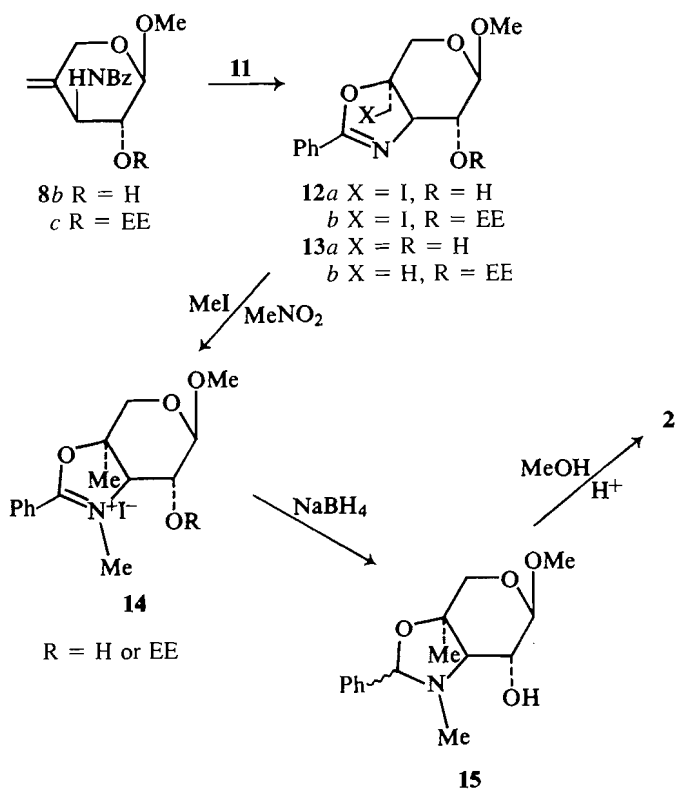

SCHEME 3

Since *cis*-fusion is expected for 6/5 heterocyclic systems (19) the product was expected to establish the desired orientation at C-4 stereospecifically.

Quaternization of the nitrogen of **13***b* required heating with methyl iodide in nitromethane for 48 h (tlc). The resulting salt, presumably **14**, was reduced directly with sodium borohydride in methanol. During these two steps, the C-2 protecting group was lost, giving **15** as the product. Strangely, the unprotected alcohol **13***a* could not be *N*-methylated under identical conditions.

Hydrolysis of the oxazolidine **15** was achieved with methanol and hydrogen chloride and the resulting material had infrared and ^{1}H nmr spectra identical with those of an authentic sample of methyl α-L-garosaminide **2** (*vide infra*).

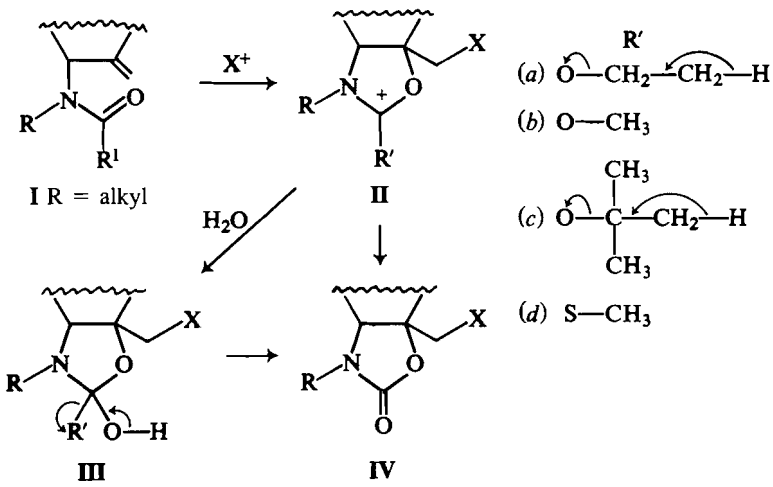

SCHEME 4

Mechanistic considerations

In spite of the success of the above route, some economy of steps was desired. An intermediate such as **I** (Scheme 4, R = Me) was preferable since the extra steps of *N*-methylation and reduction would be circumvented. The urethane group emerged as the nitrogen substituent of choice since the corresponding cationic intermediate, **II**, is stablized by three heteroatoms, and should react further to give cyclic urethane **IV** (i.e. a 2-oxazolidone).

It is appropriate to comment on the possible modes of decomposition of the carbocation intermediates in Scheme 4. These species ought to react readily with traces of water to give **III**, which should eject an alcohol to give the cyclic urethane **IV**. This mode of decomposition should not be greatly affected by the nature of the substitutent R′. However, subsequent to our preliminary report, Parker and O'Fee (20) found that methyl urethanes, for example **II***b*, gave little, if any, oxazolidone, whereas *tert*-butyl analogs, for example **II***c*, reacted very smoothly. The results with **II***a* and **II***c* are accommodated by the alternate mode of decomposition depicted in Scheme 4, in which ethylene and isobutylene, respectively, are ejected. This is more satisfying than involvement of **III**, since our work was carried out under rigorously anhydrous conditions.

The foregoing notwithstanding, it should be noted that Knapp and Patel have obtained excellent results from bromocyclization of methylurethanes and methylthiourethanes, such as **II***b* and **II***d* respectively (21).

Route 2

The *N*-methyl amino alcohol **16***a*, prepared in a manner similar to **8***a*, was treated with ethyl chloroformate, followed by ethyl vinyl ether, to yield **16***c*. Reaction of **16***c* with the iodonium salt, **11**, afforded the desired product **17***a* in 82% yield. Deiodination was effected by hydrogenolysis over palladium, and subsequent hydrolysis with pyridinium *p*-toluenesulfonate led to oxazolidone **17***c* as a crystalline substance. This material was alternatively prepared by treating urethane **18** (obtained from authentic methyl α-L-garosaminide[4]) with sodium hydride in dimethyl formamide. The two samples had identical physical constants. Hydrolysis of **17***c* with potassium hydroxide gave the previously described garosamide **2**.

Summary

The syntheses described above are reasonably successful in terms of economy of steps and overall yield. The oxazoline route yields methyl α-L-garosaminide **2** from the known epoxy uloside **3** in 8 steps with 14% overall yield. The overall yield of **2** from **3** for the oxazolidone route (Scheme 5) is 11% in 8 steps. Further use of the oxy-amination procedure is reported in the accompanying paper (16).

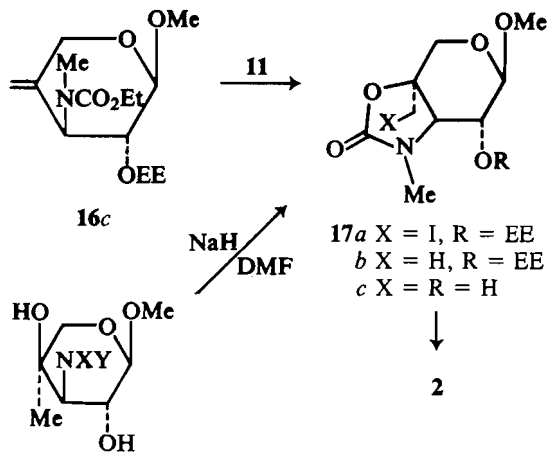

SCHEME 5

Can. J. Chem. Downloaded from www.nrcresearchpress.com by 210.87.254.105 on 09/06/12
For personal use only.

Can. J. Chem. Downloaded from www.nrcresearchpress.com by 210.87.254.105 on 09/06/12
For personal use only.

Experimental

General methods

Melting points were determined in capillary tubes in a Buchi model SMP-20 melting point apparatus, and are uncorrected. Elemental analyses were performed by Guelph Chemical Laboratories Ltd., 500 York Road, Guelph, Ont., N1H 3J4. Nuclear magnetic resonance (^{1}H nmr) spectra were determined in deuteriochloroform containing 1% tetramethylsilane (TMS) as internal standard with a Perkin– Elmer R-12B (60 MHz) or, when specifically stated, with a Varian HR-220 spectrometer. Coupling constants were obtained by measuring the spacings of spectra judged to be first order. Infrared (ir) spectra were determined on a Beckman model IR-10 spectrometer using 0.1-mm sodium chloride cells and chloroform as solvent for solids, or sodium chloride plates for thin film smears. Low resolution mass spectra were determined on a Varian MAT CH7 mass spectrometer. High resolution mass spectra (hrms) were determined on a VG 7070F.

Optical rotations were measured on a Carl Zeiss model LEP nür 370740 Lichtelektrisches Präzisionspolarimeter at 23°C.

The progress of all reactions was monitored by thin layer chromatography (tlc) which was performed on 1.3 cm × 6.6 cm aluminum sheets precoated with silica gel 60 (HF-245, E. Merck) to a thickness of 0.25 mm. The following solvent systems were used to develop the plates: (A) ethyl acetate – petroleum ether (30–60°C), (1:1); (B) diethyl ether – methylene chloride (1:19); (C) ethyl acetate. The chromatograms were viewed under an ultraviolet light, sprayed with concentrated sulfuric acid, and heated to a temperature greater than 100°C under a hot air gun. For column chromatography E. Merck Kieselgel 60 (230–400 mesh A.S.T.M.) was used. The columns were eluted under pressure.

*Methyl 2,3-anhydro-4-*C*-methylene-β-*D*-*erythro*-pentopyranoside (**5**)*

To a stirred mixture of (methyl) triphenylphosonium bromide (6.50 g, 18.2 mmol) and 50 mL dry DME under argon was added 2.2 molar n-butyllithium in hexane (6.04 mL, 13.3 mmol). The resulting suspension was stirred for 15 min, placed in an ice bath, and stirred an additional 15 min. The ketone, **3** (10) (1.74 g, 12.1 mmol), dissolved in 15 mL dry dimethoxyethane, was added dropwise. After the addition was complete the resulting mixture was stirred for 5 min, then quenched with wet diethyl ether (300 mL). The resulting slurry was filtered through Celite and washed several times with diethyl ether. The filtrate was evaporated under reduced pressure at room temperature and the residue was chromatographed with solvent system B. Epoxy olefin **5**, the only carbohydrate product, was isolated as a mobile oil (0.88 g, 51.3%); R_f 0.51 (solvent B); $[\alpha]_D^{23}$ −123.7° (*c* 1.0, chloroform); ir ν_{max}: 1450 (terminal alkene C—H bend) cm^{-1}; ^{1}H nmr δ: 3.15 (dd, 1, $J_{2,3}$ = 3.5 Hz, H-3), 3.4 (s, 3, —OCH_3), 3.62 (d, 1, H-3), 4.07–4.18 (complex ABq, 2, H-5, H-5′), 4.92 (bs, 1, H-1), 5.20–5.35 (dm, 2, =CH_2).

*Methyl 2,3-anhydro-4-*C*-methyl-β-*D*-*ribopyranoside (**6**)*

Epoxy olefin **5** (0.197 g, 1.39 mmol) was dissolved in 5 mL THF and 6 mL water, to which was added mercuric acetate (0.493 g, 1.56 mmol). The mixture was stirred at room temperature until the starting material had disappeared – typically 10 h. At this time 3.5 mL of 3 *M* aqueous sodium hydroxide and 2 mL of freshly prepared aqueous sodium borohydride (0.5 *M*, 1.0 mmol) in 3 *M* sodium hydroxide were added in quick succession. The resulting mixture was extracted 3 times with methylene chloride. The organic layers were combined, filtered to remove suspended mercury, dried over sodium sulfate, and evaporated. The sole product **6** (0.176 g, 79%) was obtained as a white solid. Recrystallization from chloroform/hexane yielded white crystals which showed mp 99–101°C; $[\alpha]_D^{23}$ −72° (*c* 1.1, chloroform). The literature (13) reports mp 103°C; $[\alpha]_D^{23}$ −79°.

*Methyl 3-azido-3,4-dideoxy-4-*C*-methylene-α-*L*-threo-pentopyranoside, (**9**)*

The starting material **5** (0.10 g, 0.70 mmol) was dissolved in 4 mL of a 3:1 ethanol/water mixture, sodium azide (0.14 g, 2.1 mmol) was added, and the mixture was stirred at room temperature. After 30 min, tlc indicated that the epoxy olefin had been consumed and replaced by **9** with trace amounts of **10**, showing R_f 0.47 and 0.32 respectively in solvent A. The reaction mixture was poured into ice water and the aqueous layer was extracted three times with methylene chloride. The combined organic washings were dried over sodium sulfate and evaporated to yield 0.92 g of a white solid (71%). The crude product exhibited the following physical data; ir ν_{max}: 3300–3500 (OH), 2120 (N_3), 1625 (C=C) cm^{-1}; ^{1}H nmr δ: 3.1 (bs, 1, OH), 3.30–4.47 (m, 5, H-1, H-2, H-3, H-5, H-5′), 3.50 (s, 3, —OCH_3), 5.15–5.30 (dm, 2, =CH_2).

*Methyl 4-*C*-azidomethyl-3,4-dideoxy-β-*D*-*glycero*-pent-3-enopyranoside (**10**)*

(a) Epoxy olefin **5** (1.0 g, 7.04 mmol) was dissolved in 25 mL of ethanol, to which was added 7.5 mL water, sodium azide (0.52 g, 8.1 mmol), and ammonium chloride (0.53 g, 9.8 mmol). The mixture was refluxed with stirring for 4 h, at which time tlc revealed **10** as the only product. The solvent was evaporated and the residue was partitioned between water and methylene chloride. The aqueous layer was separated and washed once more with methylene chloride, then the organic layers were combined, dried, and evaporated. Product **10** was obtained as a pale brown syrup (0.88 g, 67.5%); $[\alpha]_D^{23}$ −175.1° (*c* 0.6, chloroform); ir ν_{max}: 3440–3460 (OH), 2100 (N_3) cm^{-1}; ^{1}H nmr δ: 2.8 (bs, 1, —OH), 3.53 (s, 3, —OCH_3), 3.8 (s, 2, H-4a, H-4b), 3.9 (m, 1, H-2), 4.13 (s, 2, H-5, H-5′), 4.6 (d, 1, $J_{1,2}$ = 2.5 Hz, H-1), 5.9 (bs, 1, H-3); *m/e*: 143 ($M^+ - N_3$), 125 ($M^+ - N_3 - H_2O$), 94 ($M^+ - N_3 - H_2O$ – OMe).

(b) Azide **9**, upon standing at room temperature for about 24 h, or when refluxed in ethanol/water for 4 h, was converted into azide **10**.

*Methyl 3-amino-3,4-dideoxy-4-*C*-methylene-α-*L*-threo-pentapyranoside (**8***a*)*

The epoxy olefin **5** (0.389 g, 2.74 mmol) was dissolved in absolute ethanol (20 mL) and placed in a pressure vessel. The vessel was cooled in an ice bath and the solution saturated with a stream of ammonia. The pressure vessel was sealed, placed in an oil bath, and heated to 80°C. After 30 min the vessel was removed, cooled to room temperature, and the solvent was removed on a rotary evaporator. A brown solid, **8***a* (0.42 g, 96.8%), was obtained, which was suitable for subsequent manipulations. After two recrystallizations from ethanol white crystals of **8***a* were obtained with the following physical constants: mp 170.0–170.5°C; $[\alpha]_D^{23}$ −65.5° (*c* 0.7, chloroform); ir ν_{max}: 3400–3600 (NH and OH) cm^{-1}; ^{1}H nmr δ: 3.54 (s, 3, OCH_3), 3.90–4.32 (m, 3, H-1, H-5, H-5′), 5.10 (dm, 2, =CH_2). *Anal.* calcd. for $C_7H_{13}O_3N$: C 52.82, H 8.23, N 8.80; found: C 53.13, H 8.51, N 8.69.

*Methyl 3-benzamido-3,4-dideoxy-4-*C*-methylene-α-*L*-threo-pentopyranoside (**8***b*)*

The allylic amine **8***a* (0.360 g, 2.26 mmol) was dissolved in 20 mL dry chloroform. To this was added sodium bicarbonate (0.190 g, 2.26 mmol) and benzoyl chloride (0.30 mL, 2.6 mmol). After stirring for 1 h at room temperature, 20 mL of water was added, and the mixture was stirred another 15 min. The mixture was poured into a separatory funnel and the organic layer was removed. The aqueous layer was saturated with sodium chloride and extracted twice more with methylene chloride. The organic layers were combined, dried, and evaporated to dryness to give a white solid **8***b* (0.494 g, 83%) which, after recrystallization from ethanol, gave the following data: mp 202–203°C; $[\alpha]_D^{23}$ −131.3° (*c* 1.6, chloroform); ir ν_{max}: 1660 (C=O stretch) cm^{-1}; ^{1}H nmr (220 MHz) δ: 2.62 (d, 1, $J_{2,3}$ = 8 Hz, H-3), 3.50 (s, 3, —OCH_3), 3.65 (m, 1, —OH), 4.10 (ABq, 2, $J_{5,5'}$ = 13.5 Hz, H-5, H-5′), 4.60 (d, 1, $J_{1,2}$ = 4 Hz, H-1), 4.8 (dd, 1, H-2), 5.23 (d, 2, =CH_2), 7.42 (m, 3, *meta* and *para* phenyl protons), 7.75 (m, 2, *ortho* phenyl protons). *Anal.* calcd. for $C_{14}H_{17}O_5N$: C 63.87, H 6.51, N 5.32; found: C 64.10, H 6.55, N 5.25.

*2′-Phenyl-(methyl 3,4-dideoxy-4-*C*-iodomethyl-α-*L*-arabinopyranosido)-[3,4:4′,5′]-Δ$^{2'}$-oxazoline (**12***a*)*

Compound **8***b* (0.128 g, 0.49 mmol) was dissolved in 20 mL

Can. J. Chem. Downloaded from www.nrcresearchpress.com by 210.87.254.105 on 09/06/12
For personal use only.

chloroform to which was added iodonium dicollidine perchlorate **11** (17) (0.342 g, 0.735 mmol). The solution was stirred at room temperature in the dark for 4 h. Diethyl ether (100 mL) was added and the unreacted reagent was removed by filtration. The filtrate was evaporated and the residue was redissolved in methylene chloride. The methylene chloride phase was washed with 10% sodium thiosulfate, 5% hydrochloric acid, and, finally, water. The aqueous layers were washed successively with two fresh aliquots of methylene chloride. The organic layers were combined, dried over sodium sulfate, and evaporated. The crude syrup obtained was chromatographed on silica gel with solvent A to yield product **12***a* as a foam (0.147 g, 93%); R_f 0.33 (Solvent A); ir ν_{max}: 1730 (oxazoline C=N stretch), 3400 (OH) cm^{-1}; ^1H nmr δ: 3.48 (s, 3, $-OCH_3$), 3.52 (s, 2, $-CH_2I$), 4.54 (d, 1, $J_{1,2}$ = 5 Hz, H-1), 7.48 (m, 3, *meta* and *para* phenyl protons), 7.95 (m, 2, *ortho* phenyl protons). *Exact Mass* calcd. for $M^+ - OCH_3$: 357.9942; found (hrms): 357.9940; calculated for $M^+ - I$: 262.1079; found (hrms): 262.1078.

*2'-Phenyl-(methyl 3,4-dideoxy-4-*C*-methyl-α-L-arabinopyranosido)-[3,4:4',5']-Δ$^{2'}$-oxazoline (**13**a)*

Iodide **12***a* (0.347 g, 0.89 mmol) was dissolved in 20 mL reagent benzene to which was added tri-n-butyltin hydride (0.30 mL, 0.10 mmol). The reaction mixture was heated to reflux for 4 h, at which time the benzene was removed by evaporation. The resultant residue was partitioned between hexane and acetonitrile. The acetonitrile layer was washed twice more with hexane, then evaporated to give product **13***a* (0.155 g, 66%), which after one recrystallization from ethyl acetate had the following physical data: mp 208–209°C; $[\alpha]_D^{23}$ −0.6° (*c* 1.3, chloroform); ^1H nmr δ: 1.40 (s, 3, $-CCH_3$), 3.54 (s, 3, $-OCH_3$), 3.87 (ABq, 2, $J_{5,5'}$ = 11 Hz, H-5, H-5'), 4.49 (d, 1, $J_{1,2}$ = 5 Hz, H-1), 4.05 (bs, 1, —OH), 7.55 (m, 3, *meta* and *para* phenyl protons), 8.10 (m, 2, *ortho* phenyl protons). Satisfactory elemental analysis of **13***a* could not be obtained.[5]

*Methyl 3-benzamido-3,4-dideoxy-2-*O*-α-ethoxyethyl-4-*C*-methylene-α-L-*threo*-pentopyranoside (**8**c)*

The starting material **8***b* (0.116 g, 0.44 mmol) was dissolved in dry methylene chloride (40 mL) to which was added ethyl vinyl ether (0.12 mL, 1.2 mmol) and pyridinium *p*-toluenesulfonate (0.30 g, 0.13 mmol). The solution was stirred at room temperature and the reaction progress was followed by tlc. Upon completion, typically 4 h, the reaction mixture was poured into an equal volume of brine, shaken, and separated. The aqueous layer was washed twice with methylene chloride. The organic layers were combined, dried over sodium sulfate, and evaporated to yield impure **8***c*. After chromatography, in solvent A, the product **8***c* was obtained as a white solid (0.156 g, quantitative yield); it showed mp 154–155°C; R_f 0.30 (solvent A); ir ν_{max}: 1730 (amide C=O stretch) cm^{-1}; ^1H nmr δ: 1.05–1.5 (m, 6, $-OCH(CH_2)OCH_2CH_3$), 3.54 (s, 3, $-OCH_3$), 5.1 (m, 2, $=CH_2$), 7.30–8.0 (m, 5, phenyl protons). *Anal.* calcd. for $C_{18}H_{25}O_5N$: C 64.46, H 7.51, N 4.18; found: C 64.14, H 7.47, N 4.11.

*2'-Phenyl-(methyl 3,4-dideoxy-2-*O*-α-ethoxyethyl-4-*C*-iodomethyl-α-L-arabinopyranosido)-[3,4:4',5']-Δ$^{2'}$-oxazoline (**12**b)*

Compound **8***b* (0.047 g, 0.14 mmol) was treated with iodonium dicollidine perchlorate **11** (0.098 g, 0.21 mmol) as described for **12***a* above. The crude product was chromatographed with solvent A to yield compound **12***b* as an amber syrup (0.077 g, quantitative yield); R_f 0.5 (solvent A); ir ν_{max}: 1665 (oxazoline C=N stretch) cm^{-1}; ^1H nmr δ: 1.05–1.55 (m, 6, $-OCH(CH_3)OCH_2CH_3$), 3.50 (s, OCH_3), 3.65 (bs, 2, $-CH_2I$), 4.6 (m, 1, H-1), 4.95 (m, 1, $-OCH(CH_3)OCH_2CH_3$), 7.55 (m, 3, *meta* and *para* phenyl protons), 8.0 (m, 2, *ortho* phenyl protons).

[5]Compound **13***a* was hydrolysed on standing to give the crystalline amide **19**, mp 222–223°C. *Anal.* calcd. for $C_{14}H_{19}O_5N$: C 59.72, H 6.67, N 4.70; found: C 59.66, H 6.83, N 4.81.

*2'-Phenyl-(methyl 3,4-dideoxy-2-*O*-α-ethoxyethyl-4-*C*-methyl-α-L-arabinopyranosido)-[3,4:4,4'5')-Δ$^{2'}$-oxazoline (**13**b)*

Iodide **12***b* (0.214 g, 0.48 mmol) was dissolved in 20 mL reagent benzene to which was added tri-n-butyltin hydride (0.15 mL, 0.50 mmol). The reaction was heated to reflux for 4 h in the presence of AIBN (1–2 mg). The benzene was removed by rotary evaporation and the resultant residue was chromatographed using solvent A. Product **13***b* was isolated as a syrup (0.127 g, 83%); it showed R_f 0.5 (solvent A); ir ν_{max}: 1645 (oxazoline C=stretch) cm^{-1}; ^1H nmr δ: 1.0–1.45 (m, 6, $-OCH(CH_3)OCH_2CH_3$), 1.45 (s, 3, $-C(CH_3)$), 3.36 (s, 3, $-OCH_3$), 4.60 (two d, 1, H-1), 4.90 (two q, 1, $-OCH(CH_3)CH_2CH_3$).

*3'-*N*-Methyl-2'-phenyl-(methyl 3,4-dideoxy-4-*C*-methyl-α-L-arabinopyranosido)-[3,4:4',5')-oxazolidine (**15**)*

The starting material **13***b* (0.395 g, 1.18 mmol) was dissolved in nitromethane (10 mL) to which was added methyl iodide (0.20 mL, 2.36 mmol). The reaction flask was fitted with a reflux condenser and heated with stirring at 70–80°C for 24 h. At this time more methyl iodide was added (0.20 mL, 2.36 mmol), and the reaction mixture was heated an additional 24 h. Analysis by tlc indicated the replacement of starting material by a new, uv active spot at the base line. Solvent and remaining reagent were removed under reduced pressure to yield a syrupy residue, presumably **14**.

The residue was redissolved in absolute methanol (15 mL) and the solution was cooled in an ice bath. To this was added sodium borohydride (0.045 g, 1.18 mmol) and the mixture was stirred for 1 h at 5°C, with the exclusion of moisture. At this time tlc indicated that the base line material had been replaced by a more mobile compound having R_f 0.58 (solvent A). The reaction vessel was allowed to warm to room temperature and, after slow addition of small amounts of water, the contents were partitioned between equal volumes of water and methylene chloride. The layers were separated and the aqueous layer was extracted twice more with methylene chloride. The organic layers were combined, dried over sodium sulfate, and evaporated. Chromatography of the residue (solvent A) yielded solid oxazolidine **15** (0.201 g, 61.5%). Recrystallization from ethyl acetate gave pure **15** which showed mp 101.5–102.5°C; $[\alpha]_D^{23}$ −3.3° (*c* 0.6, chloroform); ir ν_{max}: 3300–3650 (OH stretch) cm^{-1}; ^1H nmr δ: 1.43 (s, 3, $-CCH_3$), 2.34 (s, 3, $-NCH_3$), 2.60 (d, 1, $J_{2,3}$ = 5 Hz, H-3), 3.10 (bs, 1, —OH), 3.31–4.10 (m, 3, H-2, H-5, H-5'), 3.43 (s, 3, $-OCH_3$), 4.58 (d, 1, $J_{1,2}$ = 4 Hz), 4.90 (s, 1, benzylidine-methine), 7.40–7.70 (m, 5, aromatic protons). *Anal.* calcd. for $C_{15}H_{21}O_4H$: C 64.50, H 7.58, N 5.01; found: C 64.75, H 7.95, N 5.41.

*Methyl 3,4-dideoxy-3-(*N*-ethoxycarbonyl-*N*-methylamino)-4-*C*-methylene-α-L-*threo*-pentopyranoside (**16**b)*

The epoxy olefin **5** (0.77 g, 5.4 mmol) was dissolved in absolute ethanol (30 mL) and placed in a pressure vessel. The vessel was cooled in an ice bath and gaseous methylamine was bubbled through the ethanol solution for 15 min. The vessel was then sealed, placed in an oil bath, and heated to 80°C. After 30 min the vessel was removed, cooled to room temperature, and the contents concentrated. The product, obtained as a heavy brown oil, was dissolved in 10 mL of chloroform. To this was added sodium bicarbonate (0.361 g, 2.2 mmol) and ethyl chloroformate (0.39 mL, 2.5 mmol). After stirring for 15 min, saturated sodium bicarbonate solution (20 mL) was added and the mixture was stirred for an additional 15 min. The aqueous and organic layers were separated and the aqueous phase was washed three times with methylene chloride. The organic layers were combined, dried, and evaporated to dryness. The product **16***b* was obtained as a beige solid (0.287 g, 55%) which, upon recrystallization from ethanol, gave the following physical data: mp 132.5–133°C; $[\alpha]_D^{23}$ −63.3° (*c* 1.0, chloroform); ir ν_{max}: 1695 (urethane C=O stretch), 3300–3600 (OH stretch) cm^{-1}; ^1H nmr δ: 1.25 (t, 2, $-OCH_2CH_3$), 2.89 (s, 3,

Can. J. Chem. Downloaded from www.nrcresearchpress.com by 210.87.254.105 on 09/06/12
For personal use only.

—NHCH_3), 3.58 (s, 3, —OCH_3), 4.9 (bd, 3, =CH_2, H-1); *m/e*: 245 (M^+), 227 ($M^+ - H_2O$), 214 (M^+ − OMe), 185 ($M^+ - C_2O_2H_4$). *Anal.* calcd. for $C_{11}H_{19}O_5N$: C 53.87, H 7.81, N 5.71; found: C 53.88, H 8.05, N 5.68.

*Methyl 3,4-dideoxy-3-(*N*-ethoxycarbonyl-*N*-methyl amino)-2-O-ethoxyethyl-4-C-methylene-α-*L*-*threo*-pentopyranoside (**16***c*)*

Urethane **16***b* (0.082 g, 0.33 mmol) was treated with ethyl vinyl ether in a similar manner as used in the preparation of **8***c*. The crude syrup obtained was chromatographed on silica gel using solvent A. Compound **16***c* (0.092 g, 86%) was obtained as a thick oil; R_f 0.52 (solvent A); ir ν_{max}: 1690 (urethane C=O stretch) cm^{-1}; ^1H nmr δ: 1.0−1.5 (m, 9, —$OCH(CH_3)OCH_2CH_3$, —OCH_2CH_3), 2.78, 2.81 (two s, 3, —NCH_3), 3.5 (two, s, 3, —OCH_3), 4.93 (bd, 4, =CH_2, H-1, —$OCH(CH_3)OCH_2CH_3$).

*3′-*N*-Methyl-2′-oxo-(methyl 3,4-dideoxy-2-O-α-ethoxyethyl-4-C-iodomethyl-α-*L*-arabinopyranosido)-[4,4:4′5′]-oxazolidone (**17**a)*

The starting material **16***c* (0.162 g, 0.051 mmol) was dissolved in chloroform, to which was added one equivalent of iodonium dicollidine perchlorate (0.202 g, 0.051 mmol). The resulting solution was stirred in the dark for five days, a fresh equivalent of iodonium dicollidine perchlorate being added per 24 h of reaction time. The reaction mixture was worked up by addition of diethyl ether. Unreacted reagent was filtered off and the filtrate was concentrated under vacuum. The residue was dissolved in methylene chloride and washed with 10% sodium thiosulfate, then 5% hydrochloric acid and, finally, water. The aqueous layers were washed successively with two fresh aliquots of methylene chloride. The organic layers were combined, dried over sodium sulfate, and evaporated to dryness to yield **17***a* (0.174 g, 82%); it showed R_f 0.46 (solvent A); ir ν_{max}: 1740 (urethane C=O stretch) cm^{-1}; ^1H nmr δ: 1.20−1.40 (m, 6, —$OCH(CH_3)OCH_2CH_3$), 2.84, 2.93 (two s, 3, —NCH_3), 3.38, 3.40 (two s, 3, —OCH_3), 3.51, 3.54 (two s, 2, —CH_2I), 4.58, 4.69 (two d, 1, H-1), 4.86 (d, 1, —$OCH(CH_3)OCH_2CH_3$).

*3-*N*-Methyl-2′-oxo-(methyl 3,4-dideoxy-2-O-ethoxyethyl-4-C-methyl-α-*L*-arabinopyranosido)-[3,4:4′,5′]-oxazolidone (**17**b)*

Compound **17***a* (0.238 g) was placed in a Parr hydrogenation flask, then dissolved in methanol/water, 9:1 (20 mL). One pellet of potassium hydroxide and 10% palladium on carbon (50 mg) were added. The mixture was shaken under 20 atm of hydrogen for 24 h (1 atm = 101.3 kPa). The reaction mixture was filtered and the filtrate was partitioned between water and methylene chloride. The organic layer was separated and washed with 5% hydrochloric acid followed by water. The aqueous layers were washed successively with two portions of methylene chloride. The combined organic layers were dried over sodium sulfate and evaporated to yield **17***b* (0.162 g, 76.8%); ir ν_{max}: 1750 (urethane C=O stretch) cm^{-1}; ^1H nmr δ: 1.1−1.45 (m, 6, —$OCH(CH_3)OCH_2CH_3$), 1.51 (s, 3, —$C(CH_3)$—), 2.92, 2.98 (two s, 3, —$N(CH_3)$—), 3.4 (s, 3, —OCH_3), 4.60, 4.72 (two d, 1, H-1), 4.90 (two q, 1, —$OCH(CH_3OCH_2CH_3)$).

*3-*N*-Methyl-2′-oxo-(methyl 3,4-dideoxy-4-C-methyl-α-*L*-arabinopyranosido)-[3,4:4′,5′]-oxazolidone (**17**c)*

(a) Starting material **17***b* (0.162 g, 0.561 mmol) was dissolved in ethanol (10 mL) to which was added pyridinium *p*-toluene sulfonate (22) (0.017 g, 0.056 mmol). The solution was warmed on a steam bath until all the starting material had reacted. The ethanol was evaporated and the residue was taken up in methylene chloride (40 mL) and brine (15 mL). The layers were separated and the aqueous portion was washed twice more with methylene chloride. The organic layers were dried and evaporated to yield solid **17***c* (0.112 g, 92.1%). Recrystallization from ethyl acetate, followed by chloroform and hexane, yielded the following physical constants: mp 136−137°C; $[\alpha]_D^{23}$ −44.3° (*c* 0.5 chloroform); ir ν_{max}: 1750 (C=O stretch) cm^{-1}; ^1H nmr (220 MHz) δ: 1.48 (s, 3, —CCH_3), 3.03 (s, 4, —NCH_3, —OH), 3.40 (d, 1, $J_{2,3}$ = 6 Hz), 3.50 (s, 3, —OCH_3), 3.75 (m, 1, H-2), 3.81 (ABq, 2, $J_{5,5'}$ = 12.5 Hz, H-5, H-5′), 4.39 (d, 1, $J_{1,2}$ = 5.5 Hz). *Anal.* calcd. for $C_9H_{15}O_5N$: C 49.76, H 6.96, N 6.45; found: C 49.66, H 6.84, N 6.33.

(b) Compound **18** (0.240 g, 0.738 mmol), derived from authentic methyl α-*L*-garosaminide (12), was dissolved in dry DMF (15 mL) and cooled in an ice bath. A small amount of 50% sodium hydride dispersion in oil (0.040 g, 0.833 mmol) was washed three times with petroleum ether (bp 30−60°C) and added to the reaction vessel. The mixture was stirred at 0°C with exclusion of moisture until tlc indicated that compound **18**, R_f 0.45 (Solvent C), had been replaced by a new, more polar product. The flask contents were partitioned between water, added slowly, and methylene chloride. The organic layer was separated, dried, and evaporated to yield a white solid (0.112 g, 70%). The material was recrystallized from ethyl acetate, followed by chloroform and hexane, to give oxazolidone **17***c* of part (a); it showed a mixture mp 134.5−136°C.

*Methyl α-*L*-garosaminide (**2**)*

(a) The starting material **15** (0.111 g, 0.398 mmol) was dissolved in absolute methanol (30 mL) to which was added methanolic hydrochloric acid (13.5%, 5 mL). The solution was stirred at room temperature, with exclusion of moisture, for 24 h, at which time tlc (solvent A) indicated the replacement of **15** by a new material at the base line. The methanol was removed under vacuum and the resulting residue was partitioned between 5% hydrochloric acid (40 mL) and methylene chloride (40 mL). The aqueous layer was separated, neutralized with 5% sodium hydroxide, and evaporated to dryness. The solid obtained was extracted three times with hot ethyl acetate. The ethyl acetate was evaporated to yield amorphous, solid methyl α-garosaminide **2** (0.054 g, 70.1%). This material refused recrystallization from ethanol, but its nmr, ir, and tlc behavior matched that of the authentic sample (12).

(b) The starting oxazolidone **17***c* (0.112 g, 0.516 mmol) was added to 15% KOH (20 mL) and the reaction vessel was fitted with a condenser. The mixture was heated to 50−60°C for 6 h, at which time tlc (solvent A) indicated the replacement of **17***c* by a new material at the base line. The solution was acidified with 10% sulfuric acid and washed once with methylene chloride. The aqueous layer was neutralized with 5% sodium hydroxide and then evaporated to dryness. The solid remaining was extracted three times with hot ethyl acetate, which was removed under vacuum to yield **2** (0.067 g, 72%) as a thick syrup. The physical constants were identical with those of the material described in part (a).

Acknowledgements

We are grateful to NSERC for support of this work by means of an operating grant, and a PRAI grant.[4] In connection with the latter we express our thanks to Bristol Laboratories, Candiac, Quebec, particularly Drs. Marcel Menard and Ivo Monkovic, for helpful discussions. We also thank Dr. J. J. Wright of Schering Corporation for generous samples of **2** and **18**.

1. M. J. Weinstein, G. M. Leudemann, E. M. Oden, and G. H. Wagman. Antimicrob. Agents Chemother. 1 (1964).
2. D. J. Cooper. Pure Appl. Chem. **28**, 121 (1971).
3. H. Reinmann, R. S. Jaret, and D. J. Cooper. J. Chem. Soc. Chem. Commun. 924 (1971).
4. P. L. J. Daniels, R. S. Jaret, T. L. Nagabhushan, and W. N. Turner. J. Antibiot. **29**, 488 (1976).

5. R. S. EGAN, R. L. DEVAULT, S. L. MUELLER, M. I. LEVENBERG, A. C. SINCLAIR, and R. S. STANASZEK. J. Antibiot. **28**, 29 (1975).
6. H. W. PAULS and B. FRASER-REID. J. Am. Chem. Soc. **102**, 3956 (1980).
7. M. GEORGES and B. FRASER-REID. Tetrahedron Lett. **22**, 4636 (1981).
8. M. GEORGES, D. MACKAY, and B. FRASER-REID. J. Am. Chem. Soc. **104**, 1101 (1982).
9. H. W. PAULS and B. FRASER-REID. J. Org. Chem. **48**, 1392 (1983).
10. H. W. PAULS and B. FRASER-REID. J. Chem. Soc. Chem. Commun. 1031 (1983).
11. W. MEYER ZU RECKENDORF and E. BISHOP. Chem. Ber. **105**, 2546 (1972).
12. J. J. WRIGHT and C. L. LUCE. J. Org. Chem. **43**, 1968 (1978).
13. H. PAULSEN and K. EBERSTEIN. Tetrahedron Lett. 1495 (1975).
14. S. JAROSZ, D. R. HICKS, and B. FRASER-REID. J. Org. Chem. **47**, 935 (1982).
15. S. WINSTEIN, L. GOODMAN, and R. BOSHAN. J. Am. Chem. Cos. **72**, 2311 (1950).
16. (*a*) M. GEORGES and B. FRASER-REID. Tetrahedron Lett. **22**, 4636 (1981); (*b*) M. GEORGES, D. MACKAY, and B. FRASER-REID. Can. J. Chem. **62**, 000 (1984).
17. R. U. LEMIEUX and A. R. MORGAN. Can. J. Chem. **43**, 2199 (1965).
18. B. FRASER-REID and D. E. ILEY. Can. J. Chem. **57**, 645 (1979).
19. E. L. ELIEL. The stereochemistry of carbon compounds. McGraw Hill, New York. 1962. p. 276.
20. K. A. PARKER and R. O'FEE. J. Am. Chem. Soc. **105**, 654 (1983).
21. S. KNAPP and D. V. PATEL. Tetrahedron Lett. **23**, 3539 (1982).
22. M. MIYASHITA, A. YOSHIKOSHI, and P. A. GRIECO. J. Org. Chem. **42**, 3772 (1977).

Can. J. Chem. Downloaded from www.nrcresearchpress.com by 210.87.254.105 on 09/06/12
For personal use only.

Stereocontrolled routes to *cis*-hydroxyamino sugars. Part VII.[1] A synthesis of holacosamine[2]

MICHAEL GEORGES,[3] D. MACKAY, AND BERT FRASER-REID[4]
Department of Chemistry, University of Waterloo, Waterloo, Ont., Canada N2L 3G1

Received October 14, 1983

MICHAEL GEORGES, D. MACKAY, and BERT FRASER-REID. Can. J. Chem. **62**, 1539 (1984).

Methyl 4,6-di-*O*-*p*-toluenesulfonyl-α-D-*threo*-hex-2-enopyranoside **4***b* reacts with methylamine at room temperature to displace the allylic sulfonate only, and the ethyl urethane of the resulting 4-*N*-methylamino sugar is cyclized with iodonium ion to give the 2-iodo-oxazolidinone, **13**. This substance, upon treatment with sodium iodide in acetone, gives the 2,6-diiodide **14***a*. Deiodination, followed by base hydrolysis, gives the *cis*-hydroxyamino precursor, which upon *N*-acetylation and *O*-methylation affords the previously known holacosaminide **1***b*.

MICHAEL GEORGES, D. MACKAY et BERT FRASER-REID. Can. J. Chem. **62**, 1539 (1984).

Le di-*O*-*p*-toluènesulfonyl-4,6 α-D-*thréo*-hexèno-2 pyrannoside de méthyle (**4***b*) réagit avec la méthylamine à la température ambiante pour déplacer uniquement le sulfonate allylique; l'éthyl uréthane du sucre *N*-méthylamino-4 qui en résulte se cyclise avec l'ion iodonium pour donner l'iodo-2 oxazolidinone (**13**). Cette substance, sous l'action de l'iodure de sodium dans l'acétone, conduit au dérivé diiodo-2,6 (**14***a*). L'élimination de l'iode, suivie d'une hydrolyse alcaline, conduit au précurseur amino-alcool-*cis* qui, par *N*-acétylation et *O*-méthylation, fournit l'holacosaminide déjà connu, **1***b*.

[Traduit par le journal]

In the accompanying paper (1) we gave full details of a new synthesis of garosamine in which the troublesome *cis*-hydroxyamino moiety and the tertiary hydroxyl group were established simultaneously by means of iodonium ion-induced cyclization of an allylic amide, for example **I**–**III**, Scheme 1. A secondary feature of this crucial process of the introduction of the iodine atom which opens the way for several additional transformations, of which reductive deiodination is one of the more obvious. Thus, a ready route to polydeoxyamino sugars is suggested, and in order to develop this chemistry we looked at the trideoxyamino sugar, holacosamine **1***a*. In this paper we give full details of this study, which was reported previously in preliminary form (2).

Holacosamine, **1***a* (Scheme 3), was first obtained from the amino glycosteroids, holacurtin, **2***a*, and holarosine, **2***b*, isolated from the leaves of *Holarrhena curtisii* which is a native plant of Malaysia (3). The sugar was subsequently isolated from the corticosteroid, mitiphylline, extracted from the leaves of *Holarrhena mitis* from Sri Lanka (4). These compounds have cardiotonic activity, and there is also some interest in them as anti-cancer drugs in view of the discovery that some glycosteroids have significant inhibitory activity against human carcinoma of the nasopharynx (5). An early synthesis of holacosamine was reported by Gero and co-workers (6), but the number of epimerizations needed to establish the proper stereorelationships, the harsh conditions for most of these reactions, and their low yield illustrate the problems associated with even such a relatively simple *cis*-hydroxyamino sugar.

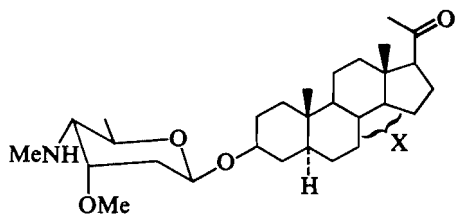

2

a X = 8β-H 14β-OH, holacurtin
b X = $\Delta^{8\text{-}14}$, holarosine

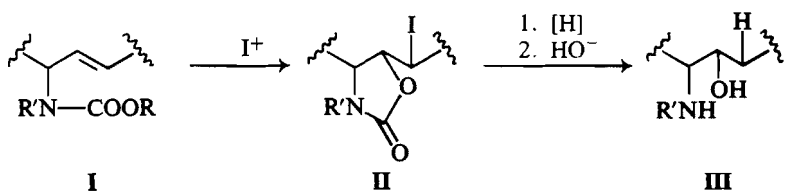

I **II** **III**

SCHEME 1

[1]For Part VI see accompanying paper, ref. 1.
[2]For a preliminary account of this work see ref. 2.
[3]Holder of NSERC Post-graduate Scholarship 1982–1983.
[4]Present address: Gross Chemical Laboratory, Duke University, Durham, NC 27706, U.S.A. Address correspondence to this author.

Can. J. Chem. Downloaded from www.nrcresearchpress.com by 210.87.254.5 on 09/06/12
For personal use only.

Application of the process depicted in **I** → **II** → **III**, Scheme 1, would require the unsaturated amino sugar **7** whose preparation from the *threo*-hex-2-eno-pyranoside **4***b* is apparent. Although the corresponding diacetate **4***a* is obtainable in one step from "triacetyl galactal" by the Ferrier rearrangement (7), considerations of economy and efficiency make the three-step sequence beginning with commercially available "triacetyl glucal", **6**, more attractive (7). As was the case in Gero's synthesis (6), we faced a double inversion sequence to establish the C-4 nitrogen in **7**. However, since our reactions would be occurring at an allylic site, much milder conditions would be required.

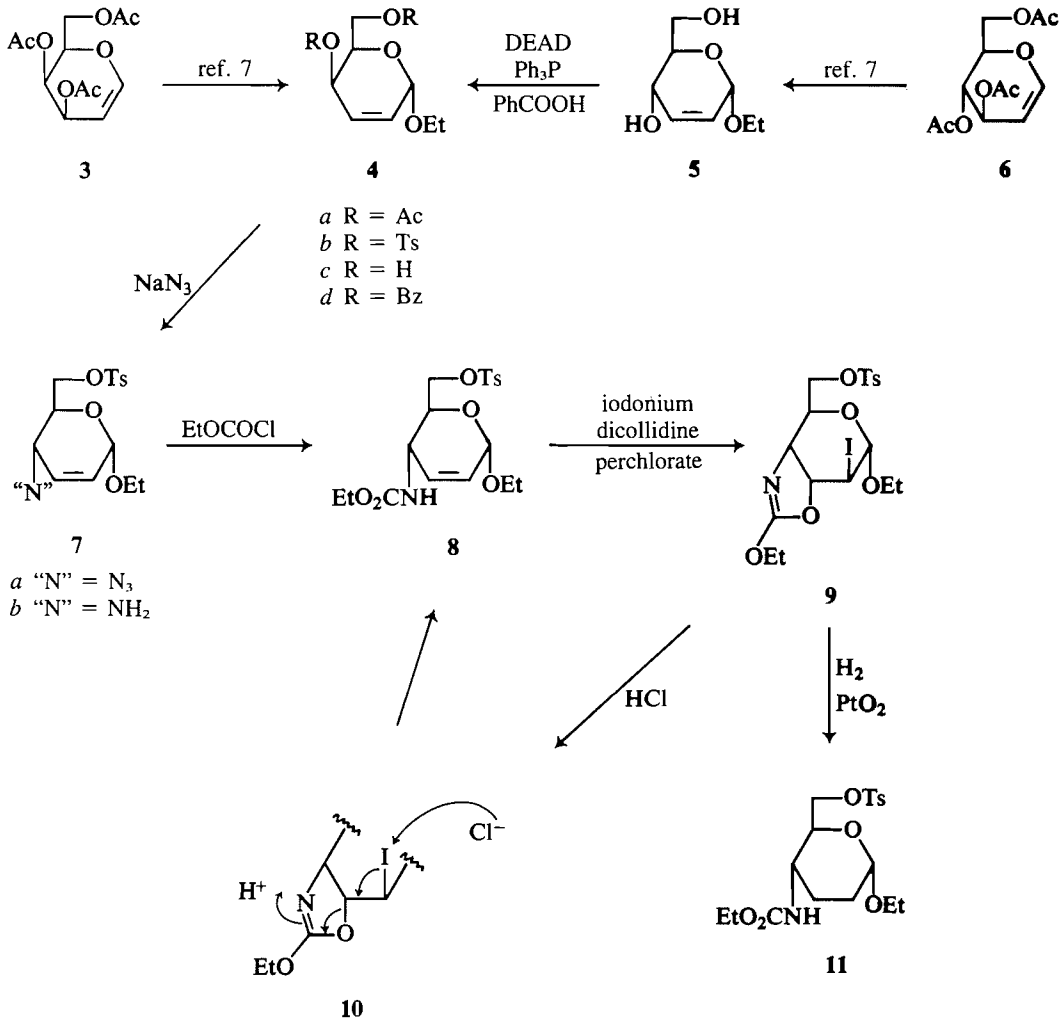

SCHEME 2

Reaction of the diol **5** under the Mitsunobu conditions (8), as modified by Galynker and Still (9), allowed for direct conversion into the disulfonate **4***b*. Although this modification (9) saves two steps in the sequence, the necessity of using five equivalents of diethyl azodicarboxylate per hydroxyl group did not make it very practical for large scale preparations and conventional sulfonation was therefore preferred. Accordingly, **5** was converted into the dibenzoate **4***d* by the Mitsunobu reaction (8), and the latter was converted into the disulfonate **4***b* via diol **4***c*. Reaction of **4***b* with sodium azide in dimethyl sulfoxide at room temperature displaced only the allylic sulfonate, and the structure of the product **7***a* was apparent from the value $J_{3,4}$ = 1 Hz. The azide was reduced to the amine **7***b* with lithium aluminium hydride in ether at −25°C. Treatment of the derived urethane, **8**, with iodonium dicollidine perchlorate (10) in methylene chloride gave the oxazoline **9**, instead of an oxazolidinone as in the garosamine synthesis (1).

Very surprisingly, hydrolysis of **9** with 0.5 *N* hydrochloric acid at room temperature for 1.5 h regenerated the allylic urethane **8**. We rationalized that this course of reaction was triggered by protonation of the nitrogen with the eventual collapse depicted in **10**. Removal of the C-2 iodine should, therefore, prevent this process, but reductive deiodination of **9** proved remarkably difficult. Hydrogenolysis did not occur with palladium as catalyst, and with platinum, two products in the ratio 7:1 were obtained, the major of which proved to be **11**. Compound **11** is probably formed by a homolytic fragmentation comparable to the heterolytic process depicted in **10**, followed by hydrogenation of the double bond.

Can. J. Chem. Downloaded from www.nrcresearchpress.com by 210.87.254.5 on 09/06/12
For personal use only.

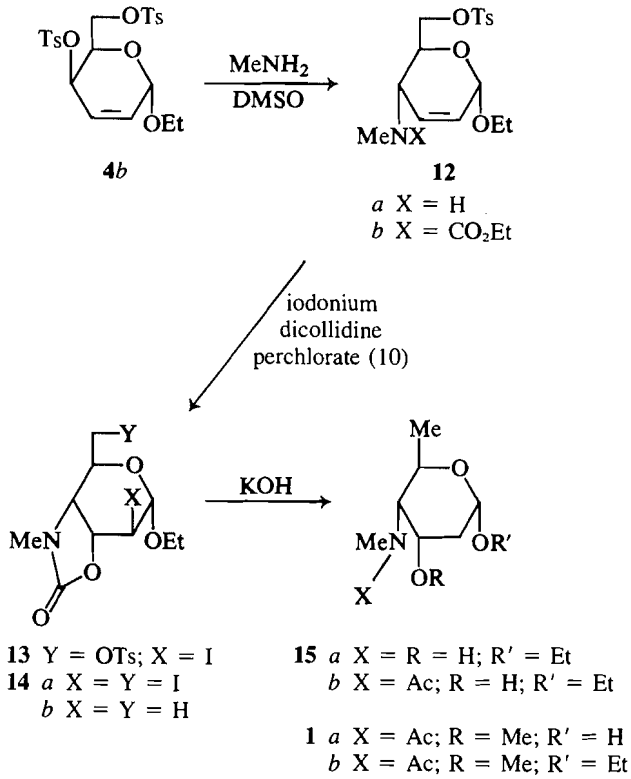

4b **12** *a* X = H; *b* X = CO_2Et

13 Y = OTs; X = I
14 *a* X = Y = I; *b* X = Y = H

15 *a* X = R = H; R′ = Et; *b* X = Ac; R = H; R′ = Et

1 *a* X = Ac; R = Me; R′ = H; *b* X = Ac; R = Me; R′ = Et

SCHEME 3

The difficulties experienced with **9** contrasted with the smooth process in the garosamine case (1), and suggested that at least part of our problem might be due to the fact that our intermediate **9** was a 2-ethoxy oxazolidine instead of an oxazolidinone. The presence of a C-4 *N*-methyl substituent, ultimately required at C-4 of **1**, would preclude the formation of such a 2-ethoxy oxazolidine, and so the ammonolysis of **4***b* was examined. The pressure vessel method used in our earlier work (1) led to decomposition, but use of dimethyl sulfoxide saturated with methylamine at room temperature afforded a 71% yield of **12***a*. Reaction of the derived urethane **12***b* with iodonium dicollidine perchlorate (10) at room temperature did give the desired oxazolidone **13**, but a second, unstable product obtained in 25% yield vitiated this result. The structure of the latter material was not determined, but patient experimentation showed that its formation could be avoided by adding the iodonium salt in small portions to **12***b* in refluxing dioxane.

When **13** was heated in refluxing acetone containing sodium iodide, the diiodourethane **14***a* was obtained and this was reduced with tri-*n*-butyltin hydride in refluxing benzene to afford the trideoxy sugar **14***b*. Hydrolysis of the oxazolidone with 5% potassium hydroxide proceeded smoothly to yield the *cis* vicinal hydroxyamine, **15***a*. *N*-Acetylation of the latter followed by *O*-methylation of the product, **15***b*, yielded *N*-acetyl holacosamine **1***b*. An attempt to procure an authentic sample of holacosamine from Gero (6) was unsuccessful. However, the synthetic sample of **1***b* gave compatible 400 MHz ^{1}H nmr and ir spectra, as well as microanalytical data (see Experimental).

Experimental

General methods

Melting points were determined in capillary tubes in a Buchi Model 510 and are uncorrected. Elemental analyses were performed by Guelph Chemical Labs, Guelph, Ontario and by Dr. F. Kasler, Department of Chemistry, University of Maryland. The ^{1}H nmr spectra were determined in deuteriochloroform with internal tetramethylsilane as the standard, unless otherwise stated, on one of the following spectrometers: Varian T-60, Bruker WP-80, or Bruker WH-400. Coupling constants were measured directly from the spectra or calculated from the peak listings. The ir spectra were determined on either a Beckman IR-10 or a Perkin–Elmer 298 spectrometer. Neat samples were smeared on sodium chloride plates and solutions were placed in sodium chloride cells. Low resoltuion ms were run on a Hitachi/Perkin–Elmer RMH-2. Optical rotations were determined on a Perkin–Elmer 241 polarimeter.

Thin layer chromatography (tlc) was performed using aluminum plates precoated with silica gel (HF-254, 0.2 mm thickness) containing a fluorescent indicator (E. Merck, CAT. 5539). The chromatograms were viewed under a uv light (254 nm), sprayed with concentrated sulfuric acid, and heated until charring occurred.

Column chromatography was carried out using silica gel (E. Merck 70–230 mesh A.S.T.M. or 230–500 mesh A.S.T.M.).

*Ethyl 2,3-dideoxy-α-D-*threo*-hex-2-enopyranoside, 4*c

To a solution of **5** (11) (1.74 g, 10 mmol) triphenylphosphine (5.76 g, 22 mmol), and benzoic acid (2.68 g, 22 mmol) in dry tetrahydrofuran (50 mL) at 23°C under argon was added, over a period of 5 min, diethyl azodicarboxylate (3.82 g, 22 mmol). The reaction mixture was stirred for 30 min, after which time the solvent was removed *in vacuo*. The resulting oily mixture was purified by medium pressure chromatography on silica gel (30:70 diethyl ether – petroleum ether 30–60°C, R_f 0.57) to afford 3.31 g (85%) of the known (12) **4***d* dibenzoate as a colourless oil; ir ($CHCl_3$) ν_{max}: 2910, 1715 (benzoate), 1614, 1600, 1310–1160, 1110–950 cm^{-1}; ^{1}H nmr (80 MHz) δ: 1.23 (t, 3H, OCH_2CH_3), 3.39–4.06 (m, 2H, OCH_2CH_3), 4.42–4.78 (m, 3H, H5, H6, H6), 5.17 (d, J = 3 Hz, 1H, H1), 5.38 (bd, J = 5.3 Hz, 1H, H4), 6.09 (dd, J = 3, 10 Hz, 1H, H2), 6.31 (dd, J = 5.1, 10 Hz, 1H, H3), 7.30–7.60 (m, 6H, aromatic), 7.94–8.13 (m, 4H, aromatic).

To a solution of **4***d* (4.36 g, 11mmol) in methanol (50 mL) at 23°C was added a catalytic amount of sodium methoxide (100 mg). The reaction mixture was stirred for 2 h, after which time the solvent was removed *in vacuo*. The resulting mixture was chromatographed on silica gel (7:93 methanol – methylene chloride, R_f 0.32) to afford 1.51 g (75%) of an oil that crystallized upon standing. Recrystallization from methylene chloride – hexane afforded the known diol **4***c* as a crystalline material, mp 75–76°C (lit. (11) mp 76–77°C).

*Ethyl 2,3-dideoxy-4,6-di-*O*-p-toluenesulfonyl-α-D-*threo*-hex-2-enopyranoside, 4*b

To a solution of **4***c* (4.00 g, 23 mmol) in dry pyridine (30 mL) cooled to −40°C, *p*-toluenesulfonyl chloride (8.70 g, 46 mmol) and dry pyridine (20 mL) were added over 20 min. After 48 h at 0°C the reaction mixture was poured into ice water, carefully neutralized with 1 *N* HCl, and extracted with methylene chloride (1 × 75, 2 × 25 mL). The methylene chloride fractions were combined, washed with a saturated aqueous sodium chloride solution, dried over sodium sulfate, and concentrated *in vacuo* to yield an oil. Medium pressure chromatography on silica gel (2:98 methanol – methylene chloride) followed by recrystallization (ether–hexane) afforded 9.52 g (86%) of pure **4***b* mp 78–79°C; R_f 0.36 (methylene chloride); $[\alpha]_D^{23}$ −11.3° (*c* 0.7, in $CHCl_3$); ir ν_{max} ($CHCl_3$): 2920, 1594 (C=C), 1464 (SO_2), 1168 (SO_2), 1097, 1000, 972 cm^{-1}; ^{1}H nmr (80 MHz) δ: 1.20 (t, 3H, OCH_2CH_3), 2.48 (s, 6H, tosyl CH_3), 3.25, 4.00 (m, 2H, OCH_2CH_3), 4.12 (2d, J = 2, 2.5, 6 Hz, 2H, H6, H6), 4.31 (ddd, J = 2.5, 6 Hz, 1H, H5), 4.67 (dd, J = 2.5, 5 Hz, 1H, H4), 4.97 (d, J = 2.5 Hz, 1H, H1), 5.82 (dd, J = 5, 10 Hz, 1H, H3), 6.03 (dd, J = 2.5, 10 Hz, 1H, H2), 7.33 (d, 4H, aromatic), 7.78 (d, 4H, aromatic). *Anal.* calcd. for $C_{22}H_{26}O_8S_2$: C 54.76, H 5.43; found: C 54.90, H 5.17.

*Ethyl 4-azido-2,3,4-trideoxy-6-*O*-p-toluenesulfonyl-α-D-*erythro*-hex-2-enopyranoside, 7*a

To a solution of **4***b* (12.7 g, 26 mmol) in dry dimethyl sulfoxide

Can. J. Chem. Downloaded from www.nrcresearchpress.com by 210.87.254.5 on 09/06/12
For personal use only.

Can. J. Chem. Downloaded from www.nrcresearchpress.com by 210.87.254.5 on 09/06/12
For personal use only.

(20 mL) under argon at 23°C was added sodium azide (2.40 g, 37 mmol). The reaction mixture was stirred for 45 min, poured into 100 mL of ice water, and extracted with ethyl acetate (1 × 100, 1 × 30 mL). The ethyl acetate fractions were combined, washed with a saturated aqueous sodium chloride solution, dried over sodium sulfate, and concentrated *in vacuo* to afford 7.20 g (77%) of **7***a* as a colourless oil; R_f 0.69 (methylene chloride); ir ν_{max} ($CHCl_3$): 2900, 2100 (N_3), 1585 (tosylate), 1430, 1350, 1270, 1220, 1155, 1100, 1084, 990, 955, 910 cm^{-1}; ^1H nmr (80 MHz) δ: 1.19 (t, 3H, OCH_2CH_3), 2.46 (s, 3H, ϕCH_3), 3.30–3.95 (m, 4H, OCH_2CH_3, H4, H5), 4.25 (bs, 2H, H6, H6), 4.95 (s, 1H, H1), 5.93 (s, 2H, H2, H3), 7.35 (bd, 2H, aromatic), 7.82 (bd, aromatic); *m/e*: 325 ($M^+ - N_2$).

*Ethyl 4-amino-2,3,4-trideoxy-6-*O-p-*toluenesulfonyl-α-D-*erythro-*hex-2-enopyranoside,* **7**b

To a suspension of lithium aluminum hydride (380 mg, 10 mmol) in dry ether (150 mL) at −25°C under an atmosphere of argon was added, over 10 min, **7***a* (7.20 g, 20 mmol) in dry ether (50 mL). The reaction mixture was stirred for 20 min. The excess lithium aluminum hydride was destroyed by the slow addition of sodium sulfate decahydrate. The resulting precipitate was removed by filtration. The filtrate was concentrated *in vacuo* to afford 6.00 g (90%) of **7***b* as a clear oil; R_f 0.52 (110:90 methanol − methylene chloride); ir ν_{max} ($CHCl_3$): 3410, 3320 (amine), 2985, 2900, 1600 (tosylate, amine), 1455, 1320, 1120, 975, 970 cm^{-1}; ^1H nmr (80 MHz) δ: 1.19 (dt, 3H, OCH_2CH_3), 1.39 (s, 2H, NH_2), 2.45 (s, 3H, CH_3), 3.21–3.87 (m, 4H, OCH_2CH_3, H4, H5), 4.26 (d, 2H, H6, H6), 4.87 (bs, 1H, H1), 5.66–5.77 (m, 2H, H2, H3), 7.32 (bd, 4H, aromatic), 7.71 (bd, 4H, aromatic); *m/e*: 283 (($M^+ + 1$)-OC_2H_5), 282 ($M^+ - OC_2H_5$).

*Ethyl 2,3,4-trideoxy-4-*N-*ethoxycarbonylamino-6-*O-p-*toluenesulfonyl-α-D-*erythro-*hex-2-enopyranoside,* **8**

To a solution of **7***b* (790 mg, 2.4 mmol) and triethylamine (0.42 mL, 3 mmol) in dry methylene chloride (15 mL) at 0°C under argon was added, over 5 min, ethyl chloroformate (0.25 mL, 2.6 mmol) in dry methylene chloride (3 mL). The mixture was stirred for 30 min and then methanol (~0.5 mL) was added to destroy any remaining ethyl chloroformate. The reaction mixture was washed with water, dried over sodium sulfate, and concentrated *in vacuo*. Purification by medium pressure chromatography on silica gel (2:3 diethyl ether − methylene chloride, R_f 0.82) afforded 828 mg (86%) of **8** as a colourless oil; ir ν_{max} ($CHCl_3$): 3440 (NH), 2900, 1725 (urethane), 1610, 1590, 1375, 1310, 1185, 1108, 1005, 985 cm^{-1}; ^1H nmr (80 MHz) δ: 1.21 (dt, 6H, OCH_2CH_3), $CO_2CH_2CH_3$), 2.45 (s, 3H, CH_3), 3.38–4.70 (m, 9H, OCH_2CH_3, $CO_2CH_2CH_3$, H4, H5, H6, H6, NH), 4.94 (s, 1H, H1), 5.77 (s, 2H, Hs, H3), 7.32 (d, 2H, aromatic), 7.80 (d, 2H, aromatic); *m/e*: 355 (($M^+ + 1$)-OC_2H_5), 354 ($M^+ - OC_2H_5$).

*2′-Ethoxy (ethyl 2,4-dideoxy-2-iodo-6-*O-p-*toluenesulfonyl-α-D-altropyranosido)-[3,4:5′,4′]-Δ²-oxazoline,* **9**

A solution of **8** (399 mg, 1 mmol) and iodonium dicollidine perchlorate (10) (702 mg, 1.5 mmol) in dry methylene chloride (7 mL) was stirred under argon at 23°C in the dark. After 6 h an additional 350 mg (0.75 mmol) of iodonium dicollidine perchlorate were added and the reaction was allowed to continue for 18 h. The reaction mixture was poured into diethyl ether (25 mL) and filtered. The filtrate was concentrated *in vacuo* to yield a reddish coloured oil. Purification by medium pressure chromatography on silica gel (10:90 diethyl ether − methylene chloride) followed by recrystallization (diethyl ether − hexane) afforded 320 mg (61%) of **9**; R_f 0.76 (3:7 diethyl ether − methylene chloride); ir ν_{max} ($CHCl_3$): 2900, 1658 (C=N), 1595, 1362, 1324, 1170, 1100, 990, 915 cm^{-1}; ^1H nmr (80 MHz) δ: 1.08–1.40 (m, 6H, 2(OCH_2CH_3)), 2.45 (s, 3H, ϕCH_3), 3.48–4.34 (m, 10 H, C2, C3, C5, C6, C6, 2(OCH_2CH_3)), 5.13 (d, 1H, H1), 7.26–7.38 (bd, 2H, aromatic), 7.73–7.86 (bd, 2H, aromatic); *m/e*: 526 ($M^+ + 1$), 525 (M^+).

*Ethyl 4-*N-*ethoxycarbonylamino-2,3,4-trideoxy-6-*O-p-*toluenesulfonyl-α-D-*erythro-*hexopyranoside,* **11**

Product **9** (120 mg, 0.20 mmol) in methanol (10 mL) and triethylamine (0.25 mL) was hydrogenated over platinum oxide (10 mg). After 2 h the reaction mixture was filtered through a bed of Celite. The filtrate was evaporated to dryness *in vacuo*. Purification by medium pressure chromatography (30:70 diethyl ether − chloroform, R_f 0.65) followed by recrystallization (methylene chloride − hexane) afforded 35 mg (38%) of **11** as crystals, mp 116–117°C; ir ν_{max}: 3418 (NH), 1710 (urethane), 1600, 1450 (tosylate), 1290, 1117, 973, 951 cm^{-1}; ^1H nmr (80 MHz) δ: 1.21 (dt, 6H, OCH_2CH_3, $CO_2CH_2CH_3$), 1.60 (s, 1H, NH), 1.68–1.86 (m, 4H, H2, H2, H3, H3), 2.43 (s, 3H, ϕCH_3), 3.22–4.57 (m, 9H, H4, H5, H6, H6, OCH_2CH_3, $CO_2CH_2CH_3$), 4.77 (bs, 1H, H1), 7.36 (2bs, 2H, aromatic), 7.79 (2bs, 2H, aromatic). *Anal.* calcd. for $C_{18}H_{27}N\,O_7S$: C 53.86, H 6.73, N 3.49; found: C 54.20, H 7.05, N 3.30.

*Ethyl 2,3,4-trideoxy-4-*N-*methylamino-6-*O-p-*toluenesulfonyl-α-D-*erythro-*hex-2-enopyranoside,* **12**a

To a solution of dry dimethyl sulfoxide saturated with methylamine (1 mL) was added **4***b* (110 mg, 0.2 mmol). The reaction mixture was allowed to stand at room temperature for 1.5 h, during which time the colour changed from light yellow to wine red. The reaction mixture was diluted with 3 mL of ice water and extracted with ethyl acetate (3 × 5 mL). The ethyl acetate fractions were combined, washed with a saturated aqueous sodium chloride solution, dried, and concentrated *in vacuo* to afford an orange-red oil. Purification by medium pressure chromatography on silica gel (8:92 methanol − methylene chloride, R_f 0.50) afforded 55 mg (71%) of **12***a* as a colourless oil: $[\alpha]_D^{23}$ +160.5° (*c* 1.1, in $CHCl_3$) ir ν_{max}: ($CHCl_3$) 3680 (NH), 3460 (NH), 2880, 2480, 1598 (C=C), 1425, 1355 (S[=O]$_2$), 1100, 995, 925 cm^{-1}; ^1H nmr (80 MHz) δ: 1.00 (s, 1H, NH), 1.22 (t, 3H, OCH_2CH_3), 1.38 (s, 3H, ϕCH_3), 1.48 (s, 3H, NCH_3), 2.48 (bd, 1H, H4), 3.34–3.95 (m, 3H, OCH_2CH_3, H5), 4.28–4.48 (m, 2H, H6, H6), 4.94 (bs, 1H H1), 5.88 (dt, J = 2 Hz, 10 Hz, 1H, H3), 6.08 (bd, J = 10 Hz, 1H, H2), 7.35 (2bs, 2H, aromatic), 7.83 (2s, 2H aromatic); *m/e*: 297 (($M^+ + 1$)-OC_2H_5), 296 ($M^+ - OC_2H_5$).

*Ethyl 2,3,4-trideoxy-4-*N-*ethoxycarbonyl-*N-*methylamino)-6-*O-p-*toluenesulfonyl-α-D-*erythro-*hex-2-enopyranoside,* **12**b

To a solution of **12***a* (1.90 g, 5.6 mmol) and triethylamine (606 mg, 6 mmol) in dry methylene chloride (35 mL) under argon at 0°C was added, over 5 min, ethyl chloroformate (0.57 mL, 6 mmol) in dry methylene chloride (10 mL). The reaction mixture was stirred for 2 h, quenched with 1 mL of methanol, washed with a saturated aqueous sodium chloride solution, dried over sodium sulfate, and concentrated *in vacuo*. Purification by medium pressure chromatography on silica gel (3:97 methanol − methylene chloride, R_f 0.73) afforded 1.80 g (79%) of **12***b* as a colourless oil: $[\alpha]_D^{23}$ +34.3° (*c* 1.1, in $CHCl_3$); ir ν_{max} ($CHCl_3$): 2887, 1680 (urethane), 1593, 1357, 1291, 1127, 959 cm^{-1}; ^1H nmr (80 MHz) δ: 1.25 (dt, 6H, OCH_2CH_3, $CO_2CH_2CH_3$), 2.46 (s, 3H, ϕCH_3), 2.75 (s, 3H, NCH_3), 3.37–3.88 (m, 2H, H4, H5), 3.88–4.31 (m, 6H, H6, H6, OCH_2CH_3, $CO_2CH_2CH_3$), 4.95 (bs, 1H, H1), 6.70 (bd, J = 10.6 Hz, 1H, H3), 6.93 (dt, J = 2.4, 10.6 Hz, 1H, H2); *m/e*: 370 (($M^+ + 2$]-OC_2H_5), 369 (($M^+ + 1$)-OC_2H_5), 368 (M^+-OC_2H_5).

*3′-*N-*methyl-2′-oxo-(ethyl 2,4-dideoxy-2-iodo-6-*O-p-*toluenesulfonyl-α-D-altropyranosido)-[3,4:5[,4′]-oxazolidone,* **13**

To a solution of **12***b* (1.20 g, 2.5 mmol) in 15 mL of refluxing dioxane under argon was added iodonium dicollidine perchlorate (1.75 g, 3.7 mmol). After 15 min a second addition of iodonium dicollidine perchlorate (0.88 g, 1,9 mmol) was made, followed by a third addition (0.88 g, 1.9 mmol) 15 min later. The reaction mixture was refluxed another 10 min, then cooled and concentrated *in vacuo*. The resulting dark oil was diluted with 75 mL of methylene chloride, washed with ice-cold 0.5 *N* hydrochloric acid, 0.5 *M* sodium thiosulfate, saturated aqueous sodium chloride, dried over sodium sulfate, and concentrated *in vacuo*. Further purification by medium pressure chromatography (diethyl ether, R_f 0.43) afforded 1.03 g (72%) of **13** as a colourless oil; $[\alpha]_D^{23}$ −2.9° (*c* 0.3, in $CHCl_3$); ir ν_{max} ($CHCl_3$): 2900, 1760 (urethane), 1590, 1600 (C=C tosylate), 1460 (tosylate), 1435 (R_2NCH_3), 1100, 995 cm^{-1}; ^1H nmr (80 MHz) δ: 1.19 (t, 3H, OCH_2CH_3), 2.48 (s, 3H, ϕCH_3), 2.85 (s, 3H, NCH_3), 3.29–4.38 (m, 7H, H2, H4, H5, H6, H6, OCH_2CH_3), 4.73 (dd, J = 8.0, 9.3 Hz, 1H,

Can. J. Chem. Downloaded from www.nrcresearchpress.com by 210.87.254.5 on 09/06/12
For personal use only.

H3), 5.12 (d, J = 6.0 Hz, 1H, H1), 7.30 (d, 2H aromatic), 7.82 (d, 2H, aromatic); *m/e*: 479 (M^+).

*3'-N-Methyl-2'-oxo-(ethyl 2,4,6-trideoxy-2,6-diiodo-α-D-altropyranosido)-[3,4:5',4]-oxazolidone, **14**a*

A solution of **13** (400 mg, 0.8 mmol) and sodium iodide (180 mg, 1.2 mmol) in dry acetone (10 mL) was refluxed for 6 h. The reaction mixture was cooled and concentrated *in vacuo*. The residue was diluted with methylene chloride (25 mL), washed with a saturated aqueous sodium chloride solution, dried over sodium sulfate, and concentrated again *in vacuo* to give a clear oil. Purification by medium pressure chromatography on silica gel (diethyl ether) followed by recrystallization (methylene chloride − hexane) afforded 280 mg (76%) of **14***a* as crystals, mp 109−110°C; R_f 0.53 (diethyl ether); $[\alpha]_D^{23}$ +7.5° (*c* 1, in $CHCl_3$); ir ν_{max} ($CHCl_3$): 3510 (carbonyl overtone), 2900, 1755 (urethane), 1590, 1421, 1373, 1348, 1125, 1098, 992, 955 cm^{-1}; ^1H nmr (400 MHz) δ: 1.24 (t, 3H, OCH_2CH_3), 2.92 (s, 3H, NCH_3), 3.29 (dd, J = 6.9, 11.2 Hz, 1H, H6), 3.52 (dd, J = 2.3, 11.2 Hz, 1H, H6), 3.58 (m, 1H, $OCH\,CH_3$), 3.78 (m, $J_{4,5}$ = 16.6 Hz, H4, H5), 3.95 (m, 1H, $OCH\,CH_3$), 4.08 (dd, J = 6.1, 9.4 Hz, 1H, H2), 4.76 (dd, J = 9.4, 8.0 Hz, 1H, H3), 5.20 (d, J = 6.1 Hz, 1H, H1). *Anal.* calcd. for $C_{10}H_{15}NO_4I_2$: C 25.71, H 3.24, N 3.00, I 54.34; found: C 25.75, H 3.30, N 3.00, I 54.92.

*3'-N-Methyl-2'-oxo-(ethyl 2,4,6-trideoxy-α-D-*ribo-hexapyranosido)-[3,4:5',4']-oxazolidone, ***14**a*

To a solution of **14***b* (250 mg, 0.5 mmol) in dry benzene (10 mL) under argon was added tri-*n*-butyltin hydride (0.4 mL, 1.5 mmol) and a catalytic amount of benzoyl peroxide. The reaction mixture was refluxed for 30 min, cooled, and concentrated *in vacuo*. The resulting oil was dissolved in acetonitrile (25 mL) and washed with hexane (1 × 15, 1 × 5 mL). The acetonitrile layer was concentrated *in vacuo* to afford an oil that crystallized upon standing. Recrystallization from methylene chloride − hexane afforded 70 mg (59%) of **14***b* as crystals, mp 67−68°C; R_f 0.35 (diethyl ether); $[\alpha]_D^{23}$ +107.1° (*c* 0.5, in $CHCl_3$); ν_{max} ($CHCl_3$): 3485 (carbonyl overtone), 2895, 1747 (urethane), 1595, 1425, 1373, 1105, 1045, 1005 cm^{-1}; ^1H nmr (80 MHz) δ: 1.25 (t, 3H, OCH_2C_3), 1.37 (d, J = 6.3 Hz, 3H, CH_3), 1.71−2.48 (m, 2H, H3, H2), 2.90 (s, 3H, NCH_3), 3.27−4.13 (m, 4H, H5, OCH_2CH_3), 4.42−4.94 (m, 2H, H1, H3). *Anal.* calcd. for $C_{10}H_{17}NO_4$: C 55.81, H 7.92, N 6.51; found: C 56.10, H 8.12, N 6.77.

*Ethyl-4-(N-methylacetamido)-2,4,6-trideoxy-α-D-*ribo-*hexopyranoside, **15**b*

A solution of **14***b* (175 mg, 0.8 mmol) in 5 mL of 5% potassium hydroxide was refluxed for 30 min. The reaction mixture was cooled and concentrated *in vacuo*. The resulting oily material was extracted with hot ethyl acetate (3 × 5 mL). The ethyl acetate fractions were combined and concentrated *in vacuo* to afford 110 mg (71%) of crude **15***a* as a clear oil; ^1H nmr (80 MHz) δ: 1.08−1.44 (m, 6H, OCH_2CH_3, CH_3), 1.80−2.33 (m, 4H, H2, H2, OH, NH), 2.45 (s, 3H, NCH_3), 3.30−4.18 (m, OCH_2CH_3, H3, H4), 4.90 (bd, 1H, H1).

To a solution of impure **15***a* (55 mg, 0.3 mmol) in dry methanol (2 mL) at 23°C under argon was added 0.25 mL of acetic anhydride. After 24 h the solvents were removed *in vacuo* to give an oil. Purification by medium pressure chromatography on silica gel (5:95 methanol − methylene chloride, R_f 0.38) afforded 55 mg (82%) of **15***b* as a colourless oil; $[\alpha]_D^{23}$ +194° (*c* 1.1, in $CHCl_3$); ir ν_{max} ($CHCl_3$): 3500 (OH), 3400, 1620 (amide), 1380, 1310, 950 cm^{-1}; ^1H nmr (80 MHz) δ: 1.10−1.30 (m, 6H, OCH_2CH_3, C—CH_3), 1197−2.23 (m, 6H, H2, OH, CH_3CO), 3.08 (d, 3H, NCH_3), 3.22−4.54 (m, 6H, OCH_2CH_3, H3, H4, H5), 4.96 (bs, 1H, H1); *m/e*: 232 (M^+ +1), 231 M^+.

*Ethyl-4-(N-methylacetamido)-3-O-methyl-2,4,6-trideoxy-α-D-*ribo-hexopyranoside, ***1**b*

To a suspension of sodium hydride (prewashed with hexane) (20 mg, 50% oil dispersion, 0.4 mmol) in dry tetrahydrofuran (3 mL) at 23°C under argon was added **15***b* (55 mg, 0.2 mmol) in dry tetrahydrofuran (2 mL). Tetra-*n*-butylammonium iodide (10 mg) was added, followed 10 min later by the addition of methyl iodide (1 mL). The reaction mixture was stirred for 2 h, quenched with sodium sulfate decahydrate, and filtered. The filtrate was concentrated *in vacuo* and then diluted with 5 mL of a saturated aqueous sodium chloride solution. The aqueous solution was extracted with diethyl ether (3 × 5 mL). The diethyl ether fractions were combined, washed with water, dried over sodium sulfate, and concentrated *in vacuo* to give an oil that crystallized upon standing. Recrystallization from hexane afforded 46 mg (79%) of **1***b* as granular crystals, mp 83−84°C; $[\alpha]_D^{23}$ +29.6° (*c* 0.6, in $CHCl_3$); R_f 0.31 (2:98 methanol − diethyl ether); ir ν_{max}: ($CHCl_3$) 3396, 1623 (amide), 1380, 1316, 943 cm^{-1}; ^1H nmr (400 Mhz, $CDCl_3$) δ: 1.17−1.84 (m, 6H, OCH_2CH_3, CH_3), 1.81 (dt, J = 4.1, 14.4 Hz, H2), 2.11 (d, 3H, $COCH_3$), 2.16 (2dd, J = 1.0, 14.2 Hz), 2.76 (d, 3H, NCH_3), 3.33 (d, 3H, OCH_3), 3.38−3.76 (m, 3H, H4, OCH_2CH_3), 4.22−4.32 (m, 2H, H3, H5), 4.80 (d, J = 4.2, 1H, H1). *Anal.* calcd. for $C_{12}H_{23}NO_4$: C 58.78, H 9.93, N 5.71; found: C 58.84, H 9.50, N 5.92.

Acknowledgement

We are grateful to NSERC and to NIH (GM 32569) for support of this work.

1. H. W. PAULS and B. FRASER-REID. Can. J. Chem. **62**, 0000 (1984).
2. M. GEORGES and B. FRASER-REID. Tetrahedron Lett. **22**, 4635 (1981).
3. M. M. JANOT, P. H. DEVISSAGUET, Q. KHUONG-HUU, J. PARELLO, N. G. BISSET, and R. GOUTAREL. C. R. Acad. Sci. Ser. C, **266**, 388 (1968).
4. M. M. JANOT, M. LEBOEUF, A. CAVE, R. O. B. WIJESEKERA, and R. GOUTAREL. C. R. Acad. Sci. Ser. C, **267**, 1050 (1968).
5. S. M. KUPCHAN, R. J. HEMINGWAY, and R. W. DOSKOTCH. J. Med. Chem. **7**, 803 (1964).
6. J. HILDESHEIM, S. D. GERO, G. KHUONG-KUU, and C. MONNERET. Tetrahedron Lett. 2849 (1969).
7. R. J. FERRIER and N. PRASAD. J. Chem. Soc. C, 570 (1969).
8. O. MITSUNOBU. Synthesis, 1 (1981).
9. I. GALYNKER and W. C. STILL. Tetrahedron Lett. **23**, 4461 (1982).
10. R. U. LEMIEUX and A. R. MORGAN. Can. J. Chem. **43**, 2199 (1965).
11. R. J. FERRIER and N. VETHAVIYASER. J. Chem. Soc. C, 1907 (1971).
12. B. FRASER-REID, S. Y.-K. TAM, and B. RADATUS. Can. J. Chem. **53**, 2005 (1975).

Condensation of thiophenols with aryl halides using metallic copper as a reactant. Intermediation of cuprous thiophenolates

TAKAKAZU YAMAMOTO[1] AND YASUHIRO SEKINE

Research Laboratory of Resources Utilization, Tokyo Institute of Technology, 4259 Nagatsuta, Midori-ku, Yokohama 227, Japan

Received November 1, 1983

TAKAKAZU YAMAMOTO and YASUHIRO SEKINE. Can. J. Chem. **62**, 1544 (1984).

The reaction of thiophenol (PhSH) with metallic copper affords CuSPh and H_2 through Cu-catalyzed dehydrogenative coupling of PhSH to PhSSPh and ensuing addition of PhSSPh to Cu. Condensation between thiophenols (ArSH) and aryl iodides or bromides (Ar'X) in the presence of Cu affords diaryl sulfides (ArSAr') in good or moderate yields (ArSH + Ar'X + Cu → ArSAr' + CuX + $1/2H_2$). Use of alkyl iodides (RI), instead of Ar'X, affords alkyl aryl sulfides (ArSR) in good yields. These condensations are considered to proceed mainly through (1) copper-catalyzed dehydrogenative coupling of ArSH to ArSSAr with evolution of H_2, (2) addition of ArSSAr to Cu giving CuSAr, and (3) coupling of CuSAr with Ar'X giving ArSAr' and CuX; temperature dependence of products, time course of the reaction, the reaction of PhSSPh with Cu, and the reaction of Ar'X with CuSPh support this view. Use of copper oxides (Cu_2O and CuO), instead of Cu, also affords diaryl sulfides in good or moderate yields.

TAKAKAZU YAMAMOTO et YASUHIRO SEKINE. Can. J. Chem. **62**, 1544 (1984).

Le thiophénol (PhSH) réagit avec le cuivre métallique en donnant du CuSPh et du H_2; cette réaction se produit via un couplage déshydrogénant, catalysé par le cuivre, du PhSH en PhSSPh qui s'additionne ensuite sur le Cu. La condensation des thiophénols (ArSH) avec les iodures ou les bromures aryliques (Ar'X) en présence de cuivre fournit les sulfures de diaryles (ArSAr') avec des rendements qui varient de bons à modérés (ArSH + Ar'X + Cu → ArSAr' + CuX + $1/2H_2$). L'utilisation d'iodures d'alkyles (RI), au lieu de Ar'X, permet d'obtenir des sulfures d'alkyles et d'aryles (ArSR) avec de bons rendements. On considère que ces condensations se font principalement par: (1) l'intermédiaire du couplage déshydrogénant, catalysé par le cuivre, de ArSH en ArSSAr avec dégagement d'hydrogène, (2) l'addition de ArSSAr sur le cuivre pour donner le CuSAr et (3) le couplage de CuSAr avec Ar'X qui donne le ArSAr' et le CuX; l'effet de la température sur la nature des produits, l'influence du temps sur le cours de la réaction, la réaction de PhSSPh avec le Cu et la réaction de Ar'X avec le CuSPh confirment cette hypothèse. L'utilisation d'oxydes de cuivre (Cu_2O et CuO), au lieu de Cu, permet également d'obtenir les sulfures de diaryles avec des rendements allant de bons à modérés.

[Traduit par le journal]

Introduction

Previously we reported effective Ullman type condensation of active hydrogen compounds, RZH (Z = N, O, C), with aryl halides, ArX, using metallic copper as a reactant (1).

[1] RZH + ArX + Cu → RZAr + CuX

The condensation was assumed to proceed through formation of intermediate CuZR and ensuing attack of ArX on CuZR. However, in the case of the active hydrogen compounds tested in our previous paper, isolation of the supposed CuZR was not feasible. Recently, we have found that a similar condensation proceeds when thiophenol is employed as the active hydrogen compound and in this case the supposed intermediate CuSPh is isolable.

The purpose of the present study is twofold: to apply the condensation reaction expressed by eq. [1] to thiophenols (ArSH), and to reveal the process giving the intermediate CuSPh.

Results and discussion

Reaction of PhSH with Cu

We first examined the reaction of thiophenol, PhSH, with Cu in the absence of ArX. As shown in Table 1, the reaction of PhSH with Cu above 150°C gives CuSPh, PhSSPh, and H_2. Table 1 includes reactions of diphenyl disulfide, PhSSPh, with Cu. Formation of CuSPh by reaction of PhSH with cuprous oxide (Cu_2O) is known (2), but formation of CuSPh by the reaction of PhSH and Cu has not been reported. CuSPh seems to be formed through direct reaction of PhSH with Cu (eq. [2]) or by an indirect route via PhSSPh (eqs. [3] and [4]).

[2] 2Cu + 2PhSH → 2CuSPh + H_2

[3] 2PhSH → PhSSPh + H_2

[4] 2Cu + PhSSPh → 2CuSPh

Occurrence of the reaction [4] was supposed by several researchers (3–5), and it is now unequivocally established as shown in Nos. 5–8 in Table 1.

At the moment, we do not have evidence to prove or disprove the direction reaction route to form CuSPh (eq. [2]). However, as for the indirect route via PhSSPh, the reaction definitely proceeds, since PhSSPh is formed in the reaction of PhSH with Cu (Nos. 1–4); we prefer the indirect route as the main reaction route. The dehydrogenative coupling of PhSH (eq. [3]) is evidently catalyzed by Cu, since heating of PhSH without Cu afforded considerably less PhSSPh. Partial formation of PhSPh at temperatures higher than 180°C is considered to be due to thermal degradation of CuSPh.

Condensation between ArSH and Ar'X

Based on the results obtained above, we analyzed the condensation of PhSH with PhBr or TolX (Tol = *p*-tolyl; X = Br, I) using metallic copper as a reactant. Figure 1 shows the temperature dependence of the products. From the results shown in Fig. 1 the following conclusions can be drawn.

1. Cu-catalyzed dehydrogenation of PhSH affords PhSSPh as the initial product. The presence of the aryl halide may assist this catalytic reaction.

2. PhSSPh reacts with Cu to afford an intermediate species,

[1]Author to whom all correspondence should be addressed.

Can. J. Chem. Downloaded from www.nrcresearchpress.com by 210.87.254.42 on 09/06/12
For personal use only.

TABLE 1. Formation of CuSPh by reactions of Cu with PhSH and PhSSPh[a]

No.	Reactant (mmol)	Cu (mmol)	Temp. (°C)	CuSPh[b] (mmol)	Other products (mmol)		
					PhSSPh	PhSPh	H_2
1	PhSH (10)	30	150	1.7	0.4	0	Small amount
2	PhSH (10)	30	180	2.1	1.4	0.1	2.0
3	PhSH (10)	30	210	3.2	2.0	0.3	2.4
4	PhSH (10)	30	240	1.7	0.7	0.6	4.0
5	PhSSPh (5)	30	150	4.9	—	0	0
6	PhSSPh (5)	30	180	5.3	—	0.3	0
7	PhSSPh (5)	30	210	5.9	—	0.4	0
8	PhSSPh (5)	30	240	5.5	—	0.9	0

[a]Reaction time = 6 h; under N_2.
[b]Based on powder X-ray pattern, increase in weight, and acidolysis of the copper product (see Experimental).

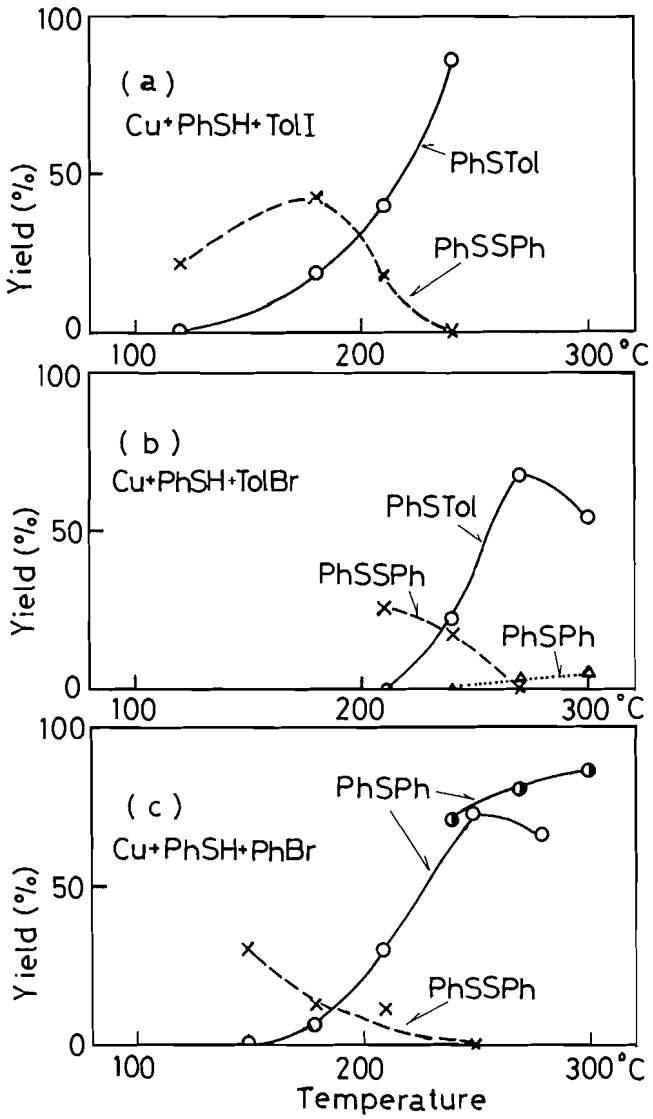

FIG. 1. Temperature dependence of yields of products in the condensation reaction of PhSH with aryl halide (Ar'X) using Cu as a reactant, under N_2 for 6 h; Cu/PhSH = 3.0. ○ (or ◑) and × show yields of PhSAr' and PhSSPh (based on PhSH), respectively. (a) Ar'X = TolI (1 mol/mol of PhSH). (b) Ar'X = TolBr (1 mol/mol of PhSH); △ shows a yield of PhSPh. (c) Ar'X = PhBr (1 mol/mol of PhSH for ○ and ×; 2 mol/mol of PhSH for ◑). Evolution of a considerable amount of H_2 was confirmed in experiments shown in Fig. 1(c).

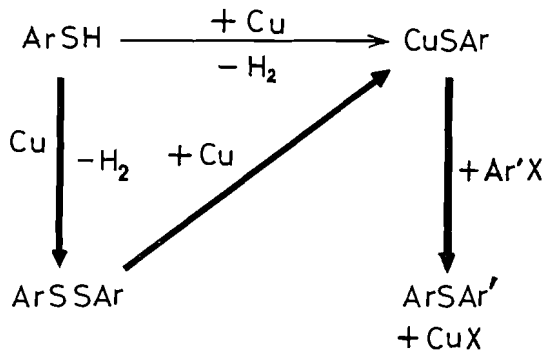

SCHEME 1

CuSPh, which further reacts with PhBr and TolX to give PhSPh and PhSTol, respectively. As discussed above, a direct reaction of PhSH with Cu also may afford the intermediate CuSPh; this situation is visualized in Scheme 1.

3. At higher temperatures (above about 250°C), degradation of CuSPh occurs to give PhSPh even in the reaction using TolX as the reactant. Thermolysis of CuSPh becomes rapid at about 250°C to give Cu_2S and PhSPh as revealed by TGA, glc, and powder X-ray diffraction pattern.

4. TolI has higher reactivity than TolBr, in agreement with the known trend that aryl iodides have higher reactivity than aryl bromides (1, 6).

In relation to Scheme 1, that CuSPh affords aryl phenyl sulfide by the reaction with aryl halides was demonstrated by Adams (1, 7) and here in Table 2, which shows no correlation between the Hammett's σ-value and reactivity of aryl bromide. Time dependence of the product of the reaction of Cu with the mixture of PhSH and PhBr (Table 3) also supports conclusions Nos. 1 and 2. Campbell reported preparation of diaryl sulfides by reactions of diaryl disulfides (e.g., PhSSPh) with mixtures of Cu and aryl halides in dimethylacetamide (3), and he assumed the addition of diaryl disulfides to Cu giving the arylthiolatocoppers. We investigated similar reactions by using no solvent and obtained diaryl sulfides from diaryl disulfides, aryl bromides or iodides, and Cu in good yields.

Table 4 shows results of condensation of thiophenols with aryl halides using Cu as a reactant. As shown in Table 4, the condensation of aryl iodides with thiophenols proceeds smoothly at 240°C to give the corresponding diaryl sulfides in good yields. The condensation of aryl bromides with thiophenols requires considerably higher temperature; it gives the

Can. J. Chem. Downloaded from www.nrcresearchpress.com by 210.87.254.42 on 09/06/12
For personal use only.

TABLE 2. Reactions of 1:1 mixtures of PhBr and p-RC_6H_4Br with CuSPh. CuSPh (1 mmol) + (PhBr (10 mmol) + p-RC_6H_4Br (10 mmol)) →

No.	p-RC_6H_4Br	σ_p value of R[a]	p-RC_6H_4SPh/PhSPh	Total yield (%/CuSPh)
1	p-$NO_2C_6H_4Br$	0.71	0.99	41
2	p-$NO_2C_6H_4Br$	0.50	1.66	42
3	p-FC_6H_4Br	0.06	0.22	24
4	p-$CH_3C_6H_4Br$	−0.17	1.56	67
5	p-$CH_3OC_6H_4Br$	−0.27	1.75	42

[a]Hammett's σ_p value of R in p-RC_6H_4Br. Reactions were carried out at 240°C.

TABLE 3. Time dependence of the product of the reaction of Cu with the mixture of PhSH and PhBr[a]

Time (h)	Product (mmol)		
	PhSSPh	PhSPh	Cu-compound[b]
3	0.9	1.9	CuSPh (major) + γ-CuBr (minor)
6	0	7.2	γ-CuBr

[a]At 240°C; Cu = 30 mmol; PhSH = 10 mmol; PhSBr = 10 mmol.
[b]Identified by powder X-ray diffraction analysis.

TABLE 4. Preparation of diaryl sulfides by reactions of thiophenols with mixtures of aryl halides (Ar'X) and metallic Cu[a]

Run	ArSH	Ar'X	Temp. (°C)	Yield of ArSAr' (%)
1	PhSH	PhI	240	87
2	PhSH	p-$CH_3C_6H_4I$	240	86
3	p-ClC_6H_4SH	PhI	240	86
4	p-$CH_3C_6H_4SH$	PhI	240	88
5	PhSH	p-$NO_2C_6H_4I$	240	43
6	PhSH	PhBr	300	86
7	PhSH	PhBr	280	65
8	PhSH	p-$CH_3C_6H_4Br$	270	67
9	p-ClC_6H_4SH	PhBr	240	23
10	p-$CH_3C_6H_4SH$	PhBr	240	29
11	PhSH	p-$NO_2C_6H_4Br$	240	41
12	PhSH	p-ClC_6H_4Br	270	54
13	PhSH	p-$CH_3OC_6H_4Br$	270	42
14	PhSH	p-FC_6H_4Br	270	24
15	PhSH	p-$CH_3COC_6H_4Cl$	240	18
16	PhSH	p-$NO_2C_6H_4Cl$	240	0

[a]Cu = 30 mmol; ArSH = 10 mmol; Ar'X = 10 mmol except for Run 2, where 20 mmol of Ar'X was employed. Reaction time = 6 h.

diaryl sulfides in good or moderate yields in cases of Runs 6, 7, 8, 11, 12, and 13, but the yield of sulfide is sometimes low, as shown in Runs 9, 10, and 14. Aryl chlorides show only low reactivities for the condensation reaction.

Use of Cu_2O or CuO, instead of Cu, in the condensation reaction also affords the corresponding diaryl sulfides as shown in Fig. 2. In the case of Cu_2O, the condensation most probably proceeds through a known facile reaction of PhSH with Cu_2O to give CuSPh (2), which, as described above, reacts with aryl halide. When CuO is employed, an oxidation product of PhSH, PhSSPh, is formed in about 50% yield per PhSH at relatively

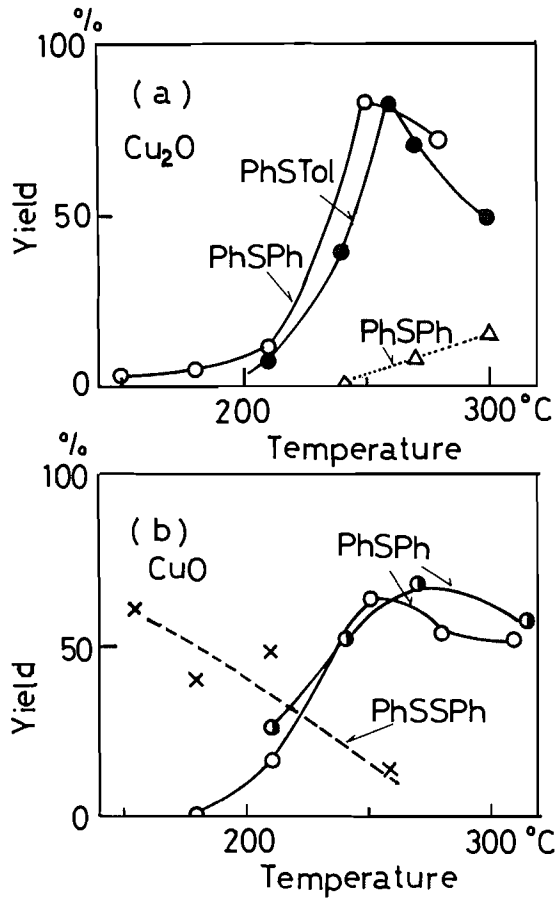

FIG. 2. Condensation using copper oxides. (a) Cu_2O = 15 mmol, PhSH = 10 mmol, PhBr = 10 mmol for ○. Cu_2O = 15 mmol, PhSH = 10 mmol, TolBr = 10 mmol for ●. △ represents yield of PhSPh in the condensation between PhSH and TolBr. (b) CuO = 30 mmol, PhSH = 10 mmol, PhBr = 10 mmol (○) or 20 mmol (◑). X shows yield of PhSSPh (PhBr = 10 mmol).

low temperatures. PhSSPh seems to be consumed in a further reaction with a mixture of aryl halide and CuO to give the diaryl disulfide. Use of alkyl iodides (RI) instead of aryl halides in the condensation reaction with thiophenols using Cu as a reactant affords alkyl aryl sulfides (ArSR) as shown in Figs. 3 and 4. The yield profile obtained at 120°C using n-alkyl iodides (Fig. 3) agrees with an order of reactivities of alkyl iodides in S_N2-type reactions (8), suggesting that the reaction proceeds through S_N2-type nucleophilic attack of CuSPh on alkyl iodide.

Experimental

Materials

Cu was prepared by reducing Cu^{2+} with Zn (9) in a Schlenk tube under an atmosphere of N_2 and stored under N_2 to avoid oxidation. Cu_2O, thiophenols, and organic halides were used as purchased from Tokyo Kasei or Wako Co. Ltd.

Analysis

Analyses of H_2, diaryl sulfides, diaryl disulfides, and other volatile organic products were carried out by gas chromatography with a Shimadzu GC-3BT gas chromatograph (carrier = He; column = SDC-550 or SSE-30 on SiO_2 purchased from Gas-chro Kogyo Co. Ltd.) using appropriate compounds (Ph−Ph, $PhCH_2Ph$, or $PhCH_2CH_2Ph$ in most cases) as internal standards. Thermogravimetric analyses were made with a Shimadzu thermoanalyzer DT-30. The ir and nmr spectra were recorded on a Hitachi 295 spectrometer and JEOL PS-100 spectrometer, respectively. Microanalyses of C, H, and

Can. J. Chem. Downloaded from www.nrcresearchpress.com by 210.87.254.42 on 09/06/12
For personal use only.

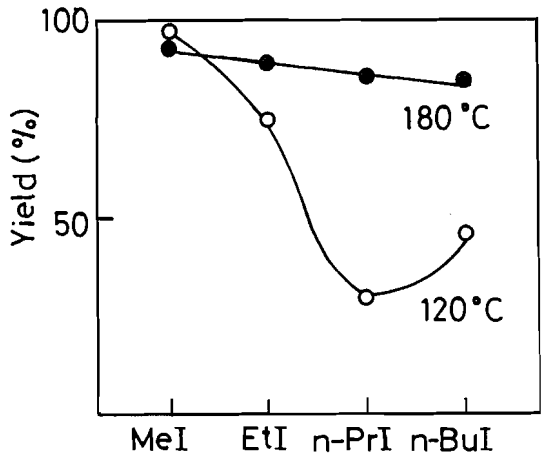

FIG. 3. Condensation between PhSH and alkyl iodides using Cu (molar ratio = 1:1:3). Temperature = 120°C (○) or 180°C (●).

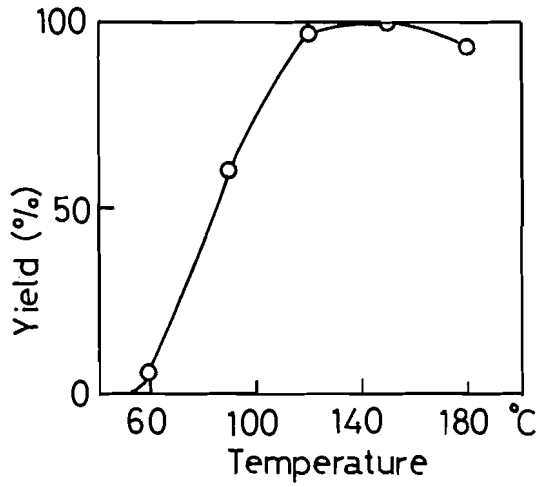

FIG. 4. Temperature dependence of yield of PhSMe in the condensation between PhSH and MeI using Cu (PhSH/MeI/Cu = 1:1:3).

N were performed with a Yanagimoto CHN Autocorder MT-2, and those of S with a Yazawa sulfur analyzer. Powder X-ray diffraction patterns were obtained with a Phillips PS-1051 (amount of sample: ca. 50 mg).

Reactions of Cu and PhSH and PhSSPh (cf. Table 1, No. 2)

A mixture of Cu (1.91 g, 30 mmol) and PhSH (1.1 g, 10 mmol) was heated in a 100-cm^3 stainless steel autoclave (Type VS-1, purchased from Taiatsu Glass Co., Ltd.) under an atmosphere of N_2. After 6 h, the reaction mixture was cooled to room temperature. Gas chromatographic analysis of the gas phase showed evolution of 2.0 mmol of H_2. Organic materials were extracted by diethyl ether and glc analysis of the extract showed formation of 1.4 mmol of PhSSPh and 0.1 mmol of PhSPh. Weighing the remaining solid showed an increase in weight of 190 mg, corresponding to conversion of 1.7 mmol of Cu to CuSPh. Powder X-ray diffraction pattern (X-ray sources: CuK_α) of the remaining solid showed only diffraction bands assigned to Cu (at $2\theta = 43.4°$ and 50.5°) and CuSPh (at $2\theta = 7.2°$, 10.2°, and 16.2°). Authentic CuSPh was prepared according to the literature (2). Acidolysis of the solid with concentrated HCl released 1.7 mmol of PhSH. In a separate experiment we confirmed that CuSPh (2) released PhSH quantitatively on acidolysis with HCl. Other results in Table 1 were obtained analogously.

Reaction of CuSPh with aryl halide (cf. Table 2)

A mixture of CuSPh (1.73 g, 10 mmol) and TolBr (1.71 g, 10 mmol) was heated in an autoclave at 270°C for 6 h under N_2. Gas–liquid chromatographic analysis showed formation of 6.8 mmol of PhSTol and 1.4 mmol of PhSPh. A similar reaction with TolCl gave 0.8 mmol of PhSTol and 4.2 mmol of PhSPh.

No. 1 in Table 2: A mixture of CuSPh (0.173 g, 1 mmol), PhBr (1.05 cm^3, 10 mmol), and p-$NO_2C_6H_4Br$ (2.01 g, 10 mmol) was heated in an autoclave at 240°C for 6 h. The glc analysis showed formation of 0.204 mmol of p-$NO_2C_6H_4SPh$ and 0.206 mmol of PhSPh. Other reactions listed in Table 2 were carried out analogously.

Condensation of thiophenols with aryl and alkyl halides using metallic copper as the reactant

No. 1 in Table 4: A mixture of Cu (1.9 g, 30 mmol), PhSH (1.1 g, 10 mmol), and PhI (1.1 cm^3, 10 mmol) in an autoclave was heated at 240°C for 6 h under N_2. The glc analysis showed formation of 8.7 mmol of PhSPh and 0.7 mmol of PhSSPh. Other condensations were carried out analogously.

1. T. YAMAMOTO and Y. KURATA. Can. J. Chem. **61**, 86 (1983).
2. R. ADAMS, W. REIFSCHNEIDER, and M. D. NAIR. Croat. Chem. Acta, **29**, 277 (1957).
3. J. R. CAMPBELL. J. Org. Chem. **27**, 2207 (1962).
4. T. YAMATO, Y. TANAKA, and T. SASADA. Kogyo Kagaku Zasshi, **61**, 252 (1958).
5. K. P. MEYER. Proc. Int. Vac. Congr. 7th (1977). p. 1985; Chem. Abstr. **89**, 62137 (1977); L. M. ROEV, L. M. ARTYNKHOUSKAYA, R. A. SVISHCHUK, V. S. PILYVASKII, and YU. YA. LIZUN. Dopov. Akad. Nauk Ukr. RSR Ser. B, Geol. Khim. Biol. Nauki, 649 (1979); Chem. Abstr. **91**, 192938k (1978).
6. H. WEINGARTEN. J. Org. Chem. **29**, 977 (1964).
7. R. ADAMS and A. FERRETTI. J. Am. Chem. Soc. **81**, 4927 (1959).
8. J. MARCH. Advanced organic chemistry. Reactions, mechanisms, and structure. McGraw–Hill, New York. 1977.
9. P. H. GORE and G. K. HUGHES. J. Chem. Soc. 1615 (1959).

Can. J. Chem. Downloaded from www.nrcresearchpress.com by 210.87.254.42 on 09/06/12
For personal use only.

Synthèses de dioxolannes α-iodés

CHRISTOPHE DAUBIÉ, CATHY BACQUET-EINHORN ET DANIEL LELANDAIS[1]

Laboratoire de Chimie Organique Structurale, Bâtiment F 7ème étage, E.R.A. 557, 4 Place Jussieu, 75230 Paris Cedex 05, France

Reçu le 3 octobre 1983

CHRISTOPHE DAUBIÉ, CATHY BACQUET-EINHORN et DANIEL LELANDAIS. Can. J. Chem. **62**, 1548 (1984).

Trois méthodes de préparation de cétals cycliques iodés sont décrites. La iodation directe des cétals par le chlorure d'iode dans l'éther conduit à des composés monoiodés avec de bons rendements. La réaction s'effectue avec une grande sélectivité quand l'un des carbones α est tertiaire.

CHRISTOPHE DAUBIÉ, CATHY BACQUET-EINHORN, and DANIEL LELANDAIS. Can. J. Chem. **62**, 1548 (1984).

Three methods of iodination of cyclic ketals are described. Direct iodination by monoiodine chloride in ether leads to very good yields in monoiodo compounds. A high selectivity is obtained when one of the α-carbon atoms is tertiary.

Can. J. Chem. Downloaded from www.nrcresearchpress.com by 210.87.254.5 on 09/06/12
For personal use only.

Dans le cadre de recherches effectuées au laboratoire sur les dérivés cétalisés de composés carbonylés (1) nous nous sommes intéressés à la synthèse de cétals cycliques α-iodés du type

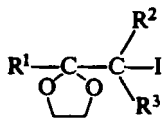

Si de tels cétals α-bromés ont déjà été décrits (2), il n'en est pas de même pour leurs analogues α-iodés. A notre connaissance seuls Goosen et McLeland (3) signalent l'obtention d'acétals cycliques α-iodés sans d'ailleurs décrire ces composés. Pourtant ce type de produits peut présenter un intérêt soit dans l'utilisation de l'iode comme marqueur, soit en synthèse. Par ailleurs ils ont déjà fourni par réduction électrochimique des γ-bisdioxolannes que nous décrirons par ailleurs.[2]

Pour préparer les cétals α-iodés nous avons tout d'abord fait appel à deux méthodes dérivées de réactions classiques, puis avons mis au point une méthode originale de iodation directe de cétals cycliques par le chlorure d'iode. Cette réaction s'est révélée simple, rapide et efficace dans la très grande majorité des cas étudiés.

Les résultats obtenus selon les trois voies sont décrits dans les tableaux 1 à 3.

Première méthode

Elle est dérivée de celle proposée par Garbisch (4) pour la synthèse directe de cétals α-bromés à partir de cétones cycliques: la cétone en solution dans l'éthylèneglycol est traitée par l'iode.

Dans notre cas, si le résultat est assez satisfaisant avec la cyclohexanone, il n'en a pas été de même avec les cétones acycliques; des composés diiodés sont obtenus si la température de réaction est un peu élevée ou du cétal non halogéné lorsqu'elle est trop basse.

En fait la manipulation est délicate à mener: d'une part il est difficile de contrôler correctement l'introduction d'iode; d'autre part, la réaction devant être initiée thermiquement, son évolution devient délicate à maîtriser par la suite.

Les rendements indiqués dans le tableau 1 sont les meilleurs que nous ayons obtenus lors de différents essais. Leur modicité et les excellents résultats obtenus sans problème avec le chlorure d'iode nous ont amenés à ne pas approfondir, dans l'immédiat, l'étude de cette méthode.

TABLEAU 1. Synthèse de dioxolannes α-iodés par iodation de cétones dans l'éthylène glycol

N°	Cétone de départ	Produit obtenu	Rdt (%)
A_2		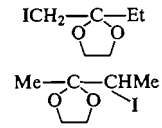	7 41
A_9	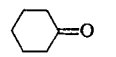	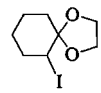	75
A_{10}	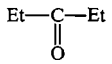	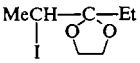	20

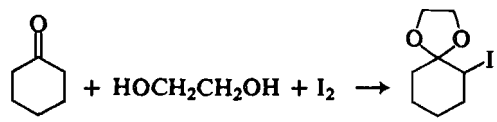

SCHÉMA 1

Notons toutefois que, lorsque deux sites d'attaque sont possibles, la réaction conduit à l'halogénure secondaire de façon prépondérante (essai A_2).

Deuxième méthode

Elle fait appel à la synthèse de cétones α-iodées par échange iode–chlore ou iode–brome au moyen de l'iodure de potassium à partir de cétones α-chlorées ou α-bromées (5, 6) suivie de leur cétalisation (7).

La première difficulté rencontrée est, dans ce cas, l'obtention des cétones α-iodées. Nous avons pu isoler les cétones α-bromées indiquées dans le tableau 2 dont la plupart n'avaient pas été entièrement décrites jusqu'ici (essais B_2, B_3, B_4, B_6, B_8, B_9). Cependant ces produits sont relativement instables et doivent être cétalisés immédiatement après leur préparation pour obtenir des rendements corrects.

Même dans ces conditions, la cétalisation s'effectue de telle sorte qu'une perte d'iode intervient durant la réaction et que les rendements chutent dès que l'on veut former un iodure secondaire.

Cette méthode reste néanmoins intéressante dans la mesure où la bromation régiosélective des cétones est bien connue (8).

[1] Auteur à qui envoyer toute correspondance.

[2] C. Daubié, C. Bacquet-Einhorn et D. Lelandais. Travail en cours.

TABLEAU 2. Synthèse de dioxolannes α-iodés par échange iode–brome sur les cétones α-bromées

N°	$R^1-C(=O)-CH(R^2)-Br$	Produits obtenus	Rdt 1*	Rdt 2†
B_0	R^1 = Me R^2 = H	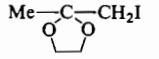	80	56
B_2	R^1 = Me R^2 = Me	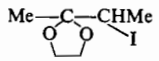	65	35
B_3	R^1 = Me R^2 = Et	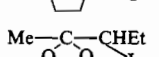	65	30
B_4	R^1 = Me R^2 = Pentyl	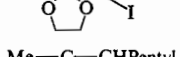	50	25
B_5	R^1 = Me R^2 = iPr	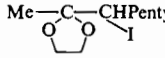	55	27
B_6	R^1 = *t*Bu R^2 = H	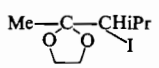	10	7
B_7	R^1 = nPr R^2 = H	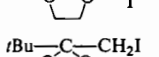	62	50
B_8	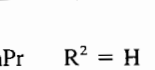	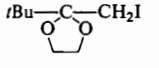	—	—
B_9		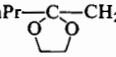	35	22

* Rdt 1: calculé par rapport à R^1COCHR^2Br.
† Rdt 2: calculé par rapport à $R^1COCH_2R^2$.

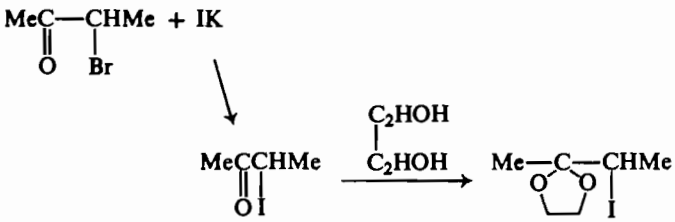

SCHÉMA 2

Il sera possible de préparer ainsi des cétals iodés différents de ceux obtenus par iodation directe par le chlorure d'iode.

Troisième méthode

Il s'agit du traitement direct des cétals cycliques (obtenus le plus souvent à partir des cétones selon la méthode de Salmi (7)) par le chlorure d'iode.

Si l'étude de la littérature montre l'intérêt croissant porté à cet halogénure mixte il est surtout utilisé pour l'iodation de composés aromatiques ou comme catalyseur de diverses réactions de chloration. Nous citerons cependant son emploi dans des études cinétiques d'halogénation de cétones (9) et surtout son intervention dans deux réactions intéressant directement (10) ou indirectement (3) des acétals. Comme nous l'avons signalé plus haut, l'une de ces réactions (3) conduit à l'obtention de petites quantités d'acétals α-iodés; cependant l'approche des auteurs est différente de celle adoptée ici.

Dans notre cas la position α des cétals cycliques s'est révélée très réactive vis à vis du chlorure d'iode. De tous les solvants utilisés, l'éther a conduit à la plus haute sélectivité, les produits monoiodés étant formés avec un rendement quasiment quantitatif (voir tableau 3).

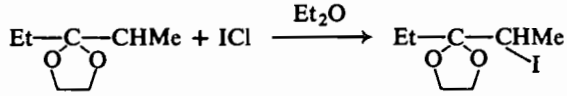

SCHÉMA 3

Les essais C_2 et C_{18} montrent la formation prépondérante d'un iodure secondaire par rapport à l'iodure primaire comme nous l'avions noté pour la première méthode.

En outre, lorsque l'un des carbones α du dioxolanne de départ est tertiaire, la réaction fournit un composé iodé sur l'autre carbone de façon totalement régiosélective (essais C_{13}, C_{17}, C_{19}). En fait la formation d'un iodure tertiaire n'a été observée en aucun cas (voir C_{20}).

Le mécanisme des réactions d'halogénation a été étudié dans le cas des chlorations et des bromations et il sort de l'objet de cet article de discuter celui de la réaction présentée ici.

Il nous semble cependant que quelques résultats observés trouvent leur source dans l'importance des effets stériques lors de cette iodation. C'est le cas, pensons nous, pour l'essai C_{15} où l'encombrement du cycle cétalique est accru, ainsi que pour l'essai C_{12} où ce sont cette fois les radicaux R^1 et R^2 qui augmentent la gêne stérique. Il est remarquable dans ce dernier cas que la réaction s'effectue avec d'excellents rendements si R^2 est un méthyle (essai C_6) au lieu d'un éthyle.

Conclusion

Les différentes méthodes décrites ici nous ont conduit à l'obtention d'un nombre important de cétals cycliques α-iodés qui sont des produits nouveaux.

Les deux premières méthodes peuvent avoir souvent leur utilité. C'est en particulier le cas pour la seconde qui profite des

Can. J. Chem. Downloaded from www.nrcresearchpress.com by 210.87.254.5 on 09/06/12
For personal use only.

TABLEAU 3. Synthèse de dioxolannes α-iodés par iodation directe de dioxolannes

N°	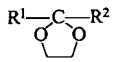		Produits obtenus		Rdt 1*	Rdt 2†
C_2	R^1 = Me	R^2 = Et	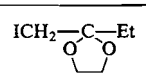 (a)	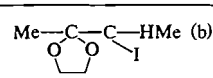 (b)	15 (a) 80 (b)	14(a) 72 (b)
C_6	R^1 = *t*Bu	R^2 = Me	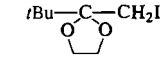		98	84
C_9	$R^1 = R^2 = (CH_2)_5$		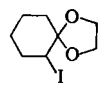		98	83
C_{10}	$R^1 = R^2$ = Et		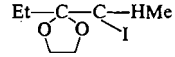		98	88
C_{11}	$R^1 = R^2$ = iBu		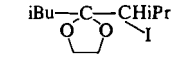		95	67
C_{12}	R^1 = *t*Bu	R^2 = Et	Produit de départ		—	—
C_{13}	$R^1 = C_6H_{11}$	R^2 = Me	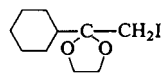		98	88
C_{14}	$R^1 = CH_2I$	R^2 = Me	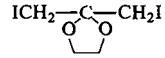		98	78
C_{15}	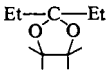		Produit de départ		—	—
C_{16}	R^1 = Me	$R^2 = CH_2CO_2Et$	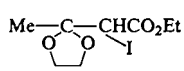		95	76
C_{17}	R^1 = Me	$R^2 = CHCO_2Et$ (Et)	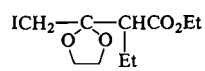		98	84
C_{18}	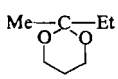		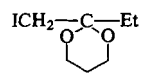 (a)	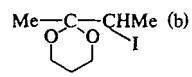 (b)	15 (a) 80 (b)	6 (a) 32 (b)
C_{19}	R^1 = Me	R^2 = iPr	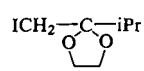		95	82
C_{20}	$R^1 = R^2$ = iPr		Produit de départ		—	—

*Rdt 1: calculé par rapport à R^1—C(O,O)—R^2.

†Rdt 2: calculé par rapport à R^1—CO—R^2.

connaissances acquises pour la bromation ou la chloration régiosélective des cétones et peut conduire ainsi à des produits que la troisième méthode ne permet pas d'atteindre (essai B_7 par exemple).

Pourtant cette troisième méthode se révèle la plus rentable, d'abord à cause des très bons rendements et de la simplicité de sa mise en oeuvre, mais aussi à cause de l'iodation quasi-totalement régiosélective observée dans certains cas.

Partie expérimentale

Les spectres rmn ont été effectués sur un appareil Bruker 80 WP en solution dans le deutérochloroforme avec pour référence interne l'hexaméthyldisiloxane.

Les échantillons pour analyse ont été séparés par chromatographie en phase vapeur sur une colonne SE 30 de 3 mètres de long.

Synthèse de cétals α-iodés selon la 1^e^ méthode

La réaction est conduite sous azote avec une agitation magnétique.

Une solution de 0,1 mol de cétone dans 60 mL d'éthylèneglycol est portée à 60°C. Quelques gouttes d'une solution de 0,1 mol d'iode dans l'éther sont alors ajoutées. Quand le milieu réactionnel est décoloré, la température est amenée à 30°C, et le reste de la solution d'iode est introduit goutte à goutte. A la fin de l'addition, l'agitation est maintenue pendant deux heures. Le milieu est alors neutralisé par du carbonate de sodium, puis dilué par 50 mL de pentane et 50 mL d'eau. Après trois extractions par 50 mL d'éther et séchage sur carbonate de sodium, la phase organique est évaporée à température ambiante. Le résidu est distillé.

Dioxolannes α-iodés

Dioxa-1,4 iodo-6 spiro[4,5] décane; A_9: $E_{0,1}$ = 80°C; δ = 4,4 à 3,8 (m, 5H), 2,3 à 1,2 (m, 8H). *Anal.* calc. pour $C_8H_{13}O_2I$: C 35,83, H 4,88, I 47,34%; trouvé: C 35,80, H 4,86, I 47,30%.

Éthyl-2 (iodo-1 éthyl)-2 dioxolanne-1,3; A_{10}: $E_{0,1}$ = 80°C; δ = 4,2 (q, 1H), 4,0 (s, 4H), 1,95 (q, 2H), 1,9 (d, 3H), 0,9 (t, 3H). *Anal.* calc. pour $C_7H_{13}O_2I$: C 32,82, H 5,11, I 49,56%; trouvé: C 32,84, H 5,09, I 49,53%.

Éthyl-2 iodométhyl-2 dioxolanne-1,3; A_2 ou C_{2a}: $E_{0,1}$ = 77°C; δ =4,0 (s, 4H), 3,2 (s, 2H), 1,9 (q, 2H), 0.9 (t, 3H). *Anal.* calc. pour $C_6H_{11}O_2I$: C 29,77, H 4,58, I 52,43%; trouvé: C 29,74, H 4,55, I 52,40%.

(Iodo-1 éthyl)-2 méthyl-2 dioxolanne-1,3; A_2 ou B_2 ou C_{2b}: $E_{0,1}$ = 75°C; δ = 4,2 (q, 1H), 4,0 (s, 4H), 1,9 (d, 3H), 1,5 (s, 3H). *Anal.* calc. pour $C_6H_{11}O_2I$: C 29,77, H 4,58, I 52,43%; trouvé: C 29,73, H 4,60, I 52,40%.

Can. J. Chem. Downloaded from www.nrcresearchpress.com by 210.87.254.5 on 09/06/12
For personal use only.

Can. J. Chem. Downloaded from www.nrcresearchpress.com by 210.87.254.5 on 09/06/12
For personal use only.

Synthèse de cétals α-iodés selon la 2e méthode

Suivant le type de cétones bromées désiré (bromation sur le carbone le moins substitué, le plus substitué, ou bromation d'une cétone cyclique) quatre méthodes de synthèses ont été utilisées (6, 8). Les cétones iodées correspondantes, obtenues selon le mode opératoire de Modaraï et Khosdel (5), sont traitées suivant le méthode de Salmi (7).

Exemple: synthèse du iodométhyl-2 propyl-2 dioxolanne-1,3: une solution de 0,1 mol de bromo-1 pentanone-2 (6) dans 50 mL d'éthanol est portée à reflux deux heures en présence de 0,12 mol d'iodure de potassium. Après refroidissement du milieu réactionnel, la solution filtrée est évaporée à froid. La cétone iodée brute est ajoutée à une solution de 100 mL de benzène contenant 0,12 mol d'éthylèneglycol et quelques milligrammes d'APTS. L'élimination totale de l'eau est observée après 12 heures de reflux. La solution benzénique est lavée deux fois avec une solution de potasse $N/10$. La phase organique décolorée est alors séchée sur carbonate de sodium et évaporée à froid. Le résidu est distillé $E_{0,1}$ = 80°C; Rdt = 62%.

Cétones iodées

Iodo-1 propanone-2: δ = 3,7 (s, 2H), 2,3 (s, 3H).

Iodo-2 cyclohexanone: δ = 4,8 (m, 1H), 3,8 à 1,5 (m, 8H).

Iodo-3 butanone-2: δ = 4,5 (q, 1H) 2,3 (s, 3H), 1,8 (d, 3H).

Iodo-3 pentanone-2: δ = 4,3 (t, 1H), 2,3 (s, 3H), 1,9 (d, 2H), 1,0 (t, 3H).

Iodo-3 octanone-2: δ = 4,4 (t, 1H), 2,3 (s, 3H), 2,2 à 1,5 (m, 2H), 1,5 à 0,7 (m, 9H).

Iodo-3 méthyl-4 pentanone-2: δ = 4,3 (d, 1H), 2,6 à 2,0 (m, 2H), 2,3 (s, 3H), 1,0 (m, 6H).

Iodo-1 diméthyl-3,3 butanone-2: δ = 3,7 (s, 2H), 1,0 (s, 9H).

Iodo-1 pentanone-2: δ = 3,7 (s, 2H), 2,8 (t, 2H), 2,0 à 1,1 (m, 2H), 0,9 (t, 3H).

Iodo-3 méthyl-3 butanone-2: δ = 2,4 (s, 3H), 2,0 (s, 6H).

Dioxolannes α-iodés

Iodométhyl-2 méthyl-2 dioxolanne-1,3; B_1: $E_{0,1}$ = 54°C; δ = 3,95 (s, 4H), 3,3 (s, 2H), 1,5 (s, 3H). *Anal.* calc. pour $C_5H_9O_2I$: C 26,33, H 3,97, I 55,65%; trouvé: C 26,28, H 3,94, I 55,63%.

(Iodo-1 éthyl)-2 méthyl-2 dioxolanne-1,3; B_2: voir première méthode.

(Iodo-1 propyl)-2 méthyl-2 dioxolanne-1,3; B_3: $E_{0,1}$ = 77°C; δ = 4,0 (s, 4H), 3,9 (t, 1H), 2,0 à 1,4 (m, 2H), 1,4 (s, 3H), 1,0 (t, 3H). *Anal.* calc. pour $C_7H_{13}O_2I$: C 32,82, H 5,11, I 49,58%; trouvé: C 32,77, H 5,10, I 49,55%.

(Iodo-1 hexyl)-2 méthyl-2 dioxolanne-1,3; B_4: $E_{0,1}$ = 115°C; δ = 4,0 (s, 4H), 3,9 (t, 1H), 2,0 à 0,7 (m, 14H). *Anal.* calc. pour $C_{10}H_{19}O_2I$: C 40,28, H 6,42, I 42,57%; trouvé: C 40,23, H 6,40, I 42,51%.

(Iodo-1 méthyl-2 propyl)-2 méthyl-2 dioxolanne-1,3; B_5: $E_{0,1}$ = 80°C; δ = 4,25 (d, 1H), 4,0 (m, 4H), 1,5 (s, 3H), 1,5 à 1,1 (m, 1H), 1,0 (d, 6H). *Anal.* calc. pour $C_8H_{15}O_2I$: C 35,56, H 5,60, I 46,98%; trouvé: C 35,58, H 5,57, I 47,01%.

Iodométhyl-2 tertiobutyl-2 dioxolanne-1,3; B_6: séparé sur SE 30; δ = 4,0 (m, 4H), 3,6 (s, 2H), 1,0 (s, 9H). *Anal.* calc. pour $C_7H_{15}O_2I$: C 32,57, H 5,85, I 49,17%; trouvé: C 32,54, H 5,83, I 49,12%.

Iodométhyl-2 propyl-2 dioxolanne-1,3; B_7: $E_{0,1}$ = 80°C; δ = 4,0 (s, 4H), 3,2 (s, 2H), 2,0 à 1,0 (m, 4H), 0,9 (t, 3H). *Anal.* calc. pour $C_7H_{13}O_2I$: C 32,82, H 5,11, I 49,58%; trouvé: C 32,85, H 5,10, I 49,52%.

Dioxa-1,4 iodo-6 spiro[4,5] décane; A_9: voir première méthode.

Synthèse de cétals α-iodés selon la 3e méthode

Les dioxolannes des cétones ont été préparés selon Salmi (7). La réaction d'iodation est conduite sous azote avec agitation magnétique.

Une solution de 0,02 mol de dioxolanne dans 10 mL d'éther anhydre est rapidement ajoutée à une solution de 0,024 mol de chlorure d'iode dans 40 mL d'éther anhydre refroidie par un bain de glace. L'évolution de la réaction est suivie par chromatographie en phase gazeuse.

Quand tout le dioxolanne de départ a disparu le milieu réactionnel est traité par une solution de potasse jusqu'à décoloration. Le mélange obtenu est extrait quatre fois par 20 mL d'éther, séché sur carbonate de sodium puis évaporé à température ambiante. Le résidu est distillé.

Dioxolannes α-iodés

Éthyl-2 iodométhyl-2 dioxolanne-1,3; C_{2a} ou A_2: voir première méthode.

(Iodo-1 éthyl)-2 méthyl-2 dioxolanne-1,3; C_{2b} ou A_2: voir première méthode.

Iodométhyl-2 tertiobutyl-2 dioxolanne-1,3; C_6 ou B_6: voir deuxième méthode.

Dioxa-1,4 iodo-6 spiro[4,5] décane; C_9 ou A_9: voir première méthode.

Éthyl-2 (iodo-1 éthyl)-2 dioxolanne-1,3; C_{10} ou A_{10}: voir première méthode.

(Iodo-1 méthyl-2 propyl)-2 isobutyl-2 dioxolanne-1,3; C_{11}: séparé sur SE 30 à 210°C; δ = 4,3 (d, 1H), 4,0 (m, 4H), 1,8 (m, 4H), 0,9 (d, 12H). *Anal.* calc. pour $C_{11}H_{21}O_2I$: C 42,31, H 6,77, I 40,65%; trouvé: C 42,28, H 6,72, I 40,66%.

Cyclohexyl-2 iodométhyl-2 dioxolanne-1,3; C_{13}: séparé sur SE 30 à 210°C; δ = 4,0 (m, 4H), 3,2 (s, 2H), 2,0 à 1,0 (m, 11H). *Anal.* calc. pour $C_{10}H_{17}O_2I$: C 40,55, H 5,78, I 42,85%; trouvé: C 40,52, H 5,74, I 42,87%.

Di(iodométhyl)-2,2 dioxolanne-1,3; C_{14}: séparé sur SE 30 à 210°C; δ = 4,0 (s, 4H), 3,2 (s, 4H). *Anal.* calc. pour $C_5H_8O_2I_2$: C 16,97, H 2,28, I 71,71%; trouvé: C 16,92, H 2,24, I 71,73%.

Iodo-2 (méthyl-2 dioxolanne-1,3 yl-2)-2 acétate d'éthyle; C_{16}: séparé sur SE 30 à 210°C; δ = 4,35 (s, 1H), 4,15 (q, 2H), 4,0 (s, 4H), 1,65 (s, 3H), 1,2 (t, 3H). *Anal.* calc. pour $C_8H_{13}O_4I$: C 32,01, H 4,37, I 42,28%; trouvé: C 32,08, H 4,39, I 42,25%.

Éthyl-2 (iodométhyl-2 dioxolanne-1,3 yl-2)-2 acétate d'éthyle; C_{17}: séparé sur SE 30 à 210°C; δ = 4,25 à 3,9 (m, 6H), 3,8 à 3,4 (m, 2H), 2,9 à 2,6 (m, 1H), 1,8 à 1,4 (m, 2H), 1,75 (t, 3H), 0,9 (t, 3H). *Anal.* calc. pour $C_{10}H_{17}O_4I$: C 36,60, H 5,22, I 38,67%; trouvé: C 36,57, H 5,18, I 38,69%.

Iodométhyl-2 éthyl-2 dioxanne-1,3; C_{18a}: séparé sur SE 30 à 210°C; δ = 3,9 (t, 4H), 3,4 (s, 2H), 2,0 à 1,5 (m, 4H), 0,9 (t, 3H). *Anal.* calc. pour $C_7H_{13}O_2I$: C 32,82, H 5,11, I 49,56%; trouvé: C 32,80, H 5,09, I 49,55%.

(Iodo-1 éthyl)-2 méthyl-2 dioxanne-1,3; C_{18b}: séparé sur SE 30 à 210°C; δ = 4,5 (q, 1H), 3,9 (t, 4H), 2,0 à 1,7 (m, 5H), 1,5 (s, 3H). *Anal.* calc. pour $C_7H_{13}O_2I$: C 32,82, H 5,11, I 49,56%; trouvé: C 32,78, H 5,10, I 49,57%.

Iodométhyl-2 isopropyl-2 dioxolanne-1,3; C_{19}: séparé sur SE 30 à 210°C; δ = 4,0 (m, 4H), 3,2 (s, 2H), 2,5 à 1,9 (m, 1H), 1,0 (d, 6H). *Anal.* calc. pour $C_7H_{13}O_2I$: C 32,82, H 5,11, I 49,56%; trouvé: C 32,83, H 5,09, I 49,54%.

1. (*a*) D. LELANDAIS, C. BACQUET et J. EINHORN. Tetrahedron, **37**, 3131 (1981); (*b*) J. EINHORN, J. L. SOULIER, C. BACQUET et D. LELANDAIS. Can. J. Chem. **61**, 584 (1983); (*c*) C. BACQUET-EINHORN, J. L. SOULIER et D. LELANDAIS. Bull. Soc. Chem. Belg. **92**, 305 (1983).
2. (*a*) A. MARQUET et J. JACQUES. Bull. Soc. Chim. Fr. 90 (1962); (*b*) M. GAUDRY et A. MARQUET. Bull. Soc. Chim. Fr. 4169 (1969).
3. A. GOOSEN et C. W. MCLELAND. J. S. Afr. Chem. Inst. **28**, 358 (1975).
4. E. W. GARBISCH, JR. J. Org. Chem. **30**, 2109 (1965).
5. B. MODARAI et E. KHOSHDEL. J. Org. Chem. **42**, 3527 (1977).
6. J. F. W. KEANA et R. R. SCHUMAKER. Tetrahedron, **26**, 5191 (1970).
7. E. J. SALMI. Chem. Ber. **71B**, 600 (1939).
8. (*a*) C. RAPPE et R. KUMAR. Arkiv Kemi, **39**, 475 (1965); (*b*) J. R. CATCHE, D. M. REY et E. R. H. JONES. J. Chem. Soc. 272 (1948); (*c*) J. COLONGE et J. C. DUBIN. Bull. Soc. Chim. Fr. 1180 (1960); (*d*) M. GAUDRY et A. MARQUET. Tetrahedron, **26**, 5617 (1970).
9. (*a*) A. GERO. J. Org. Chem. **19**, 468 (1954); 471 (1954); (*b*) J. M. CACHAZA, A. CASTRO et M. A. HERRAEZ. An. Quim. **69**, 847 (1973).
10. A. GOOSEN et C. W. MCLELAND. J. Chem. Soc. Perkin Trans. 1, **3**, 977 (1981).

Nouvelle synthèse électrochimique de γ-bisdioxolannes symétriques et dissymétriques

CHRISTOPHE DAUBIÉ, CATHY BACQUET-EINHORN ET DANIEL LELANDAIS[1]

Laboratoire de Chimie Organique Structurale, Bâtiment F, 4 Place Jussieu, 75230 Paris Cedex 05, France

Reçu le 12 août 1983

CHRISTOPHE DAUBIÉ, CATHY BACQUET-EINHORN et DANIEL LELANDAIS. Can. J. Chem. **62**, 1552 (1984).

La réduction électrochimique de dioxolannes α-iodés permet de préparer une série de γ-bisdioxolannes symétriques et dissymétriques.

CHRISTOPHE DAUBIÉ, CATHY BACQUET-EINHORN, and DANIEL LELANDAIS. Can. J. Chem. **62**, 1552 (1984).

The electrochemical reduction of α-iodinated dioxolanes leads to the preparation of a series of symmetrical and non-symmetrical γ-bisdioxolanes.

[Journal translation]

Can. J. Chem. Downloaded from www.nrcresearchpress.com by 210.87.254.105 on 09/06/12
For personal use only.

Nous avons récemment mis au point une nouvelle méthode de préparation de cétals α-iodés (1) du type

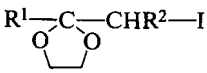

avec R^2 = H ou radical, et il nous a semblé intéressant d'étudier le comportement électrochimique de ces composés.

En effet, les iodures d'alkyle RI étant connus pour fournir un radical R· par réduction électrochimique, nous pouvions espérer dans notre cas aboutir, par dimérisation du radical intermédiaire, à des γ-bisdioxolannes qui ont déjà été l'objet de notre attention (2, 3).

Par ailleurs, l'obtention par réduction électrochimique, du dioxolanne de la cyclopropanone à partir du 2,2 bis(chlorométhyl)-1,3 dioxolanne (4) et la réactivité plus grande des dérivés iodés par rapport aux analogues chlorés confortaient cet espoir.

En fait les essais d'électrolyse menés dans des conditions analogues ou voisines (utilisation d'une concentration supérieure en dérivé halogéné destinée à favoriser la dimérisation) de celles décrites par Van Tilborg *et al.* (4) ne nous ont conduits qu'à de faibles quantités de dimère. A côté du cétal déshalogéné (80%) la réaction fournit un mélange complexe de produits (probablement issus de l'ouverture du cycle cétalique et de diverses dégradations).

Les essais d'électrolyse dans les conditions classiques ayant échoué, nous avons observé que la réaction espérée se produisait avec de bons rendements en dimère (Tableau 1) et des rendements moyens en courant en conduisant l'électrolyse de la façon suivante: (*i*) cellule à compartiment unique; (*ii*) anode en platine et cathode en platine portée à un potentiel pouvant atteindre −5 V par rapport à l'électrode de référence au calomel; (*iii*) milieu méthanolique anhydre 1 *M* en dioxolanne α-iodé et 1 *M* en potasse.

Les conditions opératoires extrêmes utilisées nous amènent, sans vouloir discuter du mécanisme, à faire quelques remarques:

1. L'électrolyse conduite en cellule à compartiments séparés – dont seul le compartiment cathodique reçoit le substrat – libère le dimère avec des rendements qui ne sont pas supérieurs à ceux observés en compartiment unique, tout en compliquant le montage.

2. L'utilisation d'une quantité équimolaire de potasse est indispensable, le substrat n'étant modifié que proportionnellement à la quantité de potasse ajoutée. L'électrolyse s'accompagne d'ailleurs d'une forte précipitation d'iodure de potassium.

3. Les dérivés bromés sont retrouvés intacts dans les mêmes conditions d'électrolyse.

4. Si les réactions électrochimiques classiques ont permis d'obtenir un peu (5%) des dimères attendus, nous avons pu observer qu'il en était de même lors de diverses réactions de type Wurtz utilisant le sodium (5). Mais les rendements sont très faibles là encore et le produit principal est le dioxolanne déshalogéné.

La méthode proposée ici semble donc satisfaisante. Elle présente cependant des limitations: en effet les acétals α-iodés ouverts fournissent essentiellement des produits de dégradation tandis que les dioxannes-1,3 α-iodés, homologues supérieurs des dioxolannes utilisés, ne conduisent qu'au dioxanne déshalogéné. Par contre, cette électrolyse s'est révélée une synthèse rentable de γ-bisdioxolannes dissymétriques.

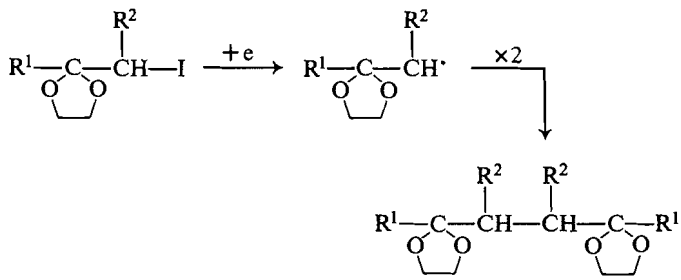

SCHÉMA 1

TABLEAU 1. Préparation de γ-bisdioxolannes symétriques

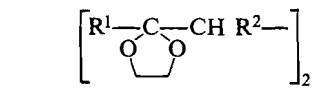

N°.	R^1	R^2	Rendement (%)
1	Me	H	70
2	*t*Bu	H	70
3	Me	Me	66
4	Me	Et	60
5	Me	iPr	69
6	Me	Pent	58
7	Ph	Me	59
8	—$(CH_2)_4$—		57

[1] Auteur à qui adresser toute correspondance.

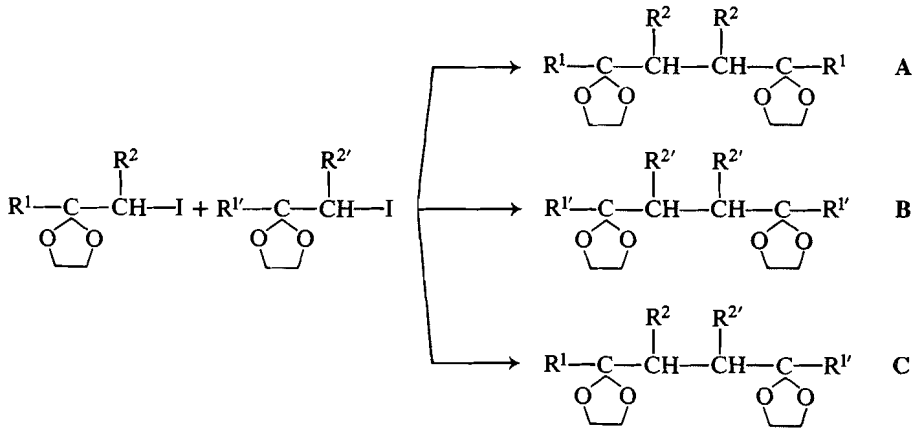

SCHÉMA 2

TABLEAU 2. Préparation de γ-bisdioxolannes dissymétriques

N°.	R^1	R^2	$R^{1'}$	$R^{2'}$	**A** (%)*	**B** (%)*	**C** (%)*
9	Me	H	Me	Me	25	22	54
10	Me	H	Me	Pent	40	20	52
11	Me	H	iBu	iPr	29	26	55
12	⬡	H	Me	Me	30	39	37
13	Me	H	Ph	Me	32	35	30
14	*t*Bu	H	iBu	iPr	40	23	50
15	Me	Me	iBu	iPr	35	25	47
16	Me	H	—$(CH_2)_4$—		22	25	53

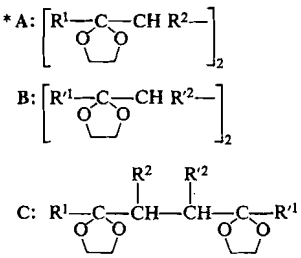

Ces produits sont obtenus en utilisant une méthode bien connue pour d'autres dimérisations radicalaires mixtes, la réaction de Kolbe en particulier (3): le cétal α-iodé le plus précieux est introduit de façon controlée durant l'électrolyse d'un excès du composé le plus accessible.

En conclusion, on peut remarquer que, si pour certains γ-bisdioxolannes (**1, 2**) les rendements sont légèrement inférieurs à ceux que nous avions obtenus par oxydation anodique d'acides β-cétaliques (2), la méthode reste compétitive vu l'accès très aisé aux produits de départ. En outre, contrairement à la réaction précédemment décrite, elle permet l'accès à des γ-bisdioxolannes substitués sur les carbones centraux, ce qui accroit considérablement la quantité de squelettes carbonés susceptibles d'être atteints par cette voie.

Enfin, sans préjuger des applications nouvelles issues d'un déblocage sélectif des cétals, en cours d'étude au laboratoire, ces γ-bisdioxolannes mènent par déblocage total à des γ-dicétones dont l'intérêt comme synthons n'est plus à démontrer.

Partie expérimentale

Les spectres rmn ont été effectués sur un appareil Brucker 80WP en solution dans le deutérochloroforme avec pour référence interne l'hexaméthyldisiloxane.

I. *Préparation des dioxolannes α-iodés*

Ils ont été synthétisés de deux façons différentes: soit par une réaction d'échange brome–iode sur la cétone bromée selon la réf. 6 suivie de la préparation du dioxolanne selon Salmi (7), composés **1**, **3–7**; soit par iodation directe des dioxolannes de cétones selon la réf. 1, composés **2** et **8**.

II. *Obtention des bisdioxolannes*

1. *Conditions d'électrolyse: mode opératoire général*

L'appareil utilisé est un potentiostat Tacussel PRT 40-5X qui permet d'imposer un potentiel fixe à la cathode. Les mesures coulométriques ont été faites à l'aide d'un intégrateur Tacussel IG5-LN monté en série sur le circuit. L'intensité du courant est vérifiée par un ampèremètre monté sur le circuit de l'anode. La cellule d'électrolyse est constituée par une cuve de verre entourée d'une jaquette permettant de maintenir une circulation d'eau de refroidissement. L'anode est une lame de platine de 3 cm^2 et la cathode une lame de platine de 9 cm^2.

Cas de γ-bisdioxolannes symétriques

Dans la cellule non divisée une solution de 0,02 mol de dioxolanne α-iodé dans 20 mL de méthanol anhydre est introduite. L'électrolyse est effectuée sous agitation magnétique et la tension imposée est comprise entre −2,5 et −5 V par rapport à l'électrode de référence au calomel, la réaction commence dès que l'on ajoute quelques pastilles de potasse. L'addition de potasse doit se faire progressivement pour éviter une trop forte intensité de courant. L'électrolyse est arrêtée après passage de 3 F/mol substrat. Le mélange réactionnel est évapo-

Can. J. Chem. Downloaded from www.nrcresearchpress.com by 210.87.254.105 on 09/06/12
For personal use only.

ré sous pression réduite, le résidu est repris par 100 mL d'un mélange 1 : 1 d'éther et de chloroforme. Le précipité jaune obtenu est filtré. Le filtrat est séché au carbonate de sodium puis évaporé.

Cas de γ-bisdioxolannes dissymétriques

Dans la cellule, une solution de 0,02 mol du dioxolanne α-iodé le plus accessible est mis en solution dans 20 mL de méthanol anhydre. L'électrolyse est démarrée dans les mêmes conditions que ci-dessus mais une solution de 0,01 mol du dioxolanne α-iodé le plus précieux dans 10 mL de méthanol est ajoutée goutte à goutte de telle sorte que toute la solution soit versée après passage de 0,01 F. La potasse est ajoutée dès l'introduction du produit le plus précieux et progressivement tout au long de l'électrolyse de manière à maintenir une intensité de courant constante. La réaction est ensuite menée comme précédemment.

2. *Produits isolés*

Bis(méthyl-2 dioxolanne-1,3 yl-2)-1,2 éthane, ***1*** *(2)*

Rendement 70%.

Bis(tertiobutyl-2 dioxolanne-1,3 yl-2)-1,2 éthane, ***2*** *(2)*

Rendement 70%.

Bis(méthyl-2 dioxolanne-1,3 yl-2)-2,3 butane, ***3*** *(2)*

Rendement 66%.

Bis(méthyl-2 dioxolanne-1,3 yl-2)-3,4 hexane, ***4***

Rendement 60%; séparé sur S.E.30 à 210°C; rmn ($CDCl_3$): 3,95 (s, 8H), 2 à 1,2 (m, 6H), 1,2 (s, 6H), 1 (t, 6H) ppm. *Anal.* calc. pour $C_{14}H_{26}O_4$: C 65,08, H 10,14; trouvée: C 65,30, H 10,08.

Bis(méthyl-2 dioxolanne-1,3 yl-2)-3,4 (diméthyl-2,5) hexane, ***5***

Rendement 69%; séparé sur S.E.30 à 210°C; rmn ($CDCl_3$): 3,9 (s, 8H), 1,8 à 1,2 (m, 4H), 1,2 (s, 6H), 0,9 (d, 12H) ppm. *Anal.* calc. pour $C_{16}H_{30}O_4$: C 67,09, H 10,56; trouvée: C 67,04, H 10,47.

Bis(méthyl-2 dioxolanne-1,3 yl-2)-6,7 dodécane, ***6***

Rendement 58%; séparé sur S.E.30 à 210°C; rmn ($CDCl_3$): 3,9 (s, 8H), 2 à 0,6 (m, 30H) ppm. *Anal.* calc. pour $C_{28}H_{38}O_4$: C 70,13, H 11,18; trouvée: C 70,08, H 11,12.

Bis(phényl-2 dioxolanne-1,3 yl-2)-2,3 butane, 7

Rendement 59%; F 115°C; rmn ($CDCl_3$): 7,5 à 7,2 (m, 10H), 4 à 3,5 (m, 8H), 2,5 à 2,1 (m, 2H), 1 à 0,8 (m, 6H) ppm. *Anal.* calc. pour $C_{22}H_{26}O_4$: C 74,55, H 7,39; trouvée: C 74,53, H 7,37.

Bis(dioxa-1,4 spiro[4,5] décyle)-6,6', 8

Rendement 57%; séparé sur S.E.30 à 210°C; rmn ($CDCl_3$): 3,95 (s, 8H), 2,2 à 1 (m, 18H) ppm. *Anal.* calc. pour $C_{16}H_{26}O_4$: C 68,05, H 9,28; trouvée: C 68,01, H 9,23.

(Méthyl-2 dioxolanne-1,3 yl-2)-2 (méthyl-2 dioxolanne-1,3 yl-2)-1 propane, ***9***

Rendement 54%; séparé sur S.E.30 à 210°C; rmn ($CDCl_3$): 3,9 (s, 8H), 2 à 1,5 (m, 3H), 1,35 (s, 3H), 1,15 (s, 3H), 1,05 (d, 3H) ppm. *Anal.* calc. pour $C_{11}H_{20}O_4$: C 61,09, H 9,32; trouvée: C 61,05, H 9,28.

(Méthyl-2 dioxolanne-1,3 yl-2)-2 (méthyl-2 dioxolanne-1,3 yl-2)-1 heptane, ***10***

Rendement 52%; séparé sur S.E.30 à 210°C; rmn ($CDCl_3$): 3,95 (s, 8H), 2 à 0,8 (m, 20H) ppm. *Anal.* calc. pour $C_{15}H_{28}O_4$: C 66,14, H 10,36; trouvée: C 66,08, H 10,32.

(Isobutyl-2 dioxolanne-1,3 yl-2)-2 (méthyl-2 dioxolanne-1,3 yl-2)-1 méthyl-3 butane, **11**

Rendement 55%; séparé sur S.E.30 à 210°C; rmn ($CDCl_3$): 3,95 (s, 8H), 2 à 1,4 (m, 7H), 1,4 (s, 3H), 1 à 0,8 (m, 12H) ppm. *Anal.* calc. pour $C_{16}H_{30}O_4$: C 67,09, H 10,56; trouvée: C 67,02, H 10,54.

(Cyclohexyl-2 dioxolanne-1,3 yl-2)-1 (méthyl-2 dioxolanne-1,3 yl-2)-2 propane, ***12***

Rendement 37%; séparé sur S.E.30 à 210°C; rmn ($CDCl_3$): 3,95 (s, 8H), 2 à 0,9 (m, 17H), 1,2 (s, 3H) ppm. *Anal.* calc. pour $C_{16}H_{28}O_4$: C 67,57, H 9,93; trouvée: C 67,54, H 9,91.

(Phényl-2 dioxolanne-1,3 yl-2)-2 (méthyl-2 dioxolanne-1,3 yl-2)-1 propane, ***13***

Rendement 30%; séparé sur S.E.30 à 210°C; rmn ($CDCl_3$): 7,5 à 7,2 (m, 5H), 4,1 à 3,6 (m, 8H), 2,2 à 1,4 (m, 3H), 1,2 (s, 3H), 0,95 (d, 3H) ppm. *Anal.* calc. pour $C_{16}H_{22}O_4$: C 69,04, H 7,97; trouvée: C 69,03, H 7,95.

(Tertiobutyl-2 dioxolanne-1,3 yl-2)-1 (isobutyl-2 dioxolanne-1,3 yl-2)-2 méthyl-3 butane, ***14***

Rendement 50%; séparé sur S.E.30 à 210°C; rmn ($CDCl_3$): 4,1 à 3,9 (m, 8H), 1,9 à 1,1 (m, 7H), 1,05 à 0,9 (m, 21H) ppm. *Anal.* calc. pour $C_{19}H_{36}O_4$: C 69,47, H 11,05; trouvée: C 69,40, H 11,03.

(Méthyl-2 dioxolanne-1,3 yl-2)-2 (isobutyl-2 dioxolanne-1,3 yl-2)-3 méthyl-4 pentane, ***15***

Rendement 47%; séparé sur S.E.30 à 210°C; rmn ($CDCl_3$): 3,9 (s, 8H), 2,1 à 1,5 (m, 6H), 1,2 (s, 3H), 1,1 à 0,8 (m, 15H) ppm. *Anal.* calc. pour $C_{17}H_{32}O_4$: C 67,96, H 10,74; trouvée: C 67,91, H 10,70.

[(Ethylenedioxy)-2,2 propyl]-6 dioxa-1,4 spiro[4,5] décane, ***16***

Rendement 53%; séparé sur S.E.30 à 210°C; rmn ($CDCl_3$): 4,1 à 3,7 (m, 8H), 2,2 à 1,1 (m, 14H) ppm. *Anal.* calc. pour $C_{13}H_{22}O_4$: C 64,44, H 9,15; trouvée: C 64,38, H 9,09.

1. C. DAUBIÉ, C. BACQUET-EINHORN et D. LELANDAIS. Can. J. Chem. **62**, 1548 (1984).
2. J. EINHORN, J. L. SOULIER, C. BACQUET et D. LELANDAIS. Can. J. Chem. **61**, 584 (1983).
3. C. BACQUET-EINHORN, J. L. SOULIER et D. LELANDAIS. Bull. Soc. Chim. Belg. **92**, 305 (1983).
4. W. J. M. VAN TILBORG, R. PLOMP, R. DE RUITER et C. J. SMIT. Recl. Trav. Chim. Pays-Bas, **99**, 206 (1980).
5. G. M. LAMPMAN et J. C. AUMILLER. Org. Synth. **51**, 55 (1971).
6. B. MODARAI et E. KHOSHDEL. J. Org. Chem. **42**, 3527 (1977).
7. E. J. SALMI. Chem. Ber. B, **71**, 1803 (1938).

Can. J. Chem. Downloaded from www.nrcresearchpress.com by 210.87.254.105 on 09/06/12
For personal use only.

Discussion on ^{13}C nuclear magnetic resonance spectra of structurally rigid cyclonucleosides. Violation of Karplus relationship between $^{3}J_{C,H}$ and dihedral angles

JUN UZAWA AND KENTARO ANZAI[1]

The Institute of Physical and Chemical Research, Wako-shi, Saitama 351, Japan

Received January 25, 1983

JUN UZAWA and KENTARO ANZAI. Can. J. Chem. **62**, 1555 (1984).

Using structurally rigid cyclonucleoside derivatives of adenosine, the effect of the oxygen functional groups on the vicinal coupling constants between carbon and hydrogen in ^{13}C nmr was investigated.

JUN UZAWA et KENTARO ANZAI. Can. J. Chem. **62**, 1555 (1984).

Faisant appel à des dérivés cyclonucléosides de l'adénosine structuralement rigides, on a étudié l'effet des groupements fonctionnels oxygénés sur les constantes de couplage vicinales entre les carbones et les hydrogènes, dans les spectres rmn du ^{13}C.

[Traduit par le journal]

Can. J. Chem. Downloaded from www.nrcresearchpress.com by 210.87.254.5 on 09/06/12
For personal use only.

Deviation from the Karplus relationship (1–3) between dihedral angles and vicinal coupling constants in ^{1}H nmr and ^{13}C nmr has attracted the attention of organic chemists. In 1965 Booth (4) reported that the proton-proton vicinal coupling constant in a structure —CH—CH(R)—, where R is an oxygen or nitrogen functional group, was influenced by the electronegativity of the hetero atom as well as its orientation in the molecule.

Schwarcz and Perlin (5) also observed the orientational effect of oxygen functional groups upon vicinal coupling constants between carbon and hydrogen using ^{13}C-enriched carbohydrate derivatives. Their findings were: when a compound has a partial structure ^{13}C—C—C(O)—H, where the ^{13}C—C and C—O bonds are located in a *trans* relationship, the vicinal coupling constant between carbon and hydrogen is smaller than that of the compound having a *cis* structure. Thus, their data showed that when the dihedral angle between the ^{13}C—C and C—H bonds is 60° the coupling constant is no longer observed, for the case of "*trans*" compounds only.

Delbaere *et al.* (6) were interested in "anomalous" vicinal coupling constants between carbon and hydrogen when they studied the cyclonucleoside derivatives of uracil, and gave an explanation for the deviation from the Karplus curve based on the bond electron density obtained by X-ray diffraction analysis.

Synthesis of the adenosine cyclonucleoside **1** from 2′,3′-*O*-isopropylidene adenosine and phenyl chloroformate was reported in a previous paper (7), where the configurational assignment at C8 was not yet accomplished. For the structural determination of **1**, long-range selective proton-decoupling (lspd) (8–11) was quite useful to extract $^{3}J_{C,H}$ from broadening peaks in ^{13}C nmr. Thus structural assignment of **1** as a 8,5′-*O*-cyclonucleoside of adenosine rather than a 2,5′-*O*-cyclonucleoside congener was possible using lspd, in spite of the uselessness of the conventional ^{13}C nmr and ^{1}H nmr spectra: i.e. the broadening peaks of a doublet at δ 98.0 ($^{1}J_{C,H}$ = 188.0 Hz), which showed the presence of a sp^{3}-carbon in the base moiety of the product, were sharpened in a triple resonance spectrum (Fig. 1) obtained by weak irradiation at H-1′ and H-5′

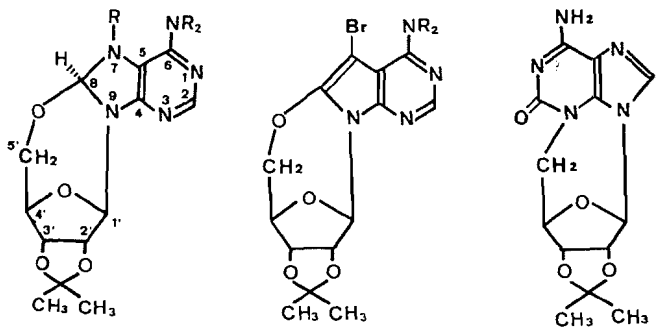

1 R = $COOC_6H_5$ **2** **3**

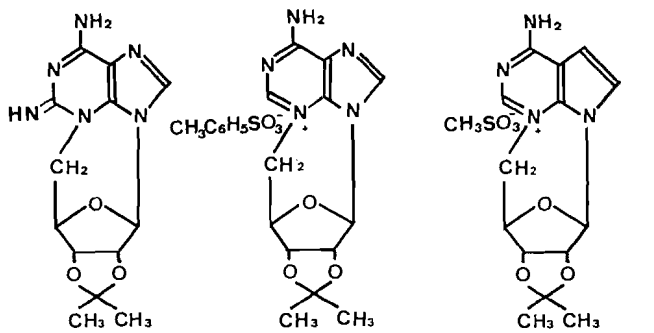

4 **5** **6**

($^{3}J_{C8,H\text{-}1'}$ = 4.9 Hz, $^{3}J_{C8,H\text{-}5'a}$ = 9.8 Hz, $^{3}J_{C8,H\text{-}5'b}$ = 4.9 Hz), thus excluding a structural assignment of the product as a 2,5′-*O*-cycloadenosine derivative.

The configuration at C8 of **1** was determined to be *R* by nOe difference spectra, which disclosed the proximity of H-8 to H-1′ (7% nOe) as well as H-5′ to H-8 (18% nOe), and gave grounds for believing that the N9—C1′—O(4′)—C4′—C5′—O(5′)—C8 seven-membered ring exists as a pseudo-

[1] Author to whom correspondence should be addressed.

Can. J. Chem. Downloaded from www.nrcresearchpress.com by 210.87.254.5 on 09/06/12
For personal use only.

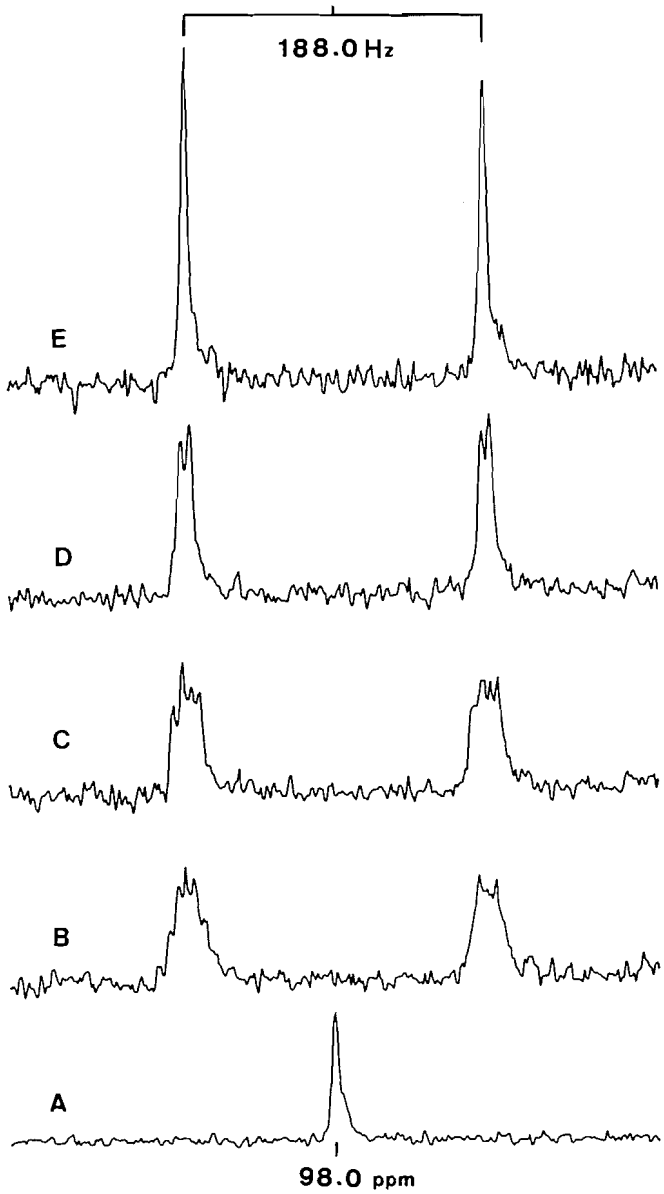

FIG. 1. Long-range selective ^1H decoupling spectra at 98.0 ppm of **1**. **A**, proton noise decoupling; **B**, gated decoupling with nOe; **C**, irradiation at H-1′; the splittings are 9.8 Hz and 4.9 Hz ($^3J_{C8,H\text{-}5'}$); **D**, irradiation at H-5′; the splitting is 4.9 Hz ($^3J_{C8,H\text{-}1'}$); **E**, irradiation at H-1′ and H-5′ simultaneously. The spectra were recorded on a JEOL FX-400 FT nmr spectrometer at 100.7 MHz. Experimental conditions; repetition, 1.8 s × 5000; data points, 32 K; spectral width, 16 kHz; power level for ^1H irradiation ($\gamma H_2/2\pi$), 100 Hz; concentration, 80 mg in 1 mL $CDCl_3$.

chair conformer as depicted in Fig. 2.[2]

Collection of $^3J_{C,H}$ in ^{13}C nmr of **1** (Table 1) led to findings that there are cases where the Karplus relationship between vicinal coupling constants and dihedral angles is not evident: e.g. coupling was not observed between C4 and H-1′, though the dihedral angle of this structurally rigid compound was measured to be 35° and a $^3J_{C,H}$ value around 3 Hz was expected based on the Karplus curve (3).

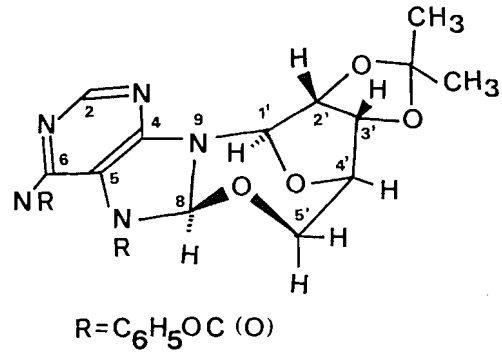

FIG. 2. Dreiding model construction of compound **1**.

TABLE 1. $^3J_{C,H}$ values (Hz)[a] of cyclonucleosides **1** to **6**

Carbon	Proton	1	2	3	4	5	6
2	5′			0	0	2.5	<1.9
	5′			0	0	0	0
4	1′	0	2.0	6.0	6.4	≃6	6.8
	5′			5~7	10.0	6~8	7.8
	5′			<2			5.9
	2	11.0	11.7			≃7	≃7
	8	4.9		≃6	10.0	≃7	≃7
5	8	2.4		11.7	9.8	11.7	8.8
6	2	13.4	10.7			11.7	11.7
8	1′	4.9	6.8	2.0	2.0	<1.5	1.9
	5′	9.8	9.8				
	5′	4.9	2.0				

[a] Reference 17.

Investigation of $^3J_{C,H}$ in other structurally rigid cyclonucleosides **2** through **6** (Table 1), which were mainly prepared in this laboratory (12–17), resulted in finding that the orientational effect of oxygen functional groups on $^3J_{C,H}$ is also similar to that observed by Schwarcz and Perlin (5) in the study on glycoside derivatives.

The chemical shifts of compounds **1** through **6** in ^{13}C nmr (Table 2)[3,4] are worth comment before entering the present theme. The polarity of the atoms located near the observed nuclei seemed to influence the chemical shift: e.g. a δ_{C5} value in **1** is 18.4 ppm lower than the corresponding δ value in **2**, being consistent with the shielding effect of N7 in **1**. Similarly, a δ_{C5} value in **5** is 14.8 ppm lower than the corresponding δ value in **6**. The $\delta_{C5'}$ values in **1** through **6** reflect a stronger polar effect of oxygen than that of nitrogen, the increase of polarity by affording charge on nitrogen, and the difference of polarity between sp^2 and sp^3 carbons. Chemical shifts of carbons on the furanose ring as well as those of the isopropylidene group are quite similar through these compounds with an exception that $\delta_{C1'}$ in **2** is 4–5 ppm higher than the other $\delta_{C1'}$ values, and the reason is not evident.

Inspection of these $^3J_{C,H}$ values of compounds **1** through **6** (Table 1),[4] which were determined unequivocally by lspd,

[2] On the contrary, if a molecular model is constructed as having *S*-configuration at C8, H-2′ and H-8 are found to be in close proximity, and the lack of nOe between these two protons also serves as another evidence for *R*-configuration.

[3] Assignment of the peaks was confirmatively done through studies on lspd, selective decoupling, and $^1J_{C,H}$.

[4] The numbering of the 7-deazaadenosine derivatives **2** and **6** is given here in a similar way to that of the adenosine derivatives for the reader's convenience.

TABLE 2. ^{13}C chemical shifts of compounds **1** to **6** ($^{13}C—^{1}H$ coupling constants)

Carbon	1	2	3	4	5	6
2	153.8 (206.3)	151.7	155.5	116.9	149.1 (215.8)	149.2 (213.8)
4	156.0	144.0	141.9	145.5	140.4	138.9
5	117.2	98.8	113.3	113.3	119.5	104.7
6	138.3	156.1	158.4	163.8	156.6	158.3
7	—	70.2	—	—	—	103.1 (181.6)
8	98.0 (188.0)	144.3	133.3 (216.1)	131.0 (214.8)	139.1 (220.7)	124.0 (195.3)
1′	91.4 (173.3)	86.2 (168.5)	90.1 (172.9)	89.8 (169.9)	90.7 (175.8)	92.2 (172.9)
2′	82.2 (158.7)	81.3 (159.9)	80.6 (159.2)	81.6 (160.2)	79.3 (160.2)	79.9 (160.2)
3′	85.2 (161.1)	84.9 (161.1)	85.3 (162.1)	85.1 (161.1)	85.2 (164.1)	85.0 (163.1)
4′	89.2 (152.6)	85.2 (153.8)	84.5 (154.3)	84.9 (155.3)	84.1 (156.3)	83.2 (155.3)
5′	69.5 (146.5)	76.0 (151.4)	50.9 (146.5)	49.3 (140.4)	57.3 (146.5)	58.0 (145.3)
$>C(CH_3)_2$	113.0	111.3	112.0	116.6	112.4	112.2
$>C(CH_3)_2$	26.3	26.0	25.8	25.9	25.7	25.6
	24.7	24.3	24.2	24.1	24.3	24.1

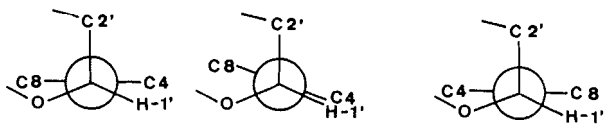

$^{3}J_{C,H}$	1	2	3 ~ 6
C4-H1'	0	2.0	6.0~6.8
C8-H1'	4.9	6.8	≤ 2.0

FIG. 3. The Newman projection of adenosine cyclonucleoside derivatives **1** to **6** through the C1′—N9 bond.

reveals that $^{3}J_{C4,H\text{-}1'}$ and $^{3}J_{C8,H\text{-}1'}$ of these adenosine cyclonucleosides are under the influence of the orientational effect of oxygen functional groups on $^{3}J_{C,H}$, and the Newman projection through C1′ and N9 as depicted in Fig. 3 will be helpful in illustrating this effect.

In conclusion, we add further proof that an oxygen atom located at a *trans* position to the observed carbon nucleus has the effect of decreasing $^{3}J_{C,H}$ and in consideration of this, lspd serves a useful purpose in the structural determination of cyclonucleosides.

1. M. KARPLUS. J. Chem. Phys. **30**, 11 (1959).
2. M. KARPLUS. J. Am. Chem. Soc. **85**, 2870 (1963).
3. F. A. L. ANET. Can. J. Chem. **39**, 789 (1961).
4. H. BOOTH. Tetrahedron Lett. 411 (1965).
5. J. A. SCHWARCZ and A. S. PERLIN. Can. J. Chem. **50**, 3667 (1972).
6. L. T. J. DELBAERE, M. N. G. JAMES, and R. U. LEMIEUX. J. Am. Chem. Soc. **95**, 7866 (1973).
7. K. ANZAI, J. B. HUNT, G. ZON, and W. EGAN. J. Org. Chem. **47**, 4281 (1982).
8. J. FEENEY, P. PARTINGTON, and G. C. K. ROBERTS. J. Magn. Reson. **13**, 268 (1974).
9. J. UZAWA and M. URAMOTO. Org. Magn. Reson. **12**, 612 (1979).
10. Y. TSUDA, S. NAKAJIMA, S. UDAGAWA, and J. UZAWA. J. Nat. Prod. **43**, 467 (1980).
11. T. NOMURA, T. FUKAI, T. NARITA, S. TERADA, J. UZAWA, Y. IITAKA, M. TAKASUGI, S. ISHIKAWA, S. NAGANO, and T. MASAMUNE. Tetrahedron Lett. **22**, 2195 (1981).
12. K. ANZAI and M. MATSUI. Bull. Chem. Soc. Jpn. **47**, 417 (1974).
13. K. ASAHI, K. ANZAI, S. SUZUKI, and H. IWASAKI. Chem. Lett. 1197 (1973).
14. K. ANZAI. Agric. Biol. Chem. **40**, 373 (1976).
15. V. M. CLARK, A. R. TODD, and J. ZUSSMAN. J. Chem. Soc. 2952 (1951).
16. W. JAHN. Chem. Ber. **98**, 1706 (1965).
17. K. ANZAI and M. MATSUI. Bull. Chem. Soc. Jpn. **46**, 618 (1973).

Can. J. Chem. Downloaded from www.nrcresearchpress.com by 210.87.254.5 on 09/06/12
For personal use only.

1,5-Acyclic stereoselection. The stereocontrolled synthesis of optically active vitamin E fourteen-carbon side chain alcohol[1]

GERVAIS BÉRUBÉ[2] AND PIERRE DESLONGCHAMPS

Laboratoire de Synthèse Organique, Département de Chimie, Faculté des Sciences, Université de Sherbrooke, Sherbrooke (Qué.), Canada J1K 2R1

Received March 22, 1984

GERVAIS BÉRUBÉ and PIERRE DESLONGCHAMPS. Can. J. Chem. **62**, 1558 (1984).

The Diels–Alder product **3** was first transformed into the symmetrical nine-membered cyclic carbonate **8**. Reaction of **8** with *l*-(−)-α-methylbenzylamine (**12**) yielded a mixture of optically active diastereoisomeric urethanes **9***a* (**9**, R = H, R′ = $C_6H_5CHCH_3NHCO$—) and **9***b* (**9**, R = $C_6H_5CHCH_3NHCO$—, R′ = H) which were separated and respectively converted into **11***a* and **11***b*. Compounds **11***a* and **11***b* were then transformed respectively into the optically active side chain alcohol **2** (R = H) of vitamine E (**1**).

GERVAIS BÉRUBÉ et PIERRE DESLONGCHAMPS. Can. J. Chem. **62**, 1558 (1984).

Le produit de Diels–Alder **3** fut transformé en carbonate symétrique cyclique à neuf membres **8**. La réaction de **8** avec la *l*-(−)-α-méthylbenzylamine a donné les uréthanes diastéréoisomériques optiquement actifs **9***a* (**9**, R = H, R′ = $C_6H_5CHCH_3$-NHCO—) et **9***b* (**9**, R = $C_6H_5CHCH_3NHCO$—, R′ = H) qui furent séparés et respectivement transformés en composés **11***a* et **11***b*. Ces derniers ont conduit par la suite à la chaîne latérale de la vitamine E, i.e. l'alcool **2** (R = H) optiquement actif.

The stereocontrolled synthesis of substituted aliphatic chains containing chiral centers, i.e. acyclic stereoselection, is presently an active field of research (1). For instance, several groups have reported (2, 3) various ways of constructing the 1,5-dimethylated aliphatic chain which is found in vitamin E (**1**) (Scheme 1) and in several other natural products like vitamin **K**, phytol, and insect pheromones (pine saw fly (4) and tsetse fly (5)).

In this communication, we wish to report a new strategy for the synthesis of the optically active side chain alcohol **2** (R = H) which has been converted into vitamin E (2).

The Diels–Alder product **3** (mp 94–95°C) which is readily available (6) from the addition of maleic anhydride to *trans,trans*-2,4-hexadiene, was chosen as starting material (Scheme 2). Esterification of **3** (CH_3OH, HCl, 95% yield) gave the *cis*-dimethylester **4**[3] (mp 49–50°C) which was converted ($CHBr_3$, NaOH, $(C_2H_5)_3NCH_2C_6H_5Cl$, 0° → 25°C, 65% yield) (7) into the dibromocyclopropane derivative **5** (mp 114–115°C). Basic hydrolysis (NaOH, H_2O–dioxane–CH_3OH, 99% yield) of **5** gave the corresponding dicarboxylic acid which upon bis-decarboxylation ($Pb(OAc)_4$, pyridine, 65°C, 84% yield) (8) yielded the cyclic olefin **6**. Cleavage of **6** ((a) O_3, CH_3OH, CH_2Cl_2, −78°C (9) and (b) $LiBH_4$, 0°C, 96% yield) gave the *meso*-dibromocyclopropyldiol **7** (mp 126–127°C).

Compound **7** was then converted ((a) dihydropyran, *p*-TsOH, C_6H_6, 84% yield, (b) CH_3Li, ether, −35°C, 96% yield (10)) into the allene derivative **10** (R = R′ = THP). Catalytic reduction (H_2, PtO_2, CH_3OH, 99% yield) and hydrolysis (*p*-TsOH, CH_3OH, 89%) of **10** (R = R′ = THP) gave *meso*-2,6-dimethylheptan-1,7-diol **11** (R = R′ = H) (3*f*).

A toluene solution of phosgene was slowly added (with a syringe pump) during a period of 10 h to a mixture of *meso*-dibromocyclopropyldiol **7**, triethylamine, and dichloromethane, to yield the nine-membered cyclic carbonate **8** (mp 96–98°C) in 80% yield (11). The lithiated derivative of *l*-(−)-α-methylbenzylamine (**12**) (*n*-BuLi, ether) was then reacted with the symmetrical cyclic carbonate **8** (THF, −78°C, 30 min, 86% yield) to yield a mixture (~1:1 ratio) of optically active diastereoisomeric urethanes **9***a* (**9**, R = H and R′ = Ur = $C_6H_5CHCH_3NHCO$—) and **9***b* (**9**, R = Ur = $C_6H_5CHCH_3$-NHCO— and R′ = H) which were separated by hplc (12). Treatment of optically active urethane **9***a* with methyllithium (ether, −35°C, 99% yield) (10) gave the corresponding allene **10***a* which on catalytic reduction (H_2, PtO_2, CH_3OH, 98% yield) furnished the optically active urethane **11***a*. Similarly, **9***b* yielded the optically active urethane **11***b* via **10***b*.

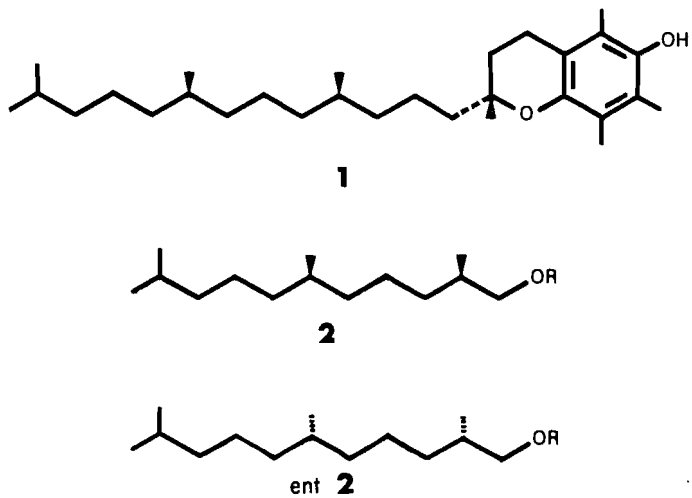

SCHEME 1

Each diastereoisomer (**11***a* and **11***b*) was then respectively converted into optically active **2** (R = H), i.e. 2*R*,6*R*,2,6,10-trimethylundecan-1-ol. The conversion **11***a* (**11**, R = H, R′ = Ur) → **2** (R = H) was carried out in the following manner: (a) *p*-TsCl, $(C_2H_5)_3N$, CH_2Cl_2, 0° → 25°C, 99% yield in tosylate **11** (R = Ts, R′ = Ur), (b) $SiHCl_3$, $(C_2H_5)_3N$, C_6H_6, 25°C (13), 76% yield in tosylate alcohol **11** (R = Ts, R′ = H; $[\alpha]_D$ +8.07° (*c* 3.025 in $CHCl_3$), (c) dihydropyran, pyridinium *p*-toluenesulfonate (PPTS), CH_2Cl_2 (14), 94% yield in THP derivative **11**

[1]A portion of this work was presented at the meeting of the "Association Canadienne-Française pour l'Avancement des Sciences" (ACFAS), May 25–27, 1983.

[2]NSERCC and FCAC predoctoral fellowships, 1981–1984.

[3]For all new substances, the spectra (ir, 250 MHz and 60 MHz ^1H nmr, ^{13}C nmr, and high resolution mass spectra) were in complete agreement with the assigned structures.

Can. J. Chem. Downloaded from www.nrcresearchpress.com by 210.87.254.6 on 09/06/12
For personal use only.

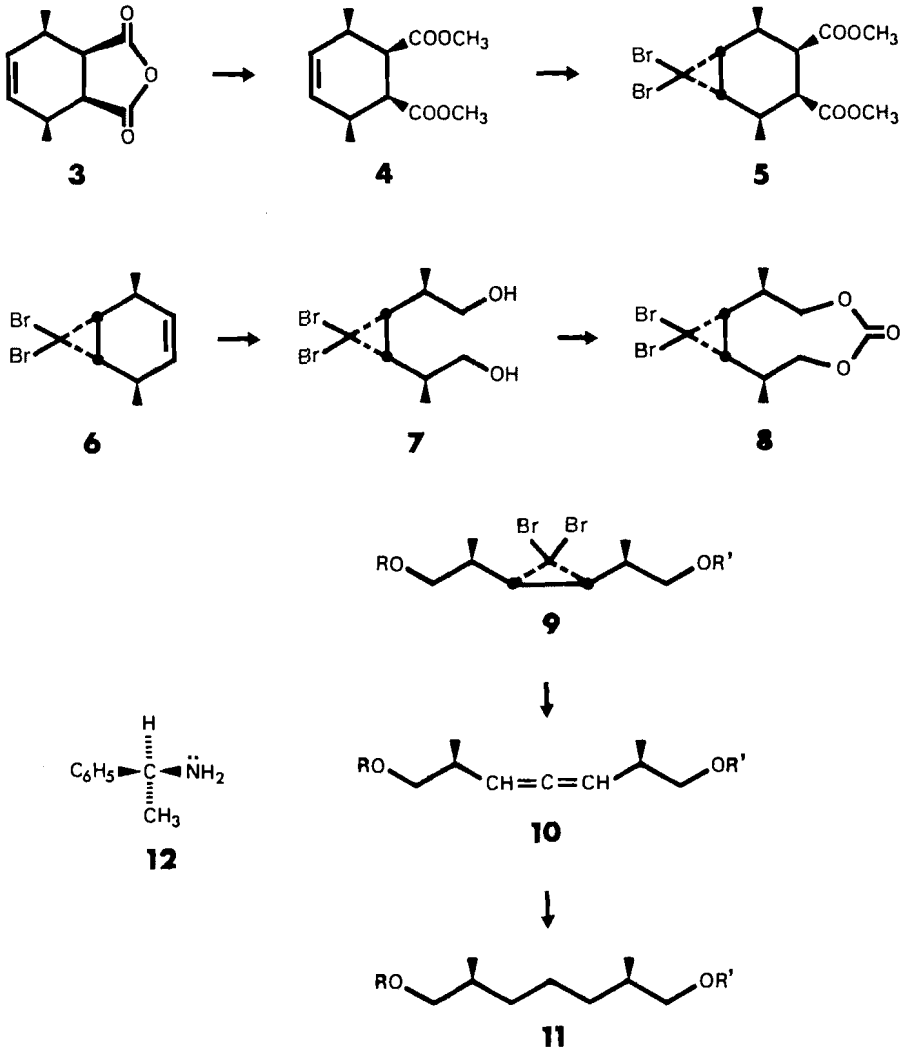

SCHEME 2

(R = Ts, R′ = tetrahydropyran), (d) $(CH_3)_2CHCH_2CH_2MgBr$, Li_2CuCl_4, THF, −78° → 25°C (15; for preparation of the reagent, see ref. 15*b*), 60% yield in **2** (R = THP), and (e) CH_3OH, PPTS, (14), 99% yield in **2** (R = H). The transformation **11***b* (**11**, R = Ur, R′ = H) → **2** (R = H) was realized via the following steps: (a) *tert*-butyldimethylsilyl (TBDMS) chloride, imidazole, THF, 25°C (16), 96% yield in **11** (R = Ur, R′ = TBDMS), (b) $SiHCl_3$, $(C_2H_5)_3N$, C_6H_6, 25°C (13), 84% yield in **11** (R = H, R′ = TBDMS), (c) *p*-TsCl, $(C_2H_5)_3N$, CH_2Cl_2, 0° → 25°C, 90% yield in **11** (R = Ts, R′ = TBDMS), (d) $(CH_3)_2CHCH_2CH_2MgBr$, Li_2CuCl_4, THF, 0° → 25°C (15), 65% yield in **2** (R = TBDMS), and (e) $(n\text{-}Bu)_4NF$, THF, 25°C (16), 68% yield in **2** (R = H).

The diastereoisomer **11***b* (**11**, R = Ur, R′ = H) was also transformed into the enantiomer of **2** (R = H) (ent-**2**) (17), i.e. 2*S*,6*S*,2,6,10-trimethylundecan-1-ol, in the following way: (a) *p*-TsCl, $(C_2H_5)_3N$, CH_2Cl_2, 0° → 25°C, 86% yield in **11** (R = Ur, R′ = Ts), (b) $SiHCl_3$, $(C_2H_5)_3N$, C_6H_6, 25°C (13), 87% yield in **11** (R = H, R′ = Ts; $[\alpha]_D$ −8.05° (*c* 3.3 in $CHCl_3$), (c) *tert*-butyldimethylsilyl chloride, imidazole, THF, 25°C (16), 88% yield in **11** (R = TBDMS, R′ = Ts), (d) $(CH_3)_2CHCH_2CH_2MgBr$, Li_2CuCl_4, THF, 0° → 25°C (15), 66% yield in ent-**2** (R = TBDMS), and (e) $n(Bu)_4NF$, THF, 25°C (16), 83% yield in ent-**2** (R = H).

The samples of 2*R*,6*R*,2,6,10-trimethylundecan-1-ol (**2**, R = H, $[\alpha]_D$ + 8.6° (*c* 2.07, hexane) obtained and that of its enantiomer (ent-**2**, R = H, $[\alpha]_D$ −8.17° (*c* 2.09, hexane) (lit. (2, 3) $[\alpha]_D$ 8.6 ± 0.6°) were shown to be enantiomerically pure by analysis (250 MHz ^1H nmr) of their corresponding Mosher's ester derivative (O-methylmandelate) (18).

The principal elements of the above synthetic strategy can be summarized as follows: (a) The readily available symmetrical Diels–Alder product **3** ensures a complete control of the relative stereochemistry of the two methyl groups. (b) Appropriate functional group modifications and insertion of a methylene group (cyclopropane and allene formation and catalytic reduction) allow the mutation from a 1,4 to a 1,5-acyclic stereoselection process. (c) The symmetrical properties of **3** permit the formation of the nine-membered cyclic carbonate **8**. (d) Reaction of the symmetrical carbonate **8** with optically active *l*-(−)-α-methylbenzylamine gave a mixture of two optically active diastereoisomers which can be separated and converted into the desired optically active fourteen-carbon side chain alcohol **2**. This last operation ensures a complete control of the absolute configuration without loss of enantiomeric materials (12).

Work is now in progress to produce more complex substituted aliphatic chains starting from compounds **9** and **10**.

Can. J. Chem. Downloaded from www.nrcresearchpress.com by 210.87.254.6 on 09/06/12
For personal use only.

Acknowledgements

This research was supported by the Natural Sciences and Engineering Research Council of Canada and by the "Ministère de l'Éducation (F.C.A.C.) du Québec".

1. (*a*) P. A. BARTLETT. Tetrahedron, **36**, 2 (1980); (*b*) C. H. HEATHCOCK. Science, **214**, 395 (1981); (*c*) S. MASAMUNE and W. CHOY. Aldrichimica Acta, **15**, 47 (1982); (*d*) S. MASAMUNE. Heterocycles. In press; (*e*) T. MUKAIYAMA. Tetrahedron. In press.
2. (*a*) N. COHEN, C. G. SCOTT, C. NEUKOM, R. J. LOPRESTI, G. WEBER, and G. SAUCY. Helv. Chim. Acta, **64**, 1158 (1981), and references cited therein; (*b*) N. COHEN, W. F. EICHEL, R. J. LOPRESTI, C. NEUKOM, and G. SAUCY. J. Org. Chem. **41**, 3505 (1976).
3. (*a*) M. KOREEDA and L. BROWN. J. Org. Chem. **48**, 2122 (1983); (*b*) G. HELMCHEN and R. SCHMIERER. Tetrahedron Lett. **24**, 1235 (1983); (*c*) C. H. HEATHCOCK and E. T. JARVI. Tetrahedron Lett. **23**, 2825 (1982); (*d*) B. M. TROST and T. P. KLUN. J. Am. Chem. Soc. **103**, 1864 (1981); (*e*) T. FUJISAWA, T. SATO, T. KAWARA, and K. OHASHI. Tetrahedron Lett. **22**, 4823 (1981); (*f*) W. C. STILL and K. P. DARST. J. Am. Chem. Soc. **102**, 7385 (1980); (*g*) B. M. TROST and T. P. KLUN. J. Org. Chem. **45**, 4256 (1980); (*h*) G. SAUCY, N. COHEN, B. L. BANNER, and D. P. TRULLINGER. J. Org. Chem. **45**, 2080 (1980); (*i*) B. M. TROST, T. P. KLUN. J. Am. Chem. Soc. **101**, 6756 (1979); (*j*) C. FUGANTI and P. GRASSELLI. J. Chem. Soc. Chem. Commun. 995 (1979); (*k*) H. G. W. LEUENBERGER, W. BOGUTH, R. BARNER, M. SCHMID, and R. ZELL. Helv. Chim. Acta, **62**, 455 (1979); (*l*) M. SCHMID and R. BARNER. Helv. Chim. Acta, **62**, 464 (1979); (*m*) R. ZELL. Helv. Chim. Acta, **62**, 474 (1979); (*n*) J. TAKAHASHI, K. MORI, and M. MATSUI. Agric. Biol. Chem. **43**, 1605 (1979); (*o*) K.-K. CHAN, A. C. SPECIAN, JR., and G. SAUCY. J. Org. Chem. **43**, 3435 (1978); (*p*) K.-K. CHAN and G. SAUCY. J. Org. Chem. **42**, 3828 (1977); (*q*) D. VALENTINE, JR., K.-K. CHAN, C. G. SCOTT, K. K. JOHNSON, K. TOTH, and G. SAUCY. J. Org. Chem. **41**, 62 (1976); (*r*) K.-K. CHAN, N. COHEN, J. P. DENOBLE, A. C. SPECIAN, JR., and G. SAUCY. J. Org. Chem. **41**, 3497 (1976); (*s*) N. COHEN, W. F. EICHEL, R. J. LOPRESTI, C. NEUKOM, and G. SAUCY. J. Org. Chem. **41**, 3512 (1976); (*t*) J. W. SCOTT, F. T. BIZARRO, D. R. PARRISH, and G. SAUCY. Helv. Chim. Acta, **59**, 290 (1976).
4. (*a*) S. BYSTRÖM, H.-E. HÖGBERG, and T. NORIN. Tetrahedron, **37**, 2249 (1981); (*b*) R. BAKER, P. WINTON, R. W. TURNER. Tetrahedron Lett. **21**, 1175 (1980); (*c*) K. MORI and S. TAMADA. Tetrahedron, **35**, 1279 (1979); (*d*) D. JEWETT, F. MATSUMURA, and H. C. COPPEL. J. Chem. Ecol. **4**, 277 (1978), and references cited therein.
5. (*a*) D. A. CARLSON, P. A. LANGLEY, and P. HUYTON. Science, **201**, 750 (1978); (*b*) P. E. SONNET, E. C. UEBEL, R. L. HARRIS, and R. W. MILLER. J. Chem. Ecol. **3**, 245 (1977), and references cited therein.
6. (*a*) O. DIELS and K. ALDER. Ann. Chem. **62**, 470 (1929); (*b*) K. ALDER and W. VOGT. Justus Liebigs Ann. Chem. **571**, 137 (1951).
7. (*a*) D. DAVALIAN, P. J. GARRATT, W. KOLLER, and M. M. MANSURI. J. Org. Chem. **45**, 4183 (1980); (*b*) M. MAKOSZA and M. WAWRZYNIEWICZ. Tetrahedron Lett. **53**, 4659 (1969).
8. (*a*) C. M. CIMARUSTI and J. WOLINSKY. J. Am. Chem. Soc. **90**, 113 (1968); (*b*) R. A. SHELDON and J. K. KOCHI. Organic reactions. Vol. 19. R. E. Krieger Publishing Co., Huntington, NY. 1975. Chapt. 4.
9. R. W. WHITE, S. W. KING, and L. O'BRIEN. Tetrahedron Lett. **39**, 3587 (1971).
10. L. SKATTEBØL. Acta Chem. Scand. **17**, 1683 (1963).
11. PL. A. PLATTNER, A. FÜRST, K. KOLLER, and W. LANG. Helv. Chim. Acta, **31**, 1455 (1948).
12. A. FISCHLI, M. KLAUS, H. MAYER, P. SCHÖNHOLZER, and R. RUEGG. Helv. Chim. Acta, **58**, 564 (1975).
13. W. H. PIRKLE and J. R. HAUSKE. J. Org. Chem. **42**, 2781 (1977).
14. M. MIYASHITA, A. YOSHIKOSHI, and P. A. GRIECO. J. Org. Chem. **42**, 3772 (1977).
15. (*a*) G. FOUQUET and M. SCHLOSSER. Angew. Chem. Int. Ed. Engl. **13**, 82 (1974); (*b*) M. TAMURA and J. KOCHI. Synthesis, 303 (1971).
16. E. J. COREY and A. VENKATESWARLU. J. Am. Chem. Soc. **94**, 6190 (1972).
17. G. QUINKERT and H. STARK. Angew. Chem. Int. Ed. Engl. **22**, 637 (1983).
18. J. A. DALE and H. S. MOSHER. J. Am. Chem. Soc. **95**, 512 (1973).

Can. J. Chem. Downloaded from www.nrcresearchpress.com by 210.87.254.6 on 09/06/12
For personal use only.

Nuclear magnetic resonance study of fluorine exchange in the $PhPF_4-PhPF_5^-$ system

CHENGRUI WANG[1] AND ALEXANDER F. JANZEN
Department of Chemistry, University of Manitoba, Winnipeg, Man., Canada R3T 2N2

Received May 13, 1983

This paper is dedicated to Professor Gerald E. Dunn on the occasion of his 65th birthday

CHENGRUI WANG and ALEXANDER F. JANZEN. Can. J. Chem. **62**, 1563 (1984).

Intermolecular fluorine exchange in the $PhPF_4-PhPF_5^-$ system has been studied by ^{31}P nmr spectroscopy. The anion $PhPF_5^-$ was prepared *in situ* from $PhPF_4$ and KF in 18-crown-6, or from $PhPF_4$ and SiF_5^-. Exchange was found to be first-order in $PhPF_4$, first-order in $PhPF_5^-$, and slowed down by donor solvents such as acetonitrile, in support of a mechanism involving a fluorine-bridged intermediate. Experimental difficulties are probably due to HF impurities.

CHENGRUI WANG et ALEXANDER F. JANZEN. Can. J. Chem. **62**, 1563 (1984).

Utilisant la rmn du ^{31}P, on a étudié l'échange intermoléculaire du fluor dans le système $PhPF_4-PhPF_5^-$. On a préparé l'anion $PhPF_5^-$ *in situ* à partir du $PhPF_4$ et du KF dans l'éther 18-couronne-6 ou à partir du $PhPF_4$ et du SiF_5^-. On a trouvé que l'échange est du premier ordre en $PhPF_4$, du premier ordre en $PhPF_5^-$ et ralenti par les solvants donneurs comme l'acétonitrile; ceci est en accord avec un mécanisme impliquant un intermédiaire avec une fluor ponté. Les difficultés expérimentales sont probablement dues à la présence d'impuretés dans le HF.

[Traduit par le journal]

Can. J. Chem. Downloaded from www.nrcresearchpress.com by 210.87.254.105 on 09/06/12
For personal use only.

Axial–equatorial fluorine exchange in phenyltrifluorophosphorane, $PhPF_3H$, is a unimolecular process with $\Delta G_{298} = 13.3 \pm 0.5$ kcal/mol. Addition of a base such as pyridine (or triethylamine) leads to intermolecular fluorine exchange with $\Delta G_{298} = 7 \pm 2$ kcal/mol. The intermolecular process is solvent-dependent and appears to involve slow reaction with base to produce $PhPF_4H^-$, followed by rapid fluorine transfer between five- and six-coordinate species, $PhPF_3H$ and $PhPF_4H^-$, via a fluorine-bridged intermediate (1). In order to establish whether a similar mechanism is responsible for intermolecular fluorine exchange in phenyltetrafluorophosphorane, $PhPF_4$, (2) we decided to carry out a ^{31}P nmr study of exchange in the $PhPF_4-PhPF_5^-$ system.

The $PhPF_5^-$ anion was prepared in two ways: either by addition of KF in 18-crown-6 to $PhPF_4$ or by addition of SiF_5^- to $PhPF_4$.

[1] $PhPF_4 + KF \text{ (in 18-crown-6)} \rightarrow K(18\text{-crown-6})^+PhPF_5^-$

[2] $PhPF_4 + Pr_4N^+SiF_5^- \rightarrow Pr_4N^+PhPF_5^- + SiF_4$

Intermolecular fluorine exchange was initiated by adding small amounts of F^- or $PhPF_5^-$ to an excess of $PhPF_4$, and the rate of exchange was studied by means of $^{31}P\{^1H\}$ nmr spectroscopy. Unlike $PhPF_3H$ (1), intramolecular exchange in $PhPF_4$ could not be slowed down, even at −110°C, therefore axial–equatorial exchange of ligands was always faster than intermolecular fluorine exchange.

If fluorine exchange in $PhPF_4-PhPF_5^-$ is a simple bimolecular process, then one should find that $a = b = 1$ in eq. [3].

$$[3] \quad \tau^{-1} = \frac{1}{4}k[PhPF_4]^{a-1}[PhPF_5^-]^b$$

A plot of $\ln \tau^{-1}$ vs. $\ln [PhPF_5^-]$ is shown in Fig. 1 and the slopes are 1.05 in toluene and 1.19 in acetonitrile, which we interpret as unity. As seen in Fig. 1, exchange is slower in acetonitrile than in toluene, in agreement with a similar effect found in the $PhPF_3H-PhPF_4H^-$ system (1) and attributed to coordination of the donor solvent to the phosphorane, thus preventing the formation of a fluorine-bridged intermediate.

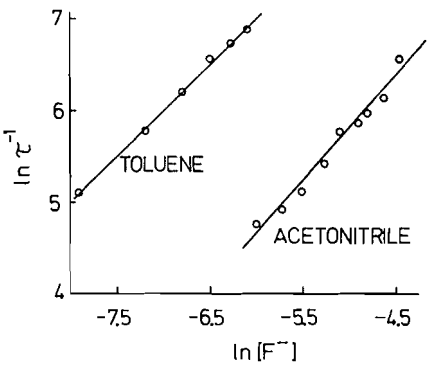

FIG. 1. Plot of $\ln \tau^{-1}$ vs. $[F^-]$ in toluene and acetonitrile solutions at 34°C and $[PhPF_4] = 0.4$ *M*. Note: $[F^-] = [PhPF_5^-]$

Experimental difficulties were encountered during studies of exchange as a function of temperature and $PhPF_4$ concentration. We attribute these difficulties to the presence of impurities which were detected in several ways: firstly, most $PhPF_4-PhPF_5^-$ samples contained varying amounts of the hydrolysis product $PhP(O)F_2$ (2, 5), detected by ^{31}P nmr. No other phosphorus-containing impurity could be detected. Secondly, plots of $\ln \tau^{-1}$ vs. $\ln [PhPF_4]$, as well as activation energy plots,

[4] $PhPF_4 + H_2O \rightarrow PhP(O)F_2 + 2HF$

did not give consistent results. ^{31}P nmr examination showed that $PhPF_4$ was free of impurities after one distillation; therefore, the most likely source of moisture was 18-crown-6 (used to solubilize KF) or $Pr_4N^+PhPF_5^-$. Water is completely removed as a result of eq. [4], and $PhP(O)F_2$ always gave sharp nonexchange-broadened lines, therefore, these species do not interfere with exchange in the $PhPF_4-PhPF_5^-$ system.

Our view is that HF is responsible for experimental difficulties, probably due to the equilibrium of eq. [5].

[5] $PhPF_5^- + HF \rightleftarrows PhPF_4 + FHF^-$

The problem of HF and H_2O impurities also arose in the $PhPF_3H-PhPF_4H^-$ study (1), but there it was solved by ensuring that samples contained a slight excess of $PhPF_2$ so that any HF would react to give $PhPF_3H$ while H_2O was removed

[1]Visiting scientist. Permanent address: Department of Chemistry, Wuhan University, Wuhan, China.

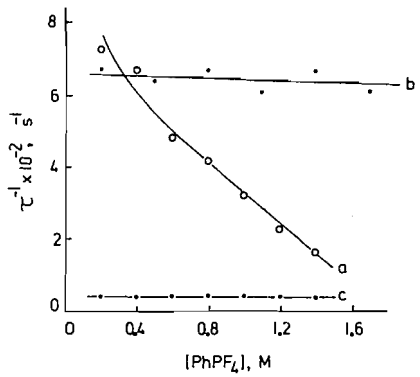

FIG. 2. Plot of τ^{-1} vs. $[PhPF_4]$ at 34°C. (*a*) $[F^-] = 8.6 \times 10^{-4}$ *M* in toluene. (*b*) $[F^-] = 6.5 \times 10^{-4}$ *M* in benzene. Note: $[F^-] = [PhPF_5^-]$ (*c*) $[PhPF_5^-] = 5.6 \times 10^{-4}$ *M* in benzene.

as PhP(O)HF. Such *in situ* removal of common impurities was not achieved in this study.

The study of exchange as a function of $PhPF_4$ concentration was repeated several times. Line (*a*) in Fig. 2, showing a decrease in rate with increasing $PhPF_4$ concentration, is a result which we ascribe to the effect of impurities. On two occasions, however, careful studies showed the rate to be independent of $PhPF_4$ concentration, as seen in lines (*b*) and (*c*). If the rate of fluorine exchange is indeed independent of $PhPF_4$ concentration ($a = 1$ in eq. [3]), and if the order is one with respect to $PhPF_5^-$ concentration, as shown in Fig. 1, then the most reasonable mechanism of exchange is a bimolecular process involving five- and six-coordinate phosphorus species and a fluorine-bridged intermediate. Such a mechanism is entirely consistent with that proposed for the $PhPF_3H-PhPF_4H^-$ system (1) and for related exchange in silicon fluorides (3).

[6] 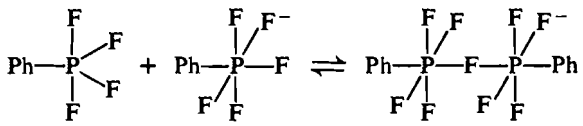

Experimental

Acetonitrile was distilled from P_2O_5 and stored over 4A molecular sieve. Toluene was distilled and stored over 4A molecular sieve. Potassium fluoride (Fisher) was dried at 100°C under vacuum for 48 h, and 18-crown-6 (Aldrich) was dried over P_2O_5 (4). $C_6H_5PF_4$ was prepared by the method of Schmutzler (5) and the fraction bp 131.5–133°C stored at 0°C prior to use. Solutions of KF in 18-crown-6 in a 1:1 molar ratio were added to $PhPF_4$ in acetonitrile or toluene in a nitrogen-filled dry box. $(n\text{-}C_3H_7)_4NSiF_5$ was prepared as described previously (6, 7).

$C_6H_5PF_4$ (4.8 g) was syringed onto $(n\text{-}C_3H_7)_4NF$ (5.4 g) (7, 8) in 50 mL acetonitrile in a nitrogen-filled dry box. Evaporation of the solvent gave crystalline $(n\text{-}C_3H_7)_4NPhPF_5$ (1.7 g), which was filtered, dried over P_2O_5 and under vacuum and identified by ^{31}P and ^{19}F nmr (2, 9).

Nuclear magnetic resonance spectra

The proton-decoupled ^{31}P nmr spectra were obtained on a Bruker WH-90 spectrometer at 36.44 MHz. Line-shape calculations were performed on an Amdahl 470-V7 computer with the IBM Fortran H (extended) compiler using a modified version of the program EXCHSYS (10, 11). The exchange probability matrix is identical to that required for the ^1H nmr study of fluorine exchange in $CH_3SiF_4^-$ (7, 11).

M_1	−2	−1	0	+1	+2
−2	$-\frac{1}{2}$	$\frac{1}{2}$	0	0	0
−1	$\frac{1}{8}$	$-\frac{1}{2}$	$\frac{3}{8}$	0	0
0	0	$\frac{1}{4}$	$-\frac{1}{2}$	$\frac{1}{4}$	0
+1	0	0	$\frac{3}{8}$	$-\frac{1}{2}$	$\frac{1}{8}$
+2	0	0	0	$\frac{1}{2}$	$-\frac{1}{2}$

Acknowledgements

We acknowledge the Natural Sciences and Engineering Research Council of Canada and the donors of the Petroleum Research Fund, administered by the American Chemical Society, for financial support of this work. We thank Mr. R. K. Marat and Dr. A. E. Lemire for assistance with the nmr line-shape analysis.

1. R. K. MARAT and A. F. JANZEN. Inorg. Chem. **19**, 798 (1980).
2. R. APPEL, I. RUPPERT, and F. KNOLL. Chem. Ber. **105**, 2492 (1972).
3. R. K. MARAT and A. F. JANZEN. Can. J. Chem. **55**, 3845 (1977).
4. R. MENGEL and W. GUSCHLBAUER. Angew. Chem. Int. Ed. **17**, 525 (1978).
5. R. SCHMUTZLER. Inorg. Chem. **3**, 410 (1964).
6. F. KLANBERG and E. L. MUETTERTIES. Inorg. Chem. **7**, 155 (1968).
7. R. K. MARAT and A. F. JANZEN. Can. J. Chem. **55**, 1167 (1977).
8. E. J. COREY and A. VENKATESWARLU. J. Am. Chem. Soc. **94**, 6190 (1972).
9. R. SCHMUTZLER and G. S. REDDY. Inorg. Chem. **4**, 191 (1965).
10. J. K. KRIEGER. Ph.D. Thesis, Massachusetts Institute of Technology. Cambridge, MA. 1971.
11. R. K. MARAT. M.Sc. Thesis. University of Manitoba, Winnipeg, Man. 1976.

Can. J. Chem. Downloaded from www.nrcresearchpress.com by 210.87.254.105 on 09/06/12
For personal use only.

The far-infrared spectra and the ring inversion vibrations of a series of methylenecyclohexanes

HAL WIESER, TRACY L. SMITHSON, NAN IBRAHIM, AND PETER J. KRUEGER
Department of Chemistry, University of Calgary, Calgary, Alta., Canada T2N 1N4

Received December 2, 1983

This paper is dedicated to Professor Gerald E. Dunn on the occasion of his 65th birthday

HAL WIESER, TRACY L. SMITHSON, NAN IBRAHIM, and PETER J. KRUEGER. Can. J. Chem. **62**, 1565 (1984).

The far-infrared spectra in the region of 50 to 400 cm^{-1} are reported for the vapours of methylenecyclohexane and the related compounds 4-methylenetetrahydro-4*H*-pyran, 4-methylenetetrahydro-4*H*-thiopyran and 3-methylenetetrahydro-4*H*-pyran. The absorptions are assigned to the three out-of-plane deformations of the six-membered rings. The observed series of Q branches are ascribed to combination sequences involving the three modes. The lowest wavenumber sequence in each compound is believed to arise from a vibration which if completely executed would take the chair conformation to its equivalent via an inversion through the planar form. With the use of a one-dimensional Hamiltonian incorporating a quadratic-quartic double minimum potential function, barriers to planarity for the rings are estimated. The similarities between these compounds and the corresponding ketones are discussed.

HAL WIESER, TRACY L. SMITHSON, NAN IBRAHIM et PETER J. KRUEGER. Can. J. Chem. **62**, 1565 (1984).

On rapporte les spectres infrarouges lointains, dans la région allant de 50 à 400 cm, des vapeurs du méthylènecyclohexane et de composés apparentés, les méthylène-4 tétrahydro 4*H*-pyranne, méthylène-4 tétrahydro 4*H*-thiopyranne et méthylène-3 tétrahydro 4*H*-pyranne. On a attribué les absorptions aux trois déformations hors du plan des cycles à 6 chaînons. On a attribué les séries de branches Q observées à des séries de combinaisons qui font intervenir les trois modes. On pense que la série de combinaisons apparaissant aux plus faibles longueurs d'onde, dans le cas de chacun des composés, provient d'une vibration qui, si elle était complètement exécutée, transformerait la conformation chaise en son équivalent par l'intermédiaire d'une inversion en passant par la forme planaire. On a évalué les barrières à la planéité du cycle en utilisant un Hamiltonien unidimensionel incorporant une fonction de potentiel quadratique-quartique à double minima. On discute des ressemblances entre ces composés et les cétones correspondantes.

[Traduit par le journal]

Can. J. Chem. Downloaded from www.nrcresearchpress.com by 210.87.254.40 on 09/06/12
For personal use only.

Introduction

We have recently had the opportunity of comparing the far-infrared spectra of conjugated and non-conjugated cyclohexenones (1) with those of the corresponding methylenecyclohexenes (2). These spectra reflected appreciable differences in the effect of the keto and vinyl groups on the out-of-plane deformation modes of the cyclohexene ring. In the conjugated compounds the magnitude of the barrier to inversion through the molecular plane depends to some degree on the extent of conjugation, the barrier being larger for the ketone (3640 vs. 2110 cm^{-1}). For the non-conjugated ketone the spectra indicated a bent ground state conformer with a relatively low barrier of 464 cm^{-1} to planar inversion. The non-conjugated methylene compound appears to exist in four equivalent bend-twist ground state conformations which can interconvert via either a twist barrier of 1476 cm^{-1} or a bend barrier of 2215 cm^{-1}, the planar structure being 3641 cm^{-1} above the ground state.

We have investigated recently also the inversion vibrations of a series of heteroatom substituted cyclohexanones as they are observed in the far-infrared spectra (3). The lowest wavenumber mode we visualized as a vibration which if completely executed would lead to the chair–chair inversion through the planar form. The observed sequences of absorptions suggest a barrier to planarity of 2940 cm^{-1} for the parent compound and diminishing barriers for the oxygen-substituted analogs, depending on the position and number of the oxygen atoms. It was of interest to us to determine to what extent the inversion modes are affected when the keto group is replaced by the vinyl group.

Cyclohexanone and methylenecylohexane are similar in several respects. Both exist in a chair conformation in the ground state (4, 5). The ketone is slightly flattened at the C=O end as determined experimentally and by molecular mechanics calculations (6). A similar effect can probably be expected also for the methylene compound, although corresponding data are not available. The free energy barriers for the chair–chair interconversion ($\Delta G^{\#}$) via one of the flexible conformations have been reported from low temperature proton nmr measurements as 17 and 35 kJ/mol (5, 7) (4.0 and 8.4 kcal/mol, or 1400 and 2940 cm^{-1}), respectively, for cyclohexanone and methylenecyclohexane. For the latter the corresponding calculated strain energy barrier is quoted as 34 kJ/mol (8.1 kcal/mol) (8). The various boat and twist-boat conformations are said to be of similar energy and about 12 kJ/mol (4) or, respectively, 20 to 24 kJ/mol (8, 9) less stable than the chair conformation (1000, or 1660 to 2000 cm^{-1}). In both compounds the process of inversion is likely to start with a torsion about the C—C bonds adjacent to the carbonyl or vinyl groups.

In the following we report the vapour phase far-infrared spectra of methylenecyclohexane (**I**) and the related compounds 4-methylenetetrahydro-4*H*-pyran (**II**), 4-methylenetetrahydro-4*H*-thiopyran (**III**), and 3-methylenetetrahydro-4-*H*-pyran (**IV**):

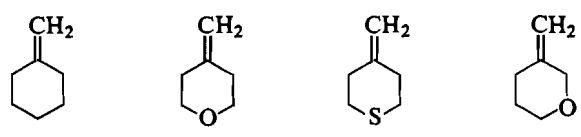

I **II** **III** **IV**

The spectra are characterized by the sequences of absorptions typical of anharmonic, large amplitude vibrations. These are assigned as far as is possible in terms of the three out-of-plane ring deformations, and barriers to planarity are suggested.

TABLE 1. Comparison of the ring inversion vibrations (in cm^{-1}) of methylenecyclohexanes and cyclohexanones

	Compound	$\nu_1(A')$	$\nu_2(A'')$	$\nu_3(A')$
I	Methylenecyclohexane	123.58	202.37	303.74
	Cyclohexanone	92.39	181.51	307.62
II	4-Methylenetetrahydro-4*H*-pyran	127.31	211.06	327.84
	Tetrahydro-4*H*-pyran-4-one	97.16	184.44	336.87
III	4-Methylenetetrahydro-4*H*-thiopyran	106.83	204	251.37
	Tetrahydro-4*H*-thiopyran-4-one	77.48	186.2	253.6
IV	3-Methylenetetrahydro-4*H*-pyran	126.35	215.06	321.17
	Tetrahydro-4*H*-pyran-3-one	90.48	186.43	336.64

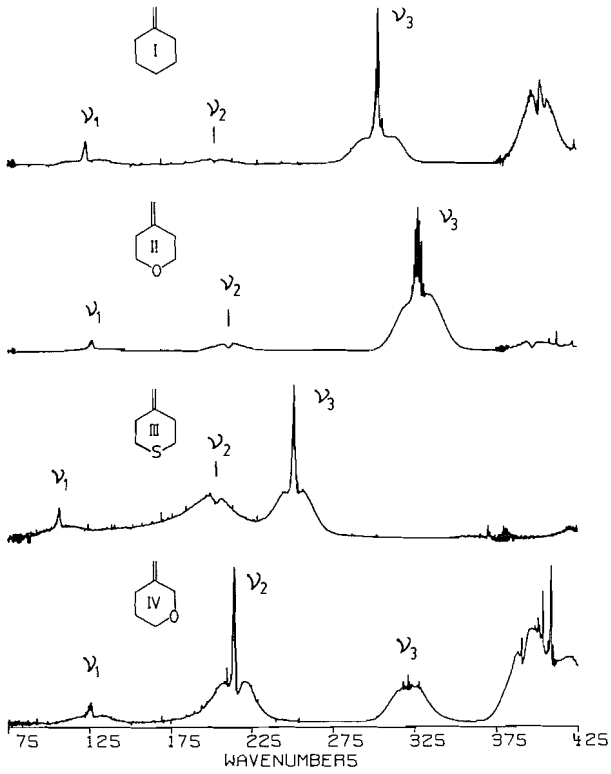

FIG. 1. Survey spectra of methylenecyclohexane and related compounds: 18 m path, reduced vapour pressures, 0.24 cm^{-1} resolution, 6 μm Mylar beamsplitter, 400 cm^{-1} Mylar (for **I** to **III**) or polyethylene (for **IV**) cut-on filter on bolometer, 400 scans.

Experimental

Methylenecyclohexane was purchased from K & K Laboratories and dried by means of refluxing over benzophenone and sodium followed by distillation. The remaining compounds were made from the corresponding ketones by means of the Wittig reaction (10) using triphenylphosphorous methylide. The ketone analogs of **II** and **III** originated from Aldrich Chemicals. The synthesis of the ketone precursor for **IV** was described previously (3). The yields after purification by preparative gc (**II** and **IV**) and distillation (**III**) were 15, 44, and 10% for **II** to **IV**, respectively. The final purity as determined by gc was at least 99% for **II** and **III**, and 85% for **IV**. The contaminant in the last mentioned was *n*-octane, apparently a by-product of the reaction with a very similar boiling point. The far-infrared spectra show no trace of this impurity.

The spectra were obtained with a Nicolet 8000 Fourier Transform Interferometer with optical paths of either 18.75 m in a 20 m Wilks multipass cell, or 45 m in a 60 m optically matched long path cell manufactured by Nicolet. The vapour pressures were adjusted to give reasonable absorbancies in the region of interest. The resolution was set at 0.07, 0.12, or 0.24 cm^{-1} with boxcar apodization. The interferograms were transformed with at least two times zero filling. Either a globar or a mercury arc was used as the light source in conjunction with a 400 or 250 cm^{-1} cut-on filter, respectively, on an Infrared Laboratories liquid helium cooled bolometer as detector operating at 4.2 K, and the appropriate Mylar beamsplitter. The mirror velocity was adjusted as required to achieve a good signal-to-noise ratio. Between 200 and 400 scans were accumulated as necessary. Calibrated against standard water absorptions the reported peak positions are believed to be accurate to at least 0.03 cm^{-1}.

Results

In the C_s symmetry point group of the molecules **I**, **II**, and **III**, the three out-of-plane deformation modes belong to $2A' + A''$. For cyclohexanone we conveniently described the two A' modes, in increasing energy, as out-of-phase (ν_1) and in-phase (ν_3) combinations of a simultaneous though not necessarily equal folding about the C2—C6 and C3—C5 axes, and the A'' mode (ν_2) as a twisting of the middle part of the chair (3). These descriptions we realize are at best approximate. They are, however, based upon extensive earlier force field calculations (11), are consistent with the vapour phase contours, the apparent band intensities, intensity changes upon oxygen substitution, and resemble the corresponding deformation coordinates suggested for cyclohexane (12, 13).

The three absorptions of the methylene compounds are shown in the survey spectra in Fig. 1. The skeletal deformations of the vinyl group, placed in other molecules near 350 and 420 cm^{-1} (14), are not assigned specifically and will not be discussed. The positions of the ring deformation modes are compared in Table 1 for the two series. As in the ketones, the ν_1 and ν_3 fundamentals in the methylene compounds show the expected C contours. As also observed for the ketones, the ν_2 mode exhibits the B contour anticipated for **I**, **II**, and **III**, whereas for **IV** the absorption takes on an A−C character and dominates the spectrum, indicating a comparatively larger dipole moment change in the twist mode. The relative intensities of ν_1 and ν_3 are reversed in the two series, that of the latter being greater for the methylenecyclohexanes. We interpret this as indicating that it is the vinyl or the carbonyl end which undergoes the larger displacement for ν_1, and the opposite end for ν_3. The positions of the fundamentals point to the same conclusions. The ν_1 absorption is shifted to higher wavenumbers by a significant amount for the methylene compounds, while ν_3 stays nearly the same. The ν_2 fundamental evidently is also shifted to higher energy as would be expected if the vibration involved partly a torsion about the C1—C2 and C1—C6 bonds.

If some interaction between the skeletal modes does take place, we would expect to find evidence to this effect primarily

Can. J. Chem. Downloaded from www.nrcresearchpress.com by 210.87.254.40 on 09/06/12
For personal use only.

Can. J. Chem. Downloaded from www.nrcresearchpress.com by 210.87.254.40 on 09/06/12
For personal use only.

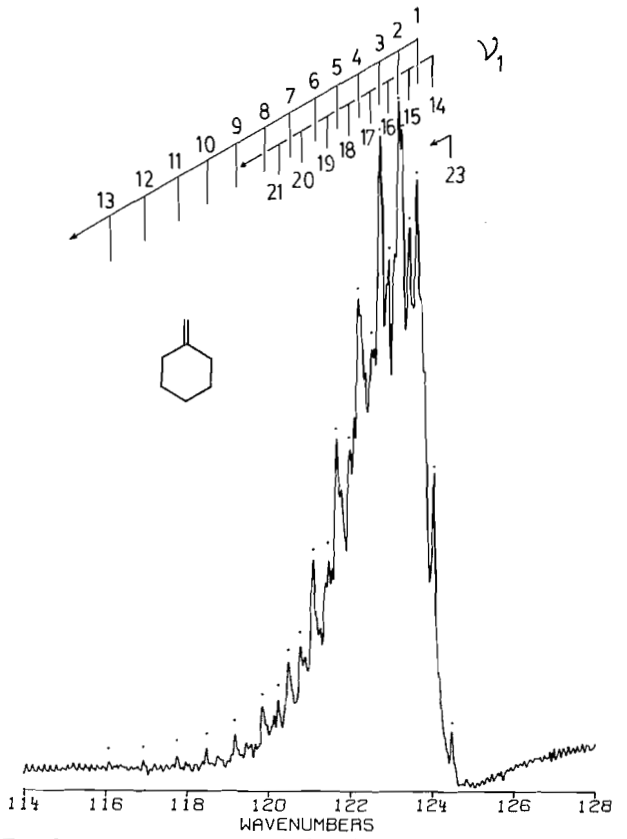

FIG. 2. Expansion of ν_1 band of methylenecyclohexane: 45 m path, reduced vapour pressure, 0.07 cm^{-1} resolution, 12 μm Mylar beamsplitter, 250 cm^{-1} cut-on filter, 200 scans.

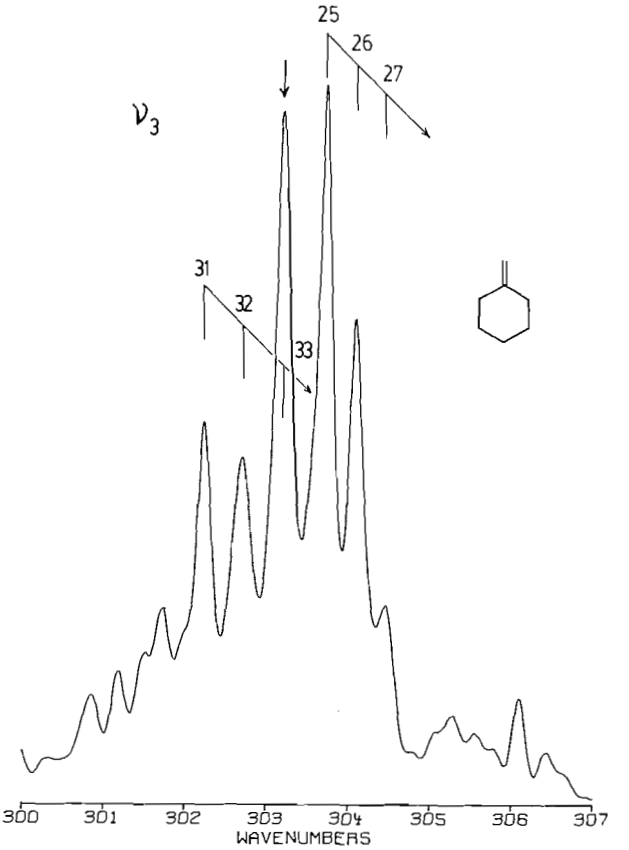

FIG. 3. Expansion of ν_3 band of methylenecyclohexane: 18 m path, reduced vapour pressure, 0.24 cm^{-1} resolution, 6 μm Mylar beamsplitter, 400 cm^{-1} Mylar cut-on filter, 200 scans.

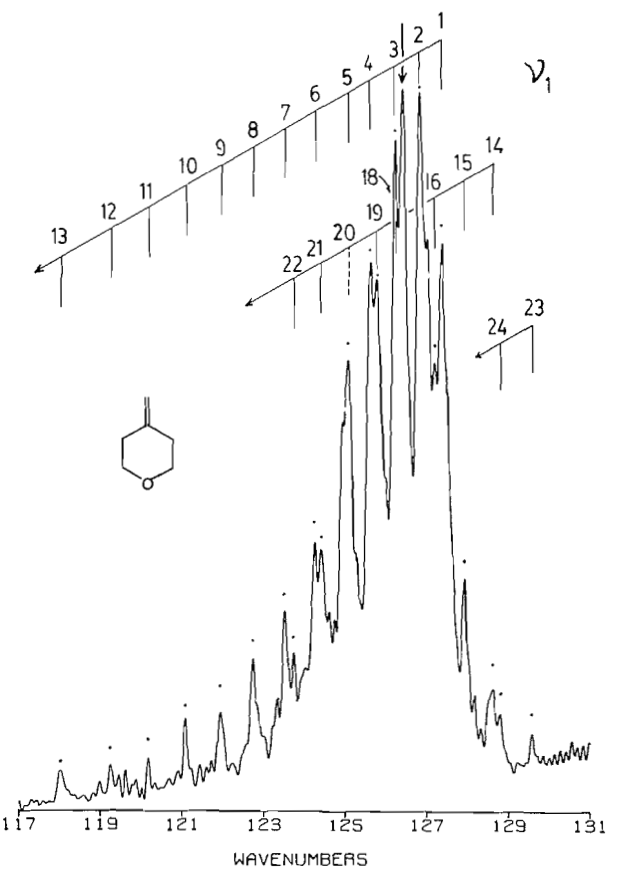

FIG. 4. Expansion of ν_1 band of 4-methylenetetrahydro-4*H*-pyran: 18 m path, reduced vapour pressure, 0.12 cm^{-1} resolution, 12 μm Mylar beamsplitter, 250 cm^{-1} cut-on filter, 400 scans.

for ν_1 and ν_3 in **I**, **II**, and **III**, and for all three modes in **IV**, as we observed for the ketones. All the corresponding absorptions in Fig. 1 show the characteristic sequences. They are expanded in Figs. 2 to 10. The ν_1/ν_3 sequences of all four compounds and the ν_1/ν_2 sequences of **IV** can be assigned as combination series, as summarized in the common energy level scheme drawn in Fig. 11. The peak positions are given in Tables 2 to 4. The peak numbers listed in these tables correspond to the labelled absorptions in the figures and the numbered transitions in the energy level diagram.

For the ketones we were able to model the ν_1 spacings successfully with a one-dimensional double minimum potential function. We suggested that this function can be thought of as representing a section through the four-dimensional potential energy surface (i.e. the potential in the three ring deformations) along the ν_1 coordinate at zero displacement of the other two. The height of the central barrier should then provide an estimate for the barrier to the chair−chair inversion through the planar structure. From Table 2 it is evident that for all four methylene compounds the one-dimensional quadratic-quartic potential successfully reproduces the transitions in the ground state of all other modes. All the energy levels shown are described properly without truncation errors by the set of basis functions used. Moreover, the potential constants, given in terms of the dimensionless coordinate, are well determined by the data, so that we are confident that the extrapolation to the barrier top does not introduce an error in the barrier height of more than 10%. The inversion sequences in the first excited state of ν_3 for **I**, **II**, and **III**, and ν_2 for **IV** yield estimates for

Can. J. Chem. Downloaded from www.nrcresearchpress.com by 210.87.254.40 on 09/06/12
For personal use only.

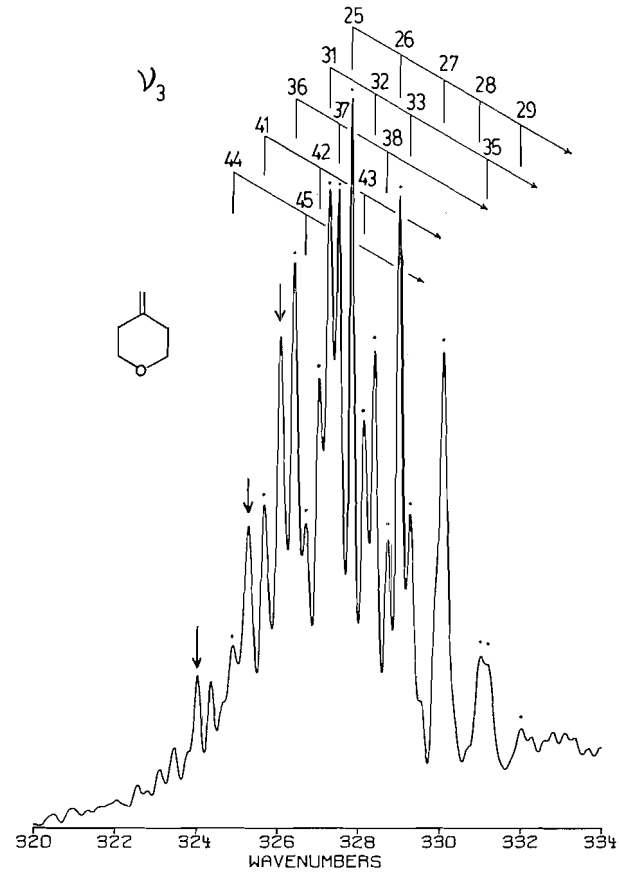

FIG. 5. Expansion of ν_3 band of 4-methylenetetrahydro-4*H*-pyran: 18 m path, reduced vapour pressure, 0.24 cm^{-1} resolution, 6 μm Mylar beamsplitter, 400 cm^{-1} cut-on filter, 400 scans.

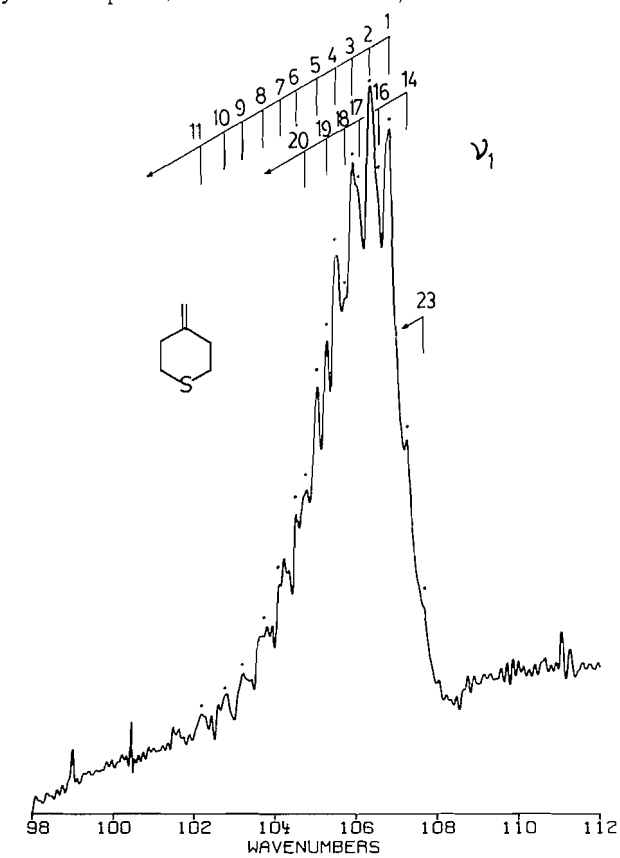

FIG. 6. Expansion of ν_1 band of 4-methylenetetrahydro-4*H*-thiopyran: 18 m path, saturated vapour pressure, 0.12 cm^{-1} resolution, 12 μm Mylar beamsplitter, 250 cm^{-1} cut-on filter, 200 scans.

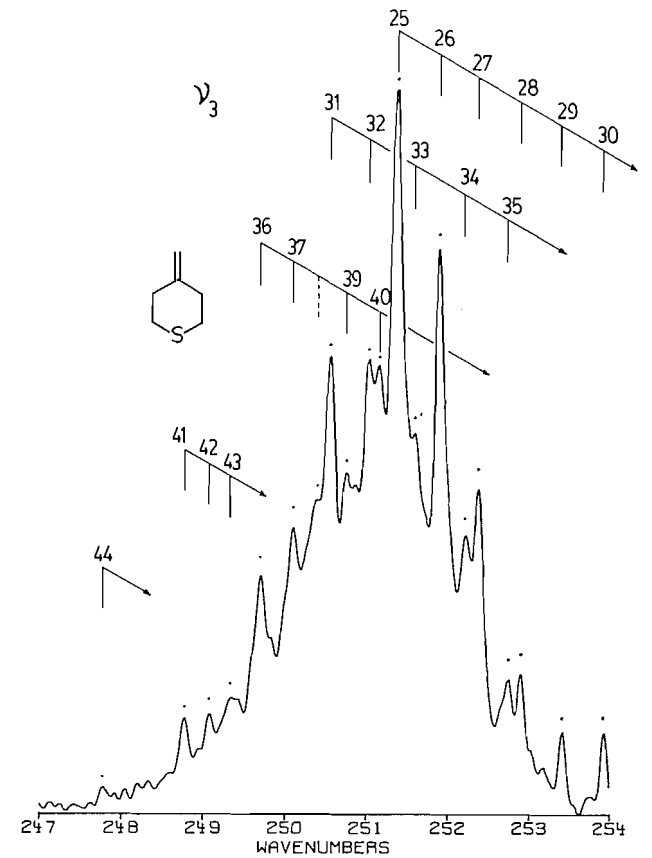

FIG. 7. Expansion of ν_3 band of 4-methylenetetrahydro-4*H*-thiopyran: 18 m path, saturated vapour pressure, 0.12 cm^{-1} resolution, 6 μm Mylar beamsplitter, 400 cm^{-1} Mylar cut-on filter, 300 scans.

the effective excited state potential constants. These, together with the barriers deduced from them, are given in Table 3.

Discussion

The location of the lowest members of the ν_1 sequences in the ground state and in the first excited state of ν_3 in all cases are assured by the combination principle. For **III**, in particular, the first five transitions in ν_1, which may appear uncertain as a result of the closeness of the series, are confirmed by the clearly assignable ν_3 sequence (cf. Figs. 6 and 7). There are several additional prominent Q branches left unassigned for **I** and **II** that cannot be part of the ν_1/ν_3 combination series (for example in Figs. 3, 4, and 5, marked with an arrow). These we believe are ν_1 transitions in various excited states of ν_2. They cannot be confirmed since the B contours of the twist mode are not resolved and no sum or difference bands are observed. For **IV**, however, where the twist band dominates, ν_1/ν_2 sequences are clearly evident (see Fig. 9).

Ideally a proper theoretical analysis for modelling the observed transitions should use an appropriate three-dimensional Hamiltonian allowing for coupling and anharmonic corrections in both the kinetic and potential energy parts. The feasibility of using such a three-dimensional analysis for ring deformations has recently been demonstrated. For 1,3-disilacyclobutane a Hamiltonian was employed which in principle is similar to that indicated in footnote *e* of Table 2, except that it is extended to include appropriate potential terms in the three coordinates as well as a kinetic energy expansion for the puckering coordinate (16). In that particular case, only the puckering mode displayed a double minimum character while the other two modes were

TABLE 2. Positions of ν_1 (cm^{-1}) in the ground state of all other modes

Transition[a] $\nu_\mu \leftarrow \nu_l$	Pk*[b] No.	I Obs.[c]	I Δ[d]	II Obs.[c]	II Δ[d]	III Obs.[c]	III Δ[d]	IV Obs.[c]	IV Δ[d]
3, 2 1, 0	1	123.58	−0.08	127.31	−0.10	106.83	0.03	126.35	−0.06
5, 4 3, 2	2	123.13	−0.02	126.76	−0.02	106.34	0.03	125.60	−0.01
7, 6 5, 4	3	122.67	0.04	126.16	0.01	105.93	−0.01	124.80	0.01
9, 8 7, 6	4	122.15	0.05	125.56	0.05	105.52	0.02	123.98	0.02
11,10 9, 8	5	121.63	0.06	125.02	0.16	105.06	0.00	123.11	0.00
13,12 11,10	6	121.07	0.04	124.23	0.03	(104.54	0.07)	122.29	0.05
15,14 13,12	7	120.49	0.00	123.50	−0.02	(104.12	−0.03)	121.23	−0.13
17,16 15,14	8	119.85	−0.09	122.73	−0.11	(103.69	0.00)	120.36	−0.09
19,18 17,16	9	(119.16	−0.22)	(121.94	−0.21)	(103.22	−0.01)	119.62	0.09
21,20 19,18	10	(118.49	−0.32)	(121.08	−0.36)	(102.81	0.05)		
23,22 21,20	11	(117.76	−0.47)	(120.17	−0.55)	(102.20	−0.08)		
25,24 23,22	12	(116.93	−0.72)	(119.23	−0.76)				
27,26 25,24	13	(116.09	−0.97)	(118.03	−1.22)				
Derived parameters[e]									
Std. dev./cm^{-1}		0.06		0.09		0.03		0.09	
$(V_2/m\gamma)/cm^{-1}$		−48.179(36)		−51.219(57)		−35.930(19)		−50.563(50)	
$(V_4/(m\gamma)^2)/cm^{-1}$		0.10110(177)		0.13040(285)		0.063041(1270)		0.16462(221)	
Barrier/cm^{-1}[f]		5740 ± 110		5030 ± 120		5120 ± 100		3880 ± 60	

[a]Quantum numbers of the upper (u) and lower (l) energy levels. Each level is doubly degenerate as reflected by the labelling.

[b]The peak numbers correspond to the observed peak positions marked in Figs. 2, 4, 6, and 8, respectively.

[c]Observed positions given in parentheses were not included in the fitting process.

[d]Observed − calculated.

[e]Evaluated with the potential function $V(q) = (V_2/m\gamma)q^2 + (V_4/m^2\gamma^2)q^4$, q the dimensionless coordinate (15). Fixed parameters: $\gamma = 4\pi^2 c\nu/h$; $\nu = 80.0\ cm^{-1}$; 125 basis functions per symmetry block for **I** to **III**, and 100 for **IV**.

[f]Uncertainties reflect the estimated standard deviations for the potential constant.

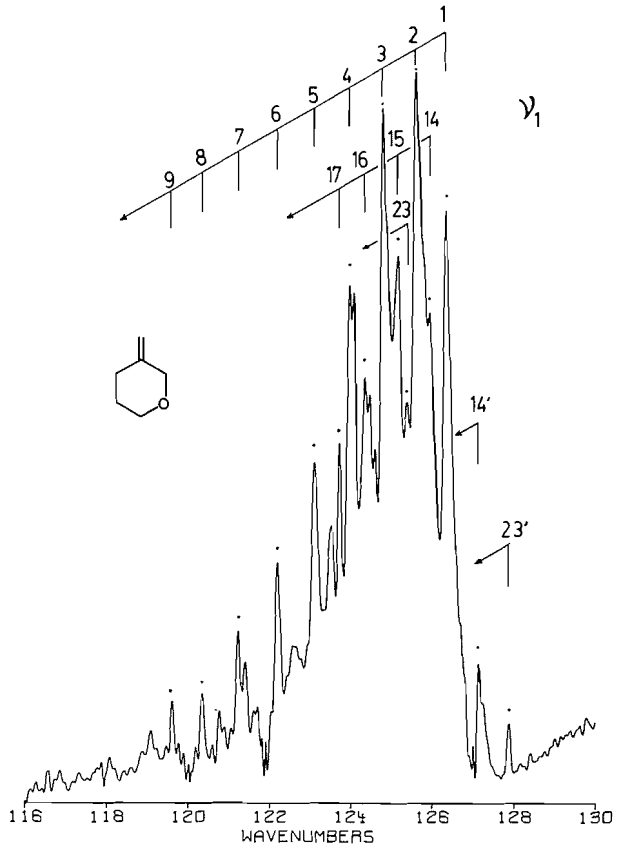

FIG. 8. Expansion of ν_1 band of 3-methylenetetrahydro-4*H*-pyran: 18 m path, saturated vapour pressure, 0.12 cm^{-1} resolution, 12 μm Mylar beamsplitter, 250 cm^{-1} cut-on filter, 300 scans. The peaks labelled with unprimed numbers 14 to 17 and 23 are combinations with ν_2, and those with primed numbers 14 and 23 are the same type of combinations with ν_3.

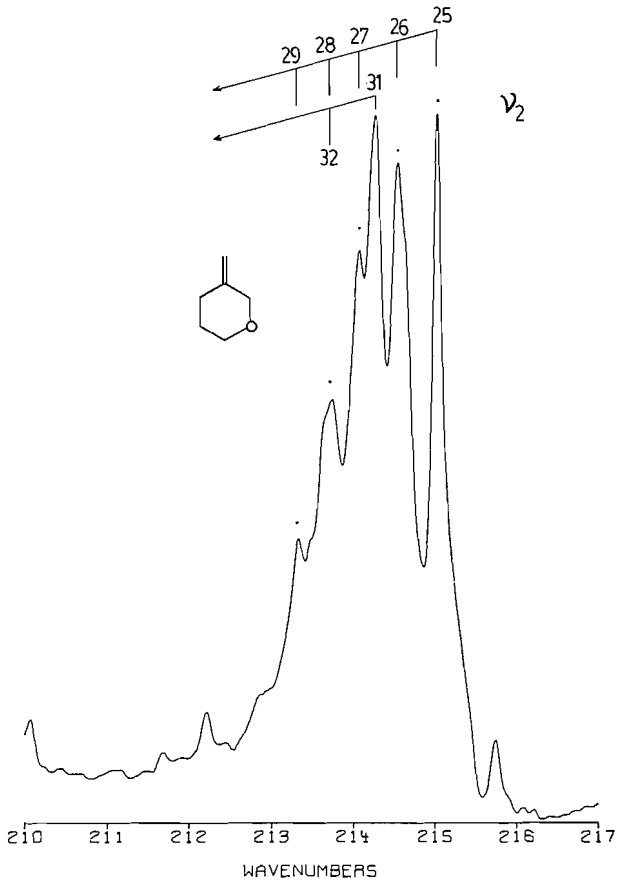

FIG. 9. Expansion of ν_2 band of 3-methylenetetrahydro-4*H*-pyran: 18 m path, reduced vapour pressure, 0.12 cm^{-1} resolution, 12 μm Mylar beamsplitter, 250 cm^{-1} cut-on filter, 300 scans.

Can. J. Chem. Downloaded from www.nrcresearchpress.com by 210.87.254.40 on 09/06/12
For personal use only.

TABLE 3. Positions of ν_1 (cm^{-1}) in the first excited state of ν_2 and ν_3

Transition[a] $\nu_u \leftarrow \nu_l$	Pk.[b] No.	**I** (ν_3) Obs.[c]	Δ[d]	**II** (ν_3) Obs.[c]	Δ[d]	**III** (ν_3) Obs.[c]	Δ[d]	**IV** (ν_2) Obs.[c]	Δ[d]
3, 2 1, 0	14	124.03	0.05	128.59	0.12	107.27	−0.03	125.95	0.01
5, 4 3, 2	15	123.39	−0.08	127.88	−0.02	(106.90)		125.19	−0.02
7, 6 5, 4	16	122.90	−0.06	127.14	−0.20	106.55	0.05	124.48	0.00
9, 8 7, 6	17	122.48	0.04	(126.76)		106.06	−0.03	123.73	0.00
11,10 9, 8	18	121.96	0.05	126.16	−0.02	105.70	0.20		
13,12 11,10	19	121.45	0.08	125.73	0.14	105.30	0.04		
15,14 13,12	20	120.78	−0.05	(124.99)		104.80	−0.04		
17,16 15,14	21	120.24	0.04	124.38	0.00				
19,18 17,16	22			123.74	−0.03				
Derived parameters[e]									
Std. dev./cm^{-1}		0.07		0.12		0.04		0.02	
$(V_2/m\gamma)/cm^{-1}$		−48.429(40)		−52.018(73)		−36.245(29)		−50.126(18)	
$(V_4/(m\gamma)^2)/cm^{-1}$		0.10118(196)		0.11930(331)		0.059252(1330)		0.14770(166)	
Barrier/cm^{-1}[f]		5800 ± 130		5670 ± 170		5540 ± 130		4250 ± 50	

[a]Quantum numbers of the upper (u) and lower (l) energy levels. Each level is doubly degenerate as reflected by the labelling.

[b]The peak numbers correspond to the observed peak positions marked in Figs. 2, 4, 6, and 8, respectively.

[c]The positions in brackets are calculated; lines cannot be measured due to overlapping bands.

[d]Observed − calculated.

[e]Evaluated with the potential function $V(q) = (V_2/m\gamma)q^2 + (V_4/m^2\gamma^2)q^4$, q the dimensionless coordinate (15). Fixed parameters: $\gamma = 4\pi^2 c\nu/h$; $\nu = 80.0\ cm^{-1}$; 125 basis functions per symmetry block for **I** and **III**, and 100 for **II** and **IV**.

[f]Uncertainties reflect the estimated standard deviations for the potential constants.

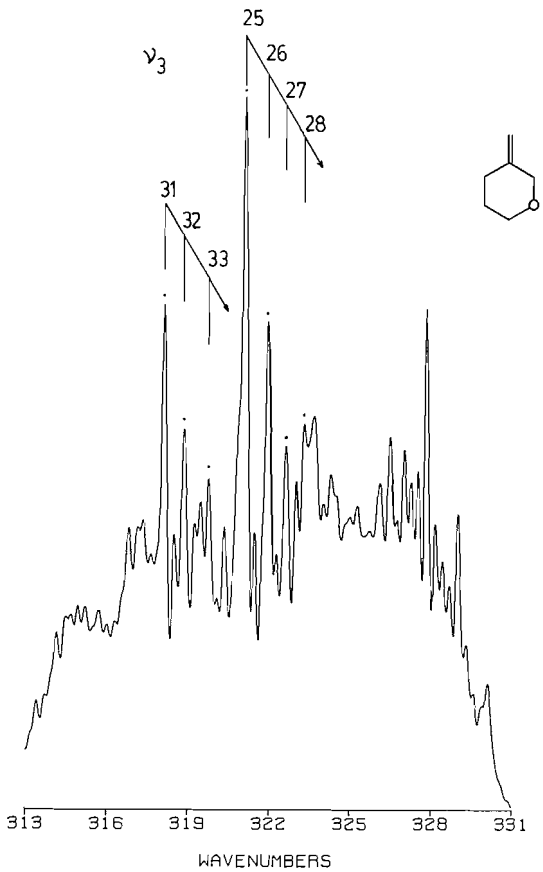

FIG. 10. Expansion of ν_3 band of 3-methylenetetrahydro-4*H*-pyran: 18 m path, reduced vapour pressure, 0.24 cm^{-1} resolution, 6 μm Mylar beamsplitter, 400 cm^{-1} polyethylene cut-on filter, 400 scans.

treated as harmonic, and the authors could take advantage of the relatively infrequent luxury of having available a wealth of combination data. More appropriate for our present case is the kind of treatment demonstrated recently with cyclohexane (17) and *p*-dioxane (18). For neither of these two molecules are the transitions sufficiently well-known experimentally to permit the evaluation of the potential parameters best fitting the observed positions, although the author states that in principle the method does not preclude a fitting procedure. For the methylenecyclohexanes and the ketone analogues we chose not to pursue such computations at this time. Notwithstanding the amount of information we do have, the set of data obviously is not complete. We have tried earlier to reproduce the ν_1 and ν_3 transitions of the ketone analogue of **II** in a two-dimensional way, albeit with a constant coordinate-independent reduced mass (3). The results were not encouraging and we accepted perforce the one-dimensional method as currently the only reasonable way of extracting the limited barrier information from the data.

At first glance it is remarkable that the one-dimensional Hamitonian with the quadratic-quartic potential function is capable of reproducing the spacings for ν_1 quite as successfully. Perhaps this success is not too surprising, however, when one considers that since the chair is the ground state conformation ν_1 must be the dominant mode, and up to a relatively high energy the other two modes correspond to anharmonic deformations in the chair's deep potential well. The spectra show the slowly diminishing sequence for ν_1 characteristic of a double minimum situation with a high barrier, while the diminishing sequences of ν_3 (and of ν_2 in the case of **IV**) are caused by the anharmonic potential environment. In order to evaluate quantitatively the extent to which the three modes are coupled, of course, would require some sort of three-dimensional analysis. For coupled they must be, at least to some extent, since the ν_1 sequences in the excited states of ν_2 and ν_3 are shifted from the

Can. J. Chem. Downloaded from www.nrcresearchpress.com by 210.87.254.40 on 09/06/12
For personal use only.

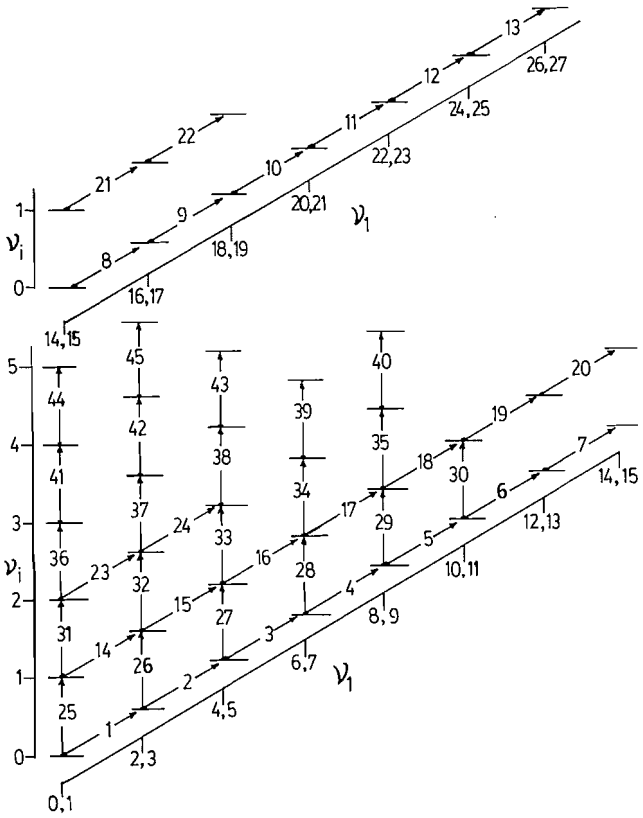

FIG. 11. Energy level diagram showing combination transitions between ν_1 and ν_i, $i = 2$ or 3. Numbered transitions correspond to the peaks labelled in Figs. 2 to 10 and in Tables 2 to 4.

ν_1 fundamental position (to lower wavenumbers for the former and to higher for the latter), and the effective potential constants for ν_1 are different in the excited states of ν_2 (**IV** only) and of ν_3 (**I**, **II**, and **III**) than those of the ground state. The question as to how the barrier to planarity which is estimated here one-dimensionally would be affected by a multidimensional approach, unfortunately cannot be answered. Neither does the present analysis provide any information about the relative stabilities of the conformers involved or the barriers to interconversion between them. Specifically this means that the inversion barriers derived from nmr measurements cannot be verified by the infrared data since these two methods determine different barriers on the potential surface.

It is noteworthy to observe the trend of negative to positive to negative deviations between the calculated and observed ν_1 transitions in Table 2. This kind of trend, as noted by Malloy (19), can result from neglecting the subtle contribution made to the anharmonicity by the kinetic energy. When we attempted to include in the fitting process a kinetic term of the form $g^{(2)}pq^2p$, q the dimensionless coordinate, p its conjugate momentum, and $g^{(2)}$ the coefficient of q^2 in the expansion of the reduced mass in terms of the deformation coordinate used as a fitting parameter, the deviations were reduced only marginally with the trend remaining, even if $g^{(2)}$ was optimized to yield the best fitting potential constants. In contrast, remarkable improvements in the fit have been demonstrated by just such a procedure in several other instances (19, 20). While anharmonic contributions from the kinetic energy may well play a role also in the present cases, they evidently are difficult to quantify. Judging by the experience made by others (e.g. 19, 21), we believe that the estimated barriers to planarity are not likely to be influenced significantly by neglecting such contributions.

TABLE 4. Other combination sequences

Transition $(\nu_i, \nu_1)_u \leftarrow (\nu_i, \nu_1)_l$	Pk.[a] No.	Position/cm^{-1} I	II	III	IV
Combinations with ν_2 ($i = 2$)					
2 3, 2 2 1, 0	23				125.39
1 1, 0 0 1, 0	25				215.06
3, 2 3, 2	26				214.57
5, 4 5, 4	27				214.10
7, 6 7, 6	28				213.76
9, 8 9, 8	29				213.35
2 1, 0 1 1, 0	31				214.30
3, 2 3, 2	32				213.76
Combinations with ν_3 ($i = 3$)					
1 3, 2 1 1, 0	14				127.14[b]
2 3, 2 2 1, 0	23	124.48	129.57	107.70	127.88[b]
5, 4 3, 2	24		128.79		
1 1, 0 0 1, 0	25	303.74	327.84	251.37	321.17
3, 2 3, 2	26	304.14	329.05	251.89	321.99
5, 4 5, 4	27	304.48	330.14	252.38	322.66
7, 6 7, 6	28		331.05	252.91	323.57
9, 8 9, 8	29		332.03	253.42	
11,10 11,10	30			253.94	
2 1, 0 1 1, 0	31	302.22	327.31	250.56	318.14
3, 2 3, 2	32	302.72	328.44	251.06	318.88
5, 4 5, 4	33	303.19	329.30	251.60	319.79
7, 6 7, 6	34			252.23	
9, 8 9, 8	35		331.10	252.73	
3 1, 0 2 1, 0	36		326.47	249.71	
3, 2 3, 2	37		327.55	250.10	
5, 4 5, 4	38		328.73		
7, 6 7, 6	39			250.76	
9, 8 9, 8	40			251.17	
4 1, 0 3 1, 0	41		325.71	248.77	
3, 2 3, 2	42		327.07	249.08	
5, 4 5, 4	43		328.18	249.40	
5 1, 0 4 1, 0	44		324.93	247.89	
3, 2 3, 2	45		326.74		

[a]Peak numbers correspond to labelled peak positions in Figs. 2 to 10, and numbered transitions in Fig. 11.
[b]Peak numbers 14′ and 23′ in Fig. 8.

Accepting the deduced values for the barriers to planarity as reasonable estimates, some interesting trends are revealed. The barriers diminish with oxygen substitution. The same trend was observed for the ketones, for which the comparative values for the analogues of **I**, **II**, and **IV** are 2940, 2772, and 1068 cm^{-1}, respectively (3). An oxygen atom in the position β to the exocyclic double bond (either C=C or C=O) evidently reduces the barrier more effectively than an oxygen in the γ position. The difference between the cyclohexanones and the methylene analogues reflects the established fact that torsion about a C—C bond adjacent to a carbonyl group is easier than when adjacent to a vinyl group.

Apart from different relative intensities reflecting differences in the dipole moment change with the coordinates, the far-infrared absorptions of the methylenecylohexanes are very similar to those of their ketone counterparts. In appears, therefore, that replacing the carbonyl group with the vinyl group does not affect dramatically the dynamics of the deformations of the cyclohexane ring.

Can. J. Chem. Downloaded from www.nrcresearchpress.com by 210.87.254.40 on 09/06/12
For personal use only.

Acknowledgements

This research is supported by a special project fund from the Alberta Environment Research Trust (to H.W.) and by Operating Grants from the Natural Sciences and Engineering Research Council of Canada (to H.W. and P.J.K.), all of which are hereby gratefully acknowledged.

1. H. WIESER, T. L. SMITHSON, and P. J. KRUEGER. J. Mol. Spectrosc. **96**, 368 (1982).
2. T. L. SMITHSON, N. IBRAHIM, and H. WIESER. Can. J. Chem. **61**, 442 (1983).
3. T. L. SMITHSON, N. IBRAHIM, and H. WIESER. Can. J. Chem. **61**, 1924 (1983).
4. R. BUCOURT. *In* Topics in stereochemistry. Vol. 8. *Edited by* E. L. Eliel and N. L. Allinger. John Wiley and Sons, New York. 1974. pp. 159–224.
5. J. T. GERIG and R. A. RIMERMAN. J. Am. Chem. Soc. **92**, 1219 (1970).
6. R. J. ABRAHAM, M. J. BOVILL, D. J. CHADWICK, L. GRIFFITHS, and F. SANCASSAN. Tetrahedron, **36**, 279 (1980).
7. F. A. L. ANET, G. N. CHMURNY, and J. KRANE. J. Am. Chem. Soc. **95**, 4423 (1973).
8. F. A. L. ANET and I. YAVARI. Tetrahedron, **34**, 2879 (1978).
9. N. L. ALLINGER, M. T. TRIBBLE, and M. A. MILLER. Tetrahedron, **28**, 1173 (1972).
10. G. WITTIG and U. SCHOELLKOPF. Org. Synth. **40**, 66 (1960).
11. H. FUHRER, V. B. KARTHA, P. J. KRUEGER, H. H. MANTSCH, and R. N. JONES. Chem. Rev. **5**, 439 (1973).
12. H. M. PICKETT and H. L. STRAUSS. J. Am. Chem. Soc. **92**, 7281 (1970).
13. J. B. HENDRICKSON. J. Am. Chem. Soc. **89**, 7047 (1967).
14. T. B. MALLOY, JR., F. FISHER, J. LAANE, and R. M. HEDGES. J. Mol. Spectrosc. **40**, 239 (1971) and references therein.
15. J. A. DUCKETT, T. L. SMITHSON, and H. WIESER. J. Mol. Spectrosc. **78**, 407 (1979).
16. P. M. KILLOUGH, R. M. IRWIN, and J. LAANE. J. Chem. Phys. **76**, 3890 (1982).
17. D. GRAVERON-DEMILLY. Mol. Phys. **44**, 491 (1981).
18. D. GRAVERON-DEMILLY. J. Chem. Phys. **79**, 81 (1983).
19. T. B. MALLOY, JR. J. Mol. Spectrosc. **44**, 504 (1972).
20. T. L. SMITHSON, J. A. DUCKETT, and H. WIESER. J. Phys. Chem. **88**, 1102 (1984).
21. L. E. BAUMAN, P. M. KILLOUGH, J. M. COOKE, J. R. VILLARREAL, and J. LAANE. J. Phys. Chem. **86**, 2000 (1982).

Can. J. Chem. Downloaded from www.nrcresearchpress.com by 210.87.254.40 on 09/06/12
For personal use only.

Determination of CNDO/2 dipole moment derivatives from interpolating polynomials

ALLAN WILLIAM TARR AND BRYAN ROGER HENRY
Department of Chemistry, University of Manitoba, Winnipeg, Man., Canada R3T 2N2

Received October 10, 1983

This paper is dedicated to Professor Gerald E. Dunn on the occasion of his 65th birthday

ALLAN WILLIAM TARR and BRYAN ROGER HENRY. Can. J. Chem. **62**, 1573 (1984).

A numerical differentiation technique is presented from which dipole moment derivatives are estimated from sets of CNDO/2 calculated dipole moment values. The dipole moment values are evaluated over a range of molecular geometries, which are obtained by distorting the molecule along CH-stretching local coordinates. The technique effectively fits the dipole moment values to an interpolating polynomial, but the utilization of difference tables and lozenge diagrams makes the explicit determination of the polynomial unnecessary.

First, second, and third order pure derivatives, and second order mixed derivatives, are estimated for methane and ethane. Several testing procedures for the numerical technique are discussed. On this basis, the accuracy of these derivatives is judged to be very good.

ALLAN WILLIAM TARR et BRYAN ROGER HENRY. Can. J. Chem. **62**, 1573 (1984).

On présente une technique de différenciation numérique qui permet d'évaluer les dérivées du moment dipolaire à partir d'un ensemble de valeurs de moments dipolaires calculés par CNDO/2. On a évalué les moments dipolaires dans un domaine de géométries moléculaires que l'on obtient en déformant la molécule le long de coordonnées locales d'élongation du C—H. La technique permet effectivement d'établir une corrélation avec les valeurs du moment dipolaire jusqu'à un polynome d'interpolation; toutefois l'utilisation de tables de différence et de diagrammes de lozange rend inutile la détermination explicite du polynome.

On a évalué, pour le méthane et pour l'éthane, les dérivées pures des premier, deuxième et troisième ordres et les dérivées mixtes du deuxième ordre. On discute de plusieurs méthodes de vérification de la technique numérique. Dans ces conditions, on estime que la précision de ces dérivées est très bonne.

[Traduit par le journal]

Can. J. Chem. Downloaded from www.nrcresearchpress.com by 210.87.254.5 on 09/06/12
For personal use only.

Introduction

The local mode model has proven to be very useful in understanding the high energy, XH-stretching overtone spectra of a wide variety of molecules (1). Although the general patterns of the overtone bands can be rationalized within this model, quantitative prediction of relative local mode intensities remains a major problem. Of central importance in understanding these intensities is the dependence of the electric dipole moment, μ, on local coordinates. The dipole moment can be expanded in a Taylor series in local coordinates, q_i

$$[1] \quad \boldsymbol{\mu} = \boldsymbol{\mu}^0 + \sum_i \boldsymbol{\mu}_i q_i + \left(\frac{1}{2}\right) \sum_{i,j} \boldsymbol{\mu}_{ij} q_i q_j + \ldots$$

where $\boldsymbol{\mu}^0$ is the electric dipole moment of a molecule at the average geometry of the vibrational ground state, and $\boldsymbol{\mu}_i = (\partial\boldsymbol{\mu}/\partial q_i)_0$ and $\boldsymbol{\mu}_{ij} = (\partial^2\boldsymbol{\mu}/\partial q_j \partial q_i)_0$ represent the derivatives of the dipole moment function, which are evaluated at the average geometry. The purpose of the present paper is to present a convenient method to obtain these dipole moment derivatives and to illustrate the application of the method to methane and ethane.

CNDO molecular orbital theory (2*a*) has been used extensively to calculate first order derivatives of the electric dipole moment (3–8). The general procedure is to distort the molecule from its equilibrium geometry along some symmetry coordinate (3–6, 8), or to move a specific atom along a Cartesian coordinate (7). The dipole moments of the molecule at several distorted geometries are calculated, and the first derivative is often obtained from the assumption that the dipole moment is linear in the distorting coordinate. Occasionally nonlinear dipole moment functions have been assumed. In one investigation of ethane, twenty values of the distorted geometry dipole moments have been fitted with a least squares procedure to a quadratic function of the Cartesian nuclear displacement (7).

Molecular orbital calculations have also been used to calculate dipole moment derivatives with respect to local coordinates (9–12). Burberry and Albrecht have determined the first and second order derivatives of the dipole moment functions of benzene and ground ($X^2\pi$) state CH radical with respect to the CH-stretching local coordinates (9). A one dimensional dipole moment function was assumed in both cases. The dipole moments of distorted geometries of benzene were determined from CNDO/S (13) calculations and were fitted to a quintic power series in the displacement. The published (14) *ab initio*, extended CI dipole moments of the CH radical, at a variety of bond lengths, were also fitted to a power series. Tamagake *et al.* have published a series of papers (10–12) in which they have calculated $\boldsymbol{\mu}_1$ and $\boldsymbol{\mu}_{11}$ for several molecules. They used *ab initio* calculations with 4-31 G (15) and 6-31 G* (16) basis sets to determine dipole moments at distorted geometries. In all cases a one dimensional dipole moment function was assumed and the dipole moments were fitted to a quadratic function in displacement. In fitting their model to experimental overtone intensities, they found an indication that $\boldsymbol{\mu}_{111}$ should not be neglected in the case of chloroform (11), and that the mixed second derivative, $\boldsymbol{\mu}_{12}$, was important in the case of 1,1-dichloroethane (12).

The numerical technique that we present in this paper effectively fits the dipole moment values to a one dimensional interpolating polynomial of high degree. However, through the use of forward difference tables and lozenge diagrams, we are able to avoid the explicit determination of the interpolating polynomial. The technique allows a straightforward determination of $\boldsymbol{\mu}_1$, $\boldsymbol{\mu}_{11}$, $\boldsymbol{\mu}_{12}$, and $\boldsymbol{\mu}_{111}$ in an efficient fashion.

Theory

1. Outline

In the calculation of dipole moments, the average geometry

Can. J. Chem. Downloaded from www.nrcresearchpress.com by 210.87.254.5 on 09/06/12
For personal use only.

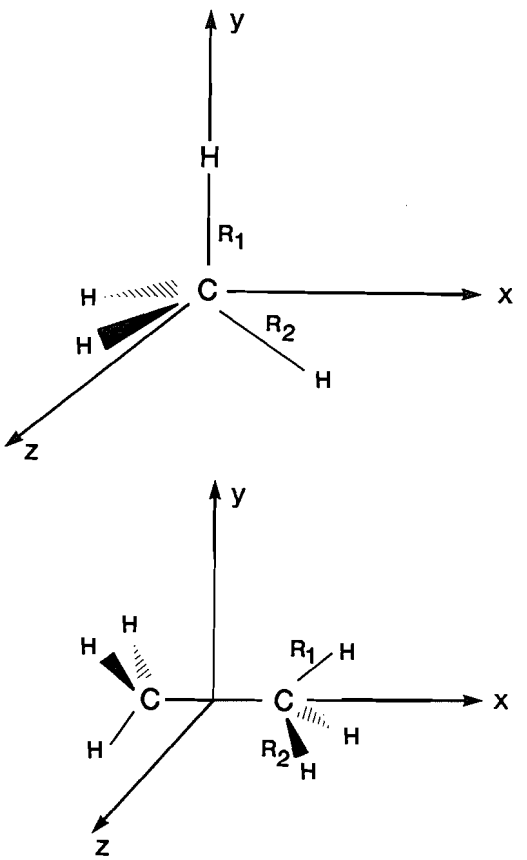

FIG. 1. Spectroscopic structures for (*a*) methane: r^0_{CH} = 1.09397 Å (22), ∠HCH = 109.47° and (*b*) ethane (23): r^0_{CH} = 1.108 Å, r^0_{CC} = 1.536 Å, ∠HCH = 108.8°, ∠CCH = 110.1°.

of the vibrational ground state of the molecule of interest is held rigid, except for the two CH bonds R_1 and R_2 (see Fig. 1). Each of these bond lengths is varied independently in a stepwise fashion. A constant stepsize of h = 0.05 Å is used for both R_1 and R_2. Trials with other stepsizes indicated that this value was the optimum one for this work (*vide infra*).

The dipole moments of the distorted molecules are calculated from the CNDO/2 program INDOFPT (17). There are several reasons why CNDO/2 is used to obtain these values. Dipole moments from CNDO/2 calculations have been found to be generally reliable, especially for hydrocarbons (2). In some instances, CNDO/2 calculations have been more successful at predicting ir intensities than *ab initio* calculations (6). In a parallel study,[1] we have compared dipole moments calculated for dichloromethane from CNDO/2, INDO (2*a*), and STO-3G (18) molecular orbital theories. The CNDO/2 and INDO calculations used the INDOFPT program (17), while the STO-3G calculation used GAUSSIAN 70 (19). The CNDO/2 calculation gave a value for the dipole moment only 3% higher than the experimental value of 1.60 ± 0.03 D (20). Values for the INDO and STO-3G calculations were approximately 7% and 40% too high, respectively.

Thus, CNDO/2 dipole moments are calculated as R_1 and R_2 are varied uniformly and independently. Bond independence is a good approximation for the molecules considered in this work. The valence electron densities of the atoms of methane, which are not involved in the R_1 stretch, vary by less than 0.25% over the full range of the R_1 stretch. Changes of a similar magnitude are observed for ethane, except for the hydrogen atom *trans* to the R_1 bond. The valence electron density at this atom decreases by 0.5% over the full extension of the R_1 bond.

In order to obtain the derivatives simply and accurately, the calculations require that for a specific R_2 value, the dipole moment must be evaluated at an odd number of R_1 values, and vice versa. It is convenient to organize the dipole moments, $\boldsymbol{\mu}(R_1, R_2)$, as a square grid, where each grid element contains the three Cartesian components of the dipole moment. The geometry distortions are performed such that the central element of the grid is $\boldsymbol{\mu}(R_1^0, R_2^0)$, where R_1^0 and R_2^0 refer to the average bond length, r_{CH}^0.

In the next section, we present a numerical technique which allows the approximation of derivatives of one dimensional functions. This technique can be used straightforwardly to estimate the pure derivatives of the dipole moment, $\boldsymbol{\mu}_1$, $\boldsymbol{\mu}_{11}$, and $\boldsymbol{\mu}_{111}$, e.g.

$$[2] \quad \boldsymbol{\mu}_1 = (\mathrm{d}\boldsymbol{\mu}(R_1, R_2^0)/\mathrm{d}R_1)_{R_1 = R_1^0}$$

where R_2 is held fixed at R_2^0. To evaluate $\boldsymbol{\mu}_{12}$, the foregoing procedure is repeated for all the selected values of R_2 to obtain a set of $\boldsymbol{\mu}_1$ values as a function of R_2. Thus the problem is reduced to one dimension, and $\boldsymbol{\mu}_{12}$ can be estimated from

$$[3] \quad \boldsymbol{\mu}_{12} = (\mathrm{d}/\mathrm{d}R_2[(\mathrm{d}\boldsymbol{\mu}(R_1, \bar{R}_2)/\mathrm{d}R_1)_{R_1 = R_1^0}])_{R_2 = R_2^0}$$

where the bar on R_2 denotes the parametric dependence of $\boldsymbol{\mu}_1$.

2. *Numerical differentiation*

Numerical derivatives can be obtained through the use of one dimensional interpolating polynomials of high degree (21). Any particular row or column of the dipole moment grid contains dipole moment values which are effectively a function of only one CH bond length. For generality, denote the set of CH bond lengths and the corresponding dipole moments as $\{x_i, f(x_i)\}$. The following constraints are imposed on the data set to increase the ease of calculation and accuracy of the result. The x_i values are evenly spaced, i.e., $x_{i+1} = x_i + h$ and are odd in number, n. The point at which the derivatives are evaluated x_0, is set to be the central point in the range of x_i values.

The technique effectively fits the n data points to a polynomial of degree $(n - 1)$.

$$[4] \quad P_{n-1}(x_i) = f(x_i)$$

This interpolating polynomial is used as an approximation to the continuous function, i.e.,

$$[5] \quad P_{n-1}(x) \simeq f(x)$$

Numerical approximations of the derivatives of $f(x)$ are obtained by analytic differentiation of $P_{n-1}(x)$. Although $P_{n-1}(x)$ can be determined explicitly, the following technique does not require it.

The numerical technique can be derived through the use of symbolic operator algebra. With a constant stepsize, h, it is possible to introduce an integral index, s, where $s = (x_i - x_0)/h$. A forward difference operator, Δ, can be defined

$$[6] \quad \Delta f_s = f_{s+1} - f_s$$

in which we have used the more concise notation $f_s \equiv f(x_s)$. The forward difference operator is linear. Thus higher order difference operators can be defined by

$$[7] \quad \Delta^j f_s = \Delta^{j-1} f_{s+1} - \Delta^{j-1} f_s$$

[1] B. R. Henry, O. S. Mortensen, A. W. Tarr, and K. Ahmed. Unpublished work.

Can. J. Chem. Downloaded from www.nrcresearchpress.com by 210.87.254.5 on 09/06/12
For personal use only.

The calculated fifferences are conveniently tabulated in a (forward) difference table, e.g.,

f_s	Δf_s	$\Delta^2 f_s$	$\Delta^3 f_s$	$\Delta^4 f_s$
f_{-2}				
	Δf_{-2}			
f_{-1}		$\Delta^2 f_{-2}$		
	Δf_{-1}		$\Delta^3 f_{-2}$	
f_0		$\Delta^2 f_{-1}$		$\Delta^4 f_{-2}$
	Δf_0		$\Delta^3 f_{-1}$	
f_1		$\Delta^2 f_0$		
	Δf_1			
f_2				

[8]

and the interpolating polynomial can be written in terms of these forward differences (21). Two frequently used formulae are the Newton–Gregory forward formula

$$[9] \quad P_{n-1}(x) = \sum_{j=0}^{(1/2)(n-1)} \binom{s}{j} \Delta^j f_0$$

and the Newton–Gregory backward formula

$$[10] \quad P_{n-1}(x) = \sum_{j=0}^{(1/2)(n-1)} \binom{s+j-1}{j} \Delta^j f_{-j}$$

where

$$\binom{s}{j} = [s(s-1)(s-2)\ldots(s-j+1)]/j!$$

$$\binom{s}{0} = 1 \text{ and } \Delta^0 f_0 = f_0$$

Since x_0 has been constrained to lie at the center of the range of x values, eqs. [9] and [10] use only half of the available data. However, the coefficients of the differences in eqs. [9] and [10] can be modified to allow an interpolating polynomial to be fitted to all the available data points (21). For example, the difference table of eq. [8] is associated with the following lozenge diagram for an interpolating polynomial

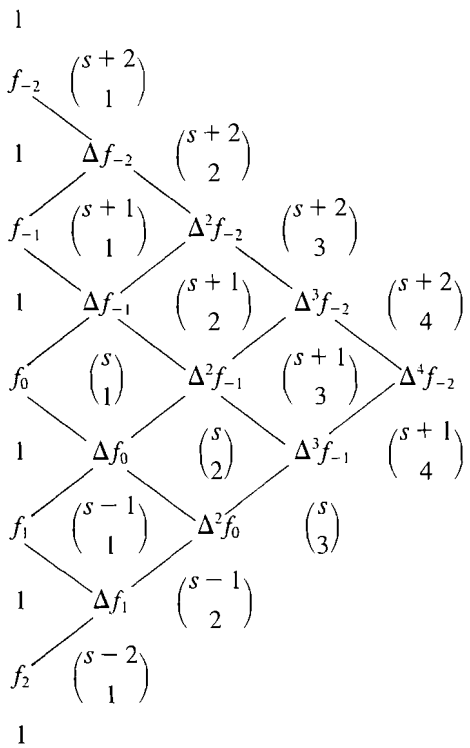

[11]

The modified Newton–Gregory forward formula can be obtained from the lozenge diagram by summing the differences along the top diagonal, with each difference multiplied by the coefficient directly above, i.e.,

$$P_4(x) = \sum_{j=0}^{4} \binom{s+2}{j} \Delta^j f_{-2}$$

The utility of the lozenge diagram, and the accompanying difference table, lies in the property that any path starting at the left and ending at the right (in this example at $\Delta^4 f_{-2}$) will generate the same interpolating polynomial, as long as a few simple rules are obeyed (21).

Lozenge diagrams can be generated from which the values of the derivatives of the interpolating polynomial may be obtained. Small lozenge diagrams for $(dP_{n-1}/dx)_{x_0}$ and $(d^2P_{n-1}/dx^2)_{x_0}$ are available in numerical analysis texts (ref. 21, for example). However, to our knowledge, lozenge diagrams for $(d^3P_{n-1}/dx^3)_{x_0}$ and large diagrams for the lower order derivatives are not available in the literature. We have calculated lozenge diagrams, capable of accepting thirteen data points, for the first, second, and third order derivatives. These results are presented in Figs. 2–4.

The lozenge diagrams are extended (or created) as follows. If the derivatives are evaluated at $x = x_0$, then $s = 0$ and the differential operator, D, can be defined as (21)

$$[12] \quad Df_0 = (1/h) \ln (1 + \Delta) f_0$$

where 1 and Δ are the unit and forward difference operators, respectively. Similarly, higher order differential operators are defined as

$$[13] \quad D^k f_0 = (1/h)^k \ln^k (1 + \Delta) f_0$$

Expansion of the differential operator in terms of the Maclaurin expansion for $\ln (1 + \Delta)$ gives

$$[14] \quad hDf_0 = \sum_{j=1}^{\infty} (-1)^{j+1} (1/j) \Delta^j f_0$$

Equation [14] generates the row of coefficients above the diagonal $\Delta^j f_0$ row in the D^1 lozenge diagram (Fig. 2) from the Newton–Gregory forward formula. The remaining coefficients can be calculated from another property of the lozenge diagram, namely, that the coefficients in a lozenge diagram behave as an upside down, backwards difference table, i.e.,

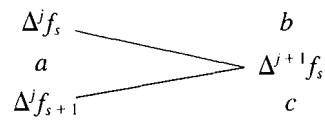

$$\Delta^{j+1} f_s = \Delta^j f_{s+1} - \Delta^j f_s$$

whereas $a = b - c$.

The coefficients above the $\Delta^j f_0$ row in the D^2 lozenge diagram (Fig. 3) are calculated by squaring the Maclaurin expansion for $\ln (1 + \Delta)$.

$$[15] \quad h^2 D^2 f_0 = [\Delta^2 - \Delta^3 + (11/12)\Delta^4 - (5/6)\Delta^5 + (137/180)\Delta^6 - (7/10)\Delta^7 + (363/560)\Delta^8 - (761/1260)\Delta^9 + (7129/12600)\Delta^{10} - (671/1260)\Delta^{11} + (83711/166320)\Delta^{12} + \ldots] f_0$$

Can. J. Chem. Downloaded from www.nrcresearchpress.com by 210.87.254.5 on 09/06/12
For personal use only.

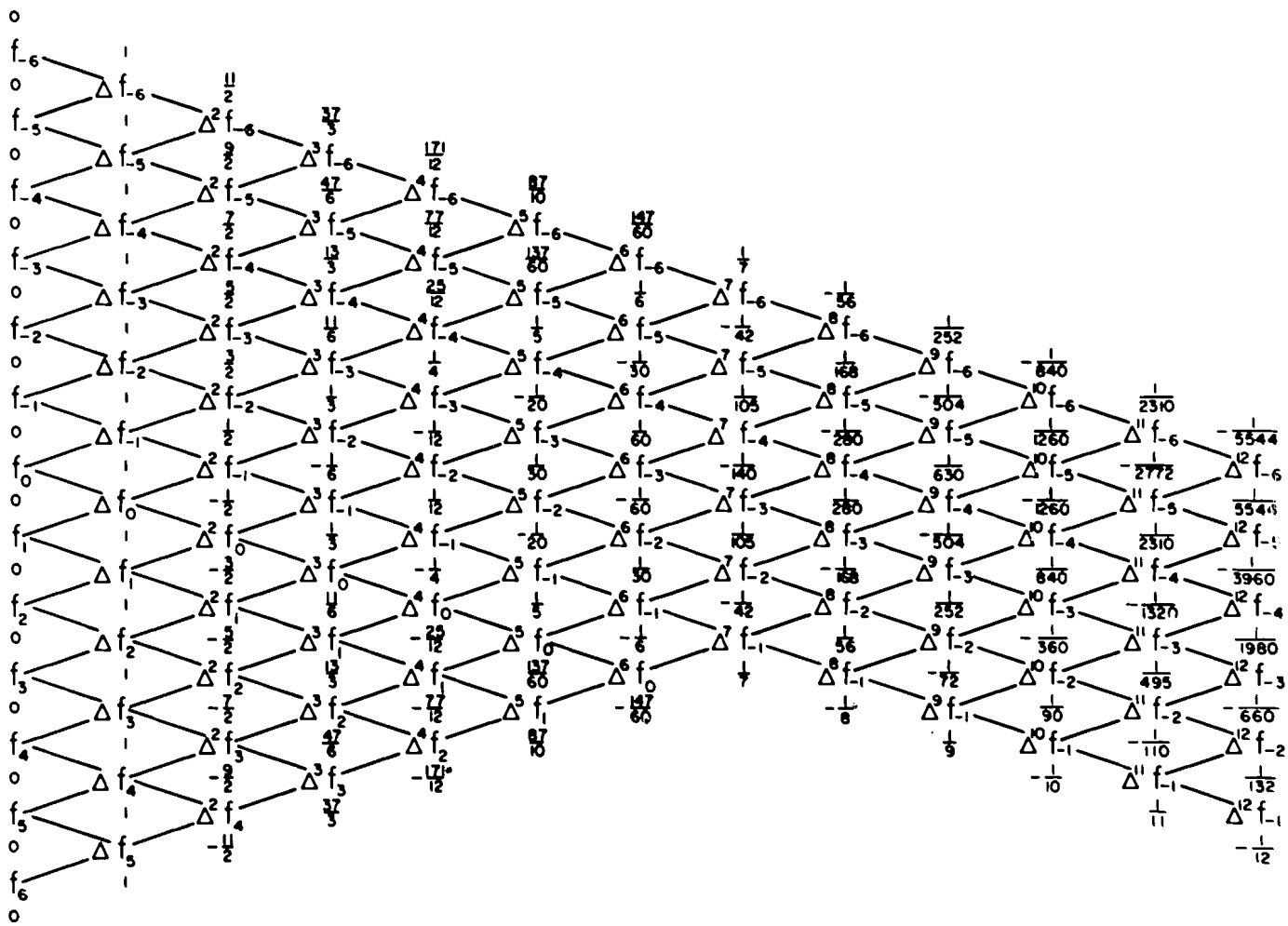

FIG. 2. Lozenge diagram for first order derivatives (hDf_s).

Similarly, the lozenge diagram in Fig. 4 was produced starting with the coefficients from

$$[16]\quad h^3D^3f_0 = [\Delta^3 - (3/2)\Delta^4 + (7/4)\Delta^5 - (15/8)\Delta^6 + (29/15)\Delta^7 - (469/240)\Delta^8 + (29531/15120)\Delta^9 - (1303/672)\Delta^{10} + (16103/8400)\Delta^{11} - (190553/100800)\Delta^{12} + \ldots]f_0$$

The derivative values are calculated from the lozenge diagrams and difference tables in a manner similar to that used to obtain the interpolating polynomial.

Results

The molecular geometry and coordinate system that we used in the calculation of the dipole moment derivatives of methane are shown in Fig. 1*a*. The equilibrium bond length, r_{CH}^0, was taken from an analysis by Herranz and Stoicheff of the high resolution spectrum of the ν_3 Raman band of methane (22). The Cartesian components of the dipole moment were calculated at nine R_1 values (R_1 = 0.89397 (0.05) 1.29397 Å with R_2 = 1.09397 Å). The Cartesian components of $\boldsymbol{\mu}_1$, $\boldsymbol{\mu}_{11}$, and $\boldsymbol{\mu}_{111}$ were estimated with the numerical procedure of the last section, and are given in Table 1. The relatively large number of R_1 values is required in order to obtain reasonable estimates of $\boldsymbol{\mu}_{111}$.

The Cartesian components of $\boldsymbol{\mu}_{12}$ were estimated from a 9 × 9 grid of dipole moment values, i.e., R_1, R_2 = 0.89397 (0.05) 1.29397 Å. The components of $\boldsymbol{\mu}_{12}$ were estimated numerically and are also given in Table 1.

TABLE 1. Local coordinate dipole moment derivatives of methane[a]

Derivatives[b]	*x*	*y*	*z*
$\boldsymbol{\mu}_1$[c] (D Å^{-1})	0	−0.5437	0
$\boldsymbol{\mu}_{11}$[c] (D Å^{-2})	0	−1.06	0
$\boldsymbol{\mu}_{12}$[d] (D Å^{-2})	0.859	0.059	0
$\boldsymbol{\mu}_{111}$[c] (D Å^{-3})	0	1.1	0

[a] The number of significant figures indicates the estimated accuracy of the derivatives of the CNDO/2 calculated dipole moment function and is not intended to imply that the derivatives of the actual dipole moment function are this well known.
[b] All derivatives were evaluated at R_1 = R_2 = 1.09397 Å.
[c] Nine data points were used (R_1 = 0.89397 (0.05) 1.29397 Å, R_2 = 1.09397 Å).
[d] 9 × 9 data point were used (R_1, R_2 = 0.89397 (0.05) 1.29397 Å).

The molecular geometry and coordinate system that we used for the ethane molecule are shown in Fig. 1*b*. The geometry was taken from an analysis by Lafferty and Plyler (23) of the rotational fine structure of the ir (ν_2 + ν_6) combination band of ethane, and from studies of the rotational fine structure of the

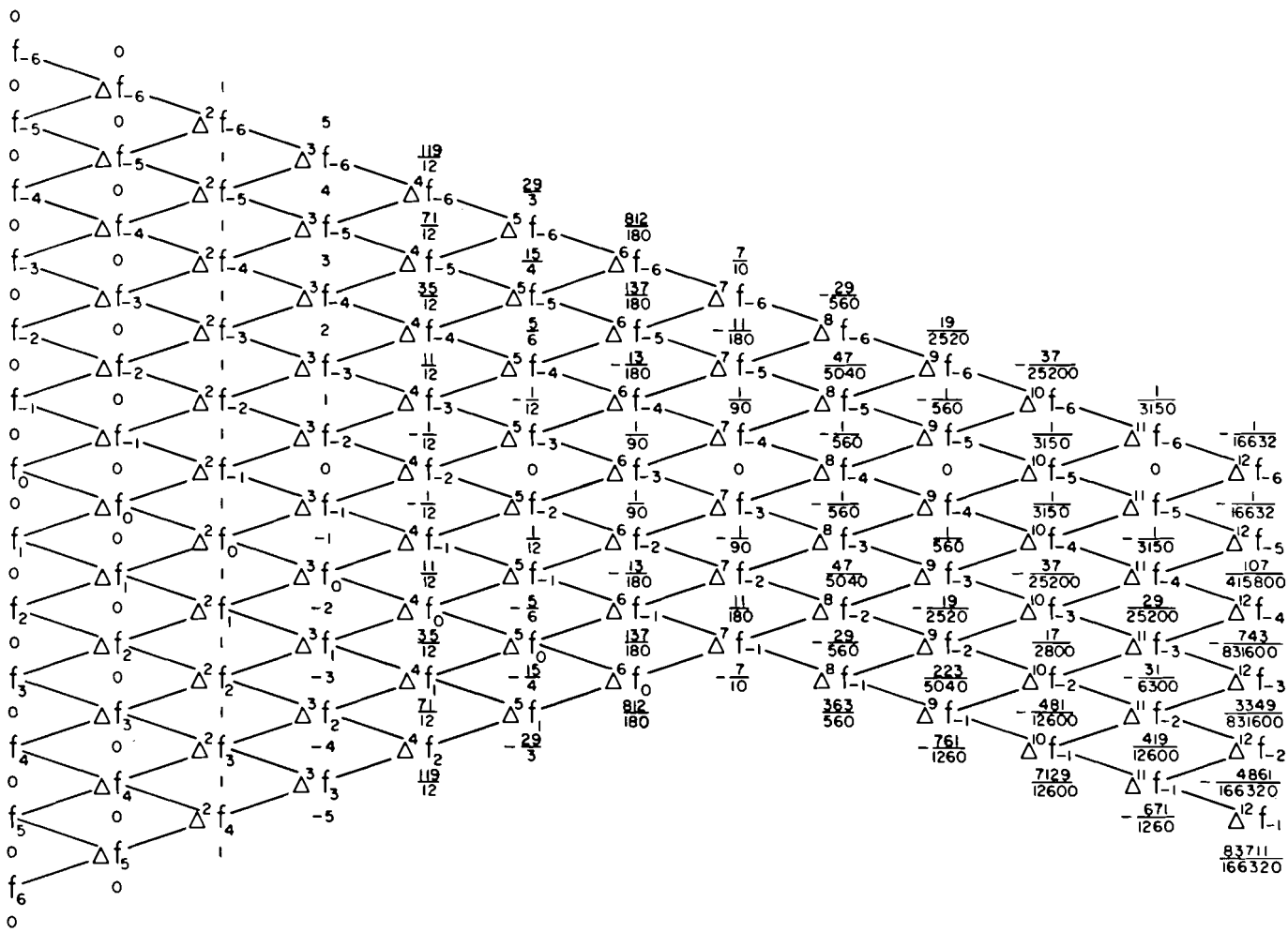

FIG. 3. Lozenge diagram for second order derivatives ($h^2D^2f_s$).

Raman ν_{11} band of ethane (24) and the ir ($\nu_2 + \nu_6$) combination band of perdeuteroethane (25). The molecule was held fixed in its low energy, staggered conformation.

The components of $\boldsymbol{\mu}_1$, $\boldsymbol{\mu}_{11}$, and $\boldsymbol{\mu}_{111}$ were estimated from the dipole moment components calculated at nine R_1 values (R_1 = 0.908 (0.05) 1.308 Å with R_2 = 1.108 Å). As in methane, a 9 × 9 grid (R_1, R_2 = 0.908 (0.05) 1.308 Å) of dipole moments was used to estimate the components of $\boldsymbol{\mu}_{12}$. The dipole moments in the upper right triangular portion of the grid, including the principal diagonal, were calculated directly. The remaining dipole moments were calculated from the transformation matrix.

$$[17]\quad \begin{bmatrix} \mu_x(a,\,b) \\ \mu_y(a,\,b) \\ \mu_z(a,\,b) \end{bmatrix} = \begin{bmatrix} 1 & 0 & 0 \\ 0 & \cos 120^\circ & \sin 120^\circ \\ 0 & \sin 120^\circ & -\cos 120^\circ \end{bmatrix} \begin{bmatrix} \mu_x(b,\,a) \\ \mu_y(b,\,a) \\ \mu_z(b,\,a) \end{bmatrix}$$

The components of the dipole moment derivatives are given in Table 2.

TABLE 2. Local coordinate dipole moment derivatives of ethane[a]

Derivatives[b]	x	y	z
$\boldsymbol{\mu}_1$[c] (D Å^{-1})	−0.3659	−0.7353	0
$\boldsymbol{\mu}_{11}$[c] (D Å^{-2})	−0.939	−1.39	0
$\boldsymbol{\mu}_{12}$[d] (D Å^{-2})	0.127	0.044	0.079
$\boldsymbol{\mu}_{111}$[c] (D Å^{-3})	0.05	0.35	0

[a] See footnote *a* of Table 1.
[b] All derivatives were evaluated at $R_1 = R_2$ = 1.108 Å.
[c] Nine data points were used (R_1 = 0.908 (0.05) 1.308 Å, R_2 = 1.108 Å).
[d] 9 × 9 data points were used (R_1, R_2 = 0.908 (0.05) 1.308 Å).

Discussion

The results of Tables 1 and 2 can be compared to other results from the literature only in a very limited sense. What other results do exist relate primarily to $\boldsymbol{\mu}_1$. Newton and Person have reported atomic polar tensors calculated from experimental ir intensities of methane (6). They reported two polar tensors due to the uncertainty in the signs of the dipole moment derivatives with respect to normal coordinates. The two values of $\boldsymbol{\mu}_1$, contained in these tensors, are -0.667 ± 0.038 D Å^{-1} and -0.52 ± 0.13 D Å^{-1}, with the former value corresponding to the preferred sign combination. The same authors also reported hydrogen polar tensors derived from CNDO/2 calculations and from the *ab initio* calculations of Meyer and Pulay (26). These tensors give $\boldsymbol{\mu}_1$ values of -0.542 D Å^{-1} and -0.845 D Å^{-1}, respectively. Kornblum has made several calculations of the values of $\boldsymbol{\mu}_1$ for the CH_n (n = 1–4) series using a STO-3G basis set (27). The preferred calculation for methane

Can. J. Chem. Downloaded from www.nrcresearchpress.com by 210.87.254.5 on 09/06/12
For personal use only.

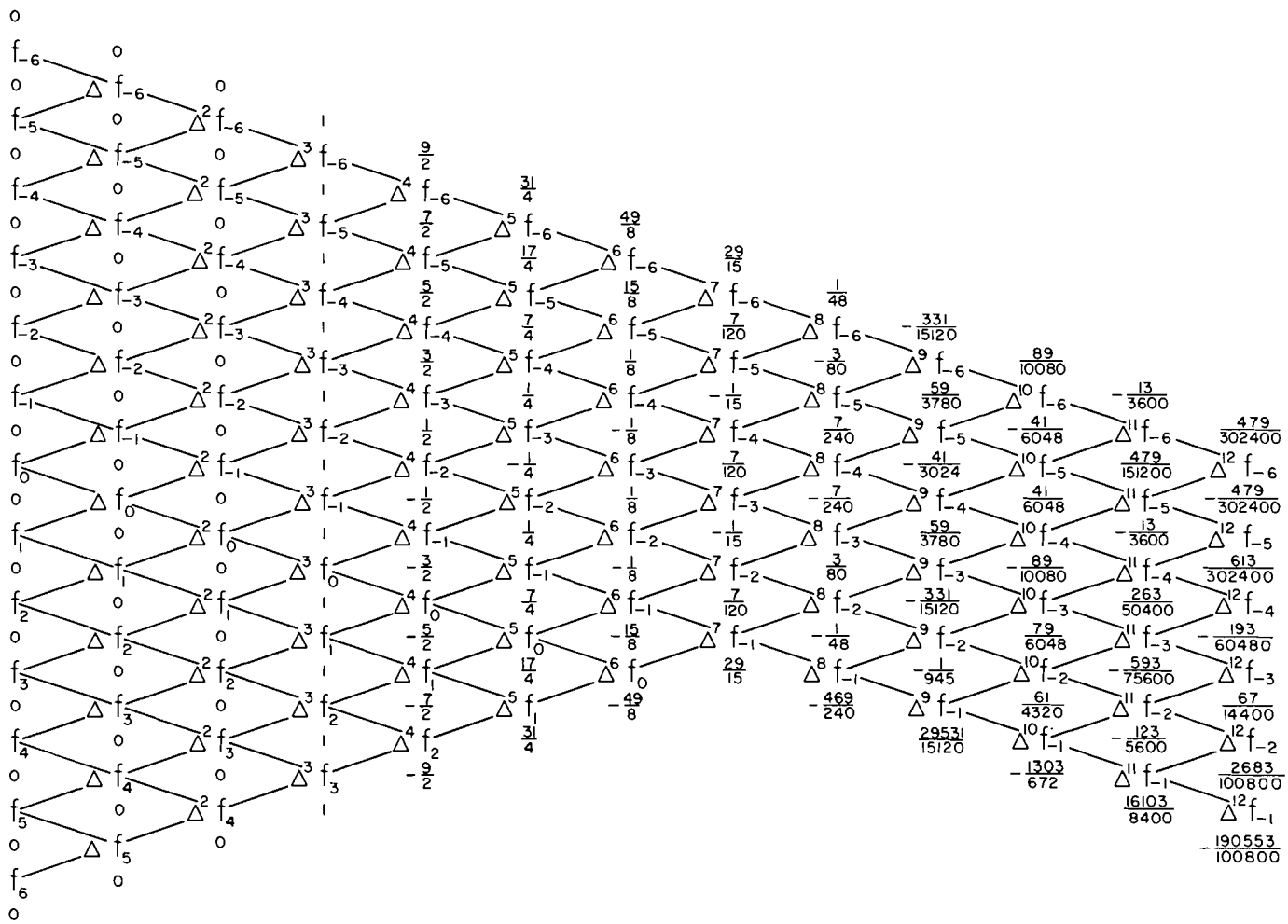

FIG. 4. Lozenge diagram for third order derivatives ($h^3D^3f_x$).

gave $\boldsymbol{\mu}_1 = -0.444$ D Å^{-1}. Tamagake *et al.* calculated values of $\boldsymbol{\mu}_1 = -0.85$ D Å^{-1} and $\boldsymbol{\mu}_{11} = -1.30$ D Å^{-2} from their 4-31G calculations on methane (10). It is not surprising that these results are in moderately good agreement with each other and with the results of Table 1. The differences primarily reflect the relative accuracy of the input data, i.e., the dipole moments, and not differences in the theoretical techniques used to obtain the dipole moment derivatives. It is this latter theme, particularly as it relates to higher order dipole moment derivatives, that is the principal concern of this work.

Thus we have evaluated our procedure using a number of internal tests. The *y*-components of the pure derivatives of the dipole moment of methane were calculated with differing numbers of dipole moment values. The results of this "convergence" test are given in Table 3. Table 3 demonstrates that an increase in the number of data points past nine has no significant effect on the values of $\boldsymbol{\mu}_1$ and $\boldsymbol{\mu}_{11}$. The value of $\boldsymbol{\mu}_{111}$ changes slightly due to round-off errors (*vide infra*). Therefore, additional values bracketing the central set of nine values do not significantly alter the form of the calculated dipole moment function at r_{CH}^0. The "convergence" of $\boldsymbol{\mu}_{12}$ was not calculated but is expected to be similar to that of $\boldsymbol{\mu}_{11}$.

The "convergence" observed in Table 3 does not guarantee the accuracy of the numerical procedure. Round-off errors due to truncation of the computer generated dipole moment values can markedly affect the values of the higher order derivatives. The round-off effects become serious when the stepsize is small enough that the truncation error is comparable to $\boldsymbol{\mu}(x + h) - \boldsymbol{\mu}(x)$.

TABLE 3. Convergence test for methane

Number of data points	$(\mu_1)_y^a$ (D Å^{-1})	$(\mu_{11})_y^a$ (D Å^{-2})	$(\mu_{111})_y^a$ (D Å^{-3})
3	−0.5432	−1.0560	—
5	−0.5436	−1.0557	1.0800
7	−0.5437	−1.0556	1.1100
9	−0.5437	−1.0556	1.1497
11	−0.5437	−1.0556	1.1844
13	−0.5437	−1.0556	1.2148

[a] All derivatives were evaluated at $R_1 = R_2 = 1.09397$ Å.

In order to determine the appropriate stepsize, and to obtain an estimate of the truncation errors, we used an analytically compact, two dimensional exponential test function, $f(x, y) = 0.036 \exp(x + y)$. The pre-exponential factor was chosen such that the $f(x, y)$ surface around (1, 1) would roughly mimic the *y*-component of the distorted geometry dipole moments of dichloromethane. Specifically, the pre-exponential factor was calculated to meet the condition that $f(1 + h, 1) - f(1, 1) = \mu_y(R_1^0 + h, R_2^0) - \mu_y(R_1^0, R_2^0)$, for $h = 0.005$ Å. Although the value of $f(1, 1) = 0.266$ did not reproduce the magnitude of the equilibrium geometry dipole moment of dichloromethane, 1.65 D, the gradients of the $\mu_y(R_1, R_2)$ and $f(x, y)$ surfaces were

Can. J. Chem. Downloaded from www.nrcresearchpress.com by 210.87.254.5 on 09/06/12
For personal use only.

Can. J. Chem. Downloaded from www.nrcresearchpress.com by 210.87.254.5 on 09/06/12
For personal use only.

similar over the regions considered when the stepsize was 0.05 Å. Thus the $f(x, y)$ test function was a good imitation of the y component of the $\mu(R_1, R_2)$ function even though the two functions were shifted from one another by a constant value. The shift constant was of no consequence in the evaluation of the numerical differentiation procedure.

Errors in numerical differentiation were obtained by comparison of the analytical and numerical derivatives of the test function. The test function values used to obtain the numerical derivatives were truncated, with rounding, to the same degree as the computer generated dipole moment values. Large errors in f_{111} resulted when the technique was tested with nine points and a stepsize of 0.005 Å. The effect of round-off error was reduced by an increase in the stepsize. With a stepsize of 0.05 Å, the values of the numerical derivatives differed by 0.01%, 3%, and 12% from the analytical values of f_1, f_{11}, and f_{111}, respectively. The mixed second derivative was not calculated with this stepsize since previous testing with $h = 0.02$ Å had shown that the quality of f_{11} and f_{12} were similar (9% and 4% low, respectively, as compared to the analytical derivatives).

An alternative to increasing the stepsize to minimize the effects of round-off error would have been a modification of the INDOFPT program to allow the generation of more precise dipole moment values. This option was not undertaken even though, in theory, the mapping of the dipole moment function would be somewhat better with a smaller stepsize. Such a modification is clearly not justified given the accuracy of the CNDO/2 calculation.

The test function was also used to investigate the type of convergence illustrated in Table 3, as the number of data points is increased. Round-off errors in a difference table increase in magnitude toward the right side of the table. Thus, as the number of data points increases, the difference table becomes larger and the round-off errors in the rightmost portion of the table increase. Therefore, round-off errors impose an effective upper limit on the number of points that can be used to estimate meaningful values of the derivatives. Calculations with the test function showed that the discrepancy between analytical and numerical derivatives increases very slowly, with increasing number of points, for f_1 and f_{11}, and by about 2% for each additional pair of points for f_{111}. A decrease in the number of data points decreases the effects of round-off errors but also decreases the accuracy of the mapping of the function. In the present work, the appropriate trade-off between these two factors was found to occur at nine points.

As we have already noted for methane (Table 3), the round-off errors do not significantly affect μ_1 and μ_{11} when up to thirteen dipole moment values are used. Similar results are obtained for ethane. The values of μ_{111} given in Tables 1 and 2 change in their least significant digit. Thus, for thirteen data points, $(\mu_{111})_y$ changes by 0.1 D Å^{-3} and 0.02 D Å^{-3} for methane and ethane, respectively.

On the basis of these tests, we conclude that numerical differentiation with interpolating polynomials gives very good estimates of theoretical dipole moment derivatives, up to at least the second order derivatives. The numerical third order derivatives, although subject to larger errors, are considered to be good estimates as well. One other observation supports this conclusion. In our calculation of the local coordinate dipole moment derivatives of dichloromethane,[1] the Cartesian coordinate system was chosen so that the z-axis bisected the Cl—C—Cl angle and the z-axis lay in the H—C—H plane. Therefore, by symmetry, $(\mu_{12})_y = 0$. The numerical value that we calculated using 9×9 data points and a stepsize of 0.05 Å was -5×10^{-7} D Å^{-2}, which provides another indication of the level of accuracy of the numerical technique.

Acknowledgements

We are grateful to the Natural Sciences and Engineering Research Council of Canada for a postgraduate fellowship (A.W.T.) and other financial assistance.

1. B. R. HENRY. *In* Vibrational spectra and structure. Vol. 10. *Edited by* J. R. Durig. Elsevier, New York. 1981. p. 269 and references therein.
2. (*a*) J. A. POPLE and D. L. BEVERIDGE. Approximate molecular orbital theory. McGraw-Hill, New York. 1970; (*b*) J. N. MURRELL and A. J. HARGET. Semi-empirical SCF MO theory of molecules. Wiley, New York. 1972. Chapt. 3 and references therein.
3. G. A. SEGAL and M. L. KLEIN. J. Chem. Phys. **47**, 4236 (1967).
4. G. JALSOVSZKY and P. PULAY. J. Mol. Struct. **26**, 277 (1975).
5. A. J. VAN STRATEN and W. M. A. SMIT. J. Mol. Spectrosc. **65**, 202 (1977).
6. J. H. NEWTON and W. B. PERSON. J. Phys. Chem. **82**, 226 (1978).
7. Z. C. KORNBLUM and T. ISHIDA. J. Chem. Phys. **69**, 1814 (1978).
8. J. PACANSKY and B. SCHRADER. J. Chem. Phys. **78**, 1033 (1983).
9. M. S. BURBERRY and A. C. ALBRECHT. J. Chem. Phys. **70**, 147 (1979).
10. K. TAMAGAKE, S. HYODO, and T. FUJIYAMA. Bull. Chem. Soc. Jpn. **55**, 1267 (1982).
11. S. HYODO, K. TAMAGAKE, and T. FUJIYAMA. Bull. Chem. Soc. Jpn. **55**, 1272 (1982).
12. K. TAMAGAKE, S. HYODO, and T. FUJIYAMA. Bull. Chem. Soc. Jpn. **55**, 1277 (1982).
13. J. DEL BENE and H. H. JAFFÉ. J. Chem. Phys. **48**, 1807 (1968); **48**, 4050 (1968); **49**, 1221 (1968); **50**, 1126 (1969).
14. G. C. LIE, J. HINZE, and B. LIU. J. Chem. Phys. **59**, 1872 (1973); **59**, 1887 (1973).
15. R. DITCHFIELD, W. J. HEHRE, and J. A. POPLE. J. Chem. Phys. **54**, 724 (1971).
16. P. C. HARIHARAN and J. A. POPLE. Theoret. Chim. Acta, **28**, 213 (1973).
17. P. A. DOBOSH. Quantum Chemistry Program Exchange, **11**, 141 (1979).
18. W. J. HEHRE, R. F. STEWART, and J. A. POPLE. J. Chem. Phys. **51**, 2657 (1969).
19. W. J. HEHRE, W. A. LATHAN, R. DITCHFIELD, M. D. NEWTON, and J. A. POPLE. Quantum Chemistry Program Exchange, **11**, 236 (1979).
20. R. C. WEAST (*Editor*). Handbook of Chemistry and Physics. 59th ed. CRC Press Inc., West Palm Beach. 1978–79. p. E-64.
21. C. F. GERALD. Applied numerical analysis. 2nd ed. Addison Wesley Publishing Company, Inc., Don Mills. 1978. Chapts. 3, 4.
22. J. HERRANZ and B. P. STOICHEFF. J. Mol. Spectrosc. **10**, 448 (1963).
23. W. J. LAFFERTY and E. K. PLYLER. J. Chem. Phys. **37**, 2688 (1962).
24. J. ROMANKO, T. FELDMAN, and H. L. WELSH. Can. J. Phys. **33**, 588 (1955).
25. H. C. ALLEN, JR. and E. K. PLYLER. J. Chem. Phys. **31**, 1062 (1959).
26. W. MEYER and P. PULAY. J. Chem. Phys. **56**, 2109 (1972).
27. Z. C. KORNBLUM. J. Chem. Phys. **75**, 5816 (1981).

The conversions of isothiazolium salts into thiophenecarboxylic ester derivatives

DAVID M. MCKINNON,[1] K. ANN DUNCAN, AND LESLEY M. MILLAR
Department of Chemistry, University of Manitoba, Winnipeg, Man., Canada R3T 2N2

Received March 4, 1983

This paper is dedicated to Professor Gerald E. Dunn on the occasion of his 65th birthday

DAVID M. MCKINNON, K. ANN DUNCAN, and LESLEY M. MILLAR. Can. J. Chem. **62**, 1580 (1984).

Several 3-aminothiophene-2-carboxylic ester derivatives are made by reaction of potassium 3-ethoxy-3-oxopropanoate with isothiazolium salts or by reaction with 2-ethoxy-2-oxoethylidenedimethylsulfurane. In the latter case deaminated products are also isolated. These products are consistent with initial nucleophilic attack on the sulfur atom of the isothiazolium salt. In one case a pyrrole derivative is formed by a novel rearrangement of an intermediate aziridine derivative. Some further derivatives of 3-benzylaminobenzo[*b*]thiophene are described.

DAVID M. MCKINNON, K. ANN DUNCAN et LESLEY M. MILLAR. Can. J. Chem. **62**, 1580 (1984).

On a préparé plusieurs esters de l'acide amino-3 thiophène carboxylique-2 en faisant réagir l'éthoxy-3 oxo-3 propanoate de potassium avec des sels d'isothizaolium ou avec l'éthoxy-2 oxo-2 éthylidènediméthyl-sulfuranne. Dans ce dernier cas, on a également isolé des produits de désamination. Ces produits correspondent à une attaque nucléophile initiale sur l'atome de soufre du sel d'isothiazolium. Dans un cas, il se forme un dérivé du pyrrole selon une nouvelle transposition d'un dérivé aziridine intermédiaire. On décrit quelques autres dérivés de le benzylamino-3 benzo[*b*]thiophène.

[Traduit par le journal]

Can. J. Chem. Downloaded from www.nrcresearchpress.com by 210.87.254.105 on 09/06/12
For personal use only.

Introduction

Nucleophilic attack by some stable carbanions at the ring sulfur atom of both monocyclic isothiazolium salts **1** and 1,2-benzisothiazolium salts has been demonstrated (1, 2). The final isolated products are frequently thiophene or benzo[*b*]thiophene derivatives respectively, formed by recyclization of initial reaction products. For example, the reaction of phenacylidenedimethylsulfurane with 2,5-diphenylisothiazolium perchlorate (**1***a*) afforded 3-anilino-2-benzoyl-5-phenylthiophene. An alternative approach to this type of compound used sodium benzoylacetate, behaving as a potential phenacyl ion, reacting with 2,5-diphenyl-3-methylthioisothiazolium perchlorate (**1***b*). In this case the final aromatization is effected by loss of a group that was originally on the isothiazolium ring. In view of the potential of aminothiophenecarboxylic acids in the synthesis of fused thiophene heterocycles, analogous to the preparation of fused heterocycles from anthranilic acid derivatives, we have investigated their preparation by methods analogous to these.

Results and discussion

Since we have earlier demonstrated that in these reactions sodium benzoylacetate functions as a potential phenacyl ion, accordingly, in this work, we used potassium 3-ethoxy-3-oxopropanoate as a source of the anion of ethyl acetate. Thus, when it was treated with 2-benzyl-3-methylthio-1,2-benzisothiazolium perchlorate (**1***c*), ethyl 3-benzylaminobenzo[*b*]thiophene-2-carboxylate (**2***b*) was obtained in high yield. This reaction likely proceeds by initial attack of the anion on the ring sulfur atom, forming an acyclic intermediate which then recyclizes, forming the thiophene by loss of methanethiol (Scheme 1, X = SCH_3). Likewise 2-methyl-3-methylthio-1,2-benzisothiazolium perchlorate (**1***d*) gave ethyl 3-methylaminobenzo[*b*]thiophene-2-carboxylate (**2***c*).

Treatment of monocyclic isothiazolium salts **1***e*,*g* similarly successfully gave the thiophene-2-carboxylic ester **3***b* in moderate yield. In these cases the final aromatization is by loss of an amine function, as these compounds lack alkylthio leaving groups in suitable positions. For the compound **1***h*, the thiophene derivative **3***c* was obtained along with methyl 3-methylamino-2-phenyldithiopropenoate (**4**). Had attack of the nucleophile occurred at carbon-5 of the salt, methanethiol would likely have been eliminated to provide a reductant, as is known for some 2,1-benzisothiazolium cation reactions (3).

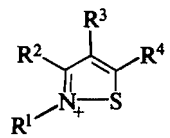

1

a R^1 = Ph; R^2 = R^3 = H; R^4 = Ph
b R^1 = Ph; R^2 = SMe; R^3 = H; R^4 = Ph
c R^1 = $PhCH_2$; R^2 = SMe; R^3, R^4 = —(CH=CH)$_2$—
d R^1 = Me; R^2 = SMe; R^3, R^4 = —(CH=CH)$_2$—
e R^1 = Ph; R^2 = H; R^3 = Ph; R^4 = H
f R^1 = Ph; R^2 = H; R^3 = Ph; R^4 = SMe
g R^1 = Me; R^2 = H; R^3 = Ph; R^4 = H
h R^1 = Me; R^2 = H; R^3 = Ph; R^4 = SMe
i R^1 = R^2 = Me; R^3 = R^4 = H

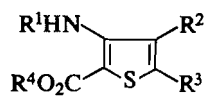

2

a R^1 = Me; R^2 = H; R^3 = Ph; R^4 = Et
b R^1 = $PhCH_2$; R^2, R^3 = —(CH=CH)$_2$—; R^4 = Et
c R^1 = Me; R^2, R^3 = —(CH=CH)$_2$, R^4 = Et
d R^1 = Ph; R^2 = Ph; R^3 = H; R^4 = Et
e R^1 = Ph, R^2 = Ph; R^3 = SMe; R^4 =Et
f R^1 = Me; R^2 = Ph, R^3 = H; R^4 = Et
g R^1 = Me; R^2 = Ph; R^3 = SMe; R^4 = Et
h R^1 = Ph; R^2 = Ph; R^3 = SMe; R^4 = Me

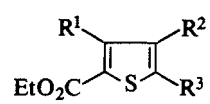

3

a R^1 = R^2 = H, R^3 = Ph
b R^1 = H, R^2 = Ph; R^3 = H
c R^1 = H, R^2 = Ph, R^3 = SMe

[1]Author to whom correspondence may be addressed.

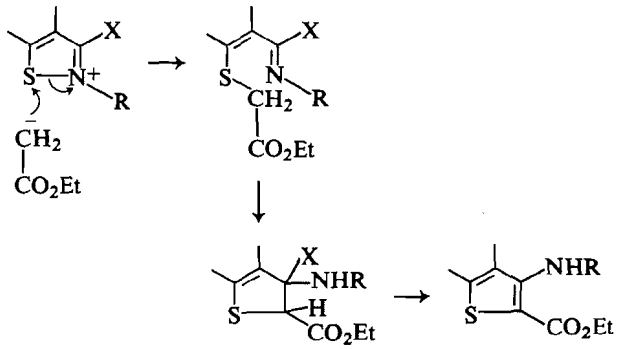

SCHEME 1

Indeed, treatment of the salt **1***h* with sodium methanethiolate did provide the aminodithioester **4** in good yield. However, we have not been able to isolate any reaction product arising from nucleophilic attack at carbon.

Another possible approach to the desired amino esters would be by using the anion of ethyl acetate stabilized as an ylid. Accodingly, 2-ethoxy-2-oxoethylidenedimethylsulfurane was treated with the five monocyclic isothiazolium salts **1***a*, *e*–*h*, and in each case we obtained the expected 3-aminothiophene-2-carboxylic ester derivatives **2***a*, *d*–*g*, i.e. products consistent with initial attack of the ylid at ring sulfur (Scheme 2). However, the intermediate **5** could form the ester **2** in several ways. One possible pathway is via an aziridine **6** (Scheme 2, path a) as suggested (4) by analogy with the known formation of aziridines from imines and sulfur ylids (5). Nevertheless, we consider that another pathway, involving a β-elimination, is more likely, especially for the formation of unsaturated esters of type **2** (Scheme 2, path b). This is discussed below.

In three cases, **1***a*, *e*, and *f* the aminoesters **2** were accompanied by products which did not contain an amino function, i.e. **3***a*, *b*, and *c* respectively. Likewise **1***h* also gave **3***c* (the nitrogen atom and substituent are lost in the reaction). One possibility is that there is some reduction stage in the reaction, involving loss of the sulfonium moiety, so that eventual aromatization ocurs by loss of amine. This reduction may be by the ethanol solvent or by a nucleophilic displacement on the exocyclic sulfur atom. Various stabilized carbanions or equivalent are known to be displaceable from the corresponding sulfides (6–8). Another possibility is that there may be bond formation between the sulfur and nitrogen atoms, producing a four-membered ring or transition state analogous to the intermediates of Wittig reactions, with final elimination of an azasulfonium ylid (Scheme 2, path c). Although the occurrence of "σ-tetravalent" sulfur in the four-membered ring is not impossible (9), there do not appear to be any earlier literature reports of a reaction such as path c, and it may represent an unusual reaction product of sulfonium ylids.

When the isothiazolium salt **1***g* was treated with ylid, the pyrrole derivative **7** was obtained as a minor product. A possible source for its formation would be the episulfide **8**, since it is known that these readily extrude sulfur, especially when aromatic structures are produced (10). The episulfide itself could be formed from the aziridine **6** by a number of possible rearrangement mechanisms. Although we have shown one ionic mechanism (Scheme 3), there are in fact a number of methods, involving other ionic mechanisms or pericyclic reactions, whereby the conversion might be effected. The pyrrole **7** has not been previously synthesized. Its structure was proved by hydrolysis and decarboxylation to the known 1-methyl-3-phenylpyrrole. While isothiazolium salts have been used in the preparation of other heterocyclic systems, these reactions have usually involved retention of the sulfur atom. This reaction therefore is of a new type, where the nitrogen atom is retained instead, and it may have potential in the synthesis of pyrrole derivatives.

Another plausible mechanism for the formation of the aziridines **6** would be from a carbene **9**, produced by α-elimination from the sulfonium ylid, such as are known (11).

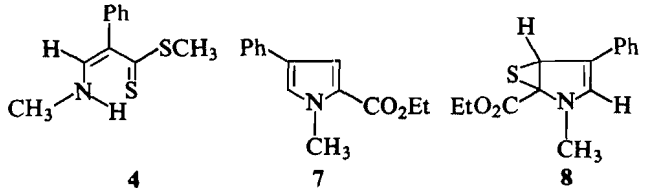

4 **7** **8**

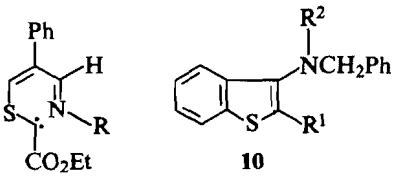

9 **10**

a R¹ = CO_2H; R^2 = H
b R¹ = H; R^2 = CO_2Et
c R¹ = CO_2Et; R^2 = CO_2Et
d R¹ = $CON(CH_2)_4$; R^2 = H

Whatever the actual mechanism for the formation of the pyrrole **7**, in each case an aziridine appears a probable inter-

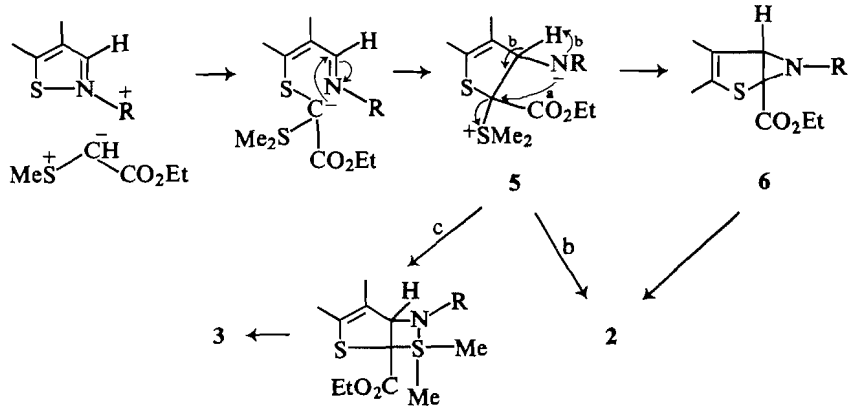

SCHEME 2

Can. J. Chem. Downloaded from www.nrcresearchpress.com by 210.87.254.105 on 09/06/12
For personal use only.

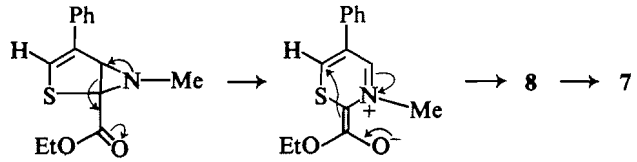

SCHEME 3

mediate. Since there appears to be little reason why any such aziridine should not convert to the corresponding pyrrole, and yet pyrrole products were not obtained from the isothiazolium salts **1***a*, *e*, *f*, we favor the β-elimination pathway (Scheme 2, path b) for these. Possibly in these cases the nitrogen atom, bearing an aryl substituent, would be less nucleophilic and less able to displace dimethyl sulfide to form the aziridine. However, in one case, **1***h*, which is an *N*-methylisothiazolium salt, no pyrrole was obtained. Other factors may therefore be implicated.

The reaction of 2,3-dimethylisothiazolium perchlorate (**1***i*) with the ylid gave a number of products which we have been unable to identify.

We attempted to produce aminothiophenecarboxylic esters using a nitrogen ylid, the anion of *N*-(2-methoxy-2-oxoethyl)-pyridinium bromide, and treatment with the isothiazolium salt (**1***f*) gave methyl 3-anilino-5-methylthio-4-phenylthiophene-2-carboxylate (**2***h*). The yield of this, however, was lower than the ester formed using the sulfonium ylid.

Since N-substituted anthranilic acids serve as synthetic precursors of isatoic anhydrides and thence 2,1-benzisothiazoles (12, 13), we attempted comparable conversions of the amino-acid **10***a*, produced by basic hydrolysis of the ester **2***b*, in an attempt to prepare thieno[3,2-*c*]isothiazole derivative. The acid **10***a* only gave the urethane **10***b* on treatment with ethyl chloroformate. The acid contains structural elements resembling anthranilic acids and thiophene-2-carboxylic acids, both of which decarboxylate readily. Treatment of **2***b* directly gave the ester **10***c*, and thionation of the amide **10***d*, prepared from the ester **2***b* and pyrrolidine, gave a complex mixture from which no thioamides, possible precursors of isothiazoles, could be isolated.

Although the nitrogen atom in compound **10***d* would be expected to have sp^2 hybridization, due to its attachment both to a thiophene ring and a carbonyl group, the neighboring benzylic protons were evident as two doublets, indicating their non-equivalency. It thus appears that steric constraints force the nitrogen atom into an sp^3 hybridization, rendering the benzylic protons diastereotopic. Rapid inversion at nitrogen is also precluded by steric hindrance.

Experimental

The ^{1}H nmr spectra were obtained in deuteriochloroform solution using tetramethylsilane as an internal standard, on a Varian model E.M. 360 spectrometer. Mass spectra were obtained on a Finnigan model 1015 spectrometer, and thick-layer chromatography (tlc) was performed on "Camag" silica gel type D.S.F.5 supplied by Terochem laboratories. Where necessary, solutions were dried over anhydrous magnesium sulfate.

*Reactions of isothiazolium salts (**1**) with potassium 3-ethoxy-3-oxopropanoate*

To the isothiazolium salt (~1 mmol) in anhydrous ethanol (10 mL) was added potassium 2-ethoxy-2-oxopropanoate (1.5 mmol) and the mixture heated gently until complete reaction (~5 min). The solutions were diluted with water and extracted with chloroform. The dried evaporated extracts were thick oils which were purified by chromatography using benzene or chloroform as eluents, depending on the polarity of products. In some cases the products crystallized on standing. For the product **2***b* no chromatography was necessary and it was crystallized from ethanol. Results are summarized in Table 1.

*Reactions of isothiazolium salts (**1**) with 2-ethoxy-2-oxoethylidene-dimethylsulfurane*

2-Ethoxy-2-oxoethyldimethylsulfonium bromide (1.5 mmol) in ethanol (10 mL) was treated with sodium ethoxide (1.5 mmol) and to the solution was added the isothiazolium salt (1 mmol). The mixtures were warmed until homogeneous and the solutions were worked up as above. Results are summarized in Table 2. In general, although both thiophenecarboxylic esters (**3**) and aminothiophenecarboxylic esters (**2**) chromatographed at similar R_f values, satisfactory separation was obtained by varying the eluents.

*Reaction of 2,4-diphenyl-3-methylthioisothiazolium perchlorate with N-(2-methoxy-2-oxoethyl)pyridinium bromide to form **2**h*

To a solution of sodium (46 mg) dissolved in ethanol (10 mL) was added the pyridinium salt (232 mg, 1.0 mmol) and the mixture swirled until homogeneous. Then the isothiazolium salt (384 mg, 1.0 mmol) was added, and the mixture warmed until homogeneous. Work-up by the procedures used above for sulfonium ylids gave the ester as an oil which crystallized on standing. It was finally recrystallized from ethanol as pale yellow needles, mp 158°C (19%).

The nmr spectrum, δ: 2.47 (3H, s, S—CH_3), 3.71 (3H, s, CO_2Me), 6.5–7.4 (10H, m, aromatic), 8.45 (broad N—H). The mass spectrum: M^+ 355, M calcd. 355. *Anal.* calcd. for $C_{19}H_{17}NO_2S_2$: C 64.23, H 4.79, N 3.94, S 18.03; found: C 64.41, H 4.82, N 3.81, S 18.22.

*Reduction of 2-methyl-5-methylthio-4-phenylisothiazolium perchlorate (**1**h) by methanethiol to methyl 3-methylamino-2-phenyldithiopropenoate (**4**)*

The salt **1***h* (1.0 mmol) was added to a sodium methanethiolate solution (prepared by passing excess methanethiol into a solution of sodium ethoxide) and the mixture warmed until homogeneous, then diluted with water. The dried chloroform extract gave yellow needles on evaporation. Recrystallization from hexane gave **4** as long yellow needles (60%). The product was identical (mixture mp, R_f, to that isolated above). The nmr spectrum, δ: 2.5 (3H, s, S—CH_3), 3.1–3.2 (3H, d, N—CH_3), 6.8–7.1 (1H, s, vinyl), and 7.2–7.5 (5H, m, aromatic).

*3-Benzylaminobenzo[b]thiophene-2-carboxylic acid (**10**a)*

The ester **2***b* (1 g, 3.02 mmol) in ethanol (10 mL) was treated with 20% aqueous sodium hydroxide solution (5 mL) and refluxed 3 h. The solvent was evaporated and the residue in water (10 mL) was adjusted to pH 4 with concentrated hydrochloric acid. The amino acid precipitated as a pale yellow powder, mp 125–126°C (94%), which was collected and dried. This was sufficiently pure for further reactions without recrystallization. The mass spectrum: M^+ 283, M calcd.: 283. *Anal.* calcd. for $C_{10}H_{13}NO_2S$: C 67.84, H 4.59, N 4.95, S 11.31; found: C 67.66, H 4.81, N 4.63, S 11.52.

*Ethyl N-benzyl-N-(3-benzo[b]thienyl)carbamate (**10**b)*

The acid **10***a* (0.707 g, 2.5 mmol) in ethyl chloroformate (10 mL) was refluxed 3 h. Evaporation of the solution yielded a viscous oil which crystallized on standing under cyclohexane. The material was recrystallized from cyclohexane as colorless needles, mp 76–78°C (85%). The nmr spectrum, δ: 1.15 and 4.20 (—CH_2—CH_3), 4.90 2H, s, CH_2—Ph), 6.99 (1H, s, the thiophene), 7.15–7.95 (9H, m, aromatic). *Anal.* calcd. for $C_{18}H_{17}NO_2S$: C 69.45, H 5.47, N 4.50, S 10.29; found: C 69.28, H 5.20, N 4.69, S 10.51.

*Reactions of ethyl 3-benzylaminobenzo[b]thiophene-2-carboxylate (**2**b) with pyrrolidine to form N-pyrrolidinyl-3-benzylamino-benzo[b]thiophene-2-carboxamide (**10**c)*

The ester **2***b* (1 g, 3.2 mmol) in pyrrolidine (10 mL) was heated in a closed vessel at 130°C for 16 h. Evaporation of the solution gave a semicrystalline oil which was crystallized from methanol as colorless

Can. J. Chem. Downloaded from www.nrcresearchpress.com by 210.87.254.105 on 09/06/12
For personal use only.

TABLE 1. Reactions of isothiazolium salts with potassium 3-ethoxy-3-oxopropanoate

Salt	Product	Yield (%)	Melting point (°C)	Formula	Analysis: Calculated C	H	N	S	Found C	H	N	S
1*c*	**2***b*	74	97–99	$C_{18}H_{17}NO_2S$	69.45	5.47	4.50	10.29	69.63	5.31	4.62	10.41
1*d*	**2***c*	89	41–42	$C_{12}H_{13}NO_2S$	61.28	5.53	5.96	13.62	61.36	5.61	5.81	13.44
1*e*	**3***d*	88	*	$C_{13}H_{12}O_2S$	67.22	5.21	—	13.80	67.28	5.31	—	13.80
1*g*	**3***d*	47	*									
1*h*	**3***c*	38	75–77	$C_{14}H_{14}O_2S_2$	60.40	5.07	—	23.03	60.27	5.09	—	22.80
1*h*	**4**	14	130–132	$C_{11}H_{13}NS$	59.15	5.87	6.27	28.71	59.14	5.83	6.16	28.74

*This product could not be crystallized.

TABLE 2. Reactions of isothiazolium salts with 2-ethoxy-2-oxoethylidenedimethylsulfurane

Salt	Product	Yield (%)	Melting point (°C)	Formula	Analysis: Calculated C	H	N	S	Found C	H	N	S
1*a*	**2***a*	9	90–91	$C_{19}H_{17}NO_2S$	70.56	5.26	4.33	9.91	70.61	5.30	4.26	9.90
	3*a*	30	‡	$C_{13}H_{12}O_2S$	67.22	5.21	—	13.80	67.26	5.29	—	13.58
1*e*	**2***d*	42	73–74	$C_{19}H_{17}NO_2S$	70.56	5.26	4.33	9.91	70.51	5.34	4.24	9.92
	3*b**	25	‡									
1*f*	**2***e*	36	122–123	$C_{20}H_{19}NO_2S_2$	65.01	5.18	3.79	17.35	64.93	5.21	3.66	17.28
	3*c**	40										
1*g*	**2***f*	52†	‡									
	7	30	53	$C_{14}H_{15}NO_2$	73.34	6.59	6.11	—	73.27	6.58	5.95	—
1*h*	**2***g*	47	99–100	$C_{15}H_{17}NO_2S_2$	58.6	5.57	4.56	20.86	58.46	5.61	4.41	20.96
	3*c**	30										

*See Table 1.

†This compound appears to decompose on standing; however, ms and nmr properties were consistent with this structure. (The mass spectrum: M^+ 261, M calcd. 261; the nmr spectrum, δ: 1.2–1.5 and 4.2–4.5 (3H, t, and 2H, q resp; CH_2—CH_3), 2.5–2.6 (3H, broad, N—CH_3), 6.6–6.8 (1H, N—H), 7.1 (1H, s, thiophene), 7.2–7.7 (5H, m, aromatic). When shaken with D_2O the broad peak at 2.5–2.6 collapsed into sharp singlet and that at 6.6–6.8 disappeared.)

‡This product was an uncrystallizable oil.

needles, mp 150–152°C (72%). The nmr spectrum, δ: 1.6–2.0 and 3.5–3.8 (two 4H, m, the pyrrolidinyl), 4.70 (2H, d, —CH_2—Ph), 7.1–8.0 (10H, m, aromatic and amino). The mass spectrum: M^+ 336, M calcd. 336. *Anal.* calcd. for $C_{20}H_{20}N_2OS$: C 71.43, H 5.95, N 8.33, S 9.52; found: C 71.52, H 6.03, N 8.54, S 9.63.

Attempted thionation of **10***c* in benzene with phosphorus pentasulfide gave only a small amount of a complex yellow oil on work-up.

Prepration of ethyl N*-benzyl-*N*-(2-ethoxycarbonylbenzo[*b*]thienyl) carbamate (**10**d)*

The ester **2***b* (1 g, 3.2 mmol) in ethyl chloroformate (5 mL) was refluxed 24 h. Evaporation of the solution gave a viscous colorless oil which did not crystallize but was purified by tlc in chloroform. The nmr spectrum, δ: 0.83–1.40 and 3.90–4.41 (two —CH_2—CH_3, superimposed), 4.60–5.25 (2H, q, the diastereotopic benzylic —CH_2—Ph), and 7.23–7.95 (9H, m, aromatic). The mass spectrum: M^+ 383, M calcd. 383. *Anal.* calcd. for $C_{21}H_{21}NO_4S$: C 65.80, H 5.48, N 3.66, S 8.36; found: C 65.88, H 5.62, N 3.49, S 8.45.

Preparation of 1-methyl-3-phenylpyrrole

The pyrrole **7** (15 mg) was refluxed 2 h in solution of potassium hydroxide (0.1 g) in 50% aqueous ethanol (5 mL). Work-up gave 1-methyl-4-phenylpyrrole-2-carboxylic acid as a colorless crystalline powder, mp 165–170°C. This was not further purified or analyzed. Heating at 180°C for 2 h gave 1-methyl-3-phenylpyrrole as a colorless crystalline sublimate, mp 43–44°C (lit. (14) mp 43–44°C) (90%).

Acknowledgements

We wish to thank the Natural Sciences and Engineering Research of Canada for financial support of this work. We also wish to thank Mr. W. Buchannon for preparation of mass spectra.

1. D. M. McKINNON, M. E. R. HASSAN, and M. S. CHAUHAN. Can. J. Chem. **55**, 1123 (1977).
2. D. M. McKINNON and M. E. HASSAN. Can. J. Chem. **51**, 3081 (1973).
3. D. M. McKINNON, K. A. DUNCAN, and M. L. MILLAR. Can. J. Chem. **60**, 440 (1982).
4. A. J. SPEZIALE, C. C. TUNG, K. W. RATTS, and A. YAO. J. Am. Chem. Soc. **87**, 3460 (1965).
5. E. J. COREY and M. CHAYKOVSKY. J. Am. Chem. Soc. **87**, 1353 (1965).
6. D. LEAVER, D. M. McKINNON, and W. A. H. ROBERTSON. J. Chem. Soc. 32 (1965).
7. Y. ISKANDER and R. TEWFIK. J. Chem. Soc. 2393 (1961).
8. D. SEEBACH, M. BRAUN, and N. DUPREY. Tetrahedron Lett. 3509 (1973).
9. H. KWART and K. G. KING. *In* Reactivity and structure concepts in organic chemistry. Vol. 3. d-Orbitals in the chemistry of silicon, phosphorus and sulfur. *Edited by* K. Hafner, J.-M. Lehn,

Can. J. Chem. Downloaded from www.nrcresearchpress.com by 210.87.254.105 on 09/06/12
For personal use only.

C. W. Rees, P. von R. Schleyer, B. M. Trost, and R. Zahradnik. Springer-Verlag, Berlin. 1977.
10. J. D. LOUDON. *In* Organic sulfur compounds. Vol. I. *Edited by* N. Kharasch. Pergamon Press, New York. 1961.
11. E. BLOCK. *In* Organic Chemistry. Vol. 37. Reactions of organosulfur compounds. *Edited by* A. T. Blomquist and H. R. Wasserman. Academic Press, New York. 1978. p. 110.
12. J. FAUST and R. MAYER. J. Prakt. Chem. **318**, 161 (1976).
13. A. H. ALBERT, D. E. O'BRIEN, and R. K. ROBINS. J. Heterocycl. Chem. **15**, 529 (1978).
14. A. PADWA, D. DEAN, and T. OINE. J. Am. Chem. Soc. **97**, 2822 (1975).

Can. J. Chem. Downloaded from www.nrcresearchpress.com by 210.87.254.105 on 09/06/12
For personal use only.

The effect of α-cyclodextrin upon the kinetics of aqueous bromination of anisole

OSWALD S. TEE[1] AND JANICE M. BENNETT[2]

Department of Chemistry, Concordia University, 1455 de Maisonneuve Ouest, Montréal, P.Q., Canada H3G 1M8

Received September 26, 1983

This paper is dedicated to Professor Gerald E. Dunn on the occasion of his 65th birthday

OSWALD S. TEE and JANICE M BENNETT. Can. J. Chem. **62**, 1585 (1984).

α-Cyclodextrin (cyclohexaamylose) (CD) reduces the rate of bromination of anisole and *p*-methylanisole in aqueous KBr solutions (0.05−0.1 *M*). This retardation is largely due to the formation of a CD − tribromide ion complex and, to a lesser extent, to the encapsulation of bromine and of the anisole substrate. For *p*-methylanisole no other effects seem to be important. However, for anisole a pathway involving free (or complexed) anisole and complexed (or free) bromine seems to be operative. The intermediacy of a ternary complex (CD−anisole−Br_2) cannot be ruled out. Both equilibrium and kinetic measurements indicate that the dissociation constant of the CD−Br_3^- complex is ~2 × 10^{-4} *M*.

OSWALD S. TEE et JANICE M BENNETT. Can. J. Chem. **62**, 1585 (1984).

L'α-cyclodextrine (cyclohexaamylose) (CD) réduit la vitesse de bromation de l'anisole et du *p*-méthylanisole dans des solutions aqueuses de KBr (0,05 à 0,1 *M*). Ce ralentissement est dû en grande partie à la formation d'un complexe CD − ion tribromure et, à un moindre degré, à l'encapsulation du brome et du substrat anisole. Il ne semble pas y avoir d'autres effets importants dans le cas du *p*-méthylanisole. Cependant, dans le cas de l'anisole, un mécanisme impliquant de l'anisole libre (ou complexé) et du brome complexé (ou libre) semble avoir une certaine importance. On ne peut écarter la participation d'un complexe ternaire intermédiaire (CD−anisole−Br_2). Des mesures d'équilibre et de cinétique indiquent que la constante de dissociation du complexe de CD−Br_3^- est d'environ 2 × 10^{-4} *M*.

[Traduit par le journal]

Can. J. Chem. Downloaded from www.nrcresearchpress.com by 210.87.254.105 on 09/06/12
For personal use only.

Cyclodextrins are toroidal-shaped molecules, composed of several glucose units, with a hydrophobic cavity (1). They form inclusion complexes with a wide variety of organic substrates (1, 2). Most studies of their ability to influence reactivity have focussed upon "model enzyme studies" (3) and, in particular, on their ability to catalyze hydrolytic reactions (1, 3−5). Much less attention has been spent on their possible effect on other classes of reaction (1, 2, 4). Notable exceptions are studies of the influence of cyclodextrins on intermolecular (6) and intramolecular Diels−Alder reactions (7), on the Reimer−Tiemann reaction (8), and on the chlorination of anisole by hypochlorous acid (9).

In the last case, the classic study of Breslow and Campbell (9), it was found that α-cyclodextrin[3] significantly raises the *para/ortho* product ratio. This effect has two origins: *o*-chlorination is suppressed due to complexation of the anisole, and *p*-chlorination is enhanced due to a process involving a hypochlorite ester of the cyclodextrin encapsulating anisole (9).

Following on from earlier work on pyridones (10), we are now studying the bromination of phenols (11). It seemed reasonable that cyclodextrins might exert significant effects on the normal course of these reactions since various phenols (and their anions) form inclusion complexes (1). Preliminary kinetic experiments with *p*-nitrophenol and phenol suggested that the situation was far more complex than anticipated. Therefore we have studied the bromination of anisole in the presence of α-cyclodextrin[3] in some detail to minimize the complexities which might be involved with an ionizable phenol.

Results and discussion

We have monitored the kinetics of bromination of anisole in aqueous solution as a function of the concentrations of anisole, α-cyclodextrin, bromide ion, and hydrogen ion using the stopped-flow method. Some experiments were also carried out with *p*-methylanisole. Before discussing these results, we first consider the various equilibria involving several species in solution and which are relevant to analysis of the kinetics.

Equilibria

For reasons given elsewhere (12), bromination reactions in aqueous solution are conveniently studied when the medium contains an excess of bromide ion. In the present work we have used [KBr] = 0.05−0.10 *M*. Therefore, the first equilibrium which must be considered is that forming tribromide ion (eq. [1]). In general, the presence of this equilibrium is easily

$$[1] \quad Br_3^- \rightleftharpoons Br^- + Br_2$$

$$K = \frac{[Br^-][Br_2]}{[Br_3^-]} = 0.0562\ M \ (13)$$

corrected for (12, 14), the fraction of free bromine given by[4]

$$[2] \quad f_B = \frac{[Br_2]}{[Br_2]_t} = \frac{K}{(K + [Br^-])}$$

However, in the present case there are added complications. It turns out that *all three species* involved in eq. [1] form complexes with α-cyclodextrin (CD) in aqueous solution and these must be accounted for.

Wojcik and Rohrbach determined the dissociation constant (K_I) of the complex between CD and bromide ion[4,5] (15). The high value indicates relatively weak binding and in many instances the complexation might be ignored. This is not the case

[1]Author to whom correspondence should be addressed.

[2]Undergraduate participant 1982−83. NSERC Summer Student, 1982.

[3]α-Cyclodextrin (cyclohexaamylose) has six glucose units joined 1,4 in its torus. Its cavity is about 7Å deep and 4.5 Å across (1).

[4]On concentration brackets a subscript "t" indicates the total concentration, a subscript "c" indicates the concentration of a species complexed with CD.

[5]The reversed square brackets are used to symbolize the cyclodextrin encapsulating the species shown between them.

Can. J. Chem. Downloaded from www.nrcresearchpress.com by 210.87.254.105 on 09/06/12
For personal use only.

[3] $]Br^-[\rightleftharpoons Br^- + CD$

$$K_I = \frac{[Br^-][CD]}{[Br^-]_c} = 0.286\ M \quad (15)$$

here; at the high concentrations of bromide ion used, the effect of equilibrium [3] upon the concentration of CD must be included. The available CD is given by:[4]

[4] $$[CD] = \frac{K_I[CD]_t}{(K_I + [Br^-])}$$

Bromine forms a stronger complex with α-cyclodextrin (eq. [5]) (9). However, under our conditions this complexation does not affect the concentration of CD appreciably since

[5] $]Br_2[\rightleftharpoons Br_2 + CD$

$$K_B = \frac{[Br_2][CD]}{[Br_2]_c} = 2.1 \times 10^{-3}\ M \quad (9)$$

$[Br_2] \leq 50\ \mu M$. However, it does contribute somewhat to the reduction of the free bromine concentration (*vide infra*).

Our initial kinetics experiments suggested the formation of a CD complex having a dissociation constant about $10^{-4}\ M$. This is too low for either bromine or anisole (9). Therefore, we carried out a uv spectral study of the effect of adding α-cyclodextrin to aqueous solutions containing bromide ion, bromine, and tribromide ion. Qualitatively, we observe an increase in the Br_3^- absorption maximum at 266 nm and a slight shift to longer wavelengths, suggesting complexation of tribromide ion and an apparent shift in the Br_3^-/Br_2 equilibrium (eq. [1]). Consistent with this we note that formation of Br_3^- is more favorable in less polar media (15). Quantitative measurements at two wavelengths (see Experimental) gave an average dissociation constant $K_T = 1.7 \pm 0.2 \times 10^{-4}\ M$ for the complex between tribromide ion and α-cyclodextrin complex. This low value indicates 10-fold stronger binding than that of

[6] $]Br_3^-[\rightleftharpoons Br_3^- + CD$

$$K_T = \frac{[Br_3^-][CD]}{[Br_3^-]_c} = 1.7 \times 10^{-4}\ M$$

of bromine (see eq. [5]), and it means that under our kinetic conditions equilibrium [6] will be of more significance than [5] in determining the free bromine concentration (see later).

The free anisole (An) concentration is governed by the constant K_A, previously determined by Breslow and Campbell (9). For *p*-methylanisole the value of K_A is 0.015 *M* (9).

[7] $]An[\rightleftharpoons An + CD$

$$K_A = \frac{[An][CD]}{[An]_c} = 3.7 \times 10^{-3}\ M \quad (9)$$

Except at the lowest CD concentrations used, we have $[CD] \gg [An]_t$ and so the fraction of free anisole is given by eq. [8].

[8] $$f_A = \frac{[An]}{[An]_t} = \frac{K_A}{(K_A + [CD])}$$

From the above discussion it is apparent that analysis of the bromination kinetics requires appropriate consideration of *five* equilibria: [1], [3], [5], [6], and [7]. Complexation of bromide ion ([3]) intrudes by reducing available cyclodextrin and can be corrected for by eq. [4]. Similarly, the encapsulation of anisole [7] can be accounted for by eq. [8]. The three remaining equilibria affect the concentration of free bromine and must be considered together.

The total bromine is given by[4]

$$[Br_2]_t = [Br_2] + [Br_3^-] + [Br_2]_c + [Br_3^-]_c$$

Therefore, the fraction of free bromine is given by eq. [9]. At zero CD this expression simplifies to eq. [2], as is appropriate.

[9] $$f_B = \frac{KK_BK_T}{(K_BK_T(K + [Br^-]) + [CD](KK_T + K_B[Br^-]))}$$

At the highest bromide ion concentration used (0.1 *M*), $K_B[Br^-] = 2.1 \times 10^{-4}\ M^2$, whereas $KK_T = 9.6 \times 10^{-6}\ M^2$ and so a simplified version of eq. [9] was also used: eq. [10]. This corresponds to the situation where the formation and complexation of Br_3^- are the major factors which reduce the free bromine concentration.

[10] $$f_B = \frac{KK_T}{(K_T(K + [Br^-]) + [Br^-][CD])}$$

Kinetics

The aqueous bromination of various anisoles has been studied by Aaron and Dubois (16). For anisole in 0.1 *M* NaBr + 1 m*M* $HClO_4$ at 25°C they obtained a second-order rate constant, $k_2^{obs} = 37\,000\ M^{-1}\ s^{-1}$. Under slightly different conditions (0.1 *M* KBr + 10 m*M* HCl) we obtain essentially the same value: $36\,400\ M^{-1}\ s^{-1}$. In each case the reported value is derived from the apparent rate constant (k_2^{app}) by correcting for the fraction of free bromine (eq. [2]) in the equilibrium [1]. For the reaction

$$An + Br_2 \xrightarrow{k_2}$$

$$\text{rate} = k_2^{app}[An][Br_2]_t = k_2[An][Br_2]$$

and so

$$k_2^{app} = k_2 f_B$$

Hence we take $k_2^{obs} = k_2^{app}/f_B$. This approach ignores any reaction via tribromide ion, which is reasonable since k_2^{obs} remains constant ($36\,400$, $34\,600$, $35\,100\ M^{-1}\ s^{-1}$) at the bromide concentrations (0.1, 0.075, 0.05 *M*) used.

We have also measured the kinetics of bromination of *p*-methylanisole and again find good agreement between our results and those of Aaron and Dubois (16) under comparable conditions.

We now consider the effect on adding α-cyclodextrin upon the kinetics of bromination of anisole and of *p*-methylanisole. These two substrates present slightly different pictures. In the case of anisole it appears that there are two bromination pathways, whereas for *p*-methylanisole only one is important. For simplicity of presentation the latter case will be dealt with first, even though it was in fact studied last.

Table 1 shows the effect of added CD[6] upon the measured values of k_2^{app} for *p*-methylanisole at two different bromide ion concentrations. In both cases k_2^{app} is substantially reduced in a manner consistent with the complexation of Br_3^-, Br_2, and the anisole, although the effect of the first of these is dominant.

If the reaction only involves *free* bromine reacting with the *free* anisole then k_2^{app} is simply governed by the fractions of these species.

[11] $$k_2^{app} = k_2 f_A f_B$$

where $f_A = [An]/[An]_t$ and $f_B = [Br_2]/[Br_2]_t$. Since both f_A and f_B depend upon the CD concentration (eqs. [8] and [9]), the form of k_2^{app} in eq. [11] is complex. However, analysis of the data can be facilitated by defining a corrected rate constant

Can. J. Chem. Downloaded from www.nrcresearchpress.com by 210.87.254.105 on 09/06/12
For personal use only.

TABLE 1. Apparent second-order rate constants for the bromination of *p*-methylanisole[a]

[KBr] (*M*)	$[CD]_t$ (m*M*)	k_2^{app} (M^{-1} s^{-1})	$10^4/k_2^{corr}$ (*M* s)
0.10	0	2220	4.50
	0.25	1590	6.21
	0.50	1190	8.20
	1.0	747	12.8
	2.0	407	22.4
	5.0	168	47.7
0.05[b]	0	3400	2.84
	0.25	2400	4.10
	0.50	1780	5.44
	1.0	1210	7.75
	2.0	678	13.0
	5.0	251	29.9

[a]At 25°C, pH = 2.08 (HCl), total I = 0.11 *M*. Each rate constant is derived from a pseudo-first-order rate constant which is the average of 3–5 runs. Values of k_2^{corr} have been corrected for substrate complexation (see eq. [12]) using the corrected [CD] (eq. [4]).
[b]With 0.05 *M* NaCl to maintain I.

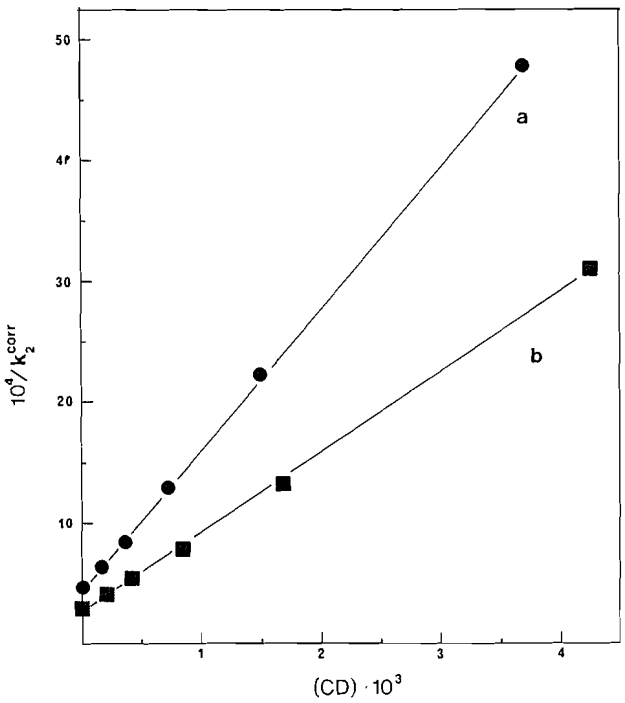

FIG. 1. Rate data for the bromination of *p*-methylanisole, plotted according to eq. [13]. Data from Table 1: (a) 0.10 *M* KBr; (b) 0.05 *M* KBr.[6]

(k_2^{corr}) which allows for the effect of complexation of the anisole, which in the present case is fairly small:

$$[12] \quad k_2^{corr} = k_2^{app}/f_A = k_2 f_B$$

The fraction f_A is taken from eq. [8]. The form of eq. [12] is still non-linear, but its reciprocal, eq. [13], is linear in the concentration of CD,[6] the fraction f_B being obtained from eq. [10].

[6]In the tables the CD concentration is that added, i.e. $[CD]_t$. In data analysis and for plots we use the value obtained after correction for the effect of Br^- (eq. [4]).

TABLE 2. Constants from fitting and direct measurements for *p*-methylanisole bromination[a]

$[Br^-]$	Method	k_2	$K_T \times 10^4$
0.10	Direct	6170[b]	1.7[c]
	Equation [13]	6590	2.3
0.05	Direct	6430[b]	1.7[c]
	Equation [13]	7430	1.8

[a]At 25°C, I = 0.11 *M*, pH = 2.08 (HCl). Units of k_2 are M^{-1} s^{-1}, of K_T are *M*.
[b]From the runs at zero [CD] (see Table 1).
[c]Measured spectrophotometrically in 0.01 *M* KBr (see Experimental) and corrected for Br^- inclusion.

TABLE 3. Apparent second-order rate constants for the bromination of anisole[a]

$[Br^-]$ (*M*)	$[CD]_t$ (m*M*)	k_2^{app} (M^{-1} s^{-1})	$10^4/k_2^{corr}$ (*M* s)
0.10	0	13100	0.763
	0.5	4930	1.84
	0.6	4600	1.94
	1.0	3160	2.64
	1.5	2310	3.33
	2.0	1620	4.41
	3.0	1220	5.12
	4.0	929	5.98
	5.0	731	6.84
	10.0	347	9.60
0.075[b]	0	14800	0.675
	0.5	6870	1.31
	0.8	5160	1.65
	1.0	4380	1.88
	2.0	2530	2.77
	5.0	1080	4.47
	10.0	553	5.76
0.05[b]	0	18600	0.537
	0.5	8890	1.01
	1.0	5690	1.43
	2.5	2840	2.24
	4.0	1850	2.82
	5.0	1500	3.10
	10.0	747	4.06

[a]As Table 1.
[b]As Table 1.

$$[13] \quad 1/k_2^{corr} = 1/k_2 f_B = \frac{(K + [Br^-])}{k_2 K} + \frac{[Br^-][CD]}{k_2 K K_T}$$

Figure 1 shows two plots[6] of the data for *p*-methylanisole corresponding to eq. [13]. They are quite linear ($r > 0.999$) and from their slopes and intercepts one can extract reasonable values of k_2 and K_T (Table 2).

From the above we conclude that α-cyclodextrin significantly reduces the rate of bromination of *p*-methylanisole due to the complexation of tribromide ion and, to a lesser extent, of bromine and the substrate itself. The only important bromination pathway is that involving free substrate and free bromine. Attempts to analyse the data in terms of two pathways, as in the case of anisole (below), led to nonsensical results, such as negative rate constants.

Table 3 presents the data obtained for anisole as a function of CD concentration[6] and at three different bromide concentrations. These data are presented graphically in Fig. 2, as plots

Can. J. Chem. Downloaded from www.nrcresearchpress.com by 210.87.254.105 on 09/06/12
For personal use only.

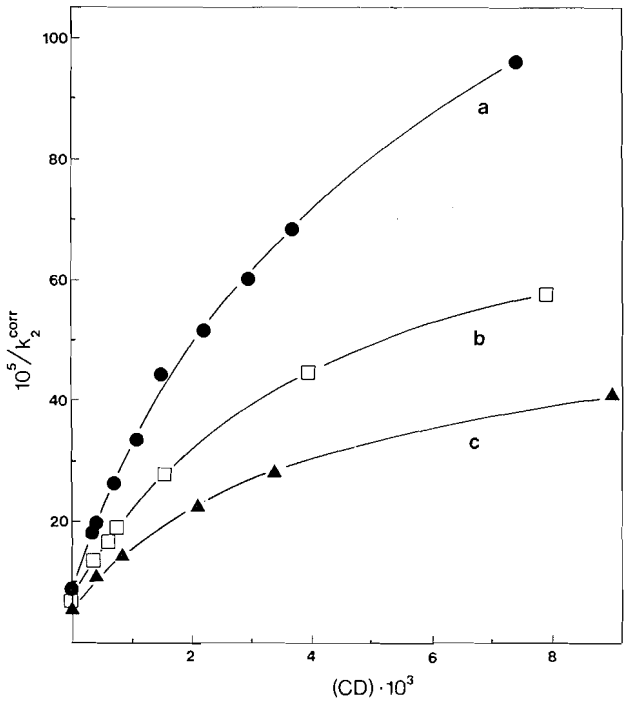

FIG. 2. Rate data for the bromination of anisole. Data from Table 3: (a) 0.10 *M* KBr; (b) 0.075 *M* KBr; (c) 0.05 *M* KBr.[6]

of $1/k_2^{corr}$ versus [CD]. Unlike the linear plots for *p*-methylanisole in Fig. 1, these plots are decidedly curved, the reason being that at higher CD concentrations k_2^{app} is larger than anticipated. As [CD] is raised from 0 to 0.01 *M*,[7] the value of k_2^{app} decreases by a factor of 38. This decrease is *smaller* than the factor of 90 which should arise due to the complexation with CD of Br_2, Br_3^-, and anisole. In other words, there appears to be a second bromination pathway which becomes important as the concentration of CD is raised.

There are various possibilities for a second process, but our results are consistent with either complexed bromine reacting with free anisole, or free bromine attacking complexed anisole. A variety of experiments were carried out to eliminate other possibilities.

At high CD concentration (0.02 *M*) the pseudo-first-order rate constants (k_1^{obs}) for bromine disappearance (see Experimental) increase monotonically with anisole concentration, showing that the transition state for the second process contains anisole. This eliminates the possibility of rate-limiting dissociation of the CD–bromine or CD – tribromide ion complexes.

Experiments were also carried out at various pHs in the range of 0–5. Both in the presence and absence of CD (0.01 *M*) the respective values of k_2^{app} remain constant. These results militate against any process involving HOBr or a hypobromite ester of the cyclodextrin (cf. ref. 9), since the formation of these from bromine is pH dependent (see eq. [14]) (17).

$$[14]\quad Br_2 + ROH \rightleftharpoons ROBr + H^+ + Br^-$$

Likewise, the experiments carried out at three different bromide concentrations are inconsistent with the involvement of

[7]Initial experiments were carried to higher CD concentrations, but then one encounters deviations due to CD affecting the Br^- concentration (eq. [3]).

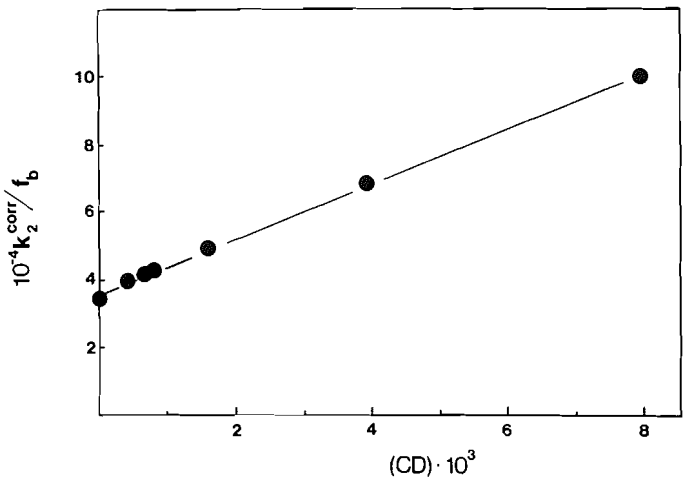

FIG. 3. Rate data for the bromination of anisole, plotted according to eq. [17]. [KBr] = 0.075 *M*.[6]

tribromide ion in the second process. They are, however, compatible with the attack of free (or complexed) bromine on complexed (or free) anisole, as we now show.

If the second process involves free bromine and complexed anisole

$$[15]\quad]An[+ Br_2 \xrightarrow{k_2'}$$

then the overall rate constant will be a weighted sum due to the two contributing pathways,

$$[16]\quad k_2^{app} = (k_2 f_A + k_2'(1 - f_A))f_B$$

where f_A is the fraction of free anisole (eq. [8]), $(1 - f_A)$ the fraction of the anisole–CD complex, and f_B is the fraction of free bromine (eq. [9] or [10]). Rearrangement of eq. [16] leads to

$$\frac{k_2^{app}}{f_A f_B} = k_2 + k_2' \frac{(1 - f_A)}{f_A}$$

which is the same as

$$[17]\quad \frac{k_2^{corr}}{f_B} = k_2 + k_2' \frac{[CD]}{K_A}$$

since $k_2^{corr} = k_2^{app}/f_A$. Figure 3 shows a plot based on eq. [17]. The data for all three bromide ion concentrations (0.1, 0.075, 0.05 *M*) show comparable linearity (r = 0.9950, 0.9980, 0.9975). The values of k_2 and k_2' obtained from the least-squares slopes and intercepts are collected in Table 4.

The data may also be analyzed by a Lineweaver–Burk type of equation (1, 9), to obtain values of k_2' and K_T. Using f_B from eq. [10], the appropriate equation for k_2^{corr} is

$$[18]\quad k_2^{corr} = \frac{(k_2 K_A + k_2'[CD])KK_T}{K_A(KK_T + K_T[Br^-] + [Br^-][CD])}$$

and the apparent rate constant in the absence of CD is defined by

$$[19]\quad k_2^u = k_2 K/(K + [Br^-])$$

From these two equations considerable manipulation leads to the Lineweaver–Burk form shown below.

$$[20]\quad \frac{1}{k_2^{corr} - k_2^u} = \frac{K_A K_T(K + [Br^-])}{[CD](k_2' KK_T - k_2^u K_A[Br^-])} + \frac{K_A[Br^-]}{(k_2' KK_T - k_2^u K_A[Br^-])}$$

Can. J. Chem. Downloaded from www.nrcresearchpress.com by 210.87.254.105 on 09/06/12
For personal use only.

TABLE 4. Constants from fitting and direct measurements for anisole bromination[a]

$[Br^-]$	Method	k_2	k_2'	$K_T \times 10^4$
0.10	Direct	36 400[b]	—	1.7[c]
	Equation [17]	36 000	26 000	—[d]
	Equation [20]	—	32 400	1.5
	Equation [21]	36 300	26 000	—[d]
0.075	Direct	34 600[b]	—	1.7[c]
	Equation [17]	38 400	37 800	—[d]
	Equation [20]	—	26 700	2.0
	Equation [21]	39 500	37 000	—[d]
0.04	Direct	35 100[b]	—	1.7[c]
	Equation [17]	38 600	38 300	—[d]
	Equation [20]	—	30 800	1.9
	Equation [21]	40 300	37 300	—[d]
	Average:	37 200	32 400	1.8

[a]As Table 2.
[b]From the runs at zero [CD] (see Table 3).
[c]As Table 2.
[d]Assumed to be the measured value of 1.7×10^{-4} M.

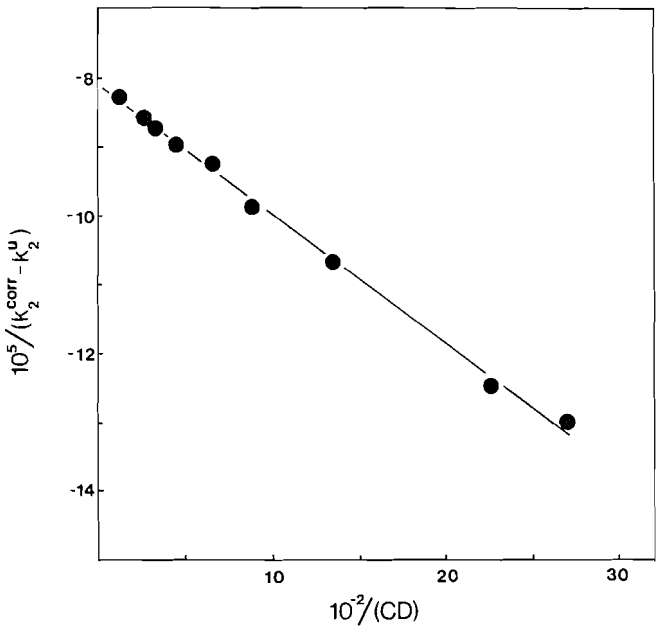

FIG. 4. Rate data for the bromination of anisole, plotted according to the Lineweaver–Burk form, eq. [20]. [KBr] = 0.1 M.[6]

Figure 4 shows a plot corresponding to this equation. The plots for all three values of $[Br^-]$ (0.1, 0.075, 0.05 M) are quite linear (r = 0.9974, 0.9999, 0.9997). From the slopes and intercepts were obtained the values of k_2' and K_T presented in Table 4.

We have also applied non-linear fitting techniques (18) to the equation appropriate to the curved plots shown in Fig. 2. The reciprocal form of k_2^{corr}, using f_B from eq. [9], is

$$[21] \quad \frac{1}{k_2^{corr}} = \frac{K_A(K_B K_T(K + [Br^-]) + [CD](KK_T + K_B[Br^-]))}{(k_2 K_A + k_2'[CD])KK_B K_T}$$

Fitting this equation with k_2 and k_2' as the disposable parameters gives the values in Table 4, and calculated curves which fit the experimental data well[8] (Fig. 2).

The values of the constants given by the three treatments show reasonable consistency and agreement[9] with those from direct measurement, where available (Table 4). They support the hypothesis that free bromine attacks encapsulated anisole (eq. [15]), but they are inconsistent with the second bromination pathway involving Br_3^-. If such a process was involved, the value of k_2' would vary in proportion to $[Br^-]$.

The second pathway might also involve free anisole and encapsulated bromine:

$$[22] \quad An +]Br_2[\xrightarrow{k_2''}$$

since this is kinetically indistinguishable from the process [15]. This is clearly seen in eq. [23], which is appropriate for the process [22], and which has the same mathematical form as eq. [17].

$$[23] \quad \frac{k_2^{corr}}{f_B} = k_2 + k_2'' \frac{[CD]}{K_B}$$

Thus to obtain estimates of k_2'' one can take the values of k_2' from Table 4 and multiply them by the factor K_B/K_A.

Assuming that the process [15] is involved, the data in Table 4 suggest that free anisole is slightly more reactive than encapsulated anisole towards free bromine ($k_2 \sim 37\,000$, $k_2' \sim 32\,000\ M^{-1}\ s^{-1}$). On the other hand, if the second process is that depicted in eq. [22], the data indicate that free bromine is about twice as reactive as the bromine–CD toward free anisole ($k_2 \sim 37\,000$, $k_2'' \sim 18\,000\ M^{-1}\ s^{-1}$).

Initially we had hoped to be able to differentiate between the processes [15] and [22] by studying *p*-methylanisole (PMA) as substrate. The conclusion that PMA has no second pathway might indicate that anisole employs the k_2' process (]An[+ Br_2 →). In encapsulated PMA the reactive *ortho* positions should be buried and unavailable for reaction (9), and so no k_2' process would be observed[10] (Scheme 1).

However, a similar steric argument might be used to invoke the k_2'' process (An +]Br_2[→) for anisole. The lack of reactivity of PMA[10] might simply reflect that its *ortho* positions cannot penetrate the CD cavity far enough to react with encapsulated bromine (Scheme 2).

In a similar way, we cannot rule out the involvement of a discrete ternary complex (CD–anisole–Br_2) (Scheme 3). Evidence for the intermediacy of such a complex in the α-cyclo-

[8]For example, for the data at $[Br^-]$ = 0.1 M the average deviation of the points is 2.4%.

[9]The agreement between the values obtained using eqs. [17] and [21] is very good. The agreement with the values of k_2' from the Lineweaver–Burk treatment (eq. [20]) is much poorer. This is not too surprising, since this treatment put heavy emphasis on the rate constant (k_2^u) at [CD] = 0, and this value gave us problems due to solubility problems (see Experimental). Moreover, the point at [CD] = 0 consistently shows the largest deviation (~10%) in the other treatments. Given that our data analysis employs various constants from various sources, we feel that the overall agreement inTable 2 and Table 4 is quite satisfactory.

[10]In principle, the inability to detect a k_2' process for PMA might simply be due to its weaker binding to CD (see above). To put this into perspective, one has to estimate what value of k_2' would be detectable under our conditions. Assuming we could detect a 20% contribution from a second process at [CD] = 0.005 M, we conclude that for PMA $k_2' < 3900\ M^{-1}\ s^{-1}$. Likewise for the alternative process we estimate $k_2'' < 550\ M^{-1}\ s^{-1}$. Both of these values are significantly lower than k_2 for PMA (~6500 $M^{-1}\ s^{-1}$).

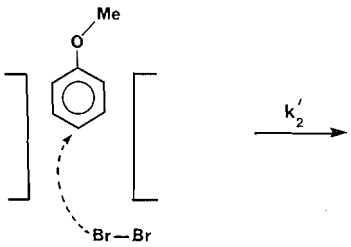

SCHEME 1

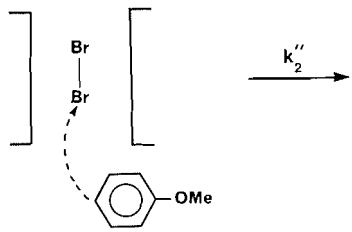

SCHEME 2

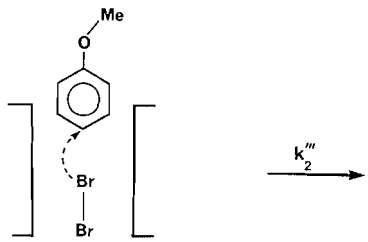

SCHEME 3

dextrin mediated Riemer-Tiemann reaction has been put forward (8). In a ternary complex involving PMA the approach of Br_2 to the *ortho* positions would again be blocked (Scheme 3).

Experimental

Anisole (Chemalog) was distilled before use. *p*-Methylanisole (Aldrich) and α-cyclodextrin hydrate (Aldrich) were used as received. Other reagents were of the analytical grade. Potassium bromide was kept in a drying oven at 110–120°C when not in use.

The anisole substrates are poorly soluble in water. Initial experiments showed poor reproducibility which was traced to this problem. For the results reported here, a stock solution of the anisole in methanol (0.05 *M*) was used and diluted with the desired aqueous medium. Immediately before use substrate solutions were shaken vigorously for several minutes. Use of a stock solution in ethanol gave odd results at low CD concentrations. This was probably due to the encapsulation of EtOH by CD (19). The solubility problems diminish with increasing CD concentration due to CD–anisole complex formation (9).

Bromine solutions were made by dilution of a small volume of a stock solution (0.1 *M* in 0.1 *M* aqueous KBr) with the desired medium. This stock solution was made by weighing a few drops of liquid bromine into 10 mL of 0.1 *M* KBr and diluting with 0.1 *M* KBr to arrive at a 0.1 *M* concentration.

Kinetic measurements normally used a substrate concentration of 5×10^{-4} *M* and a bromine concentration of 5×10^{-5} *M* (both values are after mixing in the stopped-flow). Equilibrium measurements (see below) employed bromine solutions of 10^{-4} *M* and 10^{-3} *M* for the experiments at 265 nm and 385 nm, respectively.

Most of the kinetic experiments were carried out at pH 2.08 (0.01 *M* HCl + 0.1 *M* electrolyte). The total ionic strength was maintained at 0.11 *M*, from 0.1 *M* (KBr + NaCl) + 0.01 *M* (HCl or buffer). Unlike Br^-, Cl^- apparently does not form a complex with CD (15). Experiments at pH > 2 used Perrin's (I = 0.01 *M*) buffers (20).

Kinetic methods

Rates were measured as bromine disappearance at 265 nm (Br_3^- band) using the stopped-flow apparatus (21) and acquisition system (22) described earlier. With an excess of substrate, ten-fold or more, good first-order behaviour was observed for >90% reaction; least-squares analysis of ln $(A - A_\infty)$ vs. t showed good linearity (r > 0.999). Pseudo-first-order rate constants (k_1^{obs}) were converted to apparent second-order rate constants (k_2^{app}) by division by the factor $([S] - [Br_2]_0)$ (23).

Bromine reacts with α-cyclodextrin over a period of about an hour. Accordingly, bromine was not brought into contact with CD until mixed in the stopped-flow apparatus. One drive syringe contained substrate and CD in the appropriate medium, the other contained bromine in the medium. This approach should not distort the results since the rate constants for the formation of CD inclusion compounds approach diffusion-controlled (1). Moreover, initial experiments where CD was present in both syringes gave similar results.

Equilibrium measurements

The dissociation constant K_T for the CD–Br_3^- complex was measured spectrophotometrically (9, 24). Absorbance values at two wavelengths were analyzed using the equation:

$$[24] \quad \frac{[Br_2]_t}{(A - A_0)} = \frac{K_T}{\beta\Delta\epsilon[CD]} + \frac{1}{\Delta\epsilon}$$

This is the same as the Benesi–Hildebrand equation (9, 24), except that it contains the factor β, which is the fraction of Br_3^- in the equilibrium [1]. It is given by:

$$\beta = [Br_3^-]/[Br_2]_t = [Br^-]/(K + [Br^-])$$

We used a medium containing 0.01 *M* KBr (+ 0.09 *M* NaCl), so that β = 0.151. At zero [CD] the Br_3^- band (265 nm) is small. As [CD] increases this band increases dramatically as more and more bromine becomes converted to Br_3^- and encapsulated. Even at 385 nm (bromine band) one sees an increase in absorption because the extinction coefficient of Br_3^- is greater than that of Br_2 (17).

Separate experiments at 265 nm (pH 3) and at 385 nm (pH 2) gave plots of $1/(A - A_0)$ vs. $1/[CD]_t$ showing good linearity (r = 0.9936 and 0.9998). From their slopes and intercepts (and β) we obtained $K_T = 1.58 \times 10^{-4}$ and 1.95×10^{-4} *M*, respectively. Correcting these for the free CD concentration (eq. [4]) and averaging the results gives $K_T = 1.7 \pm 0.2 \times 10^{-4}$ *M*.

Acknowledgement

The authors thank the Natural Sciences and Engineering Council of Canada for an operating grant to O.S.T. and a Summer Studentship to J.M.B.

1. M. BENDER and M. KOMIYAMA. Cyclodextrin chemistry. Springer Verlag, New York. 1978.
2. D. D. MACNICOL, J. J. MCKENDRICK, and D. R. WILSON. Chem. Soc. Rev. **7**, 83 (1978); W. SAENGER. Angew. Chem. Int. Ed. Engl. **19**, 344 (1980); I. TABUSHI. Acc. Chem. Res. **15**, 66 (1982).
3. H. DUGAS and C. PENNEY. Bioorganic chemistry. Springer Verlag, New York. 1981.
4. R. BRESLOW. Science, **218**, 532 (1982); Acc. Chem. Res. **13**, 170 (1980).
5. R. BRESLOW, G. TRAINOR, and A. UENO. J. Am. Chem. Soc. **105**, 2739 (1983); W. J. LE NOBLE, S. SRIVASTAWA, R. BRESLOW, and G. TRAINOR. J. Am. Chem. Soc. **105**, 2748 (1983), and references therein.
6. R. BRESLOW and D. C. RIDEOUT. J. Am. Chem. Soc. **102**, 7816 (1980).
7. D. D. STERNBACH and D. M. ROSSANA. J. Am. Chem. Soc. **104**,

Can. J. Chem. Downloaded from www.nrcresearchpress.com by 210.87.254.105 on 09/06/12
For personal use only.

5853 (1982).
8. M. KOMIYAMA and H. HIRAI. J. Am. Chem. Soc. **105**, 2018 (1983).
9. R. BRESLOW and P. CAMPBELL. J. Am. Chem. Soc. **91**, 3085 (1969); Bioorg. Chem. **1**, 140 (1971).
10. O. S. TEE and M. PAVENTI. J. Am. Chem. Soc. **104**, 4142 (1982); Can. J. Chem. **61**, 2556 (1983).
11. O. S. TEE, N. R. IYENGAR, and M. PAVENTI. J. Org. Chem. **48**, 759 (1983).
12. O. S. TEE and C. G. BERKS. J. Org. Chem. **45**, 830 (1980).
13. R. P. BELL and E. N. RAMSDEN. J. Chem. Soc. 1294 (1958).
14. O. S. TEE and G. V. PATIL. J. Org. Chem. **41**, 838 (1976).
15. P. B. D. DE LA MARE. Electrophilic halogenation. Cambridge University Press, Cambridge. 1976.
16. J. J. AARON and J. E. DUBOIS. Bull. Soc. Chim. Fr. 603 (1971).
17. J. M. PINK. Can. J. Chem. **48**, 1169 (1970).
18. P. R. BEVINGTON. Data reduction and error analysis for the physical sciences. McGraw–Hill, New York. 1969.
19. R. I. GELB, L. M. SCHWARTZ, M. RADEOS, R. B. EDMONDS, and D. A. LAUFER. J. Am. Chem. Soc. **104**, 6283 (1982).
20. D. D. PERRIN. Aust. J. Chem. **16**, 572 (1963).
21. O. S. TEE, D. C. THACKRAY, and C. G. BERKS. Can. J. Chem. **56**, 2970 (1978).
22. O. S. TEE, M. TRANI, R. A. MCCLELLAND, and N. E. SEAMAN. J. Am. Chem. Soc. **104**, 7219 (1982).
23. S. BANERJEE, O. S. TEE, and K. D. WOOD. J. Org. Chem. **42**, 3670 (1970).
24. H. A. BENESI and J. H. HILDEBRAND. J. Am. Chem. Soc. **71**, 2703 (1949).

Can. J. Chem. Downloaded from www.nrcresearchpress.com by 210.87.254.105 on 09/06/12
For personal use only.

Long-range $^{13}C,^{1}H$ and $^{13}C,^{19}F$ coupling constants as indicators of the conformational properties of 4-fluoroanisole, 2,3,5,6-tetrafluoroanisole, and pentafluoroanisole

TED SCHAEFER, REINO LAATIKAINEN,[1] TIMOTHY A. WILDMAN,[2] JAMES PEELING,[3] GLENN H. PENNER, JAMES BALEJA, AND KIRK MARAT

Department of Chemistry, University of Manitoba, Winnipeg, Man., Canada R3T 2N2

Received October 28, 1983

This paper is dedicated to Professor Gerald E. Dunn on the occasion of his 65th birthday

TED SCHAEFER, REINO LAATIKAINEN, TIMOTHY A. WILDMAN, JAMES PEELING, GLENN H. PENNER, JAMES BALEJA, and KIRK MARAT. Can. J. Chem. **62**, 1592 (1984).

Long-range spin–spin coupling constants over six bonds between ^{13}C nuclei in the methyl group and ring protons or ^{19}F nuclei in the *para* position are reported for 4-fluoroanisole, 2,3,5,6-tetrafluoroanisole, and pentafluoroanisole in solution. The couplings are $\sigma-\pi$ electron mediated, as indicated by INDO MO FPT computations and by measurements on anisole, 2,6-dibromoanisole, 2,6-dichloroanisole, 2,6-dibromo-4-fluoroanisole, and 2,6-dibromo-4-methylanisole. On the basis of the measured coupling magnitudes and a hindered rotor model, it is concluded that the barrier to internal rotation about the C_{sp^2}—O bond in 4-fluoroanisole lies near 6 kcal/mol, is nearly zero in the tetrafluoroanisole, and is somewhat less than 1 kcal/mol in the pentafluoroanisole. In the latter, the preferred conformation is that in which the methoxy group lies in a plane perpendicular to the pentafluorophenyl plane. Some inconclusive dynamic nmr experiments on anisole, including $T_{1\rho}$ measurements, are briefly discussed.

TED SCHAEFER, REINO LAATIKAINEN, TIMOTHY A. WILDMAN, JAMES PEELING, GLENN H. PENNER, JAMES BALEJA et KIRK MARAT. Can. J. Chem. **62**, 1592 (1984).

On rapporte les constantes de couplage à longue distance à travers six liaisons entre le noyau ^{13}C du groupe méthyle et les protons du cycle ou les noyaux ^{19}F en position *para* du fluoro-4 anisole, du tétrafluoro-2,3,5,6 anisole et du pentafluoroanisole en solution. Les couplages sont transmis par les électrons $\sigma-\pi$ comme l'indiquent des calculs d'OM INDO FPT et des mesures sur l'anisole et sur les dibromo-2,6, dichloro-2,6, dibromo-2,6 fluoro-4 et dibromo-2,6 méthyl-4 anisoles. En se basant sur l'intensité des couplages mesurés et sur un modèle rotatif encombré, on conclut que la barrière à la rotation interne autour de la liaison C_{sp^2}—O dans le fluoro-4 anisole est voisine de 6 kcal/mol alors qu'elle est voisine de zéro dans le cas du tétrafluoroanisole et quelque peu inférieure à 1 kcal/mol dans le cas du pentafluoroanisole. Dans ce dernier cas, la conformation préférée est celle où le groupe méthoxy se situe dans un plan perpendiculaire à celui du pentafluorophényle. On discute brièvement de certaines expériences de rmn dynamique sur l'anisole, y compris des mesures de $T_{1\rho}$, qui ne permettent toutefois pas de tirer de conclusions.

[Traduit par le journal]

Can. J. Chem. Downloaded from www.nrcresearchpress.com by 210.87.254.42 on 09/06/12
For personal use only.

Introduction

Various physical techniques (1–8) indicate[4] coplanar heavy atoms in the preferred conformation of anisole and imply that the barrier to internal rotation about the C_{sp^2}—O bond is strongly state dependent, and that in solution it lies between about 1.5 and 6 kcal/mol (1 cal ≡ 4.184 J). In some treatments, notably those applied to the torsional mode corresponding to oscillation about the C_{sp^2}—O bond (10, 11), a twofold hindering potential is assumed. It is also usually assumed that $2p-\pi$ conjugation accounts for the preferred planarity and that repulsion between the methyl group and the *ortho* C—H bonds perhaps introduces a fourfold component (7) to the rotational potential (the rotational barrier in phenol is twofold (12)).

The most recent calculations on anisole (7, 9) at the STO 3G MO and 4-31 G MO levels of theory imply a very shallow local minimum, if present at all, in the perpendicular conformation, but that a fourfold component does exist. The magnitude of internal barrier to rotation about the C_{sp^2}—O bond is computed (7) as 1.9 kcal/mol, to be compared with a molecular mechanics result of 1.9 kcal/mol (8). In solution this barrier must be substantially higher, as implied by the torsional data and by our coupling data below. In the solid the barrier magnitude is about 11.5 kcal/mol (1).

A technique not yet applied to this problem is the *J* method (13), in which a long-range nuclear spin–spin coupling with a known conformational dependence is related to the hindering potential and other parameters. This method has had some success in defining the low-energy conformation and the twofold internal potential of sidechains in benzene derivatives, for example in such compounds as ethylbenzene (14) and thiophenol (15, 16) derivatives. Such studies utilized couplings over four and six bonds between sidechain protons and ring protons or fluorine nuclei. More recently (17), the couplings over five bonds between sidechain protons and ring *para* carbon nuclei, as well as over six bonds between β carbon nuclei and *para* ring protons have been examined and found to be useful in the *J* method.

Now, in anisole and its derivatives suitable coupling constants would involve a ^{13}C nucleus in the methyl group, the methyl protons displaying no long-range couplings to *para* protons or fluorine nuclei. A series of experiments on anisole and its derivatives in this laboratory have yielded numerous coupling data for ^{1}H, ^{19}F, and ^{13}C nuclei. These results have not been entirely explicable for anisole, where the fourfold component of the barrier to rotation about the C_{sp^2}—O bond adds an additional complication. However, for the title compounds a reasonable explanation of these data is possible. The coupling

[1] Present address: Department of Chemistry, University of Kuopio, Kuopio 10, Finland.

[2] Present address: Division of Chemistry, National Research Council, Ottawa, Ont., Canada K1A 0R6.

[3] Present address: Department of Chemistry, University of Petroleum and Minerals, Dhahran, Saudi Arabia.

[4] The literature on anisole conformations and barrier has been reviewed in detail (9) up to July, 1982, citing some 100 publications.

TABLE 1. Relevant spin–spin coupling constants for some anisole derivatives at 305 K as degassed samples in 10-mm od tubes

	$^6J_p^{C,H}$	$^5J_m^{C,H}$	$^4J_o^{C,H}$	$^1J_\alpha^{C,H}$
Anisole	<0.05[a,f]	0.116(2)	<0.05	142.782(3)
	<0.05[b]	0.112(2)	<0.05	143.593(3)
2,6-DiCl[c]	(−)0.603(5)	0.265(7)	—	145.441(5)
2,6-DiBr[c]	(−)0.625(7)	0.264(4)	—	145.476(7)
2,6-DiBr-4-Me[c]	0.637(20)	0.264(10)	—	145.169(20)
	$^6J_p^{C,F(H)}$	$^5J_m^{C,F}$	$^4J_o^{C,F}$	
4-F[d]	0.085(5)[f]	—	—	—
2,3,5,6-Tetra-F[d]	0.331(8)[g]	0.373(46)	3.843(6)	—
Penta-F[d]	0.963(23)	0.373(46)	3.444(15)	—
4-F-2,6-diBr[e]	1.476(20)	—	—	—

[a] Enriched to 95% α-^{13}C, 200 mg in 2.5 mL of a solvent consisting of 30 v/v% C_6D_{12} in CS_2.

[b] Enriched as above, approximately 5 mol% in acetone-d_6; both samples run at 315 K in an attempt to reduce spin-lattice relaxation rates of α-^{13}C. Diethylether as solvent did not appear to alter the long-range couplings.

[c] Samples were 50 v/v% in benzene-d_6, 0.637 Hz being $^7J_p^{C,H}$.

[d] Samples were 50 v/v% in acetone-d_6.

[e] Samples were 11 mol% in acetone-d_6.

[f] Numbers in parentheses are estimated errors in the last one or two significant figures for these parameters obtained from first-order splitting patterns; in 2,5-dichloro-, 3,5-dichloro-, and 2,3,5-dichloroanisoles no evidence for couplings to *ortho* or *para* protons larger than those in the table could be found.

[g] The value of 0.331 Hz is equal to $^6J_p^{C,H}$ and was indistinguishable in magnitude from $^5J_m^{C,F}$. The ^{13}C nmr spectrum was acquired with the INEPT pulse sequence.

mechanisms for $^6J_p^{C,H}$ and $^6J_p^{C,F}$ are investigated and the observed numbers are used to show that the barrier in 4-fluoroanisole must indeed be rather large, that it is very small or zero in the tetrafluoroanisole, and that in the pentafluoroanisole the preferred conformation is perpendicular.

Experimental

Materials

Anisole-α-^{13}C was prepared by the standard method (18) in which methyl iodide containing 95 at.% ^{13}C (Merck, Sharp and Dohme) was added to a mixture of zone-refined phenol (Aldrich) and anhydrous K_2CO_3 in acetone. The product was identified by ^{1}H nmr and mass spectrometry. The 2,6-dichloro- and 2,6-dibromoanisoles came from Aldrich, as did the 4-methyl-2,6-dibromophenol used to prepare the corresponding anisole derivative using unenriched methyl iodide. The 4-fluoroanisole and the pentafluoroanisole were purchased from Aldrich, while 2,3,5,6-tetrafluoroanisole was a PCR, Inc. product.

The 2,6-dibromo-4-fluoroanisole was synthesized as follows: 8.96 g of 4-fluorophenol (Pfaltz and Bauer, 0.08 mol) were dissolved in 60 mL CS_2 containing 10 mL ether in a 250-mL round bottom flask, and 25.6 g of Br_2 (0.082 mol, ca. 8.5 mL) in 20 mL CS_2 were added dropwise at room temperature over a 0.5-h period. The mixture was stirred for 1 day and then refluxed for 3 h, reduced in volume by rotary evaporation under reduced pressure, taken up in ether, washed twice with water, dried over $MgSO_4$, and rotary-evaporated to yield 17.28 g of a crystalline solid (80%). Spectral data confirmed product identity. This 2,6-dibromo-4-fluorophenol was methylated as above (18) and the anisole derivative was submitted to mass spectral and ^{1}H nmr analysis.

Spectral data

The spectral data employed in this paper were mainly accumulated on a WH90 FT nmr spectrometer at a probe temperature maintained at 305 K, unless otherwise stated. The ^{13}C nmr spectra of the anisole derivatives were acquired using the INEPT (19) pulse sequence. A typical experiment had a 12-μs P_{90} pulse for carbon, a 43-μs P_{90} pulse for protons, $1/4J$ = 1.8 ms, and a 5-s equilibrium delay time. A spectral width of about 400 Hz and up to 1000 scans were employed. The ^{13}C nmr spectra of the fluorine derivatives were also acquired under conditions of broadband ^{1}H decoupling. The solvents and concentrations are indicated in Table 1. Variable temperature experiments were performed using the temperature controller, previously calibrated with a thermocouple.

Molecular orbital calculations

These were carried out on an Amdahl 470/V8 computer system and employed the INDO MO FPT programs (20, 21). The geometry of anisole was that recently described in another connection (22), in which the C_2C_1O angle is given by 120° + 5.0 cos θ and the COC angle by 112° + 3.0° |cos θ|. Here θ is the angle of twist about the C_{sp^2}—O bond, zero corresponding to a heavy-atom coplanar geometry. Similar calculations on 4-fluoroanisole employed a standard geometry (23). Some computations were performed in which certain off-diagonal Fock matrix elements were forced to vanish, in the manner of Barfield (24), thereby providing indications of coupling pathways.

Results and discussion

Conformational dependence of $^6J_p^{C,H}$ and $^6J_p^{C,F}$.

In anisole, $^6J_p^{C,H}$ could not be observed, as illustrated in Fig. 1, and is clearly <0.05 Hz. In the presence of two *ortho* chlorine or bromine substituents the coupling becomes 0.603(5) and 0.625(7) Hz, respectively. In 4-methyl-2,6-dibromoanisole, $^7J_p^{C,H}$ is 0.637(20) Hz. In the presence of two sizeable *ortho* substituents, X-ray diffraction data indicate a perpendicular conformation of the methoxy group (25–27). For a σ–π mechanism, in which the coupling is transmitted via the π orbitals of the benzene ring, it is expected that $^6J_p^{C,H} = -^7J_p^{C,H}$ (13, 28) in the dibromoanisole and its 4-methyl derivative. The signs of these two couplings are unknown. However, our INDO MO FPT computations in Table 2 clearly show that $^6J_p^{C,H}$ is negative and that it has a $\sin^2\theta$ dependence as expected for a σ–π mechanism. In particular, a calculational series in

Can. J. Chem. Downloaded from www.nrcresearchpress.com by 210.87.254.42 on 09/06/12
For personal use only.

Can. J. Chem. Downloaded from www.nrcresearchpress.com by 210.87.254.42 on 09/06/12
For personal use only.

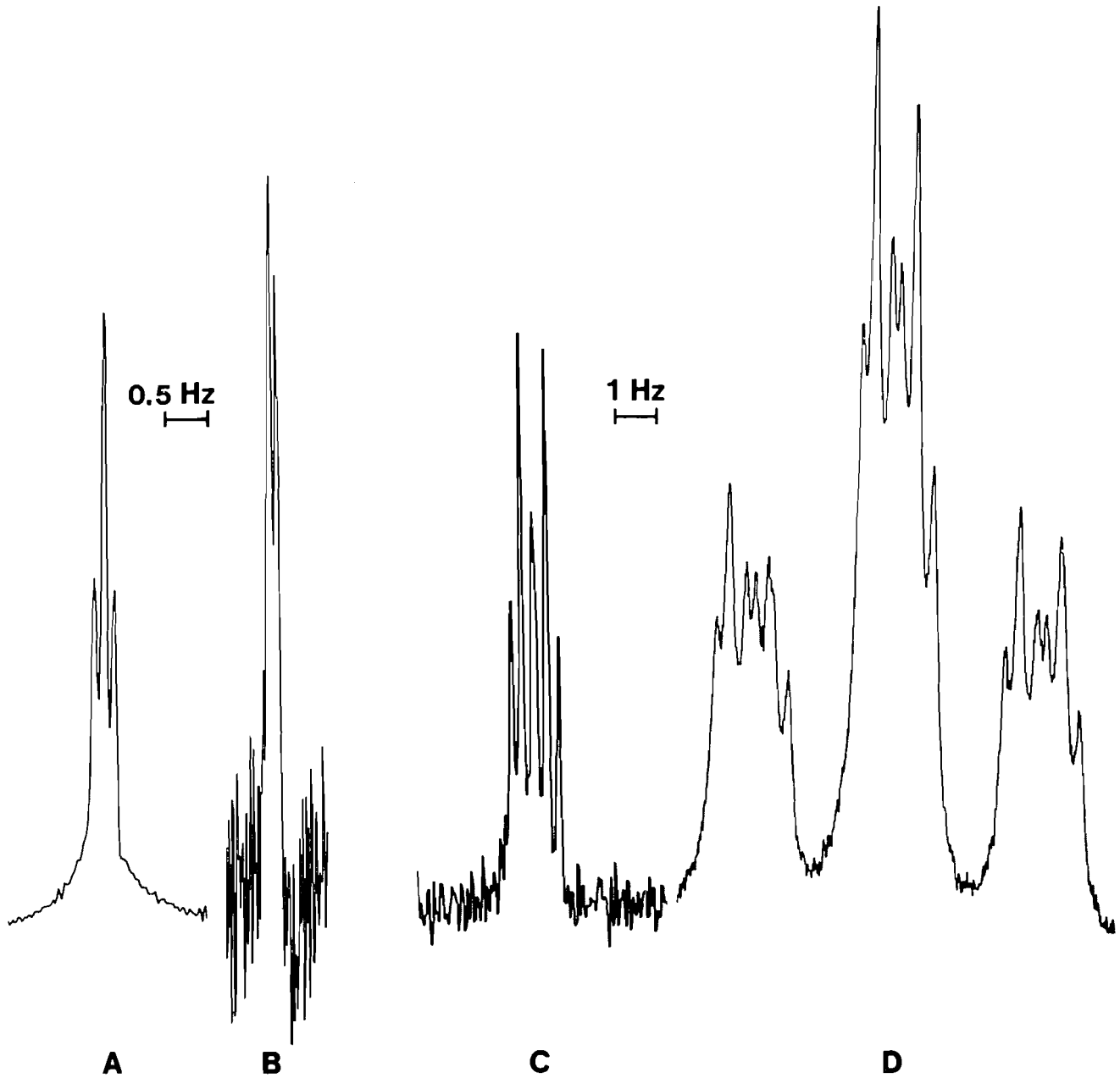

FIG. 1. In A is shown one of the multiplets of the ^{13}C nmr spectrum of the methyl group of anisole-α-^{13}C as a 2 to 4 mol% solution in CS_2 containing 30 v/v% C_6D_{12}. The spectrum was accumulated with 1020 scans using the INEPT pulse sequence on a WH90 spectrometer and a probe temperature of 315 K. The triplet arises from coupling to the *meta* protons five bonds removed and the splitting is just less than 0.12 Hz. The triplet can be reproduced by simulation of a six-spin system, with the ^1H nmr parameters taken from a full analysis of the ^1H spectrum, a linewidth at half height of 0.05 Hz for ^{13}C, and a coupling of 0.03 Hz to the *para* proton. In B is shown the ^{13}C nmr spectrum of the methyl group of 4-fluoroanisole as a 50 vol% solution in acetone-d_6 under conditions of ^1H decoupling. The splitting is very near 0.08 Hz, as determined from repeated experiments. Very similar spectra were obtained for a benzene-d_6 solution, all spectra being accumulated at 305 K and acquisition times of 41 s. In C one of the multiplets in the ^{13}C nmr spectrum of the methyl group of 2,6-dichloroanisole is shown for a 50 vol% solution in benzene-d_6; 648 scans were used with the INEPT sequences. The large "doublet" splitting is 0.60 Hz and the smaller splitting is 0.26 Hz. Part D displays the ^{13}C nmr spectrum of the methyl group of a 50 vol% solution of pentafluoroanisole in acetone-d_6 at 305 K. The protons are being decoupled. The coupling over six bonds to ^{19}F is 0.96 Hz; 1424 scans were accumulated into 32K of memory.

which the twist of the methyl group about the C_{sp^3}—O is correlated with the rotation about the C_{sp^2}—O bond, as in column *B* of Table 2, yields eq. [1].

$$[1] \quad {}^6J_p^{C,H}\,(\text{Hz}) = -0.01 - 0.626 \sin^2\theta$$

This equation reproduces the numbers in column *B* to within 0.01 Hz and also happens to agree rather closely with the magnitudes of ${}^6J_p^{C,H}$ in 2,6-dibromoanisole and of ${}^7J_p^{C,H}$ in the 4-methyl-2,6-dibromoanisole. In conjunction, the experimental and theoretical data presented here appear to warrant the conclusion that ${}^6J_p^{C,H}$ is a σ−π coupling with a simple conformational dependence. Furthermore, in column *C* of Table 2 the σ−π path at the site of the methoxy group has been interrupted by setting the relevant off-diagonal Fock matrix elements equal to zero for all SCF cycles, resulting in a marked reduction in the magnitude of the calculated coupling and there-

Can. J. Chem. Downloaded from www.nrcresearchpress.com by 210.87.254.42 on 09/06/12
For personal use only.

TABLE 2. INDO MO FPT values for $-{}^6J_p^{C,H}$ in anisole as a function of the torsion angle, θ

θ (deg)[a, b]	A[c]	B[d]	C[e]
0	0.009	0.010	0.027
7.5	0.016	0.020	0.025
15	0.039	0.049	0.024
30	0.122	0.158	0.021
45	0.243	0.310	0.016
60	0.355	0.469	0.018
75	0.443	0.594	0.016
90	0.474	0.636	0.016

[a] The geometry is described in the text and was the same as that used in a satisfactory calculation of ${}^5J_o^{H,CH_3}$ (22).

[b] θ is the angle of twist about the C_{sp^2}—O bond, zero corresponding to a planar form.

[c] No twisting of CH_3 about its O—C bond, being staggered about the *ortho* C—H bond for θ = 0.

[d] The methyl group twists so as to keep two H—H_{ortho} distances equal (correlated motion).

[e] All Fock matrix elements involving oxygen p_z, methyl carbon p_z, and methyl hydrogen 1*s* orbitals are kept at zero.

fore qualitative support of the conclusion above.

Calculations on 2-fluoroanisole, not reproduced here, suggest that ${}^6J_p^{C,H}$ changes by 0.01 Hz, at most, in the presence of the *ortho* fluorine substituent, implying that intrinsic ring substituent perturbations of this coupling are small or negligible. Consequently, ${}^6J_{90}^{C,H}$ in anisole and its derivatives will be taken as 0.63 ± 0.01 Hz in magnitude. Of course, the methoxy group in the 2,6-dibromo derivative is not *rigidly* held at θ = 90°. However, if the barrier to internal rotation in this molecule is greater than about 6 kcal/mol, then the quoted value for ${}^6J_{90}^{C,H}$ is acceptable.

Turning to ${}^6J_p^{C,H}$, INDO MO FPT calculations substantiate its $\sin^2\theta$ dependence in 4-fluoroanisole but estimate its maximum value as only 0.7 Hz. For 2,6-dibromo-4-fluoroanisole the observed value is 1.476(20) Hz. An underestimate of the magnitude of ${}^6J_p^{F,H}$ in 4-fluorotoluene is also found (28*b*). The methyl group replacement technique (25) is inapplicable as a test of the σ−π mechanism but, in line with the computations for ${}^6J_p^{F,H}$ and ${}^6J_p^{C,F}$, the latter will also be taken as a σ−π coupling. The presence of a small contribution to ${}^6J_p^{C,F}$ from a mechanism other than σ−π cannot be ruled out, nor can an intrinsic ring substituent perturbation of its magnitude. Yet the discussion below is self-consistent if these assumptions are made, namely that ${}^6J_p^{C,F} = 1.48\ \langle\sin^2\theta\rangle$, where $\langle\sin^2\theta\rangle$ is the expectation value of $\sin^2\theta$ for the hindered motion.

Conformational deductions

(i) 4-Fluoroanisole

On the assumption that ${}^6J_p^{C,F}$ is a σ−π coupling, its magnitude being 0.085 ± 0.005 Hz, one has $\langle\sin^2\theta\rangle$ as (0.085 ± 0.005)/(1.476 ± 0.020) = 0.058 ± 0.005, where the error estimate depends on the measurement errors only. For a *twofold* barrier, tables of $\langle\sin^2\theta\rangle$ as a function of temperature, reduced moment of inertia, and the barrier are available (29). In the present instance they yield the barrier as 5.6 ± 0.5 kcal/mol. If harmonic oscillator instead of free rotor functions are used as a basis, the barrier becomes 5.2 ± 0.5 kcal/mol.

The torsional modes for liquid 4-fluoroanisole gave 6.1 kcal/mol (error not given (11)), assuming a harmonic oscillator model and a twofold barrier. If, as indicated by molecular orbital calculations, the fourfold component is a significant part of the barrier in anisole and therefore no doubt also for 4-fluoroanisole, then the present results are only an approximation to the true barrier. According to the torsional frequencies, the barrier is markedly state dependent, being only about 3 kcal/mol in the gas phase. Microwave spectra confirm the preferred planar conformation of 4-fluoroanisole (30) and place a lower limit of 1.1 kcal/mol on the barrier in the gas phase and are not compatible with a perpendicular conformer of appreciable stability.

The coupling data were measured in acetone-d_6 solution and confirm the rather high barrier found from the torsional data in the liquid. The dipole moment of anisole calculated by STO 3G (9) increases by 0.15 D on going to the perpendicular conformer, from 1.18 to 1.33 D. The experimental value is 1.30 ± 0.03 D (31). Consequently a polar solvent should stabilize the perpendicular form (32), contrary to experiment.

It seems unequivocal that the barrier to rotation about the C_{sp^2}—O bond in 4-fluoroanisole is substantial. Whatever the true shape of the barrier, a small value would entail a much larger ${}^6J_p^{C,F}$ than the observed value of <0.1 Hz.

(ii) 2,3,5,6-Tetrafluoroanisole

${}^6J_p^{C,H}$ is 0.331(8) Hz and, as before, $\langle\sin^2\theta\rangle$ is (0.331 ± 0.008)/(0.630 ± 0.010) or 0.525 ± 0.020, where the ${}^6J_{90}^{C,H}$ is taken as discussed above. If the O—CH_3 bond lay rigidly in a plane perpendicular to the benzene plane, then $\langle\sin^2\theta\rangle$ would equal unity and would vanish if this bond were fixed in the molecular plane. Free rotation about the C_{sp^2}—O bond entails a value of 0.5 for $\langle\sin^2\theta\rangle$. Consequently, a value of 0.525 suggests a very small barrier of 0.1 ± 0.1 kcal/mol (from $\langle\sin^2\theta\rangle$ versus twofold barrier tables) with a slightly preferred perpendicular conformation. Whether the latter is indeed of lower energy depends rather crucially on the true value of ${}^6J_{90}^{C,H}$. The safe conclusion, whether or not there exists a fourfold component, is that the internal barrier is effectively zero.

Support for this conclusion can be adduced in three ways. First, the high resolution nmr spectra of 2,3,5,6-tetrafluoroanisole partially oriented in a nematic phase were consistent with either essentially free rotation or interconversion between 2^{n+1} equivalent positions (n = 1,2,3,...) of the methoxy group (33). This result can be taken as support for the conclusions reached above on the basis of ${}^6J_p^{CH}$. Second, if a 4-fluoro substituent reduces the $2p\ldots\pi$ conjugation of the methoxy group, pentafluoroanisole might well display an unmistakable preference for the perpendicular conformation. This aspect is discussed in the next section. Third, confirmatory evidence might be sought in the temperature dependence of ${}^5J_o^{F,CH_3}$, as can be seen in the following way.

${}^5J_o^{F,CH_3}$ is a proximate (34) coupling, as shown in unpublished work in this laboratory. Its value is +0.2 to +0.3 Hz when the methoxy group is oriented in the plane of the ring with the methyl group lying *trans* to an *ortho* C—F bond. As the methyl group approaches this C—F bond it becomes rather larger than +3 Hz. For a 4.7 mol% solution of the tetrafluoroanisole in acetone-d_6, ${}^5J_o^{F,CH_3}$ increases from 1.30 Hz at 305 K to 1.45 Hz at 192 K. Because this coupling is largest when the methyl group approaches the *ortho* C—F bond most closely, this small increase of about 10^{-3} Hz/deg implies that the perpendicular conformer is not the stable conformer. However, it is conceivable that a decrease in temperature stabilizes the planar or

Can. J. Chem. Downloaded from www.nrcresearchpress.com by 210.87.254.42 on 09/06/12
For personal use only.

a near planar conformation as the density of the polar solution increases. Note that the planar conformation of 4-fluoroanisole is apparently strongly stabilized in solution.

(iii) Pentafluoroanisole

The value of $\langle \sin^2 \theta \rangle$ is $(0.963 \pm 0.023)/(1.476 \pm 0.020)$ or 0.652 ± 0.025. It seems definite that the low-energy conformation is perpendicular. In terms of a twofold barrier, its magnitude is therefore $0.7_8 \pm 0.1_4$ kcal/mol as obtained from tables of $\langle \sin^2 \theta \rangle$ as a function of the barrier, the temperature, and the reduced moment of inertia. The torsional frequencies in the gas phase yield a twofold barrier of 0.86 kcal/mol, but do not assign the low-energy confromation, nor do photoelectron data (35). The chemical shift of ^{13}C-4 indicates a nonplanar conformation (36). Because a *para* fluorine substituent reduces the conjugative barrier in *N*-methylaniline (37) and thiophenol (15, 16), the present result is reasonable in comparison to 2,3,5,6-tetrafluoroanisole. Parenthetically, a *para* amino substituent in thiophenol induces a perpendicular low-energy conformation of the sulfhydryl group in thiophenol (16).

Additional evidence for a perpendicular conformer in pentafluoroanisole comes from the temperature dependence of $^5J_o^{F,CH_3}$. For a 5 mol% solution in acetone-d_6, this coupling *decreases* from 1.085(2) Hz at 305 K to 1.003(8) Hz at 180 K. For the reasons discussed in the previous section, this decrease is consistent with a preferred perpendicular conformer whose amplitude of oscillation about the C_{sp^2}—O bond decreases as the temperature of the sample drops.

(iv) Concerning the barrier magnitude

The large decrease in the barrier to rotation about the C_{sp^2}—O bond in the presence of the two *ortho* C—F bonds is probably a composite of steric and conjugative interactions. That two *ortho* C—F bonds can raise a barrier by steric forces is clear from 2,6-difluoroethylbenzene (38). In this molecule the twofold barrier is most likely mainly steric and is 4 to 5 kcal/mol higher than in ethylbenzene itself. Of course, in the ethylbenzene the stable conformer is perpendicular, so that the barrier increases as the *ortho* C—F bonds introduce increased repulsion with the methyl group in a planar conformer during the rotation about the C_{sp^2}—C_{sp^3} bond. In the anisole derivatives, the planar conformation is destabilized relative to the nonconjugative perpendicular conformer by the steric repulsions between the C—F bonds and the methyl group. As well, because fluorine is a π donor, the *ortho* C—F bonds will decrease the double bond character of the C_{sp^2}—O bond and therefore cause a further destabilization of the conjugative ground state. The net result is a nearly zero internal barrier in the tetrafluoroanisole. Addition of a *para* fluorine substituent to the latter further decreases the $2p-\pi$ conjugation of the methoxy group, leading to a perpendicular ground state in pentafluoroanisole. Of course, the coupling data in Table 1 and X-ray structure analysis show that *ortho* substituents larger than fluorine, such as chlorine or bromine, cause very stable perpendicular conformers in anisole.

(v) Remarks on the barrier in anisole

The discussion in previous paragraphs implies a higher barrier in anisole than in 4-fluoroanisole. The torsional data for the two liquids do not support this implication, giving 6.05 and 6.10 kcal/mol for the former and latter, respectively (11). The coupling data in Table 1 indicate a substantial barrier for anisole. In fact, a classical averaging procedure gave the result that V_2 is 6.0 kcal/mol and V_4 is very nearly zero if $^6J_p^{C,H}$ is as large as 0.036 Hz in magnitude and $^6J_{90}^{C,H}$ is -0.640 Hz with a strict $\sin^2 \theta$ dependence. The ^{13}C nmr spectrum of the methyl group in Fig. 1 suggests that $^6J_p^{C,H}$ can hardly be larger than 0.036 in magnitude. Therefore our coupling data for anisole and 4-fluoroanisole are consistent with a higher barrier in the former, the barrier in the latter being estimated above as 5.6 ± 0.5 kcal/mol.

However, a barrier as high as 6 kcal/mol should have led to a positive DNMR result using ^{13}C nmr spectra. Yet, for a dimethyl ether solution at 120 K not even a relative broadening of the C-2 and C-6 peaks was observable, and similarly for the 3,5-dichloro derivative. On the basis of known substituent effects on ^{13}C shifts (39, 40), the difference in chemical shifts between C-2 and C-6 in planar anisole at slow exchange can be hardly less than 6 ppm. It is then a simple matter to show that the free energy of activation for rotation about the C_{sp^2}—O bond must be less than 4.7 kcal/mol.

If the small $^6J_p^{C,H}$ for anisole is to be consistent with this result, the potential barrier cannot be purely twofold. The potential must increase rather rapidly as the methoxy group leaves the ring plane if $^6J_p^{C,H}$ is to be as small as observed. A rapid rise in potential can be provided by a substantial fourfold component. A coupling of -0.030 Hz can be fit with V_2 and V_4 values of 2.7 ± 0.9 and 2.2 ± 0.5 kcal/mol, respectively, yielding a maximum in the hindering potential of 3.8 kcal/mol. This number, while consistent with the DNMR result, is inconsistent with the torsional data in solution. It is noteworthy, however, that in the gas phase (1) the methoxy torsion frequency can be reproduced exactly by a V_2 of 4.8 kcal/mol and a minor contribution from V_4. Even if, as suggested (1), the V_4 component becomes more important in solution, the evidence for an increased magnitude of the barrier in solution suggests the inadequacy of the fit to the coupling data. Of course, the -0.03 Hz is only an estimate of $^6J_p^{C,H}$. It may actually be smaller in magnitude (see Fig. 1).

Because $T_{1\rho}$ measurements can give estimates of site exchange rates rather higher than those obtainable from lineshapes, an attempt to resolve the unsatisfactory situation described above involved $T_{1\rho}$ measurements (41, 42). The result of an extensive set of measurements was that the free energy of activation is less than 4.4 kcal/mol on the assumption that the shift difference between C-2 and C-6 is 6 ppm, again a negative result. Attempts at measuring this chemical shift difference in solid anisole in another laboratory have been unsuccessful so far. In the solid state, this shift is 6.0 ppm for an ethylphenyl ether derivative (43).

Because our DNMR and $T_{1\rho}$ measurements did not give positive results, they are not described here in detail.

As far as coupling constants are concerned, the anisole barrier problem remains unsatisfactory. In future, other couplings, including ^{13}C,^{13}C interactions, will be studied. Perhaps a temperature dependence of some couplings will be found and may allow a fit to a two-term potential function.

Acknowledgements

For financial help we are grateful to the Natural Sciences and Engineering Research Council of Canada, the University of Petroleum and Minerals, and to the Research Council for the Natural Sciences of the Academy of Finland.

1. H. KONSCHIN, G. TYLLI, and C. GRUNDFELT-FORSIUS. J. Mol. Struct. **77**, 51 (1981), and references therein.
2. K. S. DHAMI and J. B. STOTHERS. Can. J. Chem. **44**, 2855 (1966).

3. P. F. OESPER, C. P. SMYTH, and M. S. KHARASCH. J. Am. Chem. Soc. **64**, 937 (1942).
4. S. K. GARG and C. P. SMYTH. J. Chem. Phys. **46**, 373 (1967).
5. D. G. LISTER and N. L. OWEN. J. Chem. Soc. Faraday Trans. 2, **69**, 1304 (1973).
6. H. M. SEIP and R. SEIP. Acta Chem. Scand. **27**, 4024 (1973).
7. M. KLESSINGER and A. ZYWIETZ. J. Mol. Struct. **90**, 341 (1982), Theochem, and references therein.
8. H. DODZIUK, H. V. VOITHENBERG, and N. L. ALLINGER. Tetrahedron, **38**, 2811 (1981), and references therein.
9. T. A. WILDMAN. Ph.D. Thesis, 1982. University of Manitoba, Winnipeg, Canada.
10. N. L. OWEN and R. E. HESTER. Spectrochim. Acta, Part A, **25**, 343 (1969).
11. G. ALLEN and S. FEWSTER. *In* Internal rotation in molecules. *Edited by* W. J. Orville-Thomas. Wiley and Sons, London. 1974. Chapt. 8.
12. N. W. LARSEN and F. M. NICOLAISEN. J. Mol. Struct. **22**, 29 (1974).
13. W. J. E. PARR and T. SCHAEFER. Acc. Chem. Res. **13**, 400 (1980).
14. T. SCHAEFER, L. KRUCZYNSKI, and W. NIEMCZURA. Chem. Phys. Lett. **38**, 498 (1976).
15. T. SCHAEFER and W. J. E. PARR. Can. J. Chem. **55**, 552 (1977).
16. T. SCHAEFER and T. A. WILDMAN. Chem. Phys. Lett. **80**, 280 (1981).
17. T. SCHAEFER, J. PEELING and G. H. PENNER. Can. J. Chem. **61**, 2773 (1983).
18. L. F. FIESER and M. FIESER. Reagents in organic synthesis. Wiley and Sons, New York. 1967. pp. 682f.
19. G. MORRIS and R. FREEMAN. J. Am. Chem. Soc. **101**, 760 (1979).
20. J. A. POPLE, J. W. MCIVER, and N. S. OSTLUND. J. Chem. Phys. **49**, 2960 (1968).
21. P. A. DOBOSH. Quantum Chemistry Program Exchange, **11**, 141 (1979).
22. T. SCHAEFER and R. LAATIKAINEN. Can. J. Chem. **61**, 224 (1983).
23. J. A. POPLE and M. GORDON. J. Am. Chem. Soc. **89**, 4253 (1967).
24. M. BARFIELD. J. Am. Chem. Soc. **102**, 1 (1980).
25. M. W. WIECZOREK. Acta Crystallogr. Part B, **36**, 1515 (1980).
26. G. W. BURTON, Y. LEPAGE, E. J. GABE, and K. U. INGOLD. J. Am. Chem. Soc. **102**, 7792 (1980).
27. G. W. BURTON and K. U. INGOLD. J. Am. Chem. Soc. **103**, 6472 (1981).
28. (*a*) R. A. HOFFMAN. Mol. Phys. **1**, 326 (1958); (*b*) R. WASYLISHEN and T. SCHAEFER. Can. J. Chem. **50**, 1852 (1972).
29. R. VEREGIN. M.Sc. Thesis, 1981. University of Manitoba, Winnipeg, Canada.
30. D. G. LISTER. J. Mol. Struct. **68**, 33 (1980).
31. N. L. ALLINGER, J. J. MAUL, and M. J. HICKEY. J. Org. Chem. **36**, 2747 (1971).
32. R. J. ABRAHAM and E. BRETSCHNEIDER. *In* Internal rotation in molecules. *Edited by* W. J. Orville-Thomas. Wiley and Sons, London. 1974. Chapt. 13.
33. J. W. EMSLEY, J. C. LINDON, and D. W. STEPHENSON. J. Chem. Soc. Perkin Trans. **2**, 1794 (1975).
34. J. HILTON and L. H. SUTCLIFFE. Prog. Nucl. Magn. Reson. **10**, 27 (1925).
35. A. D. BAKER, D. P. MAY, and D. W. TRUNER. J. Chem. Soc. B, 22 (1968).
36. J. W. EMSLEY. J. Chem. Soc. A, 1459 (1968).
37. L. LUNAZZI, C. MAGAGNOLI, and D. MACCIENTELLI. J. Chem. Soc. Perkin Trans. **2**, 1704 (1980).
38. T. SCHAEFER, R. P. VEREGIN, R. LAATIKAINEN, R. SEBASTIAN, K. MARAT, and J. L. CHARLTON. Can. J. Chem. **60**, 2611 (1982).
39. R. JOST, J. SOMMER, C. ENGDAHL, and P. AHLBERG. J. Am. Chem. Soc. **102**, 7063 (1980).
40. W. KITCHING, I. DEJONGE, W. ADCOCK, and A. N. ABEYWICKREMA. Org. Magn. Reson. **14**, 502 (1980).
41. C. DEVERELL, R. E. MORGAN, and J. H. STRANGE. Mol. Phys. **18**, 553 (1970).
42. P. STILBS and M. M. MOSELEY. J. Magn. Reson. **31**, 55 (1978).
43. L. B. ALEMANY, D. M. GRANT, R. J. PUGMIRE, T. D. ALGER, and K. W. ZILM. J. Am. Chem. Soc. **105**, 2133 (1983).

Can. J. Chem. Downloaded from www.nrcresearchpress.com by 210.87.254.42 on 09/06/12
For personal use only.

On the spin trapping of cyanatyl (·NCO) radicals by nitrosodurene

DETLEF REHOREK[1] AND EDWARD G. JANZEN[2]

Guelph–Waterloo Centre for Graduate Work in Chemistry, Department of Chemistry and Biochemistry, University of Guelph, Guelph, Ont., Canada N1G 2W1

Received October 5, 1983

This paper is dedicated to Professor Gerald E. Dunn on the occasion of his 65th birthday

DETLEF REHOREK and EDWARD G. JANZEN. Can. J. Chem. **62**, 1598 (1984).

Spin trapping experiments with cyanatyl radicals and nitrosodurene show that the triazene-1,3-dioxyl radical described earlier has the structure as indicated for **I**.

DETLEF REHOREK et EDWARD G. JANZEN. Can. J. Chem. **62**, 1598 (1984).

Des expériences de piégeage de spin impliquant les radicaux cyanatyles et le nitrosodurène ont permis de démontrer que le radical triazènedioxyle-1,3 décrit antérieurement doit être représenté par la structure **I**.

[Traduit par le journal]

Can. J. Chem. Downloaded from www.nrcresearchpress.com by 210.87.254.105 on 09/06/12
For personal use only.

It has been shown that azidyl radicals (N_3·) may be trapped by nitrones to give persistent spin adducts which are easily detected by electron spin resonance (esr) at room temperature in liquid solution (1–4).

Nitrosodurene, however, gives a persistent aminoxyl (nitroxide) which appears to be the result of double spin trapping. Since hyperfine splitting due to three nitrogen nuclei, with two being magnetically equivalent, was detected, the spectrum was tentatively assigned to the triazene-1,3-dioxyl, **I**, (5):

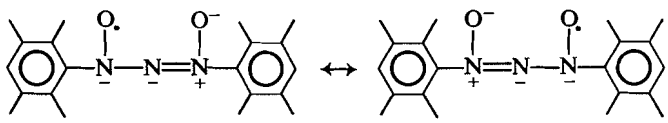

I

which is isoelectronic with the well-known seven π-electron nitronyl nitroxides (6, 7):

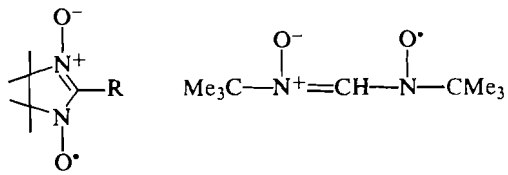

An alternate structure (**II**) with a pendant N_2 group which might have been formed by the addition of N_3· radicals to the nitrosodurene dimer, similar to the previously reported (8) reaction of iminyl radicals, has also been considered:

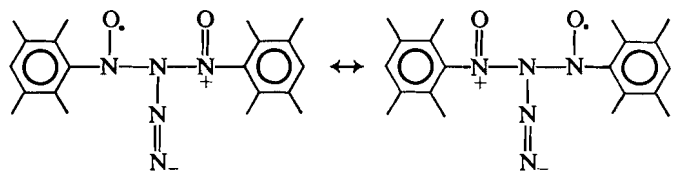

II

Although experiments with ^{15}N-labelled azide (9) confirmed the presence of two equivalent nitrogens originating from the nitrosodurene structure, **II** could not be ruled out. Since cyanatyl radicals (OCN·) are isoelectronic with azidyl radicals, a similar behaviour of these radicals towards nitrosodurene might be expected.

The esr spectra of the aminoxyls recorded during spin trapping of azidyl and cyanatyl radicals by nitrosodurene[3] together with the computer simulation are shown in Fig. 1. The hyperfine coupling constants measured from these spectra are identical within experimental error (±0.05 G). Moreover, no secondary splitting was observed with the azide spin adduct of perdeuteronitrosodurene (as might be expected from the pendant N_2 group). These findings strongly suggest that the spectrum in Fig. 1 is due to structure **I** and not **II**.

Similar results were obtained with pentamethylnitrosobenzene, whereas nitrosomesitylene gave measurable spectra with azidyl radicals only (see Table 1).

The mechanism of formation of **I** is of interest. The following route suggests itself:

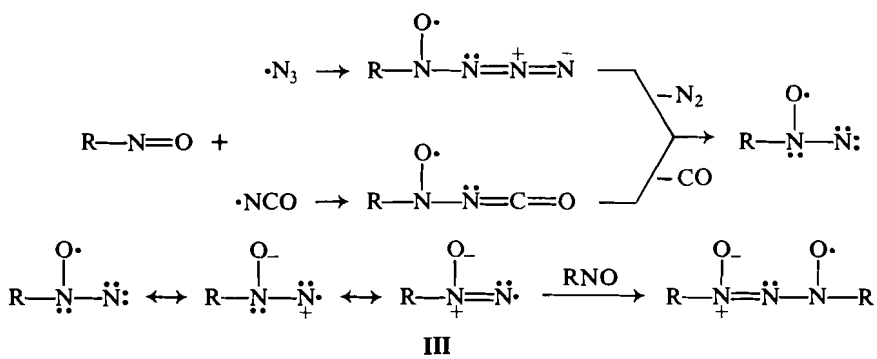

III

[1]On sabbatical leave from Sektion Chemie der Karl Marx Universität, Leipzig, DDR.

[2]Author to whom correspondence should be addressed.

[3]The pseudohalide radicals were generated by photolysis (330 nm < λ < 500 nm) of the CT complex formed between CBr_4 and tetrabutylammonium pseudohalide in dichloromethane. The nitrosoaromatics were synthesized according to the literature (10).

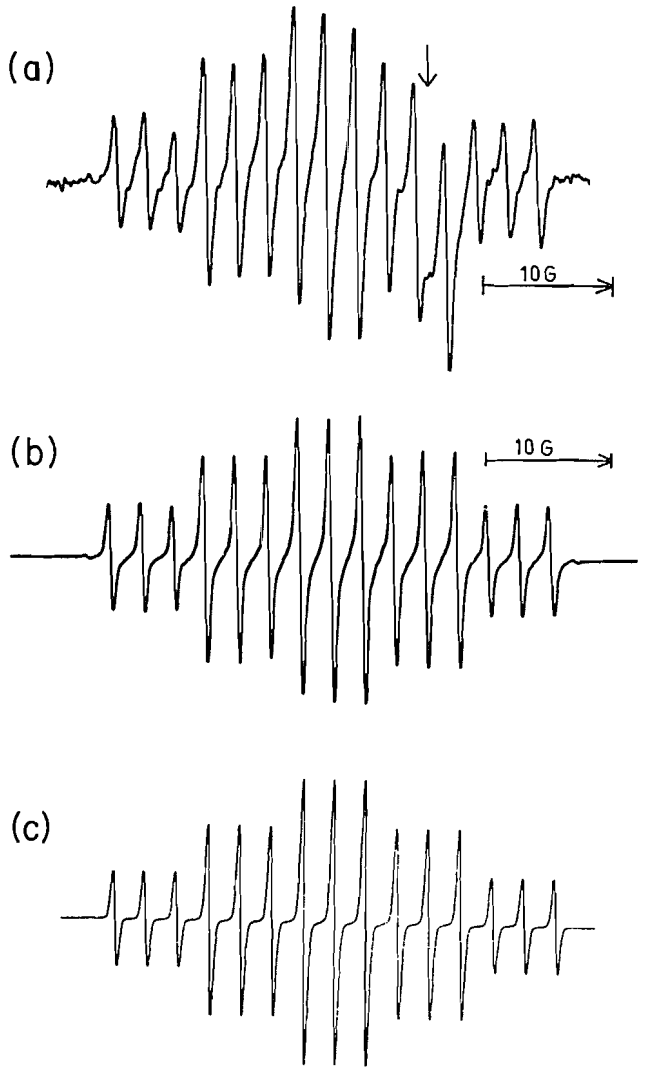

FIG. 1. The esr spectrum of bis-duryltriazene-1,3-dioxyl obtained from (a) ·NCO radicals (arrow indicates F-centre infused quartz cell); (b) $\cdot N_3$ radicals; (c) computer simulation.

III would appear to be one of the radicals expected from thermal decomposition of "azoxydurene":

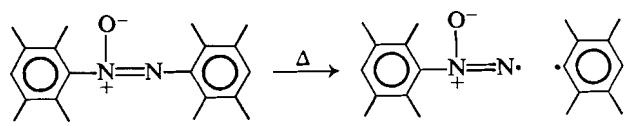

It should be noted that the signal intensity of the aminoxyls formed by spin trapping of cyanatyl radicals by nitrosodurene is much less than for azidyl radicals (about 100× less). In order to obtain sufficient esr intensity, spin trap concentrations above 0.01 *M* were needed. In contrast, both azidyl and cyanatyl radicals appear to be easily trapped by nitrones (1–4, 11).

No persistent spin adducts were obtained with thiocyanatyl and selenocyanatyl radicals and nitrosodurene.

In conclusion, the assignment of the structure of the aminoxyl obtained from nitrosodurene and azidyl radicals (**I**) has been confirmed. Nitrosodurene or nitrones can be used as detectors of azidyl radicals although nitrones are better spin traps for the detection of cyanatyl radicals.

TABLE 1. Electron spin resonance hyperfine splitting constants of diaryltriazene-1,3-dioxyls[a]

Spin trap	Radical trapped	a_N^1	a_N^2
Nitrosodurene	$\cdot N_3$	7.21 (2 N)	2.38 (1 N)
Nitrosodurene	·NCO	7.23 (2 N)	2.40 (1 N)
Pentamethylnitrosobenzene	$\cdot N_3$	7.18 (2 N)	2.38 (1 N)
Pentamethylnitrosobenzene	·NCO	7.18 (2 N)	2.40 (1 N)
Nitrosomesitylene	$\cdot N_3$	7.02 (2 N)	2.32 (1 N)

[a]In gauss; ±0.05 G; solvent CH_2Cl_2.

Acknowledgements

This work is being supported by the Natural Sciences and Engineering Research Council of Canada. Grateful acknowledgement is hereby made. We would also like to thank Dr. R. Konaka for the gift of deuterated nitrosodurene, and Henry J. Stronks for preparing the tetraalkylammonium salts.

1. L. V. OKHLOBYSTINA, V. A. TYURIKOV, B. I. SHAPIRO, YA. K. SYRKIN, and A. A. FAINZIL'BERG. Izv. Akad. Nauk SSSR, Ser. Khim. 2436 (1975).
2. W. KREMERS and A. SINGH. Can. J. Chem. **58**, 1592 (1980).
3. D. REHOREK, P. THOMAS, and H. HENNIG. Inorg. Chim. Acta, **32**, L1 (1979).
4. E. G. JANZEN, H. J. STRONKS, D. E. NUTTER, E. R. DAVIS, H. N. BLOUNT, J. L. POYER, and P. B. MCCAY. Can. J. Chem. **58**, 1596 (1980).
5. D. REHOREK and H. HENNIG. Z. Chem. **19**, 263 (1979).
6. H. G. AURICH and P. HÖHLEIN. Tetrahedron Lett. 279 (1974).
7. H. G. AURICH, S. J. DUGGAL, P. HÖHLEIN, H. G. KLINGELHÖFER, and W. WEISS. Chem. Ber. **114**, 2440 Z(1981).
8. T. SUEHIRO, S. MASUDA, and N. MOTOYAMA. Chem. Lett. 53 (1980).
9. W. KREMERS, G. W. KOROLL, and A. SINGH. Can. J. Chem. **60**, 1597 (1982).
10. L. I. SMITH and F. L. TAYLOR. J. Am. Chem. Soc. **57**, 2370 (1935); **57**, 2460 (1935).
11. T. H. WALTER, E. E. BANCROFT, G. L. MCINTIRE, E. R. DAVIS, L. M. GIERASCH, H. N. BLOUNT, H. J. STRONKS, and E. G. JANZEN. Can. J. Chem. **60**, 1621 (1982).

Can. J. Chem. Downloaded from www.nrcresearchpress.com by 210.87.254.105 on 09/06/12
For personal use only.

Heteroanthracyclines. 2. 4-Demethoxythioxanthodaunomycinone (7,8,9,10-tetrahydrobenzo(*b*)-6,7,9,11-tetrahydroxy-9-acetylthioxanthen-12-one)

CHIU-MING WONG,[1] AI-QIAO MI,[2] JIALI REN,[3] WASIMUL HAQUE, HING-YAT LAM,[4] AND KIRK MARAT
Department of Chemistry, University of Manitoba, Winnipeg, Man., Canada R3T 2N2

Received November 17, 1983

This paper is dedicated to Professor Gerald E. Dunn on the occasion of his 65th birthday

CHIU-MING WONG, AI-QIAO MI, JIALI REN, WASIMUL HAQUE, HING-YAT LAM, and KIRK MARAT. Can. J. Chem. **62**, 1600 (1984).

The title compound, a new heteroanthracyclinone was synthesized in five steps starting with 5,8-dimethoxy-2-acetyltetralin (**15**). Reaction of 2,2′-dithiosalicylic acid (**16**) with the tetralin **15** in concentrated sulfuric acid gave the tetracyclic thioxanthones **17** and **18**. Conversion of **18** to **24** by demethylation and realkylation followed by oxidation and acid hydrolysis gave the title compound **27**.

CHIU-MING WONG, AI-QIAO MI, JIALI REN, WASIMUL HAQUE, HING-YAT LAM et KIRK MARAT. Can. J. Chem. **62**, 1600 (1984).

On a synthétisé le composé mentionné dans le titre, une nouvelle hétéroanthracyclinone, en cinq étapes en utilisant la diméthoxy-5,8 acétyl-2 tétraline (**15**) comme produit de départ. La réaction de l'acide dithio-2,2′ salicylique (**16**) avec la tétraline **15** dans l'acide sulfurique concentré conduit aux thioxanthones tétracycliques **17** et **18**. La transformation de **18** en **24** par le biais d'une déméthylation et d'une réalkylation suivie d'une oxydation et d'une hydrolyse acide conduit au composé **27** mentionné dans le titre.

[Traduit par le journal]

Introduction

For the last decade, attempts to improve the therapeutic effect of the first generation anthracycline antitumor antibiotics, namely daunomycin (**1**) and adriamycin (**2**), have been rewarded with encouraging results. New anthracyclines and their derivatives, of both natural and synthetic origin, such as aclacinomycin A (**3**), 4-demethoxydaunomycin (**4**), 4-demethoxy-11-deoxydaunomycin (**5**), 11-deoxydaunomycin (**6**), and 4′-deoxydaunomycin (**7**) and many others were shown to be much more potent or slightly less toxic than the first generation antitumor anthracyclines (1). However, cardiotoxicity remains the critical side effect which severely restricts the dosages and excludes the possibility of using these drugs for long term maintenance purposes.

According to structure–activity relationship studies, the antineoplastic properties of anthracyclines could be rationalized by at least four different mechanisms. They are: intercalative binding to DNA double helix (2); superoxide formation causing DNA and chromosome cleavage (3); quinone methide formation and alkylation (4); interaction with cell membranes and possibly lipid peroxidation (5). The superoxide formation is likely to be the cause of cardiotoxicity due to the relatively low level of superoxide dismutase in the heart cells.

In our continuous effort to search for anthracycline analogues with reduced cardiotoxicity, we have proposed heteroanthracyclines for structure–activity relationship and cardiotoxicity studies and, recently, we reported the synthesis and biological activity of 4-demethoxyxanthodaunomycinone (**8**) (6). The low activity of **8** against MCF-7 human mammary cancer cells as compared to daunomycinone (**9**), which has no activity, could be an indication that a quinone methide inter-

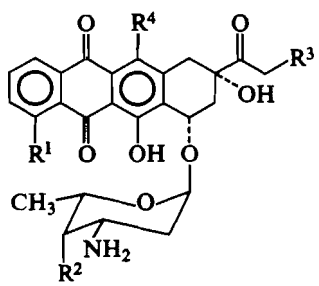

1 R¹ = OCH_3, R^2 = R^4 = OH, R^3 = H
2 R¹ = OCH_3, R^2 = R^3 = R^4 = OH
4 R¹ = R^3 = H, R^2 = R^4 = OH
5 R¹ = R^3 = R^4 = H, R^2 = OH
6 R¹ = OCH_3, R^2 = OH, R^3 = R^4 = H
7 R¹ = OCH_3, R^2 = R^3 = H, R^4 = OH

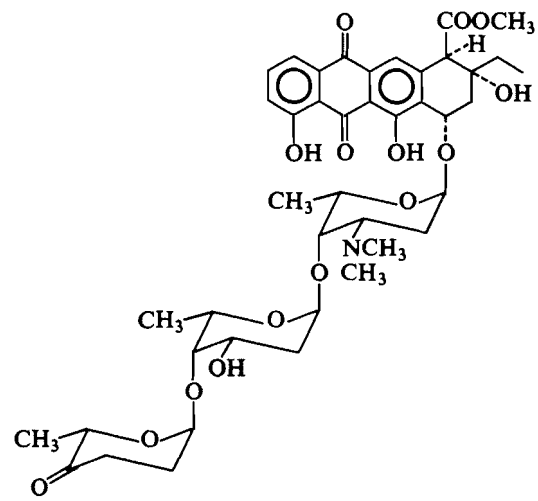

3

[1] Author to whom correspondence should be addressed.
[2] Research associate from Chengdu Institute of Organic Chemistry, Academia Sinica, Chengdu, China.
[3] Visiting scholar from Xinjiang Institute of Chemistry, Wulumuqi, Academia Sinica, China.
[4] American Leukemia Society scholar, Department of Medicine, University of Manitoba, Winnipeg, Manitoba.

Can. J. Chem. Downloaded from www.nrcresearchpress.com by 210.87.254.5 on 09/06/12
For personal use only.

Can. J. Chem. Downloaded from www.nrcresearchpress.com by 210.87.254.5 on 09/06/12
For personal use only.

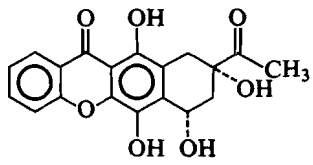

8

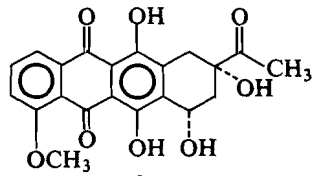

9

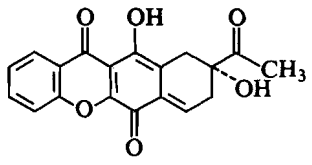

10

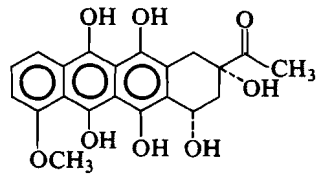

11

mediate similar to **10** (7) is a contributing factor to cytoxicity. A similar intermediate in the case of anthracyclines is still a postulate and has not been isolated or proven to exist. Nevertheless, the activity of **8** could mean that daunomycin goes through a bioreductive process to the hydroquinone intermediate **11** before it can easily form the quinone methide **12** and its cytotoxicity becomes discernible. The availability of 4-demethoxythioxanthodaunomycinone (**27**) opens the avenue further for studies of the possible quinone methide intermediate and the relationship between the quinone moiety of anthracyclines and cardiotoxicity. Furthermore, it could also serve as a precursor for the corresponding sulfone and sulfoxide analogues of anthracyclines. Although direct chemical conversion of **27** and its derivatives to the corresponding sulfoxide and sulfone has not yet been achieved, they have been synthesized in a more elaborate process and will be reported later.

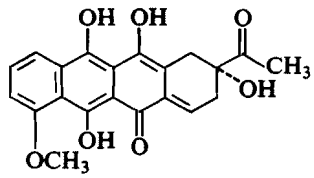

12

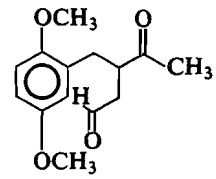

13

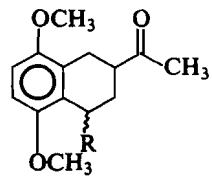

14 R = Cl
15 R = H

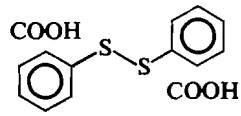

16

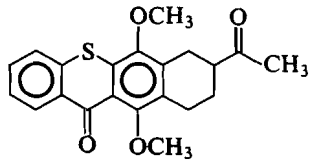

17

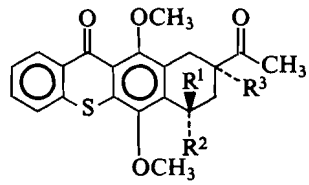

18 R¹ = R² = R³ = H
19 R¹ = H, R² = R³ = OH
20 R¹ = R³ = OH, R² = H

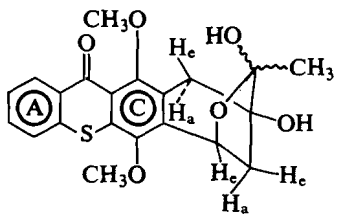

21

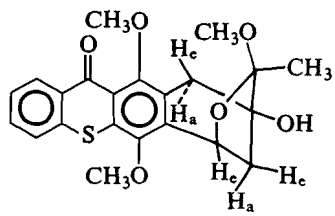

22

Results and discussion

The starting material, 3-acetyl-4-(2,5-dimethoxyphenyl)-butanal (**13**) (8), was easily converted to 1-chloro-5,8-dimethoxy-3-acetyltetralin (**14**) in a hydrogen chloride saturated dichloromethane solution at −40°C. Hydrogenolysis of **14** in ethanol in the presence of palladium on charcoal gave an overall yield of more than 75% of 5,8-dimethoxy-2-acetyltetralin (**15**). The tetracyclic skeletons **17** and **18** were conveniently assembled by condensing 2,2′-dithiosalicylic acid (**16**) with the tetralin **15** (9) in concentrated sulfuric acid in 58% yield. This process offers a route to the tetracyclic aglycone skeletons which is shorter and easier than the tedious process reported earlier in the xanthone series (6). The two isomers separated by column chromatography on silica were characterized by routine spectroscopy and elemental analyses and finally dipole moments (10, 11), which provided the only simple means to differentiate **17** from **18**. The first isomer (**17**) collected from the column has a calculated dipole moment of 3.2 D and an experimental value of 3.5 D; the second isomer (**18**) from the column has a calculated value of 4.7 D and an experimental value of 4.9 D.

Oxidation of **18** by molecular oxygen in *N,N*-dimethylformamide, *tert*-butyl alcohol, and trimethyl phosphite (12) gave directly a 3:1 mixture of the *cis*-diol **19** and the *trans*-diol **20** in 50% yield. The *cis*-geometry of **19** and the *trans*-geometry of **20** of the C_7—OH and C_9—OH together with the D-ring conformations of these two isomers could be established by detailed analysis of their high field ^{1}Hmr spectra, infrared spectra, and the formation of derivative **22**.

The high field ^{1}Hmr spectrum of **19** (Figs. 1(a) and 1(b)) shows that the C_7—H_e appearing as an octet at 5.28 ppm is coupled to C_7—OH, C_8—H_a, and C_8—H_e with J_{7c7OH} = 8.5 Hz, J_{7c8a} = 4.7 Hz, and J_{7e8e} = 2.5 Hz. The C_9—OH appears as a singlet at 4.554 ppm while the C_7—OH appears as a doublet at 4.268 ppm with J_{7OH7e} = 8.5 Hz which collapsed to a singlet when the C_7—H_e at 5.28 ppm was irradiated. The C_{10}—H_e appearing as doublet of a doublet at 3.195 ppm is geminally coupled to C_{10}—H_a with J_{10e10a} = 17.3 Hz and it is further coupled to C_8—H_e with J_{10e8e} = 1.9 Hz. The C_{10}—H_a appears only as a doublet with J_{10a10e} = 17.3 Hz at 3.06 ppm. The C_8—H_e at 2.30 ppm shows up as two triplets which are in fact doublet of a doublet of a doublet with J_{8a8e} = 14 Hz, J_{7e8e}

Can. J. Chem. Downloaded from www.nrcresearchpress.com by 210.87.254.5 on 09/06/12
For personal use only.

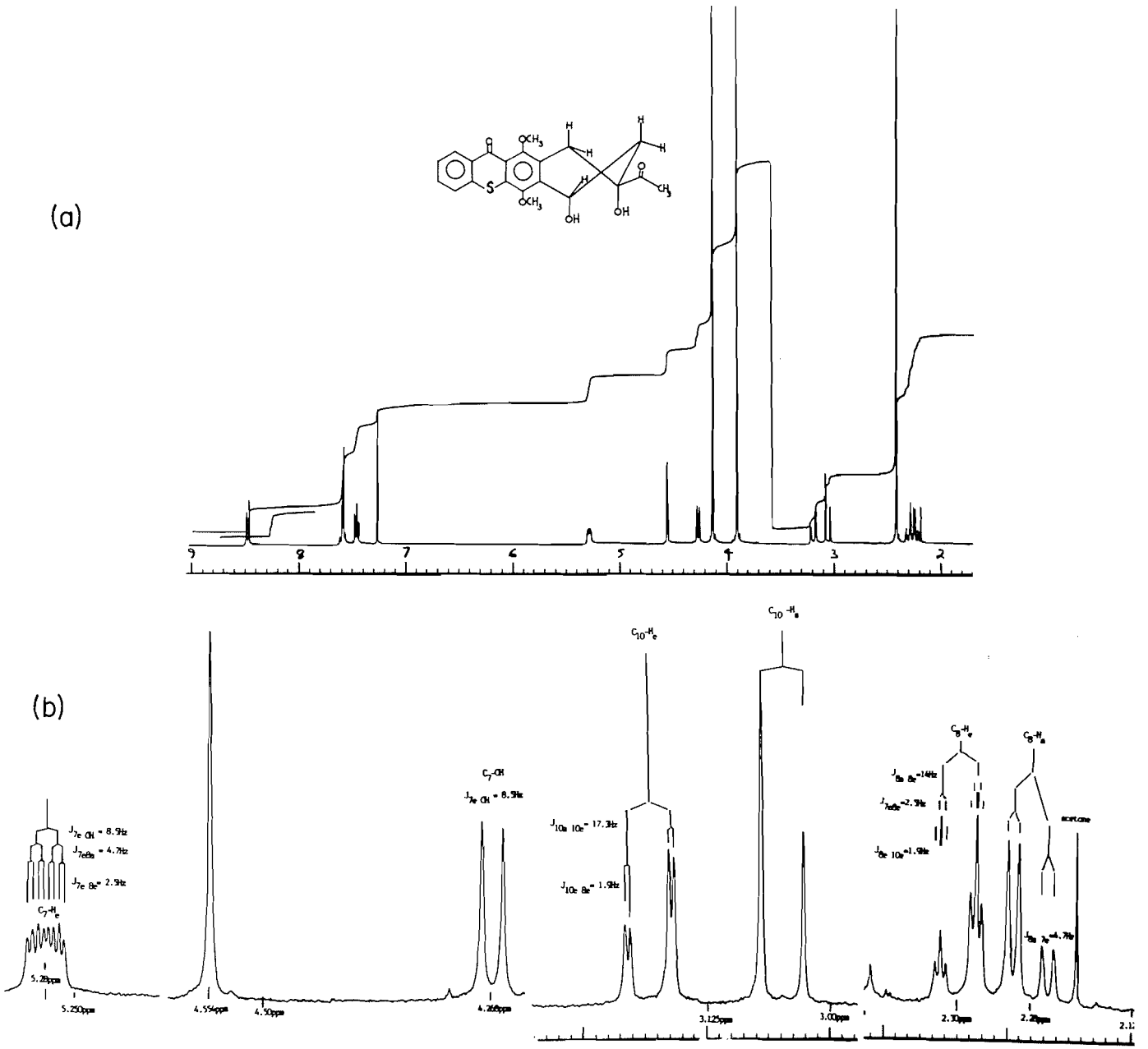

FIG. 1. (a) Bruker WH-400 ^{1}Hmr spectrum of **19**. (b) Expanded area between 5.3 and 2.1 ppm.

= 2.5 Hz, and J_{8e10e} = 1.9 Hz. The C_8—H_a appearing at 2.228 ppm is a doublet of a doublet with J_{8a8e} = 14.0 Hz, J_{8a7e} = 4.7 Hz. The infrared spectrum of **19** shows a relatively broad absorption peak at 3450 cm^{-1} while in the case of **20** two absorption peaks at 3600 cm^{-1} and 3560 cm^{-1} are present, indicating that both the C_7—OH and C_9—OH are hydrogen-bonded. This information agrees well with the D-ring conformation of **19** shown in Fig. 1(a) instead of the other possible conformation where the C_7—OH and C_9—OH are both equatorial.

The high field ^{1}Hmr spectrum of **20** shows that it exists in a slow equilibrium with the hemiketal **21**. When the C_6—OCH_3 and C_{11}—OCH_3 are replaced by other groups such as benzyloxy or methoxymethylenoxy groups, the ^{1}Hmr spectra become too complicated, or the compounds become too unstable to be thoroughly purified for detailed analyses. Only in the case of **20** can all the peaks be clearly identified, along with those of **21** (Figs. 2(a) and 2(b)). The C_7—H_e of **21** appearing as a doublet at 5.40 ppm with J_{7e8e} = 6.0 Hz is a good indication of the [3.2.1]bicyclo-hemiketal structure where the H_{7e}—C_7—C_8—H_{8a} dihedral angle is close to 90° with $J_{7e8a} \simeq 0$. The C_{10}—H_e of **21** appears at 3.323 ppm as doublet of a doublet with J_{10e10a} = 17.8 Hz and J_{10e8e} = 2.0 Hz. The C_{10}—H_a appears at 3.195 ppm as a doublet with J_{10a10e} = 17.8 Hz. Signals due to the C_9—OH and the C_{13}—OH, which disappear after deuterium exchange with deuterated methanol, appear as singlets at 3.105 ppm and 2.805 ppm respectively. The relatively high field shift of the C_{13}—OH in comparison with other hydroxy protons of **20**, **21**, and **22** could be the result of diamagnetic shielding of ring C and is in agreement with the assignment of the stereochemistry at C_{13}. The C_8—H_e appears as an octet at 2.675 ppm with J_{8e8a} = 11.0 Hz, J_{8e7e} = 2.0 Hz. The C_8—H_a, appearing at higher field than all the other C_8—H's of both **20** and **21** at 2.0 ppm as a doublet with J_{8a8e} = 11.0 Hz, is also due

Can. J. Chem. Downloaded from www.nrcresearchpress.com by 210.87.254.5 on 09/06/12
For personal use only.

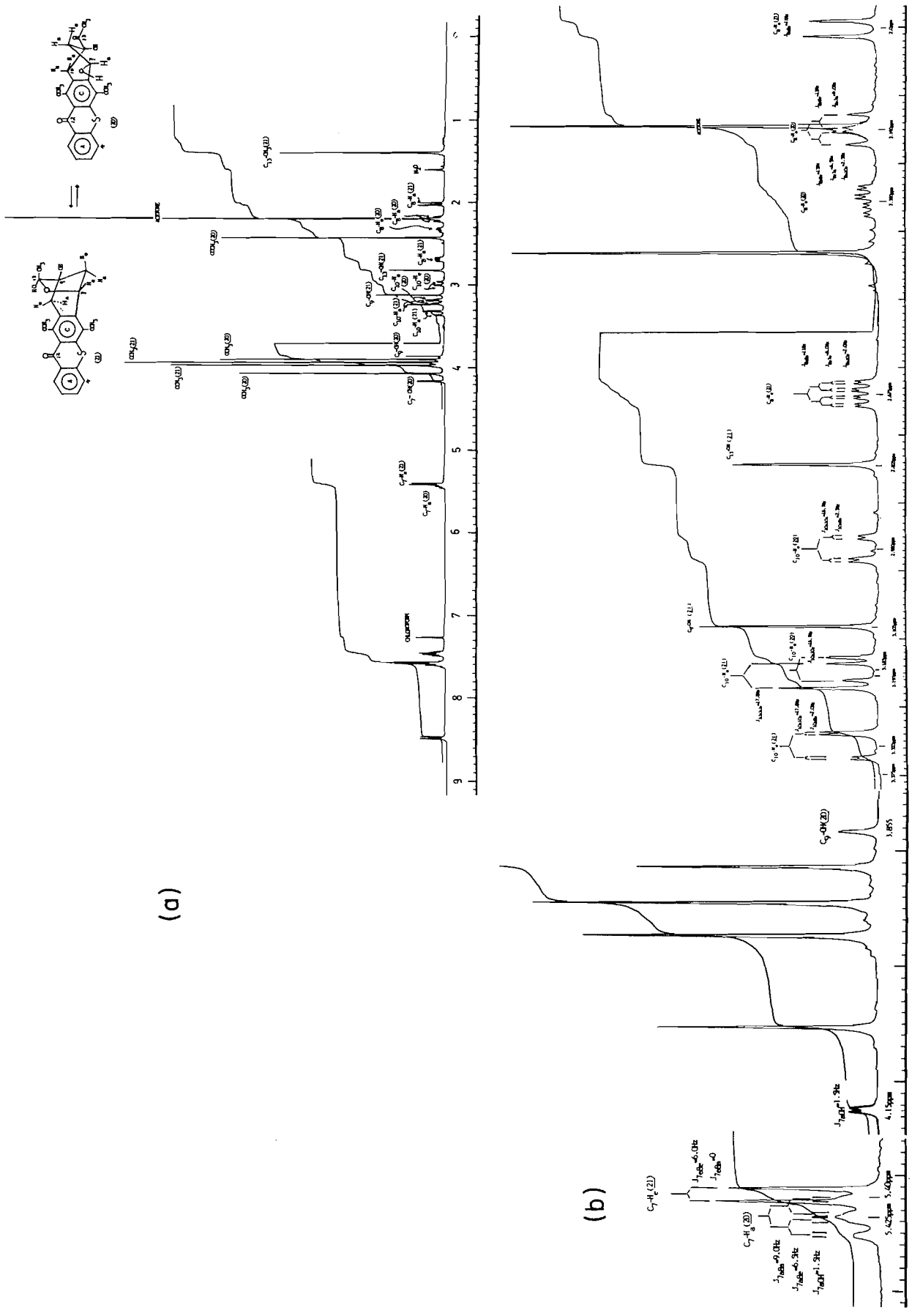

FIG. 2. (a) Bruker WH-400 ^{1}Hmr spectrum of **20** and **21** in equilibrium. (b) Expanded area between 5.5 and 2.0 ppm.

Can. J. Chem. Downloaded from www.nrcresearchpress.com by 210.87.254.5 on 09/06/12
For personal use only.

to the diamagnetic shielding of ring C of **21**.

The D-ring protons of **20** can also be easily identified. The C_7—H_a at 5.425 ppm is coupled to C_8—H_a, C_8—H_e, and C_7—OH with J_{7a8a} = 9.0 Hz, J_{7a8e} = 6.5 Hz, and J_{7aOH} = 1.5 Hz. The C_7—OH doublet at 4.15 ppm with J_{7OH7a} = 1.5 Hz and the C_9—OH at 3.855 ppm exchanged with deuterated methanol. The C_{10}—H_a appears at 3.185 ppm as a doublet with J_{10a10e} = 16.7 Hz, while the C_{10}—H_e appears as doublet of a doublet at 2.960 ppm with J_{10e10a} = 16.7 Hz and J_{10e8e} = 2.3 Hz. The C_8—H_e appearing at 2.320 ppm as an octet is coupled to C_8—H_a, C_7—H_a, and C_{10}—H_e with J_{8e8a} = 13 Hz, J_{8e7a} = 6.5 Hz, and J_{8e10e} = 2.3 Hz. The C_8—H_a appearing at 2.190 ppm as a quartet is coupled to C_8—H_e and C_7—H_a with J_{8a8e} = 13 Hz and J_{8a7a} = 9.0 Hz. The four methoxy groups of **20** and **21** show up as four singlets between 3.88 and 4.08 ppm while the acetyl group of **20** appears at 2.43 ppm and the C_{13}—CH_3 of **21** appears at 1.40 ppm. The *trans*-geometry of **20** was further established when it was converted completely into **22**. The ^{1}Hmr spectrum of **22** shows only a clean doublet for H_{7e} with J_{7e8e} = 6 Hz, in addition to a new peak at 3.35 ppm for the C_{13}—OCH_3. The peaks at 5.425 ppm (Fig. 2(b)) belonging to the C_7—H_a, together with all other peaks assigned to **20**, completely disappear. The infrared spectum of **20** shows a weak absorption at 1710 cm^{-1} which disappears after **20** is converted to **22**. While conversion of the *trans*-isomer **20** to the *cis*-isomer **19** can easily be achieved by aqueous trifluoroacetic acid, demethylation of **19** to the desired product **27** by various processes failed. It is obvious that a protecting group much less stable than a methyl group is necessary. The isomer **18** was demethylated by hot sulfuric acid to give the phenol **23** which was realkylated by chloromethyl methyl ether to form **24**. Oxidation of **24** by molecular oxygen as before gave a mixture of

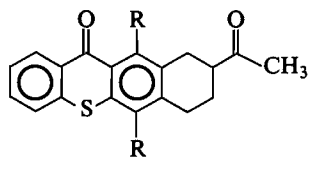

23 R = OH
24 R = OCH_2OCH_3

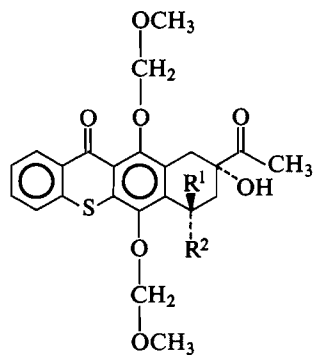

25 R^1 = H, R^2 = OH
26 R^1 = OH, R^2 = H

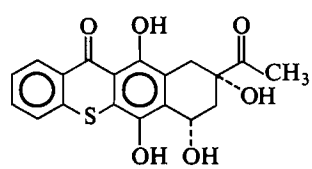

27

the *cis*-diol **25** and the *trans*-diol **26**. However, attempts to effect a clean separation of **25** from **26** under various chromatography conditions failed. Separation of **25** from **26** by preparative thin-layer chromatography on neutral alumina invariably gave only the *cis*-diol **25**, the structure of which was firmly established by detailed analysis of its high field ^{1}Hmr spectrum (Figs. 3(b) and 3(c)). The C_7—H_e at 5.328 ppm is a poorly resolved octet with J_{7e7OH} = 5.0 Hz, J_{7e8a} = 4.0 Hz, and J_{7e8e} = 3.0 Hz. The two latter coupling constants reveal that the C_7—H_{7e} bond bisects the H_{8a}—C_8—H_{8e} angle almost equally while, in the case of compound **19**, the coupling constants J_{7e8a} = 4.7 Hz and J_{7e8e} = 2.5 Hz correspond to the H_{7e}—C_7—C_8—H_{8a} and H_{7e}—C_7—C_8—H_{8e} dihedral angles of about 45° and 65°. This difference could be rationalized if, in the case of **19**, the C_7—OH proton hydrogen-bonds with the C_9—OH oxygen and, in the case of **25**, the C_7—OH proton hydrogen-bonds with the C_{16}—OCH_3 oxygen. The C_{15}—H_aH_b show up as an AB quartet at 5.281 ppm with J_{15a15b} = 6.0 Hz and $\Delta\delta_{ab}$ = 0.165 ppm. The C_{16}—H_aH_b appear as an AB quartet at 5.146 ppm with J_{16a16b} = 6.6 Hz and $\Delta\delta_{ab}$ = 0.034 ppm. The C_9—OH appears at 5.092 ppm as a singlet and the C_7—OH appears as a doublet at 4.931 ppm with J_{7OH7e} = 5.0 Hz. The C_{10}—H_aH_e appear at 3.290 as an AB quartet with J_{10a10e} = 18 Hz and $\Delta\delta_{ab}$ = 0.22 ppm. The C_{10}—H_e is further coupled to C_8—H_e with J_{10e8e} = 2.0 Hz while the C_{10}—H_a appears only as a doublet. The C_8—H_aH_b appear as an AB quartet at 2.210 ppm with J_{8a8e} = 14 Hz. The C_8—H_e is further coupled to C_7—H_e and C_{10}—H_e with J_{8e7e} = 4.5 Hz and J_{8e10e} = 2.0 Hz, while the C_8—H_a is further coupled to C_7—H_e with J_{8a7e} = 4.0 Hz, in agreement with the assigned structure.

Hydrolysis of **25** in acetone in the presence of dilute hydrochloric acid gave the desired product, 4-demethoxythioxanthodaunomycinone (**27**). The ^{1}Hmr spectrum (Fig. 4) reveals a very low field one-proton singlet at 13.98 ppm, typical of the strongly chelated proton of C_{11}—OH. The non-chelated phenolic C_6—OH appears at 6.95 ppm as a singlet. The C_7—H_e at 5.10 ppm shows up as an octet with J_{7e7OH} = 12.0 Hz, J_{7e8a} = 5.5 Hz, and J_{7e8e} = 2.7 Hz. The C_9—OH at 4.13 ppm is a singlet and the C_7—OH at 3.95 ppm is a doublet with J_{7OH7e} = 12 Hz. This relatively large coupling constant is possible if the dihedral angle of H_{7e}—C_7—O—H is close to 180°, as shown in Fig. 4. Both C_{10}—H_2 and C_8—H_2 are broad singlets at 3.02 ppm and 2.34 ppm respectively and the acetyl group appears as a sharp three-proton singlet at 2.40 ppm.

Experimental

All melting points were recorded on a Fischer–Johns apparatus and were uncorrected. Nuclear magnetic resonance spectra were recorded on a Bruker WH-90 or a Bruker WH-400 using tetramethylsilane as internal standard. Infrared spectra were recorded on a Perkin–Elmer 710 infracord and dipole moments were taken on a DM01 Kahl dipolometer. Mass spectra were recorded on a Finnigan 1015 or an A.E.I. MS-50. Elemental analyses were performed by Geller laboratories.

Preparation of 5,8-dimethoxy-2-acetyltetralin (15)

To a methylene chloride solution (150 mL) saturated with anhydrous hydrogen chloride at −30°C was added 3-acetyl-4-(2,5-dimethoxyphenyl)-butanal (**13**) (15 g) and the solution was stirred for a period of 20 min, evaporated to dryness under reduced pressure at room temperature to give the easily polymerized chlorotetralin **14**, possibly as mixture of *cis*- and *trans*-isomers which, without purification, was then hydrogenolysed in ethanol (200 mL) in the presence of Pd/C (5%) (1.5 g) under atmospheric pressure for a period of 4 h. The ethanol solution, after removal of the catalyst by filtration, was evaporated to dryness under reduced pressure to give a colorless syrupy residue which crystallized upon addition of ether. The crystalline product (7.7 g) is identical to the 5,8-dimethoxy-2-acetyltetralin (**15**) prepared previously (8).

Preparation of 7,8,9,10-tetrahydrobenzo[b]-8-acetyl-6,11-dimethoxythioxanthen-12-one (17) and 7,8,9,10-tetrahydrobenzo[b]-9-acetyl-6,11-dimethoxythioxanthen-12-one (18)

To an ice-cooled stirred concentrated sulfuric acid solution (250 mL) of 2,2′-dithiosalicyclic acid (**16**) (15 g) was added 5,8-dimethoxy-2-acetyltetralin (**15**) (5 g). The solution was stirred for a period of

Can. J. Chem. Downloaded from www.nrcresearchpress.com by 210.87.254.5 on 09/06/12
For personal use only.

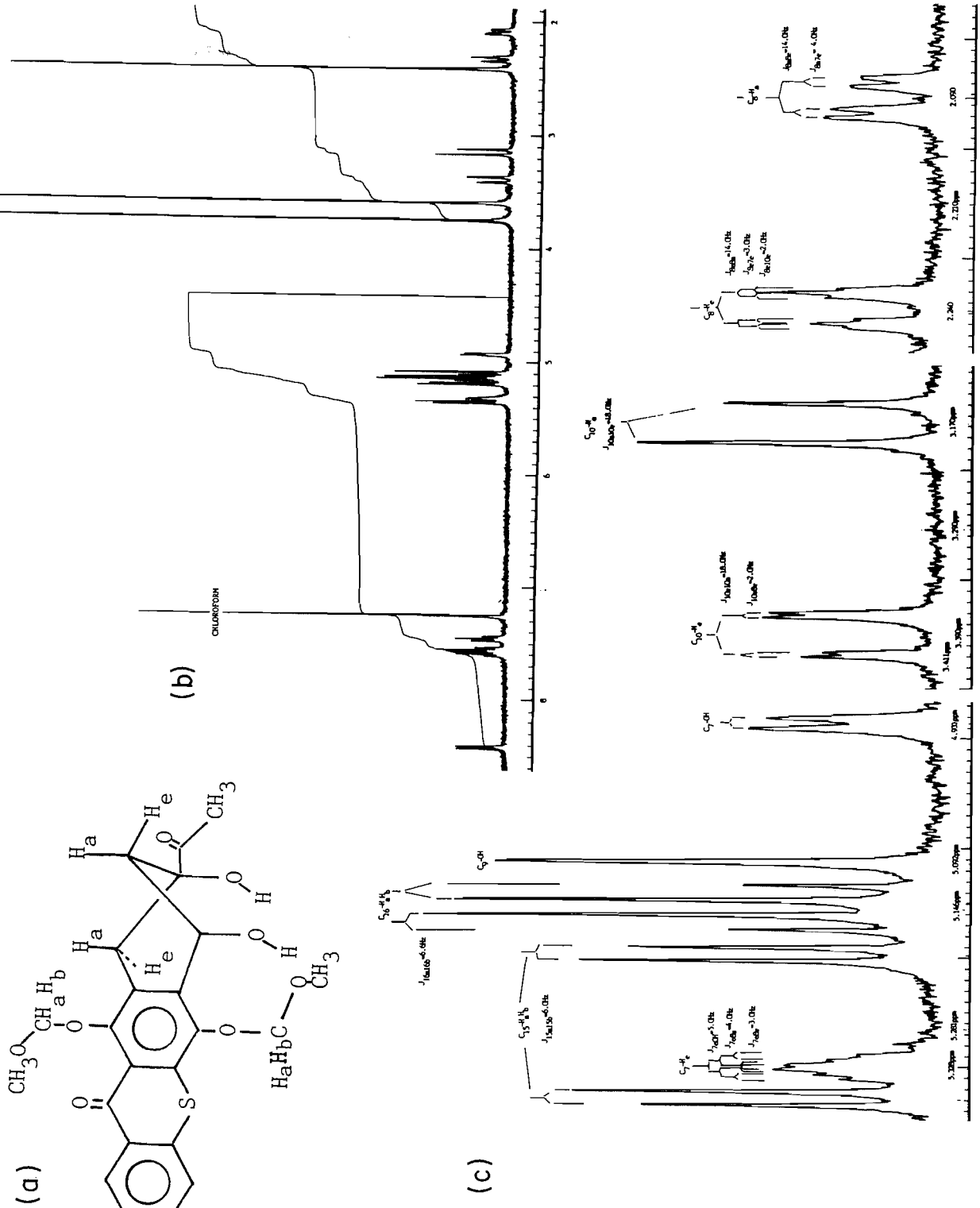

FIG. 3. (a) Compound **25**. (b) Bruker WH-400 ^{1}Hmr spectrum of **25**. (c) Expanded area between 5.4 and 2.0 ppm.

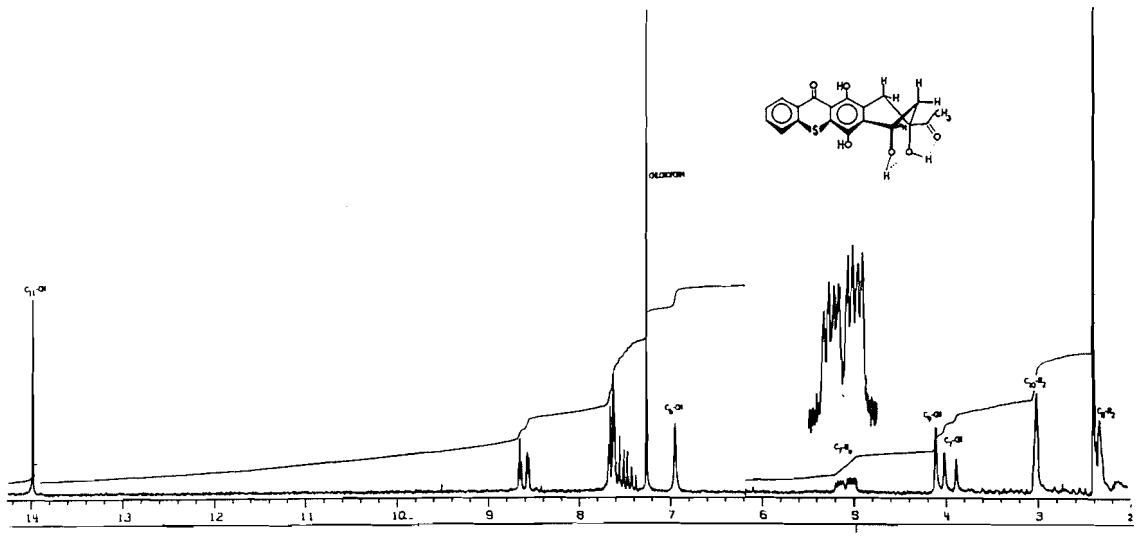

FIG. 4. Bruker WH-90 ^{1}Hmr spectrum of **27**.

6 h at room temperature and then poured into ice-water (1.5 L) and extracted exhaustively with ethyl acetate (4 × 300 mL). The combined extracts, washed with water, sodium bicarbonate solution, and dried over anhydrous magnesium sulfate, were evaporated to dryness under reduced pressure to give an orange solid residue (6.2 g) which was a mixture of mainly **17** and **18** together with a small amount of corresponding demethylated compounds. This crude product was then dissolved in acetone (200 mL) to which was added finely pulverized potassium carbonate (10 g) and methyl iodide (10 mL). The solution was stirred at 40°C for a period of 16 h, cooled, filtered, and evaporated to dryness to give a semi-solid residue which was purified by pressurized column chromatography on silica (250 g E.M. Silica Gel 60, 230 mesh) to give the crystalline products **17** (2.3 g) and **18** (2.1 g).

The first isomer **17** was purified by recrystallization from chloroform and ether, mp 142–144°C; ir (cm^{-1}): 1710 (acetyl), 1640 (phenone); ^{1}Hmr (δ ppm): 8.48 (m, 1H, C_4—H), 7.32–7.61 (m, 3H, C_1—H, C_2—H, C_3—H), 3.91 (s, 3H, OCH_3), 2.15–1.55 (m, 2H, C_8—H_2); *Mol. Wt.* (ms) calcd. for $C_{21}H_{20}O_4S$: 368.1084; found: 368.1087; dipole moment calcd.: 3.2 D; found: 3.5 D. *Anal.* calcd. for $C_{21}H_{20}O_4S$: C 68.46, H 5.43; found: 68.47, H 5.49.

The second isomer **18** was further purified by recrystallization from chloroform–ether, mp 160–162°C; ir (cm^{-1}): 1710 (acetyl), 1640 (phenone); ^{1}Hmr (δ ppm): 8.44 (m, 1H, C_1—H), 7.33–7.62 (m, 3H, C_2—H, C_3—H, C_4—H), 3.92 (s, 3H, OCH_3), 3.80 (s, 3H, OCH_3), 2.70–3.44 (m, 5H, C_7—H_2, C_9—H, C_{10}—H_2), 2.08–2.35 (m, 2H, C_8—H_2), 2.30 (s, 3H, $COCH_3$); *Mol. Wt.* (ms) calcd. for $C_{21}H_{20}O_4S$: 368.1084; found: 368.1088; dipole moment calcd.: 4.7 D; found: 4.9 D.

*Preparation of 7,8,9,10-tetrahydrobenzo[*b*]-6,11-dimethoxy-7,9-*cis*-dihydroxy-9-acetylthioxanthen-12-one (**19**) and 7,8,9,10-tetrahydrobenzo[*b*]-6,11-dimethoxy-7,9-*trans*-dihydroxy-9-acetylthioxanthen-12-one (**20**)*

The thioxanthone **18** (200 mg) was added to *N,N*-dimethylformamide (30 mL) containing *tert*-butyl alcohol (1.5 mL). The solution was warmed in a hot water bath to dissolve the thioxanthone, cooled in a Dry Ice bath at −30°C and then was added to freshly distilled trimethyl phosphite (0.5 mL) and potassium *tert*-butoxide (200 mg). Dry oxygen was introduced into the solution through a gas dispersion tube for a period of 1 h, keeping the cold bath temperature between −20°C and −30°C. Cold dilute hydrochloric acid was added dropwise until the dark brown colour of the solution disappeared. Water (150 mL) was added and the aqueous solution was extracted with ethyl acetate (3 × 150 mL). The combined ethyl acetate solution was dried over magnesium sulfate, evaporated to dryness under reduced pressure, and the residue was subjected to thick-layer chromatography over silica.

The less polar *cis*-isomer (**19**) (85 mg) was further purified by recrystallization from chloroform–ether, mp 205–208°C; ir (cm^{-1}): 3450 (*cis*-C_7—OH and C_9—OH), 1710 (acetyl), 1640 (phenone); *Mol. Wt.* (high resolution ms) calcd. for $C_{21}H_{20}O_6S$: 400.0981; found: 400.0986; ^{1}Hmr, see Figs. 1(a) and 1(b).

The more polar *trans*-isomer (**20**) (30 mg) was further purified by recrystallization from chloroform–acetone, mp 102–106°C; ir (cm^{-1}): 3600 (OH), 3560 (OH), 1715 (weak, $COCH_3$), 1645 (phenone); ^{1}Hmr, see Figs. 2(a) and 2(b).

*Preparation of ketal **22***

The *trans*-isomer **20** (160 mg) was added to benzene (60 mL) containing freshly distilled 2,2-dimethoxypropane (500 mg) and anhydrous *p*-toluenesulfonic acid (26 mg). The solution was stirred at room temperature under anhydrous condition for 24 h, washed with saturated sodium carbonate solution, dried over magnesium sulfate, and evaporated to dryness under reduced pressure. The solid residue (161 mg) was recrystallized from methylene chloride – ether, mp 123–124°C; ir (cm^{-1}): 3550 (OH), 1645 (phenone), 1590 (aromatic); ^{1}Hmr (δ ppm): 8.49 (dd of d, 1H, C_1—H, $J_{1,2}$ = 8 Hz, $J_{1,3}$ = 1.4 Hz, $J_{1,4}$ = 1.0 Hz), 7.35–7.62 (m, 3H, C_2—H, C_3—H, C_4—H), 5.31 (d, 1H, C_7—H_e, J_{7e8e} = 6.0 Hz, J_{7e8a} = 0), 3.94 (s, 3H, OCH_3), 3.92 (s, 3H, OCH_3), 3.35 (s, 3H, C_{13}—OCH_3), 3.38 (dd, 1H, C_{10}—H_e, J_{10e10a} = 20 Hz, J_{10e8e} = 1.5 Hz), 3.23 (s, 1H, C_9—OH), 3.09 (d, 1H, C_{10}—H_a, J_{10a10e} = 20 Hz), 2.64 (dd of d, 1H, C_8—H_e, J_{8e8a} = 11 Hz, J_{8e7e} = 6 Hz, J_{8e7e} = 1.5 Hz), 1.92 (d, 1H, C_8—H_a, J_{8a8e} = 11 Hz, J_{8a7e} = 0), 1.24 (s, 3H, C_{13}—CH_3); *Mol. Wt.* (high resolution ms) calcd. for $C_{22}H_{22}O_6S$: 414.1137; found: 414.1137.

*Preparation of **23***

The thioxanthone **18** (2 g) in sulfuric acid solution (80%) (200 mL) was heated with stirring in a 100°C oil-bath for 14 h. The solution was diluted with water (800 mL), extracted exhaustively with ethyl acetate (4 × 300 mL), and after routine work-up gave a dark brown solid residue which was purified by fast filtration over silica and recrystallization from acetone–ether, mp 253–254°C; ir (cm^{-1}) (Nujol: 3300 (broad, phenols), 1700 (acetyl), 1620 (chelated phenone), 1590 (aromatic); ^{1}Hmr (δ ppm): 12.1 (s, 1H, C_{11}—OH), 8.30 (dd of d, 1H, C_1—H, $J_{1,2}$ = 7 Hz, $J_{1,3}$ = 1.5 Hz, $J_{1,4}$ = 1.5 Hz), 7.30–7.80 (m, 3H, C_2—H, C_3—H, C_4—H), 5.22 (s, 1H, C_6—OH), 2.55–3.22 (m, 5H, C_7—H_2, C_9—H, C_{10}—H_2), 2.06–2.30 (m, 2H, C_8—H_2), 2.28 (s, 3H, $COCH_3$); *Mol. Wt.* (high resolution ms) calcd. for $C_{19}H_{16}O_4S$: 340.0769; found: 340.0771. *Anal.* calcd. for $C_{19}H_{16}O_4S$: C 67.04, H 4.74; found: C 67.10, H 4.77.

Can. J. Chem. Downloaded from www.nrcresearchpress.com by 210.87.254.5 on 09/06/12
For personal use only.

Can. J. Chem. Downloaded from www.nrcresearchpress.com by 210.87.254.5 on 09/06/12
For personal use only.

Preparation of ***24***

To anhydrous acetone (100 mL) containing pulverized and freshly baked potassium carbonate (5 g) was added the thioxanthone **23** (450 mg). To the dark orange solution heated in a 80°C oil bath under nitrogen was injected chloromethyl methyl ether (2.5 mL) which was dried by passing freshly distilled chloromethyl methyl ether through grade 1 neutral alumina. The acetone solution was heated under reflux for 7 h, cooled, filtered, and evaporated to dryness under reduced pressure. The residue was dissolved in methylene chloride, filtered to remove the residual potassium carbonate, and evaporated to dryness to give a syrupy residue which crystallized upon addition of ether and was recrystallized from methylene chloride – ether (360 mg), mp 126–128°C; ir (cm^{-1}): 1710 (acetyl), 1640 (phenone), 1595 and 1580 (aromatic); ^{1}Hmr (δ ppm): 8.43 (dd of d, 1H, C_1—H, $J_{1,2}$ = 7.5 Hz, $J_{1,3}$ = 1.5 Hz, $J_{1,4}$ = 1.5 Hz), 7.30–7.60 (m, 3H, C_2—H, C_3—H, C_4—H), 5.17 (s, 2H, —O—CH_2—O—), 5.11 (s, 2H, —O—CH_2—O—), 3.72 (s, 3H, OCH_3), 3.60 (s, 3H, OCH_3), 2.50–3.55 (m, 5H, C_7—H_2, C_9—H, C_{10}—H_2), 2.0–2.34 (m, 2H, C_8—H_2), 2.28 (s, 3H, $COCH_3$); *Mol. Wt.* (high resolution ms) calcd. for $C_{23}H_{24}O_6S$: 428.1294; found: 428.1293.

Preparation of ***25***

The methoxymethyl ether **24** (200 mg) was dissolved in anhydrous *N,N*-dimethylformamide (30 mL) and *tert*-butyl alcohol (1.5 mL). To the gently stirred solution kept in a cold bath of −30°C was added potassium *tert*-butoxide (200 mg) and anhydrous trimethyl phosphite (0.5 mL). Dry oxygen was introduced through a gas dispersion tube into the solution for 1 h, keeping the cold bath temperature between −20°C and −30°C. The solution was acidified to pH 8–9 by adding, dropwise, cold dilute hydrochloric acid, then was diluted with water and extracted exhaustively by chloroform. The extract, washed with water and dried over anhydrous magnesium sulfate, was evaporated to thorough dryness under reduced pressure to give a brown residue. Thin-layer chromatography of the residue over silica gave a major fraction (138 mg) which was shown by ^{1}Hmr to be a mixture of mainly **25** and possibly **26**. Further purification of this fraction by thin-layer chromatography over neutral alumina gave only the *cis*-isomer **25** (80 mg) which was further purified by recrystallization from methylene chloride – ether, mp 135–137°C; ^{1}Hmr (δ ppm): 8.425 (dd, 1H, C_1—H, $J_{1,2}$ = 8 Hz, $J_{1,3}$ = 1.1 Hz), 7.58 (m, 2H, C_3—H, C_4—H), 7.45 (dd of d, 1H, C_2—H, $J_{2,1}$ = 8 Hz, $J_{2,3}$ = 7 Hz, $J_{2,4}$ = 1.6 Hz), 5.281 (q, 2H, C_{15}—H_aH_b, J_{15a15b} = 6 Hz, Δδ = 0.165 ppm), 5.328 (dd of d, 1H, C_7—H_e, J_{7e7OH} = 5.0 Hz, J_{7e8a} = 4.0 Hz, J_{7e8e} = 3.0 Hz), 5.146 (q, 2H, C_{16}—H_aH_b, J_{16a16b} = 6.6 Hz, Δδ = 0.034 ppm), 5.092 (s, 1H, C_9—OH), 4.931 (d, 1H, C_7—OH, J_{7OH7e} = 5.0 Hz), 3.756 (s, 3H, OCH_3), 3.390 (dd, 1H, C_{10}—H_e, J_{10e10a} = 18 Hz, J_{10e8e} = 2.0 Hz), 3.170 (d, 1H, C_{10}—H_a, J_{10a10e} = 18.0 Hz), 2.416 (s, 3H, $COCH_3$), 2.240 (dd of d, 1H, C_8—H_e, J_{8e8a} = 14.0 Hz, J_{8e7e} = 3.0 Hz, J_{8e10e} = 2.0 Hz), 2.09 (dd, 1H, C_8—H_a, J_{8a8e} = 14.0 Hz, J_{8a7e} = 4.0 Hz); see Figs. 3(b) and 3(c); *Mol. Wt.* (high resolution ms) calcd. for $C_{23}H_{24}O_8S$: 460.1202; found: 460.1193.

*Preparation of 4-dimethoxythioxanthodaunomycinone (****27****)*

The *cis*-isomer **25** (65 mg) was added to acetone (15 mL) containing dilute hydrochloric acid (2 mL (5%). The acetone solution was stirred at room temperature for a period of 16 h, concentrated by removing most of the acetone under reduced pressure, diluted with water (20 mL), and extracted with ethyl acetate (4 × 30 mL). The combined ethyl acetate extracts were dried over magnesium sulfate and evaporated to dryness under reduced pressure to give a light yellow crystalline product (45 mg) which was recrystallized from acetone–ether, mp 190–192°C; ir (cm^{-1}): 3450 (*cis*-C_7—OH, C_9—OH), 1710 (acetyl), 1620, 1600 (chelated phenone), 1585 (aromatic); ^{1}Hmr (δ ppm): 14.0 (s, 1H, C_{11}—OH), 8.60 (dd of d, 1H, C_1—H, $J_{1,2}$ = 8 Hz, $J_{1,3}$ = 1.4 Hz, $J_{1,4}$ = 1.2 Hz), 7.38–7.68 (m, 3H, C_2—H, C_3—H, C_4—H), 6.95 (s, 1H, C_6—OH), 5.10 (dd of d, 1H, C_7—H_e, J_{7e7OH} = 12 Hz, J_{7e8e} = 5 Hz, J_{7e8a} = 2 Hz), 4.13 (s, s, 1H, C_9—OH), 3.95 (d, 1H, C_7—OH, J_{7OH7e} = 12 Hz), 3.02 (broad s, 2H, C_{10}—H_2), 2.40 (s, 3H, $COCH_3$), 2.34 (broad s, 2H, C_8—H_2); see Fig. 4.

Acknowledgement

Financial support from NSERC of Canada and Farmitalia Carlo Erba of Italy for this project is gratefully acknowledged.

1. F. ARCAMONE. Doxorubicin anticancer antibiotics. Med. Chem. **17**, (1981).
2. W. J. PIGRAM, W. FALBER, and L. D. HAMILTON. Nature (London), New Biol. **235**, 17 (1972).
3. N. R. BACHUR, S. L. GORDON, M. V. GEE, and H. KON. Proc. Natl. Acad. Sci. U.S.A. **76**, 954 (1979).
4. A. C. SARRORELLI. Cancer chemotherapy, ACS Symposium Series 30, A.C.S., Washington, DC. 1976.
5. T. R. TRITTON and G. YEE. Science, **217**, 248 (1982).
6. C. M. WONG, W. HAQUE, H. Y. LAM, K. MARAT, E. BOCK, and A. Q. MI. Can. J. Chem. **61**, 1788 (1983).
7. H. W. MOORE. Science, **197**, 527 (1977).
8. C. M. WONG, A. Q. MI, H. Y. LAM, and W. HAQUE. Can. J. Chem. **61**, 562 (1983).
9. W. G. PRESCOTT and S. SMILE. J. Chem. Soc. **99**, 641 (1911).
10. C. G. LEFEVRE and R. J. W. LEFEVRE. J. Chem. Soc. 196 (1937).
11. V. I. MINKIN, O. A. OSIPOV, and Y. A. ZHDANOV. Dipole moment in organic chemistry. Plenum Press, New York. 1970. p. 91.
12. C. M. WONG, A. Q. MI, W. HAQUE, and H. Y. LAM. Synth. Commun. **13**, 15 (1983).

A change in rate-determining step in the hydrolysis of cyclic ketals

ROBERT A. MCCLELLAND AND N. ESTHER SEAMAN
Department of Chemistry, University of Toronto, Toronto, Ont., Canada M5S 1A1

Received October 12, 1983

This paper is dedicated to Professor Gerald E. Dunn on the occasion of his 65th birthday

ROBERT A. MCCLELLAND and N. ESTHER SEAMAN. Can. J. Chem. **62**, 1608 (1984).

A kinetic study is reported of the hydrolysis of 2-methoxy-2-phenyltetrahydrofuran and 2-ethoxy-2-phenyltetrahydrofuran. At pH >6 the rate-determining step involves H^+-catalyzed formation of the oxocarbocation, this reaction occurring with cleavage of the exocyclic alkoxy group to produce a cyclic cation. Between pH 5 and pH 6 a change-over occurs and at pH <5, the rate-determining step in product formation is breakdown of the cyclic hemiketal intermediate, 2-hydroxy-2-phenyltetrahydrofuran. The changeover occurs because the H^+-catalyzed breakdown of this intermediate is a slower process than the H^+-catalyzed oxocarbocation-forming step. Hydroxide ion catalysis makes the hemiketal decomposition faster at higher pH. Analogous cyclic ortho esters (2-alkoxy-1,3-dioxolanes) show this same change in rate-determining step between high pH and low pH, while acyclic acetals, ketals, and ortho esters generally have the oxocarbocation-forming stage rate determining at all acidities. It is concluded that the structural features inherent in the cyclic systems are responsible for the difference. In particular, the oxocarbocation-forming stage involves exocyclic bond cleavage, giving it an entropic advantage over the hemiketal or hemiorthoester breakdown which is endocyclic.

ROBERT A. MCCLELLAND et N. ESTHER SEAMAN. Can. J. Chem. **62**, 1608 (1984).

On rapporte une étude cinétique de l'hydrolyse du méthoxy-2 phényl-2 tétrahydrofuranne et de l'éthoxy-2 phényl-2 tétrahydrofuranne. A un pH > 6, l'étape déterminante fait intervenir la formation d'un oxocarbocation qui est catalysée par H^+ et qui implique un clivage du groupe alkoxy exocyclique afin de produire un cation cyclique. A des pH compris entre 5 et 6, il se produit une transition dans le mécanisme de la réaction; à un pH inférieur à 5, l'étape déterminante est la rupture de l'hémicétal cyclique intermédiaire, l'hydroxy-2 phényl-2 tétrahydrofuranne. La transition dans le mécanisme réactionnel se produit parce que la rupture de cet intermédiaire, catalysée par H^+, est un processus plus lent que l'étape de formation de l'oxocarbocation, catalysée par H^+. La catalyse par l'ion hydroxyde fait que la décomposition de l'hémicétal se fait de plus en plus rapidement à mesure que l'on augmente le pH. Dans le cas des ortho esters cycliques analogues (alkoxy-2 dioxolannes-1,3), on observe le même type de transition entre les étapes déterminantes lorsqu'on passe des pH faibles aux pH plus élevés; par ailleurs, quel que soit le pH, la formation de l'oxocarbocation est généralement l'étape déterminante lors de l'hydrolyse des acétals acycliques, des cétals et des ortho esters. On en conclut que les caractéristiques structurales inhérentes aux systèmes cycliques sont responsables de la différence. En particulier, la formation de l'oxocarbocation qui implique le clivage de la liaison exocyclique possède un avantage entropique sur les ruptures impliquées lors de l'hydrolyse des hémicétal ou ortho ester qui sont endocycliques.

[Traduit par le journal]

Can. J. Chem. Downloaded from www.nrcresearchpress.com by 210.87.254.42 on 09/06/12
For personal use only.

A three-stage reaction mechanism is now commonly accepted (1) for the hydrolysis of acetals and ortho esters: (*i*) generation, usually in an acid-catalyzed reaction, of an oxocarbocation; (*ii*) hydration of this cation to a hemiacetal or hemiorthoester; and (*iii*) breakdown of this intermediate to products. The first reaction stage is normally the rate-

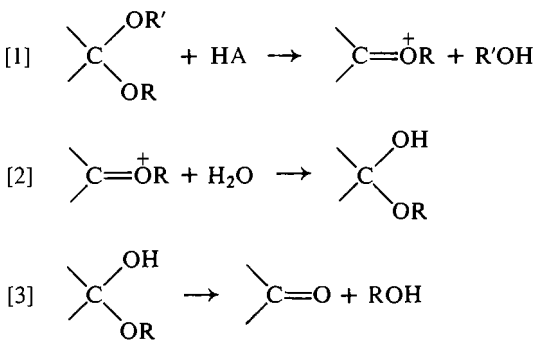

determining step, and a considerable body of information is now available for this process. Within the last ten years, however, a number of acetal derivatives (2–10) and ortho acid derivatives (10–22) have been found where a later stage is rate limiting or partially rate limiting under some conditions, and the oxocarbocation intermediate or the hemiacetal/hemiorthoester intermediate is observed as a transient intermediate. These studies not only conclusively establish the existence of these intermediates, they also supply kinetic and mechanistic information for the later stages.

Cyclic ortho esters such as **1** (2-alkyl or aryl-2-alkoxy-1,3-dioxolanes) have proved to be particularly noteworthy in this respect (11, 15). The first reaction stage involves loss of the exocyclic alkoxy group, and in acids this process is found to

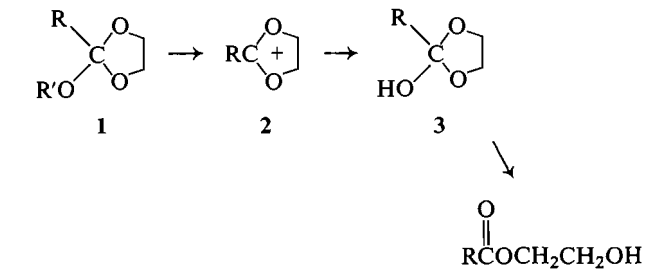

occur considerably more rapidly than the third reaction stage, the ring opening of the cyclic hemiorthoester **3**. This intermediate therefore accumulates during the hydrolysis, and the kinetics which are based on appearance of product refer directly to the kinetics of the third stage, the hemiorthoester decomposition. Acyclic ortho esters, with one exception (21), do not show this behavior, the dialkoxycarbocation-forming stage being rate determining at all acidities. The cyclic ortho esters must open a ring in the third stage, and the change in rate-determining step appears to be associated with an inherent difficulty of this process.

Can. J. Chem. Downloaded from www.nrcresearchpress.com by 210.87.254.42 on 09/06/12
For personal use only.

The oxocarbocation-forming stage is rate limiting (or mainly rate limiting (7, 8)) at all acidities with simple acyclic acetals and ketals. We considered if a change in behavior could be observed by incorporating the structural features inherent in the cyclic ortho ester **1** at this level of oxidation. We have, therefore, prepared ketal analogs and report here that they do undergo a similar change in the slow step.

Results and analysis

2-Methoxy-2-phenyltetrahydrofuran (**4**) and its 2-ethoxy derivative (**5**) were prepared by the reaction of alcoxide with the oxocarbocation (**6**), prepared as its borofluorate salt by treatment of 4-chlorobutyrophenone with silver borofluorate (23).

[5] $PhC(=O)CH_2CH_2CH_2Cl \xrightarrow{AgBF_4} Ph-C^{+}(=O)$ (**6**)

$\xrightarrow[ROH]{RO^-}$ Ph, C, O, RO

4, R = Me

5, R = Et

Hydrolysis in aqueous solution produces 4-hydroxybutyrophenone (**7**) and, presumably, ROH. The hydroxyketone exists predominantly in this form. We estimate that the concentration at equilibrium of the cyclic hemiketal **8** is less than 0.1%. This figure is arrived at through the observation that the ultraviolet (uv) spectrum of **7** in 1.0 *M* NaOH is quantitatively identical to the spectrum recorded at pH 7. The hemiketal hydroxyl group, because of the adjacent oxygen, is considerably more acidic

[6] $PhC(=O)CH_2CH_2CH_2OH$ (**7**) $\overset{K_{eq}}{\rightleftharpoons}$ Ph, C, O, HO (**8**)

K_a(app) / K_a

Ph, C, O, $^-$O (**9**)

than the hydroxyl of a simple alcohol, pK_a values for simple aldehyde hydrates and hemiacetals being in the range 12−12.5 (24−27). If there were a significant amount of the neutral hemiketal in equilibrium with the hydroxyketone, that equilibrium would shift in concentrated base because of the hemiketal ionization (see refs. 27−29 for systems where this occurs). This would show up as a decrease in uv absorbance due to the disappearance of the PhCO— chromophore (27). In quantitative terms, we define (28) K_a(app) as [**9**][H$^+$]/[**7**] and set pK_a(app) > 15, since no hemiacetal anion is observed even at pH 14. K_a(app) is equal to $K_{eq} \cdot K_a$, and if p$K_a \approx 12$, $K_{eq} < 0.001$.

The hydrolysis of the ketals **6** and **5** can proceed with cleavage, initially, of either the exocyclic or endocyclic C—O bond, and we propose that the former is occurring as it does with the

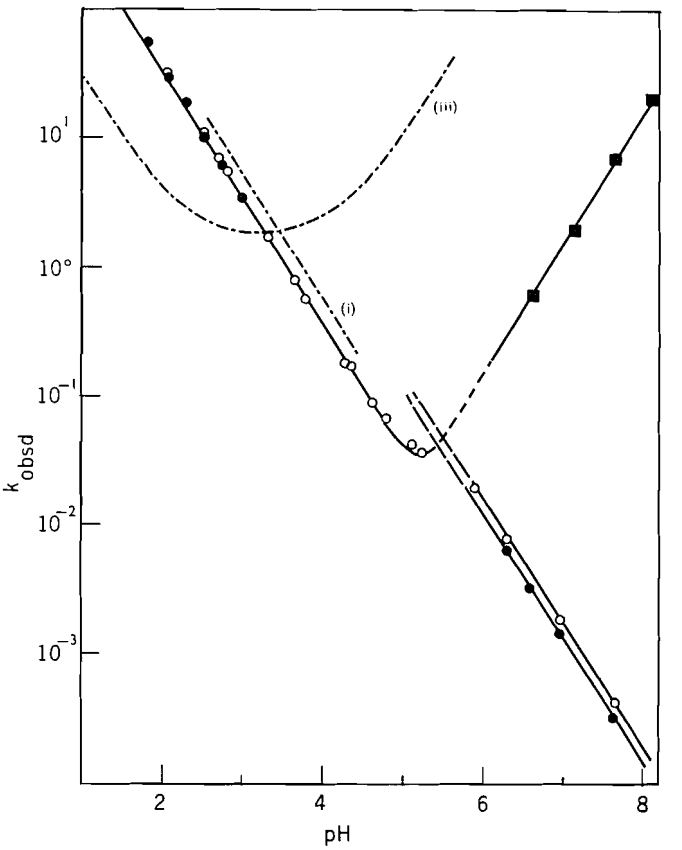

FIG. 1. Observed first-order rate constants (25°C, ionic strength = 0.1) as a function of pH. (○) 2-Methoxy-2-phenyltetrahydrofuran. (●) 2-Ethoxy-2-phenyltetrahydrofuran. (■) Stopped-flow trapping experiments with 2-ethoxy-2-phenyltetrahydrofuran. (....) 2-Methoxy-2-phenyl-1,3-dioxolane, from ref. 14. Stage (i): $k_{obsd} = 5.4 \times 10^3$ [H$^+$]. Stage (iii): $k_{obsd} = 3.0 \times 10^2$ [H$^+$] + 1.5 + 10^{10} [OH$^-$].

analogous ortho ester **1**. One piece of evidence is that the ketals in 100% H_2SO_4 produce methanol or ethanol and the oxocarbocation **6**. This cation is stable in 100% H_2SO_4 and its structure is verified by nmr comparison with the cation obtained from the chloroketone (23) (eq. [5]). The cleavage could be different in the aqueous solutions where the kinetic experiments have been conducted. However, the kinetic parameters themselves provide strong support for initial exocyclic cleavage.

Kinetic studies were conducted at constant pH and buffer concentration, using 10^{-4} *M* solutions of ketal and following the appearance of the product ketone using uv spectroscopy. In phosphate buffers of pH 6−8, the observed first-order rate constants obey the relationship $k_{obsd} = k_1^H[H^+]$ (Fig. 1), with $k_1^H = (1.35 \pm 0.08) \times 10^4\ M^{-1}\ s^{-1}$ for R = Me and $(1.65 \pm 0.04) \times 10^4\ M^{-1}\ s^{-1}$ for R = Et. Buffer catalysis is not observed, although this aspect was not investigated in detail. In HCl solutions, first-order rate constants obtained with the two ketals were identical, within experimental error (Fig. 1), obeying the relationship $k_{obsd} = k_3^H[H^+]$ with $k_3^H = (3.7 \pm 0.1) \times 10^3\ M^{-1}\ s^{-1}$.

This behavior is similar to that observed with the cyclic ortho esters **1**, and points to a change in the slow step in the overall hydrolysis between the phosphate buffers and HCl solutions. The changeover occurs because k_1^H, the rate constant for acid-catalyzed formation of the hemiketal, is greater than k_3^H, the rate constant for its acid-catalyzed decomposition. In con-

[7] 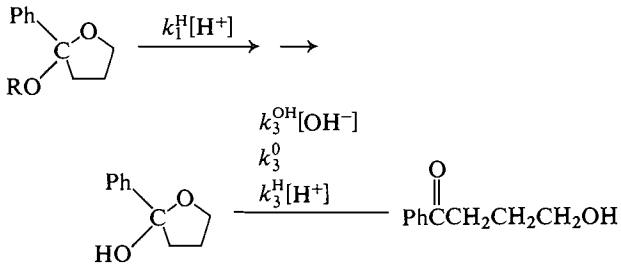

sequence, the hemiketal forms in acid solutions more rapidly than it goes on to ketone product, and it therefore accumulates as a transient intermediate during the hydrolysis. Since rate constants are based on product formation, they refer directly to the hemiketal decomposition, and k_3^H is provided by the acid kinetics. It can be noted that the acid rates are independent of the nature of the exocyclic alkoxy group, since that group is not present in the kinetically important step. This observation also provides further indication that the exocyclic group is lost in the initial reaction stage.

Hemiacetals, hemiketals, and hemiorthoesters have other pathways available for their decomposition, a pH-independent reaction (k_3^0 of eq. [7]) and an hydroxide ion catalyzed reaction (k_3^{OH}). The occurrence of these means that at high pH the oxocarbocation-forming stage, which is only acid catalyzed, must become the slow step. The changeover is depicted in Fig. 1 for a typical cyclic ortho ester, 2-methoxy-2-phenyl-1,3-dioxolane, where, because of relatively large k_3^0 and k_3^{OH} rate constants, changeover occurs near pH 3.5. With the ketals of this study, first-order rate constants measured in dilute formate and acetate buffers remain on the line extrapolated from HCl solutions even at pH 5 (Fig. 1), indicative that hemiketal decomposition is remaining rate limiting. The changeover occurs abruptly at this point and, by pH 5.8, the first-order rate constants join the high pH lines associated with a rate-determining first stage. The region between pH 5.2 and 5.5 is characterized by marked curvature in the first-order kinetic plots. This behavior is observed near the crossover point in any system which has this type of changeover, and is associated with the first-order rate constants for formation and decomposition having very similar magnitudes (14). Curved first-order kinetic plots should be obtained in all acid solutions, and the statement that stage three is the slow stage in these solutions is not exactly valid. It is true that the rate difference is rather small. However, a system of consecutive irreversible first-order reactions can be shown to have reasonable first-order kinetics in product formation in such a case, with the observed rate constant equal to the slower of the two first-order rate constants (17).

The abruptness of the changeover makes the determination of k_3^0 and k_3^{OH} difficult, and in fact it is impossible to determine which of the two processes is becoming important around pH 5 so that the hemiketal decomposition becomes more rapid than formation. The following trapping experiment, however, provides this information, as well as furnishing additional proof that hemiketal is present as a transient intermediate in acid solutions. This approach was described initially by Jensen and Lenz (7), where it was used to establish the presence of small quantities of benzaldehyde hemiacetals during hydrolysis of benzaldehyde acetals. Reacting acid solutions of these acetals were rapidly treated with excess hydroxide. This quenches any further reaction of the acetal itself, since acid is required to convert this species to the oxocarbocation and thus initiate the overall hydrolysis. However, any hemiacetal which is present as a transient intermediate is rapidly converted to the product benzaldehyde, because of the OH^--catalyzed pathway of decomposition available to such species. This was observed by Jensen and Lenz as a burst in absorbance accompanying the hydroxide quench. In our version of this experiment (8) the quenching was carried out on a stopped-flow spectrophotometer, with the pH after the quench being such that the actual conversion of hemiacetal to benzaldehyde could be monitored. This has the added benefit of providing kinetic information for this process as it occurs in the quenched solution.

In the present case the ketal **5** was added to dilute pH 5.0 buffer, and this solution rapidly placed in one syringe of a stopped-flow apparatus where it was mixed with buffers containing excess phosphate such that the pH after mixing was 7–8. A significant increase in absorbance is observed in the mixed solution, associated with the conversion to product of the hemiketal which had accumulated in the pH 5 solution. The hemiketal, of course, reacts at pH 5 as well, so that subsequent firings result in smaller absorbance changes until no change is observed at all. This experiment conclusively establishes that hemiketal is being formed as a transient intermediate in acid solutions. The rates obtained after mixing provide kinetic data for the decomposition in the high pH solutions. The following relationship is obeyed (Fig. 1): $k_{obsd} = k_3^{OH}[OH^-]$, with $k_3^{OH} = 1.4 \times 10^7\ M^{-1}\ s^{-1}$. (Buffer catalysis, probably representing general base catalysis (8), is also observed, but this point was not investigated in detail.)

Extrapolation of this rate to pH 5–5.5 reveals that it is the inception of the hydroxide ion catalyzed reaction that results in the change in slow step at this pH (Fig. 1). The rate–pH profile for hemiketal breakdown consists only of $[H^+]$-catalyzed and $[OH^-]$-catalyzed regions, with the pH-independent reaction not being able to compete at any acidity. An upper limit of $0.01\ s^{-1}$ can be set on k_2^0, based on the consideration that a value greater than this would have resulted in an observable contribution to the overall rate at pH 5.0.

Discussion

The question as to whether the third reaction stage can become rate limiting in the hydrolysis of an acetal, ketal, or ortho ester revolves around a comparison of the hydronium ion catalytic coefficients k_3^H and k_1^H. As summarized in Table 1, acyclic systems generally have $k_3^H > k_1^H$, and in such a case the first stage, formation of the oxocarbocation, must be rate determining at all acidities. Although k_3^H is sufficiently close to k_1^H with both the acetal and ketal that there is a small amount of hemiacetal/hemiketal build-up in acid solutions (7, 8), it now appears as if incorporation into a cyclic system can result in the opposite situation, $k_3^H < k_1^H$. This has now been observed with a number of cyclic ortho esters (12–14, 17, 33), and, in this study, with a cyclic ketal, and, as discussed recently by Kresge and co-workers, the effect must therefore be associated with the presence of the ring. In these cases, although oxocarbocation formation is rate limiting at high pH, a changeover occurs and breakdown of the hemiketal or hemiorthoester becomes rate limiting in acids.

We can consider why there is a difference between acyclic and cyclic systems. It is probably fair to say that the acid-catalyzed third stage, involving cleavage of a carbon–oxygen bond in a species such as HO—C—OR, is inherently going to be more rapid than the analogous cleavage when only alkoxyl

Can. J. Chem. Downloaded from www.nrcresearchpress.com by 210.87.254.42 on 09/06/12
For personal use only.

TABLE 1. Rate constants[a] for acid-catalyzed formation and breakdown of hemiacetals, hemiketals, and hemiorthoesters

Substrate (R = Me or H)	k_1^H, M^{-1} s^{-1}	k_3^H, M^{-1} s^{-1}	k_3^0, s^{-1}	k_3^{OH}, M^{-1} s^{-1}
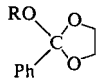	5.4×10^{3}[b]	3.0×10^{2}[b]	1.5[b]	10^{10}[c]
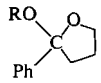	1.4×10^{4}[d]	3.7×10^{3}[d]	$<10^{-2}$[d]	1.4×10^{7}[d]
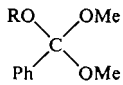	56[e]	1.9×10^{4}[f]	0.7[f]	5×10^{8}[f]
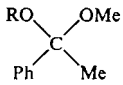	1.6×10^{3}[g]	$\approx10^{4}$[h]	Not known	$\approx3\times10^{7}$[h]
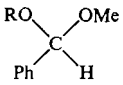	30[i]	2.6×10^{2}[j]	5.2×10^{-3}[j]	6.9×10^{5}[j]

[a]25°C, ionic strength = 0.1, in H_2O, unless otherwise noted.
[b]Reference 14.
[c]Reference 14 gives 6×10^{10} M^{-1} s^{-1}. Recent work (R. A. McClelland, unpublished) indicates a number nearer 10^{10} is more correct.
[d]This work.
[e]Reference 30.
[f]Reference 20, 50% dioxane/water.
[g]Reference 31, ionic strength = 1.0.
[h]Reference 8, based on 4-chlorophenyl. The number for k_3^H arises from the observation that a small amount of hemiketal does accumulate during ketal hydrolysis.
[i]Reference 32.
[j]Reference 5, T = 15°C.

groups are present (RO—C—OR). This seems reasonable since there should be an additional hydrogen-bonding stabilization in the developing cation in the former case ($HO{=}\overset{+}{C}$) or, in the mechanism which we prefer (20), simultaneous removal of the hydroxyl proton to assist bond breaking. We feel that it is this factor which makes $k_3^H > k_1^H$ in the acyclic systems. This same factor must, of course, also be in operation in the cyclic species, so that here there must be some additional factor responsible for the turnaround. The major difference with the cyclic system is that the third reaction stage involves cleavage of an endocyclic bond or ring opening, while the first stage involves exocyclic cleavage or the production of two species from one. This results in an entropic disadvantage to the ring opening, which we feel is the major cause behind the third stage becoming slower than the first. Support for this suggestion comes in the general observation (34) that hydrolysis reactions of 1,3-dioxolanes and 1,3-dioxanes, cyclic acetals, and ketals, where a ring must open in the first stage, are significantly slower than reactions of acyclic analogs. The difference in reactivity, moreover, appears mainly in the entropy of activation.

The k_1^H values also deserve comment. The approximately 100-fold difference in k_1^H observed between cyclic and acyclic orthobenzoates has been explained (35, 36) in terms of a steric inhibition of resonance in the dialkoxycarbocation **10** derived from the former. The aromatic ring in **10** is forced out of coplanarity with the π system associated with the charge. In the cyclic cation **11**, full planarity is possible because the methylene carbons are tied back in the ring. The observation of a similar, albeit smaller (approximately 10-fold), difference between cyclic and acyclic phenyl ketones implies that a similar effect is in operation even here. That is, there is some steric inhibition to resonance in the oxocarbocation **12** derived from an acetophenone ketal, and the π systems are not completely coplanar.

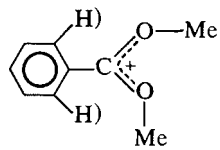

10

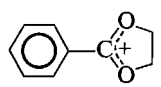

11

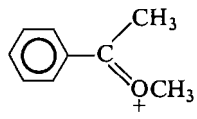

12

Experimental

Materials

Starting ketals were prepared by a modification of the method of Ward and Sherman (23). 4-Chlorobutyrophenone (0.01 mol) was slowly added to a stirred suspension of silver borofluorate (0.01 mol) in anhydrous ether (50 mL) cooled in an ice bath. After 30 min stirring at room temperature, the precipitate, which had formed from a mixture of the borofluorate salt of **6** and silver chloride, was filtered in an anhydrous environment (glove bag), washed with dry ether, and then added to a stirred solution containing an excess quantity of sodium methoxide in anhydrous methanol or ethoxide in ethanol. The silver chloride was then removed by filtration, the majority of the alcohol removed on a rotary evaporator, and a mixture of ether (100 mL) and water (100 mL) added. The ether layer was separated, washed with dilute aqueous sodium bicarbonate, and dried with sodium carbonate. After filtration, the ether was removed and the ketal obtained by distillation. Samples were stored over a small amount of anhydrous Na_2SO_3. *2-Methoxy-2-phenyltetrahydrofuran* (**4**) had bp 70°C/0.1 Torr (1 Torr = 133.32 Pa); nmr δ: 7.1–7.5 (m, 5H), 4.0 (complex

Can. J. Chem. Downloaded from www.nrcresearchpress.com by 210.87.254.42 on 09/06/12
For personal use only.

t, 2H), 3.00 (s, 3H), and 1.8–2.5 (m, 4H). *Anal.* calcd. for $C_{11}H_{14}O_2$: C 74.13, H 7.92; found: C 73.86; H 7.88. *2-Ethoxy-2-phenyltetrahydrofuran* (**5**) had bp 74°C/0.05 Torr; nmr δ: 7.1–7.5 (m, 5H), 4.0 (complex t, 2H), 3.43 (q, 2H), 1.8–2.5 (, 4H), and 1.13 (t, 3H). *Anal.* calcd. for $C_{12}H_{16}O_2$: C 74.97, H 8.39; found: C 74.91, H 8.23.

Kinetic methods

These have been described previously (8, 14). The wavelength employed in kinetic studies was 250 nm.

Acknowledgement

Continued financial support of the Natural Sciences and Engineering Research Council of Canada is gratefully acknowledged.

1. E. H. CORDES and H. G. BULL. Chem. Rev. **74**, 581 (1974).
2. A. L. MORI, M. A. PORZIO, and L. L. SCHALEGER. J. Am. Chem. Soc., **94**, 5034 (1972).
3. A. L. MORI and L. L. SCHALEGER. J. Am. Chem. Soc. **94**, 5039 (1972).
4. R. F. ATKINSON and T. C. BRUICE. **96**, 819 (1974).
5. B. CAPON, K. NIMMO, and G. P. REID. J. Chem. Soc. Chem. Commun. 871 (1976).
6. B. CAPON. Pure Appl. Chem. **49**, 1001 (1977).
7. J. L. JENSEN and P. A. LENZ. J. Am. Chem. Soc. **100**, 1291 (1978).
8. R. L. FINLEY, D. G. KUBLER, and R. A. MCCLELLAND. J. Org. Chem. **45**, 644 (1980).
9. T. J. PRZYSTAS and T. H. FIFE. J. Am. Chem. Soc. **103**, 4884 (1981).
10. R. A. MCCLELLAND and M. AHMAD. J. Am. Chem. Soc. **100**, 7027 (1978).
11. B. CAPON, J. H. GALL, and D. M. A. GRIEVE. J. Chem. Soc. Chem. Commun. 1034 (1976).
12. M. AHMAD, R. G. BERGSTROM, M. J. CASHEN, A. J. KRESGE, R. A. MCCLELLAND, and M. F. POWELL. J. Am. Chem. Soc. **99**, 4827 (1977).
13. R. A. MCCLELLAND, M. AHMAD, J. BOHONEK, and S. GEDGE. Can. J. Chem. **57**, 1531 (1979).
14. M. AHMAD, R. G. BERGSTROM, M. J. CHASEN, Y. CHIANG, A. J. KRESGE, R. A. MCCLELLAND, and M. F. POWELL. J. Am. Chem. Soc. **101**, 2669 (1979).
15. R. A. MCCLELLAND and M. AHMAD. J. Org. Chem. **44**, 1855 (1979).
16. B. CAPON and D. M. A. GRIEVE. J. Chem. Soc. Perkin Trans. 2, 300 (1980).
17. R. A. MCCLELLAND and M. ALIBHAI. Can. J. Chem. **59**, 1169 (1981).
18. B. CAPON and A. K. GHOSH. J. Am. Chem. Soc. **103**, 1765 (1981).
19. B. CAPON, A. K. GHOSH, and D. M. A. GRIEVE. Acc. Chem. Res. **14**, 306 (1981).
20. R. A. MCCLELLAND and G. PATEL. J. Am. Chem. Soc. **103**, 6908 (1981); **103**, 6912 (1981).
21. R. A. BURT, Y. CHIANG, A. J. KRESGE, and M. A. MCKINNEY. J. Am. Chem. Soc. **104**, 3685 (1982).
22. R. A. BURT, Y. CHIANG, H. K. HALL, and A. J. KRESGE. J. Am. Chem. Soc. **104**, 3687 (1982).
23. H. R. WARD and P. D. SHERMAN. J. Am. Chem. Soc. **90**, 3812 (1968).
24. J. M. LOS and L. B. SIMPSON. Recl. Trav. Chim. Pays-Bas, **75**, 267 (1956).
25. P. GREENZAID. J. Org. Chem. **38**, 3164 (1973).
26. J. M. SAYER. J. Org. Chem. **40**, 2545 (1975).
27. J. HARRON, R. A. MCCLELLAND, C. THANKACHAN, and T. T. TIDWELL. J. Org. Chem. **46**, 903 (1981).
28. O. S. TEE, M. TRANI, R. A. MCCLELLAND, and N. E. SEAMAN. J. Am. Chem. Soc. **104**, 7219 (1982).
29. R. A. MCCLELLAND and N. E. SEAMAN. J. Am. Chem. Soc. Submitted.
30. H. G. BULL, K. KOEHLER, T. C. PLETCHER, J. J. ORTIZ, and E. H. CORDES. J. Am. Chem. Soc. **93**, 3002 (1971).
31. P. R. YOUNG and W. P. JENCKS. J. Am. Chem. Soc. **99**, 8238 (1977).
32. B. CAPON and K. NIMMO. J. Chem. Soc. Perkin Trans. 2, 1113 (1975).
33. Y. CHIANG, A. J. KRESGE, H. O. LAHTI, and D. P. WEEKS. J. Am. Chem. Soc. In press.
34. A. V. WILLI. *In* Comprehensive chemical kinetics. Vol. 8. *Edited by* C. H. Bamford and C. F. H. Tipper. Elsevier, New York, NY. 1977. pp. 49–50.
35. Y. CHIANG, A. J. KRESGE, P. SALOMAA, and C. I. YOUNG. J. Am. Chem. Soc. **99**, 4494 (1974).
36. Y. CHIANG, A. J. KRESGE, and C. I. YOUNG. Finn. Chem. Lett. 13 (1978).

Can. J. Chem. Downloaded from www.nrcresearchpress.com by 210.87.254.42 on 09/06/12
For personal use only.

FOR ERRATA SEE
V. 62 # 12 1984 P. 2948

Hydrolysis mechanisms for acylhydrazines in aqueous sulfuric acid, determined using the excess acidity method[1,2]

ROBIN A. COX AND KEITH YATES

Department of Chemistry, University of Toronto, 80 St. George St., Toronto, Ont., Canada M5S 1A1

Received December 7, 1983

This paper is dedicated to Professor Gerald E. Dunn on the occasion of his 65th birthday

ROBIN A. COX and KEITH YATES. Can. J. Chem. **62**, 1613 (1984).

The excess acidity method has been applied to hydrolysis rate data for some acyl- and benzoylhydrazines, obtained as a function of medium composition in aqueous sulfuric acid mixtures. Two hydrolysis mechanisms are indicated, both involving a second proton transfer to monoprotonated substrate. In the first mechanism this transfer is to oxygen, which is the rate-determining step in dilute acid, followed by attack of a water molecule in an A-2 hydrolysis, which is rate determining in more concentrated acid. Bisulfate ion becomes the nucleophile at high acidity. The second mechanism, found at higher acid concentrations, involves rate-determining nitrogen protonation, probably concerted with C—N bond rupture, to give an acylium ion, for those substrates capable of forming one.

ROBIN A. COX et KEITH YATES. Can. J. Chem. **62**, 1613 (1984).

On a appliqué la méthode de l'acidité en excès aux données, obtenues en fonction de la composition du milieu dans des mélanges d'acide sulfurique aqueux, de vitesses d'hydrolyse de certaines acyl- et benzoyl-hydrazines. On identifie deux mécanismes d'hydrolyse impliquant tous deux un deuxième transfert de proton au substrat monoprotoné. Dans le premier mécanisme, ce transfert, qui se fait vers l'oxygène, est l'étape déterminante en milieu acide dilué et il est suivi par une attaque d'une molécule d'eau dans une hydrolyse de type A-2 qui devient l'étape déterminante en milieu acide plus concentré. A des acidités élevées, l'ion bisulfate devient le nucléophile. Le deuxieme mécanisme, observé à des concentrations d'acide encore plus élevées, fait intervenir la protonation de l'azote dans l'étape déterminante et cette protonation se produit probablement d'une façon concertée avec la rupture de la liaison C—N pour donner un ion acyllium avec les substrats susceptibles d'en former.

[Traduit par le journal]

Can. J. Chem. Downloaded from www.nrcresearchpress.com by 210.87.254.5 on 09/06/12
For personal use only.

Introduction

Recently, the excess acidity method, developed as a tool for the investigation of reaction mechanisms in strong acid media (1), was applied to rate data obtained for the hydrolysis of benzamides (2) and related compounds in sulfuric acid (3). It was found that nucleophilic attack upon oxygen-protonated amide was rate limiting, and that, as the acidity increased, the nucleophile changed from three water molecules acting in concert, in dilute acid, to one water molecule, to one bisulfate ion at high acidities (3).

It is of interest to see how far this mechanism extends to other amidic substrates, and in this paper the hydrolyses of some acyl- and benzoylhydrazines are studied. These compounds are protonated in the pH-range, as shown in reaction [1], on the amine nitrogen (4, 5), and the resulting positive

[1] 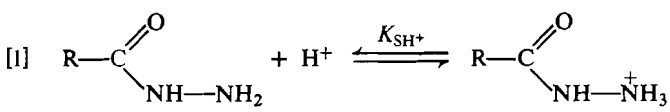

charge should alter the properties of the amide part of the molecule considerably in acidic media. Previous work on these substrates includes that of Edward *et al.*, on acetylhydrazine in HCl (6), of Mashim and Ikeda, on formylhydrazine in $HClO_4$ and H_2SO_4 (4), of Mashima *et al.*, on a number of acylhydrazines in H_2SO_4 (7), of Zarakhani *et al.*, on benzoylhydrazine in H_2SO_4 (8), and of Jagdale and Nimbalkar, on some substituted benzoylhydrazines in H_2SO_4, $HClO_4$, and HCl (9). The consensus of their conclusions is that most compounds hydrolyze by an A-2 mechanism, and that some may switch to an A-1 mechanism at high acidity.

Kinetic analysis

The excess acidity method, applied to reaction kinetics, consists of deriving rate equations based on reasonable reaction mechanisms, and determining which of them best applies to the process under consideration (1). Several examples of the method in use are now available (1, 3, 10–12). For the acylhydrazine hydrolyses under consideration here, a reasonable possibility is that given in Scheme 1, which is based on the normal amide hydrolysis mechanism (3). Monoprotonated substrate SH^+ is protonated again, on the carbonyl oxygen; insofar as the substrate is already positively charged, the possibility that this second protonation is rate determining must be considered. Diprotonated SH_2^{2+} then undergoes nucleophilic attack; one water molecule is shown as the nucleophile in Scheme 1, but several water molecules or a bisulfate ion may be involved (3, 10–12). If the second protonation is fast this second stage will probably be the slow step. Subsequent tautomerization and loss of hydrazine lead to the observed benzoic acid product (6–9).

Scheme 1, k_0 slow

[2] $$k_\psi C_{SH^+} = k_0 a_{SH} + a_{H^+}/f_\ddagger = k_0 C_{SH^+} C_{H^+} (f_{SH^+} f_{H^+}/f_\ddagger)$$

[3] $$\log (f_{SH^+} f_{H^+}/f_\ddagger) = m_0^\ddagger \log (f_{SH^+} f_{H^+}/f_{SH_2^{2+}}) = m_0^\ddagger m^* X$$

[4] $$\log k_\psi - \log C_{H^+} = \log k_0 + m_0^\ddagger m^* X$$

Using the terminology of Scheme 1, eq. [2] is obtained in the usual way (1); k_ψ is the observed pseudo-first-order rate constant, a is activity, C molar concentration, and f molar activity coefficient. Activity coefficient ratios such as those in eqs. [2] and [3] have been shown to be linear in one another (1, 13), and the slope parameters $m^\ddagger$ (subscript 0 for A-S_E2 processes, 1 for

[1]Mechanistic studies in strong acids IX. Part VIII is ref. 12.

[2]Presented in part at the 66th Chemical Conference of the Chemical Institute of Canada, Calgary, Alberta, June 1983, No. OR21-3.

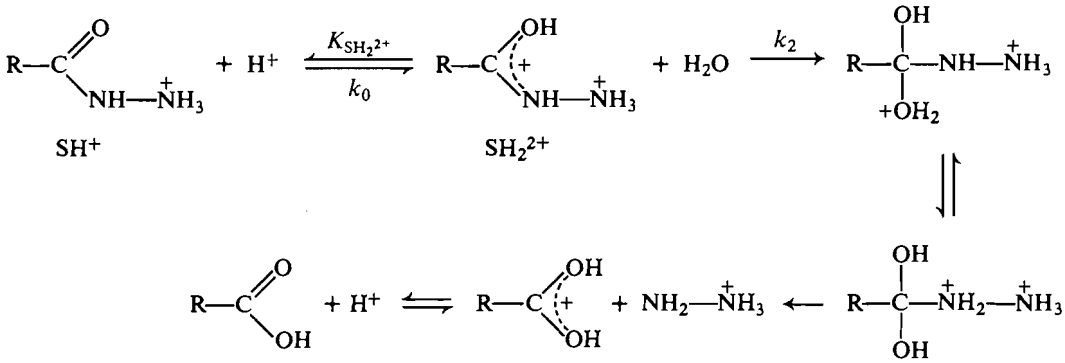

SCHEME 1

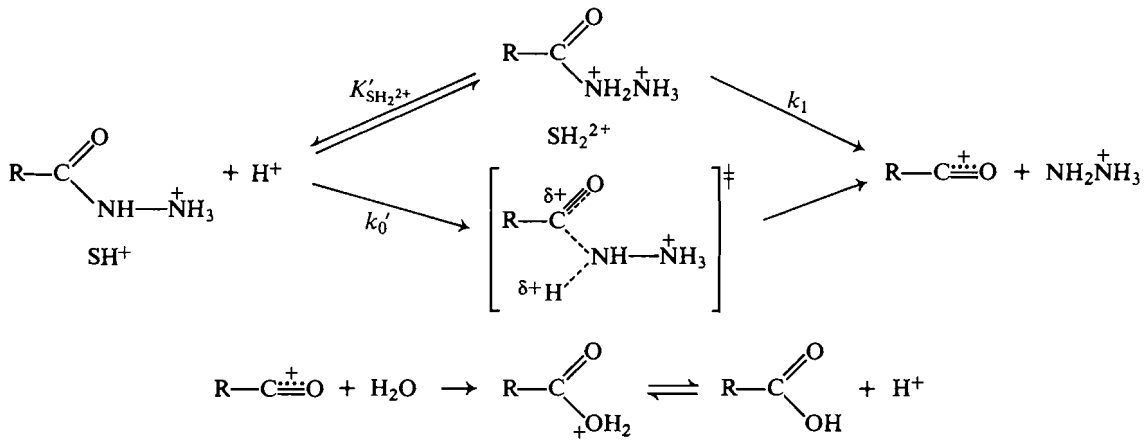

SCHEME 2

A-1, and 2 for A-2 reactions, subscripts on k similarly) and m^* are defined as in eq. [3]. $X = \log (f_{B^*} f_{H^+}/f_{B^*H^+})$ for a standard base B*; values of X and $\log C_{H^+}$ in H_2SO_4 (13), $HClO_4$ (13), and HCl (14) are available. Suitable manipulation of eqs. [2] and [3] produces eq. [4], for the rate-determining proton transfer to oxygen shown in Scheme 1. Regarding the slope parameters, $m_o^{\ddagger} < 1$ for an A-S_E2 proton transfer (1), probably about 0.5 (12), and m^* for carbonyl oxygen protonation is 0.6 or less (13). Thus a total slope against X of 0.3 or less would be expected for eq. [4].

Scheme 1, k_2 *slow*

$$k_\psi C_{SH^+} = k_2 a_{H_2O} a_{SH_2^{2+}}/f_\ddagger$$

$$K_{SH_2^{2+}} = a_{SH^+} a_{H^+}/a_{SH_2^{2+}}$$

$$k_\psi = (k_2/K_{SH_2^{2+}}) a_{H_2O} C_{H^+} (f_{SH^+} f_{H^+}/f_\ddagger)$$

[5] $$\log k_\psi - \log C_{H^+} - \log a_{H_2O} = \log (k_2/K_{SH_2^{2+}}) + m_2^{\ddagger} m^* X$$

[6] $$\log k_\psi - \log C_{H^+} - \log C_{HSO_4^-} = \log (k_2'/K_{SH_2^{2+}}) + m_2^{\ddagger\prime} m^* X$$

If the k_2 step is rate determining in Scheme 1, eq. [5] can be derived, as shown above, for the case in which the nucleophile is one water molecule. If several are involved, eq. [5] is modified by multiplying the $\log a_{H_2O}$ term by two, three, etc. (11, 12), and if the nucleophile is bisulfate, eq. [6] results. (Bisulfate activities are unavailable, but the error involved in using the concentration should be small (3, 10).) For A-2 reactions $m_2^{\ddagger} \simeq 1$ (1, 12), thus an overall slope against X of 0.6 or less should result for eqs. [5] and [6].

By analogy with ester hydrolysis (11, 12), another possible mechanism for acylhydrazines would be acylium ion formation at low water activity, as shown in Scheme 2. Here either pre-equilibrium nitrogen protonation, followed by carbon–nitrogen bond breaking, can occur, the upper A-1 process in Scheme 2, or slow nitrogen protonation, which may or may not be concerted with C—N bond rupture, may result, the lower A-S_E2 process of Scheme 2.

Scheme 2, k_1 *slow*

$$k_\psi C_{SH^+} = k_1 a_{SH_2^{2+}}/f_\ddagger = (k_1/K'_{SH_2^{2+}}) C_{SH^+} C_{H^+} (f_{SH^+} f_{H^+}/f_\ddagger)$$

[7] $$\log k_\psi - \log C_{H^+} = \log (k_1/K'_{SH_2^{2+}}) + m_1^{\ddagger} m^* X$$

Equation [7] can be derived for A-1 acylium ion formation. For A-1 processes $m_1^{\ddagger} > 1$, probably about 2–3 (1), and m^* for nitrogen protonation $\simeq 1$ (13), so an overall slope of 2–3 should be obtained.

Scheme 2, k_0' *slow*

$$k_\psi C_{SH^+} = k_0' a_{SH^+} a_{H^+}/f_\ddagger$$

[8] $$\log k_\psi - \log C_{H^+} = \log k_0' + m_0^{\ddagger\prime} m^* X$$

In this case an overall slope against X of about 0.5 would be reasonable, so eqs. [7] and [8] should be distinguishable by their slopes.

In deriving the above equations it has been assumed that the substrate is fully monoprotonated but essentially not diprotonated under the acidic reaction conditions. Since monoprotonation occurs in the range pH 2 to pH 3.5 (4, 5), the former assumption is reasonable. Brignell *et al.* (15) found that

Can. J. Chem. Downloaded from www.nrcresearchpress.com by 210.87.254.5 on 09/06/12
For personal use only.

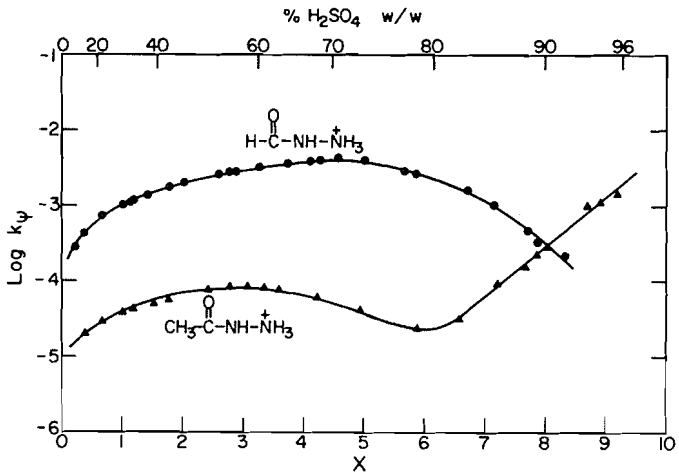

FIG. 1. Plots of log hydrolysis rate constants against acidity, for formylhydrazine and acetylhydrazine, at 25°C in aqueous sulfuric acid (7).

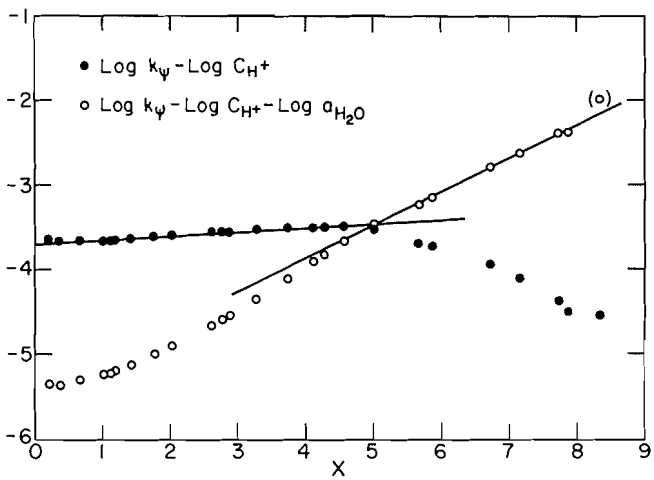

FIG. 2. Hydrolysis rate constants for formylhydrazine at 25°C, plotted according to eq. [4] (filled circles) and eq. [5] (open circles), showing the change in rate-determining step (Scheme 1).

the first and second protonation in a series of substituted phenylhydrazines were separated by at least ten H_0 units, so the latter assumption is reasonable too.

Results

Graphs of log observed rate constant against acidity (as X) for formyl- and acetylhydrazine (7) are given in Fig. 1; the other acylhydrazines behave similarly. Overall, the rate profiles resemble those for ester rather than amide hydrolysis (compare Fig. 1 with ethyl benzoate, Fig. 1 in ref. 12, for instance), and the reactions are fast compared to those of normal amides (2, 3). The formylhydrazine data are plotted according to eqs. [4] and [5] in Fig. 2. A change in rate-determining step is clearly indicated. Equation [4], the k_0 pathway in Scheme 1, is followed at acidities below about 75% H_2SO_4, and eq. [5], k_2 in Scheme 1 rate-determining, above this acidity. The slopes are in accord with the expectations noted above. The acetylhydrazine results, see Fig. 3, are similar, except that the change in rate-determining step occurs at lower acidity, about 60% H_2SO_4. At about 82% H_2SO_4 another mechanism takes over, with log k_ψ − log C_{H^+} again linear against X in this region. This is assigned to the k_0' pathway of

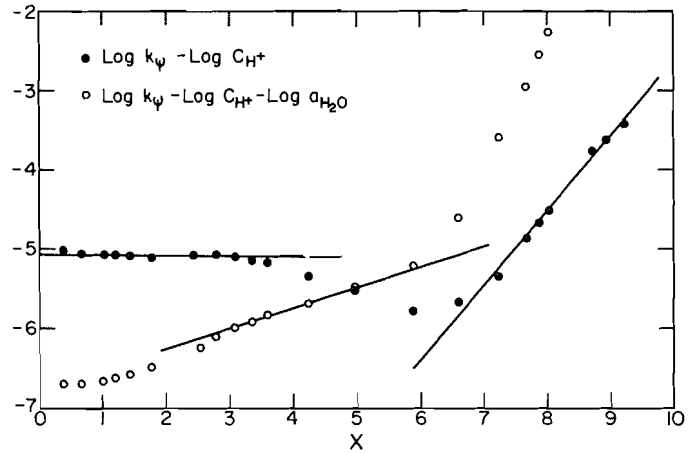

FIG. 3. Hydrolysis rate constants for acetylhydrazine at 25°C, plotted according to eqs. [4] and [8] (filled circles), and eq. [5] (open circles), showing the change of mechanism, Scheme 1 to Scheme 2.

Scheme 2, on the basis of the observed less-than-unit slope. The two mechanisms were separated, on the assumption that $k_\psi = k_{A\text{-}2} + k_{A\text{-}1}$, using the same computer program as before (3, 11, 12).

The slope and intercept values for all the acylhydrazines in the study are given in Tables 1 and 2. These include the compounds studied by Mashima *et al.* (7) at 25 and 55°C, and some results for benzoylhydrazine by Zarakhani *et al.* (8), extrapolated to 25°C as before (3, 12). Scheme 1 was followed by all the compounds examined (results in Table 1), with the nucleophile being one water molecule. In this case, the k_0 step is rate determining in the acidity region where three water molecules were involved in benzamide hydrolysis (3), so a three-water-molecule mechanism is not observed here.

Some of the compounds switch to a Scheme 2 mechanism, and the slope and intercept data of eq. [8] for these are collected in Table 2. Formylhydrazine and chloroacetylhydrazine at 55°C do not hydrolyze by Scheme 2, but at higher acidities bisulfate ion takes over as a nucleophile from water in the Scheme 1 hydrolysis. The results of fitting the data for these two compounds to eq. [6] are also shown in Table 2. For formylhydrazine at 25°C this mechanism was represented by only one data point, and details could not be obtained.

For benzoylhydrazine, one deviant point on the high acidity side was also observed; it was impossible to tell whether this represented a switch to a Scheme 2 mechanism or not, although this seems likely. Activation parameters were obtained; for k_2 these were $\Delta H^\ddagger = 21.43 \pm 0.45$ kcal/mol, and $\Delta S^\ddagger = -28.6 \pm 1.5$ eu, and for k_0, 21.02 ± 0.33 and −21.0 ± 1.1. The same data could be fitted to either eq. [4] or eq. [5] for this compound, and so both sets of results are given here and in Table 2.

Jagdale and Nimbalkar (9) studied benzoylhydrazine at 90°C, together with its *m*- and *p*-methoxy derivatives. Their results for the parent compound are in fair agreement with those of Zarakhani's group (8). Equation [5] (k_2) fits the data considerably better than eq. [4] (k_0), and gives slopes of 0.350 ± 0.008, 0.341 ± 0.008, and 0.381 ± 0.025, and intercepts of −4.768 ± 0.006, −4.591 ± 0.006, and −4.672 ± 0.020 for the *p*-OCH_3, *m*-OCH_3, and parent compounds, respectively.

All values of X, log C_{H^+}, log a_{H_2O} and log $C_{HSO_4^-}$ used were obtained from the sources previously cited, and temperature-corrected as necessary as described before (3, 10−13).

Can. J. Chem. Downloaded from www.nrcresearchpress.com by 210.87.254.5 on 09/06/12
For personal use only.

TABLE 1. Slope and intercept values of eqs. [4] and [5], for the hydrolysis of $RCONHNH_2$ in dilute sulfuric acid: Scheme 1, nucleophile water

R, T (°C)	log k_0	$m_0^{\ddagger}m^*$	log $(k_2/K_{SH_2^{2+}})^a$	$m_2^{\ddagger}m^*$
H, 25	−3.691±0.005	0.048±0.002	−3.702±0.019	0.394±0.003
CH_3, 25	−5.062±0.013	−0.005±0.007	−5.045±0.040	0.261±0.010
Ph, 25	−7.210±0.038	0.101±0.007	−7.423±0.051	0.458±0.009
H, 55	−2.667±0.006	0.016±0.002	−2.687±0.010	0.388±0.004
CH_3, 55	−4.024±0.008	0.044±0.006	−4.012±0.024	0.312±0.008
$ClCH_2$, 55	−3.826±0.007	−0.051±0.003	−3.895±0.032	0.337±0.010
CH_3CH_2, 55	−4.008±0.059	0.060±0.035	−4.053±0.018	0.332±0.006
$CH_3(CH_2)_2$, 55	−3.936±0.008	−0.030±0.006	−4.014±0.027	0.252±0.010
$CH_3(CH_2)_6$, 55	−4.289±0.041	0.017±0.028	−4.410±0.018	0.338±0.007

[a]In pure water, which is 55.346 M at 25°C and 54.716 M at 55°C. True second-order rate constants are obtained by subtracting 1.743 and 1.738, respectively, from the numbers in this column.

TABLE 2. Slope and intercept values of eqs. [8] and [6], for the hydrolysis of $RCONHNH_2$ in more concentrated sulfuric acid: Scheme 2, and Scheme 1 with nucleophile HSO_4^-

R, T (°C)	log k_0'	$m_0^{\ddagger\prime}m^*$	log $(k_2'/K_{SH_2^{2+}})^a$	$m_2^{\ddagger\prime}m^*$
H, 25	—	—	—	—
CH_3, 25	−12.09±0.17	0.948±0.021	—	—
Ph, 25	—	—	—	—
H, 55	—	—	−9.05±0.73	0.641±0.094
CH_3, 55	−8.68±0.15	0.759±0.021	—	—
$ClCH_2$, 55	—	—	−8.42±0.47	0.399±0.061
CH_3CH_2, 55	−8.36±0.14	0.739±0.020	—	—
$CH_3(CH_2)_2$, 55	−8.54±0.15	0.763±0.022	—	—
$CH_3(CH_2)_6$, 55	−8.14±0.08	0.737±0.012	—	—

[a]In a hypothetical ideal medium containing 1 M bisulfate ion.

Discussion

The excess acidity method is capable of revealing mechanistic features which other methods of analyzing kinetic data in strong acids cannot (1, 3, 12). Here the change in rate-determining step in Scheme 1 is clearly indicated by the change in the rate equation followed, eq. [4] to eq. [5], see Figs. 2 and 3. Also, the change in nucleophile in some cases, from water to bisulfate, can be seen. Mashima *et al.* (7) analyzed the same data in terms of the Bunnett–Olsen (16) and Bunnett w-parameter (17) mechanistic criteria; these showed the change in mechanism from Scheme 1 to Scheme 2, assigned as A-2 and A-1 without further specification (7). These methods proved to be ambiguous, however, in the Scheme 1 region, giving curved plots or multiple linearity, and did not show the change in rate-determining step. In the Scheme 2 acidity region the distinction between A-1 and A-S_E2 acylium ion formation, made in this work, was not apparent.

As noted above, at least for the acylhydrazines hydrolysis is faster than it is for equivalent amides (3); the extra positive charge in the substrate causes the second protonation to be difficult, as would be expected, but when SH_2^{2+} is formed it reacts very quickly. Evidently the strongly electron-withdrawing $^+NH_3$ group makes the carbon centre much more electrophilic. For instance, in Scheme 1 deprotonation of SH_2^{2+} back to SH^+ has to be slower than nucleophilic attack on it by H_2O, in order for the k_0 step to be rate determining, as it is in the low acidity region. SH_2^{2+} is resonance-stabilized, which means that the internal electron pair on the amide nitrogen is competing for the second positive charge with the external electron pairs on solvating water molecules. This effect evidently slows deprotonation enough, and the $^+NH_3$ group accelerates nucleophilic attack by water enough, to make the protonation step rate determining. At low acidities, C_{H^+} is low and protonation is rate limiting. As the acidity increases, C_{H^+} increases and a_{H_2O} decreases, and nucleophilic attack becomes the slow step.

Both mechanisms involve slow proton transfer, at least at some acidities. Slow protonation is quite common at carbon (18), and it has been observed at sulfur in strong acids (12), but rate-determining oxygen or nitrogen protonation is seen less often. Here it can be observed because the second protonation of a positively charged species is involved. In the Scheme 2 process there is no way of deciding from the data whether or not C—N bond rupture is concerted with proton transfer, but this process has precedent in the Wallach rearrangement of azoxy compounds in strong acids (19), where a symmetrical dicationic intermediate is formed by concerted proton transfer to oxygen, N—O bond cleavage, and participation of a nitrogen lone pair (20). It seems reasonable here too.

Formyl- and chloroacetylhydrazine do not react by Scheme 2. Acylium ions which are stabilized by electron-donating alkyl groups can evidently form more easily than those which have only H, or electron-withdrawing $ClCH_2$. Formylhydrazine hydrolyzes faster than the other compounds by Scheme 1. Benzoylhydrazine reacts much more slowly. Presumably this is because of the absence of stabilizing alkyl groups in the former case, and in the latter because the charge can be delocalized into the aromatic ring, reducing the susceptibility of the carbon to nucleophilic attack. Steric factors do not seem important; increasing the length of the alkyl chain makes little difference

Can. J. Chem. Downloaded from www.nrcresearchpress.com by 210.87.254.5 on 09/06/12
For personal use only.

to the rates (Table 1).

As mentioned, the benzoylhydrazine data can be fitted to either eq. [4] or eq. [5]. One data set gives a better statistical fit with eq. [4] (8), and the other with eq. [5] (9). On the basis of the activation parameters, a $\Delta S^{\ddagger}$ of -28 eu for k_2 seems much more likely than one of -21 for k_0, and so the former is tentatively assigned the rate-determining step in this case. Benzamides are more difficult to protonate than acetamides by up to one pK unit (21), but this fact may not affect the *rate* of proton transfer. Once SH_2^{2+} is formed it is resonance-stabilized, as mentioned, and thus less reactive. Thus it is not unreasonable that nucleophilic attack should be rate limiting at all acidities for these compounds.

The methoxy-substituted benzoylhydrazines studied by Jagdale and Nimbalkar (9) react in the order m-OCH_3 > H > p-OCH_3. This order is as expected, and can be rationalized by considering that inductive electron withdrawal of OCH_3, which

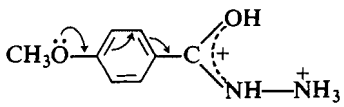

is activating to nucleophilic attack, is counteracted by mesomeric electron donation, as shown, which is deactivating, in the *para* but not the *meta* position.

Normal amides do not usually hydrolyze by forming acylium ions; the only cases of this observed so far involve β-lactams (3) and some acetanilides (22). Presumably this is because nitrogen protonation as in Scheme 2 produces a neutral NH_3 leaving group in the amide case, compared to the positive $^{+}NH_3$—NH_2 leaving group involved here, which must be much better in acidic media. Apart from this, acylhydrazines react in much the same way as normal amides do, see Scheme 1, when account is taken of the fact that they contain an extra positive charge.

Acknowledgement

Financial support of this research is by the Natural Sciences and Engineering Research Council of Canada.

1. R. A. Cox and K. Yates. Can. J. Chem. **57**, 2944 (1979).
2. C. R. Smith and K. Yates. J. Am. Chem. Soc. **93**, 6578 (1971).
3. R. A. Cox and K. Yates. Can. J. Chem. **59**, 2853 (1981).
4. M. Mashima and F. Ikeda. Bull. Chem. Soc. Jpn. **46**, 1366 (1973).
5. C. R. Lindegren and C. Niemann. J. Am. Chem. Soc. **71**, 1504 (1949).
6. J. T. Edward, H. P. Hutchison, and S. C. R. Meacock. J. Chem. Soc. 2520 (1955).
7. M. Mashima, F. Ikeda, T. Doi, and S. Nishikawa. Bull. Chem. Soc. Jpn. **54**, 3659 (1981).
8. N. G. Zarakhani, E. N. Borisova, P. P. Nechaev, and G. E. Zaikov. Izv. Akad. Nauk SSSR, Ser. Khim. 2476 (2044 in Eng. Ed.) (1981).
9. M. H. Jagdale and A. Y. Nimbalkar. Acta Cienc. Indica, **2**, 336 (1976); Gazz. Chim. Ital. **109**, 51 (1979).
10. R. A. Cox, C. R. Smith, and K. Yates. Can. J. Chem. **57**, 2952 (1979).
11. R. A. Cox, M. F. Goldman, and K. Yates. Can. J. Chem. **57**, 2960 (1979).
12. R. A. Cox and K. Yates. Can. J. Chem. **60**, 3061 (1982).
13. R. A. Cox and K. Yates. J. Am. Chem. Soc. **100**, 3861 (1978).
14. R. A. Cox and K. Yates. Can. J. Chem. **59**, 2116 (1981).
15. P. J. Brignell, C. D. Johnson, A. R. Katritzky, N. Shakir, H. O. Tarhan, and G. Walker. J. Chem. Soc. B, 1233 (1967).
16. J. F. Bunnett and F. P. Olsen. Can. J. Chem. **44**, 1917 (1966).
17. J. F. Bunnett. J. Am. Chem. Soc. **83**, 4956 (1961); **83**, 4968 (1961); **83**, 4973 (1961); **83**, 4978 (1961).
18. C. H. Rochester. Acidity functions. Academic Press, New York. 1970.
19. R. A. Cox and E. Buncel. *In* The chemistry of the hydrazo, azo and azoxy groups. *Edited by* S. Patai. Wiley, New York. 1975. p. 775.
20. R. A. Cox. J. Am. Chem. Soc. **96**, 1059 (1974).
21. R. A. Cox, L. M. Druet, A. E. Klausner, T. A. Modro, P. Wan, and K. Yates. Can. J. Chem. **59**, 1568 (1981).
22. J. W. Barnett and C. J. O'Connor. J. Chem. Soc. Perkin Trans. 2, 2378 (1972).

Can. J. Chem. Downloaded from www.nrcresearchpress.com by 210.87.254.5 on 09/06/12
For personal use only.

A spin-lattice relaxation study of the molecular reorientation of 2-methylindole as a function of viscosity and complex formation

KENNETH J. FRIESEN AND BARRY J. BLACKBURN

Department of Chemistry, University of Winnipeg, Winnipeg, Man., Canada R3B 2E9

Received February 2, 1984

This paper is dedicated to Professor Gerald E. Dunn on the occasion of his 65th birthday

KENNETH J. FRIESEN and BARRY J. BLACKBURN. Can. J. Chem. **62**, 1618 (1984).

The viscosity (η) dependence of the ^{13}C spin-lattice relaxation time (T_1) of C-3 of 2-methylindole was investigated by changing the temperature (T) and by changing the solvent system. The observed η/T dependence of the effective reorientation correlation time (calculated from T_1) is compared with those derived from theory based on hydrodynamic rotation with "stick" and with "slip" boundary conditions. This data implies that the reorientation of 2-methylindole obeys a near-slip condition in 1,2-dichloroethane. The ^{13}C T_1 of C-3 of 2-methylindole was also determined as a function of the fraction complexed with 1,3,5-trinitrobenzene (TNB) at 35°C in 1,2-dichloroethane. The observed T_1, in this case, depends on the rates of reorientation of the molecule in the free and the bound states, the rate of association of the molecules, the rate of dissociation of the complex, as well as increases in viscosity brought about by increases in the concentration of TNB. Analysis of the data, by application of the Anderson–Fryer formulation, gives a rate of reorientation in the bound state of 55 ns^{-1} at 35°C and 0.69 cP as compared to a value of 150 ns^{-1} in the free state under the same conditions.

KENNETH J. FRIESEN et BARRY J. BLACKBURN. Can. J. Chem. **62**, 1618 (1984).

Faisant varier la température (T) et le système de solvant, on a étudié l'effet de la viscosité (η) sur le temps de relaxation spin-réseau (T_1) du ^{13}C du carbone en position 3 du méthyl-2 indole. La valeur observée pour la dépendance η/T du temps de corrélation effectif de la réorientation (calculée à partir de T_1) a été comparée aux valeurs que l'on peut dériver en se basant sur une rotation hydrodynamique dans des conditions où les limites sont fixées par des "tiges" et des "lamelles". Ces donnés impliquent que, dans le dichloro-1,2 éthane, la réorientation du méthyl-2 indole obéit à une condition quasilamelaire. Opérant à 35°C, dans le dichloro-1,2 éthane, on a également déterminé la valeur T_1 du ^{13}C pour le carbone en position 3 du méthyl-2 indole en fonction de la fraction complexée avec le trinitro-1,3,5 benzène (TNB). Dans ce cas, la valeur observée pour T_1 dépend des vitesses de réorientation de la molécule dans les états libre et lié, de la vitesse d'association des molécules, de la vitesse de dissociation du complexe ainsi que des augmentations de viscosité, dues aux augmentations de concentration dans le TNB. L'analyse des données, à l'aide de la formulation de Anderson–Fryer, conduit à une vitesse de réorientation de l'état lié de 55 ns^{-1}, à 35°C et 0,69 cP, qui se compare à une valeur de 150 ns^{-1} pour l'état libre dans les mêmes conditions.

[Traduit par le journal]

Introduction

The calculations of Hu and Zwanzig (1) on rotational friction coefficients of spheroids under two sets of boundary conditions, combined with Woessner's theory (2), have proved useful in the study of molecular reorientation by nuclear magnetic relaxation methods. A good example of this, which includes a theoretical discussion, is a study (3) of the hydrodynamical rotation of triphenylene. A review article in this area, giving theoretical developments as well as experimental studies, has appeared recently (4).

Anderson and Fryer (5) have given expressions relating nuclear relaxation times to the rates of reorientation and chemical exchange of a molecule in the free and complexed state and applied them to proton relaxation data. Brevard and Lehn (6) have adapted these equations to study the molecular dynamics of complex formation by deuterium quadrupolar relaxation. A recent review (7) summarizes the latter two articles and discusses related studies.

In this paper, the effects of viscosity and complex formation with 1,3,5-trinitrobenzene on the carbon-13 spin-lattice relaxation times for C-3 of 2-methylindole-(methyl,3-$^{13}C_2$) are evaluated in light of the above-mentioned theories to give information about the molecular reorientation. Some of this data was presented earlier in a preliminary communication (8) which pointed out the usefulness of carbon-13 spin-lattice relaxation times as a probe for the study of electron donor–acceptor complexes.

Experimental

1,3,5-Trinitrobenzene and 1,2-dichloroethane were purified and 2-methylindole-(methyl,3-$^{13}C_2$) synthesized by previously reported methods (8). 1,1,2,2,-Tetrachloroethane was washed with concentrated sulfuric acid, then water, and then dried and distilled.

Solutions, prepared by weight, were transferred into 8-mm nmr tubes, degassed on a high vacuum gas line at least four times by the freeze–pump–thaw technique, and then sealed. All solutions utilizing 1,2-dichloroethane as either a pure or mixed solvent contained sufficient 1,2-dichloroethane-d_4 to provide a deuterium lock. The sample of 2-methylindole in pure 1,1,2,2,-tetrachloroethane was degassed by bubbling dry nitrogen through for about 3 min. A coaxial tube containing D_2O was added to this sample to provide the lock nucleus.

Viscosities were determined with an Ostwald viscometer and density bottle at 35°C using unenriched 2-methylindole.

Proton-decoupled ^{13}C nmr spectra were obtained on a Varian CFT-20 spectrometer. Spin-lattice relaxation times, T_1's, for C-3 of 2-methylindole-(methyl,3-$^{13}C_2$) were determined by the inversion–recovery pulse sequence ($d-180°-t_i-90°$), where t_i is a variable time, and the pulse delay, $d \geq 7T_1$. For each T_1 determination, 10–12 t_i values were used. A total of 40–50 transients was sufficient to obtain signal-to-noise > 75:1. The free induction decays were weighted to broaden the lines, otherwise seen as a doublet due to $^{13}C—^{13}C$ coupling, in order to facilitate phasing. The T_1 values, determined with semilogarithmic plots, had a precision better than 4%. Nuclear Overhauser enhancement, nOe, factors were measured using the gated proton decoupler technique with $d \geq 7T_1$.

The probe temperature, measured with a thermometer immersed in 1,2-dichloroethane and set to the same depth as the sample being studied, was maintained with a Varian CFT-20 Variable Temperature Accessory using precooled nitrogen where necessary.

Results and discussion

Effect of viscosity changes

The viscosity dependence of T_1 for C-3 of 2-methylindole

Can. J. Chem. Downloaded from www.nrcresearchpress.com by 210.87.254.6 on 09/06/12
For personal use only.

Can. J. Chem. Downloaded from www.nrcresearchpress.com by 210.87.254.6 on 09/06/12
For personal use only.

TABLE 1. Data for 2-methylindole in 1,2-dichloroethane as a function of temperature

Temp (°C)	η(cP)[a]	T_1(s)[b]	τ_c(ps)
35.0	0.68_8	6.3_7	6.92
24.2	0.79_3	5.1_5	8.56
10.5	0.95_2	4.3_0	10.25
−1.5	1.14_0	3.1_2	14.13
−12.1	1.36_0	2.4_4	18.06
−22.0	1.62_0	2.1_0	20.99

[a] Solvent viscosities from literature data (11*a*).
[b] Spin-lattice relaxation times for C-3 of 2-methylindole-(methyl,3)-$^{13}C_2$ determined with a 0.100 molal solution in 1,2-dichloroethane, 50% of which was 1,2-dichloroethane-d_4.

TABLE 2. Data for 2-methylindole in 1,2-dichloroethane/1,1,2,2-tetrachloroethane mixtures at 35°C

$[D]$[a]	X[b]	η(cP)[c]	T_1(s)[d]	τ_c(ps)
0.100	0.00	0.69_6	6.3_7	6.92
0.096	0.24_5	0.86_3	4.8_1	9.16
0.098	0.49_5	1.04_7	3.7_1	11.88
0.091	0.71_1	1.21_8	3.1_0	14.22
0.097	0.98_4	1.44_8	2.6_9	16.39

[a] Molal concentration of 2-methylindole.
[b] Mole fraction of 1,1,2,2-tetrachloroethane.
[c] Experimentally determined viscosities of solutions containing 2-methylindole.
[d] Spin-lattice relaxation times for C-3 of 2-methylindole-(methyl,3)-$^{13}C_2$.

was determined by changing the temperature as well as by changing the solvent system used.

Since nOe factors for C-3 of 2-methylindole are within experimental error of the full nOe over the entire viscosity range studied, it is assumed that this carbon is relaxed solely by the dipolar interaction with its bonded proton. In the region of motional narrowing and under conditions of complete proton decoupling the dipolar ^{13}C relaxation rate, $1/T_1$, of a carbon nucleus containing one bonded proton is related (9) to the effective molecular correlation time, τ_c, according to

$$[1] \quad 1/T_1 = \hbar^2\gamma_C^2\gamma_H^2 r^{-6}\tau_c$$

where $2\pi\hbar$ is Planck's constant, γ_C and γ_H are the magnetogyric ratios of ^{13}C and ^1H nuclei, and r is the C—H bond length.

Table 1 summarizes the T_1 data for C-3 of 2-methylindole as a function of temperature. The effective molecular correlation times were calculated from the T_1 data by eq. [1] using $r = 1.08$ Å for the required C—H bond length in 2-methylindole (10). The viscosities of 1,2-dichloroethane as a function of temperature, also given in Table 1, were obtained from the literature (11*a*); it was assumed that the small amount of 2-methylindole (0.10 molal) and the use of 50% 1,2-dichloroethane-d_4 would not significantly affect these solvent values. A least-squares fit of the data to (3, 4, 12)

$$[2] \quad \tau_c = C\,\eta/T + b$$

where η is the viscosity, T is the temperature in K, and b is the intercept, gives the experimental η/T dependence of τ_c as C_{exp} = 3.46 ns K/cP, with a correlation coefficient of 0.995.

Variation of the viscosity was also accomplished by using different mixtures of 1,2-dichloroethane and 1,1,2,2-tetrachloroethane as the solvent. 1,1,2,2-Tetrachloroethane was chosen since its dielectric constant (ϵ = 7.83 at 25°C) (11*b*) matched that of 1,2-dichloroethane (ϵ = 10.13 at 25°C) (11*b*) fairly well, it provided a sufficient range in viscosity, and because of a reasonable structural similarity to 1,2-dichloroethane. The changes in the solvent, other than viscosity, should therefore not be great on mixing this component with 1,2-dichloroethane. The T_1's of C-3 of 2-methylindole at 35°C as a function of solvent mixture are given in Table 2; also given in this table are the experimentally determined viscosities and the correlation times calculated by eq. [1]. These correlation times show a η/T dependence (according to eq. [2]) of C_{exp} = 3.96 ns K/cP, with a correlation coefficient of 0.996.

The use of a hydrodynamical model in a study of this type is common (4, 13). In order to apply such a model of molecular reorientation to the rotational behaviour of 2-methylindole in solution, an approximation of the molecular geometry is necessary. A space-filling model suggests that 2-methylindole may be approximated by an oblate spheroid. Using the van der Waals radius of carbon, 1.7 Å, as an approximation (3, 14) of the semi-minor axis, c, and the sum of the van der Waals volume increments of all the atoms in this molecule (15), 126.8 Å^3, as an approximation of the molecular volume, V, the semi-major axis, a, is calculated to be 4.22 Å. This value of a is regarded as a lower limit, as using $V = 4\pi a^2 c/3$ to calculate a implicitly assumes unfilled spaces between peripheral atoms as part of the volume. A scale diagram of 2-methylindole was drawn using the bond lengths and angles of L-tryptophan hydrochloride (16) determined by X-ray crystallography. If van der Waals radii of the outer atoms are included (3), this diagram suggests that 5.55 Å is the maximum radius that would be swept out by rotation in the plane of the molecule; therefore a = 5.55 Å was taken as an upper limit. We consider the average of these two limits, 4.9 Å, to be a reasonable approximation.

Molecular reorientation was considered under two different boundary conditions. Under "stick" boundary conditions, which assumes that the solvent sticks to the surface of and therefore rotates with the solute, the viscosity-dependent term in eq. [2] can be theoretically calculated for a spheroid (2, 3) by

$$[3] \quad \tau_{stick} = \frac{\zeta_1}{24\,kT} + \frac{3\zeta_1}{8\,kT[1 + (2\zeta_1/\zeta_3)]}$$

where T is the temperature, k is the Boltzmann constant, and ζ_1 and ζ_3 are rotational friction coefficients ($\zeta_1 = \zeta_2$ for a spheroid) which are calculated from the geometry of the spheroid and the viscosity. The equations for ζ_1 and ζ_3 and a discussion relevant to them are given in ref. 3. Substitution for the rotational friction coefficients and rearranging gives τ_{stick} proportional to η/T and the proportionality constant can be calculated from the geometry of the molecule. Using a = 4.9 Å and c = 1.7 Å yields a η/T dependence, C_{stick}, of 19.7 ns K/cP. (For a = 4.22 Å and c = 1.7 Å, C_{stick} = 13.2 ns K/cP.)

Under slip boundary conditions the solvent is considered to slip by the surface of the rotating molecule and resistive forces are due only to the displacement of fluid as the body rotates. For rotation *of* the symmetry axis of spheroids, Hu and Zwanzig (1) have calculated the ratio ζ_{slip}/ζ_1 as a function of the ratio of the lengths of the semiaxes. The rotational friction coefficient corresponding to ζ_3 will be zero since rotation *about* the

TABLE 3. The calculated and experimental values of C, the η/T dependence, for τ_c of 2-methylindole

		C (ns K/cP)
Stick	a = 4.22 Å	13.2
	a = 4.90 Å	19.7
Slip	a = 4.22 Å	1.16
	a = 4.90 Å	2.13
Experimental	Solvent variation	3.96
	Temperature variation	3.46

TABLE 4. Spin-lattice relaxation times for C-3 of 2-methylindole as a function of the fraction complexed at 35°C in 1,2-dichloroethane

$[D]^a$	$[A]^b$	η(cP)^c	T_1(s)^d	α^e
0.100	—	0.68_6	6.6_0	0.00
0.099	0.101	0.72_0	5.1_6	0.106
0.100	0.360	0.81_1	3.7_8	0.300
0.102	0.365	0.81_4	3.5_6	0.303
0.100	0.555	0.88_3	3.1_7	0.401
0.100	1.153	1.13_0	2.1_5	0.587
0.103	1.588	1.34_6	1.7_2	0.664

[a,b] Initial concentrations of 2-methylindole and 1,3,5-trinitrobenzene, respectively, in mol (kg solvent)$^{-1}$.

[c] Experimentally determined solution viscosities.

[d] Spin-lattice relaxation times for C-3 of 2-methylindole-(methyl,3)-$^{13}C_2$.

[e] The fraction of 2-methylindole complexed.

symmetry axis of an oblate spheroid does not displace any fluid. Under this condition the right hand side of eq. [3] is dominated by the first term so that the viscosity-dependent term in eq. [2] can be calculated for the slip condition by

$$[4] \quad \tau_{slip} = \frac{R\zeta_1}{24\ kT}$$

where R is the ratio ζ_{slip}/ζ_1 obtained from the work of Hu and Zwanzig (1). Substituting and rearranging gives τ_{slip} proportional to η/T. Using a = 4.9 Å and c = 1.7 Å yields a η/T dependence, C_{slip}, of 2.13 ns K/cP. (For a = 4.22 Å and c = 1.7 Å, C_{slip} = 1.16 ns K/cP.)

Comparison of the experimentally determined η/T dependence of the effective molecular correlation time with the results of the slip and stick treatments (see Table 3) implies that the molecular reorientation of 2-methylindole much more nearly approximates slip conditions than stick conditions. The slip boundary condition will disturb less solvent and will therefore show a smaller viscosity dependence and faster rate of reorientation. The stick boundary condition predicts too much friction to rotation for the case at hand and therefore shows a viscosity dependence that is too high. In spite of the difficulty in defining the geometry due to the lack of symmetry in 2-methylindole, the model does provide a qualitative picture of the reorientation of 2-methylindole in 1,2-dichloroethane. The solvent is not expected to interact strongly with 2-methylindole since it will not hydrogen bond to the solute. Therefore the amount of "stick" is expected to be minimal, which is in agreement with observations.

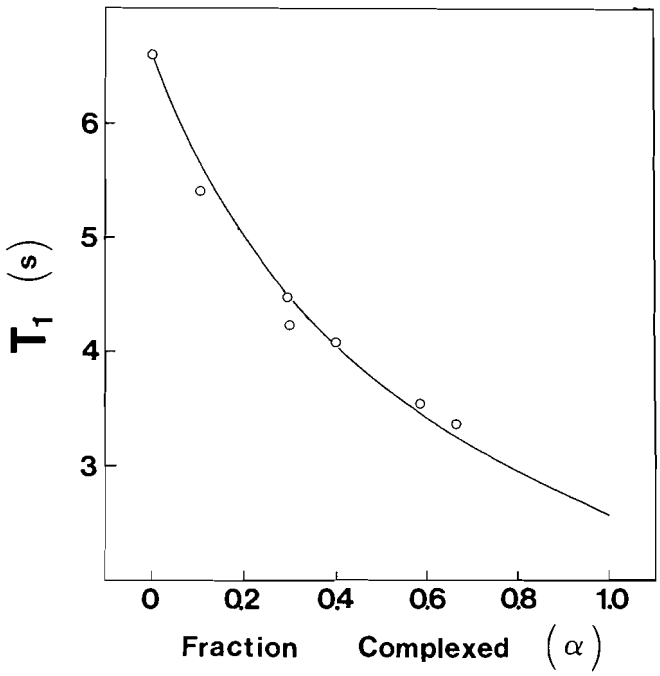

FIG. 1. The dependence of T_1 (corrected for the effects of viscosity) of C-3 of 2-methylindole on the fraction complexed, showing the experimental points and the theoretical curve providing the best fit.

Effect of complex formation

The experimental dependence of T_1 of C-3 of 2-methylindole on the fraction complexed (see Table 4) was determined by measuring the relaxation time as a function of the concentration of 1,3,5-trinitrobenzene (TNB) while keeping the concentration of 2-methylindole essentially constant. The fraction complexed, α, was calculated from the initial concentrations and an equilibrium constant of 1.3 kg solvent mol^{-1}, assuming 1:1 complex formation only (see ref. 8). (The equilibrium constant was obtained by standard methods (17) from the chemical shift changes, of C-2 and the methyl carbon of 2-methylindole, which result from complex formation with TNB.) Figure 1 shows the observed T_1, corrected to account for the changes in viscosity as TNB is added, as a function of the fraction complexed. The reference viscosity chosen is that of the solution containing no TNB.

Since nOe factors for all solutions are within experimental error of the full nOe, relaxation of C-3 is dominated by dipolar interaction with the directly attached proton. The dipolar spin-lattice relaxation time of a nucleus undergoing exchange between the free and complexed state will depend on the rates of reorientation of the free molecule (k_1) and the complex (k_2), as well as the rate of association (k_3) of the molecules and the rate of dissociation (k_4) of the complex. Utilizing the equations of Anderson and Fryer (5), the ^{13}C dipolar relaxation rate, $1/T_1$, can be written as a function of these rate constants and the fraction complexed. In the region of motional narrowing and under conditions of complete proton decoupling

$$[5] \quad 1/T_1 = B[(Q_+/\lambda_+) + (Q_-/\lambda_-)]$$

where $B = \hbar^2\gamma_C^2\gamma_H^2 r^{-6}$ and Q_+, Q_-, λ_+, and λ_- are complex functions of k_1, k_2, k_3, k_4, and the fraction complexed which are given in the work of Anderson and Fryer (5). (As pointed out by Brevard and Lehn (6) a minus sign should replace the plus sign in the brackets of the Q_+ and Q_- expressions.) Using this relationship, T_1 can be calculated as a function of the fraction

Can. J. Chem. Downloaded from www.nrcresearchpress.com by 210.87.254.6 on 09/06/12
For personal use only.

TABLE 5. Relaxation times and rate constants[a] for 2-methylindole and its complex with 1,3,5-trinitrobenzene at 35°C and 0.69 cP in 1,2-dichloroethane

T_D[b] (s)	T_{AD}[c] (s)	k_1 (ns^{-1})	k_2 (ns^{-1})	k_3 (kg mol^{-1} ns^{-1})	k_4 (ns^{-1})
6.6	2.4	150	55	18	14

[a] See text for definitions of k_1, k_2, k_3, and k_4.
[b, c] Spin-lattice relaxation times for C-3 of 2-methylindole-(methyl,3)-$^{13}C_2$ in the free and complexed state respectively.

complexed for a given set of rate constants.

This T_1 expression can be reduced to an equation containing two unknowns. In the region of motional narrowing and under conditions of complete proton decoupling, T_1 is related to the effective molecular correlation time for reorientational motion by eq. [1]. Therefore, the T_1 of C-3 of 2-methylindole in the solution containing no TNB was used to calculate the rate of reorientation of free 2-methylindole as $k_1 = (\tau_c)^{-1}$ (6). By using the equilibrium constant of 1.3 kg solvent mol^{-1}, determined as described above, a substitution can be made for k_3, since $K = k_3/k_4$.

The computer program of Brevard and Lehn (6, private communication with J. M. Lehn), based on the deuterium quadrupolar relaxation version of eq. [5], was modified for ^{13}C dipolar relaxation and to take into account the effects of viscosity on the experimental T_1's. This program was used to generate a series of theoretical curves of T_1 as a function of the fraction complexed. For each k_2 (rate of reorientation of the complex) tested, k_4 (rate of dissociation of the complex) was varied such that k_4/k_2 covered the range from 10^{-5} to 10^4. Best fits with the experimental data are given by k_2 of 55 ± 5 ns^{-1}. The theoretical curve best fitting the experimental points is shown in Fig. 1.

The results, summarized in Table 5, show that the overall rotational motion of 2-methylindole decreases considerably due to complex formation ($k_1/k_2 \sim 3$). The rates of formation and dissociation of the complex, k_3 and k_4, are slower than the rates of reorientation of 2-methylindole in the free, k_1, and bound state, k_2. The lifetime of the complex, $(k_4)^{-1}$, is therefore longer than the correlation time for rotational motion of the complex, $(k_2)^{-1}$. This implies that the complex experiences considerable rotational motion prior to dissociation. Thus, by the classification of ref. 7, this is a true complex and not merely a collision complex.

In the limiting case for slow exchange relative to the rates of molecular reorientation in the free and complexed environments (k_3, $k_4 \ll k_1$, k_2), eq. [5] simplifies to (5)

$$[6] \quad 1/T_1 = (1 - \alpha)/T_D + \alpha/T_{AD}$$

where T_D and T_{AD} represent the dipolar spin-lattice relaxation times of the free and complexed molecules respectively. A simplification in eq. [5] also occurs (5) in the limiting case for fast exchange relative to the rates of reorientation (k_3, $k_4 \gg k_1$, k_2). The results in Table 5 show that the system under investigation is best defined as having an intermediate rate of exchange relative to k_1 and k_2.

Our previous treatment of the 2-methylindole/TNB system (8), which assumed slow exchange relative to k_1 and k_2, gave $T_{AD} = 3.0$ s. The difference between this value and T_{AD} of 2.4 s obtained here may be attributed to this assumption.

Acknowledgments

We thank our colleagues Brian Pettitt and Rod Wasylishen for valuable discussions and the University of Winnipeg for financial assistance.

1. C.-M. HU and R. ZWANZIG. J. Chem. Phys. **60**, 4354 (1974).
2. D. E. WOESSNER. J. Chem. Phys. **37**, 647 (1962).
3. R. E. WASYLISHEN, B. A. PETTITT, and W. DANCHURA. Can. J. Chem. **55**, 3602 (1977).
4. R. T. BOERÉ and R. G. KIDD. *In* Annual reports on nmr spectroscopy. Vol. 13. *Edited by* G. A. Webb. Academic Press, London. 1982. p. 319.
5. J. E. ANDERSON and P. A. FRYER. J. Chem. Phys. **50**, 3784 (1969).
6. CH. BREVARD and J. M. LEHN. J. Am. Chem. Soc. **92**, 4987 (1970).
7. P. LASZLO. *In* Progress in nmr spectroscopy. Vol. 13. *Edited by* J. W. Emsley, J. Feeney, and L. H. Sutcliffe. Pergamon Press, Oxford. 1980. p. 257.
8. B. J. BLACKBURN and K. J. FRIESEN. Org. Magn. Reson. **9**, 113 (1977).
9. A. ABRAGAM. The principles of nuclear magnetism. Oxford University Press, London. 1961. Chapt. VIII.
10. J. A. POPLE and D. L. BEVERIDGE. Approximate molecular orbital theory. McGraw–Hill, New York. 1970.
11. International Critical Tables. McGraw–Hill, New York. (*a*) Vol. 7. 1930. p. 213. (*b*) Vol. 6. 1929. p. 84.
12. D. R. BAUER, J. I. BRAUMAN, and R. PECORA. J. Am. Chem. Soc. **96**, 6840 (1974).
13. A. KRATOCHWILL. *In* Nuclear magnetic resonance: a specialist periodical report. Vol. 12. *Edited by* G. A. Webb. The Royal Society of Chemistry, London. 1983. p. 96.
14. C. K. PROUT and J. D. WRIGHT. Angew. Chem. Int. Ed. Engl. **7**, 659 (1968).
15. J. T. EDWARD. J. Chem. Educ. **47**, 261 (1970).
16. A. R. KATRITZKY (*Editor*). Physical methods in heterocyclic chemistry. Vol. 5. Academic Press, New York. 1972.
17. R. C. GRIFFITH, D. M. GRANT, and J. D. ROBERTS. J. Org. Chem. **40**, 3726 (1975).

Can. J. Chem. Downloaded from www.nrcresearchpress.com by 210.87.254.6 on 09/06/12
For personal use only.

A trihydroxy acyclonucleoside series[1]

KELVIN K. OGILVIE,[2] NGHE NGUYEN-BA, AND RAYMOND G. HAMILTON
Department of Chemistry, McGill University, Montreal, P.Q., Canada H3A 2K6

Received December 8, 1983

This paper is dedicated to Professor Gerald E. Dunn on the occasion of his 65th birthday

KELVIN K. OGILVIE, NGHE NGUYEN-BA, and RAYMOND G. HAMILTON. Can. J. Chem. **62**, 1622 (1984).

An acyclonucleoside structure (**Z**) has been developed which possesses three hydroxymethyl groups attached to the carbon which is analogous to the 4′-carbon of natural nucleosides. The presence of the third hydroxymethyl group significantly reduces activity against herpesviruses as compared to the dihydroxymethyl (BIOLF-62) and monohydroxymethyl (acyclovir) models.

KELVIN K. OGILVIE, NGHE NGUYEN-BA et RAYMOND G. HAMILTON. Can. J. Chem. **62**, 1622 (1984).

On a développé une structure acyclonucléoside (**Z**) comportant un carbone portant trois groupes hydroxyméthyles qui est analogue au carbone 4′ des nucléosides naturels. Si on la compare aux modèles dihydroxyméthylés (BIOLF-62) et monohydroxyméthylés (acyclovir), on note que la présence d'un troisième groupe hydroxymèthyle réduit d'une façon importante l'activité contre les virus herpès.

[Traduit par le journal]

Can. J. Chem. Downloaded from www.nrcresearchpress.com by 210.87.254.40 on 09/06/12
For personal use only.

Introduction

Nucleoside analogues represent an important group of biologically active molecules (1). We have developed an analogue structure **Y** (2–6, the "glycerosides"), members of which have shown pronounced antiviral activity (5, 7–12). As part of our overall program to determine the limits on structural changes to the side chain with regard to optimal biological activity, we have introduced specific changes at the 3′-position. One such structural change involves the introduction of an additional hydroxymethyl group at the 3′-position (analogous to the 4′-position of natural nucelosides). In this report we wish to describe the synthesis of compound **Z** where B = adenine, cytosine, guanine, 6-chloropurine, and thymine. When B = guanine, the series **X**, **Y**, and **Z** represent a progression of hydroxymethyl modification at the 4′-position. The order of activity against herpesviruses is **Y** > **X** ≫ **Z** where **X** is acyclovir (1, 13).

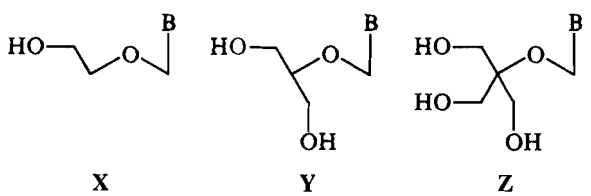

X **Y** **Z**

Discussion and results

The key intermediate in the synthesis is compound **5**. The route to compound **5** is outlined in Scheme 1. The starting material, 1,3-dibenzyloxy-2-propanol (**1**), is readily available (5) and is easily oxidized to the ketone **2** using *N*-chlorosuccinimide and dimethyl sulfide (14). Other common oxidizing agents such as pyridinium chlorochromate, pyridinium dichromate, and Jones reagent were less successful. Compound **2** was smoothly converted into the epoxide **3** in high yield using trimethylsulfoxonium iodide (15). Sodium hydride was very effective in this reaction provided that rigorously anhydrous conditions were maintained; otherwise a number of by-products formed. However, *n*-butyllithium gave good yields consistently. The epoxide ring of **3** was opened by the attack of benzylate anion at the least hindered site to produce the desired 1,3-dibenzyloxy-2-benzyloxymethyl-2-propanol (**4**).

In preparing the glyceroside series **Y** we had activated the intermediate alcohol by conversion to the chloromethyl ether. This conversion requires formaldehyde under strongly acidic conditions (HCl). When applied to **4**, a product was obtained which was quite unstable because of the adjacent tertiary carbon system. To avoid the acidic conditions we attempted the synthesis of the thiomethyl ether system **5**. The alcohol **4** was smoothly converted to the stable product **5** using acetic anhydride in DMSO (16). The thiomethyl ether system is readily activated by iodine, allowing nucleophilic attack at the methylene position. As a result, compound **5** was coupled to purines and pyrimidines using the silylated base procedure (3, 17–19) to produce the desired compounds of general structure **Z** as outlined in Scheme 2.

As usual, the guanine derivative (**12**) was produced in the lowest yield. However, the process was unexpectedly easy to carry out. The N-7 isomer is produced in significant quantity along with the N-9 isomer. Fortunately, in the method used (beginning with *N*-acetylguanine), the N-7 isomer crystallizes from solution after removal of the *N*-acetyl group from the direct condensation product. This greatly facilitates an otherwise tedious separation process. This route to the guanine derivative was prompted by a similar and earlier success in the synthesis of the guanine derivative of **Y** (BIOLF-62).[3]

The route chosen to the adenine derivative **9** involved 6-chloropurine in the condensation step. Using the conditions described (48 h condensation time), very little of the N-7 isomer is present at the end of the reaction. The chlorine at position 6 is readily displaced by ammonia to give the adenine derivative **9**.

All of the compounds were identified by their spectral characteristics. In this regard the ^{13}C chemical shift data (Table 1) and the uv data (Table 2) are most useful. These identifications are confirmed by comparison of these results to those from the series **Y** compounds (3–6).

The compounds described in this report have been subjected to testing against herpesviruses. Only the guanine derivative **12** had an ED-50 of less than 100 μg/mL with HSV-1. The ED-50

[1] Part VI in a series on antiviral and ring-open nucleoside analogues. Part V is ref. 5.

[2] Author to whom correspondence may be addressed.

[3] Unpublished results.

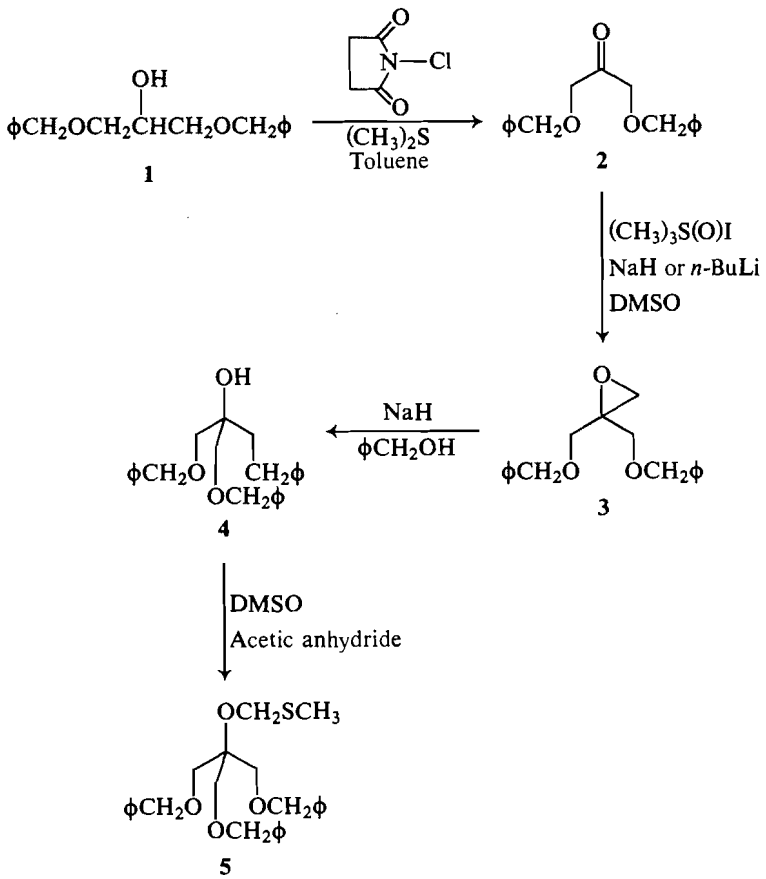

SCHEME 1

TABLE 1. ^{13}C nuclear magnetic resonance data (δ, ppm) of acyclonucleosides[a]

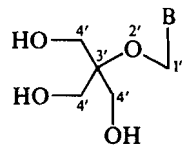

Compound	Base ring	C-2	C-4	C-5	C-6	C-8	C-1′	C-3′	C-4′
6	Cytosine	154.62	165.03	94.41	146.63		72.51	81.25	59.89
7	Thymine[b]	151.01	164.33	109.09	140.76		71.00	81.04	60.27
8	6-Chloropurine	149.06	151.71	130.83	151.71	147.61	67.93	82.06	60.38
9	Adenine	151.38	149.06	118.69	155.21	141.84	67.34	81.79	60.16
12	Guanine	153.92	150.95	116.43	156.99	137.95	66.90	81.42	60.38
13	Guanine	153.27	160.34	107.69	155.16	144.42	69.92	81.32	60.81

[a] Spectra were obtained in DMSO-d_6 on a Bruker WH90 spectrometer.
[b] The C-5 methyl group appeared at 11.93 ppm.

value of **12** at 54 μg/mL is substantially below that of BIOLF-62 (**Y**, B = guanine) where the ED-50 vs. HSV-1 is 0.2 μg/mL.

Experimental

General methods

Products from preparative scale reactions were isolated by column chromatography using Merck silica gel 60 (230–400 mesh) packed in glass columns (15 g of silica per gram of crude material). Thin-layer chromatographic data (R_f values) are recorded from Merck Kieselgel 60F254 analytical sheets. Solvent A consists of isopropyl alcohol – concentrated ammonium hydroxide – water (7:1:2). Purine bases were purchased from Sigma Chemical Co. Ultraviolet spectra were recorded on a Cary 17 spectrometer. Nuclear magnetic resonance spectra were recorded using a Bruker WH-90, a Varian XL-200, and a Varian T60A spectrometer.

1,3-Dibenzyloxyacetone (2)

N-chlorosuccinimide (43 g) was suspended in 500 mL of toluene (Spectrograde) and the mixture was cooled in an ice bath. Dimethyl sulfide (35 mL) was added and a white precipitate formed immediately. The mixture was then cooled to −25°C in a dry ice – carbon tetrachloride bath. 1,3-Dibenzyloxy-2-propanol (60 g) in toluene (50 mL) was added to the mixture via syringe through a serum cap. The mixture was kept under nitrogen for 2 h, whereupon triethylamine (45 mL) was added and the cooling bath was removed. After a further 25 min the solution was collected by filtration. The residue was washed with ether (500 mL). The filtrate and washings were combined, neutralized with 5% aqueous HCl, washed with saturated sodium chloride

Can. J. Chem. Downloaded from www.nrcresearchpress.com by 210.87.254.40 on 09/06/12
For personal use only.

Can. J. Chem. Downloaded from www.nrcresearchpress.com by 210.87.254.40 on 09/06/12
For personal use only.

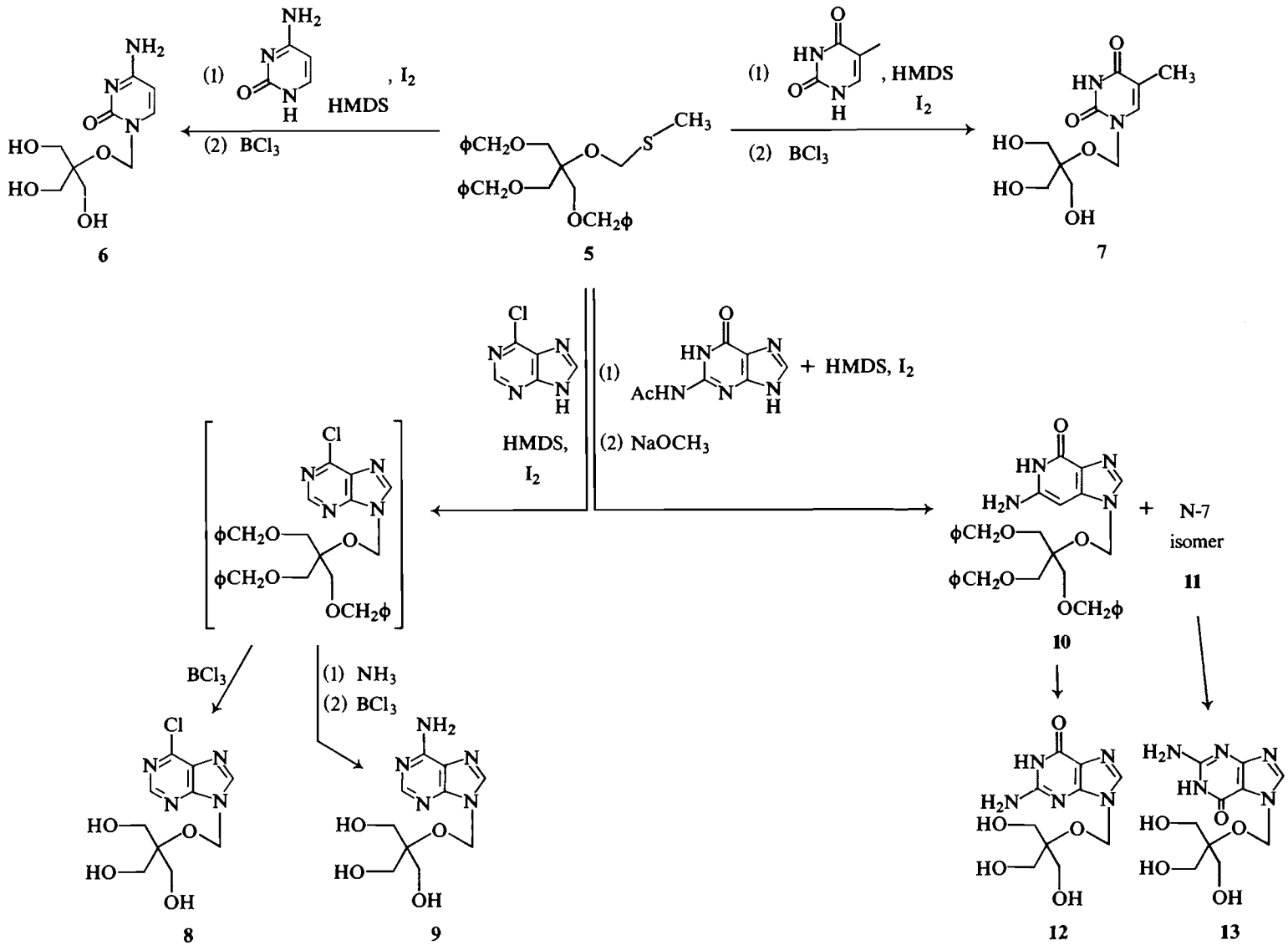

6 5 7 8 9 10 11 12 13

SCHEME 2

TABLE 2. Ultraviolet spectral data of acyclonucleosides

Compound	Base ring	λ_{max}, nm (ε) pH 1	pH 7	pH 14
6	Cytosine	276(10 000)	267(6 600)	267(7 200)
7	Thymine	265(11 500)	265(11 300)	264(9 200)
8	6-Chloropurine	263(7 400)	264(8 400)	264(6 900)
9	Adenine	257(12 400)	258(12 600)	258(12 500)
12	Guanine	254(11 800)	250(12 300)	254(11 300)
		274(8 200)	270(8 900)	266(10 900)
13	Guanine	250(9 500)	240(6 800)	282(7 700)
		268(7 500)	284(7 700)	

in water and with water, and finally dried over magnesium sulfate. The solvents were removed at reduced pressure (liquid nitrogen trap for dimethyl sulfide) and the resulting oil was distilled in a Kugelrohr apparatus. The product (50 g, 83%) was obtained in the fraction boiling at 140–155°C (0.05 Torr) (1 Torr = 133.32 Pa). Normal high vacuum distillation was not satisfactory as the product decomposes at high temperature. The ^{1}Hmr spectrum ($CDCl_3$ + TMS) showed signals at δ (ppm) of 4.16 (s, 4H, —C(=O)—CH_2—O—), 4.50 (s, 4H, —$CH_2\phi$), and 7.23 (s, 10H, ϕ). This material was used directly in the subsequent experiment.

2,2-Dibenzyloxymethylethylene oxide (3)

Trimethylsulfoxonium iodide (25.3 g, 0.115 mol) was dissolved in dry DMSO (350 mL). *n*-Butyllithium (66 mL, 1.65 *M* in hexane) was added via syringe to the mixture kept under nitrogen. The mixture was stirred for 25 min and then cooled to room temperature, at which point compound **2** (26.7 g, 0.098 mol) in DMSO (10 mL) was added via syringe. The mixture was stirred for a further 45 min and then poured into 1 L of cold water. The product was extracted into ether (3 × 300 mL). The organic layer was washed with saturated NaCl solution and dried over magnesium sulfate. Solvents were removed at reduced pressure and the residue was distilled in a Kugelrohr apparatus. The product (bp 120–135°C/0.05 Torr) was obtained in 82% yield (23 g). The ^{1}Hmr spectrum ($CDCl_3$ + TMS) showed signals at δ (ppm) of 2.66 (s, 2H, CH_2), 3.80 (4H, —CH_2—), 4.50 (s, 4H, —$CH_2\phi$), and 7.20 (s, 10H, ϕ).

1,3-Dibenzyloxy-2-benzyloxymethyl-2-propanol (4)

To benzyl alcohol (150 mL) in a three-neck flask (500 mL) was added sodium hydride (2.4 g, 0.1 mol obtained by washing 4 g of 60% sodium hydride dispersion in oil with hexane) in portions under a nitrogen atmosphere. The resulting mixture was stirred for 1 h. Compound **3** (22.5 g, 0.08 mol) in benzyl alcohol (20 mL) was added via syringe. The reaction mixture was heated at 90–95°C for 18 h. After cooling to room temperature, the mixture was poured into 500 mL of cold water and the solution was neutralized with 5% aqueous HCl. The product was extracted into ether (2 × 300 mL) and the combined extracts were washed with water and saturated NaCl solution. After drying over magnesium sulfate the solvent was removed to leave an oil which was distilled in a Kugelrohr apparatus. The fraction boiling at 190–210°C (0.1 Torr) contained the desired product (26.7 g, 86%). The ^{1}Hmr spectrum ($CDCl_3$ + TMS) showed signals of δ (ppm) of 2.80 (s, 1H, —OH), 3.53 (s, 6H, —CH_2O—), 4.46 (s, 6H, —$CH_2\phi$), and 7.20 (s, 15H, ϕ). This material was used directly in the subsequent experiment.

The methylthiomethyl ether 5

Compound **4** (28 g) was dissolved in 100 mL of dry DMSO (100 mL) followed by the addition of acetic anhydride (100 mL). The solution was stirred at room temperature for 48 h. The solvents were removed at reduced pressure and the residue was dissolved in 300 mL of ether. After washing with water and saturated NaCl solution, the ether solution was dried over magnesium sulfate and again concentrated to an oil at reduced pressure. The product (27.3 g, 84%) was collected in the fraction boiling at 190–210°C (0.1 Torr) on distillation in a Kugelrohr apparatus. The ^{1}Hmr spectrum ($CDCl_3$ + TMS) showed signals at δ (ppm) of 2.20 (s, 3H, —SCH_3), 3.70 (s, 6H, —CH_2O), 4.53 (s, 3H, —$CH_2\phi$), 4.83 (s, 2H, —CH_2S—), and 7.30 (s, 15H, ϕ). The product **5** was stable on standing and was used directly in the condensation reactions described below.

Standard procedure for the condensation of 5 with purines and pyrimidines. Reaction condition 1

The purine or pyrimidine base (10 mmol) was heated at reflux in HMDS (50 mL) to which ammonium sulfate (200 mg) had been added. Reflux was continued until the solution became clear (30 min for 6-chloropurine; 3 h for cytosine and thymine; 18 h for *N*-acetylguanine). At this point the excess HMDS was removed by distillation at reduced pressure. Atmospheric pressure was restored using nitrogen and the solid residue was dissolved in 75 mL of freshly distilled THF. Compound **5** (4.52 g, 10 mmol) dissolved in dry THF (15 mL) is added, followed by 5 g of oven activated molecular sieves (type 4A). Iodine (2.54 g) was added and the solution was stirred at room temperature for 48 h. (A nitrogen atmosphere was maintained at all times. For the *N*-acetylguanine reaction, the solution was stirred at room temperature for 24 h, followed by heating at a gentle reflux for 6 h.) Sodium sulfite solution (150 mL, 5% aqueous) was added and the resulting solution was extracted with methylene chloride (3 × 200 mL). The combined extracts were washed with saturated NaCl solution and water and then dried over magnesium sulfate. The solvent was removed at reduced pressure and the residue was flash-chromatographed on silica gel. The specific solvents for each base and the properties of the product are described below.

Standard procedure for the removal of the benzyl groups. Reaction condition 2

The product (2 g) from reaction condition 1 (the tribenzyl product) was dissolved in methylene chloride (50 mL) and the solution was coolled to −78°C. A 1 *N* solution of BCl_3 in methylene chloride (23 mL) was added via syringe and under a nitrogen atmosphere. The mixture was stirred at −78°C for 3 h. A solution of methanol and methylene chloride (1:1, 50 mL) was added and the cooling bath was removed. The clear solution was neutralized with triethylamine or sodium bicarbonate and stirred for an additional 35 min. The solvent was removed at reduced pressure, water (20 mL) was added, and again the solvent was removed at reduced pressure. This process was repeated three times, followed by the evaporation of absolute ethanol (30 mL). At this point variations in the work-up occurred. The remaining procedures are described for the individual compounds listed below.

1-[[1,3-Dihydroxy-2-(hydroxymethyl)-2-propoxy]methyl]cytosine 6

Reaction condition 1 (from cytosine)

The product was isolated by flash chromatography using chloroform – ethyl acetate – ethanol (4:5:1) as eluant. The yield of the

Can. J. Chem. Downloaded from www.nrcresearchpress.com by 210.87.254.40 on 09/06/12
For personal use only.

Can. J. Chem. Downloaded from www.nrcresearchpress.com by 210.87.254.40 on 09/06/12
For personal use only.

tribenzylated product was 3.5 g (58%). The product had an R_f of 0.31 in chloroform–methanol (9:1). The ^{1}Hmr spectrum ($CDCl_3$ + TMS) showed signals at δ (ppm) of 3.66 (s, 6H, —CH_2O—), 4.50 (2, 6H, —$CH_2\phi$), 5.40 (s, 2H, —NCH_2O—), 5.73 (d, 1H, J = 6 Hz, H-5), 7.30 (s, total 16H, 15 from φ and H-6 buried under aromatic H's).

Reaction condition 2

The above product was treated as described in the general procedure. The residue so obtained was extracted with chloroform (30 mL) under stirring and the solution was filtered through Celite. The Celite was washed twice with chloroform (2 × 20 mL) which removed the triethylamine hydrochloride. The Celite was then washed with 150 mL of hot methanol. The methanol solution was concentrated at reduced pressure and the residue was crystallized from methanol–ether to give the desired product **6** (72%, mp 198–200°C, R_f in solvent A of 0.53). The ^{1}Hmr spectrum (DMSO-d_6 + TMS) showed signals at δ (ppm) of 3.50 (s, 6H, —CH_2—OH), 5.23 (s, 2H, —NCH_2O—), 5.80 (d, 1H, H-5, $J_{5,6}$ = 6 Hz), 7.73 (d, 1H, H-6, $J_{5,6}$ = 6 Hz), and 7.73 (broad, 2H, —NH_2). The ^{13}C chemical shifts are recorded in Table 1. The uv characteristics are collected in Table 2. *Anal.* calcd. for $C_9H_{15}N_3O_5 \cdot 1/2H_2O$: C 42.52, H 6.29, N 16.53; found: C 42.62, H 6.15, N 16.62.

1-[[1,3-Dihydroxy-2-(hydroxymethyl)-2-propoxy]methyl]thymine 7

Reaction condition 1 (from thymine)

The tribenzyl product was recovered as an oil in 74% yield from flash chromatography using ethyl acetate – hexane (1:1) as eluant. The ^{1}Hmr spectrum ($CDCl_3$ + TMS) showed signals at δ (ppm) of 1.70 (s, 3H, —CH_3), 3.63 (s, 6H, —CH_2O—), 4.46 (s, 6H, —$CH_2\phi$), 5.30 (s, 2H, —NCH_2O—), 7.10 (m, 1H, H-6), and 7.20 (s, 15H, φ). The compound had λ_{max} of 263 nm in methanol. This intermediate was subjected directly to the general reaction condition 2.

Reaction condition 2

The residue was stirred with 30 mL of hot methanol and filtered. Silica gel (5 g) was added and the resulting slurry was concentrated in a rotary evaporator and the silica was dried under high vacuum overnight. This silica was placed on top of a prepared silica gel column which was then eluted with methylene chloride – methanol (4:1). The desired product **7** was obtained in 70% yield (mp 165–167°C). The product had an R_f of 0.48 in methylene chloride – methanol (4:1). The ^{1}Hmr spectrum (DMSO-d_6 + TMS) showed signals at δ (ppm) of 1.80 (s, 3H, —CH_3), 3.55 (s, 6H, —CH_2O—), 4.50 (broad, 3H, —OH), 5.23 (s, 2H, —NCH_2O—), and 7.53 (s, 1H, H-6). The ^{13}C spectral properties and the uv data are collected in Tables 1 and 2, respectively. *Anal.* calcd. for $C_{10}H_{16}N_2O_5$: C 46.16, H 6.19, N 10.76; found: C 46.00, H 6.08, N 10.71.

9[[1,3-Dihydroxy-2-(hydroxymethyl)-2-propoxy]methyl]-6-chloropurine 8

Reaction condition 1 (from 6-chloropurine)

The residue was flash chromatographed on silica gel using ethyl acetate – hexane (1:1). The tribenzyl product was obtained as an oil in 55% yield with R_f of 0.38 in the eluting solvent. The uv spectrum (methanol) showed λ_{max} at 263 nm. The ^{1}Hmr spectrum ($CDCl_3$ + TMS) showed signals at δ (ppm) of 3.63 (s, 6H, —CH_2O—), 4.43 (s, 6H, —$OCH_2\phi$), 5.90 (s, 2H, —NCH_2O—), 7.20 (s, 15H), 8.20 (s, 1H, H-2), and 8.66 (s, 1H, H-8).

A trace amount of another product, assumed to be the N-7 isomer, was also obtained. This material had R_f 0.22 in the eluting solvent and a λ_{max} of 267 nm in methanol. The ^{1}Hmr spectrum of this product ($CDCl_3$ + TMS) showed signals at δ (ppm) of 3.70 (s, 6H, —CH_2O—), 4.40 (s, 6H, —$OCH_2\phi$), 6.0 (s, 2H, —NCH_2O—), 7.30 (s, 15H, φ), 8.30 (s, 1H, H-2), and 8.80 (s, 1H, H-8).

Reaction condition 2

The residue (obtained by starting with the desired N-9 product from reaction condition 1) was extracted with warm methanol. The solution was filtered and treated with 5 g of silica gel as described for compound **7**. The column was eluted with methylene chloride – methanol (4:1). The desired product **8** was crystallized from methanol–ether in 65% yield (mp 158–160°C) and had R_f of 0.58 in the eluting solvent. The ^{1}Hmr spectrum (DMSO-d_6 + TMS) showed signals at δ (ppm) of 3.66 (s, 6H, —CH_2OH), 4.66 (t, 3H, —OH), 6.00 (s, 2H, —NCH_2O—), 8.83 (s, 1H, H-2), and 8.86 (s, 1H, H-8). The ^{13}C spectral data and the uv data are collected in Tables 1 and 2 respectively. *Anal.* calcd. for $C_{10}H_{13}ClN_4O_4 \cdot 1/2H_2O$: C 40.34, H 4.74, N 18.82; found: C 40.72, H 4.38, N 18.60.

9-[[1,3-Dihydroxy-2-(hydroxymethyl)-2-propoxy]methyl]adenine 9

The N-9 product of reaction condition 1 from the 6-chloropurine condensation was heated in a steel bomb at 125°C for 17 h in saturated (at 0°C) methanolic ammonia (15 mL/g of starting material). The bomb was cooled to room temperature, the solvents were evaporated, and the product obtained by chromatography on silica gel using methylene chloride – methanol (9:1) as eluant. The product was obtained in 88% yield and had λ_{max} (methanol) at 257 nm and an R_f of 0.68 in the eluting solvent. The ^{1}Hmr spectrum ($CDCl_3$ + TMS) showed signals at δ (ppm) of 3.70 (s, 6H, —CH_2O—), 4.40 (s, 6H, —$OCH_2\phi$), 5.80 (s, 2H, —NCH_2O—), 6.20 (b, 2H, —NH_2), 7.30 (s, 15H, φ), 8.0 (s, 1H, H-2), and 8.30 (s, 1H, H-8).

This material was subjected to reaction condition 2 and the product was obtained by silica gel chromatography using methylene chloride – methanol (4:1). The product **9** (76%) had mp 206–209°C and an R_f of 0.17 in the eluting solvent. The ^{1}Hmr spectrum (DMSO-d_6 + TMS) showed signals at δ (ppm) of (bs, 6H, —CH_2OH), 5.80 (s, 2H, —NCH_2O—), 7.40 (b, 2H, —NH_2), 8.20 (s, 1H, H-2), and 8.30 (s, 1H, H-8). The ^{13}C spectral data and the uv data are collected in Tables 1 and 2 respectively. *Anal.* calcd. for $C_{10}H_{15}N_5O_4 \cdot 1/2H_2O$: C 43.16, H 5.79, N 25.17; found: C 43.41, H 5.81, N 25.26.

*9-[[1,3-Dihydroxy-2-(hydroxymethyl)-2-propoxy]methyl]guanine (**11**) and 7-[[1,3-dihydroxy-2-(hydroxymethyl)-2-propoxy]-methyl]guanine (**12**)*

Reaction condition 1

The starting material in this condensation was *N*-acetylguanine. The residue from reaction condition 1 was flash-chromatographed on silica gel using chloroform – ethyl acetate – ethanol (4:5:1). An oil was obtained (43%) which according to ^{1}Hmr was a mixture of the N-9 and N-7 isomers (3:2).

The mixture was dissolved in dry methanol (50 mL) and this solution was added to methanol (100 mL) containing sodium (500 mg). This solution was heated at reflux for 3 h. After cooling to room temperature the solution was carefully neutralized using glacial acetic acid. White crystals formed during the neutralization and these were collected by filtration and found to be the pure N-7 isomer (**11**) in 9% overall yield (mp 215–218°C). The filtrate was concentrated and chromatographed on silica gel using methylene chloride – methanol (9:1). The N-9 isomer (**10**) was obtained in 15% overall yield (mp 185°C (dec.)).

The ^{1}Hmr spectrum of N-9 isomer **10** (DMSO-d_6 + TMS) showed signals at δ (ppm) of 3.6 (s, 6H, —CH_2O—), 4.53 (s, 6H, —$CH_2\phi$), 5.60 (s, 2H, —NCH_2O—), 6.46 (b, 2H, —NH_2), 7.3 (s, 15H, φ), 7.66 (s, 1H, H-8), and 9.14 (b, 1H, H-1). The ^{1}Hmr spectrum of the N-9 isomer (**11**) under the same conditions showed signals at δ (ppm) of 3.63 (s, 6H, —CH_2O—), 4.53 (s, 6H, —$CH_2\phi$), 5.86 (s, 2H, —NCH_2O—), 6.23 (b, 2H, —NH_2), 7.33 (s, 15H, φ), and 7.96 (s, 1H, H-8).

*Reaction condition 2 on **10***

The N-9 isomer from above (**10**) was subjected to the standard conditions. The residue obtained crystallized from 95% ethanol to give pure **12** in 77% yield (mp >300°C). The R_f in solvent A on tlc was 0.51. The ^{1}Hmr spectrum of **12** (DMSO-d_6 + TMS) showed signals at δ (ppm) of 3.60 (s, 6H, —CH_2OH), 5.63 (s, 2H, —NCH_2O—), 6.53 (b, 2H, —NH_2), 7.90 (s, 1H, H-8), and 10.80 (b, 1H, H-1). The ^{13}C and uv data are collected in Tables 1 and 2 respectively. *Anal.* calcd. for $C_{10}H_{15}N_5O_5$: C 42.10, H 5.26, N 24.56; found: C 41.89, H 5.19, N 24.83.

*Reaction condition 2 on **11***

The N-7 isomer from above (**11**) was subjected to the standard

conditions. The dry white residue from the reaction was treated with chloroform and filtered through Celite. The Celite was washed with chloroform (2 × 20 mL). The Celite was then poured into 200 mL of water which was brought to the boiling point and filtered. The filtrate was lyophilized to yield a white powder (78% yield, R_f on tlc in solvent A of 0.53). The ^{1}Hmr spectrum of **13** in (DMSO-d_6 + TMS) showed signals at δ (ppm) of 3.50 (s, 6H, —CH_2OH), 5.70 (s, 2H, —NCH_2O—), 6.40 (b, 2H, —NH_2), and 8.10 (s, 1H, H-8). The ^{13}C and uv data are collected in Tables 1 and 2 respectively. *Anal.* calcd. for $C_{10}H_{15}N_5O_5$: C 42.10, H 5.26, N 24.56; found: C 42.39, H 5.40, N 24.67.

Acknowledgements

We are grateful for financial support from Bio Logicals Inc. and the Natural Sciences and Engineering Research Council of Canada. We are indebted to Dr. K. O. Smith for the antiviral tests.

1. R. T. WALKER, E. DE CLERCQ, and F. ECKSTEIN (*Editors*). Nucleoside analogues. Plenum Press, New York. 1978.
2. K. K. OGILVIE and M. F. GILLEN. Tetrahedron Lett. **21**, 327 (1980).
3. K. K. OGILVIE, U. O. CHERIYAN, B. K. RADATUS, K. O. SMITH, K. S. GALLOWAY, and W. L. KENNELL. Can. J. Chem. **60**, 3005 (1982).
4. K. K. OGILVIE, R. G. HAMILTON, M. F. GILLEN, B. K. RADATUS, K. O. SMITH, and K. S. GALLOWAY. Can. J. Chem. **62**, 16 (1984).
5. K. K. OGILVIE, N. NGUYEN-BA, M. F. GILLEN, B. K. RADATUS, U. O. CHERIYAN, H. R. HANNA, K. O. SMITH, and K. S. GALLOWAY. Can. J. Chem. **62**, 241 (1984).
6. K. K. OGILVIE, D. M. DIXIT, B. K. RADATUS, and K. O. SMITH. Nucleosides Nucleotides, **2**, 147 (1983).
7. K. O. SMITH, K. S. GALLOWAY, W. L. KENNEL, K. K. OGILVIE, and B. K. RADATUS. Antimicrob. Agents Chemother. **22**, 55 (1982).
8. K. O. SMITH, K. S. GALLOWAY, K. K. OGILVIE, and U. O. CHERIYAN. Antimicrob. Agents Chemother. **22**, 1026 (1982).
9. K. O. SMITH, K. S. GALLOWAY, S. L. HODGES, K. K. OGILVIE, B. K. RADATUS, S. S. KALTER, and R. L. HEBERLING. Am. J. Vet. Res. **44**, 1032 (1983).
10. A. K. FIELD, H. PERRY, R. LIOU, H. BULL, R. L. TOLMAN, and J. D. KARKAS. Biochem. Biophys. Res. Commun. **116**, 360 (1983).
11. Y.-C. CHENG, E.-S. HUANG, J.-C. LIN, E.-C. MAR, J. S. PAGANO, G. E. DUTSCHMAN, and S. P. GRILL. Proc. Natl. Acad. Sci. U.S.A. **80**, 2767 (1983).
12. J. C. MARTIN, C. A. DVORAK, D. F. SMEE, T. R. MATTHEWS, and J. P. H. VERHEYDEN. J. Med. Chem. **26**, 759 (1983).
13. H. J. SCHAEFFER, L. BEAUCHAMP, P. DE MIRANDA, G. B. ELION, D. J. BAUER, and P. COLLINS. Nature, **272**, 583 (1978).
14. E. J. COREY and C. U. KIM. J. Am. Chem. Soc. **94**, 7586 (1972).
15. E. J. COREY and M. CHAYKOVSKY. Org. Synth. **49**, 78 (1969).
16. K. YAMADA, K. KATO, H. NAGASE, and Y. HIRATA. Tetrahedron Lett. **17**, 65 (1976).
17. T. NISHIMURA, B. SHIMIZU, and I. IWAI. Chem. Pharm. Bull. Jpn. **11**, 1470 (1963).
18. E. WITTENBURG. Z. Chem. **4**, 303 (1964).
19. G. RITZMANN and W. PFLEIDERER. Chem. Ber. **106**, 1401 (1973).

Can. J. Chem. Downloaded from www.nrcresearchpress.com by 210.87.254.40 on 09/06/12
For personal use only.

Studies of azo and azoxy dyestuffs. Part 17.[1] Synthesis and structure determination of isomeric α and β phenylazoxypyridines, *N*-oxides, and methiodides. A reexamination of the oxidation of phenylazopyridines and X-ray structure analyses of 4-(phenyl-α-azoxy)pyridinium methiodide and 4-(phenyl-β-azoxy)pyridine-*N*-oxide[2]

E. BUNCEL AND S. R. KEUM
Department of Chemistry, Queen's University, Kingston, Ont., Canada K7L 3N6

M. CYGLER
Department of Biochemistry, University of Alberta, Edmonton, Alta., Canada T6G 2H7

AND

K. I. VARUGHESE AND G. I. BIRNBAUM
Division of Biological Sciences, National Research Council of Canada, Ottawa, Ont., Canada K1A 0R6

Received December 5, 1983

This paper is dedicated to Professor Gerald E. Dunn on the occasion of his 65th birthday

E. BUNCEL, S. R. KEUM, M. CYGLER, K. I. VARUGHESE, and G. I. BIRNBAUM. Can. J. Chem. **62**, 1628 (1984).

In an extension of Wallach rearrangement studies into the phenylazoxypyridine series, an investigation of 4-, 3-, and 2-phenylazoxypyridines, the *N*-oxides, and methiodides is reported. Oxidation of 4- and 3-phenylazopyridine with peracetic acid gives rise to the α and β phenylazoxypyridine-*N*-oxides, contrary to previous literature reports on the obtention solely of the α isomers. 2-Phenylazopyridine, however, yields only the 2-(phenyl-α-azoxy)pyridine-*N*-oxide. These results are rationalized on the basis of field, resonance, and steric effects. An unprecedented reactivity difference has been observed in the reactions of the α,β isomers of phenylazoxypyridines under conditions of the Wallach rearrangement. This reactivity difference permits the isolation of the α-azoxy isomers from the α,β mixtures. Unequivocal confirmation of the structures has been obtained from X-ray crystal structure determinations of two representative compounds in this series, viz. 4-(phenyl-β-azoxy)-pyridine-*N*-oxide (**11**) and 4-(phenyl-α-azoxy)pyridinium methiodide (**12**), which itself was formed by deoxygenation of 4-(phenyl-α-azoxy)pyridine-*N*-oxide, followed by methylation with methyl iodide. The crystal structure of **11** was solved by direct methods and refined by block-diagonal least squares to $R = 0.041$ for 2479 observed reflections. The asymmetric unit contains two independent molecules, both of which are planar. The structure of **12** was determined by the heavy-atom method and refined by full-matrix least squares to $R = 0.043$ for 1718 observed reflections. The molecules are not planar, the pyridine ring being rotated by 36.5° from the phenylazoxy plane. Evidence is presented for the existence of intramolecular C—H···O and C—H···N bonds in crystal structures of *trans*-azoxyarenes. The carbon atoms involved in these hydrogen bonds are *ortho* to the azoxy group and can act as proton donors as a result of the inductive effect of the adjacent nitrogen.

E. BUNCEL, S. R. KEUM, M. CYGLER, K. I. VARUGHESE et G. I. BIRNBAUM. Can. J. Chem. **62**, 1628 (1984).

Dans le but de poursuivre les études sur la transposition de Wallach dans la série des phénylazoxypyridines, on rapporte une étude réalisée sur les phénylazoxy-4, phénylazoxy-3 et phénylazoxy-2 pyridines, et leurs *N*-oxydes et les iodométhylates. L'oxydation des phénylazo-4 et phénylazo-3 pyridines par l'acide peracétique conduit aux α ainsi qu'aux β *N*-oxydes de phénylazoxypyridines; ce résultat diffère de ce qui a été rapporté antérieurement, à savoir qu'on avait alors obtenu uniquement l'isomère α. Cependant, la phénylazo-2 pyridine donne uniquement le *N*-oxyde de la (phényl-α azoxy)-2 pyridine. On rationalise ces résultats en se basant sur les effets du champ, de résonance, et les effets stériques. On a observé une différence de réactivité inhabituelle au cours de la réaction des isomères α et β des phénylazoxypyridines dans les conditions de la transposition de Wallach. Cette différence de réactivité permet d'isoler l'isomère α azoxy d'un mélange contenant les isomères α et β. On a confirmé les structures d'une manière univoque en se basant sur la détermination des structures cristallines, par diffraction de rayons-X, de deux composés représentatifs de la série, à savoir: le *N*-oxyde de (phényl-β azoxy)-4 pyridine (**11**) et l'iodométhylate de (phényl-α azoxy)-4 pyridinium (**12**); ce dernier composé se forme d'ailleurs lui-même par une désoxygénation du *N*-oxyde de la (phényl-α azoxy)-4 pyridine suivie d'une méthylation par l'iodure de méthyle. On a résolu la structure cristalline du composé **11** par des méthodes directes et on l'a affinée par la méthode des moindres carrés (approximation diagonale) jusqu'à une valeur de $R = 0{,}041$ pour 2479 réflexions observées. L'unité asymétrique contient deux molécules indépendantes qui sont planes. On a déterminé la structure du composé **12** par la méthode de l'atome lourd et on l'a affinée par la méthode des moindres carrés (matrice entière) jusqu'à une valeur de $R = 0{,}043$ pour 1718 réflexions observées. Les molécules ne sont pas planes; le cycle de la pyridine est décalé de 36,5° par rapport au plan du groupe phénylazoxy. On présente des données suggérant l'existence de liaisons intramoléculaires C—H···O et C—H···N dans les structures cristallines des azoxyarènes-*trans*. Les atomes de carbones impliqués dans ces liaisons hydrogènes sont en *ortho* du groupe azoxy et peuvent agir comme donneurs de protons en raison de l'effet inductif de l'atome d'azote adjacent.

[Traduit par le journal]

Introduction

As an extension of our studies (1–4) of the acid-catalyzed Wallach rearrangement of azoxybenzene to *p*-hydroxyazobenzene (eq. [1]), and related processes, we have undertaken an investigation of the phenylazoxypyridine series. These systems would constitute the first incursion of Wallach rear-

[1] 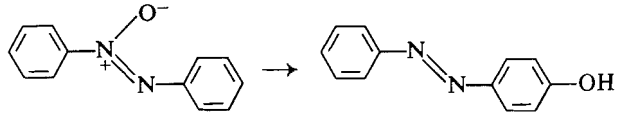

1 **2**

[1]Part 16: see ref. 59.
[2]NRCC No. 23486.

Can. J. Chem. Downloaded from www.nrcresearchpress.com by 210.87.254.105 on 09/06/12
For personal use only.

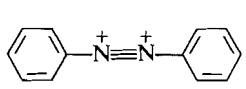

3

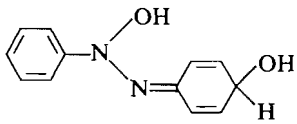

4

rangement studies into the heterocyclic series and, as well, would provide a critical test of previously proposed mechanisms (5–16) for this process, for example concerning formation of the key intermediates **3** and **4**.

Another point of interest in the phenylazoxypyridine series relates to the difference in reactivities that one might expect for α and β isomers, for example 4-(phenyl-α-azoxy)pyridine **5** and 4-(phenyl-β-azoxy)pyridine **6**.

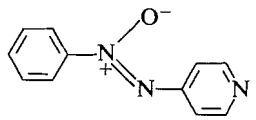

5

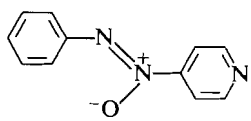

6

At the outset of our work there was no study extant which reported the formation of a β phenylazoxypyridine. The oxidation of 4-phenylazopyridine with peracetic acid was reported (17) to give rise only to the 4-(phenyl-α-azoxy)pyridine-*N*-oxide, none of the isomeric β product being obtained. Similarly, only 3-(phenyl-α-azoxy)pyridine-*N*-oxide and 2-(phenyl-α-azoxy)pyridine-*N*-oxide were reported as formed in related reactions (18–20). These results are somewhat surprising since the oxidation of unsymmetrical azobenzene derivatives generally gives rise to a mixture of the isomeric α- and β-azoxybenzenes in a ratio of ca. 1:1 (21–24), except when a bulky substituent is present on one ring in which case one azoxy isomer is obtained predominantly (25).

In the present work we have found, however, that the peracetic acid oxidation of 4- and 3-phenylazopyridine gives rise to both α- and β-azoxy *N*-oxides, though only the α isomer is formed in the case of 2-phenylazopyridine. The characterization of these compounds and their structure determination forms the substance of the present paper.

Results and discussion

Synthetic strategy

The following synthetic strategy was devised in order to facilitate the efficient synthesis of the desired families of compounds, that is the α/β 4-, 3-, and 2-phenylazoxypyridines, the *N*-oxides, and methiodides.

1. The mixture of α,β phenylazoxypyridine-*N*-oxides obtained in the peracetic oxidation of the phenylazopyridines was separated into its constituents by hplc. Prior to use of the hplc method, repeated crystallization from ethanol or use of column chromatography proved to be unsuccessful as methods of separation.

2. The resulting α and β phenylazoxypyridine-*N*-oxides were separately deoxygenated (phosphorus trichloride) to yield the parent phenylazoxypyridines.

3. Methylation of the latter (methyl iodide) gave the respective methiodides in straightforward manner.

The physical properties of the families of compounds thus obtained, together with the elemental analyses, are given in Tables 1 and 2.

The uv absorption data of the various azoxy compounds synthesized in this work are included in Table 1. The absorption maxima ($\pi-\pi^*$) show only slight bathochromic or hypsochromic shifts with respect to azoxybenzene (λ_{max} 323 nm in EtOH). This is not surprising since these compounds can be classified as even, heteroconjugated systems (26) and introduction of a heteroatom into the axoxybenzene π system does not alter significantly the lowest $\pi-\pi^*$ transition. Further discussion of the uv characteristics has been given elsewhere (27).

The nmr characteristics of the families of compounds together with a full interpretation will be described in a future paper. The structural assignments based on the nmr results are in complete agreement with the assignments given in this paper as a result of the X-ray structure determinations (*vide infra*) and other considerations.

Orientation in oxidation

In the oxidation of phenylazopyridines by peracid, the site of the attack will be determined by the relative electron densities at the various nitrogen centres since the peroxide function acts as an electrophilic reagent (28). It is hence expected that when more than one site of attack is possible, the position of attack in peracid oxidation will follow the same order as found in protonation (29, 30). This expectation should probably hold even though the former process is governed by kinetic considerations and the latter by thermodynamic. One would then predict that mono-oxidation will occur on the pyridine nitrogen as the basicity of this center (pK_a 4.4 (27)) is much greater than that of the azo function (pK_a −5.1 (27)). In fact, oxidation of 4-phenylazopyridine by perbenzoic acid (17) or *m*-chloroperbenzoic acid (present work) under mild conditions occurs almost exclusively on the pyridine function to yield 4-phenylazopyridine-*N*-oxide.

Further oxidation of 4-phenylazopyridine-*N*-oxide should occur on the azo nitrogen with the greatest electron density, and this is expected to be the nitrogen adjacent to the benzene ring. The azo nitrogen adjacent to the heterocyclic ring will be depleted of electron density as a result of a field effect between this center and the N^+-O^- dipole. There could also be the possibility of a partial positive charge on this nitrogen as indicated by structure **7***a*. The nitrogen adjacent to the benzene ring could take on either partial positive charge as indicated in **7***b*, or partial negative charge as in **7***c*. Crystal structure results presented subsequently on an azoxy analogue (**11**) suggest that contribution by **7***c* should be the more likely.

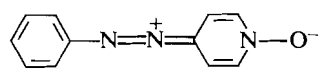

7*a*

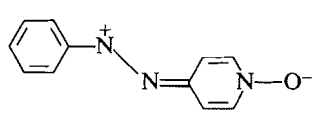

7*b*

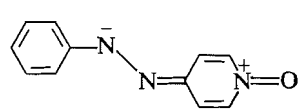

7*c*

Whereas the above considerations refer to initial state effects, one can invoke also a transition state effect which would lead to the result of preferential attack by electrophilic oxygen on the nitrogen removed from the heterocyclic ring. Thus, to the extent that the transition state structure resembles the product in its electronic configuration, there will be partial delocalization of charge as shown by **8***a* ↔ **8***b*. This type of delocalization is not possible if the nitrogen adjacent to the

Can. J. Chem. Downloaded from www.nrcresearchpress.com by 210.87.254.105 on 09/06/12
For personal use only.

Can. J. Chem. Downloaded from www.nrcresearchpress.com by 210.87.254.105 on 09/06/12
For personal use only.

TABLE 1. Melting points, analytical and uv data in ethanol for the isomeric α- and β-phenylazoxypyridine compounds

Compound	Melting point	(lit.)	Analyses								Ultraviolet	
			Calcd.				Found				λ_{max} (nm)	log ε (EtOH)
			C	H	N	I	C	H	N	I		
4-(Phenyl-α-azoxy)pyridine	87–88	(80[19])	66.33	4.52	21.11		66.08	4.62	20.98		302	3.60
											225	4.11
3-(Phenyl-β-azoxy)pyridine	67–68		66.33	4.52	21.11		66.03	4.55	20.87		329	4.13
											234	4.01
3-(Phenyl-α-azoxy)pyridine	64–65	(61–62[19])	66.33	4.52	21.11		66.12	4.49	20.94		318	4.22
											225	4.03
3-(Phenyl-β-azoxy)pyridine	80–81		66.33	4.52	21.11		66.12	4.50	20.95		326	4.09
											238	4.12
2-(Phenyl-α-azoxy)pyridine	30–31	(30–31[19])	66.33	4.52	21.11						320	4.05
											268	3.97
4-(Phenyl-α-azoxy)pyridine-*N*-oxide	144–145	(142[19])	61.40	4.18	19.53		61.05	4.22	19.30		367	4.38
											289	3.91
4-(Phenyl-β-azoxy)pyridine-*N*-oxide	146–147		61.40	4.18	19.53		61.20	4.06	19.25		349	4.38
											232	4.12
3-(Phenyl-α-azoxy)pyridine-*N*-oxide	124–126	(85–87[19])	61.40	4.18	19.53		61.39	4.17	19.60		308	4.20
											278	4.34
3-(Phenyl-β-azoxy)pyridine-*N*-oxide	134–135		61.40	4.18	19.53		60.97	3.99	19.42		331	4.17
											278	4.34
2-(Phenyl-α-azoxy)pyridine-*N*-oxide	136–137	(137–138[19])	61.40	4.18	19.53		61.37	4.29	19.71		330	3.89
											268	4.29
4-(Phenyl-α-azoxy)pyridinium methiodide	212–213 (dec.)		42.24	3.52	12.32	37.22	41.92	3.58	12.24	37.13	333	4.15
3-(Phenyl-α-azoxy)pyridinium methiodide	165–167		42.24	3.52	12.32	37.22	42.15	3.65	12.03	36.86	318	4.21
2-(Phenyl-α-azoxy)pyridinium methiodide	185–187		42.24	3.52	12.32	37.22	42.77	3.60	12.41	36.97	384	4.01

TABLE 2. Characterization of phenylazopyridinium methiodides

Compound	Yield (%)	Melting point (°C)	(lit.)	*Anal.*[a] found C	H	N	I
4-Phenylazopyridinium methiodide	93	188–189	(188[53])	43.90	3.70	13.10	39.00
3-Phenylazopyridinium methiodide	92	155–157		44.10	3.68	13.20	39.30
2-Phenylazopyridinium methiodide	86	161–162	(162–163[54])	43.90	3.68	13.10	38.96

[a]*Anal.* calcd.: C 44.30, H 3.69, N 12.90, I 39.10%.

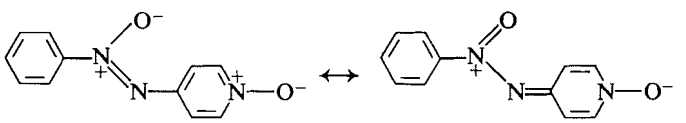

8*a* **8***b*

heterocyclic ring undergoes attack by electrophilic oxygen.

The direct field effect will increase in importance as one proceeds to 3-phenyl- and to 2-phenylazopyridine-*N*-oxides. The resonance effect, on the other hand, will operate in the latter case but not in the former. In addition to the field and resonance effects, a steric effect may also operate due to interaction between the approaching peracid molecule, especially with the more sterically demanding perbenzoic or *m*-chloroperbenzoic acids, and the protonated/solvated *N*-oxide function. This steric factor is clearly expected to be greatest in the case of the reaction of 2-phenylazopyridine-*N*-oxide, and this should serve to further decrease the availability towards oxygenation of the nitrogen site adjacent to the heterocyclic ring.

Our observations are in qualitative agreement with the above considerations, since both the 4- and 3-phenylazopyridines, on oxidation with peracetic acid, have been found to give rise predominantly to the α-phenylazoxypyridine-*N*-oxides. That oxidation occurs sequentially is indicated by the fact that the respective phenylazopyridine-*N*-oxides have been isolated in small yield in these reactions. On the other hand, the latter compounds are the major products when oxidation is performed with *m*-chloroperbenzoic acid. Reaction of 2-phenylazopyridine with peracetic acid gave rise only to 2-(phenyl-α-azoxy)-2-pyridine-*N*-oxide, indicating that in this case a combination of field and steric effects prevails, resulting in complete exclusion of the β isomer (30).

Reactivity differences of isomers in Wallach rearrangement: a novel method of isomer separation

A preliminary study has revealed an apparently unprecedented difference in the reactivities of α and β 4-phenylazoxypyridine-*N*-oxides under Wallach rearrangement conditions. In fact, under conditions that the β isomer reacted readily (95–100% H_2SO_4), to yield 4-(*p'*-hydroxyphenylazo)pyridine-*N*-oxide, no detectable rearrangement could be observed for the α isomer (31).

This observation could be utilized in the present work to separate the pure α isomers from the α,β mixtures in the case of 4- and 3-phenylazoxypyridines and their *N*-oxides. In practice, the α,β azoxy mixture was allowed to react in the acid medium until rearrangement of the β isomer was essentially complete (≥95%) and the unreacted α-azoxy isomer was isolated following work-up (see Experimental). The rearrangement products, i.e. 4(3)-(*p'*-hydroxyphenylazo)pyridines and *N*-oxides, could readily be separated by their solubility in aqueous base through formation of the azophenolate salt, leaving the unreacted α-azoxy compound in the organic phase. In each case, the α isomer thus obtained had properties identical to that of the compound obtained by hplc separation of the α,β mixture in the peracetic acid oxidation. Since α,β azoxy isomers are generally difficult to separate by normal procedures (23–25), the present method for obtaining one isomer in pure form is noteworthy, though based on serendipitous circumstances.

Structural considerations in phenylazoxypyridine series

Structural identification of the phenylazoxypyridine isomers in the work of Colonna, Risaliti, and Pentimalli (17–20) was based on the classical method first devised by Angeli (32). The principle of this method is that the $N^+—O^-$ dipole of the azoxy function "protects" the phenyl ring adjacent to $N^+—O^-$ from electrophilic attack, e.g. in bromination or nitration (33). Moreover, the pyridine ring would itself be deactivated, relative to a phenyl ring, towards electrophilic attack (34, 35).

The reaction sequence thus used by Colonna *et al.* (17) to assign the structure is shown in Scheme 1, which uses the oxidation of 3-phenylazopyridine for illustration. The finding that the product from the peracid oxidation did not undergo bromination was used as the main evidence for assignment of structure as the α isomer.

However, caution is required when applying the classical method to the present systems. Considering the possible resonance structures **9***a*, **9***b*, and **9***c*, to the extent that **9***b* would be contributing, the benzene ring would be activated towards electrophilic attack; however, contribution by **9***c* would result in deactivation. It seems reasonable that **9***c* would indeed be an important contributor, in which case compound **9** could be unreactive towards electrophilic substitution, even though it is the β isomer. This would cause the classical method to be inconclusive as a way of differentiating between α and β isomers in the phenylazoxypyridine series.

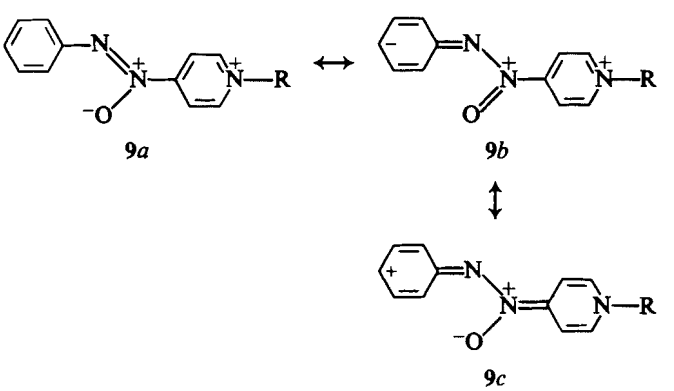

9*a* **9***b* **9***c*

One can contrast this situation and the one that obtains with 4-β-nitroazoxybenzene, which does undergo electrophilic sub-

Can. J. Chem. Downloaded from www.nrcresearchpress.com by 210.87.254.105 on 09/06/12
For personal use only.

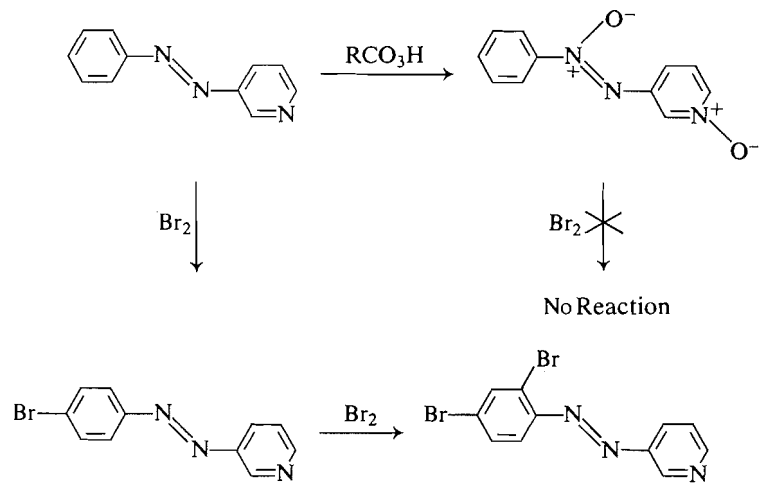

SCHEME 1

stitution. Of the analogous resonance structures **10***a*, **10***b*, and **10***c*, one would expect that contribution by **10***b* would outweigh that by **10***c*. In **10***c* the barrier to rotation about the C_4—NO_2 bond should be low, contrasting with **9***c* where the positive nitrogen pole forms part of the π-system of the hetero ring. Bromination of **10** is hence expected to occur at the benzene ring. Thus analogy between the pyridine and nitro functionalities is of limited utility in predicting reactivities of the present series of compounds.

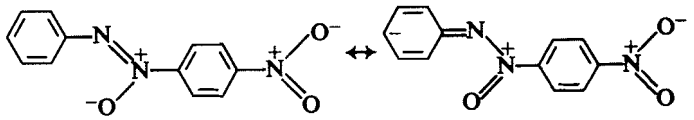

10*a* **10***b*

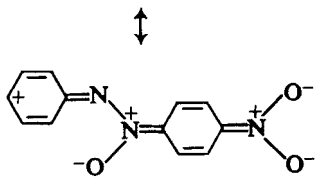

10*c*

Unequivocal structure proof in the present system can be obtained from X-ray structure determinations. This aspect of the work is described in detail in the following section, but the main conclusion can be drawn here. Structure analysis was effected for two representative compounds which could be obtained in satisfactory crystalline form, viz. 4-(phenyl-β-azoxy)pyridine-*N*-oxide (**11**) and 4-(phenyl-α-azoxy)pyridinium methiodide (**12**), the latter being obtained by deoxygenation of the corresponding *N*-oxide, followed by methylation with methyl iodide. Since the α and β phenylazoxypyridine-*N*-oxides are the precursors of the α and β phenylazoxypyridines, as well as of the corresponding pyridinium methiodides, it follows that the X-ray structure analyses provide sufficient basis for correlating the structures of the various compounds investigated in this work.

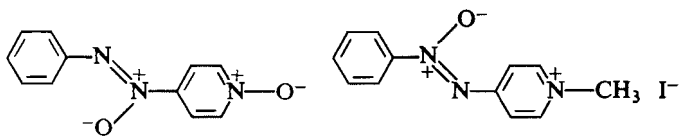

11 **12**

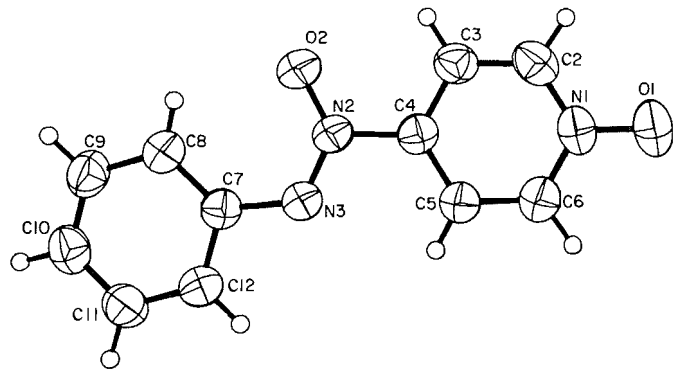

FIG. 1. The numbering system in **11**.

Results of X-ray analyses

The final atomic parameters in **11** and in **12** are listed in Tables 3 and 4, respectively. Figures 1 and 2 show the atomic numbering system in the two molecules.

The bond lengths and bond angles in **11** (mols A and B) are listed in Table 5. Since the distances appeared somewhat shorter than expected, we applied to them corrections for thermal vibration (36). The average correction was 0.007 Å (2σ) and the largest one 0.011 Å. The agreement between equivalent bond lengths in the two independent molecules A and B is excellent, both for the uncorrected and the corrected values: the average difference is 0.004 Å and the largest one 0.008 Å. Consequently, we feel justified in averaging these values, and in the subsequent discussion of this structure we will be referring to averaged corrected bond lengths. These bond lengths are also given in Table 5.

Both molecules are almost planar: the dihedral angles between six-membered rings are 5.6 and 3.6° for molecules A and B, respectively. All molecules pack in the crystal with their long axes almost parallel to *c* (Fig. 3). We note some stacking of the aromatic rings as well as some dipole–dipole interactions between adjacent N → O groups. The order of packing is −A−A−B−B− and the stacking distances between the A−A and B−B pairs are 3.14 and 3.30 Å, respectively.

The bond lengths and bond angles in **12** are listed in Table 6. Their estimated standard deviations are 2–3 times larger than in **11** owing to the presence of the heavy iodide ion. The molecules are not planar, the pyridine ring being rotated by

Can. J. Chem. Downloaded from www.nrcresearchpress.com by 210.87.254.105 on 09/06/12
For personal use only.

Can. J. Chem. Downloaded from www.nrcresearchpress.com by 210.87.254.105 on 09/06/12
For personal use only.

TABLE 3. Final atomic parameters for 4-(phenyl-β-azoxy)pyridine-*N*-oxide[a] (**11**)

Atom	*x*	*y*	*z*	U_{eq}/U
O(1A)	9220(1)	−2299(4)	45604(7)	775
O(2A)	8179(2)	2700(4)	64153(8)	816
N(1A)	9082(1)	−1579(4)	50109(8)	572
N(2A)	8599(1)	746(3)	64531(7)	502
N(3A)	8890(1)	−625(3)	68731(7)	511
C(2A)	8617(2)	474(5)	50111(9)	621
C(3A)	8460(2)	1259(4)	54790(9)	556
C(4A)	8776(1)	−82(4)	59575(9)	490
C(5A)	9252(2)	−2183(4)	59597(9)	556
C(6A)	9403(2)	−2906(4)	54817(10)	598
C(7A)	8724(1)	−84(4)	73724(8)	489
C(8A)	8272(2)	1891(4)	75010(10)	588
C(9A)	8156(2)	1995(5)	80195(11)	665
C(10A)	8488(2)	213(5)	84051(10)	637
C(11A)	8946(2)	−1721(5)	82856(10)	642
C(12A)	9064(2)	−1874(4)	77722(10)	586
O(1B)	4194(2)	−483(4)	71934(8)	851
O(2B)	3262(2)	2769(3)	92418(8)	820
N(1B)	4072(1)	−170(4)	76690(8)	609
N(2B)	3630(1)	813(3)	91912(7)	492
N(3B)	3891(1)	−865(3)	95417(7)	482
C(2B)	3639(2)	1798(5)	77646(10)	665
C(3B)	3487(2)	2144(4)	82590(10)	596
C(4B)	3787(1)	423(4)	86669(8)	483
C(5B)	4230(2)	−1598(4)	85706(9)	565
C(6B)	4375(2)	−1842(5)	80711(10)	624
C(7B)	3743(1)	−740(4)	100590(8)	472
C(8B)	3293(2)	1041(4)	102574(10)	564
C(9B)	3192(2)	766(5)	107737(11)	659
C(10B)	3530(2)	−1215(5)	110967(10)	633
C(11B)	3973(2)	−2978(5)	109007(10)	617
C(12B)	4080(2)	−2764(4)	103868(9)	563
H(2A)	843(2)	132(5)	467(1)	72(7)
H(3A)	814(2)	270(5)	548(1)	65(6)
H(5A)	945(2)	−316(5)	627(1)	61(6)
H(6A)	974(2)	−432(6)	546(1)	81(9)
H(8A)	808(2)	316(5)	726(1)	57(6)
H(9A)	785(2)	334(6)	811(1)	86(9)
H(10A)	837(2)	29(5)	875(1)	70(7)
H(11A)	918(2)	−296(6)	857(1)	82(9)
H(12A)	937(2)	−319(5)	768(1)	63(6)
H(2B)	344(2)	288(5)	748(1)	72(7)
H(3B)	319(2)	353(6)	833(1)	80(9)
H(5B)	448(2)	−279(6)	886(1)	79(9)
H(6B)	473(2)	−313(5)	800(1)	66(7)
H(8B)	309(2)	250(5)	1005(1)	60(6)
H(9B)	290(2)	204(5)	1091(1)	72(7)
H(10B)	346(2)	−136(5)	1145(1)	67(7)
H(11B)	418(2)	−439(6)	1111(1)	76(7)
H(12B)	437(2)	−395(5)	1023(1)	62(6)

[a]The *z* coordinates of the nonhydrogen atoms were multiplied by 10^5, their other parameters by 10^4. All hydrogen atom parameters were multiplied by 10^3.

TABLE 4. Final atomic parameters for 4-(phenyl-α-azoxy)pyridinium methiodide (**12**)

Atom	*x*	*y*	*z*	U_{eq}/U
I(1)	0.24413(4)	0.21319(3)	0.17571(3)	0.0459
O(1)	0.0824(7)	0.3312(4)	0.7487(4)	0.056
N(1)	0.2412(6)	−0.2036(4)	0.8593(5)	0.038
N(2)	0.2866(6)	0.2409(4)	0.5785(8)	0.040
N(3)	0.1998(6)	0.3457(5)	0.6212(5)	0.042
C(1)	0.2329(10)	−0.3648(6)	0.9513(8)	0.052
C(2)	0.2642(8)	−0.1549(6)	0.7088(6)	0.048
C(3)	0.2762(8)	−0.0075(5)	0.6195(6)	0.041
C(4)	0.2564(7)	0.0942(6)	0.6849(5)	0.037
C(5)	0.2311(8)	0.0409(6)	0.8443(6)	0.048
C(6)	0.2239(8)	−0.1105(6)	0.9273(7)	0.050
C(7)	0.2402(7)	0.4948(5)	0.5069(5)	0.037
C(8)	0.3739(8)	0.5151(5)	0.3652(5)	0.044
C(9)	0.4132(8)	0.6598(6)	0.2608(6)	0.051
C(10)	0.3174(11)	0.7779(6)	0.2953(8)	0.054
C(11)	0.1827(10)	0.7560(7)	0.4306(8)	0.061
C(12)	0.1417(9)	0.6132(6)	0.5429(7)	0.051
H(21)	0.274(8)	−0.230(8)	0.672(7)	0.050(16)
H(31)	0.286(8)	0.032(6)	0.504(5)	0.058(16)
H(51)	0.207(10)	0.110(7)	0.894(8)	0.065(19)
H(61)	0.231(7)	−0.148(5)	1.030(6)	0.030(11)
H(81)	0.433(4)	0.417(4)	0.354(4)	0.041(10)
H(91)	0.487(10)	0.669(9)	0.156(10)	0.083(20)
H(101)	0.361(8)	0.870(7)	0.226(7)	0.043(14)
H(111)	0.109(10)	0.834(7)	0.455(10)	0.083(22)
H(121)	0.048(8)	0.608(5)	0.625(6)	0.032(12)
H(11)	0.291(9)	−0.382(7)	0.831(8)	0.054(16)
H(12)	0.096(8)	−0.379(6)	0.991(6)	0.040(13)
H(13)	0.325(14)	−0.392(11)	1.024(12)	0.094(29)

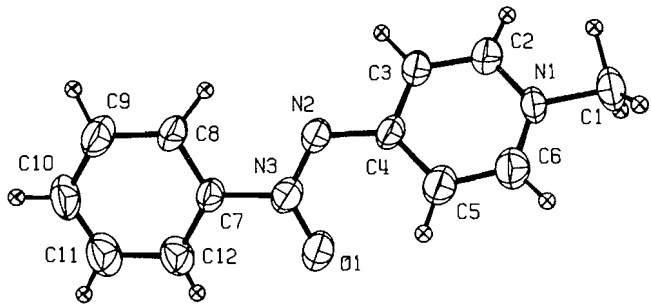

FIG. 2. The numbering system in **12**.

about 37° from the phenylazoxy group. The packing of the molecules in the crystal is shown in Fig. 4. Phenyl rings and azoxy groups are stacked parallel to each other at a distance of 3.48 Å, giving rise to considerable overlap.

Discussion of crystal structures

Bond lengths

No crystal structure of a phenylazoxypyridine has yet been reported in the literature, but derivatives of azobenzene and azoxybenzene have been studied. Among the latter are several *trans* (37–40) and one *cis* isomer (41) (structures **13**–**17**). Some of the authors have compiled geometrical details of the azoxy group in previously determined structures and attempted to interpret them (40, 41). Such attempts have been generally unsuccessful owing to the low precision or low accuracy of some of the structure determinations. In particular, the two earliest studies, those of *p*-azoxyanisole (37) and ethyl *p*-

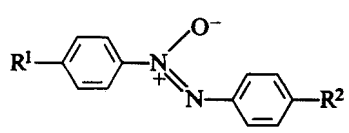

13 $R^1 = R^2 = OCH_3$
14 $R^1 = R^2 = CO_2C_2H_5$
15 $R^1 = N(CH_3)_2$, $R^2 = H$
16 $R^1 = R^2 = O(CH_2)_6CH_3$

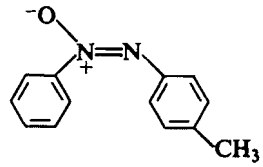

17

Can. J. Chem. Downloaded from www.nrcresearchpress.com by 210.87.254.105 on 09/06/12
For personal use only.

TABLE 5. Bond lengths (Å) and bond angles (deg) in **11**[a]

Bond	Length			Bonds	Angle	
	Mol. A	Mol. B	Corr.[b]		Mol. A	Mol. B
N(1)—O(1)	1.299	1.298	1.302	O(1)—N(1)—C(2)	120.4	120.7
N(1)—C(2)	1.349	1.347	1.357	O(1)—N(1)—C(6)	119.7	119.7
C(2)—C(3)	1.365	1.368	1.371	C(2)—N(1)—C(6)	119.9	119.6
C(3)—C(4)	1.374	1.379	1.387	N(1)—C(2)—C(3)	121.4	121.7
C(4)—C(5)	1.379	1.381	1.389	C(2)—C(3)—C(4)	119.2	118.7
C(5)—C(6)	1.374	1.369	1.376	C(3)—C(4)—C(5)	119.7	119.8
C(6)—N(1)	1.355	1.351	1.363	C(4)—C(5)—C(6)	119.7	119.1
C(4)—N(2)	1.453	1.450	1.455	C(5)—C(6)—N(1)	120.4	121.1
N(2)—O(2)	1.254	1.258	1.265	C(3)—C(4)—N(2)	119.1	118.4
N(2)—N(3)	1.270	1.266	1.274	C(5)—C(4)—N(2)	121.3	121.8
N(3)—C(7)	1.410	1.411	1.415	C(4)—N(2)—O(2)	116.8	116.2
C(7)—C(8)	1.398	1.396	1.406	C(4)—N(2)—N(3)	115.2	115.4
C(8)—C(9)	1.391	1.383	1.391	O(2)—N(2)—N(3)	128.1	128.4
C(9)—C(10)	1.373	1.376	1.382	N(2)—N(3)—C(7)	120.7	120.9
C(10)—C(11)	1.375	1.379	1.386	N(3)—C(7)—C(8)	129.2	128.6
C(11)—C(12)	1.382	1.378	1.384	N(3)—C(7)—C(12)	111.7	112.2
C(12)—C(7)	1.399	1.401	1.408	C(12)—C(7)—C(8)	119.1	119.2
				C(7)—C(8)—C(9)	118.9	119.2
				C(8)—C(9)—C(10)	120.4	121.5
				C(9)—C(10)—C(11)	120.4	119.4
				C(10)—C(11)—C(12)	119.6	120.6
				C(11)—C(12)—C(7)	119.1	120.2

[a]The esd's are 0.003–0.004 Å and 0.17–0.26°.
[b]Averages for molecules A and B after correction for thermal vibration.

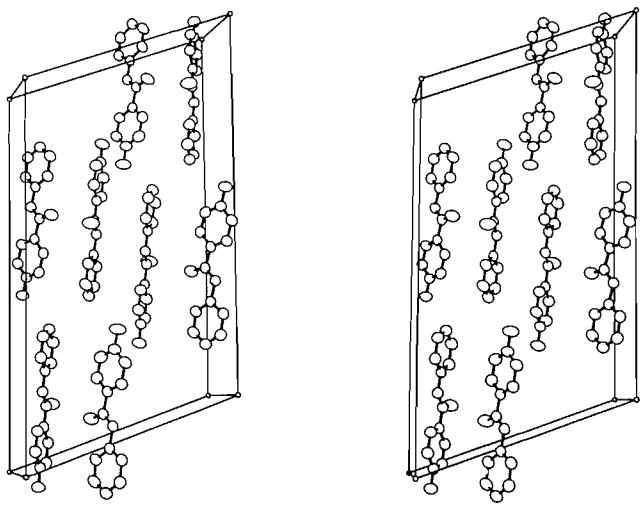

FIG. 3. Packing diagram of **11**. The directions of the axes are $a \leftarrow$, $b \odot$, $c \uparrow$. Bonds in molecule A are shaded.

azoxybenzoate (38), produced results which were incompatible with subsequent X-ray analyses: the C—N(O) bonds were unusually long (1.496, 1.570 Å) while the N(O)=N bonds were unusually short (1.218, 1.155 Å). However, a critical reading of these publications reveals several disturbing details: the *R* values (9.1 and 9.3%) were rather high, considering that the data had been collected on a diffractometer; in the *p*-azoxyanisole structure the final difference Fourier map showed two extraneous peaks, indicating the possibility of disorder; in both structures there were atoms with unusually high and (or) low temperature parameters, but no corrections were made for thermal vibration. In view of these facts, we feel justified in ignoring the distances found in these two structure analyses.

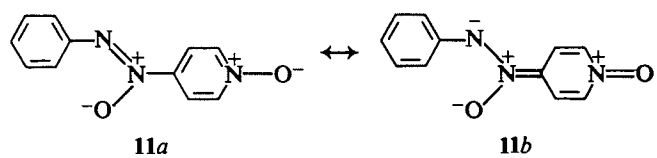

11*a* **11***b*

The bond lengths in the azoxy group (Table 7) can now be interpreted on the basis of substitution and electron delocalization. The N=N bond lengths (1.26–1.28 Å) are intermediate between those found in azobenzenes (1.23–1.25 Å) and those in diazoxy compounds (1.31–1.32 Å) in which both nitrogen atoms carry an oxygen (42). Similarly, the C—N(O) bond length in azoxy groups is 1.44–1.47 Å while the C—N bonds are in the 1.41–1.43 Å range, both in azo- (43) and in azoxybenzenes (39–41). No N—O bonds deviate significantly from the average observed value of 1.266 Å.

The bond lengths in **11** indicate a significant contribution of a quinonoid resonance form to the structure. This is borne out by a comparison of the bond lengths in the pyridine *N*-oxide moiety with the results of the highly precise, low-temperature (30 K) X-ray analysis of *p*-nitropyridine *N*-oxide (44). With the exception of the somewhat short N(1)—C(2) value of 1.357 Å, all bond lengths in the two structures agree within 0.007 Å (2σ). In both structures the C—C bonds parallel to the molecular axis are significantly shorter than the other C—C ring bonds. In *p*-nitropyridine *N*-oxide (**18**) there will be similar charge delocalization, with contribution by the resonance form **18***b*.

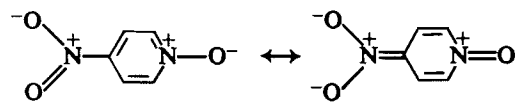

18*a* **18***b*

TABLE 6. Bond lengths (Å) and bond angles (deg) in **12**

(a) Bond lengths

Bond	Length	Bond	Length	Bond	Length
N(1)—C(2)	1.343(7)	N(1)—C(1)	1.479(7)	C(7)—C(8)	1.396(7)
C(2)—C(3)	1.363(8)	N(2)—C(4)	1.406(7)	C(8)—C(9)	1.393(8)
C(3)—C(4)	1.383(7)	N(2)—N(3)	1.281(6)	C(9)—C(10)	1.374(9)
C(4)—C(5)	1.420(8)	N(3)—O(1)	1.255(6)	C(10)—C(11)	1.352(11)
C(5)—C(6)	1.385(9)	N(3)—C(7)	1.454(7)	C(11)—C(12)	1.403(10)
C(6)—N(1)	1.330(7)			C(12)—C(7)	1.390(7)

(b) Bond angles

Bonds	Angle	Bonds	Angle
C(1)—N(1)—C(2)	118.9(5)	N(2)—N(3)—O(1)	126.4(4)
C(1)—N(1)—C(6)	119.5(5)	N(2)—N(3)—C(7)	115.4(4)
C(2)—N(1)—C(6)	121.6(4)	O(1)—N(3)—C(7)	118.2(4)
N(1)—C(2)—C(3)	120.7(5)	N(3)—C(7)—C(8)	119.7(4)
C(2)—C(3)—C(4)	119.9(5)	N(3)—C(7)—C(12)	118.2(5)
C(3)—C(4)—C(5)	118.6(5)	C(12)—C(7)—C(8)	122.1(5)
C(4)—C(5)—C(6)	118.2(5)	C(7)—C(8)—C(9)	117.9(5)
C(5)—C(6)—N(1)	120.9(5)	C(8)—C(9)—C(10)	120.6(6)
C(3)—C(4)—N(2)	113.9(4)	C(9)—C(10)—C(11)	120.7(6)
C(5)—C(4)—N(2)	127.4(4)	C(10)—C(11)—C(12)	121.5(7)
C(4)—N(2)—N(3)	118.2(4)	C(11)—C(12)—C(7)	117.2(6)

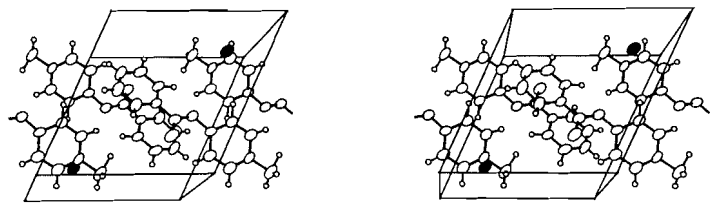

FIG. 4. Packing diagram of **12**. The directions of the axes are a ⊙, b →, c ↑. The iodide ion is shaded.

The bond lengths in the phenyl ring also differ from normal values. Near the substituted atom the bonds are longer than usual, but further away from it they are significantly shorter. This is a clear indication of the inductive effect of the substituent which causes the σ electrons to be displaced away from the substituted carbon atom (45).

A quinonoid resonance form might at first sight be expected to contribute to the structure of **12** as well. However, in view of the rotation of the pyridine ring from the phenylazoxy group (see above), that contribution cannot be very large. This can be attributed to the fact that structure **12***b* does not contain the

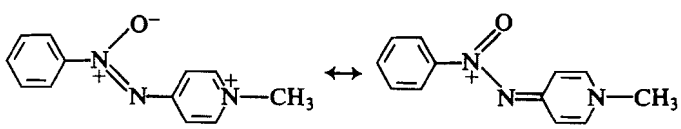

12*a* **12***b*

stabilizing features associated with the quinonoid moiety of **11***b* or **18***b*, namely delocalization of the negative charge onto two electronegative atoms (O, N in **11***b*; O, O in **18***b*). Although the lower precision of the results obtained with **12** precludes a rigorous analysis, we can state that the observed bond lengths agree qualitatively with expected values.

C—H···O and C—H···N bonds

In their discussion of the structure of *p*-azoxyanisole, Krigbaum *et al.* (37) noted the short distances (2.27 and 2.31 Å) between the oxygen atom of the azoxy group and the hydrogen atoms H_B and H_C, respectively (Fig. 5). Nevertheless, they found "little evidence for the existence of hydrogen bonds" between these atoms. Other authors (39, 40) have not commented on short H···O distances. There is no doubt, however, that intramolecular C—H···O and C—H···N bonds are common features in molecules in which two aromatic rings are attached to a *trans* azoxy group. In a recent review of 113 crystal structures determined by neutron diffraction, Taylor and Kennard (46) cite 59 (C—)H···O contacts ≤2.400 Å, i.e. at least 0.3 Å shorter than the sum of the van der Waals radii of hydrogen and oxygen, as well as 11 (C—)H···N contacts with H···N distances in the range of 2.522–2.721 Å. In intramolecular hydrogen bonds the C—H···O angles were in the range 90.7–155.7°. These results, and the conclusions based on them, are highly significant since hydrogen atom coordinates obtained from neutron diffraction studies are ~10 times more precise than those obtained from X-ray analyses. On the other hand, it has been shown (47) that very reliable information about the geometry of a hydrogen bond can be obtained even from an X-ray analysis if one extends an observed O—H bond length to the real distance known from neutron diffraction (0.97 Å). Using corrected values of 1.09 Å for C(ar)—H bonds (48), we calculated H···O and H···N distances as well as C—H···O and C—H···N angles in our structures, as well as in previously determined crystal structures of azoxybenzenes.

Can. J. Chem. Downloaded from www.nrcresearchpress.com by 210.87.254.105 on 09/06/12
For personal use only.

TABLE 7. Geometry of azoxyarenes[a]

Parameters	**11**[b]	**12**	**15**	**16**	**17**
C—N(O)	1.455(2)	1.454(7)	1.441(9)	1.458(2)	1.470(2)
N—O	1.265(2)	1.255(6)	1.275(8)	1.266(2)	1.264(2)
N=N	1.274(2)	1.281(6)	1.262(8)	1.257(2)	1.265(2)
N—C	1.415(2)	1.406(7)	1.414(9)	1.420(2)	1.427(3)
$H_A \cdots N$	2.44	2.39	2.43	2.28	—
$H_B \cdots O$	2.33	2.40	2.44	2.35	—
$H_C \cdots O$	2.14	2.33	2.26	2.21	—
α	121.5(2)	119.7(4)	120.3(8)	122.0(2)	119.0(5)
β	118.7(2)	118.2(5)	119.8(8)	118.6(2)	118.3(5)
γ	115.3(2)	115.4(4)	118.4(7)	115.4(2)	125.0(5)
δ	116.5(2)	118.2(5)	114.5(7)	117.1(2)	114.3(5)
ϵ	128.2(2)	126.4(4)	126.8(7)	127.5(2)	120.5(5)
ζ	120.8(2)	118.2(4)	118.8(7)	120.2(2)	119.2(5)
η	112.0(2)	113.9(4)	120.3(8)	113.0(2)	123.4(5)
θ	128.9(2)	127.4(4)	119.8(8)	129.8(2)	116.5(5)
ι	93	94	95	104	—
κ	97	94	90	96	—
λ	114	103	107	108	—

[a]See Fig. 5 for definitions. All C(ar)—H bonds normalized to 1.09 Å.
[b]Averages of molecules A and B after corrections for thermal vibration.

The results, listed in Table 7, show that the distances and angles are in very good agreement with those found by Taylor and Kennard (46). It will be noted that all protons participating in these intramolecular hydrogen bonds are bonded to carbon atoms which are *ortho* to the azoxy group. We should also point out that we found *intermolecular* C—H···O bonds involving *ortho* carbon atoms in *cis*-azobenzene dioxide (42) and in *cis*-4-(phenyl-α-azoxy)toluene (41). The electron density at these carbon atoms is decreased owing to the inductive effect of the adjacent nitrogen (see above) which enhances their ability to act as proton donors. Thus, it was found (46) that in *p*-nitropyridine *N*-oxide a carbon atom *ortho* to the nitro group participates in a fairly strong hydrogen bond (H···O 2.145 Å). Another C—H···O bond found in that structure involves a carbon atom *ortho* to the positively charged ring nitrogen. Such carbons are especially likely to form C—H···X bonds (46), and in the crystal structure of **11** we observe that in each independent molecule C(6) donates its proton to O(1) in another molecule. The H···O distances are 2.34 and 2.13 Å and the C—H···O angles are 173 and 165°, respectively.

Bond angles and torsion angles

The geometry of *trans*-azoxyarenes reveals various distortions of bond angles which are necessary in order to avoid excessively short nonbonded interatomic contacts. An indication of the crowding is the H···O and H···N distances in the intramolecular hydrogen bonds. Of the 59 (C—)H···O contacts listed by Taylor and Kennard (46), 56 are longer than the $H_C \cdots O$ distance of 2.14 Å in **11** (Table 7) and about half are longer than 2.33 Å, the $H_B \cdots O$ distance. Moreover, none of the (C—)H···N distances listed there is as short as the $H_A \cdots N$ distances in Table 7. An inspection of the bond angles in Table 7 enables us to formulate several observations about *trans*-azoxyarenes. The sums (α + γ) and (β + δ) are approximately 236° each, but the former is usually somewhat larger, reflecting the fact that the van der Waals radius of N is slightly larger than that of O. Since in all cases the aromatic ring attached to N(O) is more or less in the plane of the azoxy group, these sums have to be balanced in order to prevent either N or O from being too close to one of the *ortho* hydrogen atoms. The $H_C \cdots O$ distance

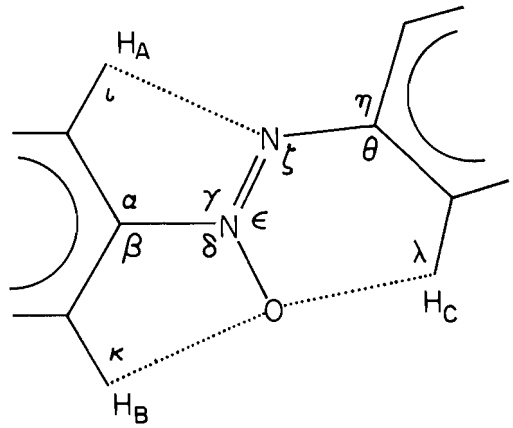

FIG. 5. Geometry of azoxyarenes.

would be prohibitively short if not for a rotation of the aromatic ring about the N—C bond (0–36.5°, Table 8) and for an increase of ϵ vs. γ and θ vs. η. Table 8 shows that in most structures the two aromatic rings are not coplanar; this is probably attributable to the fact that rotation about a bond is energetically more favourable than distortion of a bond angle. The exact planarity of **14** probably reflects a higher contribution of the quinonoid structure which results from a delocalization of electrons to the carbonyl oxygen of the ester group.

It is well known that bond angles in aromatic rings are affected by ring substitution. These distortions, caused by withdrawal or release of π and (or) σ electrons, have been compiled for various substituents (49) but not for an azoxy group. We note, however, that in the phenyl ring of **11** the deviations from 6/*mmm* symmetry agree qualitatively with those calculated for an N=NR substituent. In the structure of **12** the angular distortions are larger and fairly similar to those caused by an NO_2 substituent. We can also derive the distortion effect of an N(O)=N(C_6H_5) substituent by subtracting the known corrections due to an NO_2 group (49*b*) from the angles found in *p*-nitropyridine *N*-oxide (44). This gives us the angles in unsubstituted pyridine *N*-oxide, and the difference between

Can. J. Chem. Downloaded from www.nrcresearchpress.com by 210.87.254.105 on 09/06/12
For personal use only.

TABLE 8. Torsion angles in *trans*-azoxyarenes

Azoxyarene	C—C—N(O)=N	C—N(O)=N—C	N(O)=N—C—C
11 mol. A	−1.7	177.1	−1.5
mol. B	−2.8	177.5	2.4
12	−3.3	178.8	−36.5
13	−3.6	175.8	−20.1
14	−0.8	180.0	0.0
15	2.1	177.9	31.3
16	3.1	179.8	10.0

them and the angles in the pyridine ring in **11** yields the following corrections for N(O)=N(C_6H_5): +1.3, −1.0, +0.3, and +0.4° for the *ipso*, *ortho*, *meta*, and *para* atoms, respectively. The correlation between the first two values is exactly as calculated by Domenicano and Murray-Rust (49*a*).

One of the most interesting differences between the crystal structures of the α- and β-azoxy isomers is that whereas in the β compound **11** the pyridine ring and the benzene ring are practically coplanar, in the α compound **12** the two rings deviate appreciably from coplanarity (see Table 8). It was noted also that the bond lengths found in **11** were indicative of significant contribution by the quinonoid resonance forms **11***b*. It follows on inspection of the structure **11***b* that the negative charge on the azo nitrogen will be further delocalized over the benzene ring, implying coplanarity between the latter and the pyridine ring, as found experimentally. However, in the case of **12**, contribution via the quinonoid form **12***b* was not considered to be important. The deviation from coplanarity of the two rings in the case of **12** would then result from the short N···H and O···H contacts, which appear to be characteristic of *trans*-azoxyarenes in general (Table 7 and Fig. 5).

Experimental

Melting points were determined on a Fisher–Johns block and are uncorrected. The uv spectra were taken on a Beckman DU-8 spectrophotometer. Column chromatography was carried out using basic alumina (Sigma). The hplc separations were performed using silica gel columns (Merck) fitted to a fluid metering pump, pulse dampener (FMI), uv detector, and fractionator (Gilson).

Aminopyridines (Aldrich) were used as received. 30% H_2O_2 was procured from Mallinckrodt. Nitrosobenzene was prepared by the method of Vogel (50), kept in a dry box, and sublimed before use.

Phenylazopyridines

The 4-, 3-, and 2-phenylazopyridines were prepared by condensation of nitrosobenzene with 4-, 3-, and 2-aminopyridine, respectively, according to the procedure of Brown and Grammeman (51) and purified by column chromatography with benzene as eluent. Recrystallization from hexane yielded 4-phenylazopyridine, mp 97–98°C (lit. (19) mp 98–99°C); 3-phenylazopyridine, mp 51–52°C (lit. (19) mp 53–54°C); and 2-phenylazopyridine, mp 32–34°C (lit. (19) mp 32°C).

m-*Chloroperbenzoic acid oxidation of phenylazopyridines*

Oxidation of 4-, 3-, and 2-phenylazopyridine by the method of Badger and Lewis (52) using *m*-chloroperbenzoic acid yielded the 4-, 3-, and 2-phenylazopyridine-*N*-oxides. The reaction products were purified by column chromatography eluting with ethyl acetate/methylene chloride, and recrystallized from hexane yielding 4-phenylazopyridine-*N*-oxide, mp 149–150°C (lit. (19) mp 150°C); 3-phenylazopyridine-*N*-oxide, mp 86–88°C (lit. (19) mp 87–88°C); and 2-phenylazopyridine-*N*-oxide, mp 108–109°C (lit. (19) mp 109–110°C).

Peracetic acid oxidation of phenylazopyridines

2-Phenylazopyridine, on reaction with H_2O_2/glacial acetic acid following the method of Colonna, Risaliti, and Pentimalli (17–19), gave, after column chromatography and recrystallization from ethanol, yellow crystals of 2-(phenyl-α-azoxy)pyridine-*N*-oxide, mp 136–137°C (lit. (19) mp 137–138°C), and a small quantity of 2-phenylazopyridine-*N*-oxide.

Oxidation of 4- and 3-phenylazopyridines yielded small amounts of phenylazopyridine-*N*-oxides and mixtures of the α and β phenylazoxypyridine-*N*-oxides. The latter were separated by hplc using toluene/ethyl acetate/methanol (4:2:1) as the eluent solvent mixture and monitoring the separation by tlc. The α,β mixture of 4-phenylazoxypyridine-*N*-oxides (3.00 g) yielded 1.50 g of pure 4-(phenyl-α-azoxy)pyridine-*N*-oxide, mp 144–145°C (lit. (19) mp 142°C), and 0.85 g of pure 4-(phenyl-β-azoxy)pyridine-*N*-oxide, mp 146–147°C. Similarly, 5.50 g of the α,β mixture of 3-phenylazoxypyridine-*N*-oxides yielded 3.14 g of pure 3-(phenyl-α-azoxy)pyridine-*N*-oxide, mp 124–126°C (lit. (19) mp 85–87°C), and 1.05 g of pure 3-(phenyl-β-azoxy)pyridine-*N*-oxide, mp 134–135°C. Based on the recovered yields, the product ratios in the oxidation are calculated as: 4-phenylazoxypyridine-*N*-oxide, α/β ≃ 2:1; 3-phenylazoxypyridine-*N*-oxide, α/β ≃ 3:1.

Phenylazoxypyridines

The 4-, 3-, and 2-phenylazoxypyridine-*N*-oxides obtained as above were selectively deoxygenated on the *N*-oxide function with phosphorus trichloride according to the procedure of Pentimalli (19). The products, recrystallized from petroleum ether, had the mp values: 4-(phenyl-α-azoxy)pyridine, 87–88°C (lit. (19) mp 80°C); 4-(phenyl-β-azoxy)pyridine, 67–68°C; 3-(phenyl-α-azoxy)pyridine, 64–65°C (lit. (19) mp 59–61°C); 3-(phenyl-β-azoxy)pyridine, 80–81°C; 2-(phenyl-α-azoxy)pyridine, 30–31°C (lit. (19) mp 30–31°C).

Phenylazoxypyridinium methiodides

Methylation of the phenylazoxypyridines with methyl iodide yielded the pyridinium methiodides. As one example of the procedure, a solution of 2-(phenyl-α-azoxy)pyridine (1.80 g) in 30 mL ethanol was heated under reflux with 5.0 g methyl iodide for 5 h. The red crystals obtained on cooling were recrystallized from ethanol to yield 1.85 g of 2-(phenyl-α-azoxy)pyridinium methiodide, mp 185–187°C.

Phenylazopyridinium methiodides

These were obtained in 86–93% yield by methylation of the phenylazopyridines as described above. The characteristics of the products and analytical data are given in Table 2.

Isolation of α isomers from Wallach rearrangement of α,β azoxy mixtures

The isolation of 3-(phenyl-α-azoxy)pyridine following reaction of the mixture of α,β isomers in 99.5% H_2SO_4 is described as a representative example. The sample used was obtained by deoxygenation (PCl_3) of an α,β mixture of 3-phenylazoxypyridine-*N*-oxides resulting from the peracetic acid oxidation of 3-phenylazopyridine and originated prior to use of the hplc method for isomer separation.

The α,β mixture of 3-phenylazoxypyridines (0.070 g) was dissolved in 300 mL of preheated (50°C) 99.47% H_2SO_4 in a round-bottom flask, which was wrapped in aluminum foil and placed in a thermostatted bath at 50°C. After 20 min, corresponding to >95% reaction for the β isomer, the solution was cooled to 0°C, diluted 10-fold with water while keeping the temperature below 5°C, and transferred to a liquid–liquid extractor containing 400 mL of methyl-

Can. J. Chem. Downloaded from www.nrcresearchpress.com by 210.87.254.105 on 09/06/12
For personal use only.

Can. J. Chem. Downloaded from www.nrcresearchpress.com by 210.87.254.105 on 09/06/12
For personal use only.

ene chloride. After extraction had proceeded for 20 h, the CH_2Cl_2 solution was concentrated to 100 mL and extracted with 1 *N* NaOH in a separatory funnel. The basic extract was carefully neutralized with 1 *N* HCl which caused the hydroxyazo product to precipitate. The solid material was filtered and recrystallized from ethanol, yielding 3-(*p'*-hydroxyphenylazo)pyridine, mp 220–221°C. The CH_2Cl_2 solution from the extraction was dried ($MgSO_4$), evaporated to dryness, and the residue dissolved in 20 mL of methanol/ethyl acetate/toluene (1:2:4). Development on a preparative tlc plate and recrystallization of the product thus obtained from petroleum ether yielded the 3-(phenyl-α-azoxy)pyridine, mp 64–65°C.

X-ray analysis of ***11***

Crystals are yellowish in color and the one chosen for data collection was a rectangular parallelopiped with dimensions 0.075 × 0.17 × 0.5 mm. All X-ray measurements were carried out on a CAD-4 diffractometer. Systematic absences indicated the space group to be $P2_1/c$. The unit cell dimensions were obtained from a least-squares refinement of the angular settings of 24 reflections with 2θ values between 80° and 90°. The volume and the density indicated that there are two molecules per asymmetric unit.

$C_{11}H_9N_3O_2$ mw = 215.2

Monoclinic, space group $P2_1/c$, a = 14.984(1), b = 5.627(1), c = 25.484(1) Å, β = 109.93(1)°, Z = 8, D_m = 1.41, D_c = 1.415 g cm^{-3} (21°C), CuKα$_1$, λ = 1.54051, CuKα$_2$, λ = 1.54433 Å, F(000) = 896, V = 2019.8 Å^3, μ = 8.5 cm^{-1}.

The density was measured by flotation in a mixture of bromobenzene and chlorobenzene.

A total of 4136 unique reflections (2θ < 150°) was measured (ω–2θ scan) with Ni-filtered CuKα radiation. Three standard reflections were monitored at regular intervals; their intensities did not show any systematic changes. Of the measured reflections, 2484 had intensities greater than 2σ(I) and were considered observed. The structure was solved by direct methods with the aid of the program MULTAN (55) and refined by block-diagonal least squares. Sixteen hydrogens were located on a difference map and the remaining two from stereochemical considerations. Hydrogen parameters were refined isotropically while those for nonhydrogen atoms were refined using anisotropic thermal parameters. All C—H bonds were in the range 0.92–0.97 Å. The quantity minimized in the refinements was $w(|F_o| - |F_c|)^2$ where $w = [(12/|F_o|) \sin\theta]^{1/2}$ for $|F_o| < 12$ and $w = [(|F_o|/12) \sin\theta]^{1/2}$ for $|F_o| > 12$.

During the final stages of the refinement it was noticed that five reflections (400, 410, 112, 211, and 217) were seriously affected by extinction and they were given zero weights in the least-squares calculations. The final R and R_w are 0.041 and 0.045 for the 2479 reflections used in the least-squares refinement. All scattering factors were taken from ref. 56 and all calculations, apart from MULTAN 78 (55), were carried out with programs written by Ahmed *et al.* (57). Lists of anisotropic temperature parameters and of observed and calculated structure factors are available.[3]

X-ray analysis of ***12***

Red prisms were obtained from ethanol solution. They belong to the triclinic space group $P\bar{1}$. The crystal data are as follows:

$[C_{12}H_{12}N_3O]^+ I^-$ fw = 313.14

$P\bar{1}$, a = 7.477(1), b = 9.939(1), c = 10.073(1) Å, α = 65.39(1), β = 70.38(1), γ = 79.92(1)°, V = 640.51 Å^3, Z = 2, D_c = 1.62 g cm^{-3}, λ(CuKα) = 1.54178 Å, μ(CuKα) = 198.7 cm^{-1}.

A crystal with dimensions 0.11 × 0.26 × 0.28 mm was used for data collection. A total of 1756 independent reflections with 2θ < 128° were measured on a Syntex $P2_1$ diffractometer, using Ni-filtered CuKα radiation. The ω/2θ scan technique was employed with the scan width Δ(2θ) = (1.6 + 0.28 tan θ)° and the scan speed varying in the range 2.0 to 10.0°/min. Three reflections were monitored every 60 reflections and were used for appropriate scaling. Of the measured reflections, 1718 were above the threshold of 2.5σ(I_{net}). The intensities were corrected for Lorentz and polarization factors. An absorption correction was calculated analytically and first checked on several reflections, randomly distributed in the reciprocal space, for which the intensities were measured over the full range of ψ angles (every 10°). After applying the correction, the intensities of these reflections were scattered by less than 5% from their mean values. The absorption correction for all measured data varied in the range 0.047 to 0.252.

The position of the iodine atom was derived from a Patterson map. The Fourier map, calculated with phases from the iodine atom, revealed all nonhydrogen atoms. The structure was refined by the full-matrix least-squares procedure with first isotropic and later anisotropic temperature factors. All hydrogen atoms were located on a difference map and were included in the refinement with isotropic temperature factors. Three reflections with low θ angles and large $|F_o|$ were affected by extinction and were given zero weight in the refinement. The weighting scheme $w^{-1} = \sigma^2_{stat}(F) + k^2F_o^2$, with k = 0.0035, was used in the last few cycles of refinement. At convergence the residual indices were: R = 0.0432 and R_w = 0.0614. The average parameter shift in the last cycle of the refinement was 0.08 and the maximum was 0.42.

All scattering factors were taken from ref. 56 and all calculations were performed with the program SHELX (58). Lists of anisotropic temperature parameters and of observed and calculated structure factors are available.[3]

[3]These lists may be obtained at a nominal charge from the Depository of Unpublished Data, CISTI, National Research Council of Canada, Ottawa, Ont., Canada K1A 0S2.

Acknowledgements

We thank the Natural Sciences and Engineering Research Council of Canada for support of this work via an operating grant (E.B.) and a scholarship (S.R.K.). Discussions with Dr. N. J. Bunce are also acknowledged.

1. E. BUNCEL. Acc. Chem. Res. **8**, 132 (1975).
2. R. A. COX and E. BUNCEL. J. Am. Chem. Soc. **97**, 1871 (1975).
3. R. A. COX, A. DOLENKO, and E. BUNCEL. J. Chem. Soc. Perkin Trans. 2, 471 (1975).
4. D. L. H. WILLIAMS and E. BUNCEL. *In* Cationic aromatic rearrangements. Isotopes in organic chemistry. Vol. 5. *Edited by* E. Buncel and C. C. Lee. Elsevier, Amsterdam. 1980.
5. P. H. GORE. Chem. Ind. (London), 191 (1959).
6. C. S. HAHN and H. H. JAFFÉ. J. Am. Chem. Soc. **84**, 946 (1962).
7. C. S. HAHN, K. W. LEE, and H. H. JAFFÉ. J. Am. Chem. Soc. **89**, 4975 (1967).
8. D. DUFFEY and E. C. HENDLEY. J. Org. Chem. **33**, 1918 (1968).
9. D. DUFFEY and E. C. HENDLEY. J. Org. Chem. **35**, 3579 (1970).
10. I. SHIMAO, K. FUJIMORI, and S. OAE. Bull. Chem. Soc. Jpn. **55**, 546 (1982).
11. I. SHIMAO and S. OAE. Bull. Chem. Soc. Jpn. **56**, 643 (1983).
12. J. YAMAMOTO, H. AIMI, Y. MASUDA, T. SUMIDA, M. UMEZU, and T. MATUURA. J. Chem. Soc. Perkin Trans. 2, 1565 (1982).
13. J. YAMAMOTO, T. SAKAMOTO, K. KUSUNOKI, M. UMEZU, and T. MATUURA. Nikon Kagaku Kaishi, 66 (1977).
14. E. BUNCEL and B. T. LAWTON. Can. J. Chem. **43**, 862 (1965).
15. E. BUNCEL and W. M. J. STRACHAN. Can. J. Chem. **48**, 377 (1970).
16. E. BUNCEL, R. A. COX, and A. DOLENKO. Tetrahedron Lett. 215 (1975).
17. M. COLONNA, A. RISALITI, and L. PENTIMALLI. Gazz. Chim. Ital. **86**, 1067 (1956).
18. M. COLONNA and A. RISALITI. Gazz. Chim. Ital. **85**, 1148 (1955).
19. L. PENTIMALLI. Ann. Chim. (Rome), **55**, 435 (1965).
20. L. PENTIMALLI. Tetrahedron, **5**, 27 (1959).
21. C. S. HAHN and H. H. JAFFÉ. J. Am. Chem. Soc. **84**, 949 (1962).
22. R. STEINRASSER and L. POHL. Tetrahedron Lett. 1921 (1971).
23. B. T. NEWBOLD. *In* The chemistry of hydrazo, azo and azoxy

groups. *Edited by* S. Patai. Wiley, New York. 1975. Chapt. 14.
24. N. J. BUNCE, J. P. SCHOCH, and M. C. ZERNER. J. Am. Chem. Soc. **99**, 7986 (1977).
25. M. A. BERWICK and R. E. RONDEAU. J. Org. Chem. **37**, 2409 (1972).
26. M. J. S. DEWAR and R. C. DOUGHERTY. The PMO theory of organic chemistry. Plenum Press, New York. 1975. Chapt. 3.
27. S. R. KEUM. Ph.D. Thesis, Queen's University, Kingston, 1982.
28. R. CURCI and G. MODENA. Tetrahedron, **22**, 1227 (1966).
29. R. A. COX and E. BUNCEL. *In* The chemistry of hydrazo, azo and azoxy groups. *Edited by* S. Patai. Wiley, New York. 1975, Chapt. 18.
30. E. BUNCEL and S. R. KEUM. Heterocycles, **20**, 1951 (1983).
31. E. BUNCEL and S. R. KEUM. J. Chem. Soc. Chem. Commun. 578 (1983).
32. A. ANGELI. Gazz. Chim. Ital. **46**, II, 67 (1916); **46**, II, 78 (1916).
33. E. BUNCEL. *In* Mechanisms of molecular migrations. Vol. 2. *Edited by* B. S. Thyagarajan. Wiley, New York. 1968. p. 61.
34. P. B. D. DE LA MARE and J. H. RIDD. Aromatic substitution – nitration and halogenation. Academic Press, New York. 1969.
35. A. R. KATRITZKY and C. D. JOHNSON. Angew. Chem. Int. Ed. Engl. **6**, 608 (1967).
36. V. SCHOMAKER and K. N. TRUEBLOOD. Acta Crystallogr. Sect. B, **24**, 63 (1968).
37. W. R. KRIGBAUM, Y. CHATANI, and P. G. BARBER. Acta Crystallogr. Sect. B, **26**, 97 (1970).
38. W. R. KRIGBAUM and P. G. BARBER. Acta Crystallogr. Sect. B, **27**, 1884 (1971).
39. J. BROWNING, D. A. R. HAPPER, and B. R. PENFOLD. J. Cryst. Mol. Struct. **4**, 187 (1974).
40. (*a*) A. J. LEADBETTER and M. A. MAZID. Mol. Cryst. Liq. Cryst. **51**, 85 (1979); (*b*) M. COTRAIT, P. MARSAU, and M. PESQUER. Acta Crystallogr. Sect. B, **35**, 1102 (1979).
41. L. HOESCH and H. P. WEBER. Helv. Chim. Acta, **60**, 3015 (1977).
42. D. A. DIETERICH, I. C. PAUL, and D. Y. CURTIN. J. Am. Chem. Soc. **96**, 6372 (1974).
43. (*a*) J. B. WETHERINGTON, K. D. HOLMES, JR., and J. W. MONCRIEF. Acta Crystallogr. Sect. B, **30**, 246 (1974); (*b*) J. S. PRASAD. Acta Crystallogr. Sect. B, **35**, 1404 (1979); (*c*) J. S. PRASAD. Acta Crystallogr. Sect. B, **35**, 1407 (1979).
44. Y. WANG, R. H. BLESSING, F. K. ROSS, and P. COPPENS. Acta Crystallogr. Sect. B, **32**, 572 (1976).
45. S. FORTIER, G. I. BIRNBAUM, G. W. BUCHANAN, and B. A. DAWSON. Can. J. Chem. **58**, 191 (1980).
46. R. TAYLOR and O. KENNARD. J. Am. Chem. Soc. **104**, 5063 (1982).
47. G. A. JEFFREY and S. TAKAGI. Acc. Chem. Res. **11**, 264 (1978).
48. P. COPPENS and M. S. LEHMANN. Acta Crystallogr. Sect. B, **32**, 1777 (1976).
49. (*a*) A. DOMENICANO and P. MURRAY-RUST. Tetrahedron Lett. 2283 (1979); (*b*) R. NORRESTAM and L. SCHEPPER. Acta Chem. Scand. Ser. A, **35**, 91 (1981).
50. A. I. VOGEL. Practical organic chemistry. 3rd ed. Longmans, London. 1956. p. 630.
51. E. V. BROWN and G. R. GRANNEMAN. J. Am. Chem. Soc. **97**, 621 (1975).
52. G. M. BADGER and G. E. LEWIS. J. Chem. Soc. 2151 (1953).
53. A. HANTZSCH and A. BURAWOY. Chem. Ber. **63B**, 1760 (1930); **63B**, 1775 (1930).
54. R. W. FAESSINGER and E. V. BROWN. J. Am. Chem. Soc. **73**, 4606 (1951).
55. P. MAIN, S. E. HULL, L. LESSINGER, G. GERMAIN, J.-P. DECLERCQ, and M. M. WOOLFSON. MULTAN 78, University of York, England, and University of Louvain, Belgium, 1978.
56. International tables for X-ray crystallography. Vol. IV. Kynoch Press, Birmingham. 1974.
57. F. R. AHMED, S. R. HALL, M. E. PIPPY, and C. P. HUBER. J. Appl. Crystallogr. **6**, 309 (1973).
58. G. M. SHELDRICK. SHELX 76. A program for crystal structure determination. University of Cambridge, England. 1976.
59. E. BUNCEL and S. R. KEUM. Tetrahedron, **39**, 1091 (1983).

Can. J. Chem. Downloaded from www.nrcresearchpress.com by 210.87.254.105 on 09/06/12
For personal use only.

The conformational analysis of leukotriene D_4 in aqueous solution based on high-field nuclear magnetic resonance measurements[1]

MAKIKO SUGIURA,[2] HELMUT BEIERBECK, AND GEORGE KOTOVYCH
Department of Chemistry, University of Alberta, Edmonton, Alta., Canada T6G 2G2

AND

PATRICE C. BÉLANGER
Merck–Frosst Canada Inc., P.O. Box 1005, Pointe-Claire/Dorval, P.Q., Canada H9R 4P8

Received December 16, 1983

This paper is dedicated to Professor G. E. Dunn on the occasion of his 65th birthday

MAKIKO SUGIURA, HELMUT BEIERBECK, GEORGE KOTOVYCH, and PATRICE C. BÉLANGER. Can. J. Chem. **62**, 1640 (1984).

The conformational analysis of LTD_4 in D_2O was carried out based on the analysis of vicinal proton–proton coupling constants, nonselective proton longitudinal relaxation times, and nuclear Overhauser effect data. The H6—C6 to C12 region of the molecule is *transoid*, the predominant rotamer about C5—C6 is *gauche*, and two rotamers can be used to describe the rotation about C12—C13. There are three rotamers that can be used to describe the rotation about the C21—C22 bond of cysteine. Finally, chelation between an Yb^{3+}, shift reagents and LTD_4 was not observed.

MAKIKO SUGIURA, HELMUT BEIERBECK, GEORGE KOTOVYCH et PATRICE C. BÉLANGER. Can. J. Chem. **62**, 1640 (1984).

Faisant appel à une analyse des constantes de couplage proton–proton vicinales, des temps de relaxation longitudinaux non-sélectifs des protons et de données d'effet Overhauser nucléaire, on a réalisé une analyse conformationnelle du LTD_4 dans le D_2O. La région H6—C6 à C12 de la molécule est *transoide*, le rotamère prédominant autour de la liaison C5—C6 est *gauche* et deux rotamères peuvent être utilisés pour décrire la rotation autour de la liaison C12—C13. On peut utiliser trois rotamères pour décrire la rotation autour de la liaison C21—C22 de la cystèine. Finalement, on n'a pas pu observé de chélation entre le Yb^{3+}, un réactif de contact, et le LTD_4.

[Traduit par le journal]

Introduction

The metabolism of arachidonic acid involves its oxygenation via two enzymic systems. Cyclooxygenase transforms arachidonic acid into the prostaglandins, the thromboxanes, and prostacyclin, and lipoxygenases give rise to a new class of eicosanoids, the leukotrienes. In this metabolic process, 5-lipoxygenase oxidizes arachidonic acid to form 5(*S*)-hydroperoxy-6*E*-8,11,14*Z*-eicosatetraenoic acid (5-HPETE), which is then converted to 5*S*-5,6-epoxy(7*Z*,9*Z*,11*E*,14*E*)-eicosatetraenoic acid, leukotriene A_4 (LTA_4) (1, 2).

Leukotriene A_4 may be further metabolized by two enzymic pathways or may be chemically hydrolysed by a non-enzymic pathway. The first enzymic pathway (2, 3) involves insertion of H_2O to produce leukotriene B_4 ((5*S*,12*R*)-5,12-dihydroxy-(6*Z*,8*E*,10*E*,14*Z*)-eicosatetraenoic acid) (LTB_4). Two other 5,12-dihydroxyeicosatetraenoic acids can also be produced by the nonenzymic hydrolysis of leukotriene A_4. In this case, the double bonds in the triene structure are all *trans* and the hydroxyl groups have the configuration 5*S*,12*S* or 5*S*,12*R*. A fourth 5,12-dihydroxyeicosatetraenoic acid may be produced by a dual lipoxygenase attack and in this case the triene structure has the configuration *trans, cis, trans* and the hydroxyl groups are 5*S*,12*S*.

Leukotriene B_4 is a potent stimulator of the movement of leucocytes in vitro and can also induce vascular permeability changes. The role of LTB_4 as a mediator of leucocyte function has recently been reviewed (4).

The second enzymic pathway involves conjugation with glutathione to produce leukotriene C_4 (LTC_4) ((5*S*)-hydroxy-(6*R*)-*S*-glutathionyl-7,9-*trans*-11,14-*cis*-eicosatetraenoic acid) which is then metabolized to form leukotrienes D_4 (Fig. 1) and E_4 (5, 6). These compounds collectively account for the biological activity known as Slow Reacting Substance of Anaphylaxis (SRS-A). These leukotrienes possess potent biological properties and can contract certain smooth muscle preparations, constrict coronary and cerebral arteries, and may induce changes in vascular permeability and mucous production. They may therefore be important mediators of human diseases such as bronchial asthma. This research has now been well reviewed (7–11). The geometrical assignments of the double bonds of the different leukotrienes as well as the stereochemical assignments have been made possible by total syntheses and subsequent comparison of synthetic and natural products (12–20).

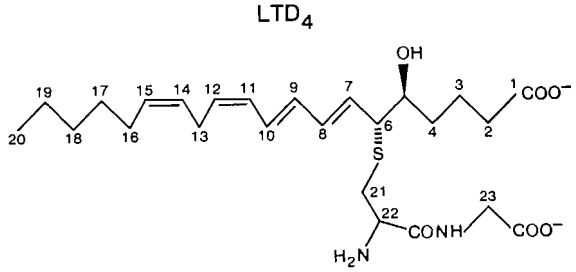

FIG. 1. The structure of LTD_4.

In the present study, our objective is to obtain the possible conformations of LTD_4 in aqueous solution. The determination of such a conformation is very important as it could be used in the design of analogs of LTD_4. It could also lead to a better understanding of the structure–activity relationships (21, 22) and of the interaction of LTD_4 with its specific receptor. Some nmr studies have been reported on derivatives of leukotrienes (23–26) and the deprotected LTD_4 in methanol solution (26), but only LTB_4 has been studied in an aqueous system (27). The

[1] This is paper No. 12 in a series of high-field nmr studies on the eicosanoids.

[2] Present address: Kobe Women's College of Pharmacy, Kobe, Japan.

Can. J. Chem. Downloaded from www.nrcresearchpress.com by 210.87.254.42 on 09/06/12
For personal use only.

TABLE 1. Proton chemical shifts and coupling constants for LTD_4 in D_2O (0.0025 *M*, pH ~9.0)

	δ_H (ppm)	*J* (Hz)
H-2	2.17	
H-3	1.5–1.6	
H-4	1.4–1.5	
H-4′	1.6–1.7	
H-5	~3.80	$J_{5,6} = 4.1$
H-6	3.45	$J_{6,7} = 10.1$, $J_{6,8}$ or $J_{6,9} \leq 1.0$
H-7	5.67	$J_{7,8} = 14.6$, $J_{7,10} \simeq 1.0$
H-8	6.33	$J_{8,9} = 10.4$
H-9	6.35	$J_{9,10} = 14.5$
H-10	6.70	$J_{10,11} = 11.2$
H-11	6.11	$J_{11,12} = 11.2$
H-12	5.56	$J_{12,13} = J_{12,13'} = 8.5$ $J_{12,14} \simeq 0.9$
H-13 H-13′	2.99	$(J_{13,13'} = -16)$,[a] $J_{13,15} = J_{13',15} \simeq 1.0$ $J_{13,14} = J_{13',14} = 7.1$
H-14	5.46	$J_{14,15} = 10.7$
H-15	5.52	$J_{15,16} = 7.3$
H-16	2.10	
H-17	~1.34	
H-18, 19	~1.28	
H-20	0.84	
H-21	2.66	$J_{21,21'} = -13.7$
H-21′	2.84	$J_{21,22} = 7.1$, $J_{21',22} = 5.4$
H-22	3.55	
H-23	3.71	$J_{23,23'} = -17.4$
H-23′	3.81	

[a] Assumed value in the computer analysis.

small amount of material available and its stability are responsible for the scarcity of these important studies, and the nature of these derivatives makes it nearly impossible to obtain crystals suitable for X-ray analysis. Hence we have carried out an extensive proton nmr investigation of LTD_4 in aqueous solution. The experiments involve a pH-dependent study of the chemical shifts, proton longitudinal nonselective relaxation time measurements, nuclear Overhauser enhancements, and an analysis of the coupling constants. These data were combined with conformational studies of model compounds and, in this manner, the preferred conformations for LTD_4 are evaluated.

Experimental

The potassium salt of LTD_4 was synthesized by Merck–Frosst Canada, Inc., Pointe Claire, Quebec, Canada (28). The nmr measurements were carried out in D_2O (100%, Aldrich), which was vacuum distilled. The leukotriene was received as a solution in water, which was removed under vacuum. D_2O was then added, the samples were degassed, and then pumped to dryness twice. In this way the residual HDO peak was minimized. Fresh 100% D_2O was then added (0.4 mL) and the solutions were degassed four times using the freeze–pump–thaw technique and then sealed. All glassware was cleaned extensively, including a nitric acid wash, to eliminate paramagnetic impurities.

The proton magnetic resonance measurements were carried out in the Fourier transform mode using the Bruker WH-400/DS nmr spectrometer and the Aspect 2000 Data System, utilizing 16K of data memory for the nOe and the relaxation time measurements. Up to 64 K of memory were used in evaluating the chemical shifts and coupling constants. The deuterium resonance of the solvent D_2O was used as the lock signal. The proton longitudinal nonselective relaxation times (T_1^{NS}) were obtained using the (180°–τ–90°–t) two-pulse sequence. Usually about 10 τ values were included in the analysis of the data, based on the initial slope of a plot of ln ($M_\infty - M_\tau$) vs. τ.

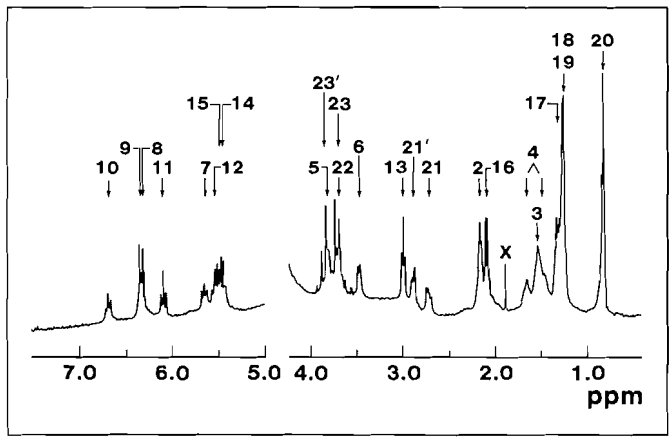

FIG. 2. The general spectrum of LTD_4 in aqueous solution (pH ~8).

These *M* values were obtained from the measurement of the sum of the peak heights of a multiplet corresponding to a given proton, and for some protons peak areas were measured by weighing out the peaks. As well, two M_∞ values were measured for maximum accuracy. The relaxation times were obtained from a computer analysis of the data using a least-squares program.

The steady-state nOe difference experiments were carried out following procedures described previously (29). Saturation power levels were determined by measuring the minimum power necessary to completely suppress a given multiplet. The reported nOe's are the average values for two or three experiments. Subspectral analyses were carried out with the Bruker PANIC program.

For the pH studies, phosphate and borax buffer solutions were prepared in D_2O at pH's of 6 to 9. The buffer concentrations were ~0.005 *M*. About 70 μg LTD_4 was then added to 0.4 mL of buffer solution, and the concentration of LTD_4 in each solution was about 3.5×10^{-4} *M*. Duplicate buffer solutions were prepared with a trace of DSS to be used as a reference. After the spectrum was obtained on LTD_4, the reference sample was placed in the probe, the lock signal adjusted to the same spectral reference, and in this way the chemical shifts were calibrated. Shifts at eight pH values were determined to confirm that at pH ~9 only one predominant species is present in solution. At pH ~9.0 the NH_2 group is deprotonated.

The chemical shifts reported in Table 1 are with respect to external DSS.

Results

The assignment of the proton multiplets was carried out following standard decoupling techniques and these are shown in Fig. 2. The chemical shifts and coupling constants are listed in Table 1 and two examples of the computer fit to the data are shown in Fig. 3. Comparing our chemical shifts in Table 1 with those previously reported in CD_3OD (26), a solvent effect on the shifts is observed.

To check for aggregation, chemical shifts were measured, at pH ~8, on ~3×10^{-3} *M* and ~3.6×10^{-4} *M* solutions with good agreement in the first-order chemical shifts. Hence the relaxation time data in Table 2 and the nOe data in Table 3 were obtained under conditions where intermolecular association is not present. In the case of prostaglandin $F_{2\alpha}$ (30), hydrophobic interactions were not present at concentrations below 0.02 *M* and this is also apparent with prostacyclin and its analogs (31). Consequently, the present studies are carried out at a concentration where aggregation is minimal. As well, the pK_a for the cysteine amino group is determined to be ~7.5 and the NH_2 group is not protonated for all of the data reported in the tables for aqueous solutions at a pH ~9.

Can. J. Chem. Downloaded from www.nrcresearchpress.com by 210.87.254.42 on 09/06/12
For personal use only.

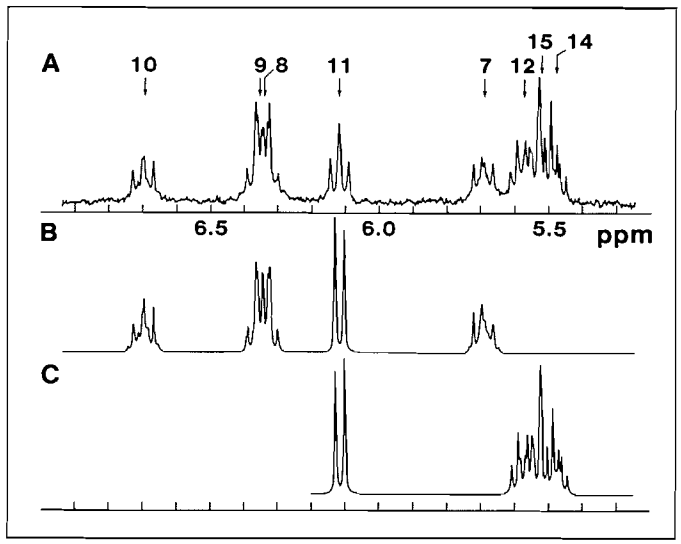

FIG. 3. A. The low-field region of LTD_4 in aqueous solution (pH ~9) with couplings to H16 removed. B. A 6-spin computer fit for H6 to H11. C. A 6-spin computer fit for H11 to H15.

TABLE 2. Proton nonselective relaxation times for LTD_4 in D_2O (0.0025 *M*, pH ~9.0)[a]

	T_1^{NS} (obs)	T_1^{NS} (calcd)
H2	0.64	
H-6	0.48	0.58
H7	1.13	1.12
H8[b]	0.88	0.98
H9[b]	0.88	0.98
H10	0.81	0.65
H11	1.11	1.00
H13	0.47	
H16	0.83	
H21	0.40	
H21′	0.40	
H23	1.02	

[a] The fit to the data was obtained using a correlation time of 0.33 ns.
[b] Values of T_1's were determined simultaneously because of multiplet overlap.

In Table 1, the chemical shifts for protons H-2 to H-4, and H-17 to H-20 are reported to first order, whereas the remainder of the chemical shifts, and the coupling constants, were determined from a computer fit to the data. Several simulations were carried out, namely (a) decoupling H-6 and fitting the spectra for H-7 to H-11; (b) decoupling H-16 and fitting H-11 to H-15; (c) decoupling H-8 and fitting the spectra for H-5 to H-7; (d) decoupling H-13 and fitting H-11 to H-16, and (e) fitting the amino acid proton spectra.

The approach that was chosen to elucidate the possible conformations of LTD_4 in solution is based on the Karplus analysis of the coupling constants combined with proton nuclear Overhauser effect (nOe) measurements and proton nonselective relaxation time measurements (T_1^{NS}). The application of the Karplus equation to conformational analysis has been well documented (32, 33). The proton nOe and relaxation time measurements were carried out since these data are extremely sensitive to the interproton distances (34, 35). For proton–proton intramolecular dipolar relaxation, the spin-lattice transition probabilities are W_0^{ij}, W_1^{ij}, and W_2^{ij}, respectively, for zero-, single-, and double quantum transitions involving the nuclear spins i and j. These are given as follows:

$$[1] \quad W_0^{ij} = \frac{1}{10}\gamma^4\hbar^2\tau_c/r_{ij}^6$$

$$[2] \quad W_1^{ij} = \frac{3}{20}\gamma^4\hbar^2\tau_c/(1 + \omega^2\tau_c^2)\,r_{ij}^6$$

$$[3] \quad W_2^{ij} = \frac{6}{10}\gamma^4\hbar^2\tau_c/(1 + 4\omega^2\tau_c^2)\,r_{ij}^6$$

The relaxation rates are defined as

$$[4] \quad \sigma_{ij} = W_2^{ij} - W_0^{ij}$$

$$[5] \quad \rho_{ij} = W_0^{ij} + 2W_1^{ij} + W_2^{ij}$$

where σ_{ij} is the cross-relaxation term and ρ_{ij} is the direct relaxation term for a proton pair. The interproton distance is r_{ij}, ω is the Larmor frequency, and τ_c is the correlation time for molecular reorientation. The magnetogyric ratio is γ and $\hbar$ is Planck's constant h divided by 2π.

The nuclear Overhauser effect (nOe) is an excellent probe of molecular conformation because it depends on the interproton distance r_{ij}^6. It is defined as the fractional enhancement of nucleus d on saturating nucleus s ($f_d(s)$) and comprises a term (first) for *direct* interactions and one (second) for *indirect* interactions (35–37).

$$[6] \quad f_d(s) = \sum_s N_s\sigma_{ds}/R_d - \sum_{n\neq d,s} N_n\sigma_{dn}f_n(s)/R_d$$

where N_i is the number of equivalent nuclei i. The total direct relaxation rate is R_d:

$$[7] \quad R_d = \sum_n N_n\rho_{dn} + p^*$$

The nonselective relaxation time is T_1^{NS} and is defined as:

$$[8] \quad T_1^{NS} = \frac{1}{R_d + S_d}, \text{ where } S_d = \sum_n N_n\sigma_{dn}$$

On the basis of these equations, a computer program was written which optimizes the nOe and the T_1^{NS} data for a given conformation. The optimum value of τ_c is thus obtained. Several possible conformations are used as input, based on the Karplus analysis of the coupling constants. The internuclear distances are estimated from Dreiding models. This approach has now been successfully applied to the study of leukotriene B_4 (27).

The molecular modeling was carried out in the following manner for LTD_4 in aqueous solution at pH ~9.0. Carbon atoms C1 to C6 and C15 to C20 are *trans*, as expected. The triene portion of the molecule from C6 to C12 is also *trans* (24, 26, 27), and the present study supports this conclusion. The coupling constants observed for olefinic protons across a connecting single bond are J(H6—H7) = 10.1 Hz, J(H8—H9) = 10.4 Hz, J(H10—H11) = 11.2 Hz. The coupling constants indicate that the olefinic protons about interconnecting single bonds are *transoid*.

To estimate the possible rotamers about C4—C5, coupling

Can. J. Chem. Downloaded from www.nrcresearchpress.com by 210.87.254.42 on 09/06/12
For personal use only.

TABLE 3. The nuclear Overhauser effect for LTD_4 in D_2O (0.0025 *M*, pH ~9.0)[a]

	Observed							
Sat'd	H-5	H-7	H-8	H-9	H-10	H-12	H-13	H-14
H-2	Small			Small				
H-8, 9		6.0% (7.7%)			4.0% (4.5%)			
H-10			4.5% (5.1%)				1.8% (1.2%)	
H-11						8% (7.2%)		
H-13					7.7% (7.6%)	7.4% (5.1%)		11.0%

[a]These data were optimized using a correlation time of 0.33 ns. Values in brackets represent the calculated nOe's.

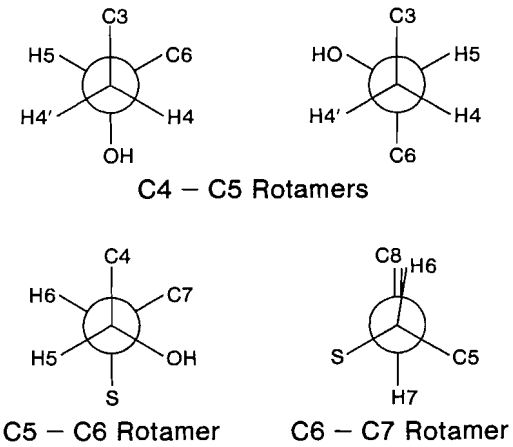

FIG. 4. The possible rotamers about C4—C5, C5—C6, and C6—C7.

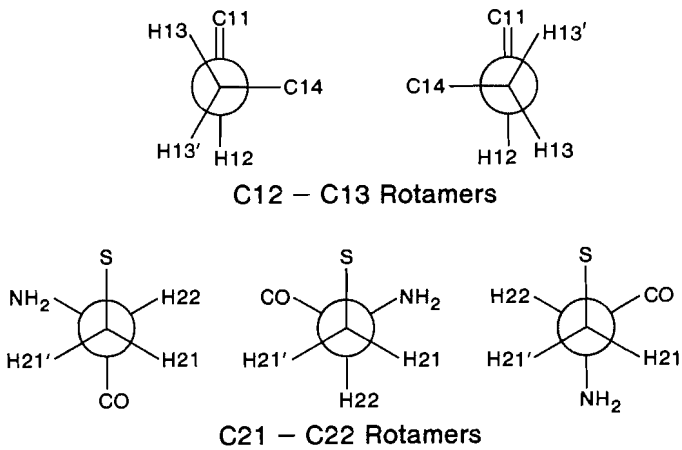

FIG. 5. The possible rotamers about C12—C13, and C21—C22.

constants *J*(H4—H5) are required, but could not be evaluated from the spectra. The two rotamers used in the present analysis (Fig. 4) are the same as were evaluated for LTB_4 where the coupling constants could be measured *J*(H4—H5) = 6.3 Hz (27). The C4—C5—C6—C7 dihedral angle is 60°, in agreement with *J*(H5—H6) of 4.1 Hz (Fig. 4) (26). A value of 4.1 Hz may indicate the presence of a *transoid* conformer, but the predominant conformer is still *gauche*.

The H6—C6—C7—H7 dihedral angle is chosen as 180° because the coupling constant is 10.1 Hz and this leads to a *trans* orientation between the methine protons at C6 and C7 (26). As well, for rotational isomerism about sp^2–sp^3 carbon–carbon single bonds, the preferred conformation (Fig. 4) is the one where the C—H bond at the sp^3 center eclipses the C=C double bond (38–40), and this places H6 and H7 in a *trans* orientation.

In considering the rotamers about C12—C13 (Fig. 5) the preferred rotamers again are expected to be the ones where CH(13) and CH(13′) eclipse the C11=C12 double bond. However, this leads to a steric interaction between H-10 and H-13 (or H-13′) because of the extra *cis* double bond substitution, and the calculated T_1^{NS} for H10 is too short. In the present analysis, two preferred rotamers are used, as shown in Fig. 5 with the C11—C14 bonds perpendicular. In this way, the stabilization due to the eclipsed conformation is still present, but is decreased by the H10—H13 interaction. This gives a more reasonable fit to the T_1^{NS} data. The H12—H13 and H12—H13′ dihedral angles are then equal to 150° and 30°. A coupling constant *J*(H12—H13) of ~9 Hz is expected and a coupling of 8.5 Hz is observed. Finally, even though the data are not sufficient to prove the presence of these two rotamers about C13—C14 and C15—C16, the above analysis can be extended to rotation about these bonds. In considering the amino acid substituent, the choice of the C5—C6—S—C21 dihedral angle and the C6—S—C21—C22 dihedral angle does not affect the nmr data, especially since an nOe is not observed between H6 and H21. Hence in considering the rotation about C6 and S, C5 was placed *trans* to C21, and for rotation about S—C21, C6 was placed *trans* to C22.

To calculate the rotamers associated with the amino acid cysteinyl glycine side chain, a pH dependence of coupling constants for this dipeptide was carried out[3] following the procedure of Fujiwara *et al.* (41). It was found that at pH 9.27, the populations of the three rotamers are about 0.25, 0.33, and 0.42. In rotamer 1, the sulphur is *trans* to CO, whereas in rotamer 2 the sulphur is *trans* to the NH_2 group and in rotamer three the sulphur is *trans* to H22 (Fig. 5). The coupling constants at this pH are 7.2 and 5.4 Hz for *J*(H21—H22) and *J*(H21—H22′). For LTD_4 the coupling constants are 7.1 Hz and 5.4 Hz, indicating a distribution of rotamers about the C21—C22 bond in LTD_4 similar to that for free cysteinyl glycine.

In analyzing the T_1 and nOe data by themselves, several

[3] P. C. Bélanger, unpublished data.

Can. J. Chem. Downloaded from www.nrcresearchpress.com by 210.87.254.42 on 09/06/12
For personal use only.

models were tried and, because of the large number of possible rotamers, it was impossible to determine the allowed conformations. However, with the aid of the Karplus analysis of the coupling constants, the T_1^{NS} and nOe data can be used to confirm the possible conformations. A fit to the T_1^{NS} (Table 2) and nOe data (Table 3) was obtained for the above mentioned conformations. The reorientational correlation time τ_c for the C—H vectors for the planar C6 to C12 portion of the molecule is taken to be isotropic, in agreement with the data for prostacyclin (31) and prostaglandin $F_{2\alpha}$ (30). The optimized fit to the nOe data is achieved with $\tau_c = 0.33 \pm 0.05$ ns (95% confidence limits). This correlation time was then used to obtain the best fit to the T_1^{NS} data, which are not very sensitive to a change in the correlation time.

Because of the availability of potential metal ion ligands at C5(OH), S, C=O groups, and COO^-, it was thought that chelation with a metal ion may be observed. However, on adding up to 40% $YbCl_3$, a shift reagent, no chemical shifts were observed.

Discussion

One of the important conclusions of the present study is based on the coupling constants and confirms the observation (26) that H6—C6 to C12 is *transoid*. The coupling constants presented in Table 1 are the first to be published on unprotected LTD_4 in aqueous solution. The *transoid* conformation is supported by the fit to the T_1 data and the nOe data for the region of the molecule that can be represented by a single isotropic correlation time. A comparison of the data indicates that the calculated and experimental values are within 10% of each other.

Because the LTD_4 molecule is flexible, an analysis of all of the available parameters must be undertaken in order to evaluate the preferred conformations for LTD_4. This includes an analysis of the coupling constants, the T_1^{NS}, and the nOe data. Using this combined approach, the conformational analysis of a complex molecule such as LTD_4 is possible. The predominant rotamer about C5—C6 has C4 and C7 *gauche*. Secondly, H6 and H7 are *trans*, and there are two rotamers about C12—C13. As nOe's were not observed between H21 and H-6, conclusions cannot be drawn about the C5—C6—S—C21 and C6—S—C21—C22 dihedral angles. Finally, the conformers at pH 9 for the C21—C22 bond of cysteine in LTD_4 are calculated by comparing the H21—H22 coupling constants with the model compound cysteine-glycine, and three rotamers are predicted.

Acknowledgements

The authors wish to thank Drs. M. Bernstein, R. N. Young, and J. Rokach for helpful discussions and Merck–Frosst Canada, Inc., the Natural Sciences and Engineering Research Council of Canada, and the University of Alberta for financial assistance.

1. P. BORGEAT, M. HAMBERG, and B. SAMUELSSON. J. Biol. Chem. **251**, 7816 (1976), and correction **252**, 8772 (1977).
2. P. BORGEAT and B. SAMUELSSON. Proc. Natl. Acad. Sci. U.S.A. **76**, 3213 (1979); **76**, 2148 (1979).
3. P. BORGEAT and B. SAMUELSSON. J. Biol. Chem. **254**, 2643 (1979).
4. A. W. FORD-HUTCHINSON. Agents Actions Suppl. **12**, 154 (1983).
5. R. C. MURPHY, S. HAMMARSTROM, and B. SAMUELSSON. Proc. Natl. Acad. Sci. U.S.A. **76**, 4275 (1979).
6. S. HAMMARSTROM, R. C. MURPHY, B. SAMUELSSON, D. A. CLARK, C. MIOSKOWSKI, and E. J. COREY. Biochem. Biophys. Res. Commun. **91**, 1266 (1979).
7. J. G. ATKINSON and J. ROKACH. Synthesis of the leukotrienes and other lipoxygenase-derived products. CRC Press Inc., Boca Raton, U.S.A. 1984.
8. B. SAMUELSSON. Angew. Chem. Int. Ed. Engl. **21**, 902 (1982).
9. E. J. COREY. Experientia, **38**, 1259 (1982).
10. P. J. PIPER. Eur. J. Resp. Dis. **63**, S122, 55 (1982).
11. R. M. GREEN and P. F. LAMBETH. Tetrahedron, **39**, 1687 (1983).
12. E. J. COREY, D. A. CLARK, G. GOTO, A. MARFAT, C. MIOSKOWSKI, B. SAMUELSSON, and S. HAMMARSTROM. J. Am. Chem. Soc. **102**, 1436 (1980).
13. E. J. COREY, A. MARFAT, G. GOTO, and F. BRION. J. Am. Chem. Soc. **102**, 7984 (1980).
14. J. ROKACH, Y. GIRARD, Y. GUINDON, J. G. ATKINSON, M. LARUE, R. N. YOUNG, P. MASSON, and G. HOLME. Tetrahedron Lett. **21**, 1485 (1980).
15. S. HAMMARSTROM, B. SAMUELSSON, D. A. CLARK, G. GOTO, A. MARFAT, C. MIOSKOWSKI, and E. J. COREY. Biochem. Biophys. Res. Commun. **92**, 946 (1980).
16. R. A. LEWIS, J. M. DRAZEN, K. F. AUSTEN, D. A. CLARK, and E. J. COREY. Biochem. Biophys. Res. Commun. **96**, 271 (1980).
17. M. ROSENBERGER and C. NEUKOM. J. Am. Chem. Soc. **102**, 5425 (1980).
18. H. R. MORRIS, G. W. TAYLOR, J. ROKACH, Y. GIRARD, P. J. PIPER, J. R. TIPPINS, and M. H. SAMHOUN. Prostaglandins, **20**, 601 (1980).
19. R. A. LEWIS, K. F. AUSTEN, J. M. DRAZEN, D. A. CLARK, A. MARFAT, and E. J. COREY. Proc. Natl. Acad. Sci. U.S.A. **77**, 3710 (1980).
20. J. ROKACH, R. N. YOUNG, M. KAKUSHIMA, C. K. LAU, R. SEGUIN, R. FRENETTE, and Y. GUINDON. Tetrahedron Lett. **22**, 979 (1981).
21. J. M. DRAZEN, R. A. LEWIS, K. F. AUSTEN, M. TODA, F. BRION, A. MARFAT, and E. J. COREY. Proc. Natl. Acad. Sci. U.S.A. **78**, 3195 (1981).
22. R. A. LEWIS, J. M. DRAZEN, K. F. AUSTEN, M. TODA, F. BRION, A. MARFAT, and E. J. COREY. Proc. Natl. Acad. Sci. U.S.A. **78**, 4579 (1981).
23. D. M. RACKHAM, S. E. MORGAN, J. W. PASCHAL, and T. K. ELZEY. Spectrosc. Lett. **14**, 589 (1981).
24. E. J. COREY, P. B. HOPKINS, A. E. BARTON, B. BANGERTER, and P. BORGEAT. Tetrahedron Lett. **38**, 2653 (1982).
25. S. R. BAKER, W. B. JAMIESON, S. W. MCKAY, S. E. MORGAN, D. M. RACKHAM, W. S. ROSS, and P. R. SHRUBSALL. Tetrahedron Lett. **21**, 4123 (1980).
26. P. LOFTUS and P. R. BERNSTEIN. J. Org. Chem. **48**, 40 (1983).
27. M. SUGIURA, H. BEIERBECK. P. BÉLANGER, and G. KOTOVYCH. J. Am. Chem. Soc. In press.
28. J. ROKACH, R. N. YOUNG, M. KAKUSHIMA, C.-K. LAU, R. SEQUIN, R. FRENETTE, and Y. GUINDON. Tetrahedron Lett. **22**, 979 (1981).
29. G. KOTOVYCH and G. H. M. AARTS. Can. J. Chem. **58**, 2649 (1980).
30. W. W. CONOVER and J. FRIED. Proc. Natl. Acad. Sci. U.S.A. **71**, 2157 (1974).
31. M. SUGIURA, H. BEIERBECK, and G. KOTOVYCH. J. Am. Chem. Soc. In press.
32. V. F. BYSTROV. Prog. Nucl. Magn. Reson. Spectrosc. **10**, 41 (1976).
33. G. GOVIL and R. V. HOSUR. Conformation of biological molecules. *In* NMR, Basic principles and progress. Vol. 20. Springer Verlag, Berlin. 1982.
34. I. SOLOMON. Phys. Rev. **99**, 559 (1955).
35. J. M. NOGGLE and R. E. SCHIRMER. The nuclear Overhauser

Can. J. Chem. Downloaded from www.nrcresearchpress.com by 210.87.254.42 on 09/06/12
For personal use only.

effect. Chemical applications. Academic Press, New York. 1971.
36. A. A. BOTHNER-BY and P. E. JOHNER. Biophys. J. **24**, 779 (1978).
37. N. R. KRISHNA, D. G. AGRESTI, J. D. GLICKSON, and R. WALTER. Biophys. J. **24**, 791 (1978).
38. G. J. KARABATSOS and D. J. FENOGLIO. Top. Stereochem. **5**, 167 (1970).
39. A. A. BOTHNER-BY, C. NAAR-COLIN, and H. GUNTHER. J. Am. Chem. Soc. **84**, 2748 (1962).
40. H. KISHI. Aldrichimica Acta, **13**, 23 (1980).
41. S. FUJIWARA, G. FORMICKA-KOZLOWSKA, and H. KOZLOWSKI. Bull. Chem. Soc. Jpn. **50**, 3131 (1977).

Can. J. Chem. Downloaded from www.nrcresearchpress.com by 210.87.254.42 on 09/06/12
For personal use only.

Substituent effects on rates of formation of methoxy-substituted carbonyl ylides from 2-aryl-2-methoxy- and 5-aryl-2-methoxy-Δ^3-1,3,4-oxadiazolines

MICHEL BÉKHAZI, PETER J. SMITH,[1] AND JOHN WARKENTIN
Department of Chemistry, McMaster University, Hamilton, Ont., Canada L8S 4M1

Received December 2, 1983

This paper is dedicated to Professor Gerald E. Dunn on the occasion of his 65th birthday

MICHEL BÉKHAZI, PETER J. SMITH, and JOHN WARKENTIN. Can. J. Chem. **62**, 1646 (1984).

2-Aryl-2-methoxy-5,5-dimethyl-Δ^3-1,3,4-oxadiazolines (**4**) and 5-aryl-2-methoxy-2,5-dimethyl-Δ^3-1,3,4-oxadiazolines (**5**) were synthesized. Compounds **4** decompose in solution with first order kinetics. Rate constants are correlated with Hammett substituent constants (σ^-) with $\rho(49.2°C) = 0.74$ and 0.89 for CCl_4 and CD_3OD, respectively. The final products from **4** indicate that thermolysis involves the cleavage of both C—N bonds, to form N_2 and, initially, a carbonyl ylide. Compounds **5**, which were obtained as mixtures of *cis/trans* isomers containing several impurities, and which therefore gave poorer kinetic data, decomposed in $CDCl_3$ solution with $\rho(45°C) \simeq 1.1$. Carbonyl ylide intermediates, similar to those from the closely-related compounds **4**, were assumed on the basis of analogy and on the basis of partial identification of products. The effects of *para* substituents in the aryl groups of **4** and **5** show that the transition states have greater electron density at C-2 of **4** and at C-5 of **5** than do the starting materials. In spite of the increase in electron density at C-2 of **4**, the transition state must be less polar, overall, than the ground state because rate constants for thermolysis of **4** in methanol are smaller than those for CCl_4 solvent. A plausible explanation for the substituent effects and the solvent effects is that the loss of N_2 is concerted, with a transition state resembling more closely a spin paired 1,3-diradical than a 1,3-dipole. Alternative stepwise mechanisms, in which C2—N3 bond scission of **4** and C5—N4 bond scission of **5** are the rate-determining steps, leading to 1,5-diradical intermediates, can not be excluded on the basis of the evidence.

MICHEL BÉKHAZI, PETER J. SMITH et JOHN WARKENTIN. Can. J. Chem. **62**, 1646 (1984).

On a synthétisé les aryl-2 méthoxy-2 diméthyl-5,5 Δ^3 oxadiazolines-1,3,4 (**4**) et aryl-5 méthoxy-2 diméthyl-2,5 Δ^3 oxadiazolines-1,3,4 (**5**). Les composés **4** se décomposent en solution avec une cinétique d'ordre un. On a relié les constantes de vitesse aux constantes de substitution de Hammet (σ^-) et les valeurs de ρ à 49,2°C sont respectivement 0,74 et 0,89 pour le CCl_4 et le CD_3OD. Les produits finals obtenus à partir du composé **4** indiquent que la thermolyse implique le clivage des deux liaisons C—N pour former du N_2 et, initialement, un ylure de carbonyle. Les composés **5**, que l'on obtient sous la forme de mélanges d'isomères *cis/trans* contenant plusieurs impuretés et qui par conséquent donnent de mauvaises donnés cinétiques, se décomposent en solution dans le $CDCl_3$ et la valeur de ρ à 45°C est égale à 1,1. En se basant sur l'analogie des réactions et sur une identification partielle des produits, on fait l'hypothèse qu'il existe aussi dans ces cas des ylures de carbonyle intermédiaires semblables à ceux observés dans le cas des composés **4** qui leur sont très voisins. Les effets des substituants en position *para* des groupes aryles des composés **4** et **5** montrent que, par rapport aux produits de départ, les états de transition ont une plus grande densité électronique en C-2 dans les composés **4** et en C-5 dans les composés **5**. En dépit d'une augmentation de la densité électronique en C-2, dans les composés **4**, l'état de transition doit être, dans l'ensemble, moins polaire que l'état fondamental puisque les constantes de vitesse de la thermolyse des composés **4** dans le méthanol sont plus faibles que celles dans le CCl_4. Une perte de N_2 concertée, avec un état de transition ressemblant de très près à un diradical-1,3 de spin pairé plutôt qu'à un dipole, constitue une explication plausible des effets de substituant et de solvant. Les preuves obtenues n'excluent pas la possibilité d'un mécanisme par étapes dans lequel la scission de la liaison C2—N3 des composés **4** et de la liaison C5—N4 des composés **5** constituerait l'étape déterminante et conduirait à la formation de diradicaux-1,5 intermédiaires.

[Traduit par le journal]

Introduction

Cycloaddition and cycloreversion reactions have had a very large impact on several areas of chemistry, including synthesis and both the theoretical and the experimental aspects of mechanism.[2] In general, cycloadditions are used to prepare stable end products while cycloreversions are of greatest interest as routes to reactive intermediates, such as diradicals, carbenes, and ylides. Mechanistic interest in both classes of reactions has centered around the question of the timing of the bond-forming or bond-breaking processes that are involved. In principle, mechanistic information can be obtained by studying either a cycloaddition or its reverse, because the transition state must be the same for either direction of the reaction. In practice, there are many cases where only one choice is available. Cycloadditions to N_2, for example, do not occur readily, although the reverse process, cycloelimination of N_2, is a well-known and much studied reaction (8–10).

Although many studies of the mechanisms of extrusion of nitrogen from cyclic compounds have been reported, there is continued activity and interest in the area because of the apparent variety of mechanisms that are applicable. That variety can be illustrated with the 1-pyrazoline system for which, depending on the substituents, an ion pair mechanism (11), eq. [1], and a range of diradicaloid mechanisms have been proposed. The latter family includes planar 1,3-diradicals (12–16), nonplanar 1,3-diradicals (or π-cyclopropanes) (17), and 1,5-diradicals of the alkyl diazenyl type (18–20). Finally, it has been pointed out that, for monocyclic 1,3-dialkyl pyrazolines at least, it may not be possible to describe the cycloelimination of N_2 (and the subsequent chemistry, if there

[1] Department of Chemistry, University of Saskatchewan, Saskatoon, Saskatchewan.

[2] The literature on these subjects is very extensive. For review articles on cycloadditions and cycloreversions see refs. 1–7 and 8–10, respectively. The list is not exhaustive and some of the review articles deal also with additional material that does not fit into either category. Moreover, the separation of reviews into those on cycloaddition and those on cycloreversion is somewhat arbitrary in a few instances because of overlap of the topics.

Can. J. Chem. Downloaded from www.nrcresearchpress.com by 210.87.254.105 on 09/06/12
For personal use only.

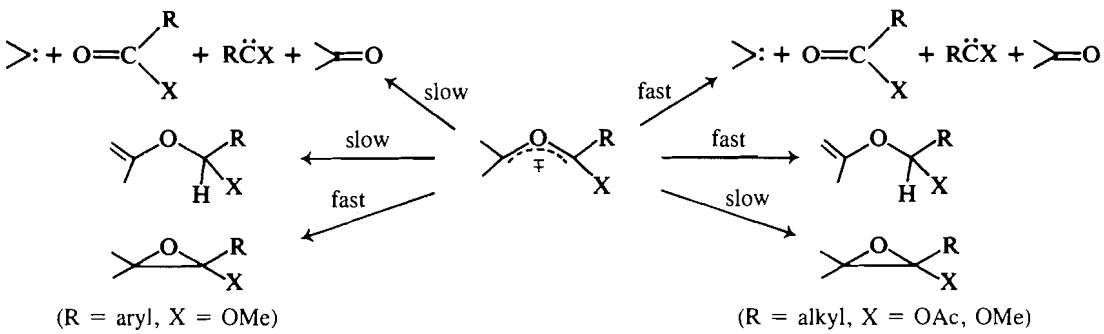

SCHEME 1

[1] 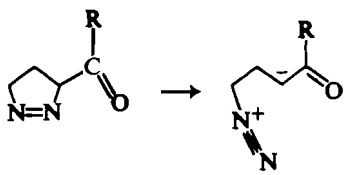

are discreet steps) with conventional mechanistic terminology (21).

Mechanisms of thermolysis of Δ^3-1,3,4-oxadiazolines (oxy analogues of pyrazolines) have not been studied extensively. Small solvent effects and small aryl substituent effects on the rate constants for thermolysis of **1** were interpreted in terms of concerted extrusion of N_2 (22), leading to a carbonyl ylide (eq. [2]). Although dipolar contributors to **2** suggest that the

[2] 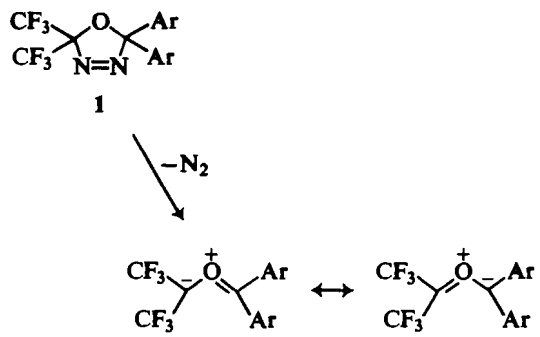

1 **2**

benzylic carbon ought to become negative at the transition state for concerted decomposition, aryl substituent effects were correlated with σ^+ constants with $\rho^+ = -0.50$, suggesting development of positive charge there. Stepwise scission of the C—N bonds in the thermolysis of **3** (eq. [3]) was proposed (23), in part to account for the presence of oxirane among the reaction products from **3***a* but not among those from **3***b*. Although

[3] 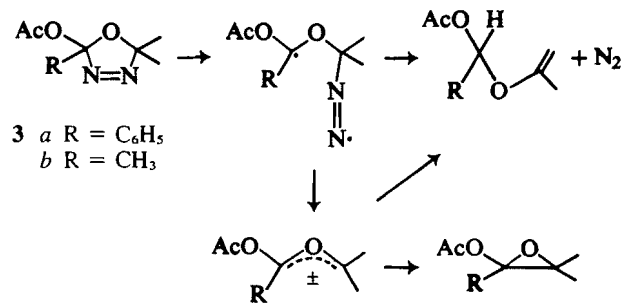

3 *a* R = C_6H_5
b R = CH_3

that mechanism could account for some additional features, such as very low yields of cycloadduct from thermolysis of compounds like **3***b* in the presence of neat acrylonitrile, it has been pointed out (10) that the rate factor (k_{3a}/k_{3b}) is smaller than might be expected for a stepwise mechanism. Moreover, it has been found subsequently that both trialkylacetoxy- (24) and trialkylalkoxy-substituted carbonyl ylides (25, 26) can fragment to carbenes and carbonyl compounds more rapidly (27) than they can close to oxiranes. An intramolecular 1,4-hydrogen shift is also fast relative to oxirane formation, in some systems. On the other hand, an aryl substituent at the ylide carbon which bears the alkoxy group slows or stops both ylide fragmentation and intramolecular H-transfer (27). Those results, summarized in Scheme 1, can be interpreted in terms of ylide chemistry alone without invoking a diazenyl diradical intermediate (23) as the precursor of that ylide. However, in view of recent evidence for stepwise homolysis of a number of unsymmetric (28) and symmetric (29, 30) acyclic azo compounds, it would be premature to dismiss the diazenyl diradical mechanism of oxadiazoline thermolysis entirely at this time.

In view of the considerable potential of carbonyl ylides, not only as intermediates for cycloadditions but also as sources of carbenes (24–27), we began studies aimed at elucidating the mechanisms of ylide formation from oxadiazolines and of intramolecular and intermolecular ylide reactions.[3] We report here some substituent effects and solvent effects on rate constants for unimolecular thermolysis of oxadiazolines **4** and **5**.

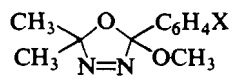

4 *a* X = *p*-OCH_3
b X = *p*-CH_3
c X = H
d X = *p*-Cl
e X = *p*-CF_3
f X = *p*-NO_2

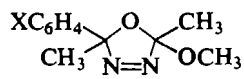

5 *a* X = *p*-OCH_3
b X = H
c X = *p*-Br

Methods, results, and discussion

2-Methoxyoxadiazolines **4** were synthesized by oxidation of the appropriate hydrazones with lead tetraacetate (LTA) in methanol, eq. [4] (24–27, 31, 32). The corresponding 2-acetoxyoxadiazolines (eq. [4]), which are always obtained as

[3] Ylide chemistry is being investigated wih the use of laser flash spectroscopy, in collaboration with Drs. J. C. Scaiano and W. J. Leigh.

Can. J. Chem. Downloaded from www.nrcresearchpress.com by 210.87.254.105 on 09/06/12
For personal use only.

Can. J. Chem. Downloaded from www.nrcresearchpress.com by 210.87.254.105 on 09/06/12
For personal use only.

TABLE 1. Oxadiazolines **4**[a] and **5**

Compound	Yield (%)	^{1}H nmr ($CDCl_3$, TMS)	^{13}C nmr ($CDCl_3$, TMS)	
4*a*	59	1.40 (s, 3H), 1.56 (s, 3H) 3.06 (s, 3H), 3.67 (s, 3H) 6.73 (d, 2H), 7.43 (d, 2H)	24.06 (CH_3) 24.50 (CH_3) 50.74 (OCH_3) 55.28 (OCH_3) 113.69 (Ar)	121.81 (C-5) 127.81 (Ar) 128.24 133.22 (C-2) 160.24 (Ar)
4*b*	55	1.40 (s, 3H), 1.56 (s, 3H) 2.30 (s, 3H), 3.08 (s, 3H) 7.10 (d, 2H), 7.50 (d, 2H)	24.35 (CH_3) 24.20 (CH_3) 24.57 (CH_3) 50.89 (OCH_3) 122.03 (C-5)	126.80 (Ar) 129.27 (Ar) 132.85 (C-2 or Ar) 133.84 (Ar or C-2) 139.72 (Ar)
4*c*	47	1.43 (s, 3H), 1.60 (s, 3H) 3.13 (s, 3H) 7.14–7.70 (m, 5H)	24.13 (CH_3) 24.50 (CH_3) 50.96 (OCH_3) 122.17 (C-5) 126.78 (Ar)	128.54 (Ar) 129.71 (Ar) 133.29 (C-2) 135.70 (Ar)
4*d*	55	1.41 (s, 3H), 1.60 (s, 3H) 3.10 (s, 3H) 7.27 (d, 2H), 7.55 (d, 2H)	24.05 (CH_3) 24.35 (CH_3) 50.82 (OCH_3) 122.32 (C-5) 128.17 (Ar)	128.61 (Ar) 132.63 (C-2) 134.17 (Ar) 139.72 (Ar)
4*e*	54	1.43 (s, 3H), 1.61 (s, 3H) 3.10 (s, 3H) 7.26–7.83 (m, 4H) ^{19}F nmr: 62.66 (s)	24.34 (CH_3) 24.56 (CH_3) 51.10 (OCH_3) 122.97 (C-5)	125.61 (Ar) 127.43 (Ar) 132.69 (C-2) 139.64 (Ar)
4*f*	29	1.43 (s, 3H), 1.67 (s, 3H) 3.14 (s, 3H) 7.58 (d, 2H), 8.03 (d, 2H)	24.35 (CH_3) 24.38 (CH_3) 51.11 (OCH_3) 123.70 (C-5 or Ar) 123.78 (Ar or C-5)	128.03 (Ar) 132.19 (C-2) 142.50 (Ar) 148.35 (Ar)

Compound	Yield (%)	^{1}H nmr
5*a* (*cis*/*trans* isomer plus impurities)	40[b]	1.42 (s, 3H), 1.63 (s, 3H), 1.69 (s, 3H), 1.79 (s, with shoulder), 1.77 (3.8H, total), 1.99 (s, 0.8H, acetoxy imp), 2.03 (s, 0.5 H, acetoxy imp), 2.75 (s, 3H), 3.10 (s, 1.1H, imp), 3.17 (s, 3.1H), 3.72 (s, 6.7H, *p*-OCH_3)[c,d]
5*b* (*cis*/*trans* isomers plus impurities)	40[b]	1.46 (s, 3H), 1.53 (s, 0.7H, imp), 1.70 (s, 3H), 1.78 (s, 0.8H, imp), 1.86 (s, 3.1H), 1.88 (s, 0.6H, imp), 2.04 (s, 1.1H, imp), 2.05 (s, 0.9H, imp), 2.24 (s, 0.7H, imp), 2.54 (s, 0.9H, imp), 2.78 (s, 3H), 3.16 (s, 3H), 3.22 (s, 3.6H)[c,e]
5*c* (*cis*/*trans* isomers plus impurities)	40[b]	1.41 (s, 2.8H), 1.44 (s, 3H), 1.63 (s, 2.7H), 1.70 (s, 3.1H), 1.72 (sh on peak at δ 1.70, 1.6H, imp), 1.79 (s, 3.6H), 2.03 (s, 4.3H), 2.49 (s, 2.2H), 2.74 (s, 3H), 3.10 (s, 5.6H), 3.18 (s, 3H)[c,f]

[a] All compounds **4** had a band in each of the following ranges of the infrared spectrum (cm^{-1}, CCl_4): 1452–1467, 1380–1382, 1365–1368, 1276–1282, 1230–1238, 1195–1197, 1107–1115.

[b] The yield is a rough estimate only, because of the impure state of the product.

[c] In $CDCl_3$ with ref. CH_2Cl_2, δ 5.22.

[d] Peaks at δ 1.42 to δ 1.79 were assigned to methyl groups at C-2 and C-5 of a 1:1 mixture of *cis* and *trans* isomers. Signals at δ 2.75 and 3.17 were assigned to methoxy groups at C-2 in the isomers. The δ 2.75 signal was assigned to the isomer in which the 2-methoxy- and 5-(4-methoxyphenyl) substituents are *cis*. Signals from *p*-methoxy groups of the two isomers are overlapped at δ 3.72, where there is also a contribution from impurities, presumably 2-acetoxy analogues. The aryl region of the spectrum closely resembled that of **4***a* and is not listed. Integrals are listed relative to the four singlets of equal intensity which were assigned "3H".

[e] The singlet at δ 2.78, assigned to the 2-OCH_3 group *cis* to the 5-aryl group, was used as the reference for integration by assigning to it the value "3H".

[f] The reference signal for integration was that at δ 2.74 (see footnote *e*). The singlets at δ 1.44, 2.03, and 3.10 may arise from the products of decomposition of **5***c*. Those three signals remained intense in samples taken to completion of thermolysis.

[4] $(CH_3)_2C{=}NNHCOC_6H_4X$

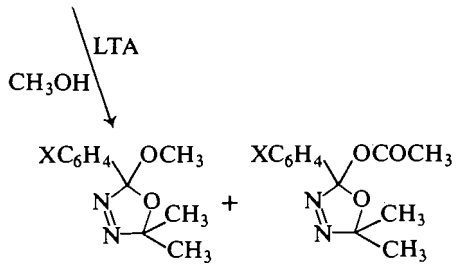

4

coproducts, were destroyed by saponification (24–27, 31) and the residual methoxy compounds were purified by column chromatography (Experimental).

Compounds **5**, which were obtained by analogous oxidation of acetyl hydrazones of acetophenones, proved to be very difficult to obtain in pure form. Acyl hydrazones of acetophenones oxidize more slowly than do those of dialkyl ketones while, at the same time, the oxidation products from the former (2,5-dialkyl-5-aryl-2-alkoxyoxadiazolines) are somewhat more labile than those from the latter (5,5-dialkyl-2-alkoxyoxadiazolines). It was not possible, therefore, to find conditions for the preparation of **5** which did not lead to mixtures of **5**, starting material, and products from thermolysis of **5**. Moreover, the oxidative cyclizations gave **5** and the acetoxy analogue as mixtures of *cis/trans* isomers. Consequently, all experiments with **5** had to be carried out with materials of low purity (ca. 60–80%) and only three members of the series could be obtained at that level of purity. Table 1 lists the spectral data of compounds **4** and of mixtures containing **5**.

Attempts to prepare 5,5-diaryl-2-methoxy-2-methyl oxadiazolines (**6**), to avoid the problem of *cis/trans* isomeric mixtures, were even less rewarding. Acyl hydrazones of benzophenones are still less reactive toward lead tetraacetate than their acetophenone counterparts and the derived oxadiazolines (**6**) appear to be very labile. As a result, conditions which lead to formation of **6** also permitted their rapid thermolysis and no measurements at all could be made on **6**. Hoffmann and Luthardt have reported that the analogous 2,5- and 5,5-diaryl-2-acetoxyoxadiazolines decompose quite rapidly at 0°C (33).

Thermolysis of oxadiazolines was followed by ^1H nmr spectroscopy using peak areas from the electronic integrator, normalized to that of an internal standard such as CH_2Cl_2. Good fits to the first order rate law were obtained, with correlation coefficients typically better than 0.998 for **4**. In the case of **5**, where the substrates were complex mixtures containing geometric isomers of **5**, geometric isomers of the corresponding 2-acetoxy compounds, and products from their decomposition during preparation of the sample, it was important to follow the decay of an appropriate signal in the ^1H nmr spectrum. Fortunately each of the mixtures containing **5***a*–**5***c* gave a distinctive signal (δ 2.75, 2.78, and 2.74, respectively), assignable to a methoxy group at C-2 shielded by a *cis* aryl group at C-5. The spectra of t_∞ samples were free of signals near δ 2.75. There was assurance, therefore, not only that what was being monitored was the concentration of a methoxyoxadiazoline and not that of an acetoxy analogue, but also that the measured rates pertained to the same geometric isomer of the family **5**.

Before beginning a discussion of the substituent and solvent effects on rates we turn briefly to the evidence for the existence of a carbonyl ylide intermediate in the thermolysis of 1,3,4-oxadiazolines. That evidence comes from the finding that oxiranes and/or enol ethers (22, 25, 32) are formed from an intermediate which can be diverted away from those products by methanol (22, 25, 34) and, in some cases, by reactive dipolarophiles (27, 32, 33*b*, 35). Moreover, the compounds resulting from interception of the intermediate have structures expected on the basis of the assumption that the intermediate is a carbonyl ylide, eqs. [5], [6].

[5]

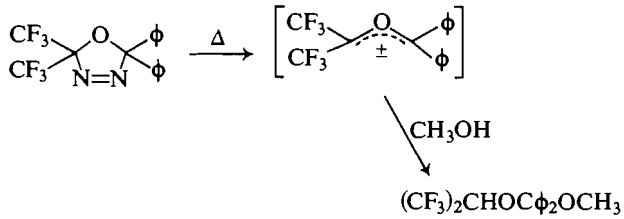

[6]

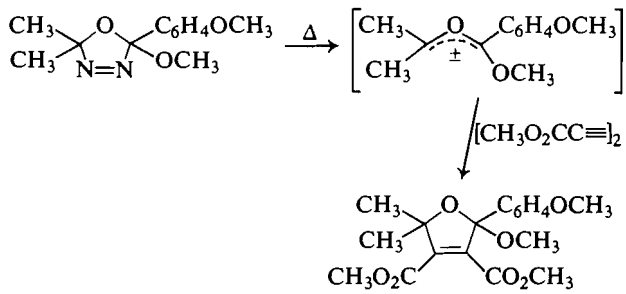

Similar adducts have been obtained by trapping intermediates from non-oxadiazoline sources (36–40), including oxiranes, from which initial intermediates other than carbonyl ylides are particularly hard to imagine.

Oxadiazoline **4***a* had been decomposed earlier (27) in CD_3OD at 79.5°C. The absence of acetone, methyl *p*-methoxybenzoate, and 2-methoxy-2-(4-methoxyphenyl)-3,3-dimethyloxirane reported earlier (27) was noted also in the present study at 49.2°C. Similar results were obtained for other members of the family **4**.

Thermolysis of **4** in CCl_4 gave a complex mixture of products, some of which were not identified. For example, **4***c* gave acetone and methyl benzoate as major products, as well as isopropyl benzoate and at least five additional minor products. 2-Methoxy-2-phenyl-3,3-dimethyloxirane, the expected product of cyclization of a carbonyl ylide intermediate, was not found. That compound was synthesized independently and shown to be thermally stable at temperatures higher than those used for thermolysis of **4** (Experimental section). The fact that oxirane was not found among the products from **4***c*, under conditions that do not cause thermal ring opening of that oxirane, suggests at first that oxirane was not formed. Such a conclusion is probably not warranted, however, because of the possibility that one of the unidentified minor products (a trace amount of HCl for example) acts as a catalyst for ring opening of the oxirane.

Although compounds from the family **5** had not been studied previously, and ylide intermediates had therefore not been demonstrated for them specifically, it was possible to detect an ylide-derived product in the t_∞ samples. In the case of **5***b*, for example, the ^1H nmr spectrum of the thermolysis products

Can. J. Chem. Downloaded from www.nrcresearchpress.com by 210.87.254.105 on 09/06/12
For personal use only.

Can. J. Chem. Downloaded from www.nrcresearchpress.com by 210.87.254.105 on 09/06/12
For personal use only.

included a pair of doublets from vinylic protons (δ 4.8 and 4.3) and a quartet at low field (δ 6.5) characteristic of $H_2C{=}C(Ar)OCH(CH_3)OR$. Although it was not possible to determine whether that minor product had come from **5***b* (R = CH_3) or from the acetoxy analogues present as impurities (R = $COCH_3$), it does not really matter because the mechanistic analogy between 2-methoxy- and 2-acetoxyoxadiazolines is quite well established (24–27).

There is little doubt then that Δ^3-1,3,4-oxadiazolines, in general, undergo thermolysis via carbonyl ylide intermediates and the remaining mechanistic questions are whether the transition state for the rate-determining step involves one or two C—N bond scissions and whether that transition state is dipolar or diradical in character.

The results (Table 2) suggest that the extrusion of N_2 from 2-alkoxy-Δ^3-1,3,4-oxadiazolines may be a concerted process. Substitution of a phenyl group at either C-2 or C-5 leads to an enhanced thermolysis rate constant. Thus, at C-2 the enhancement factors are 3.6 in CCl_4 and 6.4 in CD_3OD at a temperature that is 30° lower than that used for the 2-methyl analogue. The true rate factors can be estimated by assuming that rate constants for **4** would double with every 10° increment in the temperature, for temperatures near 50°C. That assumption leads to estimates of 29 and 51 for the phenyl group effect at C-2, in CCl_4 and in CD_3OD, respectively. Similarly, the rate factor caused by phenyl-for-methyl substitution at C-5 is estimated to be 125. The most likely reason for those effects is that both the C-2 to N-3 and the N-4 to C-5 bonds break in the rate-determining step.[4]

The effects of *p*-substituents in aryl groups at C-2 and at C-5 (Table 2) are similar. In each case electron-withdrawing groups enhance the thermolysis rate constant, indicating that C-2 and C-5 become more electron-rich as the substrates pass from their ground states to the transition states. That is the result that would be expected from a mechanism involving an ylide-like transition state, as the following dipolar contributors to the ylide structure suggest. It was pointed out in the Introduction

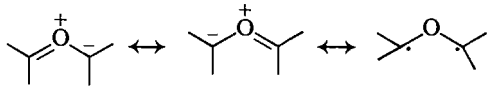

that a previous study (22), with oxadiazoline **1** (eq. [2]), gave the opposite result. In that case the substituent effects indicated that the benzylic carbon became more positive in the transition state than it had been in the ground state. Although that result may appear to be at odds with a concerted mechanism leading to a carbonyl ylide intermediate, it can be rationalized within that mechanistic framework. A highly unsymmetric ylide like **2** might well have a charge distribution described largely by

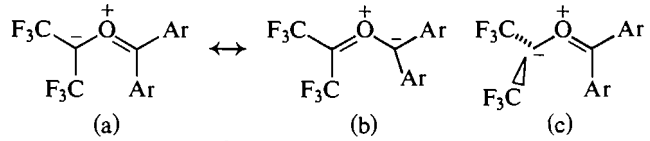

(a) (b) (c)

2

TABLE 2. First order rate constants for thermolysis of oxadiazolines **4** and **5**, at 49.2°C and at 45°C, respectively[a]

Compound	Solvent	$k \times 10^5$ (s^{-1})	σ_p^- of X[b]
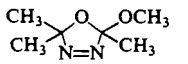	CCl_4	1.39[c]	
	CD_3OD	0.49[c]	
4*a* (*p*-OCH_3)	CCl_4	2.57	−0.27
	CD_3OD	1.57	
4*b* (*p*-CH_3)	CCl_4	3.68	−0.17
	CD_3OD	2.05	
4*c* (H)	CCl_4	5.00	0
	CD_3OD	3.16	
4*d* (*p*-Cl)	CCl_4	7.56	0.23
	CD_3OD	4.76	
4*e* (*p*-CF_3)	CCl_4	12.4	0.65
	CD_3OD	9.68	
4*f* (*p*-NO_2)	CCl_4	39.5	1.24
	CD_3OD	38.3	
5*a* (*p*-OCH_3)	$CDCl_3$	9.9	−0.27
5*b* (H)	$CDCl_3$	22	0
5*c* (*p*-Br)	$CDCl_3$	41	0.23

[a] Water bath (49.20 ± 0.05°C) for compounds **4** and probe (45 ± 1°C) for compounds **5**.

[b] These values were taken to be the same as σ_p-values except for the NO_2 group, for which $\sigma_p = 0.78$, and the CF_3 group, for which $\sigma_p = 0.54$ (41). The correlation coefficients for the Hammett plot for **4**, using σ_p values, were 0.979 (CCl_4) and 0.978 (CD_3OD). Corresponding correlation coefficients from use of σ_p^--values were 0.995 and 0.998.

[c] At 79.5°C.

contributor (a), with only a small weighting accorded to contributor (b). Alternatively, the ground state of **2** could be twisted, like the 0°,90° conformation (c), in which also the aryl substituents would "see" the benzylic carbon as a positive site. Whatever the reason for the negative ρ-value of Shimizu and Bartlett (22), there is no doubt that the present results, indicating accumulation of *negative* charge at C-2 of **4** and at C-5 of **5** and thereby suggesting that, for each one, negative charge accumulates at *both ends* of the 1,3-fragment, are much more in keeping with expectations based on the classical valence bond structure of a simple carbonyl ylide.

Although the sense of charge redistribution that accompanies extrusion of nitrogen is unmistakable, the ρ-values are quite small[5,6] and it follows that relatively little negative charge develops at C-2 of **4** and at C-5 of **5**. This point is supported strongly by the solvent effects on rates of thermolysis of **4**. For all compounds **4** the rate constants for thermolysis in methanol were slightly smaller than those pertaining to CCl_4 solvent. Such a dependence is a common feature of the thermolysis kinetics of *cis* azo compounds (10, 42, 43). The explanation, in terms of preferential solvation of the polar ground state relative to solvation of the radical-pair-like transition state, can be invoked also for **4** and **5**. The oxadiazolines must have substantial local dipoles with the positive ends at C-2 and C-5, each of which bears an electron-withdrawing azo nitrogen and

[4] It would be desirable to determine rate constants for thermolysis of 2,5-diaryl-2-methoxyoxadiazolines, of course, to ascertain whether or not the aryl groups have additive effects. In view of our difficulties with the purification of **5** we hold out little hope of success for the preparation of 2,5-diaryl analogues in a pure state, using current methodology.

[5] For a list of ρ-values for reactions of known mechanism, see ref. 42. For example, displacement of Cl from 1-chloro-2-nitro-4-X benzenes by methoxide in methanol is correlated with σ^--values for X, with ρ (50°C) = 3.9.

[6] With only three points in hand, the ρ-value for **5** is not very reliable, of course.

Can. J. Chem. Downloaded from www.nrcresearchpress.com by 210.87.254.105 on 09/06/12
For personal use only.

one or two alkoxy groups. Since the dipole vectors from the azo and alkoxy substituents are additive, the oxadiazolines must be more polar than a simple *cis* azo compound and therefore at least as strongly solvated in polar media. Concerted loss of nitrogen from **4** or **5** would cause a larger reduction of substrate polarity than would the first step of a stepwise mechanism, in which one dipolar centre is effectively retained. The concerted mechanism therefore accommodates the solvent effect particularly well, especially if compensating polarity in the ylide product is poorly developed at the transition state.

In summary, the following description of the transition state appears to fit the information best. Both C—N bonds are partially severed and the C—O—C portion of the 5-membered ring has made some progress, by conrotatory motion, toward the 0°,0° ground state geometry of the carbonyl ylide product. Relatively little resonance stabilization, which requires full coplanarity if it is to be important, has accrued and, as a result, there is only a little ylide-like charge separation.

An alternative picture would have the transition state more product-like and would explain away the small ρ-value by invoking largely diradical character for the ylide itself, and therefore also for the transition state leading to it. Support for the view that many 1,3-dipoles are really more diradicaloid than dipolar comes from theory (44–46) and awaits experimental testing.

Experimental

2-Methoxy-2-(4-methoxyphenyl)-5,5-dimethyl-Δ^3-1,3,4-oxadiazoline **4***a*

To an ice-cold solution of lead tetraacetate (4.8 g, 10.8 mmol) in dry methanol (30 mL) was added acetone-N-(4-methoxybenzoyl)-hydrazone (2.0 g, 9.7 mmol), with stirring. When the yellow colour of the solution had been discharged, potassium hydroxide (pellets, 1 g) was added and the reaction mixture was stirred for 2 h at ice temperature. Much of the methanol was removed with a rotary evaporator without heating, water was added, and the aqueous solution/suspension was extracted with dichloromethane. After the extract had been dried over calcium chloride, the solvent was evaporated and the residue was chromatographed on basic alumina in a water-cooled column (ca. 10°C) using ether (5%) in hexane. The first fraction eluted was **4***a* (1.4 g, 59% yield); ms (ei mode, *m/z*): 135 ($CH_3OC_6H_4CO^+$), 107 ($CH_3OC_6H_4^+$), 92 ($C_6H_4O^+$); nmr spectra in Table 1.

2-Methoxy-5,5-dimethyl-2-(4-methylphenyl)-Δ^3-1,3,4-oxadiazoline **4***b*

The procedure described above for the preparation of **4***a* was followed. Oxidation of acetone-N-(4-methylbenzoyl)hydrazone afforded **4***b* in 55% yield; ms (ei mode, *m/z*): 150 ($CH_3C_6H_4CO_2CH_3^+$), 119 ($CH_3C_6H_4CO^+$), 91 ($C_7H_7^+$); nmr spectra in Table 1.

2-Methoxy-5,5-dimethyl-2-phenyl-Δ^3-1,3,4-oxadiazoline **4**c

This material was obtained in 47% yield by the procedure already described; ms (ei mode, *m/z*): 136 ($C_6H_5CO_2CH_3^+$), 105 ($C_6H_5CO^+$), 77 ($C_6H_5^+$); nmr spectra in Table 1.

2-(4-Chlorophenyl)-2-methoxy-5,5-dimethyl-Δ^3-1,3,4-oxadiazoline **4**d

Oxidation of acetone-*p*-chlorobenzoyl hydrazone as described above for analogues gave **4***d* in 55% yield; ms (ei mode, *m/z*): 141, 139 ($ClC_6H_4CO^+$); 113, 111 ($C_6H_4Cl^+$); nmr spectra in Table 1.

2-(4-Trifluoromethylphenyl)-2-methoxy-5,5-dimethyl-Δ^3-1,3,4-oxadiazoline **4**e

Compound **4***e* was obtained in 54% yield by the general procedure; ms (ei mode, *m/z*): 173 ($CF_3C_6H_4CO^+$), 145 ($CF_3C_6H_4^+$); nmr spectra in Table 1.

2-Methoxy-5,5-dimethyl-2-(4-nitrophenyl)-Δ^3-1,3,4-oxadiazoline **4**f

The general procedure afforded **4***f* in low yield (29%); ms (ei mode, *m/z*): 150 ($O_2NC_6H_4CO^+$), 104 ($C_6H_4CO^+$), 76 ($C_6H_4^+$); nmr spectra in Table 1.

2-Methoxy-5-(4-methoxyphenyl)-2,5-dimethyl-Δ^3-1,3,4-oxadiazoline **5**a *(*cis *and* trans *isomers containing 2-acetoxy analogues)*

p-Methoxyacetophenone-N-acetylhydrazone (1.0 g, 4.9 mmol) was added to an ice-cold solution of lead tetraacetate (3.02 g, 7.2 mmol, washed free of acetic acid with 30–60°C petroleum ether) in absolute methanol (50 mL). The resulting solution was placed in a freezer compartment (−33°C) where it was kept for 24 h. The solution was then kept at 0°C for 7 h, during which time it became colourless. A few pellets of KOH were added and stirring was continued, at 0°C, for 4 h more. A white precipitate was formed during that period. Cold water and cold dichloromethane were added and the resulting mixture was filtered through Celite. The methylene chloride layer was separated, washed with water, and dried in the refrigerator over $CaCl_2$. Evaporation of most of the solvent with a rotary evaporator and addition of $CDCl_3$ at room temperature gave a solution from which gas was evolved slowly (bubbles); ^{1}H nmr spectrum in Table 1.

2-Methoxy-2,5-dimethyl-5-phenyl-Δ^3-1,3,4-oxadiazoline **5**b *(*cis *and* trans *isomers containing 2-acetoxy analogues*

Oxidation of acetophenone-N-acetylhydrazone, by the procedure described above for preparation of **5***a*, gave a solution ($CDCl_3$) containing **5***b* from which gas was evolved at room temperature; ^{1}H nmr spectrum in Table 1.

5-(4-Bromophenyl)-2-methoxy-2,5-dimethyl-Δ^3-1,3,4-oxadiazoline **5**c *(*cis *and* trans *isomers containing 2-acetoxy analogues)*

Oxidation of *p*-bromoacetophenone-N-acetylhydrazone by the procedure described for preparation of **5***a* afforded a solution of crude **5***c* from which gas was evolved slowly at room temperature; ^{1}H nmr spectrum in Table 1.

Kinetics of thermolysis of **4**

An oxadiazoline **4** (20 mg) was dissolved in 0.5 mL of the solvent (CD_3OD or CCl_4) containing a small amount of CH_2Cl_2, which served as internal standard for integration. The solution was transferred to an nmr tube fitted with a ground glass joint and it was subjected to three cycles of freeze–pump–thaw degassing at 10^{-2} Torr (1 Torr = 133 Pa) before the tube was sealed.

Temperature was controlled with a water bath at 49.2 ± 0.05°C. The tube was withdrawn from the bath and chilled before an analysis of the contents by ^{1}H nmr spectroscopy. Time spent by a tube outside the bath, which included a brief period in the spectrometer probe at ca. 35°C, was not counted.

Progress of the reaction was followed by integrating the signal from the 2-methoxy substituent of the substrate and that from the internal standard. A plot of ln (relative integral) against time was linear. Typically, a reaction was followed to 80% or more of completion and each compound was thermolyzed at least twice in each solvent.

Kinetics of thermolysis of **5**

A solution of **5** in $CDCl_3$ containing CH_2Cl_2, which was prepared in order to acquire the ^{1}H nmr spectrum (see synthesis of **5***a*), was used directly for the kinetic studies. The sample was kept in the probe (T = 45°C), in a tightly-capped nmr tube, for the duration of the kinetic run (about two half-lives), during which time 14 to 20 readings were taken of the integral of the signal being monitored (**5***a*, δ 2.75; **5***b*, δ 2.78; **5***c*, δ 2.74) and of the integral of the signal from CH_2Cl_2. Correlation coefficients for plots of ln (relative integral) against time had the values 0.988, 0.996, and 0.994 for **5***a*, **5***b*, and **5***c*, respectively.

α-Bromoisobutyrophenone

Isobutyrophenone (1.48 g, 0.010 mol) in CCl_4 (10 mL) containing acetic acid (1 mL) was treated with Br_2 (1.60 g, 0.010 mol). Ether was added and the resulting solution was washed with aqueous sodium bicarbonate and with brine before it was dried over $MgSO_4$. Filtration, followed by evaporation of the solvents, left 2.27 g (98%) of crude

bromoketone: ^{1}H nmr (δ, CCl_4, TMS): 2.00 (s, 6H), 7.45 (m, 3H), 8.16 (m, 2H).

2-Methoxy-2-phenyl-3,3-dimethyloxirane

Following the procedure of Stevens and Dykstra (47) a solution of α-bromoisobutyrophenone (2.27 g, 0.010 mol) in methanol (15 mL) was heated to reflux and sodium methoxide (0.010 mol) in methanol (10 mL) was added. The resulting solution was refluxed for 10 min before it was poured onto ice. Extraction of the aqueous methanol with hexane, followed by drying and evaporation of the hexane, left the title compound (1.58 g, 90%) as an oil; ^{1}H nmr (δ, CCl_4, TMS): 0.97 (s, 3H), 1.47 (s, 3H), 3.17 (s, 3H), 7.36 (m, 5H). Singlets at δ 1.03, 1.20, 1.57, and 3.30, from impurities, accounted for about 8% of the total integral.

Thermal stability of 2-methoxy-2-phenyl-3,3-dimethyloxirane in benzene and in carbon tetrachloride

The oxirane described above (20 mg), dissolved in benzene (0.5 mL) and sealed into an nmr tube, was heated at 80°C in an oil bath for 96 h. The ^{1}H nmr spectrum at the end of the heating period was indistinguishable from that of the unheated sample, indicating that the oxirane is persistent at 80°C in benzene; ^{1}H nmr (C_6H_6 solvent, rel. C_6H_6 at δ 7.40): 1.10 (s, 3H), 1.76 (s, 3H), 3.33 (s, 3H), ArH obscured by solvent.

A similar sample, but containing also dimethyl acetylenedicarboxylate (56 mg) to test for reversible formation of ylide, was not altered after 96 h at 80°C as judged from the ^{1}H nmr spectrum.

An analogous sample of the oxirane in CCl_4 solvent that had been washed with bicarbonate, dried, and distilled, was not affected by heating for 100 h at 50°C or for 90 h at 80°C.

Acknowledgments

Financial support of this work, from the Natural Sciences and Engineering Research Council of Canada, is gratefully acknowledged. We extend thanks to Dr. P. A. Risbood for the synthesis of 2-methoxy-2-phenyl-3,3-dimethyloxirane and to Mr. E. Y. Osei-Twum for testing its thermal stability.

1. I. R. Dunkin. *In* Org. React. Mech. *Edited by* A. C. Knipe and W. E. Watts. Wiley, New York. 1981. Chapt. 13.
2. I. R. Dunkin. *In* Org. React. Mech. *Edited by* A. C. Knipe and W. E. Watts. Wiley, New York. 1980. Chapt. 13.
3. R. Huisgen. Pure Appl. Chem. **53**, 171 (1981).
4. R. Huisgen. Pure Appl. Chem. **52**, 2283 (1980).
5. J. Sauer and R. Sustmann. Angew. Chem. Int. Ed. Engl. **19**, 779 (1980).
6. K. N. Houk. Top. Curr. Chem. **79**, 1 (1979).
7. R. M. Kellogg. Tetrahedron, **32**, 2165 (1976).
8. G. Bianchi, C. D. Micheli, and R. Gandolfi. Angew. Chem. Int. Ed. Engl. **18**, 721 (1979).
9. H. Maier and K. Zeller. Angew. Chem. Int. Ed. Engl. **16**, 835 (1977).
10. P. S. Engel. Chem. Rev. **80**, 99 (1980).
11. M. J. Begley, F. M. Dean, L. E. Houghten, R. S. Johnson, and K. B. Park. J. Chem. Soc. Chem. Commun. 461 (1978).
12. M. Schneider and H. Ströhacker. Tetrahedron, **32**, 619 (1976).
13. C. G. Overberger, N. Weinshenker, and J. P. Anselme. J. Am. Chem. Soc. **86**, 5364 (1964).
14. M. Schneider. Angew. Chem. Int. Ed. Engl. **14**, 707 (1967).
15. R. J. Crawford and D. M. Cameron. Can. J. Chem. **45**, 691 (1967).
16. R. J. Crawford and M. Ohno. Can. J. Chem. **52**, 3134 (1974).
17. R. J. Crawford and A. Mishra. J. Am. Chem. Soc. **88**, 3963 (1966).
18. W. R. Roth and M. Martin. Justus Liebigs Ann. Chem. **702**, 1 (1967).
19. W. R. Roth and M. Martin. Tetrahedron Lett. 4695 (1967).
20. P. C. Hiberty and Y. Jean. J. Am. Chem. Soc. **101**, 2538 (1979).
21. T. C. Clarke, L. A. Wendling, and R. G. Bergman. J. Am. Chem. Soc. **99**, 2740 (1977).
22. N. Shimizu and P. D. Bartlett. J. Am. Chem. Soc. **100**, 4260 (1978).
23. D. W. K. Yeung, G. A. MacAlpine, and J. Warkentin. J. Am. Chem. Soc. **100**, 1962 (1978).
24. M. Békhazi and J. Warkentin. J. Org. Chem. **47**, 4870 (1982).
25. M. Békhazi and J. Warkentin. J. Am. Chem. Soc. **103**, 2473 (1981).
26. M. Békhazi and J. Warkentin. J. Am. Chem. Soc. **105**, 1289 (1983).
27. M. Békhazi and J. Warkentin. Can. J. Chem. **61**, 619 (1983).
28. P. S. Engel and D. B. Gerth. J. Am. Chem. Soc. **105**, 6849 (1983).
29. J. J. Dannenberg and D. Rocklin. J. Org. Chem. **47**, 4529 (1982).
30. R. C. Neuman and G. A. Binegar. J. Am. Chem. Soc. **105**, 134 (1983).
31. M. Békhazi and J. Warkentin. J..Am. Chem. Soc. **105**, 5675 (1983).
32. R. W. Hoffmann and H. J. Luthardt. Tetrahedron Lett. 411 (1966).
33. (*a*) R. W. Hoffmann and H. J. Luthardt. Chem. Ber. **101**, 3851 (1968); (*b*) Chem. Ber. **101**, 3861 (1968).
34. S. W. Ege, J. E. Gess, A. Thomas, P. Umrigar, G. W. Griffin, P. K. Das, A. M. Trozzolo, and T. M. Leslie. J. Chem. Soc. Chem. Commun. 1263 (1980).
35. P. Rajagopalan and B. G. Advani. Tetrahedron Lett. 2689 (1967).
36. C. W. Martin, J. A. Landgrebe, and E. Rapp. Chem. Commun. 1438 (1971).
37. M. Hamaguchi and T. Ibata. Tetrahedron Lett. 4475 (1974).
38. A. Dahmen, H. Hamberger, R. Huisgen, and V. Markowski. Chem. Commun. 1192 (1971).
39. T. Do-Minh, A. M. Trozzolo, and G. W. Griffin. J. Am. Chem. Soc. **92**, 1402 (1970).
40. D. R. Arnold and L. A. Karnischky. J. Am. Chem. Soc. **92**, 1404 (1970).
41. J. Shorter. Correlation analysis in organic chemistry. Clarendon Press, Oxford. 1973. Chapt. 2.
42. A. Schulz and C. Rüchardt. Tetrahedron Lett. 3883 (1976).
43. W. Duismann and C. Rüchardt. Chem. Ber. **111**, 596 (1978).
44. R. D. Harcourt and W. Roso. Can. J. Chem. **56**, 1093 (1978).
45. L. B. Harding and W. A. Goddard III. J. Am. Chem. Soc. **100**, 7180 (1978).
46. P. C. Hiberty and G. Ohanessian. J. Am. Chem. Soc. **104**, 66 (1982).
47. C. L. Stevens and S. J. Dykstra. J. Am. Chem. Soc. **75**, 5975 (1953).

Can. J. Chem. Downloaded from www.nrcresearchpress.com by 210.87.254.105 on 09/06/12
For personal use only.

Electron spin resonance study of the hyperfine splitting constants of naturally abundant carbon-13 and nitrogen-15 in diphenylmethyl *tert*-butyl aminoxyl (nitroxide). Solvent and temperature effects

EDWARD G. JANZEN[1]

Department of Chemistry and Biochemistry, Guelph–Waterloo Centre for Graduate Work in Chemistry, University of Guelph, Guelph, Ont., Canada N1G 2W1

Received December 2, 1983

This paper is dedicated to Professor G. E. Dunn on the occasion of his 65th birthday

EDWARD G. JANZEN. Can. J. Chem. **62**, 1653 (1984).

The β-^{13}C and ^{15}N hyperfine splitting constants in the phenyl radical adduct of phenyl *tert*-butyl nitrone (PBN), diphenylmethyl *tert*-butyl aminoxyl, have been measured as a function of solvent and temperature.

EDWARD G. JANZEN. Can. J. Chem. **62**, 1653 (1984).

Opérant à diverses températures et dans divers solvants, on a mesuré les constantes de couplage hyperfin du β-^{13}C et du ^{15}N des adduits du radical phényle avec la phényl *tert*-butyl nitrone (PBN) nommément le diphénylméthyl *tert*-butyl aminoxyle.

[Traduit par le journal]

Introduction

In previous publications the β-^{13}C hyperfine splitting constants (hfsc's) of the cyanyl (1) and trichloromethyl (2) radical adducts of phenyl *tert*-butyl nitrone (PBN) have been reported:

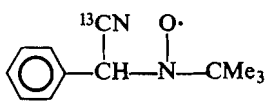

a_N = 15.02, a_β^H = 2.03, $a_\beta^{C\text{-}13}$ = 9.85 G
(in CH_3CN)

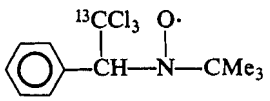

a_N = 14.10, a_β^H = 1.74, $a_\beta^{C\text{-}13}$ = 9.68 G
(in lipid or organic phase)

Since the β-^{13}C hfsc for the methyl adduct is considerably smaller (3), it was of interest to investigate the β-^{13}C hfsc

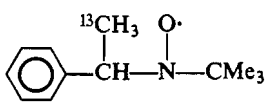

a_N = 14.6, a_β^H = 3.6, $a_\beta^{C\text{-}13}$ = 3.15 G
(in benzene)

for the phenyl adduct where the time-average conformation of the diphenylmethyl group is more readily assigned:

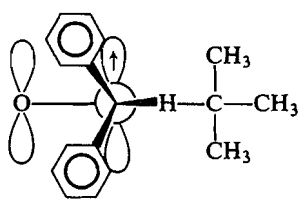

Experimental

Diphenylmethyl *tert*-butyl aminoxyl was prepared in an inert solvent (benzene or acetonitrile) by allowing phenylazotriphenylmethane to decompose in the presence of PBN under nitrogen (4) (overnight at room temperature or about 1 h at 50–70°C in a water bath):

$$(C_6H_5)_3CN_2C_6H_5 \rightarrow (C_6H_5)_3C\cdot + N_2 + C_6H_5\cdot$$

$$C_6H_5\cdot + PBN \rightarrow (C_6H_5)_2CHN(O\cdot)C(CH_3)_3$$

The solution was subsequently exposed to air to remove the signal due to the triphenylmethyl radicals:

$$2(C_6H_5)_3C\cdot + O_2 \rightarrow (C_6H_5)_3COOC(C_6H_5)_3$$

In order to obtain the spectrum in a different solvent, the solvent (benzene or acetonitrile) was evaporated and the new solvent added. Sample solutions were thoroughly purged with nitrogen to remove oxygen (15–20 min vigorous bubbling) before esr experiments were attempted.

An IBM ER200D-SRC spectrometer with an ASPECT data system was used. Although strong signals were obtained, the spectra were accumulated for display on the screen (3–5 scans were sufficient). The cursor was used to locate the maxima and minima of both the parent and satellite peaks (the latter at appropriately higher amplification of stored signal). Peak positions were calculated by computer and recorded in gauss by the printer.

The method used in calculating the hyperfine splittings is given below (see Figs. 1 and 2):

N-14, average of 8 spaces:
3T − 1T,3B − 1B,4T − 2T,4B − 2B,5T − 3T,5B − 3B,6T − 4T,6B − 4B

β-H, average of 6 spaces:
2T − 1T,2B − 1B,4T − 3T,4B − 3B,6T − 5T,6B − 5B

α-^{13}C, 2 × average of 6 spaces:
1T − 1S,1S − 2B,3T − 1S,1S − 4B,5T − 1S,1S − 6B

β-^{13}C, 2 × average of 6 spaces:
1T − OS,OS − 2B,3T − OS,OS − 4B,5T − OS,OS − 6B

N-15, sum of 2 spaces:
(4B − NF) + (NF − 3T)

The repeatability was better than ±0.005 G for N-14 and β-H hfsc's and better than ±0.05 G for α-C-13 and β-C-13 hfsc's. Because the high-field spacing is larger than the low-field spacing for the nitrogen triplet these measurements were averaged.

[1] All experimental work was peformed at the West Coast Customer Centre of IBM Instruments Inc., 40 W. Brokaw Rd., San Jose, CA 95110, U.S.A.

Can. J. Chem. Downloaded from www.nrcresearchpress.com by 210.87.254.40 on 09/06/12
For personal use only.

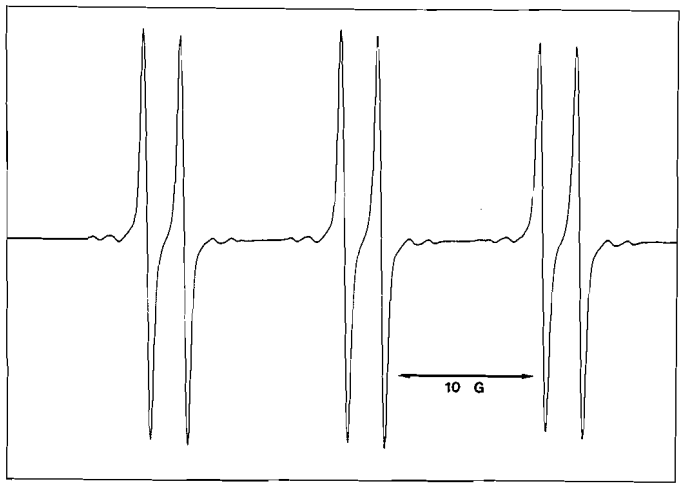

FIG. 1. Electron spin resonance spectrum of diphenylmethyl *tert*-butyl aminoxyl in acetonitrile at room temperature.

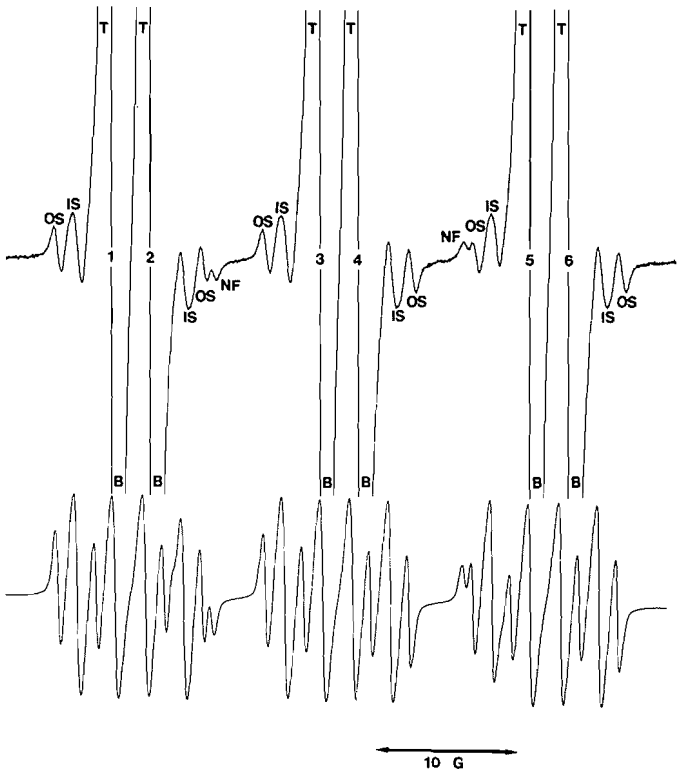

FIG. 2. Electron spin resonance spectrum from Fig. 1 at higher spectrometer gain with computer simulated esr spectrum of a mixture of two aminoxyls: one with N-14, β-H, β-C-13 and the other with N-15 and β-H only.

Results

A typical spectrum consisting of a triplet of doublets due to diphenylmethyl *tert*-butyl aminoxyl is shown in Fig. 1. Satellite peaks are clearly evident. At higher spectrometer gain (Fig. 2) these peaks are strong enough for accurate measurements. Intensity comparisons show that the outside peaks (OS) are due to 2 equivalent ^{13}C atoms and the "extra" two peaks in the spectrum are due to ^{15}N-hfs (marked NF). The OS peaks are assigned to the β-carbons of the phenyl groups of the diphenylmethyl group since the small dihedral angle of the carbon–phenyl bonds (~30° av.) should give the largest β-^{13}C hfsc in the molecule. The inside pair of satellites (IS) are due to 5 approximately equivalent ^{13}C atoms, namely the methyl groups of the *tert*-butyl function and the two α-carbon atoms attached to the nitroxyl nitrogen. This assignment is supported by the fact that in di-*tert*-butyl aminoxyl the α- and β-^{13}C hfsc's are almost the same (5), e.g. $a_{\alpha}^{C\text{-}13} = 4.38$, $a_{\beta}^{C\text{-}13} = 4.35$ G in benzene.

TABLE 1. Hyperfine splitting constants at room temperature

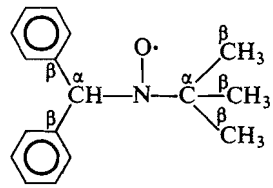

Solvent	$a_{N\text{-}15}$	$a_{N\text{-}14}$	a_{β}^{H}	$a_{\beta\text{-}\phi}^{C\text{-}13}$	$a_{\alpha}^{C\text{-}13}$	$\simeq a_{\beta\text{-}t\text{-}Bu}^{C\text{-}13}$
Hexane	—	14.25	2.10	7.38		—
Toluene	—	14.39	2.17	7.41		—
Benzene	20.37	14.41	2.19	7.41		4.63
Pyridine	20.48	14.59	2.44	7.46		4.86
Methylene chloride	—	14.72	2.69	7.43		—
Acetonitrile	20.65	14.72	2.72	7.50		4.88
Methanol	21.31	15.15	3.12	7.47		—
Water	22.39	16.02	4.23	7.65		—

The same spectrum could be obtained in various solvents, although the OS and NF peaks were sometimes overlapped (e.g. in hexane). On the other hand, the IS peak divided into two peaks in some solvents (e.g. in water) with an apparent intensity ratio of 2:3.

The splitting parameters obtained in eight solvents are given in Table 1. It is evident that all hyperfine coupling constants increase with increase in polarity of the solvent. This observation agrees with the data published for di-*tert*-butyl aminoxyl (5).

The hyperfine splitting constants of diphenylmethyl *tert*-butyl aminoxyl as a function of temperature in four solvents are given in Table 2. The N- and β-H hfsc's increase as a function of temperature in all solvents studied. In contrast, the β-^{13}C hfsc's decrease with increase in temperature in every solvent.

Discussion

In a previous publication (6) the solvent effect on the N- and β-H hfsc of diphenylmethyl *tert*-butyl aminoxyl was reported for 30 solvents. It was found that both the N- and β-H hfsc's increased approximately linearly with solvent polarity. Since the magnitude of the N-hfsc is itself a measure of the solvent polarity (7), the β-hfsc could be plotted against the N-hfsc and a good linear relationship was obtained.

A plot of both the β-H and the β-^{13}C-phenyl hfsc's against the N-hfsc is given in Fig. 3. The increase in β-H and β-^{13}C hfsc with increase in N-hfsc is attributable to the increase in spin density on the nitrogen atom of the nitroxyl function caused by the more polar solvent:

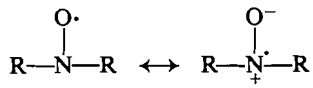

However, the change in β-^{13}C-phenyl hfsc with increase in polarity of solvent is much less than the change in the β-H hfsc

Can. J. Chem. Downloaded from www.nrcresearchpress.com by 210.87.254.40 on 09/06/12
For personal use only.

TABLE 2. Hyperfine splitting constants of diphenylmethyl *tert*-butyl aminoxyl

Temperature (K)	Toluene			Methylene chloride			Acetonitrile			Methanol		
	a_N	a_β^H	a_β^{C-13}	a_N	a_β^H	a_β^{C-13}	a_N	a_β^H	a_β^{C-13}	a_N	a_β^H	a_β^{C-13}
180				14.67	2.68					15.03	3.06	
190				14.68	2.66	7.52				15.07	3.02	
200				14.69	2.66	7.54				15.09	3.02	
210				14.69	2.66	7.54				15.10	3.04	7.51
220	14.28	1.98	7.45	14.70	2.67	7.55				15.09	3.06	7.49
230	14.31	2.00	7.43	14.69	2.67	7.54				15.12	3.08	7.49
240	14.31	2.04	7.43	14.70	2.68	7.52	14.68	2.68	7.54	15.12	3.09	7.52
250	14.32	2.06	7.44	14.70	2.68	7.52	14.67	2.69	7.54	15.13	3.10	7.50
260	14.33	2.09	7.45	14.70	2.68	7.51	14.68	2.70	7.52	15.14	3.11	7.47
270	14.35	2.11	7.41	14.71	2.68	7.48	14.69	2.71	7.49	15.14	3.11	7.50
280	14.36	2.14	7.41	14.70	2.68	7.48	14.71	2.71	7.45	15.15	3.13	7.47
290	14.37	2.16	7.44				14.72	2.72	7.45	15.15	3.13	7.49
300	14.39	2.17	7.41	14.72	2.69	7.43	14.73	2.72	7.49	15.16	3.13	7.47
310							14.74	2.74	7.39			
320							14.74	2.75	7.43			
330							14.76	2.75	7.36			
340							14.77	2.76	7.43			
350							14.78	2.77	7.37			

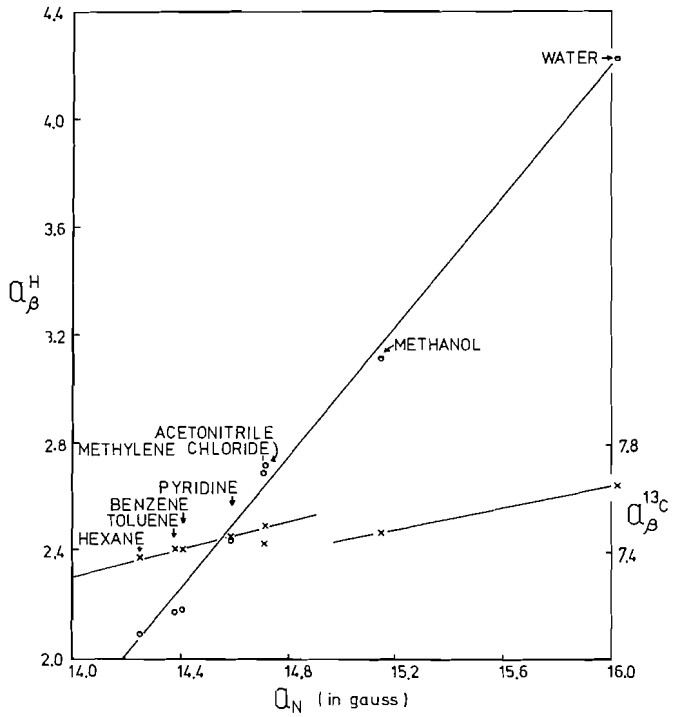

FIG. 3. Plot of a_β^H vs. a_N (in gauss) for diphenylmethyl *tert*-butyl aminoxyl in solvents indicated (left vertical); plot of a_β^{C-13} vs. a_N for same (right vertical).

when plotted against the N-hfsc. In addition there seems to be a discontinuity in the plot so that the points for the β-^{13}C-phenyl hfsc in the two protic solvents (methanol and water) seem to fall off the line marked by the other six solvents. This difference is small but has been seen in another example.[2]

If it is assumed that the Heller–McConnell equation applies for both the proton and the carbon atoms, the smaller values for the β-^{13}C hfsc's must be atrributable to the smaller magnitude of B in the case of carbon. This value can be calculated from the β-^{13}C hfsc in di-*tert*-butyl aminoxyl (5). (a_β^{C-13} = 4.50 G in CH_2Cl_2). If:

$$a_\beta^{C-13} = [B_0^{C-13} + B^{C-13} (\cos \theta_{C-13})^2]\rho_N$$

and $B_0^{C-13} \simeq$ zero, $(\cos \theta_{C-13})^2 \rightarrow \frac{1}{2}$ for freely rotating groups, and $\rho_N \simeq 0.45 \pm 0.05$, then $B^{C-13} = 20 \pm 2$. Then:

$$a_\beta^{C-13} \simeq 18\text{–}22 (\cos \theta)^2 \rho_N$$

For aminoxyls:

$$a_\beta^{C-13} \simeq 7\text{–}11 (\cos \theta)^2 \text{ for } \rho_N = 0.40\text{–}0.50$$

As a check, the predicted value of a_β^{C-13} for the β-carbons of the phenyl groups of diphenylmethyl *tert*-butyl aminoxyl is about 5–8 gauss, assuming $\theta \simeq 30°$, which is in good agreement with experiment.

Using this value it is clear that in the cyanyl and trichloromethyl adducts, where $a_\beta^{C-13} \simeq 10$ gauss, the CN and CCl_3 groups must almost eclipse the *p*-orbital of the nitrogen atom of the nitroxyl function:[3]

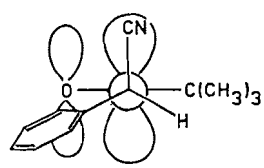

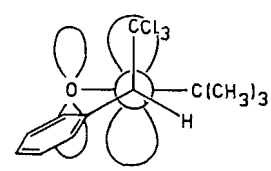

On the other hand, the smaller β-^{13}C hfsc in the methyl adduct (3.15 gauss) must mean that the most stable time-average conformation is quite different. Thus from the equation

$$3.15 \simeq 20 \pm 2 (\cos \theta)^2 (0.45 \pm 0.05)$$

it is possible to estimate that $\theta_\beta^{C-13} = 53 \pm 4°$ for the methyl adduct of PBN.

[2] Unpublished results of C. M. DuBose.

[3] The β-^{13}C hfsc's for aminoxyls with polar groups in the β-position will be the subject of further publications.

Can. J. Chem. Downloaded from www.nrcresearchpress.com by 210.87.254.40 on 09/06/12
For personal use only.

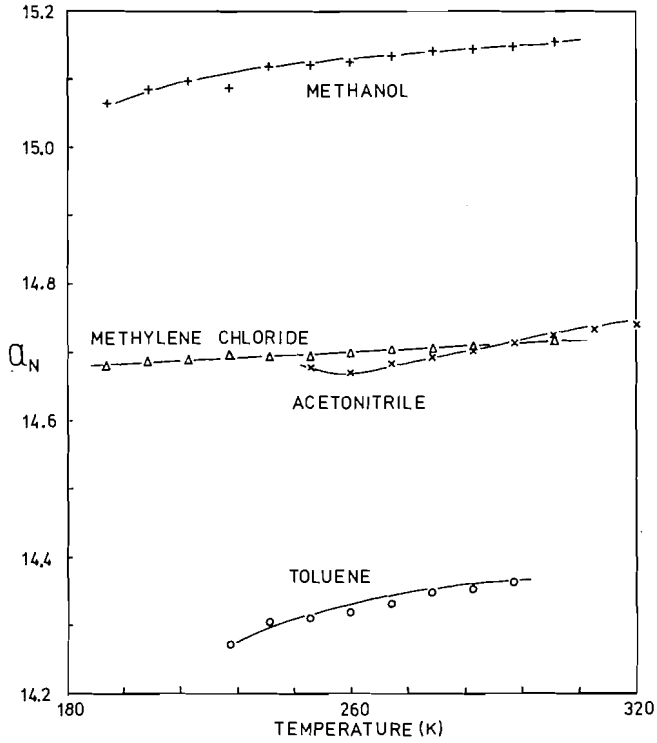

FIG. 4. Plot of a_N vs. temperature (K) for diphenylmethyl *tert*-butyl aminoxyl in four solvents (as indicated).

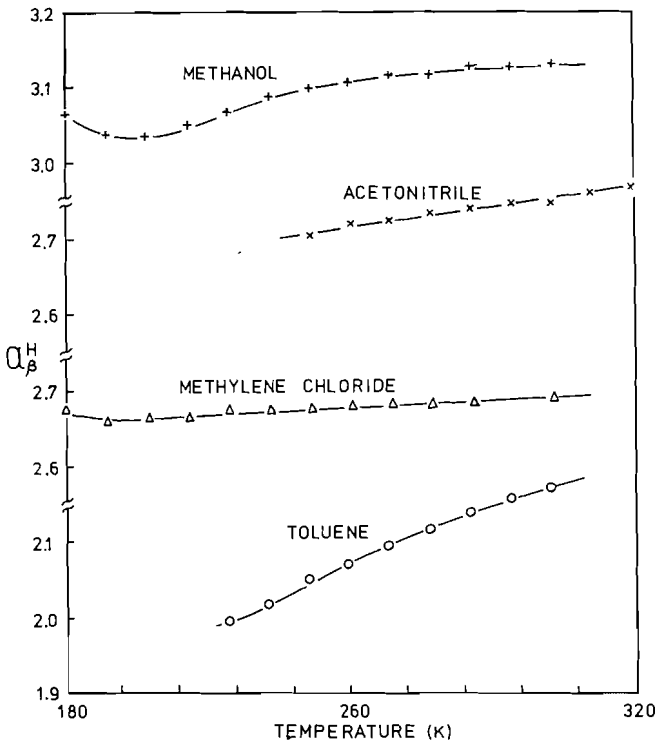

FIG. 5. Plot of a_β^H vs. temperature (K) for diphenylmethyl *tert*-butyl aminoxyl in four solvents (as indicated).

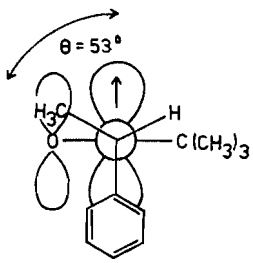

A plot of the N-hfsc as a function of temperature is shown in Fig. 4. The plots all show that the N-hfsc increases slightly with increase in temperature. Slight curvature may be present, which is in the same direction for methanol, methylene chloride, and toluene, but spectra due to slightly immobilized aminoxyls were obtained at low temperatures. According to Bullock and Howard (8), aminoxyls which are planar or almost planar show this temperature effect, i.e. the N-hfsc increases with increase in temperature. This is because, as the temperature is raised, the groups around the nitrogen atom spend more time above and below the $C_2NO\cdot$ plane. Thus the N-hfsc increases because the *s*-character of the orbital containing the unpaired electron is greater in a nonplanar nitroxyl function. However, Griller (9) has found that in some solvents (cyclopentane and ethanol) the change in N-hfsc for di-*tert*-butyl aminoxyl as a function of temperature can be attributed to volume change in the solvent.

A plot of the β-H hfsc as a function of temperature is given in Fig. 5. The β-H hfsc's increase with increase in temperature with different slopes as a function of solvent. The plot is almost flat for methylene chloride, whereas the slope is greatest for toluene and acetonitrile.

The increase in the β-H hfsc is expected with increase in temperature if the oscillation of the diphenylmethyl group is

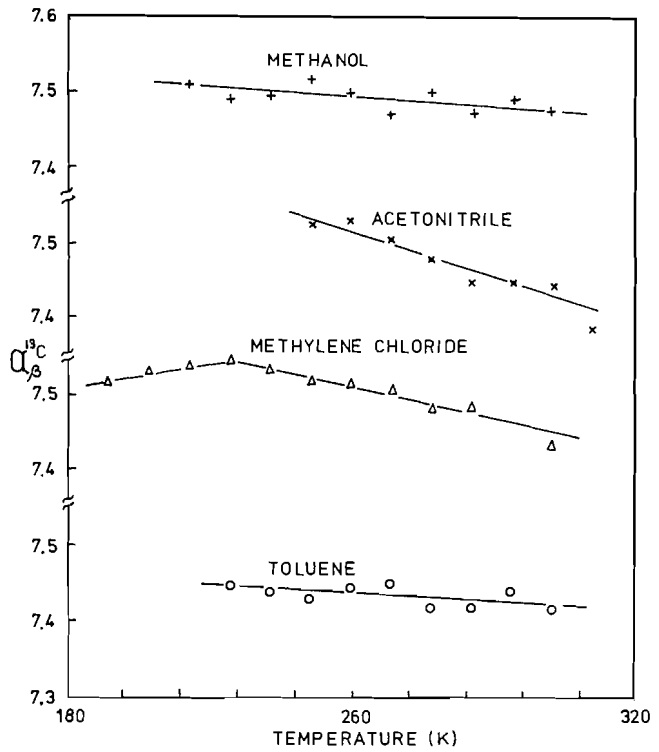

FIG. 6. Plot of $a_\beta^{C\text{-}13}$ vs. temperature (K) for diphenylmethyl *tert*-butyl aminoxyl in four solvents (as indicated).

increased at higher temperatures. This places the C—H bond above and below the eclipsing C—N bond at smaller dihedral angles to the *p*-orbital on nitrogen. Since the magnitude of deviation from planarity of the nitroxyl function also increases with increase in temperature, these motions may be correlated:

Can. J. Chem. Downloaded from www.nrcresearchpress.com by 210.87.254.40 on 09/06/12
For personal use only.

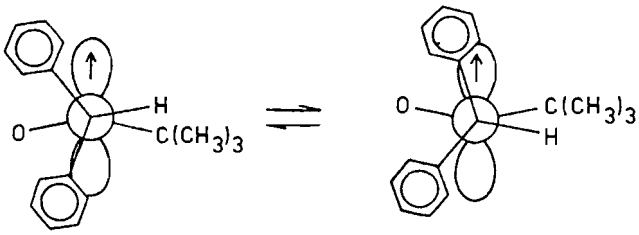

Figure 6 shows the plot of the β-^{13}C hfsc as a function of temperature. In each solvent the magnitude of the β-^{13}C hfsc decreases with increase in temperature. The slopes are different for each solvent but little, if any, curvature is found.

In order to account for the fact that the β-^{13}C hfsc decreases with increase in temperature, a plot of $(\cos\theta)^2$ as a function of θ should be considered:

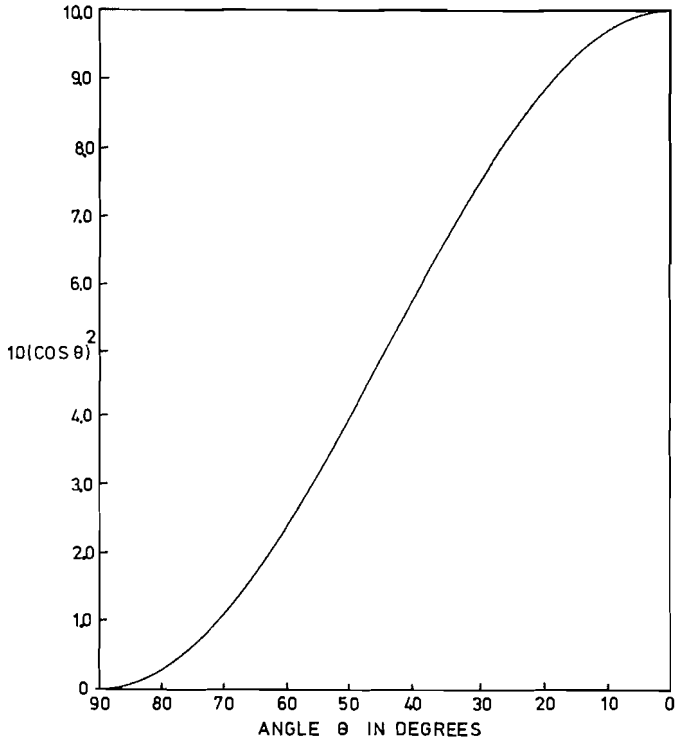

It is expected that when $\theta < 45°$, larger oscillations will bring about smaller hfsc's, as found for the β-^{13}C hfsc's in diphenylmethyl *tert*-butyl aminoxyl. On the other hand, when $\theta > 45°$, increasing the temperature should lead to larger hfsc's, as found for the β-H hfsc's of the same aminoxyl as shown in Fig. 5. However, specific solvent effects seem to exist. The differences in the slopes of the plots of the β-H and β-C-13 hfsc's as a function of temperature in different solvents may be the result of small changes in θ from one solvent to another.[4]

In conclusion, the reported results indicate that the β-H and β-C-13 hfsc's in diphenylmethyl *tert*-butyl aminoxyl respond to solvent and temperature in predictable ways, i.e. both increase with increase in solvent polarity, and the β-H hfsc increases with increase in temperature while the β-C-13 hfsc decreases with increase in temperature. It is noteworthy that the effect of temperature on the hfsc's of diphenyl *tert*-butyl aminoxyl is *very* small, and in any case much smaller than the effect of solvent polarity.

Acknowledgements

The author gratefully acknowledges the help of Mr. Uwe M. Oehler in discussions and preparation of this manuscript. The author also wishes to thank Dr. D. D. Thomas and IBM Instruments Inc. for arranging a 6-month stay in the West Coast Customer Center where this work was done.

1. E. G. JANZEN, and H. J. STRONKS. J. Phys. Chem. **85**, 3952 (1981).
2. J. L. POYER, P. B. MCCAY, E. K. LAI, E. G. JANZEN, and E. R. DAVIS. Biochem. Biophys. Res. Commun. **94**, 1154 (1980).
3. P. SCHMID and K. U. INGOLD. J. Am. Chem. Soc. **100**, 2493 (1978).
4. E. G. JANZEN and C. A. EVANS. J. Am. Chem. Soc. **97**, 205 (1975).
5. R. BRIERE, G. CHAPELET-LETOURNEUX, H. LEMAIRE, and A. RASSAT. Mol. Phys. **20**, 211 (1971).
6. E. G. JANZEN, G. A. COULTER, U. M. OEHLER, and J. P. BERGSMA. Can. J. Chem. **60**, 2725 (1982).
7. B. R. KNAUER and J. J. NAPIER. J. Am. Chem. Soc. **98**, 4395 (1976).
8. A. T. BULLOCK and C. B. HOWARD. J. Chem. Soc. Faraday Trans. 1, **76**, 1296 (1980).
9. D. GRILLER. J. Am. Chem. Soc. **100**, 5240 (1978).
10. A. H. REDDOCH and S. KONISHI. J. Chem. Phys. **70**, 2121 (1979).

[4] For a discussion of specific solvent effects on aminoxyls see, for example, ref. 10.

Can. J. Chem. Downloaded from www.nrcresearchpress.com by 210.87.254.40 on 09/06/12
For personal use only.

Enthalpies of fusion and heat capacities for $H_2{}^{18}O$ ice and $H_2{}^{18}O$ tetrahydrofuran clathrate hydrate in the range 100–270 K[1]

Y. P. HANDA

Division of Chemistry, National Research Council of Canada, Ottawa, Ont., Canada K1A 0R9

Received January 10, 1984

Y. P. HANDA. Can. J. Chem. **62**, 1659 (1984).

Heat capacities between 100 and 270 K and enthalpies of fusion for $H_2{}^{18}O$ and tetrahydrofuran clathrate hydrate THF·16.9$H_2{}^{18}O$ have been determined using a heat flow calorimeter. The results are compared with the corresponding systems containing $H_2{}^{16}O$. The isotope effects on heat capacities, enthalpies of fusion, and temperature of fusion have been used to calculate ^{18}O fractionation factors, α, for the solid–liquid equilibrium in water and the hydrate. For $H_2{}^{18}O$, $\alpha = 1.0032 \pm 0.0007$ at 273.2 K and for THF·16.9$H_2{}^{18}O$, $\alpha = 1.0037 \pm 0.0006$ at 277.3 K.

Y. P. HANDA. Can. J. Chem. **62**, 1659 (1984).

Faisant appel à un calorimètre à écoulement de chaleur et opérant entre 100 et 270 K, on a déterminé les capacités calorifiques et les enthalpies de fusion du $H_2{}^{18}O$ et du clathrate THF·16,9$H_2{}^{18}O$. On a comparé les résultats à ceux obtenus avec les systèmes correspondants contenant du $H_2{}^{16}O$. On a utilisé les effets isotopiques sur les capacités calorifiques, les enthalpies de fusion et la température de fusion pour calculer les facteurs de fractionnement, α, du ^{18}O, pour l'équilibre solide–liquide dans l'eau et dans l'hydrate. Pour le $H_2{}^{18}O$ la valeur de $\alpha = 1{,}0032 \pm 0{,}0007$ à 273,2 K et pour le THF·16,9$H_2{}^{18}O$, $\alpha = 1{,}00037 \pm 0{,}0006$ à 277,3 K.

[Traduit par le journal]

Introduction

There have been several studies of deuterium isotope effect on the thermophysical properties of ice (1, 2) and clathrate hydrates (3, 4). The ^{18}O isotope effect on the thermal properties of these systems does not appear to have been reported in the literature. In this paper we make an experimental assessment of this effect for the systems $H_2{}^{18}O$–$H_2{}^{16}O$ and THF·16.9$H_2{}^{18}O$ –THF·16.9$H_2{}^{16}O$ where THF is tetrahydrofuran containing the ordinary oxygen. The results have also been used to calculate the ^{18}O fractionation factors in the two systems.

Experimental

Apparatus

An automated Tian-Calvet heat flow calorimeter (SETARAM, Model BT) operating under digital control was used in the temperature scanning mode using scan rates of 9 K h^{-1} for heat capacity measurements and 3 K h^{-1} for enthalpy of fusion measurements. The details of the calorimeter and the operating technique are given elsewhere (5). Heat capacities and enthalpies of fusion are precise to 0.5% and 0.3%, respectively, and temperatures of fusion to 0.05 K.

Samples

Normalized $H_2{}^{18}O$ was obtained from MSD Isotopes, Montreal, with specified composition of 97.17 atom% ^{18}O, 0.28 atom% ^{17}O, and 2.55 atom% ^{16}O. Ice was made from degassed water by slow freezing, followed by thermal annealing at 265 K for 24 h and at 80 K for 12 h.

Uninhibited THF was obtained from Anachemia. It was analysed using a Finnigan 4010 GC/MS and a Perkin Elmer 3920 gas chromatograph and found to be 99.9 mol% pure. It was used without further purification. A solution of composition THF·16.9$H_2{}^{18}O$ was prepared in the calorimeter cell from degassed components. The hydrate was prepared by cycling the temperature of the cell between 263 and 243 K at 24 h intervals for 7 days.

Results and discussion

Clathrate hydrates are non-stoichiometric compounds. In this paper, extensive thermodynamic properties of these compounds refer to that amount of the substance containing 1 mol of water.

Heat capacities

From the calorimetric runs, heat capacities for $H_2{}^{18}O$ and THF·16.9$H_2{}^{18}O$ in the range 100–270 K were obtained at 1 K intervals. By assuming that (*1*) our sample of water is an ideal solution of the three isotopic species $H_2{}^{16}O$, $H_2{}^{17}O$, and $H_2{}^{18}O$; (*2*) molar heat capacity of $H_2{}^{17}O$ is an arithmetic mean of molar heat capacities of $H_2{}^{16}O$ and $H_2{}^{18}O$; (*3*) C_p of water of natural isotopic composition is the same as that of pure $H_2{}^{16}O$, heat capacities pertaining to 100% ^{18}O content were calculated for water using present results and C_p data for ordinary water obtained with the same apparatus (5). Similarly C_p values for THF·16.9$H_2{}^{18}O$ pertaining to 100% ^{18}O content of water were obtained using present results and C_p data for THF·16.9$H_2{}^{16}O$ reported previously (5). For both systems, the correction for the ^{18}O content in the temperature range 100–270 K amounted to 0.4% or less.

The results at selected temperatures are given in Table 1. C_p values in the range 100–270 K (a total of 171 data points) were fitted to a smoothing polynomial by the method of least squares. Each data point was assigned unit weight. The choice of the number of parameters for the fit was based on the application of the *F*-test to the changes of the variance. For $H_2{}^{18}O$ the fit is

$$[1]\quad C_p/(\text{J K}^{-1}\text{ mol}^{-1}) = -0.934 + 0.2394\,(T/\text{K}) - 7.614 \times 10^{-4}\,(T/\text{K})^2 + 1.562 \times 10^{-6}\,(T/\text{K})^3$$

with a standard deviation of 0.12 J K^{-1} mol^{-1}. For THF·16.9$H_2{}^{18}O$ the fit is

$$[2]\quad C_p/(\text{J K}^{-1}\text{ (mol H}_2\text{O)}^{-1}) = 4.951 + 0.2375\,(T/\text{K}) - 9.363 \times 10^{-4}\,(T/\text{K})^2 + 2.274 \times 10^{-6}\,(T/\text{K})^3$$

with a standard deviation of 0.15 J K^{-1} (mol $H_2O)^{-1}$.

The results as represented by eqs. [1] and [2] are plotted in Fig. 1. For comparison, the heat capacities for $H_2{}^{16}O$ and THF·16.9$H_2{}^{16}O$ taken from our previous work (5) are also shown. For water, heat capacities of the ^{18}O system, $C_p{}^{18}$, are higher than that of the ^{16}O system, $C_p{}^{16}$, over the entire temperature range 100–270 K. The ^{18}O effect is 7% at 100 K, decreases with increase in temperature until at 200 K the effect

[1] NRCC No. 23333.

Can. J. Chem. Downloaded from www.nrcresearchpress.com by 210.87.254.6 on 09/06/12
For personal use only.

Can. J. Chem. Downloaded from www.nrcresearchpress.com by 210.87.254.6 on 09/06/12
For personal use only.

TABLE 1. Experimental heat capacities of ice and THF hydrate at selected temperatures

	C_p/(J K^{-1} (mol H_2O)$^{-1}$)	
T/K	$H_2{}^{18}O$	THF·16.9$H_2{}^{18}O$
100	16.93	21.83
110	18.31	22.85
120	19.57	23.92
130	20.82	24.99
140	21.98	25.84
150	23.08	27.32
160	24.26	28.29
170	25.58	29.43
180	26.54	30.74
190	27.76	31.83
200	29.00	33.00
210	30.38	34.50
220	31.48	36.13
230	32.93	37.56
240	34.35	39.39
250	35.59	41.35
260	37.15	43.00
270	39.69	46.26

is 2.5%. In the range 200–270 K, the effect remains constant at 2.5%.

From very precise measurements and extensive thermal conditioning of the samples, Haida *et al.* (2, 6) have shown that C_p of both H_2O and D_2O shows anomalous behavior in the region 100–140 K. This has been attributed to relaxation of the disordered configuration of the protons or deuterons in their respective lattices. Our C_p measurements on $H_2{}^{16}O$ and $H_2{}^{18}O$ also show a slight anomaly at around 115 K similar to the one observed for H_2O and D_2O. The magnitude of the anomaly is, however, within experimental precision. Such a result is expected in view of the limited thermal conditioning of our samples.

Due to the ice-like nature of clathrate hydrates (7), the ^{18}O isotope effect on the heat capacity of tetrahydrofuran hydrate will be expected to be similar to that in ice. However, as seen in Fig. 1, in the range 100–140 K, $C_p{}^{18}$ of THF hydrate is higher than its $C_p{}^{16}$ by only 1.6% and above 140 K the heat capacities of the two systems are virtually the same.

Enthalpies of fusion

The measured enthalpies of fusion, $\Delta_{fus}H$, were corrected to 100% ^{18}O content of water by making the same assumptions as in the case of heat capacities and using $\Delta_{fus}H^{16}$ for $H_2{}^{16}O$ and THF·16.9$H_2{}^{16}O$ reported previously (5). The correction in both systems amounted to 0.3%.

For $H_2{}^{18}O$ we obtained values of 6034.5 J mol^{-1} and 273.50 K for the enthalpy of fusion, $\Delta_{fus}H^{18}$, and fusion temperature, $T_{fus}{}^{18}$, respectively. The corresponding values for $H_2{}^{16}O$ are $\Delta_{fus}H^{16}$ = 6013.5 J mol^{-1} and $T_{fus}{}^{16}$ = 273.20 K as reported previously (5). The isotope effect on fusion temperature δT (= $T_{fus}{}^{18} - T_{fus}{}^{16}$) is 0.30 K and agrees well with literature value of (0.28 ± 0.02) K reported by Steckel and Szapiro (8). The isotope effect on the enthalpy of fusion δH (= $\Delta_{fus}H^{18} - \Delta_{fus}H^{16}$) is (21 ± 25) J mol^{-1}. From temperature dependences of the directly measured vapor pressure isotope effects in the solid and liquid phases Jakli and Staschewski (9) obtained for δH a value of −46 J mol^{-1}. Other literature values for δH quoted by Jakli and Staschewski (9) and also obtained from temperature dependences of vapor pressures are −42 and 33 J mol^{-1}. The present result tends to favor the latter value.

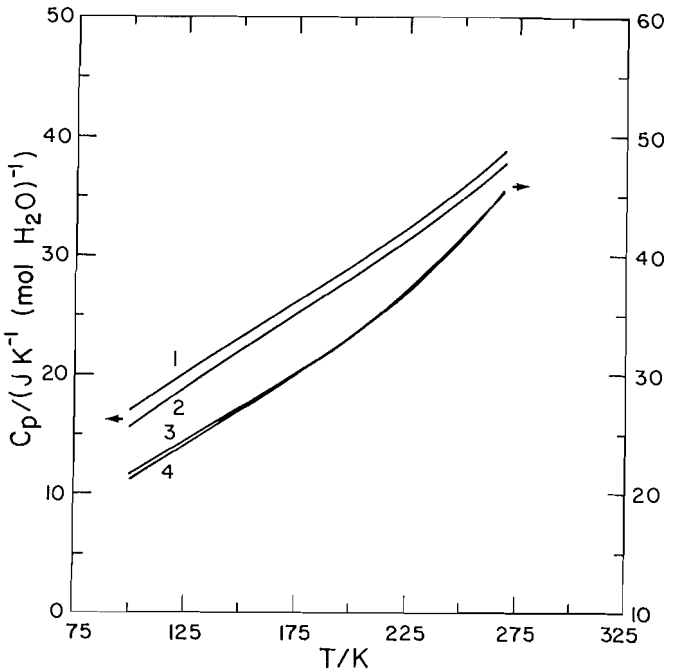

FIG. 1. Smoothed heat capacities vs. temperature for ice and tetrahydrofuran clathrate hydrate. Curve *1*: $H_2{}^{18}O$ from eq. [1]; curve *2*: $H_2{}^{16}O$ from ref. 5; curve *3*: THF·16.9$H_2{}^{18}O$ from eq. [2]; curve *4*: THF·16.9$H_2{}^{16}O$ from ref. 5. Curves *1* and *2* refer to the ordinate on the left and *3* and *4* to the ordinate on the right.

For THF·16.9$H_2{}^{16}O$ the values of $\Delta_{fus}H^{16}$ and $T_{fus}{}^{16}$ are 5526.6 J (mol H_2O)$^{-1}$ and 277.65 K, respectively. The corresponding values for THF·16.9$H_2{}^{16}O$ are 5842.3 J (mol H_2O)$^{-1}$ and 277.30 K (5), thus giving δT = 0.35 K and δH = −315.7 J (mol H_2O)$^{-1}$. As in the case of heat capacities, the isotope effect on the enthalpy of fusion for tetrahydrofuran hydrate is quite different than for ice.

Fractionation factors

Fractionation of $H_2{}^{18}O$ between the solid and the liquid phases can be represented by the hypothetical process

[3] $H_2{}^{16}O(s) + H_2{}^{18}O(l) \rightleftarrows H_2{}^{16}O(l) + H_2{}^{18}O(s)$

where s represents the solid phase and l the liquid phase. When $H_2{}^{18}O$ is present as the infinitely dilute component in $H_2{}^{16}O$ (as in the case of natural water) and assuming that $H_2{}^{18}O$ and $H_2{}^{16}O$ form ideal solutions both in the solid and the liquid phases, the fractionation factor, α, for reaction [3] at temperature T can be written as (10)

$$[4]\quad R \ln \alpha = \frac{1}{T}(\delta H - \Delta C_p \cdot \delta T) - \delta S + \Delta C_p \ln (T_{fus}{}^{18}/T_{fus}{}^{16})$$

where

$$[5]\quad \alpha = (x^{18}/x^{16})_s/(x^{18}/x^{16})_l$$

x being the mole fraction. In eq. [4], δS is the isotope effect on the entropy of fusion ($\delta S = \Delta_{fus}S^{18} - \Delta_{fus}S^{16}$) and ΔC_p is the difference between heat capacity of the liquid and solid phases. In the derivation of eq. [4] it has been assumed that $\Delta C_p{}^{18} = \Delta C_p{}^{16}$ and further that ΔC_p is constant between T and the fusion

temperature of the pure component. Equation [4] thus requires pure component properties only. For H_2O, ΔC_p = 37.7 J K^{-1} mol^{-1} at 273.2 K calculated by using the C_p values for liquid $H_2{}^{16}O$ as suggested by Kell (11) and for $H_2{}^{16}O$ ice extrapolated from the results reported previously (5). Substituting the various values in eq. [4] gives, for H_2O, $\alpha = 1.0032 \pm 0.0007$ at 273.2 K. The uncertainty in α was calculated assuming uncertainties of 1% in $\Delta_{fus}H$, 2% in ΔC_p, and 0.05 K in fusion temperatures. The major source of error in α is the uncertainty associated with fusion temperature. Our value of α compares well with the literature values of 1.0030 (12), 1.0028 ± 0.0001 (13), and 1.00268 ± 0.00003 (14) obtained by direct freezing experiments and values of 1.0035 ± 0.0003 (9), 1.0034 ± 0.0003 (15), and 1.0030 ± 0.0003 (16) obtained from vapor pressure isotope effects.

To calculate ΔC_p for THF hydrate, C_p for the solid phase was obtained by extrapolating the results for THF·$16.9H_2{}^{16}O$ reported previously (5) and for the liquid phase of the same composition calculated by using heat capacity of water (11), THF (17), and excess heat capacity for H_2O + THF (18) and assuming no temperature dependence for the excess heat capacity. For the THF hydrate ΔC_p = 41.9 J K^{-1} (mol $H_2O)^{-1}$ at 277.3 K. As in the case of water, substituting various values in eq. [4] and assuming negligible error in the composition of the hydrate, we obtain for THF hydrate $\alpha = 1.0037 \pm 0.0006$ at 277.3 K. The literature value for THF hydrate of same composition as the present is 1.00268 ± 0.00003 (14) obtained by direct freezing experiments.

Davidson *et al.* (14), using direct freezing technique, found α for ice and THF hydrate to be the same. In the present case, α for the THF hydrate at 277.3 K is slightly higher than α for ice at 273.3 K, though within the limits of precision of the results this claim is speculative at best. Stupin and Gurikov (4) found that the deuterium isotope effect on the thermal and electrical properties of clathrate hydrates depends on the nature of the hydrate former. It would be interesting to see if this is true of the ^{18}O fractionation factors also.

Acknowledgement

The author thanks Mr. M. Bednas for analysing the tetrahydrofuran used in this work.

1. G. JANCSO and W. A. VAN HOOK. Chem. Rev. **74**, 689 (1974).
2. O. HAIDA, H. SUGA, and S. SEKI. J. Glaciology, **22**, 155 (1979).
3. D. R. HAFEMANN and S. L. MILLER. J. Phys. Chem. **73**, 1398 (1969).
4. D. YU. STUPIN and YU. V. GURIKOV. Russ. J. Phys. Chem. **53**, 909 (1979).
5. Y. P. HANDA, R. E. HAWKINS, and J. J. MURRAY. J. Chem. Thermodyn. In press.
6. O. HAIDA, T. MATSUO, H. SUGA, and S. SEKI. J. Chem. Thermodyn. **6**, 815 (1974).
7. D. W. DAVIDSON. *In* Water: a comprehensive treatise. Vol. 2. *Edited by* F. Franks. Plenum Press, New York. 1973. Chapt. 3.
8. F. STECKEL and S. SZAPIRO. Trans. Faraday Soc. **59**, 331 (1963).
9. G. JAKLI and D. STASCHEWSKI. J. Chem. Soc. Faraday Trans. I. **73**, 1505 (1977).
10. R. E. WESTON. Geochim. Cosmochim. Acta, **8**, 281 (1955).
11. G. S. KELL. J. Chem. Eng. Data, **20**, 97 (1975).
12. J. R. O'NEIL. J. Phys. Chem. **72**, 3683 (1968).
13. T. SUZUOKI and T. KIMURA. Mass Spectrosc. **21**, 229 (1973).
14. D. W. DAVIDSON, D. G. LEAIST, and R. HESSE. Geochim. Cosmochim. Acta. **47**, 2293 (1983).
15. M. MAJOUBE. J. Chim. Phys. Physicochim. Biol. **68**, 1423 (1971).
16. J. PUPEZIN, G. JAKLI, G. JANCSO, and W. A. VAN HOOK. J. Phys. Chem. **76**, 743 (1972).
17. B. V. LEBEDEV, I. B. RABINOVICH, V. I. MILOV, and V. YA LITYAGOV. J. Chem. Thermodyn. **10**, 321 (1978).
18. O. KIYOHARA, P. J. D'ARCY, and G. C. BENSON. Can. J. Chem. **57**, 1006 (1979).

Can. J. Chem. Downloaded from www.nrcresearchpress.com by 210.87.254.6 on 09/06/12
For personal use only.

The synthesis, crystal and molecular structure of 1,1,3,3-tetramethylimidazolidinium diiodide methylene dichloride solvate, $(C_7H_{18}N_2)I_2 \cdot CH_2Cl_2$

MASOOD A. KHAN, CLOVIS PEPPE, AND DENNIS G. TUCK

Department of Chemistry, University of Windsor, Windsor, Ont., Canada N9B 3P4

Received May 19, 1983[1]

MASOOD A. KHAN, CLOVIS PEPPE, and DENNIS G. TUCK. Can. J. Chem. **62**, 1662 (1984).

A simple preparation of the title compound, its crystal structure, and nmr spectra are reported. The compound crystallizes in the space group $P2_1/n$, with a = 8.109(2) Å, b = 16.183(4) Å, c = 11.968(4) Å, β = 93.45(2)°, V = 1567.7(7) Å^{-3}, ρ = 1.987 g cm^{-3}, Z = 4 (MoK$_\alpha$, λ = 0.71069 Å). The structure was solved by the heavy atom method and refined to the final R = 0.0415 for 1261 "observed" reflections. The structure consists of five-membered cyclic $C_7H_{18}N_2^{2+}$ cations, iodide anions, and methylene dichloride molecules which are held loosely in the lattice.

MASOOD A. KHAN, CLOVIS PEPPE et DENNIS G. TUCK. Can. J. Chem. **62**, 1662 (1984).

On rapporte une préparation simple du composé mentionné dans le titre, de même que sa structure cristalline ainsi que son spectre rmn. Le composé cristallise dans le groupe d'espace $P2_1/n$, avec a = 8,109(2), b = 16,183(4), c = 11,968(4) Å, β = 93,45(2)°, V = 1567,7(7) Å^{-3}, ρ = 1,987 g/cm^{-3}, Z = 4 (MoK$_\alpha$, λ = 0,71069 Å). On a résolu la structure par la méthode des atomes lourds et on l'a affiné jusqu'à une valeur finale de R = 0,0415 pour les 1261 réflexions observées. La structure comporte des cations cycliques à cinq chaînons, $C_7H_{18}N_2^{2+}$, des anions iodures et des molécules de dichlorure de méthylène qui sont retenues d'une façon lâche dans la maille.

[Traduit par le journal]

Introduction

In a recent paper from this laboratory (1), we described the preparation and properties of solution of indium(I) halides (InX; X = Cl, Br, I) in mixtures of aromatic solvents and neutral bases. One reaction of particular interest corresponds to the oxidative insertion of the $In^{I}X$ (X = Cl, Br, I) solute species into the In^{III}—X bonds of indium trihalides (2). While studying these processes in a solvent system consisting of a mixture of toluene/methylene dichloride/*N,N,N′,N′*-tetramethyl-1,2-ethanediamine (tmen), we observed that tmen reacts slowly with CH_2Cl_2 to form 1,1,3,3-tetramethylimidazolidinium dichloride, $(C_7H_{18}N_2)Cl_2$. The reaction between InI and $InCl_3$ gave, *inter alia*, the crystalline diiodide derivative of the cyclic diammonium cation as the methylene dichloride solvate $(C_7H_{18}N_2)I_2 \cdot CH_2Cl_2$ (**1**).

Quaternisation reactions of *N,N,N′,N′*-tetramethyl-α,ω-diaminoalkanes with α,ω-dihaloalkanes have been previously studied in some detail (3, 4), since they lead to the formation of ionene polymers which are believed to have a sufficiently high positive charge concentration to produce organic materials of high electronic conductivity. In addition to the polymeric products, such reactions also produce cyclic diammonium compounds, and ring systems containing 5 to 14 atoms have been isolated, depending on the nature of the diamine and the dihaloalkane (4). The reaction of tmen with CH_2Br_2 was reported to give the bromide analogue of compound **1** (4), but to our knowledge similar reactions involving methylene dichloride have not been reported.

Experimental

Preparative

1,1,3,3-Tetramethylimidazolidinium dichloride

A total of 4 mL of tmen was added to 50 mL of CH_2Cl_2–toluene (1:1, v/v) and the solution kept at room temperature; the crystals which deposited after 3–15 days were shown to be $[C_7H_{18}N_2]Cl_2$. Found: Cl 35.1; calcd. 35.3. ^{1}H nmr (DCl solution, external TMS) 4.24 s, 6H; 5.10 s, 2H; 5.97 s, 1H.

1,1,3,3-Tetramethylimidazolidinium diiodide methylene dichloride solvate (1)

Equimolar quantities of InI and $InCl_3$ (5.0 mmol) were suspended in 50 mL of CH_2Cl–toluene (1:1, v/v) and cooled to −20°C under an atmosphere of dry nitrogen; tmen (4 mL) was then added and the temperature allowed to rise slowly to ambient (ca. 3 h). A clear yellow solution was obtained, and was kept at room temperature for one week, after which crystals of **1** began to deposit. The crystals were filtered and dried *in vacuo*. Found: I 56.4, calcd. 54.1. ^{1}H nmr (DCl solution, external TMS) 4.30 s, 6H; 5.13 s, 2H; 6.01 br, 2H; this last resonance is the apparent superposition of the coincident resonances from CH_2Cl_2 and the bridging $\overset{+}{N}$—CH_2—$\overset{+}{N}$ group of the cation.

X-ray studies

Crystals of the title compounds are colourless prisms. A crystal with approximate dimensions 0.12 × 0.18 × 0.23 mm was sealed in a thin-walled glass capillary and used for subsequent data collection on a Syntex $P2_1$ diffractometer (Table 1). Details of the procedure for data collections and processing were described elsewhere (5). Since crystal decomposition was rapid even in the capillary, variable scan speeds of 4.88–9.77°/min were used, and data collection was terminated at $2\theta_{max}$ = 40°. During the data collection, the averaged intensity decrease of three monitor reflections was 53%, and this was corrected for by applying a scale factor based on the averaged intensity decrease. The systematic absences ($0k0$, $k = 2n$; $h0l$, $h + l = 2n$) identified the space group as $P2_1/n$, a non-standard setting of $P2_1/c$ (C_{2h}^5, No. 14, with the equipoints $\pm(x, y, z)$ and $\pm(\frac{1}{2} + x, \frac{1}{2} - y, \frac{1}{2} + z)$). The data were corrected for Lorentz and polarization effects; absorption corrections could not be applied because of the rapid crystal decomposition.

The position of iodine atoms were obtained from a sharpened Patterson synthesis, and a difference Fourier map based on the iodine atoms gave the positions of all the remaining non-hydrogen atoms. The structure was refined anisotropically by full-matrix least-squares method and converged at R = 0.0487. At this stage, a difference map showed peaks at some plausible hydrogen atom locations. All hydrogen atoms were then included in the idealized positions, with C—H = 0.95 Å. After six more cycles of refinement convergence was achieved, with the final R = 0.0415 and the final R_w = 0.0469 for 1261 unique "observed" reflections. The function minimized during least-squares calculations was $\Sigma w(|F_o| - |F_c|)^2$ and a weighting scheme of the form $w = 1/[\sigma^2(F) + 0.001F^2]$ was employed. In the last cycle of refinement the largest shift/error ratio was 0.05. The final difference map had no features of any chemical significance, the

[1] Revision received March 14, 1984.

Can. J. Chem. Downloaded from www.nrcresearchpress.com by 210.87.254.105 on 09/06/12
For personal use only.

Can. J. Chem. Downloaded from www.nrcresearchpress.com by 210.87.254.105 on 09/06/12
For personal use only.

TABLE 1. Summary of crystal data, intensity collection, and structural refinement for $(C_7H_{18}N_2)I_2 \cdot CH_2Cl_2$, $C_8H_{20}Cl_2I_2N_2$

Cell constants	a = 8.109(2) Å, b = 16.183(4) Å c = 11.968(4) Å, β = 93.45(2)°
Cell volume	1567.7(7) Å^3
Space group	$P2_1/n$ (non-standard setting of No. 14)
Z	4
M_r	468.98
ρ(calcd)	1.987 g cm^{-3}
F(000)	888
Absorption coefficient	40.4 cm^{-1}
Crystal dimensions	0.12 × 0.18 × 0.23 mm
Radiation	MoK$_\alpha$ (λ = 0.71069 Å)
2θ angle	4–40°
Scan type	coupled θ (crystal)/2θ (counter)
Scan width	K$_{\alpha1}$ − 1° to K$_{\alpha2}$ + 1°
Scan speed	4.88–9.77° min^{-1}
Background time/scan time	0.5
Total reflections measured	1670
Unique average data	1261
No. of parameters (NP)	127
$R = (\Sigma\Delta/\Sigma\lvert F_o\rvert)$	0.0415
$R_w = [\Sigma w\Delta^2/\Sigma wF_o^2]^{1/2}$	0.0469

TABLE 2. Positional thermal parameters for non-hydrogen atoms[a]

Atom	x	y	z	$\bar{U}_{eq}$ (Å^2 × 10^3)[b]
I(1)	0.27498(8)	0.12961(4)	0.93963(5)	46.0(6)
I(2)	0.16649(8)	0.12063(4)	0.46365(5)	43.2(6)
Cl(1)	0.3491(3)	0.4949(1)	0.3308(2)	46(2)
Cl(2)	0.2688(4)	0.3404(2)	0.2153(3)	73(2)
N(1)	0.1266(8)	0.4101(4)	0.8023(5)	28(4)
N(2)	0.2755(8)	0.3369(4)	0.6632(5)	30(4)
C(1)	0.0106(11)	0.3569(5)	0.7302(8)	42(6)
C(2)	0.1187(10)	0.2903(5)	0.6906(7)	38(6)
C(3)	0.2815(11)	0.4126(5)	0.7386(8)	34(6)
C(4)	0.4059(11)	0.4233(5)	0.2296(7)	46(6)
C(11)	0.1625(12)	0.3738(5)	0.9160(8)	47(7)
C(12)	0.0557(12)	0.4955(5)	0.8105(8)	52(7)
C(21)	0.2681(13)	0.3659(5)	0.5427(7)	49(7)
C(22)	0.4238(11)	0.2827(6)	0.6849(8)	57(7)

[a] The esd of the last digit is given in parentheses.

[b] U_{eq} is calculated from the refined anisotropic thermal parameters (deposited material) ($U_{eq} = (1/3)\sum_{i=1}^{3}(\text{rmsd})_i^2$, with rmsd values taken from the ORTEP output).

largest peak being 0.8 e Å^3 and close to I(2).

All calculations were done on the IBM 3031 computer. The programmes used during structural analysis include CHECK, PROC, ABSORB, SHELX, XANADU, and ORTEP (6). Scattering factors for all the non-hydrogen atoms, including anomalous dispersion correction terms for Cl and I ($\Delta f'$ and $\Delta f''$), were taken from ref. 7, and scattering factors for hydrogen atom were obtained from ref. 8.

Positional and thermal parameters are given in Table 2, and the bond distances and angle are listed in Table 3. Tables of observed and calculated structure factor amplitudes, anisotropic thermal parameters, and hydrogen atom coordinates are available as Supplementary Data.[2] Figure 1 shows the cation with the atomic numbering scheme, and Fig. 2 gives the unit cell packing; hydrogen atoms are omitted from Fig. 2 for the sake of clarity.

[2] A complete set of data is available, at a nominal charge, from the Depository of Unpublished Data, CISTI, National Research Council of Canada, Ottawa, Ont., Canada K1A 0S2.

TABLE 3. Bond distances (Å) and angles (deg) in $(C_7H_{18}N_2)I_2 \cdot CH_2Cl_2$

Bond	Distance
(*a*) 1,1,3,3-Tetramethylimidazolidinium dication	
N(1)—C(1)	1.51(1)
N(1)—C(3)	1.51(1)
N(1)—C(11)	1.50(1)
N(1)—C(12)	1.50(1)
N(2)—C(2)	1.53(1)
N(2)—C(3)	1.52(1)
N(2)—C(21)	1.52(1)
N(2)—C(22)	1.50(1)
C(1)—C(2)	1.48(1)
(*b*) Dichloromethane	
C(4)—Cl(1)	1.758(9)
C(4)—Cl(2)	1.744(9)

Bonds	Angle
(*a*) 1,1,3,3-Tetramethylimidazolidinium dication	
C(1)—N(1)—C(3)	103.7(6)
C(1)—N(1)—C(11)	112.1(7)
C(1)—N(1)—C(12)	109.6(7)
C(11)—N(1)—C(12)	110.9(6)
C(11)—N(1)—C(3)	110.4(7)
C(12)—N(1)—C(3)	110.0(6)
C(2)—N(2)—C(3)	105.5(5)
C(2)—N(2)—C(21)	111.7(7)
C(2)—N(2)—C(22)	110.0(6)
C(21)—N(2)—C(22)	109.4(7)
C(21)—N(2)—C(3)	108.3(6)
C(22)—N(2)—C(3)	111.9(6)
N(1)—C(1)—C(2)	103.8(7)
N(2)—C(2)—C(1)	103.0(6)
N(1)—C(3)—N(2)	106.3(6)
(*b*) Dichloromethane	
Cl(1)—C(4)—Cl(2)	112.5(5)

Results and discussion

Preparative

Although methylene chloride is normally regarded as an unreactive solvent, it slowly quaternises both nitrogen sites of the tmen molecule, apparently by nucleophilic attack of the basic nitrogen at the carbon atom of CH_2Cl_2. This seems to be the first report on this reaction, although the use of such a process was mentioned before in the process of coagulation of polymers (9); no structural details were given in that publication. The unusual preparative route to the diiodide derivative can be regarded simply as exchange of the chloride anions of the initially formed dichloride salt with iodide ions from the indium–iodide compounds present in the solution. We attempted to prepare the diiodide salt of the cyclic cation from a reaction between equimolar quantities of tmen and CH_2I_2 in toluene. The ^{1}H nmr spectrum of the product isolated consists of a complex spectrum in the range 3.58–5.97 ppm from TMS (aq. DCl solution) suggesting the formation of a polymeric linear derivative as well as the cyclic dication.

Structural

The crystal structure of **1** consists of discrete dipositive cations, iodide anions, and loosely held CH_2Cl_2 solvent molecules (Fig. 1). Crystals of **1** are unstable because of the loss of

Can. J. Chem. Downloaded from www.nrcresearchpress.com by 210.87.254.105 on 09/06/12
For personal use only.

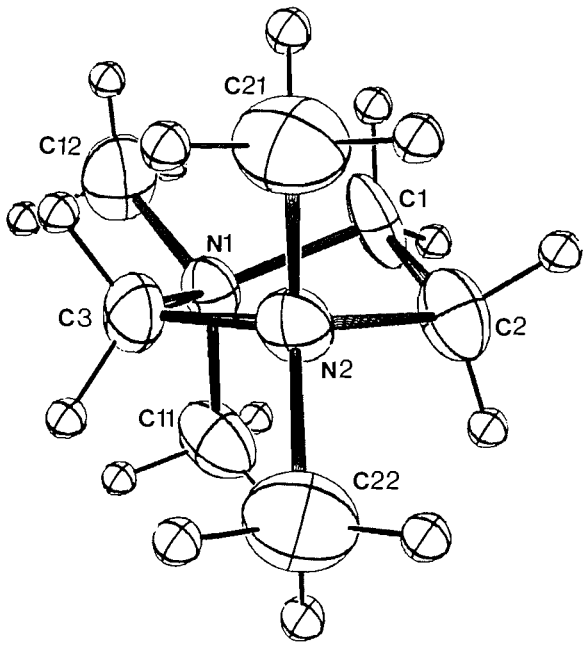

FIG. 1. The molecular structure of the 1,1,3,3-tetramethylimidazolidinium cation, $C_7H_{18}N_2^{2+}$.

TABLE 4. Torsion angles (deg)[a]

Atoms	Angle
C(3)—N(1)—C(1)—C(2)	40.0
C(1)—N(1)—C(3)—N(2)	−22.4
N(1)—C(3)—N(2)—C(2)	−2.7
N(1)—C(1)—C(2)—N(2)	−41.4
C(1)—C(2)—N(2)—C(3)	27.1

[a] Esd 0.7°.

TABLE 5. ^1H and ^{13}C nmr spectra of $C_7H_8N_2X_2$ salts (ppm from TMS)

	X = Cl		X = I[a]	
Site	^1H	^{13}C	^1H	^{13}C
C(1,2)	4.48 (2H)	63.9	4.51 (2H)	64.0
C(3)	5.40 (1H)	90.5	5.43 (1H)	90.5
C(11,12,21,22)	3.58 (6H)	56.4	3.61 (6H)	56.7

[a] Spectra of compound after loss of occluded CH_2Cl_2.

these solvent molecules from the lattice, and the proton nmr spectrum of the decomposed crystals showed the set of three singlets characteristic of the cyclic dication. The crystal instability encountered during data collection is therefore caused by the loss of the occluded solvent molecule rather than by decomposition of the dication.

Figure 2 shows the structure of the dication. The five-membered ring has the usual envelope conformation, as demonstrated by the torsion angles in Table 4. The plane is formed by the atoms N(1), N(2), C(2), and C(3) (maximum deviation, at C(3), 0.016(9) Å) and the C(1) atom is 0.61(9) Å out of plane. The dihedral angle between the planes N(1), C(1), C(2), and N(1), C(3), N(2), C(2) is 41.3°. The bond lengths in the dication are in agreement with literature values, with the exception of a significant shortening to 1.48(1) Å at C(1)—C(2).

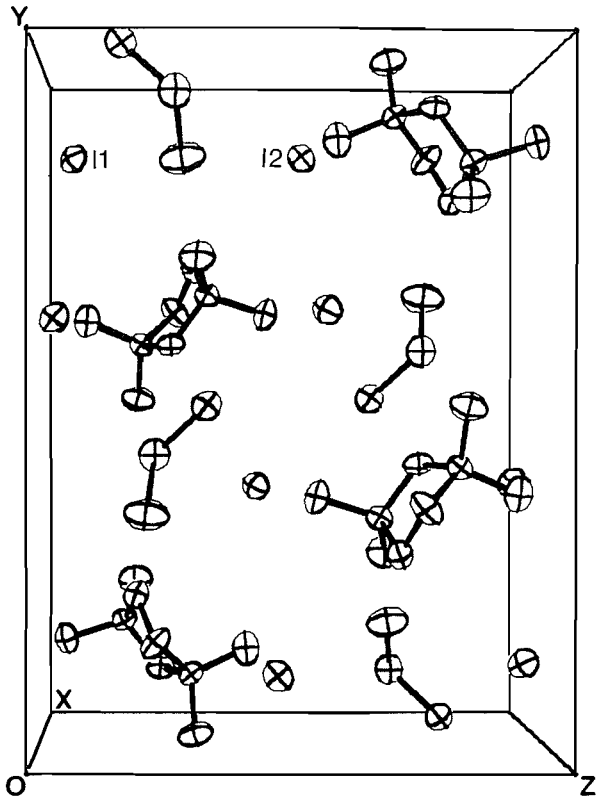

FIG. 2. The unit cell packing of $(C_7H_{18}N_2)I_2 \cdot CH_2Cl_2$, with hydrogen atoms omitted.

Similar values have been observed for this C—C bond length in molecules in which tmen acts as a bidentate ligand (10). The bond angles in the ring range between 103.0 and 106.3°, similar to the values reported for the dicarboxylic acid derivative of cyclopentane (11). There are no significant interionic interactions, the shortest such distance being 3.872(5) Å between I(1) and C(1). The C—Cl(1, 2) bond lengths, and the Cl—C—Cl angle in CH_2Cl_2 call for no comment.

Nuclear magnetic resonance spectroscopy

In view of the unusual C—C bond length in the dication, we re-examined the nmr spectra of the $C_7H_8N_2X_2$ salts, recording ^1H spectra in D_2O (c.f. DCl values reported in Preparative Section) and ^{13}C spectra in D_2O/dioxane. The results, relative to TMS in both cases, are shown in Table 5, which uses the atomic numbering scheme of Fig. 1 for identification. The ^1H results are similar to those reported for the 1,1,4,4-tetramethylpiperazonium cation (4), for which the N—CH_3 groups have the ^1H resonance at 3.4 ppm, and the ring CH_2 resonance at 4.05 ppm (from TMS). Analogous frequencies have been found for N-methyl cationic derivatives of quinucleodine (12). It therefore appears that the nmr spectrum of the dication is similar to those of related compounds, so that the relatively short C(1)—C(2) bond in the ring does not result in any unusual spectroscopic properties.

Acknowledgements

This work was supported in part by Operating Grants from the Natural Sciences and Engineering Research Council of Canada. One of us (C.P.) thanks the Conselho Nacional de Desenvolvimento Cientifico e Tecnológico (Brasil) for the award of a scholarship.

1. C. PEPPE, D. G. TUCK, and L. VICTORIANO. J. Chem. Soc. Dalton Trans. 2165 (1982).
2. C. PEPPE and D. G. TUCK. Unpublished results.
3. H. NOGUCHI and A. REMBAUM. J. Polym. Sci. Part B, **7**, 383 (1969).
4. H. NOGUCHI and A. REMBAUM. Polym. Prepr. Am. Chem. Soc. Div. Polym. Chem. **10**, 718 (1969).
5. M. A. KHAN, R. C. STEEVENSZ, D. G. TUCK, J. G. NOLTES, and P. W. R. CORFIELD. Inorg. Chem. **19**, 3407 (1980).
6. M. A. KHAN, C. PEPPE, and D. G. TUCK. Unpublished results.
7. International Tables for X-ray Crystallography. Vol. IV, Kynoch Press, Birmingham. 1974. pp. 99 and 149.
8. R. F. STEWART, E. R. DAVIDSON, and W. T. SIMPSON. J. Chem. Phys. **42**, 3175 (1965).
9. W. HUFENREUTER, W. ZILL, J. BAUER, and M. HARWART. East German Patent 139264 (1979); Chem. Abstr. **93**, 115699 (1980).
10. M. A. KHAN, C. PEPPE, and D. G. TUCK. Unpublished results.
11. E. BENEDETTI, P. CORRADINI, and C. PEDONE. J. Phys. Chem. **76**, 790 (1972).
12. J. AKUOKO and G. W. WOOD. Private communication.

Can. J. Chem. Downloaded from www.nrcresearchpress.com by 210.87.254.105 on 09/06/12
For personal use only.

Diterpenoids from the brown alga *Dictyota binghamiae*

CHARLES PATHIRANA AND RAYMOND J. ANDERSEN[1]

Departments of Chemistry and Oceanography, University of British Columbia, Vancouver, B.C., Canada V6T 1W5

Received December 13, 1983

CHARLES PATHIRANA and RAYMOND J. ANDERSEN. Can. J. Chem. **62**, 1666 (1984).

Extracts of the brown alga *Dictyota binghamiae* contain three previously known and three new diterpenoids. The known compounds, pachydictyol A (**1**), dictyoxide (**7**), and the diacetal **16**, were identified by comparison of their spectral data with published values. The structures of the new diterpenoids, dictyol G acetate (**12**), dictyoxide A (**13**), and dictyotriol A diacetate (**15**), were proposed on the basis of their spectral data and the structures of acetate **12** and ether **13** were confirmed by chemical interconversion.

CHARLES PATHIRANA et RAYMOND J. ANDERSEN. Can. J. Chem. **62**, 1666 (1984).

Les extraits de l'algue brune *Dictyota binghamiae* contiennent trois diterpènes déjà connus et trois nouveaux. On a identifié les composés connus, le pachydictyol A (**1**), le dictyoxyde (**7**) et le diacétal **16** grâce à une comparaison de leurs données spectrales avec les valeurs rapportées dans la littérature. On a proposé des structures pour les nouveaux diterpènes, l'acétate de dictyol G (**12**), le dictyoxyde A (**13**) et le diacétate de dictyotriol A (**15**) en se basant sur leurs données spectrales et les structures de l'acétate **12** et de l'éther **13** ont été confirmées par une conversion chimique.

[Traduit par le journal]

Introduction

Species of brown algae belonging to the family *Dictyotaceae* have been a rich source of diterpenoids containing the perhydroazulene ring system. Pachydictyol A (**1**), which was isolated by Hirschfeld *et al.* (1) from *Pachydictyon coriaceum*, was the first member of this family to be reported. Subsequently a number of oxygenated derivatives of Pachydictyol A have been described. These include dictyol A (**2**), B (**3**), C (**4**), and D (**5**) isolated from the Mediterranean alga *Dictyota dichotoma* var *implexa* (2), dictyol E (**6**) and dictyoxide (**7**) isolated from *Dilophus ligulatus* (2*b*, 3), dictyotadiol (**8**) and dictyol B acetate (**9**) isolated from the British *Dictyota dichotoma* (4), and dictytriol (**10**) and dictyone (**11**) isolated from a Japanese collection of *Dictyota dichotoma* (5). We have examined extracts of *Dictyota binghamiae* which was collected subtidally in Barkley Sound, British Columbia and we wish to describe herein the isolation of three previously known and three new diterpenoids from the alga.

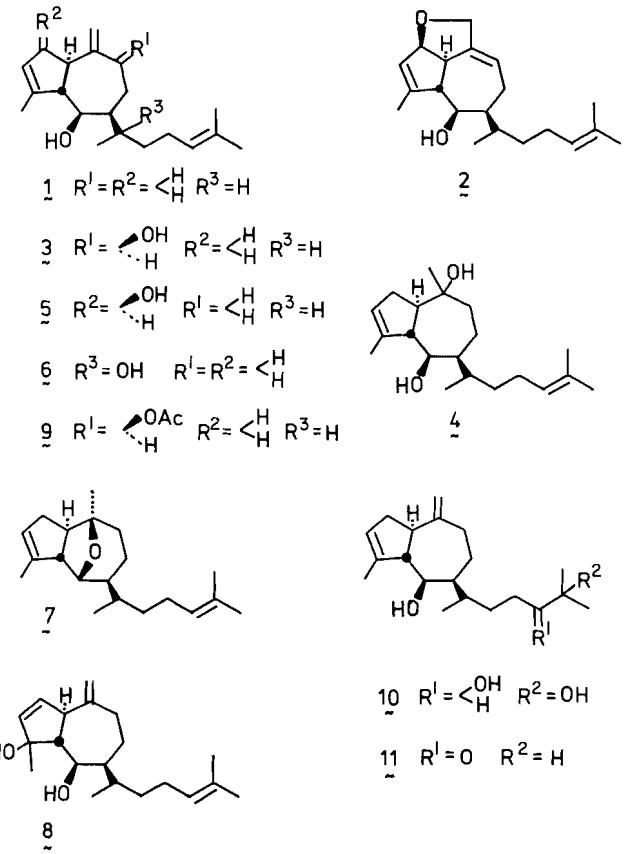

Results and discussion

Initial collections of *D. binghamiae* were dried in a convection oven at 50°C prior to powdering in a Wiley mill and soxhlet extraction with hexane. The crude hexane extract was fractionated by flash chromatography using a series of step gradients involving hexane, chloroform, and ethyl acetate. Fractions eluting with chloroform and chloroform – ethyl acetate mixtures contained the diterpenoids. Final purification of the individual compounds was achieved by radial thin layer chromatography and hplc. Later collections of *D. binghamiae* were extracted with methanol immediately after collection. The hexane soluble portion of the concentrated methanol extracts contained the diterpenoids, which were purified by radial tlc and hplc as before.

Five pure diterpenoids were obtained from the oven dried alga. Two previously known diterpenoids, pachydictyol A (**1**) and dictyoxide (**7**), were obtained as pale yellow oils. The spectral data for both substances were in excellent agreement with published values (1, 3).

Dictyol G acetate (**12**) was obtained as an optically active ($[\alpha]_D^{22}$ +50°) colorless oil from preparative reverse phase hplc. High resolution mass spectrometry showed that it had a molecular formula of $C_{22}H_{34}O_3$. Its ir spectrum contained hydroxyl (3500 cm^{-1}) and carbonyl (1725 cm^{-1}) absorption bands. A three-proton resonance at δ 2.02 (s) ppm in the ^1H nmr spectrum, and a significant fragment ion at *m/z* 286 ($M^+ - CH_3CO_2H$) in the mass spectrum, indicated the presence of an acetate ester. The ^1H and ^{13}C nmr spectra of acetate **12** also clearly indicated that it had the same substituted bicyclic ring system as pachydictyol A (**1**) (see Table 1) and thus the acetoxy substituent had to be attached to the side chain. A deshielded resonance at δ 5.57 ppm (dt, 1H, J = 8, 4 Hz) in the ^1H nmr spectrum of **12**, which was not present in the ^1H nmr spectrum

[1] Author to whom correspondence may be addressed.

Can. J. Chem. Downloaded from www.nrcresearchpress.com by 210.87.254.6 on 09/06/12
For personal use only.

TABLE 1. ^{1}H nuclear magnetic resonance data for *Dictyota binghamiae* diterpenoids (400 MHz, $CDCl_3$)

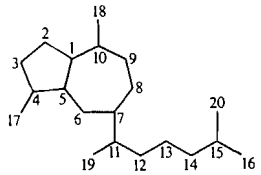

Carbon	Pachydictyol A (**1**)	Dictyoxide (**7**)	Dictyoxide A (**13**)	Dictyol G acetate (**12**)	Dictyotriol A diacetate (**15**)
1	2.67 q, J = 10 Hz	2.41 dt, J = 12, 6 Hz	2.62 q, J = 9 Hz	—	2.79 q, J = 10 Hz
2	2.62 m	—	—	2.49 m	2.49 m
3	5.33 br s	5.50 br s	5.37 br s	5.33 br s	5.34 br s
5	2.32 br t	2.63 br d, J = 12 Hz	2.75 br t, J = 10 Hz	2.33 br t	2.33 m
6	3.92 br d, J = 8 Hz	3.97 m	3.74 dd, J = 10, 4 Hz	3.93 br d, J = 8 Hz	3.87 dd, J = 3, 8 Hz
7	—	—	—	—	2.02 dd, J = 10, 3 Hz
8	—	—	—	—	1.92 ddd, J = 15, 10, 2 Hz
					1.76 dd, J = 15, 6 Hz
9	—	—	—	—	5.59 dd, J = 6, 2 Hz
11	—	—	—	—	1.86 m
12	—	—	1.14 q, J = 12 Hz	1.93 m	4.92 m
13	—	—	4.45 ddd, J = 12, 8, 4 Hz	5.57 dt, J = 8, 4 Hz	—
14	5.12 br t, J = 6 Hz	5.09 br t, J = 8 Hz	5.20 br d, J = 8 Hz	5.12 br d, J = 8 Hz	5.10 t, J = 7 Hz
16	1.61 br s	1.60 br s	1.65 br s	1.72 d, J = 1.5 Hz	1.64 br s
17	1.81 br s	1.78 br s	1.79 br s	1.82 d, J = 1 Hz	1.82 d, J = 1 Hz
18	4.75 s	1.25 s	4.82 s	4.75 s	5.10 s
	4.74 br s		4.79 s	4.73 s	5.03 s
19	1.00 d, J = 7 Hz	0.90 d, J = 7 Hz	0.95 d, J = 7 Hz	1.04 d, J = 7 Hz	0.94 d, J = 7 Hz
20	1.69 br s	1.68 br s	1.70 br s	1.74 d, J = 1.5 Hz	1.70 br s

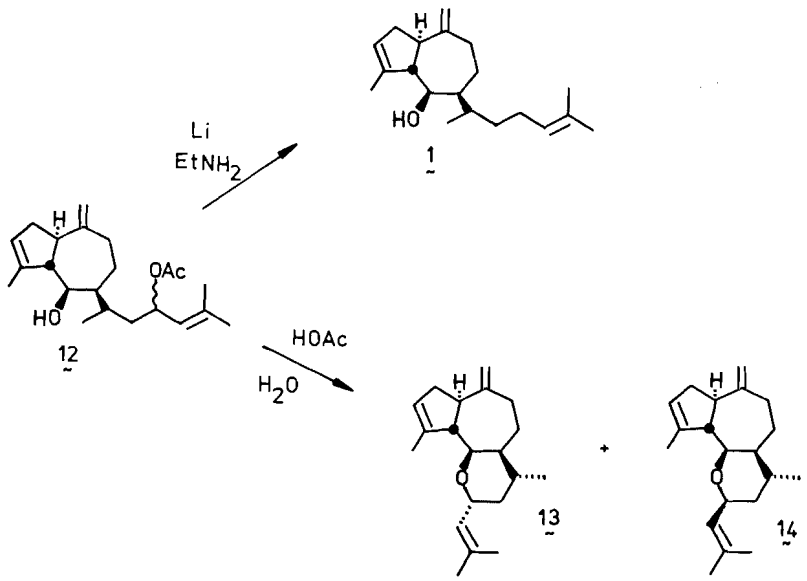

SCHEME 1

of pachydictyol A (**1**), could be assigned to a methine proton α to the acetoxy functionality. The chemical shift of the methine proton implied that it must also be allylic, and a double resonance experiment showed that it was spin coupled to the olefinic proton on C14 (δ 5.12, bd, J = 8 Hz). Thus the acetoxy functionality in **12** must be attached to C13. Reduction of dictyol G acetate (**12**) with lithium in ethylamine gave pachydictyol A (**1**) which was identical to an authentic sample by tlc and ^{1}H nmr comparison (see Scheme 1).

Dictyoxide A (**13**) was obtained as an optically active ($[\alpha]_D^{22}$ −5.6°) pale yellow oil that had the molecular formula $C_{20}H_{30}O$. Its ir spectrum showed an absence of either hydroxyl or carbonyl absorptions and its ^{13}C nmr spectrum contained two resonances at δ 79.5 and 68.6 ppm, appropriate for the carbon atoms of an ether functionality. Six additional carbon resonances at δ 152.0, 142.0, 133.5, 126.8, 124.9, and 106.8 ppm could be assigned to three olefin functionalities. Since the molecular formula of **13** requires six sites of unsaturation, we could conclude that it must be tricyclic. The ^{1}H nmr spectrum of **13** showed methyl resonances at δ 0.95 (d, 3H, J = 7 Hz), 1.65 (bs, 3H), 1.79 (bs, 3H), and 1.70 (bs, 3H) ppm that were virtually identical to those observed for the three olefinic and

Can. J. Chem. Downloaded from www.nrcresearchpress.com by 210.87.254.6 on 09/06/12
For personal use only.

Can. J. Chem. Downloaded from www.nrcresearchpress.com by 210.87.254.6 on 09/06/12
For personal use only.

one aliphatic methyl groups in pachydictyol A (**1**) (see Table 1). In addition, olefinic proton resonances at δ 5.37 (bs, 1H), 4.82 (bs, 1H), and 4.79 (bs, 1H) ppm were similar to those observed for their counterparts on C3 and C18 in **1**. The above evidence led to the hypothesis that dictyoxide **A** (**13**) had the same carbon skeleton as pachydictoyl A (**1**) but that the alcohol functionality in **1** was replaced by a cyclic ether in **13**. We assumed that one point of attachment of the cyclic ether was C6 and assigned a resonance at δ 3.74 ppm (dd, 1H, J = 10, 4 Hz) to the methine proton on that carbon. A downfield resonance at δ 4.45 ppm (ddd, 1H, J = 12, 8, 4 Hz) was assigned to a methine proton on the second ether carbon. This methine proton was shown via a double resonance experiment to be spin coupled to the olefinic proton on C14 (δ 5.20, bd, IH, J = 8 Hz) and hence C13 had to be the second point of attachment of the cyclic ether.

The constitution of dictyoxide A was confirmed by treatment of dictyol G acetate (**12**) with aqueous acetic acid which gave a 20% yield of **13** (see Scheme 1) and a very low yield of a second compound which was tentatively assigned the epimeric structure **14**. An analysis of the coupling constants observed for H13 and H12α in ether **13** revealed that the tetrahydropyran ring assumed a chair conformation and allowed us to assign the relative configuration at C13. H13 shows an 8-Hz vicinal coupling to H14, a 4-Hz axial, equatorial coupling to H12β and a 12-Hz axial, axial coupling to H12α. Therefore H13 must be axial and the vinyl residue must be equatorial. H12α appears as a quartet at δ 1.14 ppm with a 12-Hz coupling constant. It must therefore be coupled to H12β with a 12-Hz geminal coupling and to an axial proton on C11. Thus the C19 methyl must be equatorial and *cis* to the C13 vinyl substituent. Since the relative stereochemistry at C11 in pachydictyol A is known, we can conclude that dictyoxide A (**13**) adopts the conformation shown in Fig. 1. We were unable to adequately characterize the epimer **14** due to a very limited sample size, but its ^{1}H nmr spectrum was consistent with the proposed structure.

Dictyotriol A diacetate (**15**) was obtained as an optically active ($[\alpha]_D^{22}$ + 12.5°) colorless oil that had a molecular formula of $C_{24}H_{36}O_5$. Its ir spectrum showed hydroxyl (3450 cm^{-1}) and

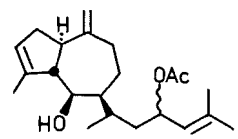

12

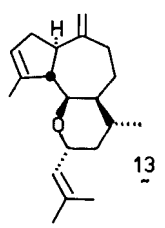

13

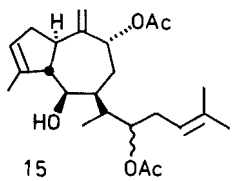

15

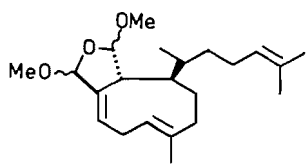

16

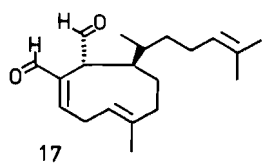

17

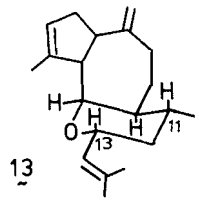

13

FIG. 1.

carbonyl (1730 cm^{-1}) absorption bands. Two singlet methyl resonances at δ 2.06 and 2.07 ppm in the ^{1}H nmr of **15** indicated that it was a diacetate. The remainder of the ^{1}H nmr suggested that diacetate **15** had the same carbon skeleton as pachydictyol A (**1**) and that the $\Delta^{3,4}$, $\Delta^{10,18}$, $\Delta^{14,15}$, and C6 hydroxy functionalities were intact (see Table 1). Two resonances at δ 4.92 (m, 1H) and 5.59 (dd, 1H, J = 2, 6 Hz) ppm could be assigned to methine protons α to the acetoxy functionalities. This implied that the acetates were both esters of secondary alcohols, one of them allylic. Irradiation of the allylic methine proton (δ 5.50 ppm) did not change either the C3 or C14 olefinic proton resonances (δ 5.34 and 5.10 ppm) but it did simplify the H8α resonance to a broad doublet (δ 1.76 ppm, J = 15 Hz) and the H8β resonance to a doublet of doublets (δ 1.92 ppm, J = 15, 8 Hz). Decoupling further demonstrated a 1.5-Hz W coupling between H8α and H6, confirming the assignment of the former resonance. The allylic acetate must therefore be on C9 and it was assigned the α configuration because both the multiplicity and chemical shift of the α acetoxy methine proton were substantially different than those reported for dictyol B acetate (**9**) in which the C9 acetate is β (**9**: H9α, δ 5.16 ppm, t, J = 7 Hz (4)). The stereochemistry at C9 was confirmed by demonstrating a difference nOe in H5, H8β, and H8α when the H9 methine proton was irradiated.

Placement of the second acetoxy functionality on C12 followed from the fact that it had to be on a non-allylic secondary carbon which, according to decoupling experiments, was not vicinal to the C9 acetate. Further support for the positions of both acetoxy functionalities could be found in a ^{1}H 2D nmr COSY experiment (7) (see Fig. 2).[2] Clearly visible are the (14/13, 13′) and (12/13, 13′) off-diagonal peaks which would be expected if diacetate **15** contains a C12 acetoxy. It is also possible to follow the required coupling sequence from the C9 acetoxy α methine proton to the C6 carbinol methine proton. Thus starting at C9 we find the off-diagonal elements (9/8α), (9/8β), (7/8β), and (6/7).

The methanol extracted *D. binghamiae* was found to contain pachydictyol A (**1**), dictyoxide (**7**), dictyol G acetate (**12**), dictyotriol A diacetate (**15**), and **16**, a dimethoxy derivative of dictyodial (**17**) (6). A mixture of acetals **16**, which were epimeric at C19, have previously been reported from the Japanese alga *Pachydictyon coriaceum* (6). We isolated only a single epimer and we have not determined the configuration at C19. It appears that the diacetal **16** is an artifact formed from the reaction of dictyodial (**17**) with methanol. Our failure to find dictyoxide A (**13**) in the methanol extracted *D. binghamiae* also seems to indicate that it is an artifact formed from dictyol G acetate (**12**) during oven drying of the algae.

[2] Identification of the off-diagonal peaks in the COSY spectrum is made by listing the identities of the individual protons, that resonating downfield listed first.

Can. J. Chem. Downloaded from www.nrcresearchpress.com by 210.87.254.6 on 09/06/12
For personal use only.

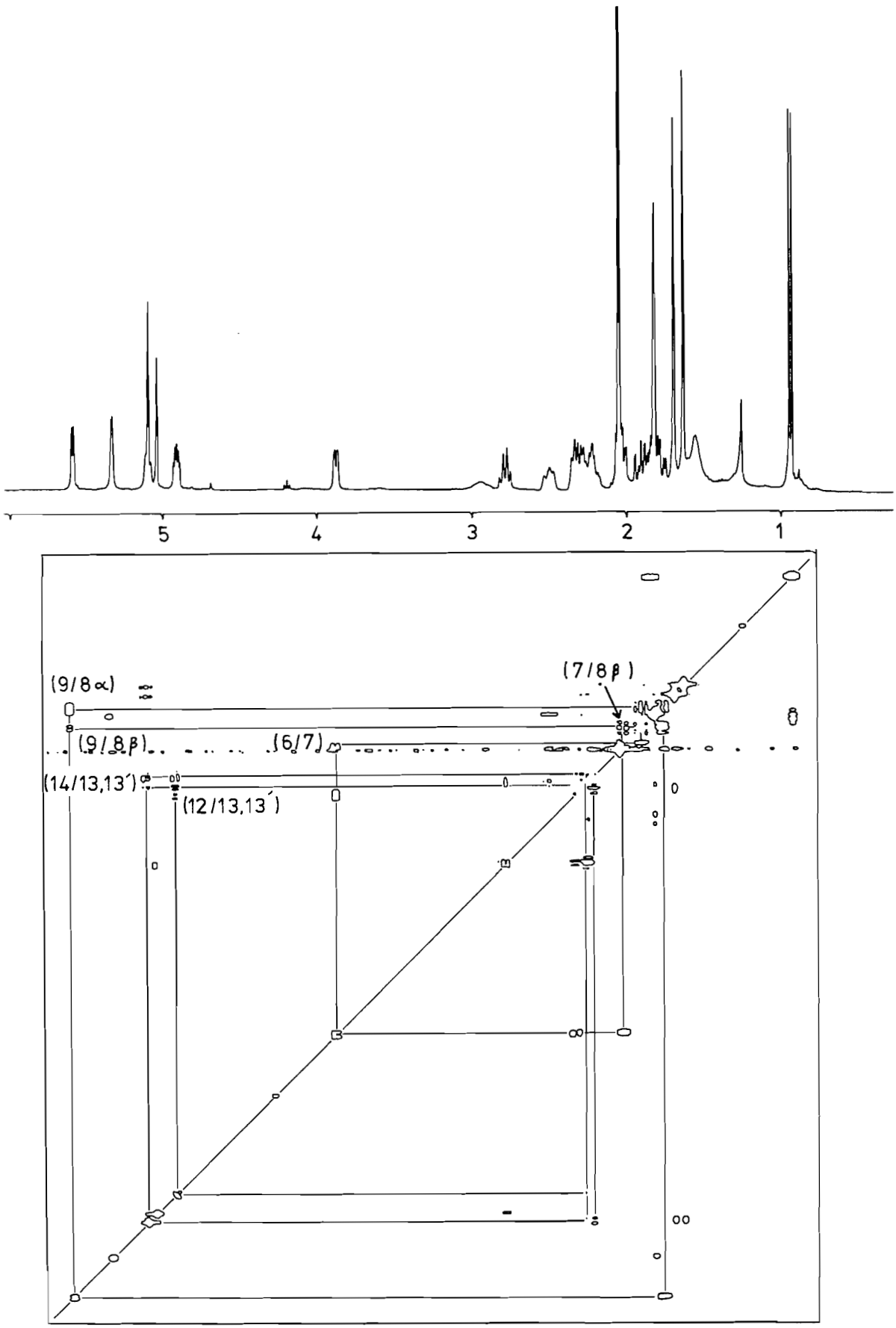

FIG. 2. Contour plot of the COSY two-dimensional nmr spectrum of dictyotriol A diacetate (**15**) in $CDCl_3$ at 400 MHz. Off-diagonal responses establishing proton spin-coupling connectivities are labelled with the protons involved, the downfield resonance listed first. Only the connectivities required to demonstrate the positions of the acetate functionalities are shown.

Can. J. Chem. Downloaded from www.nrcresearchpress.com by 210.87.254.6 on 09/06/12
For personal use only.

Experimental

The ^1H and ^{13}C nmr spectra were recorded on Bruker WH 400 and WP80 spectrometers. TMS was used as an internal standard. Low resolution mass spectra where recorded on an AEI MS902 spectrometer and high resolution mass spectra were recorded on an AEI MS 50 spectrometer. The ir spectra were recorded on a Perkin–Elmer model 710 B spectrometer and optical rotations were measured on a Perkin–Elmer 141 polarimeter using a 1-dm cell. Melting points were obtained on a Fisher–Johns apparatus and values are uncorrected. Merck silica gel 230–400 mesh was used for flash chromatography, Merck silica gel PF 254 with $CaSO_4 \cdot 1/2\ H_2O$ Type 60 was used for radial tlc and a Whatman Magnum 9-ODS 3 column was used for preparative hplc. All chromatography solvents were hplc grade.

Collection data

Dictyota binghamiae was collected by hand using SCUBA (−3 to −5 m) in shallow bays off Dixon Island and Execution Rock in Barkley Sound, British Columbia.

Extraction and chromatography

Oven dried (50°C, 24 h) and powdered (Wiley mill) alga (135 g) was soxhlet extracted with hexane to give 2.3 g of crude oil after evaporation.

Methanol extracted alga was homogenized in an industrial blender with the solvent and extracted at room temperature for one to three days. The homogenate was filtered and the filtrate was evaporated *in vacuo* to give an aqueous suspension which was exhaustively extracted with hexane. Concentration of the hexane *in vacuo* gave a crude oil.

The crude hexane extracts were fractionated by step gradient flash chromatography using the following solvent sequence: (*i*) hexane; (*ii*) hexane/chloroform, 1:1; (*iii*) chloroform; (*iv*) chloroform/ethyl acetate, 9:1; (*v*) chloroform/ethyl acetate, 1:1. The chloroform eluted componenets from the flash chromatography were further purified by radial tlc (hexane/ethyl acetate, 95:5) to give crude samples of pachydictyol A (**1**), dictyoxide (**7**), and dictyoxide A (**13**) and a pure sample of diacetal **16**. Final purification of **1**, **7**, and **13** was accomplished by reverse phase hplc (**1** and **7**; water/acetonitrile, 20:80: **13**; water/ethanol, 20:80). The chloroform/ethyl acetate eluted components from the flash chromatography were further purified by radial tlc (hexane/ethyl acetate, 85:15) and reverse phase hplc (water/ethanol, 20:80) to give pure dictyol G acetate (**12**) and dictyotriol A diacetate (**15**).

Pachydictyol A (1): obtained as a pale yellow oil (ca. 0.013%); ir ($CHCl_3$): 3300, 3050–2850, 1460, 1400 cm^{-1}; ^1H nmr (400 MHz, $CDCl_3$) δ: 5.33 (br s, 1H), 5.12 (br t, 1H, J = 6 Hz), 4.75 (s, 1H), 4.74 (br s, 1H), 3.92 (br d, 1H, J = 8 Hz), 2.67 (q, 1H, J = 10 Hz), 2.62 (m, 1H), 2.49 (m, 1H), 2.32 (m, 1H), 1.81 (m, 3H), 1.69 (br s, 3H), 1.61 (br s, 3H), 1.00 (d, 3H, J = 7 Hz) ppm; ^{13}C nmr (100.6 MHz, $CDCl_3$) δ: 152.60, 141.48, 131.46, 124.81, 124.02, 107.15, 75.23, 60.58, 47.79, 46.24, 40.54, 35.17, 34.93, 34.01, 25.71, 25.66, 23.61, 17.66, 17.54, 15.80 ppm; ms m/z (rel. intensity): 288(M^+, 47), 270(19), 255(5), 203(20), 175(13), 159(56), 109(25), 91(32), 69(73), 41(100), 28(93). *Exact Mass* calcd. for $C_{20}H_{32}O$: 288.2454; found (hrms): 288.2453.

Dictyoxide (7): obtained as a pale yellow oil (ca. 0.008%). ^1H nmr (400 Hz, $CDCl_3$) δ: 5.50 (br s, 1H), 5.09 (t, 1H, J = 8 Hz), 3.97 (m, 1H), 2.63 (br d, 1H, J = 12 Hz), 2.41 (dt, 1H, J = 12, 6 Hz), 2.04 (m, 2H), 2.00–1.85 (m, 2H), 1.82–1.70 (m, 1H), 1.78 (br s, 3H), 1.68 (br s, 3H), 1.60 (br s, 3H), 1.65–1.45 (m, 5H), 1.37 (m, 1H), 1.25 (s, 3H), 1.10 (m, 1H), 0.90 (d, 3H, J = 7 Hz) ppm; ^{13}C nmr (100.6 MHz, $CDCl_3$) δ: 141.37, 130.57, 124.87, 123.66, 77.33, 74.19, 63.12, 61.30, 38.79, 38.38, 37.29, 34.51, 29.82, 26.32, 25.55, 22.23, 20.41, 17.63, 16.44, 15.91 ppm; ms m/z (rel. intensity): 288(M^+, 18), 270(5), 255(3), 207(16), 178(17), 159(14), 121(39), 107(46), 69(50), 55(36), 43(54), 41(64), 28(100). *Exact Mass* calcd. for $C_{20}H_{32}O$: 288.2454; found: 288.2465.

Dictyol G acetate (12): obtained as a colorless oil (ca. 0.015%); $[\alpha]_D^{22}$ +50.0° (*c* 0.13, $CHCl_3$); ir (film): 3500 (OH), 3100–2850, 1725 (C=O), 1460, 1386, 1250 cm^{-1}; ^1H nmr (400 MHz, $CDCl_3$) δ: 5.57 (dt, 1H, J = 4 Hz), 5.33 (br s, 1H), 5.12 (br d, 1H, J = 8 Hz), 4.75 (s, 1H), 4.73 (s, 1H), 3.93 (br d, 1H, J = 8 Hz), 2.70–1.45 (m, 12H), 2.02 (s, 3H), 1.82 (d, 3H, J = 1.0 Hz), 1.74 (d, 3H, J = 1.5 Hz), 1.72 (d, 3H, J = 1.3 Hz), 1.27 (m, 1H), 1.04 (d, 3H, J = 7 Hz) ppm; ^{13}C nmr (100.6 MHz, $CDCl_3$) δ: 170.48, 152.38, 141.36, 136.33, 124.51, 124.13, 107.21, 74.93, 70.58, 60.47, 48.03, 46.21, 40.45, 40.37, 33.99, 32.11, 25.62, 23.84, 21.25, 18.35, 18.12, 15.82 ppm; ms m/z (rel. intensity): 346(M^+), 286(30), 268(20), 186(26), 159(21), 145(16), 133(17), 120(35), 109(50), 91(21), 82(100), 69(21), 55(23), 43(40). *Exact Mass* calcd. for $C_{22}H_{34}O_3$: 346.2509; found (hrms): 346.2487.

Dictyoxide A (13): obtained as a pale yellow oil (ca. 0.010%); $[\alpha]_D^{22}$ −5.6° (*c* 0.16, $CHCl_3$); ir (film): 2980, 2920, 1620, 1520, 1470, 1350, 1240 cm^{-1}; ^1H nmr (400 MHz, $CDCl_3$) δ: 5.37 (br s, 1H), 5.20 (br d, 1H, J = 8 Hz), 4.82 (s, 1H), 4.79 (s, 1H), 4.45 (ddd, 1H, J = 12, 8, 4 Hz), 3.74 (dd, 1H, J = 10, 4 Hz), 2.75 (br t, 1H, J = 10 Hz), 2.62 (q, 1H, J = 9 Hz), 2.58–2.18 (m, 5H), 1.84 (m, 1H), 1.79 (br s, 3H), 1.70 (br s, 3H), 1.65 (br s, 3H), 1.70–1.50 (m, 3H), 1.14 (q, 1H, J = 12 Hz), 0.95 (d, 3H, J = 7 Hz) ppm; ^{13}C nmr (100.6 MHz, $CDCl_3$) δ: 151.95, 142.97, 133.46, 126.84, 124.90, 106.81, 79.49, 68.55, 53.59, 46.64, 45.53, 39.67, 34.34, 34.21, 29.45, 25.78, 25.09, 20.21, 18.34, 17.26 ppm; ms m/z (rel. intensity): 286(M^+), 268(23), 177(23), 159(20), 145(20), 120(40), 109(63), 91(40), 82(66), 69(57), 67(54), 43(49), 41(91), 28(100). *Exact Mass* calcd. for $C_{20}H_{30}O$: 286.2298; found (hrms): 286.2298.

Dictyotriol A diacetate (15): obtained as a colorless oil (ca. 0.031%); $[\alpha]_D^{22}$ +12.5° (*c* 0.11, $CHCl_3$); ir (film): 3450 (OH), 3050–2850, 1730–1700 (C=O), 1450, 1380, 1250, 1030, 1000, 980 cm^{-1}; ^1H nmr (400 MHz, $CDCl_3$) δ: 5.59 (dd, 1H, J = 2, 6 Hz), 5.34 (br s, 1H), 5.10 (s, 1H), 5.10 (t, 1H, J = 7 Hz), 5.03 (s, 1H), 4.92 (m, 1H), 3.87 (dd, 1H, J = 3, 8 Hz), 2.95 (br s, 1H), 2.79 (q, 1H, J = 10 Hz), 2.49 (m, 1H), 2.40–2.15 (m, 4H), 2.07 (s, 3H), 2.06 (s, 3H), 2.02 (dd, 1H, J = 3, 10 Hz), 1.92 (ddd, 1H, J = 2, 10, 15 Hz), 1.86 (m, 1H), 1.82 (m, 3H), 1.76 (dd, 1H, J = 6, 15 Hz), 1.70 (br s, 3H), 1.64 (br s, 3H), 0.94 (d, 3H, J = 7 Hz) ppm; ms m/z (rel. intensity): 404(M^+), 344(10), 284(23), 266(8), 157(35), 109(33), 69(42), 43(100). *Exact Mass* calcd. for $C_{24}H_{36}O_5$: 404.2564; found (hrms): 404.2570.

Diacetal 16: obtained as a pale yellow oil; ^1H nmr (400 MHz, $CDCl_3$) δ: 5.85 (d, 1H, J = 8 Hz), 5.45 (dd, 1H, J = 3, 12 Hz), 5.16 (s, 1H), 5.13 (t, 1H, J = 6 Hz), 5.08 (s, 1H), 3.38 (s, 3H), 3.32 (s, 3H), 3.07 (br dd, 1H, J = 12, 16 Hz), 2.64 (ddd, 1H, J = 3, 8, 16 Hz), 2.27 (br s, 1H), 2.21 (br d, 1H, J = 12 Hz), 2.05–1.85 (m, 5H), 1.72 (br s, 3H), 1.67 (br s, 3H), 1.60 (br s, 3H), 1.70–1.55 (m, 2H), 1.22 (q, 2H, J = 8 Hz), 0.99 (d, 3H, J = 7 Hz) ppm; ms m/z (rel. intensity): 348(M^+), 316(14), 284(18), 201(18), 159(57), 145(95), 109(90), 69(85), 41(100). *Exact Mass* calcd. for $C_{22}H_{36}O_3$: 348.2666; found (hrms): 348.2649.

Acid hydrolysis of dictyol G acetate (12)

Dictyol G acetate (**12**) (5 mg) was dissolved in aqueous HOAc (30%, 1 mL) with a few drops of CH_3CN and the reaction mixture was stirred at room temperature for 24 h. It was then freeze-dried and the products were separated by tlc (hexane/ethyl acetate 85:15) to give dictyoxide A (**13**) (0.9 mg, R_f 0.56) and its epimer (**14**). Compound **14**: ^1H nmr ($CDCl_3$, 400 MHz) δ: 1.16 (d, 1H, J = 7 Hz), 1.68 (s, 3H), 1.71 (s, 3H), 3.71 (dd, 1H, J = 4, 9 Hz), 4.22 (ddd, 1H, J = 12, 8, 4 Hz), 4.69 (bs, 2H), 5.14 (bd, 1H, J = 8 Hz), 5.35 (bs) ppm.

Li/EtNH$_2$ reduction of dictyol G acetate (12)

Dictyol G acetate (**12**) (20 mg) was dissolved in ethylamine (1.5 mL, anhydrous) and into that freshly cut Li was added in excess and stirred for 20 min. The solvent was then evaporated under vacuum and the products were separated by tlc (hexane/ethyl acetate, 95:5). The product, pachydictyol A (**1**) (2.9 mg) was identified by ^1H nmr and tlc.

Acknowledgements

The authors would like to thank Mike LeBlanc, Terry

Klinger, and the staff of the Bamfield Marine Station for assistance with collecting *Dictyota binghamiae*. Financial support was provided by the Natural Sciences and Engineering Research Council of Canada. We wish to thank Dr. J. Sims and Dr. W. Fenical for authentic samples of pachydictyol A and Dr. S. O. Chan for performing the 2D nmr COSY experiment.

1. D. R. HIRSCHFELD, W. FENICAL, G. H. Y. LIN, R. M. WING, P. RADLICK, and J. J. SIMS. J. Am. Chem. Soc. **95**, 4049 (1973).
2. (*a*) E. FATTORUSSO, S. MAGNO, L. MAYOL, C. SANTACROCE, D. SICA, V. AMICO, G. ORIENTE, M. PIATTELLI, and C. TRINGALI. J. Chem. Soc. Chem. Commun. 575 (1976); (*b*) B. DANISE, L. MINALE, R. RICCIO, V. AMICO, G. ORIENTE, M. PIATTELLI, C. TRINGALI, E. FATTORUSSO, S. MAGNO, and L. MAYOL. Experientia, **33**, 413 (1977).
3. V. AMICO, G. ORIENTE, M. PIATTELLI, and C. TRINGALI. Phytochemistry, **18**, 1895 (1979).
4. D. J. FAULKNER, B. N. RAVI, J. FINER, and J. CLARDY. Phytochemistry, **16**, 991 (1977).
5. N. ENOKI, R. ISHIDA, S. URANO, M. OCHI, T. TOKOROYAMA, and T. MATSUMOTO. Chem. Lett. 1837 (1982).
6. M. ISHITSUKA, T. KUSUMI, J. TANAKA, and H. KAKISAWA. Chem. Lett. 1517 (1982).
7. (*a*) R. FREEMAN, A. MORRIS, and A. J. BAX. Magn. Reson. **42**, 164 (1981); (*b*) M. A. BERNSTEIN, L. D. HALL, and S. SUKUMAR. Carbohydr. Res. **103**, C1–C6 (1982).

Can. J. Chem. Downloaded from www.nrcresearchpress.com by 210.87.254.6 on 09/06/12
For personal use only.

A nuclear magnetic resonance study of the kinetics and equilibria for the oxidation of penicillamine and *N*-acetylpenicillamine by glutathione disulfide

DALLAS L. RABENSTEIN[1] AND YVON THERIAULT
Department of Chemistry, University of Alberta, Edmonton, Alta., Canada T6G 2G2

Received February 6, 1984

DALLAS L. RABENSTEIN and YVON THERIAULT. Can. J. Chem. **62**, 1672 (1984).

The kinetics and equilibria of the oxidation of penicillamine by glutathione disulfide to form, in the first step, penicillamine–glutathione mixed disulfide and glutathione and, in the second step, penicillamine disulfide and glutathione have been studied over the pH range 4–9 by ^{1}H nmr. The reactive species are found to be penicillamine with its amino group protonated and its thiol group deprotonated and glutathione disulfide and penicillamine–glutathione mixed disulfide with their two amino groups protonated. The rate and equilibrium constants for the first step are much larger than those for the second step, indicating a small tendency for penicillamine to form its symmetrical disulfide by thiol/disulfide exchange reactions. This and the smaller reducing power of penicillamine as compared to glutathione are attributed to steric hindrance from the methyl groups adjacent to the sulfur. The kinetics and equilibria of the oxidation of *N*-acetylpenicillamine by glutathione disulfide were studied at neutral pH. Conditional equilibrium and rate constants for the oxidation of penicillamine by glutathione disulfide at pH 7.4 are presented and discussed in terms of the metabolism of penicillamine.

DALLAS L. RABENSTEIN et YVON THERIAULT. Can. J. Chem. **62**, 1672 (1984).

Faisant appel à la rmn du ^{1}H et travaillant dans un intervalle de pH allant de 4 à 9, on a déterminé les cinétiques et les équilibres d'oxydation de la pénicillamine par le disulfure de glutathion qui, dans une première étape, conduit à la formation de glutathion et d'un sulfure mixte de pénicillamine et de glutathion et, dans une deuxième étape, donne le disulfure de pénicillamine et du glutathion. On a trouvé que les espèces réactives sont d'une part la pénicillamine dans laquelle le groupe amino est protoné et le groupe thiol est déprotoné et d'autre part le disulfure de glutathion et le disulfure mixte de pénicillamine et de glutathion dans lesquels les groupes amino sont protonés. Les constantes de vitesse et d'équilibre de la première étape sont beaucoup plus élevées que celles de la deuxième étape; ceci indique que la tendance de la pénicillamine à former son disulfure symétrique par des réactions d'échanges entre thiols et disulfures est faible. On attribue cette tendance et le pouvoir réducteur plus faible de la pénicillamine par rapport au glutathion, à l'encombrement stérique des groupes méthyles adjacents au soufre. On a étudié, à un pH neutre, les cinétiques et les équilibres d'oxydation de la *N*-acétylpénicillamine par le disulfure de glutathion. On présente des constantes de vitesse et d'équilibre conditionnels pour l'oxydation de la pénicillamine par le disulfure de glutathion à un pH de 7,4 et on en discute en fonction du métabolisme de la pénicillamine.

[Traduit par le journal]

Introduction

The metabolism and biological functions of thiols depend to a large extent on the ease with which they are oxidized. There are several reactions by which they are oxidized in biological systems, including oxidation by disulfides via thiol/disulfide exchange as described by eqs. [1] and [2] (1, 2).

[1] $RSH + R'SSR' \rightleftarrows RSSR' + R'SH$

[2] $RSH + RSSR' \rightleftarrows RSSR + R'SH$

In this paper, we present the results of a ^{1}H nmr study of the oxidation of D-penicillamine (PSH, **1**) and *N*-acetyl-D,L-penicillamine (N-PSH) by glutathione disulfide (GSSG, **2**). PSH is widely used in medicine (3–6) for the treatment of Wilson's disease (7), heavy metal poisoning (8, 9), cystinuria (10), and rheumatoid arthritis (4). The primary pathway of PSH metabolism is via disulfide formation (3), and its pharmacological and therapeutic actions are largely explained by its ability to take part in thiol/disulfide exchange reactions (3, 5, 6). For example, the molecular basis for the treatment of cystinuria by PSH is the formation of the more soluble penicillamine–cysteine mixed disulfide from insoluble cystine by thiol/disulfide exchange (10). Also, the depolymerization and loss of serological activity of rheumatoid factor on reaction with PSH in vitro is by thiol/disulfide exchange involving disulfide bonds in rheumatoid factor (11).

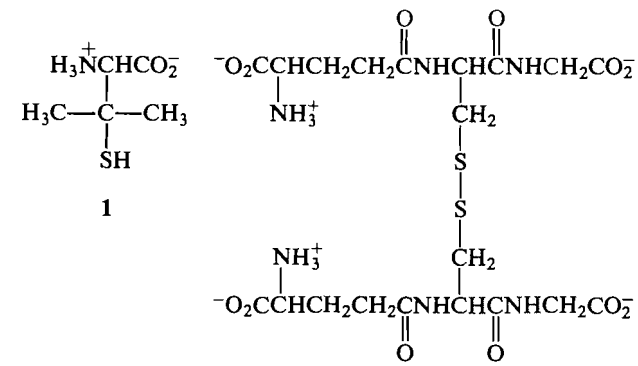

1

2

Despite their importance, there have been few reports on the kinetics and equilibria of the oxidation of PSH by thiol/disulfide exchange reactions (5, 12, 13). In this study, we have obtained kinetic and equilibrium data for the reaction of PSH with GSSG and of GSH with PSSP over a wide range of solution pH by ^{1}H nmr. Resolved resonances are obtained for the various PSH-containing species, making it possible to characterize separately the two stepwise thiol/disulfide exchange reactions involved in the overall oxidation of thiol to disulfide. Results on the kinetics and equilibria for the reaction of N-PSH with GSSG at neutral pH are also reported. Glutathione disulfide was chosen for this study because it occurs naturally in biological systems (1, 2), it may be involved in the metabolism of PSH (5), and, with the cystine placed between two amino acid residues, it serves to a first approximation as a model for disulfide bonds in proteins.

Experimental

D-Penicillamine, glutathione, glutathione disulfide, and *N*-acetyl-

[1]Author to whom correspondence should be addressed.

Can. J. Chem. Downloaded from www.nrcresearchpress.com by 210.87.254.6 on 09/06/12
For personal use only.

Can. J. Chem. Downloaded from www.nrcresearchpress.com by 210.87.254.6 on 09/06/12
For personal use only.

D,L-penicillamine were obtained from Sigma Chemical Co. D-Penicillamine disulfide was obtained from Aldrich Chemical Co. For most experiments, the thiols and disulfides were used as received. In several experiments, solutions of penicillamine were electrolyzed over a Hg pool electrode (14) to reduce traces (<1%) of penicillamine disulfide.

The pH measurements were made at 25°C with a Fisher Accumet pH meter equipped with a standard glass electrode and a fiber-tipped, saturated calomel reference electrode, or a microcombination electrode. The pH meter was calibrated with standard solutions having nominal pH values of 4.00, 7.00, and 10.00 at 25°C. The exact pH value of each standard solution was established, and checked periodically, by comparison with freshly prepared NBS pH standard solutions. In some of the experiments done in sealed nmr tubes, the pH was determined from the chemical shifts of resonances for the C2 and C4,5 hydrogens of imidazole, which was added to the solution as a pH indicator (15). The pH is related to the observed chemical shift, δ_{obs}, for C2H and C4,5H, respectively, by:

$$[3] \quad pH = 7.28 + \log\left(\frac{\delta_{obs} - 8.700}{7.7820 - \delta_{obs}}\right)$$

$$[4] \quad pH = 7.27 + \log\left(\frac{\delta_{obs} - 7.4892}{7.1380 - \delta_{obs}}\right)$$

Accurate pH values can be obtained from the imidazole chemical shifts over the pH range 6.3−8.3; at lower and higher pH values, the chemical shifts approach those of HIm^+ and Im, respectively, and are not sensitive to changes in pH.

The ^1H nmr spectra were measured at 200 MHz and 25°C on a Bruker WH-200 nmr spectrometer operating in the pulse/Fourier transform mode. The nmr spectra were obtained on aqueous solutions. To avoid the dynamic range problem, the water resonance was reduced in intensity by saturating it with a decoupler pulse applied at the water resonance frequency for 2 s prior to the observation pulse. The spectrometer was run in the unlocked mode because the magnet shows no detectable drift over the time required to obtain a spectrum. The ^1H chemical shifts were measured relative to the methyl resonance of *tert*-butanol (TBA), which was added to the solutions at a concentration of 0.001−0.01 *M*, depending on the thiol and disulfide concentrations. The chemical shifts are reported relative to the methyl resonance of sodium-2,2-dimethyl-2-silapentane-5-sulfonate (DSS); the resonance for TBA is 1.2397 ppm to high frequency from that of DSS. So that quantitative information could be obtained from resonance intensities, the repetition time was at least 5 times the longest T_1 of the methyl resonances of interest. The T_1 values of the methyl resonances were measured by the inversion−recovery method, and ranged from 0.3−1 s.

Solutions were prepared in water which had been purified by distilling it twice and then passing it through a Barnstead D8902 Ultrapure mixed bed ion-exchange resin. KCl (1 *M*) and EDTA (0.003 *M*) were added for ionic strength control and to complex traces of heavy metals which would catalyze the air oxidation of thiols (16). Previous studies have shown that EDTA has no effect on the rates of thiol/disulfide exchange (16). The solvent mixture was deoxygenated by bubbling with argon or nitrogen before addition of thiol to minimize oxidation by dissolved oxygen. Inert gas was also blown over the solution during adjustment of pH, and nmr tubes were flushed with the gas before transfer of an aliquot of solution to the tube. This method of solution preparation was satisfactory for solutions which came to equilibrium within a few hours after mixing of the thiol and disulfide. For those systems which reacted more slowly, the sample solution was degassed by taking the sample, in an nmr tube, through at least three freeze−pump−thaw cycles on a vacuum line. The nmr tube was then sealed while still on the vacuum line.

Several procedures were used to obtain the kinetic data. (*i*) In cases where the system came to equilibrium within a few hours and the pH was one at which resolved resonances are observed for the reactants and products, spectra were measured at preselected times while the sample remained continuously in the spectrometer. (*ii*) When the reaction was either too fast or the pH was one at which the resonances of interest were not resolved, aliquots were taken from a reaction vial as a function of time and quenched by lowering the pH to 0.5−2 with HCl. Spectra were measured for all the aliquots once the reaction was completed. (*iii*) When the reaction came to equilibrium very slowly, the sample was sealed in an nmr tube and stored at 25°C. Spectra were taken hourly, daily, or weekly as necessary to characterize the time course.

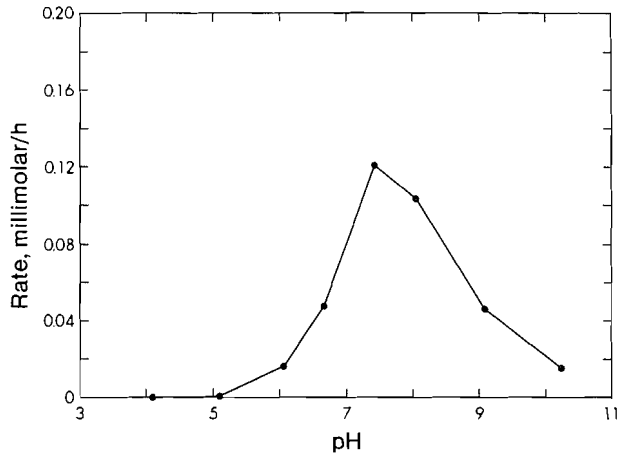

FIG. 1. Initial rate of air oxidation of PSH (0.0042 *M*) to PSSP as a function of pH.

Results

Air oxidation of penicillamine

Thiols are easily air oxidized to disulfides. Since air oxidation would lead to errors in the equilibrium and kinetic parameters measured for the thiol/disulfide exchange reactions, the air oxidation of PSH was studied. The procedure involved adjusting the pH of 0.0042 *M* PSH solutions to selected values in the pH range 4−10, placing aliquots in loosely stoppered vials, and then removing 0.5-mL portions for nmr analysis as a function of time for up to six days. The rate of decrease in PSH concentration was found to be dependent on solution pH, and independent of PSH and PSSP concentrations. The pH dependence of the initial rate is plotted in Fig. 1. As the pH is increased from 4, the initial rate increases, reaches a maximum at pH 7.5, and then decreases as the pH is increased further. The pH−rate profile in Fig. 1 is similar to that observed for the oxidation of GSH to GSSG (17). To test the efficiency of the freeze−pump−thaw technique for removing oxygen from sample solutions, a sealed tube containing a pH 8 solution (near the maximum in Fig. 1) of 0.060 *M* PSH was prepared by this procedure. After 10 days, no PSSP was detected in the ^1H nmr spectrum. After 33 days, approximately 3% of the PSH had been oxidized.

Penicillamine−glutathione disulfide nuclear magnetic resonance spectra

In Fig. 2 is shown the 200-MHz ^1H nmr spectrum of a solution prepared by reacting PSH with GSSG at pH 7.9 for 5 min, and then adjusting the pH to 4.06. The initial concentrations were 0.13 *M* PSH and 0.12 *M* GSSG. As is shown later, no PSSP is formed under these reaction conditions. The formation of PSSG is indicated by the appearance of an additional pair of methyl resonances in the 1.3−1.8 ppm region,[2]

[2]The chemical shifts of the ^1H resonances for the two methyl groups of PSH, and of PSSG, are different due to the asymmetric center at C_α.

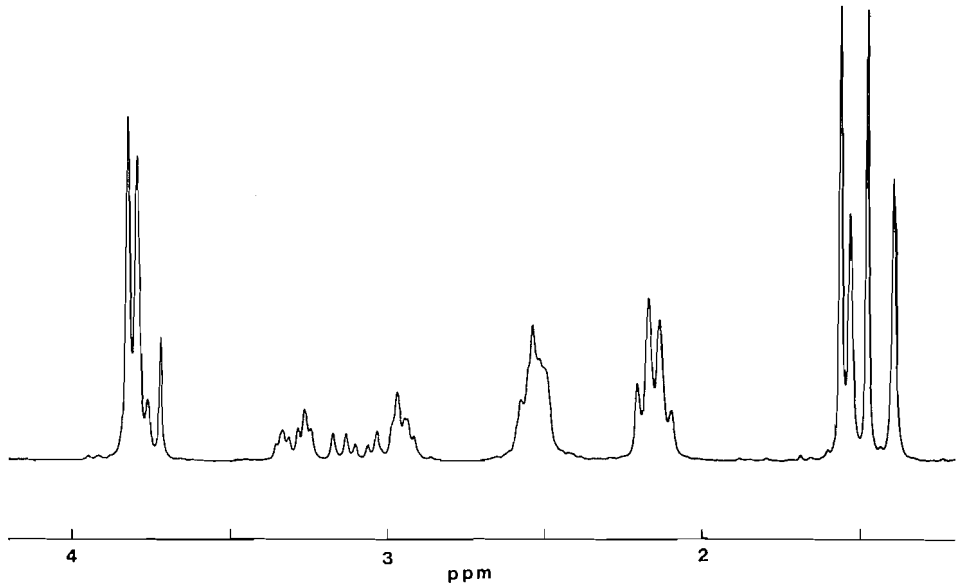

FIG. 2. 200-MHz ^{1}H nmr spectrum of mixture prepared by reacting 0.13 *M* PSH with 0.12 *M* GSSG.

and by additional resonances for C_α and C_β protons in the 3–4 ppm region. There is extensive overlap of resonances in the 3–4 ppm region, making it difficult to characterize the mixture using these resonances. However, the methyl resonances are singlets, and the resonances for the various penicillamine-containing species are reasonably well resolved over a wide range of pH, as shown in Figs. 3 and 4. The initial concentrations in the solution used to obtain the spectra in Fig. 3 were 0.02 *M* PSH, 0.01 *M* PSSP, 0.01 *M* GSSG, and 0.007 *M* TBA. The assignments were made by comparison with spectra obtained over the same pH range for solutions of PSH and PSSP. The chemical shift data plotted in Fig. 4 for PSH and PSSP were obtained from these experiments, while those for PSSG were obtained from spectra similar to those shown in Fig. 3. Since there is at least one resolved methyl resonance for each of the three penicillamine-containing species over a wide range of pH, these resonances were used to characterize the equilibria and kinetics of the oxidation of PSH by GSSG and of GSH by PSSP.

Penicillamine–glutathione thiol/disulfide exchange kinetics

The oxidation of PSH by GSSG takes place via two thiol/disulfide exchange reactions:

$$[5]\quad PSH_t + GSSG_t \underset{k_{2c}}{\overset{k_{1c}}{\rightleftharpoons}} PSSG_t + GSH_t$$

$$[6]\quad PSH_t + PSSG_t \underset{k_{4c}}{\overset{k_{3c}}{\rightleftharpoons}} PSSP_t + GSH_t$$

where k_{1c}–k_{4c} are conditional rate constants and $[PSH]_t$, $[PSSG]_t$, etc., represent the sums of the concentrations of the various protonated forms of PSH, PSSG, etc. at a particular pH. The rate of the second reaction is much slower than the first, and thus the kinetics of the two reactions were studied separately. The kinetics of the first reaction were studied over the pH range 4 to 9, using concentrations of reactants ranging from 0.0015 *M* to 0.024 *M*. Altogether, twenty kinetic experiments were performed by the methods described in the experimental section.

Typical time course spectra are shown in Fig. 5. The data at pH 3.96 indicate that, although thiol/disulfide exchange to form PSSG does take place, it is slow at this pH. However, there is no PSSP detected, even after 8 days. The second time course series in Fig. 5 indicates that the reaction of PSH with GSSG is somewhat faster at pH 6.61. Also, resonances due to PSSP are detected after 37 min. Comparison with time course spectra obtained for solutions of similar pH and concentration in degassed, sealed nmr tubes indicate this PSSP is formed by air oxidation. Rate constant k_{1c} was calculated from time course data taken before the appearance of PSSP.

The reaction of PSH with GSSG was found to be first order in the concentration of PSH and first order in the concentration of GSSG. The rate equation for the reaction represented by eq. [5] is:

$$[7]\quad \frac{d[PSSG]}{dt} = k_{1c}[PSH]_t[GSSG]_t - k_{2c}[PSSG]_t[GSH]_t$$

Rate constant k_{1c} was evaluated by fitting time course data by nonlinear least-squares calculations (18) to eq. [8], which is obtained from the integrated form of the rate expression for a second order, reversible reaction.

$$[8]\quad X = \frac{A_0B_0X_e\left(1 - \exp\left(\frac{k_{1c}t}{A}\right)\right)}{X_e(A_0 + B_0) - A_0B_0\left(1 + \exp\left(\frac{k_{1c}t}{A}\right)\right)}$$

where

$$[9]\quad A = \frac{X_e}{2A_0B_0 - X_e(A_0 + B_0)}$$

X and X_e are the concentrations of PSSG at time t and at equilibrium, and A_0 and B_0 the initial concentrations of PSH and GSSG. k_{1c} and X_e were both treated as unknowns in the nonlinear least-squares calculations. Typical time course data for the formation of PSSG at pH 3.96 and 9.01 are shown in Fig. 6. Values of k_{1c} = 0.0263 ± 0.0013 L/mol-min and $[PSSG]_e$ = 0.00779 ± 0.00020 *M* were obtained from the nonlinear least-squares fit of the pH 3.96 data; values of 146 ±

Can. J. Chem. Downloaded from www.nrcresearchpress.com by 210.87.254.6 on 09/06/12
For personal use only.

Can. J. Chem. Downloaded from www.nrcresearchpress.com by 210.87.254.6 on 09/06/12
For personal use only.

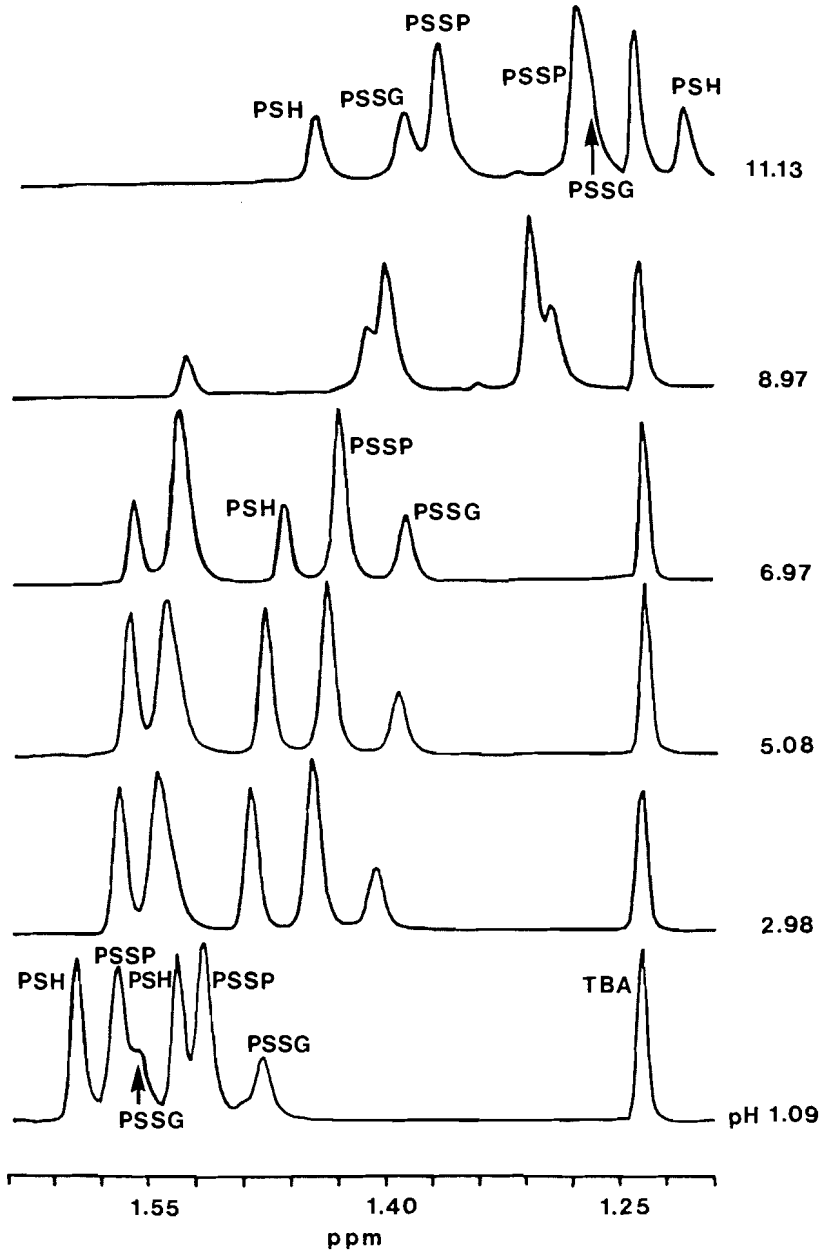

FIG. 3. Portions of the 200-MHz ^{1}H nmr spectra of a solution prepared from 0.02 *M* PSH, 0.01 *M* PSSP, 0.01 *M* GSSG, and 0.007 *M* TBA as a function of pH. The resonances are from methyl groups.

12 L/mol-min and 0.000761 ± 0.00004 *M* were obtained from the pH 9.01 data. The solid curves through the experimental points in Fig. 6 are the theoretical curves predicted by these parameters. The values obtained for k_{1c} from the twenty kinetic experiments are plotted in Fig. 7.

Thiol/disulfide exchange reactions proceed via the thiolate anion (19–27). There are two thiolate species possible for PSH: PS^-, in which the thiol group is deprotonated and the amino group protonated, and PS^{2-}, in which both groups are deprotonated. Both are present at low concentrations over the pH range 4–7; however, the dependence of their fractional concentrations on pH is different. The logarithms of their fractional concentrations (α), along with that of the form having both groups protonated (PSH^0), are plotted as a function of pH in Fig. 7. Over the pH range 4–7, the slope of the log α_{PSH^0} vs. pH plot is zero, that of the log α_{PS^-} vs. pH plot is one, and that of the log $\alpha_{PS^{2-}}$ vs. pH plot is two. The slope of the log k_{1c} vs. pH plot is one, indicating PS^- to be the reactive species.

There is also the possibility that the rate constant depends on the protonation state of GSSG. However, the pH dependence of log k_{1c} indicates that either the rate constant is the same for the various GSSG species present over the pH range studied or the fractional concentration of the GSSG species involved in the reaction is constant. Over this pH range, the fractional concentration of the species $GSSG^{2-}$, in which the four carboxylic acid groups are deprotonated and the two amino groups protonated, is nearly one while that of the other species varies over several orders of magnitude, indicating $GSSG^{2-}$ to be the predominant species involved.

The kinetics of the reaction of GSH with PSSP were studied over the pH range 5–8, either by following the time course for a reaction mixture in an nmr tube or by removing aliquots from a reaction vial as a function of time, quenching the reaction by lowering the pH, and then analyzing the mixture by nmr.

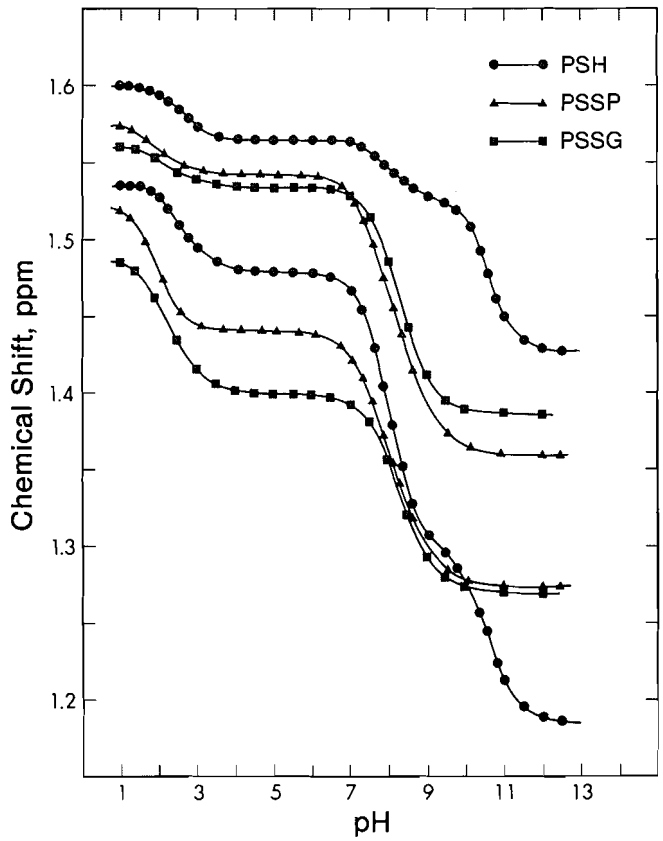

FIG. 4. pH dependence of the chemical shifts of the methyl resonances for PSH, PSSG, and PSSP.

Higher reactant concentrations (typically 0.1 *M*) were used due to the slowness of the reaction, and the length of time over which the progress of the reaction could be followed was limited to ~50 h due to air oxidation of thiols. The values obtained for k_{4c} were (pH, k_{4c}): 5.11, 0.00025 L/mol-min; 5.74, 0.00094 L/mol-min; 6.54, 0.0040 L/mol-min; 7.03, 0.0052 L/mol-min; 7.35, 0.012 L/mol-min; 8.03, 0.021 L/mol-min.

The general pH dependence of k_{4c} is similar to that observed for k_{1c}, and a comparison with the pH dependencies of the fractional concentrations of the various thiol-deprotonated forms of GSH indicates the thiol-deprotonated, amino-protonated form (GS^{2-}) to be the reactive species. Over this same pH range, PSSP is present predominantly in the amino-protonated form. Thus, the exchange reactions which occur are:

$$[10]\quad PS^- + GSSG^{2-} \underset{k_2}{\overset{k_1}{=}} PSSG^- + GS^{2-}$$

$$[11]\quad PS^- + PSSG^- \underset{k_4}{\overset{k_3}{=}} PSSP + GS^{2-}$$

where k_1–k_4 are pH independent rate constants.

Rate constant k_1 is related to the conditional rate constant k_{1c} by eq. [12].

$$[12]\quad k_{1c} = k_1\left(\frac{k_{a12}a_H}{a_H^2 + a_H K_{A2} + K_{A2}K_{A3}}\right)$$

where K_{A2} and K_{A3} are acid dissociation constants for PSH and a_H is calculated directly from the pH meter reading. k_{a12} is the microscopic acid dissociation constant for the deprotonation of the thiol group of the PSH species in which both the amino and thiol groups are protonated (28). A value of 190 ± 7 L/mol-min was obtained for k_1 by fitting the k_{1c} data at pH > 5 to eq. [12]. The solid line through the experimental points in Fig. 7 is the theoretical curve predicted by this value for k_1.

Rate constant k_4 was calculated from the values for k_{4c} using eq. [13].

$$[13]\quad k_{4c} = k_4\left(\frac{k_{a123}a_H}{a_H^2 + K_{A3}a_H + K_{A3}K_{A4}}\right)$$

where K_{A3} and K_{A4} are acid dissociation constants for GSH and k_{a123} is the microscopic acid dissociation constant for deprotonation of the thiol group from the carboxyl-deprotonated, amino- and thiol-protonated form of GSH (29). The value obtained for k_4 is 1.30 ± 0.34 L/mol-min.

Penicillamine–glutathione thiol/disulfide exchange equilibria

The equilibrium constants for the reactions represented by eqs. [10] and [11] are defined as:

$$[14]\quad K_1 = \frac{[PSSG^-][GS^{2-}]}{[PS^-][GSSG^{2-}]}$$

$$[15]\quad K_2 = \frac{[PSSP]^-[GS^{2-}]}{[PS^-][PSSG^-]}$$

where PS^- and GS^{2-} are the amino-protonated, thiol-deprotonated forms of PSH and GSH, and $GSSG^{2-}$, $PSSG^-$, and PSSP the amino-protonated forms of GSSG, PSSG, and PSSP. K_1 and K_2 were determined from the conditional (pH-dependent) equilibrium constants K_{1c} and K_{2c} for reactions [5] and [6]. K_1 and K_2 are related to K_{1c} and K_{2c} by:

$$[16]\quad K_1 = K_{1c}\frac{\alpha_1\alpha_2}{\alpha_3\alpha_4}$$

$$[17]\quad K_2 = K_{2c}\frac{\alpha_2\alpha_5}{\alpha_1\alpha_3}$$

where α_1 is the fraction of $PSSG_t$ that is in the form $PSSG^-$, α_2 the fraction of GSH_t that is GS^{2-}, α_3 the fraction of PSH_t that is PS^-, α_4 the fraction of $GSSG_t$ that is $GSSG^{2-}$, and α_5 the fraction of $PSSP_t$ that is in the form PSSP. α_1–α_5 can be calculated from the acid dissociation constants for the various species (30).[3]

K_{1c} and K_{2c} were determined over a wide range of solution conditions from the equilibrium concentrations of PSH_t, etc., which were determined from the intensities of the methyl resonances. First, the concentrations of PSH, PSSG, and PSSP, if present, were calculated from the initial PSH concentration and the relative areas of the methyl resonances, and then the concentrations of GSH and GSSG were obtained by difference. Equilibrium data were obtained from reactions carried out (*i*) in D_2O under an argon atmosphere, (*ii*) in H_2O under an argon atmosphere, and (*iii*) in H_2O in sealed nmr tubes which were degassed by the freeze–pump–thaw technique before sealing. The experiments in (*iii*) were found to be necessary for the measurement of K_{2c}, because the kinetics of the reaction represented by eq. [6] are slow and, at the long reaction times required to reach equilibrium, it was found that air oxidation

[3]For example, $\alpha_1 = [PSSG^-]/[PSSG]_t = a_H^2/(a_H^2 + K_{A4}a_H + K_{A4}K_{A5})$ where K_{A4} and K_{A5} are the last two acid dissociation constants for PSSG (30).

Can. J. Chem. Downloaded from www.nrcresearchpress.com by 210.87.254.6 on 09/06/12
For personal use only.

Can. J. Chem. Downloaded from www.nrcresearchpress.com by 210.87.254.6 on 09/06/12
For personal use only.

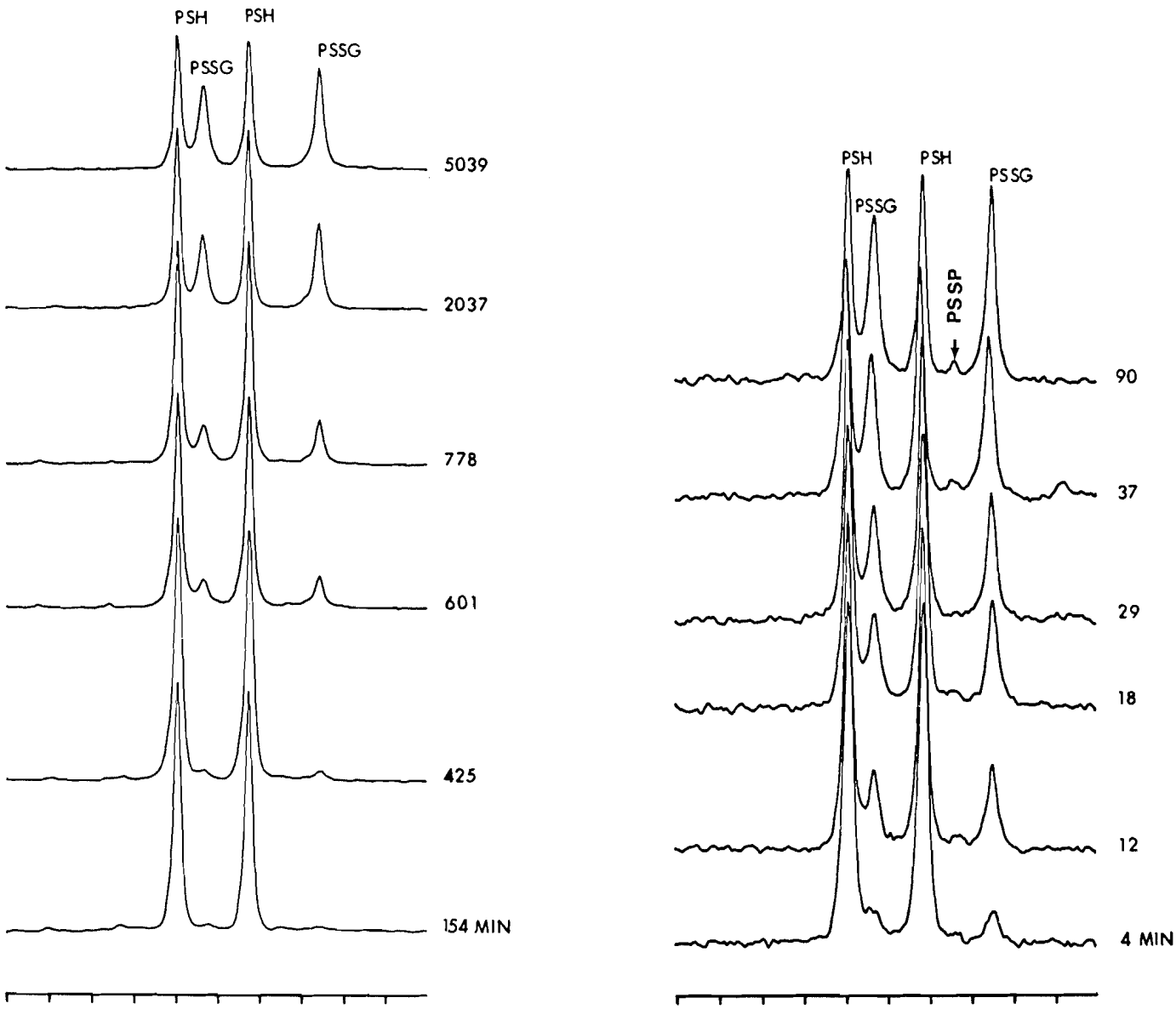

FIG. 5. 200-MHz ^{1}H nmr spectra obtained as a function of time for the reaction of PSH with GSSG. (Left) Initial concentrations of PSH and GSSG, 0.0160 *M*, pH = 3.96. (Right) Initial concentrations of PSH and GSSG, 0.00400 *M*, pH = 6.61.

of PSH and GSH leads to irreproducible results for K_{2c} in experiments (*i*) and (*ii*).

K_{1c} was measured at 15 pH values, covering the pH range 3.8−10.5, in experiment (*i*), at 9 pH values covering the pH range 7.2−10.0, in experiment (*ii*), and at 12 pH values covering the pH range 4.2−10.0 in experiment (*iii*). In experiments (*i*) and (*ii*), spectra were measured within 24 h of mixing the reactants. Beyond this time, PSSP and PSSG resonances increase due to air oxidation. The reaction represented by eq. [5] is sufficiently fast at the concentrations and pH values used that it has come to equilibrium within this time. However, the reaction represented by eq. [6] is much slower and has not reached equilibrium.

K_{2c} was measured as a function of pH in experiment (*iii*). To ensure that both reactions had come to equilibrium, spectra were measured for each of the solutions in sealed nmr tubes every few days for approximately one month.

A value of 0.56 ± 0.02 was calculated for K_1 and a value of 0.0143 ± 0.0014 for K_2 from the K_{1c} and K_{2c} values with eqs. [16] and [17]. With these values for K_1 and K_2 and the values determined for k_1 and k_4, k_2 and k_3 are calculated to be 340 ± 20 L/mol-min and 0.019 ± 0.005 L/mol-min respectively.

pH-independent equilibrium constants for the reactions written in terms of all the reactants and products in their fully deprotonated forms can also be calculated from the values for K_{1c} and K_{2c}. The values obtained are 34.8 ± 0.9 for the first reaction and 0.99 ± 0.10 for the second reaction.

N-*Acetylpenicillamine − glutathione disulfide reactions*

The kinetics and equilibria of the oxidation of *N*-acetyl-D,L-penicillamine (N-PSH) by GSSG were studied for comparison with the results obtained for the oxidation of PSH by GSSG. In Fig. 8 are shown ^{1}H nmr spectra for the penicillamine methyl protons in a solution containing N-PSH and GSSG at pH 6.58 as a function of time. One pair of resonances is observed for the two penicillamine methyl groups of N-PSH, whereas two pairs of resonances are observed for the N-PSH methyl groups in the mixed disulfide due to the two different

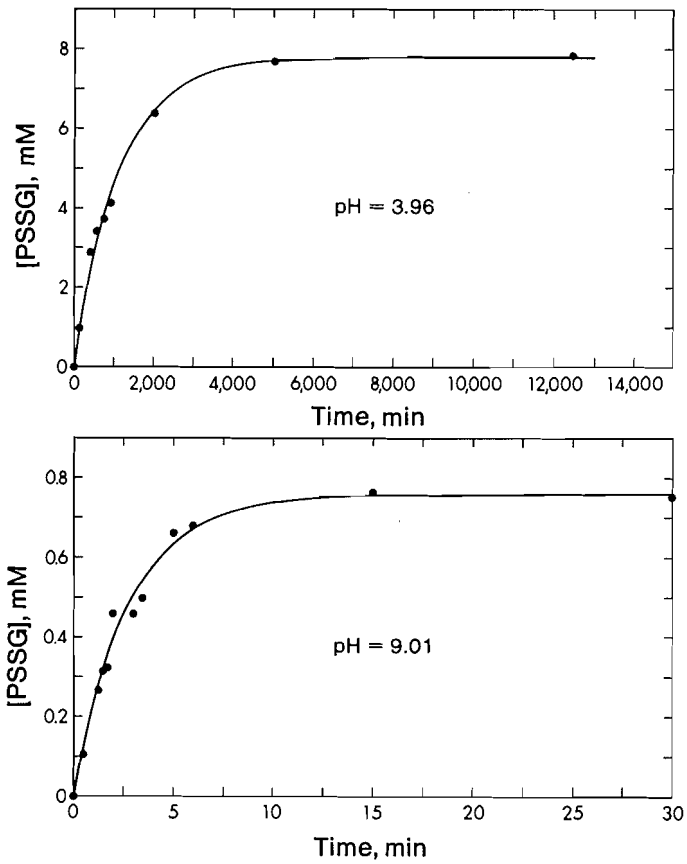

FIG. 6. Kinetic data for the formation of PSSG by reaction of PSH with GSSG at pH 3.96 and 9.01. At pH 3.96, the initial concentrations of PSH and GSSG were 0.0160 *M*. At pH 9.01, the initial concentrations were 0.00143 *M* PSH and 0.00137 *M* GSSG. The solid curves through the points are theoretical curves calculated with the rate parameters obtained from the data as described in the text.

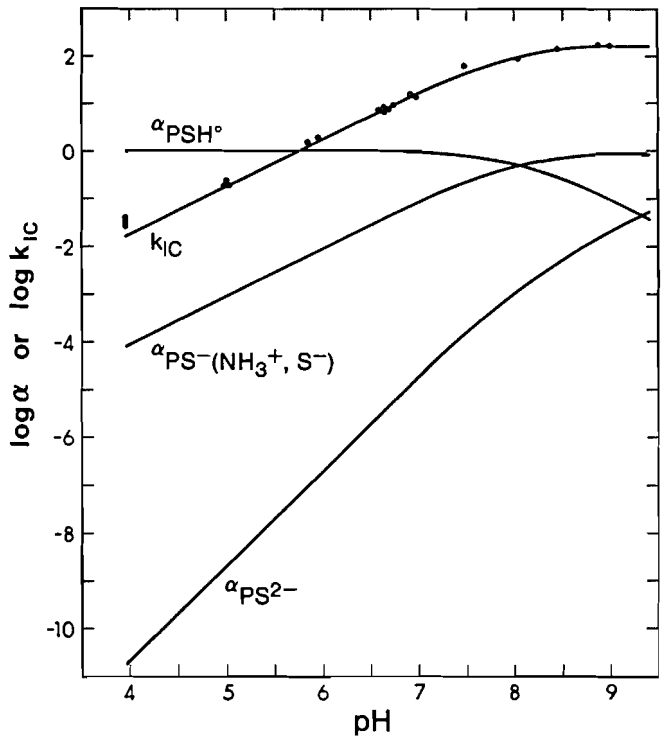

FIG. 7. The logarithm of the fractional concentrations (α) of the fully protonated (PSH^0), amino-protonated, thiol-deprotonated (PS^-), and amino-deprotonated, thiol-deprotonated (PS^{2-}) forms of PSH, and of the conditional rate constant k_{1c} as a function of pH. The solid curve through the experimental points is the theoretical curve predicted by the pH-independent rate constant k_1, as described in the text.

configurations which form: *N*-acetyl-D-penicillamine-glutathione mixed disulfide and *N*-acetyl-L-penicillamine-glutathione mixed disulfide.[4] Since the *N*-acetyl-D,L-penicillamine is a racemic mixture, the two pairs of resonances from the mixed disulfide are of equal intensity.

Using procedures similar to those described above, K_{1c}, defined by eq. [5], was found to be 2.55 ± 0.15 at pH 6.95, 2.60 ±0.13 at pH 7.44, and 2.79 ± 0.13 at pH 8.02. A value of 0.747 ± 0.012 L/mol-min was measured for the conditional rate constant k_{1c} at pH 6.58. Assuming the reactive species in the thiol/disulfide exchange reaction between N-PSH and GSSG at pH 6.58 to be the carboxyl and thiol-deprotonated form of N-PSH and the $GSSG^{2-}$ form of GSSG, a value of 3660 L/mol-min is calculated for rate constant k_1 from the value measured for k_{1c} at pH 6.58 and a pK_a of 10.27 for the thiol group of N-PSH (31). A pH-independent equilibrium constant cannot be calculated from the K_{1c} values because the acid dissociation constants of the mixed disulfide are not known.

Discussion

It is well established that thiol/disulfide exchange reactions are mechanistically simple S_N2 displacement reactions (19, 20), and that they proceed via the thiolate anion (19–27). For both PSH and GSH, there are two thiolate species possible, PS^- and GS^{2-}, in which the thiol group is deprotonated and the amino group protonated, and PS^{2-} and GS^{3-}, in which both groups are deprotonated. The pH dependence of the conditional rate constants indicate that PS^- and GS^{2-} are the reactive species.

Equations [10] and [11] describe the two steps in the oxidation of PSH by GSSG in terms of the species involved, and eq. [18] describes the overall reaction.

[18] $2PS^- - GSSG^{2-} \rightleftarrows PSSP + 2GS^{2-}$

The equilibrium constant for the overall reaction, K_3, is calculated to be 8.0×10^{-3} using the relation $K_3 = K_1K_2$. If the position of equilibrium in the two stepwise reactions was governed by random distribution, K_1 and K_2 would be 2 and 0.5 respectively, and K_3 would equal 1. The values obtained for K_1 and K_2 differ from these values by factors of ~4 and ~35 respectively. For comparison, Gorin and Doughty (27) reported values of $K_1 = 1.27$ and $K_2 = 0.27$ at pH 6.6 and 25°C for the reaction of cysteine with glutathione disulfide. Penicillamine differs from cysteine in that the thiol group of penicillamine is adjacent to two bulky methyl groups, which hinder its reactivity (5). The large difference between k_1 and k_3 indicates this is particularly true in the reaction of PS^- and PSSG, in which there also are two methyl groups adjacent to the specific disulfide sulfur at which the reaction occurs. The large difference between k_4 and k_2 suggests that the methyl groups also hinder the access of thiolate groups to the disulfide group of PSSP. Steric effects on thiol/disulfide exchange reac-

[4]The glutamic acid and cysteine residues in glutathione are both of the L-configuration.

Can. J. Chem. Downloaded from www.nrcresearchpress.com by 210.87.254.6 on 09/06/12
For personal use only.

Can. J. Chem. Downloaded from www.nrcresearchpress.com by 210.87.254.6 on 09/06/12
For personal use only.

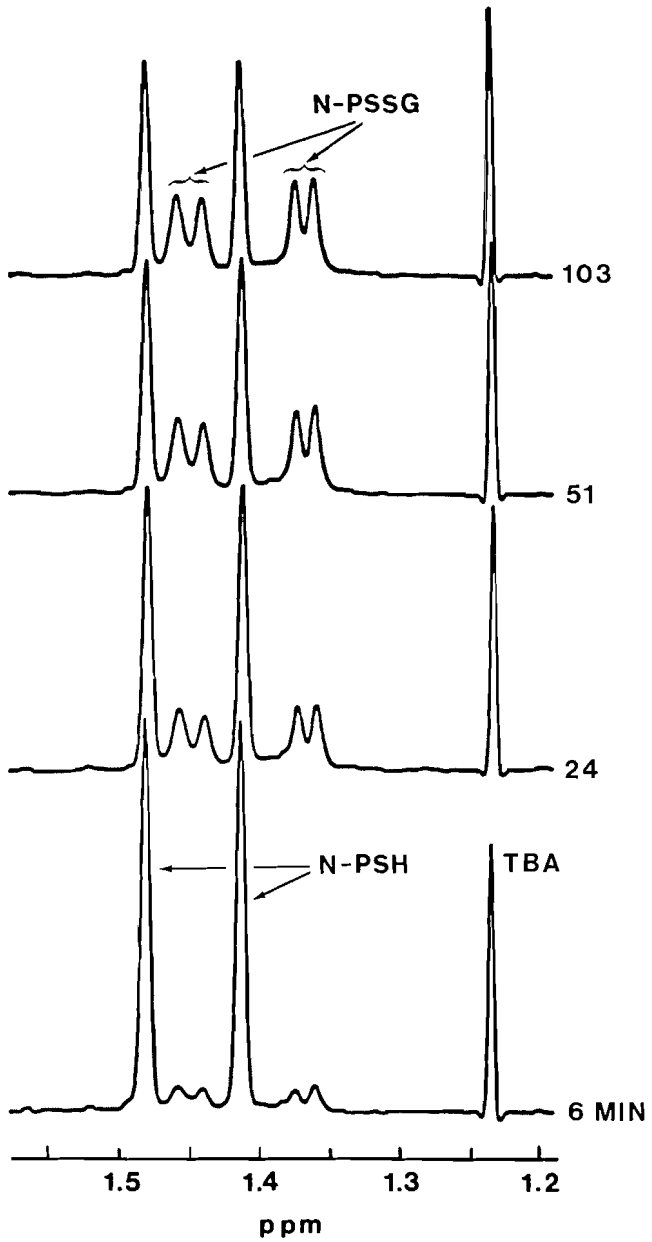

FIG. 8. Portions of the 200-MHz ^{1}H nmr spectra obtained as a function of time for the reaction of N-PSH with GSSG. Initial concentrations N-PSH = 0.0365 *M* and GSSG = 0.0348 *M*. TBA = 0.004 *M*, pH = 6.58. The resonances are from methyl groups.

tions have been observed previously for related systems. Equilibrium constants for thiol/disulfide exchange involving a series of alkyl thiols and disulfides differ from the statistically predicted values by a factor of 2 or less, except for the reaction of *tert*-butyl thiol with n-butyl *tert*-butyl mixed disulfide (32). Also, exchange equilibrium constants for the reaction of a series of 2-aminoethane thiols with 4,4′-dithiobis(benzenesulfonate) are near statistical values except for those having two methyl groups next to the thiol (26). Weber *et al.* found that the rate of reaction of GSH with RSSC, where R is an alkyl group and CS is cysteine, to form RSH and the cysteine–glutathione mixed disulfide is slowest when R is *tert*-butyl and isopropyl (33).

At physiological pH, thiol groups are almost completely protonated and the reactive thiol-deprotonated species PS^- and

TABLE 1. Conditional equilibrium and rate constants for penicillamine–glutathione thiol/disulfide exchange at pH 7.4

Constant	Value
K_{1c}	1.36
K_{2c}	0.039
K_{3c}	0.053
k_{1c}	36.6 L/mol-min
k_{2c}	26.9 L/mol-min
k_{3c}	0.00047 L/mol-min
k_{4c}	0.012 L/mol-min

GS^{2-} represent a minor fraction of the total PSH and GSH. Also, since the pK_A's of the thiol groups of PSH and GSH are different, the fraction of PSH present as PS^- is different from the fraction of GSH present as GS^{2-}. Thus, at physiological pH, the conditional equilibrium and rate constants are different from the above values for K_1–K_3 and k_1–k_4. The conditional equilibrium and rate constants calculated from these values for a pH of 7.4 are listed in Table 1. The corresponding values for the reaction of N-PSH with GSSG at pH 7.4 are K_{1c} = 2.6, k_{1c} = 4.9 L/mol-min, and k_{2c} = 1.9 L/mol-min. This value for k_{1c} is less than that for PSH, even though k_1 is larger for N-PSH, because the fraction of the N-PSH in which the thiol group is deprotonated at pH 7.4 is less.

The small value for K_{2c} in Table 1 indicates that the tendency to form PSSP from the mixed disulfide is small. The small value for k_{3c} suggests that the PSSP found as a metabolite of penicillamine (3) is formed not by thiol/disulfide exchange but by other oxidation reactions. It has been proposed that, in cells, the nonenzymatic reduction of PSSP by GSH followed by the enzyme catalyzed reduction of GSSG to GSH is an efficient system for the reduction of PSSP (5). However, the small value obtained for k_{4c} in this study suggests that, once formed, reduction of PSSP by other thiols, including GSH and protein thiols, will be of minor importance in the metabolism of penicillamine.

The overall conditional equilibrium constant K_{3c} is related to the difference between the formal electrode potentials $E^{0\prime}$ of the GSSG/GSH and PSSP/PSH couples according to eq. [19].

$$[19]\quad E^{0\prime}_{GSSG/GSH} - E^{0\prime}_{PSSP/PSH} = \frac{RT}{nF} \ln K_{3c}$$

Values reported for $E^{0\prime}_{GSSG/GSH}$ are −0.205 V vs. the standard hydrogen electrode at 30°C and pH 7 (20) and −0.24 V at 40°C and pH 7 (34). Using the value given for K_{3c} in Table 1, $E^{0\prime}_{GSSG/GSH} - E^{0\prime}_{PSSP/PSH}$ is calculated to be −0.0378 V. For comparison, $E^{0\prime}_{GSSG/GSH} - E^{0\prime}_{CSSC/CSH}$, where CSSC is cystine, is reported to be in the range −0.013 to −0.018 V at pH 6.6–7.0 (21, 23, 27). The stepwise equilibrium constants for thiol/disulfide exchange indicate that the lower reducing power of PSH as compared to cysteine is due to the much smaller tendency of penicillamine to form its symmetrical disulfide from its unsymmetrical, mixed disulfides.

Acknowledgements

This research was supported by the Natural Sciences and Engineering Research Council of Canada, the Alberta Heritage Foundation for Medical Research, and the University of Alberta. Financial support of Y.T. by an AHFMR Studentship is gratefully acknowledged.

1. P. C. JOCELYN. Biochemistry of the SH group. Academic Press, London. 1972. p. 121.
2. Y. M. TORCHINSKY. Sulfur in proteins. Pergamon Press, New York. 1981. p. 57.
3. J. C. CRAWHALL, D. LECAVALIER, and P. RYAN. Pharm. Drug Dispos. **1**, 73 (1979).
4. F. M. ANDREWS, A. J. CAMP, A. T. DAY, A. M. FREEMAN, D. N. GOLDING, J. R. GOLDING, A. G. S. HILL, E. LEWIS-FANING, and W. H. LYLE. Lancet, **1**, 275 (1973).
5. E. JELLUM and S. SKREDE. *in* Penicillamine research in rheumatoid disease. *Edited by* E. Munthe. Fabritius and Sonner, Oslo. 1976. p. 68.
6. M. FRIEDMAN. Proc. R. Soc. Med. **70** (Suppl. 3), 50 (1977).
7. J. M. WALSHE. Am. J. Med. **21**, 487 (1956).
8. A. GOLDBERG, J. A. SMITH, and A. LOCKHEAD. Br. J. Med. **1**, 1270 (1963).
9. J. T. MACGREGOR and T. W. CLARKSON. Adv. Exp. Med. Biol. **48**, 463 (1974).
10. J. C. CRAWHALL, E. F. SCOWEN, and R. W. E. WATTS. Br. Med. J. **1**, 588 (1963).
11. R. HEIMER and M. FEDERICO. Clin. Chim. Acta, **25**, 41 (1958).
12. A. PIHL and L. ELDJARN. Proc. 4th Intl. Congr. Biochemistry, Vienna Vol. 13. p. 43. 1958.
13. A. PIHL, L. ELDJARN, and K. F. NAKKEN. Acta Chem. Scand. **12**, 1357 (1958).
14. R. SAETRE and D. L. RABENSTEIN. Anal. Chem. **50**, 276 (1978).
15. D. L. RABENSTEIN and A. A. ISAB. Anal. Biochem. **121**, 423 (1982).
16. J. F. ROESLER, J. LESLIE, and G. GORIN. J. Org. Chem. **29**, 1488 (1964).
17. M. DIXON and H. E. TUNNICLIFFE. Proc. R. Soc. B, **94**, 266 (1923).
18. J. L. DYE and V. A. NICELY. J. Chem. Educ. **48**, 443 (1971).
19. J. M. WILSON, and R. J. BAYER, and D. J. HUPE. J. Am. Chem. Soc. **99**, 7922 (1977).
20. R. P. SZAJEWSKI and G. M. WHITESIDES. J. Am. Chem. Soc. **102**, 2011 (1980).
21. I. M. KOLTHOFF, W. STRICKS, and R. C. KAPOOR. J. Am. Chem. Soc. **77**, 4733 (1955).
22. L. ELDJARN and A. PIHL. J. Am. Chem. Soc. **79**, 4589 (1957).
23. P. JOCELYN. Eur. J. Biochem. **2**, 327 (1967).
24. A. PIHL, L. ELDJARN, and K. NAKKEN. Acta Chem. Scand. **12**, 1357 (1958).
25. L. ELDJARN and A. PIHL. J. Biol. Chem. **225**, 499 (1957).
26. G. GORIN, G. DOUGHTY, and R. GIDEON. J. Chem. Soc. B, 729 (1967).
27. G. GORIN and G.DOUGHTY. Arch. Biochem. Biophys. **126**, 547 (1968).
28. R. S. REID and D. L. RABENSTEIN. Can. J. Chem. **59**, 1505 (1981).
29. D. L. RABENSTEIN. J. Am. Chem. Soc. **95**, 2797 (1973).
30. Y. THERIAULT, B. V. CHEESMAN, A. P. ARNOLD, and D. L. RABENSTEIN. Can. J. Chem. **62**, 1312 (1984).
31. S. J. BACKS and D. L. RABENSTEIN. Inorg. Chem. **20**, 410 (1981).
32. G. DALMAN, J. MCDERMED, and G. GORIN. J. Org. Chem. **29**, 1480 (1964).
33. U. WEBER, P. HARTTER, and L. FLOHÉ. Hoppe-Seyler's Z. Physiol. Chem. **351**, 1389 (1970).
34. J. ROST and S. RAPOPORT. Nature, **201**, 185 (1964).

Can. J. Chem. Downloaded from www.nrcresearchpress.com by 210.87.254.6 on 09/06/12
For personal use only.

Etude du système acridine orange – poly(C) et de son interaction avec les complexes du palladium(II)

ROBERT MÉNARD ET MIKLOS ZADOR

Département de Chimie, Université de Montréal, C.P. 6210, Succ. A, Montréal (Qué.), Canada H3C 3V1

Reçu le 6 décembre 1983

ROBERT MÉNARD et MIKLOS ZADOR. Can. J. Chem. **62**, 1681 (1984).

Le complexe formé entre l'acridine orange (AO) et l'acide polycytidylique (poly(C)) a été étudié par spectrophotométrie et spectrofluorimétrie. Le complexe a été caractérisé par sa stoechiométrie, sa structure et les paramètres thermodynamiques de sa formation. Les résultats sont en accord avec une agrégation externe des molécules protonées de colorant le long de la chaîne du poly(C) chargée négativement et indiquent qu'environ deux molécules d'AO peuvent se fixer, par unité de nucléotide, au poly(C). La cinétique de la réaction de ce complexe avec un complexe de Pd(II) a été étudiée par la méthode du flux-stoppé. L'addition de (dien)Pd(II) au complexe AO–poly(C) conduit à la dissociation de celui-ci, due à la fixation du complexe de Pd(II) au site N3 de la base cytosine du poly(C). La constante de vitesse de libération de l'AO, extrapolée à une concentration d'AO nulle, correspond à la constante de vitesse pour la fixation du (dien)Pd(II) sur le poly(C). Ceci indique que l'AO peut être utilisé comme indicateur lors de cette réaction et permet de réaliser l'étude cinétique à des concentrations très faibles ($\leq 5 \times 10^{-6}$ *M*).

ROBERT MÉNARD and MIKLOS ZADOR. Can. J. Chem. **62**, 1681 (1984).

The complex formed between acridine orange (AO) and polycytidylic acid (poly(C)) was studied by spectrophotometry and spectrofluorometry. The complex was characterized by its stoichiometry, structure, and the thermodynamic parameters of its formation. The results are in agreement with an external aggregation of the protonated dye along the negatively charged poly(C) chain and indicate that approximately two AO molecules are bound per nucleotide unit of poly(C). The kinetics of the reaction between this complex and a Pd(II) complex was studied by the stopped-flow method. The addition of (dien)Pd(II) to the AO–poly(C) complex leads to the dissociation of the latter, due to fixation of the Pd(II) complex to the N3 site of the cytosine base of poly(C). The rate constant for the AO liberation, extrapolated at zero AO concentration, corresponds to the rate constant of Pd(II) fixation on poly(C). This indicates that AO can be used as an indicator for this reaction and allows kinetic studies at very low concentrations ($\leq 5 \times 10^{-6}$ *M*).

Can. J. Chem. Downloaded from www.nrcresearchpress.com by 210.87.254.6 on 09/06/12
For personal use only.

Introduction

L'acridine orange (AO) et la proflavine (PF) sont tous deux des agents mutagènes (1,2), ce qui est généralement attribué à leur interaction avec les acides nucléiques. L'activité biologique de ces colorants basiques et le fait que la plupart des dérivés de l'acridine sont fluorescents sont les raisons qui expliquent l'immense intérêt porté envers ces molécules. Plusieurs études ont été effectuées sur l'interaction entre les acridines et les acides nucléiques (3–7) ou d'autres polynucléotides et polyélectrolytes synthétiques (8–16).

Il existe principalement deux types de liaison entre l'AO (ou la PF) et les polynucléotides. Le premier type correspond à l'empilement des molécules de colorant le long de la chaîne, mais à l'extérieur des hélices (8). Le deuxième type implique l'intercalation du colorant entre deux paires de bases d'une double hélice (17). On observe aussi dans certains cas, comme en présence d'un polynucléotide à simple brin comme l'ADN dénaturé, une intercalation partielle (18). L'importance relative de ces complexes dépend de la structure du polymère (double hélice, simple hélice; natif, dénaturé), du rapport [polynucléotide]/[colorant], de la force ionique, etc.

Ce travail est consacré à l'étude de l'interaction entre un polynucléotide à simple brin, l'acide polycytidylique (poly(C)) et l'acridine orange. Cette interaction nous intéresse en vue de l'utilisation de l'AO comme indicateur lors de l'étude cinétique de réactions entre des polynucléotides et divers complexes d'ions métalliques tels ceux du Pd(II) et du Pt(II). La faible solubilité des polynucléotides ou des complexes formés est souvent la source de nombreux problèmes rencontrés lors de l'étude de ces réactions. L'utilisation d'un colorant fluorescent permettant de travailler à très faible concentration peut donc possiblement ouvrir la voie à de nombreuses études cinétiques quantitatives de ces systèmes.

La fluorescence de l'AO a déjà été utilisée avec succès pour étudier la réaction entre l'AO et l'ADN à des concentrations très basses (19). Dans le cas présent, l'AO est utilisé uniquement comme indicateur pour permettre la détermination des paramètres cinétiques de la réaction entre le poly(C) et des complexes du Pd(II). Pour vérifier la validité d'une telle méthode, la caractérisation du complexe AO–poly(C) et de son interaction avec le complexe du Pd(II) est indispensable.

Partie expérimentale

L'acridine orange (diméthylamino-3,6 acridine) a été obtenu sous forme de l'hydrochlorure de Eastman Kodak Co. et la proflavine (diamino-3,6 acridine) de Sigma Chemical Co. sous forme d'hémisulfate. L'AO et la PF ont été recristallisés plusieurs fois de mélanges méthanol–éther (~1:3) et éthanol–eau (1:1) respectivement.

L'acide polycytidylique (poly(C)) provenait de chez Sigma Chemical Co. et l'acide polyadénylique (poly(A)) de Miles Laboratories Inc. Tous deux sont des produits de haute pureté et furent utilisés sans purification supplémentaire. Le [(dien)PdCl]Cl (dien: diéthylènetriamine) a été synthétisé selon une méthode légèrement modifiée de celle décrite dans la littérature (20). Le complexe $[(dien)Pd(H_2O)](NO_3)_2$ a été préparé en précipitant les chlorures d'une solution de [(dien)PdCl]Cl sous forme de AgCl par addition de $AgNO_3$. Le précipité est retiré par filtration et la solution amenée à un volume connu.

L'AO et la PF sont photosensibles et peuvent en plus s'adsorber sur le verre et le quartz. Pour ces raisons, des précautions particulières ont été prises pour s'assurer de la fiabilité de nos résultats. Les solutions mères de colorant ont été conservées dans des bouteilles opaques en Teflon noir à 6°C. Dans ces conditions, les colorants étaient stables pendant plusieurs semaines. Les solutions diluées ont été fraîchement préparées et gardées à l'abri de la lumière. La verrerie normalement utilisée a été remplacée par du matériel de plastique. Les ballons jaugés, béchers et pipettes étaient en polypropylène et les cuvettes pour la spectrophotométrie en polystyrène transparent (Sarstedt Canada Inc.). Le seul contact avec du verre se produisait lors de

l'ajustement du pH où des électrodes en verre furent utilisées.

Les spectres d'absorption ont été enregistrés à l'aide d'un spectrophotomètre Perkin–Elmer modèle 552 tandis qu'un fluorimètre Fluorispec modèle SF-1 de Baird-Atomic Inc. a été utilisé pour les mesures de fluorescence. La cinétique des réactions entre le complexe AO–poly(C) et (dien)Pd(II) a été suivie par spectrophotométrie à flux-stoppé au moyen d'un Dionex modèle D-130 combiné à un système d'acquisition des données construit dans notre laboratoire (21). Les constantes de vitesse d'ordre deux ont été obtenues par traitement de moindres carrés de l'équation intégrée correspondante.

Toutes les mesures ont été effectuées à pH 7 et 25°C sauf lorsque spécifié autrement. Dans ces conditions, l'acridine orange est protoné (pK_a = 10,2) et les groupements phosphate des polynucléotides sont chargés négativement ($pK_a \approx 1$ (22)).

Résultats

L'étude spectrophotométrique montre que, comme pour la dimérisation, la fixation de l'AO sur le poly(C) s'accompagne de variations dans les spectres d'absorption et de fluorescence. Les spectres d'absorption pour l'AO seul et un présence de concentrations croissantes de poly(C) sont illustrés à la figure 1(a). On remarque l'absence de point d'isoabsorbance (isosbestique), ce qui indique la présence de plus de deux espèces en solution.

Dans le cas de l'AO seul (courbe 1) on observe deux maximums dans la région du visible: un premier à 492 nm attribué au monomère libre en solution et un deuxième, sous forme d'un épaulement à environ 465 nm, qui prédomine dans les solutions d'AO à concentration élevée, attribué au dimère $(AO)_2$ (5, 8, 23). Lors de l'addition de poly(C), ces bandes diminuent d'intensité (courbes 2–4), indiquant l'interaction avec le poly(C). A concentration en poly(C) élevée (courbe 4) on distingue clairement l'apparition d'une nouvelle bande vers 438 nm et on l'attribue à l'agrégation de l'AO sur la chaîne du poly(C) (5, 8). La position de cette bande exclue l'intercalation pour laquelle le maximum devrait se situer, d'après la littérature, vers 502 nm (7). L'addition du poly(C) à l'AO entraîne aussi une désactivation de fluorescence à 530 nm sans déplacement du maximum (Fig. 1(b)). L'intercalation conduirait plutôt à une augmentation de fluorescence (19).

Les variations d'absorbance ont été étudiées en fonction du rapport p = [poly(C)]/[AO] ([poly(C)] exprimée en mol L^{-1} d'unité de mononucléotide), de l'acidité et de la force ionique pour caractériser le complexe formé, notamment sa stoechiométrie, sa structure et les paramètres thermodynamiques de sa formation.

Premièrement, on remarque que le complexe AO–poly(C) est fortement influencé par la force ionique de la solution. L'absorbance à 492 nm de la solution contenant le complexe AO–poly(C), à un rapport p = 1,0, augmente considérablement lors de l'addition de $NaNO_3$ (ou de NaCl) (Fig. 2(a)). Ceci indique l'apparition d'AO libre provenant de la dissociation du complexe. Ce comportement est caractéristique aux complexes de type externe dont la formation est due aux interactions électrostatiques des ions positifs avec les sites phosphate de la chaîne chargés négativement (5, 8).

Un effet spécifique apparaît lors de l'addition d'ions Mg^{2+} à force ionique constante. Dans ce cas, la dissociation du complexe AO–poly(C) apparaît pour de petites quantités de $MgCl_2$ ajouté (~0,01 M) malgré une force ionique relativement élevée de 0,1 M (Fig. 2(b)). Cet effet est attribué à la fixation préférentielle (comparé aux ions Na^+) d'ions Mg^{2+} par les sites phosphate.

Comme on peut le voir sur la figure 2(c), l'addition du

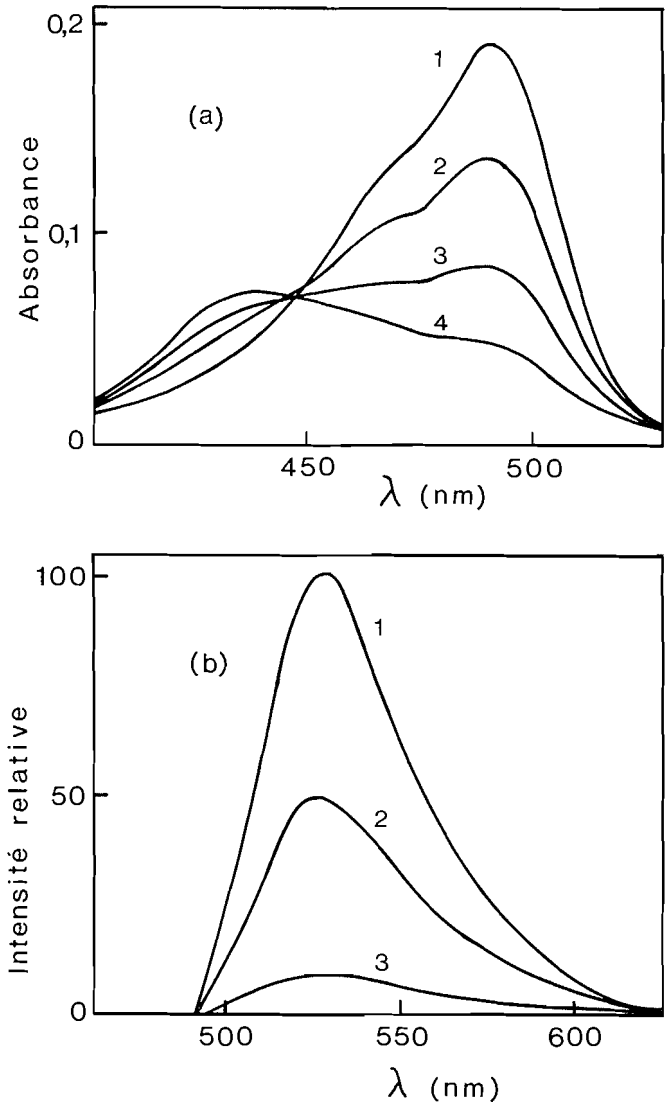

FIG. 1. Spectres d'absorption (a) et de fluorescence (b) de l'acridine orange à diverses concentrations de poly(C) ajouté. Conditions: (a) AO $5,0 \times 10^{-6}$ M, $NaNO_3$ 0,009 M, NaCl 0,001 M, pH 7, poly(C) ajouté: (1) 0, (2) $1,5 \times 10^{-6}$ M, (3) $2,5 \times 10^{-6}$ M, (4) $5,0 \times 10^{-6}$ M; (b) AO $1,0 \times 10^{-5}$ M, λ_{exc} = 490 nm, pH 7, poly(C) ajouté: (1) 0, (2) $5,0 \times 10^{-6}$ M, (3) $1,0 \times 10^{-5}$ M.

complexe (dien)$Pd(H_2O)^{2+}$ entraîne également la dissociation du AO–poly(C) et ceci à des concentrations beaucoup plus faibles ($<10^{-5}$ M). Cependant, dans ce dernier cas l'effet est indirect et provient de la fixation de (dien)Pd(II) sur le site N3 de la base cytosine. Il est connu que la fixation du (dien)Pd(II) se fait sur le site N3 dans le cas de la cytidine (24). Lors de cette réaction la bande à λ = 268 nm, correspondant au groupe cytosine, subit une augmentation d'intensité et un léger déplacement vers le rouge. Les mêmes phénomènes sont observés dans le cas du poly(C) et il est permis de supposer que le même site N3 soit impliqué. La fixation du (dien)Pd^{2+} conduit à la diminution du champ électrique de la chaîne phosphate chargée négativement et entraîne la libération de l'AO. Le même effet a été observé en fluorescence. Dans les deux cas, l'addition de concentrations suffisantes de (dien)$Pd(H_2O)^{2+}$ conduit au spectre de l'AO libre. Des tests effectués montrent que l'addition de (dien)Pd(II) n'influence pas les spectres d'absorption et de fluorescence de l'AO en absence de poly(C), ce qui indique

Can. J. Chem. Downloaded from www.nrcresearchpress.com by 210.87.254.6 on 09/06/12
For personal use only.

Can. J. Chem. Downloaded from www.nrcresearchpress.com by 210.87.254.6 on 09/06/12
For personal use only.

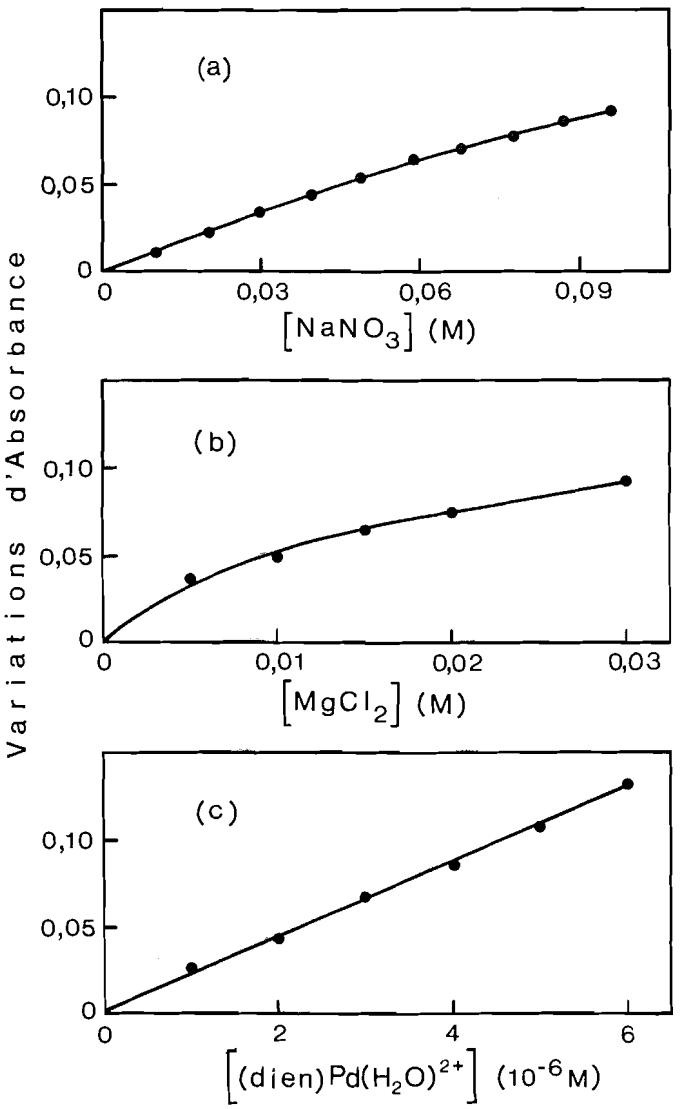

FIG. 2. Variations de l'absorbance à 492 nm du système AO–poly(C) lors de l'addition de $NaNO_3$ (a), $MgCl_2$ (b) et $[(dien)Pd(H_2O)](NO_3)_2$ (c). Conditions: (a) AO = poly(C) = $1{,}0 \times 10^{-5}$ *M*, pH 7; (b) AO = poly(C) = $1{,}0 \times 10^{-5}$ *M*, force ionique constante (0,1 *M*, ajustée avec $NaNO_3$), pH 7; (c) AO = poly(C) = $2{,}0 \times 10^{-5}$ *M*, force ionique constante (0,1 *M* $NaNO_3$), pH 7.

l'absence d'interaction Pd(II)–AO.

L'augmentation de l'acidité du milieu s'accompagne de l'augmentation de l'absorbance à 492 nm. A pH bas (<2) le spectre et l'absorbance correspondent à ceux de l'AO libre. La protonation du poly(C) au site N3 de la cytosine conduit donc, de la même façon que lors de la fixation du (dien)Pd(II), à la dissociation du complexe AO–poly(C). La courbe de titrage spectrophotométrique ne correspond pas à un équilibre acide–base simple. Les écarts se situent surtout entre pH 4 à 6 et peuvent être attribués à la formation de la double hélice du poly(C) semi-protoné.

Les variations d'absorbance en fonction du rapport *p* sont présentées à la figure 3. On observe une diminution graduelle d'absorbance jusqu'à $p \approx 1$, ensuite l'absorbance ne varie pratiquement plus. L'allure de la courbe montre qu'à l'addition des premières quantités de poly(C) ($p \leq 0{,}4$), la diminution d'absorbance est plus rapide que celle prévue pour un complexe, même très stable, de stoechiométrie 1:1. Par exemple,

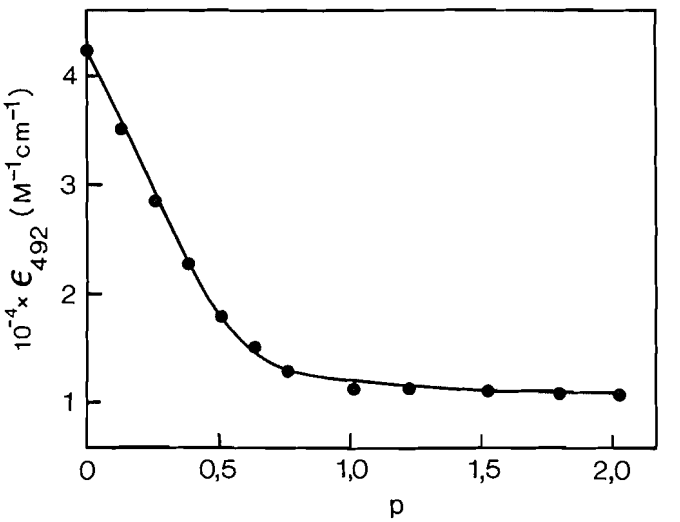

FIG. 3. Titrage spectrophotométrique à 492 nm de l'AO par le poly(C). Les points représentent les résultats expérimentaux et la ligne continue, la valeur calculée (voir texte). Conditions: AO $2{,}00 \times 10^{-5}$ *M*, NaCl 0,1 *M*, pH 7.

pour $p = 0{,}381$ l'absorbance est abaissée de 0,845 à 0,455 alors que pour le complexe 1:1 stable on calcule une valeur de 0,603. Ce phénomène est aussi visible sur les spectres de la figure 1(a). Ceci montre clairement qu'il y a plus d'une molécule d'AO fixée par unité de nucléotide dans ces conditions (excès de l'AO).

Les paramètres thermodynamiques de l'interaction AO–poly(C) ont été déterminés en utilisant le modèle de Schwarz (25) qui a été appliqué avec succès à l'interaction de colorants acridines avec l'acide L-glutamique (11, 12) et d'autres polyanions linéaires présentant des sites de liaison équivalents (14, 15).

D'après ce modèle, on représente par *g* le nombre de sites de liaison d'AO par unité de nucléotide du poly(C). Deux constantes d'équilibre sont utilisées, $K^{\ddagger}$ pour le processus de nucléation c.-à-d. fixation d'une molécule d'AO sur la chaîne et *K* pour le processus de croissance d'agrégat impliquant l'empilement de molécules d'AO sur des sites adjacents de façon coopérative. Le facteur de coopérativité *q* est défini par $q = K/K^{\ddagger}$. Cette coopérativité est due à l'interaction de molécules d'AO voisines, stabilise l'agrégat et favorise sa croissance. Ce phénomène est important dans le cas de l'AO tel que montré par sa constante de dimérisation élevée en solution aqueuse (12, 23).

Le titrage spectrophotométrique a été effectué pour des rapports [poly(C)]/[AO] assez petits ($p \leq 2$). Dans ces conditions, le système peut être décrit convenablement en utilisant seulement *K* et *g*. Les variations d'absorptivité molaire à $\lambda =$ 492 nm sont dues à des variations des fractions de chaque espèce en solution lors de l'addition du poly(C). L'additivité de l'absorbance et les bilans de matière des espèces en solution conduisent, d'après Schwartz *et al.* (11), à l'équation [1]:

$$[1] \quad \epsilon = \epsilon_{st} + (\epsilon_a - \epsilon_{st})\bar{\gamma}_a + 2(\epsilon_d - \epsilon_{st})K_d c_a^0 \bar{\gamma}_a^2$$

où ϵ, ϵ_a, ϵ_d, ϵ_{st}: absorptivités molaire expérimentale, du monomère libre, du dimère libre et du complexe AO–poly(C) respectivement; K_d: constante de dimérisation de l'AO; c_a^0: concentration totale d'AO; $\bar{c}_a$: concentration de monomère libre à l'équilibre; $\bar{\gamma}_a = \bar{c}_a/c_a^0$: fraction des molécules d'AO sous forme de monomère à l'équilibre.

Can. J. Chem. Downloaded from www.nrcresearchpress.com by 210.87.254.6 on 09/06/12
For personal use only.

La façon de déterminer les divers paramètres de cette équation ainsi que la valeur de g est légèrement différente des méthodes graphiques utilisées par Schwarz. En étudiant la dimérisation de l'AO en fonction de sa concentration, ϵ_a, ϵ_d et K_d peuvent être évalués. Des valeurs de $\epsilon_a = 57\,900$ L mol^{-1} cm^{-1}, $\epsilon_d = 5000$ L mol^{-1} cm^{-1} et $K_d = 1{,}5 \times 10^4\ M^{-1}$ ont été obtenues. La valeur de ϵ_{st} est déterminée sur la figure 3 en prenant $\epsilon_{st} = \epsilon$ pour $p \rightarrow \infty$, soit 10 400 L mol^{-1} cm^{-1}. Connaissant K_d et les valeurs des diverses absorptivités molaire on peut calculer $\bar{\gamma}_a$, par l'équation [1], pour diverses valeurs de p en utilisant les résultats expérimentaux.

On doit ensuite déterminer le paramètre g dont la connaissance est nécessaire pour l'obtention de la constante d'équilibre K. On peut obtenir g à partir de la variation de γ_a^*en fonction du rapport p. γ_a^* représente la fraction totale d'AO non-lié au polymère (monomère ou dimère libres) et est donné par l'équation [2]:

$$[2] \quad \gamma_a^* = \bar{\gamma}_a + 2K_d c_a^0 \bar{\gamma}_a^2$$

La loi de la conservation de la matière relie γ_a^* à p par l'équation [3]:

$$[3] \quad \gamma_a^* = 1 - \bar{\theta} g p$$

où $\bar{\theta}$: fraction des sites de liaison occupés par l'AO à l'équilibre. Comme en présence d'un grand excès d'AO (valeurs de p faibles) on tend vers $\bar{\theta} = 1$, on peut obtenir g comme la pente de la droite γ_a^* vs. p passant par les premiers points. Les résultats conduisent à $g = 2{,}05$ pour le système AO−poly(C). Cette valeur implique qu'il y a plus d'un AO qui se lie par unité de nucléotide sur le poly(C).

La détermination de la constante d'équilibre K a été effectuée par simulation à l'ordinateur. Cette constante est définie par l'équation [4].

$$[4] \quad K = \frac{\bar{c}_{st}}{\bar{c}_a \cdot \bar{c}_p}$$

où $\bar{c}_{st}$: concentration du complexe AO−poly(C) à l'équilibre; $\bar{c}_p$: concentration du poly(C) libre à l'équilibre. En remplaçant $\bar{c}_{st}$ et $\bar{c}_p$ par leurs valeurs en termes de $\bar{c}_a$ et en réarrangeant l'équation résultante, on obtient:

$$[5] \quad (2K_dK)\bar{c}_a^3 + (2K_d + K)\bar{c}_a^2 + (Kgc_p^0 + 1 - Kc_a^0)\bar{c}_a - c_a^0 = 0$$

où c_p^0: concentration totale de poly(C).

La méthode de simulation consiste à résoudre cette équation du troisième degré pour une valeur de K à diverses valeurs de c_p^0. Les valeurs de $\bar{c}_a$ et donc de $\bar{\gamma}_a$ ainsi obtenues sont introduites dans l'équation [1] ce qui conduit à la courbe calculée de ϵ vs. p. Celle-ci est ensuite comparée à l'ensemble des résultats expérimentaux. Différentes valeurs de K conduisent à des courbes différentes. Tel que montré par la figure 3, l'accord entre la courbe calculée et les points expérimentaux est excellent pour $K = 1{,}3 \times 10^6\ M^{-1}$. Des accords nettement moins bons sont obtenus pour des valeurs de K de $1 \times 10^6\ M^{-1}$ et $2 \times 10^6\ M^{-1}$ ce qui montre la sensibilité de la méthode.

L'interaction du poly(C) avec la proflavine a été étudiée de façon similaire. Comme l'interaction n'est pas suffisamment forte à une force ionique de 0,1 M, ces expériences ont du être effectuées à force ionique beaucoup plus basse (0,001 M). Les résultats sont donnés au tableau 1. Les valeurs de ϵ_d et K_d pour la proflavine ont été tirées de la littérature (11). Il n'est pas nécessaire de connaître avec précision ces deux paramètres à cause de la très faible quantité de dimère présent dans le cas de la PF dans ces conditions, dû à la faible valeur de K_d (~525 M^{-1}). A titre de comparaison, le complexe AO−poly(A) a aussi été étudié. Les résultats sont résumés au tableau 1.

TABLEAU 1. Paramètres thermodynamiques de divers systèmes colorant−polynucléotide

Système	μ (M)	g	K (M^{-1})
AO−poly(C)	0,1	2,05	$1{,}3\times10^6$
AO−poly(A)	0,1	1,40	$2{,}0\times10^6$
PF−poly(C)	0,001	1,15	$5{,}0\times10^6$

La cinétique de la réaction entre AO−poly(C) et le complexe de Pd(II) a ensuite été étudiée et comparée à la réaction entre le poly(C) et (dien)Pd(II) en absence d'AO. Dans ce deuxième cas, la réaction a été suivie en étudiant l'augmentation d'absorbance de la bande à $\lambda = 268$ nm du poly(C) lors de la fixation du complexe de Pd(II). Les concentrations de poly(C) et de (dien)Pd(II) étaient de $5 \times 10^{-5}\ M$ et $2{,}5 \times 10^{-5}\ M$ respectivement en absence d'AO et de $5 \times 10^{-6}\ M$ et $2{,}5 \times 10^{-6}\ M$ en présence de l'AO. Il est à noter que l'utilisation de l'AO permet de travailler à des concentrations 10 fois plus faibles qu'en absence de colorant. Ces mesures ont été faites en absorbance pour des raisons pratiques. On peut prévoir cependant qu'en utilisant la fluorescence de l'AO on pourrait descendre à concentration encore plus basse.

Ces réactions ont été étudiées à force ionique constante (μ = 0,1 M), pH 7 et à deux concentrations en ion chlorure différentes (0,001 M et 0,01 M). Le complexe de palladium est sous forme de (dien)Pd$(H_2O)^{2+}$ à très faible concentration en chlorure et sous forme de (dien)PdCl$^+$ en présence de concentrations en chlorure plus élevées. L'espèce (dien)Pd$(H_2O)^{2+}$ est plus réactive que le (dien)PdCl$^+$. Aucune réaction n'a été détectée entre les complexes de Pd(II) et l'AO. Les réactions sont représentées par les équations [6] et [7]:

$$[6] \quad \text{(dien)Pd(II)} + \text{poly(C)} \xrightarrow{k} \text{(dien)Pd(II)−poly(C)}$$

$$[7] \quad \text{(dien)Pd(II)} + \text{AO−poly(C)} \xrightarrow{k_{AO}} \text{(dien)Pd(II)−poly(C)} + \text{AO}$$

Les valeurs de k_{AO} obtenues sont légèrement plus faibles que les valeurs de k correspondantes et diminuent avec l'augmentation de la concentration de l'AO. Ceci est attribuable au fait que l'AO est chargé positivement et sa fixation sur le poly(C) neutralise les charges négatives du poly(C). L'interaction favorable entre le poly(C) négatif et le (dien)Pd(II) positif perd donc de l'importance lorsque la quantité d'AO fixé sur le poly(C) augmente ce qui conduit à une diminution de la vitesse de réaction. Cependant, une extrapolation linéaire à [AO] = 0 donne des valeurs de constante de vitesse très près de celles obtenues en absence d'AO. Ces valeurs sont données au tableau 2.

La constante de vitesse de la réaction entre (dien)Pd(II) et le poly(C) à pH 4,5 ne peut être déterminée à cause de la faible solubilité du produit à ce pH. Cependant, avec l'AO comme indicateur, la réaction a pu être étudiée. La constante de vitesse ainsi obtenue à pH 4,5 est environ 12 fois plus faible que pour la même réaction à pH 7 (900 M^{-1} s^{-1} à pH 4,5 vs. 11 000 M^{-1} s^{-1} à pH 7). Ceci est attribuable à deux facteurs principalement: (*i*) l'influence défavorable de la protonation sur les sites N3 et (*ii*) la structure secondaire particulière, à pH 4,5 (26), impliquant une double hélice due à la formation de ponts hydrogène

TABLEAU 2. Constantes de vitesse des réactions avec et sans indicateur

$[Cl^-]$ (M)	k^*_{AO} (M^{-1} s^{-1})	k (M^{-1} s^{-1})
0,001	$2,2(\pm0,4)\times10^4$	$2,3(\pm0,2)\times10^4$
0,010	$1,1(\pm0,1)\times10^4$	$1,0(\pm0,1)\times10^4$

*Les valeurs de k_{AO} sont extrapolées, comme décrit dans le texte.

entre les sites N3 protonés d'un brin et les sites non-protonés de l'autre.

Discussion

L'interaction du poly(C) avec l'acridine orange se décrit très bien en considérant uniquement la formation de complexes externes impliquant l'interaction électrostatique du colorant protoné avec les sites phosphate. La possibilité de contact étroit entre l'AO et les bases cytosine est à toute fin pratique à éliminer si on considère, d'une part, l'absence de la bande caractéristique de ce type d'interaction à $\lambda = 502$ nm dans le spectre d'absorbance et, d'autre part, l'absence d'exaltation de fluorescence à 530 nm caractéristique de l'intercalation. La désactivation de fluorescence observée a été, en général, reliée à la formation du complexe externe comme le sont l'hypochromicité et l'effet hypsochrome (blue shift) observés pour les mesures d'absorbance.

Ces phénomènes sont dus à la structure secondaire du poly(C), qui est à simple hélice et, en partie, au fait que les bases pyrimidiques, telle la cytosine, offrent un recouvrement moins favorable avec le colorant polyaromatique que les bases puriques.

L'influence de divers facteurs expérimentaux tels la force ionique, la présence d'ions Mg^{2+} et de complexes de Pd(II), indique que l'interaction est due, au moins en partie, à des forces de type électrostatique entre la chaîne chargée négativement et l'AO protoné chargé positivement.

Toutefois la valeur élevée des constantes d'équilibre, comparée à celles d'ions métalliques, montre qu'il y a un terme important dans l'énergie libre totale dû à l'interaction entre molécules de colorant voisines. Ceci produit un effet coopératif contribuant à renforcer l'interaction. Cette stabilisation supplémentaire est particulièrement importante dans le cas de l'AO qui possède une forte tendance à former des agrégats en solution. Ceci explique, par exemple, qu'il faut une concentration élevée d'ion Mg^{2+} ($\sim0,01$ M) pour déplacer significativement des sites phosphate l'AO qui est à une concentration de loin inférieure (10^{-5} M) même si, à cause de sa charge +2, le Mg^{2+} devrait avoir une interaction électrostatique plus forte que l'AO.

L'importance de l'interaction entre molécules de colorant sur la stabilité du complexe colorant–polynucléotide est aussi mise en évidence lors de l'étude du système PF–poly(C). La proflavine est un colorant qui a une constante d'équilibre de dimérisation beaucoup plus faible que l'AO. En conséquence, l'interaction de cycles voisins sur le poly(C) apporte peu de stabilité supplémentaire au complexe formé. Ceci explique qu'à une force ionique de 0,1 M, le complexe PF–poly(C) ne se forme pas tandis que dans le cas de l'AO il se forme facilement. Pour avoir un complexe PF–poly(C), il faut descendre à force ionique beaucoup plus faible (0,001 M) afin d'accroître la force de la liaison électrostatique et stabiliser ainsi le complexe.

La tendance à l'agrégation de l'AO se reflète aussi dans la valeur de g obtenue pour le système AO–poly(C). En effet, celle-ci indique qu'il y a environ deux molécules d'AO fixées par unité de nucléotide sur le poly(C). Cependant, pour le système AO–poly(A), à la même force ionique, une valeur de $g = 1,40$ a été obtenue. Ceci est dû au fait que la structure des polymères impliqués influence beaucoup la stoechiométrie des complexes formés.

Bradley et Wolf (8) ont déjà proposé que l'agrégation serait plus importante pour les polymères pouvant assumer des positions optimales, permettant une meilleure interaction entre les cycles de colorant voisins. La distance entre deux bases consécutives dans la direction de l'axe, à pH 7, est de 3.98 Å pour le poly(C) (27) et 3.5 Å pour le poly(A) (28). Ceci est une conséquence du fait que l'interaction d'empilement entre deux bases adénine est supérieure à celle entre deux cytosines à cause de la plus grande surface des bases puriques. Pour la même raison, le poly(C) est probablement aussi plus flexible que le poly(A) et peut, à cause de ces caractéristiques, accommoder un plus grand nombre de molécules d'AO le long de sa chaîne que le poly(A). En fait, les spectres visible sont aussi différents et la bande à 438 nm est absente dans le cas du poly(A) où seule la bande à $\lambda = 465$ nm apparaît. Ceci indique un mode de recouvrement différent, probablement moins important, dans le cas du poly(A).

Il est à noter que d'autres chercheurs ont obtenu une valeur de $g \approx 1$ pour le système AO–poly(A) en absence d'électrolyte ajouté, ce qui peut être expliqué par la répulsion trop importante de molécules voisines dans ces conditions. Nos résultats à force ionique élevée (0,1 M) ne peuvent pas être décrits en considérant une valeur de $g = 1$.

L'AO possède donc les propriétés recherchées au départ pour son utilisation comme indicateur. L'absorbance de ce colorant est assez élevée pour nous permettre de travailler à faible concentration ce qui est encore plus vrai lorsqu'on utilise la fluorescence. Il se lie au poly(C) avec un spectre d'absorbance et de fluorescence différents de ceux de l'AO libre en solution. En plus, le colorant protoné est inerte envers le palladium.

Lors de l'étude de la cinétique de la réaction entre le poly(C) et le complexe de Pd(II), par l'entremise de l'indicateur, on peut suivre les variations dans le spectre de l'AO en fonction du temps dues à sa libération. Cependant, l'étape lente du processus doit être la réaction du Pd(II) sur le poly(C) et non la dissociation du complexe AO–poly(C), ce qui a été démontré, étant donné que la valeur de la constante de vitesse extrapolée à [AO] = 0 (k_{AO}) est en accord avec celle obtenue sans indicateur. La formation et la dissociation du complexe AO–poly(C) sont trop rapides pour être observables par flux-stoppé et on peut prévoir que la fixation du (dien)Pd^{2+} sur le site N3 de la cytosine accélère encore la dissociation. Les polynucléotides à plusieurs brins, tels l'ADN, permettent l'intercalation de plusieurs colorants. Dans le cas du bromure d'éthidium, un colorant souvent utilisé, la formation du complexe intercalé est inhibée par les complexes du Pt(II) (29), ce qui est attribué à l'interaction de ceux-ci avec les sites azotés. Ce colorant peut également servir à l'étude de compétition avec des ions métalliques (30). Cependant, l'intercalation produit une perturbation des sites basiques de la double-hélice. Pour cette raison l'AO, formant un complexe externe, le seul observé dans le cas du poly(C) à simple brin, est un indicateur plus avantageux pour l'étude de la fixation d'ions métalliques sur les polynucléotides.

Can. J. Chem. Downloaded from www.nrcresearchpress.com by 210.87.254.6 on 09/06/12
For personal use only.

La précision de cette méthode faisant appel à l'AO (~10−20%) est suffisante pour étudier des variations importantes de réactivité tel qu'illustré par le changement dû à la protonation des sites N3 à pH 4.5. La méthode peut avoir des applications intéressantes dans la caractérisation cinétique de réactions impliquant des molécules peu solubles ou de celles se déroulant sans variation de propriété physique facilement mesurable.

Remerciements

Nous tenons à remercier le Conseil de recherches en sciences naturelles et en génie du Canada et le Fonds F.C.A.C. (Québec) pour l'aide financière et les bourses d'études supérieures (R.M.) accordées.

1. S. BRENNER, L. BARNETT, F. H. C. CRICK et A. ORGEL. J. Mol. Biol. **3**, 121 (1961).
2. A. ORGEL et S. BRENNER. J. Mol. Biol. **3**, 762 (1961).
3. A. R. PEACOCKE et J. N. H. SKERRETT. Trans. Faraday Soc. **52**, 261 (1956).
4. A. L. STONE et D. F. BRADLEY. J. Am. Chem. Soc. **83**, 3627 (1961).
5. A. BLAKE et A. R. PEACOCKE. Biopolymers, **6**, 1225 (1968).
6. R. W. ARMSTRONG, T. KURUCSEV et U. P. STRAUSS. J. Am. Chem. Soc. **92**, 3174 (1970).
7. E. FREDERICQ et C. HOUSSIER. Biopolymers, **11**, 2281 (1972).
8. D. F. BRADLEY et M. K. WOLF. Proc. Natl. Acad. Sci. **45**, 944 (1959).
9. G. G. HAMMES et C. D. HUBBARD. J. Phys. Chem. **70**, 1615 (1966).
10. G. G. HAMMES et C. D. HUBBARD. J. Phys. Chem. **70**, 2889 (1966).
11. G. SCHWARZ, S. KLOSE et W. BALTHASAR. Eur. J. Biochem. **12**, 454 (1970).
12. G. SCHWARZ et W. BALTHASAR. Eur. J. Biochem. **12**, 461 (1970).
13. M. DOURLENT et C. HÉLÈNE. Eur. J. Biochem. **23**, 86 (1971).
14. G. SCHWARZ et S. KLOSE. Eur. J. Biochem. **29**, 249 (1972).
15. V. VON TSCHARNER et G. SCHWARZ. Biophys. Struct. Mech. **5**, 75 (1979).
16. T. IMAE, S. HAYASHI, S. IKEDA et T. SAKAKI. Int. J. Biol. Macromol. **3**, 259 (1981).
17. L. S. LERMAN. J. Mol. Biol. **3**, 18 (1961).
18. S. ICHIMURA, M. ZAMA, H. FUJITA et T. ITO. Biochim. Biophys. Acta, **190**, 116 (1969).
19. M. SAKODA, K. HIROMI et K. AKASAKA. J. Biochem. **71**, 891 (1972).
20. W. H. BRADDLEY et F. BASOLO. J. Am. Chem. Soc. **88** , 2944 (1966).
21. K. THAMMAVONG et M. ZADOR. J. Phys. E, **9**, 1041 (1976).
22. J. K. BARTON et S. J. LIPPARD. Met. Ions Biol. **1**, 39 (1980).
23. V. ZANKER. Z. Physik. Chem. **199**, 225 (1952).
24. F. D. ROCHON, P. C. KONG, B. COULOMBE et R. MELANSON. Can. J. Chem. **58**, 381 (1980).
25. G. SCHWARZ. Eur. J. Biochem. **12**, 442 (1970).
26. C. H. CHOU et G. J. THOMAS, JR. Biopolymers, **16**, 765 (1977).
27. A. GULIK. H. INOUE et V. LUZZATI. J. Mol. Biol. **53**, 221 (1970).
28. J. WITZ et V. LUZZATI. J. Mol. Biol. **11**, 620 (1965).
29. M. HOWE-GRANT, K. C. WU, W. R. BAUER et S. J. LIPPARD. Biochemistry, **15**, 4339 (1976).
30. J.-B. LEPECQ et C. PAOLETTI. J. Mol. Biol. **27**, 87 (1967).

Can. J. Chem. Downloaded from www.nrcresearchpress.com by 210.87.254.6 on 09/06/12
For personal use only.

The sulfohaloform reaction revisited and revised

JAMES CLAYTON BAUM, WILLIAM RAYNE HARDSTAFF, RICHARD FRANCIS LANGLER,[1] AND ANTHONY MAKKINJE
Department of Chemistry, Florida Institute of Technology, Melbourne, FL 32901, U.S.A.

Received November 20, 1983

JAMES CLAYTON BAUM, WILLIAM RAYNE HARDSTAFF, RICHARD FRANCIS LANGLER, and ANTHONY MAKKINJE. Can. J. Chem. **62**, 1687 (1984).

A study of the aqueous chlorinolyses of a series of benzylic dithioacetals along with related α-chlorobenzylic sulfides is reported. These results require a modification of our previously proposed sulfohaloform reaction, so that thionium ion intermediates which have at least one alkyl group on sp^2 carbon follow a different pathway.

JAMES CLAYTON BAUM, WILLIAM RAYNE HARDSTAFF, RICHARD FRANCIS LANGLER et ANTHONY MAKKINJE. Can. J. Chem. **62**, 1687 (1984).

On rapporte une étude sur la chloronolyse, en milieu aqueux, d'une série de dithioacétals benzyliques et des sulfures α-chlorobenzyliques apparentés. Pour expliquer ces résultats, il faut modifier le mécanisme de réaction sulfohaloformique que nous avons proposé antérieurement de façon à ce que les ions thionium intermédiaires qui portent au moins un groupe alkyle sur le carbone sp^2 suivent une voie différente.

[Traduit par le journal]

Can. J. Chem. Downloaded from www.nrcresearchpress.com by 210.87.254.40 on 09/06/12
For personal use only.

Introduction

Some time ago, we published an examination of the pathway followed by dialkyl sulfides upon chlorinolysis in aqueous acetic acid (1). The study involved a detailed examination of sulfides and led to a proposed general pathway which we called the sulfohaloform reaction. We have subsequently carried out studies on the regiochemistry of the first step in aprotic media (2, 3) as well as an examination of steric effects in the cleavage step (4) in aqueous acetic acid.

The first step in the sulfohaloform pathway is believed to proceed as shown in Scheme 1. The proposed intermediacy of α-chloro-chlorosulfonium cations (derived from α-chloro-sulfides) in the sulfohaloform reaction rested on the following evidence: the chlorinolysis of the corresponding chlorine-free sulfoxides furnished different products from those obtained by chlorinolysis of the chlorine-free sulfides, thus ruling out sulfoxides as the first formed intermediates. The disturbing feature of the original proposal is the apparent inability of the thionium ion[2] intermediates, formed in the second step, to undergo hydrolysis.

We have subsequently developed benzylic sulfides as precursors for sulfonyl chlorides (8). While we did not establish whether aqueous chlorinolysis of benzylic sulfides proceeds by S_N1 dissociation of the intermediate chlorosulfonium cations or by the intermediacy of the corresponding sulfoxides with unimolecular dissociation of the corresponding oxochlorosulfonium cations, we did demonstrate that these reactions proceed without Pummerer rearrangement (see Scheme 1). We decided to generate benzylic thioniums ions, **A**, in order to determine whether they have any tendency to hydrolyze during exhaustive

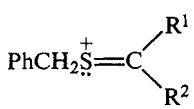

A

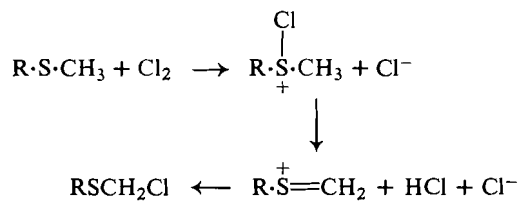

SCHEME 1

aqueous chlorinolyses. Such species, if hydrolyzed, would give rise to α-hydroxy sulfides which could dissociate to furnish phenylmethanethiol which would be transformed into phenylmethanesulfonyl chloride in aqueous acetic acid saturated with Cl_2. On the other hand, if they undergo exclusive nucleophilic attack by chloride ions, the intermediate α-chlorosulfide would be transformed into the corresponding α-chlorosulfonyl chloride and benzyl chloride (8).

Simple alkyl benzylic sulfides are ruled out as precursors since (*i*) they appear to undergo dissociation into sulfenyl chlorides and benzyl cations after chlorosulfonium cation formation (8), and (*ii*) any thionium ion intermediates would form by abstraction of a benzylic proton rather than abstraction of a proton from the alkylated α-carbon (2, 3).

To circumvent these problems we have decided to employ some dithioacetals, **B**, as precursors. Such substrates are

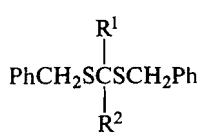

B

known to cleave pursuant to chlorosulfonium cation formation (9). The corresponding S-hydroxysulfonium sulfides are also known to dissociate in a parallel process (10). The expected mechanism for thionium ion formation is shown in Scheme 2.

Results and discussion

To begin our study of the simplest system, we have prepared and chlorinated benzyl chloromethyl sulfide, which gave results consistent with our previous report (8):

[1] Author to whom correspondence should be addressed.

[2] Durst *et al.* have called R·SO·CHR an oxosulfenium ion (5). We have called RSCHR a sulfenium ion (6) while Trost *et al.* call it a thionium ion (7). A referee of this paper has pointed out that the term sulfenium ion has also been applied to RS^+. To avoid confusion we shall refer to the first two species as oxothionium and thionium ions respectively.

TABLE 1. Chlorinolysis of 1 g $PhCH_2 \cdot S \cdot CHClCH_3$ (**6**)

Volume of Cl_2/H_2O* (mL)	Volume of Cl_2/HOAc† (mL)	Volume of HOAc (mL)	$(PhCH_2S)_2$ (%)	$(PhCH_2S)_2CHCH_3$ (%)	$PhCH_2SO_2Cl$ (%)	$PhCH_2Cl$ (%)	$PhCH_2OAc$ (%)
10	—	50	8.8	69.2	—	—	—
10	25	25	10.1	17.8	30.9	18.0	20.6
10	50	—	—	—	52.0	24.5	26.5

* H_2O was saturated with Cl_2 at ambient temperature.
† HOAc was saturated with Cl_2 at ambient temperature.

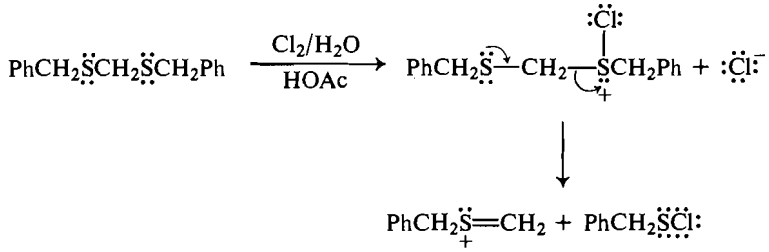

SCHEME 2

[1] $PhCH_2SH + CH_2O \xrightarrow{HCl} PhCH_2SCH_2Cl$ (**1**)

$\xrightarrow[HOAc]{Cl_2/H_2O} PhCH_2Cl$ (38%) + $ClCH_2SO_2Cl$ (54%) (**2**)

+ $PhCH_2SO_2Cl$ (9.4%) + $PhCH_2OAc$ (16%)

We have, subsequently, subjected bis(thiobenzyl)methane to exhaustive aqueous chlorinolysis which furnished the results shown in eq. [2]

[2] $(PhCH_2S)_2CH_2$ (**3**) $\xrightarrow[HOAc]{Cl_2/H_2O}$ $PhCH_2SO_2Cl$ (**4**) (38%)

+ $ClCH_2SO_2Cl$ (**2**) (53.6%) + $PhCH_2Cl$ (73.9%) + $PhCH_2OAc$ (9.8%)

The results shown in eq. [2] are in complete accord with our previous results on methyl sulfides as well as with our expectation that dithioacetals will dissociate to furnish thionium ions and sulfenyl chlorides following chlorosulfonium cation formation (*vide* Scheme 2). We note that these results (*i*) support our past proposal (1) that unsubstituted thionium ions react with chloride ions in preference to water molecules, (*ii*) offer further support to Wilson's proposal (11) that thionium ions are intermediates in the chlorinolyses of simple sulfides, and (*iii*) offer additional support to our contention (2) that thionium ions are unable to isomerize to the more stable regioisomeric thionium ions under normal conditions (2, 6).

We then chlorinated 1,1-bis(thiobenzyl)ethane **5** (eq. [3]) and α-chloroethyl benzyl sulfide **6** (eq. [4]).

[3] $(PhCH_2S)_2CHCH_3 + Cl_2/H_2O/HOAc \rightarrow 2\ PhCH_2SO_2Cl$
5 **4** (73%)

[4] $PhCH_2SCHClCH_3 + Cl_2/H_2O \xrightarrow{HOAc} PhCH_2SO_2Cl$
6 **4** (73.3%)

These results suggest the intermediacy of the thionium ion derived from **6** via unimolecular dissociation followed by hydrolysis *prior to* reaction with Cl_2. Since we were concerned that significant hydrolysis may have occurred before the introduction of Cl_2, and because we wished to learn more about the course of the conversion of **6** → **4**, we have undertaken a series of partial chlorinolyses of **6** in which chlorine was introduced *before* the sulfide. The results of this series of partial chlorinolyses are presented in Table 1, and show that α-alkyl-α-chlorosulfides dissociate to form chlorine-free thionium ions (in aqueous acetic acid) faster than they react with limited amounts of Cl_2 to furnish chlorosulfonium cations, clearly ruling out α-chloro-chlorosulfonium cations as principal intermediates in the chlorinolysis of dialkyl sulfides.

While it remains unclear whether α-chlorosulfides intervene in these reactions, it is clear that hydrolysis of the chlorine-free thionium ion is the principal pathway by which the reactions proceed.

To complete our study of these systems we have chlorinated the dithioketal **7** as depicted in eq. [5].

[5] $(PhCH_2S)_2C(CH_3)_2$ (**7**) $\xrightarrow[HOAc]{Cl_2/H_2O}$ 2 $PhCH_2SO_2Cl$ (**4**) (88%)

The change in behaviour of unalkylated thionium ions vs. alkylated thionium ions vis-à-vis hydrolysis could have been anticipated on the grounds that alkyl groups are more electron releasing than hydrogen atoms. In order to see whether selected thionium ions have gas phase stabilities which parallel their ease of formation in solution, or whether solvent effects must be invoked to rationalize the apparently greater facility of alkylated thionium ion formation, we have undertaken a modest MNDO study of the appropriate species **A**.[3]

[3] We intend the present MNDO study to supplement the one we have recently published (6).

Can. J. Chem. Downloaded from www.nrcresearchpress.com by 210.87.254.40 on 09/06/12
For personal use only.

TABLE 2. MNDO heats of formation and substituent effects on energetics of thionium ion formation

Sulfides	ΔH_f (kcal/mol)	Thionium ions	ΔH_f (kcal/mol)	$\Delta\Delta H_f$	$\Delta\Delta H_r$
CH_3SCH_3	−17.4	$CH_3\overset{+}{S}=CH_2$	207.1	224.5	—
$PhCH_2SCH_3$	10.3	$PhCH_2\overset{+}{S}=CH_2$	226.5	216.2	−8.3
$PhCH_2SCH_2CH_3$	4.5	$PhCH_2\overset{+}{S}=CHCH_3$	211.7	207.2	−17.3
$PhCH_2SCH(CH_3)_2$	2.0	$PhCH_2\overset{+}{S}=C(CH_3)_2$	202.2	200.2	−24.3

TABLE 3. MNDO results on selected thionium ions

Thionium ion	ΔH_f (kcal/mol)	π Bond order CS	π Electron population S
$PhCH_2\overset{+}{S}=CH_2$	226.5	0.87	1.48
$PhCH_2\overset{+}{S}=CHCH_3$	211.7	0.82	1.53
$PhCH_2\overset{+}{S}=C(CH_3)_2$	202.2	0.78	1.57

MNDO calculations – method and results

Computations on a selected series of thionium ions and their corresponding sulfides were done using the MNDO (Modified Neglect of Differential Overlap) semi-empirical method described previously (6). Geometries were fully optimized except that the phenyl rings were constrained to be planar, with equal C—C bond lengths, C—H bond lengths, and 120° HCC and CCC bond angles.

The calculated heats of formation for the compounds studied are listed in Table 2. The ΔH_f's are consistent with our earlier results (6) except that the sulfide geometry is slightly more stable (0.2 kcal) with the Ph—C bond *trans*, instead of *cis*, to The $\overset{+}{S}$—CH_3 bond in benzyl methyl sulfide. This added stability for the phenyl-substituted sulfides increases with alkyl substitution. The important point is that the stability of the phenyl-substituted thionium ion increases with alkylation of the sp^2 carbon, as indicated by the decreasing ΔH_f's.

The CS π bond orders and π electron populations at S are tabulated for the thionium ions in Table 3. As the thionium ion stability increases, the π bond order decreases and the π electron population at S increases. These trends agree with our previous calculations (6) and indicate that the electron-releasing alkyl substituent is acting through the thionium ion π system to stabilize the system.

Mechanistic and pathway conclusions

The calculated ΔH_f values for the appropriate sulfides and the corresponding thionium ions (see Table 2) permit one to obtain $\Delta\Delta H_f$ values for the reaction shown in eq. [6] relative to the reaction in eq. [7].

[6] $ZYCHSCH_2PH \rightarrow ZYC = \overset{+}{S}CH_2Ph + \bar{H}$

[7] $CH_3SCH_3 \rightarrow CH_2 = \overset{+}{S}CH_3 + \bar{H}$

Calculated $\Delta\Delta H_f$ results, reflecting the impact on thionium ion energetics of progressively incoprorating methyl groups on sp^2 carbon, are presented in Table 2. These results indicate that solvent effects, while potentially important, do not need to be invoked to make calculated gas phase stabilities compatible with our solution phase results. The higher presumed inherent reactivity of **A** ($R^1 = R^2 = H$) over the other thionium ions, previously advanced to rationalize the preference for the unsubstituted thionium ion for chloride ions over water molecules, is compatible with our MNDO results. Scheme 3 presents our conclusions about the pathway followed by dialkyl sulfides upon exhaustive aqueous chlorinolysis.

The original version of the sulfohaloform reaction (1) was based on an extrapolation of detailed study of aqueous chlorinolyses of α-polychloromethyl sulfides and sulfoxides. The first intermediate for this reaction is shown in eq. [8] (X = Cl).

[8] $XCH_2SR \xrightarrow{Cl_2/H_2O} XCH_2\overset{\bar{O}}{\underset{|}{S}}R^+$

Since that time, similar behaviour has been observed for sulfides bearing an α-sulfonyl group (4) or two α-fluorine atoms (12). Parallel behaviour has also been suggested for sulfides bearing an α-carboxyl group (13). The intermediacy of the corresponding sulfoxide in the aqueous chlorinolysis of a sulfide is clearly the result of hydrolysis of the first formed chlorosulfonium cation (depicted in Scheme 1). The hydrolysis is evidently faster than the competing elimination reaction which would otherwise produce a thionium ion.

We conclude that aqueous chlorinolysis of sulfides is not as simple as originally proposed. The following facts have emerged: (*i*) highly electronegative substituents attached to an α-carbon in the sulfide substrate accelerate hydrolysis of the first formed chlorosulfonium chloride salt leading to formation of a sulfoxide, (*ii*) sulfides without strongly electronegative α-groups form thionium ions which react preferentially with the chloride counter ions leading to formation of an α-chlorosulfide, and (*iii*) the presence of inductive stabilizers (i.e., alkyl groups) on sp^2 carbon results in the intermediacy of thionium ions which hydrolyze. Scheme 4 presents this more complex array of pathways as The Revised Sulfohaloform Reaction.

Experimental

Aqueous chlorinolysis of 1

Crude benzyl chloromethyl sulfide (6.935 g) (14) was dissolved in glacial acetic acid (25 mL) and water (3 mL). Cl_2 (ca. 200 mL/min) was bubbled into the reaction mixture for 2 h. The reaction mixture was maintained between 20 and 30°C with an ice/water bath as necessary. Methylene chloride (100 mL) and water (50 mL) were added and the layers separated. The organic layer was washed with 2.5% w/v sodium hydroxide (two 50-mL aliquots). The organic layer was dried ($MgSO_4$) and concentrated, affording a crude mixture which contained phenylmethanesulfonyl chloride (0.728 g), chloromethanesulfonyl chloride (3.182 g), benzyl chloride (1.930 g), and benzyl acetate (0.970 g). The bulk of the phenylmethanesulfonyl chloride crystallized from the crude and was filtered off. It was shown to be identical to authentic material by ir, nmr, and tlc.

The filtered concentrated crude was chromatographed on silica gel (400 g) employing carbon tetrachloride elution (100-mL fractions). Fractions 12–18 were concentrated and combined, affording benzyl chloride which was identical to authentic material by nmr, ir, and tlc.

Can. J. Chem. Downloaded from www.nrcresearchpress.com by 210.87.254.40 on 09/06/12
For personal use only.

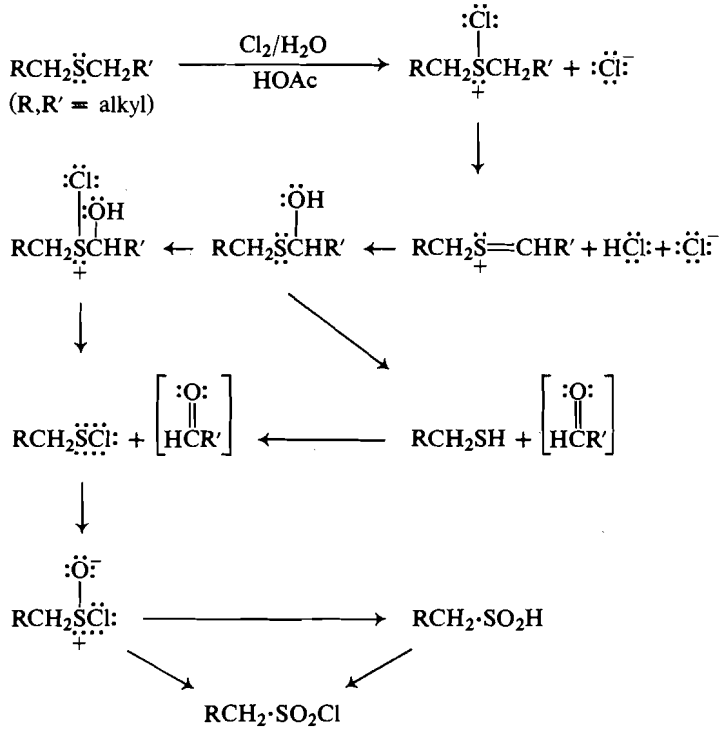

SCHEME 3

Fractions 37–40 were concentrated and combined, affording clean chloromethanesulfonyl chloride which was identical with authentic material by ir and nmr.

Aqueous chlorinolysis of ***3***

Bis(thiobenzyl)methane **3** (5.007 g) was suspended in glacial acetic acid (25 mL) and water (5 mL). The reaction mixture was chlorinated and worked up as described above. Phenylmethanesulfonyl chloride (1.394 g) crystallized from the crude and was shown to be identical with authentic material by mp, ir, and nmr.

The filtered concentrated crude mixture was rectified at reduced pressure, affording a mixture (bp 120–130°C/100 Torr) (1 Torr = 133.3 Pa) which contained chloromethanesulfonyl chloride (1.532 g), benzyl acetate (0.289 g), and benzyl chloride (1.729 g). The identity of the components was established by the addition of authentic compounds which, in each case, increased the intensity of the expected signals in the nmr spectrum of the mixture.

Aqueous chlorinolysis of ***5***

1,1-Bis(thiobenzyl)ethane **5** (5.002 g) was added to glacial acetic acid (25 mL) and water (5 mL). The reaction mixture was chlorinated and worked up as described above. The residue (5.050 g) was shown to be identical to authentic phenylmethanesulfonyl chloride by nmr, tlc, and mp.

Preparation of $PhCH_2SCH{=}CH_2$

Sodium metal (0.8025 g) was dissolved in refluxing 2-propanol (30 mL). A solution of $PhCH_2SCH_2CH_2Cl$ (6.038 g) (15) in 2-propanol (30 mL) was added and the reaction mixture refluxed for 1 h. Water (60 mL) was added and the resultant mixture washed with chloroform (four 60-mL portions). The combined organic layers were dried and concentrated. The residue was rectified at reduced pressure, affording clean benzyl vinyl sulfide (3.166 g, bp 52–56°C/0.4 Torr) which had ir ($CHCl_3$): 1585 cm^{-1}; nmr ($CDCl_3$) δ: 3.86 (2H, s), 5.20 (1H, d, J_{AX} ≃ 15 Hz), 5.26 (1H, d, J ≃ 11 Hz), 6.36 (1H, q, J_{AX} = 15 Hz, J_{BX} = 11 Hz); Cmr ($CDCl_3$) δ: 35.71, 111.01, 126.73, 128.10, 128.34, 131.66, 136.75; ms *m/e*: 150 (M^+, 28.6%) and 91 (100%).

Preparation of ***6***

Benzyl vinyl sulfide (5.006 g) was dissolved in carbon tetrachloride (50 mL). HCl (ca. 200 mL/min) was bubbled into the reaction mixture for 1 h. The solvent was evaporated and the residue rectified at reduced pressure, affording $PhCH_2SCHClCH_3$ (3.847 g, bp 92–93°C/0.9 Torr) which had nmr ($CDCl_3$) δ: 1.86 (3H, d), 3.90 (2H, s), 4.96 (1H, q), and 7.33 (5H, s); ms *m/e*: 188 (5.8%), 186 (M^+, 17.6%), 151 (25%), and 91 (100%).

Exhaustive aqueous chlorinolysis of ***6***

The chlorosulfide (5.0160 g) was added to glacial acetic acid (25 mL) and water (5 mL). The reaction mixture was chlorinated and worked up as described above. An nmr of the crude showed no observable α-chloroethanesulfonyl chloride present. The residue was crystallized from carbon tetrachloride, affording phenylmethanesulfonyl chloride (3.747 g) which was identical with authentic material by ir, nmr, mp, and mixture mp.

Controlled aqueous chlorinolysis of ***6***

A series of chlorinolyses of **6** were conducted. The results are presented in Table 1. Details below are provided for the second run.

Water (10 mL) was saturated with Cl_2 at ambient temperature. Glacial acetic acid (25 mL) was saturated with Cl_2 at room temperature. The chlorosulfide **6** (1.0084 g) was added to the Cl_2/H_2O, $HOAc/Cl_2$, and glacial acetic acid (25 mL) and the reaction mixture stirred at ambient temperature for 0.5 h. Water (50 mL) was added and the resultant mixture washed with chloroform (three 75-mL aliquots). The combined organic layers were washed with 2.5% w/v sodium hydroxide (four 50-mL aliquots). The organic layer was dried and concentrated, affording a residue which contained benzyl acetate (0.164 g), phenylmethanesulfonyl chloride (0.3116 g), benzyl chloride (0.1205 g), dibenzyl disulfide (0.066 g), and 1,1-bis(thiobenzyl)ethane (0.129 g).

The crude residue was chromatographed on silica gel (100 g) employing carbon tetrachloride elution (100-mL fractions). Fraction 4 contained benzyl chloride and dibenzyl disulfide. The presence of benzyl chloride was confirmed by the addition of authentic material and observing the change in intensity of the appropriate signals in the nmr spectrum of the mixture. Fraction 5 afforded clean dibenzyl disulfide which was identical to authentic material by ir, nmr, and tlc. Fractions 6–10 were combined and concentrated, affording

Can. J. Chem. Downloaded from www.nrcresearchpress.com by 210.87.254.40 on 09/06/12
For personal use only.

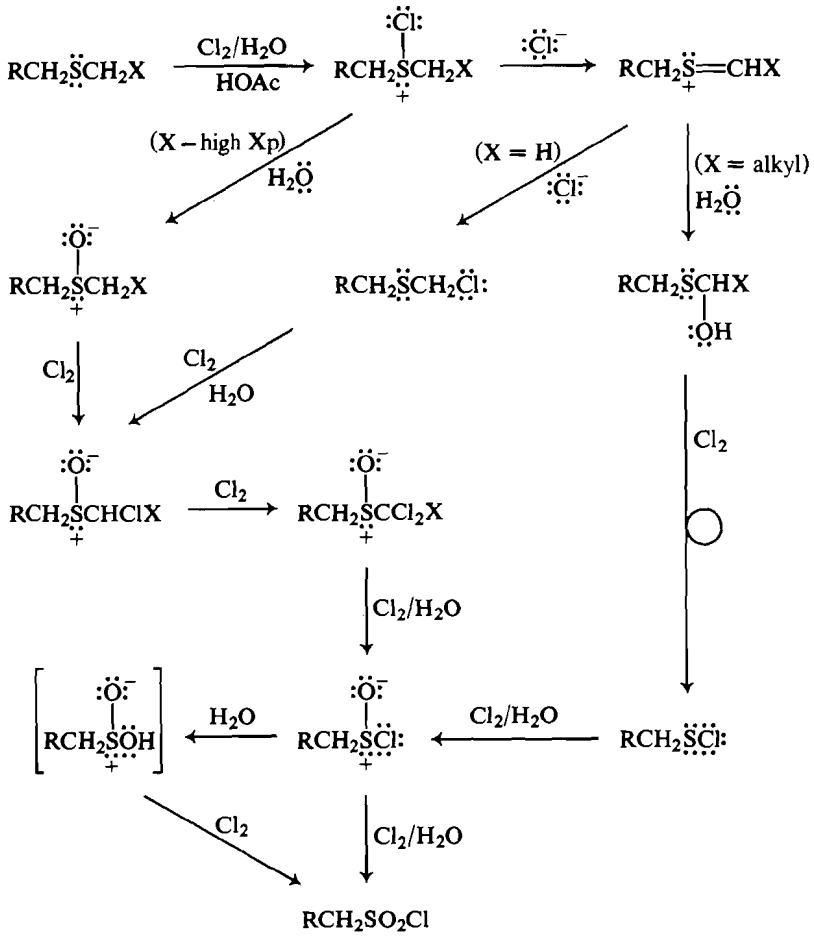

SCHEME 4. The revised sulfohaloform reaction

1,1-bis(thiobenzyl)ethane which was identical with authentic material by ir, nmr, and tlc. Fractions 13–18 were combined and concentrated, affording phenylmethanesulfonyl chloride which was identical to authentic material by ir, nmr, and tlc. Fraction 31 was combined with a final elution with diethyl ether (400 mL). Upon concentration of this eluent, benzyl acetate was obtained which was identical with authentic material by ir, nmr, and tlc.

Aqueous chlorinolysis of 7

2,2-Bis(thiobenzyl)propane (1.0190 g) was added to glacial acetic acid (50 mL) and water (10 mL). The reaction mixture was chlorinated and worked up as described above, furnishing clean crystalline phenylmethanesulfonyl chloride (1.1948 g).

Acknowledgments

The authors are indebted to Dr. J. H. Kim who ran the mass spectra and Dr. D. L. Hooper who ran the ^{13}C nmr spectrum. We are grateful to Mount Allison University for financial support in the early stages of the work and to the Florida Institute of Technology for financial support in the latter stages of the work and for the use of F.I.T. computing facilities.

1. J. S. GROSSERT and R. F. LANGLER. Can. J. Chem. **55**, 407 (1977).
2. T. P. AHERN, D. G. KAY, and R. F. LANGLER. Can. J. Chem. **56**, 2422 (1978).
3. J. R. HANCOCK, W. R. HARDSTAFF, P. A. JOHNS, R. F. LANGLER, and W. S. MANTLE. Can. J. Chem. **61**, 1472 (1983).
4. D. G. KAY, R. F. LANGLER, and J. E. TRENHOLM. Can J. Chem. **57**, 2185 (1979).
5. T. DURST, K. C. TIN, and M. J. V. MARCIL. Can J. Chem. **51**, 1704 (1973).
6. J. L. GINSBURG and R. F. LANGLER. Can J. Chem. **61**, 589 (1983).
7. B. M. TROST, M. VAULTIER, and M. L. SANTIAGO. J. Am. Chem. Soc. **102**, 7029 (1980).
8. R. F. LANGLER. Can J. Chem. **54**, 498 (1976).
9. H. BOHME and H. GRAN. Justus Liebigs Ann. Chem. **577**, 68 (1952).
10. R. KUHN and F. A. NEUGEBAUER. Ber. Dtsch. Chem. Ges. **94**, 2629 (1961).
11. G. E. WILSON, JR. and M. G. HUANG. J. Org. Chem. **35**, 3002 (1970).
12. G. G. I. Moore. J. Org. Chem. **44**, 1708 (1979).
13. R. F. LANGLER, Z. A. MARINI, and E. S. SPALDING. Can. J. Chem. **57**, 3193 (1979).
14. L. A. PAQUETTE, L. S. WITTENBROOK, and K. SCHREIBER. J. Org. Chem. **33**, 1080 (1968).
15. H. O. FONG, W. R. HARDSTAFF, D. G. KAY, R. F. LANGLER, R. H. MORSE, and D. N. SANDOVAL. Can. J. Chem. **57**, 1206 (1979).

Can. J. Chem. Downloaded from www.nrcresearchpress.com by 210.87.254.40 on 09/06/12
For personal use only.

Diffusion in aqueous solutions of sulfuric acid

DEREK G. LEAIST

Department of Chemistry, University of Western Ontario, London, Ont., Canada N6A 5B7

Received January 16, 1984

DEREK G. LEAIST. Can. J. Chem. **62**, 1692 (1984).

Diffusion of sulfuric acid in aqueous solution has been measured by a conductimetric technique at 25°C over the concentration range from 0.00035 to 0.2 mol dm^{-3}. At the lower end of this range, dissociation of bisulfate to sulfate and hydrogen ions produces a sharp increase in the rate of diffusion of the sulfuric acid component. Expressions are developed to predict the concentration dependence of the diffusion coefficient in terms of the mobilities of the diffusing ions and the degree of bisulfate dissociation. The treatment includes electrophoretic corrections that are derived from Onsager–Fuoss theory for the unsymmetrical, multi-ion electrolyte. At low concentrations where theory applies the observed diffusion coefficients are lower than the predicted values.

DEREK G. LEAIST. Can. J. Chem. **62**, 1692 (1984).

Opérant à 25°C et à des concentrations allant de 0.00035 à 0.2 mol dm^{-3} et faisant appel à une technique conductométrique, on a mesuré la diffusion de l'acide sulfurique en solution aqueuse. Aux concentrations les plus basses, la dissociation du bisulfate en ions sulfate et hydrogène provoque une importante augmentation de la vitesse de diffusion de l'acide sulfurique. On a mis au point des expressions qui permettent de prévoir l'effet de la concentration sur le coefficient de diffusion en fonction des mobilités des ions qui diffusent et du degré de dissociation du bisulfate. Le traitement comporte des corrections électrophorétiques que l'on a déduit de la théorie de Onsager–Fuoss relative aux électrolytes multi-ioniques non symétriques. Aux faibles concentrations où la théorie s'applique, les coefficients de diffusion observés sont plus faibles que les valeurs prévues.

[Traduit par le journal]

Can. J. Chem. Downloaded from www.nrcresearchpress.com by 210.87.254.5 on 09/06/12
For personal use only.

Introduction

Industrial applications have prompted extensive inquiry into the physicochemical properties of aqueous solutions of sulfuric acid. Below 0.1 mol dm^{-3}, the properties of this system are complicated by the dissociation of bisulfate to sulfate and hydrogen ions. The purpose of this research is to establish the diffusional behavior of sulfuric acid at low concentrations where bisulfate dissociation is appreciable.

Previous studies (1–5) have shown that dissociation affects diffusion in two important ways. First, by increasing the number of dissolved particles per mol of solute, dissociation will increase the free energy gradient that drives the diffusion process. On the other hand, because a single species can move through the solution with less frictional resistance than two separate daughter species, dissociation will tend to reduce the overall mobility of the solute component. In the case of aqueous sulfuric acid, accurate activity data (6) are available for the evaluation of the first effect. In order that the second effect can be analyzed, we develop expressions for the mobility of the acid in terms of the degree of dissociation and the mobility of the diffusing ions.

At low concentrations, ionic mobilities can be estimated from limiting ionic conductivities with appropriate corrections for the well-known electrophoretic effect. Although convenient expressions can be developed to calculate these corrections for binary diffusion in solutions of strong electrolytes (7*a*, 8), the treatment of the electrophoretic effect in the case of a complex electrolyte such as sulfuric acid is significantly more difficult. For example, when three or more ionic species are present, we can no longer make the simplifying assumption that the diffusion velocities of the ions are identical. In this investigation we extend electrophoretic calculations to binary diffusion of an incompletely-dissociated, multi-ion electrolyte.

No diffusion measurements appear to have been made for aqueous sulfuric acid below 0.1 mol dm^{-3}. We report diffusion coefficients that were determined in this region by a conductimetric technique, and compare the results with values predicted by the equations which were developed.

Experimental

Savino and Vitagliano (10) have used Gouy interferometry to measure accurate diffusivities for aqueous sulfuric acid at concentrations from 0.1 to 4.8 mol dm^{-3}. Unfortunately, optical techniques are less reliable at lower concentrations. There, changes in the refractive index become too small to be measured with the required precision. Furthermore, the strong concentration dependence of the diffusion coefficient presents serious difficulties in the analysis of the interference patterns.

Procedure

The diffusion coefficients reported here were measured at 25°C by a conductimetric technique similar to the one developed by Harned and co-workers, especially for the study of dilute salt solutions (9,11). A syringe fitted with a long needle was used to introduce a small volume of sulfuric acid solution (0.1 to 0.5 mol dm^{-3}) into the bottom of a cylindrical chamber (1.270 cm diameter, 4.572 (±0.002) cm height) filled with conductivity water. As the acid diffused upward, its rate of diffusion was monitored by the change in the electrical conductance of the solution measured with pairs of small electrodes positioned at levels one-sixth of the distance from the top and bottom of the chamber. Conductance readings were taken for three consecutive days beginning one-and-a-half days after the introduction of electrolyte. By this time the concentration gradient along the column was very small. This helped to ensure that the measured diffusion coefficient corresponded to the differential value at the final cell concentration (9).

The diffusion cells used in this work were bored from a polypropylene rod. Platinum electrodes (1 mm diameter, cell constant ~10 cm^{-1}) were cemented with epoxy into holes drilled at the appropriate levels. The top of each chamber was sealed with a glass slide lubricated with a mixture of equal parts of Vaseline and Apiezon M grease. Further details of the equipment and procedure have been described (12).

Materials

Reagent grade sulfuric acid was used without further purification. Stock solutions of acid were made up from deionized, doubly-distilled water (conductivity 0.8×10^{-6} ohm^{-1} cm^{-1}). Concentrations of acid were determined by titration against standardized base.

Analysis of experimental data

Integration of the diffusion equation for restricted diffusion in a column of height a gives the Fourier expression (9)

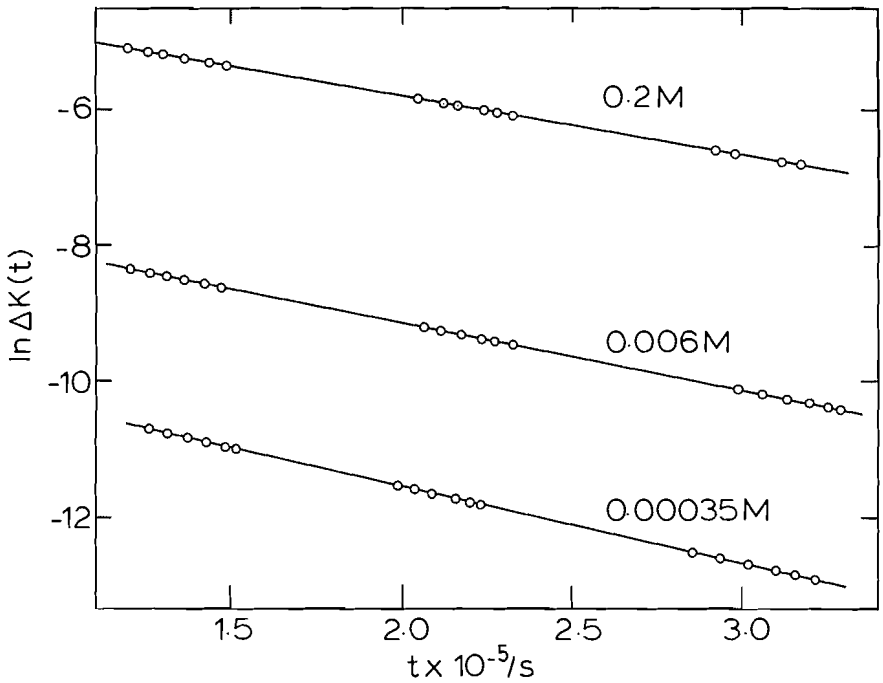

FIG. 1. Logarithm of the difference in conductance (in ohm^{-1}) plotted against the time for 0.2, 0.006, and 0.00035 mol dm^{-3} sulfuric acid.

$$[1] \quad \Delta c(t) = \sum_{n=1}^{\infty} A_n \sin(n\pi/2) \sin(n\pi/3) \exp(-n^2\pi^2 Dt/a^2)$$

for the difference in concentration between levels $a/6$ and $5a/6$ above the base of the column. D is the diffusion coefficient, t is the elapsed time since the introduction of electrolyte, and A_n are constants. The expression for $\Delta c(t)$ converges very rapidly; for $t \gtrsim a^2/20D$, only the first term in the series is significant.

$$[2] \quad \Delta c(t) = (\sqrt{3}A_1/2) \exp(-\pi^2 Dt/a^2)$$

In the present experiments, we followed $\Delta c(t)$ by measurement of the conductance difference defined by (9, 11, 12)

$$[3] \quad \Delta K(t) = (k_B/k_T)K_B(t) - K_T(t)$$

where $K_B(t)$ and $K_T(t)$ denote conductances measured at the bottom (B) and top (T) electrode positions, and k_B/k_T is the ratio of cell constants for the bottom and top pairs of electrodes. (This ratio is required to correct for imperfections in cell construction that lead to small discrepancies in electrode dimensions.) If diffusion is allowed to proceed until the concentration gradient in the cell is small, $\Delta K(t)$ will be proportional to $\Delta c(t)$. With this simplification, computation of D from conductance data is straightforward:

$$[4] \quad D = -\frac{a^2}{\pi^2} \frac{\mathrm{d} \ln \Delta K(t)}{\mathrm{d}t}$$

Calculations based on published conductivities for aqueous sulfuric acid (13) indicated that $\Delta K(t)$ is effectively proportional to $\Delta c(t)$ provided $t > 120\,000$ s. Conductance readings were taken at times long enough to satisfy this criterion; D values then were computed by least-squares analysis of the slope of $\ln \Delta K(t)$ plotted against t.

Results

Representative plots of $\ln \Delta K(t)$ against t are shown in Fig. 1. Over each three-day period during which conductivity readings were taken, the slope, and hence D, are constant within experimental error (±0.5%). This confirmed that $\Delta K(t)$ was proportional to $\Delta c(t)$, and also that the measured diffusion coefficients were in fact differential values.

The results of the diffusion measurements are recorded in column 4 of Table 1. At low concentrations the diffusion coefficient increases sharply as the bisulfate is converted to the more rapidly moving sulfate and hydrogen ions. Above 0.1 mol dm^{-3}, the present conductimetric data overlap the optical data of Savino and Vitagliano (10). Agreement between the two sets of data is very good, well within their combined uncertainties.

There was no evidence for adsorption of ions onto the walls of the diffusion cells. Indeed, the polypropylene cells worked well at concentrations as low as 0.00035 mol dm^{-3}, an order of magnitude lower than concentrations achieved in earlier studies of acid diffusion in which glass cells (14, 15) were used. Below this limit, however, it appeared that the density gradient was too small to fully stabilize the column of solution against convection for the required five day duration of the experiment.

Discussion

Aqueous sulfuric acid diffuses as H^+, HSO_4^-, and SO_4^{2-}, in proportions that vary with concentration. Because the rate of equilibration of the bisulfate dissociation reaction

$$HSO_4^- \rightleftarrows H^+ + SO_4^{2-}$$

is virtually instantaneous compared to the duration of a diffusion run, we can assume that the equilibrium of the reaction holds at each point along the diffusion path. In addition, the ionic flows must satisfy the requirement that the electric current vanishes for pure diffusion. In view of these dual constraints imposed on the three ionic flows, only one diffusional flow can be independent. Therefore, we may use the binary equations

$$[5] \quad J = -D\nabla c$$

$$[6] \quad J = -L\nabla\mu$$

to describe the isothermal diffusion of aqueous sulfuric acid. J, c, and μ refer to the molar flux, concentration (in mol per unit volume), and chemical potential of the H_2SO_4 component.

The transport coefficients D and L are related by $D = L\partial\mu/\partial c$. If we adopt the expression (6)

Can. J. Chem. Downloaded from www.nrcresearchpress.com by 210.87.254.5 on 09/06/12
For personal use only.

TABLE 1. Experimental transport coefficients and supplementary data for aqueous Sulfuric Acid at 25°C

c (10^{-3} mol dm^{-3})	α	$1 + c\,\mathrm{d} \ln y_{\pm}/\mathrm{d}c$	D (10^{-9} m^2 s^{-1})	L/c (10^{-12} m s^{-1} N^{-1} mol^{-1})
0.35	0.95	0.934	2.402	0.346
0.70	0.91	0.900	2.342	0.350
1.00	0.88	0.878	2.310	0.354
1.58	0.83	0.850	2.268	0.359
3.00	0.75	0.804	2.166	0.362
4.57	0.68	0.774	2.112	0.367
6.00	0.64	0.755	2.074	0.369
8.00	0.60	0.735	2.034	0.372
10.8	0.55	0.719	1.978	0.370
19.5	0.45	0.691	1.933	0.376
28.2	0.40	0.676	1.896	0.377
37.0	0.37	0.665	1.874	0.379
40.0	0.36	0.662	1.875	0.381
80.0	0.29	0.655	1.828	0.375
100.0	0.27	0.656	1.818	0.372
101.2	0.27	0.656	1.825[a]	0.374
150.0	0.25	0.658	1.811	0.370
197.8	0.23	0.660	1.811[a]	0.367
200.0	0.23	0.660	1.800	0.369

[a] These data obtained by the Gouy method (10).

[7] $\mu = \mu^0 + RT \ln (4c^3 y_{\pm}^3)$

for μ, we obtain

[8] $$D = 3RT\left(\frac{L}{c}\right)\left(1 + c\frac{\mathrm{d} \ln y_{\pm}}{\mathrm{d}c}\right)$$

where $y_{\pm}$ is the stoichiometric mean ionic activity coefficient on the molar concentration scale.

The term $c\,\mathrm{d} \ln y_{\pm}/\mathrm{d}c$ can be evaluated by the differentiation of Pitzer's equation (6) for the activity coefficient of aqueous sulfuric acid.[1] The thermodynamic factor $1 + c\,\mathrm{d} \ln y_{\pm}/\mathrm{d}c$ calculated in this manner takes values listed in the third column of Table 1. In column 2 are recorded values for the degree of dissociation of the bisulfate ion

[9] $\alpha = c_{SO_4^{2-}}/(c_{HSO_4^-} + c_{SO_4^{2-}})$

calculated[1] from

[10] $$K_{a2} = \frac{(1+\alpha)\alpha c}{1-\alpha}\frac{y_{H^+} y_{SO_4^{2-}}}{y_{HSO_4^-}} = 0.0105 \text{ mol dm}^{-3}$$

Below about 0.01 mol dm^{-3}, we see that the thermodynamic factor increases markedly as more bisulfate undergoes dissociation. Indeed, thermodynamics accounts for most of the concentration dependence of the diffusion coefficient in this region. If the electrolyte was fully ionized, the thermodynamic factor would of course be much less sensitive to concentration. In the case of a strong electrolyte such as aqueous calcium chloride, for example, $1 + c\,\mathrm{d} \ln y_{\pm}/\mathrm{d}c$ takes values 0.900, 0.929, and 0.947 at 0.005, 0.002, and 0.001 mol dm^{-3} (17, 18), while the corresponding values for aqueous sulfuric acid are 0.767, 0.833, and 0.879.

Also listed in Table 1 (column 5) are the values for L/c, the molar mobility of aqueous H_2SO_4, that were derived from the diffusion data by use of eq. [8]. It is of interest to note that the mobility of the acid actually decreases with the degree of dissociation, even though the highly mobile hydrogen ions are generated. As mentioned earlier, the reduced mobility is interpreted on the grounds that diffusion of H^+ and SO_4^{2-} is subject to more frictional resistance than diffusion of a single HSO_4^- species. As we will see later, this behavior is nearly masked by an exceptionally large electrophoretic effect.

In order to analyze diffusion of sulfuric acid in greater detail, we will use the expression derived by Creeth and Stokes (19) for the diffusion coefficient of an incompletely-dissociated 2:1 or 1:2 electrolyte

[11] $$D = 3\frac{\alpha(1+\alpha)D_1D_2 + (1-\alpha^2)D_1D_3 + \alpha(1-\alpha)D_2D_3}{(1+\alpha)D_1 + 4\alpha D_2 + (1-\alpha)D_3} \times \left(1 + c\frac{\mathrm{d} \ln y_{\pm}}{\mathrm{d}c}\right)$$

The D_i in the preceding equation refer to the diffusivities of the ions, which we number as follows: $H^+ = 1$, $SO_4^{2-} = 2$, and $HSO_4^- = 3$. As a first approximation, we will ignore the electrophoretic effect. As well, let us assume that the ionic diffusivities are independent of concentration and are given by their limiting values. Accurate values for the latter quantities can be calculated from conductivity data by the use of the relationship

[12] $$D_i^0 = \frac{RT}{F^2}\frac{\lambda_i^0}{z_i^2}$$

where R is the gas constant, T is the absolute temperature, F is the Faraday, λ_i^0 are the limiting ionic molar conductivities, and z_i are the ionic valencies. From the literature values (7*b*, 20–23) $\lambda_1^0 = 0.034981$, $\lambda_2^0 = 0.01600_4$, and $\lambda_3^0 = 0.00512$ m^2 ohm^{-1} mol^{-1}, we calculate $D_1^0 = 9.315 \times 10^{-9}$, $D_2^0 = 1.065 \times 10^{-9}$, and $D_3^0 = 1.363 \times 10^{-9}$ m^2 s^{-1}. Upon substitution of the

[1] Published densities (16) were used to convert the reported (6) molal activity coefficients γ_i to the molar activity coefficients y_i by the use of the relationship $y_i = m_i\rho_0\gamma_i/c_i$. m is sulfuric acid molality and ρ_0 is the density of the pure solvent.

Can. J. Chem. Downloaded from www.nrcresearchpress.com by 210.87.254.5 on 09/06/12
For personal use only.

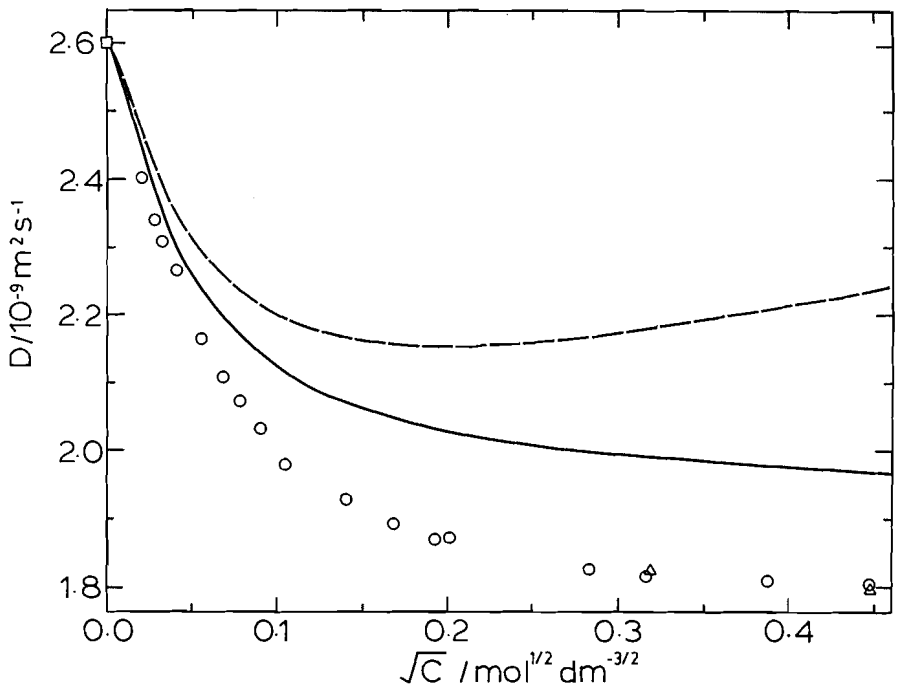

FIG. 2. Comparison of calculated diffusion coefficients with observed values for aqueous sulfuric acid at 25°C: dashed curve, eq. [11] without electrophoretic corrections; solid curve, eq. [11] with electrophoretic corrections; circles, present conductimetric data; triangles, optical data of Savino and Vitagliano (10).

limiting ionic diffusivities into eq. [11], the calculated D values shown by the dashed curve in Fig. 2 are obtained; the measured values are plotted as circles and triangles. At zero concentration, D is given by the limiting Nernst value for fully dissociated $2H^+ + SO_4^{2-}$

$$[13]\quad D^0 = \frac{3D_1^0 D_2^0}{D_1^0 + 2D_2^0} = 2.600 \times 10^{-9}\ \mathrm{m^2\ s^{-1}}$$

It is evident from Fig. 2 that the observed diffusion coefficients fall well below the dashed curve, even at the lowest concentrations accessible to the experiment. At low ionic strength, this discrepancy can be attributed to the neglect of the electrophoretic correction which appears to be large and negative for the system under discussion. At 0.01 mol dm^{-3}, for example, the observed diffusion coefficient is about 10% lower than the predicted value. Since one of the ions in the mixture (H^+) is considerably more mobile than the others, a negative electrophoretic effect is to be expected (see ref. 14 for the diffusion of aqueous hydrochloric acid). However, the size of the correction — an order of magnitude larger than corrections observed for other aqueous electrolytes (24) — is striking.

The theory developed by Onsager and Fuoss (25, 26) gives an accurate description of diffusion in binary solutions of strong 1:1 electrolytes at low ionic strength (7, 11, 14, 24). For higher-valency electrolytes, agreement between theory and experiment is only moderately good (7, 11). For the latter systems, however, the comparison is difficult to make, owing to the lack of accurate activity coefficients at low concentrations as well as uncertainties regarding the formation of ion-pairs.

Can the Onsager–Fuoss theory account for the diffusion behavior observed for dilute aqueous sulfuric acid? To answer this question we now turn to the problem of calculating electrophoretic corrections for binary diffusion in a solution of a complex, multi-ion electrolyte. Such electrolytes are invariably unsymmetrical. Therefore, following Robinson and Stokes (7*a*, 18), only the first-order corrections (proportional to $c^{1/2}$) will be included in the analysis since the higher-order terms imply an ionic distribution function that is inconsistent with the Poisson equation. Because of this limitation, good agreement is not to be expected. Nevertheless, the electrophoretic effect observed for aqueous sulfuric acid is large and unambiguous so that prediction of the effect for this system will constitute a clear test of theory.

In the limit of infinite dilution, the velocity v_i of a migrating ion is given by

$$[14]\quad v_i = \omega_i k_i$$

where ω_i is the limiting mobility

$$[15]\quad \omega_i = \lambda_i^0 / F z_i^2$$

and k_i is the force acting on the ion, which, in the case of pure diffusion, equals the negative gradient of the ion's electrochemical potential

$$[16]\quad k_i = -\nabla \tilde{\mu}_i$$

At non-zero concentrations, a force which would impart velocity v_i in the absence of ion–ion interactions actually produces a velocity $v_i + \Delta v_i$ where Δv_i is the electrophoretic contribution to the diffusion velocity. Provided Δv_i is small compared to v_i, the ionic diffusivities can be corrected for the effects of electrophoresis simply by multiplying each limiting ionic diffusivity by the factor $1 + (\Delta v_i / v_i)$. We obtain the expression

$$[17]\quad D_i = (1 + \delta_i) D_i^0$$

in which, for convenience, δ_i is an abbreviation for $\Delta v_i / v_i$ (7*a*).

According to the Onsager–Fuoss theory (24, 25), the δ_i values are given by

$$[18]\quad \delta_i = -\frac{\kappa}{6\pi\eta\omega_i} \sum_\sigma \frac{z_i u_\sigma}{z_\sigma} \left(\frac{k_\sigma}{k_i}\right)$$

Can. J. Chem. Downloaded from www.nrcresearchpress.com by 210.87.254.5 on 09/06/12
For personal use only.

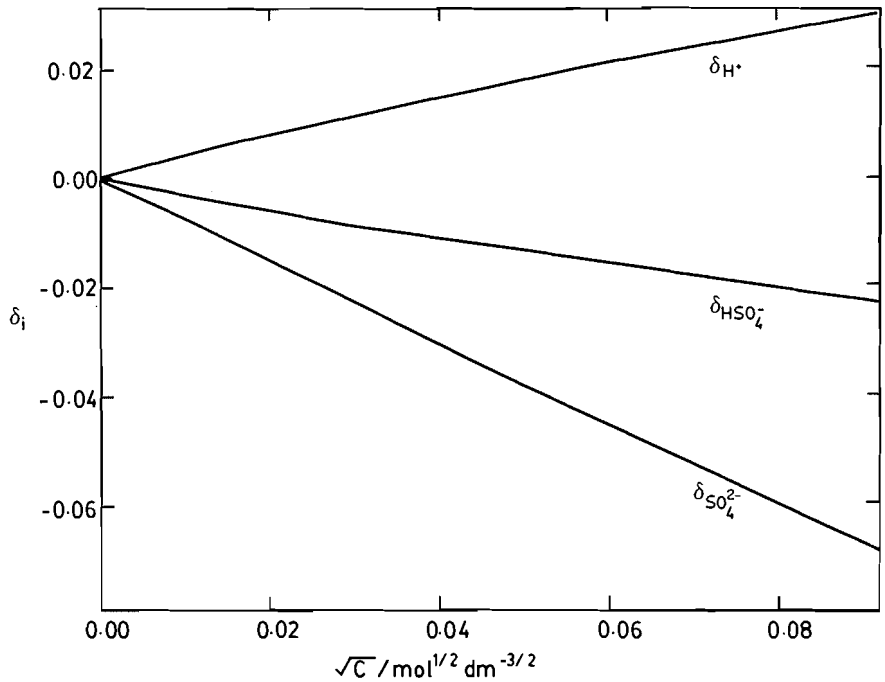

FIG. 3. Electrophoretic corrections plotted against the square root of the concentration.

where η is the viscosity of the pure solvent, u_σ stands for the fraction of the ionic strength contributed by ion σ

$$[19]\quad u_i = \tilde{c}_i z_i^2 / \sum_\sigma \tilde{c}_\sigma z_\sigma^2$$

and κ is the reciprocal Debye length given in the usual notation by

$$[20]\quad \kappa = \left[\frac{4\pi N e^2}{1000 \epsilon kT} \sum_\sigma \tilde{c}_\sigma z_\sigma^2\right]^{1/2}$$

In the preceding equations, $\tilde{c}_i$ refers to the concentration of ion i in mol per unit volume. The summations run over all ionic species present in solution.

For aqueous solutions of sulfuric acid, we have $\tilde{c}_1 = (1 + \alpha)c$, $\tilde{c}_2 = \alpha c$, and $\tilde{c}_3 = (1 - \alpha)c$ for H^+, SO_4^{2-}, and HSO_4^-, respectively. In order to compute the electrophoretic corrections, all that remains is to determine the force ratios k_σ/k_i that appear in eq. [18]. This is easily accomplished if we recall the constraints on the ionic flows, namely, local equilibrium of the dissociation reaction

$$[21]\quad \tilde{\mu}_3 = \tilde{\mu}_1 + \tilde{\mu}_2$$

and the electroneutrality requirement

$$[22]\quad \tilde{c}_1 \nu_1 = 2\tilde{c}_2 \nu_2 + \tilde{c}_3 \nu_3$$

From eqs. [21] and [22] we find

$$[23]\quad k_3 = k_1 + k_2$$

$$[24]\quad \tilde{c}_1 \omega_1 k_1 = 2\tilde{c}_2 \omega_2 k_2 + \tilde{c}_3 \omega_3 k_3$$

and hence

$$[25]\quad \frac{k_1}{k_2} = \frac{2\tilde{c}_2 \omega_2 - \tilde{c}_3 \omega_3}{\tilde{c}_1 \omega_1 - \tilde{c}_3 \omega_3}$$

$$[26]\quad \frac{k_2}{k_3} = \frac{\tilde{c}_1 \omega_1 - \tilde{c}_3 \omega_3}{\tilde{c}_1 \omega_1 + 2\tilde{c}_2 \omega_2}$$

$$[27]\quad \frac{k_3}{k_1} = \frac{2\tilde{c}_2 \omega_2 + \tilde{c}_1 \omega_1}{2\tilde{c}_2 \omega_2 - \tilde{c}_3 \omega_3}$$

The electrophoretic corrections δ_i are obtained by substitution of eqs. [25]–[27] into eq. [18]. In Fig. 3, δ_i values calculated in this manner for dilute sulfuric acid are plotted against the square root of the concentration. (The calculations are based on the values $\eta = 8.90 \times 10^{-4}$ kg m^{-1} s^{-1} for the viscosity and $\epsilon = 78.3$ for the dielectric constant of water at 25°C (7*c*).) When the corrected ionic diffusivities are substituted into eq. [11], we obtain the calculated values for the diffusion coefficient of sulfuric acid shown by the continuous curve in Fig. 2. As anticipated, inclusion of the electrophoretic corrections lowers the predicted diffusion coefficient. Although this brings the predictions into closer agreement with the experimental results, especially at the lower concentrations investigated, the observed electrophoretic effect is twice as large as the effect predicted by theory. This is true even at the very low concentrations ($\lesssim$0.005 mol dm^{-3}) where the theory is expected to apply (27, 28) and where complications arising from viscosity changes of the solutions are negligible. Without obvious reasons to dismiss the experimental results, we conclude that theory in its present form can provide only a qualitative description of diffusion in dilute solutions of sulfuric acid.

Values of the thermodynamic factor $1 + c\,\mathrm{d}\ln y_\pm/\mathrm{d}c$ and the limiting ionic conductances used to predict D are well established. On the other hand, values of α, the degree of dissociation of HSO_4^-, are not accurately known. Since the values of α used here were calculated from eq. [10], they depend on the values used for both the activity coefficient ratio $y_{H^+} y_{SO_4^{2-}}/y_{HSO_4^-}$ and K_{a2}. Because estimates of the activity coefficient of a divalent ion in a mixture are required, evaluation of the former is difficult. For K_{a2}, we used the value 0.0105 mol dm^{-3} recommended by Pitzer, Roy, and Silvester (6) in their comprehensive correlation of extensive emf and osmotic data. In another study, however, Covington, Dobson, and Wynne-

Can. J. Chem. Downloaded from www.nrcresearchpress.com by 210.87.254.5 on 09/06/12
For personal use only.

Jones (29) determined $K_{a2} = 0.0106$. From conductance studies, Kerker (30) obtained $K_2 = 0.0102$, while Dunsmore and Nancollas (31) obtained $K_2 = 0.0105$. Young, Maranville, and Smith (32) determined the slightly higher value $K_{a2} = 0.0120$ from analysis of Raman spectra.

Uncertainties in the values of K_{a2} and $y_{H^+}y_{SO_4^{2-}}/y_{HSO_4^-}$ will lead to errors in the values we have used for α. If we have underestimated α, the calculated values of the mobility, then D will be too high. This might contribute to the poor agreement between theory and experiment shown in Fig. 2.

In order to examine this possibility in greater detail, consider the data point obtained at 0.001 mol dm^{-3} H_2SO_4. From Fig. 2, we see that the predicted value of D is about 2% higher than the observed value. If we repeat the calculation of D with a value of K_{a2} that is 10% larger than 0.0105 (or a value of $y_{H^+}y_{SO_4^{2-}}/y_{HSO_4^-}$ 10% smaller than the value recommended by Pitzer and Silvester), the value calculated for D will be only 0.4% lower than shown in Fig. 2. At 0.003 mol dm^{-3} where the observed D value is 3.5% below the predicted value, a 10% increase in K_a (or a 10% decrease in $y_{H^+}y_{SO_4^{2-}}/y_{HSO_4^-}$) will produce a 0.6% decrease in the predicted D value. Therefore, the discrepancy between theory and experiment is much too large to be explained by errors made in the values used for α.

Finally, it may be mentioned that Onsager and Fuoss (25) and Harned (24) have proposed that the second-order terms (proportional to $c \ln c$) be included in the calculation of electrophoretic corrections for unsymmetrical electrolytes, even though this procedure is known to be inconsistent (7*a*, 18). When we calculated the second-order correction for aqueous sulfuric acid, we found that it was large and *positive*. In fact, it practically cancelled out the first-order correction. Since inclusion of the second-order terms makes the discrepancy between theory and experiment significantly larger, the present investigation provides evidence that only first-order terms should be included in the treatment of the electrophoretic effect for unsymmetrical electrolytes.

Acknowledgment

I am indebted to Tom Richards for assistance with the diffusion measurements. This research was sponsored by the Natural Sciences and Engineering Research Council of Canada.

1. H. S. HARNED and R. M. HUDSON. J. Am. Chem. Soc. **73**, 3781 (1951); **73**, 5880 (1951).
2. B. F. WISHAW and R. H. STOKES. J. Am. Chem. Soc. **76**, 2065 (1954).
3. G. T. A. MULLER and R. H. STOKES. Trans. Faraday Soc. **53**, 642 (1957).
4. V. VITAGLIANO and P. A. LYONS. J. Am. Chem. Soc. **78**, 4538 (1956).
5. C. W. GARLAND, S. TONG, and W. H. STOCKMAYER. J. Phys. Chem. **69**, 1718 (1965).
6. K. S. PITZER, R. N. ROY, and L. F. SILVESTER. J. Am. Chem. Soc. **99**, 4930 (1977).
7. R. A. ROBINSON and R. H. STOKES. Electrolyte solutions. 2nd ed. Academic Press, New York. 1959. (*a*) Chapt. 11; (*b*) Appendix 6.1; (*c*) Appendix 1.1.
8. H. S. HARNED and B. B. OWEN. Physical chemistry of electrolytic solutions. 2nd ed. Reinhold Publishing Corp., New York. 1950. Chapt. 6.
9. H. S. HARNED and R. L. NUTTALL. J. Am. Chem. Soc. **69**, 736 (1947).
10. M. R. SAVINO and V. VITAGLIANO. Ric. Sci. Rend. Sez. A, **2**, 341 (1962).
11. T. A. RENNER and P. A. LYONS. J. Phys. Chem. **78**, 1667 (1974).
12. D. G. LEAIST and P. A. LYONS. Aust. J. Chem. **33**, 1869 (1980).
13. International critical tables. Vol. III. McGraw-Hill Book Co., New York. 1929. p. 242.
14. J. A. HARPST, E. HOLT, and P. A. LYONS. J. Phys. Chem. **69**, 2333 (1965).
15. V. M. M. LOBO and M. H. S. F. TEIXEIRA. Electrochim. Acta, **24**, 565 (1979).
16. I. M. KLOTZ and C. F. ECKERT. J. Am. Chem. Soc. **64**, 1878 (1942).
17. H. G. MCLEOD and A. R. GORDON. J. Am. Chem. Soc. **68**, 58 (1946).
18. R. H. STOKES. J. Am. Chem. Soc. **75**, 4563 (1953).
19. J. M. CREETH and R. H. STOKES. J. Phys. Chem. **64**, 946 (1960).
20. L. S. DARKEN and H. F. MEIER. J. Am. Chem. Soc. **64**, 621 (1942).
21. V. SIVERTZ, R. E. REITMEIER, and H. V. TARTAR. J. Am. Chem. Soc. **62**, 1379 (1940).
22. I. L. JENKINS and C. B. MONK. J. Am. Chem. Soc. **72**, 2695 (1950).
23. M. KERKER. J. Am. Chem. Soc. **79**, 3664 (1957).
24. H. S. HARNED. Discuss. Faraday Soc. **24**, 9 (1957).
25. L. ONSAGER and R. M. FUOSS. J. Phys. Chem. **26**, 2689 (1932).
26. M. S. CHEN and L. ONSAGER. J. Phys. Chem. **81**, 2017 (1977).
27. H. S. HARNED and F. M. POLESTRA. J. Am. Chem. Soc. **76**, 2064 (1954).
28. H. S. HARNED and H. W. PARKER. J. Am. Chem. Soc. **77**, 265 (1955).
29. A. K. COVINGTON, J. V. DOBSON, and W. F. K. WYNNE-JONES. Trans. Faraday Soc. **61**, 2057 (1965).
30. M. KERKER. J. Am. Chem. Soc. **79**, 3664 (1957).
31. H. S. DUNSMORE and G. H. NANCOLLAS. J. Phys. Chem. **68**, 1579 (1964).
32. T. F. YOUNG, L. F. MARANVILLE, and H. M. SMITH. The Structure of electrolytic solutions. *Edited by* W. J. Hamer. Wiley, New York. 1959. Chapt. 4.

Can. J. Chem. Downloaded from www.nrcresearchpress.com by 210.87.254.5 on 09/06/12
For personal use only.

Zinc(II) and cadmium(II) compounds with the 2-[(dimethylamino)methyl]phenyl ligand

AKHTAR OSMAN, RICHARD G. STEEVENSZ, AND DENNIS G. TUCK
Department of Chemistry, University of Windsor, Windsor, Ont., Canada N9B 3P4

AND

HARRY A. MEINEMA AND JAN G. NOLTES
Institute of Applied Chemistry TNO, P.O. Box 5009, 3502 JA Utrecht, The Netherlands

Received October 31, 1983

AKHTAR OSMAN, RICHARD G. STEEVENSZ, DENNIS G. TUCK, HARRY A. MEINEMA, and JAN G. NOLTES. Can. J. Chem. **62**, 1698 (1984).

The compounds L_2M (M = Zn, Cd; L = 2-[(dimethylamino)methyl]phenyl ligand) are obtained by reacting MCl_2 with LiL. The organometallic halides have been prepared, either by a similar route (LZnCl), or by the direct electrochemical oxidation of cadmium metal in the presence of 1-bromo-2-[(dimethylamino)methyl]benzene (LCdBr). The latter can be converted to LCdMe or LCdPh. Proton nmr spectroscopy shows that both L_2Zn and L_2Cd undergo rapid intramolecular bond fission and formation at the M + NMe_2 site. For L_2Cd, studies of the Cd—C—C—H coupling show that the Cd—C_6H_5 bond undergoes rapid homo-exchange at room temperature.

AKHTAR OSMAN, RICHARD G. STEEVENSZ, DENNIS G. TUCK, HARRY A. MEINEMA et JAN G. NOLTES. Can. J. Chem. **62**, 1698 (1984).

On obtient les composés L_2M (M = Zn, Cd; L = ligand [(diméthylamino) méthyl]-2 phényl) en faisant réagir MCl_2 avec LiL. On a préparé les halogénures organométalliques soit par une route semblable (LZnCl) soit par l'oxydation électrochimique directe du cadmium métallique en présence de bromo-1 [(diméthylamino) méthyl]-2 benzène (LCdBr). On peut transformer ce dernier soit en LCdMe ou en LCdPh. La rmn du ^1H démontre que le L_2Zn ainsi que le L_2Cd subissent chacun des fissions et des formations de liaisons intramoléculaires rapides au niveau du site M+ NMe_2. Dans le cas du L_2Cd, les études du couplage Cd—C—C—H démontrent que la liaison Cd—C_6H_5 subit un échange homolytique rapide à la température ambiante.

[Traduit par le journal]

Introduction

Metal complexes of the potentially bidentate 2-[(dimethylamino)methyl]phenyl ligand (= L) have been the subject of a number of recent publications. Many of these compounds are derivatives of metals formally in a d^{10} configuration, such as tin(IV) (1), germanium(IV) (2), indium(III) (3, 4), thallium(III) (5), mercury(II) (6), and copper(I) (7). Particular attention has been paid to the coordination environment of the metal, both in the solid state (e.g., Sn (8), In (3), Cu (9)) and in solution (e.g. In (4), Hg (6), Cu (10)). We now report studies of ML_2 (M = Zn, Cd) and some related species.

Experimental

General

All reactions were carried out in an atmosphere of dry nitrogen. Solvents were purified and dried over sodium. Powdered zinc or cadmium chloride was dried at 150−160°C for 3−4 h. All other reagents were used as supplied.

Proton nmr spectra were recorded on JEOLCO C-60 HL or Varian EM-360 spectrometers at ambient temperature (30°C) unless otherwise stated. Infrared spectra were recorded on a Beckman IR-12 instrument using KBr cells. Mass spectra were obtained on a Varian MAT CH5 DF instrument, interfaced to an INCOS 2000 data system, and operating in either electron impact or field ionisation modes.

Metal analysis was by atomic absorption spectrophotometry.

Preparation of o-*lithio*-N,N′-*dimethylbenzylamine (LiL)*

A 5 mL portion (11 mmol) of *n*-butyllithium in hexane (2.24 mol L^{-1}) was added in one operation to 1.35 g (10 mmol) of *N*,*N*′-dimethylbenzylamine dissolved in diethyl ether (60 mL), all at room temperature. The reaction mixture was stirred for at least 18 h at room temperature before using the resultant yellow suspension of LiL in further preparative work.

Preparation of bis{2-[(dimethylamino)methyl]phenyl}zinc (L_2Zn)

Powdered anhydrous zinc chloride (0.68 g, 5.0 mmol) was slowly added over 2 h to a freshly prepared suspension of LiL (10 mmol) in 80 mL diethylether. The mixture was stirred for a further 4 h, insoluble material (LiCl) removed by filtration, and the solution phase concentrated. The addition of benzene to this concentrate removed any remaining traces of LiCl, after which the solution was again concentrated; petroleum ether (30−60°C) was then added with cooling to precipitate colourless crystals of $Zn[C_6H_4CH_2N(CH_3)_2\text{-}2]_2$. *Anal.* calcd.: Zn 19.6; found: Zn 19.2. ^1H nmr ($CDCl_3$/TMS) δ = 7.4−6.9 ppm, m (2.1H), C_6H_4; δ = 4.10 ppm, s (1.0H), NCH_2; δ = 2.62 ppm, s (3.1H), $N(CH_3)_2$.

Preparation of bis{2-[(dimethylamino)methyl]phenyl} cadmium (L_2Cd)

Anhydrous $CdCl_2$ (0.9 g, 0.50 mmol) was slowly (ca. 1.5 h) added to a freshly prepared suspension of 2-[(dimethylamino)methyl]phenyl lithium (10 mmol) in 60 mL of ether at room temperature. The mixture was then stirred for a further 3 h, by which time the reaction mixture contained a light grey suspension. The insoluble material was filtered off and the organic solution concentrated to a yellow oil. This oil was dissolved in 10 mL benzene and the murky solution filtered and again concentrated to a thick yellow liquid. The resulting oil was treated dropwise with 5−10 mL petroleum ether (30−60°C) and immediately cooled by rapid evaporation of a small portion of solvent *in vacuo*, which afforded white crystals of $Cd[C_6H_4CH_2N(CH_3)_2\text{-}2]_2$ which were collected, washed with cold petroleum ether (30−60°C), and dried *in vacuo*. Yield 0.3 g (16.0%). *Anal.* calcd.: Cd 29.5; found: Cd 29.0. ^1H nmr (C_6D_6/TMS) δ = 7.6−7.0 ppm, m (2.1H), C_6H_4; δ = 3.20 ppm, s (1.0H), NCH_2; δ = 1.93 ppm, s (3.0H), $N(CH_3)_2$.

Preparation of 2-[(dimethylamino)methyl]phenylzinc chloride (LZnCl)

Anhydrous $ZnCl_2$ (1.36 g, 10 mmol) was slowly added over 3 h to a suspension of 2-[(dimethylamino)methyl]phenyl lithium (10 mmol) in 100 mL diethylether. An exothermic reaction took place, requiring the reaction vessel to be cooled in an ice bath. The reaction mixture was stirred for 3−4 h, and then worked up using the procedures outlined above for ZnL_2. The yield of $ClZn[C_6H_4CH_2N(CH_3)_2\text{-}2]$ was 0.6 g (28%). *Anal.* calcd.: Zn 27.8, Cl 15.1; found: Zn 28.3, Cl 14.4.

Can. J. Chem. Downloaded from www.nrcresearchpress.com by 210.87.254.105 on 09/06/12
For personal use only.

^{1}H nmr ($CDCl_3$/TMS) δ = 7.6–6.9, m (1.9H), C_6H_4; δ = 3.98, s (1.0H), CH_2; δ = 2.50, s (3.0H), $N(CH_3)_2$.

Preparation of 1-bromo-2-[(dimethylamino)methyl]benzene (LBr)

1, α-dibromotoluene (CARE!) (48 g, 0.19 mol) was slowly added to a preheated (50°C) aqueous solution of dimethylamine (32 g, 0.71 mol, in 55 mL). The temperature was then held at 70°C for 2 h, after which a second 0.71 mol portion of 40% aqueous dimethylamine was added and the mixture heated for a further 3.5 h. The green–yellow organic layer was separated and the aqueous layer washed several times with benzene. The combined organic phase and benzene extracts were dried over anhydrous sodium sulphate, concentrated, and distilled, to yield $BrC_6H_4CH_2N(CH_3)_2$ as a colourless liquid (bp 60°C at 0.1 mm) (11). Yield 34.0 g (78%). ^{1}H nmr ($CDCl_3$/TMS) δ = 7.6–6.8, m (2.2H), C_6H_4; δ = 2.20 (3.0H), $N(CH_3)_2$.

Electrochemical preparation of 2-[(dimethylamino)methyl]-phenylcadmium bromide (LCdBr)

The electrochemical synthesis was carried out in the two-arm cell described in earlier papers (12, 13). The solution (see below) was placed in one arm, where it was repeatedly frozen, evacuated, and melted in order to remove all traces of oxygen. The degassed solution was then decanted *in vacuo* into the other arm, in which a piece of cadmium metal was suspended on a thin platinum wire entering the vessel through a Teflon plug situated in a standard taper neck. The cadmium then formed the anode of an electrochemical, non-aqueous cell; the cathode was a tungsten wire fused into the wall of the tube.

A solution of 1-bromo-2-[(dimethylamino)methyl]benzene (typically 1 g) in acetonitrile/benzene (ca. 8 mL; 2/1 v/v mixture) containing approximately 10 mg tetraethylammonium perchlorate was degassed in the manner described, and transferred to the electrochemical cells. The cadmium (ca. 5 g) was electrochemically oxidised for 5–6 h, during which time the white solid produced at the anode deposited in the bottom of the cell. The cell was opened, the solid collected by filtration under nitrogen, and the product washed with benzene and diethyl ether. In two separate experiments, 98 mg and 75 mg of cadmium were lost from the anode, and 186 mg and 154 mg of product obtained, representing yields of 65–70%. The product was $BrCd[C_6H_4CH_2N(CH_3)_2$-2], which is only slightly soluble in acetonitrile, chloroform, benzene, or acetone, and soluble in warm pyridine. *Anal.* calcd.: Cd 34.4, Br 24.5; found: Cd 34.7, Br 24.5.

Preparation of {2-[(dimethylamino)methyl]phenyl}methylcadmium (LCdMe)

LCdBr (100 mg, 0.34 mmol) was refluxed with an equimolar quantity of MeLi in 5 mL of benzene/diethyl ether (1/1 v/v) under nitrogen for 3–4 h with mechanical stirring. The white product thus formed was collected by filtration, washed several times with diethyl ether to remove residual LiBr, and dried *in vacuo*. Yield of $CH_3Cd[C_6H_4CH_2N(CH_3)_2$-2] 76 mg (84%). *Anal.* calcd.: Cd 43.0; found: Cd 41.9. The compound is insoluble in acetone, acetonitrile, or cold benzene, but slightly soluble in hot benzene; the insolubility prevented us from recording nmr spectra.

Preparation of {2-[(dimethylamino)methyl]phenyl}phenylcadmium (LCdPh)

Procedures similar to those just described, using PhLi (0.35 mmol) and LCdBr (107 mg, 0.33 mmol) yielded 95 mg of $C_6H_5Cd[C_6H_4N(CH_3)_2$-2]. Yield 89%. *Anal.* calcd.: Cd, 34.7; found: Cd 34.9. The solubilities of this compound are similar to those of the methyl analogue.

Results and discussion

Preparative

The preparation of L_2Zn and L_2Cd via the lithio derivative of the parent amine represents a logical extension of earlier syntheses of this type, and calls for little further comment. Three experimental points observed in the cadmium work are worth noting. Firstly, L_2Cd was obtained in pure form only when solid $CdCl_2$ was added to the organolithium suspension; addition in the reverse order causes the reaction to proceed in a less selective manner, as indicated by the isolation of various unidentifiable products whose presence caused difficulty in the purification of L_2Cd. Secondly, the particular cadmium halide chosen is important. Cadmium chloride was preferred, since the complete removal of LiCl could be achieved by the addition of benzene and subsequent filtration; when $CdBr_2$ was used, L_2Cd was contaminated with trace amounts of LiBr. Thirdly, pieces of grey material, presumed to be cadmium metal, were observed in the solution during the course of the reaction; analysis showed that the insoluble byproducts (theoretically CdX_2) contained up to 37.0% cadmium. This last observation is in keeping with the observed instability of the L_2Cd compound, which decomposes in air, and to a lesser extent in non-aqueous solvents.

The synthesis of LZnCl was accomplished by the reaction of $ZnCl_2$ with 1 mol of LiL. For LCdBr, we found it convenient to carry out a direct electrochemical synthesis, using anodic cadmium, to achieve what is effectively the insertion of the metal into the C—Br bond of 1-bromo-2-[(dimethylamino)-methyl]benzene. This process parallels earlier work on the direct synthesis of other RCdX compounds by electrochemical methods (14–17). The organocadmium compound LCdBr is a useful starting material for further synthetic work, exemplified by the synthesis of $LCdCH_3$ and $LCdC_6H_5$ from the reaction of LCdBr with the appropriate alkyl or aryl–lithium compounds.

Finally we note briefly a reaction which has yet to be explored in detail, and which depends on the reactivity of the phenyl-ring proton *ortho* to the $CH_2N(CH_3)_2$ group in $C_6H_5CH_2N(CH_3)_2$. The reactivity at this site is, of course, demonstrated by the smooth lithiation to give LiL (see above). When a solution of C_2H_5CdI in acetonitrile, prepared by the electrochemical oxidation of cadmium into a solution of C_2H_5I (14, 15) was reacted with HL, gas was evolved in accordance with the equation

$$[1] \quad C_2H_5CdI + HL \rightarrow C_2H_6 + LCdI$$

(wt. of C_2H_5CdI), calculated from cadmium dissolved, 0.36 g 1.34 mmol; vol. of gas collected, corrected to STP, 30.5 mL, 1.36 mmol and a colourless solid precipitated. Analytical results immediately after isolation of this solid. (*Anal.* calcd. for LCdI: Cd 30.1; I 34.0; found: Cd 30.6, I 34.5) confirmed the stoichiometry of reaction [1] but results 24 h later showed that subsequent decomposition had occurred. Despite this, the initial reaction [1] above suggests that alkane elimination between an organometallic halide RMX and LH may be a useful route to LMX compounds.

Nuclear magnetic resonance spectroscopy

The ^{1}H nmr spectra reported in the Experimental section serve to characterise the compounds in question. Benzene was the solvent of choice, both because of suitable solubilities and because some of the LZn and LCd complexes were found to undergo decomposition in CCl_4 and $CDCl_3$. We observed significant solvent shifts of the proton resonances between C_6D_6 and $CDCl_3$; for example, with L_2Cd, NCH_2 is found at 3.50 ($CDCl_3$) or 3.25 (C_6D_6) ppm, and NCH_3 at 2.31 ($CDCl_3$) or 1.93 (C_6D_6) ppm. Other 2-dimethylaminophenyl metal complexes show similar effects in these solvents (e.g. L_2InCl (4), LMe_2SnBr (1), and the origin of these solvent shifts has been discussed elsewhere (18)).

Nuclear magnetic resonance spectroscopy is a useful tool for obtaining information about the nature of the intramolecular

Can. J. Chem. Downloaded from www.nrcresearchpress.com by 210.87.254.105 on 09/06/12
For personal use only.

coordination in LM compounds (19). The L_2M complexes (L = Zn, Cd) may occur as 2-, 3-, or 4-coordinate species. For L_2Zn at ambient temperatures, and for L_2Cd at 25°C and −50°C, both the NCH_2 and NCH_3 sets of protons give rise to singlets ($CDCl_3$ solution). These NCH_2 and NCH_3 moieties lack a molecular symmetry plane in a four-coordinate ML_2 complex, so that anisochronous resonances should be observed. The experimental observation that these resonances appear as singlets points to a rate-determining Cd—N bond dissociation which is fast on the nmr time-scale even at −50°C. Rapid pyramidal inversion at nitrogen clearly cannot take place while nitrogen is coordinate to the metal. That the equilibrium [2] should lie well

[2] 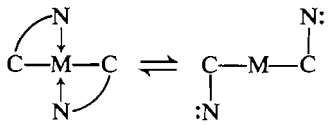

to the right is not surprising, since the strain involved in the formation of a pseudo-tetrahedral MC_2N_2 kernel must be considerable for both zinc and cadmium, given that the bite angle N—M—C in related complexes has been found consistently to be close to 75° (e.g., 75.3° in Ph_2LSnBr (8), 73° in CpLTi (20), and 77 ° in L_2InCl (3)). Recently van Koten *et al.* (6) have used the chiral labelling technique (10) to show that the Hg—N coordination is stable on the nmr time scale at −70°C in LHgX compounds (X = Cl, OAc), but becomes labile at higher temperatures.

Although the ^1H nmr spectrum of L_2Cd gives little definitive information about the Cd—N coordination beyond the high lability of the bond, it does reveal an interesting dynamic effect in the Cd—C(aryl) bond. The phenyl/hydrogen atom *ortho* to this bond appears as a broad singlet (half-width ~20 Hz) at 24°C, but at −40°C one observes a triplet with satellites at a separation of 47 Hz, corresponding to the coupling of this proton with the cadmium isotopes ^{111}Cd (spin 1/2, 12.75%) and ^{113}Cd (spin 1/2, 12.76%), with J(Cd—C—C—H) similar to that reported for other organocadmium compounds (21). These satellites coalesce into the main peak at room temperature. Although we have not investigated this phenomenon in detail, it is compatible with ligand exchange between CdL_2 units which is slow on the nmr time scale at low temperatures.

[3] $CdL_2 + CdL_2^* \rightleftharpoons 2LCdL^*$

which is slow on the nmr time scale at low temperatures. Such homo-exchange has been extensively studied for dialkylcadmium compounds (21), but does not appear to have been observed previously for diaryl derivatives.

Mass spectrometry

As part of a programme of investigations into the mass spectrometric behaviour of organometallic compounds (22), we have recorded the electron impact (EI) and field desorption (FD) mass spectra of CdL_2, and for comparison the EI spectrum of LBr.

The dominant peak for LBr is at m/e = 170 + 172, corresponding to $C_7H_7Br^+$ (Br = 79 or 81); a variety of lower m/e values include strong peaks at 86($C_5H_{12}N^{+\cdot}$), 84($C_5H_{10}N^{+\cdot}$), and 28 ($C_2H_4^{+\cdot}$). The EI mass spectrum of CdL_2 shows no molecular ion, and the highest significant m/e values are at 135 ($LH^{+\cdot}$) and 134 (L^+). The most intense peak at m/e = 58($NC_3H_8^+$), with a significant intensity at m/e = 44($NC_2H_6^+$). The only cadmium-containing peaks are those in the region 110−114, corresponding to the various isotopic forms of $Cd^{+\cdot}$. The EI-induced decomposition of the CdL_2 complex and that of LBr clearly differ significantly.

The FD spectrum of CdL_2 reveals the ions formed in the low energy ionisation processes of this mode of mass spectrometry. No Cd^+ ions were detected, and m/e values up to ~800 were recorded. Such ions, which result from ionisation of aggregates, are not uncommon in FD mass spectrometry (22). More importantly, a series of ions at m/e = 378−386 clearly arise from the various isotopic forms of CdL_2^+. Other ions derived from the parent molecule correspond to $[CdL_2 - 2CH_3]^+$ and $[CdL_2 - N(CH_3)_2]^+$. The ions HL_2^+, $L_2CH_3^+$, $[L_2 - CH_3]^+$, $[CdL - CH_3]^+$, and $CdC_6H_5NCH_2^+$ are also prominent. The spectrum clearly does not give that small number of easily identifiable peaks which is generally an important advantage of the FDMS method. On the other hand, it does indicate the variety of stable positive ions which can be derived from CdL_2 by various transfer and abstraction processes.

Acknowledgements

J.G.N. and D.G.T. gratefully acknowledge support of this work by NATO (Grant No. 1247).

1. G. VAN KOTEN, C. A. SCHAAP, and J. G. NOLTES. J. Organomet. Chem. **99**, 157 (1975).
2. C. BRELIÈRE, F. CARRÉ, R. J. P. CORRIU, A. DESAXCE, M. POIRIER, and G. ROYO. J. Organomet. Chem. **205**, C1 (1981).
3. M. A. KHAN, R. C. STEEVENSZ, D. G. TUCK, J. G. NOLTES, and P. W. R. CORFIELD. Inorg. Chem. **19**, 3407 (1980).
4. J. T. B. H. JASTRZEBSKI, G. VAN KOTEN, D. G. TUCK, H. A. MEINEMA, and J. G. NOLTES. Organometallics, **1** 1492 (1982).
5. A. F. M. J. VAN DER PLOEG, G. VAN KOTEN, and K. J. VRIEZE. J. Organomet. Chem. **222**, 155 (1981).
6. A. F. M. J. VAN DER PLOEG, C. E. M. VAN DER KOLK, and G. VAN KOTEN. J. Organomet. Chem. **212**, 283 (1981).
7. G. VAN KOTEN, A. J. LEUSINK, and J. G. NOLTES. J. Organomet. Chem. **84**, 117 (1975).
8. G. VAN KOTEN, J. G. NOLTES, and A. L. SPEK. J. Organomet. Chem. **118**, 183 (1976).
9. G. VAN KOTEN and J. G. NOLTES. J. Organomet. Chem. **84**, 129 (1975).
10. G. VAN KOTEN and J. G. NOLTES. J. Am. Chem. Soc. **101**, 6593 (1979).
11. B. GOGOLIMSKA and I. GRUDA. Acta Polon. Pharm. **20**, 147 (1963).
12. J. J. HABEEB and D. G. TUCK. J. Organomet. Chem. **139**, C17 (1977).
13. D. G. TUCK. Pure Appl. Chem. **51**, 2005 (1979).
14. J. J. HABEEB, A. OSMAN, and D. G. TUCK. Chem. Commun. 379 (1976).
15. J. J. HABEEB and D. G. TUCK. J. Organomet. Chem. **146**, 213 (1978).
16. A. OSMAN and D. G. TUCK. J. Organomet. Chem. **169**, 255 (1979).
17. J. J. HABEEB, A. OSMAN, and D. G. TUCK. Inorg. Chem. Acta, **35**, 105 (1979).
18. A. MACKOR and H. A. MEINEMA. Rec. Trav. Chim. Pays-Bas, **91**, 911 (1972).
19. G. VAN KOTEN, J. T. B. H. JASTRZEBSKI, J. G. NOLTES, W. M. G. F. PONTENAGEL, J. KROON, and A. L. SPEK. J. Am. Chem. Soc. **100**, 5021 (1978).
20. W. F. J. VAN DER WAL and H. R. VAN DER WAL. J. Organomet. Chem. **153**, 335 (1978).
21. N. S. HAM and T. MOLE. Progress in nuclear magnetic resonance spectroscopy. *Edited by* J. W. Emsley, J. Feeney, and L. H. Sutcliffe. Vol. 4. Pergamon Press, London. 1969. p. 156.
22. D. G. TUCK, G. W. WOOD, and S. ZHANDIRE. Can. J. Chem. **58**, 833 (1980).

Can. J. Chem. Downloaded from www.nrcresearchpress.com by 210.87.254.105 on 09/06/12
For personal use only.

The direct electrochemical synthesis of some thorium(IV) nitrate complexes

N. KUMAR AND DENNIS G. TUCK

Department of Chemistry, University of Windsor, Windsor, Ont., Canada N9B 3P4

Received January 30, 1984

N. KUMAR and DENNIS G. TUCK. Can. J. Chem. **62**, 1701 (1984).

The electrochemical oxidation of thorium in either nitric acid/tri-*n*-butyl phosphate (TBP) or dinitrogen tetroxide/ethyl acetate/acetonitrile media gives rise to non-aqueous solutions of thorium(IV) nitrate species. The only neutral adduct which could be obtained from HNO_3/TBP solution was $Th(NO_3)_4.8dmso$ (dmso = dimethylsulphoxide). Salts of $[Th(NO_3)_6]^{2-}$ with Et_4N^+, $[(bpyH)_3NO_3]^{2+}$, and $[(phenH)_3NO_3]^{2+}$ (bpy = 2,2′-bipyridine; phen = 1,10-phenanthroline) were also prepared by this route. Solutions in N_2O_4/EtOAc/CH_3CN yield $Th(NO_3)_4$, and neutral adducts with dmso, bpy, phen, Ph_3PO, and pyridine-*N*-oxide.

N. KUMAR et DENNIS G. TUCK. Can. J. Chem. **62**, 1701 (1984).

L'oxydation électrochimique du thorium soit dans l'acide nitrique/phosphate de tri-*n*-butyle (PTB) ou par le tétroxyde d'azote/acétate d'éthyle/acétonitrile conduit à la formation de nitrate de thorium(IV) en solutions dans des milieux non-aqueux. Le seul adduit neutre que l'on a pu obtenir à partir d'une solution de HNO_3/PTB est le $Th(NO_3)_4.8dmso$ (dmso = diméthylsulfoxyde). Utilisant cette méthode, on a aussi préparé les sels de $[Th(NO_3)_6]^{2-}$ avec les cations Et_4N^+, $[(bpyH)_3NO_3]^{2+}$ et $[(phenH)_3NO_3]^{2+}$ (bpy = bipyridine-2,2′; phen = phénanthroline-1,10). Des solutions dans le N_2O_4/EtOAc/CH_3CN conduisent au $Th(NO_3)_4$ et à des adduits neutres avec le dmso, la bpy, la phen, la Ph_3PO et la *N*-oxyde de la pyridine.

[Traduit par le journal]

Can. J. Chem. Downloaded from www.nrcresearchpress.com by 210.87.254.6 on 09/06/12
For personal use only.

Introduction

In previous papers from this laboratory (1, 2), we have described the direct electrochemical synthesis of thorium(IV) and (II) halides, some neutral adducts, and anionic thorium(IV) halide complexes. As part of the continuing exploration of the application of the electrochemical oxidation of metals, we now report that solutions of thorium(IV) nitrate species and various solid derivatives can also be prepared in this manner.

Thorium metal is not attacked by aqueous nitric acid, and in fact is rendered impassive to oxidation by such treatment (3*a*). The route to the hydrates of thorium(IV) nitrate is via the hydroxide (3*b*). Anhydrous thorium(IV) nitrate has been prepared by dissolving $ThCl_4$ in ethyl acetate/dinitrogen tetroxide, followed by thermal decomposition of the N_2O_4 adduct so formed (5); thorium is not attacked by solutions of N_2O_4 in organic solvents (6). The method of direct electrochemical synthesis is based in part on the use of non-aqueous electrolyte phases (7), and we have found that thorium(IV) nitrate species can be prepared by carrying out the oxidation of the metal into solutions of dinitrogen tetroxide in ethyl acetate/acetonitrile mixtures, or into solutions of nitric acid in tri-*n*-butyl phosphate. This latter solvent system was selected because of its relevance to the solvent extraction methods commonly used in the industrial scale purification of heavy elements.

Experimental

Materials

Thorium metal, supplied in the form of rod (7.9 mm diameter, Alfa) was sliced into discs, 2–4 mm thick. Acetone was dried over anhydrous magnesium sulphate and molecular sieves, acetonitrile over phosphorus pentoxide, and ethyl acetate over calcium hydride. Dinitrogen tetroxide (Matheson) was dried by passing the gas over phosphorus pentoxide.

Tetraethylammonium nitrate was prepared by reacting equimolecular amounts of tetraethylammonium bromide and silver nitrate in aqueous solution. Tri-*n*-butyl phosphate (TBP) was purified by the method reported earlier (8). Other reagents were used without further purification. All experimental operations were performed in an atmosphere of dry nitrogen. All work was at room temperature (20°C) unless otherwise noted.

Thorium was determined by titration against solutions of EDTA, using Alizarin S as indicator (9). Nitrate was determined gravimetrically as nitron nitrate (10).

Infrared spectra were recorded as Nujol mulls on a Perkin Elmer IR-18 spectrophotometer in the range 100–4000 cm^{-1}.

Electrochemical oxidation with HNO_3/TBP

Equilibration of equal volumes of TBP and 10 *M* aqueous nitric acid yields an organic phase containing 3.6 mol L^{-1} HNO_3 (c.f. ref. 8). This solution was separated from the aqueous layer and used without further treatment in the electrochemical synthesis.

In a typical experiment, 50 mL of HNO_3/TBP was placed in a 100 mL tall-form beaker. A platinum foil (1 × 1 cm^2) served as the cathode; the anode was a thorium disc (1.14 g, 4.9 mmol) suspended on a platinum wire. A current of 10 mA was passed through this cell for 45 h, after which time it was found that 0.77 g of thorium had been removed from the anode (see Table 1 for details). The solution phase was filtered through a sinter to remove suspended particles of thorium; addition of organic solvents such as acetone, diethyl ether, or benzene to the resultant clear solution did not cause any precipitation. Heating resulted in the evolution of thick brown fumes, but again no precipitate was formed. The addition of certain ligands to the solution yielded either neutral or anionic thorium(IV) nitrate complexes.

Anionic complexes from HNO_3/TBP media

(*a*) A solution of tetraethylammonium nitrate (0.77 g, 4.2 mmol) in ethanol (5 mL) was added to an electrochemically prepared solution of thorium (0.41 g, 1.8 mmol) in 40 mL HNO_3/TBP (HNO_3 3.6 *M*). The white solid which precipitated immediately was collected, washed three times with diethyl ether, and dried *in vacuo*. Analysis (Table 2) and infrared spectroscopy identified this product as $(Et_4N)_2[Th(NO_3)_6]$.

(*b*) 2,2′-Bipyridine (bpy) (0.42 g, 3 mmol) in ethanol (10 mL) was added to a solution of thorium (0.15 g, 0.65 mmol) in HNO_3/TBP. The mixture was stirred for 2 h at room temperature, after which the volume was reduced *in vacuo*. The white product which precipitated was collected, washed (diethyl ether), dried, and recrystallised from acetone/toluene (1:1, v/v). The colourless crystals were shown analytically and by X-ray crystallography (11) to be $[(bpyH)_3NO_3][Th(NO_3)_6]$.

(*c*) A similar reaction with 1,10-phenanthroline (phen) yielded pale pink crystals analysed as $[(phenH)_3NO_3][Th(NO_3)_6]$.

Neutral complexes from HNO_3/TBP media

(*a*) Dimethylsulphoxide (2 g, 25 mmol) was added to a HNO_3/TBP

TABLE 1. Typical experimental conditions for electrochemical oxidation of thorium in HNO_3 or N_2O_4 media

Solvent[a]	Mass HNO_3/N_2O_4 (g)	Initial voltage (V)	Current (mA)	Time of electrolysis (h)	Mass Th dissolved (g)	E_F (mol F^{-1})
TBP/HNO_3	11.3	8	10	45	0.77	0.19
TBP/HNO_3/acetone (1:7)	1.6	20	10	28	0.49	0.21
N_2O_4/MeCN/EtOAc (MeCN:EtOAc = 2:3)	2.4	10	10	27	0.32	0.16

[a]TBP = tri-*n*-butyl phosphate.

TABLE 2. Analytical and other results for thorium(IV) nitrate complexes

Compound	Colour	M.pt.[a] (°C)	Yield[b] (%)	Analysis, found (calcd.) (%) Th	NO_3
$Th(NO_3)_4$	Colourless	~55	55	47.9(48.3)	52.8(51.7)
$Th(NO_3)_4$.6dmso[c]	Colourless[d]		93	24.9(24.4)	26.8(26.2)
$Th(NO_3)_4$.8dmso	Colourless	68	50	20.6(21.3)	22.6(22.8)
$Th(NO_3)_4$.2Ph_3PO	Colourless	264–266 (262–266)	65	22.6(22.1)[e]	
$Th(NO_3)_4$.8pyNO[c]	Colourless	145–150 (150–155)	60	18.4(18.7)	20.6(20.0)
$Th(NO_3)_4$.2bpy[c]	Pale pink	205 (decom.)	68	29.6(29.3)	30.5(31.3)
$Th(NO_3)_4$.2phen[c]	Pale pink[d]		82	28.5(28.3)	29.5(30.2)
$(Et_4N)_2[Th(NO_3)_6]$	Colourless[d]		74	26.4(26.4)	42.2(43.0)
$[(bpyH)_3NO_3][Th(NO_3)_6]$[c]	Colourless	120	80	20.8(20.4)	37.1(38.2)
$(phenH)_3NO_3][Th(NO_3)_6]$[c]	Pale pink	152	76	18.6(19.2)	35.2(35.9)

[a]Literature values in parentheses.
[b]Based on Th metal dissolved electrochemically.
[c]dmso = dimethylsulphoxide; pyNO = pyridine-*N*-oxide; bpy = 2,2′-bipyridine; phen = 1,10-phenanthroline.
[d]Not determined.
[e]Compound difficult to dissolve; Th determined gravimetrically as ThO_2.

phase containing 0.15 g (0.6 mmol) thorium, and the mixture stirred for 4 h at room temperature. The precipitate which formed during this period was collected, washed with diethyl ether, and dried *in vacuo*. The product is the extremely hygroscopic $Th(NO_3)_4$.8dmso.

(*b*) We were unable to obtain any well-defined complexes on using urea, pyridine, triphenyl phosphine, or triphenylphosphine oxide under conditions similar to those used for dimethylsulphoxide. It seems probable that the high concentration of HNO_3 effectively prevented the formation of such complexes, and attempts were therefore made to run the electrochemical experiment at a lower concentration of HNO_3 by diluting the original HNO_3/TBP (3.6 *M*) solution. Acetone was found to be the most suitable diluent, but the addition of neutral complexing agents to such solutions did not yield adducts, the only exception again being in the case of dmso (see below).

Electrochemical oxidation with diluted HNO_3/TBP media

A solution (10 mL) of HNO_3/TBP (3.6 *M* HNO_3) was diluted with 65 mL of acetone, and this mixture then used as the electrolyte phase in the usual way. After completion of the electrolysis (Table 1), the reaction mixture was filtered, reduced in volume to 10 mL under reduced pressure, and treated with solid Na_2CO_3 (4 g) to neutralize any free nitric acid. The resultant solution was then stirred for 2 h with dmso (2 g) in acetone (50 mL). Addition of diethyl ether (30 mL) and pumping *in vacuo* produced a white precipitate of $Th(NO_3)_4$.6dmso, which was collected, washed with diethyl ether, and dried *in vacuo*.

Electrochemical oxidation with N_2O_4 solutions

The cell, a 100 mL tall-form beaker, contained 50 mL of ethyl acetate/acetonitrile (3:2 v/v). Dinitrogen tetroxide was condensed into this solution, cooled to 0°C, until (typically) 2 mL of liquid N_2O_4 (32 mmol) was present. Electrolysis under the conditions summarized in Table 1 caused oxidation of the thorium anode. The final solution phase was filtered (glass sinter) and the volume of the filtrate reduced to 10 mL. Addition of diethyl ether (40 mL) brought down a small quantity of white solid, which was removed by filtration. The resultant solution (*A*) was used for the preparation of $Th(NO_3)_4$ and a number of neutral adducts as described below.

Thorium tetranitrate

The solution *A* was concentrated slowly *in vacuo*, finally yielding an oily product. Repeated cycles of freezing (liquid nitrogen), pumping *in vacuo*, and melting gave a solid which was washed twice with diethyl ether; this product is the colourless, amorphous, and extremely hygroscopic $Th(NO_3)_4$.

Neutral adducts of $Th(NO_3)_4$

Solution *A* (10 mL) containing 0.4 g (1.7 mmol) thorium, as calculated from the weight loss of the anode, was diluted with acetonitrile to 50 mL. Addition of excess 2,2′-bipyridine (0.52 g, 3 mmol) was followed by stirring (2–3 h); the solution was concentrated to 5 mL, and benzene (15 mL) added to produce a pale pink precipitate which was collected by filtration, washed with ether (20 mL), and dried *in vacuo*. This product is $Th(NO_3)_4$.2bpy. Similar reactions with 1,10-phenanthroline yielded $Th(NO_3)_4$.2phen.

Triphenylphosphine oxide (TPPO) (1 g, 3.6 mmol) in acetonitrile (10 mL) was added to a sample of solution *A* (25 mL; 0.51 g Th, 2.2 mmol). The mixture was refluxed for 2 h, and excess solvent removed *in vacuo*, yielding a sticky solid which was recrystallised from hot benzene, when crystals of $Th(NO_3)_4$.2TPPO were obtained. With pyridine-*N*-oxide (pyNO) the refluxing was not necessary, and $Th(NO_3)_4$.8pyNO crystallised on concentrating the reaction mixture.

Can. J. Chem. Downloaded from www.nrcresearchpress.com by 210.87.254.6 on 09/06/12
For personal use only.

TABLE 3. Infrared absorptions (cm^{-1}) for NO_3 group in thorium(IV) nitrate complexes

Compound	ν_1	ν_2	ν_3	ν_4	ν_5	ν_6	Th—O_2NO
$Th(NO_3)_4$	1630m, 1570s	1015m	805m	1310w,1280s	745m	—	236s
$Th(NO_3)_4$.6dmso	1498s	1028m	820m	1280	736m	720m	192vs
$Th(NO_3)_4$.8dmso	1500s	1024m	822m	1285m	740m	715m	205s
$Th(NO_3)_4$.2Ph_3PO	1540s	1015m	802m	1275	740m	—	220vs
$Th(NO_3)_4$.8pyNO	—	1022w	—	1350sh	—	—	—
$Th(NO_3)_4$.2pby	1520m	1035m	808m	1300−1275br	740m	722m	210br
$Th(NO_3)_4$.2phen	1515s	1025s	810w	1280	740m	722m	210br
$(Et_4N)_2[Th(NO_3)_6]$	1520s,br	1020s	820m	1270	738m	718w	212s,br
$[(bphH)_3NO_3][Th(NO_3)_6]$	1502s	1020m	805m	1295s	735s	708m	220m,br
$[(phenH)_3NO_3][Th(NO_3)_6]$	1505s	1020s	818m	1275s	736m	728w	218sh

Results and discussion

Preparative

The electrochemical oxidation of thorium metal into either HNO_3/TBP or N_2O_4/EtOAc/MeCN is a straightforward process, yielding solutions of thorium(IV) which serve as the source of a number of anionic and neutral derivatives. The electrochemical efficiency, E_F, defined as moles of metal dissolved per Faraday of electricity, is ~0.2 mol F^{-1} for all systems studied. The electrochemical oxidation in those halide systems in which the products are thorium(IV) compounds is close to Faradaic behaviour (E_F = 0.25 mol F^{-1}), but values of E_F ~0.2 were found for β-diketonate systems (1). There is no other electrochemical work in nitrate media against which to compare the present results.

With TBP/HNO_3, the resultant highly acidic solutions of thorium(IV) yield salts of the anionic $[Th(NO_3)_6]^{2-}$ complex, even with the potentially bidentate neutral ligands bpy and phen. Protonation of these ligands gives salts of this anion with the unusual $[(bpyH)_3NO_3]^{2+}$ and $[(phenH)_3NO_3]^{2+}$ cations, one of which has been characterised by X-ray crystallography (11). A salt with the more conventional Et_4N^+ cation can also be obtained in this way, and there are a number of reports in the literature of salts with other cations, including diprotonated 1,10-phenanthroline (12). This last species was obtained in the present work via solutions of nitric acid.

Dimethylsulphoxide was the only neutral ligand to yield an adduct of $Th(NO_3)_4$ from such acidic media. With N_2O_4/organic solvent solutions, the electrochemical method provides a route to $Th(NO_3)_4$ itself, and to neutral complexes with both bidentate and monodentate ligands. The 1:2 adducts with triphenylphosphine oxide (12−14) and pyridine-*N*-oxide (15) are apparently identical to those reported by previous workers. The 1:8 adduct with dmso is different in stoichiometry from the compounds described in the literature (12, 16−18), but it may well be that reaction conditions affect the nature of the product, as evidenced by the preparation of both $Th(NO_3)_4$.8dmso and $Th(NO_3)_4$.6dmso from different media in the present work. The 1:2 adduct with 1,10-phenanthroline has been reported previously by Smith and Wassef (1). and the bpy compound extends this series.

Infrared spectroscopy

The vibrational spectra of the nitrate ion in the free state and in its various modes of ligation have been the subject of considerable discussion, and we follow the assignments by Hester and Grossman (19), Bullock (20), and Addison *et al.* (4). The results (Table 3) for $Th(NO_3)_4$ are similar to those reported by Ferraro and Walker (5). The remaining compounds show infrared absorptions similar to those given by Alvey, Bagnall, and Brown (16) and are accordingly formulated as complexes of covalent bidentate nitrate, a conclusion confirmed for $[(bpyH)_3NO_3][Th(NO_3)_6]$ by X-ray crystallography (11). In the case of $Th(NO_3)_4$.8dmso and $Th(NO_3)_4$.6dmso, bands at 840 and 1350 cm^{-1} have been taken to indicate the presence of ionic nitrate (16) in the lattice, in addition to that which is coordinated to the metal; the variation in stoichiometry with reaction conditions may well centre upon the competition between nitrate and dmso for the available coordination sites. The pyridine-*N*-oxide complex shows no evidence of coordinated nitrate, in agreement with the results published by Richard and Woollard (15).

The contributions made to these spectra by the neutral ligands are in keeping with results in the literature. ν(S=O) is at 950 or 960 cm^{-1} in $Th(NO_3)_4$.8dmso and $Th(NO_3)_4$.6dmso, respectively, ν(N=O) is at 1220 cm^{-1} in the pyNO complex, and ν(P=O) is at 1056 cm^{-1} in the Ph_3PO adduct. All the compounds show far infrared absorptions at 220 ± 20 cm^{-1}, attributed to ν(Th—O_2NO).

These results in general give little information on the actual coordination numbers at thorium in the compounds prepared. By analogy with $[Th(NO_3)_6]^{2-}$, the bpy and phen adducts likely involve twelve-coordinate thorium, but further work will be required to establish the coordination kernel in the other neutral adducts.

Acknowledgement

This work was supported by an Operating Grant from the Strategic Grants programme of the Natural Sciences and Engineering Research Council of Canada.

1. N. KUMAR and D. G. TUCK. Can. J. Chem. **60**, 2579 (1982).
2. N. KUMAR and D. G. TUCK. Inorg. Chem. **22**, 1951 (1983).
3. L. I. KATZIN. The actinide elements. *Edited by* G. T. Seaborg and J. J. Katz. McGraw-Hill, New York. 1954. (*a*) p. 76; (*b*) p. 81.
4. C. C. ADDISON, N. LOGAN, S. C. WALLWORK, and C. D. GARNER. Q. Rev. **25**, 289 (1971).
5. J. R. FERRARO and A. WALKER. J. Chem. Phys. **45**, 550 (1966).
6. J. R. FERRARO, L. I. KATZIN, and G. GIBSON. J. Am. Chem. Soc. **77**, 327 (1955).
7. D. G. TUCK. Pure Appl. Chem. **51**, 2005 (1979).
8. D. G. TUCK. J. Chem. Soc. 2783 (1958).
9. J. J. FRITZ and J. J. FORD. Anal. Chem. **25**, 1640 (1953).
10. W. F. HILDEBRAND. Applied inorganic analysis. 2nd ed. John Wiley, New York. 1953. p. 788.
11. M. A. KHAN, N. KUMAR, and D. G. TUCK. Can. J. Chem. In press.
12. B. A. SMITH and M. A. WASSEF. J. Chem. Soc. (A) 1817 (1968).

Can. J. Chem. Downloaded from www.nrcresearchpress.com by 210.87.254.6 on 09/06/12
For personal use only.

13. J. G. H. DUPREEZ and C. P. J. VAN VUREN. J. Inorg. Nucl. Chem. **36**, 81 (1974).
14. MAZHAR-UL-HAQUE, C. N. CAUGHLAN, F. A. HART, and R. VANNICE. Inorg. Chem. **10**, 115 (1971).
15. C. E. F. RICKARD and D. C. WOOLLARD. Inorg. Nucl. Chem. Lett. **14**, 207 (1978).
16. P. J. ALVEY, K. W. BAGNALL, and D. BROWN. J. Chem. Soc. Dalton Trans. 2326 (1973).
17. P. J. ALVEY, K. W. BAGNALL, D. BROWN, and O. V. LOPEZ. J. Chem. Soc. Dalton Trans. 1277 (1975).
18. A. K. MOLODKIN, O. M. IVANOVA, Z. V. BETYAKOVA, and L. E. KOLESNIKOVA. Russ. J. Inorg. Chem. **15**, 1682 (1970).
19. R. W. HESTER and W. L. GROSSMAN. Inorg. Chem. **5**, 1308 (1966).
20. J. I. BULLOCK. J. Inorg. Nucl. Chem. **29**, 2257 (1967).

Can. J. Chem. Downloaded from www.nrcresearchpress.com by 210.87.254.6 on 09/06/12
For personal use only.

Synthesis and structural characterization of bis(tropolonatodimethylgallium), $[(C_7H_5O_2)Ga(CH_3)_2]_2$

STEVEN J. RETTIG, ALAN STORR, AND JAMES TROTTER

Department of Chemistry, University of British Columbia, 2036 Main Mall, Vancouver, B.C., Canada V6T 1Y6

Received October 26, 1983

STEVEN J. RETTIG, ALAN STORR, and JAMES TROTTER. Can. J. Chem. **62**, 1705 (1984).

Details of the synthesis, physical properties, and solid-state structure of $[(C_7H_5O_2)Ga(CH_3)_2]_2$ are reported. Crystals of bis(tropolonatodimethylgallium) are monoclinic, a = 10.2669(9), b = 9.3237(3), c = 10.8671(10) Å, β = 112.896(4)°, Z = 2, space group $P2_1/n$ (22°C, λ = 0.70930 Å). The structure was solved by conventional heavy-atom techniques and was refined by full-matrix least-squares procedures to R = 0.034 and R_w = 0.037 for 1746 reflections with $I \geq 3\sigma(I)$. The centrosymmetric binuclear dimer features five-coordinate gallium atoms having irregular trigonal bipyramidal coordination geometry and a planar four-membered Ga_2O_2 ring. Important bond lengths (corrected for libration) are Ga—O(equatorial) = 1.972(2), Ga—O(axial) = 2.025(2) and 2.551(2) Å, and Ga—C = 1.951(4) and 1.954(4) Å.

STEVEN J. RETTIG, ALAN STORR et JAMES TROTTER. Can. J. Chem. **62**, 1705 (1984).

On rapporte les détails relatifs à la synthèse, aux propriétés physiques et à la structure à l'état solide du $[(C_7H_5O_2)Ga[CH_3)_2]_2$. Les cristaux du bis(tropolonatodiméthylgallium) sont monocliniques, a = 10,2669(9), b = 9,3237(3), c = 10,8671(10) Å, β = 112,896(4)°, Z = 2, groupe d'espace $P2_1/n$ (22°C, λ = 0,70930 Å). On a résolu la structure par les techniques conventionnelles des atomes lourds et on l'a affiné par la méthode des moindres carrés (matrice complète) jusqu'à des valeurs de R = 0,034 et R_w = 0,037 pour 1746 réflexions avec $I \geq 3\sigma(I)$. Le dimère binucléaire centrosymétrique comporte des atomes de gallium penta-coordonnés possédant une géométrie de coordination bipyramidale trigonale irrégulière et un cycle plan à quatre chaînons de Ga_2O_2. Les longueurs de liaisons importantes (corrigées pour la libration) sont: Ga—O (équatorial) = 1,972(2), Ga—O(axial) = 2,025(2) et 2,551(2) Å et Ga—C = 1,951(4) et 1,954(4) Å.

[Traduit par le journal]

Can. J. Chem. Downloaded from www.nrcresearchpress.com by 210.87.254.105 on 09/06/12
For personal use only.

Introduction

As part of our continuing study of compounds containing five-coordinate gallium atoms (1–6) we have synthesized and structurally characterized the compound bis(tropolonatodimethylgallium), $[(C_7H_5O_2)Ga(CH_3)_2]_2$. The choice of tropolone as the "active hydrogen" compound in this study was dictated by three considerations. Firstly, it was hoped to incorporate the tropolonato moiety in a mixed pyrazolyl gallate anionic ligand, secondly, we wished to extend our studies of five-coordinate gallium systems having three oxygen atoms in the coordination sphere about gallium and, finally, tropolone and its derivatives have been recently cited as antibiotic potentiators (7). Although the first objective was not fulfilled, the bis(tropolonatodimethylgallium) compound was isolated in high yield and shown to consist of dimer units in the solid state, displaying the familiar Ga_2O_2 central bridging unit and irregular trigonal bipyramidally coordinated gallium atoms. In dilute solution and in the gas phase, however, the compound exists solely as the monomeric species.

Experimental

Air-sensitive materials were handled in oxygen-free dry nitrogen. Tetrahydrofuran (THF) was dried by refluxing over sodium/benzophenone and used immediately following distillation. Tropolone (Aldrich) was used as supplied. Trimethylgallium was prepared as described earlier (8). 3,5-Dimethylpyrazole (pz″H) (Aldrich) and sodium hydride (Alfa) were used as supplied.

Attempted preparation of $Na^+[Me_2Gapz''(C_7H_5O_2)]^-$

$$Na^+[Me_3Gapz'']^- + C_7H_6O_2 \rightarrow Na^+[Me_2Gapz''(C_7H_5O_2)]^- + MeH$$

Trimethylgallium (2.156 g, 18.8 mmol) in THF was added to Napz″ (2.218 g, 18.8 mmol) (made from NaH + pz″H) in the same solvent. To the clear colorless solution of $Na^+[Me_3Gapz'']^-$ so formed was added tropolone (2.293 g, 18.8 mmol) in THF. An immediate formation of yellowish precipitate was observed. The mixture was refluxed for approximately 40 h and then filtered. The pale yellow solid precipitate was isolated and shown by elemental analysis to be sodium tropolonate, $Na^+C_7H_5O_2^-$. The soluble reaction product from the reaction was shown to be the $[Me_2Ga(\mu\text{-}pz'')]_2$ dimer (9).

Preparation of bis(tropolonatodimethylgallium), $[(C_7H_5O_2)Ga(CH_3)_2]_2$

Trimethylgallium (1.945 g, 16.96 mmol) in THF was added to tropolone (2.068 g, 16.95 mmol) in the same solvent. A vigorous evolution of methane occurred on mixing the two reactants. On cessation of gas evolution the solvent was removed under vacuum from the clear product solution. The solid obtained was recrystallized from benzene to yield colorless air-stable crystals of the product. *Anal.* calcd. for $[(C_7H_5O_2)Ga(CH_3)_2]_2$: C 48.93, H 4.98; found: C 48.61, H 5.16. ^1H nmr (C_6D_6, τ values refer to $\tau_{C_6H_6}$ = 2.84 ppm): 9.90 s ($GaMe_2$, 6), 6.32 t (J = 10 Hz, 1), 4.84 t (J = 10 Hz, 2), 2.84 d (J = 10 Hz, 2). The mass spectrum of the compound displayed weak signals due to the monomer parent ion $(C_7H_5O_2)Ga(CH_3)_2^+$ (= P^+) (4%), the strongest signals arising from the $P - Me^+$ ion (100%) and the $P - 2Me^+$ ion (13%). Mol. wt. calcd. for $(C_7H_5O_2)Ga(CH_3)_2$: 220.9; found (cryoscopy in benzene solution): 222.

X-ray crystallographic analysis of bis(tropolonatodimethylgallium)

A crystal bounded by the six faces (followed by their distances in mm from a common origin): ±(1 0 −1), 0.200, ±(0 1 1), 0.150, ±(1 −1 1), 0.138 was mounted in a general orientation. Unit-cell parameters were refined by least-squares on 2 sin θ/λ values for 25 reflections (2θ = 40–45°) measured on a diffractometer with Mo–$K\alpha$ radiation ($\lambda(K\alpha_1)$ = 0.70930, $\lambda(K\alpha_2)$ = 0.71359 Å). Crystal data at 22°C are:

$C_{18}H_{22}Ga_2O_4$ fw = 441.82

Monoclinic, a = 10.2669(9), b = 9.3237(3), c = 10.8671(10) Å, β = 112.896(4)°, V = 958.3(1) Å^3, Z = 2, ρ_c = 1.531 g cm^{-3}, F(000) = 448, μ(Mo − $K\alpha$) = 27.3 cm^{-1}. Absent reflections: $h0l$, $h + l$ odd, and $0k0$, k odd, uniquely indicate the space group $P2_1/n$ [nonstandard setting of $P2_1/c$, C_{2h}^5, No. 14, equivalent positions: ±(x, y, z; 1/2 − x, 1/2 + y, 1/2 − z)].

Intensities were measured with graphite-monochromated Mo − $K\alpha$ radiation on an Enraf-Nonius CAD4-F diffractometer. An ω–2θ scan at 1.18–10.06° min^{-1} over a range of (0.60 + 0.35 tan θ) degrees in ω (extended by 25% on both sides for background measurement) was employed. Data were measured to 2θ = 65°. The intensities of three

Can. J. Chem. Downloaded from www.nrcresearchpress.com by 210.87.254.105 on 09/06/12
For personal use only.

check reflections, measured every 3600 s throughout the data collection, showed uniform decreases to final values 10% less than the initial values, the intensities being scaled accordingly. After data reduction,[1] an absorption correction was applied using the Gaussian integration method (10, 11). Transmission factors ranged from 0.353 to 0.524 for 184 integration points. Of the 3445 independent reflections measured, 1746 (50.7%) had intensities greater than $3\sigma(I)$ above background where $\sigma^2(I) = S + 2B + (0.04(S - B))^2$ with S = scan count and B = normalized background count.

The coordinates of the Ga atom were determined from the Patterson function and those of the O and C atoms from a subsequent difference map. After full-matrix least-squares refinement of the non-hydrogen atoms with anisotropic thermal parameters to $R = 0.063$, a difference map gave the positions of all 11 independent hydrogen atoms which were refined with isotropic thermal parameters in subsequent cycles of refinement. The scattering factors of ref. 12 were used for non-hydrogen atoms and those of ref. 13 for hydrogen atoms. Anomalous scattering factors from ref. 14 were used for the Ga atoms. The weighting scheme, $w = 1/\sigma^2(F)$ where $\sigma^2(F)$ is derived from the previously defined $\sigma^2(I)$, gave uniform average values of $w(|F_o| - |F_c|)^2$ over ranges of both $|F_o|$ and $\sin\theta/\lambda$ and was employed in the final stages of refinement. Reflections with $I < 3\sigma(I)$ were not included in the refinement. An isotropic Type I extinction correction (Thornley-Nelmes definition of mosaic anisotropy with a Lorentzian distribution) was applied (15–17). The final value of g was $5.8(5) \times 10^4$. Convergence was reached at $R = 0.034$ and $R_w = 0.037$ for 1746 reflections with $I \geq 3\sigma(I)$. For all 3445 reflections $R = 0.097$. The function minimized was $\Sigma w(|F_o| - |F_c|)^2$, $R = \Sigma||F_o| - |F_c||/\Sigma|F_o|$ and $R_w = (\Sigma w(|F_o| - |F_c|)^2/\Sigma w|F_o|^2)^{1/2}$.

On the final cycle of refinement the mean and maximum parameter shifts corresponded to 0.04 and 0.72σ, respectively. The largest shift was associated with the thermal parameter of H(2c). The mean error in an observation of unit weight was 1.575. A final difference map showed maximum fluctuations of $\pm 0.26(13)$ e Å^{-3}. The final positional and thermal parameters appear in Tables 1 and 5, respectively.[2] Measured and calculated structure factors have been placed in the Depository of Unpublished Data.[2]

The ellipsoids of thermal motion for the non-hydrogen atoms are shown in Fig. 1. The thermal motion has been analysed in terms of the rigid-body modes of translation, libration, and screw motion (18). The rms standard error in the temperature factors σU_{ij} (derived from the least-squares analysis) is 0.0015 Å^2. Analysis of the entire dimer indicated significant independent motion of the "$GaMe_2$" units. Independent analyses were carried out for two molecular fragments, the Ga coordination group and the tropolone moiety (rms $\Delta U_{ij} = 0.0016$ and 0.0017 Å^2, respectively). The appropriate bond distances have been corrected for libration (18, 19), using shape parameters q^2 of 0.08 for all atoms involved. Corrected bond lengths appear in Table 2 along with the uncorreeted values; corrected bond angles do not differ by more than 1σ from the uncorrected values given in Table 3. Intra-annular torsion angles defining the conformation of the tropolone ring are listed in Table 4. Bond lengths and angles involving hydrogen and a complete listing of torsion angles (tables 6–8) are included as supplementary material.[2]

TABLE 1. Final positional (fractional $\times 10^4$, Ga $\times 10^5$, H $\times 10^3$) and isotropic thermal parameters ($U \times 10^3$ Å^2) with estimated standard deviations in parentheses

Atom	x	y	z	U_{eq}/U_{iso}
Ga	32135(3)	42110(3)	42483(3)	50
O(1)	4166(2)	5887(2)	5312(2)	53
O(2)	1561(2)	5226(2)	4432(2)	58
C(1)	2783(6)	4432(7)	2352(4)	82
C(2)	3485(5)	2536(4)	5390(5)	68
C(3)	3374(2)	6789(3)	5624(2)	42
C(4)	1872(2)	6387(3)	5107(2)	45
C(5)	800(3)	7164(3)	5310(3)	54
C(6)	856(4)	8435(4)	5963(3)	60
C(7)	1988(4)	9308(4)	6645(3)	61
C(8)	3378(4)	9100(3)	6840(3)	56
C(9)	3977(3)	7978(3)	6395(3)	50
H(5)	−2(4)	674(4)	497(4)	66(9)
H(6)	1(4)	864(4)	592(3)	64(9)
H(7)	189(4)	1006(5)	704(3)	75(10)
H(8)	408(4)	971(4)	738(3)	60(8)
H(9)	491(3)	800(3)	665(3)	59(9)
H(1a)	316(9)	520(11)	234(10)	186(39)
H(1b)	325(6)	386(6)	202(5)	110(17)
H(1c)	199(10)	460(9)	199(7)	183(35)
H(2a)	283(10)	224(8)	511(10)	146(38)
H(2b)	390(4)	185(5)	517(4)	86(12)
H(2c)	386(5)	274(5)	636(5)	161(16)

*U_{eq} = (1/3)trace (U_{diag}).

TABLE 2. Bond lengths (Å) with estimated standard deviations in parentheses

Bond	Length		Bond	Length	
	Uncorr.	Corr.		Uncorr.	Corr.
Ga —O(1)	1.963(2)	1.972	C(3)—C(4)	1.469(3)	1.478
Ga —O(2)	2.020(2)	2.025	C(3)—C(9)	1.382(4)	1.387
Ga —C(1)	1.943(4)	1.951	C(4)—C(5)	1.405(4)	1.411
Ga —C(2)	1.946(4)	1.954	C(5)—C(6)	1.371(4)	1.375
Ga —O(1)′	2.545(2)	2.551	C(6)—C(7)	1.376(5)	1.382
O(1)—C(3)	1.303(3)	1.308	C(7)—C(8)	1.372(5)	1.377
O(2)—C(4)	1.276(3)	1.279	C(8)—C(9)	1.392(4)	1.397

*Here and elsewhere primed atoms are related to those in Table 1 by inversion through the centre of symmetry at 1/2, 1/2, 1/2.

Results and discussion

The title compound, bis(tropolonatodimethylgallium), represents the second example of a complex having a five-coordinate gallium centre which does not include nitrogen in the pentacoordination sphere about the metal atom (the Ga atom is coordinated to three oxygen and two carbon atoms). As with the salicylaldehydatodimethylgallium dimer, $(SalGaMe_2)_2$, the first such example (3), the present compound is not associated in either the gas phase or in dilute solution. Thus the mass spectrum of the compound gives no signals at m/e values higher than those corresponding to the monomer ion or its ions arising from predictable fragmentation patterns. In dilute benzene solution, molecular weight measurements indicate the monomer species to be present. The ^{1}H nmr pattern in C_6D_6, consisting of a singlet for the "$GaMe_2$" protons and a triplet: triplet:doublet pattern for the protons of the tropolonato moiety, is also consistent with a monomeric species in solution.

The solid state structure consists of well-separated dimeric units in which each five-coordinate Ga atom is in an irregular trigonal bipyramidal environment. Space group symmetry re-

[1]The computer programs used include locally written programs for data processing and locally modified versions of the following: ORFLS, full-matrix least-squares, and ORFFE, function and errors, by W. R. Busing, K. O. Martin and H. A. Levy; FORDAP, Patterson and Fourier syntheses, by A. Zalkin; ORTEP II, illustrations, by C. K. Johnson.

[2]The structure factor table, Table 5 (anisotropic thermal parameters) and other material mentioned in the text are available, at a nominal charge, from the Depository of Unpublished Data, CISTI, National Research Council of Canada, Ottawa, Canada K1A 0S2.

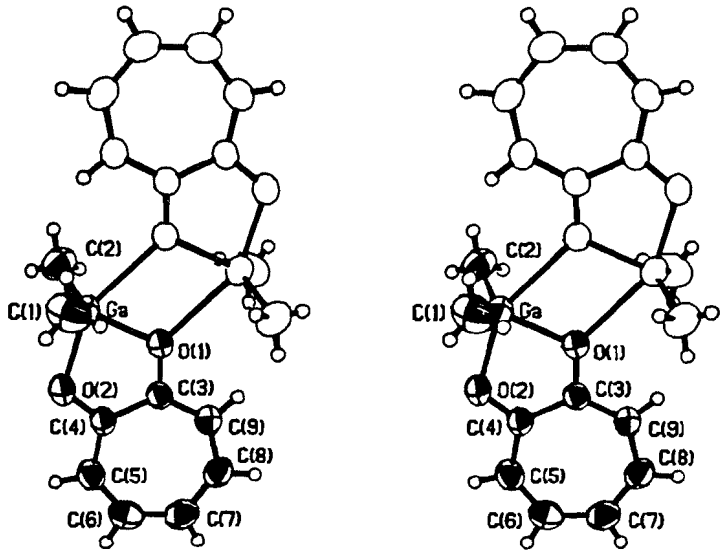

FIG. 1. Stereoscopic view of bis(tropolonatodimethylgallium). 50% probability thermal ellipsoids are shown for the non-hydrogen atoms. Hydrogen atoms have been assigned artificially small thermal parameters for the sake of clarity.

TABLE 3. Bond angles (deg) with estimated standard deviations in parentheses

Bonds	Angle (deg)	Bonds	Angle (deg)
O(1)—Ga —O(2)	79.27(8)	Ga —O(2)—C(4)	114.96(15)
O(1)—Ga —C(1)	113.3(2)	O(1)—C(3)—C(4)	113.9(2)
O(1)—Ga —C(2)	110.38(15)	O(1)—C(3)—C(9)	119.8(2)
O(1)—Ga —O(1)′	70.73(8)	C(4)—C(3)—C(9)	126.3(2)
O(2)—Ga —C(1)	101.6(2)	O(2)—C(4)—C(3)	115.3(2)
O(2)—Ga —C(2)	103.33(15)	O(2)—C(4)—C(5)	119.4(2)
O(2)—Ga —O(1)′	149.99(7)	C(3)—C(4)—C(5)	125.3(2)
C(1)—Ga —C(2)	132.7(2)	C(4)—C(5)—C(6)	130.5(3)
C(1)—Ga —O(1)′	89.5(2)	C(5)—C(6)—C(7)	130.3(3)
C(2)—Ga —O(1)′	88.43(14)	C(6)—C(7)—C(8)	127.6(3)
Ga —O(1)—C(3)	116.6(2)	C(7)—C(8)—C(9)	128.7(3)
Ga —O(1)—Ga′	109.27(8)	C(3)—C(9)—C(8)	131.2(3)
C(3)—O(1)—Ga′	134.10(15)		

TABLE 4. Intra-annular torsion angles (deg) standard deviations in parentheses

Atoms	Torsion angle (deg)
C(9)—C(3)—C(4)—C(5)	0.5(4)
C(3)—C(4)—C(5)—C(6)	2.1(5)
C(4)—C(5)—C(6)—C(7)	−2.0(6)
C(5)—C(6)—C(7)—C(8)	−0.2(6)
C(6)—C(7)—C(8)—C(9)	0.6(6)
C(7)—C(8)—C(9)—C(3)	1.5(6)
C(4)—C(3)—C(9)—C(8)	−2.6(5)

quires each dimer to possess a centre of symmetry. The dimerization occurs via the formation of a four-membered Ga_2O_2 ring in which each oxygen atom occupies an equatorial coordination site of one Ga atom and an axial site of the other. This type of dimerization has been noted for $(SalGaMe_2)_2$ (3), $(Me_2NCH_2CH_2OGaR_2)_2$ (R = H, Me) (5), and $[MeN(CH_2CH_2O)_2GaH]_2$ (6). The terminal tropolonato O atoms occupy the other axial positions while methyl groups complete the equatorial planes. The angle between the axial substituents, 149.99(8)°, is similar to the values of 150−152° found for the "ethanolamine" complexes (5, 6) in which five-membered chelate rings are also fused to the central Ga_2O_2 ring, but considerably smaller than the value of 164.4(1)° in $(SalGaMe_2)_2$ which contains six-membered chelate rings. The Ga atom is displaced by 0.2111(3) Å toward O(2) from the plane of the equatorial substituents. The system of five fused rings is planar to within 0.018(3) Å. The small but significant deviation from planarity arises in the tropolone ring which is significantly nonplanar (χ^2 = 84.6, maximum deviation 0.015(3) Å), the four-membered ring being exactly planar and the five-membered chelate ring being planar within experimental error (χ^2 = 7.5, maximum deviation 0.0035(21) Å).

The Ga—O distances[3] involving the bridging tropolonato O atom (1.972(2) and 2.551(2) Å for the equatorial and axial bonds, respectively) are significantly longer than those observed earlier for related molecules. In $(Me_2NCH_2CH_2OGaR_2)_2$ (R = H, Me) and $[MeN(CH_2CH_2O)_2GaH]_2$ which contain bridging alkoxide groups, the corresponding bond lengths are in the ranges 1.911(3)−1.960(8) Å and 2.018(2)−2.078(3) Å,

[3]Libration-corrected bond lengths (esd's assumed equal to those associated with the uncorrected values) are employed throughout the discussion and are compared with similarly treated distances except in the case of $(Me_2NCH_2CH_2OGaH_2)_2$ (5).

Can. J. Chem. Downloaded from www.nrcresearchpress.com by 210.87.254.105 on 09/06/12
For personal use only.

respectively. The corresponding distances in $(SalGaMe_2)_2$ involving a bridging phenoxide moiety are 1.933(3) and 2.469(3) Å. The axial Ga—O bond to the terminal tropolonato O atom of 2.025(2) Å is similar to those quoted above for the bridging alkoxide groups and significantly shorter than the value of 2.127(3) Å for the aldehyde O atom in $(SalGaMe_2)_2$. A similar trend in B—O bond lengths has been noted for the tetrahedral tropolonato- (20), salicylaldehydato- (21), and aminoethanolatodiarylboron complexes (22–25). These findings are consistent with the known donor properties of these oxygen-containing ligands. The Ga—C distances are in good agreement with those reported earlier (1–6).

The observed geometry of the tropolonate ligand is intermediate between that in tropolone itself (26), in which there is partial localization of the double bonds, and the fully delocalized and symmetric structure such as that observed in the boron complex $(C_7H_5O_2)BPh_2$ (20). The structural inequivalence of the tropolonato oxygen atoms leads to a small alternation of bond lengths in the seven-membered ring (similar to that observed in the structure of $[(C_7H_5O_2)TlPh_2]_2$ (27)), although this can occur in the absence of structural differences as in the case of the square planar complex $(C_7H_5O_2)_2Cu$ (28) in which each ligand is bidentate and chelating. As expected,the two C—O distances differ significantly and both of these values (1.279(3) and 1.308(3) Å) are shorter than the mean C—O distance of 1.313(2) Å in the boron compound, consistent with relatively stronger O—B bonding than O—Ga bonding in these two tropolonate complexes. The shorter C—O bonds in the present structure are balanced by a significant lengthening of the unique C(3)—C(4) bond to 1.478(3) Å from the value of 1.446(2) Å in the boron compound. In tropolone itself, the C—O and unique C—C distances are 1.263(3), 1.333(3), and 1.454(4) Å, respectively. The average C—C distance for the remaining six tropolonato ring bonds is 1.388(13) Å compared to 1.385(26) Å in tropolone and 1.385(5) Å in the diphenylboron chelate. The mean short and long C—C bonds average 1.380(6) and 1.397(15) Å respectively, compared to corresponding values of 1.364(20) and 1.405(10) Å in tropolone (26).

Acknowledgments

We thank the Natural Sciences and Engineering Research Council of Canada for financial support and the University of British Columbia Computing Centre for assistance.

1. K. S. CHONG, S. J. RETTIG, A. STORR, and J. TROTTER. Can. J. Chem. **59**, 94 (1981).
2. K. R. BREAKELL, S. J. RETTIG, A. STORR, and J. TROTTER. Can. J. Chem. **55**, 4174 (1977).
3. S. J. RETTIG, A. STORR, and J. TROTTER. Can. J. Chem. **54**, 1278 (1976).
4. S. J. RETTIG, A. STORR, and J. TROTTER. Can. J. Chem. **53**, 753 (1975).
5. S. J. RETTIG, A. STORR, and J. TROTTER. Can. J. Chem. **53**, 58 (1975).
6. S. J. RETTIG, A. STORR, and J. TROTTER. Can. J. Chem. **52**, 2206 (1974).
7. Chemical and Engineering News. Aug. 31. 1981. p. 9.
8. A. STORR and B. S. THOMAS. Can. J. Chem. **48**, 3667 (1970).
9. D. F. RENDLE, A. STORR, and J. TROTTER. Can. J. Chem. **53**, 2944 (1975).
10. P. COPPENS, L. LEISEROWITZ, and D. RABINOVICH. Acta Crystallogr. **18**, 1035 (1965).
11. W. R. BUSING and H. A. LEVY. Acta Crystallogr. **22**, 457 (1967).
12. D. T. CROMER and J. B. MANN. Acta Crystallogr. Sect. A, **24**, 321 (1968).
13. R. F. STEWART, E. R. DAVIDSON, and W. T. SIMPSON. J. Chem. Phys. **42**, 3175 (1965).
14. D. T. CROMER and D. LIBERMAN. J. Chem. Phys. **53**, 1891 (1970).
15. P. J. BECKER and P. COPPENS. Acta Crystallogr. Sect. A, **30**, 129 (1974); **30**, 148 (1974); **31**, 417 (1975).
16. P. COPPENS and W. C. HAMILTON. Acta Crystallogr. Sect. A, **26**, 71 (1970).
17. F. R. THORNLEY and R. J. NELMES. Acta Crystallogr. Sect. A, **30**, 748 (1974).
18. V. SCHOMAKER and K. N. TRUEBLOOD. Acta Crystallogr. Sect. B, **24**, 63 (1968).
19. D. W. J. CRUICKSHANK. Acta Crystallogr. **9**, 747 (1956); **9**, 754 (1956); **14**, 896 (1961).
20. S. J. RETTIG and J. TROTTER. Can. J. Chem. **60**, 2957 (1982).
21. S. J. RETTIG and J. TROTTER. Can. J. Chem. **54**, 1168 (1976).
22. S. J. RETTIG and J. TROTTER. Can. J. Chem. **51**, 1288 (1973).
23. S. J. RETTIG and J. TROTTER. Acta Crystallogr. Sect. B, **30**, 2139 (1974).
24. S. J. RETTIG and J. TROTTER. Can. J. Chem. **54**, 3130 (1976).
25. S. J. RETTIG and J. TROTTER. Can. J. Chem. **61**, 2334 (1983).
26. H. SHIMANOUCHI and Y. SASADA. Acta Crystallogr. Sect. B, **29**, 81 (1973).
27. R. T. GRIFFIN, K. HENRICK, R. W. MATTHEWS, and M. MCPARTLIN. J. Chem. Soc. Dalton Trans. 1550 (1980).
28. W. M. MACINTYRE, J. M. ROBERTSON, and R. F. ZAHROBSKY. Proc. R. Soc. Sect. A, **269**, 161 (1965).

Can. J. Chem. Downloaded from www.nrcresearchpress.com by 210.87.254.105 on 09/06/12
For personal use only.

Studies of intramolecular Diels–Alder reactions: preparation of methyl spiro[2.4]hepta-4,6-dien-1-yl esters and their internal cycloaddition reactivity

GERARD GALLACHER, ANG SER NG, SAMUEL K. ATTAH-POKU, KAZIMIERZ ANTCZAK, SANDRA J. ALWARD, JOHN F. KINGSTON, AND ALEX G. FALLIS

Department of Chemistry, Memorial University of Newfoundland, St. John's, Nfld., Canada A1B 3X7

Received January 9, 1984

GERARD GALLACHER, ANG SER NG, SAMUEL K. ATTAH-POKU, KAZIMIERZ ANTCZAK, SANDRA J. ALWARD, JOHN F. KINGSTON, and ALEX G. FALLIS. Can. J. Chem. **62**, 1709 (1984).

Different routes to the spiro[2.4]hepta-4,6-dien-1-yl esters **5**, **6**, **7**, **26**, and **28** are described and their intramolecular Diels–Alder reactivity examined. A sidechain oxygen substituent is essential for cyclization although its exact role in the cycloaddition remains obscure. The trienes **5**, **6**, and **28** cyclize to the tetracyclo[5.4.0^{1,7}.0^{4,6}.0^{6,10}]undecenes **9**, **10**, and **30** which are useful synthetic intermediates for the preparation of sesquiterpenes.

GERARD GALLACHER, ANG SER NG, SAMUEL K. ATTAH-POKU, KAZIMIERZ ANTCZAK, SANDRA J. ALWARD, JOHN F. KINGSTON et ALEX G. FALLIS. Can. J. Chem. **62**, 1709 (1984).

On décrit différentes voies d'accès aux esters spiro[2.4]heptadiène-4,6 yles-1 **5**, **6**, **7**, **26** et **28** et on étudie leur réactivité lors de réactions de Diels–Alder intramoléculaires. Un substituant oxygène sur la chaîne latérale est essentiel pour obtenir une cyclisation; toutefois le rôle exact de l'oxygène dans la cycloaddition demeure obscur. Les triènes **5**, **6** et **28** se cyclisent en tétracyclo[5.4.0^{1,7}.0^{4,6}.0^{6,10}] undécènes **9**, **10** et **30** qui sont des intermédiaires utiles pour la préparation de sesquiterpènes.
[Traduit par le journal]

Can. J. Chem. Downloaded from www.nrcresearchpress.com by 210.87.254.40 on 09/06/12
For personal use only.

Introduction

The Diels–Alder reaction occupies a position of prominence in the arsenal of the synthetic organic chemist, as a consequence of its good yields, mild reaction conditions, high stereoselectivity, and predictability. However, several features of the intramolecular reaction are imperfectly understood, and further refinement is required if these cycloadditions are to be used with confidence at key stages of a total synthesis. Nevertheless, the synthetic potential of the intramolecular version of this reaction, in which the diene and dienophile are constrained in the same molecule, is considerable and in recent years has been applied to a variety of synthetic objectives with notable success (for reviews, see ref. 1). When the reacting components are themselves cyclic, and (or) have ring substituents, complex multicyclic arrays (Scheme 1) such as those contained in drugs and natural products can be constructed. Often the syntheses of molecules of this complexity are more difficult and lengthy by other routes.

In order to use these cycloadditions synthetically one must be able to predict the feasibility of the cyclization with various substitution patterns in both the reacting units themselves and the sidechain connecting them. An understanding of how these factors and related structural features influence the rate and stereoselectivity of the reaction is also essential. Recent studies by Boeckman and Ko (2) have shown that a fourfold change in rate is induced by sidechain geminal dimethyl functionality in the preparation of a tetrahydrohydrindan. The rate is also enhanced by conjugation of the dienophile with nitrile rather than ester although, as Roush *et al.* (3) have also found, the steric demands of the dienophile (*E* or *Z*) have little influence on the stereochemistry of the new rings. Sidechain substituents also play a key role in the cyclization of furans and several cases which fail to cyclize have been reported (4). In general, geminal substitution at the second carbon in the chain was required for the cycloaddition to proceed.

Among the diverse structures produced in nature the bridged sesquiterpenes longifolene (5) and sativene (copacamphene) (6) occupy a prominent position. Both have been the object of a variety of synthetic approaches (longifolene syntheses (7*a*) and sativene syntheses (7*b*)) and have served as a challenge for

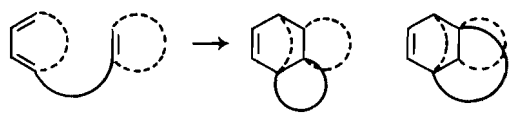

SCHEME 1

SCHEME 2

new synthetic methodology. Recently the interesting marine natural products sinularene (8) and 12-acetoxy sinularene (9) were isolated from soft corals and shown to possess a related bridged bicyclo[2.2.1]heptane skeleton.[1]

In principle these structures could be prepared using an intramolecular Diels–Alder reaction between a cyclopentadiene and an appropriately substituted sidechain. However, as an early approach to longifolene showed (11), the propensity of cyclopentadienes to undergo facile 1,5-sigmatropic rearrangement takes precedence (Scheme 2), and for this strategy to be successful either the rearrangement has to be blocked or the reaction must be conducted under conditions where cycloaddition can compete efficiently with rearrangement (for a successful intermolecular example, see ref. 12). Unfortunately, blocking the sigmatropic reaction is not necessarily straightforward since it has been found (13)[2] that even chlorine

[1] While this work was in progress two syntheses of sinularene were reported (10) and, since acceptance of this manuscript, 12-acetoxy-sinularene has also been prepared (26).

[2] In related studies we are examining the migratory aptitudes of 5-seleno and 5-thiocyclopentadienes in order to use these compounds and the stabilized anions derived from them for a variety of synthetic objectives. As we have pointed out elsewhere (25), an alternative solution employs a "brexane" intermediate followed by a ring expansion. This approach has been used by Snowden in a synthesis of sativene (see 7*b*).

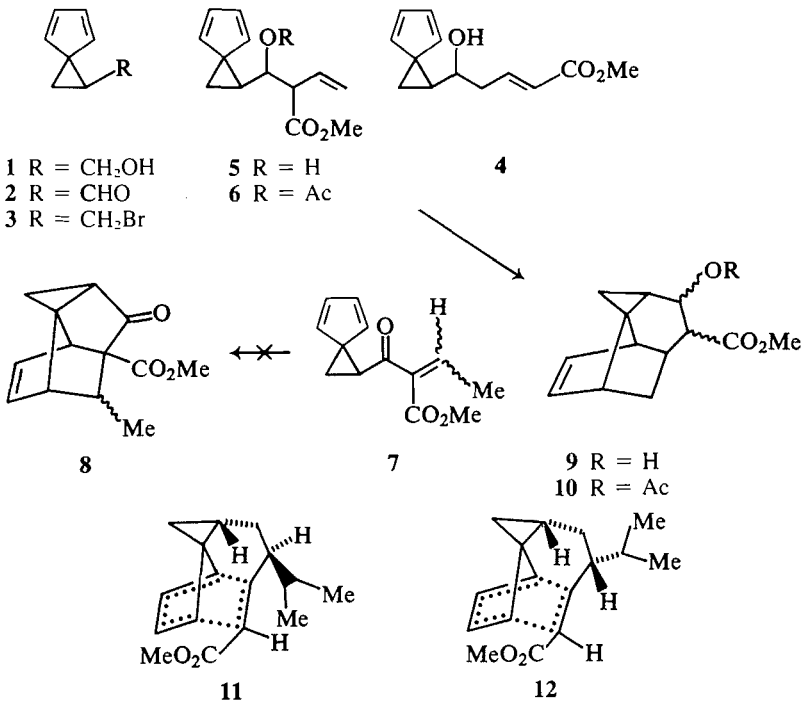

migrates prior to cyclization in a related cyclopentadiene. Synthesis of a suitable spiro[2.4]heptadiene of type **A** should permit formation of the tetracyclic compound(s) **B** (described herein), since the sigmatropic rearrangement is blocked by the cyclopropane moiety, and with the appropriate substitution pattern controlled cyclopropane ring opening (hydrogenolysis, solvolysis, dissolving metal reductions, Lewis acid catalysis, etc.) should provide a general entry into the desired tricyclo[4.4.$0^{1,6}$.$0^{5,9}$]decane and tricyclo[5.4.$0^{1,7}$.$0^{6,10}$]undecane ring systems (Scheme 3) (see following paper).

Results and discussion

In order to bring these ideas to fruition, and as initial efforts to add diazocyclopentadiene to suitable olefins were not encouraging, the spiro-alcohol **1** was prepared from sodium cyclopentadiene and epichlorohydrin according to the procedure of Bangert and Boekelheide (14) and oxidized with active MnO_2 to the aldehyde **2** (83%). This aldehyde was rather unstable but could be briefly stored in solution at −20°C. In its ^{1}H nmr spectrum the aldehydic hydrogen appeared as a doublet, J = 5 Hz at δ 9.30, coupled to the tertiary cyclopropyl proton which gave rise to a complex multiplet at δ 2.87. The Grignard reagent derived from bromomethyl crotonate was next added to the aldehyde. In order to minimize self condensation the aldehyde was added dropwise during Grignard formation and the product could be isolated in 63% yield after chromatography. Crotyl Grignard reagents frequently afford a mixture of α- and γ-substitution products (15). In this instance a single regiochemical isomer was obtained. Vinyl groups usually display a characteristic ABC pattern in their ^{1}H nmr spectra at approximately δ 5 ppm. Although the appearance in this case was atypical (complex overlapping multiplet), the chemical shift was in the correct range, suggesting the structure was **5** rather than **4**.[3] Oxidation of **5** in dimethylsulfoxide containing di-

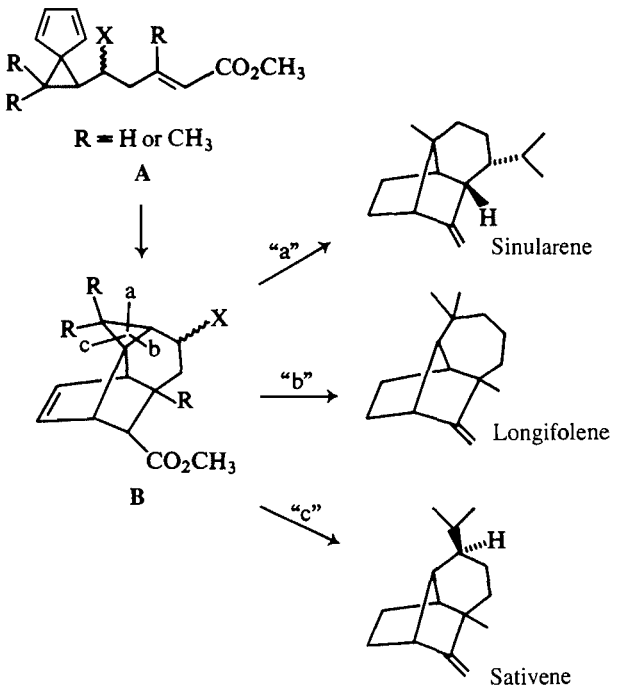

SCHEME 3

cyclohexyldicarbodiimide and trifluoroacetic acid provided a new ketone **7** whose spectral features were consistent with a conjugated system and confirmed the assignment of structure **5** to the triene. The ^{1}H nmr spectrum of **7** contained two overlapping vinyl methyl doublets at δ 1.82 and 1.89, J = 9 Hz, indicating, as did the methoxyl resonances at 3.64 and 3.70, that an ~1:1 mixture of E and Z isomers was present. The β-olefinic proton multiplet was shifted to low field 6.83, as expected for hydrogens on a conjugated double bond. Molecular models suggested that internal cyclization of this triene would be difficult in view of the contiguous sp^2 hybridized centres in the sidechain and the limited rotational freedom this

[3] Please note that this assignment differs from our preliminary communication and that the substituents were attached incorrectly to C_{11} rather than C_2 of the adducts (16).

Can. J. Chem. Downloaded from www.nrcresearchpress.com by 210.87.254.40 on 09/06/12
For personal use only.

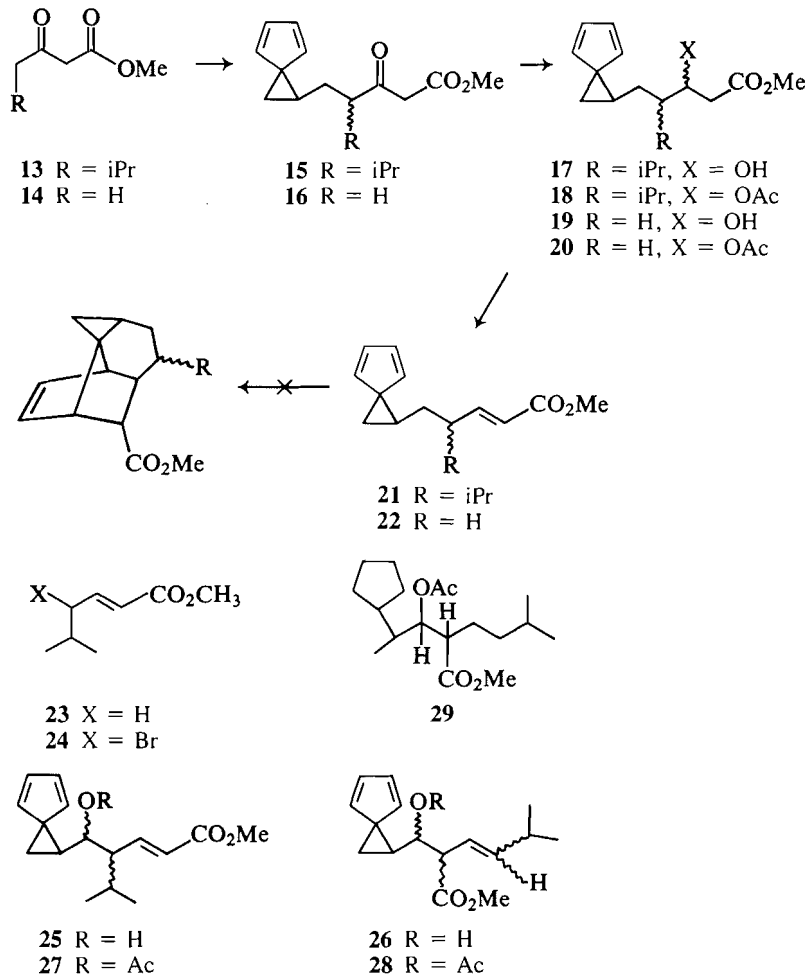

Can. J. Chem. Downloaded from www.nrcresearchpress.com by 210.87.254.40 on 09/06/12
For personal use only.

imparts. This was confirmed experimentally. In contrast, the hydroxy-triene **5** underwent intramolecular cycloaddition (53%, 60% based on reacted triene) at 180°C in refluxing *p*-dichlorobenzene or, alternatively, in a sealed tube in toluene. This demonstrated the feasibility of this approach to the natural products but clearly a different substitution pattern was required.

In order to provide a direct route to sinularene it seemed appropriate to carry the isopropyl function in the sidechain. It appeared that this would introduce the interesting possiblity of controlling the stereochemistry of the isopropyl substituent as a consequence of steric interactions in the Diels–Alder transition state. It can be seen that the non-bonded interactions between the developing *exo* hydrogen and the isopropyl substituent are reduced in **12** compared to **11** and should clearly favour preferential cyclization to the required stereoisomer, although interaction between the bridgehead hydrogen and the isopropyl group in **12** may partially counteract this effect.

In order to test this possibility the desired triene ester **21** was synthesized in the following manner. Treatment of alcohol **1** with triphenylphosphine dibromide in acetonitrile afforded (73%) bromide **3** which was added to the dianion derived from methyl 5-methyl-3-oxo hexanoate (**13**) (17) to give the keto-ester **15**. Selective reduction of the ketone was achieved with sodium borohydride (70%) and the alcohol **17** converted to its acetate **18** under standard conditions with acetic anhydride in pyridine (88%). Direct dehydration of the alcohol with phosphorus oxychloride gave a mixture of α,β and β,γ unsaturated esters, a difficulty which was avoided when the diester **18** was treated with potassium *tert*-butoxide at room temperature for 50 min (18) to afford the triene **21** (82%). Unfortunately no conditions, thermal or Lewis acid catalysis, could be found to effect cyclization of **21** without decomposition of the sensitive spirocyclopentadiene moiety. In order to be certain a small amount of cyclized material was not overlooked, the diastereomers were separated by flash chromatography and studied individually, but cycloaddition did not occur.

In view of the fact that triene **5** cyclizes while **21** does not, it appears that both diastereomers of **21** experience adverse steric crowding during the attempted cycloaddition. Thus removal of the isopropyl substituent should facilitate cyclization. In an effort to learn more about these conformational effects, the unsubstituted triene **22** was synthesized by alkylation of the dianion of methyl acetoacetate with bromide **3** to give **16**. The double bond was introduced by reduction to the alcohol **19** followed by acetylation and elimination by the same procedure as utilized above. To our amazement, and disappointment, **22** showed no inclination to cyclize and after 65 h at 195°C in a sealed tube in toluene was recovered unchanged. The double bond is clearly conjugated since the dienophilic protons for **22** appear as separate signals, the β proton as a multiplet centred at δ 6.75, the α proton as a distorted doublet of triplets centred at δ 5.6.

Why does **5** undergo the desired cyclization while **21** and **22** do not? It appears that the alcohol **5** prefers a conformation in which the dienophile is folded underneath the cyclopentadiene

Can. J. Chem. Downloaded from www.nrcresearchpress.com by 210.87.254.40 on 09/06/12
For personal use only.

ring in an alignment which approximates that required for cycloaddition. Partial support for this contention is provided by the ^{1}H nmr spectrum of **5**, referred to above, in which the standard vinyl pattern appears to be affected by its proximity to the cyclopentadiene system. The hydroxyl function clearly exerts a beneficial influence but intramolecular hydrogen bonding with the ester cannot be the dominant factor since when the acetate **6**, prepared from **5**, was heated (175°C, 45 h, toluene, 66%), cyclization occurred even though the opportunity for hydrogen bonding was absent. This cycloaddition also proceeded readily under catalytic conditions with aluminum chloride at 23°C in dichloromethane for 3 h (75%).

Stereochemical influences of a similar type have been observed previously. For example, in the synthesis of patchouli alcohol it was found (19) that only one diastereomer of 1-(3-methyl-4-penten-1-yl)-2,6-trimethyl-2,5-cyclohexadien-1-ol would undergo an intramolecular Diels–Alder reaction and neither of them would cyclize unless a little potassium *tert*-butoxide was added! Unfortunately we have not uncovered a similar trick, and scrutiny of molecular models does not provide a reliable predictive guide to the relative ease of cyclization. In the above cases the approach of the reactive centres within the required 2.2 Å distance (20) seems readily achievable, but subtle conformational barriers intervene. Apparently the hydroxyl or acetoxy substituent holds the molecule in a folded conformation which either relieves a non-bonded interaction, although this is difficult to discern from models, or more likely the oxygen lone pair exerts a subtle but beneficial stereoelectronic effect of the barrier to cyclization is lowered and cycloaddition occurs before decomposition of the sensitive spiro-cyclopentadiene moiety. If this analysis is correct, then trienes such as **25** or **26** which contain the requisite sidechain hydroxyl function should exist preferentially in a folded conformation and undergo intramolecular cyclization. This has been shown to be the case for **26** and **28**.

Condensation of isovaleraldehyde with methyl (triphenylphosphoranylidene)acetate provided the unsaturated ester **23** (93%), which upon treatment with *N*-bromosuccinimide in refluxing carbon tetrachloride gave the allylic bromide **24** (80%). Grignard addition as outlined above with aldehyde **2** afforded a new triene. Generally bulky crotyl reagents and a sterically hindered carbonyl group favour the formation of the γ-substitution product. However, the ^{1}H nmr spectrum of this material contained no signals below the multiplets for the cyclopentadiene hydrogens, suggesting the product possessed structure **26**. This was confirmed by reducing the corresponding acetate **28** (H_2, 10% Pd/C, 2.5 atm., methanol) to the saturated ester **29**. Proton decoupling experiments established that the protons on the acetate and ester-bearing carbons were coupled to each other, a situation which could not have arisen from structure **27**. Additional support was provided in the 400-MHz spectrum of the triene acetate **28** obtained at the University of Alberta which revealed that the tertiary-isopropyl hydrogen was coupled to the neighbouring olefinic protons.

This condensation introduces two new chiral centres into the aldehyde **2** which is itself racemic. As illustrated for the *S*-aldehyde (Scheme 4), the Grignard can approach the carbonyl group from either the top or bottom face (shown) and in principle the ester function may be either *syn* or *anti* to the aldehydic hydrogen. It was anticipated that the Grignard reagent would be oriented on the same side as this hydrogen, partly because of the gorup's steric bulk, and, equally important, because the delocalized π system of the Grignard reagent

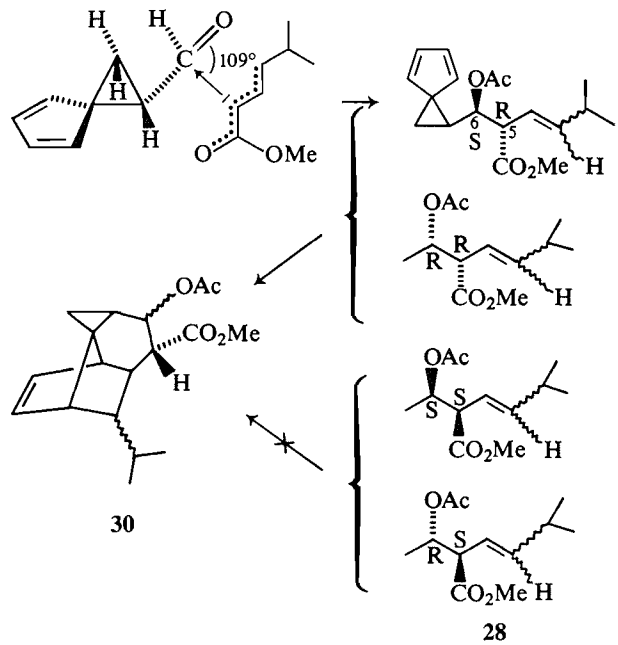

SCHEME 4

would likely align itself preferentially with the π system of the diene. Attack from the bottom thus generates the $C_6(S)C_5(R)$ triene whereas a topside approach will give the $C_6(R)C_5(R)$ diastereomer. Experimentally the coupled product was separated by flash chromatography into four diastereomers (~1:1:6:6), although the *E* and *Z* olefins could not be resolved. The major components, comprising 84% of the product, were assumed to be the C_6C_5 *SR* and *RR* isomers. The minor diastereomers refused to cyclize and direct cyclization (180°C, 24 h, *p*-dichlorobenzene, ~10%) of the major trienes was accompanied by extensive decomposition. However, the acetates **28** were more stable and cyclized cleanly (180°C, 24 h, 89% based on cyclized **28**) to the requisite tetracyclic diesters **30**. The formation of these adducts confirms the conclusions implied above since the fact that the minor *R,S* and *S,S* trienes failed to cyclize suggests that non-bonded interactions of the type depicted in **11** do play a dominant role.

The acetate cycloadditions (**28**, *R,R*; *S,R*) may also be catalyzed with $AlCl_3$ (1.1 equiv., 23°C, CH_2Cl_2 25%) under mild conditions, although polymerization competes. These results add to the growing list of intramolecular Diels–Alder reactions which may be catalyzed with Lewis acids (21), although unfortunately in all cases examined other catalysts ($EtAlCl_2$, $SnCl_4$, $FeCl_3$, $BF_3 \cdot Et_2O$, −78° to 23°C) promoted decomposition rather than cyclization. It should be noted that, for **28** and example **6** above, these cycloadditions differ from the normal situation in which the Lewis acid alters the electron density of the double bond by coordination with the dienophile. Instead, complexation with the oxygen and ester sidechain functionality resulted in a beneficial conformational bias which facilitated cyclization.

In conclusion, a C_5-oxygen substituent is essential for successful cyclization of these trienes, although further work is required to ascertain the exact origin of this effect, and whether an ester substituent plus both cyclopropane and diene units are essential. However, orbital proximity effects in rigid systems are well documented (22) and through space interactions of oxygen lone pair orbitals are known to influence conformer populations (23). These concepts are being applied to the syn-

Can. J. Chem. Downloaded from www.nrcresearchpress.com by 210.87.254.40 on 09/06/12
For personal use only.

thesis of sinularene and are currently being extended to an asymmetric synthesis of (+)-longifolene, commencing with ascorbic acid, utilizing the synthetically useful way we have developed of blocking the 1,5-sigmatropic rearrangement of cyclopentadienes, and taking advantage of the conditions described under which hydroxyl-bearing trienes undergo cycloaddition.

Experimental

Melting points were determined in capillary tubes with a Thomas–Hoover Uni-Melt apparatus or a Fischer–John's melting point apparatus and are uncorrected. Infrared spectra were recorded on a Perkin–Elmer 237B or 451 grating spectrophotometer, and were calibrated with the 2850 and 1601 cm^{-1} bands of polystyrene film. Ultraviolet spectra were recorded on a Perkin–Elmer 202 uv–visible spectrophotometer and were calibrated with the 279.4-nm band of a Holmium oxide filter. Proton magnetic resonance spectra were measured at 80 MHz with a Bruker model WP80 spectrometer employing a chloroform lock or at 60 MHz qith a Varian model EM-360 spectrometer. Signal positions are reported in ppm downfield from tetramethylsilane (δ scale) as an internal standard, the number of protons, multiplicity, coupling constants, and proton assignments are indicated in parentheses. Mass spectra were determined on a V.G. Micromass 7070 HS instrument using an ionization energy of 70 eV. Gas–liquid chromatograph analyses were conducted on a Hewlett Packard 402B gas chromatograph equipped with a column (3 m × 6 mm id) containing 1.5% OV-17 supported on Gas Chrom Q using helium as the carrier gas. Thin-layer chromatographic analyses were carried out on commercial precoated silica gel plates with fluorescent indicator (Eastman Kodak silica gel 13181). Preparative thin-layer chromatography was conducted on 20 × 20 cm glass plates coated with silica gel $PF_{254+366}$ type 60 (E. Merck). Flash chromatography used BDH silica gel Kieselgel 60, 230–400 mesh (24).

Solutions in organic solvents were dried over anhydrous magnesium sulphate and stripped of solvent with a Büchi rotary evaporator connected to a water aspirator. Unless otherwise indicated, all reactions were conducted under argon.

1-Carboxaldehydespiro[2.4]hepta-4,6-diene (2)

The spiro-alcohol **1** (12) (2 g, 18 mmol) was dissolved in dichloromethane (25 mL) – chloroform (50 mL) and freshly prepared active MnO_2 (30 g) added. The mixture was stirred under reflux for 12 h, cooled to room temperature, and diluted with ether (100 mL). The mixture was stirred for a further 15 min, filtered, the solid washed thoroughly with ether (250 mL), and the combined filtrate concentrated to afford the aldehyde **2** (1.8 g, 83%) as a pale yellow liquid: ir (KBr): 2825 (H—CO), 2720 (H—CO), 1704 (C=O) cm^{-1}; ^1H nmr (CCl_4) δ: 2.17 (2H, m, cyclopropyl H), 2.87 (1H, m, cyclopropyl H), 5.95 (1H, m, cyclopentadienyl H, C-4), 6.28 (1H, m, cyclopentadienyl H, C-7), 6.47 (2H, m, cyclopentadienyl H), 9.30 (1H, d, J = 5 Hz, H—CO).

The aldehyde was further characterized as its semicarbazone, mp 168–169°C (methanol–water). *Anal.* calcd. for $C_9H_{11}N_3O$: C 61.00, H 6.26, N 23.71; found: C 61.01, H 6.57, N 23.74.

1-Bromomethylspiro[2.4]hepta-4,6-diene (3)

Triphenylphosphine dibromide was prepared from triphenylphosphine (6.82 g, 26 mmol) suspended in dry acetonitrile (100 mL), stirred magnetically in a 250-mL round bottomed flask which was cooled in an ice bath during the dropwise addition of bromine (1.28 mL, 25 mmol). Pyridine (2.0 mL, 25 mmol) was added to the stirred white suspension, followed by the alcohol **1** (3.0 g, 24.6 mmol) to give a clear light yellow solution. Stirring was continued for a further 10 min at 0°C after addition was complete, and the solvent removed under reduced pressure. The dark orange residue so obtained was triturated with petroleum ether (3 × 100 mL), concentrated, and set at −20°C to precipitate triphenylphosphine oxide. Rapid column chromatography (sintered glass funnel packed with silica gel and elution with petroleum ether under water aspirator suction) afforded the bromide **3** (3.7 g, 81%); ^1H nmr (CCl_4) δ: 1.5–2.0 (2H, m, cyclopropyl H), 1.41 (1H, m, cyclopropyl H), 3.40 (2H, m, —CH_2—Br), 5.91 (2H, m, cyclopentadienyl H), 6.44 (2H, m, cyclopentadienyl H).

3-Carbomethoxy-4-hydroxy-4-(spiro[2.4]hepta-4,6-dien-1-yl)butene (5)

Magnesium (6 g, 247 mmol) was added to dry THF (300 mL) in a three-necked 1-L flask equipped with a paddle stirrer. Methyl 4-bromocrotonate (19.1 g, 107 mmol, Aldrich) in THF (100 mL) was added in small portions until the Grignard commenced, after which the remaining bromide and aldehyde **2** (8.7 g, 72.5 mmol) were added dropwise simultaneously. Once the vigorous reaction had subsided, the reaction was stirred for a further 2 h at room temperature and poured into saturated aqueous NH_4Cl solution (200 mL). After ether extraction (3 × 100 mL), the combined extracts were dried, concentrated, and purified by flash chromatography (20% ethyl acetate/petroleum ether). This initially afforded 3.8 g of product and rechromatography of the impure fractions yielded an additional 4.6 and 1.5 g for a total of 9.9 g (63%) of the triene alcohol **5**; uv (CH_3OH): 198 (ε = 6500), 224 (ε = 7500), 258 sh (ε = 2300) nm; ir (film): 3470 (br, OH), 1730 (C=O), 1643 (C=C) cm^{-1}; ^1H nmr (CCl_4) δ: 1.6–2.3 (3H, m, cyclopropyl H), 2.7–3.2 (1H, m, CH—C=), 3.63 (3H, s, OCH_3), 3.70 (1H, m, H—C—OH), 4.6–5.5 (3H, m, CH=CH_2), 5.88 (1H, m, cyclopentadienyl H), 6.28 (3H, m, cyclopentadienyl H). *Exact Mass* calcd. for $C_{13}H_{16}O_3$: 220.1099; found: 220.1101.

3-Carbomethoxy-4-(spiro[2.4]hepta-4,6-dien-1-yl)-2-buten-4-one (7)

The alcohol **5** (152 mg, 0.69 mmol) was dissolved in anhydrous DMSO (1.2 mL) and benzene (2.4 mL) contaning dicyclohexyldicarbodiimide (434 mg, 2.1 mmol, Aldrich) and pyridine (57 mg, 0.71 mmol). Trifluoroacetic acid (49 mg, 0.43 mmol) was added to the stirred solution and stirring was continued for 19 h at 22°C. Dicyclohexylurea was precipitated by the addition of ethyl acetate (10 mL), the mixture filtered, the residue washed with ethyl acetate, the combined filtrates washed with water (4 × 3 mL), dried over potassium carbonate, filtered, and concentrated. The residual brown oil was purified by tlc ($CHCl_3$) to give the keto-ester **7** as a yellow oil, 80 mg (53%); ir ($CHCl_3$): 1720 (C=O), 1685 (sh, C=O) cm^{-1}; ^1H nmr ($CDCl_3$) δ: 1.82, 1.89 (3H, d, J = 9 Hz, =$CHCH_3$), 2.50 (1H, m, cyclopropyl H), 3.23 (1H, t, J = 7 Hz, cyclopropyl H by C=O), 3.64, 3.70 (3H, s, OCH_3), 5.95 (2H, m, cyclopentadienyl H), 6.35 (2H, m, cyclopentadienyl H), 6.83 (1H, m, J = 9 Hz, HMeC=).

3-Carbomethoxy-4-acetoxy-4-(spiro[2.4]hepta-4,6-dien-1-yl)butene (6)

The alcohol **5** (265 mg, 1.2 mmol) was dissolved in pyridine (5 mL) cooled to 0°C in an ice bath and acetic anhydride (2 mL) added. The reaction was stirred at room temperature for 15 h and poured onto ice/water. The aqueous solution was extracted with ether (2 × 50 mL), the combined extract washed with 3 *M* HCl, saturated aqueous sodium bicarbonate solution, brine, and dried. Purification by preparative tlc on silica gel (20% ethyl acetate/petroleum ether) gave the acetate **6** (255 mg, 82%); ir (film): 1745 (C=O), 1645 (C=C) cm^{-1}; ^1H nmr (CCl_4) δ: 1.3–2.3 (3H, m, cyclopropyl H), 1.95 (3H, s, CH_3—CO), 2.86 (1H, dd, J = 4, 9 Hz, HC—C=), 3.50, 3.53 (3H, s, OCH_3), 4.65 (1H, m, H—C—OAc), 4.8–5.6 (3H, m, CH=CH_2), 5.79 (1H, m, cyclopentadienyl H), 6.21 (3H, m, cyclopentadienyl H). *Exact Mass* calcd. for $C_{15}H_{18}O_4$: 262.1205; found: 262.1207.

2-Carbomethoxytetracyclo[5.4.0^{1,7}.0^{4,6}.0^{6,10}]undec-8-en-3-ol (9)

The triene alcohol **5** (3.8 g, 17.6 mmol) was placed in a 250-mL round bottom flask and solid *para*-dichlorobenzene (approximately 200 g) and boiling stones added. The reaction mixture was refluxed for 6 h and the solvent removed under reduced pressure. Flash chromatography (30% ethyl acetate/petroleum ether) of the remaining oil afforded 0.45 g of recovered triene and the tetracyclic alcohol **9** (2.0

Can. J. Chem. Downloaded from www.nrcresearchpress.com by 210.87.254.40 on 09/06/12
For personal use only.

g, 60% based on reacted triene). Smaller scale runs were conducted in sealed tubes in toluene at 175°C for 5 h but yields were usually lower, 35–40%; ir (film): 3415 (br, OH), 1730 (C=O) cm^{-1}; ^1H nmr (CCl_4) δ: 0.49 (1H, m, cyclopropyl H), 1.0 (2H, m, cyclopropyl H), 1.6–2.0 (3H, m), 2.28 (2H, br s, bridgehead H), 2.71 (1H, d, J = 8.5 Hz, H—CCO_2CH_3), 3.50 (1H, m, H—C—OH), 3.61 (3H, s, OCH_3), 5.79 (1H, m, cyclopentadienyl H), 6.02 (1H, m, cyclopentadienyl H). *Exact Mass* calcd. for $C_{13}H_{16}O_3$: 220.1099; found: 220.1098.

*3-Acetoxy-2-carbomethoxytetracyclo[5.4.0^{1,7}.0^{4,6}.0^{6,10}]undec-8-ene (**10**)*

The triene acetate **6** (200 mg, 0.78 mmol) was dissolved in toluene (10 mL) flushed with argon and heated in a sealed tube at 175°C for 4.5 h. After the removal of the solvent under reduced pressure the product was purified by tlc (twice) (10% ethyl acetate/petroleum ether) to give 55 mg of recovered starting material and the tetracyclic acetate **10** (95 mg, 66% based on reacted triene); ir (film): 1740 (esters) cm^{-1}; ^1H nmr ($CDCl_3$) δ: 0.39 (1H, m, cyclopropyl H), 1.18 (2H, complex, cyclopropyl H), 1.65 (2H, m, cyclohexyl H), 1.78 (1H, m), 2.01 (3H, s, $COCH_3$), 2.39 (2H, m, bridgehead H), 2.82 (1H, d, J = 8 Hz, H—C—CO_2CH_3), 3.64 (3H, s, OCH_3), 4.57 (1H, J = 7 Hz, H—C—OAc), 5.89 (1H, br m, cyclopentadienyl H), 6.15 (1H, br m, cyclopentadienyl H).

Cyclization proceeded in 75% yield in dichloromethane at 22°C (3 h) in the presence of $AlCl_3$ (1.2 equiv).

*Methyl 4-isopropyl-5-(spiro[2.4]hepta-4,6-dien-1-yl)-3-oxopentanoate (**15**)*

Methyl 5-methyl-3-oxohexanoate (**13**) (prepared from methyl acetoacetate and 2-iodopropane (17)) (1.4 g, 8.4 mmol) was added dropwise to a THF (25 mL) suspension of sodium hydride (598 mg, 60%) maintained at 0°C contained in a serum capped 100-mL flask equipped with pressure equalizing dropping funnel and magnetic stirring bar. After 10 min further stirring a hexane solution of *n*-butyllithium (6.5 mL, 14 mmol) was added dropwise creating a yellow–orange solution which was stirred at 0°C for a further 10 min. The bromide **3** (2.6 g, 14 mmol) dissolved in THF (5 mL) was added dropwise causing the colour of the dianion to fade and the reaction was slowly allowed to warm to room temperature (0.5 h). The reaction was cooled to 0°C, quenched with 3 *M* HCl (15 mL), ether (50 mL) added, and the reaction mixture poured into water/ether (1:1, 50 mL) and extracted with ether (2 × 50 mL). The combined extracts were washed with pH 7 buffer (3 × 20 mL), dried, and purified by flash chromatography (7.5% ethyl acetate/petroleum ether) to afford the keto-ester **15** (850 mg, 36%); ir (film): 1750 (CO_2CH_3), 1713 (C=O) cm^{-1}; ^1H nmr (CCl_4) δ: 0.93 (6H, overlapping singlets, $(CH_3)_2C$), 1.1–2.3 (7H, complex), 3.18, 3.29 (2H, s, OC—CH_2CO; 4.59, 4.87, s, enol H), 3.63, 3.69 (3H, s, OCH_3), 5.98 (2H, m, cyclopentadienyl H), 6.35 (2H, m, cyclopentadienyl H). *Exact Mass* calcd. for $C_{16}H_{22}O_3$: 262.1569; found: 262.1570.

*Methyl 5-(spiro[2.4]hepta-4,6-dien-1-yl)-3-oxopentanoate (**16**)*

Following the procedure outlined above, methyl acetoacetate (**14**) (4.6 g, 40 mmol, Eastman) was converted to its dianion and alkylated with the bromide **3** (3.7 g, 20 mmol) to give, after work-up and flash chromatography (15% ethyl acetate/petroleum ether), the keto-ester **16** (1.90 g, 43%); ir (film): 1748 (CO_2CH_3), 1718 (C=O) cm^{-1}; ^1H nmr (CCl_4) δ: 1.15–2.55 (7H, complex m), 3.19 (2H, s, OC—CH_2—CO), 3.59 (3H, s, OCH_3), 5.85 (1H, m, cyclopentadienyl H), 6.05 (1H, m, cyclopentadienyl H), 6.30 (2H, m, cyclopentadienyl H). *Exact Mass* calcd. for $C_{13}H_{16}O_3$: 220.1099; found: 220.1095.

*Methyl 4-isopropyl-3-hydroxy-5-(spiro[2.4]hepta-4,6-dien-1-yl)-pentanoate (**17**)*

The keto-ester **15** (2.09 g, 7.8 mmol) was dissolved in methanol (35 mL) and, after cooling to −40°C (CCl_4/solid CO_2 bath), sodium borohydride (300 mg) was added. The reaction was stirred at this temperature for 2 h and brine (25 mL) and water (25 mL) added. The solution was extracted with ether (4 × 40 mL), washed with brine, dried, and the alcohol-ester **17** obtained after flash chromatography (75% ethyl acetate/petroleum ether) (1.45 g, 70%); ir (film): 3500 (br, OH), 1735 (C=O) cm^{-1}; ^1H nmr (CCl_4) δ: 0.90 (6H, d, J = 6 Hz, $(CH_3)_2$—), 1.1–2.1 (7H, complex), 2.33 (2H, dm, J = 6 Hz, CH_2—CO), 2.77 (1H, br s, OH), 3.61 (3H, s, OCH_3), 3.95 (1H, br m, H—C—OH), 5.88 (1H, m, cyclopentadienyl H), 6.20 (3H, complex m, cyclopentadienyl H). *Exact Mass* calcd. for $C_{16}H_{24}O_3$: 264.1725; found: 264.1718.

In addition 0.45 g (22%) of a single diastereomer of the starting keto-ester **15** was separated, which was reduced separately and converted to the triene **21**.

*Methyl 3-hydroxyl-5-(spiro[2.4]hepta-4,6-dien-1-yl)pentanoate (**19**)*

The keto-ester **16** (1.9 g, 8.6 mmol) was reduced at −40°C using the procedure outlined above to afford, after flash chromatography (30% ethyl acetate/petroleum ether) the alcohol **19** (1.58 g, 83%); ir (film): 3425 (br OH), 1740 (C=O) cm^{-1}; ^1H nmr (CCl_4) δ: 1.2–2.0 (7H, complex), 2.20 (2H, br d, J = 6.5 Hz, CH_2—CO), 2.79 (1H, br s, OH), 3.61 (3H, s, OCH_3), 3.82 (1H, br m, H—C—OH), 5.85 (1H, dt, J = 5, 2 Hz, cyclopentadienyl H), 6–6.45 (3H, complex m, cyclopentadienyl H). *Exact Mass* calcd. for $C_{13}H_{18}O_3$: 222.1256; found: 222.1250.

*Methyl 4-isopropyl-3-acetoxy-5-(spiro[2.4]hepta-4,6-dien-1-yl)-pentanoate (**18**)*

Acetylation of the alcohol **17** (1.2 g, 4.5 mmol) was conducted with acetic anhydride – pyridine as outlined above to afford the diester **18** (1.22 g, 89%) after flash chromatography (15% ethyl acetate/petroleum ether); ir (film): 1747 (C=O) cm^{-1}; ^1H nmr (CCl_4) δ: 0.94 (6H, d, J = 6 Hz, $(CH_3)_2$—), 1.1–2.2 (7H, complex), 1.93 (3H, s, CH_3CO), 2.41 (2H, d, J = 6 Hz, CH_2—CO), 3.56 (3H, s, OCH_3), 5.17 (1H, br m, H—C—OAc), 5.99 (2H, m, cyclopentadienyl H), 6.29 (2H, m, cyclopentadienyl H). *Exact Mass* calcd. for $C_{18}H_{26}O_4$: 306.1830; found: 306.1842.

*Methyl 3-acetoxy-5-(spiro[2.4]hepta-4,6-dien-1-yl)pentanoate (**20**)*

Acetylation of the alcohol **19** (500 mg, 2.3 mmol) was conducted with acetic anhydride – pyridine as outlined above to give the diester **20** (560 mg, 94%) after flash chromatography (15% ethyl acetate/petroleum ether); ir (film): 1745 (C=O) cm^{-1}; ^1H nmr (CCl_4) δ: 1.1–2.0 (7H, complex), 1.92 (3H, s, CH_3—CO), 2.40 (2H, d, J = 6 Hz, CH_2—CO), 3.57 (3H, s, OCH_3), 5.96 (1H, m, H—C—OAc), 5.85 (1H, m, cyclopentadienyl H), 6.00 (1H, m, cyclopentadienyl H), 6.30 (2H, m, cyclopentadienyl H). *Exact Mass* calcd. for $C_{15}H_{20}O_4$: 264.1362; found: 264.1358.

*Methyl 4-isopropyl-5-(spiro[2.4]hepta-4,6-dien-1-yl)pentanoate (**21**)*

The acetate **18** (600 mg, 1.7 mmol) was dissolved in dry *tert*-butyl alcohol (2 mL). A freshly prepared 1 *M* solution of potassium *tert*-butoxide in *tert*-butyl alcohol (0.95 mL) was added dropwise to the stirred solution. After 1 h at room temperature the reaction was poured onto ice/water (30 mL), extracted with ether (2 × 50 mL), the combined extracts washed with water until neutral, dried, and purified by flash chromatography (7.5% ethyl acetate/petroleum ether) to give the triene **21** (335 mg, 82%); ir (film): 1727 (C=O), 1659 (C=C) cm^{-1}; ^1H nmr (CCl_4) δ: 0.86 (6H, d, J = 6.5 Hz, $(CH_3)_2C$), 1.0–2.2 (7H, br complex m), 3.58 (3H, s, OCH_3), 5.49 (1H, dd, J = 15, 8 Hz, C=CH—CO), 5.7–6.4 (4H, m, cyclopentadienyl H), 6.55 (1H, dd, J = 15, 8 Hz, CH=C—CO). In cyclization attempts the triene **21** decomposed above 215°C, and at room temperature in the presence of Lewis acids, while 65 h in xylene in a sealed tube at 200°C produced no cyclized product.

*Methyl 5-(spiro[2.4]hepta-4,6-dien-1-yl)pentanoate (**22**)*

Utilizing the analogous basic elimination procedure outlined above the acetate **20** was converted to the triene **22**. This triene **22** was recovered unchanged after 65 h at 195°C in a sealed tube in toluene; ir (film): 1727 (C=O), 1662 (C=C) cm^{-1}; ^1H nmr (CCl_4) δ: 1.25–2.4 (7H, complex), 3.60 (3H, s, OCH_3), 5.59 (1H, d t, J = 15, 7 Hz, C=CH—CO), 5.75–6.4 (4H, m, cyclopentadienyl H), 6.78 (1H, d t, J = 15, 7 Hz, CH=C—CO).

Can. J. Chem. Downloaded from www.nrcresearchpress.com by 210.87.254.40 on 09/06/12
For personal use only.

E-*Methyl 5-methyl-2-hexenoate (23)*

Isovaleraldehyde (1.0 g, 9.8 mmol, Aldrich) in dichloromethane (15 mL) was added to a tetrahydrofuran solution (15 mL) containing methyl(triphenylphosphorylidine)acetate (3.6 g, 10.8 mmol, Aldrich) and stirred under nitrogen at room temperautre for 1 h. After filtration, concentration, and trituration with petroleum ether the product was distilled, 90–91°C/20 Torr (1 Torr = 133.3 Pa), to give the ester **23**, (1.32 g, 95%); ir (film): 1722 (C=O), 1650 (C=O) cm^{-1}; ^1H nmr (CCl_4) δ: 0.90 (6H, d, J = 6.5 Hz, $(CH_3)_2$), 1.60 (1H, m, H—C$(CH_3)_2$), 2.01 (2H, m, J ~ 6 Hz, —CH_2—), 3.57 (3H, s, OCH_3), 5.60 (1H, d, J = 16 Hz, =CHCO), 6.71 (1H, dt, J = 16, 8 Hz, CH=C—CO).

E-*Methyl 5-methyl-4-bromo-2-hexenoate (24)*

N-Bromosuccinimide (1.38 g, 7.8 mmol, recrystallized, Fisher) was added to carbon tetrachloride (15 mL) followed by ester **23** (1.0 g, 7.0 mmol) in carbon tetrachloride (25 mL) and azoisobutylnitrile (0.010 g). The mixture was stirred under reflux for 18 h, filtered, concentrated, and the residue purified by distillation, bp 58–60°C/0.04 Torr, to give **24** (1.23 g, 78%); ir (film): 1722 (C=O), 1650 (C=O) cm^{-1}; ^1H nmr (CCl_4) δ: 0.90 (6H, d, J = 6 Hz, $(CH_3)_2C$), 1.95 (1H, m, J ~ 6 Hz, H—C$(CH_3)_2$), 3.68 (3H, s, OCH_3), 4.37 (1H, dd, J = 10, 6 Hz, H—C—Br), 5.80 (1H, d, J = 16 Hz, =CHCO), 6.67 (1H, dd, J = 10, 16 Hz, CH=C—CO). *Exact Mass* calcd. for $C_8H_{13}BrO_2$: 220.0098 and 222.0078; found: 220.0157 and 222.0074.

2-Methyl-5-carbomethoxy-6-hydroxy-6-(spiro[2.4]hepta-4,6-dien-1-yl)-3-hexene (26)

Magnesium (3.91 g, 163 mmol) was added to dry THF (150 mL) in a three-necked 500-mL flask equipped with a paddle stirrer. The bromo-ester **24** (19 g, 85.5 mmol) was added in small portions until the Grignard commenced, after which the remaining bromide and aldehyde **2** (9.79 g, 75 mmol) in THF (100 mL) were added dropwise simultaneously. Once the vigorous reaction had subsided the reaction was stirred for a further 2 h at room temperature and poured into saturated aqueous NH_4Cl solution (100 mL). After ether – ethyl acetate extraction (1 : 1, 3 × 100 mL), the combined extracts were dried, concentrated, and purified by flash chromatography (10% ethyl acetate/petroleum ether). This afforded a total yield of 17.96 g (91%) separated into the four C_6C_5 diastereomers as follows.

(a) *SS*,[4] 1.23 g (6.2%); ir (film): 3400–3500 (br, OH) 1725 (C=O) cm^{-1}; ^1H nmr (CCl_4) δ: 1.00 (6H, d, J = 6.5 Hz, $(CH_3)_2C$), 1.4–2.5 (4H, complex, cyclopropyl H, H—C$(CH_3)_2$), 3.21 (1H, m, CH—C=), 3.70 (3H, s, OCH_3), 3.78 (1H, br s, H—C—OH), 5.53 (2H, m, CH=CH), 6.00 (1H, m, cyclopentadienyl H), 6.38 (3H, m, cyclopentadienyl H).

(b) *RS*, 1.63, (8.3%); ir (film): 3400–3500 (br, OH), 1725 (C=O) cm^{-1}; ^1H nmr (CCl_4) δ: 0.99 (6H, d, J = 6.5 Hz, $(CH_3)_2C$), 1.5–2.5 (4H complex, cyclopropyl H, H—C$(CH_3)_2$), 3.20 (1H, m, CH—C=), 3.70 (3H, s, OCH_3), 3.81 (1H, br s, H—C—OH), 5.31–5.39 (2H, m, CH=CH), 6.01 (1H, m, cyclopentadienyl H), 6.40 (3H, m, cyclopentadienyl H).

(c) *SR*, 7.92 g (40.3%); ir (film): 3400–3500 (br, OH), 1735 (C=O), 1635 (sh, C=C) cm^{-1}; ^1H nmr (CCl_4) δ: 0.95 (6H, dd, J = 6.5 Hz, $(CH_3)_3C$—), 1.81 (2H, m, cyclopropyl H), 2.16 (2H, m, J = 6.5 Hz, cyclopropyl H, H—C$(CH_3)_2$), 2.85 (1H, m, CH—C=), 3.63 (3H, s, OCH_3), 3.80 (1H, dd, J = 4.9 Hz, H—C—OH), 5.30 (2H, m, CH=CH), 5.98 (1H, m, cyclopentadienyl H), 6.13 (1H, m, cyclopentadienyl H), 6.44 (2H, m, cyclopentadienyl H).

(d) *RR*, 7.18 g (36.5%); ir (film): 3400–3500 (br, OH), 1735 (C=O) cm^{-1}; ^1H nmr (CCl_4) δ: 1.02 (6H, d, J = 6.5 Hz), 1.90 (2H, m, cyclopropyl H), 2.22 (2H, m, cyclopropyl H, H—C$(CH_3)_2$), 3.15 (1H, br t, J ~ 7 Hz, CH—C=), 3.80 (3H, s, OCH_3), 3.90 (1H, m, H—C—OH), 5.3–5.8 (2H, m, CH=CH), 6.00 (1H, m, cyclopentadienyl H), 6.25 (1H, m, cyclopentadienyl H), 6.44 (2H, m, cyclopentadienyl H).

2-Methyl-5-carbomethoxy-6-acetoxy-6-(spiro[2.4]hepta-4,6-dien-1-yl)-3-hexene (28)

Acetic anhydride (1.08 g, 1 mL, 10.5 mmol) was added dropwise to a cold (0°C, external ice bath) solution of the appropriate alcohol **26** (1.0 g, 3.8 mmol) in dry pyridine (10 mL). The reaction mixture was stirred at 22°C for 12 h, poured into ice-cold 10% aqueous HCl – ether, the ether layer separated, washed with 10% aqueous hydrochloric acid, brine, dried, filtered, concentrated, and purified by flash chromatography (10% ethyl acetate/*n*-hexane) to give the individual acetates **28**, 1.06 g (91%); ir ($CHCl_3$): 1727 (C=O) cm^{-1}; (a) *SS*, ^1H nmr (CCl_4) δ: 0.91 (3H, s, CH_3), 1.03 (3H, s, CH_3), 1.78 (3H, s, CH_3CO), 3.09 (1H, br t, J ~ 7 Hz, CH—C=), 3.61 (3H, s, OCH_3), 4.79 (H, dd, J = 7, 8 Hz, CHOAc), 5.35 (2H, m, CH=CH), 5.90 (2H, m, cyclopentadienyl H), 6.23 (2H, m, cyclopentadienyl H); (b) *RS*, ^1H nmr (CCl_4) δ: 0.92 (3H, s, CH_3), 1.02 (3H, s, CH_3), 1.93 (3H, s, CH_3CO), 3.09 (1H, br t, J ~ 8 Hz, CH—C=), 3.61 (3H, s, OCH_3), 5.00 (1H, t, J = 8 Hz, CHOAc), 5.29 (2H, m, CH=CH), 5.81 (1H, m, cyclopentadienyl H), 6.10 (1H, m, cyclopentadienyl H), 6.28 (2H, m, cyclopentadienyl H). *Exact Mass* calcd. for $C_{18}H_{24}O_4$: 304.1674; found: 304.1642. (c) *SR*, ^1H nmr (CCl_4) δ: 0.86 (3H, s, CH_3), 1.00 (3H, s, CH_3), 1.99 (3H, s, CH_3CO), 2.80 (1H, m, CHC=), 3.62 (3H, s, OCH_3), 4.8–5.25 (3H, m, CHOAc, CH=CH), 5.84 (1H, m, cyclopentadienyl H), 6.25 (3H, m, cyclopentadienyl H). *Exact Mass* calcd. for $C_{18}H_{24}O_4$: 304.1674; found: 304.1666. (d) *RR*, ^1H nmr (CCl_4) δ: 0.84 (3H, s, CH_3), 0.94 (3H, s, CH_3), 2.00 (3H, s, CH_3CO), 3.10 (1H, dd, J ~ 8 Hz, CHC=), 3.59 (3H, s, OCH_3), 4.85–5.5 (3H, m, CHOAc, CH=CH), 5.89 (1H, m, cyclopentadienyl H), 6.35 (3H, m, cyclopentadienyl H); (400 MHz, $CDCl_3$) δ: 0.85, 0.89 (3H, d, J = 7 Hz, $(CH_3)_2$), 1.68 (1H, dd, J = 4.5, 8.5 Hz, cyclopropyl H), 1.84 (1H, dd, J = 4.5, 7.5 Hz, cyclopropyl H), 2.03 (1H, m, H—CMe_2), 2.08 (3H, s, CH_3CO), 2.16 (1H, m, cyclopropyl H), 3.22 (1H, br t, J ~ 2.9 Hz, CHC=), 3.66 (3H, s, OCH_3), 5.00 (1H, m, J = 2, 9, 16 Hz, HC=C), 5.18 (1H, dd, J = 1, 9 Hz, HC—OAc), 5.48 (1H, m, J = 1, 6, 16 Hz, C=CHiPr), 6.00 (1H, m, cyclopentadienyl H), 6.38 (1H, m, cyclopentadienyl H), 6.43 (1H, m, cyclopentadienyl H), 6.52 (1H, m, cyclopentadienyl H). Decoupling the isopropyl methyl signals revealed the location of the methine proton (2.03) which was itself coupled to the olefinic signal at 5.48. *Exact Mass* calcd. for $C_{18}H_{24}O_4$: 304.1674; found: 304.1661.

2-Pentyl-3-acetoxy-4-carbomethoxy-7-methyloctane (29)

Acetate **28** (0.5 g, 1.65 mmol) was dissolved in anhydrous methanol (25 mL), catalyst added (100 mg, 10% Pd/C), and the mixture placed in a Paar apparatus under 2.5 atm of hydrogen for 7 h. The catalyst was removed by filtration, washed with methanol, and the combined filtrate and methanol washings concentrated and subjected to flash chromatography (10% ethyl acetate/*n*-hexane) to give the diastersomeric esters **29**, 0.47 g (93%); ir (film): 1735 (esters) cm^{-1}; ^1H nmr (CCl_4) δ: 0.87, 0.99 (9H, overlapping doublets, J ~ 7 Hz, CH_3's), 2.02, (3H, s, CH_3CO), 2.53 (1H, m, CH—C=O), 3.67 (3H, s, OCH_3), 5.22 (1H, dd, J ~ 9 Hz, CHOAc). Decoupling experiments indicated that the signals at 2.53 and 5.22 were coupled to each other.

2-Carbomethoxy-11-isopropyltetracyclo[5.4.0^{1,7}.0^{4,6}.0^{6,10}]undec-8-en-3-acetate (30)

The triene acetate **28** (1.02 g, 3.35 mmol) was refluxed under nitrogen in *p*-dichlorobenzene (40 mL) for 20 h, the solvent removed under reduced pressure, and the residual oil purified by flash chromatography (4% ethyl acetate/*n*-hexane) to give the adduct **30**, 0.615 g (60%), and recovered triene **28**, 0.30 g (29%); ^1H nmr (CCl_4) δ: 0.39 (1H, m, J ~ 7 Hz, cyclopropyl H), 1.95 (3H, s, CH_3CO), 2.30 (2H, br s, bridgehead H), 2.84 (1H, d, J = 9 Hz, $CHCO_2Me$), 3.62 (3H, s, OCH_3), 4.57 (1H, t, J = 8.5 Hz, CHOAc), 5.98 (2H, br s, CH=CH). *Exact Mass* calcd. for $C_{18}H_{24}O_4$: 304.1674; found: 304.1672.

Alternatively the triene **28** (0.818 g, 2.69 mmol) was dissolved in

[4] These configurational assignments are tentative since the diastereomers have not been degraded to a compound of known absolute configuration.

dichloromethane (10 mL) and a solution (dichloromethane/ether, 2:1, 30 mL) of aluminium chloride (0.430 g, 3.22 mmol) added. The reaction mixture was stirred for 0.5 h, pyridine (3 mL) added, the solvent removed, and the residue purified by flash chromatography (10% ethyl acetate/*n*-hexane) to afford **30**, 0.205 g (25%).

The cyclization of the acetate isomers **28** was examined individually but only the C_6C_5 *RR* and *SR* diastereomers afforded the Diels–Alder adduct **30**.

Acknowledgements

We are grateful to Memorial University of Newfoundland and the Natural Sciences and Engineering Research Council of Canada for financial support of this research; D. Jamieson, R. J. Andersen, and B. Gregory for high resolution mass spectra; E. G. Breitholle, W. H. J. Tam, N. C. Wang, and L. Taylor for preliminary experiments, F. Chau for technical assistance, and H. J. Liu (University of Alberta) for 400 MHz ^{1}H nmr spectra.

1. A. G. FALLIS. Can. J. Chem. **62**, 183 (1984); E. CIGANEK. Org. React. In press; G. BRIEGER and J. N. BENNETT. Chem. Rev. **80**, 63 (1980); W. OPPOLZER. Angew. Chem. Int. Ed. Engl. **16**, 10 (1977).
2. R. K. BOECKMAN and S. S. KO. J. Am. Chem. Soc. **104**, 1033 (1982).
3. W. R. ROUSH, H. R. GILLIS, and A. I. KO. J. Am. Chem. Soc. **104**, 2269 (1982).
4. D. D. STERNBACH and D. M. ROSSANA. Tetrahedron Lett. **23**, 303 (1982).
5. G. OURISSON. Bull. Soc. Chim. Fr. 895 (1955); J.-C. THIERRY and R. WEISS. Tetrahedron Lett. 2663 (1969).
6. P. DE MAYO and R. E. WILLIAMS. J. Am. Chem. Soc. **87**, 3275 (1965); L. A. SMEDMAN, E. ZAVARIN, and R. TERANISHI. Phytochem. 1457 (1969).
7. (*a*) E. J. COREY, M. OHNO, R. B. MITRA, and P. VATAKENCHERRY. J. Am. Chem. Soc. **86**, 478 (1964); J. E. MCMURRY and S. J. ISSER. J. Am. Chem. Soc. **94**, 7132 (1972); R. A. VOLKMANN, G. C. ANDREWS, and W. S. JOHNSON. J. Am. Chem. Soc. **97**, 4777 (1975); W. OPPOLZER and T. GODEL. J. Am. Chem. Soc. **100**, 2583 (1978); W. OPPOLZER. Pure Appl. Chem. **53**, 1181 (1981); (*b*) J. E. MCMURRY. J. Am. Chem. Soc. **90**, 6821 (1968); G. L. HODGSON, D. F. MACSWEENEY, and T. MONEY. J. Chem. Soc. Perkin Trans. 1, 2113 (1973); E. PIERS, M. B. GERAGHTY, R. D. SMILLIE, and M. SAUCY. Can. J. Chem. **53**, 2849 (1975); H. HAGIWARA, M. MIYASHITA, H. UDA, and A. YOSHIKOSHI. Bull. Chem. Soc. Jpn. **48**, 3723 (1975); P. BAKUZIS, O. O. S. CAMPOS, and M. L. F. BAKUZIS. J. Org. Chem. **41**, 3261 (1976); M. YANAGIYA, K. KANEKO, T. KAJI, and T. MATSUMOTO. Tetrahedron Lett. 1761 (1979); W. OPPOLZER. Pure Appl. Chem. **53**, 1181 (1981); R. L. SNOWDEN. Tetrahedron Lett. **22**, 101 (1981).
8. C. M. BEECHAM, C. DJERASSI, and H. EGGERT. Tetrahedron, **34**, 2503 (1978).
9. J. C. BRAEKMAN, D. DALOZE, A. DUPONT, B. TURSCH, J. P. DE CLERCQ, G. GERMAIN, and M. VAN MEERSSCHE. Tetrahedron, **37**, 179 (1981).
10. P. A. COLLINS and D. WEGE. Aust. J. Chem. **32**, 1819 (1979); W. OPPOLZER, H. F. STRAUSS, and D. P. SIMMONS. Tetrahedron Lett. **23**, 4673 (1982).
11. G. BRIEGER. J. Am. Chem. Soc. **85**, 3783 (1963).
12. E. J. COREY, N. M. WEINSHENKER, T. K. SCHAAF, and W. HUBER. J. Am. Chem. Soc. **91**, 5675 (1969); E. J. COREY, U. KOELLIKER, and J. NEUFFER. J. Am. Chem. Soc. **93**, 1489 (1971).
13. R. S. GLASS, J. D. HERZOG, and R. L. SOBCZAK. J. Org. Chem. **43**, 3209 (1978).
14. K. BANGERT and V. BOEKELHEIDE. Tetrahedron Lett. 1119 (1963); cf., H. SCHALTEGGER. Helv. Chim. Acta, **45**, 1368 (1962).
15. R. A. BENKESER. Synthesis, **3**, 347 (1971).
16. S. K. ATTAH-POKU, G. GALLACHER, A. S. NG, L. E. B. TAYLOR, S. J. ALWARD, and A. G. FALLIS. Tetrahedron Lett. **24**, 677 (1983).
17. S. N. HUCKIN and L. WEILER. J. Am. Chem. Soc. **96**, 1082 (1974).
18. K. H. FUNG, K. J. SCHMALZL, and R. N. MIRRINGTON. Tetrahedron Lett. 5017 (1969).
19. F. NÄF, R. DECORZANT, W. GIERSCH, and G. OHLOFF. Helv. Chim. Acta, **64**, 1387 (1981).
20. R. F. TOWNSHEND, G. RAMUNNI, G. SEGAL, W. J. HEHRE, and L. SALEM. J. Am. Chem. Soc. **98**, 2190 (1976).
21. W. R. ROUSH and A. G. MYER. J. Org. Chem. **46**, 1509 (1981); W. R. ROUSH, H. R. GILLIS, and A. I. KO. J. Am. Chem. Soc. **104**, 2269 (1982); H. R. GILLIS, JR. Ph.D. Thesis, Mass. Inst. of Technology, 1982; G. STORK and D. H. SHERMAN. J. Am. Chem. Soc. **104**, 3738 (1982).
22. H. D. MARTIN and B. MAYER. Angew. Chem. Int. Ed. Engl. **22**, 283 (1983).
23. P. DESLONGCHAMPS. Stereoelectronic effects in organic chemistry. Pergamon Press, Oxford. 1983.
24. W. C. STILL, M. KAHN, and A. MITRA. J. Org. Chem. **43**, 2923 (1978).
25. A. G. FALLIS and E. G. BREITHOLLE. Abstract M1, Int. Symposium on Stereochemistry, Kingston, Ont., Canada, June 27 – July 2, 1976.
26. W. OPPOLZER, T. BEGLEY, and A. ASHCROFT. Tetrahedron Lett. **25**, 825 (1984).

Can. J. Chem. Downloaded from www.nrcresearchpress.com by 210.87.254.40 on 09/06/12
For personal use only.

A general synthesis of the tricyclo[4.4.0^{1,6}.0^{5,9}]decane (sinularene) and tricyclo[5.4.0^{1,7}.0^{6,10}]undecane (longifolene) ring systems by selective cleavage of bridged-ring cyclopropyl ketones

SAMUEL K. ATTAH-POKU, KAZIMIERZ ANTCZAK, SANDRA J. ALWARD, AND ALEX G. FALLIS
Department of Chemistry, Memorial University of Newfoundland, St. John's, Nfld., Canada, A1B 3X7

Received January 9, 1984

SAMUEL K. ATTAH-POKU, KAZIMIERZ ANTCZAK, SANDRA J. ALWARD, and ALEX G. FALLIS. Can. J. Chem. **62**, 1717 (1984).

The reactivity of the tetracyclic cyclopropyl compounds **1**, **8**, **9**, **10**, and **15** has been investigated and general routes to the "sinularene" and "longifolene" skeletons developed. Hydrogenolysis cleaves the least substituted cyclopropane bond ("a") to give the tricyclo[4.4.0^{1,6}.0^{5,9}]decane (sinularene) ring systems **5** and **6**. Lithium–ammonia and zinc – zinc chloride reduction affords both tricyclic ketones **11** and **13** and **12** and **14** while chromium sulphate in 1 : 1 dimethyl formamide/water gives the tricyclo[5.4.0^{1,7}.0^{6,10}]undecene (longifolene) skeleton **14** exclusively (cleavage of bond "b") from ketone **9**.

SAMUEL K. ATTAH-POKU, KAZIMIERZ ANTCZAK, SANDRA J. ALWARD et ALEX G. FALLIS. Can. J. Chem. **62**, 1717 (1984).

On a étudié la réactivité des composés tétracycliques contenant des cyclopropyles, **1**, **8**, **9**, **10** et **15** et on a mis au point des voies d'accès générales aux squelettes "sinularène" et "longifolène". Par hydrogénolyse, on clive la liaison la moins substituée ("a") du cyclopropane et l'on obtient les systèmes tricyclo[4.4.0^{1,6}.0^{5,9}]décane (sinularène) **5** et **6**. La réduction par l'ammoniac et le lithium ou par le zinc et le chlorure de zinc fournissent les deux cétones tricycliques **11** et **13**, **12** et **14**; toutefois la réduction par le sulfate de chrome dans un mélange 1 : 1 de diméthylformamide/eau conduit exclusivement au squelette tricyclo[5.4.0^{1,7}.0^{6,10}]undécène (longifolène) **14** à partir de la cétone **9** (clivage de la liaison "b").

[Traduit par le journal]

Introduction

Controlled cleavage of cyclopropane intermediates provides a useful method for the total synthesis of multicyclic natural products and has been successfully employed in the stereocontrolled syntheses of (±) hinesol and (±) epihinesol (1), and (−)-acorenone B and (±) α-chamigrene (2). The preceding paper (3) outlines our general approach, using an intramolecular Diels–Alder sequence, to the tricyclic skeletons represented in nature by sinularene, longifolene, and sativene (copacamphene) (Scheme 1). This strategy requires, after construction of the appropriate tetracyclic precursor, selective cyclopropane bond cleavage (a, b, or c) to afford the desired tricyclic ring systems. The results of these studies, which permit controlled rupture of bond "a" or "b", are outlined below (4).[1]

Results and discussion

At the outset of this study it was anticipated that the strain inherent in the three-membered ring confined in the tetracyclo[5.4.0^{1,7}.0^{4,6}.0^{6,10}]undecene skeleton **1** would facilitate cleavage under a variety of conditions. In addition, during solvolysis procedures the presence of the double bond should help stabilize the presumed "C_7-norbornyl type" carbonium ion intermediates for a synthetic sequence leading to the "longifolene" ring system. Unfortunately, in practice neither of these objectives was experimentally feasible and treatment of the alcohol **1** or its tosylate (both epimers separately) under a variety of acidic and solvolytic conditions failed to provide ring-opened products in spite of related literature precedent (5). Similarly, reaction of the bromide with magnesium, lithium, and zinc salts did not afford the desired ring-opened olefins although these reactions proceed readily with less complex systems (6). Likewise, the phosphonate prepared from **1** underwent reduction with lithium napthalide but carbon–carbon bond cleavage did not result. Although disappointing, this latter result is not entirely surprising since the best success with this reagent has been achieved for cyclobutane ring fission (7).

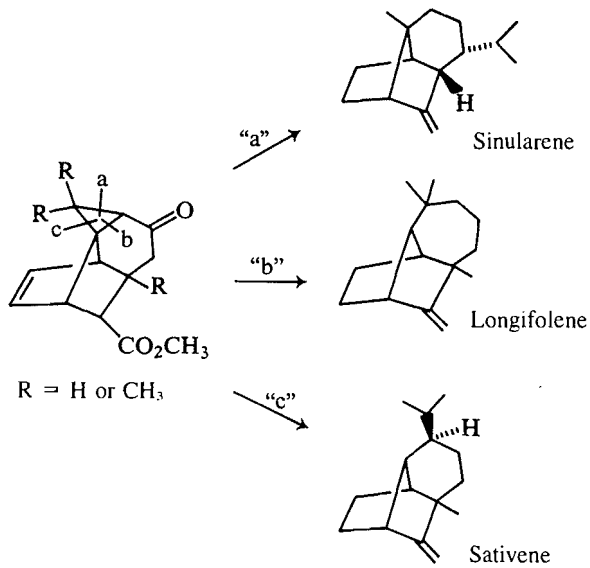

SCHEME 1

It is well established that hydrogenolysis of cyclopropanes gives, as the predominant products, compounds which result from preferential cleavage of the least substituted bond (8). Treatment of alcohol **1** with hydrogen at 3 atm (1 atm = 101.3 kPa) in acetic acid in the presence of PtO_2 catalyst afforded a 90% yield of **5** resulting, as expected, from rupture of the least substituted bond "a", to give the tricyclo[4.4.0^{1,6}.0^{5,9}]decane (sinularene) compound as the only product.

In contrast to the general lack of reactivity of the compounds above, further activation of the cyclopropane unit, achieved by Jones' oxidation of the alcohol **1** to the cyclopropyl ketone **8**, provided a system very susceptible to cleavage. Hydrogenolysis occurred under mild conditions in methanol at room temperature using 10% Pd/C catalyst to give the "sinularene"

[1] Please note that the substituents in our preliminary communication were attached incorrectly to C_{11} rather than C_2 of the adducts.

Can. J. Chem. Downloaded from www.nrcresearchpress.com by 210.87.254.105 on 09/06/12
For personal use only.

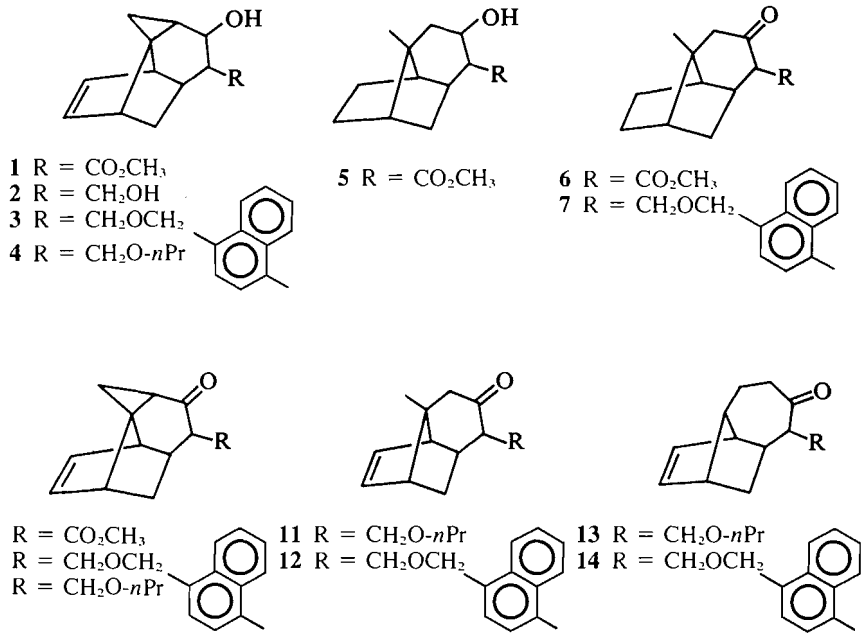

ketone **6** exclusively (95%).

Dissolving metal reductions of cyclopropyl ketones are subject to a variety of influences. Cleavage of the most substituted σ bond is frequently favoured, as this will afford the more thermodynamically stable carbanion intermediate although, in this case, it would involve the formation of a bridgehead carbanion. An important stereoelectronic factor concerns the relative orientation of the cyclopropane bonds and the carbonyl function. In general a preference is observed for cleavage of the cyclopropane bond which overlaps most efficiently with the π orbital of the carbonyl group (9). Molecular models imply that the difference between the least (a) and most substituted (b) bonds relative to the carbonyl is modest with a slight preference in favour of fission of "a" although a mixture of products is likely to result. In keeping with this analysis, lithium–ammonia reduction of **10**, in the presence of *tert*-butyl alcohol, afforded a mixture of the sinularene (74%) and longifolene (21%) type ketones **11** and **13**.

Often the metal and the solvent influence the course of these reactions and it was of interest to discover that zinc and chromium changed the above ratio. Treatment of **9** with zinc in methanol in the presence of zinc chloride (10) afforded the sinularene type ketone **12** (25%) as the minor and the longifolene type ketone **14** (75%) as the major products. The dominance of the longifolene product suggests that an intermediate salt of type **20**, in which the double bond plays a coordinating role, may be involved.

Solutions containing salts of chromium(II) ion are known to reduce conjugated enones under certain conditions (11, 12) but the reactions of cyclopropyl ketones under these conditions do not appear to have been investigated. Exposure of **9** to a solution of $CrSO_4$ in 2:1 dimethylformamide – water afforded the longifolene type ketone **14** (84%) as the only product. In contrast, the saturated ketone **15** gave a mixture of both **7** and **19** (20:80) under identical reaction conditions and reacted more slowly. It appears that the double bond exerts a beneficial influence in directing cleavage of the most substituted bond ("b"). Cyclopropyl methyl ketone reacted very sluggishly under these conditions to give a low yield of 2-pentanone, thus further establishing the importance of the double bond. It is

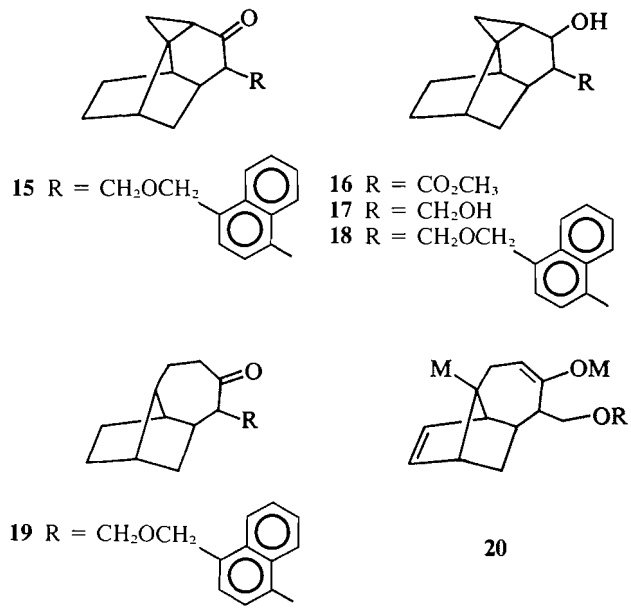

likely that a more active form of Cr(II), possibly as a diamine complex (12), will be required for chromium to be generally useful for cyclopropane cleavage. In keeping with mechanistic studies by House and Kinlock (12), an intermediate species such as **20**, in which the solvated chromium at the bridgehead is favourably disposed for interaction with the π system of the olefin, accounts for our results. In a related case, recent calculations (13) have indicated that the lithium in 7-lithionorbornadiene is strongly coordinated to the neighbouring π bond and bicyclic nickelocene complexes display similar stabilization (14).

The compounds required for this study were prepared from the intramolecular Diels–Alder adduct **1** (3). Lithium aluminum hydride reduction of ester **1** gave the diol **2** in which the primary alcohol group could be selectively protected with either 1-chloromethyl-4-methylnaphthalene or 1-chloropropane in the presence of sodium hydride to give **3** and **4** respectively. Jones' oxidation of the appropriate alcohols **1**, **3**, and **4** pro-

Can. J. Chem. Downloaded from www.nrcresearchpress.com by 210.87.254.105 on 09/06/12
For personal use only.

Can. J. Chem. Downloaded from www.nrcresearchpress.com by 210.87.254.105 on 09/06/12
For personal use only.

TABLE 1. Product distribution from reductive cyclopropane cleavage

Compound	Reagent	Products	
		"Sinularene type"	"Longifolene type"
1	$H_2/PtO_2/HOAc$ 3 atm	**5** (90%)	0
8	$H_2/Pd/C/MeOH$ 1 atm	**6** (95%)	0
10	$Li/NH_3/t$BuOH	**11** (74%)	**13** (21%)
9	$Zn/ZnCl_2/MeOH$	**12** (25%)	**14** (75%)
9	$CrSO_4/Zn$ DMF/H_2O	0	**14** (84%)
15	$CrSO_4/DMF/H_2O$	**7** (20%)	**19** (79%)

vided the ketones **8**, **9**, and **10**. Compound **15** was prepared in a similar manner from a sample of **1** in which the double bond was first saturated by hydrogenation over 10% Pd/C in methanol at room temperature to give **16**, followed by lithium aluminum hydride reduction to **17**, selective ether formation to give **18**, and Jones' oxidation.

As summarized in Table 1, these ring-opening studies allow controlled cyclopropane ring cleavage to either the tricyclo[4.4.$0^{1,6}$0^{5,9}]decane (sinularene) skeleton under hydrogenolysis conditions or to the tricyclo[5.4.$0^{1,7}$.$0^{6,10}$]undecane (longifolene) ring system using chromium sulphate. This methodology has laid the groundwork for our approach to the total synthesis of sinularene and we are currently engaged in further extensions of this chemistry via a total synthesis of chiral longifolene from ascorbic acid (Vitamin C).

Experimental

Melting points were determined in capillary tubes with a Thomas–Hoover Uni-Melt apparatus or a Fischer–John's melting point apparatus and are uncorrected. Infrared spectra were recorded on a Perkin–Elmer 237B or 451 grating spectrophotometer, and were calibrated with the 2850 and 1601 cm^{-1} bands of polystyrene film. Ultraviolet spectra were recorded on a Perkin–Elmer 202 uv–visible spectrophotometer and were calibrated with the 279.4-nm band of a Holmium oxide filter. Proton magnetic resonance spectra were measured at 80 MHz with a Bruker model WP80 spectrometer employing a chloroform lock or at 60 MHz with a Varian model EM-360 spectrometer. Signal positions are reported in ppm downfield from tetramethylsilane (δ scale) as an internal standard; the number of protons, multiplicity, coupling constants, and proton assignments are indicated in parentheses. Mass spectra were determined on a V.G. Micromass 7070 HS instrument using an ionization energy of 70 eV. Gas–liquid chromatographic analyses were conducted on a Hewlett Packard 402B gas chromatograph equipped with a column (3 m × 6 mm id) containing 1.5% OV-17 supported on Gas Chrom Q using helium as the carrier gas. Thin-layer chromatographic analyses were carried out on commercial precoated silica gel plates with fluorescent indicator (Eastman Kodak silica gel 13181). Preparative thin-layer chromatography was conducted on 20 × 20 cm glass plates coated with silica gel $PF_{254+366}$ type 60 (E. Merck). Flash chromatography used BDH silica gel Kieselgel 60, 230–400 mesh (15).

Solutions in organic solvents were dried over anhydrous magnesium sulphate and stripped of solvent with a Büchi rotary evaporator connected to a water aspirator. Unless otherwise indicated, all reactions were conducted under argon.

2-Carbomethoxy-5-methyltricyclo[4.4.$0^{1,6}$.$0^{5,9}$]decan-3-ol (5)

The cyclopropyl alcohol **1** (0.25 g, 1.1 mmol) (3) in acetic acid (20 mL), to which 10% PtO_2/C (10 mg) had been added, was placed in a Parr apparatus under 3 atm of hydrogen for 12 h at room temperature. The reaction mixture was diluted with ether (50 mL), filtered, and the filtrate neutralized with saturated aqueous sodium bicarbonate solution and extracted with ether. The ethereal extracts were washed with brine, dried, filtered, concentrated, and the product purified by flash chromatography (20% ethyl acetate/petroleum ether) to give **5** (0.225 g, 90%); ir ($CHCl_3$): 3480 (br, OH), 1716 (C=O) cm^{-1}; ^{1}H nmr (CCl_4) δ: 0.96 (3H, s, CH_3), 3.20 (1H, d, J = 7 Hz, H—C—CO_2Me), 3.60 (3H, s, OCH_3), 3.98 (1H, m, J ~ 6 Hz). *Exact Mass* calcd. for $C_{13}H_{20}O_3$: 224.1412; found: 224.1406.

2-Carbomethoxytetracyclo[5.4.$0^{1,7}$.$0^{4,6}$.$0^{6,10}$]undec-8-en-3-one (8)

The tetracyclic alcohol **1** (0.5 g, 2.7 mmol) was dissolved in acetone (25 mL) and Jones reagent (2 mL, prepared from chromium trioxide (7.0 g), H_2O (50 mL), and concentrated H_2SO_4 (6.1 mL)) added dropwise. The resulting mixture was stirred at room temperature for 15 min and sodium hydrosulfide added until the yellow colour discharged. The reaction mixture was filtered, and the filtrate concentrated to ~1 mL and extracted with ether. The ether extracts were washed with brine, dried, concentrated, and purified by flash chromatography (16% ethyl acetate/petroleum ether) to give the keto-ester **8** (0.439 g, 88%); ir (film): 1740 (CO_2CH_3), 1717 (C=O) cm^{-1}; ^{1}H nmr ($CDCl_3$) δ: 1.1–2.3 (6H, complex), 2.65 (2H, br s, bridgehead H), 3.53 (1H, br s, H—C—CO_2CH_3), 3.70 (3H, s, OCH_3), 6.13 (2H, br m, HC=CH). *Exact Mass* calcd. for $C_{13}H_{14}O_3$: 218.0943; found: 218.0944.

2-Carbomethyoxy-5-methyltricyclo[4.4.$0^{1,6}$.$0^{5,9}$]decan-3-one (6)

(a) *Oxidation of 5*

Jones reagent (1 mL) was added dropwise over 5 min to a stirred solution of the alcohol **5** (0.25 g, 1.2 mmol) in acetone (20 mL). Stirring was continued for a further 10 min, 2-propanol (1 mL) was added to consume excess oxidant, the reaction mixture concentrated, the residue (~2 mL) extracted with ether, the ethereal extracts washed with water, brine, dried, filtered, concentrated, and the product purified by flash chromatography (5% ethyl acetate/petroleum ether) to give the ketone **6** (0.175 g, 71%); ir ($CHCl_3$): 1733 (C=O), 1710 (C=O), 1640 (C=O), 1610 (C=O) cm^{-1}; ^{1}H nmr (CCl_4) δ: 1.03 (3H, s, CH_3), 3.06 and 3.29 (1H, d, J = 3 Hz, br s, $W_{1/2}$ = 4 Hz, H—C—CO_2CH_3), 3.65 (3H, s, OCH_3). *Exact Mass* calcd. for $C_{13}H_{18}O_3$: 222.1256; found: 222.1227.

(b) *Reduction of 8*

Hydrogenation of cyclopropyl ketone **8** (0.25 g, 1.1 mmol) was conducted in methanol (10 mL) using 10% Pd/C (20 mg) at atmospheric pressure and room temperature for 12 h. The reaction mixture was filtered, concentrated, and purified by flash chromatography (5% ethyl acetate/petroleum ether) to give ketone **6** (0.238 g, 95%).

2-Hydroxymethyltetracyclo[5.4.$0^{1,7}$.$0^{4,6}$.$0^{6,10}$]undec-8-en-3-ol (2)

The hydroxy-ester **1** (4.37 g, 19.7 mmol) (3) in ether (50 mL) was added dropwise to a cold (0°C), stirred, suspension of lithium aluminum hydride (2.24 g, 59 mmol, Aldrich) in ether (50 mL). After addition was complete the ice-bath was removed and the reaction mixture stirred at room temperature for 2 h, the ice bath replaced, and water (5 mL) added cautiously. This was followed by THF (200 mL) and anhydrous sodium sulfate; stirring was continued for 30 min, the mixture filtered, and the residue washed thoroughly with THF. The filtrates were concentrated and purified by flash chromatography on silica gel (60% ethyl acetate/petroleum ether) to give the diol **2** (3.63 g, 95%), mp 176–177°C; ^{1}H nmr ($CDCl_3$) δ: 0.47 (1H, m, cyclopropyl H), 0.74–2.4 (7H, complex), 3–4 (5H, complex, H—C—OH), 5.81 (1H, m, HC=C), 6.18 (1H, dd, HC=C, J = 3, 5 Hz).

2-(4-Methyl-1-methyloxynaphthyl)methyltetracyclo-[5.4.$0^{1,7}$.$0^{4,6}$.$0^{6,10}$]undec-8-en-3-ol (3)

The diol **2** (0.80 g, 4.2 mmol) in THF (10 mL) was added to a cold (0°C) stirred suspension of sodium hydride (0.50 g, 10.4 mmol, Aldrich, 60% dispersion in oil) in THF (10 mL). After 5 min hexamethylphosphoramide (5 mL, Aldrich) was added, followed by 1-(chloromethyl)-4-methylnapthalene (0.833 g, 4.4 mmol, Aldrich) in THF (5 mL), the ice bath was removed, and stirring continued at room

Can. J. Chem. Downloaded from www.nrcresearchpress.com by 210.87.254.105 on 09/06/12
For personal use only.

temperature for 24 h. The ice bath was replaced, water (1 mL) added slowly, and the reaction mixture poured into cold (0°C) 10% aqueous hydrochloric acid and extracted with ether (2×). The combined extracts were washed with brine, dried, filtered, concentrated, and purified by flash chromatography (15% ethyl acetate/petroleum ether) to give the hydroxy-ether **3** (1.23 g, 85%) which was recrystallized from acetone/petroleum ether (1:10), mp 142–143°C; ir ($CHCl_3$): 3560 (sh, OH), 3575 (br, OH) cm^{-1}; ^1H nmr (CCl_4) δ: 0.35 (1H, m, cyclopropyl H), 0.6–2.3 (8H, complex), 2.59 (3H, s, CH_3—Ar), 3.04 (2H, m, H—C—OH, OH), 3.47 (2H, m, CH_2—O), 4.77 (2H, s, O—CH_2Ar), 5.72 (1H, m, CH=C), 6.00 (1H, m, CH=C), 7.16 (2H, m, Ar), 7.39 (2H, m, Ar), 7.90 (2H, m, Ar). *Exact Mass* calcd. for $C_{24}H_{26}O_2$: 346.1933; found: 346.1926.

2-(1-Oxypropyl)methyltetracyclo[5.4.0^{1,7}.0^{4,6}.0^{6,10}]undec-8-en-3-ol (4)

The diol **2** (0.749 g, 3.9 mmol) was converted to the hydroxypropyl ether **4** using sodium hydride and 1-chloropropane following the procedure outlined above. Flash chromatography of the product (20% ethyl acetate/*n*-hexane) afforded **4**, 630 mg (69%); ir ($CHCl_3$): 3475 (OH), 1050–1100 (C—O) cm^{-1}; ^1H nmr (CCl_4) δ: 0.38 (1H, m, cyclopropyl H), 0.88 (3H, t, J = 7 Hz, CH_3CH_2), 2.9–3.5 (5H, m, CH_2—O, HC—OH), 5.61 (1H, m, HC=), 5.94 (1H, m, HC=). Further elution (60% ethyl acetate/*n*-hexane) gave 135 mg (18%) of the unreacted diol **2**.

2-(4-Methyl-1-methyloxynaphthyl)methyltetracyclo-[5.4.0^{1,7}.0^{4,6}.0^{6,10}]undec-8-en-3-one (9)

Jones reagent (1.5 mL) was added dropwise over 10 min to a stirred solution of the alcohol **3** (0.50 g, 2.3 mmol) in acetone (50 mL). Stirring was continued for a further 5 min, 2-propanol was added until the yellow colour was discharged, the reaction mixture filtered, the residue washed with ether, the filtrate concentrated, and further ether added. The ethereal solution was washed with water, brine, dried, filtered, concentrated, and the product purified by flash chromatography (10% ethyl acetate/petroleum ether) to give **9** (0.348 g, 70%) which was recrystallized from carbon tetrachloride/petroleum ether, mp 135–136°C; ir ($CHCl_3$): 1704 (C=O) cm^{-1}; ^1H nmr ($CDCl_3$) δ: 2.68 (3H, s, CH_3—Ar), 3.67 (2H, m, CH_2O), 4.89 (2H, s, O—CH_2Ar), 5.88 (1H, m, CH=C), 6.12 (1H, m, CH=C), 7.21 (2H, m, Ar), 7.43 (2H, m, Ar), 7.98 (2H, m, Ar). *Exact Mass* calcd. for $C_{24}H_{24}O_2$: 344.1776; found: 344.1781.

2-(1-Oxypropyl)methyltetracyclo[5.4.0^{1,7}.0^{4,6}.0^{6,10}]undec-8-en-3-one (10)

Oxidation of alcohol **4** (319 mg, 1.36 mmol) was accomplished as outlined above to give, after flash chromatography (15% ethyl acetate/*n*-hexane), the ketone **10**, 260 mg (82%); ir ($CHCl_3$): 1700 (C=O), 1115 (C—O) cm^{-1}; ^1H nmr (CCl_4) δ: 0.91 (3H, t, J = 7 Hz, CH_3CH_2), 2.55 (2H, br m, CH_2C=O), 3.14–3.74 (4H, m, CH_2—O), 5.97 (1H, m, HC=), 6.10 (1H, m, HC=C).

2-(4-Methyl-1-methyloxynaphthyl)methyl-5-methyltricyclo-[4.4.0^{1,6}.0^{5,9}]decan-3-one (7)

Hydrogenation of cyclopropyl ketone **9** (0.50 g, 1.45 mmol) was conducted in methanol/ethyl acetate (1:1, 50 mL) with 10% Pd/C (50 mg) at atmospheric pressure and 23°C for 12 h. Filtration, concentration, and flash chromatography (10% ethyl acetate/petroleum ether) afforded the ketone **7** (0.353 g, 70%); ir ($CHCl_3$): 1706 (C=O) cm^{-1}; ^1H nmr ($CDCl_3$) δ: 0.81 (3H, s, CH_3), 2.62 (3H, s, CH_3Ar), 3.60 (2H, d, J = 7 Hz, —CH_2—O), 4.73 (2H, s, O—CH_2—Ar), 7.19 (2H, m, Ar), 7.38 (2H, m, Ar), 7.88 (2H, m, Ar). *Exact Mass* calcd. for $C_{24}H_{28}O_2$: 348.2089; found: 348.2083.

Zinc Reduction of Ketone 9

Zinc powder (78.5 mg, 1.2 mmol) and zinc chloride (16 mg, 0.12 mmol) were added to a methanol solution (5 mL) of the cyclopropyl ketone **9** (40 mg, 0.12 mmol) and stirred at 23°C for 18 h. Ethyl acetate (20 mL) was added, the mixture was filtered, concentrated, extracted with ether, the combined extracts washed with water, brine, dried, filtered, concentrated, and the product purified by flash chromatography (10% ethyl acetate/petroleum ether) to afford **14** (30 mg, 75%) and **12** (10 mg, 25%). Hydrogenation of the minor component **12** (10% Pd/C, MeOH, 23°C) gave **19**.

2-(4-Methyl-1-methyloxynaphthyl)methyltricyclo[5.4.0^{1,7}.0^{6,10}]-undec-8-en-3-one (14)

Chromium(II) sulfate (0.73 g, 1.6 mmol) and zinc powder (0.5 g, 7.7 mmol) were added to the cyclopropyl ketone **9** (49 mg, 0.14 mmol) in dimethylformamide/water (2:1) (13 mL) and stirred at room temperature for 1 h. Ether (20 mL) was added, the reaction mixture was filtered, the organic phase separated, washed with brine, dried, filtered, concentrated, and the product purified by flash chromatography (15% ethyl acetate/petroleum ether) to give ketone **14** (42 mg, 84%).

Alternatively the reduction was conducted in dimethylformamide–water (12:1) (13 mL) with added chromium(II) sulfate solution (5 mL, 0.02 *M*) for 1 h at room temperature and worked up as above to give **14** (40 mg, 80%); ir ($CHCl_3$): 1710 (C=O) cm^{-1}; ^1H nmr ($CDCl_3$) δ: 2.64 (3H, s, CH_3Ar), 3.75 (2H, m, CH_2—O), 4.81 (2H, s, O—CH_2Ar), 5.84 (1H, m, CH=C), 6.14 (1H, m, CH=C), 7.19 (2H, m, Ar), 7.45 (2H, m, Ar), 7.97 (2H, m, Ar).

Lithium/ammonia reduction of ketone 8

A THF solution (5 mL) containing *tert*-butyl alcohol (240 mg, 3.25 mmol) and the cyclopropyl ketone **8** (150 mg, 0.65 mmol) was added to a stirred solution of lithium (45 mg, 6.5 mmol) in liquid ammonia at −78°C. After 1 h the carbon dioxide – acetone bath was removed and the reaction mixture warmed to room temperature (~1 h). Ether (30 mL) was added followed by methanol (2 mL) and water (10 mL), the reaction acidified with 10% aqueous hydrochloric acid, the mixture extracted with ether, the ether extracts washed with brine, dried, filtered, concentrated, and the products purified by flash chromatography (10% ethyl acetate/petroleum ether) to give the bridged cyclohexanone **11**, 112 mg (74%); ir ($CHCl_3$): 1700 (C=O) cm^{-1}; ^1H nmr (CCl_4) δ: 0.91 (3H, t, J = 7 Hz, CH_3—CH_2), 1.02 (3H, s, CH_3—C), 2–2.8 (6H, complex, bridgehead H, CH_2C=O), 3.40 (4H, m, CH_2—O), 6.01 (2H, br s, CH=CH), and the bridged cycloheptanone **13**, 32 mg (21%); ir ($CHCl_3$): 1695 (C=O) cm^{-1}; ^1H nmr ($CDCl_3$) δ: 0.7–1.9 (10H, complex), 1.9–2.9 (6H, complex, bridgehead H, CH_2C=O), 3.48 (4H, m, CH_2—O), 5.94 (2H, br s, CH=CH).

2-(4-Methyloxynaphthyl)methyltetracyclo[5.4.0^{1,7}.0^{4,6}.0^{6,10}]-undecan-3-one (15)

Jones reagent (0.75 mL) was added dropwise over 5 min to a stirred solution of the alcohol **18** (0.25 g, 1.1 mmol) in acetone (25 mL). Stirring was continued for a further 5 min, 2-propanol (0.5 mL) was added to decompose excess oxidant, the reaction mixture concentrated, the residue extracted with ether, the ethereal extracts washed with water, brine, dried, filtered, concentrated, and the product purified by flash chromatography (10% ethyl acetate/petroleum ether) to afford the ketone **15** (0.199 g, 80%), mp 78–80°C; ir ($CHCl_3$): 1705 (C=O) cm^{-1}; ^1H nmr (CCl_4) δ: 2.53 (3H, s, CH_3—Ar), 3.38 (2H, m, CH_2—O), 4.65 (2H, s, OCH_2Ar), 7.05 (2H, m, Ar), 7.25 (2H, m, Ar), 7.78 (2H, m, Ar). *Exact Mass* calcd. for $C_{24}H_{26}O_2$: 346.1933; found: 346.1974.

Chromium reduction of cyclopropylketone 15

A solution of chromium(II) sulphate in water (5 mL, 0.02 *M*) was added dropwise to a DMF solution (10 mL) of the cyclopropylketone **15** (40 mg, 0.12 mmol) and the reaction stirred at 23°C for 4 h. The reaction mixture was extracted with ether, the combined extracts washed with water, brine, dried, filtered, concentrated, and the products purified by flash chromatography (10% ethyl acetate/petroleum ether) to give **7** (8.0 mg, 20%) and **19** (32 mg, 79%); ^1H nmr ($CDCl_3$) δ: 2.68 (3H, s, CH_3Ar), 3.3–3.9 (2H, m, CH_2—O), 4.91 (2H, s, OCH_2Ar), 7.30 (2H, m, Ar), 7.53 (2H, m, Ar), 8.07 (2H, m, Ar).

2-Hydroxymethyltetracyclo[5.4.0^{1,7}.0^{4,6}.0^{6,10}]undecan-3-ol (17)

The unsaturated hydroxy-ester **1** (0.50 g, 2.2 mmol) was hydrogenated in methanol (25 mL) containing 10% Pd/C (25 mg) at 23°C

for 4 h. The reaction mixture was diluted with ether (50 mL), filtered, concentrated, and purified by flash chromatography (20% ethyl acetate/petroleum ether) to give the saturated hydroxy-ester **16** (0.48 g, 95%); ir ($CHCl_3$): 3560 (OH), 3400–3500 (br sh, OH), 1725 (sh, C=O), 1705 (C=O) cm^{-1}; ^1H nmr ($CDCl_3$) δ: 0.48 (1H, m, cyclopropyl H), 2.92 (1H, s, CH—CO_2Me), 3.57 (1H, m, H—C—OH), 3.69 (3H, s, OCH_3). The hydroxy-ester (0.44 g, 1.97 mmol) in ether (5 mL) was added dropwise to a stirred suspension of lithium aluminum hydride (0.224 g, 5.9 mmol) in ether (5 mL) at 0°C. Once addition was complete the ice-bath was removed and the reaction stirred at room temperature for 1.5 h, the reaction cooled, and water (0.5 mL) added carefully followed by anhydrous THF (20 mL) and anhydrous sodium sulphate. The mixture was stirred for a further 0.5 h, filtered, the residue washed thoroughly with THF, and the filtrate concentrated and purified by flash chromatography (60% ethyl acetate/petroleum ether) to give **17** (0.34 g, 90%); ir ($CHCl_3$): 3585 (OH), 3350–3450 (br, OH) cm^{-1}; ^1H nmr (CCl_4) δ: 0.59 (1H, m, cyclopropyl H), 3.73 (2H, br d, J = 5 Hz, CH_2—O), 4.45 (1H, br t, J = 4 Hz, HC—O).

2-(4-Methyl-1-methyloxynaphthyl)methyltetracyclo-[5.4.0^{1,7}.0^{4,6}.0^{6,10}]undecan-3-ol (18)

The diol **17** (0.80 g, 4.2 mmol) in THF (10 mL) was added to a cold (0°C) stirred suspension of sodium hydride (0.5 g, 10.4 mmol, Aldrich 60% dispersion in oil) in THF (10 mL). After 5 min hexamethylphosphoramide (5 mL, Eastman) was added, followed by 1-(chloromethyl)-4-methyl naphthalene (0.832 g, 4.4 mmol, Aldrich) in THF (5 mL), the ice bath was removed, and stirring continued at room temperature for 24 h. The ice bath was replaced, water (1 mL) added slowly, and the reaction mixture poured into cold (0°C) 10% aqueous hydrochloric acid and extracted with ether (2×). The combined extracts were washed with brine, dried, filtered, concentrated, and purified by flash chromatography (15% ethyl acetate/petroleum ether) to give the hydroxy-ether **18** (1.02 g, 70%); ir ($CHCl_3$): 3575 (sh, OH), 3450–3500 (OH) cm^{-1}; ^1H nmr ($CDCl_3$) δ: 0.45 (1H, m, cyclopropyl H), 0.65–2.0 (12H, complex), 2.60 (3H, s, CH_3—Ar), 2.88 (1H, br, s, OH), 3.17 (1H, m, H—C—OH), 3.49 (2H, m, CH_2—O), 4.84 (2H, s, O—CH_2Ar), 7.16 (2H, m, Ar), 7.43 (2H, m, Ar), 7.96 (2H, m, Ar). *Exact Mass* calcd. for $C_{24}H_{28}O_2$: 348.2089; found: 348.2092.

Acknowledgements

We are grateful to Memorial University of Newfoundland and the Natural Sciences and Engineering Research Council of Canada for financial support of this research, B. Gregory for high resolution mass spectra, F. Chau for technical assistance, and J. F. Kingston for fruitful discussions.

1. J. LAFONTAINE, M. MONGRAIN, M. SERGENT-GUAY, L. RUEST, and P. DESLONGCHAMPS. Can. J. Chem. **58**, 2460 (1980).
2. J. D. WHITE, J. F. RUPPERT, M. A. AVERY, S. TORII, and J. NOKAMI. J. Am. Chem. Soc. **103**, 1813 (1981).
3. G. GALLACHER, A. S. NG, S. K. ATTAH-POKU, K. ANTCZAK, S. J. ALWARD, and A. G. FALLIS. Can. J. Chem. **62**, 1709 (1984).
4. S. K. ATTAH-POKU, S. J. ALWARD, and A. G. FALLIS. Tetrahedron Lett. **24**, 681 (1983).
5. S. F. BRADY, M. A. ILTON, and W. S. JOHNSON. J. Am. Chem. Soc. **90**, 2882 (1968); M. MONGRAIN, J. LAFONTAINE, A. BELANGER, and P. DESLONGCHAMPS. Can. J. Chem. **48**, 3273 (1970); J. D. WHITE and J. F. RUPPERT. J. Am. Chem. Soc. **103**, 1808 (1981).
6. J. P. MCCORMICK and D. L. BARTON. J. Org. Chem. **45**, 2566 (1980).
7. P. A. WENDER and J. C. LECHLEITER. J. Am. Chem. Soc. **100**, 4321 (1978).
8. J. ALTMAN, D. BECKER, D. GINSBURG, and H. J. E. LOEWENTHAL. Tetrahedron Lett. 757 (1967); C. W. WOODWORTH, V. BUSS, and P. V. R. SCHLEYER. Chem. Commun. 569 (1968).
9. T. NORIN. Acta Chem. Scand. **19**, 1289 (1965); W. G. DAUBEN and R. E. WOLF. J. Org. Chem. **35**, 374 (1970); S. W. STALEY. *In* Selective organic transformations. Vol. 2. *Edited by* B. S. Thyagarajan. Wiley–Interscience, New York, NY. 1972. p. 309; P. DESLONGCHAMPS. Stereoelectronic Effects in organic chemistry. Pergamon Press, Oxford. 1983. p. 246.
10. J. DEKKER, F. J. C. MARTINS, and J. A. KRUGER. Tetrahedron Lett. 2489 (1975); W. S. MURPHY and S. WATTANASIN. Tetrahedron Lett. **22**, 695 (1981).
11. C. E. CASTRO, R. D. STEPHENS, and S. MOJE. J. Am. Chem. Soc. **88**, 4964 (1966).
12. H. O. HOUSE and E. F. KINLOCK. J. Org. Chem. **39**, 1173 (1974).
13. S. NAGASE and K. N. HOUK. Tetrahedron Lett. **23**, 19 (1982).
14. M. DUBECK. J. Am. Chem. Soc. **82**, 6193 (1960); C. BLEASDALE and D. W. JONES. Chem. Commun. 214 (1983).
15. W. C. STILL, M. KAHN, and A. MITRA. J. Org. Chem. **43**, 2923 (1978).

Can. J. Chem. Downloaded from www.nrcresearchpress.com by 210.87.254.105 on 09/06/12
For personal use only.

Studies on γ-irradiated aqueous solutions of amino acids with functional groups by the spin-trap high-performance liquid chromatography – electron spin resonance method

NAOHISA IGUCHI, FUMIO MORIYA,[1] KEISUKE MAKINO,[2] SOUJI ROKUSHIKA AND HIROYUKI HATANO[3]
Department of Chemistry, Faculty of Science, Kyoto University, Sakyo-ku, Kyoto 606, Japan

Received December 14, 1983

NAOHISA IGUCHI, FUMIO MORIYA, KEISUKE MAKINO, SOUJI ROKUSHIKA, and HIROYUKI HATANO. Can. J. Chem. **62**, 1722 (1984).

Aqueous solutions of L-glutamine, L-asparagine, sodium L-glutamate, sodium L-aspartate, L-serine, and L-threonine were γ-irradiated in the presence of a spin trap, 2-methyl-2-nitrosopropane. Stable spin adducts produced in the irradiated solutions were analyzed by the spin-trap hplc–esr method. The spin adducts of the following short-lived radicals were found and identified: $H_2NCOCH_2\dot{C}H_2CHCOO^-$ (**1**), $H_2NCOCH_2CH_2\dot{C}(NH_3^+)COO^-$ and $H_2NCO\dot{C}HCH_2CH(NH_3^+)COO^-$ for L-glutamine; $H_2NCO\dot{C}HCH(NH_3^+)COO^-$ (**2**) for L-asparagine; $^-OOCCH_2CH_2\dot{C}HCOO^-$ (**3**) and $^-OOC\dot{C}HCH_2CH(NH_3^+)COO^-$ for sodium L-glutamate; $^-OOCCH_2\dot{C}HCOO^-$ (**4**) and $^-OOC\dot{C}HCH(NH_3^+)COO^-$ (**5**) for sodium L-aspartate; $HO\dot{C}HCH(NH_3^+)COO^-$ and $HOCH_2\dot{C}HCOO^-$ (**6**) for L-serine; $CH_3CH(OH)\dot{C}HCOO^-$ (**7**) and $\dot{C}H_2CH(OH)CH(NH_3^+)COO^-$ for L-threonine. The free radicals, **1**, **3**, **4**, **6**, and **7**, were due to the reaction of the hydrated electron (e_{aq}^-) with these amino acids and the other adducts were due to the attack of hydroxyl radical (·OH). The two diastereomeric pairs of spin adducts of the short-lived radicals, **2** and **5**, could be individually separated by the technique utilized.

NAOHISA IGUCHI, FUMIO MORIYA, KEISUKE MAKINO, SOUJI ROKUSHIKA et HIROYUKI HATANO. Can. J. Chem. **62**, 1722 (1984).

On a irradié des solutions aqueuses de L-glutamine, de L-asparagine, de L-glutamate de sodium, de L-aspartate de sodium, de L-sérine et de L-thréonine par des rayons γ en présence d'un capteur de spin, le méthyl-2 nitroso-2 propane. Faisant appel à la méthode de clhp–rpe des spin piégés, on a analysé les adduits de spin stables produits dans les solutions irradiées. On a trouvé et on a identifié les adduits de spin des radicaux suivants à courte vie: $H_2NCOCH_2CH_2CHCOO^-$ (**1**), $H_2NCOCH_2CH_2\dot{C}(NH_3^+)COO^-$ et $H_2NCO\dot{C}HCH_2CH(NH_3^+)COO^-$ pour la L-glutamine; $H_2NCO\dot{C}HCH(NH_3^+)COO^-$ (**2**) pour la L-asparagine; $^-OOCCH_2CH_2\dot{C}HCOO^-$ (**3**) et $^-OOC\dot{C}HCH_2CH(NH_3^+)COO^-$ pour le L-glutamate de sodium; $^-OOCCH_2\dot{C}HCOO^-$ (**4**) et $^-OOC\dot{C}HCH(NH_3^+)COO^-$ (**5**) pour le L-aspartate de sodium; $HO\dot{C}HCH(NH_3^+)COO^-$ et $HOCH_2\dot{C}HCOO^-$ (**6**) pour la L-sérine; $CH_3CH(OH)\dot{C}HCOO^-$ (**7**) et $\dot{C}H_2CH(OH)CH(NH_3^+)COO^-$ pour la L-thréonine. Les radicaux libres **1**, **3**, **4**, **6** et **7** proviennent de la réaction de l'électron hydraté (e_{aq}^-) avec ces acides aminés et les autres adduits proviennent d'une attaque du radical hydroxyle (·OH). La méthode utilisée permet de séparer individuellement les deux paires d'adduits de spin diastéréoisomères des radicaux de faible temps de vie, **2** et **5**.

[Traduit par le journal]

Introduction

Spin trapping (1–8) is the method by which short-lived radicals are converted into relatively stable aminoxyl radicals by reaction with diamagnetic compounds (spin traps). By means of this unique method, the assignment of the parent short-lived radicals can be made by analyzing the electron spin resonance (esr) spectra of the spin adducts produced. Since the introduction of this method, it has been intensively used to detect short-lived free radicals produced in aqueous solutions (9–12).

The combination of the spin trapping method, where 2-methyl-2-nitrosopropane is used as a spin trap, and high-performance liquid chromatography (hplc), by which individual spin adducts are isolated from their mixture solutions, has been utilized in order to assign each short-lived free radical produced in aqueous amino acid or peptide solutions by γ-radiolysis (13–19). This is because ionizing radiation is known to form a number of short-lived free radicals in aqueous solutions by the attack of highly reactive primary species such as hydrated electrons (e_{aq}^-) (20) and hydroxyl radicals (·OH) (21) which are generated from water, and in general, therefore, esr spectra obtained from the irradiated solutions by spin trapping are highly complicated. By the separation of the spin adducts followed by their esr analysis, a number of free radicals from the amino acids and peptides (glycine (16), L-alanine (16), L-valine (14), L-leucine (15), L-isoleucine (15), DL-methionine (13), L-proline (18), *trans*-4-hydroxy-L-proline (18), glycylglycine (17), glycyl-L-alanine (17), L-alanylglycine (19), L-alanyl-L-alanine (19), and so on), many of which had not been found before this combination was used, could be detected and assigned. In addition, the spin adducts produced in the irradiated aqueous MNP solution have been separated and assigned to the structures so that the identification of the spin adducts from amino acids and peptides can be made more unambiguous (22). It has also been demonstrated previously that some of the esr spectra from the amino acids and peptides showed extreme complexity due to the structural specificities of the spin adducts and that, in such cases, changes in the pH and D_2O replacement of the sample solution were useful for the unambiguous assignment. The hyperfine splittings (hfs) due to the atoms adjacent to functional groups such as amino or carboxyl groups were found to be changed by such treatments.

In the present study, amino acids with additional functional groups (L-glutamine, L-asparagine, L-glutamic acid, L-aspartic acid, L-serine, and L-threonine) were γ-irradiated in aqueous solutions, producing short-lived free radicals. These radicals were investigated by this combination hplc–esr method coupled with the changes in conditions of the sample solutions. Previously, only a few spin adducts from these amino acids could be assigned because of the high complexity of the obtained esr spectra arising from the overlapping of the esr components of several spin adducts present in the same sample

[1] Present address: Department of Chemistry, Kobe University of Commerce, Tarumi-ku, Kobe 655, Japan.

[2] Present address: Department of Textile Science, Kyoto Institute of Technology, Sakyo-ku, Kyoto 606, Japan.

[3] Author to whom correspondence may be addressed.

Can. J. Chem. Downloaded from www.nrcresearchpress.com by 210.87.254.40 on 09/06/12
For personal use only.

Can. J. Chem. Downloaded from www.nrcresearchpress.com by 210.87.254.40 on 09/06/12
For personal use only.

solution (10, 11). Therefore, it will be interesting if other unidentified free radicals from these amino acids can be analyzed by the method we have proposed. Also, since these amino acids are frequently located in the active center of various enzymes, such assignment is believed to be useful in understanding their inactivation caused by radiolysis.

Experimental

2-Methyl-2-nitrosopropane (MNP) used in this study was synthesized by the method proposed previously by Stowell (23). D_2O (99.8%) was obtained from E. Merck Co. Amino acids and all other reagents were purchased from Nakarai Chemicals (Kyoto, Japan). These compounds were used without further purification.

Aqueous MNP solutions (5 mg/mL) were prepared by stirring for 1 h at 45°C in the dark (22). L-glutamine (Gln), L-asparagine (Asn), L-serine (Ser), and L-threonine (Thr) (0.2 *M*) were dissolved into the MNP solutions. The sample solutions, with the exception of Asn, were cooled by ice and irradiated with ^{60}Co γ-rays at a dose rate of 4 kGy/h to a total dose of 3 kGy without deaeration. Aqueous solutions containing Asn were irradiated at room temperature. In the case of sodium L-glutamate (Na-Glu) and sodium L-aspartate (Na-Asp), saturated solutions were irradiated.

Immediately after the irradiation, the concentration of phosphoric ion in the irradiated solution was adjusted to 0.2 *M* by 2.0 *M* sodium phosphate buffer. A quantity of 1.0 mL (in the cases of Na-Glu and Na-Asp: 0.2 mL) of the solution was loaded on a 0.75 × 60 cm cation-exchange column (IEX-210SC of Toyo Soda). The high-performance liquid chromatograph used was a Toyo Soda HLC-803. The eluate was passed through ultraviolet uv (JASCO UVIDEC 100) and esr detectors and collected in the fraction tubes. The wavelength of the uv detector was 240 nm. The esr spectrometer was a JEOL PE-3X (X-band, 100-kHz field modulation). For the detection of radicals during chromatography, the magnetic field was fixed at the positions indicated by the vertical arrows, as shown in Fig. 1. The field modulation was used at a high amplitude of 1 mT to cover a wide range. A quartz flow cell (0.6-mm id) was fixed in the esr cavity. The eluent employed for the separation was 0.2 *M* Na_2HPO_4–Na_2HPO_4 buffer (pH 6.8). Each part in the chromatographic system was connected with 0.25-mm id Teflon tube. The chromatographic conditions were as follows: flow rate, ca. 0.3 mL/min (in the cases of Na-Glu and Na-Asp, ca. 0.1 mL/min); pressure, ca. 10 kg/cm^2; temperature, ca. 25°C. The esr spectra of the fractions containing the spin adducts were obtained at ca. 25°C in the dark. In some cases, the second derivative spectra (80 Hz modulation) were measured to obtain further information. The pH adjustment, which was employed to study the spectral changes depending on the pH of the solutions, was performed using dilute HCl or NaOH. Some of the fractions were lyophilized and then added to D_2O in order to determine the hyperfine splittings arising from the exchangeable hydrogens. Hyperfine splitting constants (hfsc's) were measured by using Mn^{2+} in MgO as a reference. The simulation of the esr spectra was achieved by using a JEOL JEC-980A minicomputer.

For other experimental details refer to previous works (13–19).

Results and discussion

By the method of combination of spin trapping with MNP and hplc separation of the resulting spin adducts, several individual esr spectra were obtained for each amino acid, and it was found that the parent radicals were produced by the deamination reaction due to the attack of e^-_{aq} or by the H-abstraction reaction caused by ·OH. The hfsc's obtained from the spectra and by the computer simulation are all listed in Table 1.

L-Glutamine

The esr spectrum obtained from the γ-irradiated aqueous solution containing Gln and MNP is shown in Fig. 1(a). The spectrum is composed of the several overlapping esr signals of the spin adducts, which are produced by the reactions of MNP with short-lived radicals from Gln as well as from MNP. By the chromatographic separation of this sample solution, five peaks (elution volumes: 9.8 mL, 14.8 mL, 16.8 mL, 18.0 mL, and 20.5 mL, respectively) were detected by esr. However, analyzable esr signals could not be obtained from the fractions of the second and fourth peaks. Figures 2(a)–(c) show the esr spectra obtained from the first, third, and fifth peaks, respectively.

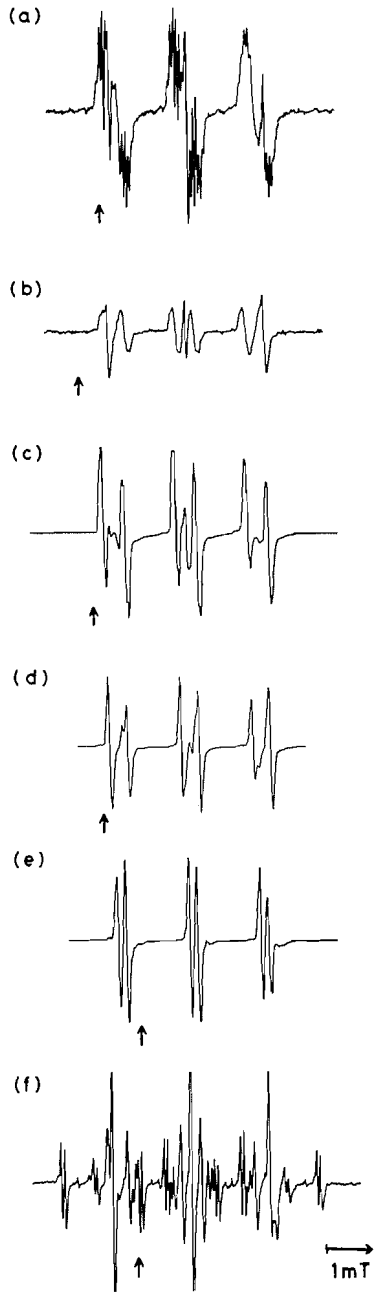

FIG. 1. Electron spin resonance spectra obtained from the γ-irradiated aqueous solutions of (a) Gln, (b) Asn, (c) Na-Glu, (d) Na-Asp, (e) Ser, and (f) Thr. During chromatography the magnetic fields were fixed at the positions indicated by the vertical arrows and the modulation amplitude was set to 1 mT. The esr settings are as follows: modulation amplitude, 0.02 mT; receiver gain, 5.0 × 10^2 for (a), (b), and (f), 1.0 × 10^2 for (c), (d), and (e); time constant, 0.03 s for (a), (b), (e), and (f), 0.01 s for (c) and (d); scan time, 8 min for (a), (b), (e), and (f), 4 min for (c) and (d).

TABLE 1. The hyperfine splitting constants (mT) of the spin adducts

Amino acid	Spin adduct	pH	a(N)	a(βH)	a(βN)	a(γN)	a(γN)	a(δH)
Gln	**1**	6.8	1.56	0.47		0.055 (2H)		
	2	6.8	1.60		0.10	0.14		
						0.10		
						0.05 (3H, amino)		
		11.0	1.61		0.10	0.135		
						0.10		
	3	6.8	1.53	0.40		0.06 (2H)	0.06	0.06 (amide)
		11.0	1.55	0.34		0.07 (2H)	0.07	0.07 (amide)
Asn	**4***a*	1.3	1.51	0.53				
		6.8	1.51	0.41		0.11		
		11.0	1.52	0.33			0.075 (amino or amide)	
								0.075 (amide)
	4*b*	6.8	1.51	0.36				
Na-Glu	**6**	6.8	1.56	0.45		0.055 (2H)		
	7	1.6	1.53	0.28				
		6.8	1.57	0.48		0.055 (2H)		
		12.0	1.55	0.44		0.06 (2H)		
Na-Asp	**8**	6.8	1.57	0.58		0.06 (2H)		
	9*a*	1.6	1.50	0.34				
		6.8	1.53	0.39				
		11.0	1.54	0.49				
	9*b*	1.6	1.52	0.25		0.07		
		6.8	1.57	0.32		0.07		
		11.0	1.56	0.44		0.06		
Ser	**10**	5.4	1.50	0.17				
	11	1.6	1.54	0.26		0.03 (2H)		
		6.8	1.56	0.44		0.04 (2H)		
Thr	**12**	1.5	1.53	0.27				
		6.8	1.56	0.42				
	13	6.8	1.63	1.51		0.08		
				0.68				
		11.0	1.65	1.57		0.08		
				0.64				

In the spectrum shown in Fig. 2(a), which was obtained from the fraction giving the first peak, each component of the primary triplet, which is due to the aminoxyl nitrogen, splits into 2 × 3 secondary lines due to a β-hydrogen and two equivalent γ-hydrogens. This spectrum was not changed at the alkaline pH. Consequently, this esr spectrum was assigned to the spin adduct (**1**), which is due to the reaction of the hydrated electron (e^-_{aq}) with the Gln, and called the deamino adduct.

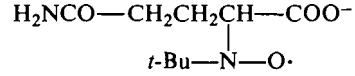

1

The spectra produced by the fraction giving the third peak were measured in H_2O and D_2O, as shown in Figs. 3(a) and (b), respectively, where the $M_1 = 0$ components of each spectrum are represented. In D_2O, the second derivative of the spectrum was also obtained. The spectrum consists of 11 lines in H_2O whereas there are 10 lines in D_2O. The spectral change depending on the solvents indicates that the spectrum in H_2O involves hyperfine splittings due to at least one exchangeable hydrogen of the amino group or the amide group of the spin adduct. Also, a spectrum obtained in a basic solution (pH 11) was different from that at the neutral pH, which suggests the presence of the amino group near the aminoxyl group. The computer simulations for the esr spectra at neutral pH were carried out. In Figs. 3(a) and (b), the simulated spectra at pH 7 in H_2O and at pH 7 in D_2O are depicted, respectively, together with their original spectra. The parameters used for the simulations were as follows: a(βN) = 0.10 mT, a(γH-1) = 0.14 mT, a(γH-2) = 0.10 mT, a(γH) = 0.04 mT (three amino hydrogens) and Lorentzian peak-to-peak line width = 0.04 mT for the form in H_2O. In the case of the structure in D_2O, the values for the amino hydrogens were replaced by zero (the splitting constant due to a deuterium was too small to be observed, compared to that due to a hydrogen). The other values used were the same as those utilized for the form in H_2O. Consequently, the spectrum in Fig. 3(a) was assigned to the spin adduct **2**. The parent free radical of this adduct was formed by the attack of hydroxyl radical (·OH) to the Gln.

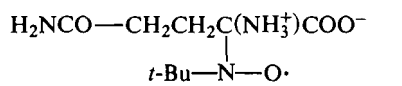

2

Figures 3(c) (in H_2O) and (d) (in D_2O) show the $M_1 = 0$ components of the esr spectra obtained from the fifth peak. The spectral pattern consisting of 2 × 6 lines in H_2O changed to 2 × 5 lines in D_2O. Assuming that the spectral change dependent on the solvent is due to the change in the splittings arising from one of the two exchangeable amide hydrogens (δ-hydrogens, (24)), the spin adduct in the fraction was assigned to the structure **3**. In order to make this assignment more unambiguous, computer simulation was made for the spectra shown in Figs.

Can. J. Chem. Downloaded from www.nrcresearchpress.com by 210.87.254.40 on 09/06/12
For personal use only.

Can. J. Chem. Downloaded from www.nrcresearchpress.com by 210.87.254.40 on 09/06/12
For personal use only.

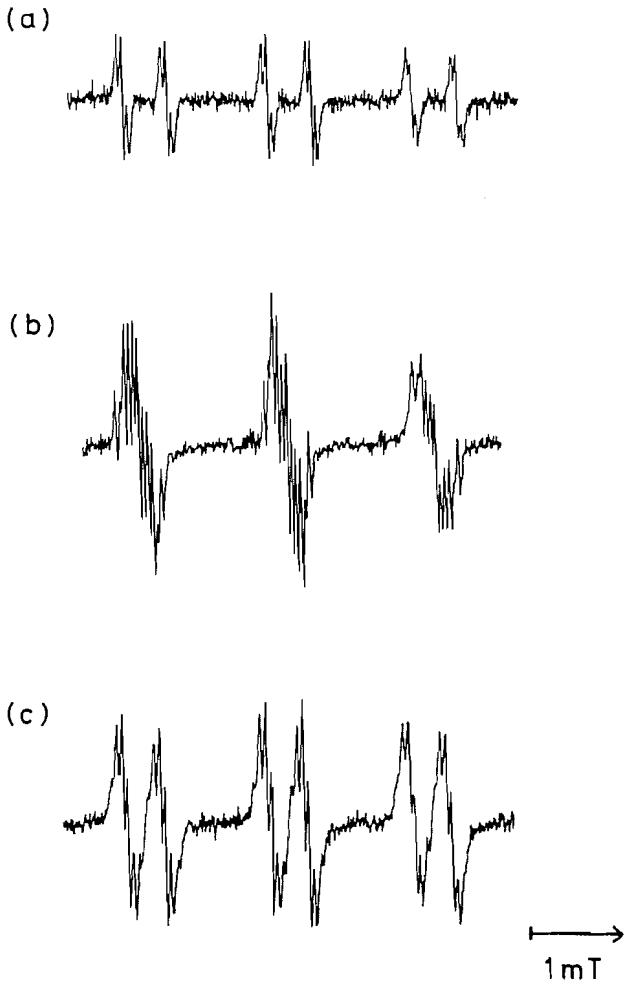

FIG. 2. Electron spin resonance spectra of the spin adducts from Gln. Figures (a)–(c) were obtained from the fractions giving the first, third, and fifth peaks in the esr chromatogram, respectively. The esr measurements were carried out at pH 6.8 in H_2O. The esr settings are as follows: modulation amplitude, 0.025 mT for (a) and (c), 0.02 mT for (b); receiver gain, 1.0×10^3; time constant, 0.1 s; scan time, 16 min.

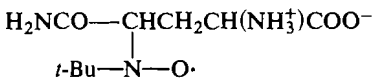

3

3(c) and 3(d) and good agreement between the spectra and the simulation spectra could be obtained. The esr parameters used for the simulation of the spectrum in H_2O were as follows: $a(\beta H) = 0.40$ mT, $a(\gamma H) = 0.06$ mT (2H), $a(\gamma N) = 0.06$ mT (amide nitrogen), $a(\delta H) = 0.06$ mT (amide hydrogen). The values used for the spectrum in D_2O were the same as those for the spectrum in H_2O except that the hfsc for the amide hydrogen was replaced by zero.

L-Asparagine

The esr spectrum shown in Fig. 1(b) was obtained from aqueous Asn solution with MNP just after the γ-irradiation. By chromatographic separation, three peaks (elution volumes were: 11.9 mL, 19.6 mL, and 27.4 mL, respectively) appeared in the esr chromatogram. The fractions of these peaks lead to the esr spectra shown in Figs. 4(a)–(c).

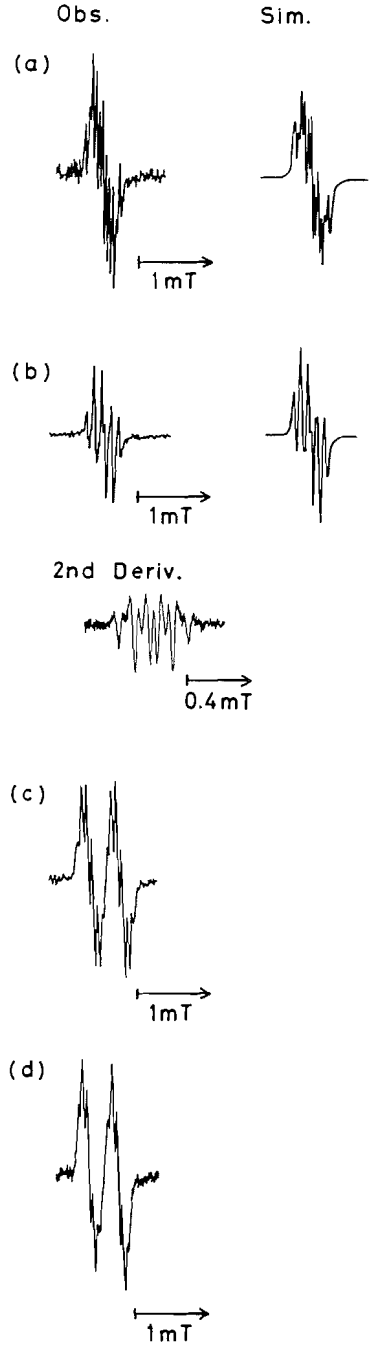

FIG. 3. (a) The $M_I = 0$ component of the esr spectrum in Fig. 2(b) and its simulation spectrum. The esr settings are as follows: modulation amplitude, 0.02 mT; receiver gain, 1.0×10^3; time constant, 0.1 s; scan time, 16 min. The esr parameters for the simulation spectrum refer to the text. (b) The $M_I = 0$ component (first and second derivatives at pH 6.8 in D_2O) of the esr spectrum of the spin adduct in Fig. 2(b) and the simulation for the first derivative. The esr settings are as follows: first derivative: modulation amplitude, 0.02 mT; receiver gain, 1.0×10^3; time constant, 0.3 s; scan time, 32 min; second derivative, modulation amplitude (100 kHz and 80 Hz), 0.02 mT; receiver gain (100 kHz), 1.0×10^4; receiver gain (80 Hz), 5.0; time constant, 1 s; scan time, 64 min. (c) The $M_I = 0$ component of the esr spectrum in Fig. 2(c). The esr settings are as follows: modulation amplitude, 0.025 mT; receiver gain, 1.0×10^3; time constant, 0.1 s; scan time, 16 min. (d) The $M_I = 0$ component (at pH 6.8 in D_2O) of the esr spectrum of the spin adduct in Fig. 2(c). The esr settings are as follows: modulation amplitude, 0.025 mT; receiver gain, 2.0×10^3; time constant, 1 s; scan time, 16 min.

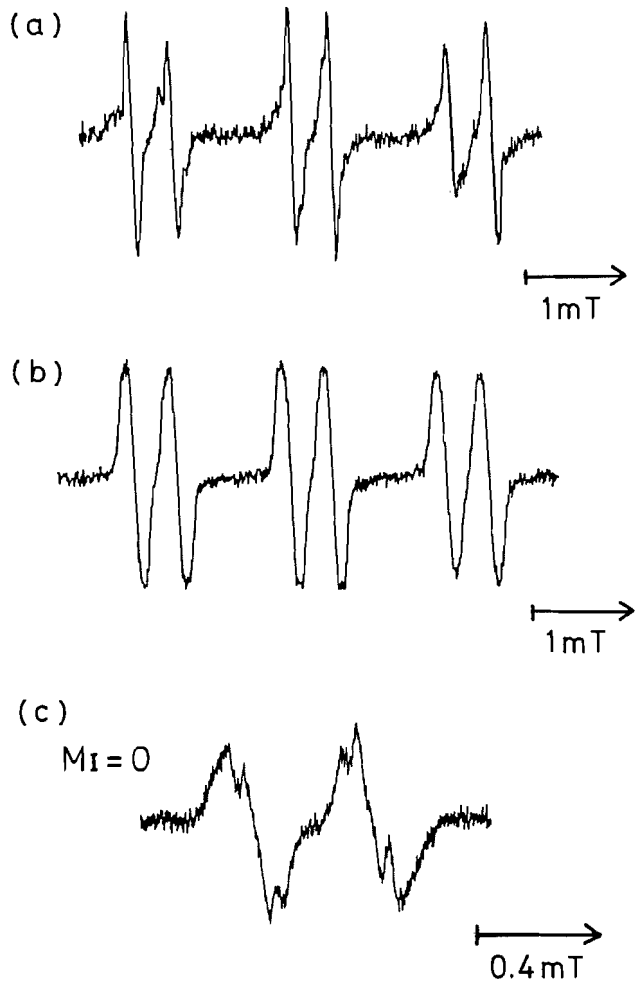

FIG. 4. Electron spin resonance spectra of the spin adducts from Asn. Figures (a) and (b) were obtained from the fractions giving the first and second peaks in the esr chromatogram, respectively. Figure (c) is the $M_I = 0$ component of expanded spectrum obtained from the third fraction. The esr measurements were carried out at pH 6.8 in H_2O for (a) and (b), while at pH 6.8 in D_2O for (c). The esr settings are as follows: modulation amplitude, 0.02 mT; receiver gain, 2.0×10^3 for (a), 1.0×10^3 for (b), 5.0×10^3 for (c); time constant, 1 s for (a), 0.3 s for (b), 3 s for (c); scan time, 64 min for (a), 32 min for (b), 128 min for (c).

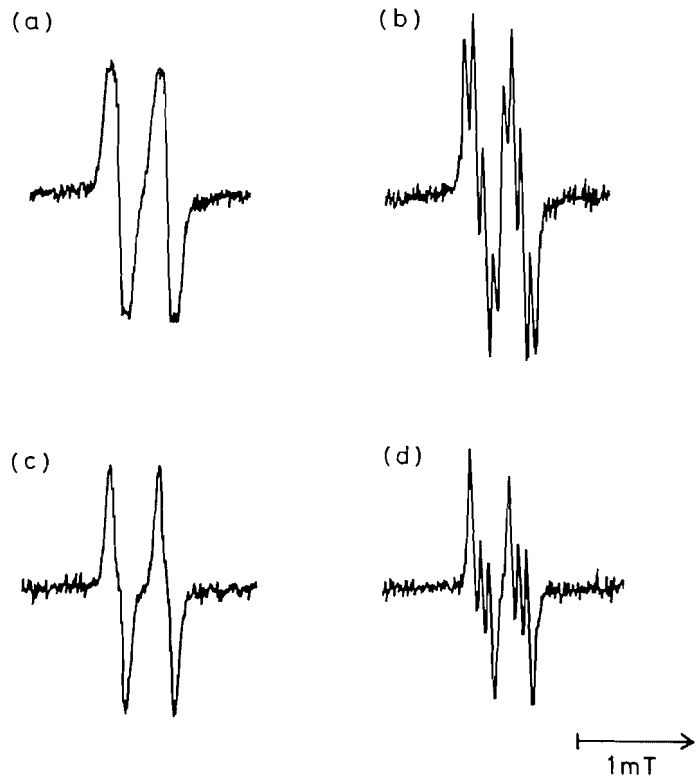

FIG. 5. The $M_I = 0$ components of the esr spectra of the spin adduct in Fig. 4(b) which were obtained at (a) pH 6.8 in H_2O, (b) pH 11.0 in H_2O, (c) pH 6.8 in D_2O, and (d) pH 11.0 in D_2O. The esr settings are as follows: modulation amplitude, 0.02 mT; receiver gain, 1.0×10^3 for (a), (c), and (d), 7.1×10^2 for (b); time constant, 0.3 s for (a), (c), and (d), 0.1 s for (b); scan time, 32 min for (a), (c), and (d), 16 min for (b).

The spectrum represented in Fig. 4(a) (the first peak) consists of more than two spectra, so satisfactory identification could not be made. The spectrum shown in Fig. 4(b) (the second peak) is composed of only broad 3×2 lines. However, the spectra at pH 11 in H_2O and in D_2O involve further fine splittings as represented in Figs. 5(b) and 5(d). The esr spectrum at pH 11 in H_2O consists of two lines split into a quartet with an intensity ratio of 1:2:2:1, while the spectrum at pH 11 in D_2O has 2×3 secondary lines with an intensity ratio of 1:1:1. It is likely that the 4 secondary lines in the spectrum at pH 11 in H_2O are due to an amide nitrogen and one of two amide hydrogens, whereas the three lines appearing in the spectrum at pH 11 in D_2O are produced from only an amide nitrogen. Also, this marked spectral change caused by the pH variation indicates that this spin adduct retained the amino group. Consequently this spectrum was assigned to the spin adduct **4***a*.

The spectrum obtained from the third peak had a triplet split

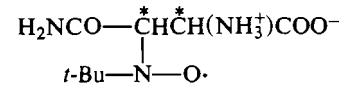

4*a*

into doublets. The signal intensity of this spectrum was not enough to observe further splittings because of the low concentration of the adduct in the fraction. However, in the case of the spectrum in D_2O, secondary splitting of 2×3 lines could be observed as shown in Fig. 4(c). This result indicates that the adduct has a γ-nitrogen, or a γ-hydrogen and a γ-nitrogen whose hfsc is not equal to, but slightly different from, that of the γ-hydrogen, or two equivalent γ-hydrogens, as well as a β-hydrogen. This implies that the esr spectrum could be assigned to the structure **4***b* or **5**. In the case of the adduct **4***b*,

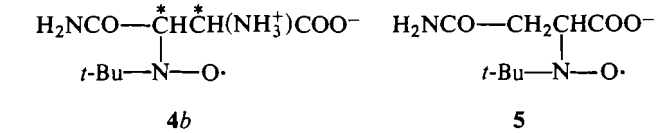

4*b* **5**

which can be produced by the H-abstraction from the Asn caused by ·OH attack, the γ-hfs is produced from a γ-hydrogen and a γ-nitrogen. The adduct **5** can be produced by the deamination reaction of Asn and the γ-hfs arises from two equivalent γ-hydrogens. Generally, deamino adducts of amino acids have a primary splitting $a(N) = 1.56$ or 1.57 mT, due to an aminoxyl nitrogen, while this adduct has a primary splitting

Can. J. Chem. Downloaded from www.nrcresearchpress.com by 210.87.254.40 on 09/06/12
For personal use only.

Can. J. Chem. Downloaded from www.nrcresearchpress.com by 210.87.254.40 on 09/06/12
For personal use only.

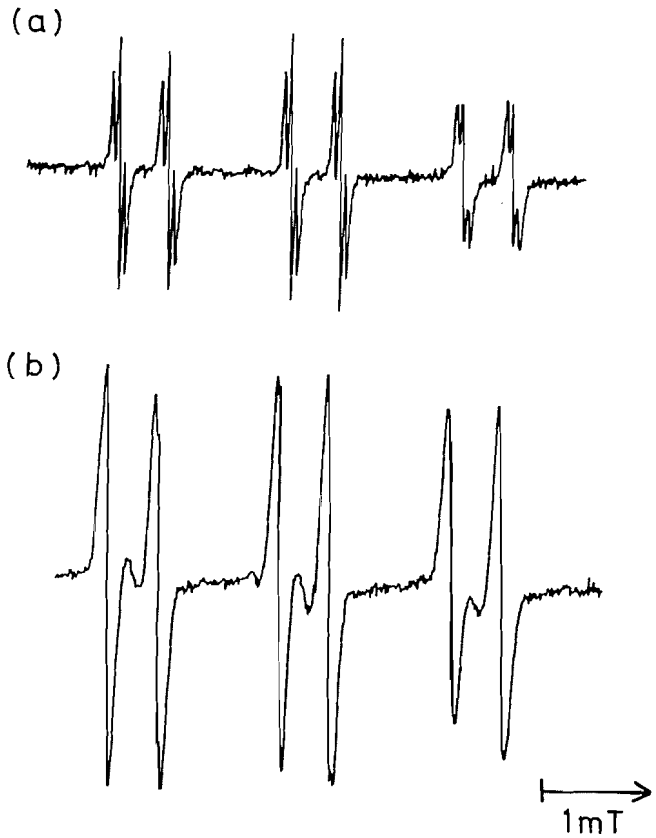

FIG. 6. Electron spin resonance spectra of the Na-Glu spin adducts obtained from the fractions giving the first (a) and second (b) peaks. They were observed at pH 6.8. The esr settings are as follows: modulation amplitude, 0.02 mT; receiver gain, 5.0×10^2; time constant, 0.1 s; scan time, 16 min.

a(N) = 1.51 mT. In addition, adducts which do not have amino groups are eluted approximately at the void volume of the column, while this peak was eluted considerably late. Considering these facts, this spectrum was assigned to the adduct ***4b***. Since the structure ***4b*** is the same as ***4a***, these two species are diastereomeric spin adducts of each other (the carbon atoms asterisked are the chiral centers).

Sodium L-glutamate

The γ-irradiated aqueous Na-Glu solution containing MNP produced the esr spectrum shown in Fig. 1(c). The chromatographic separation of the solution at low flow rate of 0.1 mL/min gave two bands (elution volumes: 10.1 mL and 10.6 mL, respectively) in the esr chromatogram. The retention volumes of these bands are small. This is due to the existence of two carboxyl groups in the molecules. The spectra obtained from the fractions are shown in Figs. 6(a) and (b), respectively.

The spectrum shown in Fig. 6(a) (the first peak) has 2 × 3 secondary splitting due to a β-hydrogen and two equivalent γ-hydrogens. There are two possibilities for the assignment of the adduct. One possible structure is **6**. The other one is **7**. Since the observed spectra were not changed in the alkaline

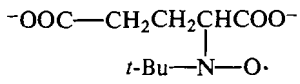

6

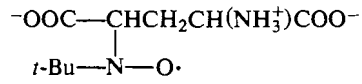

7

solution and since the adduct was eluted fast at the void volume, the spectra could be assigned to the adduct **6**, which does not have an amino group.

The spectrum in Fig. 6(b) (the second peak) consists of relatively broad 2 × 3 splittings. The hfsc's of the adduct are reversibly varied by the pH alteration as shown in Table 1 (at pH 1.6, 6.8, 12.0). The change in the alkaline pH range indicates the existence of an amino group in the adduct. Also, the large change in the acidic range implies that the adduct has a carboxyl group adjacent to the carbon on which there is a β-hydrogen of the adduct. The fast elution of this adduct may be due to the existence of the two carboxyl groups. Consequently, the spectrum was assigned to the spin adduct **7**. A little skew observed in the spectrum is probably due to the presence of some other radicals.

Sodium L-aspartate

The esr spectrum represented in Fig. 1(d) was produced by the γ-irradiated Na-Asp solution. Figures 7(a)–(c) show the spectra obtained from the three peaks (elution volumes were: 10.9 mL, 11.3 mL, and 12.9 mL, respectively) appearing in the esr chromatogram. Those bands were also eluted fast.

The esr spectrum from the first peak (Fig. 7(a)), which appeared at the void volume, was not changed at the alkaline pH at all, indicating that the structure of the adduct is **8**.

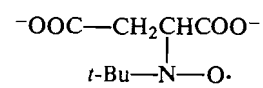

8

The spectrum obtained from the fraction of the second peak, which is shown in Fig. 7(b), consists of a secondary doublet due to a β-hydrogen. The hfs constants of the adduct are varied by the pH alteration as shown in Table 1 (pH 1.6, 6.8, and 11.0). Since this change of the hfsc's in the alkaline pH range indicates that this adduct has an amino group, this spectrum was assigned to the structure ***9a***. The splittings arising from a γ-hydrogen and γ-nitrogen could overlap to produce no fine structure.

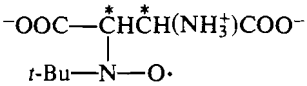

9a

The fraction due to the third peak led to the spectrum shown in Fig. 7(c) and this spectrum was changed to that in Fig. 7(d) in D_2O. In both cases, the spectra consist of 2 × 2 secondary splittings due to a β-hydrogen and a γ-hydrogen. The difference of the line widths between the spectra implies that the spin adduct has amino hydrogens exchangeable to H_2O. The spectra were found to be reversibly changed in the acidic and alkaline pH ranges as well as the second peak. The structure of the adduct was assigned to ***9b***. Since ***9a*** and ***9b*** are the same, they

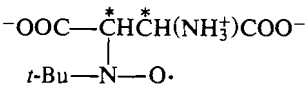

9b

are a pair of the diastereomeric spin adducts, which were eluted separately in the esr chromatogram.

L-Serine

The esr spectrum obtained from the γ-irradiated aqueous

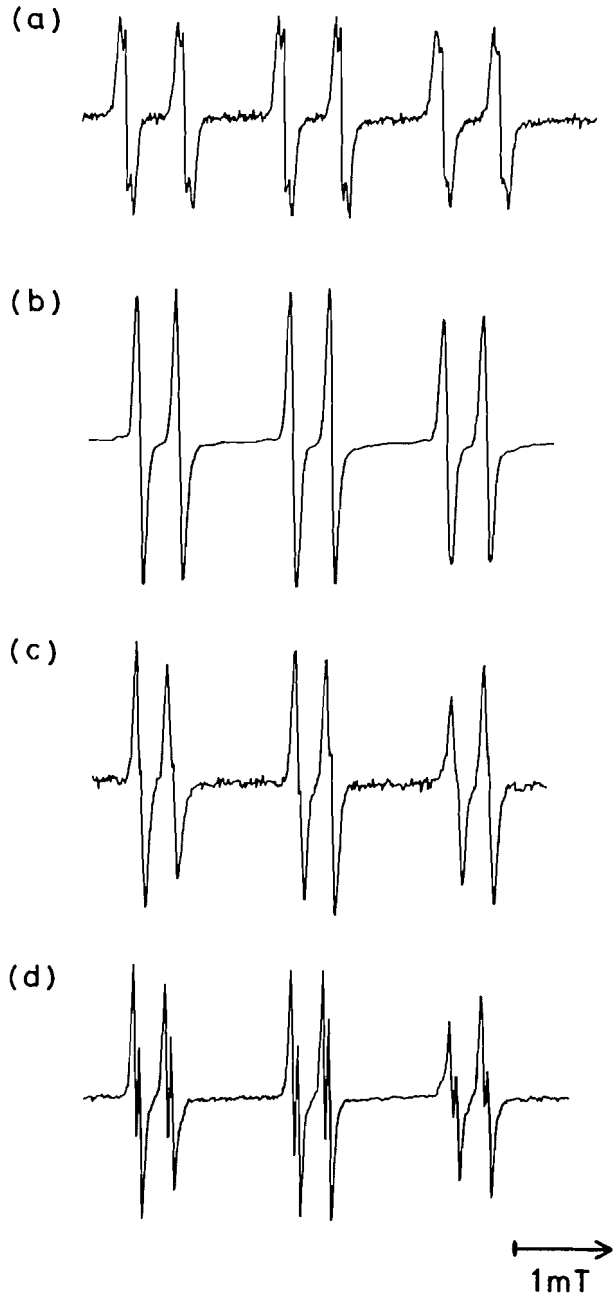

FIG. 7. Electron spin resonance spectra of the Na-Asp spin adducts obtained at pH 6.8 in H_2O from the fractions giving the first (a), second (b), and third (c) peaks. Figure (d) was obtained at pH 6.8 in D_2O from the third fraction. The esr settings are as follows: modulation amplitude, 0.02 mT; receiver gain, 5.0×10^2 for (a) and (c), 1.0×10^2 for (b), 2.5×10^2 for (d); time constant, 0.1 s for (a) and (c), 0.03 s for (b) and (d); scan time, 16 min for (a), 8 min for (b), (c), and (d).

L-serine solution is shown in Fig. 1(e). The main component of the spectrum is composed of 3 × 2 lines and was assigned to the spin adduct **10**. This adduct was unstable, decaying with a half life of about 10 min.

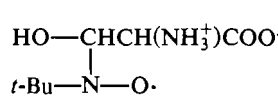

10

The esr chromatogram obtained from this solution exhibited only one analyzable peak (elution volume: 11.9 mL). The spectrum from the peak is shown in Fig. 8(a). Since this is a typical spectrum of a deamino adduct, the structure of this adduct is **11**. The peak due to the adduct **10** did not appear in the chromatogram because the adduct was unstable on the column.

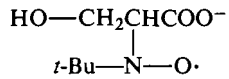

11

L-Threonine

The esr spectrum of aqueous L-threonine solution just after the γ-irradiation is represented in Fig. 1(f). By the chromatographic analysis, two spin adducts (elution volumes: 12.1 mL and 18.2 mL) were detected. Their esr spectra are shown in Figs. 8(b) and (c).

The esr spectrum depicted in Fig. 8(b) (the first peak) was assigned to the structure **12**, which is a deamino adduct. Splitting due to a γ-hydrogen is not seen in the spectrum, probably because of the overlapping of two similar spectra arising from the existence of a pair of diastereomeric spin adducts.

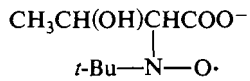

12

The esr spectrum shown with its stick diagram in Fig. 8(c) was obtained from the fraction of the second peak. This spectral pattern, consisting of three sets of two sharp outer lines and two broad inner lines, is typical of a radical whose structure is *t*-Bu—N(O·)—CH_2—C*XYZ which has a methylene group between the chiral center and the aminoxyl group (25). Consequently, this spectrum was assigned to **13**.

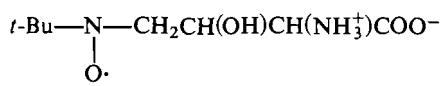

13

In summary, by the spin-trap hplc–esr method, three, two, two, three, two, and two spin adducts were found to be produced from Gln, Asn, Na-Glu, Na-Asp, Ser, and Thr, respectively. The assignments were made more unambiguous by the observation of the spectral changes which were caused by changing the nature of the solutions. All of the spectral changes observed here were determined to be reversible. Some spin adducts detected in this study were not previously assigned unambiguously. In the present work, the relative spin adduct concentration in the radiolytic mixture could not be determined. Since spin adducts start decaying at a different rate immediately after the irradiation, although it is very slow, it seems to be quite difficult to estimate the concentration of each spin adduct even after the separation, although most of the spin adducts have been found to be more stable on the chromatographic column than in solution. Also, the facts that the chromatographic band widths of each spin adduct are not equal in most cases and that some chromatographic bands overlap with each other, so that esr measurments can not be performed

Can. J. Chem. Downloaded from www.nrcresearchpress.com by 210.87.254.40 on 09/06/12
For personal use only.

Can. J. Chem. Downloaded from www.nrcresearchpress.com by 210.87.254.40 on 09/06/12
For personal use only.

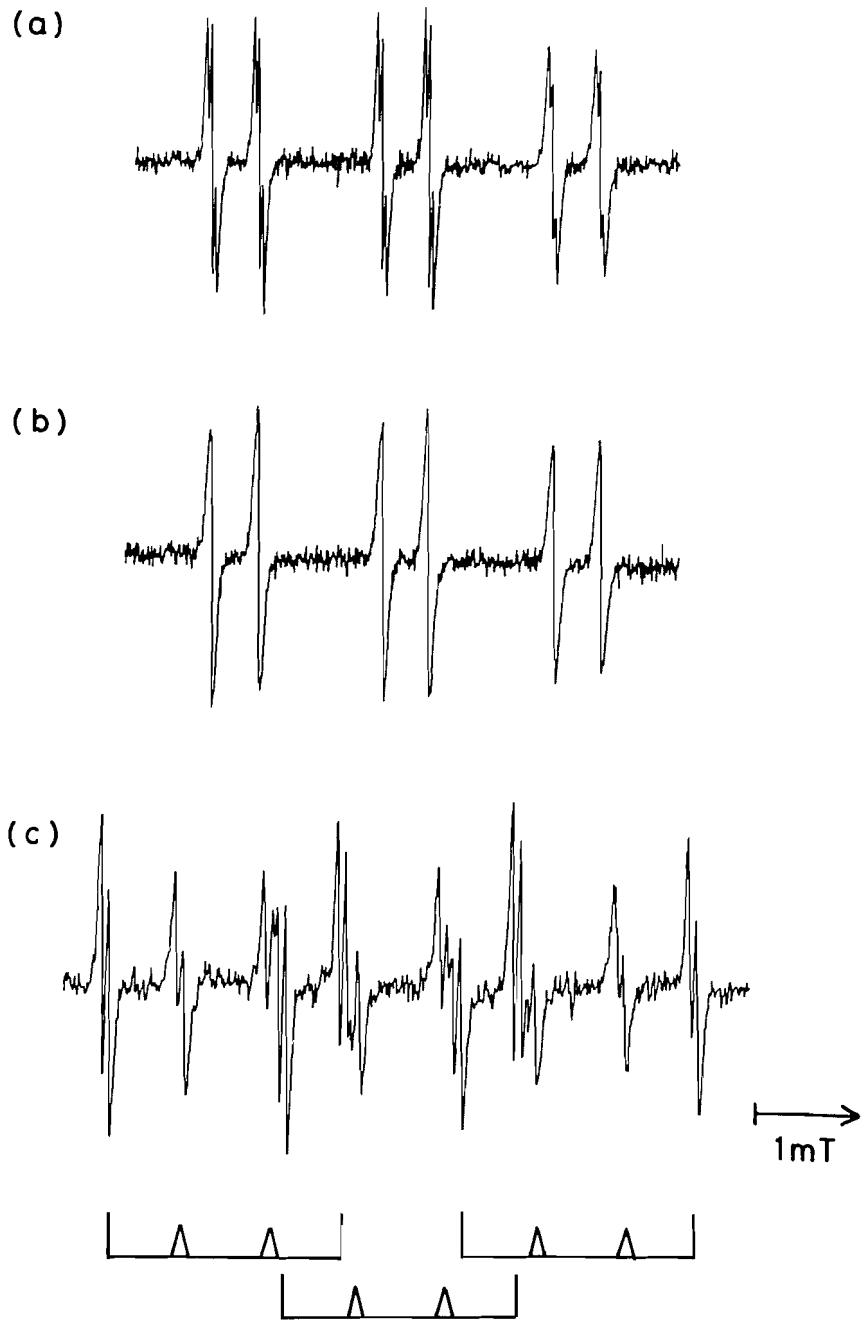

FIG. 8. Electron spin resonance spectra obtained at pH 6.8 from the spin adduct of Ser separated by hplc (a) and those of Thr ((b) and (c): the first and second peaks, respectively). The esr settings are as follows: modulation amplitude, 0.02 mT for (a) and (b), 0.04 mT for (c); receiver gain, 1.0×10^3 for (a) and (b), 3.2×10^3 for (c); time constant, 0.1 s for (a) and (b), 1 s for (c); scan time, 16 min for (a) and (b), 32 min for (c).

at the highest concentration of the spin adducts, prevent the estimation. However, this does not mean that a significant number of the spin adducts produced by the irradiation were left undetected. For instance, in the previous paper (15), all of the spin adducts produced by the H-abstraction from the possible carbons of L-isoleucine could be detected by the method. The estimation of the relative concentration remains as a problem we should overcome in the future. Also, the estimation of the parent short-lived radical concentration is a future problem, because the estimated relative concentration of the spin adduct involves both the reaction rate of each parent radical with a spin trap and the radiolytic yield of the parent radical.

1. E. G. JANZEN and B. J. BLACKBURN. J. Am. Chem. Soc. **90**, 5909 (1968).
2. E. G. JANZEN. Acc. Chem. Res. **4**, 31 (1971), and references therein.
3. E. G. JANZEN. *In* Free radicals in biology. Vol. 4. *Edited by* W. A. Pryor. Academic Press, New York. 1980. Chapt. 4, and references therein.
4. M. J. PERKINS. Adv. Phys. Org. Chem. **17**, 1 (1980), and references therein.
5. C. LAGERCRANTZ and S. FORSHULT. Nature, **218**, 1247 (1968).
6. C. LAGERCRANTZ. J. Phys. Chem. **75**, 3466 (1971).
7. F. P. SARGENT, E. M. GARDY, and H. R. FALK. Chem. Phys. Lett. **24**, 120 (1974).

8. E. A. EVANS. Aldrichimica Acta, **12**, 23 (1979), and references therein.
9. H. TANIGUCHI and H. HATANO. Chem. Lett. (Jpn.) 531 (1974).
10. S. RUSTGI, A. JOSHI, H. MOSS, and P. RIESZ. Int. J. Radiat. Biol. **31**, 415 (1977).
11. S. RUSTGI, A. JOSHI, P. RIESZ, and F. FRIEDBERG. Int. J. Radiat. Biol. **32**, 533 (1977).
12. S. N. RUSTGI and P. RIESZ. Int. J. Radiat. Biol. **34**, 301 (1978).
13. K. MAKINO. J. Phys. Chem. **83**, 2520 (1979).
14. K. MAKINO. J. Phys. Chem. **84**, 1016 (1980).
15. K. MAKINO. J. Phys. Chem. **84**, 1968 (1980).
16. F. MORIYA, K. MAKINO, N. SUZUKI, S. ROKUSHIKA, and H. HATANO. J. Phys. Chem. **84**, 3085 (1980).
17. F. MORIYA, K. MAKINO, N. SUZUKI, S. ROKUSHIKA, and H. HATANO. J. Phys. Chem. **84**, 3614 (1980).
18. N. SUZUKI, K. MAKINO, F. MORIYA, S. ROKUSHIKA, and H. HATANO. J. Phys. Chem. **85**, 263 (1981).
19. F. MORIYA, K. MAKINO, N. SUZUKI, S. ROKUSHIKA, and H. HATANO. J. Am. Chem. Soc. **104**, 830 (1982).
20. M. ANBAR, M. BAMBENEK, and A. B. ROSS. Natl. Stand. Ref. Data Ser. Natl. Bur. Stand. No. 43, 1973.
21. L. M. DORFMAN and G. E. ADAMS. Natl. Stand. Ref. Data Ser. Natl. Bur. Stand. No. 46, 1973.
22. K. MAKINO. J. Phys. Chem. **84**, 1012 (1980).
23. J. C. STOWELL. J. Org. Chem. **36**, 3055 (1971).
24. E. G. JANZEN, E. R. DAVIS, and D. E. NUTTER, JR. Tetrahedron Lett. 3309 (1978).
25. B. C. GILBERT and M. TRENWITH. J. Chem. Soc. Perkin Trans. 2, 1834 (1973).

Can. J. Chem. Downloaded from www.nrcresearchpress.com by 210.87.254.40 on 09/06/12
For personal use only.

The gas-phase photolysis of 2-methyl-1,3-butadiene at 123.6 nm

VALERIE I. LANG AND RICHARD D. DOEPKER

Department of Chemistry, University of Miami, Miami, FL 33124, U.S.A., and Department of Chemistry, Eastern Washington University, Cheney, WA 99004, U.S.A.

Received January 23, 1984

VALERIE I. LANG and RICHARD D. DOEPKER. Can. J. Chem. **62**, 1731 (1984).

The gas-phase photolysis of 2-methyl-1,3-butadiene has been investigated using krypton (123.6 nm) resonance radiation. The observed neutral products of the primary decomposition were vinylacetylene, ethylene, acetylene, methylacetylene, propylene, allene, 2-methy-1-buten-3-yne, pentatriene/1-penten-3-yne, 1,3-butadiene, 2-butyne and butatriene, listed in decreasing order of concentration. There was also evidence of the presence of several radical fragments: CH_2/CH_3, C_2H_3, C_3H_3, and C_4H_5. Quantum yields for each of the products were determined in the photolysis of 2-methyl-1,3-butadiene, performed both in the presence and the absence of additives. Nitric oxide and oxygen were employed as radical scavengers, while hydrogen sulfide and hydrogen iodide were used as radical interceptors. Twelve primary, neutral molecule, reaction channels were proposed and the quantum efficiency assigned for each. The ionization efficiency of 2-methyl-1,3-butadiene was established as $n = 0.55$ at 10.03 eV. No products formed exclusively via an ion–molecule pathway were identified and therefore the fate of the $C_5H_8^+$ ion was not determined.

VALERIE I. LANG et RICHARD D. DOEPKER. Can. J. Chem. **62**, 1731 (1984).

Faisant appel à la radiation de résonance du krypton (123,6 nm), on a étudié la photolyse en phase gazeuse du méthyl-2 butadiène-1,3. La décomposition primaire donne, dans l'ordre décroissant de leur importance, les produits neutres suivants: vinylacétylène, éthylène, acétylène, méthylacétylène, propylène, allène, méthyl-2 butène-1 yne-3, pentatriène/pentène-1 yne-3, butadiène-1,3, butyne-2 et butatriène. On trouve également plusieurs fragments radicalaires CH_2/CH_3; C_2H_3; C_3H_3 et C_4H_5. On a déterminé les rendements quantiques de chacun des produits obtenus lors des photolyses du méthyl-2 butadiène-1,3 réalisées en présence et en l'absence d'additifs. On a utilisé l'oxyde nitrique et l'oxygène comme pièges de radicaux alors que le sulfure d'hydrogène et l'iodure d'hydrogène ont été utilisés comme intercepteurs de radicaux. On propose 12 voies réactionnelles primaires pour les réactions conduisant aux molécules neutres et on a calculé pour chacune d'elles l'efficacité quantique. On a établi que, pour une énergie de 10,03 eV, l'efficacité d'ionisation (n) du méthyl-2 butadiène-1,3 s'établit à 0,55. On n'a identifié aucun produit provenant uniquement d'une réaction ion–molécule et, par conséquent, on n'a pas déterminé le sort de l'ion $C_5H_8^+$.

[Traduit par le journal]

Introduction

The ultraviolet photochemistry of 2-methyl-1,3-butadiene has been of interest to the Environmental Protection Agency (1, 2) since the volatile hydrocarbons were detected as a foliage emission in ambient forest atmopshere (3, 4). Smog chamber simulation using ultraviolet radiation at lower atmosphere sunlight wavelengths (between 290–380 nm) were undertaken by Arnts and Gay (1). They compared the oxidant-forming potential of naturally emitted terpenes and the hemiterpene isoprene with that of hydrocarbon emissions from autombile exhaust.

Srinivason and Boué (5, 6) studied the mercury $^3P_1$ (254 nm) sensitized isomerization of gas phase linear 1,3-diene to cyclopropane derivatives. At room temperature (25°C), the formation of 2,3-dimethylcyclopropene and 3,3-dimethylcyclopropene from 2-methyl-1,3-butadiene (isoprene) was a linear function with time, with the intercept at the origin. The photoisomerization of isoprene to these products was found to be a primary process.

Many of the photochemical reactions of 1,3-diene in general can be rationalized in terms of a diradical intermediate with a cyclopropane-like structure (5, 6*b*). In the case of 2-methyl-1,3-butadiene, formation of the diradical intermediate is followed by a 1,3-hydrogen shift to give the final products 3,3-dimethylcyclopropene and 2,3-dimethylcyclopropene. At a reaction pressure of 10 Torr, the two dimethylcyclopropenes thermally decompose to give 2-methylmethylenecyclopropane, 1,2-pentyne, 3-methyl-1-butyne, and one unidentified product. However, at 300 Torr, the only products were 2,3-dimethyl- and 3,3-dimethylcyclopropenes.

Prior to the present investigation, the photochemistry of 2-methyl-1,3-butadiene was studied between 147.0 nm and its absorption threshold (ca. 255 nm) by Collin *et al.* (7). When isoprene (2-methyl-1,3-butadiene) was irradiated with 230–255 nm photons ethylene, acetylene, propyne, allene, and 1,4-pentadiene were found. The radiation-produced yields decreased with increasing pressure. Stern–Volmer plots indicated that the photoexcited parent molecule produced by 230–255 nm radiation is collisionally stabilized at high pressures.

As the incident energy is increased with wavelengths of 174 and 163 nm less pressure dependency was observed, and at 147.0 nm none was found, within the pressure ranges used in the study. Eight primary reaction channels were proposed for the fragmentation of 2-methyl-1,3-butadiene at these three wavelengths. At 147.0 nm the products reported by Collin *et al.* (7) were methane, acetylene, ethylene, ethane, propylene, methylacetylene, allene, vinylacetylene, isobutene, and 2-methyl-1-buten-3-yne. Vinylacetylene was found to be the major product at 147.0 nm with a quantum yield of 0.66.

The most frequently quoted first ionization potential of 2-methyl-1,3-butadiene of 8.84 eV was reported by Watanabe *et al.* (8) and Franklin *et al.* (9). More recently Worley and Webb (10) have measured the ionization energy as 8.87 eV using photoelectron spectra of the diene. In the mass spectrum of isoprene obtained by Holmes (11), the appearance potentials were 8.84 eV for the $C_5H_8^+$ ion and 10.5 eV for the $C_5H_7^+$ ion.

Collin, Bertrand, and Gagnon (12) reported the ionization efficiencies of several unsaturated hydrocarbons at 123.6 nm (10.0 eV) and 104.8–106.7 nm (11.6–11.8 eV). At 10.03 eV, the ionization efficiencies (n) values were within limit $n < 0.27$ for monoolefins; $n = 0.30–0.45$ for diolefins; $n > 0.45$ for acetylenic type compounds. The reported ionization efficiency

Can. J. Chem. Downloaded from www.nrcresearchpress.com by 210.87.254.105 on 09/06/12
For personal use only.

TABLE 1. Photolysis of 2-methyl-1,3-butadiene at 123.6 nm

Product	Quantum yield with isoprene in Torr and additives in Torr				
	1.0 NO, 0.1	0.3 NO, 0.03	4.0 NO, 0.4	1.0 NO, 0.1 N_2, 68	1.0 NO, 0.1 N_2, 126
CH_4	0.01 ± 0.007[a]	0.01	0.01	0.01	0.01
C_2H_2	0.07 ± 0.022	0.08	0.08	0.08	0.07
C_2H_4	0.08 ± 0.007	0.08	0.09	0.07	0.07
C_3H_6	0.02 ± 0.001	0.02	0.03	0.03	0.03
C_3H_4[b]	0.04 ± 0.003	0.04	0.05	0.05	0.05
C_3H_4[c]	0.02 ± 0.002	0.02	0.03	0.02	0.03
C_4H_4[d]	0.17 ± 0.020	0.17	0.18	0.17	0.17
1,3-C_4H_6	0.01 ± 0.003	0.01	0.01	0.01	0.01
C_5H_6[e]	0.02 ± 0.001	0.02	0.03	0.03	0.03
C_4H_6[f]	0.01 ± 0.003	0.01	0.01	0.01	0.01
C_4H_4[g]	0.01 ± 0.005	0.02	0.03	0.01	0.01
C_5H_6[h]	0.02 ± 0.006	0.02	0.02	0.01	0.01

[a] Average values with standard deviation based on 14 individual experiments
[b] Methylacetylene.
[c] Allene.
[d] Vinylacetylene.
[e] 2-Methyl-1-buten-3yne.
[f] 2-Butyne.
[g] Butatriene.
[h] Pentatriene and/or 1-penten-3yne.

of 2-methyl-1,3-butadiene was 0.33.

In the present study an attempt has been made to extend the work of Collin *et al.* (7) by investigating the vacuum-ultraviolet photochemistry of 2-methyl-1,3-butadiene above its ionization energy. This work attempts to evaluate the primary reaction channels at 123.6 nm and to examine the effect of ionization on the product distribution.

Experimental

Materials

2-Methyl-1,3-butadiene (isoprene), obtained from K and K Laboratories, was purified by vapor chromatography using a 25 ft., 30% (W/W) squalene on chromosorp P column operated at room temperature. Analysis of the resulting isoprene disclosed an impurity of 0.03% *trans*-2-butene. Low temperature trap-to-trap distillation techniques were used to purify HI, NO, H_2S, and CH_3I while other additives were obtained commercially and used without further purification.

Irradiation and analysis

The vacuum-ultraviolet photolysis was investigated at room temperature (25°C) in a standard static system using a 600 cm^3 reaction vessel and a titanium "gettered" krypton (123.6 nm) resonance lamp. A CaF_2 was used to filter out the dual 116.5 nm Kr resonance line. Irradiation procedures, including photoionization, and mercury photosensitized procedures have been reported previously (13). Analysis was performed by vapor chromatography (25 ft., 30% squalane at 60°C) equipped with a flame ionization detector.

Actinometry

The chemical actinometer used in this study was cyclopentene $\Phi_{C_2H_4} = 0.19$ (13*b*, 14). The ionization efficiency (n) of 0.16 was assumed for cyclopentene (13*b*, 14) at 123.6 nm. These two values were used to determine the quantum yields and the ionization efficiency of isoprene.

Results

The quantum yields of the products of the 123.6 nm photolysis of 2-methyl-1,3-butadiene are reported in Tables 1 and 2. The data are representative of those collected under a variety of experimental conditions. In the absence of additive, the product yield remained essentially constant when the amount of isoprene was varied between 0.5 and 5.0 Torr. As can be noted in Table 1, there was no pressure effect when samples of isoprene between 0.3 and 5.0 Torr were photolyzed in the presence of 10% NO or O_2, even with the addition of between 37 and 149 Torr of nitrogen.

Oxygen was not as useful a radical scavenger as NO in preventing ethane formation and in removing the C_5 radical species. Hydrogen iodide was found to be a more effective radical interceptor than hydrogen sulfide, as previously noted by Ausloos *et al.* (15). The optimum concentration for HI was 7% while varying the amount of H_2S from 5 to 15% did not improve its efficiency to any appreciable extent. However, the use of HI presented difficulties in quantifying the yields of certain products. At room temperature (25°C) and 30 min reaction times, a thermal addition reaction of HI to 2-methyl-1,3-butadiene produced 3-methyl-1-butene, 2-methyl-1-butene, and 2-methyl-2-butene. Collin (7) suggested also such a complication with two of the C_5H_{10} isomers which he based on an observation of Gorton and Walsh (16).

In order to investigate a possible H-atom mechanism for the formation of the C_5H_{10} isomers, the $Hg(^3P_1)$ sensitized photolysis of H_2 (16.5 Torr) in the presence of 2-methyl-1,3-butadiene (0.5 Torr) was performed. The products of this photolysis was 2-methyl-2-butene, 2-methyl-1-butene, and 3-methyl-1-butene given in decreasing order of importance. Further 123.6 nm studies were made in which the additive CH_3I (10%) was used to participate in a competitive reaction for the available H- atoms (17), thus reducing the yield of the C_5H_{10} compounds (Table 2).

The ionization energy of 2-methyl-1,3-butadiene 8.84 eV (18) is below the photon energy of the Kr (10.0 eV) resonance lamp. The ionization efficiency for isoprene was determined to be $n = 0.55 \pm 0.03$ at 123.6 nm. No products formed exclusively through an ion–molecule pathway were identified.

Can. J. Chem. Downloaded from www.nrcresearchpress.com by 210.87.254.105 on 09/06/12
For personal use only.

TABLE 2. Photolysis of 2-methyl-1,3-butadiene at 123.6 nm

Products	Quantum yields with isoprene in Torr and additive in Torr					
	1.0 None	1.0 O_2, 0.1	1.0 HI, 0.07	1.0 H_2S, 0.10	1.0 H_2S, 0.15	1.0 CH_3I, 0.1
CH_4	0.02	0.02	0.31	0.28	0.33	0.03
C_2H_2	0.07	0.07	0.09	0.08	0.08	0.07
C_2H_4	0.07	0.08	0.12	0.12	0.12	0.09
C_2H_6	0.05	0.05	0.01	0.02	0.02	0.06
C_3H_6	0.02	0.02	0.04	0.04	0.04	0.02
C_3H_4[a]	0.03	0.04	0.05	0.04	0.04	0.04
C_3H_4[b]	0.02	0.02	0.03	0.02	0.02	0.02
C_4H_4[c]	0.15	0.17	0.17	0.17	0.17	0.17
1,3-C_4H_6	0.02	0.02	0.05	0.03	0.03	0.02
1,2-C_4H_6	0.01	0.00	0.01	0.00	0.00	0.00
C_5H_6, C_5H_{10}	0.02	0.02	0.08[d,e]	0.02	0.02	0.01
C_4H_6[f]	0.01	0.01	0.01	0.02	0.02	0.00
C_4H_4, C_5H_{10}	0.01	0.01	0.07[g,h]	0.02	0.02	0.00
C_5H_{10}[i]	0.02	0.00	0.34	0.01	0.01	0.00
C_5H_6[j]	0.03	0.02	0.02	0.02	0.02	0.02
C_5H_4[k]	0.03	0.02	0.00	0.02	0.02	0.03

[a] Methylacetylene.
[b] Allene.
[c] Vinylacetylene.
[d] 2-Methyl-1-buten-3-yne (0.06).
[e] 3-Methyl-1-butene (0.02).
[f] 2-Butyne.
[g] Butatriene (0.01).
[h] 2-Methyl-1-butene (0.06).
[i] 2-Methyl-2-butene.
[j] Pentatriene and/or 1-penten-3-yne.
[k] Unidentified.

Discussion

The most abundant stable product in the 123.6 nm photolysis of 2-methyl-1,3-butadiene is vinylacetylene, $\Phi = 0.17$. Collin *et al.* (7) reported the highest quantum yield for vinylacetylene at 147.0 nm but with ethylene becoming the major product at both 163 nm and 174 nm. The cleavage of the methyl from the #2 carbon of the parent molecule and the elimination of a hydrogen atom from the #1 carbon results in the formation of vinylacetylene (reaction [1]). Similarly, the elmination of a hydrogen atom from the #3 carbon should lead to butatriene, $\Phi = 0.01$ (reaction [2])

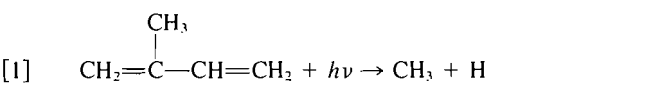

[1] $CH_2{=}C(CH_3){-}CH{=}CH_2 + h\nu \rightarrow CH_3 + H + HC{\equiv}C{-}CH{=}CH_2$

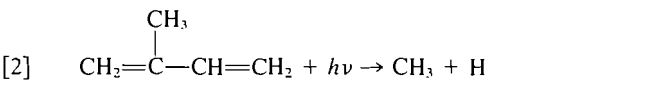

[2] $CH_2{=}C(CH_3){-}CH{=}CH_2 + h\nu \rightarrow CH_3 + H + H_2C{=}C{=}C{=}CH_2$

Since no pressure effect was observed in the formation of vinylacetylene or butatriene, it can be assumed that the elimination of both the hydrogen atom and the methyl radical must occur within the time of a few molecular vibrations. If it is assumed that reaction channels 1 and 2 are the only source of C_4H_4, then $\phi_1 = 0.17$ and $\phi_2 = 0.01$.

The elimination of the #1 methylene in conjunction with a carbon 3 to 4 hydrogen migration leads to the formation of 2-butyne (reaction [3]).

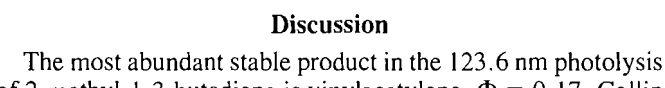

[3] $CH_2{=}C(CH_3){-}CH{=}CH_2 + h\nu \rightarrow CH_3{-}C{\equiv}C{-}CH_3 + CH_2$

1,3-Butadiene would result from a similar methylene elimination but coupled with a hydrogen atom migration from the methyl group to the #2 carbon (reaction [4]).

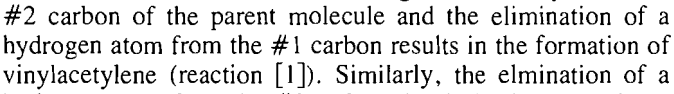

[4] $CH_2{=}C(CH_3){-}CH{=}CH_2 + h\nu \rightarrow CH_2{=}CH{-}CH{-}CH_2 + CH_2$

As is found in Table 1, the quantum yield for both 2-butyne and 1,3-butadiene are $\Phi_{C_4H_6\text{-yne}} = \Phi_{C_4H_6\text{-}1,3} = 0.01$. The primary quantum efficiencies for the reaction channels 3, and 4 are $\phi_3 = \phi_4 = 0.01$.

It is interesting to note that 1,2-butadiene was not found as a product in the NO or O_2 scavengered 123.6 nm photolysis. Although this product would result from a process involving a methylene elimination and a hydrogen 3 to 2 migration, it appears to be an unfavorable product.

The elimination of two hydrogen atoms (or molecular hydrogen) from the parent isoprene results in the formation of 2-methyl-1-butene-3-yne, $\Phi = 0.02$ via reaction channel [5].

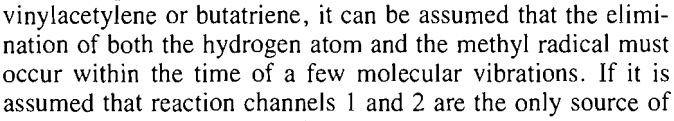

[5] $CH_2{=}C(CH_3){-}CH{=}CH_2 + h\nu \rightarrow CH_2{=}C(CH_3){-}C{\equiv}CH + 2\,H(H_2)$

Based on the formation of 2-methyl-1-buten-3-yne, the primary quantum efficiency for reaction channel is, $\phi_5 = 0.02$. If

Can. J. Chem. Downloaded from www.nrcresearchpress.com by 210.87.254.105 on 09/06/12
For personal use only.

methyl migration should occur, pentatriene or 1-penten-3-yne may be produced (reaction [6]).

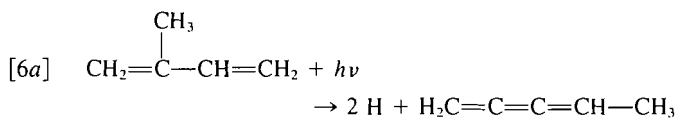

$$[6a]\quad CH_2{=}C(CH_3){-}CH{=}CH_2 + h\nu \rightarrow 2\,H + H_2C{=}C{=}C{=}CH{-}CH_3$$

$$[6b]\quad \rightarrow 2\,H + H_2C{=}CH{-}C{\equiv}C{-}CH_3$$

Analysis methods employed in this study were unable to distinguish between these two products. The primary quantum efficiency for reaction channel [6] should be equal to the scavengered quatum yield of these two C_5H_6 compounds, Table 1, $\phi_6 = 0.02$.

The appearance of propylene as a product even when scavengers are present, and the absence of a pressure effect, indicate that a primary process must exist leading to the formation of propylene. Hydrogen migration coupled with a carbon–carbon cleavage should lead to the formation of propylene and acetylene via reaction channel [7].

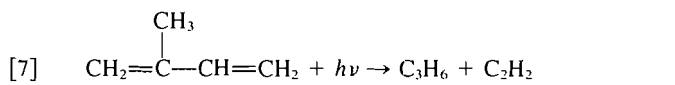

$$[7]\quad CH_2{=}C(CH_3){-}CH{=}CH_2 + h\nu \rightarrow C_3H_6 + C_2H_2$$

The fact that the propylene yield increased from 0.02 to 0.04 when HI or H_2S is introduced to the reaction system suggests the formation of a C_3H_5 radical. The fact that both H_2S and HI addition leads to the same quantum yield shows the C_3H_5 radical to be a vinyl radical (18), reaction [8].

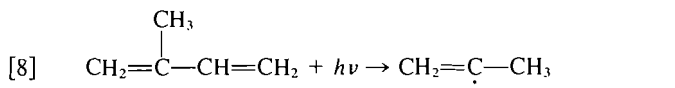

$$[8]\quad CH_2{=}C(CH_3){-}CH{=}CH_2 + h\nu \rightarrow CH_2{=}\dot{C}{-}CH_3 + C_2H_2 + H$$

Considering both reaction channels [7] and [8], the quantum influence of each process is, $\phi_7 = \phi_8 \simeq 0.02$. It must be noted that the $\Phi_{C_3H_2} = 0.08$, independent of pressure and additive. Since only 0.04 is accounted for by reaction channels [7] and [8], a third source of acetylene must be present. A key to this process can be found in Table 2, where it can be noted that the quantum yield of ethylene increases by nearly 0.04 when HI or H_2S is present. ($\Phi_{C_2H_4} = 0.08$, W/NO; $\Phi_{C_2H_4} = 0.12$ W/HI or H_2S). A logical reaction channel then would appear to lead to the formation of acetylene and a vinyl radical. A methyl elimination and a carbon–carbon cleavage should result in the formation of acetylene and a vinyl radical, reaction [9].

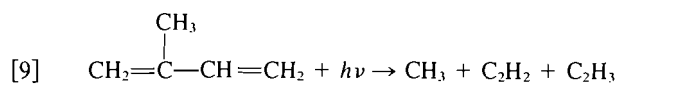

$$[9]\quad CH_2{=}C(CH_3){-}CH{=}CH_2 + h\nu \rightarrow CH_3 + C_2H_2 + C_2H_3$$

If the total formation of acetylene can be limited to reaction channels [7], [8], and [9], then the quantum efficiency of reaction channel [9] would be $\phi_9 = 0.04$, which is comparable to the vinyl radical yield of $\Phi_{C_2H_3} = 0.04$.

The elimination of molecular ethylene should result in the formation of methylacetylene or allene, depending on which hydrogen atom migrates, reaction [10].

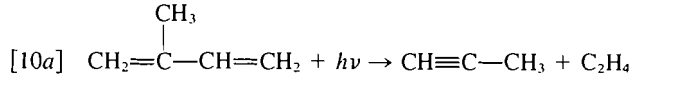

$$[10a]\quad CH_2{=}C(CH_3){-}CH{=}CH_2 + h\nu \rightarrow CH{\equiv}C{-}CH_3 + C_2H_4$$

$$[10b]\quad \rightarrow CH_2{=}C{=}CH_2 + C_2H_4$$

The quantum yield of ethylene is $\Phi_{C_2H_4} = 0.08$, while the yield of methylacetylene is $\Phi = 0.04$, and allene $\Phi = 0.02$ is $\Phi_{C_3H_4} = 0.06$. Assuming that reaction channel [10*a*] and [10*b*] are the only path for the formation of the C_3H_4 isomers, then $\phi_{10a} = 0.04$ and $\phi_{10b} = 0.02$. The excess quantum yield of 0.02 for ethylene suggests a reaction channel that simultaneously produces a propargyl radical with ethylene, reaction [11].

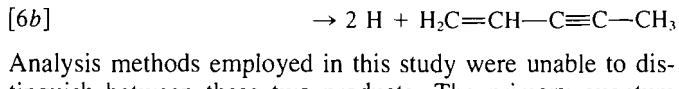

$$[11]\quad CH_2{=}C(CH_3){-}CH{=}CH_2 + h\nu \rightarrow C_2H_4 + C_3H_3 + H$$

Although there is no evidence of the C_3H_3 radical in this study, past studies in this laboratory have indicated that this species is not generally intercepted by H_2S nor HI. A maximum quantum efficiency for reaction [11] must be equal to the excess ethylene, or, $\phi_{11} = 0.02$.

Tables 1 and 2 reveal that the formation of 1,3-butadiene increases from 0.01 with NO present to a value of 0.05 when HI is added to the photolysis mixture likewise the fact that 1,2-butadiene is absent when NO is present shows a quantum yield of 0.01 when the radical interceptor HI is present. These observations are consistent with the formation of C_4H_5 radical systems. Two possible mechanisms could be postulated (reaction [12]).

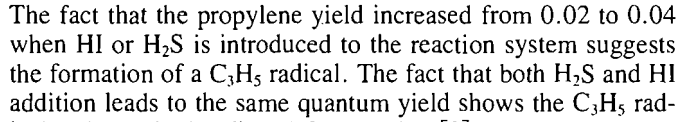

$$[12a]\quad CH_2{=}C(CH_3){-}CH{=}CH_2 \rightarrow CH_2{=}\dot{C}{-}CH{=}CH_2 + CH_3$$

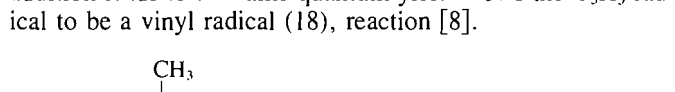

$$[12b]\quad CH_2{=}C(CH_3){-}CH{=}CH_2 \rightarrow C_4H_5 + H + CH_2$$

At present, there is no information available that

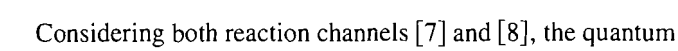

$$[13]\quad C_4H_5 + HI \rightarrow C_4H_6 + I$$

could distinguish between the two processes.

Considering the total methyl/methylene production of approximately $\Phi_{CH_3/CH_2} \simeq 0.31$ (Table 2), it is possible that the sum of the methyl/methylene formation (reactions [1]–[4], [9], and [12]) predicts a value of the total quantum yield for CH_3/CH_2 as

$$\begin{aligned}\Phi_{CH_3} &= \phi_1 + \phi_2 + \phi_3 + \phi_4 + \phi_9 + \phi_{12}\\ &= 0.17 + 0.01 + 0.01 + 0.01 + 0.04 + 0.05\\ &= 0.29\end{aligned}$$

This value is in good agreement with the experimental value of approximately 0.31.

It is apparent that the formation of 2-methyl-2-butene, 1-methyl-1-butene, and 1-methyl-3-butene were formed through a secondary process involving the addition of a hydrogen atom to a parent isoprene molecule (reactions [14] and [15]).

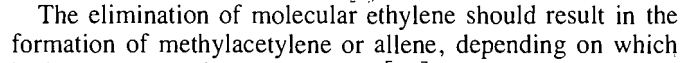

$$[14]\quad C_5H_8 + H\cdot \rightarrow C_5H_9\cdot$$

$$[15]\quad C_5H_9\cdot + RH \rightarrow C_5H_{10} + R\cdot$$

The total quantum yield for these three products in the presence of HI is $\Phi_{C_5H_{10}} = 0.42$, which is much greater than that predicted by the sum of all hydrogen atoms producing reaction channels, $\Phi_H = 0.30$. It must be recalled that HI addition to isoprene (7) leads to these products in a process that is *not* I_a-dependent, therefore this reported $\Phi_{C_5H_{10}} = 0.42$ value is completely unreliable.

Can. J. Chem. Downloaded from www.nrcresearchpress.com by 210.87.254.105 on 09/06/12
For personal use only.

TABLE 3. Quantum yields for the primary reaction channels of the 123.6 nm photolysis of 2-methyl-1,3-butadiene

	Reaction	ϕ	$\phi_{Neutral}$
[1]	$CH_2{=}C(CH_3){-}CH{=}CH_2 + h\nu \rightarrow CH_3 + H + HC{\equiv}C{-}CH{=}CH_2$	0.17	0.38
[2]	$\rightarrow CH_3 + H + H_2C{=}C{=}C{=}CH_2$	0.01	0.02
[3]	$\rightarrow CH_2 + CH_3{-}C{\equiv}C{-}CH_3$	0.01	0.02
[4]	$\rightarrow CH_2 + CH_2{=}CH{-}CH{=}CH_2$	0.01	0.02
[5]	$\rightarrow 2\,H + CH_2{=}C(CH_3){-}C{\equiv}CH$	0.02	0.04
[6]	$\rightarrow 2\,H + \{H_2C{=}C{=}CH{-}CH_3,\ H_2C{=}CH{-}C{\equiv}C{-}CH_3\}$	0.02	0.04
[7]	$\rightarrow C_2H_2 + C_3H_6$	0.02	0.04
[8]	$\rightarrow C_2H_2 + H + CH_2{=}C(CH_3){-}CH_3$	0.02	0.04
[9]	$\rightarrow C_2H_2 + CH_3 + C_2H_3$	0.04	0.09
[10]	$\rightarrow C_2H_4 + \{CH{\equiv}C{-}CH_3,\ CH_2{=}C{=}CH_2\}$	0.06	0.13
[11]	$\rightarrow C_2H_4 + C_3H_3 + H$	0.02	0.04
[12]	$\rightarrow C_4H_5 + CH_3/CH_2 + H$	0.05	0.11
[16]	$\rightarrow C_5H_8^+ + e^-$	0.55	—
		1.00	0.97

Summary and conclusion

The 123.0 nm photolysis of 2-methyl-1,3-butadiene may be described in 12 primary, neutral molecule, reaction channels and an ionization process, (reaction [16]).

[16] $C_5H_8 + h\nu \rightarrow C_5H_8^+ + e^-$

The quantum yields assigned through this study are summarized in Table 3 with an estimated accuracy of better than 10%. Although the neutral molecule decomposition of 2-methyl-1,3-butadiene is consistent with the investigation of Collin *et al.* (7), the ionization efficiency reported here $n = 0.55$ is considerably higher than reported by Collin (7), $n = 0.33$ at 123.6 nm.

1. R. R. ARNTS and B. W. GAY. EPA-600/3-79-081 U.S. Environmental Protection Agency, Research Triangle Park, North Carolina. 1979.
2. H. H. WESTBURG and R. A. RASMUSSEN. Chemosphere, **4**, 1963 (1972).
3. R. L. SEILA. EPA-600/3-79-010, U.S. Environmental Protection Agency, Research Triangle Park, NC. 1979.
4. R. A. RASMUSSEN. (*a*) Env. Sci. Tech. **4**, 667 (1970); (*b*) J. Air Pollution Control Asso. **22**, 537 (1972).
5. R. SRINIVASON and S. BOUÉ. Tetrahedron Lett. **3**, 203 (1970).
6. R. SRINIVASON. (*a*) Adv. Photochem. **4**, 113 (1966); (*b*) J. Am. Chem. Soc. **90**, 4498 (1968).
7. G. J. COLLIN, P. DEMERS, and M. GAGNON-DESLAURIERS. Can. J. Chem. **56**, 1864 (1978).
8. K. WATANABE, T. NAKAYAMA, and J. MOTTLE. J. Quant. Spectrosc. Radiat. Transfer, **2**, 369 (1962).
9. J. L. FRANKLIN, J. G. DILLARD, H. M. ROSENSTOCK, J. T. HERON, K. DROXL, and F. H. FIELD. NSRDS-NBS **26**, 1969.
10. S. D. WORLEY and T. R. WEBB. J. Electron Spectrosc. Related Phenom. **18**, 189 (1980).
11. J. L. HOLMES. Org. Mass Spectrom. **8**, 247 (1974).
12. G. J. COLLIN, C. BERTRAND AND H. GAGNON. J. Chim. Phys. **72**, 719 (1975).
13. (*a*) E. LOPEZ and R. D. DOEPKER. J. Phys. Chem. **82**, 752 (1978); (*b*) C. K. TU and R. D. DOEPKER. J. Photochem. **3**, 13 (1974); (*c*) K. L. HILL and R. D. DOEPKER. J. Phys. Chem. **76**, 3153 (1972).
14. R. LESCLAUX, S. SEARLES, L. W. SIECK, and P. AUSLOOS. J. Chem. Phys. **54**, 3411 (1971).
15. P. AUSLOOS, R. E. REBBERT, and S. G. LIAS. J. Photochem. **2**, 267 (1973).
16. P. J. GORTON and R. WALSH. J. Chem. S. Chem. Commun. 782 (1972).
17. K. L. HILL and R. D. DOEPKER. J. Phys. Chem. **76**, 1112 (1972).
18. G. J. COLLIN and A. WIECKOWSKI. J. Photochem. **8**, 103 (1978).

Can. J. Chem. Downloaded from www.nrcresearchpress.com by 210.87.254.105 on 09/06/12
For personal use only.

The variation in the second hyperpolarisability of cyclobutane and cyclopentane through inversion, and an analysis of the contributions to this property

J. WAITE AND M. G. PAPADOPOULOS

Theoretical and Physical Chemistry Institute, National Hellenic Research Foundation, Vas. Constantinou 48, Athens 501/1, Greece

Received December 20, 1983

J. WAITE and M. G. PAPADOPOULOS. Can. J. Chem. **62**, 1736 (1984).

An extended basis CNDO-coupled-Hartree–Fock procedure has been used to determine the second hyperpolarisability of cyclobutane and cylopentane in both the puckered and planar forms. Analysis of the dependence of the hyperpolarisability on geometric elements (bond lengths, angles etc.) as well as its variation with change in configuration have been presented. The contribution of the multicenter interactions to the hyperpolarisability of C_4H_8 has been evaluated and its implications discussed.

J. WAITE et M. G. PAPADOPOULOS. Can. J. Chem. **62**, 1736 (1984).

On a utilisé une méthode CNDO avec base élargie-couplée à une procédure de Hartree–Fock pour déterminer la deuxième hyperpolarisabilité du cyclobutane et du cyclopentane tant dans leurs formes planes que plissées. On rapporte une analyse de la dépendance de l'hyperpolarisabilité sur les éléments géométriques (longueurs des liaisons, angles, etc) ainsi que sa variation avec des changements dans la configuration. On a évalué les contributions des interactions entre plusieurs centres sur l'hyperpolarisabilité du C_4H_8 et on discute de leurs implications.

[Traduit par le journal]

Can. J. Chem. Downloaded from www.nrcresearchpress.com by 210.87.254.5 on 09/06/12
For personal use only.

Introduction

The second hyperpolarisability is a molecular constant, describing the non-linear response of an atom or molecule to an electric field. It is defined by eq. [1]:

$$[1]\quad E(F) = E^{(0)} - \mu_\alpha F_\alpha - \frac{1}{2}\alpha_{\alpha\beta}F_\alpha F_\beta - \frac{1}{3!}\beta_{\alpha\beta\gamma}F_\alpha F_\beta F_\gamma - \frac{1}{4!}\gamma_{\alpha\beta\gamma\delta}F_\alpha F_\beta F_\gamma F_\delta - \ldots.$$

where $E(F)$ is the electronic energy of the molecule in the presence of the uniform electric field, F; $E^{(0)}$ is the unperturbed electronic energy; μ_α is the α component of the permanent dipole moment; $\alpha_{\alpha\beta}$ is the $\alpha\beta$ component of the polarisability; $\beta_{\alpha\beta\gamma}$ is the $\alpha\beta\gamma$ component of the first hyperpolarisability; $\gamma_{\alpha\beta\gamma\delta}$ is the $\alpha\beta\gamma\delta$ component of the second hyperpolarisability; and α, β, γ, δ are suffixes denoting cartesian components.

The importance of hyperpolarisabilities in the understanding of many non-linear processes and the design of materials with predefined properties has been discussed by many authors (1–6). However, it is noted that both the experimental and the theoretical evaluation of the second hyperpolarisability encounters difficulties (7, 8). A rigorous computational treatment of this property requires an accurate knowledge of the excited states which are currently available only for very small systems and even then with considerable effort (8). It is thus not surprising that rigorous *ab initio* methods have only been applied to H_2 (9, 10), HF (11–13), and H_2O (14). On larger systems, however, semiempirical methods have been employed (15–18). The level of approximations has been usually Hückel, CNDO, or INDO; while the electric field has been considered by some variant of FPT (Finite Perturbation Theory) or PT (Perturbation Theory).

One of the aspects which has not yet been treated systematically is the dependence of the average second hyperpolarisability, γ, on geometric elements (bond lengths, bond angles, etc.), for systems larger than H_2 (10). This is a matter of importance since the computed values which are determined employing fixed geometries are compared with experimental values that may be determined from conformational mixtures or rotationally averaged structures.

A question related to the rationalization and interpretation of both the theoretical and experimental hyperpolarisability results is the importance of multicenter interactions (that is interactions, which are essentially defined in terms of the charge cloud as a whole) as well as the extent to which the hyperpolarisability can be approximated by a sum of terms and interactions associated with specific parts of the molecule. The above stated problems have been investigated employing C_4H_8, its fragments, and C_5H_{10} as test models.

Method

We have employed a computational procedure (CHF–PT–EB–CNDO, for Coupled Hartree–Fock – Perturbation Theory – Extended Basis – Complete Neglect of Differential Overlap) which has successfully predicted the polarisabilities and hyperpolarisabilities of some alkanes (16), polyenes (17), and aromatics (18). This technique relies on (*a*) a CNDO (19) wave function formed from a properly optimized basis set, and (*b*) a self-consistent perturbation theory, that was developed by McWeeny and his co-workers, and which applies directly to the Fock–Dirac density matrix (20).

The following basis set has been used for the computations (16): C: $2s(1.625)$, $2p(1.625)$; and H: $1s(1.0)$, $2s(0.5)$, $2p(0.5)$. These atomic orbitals have been used to calculate α (the average polarisability) and γ of CH_4, C_2H_6 (four conformations), C_3H_6 and C_3H_8 (two conformations) wih average errors, in comparison to the experimental results, of 4.7% and 23.1% respectively (16). These data illustrate the aptitude of the employed basis set to satisfactorily reflect changes in polarisation induced by variation in geometry.

This observation is of importance because it demonstrates that both the first and second order correction to the density matrix are succesfully described and this allows one to think that the proposed values will have an error not exceeding 30% of an experimentally determined value, when it becomes available.

This is a reasonable degree of accuracy since the experimentally derived information may be uncertain due to dispersion (21), geometrical averaging and other effects by more than 20% (17).

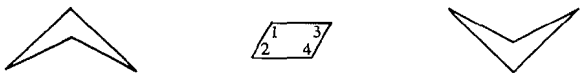

FIG. 1. Puckered and planar structures of cyclobutane which undergoes a rapid inversion between the two D_{2d} forms (23).

TABLE 1. Second hyperpolarisability of CH_2 in au as a function of the C—H bond length (R) and ∠HCH bond angle

	Hyperpolarisability[e]				
R (au)	90°	105.4°[a]	108°[d]	120°	145°
2.06	1843	1847	1847	1842	1787
2.08[a]	1887	1892	1892	1887	1831
2.10[b]	1949	1956	1956	1951	1893
2.14[c]	2045	2053	2054	2050	1988
2.20	2208	2221	2222	2220	2154
2.50	3302	3363	3370	3391	3320
3.00	6532	6854	6901	7085	7232

[a] These are the equilibrium bond lengths and angles found by *ab initio* (basis set: 4-31G) calculations for the singlet state of CH_2 (22).
[b] CH bond length in C_5H_{10} (24).
[c] CH bond length in C_4H_8 (27).
[d] ∠HCH in C_4H_8.
[e] The conversion factors for the unit of hyperpolarisability to SI and esu are: 1 au ≃ 0.503717×10^{-39} esu ≃ 0.623597×10^{-64} C^4 m^4 J^{-3}.

The average value of the second hyperpolarisability, γ, is given by (1):

$$[2] \quad \gamma = \frac{1}{5}(\gamma_{xxxx} + \gamma_{yyyy} + \gamma_{zzzz} + 2\gamma_{xxyy} + 2\gamma_{xxzz} + 2\gamma_{yyzz})$$

where x, y, and z denote cartesian components, and the individual tensors, $\gamma_{\alpha\alpha\beta\beta}$, are computed from the requisite perturbed density matrices (16, 17, 20) (Fig. 1).

Results and discussion

A. Dependence of γ on geometry elements

Cyclobutane and cyclopentane may be considered as made up of CH_2 units, while the general cycloalkane can be described by $(CH_2)_n$, where $n = 3, 4, 5, \ldots$. Thus we start our analysis by considering how the γ of CH_2 changes as a function of the C—H bond length and the bond angle ∠HCH.

The results of Table 1 show: (*a*) Variation of C—H(∠HCH = 105.4°, constant) from 2.06 au to 2.2 au leads to a maximum difference from the equilibrium value (C—H = 2.08 au, ∠HCH = 105.4° (22)) which is equal to 17.4%. It is further observed that γ increases with the bond length (Table 1). This can be rationalized by considering that lengthening of the bond makes the charge cloud more diffuse and thus more easy to polarise. (*b*) For variations of ∠HCH(C—H = 2.08 au, constant) γ has a maximum difference from the equilibrium value equal to 3.2%.

On the whole variation of the ∠HCH angle does not produce large effects on γ, which is shown to be more sensitive to the variation of the C—H bond length.

This finding implies that the variation of the internuclear distance has a larger effect on the rearrangement of the charge cloud, and in particular its outer regions, than the variation of the angle between the internuclear vectors. Further insight in the property change induced by structure variations is gained by considering the hyperpolarisability of the puckered and the planar configurations of C_4H_8 (23) and C_5H_{10} (24).

It is observed that the difference γ (puckered) − γ (planar) takes the values ≃ 2300 au and ≃ 1200 au for C_4H_8 and C_5H_{10}, respectively.

It is also noted that the difference α (puckered) − α (planar) takes the values 1.3 au and 0.7 au correspondingly.

Now, considering that α is proportional to the molecular volume, (18, 25), it appears that the larger hyperpolarisability of the puckered configuration with respect to that of the planar, for both C_4H_8 and C_5H_{10}, is associated with the larger volume. This is an interesting correlation because the second hyperpolarisability is thus associated with the volume — a well known property. Further, since this finding is in agreement with a similar observation in aromatic molecules (18), it seems that the molecular volume may be used as "thumb-rule" indicating, at least, the ordering of hyperpolarisabilities.

From the above variations of γ, induced by changes in the structure, the following are further noted. Firstly, for small changes of the bond length, like those which are normally found between assumed bond lengths and experimentally determined ones, the overall change in the molecular γ is usually less than 10% as computations on a large number of molecules have shown (16–18). This remark provides a justification for the use of standard geometric models at this level of approximation, where, on average, accuracy of around 30% is a worthy goal (17). Secondly, variation in γ induced by configuration changes are usually small. Thus fixed geometry models allow one to form a reasonably accurate estimate of the magnitude of experimental values, determined from mixtures of conformers, rotamers, etc.

B. An analysis of the contributions to γ

In order to evaluate the contribution of the multicenter interactions and the importance of considering the charge cloud as a whole we have approximated the second hyperpolarisability of a cycloalkane to a sum of (*a*) the values of the constituent CH_2 units, (*b*) the contributions due to all the pair wise interactions bonded and non-bonded, of these methylene units, γ_{pair}, and (*c*) a term, γ_{rem}, which gives a semi-quantitative measure of the multicenter interactions not included in the previous terms. This scheme is defined by the following equations:

$$[3] \quad \gamma = n\gamma_{CH_2} + \gamma_{int}$$

$$[4] \quad \gamma_{int} = \gamma_{pair} + \gamma_{rem}$$

where n is the number of CH_2 units from which the compound is constructed. In the analysis which follows we used for γ of CH_2 the value 2054 au (Table 1).

Application of eqs. [3] and [4], and the results in Table 2, give:

A. C_4H_8 (planar)

$4\gamma_{CH_2} = 8216$ au

$\gamma_{pair} = (4 \times 720 - 2 \times 670)$ au $= 1540$ au

$\gamma_{rem} = (14160 - 8216 - 1540)$ au $= 4404$ au

B. Fragment (123)

This fragment is defined in the footnote of Table 2.

$3\gamma_{CH_2} = 6162$ au

$\gamma_{pair} = (2 \times 720 - 670)$ au $= 770$ au

$\gamma_{rem} = (8650 - 6932)$ au $= 1718$ au

Can. J. Chem. Downloaded from www.nrcresearchpress.com by 210.87.254.5 on 09/06/12
For personal use only.

Can. J. Chem. Downloaded from www.nrcresearchpress.com by 210.87.254.5 on 09/06/12
For personal use only.

TABLE 2. The second hyperpolarisability, in au, of cyclobutane, its fragments, and cyclopentane

Fragment or molecule[g]	γ
(123)[a]	8650, 8018 ± 1604[e]
(14)[b]	3330
(12)[b]	4720
(34)[c]	4700
(14)[c]	4710
(23)[c]	3350
C_4H_8 (puckered)[d]	16410
C_4H_8 (planar)[d]	14160
C_5H_{10} (planar)	18860
C_5H_{10} (puckered)[f]	19870

[a] Fragment of C_4H_8 (planar).
[b] Pair of methylene units defined from C_4H_8 (planar).
[c] Pair of methylene units defined from C_4H_8 (puckered).
[d] Geometry from ref. 27.
[e] Experimental value (28). The theoretical value (8650 au) has been calculated employing a geometry, that corresponds to the fragment of C_4H_8, and which is rather strained in comparison with the equilibrium geometry of cyclopropane to which the experimental value refers (16).
[f] Geometry is from ref. 24.
[g] Note: the numbers within parentheses denote the relevant CH_2 units of C_4H_8 (Fig. 1). For example (12) means the pair of methylene units — the numbers define the relevant carbon atoms — having the same spatial position as in the parent molecule.

C. C_4H_8 (puckered)

$$4\gamma_{CH_2} = 8216 \text{ au}$$

$$\gamma_{pair} = (4 \times 700 + 710 - 650) \text{ au} = 2860 \text{ au}$$

$$\gamma_{rem} = (16410 - 2860 - 8216) \text{ au} = 5334 \text{ au}$$

From the above results we note that: (*a*) The large contribution γ_{int} makes to the overall γ is a quantitative manifestation of the considerable changes, which are induced in the outer regions of the CH_2 charge clouds, when they merge to form a compound. An acceptable basis set has to be capable of reflecting this distortion of the charge. However, most basis sets, with constraints on the size, and which are optimized for energy, do not guarantee an adequate description of the molecular polarisation (26). Thus one of the most chemically satisfactory and computationally economical solutions is to optimize the A.O. set with respect to some judiciously chosen compounds for which the experimental values of γ are known in order to study other structurally similar molecules. This option is the cornerstone of our computational technique (16–18). (*b*) It is observed that $\gamma_{pair} \neq \gamma_{int}$. In fact γ_{rem} contributes 20% to the hyperpolarisability of the fragment (123), while it contributes 31% and 33% to the hyperpolarisability of the planar and puckered forms of C_4H_8, respectively. These large contributions demonstrate the importance of the multicenter contributions and more specifically underline the significance of treating the charge cloud as a whole, because otherwise large contributions may be lost. At this point it may be noted that one may manage to fit a series of hyperpolarisability results employing some bond or atom constants. However, it is to be stated that any model which is likely to promote our understanding has to give due consideration to the fact that the nonlinearity of the various functional groups greatly depends on their intra-molecular environment, (which has been amply demonstrated by the large contribution of γ_{rem} to γ) much more, in fact, than for the dipole moment or the polarisability, (16–18). This remark defines, also, an essential condition which has to be satisfied by an additivity scheme in order to be successful.

Conclusions

In this work we have presented the second hyperpolarisabilities of C_4H_8 and C_5H_{10} which are not currently available in the literature. These results were associated with an estimate of the error (30%), which is considered to be reasonable. A critical appraisal of standard geometric models, often employed in semiempirical calculations, as well as of fixed geometry models used to approximate values determined from experimental samples, has been presented. Further, the conformational change in the hyperpolarisability has been associated with the change in molecular volume. This correlation allows the ready comprehension of γ. It also points to a possible route for the evaluation of this property, from quantities easier to determine, by employing, perhaps, a scheme similar to that in ref. 18.

Analysis of the hyperpolarisability results for C_4H_8 demonstrates the importance of the multicenter interactions and illustrates that this non-linearity is most profitably approached as a property of the outer reaches of the charge cloud treated as a whole.

1. A. D. BUCKINGHAM and B. J. ORR. Q. Rev. London, **21**, 195 (1967).
2. D. A. DIXON, R. A. EADES, and D. G. TRUHLAR. J. Phys. B**12**, 2741 (1979).
3. H. F. HAMEKA. J. Chem. Phys. **67**, 2935 (1977).
4. E. F. MCINTYRE and H. F. HAMEKA. J. Chem. Phys. **68**, 3481 (1978).
5. J. A. MORRELL, A. C. ALBRECHT, K. H. LEVIN, and C. L. TANG. J. Chem. Phys. **71**, 5063 (1979).
6. J. A. MORRELL and A. C. ALBRECHT. Chem. Phys. Lett. **64**, 46 (1979).
7. J. MUSZYNSKA, D. PAPIEROWSKA, J. PIPIN, and W. WOZNICKI. Int. J. Quant. Chem. **22**, 1153 (1982).
8. R. M. GLOVER and F. WEINHOLD. J. Chem. Phys. **65**, 4913 (1976).
9. D. M. BISHOP and L. M. CHEUNG. Phys. Rev. A**20**, 1310 (1979).
10. R. M. BERNS and P. E. S. WORMER. Mol. Phys. **44**, 1215 (1981).
11. R. J. BARTLETT and G. D. PURVIS, III. Phys. Rev. A**20**, 1313 (1979).
12. R. J. BARTLETT and G. D. PURVIS, III. Phys. Script. **21**, 255 (1980).
13. P. A. CHRISTIANSEN and E. A. MCCULLOUGH, JR. Chem. Phys. Lett. **63**, 570 (1979).
14. G. D. PURVIS III and R. J. BARTLETT. Phys. Rev. A**23**, 1594 (1981).
15. O. ZAMANI-KHAMIRI and H. F. HAMEKA. J. Chem. Phys. **73**, 5693 (1980); E. F. MCINTYRE and H. F. HAMEKA. J. Chem. Phys. **70**, 2215 (1979); **68**, 5534 (1978); **69**, 4814 (1978); J. ZYSS and BERTHIER. J. Chem. Phys. **77**, 3635 (1982); J. ZYSS. J. Chem. Phys. **70**, 333 (1979).
16. C. A. NICOLAIDES, M. G. PAPADOPOULOS, and J. WAITE. Theoret. Chim. Acta, **61**, 427 (1982).
17. M. G. PAPADOPOULOS, J. WAITE, and C. A. NICOLAIDES. J. Chem. Phys. **77**, 2527 (1982).
18. J. WAITE, M. G. PAPADOPOULOS, and C. A. NICOLAIDES. J. Chem. Phys. **77**, 2536 (1982).
19. J. A. POPLE and D. L. BEVERIDGE. Approximate molecular orbital theory. McGraw-Hill, New York. 1970.

20. R. MCWEENY. Phys. Rev. **126**, 1028 (1962); G. DIERCKSEN and R. MCWEENY. J. Chem. Phys. **44**, 3554 (1966); J. L. DODDS, R. MCWEENY, W. T. RAYNES, and J. P. RILEY. Mol. Phys. **33**, 611 (1977).
21. J. F. WARD and D. S. ELLIOTT. J. Chem. Phys. **69**, 5438 (1978).
22. W. A. LATHAN, W. J. HEHRE, and J. A. POPLE. J. Am. Chem. Soc. **93**, 808 (1971).
23. J. S. WRIGHT and L. SALEM. J. Am. Chem. Soc. **94**, 322 (1972).
24. W. J. ADAMS, H. J. GEISE, and L. S. BARTELL. J. Am. Chem. Soc. **92**, 5013 (1970).
25. M. T. KHIMENKO, N. N. GRITSENKO, and V. V. ALEKSADROV. Russ. J. Phys. Chem. **49**, 1407 (1975).
26. P. G. MEZEY and E. C. HAAS. J. Chem. Phys. **77**, 870 (1982).
27. S. MEIBOM and L. C. SNYDER. J. Chem. Phys. **52**, 3857 (1970).
28. A. D. BUCKINGHAM, M. P. BOGAARD, D. A. DUNMUR, C. P. HOBBS, and B. J. ORR. Trans. Faraday Soc. **66**, 1548 (1970).

Can. J. Chem. Downloaded from www.nrcresearchpress.com by 210.87.254.5 on 09/06/12
For personal use only.

Etude par activation collisionnelle des ions $[C_4H_7O]^+$ provenant des ions penténols et méthylcetones $[C_5H_{10}O]^{\cdot+}$ métastables

G. Bouchoux et Y. Hoppilliard
Laboratoire de Synthèse Organique, Ecole Polytechnique, 91128 Palaiseau Cedex, France

et

R. Flammang, A. Maquestiau et P. Meyrant
Laboratoire de Chimie Organique, Université de l'Etat, 19, avenue Maistriau, 7000 Mons, Belgique

Reçu le 22 juin 1983[1]

G. Bouchoux, Y. Hoppilliard, R. Flammang, A. Maquestiau et P. Meyrant. Can. J. Chem. **62**, 1740 (1984).

Les ions $[C_4H_7O]^+$ résultant de la perte de CH_3 à partir de la pentanone-2 (**1**), la méthyl-3-butanone (**2**), le méthyl-2-butène-3-ol-2 (**3**), le pentène-3-ol-2- (**4**) et le méthyl-3-butène-3-ol-2 (**5**) ont été étudiés par activation collisionnelle. Un spectromètre de masse à triple secteur a été utilisé afin de distinguer les ions fragments formés dans la source et dans la première région libre de champ. Les spectres de dissociations induites par collisions confirment ou éclairent les points suivants: (*i*) dans la source, l'élimination du CH_3 occupant la position 1 des molécules **1**−**5** conduit respectivement aux ions $[n\text{-}C_3H_7CO]^+$ (**a**), $[i\text{-}C_3H_7CO]^+$ (**b**), $[CH_3COHCHCH_2]^+$ (**c**), $[CH_3CHCHCHOH]^+$ (**d**) et $[CH_2C(CH_3)CHOH]^+$ (**e**), tandis que la perte de méthyle à partir de la chaîne produit compétitivement l'ion **c** pour les cinq précurseurs; (*ii*) en région libre de champ, les ions **1**, **3**, **4** et **5** conduisent à un même mélange de structures **a**, **b** et **c**, l'ion **2** conduit à l'ion acylium **b** de façon prépondérante. Les mécanismes et la thermochimie des réactions d'isomérisation des ions $[C_5H_{10}O]^{\cdot+}$ **1**−**5** sont discutés.

G. Bouchoux, Y. Hoppilliard, R. Flammang, A. Maquestiau, and P. Meyrant. Can. J. Chem. **62**, 1740 (1984).

The $[C_4H_7O]^+$ ions arising from 2-pentanone (**1**), 3-methylbutanone (**2**), 2-methylbut-3-en-2-ol (**3**), pent-3-en-2-ol (**4**), and 3-methylbut-3-en-2-ol (**5**) by methyl loss were studied by collisional activation. A triple sector (E/B/E) mass spectrometer was used to distinguish between fragment ion structures produced in the source and in the first field free region. The collision induced dissociations confirm or demonstrate that: (*i*) in the source, the methyl originally on the position 1 in compounds **1**−**5** is lost to give, respectively, $[n\text{-}C_3H_7CO]^+$ (**a**), $[i\text{-}C_3H_7CO]^+$ (**b**), $[CH_3COHCHCH_2]^+$ (**c**), $[CH_3CHCHCHOH]^+$ (**d**), and $[CH_2C(CH_3)CHOH]^+$ (**e**), while the methyl loss from the side chain gives, competitively, ion **c** for the five precursors; (*ii*) in the first field free region molecular ions **1**, **3**, **4**, and **5** produce an identical mixture of structures **a**, **b**, and **c**; the molecular ion **2** leads essentially to acylium ion **b**. The mechanisms and the thermochemistry of the isomerization path of **1**−**5** are discussed.

Introduction

L'élimination de CH_3 est la fragmentation principale des ions moléculaires $[C_5H_{10}O]^{\cdot+}$ métastables **1**−**5** (1−4), (Schéma 1); pour ces cinq exemples elle est en compétition avec la perte d'une molécule d'éthylène:

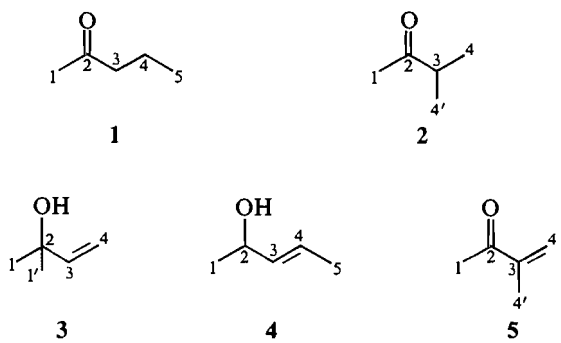

1 **2** **3** **4** **5**

Schéma 1

L'étude des spectres de masse des molécules **1**−**5** spécifiquement deutériées démontre que le radical méthyle éliminé provient aussi bien du groupement acétyle que de la chaîne propyle dans le cas de **1** (2) et **2** (3), du radical propényle pour les alcools **4** (4) et **5** (4) et du radical vinyle pour **3** (4).

Les mécanismes des réactions $[C_5H_{10}O]^{\cdot+} \rightarrow [C_4H_7O]^+ + CH_3^{\cdot}$ se produisant dans la source du spectromètre de masse ont alors été établis après examen des spectres de dissociations unimoléculaires des ions fragments $[C_4H_7O]^+$. Dans aucune des études citées, la structure des ions fragments formés en région libre de champ (RLC) n'a été directement établie. L'argumentation repose toujours sur l'utilisation du marquage isotopique et de ses conséquences sur le spectre de dissociation unimoléculaire de l'ion $M^{\cdot+}$ et sur les charactéristiques structurales des ions fragments formés dans la source. Le but du présent travail est tout d'abord d'apporter avec les spectres de collisions d'ions $[C_4H_7O]^+$ provenant de divers précurseurs, un nouveau moyen d'identification des structures **a**−**e** (Schéma 2) dont les décompositions unimoléculaires ont par ailleurs été décrites par Williams *et al.* (5) (pour **a**, **b**):

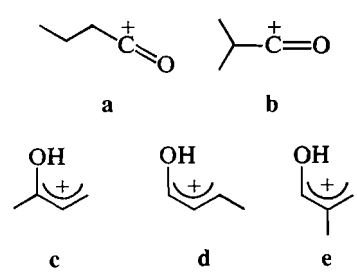

a **b** **c** **d** **e**

Schéma 2

Cette technique est ensuite utilisée sur les ions $[C_4H_7O]^+$ provenant de **1**−**5** dans la première région libre de champ d'un spectromètre de masse à triple secteur (E/B/E).

Ces résultats seront comparés aux données énergétiques associées aux réactions d'isomérisation et de dissociation des ions $[C_5H_{10}O]^{\cdot+}$ (**1**−**5**).

[1]Revision reçue le 9 février 1984.

Can. J. Chem. Downloaded from www.nrcresearchpress.com by 210.87.254.6 on 09/06/12
For personal use only.

TABLEAU 1. Spectres CID–MIKE[a] des ions $[C_4H_7O]^+$ formés dans la source à partir des précurseurs **6**–**13** (spectres étalons des ions $[C_4H_7O]^+$ **a**–**e**)

	Précurseurs	Structure $[C_4H_7O]^+$	[b]	*m/z*, A						*m/z*, B					ΣB =	*m/z*, C				
				56	55	53	51	50	ΣA	45	43	42	41	39	1000	31	29	27	26	ΣC
6		**a**	Z	16	74	(10)	3	7	*30*	—	(407)	36	32	32		—	11	67	22	*130*
			M	20	70	(8)	4	5	*33*	—	(674)	45	31	24		—	18	67	15	*48*
7		**b**	Z	71	21	(15)	3	6	*15*	—	(1100)	22	32	45		—	4	68	28	*53*
			M	73	18	(12)	4	4	*27*	—	(1550)	34	30	36		—	6	69	25	*20*
8	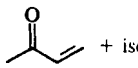 + isobutane	**c**	Z	9	59	(23)	16	17	*570*	4	(144)	27	29	40		12	17	53	18	*790*
11	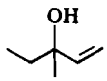	**c**	M	9	60	(71)	17	14	*500*	5	(311)	27	36	31		13	15	58	14	*195*
9		**d**	Z	10	36	(79)	27	26	*470*	1	(18)	10	36	53		18	28	42	12	800
12	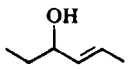	**d**	M	6	44	(203)	30	20	*370*	1	(198)	14	44	42		18	25	49	7	180
10	+ isobutane	**e**	Z	11	47	(31)	20	22	*260*	3	(46)	10	35	52		15	35	40	11	*590*
13	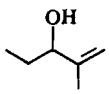	**e**	M	9	54	(65)	20	16	*140*	2	(330)	14	41	42		17	31	44	8	*100*

[a]Les intensités de pics ont été normalisées pour chaque massif en excluant la contribution des pics indiqués entre parenthèses (composantes unimoléculaires). Les participations globales de chaque massif au spectre complet sont les termes: ΣA, ΣB et ΣC; elles comprennent cette fois les pics placés entre parenthèses, elles sont rapportées à $\Sigma B = 1000$.

[b]Z = spectromètre de masse VG.ZAB.2F; M = spectromètre AEI.KRATOS.MS 902 modifié.

Resultats et discussion

1. *Spectres CID–MIKE*[2] *des ions a–e*

Les esters méthyliques **6** et **7** (Schéma 3) conduisent aux ions acylium **a** et **b** par simple rupture d'une liaison C—O. Les spectres MIKE des ions $[\mathbf{6}\text{-}OCH_3]^+$ et $[\mathbf{7}\text{-}OCH_3]^+$ ne comportent qu'un pic correspondant à l'élimination exclusive de CO (2), les énergies cinétiques $T_{0.5}$ sont très différentes (5) (respectivement 18 meV et 2 meV, VG.ZAB.2F) permettant de distinguer aisément les deux structures **a** et **b**.

Les ions **c**, **d** et **e** peuvent être formés soit par protonation des composés carbonylés **8**, **9** et **10**, soit par fragmentation des alcools **11**, **12** et **13** (Schéma 3). Les décompositions unimoléculaires des ions $[C_4H_7O]^+$ ainsi formés conduisent à deux pics *m/z* 53 ($-H_2O$) et *m/z* 43 ($-CO$ et $-C_2H_4$).

Le profil du pic $[C_4H_7O]^+ \rightarrow [C_2H_3O]^+ + C_2H_4$ est caractéristique de la structure de l'ion précurseur, "dish-topped" pour **c** ($T_{0.5}$ = 400 meV), "composite" pour **d**.

Les spectres CID–MIKE des ions $[C_4H_7O]^+$ formés dans la source à partir des molécules **6**–**13** sont rassemblés sur le tableau 1.

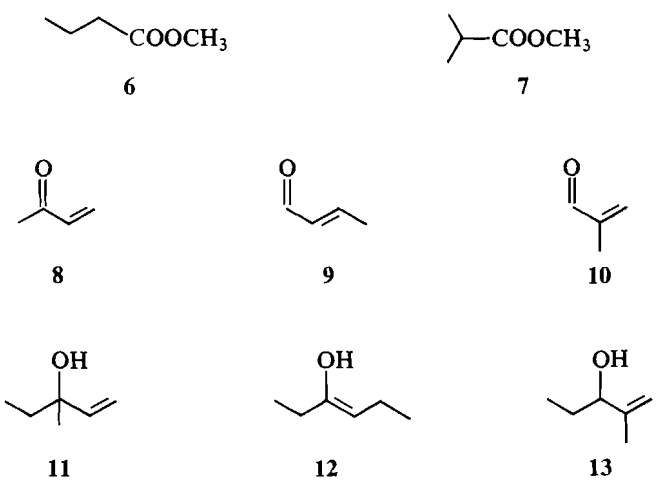

SCHÉMA 3

Le comportement des ions **a** et **b** est très largement dominé par l'élimination de 28 u.m.a. également observée sur les spectres MIKE. Parmi les fragmentations exclusivement induites par collisions, la présence pratiquement isolée du pic *m/z* 27 au coeur du massif C est caractéristique des ions acylium **a** et **b**. Seul **a** donne un pic *m/z* 29 appréciable et pour aucune des deux structures on ne détecte de pic *m/z* 31. Dans le massif B, on notera l'abondance particulière des ions *m/z* 42, ce pic surpasse *m/z* 39 dans le cas de **a**. Enfin dans la zone *m/z*

[2]On utilisera les acronymes anglosaxons MIKE (Mass Analysed Ion Kinetic Energy Spectra) et CID (Collision Induced Dissociations) – MIKE afin de désigner la technique expérimentale consistant à analyser, à l'aide d'un secteur électrique, les ions produits par la dissociation unimoléculaire (ou induite par collision) d'un ion précurseur sélectionné par un secteur magnétique (voir par exemple la référence 15).

Can. J. Chem. Downloaded from www.nrcresearchpress.com by 210.87.254.6 on 09/06/12
For personal use only.

TABLEAU 2. Spectre MIKE[a] de la pentanone 1,1,1,3,3-d_5

Fragment neutre éliminé	CH_3	CH_2D	CHD_2	CD_3	C_2H_4	C_2H_3D	$C_2H_2D_2$	C_2HD_3
Abondance (%)	65	27	18	70	43	100	47	8

[a]Mesures effectuées sur VG.ZAB.2F, 70 eV.

56−50 (A) la présence d'un pic intense m/z 56 est spécifique de l'ion **b**.

Les spectres des ions **c**, **d** et **e** sont assez différents de ceux des ions acylium, des pics nouveaux apparaissent (m/z 45, 31) ou prennent une plus grande importance (m/z 53, 51, 50, 29) et rendent identifiables les deux catégories d'ions $[C_4H_7O]^+$. La structure **c** se distingue par les intensités plus importantes des pics m/z 55 et m/z 27 au sein de leurs massifs respectifs. Les spectres des ions **d** et **e** présentent des massifs C et B extrêmement proches, la distinction entre ces deux structures est en revanche réalisable à partir des pics m/z 50−56 (le rapport m/z 55:m/z 51 est plus faible pour la structure **d**: 1,3 contre 2,5 pour **e** et 3,8 pour *c*), le pic m/z 53 domine cette région du spectre.

2. *Structure des ions $[C_4H_7O]^+$ provenant de 1 et 5*

2.1 *La pentanone-2 (1)*

La perte du méthyle occupant initialement la position 1 et celle d'un groupement CH_3 contenant trois hydrogènes de la chaîne propyle a été mise en évidence à partir des dérivés spécifiquement deutériés **1** 5,5,5-d_3 (1) et **1** 1,1,1,3,3-d_5 (2). Ces éliminations compétitives se produisent aussi bien dans la source qu'en région libre de champ du spectromètre de masse. Les ions fragments formés dans la source ont été identifiés par Krenmayr (2); à partir de **1** 1,1,1,3,3-d_5 l'élimination de CD_3 conduit à l'ion acylium **a** tandis que l'ion $[M - CH_3]^+$ correspond à **c**. Ces déductions sont basées sur le rapport des éliminations de CO et de $C_2(H,D)_4$ se produisant en première RLC d'un spectromètre à double focalisation Varian SM-IB.

Les spectres MIKE (VG.ZAB.2F) des ions $[M - CH_3]^+$ et $[M - CD_3]^+$ provenant de **1** 1,1,1,3,3-d_5 confirment les conclusions précédentes. L'ion $[M - CD_3]^+$ conduit exclusivement à $[C_3H_5D_2]^+$, le pic métastable est gaussien et sa largeur à mi-hauteur correspond à $T_{0.5}$ = 17 meV en accord avec la structure **a**.

L'ion $[M - CH_3]^+$ élimine essentiellement $C_2H_2D_2$, le pic métastable correspondant est large à sommet creux, ce profil est caractéristique ($T_{0.5}$ = 410 meV (3, 4, 6)) de la structure **c**.

Enfin le comportement de l'ion **1** 1,1,1,3,3-d_5 métastable est rapporté sur le tableau 2, un échange H/D non négligeable précède l'élimination de méthyle. On constate toutefois que les contributions des ions non échangés $[M - CH_3]^+$ et $[M - CD_3]^+$ prédominent et possèdent des valeurs comparables. Par analogie avec les fragmentations se déroulant dans la source, ces données peuvent s'interpréter par la formation compétitive d'ions **a** et **c**. L'échange partiel H/D constaté pour l'élimination de méthyle est accentué lorsque le fragment neutre expulsé est une molécule d'éthylène. La distribution $[M - C_2(H,D)_4]^{+\bullet}$ observée (Tableau 2) correspond à une répartition du type H_3D_3 sur laquelle on effectue un prélèvement de deux atomes (H_2HD/D_2 = 0,2:0,6:0,2). Cette observation, qui indique par conséquent que les échanges H/D qui précèdent l'élimination d'éthylène n'impliquent que les positions 1 et 5 (Schéma 4), est en accord avec les résultats de Beynon *et al.* (1) concernant le précurseur **1** 5,5,5-d_3:

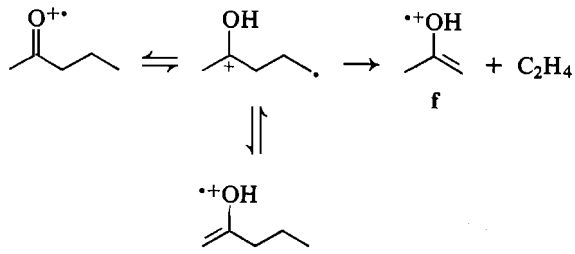

SCHÉMA 4

Les spectres CID−MIKE des ions $[1\text{-}CH_3]^+$ produits dans la source et en région libre de champ (Tableau 3) présentent de grandes similitudes. Par rapport au spectre de l'ion **a** ($[6\text{-}OCH_3]^+$, Tableau 1) on distingue une augmentation d'intensité des pics m/z 51 et 50, une abondance plus élevée du massif A et surtout l'apparition des pics m/z 45 et 31 qui trahissent la présence de la structure hydroxycarbénium **c** aussi bien parmi les ions $[1\text{-}CH_3]^+$ formés dans la source qu'en RLC. En RLC on constatera également un léger enrichissement du massif A en ions m/z 56 qui pourrait s'expliquer par l'apparition d'ions acylium **b**, à côté des structures **a** et **c** à partir de l'ion moléculaire **1** métastable.

Ajoutons enfin que l'évolution du rapport $[1a\text{-}CH_3]^+/[1a\text{-}CD_3]^+$ (0,4 en source et 0,9 en RLC) indique une plus large participation des ions de type **c** en RLC. Il se dégage de ces observations que les trajets de dissociation de **1** conduisant aux ions **a**, par simple fragmentation, et aux ions **b** et **c**, après isomérisation de l'ion moléculaire, possèdent des énergies critiques extrêmement proches.

2.2 *La méthyl-3-butanone (2)*

Il est établi que les ions de source $[2a\text{-}CD_3]^+$ et $[2a\text{-}CH_3]^+$ (**2***a*: 1,1,1,3-d_4 méthyl-3-butanone) sont, pour les premiers constitués d'un mélange d'ions **b** (majoritaire) et **e**, tandis que les seconds sont exclusivement des ions **c** (3).

Les ions $[2\text{-}CH_3]^+$ formés en source possèdent un spectre CID−MIKE très proche de celui de l'ion **b** ($[7\text{-}OCH_3]^+$, Tableau 1), la présence des pics m/z 45 et 31 témoigne de l'existence d'ions hydroxycarbénium **c**.

Un changement notable apparaît sur le spectre CID−MIKE des ions $[2\text{-}CH_3]^+$ formés en RLC, les pics m/z 45 et 31 disparaissent au profit de m/z 56: il ne subsiste pratiquement plus que la structure acylium **b** en RLC. Cette conclusion explique également la modification du rapport $[2a\text{-}CH_3]^+/[2a\text{-}CD_3]^+$ (0,5 dans la source contre 0,16 en RLC (3)). Il faut déduire de ce résultat que le processus de dissociation de l'ion **2** nécessitant le moins d'énergie est la simple élongation de la liaison C—C conduisant à **b** + $CH_3^\bullet$.

2.3 *Les penténols 3, 4 et 5*

On constate tout d'abord qu'aucune différence n'est décelable entre les spectres CID−MIKE des ions $[C_4H_7O]^+$ provenant de **3**, **8** et **11** dans la source (Tableaux 1 et 3): les ions $[3\text{-}CH_3]^+$ sont donc essentiellement des ions **c**. Ce résultat est en accord

Can. J. Chem. Downloaded from www.nrcresearchpress.com by 210.87.254.6 on 09/06/12
For personal use only.

TABLEAU 3. Spectres CID–MIKE[a] des ions $[C_4H_7O]^+$ provenant des composés **1**–**5**, **4***a* et **5***a* dans la source (S) ou dans la première région libre de champ (RLC)

Précurseurs	Région	*m/z*, A						*m/z*, B					$\Sigma B =$	*m/z*, C				
		56	55	53	51	50	ΣA	45	43	42	41	39	1000	31	29	27	26	ΣC
1 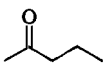	S	18	64	(61)	10	8	*78*	2	(1040)	39	33	26		7	18	60	15	*40*
	RLC	24	54	(27)	11	10	*255*	3	(220)	38	25	33		9	18	60	13	*170*
2	S	41	21	(29)	4	4	*100*	1	(607)	36	29	34		4	9	67	20	*52*
	RLC	73	19	(9)	4	5	*96*	—	(378)	39	25	35		1	6	69	23	*66*
3	S	7	61	(69)	16	15	*500*	4	(270)	27	37	31		14	16	56	14	*200*
	RLC	15	57	(26)	15	12	*430*	5	(203)	31	29	35		11	15	60	14	*248*
4 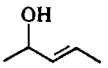	S	8	57	(108)	19	16	*410*	3	(270)	20	42	35		17	19	52	11	*158*
	RLC	16	55	(20)	16	14	*365*	4	(200)	34	28	33		13	15	59	13	*203*
4*a* 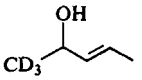	S	9	50	(186)	24	17	*325*	1	(285)	19	44	36		19	25	46	10	*116*
	RLC	24	55	(21)	12	8	*115*	1	(233)	41	29	29		5	17	63	15	*116*
5	S	10	58	(75)	18	14	*350*	4	(311)	22	38	36		16	20	53	11	*152*
	RLC	15	58	(22)	13	13	*360*	3	(188)	36	30	31		10	14	59	16	*215*
5*a* 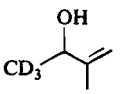	S	13	53	(93)	18	16	*160*	2	(403)	19	41	38		17	28	46	10	*86*
	RLC	33	49	(20)	10	7	*97*	—	(245)	40	29	30		3	19	63	15	*110*

[a]Voir Tableau 1.

avec la formation pratiquement exclusive (95%) d'ions $[M - CD_3]^+$ à partir de **3***a* $(CD_3)_2COHCHCH_2$ (4) dans la source du spectromètre de masse. Dans le cas des précurseurs **4** et **5**, Zwinselman *et al.* (4) constatent que les ions de source $[M - CH_3]^+$ proviennent, pour ≈60% d'une élimination de CH_3 à partir de la chaîne propényle pour donner l'ion **c**, et pour ≈40% de la perte du méthyle occupant la position 1 conduisant ainsi aux ions **d** et **e**. Les spectres CID–MIKE des ions de source $[\mathbf{4}\text{-}CH_3]^+$ et $[\mathbf{5}\text{-}CH_3]^+$ sont assez proches, ils s'interprètent par l'existence de deux mélanges d'ions dominés par la structure **c** comme en témoigne en particulier la répartition des intensités de pics *m/z* 31–27 et la ressemblance étroite avec le spectre CID–MIKE de $[\mathbf{3}\text{-}CH_3]^+$. Les ions $[C_4H_7O]^+$ provenant des dérivés **4***a* et **5***a* permettent de contrôler l'identité du second constituant de chaque mélange d'ions $[\mathbf{4}\text{-}CH_3]^+$ et $[\mathbf{5}\text{-}CH_3]^+$:

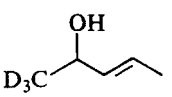

4*a*

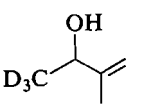

5*a*

Il existe un rapprochement certain entre les spectres CID–MIKE des ions de source $[\mathbf{4}a\text{-}CD_3]^+$ (Tableau 3) et **d** ($[\mathbf{12}\text{-}C_2H_5]^+$, Tableau 1) d'une part, et $[\mathbf{5}a\text{-}CH_3]^+$ (Tableau 3) et **e** ($[\mathbf{13}\text{-}C_2H_5]^+$, Tableau 1) d'autre part. Les spectres CID–MIKE des ions $[\mathbf{4}a\text{-}CH_3]^+$ et $[\mathbf{5}a\text{-}CH_3]^+$ sont identiques (Fig. 1); ils confirment la formation d'une structure commune de type **c** par élimination de CH_3 à partir de la chaîne propényle.

Les spectres d'activation collisionnelle apportent donc une confirmation aux conclusions de Zwinselman *et al.* (4) concernant les ions **3**, **4** et **5** de courte durée de vie ($\tau \leq 10^{-6}$ s).

En région libre de champ, **3***a* conduit à 75% d'ions $[M - CD_3]^+$ et 25% d'ions $[M - CH_3]^+$, ces pourcentages deviennent respectivement 65% et 35% pour les ions **4***a* et **5***a* métastables (4). On constate (Tableau 3) que les ions $[\mathbf{3}\text{-}CH_3]^+$, $[\mathbf{4}\text{-}CH_3]^+$ et $[\mathbf{5}\text{-}CH_3]^+$ formés en RLC possedent des spectres identiques. Ces trois spectres sont de plus assez semblables à celui des ions $[\mathbf{1}\text{-}CH_3]^+$ produits eux aussi en RLC. Compte tenu des résultats présentés lors de l'étude du composé **1**, il faut conclure ici à la production d'un mélange d'ions **a**, **b** et **c** à partir des penténols **3**, **4** et **5** métastables.

La composition du mélange peut être déduite des spectres des ions fragments issus de **4***a* et **5***a*. Les spectres CID–MIKE des ions $[\mathbf{4}a\text{-}CD_3]^+$ et $[\mathbf{5}a\text{-}CD_3]^+$ formés en RLC (Tableau 3) sont identiques. Par rapport aux spectres des ions de source, on constate le diminution importante des pics *m/z* 31, 50 et 51 et l'augmentation des pics *m/z* 56, 42 et 27 due à une très nette prédominance de structure acylium, un mélange d'ions **a** (majoritaires) et **b**.

Les ions $[\mathbf{4}a\text{-}CH_3]^+$ et $[\mathbf{5}a\text{-}CH_3]^+$ formés en RLC donnent des spectres CID–MIKE identiques entre eux et identiques à ceux qui ont été présentés sur la figure 1 pour les ions de source et dont la structure **c** est établie (4). Il ne fait donc aucun doute que l'élimination de méthyle à partir de la chaîne propényle conduit à l'ion **c**.

L'essentiel de la discussion précédente peut se résumer comme suit.

(a) Dans la source du spectromètre de masse, l'élimination du CH_3 occupant la position 1 des molécules **1**, **2**, **3**, **4** et **5** conduit respectivement aux ions **a**, **b**, **c**, **d** et **e** (ce dernier étant également formé à partir de **2**), tandis que, pour les cinq précurseurs, la perte de méthyle de la chaîne produit compétitivement l'ion **c**.

(b) En région libre de champ, les ions **1**, **3**, **4** et **5** conduisent à un même mélange d'ions **a**, **b** (minoritaire) et **c**; seul **2** possède un comportement distinct, la formation de l'ion acylium **b** étant prépondérante.

Can. J. Chem. Downloaded from www.nrcresearchpress.com by 210.87.254.6 on 09/06/12
For personal use only.

Can. J. Chem. Downloaded from www.nrcresearchpress.com by 210.87.254.6 on 09/06/12
For personal use only.

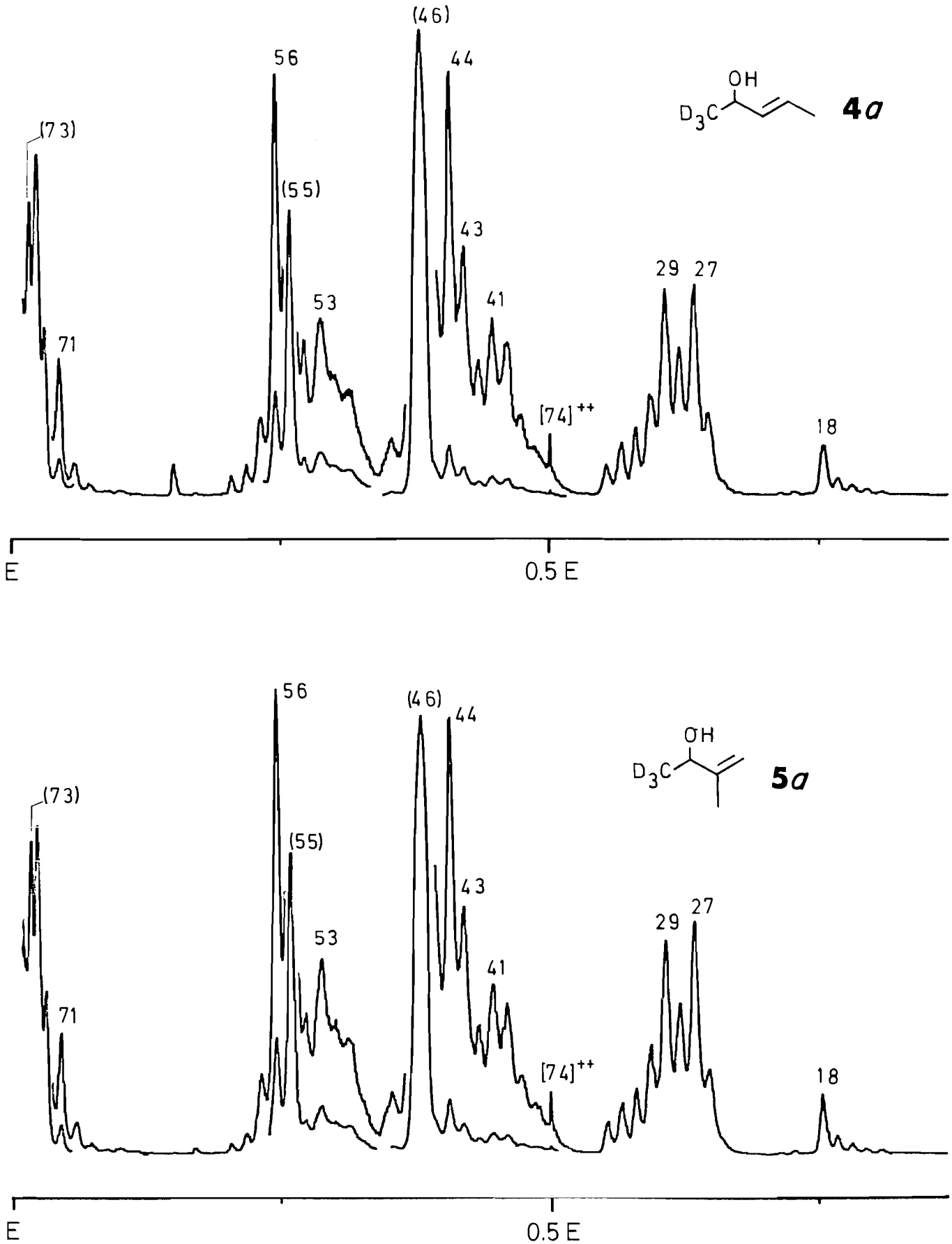

FIG. 1. Spectres CID–MIKE des ions $[\mathbf{4}a\text{-}CH_3]^+$ et $[\mathbf{5}a\text{-}CH_3]^+$ formés dans la source du spectromètre de masse MS.902.

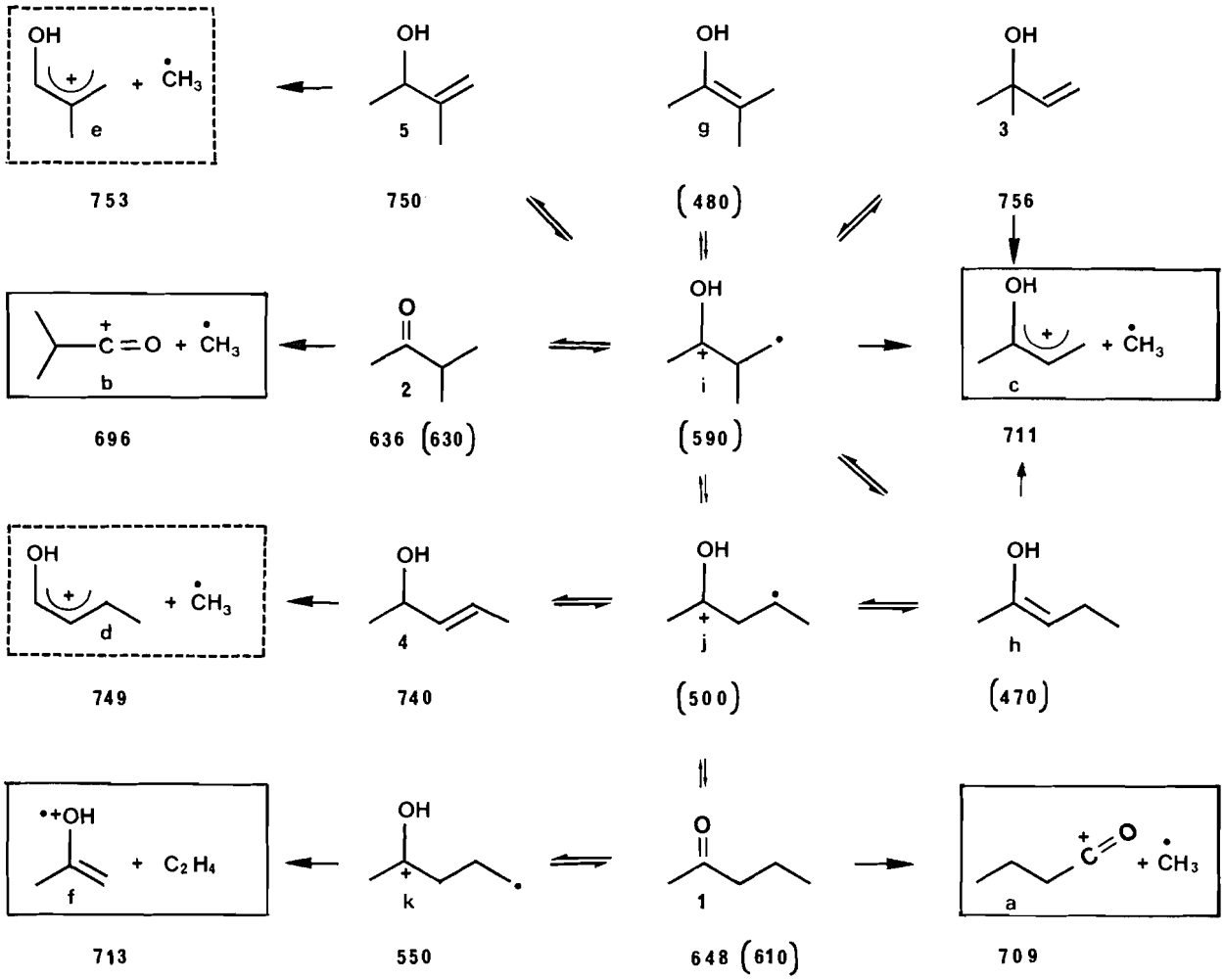

FIG. 2. Schéma d'isomérisation et de fragmentation des ions $[C_5H_{10}O]^{\cdot+}$. Les fragments encadrés d'un trait plein sont préférentiellement formés en RLC, les traits pointillés correspondent aux ions produits principalement dans la source. Les ΔH_f^0 sont exprimés en kJ mol^{-1} (entre parenthèses valeurs calculées par la méthode MINDO/3).

TABLEAU 4. Energies d'apparition (E.A. en eV) des principaux ions fragments issus de **6** et **7**[a]

	Précurseur	E.A. (m/z 71)	E.A. (m/z 74)	E.A. (m/z 87)
6	CO_2CH_3	10,8	[10,2]	10,8
7	CO_2CH_3	10,7	—	10,5

[a]Mesures effectuées sur Varian.MAT.CH5 par la méthode semi-logarithmique. Après calibration, l'échelle des énergies a été calée sur E.A. (m/z 74) = 10,2 eV (10), la reproductibilité des mesures est de l'ordre de 0,05 eV.

3. *Mécanismes et thermochimie*

L'observation des deux pics d'intensités voisines m/z 71 $[M - CH_3]^+$ et m/z 58 $[M - C_2H_4]^{\cdot+}$ sur les spectres MIKE des ions moléculaires **1**–**5** indique que les deux fragmentations possèdent des énergies critiques similaires. La thermochimie des ions **1**–**5** et de leurs dissociations conduisant à (**a**–**e**) + CH_3· (Schéma 2) et à **f** + C_2H_4 (Schéma 3) est connue (7–9). Les ΔH_f^0 des ions $[C_4H_7O]^+$ hydroxycarbénium proviennent de mesures d'affinités protoniques (7), les valeurs de ΔH_f^0 (**a**) et ΔH_f^0 (**b**) ont été déduites des énergies de photodissociation des ions moléculaires **1** et **2** (8). L'exactitude de ces deux derniers chiffres repose sur l'hypothèse de la formation exclusive des ions **a** et **b** au seuil thermodynamique en partant de **1** et **2**. Or il vient d'être établi que les ions **a** et **b** ne sont pas les seuls produits de l'élimination de CH_3 sous impact électronique à 70 eV.

Les ions **a** et **b** ont par conséquent été générés à partir des esters **6** et **7**. Les mesures d'énergie d'apparition consignées dans le tableau 4 conduisent aux estimations:

$$\Delta H_f^0 \text{ (a)} = 580 \pm 5 \text{ kJ mol}^{-1}$$

$$\Delta H_f^0 \text{ (b)} = 565 \pm 5 \text{ kJ mol}^{-1}$$

en utilisant ΔH_f^0 (**6**) = −451 kJ mol^{-1} (10), ΔH_f^0 (**7**) = −456 kJ mol^{-1} (chiffre obtenu en combinant ΔH_f^0 (**6**) et les incréments d'enthalpies des groupes n-C_3H_7 et iso-C_3H_7 (11)) et ΔH_f^0 (CH_3·) = 142 kJ mol^{-1}. Les valeurs obtenues ici sont très légèrement supérieures aux appréciations antérieures (ΔH_f^0 (**a**) = 567 kJ mol^{-1} et ΔH_f^0 (**b**) = 554 kJ mol^{-1} (8, 9)). Aucune correction aux mesures du tableau 4 n'a été effectuée en vue d'éliminer un déplacement cinétique compétitif éventuellement responsable de l'écart observé. Néanmoins ces chiffres confirment d'une part la plus grande stabilité de l'ion acylium ramifié **b**, et, d'autre part, l'extrême proximité des valeurs de ΔH_f^0 (**a**) et ΔH_f^0 (**c**) (569 ± 12 kJ mol^{-1} (7)).

Can. J. Chem. Downloaded from www.nrcresearchpress.com by 210.87.254.6 on 09/06/12
For personal use only.

Can. J. Chem. Downloaded from www.nrcresearchpress.com by 210.87.254.6 on 09/06/12
For personal use only.

La formation d'un ion $[\mathbf{3}\text{-}CH_3]^+$ de structure diméthylcétène protoné sur l'atome d'oxygène $[(CH_3)_2CCOH]^+$ (**1**) a été envisagée (4). Aucune donnée expérimentale ne permet de situer le ΔH_f^0 de cet ion, en revanche un calcul d'orbitales moléculaires a été entrepris. Ainsi les méthodes MINDO/3 (12) et MNDO (13) situent l'ion **1** 90 kJ mol^{-1} au-dessus de l'ion hydroxycarbenium **c**, la production de **1**, principalement en RLC, semble devoir être rejetée.

Un nombre restreint de réactions d'isomérisation des ions moléculaires **1**−**5** permet d'expliquer l'apparition des divers ions fragments **a**−**f** (Fig. 2). La formation des ions $[M - CH_3]^+$ de type **a** et **c** en compétition avec l'ion $[M - C_2H_4]^+$ de structure **f** à partir de **1**, **3**, **4** et **5** en RLC coïncide avec les valeurs identiques des ΔH_f^0 des produits de ces fragmentations, soit environ 710 kJ mol^{-1}. En conséquence, lorsque ces fragmentations sont globalement endothermiques, comme cela est le cas pour **1**, les réactions d'isomérisation correspondantes passent par des états de transition dont les ΔH_f^0 sont inférieurs à 710 kJ mol^{-1}. Il s'agit: de la migration 1,2 d'hydrogène (**h** ⇄ **j**); du transfert 1,2 du groupement CH_3COH (**i** ⇄ **j**) qui, à côté de l'enchaînement **i** ⇄ **h** ⇄ **j**, permet de rendre compte de l'isomérisation de la chaîne propyle avec un bilan énergétique plus favorable (14); et enfin des migrations 1,4 et 1,5 d'hydrogène (**1** ⇄ **j**, **1** ⇄ **k**).

On constate que l'état final de plus basse enthalpie, **b** + CH_3, n'est atteint de manière appréciable qu'à partir de l'ion moléculaire **2** métastable. Comme cela a été suggéré (3), ce comportement particulier s'explique par la présence d'une barrière d'isomérisation interdisant aux ions intermédiaires **i** (produits par **1**, **3**, **4** et **5**) l'accès à la structure **2**.

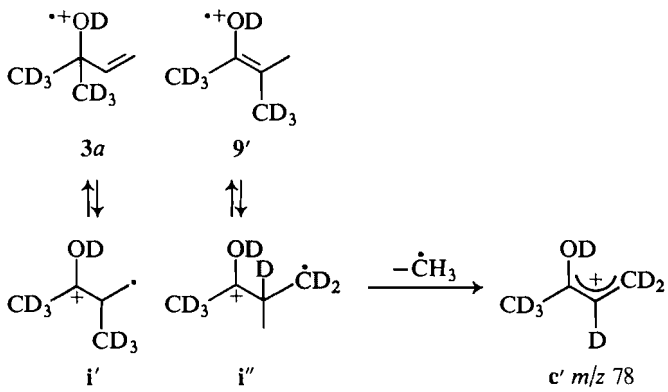

SCHÉMA 5

Ajoutons que l'isolement de **2** se traduit également par une moindre importance du pic m/z 58 sur le spectre MIKE de cet ion moléculaire (m/z 58: m/z 71 = 0,2 pour **2**, contre 0,6 pour les autres précurseurs **1**, **3**, **4** et **5**).

Le processus d'isomérisation **3** ⇄ **i** ⇄ **g** apporte une explication simple à l'élimination de CH_3 donnée en RLC partant de $[(CD_3)_2C(OD)CHCH_2]^{+\bullet}$ (4) (**3***a*) (Schéma 5). La formation d'un ion de type **c** est en effet attestée par les spectres CID−MIKE des ions $[\mathbf{3}\text{-}CH_3]^+$. Ajoutons que l'étape **3** ⇄ **i** autorise l'enchaînement d'isomérisation ultérieur conduisant à l'ion acylium **a** et à **f** + C_2H_4.

Partie expérimentale

Les spectres d'activation collisionnelle (gaz cible = hélium) des ions $[C_4H_7O]^+$ ont été relevés sur un spectromètre VG-ZAB-2F et sur un spectromètre AEI-MS.902.S modifié par l'adjonction d'un secteur électrique entre le secteur magnétique et le collecteur (E/B/E (15)). La tension d'accélération des ions a été réglée de façon à conférer une énergie cinétique voisine de 6,7 kV à tous les ions $[C_4H_7O]^+$ quelle que soit leur origine.

Les composés **1**−**5** et **8**−**10** sont d'origine commerciale tandis que **6** et **7** résultent d'une estérification. Les composés **11**, **13**, **4***a* et **5***a* sont issus de réactions de Grignard sur les cétones ou aldéhydes appropriés. La pentanone 1,1,1,3,3-d_5 a été obtenue après deux cycles d'échanges H/D dans $D_2O/BaCO_3$ (10%).

1. J. H. BEYNON, R. M. CAPRIOLI et R. G. COOKS. Org. Mass Spectrom. **9**, 1 (1974).
2. P. KRENMAYR. Monatsh. Chem. **106**, 925 (1975).
3. G. BOUCHOUX, Y. HOPPILLIARD et P. JAUDON. J. Chem. Res. (S), 148 (1983).
4. J. J. ZWINSELMAN, N. M. M. NIBBERING, N. E. MIDDLEMISS, J. H. VAJDA et A. G. HARRISON. Int. J. Mass Spectrom. Ion Phys. **38**, 163 (1981).
5. D. H. WILLIAMS, B. J. STAPLETON et R. D. BOWEN. Tetrahedron Lett. 2919 (1978).
6. A. G. HARRISON, N. E. MIDDLEMISS et J. H. VAJDA. Adv. Mass Spectrom. **8**, 853 (1980).
7. J. H. VAJDA et A. G. HARRISON. Int. J. Mass Spectrom. Ion Phys. **30**, 293 (1979).
8. E. MURAD et M. G. INGHRAM. J. Chem. Phys. **40**, 3263 (1964).
9. G. MOUVIER et R. HERNANDEZ. Org. Mass Spectrom. **10**, 958 (1975).
10. J. L. HOLMES et F. P. LOSSING. J. Am. Chem. Soc. **102**, 1591 (1980).
11. S. W. BENZON. Thermochemical kinetics. John Wiley, New York. 1968.
12. R. C. BINGHAM, M. J. S. DEWAR et D. H. LO. J. Am. Chem. Soc. **97**, 1285 (1975).
13. M. J. S. DEWAR et W. THIEL. J. Am. Chem. Soc. **99**, 4899 (1977).
14. G. BOUCHOUX, R. FLAMMANG, Y. HOPPILLIARD, A. MAQUESTIAU et P. MEYRANT. Org. Mass Spectrom. **18**, 340 (1983).
15. A. MAQUESTIAU, P. MEYRANT et R. FLAMMANG. Org. Mass Spectrom. **17**, 96 (1982).

Total synthesis of *d,l*-coronafacic acid by an intermolecular Diels–Alder approach

HSING-JANG LIU AND MONTSE LLINAS-BRUNET
Department of Chemistry, University of Alberta, Edmonton, Alta., Canada T6G 2G2

Received February 27, 1984

HSING-JANG LIU and MONTSE LLINAS-BRUNET. Can. J. Chem. **62**, 1747 (1984).

An efficient total synthesis of *d,l*-coronafacic acid (**2**) has been achieved from 4-cyclopentene-1,3-dione (**4**). The synthesis involves keto ester **7** as a key intermediate that is conveniently prepared by the Diels–Alder addition of enedione **4** to ethyl 4-ethyl-2,4-pentadienoate (**5**).

HSING-JANG LIU et MONTSE LLINAS-BRUNET. Can. J. Chem. **62**, 1747 (1984).

Utilisant la cyclopentène-4 dione-1,3 (**4**) comme produit de départ, on a réalisé une synthèse totale efficace de l'acide (*d,l*)-coronafacique (**2**). Le céto-ester **7**, l'intermédiaire clé dans cette synthèse, se prépare facilement par une addition de Diels–Alder de l'ènedione **4** sur l'éthyl-4 pentadiène-2,4 oate d'éthyle (**5**).

[Traduit par le journal]

In 1977, Ichihara *et al.* (1) reported the isolation, from culture broth of *Pseudomonas coronafacience var. atropurpurea*, of a phytotoxic compound (2) named coronatine. These investigators were also able to rigorously establish the structure (1) and the absolute stereochemistry (3, 4) of the dextrorotatory phytotoxin as **1**. Hydrolysis of coronatine (**1**) gave (+)-coronafacic acid (**2**) and (+)-coronamic acid (**3**). Conversely, condensation of coronafacic acid (**2**) via the corresponding acid chloride and coronamic acid (**3**) gave rise to the parent molecule **1** (3). Coronafacic acid (**2**), which was found to be also present in the culture broth of the phytopathogenic bacterium (1), has been the subject of considerable synthetic activity and several total syntheses have been accomplished during the past few years (5). We wish to describe an efficient total synthesis of the racemic coronafacic acid (**2**) based on a fundamentally different approach.

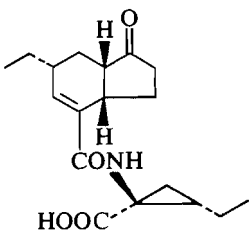

1

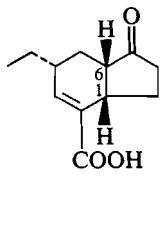

2

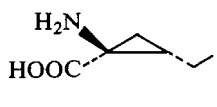

3

As illustrated in Scheme 1, the synthesis began with a Diels–Alder reaction whereby the complete carbon framework of the target molecule was conveniently assembled. 4-Cyclopentene-1,3-dione (**4**) was chosen as the dienophile for its high dienophilicity and for its symmetry, as the use of unsymmetrical 2-cyclopentenones is expected to produce adducts such as **6** possessing the undesirable regiochemistry according to the *ortho* and *para* rules (6) governing the Diels–Alder reaction. In refluxing toluene, the cycloaddition of enedione **4** and ethyl 4-ethyl-2,4-pentadienoate (**5**) (7) proceeded smoothly to give a 67% yield of the crystalline adduct **7**,[1] mp 86–88°C. The nmr spectrum showed that the compound was completely enolized in chloroform solution and that the two stable enols were in a ratio of ca. 5:1.

Treatment of the lithium salt of diketone **7**, generated *in situ* using lithium hydride as a base, with phenyl dichlorophosphate and lithium chloride in tetrahydrofuran in the presence of a small amount of hexamethylphosphoramide[2] at room temperature overnight resulted in the formation of two isomeric chlorides **8** and **9** in 3:2 ratio and in a total yield of 64%. The two isomers were separated by high pressure liquid chromatography and their regiochemistry was individually assigned on the basis of the following observations. In the nmr spectrum, the C-1 proton of the major isomer appeared at δ 3.51 as a doublet of doublets of doublets of doublets with coupling constants of 7, 7, 2.5, and 2 Hz. This proton was shown by spin decoupling experiments to be coupled to the enone vinyl proton which appeared at δ 6.21 as a doublet with a small coupling constant of 2 Hz. On the other hand, the enone vinyl proton (doublet at δ 6.23) of the minor isomer was found to be coupled with a coupling constant of 2 Hz to the C-1 proton at δ 3.78 (ddd, $J = 7$, $J' = J'' = 2$ Hz).

The isomeric chlorides **8** and **9** were individually transformed to the desired keto ester **10** as follows. The conversion of **9** into **10** was straightforward; on hydrogenation in benzene in the presence of 5% palladium on carbon and sodium bicarbonate,[3] the former compound underwent selective reduction to give an 83% yield of keto ester **10** as a mixture of two stereoisomers (~9:1). For the transformation of **8** → **10**, initial studies were intended to proceed via the intermediacy of alcohol **11** that could be easily prepared by the reduction of **8** with sodium borohydride in ethanol. Unfortunately, alcohol **11** underwent extensive decomposition when treated with a variety of acids and with titanium tetrachloride and failed to give any detectable amount of the desired product **16**. To circumvent this difficulty, chloride **8** was subjected to the treatment with silver nitrate in hot methanol[4] and the resulting esters **12** and **13**, obtained in 82% yield and in ca. 9:1 ratio, were reduced with lithium aluminum hydride.[5] Acidic work-up using hydro-

[1]The assignment of its stereochemistry follows from the *endo*-rule and the *cis*-principle (6).

[2]This procedure was developed after several unsuccessful attempts were made to effect the transformation using known methods (8). We are currently examining the generality of this procedure for the conversion of β-dicarbonyl compounds to β-halo-α,β-unsaturated carbonyl compounds. Results will be reported elsewhere.

[3]When the catalytic hydrogenation reaction was carried out in the absence of sodium bicarbonate, a substantial amount of the fully saturated compound (dihydro derivative of **10**) was formed.

[4]When performed in ethanol, the reaction was very slow and gave a poor yield of ester **12**.

[5]Selective reduction of the enone carbonyl with sodium borohydride and with lithium tri-*tert*-butoxyaluminum hydride was attempted without much success.

Can. J. Chem. Downloaded from www.nrcresearchpress.com by 210.87.254.5 on 09/06/12
For personal use only.

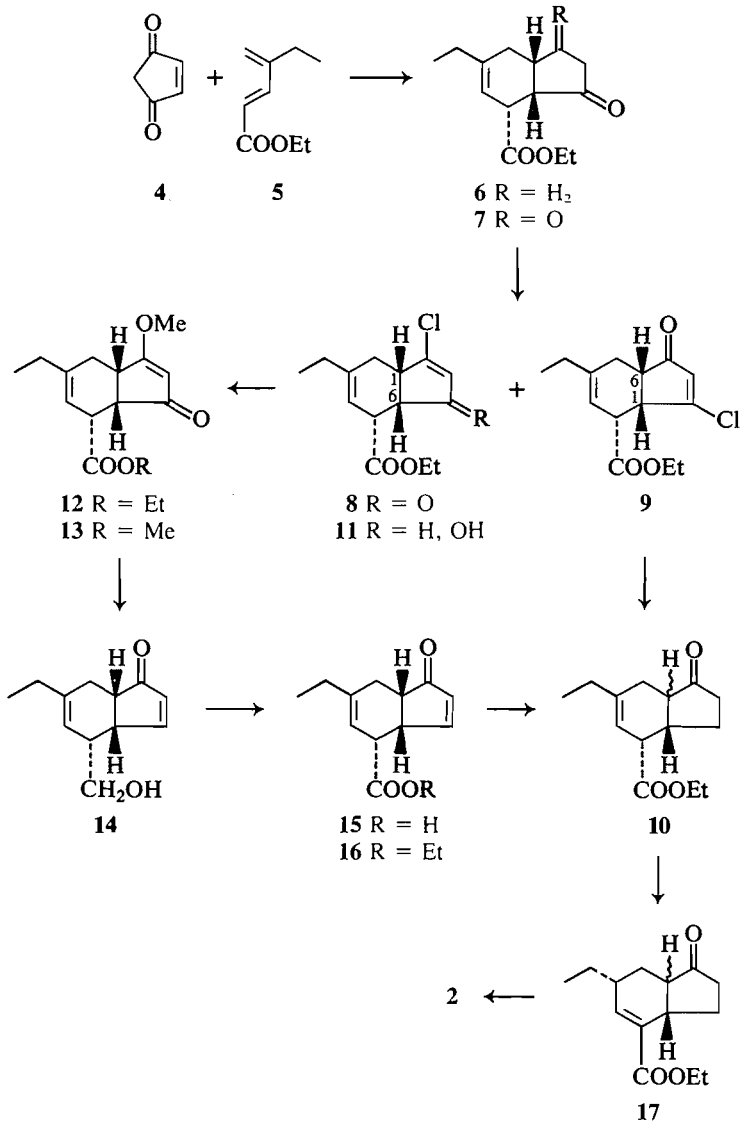

SCHEME 1

chloric acid gave a 70% yield of alcohol **14**. Jones oxidation of **14** followed by esterification of the resulting acid **15** with potassium carbonate and ethyl iodide in refluxing acetone (9) gave rise to enone ester **16** in 65% yield. Subsequent hydrogenation of this compound, carried out in ethyl acetate using 5% Pd/C as a catalyst, resulted in the selective saturation of the less substituted carbon–carbon double bond to furnish, in 92% yield, the epimeric keto esters **10** identical with those obtained previously from the minor chloride **9** (*vide supra*). Thus, by a total of seven operations, diketone **7** was converted to **10** in an overall yield of 35%.

To effect the isomerization of the double bond, the mixture of epimeric keto esters **10** was subjected to treatment with sodium ethoxide in ethanol at room temperature. Hydrolysis of the resulting α,β-unsaturated esters **17** (71% yield) in refluxing aqueous hydrochloric acid gave, in 73% yield, a solid material consisting of coronafacic acid (**2**) and its C-6 epimer[6] in ca. 4:1 ratio as determined by nmr analysis. Recrystallization of this solid material from ether–hexane gave pure *d,l*-coronafacic acid (**2**) (mp 121–125°C) identical in all respects with an authentic sample.

Experimental

General

Melting points were determined on a Kofler hot stage apparatus and are uncorrected. Elemental analyses were performed by the Microanalytical Laboratory of this department. Infrared spectra (ir) were recorded on a Nicolet 7-199 FT-IR spectrophotometer. Nuclear magnetic resonance spectra (nmr) were recorded on a Bruker WH-200 or WH-400 spectrometer and were obtained on solutions in deuteriochloroform with tetramethylsilane as internal reference. Mass spectra (ms) were recorded using A.E.I. model MS12 or MS50 mass spectrometers. Anhydrous magnesium sulfate was used for drying organic solutions.

2-Carbethoxy-4-ethylbicyclo[4.3.0]non-3-ene-7,9-dione (7)

A solution of 4-cyclopentene-1,3-dione (**4**) (290 mg, 3 mmol) and ethyl 4-ethyl-2,4-pentadienoate (**5**) (1.175 g, 7.6 mmol) in toluene (20 mL) was refluxed for 30 h under an atmosphere of nitrogen. The resulting solution was concentrated under reduced pressure. The residue was chromatographed on silica gel. Elution with a solution of 10%

[6]This compound was also isolated directly from the culture broth of *Pseudomonas coronafacience var. atropurpurea* (1). Its epimerization to **2** during the recrystallization of **2** and vice versa have been observed previously (1).

Can. J. Chem. Downloaded from www.nrcresearchpress.com by 210.87.254.5 on 09/06/12
For personal use only.

Can. J. Chem. Downloaded from www.nrcresearchpress.com by 210.87.254.5 on 09/06/12
For personal use only.

petroleum ether in ethyl acetate gave diketone **7** (500 mg; 67% yield): mp 86–88°C (ether – petroleum ether); ms M^+ 250.1202 (calcd. for $C_{14}H_{18}O_4$: 250.1205). The compound existed completely in two enol forms (~5:1) in chloroform solution as indicated by the following spectral data: ir ($CHCl_3$ cast): 3440 (OH), 1730 (ester), 1642, and 1549 (β-hydroxy-α,β-unsaturated ketone) cm^{-1}; nmr: two sets of signals with the major at δ: 6.04 (br s, 1H, —OH), 5.58 (dd, 1H, J = 6, J' = 1 Hz, =CH—), 5.26 (s, 1H, =CHCO—), 4.24 (q, 2H, J = 7 Hz, —OCH_2—), 2.06 (q, 2H, J = 7 Hz, —CH_2CH_3), 1.34 (t, 3H, J = 7 Hz, —OCH_2CH_3), and 0.99 (t, 3H, J = 7 Hz, —CH_3) and the minor at δ: 6.04 (br s, 1H, —OH), 5.62 (d, 1H, J = 8 Hz, =CH—), 5.29 (s, 1H, =CHCO—), 4.29 (q, 2H, J = 7 Hz, —OCH_2—), 2.09 (q, 2H, J = 7 Hz, —CH_2CH_3), 1.36 (t, 3H, J = 7 Hz, —OCH_2CH_3), and 0.96 (t, 3H, J = 7 Hz, —CH_3). *Anal.* calcd. for $C_{14}H_{18}O_4$: C 67.17, H 7.25; found: C 67.01, H 7.07.

5-Carbethoxy-9-chloro-3-ethylbicyclo[4.3.0]nona-3,8-dien-7-one (8) and 2-carbethoxy-9-chloro-4-ethylbicyclo[4.3.0]nona-3,8-dien-7-one (9)

At 0°C, to a solution of diketone **7** (1.03 g, 4.1 mmol) in tetrahydrofuran (15 mL) under a nitrogen atmosphere, were added lithium hydride (43 mg, 5.4 mmol) and hexamethylphosphorous triamide (0.94 mL, 5.2 mmol) with stirring. After 10 min, phenyl dichlorophosphate (1.36 mL, 9.1 mmol) and lithium chloride (380 mg, 9 mmol) were added. The reaction mixture was stirred at room temperature for 16 h. Ice-cold water and dilute hydrochloric acid were added and the resulting mixture was extracted with chloroform. The extracts were washed with water, dried, filtered, and concentrated. Flash chromatography (10) of the residue on silica gel, eluting with 8% ethyl acetate in *n*-hexane, gave a 3:2 mixture (nmr analysis) of chlorides **8** and **9** (707 mg; 64% yield). The mixture was separated by preparative high pressure liquid chromatography on a Waters Associates Prep LC/System 500 using one silica gel cartridge and eluting with 7% ethyl acetate in *n*-hexane. Fractions were collected by shaving the leading and trailing edges of the single peak and recycling the central portion. The combined "leading edge" fractions were concentrated to give pure chloride **8** (178 mg); ir (neat): 1716 (ester and ketone) and 1591 (C=C) cm^{-1}; nmr δ: 6.21 (d, 1H, J = 2 Hz, =CHCO—), 5.53 (tdd, 1H, J = 7, J' = 2, J'' = 1 Hz, —CH=), 4.15, 4.13 (both q, 1H each, J = 7 Hz each, —OCH_2—), 3.61 (dd, 1H, J = 7, J' = 2 Hz, —CHCOO—), 3.51 (dddd, 1H, $J = J'$ = 7, J'' = 2,5, J''' = 2Hz, —CHCCl=), 3.23 (dd, 1H, J = 7, J' = 2 Hz, —CHCO—), 2.47 (ddd, 1H, J = 16, J' = 7, J'' = 2 Hz, —C*H*H—), 2.29 (dd, 1H, J = 16, J' = 2.5 Hz,—C*H*H—), 1.98, 1.96 (both dq, 1H each, J = 7, J' = 1 Hz each, —CH_2CH_3), 1.26 (t, 3H, J = 7 Hz, —OCH_2CH_3), and 0.94 (t, 3H, J = 7 Hz, —CH_3); ms: M^+ 270.0842 and 268.0865 (calcd. for $C_{14}H_{17}ClO_3$: 270.0837 and 268.0865). *Anal.* calcd. for $C_{14}H_{17}ClO_3$: C 62.55, H 6.38, Cl 13.20; found: C 62.50, H 6.58, Cl 12.89. The "trailing edge" fractions were combined and concentratd to give chloride **9** (196 mg); ir (neat): 1716 (ester and ketone) and 1593 (C=C) cm^{-1}; nmr δ: 6.23 (d, 1H, J = 2 Hz, =CHCO—), 5.43 (dd, 1H, J = 7, J' = 2 Hz, —CH=), 4.17 (q, 2H, J = 7 Hz, —OCH_2—), 3.78 (ddd, 1H, J = 7, $J' = J''$ = 2 Hz, —CHCCl=), 3.53 (dd, 1H, J = 7, J' = 2 Hz, —CHCOO—), 2.96 (ddd, 1H, $J = J'$ = 7, J'' = 4 Hz, —CHCO—), 2.32 (m, 2H, —CH_2—), 1.99 (q, 2H, J = 7 Hz, —CH_2CH_3), 1.28 (t, 3H, J = 7 Hz, —OCH_2CH_3), and 0.94 (t, 3H, J = 7 Hz, —CH_3); ms: M^+ 270.0850 and 268.0875 (calcd. for $C_{14}H_{17}ClO_3$: 270.0837 and 268.0865). The remaining material was recovered as a mixture of **8** and **9**.

2-Carbethoxy-4-ethylbicyclo[4.3.0]non-3-en-7-one (10) from chloride 9

To a solution of chloride **9** (48 mg, 0.18 mmol) in benzene (1.2 mL) were added sodium bicarbonate (15 mg, 0.18 mmol) and 5% Pd/C (4.8 mg). After stirring under an atmosphere of hydrogen for 4 h, the reaction mixture was filtered and concentrated. Flash chromatography of the residue on silica gel, eluting with 5% ethyl acetate in *n*-hexane, gave a mixture of epimeric keto esters **10** (35 mg; 83% yield); ir (neat): 1732 (ketone and ester) cm^{-1}; nmr δ: 5.44, 5.37 (both br s, ~1:9, total 1H, —CH=), 4.18 (q, 2H, J = 7 Hz, —OCH_2—), 1.33, 1.34 (both t, ~9:1, total 3H, J = 7 Hz each, —OCH_2CH_3), and 1.03 (t, 3H, J = 7 Hz, —CH_3); ms: M^+ 236.1410 (calcd. for $C_{14}H_{20}O_3$: 236.1413). *Anal.* calcd. for $C_{14}H_{20}O_3$: C 71.14, H 8.54; found: C 70.85, H 8.54.

5-Carbethoxy-3-ethyl-9-methoxybicyclo[4.3.0]nona-3,8-dien-7-one (12) and 5-carbomethoxy-3-ethyl-9-methoxybicyclo[4.3.0]nona-3,8-dien-7-one (13)

Chloride **8** (381 mg, 1.42 mmol) was dissolved in methanol (10 mL) under a nitrogen atmosphere in a flask wrapped in aluminum foil to exclude light. Silver nitrate (482 mg, 2.84 mmol) was introduced and the reaction mixture heated at 70°C for 19 h. Filtration and concentration gave the crude product which was subjected to flash chromatography on silica gel. Elution with 35% ethyl acetate in *n*-hexane gave ethyl ester **12** (276 mg; 74% yield); ir (neat): 1724 (ester), 1698 (ketone), and 1600 (C=C) cm^{-1}; nmr δ: 5.53 (tdd, 1H, J = 7, J' = 2, J'' = 1 Hz, —CH=), 5.32 (d, 1H, J = 1 Hz, =CHCO—), 4.16, 4.14 (both q, 1H each, J = 7 Hz each, —OCH_2—), 3.86 (s, 3H, —OCH_3), 3.62 (dd, 1H, J = 7 Hz, J' = 2 Hz, —CHCOO—), 3.33 (dddd, $J = J'$ = 7, J'' = 3, J''' = 1 Hz, —C*H*CH_2—), 3.15 (dd, 1H, J = 7, J' = 2 Hz, —CHCO—), 2.39 (ddd, 1H, J = 16, J' = 7, J'' = 2 Hz, —C*H*H—), 2.24 (dd, 1H, J = 16, J' = 3 Hz, —C*H*H—), 1.98, 1.96 (both dq, 1H each, J = 7, J' = 1 Hz each, —CH_2CH_3), 1.27 (t, 3H, J = 7 Hz, —OCH_2CH_3), and 0.94 (t, 3H, J = 7 Hz, —CH_3); ms: M^+ 264.1365 (calcd. for $C_{15}H_{20}O_4$: 264.1362). Further elution with the same solvent system gave methyl ester **13** (24 mg; 8% yield); ir (neat): 1735 (ester) 1695 (ketone), and 1598 (C=C) cm^{-1}; nmr δ: 5.56 (br d, 1H, J = 7 Hz, —CH=), 5.30 (s, 1H, =CHCO—), 3.83 (s, 3H, —OCH_3), 3.71 (s, 3H, —$COOCH_3$), and 0.93 (t, 3H, J = 7 Hz, —OCH_2CH_3); ms: M^+ 250.1210 (calcd. for $C_{14}H_{18}O_4$: 250.1205).

4-Ethyl-2-hydroxymethylbicyclo[4.3.0]nona-3,8-dien-7-one (14)

At −20°C, to a solution of esters **12** and **13** (11:1; 389 mg, 1.48 mmol) in ether (8 mL) under a nitrogen atmosphere was added lithium aluminum hydride (112 mg, 2.95 mmol). After stirring for 20 min, the reaction mixture was allowed to warm up to −5°C. Water (2 mL) was slowly added. The resulting mixture was acidified with 1 *N* hydrochloric acid, stirred at 0°C for 45 min, and extracted with methylene chloride. The organic solution was dried, filtered, and concentrated. Flash chromatography of the residue on silica gel, eluting with 45% ethyl acetate in *n*-hexane gave alcohol **14** (198 mg; 70% yield); ir (neat): 3425 (OH), 1704 (C=O), and 1585 (C=C) cm^{-1}; nmr δ: 7.64 (dd, 1H, J = 6, J' = 3 Hz, —C*H*=CHCO—), 6.17 (dd, 1H, J = 6, J' = 2 Hz, =CHCO—), 5.35 (d, 1H, J = 5 Hz, —CH=), 3.75, 3.69 (both dd, 1H each, J = 18, J' = 6 Hz each, —CH_2O—), 2.03 (q, 2H, J = 7 Hz, —CH_2CH_3), and 0.98 (t, 3H, J = 7 Hz, —CH_3); ms: M^+ 192.1143 (calcd. for $C_{12}H_{16}O_2$: 192.1150). *Anal.* calcd. for $C_{12}H_{16}O_2$: C 74.97, H 8.39; found: C 74.78, H 8.57.

2-Carboxy-4-ethylbicyclo[4.3.0]nona-3,8-dien-7-one (15) and 2-carbethoxy-4-ethylbicyclo[4.3.0]non-3,8-dien-7-one (16)

At 0°C, to a solution of alcohol **14** (131 mg, 0.68 mmol) in acetone (4 mL) was added dropwise 1 mL of 8 *N* Jones reagent (11) with stirring. After 1 h, the reaction mixture was diluted with water and extracted with ethyl acetate. Drying, filtration, and concentration gave 120 mg of acid **15** (ir ($CHCl_3$ cast): 3060 (acid), 1700 (acid and ketone), and 1590 (C=C) cm^{-1}). This compound, without purification, was dissolved in acetone (4 mL) and potassium carbonate (161 mg, 1.17 mmol) was added. The mixture was stirred at room temperature under a nitrogen atmosphere for 1 h and iodoethane

Can. J. Chem. Downloaded from www.nrcresearchpress.com by 210.87.254.5 on 09/06/12
For personal use only.

(0.7 mL, 8.75 mmol) was then introduced. After heating at reflux for 16 h, the reaction mixture was poured into ice-cold water and extracted with methylene chloride. The organic solution was dried, filtered, and concentrated. Flash chromatography of the residue on silica gel, eluting with 8% ethyl acetate in *n*-hexane, gave enone ester **16** (103 mg; 65% yield from alcohol **14**); ir (CH_2Cl_2 cast): 1730 (ester), 1712 (ketone), 1590 (C=C) cm^{-1}; nmr δ: 7.62 (dd, 1H, J = 6, J' = 3 Hz, —C*H*=CHCO—), 6.26 (dd, 1H, J = 6, J' = 2 Hz, =CHCO—), 5.51 (dd, J = 7, J' = 2 Hz, —CH=), 4.22 (q, 2H, J = 7 Hz, —OCH_2—), 2.05 (q, 2H, J = 7 Hz, —CH_2CH_3), 1.31 (t, 3H, J = 7 Hz, —OCH_2CH_3), and 0.99 (q, 3H, J = 7 Hz, —CH_3); ms: M^+ 234.1256 (calcd. for $C_{14}H_{18}O_3$: 234.1256).

*Keto esters **10** from enone ester **16***

Enone ester **16** (85 mg, 0.36 mmol) was dissolved in ethyl acetate (3 mL) and 5% Pd/C (9 mg) was added. The mixture was stirred under an atmosphere of hydrogen at room temperature for 1 h. Filtration and concentration gave the crude product, which was purified by flash chromatography on silica gel. Elution with 5% ethyl acetate in *n*-hexane gave a mixture of keto esters **10** (78 mg; 92% yield) identical with that obtained previously from chloride **9**.

*2-Carbethoxy-4-ethylbicyclo[4.3.0]non-2-en-7-one (**17**)*

At 0°C, to a solution of keto esters **10** (35 mg, 0.15 mmol) in ethanol (1.5 mL) was added sodium hydride (80% oil dispersion; 10 mg, 0.33 mmol). After stirring at room temperature under a nitrogen atmosphere for 16 h, the reaction mixture was diluted with ice-cold water, acidified with dilute hydrochloric acid, and extracted with methylene chloride. The organic solution was dried, filtered, and concentrated. Flash chromatography of the residue on silica gel, eluting with 5% ethyl acetate in *n*-hexane, gave a mixture of epimeric esters **17** (25 mg; 71% yield); ir ($CHCl_3$ cast): 1742 (ketone), 1711 (ester), and 1642 (C=C) cm^{-1}; nmr δ: 6.98, 6.92 (2:5; both br s, total 1H, —CH=), 4.21 (m, 2H, —OCH_2—), 1.32, 1.27 (5:2; both t, total 3H, J = 7 Hz each, —OCH_2CH_3), 1.01, and 0.99 (5:2; both t, total 3H, J = 7 Hz each, —CH_3); ms: M^+ 236.1408 (calcd. for $C_{14}H_{20}O_3$: 236.1412). *Anal.* calcd. for $C_{14}H_{20}O_3$: C 71.16, H 8.53; found: C 71.14, H 8.53.

d,l-*Coronafacic acid (**2**)*

A solution of esters **17** (20 mg, 0.085 mmol) in 2.4 *N* aqueous hydrochloric acid (1.5 mL) was heated at reflux under a nitrogen atmosphere for 5.5 h. After cooling to room temperature, the resulting solution was diluted with water (2 mL) and extracted with ethyl acetate. The extracts were dried, filtered, and concentrated. Flash chromatography of the residue on silica gel, eluting with 40% ethyl acetate in *n*-hexane, gave 13 mg (73% yield) of a 4:1 (nmr integration) mixture of coronafacic acid (**2**) and its C-6 epimer. In the nmr spectrum, the vinyl proton of the latter compound appeared as a doublet of doublets (J = 4, J' = 2 Hz) at δ 7.12 in agreement with the reported value (1). Recrystallization of the mixture resulted in partial epimerization of the minor isomer to coronafacic acid (**2**) and gave 11 mg of the latter compound in crystalline form, mp 121–125°C. Concentration of the mother liquid gave 2 mg of a 1:1 mixture of **2** and its C-6 epimer. The ir, nmr, and mass spectra of the synthetic coronafacic acid were found to be identical with those of an authentic sample and displayed the following characteristic features: ir ($CHCl_3$ cast): 3040, 2634, 2532, 1685 (acid), 1741 (ketone), and 1634 (C=C) cm^{-1}; nmr δ: 7.06 (br s, 1H, —CH=) and 1.01 (t, 3H, J = 7 Hz, —CH_3); ms: M^+ 208.1104 (100%; calcd. for $C_{12}H_{16}O_3$: 208.1099).

Acknowledgements

We are grateful to the Natural Sciences and Engineering Research Council of Canada and the University of Alberta for financial support and to Professor S. Sakamura of Hokkaido University for an authentic sample of *d,l*-coronafacic acid.

1. A. Ichihara, K. Shiraishi, H. Sato, S. Sakamura, K. Nishiyama, R. Sakai, A. Furusaka, and T. Matsumoto. J. Am. Chem. Soc. **99**, 636 (1977).
2. K. Nishiyama, R. Sakai, A. Ezuka, A. Ichihara, K. Shiraishi, M. Ogasawara, H. Sato, and S. Sakamura. Ann. Phytopath. Soc. Jpn. **42**, 613 (1976); K. Nishiyama, R. Sakai, A. Ezuka, A. Ichihara, K. Shiraishi, and S. Sakamura. Ann. Phytopath. Soc. Jpn. **43**, 219 (1977).
3. A. Ichihara, K. Shiraishi, S. Sakamura, K. Nishiyama, and R. Sakai. Tetrahedron Lett. 269 (1977).
4. A. Ichihara, K. Shiraishi, S. Sakamura, A. Furusaki, N. Hashiba, and T. Matsumoto. Tetrahedron Lett. 365 (1979).
5. A. Ichihara, R. Kimura, K. Moriyasu, and S. Sakamura. Tetrahedron Lett. 4331 (1977); M. E. Jung and J. P. Hudspeth. J. Am. Chem. Soc. **102**, 2463 (1980); A. Ichihara, R. Kimura, S. Yamada, and S. Sakamura. J. Am. Chem. Soc. **102**, 6353 (1980); M. E. Jung and K. M. Halweg. Tetrahedron Lett. **22**, 2735 (1981); M. Nakayama, S. Ohira, Y. Okamura, and S. Soga. Chem. Lett. 731 (1981).
6. A. S. Onishchenko. Diene synthesis. Israel Program for Scientific Translation, Jerusalem. 1964.
7. R. J. Sundberg, P. A. Bukowick, and F. O. Holcombe. J. Org. Chem. **32**, 2938 (1967).
8. E. Piers, J. R. Grierson, C. K. Lau, and I. Nagakura. Can. J. Chem. **60**, 210 (1981), and references therein.
9. H. J. Liu and P. C. L. Yao. Can. J. Chem. **55**, 822 (1977).
10. W. C. Still, M. Kahn, and A. Mitra. J. Org. Chem. **43**, 2923 (1978).
11. D. Djerassi, R. R. Engle, and A. Bowers. J. Org. Chem. **21**, 1547 (1956).

Aliphatic diazo compounds. XIV. The synthesis of 7-substituted 3-diazo-2-norbornanones and the infrared and proton and carbon-13 nuclear magnetic resonance spectra of these diazo ketones and their precursors[1]

PETER YATES AND JOHN DAVID KRONIS
Lash Miller Chemical Laboratories, University of Toronto, Toronto, Ont., Canada M5S 1A1

Received December 14, 1983

PETER YATES and JOHN DAVID KRONIS. Can. J. Chem. **62**, 1751 (1984).

syn- and *anti*-7-Isopropyl-2-norbornanone (**5** and **6**) were prepared by catalytic hydrogenation of 7-isopropylidene-2-norbornanone; *syn*- and *anti*-7-benzhydryl-2-norbornane (**9** and **10**) were prepared in analogous fashion. Ketones **5** and **6** and *syn*- and *anti*-7-*tert*-butyl-2-norbornanone (**7** and **8**) were converted to the corresponding 3-diazo-2-norbornanones **1**–**4** via the monotosylhydrazones **44**–**47** of the corresponding α-diketones **40**–**43**. The ^1H and ^{13}C nmr spectra of **1**–**10**, **40**–**47**, and their precursors have been analyzed. The ^1H nmr spectra of the diazo ketones **1**–**4** have their C-1 and C-4 bridgehead proton signals shifted to higher and lower field, respectively, relative to the bridgehead signals of the corresponding diketones. The ^{13}C nmr spectra of all pairs of bicyclic epimers shown γ-*gauche* shielding effects by the 7-substituent at (sp^3) C-3 in the *syn* compounds and at C-5 and C-6 in the *anti* compounds. A converse effect is found at (sp^2) C-2 (and C-3 in the diketones). Comparison of the magnitude of the shielding effects of C-7 methyl, isopropyl, benzhydryl, and *tert*-butyl substituents gives evidence of δ deshielding effects at C-3 in the *syn* compounds and at C-5 and C-6 in the *anti* compounds by methyl substituents on C-8.

PETER YATES et JOHN DAVID KRONIS. Can. J. Chem. **62**, 1751 (1984).

On a préparé les isopropyl-7 norbornanones-2 *syn* et *anti* (**5** et **6**) par hydrogénation catalytique de l'isopropylidène-7 norbornanone-2; on a préparé les benzhydryl-7 norbornanones-2 *syn* et *anti* (**9** et **10**) d'une manière semblable. On a transformé les cétones **5** et **6** ainsi que les *tert*-butyl-7 norbornanones-2 *syn* et *anti* (**7** et **8**) en leurs diazo-3 norbornanones-2 correspondantes (**1**–**4**) par le biais des monotosylhydrazones **44**–**47** des α-dicétones correspondantes **40**–**43**. On a analysé les spectres rmn du ^1H et du ^{13}C des composés **1**–**10** et **40**–**47** et de leurs précurseurs. Dans les spectres rmn du ^1H des diazocétones **1**–**4**, les signaux des protons en tête de pont (C-1 et C-4) sont déplacés respectivement vers des champs plus haut et plus bas, par rapport aux signaux des protons dans les positions équivalentes des dicétones correspondantes. Les spectres rmn du ^{13}C de chacune des paires d'épimères bicycliques présentent tous des effets de blindage γ-*gauche*, dus aux substituants en position 7 et affectant la position C-3 (sp^3) des composés *syn* et les positions C-5 et C-6 des composés *anti*. On observe un effet inverse au niveau de C-2 (sp^2) (et de C-3 dans les dicétones). Une comparaison de l'amplitude des effets de blindage provoqués par les substituants méthyle, isopropyle, benzhydryle et *tert*-butyle en C-7 suggère que les substituants méthyles en C-8 provoquent des effets de déblindage δ en C-3 dans les composés *syn* et en C-5 et C-6 dans les composés *anti*.

[Traduit par le journal]

Can. J. Chem. Downloaded from www.nrcresearchpress.com by 210.87.254.5 on 09/06/12
For personal use only.

In connection with our studies on the acid-catalyzed decomposition of α-diazo ketones (1, 2), we required pairs of 3-diazo-2-norbornanones with bulky *syn*- and *anti*-7 substituents. We describe here the synthesis of the diazo ketones **1**–**4**, prepared for this purpose, and discuss their ^1H and ^{13}C nmr spectra together with those of their precursors, which reveal features of intrinsic interest in addition to providing evidence for the structural assignments. We also discuss the synthesis and spectra of the *syn*- and *anti*-7-substituted 2-norbornanones **9** and **10**, which were not converted to the corresponding 3-diazo-2-norbornanones, but which are closely related to the 2-norbornanones **5**–**8** that were the precursors of **1**–**4**. In addition we include an account of the synthesis and spectra of the tricyclo[2.2.1.$0^{2,6}$]heptan-3-ones **11**–**14**, which were prepared from **1**–**4** for the purpose of comparison with products obtained by the acid-catalyzed decomposition of the latter.

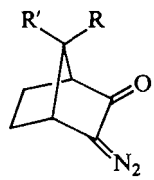

1 R = $CH(CH_3)_2$, R′ = H
2 R = H, R′ = $CH(CH_3)_2$
3 R = $C(CH_3)_3$, R′ = H
4 R = H, R′ = $C(CH_3)_3$

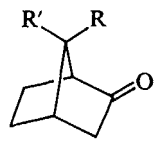

5 R = $CH(CH_3)_2$, R′ = H
6 R = H, R′ = $CH(CH_3)_2$
7 R = $C(CH_3)_3$, R′ = H
8 R = H, R′ = $C(CH_3)_3$
9 R = $CH(C_6H_5)_2$, R′ = H
10 R = H, R′ = $CH(C_6H_5)_2$

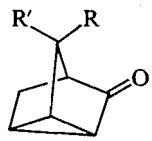

11 R = $CH(CH_3)_2$, R′ = H
12 R = H, R′ = $CH(CH_3)_2$
13 R = $C(CH_3)_3$, R′ = H
14 R = H, R′ = $C(CH_3)_3$

Synthesis of the 2-norbornanones and 3-diazo-2-norbornanones

A conceptually simple route to 7-substituted 2-norbornanones involves Diels–Alder addition of ketene to 5-substituted cyclopentadienes. In practice, this approach is complicated by several factors. First, the well-known tendency of ketene to participate in [2 + 2] rather than [4 + 2] cycloaddition reactions makes it necessary to use a ketene equivalent with subsequent conversion of the adduct to a carbonyl compound. Second, the 5-substituted cyclopentadienes very readily tautomerize to their 1- and 2-substituted isomers, which are usually highly favoured thermodynamically relative to the 5-substituted isomer (3). This problem is particularly acute in the case of relatively unreactive dienophiles, a class into which most ketene equivalents fall; however, Corey *et al.* (4) have successfully overcome it in some instances by the use of anhydrous cupric tetrafluoroborate as a catalyst for the Diels–Alder

[1] For part XIII, see ref. 1.

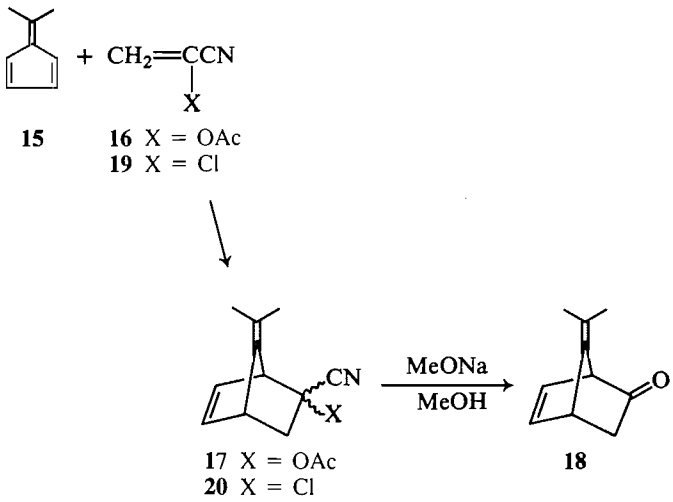

SCHEME 1

reaction, permitting the latter to be carried out at 0°C. Third, in reactions of this type one stereoisomer is often formed exclusively or predominantly (4, 5), making them impracticable for the synthesis of both *syn*- and *anti*-7-substituted 2-norbornanones.

We therefore adopted an approach based on earlier work by DePuy and Story (6), who carried out the Diels–Alder reaction of 6,6-dimethylfulvene (**15**) with the ketene equivalent 2-acetoxyacrylonitrile (**16**) to give the adducts **17**, which were converted to the dienone **18** with methanolic sodium methoxide (Scheme 1). Use of a fulvene rather than a cyclopentadiene as the diene obviates the problem of tautomerization and it appeared that **18** could serve as a source of both **5** and **6**. In fact when we prepared **18** by this method and hydrogenated it we obtained a product which was subsequently shown to be a mixture of **5** and **6**. However, this method was impracticable for the preparation of **5** and **6** on the large scale because of the high cost of 2-acetoxyacrylonitrile. We therefore undertook to develop an improved synthesis utilizing the very much more economical ketene equivalent, 2-chloroacrylonitrile (**19**). Reaction of **15** with an excess of **19** in benzene at 40°C for 51 days afforded an 82% yield of a mixture of the stereoisomeric α-chloro nitriles **20**; unfortunately, this reaction was not catalyzed by cupric tetrafluoroborate.

Attempted hydrolysis of this mixture with potassium hydroxide in dimethyl sulfoxide (7) resulted in the formation of a complex mixture of predominantly acidic products, which were not identified. They may include products of type **21***a*, whose formation has been observed in other cases (8, 9), but also include compounds containing vinyl hydrogen atoms, as shown by ^{1}H nmr spectroscopy. The latter could arise via Haller–Bauer cleavage (10) of the desired product **18** to acids of type **21***b* – a process that should be facilitated by the presence of two ethylenic double bonds in a β,γ relationship to the carbonyl group (*vide infra*).

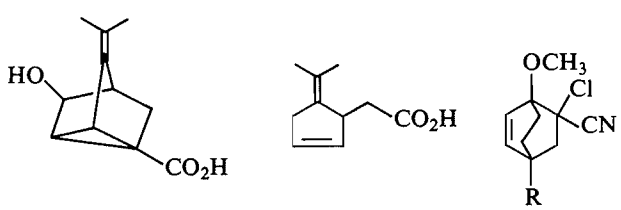

21*a* **21***b* **22**

Evans *et al.* (11) have found that sodium sulfide nonahydrate in boiling ethanol can be used to effect the transformation of chloro nitriles of type **22** to the corresponding bicyclo-[2.2.2]octenones. To determine whether this procedure was likely to be applicable to the synthesis of bicyclo[2.2.1]hept-5-en-2-ones we prepared the chloro nitriles **23***a* and **23***b* by a modification of a known procedure (12); they were obtained as a 4:1 mixture, as shown by ^{1}H nmr spectroscopy (*vide infra*). Treatment of this mixture with sodium sulfide nonahydrate in boiling ethanol gave no 5-norbornen-2-one (**24**), but a 65% yield of a crystalline product, shown to be the chloro amide **25** by its spectra (see Experimental) and the fact that it is formed from a 4:1 mixture of **23***a* and **23***b*.

23*a* X = CN, Y = Cl
23*b* X = Cl, X = CN
24 X, Y = O

25

The synthesis of **5** and **6** was pursued by avoiding the intermediacy of the dienone **18** as shown in Scheme 2. The dienes **20** could be hydrogenated exclusively at the endocyclic double bond to give **26**, which on treatment with potassium hydroxide in dimethyl sulfoxide gave the ketone **27** in 80% yield. The fact that the hydrolysis reaction proceeds well in the case of **26** but not **20** lends strength to our earlier interpretation of its failure in the latter case. The high chemoselectivity in the partial hydrogenation of **20** contrasts with the low selectivity reported in the case of **18** (6); this must reflect steric inhibition of approach by the catalyst to the face of the exocyclic double bond that is *syn* to the *exo* chloro or cyano substituent.

Catalytic hydrogenation of the ketone **27** proceeded slowly and cleanly to give a 94% yield of a 3:2 mixture of the *syn* and *anti* ketones **5** and **6**, as determined by gas chromatographic analysis. These could not be separated by liquid chromatography but were separated by the exclusive precipitation of the *anti* isomer as its 2,4-dinitrophenylhydrazone (2,4-DNP) **28**. This selectivity was expected on the basis of the known high propensity of 2-norbornanones lacking a *syn*-7 substituent to undergo *exo* nucleophilic attack at the carbonyl group (13), and permits unambiguous assignment of stereochemistry to the individual epimers. The unchanged *syn* isomer was isolated from the filtrate in 89% recovery, while the *anti* isomer was obtained in 88% recovery by treatment of **28** with titanium chloride by the method of McMurry and Silvestri (14).[2]

The synthesis of the benzhydryl compounds **9** and **10** (Scheme 3) resembled that of their isopropyl analogues **5** and **6**. Reaction of 6,6-diphenylfulvene (**29**) with 2-chloroacrylonitrile gave a crystalline mixture of adducts **30**, which could again be hydrogenated exclusively at the endocyclic ethylenic double bond to give the dihydro compounds **31**. Hydrolysis of **31** with potassium hydroxide and dimethyl sulfoxide at room temperature for 48 h gave the ketone **32** as a minor product only; the major product was an acid, assigned structure **33** on the basis of its composition and spectra (see Experimental). The acid **33** is considered to arise by Haller–Bauer

[2] Since the initiation of this work the synthesis of mixtures of *syn*- and *anti*-7-*n*-alkyl-substituted 2-norbornanones from fulvenes and 2-chloroacrylonitrile has been reported in the patent literature (15).

Can. J. Chem. Downloaded from www.nrcresearchpress.com by 210.87.254.5 on 09/06/12
For personal use only.

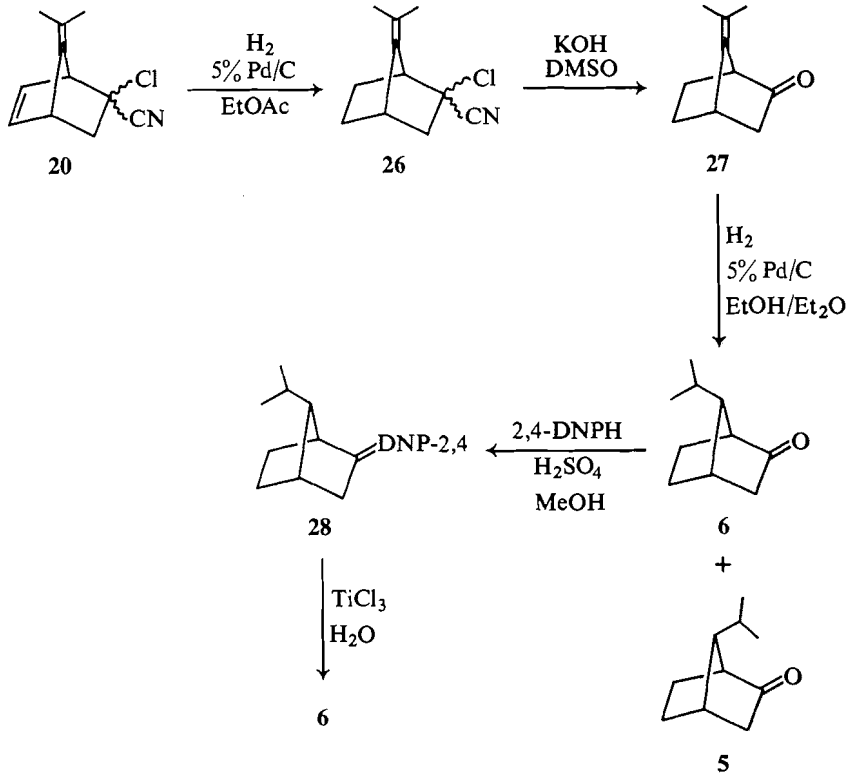

SCHEME 2

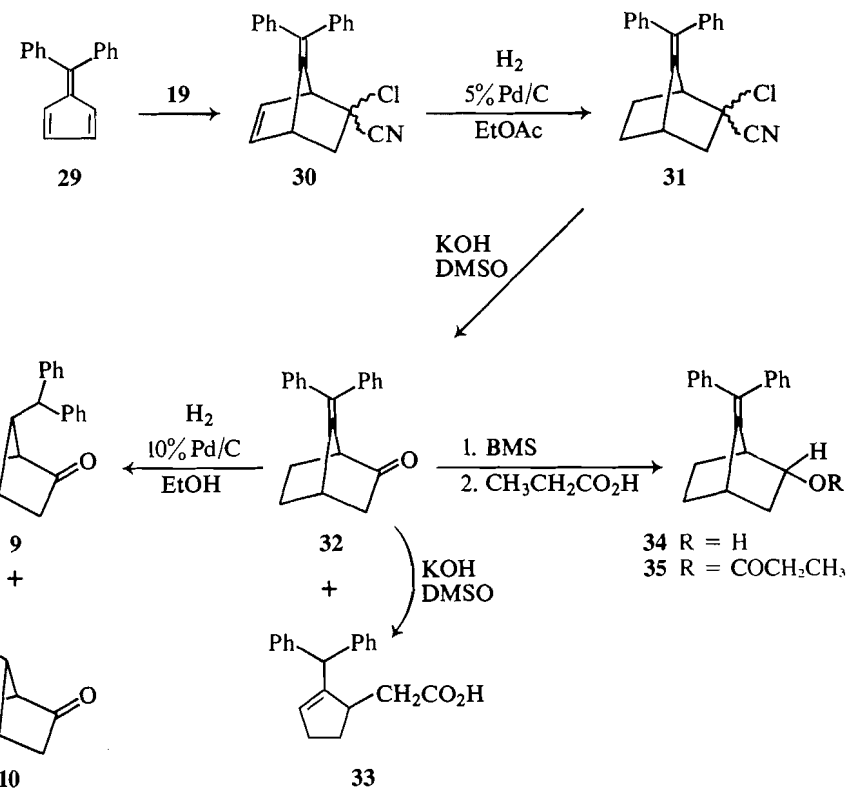

SCHEME 3

cleavage of the ketone **32**, as proposed above in the case of **18**; here facilitation of the cleavage is attributable to additional stabilization of the intermediate allylic anion by the phenyl substituents. That **32** can serve as the source of **33** was demonstrated by the fact that the latter is formed on treatment of **32** with potassium hydroxide and dimethyl sulfoxide. It was found possible to increase the yield of the desired product **32** to 86% by reducing the reaction time for the hydrolysis of **31** to 13 h. Catalytic hydrogenation of **32** gave a 92% yield of a mixture of the *syn* and *anti* ketones **9** and **10**, which in this case, unlike

Can. J. Chem. Downloaded from www.nrcresearchpress.com by 210.87.254.5 on 09/06/12
For personal use only.

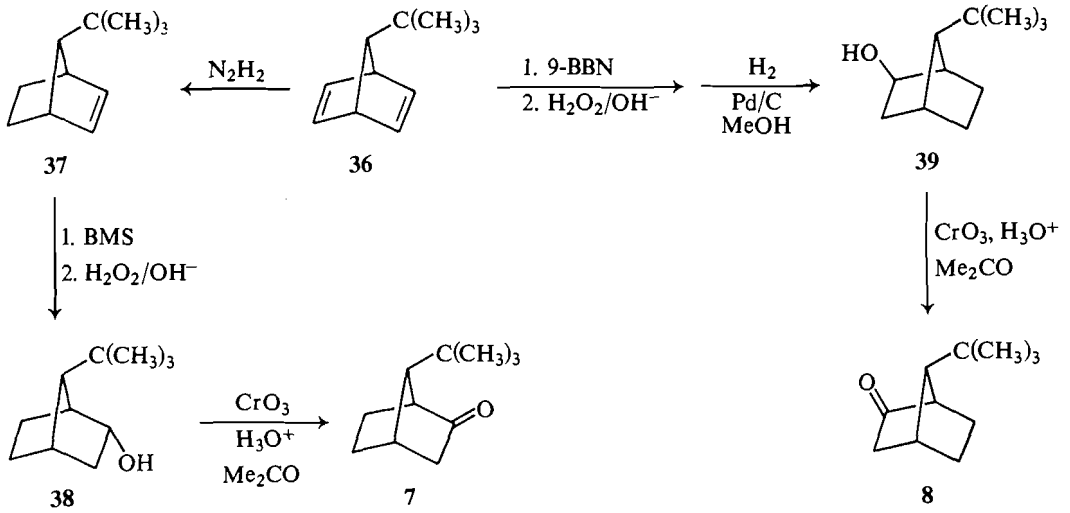

SCHEME 4

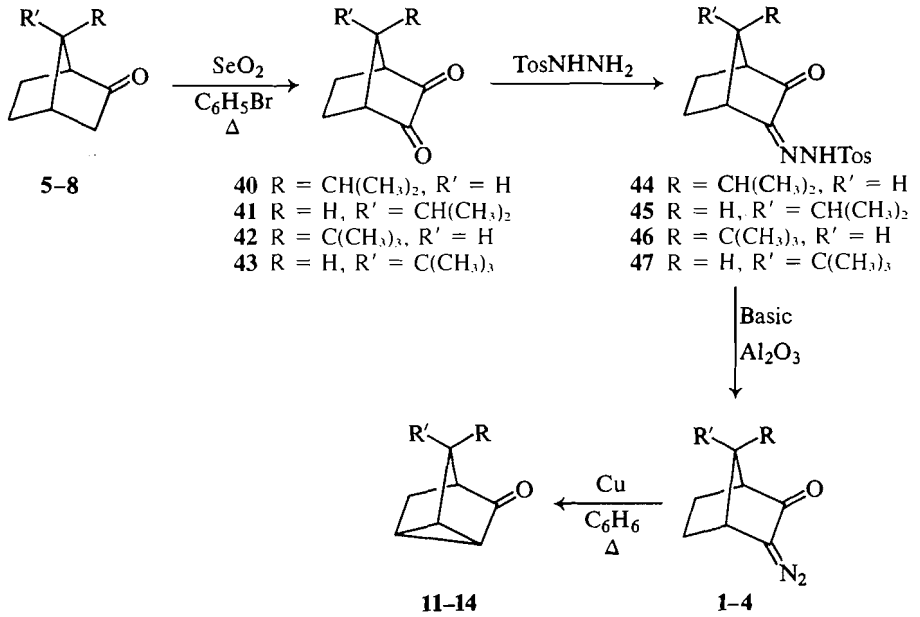

SCHEME 5

that of **5** and **6**, could be separated by liquid chromatography: individual stereochemical assignments were based on spectroscopic considerations (*vide infra*).

Initially, unexpected difficulties were encountered in the catalytic hydrogenation of **32** and the reduction of the ethylenic double bond by borane – methyl sulfide (BMS) (16) was investigated; it was anticipated that reduction of the carbonyl group would also occur, but considered that this could readily be regenerated. However, treatment of **32** with two equivalents of BMS in diglyme followed by protonolysis in boiling propionic acid gave **34**, in which only the carbonyl group had been reduced; this was accompanied by a minor product which is tentatively assigned structure **35**, the propionate of **34**.

The *tert*-butyl compounds **7** and **8** were prepared by oxidation of the alcohols **38** and **39**, respectively, with Jones reagent (Scheme 4). The alcohols were prepared from 7-*tert*-butylnorbornadiene (**36**) by the methods of Baird and Surridge (17), the only modification being hydroboration of *syn*-7-*tert*-butylnorbornene (**37**) with BMS rather than with 9-borabicyclo[3.3.1]nonane (9-BBN) – an expedient that gave an improved yield of **38**.

The general method used for the conversion of the 2-norbornanones **5**–**8** to the corresponding 3-diazo-2-norbornanones **1**–**4** was that of Scheme 5. A variety of conditions have been reported for the oxidation of ketones to α-diketones with selenium dioxide (18). In the cases studied here the best yields were obtained with the use of bromobenzene as solvent. The yields of the *anti*-7-substituted 2,3-norbornanediones **41** and **43** were lower than those of the *syn*-7 compounds **40** and **42**, presumably because of their greater susceptibility to further oxidation. Conversion of the α-diketones to their monotosylhydrazones **44**–**47** proceeded in good yield except in the case of the *syn*-*tert*-butyl compound, which gave a 45% yield. The *syn* compounds were obtained as their *Z* isomers, but the *anti* compounds were formed as mixtures of *Z* and *E* isomers, e.g., **45***Z* and **45***E*, which made recrystallization difficult. These mixtures could be converted to the single *Z* isomers by chromatography on silica gel. On one occasion **45***E* was iso-

Can. J. Chem. Downloaded from www.nrcresearchpress.com by 210.87.254.5 on 09/06/12
For personal use only.

TABLE 1. ^{1}H nuclear magnetic resonance spectra of α-chloro nitriles

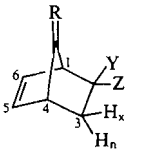

	R	Y	Z	$^H\delta$ (ppm)[a] H-1	H-3x	H-3n	H-4	H-5	H-6	$\Delta^H\delta$ (ppm) 1,4	6,5
20*a*	$C(CH_3)_2$	CN	Cl	3.93	2.67 (dd)[b]	1.69 (d)[b]	3.50	6.22	6.55	0.43	0.33
20*b*	$C(CH_3)_2$	Cl	CN	3.78	2.2[c]	2.2[c]	3.50	6.33	6.61	0.28	0.28
30*a*	CPh_2	CN	Cl	3.93	2.93 (dd)[b]	1.85 (d)[b]	3.58	6.33	6.65	0.35	0.32
30*b*	CPh_2	Cl	CN	3.77	2.4[c]	2.4[c]	3.52	6.34	6.59	0.25	0.25
23*a*[d]	H_2	CN	Cl	3.48	2.70	1.71	3.08	6.13	6.38	0.40	0.25
23*b*[d]	H_2	Cl	CN	3.32	2.28	2.28	3.08	6.21	6.43	0.24	0.22
48[e]	CH_2CH_2	CN	Cl	2.89	2.85	1.90	2.44	6.21	6.48	0.45	0.27

[a] In $CDCl_3$; the relative intensities of the signals are in accord with the assignments.
[b] For **20***a*: $J_{3x,3n}$ = 13 Hz, $J_{3x,4}$ = 4 Hz; **30***a*: $J_{3x,3n}$ = 13.5 Hz, $J_{3x,4}$ = 4 Hz.
[c] Overlapping signals.
[d] Reference 21.
[e] Reference 9.

lated by fractional crystallization. The conversion of **44**–**47** to the corresponding diazo ketones **1**–**4** was accomplished in high yield by chromatography on basic alumina according to the method of Meinwald *et al.* (19).

The tricyclic ketones **11**–**14** were prepared in 65–96% yield from the corresponding diazo ketones **1**–**4** by treatment with an excess of copper in boiling benzene (1, 20) (Scheme 5).

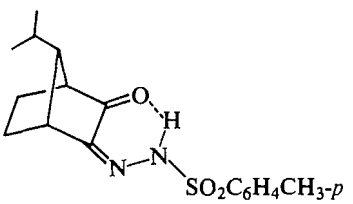

45*Z*

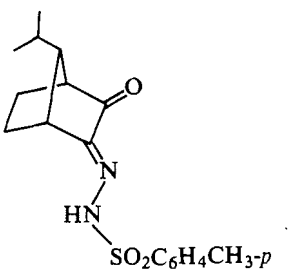

45*E*

Infrared and ^{1}H nuclear magnetic resonance spectra

Selected signals in the ^{1}H nmr spectra of the α-chloro nitriles **20** and **30** together with those of **23** are given in Table 1. Paasivirta and Kuusisto (21) have reported ^{1}H nmr assignments for each of the epimers **23***a* and **23***b*, which they separated and individually identified. The structural and ^{1}H nmr spectroscopic assignments for **20***a*, **20***b*, **30***a*, and **30***b* were made by comparison of their spectra with those of **23***a* and **23***b*. The epimers **30***a* and **30***b* were separated by fractional crystallization; the epimers **20***a* and **20***b* could not be separated, but the ^{1}H nmr signals of the individual epimers were identified on the basis of their relative intensities. The differences of the chemical shifts of the H-1 protons of the epimeric pairs **23***a* and **23***b*, **20***a* and **20***b*, and **30***a* and **30***b* lie in the range 0.15–0.16 ppm, whereas the differences for the H-4 protons are much smaller (0.00–0.06 ppm), as expected. As a result the separation of the bridgehead proton signals ($\Delta\delta_{1,4}$) for **23***a*, **20***a*, and **30***a* lies in the range 0.35–0.40 ppm while for their epimers **23***b*, **20***b*, and **30***b*, $\Delta\delta_{1,4}$ = 0.24–0.28. Furthermore, while the *exo*-3 and *endo*-3 protons of **23***a*, **20***a*, and **30***a* give rise to distinct signals as the AM part of an AMX system and can be individually assigned on the basis of the magnitude of their coupling with the adjacent bridgehead proton (H-4), the corresponding protons of **23***b*, **20***b*, and **30***b* give rise to complex signals as the AB part of an ABX system. Cantello *et al.* (9) have used a similar analysis in assigning structure **48** to the major adduct (94%) from the reaction of spiro[2.4]hepta-4,6-diene with 2-chloroacrylonitrile. It is noteworthy that in all cases the *endo*-2-chloro-*exo*-2-cyano epimer is formed predominantly: **23** (4:1), **20** (3:1), **30** (2.5:1), **48** (16:1).

Salient features in the ir and ^{1}H nmr spectra of the 2-norbornanones **5**–**10** are given in Table 2. All of these ketones give rise to carbonyl-stretching bands at 5.71–5.72 μm, characteristic of five-membered cyclic ketones, and CH deformation bands at 7.05–7.09 μm, characteristic of the —CH_2CO— grouping; the compounds with isopropyl and *tert*-butyl substituents also give rise to CH deformation bands that are characteristic of these substituents. It is of interest that while the ir spectra of **5** and **6**, as for the other members of this series, show a single band in the carbonyl stretching region, the spectra of their unsaturated precursors **18** and **27** each show two bands at 5.72–5.73 (s) and 5.80–5.81 (w) μm.

Although the individual structural assignments for compounds **5** and **6** immediately follow from their difference in reactivity with 2,4-dinitrophenylhydrazine, and those for **7** and **8** from their methods of synthesis, those for **9** and **10** rest solely on comparison of their ^{1}H and ^{13}C nmr spectra. Doublets (J = 12 Hz) at δ 3.58 and 3.77 ppm are assigned to the $(C_6H_5)_2CH$ protons in the two compounds, and the compound with the higher field signal is considered to be the *syn*-7 isomer **9**, whose benzhydryl proton is expected to be shielded by the carbonyl group relative to the benzhydryl proton of **10** (22). The same effect may be invoked to account for the shielding of the *syn*-7-*tert*-butyl protons of **7** relative to those of **8**. Examination of molecular models suggests that the most favorable conformation for the benzhydryl group in **9** and **10** is of type **50**, in which the dihedral angle between the benzyhydryl CH bond and the C-7 CH bond approaches 180°, which is in accord with the observed 12-Hz coupling constants. It is expected that the isopropyl compounds **5** and **6** will adopt similar conformations, and this could account for the fact that the methyl signals of **5** are not upfield of those of **6**. It may be noted that in each case the methyl groups give rise to two doublets, reflecting their diastereotopism.

Can. J. Chem. Downloaded from www.nrcresearchpress.com by 210.87.254.5 on 09/06/12
For personal use only.

TABLE 2. Infrared and ^{1}H nuclear magnetic resonance spectra of 2-norbornanones

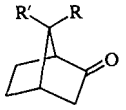

	R	R′	λ_{max} (μm)[a] C=O	$COCH_2$	$CH(CH_3)_2$	$C(CH_3)_3$	$^H\delta$ (ppm)[b] $CH(CH_3)_2$[c]	$C(CH_3)_3$	$CHPh_2$[d]
5	$CH(CH_3)_2$	H	5.71	7.05	7.20, 7.30	—	0.92 (d), 0.97 (d)	—	—
6	H	$CH(CH_3)_2$	5.71	7.08	7.21, 7.31	—	0.90 (d), 0.94 (d)	—	—
7	$C(CH_3)_3$	H	5.72	7.07	—	7.34	—	0.97 (s)	—
8	H	$C(CH_3)_3$	5.71	7.08	—	7.35	—	1.02 (s)	—
9	$CHPh_2$	H	5.72	7.07	—	—	—	—	3.58 (d)
10	H	$CHPh_2$	5.71	7.09	—	—	—	—	3.77 (d)

[a] In CCl_4.
[b] See footnote *a* in Table 1.
[c] J = 5–5.5 Hz.
[d] J = 12 Hz.

TABLE 3. Infrared and ^{1}H nuclear magnetic resonance spectra of 2,3-norbornanediones

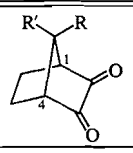

	R	R′	λ_{max} (μm)[a] C=O	$CH(CH_3)_2$	$C(CH_3)_3$	$^H\delta$ (ppm)[b] $CH(CH_3)_2$[c]	$C(CH_3)_3$	H-1,4[d]
40	$CH(CH_3)_2$	H	5.61, 5.68	7.21, 7.30	—	0.98 (d)	—	3.02 (m)
41	H	$CH(CH_3)_2$	5.60, 5.68	7.20, 7.30	—	0.98 (d)	—	2.93 (m)
42	$C(CH_3)_3$	H	5.63, 5.70	—	7.32	—	0.94 (s)	3.07 (m)
43	H	$C(CH_3)_3$	5.60, 5.69	—	7.33	—	1.08 (s)	3.05 (m)
51[e]	H	H	5.62, 5.70	—	—	—	—	3.06 (m)

[a] In CCl_4.
[b] See footnote *a* in Table 1.
[c] J = 5 Hz.
[d] $W_{1/2}$ = 6–7 Hz.
[e] References 24 and 42.

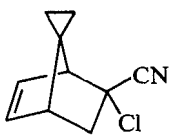

48

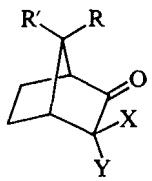

49 R = R′ = X = Y = H
51 R = R′ = H, X, Y = O
52 R = CH_3, R′ = X = Y = H
53 R = X = Y = H, R′ = CH_3

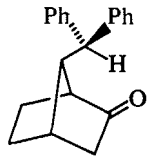

50

The ir spectra of the 2,3-norbornanediones **40**–**43** (Table 3) show two bands in the carbonyl-stretching region at 5.60–5.63 and 5.68–5.70 μm resulting from vibrational coupling, as has been observed previously for compounds of this type (23). In the ^{1}H nmr spectra of **40** and **41** the methyl proton signals appear as simple doublets, since the methyl groups in each compound are no longer diastereotopic. As in the case of the monoketones the *tert*-butyl methyl signal of the *syn* isomer **42** is shifted upfield relative to that of the *anti* isomer **43**, while there is no significant difference in the chemical shifts of the isopropyl methyl signals of **40** and **41**. Two-proton multiplets at δ 2.93–3.07 ppm in the spectra of **40**–**43** are assigned to the bridgehead protons (H-1,4) on the basis of earlier assignments for the bridgehead proton signals of 2,3-norbornanedione (**51**) (δ 3.06 ppm (24)), and related compounds (23).

The monotosylhydrazones **44**–**47** were normally isolated as their *Z* isomers. This stereochemical assignment is based on their ir and ^{1}H nmr spectra (Table 4). Strong intramolecular hydrogen bonding in these isomers results in sharp N—H stretching bands at 3.09–3.10 μm and carbonyl-stretching bands at 5.79–5.81 μm in their ir spectra. These spectra may be contrasted with the ir spectrum of the *E* isomer of **45** (*vide supra*), in which the NH stretching band is considerably broader and the carbonyl-stretching band appears at 5.70 μm. The intramolecular hydrogen bonding in the *Z* isomers is also vouchsafed by NH signals at δ 11.3–11.6 ppm in their ^{1}H nmr spectra (cf. **45***E*: δ 8.73 ppm).

The ir spectra of the α-diazo ketones **1**–**4** (Table 5) show the three characteristic strong bands associated with this functionality (25) at 4.83–4.84, 5.89–5.90, and 7.34–7.37 μm; in addition they all show a medium intensity band in the 9.1–9.3 μm region, which we have not assigned. Their ^{1}H nmr spectra show that one of the bridgehead proton signals is shifted downfield (Δδ 0.35–0.42 ppm) and the other upfield (Δδ −0.35 – −0.44 ppm) relative to the two equivalent bridgehead proton signals of the corresponding diketones **40**–**43**. An analogous effect has been observed previously for other 3-diazo-2-norbornanones (23) and the assignments made in the latter cases permit the assignment of the individual H-1 and H-4 signals given in Table 5. The diastereotopic relationship of the iso-

Can. J. Chem. Downloaded from www.nrcresearchpress.com by 210.87.254.5 on 09/06/12
For personal use only.

TABLE 4. Infrared and ^{1}H nuclear magnetic resonance spectra of 2,3-norbornanedione monotosylhydrazones

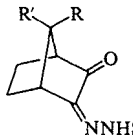

	R	R'	λ_{max} (μm)[a] NH	C=O	SO_2	$^H\delta$ (ppm)[b,c] $CH(CH_3)_2$	$C(CH_3)_3$	H-1[d]	H-4[d]	NH
44*Z*	$CH(CH_3)_2$	H	3.09	5.79	8.54	0.87 (br s)	—	2.73 (m)	2.97 (m)	11.49 (br s)
45*Z*	H	$CH(CH_3)_2$	3.10	5.79	8.55	0.89 (d)	—	2.71 (m)	2.96 (m)	11.46 (br s)
45*E*	H	$CH(CH_3)_2$	3.1 (br)	5.70	8.61	0.88 (d)	—	2.69 (m)	3.28 (m)	8.73 (br s)
46*Z*	$C(CH_3)_3$	H	3.09	5.81	8.55	—	0.75	2.74 (m)	3.03 (m)	11.57 (br s)
47*Z*	H	$C(CH_3)_3$	3.09	5.80	8.57	—	1.02	2.81 (m)	3.08 (m)	11.34 (br s)

[a] In CCl_4.
[b] See footnote *a* in Table 1.
[c] Tosyl proton signals: 2.42–2.45 (s, CH_3), 7.24–7.38 (dd, J = 8.5 Hz, H-3′,5′), 7.74–7.83 (dd, J = 8.5 Hz, H-2′,6′).
[d] $W_{1/2}$ = 6–8 Hz.

TABLE 5. Infrared and ^{1}H nuclear magnetic resonance spectra of 3-diazo-2-norbornanones

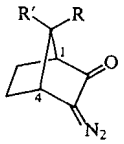

	R	R'	λ_{max} (μm)[a] CN_2	C=O	CN_2	[c]	$^H\delta$ (ppm)[b] $CH(CH_3)_2$[d]	$C(CH_3)_3$	H-1[e]	H-4[f]
1	$CH(CH_3)_2$	H	4.84	5.90	7.35	9.11	0.93 (d) 0.99 (d)	—	2.58 (m)	3.37 (m)
2	H	$CH(CH_3)_2$	4.83	5.90	7.37	9.29	0.88 (d) 0.93 (d)	—	2.57 (m)	3.30 (m)
3	$C(CH_3)_3$	H	4.83	5.89	7.34	9.12	—	1.01 (s)	2.63 (m)	3.42 (m)
4	H	$C(CH_3)_3$	4.83	5.89	7.36	9.26	—	1.00 (s)	2.70 (m)	3.47 (m)
54[g]	H	H	4.80	5.91	7.35	9.10	—	—	2.62 (m)	3.50 (m)

[a] In CCl_4.
[b] See footnote *a* in Table 1.
[c] Unassigned band.
[d] J = 5 Hz.
[e] $W_{1/2}$ = 6–7 Hz.
[f] $W_{1/2}$ = 4.5–5 Hz.
[g] Reference 24; ^{1}H nmr spectrum in CCl_4.

propyl methyl groups in **1** and **2** is readily apparent as in the case of **5** and **6** (in the case of the tosylhydrazones **44** and **45** the methyl signals were broad and poorly defined, presumably as a result of a reduced chemical shift difference between the methyl groups).

The ir and ^{1}H nmr spectra of the tricyclic ketones **11**–**14** are given in Table 6. In accord with expectation their carbonyl-stretching bands appear at shorter wavelength (Δλ 0.04–0.05 μm) than the corresponding bands of the bicyclic ketones **5**–**8**. Their methyl proton signals show analogous relationships to those of **5**–**8** and their chemical shifts are not greatly affected by the presence of the cyclopropane ring. Although most of the remaining signals give rise to overlapping multiplets, it is possible to make the assignments for H-2 given in Table 6, based on the coupling pattern of the signals and comparison with the spectra of related tricyclic ketones (26).

^{13}C Nuclear magnetic resonance spectra

Assignments for the signals in the ^{13}C nmr spectra of most of the compounds prepared in the present work are given in Tables 7–10. These assignments are based on comparison with the spectra of closely related compounds, single frequency off-resonance decoupled (sford) spectra, and consideration of well-established substituent effects.

The assignments were readily made in the case of the 2-norbornanones **5**–**8** on the basis of the extensive earlier work by Roberts (27) and Stothers (28, 29) and their co-workers on the spectra of such compounds. In Table 7 these assignments are compared with those for 2-norbornanone (**49**) (29) and *syn*-7- (**52**) and *anti*-7-methyl-2-norbornanone (**53**) (27), and in Table 8 the substituent effects of the 7-alkyl substituents are listed. The well-known γ-*gauche* shielding effect of the C-7 alkyl substituent at C-3 in all of the *syn*-7 compounds is readily apparent,[3] and to a lesser degree at C-5 and C-6 in the *anti*-7 isomers, with the interesting exception of C-5 in the *anti*-7-*tert*-butyl compound **8** (*vide infra*). Conversely, C-3 is deshielded by the 7-alkyl substituent in the *anti* isomers and C-5 and C-6 are deshielded in the *syn* isomers. This type of γ deshielding effect has been less commonly documented than the γ-*gauche*

[3] However, this effect is reversed at the carbonyl carbon (C-2) (*vide infra*).

Can. J. Chem. Downloaded from www.nrcresearchpress.com by 210.87.254.5 on 09/06/12
For personal use only.

TABLE 6. Infrared and ^{1}H nuclear magnetic resonance spectra of tricyclo[2.2.1.0^{2,6}]heptan-3-ones

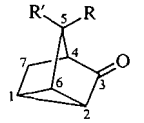

	R	R′	λ_{max} (μm)[a] C=O	λ_{max} (μm)[a] $CH(CH_3)_2$	λ_{max} (μm)[a] $C(CH_3)_3$	$^H\delta$ (ppm)[b] $CH(CH_3)_2$[c]	$^H\delta$ (ppm)[b] $C(CH_3)_3$	$^H\delta$ (ppm)[b] H-2[d]
11	$CH(CH_3)_2$	H	5.67	7.20, 7.33	—	0.93 (d), 1.04 (d)	—	1.21 (t)
12	H	$CH(CH_3)_2$	5.67	7.23, 7.33	—	0.82 (d), 0.99 (d)	—	1.37 (t)
13	$C(CH_3)_3$	H	5.67	—	7.33	—	0.95 (s)	1.27 (t)
14	H	$C(CH_3)_3$	5.67	—	7.35	—	0.98 (s)	1.43 (t)
57[e]	H	H	5.68	—	—	—	—	1.14 (t)

[a] In CCl_4.
[b] See footnote *a* in Table 1.
[c] J = 5–6 Hz.
[d] J = 5–5.5 Hz.
[e] In CCl_4; ref. 26.

TABLE 7. ^{13}C nuclear magnetic resonance spectra of 2-norbornanones, 2,3-norbornanediones, 2,3-norbornanedione tosylhydrazones, and 3-diazo-2-norbornanones

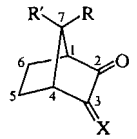

	X	R	R′		$^C\delta$ (ppm)[a] C-1	C-2	C-3	C-4	C-5	C-6	C-7	C-8	CH_3
5	H_2	$CH(CH_3)_2$	H		52.7	218.0	40.8	36.8	28.7	24.4	58.2	26.4	21.8, 22.3
6		H	$CH(CH_3)_2$		52.1	217.2	47.3	36.9	25.0	21.6	56.8	24.8	20.5, 21.6
7		$C(CH_3)_3$	H		50.8	218.7	42.1	36.8	30.0	24.8	61.4	31.6	29.9
8		H	$C(CH_3)_3$		51.8	216.0	49.3	37.8	27.2	23.2	59.3	32.1	29.8
9		$CHPh_2$	H		52.9	217.5	40.8	37.3	28.5	24.0	54.7	50.2	—
10		H	$CHPh_2$		52.5	216.6	47.3	37.6	25.0	21.5	53.3	48.7	—
49[b]		H	H		49.7	217.4	45.1	35.3	27.1	24.2	37.6	—	—
52[c]		CH_3	H		55.2	216.3	40.3	40.0	29.1	24.5	43.9	12.9	—
53[c]		H	CH_3		54.3	215.3	47.3	40.2	24.9	21.3	42.8	12.1	—
24[d]		H	H	Δ^5	55.8	214.7	37.1	40.0	142.7	130.4	50.8	—	—
27		$=C(CH_3)_2$			51.5	214.0	47.8	37.0	27.2	24.2	119.1	137.4	20.3, 20.7
18		$=C(CH_3)_2$		Δ^5	58.0	210.6	40.4	42.1	143.0	131.0	115.2	146.3	19.4, 19.8
32		$=CPh_2$			53.4	211.7	48.0	38.0	27.0	24.0	131.6	143.6	—
40	O	$CH(CH_3)_2$	H		51.9	202.7	202.7	51.9	24.3	24.3	53.4	28.6	21.8, 21.8
41		H	$CH(CH_3)_2$		49.5	201.8	201.8	49.5	21.4	21.4	50.8	23.8	20.5, 20.5
42		$C(CH_3)_3$	H		50.4	203.2	203.2	50.4	24.7	24.7	58.5	31.7	29.1
43		H	$C(CH_3)_3$		50.6	200.1	200.1	50.6	23.1	23.1	52.0	33.0	29.7
51		H	H		48.5	202.0	202.0	48.5	23.9	23.9	31.7	—	—
44*Z*	T[e]	$CH(CH_3)_2$	H		53.1	203.0	149.9	45.0	26.9	24.0	57.5	27.5	21.7, 21.8
45*Z*		H	$CH(CH_3)_2$		51.9	202.5	150.7	43.9	23.9	21.2	54.7	24.4	20.2, 20.7
45*E*		H	$CH(CH_3)_2$		51.3*	201.6	156.4	39.7	22.7†	22.0†	52.9*	24.1†	20.2, 20.9
46*Z*		$C(CH_3)_3$	H		51.5	203.4	150.8	43.7	27.4	24.4	61.4	31.5	29.0
47*Z*		H	$C(CH_3)_3$		51.5	201.2	151.3	44.6	25.7	22.8	56.9	32.5	29.6
1	N_2	$CH(CH_3)_2$	H		52.6	200.8	59.5	42.5	29.2	24.9	60.3	26.4	21.6, 22.2
2		H	$CH(CH_3)_2$		51.4	201.0	63.5	41.3	26.0	22.2	59.1	25.4	20.1, 20.9
3		$C(CH_3)_3$	H		51.0	201.1	60.1	40.7	30.0	25.5	63.1	31.5	29.4
4		H	$C(CH_3)_3$		51.1	201.0	65.0	42.5	27.9	24.0	61.5	32.1	29.4
54		H	H		49.5	200.6	62.1[g]	39.7	28.6	24.3	40.1	—	—

[a] In $CDCl_3$; the signal multiplicities in sford spectra are in accord with the assignments.
[b] Reference 29.
[c] Reference 27.
[d] Reference 36.
[e] T = $NNHSO_2C_6H_4CH_3$-*p*.
[f] The sford spectrum of **45*E*** was not obtained; the individual assignments of sets of signals marked with an asterisk or a dagger are uncertain.
[g] Very weak signal; identification tentative.

Can. J. Chem. Downloaded from www.nrcresearchpress.com by 210.87.254.5 on 09/06/12
For personal use only.

TABLE 8. Substituent effects in 7-substituted 2-norbornanones, 2,3-norbornanediones, and 3-diazo-2-norbornanones

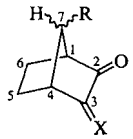

		Δδ (ppm)[a]						
		β		γ				α
X	R	C-1	C-4	C-2	C-3	C-5	C-6	C-7
H_2	*syn*-CH_3	+5.5	+4.7	−1.1	−4.8	+2.0	+0.3	+6.3
	anti-CH_3	+4.6	+4.9	−2.1	+2.2	−2.2	−2.9	+5.2
	syn-$CH(CH_3)_2$	+3.0	+1.5	+0.6	−4.3	+1.6	+0.2	+20.6
	anti-$CH(CH_3)_2$	+2.4	+1.6	−0.2	+2.2	−2.1	−2.6	+19.2
	syn-$C(CH_3)_3$	+1.1	+1.5	+1.3	−3.0	+2.9	+0.6	+23.8
	anti-$C(CH_3)_3$	+2.1	+2.5	−1.4	+4.2	+0.1	−1.0	+21.7
	syn-$CHPh_2$	+3.2	+2.0	+0.1	−4.3	+1.4	−0.2	+17.1
	anti-$CHPh_2$	+2.8	+2.3	−0.8	+2.2	−2.1	−2.7	+15.7
O	*syn*-$CH(CH_3)_2$	+3.4		+0.7		+0.4		+21.7
	anti-$CH(CH_3)_2$	+1.0		−0.2		−2.5		+19.1
	syn-$C(CH_3)_3$	+1.9		+1.2		+0.8		+26.8
	anti-$C(CH_3)_3$	+2.1		−1.9		−0.8		+20.3
N_2	*syn*-$CH(CH_3)_2$	+3.1	+2.8	+0.2	−2.6	+0.6	+0.6	+20.2
	anti-$CH(CH_3)_2$	+1.9	+1.6	+0.4	+1.4	−2.6	−2.1	+19.0
	syn-$C(CH_3)_3$	+1.5	+1.0	+0.5	−2.0	+1.4	+1.2	+23.0
	anti-$C(CH_3)_3$	+1.6	+2.8	+0.4	+2.9	−0.7	−0.3	+21.4

[a] In $CDCl_3$; $\Delta\delta = {}^{C}\delta$ (7-substituted compound) − ${}^{C}\delta$ (unsubstituted compound).

shielding effect, but downfield γ shifts have been observed involving antiperiplanar axial substituents in compounds containing a fused or bridged cyclohexane ring (30, 31).

The consistent trends observed in the substituent effects in the spectra of compounds **5**–**8**, **52**, and **53** were applied to make individual stereochemical assignments for the benzhydryl compounds **9** and **10**. The results confirmed the assignments made on the basis of their ^{1}H nmr spectra and the chemical shift assignments and substituent effects for these compounds are also given in Tables 7 and 8. Comparison of all of these data shows that there is an attenuation of the γ-*gauche* effect of a 7-alkyl group at C-3 in the *syn* series and at C-5 and C-6 in the *anti* series, with increasing substitution on the γ carbon. Thus the shielding effects fall off in the order $CH_3 > CH(CH_3)_2 \simeq CH(C_6H_5)_2 \gg C(CH_3)_3$. This is attributable to a δ deshielding effect by these substituents, an effect that has been observed previously for hydroxyl substituents and attributed, at least in part, to steric interaction (32, 33). Since γ-*gauche* substituents produce upfield shifts and sterically interacting δ substituents produce small downfield shifts, the shielding effect of a *gauche tert*-butyl group is expected to be less than that of a *gauche* methyl group (34), as observed. In general the δ deshielding effect does not override the γ shielding effect of the isopropyl and *tert*-butyl groups at C-3, C-5, and C-6 in the present cases, except in the case of the negligible deshielding effect at C-5 of the *anti-tert*-butyl group in **8**. The δ effects are much larger for the *tert*-butyl group than the isopropyl and benzhydryl groups. If the effect is primarily steric in origin, this circumstance would be nicely accommodated by our earlier proposal of preferred conformations of type **50** for the latter groups. This interpretation must be treated with caution, since it is possible that the δ effect is not primarily steric in nature and devolves from removal of a γ hydrogen, in analogy to the proposal of Saunders and ApSimon and their co-workers that the γ effect arises from removal of a β hydrogen (30, 35).

Spectroscopic assignments for the unsaturated ketones **18**, **27**, and **32** prepared in the present work are included in Table 7, together with those for 5-norbornen-2-one (**24**) (36). The introduction of Δ^5 β,γ-unsaturation into 2-norbornanones has been observed previously to lead to shielding of the carbonyl carbon; it has also been observed that C-6 is shielded and C-5 is deshielded with respect to the corresponding olefins (29). These effects have been attributed in part to homoconjugation (37). Introduction of a second β,γ ethylenic bond as in **18** can be seen to lead to appreciable further deshielding of the carbonyl carbon, perhaps as a result of "cross-homoconjugation". The individual assignments for the olefinic carbon atoms of the exocyclic double bonds in **18**, **27**, and **32** were made in analogy to those for C-5 and C-6 in **24**.

The ^{13}C nmr spectral assignments for the diketones **40**–**43** and **51**, the tosylhydrazones **44**–**47**, and the diazo ketones **1**–**4**, **54**, and **55** (38) are also given in Table 7. In order to make the assignments for C-1(4) and C-7 for the diketones, the relative signal intensities were considered together with general trends observed in the spectra of the other classes of compounds; in each case the signal assigned to C-1(4) had a significantly higher intensity than that assigned to C-7.

The assignments of signals for the diazo ketones were facilitated by comparison with the chemical shift values for C-5 versus C-6 and C-1 versus C-4 in 4-methyl-3-diazocamphor (**55**) (38). The assignments for the tosylhydrazones were made in analogy to those for the other types of compounds. The carbonyl signals for all the compounds other than the monoketones in Table 7 are shifted by 15–17 ppm to higher field relative to their parent monoketones as a result of conjugative and inductive effects. The diazo carbon signals (C-3) of the diazo ketones appear at remarkably high field for the sp^2 carbon, as has been observed for other α-diazo ketones (38, 39), presumably as a result of the high electron density at this carbon (cf. **56***a*) and the partial triple bond nature of the C—N

Can. J. Chem. Downloaded from www.nrcresearchpress.com by 210.87.254.5 on 09/06/12
For personal use only.

TABLE 9. ^{13}C nuclear magnetic resonance spectra of tricyclo[2.2.1.$0^{2,6}$]heptan-3-ones

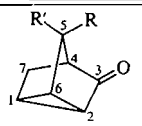

	R	R′	$^{c}\delta$ (ppm)[a, b] C-1	C-2	C-3	C-4	C-5	C-6	C-7	C-8	CH_3
11	$CH(CH_3)_2$	H	20.4*	16.7*	214.8	41.5	52.8	24.0*	32.2	28.6	21.7, 21.8
12	H	$CH(CH_3)_2$	20.3*	21.7*	213.3	41.1	50.8	23.5*	27.9	27.4	19.7, 20.8
13	$C(CH_3)_3$	H	17.9*	17.3*	215.6	40.0	56.8	20.8*	33.0	32.0	28.4
14	H	$C(CH_3)_3$	22.1*	22.5*	213.2	42.1	53.6	23.1*	29.3	32.5	29.0
57	H	H	18.9	16.9	213.8	37.3	31.3	18.9	31.3	—	—

[a] See footnote *a* in Table 7.
[b] Note that C-1, C-5, C-6, and C-7 correspond to C-5, C-7, C-4, and C-6, respectively, in 2-norbornanone (Table 7).
[c] Individual assignments for signals marked with asterisks are uncertain.

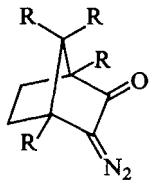

54 R = H
55 R = CH_3

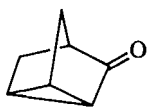

57

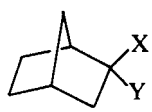

58*a* X = CN, Y = Cl
58*b* X = Cl, Y = CN

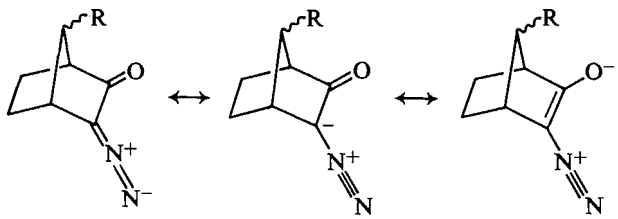

56*a* **56***b*

bond (cf. **56***a* and **56***b*).

Similar γ and δ effects to those that have been described for the 2-norbornanone series are also apparent in the spectra of the diketones, tosylhydrazones, and diazo ketones (Table 8). It was noted earlier that the chemical shift relationships of the carbonyl carbons (C-2) of the *syn*-7 and *anti*-7 2-norbornanones do not follow those of the sp^3 carbons C-3,[4] C-5, and C-6. The same holds true of the other types of compounds in Table 8, the carbonyl carbon in each *anti*-7 compound being shielded relative to that in its *syn* isomer. The origin of this effect is unclear, since it is unknown whether it is associated with the hybridization, polarization, and (or) lack of hydrogen atoms at the carbonyl carbon. However, comparision of the carbonyl carbon shifts in the *syn*-7-isopropyl (and benzhydryl) compounds with those of the corresponding *syn*-7-*tert*-butyl compounds shows δ deshielding effects in the latter, albeit smaller than those observed at C-3.[4]

The ^{13}C nmr spectra of the tricyclic ketones **11**–**14** and the parent ketone **57** (40) are given in Table 9. The signals of the cyclopropyl carbons could not be individually assigned with rigour. In analogy with C-6 in the bicyclic ketones and their derivatives, C-7[5] in the tricyclic ketones is shielded in the *anti* compounds relative to the *syn* compounds and the carbonyl carbon is deshielded in the *syn* compounds relative to their *anti* isomers. Although the uncertainty of the individual cyclopropyl carbon assignments makes detailed comparison unfeasible, it is possible to conclude that none of the cyclopropyl carbon signals of the *anti*-5-*tert*-butyl compound are at higher field than those of its *syn*-5 isomer. Thus in these tricyclic systems, C-1, unlike C-5 in the bicyclic systems, is not shielded in the *anti*-5 relative to the *syn*-5 compound. This is attributable to the change in geometry and (or) hybridization when this carbon is incorporated into a cyclopropane ring.

The ^{13}C nmr spectra of the α-chloro nitriles previously referred to and of **58***a* and **58***b*, prepared by catalytic hydrogenation of the mixture of **23***a* and **23***b* (12), are given in Table 10. Both the cyano and chloro substituent effects are known for the *exo*- and *endo*-monosubstituted norbornene system (41). The assignments for the epimeric chloro nitriles **23***a* and **23***b* were made from their sford spectra and comparison of the calculated chemical shifts with the observed shifts. The assignments for the individual members of the other pairs of epimeric chloro nitriles then follow as in Table 10. In general the γ-*gauche* effect at C-6 and C-7 of the substituents at C-2 is consistent, irrespective of their sp^2 or sp^3 nature, with a 2-*exo*-chloro substituent shielding C-7 more than a 2-*exo*-cyano substituent; the only exception is in the case of the benzhydrylidene epimers **30***a* and **30***b* whose C-7 signals have identical chemical shifts. As expected from the work of Stothers *et al.* (29), the cyano carbon exhibits a configurationally dependent chemical shift with the *endo* cyano carbon shielded with respect to the *exo* cyano carbon for each pair of epimers.

Experimental[6]

Melting points were determined on a Fisher–Johns melting point apparatus and are uncorrected. The ir spectra were recorded in CCl_4 solution with a Perkin–Elmer 137 spectrometer, unless otherwise specified; bands are strong and sharp unless denoted as m (medium), w (weak), or br (broad). The ^1H and ^{13}C nmr spectra were recorded in $CDCl_3$ solution with Varian T-60 and Varian CFT-20 or XL-100 spectrometers, respectively. Mass spectra were recorded at 70 eV with a Bell and Howell CEC 21-490 single focussing mass spectrometer; exact mass measurements were made with an AE1-MS 902 double focussing mass spectrometer. Gas chromatographic (gc) analyses were carried out on a Varian Aerograph Series 2700 gas chromatograph, equipped with a flame ionization detector, and linked with a Varian CDS-111 integrator. The injector port temperature was 270°C, the detector temperature was 290°C, and the column tem-

[4] The effects at C-2 and C-3 in the diketones are of course identical owing to symmetry.
[5] See footnote 2 in Table 9.
[6] Spectroscopic data are given only where they supplement the data given in Tables 1–10.

Can. J. Chem. Downloaded from www.nrcresearchpress.com by 210.87.254.5 on 09/06/12
For personal use only.

TABLE 10. ^{13}C nuclear magnetic resonance spectra of α-chloro nitriles

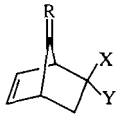

				$^{C}\delta$ (ppm)[a]									
	R	X	Y	C-1	C-2	C-3	C-4	C-5	C-6	C-7	C-8	CH_3	CN
20*a*	$C(CH_3)_2$	CN	Cl	55.0	54.8	46.3	42.8	139.9	132.1	116.3	142.7	19.6, 19.7	120.7
20*b*		Cl	CN	55.6	55.8	47.2	42.2	142.7	132.9	115.9	142.2	19.7, 19.8	119.9
30*a*	CPh_2	CN	Cl	56.0	54.7	46.0	44.3	140.6	132.3	127.6	146.9	—	120.4
30*b*		Cl	CN	56.8	55.8	46.9	43.9	143.5	133.0	127.6	146.9	—	119.5
23*a*	H_2	CN	Cl	55.4	56.6	45.7	42.9	139.4	131.9	48.5	—	—	121.2
23*b*		Cl	CN	56.2	56.8	46.9	42.6	142.1	132.5	47.0	—	—	120.0

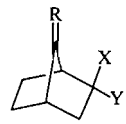

	R	X	Y										
26*a*	$C(CH_3)_2$	CN	Cl	49.1	57.6	48.4	36.8	28.2	22.6	122.4	136.3	20.7	120.8
26*b*		Cl	CN	50.0	58.3	50.0	36.2	27.3	24.8	121.9	135.9	20.7	119.7
31*a*	CPh_2	CN	Cl	50.4	57.3	48.2	38.3	28.3	22.3	133.8	~141	—	120.5
58*a*	H_2	CN	Cl	49.8	59.4	48.5	36.9	28.1	23.1	38.5	—	—	121.1
58*b*		Cl	CN	50.7	59.6	50.5	37.0	27.5	25.3	36.4	—	—	119.8

[a] See footnote *a* in Table 7.

perature was 110°C. The carrier gas was nitrogen at a flow rate of 30 mL/min. A 6-ft glass column (od 1/4 in., id 2 mm) packed with 3% OV-17 on 80/100 Chromosorb W(HP) was used. Solutions in organic solvents were dried over anhydrous Na_2SO_4 and the solvents were evaporated with a rotary evaporator at water aspirator pressure.

*6,6-Dimethylfulvene (**15**)*

6,6-Dimethylfulvene (**15**) was prepared according to the procedure of Freiesleben (43). A mixture of freshly distilled cyclopentadiene (89.57 g, 1.357 mol), acetone (78.82 g, 1.359 mol), and aqueous 40% methylamine (15.78 g, 0.2036 mol) was vigorously stirred for 4.5 h. The organic layer was separated, washed with water (2 × 60 mL) and saturated aqueous sodium chloride (60 mL), and fractionally distilled through a Vigreux column (46 cm), affording **15** (132 g, 92%) as a bright yellow liquid, bp 42°C (8 Torr) (lit. (43) bp 44–46°C (10 Torr)) (1 Torr = 133.3 Pa).

*7-Isopropylidenebicyclo[2.2.1]hept-5-en-2-one (**18**)*

The title compound **18** was prepared according to the procedure of DePuy and Story (6). Freshly distilled 2-acetoxyacrylonitrile (bp 60°C (10 Torr); 5.0 g, 45 mmol) was added dropwise with stirring over 1.5 h to 6,6-dimethylfulvene (10.0 g, 94 mmol). The solution was then heated at 55°C under a nitrogen atmosphere for 12 days. The excess dimethylfulvene was evaporated at reduced pressure with warming (40°C (0.04 Torr)) and the residue was triturated with cold pentane to give a yellow crystalline solid. Recrystallization from pentane afforded the single epimer *endo*-2-acetoxy-7-isopropylidenebicyclo-[2.2.1]hept-5-ene-*exo*-2-carbonitrile (**17***a*) (5.01 g, 51%); ir λ_{max}: 5.69, 6.95 (w), 7.43 (m), 7.59 (w), 8.18, 8.43 (w), 8.56 (m), 9.64 (m) μm; ^1H nmr δ: 1.57 (d, J = 13 Hz, 1H), 1.63 (s, 3H), 1.68 (s, 3H), 2.03 (s, 3H), 3.58 (dd, J = 13, 4 Hz, 1H), 3.45 (m, $W_{1/2}$ = 7 Hz, 1H), 4.21 (m, $W_{1/2}$ = 6 Hz, 1H), 6.07 (dd, J = 6, 3 Hz, 1H), 6.57 (dd, J = 6, 3 Hz, 1H).

The acetoxy carbonitrile **17***a* (2.0 g, 9.2 mmol) was stirred with 1 *N* methanolic sodium methoxide (17.7 mL) at ambient temperature for 3 h. Ice and water (60 mL) were added and the mixture was extracted with several portions of dichloromethane. The combined dichloromethane extracts were dried, filtered, and evaporated to give 7-isopropylidenebicyclo[2.2.1]hept-5-en-2-one (**18**). Distillation at 40°C (0.2 Torr) afforded **18** (680 mg, 50%) as a clear, colorless liquid (lit. (6) bp 46°C (0.3 Torr)); ir λ_{max}: 5.73, 5.81 (w), 7.31 (w), 8.98 (m) μm; ^1H nmr δ: 1.63 (s, 3H), 1.67 (s, 3H), 2.05 (m, $W_{1/2}$ = 4 Hz, 2H), 3.60 (m, $W_{1/2}$ = 13 Hz, 2H), 6.24 (m, $W_{1/2}$ = 11 Hz, 1H), 6.67 (dd, J = 6, 3 Hz, 1H).

*Hydrogenation of **18**. Formation of* syn- *and* anti-*7-isopropylbicyclo-[2.2.1]heptan-2-one (**5** and **6**)*

Compound **18** (962 mg, 6.50 mmol) was hydrogenated in a mixture of ethanol (5 mL) and ether (5 mL) over 5% Pd/C (15 mg) at ambient temperature and 1 atm (1 atm = 101.3 kPa) pressure until the uptake of hydrogen ceased (285 mL; 30.5 h). The mixture was filtered and the solvent was evaporated to give the crude product. Distillation at 106°C (15 Torr) afforded a mixture of epimers **5** and **6** (929 mg, 94%) as a clear, colorless liquid, bp 85°C (6 Torr), which was shown by gc and spectroscopic comparison to be identical to the mixture isolated from the hydrogenation of **27** (*vide infra*).

endo-*2-Chloro-7-isopropylidenebicyclo[2.2.1]hept-5-ene*-exo-*2-carbonitrile (**20**a) and* exo-*2-chloro-7-isopropylidenebicyclo-[2.2.1]hept-5-ene*-endo-*2-carbonitrile (**20**b)*

Freshly distilled **15** (bp 42°C (10 Torr); 97 g, 0.92 mol) was added dropwise with stirring to a solution of distilled 2-chloroacrylonitrile (bp 46°C (170 Torr); 129 g, 1.47 mol) in anhydrous benzene (200 mL). After the addition, the mixture was allowed to stand at 40°C in the dark under a nitrogen atmosphere for 51 days. The solvent and volatile components were evaporated and the resulting dark oil was distilled at 70°C (0.05 Torr) to give a clear, yellow liquid. Fractional distillation through a Vigreux column (12 cm) afforded a mixture of epimeric adducts **20***a* and **20***b*, bp 50°C (0.01 Torr), as a clear, pale yellow liquid (145 g, 82%) which solidified at −20°C. Crystallization from hexane gave a mixture of **20***a* and **20***b* as a white crystalline solid, mp 31–35°C; ir λ_{max}: 4.43 (w), 6.95, 7.31, 7.61 (m), 10.41, 11.41 (m) μm; *m/e*: 193 (1; M^+), 158 (5), 106 (100). *Anal.* calcd. for $C_{11}H_{12}ClN$: C 68.22, H 6.25, N 7.23, Cl 18.31; found: C 68.28, H 6.38, N 7.12, Cl 18.24. The adducts **20***a* and **20***b* were formed in a ratio of ~3:1 as determined by ^1H nmr spectroscopy.

*2-Chlorobicyclo[2.2.1]hept-5-ene-2-carbonitriles (**23**a and **23**b)*

The title compounds were prepared according to a modification of the procedure of Krieger (12). Freshly distilled cyclopentadiene (15.5

Can. J. Chem. Downloaded from www.nrcresearchpress.com by 210.87.254.5 on 09/06/12
For personal use only.

Can. J. Chem. Downloaded from www.nrcresearchpress.com by 210.87.254.5 on 09/06/12
For personal use only.

g, 235 mmol) was added dropwise with stirring to a solution of distilled 2-chloroacrylonitrile (41.0 g, 469 mmol) in anhydrous benzene (80 mL). After the addition the solution was allowed to stand at 40°C in the dark under a nitrogen atmosphere for 8 weeks. The volatile components of the mixture were evaporated and the residue was fractionally distilled affording a mixture of the epimeric adducts **23***a* and **23***b*, bp 32°C (0.01 Torr), as clear, colorless crystals (30.7 g, 85%), mp 38–41°C (lit. (12, 9) mp 45–47°C, 36–38°C). The adducts **23***a* and **23***b* were present in an ~4:1 ratio as determined by ^{1}H nmr spectroscopy (lit. (9) 4:1 ratio).

endo-2-*Chlorobicyclo[2.2.1]hept-5-ene*-exo-2-*carboxamide* (**25**)

A solution of the mixture of **23***a* and **23***b* (616 mg, 4.01 mmol) and sodium sulfide nonahydrate (963 mg, 4.01 mmol) in 95% ethanol (25 mL) was boiled under reflux overnight. The mixture was diluted with water and extracted with ether (4 × 25 mL). The combined ethereal extracts were washed with water and saturated aqueous sodium chloride, dried, filtered, and evaporated to give a white crystalline solid. Recrystallization from water afforded a single epimer **25** (447 mg, 65%) as white crystals, mp 114–115°C; ir λ_{max} ($CHCl_3$): 2.92 (w), 3.02 (w), 5.92, 6.36 (m), 7.40 (m) μm; ^{1}H nmr δ: 1.37–2.00 (m, 3H), 2.38–2.97 (m, 2H), 3.27 (m, 1H), 6.20 (dd, J = 5.5, 3 Hz, 1H), 6.32 (br s, 2H, absent after D_2O treatment), 6.40 (dd, J = 5.5, 2.5 Hz, 1H); ^{13}C nmr δ: 175.0 (s), 139.2 (d), 134.8 (d), 74.7 (s), 54.3 (d), 48.4 (t), 42.6 (d), 42.3 (t); m/e: 173 (2.5; $(M + 2)^+$), 171 (6; M^+), 66 (100). *Anal.* calcd. for $C_8H_{10}ClNO$: C 55.99, H 5.87, N 8.16, Cl 20.66; found: C 55.94, H 5.83, N 7.93, Cl 20.53.

endo-2-*Chloro-7-isopropylidenebicyclo[2.2.1]heptane*-exo-2-*carbonitrile* (**26**a) *and* exo-2-*chloro-7-isopropylidenebicyclo[2.2.1]heptane*-endo-2-*carbonitrile* (**26**b)

A mixture of **20***a* and **20***b* (80.0 g, 413 mmol) was hydrogenated in ethyl acetate (400 mL) over 5% Pd/C (6 g) at ambient temperature and 1 atm pressure until 1 equiv. of hydrogen was consumed (10.6 L; 19 h). Filtration followed by evaporation gave a yellow oil, which upon distillation at 65°C (0.01 Torr) afforded a mixture of **26***a* and **26***b* (78.7 g, 97%) as a clear, colorless liquid, which solidified at −20°C. Crystallization from hexane gave **26***a* as colorless crystals, mp 47.5–49°C; ir λ_{max}: 4.45 (w), 6.93 (m), 7.30 (m), 7.64 (w), 8.45 (w), 8.71 (m), 10.60 (m) μm; ^{1}H nmr δ: 1.34–2.78 (m), 1.74 (s), 1.78 (s), 3.14 (m); m/e: 197 (9; $(M + 2)^+$), 195 (26; M^+), 160 (24). *Anal.* calcd. for $C_{11}H_{14}ClN$: C 67.51, H 7.21, N 7.16, Cl 18.12; found: C 67.26, H 7.21, N 7.12, Cl 18.12.

7-Isopropylidenebicyclo[2.2.1]heptan-2-one (**27**)

A hot solution of potassium hydroxide (85.6%; 66.9 g, 1.023 mol) in water (30 mL) was added in one portion to a vigorously stirred solution of a mixture of **26***a* and **26***b* (51.3 g, 0.262 mol) in dimethyl sulfoxide (180 mL). The mixture was stirred in the dark under a nitrogen atmosphere for 15 h and then steam distilled until 1 L of distillate had been collected. The distillate was transferred to a separatory funnel with ether (100 mL). The layers were separated and the aqueous layer was extracted with ether (2 × 100 mL). The combined organic layers were washed with water (100 mL) and saturated aqueous sodium chloride (100 mL), dried, filtered, and evaporated to give the product. Distillation at 80°C (6 Torr) afforded **27** (31.5 g, 80%) as a clear, colorless liquid; ir λ_{max}: 5.72, 5.80 (w), 6.91 (w), 7.12 (w), 7.30 (w), 8.85 (w), 9.37 (w) μm; ^{1}H nmr δ: 1.67 (s, 3H), 1.73 (s, 3H), 1.30–2.73 (m, 6H), 3.08 (m, $W_{1/2}$ = 7 Hz, 2H); m/e: 150 (26; M^+).

syn- *and* anti-7-*Isopropylbicyclo[2.2.1]heptan-2-one* (**5** *and* **6**)

Compound **27** (46.4 g, 309 mmol) was hydrogenated in absolute ethanol (125 mL) and ether (125 mL) over 5% Pd/C (3 g) at ambient temperature and 1 atm pressure until the uptake of hydrogen ceased (7.5 L; 61.5 h). Filtration followed by evaporation gave the crude product, which upon distillation through a Vigreux column (12 cm) afforded a mixture of **5** and **6**, bp 85°C (6 Torr), as a clear, colorless liquid (44.3 g, 94%). Gas chromatographic analysis showed this to be a 3:2 mixture of *syn* (R_t = 3.6 min) and *anti* (R_t = 4.2 min) isomers.

Separation of syn- *and* anti-7-*isopropylbicyclo[2.2.1]heptan-2-one* (**5** *and* **6**)

(i) anti-7-*Isopropylbicyclo[2.2.1]heptan-2-one 2,4-dinitrophenylhydrazone* (**28**)

A solution of a mixture of **5** and **6** (70:30; 15.2 g, 100 mmol) in methanol (10 mL) was added in one portion to a filtered solution of 2,4-dinitrophenylhydrazine (6.90 g, 34.8 mmol) in methanol (140 mL) and concentrated sulfuric acid (9 mL). After 3 h at ambient temperature the mixture was cooled in ice and the resulting precipitate was collected by suction filtration through sintered glass and washed thoroughly with water until the washings were no longer acidic. The filtrate and washings were kept for procedure *(ii)* (*vide infra*). The orange solid was dissolved in a boiling mixture of absolute ethanol (1.1 L) and ether (500 mL). The solution was concentrated to a volume of 1.2 L and left at ambient temperature overnight. Cooling in ice afforded **28** (8.05 g) as a bright orange powder. Concentration of the mother liquor to a volume of 200 mL followed by cooling in ice afforded a further crop of product (1.24 g, 93% total based on *anti* isomer), mp 176–178°C; ir λ_{max}: 6.17 (m), 6.26 (m), 6.73 (w), 7.50, 7.14 (m) μm; ^{1}H nmr δ: 0.98 (d, J = 5 Hz, 6H), 1.13–2.43 (m, 8H), 2.57 (m, $W_{1/2}$ = 7 Hz, 1H), 2.91 (m, $W_{1/2}$ = 6 Hz, 1H), 7.88 (d, J = 10 Hz, 1H), 8.29 (dd, J = 10, 2.5 Hz, 1H), 9.08 (d, J = 2.5 Hz, 1H), 10.72 (br s, 1H); m/e: 332 (100; M^+). *Anal.* calcd. for $C_{16}H_{20}N_4O_4$: C 57.82, H 6.07, N 16.86; found: C 57.71, H 6.08, N 16.73.

(ii) syn-7-*Isopropylbicyclo[2.2.1]heptan-2-one* (**5**)

Pyruvic acid (1 g) was added to the filtrate from *(i)*. After 30 min the solution was combined with the water washings from *(i)* and water (800 mL) was added. The mixture was extracted with ether (4 × 150 mL). The combined ethereal extracts were washed with aqueous 4% sodium chloride (2 × 50 mL), dried, filtered, and evaporated to give an orange liquid (10.33 g). Distillation at 68°C (3 Torr) afforded **5** (9.52 g, 89%) as a clear, colorless liquid (gc analysis indicated the presence of <1% *anti* isomer); m/e: 152 (33; M^+), 109 (44). *Anal.* calcd. for $C_{10}H_{16}O$: C 78.90, H 10.59; found: C 78.56, H 10.58.

(iii) anti-7-*Isopropylbicyclo[2.2.1]heptan-2-one* (**6**)

An aqueous 20% solution of titanium trichloride (prepared in a glove box under a nitrogen atmosphere by the careful addition of titanium trichloride (Apache Chemicals) to degassed water; 500 mL, 648 mmol) was added slowly under a nitrogen atmosphere to a stirred solution of **28** (12.0 g, 36.1 mmol) in anhydrous 1,2-dimethoxyethane (600 mL). The mixture was stirred for 5 h and then steam distilled until 1.6 L of distillate had been collected. The distillate was extracted with dichloromethane (4 × 150 mL). The combined extracts were washed with saturated aqueous sodium chloride, dried, filtered, and evaporated to give the crude product (5.56 g). Distillation at 26°C (0.2 Torr) afforded **6** (4.82 g, 88%) as a clear, colorless liquid, which was 99.6% pure as shown by gc analysis (R_t = 4.4 min); m/e: 152 (29; M^+), 109 (44). *Anal.* calcd. for $C_{10}H_{16}O$: C 78.90, H 10.59; found: C 78.64, H 10.61.

syn-7-tert-*Butylbicyclo[2.2.1]heptan-2-one* (**7**)

syn-7-*tert*-Butylbicyclo[2.2.1]heptan-*endo*-2-ol (**38**) was prepared from *syn*-7-*tert*-butylnorbornene (**37**) by the method of Baird and Surridge (17) except that borane – methyl sulfide complex was used for the reduction of **37** rather than 9-borabicyclo[3.3.1]nonane (9-BBN).

To an ice-cold solution of **38** (3.89 g, 23.2 mmol) in acetone (50 mL) was added dropwise with stirring a solution of Jones reagent until an orange-brown color persisted. Isopropyl alcohol (5 drops) was added to give a green color, the mixture was filtered by suction, and the filtrate was evaporated to give a green oil. The oil was extracted with dichloromethane (2 × 20 mL) and the combined extracts were washed with aqueous 4% sodium bicarbonate, dried, filtered, and evaporated to give a pale green liquid (3.26 g). Distillation at 100°C (14 Torr) afforded **7** (3.12 g, 81%) as a clear, colorless liquid; ^{1}H nmr δ: 0.97 (s, 9H), 1.12–2.35 (m, 7H), 2.55 (m, 2H); m/e: 166 (50; M^+), 109 (93). *Anal.* calcd. for $C_{11}H_{18}O$: C 79.46, H 10.91; found: C 79.30, H 10.95.

Can. J. Chem. Downloaded from www.nrcresearchpress.com by 210.87.254.5 on 09/06/12
For personal use only.

anti-7-tert-*Butylbicyclo[2.2.1]heptan-2-one (8)*

To an ice-cold solution of *anti*-7-*tert*-butylbicyclo[2.2.1]heptan-*exo*-2-ol (**39**) (prepared by the procedure of Baird and Surridge (17); 1.98 g, 11.8 mmol) in acetone (45 mL) was added dropwise with stirring a solution of Jones reagent until an orange-brown color persisted. Isopropyl alcohol (5 drops) was added to give a green color, the mixture was filtered by suction, and the filtrate was evaporated to give a green oil. The oil was extracted with dichloromethane (2 × 15 mL). The combined extracts were dried over anhydrous sodium sulfate and a small amount of sodium bicarbonate, filtered, and evaporated to give an oil which crystallized at −20°C. Recrystallization from hexane at −20°C afforded **8** (1.42 g) as clear, colorless crystals. Evaporation of the mother liquor followed by sublimation at ambient temperature (0.01 Torr) with a Dry Ice – acetone condenser afforded further product (150 mg; 80% total), mp 30–32°C; ^{1}H nmr δ: 1.02 (s, 9H), 1.17–2.43 (m, 7H), 2.60 (m, 2H); *m/e*: 166 (27; M^+), 109 (59). *Anal.* calcd. for $C_{11}H_{18}O$: C 79.46, H 10.91; found: C 79.30, H 11.00.

6,6-Diphenylfulvene (29)

6,6-Diphenylfulvene (**29**) was prepared by a modification of the procedure of Wagner and Hunt (44) suggested by Poos *et al.* (45). To a warm solution of benzophenone (82.7 g, 454 mmol) in ethanolic sodium ethoxide (prepared by the addition of freshly cut sodium metal (10.4 g, 454 mmol) to anhydrous ethanol (325 mL)) was added freshly distilled cyclopentadiene (50.0 g, 757 mmol) slowly with stirring over 0.5 h under a nitrogen atmosphere. The mixture was stirred for a further 3 h and cooled in ice, and the resulting crystals were collected by suction filtration. Recrystallization from absolute ethanol afforded **29** (85.3 g, 82%) as large, red crystals, mp 76–78°C (lit. (44) mp 81–82°C).

7-Benzhydrylidene-endo-*2-chlorobicyclo[2.2.1]hept-5-ene*-exo-*2-carbonitrile (30*a*) and 7-benzhydrylidene*-exo-*2-chlorobicyclo-[2.2.1]hept-5-ene*-endo-*2-carbonitrile (30*b*)*

A solution of **29** (34.5 g, 150 mmol) in anhydrous benzene (150 mL) was added dropwise with stirring to a solution of distilled 2-chloroacrylonitrile (bp 46°C (170 Torr); 26.3 g, 301 mmol) in anhydrous benzene (100 mL). After the addition the mixture was allowed to stand at 40°C in the dark under a nitrogen atmosphere for 11 weeks. The volume of the solution was reduced to 25% of the original volume and the concentrate was cooled to 5°C. The tawny precipitate was collected by suction filtration and the filtrate was concentrated and cooled to give a further crop of product (32.2 g total, 68%). The crude product was treated with activated charcoal in boiling heptane. Gravity filtration of the hot solution followed by cooling of the filtrate afforded a white crystalline solid consisting of a mixture of **30***a* and **30***b* in a ratio of 2.5:1 as determined by ^{1}H nmr spectroscopy. The mixture was usually directly subjected to hydrogenation. Fractional crystallization of the mixture from absolute ethanol provided a pure sample of each adduct. Sublimation of *exo*-carbonitrile **30***a* at 90°C (0.005 Torr) afforded a white crystalline solid, mp 134–137°C; ir λ_{max}: 4.48 (w), 6.70 (m), 6.95, 7.57 (m), 9.35 (m), 9.71 (m), 10.36 μm; *m/e*: 319 (1; $(M + 2)^+$), 317 (3; M^+), 230 (100). *Anal.* calcd. for $C_{21}H_{16}ClN$: C 79.36, H 5.07, N 4.41, Cl 11.16; found: C 79.40, H 4.93, N 4.45, Cl 11.25.

Sublimation of *endo*-carbonitrile **30***b* at 90°C (0.005 Torr) afforded a white crystalline solid, mp 130–132°C; ir λ_{max}: 4.48 (w), 6.71, 6.94, 7.57, 9.32 (m), 9.46 (m), 9.72 (m), 10.22 (m) μm; *m/e*: 319 (0.5; $(M + 2)^+$), 317 (2; M^+), 230 (100). *Anal.* calcd. for $C_{21}H_{16}ClN$: C 79.36, H 5.07, N 4.41, Cl 11.16; found: C 79.22, H 5.10, N 4.57, Cl 11.09.

7-Benzhydrylidene-endo-*2-chlorobicyclo[2.2.1]heptane*-exo-*2-carbonitrile (31*a*) and 7-benzhydrylidene*-exo-*2-chlorobicyclo[2.2.1]heptane*-endo-*2-carbonitrile (31*b*)*

A mixture of **30***a* and **30***b* (3.18 g, 10.0 mmol) was hydrogenated in ethyl acetate (60 mL) over 5% Pd/C (125 mg) at ambient temperature and 1 atm pressure until one equivalent of hydrogen was consumed (240 mL; 2.25 h). Filtration followed by evaporation gave an oil which solidified under high vacuum affording a mixture of **31***a* and **31***b* (3.12 g, 98%). This was usually directly subjected to hydrolysis without further purification. An analytical sample of one of the epimers, considered to be **31***a*, was obtained by crystallization from heptane followed by sublimation at 80°C (0.005 Torr), as a white crystalline solid, mp 86–88°C; ir λ_{max} ($CHCl_3$): 4.50 (w), 5.12 (w), 5.28 (w), 5.52 (w), 5.72 (w), 6.24, 6.32 (w), 6.73 (m), 6.95, 7.59 (m), 8.73 (m), 9.28, 10.51, 11.03 (m), 11.47 (m) μm; ^{1}H nmr δ: 1.44–3.14 (m, 8H), 7.28 (m, 10H); *m/e*: 321 (29; $(M + 2)^+$), 319 (75; M^+), 284 (35). *Anal.* calcd. for $C_{21}H_{18}ClN$: C 78.86, H 5.67, N 4.38, Cl 11.08; found: C 79.14, H 5.85, N 4.33, Cl 11.08.

7-Benzhydrylidenebicyclo[2.2.1]heptan-2-one (32)

A hot solution of potassium hydroxide (86.3%; 1.51 g, 23.2 mmol) in water (1.5 mL) was added in one portion to a vigorously stirred solution of a mixture of **31***a* and **31***b* (2.50 g, 7.82 mmol) in dimethyl sulfoxide (20 mL). The mixture was stirred in the dark under a nitrogen atmosphere for 13 h, diluted with water (100 mL), and extracted with ether (6 × 50 mL). The combined ethereal extracts were washed with aqueous sodium bicarbonate (2 × 50 mL) and saturated aqueous sodium chloride (50 mL), dried, filtered, and evaporated to give **32** (1.84 g, 86%) as a yellowish-white foam. Sublimation at 75°C (0.01 Torr) gave a transparent gum which solidified on standing. Crystallization from methanol or hexane afforded **32** as a white crysalline solid, mp 100–102°C; ir λ_{max}: 5.71, 6.67 (w), 6.93 (w), 7.11 (w), 7.31 (w) μm; ^{1}H nmr δ: 1.43–2.71 (m, 6H), 3.19 (m, $W_{1/2}$ = 6 Hz, 2H), 7.23 (m, 10H); ^{13}C nmr δ: 211.7 (s), 143.6 (s), 131.6 (s), 53.4 (d), 48.0 (t), 38.0 (d), 27.0 (t), 24.0 (t); *m/e*: 274 (100; M^+). *Anal.* calcd. for $C_{20}H_{18}O$: C 87.56, H 6.61; found: C 87.44, H 6.65.

*Formation of (2-benzhydryl-2-cyclopentenyl)acetic acid (33) from 31*a *and 31*b

Hydrolysis of a mixture of **31***a* and **31***b* (45.6 g, 133 mmol) dissolved in dimethyl sulfoxide (400 mL) with a hot solution of potassium hydroxide (87.3%; 25.6 g, 399 mmol) in water (9 mL) for 48 h gave a very poor yield of ketone **32** after work-up as above. The original aqueous phase from the work-up was acidified with concentrated sulfuric acid and extracted several times with ether. The combined ethereal extracts were washed with water and saturated aqueous sodium chloride, dried, filtered, and evaporated to give a brown foam. The foam was applied to a Florisil plug and eluted with dichloromethane. Evaporation of the solvent followed by treatment with boiling hexane and cooling to −20°C afforded **33** as a white crystalline solid, mp 91–92°C; ir λ_{max}: 3–4 (br), 5.66 (w), 5.84, 6.69 (w), 6.89 (w), 7.10 (w) μm; ^{1}H nmr δ: 1.37–3.23 (m, 7H), 4.66 (m, $W_{1/2}$ = 5 Hz, 1H), 5.07 (m, $W_{1/2}$ = 5.5 Hz, 1H), 7.07 (m, 10H), 11.25 (br s, 1H); ^{13}C nmr δ: 179.6 (s), 148.1 (s), 143.2 (s), 141.3 (s), 130.4 (d), 128.9 (d), 128.5 (d), 128.1 (d), 126.6 (d), 126.2 (d), 51.6 (d), 43.1 (d), 38.1 (t), 30.7 (t), 30.5 (t); *m/e*: 292 (78; M^+), 232 (73). *Anal.* calcd. for $C_{20}H_{20}O_2$: C 82.16, H 6.90; found: C 82.04, H 6.90.

Formation of 33 from 32

A hot solution of potassium hydroxide (87.3%; 300 mg, 4.68 mmol) in water (0.5 mL) was added in one portion to a vigorously stirred solution of **32** (272 mg, 0.99 mmol) in dimethyl sulfoxide (8 mL). The mixture was stirred in the dark at ambient temperature under a nitrogen atmosphere for 36 h, diluted with water, and extracted several times with dichloromethane. The extracts were discarded, and the aqueous phase was acidified with concentrated sulfuric acid and extracted several times with dichloromethane. The combined extracts were dried, filtered, and evaporated to give an oil (202 mg). Sublimation at 110°C (0.01 Torr) afforded a glass (79 mg, 27%) which was shown to consist largely of **33** by ^{1}H nmr spectroscopic comparison.

syn- *and* anti-*7-Benzhydrylbicyclo[2.2.1]heptan-2-one (9 and 10)*

Compound **32** (2.15 g, 7.85 mmol) was hydrogenated in absolute ethanol (30 mL) over 10% Pd/C (60 mg) at ambient temperature and 1 atm pressure until the uptake of hydrogen ceased (200 mL; 48 h). Filtration followed by evaporation gave a mixture of **9** and **10** (2.00 g, 92%) as a colorless oil. The oil was applied to a column of silica gel (125 g) and eluted with benzene (20-mL fractions were collected).

Can. J. Chem. Downloaded from www.nrcresearchpress.com by 210.87.254.5 on 09/06/12
For personal use only.

The majority of fractions contained a mixture of *syn* (R_f = 0.3) and *anti* isomers (R_f = 0.2). The final fractions consisted of only the *anti* isomer **10** (68 mg) which was purified further by sublimation at 65°C (0.025 Torr), affording a glass, followed by treatment with boiling hexane and cooling to −20°C to give **10** as a white crystalline solid, mp 80–82°C; ^{1}H nmr δ: 1.25–2.42 (m, 8H), 2.68 (br d, J = 12 Hz, 1H), 3.77 (d, J = 12 Hz, 1H), 7.23 (s, 5H), 7.26 (s, 5H); *m/e*: 276 (21; M^+). *Anal.* calcd. for $C_{20}H_{20}O$: C 86.92, H 7.29; found: C 86.88, H 7.35.

The fractions containing mixtures of isomers were combined and evaporated to give a colorless oil, which on treatment with boiling hexane and cooling to −20°C afforded the *syn* isomer **9** (522 mg) as a white crystalline solid, mp 130–131.5°C; ^{1}H nmr δ: 1.23–2.36 (m, 8H), 2.63 (br d, J = 12 Hz, 1H), 3.58 (d, J = 12 Hz, 1H), 7.13 (s, 5H), 7.19 (s, 5H); *m/e*: 276 (24; M^+). *Anal.* calcd. for $C_{20}H_{20}O$: C 86.92, H 7.29; found: C 86.78, H 7.26.

syn-7-*Isopropylbicyclo[2.2.1]heptane-2,3-dione* (**40**)

A mixture of **5** (8.00 g, 52.6 mmol) in distilled bromobenzene (bp 56°C (20 Torr); 180 mL) and powdered selenium dioxide (14.6 g, 132 mmol) was boiled under reflux with vigorous mechanical stirring under a nitrogen atmosphere. The reaction was monitored by examination of the ^{1}H nmr spectra of aliquots, which showed a signal at δ 3.02 attributed to the bridgehead protons of the product. After 39 h the yellow mixture was cooled and filtered through Celite with suction. The residual black selenium was washed well with benzene until the washings became colorless. Evaporation of solvent from the combined filtrate and washings under high vacuum left a red oil, which was treated with hot hexane (150 mL). Gravity filtration of the hot solution and cooling the filtrate to −20°C afforded **40** (6.04 g, 69%) as a bright yellow powder. Crystallization from hexane followed by sublimation at ambient temperature (0.005 Torr) gave yellow crystals, mp 88.5–90°C; ^{1}H nmr δ: 0.98 (d, J = 5 Hz, 6H), 1.12–2.55 (m, 6H), 3.02 (m, $W_{1/2}$ = 6.5 Hz, 2H); *m/e*: 166 (39; M^+), 123 (84). *Anal.* calcd. for $C_{10}H_{14}O_2$: C 72.26, H 8.49; found: C 72.15, H 8.52.

anti-7-*Isopropylbicyclo[2.2.1]heptane-2,3-dione* (**41**)

A mixture of **6** (2.00 g, 13.2 mmol) in distilled bromobenzene (bp 56°C (20 Torr); 130 mL) and powdered selenium dioxide (3.65 g, 32.9 mmol) was heated at 140°C with vigorous mechanical stirring under a nitrogen atmosphere. The reaction was monitored by examination of the ^{1}H nmr spectra of aliquots, which showed a signal at δ 2.93 attributed to the bridgehead protons of the product. After 21 h further selenium dioxide (1.4 g) was added. After a total of 33.5 h of heating, the yellow mixture was cooled and worked up as for **40** to give a red oil, which was treated with hot hexane (100 mL). Gravity filtration of the hot solution and cooling the filtrate to −20°C afforded **41** (912 mg) as bright yellow crystals. Evaporation of the mother liquor followed by two sublimations at ambient temperature (0.01 Torr) gave a further crop of product (254 mg; 53% total), mp 68.5–70°C; ^{1}H nmr δ: 0.98 (d, J = 5 Hz, 6H), 1.08–2.42 (m, 6H), 2.93 (m, $W_{1/2}$ = 6 Hz, 2H); *m/e*: 166 (28; M^+); 123 (22). *Anal.* calcd. for $C_{10}H_{14}O_2$: C 72.26, H 8.49; found: C 72.06, H 8.47.

syn-7-tert-*Butylbicyclo[2.2.1]heptane-2,3-dione* (**42**)

Compound **7** (4.00 g, 24.1 mmol) in distilled bromobenzene (bp 42°C (10 Torr); 125 mL) was oxidized with powdered selenium dioxide (6.69 g, 60.3 mmol) as in the case of **5**, with monitoring of a ^{1}H nmr signal at δ 0.94 attributed to the *tert*-butyl protons of the product. After 70 h, the yellow mixture on work-up as before gave a yellow solid, which was treated with hot hexane (75 mL). Gravity filtration of the hot solution and cooling the filtrate to −20°C afforded **42** (2.62 g) as bright yellow elongated plates. Concentration of the mother liquor and cooling to −20°C afforded a further crop of product (53 mg; 73% total), mp 97.5–99°C; ^{1}H nmr δ: 0.94 (s, 9H), 1.19–2.49 (m, 5H), 3.07 (m, $W_{1/2}$ = 7 Hz, 2H); *m/e*: 180 (14; M^+), 123 (80). *Anal.* calcd. for $C_{11}H_{16}O_2$: C 73.30, H 8.95; found: C 73.23, H 9.03.

anti-7-tert-*Butylbicyclo[2.2.1]heptane-2,3-dione* (**43**)

Compound **8** (2.41 g, 14.5 mmol) in distilled bromobenzene (170 mL) was oxidized with selenium dioxide (6.50 g, 58.6 mmol) as in the case of **6**, with monitoring of a ^{1}H nmr signal at δ 1.08 attributed to the *tert*-butyl protons of the product. After 25 h further selenium dioxide (1.00 g) was added. After a total of 41 h of heating, the yellow mixture was worked up as before to give a red oil. The oil was distilled in a Kugelrohr apparatus at 60°C (0.025 Torr) with cold water cooling of the receiver bulb to afford a yellow solid (1.51 g). Crystallization from hexane (25 mL) wih cooling to −20°C afforded **43** (800 mg) as a bright yellow powder. Concentration of the mother liquor and cooling to −20°C gave a further crop of product (288 mg). Further concentration of the mother liquor and cooling to −20°C gave a third crop, which after sublimation at ambient temperature (0.025 Torr) afforded a further 180 mg of product (49% total), mp 65–67°C; ^{1}H nmr δ: 1.08 (s, 9H), 1.46–2.54 (m, 5H), 3.05 (m, $W_{1/2}$ = 6.5 Hz, 2H); *m/e*: 180 (12; M^+), 123 (22). *Anal.* calcd. for $C_{11}H_{16}O_2$: C 73.30, H 8.95; found: C 73.11, H 8.88.

syn-7-*Isopropylbicyclo[2.2.1]heptane-2,3-dione, (Z)-monotosylhydrazone* (**44***Z*)

To a warm solution of **40** (3.00 g, 18.1 mmol) in glacial acetic acid (10 mL) was added in one portion a warm solution of *p*-toluenesulfonylhydrazine (3.37 g, 18.1 mmol) in glacial acetic acid (10 mL). After the mixture had stood at 5°C overnight, the crystals that had separated were collected by suction filtration and washed thoroughly with water, affording **44***Z* (5.18 g, 86%). Recrystallization from a mixture of methanol (40 mL) and acetonitrile (10 mL) gave greenish-yellow crystals, mp 166.5–168.5°C; ^{1}H nmr δ: 0.87 (br s, 6H), 0.97–2.26 (m, 6H), 2.43 (s, 3H), 2.73 (m, $W_{1/2}$ = 7 Hz, 1H), 2.97 (m, $W_{1/2}$ = 6 Hz, 1H), 7.24 (d, J = 8.5 Hz, 2H), 7.74 (d, J = 8.5 Hz, 2H), 11.49 (br s, 1H); *m/e*: 179 (26; $(M - C_7H_7SO_2)^+$), 150 (14). *Anal.* calcd. for $C_{17}H_{22}N_2O_3S$: C 61.05, H 6.63, N 8.38; found: C 60.96, H 6.65, N 8.27.

anti-7-*Isopropylbicyclo[2.2.1]heptane-2,3-dione, (Z)-monotosylhydrazone* (**45***Z*)

A solution of **41** (207 mg, 1.25 mmol) and *p*-toluenesulfonylhydrazine (232 mg, 1.25 mmol) in dry dichloromethane (15 mL) was boiled under reflux overnight. Evaporation of the solvent and examination of the ^{1}H nmr spectrum of the resulting yellow oil indicated the presence of a mixture of *Z*- and *E*-monotosylhydrazones. Application of the crude material to a plug of silica gel (15 g) and elution with dichloromethane converted the mixture to the single *Z* isomer. Evaporation of solvent gave a pale green oil which was treated wih boiling ether/hexane. Cooling to −20°C afforded **45***Z* (323 mg, 77%) as greenish-yellow crystals, mp 115–117°C; ^{1}H nmr δ: 0.89 (d, J = 4 Hz, 6H), 1.02–2.18 (m, 6H), 2.43 (s, 3H), 2.71 (m, $W_{1/2}$ = 8 Hz, 1H), 2.96 (m, $W_{1/2}$ = 6 Hz, 1H), 7.30 (d, J = 8.5 Hz, 2H), 7.80 (d, J = 8.5 Hz, 2H), 11.46 (br s, 1H); *m/e*: 179 (2; $(M - C_7H_7SO_2)^+$), 150 (14). *Anal.* calcd. for $C_{17}H_{22}N_2O_3S$: C 61.05, H 6.63, N 8.38; found: C 61.30, H 6.79, N 8.28.

anti-7-*Isopropylbicyclo[2.2.1]heptane-2,3-dione, (E)-monotosylhydrazone* (**45***E*)

To a warm solution of **41** (350 mg, 2.11 mmol) in glacial acetic acid (2.5 mL) was added in one portion a warm solution of *p*-toluenesulfonylhydrazine (393 mg, 2.11 mmol) in glacial acetic acid (2 mL). After the solution had stood overnight at ambient temperature, the solvent was evaporated and the resulting yellow oil was treated with hot methanol (6 mL). Cooling to −20°C gave **45***E* (138 mg, 20%) as a white powder, mp 155–158°C; ^{1}H nmr δ: 0.88 (d, J = 5 Hz, 6H), 1.03–2.18 (m, 6H), 2.43 (s, 3H), 2.69 (m, $W_{1/2}$ = 6.5 Hz, 1H), 3.28 (m, $W_{1/2}$ = 6 Hz, 1H), 7.38 (d, J = 8 Hz, 2H), 7.83 (d, J = 8 Hz, 2H), 8.73 (br s, 1H).

syn-7-tert-*Butylbicyclo[2.2.1]heptane-2,3-dione, (Z)-monotosylhydrazone* (**46***Z*)

A solution of **42** (540 mg, 3.00 mmol) and *p*-toluenesulfonylhydrazine (558 mg, 3.00 mmol) in dry methanol (12 mL) was boiled under reflux for 48 h. The mixture was cooled to −20°C and the crystals that separated were collected by suction filtration. Recrystallization from methanol afforded **46***Z* (464 mg, 45%) as greenish-yellow crystals, mp 147–148°C; ^{1}H nmr δ: 0.75 (s, 9H),

Can. J. Chem. Downloaded from www.nrcresearchpress.com by 210.87.254.5 on 09/06/12
For personal use only.

1.25–2.18 (m, 5H), 2.42 (s, 3H), 2.74 (m, $W_{1/2}$ = 6 Hz, 1H), 3.03 (m, $W_{1/2}$ = 6 Hz, 1H), 7.30 (d, J = 8.5 Hz, 2H), 7.82 (d, J = 8.5 Hz, 2H), 11.57 (br s, 1H); *m/e*: 193 (2; $(M - C_7H_7SO_2)^+$). *Anal.* calcd. for $C_{18}H_{24}N_2O_3S$: C 62.04, H 6.94, N 8.04; found: C 62.15, H 7.09, N 8.07.

anti-7-tert-*Butylbicyclo[2.2.1]heptane-2,3-dione, (Z)-monotosylhydrazone (47Z)*

A solution of **43** (500 mg, 2.78 mmol) and *p*-toluenesulfonylhydrazine (517 mg, 2.78 mmol) in anhydrous benzene (60 mL) was boiled under reflux overnight in a 100-mL flask equipped with a Dean–Stark water separator. The solution was cooled and the solvent was evaporated to give a yellow oil which could not be crystallized. The oil was applied to a plug of silica gel (30 g) and eluted with dichloromethane. Evaporation of solvent gave a pale green oil which was treated with boiling ether/hexane. Cooling to −20°C afforded **47Z** (877 mg, 91%) as greenish-yellow crystals, mp 143–145°C; ^{1}H nmr δ: 1.02 (s, 9H), 1.17–2.30 (m, 5H), 2.45 (s, 3H), 2.81 (m, $W_{1/2}$ = 7 Hz, 1H), 3.08 (m, $W_{1/2}$ = 7 Hz, 1H), 7.32 (d, J = 8.5 Hz, 2H), 7.83 (d, J = 8.5 Hz, 2H), 11.34 (br s, 1H); *m/e*: 349 (4; $(M + 1)^+$), 193 (80; $(M - C_7H_7SO_2)^+$), 165 (15). *Anal.* calcd. for $C_{18}H_{24}N_2O_3S$: C 62.14, H 6.94, N 8.04; found: C 61.99, H 6.99, N 8.08.

Reaction of monotosylhydrazones 44Z–47Z with basic alumina. Preparation of α-diazo ketones 1–4

General procedure

A solution of vacuum-dried monotosylhydrazone (239 mg – 1.2 g, 0.687–3.6 mmol) in the minimum amount of dry dichlorethane (distilled from calcium hydride) was applied to a column (diameter 1.2 or 2 cm) of activated basic alumina (Fisher A 540; 23–100 g) packed in dichloromethane. The solution was adsorbed well into the column, which was left sealed overnight in the dark with 2 mL of solvent above the adsorption bed. Elution of the product with dichloromethane (100–300 mL) followed by evaporation of the solvent gave the diazo ketone as a bright yellow oil which solidified at −20°C.

3-Diazo-syn-7-*isopropylbicyclo[2.2.1]heptan-2-one (1)*

The yield of **1** was 96%. Sublimation at 40°C (0.01 Torr) gave bright yellow crystals, mp 57–58°C; ^{1}H nmr δ: 0.93 (d, J = 5 Hz, 3H), 0.99 (d, J = 5 Hz, 3H), 1.32–2.18 (m, 6H), 2.58 (m, $W_{1/2}$ = 7 Hz, 1H), 3.37 (m, $W_{1/2}$ = 5 Hz, 1H); *m/e*: 178 (25; M^+). *Anal.* calcd. for $C_{10}H_{14}N_2O$: C 67.39, H 7.92, N 15.72; found: C 67.50, H 7.93, N 15.80.

3-Diazo-anti-7-*isopropylbicyclo[2.2.1]heptan-2-one (2)*

The yield of **2** was 83%. Sublimation at ambient temperature (0.025 Torr) gave bright yellow crystals, mp 42–43°C; ^{1}H nmr δ: 0.88 (d, J = 5 Hz, 3H), 0.93 (d, J = 5 Hz, 3H), 1.02–2.15 (m, 6H), 2.57 (m, $W_{1/2}$ = 6 Hz, 1H), 3.30 (m, $W_{1/2}$ = 4.5 Hz, 1H); *m/e*: 178 (22; M^+). *Anal.* calcd. for $C_{10}H_{14}N_2O$: C 67.39, H 7.92, N 15.72; found: C 67.52, H 7.95, N 15.71.

syn-7-tert-*Butyl-3-diazobicyclo[2.2.1]heptan-2-one (3)*

The yield of **3** was 92%. Sublimation at ambient temperature (0.01 Torr) gave bright yellow crystals, mp 56–57°C; ^{1}H nmr δ: 1.01 (s, 9H), 1.22–2.48 (m, 5H), 2.63 (m, $W_{1/2}$ = 6.5 Hz, 1H), 3.42 (m, $W_{1/2}$ = 5 Hz, 1H); *m/e*: 192 (22; M^+). *Anal.* calcd. for $C_{11}H_{16}N_2O$: C 68.72, H 8.39, N 14.57; found: C 68.67, H 8.31, N 14.48.

anti-7-tert-*Butyl-3-diazobicyclo[2.2.1]heptan-2-one (4)*

Sublimation of the crude product at 32°C (0.025 Torr) afforded **4** (95%) as a bright yellow powder, mp 35–36°C; ^{1}H nmr δ: 1.00 (s, 9H), 1.42–2.42 (m, 5H), 2.70 (m, $W_{1/2}$ = 6 Hz, 1H), 3.47 (m, $W_{1/2}$ = 5 Hz, 1H); *m/e*: 192 (18; M^+). *Anal.* calcd. for $C_{11}H_{16}N_2O$: C 68.72, H 8.39, N 14.57; found: C 68.82, H 8.39, N 14.48.

Copper-catalyzed decomposition of α-diazo ketones 1–4. Preparation of tricyclic ketones 11–14

General procedure

To a solution of the α-diazo ketone (0.87 mmol) in anhydrous benzene (degassed by passage of argon for 30 min; 400 mL) in a 1-L flask that had been oven-dried and cooled under a stream of argon, was added powdered copper (Fisher, electrolytic metal, washed with ether and hexane, and vacuum dried prior to use; 9.8 g). The mixture was boiled gently under reflux with vigorous stirring under an argon atmosphere. The reaction was conveniently monitored by examination of the ir spectra of aliquots, which showed the disappearance of the band at 4.84 μm attributed to the diazo group of the starting material. After 5 h[7] the mixture was cooled and filtered, and the copper was washed well with benzene. Evaporation of the combined filtrate and washings afforded the tricyclic ketone as a highly volatile pale green liquid which was purified by distillation at 50°C (10 Torr) to afford a clear, colorless liquid in each case.

syn-5-*Isopropyltricyclo[2.2.1.0^{2,6}]heptan-3-one (11)*

The yield of **11** was 96%; ^{1}H nmr δ: 0.93 (d, J = 5 Hz, 3H), 1.04 (d, J = 5 Hz, 3H), 1.21 (t, J = 5 Hz, 1H), 1.32–2.15 (m, 7H); *m/e*: 150 (28; M^+), 107 (55), 79 (100). *Anal.* calcd. for $C_{10}H_{14}O$: C 79.96, H 9.39; found: C 79.80, H 9.44.

anti-5-*Isopropyltricyclo[2.2.1.0^{2,6}]heptan-3-one (12)*

The yield of **12** was 75%; ^{1}H nmr δ: 0.82 (d, J = 6 Hz, 3H), 0.99 (d, J = 6 Hz, 3H), 1.37 (t, J = 5.5 Hz, 1H), 1.68–2.13 (m, 7H); *m/e*: 150 (51; M^+), 107 (34), 79 (100). *Mol. Wt.* calcd. for $C_{10}H_{14}O$: 150.1044; found (ms): 150.1040.

syn-5-tert-*Butyltricyclo[2.2.1.0^{2,6}]heptan-3-one (13)*

The yield of **13** was 88%; ^{1}H nmr δ: 0.95 (s, 9H), 1.27 (t, J = 5 Hz, 1H), 1.58–2.05 (m, 6H); *m/e*: 164 (34; M^+), 107 (40), 79 (100). *Anal.* calcd. for $C_{11}H_{16}O$: C 80.44; H 9.82; found: C 80.13, H 9.95.

anti-5-tert-*Butyltricyclo[2.2.1.0^{2,6}]heptan-3-one (14)*

The yield of **14** was 65%; ^{1}H nmr δ: 0.98 (s, 9H), 1.43 (t, J = 5 Hz, 1H), 1.67–2.27 (m, 6H); *m/e*: 164 (46; M^+), 107 (88), 79 (100). *Mol. Wt.* calcd. for $C_{11}H_{16}O$: 164.1201; found (ms): 164.1202.

Acknowledgements

We thank the Natural Sciences and Engineering Research Council of Canada for support of this work and Messrs. Baldev Gambhir and Nick Plavac for technical assistance.

1. P. YATES and G. F. HAMBLY. Can. J. Chem. **57**, 1668 (1979).
2. P. YATES and J. D. KRONIS. Tetrahedron Lett. **24**, 2419 (1983); J. D. KRONIS, M. F. POWELL, and P. YATES. Tetrahedron Lett. **24**, 2423 (1983); R. A. BLATTEL and P., YATES. Tetrahedron Lett. 1069 (1972); 1073 (1972); P. YATES and J. D. FENWICK. J. Am. Chem. Soc. **93**, 4618 (1971); P. YATES and R. J. CRAWFORD. J. Am. Chem. Soc. **88**, 1561 (1966).
3. V. A. MIRONOV, E. V. SOBOLEV, and A. N. ELIZAROVA. Tetrahedron, **19**, 1939 (1963); S. MCLEAN and P. HAYNES. Tetrahedron, **21**, 2313 (1965); **21**, 2329 (1965).
4. E. J. COREY, U. KOELLIKER, and J. NEUFFER. J. Am. Chem. Soc. **93**, 1489 (1971).
5. H. AUKSI and P. YATES. Can. J. Chem. **59**, 2510 (1981).
6. C. H. DEPUY and P. R. STORY. J. Am. Chem. Soc. **82**, 627 (1960).
7. P. K. FREEMAN, D. M. BALLS, and D. J. BROWN. J. Org. Chem. **33**, 221 (1968).
8. J. PAASIVIRTA and H. KRIEGER. Suom. Kemistil. B, **38**, 182 (1965).
9. B. C. C. CANTELLO, J. M. MELLOR, and C. F. WEBB. J. Chem. Soc. Perkin Trans. 2, 22 (1974).
10. K. E. HAMLIN and A. W. WESTON. Org. React. **9**, 1 (1957).
11. D. A. EVANS, W. L. SCOTT, and L. K. TRUESDALE. Tetrahedron Lett. 121 (1972).
12. H. KRIEGER. Suom. Kemistil. B, **36**, 68 (1963).
13. H. C. BROWN and J. MUZZIO. J. Am. Chem. Soc. **88**, 2811 (1966).
14. J. E. MCMURRY and M. SILVESTRI. J. Org. Chem. **40**, 1502 (1975).
15. T. FUJISAWA, T. KOHORI, A. FUKUSHIMA, and K. SAKAI. Jpn.

[7] The time required for complete reaction is greatly dependent on the efficiency of stirring.

Patent, Kokai Tokkyo Koho, No. 79 41,859 (1979); Chem. Abstr. **91**, 57226m (1979).
16. C. F. LANE. J. Org. Chem. **39**, 1437 (1974).
17. W. C. BAIRD, JR. and J. H. SURRIDGE. J. Org. Chem. **37**, 304 (1972); **37**, 1182 (1972).
18. N. RABJOHN. Org. React. **24**, 261 (1976).
19. J. MEINWALD, P. G. GASSMAN, and J. J. HURST. J. Am. Chem. Soc. **84**, 3722 (1962).
20. P. YATES, F. X. GARNEAU, and G. F. HAMBLY. Pol. J. Chem. **53**, 163 (1979).
21. J. PAASIVIRTA and R. KUUSISTO. Suom. Kemistil. B, **40**, 291 (1967).
22. L. M. JACKMAN and S. STERNHELL. Applications of nuclear magnetic resonance spectroscopy in organic chemistry. 2nd ed. Pergamon Press, Oxford. 1969. p. 88.
23. P. YATES and G. F. HAMBLY. Can. J. Chem. **57**, 1656 (1979).
24. R. J. CRAWFORD. Ph.D. Thesis, University of Toronto, 1965.
25. P. YATES, B. L. SHAPIRO, N. YODA, and J. FUGGER. J. Am. Chem. Soc. **79**, 5756 (1957).
26. P. P. GALIFFI. M.Sc. Thesis, University of Toronto, 1970; J. D. FENWICK. Ph.D. Thesis, University of Toronto. 1970.
27. J. B. GRUTZNER, M. JAUTELAT, J. B. DEUCE, R. A. SMITH, and J. D. ROBERTS. J. Am. Chem. Soc. **92**, 7107 (1970).
28. S. H. GROVER and J. B. STOTHERS. Can. J. Chem. **52**, 870 (1974).
29. J. B. STOTHERS, C. T. TAN, and K. C. TEO. Can. J. Chem. **51**, 2893 (1973).
30. H. BEIERBECK and J. K. SAUNDERS. Can. J. Chem. **54**, 2985 (1976).
31. W. A. AYER, L. M. BROWNE, S. FUNG, and J. B. STOTHERS. Can. J. Chem. **54**, 3273 (1976).
32. S. H. GROVER, J. P. GUTHRIE, J. B. STOTHERS, and C. T. TAN. J. Magn. Reson. **10**, 227 (1973).
33. J. B. STOTHERS, C. T. TAN, and K. C. TEO. Can. J. Chem. **54**, 1211 (1976).
34. J. G. BATCHELOR. J. Magn. Reson. **18**, 212 (1975).
35. H. BEIERBECK, J. K. SAUNDERS, and J. W. APSIMON. Can. J. Chem. **55**, 2813 (1977).
36. J. B. STOTHERS, J. R. SWENSON, and C. T. TAN. Can. J. Chem. **53**, 581 (1975).
37. G. E. LANGFORD, H. AUKSI, J. A. GOSBEE, F. N. MACLACHLAN, and P. YATES. Tetrahedron, **37**, 1091 (1981).
38. D. G. MORRIS and A. M. MURRAY. J. Chem. Soc. Perkin Trans. 2, 1579 (1976).
39. J. FIRL, W. RUNGE, and W. HARTMANN. Angew. Chem. Int. Ed. Engl. **13**, 270 (1974).
40. G. E. HAWKES, K. HERWIG, and J. D. ROBERTS. J. Org. Chem. **39**, 1017 (1974); N. H. WERSTIUK, R. TAILLEFER, R. A. BELL, and B. SAYER. Can. J. Chem. **51**, 3010 (1973); D. P. KELLY and H. C. BROWN. J. Am. Chem. Soc. **97**, 3897 (1975); E. LIPPMAA, T. PEHK, and J. PAASIVIRTA. Org. Magn. Reson. **5**, 277 (1973).
41. N. K. WILSON and J. B. STOTHERS. *In* Topics in stereochemistry. Vol. 8. *Edited by* E. L. Eliel and N. L. Allinger. Wiley–Interscience, New York. 1974.
42. K. ALDER, H. K. SCHAFER, H. ESSER, H. KRIEGER, and R. REUBKE. Justus Liebigs Ann. Chem. **593**, 23 (1955).
43. N. FREIESLEBEN. Ger. Patent No. 1,146,050 (1963); Chem. Abstr. **59**, 9914 (1963).
44. E. C. WAGNER and W. C. HUNT. J. Chem. Educ. **28**, 309 (1951).
45. G. I. POOS, M. M. LEHMAN, E. B. LANDIS, and J. D. ROSENEAU. J. Med. Chem. **5**, 883 (1962).

Can. J. Chem. Downloaded from www.nrcresearchpress.com by 210.87.254.5 on 09/06/12
For personal use only.

An improved synthesis of *m*-diazirinophenol

PIERRE LEBLANC AND GERHARD E. GERBER
Department of Biochemistry, McMaster University, Hamilton, Ont., Canada L8N 3Z5

Received July 27, 1983[1]

PIERRE LEBLANC and GERHARD E. GERBER. Can. J. Chem. **62**, 1767 (1984).

The published synthesis of phenolic diazirine was shown to result in products which were chlorinated during the hypochlorite oxidation while the desired unchlorinated product was lost during the usual work-up. A superior synthesis is described: inclusion of pyridine during the oxidation step prevents the chlorination; the desired volatile diazirine was isolated in good yield using silica gel and reverse phase high pressure liquid chromatography.

PIERRE LEBLANC et GERHARD E. GERBER. Can. J. Chem. **62**, 1767 (1984).

On a démontré que la méthode proposée dans la littérature pour la préparation de diazirine phénolique conduit d'une part, à la formation de produits qui ont été chlorés au cours de l'oxydation par l'hypochlorite alors que d'autre part, le produit non chloré désiré est perdu lors de la purification par les méthodes usuelles. On propose une synthèse supérieure qui implique l'inclusion de pyridine au cours de l'étape d'oxydation afin de prévenir la chloration; on a isole la diazirine volatile désirée avec de bons rendements en faisant appel à des chromatographies liquide à haute pression avec phase inversée et sur gel de silice.

[Traduit par le journal]

Can. J. Chem. Downloaded from www.nrcresearchpress.com by 210.87.254.40 on 09/06/12
For personal use only.

Introduction

The phenolic diazirine group was introduced (1) as a potential photoactivable biological probe and has been incorporated into a number of biological systems (2–6). It has recently been attached to the ω-position in a series of tritiated fatty acids and these have been used to identify integral membrane proteins (6, 7) and to characterize the regions of such proteins which are buried within the hydrocarbon region of the bilayer (7). Further, we have shown that these fatty acid analogues can be biologically attached to the recently discovered (8, 9) membrane proteins which are normally acylated by fatty acids. These fatty acids thus afford photoaffinity derivatives of such membrane proteins (6, 7). Consequently, the *m*-diazirinophenolic group has a wide range of biological applications.

In the course of our synthesis of this probe by the published procedures (1, 6), we found that the yield of the desired diazirine was very low and that the products obtained were mostly chlorinated isomers. It had been suggested earlier (10) that removal of HCl generated during hypochlorite oxidations prevents the formation of chlorine and thus avoids chlorination. We therefore report a superior synthesis of the *m*-diazirinophenol, using pyridine to remove the generated HCl as the pyridinium hydrochloride salt.

Experimental

General

Dimethyl formamide (DMF) and methanol were hplc grade. The petroleum ether fraction used was the one boiling between 30–60°C. All other solvents used were reagent grade. Technical grades of both *m*-hydroxybenzaldehyde and chloromethyl methyl ether were purchased from Aldrich. *tert*-Butyl hypochlorite was freshly prepared and assayed as described (11). Thin layer chromatography (tlc) was carried out on silica gel using the following solvent systems: system A, diethyl ether – petroleum ether 1:1 (v/v); system B, diethyl ether – petroleum ether 1:4 (v/v). Elemental analyses were performed by Galbraith Laboratories, Knoxville.

Methoxymethylene ether of m-*hydroxy benzaldehyde (2)*

The *m*-hydroxy benzaldehyde (0.50 mol) was reacted at 0°C with 1.1 equivalent of sodium hydride in suspension in DMF. When the evolution of H_2 had stopped, an excess (0.55 mol) of chloromethyl methyl ether was added dropwise. The mixture was stirred at 0°C for 2 h and the resulting methoxymethylene ether obtained by vacuum distillation (62 g; 75%); bp 125–127°C at 4 Torr (1 Torr = 133.3 Pa); tlc: R_f 0.44 in system A; nmr δ (TMS): 3.23 (s, 3H, CH_3—O—), 4.97 (s, 2H, —O—CH_2—O—), 6.87–7.27 (m, 4H, aromatic), 9.53 (s, 1H, —C(=O)—H).

*1,3,5-Tri-(*m-*methoxymethylene phenyl ether)-2,4,6-triazabicyclo-[3.1.0]hexane (4)*

Chloramine was prepared by the cautious addition of *tert*-butyl hypochlorite (0.33 mol) to 10 *N* methanolic ammonia (280 mL) in a flask cooled by Dry Ice. The *m*-methoxymethylene benzaldehyde (**2**, 50 g) was added and the solution allowed to warm to room temperature during a reaction time of 36 h. The ammonia was allowed to evaporate and the solvent was removed by rotary evaporation under reduced pressure. The oily product was used directly without further characterization.

*Synthesis of 3-(*m-*methoxymethylene ether phenyl)-3*H*-diazirine in the absence of pyridine*

The triazabicyclohexane (**4**) prepared as described above starting with 30 g (0.18 mol) of the benzaldehyde (**2**) was an oily residue which was immediately dissolved in 40 mL of methanol and brought to 0°C. A solution of *tert*-butyl hypochlorite (0.09 mol) in *tert*-butyl alcohol (16 mL) was added dropwise and the reaction allowed to proceed for 2 h. Aliquots of the mixture were analyzed on hplc using a μ Bondapak C_{18} column with a solvent system consisting of 65% methanol–water. The mixture was poured into 1 L of a 10% solution of sodium metabisulfite and extracted 4 times with an equal volume of petroleum ether. The extracts were combined, subjected to silica gel chromatography using petroleum ether, and the fractions having absorbance at 360 nm were pooled. Evaporation of the ether afforded a yellow–green oil (1.95 g). The hplc analysis described in Fig. 2(a) identified products **5***a*, **5***b*, **5***c*, and **5***d* having retention times of 7.7, 11.5, 14.4, and 17.5 min respectively. Each of these components was obtained in pure form by preparative hplc on a μ Bondapak C_{18} column isocratically eluted with 55% methanol in water.

The peak eluting at 7.7 min (product **5***a*) was the desired diazirine (240 mg; 2%); ν_{max} (neat): 2930, 2860, 1605, 1580, 1490, 1450, 1400, 1350, 1320, 1278, 1250, 1210, 1150, 1080, 1030, 1000, 990, 920, 870, 770, 690 cm^{-1}; vis (cyclohexane), λ_{max}: 358 nm (ε 360); nmr δ (TMS): 1.98 (s, 1H, 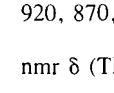), 3.38 (s, 3H, CH_3—O—), 5.03 (s, 2H, —O—CH_2—O—), 6.37–6.53 (m, 2H, aromatic),

[1]Revision received March 12, 1984.

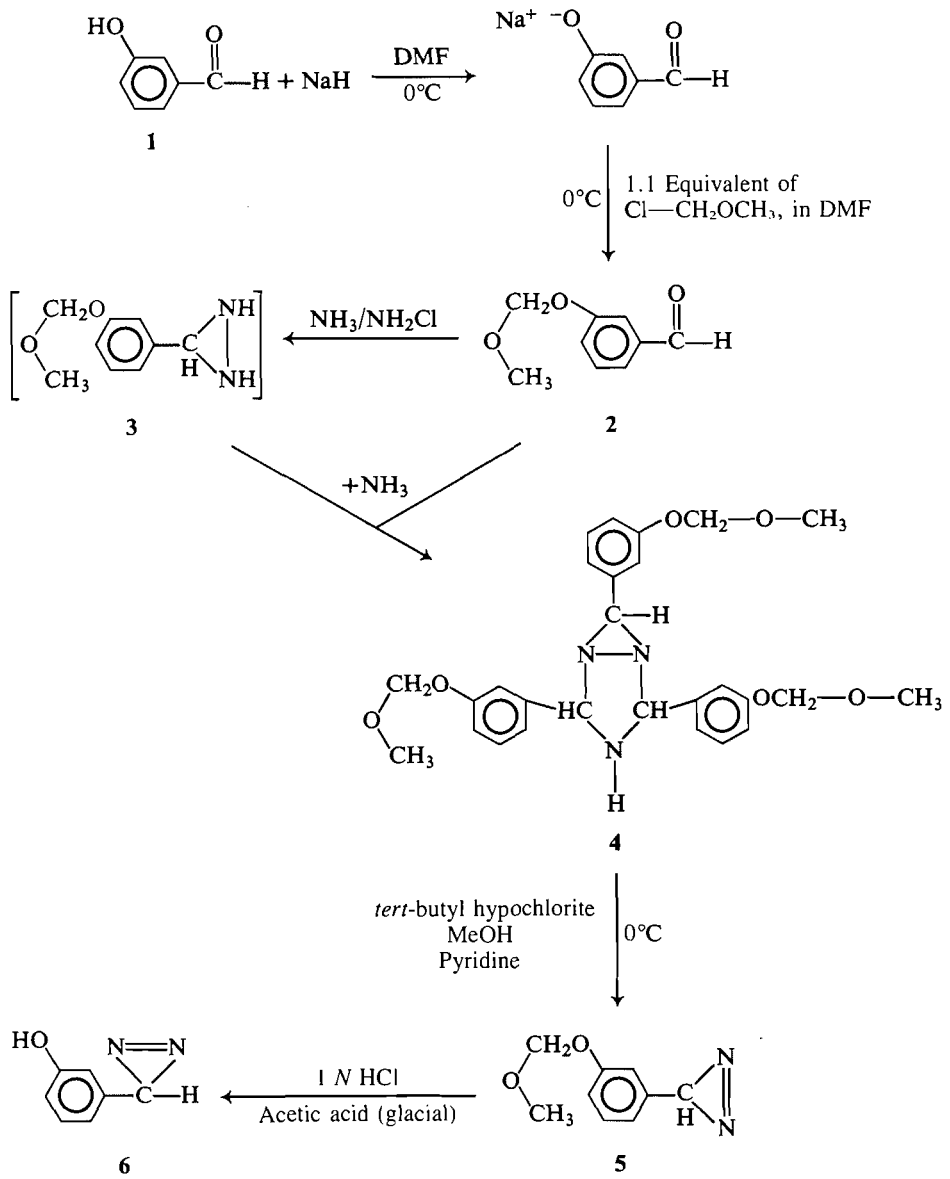

FIG. 1. Scheme for the synthesis of *m*-diazirinophenol.

6.83–7.23 (m, 2H, aromatic).

The peak observed on hplc, at 11.5 min (product **5***b*) was recovered as an oil (560 mg; 4.4%) and shown to be a chlorinated product; ν_{max} (neat): 2960, 2830, 1620, 1600, 1580, 1489, 1430, 1400, 1347, 1290, 1250, 1210, 1175, 1150, 1085, 1050, 1010, 980, 920, 815, 780, 750, 725, 625 cm^{-1}; vis (cyclohexane), λ max: 358 (ε 350); nmr δ (TMS): 2.03 (s, 1H, 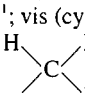), 3.52 (s, 3H, CH_3—O—), 5.20 (s, 2H, —O—CH_2—O—), 6.44 (dd, 1H, J_{ortho} = 8.2 Hz, J_{meta} = 2.0 Hz, aromatic), 6.75 (d, 1H, J_{meta} = 2.0 Hz, aromatic), 7.29 (d, 1H, J_{ortho} = 8.2 Hz, aromatic). *Anal.* calcd. for $C_9H_9N_2ClO_2$: C 50.83, H 4.27, N 13.17, Cl 16.67, O 15.05; found: C 51.27, H 4.70, N 11.20, Cl 17.78, O 14.86.

The peak eluting from hplc at 14.4 min (product **5***c*) was recovered as an oil (270 mg; 2.1%) and shown to be a chlorinated product; nmr δ (TMS): 2.54 (s, 1H, 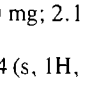), 3.50 (s, 3H, CH_3—O—), 5.24 (s, 2H, —O—CH_2—O—), 6.79 (dd, 1H, J_{ortho} = 6.8 Hz, J_{meta} = 2.5 Hz, aromatic), 7.06 (m, 2H, J_{ortho} = 6.8 Hz, J_{ortho} = 8.3 Hz, J_{meta} = 2.5 Hz, aromatic).

The peak observed on hplc at 17.5 min (product **5***d*) was recovered as an oil (700 mg; 5.5%) and shown to be a chlorinated product; ν_{max} (neat): 2930, 2860, 2830, 1620, 1600, 1571, 1475, 1425, 1400, 1345, 1305, 1278, 1238, 1210, 1170, 1150, 1140, 1080, 1060, 1010, 920, 870, 810, 640 cm^{-1}; vis (cyclohexane), λ_{max}: 358 (ε 289); nmr δ (TMS): 2.45 (s, 1H, 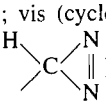), 3.39 (s, 3H, CH_3—O—), 5.02 (s, 2H, —O—CH_2—O—), 5.90 (d, 1H, J_{meta} = 2.9 Hz, aromatic), 6.88 (dd, 1H, J_{ortho} = 8.8 Hz, J_{meta} = 2.9 Hz, aromatic), 7.25 (d, 1H, J_{ortho} = 8.8 Hz, aromatic). *Anal.* calcd. for $C_9H_9N_2ClO_2$: C 50.83, H 4.27, N 13.17, Cl 16.67, O 15.05; found: C 51.86, H 4.86, N 11.25, Cl 17.05, O 15.27.

*Synthesis of 3-(*m*-methoxymethylene ether phenyl)-3*H*-diazirine in the presence of pyridine*

The triazabicyclohexane (**4**), prepared as described above starting with 50 g (0.33 mol) of the benzaldehyde (**2**) was dissolved in 60 mL of methanol and brought to 0°C. After addition of pyridine (0.51 mol), *tert*-butyl hypochlorite (0.17 mol in 20.0 mL of *tert*-butyl alcohol) was added dropwise over a period of 10 min. The reaction was allowed to proceed for 2 h. The mixture was then processed as described above

Can. J. Chem. Downloaded from www.nrcresearchpress.com by 210.87.254.40 on 09/06/12
For personal use only.

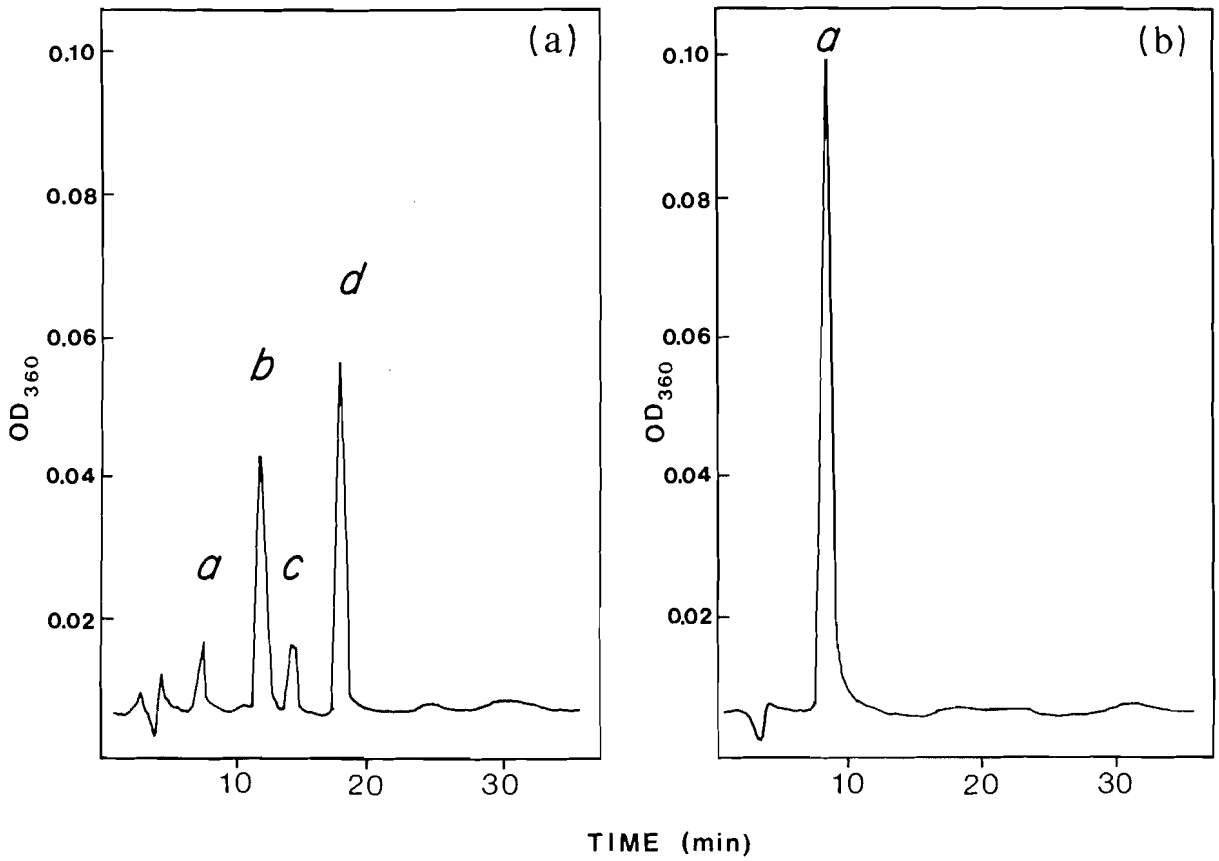

FIG. 2. High pressure liquid chromatographic analyses of the oxidation products (**5**) in the absence (a) and the presence (b) of pyridine. The reaction conditions were as described in the experimental section for the oxidation of the triazabicyclohexane. An aliquot (10 μL) of the reaction mixture was injected after 45 min, on a C_{18} reverse-phase hplc column using 65% methanol in water as an eluting solvent. The eluates were monitored using an ISCO detector equipped with a 340–365 nm filter.

Can. J. Chem. Downloaded from www.nrcresearchpress.com by 210.87.254.40 on 09/06/12
For personal use only.

for the oxidation of the triazabicyclohexane (**4**) in the absence of pyridine. Final purification was achieved by preparative hplc on a μ Bondapak C_{18} column using 55% methanol–water as solvent. After extraction into diethyl ether and drying, a pale yellow–green oil was obtained (4.30 g; 24%); tlc: R_f 0.35 in system B; ν_{max} (neat): 2930, 2860, 1605, 1580, 1490, 1450, 1400, 1350, 1320, 1278, 1250, 1210, 1150, 1080, 1030, 1000, 990, 920, 870, 770, 690 cm^{-1}; vis (cyclohexane), λ_{max}: 358 nm (ε 360); nmr δ (TMS): 1.98 (s, 1H, 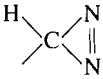), 3.38 (s, 3H, CH_3—O—), 5.03 (s, 2H, —O—CH_2—O—), 6.37–6.53 (m, 2H, aromatic), 6.83–7.23 (m, 2H, aromatic). *Anal.* calcd. for $C_9H_{10}N_2O_2$: C 61.01, H 5.12, N 15.81, O 18.06; found: C 61.25, H 6.46, N 14.45, O 17.82, Cl none.

m-*Diazirinophenol* (*6*a)

The procedure was adapted from the one described (2). The dry diazirine (*5a*) (17 mmol) was dissolved in glacial acetic acid (51 mL); 1 *N* aqueous HCl (9.58 mL) was added and allowed to react for 2 h. The mixture was then transferred to 1.8 L of 1 *N* sodium bicarbonate and the crude *m*-diazirinophenol isolated by extraction into diethyl ether. The pure *m*-diazirinophenol generated was isolated by column chromatography on silica gel using petroleum ether and diethyl ether (95:5, v/v), followed by preparative hplc using an isocratic solvent system (25% methanol in water). The resulting unchlorinated phenolic diazirine was obtained as an oil (3.0 g, 90% yield); vis (cyclohexane), λ_{max}: 358 nm (ε 360); nmr δ (TMS): 1.98 (s, 1H, 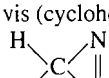), 5.47 (s, broad, 1H, arom-OH), 6.32 (dd, 1H, J_{meta} = 1.6 Hz, J_{meta} = 2.6 Hz, aromatic), 6.49 (ddd, 1H, J_{ortho} = 7.7 Hz, J_{meta} = 1.0 Hz, J_{meta} = 1.7 Hz, aromatic), 6.76 (ddd, 1H, J_{ortho} = 8.1 Hz, J_{meta} = 1.0 Hz, J_{meta} = 2.6 Hz, aromatic), 7.16 (t, 1H, J_{ortho} = 7.9 Hz, aromatic). *Anal.* calcd. for $C_7H_6N_2O$: C 62.88, H 4.51, N 20.88, O 11.93; found: C 61.98, H 4.36, N 16.40, O 13.13, Cl none.

Results and discussion

Our synthetic approach closely resembles that of Smith and Knowles (1) in that we form the triazabicyclohexane intermediate (**4**) prior to oxidative cleavage via *tert*-butyl hypochlorite (Fig. 1). Attempts at improving the yield of (*5a*) by other oxidation methods failed to produce a significant yield of the diazirine with *para*-substituted arylbicyclohexanes (1). The yields of the isolated *m*-diazirinophenol were typically in the range of 2–5% after oxidation of the triazabicyclohexane. We therefore studied the oxidation using hplc and the characteristic absorption at 360 nm of the diazirine to monitor the reaction, as shown in Fig. 2. The standard oxidation conditions resulted in a number of products as shown in Fig. 2(a). These products were isolated by preparative hplc and their nmr and vis spectra were determined. The small peak eluting at 7.7 min (Fig. 2(a)) contained product *5a* and had the nmr and vis characteristics expected for the desired diazirine. The products *5b*, *5c*, and *5d*, eluted at 11.5, 14.5, and 17.5 min respectively, had similar uv–vis spectra; however, their nmr spectra indicated the loss of an aromatic proton (3H aromatic for products *5b*, *5c*, and *5d*). Elemental analysis of these products was complicated by the fact that they were light- and heat-sensitive oils; however, the results unequivocally showed that these were all isomeric

TABLE 1. ^{1}H nuclear magnetic resonance shifts (δ ppm) of the chlorinated and unchlorinated diazirines

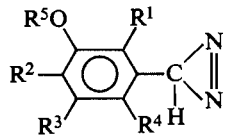

Compounds	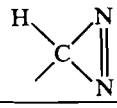	R^5		Aromatic protons			
		CH_3—O—CH_2—	H	R^1	R^2	R^3	R^4
*5*a*	1.98	3.38 s, 3H 5.03 s, 2H	—	6.37– 7.23 (4H, m)	6.37– 7.23 (4H, m)	6.37– 7.23 (4H, m)	6.37– 7.23 (4H, m)
5*b*	2.02	3.51 s, 3H 5.22 s, 2H	—	6.75 d (J_m = 2.0)	Cl	7.29 d (J_o = 8.2)	6.44 dd (J_o = 8.2, J_m = 2.0)
5*c*	2.54	3.53 s, 3H 5.26 s, 2H	—	Cl	7.12 dd (J_o = 6.9, J_m = 2.5)	7.09 dd (J_o = 6.9, 8.3)	5.93 dd (J_o = 6.8, J_m = 2.5)
5*d*	2.45	3.39 s, 3H 5.02 s, 2H	—	5.90 d (J_m = 2.9)	6.88 dd (J_o = 8.8, J_m = 2.9)	7.25 d (J_o = 8.8)	Cl
†6*a*	1.98	—	5.42	6.32 dd (J_m = 1.6, J_m = 2.6)	6.49 ddd (J_o = 7.7, J_m = 1.0, J_m = 2.6)	7.16 t (J_o = 7.9)	6.76 ddd (J_o = 8.1, J_m = 1.0, J_m = 2.6)

*5*a*, *b*, *c*, and *d* are products from oxidation in absence of pyridine.
†6*a* is derived from oxidation in presence of pyridine.

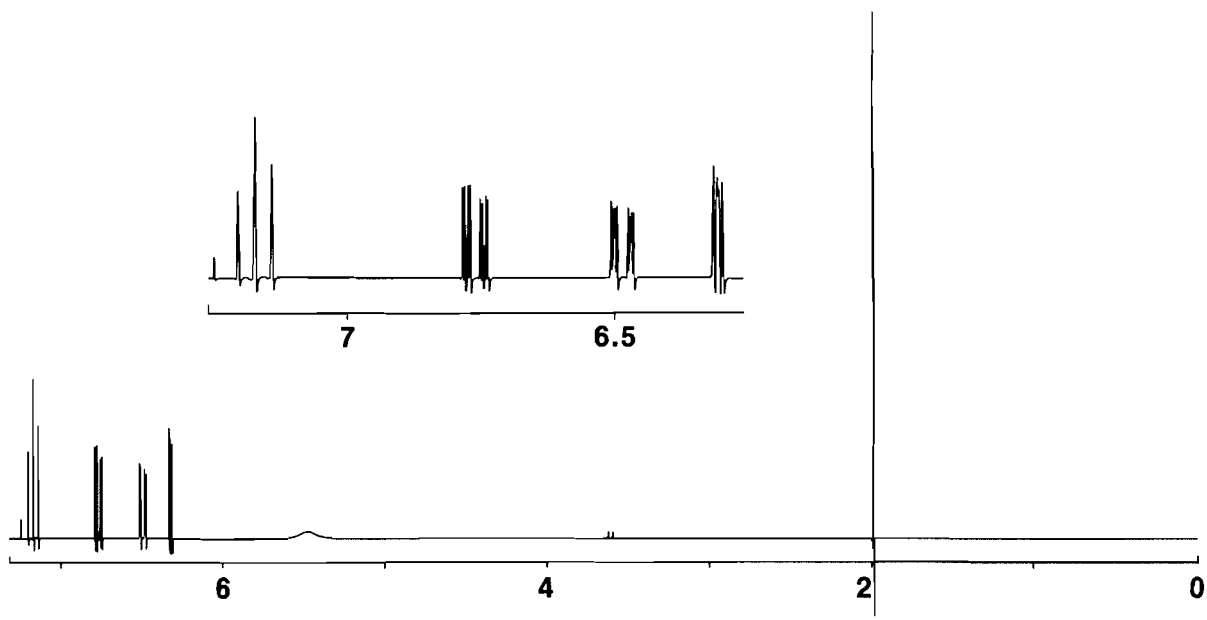

FIG. 3. The ^{1}H nmr spectrum ($CDCl_3$) of the unchlorinated *m*-diazirinophenol **6***a*.

forms of monochlorinated *m*-diazirinophenol.

Analysis of the nmr spectra using high resolution (250 MHz) nmr and spin decoupling indicated that products **5***b*, **5***c*, and **5***d* were chlorinated on the phenyl ring in positions R^2, R^1, and R^4 respectively (Table 1). It is of particular interest to note that chlorination in positions R^1 or R^4 (products **5***c* and **5***d* respectively) has a dramatic effect on the position of the adjacent diazirine proton while chlorination in position R^2 (product **5***b*) leaves this proton relatively unaffected compared to the unchlorinated compound. Furthermore the position of the *meta* proton at R^4 (when R^1 is chlorinated) or R^1 (when R^4 is chlorinated) is shifted to higher field, while the position of the proton at R^2 is shifted to lower field under these conditions. Detailed analysis of the nmr spectra of the chlorinated products enabled us to assign the position of the aromatic protons of the pure *m*-diazirinophenol (**6***a*) (see Fig. 3 for the nmr spectrum).

It was concluded that this chlorination was the result of the generation of Cl_2 during the hypochlorite oxidation. The formation of the diaziridine (**3**) generates HCl which is oxidized to Cl_2 by the hypochlorite, as had been suggested earlier (10). The pyridine traps the hydrochloric acid as the pyridinium hydrochloride salt and consequently avoids chlorination of the desired product. When the oxidation was performed in the presence of pyridine, the only diazirine-containing product

Can. J. Chem. Downloaded from www.nrcresearchpress.com by 210.87.254.40 on 09/06/12
For personal use only.

formed was eluted in the region of the desired material on hplc, as shown in Fig. 2(b); the chlorinated products **5***b*, **5***c*, and **5***d* normally eluted at 11.5, 14.5, and 17.5 min respectively were entirely absent. The pyridine thus prevented the formation of undesired products and the yield of the desired phenyldiazirine (**5***a*) was greatly improved. Removal of the methoxy methylene group afforded the pure *m*-diazirinophenol (**6***a*).

It should also be noted that the isolated yield of the unchlorinated diazirine was affected by the work-up, since it was found to be volatile while the chlorinated isomers were not. Purification by fractional distillation was avoided due to the potentially explosive properties of the diazirine; the desired pure diazirine was therefore obtained by preparative hplc, extraction into diethyl ether, and drying under nitrogen. This procedure resulted in isolated yields of 24 to 30% of the desired diazirine.

It is interesting to note that in the unchlorinated *m*-diazirinophenol, the diazirine proton is observed at δ 1.98 while the position previously reported (6) was at δ 2.4. The compound actually reported in the literature therefore likely corresponded to the major chlorinated isomer (product **5***d*, Table 1). Our previous studies used the unchlorinated *m*-diazirinophenol isolated by hplc from the crude product obtained in the absence of pyridine (5). We have shown that fatty acid analogues synthesized using this diazirine are readily incorporated into phospholipids and proteins of mammalian cells in culture (5, 7). The failure of others (12) to observe biosynthetic utilization of these fatty acids may thus be due to their use of a chlorinated isomer. In order to use these probes for biological experiments it is clearly important to avoid the chlorination.

Acknowledgements

We thank Dr. D. W. Hughes for the high resolution nmr spectroscopy. This investigation was supported by grants to G. E. Gerber by the Medical Research Council of Canada. G. E. Gerber is a MRC Scholar. P. Leblanc holds an Ontario Graduate Scholarship.

1. R. A. G. SMITH and J. R. KNOWLES. J. Chem. Soc. Perkin Trans. **2**, 686 (1975).
2. C. M. GUPTA, R. RADHAKRISHNAN, G. E. GERBER, W. L. OLSEN, S. C. QUAY, and H. G. KHORANA. Proc. Natl. Acad. Sci. U.S.A. **76**, 2595 (1979).
3. H. BAYLEY and J. R. KNOWLES. Biochemistry, **17**, 2414 (1978).
4. J. BRUNNER, H. SENN, and F. M. RICHARDS. J. Biol. Chem. **255**, 3313 (1980).
5. P. LEBLANC, J. CAPONE, and G. E. GERBER. J. Biol. Chem. **257**, 14586 (1982).
6. C. M. GUPTA, R. RADHAKRISHNAN, and H. G. KHORANA. Proc. Natl. Acad. Sci. U.S.A. **74**, 4315 (1977).
7. J. CAPONE, P. LEBLANC, G. E. GERBER, and H. P. GHOSH. J. Biol. Chem. **258**, 1395 (1983).
8. M. F. G. SCHMIDT, M. BRACHA, and M. J. SCHLESINGER. Proc. Natl. Acad. Sci. U.S.A. **76**, 1687 (1979).
9. M. J. SCHLESINGER, A. I. MAGEE, and M. F. G. SCHMIDT. J. Biol. Chem. **255**, 10021 (1980).
10. C. A. GROB and H. J. SCHMID. Helv. Chim. Acta, **36**, 1763 (1953).
11. M. J. MINTZ and C. WALLING. Org. Synth. **49**, 9 (1969).
12. W. L. OLSEN, M. SCHAECHTER, and H. G. KHORANA. J. Bacteriol. **137**, 1443 (1979).

Can. J. Chem. Downloaded from www.nrcresearchpress.com by 210.87.254.40 on 09/06/12
For personal use only.

Polarographic redox potentials of diazotized polycyclic aromatic amines and the absolute electrode potentials[1]

RICHARD M. ELOFSON, FAHMI F. GADALLAH, KARLO F. SCHULZ, AND JAMES K. LAIDLER
Alberta Research Council, 11315 – 87 Avenue, Edmonton, Alta., Canada T6G 2C2

Received December 20, 1983

RICHARD M. ELOFSON, FAHMI F. GADALLAH, KARLO F. SCHULZ, and JAMES K. LAIDLER. Can. J. Chem. **62**, 1772 (1984).

The half-wave potentials ($E_{1/2}$) of polycyclic diazonium salts as well as those of the parent hydrocarbons, the corresponding aldehydes, and the nitro compounds, when plotted against the coefficient of the energy of either the lowest vacant orbital $-m_{m-1}$ or the coefficient of the highest occupied orbital $+m_m$ of the parent hydrocarbon tend toward the midpoint potential, E_m, equal to −0.31 V vs. sce as established by Parker. The polarographic results are correlated with ^{13}C nmr results with comments on solvation energies.

RICHARD M. ELOFSON, FAHMI F. GADALLAH, KARLO F. SCHULZ et JAMES K. LAIDLER. Can. J. Chem. **62**, 1772 (1984).

On a dressé un graphique mettant en opposition d'une part les potentiels à demi-vague ($E_{1/2}$) de sels de diazonium de dérivés polycycliques, de leurs hydrocarbures, des aldéhydes et des dérivés nitro correspondants et d'autre part le coefficient de l'énergie soit de l'orbitale basse vacante ($-m_{m-1}$) ou le coefficient de l'orbitale haute occupée ($+m_m$) de l'hydrocarbure de base. Ces courbes tendent vers un potentiel à mi-point, E_m, qui est égal à −0,31 V vs. sce tel qu'établi par Parker. On peut établir une corrélation entre les résultats polarographiques et les résultats de rmn du ^{13}C qui reflète sur les énergies de solvatation.

[Traduit par le journal]

Introduction

In 1969, we reported the results of our work on the effect of substituents on the half-wave reduction potentials of aryl diazonium tetrafluoroborates in the aprotic solvent sulfolane (1). These results produced a good Hammett plot [1]. Only one reversible, one electron-reduction wave was observed.

[1] $E_{1/2} = (0.229\sigma + 0.314)$ V vs. sce

These findings led to electrochemical techniques for arylations (2) and Pschorr reactions (3). The positive reduction potentials agree well with the strong electrophilicity of diazotized aromatic amines (4).

These studies have now been extended to include a number of diazotized polycyclic aromatic amines. The results are discussed in terms of the absolute scale of electrode potentials suggested by Parker (5), and by the molecular orbital theory.

Experimental

Experimental conditions were those previously described (1). However, a new polarograph (Princeton Applied Research Model 170) operating in the three electrode configuration was used. The diazonium salts were prepared from the corresponding amines by diazotization in dilute sulfuric acid. The diazotized amines were precipitated as the tetrafluoroborate salts and recrystallized repeatedly from dry methanol–ether mixtures. Because halide ions form complexes with diazonium cations at the mercury surface (a subsequent paper will elaborate on the nature of these complexes), halide ions must be rigourously excluded if meaningful results are to be obtained.

^{13}C nmr spectra were obtained using a Bruker WP80 spectrometer operating at 20.1 MHz. The corresponding amines were diazotized in the usual manner and, because of solubility considerations, converted to chloride salts which were examined in a 20% D_2O/H_2O mixture. The chemical shifts were established based on a measured chemical shift for methanol of 50.498 ppm at 5°C in a mixture of methanol in $CDCl_3$ and TMS. A spectra reference number based on methanol in 20% D_2O in H_2O was then established. The results were within 1 ppm for comparable compounds in the previous study (16).

Results

The half-wave potentials obtained for nine polycyclic diazonium salts are presented in Table 1. Figure 1 includes the data from Table 1 and a selection of half-wave potentials of polycyclic hydrocarbons, aldehydes (6), and a few nitro compounds (Table 2). The half-wave potentials of the nitro derivatives were also determined in this laboratory.

The potentials are plotted against the coefficient of the lowest vacant orbital $-m_{m+1}$ or the coefficient of the highest occupied orbital $+m_m$ of the parent hydrocarbon. Correlations *VI* and *VII* are the oxidation potentials of these hydrocarbons as determined by Lund (7) and by Parker (5), respectively. As may be seen from Fig. 1, these plots tend toward Parker's midpoint potential E_m of −0.31 V vs. sce as the energy coefficient of the parent hydrocarbon tends toward zero.

TABLE 1. Half-wave potentials of aryldiazonium salts*

Parent compound	$-E_{1/2}$ vs. sce (V)
Aniline	0.295
4-Aminobiphenyl	0.275
1-Aminonaphthalene	0.260
2-Aminonaphthalene	0.260
1-Aminoanthracene	0.230
2-Aminoanthracene	0.235
9-Aminoanthracene	0.240
2-Aminophenanthrene	0.230
3-Aminophenanthrene	0.220
9-Aminophenanthrene	0.235

* 1.17×10^{-3} *M* in 0.4 *M* tetrabutylammonium perchlorate in sulfolane.

TABLE 2. Half-wave potentials of selected nitro compounds

Compound	$-E_{1/2}$ vs. sce (V)
Nitrobenzene	1.070
1-Nitronaphthalene	0.990
9-Nitroanthracene	0.905

[1] Alberta Research Council Contribution No. 1264.

Can. J. Chem. Downloaded from www.nrcresearchpress.com by 210.87.254.5 on 09/06/12
For personal use only.

Can. J. Chem. Downloaded from www.nrcresearchpress.com by 210.87.254.5 on 09/06/12
For personal use only.

Discussion

Working with a platinum electrode in acetonitrile, Parker found that for alternate aromatic hydrocarbons (AAH) $E_{1/2(red)} + E_{1/2(oxid)}$ is equal to -0.31 V vs. sce. This result was interpreted to indicate that the solvation energy of all the anions and cations of the series were the same. This can hardly be true for the series of aldehydes, nitro compounds, and diazonium salts as described in Fig. 1, which would be expected to obey the Born equation (8) [2] where the symbols

$$[2] \quad (\Delta G^0) = (1 - 1/D)\, Ne^2/2r_c$$

have the usual meaning and r_c is the mean effective radius of the ion. Since the degree of solvation is dependent on the mean diameter of the solute molecules, the solvation energy should be larger for smaller molecules. This fact would tend to increase either positive or negative slopes of the correlations in Fig. 1 to such an extent that all correlations might intersect at about -0.31 V vs. sce at the values of the energy coefficients equal to zero ($-m_{m+1}$ or $+m_m$ equals 0 for graphite by definition) if corrections could be made for solvation energies. In any event, these correlations lead us to support Parker's idea that the midpoint potential E_m is an important zero point against which to measure the energy change of an electrode reaction in organic systems. This is related to the "absolute" electrode potential as shown by Parker (5), where ϕ is the work function of graphite and equal to 4.39 V. This is shown in [3].

$$[3] \quad E_{absolute} = E_m - \phi$$

The first of the correlations in Fig. 1 was observed by Maccoll (9). He noted the linearity of the half-wave reduction potentials of polycyclic aromatic hydrocarbons plotted against the coefficient of the molecular orbital resonance integral in the expression for the lowest unoccupied orbital. This coefficient correlates with the maximum of the longest wave length electronic absorption spectra. In terms of the scale of Fig. 1, this became [4].

$$[4] \quad E_{1/2} = (2.368\, m_{m+1} - 0.924) \text{ V vs. sce}$$

This well-known correlation and prediction are to be expected of the classical formula proposed by Bamberger and by

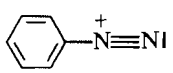

Hantzsch (10), for the reduction of aryldiazonium salts suggests that the slope of the plot for polycyclic diazonium salts should also be positive according to [5].

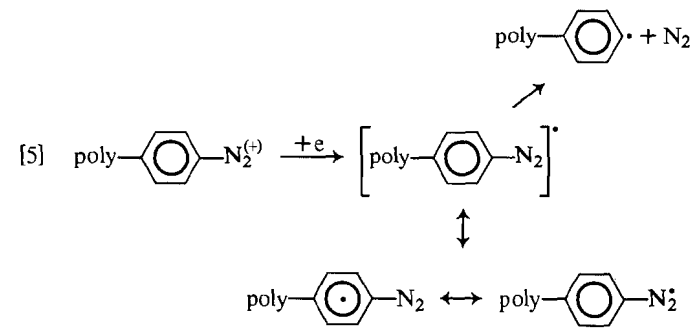

However, this is not the case. Instead, the equation for correlation V in Fig. 1 is [6].

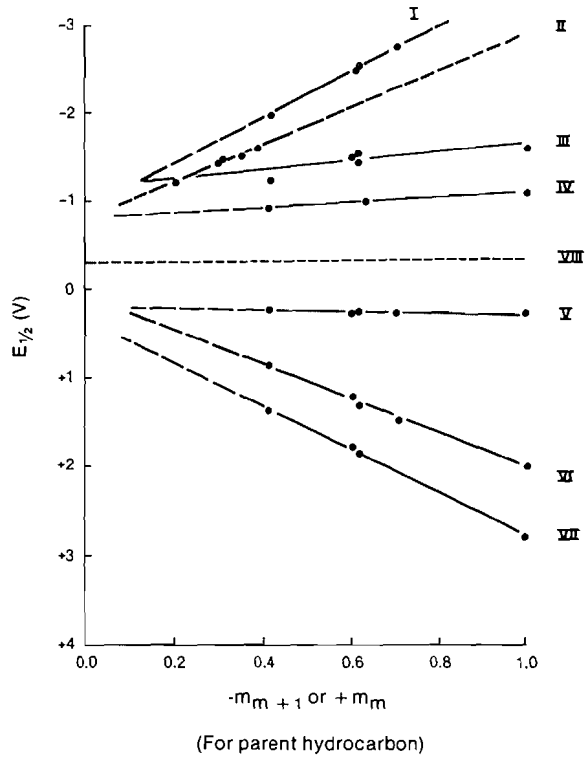

FIG. 1. *I*, $E_{1/2}$ vs. sce; polyArH $\xrightarrow{+e}$ polyArH($\dot{-}$) vs. $-m_{m+1}$ of parent hydrocarbon in aqueous dioxane, Hg electrode where applicable results agree with Parker, Pt electrode. *II*, $E_{1/2}$ vs. sce; polyArCHO $\xrightarrow{+e}$ vs. $-m_{m+1}$ of polyArCHO in 50% ethanol, Hg electrode. *III*, $E_{1/2}$ vs. sce; polyArCHO $\xrightarrow{+e}$ polyArCHO($\dot{-}$) vs. $-m_{m+1}$ of parent hydrocarbon in 50% ethanol, Hg electrode. *IV*, $E_{1/2}$ vs. sce; polyArNO$_2$ $\xrightarrow{+e}$ polyArNO$_2$($\dot{-}$) vs. $-m_{m+1}$ of parent hydrocarbon in sulfolane, Hg electrode. *V*, $E_{1/2}$ vs. sce; polyArN$_2^+$ $\xrightarrow{+e}$ polyArN$_2$(·) vs. $-m_{m+1}$ of parent hydrocarbon in sulfolane, Hg electrode. *VI*, $E_{1/2}$ vs. Ag$^+$; polyArH $\xrightarrow{-e}$ polyArH($\overset{+}{\cdot}$) vs. $-m_m$ of parent hydrocarbon in acetonitrile, Pt electrode (Lund). *VII*, $E_{1/2}$ vs. sce; polyArH $\xrightarrow{-e}$ polyArH($\overset{+}{\cdot}$) vs. $-m_m$ of parent hydrocarbon in acetonitrile, Pt electrode (Parker). *VIII*, E_m vs. sce; mid-point potential of aromatic hydrocarbons in acetonitrile (Parker).

$$[6] \quad E_{1/2} = (-0.105\, m_{m+1} + 0.215) \text{ V vs. sce}$$

A correction for solvation factors would tend to increase the negativity of the slope, thus, correlation V may be taken as either midway between *I* and *VII* or closer to *VII* if solvation effects are considered.

Accepting the fact that this electrochemical system is reversible, V could be written as:

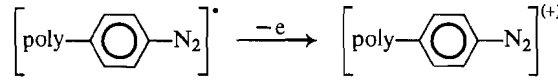

Va

and since the correlations *VI* or *VII* are written as oxidations for polyaromatics,

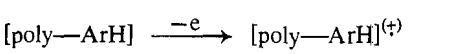

VI or *VII*

it seems reasonable that *VI* or *VII* might correlated with V. Alternatively, since polyaromatics are easier to oxidize than benzene, the reverse should follow, viz. the reduction of the highly oxidized benzene diazonium salt should release more energy (be more electrophilic) than polycyclic diazonium salts.

On the other hand, the reduction of aryldiazonium salts can be represented by [5], where correlation *I* should dominate. Combining *I* and *VI* or *VII*, the low negative slope of correlation *V* is not too surprising.

To further check the low slope of correlation *V*, ^{13}C nmr of a number of diazonium salts were determined. Many workers (11–15) have noted the shielding at the C_1 position of these salts increases when electron-donating groups are substituted in the ring, particularly in the *para* position. The results also correlate with σ or σ^+ and with $E_{1/2}$. This means that a decrease in the electrophilicity of a diazonium salt is due to increase in shielding at C_1. The relation between electrophilicity ($E_{1/2}$) and $^{13}C_1$ shielding (ppm) is shown in Table 3.

The equation for this correlation is given by:

$$[7] \quad E_{1/2} = (0.00650\delta - 0.452)\ \text{V}$$

with a correlation coefficient of 0.981. Or omitting *p*-phenyl from the correlation, the equation becomes

$$[7a] \quad E_{1/2} = (0.00665\delta - 0.467)\ \text{V}$$

These results indicate that the observed small negative slope of *V* is real.

In a recent study of *p*-substituted benzene diazonium salts (16), the equation was given by the relation

$$[8] \quad E_{1/2} = (0.0161\delta - 1.52)\ \text{V}$$

with a correlation coefficient of 0.982, where δ is the $^{13}C_1$ chemical shifts in ppm from TMS.

If the solvation effects of *p*-substituted benzene diazonium salts are assumed to be equal because of similar geometry, the slope of correlation *V* could reasonably be increased 2.42 times, as predicted earlier, to correct for the increase in mean diameter of the polycyclic diazonium salts. Also the scatter in the values of 1- and 2-naphthalene diazonium salts, Table 3, agree with the assumption that the diazonium moiety in the 2 position might be more solvated than that in the 1 position due to steric considerations.

The representation of diazonium salts shown in the conventional canonical structures **A**, **B**, **C**, and **D** (11) should be discussed in terms of correlation *V*. $^{13}C_1$ chemical shift rules out structure **C** as a significant contribution to the ground state (16).

[9]

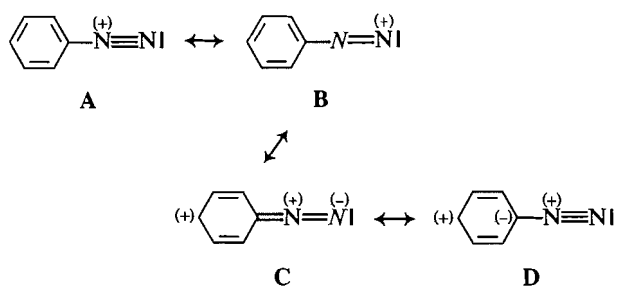

A **B** **C** **D**

Also X-ray (17) evidence rules out the same structure (18). Structure **D** (11), in particular, accounts for the increased magnetic shielding as the electophilicity of the cation decreases, and also agrees with the fact that electrochemical reduction of the cation in aprotic solvents results in a one-electron transfer to yield the aryl radical and nitrogen as the only products. In terms of energy requirements, the compressed C_1—C_4 (18, 19) distance of 2.680 Å for the benzenediazonium cation ($E_{1/2}$ = 0.295 V) shown by X-ray measurements compared to 2.795 Å units in benzene is probably less pronounced in polycyclic aryldiazonium salts. Hence the energy gained by the addition of an electron, which should relieve this compression, would be less for the polycyclic structures. A recent determination of the C_1—C_4 distance in *p*-diethylamino benzene diazonium hexafluorophosphate of 2.77 Å units with $E_{1/2}$ equal to −0.095 V makes this point rather dramatically (20).

TABLE 3. Half-wave potentials and chemical shifts $^{13}C_1$ nmr of aryldiazonium chlorides in 20% D_2O

Diazonium salt of	$^{13}C_1$ chemical shift (ppm)	$-E_{1/2}$ vs. sce (V)
Benzene	115.2	0.295
p-Phenylbenzene	111.0	0.275
2-Naphthyl	109.5	0.260
1-Naphthyl	108.1	0.260
2-Anthracene	105.6	0.235
1-Anthracene	105.6	0.230
9-Phenanthrene	105.9	0.235

One further observation gained from Fig. 1: as the substituent constant becomes more positive, the slope of the correlation decreases until it becomes negative for the substituent —N_2^+, which has the highest known constant, +1.88 (15). The negative slope, as discussed earlier, correlates with a buildup of negative charge or increase in electron density as indicated by increased magnetic shielding C_1. The apparent inability of this charge to dissipate by hybridization, as indicated by lack of the resonance structure **C** in the ground state, may account for many of the unusual properties of diazonium salts.

Acknowledgements

Thanks are due to Cheryl Goulet and Wendy Wade of our laboratories for the determination of the ^{13}C chemical shifts.

1. R. M. ELOFSON and F. F. GADALLAH. J. Org. Chem. **34**, 854 (1969).
2. F. F. GADALLAH and R. M. ELOFSON. J. Org. Chem. **34**, 3335 (1969); R. M. ELOFSON, F. F. GADALLAH, and K. F. SCHULZ. J. Org. Chem. **36**, 1526 (1971).
3. R. M. ELOFSON and F. F. GADALLAH. J. Org. Chem. **36**, 1769 (1971); F. F. GADALLAH, A. A. CANTU, and R. M. ELOFSON. J. Org. Chem. **38**, 2386 (1973).
4. R. M. ELOFSON, F. F. GADALLAH, A. A. CANTU, and K. F. SCHULZ. Can. J. Chem. **52**, 2430 (1974).
5. V. D. PARKER. J. Am. Chem. Soc. **96**, 5656 (1974); **98**, 98 (1976); V. D. PARKER and O. HAMMERICH. Acta Chem. Scand. B**31**, 883 (1977).
6. A. STREITWIESER. Molecular orbital theory for organic chemists. John Wiley and Sons. New York. 1961. Chapt. 7.
7. H. LUND. Acta Chem. Scand. **11**, 1323 (1957).
8. R. M. HEDGES and F. A. MATSEN. J. Chem. Phys. **28**, 950 (1958).
9. A. MACCOLL. Nature, **163**, 178 (1949).
10. H. ZOLLINGER. Azo and diazo chemistry, aliphatic and aromatic compounds. Interscience Publisher, Inc., New York. 1961. p. 39.
11. G. A. OLAH and J. L. GRANT. J. Am. Chem. Soc. **97**, 1546 (1975).
12. R. O. DUTHALER, H. G. FORSTER, and J. D. ROBERTS. J. Am. Chem. Soc. **100**, 4974 (1978).
13. S. H. KORZENIOWSKI, A. LEOPOLD, J. R. BEADLE, M. F. AHERN, W. A. SHEPPARD, R. K. KHANNA, and G. W. GOKEL. J. Org. Chem. **46**, 2153 (1981).
14. C. CASEWIT, J. D. ROBERTS, and R. A. BARTSCH. J. Org. Chem. **47**, 2875 (1982).

Can. J. Chem. Downloaded from www.nrcresearchpress.com by 210.87.254.5 on 09/06/12
For personal use only.

15. Y. A. USTYNYUK, O. A. SUBBOTIN, L. M. BUCHNEVA, V. N. GRUZDNEVA, and L. A. KAZITSYNA. Dokl. Akad. Nauk SSSR, **227**, 175 (1976). (Engl. Transl.)
16. R. M. ELOFSON, N. CYR, J. K. LAIDLER, K. F. SCHULZ, and F. F. GADALLAH. Can. J. Chem. **62**, 92 (1984).
17. CHR. ROMMING. Acta Chem. Scand. **17**, 1444 (1963).
18. M. CYGLER, M. PRZYBYLSKA, and R. M. ELOFSON. Can. J. Chem. **60**, 2852 (1982).
19. CHR. ROMMING. Acta Chem. Scand. **26**, 523 (1972).
20. M. PRZYBYLSKA, R. BALL, and R. M. ELOFSON. Private communication.

Can. J. Chem. Downloaded from www.nrcresearchpress.com by 210.87.254.5 on 09/06/12
For personal use only.

Spectrophotometric study of the dissociation of *p*-nitroanilinium ion in a binary aqueous-dipolar aprotic solvent system (H_2O + acetonitrile) at 25°C: effect of the solvent

A. L. DE[1] AND T. K. DE

Department of Chemistry, Presidency College, Calcutta-700073, India

Received October 24, 1983

A. L. DE and T. K. DE. Can. J. Chem. **62**, 1776 (1984).

Thermodynamic dissociation constants ($_sK$) of *p*-nitroanilinium ion (BH^+) have been determined at 25°C in aqueous solutions containing 20, 40, 60, and 80 wt% acetonitrile (ACN) by spectrophotometric measurements. Standard Gibbs energies of transfer, ΔG_t^0(B) of *p*-nitroaniline (B) from water to other solvents have been evaluated from the measurement of solubilities at 25°C. Solvent effect on the dissociation of the acid (BH^+), $\delta(\Delta G^0) = 2.303RT[p(_sK) - p(_wK)]$, results in a characteristic minimum with a change in the solvent composition. The result in this protic – dipolar aprotic mixture (H_2O + ACN) has been compared with that in aqueous mixture of protic solvent (H_2O + ethylene glycol) available from literature. The solvent effect has been discussed in terms of the standard Gibbs energies of transfer ΔG_t^0 from water to aqueous mixtures of organic co-solvent of the uncharged base (B), the hydrochloride of the base (BHCl), and hydrochloric acid (HCl) and also in terms of the individual species involved in the dissociation process. The results indicate that solvent effect on dissociation is an involved process, guided by the combined effects of various types of solute–solvent interactions of the Brønsted acid and its conjugate base in addition to the relative solvent basicities.

A. L. DE et T. K. DE. Can. J. Chem. **62**, 1776 (1984).

Faisant appel à des mesures spectrophotométriques et opérant à 25°C, on a étudié la constante thermodynamique de dissociation ($_sK$) de l'ion *p*-nitroanilinium (BH^+) dans des solutions aqueuses contenant 20, 40, 60 et 80% en poids d'acétonitrile (ACN). Utilisant des mesures de solubilité à 25°C, on a évalué les énergies standard de dissociation de Gibbs ΔG_t^0(B) de la *p*-nitroaniline (B) dans l'eau et dans d'autres solvants. L'effet du solvant sur la dissociation de l'acide (BH^+): $\delta(\Delta G^0) = 2{,}303RT[p(_sK) - p(_wK)]$ conduit à un minimum caractéristique lorsqu'on change la composition du solvant. On a comparé les résultats obtenus à l'aide de ce mélange protique/aprotique dipolaire (H_2O + ACN) avec ceux obtenus antérieurement dans un mélange aqueux d'un solvant protique (H_2O + éthylèneglycol) et rapportés dans la littérature. On discute de l'effet du solvant en termes des énergies de transfert standard de Gibbs, ΔG_t^0, de l'eau à des mélanges aqueux de co-solvants organiques pour la base libre (B), pour son chlorhydrate (BHCl) et pour l'acide chlorhydrique (HCl); on discute aussi de l'effet du solvant en termes des espèces individuelles impliquées dans le processus de la dissociation. Les résultats indiquent que l'effet du solvant sur la dissociation est un processus complexe qui est guidé par l'effet combiné de divers types d'interactions soluté–solvant de l'acide de Brønsted et de sa base conjuguée en plus des basicités relatives du solvant.

[Traduit par le journal]

Can. J. Chem. Downloaded from www.nrcresearchpress.com by 210.87.254.105 on 09/06/12
For personal use only.

Introduction

Dissociation constants of *p*-nitroanilinium ion (BH^+) were reported earlier in aqueous mixtures of protic solvents like ethylene glycol (EG) (1), methanol (2, 3), and acetic acid (4). This paper reports a study of the dissociation constants of *p*-nitroanilinium ion at 25°C in a series of aqueous mixtures of a dipolar aprotic solvent (5) acetonitrile (ACN), a solvent system of different nature. In contrast to previous studies, the contribution of the base *p*-nitroaniline (B) to the dissociation behaviour of the acid BH^+ in this solvent system was considered. This contribution was determined (1, 6) from measurement of the solubilities of the base in water as well as in various solvent mixtures.

Experimental

Purification (5) of ACN (L.R., B.D.H) and water, and the preparation (1) of solvents as well as solutions of HCl have been described earlier. *p*-Nitroaniline (AnalR) was purified by two crystallizations from aqueous ethanol (95% v/v) and then dried *in vacuo*. The dissociation constants ($_sK$) of *p*-nitroanilinium ion (BH^+) in the aqueous mixtures of ACN were determined spectrophotometrically using unbuffered solutions of HCl at different concentrations in a manner essentially similar to that described earlier (1, 2, 7–9). The $p(_sK)$ values were obtained by linear extrapolation of the plots of $p(_sK)'$ of eq. [1] against μ to $\mu = 0$

$$[1] \quad p(_sK)' = -\log m_{SH_2^+} - \log \frac{\alpha}{1-\alpha} = p(_sK) + \log \frac{\gamma_{SH_2^+}\gamma_B}{\gamma_{BH^+}} = p(_sK) + f(\mu)$$

where α and $(1 - \alpha)$ are the fractions of the indicator species present in the neutral form (B) and the ionic form (BH^+), respectively, and $m_{SH_2^+}$ is the effective molality of H^+ in the solution. A series of solution was prepared by adding weighed amounts of HCl solutions and the solvent to weighed amounts of the *p*-nitroaniline (B) solutions. The spectral absorbances were determined at 25 ± 0.2°C with a UNICAM SP 500 model spectrophotometer (England) with 1 cm quartz cells at 380 nm where the absorbance shows a maximum for the base form (2). The limiting absorbances of the acidic form at 380 nm, though small, were taken into account and the absorbance readings were corrected where necessary for the identical total concentration of the indicator (*p*-nitroaniline). The limiting absorbances (1, 2) of the acidic and basic forms of *p*-nitroaniline were measured in very concentrated HCl solutions (6 *M*) and in very dilute sodium hydroxide solutions (0.001 *M*). The values of $\alpha/(1 - \alpha) = (D - D_1)/(D_2 - D)$ were obtained from the optical densities, D_1, D_2, and D of the completely acid form (BH^+), completely base form (B), and the mixture of the two forms measured at an identical concentration of the indicator in the same cell. The molality of the *p*-nitroanilinium ion at equilibrium was negligibly small with respect to the molality of HCl, so that $-\log m_{SH_2^+}$ was virtually the same as that of $-\log m_{HCl}$ in most cases. The values of μ were taken to be equal to $m_{HCl}d_s$, where d_s is the density (5) of the solvent.

The standard Gibbs energies of transfer of the uncharged base, B, from water to aqueous mixtures of ACN were computed by the method described earlier (1, 6, 10), using the relation $\Delta G_t^0(B) = RT \ln (_wN_B/_sN_B)$ where $_wN_B$ and $_sN_B$ are the solubilities of the base in water and respective solvents (SH) on the mole fraction scale. Solubilities of B were determined at 25°C by the same method described earlier (1). As for uncharged solutes such as benzoic acid (11), tris(hydroxymethyl)aminomethane (1, 6), and nitroanilines (1, 8) in different

[1] To whom all correspondence should be addressed.

TABLE 1. Data for spectrophotometric determination of $p({}_sK)$ for *p*-nitroanilinium ion in acetonitrile-water solvent system at 25°C; percentages are % (w/w) of acetonitrile

m_{HCl}	$-\log \frac{\alpha}{1-\alpha}$	$p({}_sK)'$	m_{HCl}	$-\log \frac{\alpha}{1-\alpha}$	$p({}_sK)'$
20%; [indicator] = 1.71×10^{-5} *M*			60%; [indicator] = 2.21×10^{-5} *M*		
0.6276	0.339	0.601	1.053	0.124	0.102
0.5332	0.309	0.582	0.8763	0.004	0.061
0.4486	0.236	0.584	0.6907	−0.168	−0.007
0.3583	0.129	0.575	0.5214	−0.346	−0.063
0.2664	−0.024	0.550	0.3476	−0.561	−0.102
0.1772	−0.233	0.518	0.1667	−0.963	−0.184
0.0902	−0.538	0.507	0.1023	−1.182	−0.192
		$p({}_sK) = 0.50$			$p({}_sK) = -0.22$
40%; [indicator] = 2.01×10^{-5} *M*			80%; [indicator] = 2.03×10^{-5} *M*		
1.009	0.035	0.301	1.0635	0.249	0.223
0.8643	0.198	0.261	0.8467	0.085	0.157
0.7181	0.081	0.225	0.6333	−0.117	0.081
0.5724	−0.040	0.202	0.4224	−0.331	0.043
0.4258	−0.216	0.155	0.2081	−0.727	−0.045
0.2855	−0.424	0.120	0.1123	−1.022	−0.072
0.1379	−0.768	0.092			
		$p({}_sK) = 0.06$			$p({}_sK) = -0.10$

aquo-organic solvents, the validity of this relation depends on the assumption that the ratio of activity coefficients of the uncharged base in the saturated solutions in the mixed solvent and in water is unity.

Results

The values of $-\log [\alpha/(1-\alpha)]$, the molalities of HCl and the values of $p({}_sK)'$ are shown in Table 1. The $p({}_sK)$ values obtained in the different solvent mixtures are recorded at the bottom of the column of $p({}_sK)'$ in Table 1. The uncertainties in the $p({}_sK)$ values are of the order of ±0.005 unit. The solubilities of B and the $\Delta G_t^0(B)$ values at 25°C are recorded in Table 2. The maximum uncertainties in the $\Delta G_t^0(B)$ values are ±0.04 kJ mol^{-1}.

Discussion

As a basis for comparison (12) in different solvent mixtures, the $p({}_sK)$ values in the molal scale (Table 1) have been converted into the mole fraction scale, $p({}_sK)^N$, by the usual relation (13) and are recorded in Table 3. The solvent effect on the dissociation of BH^+ ion, $\delta(\Delta G^0)$ has been calculated (1, 8) using eq. [2]

$$[2] \quad \delta(\Delta G^0) = {}_s\Delta G^0 - {}_w\Delta G^0 = 2.303RT[p({}_sK)^N - p({}_wK)^N]$$

The values of $\delta(\Delta G^0)$ are recorded in Table 3.

Variation of $\delta(\Delta G^0)$ values with mol% ACN is shown in Fig. 1. For comparison, the corresponding variation in the water – ethylene glycol (H_2O + EG) solvent system obtained from literature (1) (Table 4) is also shown. In both cases the value of $\delta(\Delta G^0)$ decreases as the proportion of organic co-solvent increases and passes through a minimum, the decrease is greater in the case of H_2O + ACN. This indicates a greater solvent effect in the H_2O + ACN system as compared to that in H_2O + EG. The solvent effect can be expressed (1, 8, 14) in the form of eq. [3]

$$[3a] \quad \delta(\Delta G^0) = \Delta G_t^0(H^+) + \Delta G_t^0(B) - \Delta G_t^0(BH^+)$$

$$[3b] \quad = \Delta G_t^0(HCl) + \Delta G_t^0(B) - \Delta G_t^0(BHCl)$$

TABLE 2. Solubilities and standard Gibbs energies of transfer, $\Delta G_t^0(B)$ of *p*-nitroaniline in acetonitrile–water solvents at 25°C (ΔG^0 values are in mole fraction scale)

Wt% ACN	Mol% ACN	$10^2 m_B$[a]	$10^4 N_B$[b]	$\Delta G_t^0(B)/(kJ\ mol^{-1})$
0	0	0.4267[c]	0.7686[c]	0
20	9.89	4.304	8.724	−6.02
40	22.66	29.45	67.97	−11.11
60	39.71	89.91	238.2	−14.22
80	63.74	172.3	542.1	−16.25

[a] m_B = solubility in mol per kg of solvent.
[b] N_B = mole fraction of the base in the saturated solution.
[c] Reference 1.

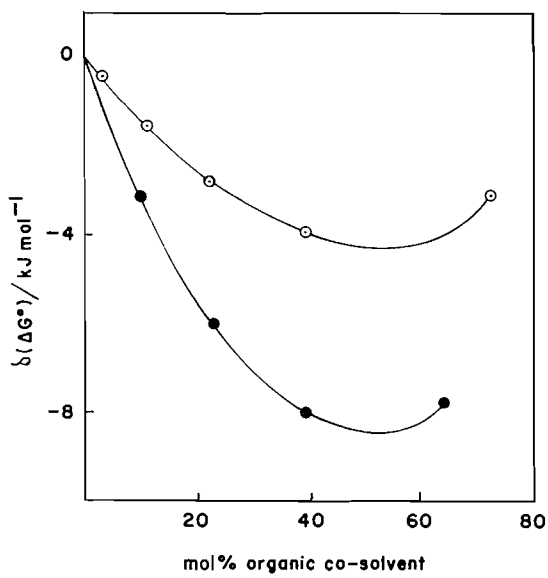

FIG. 1. Variation of $\delta(\Delta G^0)$ for *p*-nitroanilinium ion in ACN + H_2O [●] and EG + H_2O [⊙] mixtures at 25°C.

Can. J. Chem. Downloaded from www.nrcresearchpress.com by 210.87.254.105 on 09/06/12
For personal use only.

TABLE 3. Values of $p({}_sK)^N$ and $\delta(\Delta G^0)$ for *p*-nitroanilinium ion and standard Gibbs energies of transfer in acetonitrile–water solvent system at 25°C (ΔG^0 values are given in kJ mol^{-1} (mole fraction scale))

Wt% ACN	Mol% ACN	$p({}_sK)^N$	$\delta(\Delta G^0)$	ΔG_t^0(BHCl)	ΔG_t^0(HCl)[a]	ΔG_t^0(B) − ΔG_t^0(BHCl)
0	0	2.744[b]	0	0	0	0
20	9.89	2.193	−3.14	−2.18	0.7	−3.84
40	22.66	1.694	−5.99	−2.92	2.2	−8.19
60	39.71	1.346	−7.98	−1.24	5.0	−12.98
80	63.74	1.386	−7.75	3.20	11.7	−19.45

[a]References 5, 19.
[b]Reference 1; B = *p*-nitroaniline.

TABLE 4. Values of $\delta(\Delta G^0)$* for *p*-nitroanilinium ion and standard Gibbs energies of transfer* in ethylene glycol-water solvent system at 25°C (ΔG^0 values are given in kJ mol^{-1} (mole fraction scale))

Wt% EG	Mol% EG	$\delta(\Delta G^0)$	ΔG_t^0(B)	ΔG_t^0(BHCl)	ΔG_t^0(HCl)	ΔG_t^0(B) − ΔG_t^0(BHCl)
10	3.12	−0.41	−0.88	−0.14	0.33	−0.74
30	11.06	−1.50	−2.63	−0.41	0.71	−2.22
50	22.50	−2.82	−5.03	−1.16	1.05	−3.87
70	40.39	−3.87	−7.84	−2.21	1.76	−5.63
90	72.36	−3.09	−11.81	−3.69	5.02	−8.12

*Reference 1; B = *p*-nitroaniline.

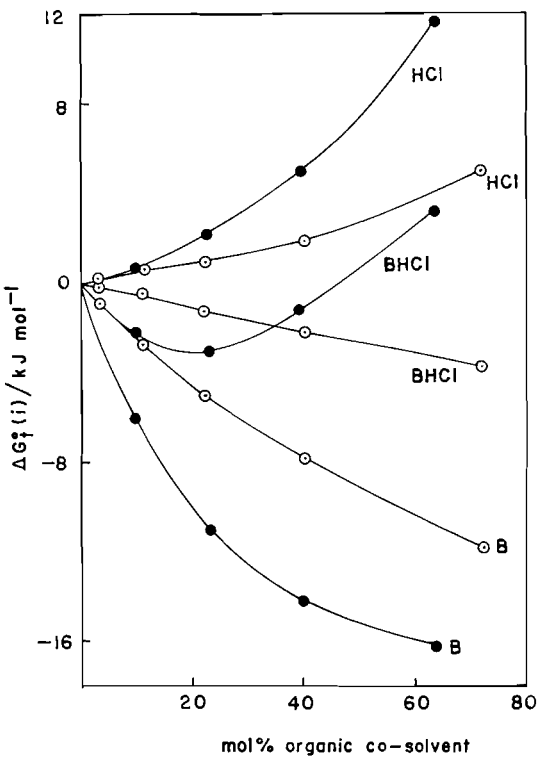

FIG. 2. Variation of $\Delta G_t^0(i)$ of some species in ACN + H_2O [●] and EG + H_2O [⊙] mixtures at 25°C. B = *p*-nitroaniline; BHCl = *p*-nitroanilinium chloride.

where ΔG_t^0(i) is the Gibbs energy change accompanying the transfer of one mole of species i from the standard state in water to the standard state in the solvent concerned, both on the mole fraction scale. The characteristic minimum in the $\delta(\Delta G^0)$ curve for a BH^+ type acid has been observed in aqueous mixtures of other protic solvents like acetic acid (4), methanol (3, 9), and the solvent effect in such cases are also smaller (not shown in Fig. 1) than that observed for the H_2O + ACN solvent system. The contribution of uncharged base was ignored in these cases and the result has been attributed to enhanced basicity of the media (4, 9, 15) resulting from a breakdown of the water structure. The contribution of base has been considered in the work by Bates *et al.* (6), Kundu *et al.* (1), and De (8, 10). The importance of the quantity ΔG_t^0(B) may be seen from Table 2.

Figure 2 illustrates the variation of ΔG_t^0(B) with mol% ACN. For comparison, the corresponding variation in H_2O + EG is also shown. There is an initial sharp decrease of ΔG_t^0(B) with mol% ACN followed by somewhat less downward trend. The values in H_2O + EG, however, decrease gradually with increase in mol% EG and are always much less negative compared to those in H_2O + ACN. The ΔG_t^0(B) values in H_2O + acetic acid (16) and H_2O + methanol (16) are also found to be much less negative. In the H_2O + EG system, the decrease in ΔG_t^0(B) has been primarily attributed (1) to the dispersion interaction of the benzene nucleus with the organic component of the solvent mixtures. In H_2O + ACN, the dispersion interaction also operates to stabilize B and this interaction possibly reaches saturation at around 0.3 mole fraction ACN, beyond which the rate of decrease in ΔG_t^0(B) falls significantly. As EG is a slightly more polarisable molecule than ACN (17) the dispersion interactions should be less in H_2O + ACN. However, the effect of forming a cavity may explain the large negative ΔG_t^0(B) values in H_2O + ACN. Since EG + H_2O are both hydroxylic solvents and because the activity of H_2O is unusually high in its mixture with ACN (18), it can be expected that H_2O + EG mixtures are more associated than H_2O + ACN mixtures. Consequently, it can be assumed that much less energy will be required to create a cavity for the accommodation of B in H_2O + ACN compared to that in H_2O + EG, thus making the cavity formation contribution to the total ΔG_t^0(B) for B more negative in the H_2O + ACN solvent system. This may explain the observed relative order of total ΔG_t^0(B) in these two solvent systems.

The values of ΔG_t^0(BHCl) calculated from eq. [3*b*] are recorded in Table 3. The ΔG_t^0(HCl) values required for calculation of ΔG_t^0(BHCl) were obtained from the literature (5, 19). The variation of ΔG_t^0(BHCl) and ΔG_t^0(HCl) (Table 3) with

Can. J. Chem. Downloaded from www.nrcresearchpress.com by 210.87.254.105 on 09/06/12
For personal use only.

TABLE 5. Values of standard Gibbs energies of transfer of H^+ and BH^+ from water to aquo-organic solvents at 25°C (ΔG^0 values are given in kJ mol^{-1} (mole fraction scale))

Wt% CH_3CN	$\Delta G_t^0(H^+)^a$	$\Delta G_t^0(BH^+)$	Wt% EG	$\Delta G_t^0(H^+)^b$	$\Delta G_t^0(BH^+)$
20	−2.9	−5.78	30	−1.2	−2.33
40	−4.2	−9.32	50	−1.0	−3.21
60	−3.9	−10.14	70	−2.2	−6.17
80	−2.6	−11.10	90	−0.7	−9.42

[a] Reference 5.
[b] Reference 21.

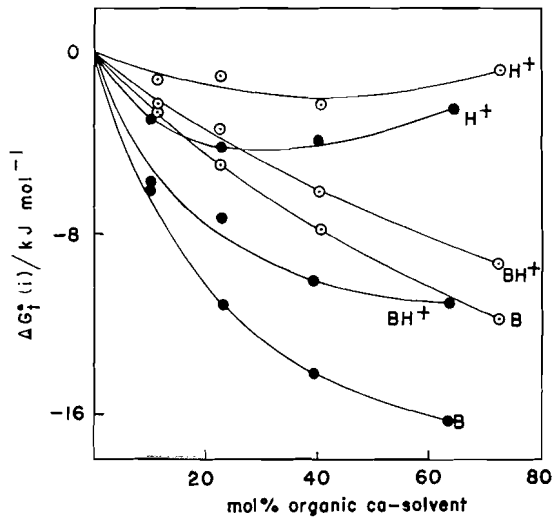

FIG. 3. Variation of $\Delta G_t^0(i)$ of some species in ACN + H_2O [●] and EG + H_2O [⊙] mixtures at 25°C; B = *p*-nitroaniline; BH^+ = *p*-nitroanilinium ion.

mol% ACN is shown in Fig. 2. For comparison, similar variations of ΔG_t^0(BHCl) and of ΔG_t^0(HCl) in H_2O + EG (Table 4) are also shown. It is observed that the ΔG_t^0(BHCl) value decreases sharply with the increase in mol% ACN at the beginning, passes through a minimum, and ultimately becomes positive. In contrast, the ΔG_t^0(BHCl) value decreases monotonically with the increase in mol% EG. The ΔG_t^0(HCl) value for both solvent systems increases with an increase in mol% organic co-solvent, but the rise in H_2O + ACN is greater at higher mol% ACN. Tables 3 and 4 show that the $\Delta G_t^0(B) - \Delta G_t^0$(BHCl) values for both solvent systems are increasingly negative with increase in mol% organic co-solvent and the minimum in $\delta(\Delta G^0)$ results from the increase in ΔG_t^0(HCl) and the simultaneous decrease of $\Delta G_t^0(B) - \Delta G_t^0$(BHCl) (vide eq. [3*b*]).

Equation [3*a*] shows that $\Delta G_t^0(B)$, $\Delta G_t^0(H^+)$, and $\Delta G_t^0(BH^+)$ are jointly responsible for the solvent effect. Values of $\Delta G_t^0(H^+)$ in the H_2O + EG system obtained by different extra-thermodynamic assumptions are available in the literature (20, 21); but since reference electrolyte (RE) method has proven to be the most sound, reasonable, and consistent (22, 23) we have utilized $\Delta G_t^0(H^+)$ values obtained by RE method for both solvent systems (5, 21) to calculate $\Delta G_t^0(BH^+)$ values which are given in Table 5. It is observed from Fig. 3 that the relative trend of $\Delta G_t^0(BH^+)$ in the two solvent systems are qualitatively similar to that of $\Delta G_t^0(B)$ and the reasons are probably similar to those advanced for the base. Comparison shows that the values of $\Delta G_t^0(BH^+)$ are less negative than those of $\Delta G_t^0(B)$ at every solvent composition in both the solvent systems. As the dielectric constant values of the solvents decrease with increase in concentration of organic co-solvent, the free energy transfer of BH^+ due to Born-type electrostatic interaction should be positive (24, 25) and this ion destabilizing effect acting in opposition should make $\Delta G_t^0(BH^+) > \Delta G_t^0(B)$.

The relative values of $\Delta G_t^0(H^+)$ in the two solvent systems have been described earlier (5). $\Delta G_t^0(H^+)$ may be taken as a measure of the basicity of the solvent SH with respect to that of water (1, 26). More negative values of $\Delta G_t^0(H^+)$ in H_2O + ACN (Table 5) results from the more extensive water structure breaking ability of ACN than EG, thereby releasing more "basic" monomeric water (26).

The solvent effect on the dissociation of *p*-nitroanilinium ion is found to be an involved process and is the combined effects of various types of solute–solvent interactions of the Brønsted acid and its conjugate base in addition to the relative solvent basicities.

1. K. K. KUNDU, A. L. DE, and M. N. DAS. J. Chem. Soc. Perkin II, 2063 (1972).
2. D. ROSENTHAL, H. B. HETZER, and R. G. BATES. J. Am. Chem. Soc. **86**, 549 (1964).
3. R. GABORIAND and R. SCHAAL. Compt. Rend. Acad. Sci. Paris, **263**, 353 (1966).
4. K. A. BONI and H. A. STROBEL. J. Phys. Chem. **70**, 3771 (1966).
5. K. DAS, A. K. DAS, and K. K. KUNDU. Electrochim. Acta, **26**, 471 (1981).
6. P. SCHINDLER, R. A. ROBINSON, and R. G. BATES. J. Res. Natl. Bur. Stand. **72**A, 141 (1968).
7. K. K. KUNDU, A. L. DE, and M. N. DAS. J. Chem. Soc. Dalton, 386 (1972).
8. A. L. DE. Electrochim. Acta, **28**, 1643 (1983).
9. E. E. SAGER, R. A. ROBINSON, and R. BATES. J. Res. Natl. Bur. Stand. **68**A, 305 (1964).
10. A. L. DE. Electrochim. Acta, **29**, 683 (1984).
11. K. DAS, A. K. DAS, K. BOSE, and K. K. KUNDU. J. Phys. Chem. **82**, 1242 (1978).
12. R. A. ROBINSON and R. H. STOKES. Electrolyte solution. 2nd ed. Butterworths, London. 1965.
13. H. S. HARNED and B. B. OWEN. The physical chemistry of electrolyte solutions. 3rd ed. Reinhold, New York. 1958.
14. A. L. DE. Ind. J. Chem., **22**A, 932 (1983).
15. R. G. BATES and R. A. ROBINSON. *In* Chemical physics of ionic solutions. *Edited by* B. E. Conway and R. G. Barradas. John Wiley and Sons, New York. 1966.
16. A. L. DE. Unpublished results.
17. A. J. PARKAR. Chem. Rev. **69**, 1 (1969).
18. T. R. STENGLE, YU E. PAN, and C. H. LANGFORD. J. Am. Chem. Soc. **74**, 9037 (1972).
19. R. SMITS, D. L. MASSART, J. JULLIARD, and J. P. MOREL. Electrochim. Acta, **21**, 431 (1976).
20. K. K. KUNDU, A. K. RAKSHIT, and M. N. DAS. Electrochim. Acta, **17**, 1921 (1972).
21. A. K. DAS and K. K. KUNDU. Ind. J. Chem. **16**A, 467 (1978).
22. J. I. KIM. J. Phys. Chem. **82**, 191 (1978).
23. M. H. ABRAHAM and A. NASEHZADEH. Can. J. Chem. **57**, 71 (1979); **57**, 2004 (1979).
24. M. BORN. Z. Physik, **1**, 45 (1920).
25. J. O'M BOCKRIS. *In* Modern aspects of electrochemistry. *Edited by* J. O'M Bockris. Vol. 1. Butterworths, London. 1954. Chapt. 2.
26. R. G. BATES. *In* Hydrogen-bonded solvent system. *Edited by* A. K. Covongton and P. Jones. Taylor and Francis, London. 1968.

Can. J. Chem. Downloaded from www.nrcresearchpress.com by 210.87.254.105 on 09/06/12
For personal use only.

Hydride transfer reactions. A kinetic study of oxidation of 2- and 3-methoxy-N-methylacridans by some π acceptors and a one-electron oxidant

ALLAN K. COLTER, PETER PLANK, JOHN P. BERGSMA, ROY LAHTI, ANDRÉ A. QUESNEL, AND A. GREGG PARSONS
Guelph–Waterloo Centre for Graduate Work in Chemistry, University of Guelph, Guelph, Ont., Canada N1G 2W1

Received January 9, 1984

ALLAN K. COLTER, PETER PLANK, JOHN P. BERGSMA, ROY LAHTI, ANDRÉ A. QUESNEL, and A. GREGG PARSONS. Can. J. Chem. **62**, 1780 (1984).

Relative rates of oxidation of N-methylacridan (**1***a*), 2-methoxy-N-methylacridan (**1***b*), and 3-methoxy-N-methylacridan (**1***c*) have been investigated as a probe of transition state structure in hydride transfer reactions. Oxidants investigated cover a 2×10^7-fold (with **1***a*) to 2×10^8-fold (with **1***c*) range of reactivity, and include the π acceptors 1,4-benzoquinone (BQ), *p*-chloranil (CA), 2,3-dicyano-1,4-benzoquinone (DCBQ), 7,7,8,8-tetracyanoquinodimethane (TCNQ), and tetracyanoethylene (TCNE) in acetonitrile (AN), BQ in 50:50 (v/v) AN–water, and the one-electron oxidant tris(2,2′-bipyridyl)cobalt(III), $Co(bipy)_3^{3+}$, in AN, all at 25°C. For all of the π acceptors except TCNE the order of reactivity, **1***c* > **1***b* > **1***a*, (DH) indicates a transition state resembling the corresponding acridinium ion product (D^+), while the order of reactivity with $Co(bipy)_3^{3+}$, **1***b* > **1***c* > **1***a*, indicates a transition state resembling the acridan radical cation ($DH^{+\cdot}$). The order of reactivity observed with TCNE, **1***b* ≈ **1***c* > **1***a*, is tentatively interpreted as indicating a transition state resembling the corresponding 9-acridanyl radical (D·).

ALLAN K. COLTER, PETER PLANK, JOHN P. BERGSMA, ROY LAHTI, ANDRÉ A. QUESNEL et A. GREGG PARSONS. Can. J. Chem. **62**, 1780 (1984).

On a étudié les vitesses relatives d'oxydation du N-méthylacridan (**1***a*), du méthoxy-2 N-méthylacridan (**1***b*) et du méthoxy-3 N-méthylacridan (**1***c*) comme méthode de déterminer la structure de l'état de transition lors de réactions de transfert d'hydrure. Les oxydants étudiés couvrent des intervalles de réactivité allant de 1 á 2×10^7 (pour le composé **1***a*) et jusqu'à 2×10^8 (pour le composé **1***c*); ils contiennent des accepteurs π comme la benzoquinone-1,4 (BQ), le *p*-chloranil (CA), la dicyano-2,3 benzoquinone-1,4 (DCBQ), le tétracyano-7,7,8,8 quinodiméthane (TCNQ) et le tétracyanoéthylène (TCNE) dans l'acétonitrile (AN), la BQ dans AN–eau (50:50, v/v) et finalement, un oxydant procédant par le biais d'un électron, le tris(bipyridyl-2,2′) cobalt(III), $Co(bipy)_3^{3+}$, dans AN; toutes ces oxydations ont été réalisées à 25°C. Pour tous les accepteurs π, à l'exception du TCNE, l'ordre de réactivité, **1***c* > **1***b* > **1***a*, (DH) indique que l'état de transition ressemble au produit, soit l'ion acridinium correspondant (D^+), tandis que l'ordre de réactivité observé avec le $Co(bipy)_3^{3+}$, **1***b* > **1***c* > **1***a*, indique que l'état de transition ressemble au cation radicalaire acridan ($DH^{+\cdot}$). On croit que l'ordre de réactivité observé avec le TCNE, **1***b* ≈ **1***c* > **1***a*, suggère l'existence d'un état de transition ressemblant au radical acridanyl-9 correspondant (D·).

[Traduit par le journal]

Introduction

The mechanisms of hydride transfer reactions of nicotinamide coenzyme models continue to attract considerable interest (1,2, and references cited). The focus of much of the current interest and controversy is the experimental distinction between a one-step hydride transfer mechanism and stepwise mechanisms involving an initial single-electron transfer. This distinction, for oxidants capable of reacting as either a hydride or electron acceptor, has proven to be very elusive. Unambiguous evidence for radical intermediates in oxidation of dihydropyridine analogs by two-electron oxidants has been obtained only with oxidants of very high oxidizing strength (3). The spectrum of mechanisms possible for hydride transfer reactions is presently poorly defined, and for most particular examples it remains difficult to specify the mechanism with any confidence.

In an earlier study (1) we examined substituent effects in oxidation of a series of N-(substituted benzyl)acridans with three benzoquinone and two cyanomethylene π acceptors covering a 10^7-fold range of reactivity. The sensitivity of the rate to electronic substituent effects as measured by the Hammett ρ value showed a 2.2-fold variation with acceptor, but no clear pattern interpretable on the basis of a change in mechanism was discernible.

In this paper we report the results of an investigation of the relative rates of oxidation of N-methylacridan (NMA, **1***a*), 2-methoxy-N-methylacridan (2-MeO-NMA, **1***b*), and 3-methoxy-N-methylacridan (3-MeO-NMA, **1***c*) to the corresponding N-methylacridinium ions (**2***a*, *b*, and *c*) by the same five π acceptors and by the one-electron oxidant tris(2,2′-bipyridyl)cobalt(III), $Co(bipy)_3^{3+}$. This study was prompted by the following considerations: 2-MeO-NMA, because of the *para* relationship between two +R groups (4) (—N(H)—CH_3 and —O—CH_3), was expected to have a lower ionization energy than 3-MeO-NMA, in which these groups have a *meta*

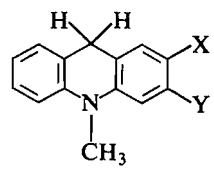

1

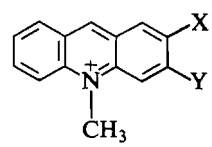

2

a X = Y = H
b X = OCH_3, Y = H
c X = H, Y = OCH_3

relationship (5). However, because of the possibility of delocalization of the positive charge in **2***c* (but not in **2***b*) onto the methoxy group (structure **3**), 3-MeO-NMA should lose a hydride more easily than 2-MeO-NMA. Thus, in contrast to the

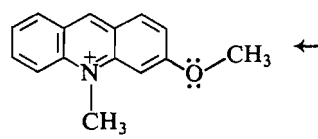

2*c*

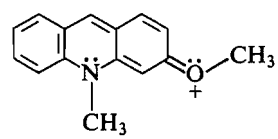

3

Can. J. Chem. Downloaded from www.nrcresearchpress.com by 210.87.254.105 on 09/06/12
For personal use only.

Can. J. Chem. Downloaded from www.nrcresearchpress.com by 210.87.254.105 on 09/06/12
For personal use only.

TABLE 1. Comparison of properties of N-methylacridans

Compound	Charge-transfer maxima, nm[a] TNB	TNF	E_{pa}, V[c]
1*a*	507	518	—
1*b*	550	563	0.65
1*c*	514	520[b]	0.75

[a] Benzene solvent, concentrations: TNB, 0.1 *M*; TNF 0.08 *M*; **1***a*, *b*, and *c*, 0.05 *M*. λ_{max} uncertain by ±5 nm except as noted.
[b] ±10 nm.
[c] Anodic peak potential vs. SCE, Pt electrode, sweep rate 0.184 V s^{-1}; acetonitrile solvent with 0.1 *M* tetraethylammonium perchlorate electrolyte.

remote substituent effects in the N-benzylacridans, the response to substitution of H by methoxy at positions 2- and 3- was expected to depend strongly on whether the transition state more closely resembles the radical cation, $\mathbf{1}^{\ddagger}$, or the acridinium ion product, **2**.

Results

In order to obtain an experimental measure of the relative ease of one-electron oxidation of **1***a*, *b*, and *c*, the charge-transfer absorption maxima of their complexes with the π acceptors 1,3,5-trinitrobenzene (TNB) and 2,4,7-trinitro-9-fluorenone (TNF) were measured (Table 1). In all solutions containing both π donor and π acceptor, a broad maximum appeared to the long wavelength side of the separate donor and acceptor spectra. A more extensive investigation of several complexes of **1***a* (6) has established that the band at 507 nm in mixtures of **1***a* and TNB is a charge-transfer band. For complexes of a series of related donors with a common π acceptor the energy of the lowest-energy charge-transfer maximum is linearly related to the ionization energy (7) or to the standard one-electron oxidation potential (7, 8) of the donor.

The standard one-electron oxidation potential, $E^0(DH/DH^{\ddagger})$ for acridans or dihydronicotinamides cannot be measured accurately electrochemically because of the irreversibility of the oxidation on the time scale of the electrochemical measurements (9, 10). The initial one-electron oxidation of **1***a* is followed by irreversible loss of a proton to yield the N-methyl-9-acridanyl radical, which is rapidly oxidized by a second electron transfer to **2***a*. Cyclic voltammograms for **1***b* and **1***c* closely resemble those reported for **1***a*; anodic peak potentials (Table 1) measured under identical conditions again indicate that **1***b* should undergo a chemical one-electron oxidation more easily than **1***c*.

To obtain a measure of the relative stabilities of **2***a*, *b*, and *c* relative to **1***a*, *b*, and *c*, equilibrium constants, K_{R^+}, for pseudobase formation [1] (11) were measured for **2***a*, *b*, and *c*

[1] 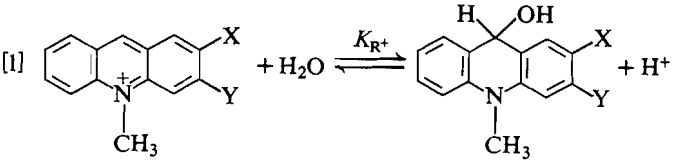

2 **4**

(as their iodide salts) (Table 2). With the methoxyacridinium salts **2***b* and *c* these determinations were complicated by disproportionation to the corresponding N-methylacridone (**5**) and N-methylacridan (**1**) at pH's above 10 (11, 12). This complication adds some uncertainty to the measured pK_{R^+} values (±0.08 p*K* units maximum) but not enough to affect the

TABLE. 2. pK_{R^+} values for N-methylacridinium ions[a]

Compound	pK_{R^+} ± std. dev.
2*a*	10.00 ± 0.02
2*b*	11.05 ± 0.07
2*c*	11.70 ± 0.04

[a] Temperature 25.0°C. Corrected to zero ionic strength.

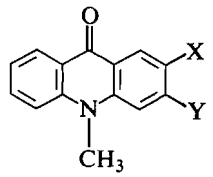

5

qualitative order of pK_{R^+} values or the conclusion that **1***c* should be a better hydride donor than **1***b*.

Rates of oxidation of **1***a*, *b*, and *c* by the π acceptors **6**–**10**

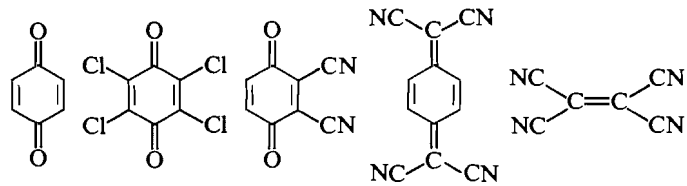

6, BQ **7**, CA **8**, DCBQ **9**, TCNQ **10**, TCNE

in acetonitrile (AN) and by 1,4-benzoquinone (BQ) in 50:50 (v/v) AN–water were measured at 25°C. In addition, rates of oxidation by the one-electron oxidant $Co(bipy)_3^{3+}$ (as the perchlorate salt) were measured in AN at 25°C.

Quantitative oxidation of **1** to **2** was confirmed by uv–visible spectral examination of reaction solutions for all oxidants except TCNQ, where the spectrum of **2** is masked by that of the radical anion reduction product, $TCNQ^{\cdot-}$. Isolation of **2***a* as the perchlorate or chloride salt in oxidation of **1***a* by all five π acceptors has been described earlier (6). The salts $\mathbf{2}b^+ClO_4^-$ and $\mathbf{2}c^+ClO_4^-$ are isolable in quantitative yield by oxidation of **1***b* and **1***c* by 2,3-dicyano-5,6-dichloro-1,4-benzoquinone (DDQ) following the procedure described earlier for NMA (6).

The corresponding reduction product of each π acceptor, A, is as described earlier (1, 6, 13) for oxidation of NMA, namely AH_2 from BQ + acetic acid, and $A^{\cdot-}$ + $0.5AH_2$ from DCBQ, TCNQ, and TCNE. CA leads to a mixture of $A^{\cdot-}$, AH^-, and AH_2 in AN but to 100% (±5%) AH_2 in AN – 0.1 *M* acetic acid (Experimental). The reduction products of the π acceptors, as well as the overall stoichiometry, depend on the extent to which the rapid reaction of the product of hydride transfer, AH^-, with unreacted acceptor ($2AH^- + A \rightleftharpoons AH_2 + 2A^{\cdot-}$) occurs, but shed no light on the mechanism of hydride transfer (1, 6, 13). With $Co(bipy)_3^{3+}$ 2 moles of Co(II), determined by spectrophotometric analysis as $CoCl_4^{2-}$, are formed per mole of **1** oxidized (Experimental). The stoichiometry is therefore as represented by [2], where DH is the hydride donor, **1**.

[2] $DH + 2Co(bipy)_3^{3+} \rightarrow D^+ + H^+ + 2Co(bipy)_3^{2+}$

TABLE 3. Rates of oxidation of NMA, 2-MeO-NMA, and 3-MeO-NMA[a]

Oxidant	[Oxidant], M	k (M^{-1} s^{-1})[b] NMA	2-MeO-NMA	3-MeO-NMA	Relative rates
BQ[c]	$(0.64-2.8) \times 10^{-1}$	5.67×10^{-4}	1.31×10^{-3}	5.07×10^{-3}	1.0:2.3:8.9
BQ[d]	$(1.8-9.9) \times 10^{-2}$	2.54×10^{-2}	1.10×10^{-1}	3.34×10^{-1}	1.0:4.3:13
TCNQ	2.0×10^{-3}	2.35×10^{-1}	3.09	8.35	1.0:13:36
CA[e]	$(0.12-4.2) \times 10^{-3}$	1.18×10	8.43×10	4.46×10^{2}	1.0:7.1:38
TCNE	4.2×10^{-3}	1.09×10^{2}	2.53×10^{3}	2.52×10^{3}	1.0:23:23
DCBQ	$(0.58-2.5) \times 10^{-3}$	1.15×10^{4}	1.28×10^{5}	1.16×10^{6}	1.0:11:101
$Co(bipy)_3^{3+}$[f]	$(0.69-1.4) \times 10^{-3}$	2.47×10^{-1}	1.94×10	3.57×10^{-1}	1.0:79:1.4

[a] Temperature 25.0°C. Solvent acetonitrile unless otherwise stated. [Acridan] = $1.6 \times 10^{-5} - 1.3 \times 10^{-4}$ M.
[b] Averages of 3 to 9 values. Reproducibilities ±2% with BQ and CA, ±4% with TCNE and TCNQ, ±10% with DCBQ and $Co(bipy)_3^{3+}$.
[c] 1.0×10^{-2} M acetic acid added.
[d] 50:50 (v/v) acetonitrile–water containing 0.01 M acetic acid.
[e] 0.1 M acetic acid added.
[f] 1×10^{-3} M 2,2′-bipyridyl added.

The kinetic results are summarized in Table 3. Rate measurements with all oxidants except CA and $Co(bipy)_3^{3+}$ were carried out under pseudo first-order conditions using a 30-fold or greater excess of oxidant. With CA and some of the $Co(bipy)_3^{3+}$ rates, lower molar ratios of oxidant to acridan were used and the data analyzed using the appropriate integrated second-order rate equation. A first-order dependence on both acridan and acceptor concentration is well established by this and earlier work (1, 6). Rate constants for **1***a* listed in Table 3 agree closely with those reported earlier except for DCBQ where the value reported earlier (6) is about 25% lower. Further investigations of $Co(bipy)_3^{3+}$ oxidations of acridans and dihydronicotinamides have been carried out and are in progress; the results will be reported separately.

Discussion

The reactivity pattern observed for $Co(bipy)_3^{3+}$ is consistent with a mechanism involving rate-determining electron transfer. By analogy with the mechanism of electrochemical oxidation of dihydropyridines (9, 10) the following mechanism is tentatively proposed:

$$DH + Co(bipy)_3^{3+} \underset{k_{-1}}{\overset{k_1}{\rightleftharpoons}} DH^{\ddagger} + Co(bipy)_3^{2+}$$

$$[3] \quad DH^{\ddagger} + bipy \xrightarrow{k_2} D^{\cdot} + bipyH^{+}$$

$$D^{\cdot} + Co(bipy)_3^{3+} \xrightarrow{fast} D^{+} + Co(bipy)_3^{2+}$$

If the main features of this mechanism are correct, k_2[bipy] must be much greater than k_{-1}[$DH^{\ddagger}$][$Co(bipy)_3^{3+}$] under the conditions of our measurements because a 20-fold increase in [bipy] (to 2×10^{-2} M) has no measurable effect on the rate.

The results of earlier studies of oxidations of NMA by π acceptors (6), particularly the variation of kinetic isotope effect with acceptor reactivity for structurally-related acceptors, are most easily accommodated by a one-step hydride transfer mechanism [4] or by a three-step electron–proton–electron mechanism [5] in which proton transfer is rate determining:

$$[4] \quad DH + A \rightarrow D^{+} + AH^{-}$$

$$[5] \quad DH + A \underset{k_{-1}}{\overset{k_1}{\rightleftharpoons}} DH^{\ddagger}A^{\cdot-} \xrightarrow[k_2]{slow} D{\cdot}AH{\cdot} \xrightarrow{fast} D^{+} + AH^{-}$$

We have argued earlier (1) that the radical cation – radical anion pair intermediate, $DH^{\ddagger}A^{\cdot-}$, of [5] is too high in energy to be an intermediate in oxidation of NMA by either BQ or CA in AN but that it cannot be excluded on this basis in oxidation of NMA by TCNQ, TCNE, or DCBQ. Indeed, successful trapping of the N-methyl-9-acridanyl radical (D·) in oxidation of NMA by DCBQ (3) is evidence that at least part of this reaction occurs by mechanism [5].

The transition state in [4] should be between DH (+A) and D^{+} (+AH^{-}) in structure and hence should reflect the energy of D^{+} (i.e., **2**) relative to DH (**1**). Values of K_R^{-1} (i.e., formation of D^{+} from **4**) from **2***a*, *b*, and *c*, relative to that of **2***a*, are, respectively, (1.0):11:50 in aqueous solution. Although the relative rates in Table 3 show some interesting and complex variations, it is clear that this pattern is maintained at least qualitatively for all of the π acceptors except TCNE. For four of the five π acceptors, therefore, D^{+} is a much better model for the transition state than $DH^{\ddagger}$.

The predictions of mechanism [5] are less clear. On the simplest level, the transition state should lie between $DH^{\ddagger}A^{\cdot-}$ and D·AH· in structure. Unfortunately we have no experimental model for the energy of D· relative to DH, though differences will surely be much smaller than the differences in the energies of $DH^{\ddagger}$ and D^{+} for the three systems compared. The relative rates of oxidation by TCNE appear to be at least consistent with [5].

Aside from the qualitative order of reactivities, two further points are worth noting. First, for the three benzoquinones, the effects of substitution increase in the order BQ < CA < DCBQ, that is, in order of increasing ease of reduction. Second, in oxidation by BQ, an increase in substituent effects is observed in changing from AN to 50:50 (v/v) AN–water solvent. Similar trends in more remote substituent effects were observed in oxidation of N-(substituted benzyl)acridans under identical conditions (1). At the same time, either an increase in acceptor strength or an increase in ion-solvating ability is accompanied by a decrease in the primary deuterium kinetic isotope effect in oxidation of NMA (6). Taken together, these results appear to require an increase in positive charge development with decreasing bond weakening. Such a trend is not in accord with the predicted changes in transition state structure along the reaction coordinate (i.e., the changes predicted by application of the Hammond postulate (14, 15)) for either mechanism [4] or mechanism [5]. If, however, bond breaking

Can. J. Chem. Downloaded from www.nrcresearchpress.com by 210.87.254.105 on 09/06/12
For personal use only.

Can. J. Chem. Downloaded from www.nrcresearchpress.com by 210.87.254.105 on 09/06/12
For personal use only.

and formation occur within a face-to-face charge-transfer complex (1, 6), increased acceptor electron affinity or ion solvation could result in increased π electron transfer from hydride donor to π acceptor in the transition state. Further work is required to test this idea, particularly to establish whether the observed pattern of substituent and isotope effects requires $\pi-\pi$ complexing.

Experimental

Melting points were measured in open capillary tubes and are uncorrected. Proton nmr spectra were measured using Varian T60 or A60 spectrometers. Chemical shifts are reported in δ units, with tetramethylsilane as internal standrad. Ultraviolet–visible spectra were obtained using Beekman 24 or Cary 118C spectrophotometers. Elemental microanalyses were performed by Guelph Chemical Laboratories, Guelph, Ontario. Electrochemical measurements were carried out by Mr. Henry J. Stronks using apparatus and methods described in the literature (16).

Reagents and solvents

BQ, CA, TCNE, TCNQ, DCBQ, and NMA were obtained and purified as previously described (6). $Co(bipy)_3(ClO_4)_3 \cdot 3H_2O$ was synthesized as described by Burstall and Nyholm (17). The recrystallized product was further purified by ion exchange chromatography on C-25-120 Sephadex cation exchange resin, eluting with aqueous NaCl. The complex was precipitated as the perchlorate salt by addition of $HClO_4$. *Anal.* calcd. for $C_{30}H_{24}O_{12}N_6Cl_3Co \cdot 3H_2O$: C 40.95, H 3.44, N 9.55; found: C 41.03, H 3.29, N 9.50. Borax buffers (pH 9.0–9.4), carbonate buffers (pH 9.6–11.8), phosphate buffers (pH 11.0–11.8), and potassium chloride – sodium hydroxide solutions (pH 12.0–12.6) used in the pK_{R^+} determinations were prepared from Fisher Scientific sodium hydroxide solutions, and Fisher Certified reagent grades sodium tetraborate, sodium bicarbonate, sodium dihydrogen phosphate, and potassium chloride, following Bates (18). Reagent grade acetonitrile was further purified for kinetic measurements as previously described (6).

2-Methoxy-N-methylacridan (2-MeO-NMA) was obtained in 90–100% crude yield by sodium borohydride reduction of 2-methoxy-N-methylacridinium iodide, as described for reduction of N-methylacridinium salts (6). One crystallization from methanol–water afforded material having mp 84.5–85.5°C and showing a single component by tlc analysis (silica gel); nmr ($CDCl_3$) δ: 3.33 (s, 3H, N—CH_3), 3.77 (s, 3H, OCH_3), 3.87 (s, 2H, 9-methylene), 6.7–7.5 (m, 7H, aromatic). *Anal.* calcd. for $C_{15}H_{15}NO$: C 79.97, H 6.71, N 6.22; found: C 80.27, H 6.72, N 6.24.

2-Methoxy-N-methylacridinium iodide was prepared by refluxing 2-methoxyacridine with an excess of methyl iodide in benzene solution (typically 1.8 mL of benzene per gram of acridine). The orange-red precipitate was washed with ether to yield the product in yields up to 80% of theory, mp 240–241°C (dec.); uv (acetonitrile) λ_{max}: 367 nm (log ϵ = 4.19). *Anal.* calcd. for $C_{15}H_{14}NOI$: C 51.30, H 4.02, N 3.99; found: C 50.98, H 4.05, N 3.84.

2-Methoxyacridine was prepared by a four-step procedure beginning with reaction of 2-chlorobenzoic acid with *p*-anisidine to form 4′-methoxydiphenylamine-2-carboxylic acid (19), followed by ring closure to 9-chloro-2-methoxyacridine using phosphorus oxychloride (20). Catalytic hydrogenation of 9-chloro-2-methoxyacridine following Albert's procedure for hydrogenation of 9-chloroacridine (21) led to 2-methoxyacridan in 95% yield. Crystallization from 95% ethanol led to about 75% recovery of material of mp 140–144°C (lit. (22) mp 139.6–140.5°C); nmr ($CDCl_3$) δ: 3.74 (s, 3H, OCH_3), 4.04 (s, 2H, 9-methylene), 5.8 (bs, 1H, N—H), 6.5–7.3 (m, 7H, aromatic). Finally, 2-methoxyacridan was oxidized to 2-methoxyacridine as follows. A solution of 2.88 g (1.17×10^{-2} mol) of *p*-chloranil in 140 mL of benzene was slowly added to a solution of 2.25 g (1.17×10^{-2} mol) of 2-methoxyacridan in 50 mL of benzene. Dry HCl gas was passed through the mixture until the brown precipitate turned yellow. The yellow 2-methoxyacridinium chloride was neutralized with aqueous sodium bicarbonate and extracted into 100 mL of chloroform. The chloroform extract was washed many times with aqueous sodium bicarbonate, dried over magnesium sulfate, filtered, and the chloroform removed by evaporation. The residue was crystallized from cyclohexane yielding 1.33 g (60%) of 2-methoxyacridine, mp 104–105°C (lit. (23) mp 104°C).

3-Methoxy-N-methylacridan (3-MeO-NMA) was prepared in 95% crude yield by reduction of 3-methoxy-N-methylacridinium iodide as described for 2-MeO-NMA. Crystallization from methanol led to product of mp 72.5–73.5°C; nmr ($CDCl_3$) δ: 3.38 (s, 3H, N—CH_3), 3.9 (s, 5H, OCH_3 and 9-methylene), 6.3–7.3 (m, 7H, aromatic). *Anal.* calcd. for $C_{15}H_{15}NO$: C 79.97, H 6.71, N 6.22; found: C 79.70, H 6.86, N 6.23.

3-Methoxy-N-methylacridinium iodide was prepared in 93% yield from 3-methoxyacridine as described for the 2-isomer, mp 231–233°C (dec.); uv (acetonitrile) λ_{max}: 366 nm (log ϵ = 4.45). *Anal.* calcd. for $C_{15}H_{14}NOI$: C 51.30, H 4.02, N 3.99; found: C 50.89, H 4.09, N 3.81.

3-Methoxyacridine was prepared by a four-step procedure analogous to that used for 2-methoxyacridine, beginning with reaction of 2-chlorobenzoic acid with *m*-anisidine to form 3′-methoxydiphenylamine-2-carboxylic acid (24) and ring closure to 9-chloro-3-methoxyacridine (20, 24, 25). Catalytic hydrogenation (21) led to 3-methoxyacridan in 96% yield. Crystallization from methanol led to product of mp 133.5–136°C; nmr ($CDCl_3$) δ: 3.79 (s, 3H, OCH_3), 4.01 (s, 2H, 9-methylene), 5.9 (bs, 1H, N—H), 6.2–7.3 (m, 7H, aromatic). 3-Methoxyacridine was obtained in 77% yield by *p*-chloranil oxidation of 3-methoxyacridan as described for 2-methoxyacridine. Purification by chromatography on neutral alumina led to product of mp 89–91°C (lit. (26) mp 89–90°C). Both 2-methoxyacridine and 3-methoxyacridine were also prepared in overall 40% yield from the 9-chloroacridines through the 9-(2-*p*-toluenesulfonylhydrazino)acridine following Albert and Royer (27).

Kinetic measurements

Kinetics of oxidation were measured spectrophotometrically using methods and instrumentation described earlier (1, 6). The progress of the reaction was followed at the N-methylacridinium ion maximum (357.5 nm for **2***a*, and 367 nm for **2***b*, *c*) for all oxidants except TCNQ, where the formation of $TCNQ^{\cdot-}$ was followed at 680 nm. To minimize errors in relative rates (Table 3), rates of oxidation of **1***a*, *b*, and *c* were compared using the same acceptor stock solution. Measurements were carried out under pseudo first-order conditions using a 30-fold or greater molar excess of acceptor with BQ, TCNQ, TCNE, DCBQ, and some of the Co(III) oxidations. With CA and most of the Co(III) rates, smaller molar ratios (2 to 30) of acceptor to donor were used and the data analyzed using the appropriate integrated second-order rate equation. For a reaction of stoichiometry represented by

$$DH + \alpha A \rightarrow D^+ + \alpha(AH^-, AH_2, \text{or } A^{\cdot-})$$

this equation is

$$[6] \quad k_2 t = \frac{1}{[A]_0 - \alpha[DH]_0} \ln \frac{[DH]_0([A]_0 - \alpha[D^+])}{[A]_0([DH]_0 - [D^+])}$$

where the symbol $[\,]_0$ refers to initial concentration, and α is the number of moles of acceptor consumed per mole of donor. Values of k_2 were obtained as $1/([A]_0 - \alpha[DH]_0)$ times the slope of a plot of $\ln([A]_0 - \alpha[D^+])/([DH]_0 - [D^+])$ vs. t. In terms of measured optical densities (OD) at $t = 0$, t, and ∞ this function takes the form $\ln\{(OD_\infty - OD_0)[A]_0 - \alpha(OD_t - OD_0)[DH]_0\}/(OD_\infty - OD_t)[DH]_0$. Such second-order plots, as well as first-order plots with large excesses of oxidant, A, were linear through at least 85% reaction. The value of α was established as 2 for the Co(III) oxidations and as 1 for oxidation by CA in AN – 0.1 *M* acetic acid (below). The second-order rate constant obtained in this way for oxidation of NMA with CA (11.8 M^{-1} s^{-1}) is in good agreement with the value obtained earlier (11.7 (6)) using pseudo first-order conditions.

The stoichiometric ratio α in oxidation of NMA with CA in AN is

between 1 and 1.5 as a result of incomplete reaction of the hydroquinone monoanion, AH^-, with unreacted acceptor, A (6):

$$2AH^- + A \rightleftharpoons AH_2 + 2A^{\cdot-}$$

However, this reaction can be suppressed by protonation of AH^-. In AN – 0.1 *M* acetic acid, spectrophotometric examination of reactions of a limiting concentration of CA with a two-fold molar excess of NMA established that under these conditions 1.00 mol of CA yields 1.00 ± 0.05 mol of D^+, i.e., that $\alpha = 1.00 \pm 0.05$.

The stoichiometric ratio in oxidation of the three donors by $Co(bipy)_3^{3+}$, measured by spectrophotometric analysis of reaction mixtures for Co(II) (as $CoCl_4^{2-}$) is 2.00 ± 0.05. The following experiment is typical. A 1.00 mL aliquot of $Co(bipy)_3(ClO_4)_3$-bipy solution (5.58×10^{-3} and 1.81×10^{-2} *M*, respectively) + 100 μL of NMA solution (2.56×10^{-3} *M*) was allowed to react for 22.5 h at 25°C, and diluted to 5.00 mL with 12 *M* aqueous HCl. The spectrum of the solution from 580–720 nm matched the published spectrum of $CoCl_4^{2-}$ (28). The optical density at the 681.5 nm maximum was 0.0564, corresponding to an apparent extinction coefficient of 551, assuming formation of 2 Co(II) per NMA. Similar measurements using 1.00 mL of 2.800×10^{-3} *M* $Co(bipy)_3(ClO_4)_2$ solution in place of the reaction mixture yielded an apparent molar extinction coefficient of 547 ± 14 at 681.5 nm. Beer's Law is obeyed (within ±5%) in the concentration range examined ($1 - 6 \times 10^{-4}$ *M*) and the analysis is unaffected by the presence of Co(III) salt. Similar results were obtained with 2-MeO- and 3-MeO-NMA. Although conversion of Co(II) to $CoCl_4^{2-}$ is incomplete in concentrated aqueous HCl (28), the apparent extinction coefficient is constant within ±5% for the solvent mixtures (ca. 1:50 (v/v) AN–HCl to ca. 2:25 (v/v) AN–HCl) examined.

Final absorbances were constant to 10–20 half-lives in all rates. The spectra of the reaction mixtures indicated quantitative (±5%) conversion of DH to D^+ with BQ, CA, TCNE, DCBQ, and $Co(bipy)_3^{3+}$ and production of the theoretical quantity of $TCNQ^{\cdot-}$ with TCNQ.

pK_{R^+} measurements

"Mixed" pK_{R^+} values (29) were determined by spectrophotometric measurement of $[DOH]/[D^+]$ in solutions of measured pH as previously described (1). Stock solutions of the iodide salts were ca. 7×10^{-4} *M*. The numbers of independent determinations averaged, the pH ranges, and analytical wavelengths were: $2a^+I^-$, 22, 9.228–11.196, 357.2 nm; $2b^+I^-$, 13, 9.596–11.911, 367.2 nm; $2c^+I^-$, 16, 10.386–12.176, 366.2 nm. Optical densities of solutions of the 2-MeO and 3-MeO salts in buffers of pH above 10 decreased significantly over a 5-min time period following the first measurement. Since the decreases were approximately linear with time over this period, initial optical densities were obtained by linear extrapolation of readings taken at 3, 4, 5, 6, and 7 min after the time of mixing. Optical densities of solutions in 0.1 *M* NaOH increased with time, extrapolating to approximately zero at zero time. Repeated spectral scans of solutions in aqueous NaOH and the basic buffers showed that the optical density changes are due to the well-documented disproportionation of the cation to the corresponding acridone and acridan (11, 12). Thus, absorption maxima appeared at 405 and 424 nm ($2b^+I^-$) and at 321, 376, and 390 nm ($2c^+I^-$), characteristic of the 2- and 3-methoxy-N-methylacridones (**5***b* and *c*), respectively (30). The disproportionation reactions were not investigated further. As a consequence of the uncertainties in measured optical densities, the pK_{R^+} values are considered to be uncertain to about ±0.08 (maximum range of measured values). Agreement between pK_{R^+} values measured at pH's where disproportionation is slow and values measured at higher pH's supports the validity of the procedure. Mixed pK_{R^+} values were corrected to zero ionic strength as previously described (1).

Acknowledgements

Financial support from the Natural Sciences and Engineering Research Council of Canada is gratefully acknowledged. We wish to thank R. J. Balahura for use of stopped flow equipment and for helpful discussions, H. J. Stronks for assistance with the electrochemical measurements, and C. C. Lai and A. Effio for technical assistance.

1. A. K. COLTER, C. C. LAI, T. W. WILLIAMSON, and R. E. BERRY. Can., J. Chem. **61**, 2544 (1983).
2. M. F. POWELL and T. C. BRUICE. J. Am. Chem. Soc. **105**, 7139 (1983).
3. C. C. LAI and A. K. COLTER. J. Chem. Soc. Chem. Commun. 1115 (1980).
4. E. S. GOULD. Mechanism and structure in organic chemistry. Holt, Rinehart and Winston, New York. 1959. p. 217.
5. D. W. TURNER. *In* Advances in physical organic chemistry. Vol. IV. *Edited by* V. Gold. Academic Press, New York. 1966. p. 31.
6. A. K. COLTER, G. SAITO, and F. J. SHAROM. Can. J. Chem. **55**, 2741 (1977).
7. R. FOSTER. Organic charge-transfer complexes. Academic Press, New York. 1969. p. 42.
8. E. S. PYSH and N. C. YANG. J. Am. Chem. Soc. **85**, 2124 (1963).
9. E. STURM, H. KIESELE, and E. DALTROZZO. Chem. Ber. **111**, 227 (1978).
10. W. J. BLAEDEL and R. G. HAAS. Anal. Chem. **42**, 918 (1970).
11. J. W. BUNTING. *In* Advances in heterocyclic chemistry. Vol. 25. *Edited by* A. R. Katritzky and A. J. Boulton. Academic Press, New York. 1979. p. 1.
12. J. W. BUNTING and S. H. KABIR. J. Org. Chem. **43**, 3662 (1978).
13. G. SAITO and A. K. COLTER. Tetrahedron Lett. **38**, 3325 (1977).
14. E. R. THORNTON. J. Am. Chem. Soc. **89**, 2915 (1967).
15. T. H. LOWRY and K. S. RICHARDSON. Mechanism and theory in organic chemistry. 2nd ed. Harper and Row, New York. 1981. p. 199.
16. G. L. MCINTIRE, H. N. BLOUNT, H. J. STRONKS, R. V. SHETTY, and E. G. JANZEN. J. Phys. Chem. **84**, 916 (1980).
17. F. H. BURSTALL and R. S. NYHOLM. J. Chem. Soc. 3570 (1952).
18. R. G. BATES. Determination of pH. 2nd ed. John Wiley and Sons, New York. 1972. pp. 462–463.
19. W. BORSCHE, F. RUNGE, and W. TRAUTNER. Chem. Ber. **66**, 1315 (1933).
20. K. GLEU and S. NITZCHE. J. Prakt. Chem. **153**, 200 (1939).
21. A. ALBERT and J. B. WILLIS. J. Soc. Chem. Ind. London, **65**, 26 (1946).
22. V. S. FEDOROV. Zh. Obsch. Khim. **26**, 591 (1956).
23. K. LEHMSTEDT, W. BRUNS, and K. KLEE. Chem. Ber. **69**, 2399 (1936).
24. K. LEHMSTEDT and K. SCHRADER. Chem. Ber. **70**, 838 (1937).
25. A. ALBERT. The acridines. 2nd ed. Edward Arnold Ltd., London. 1966. p. 53.
26. S. M. SHERLIN, G. I. BRAZ, A. Y. JAKUBOVICH, E. I. VOROBJEVA, and F. E. RABINOVICH. Zh. Obshch. Khim. **8**, 884 (1968).
27. A. ALBERT and R. ROYER. J. Chem. Soc. 1148 (1949).
28. F. A. COTTON, D. M. L. GOODGAME, and M. GOODGAME. J. Am. Chem. Soc. **83**, 4690 (1961).
29. A. ALBERT and E. P. SERJEANT. The determination of ionization constants. Chapman and Hall, London. 1971. p. 44.
30. R. D. BROWN and F. N. LAHEY. Aust. J. Sci. Res. Ser. A, **3**, 593 (1950).

Can. J. Chem. Downloaded from www.nrcresearchpress.com by 210.87.254.105 on 09/06/12
For personal use only.

Radical ions in photochemistry. 15. The photosubstitution reaction between dicyanobenzenes and alkyl olefins

ROBERT M. BORG, DONALD R. ARNOLD,[1] AND T. STANLEY CAMERON
Department of Chemistry, Dalhousie University, Halifax, N.S., Canada B3H 4J3

Received August 18, 1983[2]

ROBERT M. BORG, DONALD R. ARNOLD, and T. STANLEY CAMERON. Can. J. Chem. **62**, 1785 (1984).

The photosubstitution (electron transfer) reaction between 1,4-dicyanobenzene (**1**) and 2,3-dimethyl-2-butene (**2**), which gives 1-(4-cyanophenyl)-2,3-dimethyl-2-butene (**3**) and 3-(4-cyanophenyl)-2,3-dimethyl-1-butene (**4**), has been extended to other dicyanobenzene–olefin mixtures. Substitution of a cyano group occurs when both **1** or 1,2-dicyanobenzene (**5**) are irradiated in acetonitrile solution, in the presence of **2** or cyclohexene (**16**). Under comparable conditions, 1,3-dicyanobenzene (**6**) failed to react. Little or no substitution was observed in any case when the olefin was methylpropene (**19**). The results for **1** and **5** are in agreement with empirical free energy calculations (Weller equation) for the electron transfer process which, however, fail to explain the general lack of reactivity of 1,3-dicyanobenzene. Phenanthrene (**11**) has been shown to photosensitize the photosubstitution reaction between dicyanobenzenes and **2**. Under these conditions the olefin reacts with **6** predominantly at the 4-position, resulting in overall substitution of a hydrogen atom. This reaction occurs regiospecifically, resulting in the formation of only one of the two possible isomeric side chains. The mechanistic details of these reactions have been substantiated by means of deuterium labelling studies. The aromatic nitriles also undergo photosubstitution by **2**, in acetonitrile–methanol solution, resulting in methanol-incorporated products. Whereas reaction with **1** or **5** results in substitution of a cyano group, **6** was observed to give isomeric dicyanocyclohexenes, resulting from initial reaction at the 4-position, followed by reduction. A detailed mechanism for this secondary photoreduction has been substantiated by deuterium labelling studies. The anomalous behaviour of 1,3-dicyanobenzene has been attributed to a difference in the reactivity of the radical anion.

ROBERT M. BORG, DONALD R. ARNOLD et T. STANLEY CAMERON. Can. J. Chem. **62**, 1785 (1984).

La réaction de photosubstitution (transfert d'électron) entre le dicyano-1,4 benzène (**1**) et le diméthyl-2,3 butène-2 (**2**), qui donne le (cyano-4 phényl)-1 diméthyl-2,3 butène-2 (**3**) et le (cyano-4 phényl)-3 diméthyl-2,3 butène-1 (**4**), est étendue à d'autres mélanges de dicyanobenzène et d'oléfines. Il se produit une substitution d'un groupe cyano lorsque soit le composé **1** ou le dicyano-1,2 benzène (**5**) sont irradiés, en solution dans l'acétonitrile, en présence du composé **2** ou du cyclohexène (**16**). Dans des conditions comparables, le dicyano-1,3 benzène (**6**) ne réagit pas. Lorsque l'oféfine est le méthylpropène (**19**), on n'observe pratiquement pas de substitution. Les résultats obtenus dans le cas des composés **1** et **5** sont en accord avec des calculs empiriques d'énergies libres (équation de Weller) pour le processus de transfert d'électron, qui n'explique cependant pas le manque général de réactivité du dicyano-1,3 benzène. On a montré que le phénanthrène (**11**) photosensibilise la réaction de photosubstitution entre les dicyanobenzènes et le composé **2**. Dans ces conditions, l'oléfine réagit principalement avec la position 4 du composé **6** et il en résulte, dans l'ensemble, une substitution nette d'un hydrogène. Cette réaction est régiospécifique et conduit uniquement à la formation de l'une des deux chaînes latérales possibles. Des études impliquant des marquages par le deutérium permettent de confirmer les détails mécanistiques de ces réactions. Les nitriles aromatiques, en solution dans des mélanges d'acétonitrile et de méthanol, subissent aussi des photosubstitutions par **2**; il y a formation de produits ayant incorporé du méthanol. Alors que la réaction des composés **1** ou **5** conduit à la substitution d'un groupe cyano, on a observé que le composé **6** donne des dicyanocyclohexènes isomères qui résultent d'une réaction initiale en position 4, suivie d'une réduction. Des études impliquant des marquages par du deutérium ont permis de confirmer le mécanisme détaillé de cette photoréduction secondaire. On attribue le comportement anormal du dicyano-1,3 benzène à la différence de réactivité de l'anion radical.

[Traduit par le journal]

Introduction

The photochemistry of aromatic nitriles in the presence of olefins has been an area of intense research activity during recent years (1). This is primarily due to the variety of potentially useful reactions that are known to occur, depending upon reaction conditions, such as solvent polarity and the oxidation or reduction potentials of the reactants. In nonpolar solvents, such as hexane, exciplex formation is predominant and often results in [2e+2e] cycloaddition to the nitrile bond (1*b*, *c*) or to the aromatic ring (1*a*, *f*, *h*). In more polar solvents, such as acetonitrile, full electron transfer can occur; radical ions are then the primary reactive species (1*d*, *e*, *g*; for a recent review on the reactions of radical ions generated photochemically, see ref. 2). These can react with one another, or with some other species in solution.

Several examples of the co-reaction of photochemically generated radical ion pairs have been reported (2), but few of these involve substitution of the nitrile function on the acceptor by an olefin (3–5). Recently we have described (1*c*) the photosubstitution reaction between 1,4-dicyanobenzene, (**1**), and 2,3-dimethyl-2-butene, (**2**), which gives the substituted benzonitriles, **3** and **4** (Fig. 1). Our interest in this reaction was renewed by an observation made during our recent studies into the photosensitized (electron transfer) [2e+4e] cycloaddition of phenylated olefins (6). We noticed that, while both 1,4- and 1,2-dicyanobenzene (**1** and **5** respectively) are good sensitizers of the reaction, on the other hand, in the presence of 1,3-dicyanobenzene, (**6**), no reaction was observed.[3] This behaviour is unusual because successful uses of **6** as a photosensitizer (electron transfer) have been reported in the literature (7). However, a similar trend in reactivity has been observed in the photosubstitution (electron transfer) of dicyanobenzenes by triethylamine (8). We wondered whether this anomalous be-

[1] Author to whom all correspondence should be addressed.
[2] Revision recived March 12, 1984.
[3] R. M. Borg and D. R. Arnold, unpublished results.

Can. J. Chem. Downloaded from www.nrcresearchpress.com by 210.87.254.42 on 09/06/12
For personal use only.

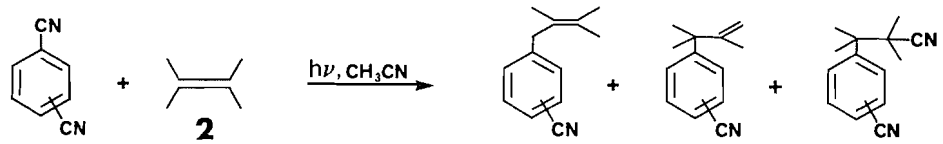

5 1,2- **7** 16(21)*% **8** 18(24)*% **12** trace

6 1,3- **9** trace **10** trace —

1 1,4- **3** 10(23)*% **4** 18(42)*% **13** trace

*Yields in the presence of Phenanthrene (**11**)

FIG. 1

haviour would also be reflected in the reactivity of **6** towards photosubstitution by **2**. Furthermore, since the scope and limitations of this photosubstitution reaction have not yet been defined, and since products such as **3** and **4** are not readily accessible by more classical synthetic procedures, we decided the reaction warrants further study.

This paper, therefore, describes the results obtained when other dicyanobenzene–olefin mixtures are irradiated, as well as the dramatic improvement in the efficiency of the reaction through the use of photosensitization (electron transfer). The variation that results when a nucleophilic solvent such as methanol is used will also be discussed.

Results

Ultraviolet irradiation of a solution of 1,2-dicyanobenzene (**5**) and **2** in acetonitrile, through Pyrex ($\lambda > 280$ nm), resulted in a clear yellow solution from which the photosubstitution products, 1-(2-cyanophenyl)-2,3-dimethyl-2-butene (**7**) and 3-(2-cyanophenyl)-2,3-dimethyl-1-butene (**8**), were isolated by column chromatography. Under similar conditions, 1,3-dicyanobenzene (**6**) reacted very slowly to give only traces of the analogous 1,3-substituted products **9** and **10** (Fig. 1).

The photosubstitution reaction is quite inefficient (i.e. long irradiation times are required) when the cyanoaromatic is irradiated directly. A dramatic enhancement in efficiency was observed upon the addition of phenanthrene (**11**). Thus, for the reaction of 1,4-dicyanobenzene (**1**) with **2**, whereas the previously reported yields of the products **3** and **4** were 10% and 18% respectively (*1e*), in the presence of **11** these increased to 23% and 42%, and the irradiation time was shortened considerably (less than one-half). Similarly, yields of **7** and **8** were improved (Fig. 1). Phenanthrene recovery was generally better than 80%. Traces of the cyanated side-chain products **12** and **13** were also obtained. Use of naphthalene instead of **11** resulted in no significant enhancement in the rate of conversion, while the addition of anthracene was observed to slow down the reaction. Dinitrile **6** also reacts faster with **2** in the presence of **11**. However, in this case, the olefins **9** and **10** were not the major products. Instead, a colourless crystalline solid was isolated which was characterized as having the structure 1-(2,4-dicyanophenyl)-2,3-dimethyl-2-butene (**14**). Only this isomer was formed; no trace of **15** was detected (Fig. 2).

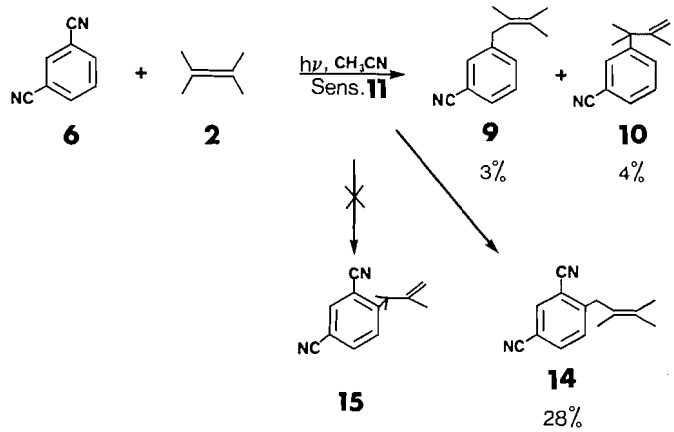

FIG. 2

The ultraviolet absorption spectra of all three dicyanobenzenes tail off at 300 nm. No reaction occurred if the irradiation was carried out through a long wavelength filter ($\lambda >$ 300 nm) unless **11** was present.

Both **1** and **5** reacted with cyclohexene (**16**) when irradiated in acetonitrile solution, but the transformation proceeded more slowly than with **2** as the olefin. Nevertheless, the photolysates were relatively clean and the desired photosubstitution products **17** and **18** (Fig. 3) were readily isolated by column chromatography. When **11** was used as a photosensitizer, the material balance of the reaction was improved in both cases. No reaction was observed between **6** and **16**, even in the presence of **11** and after prolonged irradiation.

All three dicyanobenzenes remained inert when irradiated in the presence of methylpropene (**19**) in acetonitrile solution. This was also the case in the presence of added **11**.

The photosensitized reactions illustrated in Figs. 1 and 2 were repeated with 2,3-dimethyl-2-butene-d_{12}. The substitution products were isolated and examined for deuterium incorporation by ^{13}C nmr spectroscopy.

Switching from pure acetonitrile as the solvent to a 3:1 mixture (by volume) of acetonitrile–methanol had the effect of accelerating the photolysis, which now proceeded with the incorporation of methanol in the products. Thus, the irradiation of **1** in the presence of **2** and **11**, followed by the usual work-up, afforded the ether **20** (Fig. 4) in 70% isolated yield. Similarly,

Can. J. Chem. Downloaded from www.nrcresearchpress.com by 210.87.254.42 on 09/06/12
For personal use only.

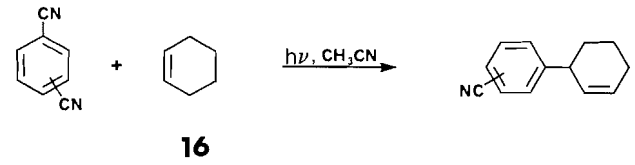

FIG. 3

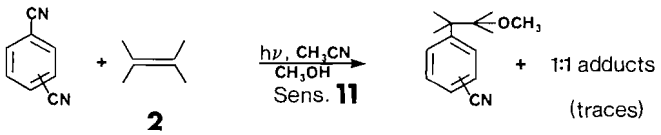

FIG. 4

the 1,2-substituted ether **21** was obtained in 45% yield from reaction of **5**. Control experiments established that these reactions proceeded in an identical fashion in the absence of **11**, except that longer irradiation times were required and yields were somewhat lower.

In the presence of methanol and **11**, the photo-induced reaction between **6** and **2** results in a complex mixture of products. Compound **22** (Fig. 5), analogous to the ethers **20** and **21**, was only a minor product. Instead, three isomeric crystalline compounds, **23–25** (Fig. 5), were obtained. The structure of these products rests firmly on the X-ray crystallographic analysis. Stereoscopic views of the molecules in the final structure are given in Fig. 6.

The relative ratios of these compounds was found to be dependent on the irradiation time. At low conversion (50%), yields of **23**, **24**, and **25** were 5%, 20%, and 26%, respectively. At higher conversion (75%), these figures changed to 0%, 7%, and 15%. Once again, in the absence of **11**, the reaction proceeded similarly, except that longer irradiation times were required, and a poorer material balance was obtained. The photolysis was also carried out with methanol-d_1 in the place of normal methanol. The products were isolated and analysed for deuterium incorporation by 360-MHz ^{1}Hmr spectroscopy.

The addition of methanol to the solvent has practically no effect on the efficiency of reaction between 1,4-dicyanobenzene (**1**) and methylpropene (**19**). However, prolonged irradiation does result in the formation of traces of the ether **26** (Fig. **7**). The addition of **11** results in the quenching of the formation of **26**. No trace of **27** could be detected. In view of the low yields obtained from this reaction, the photolyses involving **5** and **6** were not attempted.

Structural assignments

The structures assigned to the sixteen new compounds reported here (**7–10**, **12–14**, **17**, **18**, and **20–26**) are based predominantly on the ^{1}Hmr, ^{13}Cmr, infrared, and mass spectral data, as well as elemental analyses. The aliphatic region in the 80-MHz ^{1}Hmr spectra of **7** and **9** exhibits resonances corresponding to three vinyl methyl, and one vinyl methylene, groups. These are all broadened as a result of the homoallylic coupling typical of these systems (9). The isomers **8** and **10** show the ABX_3-type coupled system expected for the vicinal methylene (AB) at 4.8 ppm and methyl (X_3) at 1.7 ppm. The aromatic region in the ^{1}Hmr spectra of the four isomers is too complex at 80 MHz to allow conclusive deductions about substitution patterns to be made. However, the infrared spectra of these compounds are informative in this respect. The out-of-plane CH bending mode absorptions at 760 cm^{-1}, typical of 1,2-disubstituted aromatics (10), are prominent in the spectra of both **7** and **8** while, for **9** and **10**, bands at 790 cm^{-1} and 690 cm^{-1} are consistent with 1,3-disubstitution (10). The spectral data reported elsewhere (1*e*) for the corresponding 1,4-disubstituted isomers, **3** and **4**, render the above assignments more definitive.

Compound **14** was shown to have retained both cyano functions present in the starting material by the presence of two singlet resonances in the ^{13}Cmr spectrum at 117 and 116 ppm, typical of *sp*-hybridized carbon atoms in aromatic nitriles (11). Furthermore, the 360-MHz proton spectrum readily demonstrated the presence of an ABX system in the aromatic region with coupling constants that are consistent with 1,2,4-trisubstitution. The presence of a band of medium intensity at 860 cm^{-1} in the infrared spectrum confirmed this (10).

The cyclohexenylcyanobenzenes, **17** and **18**, were shown to be substituted at the 3-position of the cyclohexene ring (and not at the 1- or 4-position). In the mass spectra of **17** and **18**, a prominent peak at *m/e* 155 is indicative of a loss of 28 mass units, ethylene. This is consistent with 1- or 3-substitution, but not with 4-substitution. A weak absorption at 1650 cm^{-1} in the infrared spectrum, as well as no significant absorption above 290 nm in the ultraviolet spectrum, indicates a carbon–carbon double bond that is unconjugated with the aromatic ring. The presence of two vinyl protons, revealed by ^{1}Hmr and ^{13}Cmr spectroscopy, confirms that **17** and **18** are indeed 3-substituted cyclohexenes. Finally, 1,2- and 1,4-substitution on the aromatic ring is once again supported by infrared spectroscopy.

The proton magnetic resonances of the ethers **20–22** are predictably simple in the aliphatic region and the chemical shifts of the resonances compare favourably with those reported for similar compounds (1*d*, *g*). The mass spectra of all three isomers exhibit a weak peak at *m/e* 217, corresponding to an MH^+ ion, but no molecular ion. This behaviour is typical of ethers (12). The lower molecular mass region of the spectrum is dominated by the presence of an intense base peak at *m/e* 73. This may be attributed to cleavage of the side chain to give a stabilized cation as well as an also stable cyanocumyl radical; this is in good agreement with the proposed structure. It is interesting to note that while in the mass spectra of the aforementioned ethers the base peak occurs at *m/e* 73, for the similarly-structured compounds **12** and **13** (Fig. 1), the cyanocumyl cation at *m/e* 144 is the predominant ion, due to the relative instability of the alternative cyano-substituted cationic centre.

Cyclohexenes **23–25** were characterized conclusively by means of X-ray crystallography. Nevertheless, since a detailed mechanism for the formation of these compounds relies heavily on deuterium incorporation studies (*vide infra*), a complete analysis of the 360-MHz ^{1}Hmr spectra of these products was necessary. The spectral assignments are based primarily on

Can. J. Chem. Downloaded from www.nrcresearchpress.com by 210.87.254.42 on 09/06/12
For personal use only.

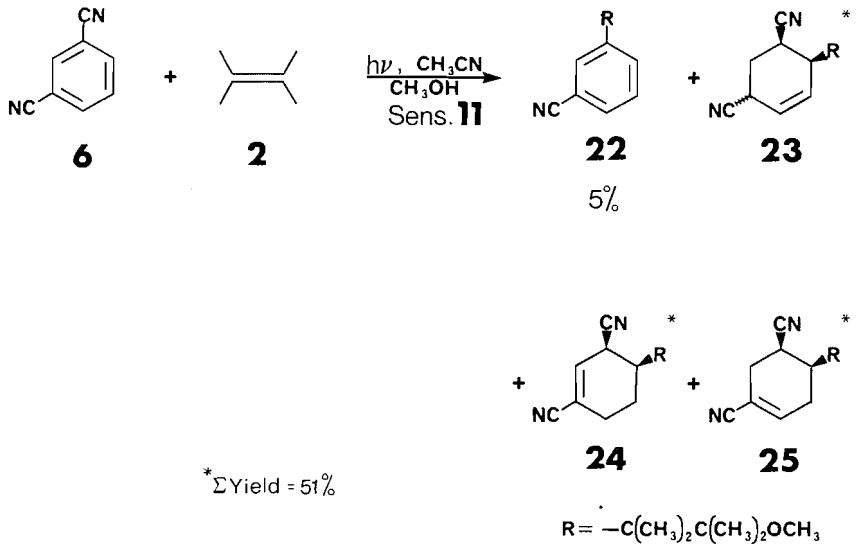

FIG. 5

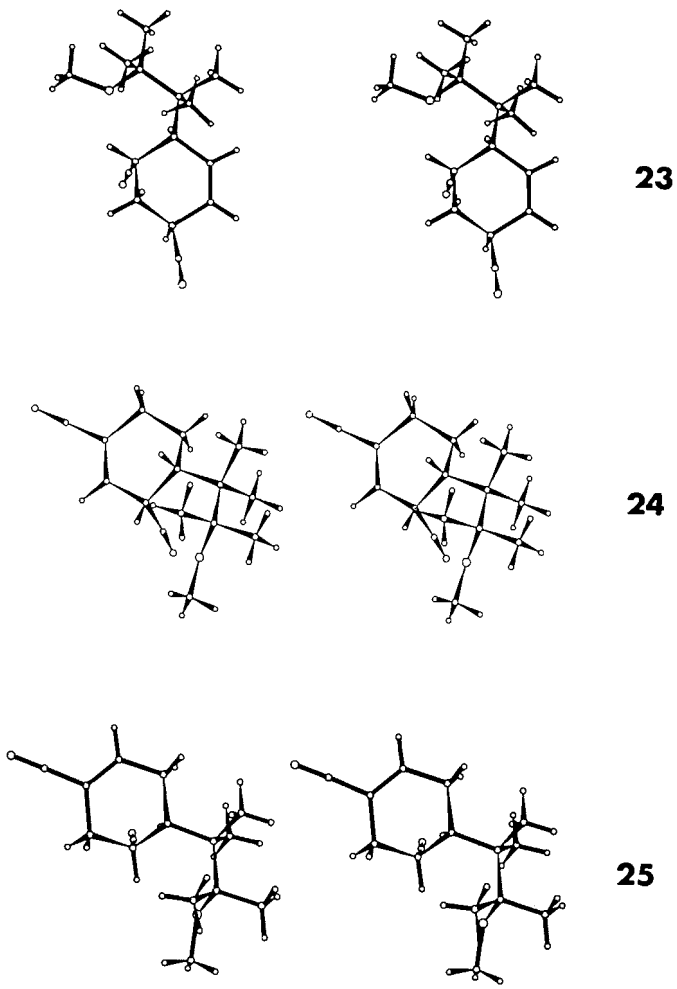

FIG. 6. Stereoscopic views of **23**, **24**, and **25**.

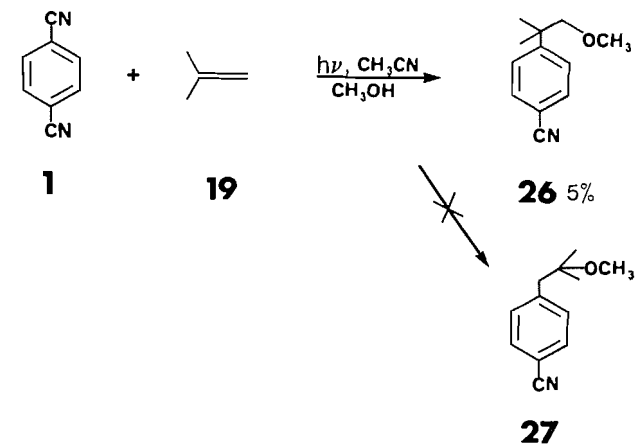

FIG. 7

X-ray data (supplementary material available). These data demonstrate that the bulky side chain present in **23**–**25** exists predominantly in an equatorial position.

The results for compound **23** will be presented here as an example. In compound **23**, since the side chain is in a pseudo-equatorial position (13), H_3 and H_6 are pseudo-axial, while H_5 is equatorial. The two high-field multiplets, centered at 2.50 and 2.09 ppm, are due to H_{4e} and H_{4a}, respectively. Analysis of these systems indicates a large coupling constant ($J_{4a,4e}$ = 13.3 Hz), typical of geminal coupling in six-membered rings (ref. 10, p. 275). The lower field resonance is assigned unambiguously to H_{4e} on the basis of the observed small coupling of 1.6 Hz magnitude with H_2. According to the X-ray data, H_{4e} and H_2 are in the correct orientation for this long-range "W-type" coupling (ref. 10, pp. 334–341). Having identified H_{4a}, $H_{3a'}$ can now easily be recognized at 3.7 ppm, due to the large coupling ($J_{3a',4a}$ = 11.9 Hz) associated with axial–axial vicinal coupling (ref. 10, p. 288). This is further substantiated by the observed small (<2 Hz) vicinal coupling, $J_{3a',2}$. Of the two remaining high field multiplets, H_{5e} is assigned to 3.42 ppm, since this resonance clearly is coupled to both H_{4e} and H_{4a}, as well as to $H_{6a'}$ ($J_{5e,6a'}$ = 3.8 Hz). This assignment seems even more reasonable on a chemical shift basis, since H_{5e} is geminal to a cyano substituent. All other coupling constants are also consistent with these assignments.

In the 360-MHz ^{1}Hmr spectrum of **23** prepared in methanol-d_1, positions 3 and 5 are completely deuterated, as is indicated clearly by the absence of the resonances assigned to $H_{3a'}$ and

Can. J. Chem. Downloaded from www.nrcresearchpress.com by 210.87.254.42 on 09/06/12
For personal use only.

TABLE 1. The fluorescence quenching of dicyanobenzenes by alkyl olefins in acetonitrile

Fluorophor	τ, ns	k_q, M^{-1} s^{-1} × 10^{10} 2	16	19
1,2-Dicyanobenzene (**5**)	5.7	2.0	1.6	1.0
1,3-Dicyanobenzene (**6**)	13.9	1.7	1.3	1.1
1,4-Dicyanobenzene (**1**)	8.8	1.5	1.5	1.3

H_{5e}. Furthermore, H_{4a} is also no longer visible, and the resonances due to H_1, H_2, $H_{6a'}$, and H_{4e} are now simplified considerably by the absence of the relevant spin–spin coupling.

A similar analysis of the 360-MHz ^{1}Hmr spectra of natural abundance and deuterated cyclohexenes **24** and **25** led to the deuterium substitution pattern assignments illustrated in Fig. 19.

A few other features in the spectral data of cyclohexenes **23**–**25** are worth mentioning. The infrared absorption spectra of **24** and **25** indicate the presence of two cyano stretching frequencies, corresponding to conjugated and unconjugated triple bonds. As expected, **23** shows only one such absorption at 2235 cm^{-1}. The mass spectra of these compounds are similar to those of the ethers **20**–**22** in that all three exhibit a weak MH^+ ion as well as an intense peak at *m/e* 73 which once again dominates the spectrum. However, fragments at *m/e* 115 and 84, presumably due to the methoxytetramethylethyl cation and tetramethylethyl radical cation, respectively, are now also quite prominent. Evidently, fragmentation of the entire side chain as a whole is preferred in the cyclohexenes, where the formation of a cyanocumyl radical is no longer feasible.

The ether **26** was distinguished from the regioisomeric form **27** on the basis of mass spectral and ^{13}Cmr data. The observed base peak at *m/e* 45 is indicative of cleavage at the side chain to give the methoxymethylene cation (as well as a cyanocumyl radical). Compound **27**, on the other hand, would be expected to give an intense peak at *m/e* 73, by analogy with the data presented for the above compounds. No such fragment was observed. An MH^+ ion at *m/e* 190 is also evident. Finally, the ^{13}Cmr magnetic resonances at 81.8 (t) and 39.4 (s) ppm are in agreement with those reported for compounds with the same side-chain composition as in **26** (15).

Photophysical studies

Rate constants for fluorescence quenching of the dicyanobenzenes by olefins **2**, **16**, and **19** were obtained from Stern–Volmer type plots of fluorescence intensity. These results are presented in Table 1. The singlet fluorescence lifetimes in degassed acetonitrile were obtained by a single photon counting technique. No exciplex emission could be detected during the quenching experiments, even at high concentrations of quencher.

The ultraviolet absorption and fluorescence emission spectra of the dicyanobenzenes, **1**, **5**, **6** and phenanthrene (**11**) in acetonitrile were measured. The emission spectra were normalized and the singlet energies of the compounds were estimated from the interesection of absorption and emission spectra. The results are presented in Table 2.

Discussion

Although the photosubstitution (electron transfer) of dicyanobenzenes by olefins is by no means a general reaction, the results just presented indicate that the method provides some synthetic utility, even in the low yield cases, since alternative synthesis of the products is not straightforward.

One of the most interesting observations to emerge from the results is the unique behaviour of 1,3-dicyanobenzene (**6**) when compared with the 1,2- and 1,4-isomers. Not only does **6** react at least ten times slower than **1** and **5** under comparable conditions, it also yields main products that are quite different. This anomalous behaviour is especially peculiar in the light of photophysical studies that show that all three isomers behave similarly.

Irradiations in acetonitrile solution

The mechanistic scheme previously proposed (1*e*) for the photosubstitution reaction in acetonitrile is outlined in Fig. 8. With reference to this scheme, the primary step in the reaction is excitation of the cyanoaromatic to the first excited singlet state. All three dicyanobenzenes absorb at wavelengths shorter than 300 nm and, under the conditions of the experiment (Pyrex, $\lambda > 280$ nm), they are expected to act as the principal absorbing species in solution. Upon encountering an olefin, electron transfer to the excited acceptor may occur, and the resulting radical ion pair is then able to proceed via the two mechanistic pathways depicted in the scheme. A similar mechanism is expected for reaction with cyclohexene (**16**), except that in this case only one product is, of course, possible.

Evidence for the involvement of the first excited singlet state of the dicyanobenzenes in the primary step of the reaction stems from the measured fluorescence lifetimes, and Stern–Volmer type plots. The quenching rate constants (Table 1) are all close to the diffusion-controlled limit[4] for acetonitrile solutions. This fluorescence quenching, combined with the fact that little or no reaction is observed when the irradiations are carried out in a nonpolar solvent (such as benzene) is strongly suggestive of an electron transfer mechanism.

The Weller (17) equation was used to estimate the free energy change associated with electron transfer from the olefins to the first excited singlet state of the dicyanobenzenes (Table 2). The calculations suggest that the transfer should be exergonic in all cases involving 2,3-dimethyl-2-butene (**2**) and cyclohexene (**16**), but unfavourable when methylpropene (**19**) is the donor. These values are consistent with the experimentally observed results for **1** and **5**, i.e. reasonably fast reaction with **2**, slower with **16**, and no reaction at all with **19**. However, they fail to explain why 1,3-dicyanobenzene (**6**) reacts so slowly when irradiated in the presence of **2** and, moreover, why it does not react at all with **16** since, in both cases, ΔG_{calc} is negative. It is conceivable that electron transfer to the first excited singlet of **6** is indeed occurring, especially in view of the diffusion-controlled quenching observed; but back electron transfer (18) is an efficient deactivation pathway. This process is probably the main reason for the low quantum yields frequently observed in photoreactions involving radical ion pairs generated in the singlet state (19).

A surprising feature of the data presented in Table 1 is the diffusion-controlled fluorescence quenching observed for all three dicyanobenzenes by methylpropene (**19**). In view of the observed lack of reaction and the positive values for ΔG_{calc} in the electron transfer step (Table 2), this result was unexpected. In these cases, a quenching mechanism other than full electron

[4] The limit is 1.7×10^{10} M^{-1} s^{-1} at 25°C using the Debye equation (16*a*): $k_d = 2 \times 10^5\ T/\eta$. At 25°C, η for acetonitrile = 0.345 cP (16*b*).

Can. J. Chem. Downloaded from www.nrcresearchpress.com by 210.87.254.42 on 09/06/12
For personal use only.

TABLE 2. The calculated free energy change for the electron transfer process

Acceptor	$-E^{red}_{1/2}$,[a] V	Singlet energy[c] kJ mol^{-1}	ΔG_{calc} for electron transfer[d] kJ mol^{-1}		
			2	**16**	**19**
1,2-Dicyanobenzene (**5**)	2.05	408	−92	−25	+6
1,3-Dicyanobenzene (**6**)	2.2[b]	418	−91	−24	+7
1,4-Dicyanobenzene (**1**)	2.00	408	−97	−29	+2

[a]Cyclic voltammetry on Pt electrode, tetraethylammonium perchlorate (TEAP, 0.1 *M*) in acetonitrile solution, vs. Ag/0.1 *M* $AgNO_3$.

[b]The electron transfer process was irreversible. Value taken as 0.029 V before the cathodic peak potential (ref. 41).

[c]Estimated from the intersection of the ultraviolet absorption and fluorescence emission spectra.

[d]Calculated from the Weller equation (17). The oxidation potentials of **2** and **16** are +1.28 V and +1.98 V, respectively (cyclic voltammetry, vs. Ag, this work). The oxidation potential of **19** (+2.3 V) was estimated from the ionization potential using the equation $E^{ox}_{1/2} = 0.827$ I.P. − 5.40 V (ref. 14).

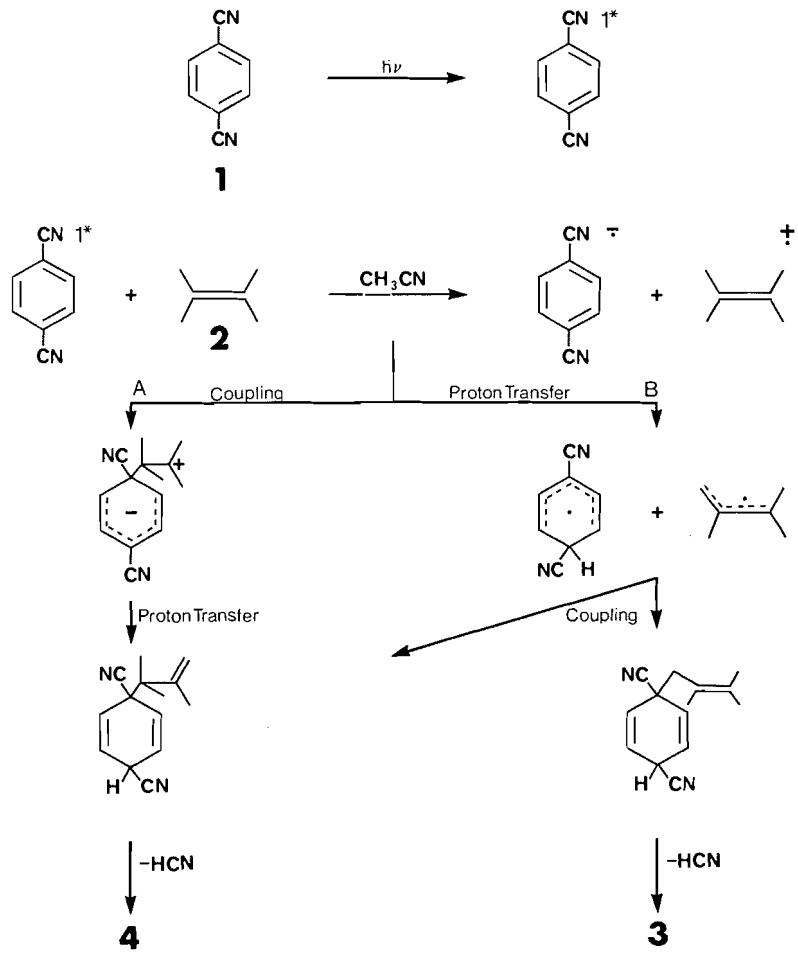

FIG. 8

transfer (e.g. exciplex formation) may be operative. The best evidence for the formation of an exciplex would be to observe emission from it. However, emission could not be detected from solutions of the dicyanobenzenes in acetonitrile, even when the fluorescence of these compounds was strongly quenched by any of the olefins investigated. Weak emission was observed when hexane was the solvent; especially when 1,3-dicyanobenzene (**6**) was the fluorophor and **2** was the quencher. It therefore seems plausible that ionic dissociation of the exciplexes in acetonitrile, followed by rapid back electron transfer, provides an efficient pathway for deactivation of the excited singlet state of the aromatic nitriles.

These photosubstitution reactions are generally inefficient, especially in the case of 1,3-dicyanobenzene (**6**). The use of phenanthrene (**11**) as a photosensitizer dramatically improved the efficiencies of some of the reactions, and material balances were enhanced. Other workers (4*a*, 7*a*, 20) have reported that **11**, as well as other aromatic hydrocarbons, act as sensitizers in photoreactions involving radical ion formation. They propose that the role these compounds play is that of a "radical

Can. J. Chem. Downloaded from www.nrcresearchpress.com by 210.87.254.42 on 09/06/12
For personal use only.

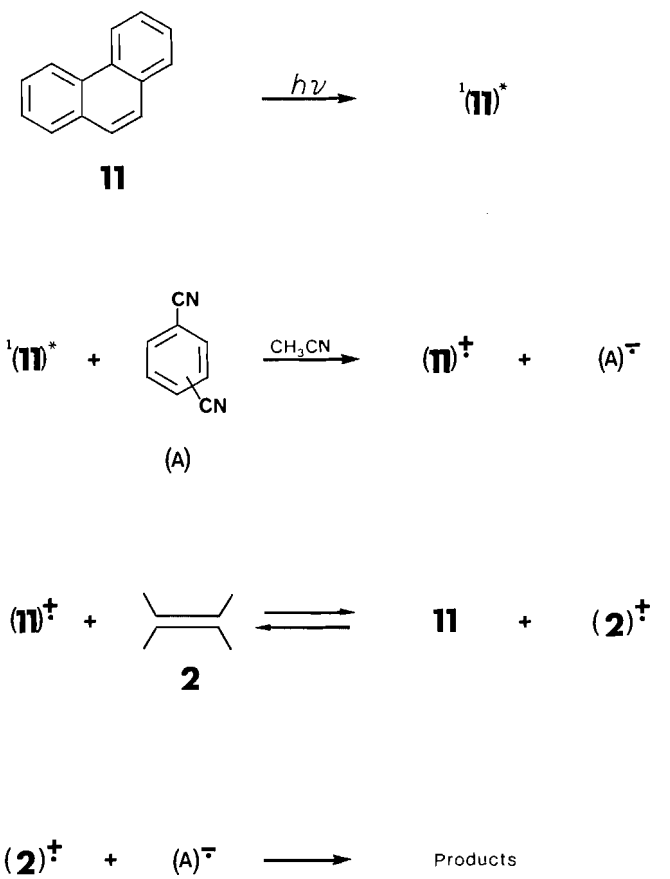

FIG. 9

cation transfer agent", as is depicted in Fig. 9, where the mechanistic scheme has been applied to the photosubstitution reaction.

According to the scheme, since **11** absorbs at longer wavelengths that the dicyanobenzenes, it now acts as the principle chromophore, resulting in the formation of the first excited singlet state (^{1}**11***). This then transfers an electron to ground state dicyanobenzene to form a radical ion pair which, in the polar acetonitrile solvent, leads to solvent separated ions. The encounter of the phenanthrene radical cation (**11**$^{\cdot+}$) with **2** could then result in a radical cation transfer. Such a transfer is feasible, but would be reversible, since **11** and **2** have similar oxidation potentials ($E^{ox}_{1/2}$ = +1.31 V and +1.28 V, respectively). This process has analogy in the well-known redox catalysis in organic electrochemistry (21). The resulting radical cation of **2** would then proceed to products according to the scheme given earlier (Fig. 8). Terms such as "co-sensitization" (20) or "redox photosensitization" (4*b*) have also been used to describe this mode of photosensitization.

There is ample evidence in the literature for the proposed electron transfer step between **11** and 1,4-dicyanobenzene (**1**). The radical cations of both pyrene (22) and **11** (7*a*) have been detected by means of laser flash photolysis in acetonitrile in the presence of **1**. Furthermore, Pac and co-workers (4*b*) have calculated the theoretical free energy change for the transfer process, using the Weller equation, and came to the conclusion that transfer from the excited singlet state of several aromatic hydrocarbons to **1** should be a highly favoured process. This was further substantiated by their observation that fluorescence from the hydrocarbons in polar solvents was quenched at the

TABLE 3. Calculated free energy change for electron transfer from the first excited singlet of phenanthrene

Acceptor	ΔG_{calc} for electron transfer,[a] kJ mol^{-1}
1,2-Dicyanobenzene (**5**)	−27
1,3-Dicyanobenzene (**6**)	−13
1,4-Dicyanobenzene (**1**)	−32

[a]Using the Weller equation (17). The reduction potentials of the acceptors are listed in Table 2. The oxidation potential of phenanthrene is +1.31 V vs. Ag.

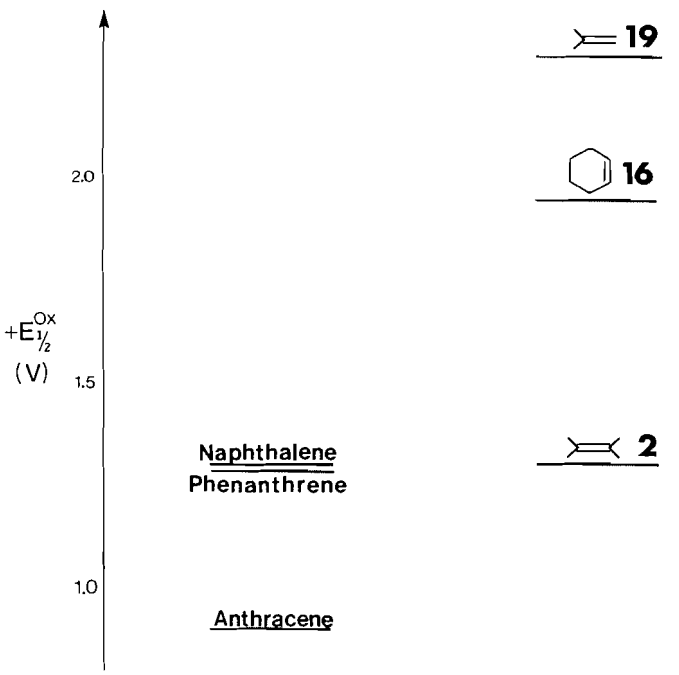

FIG. 10. The relative oxidation potentials of the aromatic hydrocarbons and the alkyl olefins.

diffusion-controlled rate by **1** (4*b*). Table 3 lists the calculated ΔG values for electron transfer from the excited singlet of phenanthrene (**11**) ($^1\Delta E_{0-0}$ = 346 kJ mol^{-1}) to the dicyanobenzenes. The values indicate that the above arguments should also apply to 1,2- and 1,3-dicyanobenzene.

Naphthalene and anthracene were also tried in the present system. Naphthalene neither sensitized nor quenched the reaction while anthracene slowed down the photolysis considerably. This, in spite of the fact that ΔG_{calc} for electron transfer to **1** from the first excited singlet of both hydrocarbons is negative (4*b*). The reason for this becomes clearer when one considers the relative oxidation potentials of these aromatic hydrocarbons compared to that of the olefins, as is illustrated in Fig. 10.

Reversible radical cation transfer to **2** or **16** is feasible from both phenanthrene (**11**) or naphthalene. However, since the main factor increasing the reaction efficiency is more effective use of light, naphthalene is not as useful a photosensitizer (electron transfer) as is phenanthrene. The absorption spectrum of **11** tails out to 360 nm while naphthalene does not absorb much above 330 nm. Since the anthracene molecule is an even longer-wavelength chromophore than **11**, it would be expected to be a more effective photosensitizer. However, as Fig. 10 indicates, transfer from the anthracene radical cation to the olefin is endothermic in all cases and this aromatic hydrocarbon

Can. J. Chem. Downloaded from www.nrcresearchpress.com by 210.87.254.42 on 09/06/12
For personal use only.

Can. J. Chem. Downloaded from www.nrcresearchpress.com by 210.87.254.42 on 09/06/12
For personal use only.

therefore acts as a quencher of the reaction. For the same reason, **11** does not photosensitize the reaction between 1,4-dicyanobenzene (**1**) and methylpropene (**19**) in acetonitrile solution, and actually quenches the formation of the ether **26** when **1** and **19** are irradiated in acetonitrile–methanol.

In most of the reported examples of related photosensitizations (4*a*, 7*a*, 20), the aromatic hydrocarbon was largely recovered after reaction. However, during the course of the irradiations described here some conversion (20%) of **11** to 9-cyanophenanthrene (**28**) and 9-cyano-9,10-dihydrophenanthrene (**29**) was observed. The formation of these side products can be explained by attack of cyanide ion on the radical cation of phenanthrene.

The photosensitized (electron transfer) cyanation of aromatic hydrocarbons has been well characterized by Pac and coworkers (7*b*). Formation of these derivatives provides further evidence for the involvement of the radical cation of **11** in the photosubstitution reaction, as well as demonstrating the presence of cyanide ion. Other evidence for the release of cyanide ion is the isolation of traces of **12** and **13** (Fig. 1). It seems likely that these compounds result from the nucleophilic interception of the radical cation of 2,3-dimethyl-2-butene (**2**) by cyanide ion. This point will be discussed in more detail below.

It was originally intended that the use of phenanthrene as a photosensitizer (electron transfer) would not only improve the yields and efficiencies of the photosubstitution reactions involving 2,3-dimethyl-2-butene (**2**) but that this would also result in a dramatic change in the ratio of products containing a terminal olefinic side chain (i.e. such as **4** and **8**, Fig. 1) to those containing the more heavily-substituted olefinic side chain (**3** and **7**). This was not so; within experimental error, no change in this ratio could be observed. Apparently, the final outcome of the photolysis is independent of whether the aromatic nitrile–olefin radical ion pair is formed in proximity or not. This is surprising, since one would expect that the use of phenanthrene to generate the radical cation of **2** would result in a different partitioning in the mechanistic pathway illustrated in Fig. 8. Presumably, less radical ion coupling (pathway A) would take place because $\mathbf{2}^{\cdot+}$ would deprotonate (to solvent) to form the relatively stable tetramethylallyl radical before encountering a dicyanobenzene radical anion molecule (pathway B).

A possible interpretation of these results is that the radical cation of **2** is in equilibrium with the allylic radical via deprotonation to the solvent. Thus, provided this equilibrium is established quickly enough, the same partitioning of product formation would be observed, both in the presence and absence of phenanthrene as a photosensitizer (electron transfer).

The deprotonation of $\mathbf{2}^{\cdot+}$ is a topic of particular interest. We have calculated a pK_a of $\mathbf{2}^{\cdot+}$ of around −4 in acetonitrile; deprotonation to this solvent might therefore be thermodynamically feasible (23). However, it is interesting to note that during studies of related systems involving **30**[5] and **31**[6] (Fig. 11), we found no evidence for the reversible deprotonation of these radical cations. The reason for this is not yet clear, and a thorough study of the kinetic versus thermodynamic acidities of these systems is continuing.

One further piece of experimental evidence pertaining to the mechanism of the photosubstitution reaction is available. In order to investigate the proposal that $\mathbf{2}^{\cdot+}$ protonates the radical

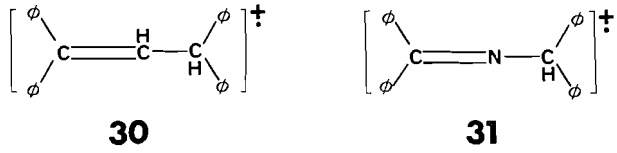

30 **31**

FIG. 11

anion of dicyanobenzene (pathway B, Fig. 8), irradiations were carried out in the presence of perdeutero-2,3-dimethyl-2-butene. Analysis of the products by ^{13}Cmr spectroscopy (see Experimental) indicated that *no deuterium was incorporated at any of the aromatic ring positions*. In the case of the 1,2- and 1,4-disubstituted products, **7** and **8**, and **3** and **4**, respectively, this can be explained if it is assumed that deuteration (protonation) via $\mathbf{2}^{\cdot+}$ occurs at the *ipso*-position, as illustrated in Fig. 8. Thus, elimination of DCN(HCN) would have to occur in the rearomatization step. However, this scheme cannot be applied to account for the lack of deuterium incorporation at the aromatic ring positions of **9** and **10**. This is because close inspection of the system involving 1,3-dicyanobenzene (**6**) reveals that protonation (deuteration) at positions other than *ipso* must occur if 1,3-disubstituted products are to be formed (Fig. 12).

The results just presented raise serious doubts about the details of the scheme originally proposed for the photosubstitution reaction (Fig. 8). This is even more so when one considers that it should be feasible to isolate intermediates such as the 1,4-cyclohexadienes proposed in the scheme. No such compounds were ever observed. It therefore seems necessary to invoke a mechanistic pathway that does not require protonation of the radical anion of dicyanobenzene by $\mathbf{2}^{\cdot+}$. Such a scheme (Fig. 13) involves a fast radical cation – allylic radical equilibrium. Two different processes then occur; radical ion coupling and loss of a proton and cyanide ion (not necessarily in that order) would result in the formation of terminal olefinic products. On the other hand, allylic radical – radical anion coupling, followed by loss of cyanide would give predominantly the tetrasubstituted olefins. This scheme can account for the product ratio being independent of the mode of formation of $\mathbf{2}^{\cdot+}$, as well as the fact that no deuterium is incorporated on the aromatic rings.

The formation of the trisubstituted product **14** (Fig. 2) is also accounted for, in part, by this mechanism. This compound probably results from coupling of the allylic radical with the radical anion of **6** at the 4-position of the aromatic ring, rather than at the 1-position. The intermediate anion thus generated would be stabilized by both cyano functions, thus explaining its preferential formation. Protonation would result in the 1,3-cyclohexadiene intermediate **32** (Fig. 14). The process would be analogous to the reaction of 9-cyanophenanthrene (**28**) with **2**, reported by Lewis and DeVoe (1*g*) (Fig. 15).

Two problems with the proposed overall mechanism now become apparent. If compound **32** was indeed an intermediate, instead of losing hydrogen cyanide to give the 1,4-substitution product **3**, it would have to be preferentially oxidized to **14** via some undetermined process. Since no amount of reduced material resulting from this was isolated, this result is not easily explained. Furthermore, attempts to isolate **32** failed. However, evidence pertaining to the existence of an intermediate such as **32** is provided by the results obtained when the photosubstitution reaction is carried out in a more nucleophilic solvent.

[5] D. D. M. Wayner and D. R. Arnold, unpublished results.
[6] J. Goodin and D. R. Arnold, unpublished results.

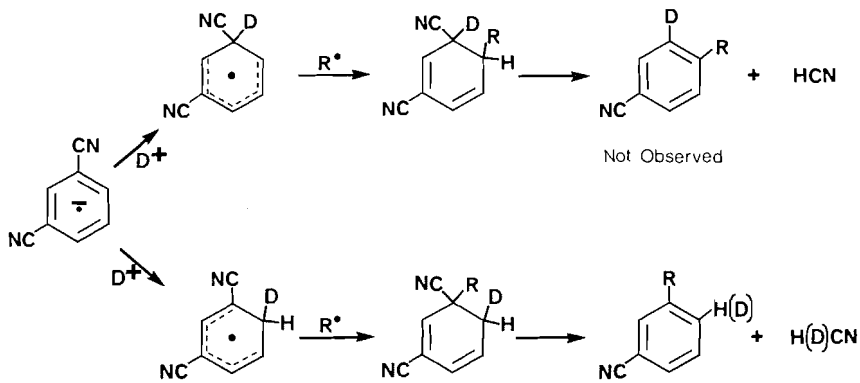

FIG. 12

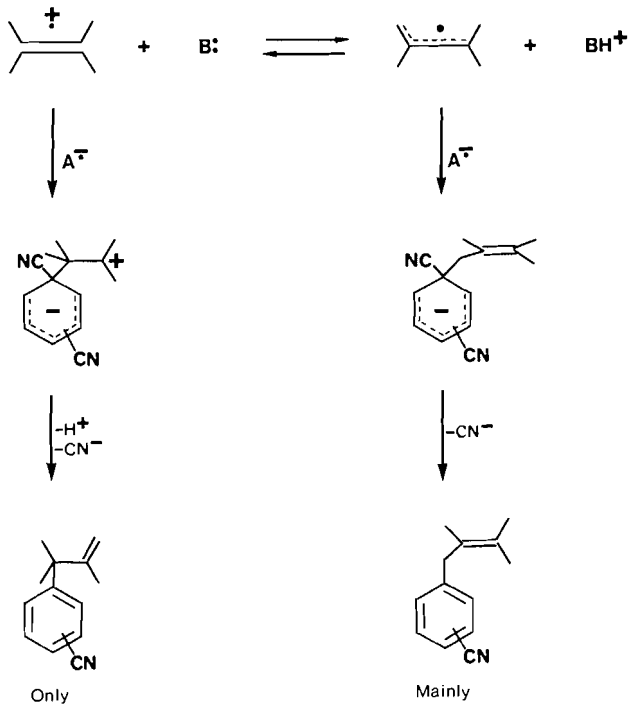

FIG. 13

Finally, another, and perhaps more serious, defect with the latest proposed scheme is that the terminal olefin **15** (Fig. 2) is never isolated. There is no apparent reason for this, since radical ion pair coupling at the 4-position of $\mathbf{6}^{\bullet+}$, followed by protonation, should lead to the same type of intermediate as **32**. At the present time, no reasonable explanation can be offered for the lack of formation of compound **15**. However, it is interesting to note that the observed regiospecificity, resulting in the predominant formation of **14** (and not **15**), has analogy in the 9-cyanophenanthrene system described above (Fig. 15).

Irradiation in acetonitrile–methanol

The mechanistic scheme proposed for the formation of the ethers **20** and **21** is shown below (Fig. 16).

The primary step is similar to that proposed for related systems (1*g*, 4*a*, 19), i.e., the photochemically generated radical cation of **2** is intercepted by the nucleophilic solvent to give the radical **33**. This couples with the radical anion of dicyanobenzene at the *ipso*-position. Loss of cyanide ion yields the observed products. The enhanced efficiencies (i.e. irradiation times were shorter, and material balances much improved) of formation of these ethers, when compared to the reactions observed in acetonitrile alone, are no doubt a result of "trapping" of the radical cation $\mathbf{2}^{\bullet+}$ by methanol, thus preventing energy-wasting back electron transfer from occurring.

It is interesting to compare the behaviour of the radical cation of **2** with that of aryl-substituted olefins, in the presence of methanol. We have previously reported (6*a*, 24) the photosensitized (electron transfer) *anti*-Markovnikov addition of alcohols to olefins such as 1,1-diphenylethylene (**34**). The proposed primary process in these reactions is the same as that illustrated in Fig. 16. However, following the interception of the olefinic radical cation by methanol, a divergence in behaviour is observed. Whereas **33** couples with the radical anion of the aromatic nitrile, the corresponding benzylic radical **35** is reduced by this radical anion and subsequent protonation of the resulting anion leads to the observed product, **36** (Fig. 17).

This difference in behaviour may be attributed to the relative ease of reduction of radical **35**, when compared to **33**. Breslow and co-workers (25) have provided approximate values for the reduction potentials of the benzyl and allyl radicals; these are $E^{red}_{1/2} = -1.0$ V and -1.2 V (vs. Ag), respectively. Unfortunately, the corresponding value for an alkyl radical is not available. However, since the reported gas-phase electron affinity of a benzyl radical (26*a*) is 85 kJ mol^{-1}, and the corresponding values for the allyl (26*a*) and methyl (26*b*) radicals are 53 and 8 kJ mol^{-1}, respectively, the reduction potential of the methyl radical can be estimated by extrapolation. The value is $E^{red}_{1/2} = -1.5$ V (vs. Ag). Thus, while it is considerably easier to reduce a benzyl radical than methyl, it should be feasible for dicyanobenzene ($E^{red}_{1/2} = -2.2$ to -2.0 V) to back electron transfer in every case. However, methyl radical has been considered here; a tertiary radical such as **33** is certainly less easily reduced.

Lewis and DeVoe (1*g*) have reported the formation of substantial amounts of the ethers **37***a* and **37***b* during the course of irradiations involving the generation of $\mathbf{2}^{\bullet+}$ in methanol. These are clearly the result of disproportionation of the radical **33**

37a **37**b

since these workers observed that **37***a* and **37***b* were formed in roughly equal amounts. Thus it appears certain that **37***b* does *not* arise via a pathway similar to that illustrated in Fig. 17.

The cyanated side-chain compounds, **12** and **13** (Fig. 1), are probably formed via an identical route to that shown in Fig. 16,

Can. J. Chem. Downloaded from www.nrcresearchpress.com by 210.87.254.42 on 09/06/12
For personal use only.

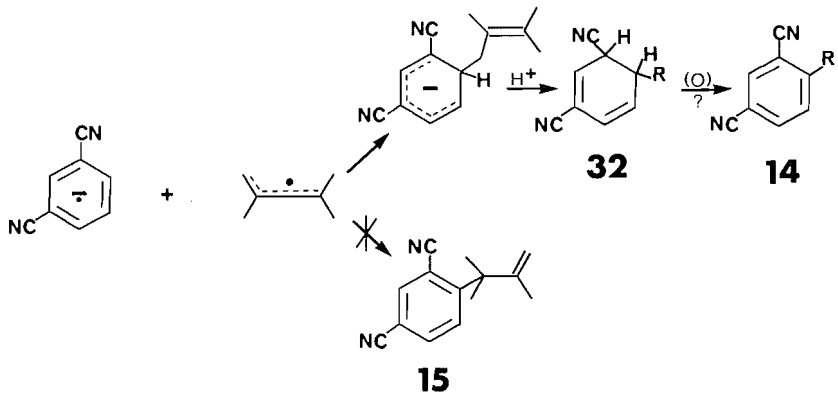

FIG. 14

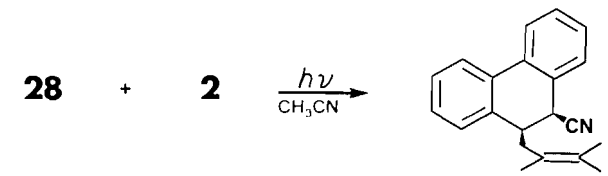

FIG. 15

except that the nucleophile is now cyanide ion, formed as a consequence of the photosubstitution reaction. Finally, it is noteworthy that while considerable amounts of 9-cyanophenanthrene (**28**) and 9-cyano-9,10-dihydrophenanthrene (**29**) were isolated from the phenanthrene-photosensitized reactions in acetonitrile solution, no trace of 9-methoxyphenanthrene or the 9-methoxydihydro derivative could be detected in the present system. Apparently the radical cation of phenanthrene (**11**) is not as susceptible to nucleophilic attack by methanol as by cyanide. This has been noted by others (4*b*) and is another added benefit to the synthetic potentiality of **11**. Obviously, however, photosensitization (electron transfer) by **11** cannot be used for the photocyanation of olefins (27).

When the irradiation of 1,3-dicyanobenzene (**6**) in the presence of **2** and **11** in acetonitrile–methanol solution was first attempted, it was expected that the major product would be **38**. This seemed like a logical prediction in view of the previous results. The eventual isolation of the cyclohexenes **23–25** as major products therefore came as a surprise since neither **1** nor **5** yielded analogous products. Compounds **23–25** are reduction products of the intermediates that would give **38**. A photochemical system such as dicyanobenzene–phenanthrene in a protic solvent is potentially a reducing medium for any substrates with a reduction potential low enough to be reduced by the dicyanobenzene radical anion (28). A few similar photochemical systems have been reported. Barltrop (29) has carried out extensive investigations on the photoreduction of aromatic systems in protic solvents, in the presence of triethylamine. Similar photoreductions (electron ttransfer) of 9-cyanophenanthrene (1*g*) and α-phenylcinnamonitrile (19) have been described in the literature.

The mechanistic scheme envisaged for the formation of cyclohexenes **23–25** is illustrated in Fig. 18. Coupling of the methoxytetramethylethyl radical **33** with $\mathbf{6}^{\bullet-}$ at the 4-position, followed by protonation, results in the 1,3-cyclohexadiene **39**. Two successive electron transfer – protonation steps to the latter would then result in the formation of the observed products.

The first electron transfer to **39** from the radical anion of **6** seems a reasonable step when one considers the reported reduction potential of crotonitrile ($E^{red}_{1/2} = -0.97$ V vs. Ag/Ag^+ in DMF) (30), a suitable model for **39**. Since the reduction potential of **6** is $E^{red}_{1/2} = -2.2$ V (Table 2), electron transfer from $\mathbf{6}^{\bullet-}$ to **39** is possible. This implies that electron transfer from the excited singlet of phenanthrene **11** is also a feasible process. However, control experiments established that **11** is not essential to the formation of **23–25**. Either this step does not occur or, more likely, both are operative.

In view of the protic solvent, it seems likely that protonation of the resulting radical anion of **39**, to give a radical, occurs rapidly. This radical, being stabilized by a cyano function and (or) being allylic, should also be reduced easily by $\mathbf{6}^{\bullet-}$ whenever such an encounter does occur. Protonation of the resulting anion would lead to the observed products.

The substitution pattern and stereochemistry of deuterium incorporation, is in good agreement with this scheme, Fig. 19. Formation of **23**, for example, would involve coupling of the methoxytetramethylethyl radical **33** with $\mathbf{6}^{\bullet-}$ at the 4-position to give a cyano-substituted cyclohexadienyl anion which would be protonated (deuterated) preferably from the side opposite to the bulky substituent. This establishes the *cis*-configuration in **39** that is retained in **23**, **24**, and **25**. Further reduction by two successive electron transfer/protonation (deuteration) steps would then follow. The stereochemical outcome of protonation (deuteration) in the latter two stages is dependent on the position of attack. Thus, protonation (deuteration) at positions that are γ, γ′, or δ to the bulky side chain would proceed via the expected (31) *axial* approach (thus resulting in *axial* deuterium incorporation). A similar result has been observed by McCullough *et al.* (1*d*). On the other hand, protonation (deuteration) cannot occur via axial attack at the carbon atom β′ to the side chain (i.e. *cis*), due to steric hindrance. *Equatorial* deuterium incorporation is therefore observed at this position (i.e. in compounds **24** and **25**, Fig. 19).

These deuterium incorporation results are therefore in good agreement with the overall mechanistic scheme proposed for the formation of compounds **23–25**. Furthermore, the inferred existence of cyclohexadiene **39** lends some credibility to the suggestion that the analogous compound **32** (Fig. 14) is a precursor to the trisubstituted product **14**.

The relative ratio of **23** to **25** was observed to be dependent on the irradiation time. Since no "scrambling" of deuterium over the ring positions in these compounds was observed, interconversion between the isomers (or intermediates leading to them) can be ruled out. The change in product ratios may then

Can. J. Chem. Downloaded from www.nrcresearchpress.com by 210.87.254.42 on 09/06/12
For personal use only.

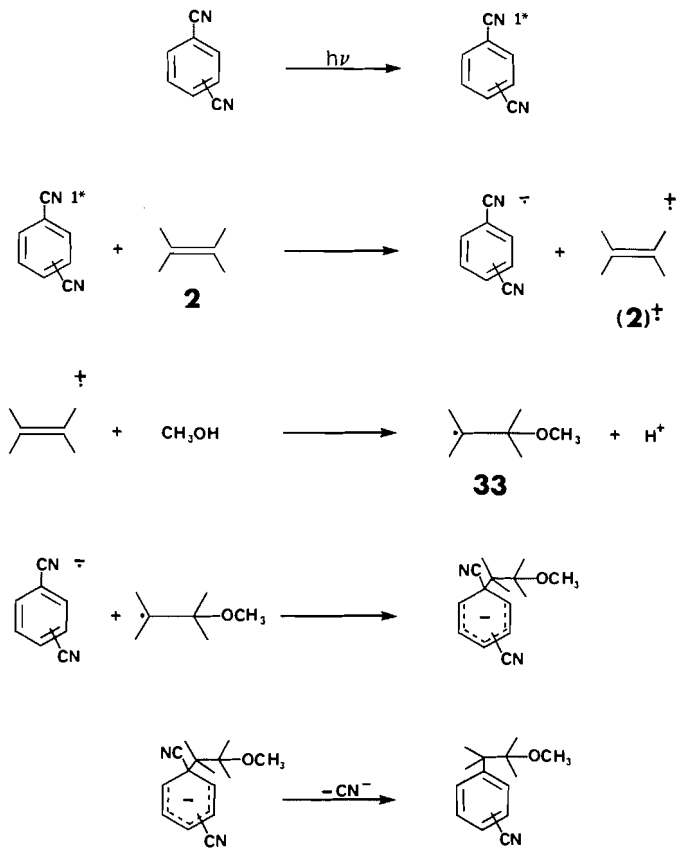

FIG. 16

be the result of secondary photolysis which leads to unidentified products. The incorporation of three atoms of deuterium per molecule is noteworthy since this indicates that methanol is the deuterating (protonating) species and that protonation via the radical cation of 2,3-dimethyl-2-butene (**2**) is not significant. Furthermore, *reduction involving hydrogen atom transfer must be of minor importance*. This result contrasts with that obtained by Mariano and colleagues (32) from their investigations into a secondary photoreduction step they observed during the photocyclization (electron transfer) of the pyridinium salt **40** (Fig. 20). The formation of **41** was rationalized in terms of a photoreduction (electron transfer) of the primary photoproduct, indolizidine (**42**). By means of deuterium studies, the authors came to the conclusion that *hydrogen atom transfer from the solvent plays an important part in the photoreduction process* (Fig. 21).

The difference between the two systems is not too surprising if one considers the electron affinity and reactivity of an allylic/cyano-stablized radical intermediate (Fig. 19) when compared to the radicaloid moiety **43**. Clearly, it is preferable for the latter species to abstract a hydrogen atom from the solvent, rather than undergo reduction to an α-amino anion. Therefore, methanol is not the reducing species in the 1,3-dicyanobenzene system being considered. Obviously, the formation of photoreduction products requires the genesis of an equivalent amount of oxidized material (such as formaldehyde (**44**) in Fig. 21). Such a compound was not identified. In view of the low material balance (50%) for this reaction, this is perhaps not too significant.

It is noteworthy that deuterium could not be detected in 1,3-dicyanobenzene (**6**) recovered from the irradiation in the presence of 2,3-dimethyl-2-butene (**2**) in acetonitrile – methanol-d_1. Thus, either the radical anion of **6** is not basic enough to be protonated by methanol, or such a process occurs irreversibly and leads to unidentified products. Finally, the lack of deuterium incorporation in the minor product **22** (Fig. 5), also isolated from the irradiation in acetonitrile – methanol-d_1, supports the mechanistic pathway shown in Fig. 16.

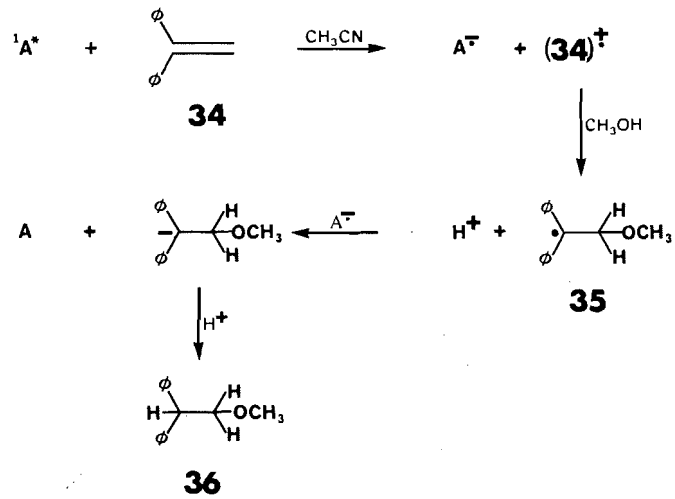

FIG. 17

The ether **26** (Fig. 7) was obtained by the irradiation of 1,4-dicyanobenzene (**1**) in the presence of **19** in acetonitrile–methanol solution. Formation of **26** is interesting because this compound results from competition between interception of the radical cation of **19** by solvent and back electron transfer in the radical ion pair. The latter process predominates in the absence

Can. J. Chem. Downloaded from www.nrcresearchpress.com by 210.87.254.42 on 09/06/12
For personal use only.

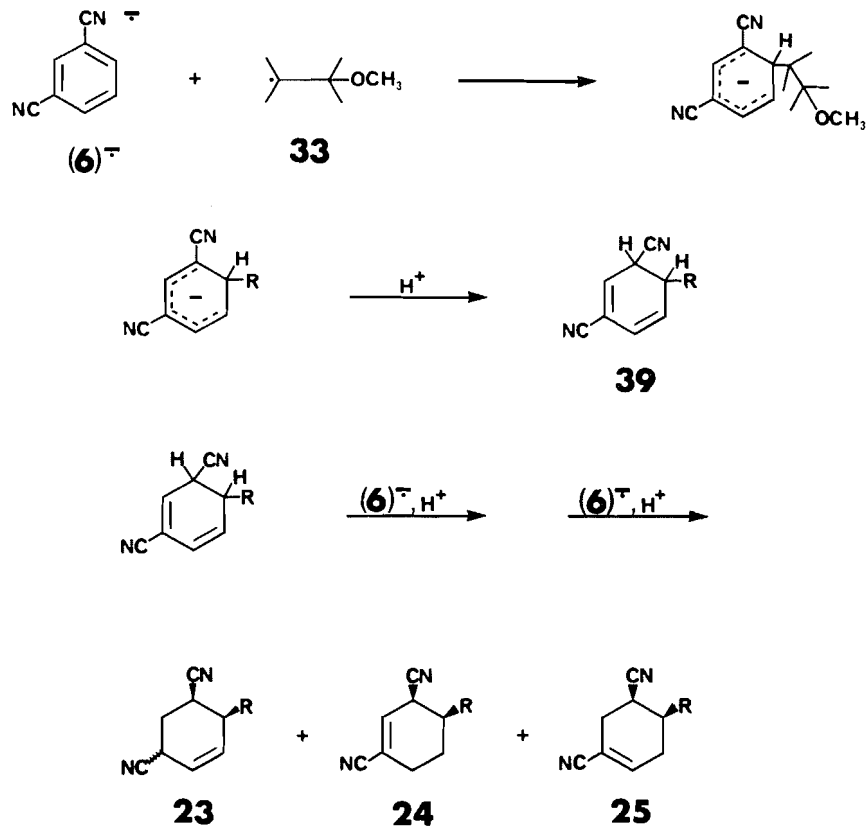

FIG. 18

of methanol and no reaction is then apparent. It is noteworthy that the observed regiospecificity (**27** was not detected, Fig. 7) has analogy in a related system (33), and provides evidence against a radical ion pair coupling (i.e. "zwitterion") mechanism occurring in methanol.

While some aspects of the mechanistic details of the photosubstitution (electron transfer) reaction still need clarification, the results clearly demonstrated the scope and limitations of the method. Efficient substitution is limited mainly to 1,2- and 1,4-dicyanobenzenes, but other polycyano-substituted aromatic hydrocarbons may also yield useful products. The use of phenanthrene as a photosensitizer has enhanced the scope of these reactions. The addition of methanol to the solvent not only renders the photolysis more efficient, but results in the incorporation of an ether function on the alkyl side chain which may serve as a useful "handle" in subsequent transformations.

The photosubstitution of dicyanobenzenes is limited to alkenes with an oxidation potential similar to, or less than, that of cyclohexene ($E^{ox}_{1/2} = +1.95$ V vs. Ag). Furthermore, the use of olefins that lead to a nonsymmetrical allylic-stabilized radical would increase the number of possible products, separation of which may not be a trivial problem.

One of the objectives of this work was to determine whether the anomalous behaviour of 1,3-dicyanobenzene (**6**), observed in other systems when compared to the 1,2- and 1,4-isomers, would also appear here. Clearly, this was the case once again and the anomaly may be attributed to a difference in the reactivity of the radical anion of **6**.

Evidence for this difference also stems from the electrochemical reduction of the dicyanobenzenes. The reduction of 1,2- and 1,4-dicyanobenzene (**5** and **1**) as electrochemically reversible, indicating their radical anions are stable within the time scale of the sweep. On the other hand, the reduction of 1,3-dicyanobenzene (**6**) is irreversible.

The irreversible electrolytic reduction of **6** in dimethylformamide (DMF) has also been reported by Baranski and Fawcett (34), who attributed the phenomenon to rapid reaction of an unstable radical anion, $\mathbf{6}^{\bullet -}$. However, Fraenkel and coworkers (35) have reported that the electron spin resonance (esr) spectrum of $\mathbf{6}^{\bullet -}$, generated electrochemically in DMF, was very persistent and thus the species causing it was quite stable. However, it was also observed that the signal was very weak when compared to that given by the radical anions of **5** and **1**, generated under identical conditions. Furthermore, the authors expressed less confidence in assigning the spectrum unequivocally to $\mathbf{6}^{\bullet -}$. There is, therefore, good reason to doubt whether this species was actually being observed. The radical anion of **6** has, however, been generated by alkali-metal reduction in tetrahydrofuran (36) and the measured electronic absorption spectrum was in good agreement with theoretical calculations. Similar results were obtained for **5** and **1**. Therefore all three dinitriles behave similarly under alkali-metal reduction conditions.

A possible interpretation of these results is that, in the electrochemical system, more than one electron is being transferred during the reduction of **6** (for example, to form the dianion), while true one-electron reduction is occurring in the chemical (as well as photochemical) system. This leads to the proposal that the radical anions of all three dicyanobenzenes can indeed be generated chemically, electrochemically, or photochemically, but the difference in the reactivity of $\mathbf{6}^{\bullet -}$, when compared to $\mathbf{5}^{\bullet -}$ or $\mathbf{1}^{\bullet -}$, causes this species to behave differently photochemically, and possibly to be further reduced in the electrochemical system. It is hoped that future photophysical,

Can. J. Chem. Downloaded from www.nrcresearchpress.com by 210.87.254.42 on 09/06/12
For personal use only.

Can. J. Chem. Downloaded from www.nrcresearchpress.com by 210.87.254.42 on 09/06/12
For personal use only.

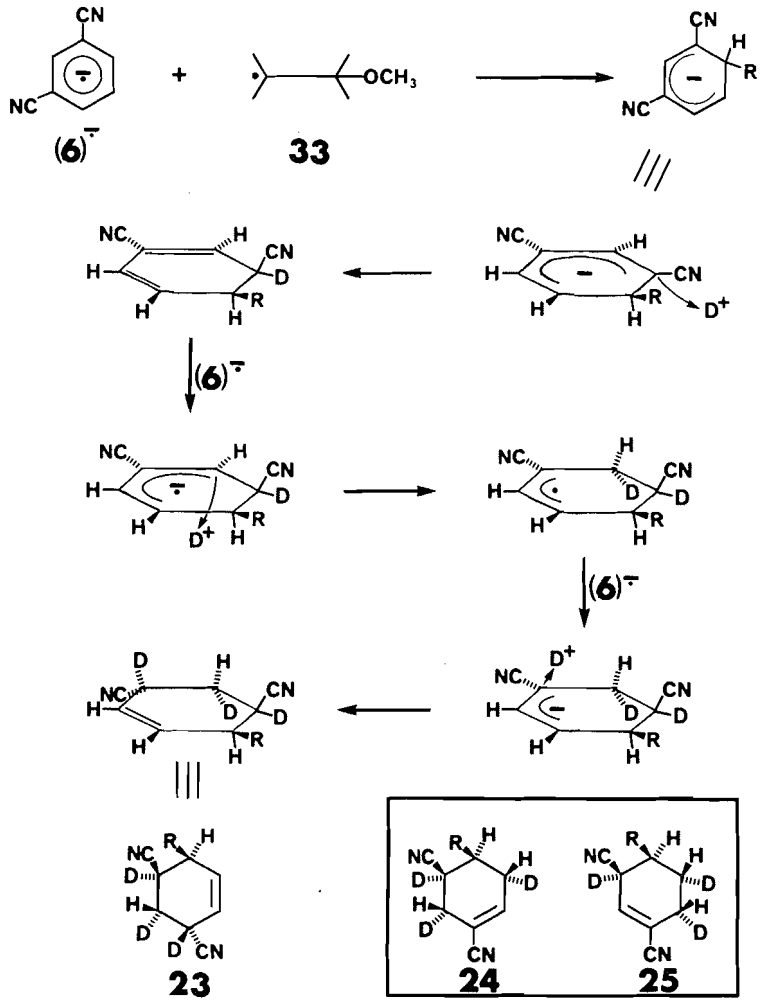

FIG. 19

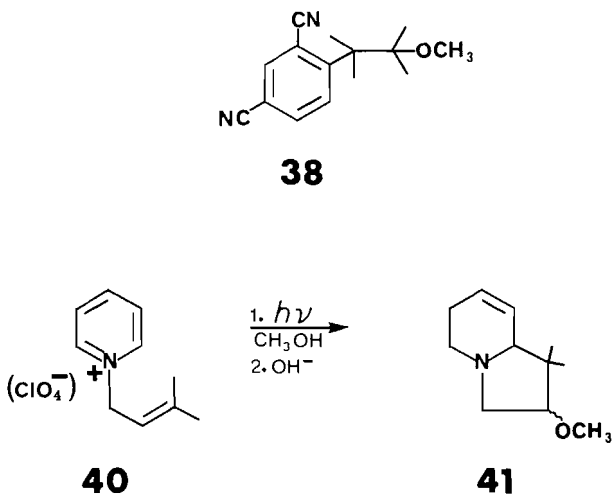

FIG. 20

electrochemical, esr spectral, and theoretical studies will shed some light on the reason(s) for this difference.

Experimental

General

Acetonitrile (Fisher, A.C.S. grade) for preparative work, as well as for photophysical and electrochemical studies, was purified by successive distillations from sodium hydride and phosphorous pentoxide, followed by passing through a basic alumina column and refluxing over calcium hydride and under nitrogen for 24 h, before distillation and storage over 3 Å molecular sieves. Dicyanobenzenes (Aldrich) were recrystallized four times from 95% ethanol and vacuum sublimed before use. 2,3-Dimethyl-2-butene (Aldrich 99+%) was used as received. Cyclohexene (Eastman) was passed through alumina and fractionally distilled before use. Methylpropene was obtained from Matheson and was of a minimum 99.8% purity. Methanol (Fisher, A.C.S. grade) was distilled and stored over 3 Å molecular sieves. Perdeutero-2,3-dimethyl-2-butene was prepared from the reaction between pinacol-d_{12} and triethyl orthoformate (37). The pinacol was synthesized by the reductive coupling of acetone-d_6 (Stohler Isotope Chemicals, 99.7% atom D), in the presence of magnesium (38).

All melting points are uncorrected. Elemental analyses were performed by Microanalysis Laboratories Limited, Toronto, Ontario, and agreed to within 0.3 of the calculated values for carbon and hydrogen and within 0.5 for nitrogen. Mass spectra were recorded on a Du Pont CEC Model 21-104 mass spectrometer, while accurate molecular ion masses were determined on a MAT Model 311A instrument.

X-ray data for the determination of structures was collected on an Enrauf–Nonius CAD-4 four circle diffractometer with automatic data collection utilizing a PDP8/a computer system (Digital Equipment Corporation). Subsequent computer operations were carried out on the Dalhousie Computer Centre's CYBER 170–720 (Control Data).

Infrared spectra were recorded on an air-purged Perkin–Elmer 180 grating spectrometer and are reported in wave numbers, calibrated against the 1602 cm^{-1} polystyrene absorption. Ultraviolet–visible absorption spectra were recorded on a Cary–Varian 219 spectrometer

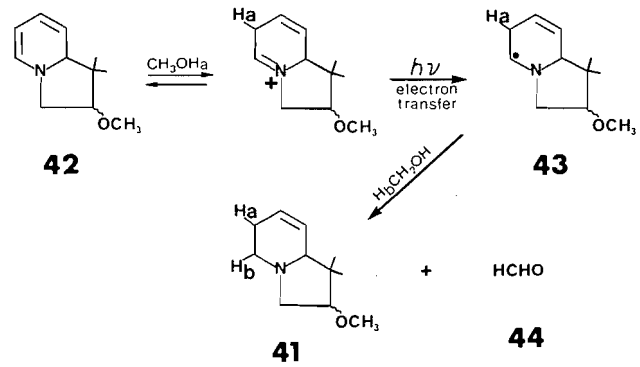

FIG. 21

and are reported in nanometers. The ^{1}Hmr and ^{13}Cmr spectra were obtained either on a Varian CFT-20 Fourier Transform nmr spectrometer or, where specified, on a Nicolet Model 360 NB spectrometer, coupled to an Oxford Instruments superconducting magnet and a Nicolet 192 kword data acquisition system. The solvents used were deuterochloroform or benzene-d_6. Tetramethylsilane or deuterochloroform were used as internal standards. Deuterium incorporation studies on compounds **23**–**25** were performed by ^{1}Hmr spectroscopy on the 360-MHz instrument. All other deuterium studies were carried out by ^{13}Cmr spectroscopy on a Varian XL-100 Fourier Transform nmr spectrometer, coupled to a Nicolet 1280 data system. Spectra were run in hexafluorobenzene/deuterochloroform (1:2) solution to which had been added 5 mg/mL chromium acetyl acetonate as a relaxation reagent. Spectra were acequired under total decoupling conditions from both ^{1}H and ^{2}H. Hexafluorobenzene was used as an internal standard (fluorine resonance). Chemical shifts were compared to those obtained for the natural abundance compounds under identical conditions. Differences of less than 0.4 ppm were considered as insignificant, i.e. deuterium substitution at that particular carbon atom was absent.

Measured oxidation and reduction potentials were obtained by cyclic voltammetry using a Princeton Applied Research Model 173 potentiostat/galvanostat, coupled to a Model 175 universal programmer. The working electrode was a platinum sphere, while the counter electrode was a platinum wire. A silver/silver nitrate (0.1 *M* in acetonitrile) electrode served as a reference potential. The electrolyte used was 0.1 *M* tetraethylammonium perchlorate (Eastman, recrystallized four times from 50% ethanol) in acetonitrile. The solutions were purged with dry nitrogen prior to each run, and a nitrogen atmosphere was maintained during the measurements. Substrate concentrations were typically 0.005 *M*. The voltammagrams were scanned at 20 mV s^{-1}, 100 mV s^{-1}, and 200 mV s^{-1}. The half-wave potentials were calculated as the average of the midpoints between the forward and reverse waves for the 100 mV s^{-1} scans. If the electron transfer process was not reversible, the half-wave was taken as 0.028 V before the anodic peak potential, or 0.029 V before the cathodic peak potential, at the 100-mV s^{-1} scan rate.

Fluorescence (emission) spectra were obtained on an Aminico–Bowman spectrophotofluorometer. Fluorescence quenching rate constants were obtained from Stern–Volmer type plots of fluorescence intensity, using a linear regression programme to estimate the best lines. Correlation coefficients (r^2) were always better than 0.99, except for the case of quenching by methylpropene (gaseous at room temperature) where values greater than 0.97 were considered acceptable. All solutions were degassed by four freeze–thaw cycles on a mercury-free vacuum line. Singlet energies were estimated from the intersection of the normalized absorption and emission spectra in acetonitrile. Singlet lifetime measurements were carried out on a Photochemical Research Associates single photon counting instrument. All photophysical and electrochemical measurements were carried out at room temperature.

Irradiations were carried out in 2-cm id Pyrex tubes using a General Electric Co. 1-kW medium pressure mercury lamp with a quartz cooling jacket immersed in a constant temperature bath at 10°C. Tube distance from the lamp was 6 cm. All samples were purged with nitrogen for 30 min prior to irradiation. Reaction mixtures were chromatographed on a low pressure liquid chromatography (lplc) system. This consisted of a Glenco Scientific Inc. glass column (2.5-cm id × 1 m), packed with 200 g of silica gel (Merck, 60 PF-254, for preparative layer chromatography) and coupled to a helium-pressurized solvent delivery system capable of near-linear solvent changes. The solvents used were distilled hexanes, changing gradually to distilled methylene chloride, followed by elution by the latter solvent alone. Fractions were monitored by an Instrumentation Specialities Co. Model UA-5 absorbance monitor (254 and 280 nm) and (or) by gas chromatography. Isolated compounds were further purified by lplc, as well as by several recrystallizations or by preparative gas chromatography.

Typically, 1 g (8 mmol) of the dicyanobenzene and 12 mmol of olefin (as well as 0.3 g (1.5 mmol) of phenanthrene where applicable) were dissolved in 25 mL of acetonitrile (or acetonitrile–methanol, 3:1 by volume) and irradiated. The course of the reactions was monitored by gas chromatography (gc) on a PYE Unicam Series 104 chromatograph equipped with a flame ionization detector. The column used was a 5 ft × 1/16 in. glass capillary packed with a 20% loading of SE-30 on Chromosorb W 60/80 mesh (Chromatographic Specialties Ltd.) with nitrogen as a carrier gas. When no further change was observed, solvent was removed by evaporation and the reaction mixture chromatographed as described earlier. All % yields reported are based on consumed dicyanobenzene.

The irradiation of 1,2-dicyanobenzene in the presence of 2,3-dimethyl-2-butene, in acetonitrile solution

Irradiation time: 140 h.

1-(2-Cyanophenyl)-2,3-dimethyl-2-butene (**7**): 0.10 g, 16%; ir (neat film), ν_{max}; 3070 (w), 2990 (m), 2920 (s), 2860 (m), 2225 (s), 1600 (m), 1485 (s), 1375 (m), 1125 (m), 760 (s), 700 (w); uv, λ_{max} (log ϵ_{max}), (hexane): 283 (3.16), 275 (3.10), 268 (sh, 2.93), 223 (3.96); ^{1}Hmr ($CDCl_3$), δ_{TMS}: 7.67–7.13 (m, 4H), 3.63 (s, br, 3H), 1.76 (s, br, 6H), 1.59 (s, br, 3H); ^{13}Cmr ($CDCl_3$), δ_{CDCl_3}: 144.9 (s), 132.6 (2 resonances, d), 128.7 (d), 127.8 (s), 126.2 (d), 124.1 (s), 118.0 (s), 112.8 (s), 38.2 (t), 20.6 (q), 20.5 (q), 18.1 (q); ms, 70 eV, *m/e* (relative intensity): 185 (M^+, 78), 171 (21), 170 (100), 143 (48), 142 (21), 116 (42). *Anal.* calcd. for **7**, $C_{13}H_{15}N$: C 84.28, H 8.16; found: C 84.11, H 8.09.

3-(2-Cyanophenyl)-2,3-dimethyl-1-butene (**8**): 0.11 g, 18%; ir (neat film), ν_{max}: 3070 (w), 2990 (s), 2225 (s), 1645 (m), 1600 (m), 1475 (s), 1445 (s), 1380 (m), 899 (s), 770 (s); uv, λ_{max} (log ϵ_{max}), (hexane): 282 (3.07), 270 (sh, 2.82), 226 (3.95); ^{1}Hmr ($CDCl_3$), δ_{TMS}: 7.60–7.25 (m, 4H), 5.03–4.99 (m, 1H, A part of an ABX_3 system, J_{AB} = 1.2 Hz, J_{AX} = 1.5 Hz), 4.85–4.83 (M, 1H, B part, J_{AB} = 1.2 Hz, J_{BX} = 0.5 Hz), 1.66 (m, 3H, X_3), 1.57 (s, 6H); ^{13}Cmr ($CDCl_3$), δ_{CDCl_3}: 151.6 (s), 149.9 (s), 135.2 (d), 132.3 (d), 126.8 (d), 126.2 (d), 118.9 (s), 112.6 (t), 111.7 (s), 44.5 (s), 27.9 (2 resonances, q), 20.0 (q); ms, 70 eV, *m/e* (relative intensity): 185 (M^+, 32), 170 (100), 144 (27), 143 (24), 142 (20), 129 (18), 116 (38). *Anal.* calcd. for **8**, $C_{13}H_{15}N$: C 84.28, H 8.16; found: C 84.51, H 8.32.

2-Cyano-3-(2-cyanophenyl)-2,3-dimethylbutane (**12**): traces; ir (neat film), ν_{max}: 3070 (w), 2990 (s), 2225 (sh, m), 2220 (s), 1595 (m), 1480 (br, s), 1460 (s), 1385 (s), 1375 (m), 1145 (s), 765 (s); uv, λ_{max} (log ϵ_{max}), (hexane): 282 (3.20), 274 (3.14), 270 (sh, 2.96), 266 (2.92), 234 (sh, 3.93), 226 (4.05); ^{1}Hmr ($CDCl_3$), δ_{TMS}: 7.78–7.60 (m, 4H), 1.78 (s, 6H), 1.38 (s, 6H); ^{13}Cmr ($CDCl_3$), δ_{CDCl_3}: 146.4 (s), 135.9 (d), 132.2 (d), 130.5 (d), 127.3 (d), 123.9 (s), 117.9 (s), 112.2 (s), 43.8 (s), 42.0 (s), 25.6 (q), 23.3 (q); ms, 70 eV, *m/e* (relative intensity): 212 (M^+, weak), 197 (M − 15, weak), 144 (100), 128 (5), 127 (3), 117 (15), 116 (45), 115 (10). *Exact Mass* of **12**: $C_{14}H_{16}N_2$ requires 212.13135; found: 212.13177. Recovered **5**: 0.29 g, 71% consumption.

The irradiation of 1,2-dicyanobenzene in the presence of 2,3-dimethyl-2-butene, in benzene solution

The above experiment was repeated with benzene as a solvent, in the place of acetonitrile. Monitoring by gas chromatography indicated

Can. J. Chem. Downloaded from www.nrcresearchpress.com by 210.87.254.42 on 09/06/12
For personal use only.

Can. J. Chem. Downloaded from www.nrcresearchpress.com by 210.87.254.42 on 09/06/12
For personal use only.

that only traces of **7** and **8** were formed under these conditions, even after prolonged irradiation.

The irradiation of 1,2-dicyanobenzene and 2,3-dimethyl-2-butene in acetonitrile solution, in the presence of phenanthrene as a photosensitizer (electron transfer)

Irradiation time: 24 h. Recovered sensitizer **11**: 0.22 g, 73% recovery. Compound **7**: 0.30 g (21%). Compound **8**: 0.350 g (24%).

9-Cyanophenanthrene (**28**): 0.03 g; mp 107–108°C (ethanol) (lit. (39) mp 110°C). This compound also possessed an identical ^{1}Hmr spectrum to that reported in ref. 40.

9-Cyano-9-10-dihydrophenanthrene (**29**): 0.025 g; mp 85–85.5°C (ethanol/H_2O) (lit. (7*b*) mp 84–85°C). The ^{1}Hmr spectrum of this compound was identical to that reported in the literature (7*b*). Compound **12**: 0.15 g (9%). Recovered **5**: 0.0 g, 100% conversion.

The irradiation of 1,2-dicyanobenzene and 2,3-dimethyl-2-butene in acetonitrile solution, in the presence of phenanthrene; irradiation through a Corning CS-7-51 filter

In each of two nmr tubes (Pyrex, 5 mm) was placed a mixture of 25 mg (0.2 mmol) 1,2-dicyanobenzene (**5**), 25 mg (0.3 mmol) of 2,3-dicyanobenzene (**5**), 25 mg (0.3 mmol) of 2,3-dimethyl-2-butene (**2**), and 0.5 mL acetonitrile. To one tube was also added 7.5 mg (0.04 mmol) of phenanthrene (**11**). Both tubes were then irradiated simultaneously through a Corning CS-7-51 light filter (λ_{cutoff} = 300 nm). The course of the reactions was monitored by gc. It was observed that formation of **7** and **8** was fairly rapid in the tube containing the sensitizer. Little reaction was observed in the other tube.

Irradiation of 1,2-dicyanobenzene and 2,3-dimethyl-2-butene in acetonitrile solution, in the presence of various polynuclear aromatic hydrocarbons as photosensitizers (electron transfer)

In each of four nmr tubes (Pyrex, 5 mm) was placed a mixture of 25 mg (0.2 mmol) 1,2-dicyanobenzene (**5**), 25 mg (0.3 mmol) of 2,3-dimethyl-2-butene (**2**), and 0.5 mL acetonitrile. To tubes 2, 3, and 4 were added 0.04 mmol of anthracene, naphthalene, and phenanthrene (**11**), respectively. All four tubes were irradiated simultaneously and the formation of the substitution products, **7** and **8**, was monitored by gc. It was observed that, relative to tube number 1 (i.e. no photosensitizer), the rate of product formation was enhanced by phenanthrene, but was not affected by the presence of naphthalene. Considerable quenching of the reaction was observed in the tube containing anthracene.

Irradiation of 1,3-dicyanobenzene in the presence of 2,3-dimethyl-2-butene, in acetonitrile solution

Irradiation time: 14 days.

1-(3-Cyanophenyl)-2,3-dimethyl-2-butene (**9**) and *3-(3-cyanophenyl)-2,3-dimethyl-1-butene* (**10**): 0.03 g (15%) of a mixture that could not be separated by column chromatography. Separation was achieved by means of preparative gas chromatography on a 6 ft × 3/8 in. aluminum column, packed with Chromosorb W loaded with 20% SE-30 (190°C). The isomers were present in the ratio of **9**/**10** as 1:1.2. Isomer **9**: ir (neat film), ν_{max}: 2990 (m), 2910 (s), 2855 (m), 2225 (s), 1595 (w), 1560 (m), 1480 (m), 1430 (br, m), 1370 (m), 1115 (w), 790 (s), 730 (m), 685 (s); uv, λ_{max} (log ϵ_{max}), (hexane): 282 (3.09), 274 (3.05), 266 (sh, 2.88), 212 (4.11); ^{1}Hmr ($CDCl_3$), δ_{TMS}: 7.38 (br, 4H), 3.41 (br, 2H), 1.75 (br, 6H), 1.57 (br, 3H); ^{13}Cmr ($CDCl_3$), δ_{CDCl}: 142.4 (s), 132.9 (d), 131.7 (d), 129.4 (d), 128.9 (d), 127.2 (s), 124.8 (s), 119.1 (s), 112.2 (s), 39.5 (t), 20.5 (2 resonances, q), 18.2 (q); ms, 70 eV, *m/e* (relative intensity): 185 (M^+, 49), 171 (14), 170 (100), 143 (10), 142 (24), 116 (16). *Anal.* calcd. for **9**, $C_{13}H_{15}N$: C 84.28, H 8.16; found: C 84.11, H 8.08. Isomer **10**: ir (neat film), ν_{max}: 3080 (w), 2970 (s), 2225 (s), 1640 (m), 1595 (w), 1575 (m), 1480 (s), 1440 (m), 1415 (m), 1375 (m), 1360 (w), 1175 (m), 895 (s), 795 (s), 690 (s); uv, λ_{max} (log ϵ_{max}), (hexane): 281 (3.02), 273 (2.99), 266 (2.82), 230 (4.03), 226 (4.06), 220 (4.06); ^{1}Hmr ($CDCl_3$), δ_{TMS}: 7.58–7.41 (m, 4H), 5.01–4.92 (m, 2H), 1.49 (br, 3H), 1.42 (s, 6H); ^{13}Cmr ($CDCl_3$), δ_{CDCl_3}: 151.0 (s), 149.9 (s), 130.6 (d), 129.8 (d), 129.4 (d), 128.8 (d), 119.1 (s), 112.1 (s), 110.7 (d), 43.9 (s), 28.0 (2 resonances, q), 19.9 (q); ms, 70 eV, *m/e* (relative intensity): 185 (M^+, 31), 171 (14), 170 (100), 144 (23), 143 (16), 142 (30), 116 (38). *Anal.* calcd. for **10**, $C_{13}H_{15}N$: C 84.28, H 8.16; found: C 84.21, H 8.06. Recovered **6**: 0.7 g, 30% conversion.

Irradiation of 1,3-dicyanobenzene and 2,3-dimethyl-2-butene in acetonitrile solution, in the presence of phenanthrene as a photosensitizer (electron transfer)

Irradiation time: 7 days. Recovered sensitizer: 0.2 g, 67% recovery. Compounds **9** and **10**: 0.06 g (7%).

1-(2,4-Dicyanophenyl)-2,3-dimethyl-2-butene (**14**): 0.30 g (28%); mp 90–90.5°C (95% ethanol); ir (KBr), ν_{max}: 3110 (w), 3070 (m), 3040 (w), 2995 (m), 2920 (s), 2860 (m), 2230 (s), 1605 (m), 1490 (s), 1450 (br, m), 1400 (m), 1373 (m), 1160 (m), 910 (m), 880 (w), 860 (m), 830 (w); uv, λ_{max} (log ϵ_{max}) (ethanol): 293 (3.13), 283 (3.10), 275 (3.05), 234 (4.13); ^{1}Hmr (360 MHz, $CDCl_3$), δ_{TMS}: 7.91 (dd, 1H, A part of an ABX system, J_{AB} = 1.8 Hz, J_{AX} = 0.6 Hz), 7.78–7.75 (dd, 1H, B part centered at 7.77 ppm, J_{BX} = 8.2 Hz), 7.39–7.36 (dd, 1H, X part centered at 7.38), 3.69 (s, 2H), 1.78 (s, 3H), 1.76 (s, 3H), 1.60 (s, 3H); ^{13}Cmr ($CDCl_3$), δ_{CDCl_3}: 150.2 (s), 135.8 (d), 135.5 (d), 129.8 (d), 129.3 (s), 122.7 (s), 116.7 (s), 115.8 (s), 114.3 (s), 110.9 (s), 38.5 (t), 20.6 (q), 20.4 (q), 18.2 (q); ms, 70 eV, *m/e* (relative intensity): 210 (M^+, 43), 195 (100), 180 (9), 170 (41), 169 (27), 168 (23), 155 (30), 141 (20). *Anal.* calcd. for **14**, $C_{14}H_{14}N_2$: C 79.96, H 6.71; found: C 79.96, H 6.64. Recovered **6**: 0.36 g, 64% conversion.

Irradiation of 1,4-dicyanobenzene and 2,3-dimethyl-2-butene in acetonitrile solution, in the presence of phenanthrene as a photosensitizer (electron transfer)

Irradiation time: 35 h. Recovered sensitizer **11**: 0.23 g, 77% recovery. Compounds **3** and **4**: 0.85 g (23%, 42% respectively). The spectral data of these two main products have been presented elsewhere (ref. 1*e*). 9-Cyanophenanthrene (**28**), and 9-cyano-9,10-dihydrophenanthrene (**29**): traces. Recovered **1**: 0.11 g, 90% conversion.

2-Cyano-3-(4-cyanophenyl)-2,3-dimethylbutane (**13**): 0.07 g (5%); ir (KBr), ν_{max}: 3070 (w), 2980 (s), 2930 (m), 2225 (s), 1605 (m), 1510 (m), 1470 (m), 1460 (m), 1405 (m); 1385 (m), 1195 (w), 1145 (m), 1090 (m), 1020 (w), 840 (m), 680 (m); uv, λ_{max} (log ϵ_{max}), (ethanol): 279 (2.91), 271 (2.96), 267 (sh, 2.89), 260 (sh, 2.78), 238 (4.24), 231 (4.30); ^{1}Hmr ($CDCl_3$), δ_{TMS}: 7.61 (s, 4H), 1.54 (s, 6H), 1.24 (s, 6H); ^{13}Cmr ($CDCl_3$), δ_{CDCl_3}: 149.1 (s), 131.4 (d), 128.4 (d), 124.1 (s), 118.3 (s), 110.6 (s), 42.2 (s), 40.4 (s), 23.9 (q), 23.0 (q); ms, 70 eV, *m/e* (relative intensity): 212 (M^+, weak), 197 (M − 15, weak), 144 (100), 116 (43), 104 (9). *Exact Mass* of **13**: $C_{14}H_{16}N_2$ requires 212.13135; found: 212.13136.

Irradiation of 1,2-dicyanobenzene in the presence of cyclohexene, in acetonitrile solution

Irradiation time: 10 days.

3-(2-Cyanophenyl)cyclohexene (**17**): 0.18 g (31%); ir (neat film), ν_{max}: 3060 (w), 3020 (m), 2930 (s), 2855 (m), 2835 (w), 2220 (s), 1650 (w), 1595 (w), 1480 (m), 1445 (s), 1430 (w), 760 (s), 740 (w), 720 (m), 680 (w), 660 (m); uv, λ_{max} (log ϵ_{max}), (hexane): 283 (3.37), 274 (3.26), 270 (sh, 3.08), 268 (3.06), 223 (4.09); ^{1}Hmr ($CDCl_3$), δ_{TMS}: 7.64–7.24 (m, 4H), 6.00–5.67 (m, 2H), 3.90–3.80 (br, 1H), 2.33–1.41 (m, 6H); ^{13}Cmr ($CDCl_3$), δ_{CDCl_3}: 150.1 (s), 132.8 (d), 132.6 (d), 129.9 (d), 128.1 (d), 127.9 (d), 126.4 (d), 117.9 (s), 111.9 (s), 39.9 (d), 31.4 (t), 24.6 (t), 20.7 (t); ms, 70 eV, *m/e* (relative intensity): 183 (M^+, 100), 168 (42), 155 (50), 154 (50), 140 (35), 129 (22), 128 (28), 127 (28), 116 (28), 115 (35). *Anal.* calcd. for **17**, $C_{13}H_{13}N$: C 85.20, H 7.15; found, C 85.22, H 7.19. Recovered **5**: 0.58 g, 42% conversion.

Irradiation of 1,3-dicyanobenzene in the presence of cyclohexene, in acetonitrile solution

No reaction could be observed by gas chromatography, even after prolonged irradiation (18 days). The usual work-up afforded the starting material **6** only. Recovery was 0.7 g (70%).

Irradiation of 1,4-dicyanobenzene in the presence of cyclohexene, in acetonitrile solution

Irradiation time: 10 days.

3-(4-Cyanophenyl)cyclohexene (**18**): 0.28 g (31%); ir (neat film)

Can. J. Chem. Downloaded from www.nrcresearchpress.com by 210.87.254.42 on 09/06/12
For personal use only.

ν_{max}: 3020 (m), 2930 (s), 2860 (m), 2840 (m), 2225 (s), 1650 (w), 1605 (s), 1505 (s), 1445 (m), 1415 (m), 1300 (m), 900 (m), 880 (m), 830 (s); uv, λ_{max} (log ϵ_{max}), (hexane): 277 (2.47), 273 (2.62), 271 (2.60), 266 (2.79), 2.58 (2.70), 241 (4.24), 234 (4.29); ^{1}Hmr ($CDCl_3$), δ_{TMS}: 7.63–7.25 (AB quartet, centered at 7.44), 5.91–5.66 (m, 2H), 3.48–3.41 (br, 1H), 2.22–1.55 (m, 6H); ^{13}Cmr ($CDCl_3$), δ_{CDCl_3}: 152.1 (s), 132.0 (d), 129.4 (d), 128.4 (d), 128.3 (d), 118.9 (s), 109.7 (s), 41.7 (d), 32.1 (t), 24.7 (t), 20.7 (t); ms, 70 eV, *m/e* (relative intensity): 183 (M^+, 75), 155 (66), 140 (86), 130 (100), 116 (79), 102 (57). *Anal.* calcd. for **18**, $C_{13}H_{13}N$: C 85.20, H 7.15; found: C 84.89, H 6.89. Recovered **1**: 0.37 g, 63% conversion.

Irradiation of 1,4-dicyanobenzene and cyclohexene in acetonitrile solution in the presence of phenanthrene as a photosensitizer (electron transfer)

Irradiation time: 8 days. Recovered sensitizer **11**: 0.05 g, 17% recovery. Compound **18**: 0.26 g (56%).[7] 9-Cyanophenanthrene (**28**): 0.04 g. 9-Cyano-9,10-dihydrophenanthrene (**29**): 0.11 g. Recovered **1**: 0.69, 31% conversion.

Irradiation of 1,4-dicyanobenzene in the presence of methylpropene, in acetonitrile solution.

No reaction was observed between **1** and **19**, even after prolonged irradiation (10 days). The usual work-up resulted in the recovery (0.65 g, 65% recovery) of **1**. The same results were obtained when phenanthrene (**11**) was used as a photosensitizer (electron transfer).

The detection of exciplex emission from solutions of dicyanobenzene and 2,3-dimethyl-2-butene in hexane

To solutions of the dicyanobenzene (10^{-3} *M*) in hexane, in a 1-cm path-length fluorescence cell, was added 2,3-dimethyl-2-butene (**2**), in 1-μL portions, while the fluorescence (emission) spectrum of the cyanoaromatic was monitored simultaneously. Quenching of the fluorescence was observed in all three cases, together with the concurrent rise of a weak new emission maximum. The approximate position of this exciplex emission was 380 nm in the case of 1,2- and 1,4-dicyanobenzene, and 385 nm for the 1,3-dicyanobenzene/olefin system. Similar results were obtained when cyclohexene (**16**) or methylpropene (**19**) were the quenchers. However, the very low intensities of the exciplex emission rendered the determination of the emission maxima difficult.

Irradiation of 1,2-dicyanobenzene and 2,3-dimethyl-2-butene in acetonitrile–methanol solution, in the presence of phenanthrene as a photosensitizer (electron transfer)

Irradiation time: 22 h. Recovered sensitizer **11**: 0.15 g, 50% recovery. Compounds **7** and **8**: traces. 9-Cyanophenanthrene (**28**): 0.03 g. 9-Cyano-9,10-dihydrophenanthrene (**29**): 0.19 g.

3-(2-Cyanophenyl)-2-methoxy-2,3-dimethylbutane (**21**): 0.25 g (45%); ir (neat film), ν_{max}: 3070 (w), 2990 (s), 2960 (sh, s), 2830 (m), 2220 (s), 1595 (m), 1480 (s), 1375 (s), 1365 (m), 1155 (s), 1080 (s), 1065 (s), 760 (s); uv, λ_{max} (log ϵ_{max}), (hexane): 282 (3.09), 273 (3.08), 266 (sh, 2.87), 233 (sh, 3.90), 226 (4.01); ^{1}Hmr ($CDCl_3$), δ_{TMS}: 7.68–7.29 (m, 4H), 3.15 (s, 3H), 1.59 (s, 6H), 1.06 (s, 6H); ^{13}Cmr ($CDCl_3$), δ_{CDCl_3}: 149.8 (s), 135.4 (d), 130.7 (d), 130.3 (d), 125.8 (d), 119.9 (s), 113.7 (s), 78.5 (s), 48.7 (q), 47.2 (s), 25.2 (q), 19.5 (q); ms, 70 eV, *m/e* (relative intensity): 218 (MH^+, 2), 202 (63), 186 (69), 171 (21), 170 (46), 145 (19), 144 (67), 143 (42), 130 (71), 129 (27), 128 (38), 127 (19), 117 (27), 116 (100), 115 (46), 103 (27), 102 (33), 73 (intense, >300). *Anal.* calcd. for **21**, $C_{14}H_{19}NO$: C 77.38, H 8.81, N 6.45; found: C 77.26, H 8.76, N 6.38. Recovered **5**: 0.67 g, 31% conversion. Compound **12**: 0.03 g (5%).

Irradiation of 1,4-dicyanobenzene and 2,3-dimethyl-2-butene in acetonitrile–methanol solution, in the presence of phenanthrene as a photosensitizer (electron transfer)

Irradiation time: 23 h. Recovered sensitizer **11**: 0.24 g, 80% recovery. Compounds **3** and **4**: traces.

[7] The increase in yield was due to a material balance improvement.

3-(4-Cyanophenyl)-2-methoxy-2,3-dimethylbutane (**20**): 1.18 g (70%); ir (neat film), ν_{max}: 2980 (s), 2940 (s), 2825 (m), 2225 (s), 1605 (m), 1505 (m), 1470 (br, m), 1400 (m), 1390 (m), 1375 (s), 1365 (m), 1150 (s), 1110 (m), 1090 (s), 1065 (s), 840 (m), 820 (w); uv, λ_{max} (log ϵ_{max}), (hexane): 278 (2.72), 272 (2.75), 269 (2.26), 266 (2.80), 258 (2.69), 239 (4.21), 232 (4.26); ^{1}Hmr ($CDCl_3$), δ_{TMS}: 7.54 (br, s, 4H), 3.10 (s, 3H), 1.37 (s, 6H), 0.99 (s, 6H); ^{13}Cmr ($CDCl_3$), δ_{CDCl_3}: 153.1 (s), 130.4 (d), 129.3 (d), 119.1 (s), 109.1 (s), 78.1 (s), 49.2 (q), 45.8 (s), 24.1 (q), 19.6 (q); ms, 70 eV, *m/e* (relative intensity): 218 (M^+, 1), 202 (53), 186 (10), 170 (23), 144 (40), 143 (23), 142 (27), 130 (93), 128 (27), 116 (100), 115 (17), 89 (23), 77 (27), 74 (93), 73 (intense, >300). *Anal.* calcd. for **20**, $C_{14}H_{19}NO$: C 77.38, H 8.81, N 6.45; found: C 77.21, H 8.82, N 6.32. Recovered **1**: 0.0 g, 100% conversion.

Irradiation of 1,3-dicyanobenzene and 2,3-dimethyl-2-butene in acetonitrile–methanol solution, in the presence of phenanthrene as a photosensitizer (electron transfer)

Irradiation time: 18 h. Recovered sensitizer **11**: 0.30 g, 98% recovery.

3-(3-Cyanophenyl)-2-methoxy-2,3-dimethylbutane (**22**): 0.04 g (4%); ir (neat film), ν_{max}: 3075 (w), 2990 (s), 2960 (s), 2830 (m), 2225 (s), 1599 (w), 1570 (m), 1480 (br, s), 1415 (m), 1390 (m), 1375 (s), 1365 (s), 1150 (s), 1065 (s), 795 (s), 695 (s); uv, λ_{max} (log ϵ_{max}), (hexane): 280 (2.14), 272 (2.91), 265 (2.75), 230 (4.00), 226 (4.04); ^{1}Hmr ($CDCl_3$), δ_{TMS}: 7.77–7.39 (m, 4H), 3.11 (s, 3H), 1.37 (s, 6H), 0.99 (s, 6H); ^{13}Cmr ($CDCl_3$), δ_{CDCl_3}: 148.8 (s), 133.0 (d), 132.4 (d), 129.0 (d), 127.5 (d), 119.5 (s), 110.9 (s), 78.0 (s), 49.2 (q), 45.4 (s), 24.1 (q), 19.6 (q); ms, 70 eV, *m/e* (relative intensity): 218 (MH^+, 3), 202 (29), 186 (8), 170 (16), 144 (33), 143 (16), 142 (20), 130 (61), 129 (15), 128 (26), 127 (11), 117 (13), 116 (100), 115 (20), 102 (33), 89 (21), 77 (42), 76 (17), 75 (21), 74 (72), 73 (intense, >300). *Anal.* calcd. for **22**: $C_{14}H_{19}NO$: C 77.38, H 8.81, N 6.45; found: C 77.51, H 8.73, N 6.42. Recovered **6**: 0.51 g, 49% conversion.

3,5-Dicyano-6-(2-methoxy-1,1,2-trimethylpropyl)cyclohexene (**23**): 0.05 g (5%); mp 85–86°C (95% ethanol); ir (KBr), ν_{max}: 3040 (w), 2980 (s), 2940 (m), 2830 (w), 2235 (m), 1640 (br, w), 1465 (br, m), 1375 (s), 1370 (m), 1150 (s), 1125 (m), 1060 (s), 780 (m), 680 (m); uv, λ_{max} (log ϵ_{max}), (ethanol): no absorption above 240 nm; ^{1}Hmr (360 MHz, $CDCl_3$), δ_{TMS}: 6.15–6.11 (H_1, br d, $J_{1,2}$ = 10.5, $J_{1,3a'} < 2$, $J_{1,5e} < 2$, $J_{1,6a'}$ = 2.0), 5.73–5.70 (H_2, br d, $J_{2,3a'} < 2$, $J_{2,4e}$ = 1.6, $J_{2,6a'} < 2$), 3.77–3.67 ($H_{3a'}$, m, $J_{3a',4e}$ = 5.0, $J_{3a',4a}$ = 11.9), 3.44–3.41 (H_{5e}, m, $J_{4a,5e}$ = 3.0, $J_{4e,5e}$ = 5.0, $J_{5e,6a'}$ = 3.8), 3.21 (OCH_3, s), 2.65–2.62 ($H_{6a'}$, m), 2.53–2.45 (H_{4e}, m, $J_{4a,4e}$ = 13.3), 2.13–2.05 (H_{4a}, ddd), 1.14 (2 × CH_3, s), 1.09 (CH_3, s), 1.03 (CH_3, s); ^{13}Cmr ($CDCl_3$), δ_{CDCl_3}: 132.6 (d), 120.7 (d), 120.3 (s), 119.9 (s), 80.3 (s), 48.5 (q), 42.9 (s), 42.4 (d), 30.8 (t), 28.0 (d), 24.9 (d), 22.0 (q), 19.4 (q), 19.1 (q), 18.7 (q); ms, 70 eV, *m/e* (relative intensity): 247 (MH^+, 1), 231 (M − 15, 27), 215 (5), 214 (17), 199 (17), 117 (93), 100 (69), 85 (39), 84 (44), 83 (100), 74 (75), 73 (intense, >150). *Anal.* calcd. for **23**, $C_{15}H_{22}N_2O$: C 73.13, H 9.00, N 11.37; found: C 73.29, H 9.31, N 11.11.

X-ray data for 23

Triclinic; a = 6.558 (10), b = 9.627 (4), c = 11.967 (3) Å; α = 101.584° (28), β = 87.429° (50), γ = 98.208° (67). Spacegroup *P*, Z = 2; 1999 unique reflections of which 1044 had $I > 3\sigma(I)$. The final refinement converged at R = 0.0342 (0.0954 on full data). MoKα, λ = 0.70926 Å, 20°C. (Supplemental material is available.)

cis-*1,3-Dicyano-4-(2-methoxy-1,1,2-trimethylpropyl)cyclohexene* (**24**): 0.19 g (20%); mp: 131°C (95% ethanol); ir (KBr), ν_{max}: 3050 (w), 2990 (s), 2890 (m), 2840 (w), 2235 (m), 2220 (m), 1645 (w), 1465 (br, m), 1395 (m), 1360 (s), 1340 (s), 1155 (s), 1070 (s); uv, λ_{max} (log ϵ_{max}), (ethanol): 206 (4.05); no absorption above 240 nm; ^{1}Hmr (360 MHz, $CDCl_3$), δ_{TMS}: 6.53–6.50 (H_2, m, $J_{2,3e'}$ = 6.1, $J_{2,6a'}$ = 2.0, $J_{2,6e'}$ = 2.0), 3.78–3.75 ($H_{3e'}$, m, $J_{3e',4a}$ = 3.9, $J_{3e',5e}$ = 2.0, $J_{3e',6e'} < 1$), 3.21 (OCH_3, s), 2.51–2.44 ($H_{6e'}$, br dd, $J_{5e,6e'} < 2$, $J_{5a,6e'}$ = 5.1, $J_{6a',6e'}$ = 18.3), 2.37–2.27 ($H_{6a'}$, m, $J_{5e,6a'}$ = 6.1, $J_{5a,6a'}$ = 11.4), 2.14–2.08 (H_{5e}, br dd, $J_{4a,5e} < 2$, $J_{5e,5a}$ = 12.7, $J_{5e,6e'} < 2$), 1.82–1.79 (H_{4a}, br dd, $J_{4a,5a}$ = 12.2), 1.76–1.65 (H_{5a}, m), 1.14

Can. J. Chem. Downloaded from www.nrcresearchpress.com by 210.87.254.42 on 09/06/12
For personal use only.

(CH_3, s), 1.10 (2 × CH_3, s), 0.98 (CH_3, s); ^{13}Cmr ($CDCl_3$), δ_{CDCl_3}: 138.7 (d), 118.3 (s), 117.7 (s), 116.6 (s), 80.4 (s), 48.5 (q), 42.7 (s), 40.5 (d), 30.9 (t), 28.9 (d), 22.7 (q), 22.0 (t), 19.6 (q), 18.9 (q), 17.8 (q); ms, 70 eV, *m/e* (relative intensity): 247 (MH^+, 1), 231 (M − 15, 85), 215 (M − 31, 4), 199 (7), 187 (18), 116 (14), 115 (100), 100 (38), 85 (44), 84 (62), 83 (68), 74 (93), 73 (intense, > 200). *Anal.* calcd. for **24**, $C_{15}H_{22}N_2O$: C 73.13, H 9.00, N 11.37; found: C 73.21, H 9.09, N 11.03.

X-ray data for ***24***

Orthorhombic; a = 10.013 (4), b = 11.541 (2), c = 26.362 (6) Å; $\alpha = \beta = \gamma = 90°$. Spacegroup P_{bca}, Z = 8; 1964 unique reflections of which 943 had $I > 3\sigma(I)$. The final refinement converged at R = 0.0357 (0.855 on full data). MoKα, λ = 0.70926 Å, 20°C. (Supplemental material is available.)

cis-*1,5-Dicyano-4-(2-methoxy-1,1,2-trimethylpropyl)cyclohexene* (**25**): 0.24 g (25%); mp 165.5°C (95% ethanol); ir (KBr), ν_{max}: 3000 (s), 2980 (s), 2970 (s), 2940 (s), 2860 (s), 2830 (m), 2230 (s), 2210 (s), 1680 (m), 1470 (m), 1440 (m), 1425 (m), 1400 (m), 1380 (s), 1370 (s), 1315 (w), 1145 (s), 1040 (s), 845 (s), 795 (m); uv, λ_{max} (log ϵ_{max}), (ethanol): 206 (3.81); no absorption above 235 nm; ^{1}Hmr (360 MHz, C_6D_6), $\delta_{C_6H_6}$: 6.00–5.97 (H_2, m), 3.19–3.16 (H_{5e}, m, $J_{4a,5e}$ = 2.1, $J_{5e,6a'}$ = 5.2, $J_{5e,6e'}$ = 2.5), 2.75 (OCH_3, s), 2.01–1.90 ($H_{3a'}$, $H_{6e'}$, m, $J_{3a',4a}$ = 12.1), 1.68–1.59 ($H_{3e'}$, $H_{6a'}$, m, $J_{3e',4a}$ = 4.1), 1.27–1.22 (H_{4a}, ddd), 0.86 (CH_3, s), 0.70 (CH_3, s), 0.58 (CH_3, s), 0.48 (CH_3, s); ^{13}Cmr ($CDCl_3$), δ_{CDCl_3}: 146.2 (d), 120.9 (s), 118.1 (s), 108.6 (s), 80.8 (s), 48.5 (q), 42.3 (s), 39.2 (d), 32.5 (t), 27.0 (d), 26.4 (t), 22.4 (q), 11.5 (q), 19.2 (q), 18.3 (q); ms, 70 eV, *m/e* (relative intensity): 231 (M − 15, 39), 215 (5), 115 (31), 104 (29), 100 (24), 91 (17), 85 (40), 84 (100), 74 (63), 73 (intense, > 200). *Anal.* calcd. for **25**, $C_{15}H_{22}N_2O$: C 73.13, H 9.00, N 11.37; found: C 73.21, H 9.12, N 10.89.

X-ray data for ***25***

Monoclinic; a = 9.231 (1), b = 6.884 (2), c = 22.973 (3) Å; $\alpha = 90°$, $\beta = 101.946°$ (11), $\gamma = 90°$. Spacegroup $P2_1/C$, Z = 4; 1946 unique reflections of which 981 had $I > 3\sigma(I)$. The final refinement converged at R = 0.0333 (0.1104 on full data). MoKα, λ = 0.70926 Å, 20°C. (Supplemental material is available).

Irradiation of 1,3-dicyanobenzene and 2,3-dimethyl-2-butene in acetonitrile–methanol solution, in the presence of phenanthrene as a photosensitizer (electron transfer): irradiation for a prolonged period

The experiment described above was repeated except that a longer irradiation time was employed (5 days). The usual work-up afforded the following compounds. Recovered sensitizer **11**: 0.22 g, 73% recovery. 9-Cyanophenanthrene (**28**) and 9-cyano-9,10-dihydrophenanthrene (**29**): traces. Compound **22**: 0.06 g (5%). Recovered **6**: 0.28 g, 73% conversion. Compound **23**: traces. Compound **24**: 0.10 g (7%). Compound **25**: 0.21 g (15%).

Irradiation of 1,3-dicyanobenzene in the presence of 2,3-dimethyl-2-butene, in acetonitrile–methanol

Irradiation time: 14 days. Recovered **6**: 0.49 g, 51% conversion. Compound **23**: trace. Compound **24**: 0.05 g (5%). Compound **25**: 0.041 g (4%).

Irradiation of 1,4-dicyanobenzene in the presence of methylpropene, in acetonitrile–methanol solution

Irradiation time: 20 days.

2-(4-Cyanophenyl)-1-methoxy-2-methylpropane (**26**): 0.02 g (4%); ir (neat film), ν_{max}: 2970 (s), 2930 (s), 2870 (s), 2930 (m), 2920 (m), 2225 (s), 1605 (s), 1505 (s), 1395 (s), 1365 (m), 1200 (m), 1115 (s), 1095 (s), 960 (m), 835 (s); uv, λ_{max} (log ϵ_{max}), (hexane): 277 (2.60), 272 (2.66), 269 (sh, 2.65), 266 (2.73), 260 (sh, 2.61), 2.58 (2.63), 238 (4.20), 228 (4.26); ^{1}Hmr ($CDCl_3$), δ_{TMS}: 7.54–7.51 (4H, AB quartet), 3.40 (s, 2H), 3.28 (s, 3H), 1.32 (s, 6H); ^{13}Cmr ($CDCl_3$), δ_{CDCl_3}: 153.1 (s), 131.6 (d), 126.8 (d), 118.8 (s), 109.4 (s), 81.8 (t), 59.1 (q), 39.4 (s), 25.7 (q); ms, 70 eV, *m/e* (relative intensity): 190 (MH^+, 37), 159 (21), 144 (69), 143 (13), 128 (9), 116 (61), 115 (8), 104 (13), 89 (9), 45 (100). *Anal.* calcd. for **26**: $C_{12}H_{15}NO$: C 76.15, H 7.99, N 7.40; found: C 76.11, H 8.21, N 7.03.

No reaction was observed when the above irradiation was repeated in the presence of phenanthrene (**11**).

Acknowledgements

This work was supported by a grant from the Natural Sciences and Engineering Research Council of Canada. A Scholarship (R.M.B.) from the Canadian Commonwealth Scholarship and Fellowship Committee is gratefully acknowledged. We thank Dr. D. L. Hooper at the Atlantic Regional Magnetic Resonance Centre at Dalhousie University for running the 360-MHz nmr spectra, as well as Dr. J. Walter at the Atlantic Regional Laboratories, National Research Council, for his help in the deuterium incorporation studies by ^{13}C nmr spectroscopy.

1. (*a*) G. Buchi, J. G. Atkinson, D. E. Ayer, and E. W. Robb. J. Am. Chem. Soc. **85**, 2257 (1963); (*b*) N. C. Yang, B. Kim, W. Chiang, and T. Hamada. J. Chem. Soc. Chem. Commun. 729 (1976); (*c*) T. S. Cantrell. J. Org. Chem. **42**, 4238 (1977); (*d*) J. J. McCullough, R. C. Miller, and W. S. Wu. Can. J. Chem. **55**, 2909 (1977); (*e*) D. R. Arnold, P. C. Wong, A. J. Maroulis, and T. S. Cameron. Pure Appl. Chem. **52**, 2609 (1980); (*f*) J. J. McCullough, W. K. MacInnis, C. J. L. Lock, and R. Faggiani. J. Am. Chem. Soc. **104**, 4644 (1982); (*g*) F. D. Lewis and R. J. DeVoe. Tetrahedron, **38**, 1069 (1982); (*h*) C. Pac, M. Yasuda, K. Shima, and H. Sakurai. Bull. Chem. Soc. Jpn. **55**, 1605 (1982), and references cited therein.
2. S. L. Mattes and S. Farid. Organic photochemistry. Vol. 6. *Edited by* A. Padwa. Marcel Dekker, New York. 1983 pp. 233–326.
3. M. Kajima, H. Sakuragi, and N. Tokumaru. Tetrahedron Lett. 2889 (1981).
4. (*a*) C. Pac, A. Nakasone, and H. Sakurai. J. Am. Chem. Soc. **99**, 5806 (1977); (*b*) T. Majima, C. Pac, A. Nakasone, and H. Sakurai. J. Am. Chem. Soc. **103**, 4499 (1981).
5. R. Bernardi, T. Caronna, S. Morrocchi, P. Traldi, and B. M. Vittimberga. J. Chem. Soc. Perkin Trans. 1, 1607 (1981).
6. (*a*) R. A. Neunteufel and D. R. Arnold. J. Am. Chem. Soc. **95**, 4080 (1973); (*b*) A. J. Maroulis and D. R. Arnold. J. Chem. Soc. Chem. Commun. 351 (1979); (*c*) D. R. Arnold, R. M. Borg, and A. Albini. J. Chem. Soc. Chem. Commun. 138 (1981).
7. (*a*) T. Asanuma, T. Gotoh, A. Tsuchida, M. Yamamoto, and Y. Nishijima. J. Chem. Soc. Chem. Commun. 485 (1977); (*b*) M. Yasuda, C. Pac, and H. Sakurai. J. Chem. Soc. Perkin Trans. 1, 746 (1981).
8. M. Ohashi, K. Miyake, and K. Tsujimoto. Bull. Chem. Soc. Jpn. **53**, 1683 (1980).
9. L. M. Jackman and S. Sternhell. *In* Applications of nuclear magnetic resonance spectroscopy. 2nd ed. *Edited by* D. H. R. Barton and W. Doering. Pergamon Press, New York. 1969. p. 325.
10. L. J. Bellamy. *In* The infra-red spectra of complex molecules. 2nd ed. Methuen, London. 1966. pp. 77–79.
11. J. B. Stothers. *In* Carbon-13 NMR spectroscopy. Academic Press, London. 1972. p. 307.
12. F. W. McLafferty. Anal. Chem. **29**, 1782 (1957).
13. (*a*) E. L. Eliel. *In* Stereochemistry of carbon compounds. McGraw–Hill, New York. 1962. p. 239. (*b*) W. G. Dauben and K. S. Pitzer. *In* Steric effects in organic chemistry. *Edited by* M. S. Newman. Wiley, New York. 1956. pp. 38–39.
14. W. C. Nerkham, G. R. Dimeler, and M. M. Desmond. J. Electrochem. Soc. **111**, 1190 (1964).
15. J. L. Stavinoha and P. S. Mariano. J. Am. Chem. Soc. **103**, 3136 (1981).

16. (*a*) P. J. W. DEBYE. Trans. Electrochem. Soc. **82**, 265 (1942); (*b*) R. C. WEAST (*Editor*). Handbook of chemistry and physics. 63rd ed. Chemical Rubber Co., Cleveland, OH. 1982.
17. D. REHM and A. WELLER. Isr. J. Chem. **8**, 259 (1970).
18. (*a*) F. SCANDOLA, V. BALZANI, and G. B. SCHUSTER. J. Am. Chem. Soc. **103**, 2519 (1981); (*b*) A. WELLER. Pure Appl. Chem. **54**, 1885 (1982).
19. F. D. LEWIS, R. J. DEVOE, and D. B. MACBLANE. J. Org. Chem. **47**, 1392 (1982).
20. (*a*) S. FARID, S. E. HARTMAN, and T. R. EVANS. *In* The exciplex. *Edited by* M. Gordon and W. R. Ware. Academic Press, New York. 1975. p. 327; (*b*) A. P. SCHAPP, L. LOPEZ, S. D. ANDERSON, and S. D. GAGNON. Tetrahedron Lett. **23**, 5493 (1982).
21. C. P. ANDRIEUX, C. BLOCMAN, J. M. DUMAS-BOUCHIAT, F. M'HALLA, and J. M. SAVEANT. J. Electroanal. Chem. **113**, 19 (1980).
22. T. HINO, H. MASUHARA, and N. MATAGA. Bull. Chem. Soc. Jpn. **49**, 394 (1970).
23. (*a*) A. M. DE P. NICHOLAS and D. R. ARNOLD. Can. J. Chem. **60**, 2165 (1982); (*b*) A. M. DE P. NICHOLAS, R. J. BOYD, and D. R. ARNOLD. Can. J. Chem. 3011 (1982).
24. (*a*) Y. SHIGEMITSU and D. R. ARNOLD. J. Chem. Soc. Chem. Commun. 407 (1975); (*b*) D. R. ARNOLD and A. J. MAROULIS. J. Am. Chem. Soc. **98**, 5931 (1976).
25. B. JAUN, J. SCHWARZ, and R. BRESLOW. J. Am. Chem. Soc. **102**, 5741 (1980).
26. (*a*) A. H. ZIMMERMAN and J. I. BRAUMAN. J. Am. Chem. Soc. **99**, 3565 (1977); (*b*) C. B. ELLISON, P. C. ENGELKING, and W. C. LINEBERGER. J. Am. Chem. Soc. **100**, 2556 (1978).
27. A. J. MAROULIS, Y. SHIGIMITSU, and D. R. ARNOLD. J. Am. Chem. Soc. **100**, 535 (1978).
28. A. J. BIRCH. Rev. **4**, 69 (1950).
29. J. A. BARLTROP. Pure Appl. Chem. **33**, 179 (1973).
30. I. G. SEVAST'YANOVA and A. P. TOMILOV. Zh. Obshoh. Khim. (Engl.) **33**, 2741 (1963).
31. H. O. HOUSE. *In* Modern synthetic reactions. *Edited by* R. Breslow. Benjamin, California. 1972. pp. 586–595.
32. U. C. YOON, S. L. QUILLEN, P. S. MARIANO, R. SWANSON, J. L. STAVINOHA, and E. BAY. J. Am. Chem. Soc. **105**, 1204 (1983).
33. P. S. MARIANO, J. L. STAVINOHA, G. PEPE, and E. F. MEYER, JR. J. Am. Chem. Soc. **100**, 7114 (1978).
34. A. BARANSKI and W. R. FAWCETT. J. Electroanal. Chem. **100**, 185 (1979).
35. P. H. RIEGER, I. BERNAL, W. H. REINMUTH, and G. K. FRAENKEL. J. Am. Chem. Soc. **85**, 683 (1963).
36. A. ISHITANI and S. NAGAKURA. Theor. Chim. Acta, (Berl). **4**, 236 (1966).
37. (*a*) G. CRANK and F. W. EASTWOOD. Aust. J. Chem. **17**, 1392 (1964); (*b*) K. P. KOPECKY and J. H. VAN DE SANDE. Can. J. Chem. **50**, 4034 (1972).
38. R. ADAMS and E. W. ADAMS. Org. Synth. Coll. Vol. **1**, 451 (1941).
39. J. E. CALLEN, C. E. DORNFELD, and G. H. COLEMAN. Org. Synth. Coll. Vol. **III**, 212 (1958).
40. W. SIMONS (*Editor*). The Sadtler handbook of proton NMR spectra. Sadtler Research Laboratories, Philadelphia. 1978. Spectrum Number 1001.
41. R. S. NICHOLSON and I. SHAIN. Anal. Chem. **36**, 706 (1964).

Can. J. Chem. Downloaded from www.nrcresearchpress.com by 210.87.254.42 on 09/06/12
For personal use only.

Structure–activity studies of β-carbolines. 2. Crystal and molecular structures of *N*-ethyl-3-carbamoyl-β-carboline

ALASTAIR K. S. MUIR AND PENELOPE W. CODDING[1]

Departments of Chemistry and Pharmacology and Therapeutics, University of Calgary, Calgary, Alta., Canada T2N 1N4

Received January 17, 1984

ALASTAIR K. S. MUIR and PENELOPE W. CODDING. Can. J. Chem. **62**, 1803 (1984).

The crystal and molecular structures of *N*-ethyl-3-carbamoyl-β-carboline, $C_{14}H_{13}N_3O$, a synthetic ligand of the benzodiazepine receptor are reported. The space group is $C2/c$ with $a = 16.220(4)$, $b = 7.728(4)$, $c = 19.623(6)$ Å, $\beta = 104.16(1)°$, $Z = 8$. The carboxyamide side chain assumes an extended conformation and is almost coplanar with the β-carboline skeleton. The observed molecular conformation is compared to the current model for the receptor binding site. Hydrogen bonding and aromatic ring stacking determine the molecular packing arrangement.

ALASTAIR K. S. MUIR et PENELOPE W. CODDING. Can. J. Chem. **62**, 1803 (1984).

On rapporte les structures cristalline et moléculaire de la *N*-éthyl carbamoyl-3 β-carboline, $C_{14}H_{13}N_3O$, un ligand synthétique du récepteur benzodiazépine. Le groupe d'espace est $C2/c$ avec $a = 16{,}220(4)$, $b = 7{,}728(4)$, $c = 19{,}623(6)$ Å, $\beta = 104{,}16(1)°$, $Z = 8$. La chaîne latérale carboxyamide assume une conformation allongée et elle est pratiquement coplanaire avec le squelette de la β-carboline. On compare la conformation moléculaire observée avec le modèle couramment accepté pour le site de liaison du récepteur. L'arrangement de l'empilement moléculaire est déterminé par les liaisons hydrogènes et par l'entassement des noyaux aromatiques.

[Traduit par le journal]

Introduction

Anti-anxiety drugs of the benzodiazepine family are heavily prescribed and hence are the subject of a large number of studies. In the past few years, a natural receptor for benzodiazepines has been identified in brain tissue (1). This finding motivated an extensive search for the endogenous ligand for the receptor. Of the many supposed ligands, several derivatives of β-carboline (**1**) have had the highest affinity for the benzodiazepine (BZD) receptor.

The β-carbolines (1) have been identified in brain tissue and in urine (2, 3); unfortunately, the actual derivatives that have been identified, 3-alkyl esters, are apparently formed in the isolation procedure. The actual endogenous congener of the 3-carboxy-β-carboline is still sought. Pharmacological tests indicate that some of the β-carbolines with affinity for the BZD receptor are antagonists of the action of the benzodiazepines and are therefore anxiogenic in nature. This finding leads to speculation that the physiological function of the BZD receptor involves alertness and other related attributes. The structure–activity data on these compounds show that the most active β-carbolines are unsaturated and uncharged (4–7); the most active synthetic structures are the 3-hydroxymethyl or 3-ethyl ester derivatives (6). It is possible that the natural side chain on C-3 is a link to a peptide; indeed, the β-carboline skeleton is related to tryptophan and may have similar biological origins.

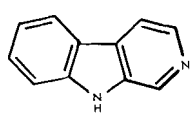

1

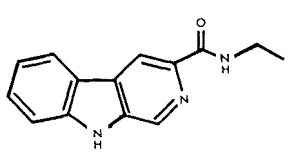

2

To model this peptide link and to develop β-carbolines that are more resistant to enzymic hydrolysis, Coutts, Micetish, and co-workers (5) prepared 3-carboxamide derivatives of β-carboline for testing. In in vitro tests, these amides are less potent inhibitors of ^{3}H-flunitrazepam binding than the alkyl esters, but they still have significant activity. The amides may also have longer half-lives in vivo so that their effect may be comparable to the esters. These amide compounds are of interest because of the possibility of electron delocalization over the entire carboxyamide. This would change the charge density on the carbonyl oxygen atom. The hydrogen bonding capability of the side chain would then be different in amides from that in esters.

Since the β-carbolines and the benzodiazepines bind to the same receptor they must share at least some components of the same pharmacophoric unit. A model for β-carboline and benzodiazepine binding has been developed through distance geometry analysis (8); this method correlates binding free energies with patterns of atom–atom distances within average, rigid molecular structures. The binding site model developed from these considerations found 4 affinity sites and a restriction site for the β-carbolines. The binding site for the side chain in the 3 position did not reflect the variation in activity observed when that group is changed from ester to amide to hydroxymethyl; the binding was proposed to involve only the terminal methyl atom of the *ethyl* ester side chain.

In this work the three-dimensional structure of *N*-ethyl-3-carbamoyl-β-carboline (**2**) is described. The structure is examined with respect to the bonding of the carboxyamide group and the fit to the binding site model developed by Crippen (8). In an earlier paper (9), the structure of the most active of the saturated β-carbolines was reported, 3-carboxyltetrahydroharmane. (All of the saturated β-carbolines are less active than the unsaturated compounds.) The differences in the two types of molecular skeletons will be examined and related to their potential as ligands for the benzodiazepine receptor.

Experimental

A sample of the title compound was provided by R.T. Coutts and R.G. Micetish of the Faculty of Pharmacy, University of Alberta. The compound was crystallized by slow evaporation of a 50:50 mixture of ethanol and water. A colorless, rectangular crystal (0.15 × 0.20 ×

[1] Author to whom correspondence should be addressed.

Can. J. Chem. Downloaded from www.nrcresearchpress.com by 210.87.254.6 on 09/06/12
For personal use only.

Can. J. Chem. Downloaded from www.nrcresearchpress.com by 210.87.254.6 on 09/06/12
For personal use only.

TABLE 1. The atomic coordinates ($\times 10^4$) and $B_{equivalent}$ values ($\times 10$) for the carbon, nitrogen, and oxygen atoms. B_{eq} is calculated from $\frac{1}{3}$ the trace of the B_{ij} matrix

Atom	x/a	y/b	z/c	B_{eq}
C(1)	7975(1)	−5593(3)	−4856(1)	37
N(2)	7287(1)	−4919(2)	−4705(1)	36
C(3)	6709(1)	−4123(2)	−5225(1)	31
C(4)	6780(1)	−3993(2)	−5908(1)	33
C(5)	7517(1)	−4239(3)	−7381(1)	44
C(6)	8001(1)	−4526(3)	−7856(1)	51
C(7)	8780(1)	−5378(3)	−7645(1)	51
C(8)	9089(1)	−5973(3)	−6974(1)	43
N(9)	8759(1)	−6116(2)	−5794(1)	37
C(10)	8101(1)	−5519(2)	−5530(1)	32
C(11)	7496(1)	−4707(2)	−6069(1)	30
C(12)	7814(1)	−4813(2)	−6694(1)	34
C(13)	8595(1)	−5687(2)	−6494(1)	35
C(31)	5946(1)	−3375(2)	−5031(1)	34
O(32)	5384(1)	−2621(2)	−5468(1)	46
N(32)	5912(1)	−3597(2)	−4370(1)	41
C(33)	5197(1)	−3025(3)	−4101(1)	44
C(34)	5282(2)	−3657(4)	−3367(1)	62

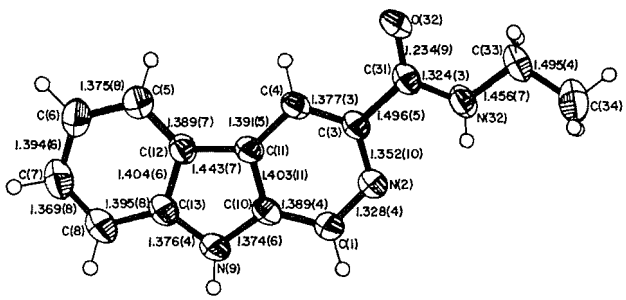

FIG. 1. The atomic labeling scheme and bond distances for the carbon, oxygen, and nitrogen atoms of *N*-ethyl-3-carbamoyl-β-carboline. The estimated standard deviations are in parenthesis. The drawing was made with the program ORTEP (24).

0.20 mm) was used for data collection on an Enraf Nonius CAD4F diffractometer with a graphite monochromator. Crystal data: $C_{14}H_{13}N_3O$ fw = 239.28 Monoclinic, $C2/c$, a = 16.220(4), b = 7.728(4), c = 19.623(6) Å, β = 104.16(1)°, V = 2385.0 Å^3, Z = 8, ρ_c = 1.333 g cm^{-3}, T = 20°C, MoKα, λ = 0.71069 Å, θ_{max} = 30°, 3472 unique reflections, 1133 observed, μ = 0.94 cm^{-1}. Lattice and space group determination and data collection procedures were as described previously (9). Lorentz and polarization corrections were applied.

The structure was solved using MULTAN 78 (10) and difference Fourier syntheses to complete the model. Full-matrix least-squares refinement of the coordinates and isotropic temperature factors converged to an R ($\Sigma||F_o| - |F_c||/\Sigma|F_o|$) value of 0.115. Successive difference Fourier syntheses then revealed the positions of the hydrogen atoms.

Hydrogen atoms were assigned isotropic thermal parameters that were 20% larger than those of the atom to which they were bonded and were included in the model; however, only their positional parameters were refined. The weighting scheme used in the refinement was $w = [[\sigma(F)]^2 + 0.001\ F^2]^{-1}$. The full-matrix least-squares refinement of the positional and anisotropic thermal parameters of the non-hydrogen atoms and the positional parameters of the hydrogen atoms converged with a maximum shift/error of 0.002, R = 0.032, and $R_w(\Sigma w(|F_o| - |F_c|)^2/\Sigma wF_o^2)^{1/2}$ = 0.038. The standard deviation of an observation of unit weight was 0.98; the largest peak in a final difference Fourier synthesis was 0.23 eÅ^{-3} and was associated with the C(11)—C(12) bond. The function minimized was $w(|F_o| - |F_c|)^2$ and the 2206 reflections used in the final refinement were the 1133 observed reflections and the 1073 unobserved reflections that had $F_c^2 > 2.5\sigma(I_o)$. Atomic coordinates are given in Table 1[2] with the atoms labeled as in Fig. 1. The bond distances for the carbon, nitrogen, and oxygen atoms are given in Fig. 1. The XRAY 76 system (11) of programs as used and the scattering factors were those of Cromer and Mann (12).

Results and discussion

Figure 1 shows the molecular structure of *N*-ethyl-3-carbamoyl-β-carboline. The carboxyamide side chain adopts an extended conformation as exemplified by the torsion angles: C(3)—C(31)—N(32)—C(33) = −177.0(2)° and C(31)—N(32)—C(33)—C(34) = 172.4(2)°. An *anti* arrangement of carbonyl oxygen atom (O(32)) and ring nitrogen atom (N(2)) across the C(3)—C(31) partial double bond is observed in this structure. Table 2 tabulates the N—C—C—O torsion angle for the 10 published examples of crystal structures containing a 2-carbamoylpyridine fragment and for this structure. In all but one case, the pyridinyl nitrogen atom is *anti* to the carbonyl oxygen atom; in the exception, α-picolinamide (15), the conformation deviates from this *antiperiplanar* conformation by only 18°. This consistent observation of one conformation for this fragment is important for the development of a model for the binding of β-carbolines to the benzodiazepine receptor because it has been established that activity is greatly dependent on the presence and the type of oxygen substituent on the carbon atom attached to the ring at C(3). The model for β-carboline binding that has been developed by distance constraint analysis (8) uses a different conformation for this group, i.e. *synclinal*, and this conformation has not been observed in any amide structure.

The ring system of the β-carboline nucleus is planar; the standard deviation for the 13 atom plane is 0.021 Å. The carboxyamide side chain lies approximately in this plane; the methyl carbon atom, C(34), shows the only significant deviation, 0.204 Å, from the plane. The carboxyamide group is also planar (σ = 0.003 Å) and the angle between the carboxyamide plane and the β-carboline is 0.6°. This coplanarity is evidence for an extensive delocalization of electrons throughout the entire π system of the β-carboline and carboxyamide group. In contrast, in the tetrahydroharmane molecule (9), the angle between the plane of the indole fragment and the carboxylic acid fragment was 58.9°.

The bond distances for the β-carboline ring are comparable to those found in other determinations of this unsaturated skeleton (21, 22) and are indicative of the aromatic nature of the ring system. The carboxyamide group shows the delocalization known to be typical of peptide linkages with distances C(31)—O(32) of 1.234(9) Å and for C(31)—N(32) of 1.324(3) Å. These values are also consistent with those observed in the other 10 examples of the 2-carbamoyl-pyridine fragment as shown in Table 2. In addition, the connecting C(3)—C(31) bond is considerably shortened, 1.496(5) Å, which suggests an overlap of the two π-systems. Both the bond distances and the overall planarity of the molecule are evidence for a delocalized π-system for the ring and carboxyamide por-

[2] Tables of the anisotropic thermal parameters, the bond angles for the non-hydrogen atoms, hydrogen atom parameters, and the observed and final calculated structure amplitudes are available, at a nominal charge, from the Depository of Unpublished Data, CISTI, National Research Council of Canada, Ottawa, Ontario, Canada K1A 0S2.

TABLE 2. Geometry of 2-carbamoyl-pyridine fragments

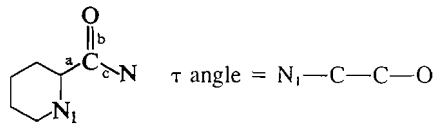

τ angle = N_1—C—C—O

	Distances (Å)			Angle (°)	
	a	*b*	*c*	τ	Ref.
2,6-Diacetylpyridine	1.505	1.221	1.357	171.5	13
bis(picolinoylhydrazone)*	1.509	1.217	1.359	176.6	
4-Methylquinoline-2-carboxamide	1.503	1.239	1.319	176.0	14
α-Picolinamide	1.519	1.234	1.322	−162.0	15
N-Pyridoxylidene-N′-picolinoylhydrazine hydrochloride	1.503	1.227	1.353	180.0	16
2-(*N*-Methylcarboxamido) quinoline	1.509	1.227	1.322	179.1	17
Quinoline-2-carboxamide	1.499	1.234	1.329	−177.5	18
Quinoline-2-carboxamide hemihydrate*	1.500	1.228	1.334	−176.3	19
	1.515	1.227	1.328	173.2	
Virginamycin factor S	1.447	1.260	1.314	179.0	20
This work	1.496	1.234	1.324	179.9	
Average	1.50(2)	1.23(1)	1.33(1)	176(5)†	

* This crystal had two unique fragments.

† The absolute values of the torsion angle were averaged. This value is 176(3)° if α-picolinamide is omitted from the average.

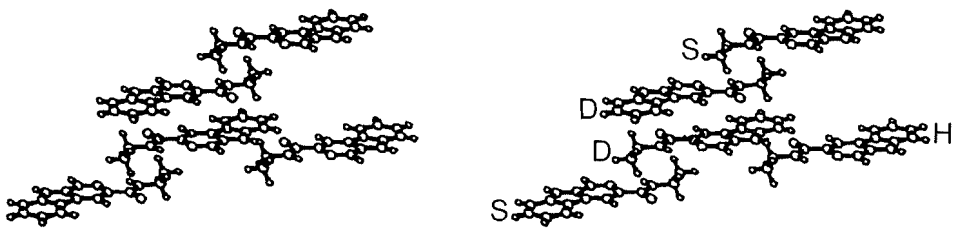

FIG. 2. A stereodrawing showing the close intermolecular contacts in the crystal. These are a dimer (D) contact, a side chain contact (S), and a hydrogen bond (H). The drawing was made with the program PLUTO (25).

tion of the side chain. Pharmacological testing has established that the fully aromatic β-carbolines are more active than their saturated congeners. Together, the two findings suggest that a π−π interaction with components of the receptor may play a role in the binding of these molecules. The delocalization of electrons into the side chain will change the energy of the π levels of the β-carboline and affect their possible interactions with portions of the receptor.

Often the intermolecular interactions in a crystal can be viewed as models for the types of forces that are important for binding to the receptor molecule (23). In this crystal, hydrogen bonding is one determinant of the packing. The bond is formed between molecules related by the face-centering of the crystal lattice; i.e., between N(9) and O(32) at $(1/2 + x, y - 1/2, z)$. This is shown in Fig. 2 as the contact between the lower molecule labeled D and the molecule labeled H. The bond is relatively weak, since the H(9)...O(32) distance is long at 1.96(2) Å, and the N(9)—H(9)...O(32) angle is 154(2)°. In paper 1 of this series (9) it was reported that the carboxylic acid derivative of β-carboline has extensive hydrogen bonding as part of the crystal environment. In both of these examples of 3-substituted β-carbolines, the oxygen atoms have functioned as hydrogen bond acceptors. Since it is known (6) that an oxygen-substituted side chain at position 3 of the β-carboline ring is necessary for maximal activity at the benzodiazepine receptor, it would appear that hydrogen-bond formation must be part of the interaction with the receptor. Rather surprisingly, the model developed by Crippen (8) does not include this site as a significant component of the binding features of these molecules.

Figure 2 shows some of the key features of the packing of the molecules of *N*-ethyl-3-carbamoyl-β-carboline. The molecules stack in dimers (labeled D) that are related by the inversion center at $(-1/2, -1/2, 0)$ and are separated by ca. 3.5 Å. The dimer stacks the carboxamide π-system over the π-system of the A ring of the β-carboline. The closest atom–atom distance is 3.464(8) Å from C(4) to N(2). The dimers are stacked in a ribbon through the operation of the center of symmetry at the cell origin. This dimer-to-dimer interaction places the carboxamide side chains in proximity, with the closest approach between C(33)—O(32) at 3.537(4) Å. In Fig. 2, this interaction is shown above and below the dimer by the molecules labeled S. The cell contains several ribbons that have a close contact of 3.74(1) Å between the methyl carbon atoms (C(34)) of the side chains in two neighboring ribbons, one at (x, y, z) and the other at $(1 - x, y, -z - 1/2)$. Close stacking of π-systems is

Can. J. Chem. Downloaded from www.nrcresearchpress.com by 210.87.254.6 on 09/06/12
For personal use only.

important in this crystalline environment. The higher activity of unsaturated β-carboline derivatives and this packing arrangement are consistent with a $\pi-\pi$ interaction between these molecules and the benzodiazepine receptor.

In summary, analysis of this structure and the previous one in this series (9) has led to the identification of a hydrogen bond *acceptor* site as a part of the receptor binding features of β-carbolines. This site has not been identified in the model of β-carboline binding (8). In addition, analysis of the bonding and the crystalline environment of the title compound and like molecules has indicated that a single side chain conformation as well as electron delocalization and $\pi-\pi$ interactions are important in the unsaturated β-carboline amides.

Acknowledgements

This research was supported by the Alberta Heritage Foundation for Medical Research (Studentship to A.K.S.M. and Scholarship and Establishment grant to P.W.C.) and the Medical Research Council of Canada (Grant No. MA-8087 to P.W.C.).

The authors wish to thank R.T. Coutts and R.G. Micetish for kindly supplying the compound, M.F. Richardson of Brock University for assistance with computerized structural searches, and K.A. Kerr for use of the diffractometer.

1. J. F. TALLMAN, S. M. PAUL, P. SKOLNICK, and D. W. GALLAGER. Science, **207**, 274 (1980).
2. N. S. BUCKHOLTZ. Life Sci. **27**, 893 (1980), and references cited therein.
3. C. BRAESTRUP, M. NIELSEN, and C. E. OLSEN. Proc. Natl. Acad. Sci. U.S.A. **77**, 2288 (1980).
4. H. A. ROBERTSON, R. T. COUTTS, A. BENDERLY, R. A. LOCOCK, and I. L. MARTIN. Eur. J. Pharmacol. **76**, 281 (1981).
5. R. A. LOCOCK, G. B. BAKER, R. G. MICETICH, R. T. COUTTS, and A. BENDERLY. Prog. Neuro-Psychopharmacol. Biol. Psychiat. **6**, 407 (1982).
6. M. CAIN, R. W. WEBER, F. GUZMAN, J. M. COOK, S. A. BARKER, K. C. RICE, J. N. CRAWLEY, S. M. PAUL, and P. SKOLNICK. J. Med. Chem. **25**, 1081 (1982).
7. K. L. LIPPKE, W. G. SCHUNACK, W. WENNING, and W. E. MÜLLER. J. Med. Chem. **26**, 499 (1983).
8. G. M. CRIPPEN. Mol. Pharmacol. **22**, 11 (1982).
9. P. W. CODDING. Can. J. Chem. **61**, 529 (1983).
10. G. GERMAIN, P. MAIN, and M. M. WOOLFSON. Acta Crystallogr. Sect. A, **27**, 368 (1971).
11. J. M. STEWART. The X-ray system of crystallographic programs. Computer Science Center, University of Maryland, College Park, MD. 1976.
12. D. T. CROMER and J. B. MANN. Acta Crystallogr. Sect. A, **24**, 321 (1968).
13. C. PELIZZI and G. PELIZZI. Acta Crystallogr. Sect. B, **35**, 126 (1979).
14. M. GDANEIC, M. JASKOLSKI, and Z. KOSTURKIEWICZ. Pol. J. Chem. **54**, 1539 (1980).
15. T. TAKANO, Y. SASADA, and M. KADUO. Acta Crystallogr. **21**, 514 (1966).
16. P. DOMIANO, A. MUSATTI, C. PELIZZI, and G. PREDIEU. Cryst. Struct. Commun. **7**, 751 (1978).
17. M. GDANIEC and T. DZIEMBOWSKA. Pol. J. Chem. **54**, 87 (1980).
18. M. GDANIEC, M. JASKOLSKI, and Z. KOSTURKIEWICZ. Acta Crystallogr. Sect. B, **33**, 3558 (1977).
19. M. GDANIEC, M. JASKOLSKI, and Z. KOSTURKIEWICZ. Acta Crystallogr. Sect. B, **33**, 2284 (1977).
20. J. P. DECLINCQ, G. GERMAIN, M. VAN MEERSSCHE, S. E. HULL, and M. J. IRWIN. Acta Crystallogr. Sect. B, **34**, 3644 (1978).
21. Y. KOKOMORI, K. SEKIDO, T.-S. WU, H.-J. TIEN, and S. HIROKAWA. Bull. Chem. Soc. Jpn. **55**, 2236 (1982).
22. M. LEBOEUF, A. CAVÉ, P. FORGACS, J. PROVOST, A. CHIARONI, and C. RICHE. J. Chem. Soc. Perkin Trans. 1, **207**, 1205 (1982).
23. G. GILLI, P. A. BOREA, V. BERTOLASI, and M. SACERDOTI. *In* Molecular structure and biological activity. *Edited by* J.F. Griffin and W.L. Duax. Elsevier Biomedical, New York. 1982. p. 259.
24. C. K. JOHNSON. ORTEP Report ORNL-3794, Oak Ridge National Laboratory, Oak Ridge, TN. 1965.
25. S. MOTHERWELL. PLUTO, University Chemical Laboratory, Cambridge, England. 1979.

Can. J. Chem. Downloaded from www.nrcresearchpress.com by 210.87.254.6 on 09/06/12
For personal use only.

Complexation par transfert de charge de la chlorpromazine en présence d'iode; action thyroïdienne sécondaire de cette molécule

ANNE-CATHERINE ABSIL, JACQUES BUXERAUD ET CLAUDE RABY

Laboratoire de Chimie Thérapeutique, Faculté de Médecine et de Pharmacie, 2, rue du Docteur Marcland, 87032 Limoges Cedex, France

Reçu le 30 septembre 1983[1]

ANNE-CATHERINE ABSIL, JACQUES BUXERAUD et CLAUDE RABY. Can. J. Chem. **62**, 1807 (1984).

L'interaction moléculaire entre l'iode et la chlorpromazine est étudiée par spectroscopie électronique. L'iode forme avec la chlorpromazine un complexe de transfert de charge, de stoechiométrie 1:1 et de type $n-\sigma$. Les valeurs de la constante de formation (K_c à 20°C = 3166 ± 19 L mol^{-1}), les paramètres thermodynamiques (ΔH^0 = −11,22 ± 0,11 kcal mol^{-1}; ΔS^0 = −22,29 ± 0,38 cal mol^{-1} K^{-1}) traduisent une forte interaction donneur−accepteur, comparable à celle obtenue avec les amines tertiaires. La constante de formation est comparée avec celles obtenues pour les molécules antithyroïdiennes. La chlorpromazine possèderait une activité sur l'hormonogénèse thyroïdienne.

ANNE-CATHERINE ABSIL, JACQUES BUXERAUD, and CLAUDE RABY. Can. J. Chem. **62**, 1807 (1984).

Molecular interaction between iodine and chlorpromazine is investigated by electron spectroscopy. Iodine forms a charge transfer complex with chlorpromazine, with 1:1 stoichiometry and of the $n-\sigma$ type. The values of the formation constant (K_c at 20°C = 3166 ± 19 L mol^{-1}) and thermodynamic parameters (ΔH^0 = −11.22 ± 0.11 kcal mol^{-1}, ΔS^0 = −22.29 ± 0.38 cal mol^{-1} K^{-1}) show a strong donor−acceptor interaction, comparable to that obtained with tertiary amines. The formation constant is compared to those obtained with antithyroid molecules. Chlorpromazine appears to have no effect on the intrathyroid cycle of iodine.

Introduction

Il est bien connu que les amines tertiaires, en particulier la triéthylamine, sont capables de former des complexes par transfert de charge avec l'iode. Ces complexes ont été étudiés qualitativement et quantitativement (1). La valeur de la constante de formation de complexe et les paramètres thermodynamiques ont permis de révéler une forte interaction donneur−accepteur.

Une étude semblable, effectuée sur les médicaments antithyroïdiens, a permis d'établir une corrélation entre les valeurs de constante K_c et l'activité antithyroïdienne (2). Cette relation structure−activité a permis de classer toutes les molécules antithyroïdiennes connues. La fixation de l'iode par formation de complexe serait donc un des mécanismes d'action des antithyroïdiens de synthèse.

La similitude d'action de la triéthylamine et des médicaments antithyroïdiens vis-à-vis de l'iode, nous a amené à nous intéresser aux nombreuses molécules médicamenteuses non antithyroïdiennes, mais possédant dans leur structure une fonction amine tertiaire. Il semble, en effet, intéressant d'étudier la formation de complexes entre de telles molécules et l'iode, afin de déterminer si ces molécules possèdent une activité antithyroïdienne secondaire méconnue à ce jour. Nous rapportons ici l'étude de l'interaction moléculaire chlorpromazine−iode. La chlorpromazine est un dérivé phénothiazinique à chaîne latérale portant un azote tertiaire permettant d'assimiler cette molécule à la famille chimique des amines tertiaires.

Partie expérimentale

Produits

L'iode est un produit suprapur bisublimé Merck 4763. Il est utilisé sans aucune purification et conservé à l'obscurité dans un dessiccateur contenant de l'anhydride phosphorique.

La chlorpromazine est un produit commercialisé sous forme de chlorhydrate. Ce chlorhydrate est transformé en base selon le procédé suivant: dans une ampoule à décanter, on introduit une prise d'essai exactement pesée, voisine de 0,30 g.

Après addition de 20 mL d'eau distillée et 10 mL de solution d'hydroxyde de sodium N, on pratique plusieurs extractions chloroformiques successives de la base ainsi libérée. Les phases chloroformiques sont recueillies et évaporées sous vide. La chlorpromazine base est purifiée par hplc; elle se présente sous la forme d'un produit huileux.

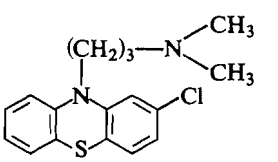

Chloro-3 (diméthylamino-3 propyl)-10 phénothiazine

Le solvant, tétrachlorure de carbone, est un produit Merck Uvasol pour spectroscopie utilisé sans aucune purification. Sa faible teneur en eau (maximum 0,01%) ne perturbe en aucun cas la formation du complexe chlorpromazine−iode.

Matériel

Les spectres électroniques sont enregistrés à l'aide d'un spectrophotomètre double faisceau Perkin−Elmer 554 uv−visible équipé d'un porte cuve thermostaté à effet Peltier (température contrôlée à ± 0,1°C). Les cuves utilisées sont en quartz, leur parcours optique est de 1 cm.

Protocole

Les solutions d'iode à des concentrations (M) de l'ordre de 10^{-4} sont préparées extemporanément par gravimétrie. Les différentes solutions de chlorpromazine sont préparées extemporanément par volumétrie à partir d'une solution mère obtenue par gravimétrie. Les solutions de complexes sont réalisées directement dans les cuves du spectrophotomètre en mélangeant 1,5 mL de solution de chlorpromazine et 1,5 mL de solution d'iode.

Les absorbances de ces solutions de complexe sont enregistrées immédiatement à différentes longueurs d'onde. De nouveaux spectres sont effectués après plusieurs heures de contact afin d'apprécier la stabilité du complexe chlorpromazine−iode.

Les paramètres thermodynamiques sont calculés en suivant l'évolution de l'absorbance d'une série de solutions en fonction de la température (10, 15, 20, 25, 30, 35 et 40°C). Les concentrations des solutions n'ont pas été corrigées dans cet intervalle de température

[1]Revision reçue le 3 avril 1984.

Can. J. Chem. Downloaded from www.nrcresearchpress.com by 210.87.254.6 on 09/06/12
For personal use only.

Can. J. Chem. Downloaded from www.nrcresearchpress.com by 210.87.254.6 on 09/06/12
For personal use only.

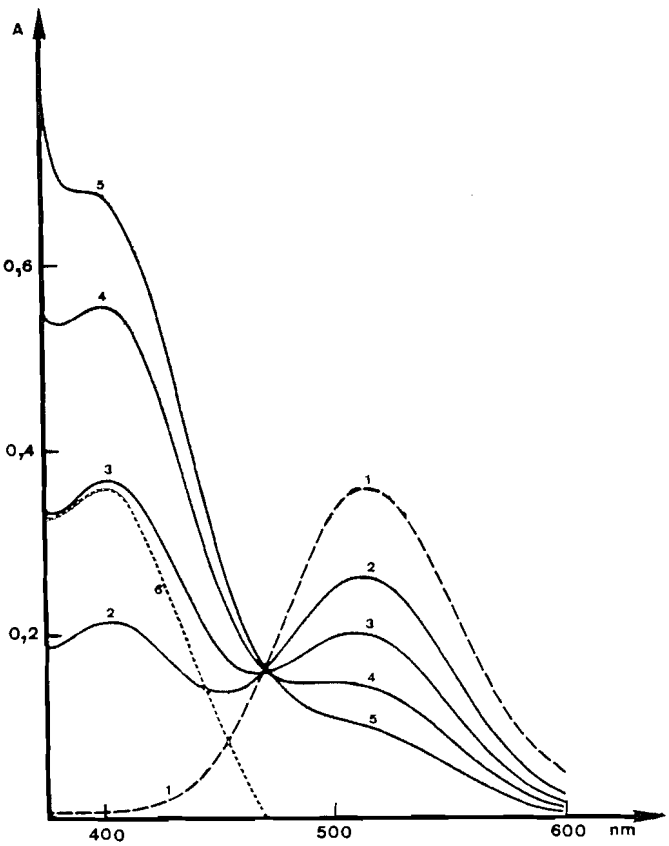

FIG. 1. Spectres d'absorption dans le visible du complexe chlorpromazine–iode (solvant tétrachlorure de carbone; température: 20 ± 0,1°C; cellules de quartz de 10 mm). La concentration de l'iode est fixée à $3{,}839 \times 10^{-4}$ *M*. Les concentrations (*M*) de la chlorpromazine sont: (1) 0; (2) $2{,}065 \times 10^{-4}$; (3) $4{,}13 \times 10^{-4}$; (4) $8{,}26 \times 10^{-4}$; (5) $1{,}377 \times 10^{-3}$. La courbe 6 représente l'absorption visible du complexe calculée pour la solution 3.

(Δ (°C) = 30). Après enrégistrement des absorbances de solutions de complexe à six températures, un retour à la température initiale permet de vérifier que les nouvelles absorbances lues restent inchangées par rapport aux absorbances initiales.

Résultats

Etude dans la région du visible

Aux concentrations utilisées variant de $0{,}207 \times 10^{-3}$ à $1{,}377 \times 10^{-3}$ *M*, le donneur est totalement transparent aux longueurs d'ondes étudiées, c'est à dire entre 420 et 515 nm.

L'adjonction d'une solution d'iode aux solutions de donneur entraîne une perturbation de la bande visible de l'iode à 515 nm: elle est déplacée vers les basses longueurs d'onde (effet hypsochrome) (fig. 1). Ces nouvelles bandes, "blue shifted bands", sont attribuées à la complexation de l'halogène, elles se recoupent en un point isobestique situé à 470 nm. Le pic du complexe est repéré à 405 nm en plaçant dans le faisceau de référence une cuve contenant une solution d'halogène à la même concentration que dans le complexe. L'enregistrement spectrophotométrique, à différentes températures, de la "blue shifted band" pour la solution de complexe montre que l'intensité de ces bandes décroit fortement avec une élévation de la température (fig. 2).

La stabilité des complexes est étudiée en réalisant de nouveaux enregistrements après 24 h. Il apparaît de nouvelles bandes d'absorption à 290 et 360 nm caractérisant la présence d'ions I_3^-. Les changements sont d'autant plus importants que

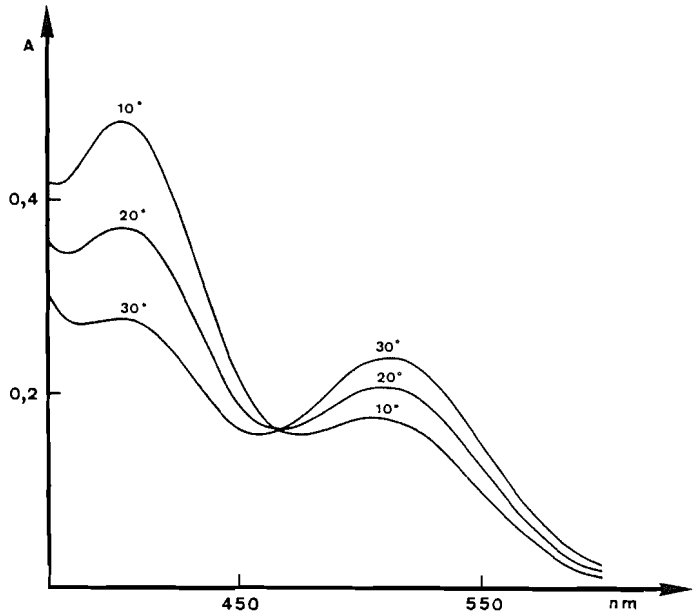

FIG. 2. Influence de la température sur la bande de l'iode complexé par la chlorpromazine dans CCl_4. Les concentrations en iode et en chlorpromazine sont respectivement: $3{,}839 \times 10^{-4}$ *M* et $4{,}13 \times 10^{-4}$ *M*.

les concentrations en donneur sont élevées.

L'étude mathématique de la transition $\pi_g \rightarrow \sigma_u$ de l'halogène, l'analyse des absorbances dans les spectres, l'existence d'un seul point isobestique, l'alignement parfait des points expérimentaux sur les droites de régression linéaire (fig. 3) confirment la présence d'un complexe de stoechiométrie 1:1. D'autre part, un contrôle matriciel de Liptay (3) à 420, 425, 430 et 435 nm a permis de s'assurer de la présence d'un seul complexe. Pour cela, les absorbances d'une série de solutions de complexes sont enregistrées. Une correction est apportée en soustrayant, pour chacune de ces absorbances lues, l'absorbance de l'iode non complexé calculée mathématiquement. Le donneur n'absorbant pas dans cette région, seule l'absorption due à l'iode est à soustraire.

$$[1] \quad A_{corr} = A_{obs} - \epsilon_{I_2}[I_2]$$

A_{corr} est l'absorbance corrigée du complexe, A_{obs} est l'absorbance du mélange donneur–iode, ϵ_{I_2} le coefficient d'absorption molaire de l'iode, $[I_2]$ la concentration d'iode non complexé, déterminée facilement à 515 nm (ϵ_{I_2} à 515 nm = 917 L mol^{-1}).

Les valeurs des absorbances corrigées du complexe ainsi obtenues pour différentes solutions à plusieurs longueurs d'onde sont disposées sous la forme d'une matrice. Cette matrice est ensuite normalisée sur la longueur d'onde 420 nm (tableau 1). En présence d'un seul complexe, toutes les colonnes sont égales aux erreurs expérimentales prés.

Pour déterminer les constantes de formation de complexe K_c et les coefficients d'absorption molaire ϵ_c la méthode de Benesi–Hildebrand–Scott (12, 13) n'a pu être utilisée, cette méthode s'appliquant lorsque les concentrations initiales en donneur sont très largement supérieures à celles de l'accepteur. L'équation [2] est donc utilisée (4, 11).

$$[2] \quad K_c = \frac{[C]}{([A_0] - [C])([D_0] - [C])}$$

où [C] est la concentration du complexe, $[A_0]$ la concentration

Can. J. Chem. Downloaded from www.nrcresearchpress.com by 210.87.254.6 on 09/06/12
For personal use only.

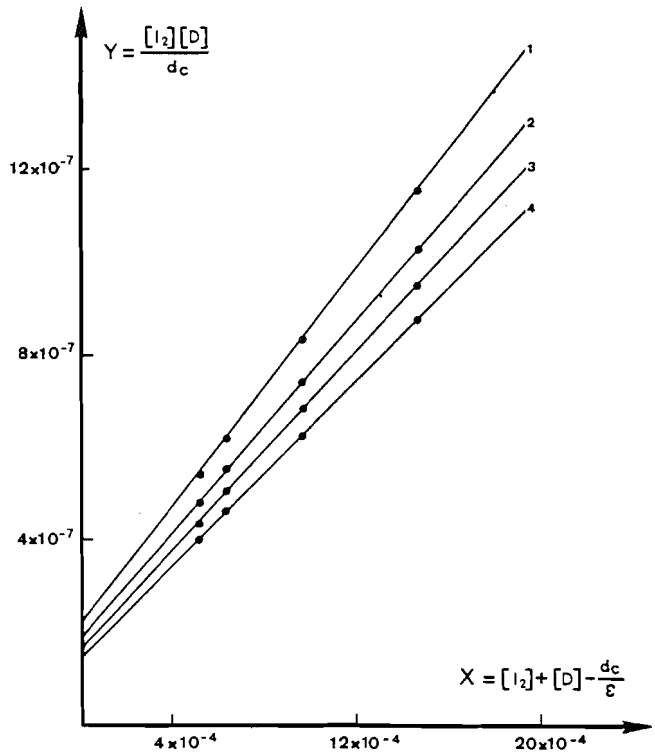

FIG. 3. Relation entre $[I_2][D]/d_c$ et $[I_2] + [D] - d_c/\epsilon_c$ pour le complexe chlorpromazine–iode à 20°C (solvant CCl_4, cuves quartz de 10 mm de parcours optique). Les droites de regression ont pour équation: (1) 435 nm, $Y = 6{,}551 \times 10^{-4} X + 2{,}093 \times 10^{-7}$ ($r = 0{,}999$); (2) 430 nm, $Y = 5{,}874 \times 10^{-4} X + 1{,}826 \times 10^{-7}$ ($r = 0{,}999$); (3) 425 nm, $Y = 5{,}338 \times 10^{-4} X + 1{,}676 \times 10^{-7}$ ($r = 0{,}999$); (4) 420 nm, $Y = 4{,}927 \times 10^{-4} X + 1{,}568 \times 10^{-7}$ ($r = 0{,}999$).

TABLEAU 1. Contrôle matriciel de Liptay effectué pour le complexe chlorpromazine–iode à 20°C

(a) Absorbances corrigées (A_{corr}) disposées sous forme de matrice*

λ (nm)	Sol. 1	Sol. 2	Sol. 3	Sol. 4
420	0,601	0,505	0,339	0,198
425	0,556	0,469	0,316	0,183
430	0,506	0,427	0,288	0,167
435	0,451	0,381	0,255	0,148

(b) Normalisation de cette matrice sur la λ 420 nm

	1	1	1	1
	0,925	0,928	0,932	0,934
	0,842	0,846	0,849	0,843
	0,750	0,754	0,752	0,747

*Les concentrations (M) des réactifs utilisées pour les 4 solutions sont: $[I_2]$ = constante = $3{,}889 \times 10^{-4}$; [chlorpromazine]: sol. 1 = $1{,}337 \times 10^{-3}$; sol. 2 = $8{,}260 \times 10^{-3}$; sol 3 = $4{,}130 \times 10^{-3}$; sol. 4 = $2{,}065 \times 10^{-4}$.

initiale de l'accepteur et $[D_0]$ la concentration initiale du donneur. Le terme [C] peut être remplacé par d_c/ϵ_c et conduire à l'éq. [3].

$$[3] \quad \frac{[A_0][D_0]}{d_c} = \left[[A_0] + [D_0] - \frac{d_c}{\epsilon_c}\right]\frac{1}{\epsilon_c} + \frac{1}{K_c\epsilon_c}$$

où la longueur d'onde étudiée d_c est l'absorbance du complexe seul, ϵ_c le coefficient d'absorption molaire du complexe et K_c la constante de formation du complexe. La résolution de l'éq. [3] par la méthode des moindres carrés nécessitant la connaissance de la valeur de ϵ_c fait appel à un procédé par itérations qui a été programmé sur ordinateur. La représentation graphique du terme $[A_0][D_0]/d_c$ en fonction de $[A_0] + [D_0] - d_c/\epsilon_c$ conduit à une droite de pente $1/\epsilon_c$ et d'intercept $1/K_c\epsilon_c$ (fig. 3). Les constantes de formation K_c et les coefficients d'absorption molaire ϵ_c du système chlorpromazine–iode sont rassemblés dans le tableau 2. Les valeurs obtenues (K_c à 20°C = 3166 ± 19 L mol^{-1}) sont en accord avec une forte interaction iode–chlorpromazine.

TABLEAU 2. Constantes de formation K_c et coefficients d'absorption molaire ϵ_c pour le complexe chlorpromazine–iode en solution dans le tétrachlorure de carbone à 10, 15, 20, 25, 30, 35 et 40°C

t (°C)	λ (nm)	K_c* (L mol^{-1})	$\bar{K}_c$	ϵ_c* (L mol^{-1} cm^{-1})
10	420	5931	6020±67	2070
	425	6034		1891
	430	6092		1699
	435	6024		1513
15	420	4258	4282±66	2051
	425	4320		1895
	430	4348		1700
	435	4201		1517
20	420	3141	3166±19	2028
	425	3186		1870
	430	3170		1700
	435	3168		1520
25	420	2208	2221±22	2025
	425	2198		1875
	430	2241		1705
	435	2238		1519
30	420	1591	1635±30	2069
	425	1646		1914
	430	1656		1750
	435	1647		1537
35	420	1195	1216±27	2045
	425	1206		1887
	430	1207		1715
	435	1256		1524
40	420	892	893±4	2036
	425	888		1876
	430	893		1710
	435	897		1518

*Evaluation à partir de la bande visible du complexe par la méthode déjà décrite, à partir de 4 solutions de complexe chlorpromazine–iode. Pour chaque solution de complexe, la concentration d'iode est constante égale à $3{,}839 \times 10^{-4}$ M et la concentration du donneur varie ($0{,}207 \times 10^{-3}$ M; $0{,}413 \times 10^{-3}$ M; $0{,}826 \times 10^{-3}$ M et $1{,}377 \times 10^{-3}$ M).

Le coefficient d'absorption molaire du complexe ϵ_c à 405 nm, maximum d'absorption de la "blue shifted band" n'a pas pu être déterminé. En effet, l'absorbance encore non négligeable des ions I_3^- à 405 nm vient interférer avec l'absorbance du complexe dans la région du visible.

La représentation graphique de $R \ln K_c$ en fonction de $1/T$ conduit à une droite dont la pente donne la valeur de ΔH^0 et l'intercept celle de ΔS^0 (fig. 4). Les paramètres thermodynamiques, en accord avec la formation de complexes, sont rassemblés dans le tableau 3.

Etude dans la région de l'ultraviolet

L'absorption dans l'ultraviolet de la chlorpromazine à une concentration de $1{,}377 \times 10^{-5}$ M en solution dans le tétra-

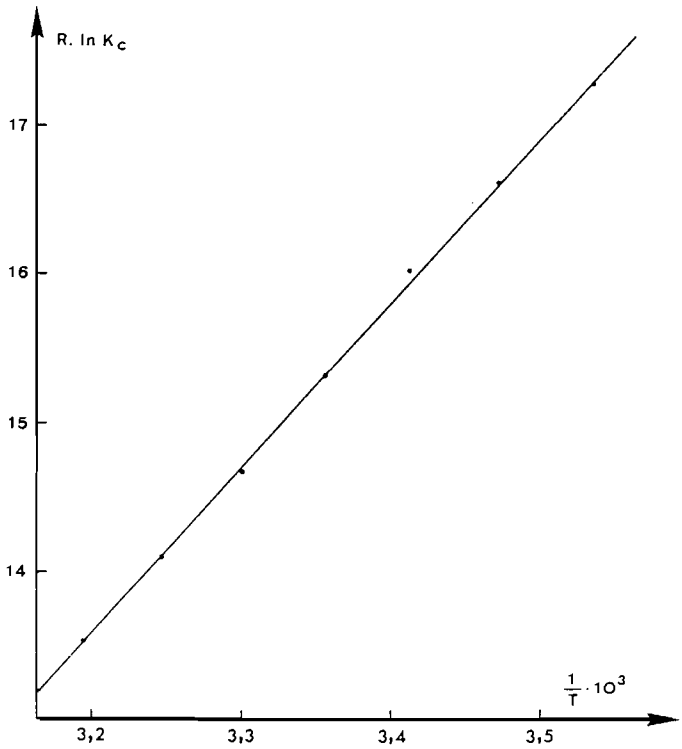

FIG. 4. Détermination des paramètres thermodynamiques du complexe chlorpromazine–iode. La droite de régression linéaire a pour équation $Y = 11{,}22\ X - 22{,}29$ ($r = 0{,}999$).

TABLEAU 3. Paramètres thermodynamiques obtenus pour les complexes chlorpromazine–iode et triéthylamine–iode

Paramètre	$[I_2]$ [Chlorpromazine]	$[I_2]$ [Triéthylamine]*
$-\Delta H^0$ kcal mol^{-1}	11,22±0,11	12,12±0,72
$-\Delta S^0$ cal mol^{-1} K^{-1}	22,29±0,38	−23,87±2,39
$-\Delta G^0$ kcal mol^{-1}	4,700±0,003 (à 293 K)	5,10±0,02 (à 293,5 K)

*Réference 1.

chlorure de carbone fait apparaître un pic principal à 259 nm (log ϵ = 4,43) et une large bande d'intensité plus faible dont le maximum est situé à 310 nm (log ϵ = 3,63).

La formation du complexe chlorpromazine–iode provoque des perturbations du spectre électronique ultraviolet avec apparition d'une nouvelle bande (fig. 5). Cette nouvelle bande est obtenue d'abord graphiquement en plaçant dans le faisceau de référence une concentration de donneur équivalente à celle se trouvant dans le complexe, puis mathématiquement en soustrayant l'absorption due à l'iode. Cette bande peut être déterminée avec plus de précision. En effet la détermination des concentrations en accepteur libre et en donneur libre est possible en faisant intervenir les constantes K_c obtenues dans le visible. Puis en soustrayant mathématiquement les absorptions respectives de l'iode et de la chlorpromazine non complexé, à partir de l'absorption lue directement pour la solution de complexe on obtient une nouvelle bande. Cette nouvelle bande est pratiquement identique à celle obtenue précédemment. Elle peut être attribuée à la bande de transfert de charge sur laquelle vient se superposer l'absorption due aux ions I_3^- à 290 nm lui donnant ainsi un aspect asymétrique.

Le maximum de la bande de transfert de charge est repéré à

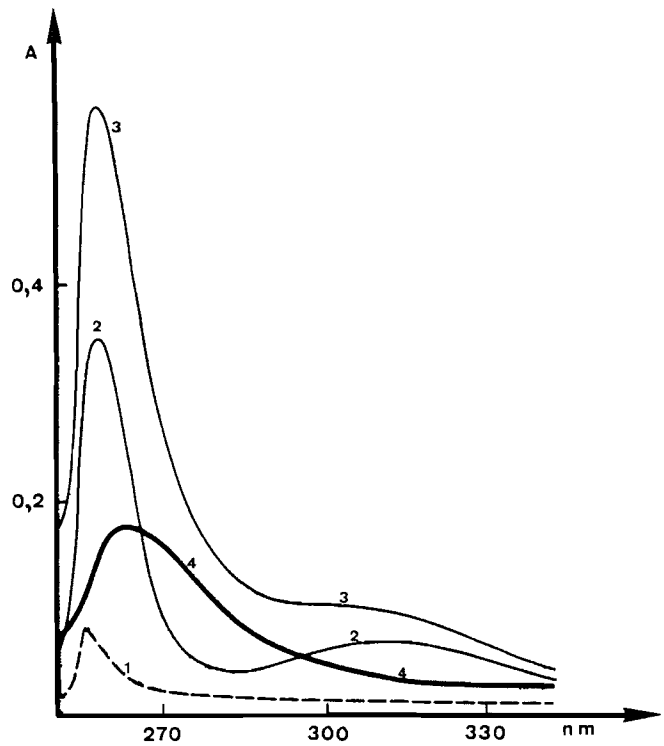

FIG. 5. Spectres d'absorption dans l'ultraviolet du complexe chlorpromazine–iode (solvant CCl_4; t: 20°C; cellules de quartz de 10 mm). Les concentrations (M) sont (1) I_2 3,839 × 10^{-4}; (2) chlorpromazine 1,377 × 10^{-5}; (3) I_2 3,839 × 10^{-4} et chlorpromazine 1,377 × 10^{-5}; (4) courbe d'absorption calculée du complexe.

264 ± 0,5 nm. Les relations de McConnell (5) et Hastings *et al.* (6) entre le potentiel d'ionisation et la fréquence du maximum de la bande de transfert de charge, permettent d'évaluer le potentiel d'ionisation de la chlorpromazine: $I_p \simeq 9{,}83 \pm 0{,}03$. Si la position du maximum d'absorption peut être repérée avec suffisamment de précision pour permettre d'évaluer le potentiel d'ionisation I_p de la chlorpromazine, par contre les absorbances de la bande de transfert de charge pour différentes concentrations ne peuvent pas être déterminées avec grande précision. En effet, l'absorption de la bande de transfert de charge se situe dans une région du spectre où absorbent aussi le donneur et les ions I_3^- formés lors de la réaction de complexation. Pour ces raisons il n'est pas possible d'entreprendre une étude thermodynamique à 264 nm. Un essai réalisé a fourni des résultats inexploitables signalés par l'obtention de coefficients de corrélation r très différents de 1 lors de la résolution de l'éq. [3] sur ordinateur.

Discussion

L'étude spectroscopique électronique confirme le caractère $n-\sigma$ des complexes iodés de transfert de charge obtenus avec la chlorpromazine. Ces complexes sont de stoechiométrie 1 : 1. Les résultats traduisent une forte interaction donneur–accepteur.

En accord avec Mulliken (7) et Popov et Deskin (8), la formation des ions I_3^- est due à la transformation d'un "outer complex" en un "inner complex" libérant des ions I^- qui viennent réagir avec l'iode moléculaire I_2 non complexé. Le schéma réactionnel est donné dans les équations [4]–[7].

[4] Chlorpromazine + $I_2 \rightleftarrows$ chlorpromazine $- I_2$
("outer complex")

Can. J. Chem. Downloaded from www.nrcresearchpress.com by 210.87.254.6 on 09/06/12
For personal use only.

TABLEAU 4. Comparaison des constantes de formation de complexes iodés obtenues avec quelques molécules antithyroïdienne, la triéthylamine et la chlorpromazine

	K_c à 20°C (L mol^{-1})	Solvant
KSCN	94 (à 22°C)*	H_2O
Mercapto-2 thiazoline	2527±118*	CCl_4
Thiourée	8825±505*	CH_2Cl_2
Tétraméthylthiourée	13215±1150*	*n*-Heptane
Mercapto-2 méthyl-1 imidazole	23194±667*	CCl_4
Triéthylamine	6315±200† (à 20,5°C)	*n*-Heptane
Chlorpromazine	3166±19	CCl_4

*Référence 2.
†Référence 1.

[5] Chlorpromazine $- I_2 \rightleftarrows$ chlorpromazine $- I^+I^-$

[6] Chlorpromazine $- I^+I^- \rightleftarrows$ [chlorpromazine $- I]^+ + I^-$ ("inner complex")

[7] $I^- + I_2 \rightleftarrows I_3^-$

La réaction selon l'éq. [5] se déroule lentement alors que les autres ont une cinétique rapide.

Les constantes K_c du complexe chlorpromazine–iode sont comparées avec celles obtenues pour la triéthylamine (1) et pour quelques molécules antithyroïdiennes (2) (tableau 4).

(*i*) La valeur de la constante K_c du complexe chlorpromazine–iode est particulièrement élevée et s'accorde avec les valeurs obtenues pour les amines tertiaires. Les paramètres thermodynamiques sont du même ordre de grandeur que ceux obtenus pour le complexe triéthylamine–iode (tableau 3). Il est donc raisonnable de penser que le transfert de charge s'effectue de la paire d'électrons libre portée par l'azote de la chaîne aminopropyle vers l'orbitale antiliante de l'iode.

(*ii*) La différence observée entre la valeur de K_c de la triéthylamine (K_c à 20,5°C = 6315 L mol^{-1}) et celle de la chlorpromazine (K_c à 20°C = 3166 L mol^{-1}) s'explique en examinant la structure tridimensionnelle de la molécule de chlorpromazine; la chaîne aminopropyle est repliée vers l'atome de chlore porté par le noyau phénothiazinique (9, 10), l'approche de l'iode vers l'azote tertiaire est donc gênée par encombrement stérique, ce qui se traduit par une diminution du caractère donneur de la chlorpromazine par rapport au caractère donneur attendu d'une amine tertiaire. Cette différence peut aussi secondairement s'expliquer par le fait que les complexes chlorpromazine–iode ont été étudiés dans CCl_4 alors que les complexes triéthylamine–iode ont été réalisés dans le *n*-heptane. Il est en effet bien connu que CCl_4 se comporte comme un accepteur vis-à-vis des amines (14). Bien que cette action soit très faible, CCl_4 est ici en très large excés et peut inhiber compétitivement de façon non négligeable la formation du complexe chlorpromazine–iode.

(*iii*) La chlorpromazine a, cependant, une constante supérieure à celle de la mercapto-2 thiazoline dont l'action antithyroïdienne est connue.

La chlorpromazine, grâce à son pouvoir de complexation de l'iode, pourraît donc perturber la synthèse des hormones thyroïdiennes et posséder une action antithyroïdienne secondaire. Une étude expérimentale chez le rat avec détermination des taux de T_3 et de T_4 et avec étude histologique des coupes de thyroïdes de rats traités par la chlorpromazine semble confirmer ce résultat.

1. S. NAGAKURA. J. Am. Chem. Soc. **80**, 520 (1958).
2. J. BUXERAUD. Thèse Doctorat ès Sciences Pharmaceutiques, Limoges n° 4 (1978).
3. W. LIPTAY. Z. Electrochem. **65**, 375 (1961).
4. J. BUXERAUD et C. RABY. C. R. Acad. Sci. Sér. C, **286**, 565 (1978).
5. H. MCCONNELL, J. S. HAM, et J. R. PLATT. J. Chem. Phys. **21**, 66 (1953).
6. S. H. HASTINGS, J. L. FRANKLIN, J. C. SCHILLER et F. A. MATSEN. J. Am. Chem. Soc. **75**, 2900 (1953).
7. R. S. MULLIKEN. J. Phys. Chem. **56**, 801 (1952).
8. A. I. POPOV et W. DESKIN. J. Am. Chem. Soc. **80**, 2976 (1958).
9. J. J. H. MCDOWELL. Acta Crystallogr. Sect. B, **25**, 2175 (1969).
10. J. J. KAUFMAN et E. KERMAN. Int. J. Quantum Chem. Quantum Biol. Symp. N° 1, 259 (1974).
11. R. P. LANG. J. Am. Chem. Soc. **84**, 1185 (1962).
12. H. A. BENESI et J. H. HILDEBRAND. J. Am. Chem. Soc. **71**, 2703 (1949).
13. R. L. SCOTT. Recl. Trav. Chim. Pays-Bas, **75**, 787 (1956).
14. W. J. LAUTENBERGER, E. N. JONES et J. G. MILLER. J. Am. Chem. Soc. **90**, 1110 (1968).

Can. J. Chem. Downloaded from www.nrcresearchpress.com by 210.87.254.6 on 09/06/12
For personal use only.

The effect of heteroatoms at the α-position of aldimines on the $^1J_{C-H}$ coupling constant at the sp^2-carbon[1]

NORBERT DE KIMPE[2,3] ROLAND VERHÉ, LAURENT DE BUYCK, AND NICEAS SCHAMP

Laboratory of Organic Chemistry, Faculty of Agricultural Sciences, State University of Gent, Coupure Links 653, B-9000 Gent, Belgium

Received December 13, 1983

NORBERT DE KIMPE, ROLAND VERHÉ, LAURENT DE BUYCK, and NICEAS SCHAMP. Can. J. Chem. **62**, 1812 (1984).

The effect of α-functionalization of a great variety of aldimines on the $^1J_{C-H}$ coupling constant at the sp^2 aldimine carbon has been determined. This comparative study includes α-*tert*-butyl, α-alkoxy-, α-phenyl-, α-hydroxy-, α-sulfenyl-, α,α-disulfenyl-, α-alkylamino-, α-chloro-, α,α-dichloro-, α-bromo-, α,α-dibromo-, and α,α,α-trichloroaldimines. Depending upon the α-heterofunctionalization the $^1J_{C-H}$ value for (*E*)-aldimines varied over a great range of about 150–178 Hz.

NORBERT DE KIMPE, ROLAND VERHÉ, LAURENT DE BUYCK et NICEAS SCHAMP. Can. J. Chem. **62**, 1812 (1984).

L'influence de la fonctionalisation en position α d'une grande varieté d'aldimines sur la valeur des constantes de couplage $^1J_{C-H}$ au niveau du sp^2-carbone de l'aldimine a été mesurée. Cette comparaison a été effectuée avec des aldimines α-*tert*-butylés, α-alkoxylés, α-phénylés, α-hydroxylés, α-sulfénylés, α,α-disulfenylés, α-alkylaminés, α-chlorés, α,α-dichlorés, α-bromés, α,α-dibromés et α,α,α-trichlorés. La grandeur de $^1J_{C-H}$ des (*E*)-aldimines varie de 150 à 178 Hz et dépend de la hétérofunctionalisation en position α du groupement imino.

Introduction

The influence of the relative stereochemistry of the nitrogen lone pair of electrons on the magnitude of spin coupling constants of proximate carbon atoms has already been studied in recent years. An important parameter related to this phenomenon is $^1J_{C-H}$, i.e. the coupling constant between a carbon atom and a hydrogen atom directly linked to it. According to a recent review on experimental and theoretical contributions in this field, the hybridization of the carbon atom plays a major role in determining the magnitude of this parameter (1). As a consequence, many classes of compounds containing the imino group —CH=N—, among others hydrazones, oximes, and simple imines (i.e. those derived from formaldehyde), have been studied theoretically in view of the influence of the nitrogen lone pair orientation on $^1J_{C-H}$ (2–4). Very few experimental data on this specific topic have been published, notably in the field of oximes (5). However, a very recent study added considerable experimental data to this subject by a study of the effect of the stereochemistry on $^1J_{C-H}$ at the sp^2 carbons of imino derivatives of aldehydes, i.e. aldoximes, aldohydrazones, and aldimines (6). The magnitudes of the coupling constant $^1J_{C-H}$ at the imino carbon of both *E* and *Z* isomers of the latter three classes of compounds have shown a consistently greater value, by about 20 Hz, for the *Z* isomer. In connection with a comprehensive study on the chemistry of α-halogenated imines (for review articles on the chemistry of α-haloimines, see ref. 7), we had occasion to study the coupling constant $^1J_{C-H}$ for a great variety of α-functionalized aldimines. Our results are discussed here and compared with the recent report of the configurational assignments of aldimines (6).

Results

Twenty-one aldimines, substituted at the α-position with various functional groups, including *tert*-butyl, phenyl and halogens (chlorine and bromine), hydroxy-, alkylthio-, alkoxy-, and alkylamino-groups, were synthesized. In addition, an α,β-unsaturated aldimine has been included in this series. The α-functionalized aldimines were prepared from aldehydes and chloral via the straightforward routes outlined in Scheme 1.

Coupling constants $^1J_{C-H}$ were measured from fully coupled spectra, obtained from 40% solutions of the aldimines in deuteriochloroform. The values, ranging between 151 and 178 Hz, are compiled in increasing order of magnitude in Table 1. The introduction of heteroatoms at the α-position of aldimines has a dramatic influence on the $^1J_{C-H}$ value. It should be stressed here that all aldimines, described by us, occurred as their *E*-stereoisomer, exclusively. This statement is based on accepted concepts of steric hindrance around an imino bond. For aldimines, there is an exclusive preference for the *E*-configuration at equilibrium (8). The barrier to *E*–*Z*-isomerization about the carbon–nitrogen double bond is very sensitive to the nature of the substituents. In some particular cases, such as for aldimines derived from *ortho*-disubstituted benzaldehydes or 9-anthrylaldehyde, a significant proportion of the *Z*-isomer has been detected at equilibrium in solution (8, 9). Such (*Z*)-aldimines may also be observed as transient intermediates after uv irradiation or may be prepared in certain cases after α-lithiation and α-alkylation by which the α-anion and the final product possess the *Z*-configuration (10). Tertiary aldimines, i.e. aldimines having an α-sp^3 carbon bearing no α-hydrogens, have not been found to show any trace of their *Z*-isomer. Because the ^{1}H nmr spectra of all our tertiary α-substituted aldimines showed only one stereoisomer (^{1}H nmr), it is reasonable to accept the *E*-stereochemistry. These findings agree with the recent study on this topic, in which no *Z*-isomer of pivaldimines (see Table 1; entry 1) could be produced or detected (6). The latter study revealed the $^1J_{C-H}$ coupling constant of (*E*)-*N*-(2,2-dimethyl-1-propylidene)isopropylamine (entry 1; Table 1) to be 150 Hz. We found a slightly higher value for α-*tert*-butylaldimines **14** and **15** (151 Hz), α,β-unsaturated aldimine **10** (153 Hz), α-alkylamino-, α-phenyl- and α-alkoxyaldimines **9**, **6**, and **11** (154.5 Hz, 155 Hz, and 155 Hz, respectively). A higher coupling constant $^1J_{C-H}$ was noticed for α-hydroxylated aldimine **16** (156.5 Hz) and α-sulfenylated aldimine **12** (158 Hz), but α,α-disulfenylated aldimines, α-chloro aldimines, and α-bromoaldimines showed

[1] This is part 34 of our series on the chemistry of α-halogenated imines. For part 33 see ref. 20.

[2] N. De Kimpe: "Bevoegdverklaard Navorser" (Research Associate) of the Belgian "Nationaal Fonds voor Wetenschappelijk Onderzoek" (National Fund for Scientific Research).

[3] Author to whom correspondence may be addressed.

Can. J. Chem. Downloaded from www.nrcresearchpress.com by 210.87.254.6 on 09/06/12
For personal use only.

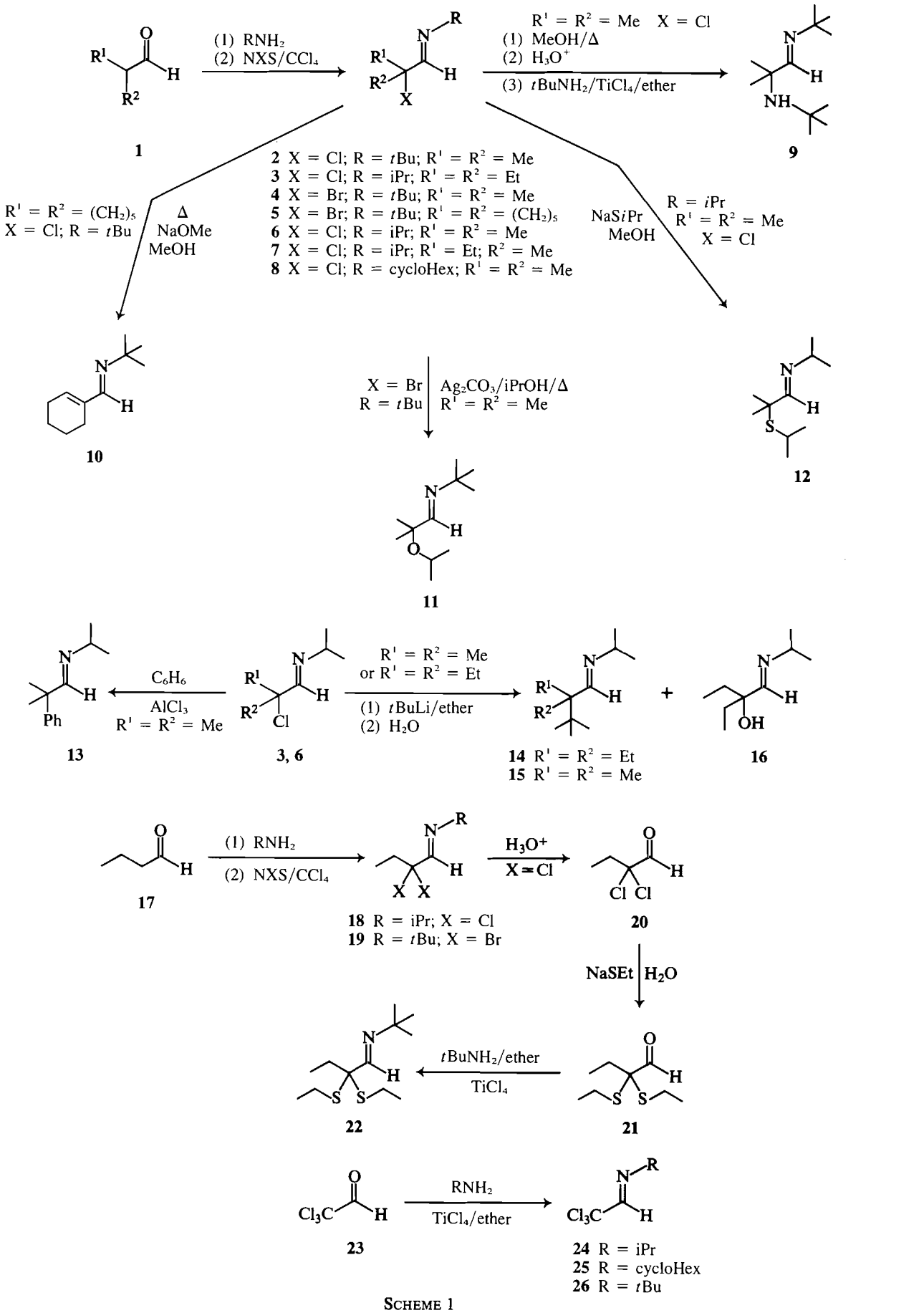

1 9 10 12 11 13 3, 6 14 15 16 17 18 19 20 22 21 23

SCHEME 1

Can. J. Chem. Downloaded from www.nrcresearchpress.com by 210.87.254.6 on 09/06/12
For personal use only.

TABLE 1. $^1J_{C-H}$ Coupling constants for α-functionalized aldimines[a]

Entry	Compound	$^1J^{E}_{C-H}$[b] (Hz)	Synthesized according to references given here
1	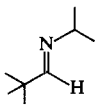 **29**	150	[c]
2	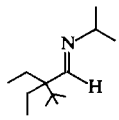 **14**	151[e]	[d]
3	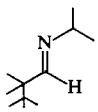 **15**	151.5	[d]
4	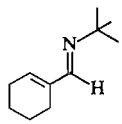 **10**	153	12
5	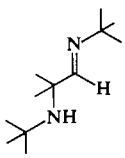 **9**	154.5[e]	12, 13
6	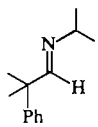 **13**	155	14
7	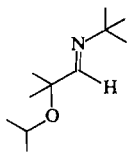 **11**	155	[d]
8	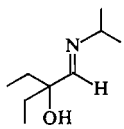 **16**	156.5[e]	[d]
9	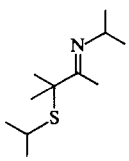 **12**	158	15
10	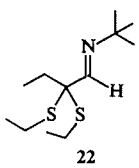 **22**	162.5	13, 16, 18
11	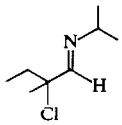 **7**	162.5	12
12	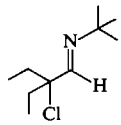 **3**	162.5	12
13	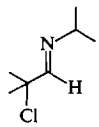 **6**	162.5	12
14	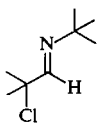 **2**	162.5	12
15	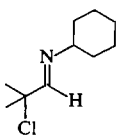 **8**	162.5	12
16	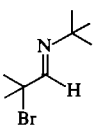 **4**	162.5	[d], 12
17	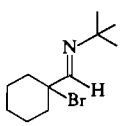 **5**	163[e]	[d], 12
18	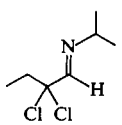 **18**	171.5	16, 17
19	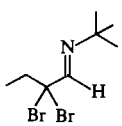 **19**	172.5	16, 17
20	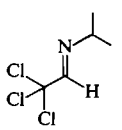 **24**	178	13

Can. J. Chem. Downloaded from www.nrcresearchpress.com by 210.87.254.6 on 09/06/12
For personal use only.

TABLE 1. (*Concluded*)

Entry	Compound	$^1J^{E}_{C-H}$ [b] (Hz)	Synthesized according to references given here	Entry	Compound	$^1J^{E}_{C-H}$ [b] (Hz)	Synthesized according to references given here
21	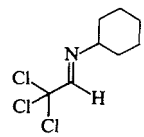 **25**	178	13	22	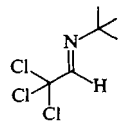 **26**	177.5	13

[a] All α-functionalized aldimines listed in this table occurred as the *E*-isomer exclusively.
[b] Accuracy ±0.5 Hz unless otherwise stated.
[c] The $^1J_{C-H}$ value of this compound originates from ref. 6.
[d] This communication.
[e] Accuracy ±1 Hz.

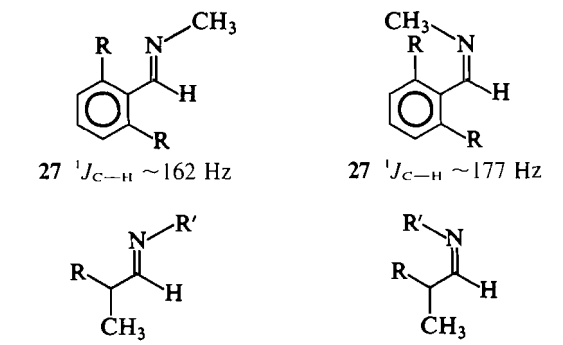

SCHEME 2

a much higher coupling constant of 162.5 Hz. The greatest coupling constants were measured for α,α-dichloroaldimine **18**, α,α-dibromoaldimine **19**, and trichloroacetaldimines (**24**–**26**) whose $^1J_{C-H}$ values mounted to 171.5 Hz, 172.5 Hz, and 177.5–178 Hz, respectively. Thus there is a marked influence of the α-substitution on the $^1J_{C-H}$ value at the sp^2 carbon of aldimines. The increasing $^1J_{C-H}$ parallels to some extent an increasing electronegativity of the α-substituents, but plotting the $^1J_{C-H}$ values versus the Higgins electronegativities (19) of the α-heteroatoms did not reveal a significant relationship. On the contrary, the *N*-substituent (R) and the geminal α,α-dialkyl groups (R^1 and R^2) did not exert an important influence on the $^1J_{C-H}$ coupling constant. This is illustrated by comparison of the data of a series of five α-chloroaldimines **2**, **3**, **6**, **7**, and **8** (R^1, R^2 = Me or Et; R = iPr, cycloHex, or *t*Bu), whose $^1J_{C-H}$ coupling constants fall within a very narrow range between 162.3 and 162.7 Hz (all values in the table have been rounded off to 162.5 Hz). The same observation is noted for α,α,α-trichloroacetaldimines **24**–**26** whose $^1J_{C-H}$ values are only very slightly influenced by the *N*-substituent (R = iPr, cycloHex, *t*Bu). This phenomenon gains interest in view of the known $^1J_{C-H}$ values for (*E*) and (*Z*) aldimines. It has been generally found that the magnitude of $^1J_{C-H}$ at the aldimine sp^2-carbon is consistently greater for the *Z*-isomer with respect to the *E*-isomer. *o*,*o*-Disubstituted benzaldimines **27** have $^1J_{C-H}$ values of about 162 Hz and 177 Hz for the *E* and *Z*-isomers, respectively (8). On the other hand, propionaldimines or isobutyraldimines **28** showed $^1J_{C-H}$ coupling constants of 151–154 Hz for the *E* isomer and 170–171 Hz for the *Z* isomers (6). The unsubstituted and simplest aldimine, i.e. methyleneamine, was recently generated at low temperature and revealed $^1J_{C-H}$ coupling constants of 163.7 Hz and 172.9 Hz (11). These data are useful for establishing stereochemical assignments in aldimines provided that both stereoisomers are available. If not, the $^1J_{C-H}$ value does not provide any conclusive information regarding the stereochemistry of aldimines because the α-substitution (especially heteroatoms) plays a major role. It has been shown in this paper that tertiairy (*E*)-aldimines show a range of $^1J_{C-H}$ values which varies from about 150 to 178 Hz. This range entirely covers the range in which $^1J_{C-H}$ values for *E* and *Z* isomers of simple aldimines (e.g. **29**) are situated, therefore pointing to the care with which such figures should be handled.

Experimental

The ^{13}C nmr spectra were recorded using a Varian FT-80 nmr spectrometer, operating at 20 MHz. The coupling constants $^1J_{C-H}$ were obtained from fully coupled spectra, using 40% solutions of aldimines in deuteriochloroform. α-Functionalized aldimines were synthesized according to the following procedures. α-Chloroaldimines **2**, **3**, **6**, **7**, and **8** were prepared by chlorination (with *N*-chlorosuccinimide in CCl_4) of aldimines, obtained from condensation of aldehydes **1** with primary amines (12). α-Bromoaldimines **4** and **5** were synthesized in an analogous way using *N*-bromosuccinimide in CCl_4. This reaction required heating of the reactants in an oil bath at 50°C for an overnight period. After completion of the reaction (nmr monitoring), the precipitated succinimide was filtered off and the solvent evaporated *in vacuo*. α-Bromoaldimine **4** had a boiling point of 58–61°C/14 Torr (1 Torr = 133.3 Pa) (yield 62%), while the α-bromoaldimine **5** decomposed on distillation *in vacuo* and was therefore used as such (purity of at least 98%). α,β-Unsaturated aldimine **10** was obtained from dehydrochlorination of the chloro analogue of α-bromoaldimine **5** using sodium methoxide in methanol under reflux (12). α-Isopropoxyaldimine **11** was synthesized by silver-induced alcoholysis of α-bromoaldimine **4** with silver carbonate (1 molar equiv.) in dry isopropanol under reflux for 16 h. Aqueous work-up afforded solvolysis product **11** as the sole product (86% yield). α-Sulfenylated aldimine **12** was produced according to our previously published procedure (15). *N*-*tert*-butyl-α-(*N*-*tert*-butyl)aminoisobutyraldimine **9** was prepared by rearrangement of α-chloroaldimine **2** with methanol into the hydrochloride of α-*tert*-butylaminoisobutyraldehyde dimethyl acetal (12), after which the latter was hydrolyzed with 4 *N* hydrochloric acid (room temperature, 16 h) in a two-phase system with dichloromethane to afford α-*tert*-butylaminoisobutyraldehyde; this aldehyde was converted into the corresponding aldimine essentially according to our published method for the preparation of α-halogenated imines from α-halogenated carbonyl compounds using primary amines in the presence of

Can. J. Chem. Downloaded from www.nrcresearchpress.com by 210.87.254.6 on 09/06/12
For personal use only.

titanium(IV) chloride (94% yield) (13). α-Phenylaldimine **13** was synthesized by Friedel–Crafts reaction of α-chloroaldimine **6** with $AlCl_3$ in benzene (14). α-*tert*-Butylated aldimines **14** and **15** were prepared by reaction of α-chloroaldimines **3** and **6** with *tert*-butyllithium in ether. The reaction mixtures were analyzed by preparative gas chromatography and afforded **14** and **15**, next to α-hydroxyaldimine **16** and coupling products, i.e. 1,4-diimines (see, for instance, footnote 1). α,α-Dichloroaldimine **18** and α,α-dibromoaldimine **19** were prepared from butanal as previously described (16, 17), except that the bromination to afford **19** required, preferentially, an overnight reaction time at 70°C. α,α-Disulfenylated aldimine **22** was obtained according to the following sequence: acidic hydrolysis of α,α-dichloroaldimine **18** afforded 2,2-dichlorobutanal **20** (16), which was converted into the protected α-ketoaldehyde **21** using sodium ethylthiolate in aqueous medium (18), after which compound **21** was transformed into α,α-disulfenylated aldimine **22** essentially according to our described procedure for the imination of α-halocarbonyl compounds (13).

N-(2,2,2-Trichloroethylidene)isopropylamine **24**, *N*-(2,2,2-trichloroethylidene)cyclohexylamine **25**, and *N*-(2,2,2-trichloroethylidene)-*tert*-butylamine **26** were prepared in analogy with the reported procedure for the synthesis of the *N*-*tert*-butyl derivative (13).

The chemical shifts (δ, $CDCl_3$) of the aldimine carbon (—*C*H=N)— of the various α-functionalized aldimines are as follows: compound **2**: 159.1 ppm; compound **3**: 162.0 ppm; compound **4**: 158.9 ppm; compound **5**: 158.6 ppm; compound **6**: 162.6 ppm; compound **7**: 162.1 ppm; compound **8**: 162.5 ppm; compound **9**: 166.1 ppm; compound **10**: 158.5 ppm; compound **11**: 162.1 ppm; compound **12**: 163.7 ppm; compound **13**: 166.3 ppm; compound **14**: 167.7 ppm; compound **15**: 168.5 ppm; compound **16**: 164.2 ppm; compound **18**: 157.5 ppm; compound **19**: 155.8 ppm; compound **22**: 157.1 ppm; compound **24**: 154.4 ppm; compound **25**: 154.5 ppm; compound **26**: 152.5 ppm.

Acknowledgements

The authors are indebted to the Belgian National Fund for Scientific Research for financial support to the laboratory.

1. P. E. HANSEN. Prog. Nucl. Magn. Reson. Spectrosc. **15**, 18 (1981).
2. T. YONEZAWA, I. MORISHIMA, K. FUKUTA, and Y. OHMORI. J. Mol. Spectrosc. **31**, 341 (1969).
3. G. E. MACIEL, J. W. MCIVER, JR., N. S. OSTLUND, and J. A. POPLE. J. Am. Chem. Soc. **92**, 1 (1970).
4. M. S. GOPINATHAN and P. T. NARASIMHAN. Mol. Phys. **22**, 473 (1971).
5. T. YONEZAWA and I. MORISHIMA. J. Mol. Spectrosc. **27**, 210 (1968).
6. R. R. FRASER and M. BRESSE. Can. J. Chem. **61**, 576 (1983).
7. N. DE KIMPE and N. SCHAMP. Org. Prep. Proced. Int. **11**, 115 (1979); N. DE KIMPE, R. VERHÉ, L. DE BUYCK, and N. SCHAMP. Org. Prep. Proced. Int. **12**, 49 (1980); N. DE KIMPE and R. VERHÉ. *In* The chemistry of halides, pseudo-halides and azides (Supplement D). *Edited by* S. Patai and Z. Rappaport. J. Wiley & Sons, Chichester, Great Britain. 1983. Chapt. 13. pp. 549–601.
8. J. BJØRGO, D. R. BOYD, C. G. WATSON, W. B. JENNINGS, and D. M. JERINA. J. Chem. Soc. Perkin Trans. 2, 1081 (1974).
9. D. R. BOYD, C. G. WATSON, W. B. JENNINGS, and D. M. JERINA. J. Chem. Soc. Chem. Commun. 183 (1972).
10. R. R. FRASER. *In* Comprehensive carbanion chemistry. *Edited by* T. Durst and E. Buncel. Elsevier-North Holland. 1982.
11. B. BRAILLON, M. C. LASNE, J. L. RIPOLL, and J.-M. DENIS. Nouv. J. Chim. **6**, 121 (1982).
12. N. DE KIMPE, R. VERHÉ, L. DE BUYCK, H. HASMA, and N. SCHAMP. Tetrahedron, **32**, 2457 (1976).
13. N. DE KIMPE, R. VERHÉ, L. DE BUYCK, L. MOËNS, and N. SCHAMP. Synthesis, 43 (1982).
14. N. DE KIMPE, R. VERHÉ, L. DE BUYCK, N. SCHAMP, and M. CHARPENTIER-MORIZE. Tetrahedron Lett. **23**, 2853 (1982).
15. N. DE KIMPE, R. VERHÉ, L. DE BUYCK, and N. SCHAMP. Synthesis, 632 (1983).
16. R. VERHÉ, N. DE KIMPE, L. DE BUYCK, and N. SCHAMP. Synthesis, 455 (1975).
17. N. DE KIMPE, R. VERHÉ, L. DE BUYCK, and N. SCHAMP. Synth. Commun. **5**, 269 (1975).
18. R. VERHÉ, N. DE KIMPE, L. DE BUYCK, and N. SCHAMP. Synthesis, 45 (1984).
19. M. L. HUGGINS. J. Am. Chem. Soc. **75**, 4123 (1953).
20. N. DE KIMPE, B. DE CORTE, R. VERHÉ, L. DE BUYCK, and N. SCHAMP. Tetrahedron Lett. **25**, 1095 (1984).

Can. J. Chem. Downloaded from www.nrcresearchpress.com by 210.87.254.6 on 09/06/12
For personal use only.

Polarography of *n*-butylthioglycolate in aqueous media, methanol, and acetonitrile

K. C. GUPTA AND KALPANA K. SHARMA
Department of Chemistry, Govt. College, Kota (Raj.), India

Received August 19, 1983[1]

K. C. GUPTA and KALPANA K. SHARMA. Can. J. Chem. **62**, 1817 (1984).

The polarographic behaviour of *n*-butylthioglycolate (RSH) at the DME in aqueous media, methanol, and acetonitrile has been investigated in the presence of 0.1 *M* KNO_3 and 0.01% thymol. The effect of pH, concentration of RSH, and drop time on the wave characteristics and the mechanism of the reaction occurring at the surface of the mercury drop have been studied. Well-defined reversible and diffusion-controlled anodic waves were obtained in aqueous media (pH 4.2), 40% methanol (pH 3.22), and 40% acetonitrile (pH 2.96). Mathematical and analytical evidence was obtained to show that the anodic wave of RSH at a dropping mercury electrode in aqueous media, 40% methanol, and 40% acetonitrile is due to the formation of the mercury complex RSHg. The dissociation constant (p*K*) of the mercapto group in *n*-butylthioglycolate is 9.6 and the diffusion coefficient in the different media are 1.17×10^{-6} cm^2 s^{-1} (in aqueous media) 1.23×10^{-6} cm^2 s^{-1} (in 40% methanol), and 2.43×10^{-6} cm^2 s^{-1} (in 40% acetonitrile). The linearity of i_d with RSH concentration provides a rapid and precise method for the determination of RSH, down to 0.4 m*M* in aqueous media, methanol, and acetonitrile.

K. C. GUPTA et KALPANA K. SHARMA. Can. J. Chem. **62**, 1817 (1984).

On a examiné le comportement polarographique, au niveau de la goutte de mercure, du thioglycolate de *n*-butyle (RSH) en solution dans l'eau, le méthanol et l'acétonitrile, en présence de KNO_3 à 0,1 *M* et de thymol à 0,01%. On a étudié l'effet du pH, de la concentration du RSH et du temps de chute sur les caractéristiques de la vague et sur le mécanisme de la réaction se produisant à la surface de la goutte de mercure. En solutions dans l'eau (pH de 4,2), dans le méthanol (40% et pH de 3,22) ou dans l'acétonitrile (40% et pH de 2,96), on a obtenu des vagues anodiques réversibles bien définies et d'autres controlées par la diffusion. On a obtenu des données qui permettent de montrer que la vague anodique du RSH qui se produit au niveau de la goutte de mercure, dans l'eau et dans des solutions à 40% de méthanol ou à 40% d'acétonitrile, est due à la formation d'un complexe de mercure RSHg. La constante de dissociation (pK) du groupe thiol du thioglycolate de *n*-butyle est égale à 9,6 et les coefficients de diffusion dans les différents milieux sont $1,17 \times 10^{-6}$ (dans l'eau), 1.23×10^{-6} (dans le méthanol à 40%) et $2,43 \times 10^{-6}$ (dans l'acétonitrile à 40%) cm^2 s^{-1}. La linéarité de i_d avec la concentration de RSH fournit une méthode précise et rapide de déterminer la concentration de RSH, jusqu'à des concentrations de 0,4 m*M*, dans des milieux aqueux, méthanoliques ou d'acétonirile.

[Traduit par le journal]

Introduction

The electrochemical behaviour of thiols, alkyl thiols, and disulphides at DME has been the subject of several polarographic investigations (1–14). Because of the increasing significance of sulphur-containing organic compounds in pharmaceutical and industrial fields, a considerable interest on their electrochemical behaviour has been shown in the past two decades, but previous electrochemical studies are limited to polarographic investigations in aqueous media. In view of the important applications of *n*-butylthioglycolate and its interesting behaviour towards complex formation with heavy metal ions, it was considered worthwhile to investigate its polarographic behaviour at a dropping mercury electrode (dme) in aqueous and aqueous – non-aqueous media, which may provide an accurate method for its quantitative determination in semimicro amounts.

Experimental

Materials and methods

Reagents

n-Butylthioglycolate (Evan's Chemetics, Inc., New York) and AnalaR (BDH) reagents KNO_3, KCl, and NaOH, methanol, acetonitrile, etc., were used. Fresh solution of *n*-butylthioglycolate was prepared in 60% non-aqueous (methanol or acetonitrile) medium. Other stock solutions used were prepared in doubly-distilled air-free conductivity water. Reagent grade acetonitrile and methanol were used after further purification (15). Freshly prepared solutions were always used to avoid the effects of aging and air oxidation. Thymol 0.01% was used as maximum suppressor.

Apparatus

A Southern manual polarograph (Surrey, England) in conjunction with the thermostated cell was used for recording current voltage curves. An external saturated calomel electrode, connected to the cell by means of agar bridge (0.3% agar + 3.0% KNO_3), served as a reference electrode. The capillary characteristics measured in KNO_3 (μ = 0.1 *M*) at $E_{d.e.}$ = −0.1 V (sce) were m = 2.98 mg, t = 2.7 (h = 45 cm) and $m^{2/3}t^{1/6}$ = 2.4436 $mg^{2/3}$ $s^{-1/2}$.

For each polarographic measurement, the solution to be polarographed was prepared in a 25.0 mL volumetric flask by the addition of known volume of the standard stock solutions to give the required concentrations of the various contents in 25.0 mL with aqueous media or 40% v/v methanol or 40% v/v acetonitrile. The cell was kept immersed in an electrically maintained thermostat and the test solution was deaerated by a stream of hydrogen. A constant inert atmosphere was maintained over the solution throughout the experiment. The ncessary correction was made for residual current in determining all diffusion current data, Thymol (0.01%) was used as the maximum suppressor and 0.1 *M* KNO_3 as supporting electrolyte.

The pH measurements were made on cambridge bench pattern (null deflection type) pH meter.

Results and discussion

Preliminary experiments showed that *n*-butylthioglycolate produces anodic wave in aqueous media, 40% v/v methanol, and 40% v/v acetonitrile at pH values between 2.5 and 8. The effects of variation of pH, RSH concentration and drop time have been studied with a view to recognize the characteristics of the wave in order to determine the mechanism of the reaction at the drop surface. Electrolysis of RSH in well-buffered medium and then polarographic analysis of the electrolysed solution were carried out.

[1]Revision received February 23, 1984.

Can. J. Chem. Downloaded from www.nrcresearchpress.com by 210.87.254.105 on 09/06/12
For personal use only.

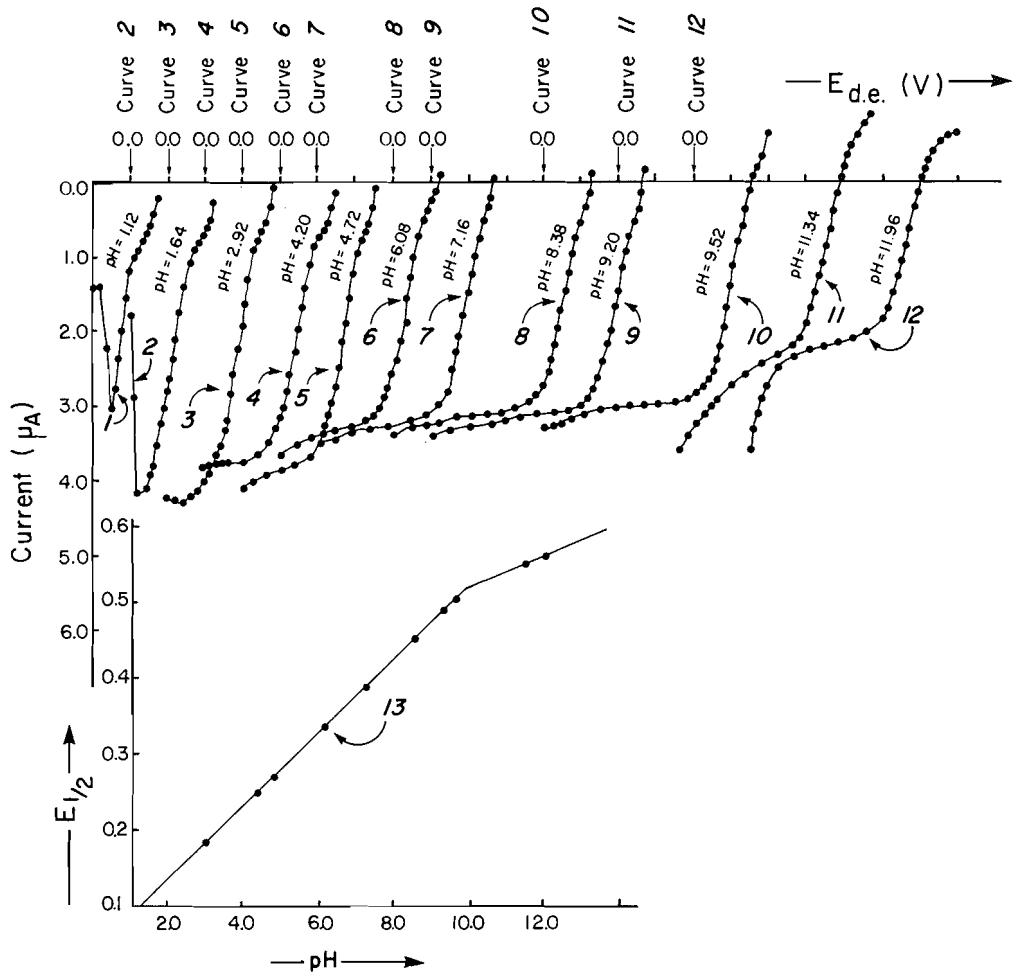

FIG. 1. Polarograms of 1.0 m*M* RSH at different pH values (curves *1*–*12*) in aqueous media, plot of $-E_{1/2}$ vs. pH (curve *13*).

Effect of pH

Polarograms of solution of 1 m*M* in *n*-butylthioglycolate at different pH values (clarks and lubs buffer) were recorded in aqueous media, 40% v/v methanol, and 40% v/v acetonitrile. The behaviour of the waves was not found to be considerably different in aqueous media (Fig. 1), 40% v/v methanol, and 40% v/v acetonitrile. It was found that reaction begins at −0.17 V and well-defined diffusion current region was not established, with the result that the waves are poorly defined below pH 2.5. However, as the pH increases the diffusion current plateau becomes more defined (curves *3*, *4*, *5*) and very well-defined anodic wave was obtained at pH 4.2 in aqueous media, at pH 3.22 in 40% v/v methanol, and at pH 2.96 in 40% v/v acetonitrile. It was observed that with the increase in pH, the waves not only start at more negative potential, but becomes irregular and irreversible in nature (curves *10*, *11*, *12*) in aqueous media. The residual current plateau disappeared in 40% v/v methanol and 40% v/v acetonitrile at pH beyond 4.5. The slow establishment of equilibrium may be regarded as the cause of irreversibility beyond certain pH in all the media studied.

The reversibility of the electrode reaction was tested by plotting log $(i_d - i)/i$ vs. $-E_{d.e.}$. The plot yielded a straight line with the slopes 0.0612 in aqueous media, 0.0603 in 40% v/v methanol and 0.0617 in 40% v/v acetonitrile within the pH range 2.5–8, producing logarithmic analysible waves. This indicates a one-electrode transfer process. The value of *n* in each of the media studied was determined by coulometric method (16) and was further checked by the De-Vries and Kroon methods (17) and found to be approximately one. All the subsequent studies were made at pH 4.20 in aqueous media, pH 3.22 in 40% methanol, and pH 2.96 in 40% acetonitrile.

Effect of concentration

Polarograms of solutions containing different concentrations of RSH (0.4–1.33 m*M*) + 0.1 *M* KNO_3 + 0.01% thymol at pH 4.2 in aqueous media, at pH 3.22 in 40% methanol, and at pH 2.96 in 40% acetonitrile were obtained. It was found that i_d/C are constant within experimental error and the mean values are 3.205 in aqueous media, 3.305 in 40% methanol, 4.617 in 40% acetonitrile. The ratio of i_d/C for methanolic-to-aqueous medium is 1.03 and acetonitrile-to-aqueous medium is 1.44. RSH can therefore be determined polarographically in 0.1 *M* KNO_3 and 0.01% thymol in aqueous, 40% v/v methanol, and 40% v/v acetonitrile.

Effect of Hg on pressure

A series of polarograms of solutions 1.0 m*M* in RSH + 0.1 *M* KNO_3 + 0.01% thymol in aqueous media (pH 4.2), 40% v/v methanol (pH 3.22), and 40% v/v acetonitrile (pH 2.96) were obtained for different heights of the mercury column. Well-defined anodic waves in aqueous media, 40% v/v methanol, and 40% v/v acetonitrile were obtained over the whole range. The constancy of i_d/h shows the diffusion-controlled nature of the wave.

Can. J. Chem. Downloaded from www.nrcresearchpress.com by 210.87.254.105 on 09/06/12
For personal use only.

Can. J. Chem. Downloaded from www.nrcresearchpress.com by 210.87.254.105 on 09/06/12
For personal use only.

Mechanism of electrode reaction

The electroxidation process indicated by the wave may involve the formation of mercurous mercaptide (one electron).

[1] $RSH + Hg \rightleftharpoons RSHg + H^+ + e^-$

or the formation of the disulphide (two electrons)

[2] $2RSH \rightleftharpoons RSSR + 2H^+ + 2e^-$

If these reactions are reversible, then the potential at any point on the wave at constant pH and 25°C should be given by

[3] $$E = E_{1/2} - 0.0591 \log \frac{i_d - i}{i}$$

for eq. [1] and

[4] $$E = E_{1/2} - \frac{0.0591}{2} \log \frac{(i_d - i)^2}{i}$$

for eq. [2].

If eq. [2] describes the wave, then a plot of $E_{d.e.}$ vs. log $(i_d - i)^2/i$ should yield straight line with a slope 0.0591/2 which is not found in the present case. On the other hand, if eq. [1] determines the wave, the plot of $E_{d.e.}$ vs. log $i_d - i/i$ should yield a straight line with a slope 0.0591, which has been found to be true for RSH in aqueous media, 40% methanol, and 40% acetonitrile in agreement with the one-electron transfer process. The values of n were further checked by other methods (16, 17).

It may therefore be inferred that the wave obtained with RSH in aqueous media, 40% methanol, 40% acetonitrile solution corresponds to the formation of mercurous mercaptide according to eq. [1]. In order to arrive at a definite reaction mechanism, solutions containing 1.0 m*M* RSH, 0.1 *M* KNO_3, and 0.01% thymol were electrolysed in different media, e.g., aqueous media (pH 4.2), 40% v/v methanol (pH 3.22), and 40% v/v acetonitrile (pH 2.96) at predetermined potentials from the respective limiting current value, in a completely inert atmosphere for 8 h. A portion of the electrolysed solution (in separate media) was then polarographed in buffered medium under identical pH values. In aqueous media, 40% methanol, and 40% acetonitrile, a cathodic wave was obtained (Figs. 2, 3, and 4, curve *2*), which corresponds to the reversible one-electron process. On passing H_2S through another portion of electrolysed solution, a black turbidity was obtained showing the presence of soluble mercury in electrolysed solution.

The presence of soluble mercury in the solution (electrolysed) was further determined by precipitating it as mercuric paraiodate (18). Further, when stationary platinum microelectrode was used, no anodic or cathodic wave was produced by RSH. This also shows that the mercury takes part in the electrode reaction. On the basis of these observations, the reaction mechanism as indicated by eq. [2] can be discarded.

In order to obtain more conclusive evidence, the following experiments were performed separately in aqueous media (pH 4.20), 40% methanol (pH 3.22), and 40% acetonitrile (pH 2.96). Solutions containing (*i*) 1.0 m*M* RSH + 0.5 m*M* $HgCl_2$; (*ii*) 1.0 m*M* RSH, (*iii*) 2.0 m*M* RSH + 0.5 m*M* $HgCl_2$, and (*iv*) chemically oxidised solution of RSH were polarographed in a buffered medium of identical pH values and similar conditions in the respective solvents. In aqueous media, 40% methanol, and 40% acetonitrile, solution *i* yielded a well-defined cathodie wave (Figs. 2, 3, and 4, curve *3*), which corresponds to one-electron reduction having $E_{1/2}$ similar to that of the anodic wave of RSH (Figs. 2, 3, and 4, curve *2*). Solution *iii*

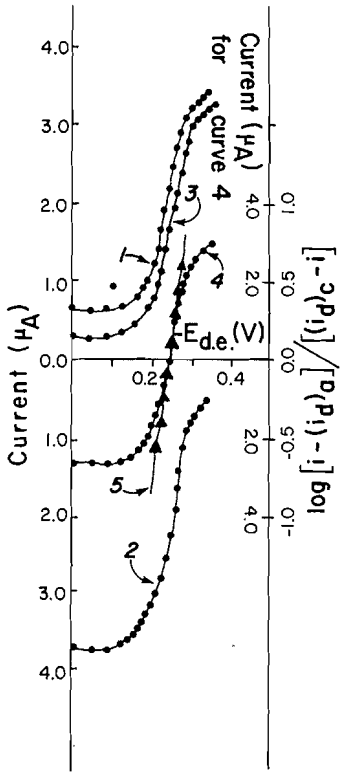

FIG. 2. Comparative anodic–cathodic $C-V$ curves of RSH and mercury–RSH complex in aqueous solution at pH 4.2. Curve *1*, 1.0 m*M* in RSH, electrolysed at large mercury pool electrode; curve 2, 1.0 m*M* in RSH; curve *3*, 1.0 m*M* in RSH + 0.5 m*M* in $HgCl_2$; curve *4*, 2.0 m*M* in RSH + 0.5 m*M* in $HgCl_2$; curve *5*, plot of $-E_{d.e.}$ vs. log $[i - (i_d)_a]/[(i_d)_c - i]$.

produced a composite wave of solution *i* and anodic wave of solution *ii*. The plot of $[i - (i_d)_a]/[(i_d)_c - i]$ for composite wave yielded a straight line with slope 0.0591 (in aqueous media), 0.0603 (in 40% methanol), 0.0624 (in 40% acetonitrile) (Figs. 2, 3, and 4, curve *5*). These observations clearly indicate that in the aqueous media, 40% methanol, and 40% acetonitrile, the anodic reaction is the anodic dissolution of mercury.

Conclusive experimental evidence was obtained by performing the following experiments with RSH and mercurous chloride. The solution containing (*i*) $HgCl_2$ and RSH in equimolar ratio and (*ii*) RSH solution saturated with Hg_2Cl_2 were polarographed under similar conditions. It was striking to note that the $C-V$ curves for the first solution showed large diffusion current at zero applied potential but the same value of slope and half-wave potential as that given by polarogram of solution *ii* and thus indicating the reduction of the same compound RSHg and the presence of the mercuric ions.

Kolthoff and co-workers (1, 4, 20, 25, and 26) considered the following reactions for the electrooxidation of mercaptan.

[5] $2RSH \rightleftharpoons RSSR + 2H^+ + 2e^-$

[6] $2RSH + Hg \rightleftharpoons Hg_2(RS)_2 + 2H^+ + 2e^-$

[7] $RSH + Hg \rightleftharpoons RSHg + H^+ + e^-$

They showed that a plot of $E_{d.e.}$ vs. log $(i_d - i)^2/i$ at 25°C should give a straight line with a slope of 0.059/2, if reactions [5] and [6] are involved (Fig. 5, curve *2*). On the other hand, if reaction [7] is involved, the plot of $E_{d.e.}$ vs. log $i_d - i/i$

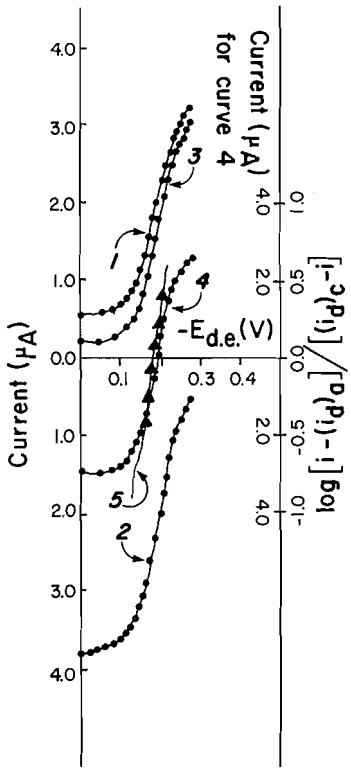

FIG. 3. Comparative anodic–cathodic $C-V$ curves of RSH and mercury–RSH complex in 40% v/v methanol at pH 3.22. Curve *1*, 1.0 m*M* in RSH, electrolysed at large mercury pool electrode; curve *2*, 1.0 m*M* in RSH; curve *3*, 1.0 m*M* in RSH + 0.5 m*M* in $HgCl_2$; curve *4*, 2.0 m*M* in RSH + 0.5 m*M* in $HgCl_2$; curve *5*, plot of $-E_{d.e.}$ vs. log $[i - (i_d)_a]/[(i_d)_c - i]$.

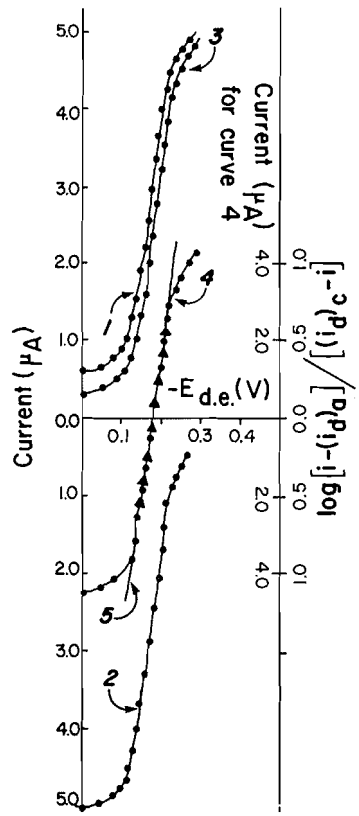

FIG. 4. Comparative anodic–cathodic $C-V$ curves of RSH and mercury–RSH complex in 40% v/v acetonitrile at pH 2.96. Curve *1*, 1.0 m*M* in RSH, electrolysed at large mercury pool electrode; cuve *2*, 1.0 m*M* in RSH; curve *3*, 1.0 m*M* in RSH + 0.5 m*M* in $HgCl_2$; curve *4*, 2.0 m*M* in RSH + 0.5 m*M* in $HgCl_2$; curve *5*, plot of $-E_{d.e.}$ vs. log $(i - (i_d)_a)/((i_d)_c - i)$.

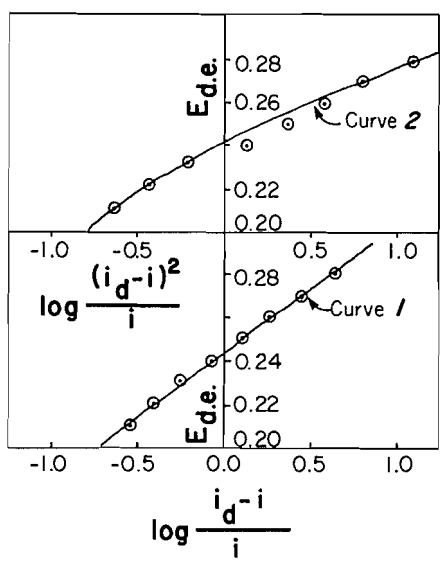

FIG. 5. Comparative plots of $E_{d.e.}$ vs. log $(i_d - i)/i$ (curve *1*) and $E_{d.e.}$ vs. log $(i_d - i)^2/i$ (curve *2*).

should give a straight line with a slope of 0.059. (Fig. 5, curve *1*). In the present case, it was found that only the analysis corresponding to reaction [7] yields a straight line with a slope equal to 0.059. Further, it was found that the half-wave potential remained constant when the RSH concentration varied from 1.33 to 0.4 m*M*. This constancy of half-wave potential is characteristic of eq. [7] but not of eqs. [5] and [6]. It may, therefore, be concluded that the anodic wave of RSH corresponds to the formation of mercurous mercaptide RSHg according to reaction [7]. This is in agreement with Kolthoff findings for cysteine and glutathione.

If this reaction is reversible the mercury in RSHg should be reversibly reducible at the dme. Experiments with RSH and mercurous chloride indicate that RSHg is not stable. In an attempt to prepare RSHg, when a solution of RSH is saturated with mercurous chloride, a whitish black precipitate, probably mixed precipitate of Hg_2Cl_2 and HgS, is obtained. Qualitative analysis of the insoluble portion showed that the presence of Hg^{2+} and polarographic analysis of the filtrate under identical conditions neither showed anodic wave nor cathodic wave except increased residual current. The formation of HgS and the absence of anodic or cathodic wave clearly reveal that mercurous chloride decomposes RSH, giving black precipitate of HgS, and that the complex RSHg is unstable.

The composite wave obtained with solution *iii* (Figs. 2, 3, and 4, curve *4*) containing RSH and $(RS)_2Hg$ has the same characteristics as the anodic wave of RSH. Figures 2, 3, and 4 give the current voltage curve of the composite wave (curve *4*) and the plot of log $[i - (i_d)_a]/[(i_d)_c - i]$ vs. $E_{d.e.}$ (curve *5*). The cathodic wave (Figs. 2, 3, and 4, curve *2*) of $(RS)_2Hg$ in the absence of RSH has the same characteristics as the composite wave mentioned above (that is, same slope (0.059) in the log plot and similar $E_{1/2}$). Experiments with $HgCl_2$ reveal that the cathodic wave results from the reduction of $(RS)_2Hg$ and it corresponds to the reduction of univalent mercury (Hg^+). The

Can. J. Chem. Downloaded from www.nrcresearchpress.com by 210.87.254.105 on 09/06/12
For personal use only.

absence of any inflection of the composite wave (solution *iii*, curve *4*) and the identical characteristics of anodic wave given by RSH and cathodic wave by $(RS)_2Hg$ suggest that the anodic wave produced by RSH is reversible and the ultimate oxidation product is $(RS)_2Hg$. The controlled potential electrolysis studies indicate that the primary electrolysis product is quickly transformed to $(RS)_2Hg$. (cf. Kolthoff).

Thus RSH is not oxidised to RSSR at the dme but depolarizes the mercury with the formation of unstable RSHg, which changes rapidly into $(RS)_2Hg$. The wave due to $(RS)_2Hg$ corresponds to the reduction of univalent mercury apparently the reactions:

[8] $(RS)_2Hg + Hg \rightleftharpoons 2RSHg$

Similar behaviour was also observed by Saxena and Gupta (3, 5) for the other sulphydril compounds. The change in solution and diffusion coefficient have been reported to affect the shape of the wave, half-wave potential, and sometimes the electrode reaction as well (21–24).

Polarograms of 1.0 m*M* in RSH + 0.1 *M* KNO_3 + 0.01% thymol in varying aqueous media, methanol, and acetonitrile composition viz. 20, 40, 60, and 80% were also recorded in buffered media of identical pH values and similar conditions. The half-wave potentials were found to shift to the more positive potential and become irreversible in nature with increased concentration of organic solvents.

We may conclude that RSH in aqueous media, 40% methanol, and 40% acetonitrile is not oxidised to RSSR at the dme, but that it depolarizes the Hg with the formation of unstable RSHg. The reduction wave of $(RS)_2Hg$ corresponds to the reduction of univalent cation.

1. I. M. KOLTHOFF and C. BARNUM. J. Am. Chem. Soc. **62**, 3061 (1940).
2. I. M. KOLTHOFF and C. BARNUM. J. Am. Chem. Soc. **63**, 520 (1941).
3. R. S. SAXENA and K. C. GUPTA. Electrochim. Acta, **13**, 1749 (1968).
4. W. STRICKS and S. K. CHAKRAVARTI. Anal. Chem. **34**, 508 (1962).
5. R. S. SAXENA and K. C. GUPTA. J. Indian Chem. Soc. **47**, 101 (1970).
6. W. F. SMYTH, G. SVEHLA, and P. ZUMAN. Anal. Chim. Acta, **52**, 129 (1970).
7. W. F. SMYTH, G. SVEHLA, and P. ZUMAN. J. Electronal. Chem. Interfacial Electrochem. **30**, 101 (1971).
8. W. F. SMYTH, G. SVEHLA, and P. ZUMAN. Anal. Chim. Acta, **51**, 463 (1970).
9. W. F. SMYTH. *In* Proceedings of the Third Analytical Chemistry Conference. Vol. 2. *Edited by* I. Buzes. Akedomial Kiado, Budapest. 1970. pp. 123–130.
10. J. K. HOWIE, J. K. KOUTS, and D. T. SAWYER. J. Am. Chem. Soc. **99**, 6323 (1977).
11. T. M. FLORENCE. J. Electroanal. Chem. Interfacial Electrochem. **97**, 237 (1979).
12. K. C. GUPTA and T. KAUR. J. Electrochem. Soc. **129**, 90 (1982).
13. R. S. SAXENA and M. C. SAXENA. Monatsh Chem. **107**, 1423 (1976).
14. K. C. GUPTA and T. KAUR. Analyst, **105**, 1124 (1980).
15. A. I. VOGEL. A text book of practical organic chemistry. ELBS, 4th ed. 1978. pp. 264, 274.
16. J. LINGANE. J. Am. Chem. Soc. **67**, 1916 (1945).
17. T. DE VRIES and J. L. KROON. J. Chem. Soc. **75**, 2484 (1953).
18. A. I. VOGEL. Quantitative inorganic analysis. 3rd ed. 1961. pp. 487, 488.
19. I. M. KOLTHOFF and C. S. MILLAR. J. Am. Chem. Soc. **63**, 1405 (1941); **63**, 2732 (1941).
20. W. STRICKS and I. M. KOLTHOFF. J. Am. Chem. Soc. **74**, 4646 (1954).
21. Z. SCHWABEK. Electrochemistry, **61**, 484 (1957); Z. Phy. Chem. (Leipzig), sonderheft, 289 (1958).
22. S. WAWZONEK and M. E. RUNNER. J. Electrochem. Soc. **99**, 457 (1952).
23. J. F. COETZEE and I. M. KOLTHOFF. J. Am. Chem. Soc. **79**, 6110 (1957).
24. R. TAKACHASCHI. Rev. Polarogr. Jpn. **9**, 116 (1961).
25. D. L. LEUSSING and I. M. KOLTHOFF. J. Electrochem. Soc. **62**, 520 (1941).
26. B. Y. GIANG, G. D. CHRISTIAN, and W. C. PURDY. J. Polarogr. Soc. **13**, 17 (1967).

Can. J. Chem. Downloaded from www.nrcresearchpress.com by 210.87.254.105 on 09/06/12
For personal use only.

The preparation and the crystal and molecular structure of $S_3N_2NH_2^+BF_4^-$; a molecular orbital study of the protonation of the trisulphur trinitride anion

CLIFFORD G. MARCELLUS AND RICHARD T. OAKLEY[1]

Guelph–Waterloo Centre for Graduate Work in Chemistry, Guelph Campus, Department of Chemistry and Biochemistry, University of Guelph, Guelph, Ont., Canada N1G 2W1

AND

A. WALLACE CORDES AND WILLIAM T. PENNINGTON

Department of Chemistry, University of Arkansas, Fayetteville, AR 72701, U.S.A.

Received January 31, 1984

CLIFFORD G. MARCELLUS, RICHARD T. OAKLEY, A. WALLACE CORDES, and WILLIAM T. PENNINGTON. Can. J. Chem. **62**, 1822 (1984).

Protonation of the trisulphur trinitride ion, $S_3N_3^-$, with tetrafluoroboric acid yields the ring-contracted *S*-amino thiodithiazyl salt, $S_3N_2NH_2^+BF_4^-$. The crystal and molecular structure of this salt has been determined by X-ray diffraction. The crystals are triclinic, space group $P\bar{1}$, with $a = 5.445(2)$, $b = 7.346(3)$, $c = 9.473(5)$ Å, $\alpha = 85.89(4)$, $\beta = 83.92(3)$, $\gamma = 82.13(3)°$, $V = 372.6(4)$ Å^3, $D_c = 2.02$ g cm^{-3}, and $Z = 2$. The structure was solved by direct methods and refined by full-matrix least-squares procedures to give a final $R = 0.060$. The structure of the five-membered ring with a single exocyclic NH_2 group bonded to sulphur is discussed in relation to other S_3N_2NR derivatives. The reasons for the instability of six-membered rings of the type S_3N_3R are discussed in the light of MNDO molecular orbital calculations on an S_3N_3H model.

CLIFFORD G. MARCELLUS, RICHARD T. OAKLEY, A. WALLACE CORDES et WILLIAM T. PENNINGTON. Can. J. Chem. **62**, 1822 (1984).

La protonation de l'ion triniture de soufre $S_3N_3^-$ par l'acide tétrafluoroborique conduit au sel $S_3N_2NH_2^+BF_4^-$ comportant le cycle *S*-aminothiodithiazyle contracté. On a déterminé la structure du cristal et la structure moléculaire de ce sel par diffraction de rayons-X. Les cristaux appartiennent au groupe d'espace triclinique $P\bar{1}$, avec $a = 5,445(2)$, $b = 7,346(3)$, $c = 9,473(5)$ Å, $\alpha = 85,89(4)$, $\beta = 83,92(3)$, $\gamma = 82,12(3)°$, $V = 372,6(4)$ Å^3, $D_c = 2,02$ g cm^{-3} et $Z = 2$. On a résolu la structure par des méthodes directes et on l'a affinée par la méthode des moindres carrés (matrice entière) jusqu'à une valeur de $R = 0,060$. On discute de la structure du cycle à 5 chaînons portant un seul groupe NH_2 exocyclique lié au soufre en relation avec les structures d'autres dérivés S_3N_2NR. On discute des raisons de l'instabilité des cycles à 6 chaînons du type S_3N_3R à la lumière des calculs d'orbitales moléculaires MNDO sur un S_3N_3H modèle.

[Traduit par le journal]

Introduction

The electronic structure of the trisulphur trinitride anion $S_3N_3^-$ has been a subject of recent discussion (1–5). While the possibility of symmetry breaking in the ground state has been suggested (2), the results of several spectroscopic (4) and theoretical (1, 3–5) studies have indicated that the species is best represented by the delocalized structure **1**. However, the threefold symmetry of the charge distribution can be lowered by chemical means. Thus the oxidation of $S_3N_3^-$ to $S_3N_3O^-$ (**2**) induces spectroscopic changes which reflect the splitting of the degenerate π^* H(ighest) O(ccupied) M(olecular) O(rbital) (6). Substitution at nitrogen by an electrophile (e.g. R^+) to produce **3** represents, at first sight, a correspondingly minor perturbation of the π-system of the anion. Nonetheless, while the existence of such species as **3** has been proposed on several occasions (7, 8), subsequent structural investigations have invariably revealed rearranged geometries based on the five-membered thiodithiazyl system **4** (9–12).

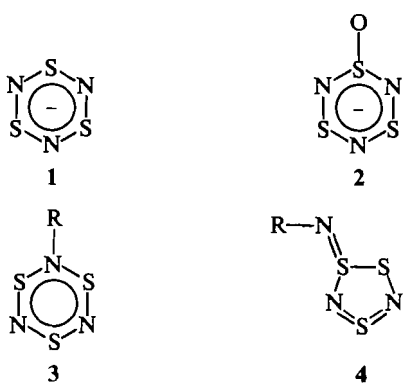

1 **2** **3** **4**

In order to investigate the apparent instability of derivatives such as **3** relative to **4**, we have examined the structural consequences of simple protonation of the $S_3N_3^-$ ion, using tetrafluoroboric acid. In this instance a rearrangement also occurs, the final product being the *S*-amino thiodithiazyl salt, $S_3N_2NH_2^+BF_4^-$ (reaction [1]). In the present paper we report the crystal and molecular structure of this salt and, using the S_3N_3H structure as a model system, present a molecular orbital interpretation of the electronic critera underlying the ring contraction process **3** to **4**. In our recent analysis of the structural consequences of the protonation of tetrasulphur tetranitride we demonstrated the importance of charge localization on the relative stabilities of different conformations of the eight-membered S_4N_4 ring (13). In the present paper these concepts are extended, and the subject of ring contraction in cyclic sulphur–nitrogen chemistry developed.

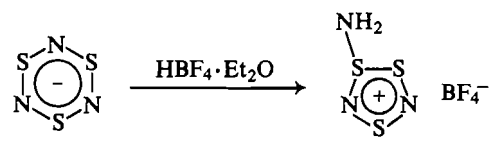

[1]

Experimental and theoretical procedures

Starting material

Tetrasulphur tetranitride S_4N_4 (14) and $PPN^+S_3N_3^-$ ($PPN^+ = [Ph_3P]_2N^+$) (15) were prepared according to published methods.

[1]To whom all correspondence should be addressed.

Can. J. Chem. Downloaded from www.nrcresearchpress.com by 210.87.254.5 on 09/06/12
For personal use only.

Can. J. Chem. Downloaded from www.nrcresearchpress.com by 210.87.254.5 on 09/06/12
For personal use only.

Tetrafluoroboric acid diethyl etherate was obtained commercially (Aldrich) and used without further purification. Methylene chloride (reagent grade) was dried by distillation from phosphorus pentoxide. Infrared spectra were recorded in Nujol mulls (CsI cell windows) using a Perkin-Elmer 467 grating spectrophotometer.

Preparation of $S_3N_2NH_2^+BF_4^-$

Method 1. An excess of $HBF_4 \cdot Et_2O$ (500 mg, 3.09 mmol) was added dropwise under an atmosphere of nitrogen to a solution of S_4N_4 (100 mg, 0.54 mmol) in 150 mL methylene chloride. The resulting deep red solution was left to stand at room temperature for 48 h, during which time the colour of the solution gradually faded to light orange, and canary yellow crystalline blocks were precipitated. The supernatant solution was decanted under nitrogen and the residual crystals washed with methylene chloride and dried *in vacuo*. The composition of these crystals was determined X-ray crystallography (*vide infra*) to be $S_3N_2NH_2^+BF_4^-$ (83 mg, 37 mmol). Infrared spectrum: 3340 (m, br), 3320 (m, br), 3070 (w), 1540 (m, br), 1250 (w), 1100–1000 (vs, br), 935 (s), 770 (w), 744 (ms), 520 (m), 470 (m, br), 380 (m).

Method 2. An excess of $HBF_4 \cdot Et_2O$ (500 mg, 3.09 mmol) was added dropwise under nitrogen to a solution of $PPN^+S_3N_3^-$ (500 mg, 0.74 mmol) in 15 mL methylene chloride. The resulting yellow solution was stored in a freezer at −20°C for one week, during which time canary yellow crystals were slowly produced. The supernatant liquid was decanted from these crystals, which were then washed with methylene chloride and dried *in vacuo*. The material was identified as $S_3N_2NH_2^+BF_4^-$ (124 mg, 0.55 mmol, 74%) by comparison of its infrared spectrum with that of a sample prepared from method 1.

X-ray analysis of $S_3N_2NH_2^+BF_4^-$

Crystals suitable for X-ray work were prepared by method 1 and sealed under argon in a glass capillary. All data were collected using an Enraf-Nonius CAD-4 diffractometer and graphite-monochromated Mo K_α (λ = 0.71073 Å) radiation. A least-squares calculation using the diffractometer settings for 25 carefully centred reflections with $22° < 2\theta < 34°$ gave the following cell dimensions (at 21°C): a = 5.445(2), b = 7.346(3), c = 9.473(5) Å, α = 85.89(4), β = 83.92(3), λ = 82.13(3)°, and V = 372.6(4) Å^3. For $S_3N_3H_2BF_4$ with mw = 227.03 and Z = 2, D_c = 2.02 g cm^{-3}, F_{000} = 224, and μ(MoKα) = 9.66 cm^{-1}.

The space group was verified by successful refinement in $P\bar{1}$ and our inability to get a better refinement in the non-centric group. A total of 3225 unique reflections were measured using $\theta-2\theta$ scans for 2θ from 2 to 70° (h = −8 to 8, k = −11 to 11, l = 0 to 15). The scan range was (1.0 + 0.35 tan θ) and the scan speeds varied from 4.0 to 20.1 deg min^{-1}. A total of 1725 reflections had $I < 3\sigma(I)$ and were considered unobserved. The intensities of three reflections (1 −1 5, −3 0 −3, 0 −4 0) which were measured periodically during the data collection varied less than 6.3% and thus indicated general crystal and electronic stability. No absorption correction was made.

The structure was solved by MULTAN 78 (16) followed by Fourier and least-squares techniques. The final full-matrix least-squares refinement based on F^2 included 108 parameters (positional and isotropic thermal parameters for hydrogen atoms) and had a parameter: reflection ratio of 1:14. The weighting scheme based on counting statistics (p = 0.07) gave no systematic variation $F/\sigma(F)$ as a function of F or sin θ. No secondary extinction correction was made. In the final cycle of refinement the maximum shift/error was 0.03, R = 0.060, R_w = 0.090, and GOF = 1.90. The final difference map had a maximum value of 0.82 e Å^{-3}. Neutral atom scattering factors corrected for real and imaginary anomalous dispersion corrections were used (17). The computer programmes used were those provided by the Enraf-Nonius SDP programme package.

Molecular orbital calculations

The M(odified) N(eglect) of D(iatomic) O(verlap) method (18) has been used by several groups for examining the electronic structures and molecular geometries of binary sulphur nitrides and related derivatives (13, 19–22). Although the method is somewhat deficient in assessing sulphur–sulphur interactions (23) it has, in several cases, been quite successful in predicting ground state geometries (e.g., S_4N_2 (19), S_3N^- (22), S_4N^- (20), $S_4N_4H^+$ (13)). In our studies on S_3N_3H and related systems we have used models with varying geometrical constraints. Numerical estimates of π-charge densities and bond orders (aps) (24) for S_3N_3H (**3**) refer to a calculation performed with full geometry optimization within the confines of C_{2v} symmetry. For the calculations related to the transformation from S_3N_3H to S_3N_2NH (i.e., **3** to **4**), no geometrical constraint was imposed save for the assumption of planarity within the five-atom SNSNS sequence. Numerical information pertaining to $S_3N_3^-$ were obtained from a calculation in which D_{3h} symmetry was imposed.[2]

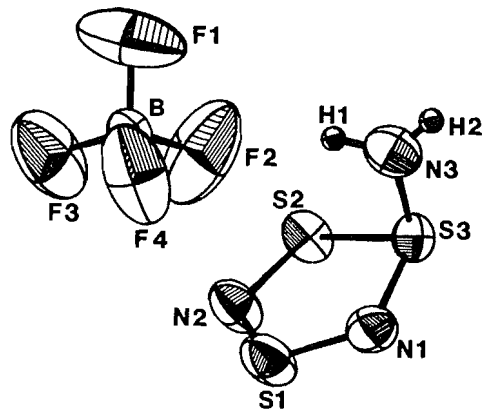

FIG. 1. ORTEP drawing (50% probability ellipsoids) of $S_3N_2NH_2^+BF_4^-$.

Discussion

Preparation of $S_3N_2NH_2^+BF_4^-$

The reaction of $S_3N_3^-$ salts with electrophiles is known to produce ring-contracted products of the type **4** (25). Accordingly the acidification of a solution of $PPN^+S_3N_3^-$ in methylene chloride with tetrafluoroboric acid diethyl etherate affords a pale yellow microcrystalline precipitate of the salt $S_3N_2NH_2^+BF_4^-$ (reaction [1]). However, a more convenient route to this compound involves the protonation of S_4N_4 with $HBF_4 \cdot Et_2O$. This latter reaction, which we have previously used to prepare $S_4N_4H^+BF_4^-$, can be modified by using more dilute solutions to prevent the precipitation of the initially formed product. Under these conditions the red colour of the solution gradually fades to orange, and yellow crystalline blocks of $S_3N_2NH_2^+BF_4^-$ are slowly formed.[3] The mechanism of this secondary reaction is open to speculation, but we note the analogy between the present results and the production of related S_3N_2NR **4** derivatives via the reaction of S_4N_4 with acid anhydrides (7, 10, 27).

Crystal structure of $S_3N_2NH_2^+BF_4^-$

Crystals of this compound consist of $S_3N_2NH_2^+$ cations and BF_4^- anions interconnected by both hydrogen bonding and charge transfer interactions. An ORTEP drawing of a single cation and anion, indicating the atom numbering scheme, is given in Fig. 1. Figure 2 illustrates the packing of the ions in the unit cell, and Fig. 3 is an ORTEP drawing of a single cation and all of the atoms which are involved in hydrogen bonding

[2]It is worth noting that when the D_{3h} restriction was lowered to C_{2v}, no significant alteration was observed in the molecular orbital distributions.

[3]A yellow crystalline compound of unknown composition has been observed in the reaction of S_4N_4 with fluorosulphuric acid (ref. 26). We suggest that this material may be $S_3N_2NH_2^+SO_3F^-$.

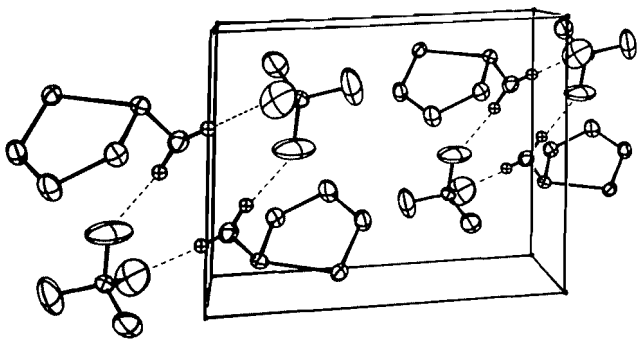

FIG. 2. Crystal packing for $S_3N_2NH_2^+BF_4^-$. The x axis is horizontal, the y axis vertical, and the origin is in the lower, left, rear corner.

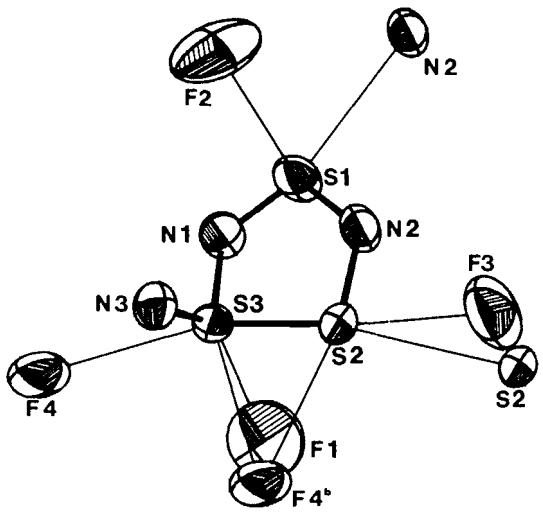

FIG. 3. ORTEP drawing (30% probability ellipsoids) of one $S_3N_2NH_2^+$ cation and all of the atoms involved in charge transfer interactions with it.

and charge transfer interactions with it. A listing of atom positions can be found in Table 1, while Table 2 provides bond distances and angles within each cation and anion. Table 3, providing temperature factors for the structure, and Table 4, which lists all the hydrogen bond and charge transfer interactions, have been deposited.[4]

Hydrogen bonds in the crystal are formed between the two hydrogen atoms of the amine group and fluorine atoms of two symmetry-related anions in the crystals (H1---F2 = 1.55(5) Å, F2 at symmetry transformation: $x - 1, y, z$; H2---F1 = 2.14(6) Å, F1 at symmetry transformation: $-x, 1 - y, -z$), forming a dimer of ion pairs about an inversion centre at $x = 0.5$, $y = 0.0$, and $z = 0.0$.

Charge transfer interactions (28) are also present, as in several related sulphur nitride salts, e.g., those of $S_3N_2^+$ (26), $S_4N_3^+$ (29). In the present case the most common interaction of this type involves transfer from a lone-pair type orbital on fluorine to an acceptor orbital (probably σ^*) on sulphur. Consistent with this interpretation all such contacts share three common features: they (*1*) are shorter than van der Waals' separations,[5] (*2*) are directed *trans* to an endocylic σ-bond (S—S or S—N), and (*3*) generate approximately tetrahedral angles with the primary covalent bonds to fluorine (i.e. B—F---S ~109°). Thus, the disulphide group of the cation is bridged by a fluorine atom (F4 at symmetry position $x - 1$, $y - 1, z$), the two S---F contacts being approximately *trans* to the S3—N1 and S2—N2 bonds. There are also interactions to these two sulphurs in directions colinear with the disulphide bond (S3---F4 of the anion at symmetry position $1 - x, 1 - y, -z$; S2---F3 of the anion at symmetry position $-x, 1 - y, 1 - z$). Finally there is a contact *trans* to the S3—N3 bond (S3---F1 of the anion at $x, y - 1, z$). For all of these interactions the primary covalent bond to the donor fluorine increases with the extent of charge transfer. For $S_3N_2NH_2^+BF_4^-$, the longest B—F bond (B—F4 = 1.342(5) Å) is almost 7σ's longer than the average of the other three B—F bonds, and involves the fluorine atom with the most numerous as well as the shortest charge transfer contacts.

TABLE 1. Atomic coordinates and B_{eq}* (Å^2) values with esd's in parentheses†

Atom	x/a	y/b	z/c	B_{eq}
S1	0.1895(2)	0.3976(2)	0.3343(2)	5.25(3)
S2	−0.1392(2)	0.1476(2)	0.3590(1)	4.01(2)
S3	0.0361(2)	0.1805(1)	0.1433(1)	3.38(2)
N1	0.2385(7)	0.3073(6)	0.1859(5)	4.23(8)
N2	−0.0212(8)	0.3081(6)	0.4262(4)	4.81(9)
N3	−0.1566(8)	0.3112(6)	0.0590(5)	4.64(9)
H1	−0.245(9)	0.401(6)	0.106(5)	4(1)
H2	−0.19(1)	0.271(8)	−0.002(7)	7(2)
B	0.5715(9)	0.7760(6)	0.2404(5)	3.37(9)
F1	0.357(1)	0.7906(9)	0.1828(6)	12.9(2)
F2	0.663(1)	0.6025(6)	0.2284(8)	12.7(2)
F3	0.518(1)	0.8150(8)	0.3745(5)	11.2(1)
F4	0.7276(9)	0.8893(5)	0.1755(5)	9.9(1)

*$B_{eq} = (4/3)(\beta_{11}a^2 + \beta_{22}b^2 + \beta_{33}c^2 + \beta_{12}ab \cos\gamma + \beta_{13}ac \cos\beta + \beta_{23}bc \cos\alpha)$.

†Hydrogen atoms were refined with isotropic thermal parameters.

TABLE 2. Selected bond distances (Å) and angles (deg) for $S_3N_2NH_2^+BF_4^-$

Atom 1	Atom 2	Distance	Atom 1	Atom 2	Atom 3	Angle
S1	N1	1.579(3)	N1	S1	N2	108.8(2)
S1	N2	1.556(3)	S3	S2	N2	97.6(1)
S2	S3	2.173(1)	S2	S3	N1	94.6(1)
S2	N2	1.615(3)	S2	S3	N3	106.1(2)
S3	N1	1.636(2)	N1	S3	N3	106.7(2)
S3	N3	1.566(4)	S1	N1	S3	118.3(2)
N3	H1	0.88(5)	S1	N2	S2	117.9(2)
N3	H2	0.71(6)	S3	N3	H1	116.(3)
B	F1	1.326(5)	S3	N3	H2	113.(4)
B	F2	1.311(5)	H1	N3	H2	128.(5)
B	F3	1.316(5)	F1	B	F2	103.6(5)
B	F4	1.342(5)	F1	B	F3	107.2(5)
			F1	B	F4	113.1(4)
			F2	B	F3	111.4(4)
			F2	B	F4	111.8(4)
			F3	B	F4	109.6(4)

[4]Tables 3 and 4 and a table of measured and calculated structure factors are available, at a nominal charge, from the Depository of Unpublished Data, CISTI, National Research Council of Canada, Ottawa, Ont., Canada K1A 0S2.

[5]S---F charge transfer interactions (Table 4) range from 3.875(3) to 3.203(4) Å.

Can. J. Chem. Downloaded from www.nrcresearchpress.com by 210.87.254.5 on 09/06/12
For personal use only.

TABLE 5. Structural parameters for S_3N_2NR rings*

Bond	Length (Å)				
	NH_2^+ (this work)	$NP_3N_3F_5$ (ref. 9)	$NCOCF_3$ (ref. 10)	NSO_2NAsPh_3 (ref. 11)	NSO_2F (ref. 12)
S2—S3	2.173(1)	2.221(2)	2.206(1)	2.230(1)	2.200(2)
S3—N1	1.636(3)	1.647(4)	1.641(4)	1.659(3)	1.644(3)
S2—N2	1.615(3)	1.629(4)	1.633(2)	1.610(3)	1.635(3)
S1—N1	1.579(3)	1.572(4)	1.589(3)	1.571(3)	1.578(3)
S1—N2	1.556(3)	1.540(4)	1.551(2)	1.548(4)	1.565(3)
Bonds	**Angle (deg)**				
	NH_2^+ (this work)	$NP_3N_3F_5$ (ref. 9)	$NCOCF_3$ (ref. 10)	NSO_2NAsPh_3 (ref. 11)	NSO_2F (ref. 12)
S2—S3—N1	94.6(1)	92.7(1)	94.0(1)	†	94.0(2)
S3—S2—N2	97.6(1)	97.8(2)	97.14(7)	†	97.5(2)
N2—S1—N1	108.8(2)	109.7(2)	109.2(2)	†	109.4(2)
S1—N1—S3	118.3(2)	119.7(2)	118.1(2)	†	119.1(2)
S1—N2—S2	117.5(2)	117.6(2)	117.95(8)	†	117.2(2)

*Atom numbering follows that shown in Fig. 1.
†Not reported.

In addition to the above anion–cation interactions, there are two cation–cation contacts which may also be of a charge transfer variety: N2 of a cation at $-x, 1-y, 1-z$ approaches S1 *trans* to the S1—N1 bond (N2---S1 = 3.222(4) Å), and there is a contact between S2 and the equivalent sulphur atom of a cation at $-x, -y, 1-z$ (S2---S2 = 3.642(2) Å).

The structure of the $S_3N_2NH_2^+$ cation

From a purely topological viewpoint, the molecular configuration of the $S_3N_2NH_2^+$ can be conveniently described as resulting from the insertion of an S—NH_2^+ group into the 6π-electron four-membered ring of disulphur dinitride.[6] The five-membered S_3N_2 ring is nearly planar, with the ring nitrogen atoms N1 and N2 displaced to opposite sides of the plane of the three sulphur atoms by 0.253(4) and 0.149(5) Å, respectively. The exocylic nitrogen atom lies 1.482(4) Å out of this plane to the side opposite N1.

The structures of a number of related five-membered S_3N_2NR rings have been determined (S_3N_2—NSO_2F, S_3N_2—$NCOCF_3$, S_3N_2—$NP_3N_3F_5$, S_3N_2—NSO_2NAsPh_3). A comparison of the S—S and S—N distances for all of these compounds, including $S_3N_2NH_2^+$, can be found in Table 5. The multiple bond character of the S—N bonds, the difference in bond lengths to S1 as opposed to S2 and S3, and the inequality of the S—N bonds to S1 are features which are common to all the S_3N_2X derivatives. The somewhat longer than normal S2—S3 bond and the lengthening of S3—N1 with respect to N2—S2 can be viewed as the result of a weakening caused by the mixing of a lone pair orbital on the exocylic nitrogen with the σ* orbitals associated with the S2—S3 and S3—N1 bonds (31). Certainly the near planarity of the S—NH_2 group in $S_3N_2NH_2^+$ (sum of angles at N3 equals 357°) and its orientation with respect to these bonds accommodates this interpretation.

*Molecular orbital analysis of the transformation **3** to **4***

Our major concern in the present study has been to understand the energetic preference for structures such as **4** over those such as **3**. Why should the latter be unstable with respect to ring contraction? Our strategy has been to carry out MNDO molecular orbital calculations on a series of model compounds based on S_3N_3H and $S_3N_3H_2^+$ formulas with the aim of evaluating the electronic factors which dictate the transformation of the **3** configuration into **4**.

TABLE 6. MNDO π-molecular orbital energies (eV) and distributions, aps* bond orders (ρ_π) and charge densities (q_π) for S_3N_3H (C_{2v} symmetry)

Orbital	Eigenvector coefficient				
	ϵ_i	N_1	S_1	N_2	S_2
$4b_1$	−1.937	−0.178	0.268	−0.512	0.547
$2a_2$	−8.708	—	0.470	−0.528	—
$3b_1$	−9.353	−0.630	0.450	0.128	−0.405
$1a_2$	−13.125	—	0.528	0.470	—
$2b_1$	−13.624	0.680	0.316	−0.216	0.494
$1b_1$	−15.876	0.329	0.354	0.417	0.541
ρ_π (total)		0.00	0.30	0.31	
q_π (total)		1.94	1.86	1.47	1.40

*See ref. 24.

It is useful to begin the analysis by considering the consequences of the protonation of the $S_3N_3^-$ ring. Table 6 provides a charge and bond order breakdown for a model S_3N_3H molecule with C_{2v} symmetry. As expected, the electronic effects of protonating the $S_3N_3^-$ ion parallel those observed in $S_4N_4H^+$ (in C_{2v} symmetry). Electron density is drawn away from the protonated nitrogen through the N—H σ-bond, and the π-system "responds" by polarizing charge back onto the protonated nitrogen. Thus the π-charge at N(H) is larger (q_π = 1.94) than in $S_3N_3^-$ (q_π(N) = 1.67), while at the unperturbed nitrogens it is somewhat less (q_π = 1.47). Further information pertinent to the strength of the π-network can be obtained from an examination of the individual π-orbitals. Figure 4 illustrates the spatial and nodal properties of these orbitals. Like its parent anion $S_3N_3^-$, S_3N_3H is a 10π-electron system. The five occupied π-orbitals can be classified into three bonding ($1b_1$, $2b_1$, and $1a_2$) and two antibonding ($3b_1$ and $2a_2$) distributions. From

[6]The distributions of the π-like orbitals in S_3N_2X derivatives have been discussed by Gleiter and co-workers (30).

Can. J. Chem. Downloaded from www.nrcresearchpress.com by 210.87.254.5 on 09/06/12
For personal use only.

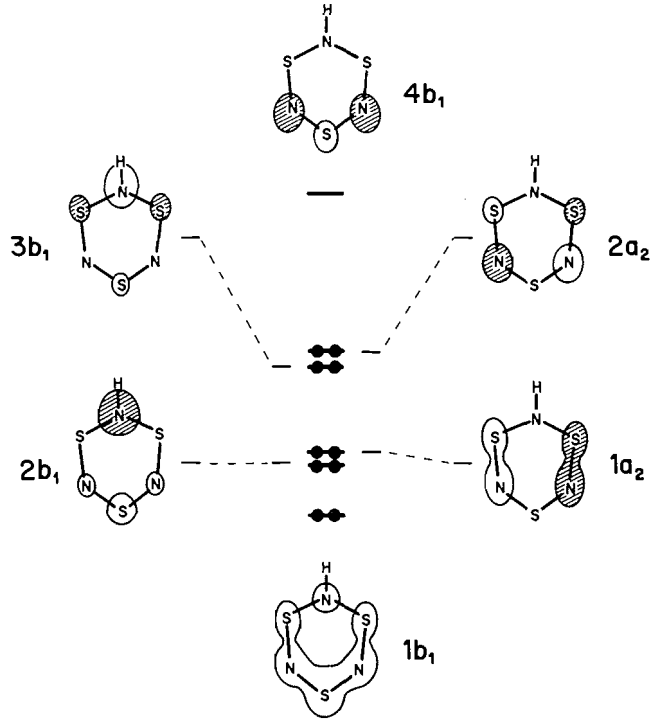

FIG. 4. Distributions and relative energies of the π-molecular orbitals (MNDO) for S_3N_3H (in C_{2v} symmetry). See Table 6 for eigenvalues.

an energetic standpoint the splitting of the formerly degenerate pairs of $S_3N_3^-$ ($2b_1$, $1a_2$ and $3b_1$, $2a_2$) is small. However, the π-bond orders, like the π-charge densities, are acutely sensitive to the electronegative perturbation caused by protonating the ring. As is indicated in Table 5, the $2b_1$ and $3b_1$ orbitals are polarized towards the protonated nitrogen, while the $1b_1$ is polarized away from it. The occupation of the $3b_1$ offsets the bonding contribution of the $2b_1$ orbital, and this effect, combined with the polarization of the $1b_1$ away from the S—N(H)—S region, leads to a weakened π-structure in the S—N(H)—S region and a strengthened S—N—S—N—S fragment. Thus the total π-bond orders (24) to the protonated nitrogen (0.00) are effectively nullified while those of the remaining S—N linkages are significantly larger (0.30, 0.31) than in $S_3N_3^-$ (0.11). In essence, the effect of protonation of $S_3N_3^-$ is to strengthen all the skeletal bonds save those to the protonated nitrogen. The latter are weakened to such an extent that some deformation is to be expected.

We have examined the energy consequences of a variety of deformations of the planar (C_{2v}) S_3N_3H model. Allowing the protonated nitrogen to move independently of the plane of the remaining five ring atoms (while the geometry at the N(H) atom is held planar) produces a chair-like conformation with a dihedral angle near 90°. The energy of this structure is ~5 kcal/mol lower than that of the C_{2v} structure. In order to simulate (and stimulate) the conversion of $S_3N_3H \rightarrow S_3N_2NH$ we performed a series of calculations in which the heat of formation was monitored as a function of d(S—S) (all other geometrical variables being optimized independently). Under these circumstances the six-membered ring structure remains the most stable until d(S—S) ≃ 2.2 Å, at which point the ring-contracted variation takes over (Fig. 5). We place little emphasis on the fact that the ring-contracted isomer **4** is predicted to be less stable (by ~20 kcal/mol) than the planar

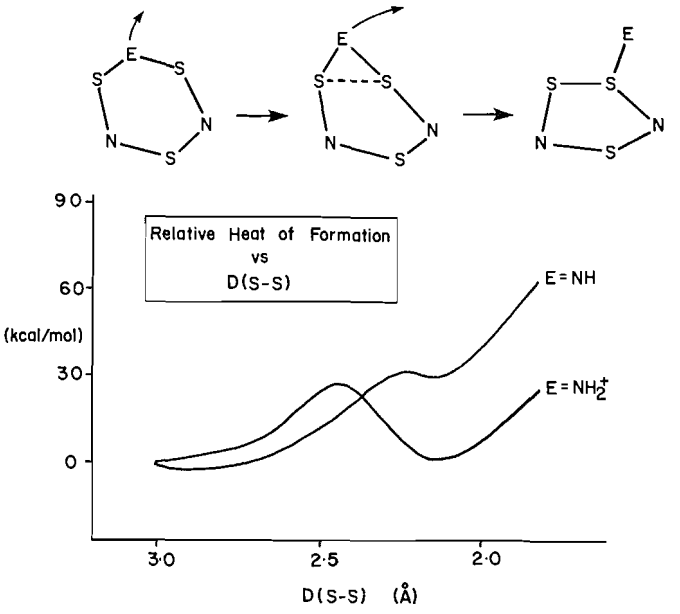

FIG. 5. Energy profile (MNDO) for the transformation of S_3N_3H and $S_3N_3H_2^+$ from six-membered to five-membered rings.

structure **3**. The discrepancy probably arises from the inadequacy of the MNDO method in assessing sulphur—sulphur interactions (23). However, we note that an analogous calculation performed on a model $S_3N_3H_2^+$ system produces a transformation **3** to **4** that is slightly exothermic (see Fig. 5). The activation energy calculated for the conversion of $S_3N_3H_2^+$ to $S_3N_2NH_2^+$ (~30 kcal/mol) probably represents a substantial overestimate of the true barrier to rearrangement. Low temperature nmr studies on the reaction of $S_3N_3^-$ with electrophiles may provide a means for measurement of this barrier.

Conclusion

It is well recognized that the π-networks of a planar binary sulphur nitrogen ring are weakened by the occupation of π* as well as π orbitals. Structural evidence on many compounds reveals that lattice forces alone are enough to cause significant molecular distortions (6). The protonation of S_4N_4 to $S_4N_4H^+$, and of $S_3N_3^-$ to S_3N_3H, effects stronger and more specific perturbations of the ring π-systems, resulting in extensive polarization of π* electron density into the skeletal bonds to the protonated nitrogens. The localized weakening of the cyclic frameworks can be alleviated in different ways; in $S_4N_4H^+$, the eight-membered ring puckers into a boat-like conformation, while in S_3N_3H a more drastic rearrangement, involving the cleavage of one of the weakened S—NH bonds, is observed. These two examples serve to illustrate that the polarizability of the π-systems of sulphur—nitrogen rings, coupled with the occupation of antibonding π-orbitals, leads to cyclic structures that will distort or even collapse upon coordination at nitrogen. The extensive chemistry of sulphur nitrides with Lewis acids and electrophiles should perhaps be interpreted in the light of these findings.

Acknowledgements

We thank the Natural Sciences and Engineering Research Council of Canada, the National Science Foundation (EPSCOR grant ISP 8011447), and the State of Arkansas for financial support.

Can. J. Chem. Downloaded from www.nrcresearchpress.com by 210.87.254.5 on 09/06/12
For personal use only.

1. (*a*) J. BOJES, T. CHIVERS, W. G. LAIDLAW, and M. TRSIC. J. Am. Chem. Soc. **101**, 4517 (1979); (*b*) T. CHIVERS, W. G. LAIDLAW, R. T. OAKLEY, and M. TRSIC. Inorg. Chim. Acta, **53**, L189 (1981).
2. A. A. BHATTACHARYYA, A. BHATTACHARYYA, and A. G. TURNER. Inorg. Chim. Acta, **45**, L13 (1980).
3. M. T. NGUYEN and T.-K. HA. J. Mol. Struct. **105**, 129 (1983).
4. J. W. WALUK and J. MICHL. Inorg. Chem. **20**, 963 (1981).
5. V. H. SMITH, J. R. SABIN, E. BRUCLAWIK, and J. MROZEK. Inorg. Chim. Acta, **77**, L101 (1983).
6. T. CHIVERS, A. W. CORDES, R. T. OAKLEY, and W. T. PENNINGTON. Inorg. Chem. **22**, 2429 (1983).
7. H. W. ROESKY and L. E. GRIMM. Ang. Chem. Int. Ed. **7**, 642 (1972).
8. W. LIDY, W. SUNDERMEYER, and W. VERBEEK. Z. Anorg. Allgem. Chem. **406**, 228 (1974).
9. I. RAYMENT, H. M. M. SHEARER, and H. W. ROESKY. J. Chem. Soc. Dalton Trans. 883 (1982).
10. R. STEUDEL, F. ROSE, R. REINHARDT, and H. BRADACZEK. Z. Naturforsch., **32B**, 488 (1977).
11. H. W. ROESKY, M. WITT, W. CLEGG, W. IDENBERG, M. NOLTENMEYER, and G. M. SHELDRICK. Ang. Chem. Int. Ed. **19**, 943 (1980).
12. B. KREBS, G. HENKEL, S. POHL, and H. W. ROESKY. Chem. Ber. **113**, 226 (1980).
13. A. W. CORDES, C. G. MARCELLUS, M. C. NOBLE, R. T. OAKLEY, and W. T. PENNINGTON. J. Am. Chem. Soc. **105**, 6008 (1983).
14. M. VILLENA-BLANCO and W. L. JOLLY. Inorg. Synth. **9**, 98 (1967).
15. T. CHIVERS, W. G. LAIDLAW, R. T. OAKLEY, and M. TRSIC. J. Am. Chem. Soc. **102**, 5773 (1980).
16. P. MAIN, S. E. HULL, L. LESSINGER, G. GERMAIN, J.-P. DECLERCQ, and M. M. WOOLFSON. Multan 78 — a system of computer programs for the automatic solution of crystal structures from X-ray diffraction data, 1978, University of York, England, and University of Louvain, Belgium.
17. D. T. CROMER and J. T. WABER. International tables for X-ray crystallography. Vol. IV. Kynoch Press; Birmingham, England. 1974.
18. M. J. S. DEWAR and W. THIEL. J. Am. Chem. Soc. **99**, 4899 (1977); **99**, 4907 (1977); QCPE (1977) No. 353 (MNDO).
19. T. CHIVERS, P. W. CODDING, W. G. LAIDLAW, S. W. LIBLONG, R. T. OAKLEY, and M. TRSIC. J. Am. Chem. Soc. **105**, 1186 (1983).
20. R. J. GLEITER and R. BARTETZKO. Z. Naturforsch. **36B**, 452 (1981).
21. (*a*) S. SENSARMA and A. G. TURNER. Inorg. Chim. Acta, **64**, L161 (1982); (*b*) A. G. TURNER. Inorg. Chim. Acta, **65**, L201 (1982); (*c*) J. J. OLEKSIK and A. G. TURNER. Inorg. Chim. Acta, **59**, 165 (1982).
22. A. W. CORDES, H. KOENIG, R. T. OAKLEY, and W. T. PENNINGTON. Inorg. Chem. **22**, 3375 (1983).
23. M. J. S. DEWAR and M. L. MCKEE. J. Comp. Chem. **4**, 84 (1983).
24. D. R. ARMSTRONG, P. G. PERKINS, and J. J. P. STEWART. J. Chem. Soc. Dalton Trans. 838 (1973).
25. J. BOJES and T. CHIVERS. Inorg. Chem. **17**, 318 (1978).
26. R. J. GILLESPIE, J. P. KENT, and J. F. SAWYER. Inorg. Chem. **20**, 3784 (1981).
27. H. W. ROESKY, W. SHAPER, O. PETERSEN, and T. MULLER. Chem. Ber. **110**, 2695 (1978).
28. (*a*) A. HORDVIK. Q. Rep. Sulfur Chem. **5**, 21 (1970); (*b*) R. E. ROSENFELD, JR., R. PARTHASARTHY, and J. D. DUNITZ. J. Am. Chem. Soc. **99**, 4860 (1972).
29. G. MOSS, T. N. GURU ROW, and P. COPPENS. Inorg. Chem. **19**, 2396 (1980) and references therein.
30. R. GLEITER, R. BARTETZKO, and P. HOFMANN. Z. Naturforsch. **35b**, 1166 (1980).
31. R. D. HARCOURT and H. M. HÜGEL. J. Inorg. Nucl. Chem. **43**, 239 (1981).

Can. J. Chem. Downloaded from www.nrcresearchpress.com by 210.87.254.5 on 09/06/12
For personal use only.

Crystal structure of 17,18,19-trisnorstemodan-3,13-dione

STEPHEN V. EVANS AND JAMES TROTTER
Department of Chemistry, University of British Columbia, Vancouver, B.C., Canada V6T 1Y6

Received September 27, 1983

STEPHEN V. EVANS and JAMES TROTTER. Can. J. Chem. **62**, 1828 (1984).

Crystals of the title compound, $C_{17}H_{24}O_2$, are monoclinic, $P2_1/c$, a = 10.395(2), b = 10.980(1), c = 13.181(3) Å, β = 113.55(1)°, Z = 4. The structure was solved by direct methods and refined by full-matrix least-squares to R = 0.051 for 1622 reflections with $I \geq 3\sigma(I)$. The molecule contains a tetracyclic system of three six-membered rings and one five-membered ring; the structure exhibits disorder of one C atom. Bond lengths and angles are normal.

STEPHEN V. EVANS et JAMES TROTTER. Can. J. Chem. **62**, 1828 (1984).

Les cristaux du composé du titre, $C_{17}H_{24}O_2$, sont monocliniques, $P2_1/c$, a = 10,395(2), b = 10,980(1), c = 13,181(3) Å, β = 113,55(1)°, Z = 4. On a résolu la structure par les méthodes directes et on a l'affinée par la méthode de moindres carrés (matrice entière) jusqu'à une valeur de R = 0,051 pour 1622 réflexions avec $I \geq 3\sigma(I)$. La molécule comprend une système tetracyclique, trois cycles de six membres et une cycle de cinq membres; et la structure présente la desordre de l'un des atomes de carbone. Les longeurs de liaisons et les angles sont normales.

Introduction

In a continuing research program aimed at the total synthesis of the structurally and physiologically interesting diterpenoid stemodin (**1**), a tetracyclic diketone possessing the stemodane carbon skeleton has been isolated (1). To establish the structure and stereochemistry conclusively before attempting conversion to (±)-stemodin, an X-ray analysis of the diketone has been undertaken, which proves structure **2**.

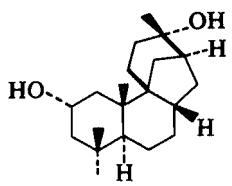

1

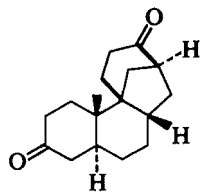

2

Experimental

Crystal data at 22°C:

$C_{17}H_{24}O_2$ fw = 260.38

Monoclinic, $P\ 2_1/c$, a = 10.395(2), b = 10.980(1), c = 13.181(3) Å, β = 113.55(1)°, Z = 4, V = 1379.1(5) Å^3, D_m = 1.26, D_c = 1.25 g cm^{-3}, $F(000)$ = 568, $\lambda(K\alpha_1)$ = 0.70930, $\lambda(K\alpha)$ = 0.71073 Å, μ = 0.9 cm^{-1}.

Intensity data were measured with Mo$K\alpha$ radiation (graphite monochromator) on an Enraf-Nonius CAD4-F diffractometer. An $\omega-2\theta$ scan was used, ω-scan angle (0.90 + 0.35 tan θ)° (extended by 25% on both sides for background measurement), scan speeds 1.55–10.06 deg min^{-1}, horizontal aperture (2.00 + tan θ) mm, vertical aperture 4 mm; three standard reflections showed no significant intensity variation during data collection. Cell parameters were refined by least-squares methods on sin θ values for 25 reflections with θ = 10–14° (the CAD4 procedure measures the peak profile and estimates the position of the α_1 peak).

A total of 3159 reflections were measured to θ = 27.5°, of which 1622 (51%) had $I \geq 3\sigma(I)$, where $\sigma^2(I) = S + 2B + [d(S - B)]^2$, with S = scan count and B = background count; previous experience indicated a value of 0.04 for d, and the appropriateness of this value was confirmed by the subsequent weighting scheme analysis. The intensities of the reflections fall off fairly rapidly with θ angle, presumably as a result of crystal quality (which might be affected by the disorder found in the structure). Most of the high angle reflections are weak, with only 30% of reflections in the range θ = 22–27.5°, but 70% of those in the range θ = 0–22°, having $I \geq 3\sigma(I)$. Lorentz and polarization factors but no absorption corrections were applied.[1]

The structure was solved by direct methods, and refined by full-matrix least-squares techniques; H atoms were located from a difference synthesis and included in the refinements, which converged to R = 0.047. Unusual geometry and large thermal anisotropy for the methylene carbon C(12) suggested disorder, which was treated by introducing two atomic positions C(12+) and C(12−) separated by about 0.67 Å, with isotropic thermal parameters and final occupancies

TABLE 1. Final positional (fractional × 10^4) and isotropic thermal parameters* (× 10^3 Å^2) with estimated standard deviations in parentheses

Atom	x	y	z	U_{eq}/U_{iso}
C(1)	7027(2)	1108(2)	9181(2)	51
C(2)	5489(3)	828(3)	8478(3)	56
C(3)	4506(2)	1212(3)	9003(2)	53
C(4)	4817(3)	2398(3)	9610(3)	55
C(5)	6375(2)	2676(3)	10245(2)	41
C(6)	6570(3)	3956(3)	10712(3)	56
C(7)	8085(3)	4167(3)	11464(3)	53
C(8)	9111(2)	3908(2)	10933(2)	39
C(9)	8852(2)	2676(2)	10297(2)	30
C(10)	7267(2)	2446(2)	9561(2)	31
C(11)	9731(2)	2628(3)	9579(2)	44
C(13)	11887(2)	2193(3)	11354(2)	51
C(14)	10932(3)	2418(2)	11922(2)	45
C(15)	10581(3)	3794(3)	11836(3)	50
C(16)	9534(2)	1781(2)	11261(2)	37
C(20)	6802(3)	3290(3)	8543(2)	47
O(1)	3481(2)	619(2)	8898(2)	74
O(2)	13079(2)	1844(2)	11821(2)	87
C(12+)	11334(4)	2580(5)	10185(3)	49(1)
C(12−)	11179(12)	1998(13)	10046(10)	47(3)

*The standard deviations for U_{eq}, calculated from the mean variance of U_{ii} divided by six (4), are all less than 0.001 Å^2; this statement has been added at the insistence of a referee.

[1]The computer programs used include locally written programs for data processing and locally modified versions of the following: MULTAN 80, multisolution program by P. Main, S. J. Fiske, S. E. Hull, L. Lessinger, G. Germain, J. P. Declercq, and M. M. Woolfson, ORFLS, full-matrix least-squares, and ORFFE, function and errors, by W. R. Busing, K. O. Martin, and H. A. Levy; FORDAP, Patterson and Fourier syntheses, by A. Zalkin; ORTEP II, illustrations, by C. K. Johnson.

Can. J. Chem. Downloaded from www.nrcresearchpress.com by 210.87.254.40 on 09/06/12
For personal use only.

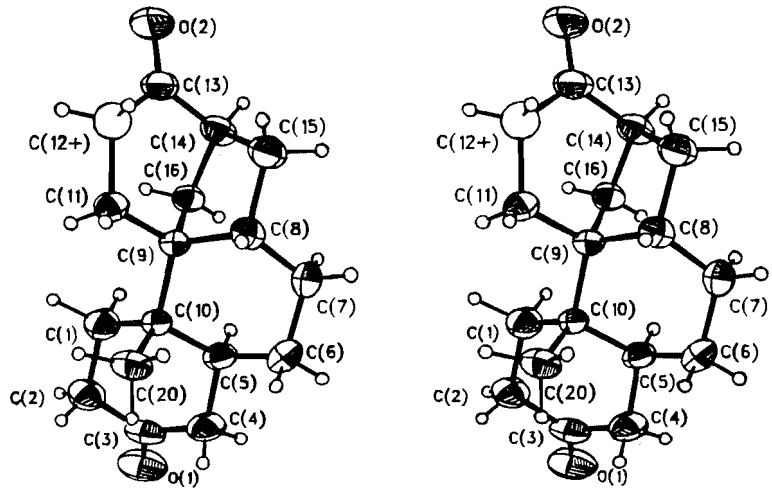

FIG. 1. Stereoview of the molecule (showing 75% occupancy C(12+)), with 50% probability thermal ellipsoids. Hydrogen atoms are not drawn to scale. The atom numbering corresponds to the chemical numbering of the stemodane skeleton; there are no atoms numbered C(17), C(18), C(19), since these methyl groups are missing in this 17,18,19-trisnor derivative.

TABLE 2. Bond lengths (Å) and angles (deg) with standard deviations in parentheses

Bond	Length (Å)	Bond	Length (Å)
C(1)—C(2)	1.525(3)	C(9)—C(10)	1.563(3)
C(1)—C(10)	1.540(3)	C(9)—C(11)	1.558(4)
C(2)—C(3)	1.506(4)	C(9)—C(16)	1.536(3)
C(3)—C(4)	1.495(4)	C(10)—C(20)	1.541(3)
C(3)—O(1)	1.209(3)	C(11)—C(12+)	1.534(5)
C(4)—C(5)	1.528(3)	C(11)—C(12−)	1.544(12)
C(5)—C(6)	1.516(4)	C(13)—O(2)	1.205(3)
C(5)—C(10)	1.551(3)	C(13)—C(12+)	1.476(5)
C(6)—C(7)	1.505(4)	C(13)—C(12−)	1.595(13)
C(7)—C(8)	1.519(4)	C(14)—C(15)	1.548(4)
C(8)—C(9)	1.557(3)	C(14)—C(13)	1.484(4)
C(8)—C(15)	1.522(3)	C(16)—C(14)	1.532(3)

Bonds	Angle (deg)	Bonds	Angle (deg)
C(2)—C(1)—C(10)	112.6(2)	C(1)—C(10)—C(5)	106.7(2)
C(1)—C(2)—C(3)	113.8(2)	C(1)—C(10)—C(9)	110.4(2)
C(2)—C(3)—C(4)	116.7(2)	C(1)—C(10)—C(20)	109.7(2)
C(2)—C(3)—O(1)	121.7(3)	C(5)—C(10)—C(9)	109.8(2)
C(4)—C(3)—O(1)	121.5(3)	C(5)—C(10)—C(20)	110.9(2)
C(3)—C(4)—C(5)	115.0(2)	C(9)—C(10)—C(20)	109.3(2)
C(4)—C(5)—C(6)	110.4(2)	C(9)—C(11)—C(12+)	117.6(3)
C(4)—C(5)—C(10)	113.5(2)	C(9)—C(11)—C(12−)	119.2(5)
C(6)—C(5)—C(10)	111.9(2)	C(11)—C(12+)—C(13)	116.3(3)
C(5)—C(6)—C(7)	110.2(2)	C(11)—C(12−)—C(13)	109.1(8)
C(6)—C(7)—C(8)	114.2(3)	C(14)—C(13)—O(2)	123.6(3)
C(7)—C(8)—C(9)	114.1(2)	C(14)—C(13)—C(12+)	114.8(2)
C(7)—C(8)—C(15)	109.0(2)	C(14)—C(13)—C(12−)	117.1(5)
C(9)—C(8)—C(15)	104.6(2)	O(2)—C(13)—C(12+)	121.2(3)
C(8)—C(9)—C(10)	112.8(2)	O(2)—C(13)—C(12−)	116.5(5)
C(8)—C(9)—C(16)	100.8(2)	C(15)—C(14)—C(13)	108.1(2)
C(8)—C(9)—C(11)	109.8(2)	C(16)—C(14)—C(13)	108.1(2)
C(10)—C(9)—C(16)	115.7(2)	C(16)—C(14)—C(15)	105.2(2)
C(10)—C(9)—C(11)	110.2(2)	C(8)—C(15)—C(14)	105.7(2)
C(16)—C(9)—C(11)	107.0(2)	C(9)—C(16)—C(14)	101.5(2)

after refinement of 75% and 25%, respectively. A fully-occupied position H(12) corresponding to overlap of two partially-occupied hydrogen positions, one from C(12+) and one from C(12−), and the other 75% occupancy H(12+) were located; no difference map peak corresponding to the second 25% occupancy H(12−) was found, not surprisingly, and no contribution was included from this quarter-hydrogen atom. Ideally this description of the disorder should be extended to neighboring atoms C(13) (the C(12−)—C(13) bond

Can. J. Chem. Downloaded from www.nrcresearchpress.com by 210.87.254.40 on 09/06/12
For personal use only.

length being rather poor) and to a smaller extent to C(11), C(9), C(14), etc. However, the reasonable anisotropic thermal parameters for these atoms, and the high correlation between the positional parameters of closely-spaced split atoms indicated that treatment of only C(12) as disordered is probably reasonably appropriate. The scattering factors of refs. 2 and 3 were used; the weighting scheme $w = 1/\sigma^2(F_0)$ gave uniform average values of $w(F_0 - F_c)^2$ over ranges of $|F_0|$ and $\sin\theta/\lambda$; the function minimized was $\sum w(F_0 - F_c)^2$, $R = \sum(F_0 - F_c)/\sum F_0$, $R_w = (\sum w(F_0 - F_c)^2/\sum wF_0^2)^{1/2}$. Final $R = 0.051$, $R_w = 0.064$ for 1622 reflections with $I \geq 3\sigma(I)$; the final R value of 0.051 for the disordered structure is slightly higher than that of 0.047 for the model with one C(12) position refined with large anisotropic thermal parameters; the disordered model is, however, more physically realistic. For all 3159 reflections to $\theta = 27.5°$, $R = 0.113$. The standard deviation in an observation of unit weight was 2.53; a final difference map showed maximum random fluctuations of ± 0.3 e Å^{-3}.

Final positional parameters are in Table 1, and thermal parameters, structure factors, and other material have been placed in the Depository of Unpublished Data.[2]

Discussion

The X-ray analysis has established the structure as **2** (Fig. 1). C(12) is disordered over two positions with 75:25 occupancies; the structural details in that region of the molecule are therefore less accurately defined. The three six-membered rings have chair conformations (with the 75% C(12+) position), considerably flattened and distorted as a result of the keto substituents and of the presence of the bridged ring system. The lower occupancy C(12−) position results in a shallow boat conformation for the C(9)—C(16) ring. The five-membered ring is best described as a half-chair, with C(9) and C(16) displaced in opposite directions from the C(8), C(15), C(14) plane.

Bond distances and angles (Table 2) are within normal ranges for such a condensed ring system. C(sp^3)—C(sp^3) = 1.505−1.563(3−5), mean 1.536, C(sp^3)—C(sp^2) = 1.476−1.506(4−5), mean 1.490 Å (omitting the distances involved in the less accurate C(12−) position), C=O = 1.205, 1.209(3) Å, angles at C(sp^3) = 101.5° at C(16), 104.6−117.6°, angles at C(sp^2) = 114.8−123.6°. Intermolecular distances correspond to van der Waals interactions.

Acknowledgements

We thank the Natural Sciences and Engineering Research Council of Canada for financial support, the University of British Columbia Computing Center for assistance, and Dr. E. Piers and I. D. Suckling for crystals and discussion.

1. E. PIERS, B. ABEYSEKERA, D. J. HERBERT, and I. D. SUCKLING. J. Chem. Soc. Chem. Commun. 404 (1982).
2. D. T. CROMER and J. B. MANN. Acta Crystallogr. Sect. A, **24**, 321 (1968).
3. R. F. STEWART, E. R. DAVIDSON, and W. T. SIMPSON. J. Chem. Phys. **42**, 3175 (1965).
4. V. SCHOMAKER and R. E. MARSH. Acta Crystallogr. Sect. A, **39**, 819 (1983).

[2]Anisotropic thermal parameters, hydrogen atom parameters, bond lengths and angles involving hydrogen atoms, torsion angles, and structure factor tables are available, at a nominal charge, from the Depository of Unpublished Data, CISTI, National Research Council of Canada, Ottawa, Ont., Canada K1A 0S2.

Can. J. Chem. Downloaded from www.nrcresearchpress.com by 210.87.254.40 on 09/06/12
For personal use only.

Reactions of NO_2 and nitrite ion with organic radicals[1]

ALLEN JOHN ELLIOT[2] AND ANITA SANDRA SIMSONS[3]

Physical Chemistry Branch, Chalk River Nuclear Laboratories, Atomic Energy of Canada Limited Research Company, Chalk River, Ont., Canada, K0J 1J0

Received October 20, 1983

ALLEN JOHN ELLIOT and ANITA SANDRA SIMSONS. Can. J. Chem. **62**, 1831 (1984).

When deoxygenated aqueous sodium nitrate solutions containing an alcohol as a hydroxyl radical scavenger are irradiated, $G(NO_2^-)$ depends on the fraction of $\dot{O}H$ which forms 1-hydroxyalkyl radicals. This arises because $\dot{N}O_2$ is not reduced to nitrite by 2- or 3-hydroxyalkyl radicals.

Helium- and N_2O-saturated sodium nitrite solutions containing different organic hydroxyl radical scavengers were irradiated. Measurements of $G(-NO_2^-)$ showed that the radicals, $\dot{C}H_2OH$ and $\dot{C}H_2C(CH_3)_2OH$, do not react with the nitrite ion as rapidly as $CO_2^{\dot{-}}$ and $(CH_3)_2\dot{C}OH$. With the latter two radicals, nitric oxide is probably formed from the reaction with the nitrite ion.

ALLEN JOHN ELLIOT et ANITA SANDRA SIMSONS. Can. J. Chem. **62**, 1831 (1984).

Lorsqu'on irrarie des solutions aqueuses désoxygénées de nitrate de sodium contenant un alcool agissant comme piège radicalaire des hydroxyles, les valeurs de $G(NO_2^-)$ dépendent de la fraction des $H\dot{O}$ qui forment des radicaux hydroxyl-1 alkyles. Ceci est dû au fait que le $\dot{N}O_2$ n'est pas réduit en nitrite par les radicaux hydroxy-2 (ou -3) alkyles.

On a aussi irradié des solutions de nitrite de sodium saturées par de l'hélium et du N_2O et contenant divers pièges pour les radicaux hydroxyles organiques. Des mesures de $G(-NO_2^-)$ ont permis de montrer que, vis-à-vis l'ion nitrite, les radicaux $HO\dot{C}H_2$ et $HOC(CH_3)_2\dot{C}H_2$ ne réagissent pas aussi rapidement que les radicaux $CO_2^{\dot{-}}$ et $HO(CH_3)_2\dot{C}$. Avec les deux derniers radicaux, il se forme probablement de l'oxyde nitrique par réaction avec l'ion nitrite.

[Traduit par le journal]

Introduction

The aqueous free radical chemistry of the oxides of nitrogen has been studied extensively by photo- and radiation-chemical techniques (1–8). In operating nuclear reactors, nitric acid and nitrate ions are formed by radiation processes both in the annulus gases (9) and the coolant circuits (10) causing corrosion of metal components. Gadolinium nitrate is used as a neutron flux control agent in the moderator of CANDU reactors. In aqueous solutions, the important reactions involving the oxides of nitrogen have been identified along with their rate constants, but the effect of organic impurities on the radiolysis of nitrate systems has received less attention although these impurities may lead to problems such as excessive hydrogen production.

In radiation chemistry studies, the nitrate ion has been used extensively to measure the yield of the solvated electron, e_{aq}^-, in aqueous solution (11–19). In the irradiation of a nitrate solution containing a hydroxyl radical scavenger such as the formate ion (11–14) or an alcohol (11, 12, 15–18), $G(NO_2^-)$ is equated to $G(e_{aq}^-)$. On examination, the literature shows that, while similar, values of $G(NO_2^-)$ are different when different $\dot{O}H$ scavengers are used, e.g., formate ion, methanol, ethanol, and 2-propanol, even after allowing for their scavenging reactivities (12). In an earlier paper from this laboratory (11), it was also noted that when the hydroxyl scavenger was formate or 2-propanol, the yield of $G(NO_2^-)$ was not linear with dose suggesting that the nitrite ion was reacting with $CO_2^{\dot{-}}$ and $(CH_3)_2\dot{C}OH$. Henglein has reported that the nitrite ion is reduced by $(CH_3)_2\dot{C}OH$ (20).

An understanding of the role of organic radicals in nitrate and nitrite chemistry is also important in other areas; the use of the nitrate–nitrite redox couple as a store for photochemical energy (21) and also in the possible formation of carcinogenic nitrosoamines by free radical processes in the body from nitrite used as a food preservative (22). In this paper, we report on the reaction, in aqueous solutions, of $\dot{N}O_2$ and NO_2^- with radicals derived from the formate ion and from a series of alcohols.

Experimental

The solute chemicals (purchased from Fisher Scientific, Baker, Anachem and BDH) were all used as supplied except for *tert*-butanol (2-methyl-2-propanol) which was recrystallized. The solutions were prepared with triply distilled water. The pH was adjusted with perchloric acid for acid solutions; a phosphate buffer (3×10^{-3} mol dm^{-3}) for pH 7, and a borate buffer (3×10^{-3} mol dm^{-3}) for pH 9. The solutions were deoxygenated by bubbling with the appropriate UHP gas and irradiated in syringes. Nitrous oxide was first passed through a RIDOX (Fisher) column to remove any traces of oxygen.

The solutions were irradiated in an AECL Gammacell at a dose rate of approximately 2.2×10^{19} eV dm^{-3} s^{-1}. In some experiments a lower dose rate of 6.4×10^{17} eV dm^{-3} s^{-1} was obtained by irradiating the samples in a water-cooled lead block. In all experiments the nitrite ion was assayed as the product formed or the solute being removed. Its concentration was determined by the diazo-method (23) using an extinction coefficient at 540 nm of 52 860 mol^{-1} dm^3 cm^{-1} for solutions containing low concentrations of hydroxyl radical scavengers. Alcohols at high concentrations affected the final optical density in the nitrite assay so standard curves were prepared in these situations.

Results

(i) Sodium nitrate solutions

Helium-saturated solutions containing 2.5×10^{-3} mol dm^{-3} sodium nitrate were irradiated at pH 6.8 along with one of the hydroxyl scavengers: *tert*-butanol, 1-butanol, 1-propanol, 2-propanol, methanol, and the formate ion. As in earlier work from these laboratories (11), $G(NO_2^-)$ values shown in Fig. 1 are the values extrapolated to zero dose. With unbuffered solutions the $G(NO_2^-)$'s were the same, within experimental error, as those given in the figure. $G(NO_2^-)$ for the nitrate–methanol solution was also unchanged when irradiated at pH 9. In this study, except for *tert*-butanol, the concentration of the organic solute was sufficient to scavenge greater than 90% of the hydrogen atoms (24). With 0.1 mol dm^{-3} and 1.0 mol dm^{-3} *tert*-butanol, about 25% and 75%, respectively, of hydrogen

[1]AECL No. 8497.

[2]To whom all correspondence should be addressed.

[3]University of Waterloo Co-operative Program Student.

Can. J. Chem. Downloaded from www.nrcresearchpress.com by 210.87.254.40 on 09/06/12
For personal use only.

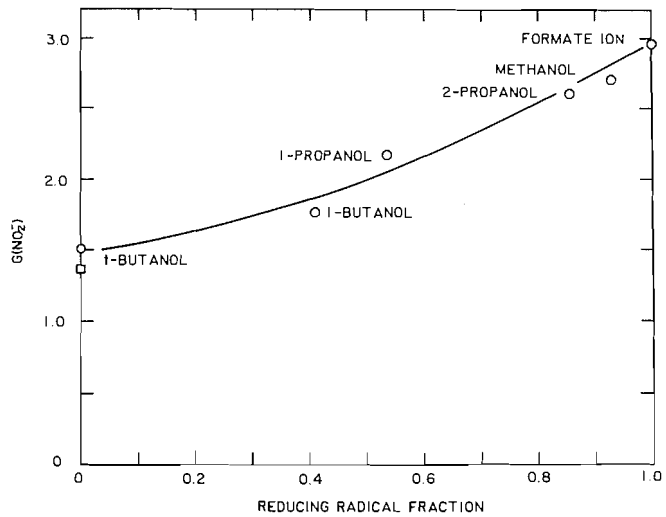

FIG. 1. $G(NO_2^-)$ as a function of the fraction of hydroxyl radicals forming reducing radicals for irradiated, helium saturated solutions containing 2.5×10^{-3} mol dm^{-3} $NaNO_3$ and 0.1 mol dm^{-3} (○) or 1 mol dm^{-3} (□) hydroxyl radical scavenger.

atoms were scavenged by the alcohol in competition with the nitrate ion. With the addition of 10^{-5} mol dm^{-3} copper(II) sulphate to 2.5×10^{-3} mol dm^{-3} sodium nitrate, 0.1 mol dm^{-3} *tert*-butanol solution, $G(NO_2^-)$ was reduced from 1.5 to 1.3.

(ii) Sodium nitrite solutions

Helium- and N_2O-saturated solutions containing sodium nitrite and various organic solutes (see Table 1) were irradiated at different pH's, dose rates, and solute concentrations. In these experiments the *G*-value for nitrite ion loss $G(-NO_2^-)$ was determined from 10–50% conversions of nitrite ion. The results are summarized in Table 1.

At pH 4.6, the formate solutions were self buffering, therefore the pH did not change during irradiation. However, at pH 4.6 with 2-propanol as the solute, the pH increased during the irradiation with the initial loss of protons, $G(-H^+)$, being about 1.3. In some experiments involving both helium- and N_2O-saturated solutions containing 0.1 mol dm^{-3} formate, NO was assayed for by the method described by Seddon and Sutton (25) but was not detected.

Henglein (20) reported that when a deoxygenated 10^{-3} mol dm^{-3} nitrite solution containing 0.2 mol dm^{-3} acetone and 0.4 mol dm^{-3} 2-propanol was irradiated, $G(-NO_2^-)$ was about 5. Since our results for 2-propanol solutions were all less than 2 (Table 1), Henglein's experiment was repeated at pH 6.8 and pH 9.4. The *G*-value for nitrite loss was 2.2 and 2.4, respectively.

(iii) Nitromethane solutions

The *G*-value for nitrite formation in a 10^{-4} mol dm^{-3} nitromethane solution, saturated with N_2O and irradiated at pH 9.5, was less than 0.2. When a helium-saturated 10^{-2} mol dm^{-3} nitromethane, 0.1 mol dm^{-3} sodium formate solution (pH 6.7) was irradiated, $G(NO_2^-)$ was less than 0.1.

Discussion

(i) Sodium nitrate solutions

A correlation exists between $G(NO_2^-)$ and the fraction of 1-hydroxyalkyl radicals formed by reaction of ·OH and ·H with the alcohol (26) present in the solution (Fig. 1). The fraction of CO_2^- formed from formate ions is taken as unity (26). These radicals are strong reducing agents and will be denoted as $\dot{R}_r$; the remaining 2- or 3-hydroxyalkyl radicals and alkoxy radicals formed will be denoted as $\dot{R}_{nr}$. In general terms, the radiolysis of deoxygenated nitrate–alcohol (or formate) solutions can be described by reactions [1]–[6].

$$[1] \quad NO_3^- + e_{aq}^- \xrightarrow{H_2O} \dot{N}O_2 + 2OH$$

$$[2] \quad RH + \dot{O}H, \dot{H} \rightarrow \dot{R}_r \text{ or } \dot{R}_{nr} + H_2O, H_2$$

$$[3] \quad \dot{N}O_2 + \dot{R}_r \rightarrow NO_2^- + R_r(-H)$$

$$[4] \quad \dot{N}O_2 + \dot{N}O_2 \rightleftharpoons N_2O_4$$

$$[5] \quad N_2O_4 + H_2O \rightarrow NO_2^- + NO_3^- + 2H^+$$

$$[6] \quad \dot{R}_r, \dot{R}_{nr} \rightarrow \text{Products}$$

Reaction [7] is too slow on the time scale of these experiments to contribute to the NO_2^- yield.

$$[7] \quad \dot{N}O_2 + \dot{R}_{nr} \rightarrow NO_2^- + R_{nr}(-H)$$

This is best illustrated by comparing $G(NO_2^-)$ for the scavengers formate and *tert*-butanol. With formate solutions, $G(NO_2^-)$ is equal to $G(e_{aq}^-)$, which indicates the strongly reducing radical CO_2^- (27) rapidly converts $\dot{N}O_2$ to NO_2^- in reaction [3]. With *tert*-butanol solutions, $G(NO_2^-)$ is approximately half $G(e_{aq}^-)$ so that reaction [7] involving the poor reducing 2-hydroxy radical cannot compete for $\dot{N}O_2$ (reaction [7]) against reactions [4] and [5] in the formation of NO_2^-. This results in two $\dot{N}O_2$ radicals forming one NO_2^- ion.

In one radiolysis experiment 10^{-5} mol dm^{-3} copper(II) sulphate was added to the 2.5×10^{-3} mol dm^{-3} sodium nitrate, 0.1 mol dm^{-3} *tert*-butanol solution to see if the copper(I) ion could reduce $\dot{N}O_2$ to NO_2^-. The copper(I) ion is formed by the overall reaction [8] from the 2-hydroxyalkyl radical (28, 29).

$$[8] \quad \dot{C}H_2—C(CH_3)_2OH + Cu^{2+} \rightarrow Cu^+ + \text{product}$$

As $G(NO_2^-)$ fell from 1.5 to 1.3 on addition of copper(II) ions, this indicates the reduction did not occur. This experiment was tried because, in the analogous iron system, the 2-hydroxy-*tert*-butanol radical was an inefficient reducing radical for the conversion of Fe(III) to Fe(II) whereas the copper(I) ion, formed by [8], was very effective (30).

Qualitatively, the results in Fig. 1 can be rationalized in terms of the fraction of strong reducing radicals formed in reaction [2] and the consequent pathways for NO_2^- formation. In reaction [3], each $\dot{N}O_2$ is converted to NO_2^- whereas by reactions [4] and [5], two $\dot{N}O_2$ are required to form one NO_2^-. However, quantitatively, for 2-propanol and methanol this explanation is not sufficient. The alcohol (or formate) concentration in these experiments is sufficient to scavenge most of the hydrogen atoms produced. Allowing for scavenging in the spur (12), in these solutions the sum of $G(\dot{O}H)$ and $G(\dot{H})$ is about four while $G(e_{aq}^-)$ is approximately three. This implies that in 2-propanol and methanol solutions, the number of 1-hydroxyalkyl radicals formed (reaction [2]) is in excess of the number of $\dot{N}O_2$ formed (reaction [1]). Hence $G(NO_2^-)$ in both cases should equal that in the formate solutions. However, this is not observed (Fig. 1) and the most likely explanation is that for these two alcohols reaction [3] cannot compete with reactions [4] and [6].

The computer code MAKSIMA CHEMIST (31) in conjunction with an optimizing routine was used to estimate values of k_3 for the formate, methanol, and 2-propanol scavengers based on reactions [1]–[6]. Most of the rate constants are known (11,

Can. J. Chem. Downloaded from www.nrcresearchpress.com by 210.87.254.40 on 09/06/12
For personal use only.

TABLE 1. $G(NO_2^-$ loss)* from irradiated solutions containing 10^{-4} mol dm^{-3} nitrite

Compound	Concentration/ mol dm^{-3}	Dose rate/ 10^{17} eV dm^{-3}	Saturating gas	$G(NO_2^-$ loss) at pH = 4.6	6.8	9.4
Sodium formate	1	220	N_2O	2.0	1.7	1.1
Sodium formate	0.1	220	N_2O	1.9	1.8	1.1
Sodium formate	0.1	220	He	—	1.8	—
Sodium formate	0.1	6.4	N_2O	—	1.6	—
Sodium formate	0.01	220	N_2O	1.9	1.3	0.7
2-Propanol	1	220	N_2O	—	1.5	—
2-Propanol	1	220	He	—	1.5	—
2-Propanol	1	6.4	N_2O	—	1.6	—
2-Propanol	0.1	220	N_2O	1.5	1.4	1.3
2-Propanol	0.1	220	He		1.8	
2-Propanol	0.1	6.4	N_2O		1.5	
2-Propanol/acetone†	0.4/0.2	220	He		2.2	2.4
Methanol	0.1	220	N_2O		0.2	
Methanol	0.1	220	He		1.8	
Methanol	0.1	6.4	N_2O		0.4	
tert-Butanol	1	220	N_2O	—	0.4	—
tert-Butanol	1	220	He	—	2.1	—
tert-Butanol	1	6.4	N_2O	—	0.4	—

*Error ± 0.1.
†$[NO_2^-] = 10^{-3}$ mol dm^{-3}.

24, 28, 32). For 2-propanol solutions the bimolecular termination rate constant for $\dot{C}H_2CH(CH_3)OH$ ($\dot{R}_{nr}$) was assumed to be the same as for the $\dot{C}H_2C(CH_3)_2OH$ radical formed from *tert*-butanol (28) and the cross termination rate constant between $\dot{C}H_2CH(CH_3)OH$ and $(CH_3)_2\dot{C}OH$ was calculated as twice the root-mean-square of the symmetrical termination rate constants (33). For methanol, reaction [9] was added, with k_9 having a value of 2.6×10^5 mol^{-1} dm^3 s^{-1} (34).

[9] $CH_3OH + CH_3\dot{O} \rightarrow \dot{C}H_2OH + CH_3OH$

Assuming that for formate, $G(NO_2^-)$ was equal to $G(e_{aq}^-)$, k_3 was estimated to be $> 5 \times 10^9$, 1.1×10^9, and 1.0×10^9 mol^{-1} dm^3 s^{-1} for formate, 2-propanol, and methanol, respectively. A similar calculation for 0.1 mol dm^{-3} *tert*-butanol indicated that the rate constant for reaction of $\dot{C}H_2C(CH_3)_2OH$ with $\dot{N}O_2$ (i.e., reaction [7]) must be less than 5×10^4 mol^{-1} dm^3 s^{-1}.

(ii) Sodium nitrite solutions

In helium-saturated nitrite solutions where e_{aq}^- as well as the organic radical derived from the $\dot{H}$ and $\dot{O}H$ scavenger are present, the values of $G(-NO_2^-)$ are similar for all solutions (Table 1). The reaction of e_{aq}^- with the nitrite ion forms nitric oxide (reaction [10]) (2, 3).

[10] $NO_2^- + e_{aq}^- \rightarrow NO_2^{2-} \xrightarrow{H_2O} NO + 2OH^-$

The similarity of $G(-NO_2^-)$ for helium- and N_2O-saturated solutions containing either formate ions or 2-propanol suggests that $CO_2^{\dot{-}}$ and $(CH_3)_2\dot{C}OH$ also reduce nitrite ions to nitric oxide. For $(CH_3)_2\dot{C}OH$ this will probably involve an adduct nitro–anion radical (35) (reaction [11]) which then dissociates to form NO_2^{2-} followed by [12].

[11] $(CH_3)_2\dot{C}OH + NO_2^- \rightarrow \dot{\bar{O}}_2N{-}C(CH_3)_2OH \rightarrow NO_2^{2-} + (CH_3)_2CO + H^+$

[12] $NO_2^{2-} \xrightarrow{H_2O} NO + 2OH^-$

This mechanism is supported by the observation that $G(-H^+)$ was approximately equal to $G(-NO_2^-)$ in the irradiation of the nitrite solution containing 2-propanol at an initial pH of 4.6. The results from irradiated nitromethane solutions which will be discussed in the next section also support reactions [11] and [12].

The low $G(-NO_2^-)$ values for N_2O-saturated nitrite solutions containing methanol or *tert*-butanol indicate that $\dot{C}H_2OH$ and $\dot{C}H_2C(CH_3)_2OH$ do not react with the nitrite ion as efficiently as $(CH_3)_2\dot{C}OH$ and $CO_2^{\dot{-}}$ at the dose rate of our experiments.

In these solutions containing formate, nitric oxide is not observed and, in all solutions, the loss of nitrite is less than a third of the total yield of radicals formed. However, nitric oxide is known to react with free radicals (36, 37) to form nitroso-compounds which are themselves excellent free radical trapping agents (38). This suggests the nitric oxide and nitroso-compounds compete effectively against the nitrite ions for the organic radicals (R) through reactions [13]–[15].

[13] $\dot{R} + NO \rightarrow RNO$

[14] $\dot{R} + RNO \rightarrow R_2\dot{N}O$ or $R\dot{N}HO + R(-H)$

[15] $\dot{R} + R_2\dot{N}O$ or $RH\dot{N}O \rightarrow$ products

For the alcohol-derived radicals, the above reactions can account for the observed results; however, with $CO_2^{\dot{-}}$ the electron transfer reaction [16] may occur.

[16] $NO + CO_2^{\dot{-}} \rightarrow NO^- + CO_2$

The subsequent reaction of $CO_2^{\dot{-}}$ with NO^- or HNO ($pK \sim 4.7$) may account for the pH dependence of $G(-NO_2^-)$ observed in these solutions (2). The radical anion of NO is known to undergo a series of reactions involving $N_2O_2^-$, $N_3O_3^-$, etc. as intermediates (2, 3).

(iii) Nitromethane solutions

Reaction [11] postulates that $(CH_3)_2\dot{C}OH$ reacts with nitrite ion to form a nitro-radical anion which decomposes to form

Can. J. Chem. Downloaded from www.nrcresearchpress.com by 210.87.254.40 on 09/06/12
For personal use only.

nitric oxide. Pulse radiolysis results (39) indicate that $HOCH_2NO_2^{\cdot-}$ (which would be formed by the reaction of $\dot{C}H_2OH$ and NO_2^-) decays by mixed first ($k \sim 80\ s^{-1}$) and second ($2k \sim 6 \times 10^6\ mol^{-1}\ dm^3\ s^{-1}$) order kinetics. The first order process (which would be the major process at our dose rates) was suggested to be the formation of the nitrite ion. The low $G(NO_2^-)$ (<0.2) observed in this study when the two nitro-anions formed in reactions [17] (40) and [18] (41) rules out this mode of decay.

$$[17]\quad \dot{O}H + CH_2{=}NO_2^- \xrightarrow{pH = 9.5} HOCH_2NO_2^{\cdot-}$$

$$[18]\quad e_{aq}^-,\ CO_2^{\cdot-} + CH_3NO_2 \xrightarrow{pH = 6.7} CH_3NO_2^{\cdot-}$$

The first order decay is most likely the formation of NO in reactions analogous to reactions [11] and [12]. The second order decay which probably entails the formation of a nitroso compound (reaction [19]) (41)

$$[19]\quad RNO_2^{\cdot-} + RNO_2^{\cdot-} \xrightarrow{2H^+} RNO + RNO_2 + H_2O$$

would not be important at the dose rates used in the nitrite solution irradiations.

Conclusions

The nitrate ion has been used extensively in radiation chemistry to measure $G(e_{aq}^-)$; however, it could be a poor choice since the measured product, the nitrite ion, can be formed by two processes depending on the radical formed from the $\dot{O}H$-scavenger. In one process $G(NO_2^-)$ equals $G(e_{aq}^-)$ (reaction [3]), while in the other $G(NO_2^-)$ is half $G(e_{aq}^-)$ (reactions [4] and [5]). The results in this paper indicate that $CO_2^{\cdot-}$ and 1-hydroxyalkyl radicals react with $\dot{N}O_2$ with rate constants greater than $10^9\ mol^{-1}\ dm^3\ s^{-1}$, whereas 2- or 3-hydroxyalkyl radicals and Cu^+ cannot reduce $\dot{N}O_2$ to the nitrite ion. The dependence of $G(NO_2^-)$ on dose for irradiated nitrite and formate (or 2-propanol) solutions can be attributed, at least in part, to the reaction of $CO_2^{\cdot-}$ and $(CH_3)_2\dot{C}OH$ with the nitrite ion.

Acknowledgement

The authors wish to acknowledge discussions with J. W. Fletcher throughout this study.

1. I. Wagner, H. Strehlow, and G. Busse. Z. Physik. Chem. **123**, 1 (1980) and references therein.
2. W. A. Seddon, J. W. Fletcher, and F. C. Sopchyshyn. Can. J. Chem. **51**, 1123 (1973).
3. M. Gratzel, S. Taniguchi, and A. Henglein. Ber. Bunsenges. Phys. Chem. **74**, 488 (1970).
4. M. Gratzel, A. Henglein, and S. Taniguchi. Ber. Bunsenges. Phys. Chem. **74**, 292 (1970).
5. M. Gratzel, A. Henglein, J. Lilie, and G. Beck. Ber. Bunsenges. Phys. Chem. **73**, 646 (1969).
6. R. K. Broszkiewicz. Bull. Acad. Pol. Sci. **24**, 221 (1976).
7. M. Faraggi, D. Zehavi, and M. Anbar. Trans. Faraday Soc. **67**, 701 (1971).
8. M. Daniels. Adv. Chem. Ser. **81**, 153 (1968).
9. J. K. Linacre and W. R. Marsh. AERE-R 10027, Harwell. 1981.
10. O. Brede, J. Bos, and E. Brasel. Radiochem. Radioanal. Lett. **50**, 45 (1981).
11. A. J. Elliot and F. C. Sopchyshyn. Can. J. Chem. **61**, 1578 (1983).
12. Z. D. Draganic and I. G. Draganic. J. Phys. Chem. **77**, 765 (1973).
13. E. Hayon. Trans. Faraday Soc. **61**, 734 (1964).
14. E. Hickel. CEA-R-4046, Saclay, France. 1970.
15. T. Sawai. Bull. Chem. Soc. Jpn. **39**, 955 (1966).
16. A. Appleby, G. Scholes, and M. Simic. J. Am. Chem. Soc. **85**, 3891 (1963).
17. J. T. Allan. J. Phys. Chem. **68**, 2697 (1964).
18. C. Baquey, J. C. Roux, and J. Sutton. J. Phys. Chem. **74**, 4210 (1970).
19. M. Haissinsky. J. Chem. Phys. **62**, 1141 (1965).
20. A. Henglein. Ber. Bunsenges. Phys. Chem. **84**, 253 (1980).
21. A. J. Frank and M. Gratzel. Inorg. Chem. **21**, 3834 (1982).
22. A. Joshi, D. M. Hinton, and G. C. Yang. Can. J. Chem. **60**, 1598 (1982).
23. W. A. Seddon. Thesis. University of Edinburgh. 1962.
24. M. Anbar, Farhataziz, and A. B. Ross. Natl. Stand. Ref. Data. Ser. (U.S. Natl. Bur. Stand.) **51** (1968).
25. W. A. Seddon and H. C. Sutton. Trans. Faraday Soc. **59**, 2323 (1963).
26. K.-D. Asmus, H. Mockel, and A. Henglein. J. Phys. Chem. **77**, 1218 (1973).
27. A. Henglein. Electroanal. Chem. **9**, 163 (1976).
28. A. B. Ross and P. Neta. Natl. Stand. Ref. Data. Ser. (U.S. Natl. Bur. Stand.) **70** (1982).
29. M. Freiberg and D. Myerstein. J. Chem. Soc. Faraday I. **76**, 1825 (1980).
30. (*a*) C. Walling and S. Kato. J. Am. Chem. Soc. **93**, 4275 (1971); (*b*) A. J. Elliot and A. S. Simsons. Unpublished results.
31. A. W. Boyd, M. B. Carver, and R. J. Dixon. Radiat. Phys. Chem. **15**, 177 (1980).
32. Farhataziz and A. B. Ross. Natl. Stand. Ref. Data. Ser. (U.S. Natl. Bur. Stand.) **59** (1977).
33. W. A. Pryor. Free radicals. McGraw-Hill, New York. 1966.
34. D. H. Ellison, G. A. Salmon, and F. Wilkinson. Proc. R. Soc. London, Ser. A. **328**, 23 (1972).
35. B. C. Gilbert, H. A. H. Laue, R. O. C. Norman, and R. C. Sealy. J. Chem. Soc. Perkin II, 1040 (1976).
36. P. Maruthamuthu and J. C. Scaiano. J. Am. Chem. Soc. **82**, 1588 (1978).
37. E. J. Burrell. J. Phys. Chem. **66**, 401 (1962).
38. E. G. Janzen. Acc. Chem. Res. **4**, 31 (1971).
39. K.-D. Asmus and I. A. Taub. J. Phys. Chem. **72**, 3382 (1968).
40. B. C. Gilbert and R. O. C. Norman. Can. J. Chem. **60**, 1379 (1982).
41. C. L. Greenstock. *In* The chemistry of amino, nitroso and nitro compounds and their derivatives. Part 1. *Edited by* S. Patai. John Wiley and Sons, 1982. p. 291.

Can. J. Chem. Downloaded from www.nrcresearchpress.com by 210.87.254.40 on 09/06/12
For personal use only.

The oxidation of alcohols by sodium ruthenate

DONALD G. LEE, LIGAYA N. CONGSON, UDO A. SPITZER, AND MERLE E. OLSON
Department of Chemistry, University of Regina, Regina, Sask., Canada S4S 0A2

Received June 27, 1983[1]

DONALD G. LEE, LIGAYA N. CONGSON, UDO A. SPITZER, and MERLE E. OLSON. Can. J. Chem. **62**, 1835 (1984).

The oxidation of 2-propanol and cyclobutanol by stoichiometric amounts of sodium ruthenate has been studied. Contrary to previously published speculations, it has been found that these reactions are not initiated by traces of perruthenate present as a contaminant in the ruthenate solutions. This conclusion is supported by both the kinetic rate law for the reaction and the products obtained from the oxidation of alcohols that would be expected to react differently with RuO_4^- and RuO_4^{2-}.

DONALD G. LEE, LIGAYA N. CONGSON, UDO A. SPITZER et MERLE E. OLSON. Can. J. Chem. **62**, 1835 (1984).

On a étudié l'oxydation du propanol-2 et du cyclobutanol par des quantités stoichiométriques de ruthénate de sodium. Contrairement aux spéculations publiées antérieurement, on a trouvé que cette réaction n'est pas initiée par des traces de perruthénate qui pourraient être présentes dans les solutions de ruthénate. Cette conclusion est basée à la fois sur la loi de la cinétique de la réaction et sur la nature des produits obtenus par oxydation des alcools qui devraient réagir différemment avec le RuO_4^- et le RuO_4^{2-}.

[Traduit par le journal]

Introduction

Sodium ruthenate may be used for the selective oxidation of primary and secondary alcohols containing carbon–carbon double bonds. The reaction has found application particularly in those cases where it is necessary to maintain basic conditions. A typical example of its use in this way appears in a recent report by Coates *et al.* in which they describe the oxidation of a number of unsaturated tricyclo lactones by alkaline RuO_4^{2-} (1). Oxidants which require neutral or acidic conditions cannot be used effectively for these reactions because the lactone ring remains closed under all but basic conditions and thus prevents oxidation of the incipient alcohol. On the other hand, the use of a number of other oxidants, such as permanganate, which function well under alkaline conditions is precluded because of their high reactivity with carbon–carbon double bonds. Other examples of the use of sodium ruthenate for the oxidation of unsaturated alcohols can also be found in the reports by Corey *et al.* (2), Nakano and Foglia (3), and Hall and co-workers (4). In addition Dauben and Cunningham have recently described the use of this reagent for the oxidation of a saturated hexacyclic alcohol (5).

In the above reactions, sodium ruthenate was prepared by the reduction of ruthenium tetroxide in aqueous sodium hydroxide solutions and used in stoichiometric quantities (6–8). However, Schroder and Griffith have also described a procedure for carrying out these reactions using catalytic quantities of ruthenium trichloride under alkaline conditions in the presence of a cooxidant, potassium persulphate (9). In these reactions it has been presumed that the cooxidant converted ruthenium(III) into RuO_4^{2-} which then oxidized the alcohols while being reduced to RuO_2. Ruthenium dioxide would then be reoxidized by cooxidant to RuO_4^{2-} and a cyclic process thus established. Dalton *et al.* have described the use of a similar process employing sodium periodate as the cooxidant for the oxidation of a number of unsaturated and saturated alcohols (10).

The exact mode of the reaction is somewhat difficult to determine because perruthenate, RuO_4^-, also forms when ruthenium tetroxide is reduced under basic conditions and Burke and Healy have pointed to the possibility that the active oxidant in these reactions might, in fact, be RuO_4^- (11). Because of the usefulness of these reactions in organic syntheses it is important to expose their mechanisms, with the expectation that greater understanding will lead to improved applications. Consequently, we have examined the stoichiometric reaction in an attempt to determine if perruthenate is also the active oxidant in the absence of a cooxidant. The results which we have obtained appear to suggest that this is not the case. Since similar products are obtained when a cooxidant is used, these results may also have implications for the catalytic reaction.

Experimental

Preparation of sodium ruthenate solutions

These solutions were prepared in three different ways. In one, ruthenium dioxide was oxidized to ruthenium tetroxide by either sodium hypochlorite or potassium periodate according to published procedures (12). The ruthenium tetroxide was then extracted into carbon tetrachloride, giving a bright yellow solution that was subsequently treated with a 1 *M* sodium hydroxide solution which reduced the RuO_4 to RuO_4^{2-} and extracted it into the aqueous layer (7). The solution of sodium ruthenate was separated and held at room temperature for at least 24 h to insure complete reduction to sodium ruthenate. Spectroscopic analysis of the solution showed that it did not contain detectable amounts of RuO_4 or RuO_4^- (13).

In a second approach RuO_2 was oxidized to RuO_4 by sodium periodate and then distilled on a stream of nitrogen into 1 *M* NaOH. After aging for 24 h this solution was found, within the limits of experimental detection, to contain only RuO_4^{2-} (13).

In a third approach RuO_2 was oxidized to RuO_4 by chromium trioxide in 1 *M* H_2SO_4 (14), extracted into carbon tetrachloride, and reduced to RuO_4^{2-} as described above.

Preparation of sodium perruthenate solutions

These solutions were also prepared by a controlled reduction of ruthenium tetroxide in cold aqueous sodium hydroxide solutions (8). Ruthenium tetroxide, prepared from the oxidation of ruthenium dioxide by sodium periodate, was carried on a stream by nitrogen into 0.3 *M* NaOH at −5°C. This solution was held at −5°C for 4 h and then extracted with 75 mL of carbon tetrachloride to remove any excess ruthenium tetroxide. The resulting green solution exhibited an absorption spectrum that was identical with that previously reported for sodium perruthenate (8).

Oxidation of cyclobutanol by sodium ruthenate

Cyclobutanol (7 mmol), prepared as previously described (15), was dissolved in 50 mL of a 0.9 *M* NaOH solution and a volume of sodium ruthenate solution containing sufficient oxidant to convert about 90% of the alcohol into ketone was added dropwise with stirring at room temperature. After 1 h the solution was gravity filtered, saturated with

[1]Revision received March 20, 1984.

Can. J. Chem. Downloaded from www.nrcresearchpress.com by 210.87.254.5 on 09/06/12
For personal use only.

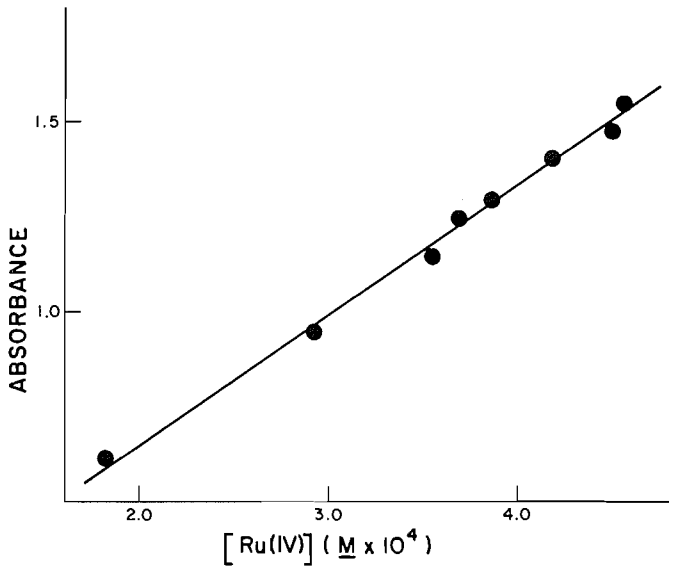

FIG. 1. Beer's Law plot for the reaction product. λ = 320 nm. Slope = 3370 M^{-1}. Intercept = −0.0090. r = 0.997. Temperature = 25.0 ± 0.1°C [NaOH] = 1.034 M.

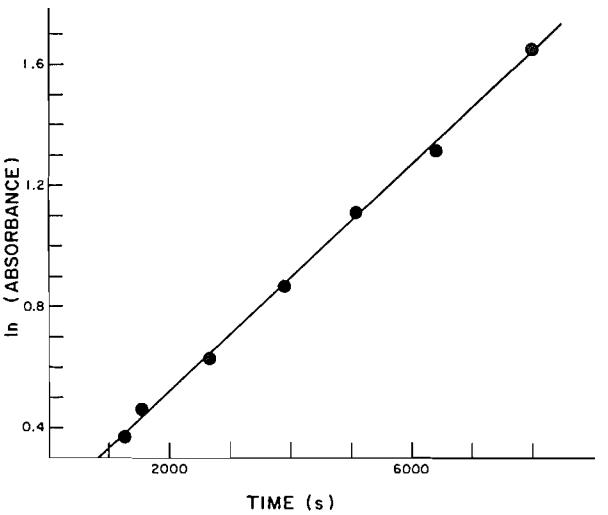

FIG. 2. Pseudo first order rate plot for the oxidation of 2-propanol by sodium ruthenate. λ = 464 nm. Temperature = 25.0 ± 0.1°C. [NaOH] = 0.951 M. [2-Propanol] = 4.16 × 10^{-3} M. r = 0.998.

sodium chloride, and extracted with eight 200-mL portions of diethyl ether. The ethereal extract was dried over anhydrous magnesium sulfate for 1 h, concentrated by rotary evaporation, and analyzed by gas chromatography. The only product detected was cyclobutanone.

Oxidation of cyclobutanol by sodium perruthenate

Two types of experiments were carried out; in one the initial reaction products which appeared to contain ruthenate ion were quenched with sodium arsenite, in the other the reaction was allowed to go to completion without external interference.

In the unquenched experiments cyclobutanol (7 mmol) in 50 mL of 0.3 M NaOH was allowed to react at −5°C with sufficient sodium perruthenate to oxidize 10−50% of the alcohol. The quenched reactions were carried out in a similar fashion with the exception that shortly after addition of oxidant the reaction was quenched with 50 mL of 0.3 M sodium arsenite. At the time of quenching the solution was a bright orange color characteristic of ruthenate ion.

When the reaction had gone to completion (as indicated by the complete disappearance of any orange color) the solution was filtered through a fine fritted filter and made acidic with sulfuric acid. Then 100 mL of a saturated solution of 2,4-dinitrophenylhydrazine in 2 M H_2SO_4 was added and allowed to react at room temperature for 24 h. The precipitate which formed was collected by filtration and dissolved in anhydrous chloroform. The filtrate was continuously extracted with ether for 48 h. The ether and chloroform solutions were combined, dried over $MgSO_4$ for 4 h and concentrated by rotary evaporation. The solid material that remained was then dissolved in a small amount of benzene, placed on an alumina column (activity III), and eluted with benzene. The bands were collected and the solvent was evaporated to yield a solid 2,4-dinitrophenylhydrazone.

In the unquenched reaction three bands were eluted. The fastest moving compound was identified as the product, cyclobutanone 2,4-dinitrophenylhydrazone, by comparison of the nmr and ir spectra (16) and melting points, 142−146°C (lit. (17) mp 147°C). The second (minor) compound was identified as acetone 2,4-dinitrophenylhydrazone from its melting point, 120−125°C (lit. (17) mp 128°C), and ir and nmr spectra. (Acetone was later shown, in a control experiment, to be present in small amounts in the solvent.) The last compound was found to be unreacted 2,4-dinitrophenylhydrazine.

Kinetics

The oxidation of 2-propanol was followed spectrophotometrically in two different ways, both of which gave rate constants that were identical within the limits of experimental uncertainty.

In the first approach, an excess of 2-propanol was added to a thermostated solution of RuO_4^{2-} and aliquots were periodically withdrawn, centrifuged to remove suspended RuO_2, and analyzed spectrophotometrically. The concentration of RuO_4^{2-} was determined by measurement of the absorbance at 464 nm (ε = 1960) (7). In a second approach, initial reaction rates were determined in the following way. Two milliliters of a ruthenate solution were added to a 1.0-cm cuvette which was in turn placed in the thermostated cell compartment of a Hewlett Packard 8450 A spectrophotometer. An excess of alcohol was added using a microliter syringe and the initial rate was determined by monitoring the increase in adsorbance at 320 nm. At this wavelength the product of the reaction (which appears to be a soluble form of ruthenium(IV) similar to the species formed during the electrochemical reduction of ruthenate (18)) conforms to Beer's Law with ε = 3370 (Fig. 1).

Although the reaction products were stable for several hours (as evidenced by the constancy of their uv−vis spectrum), ruthenium dioxide was observed to eventually precipitate. The abscissa in Fig. 1 is the concentration of product based on the assumption of a quantitative reduction of ruthenate to ruthenium(IV) oxide. The ordinate is the absorbance of the product at 320 nm before any ruthenium dioxide had precipitated.

Results

When the rate of reaction was determined by following the decrease in absorbance at λ_{max} 464 nm, linear plots of ln (absorbance) against time were obtained (Fig. 2). This indicates that the rate of reaction is first order with respect to ruthenate concentrations. When the reaction was followed by monitoring the increase in absorbance at 320 nm, the initial rates were found to be directly dependent on the concentrations of both ruthenate (Fig. 3) and 2-propanol (Table 1). This confirms that the reaction rate is first order with respect to ruthenate ion and demonstrates that it is also first order with respect to 2-propanol. The latter procedure was used for the remaining studies because the method of initial rates is known to be a more sensitive approach to kinetics (19) and because this procedure avoids the need to remove the sample from the thermostat for centrifuging before making absorbance measurements. The rate constants obtained from the use of ruthenate prepared in several different ways have been summarized in Table 1.

The yields of cyclobutanone obtainable from the oxidation of

Can. J. Chem. Downloaded from www.nrcresearchpress.com by 210.87.254.5 on 09/06/12
For personal use only.

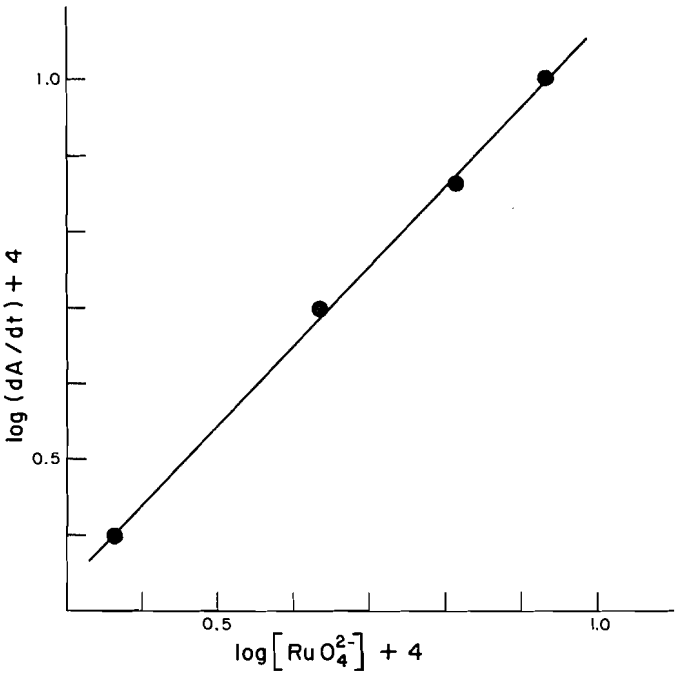

FIG. 3. Plot showing the first order dependence of the initial rate on the concentration of RuO_4^{2-}. λ = 320 nm. Slope = 1.04. Intercept = 0.12. r = 0.999. [NaOH] = 1.023 M. [2-Propanol] = 5.15 × 10^{-3} M.

cyclobutanol by sodium ruthenate and sodium perruthenate have been summarized in Table 2.

Discussion

Although most of the work described by Burke and Healy related to the catalytic reaction, they also presented some results which were taken to implicate RuO_4^- as the active oxidant in the stoichiometric reaction (11). It is as a test of this suggestion that our experiments have been conducted.

There are, in principle, two ways in which perruthenate could be produced in ruthenate solutions. The first of these is by disproportionation. This possibility can, however, be ruled out in the present case by the observation that the reaction rate is clearly first order in ruthenate concentration (Figs. 2 and 3). A reaction sequence initiated by disproportionation would require a higher order (6, 7).

As an alternative, small amounts of perruthenate could be formed from the oxidation of ruthenate by contaminants such as periodate or hypochlorite. Such compounds could easily be present in ruthenate solutions since they are used in its preparation. As described in the experimental section, ruthenium dioxide is first oxidized to ruthenium tetroxide by use of sodium periodate or sodium hypochlorite. The tetroxide is then extracted into carbon tetrachloride and reduced by treatment with aqueous base. Hence it is possible that IO_4^- or ClO^- could be carried along and be present in small amounts in the final RuO_4^{2-} solution. The reaction could then proceed by way of eq. [1]–[3].

$$[1]\quad 2RuO_4^{2-} + IO_4^- \rightarrow 2RuO_4^- + IO_3^-$$

$$[2]\quad RuO_4^- + R_2CHOH \rightarrow H_2RuO_4^- + R_2CO$$

$$[3]\quad H_2RuO_4^- + RuO_4^{2-} \rightarrow RuO_4^- + RuO_2$$

In order to determine if contaminants such as periodate could be important entities in the reaction scheme, we prepared

TABLE 1. Rates of oxidation of 2-propanol by sodium ruthenate[a]

$[RuO_4^{2-}]_i$ ($M \times 10^4$)	[2-Propanol] ($M \times 10^3$)	Initial rate ($M\ s^{-1} \times 10^7$)	k_2 ($M^{-1}\ s^{-1} \times 10^2$)
6.70	2.64	1.04±0.08	5.88±0.45
4.64	5.15	1.43±0.09	5.98±0.38
4.86[b]	5.15	1.37±0.10	5.47±0.40
4.96[c]	5.15	1.35±0.09	5.29±0.35
3.98[d]	5.15	1.22±0.08	5.95±0.39
5.50	21.6	6.68±0.42	5.62±0.35
4.54	36.1	8.92±0.57	5.44±0.35

[a]RuO_4^{2-} prepared from distilled RuO_4 unless noted otherwise. [NaOH] = 1.0 M; temperature = 25.0°C.
[b]RuO_4 extracted from a solution of sodium hypochlorite.
[c]$NaIO_4$ added to the RuO_4^{2-} solution (see text).
[d]RuO_4 prepared by oxidation of RuO_2 with chromic acid.

TABLE 2. The oxidation of cyclobutanol by ruthenate and perruthenate

Oxidant	Yield of cyclobutanone (mol)		
	Theoretical	Obtained[b]	% Yield[b]
RuO_4^{2-}	1.0	0.8–0.9	80–90
RuO_4^-	1.5	0.33–0.50	22–33
RuO_4^-[a]	0.5	0–0.01	0–2

[a]Reaction was quenched with sodium arsenite after the first stage as described in the text.
[b]Indicates the range of yields obtained from several experiments.

RuO_4^{2-} from RuO_4 that had been distilled (instead of extracted) from the solution in which it was formed. Ruthenate so prepared was found to react with 2-propanol at the same rate as that obtained by the more usual extraction procedures (Table 1).

Furthermore, if the sequence of reactions depicted in eqs. [1]–[3] is correct one would expect the reaction rate to be dependent on the amount of IO_4^- present. To test this possibility we added some sodium periodate to a solution of RuO_4^{2-} that had been prepared from distilled ruthenium tetroxide and observed spectrophotometrically the changes which occurred. As expected, some of the ruthenate was converted into perruthenate and the spectrum obtained was that of a mixture of the two (7). However, when 2-propanol was added the RuO_4^- was rapidly reduced to RuO_4^{2-} and the reduction of ruthenate then proceeded at the same rate as in those solutions which contained no periodate (Table 1).

Burke and Healy also found that ruthenate prepared using oxidants other than hypochlorite or periodate did not oxidize alcohols, with the exception of methanol. For example, they report that the use of chromic acid (which presumably would not extract into carbon tetrachloride and therefore would not be present to produce perruthenate) gave an unreactive form of ruthenate. However, in our hands, sodium ruthenate prepared by use of chromic acid reacted with 2-propanol at the same rate as all other samples of ruthenate (Table 1).

Further evidence which mitigates against the idea that perruthenate may be the active oxidant can be obtained from an examination of the products obtained in certain reactions. For example, although it is well known that perruthenate reacts rapidly with carbon–carbon double bonds (20), ruthenate solutions have often been used to oxidize unsaturated alcohols to

Can. J. Chem. Downloaded from www.nrcresearchpress.com by 210.87.254.5 on 09/06/12
For personal use only.

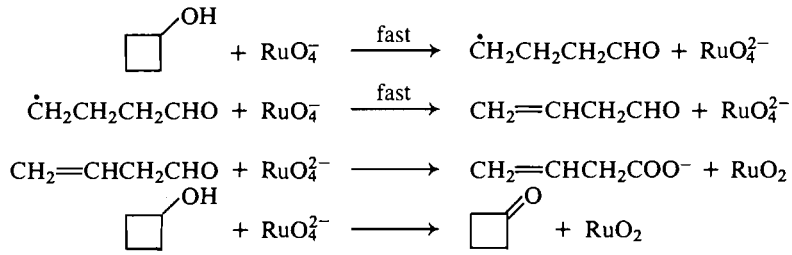

SCHEME 1

the corresponding ketones in good yields (1, 2, 4, 10, 21). If the active oxidant was actually RuO_4^-, it is to be expected that cleavage reactions would produce serious amounts of by-products. For example, Nakano and Foglia have reported a study of the oxidation of ricinoleic acid, **1**, by both perruthenate and ruthenate (3). Perruthenate was found to give *only* cleavage products while ruthenate gave mainly the corresponding keto unsaturated acid and only minor amounts of cleavage products. If perruthenate was the active oxidant in both reactions, it is to be expected that a similar array of products should have been produced, assuming that the reaction mechanism is independent of the oxidant concentration.

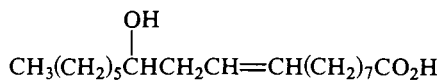

1

It is also instructive to carefully examine the products obtained from the oxidation of cyclobutanol. This compound may be used to distinguish between one- and two-electron transfer oxidants (16, 22). With 1-electron transfer agents such as chromium(IV), cerium(IV), manganese(III), and vanadium(V), carbon–carbon bond cleavage occurs and non-cyclic products are obtained. With 2-electron oxidants such as chronium(VI) and (V) cyclobutanone is the major product. When cyclobutanol was oxidized by sodium ruthenate, cyclobutanone was obtained in nearly quantitative yields (Table 2). However, when it was oxidized by sodium perruthenate the maximum yield of cyclobutanone was 33%. Furthermore, the perruthenate reaction was observed to pass through two distinct, easily observable steps; in the first (rapid) stage RuO_4^- is reduced to RuO_4^{2-} which then reacts more slowly, giving ruthenium dioxide. When this second stage was eliminated by quenching the reaction with sodium arsenite at the appropriate time, very little or no cyclobutanone was obtained (Table 2). This clearly indicates that all of the cyclobutanone from the perruthenate oxidations is formed in the second (RuO_4^{2-}) stage and that RuO_4^- acts as a one-electron oxidant.

A reaction sequence that accounts for the formation of cyclobutanone in 33% yield from the oxidation of cyclobutanol by perruthenate is summarized in Scheme 1. The plausibility of the final two steps of this sequence is enhanced by the results of control experiments which showed that ruthenate ion reacts rapidly with crotonaldehyde and cyclobutanol to give crotonic acid and cyclobutanone, respectively.

Therefore, these results appear to indicate that perruthenate is not likely the active oxidant when sodium ruthenate is used in stoichiometric quantities to oxidize alcohols. However, it is possible that perruthenate could be involved in the catalytic reaction. In fact, there is a possibility that the importance of perruthenate for these reactions may be a function of pH, since it is stable in the pH region 7–12 but rapidly reduced to ruthenate in very basic solutions (23). Consequently one might anticipate its participation to be more significant under the conditions used by Burke and Healy (0.5 *M* KOH in aqueous acetone) than under those employed, for example, by Dalton *et al.* (10) for the selective oxidation of unsaturated alcohols (1 *M* aqueous NaOH).

One factual error in the paper by Burke and Healy (11) which we have noted is found on page 1096 where they claim that Lee and van den Engh (24) have reported an isotope effect, k_H/k_D, of 4.6 for the oxidation of 2-propanol by perruthenate. No such report exists. The isotope effect quoted is for the oxidation of 2-propanol by ruthenium tetroxide.

Acknowledgements

The authors gratefully acknowledge the financial assistance of the Natural Sciences and Engineering Research Council of Canada, and of the donors of the Petroleum Research Fund, administered by the American Chemical Society and the Committee on Higher Education, Imperial Oil Limited, for support of this research.

1. R. M. COATES, P. D. SENTER, and W. R. BAKER. J. Chem. Soc. Chem. Commun. 1011 (1980); J. Org. Chem. **47**, 3597 (1982).
2. E. J. COREY, R. L. DANHEISER, S. CHANDRASEKARAN, G. E. KECK, B. GOPALAN, S. D. LARSEN, P. SIRET, and J. GRAS. J. Am. Chem. Soc. **100**, 8034 (1978).
3. Y. NAKANO and T. A. FOGLIA. J. Am. Oil. Chem. Soc. **59**, 163 (1982).
4. D. T. HALL. Thesis, University of Saskatchewan, Regina Campus, 1972; D. G. LEE, D. T. HALL, and J. CLELAND. Can. J. Chem. **50**, 3741 (1972).
5. W. G. DAUBEN and A. F. CUNNINGHAM. J. Org. Chem. **48**, 2842 (1983).
6. A. CARRINGTON and M. C. R. SYMONS. J. Chem. Soc. 284 (1960).
7. G. NOWOGROCKI and G. TRIDOT. Bull. Soc. Chim. Fr. 684 (1965); 688 (1965).
8. R. E. CONNICK and C. R. HURLEY. J. Am. Chem. Soc. **74**, 5012 (1952).
9. M. SCHRODER and W. P. GRIFFITH. J. Chem. Soc. Chem. Commun. 58 (1979).
10. A. I. DALTON, H. J. DORAN, and R. D. H. MURRAY. U.S. Patent No. 4225694 (1980).
11. L. D. BURKE and J. F. HEALY. J. Chem. Soc. Dalton Trans. 1091 (1982); J. Electroanal. Chem. Interfacial Electrochem. **124**, 327 (1981).
12. D. G. LEE and M. VAN DEN ENGH. *In* Oxidation in organic chemistry. Part B. *Edited by* W. S. Trahanovsky. Academic Press, New York. 1973. p. 177.
13. R. P. LARSEN and L. E. ROSS. Anal. Chem. **31**, 176 (1959).
14. T. D. AVTOKRATOVA. Analytical chemistry of ruthenium. Halsted, New York. 1963. p. 159.

Can. J. Chem. Downloaded from www.nrcresearchpress.com by 210.87.254.5 on 09/06/12
For personal use only.

15. D. G. LEE, U. A. SPITZER, J. CLELAND, and M. E. OLSON. Can. J. Chem. **54**, 2124 (1976).
16. J. ROČEK and A. E. RADKOWSKY. J. Org. Chem. **38**, 89 (1973).
17. Dictionary of Organic Compounds. Eyre and Spottiswoode Ltd., London. 1965.
18. K. W. LAM, K. E. JOHNSON, and D. G. LEE. J. Electrochem. Soc. **125**, 1069 (1978).
19. K. J. LAIDLER. Chemical kinetics. McGraw–Hill, New York. 1950. p. 18.
20. D. G. LEE, V. S. CHANG, and S. HELLIWELL. J. Org. Chem. **41**, 3644 (1976).
21. R. K. DWIVEDI, M. VERMA, P. KUMAR, and K. BEHARI. Tetrahedron, **39**, 815 (1983); R. K. DWIVED, H. NARAYAN, and K. BEHARI. J. Inorg. Nucl. Chem. **43**, 2893 (1981).
22. J. ROČEK and A. E. RADKOWSKY. J. Am. Chem. Soc. **95**, 7123 (1973); J. ROČEK and D. E. AYLWARD. J. Am. Chem. Soc. **97**, 5452 (1975); K. MEYER and J. ROČEK. J. Am. Chem. Soc. **94**, 1209 (1972).
23. P. EICHNER. Bull. Soc. Chim. Fr. 2051 (1967).
24. D. G. LEE and M. VAN DEN ENGH. Can. J. Chem. **50**, 2000 (1972).

Can. J. Chem. Downloaded from www.nrcresearchpress.com by 210.87.254.5 on 09/06/12
For personal use only.

Improved synthesis of *anti*-sesquinorbornene[1]

KARL R. KOPECKY AND ALAN J. MILLER
Department of Chemistry, University of Alberta, Edmonton, Alta., Canada T6G 2G2

Received April 29, 1983[2]

KARL R. KOPECKY and ALAN J. MILLER. Can. J. Chem. **62**, 1840 (1984).

Treatment of methyl hydrogen decahydro-1,4:5.8-*exo,endo*-dimethanonaphthalene-4a,8a-dicarboxylate with lead tetraacetate in benzene – acetic acid replaces the carboxyl group by an acetoxy group. Hydrolysis of this product with 25% sulfuric acid at 130°C forms 8a-hydroxydecahydro-1,4:5,8-*exo,endo*-dimethanonaphthalene-4a-carboxylic acid **10**. The reaction between **10** and benzenesulfonyl chloride in pyridine containing triethylamine at 95°C produces *anti*-sesquinorbornene **1** in 34% yield. In the absence of triethylamine **1** is converted to the hydrochloride. The iodohydroperoxide of **1** is converted by silver acetate at 0°C to the diketone in a luminescent reaction. The 1,2-dioxetane could not be isolated. Decahydro-1,4:5,8-*exo,exo*-dimethanonaphthalene-4a,8a-dicarboxylic anhydride is converted slowly by methoxide ion in methanol at 150°C to the monomethyl ester which then undergoes demethylation. The isomeric *exo,endo* anhydride undergoes reaction readily with methoxide ion at 80°C.

KARL R. KOPECKY et ALAN J. MILLER. Can. J. Chem. **62**, 1840 (1984).

La réaction du décahydro-1,4:5,8 diméthano-*exo,endo* naphtalènedicarboxylate-4a,8a de méthyle et d'hydrogène avec le tétraacétate de plomb dans un mélange de benzène – acide acétique permet de remplacer le groupe carboxyle par un groupe acétoxyle. L'hydrolyse de ce produit, avec de l'acide sulfurique à 25% et à 130°C, conduit à l'acide hydroxy-8a décahydro-1,4:5,8 diméthano-*exo,endo* naphtalène carboxylique-4a **10**. La réaction du composé **10** avec le chlorure de benzènesulfonyle, à 95°C et dans de la pyridine contenant de la triéthylamine, conduit au sesquinorbornène-*anti*, **1**, avec un rendement de 34%. En l'absence de la triéthylamine, le composé **1** se transforme en chlorhydrate. Sous l'influence de l'acétate d'argent, à 0°C, l'iodohydropéroxyde du composé **1** se transforme en une dicétone par le biais d'une réaction luminescente. On ne peut pas isoler le dioxétane-1,2. A 150°C, l'ion méthylate dans le méthanol transforme lentement l'anhydride de l'acide décahydro-1,4:5,8 diméthano-*exo,exo* naphtalènedicarboxylique-4a,8a en ester monométhyllique qui subit alors une déméthylation. L'anhydridre isomère *exo,endo* réagit facilement avec l'ion méthylate à 80°C.

[Traduit par le journal]

Can. J. Chem. Downloaded from www.nrcresearchpress.com by 210.87.254.42 on 09/06/12
For personal use only.

Introduction

It was concluded from the study (1) of a series of mono-, di-, and tricyclic-1,2-dioxetanes that C—C bond rotation was not required to accompany O—O bond rupture (2) in the thermolysis of these compounds. A study of the thermolysis of the dioxetane **2** of *anti*-sesquinorbornene **1** (3) might provide a further test of this conclusion. Examination of molecular models indicates that the perhydro-1,4:5,8-dimethanonaphthalene skeleton is very rigid. There would be no rotation about the C_{4a}—C_{8a} bond in **3**. The present paper reports an improved synthesis of **1**, some reactions of precursors to **1**, and the apparent instability of **2**.

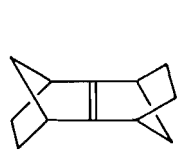

1

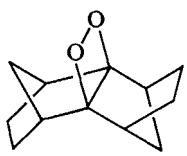

2

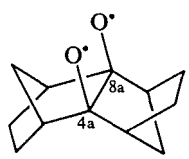

3

Results and discussion

The decarboxylation of the diacid *anti*-**9** with lead tetraacetate or by electrolysis to give **1** proceeds in poor yield (3, 4). Other methods fail completely. A modified synthesis, Chart 1, produces **1** in about the same overall yield as reported (3), but allows the convenient preparation of gram quantities of the alkene in the last step. The essential goal in the modified route to **1** was the conversion of the anhydride *anti*-**6** to the β-hydroxy acid **10** as an apparently general method for the preparation of tetrasubstituted ethylenes from β-hydroxy acids has been reported (5). In fact the conversion is straightforward. Substitution of the carboxyl group in *anti*-**7** by an acetoxy group using lead tetraacetate proceeded in 65% yield. The usual result of the treatment of a tertiary carboxylic acid with lead tetraacetate is alkene formation (6), but this is precluded in the reaction of *anti*-**7**. Hydrolysis of **8** in refluxing aqueous sulfuric acid produced a nearly quantitative yield of **10**, whose structure is assured by its ready conversion back to **8** and to the desired alkene **1**.

The reaction between the β-hydroxy acid **10** and benzenesulfonyl chloride in pyridine required a temperature at least 55°C higher than that reported (5) before any decarboxylation occurred (gas evolution) and resulted in the formation of the hydrochloride **11** of **1**. A likely route to **11** would involve hydrochlorination of initially formed **1** by pyridinium hydrochloride. Inclusion of some triethylamine in the reaction mixture completely suppresses the formation of **11** and the alkene **1** was isolated in 35% yield when the reaction was conducted at 95°C. No decarboxylation at all occurred at 55°C.

The alkene **1** is readily converted to the hydrochloride **11** upon treatment with pyridinium hydrochloride in pyridine at 70°C. These are extremely mild conditions for hydrochlorination of an unactivated alkene. The π bond has an extremely low ionization potential, 7.90 eV, as determined by photoelectron spectroscopy (7), and this results in its facile hydrochlorination.

The compound **11** is remarkably stable considering that it is a tertiary chloride. Treatment of **11** with triethylamine in pyridine at 110°C for 8 h did not produce any alkene and **11** appeared not to have reacted at all. The hydrochloride **11** reacts very slowly with silver ion in methanol. At 20°C the solution slowly becomes turbid and some starting material is still left after several hours. Either there is steric hindrance to approach

[1] This research was supported in part by a grant from the NSERC.
[2] Revision received March 28, 1984.

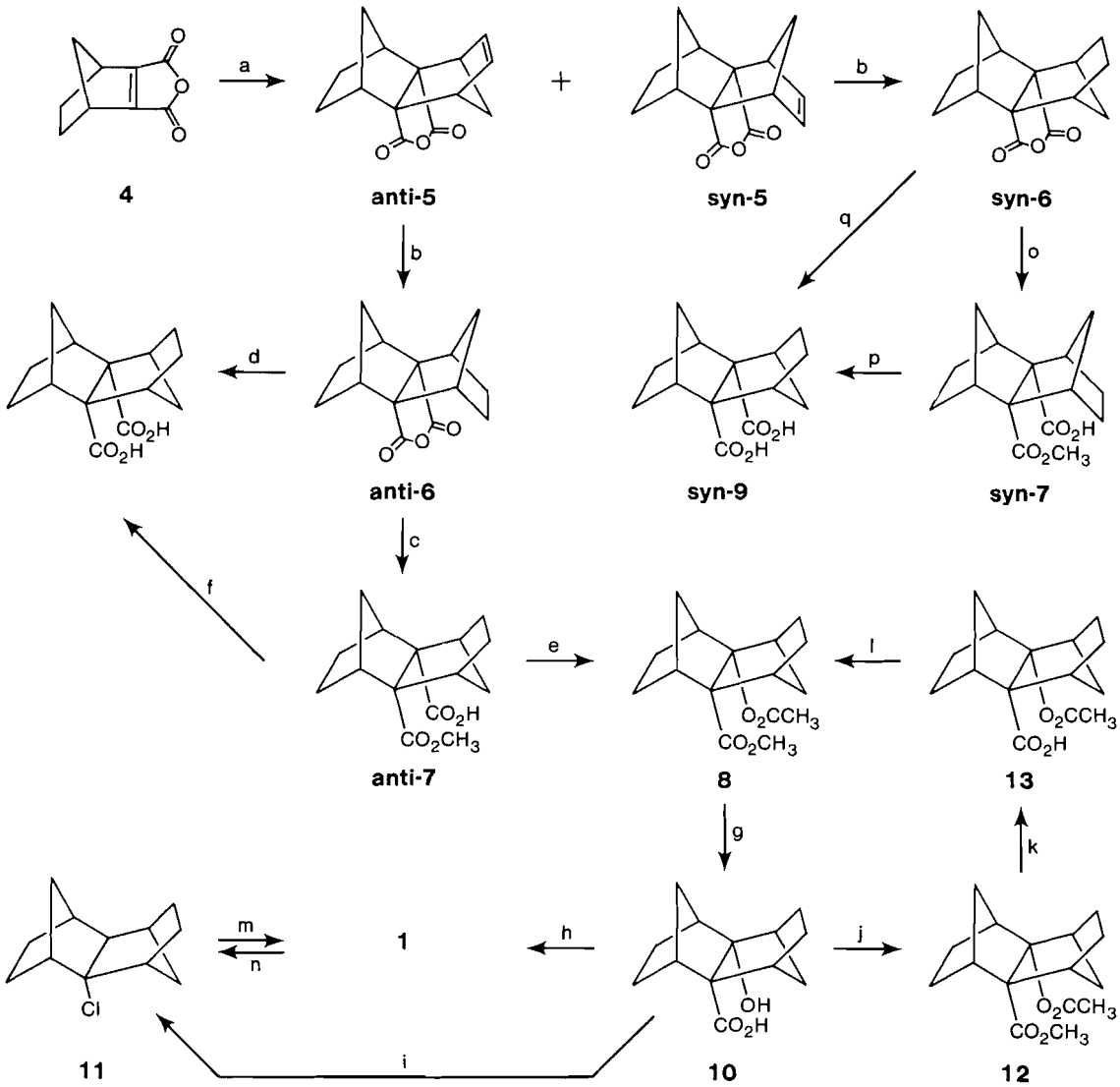

(a) $C_5H_6/C_6H_5CH_3/80°C$
(b) H_2/Pt
(c) i. $CH_3ONa/CH_3OH/80°C$;
ii. H_3O^+
(d) i. $KOH/(CH_3)_2SO/70°C$;
ii. H_3O^+
(e) $Pb(O_2CCH_3)_4/C_6H_6-HO_2CCH_3/70°C$
(f) i. $CH_3ONa/CH_3OH/150°C/8$ h;
ii. H_3O^+
(g) 25% $H_2SO_4/130°C$
(h) $C_6H_5SO_2Cl/C_5H_5N-(C_2H_5)_3N/95°C$
(i) $C_6H_5SO_2Cl/C_5H_5N/90°C$
(j) $(CH_3CO)_2O/130°C$;
(k) i. $CH_3ONa/CH_3OH/20°C$;
ii. H_3O^+
(l) $CH_3I/NaHCO_3/CH_3CON(CH_3)_2$
(m) $Mg/BrCH_2CHBrC_2H_5$
(n) $C_5H_5N\cdot HCl/C_5H_5N/70°C$
(o) i. $CH_3ONa/CH_3OH/150°C/1.5$ h;
ii. H_3O^+
(p) i. $CH_3ONa/CH_3OH/150°C/8$ h;
ii. H_3O^+
(q) i. $CH_3ONa/CH_3OH/150°C/48$ h;
ii. H_3O^+

CHART 1

of the reagents to the reaction sites in **11** or the corresponding carbocation is very unstable. Marked steric effects have been reported in reactions of other compounds with this hydrocarbon skeleton (3, 8, 9), but no instability of the carbocation has been noted.

An attempt to prove the structure of **11** by its conversion to the known (10) dihydro derivative of **1** resulted in another interesting reaction. There was no reaction between **11** and magnesium in ether but, when 1,2-dibromobutane was added to promote the reaction, **11** was converted to the alkene **1**. There was no evidence for the formation of any saturated hydrocarbon upon hydrolysis of the reaction mixture.

Some observations regarding the chemistry of other precursors to **1** and related compounds will now be described.

Relatively more *anti*-**5** than *syn*-**5** is formed when the Diels–Alder reaction between **4** and cyclopentadiene is conducted in solution at 80°C than in the silica gel catalyzed reaction at ~22°C (3). The ratios of *anti*-**5**/*syn*-**5** formed are

Can. J. Chem. Downloaded from www.nrcresearchpress.com by 210.87.254.42 on 09/06/12
For personal use only.

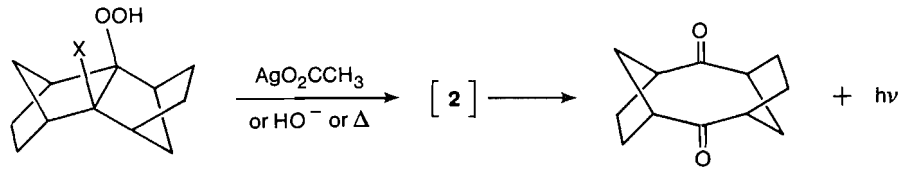

14 15

CHART 2

2.6:1 and 1.5:1, respectively. This ratio of products from the homogeneous reaction decreases from 2.8:1 to 2.2:1 as the temperature is increased from 50 to 110°C. These results suggest that the uncatalyzed reaction should result in a ~3:1 ratio of products at 20°C. There is no equilibration of *syn*-**5** to *anti*-**5** under the reaction conditions, as *syn*-**5** could be recovered unchanged after 8 h at 120°C.

The saturated anhydrides *syn*- and *anti*-**6** are very unreactive compounds. They are inert to alkoxide and methoxide ions at ambient temperatures and *syn*-**6** could not be hydrolyzed at all under a variety of conditions (3). There is a slow reaction between *syn*-**6** and methoxide ion in methanol at 150°C which produces, initially, the carboxylate ion of *syn*-**7** and then the dicarboxylate ion of *syn*-**9**. Demethylation of *anti*-**7** also occurs under these conditions. Demethylation probably results from nucleophilic attack of methoxide ion on the methyl group of the ester to form dimethyl ether, a reaction that was first observed some time ago (11). A more direct and probably easier hydrolysis of *syn*-**6** could probably be achieved by treatment with hydroxide ion in hot dimethyl sulfoxide. Hydrolysis of *anti*-**6** proceeds readily in this solvent at 70°C and also serves as a method of separating it from *syn*-**6** which is unreactive at this temperature. No attempt was made to hydrolyze *syn*-**6** at higher temperatures in this way. *Anti*-**7** is extremely difficult to hydrolyze. A slow hydrolysis occurs in the presence of aqueous hydroxide ion at 140°C.

The initial attempt to prepare the dioxetane **2** involved the photosensitized oxygenation of **1**, but **1** was found to be inert to singlet oxygen (3, 4).[3] The bromo- and iodohydroperoxides **14**, X = Br or I, of **1** were prepared and solutions of these compounds emitted light when treated with silver ion in the presence of fluorescers (a mixture of 9,10-dibromoanthracene DBA and 9,10-bis(phenylethynyl)anthracene BPEA). Luminescence from the iodohydroperoxide could be observed clearly at 0°C in a dark room and was quite bright at 20°C. Higher temperatures are required before luminescence from the bromohydroperoxide can be observed. However, the dioxetane **2** could not be isolated. If **2** is an intermediate in these reactions, it decomposes to the diketone **15** as soon as it is formed, even at 0°C. This was demonstrated by the immediate cessation of luminescence upon removal of silver acetate from a mixture also containing the iodohydroperoxide and fluorescers in dichloromethane at 0°C. No luminescence was observed when the resulting solution was quickly warmed to 25°C. Addition of some silver acetate to this solution at 20°C resulted in an immediate bright luminescence. Actually, the rigidity of the carbon skeletons of **2** and **3**, which would prevent rotation about the C_{4a}—C_{8a} bond, would tend to cause the O—O bond in **2** to be longer than the C—C bond of the dioxetane ring, much longer than the 1.48 Å as found in acyclic peroxides, and longer even than in some other strained 1,2-dioxetanes (12). The increased bond length in **2** would undoubtedly contribute to its instability and this would obscure any stabilizing effect, if there were any, of the lack of rotation about the C_{4a}—C_{8a} bond concurrent with the breaking of the O—O bond. If the luminescence results from decomposition of **2**, this is clearly the least stable tetraalkyl substituted dioxetane (13).

It was reported (4) that the energy of activation for thermolysis of **2** was ~25 kcal/mol. In view of the results just presented this value is clearly incorrect. Solutions of the bromohydroperoxide containing fluorescers become luminescent when heated to about 50°C in the absence of silver ions. The energy of activation reported was determined by measuring the intensity of the luminescence at different temperatures of benzene solutions of the bromohydroperoxide that had been treated with excess base in methanol for 20 min at 20°C. The energy of activation determined in this way thus represents the energy required to generate luminescence from the bromohydroperoxide in a process unassisted by silver ion or hydroxide ion, presumably via the dioxetane. The triplet/singlet ratio of excited states formed under these conditions was ~300:1.

Like **11**, the iodohydroperoxide **14**, X = I, is relatively unreactive toward silver ion. The reaction between the iodohydroperoxide of $\Delta^{9,10}$-octalin and silver acetate is complete within 5 min at 20°C (14), while mixtures of **14**, X = I, and silver acetate at 20°C glow clearly for more than 8 h. This corresponds to a reactivity difference of at least 100-fold.

Experimental

Melting points are uncorrected. Infrared spectra were taken on Perkin–Elmer 457 or 421 spectrometers. The ^{1}H nmr spectra were taken on a Varian A56/60 A analytical spectrometer. Mass spectra were taken on an AEI MS 50 mass spectrometer using an electron impact of 70 eV. Solutions were dried over $MgSO_4$. Elemental analyses were performed in the Microanalytical Laboratories in the Chemistry Department under the supervision of Mrs. Darlene Mahlow.

1,2,3,4,4a,5,8,8a-Octahydro-1,4:5,8-exo,exo-*dimethanonaphthalene-4a,8a-dicarboxylic anhydride and 1,2,3,4,4a,5,8,8a-octahydro-1,4:5,8*-exo,endo-*dimethanonaphthalene-4a,8a-dicarboxylic anhydride,* syn- *and* anti-*5*

A solution of 50.5 g (0.308 mol) of bicyclo[2.2.1]hept-2-ene-2,3-dicarboxylic anhydride (15) and 30 g (0.45 mol) cyclopentadiene in 300 mL toluene was heated at 80°C overnight in a pressure bottle, filtered, concentrated, and pentane added to the residue. A yield of 59.2 g (83%) of a mixture of *syn*- and *anti*-**5** crystallized. The product ratios from several reactions run at different temperatures were determined by integration of the ^{1}H nmr absorptions in C_6D_6 at δ 6.36 and 6.46, due to *anti*- and *syn*-**5**, respectively, of crude product mixtures before crystallization from which solvent was completely removed.

*Methyl hydrogen 1,2,3,4,4a,5,6,7,8,8a-decahydro-1,4:5,8-*exo,endo-*dimethanonaphthalene-4a,8a-dicarboxylate,* anti-*7*

A solution of 59.5 g (0.256 mol) of a mixture of *syn*- and *anti*-**6** in

[3] Professor P. D. Bartlett has informed us that there is now evidence that some dioxetane is formed in this reaction. An improved preparation of **1**, similar to that described here, and studies of the addition of electrophiles to **1** have also been carried out in his laboratories.

Can. J. Chem. Downloaded from www.nrcresearchpress.com by 210.87.254.42 on 09/06/12
For personal use only.

Can. J. Chem. Downloaded from www.nrcresearchpress.com by 210.87.254.42 on 09/06/12
For personal use only.

300 mL methanol containing 0.45 mol of sodium methoxide was heated at 80°C in a pressure bottle for 5 h and evaporated to dryness. Water, 200 mL, was added and the resulting mixture was filtered to yield 16.0 g (27%) of *syn*-**6**. The filtrate was extracted with ether, acidified, and the resulting mixture extracted with ether. The ether layer was dried, concentrated to 80 mL, and an equal volume of pentane added. The product crystallized at 0°C, 41.8 g (62%), mp 116–118°C; ir ν_{max} (film): 3500–2200, 1710, 1682, 1265, 1245 cm^{-1}; ^1H nmr (acetone-d_6) δ: 3.72 (s, 3H), 2.80–2.60 (br s, 2H), 2.60–2.40 (br s, 2H), 2.40–2.00 (br, overlapping acetone), 1.95–1.00 (m, 10H). *Anal.* calcd. for $C_{15}H_{20}O_4$: C 68.16, H 7.63; found: C 68.08, H 7.63.

1,2,3,4,4a,5,6,7,8,8a-Decahydro-1,4:5,8-exo,endo-*dimethano-naphthalene-4a,8a-dicarboxylic acid*, anti-***9***

A. *From* anti-***6***

A solution of 14.0 g (0.06 mol) of a mixture of *syn*- and *anti*-**6**, obtained by hydrogenation of *syn*- and *anti*-**5**, 10.0 g (0.15 mol) of KOH, and 15 mL water in 60 mL dimethyl sulfoxide was heated to 70°C for 1 h and poured into 300 mL cold water. The mixture was filtered to remove *syn*-**6** and the filtrate was acidified to give 9.2 g of *anti*-**9**, after recrystallization from pentane – ethyl acetate, mp 205–207°C (lit. (3) mp 206–209°C).

B. *From* anti-***7***

A solution of 1.6 g (6.1 mmol) *anti*-**7** in 40 mL methanol containing 52 mmol sodium methoxide was heated at 150°C overnight. Work-up yielded 1.3 g (85%) of *anti*-**9**, mp and mixture mp with authentic material 205–207°C.

1,2,3,4,4a,5,6,7,8,8a-Decahydro-1,4:5,8-exo,exo-*dimethano-naphthalene-4a,8a-dicarboxylic acid*, syn-***9***

A solution of 4.6 g (20 mmol) of *syn*-**6** in 100 mL methanol containing 0.11 mol of sodium methoxide was heated at 150°C for 2 days. Work-up yielded 4.1 g (82%) of *syn*-**9**, mp 206–208°C; ir ν_{max} (Nujol): 3700–3200, 2800–2100, 2000–1800, 1690, 1580, 1270 cm^{-1}; ^1H nmr (DMSO-d_6) δ: 10–6 (br, 2H); 2.75–2.25 (br overlapping DMSO), 1.80–1.00 (series of signals, 11H), 0.90 (s, 1H). *Anal.* calcd. for $C_{14}H_{18}O_4$: C 67.18, H 7.25; found: C 67.36, H 7.53.

Methyl hydrogen 1,2,3,4,4a,5,6,7,8,8a-decahydro-1,4:5,8-exo,exo-*dimethanonaphthalene-4a,8a-dicarboxylate*, syn-***7***

Treatment of 8.0 g of *syn*-**6** with sodium methoxide as described above at 150°C for 1.5 h afforded, after work-up, 6.8 g of recovered *syn*-**6** and 1.2 g of an acid fraction melting over a broad range which was recrystallized from ether–pentane to give 0.2 g of *syn*-**7**, mp 197–200°C; ir ν_{max} (Nujol): 3500–2300, 1720, 1635, 1305, 1260 cm^{-1}; ^1H nmr (DMSO-d_6) δ: 3.83 (s, 3H), 2.8–2.25 (br overlapping with DMSO), 1.70–1.02 (series of signals, 11H), 0.97 (s, 1H). *Anal.* calcd. for $C_{15}H_{20}O_4$: C 68.16, H 7.63; found: C 68.16, H 7.76.

This material was converted to *syn*-**9**, mp 206–208°C, by heating it at 150°C with sodium methoxide in methanol for 8 h and acidifying the cooled reaction mixture.

*Methyl 8a-acetoxy-1,2,3,4,4a,5,6,7,8,8a-decahydro-1,4:5,8-*exo,endo-*dimethanonaphthalene-4a-carboxylate*, ***8***

A solution of 42.3 g (0.16 mol) of *anti*-**7** and 75 g (0.17 mol) lead tetraacetate in 400 mL benzene and 100 mL acetic acid was heated under reflux until the original light yellow color had completely vanished (15 to 20 h), cooled, and washed with 2 × 100 mL water and then with aqueous sodium hydroxide until the washings remained basic. A black precipitate, which sometimes developed, was filtered. Unreacted *anti*-**7**, 6.2 g, was recovered from the combined basic washings. The benzene solution was washed with water, dried, concentrated to a volume of 100 mL, and the concentrate diluted with an equal volume of pentane. The product was crystallized in two crops at 2°C to yield a total of 24.7 g (65% based on recovered *anti*-**7**) of **8**, mp 120–121.5°C; ir ν_{max} (film): 3060, 2980, 2880, 1742, 1730 cm^{-1}; ^1H nmr ($CDCl_3$) δ: 3.64 (s, 3H), 3.22–3.05 (br, 1H), 2.94–2.76 (br, 1H), 2.64–2.38 (br, 2H), 2.26–1.90 (series of signals, 1H), 2.07 (s, 3H), 1.90–0.89 (series of signals 12H). *Anal.* calcd. for $C_{16}H_{22}O_4$: C 69.04, H 7.97; found: C 69.02, H 7.97.

Evaporation of the mother yielded 9.2 g of a solid which consisted of at least three compounds (tlc) and whose ^1H nmr spectrum showed absorptions in the vinyl region.

1,2,3,4,4a,5,6,7,8,8a-Decahydro-8a-hydroxy-1,4:5,8-exo,endo-*dimethanonaphthalene-4a-carboxylic acid*, ***10***

A stirred mixture of 10 g of **8** and 80 mL 4.5 *M* sulfuric acid was heated under reflux until the oily organic layer had completely solidified, ~10–12 h. This was taken up in ether and the product was crystallized from ether–pentane to give 7.6 g (95%) of **10** in two crops, mp 188–189°C (gas); ir ν_{max} (film): 3500–2000, 1678, 1475, 1278 cm^{-1}; ^1H nmr (acetone-d_6) δ: 10–7 (br, 1H), 2.80–2.55 (s, 1H), 2.55–2.25 (m, 3H), 2.25–0.95 (br, 13H). *Anal.* calcd. for $C_{13}H_{18}O_3$: C 70.24, H 8.16; found: C 70.42, H 8.20.

*Acetic 8a-acetoxy-1,2,3,4,4a,5,6,7,8,8a-decahydro-1,4:5,8-*exo,endo-*dimethanonaphthalene-4a-carboxylic anhydride*, ***12***

A solution of 2.2 g **10** in 40 mL acetic anhydride was heated under reflux for 5 h, concentrated to an oil, and the residue crystallized from ether–pentane to give 2.5 g (82%) of the acetoxy anhydride, mp 99.5–100°C; ir ν_{max} (KBr): 3070, 2980, 2880, 1800, 1745, 1725, 1365, 1250 cm^{-1}; ^1H nmr ($CDCl_3$) δ: 3.27–3.08 (br s, 1H), 2.96–2.78 (br s, 1H), 2.78–2.60 (br s, 1H), 2.60–2.90 (br s, 1H) 2.32–0.98 (series of signals 12H), 2.22 (s, 3H), 2.07 (s, 3H). *Anal.* calcd. for $C_{17}H_{22}O_5$: C 66.65, H 7.24; found: C 66.60, H 7.28.

8a-Acetoxy-1,2,3,4,4a,5,6,7,8,8a-decahydro-1,4:5,8-exo,endo-*dimethanonaphthalene-4a-carboxylic acid*, ***13***

A solution of 2.3 g (7.5 mmol) of the above anhydride in 25 mL methanol was added to a solution of 0.5 g (0.20 mmol) of sodium hydroxide in 25 mL water and the resulting homogeneous mixture allowed to stand for 30 min. The solution was concentrated to 10 mL and diluted with 15 mL water. The resulting solution was extracted with ether and acidified. The product was taken up in ether and crystallized from ether–pentane to give 1.4 g (71%) of acetoxy acid, mp 150–151°C; ir ν_{max} (film): 3500–2200, 1740, 1715, 1675, 1260 cm^{-1}; ^1H nmr ($CDCl_3$) δ: 3.30–3.12 (br s, 1H), 3.00–2.75 (br s, 2H), 2.68–2.52 (br s, 1H), 2.17 (s, 3H), 2.10–1.10 (series of signals, 12H). *Anal.* calcd. for $C_{15}H_{20}O_4$: C 68.16, H 7.63; found: C 68.39, H 7.70.

This material was converted to the acetoxy methyl ester **8** in 99% yield using a published procedure (16) for the methylation of carboxylic acids; mp and mixture mp with authentic **8**, 120–122°C.

4a-Chloro-1,2,3,4,4a,5,6,7,8,8a-decahydro-1,4:5,8-exo,endo-*dimethanonaphthalene*, ***11***

A solution of 2.2 g (10 mmol) of **10** and 3.5 g (20 mmol) benzenesulfonyl chloride in 24 mL pyridine was kept at 55°C overnight. Work-up (5) and chromatography of the neutral product (silica gel – pentane) produced a solid which was sublimed several times at 50°C/5 Torr (1 Torr = 133.3 Pa) to give 0.2 g (10%) of **11**, mp 85–87°C; ir ν_{max} (Nujol): 3060, 1295, 930, 835, 735 cm^{-1}; ^1H nmr ($CDCl_3$) δ: 3.0–0.75 (series of overlapping absorptions); *m/e*: 198 (17.4%, M^+), 196 (55.4%, M^+), 66 (100%). *Anal.* calcd. for $C_{12}H_{17}Cl$: C 73.27, H 8.71, Cl 18.02; found: C 73.40, H 8.80, Cl 18.20.

anti-*1,2,3,4,5,6,7,8-Octahydro-1,4:5,8-dimethanenaphthalene*, ***1***

A solution of 3.30 g (14.8 mmol) of **10**, 6.0 g (34 mmol) of benzenesulfonyl chloride, 6.6 g (65 mmol) of triethylamine, and 20 mL pyridine was heated at 95°C under argon for 6.5 h. Work-up (5) and chromatography of the neutral product (silica gel – pentane) gave 0.80 g (34%) of **1**, mp 64–65°C (lit. (3) mp 64–65°C).

*Conversion of **1** to **11***

A solution of 0.1 g of **1** and an excess of pyridinium hydrochloride in pyridine was heated overnight at 70°C. No **1** was left and only one product was formed (tlc) which was isolated as before and shown to be **11**; mp and mixture mp with authentic **11**, 85–87°C.

*Conversion of **11** to **1***

A mixture of 0.1 g of **11**, 0.1 g magnesium, and 2 mL ether was

treated with 0.1 g of 1,2-dibromobutane. After the exothermic reaction had subsided no starting material remained and only one product was formed (tlc) which was isolated as before and shown to be **1**; mp and mixture mp with authentic **1**, 64–65°C.

*4a-Hydroxyperoxy-8a-iodo-1,2,3,4,4a,5,6,7,8,8a-decahydro-1,4:5,8-*exo,endo*-dimethanonaphthalene,* ***14****, X = I*

To a stirred solution of 0.10 g (0.62 mmol) of **1** and 0.3 mL of 98% hydrogen peroxide in 5 mL ether at 0°C was added 0.120 g (0.32 mmol) of 1,3-diiodo-5,5-dimethylhydantoin. The mixture was stirred in subdued light for 5 min, 25 mL ether was added, and the resulting solution was shaken with ice water and with just enough aqueous bisulfite to leave the organic layer a light pink color. The organic layer was dried, concentrated at 0°C, and the residue quickly taken up in methylbutane. The pale yellow crystals which formed after 12 h at −78°C were recrystallized from methylbutane at −78°C, mp 55°C (dec.); ^{1}H nmr ($CDCl_3$) δ: 8.125 (s, 1H), 3.20 (m, 1H), 2.80 (m, 1H), 2.65–1.0 (series of m, 14H. This material is quite unstable and the crystals decompose rapidly at room temperature. The mp given is the highest of several determinations. It is stable for weeks in solution at −20°C.

anti-Tricyclo[6.2.1.^{1,8}1^{3,6}]dodecane-2,7-dione, ***15***

Method A

A solution of 20 mg **1** in 10 mL pentane at −70°C was treated with ozone. The residue remaining on evaporation of the pentane was suspended 10 mL ethanol together with 100 mg palladium on charcoal. This mixture was stirred for 30 h under hydrogen, warmed, and filtered. The ethanol was evaporated and the residue was sublimed at 120°C under 1 Torr to give 8 mg white crystals, mp 164–165°C; ir ν_{max} (Nujol): 1665, 1275, 855 cm^{-1}; ^{1}H nmr ($CDCl_3$) δ: 3.4–3.1 (m, 4H), 2.6–1.5 (series of m, 12H). *Anal.* calcd. for $C_{12}H_{16}O_2$: C 74.96, H 8.39; found: C 74.81, H 8.25.

Method B

A mixture of 15 mg of the iodohydroperoxide **14**, X = I, and 100 mg silver acetate in 2 mL dichloromethane was shaken in the dark at 22°C for 6 h and filtered. Solvent was removed to leave a small amount of residue whose ir and ^{1}H nmr spectra and R_f value on tlc were the same as those of **15** made by Method A.

Luminescence experiments

Samples of **1** were converted to the iodophydroperoxide **14**, X = I, as described above and to the bromohydroperoxide **14**, X = Br, by the usual procedure (1, 14). Crude solutions of these materials freed from hydrogen peroxide and dimethylhydantoin were used in the qualitative experiments described in the results and discussion section. A sample of the bromohydroperoxide **14**, X = Br, was treated with sodium hydroxide in methanol for 10 min at 20°C. The reaction mixture was poured into pentane, the pentane layer was washed with water, dried, concentrated to a small volume, and the residue taken up in benzene. The rate of decay of luminescence intensity from this material was measured in the usual way (14) using benzene solutions containing 10^{-2} *M* DBA and 10^{-4} *M* BPEA, as were triplet/singlet ratios using DBA and 9,10-diphenylanthracene (17).

1. K. R. KOPECKY, P. A. LOCKWOOD, R. RICO GOMEZ, and J.-Y. DING. Can. J. Chem. **59**, 851 (1981).
2. H. E. O'NEAL and W. H. RICHARDSON. J. Am. Chem. Soc. **92**, 6553 (1970).
3. P. D. BARTLETT, A. J. BLAKENEY, M. KIMURA, and W. H. WATSON. J. Am. Chem. Soc. **102**, 1383 (1980).
4. K. R. KOPECKY. Presented at the International Conference on Chemi- and Bioenergized Processes. Guarujá, S.P., Brazil. 8–10 August, 1978.
5. W. ADAM, J. BAEZA, and J.-C. LIU. J. Am. Chem. Soc. **94**, 2000 (1972).
6. R. A. SHELDON and J. K. KOCHI. *In* Organic reactions. Vol. 19. *Edited by* W. G. Dauben *et al.* John Wiley and Sons, Inc., New York. 1972. p. 279.
7. R. S. BROWN, J. M. BUSCHECK, K. R. KOPECKY, and A. J. MILLER. J. Org. Chem. **48**, 3692 (1983).
8. P. D. BARTLETT, A. M. ROOF, and W. J. WINTER. J. Am. Chem. Soc. **103**, 6520 (1981).
9. L. A. PAQUETTE and R. V. CARR. J. Am. Chem. Soc. **102**, 7553 (1980).
10. J. K. STILLE and D. A. FREY. J. Am. Chem. Soc. **81**, 4273 (1959).
11. J. F. BUNNETT, M. M. ROBINSON, and F. C. PENNINGTON. J. Am. Chem. Soc. **72**, 2378 (1950).
12. (*a*) H. NUMAN, J. H. WIERINGA, H. WYNBERG, J. HESS, and A. VOS. J. Chem. Soc. Chem. Commun. 591 (1977); (*b*) A. KREBS, A. SCHMALSTEIG, O. JARCHOW, and K.-H. KLASKA. Tetrahedron Lett. **21**, 3171 (1980); (*c*) W. ADAM, L. A. ARIAS, A. ZAHN, K. ZINNER, K. PETERS, E.-M. PETERS, and H. G. VON SCHNERING. Tetrahedron Lett. **23**, 3251 (1982).
13. P. D. BARTLETT and M. E. LANDIS. *In* Singlet oxygen. *Edited by* H. H. Wasserman and R. W. Murray. Academic Press, New York. 1979. p. 243.
14. K. R. KOPECKY, J. E. FILBY, C. MUMFORD, P. A. LOCKWOOD, and J.-Y. DING. Can. J. Chem. **53**, 1103 (1975).
15. O. DIELS and K. ALDER. Justus Liebigs Ann. Chem. **490**, 236 (1931).
16. F. A. ALVAREZ and A. N. WATT. J. Org. Chem. **33**, 2143 (1968).
17. K. R. KOPECKY and J. E. FILBY. Can. J. Chem. **57**, 283 (1979).

Can. J. Chem. Downloaded from www.nrcresearchpress.com by 210.87.254.42 on 09/06/12
For personal use only.

The influence of hydrogen bonding on the character of N—H and C=O stretching modes in 2-thiopyrrole-1,2-dicarboximide

SHANKER RAM

Department of Physics, Indian Institute of Technology, Kanpur – 2080 016, India

Received August 24, 1983[1]

SHANKER RAM. Can. J. Chem. **62**, 1845 (1984).

The infrared spectra (200–4000 cm^{-1}) of 2-thiopyrrole-1,2-dicarboximide (TPH) in solid and solution forms have been measured as a function of temperature, and a direct correlation has been obtained between the two phases and the type and extent of hydrogen bonding. It is suggested that TPH exists as cyclic dimer in the solid state (below 310 K) and in dilute solutions by the formation of two equivalent hydrogen bonds. At the transition temperature, ~310 K, the cyclic dimer undergoes to the open-cyclic dimer and persists in this structure till 410 K. In addition, the thermodynamical functions ΔG^0, ΔH^0, and ΔS^0 have been estimated using the spectral data in solution.

SHANKER RAM. Can. J. Chem. **62**, 1845 (1984).

On a mesuré, en fonction de la température, les spectres infrarouges (200–4000 cm^{-1}) du thiopyrrole-2 dicarboximide-1,2 (TPH) sous forme solide et en solution; on a obtenu une corrélation directe entre les deux phases et le type ainsi que le degré de liaison hydrogène. On suggère que, à cause de la formation de deux liaisons hydrogènes équivalentes, le THP existe à l'état de dimère cyclique tant à l'état solide (à des températures inférieures à 310 K) qu'en solutions diluées. A une température de transition d'environ ~310 K, le dimère cyclique subit une ouverture de cycle qui le transforme en dimère ouvert, forme sous laquelle il persiste jusqu'à 410 K. De plus, en se basant sur les données spectrales en solution, on a évalué les fonctions thermodynamiques ΔG^0, ΔH^0 et ΔS^0.

[Traduit par le journal]

Introduction

Pyrrole and its derivatives constitute a broad class of organic molecules with both technological and biological relevance. Recently, Agarwala and co-workers (1, 2) have reported some sulfur derivatives of pyrrole and their properties of forming molecular complexes with metal ions in different oxidation states. These studies reveal certain very fascinating aspects of coordination chemistry, e.g., the formation of Co(II) diamagnetic complexes (3–6). 2-Thiopyrrole-1,2-dicarboximide (TPH) and *N*-carbonyl pyrrole thiocarboximide (CTPH) have been found to yield oxidized products when reacted with soft metal ions (1). With these interesting features, it seems worthwhile to study the vibrational structure and spectra correlations for these compounds and their complexes.

Infrared and Raman spectra of pyrrole and its deuterated analogue have been extensively studied (7, 8) in an attempt to provide a complete vibrational analysis of the fundamental bands. This type of spectral investigation is very limited for substituted pyrroles, especially when both C=O and C=S groups are present. In a previous report (9) we have given a brief vibrational analysis of the fundamental modes of TPH in the region 200–4000 cm^{-1}. The present paper is aimed to investigate the N—H and C=O stretching bands of this compound as a function of temperature in both solid and solution forms, and to study the role which these functional groups play in the formation of the cyclic dimer, an open cyclic dimer, and the free monomers.

Experimental

The 2-thiopyrrole-1,2-dicarboximide was prepared by the literature method (10) and was recrystallized several times in aqueous ethanol to give orange–red sample of mp 140°C. Its composition and purity (99.9%) were confirmed by chemical analysis in our microanalytical laboratory. The infrared spectra of polycrystalline sample using KBr pellets were measured at different temperatures between 80 to 410 K. The temperature (below 298 K) was varied using a Specac variable temperature cell fitted with an automatic temperature control unit and liquid nitrogen as coolant. The pellet mounted on the cold finger of the low-temperature cell was first cooled to liquid-nitrogen temperature and then allowed to warm with drops of liquid nitrogen dripping on the cold finger. This gave a control of the temperature which was monitored by a thermocouple placed in contact with the pellet. For high temperature (above 298 K) studies the pellet was mounted on a home-made heating block. The reported temperatures in both (low and high) measurements are believed to be accurate to within ± 2 K.

The spectra of TPH in CCl_4 solution were measured as a function of temperature (273 to 338 K) at a fixed concentration and as a function of concentration (15 to 0.5×10^{-3} mol L^{-1}) at a fixed temperature, using a NaCl liquid cell of 0.1 cm pathlength. The temperature of the solution was controlled to within ± 1 K using a water circulating bath.

All spectra were measured on a Perkin-Elmer Model 580 infrared spectrometer.

Results and discussion

In the approximation of a C_s molecular symmetry for TPH in its ground state, the 36 normal modes of vibration would be classified as $25a' + 11a''$. In the Mulliken notation (11), the vibrations from ν_1 to ν_{25} are planar (a') and those from ν_{26} to ν_{36} are non-planar (a'') with respect to the molecular plane. For the C_s point group, the permissible site symmetries in the crystal are C_1 and C_s. The exact crystal structure of TPH is not known but our vibrational analysis for the fundamental modes (9), where two factor group components for a' vibrations and only one component for a'' vibrations were observed, suggests four molecules in the crystal unit cell located at equivalent C_s sites. In the present course of investigation, we would confine our discussion only to the N—H stretching (ν_1) and C=O stretching (ν_5) modes with an emphasis on the role which these functional groups play in the formation of hydrogen bonds.

N—H stretching bands ν_1

Infrared spectrum of the solid sample in the N—H stretching region (2800–3500 cm^{-1}) is not very sensitive to temperature between 80 and 410 K. For comparison, Fig. 1 shows the results obtained at the two extreme temperatures, 80 and 410

[1] Revision received March 16, 1984.

Can. J. Chem. Downloaded from www.nrcresearchpress.com by 210.87.254.42 on 09/06/12
For personal use only.

Can. J. Chem. Downloaded from www.nrcresearchpress.com by 210.87.254.42 on 09/06/12
For personal use only.

K. The broad band centred at about 3150 cm^{-1} includes three distinct bands of frequencies (relative integrated intensities) at 3210 (56), 3160 (78), and 3095 (52) cm^{-1} and thus indicates the presence of three different N—H stretching vibrations. The two sharper bands at 2912 and 2810 cm^{-1} are the C—H stretching vibrations of the pyrrole ring.

The spectrum of TPH in CCl_4 was measured as a function of temperature at a fixed concentration of 10.9×10^{-3} mol L^{-1} and as a function of concentration at a fixed room temperature (298 K). The results obtained at three temperatures (273, 298, and 338 K) are shown in Fig. 2. In solution, the N—H stretching bands are modified to show relatively sharp structure and all are shifted to higher frequency by about 230 cm^{-1} as compared to those in the solid. At a medium concentration of 10.9×10^{-3} mol L^{-1}, the spectrum shows four distinct bands centred at 3440, 3410, 3360, and 3320 cm^{-1}. At lower concentrations the intensities of the first two bands increase (though very little) in the same proportion but those of remaining two bands decrease continuously. The lowest frequency band (3320 cm^{-1}) disappears below $\sim 5 \times 10^{-3}$ mol L^{-1}. In our investigation, concentration could not be varied over a wide range as the solubility of TPH in CCl_4 is very small.

In a free molecule of TPH, the >N̈—H group links the >C=Ö group (a moderately stronger electron donor than the imide group) through a single valence bond. The two groups, being in very close vicinity of each other, may form both intra- and intermolecular hydrogen bonds via the H atom of imide group as shown below:

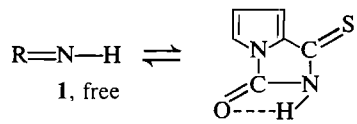

1, free

2, intra-bonded monomer

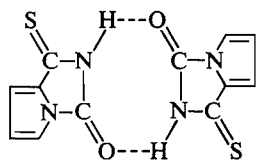

3, cyclic dimer

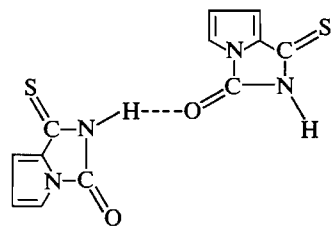

4, open-cyclic dimer

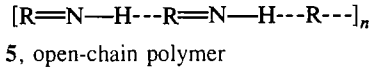

5, open-chain polymer

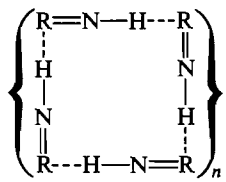

6, close-chain polymer

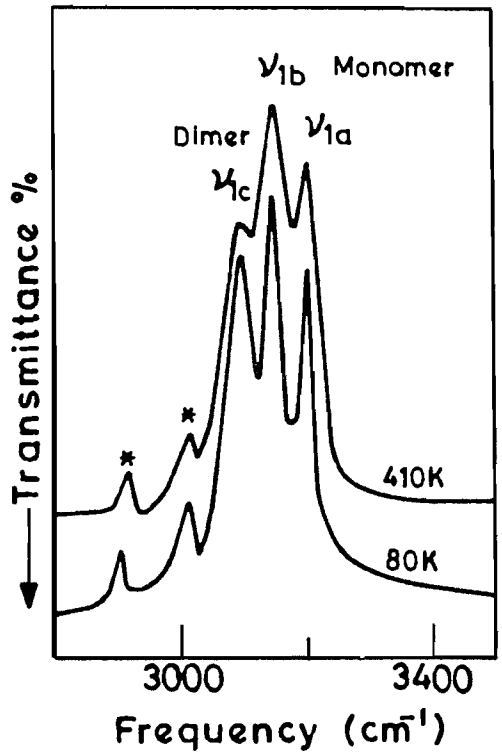

FIG. 1. N—H stretching region of TPH in pure solid phase. * C—H stretching bands.

where

R = 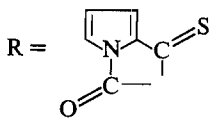

and $n = 2, 3, 4, \ldots\ldots$; indicating dimer, trimer, and other high-order polymers. In addition, the N—H group through self-association may also form intermolecular hydrogen bonds but these are extremely weak to show any effect in conventional infrared spectroscopy (12).

The formation and nature of intra- and intermolecular hydrogen bonds of polyatomic molecules in solid, liquid, and solution forms are well established and may be seen everywhere (12–16). The main purpose of this work is not, therefore, to discuss the nature of the associated species for the molecule in question, but to interprate the spectra which have a converse bearing on the nature of association. The open-chain and close-chain polymers (structures **5** and **6**) would give almost the same results and are expected to appear only in concentrated solutions of inert solvents as CCl_4 (14, 16). The interbonded dimers (structures **3** and **4**) also appear in dilute (to $\sim 1 \times 10^{-3}$ mol L^{-1}) solutions. The intrabonded bands are usually not affected much by the intermolecular separation and thus persist in solution for every dilute concentration and also in the vapour phase. Moreover, the free monomer bands (structure **1**) are very sensitive of temperature as well as of concentration, and are expected to appear strongly in dilute solutions and the band intensity increases further as temperature increases.

If the two (cyclic and open-cyclic) dimer species of TPH do not exist simultaneously (as is usually accepted for large organic molecules (13–15, 17, 18) prior to the present work), the first three prominent structures **1**, **2**, **3** (or **4**) would give at least

Can. J. Chem. Downloaded from www.nrcresearchpress.com by 210.87.254.42 on 09/06/12
For personal use only.

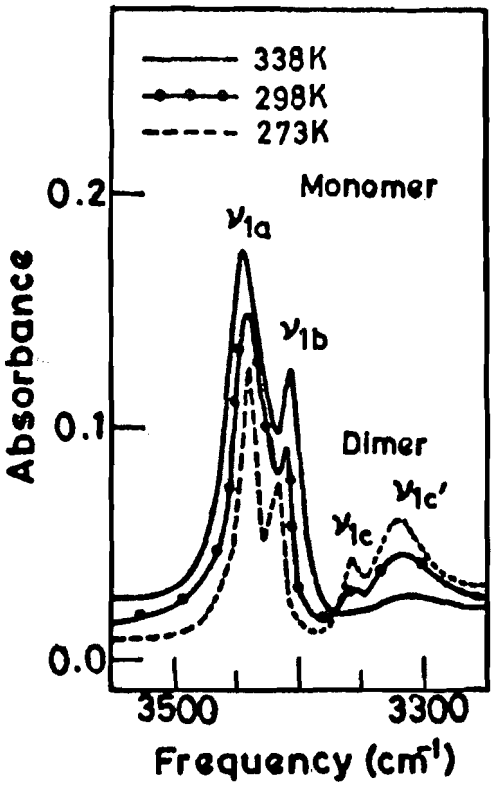

FIG. 2. N—H stretching region of TPH (in CCl_4 solution) at three different temperatures. Concentration = 10.9×10^{-3} mol L^{-1}.

four N—H stretching bands. Though Barnes *et al.* (12) have cited many examples of small inorganic molecules where both cyclic and open-cyclic dimers and other high-order polymers (trimer and tetramer) were also observed to exist simultaneously in equilibrium, the fact is that both species, in terms of vibrational bond frequencies, differ very little and identification is not so simple even if the concentration-dependence study is made in inert-gases using matrix isolation vibrational spectroscopy. Unfortunately, we do not have such sophisticated data but our investigation in CCl_4 solution also shows four different bands (see Fig. 2) which are designated as ν_{1a}, ν_{1b}, ν_{1c}, and $\nu_{1c'}$ in the order of decreasing frequency. The first two bands (ν_{1a} and ν_{1b}) are similar in structure and persist even in sufficiently dilute solutions. The intramolecular hydrogen bonding (structure **2**) usually produces very little frequency shift and therefore these two bands (which differ only by 20 cm^{-1}) are assigned to free and intrabonded N—H stretching modes, respectively. It is to be noted that in the solid state this difference is increased to ~50 cm^{-1}. The two dimeric bands ν_{1c} and $\nu_{1c'}$ are separated by ~35 cm^{-1} in solution but appear as a single band at 3095 cm^{-1} in the solid sample. These assignments are supported by the fact that the intensity of the monomer bands (ν_{1a} and ν_{1b}) increases and that of the dimer decreases as the temperature of the solution increases.

C=O stretching bands, ν_5

The evidence for intra- and intermolecular hydrogen bonds in TPH is more dramatic and clear from the C=O stretching bands, in which also the two dimeric bands (ν_{5c} and $\nu_{5c'}$) are well resolved in both the solid as well as the CCl_4 solutions (see Figs. 3 and 5).

In the spectrum of solid TPH, the relative intensity and separation of ν_{5a} (1774 cm^{-1}) and ν_{5b} (1760 cm^{-1}) are almost

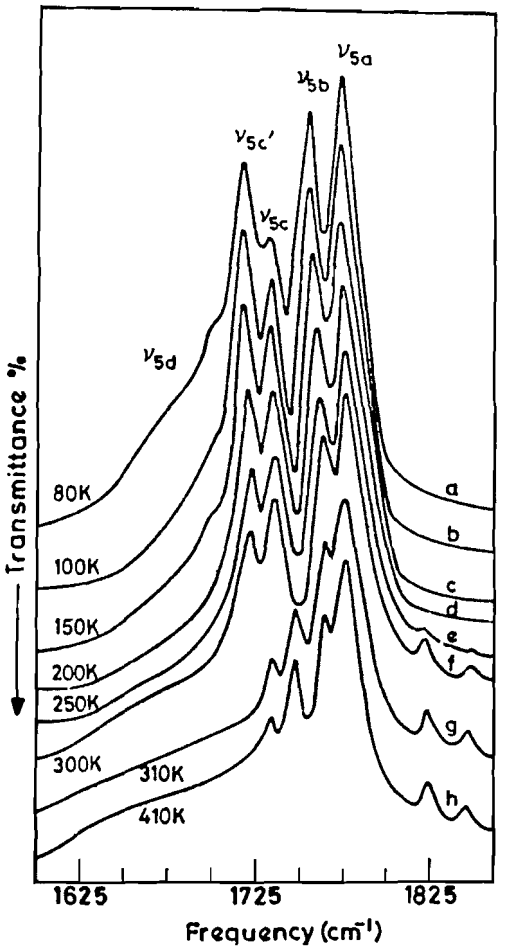

FIG. 3. The effect of temperature on the C=O stretching region of TPH in pure solid phase.

constant, though both shift by 4–10 cm^{-1} to higher frequency as the temperature rises from 80 to 410 K. On the other hand, of the two dimeric bands, ν_{5c} (1732 cm^{-1}) shows relatively lower intensity than $\nu_{5c'}$ (1717 cm^{-1}) at liquid nitrogen temperature. As temperature rises their relative intensity decreases continuously so that at 410 K, the ν_{5c} band becomes stronger than $\nu_{5c'}$, and at an intermediate temperature 250 K, both have nearly the same intensity. Moreover, the frequencies of both bands very slowly increase with temperature in the same manner from 80 to 300 K, show an abrupt increase of ~13 cm^{-1} at 310 K, and then remain constant up to 410 K. The frequency vs. temperature for these two bands is shown in Fig. 4. We believe that this indicates the presence of an open-cyclic dimer of TPH above 310 K, i.e., the C=O stretching vibrations of the open-cyclic dimer are at higher frequencies.

The solution spectra of C=O stretching region at three temperatures are shown in Fig. 5. The monomer bands are at 1796 (ν_{5a}) and 1784 (ν_{5b}) cm^{-1}, whereas those of the dimer are at 1770 (ν_{5c}) and 1764 ($\nu_{5c'}$) cm^{-1}. Both the dimer bands in dilute solutions most probably correspond to the cyclic dimer. However, the possibility of ν_{5c} and $\nu_{5c'}$ bands to belong to two different dimer species, i.e., ν_{5c} to open-cyclic dimer and $\nu_{5c'}$ to cyclic-dimer, may not be discarded. The spectra show an obvious increase in the monomer concentration and at the same time an appreciable decrease in the dimer concentration as the temperature increases from 273 to 338 K, and thus exactly resemble the spectra of N—H stretching vibration, as has been

Can. J. Chem. Downloaded from www.nrcresearchpress.com by 210.87.254.42 on 09/06/12
For personal use only.

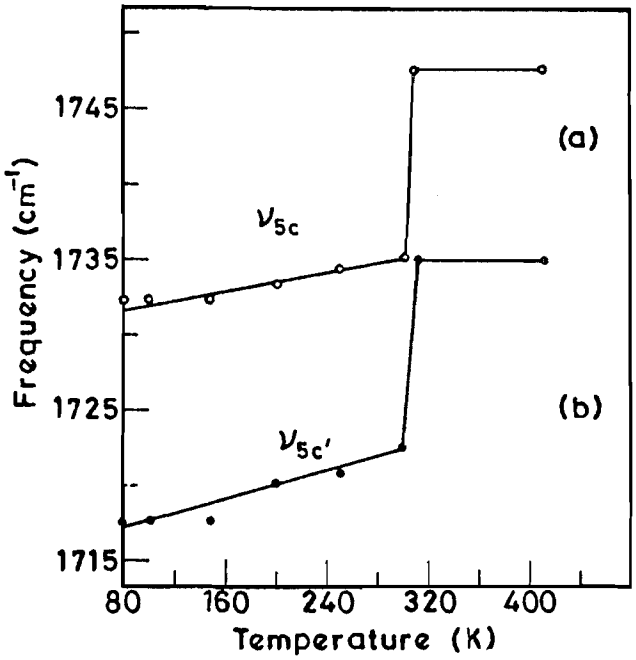

FIG. 4. C=O stretching bands of dimeric TPH vs. temperature (*a*) ν_{5c} and (*b*) $\nu_{5c'}$ bands.

discussed in the preceding section. The relatively weak and broad band centred at 1756 cm^{-1} indicates the features of a polymeric (structures **5** or **6**) C=O stretching vibration. Azima *et al.* (17) have also reported the similar results for the cyclic and open-cycle dimers existing in an equilibrium along with that of the monomer in *para*-substituted benzoic acids.

From the above observations it seems that the hydrogen bonds of TPH polymers are much stronger than those of the dimers, but it is not immediately obvious why the addition of a third (or more) unit should enhance so much the strength of the hydrogen bond which already links the first two. It occured to us that the dimers are open/cyclic chain systems with normal hydrogen bonds but that the polymers are cyclic with abnormally strong bonds derived from their special structure. There are good reasons why this should be so. If a $\rangle C{=}\ddot{O}$ group dissociates, the O^- ion is much more basic than before, and it is logical to regard the formation of a hydrogen bond which involves an extension of the C=O bond length as a step in this direction. An oxygen atom of a C=O group whose proton is engaged in a hydrogen bond should therefore be more basic than the original monomer. Similarly, the hydrogen atom of an $\rangle\ddot{N}H$ group, whose nitrogen is acting as a proton acceptor, can be expected to be more acidic than in the monomer. This must follow as the product is the same whichever end of a simple dimer is attacked by a third bonding unit. Now, it is quite understood that cyclic systems (structures **3** and **6**) will be especially enhanced in their bonding properties because of the increased acidity of the hydrogens and the increased basicity of the oxygens. Along this line and from the observations of the C=O stretching bands, we conclude that TPH forms the cyclic dimers in the solid state ($T < 310$ K) and in dilute solutions in CCl_4, but above the transition temperature 310 K, the structure most probably becomes open-cyclic. Bellamy *et al.* (17, 18) have also shown that the hydrogen-bond strengths of open-chain acid dimers of acetic (18) or oxalic acid (19) are appreciably lower than those of the corresponding cyclic forms.

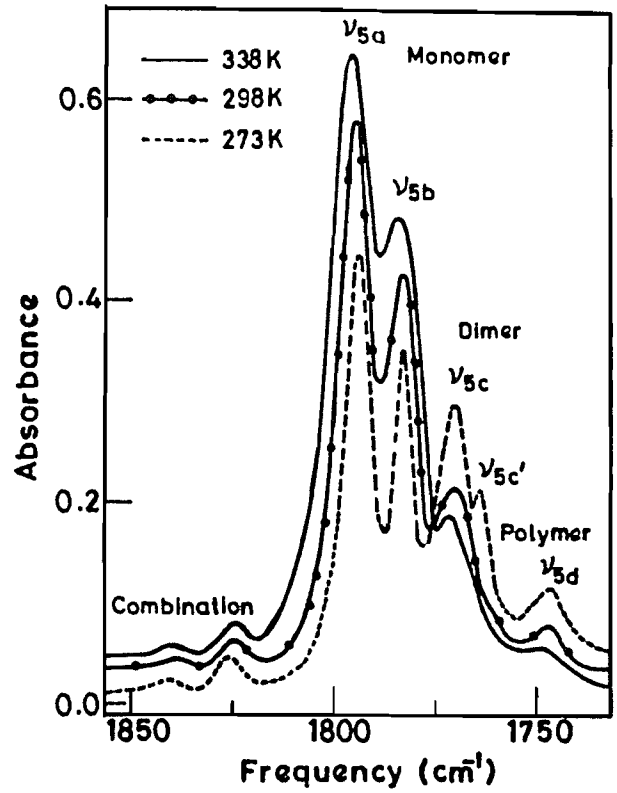

FIG. 5. The effect of temperature on the C=O stretching region of TPH in CCl_4 solution. Concentration = 10.9×10^{-3} mol L^{-1}.

Thermodynamic functions

If we assume that under our experimental conditions, the hydrogen bonding in TPH produces only the dimer and the intrabonded monomer, and that the Lambert–Beer law holds for all the three carbonyl bands, the maximum optical densities A_a, A_b, and A_c of the bands ν_{5a}, ν_{5b}, and ν_{5c} will be given by

$$[1]\quad A_a = \epsilon_a C_a l \qquad A_b = \epsilon_b C_b l \qquad A_c = \epsilon_c C_c l$$

where l is the cell length, C_a, C_b, and C_c are the concentrations of TPH present in the forms a, b, and c, respectively, and ϵ_a, ϵ_b, and ϵ_c are their respective molar extinction coefficients, each referred to one formula weight of TPH. The total concentration of TPH in the solution is

$$[2]\quad C = C_a + C_b + C_c$$

If we neglect the transformation b $\rightleftharpoons$ c, then for the chemical equilibrium, we may write

$$[3]\quad \begin{array}{ll} a \rightleftharpoons b & K_{ab} = [b]/[a] \\ a + a \rightleftharpoons c & K_{ac} = [c]/[a]^2 \end{array}$$

where K_{ab} and K_{ac} are the association constants for intrabonded monomer and interbonded dimer, respectively. In terms of K_{ab} and K_{ac}, eq. [2] becomes

$$\begin{aligned} C &= [a] + [b] + 2[c] \\ &= [a] + K_{ab}[a] + 2K_{ac}[a]^2 \end{aligned}$$

Substituting the value of $[a] = C_a$ from eq. [1], and dividing both sides by A_a/l, we get the final relation

$$[4]\quad \frac{lC}{A_a} = \frac{1}{\epsilon_a}(1 + K_{ab}) + \frac{2K_{ac}}{\epsilon_a^2}\frac{A_a}{l}$$

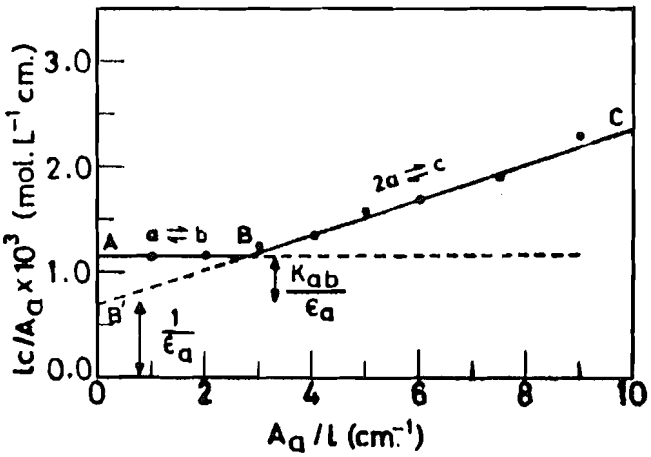

FIG. 6. Plot of lC/A_a vs. A_a/l for C=O stretching vibration of TPH in CCl_4 at 298 K. The AB curve represents a $\rightleftharpoons$ b equilibrium and that the BC curve 2a $\rightleftharpoons$ c equilibrium. The dotted lines are the extrapolated parts of the corresponding curves. $[c] = K_{ac}[a]^2 = 0$ for $A_a/l \leq 3$.

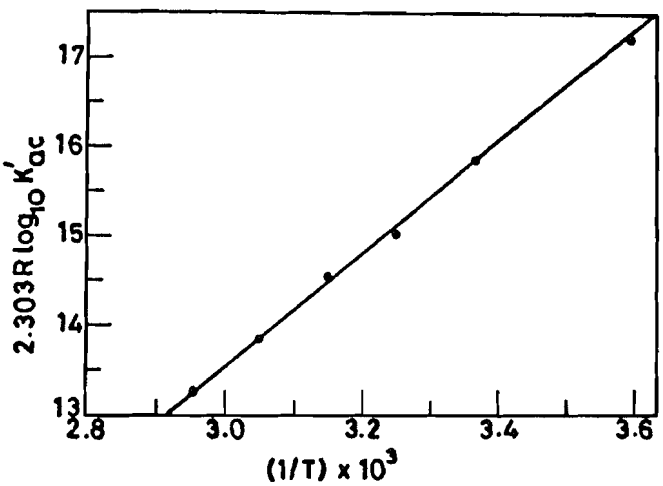

FIG. 7. Plot of $2.303R \log_{10} K'_{ac}$ vs. $1/T$ for TPH in CCl_4.

The free-monomer band ν_{5a} overlaps with the nearby intrabonded-monomer band ν_{5b}. As a result, the actual absorbance A_a would have somewhat a lower value than that read directly from the experimental peak height. This was estimated assuming that the observed doublet (of ν_{5a} and ν_{5b}) is the sum of two Lorentz curves with a slight contribution from the dimer bands. A plot of lC/A_a vs. A_a/l for the C=O stretching vibration of TPH is shown in Fig. 6. It seems reasonable to consider the plot to be linear in the two steps, AB and BC. The linearity of ABC between the points B and C indicates that in the medium of concentrated solutions of TPH in CCl_4, only the dimers and the free and intrabonded monomers are present, and the intrabonded monomers do not contribute to further hydrogen-bonded formations. Moreover, at sufficiently low concentrations, i.e., in region AB, the species existing in an equilibrium mixture are the free and the intrabonded monomers. The values of ϵ_a and K_{ac} were obtained from the intercept and the slope of the extrapolated straight line B'BC, and that of the constant K_{ab} from the difference of the intercepts of AB and B'C (i.e. OA—OB' = K_{ab}/ϵ_a) on the lC/A_a axis. The values so obtained at the room temperature are $\epsilon_a = 1430$ mol^{-1} L cm^{-1}, $K_{ac} = 0.27 \times 10^{-3}$ mol^{-1} L and $K_{ab} = 0.60$.

Assuming the ideal associated-solution model of prigogine (20) where the TPH monomer and dimer activities equal their mole fraction,

$$K'_{ac} = K_{ac}/V_0$$

in which V_0 is the molar volume of the solvent and K'_{ac} is the association constant in mole fraction unit. The standard free energy change, ΔG^0, for the formation of 1 : 1 complex is given by (21),

$$[5] \quad \Delta G^0_T = -RT \ln K'_{ac}$$

which, from the definition of $G = H - TS$, gives

$$[6] \quad 2.303\ R \log_{10} K'_{ac} = \Delta S^0 - \Delta H^0/T$$

The slope and the intercept of the plot $2.303R \log_{10} K'_{ac}$ vs. $1/T$, shown in Fig. 7, give directly the standard enthalphy ΔH^0 and the standard entropy ΔS^0 of complex formation. A least-squares analysis of these data gave $\Delta G^0_{298} = -4.75$ kcal/mol, $\Delta H^0 = -6.40$ kcal/mol, and $\Delta S^0 = -5.60$ cal/deg mol.

Acknowledgements

The author is very thankful to Professor H. D. Bist for his help and valuable discussions and to Dr. R. Saheb (Department of Chemistry) and Dr. J. S. Yadav (Department of Physics, Banaras Hindu University) for providing the sample and their infrared measurements. The financial support from the Department of Science and Technology, New Delhi, is gratefully acknowledged.

1. R. SAHEB, U. C. AGARWALA, and S. K. DIKSHIT. Ind. J. Chem. **20**A, 196 (1981).
2. T. SINGH and U. C. AGARWALA. Trans. Met. Chem. **4**, 340 (1979).
3. F. A. COTTON, T. G. DUNNE, and J. S. WOOD. Inorg. Chem. **3**, 1495 (1964).
4. B. BOSNICH, W. G. JACKSON, and S. T. D. LO. Inorg. Chem. **13**, 2598 (1974).
5. L. SINDELLARI, B. ZARLI, S. SITRAN, and E. CELON. Inorg. Chim. Acta, **64**, 80 (1982).
6. R. SAHEB, S. K. DIKSHIT, and U. C. AGARWALA. Ind. J. Chem. **22**A, 24 (1983).
7. R. C. LORD and A. F. MILLER. J. Chem. Phys. **10**, 328 (1942).
8. P. MIRONE. Gazz. Chim. Ital. **86**, 165 (1965).
9. S. RAM, O. P. LAMBA, and R. SAHEB. Ind. J. Pure Appl. Phys. In press.
10. E. P. PAPADOPOULOS. J. Org. Chem. **38**, 667 (1973).
11. R. S. MULLIKEN. J. Chem. Phys. **23**, 1997 (1955).
12. A. J. BARNES, K. SZCZEPANIAK, and W. J. ORVILLE-THOMAS. J. Mol. Struct. **59**, 39 (1980).
13. A. HALL and J. L. WOOD. Spectrochim. Acta, **23**A, 2657 (1967).
14. S. E. KRIKORIAN. Spectrochim. Acta, **37**A, 745 (1981).
15. T. GANGULY, S. MAL, and S. MUKHERJEE. Spectrochim. Acta, **39**A, 657 (1983).
16. A. D. NIKOLIC, N. L. KOBILAROV, and A. BRZIC. J. Mol. Struct. **99**, 179 (1983).
17. A. AZIMA, C. W. BROWN, and S. S. MITRA. Spectrochim. Acta, **31**A, 1475 (1975).
18. L. J. BELLAMY, R. F. LAKE, and R. J. PACE. Spectrochim. Acta, **19**, 443 (1963).
19. L. J. BELLAMY and R. J. PACE. Spectrochim. Acta, **19**, 435 (1963).
20. I. PRIGOGINE. The molecular theory of solutions. International Publisher, Inc., New York. 1957.
21. R. J. H. CLARK and R. E. HESTER. Advances in infrared and Raman spectroscopy. Vol. 2. Heyden and Sons, London. 1976. p. 223.

Can. J. Chem. Downloaded from www.nrcresearchpress.com by 210.87.254.42 on 09/06/12
For personal use only.

Thermochemical parameters for organic radicals and radical ions. Part 3. The relationship between bond dissociation enthalpy and radical stability in alkyl systems

A. MARTIN DE P. NICHOLAS AND DONALD R. ARNOLD[1]

Department of Chemistry, Dalhousie University, Halifax, N.S., Canada B3H 4J3

Received December 5, 1983

A. MARTIN DE P. NICHOLAS and DONALD R. ARNOLD. Can. J. Chem. **62**, 1850 (1984).

The relationship between radical stability and bond dissociation enthalpy (BDH) is reexamined. It is shown that relative stabilization energies of radicals are not equal to relative BDH values. *Net* stabilization energies of radicals, $SE^0[R^\cdot, RX]$ are defined relative to the R components of closed shell species RX (R(RX)). These components are chosen such that they contain the same (or, approximately the same) net charge as that of the radical ($R^\cdot$). The following results, relative to R = C_2H_5, were obtained: $R^\cdot$, $SE^0[R^\cdot, RX]$(kJ mol^{-1}) for X = R (i.e., the dimer RR), CH_3, and H; $CH_3^\cdot$, 23, 32, 37; n-$C_3H_7^\cdot$, −2, −2, −3; i-$C_3H_7^\cdot$, −9, −14, −19; *t*-$C_4H_9^\cdot$, −25, −32, −38. These results show that the methyl radical is more destabilized and the n-propyl-, i-propyl-, and *tert*-butyl radicals are more stabilized than is predicted from the corresponding relative BDH (R—X) values. The intrinsic C—H bond strengths of chosen alkanes are considered. Relative to the C—H bond in ethane, the bond in methane is found to be weaker by 8.12 kJ mol^{-1} and the primary and secondary bonds in propane and the tertiary bond in methyl propane are stronger by 2.56, 7.98, and 17.12 kJ mol^{-1} respectively.

A. MARTIN DE P. NICHOLAS et DONALD R. ARNOLD. Can. J. Chem. **62**, 1850 (1984).

On étudie de nouveau la relation existant entre la stabilité du radical et l'enthalpie de dissociation de la liaison (HDL). On montre que les énergies relatives de stabilisation des radicaux ne sont pas égales aux valeurs relatives de HDL. On a défini les énergies nettes de stabilisation des radicaux, $ES^0[R^\cdot, RX]$, par rapport aux composants R des espèces des couches complètes RX (R(RX)). On a choisi ces composants de telle sorte qu'ils contiennent la même (ou, approximativement la même) charge nette que celle du radical ($R^\cdot$). On a obtenu les résultats suivants, relatifs à R = C_2H_5: $R^\cdot$, $ES^0[R^\cdot, RX]$(kJ mol^{-1}) pour X = R (soit le dimère RR), CH_3 et H; $CH_3^\cdot$, 23, 32, 37; n-$C_3H_7^\cdot$, −2, −2, −3; i-$C_3H_7^\cdot$, −9, −14, −19; *t*-$C_4H_9^\cdot$, −25, −32, −38. Ces résultats montrent que le radical méthyle est plus déstabilisé et que les radicaux n-propyle, i-propyle et *tert*-butyle sont plus stabilisés que prévu à partir des valeurs relatives correspondantes de HBL (R—X). On considère les forces intrinsèques des liaisons C—H des alcanes choisis. Par rapport à la liaison C—H de l'éthane, on trouve que la liaison du méthane est 8,12 kJ mol^{-1} plus faible et les liaisons primaires et secondaires du propane et la liaison tertiraire du méthylpropane sont respectivement 2,56, 7,98 et 17,12 kJ mol^{-1} plus fortes.

[Traduit par le journal]

Introduction

Organic radicals are usually encountered as short-lived intermediates, rendering an accurate determination of their thermochemical parameters difficult. Most often, measured values have large uncertainties (1, 2). We have claimed previously that the presence of the effects of substituents on bond dissociation enthalpy (BDH) values cannot be attributed solely to the variation in the stability of the radicals (3). We have also suggested that a substituent scale ($\sigma_\alpha^\cdot$) based upon esr hyperfine coupling constants may reflect the component of energy that may be attributed to spin delocalization in benzyl radicals (3). In this work, we substantiate our claim that appropriate corrections (reflecting electronic effects in the R—H bonds) to relative BDH(R—H) values must be made before BDHs are used as an indication of radical stability. Simple hydrocarbon radicals are studied as representative examples. The results and conclusions are easily extended in principle to other classes of organic radicals.

Merits and ambiguities in current bond dissociation enthalpy schemes

The stability of two chemical systems can be compared only if they contain the same number of particles (electrons and nuclei, or atoms) (4, 5). For example, the free energy change, ΔG, in eq. [1], is a measure of the relative stability of the

[1] $$A + B \rightarrow C + D$$

products (C + D) with respect to the reactants (A + B). However, the stability of, say, D relative to B cannot be extracted from ΔG_1, (or ΔH_1) alone, unless the total energies of A and C are given. Moreover, even if the latter were known, individual bond contributions to the total energies of the participating species would be required before the relative importance of various factors governing the stability of one of the products (for example, a radical) can be defined in terms of one of the reactants.

The enthalpy change for the homolytic cleavage of the R—X

[2] $$RX \rightarrow R^\cdot + X^\cdot$$

bond in an organic molecule (RX) in the gaseous state, under standard conditions[2] is:

[3] $$\Delta H^0{}_2 = \Delta_f H^0(R^\cdot) + \Delta_f H^0(X^\cdot) - \Delta_f H^0(RX) = \mathrm{BDH(R—X)}$$

Equation [3] has been the basis for most definitions of the "stabilization energy" of radicals (2). This stabilization energy is conveniently derived from reactions conserving the number and nature of all chemical bonds ("isodesmic reactions" (6)).

The standard energy (or enthalpy) change $\Delta E^0{}_4$ (or $\Delta H^0{}_4$) has been defined as a measure of the interaction between X and Y (*vide infra*).

[4] $$X—Z—Y + H—Z—H \rightarrow X—Z—H + H—Z—Y$$

When Y = electron and Z = CH_2 reaction [4] yields:

[1] Author to whom all correspondence should be addressed.

[2] The standard heat of formation is symbolized by $\Delta_f H^0$ (and not $\Delta H^0{}_f$) as recommended by the IUPAC commission (5). In this paper, all species are considered in the gaseous state. However to simplify the notations used, the symbol "g" has been omitted.

Can. J. Chem. Downloaded from www.nrcresearchpress.com by 210.87.254.105 on 09/06/12
For personal use only.

TABLE 1. A correlation of gas phase bond dissociation enthalpies of R—X(BDH(R—X)) with R—H(BDH(R—H)) at 298.15 K[a, b, c]

	X											
R	H (218.0)[d]	F (79.4)[d]	Cl (121.3)[d]	Br (111.9)[d]	I (106.8)[d]	OH (39.3)	CH_3 (146.9)	C_2H_5 (108.4)	n-C_3H_7 (87.9)	i-C_3H_7 (76.1)	t-C_4H_9 (36.4)	C_6H_5 (328.9)
(146.9) CH_3	439	456[e]	350	296	238	388	378	360	361	358	351	426
(108.4) C_2H_5	410	443[e]	342	283	224	382	360	343	343	338	331	408
(87.9) n-C_3H_7	410	453	342	284	227	382	361	343	343	339	331	409
(76.1) i-C_3H_7	399	449	342	286	225	388	358	338	339	332	317	401
(36.4) t-C_4H_9	389	—	340	281	215	388	351	331	331	317	299	388
(328.9) C_6H_5	464	524	399	337	274	464	426	408	409	401	388	475
(200.0) $C_6H_5CH_2$	368	—	303	248	207	340	318	300	301	298	—	389
(163.6) $C_2H_3CH_2$	361	—	—	230	179	327	311	294	293	291	284	—
r[f]	1.0	0.70	0.91	0.94	0.95	0.89	0.97	0.98	0.98	0.99	0.99	0.99

[a] Bond dissociation enthalpies have been calculated from eq. [3]. Unless otherwise noted, the standard heat of formation of RX and R$^\cdot$ was obtained from refs. 24*a* and 2 respectively.
[b] All values are in kJ mol^{-1}.
[c] Uncertainty is in the order of 6–8 kJ mol^{-1}.
[d] Reference 28.
[e] The standard heat of formation of RX was obtained from ref. 8*b*.
[f] Correlation coefficient for the linear regression analysis of BDH(R—X)$_g$ vs. BDH(R—H)$_g$ as a function of X.

TABLE 2. The effect of the X group in RX, on relative BDH(R—X) values[a, b] in the gas phase at 298.15 K

	X											
R	H	F	Cl	Br	I	OH	CH_3	C_2H_5	n-C_3H_7	i-C_3H_7	t-C_4H_9	C_6H_5
CH_3	29	13	8	13	14	6	18	17	18	20	20	18
C_2H_5	0	0	0	0	0	0	0	0	0	0	0	0
n-C_3H_7	0	10	0	1	3	0	1	0	0	1	0	1
i-C_3H_7	−11	6	0	3	−1	6	−2	−5	−4	−6	−14	−7
t-C_4H_9	−21	—	−2	−2	−9	6	−9	−12	−12	−21	−32	−20
C_6H_5	54	81	57	54	50	82	66	65	66	63	57	67
$C_6H_5CH_2$	−42	—	−39	−35	−17	−42	−42	−43	−42	−40	—	−19
$C_2H_3CH_2$	−49	—	—	−53	−45	−55	−49	−49	−50	−47	−47	—

[a] BDH values are given in Table 1.
[b] All values are in kJ mol^{-1}.

[5*a*] $X—CH_2^\cdot + H—CH_2—H \rightarrow X—CH_2—H + H—CH_2^\cdot$

[5*b*] $R^\cdot + CH_4 \rightarrow RH + CH_3^\cdot$

ΔH^0_{5b}, has been identified as the (de)stabilization energy (RE) of a chosen radical R$^\cdot$ (eq. [6]) (7).

[6] $RE\ (R^\cdot) = \Delta H^0_{5b} = BDH(CH_3—H) - BDH(R—H)$

For π-resonance delocalized radicals, Benson's definition of stabilization energy (SE), eq. [7], has been used (8*a*), where R_SCH_3 is the fully saturated compound analogous to $R_\pi CH_3$ (8, 9).

[7] $SE\ (R_\pi CH_2^\cdot) = BDH(R_SCH_2—H) - BDH(R_\pi CH_2—H)$

The BDH methods described above (eqs. [6] and [7]) assume that the relevant relative BDH values depend only on the stability of the radicals formed (2, 7–10). This suggests that the standard enthalpy change, ΔH^0_8, given by eq. [9] should not

[8] $R^\cdot_r + RZ \rightarrow R_rZ + R^\cdot$

vary with Z (10), where R_rZ is the molecule with respect to which relative BDH values {δ(BDH(R—Z))} are measured.

[9] $\Delta H^0_8 = BDH(R—Z) - BDH(R_r—Z) = \delta(BDH(R—Z))$

However, the variation in relative BDH values (δ(ΔH^0_8)) is given by the enthalpy change for reaction [10].[3]

[10] $R_rH + RX \rightarrow R_rX + RH$

[11] $\delta(\Delta H^0_8) = \Delta H^0_8\ (Z = X) - \Delta H^0_8\ (Z = H)$
$= \delta(BDH(R—X)) - \delta(BDH(R—H))$
$= \Delta_f H^0(R_rX) - \Delta_f H^0(RX) - \Delta_f H^0(R_rH) + \Delta_f H^0(RH)$
$= \Delta H^0_{10}$

The fact that δ(ΔH^0_8) is not zero does not indicate the absence (or presence) of radical stabilizing effects, because δ(ΔH^0_8) is independent of any $\Delta_f H^0$ (radical) value (11). Indeed, the limitations of the BDH method are illustrated in Tables 1, 2, and 3.

The involvement of substituent effects on the stability of undissociated molecules is also shown in Table 4, with reference to reaction [4]. In Fig. 1, we illustrate an example of how

[3] The use of the BDH method to estimate radical stability presupposes the absence of substituent effects on the stabilities of the parent undissociated molecules. This method actually assumes that ΔH^0_{10} is zero. In Table 3 we critically assess the validity of this assumption.

Can. J. Chem. Downloaded from www.nrcresearchpress.com by 210.87.254.105 on 09/06/12
For personal use only.

Can. J. Chem. Downloaded from www.nrcresearchpress.com by 210.87.254.105 on 09/06/12
For personal use only.

TABLE 3. The standard enthalpy change,[a] $\Delta H^0_{10}(R_r = C_2H_5)$ (kJ mol^{-1}), for the reaction $C_2H_5H_{(g)} + RX_{(g)} \rightarrow C_2H_5X_{(g)} + RH_{(g)}$ at 298.15 K. The variation of BDH(R—X) values

	X										
R	H	F	Cl	Br	I	OH	CH_3	C_2H_5	i-C_3H_7	t-C_4H_9	C_6H_5
CH_3	0	−15.6[b,c]	−20.6 ± 0.8	−15.6 ± 1.4	−14.9 ± 1.3	−23.7 ± 0.5	−11.0 ± 0.6	−12.5 ± 0.7	−9.8 ± 0.8	−9.5 ± 1.2	−11.4 ± 0.7
C_2H_5	0	0	0	0	0	0	0	0	0	0	0
n-C_3H_7	0	10.1[b,c]	−0.2 ± 0.9	1.7 ± 1.2	3.0 ± 2.0	−0.5 ± 1.1	1.5 ± 0.6	−0.5 ± 0.7	0.5 ± 1.1	−0.3 ± 1.1	0.8 ± 0.9
i-C_3H_7	0	17.6[b,c]	12.4 ± 0.9	15.5 ± 1.4	12.1 ± 2.0	17.2 ± 0.6	9.5 ± 0.7	6.8 ± 0.7	5.1 ± 0.9	−2.4 ± 1.5	4.7 ± 1.2
t-C_4H_9	0	—	19.5 ± 1.4	19.6 ± 1.7	12.5 ± 2.4	27.1 ± 2.9	12.4 ± 0.9	9.4 ± 1.0	0.2 ± 1.4	−11.2 ± 1.5	1.3 ± 1.3
C_6H_5	0	27.7[b,c]	3.5 ± 0.9	0.3 ± 3.3	−4.3 ± 4.7	28.4 ± 0.9	12.3 ± 0.6	11.2 ± 0.7	9.1 ± 1.2	3.1 ± 1.4	13.8 ± 1.5
$C_6H_5CH_2$	0	—	3.3 ± 3.1	8.2 ± 4.5	25.0 ± 5.5	−0.3 ± 1.3	0.4 ± 0.7	−0.3 ± 0.9	1.8 ± 1.3	—	23.3 ± 3.1
$C_2H_3CH_2$	0	—	—	−3.7 ± 4.4	3.7 ± 2.5	−6.4 ± 2.1	0.1 ± 0.7	−0.4 ± 1.3	1.6 ± 1.9	1.6 ± 1.2	—

[a] Unless otherwise noted, ΔH^0_{10} was calculated using standard heats of formation (of species (involved) obtained from ref. 24*a*.
[b] Calculated using the standard heats of formation of $C_2H_5F(g)$ and $CH_3F(g)$ from ref. 8*b*.
[c] Uncertainty probably greater than 8 kJ mol^{-1}.

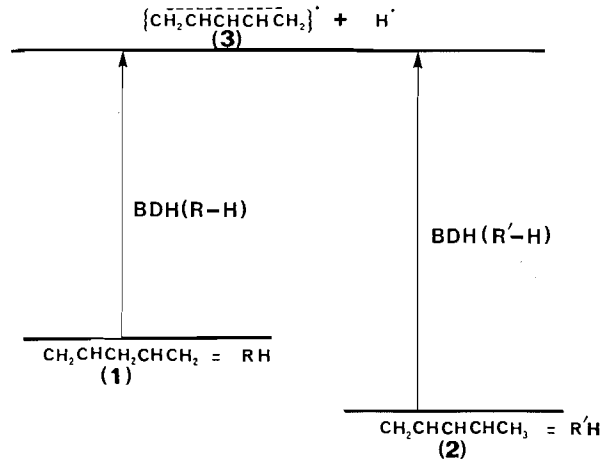

FIG. 1. A comparison of the bond dissociation enthalpies of 1,4-pentadiene (**1**) and 1,3-pentadiene (**2**). In fact, the difference in the BDH(R—H) values of **1** and **2** to give the same delocalized radical **3** has been attributed (2) to substituent effects on neutral closed shell species (i.e. extra stabilization of **2** due to its conjugated double bonds). However, the difference in the intrinsic bond strengths of the dissociated C—H bonds of **1** and **2** will also be a factor causing the unequal BDH values. It must be noted that this ambiguity will be present for all π-delocalized radicals that can be represented by at least two non-identical resonance forms.

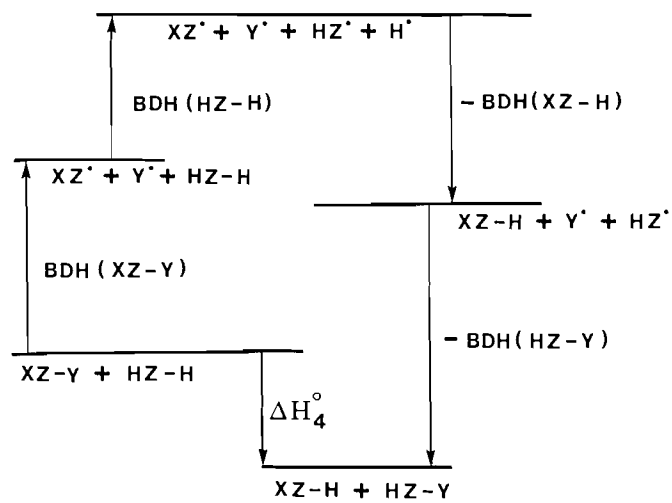

FIG. 2. A thermochemical cycle relating the enthalpy change in the isodesmic reaction [4] to BDH values of the participating species.

ambiguities can arise by equating relative BDH values to radical stability.

An analysis of the general isodesmic reaction (reaction [4])

Using the thermochemical cycle given in Fig. 2, the enthalpy change for reaction [4], ΔH^0_4, can be expressed by eq. [12], where δ(BDH(XZ—Y)) and δ(BDH(XZ—H)) are substituent effects on the BDH values of the Z—Y and Z—H bonds respectively. Equation [12]

$$[12] \quad \Delta H^0_4 = \mathrm{BDH(XZ—Y)} - \mathrm{BDH(HZ—Y)} - \mathrm{BDH(XZ—H)} + \mathrm{BDH(HZ—H)} = \delta(\mathrm{BDH(XZ—Y)}) - \delta(\mathrm{BDH(XZ—H)})$$

shows that for a fixed Y, ΔH^0_4 is a measure of only a relative interaction energy between X and Y with respect to X and H.

TABLE 4. The relative enthalpy of interaction [a,b] between two groups R and X ($\Delta H^0_{R/X}$ (kJ mol^{-1})) attached to a common moiety (CH_2) in the gas phase at 298.15 K

	X							
R	H	Cl	Br	I	OH	CH_3	C_2H_5	C_6H_5
H	0	0	0	0	0	0	0	0
CH_3	0	−20.6 ± 0.8	−15.6 ± 1.4	−14.9 ± 1.3	−23.7 ± 0.5	−11.0 ± 0.6	−12.5 ± 0.7	−11.4 ± 0.7
C_2H_5	0	−20.4 ± 0.7	−17.3 ± 1.1	−17.9 ± 2.0	−23.2 ± 1.1	−12.5 ± 0.7	−12.0 ± 0.7	−12.2 ± 0.9
C_6H_5	0	−23.9 ± 3.1	−23.8 ± 4.5	−39.9 ± 5.5	−23.4 ± 1.3	−11.4 ± 0.7	−12.2 ± 0.9	−34.7 ± 3.1
C_2H_3	0	—	−11.9 ± 4.4	−18.6 ± 2.5	−17.3 ± 2.1	−11.1 ± 0.8	−12.1 ± 1.4	−56.8 ± 8.4

[a] The standard enthalpy change at 298.15 K for the gas phase reaction $RCH_2H + HCH_2X \rightarrow RCH_2X + HCH_2H$.
[b] Calculated using standard heats of formation of species involved from ref. 24*a*.

This can also be readily seen by considering reaction [4], with Y = H, in which case $\Delta H^0_4 = 0$. It must be noted that the applicability of reaction [4] cannot be tested by the success or failure of any group additivity methods (8*b*) of obtaining the standard heat of formation of XZY from HZY, XZH, and HZH. This is because in these methods any type of interaction between X and H, say in XZH, is included in the group values for X(ZH) and ZH(X). Thus, the suitability of using reaction [4], when Y is simply an electron (or, alternatively, eq. [6]), to directly assess radical stability depends on the magnitude of the interaction between a substituent (X) and H in a molecule of the type XZH.

Factors governing bond dissociation energies

The bond dissociation energy (BDE) of a bond (C—X) at 0 K has been given by eq. [13], where ΔV is the bond potential energy (the energy needed to break the bond at 0 K when the

$$[13] \quad \mathrm{BDE(C{-}X)} = \Delta V + \Delta R + \Delta Z$$

fragments retain their valence state pertaining to bonding); ΔR is the energy change when fragments revert to the standard state at 0 K and ΔZ is the difference between the zero point energies before and after bond scission (12). Even if individual ΔV, ΔR, and ΔZ values can be estimated, the use of eq. [13] to obtain radical stabilities will be biased by effects on the parent species (C—X).

In an entirely different approach Leroy and co-workers (13) have estimated the stabilization energy (SE) of radical (or closed shell) species using

$$[14] \quad \mathrm{SE} = \Delta H_a - \Sigma N_{AB} E_{AB}$$

where ΔH_a is the heat of atomization of the species (radical or closed shell) and E_{AB}'s are standard bond energy terms derived from ΔH_a values of reference compounds. However, an unambiguous quantitative assessment of radical stability still cannot be made because it also requires an assumption regarding reference bonds.

The method

Charge effects on bond strengths

A bond by bond insight into the various factors contributing to the stability of hydrocarbons has been made possible by a suitable partitioning of the total energy of these species in terms of constituent bonds. Such an analysis in terms of electron distributions has been developed by Fliszár and co-workers (eqs. [15–19]) (14–22). Using this approach they have been able to calculate the energy of atomization, $\Delta_{at}E^*$, of several series of organic molecules at 0 K in the hypothetical vibrationless state, which shows good agreement with experiment (14–22)[4,5]. Equation [15] shows the relationship between $\Delta_{at}E^*$ and E_{ij}, where E_{ij} and E^*_{nb} give the energy contributions to $\Delta_{at}E^*$ from the iJ bond and the non-bonded interactions respectively.

$$[15] \quad \Delta_{at}E^* = \Sigma E_{ij} - E^*_{nb}$$

$$[16] \quad E_{ij} = E_{ij}(Q_i, Q_J)$$

$$[17] \quad E_{ij} = E^0_{ij} + \Delta Q_i(\partial E_{ij}/\partial Q_i)_{Q^0_i, Q^0_J} + \Delta Q_J(\partial E_{ij}/\partial Q_J)_{Q^0_i, Q^0_J}$$
$$= E^0_{ij} - \Delta q_i(\partial E_{ij}/\partial Q_i)_0 - \Delta q_J(\partial E_{ij}/\partial Q_J)_0$$

Equation [16] can be postulated, provided that for a given bond iJ the variations in Q_i and Q_J (the total electron population of the bond-forming atoms i and J respectively) due to changes in molecular environment are small. The E_{ij} terms can be expressed as standard E^0_{ij} terms (of eq. [17]) if eq. [16] is assumed (16). In eq. [17], Δq_i and Δq_J are net (i.e., $Z - Q$) atomic charges relative to standard charges q^0_i and q^0_J. By defining E_{CC} and E_{CH} with respect to the ethane CC and CH bonds and, consequently, q_C and q_H expressed relative to the net atomic charges of C and H of ethane, application of eq. [17] gives:

$$[18] \quad E_{CC} = E^0_{CC} + a_{CC}(\Delta q_{C_i} + \Delta q_{C_J})$$

$$[19] \quad E_{CH} = E^0_{CH} + a_{CH}\,\Delta q_C + a_{HC}\,\Delta q_H$$

In these equations a_{CC}, a_{CH}, and a_{HC} represent the appropriate $-(\partial E_{ij}/\partial Q_i)_0$ values of eq. [17]. *The significance of eqs. [15]–[19] is that the individual bond contributions to the differences in the relative stability of two species can be determined, if the required* a_{ij} *and* Δq *values are known (14–21).*

Useful information about charge effects on intrinsic bond strengths[6] has been obtained from the application of eqs. [15]–[19] to a variety of organic molecules. Studies by Fliszár and co-workers (14) of linear and branched paraffins and compounds containing chair or boat cyclohexane rings have given the following a_{ij} values[7,8,9] in the units kJ mol^{-1} me^{-1}: a_{HC} =

[4] The energy of atomization is symbolized by $\Delta_{at}E$ as recommended by the IUPAC commission (5).

[5] $\Delta_{at}E^* = \Sigma_i n_i[\Delta_f H^0(A_i) - 5RT/2] + \mathrm{ZPE} + (H_T - H_0) - \Delta_f H^0$ (molecule) (22).

[6] By "intrinsic" is meant the contribution of that bond to the energy of atomization of the molecule.

[7] For more details on the calculation of the a_{ij} terms see refs. 14, 19, and 20.

[8] Charge–energy relationships (eqs. [16]–[19]) are valid for small perturbations (in the order of millielectrons).

[9] The unit of charge is expressed in millielectrons and symbolized by me (14).

Can. J. Chem. Downloaded from www.nrcresearchpress.com by 210.87.254.105 on 09/06/12
For personal use only.

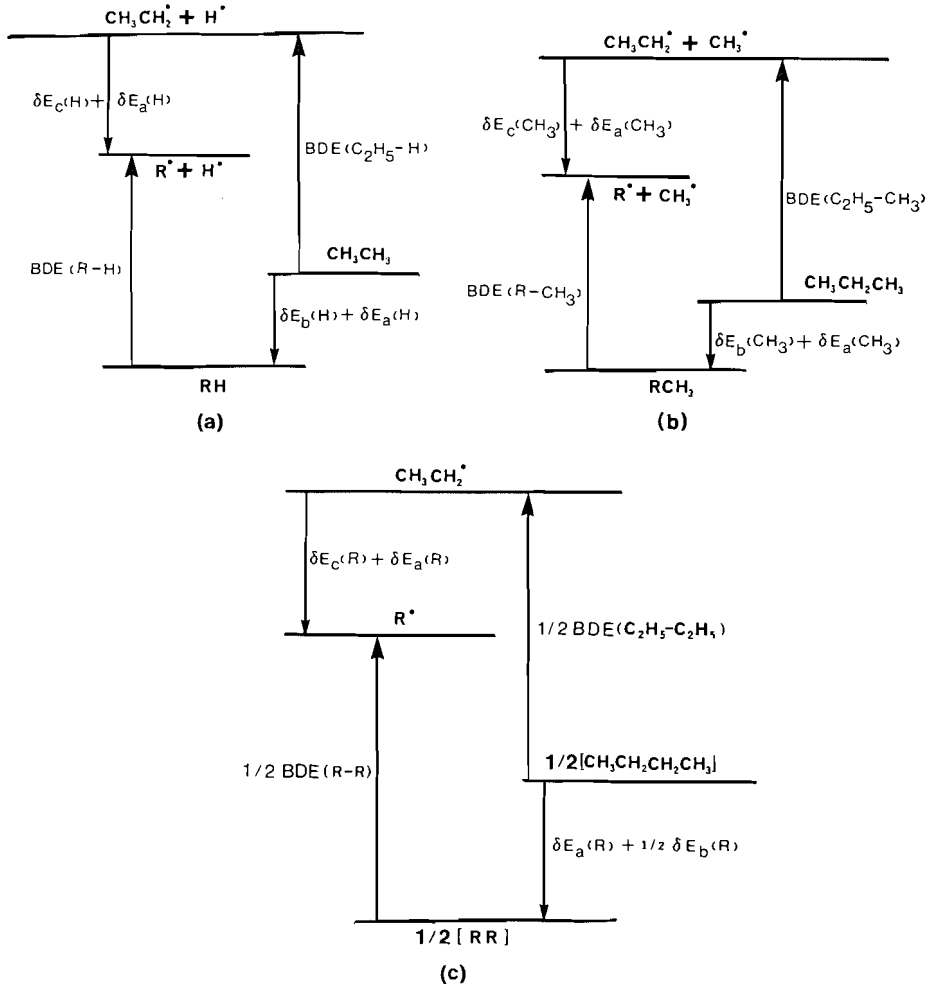

FIG. 3. A schematic representation of substituent effects on an open-shell species (CH_3CH_2) and closed shell species (CH_3CH_2X), at 0 K, in the hypothetical vibrationless state, where non-bonded interactions have been ignored. (a) X = H (b) X = CH_3 (c) X = C_2H_5. $-\delta E_a(X) = E^0\{R(RX)\} - E^0\{C_2H_5(C_2H_5X)\}$; $-\delta E_b(X) = SE^0(C^*/X)$; $-\delta E_c(X) = SE^0[R^\cdot, RX]$.

2.64, a_{CH} = 1.03, and a_{CC} = 2.04. These values indicate that 0.001 electron (= 1 me) added to hydrogen ($\Delta q_H = -1$ me) stabilized a CH bond by 2.64 kJ mol^{-1}, whereas 1 me added to carbon had a stabilizing effect of 1.03 and 2.04 kJ mol^{-1} on a CH and a CC bond, respectively (14). *Thus, any electron enrichment on a carbon atom, at the expense of the electron population at the hydrogen atoms of a CH bond in these alkanes, results in a gain in molecular stability but a concomitant weakening of that CH bond.*

The relationship between charges on atoms and stabilities provides a method of estimating substituent effects on the intrinsic C—H and C—C bond strengths of several types of organic molecules (RX) independent of the standard heat of formation of the corresponding radicals ($\Delta_f H^0(R^\cdot)$ and $\Delta_f H^0(X^\cdot)$). Next we apply this approach to assess changes in the intrinsic C—H and C—C bond strengths of a few representative alkanes. These estimations then enable the calculation of relative net stabilization energies of alkyl radicals via the use of appropriate BDH values (*vide infra*).

Relative net stabilization energies of a radical ($SE^0[R^\cdot, RX]$)

Consider the isodesmic reaction[10]

[20] $C^*(R^1R^2R^3)X + CH_3CH_2^\cdot \rightarrow [C^*(R^1R^2R^3)]^\cdot + CH_3CH_2X$

all participating species being in their hypothetical vibrationless state at 0 K. The energy change, ΔE^0_{20}, can be expressed in terms of BDE values:

[21*a*] $\Delta E^0_{20} = BDE(R—X) - BDE(CH_3CH_2—X)$

If we neglect non-bonded interactions (E^0_{nb}), from Fig. 3(a) and (b) it is clear that ΔE^0_{20}, is given by

[21*b*] $\Delta E^0_{20} = -\delta E_c(X) - \delta E_a(X) + \delta E_b(X) + \delta E_a(X)$
$= SE^0[R^\cdot, RX] - SE^0(C^*/X)$

In eq. [21*b*], $-\delta E_a(X)$ is the energy of the R component of RX, measured relative to the C_2H_5 component of C_2H_5X. Thus $-\delta E_C(X)$ is a measure of the stability of the R moiety as a radical with reference to it being a part of RX (in this paper, the R component of RX is denoted by R(RX)), and $SE^0[R^\cdot, RX]$, is referred to as a *net* stabilization energy because it is measured with reference to R(RX). Values of $-\delta E_b(X)$ (= $SE^0(C^*/X)$), are measures of the stabilization energy of the C*/X interaction in RX relative to that in C_2H_5X. Hence, it is clear that ΔE^0_{20} depends not only on effects of R^1, R^2, and R^3 (R^1, R^2, and R^3 are alkyl groups or hydrogen) on the stability of $R^\cdot$ relative to $C_2H_5^\cdot$, $SE^0[R^\cdot, RX]$, but also on $SE^0(C^*/X)$.

[10] X is a fixed group (alkyl group or hydrogen) for the series of R groups considered, where R = $C^*(R^1R^2R^3)$.

Can. J. Chem. Downloaded from www.nrcresearchpress.com by 210.87.254.105 on 09/06/12
For personal use only.

Can. J. Chem. Downloaded from www.nrcresearchpress.com by 210.87.254.105 on 09/06/12
For personal use only.

Under standard conditions, the enthalpy change for eq. [20], ΔH^0_{20} is related to $SE^0[R^\cdot, RX]$ by:

$$[22a] \quad SE^0[R^\cdot, RX] = \Delta H^0_{20} + SE^0(C^*/X) + (\Delta E^0_{nb})_{20} - \Delta(ZPE + H_T - H_0)_{20}$$

Values of $\Delta(ZPE + H_T - H_0)$ for isodesmic reactions are generally expected to be small. To a first approximation, by neglecting such effects and $(\Delta E^0_{nb})_{20}$, eq. [22*a*] simplifies to:

$$[22b] \quad SE^0[R^\cdot, RX] = \Delta H^0_{20} + SE^0(C^*/X)$$

For X = H or CH_3, the neglect of $(\Delta E^0_{nb})_{20}$ will not lead to any serious error because $\Delta E^0_{nb}(RX)$ values have been shown to be small (14, 23).

Notice that the radical R$^\cdot$ and the reference state, R(RX), contain the same number of atoms and approximately[11] the same net charge; hence their total energies or atomization energies will reflect their relative stabilities. However, the structure and charge distribution of the reference states, R(RX) (and hence $SE^0[R^\cdot, RX]$), can vary.

To test the magnitude of this variation, three types of reference states (R(RX); X = H, CH_3, and R) have been studied.

Case (i): X = H

Substitution of X = H in eq. [22*b*] gives eq. [23], where $SE^0(C^*/H^*)$ is the substituent effect on the intrinsic C*—H* bond of RH*. Equation [23] expresses $SE^0[R^\cdot, RH]$ in terms of known BDH(R—H) values and $SE^0(C^*/H^*)$ which can be calculated using eqs. [19] and [24].

$$[23] \quad SE^0[R^\cdot, RH] = \Delta H^0_{20}(X = H) + SE^0(C^*/H^*)$$

$$[24] \quad SE^0(C^*/H^*) = SE^0(C^*—(H^*)) + SE^0(H^*—(C^*)) = a_{C^*H^*}[\Delta q_{C^*}] + a_{H^*C^*}[\Delta q_{H^*}]$$

In eq. [24] $a_{C^*H^*}[\Delta q_{C^*}]$ and $a_{H^*C^*}[\Delta q_{H^*}]$ are the respective contributions to the stabilization of the C*—H* bond ($SE^0(C^*/H^*)$), from changes in the charges (in the units of me) on the C* and H* atoms relative to the carbon and hydrogen atoms of ethane. Similar equations can be developed to assess $SE^0(C^*/H^*)$ values in carbonyl compounds (19), ethers (19), and ethylenes (20).

Case (ii) X = CH_3

Substitution of X = CH_3 in eq. [22*b*] gives:

$$[25] \quad SE^0[R^\cdot, RCH_3] = \Delta H^0_{20}(X = CH_3) + SE^0(C^*/CH_3)$$

where $SE^0(C^*/CH_3)$ is the substituent effect on the interaction between C* and the whole CH_3 group (eq. [26]). Equation [25] expresses $SE^0[R^\cdot, RCH_3]$ in terms of known BDH(R—CH_3) values and $SE^0(C^*/CH_3)$, which can be calculated using eq. [26]. In eq. [26] $SE^0(Y—(Z))$ symbolizes the substituent effect on the stabilization of the Y—Z bond due to changes in the charges on the atom Y. Δq_Y symbolizes the charge on atom Y relative to that on the same atom (Y) when R = C_2H_5. Thus, (C^*/CH_3) involves the interactions in one C—C bond and three C—H bonds.

$$[26] \quad SE^0(C^*/CH_3) = SE^0\{C^*—(C)\} + SE^0\{C—(C^*)\} + 3SE^0\{C—(H)\} + 3SE^0\{H—(C)\} = a_{C^*C}[\Delta q_{C^*}] + a_{CC^*}[\Delta q_C] + 3a_{CH}[\Delta q_C] + 3a_{HC}[\Delta q_H] = a_{CC}[\Delta q_{C^*}] + 3a_{HC}[\Delta q_H] + (a_{CC} + 3a_{CH})[\Delta q_C]$$

Case (iii): X = R

The need for considering terms such as $SE^0(C^*/X)$ in eqs. [23] and [25] implies the presence of, and the variation in, charge on X (and hence R(RX)). Thus, the choice of reference state in defining radical stability using eqs. [21], [23], and [25] will be biased by this charge effect. Such charge effects can be overcome by choosing the reference state, R(RR), where $q_{R(RR)}$ is zero by symmetry. To define $SE^0[R^\cdot, RR]$, let us consider the following isodesmic reaction:

$$[27] \quad 1/2\,[C^*(R^1R^2R^3)]_2 + CH_3CH_2^\cdot \rightarrow [C^*(R^1R^2R^3)]^\cdot + 1/2\,[CH_3CH_3]_2$$

all participating species being in their hypothetical vibrationless state at 0 K.[12] ΔE^0_{27} depends not only on the effects of R^1, R^2, and R^3 (R^1, R^2, and R^3 are alkyl groups or hydrogen) on the stability of R$^\cdot$ relative to the $C_2H_5^\cdot$, $SE^0[R^\cdot, RR]$, but also on $SE^0(C^*/C^*)$ (eqs. [28] and [29]), the stabilization of the central C*—C* bond in RR relative to that in $CH_3CH_2CH_2CH_3$ (i.e. the central C—C bond in n-butane). This is illustrated in Fig. 3(c). In eq. [28] the symbolism adopted (at 0 K) is the same as in eq. [21]. Thus the descriptions of terms in eq. [21] are also applicable to eq. [28]. The standard enthalpy change for eq. [27], ΔH^0_{27}, is related to $SE^0[R^\cdot, RR]$ by:

$$[28] \quad \Delta E^0_{27} = 1/2[BDE(R—R) - BDE(CH_3CH_2—CH_2CH_3)] = SE^0[R^\cdot, RR] - 1/2\,SE^0(C^*/C^*)$$

$$[29a] \quad SE^0[R^\cdot, RR] = \Delta H^0_{27} + 1/2SE^0(C^*/C^*) + \delta(\Delta E^0_{nb})_{27} - \Delta(ZPE + H_T - H_0)_{27}$$

Values of $\Delta(ZPE + H_T - H_0)$ for isodesmic reactions are small and can be neglected in a first approximation. $(\Delta E^0_{nb})_{27}$ may not be small (for example when R = *t*-Bu (15)), but, if neglected, simplifies eq. [29*a*] to:

$$[29b] \quad SE^0[R^\cdot, RR] = \Delta H^0_{27} + 1/2\,SE^0(C^*/C^*)$$

Equation [29*b*] expresses $SE^0[R^\cdot, RR]$ in terms of known BDH(R—R) values and $SE^0(C^*/C^*)$ which can be calculated using eq. [30], where Δq_{C^*} is the charge on the C* atom of RR relative to that in RR(R = C_2H_5).

$$[30] \quad SE^0(C^*/C^*) = 2\,SE^0\{C^*—(C^*)\} = 2\,a_{CC}[q_{C^*}(RR) - q_{C^*}(n\text{-}C_4H_{10})] = 2\,a_{CC}[\Delta q_{C^*}]$$

Variation of $SE^0[R^\cdot, RX]$ with choice of X

The variation in $SE^0[R^\cdot, RX]$, for X = CH_3 and X = R (with reference to X = H), can be represented by;

$$[31a] \quad \delta(SE^0[R^\cdot, RX]) = SE^0[R^\cdot, RCH_3] - SE^0[R^\cdot, RH]$$

$$[31b] \quad \delta'(SE^0[R^\cdot, RX]) = SE^0[R^\cdot, RR] - SE^0[R^\cdot, RH]$$

Substitution of eqs. [23], [25], and [29*b*] in eq. [31] yields:

[11] The radical R$^\cdot$ is electrically neutral. But R(RX), where X ≠ R, will usually have a small net charge (q_R). For the alkanes, the magnitude of this charge is in the order of 1–10 me (see Table 9).

[12] Note that eq. [27] and eq. [20] are related by: [27] = 1/2([20](X = R) + [20](X = C_2H_5)).

$$[32a]\quad \delta(SE^0[R^\cdot, RX]) = \Delta H^0_{20}[(X = CH_3) - (X = H)] + SE^0(C^*/CH_3) - SE^0(C^*/H) = \delta(\Delta H^0_{20}) + \delta(SE^0(C^*/X))$$

$$[32b]\quad \delta'(SE^0[R^\cdot, RX]) = \Delta H^0_{27} - \Delta H^0_{20}(X = H) + 1/2\ SE^0(C^*/C^*) - SE^0(C^*/H)$$

In eq. [32] $\Delta(ZPE + H_T - H_0)$ and $\delta(\Delta E^0)_{nb}$ terms have been ignored. Although individual ΔH^0_{20} or ΔH^0_{27} values have large uncertainties (~8 kJ mol^{-1}), their difference or $\delta(\Delta H^0_{20})$ values are known more precisely (uncertainty < 1 kJ mol^{-1}) (Table 3). Thus, the differences in the $SE^0[R^\cdot, RX]$ values can be calculated using eqs. [32*a*] and [32*b*].

While individual $\Delta(ZPE + H_T - H_0)$ values for eqs. [20] and [27] are not readily calculated, their differences can usually be obtained (22). Similarly, differences in ΔE^0_{nb} values are generally estimable (14, 23). Using eqs. [21] and [29*a*], the differences in the $SE^0[R^\cdot, RX]$ values can be expressed by:

$$[33a]\quad \delta(SE^0[R^\cdot, RX]) = \delta(\Delta H^0_{20}) + \delta(SE^0(C^*/X)) - \Delta(ZPE + H_T - H_0)_{20}[(X = CH_3) - (X = H)] + (\Delta E^0_{nb})_{20}[(X = CH_3) - (X = H)]$$

$$[33b]\quad \delta'(SE^0[R^\cdot, RX]) = [\Delta H^0_{27} - \Delta H^0_{20}(X = H)] + 1/2\ SE^0(C^*/C^*) - SE^0(C^*/H) - \Delta(ZPE + H_T - H_0)_{27} + \Delta(ZPE + H_T - H_0)_{20}[X = H] + (\Delta E^0_{nb})_{27} - (\Delta E^0_{nb})_{20}[X = H]$$

From Fig. 3, it is clear that for any X the total substituent effect on the stability of a radical is a constant. Consequently, by assuming $E^0_{nb}[R(RX)]$ and $E^0_{nb}[R(RH)]$ are equal, eq. [34] is obtained.

$$[34]\quad \delta E_a(CH_3) + SE^0[R^\cdot, RCH_3] = \delta E_a(H) + SE^0[R^\cdot, RH] = \delta E_a(R) + SE^0[R^\cdot, RR]$$

The differences $\delta[E_a(CH_3) - E_a(H)]$ and $\delta[E_a(R) - E_a(H)]$ can be estimated by considering the charges on the atoms of the $R(RCH_3)$ and R(RR) relative to that in R(RH).

$$[35a]\quad \delta[E_a(CH_3) - E_a(H)] = \delta E_a(CH_3) - \delta E_a(H) = [E_a(CH_3) - E_a(H)]_R - [E_a(CH_3) - E_a(H)]_{C_2H_5}$$

$$[35b]\quad \delta[E_a(R) - E_a(H)] = [E_a(R) - E_a(H)]_R - [E_a(C_2H_5) - E_a(H)]_{C_2H_5}$$

$$[36]\quad -(E_a(X) - E_a(H))_R = \Sigma_i[(n_{C_i}a_{CC} + n_{H_i}a_{CH})\,\Delta q_{C_i}] + \Sigma_j[a_{HC}\Delta q_{H_j}] = \Sigma_i[(n_{C_i}a_{CC} + n_{H_i}a_{CH} - a_{HC})\,\Delta q_{C_i}] + a_{HC}\{q[R(RX)] - q[R(RH)]\}$$

In eq. [36] n_{C_i} and n_{H_i} are the number of carbon and hydrogen atoms attached to C_i; Δq_{C_i} and Δq_{H_j} are charges on the *i* carbon and *j* hydrogen atom of R(RX) relative to R(RH).

From eqs. [34]–[36] an expression for the $\delta(SE^0[R^\cdot, RX])$ values is obtained;

$$[37a]\quad \delta(SE^0[R^\cdot, RX]) = \delta\{E_a(CH_3) - E_a(H)\}$$

$$[37b]\quad \delta'(SE^0[R^\cdot, RX]) = \delta\{E_a(R) - E_a(H)\}$$

Results and discussion

The stabilization energy of a radical must be an invariant quantity. Tables 1 and 2 clearly show, that relative BDH values cannot be directly equated to radical stability. For example, by considering the C—OH bond cleavage it might be concluded that the stabilities of the simple alkyl radicals are in the order, $i\text{-}C_3H_7^\cdot \simeq t\text{-}C_4H_9^\cdot < C_2H_5^\cdot$. This is a complete reversal in the order of stability, $C_2H_5^\cdot < i\text{-}C_3H_7^\cdot < t\text{-}C_4H_9^\cdot$, obtained by considering C—H bond cleavage.

It might be argued that the relatively poor correlation of BDH values (when X is an electronegative atom or group) in Table 1 is due to the uncertainty in some of the data used in the analysis. However, it must be noted that a good correlation in the BDH data is a necessary but not a sufficient criterion to propose that relative BDH (R—X) values are a suitable measure of radical stability. The differences obtained in Table 2 are independent of the standard enthalpy of formation of any radical species and are equal to the ΔH^0_{10} values in Table 3. Most of these values have uncertainties that are smaller than the differences in Table 2 (24). The ambiguities in the order of stabilities inferred from Table 2 are a result of neglecting effects on the parent undissociated molecules of these radicals (see Table 4). Thus, even when more accurate determinations of BDH values are available, they will not change the apparent discrepancies in the values in Table 2 and may not significantly improve the correlation in Table 1.

The poor correlation obtained in the BDH values when X is an electronegative atom is not surprising (Table 1).[13] This is because the polarity of the $C^{\delta+}\text{---}X^{\delta-}$ bond will certainly affect the strength of the other bonds in the molecule. On dissociation of the C—X bond the effects of X on R will be absent. In addition, an X that had a partial negative charge when attached to R leaves as a neutral species. Thus, in the radical state, the R component will have to accommodate the excess electrons. Furthermore, there will be effects on the C—X bond (and, where X contains more than one atom, there will be an effect on the individual bonds in X) from the groups attached to (CX). One of the reasons for the poor correlation in Table 1 and the large ΔH^0_4 values, when X = OH, is possibly because of effects on the O—H bond.

The relatively better correlation, when X = alkyl, is probably due to the fact that substituent effects on RX are very similar in nature when X is an alkyl group or a hydrogen atom. *However, Table 2 clearly shows that even when X = alkyl the magnitude of relative BDH values changes appreciably relative to X = H.* Alternatively, it can be suggested that, due to the variation in the relative BDH values, only RH be used to define radical stability. However, such an a priori choice is unjustified, unless the effects of substituents on the intrinsic R—H bond strengths are known.

Studies by Fliszár and co-workers have shown that charge effects are the dominant factor influencing the stabilities of alkanes (14). From Table 5 it is evident that such effects can be as large as −17 kJ mol^{-1} for the tertiary C—H bond in 2-methyl propane. These effects are a result of the variation in the charges on both atoms (carbon and hydrogen) involved in the bond. In the alkanes studied, except for the primary C—H bond in propane, the variation of charge on hydrogen had a greater effect ($a_{HC}\Delta q_{H^*}$) than the corresponding variation on

[13] See for example P. D. Pacey and J. H. Wimalasena. J. Phys. Chem. In press.

Can. J. Chem. Downloaded from www.nrcresearchpress.com by 210.87.254.105 on 09/06/12
For personal use only.

TABLE 5. Charge effects[a] on the relative intrinsic C—H bond strengths in alkanes (RH), $SE^0(C^*/H^*)$ (kJ mol^{-1})

R—H*	Δq_{C^*}	$a_{CH}\Delta q_{C^*}$	Δq_{H^*}	$a_{HC}\Delta q_{H^*}$	$SE^0(C^*/H^*)$ (eq. [24])
$\overset{*}{C}H_3$—H*	1.09	1.12	2.65	7.00	8.12
$CH_3\overset{*}{C}H_2$—H*	0	0	0	0	0
$CH_3CH_2\overset{*}{C}H_2$—H*	−1.46	−1.50	−0.40	−1.06	−2.56
$\overset{*}{C}H(CH_3)_2$—H*	−1.62	−1.67	−2.39	−6.31	−7.98
$\overset{*}{C}(CH_3)_3$—H*[b]	−2.99	−3.08	−5.32	−14.04	−17.12

[a] Unless otherwise noted, charges (me) on atoms have been obtained from App. II of ref. 19.
[b] Charges on atoms calculated from Table II (n = −4.4122) of ref. 18.

TABLE 6. Charge effects[a] on the intrinsic bond strength of the C—CH_3 bond and the C—H bonds of the CH_3 group in the alkanes RCH_3

R	Δq_{C^*}	$a_{CC}\Delta q_{C^*}$	Δq_C	$(a_{CC} + 3a_{CH})\Delta q_C$	Δq_H	$3a_{HC}\Delta q_H$	$SE^0(C^*/CH_3)$[b] (eq. [26])
$\overset{*}{C}H_3$	1.62	3.30	1.46	7.49	0.40	3.17	13.96
$CH_3\overset{*}{C}H_2$	0	0	0	0	0	0	0
$CH_3CH_2\overset{*}{C}H_2$	−1.20	−2.45	0.38	1.95	−0.25	−1.98	−2.48
$\overset{*}{C}H(CH_3)_2$[b]	−1.37	−2.79	−1.27	−6.52	−0.37	−2.93	−12.24
$\overset{*}{C}(CH_3)_3$[b]	−1.66	−3.39	−2.44	−12.52	−0.95	−7.52	−23.43

[a] Unless otherwise noted, charges (me) on atoms have been obtained from ref. 19, App. II.
[b] All values are in kJ mol^{-1}.
[c] Charges on atoms calculated from Table II (n = −4.4122) of ref. 18.

TABLE 7. The relative net stabilization energies,[a] $SE^0[R^\cdot, RX]$, of alkyl radicals ($R^\cdot$) in the gas phase

			$SE^0[R^\cdot, RX]$		
$R^\cdot$	ΔH^0_{27}[b]	1/2 $SE^0(C^*/C^*)$[c] (eq. [30])	X = H (eq. [23])	X = CH_3 (eq. [25])	X = R (eq. [29b])
$CH_3^\cdot$	17.25	5.75[d]	37	32	23
$C_2H_5^\cdot$	0	0	0	0	0
n-$C_3H_7^\cdot$	−0.20	−2.14[d,e]	−3	−2	−2
i-$C_3H_7^\cdot$	−5.85	−2.84[d,f]	−19	−14	−9
t-$C_4H_9^\cdot$	−22.4	−3.04[d,f]	−38	−32	−25

[a] All values are in kJ mol^{-1}.
[b] Calculated using the standard heats of formation of RR from ref. 24a and $R^\cdot$ from ref. 2.
[c] Calculated using charges on carbon from references indicated.
[d] Reference 19, App. II.
[e] Charges for n-hexane estimated using method described in ref. 14. ^{13}C chemical shifts obtained from ref. 29.
[f] Reference 15 after multiplying by a factor (35.1/69.4) to standardize charges to q^0_C (ethane = 35.1 me).

carbon ($a_{CH}\Delta q_{C^*}$). From Table 5 we see that the C—H bond in methane is 8 kJ mol^{-1} weaker than in ethane. The primary and secondary C—H bonds of propane and the tertiary C—H bond of 2-methyl propane are found to be, respectively, 2.6, 8.0, and 17 kJ mol^{-1} more stable than the C—H bond of ethane.

Charge effects on the total interaction between a methyl group and the carbon atom at the point of attachment for selected alkanes are given in Table 6. These values show that there is a greater contribution to the total effect from charge variations on the carbon atoms than from those on the hydrogen atoms. It is also evident that the C* atom shows a greater effect in the C/CH_3 system compared to the C/H system. This is partly because $a_{CC} > a_{CH}$. The substituent effects observed on the C/CH_3 interaction is in the same order as the C/H interaction, but greater in magnitude. The variation in the relative BDH values observed for the C—CH_3 and C—H cleavages is partly due to differences in $SE^0(C^*/CH_3)$ and $SE^0(C^*/H)$ values. The $SE^0[R^\cdot, RX]$ values obtained after the appropriate BDH values have been corrected for C/H, C/CH_3, and C/C interactions are given in Table 7.

From Table 7 it is evident that, for a given $R^\cdot$, $SE^0[R^\cdot, RX]$ varies with the choice of reference state. The uncertainties in the individual $SE^0[R^\cdot, RX]$ values depend to a large extent on the error in the BDH values used to calculate ΔH^0_{20} or ΔH^0_{27}. Before discussing the relative merits of using the various $SE^0[R^\cdot, RX]$ values calculated to define radical stability, the reasons for their differences must be given careful consideration. The charge contribution to the energy differences be-

Can. J. Chem. Downloaded from www.nrcresearchpress.com by 210.87.254.105 on 09/06/12
For personal use only.

Can. J. Chem. Downloaded from www.nrcresearchpress.com by 210.87.254.105 on 09/06/12
For personal use only.

TABLE 8. Substituent effects[a] on the stabilization of the R component of RX (R(RX)) relative to R(RH)

	$(E_a(X) - E_a(H))^b$		$\delta(E_a(X) - E_a(H))$	
R	X = R	X = CH_3	X = R	X = CH_3
CH_3	24.38[c]	24.38[c]	−13.31	−5.49
C_2H_5	37.69[c]	29.87[c]	0	0
n-C_3H_7	37.91[d]	29.18[c]	0.22	−0.69
i-C_3H_7	46.38[c]	33.60[c,f]	8.69	3.73
t-C_4H_9	50.94[e]	33.69[e,f]	13.25	3.82

[a] All values in kJ mol^{-1}.
[b] Charges obtained from references indicated.
[c] Reference 19, App. II.
[d] See footnote (*e*) Table 7.
[e] See footnote (*f*) Table 7.
[f] See footnote (*b*) Table 5.

TABLE 9. Net charges[a,b] on the R component (q_R) of RH, RCH_3, and RC_2H_5

R	q_R(RH)	q_R(RCH_3)	q_R(RC_2H_5)
CH_3	9.05	0	−2.66
C_2H_5	11.70	2.66	0
n-C_3H_7	12.10	3.03	0.40
i-C_3H_7	14.09	5.04	2.40[c]
t-C_4H_9	17.02[d]	7.95	5.30[c]

[a] All charges are given in the units me.
[b] Unless indicated otherwise, charges obtained from ref. 19, App. II.
[c] See footnote (*f*) Table 7.
[d] See footnote (*b*) Table 5.

tween reference states is given in Table 8. These values show that for a given R the stabilities of the reference states are in the order R(RR) > R(RCH_3) > R(RH). This order arises because of the differences in the net charges of the reference states (Table 9).[14]

A radical, R$^\bullet$ is electrically neutral. However, Table 9 shows that q[R(RH)] and q[R(RCH_3)] have non-zero values with the exception of q[CH_3(C_2H_6)]. The closer a reference R component R(RX) is to neutrality, the more suitable it is to be used to define radical stability. This is because if q[R(RX)] is not negligible, then R(RX) and R$^\bullet$ do not have the same net charge, and their energies are not directly comparable. The rationale behind choosing R(RX) to define radical stability was to use a reference state having the identical arrangement of atoms and same net charge as R$^\bullet$ and in addition have an *inert* unpaired electron. All these conditions are met in R(RR), where q[R(RR)] is zero for all R by symmetry. R(RH) and R(RCH_3) have the limitation of having a slight deficiency in the electronic charge. Thus, conceptually the SE^0[R$^\bullet$, RR] values are the best parameters that can be used to define radical stability.

It must be noted that these SE^0[R$^\bullet$, RR] values also include stabilization due to change in hybridization (ΔR of eq. [13]). The ΔR term will include stabilization due to changes in one electron, two-electron, and nonbonded interactions. It is also interesting to consider to what extent a radical in the hypothetical sp^3 hybridized state can be stabilized. This can be obtained from[15]

$$[38] \quad SE^0[R^\bullet(sp^3), RR] = SE^0[R^\bullet, RR] - [\Delta R(R^\bullet) - \Delta R(C_2H_5^\bullet)]$$

Relative to the ethyl radical in the sp^3 state, the following SE^0[R$^\bullet$ (sp^3), RR] values in kJ mol^{-1} are obtained: CH_3, 21; i-C_3H_7, −7; t-C_4H_9, −22. These values indicate that, even in an sp^3 hybridized state, radicals are stabilized. However, the origin of this stabilization is not apparent from this study.

The dependence of the relative stabilization energies of radicals on the chosen reference state is described by δ(SE^0[R$^\bullet$, RX]) and δ'SE^0[R$^\bullet$, RX]) values in Table 10. The advantage of this approach is that these differences (δ(SE^0[R$^\bullet$, RX]) values) can be calculated independent of any $\Delta_f H^0$ (radical) values (which introduce large uncertainties). The differences in the values calculated using eqs. [32] and [33] are due to, respectively, the neglect and inclusion of (ZPE + $H_T - H_0$) and E^0_{nb} terms in the computations. The fair agreement between the two equations suggests that SE^0[R$^\bullet$, RX] calculated (eqs. [23], [25], and [28]) are reliable. However, the SE^0[R$^\bullet$, RR] value for R = i-C_3H_7 and t-C_4H_9 must be used with caution because the required (ZPE + $H_T - H_0$) and E^0_{nb} values are known with less certainty (15). Thus, the SE^0[R$^\bullet$, RR] values for these R groups may be in error. The close agreement between δ(SE^0[R$^\bullet$, RX]) (or δ') values calculated using eqs. [32] and [37] indicates the internal consistency in using linear charge–energy relationships to estimate SE^0[R$^\bullet$, RX] values.

Conclusions

The relationship between radical stability and bond dissociation enthalpies involves several factors that need careful consideration.[16] It is shown that relative BDH values cannot be directly equated to radical stability. The net stabilization energy of a radical R$^\bullet$ can be defined relative to the same R group; when present in a closed shell species RX(X is an alkyl group or hydrogen) R(RR) is found to be the most suitable reference state because (like a radical R$^\bullet$) it is electrically neutral.

SE^0[R$^\bullet$, RX] values indicate that the methyl radical is more destabilized and that the n-propyl, iso-propyl, and *tert*-butyl radicals are more stabilized, relative to the ethyl radical, than suggested from the corresponding BDH(R—X) values. This results from differences in the total C/X interactions (defined independent of any radical species) of RX as a function of R.

Finally, we have attempted to analyse critically methods of assessing radical stability, with the hope that a clearer understanding of the behaviour of these reactive species will ensue.

[14] In Table 9, the net charges of the R components RH, RCH_3, and RC_2H_5 are compared. The charges of R(RH) range from 9.05 me (the value for R = methyl) to 17.02 me (R = *tert*-butyl). The charges of R(RCH_3) and R(RC_2H_5) are of a much smaller magnitude.

[15] ΔR values were obtained from ref. 13*b*.

[16] The SE^0[R$^\bullet$, RX] values obtained in this work do not agree with the SE values reported by Leroy (13). A major reason for these differences is the use of different reference C—C (E(C—C)) and C—H (E(C—H)) bond energies and the assumption, made by Leroy, of a constant E(C—C) value for all alkanes. This work is based on the intrinsic bond energies obtained by Fliszár and co-workers for ethane: E(C—C) = 292 kJ mol^{-1}; E(C—H) = 448.1 kJ mol^{-1}. However, Leroy's work is based on E(C—C) = 355.8 kJ mol^{-1}, obtained by using an empirical scheme suggested by Laidler (25). The assumption that E(C—C) is constant is an obvious drawback of the Laidler scheme (26). In addition, the neglect of charge effects on Fajan's bond energy terms by Leroy can introduce serious error. It is noted that SE values for radicals derived from eq. [14] are measured relative to closed shell species.

TABLE 10. The variation in the relative net stabilization energies[a] of a radical R$^{\cdot}$, (SE^0[R$^{\cdot}$, RX]), with reference state[b] R(RX)

	SE^0[R$^{\cdot}$, RX] − SE^0[R$^{\cdot}$, RH]					
	X = CH_3			X = R		
R	eq. [32*a*][c]	eq. [33*a*][d]	eq. [37*a*][e]	eq. [32*b*][f]	eq. [33*b*][d]	eq. [37*b*][e]
CH_3	−5.1	−2.7	−5.5	−14.1	−12.8	−13.3
C_2H_5	0	0	0	0	0	0
n-C_3H_7	1.6	3.8	−0.7	0.3	3.0	0.2
i-C_3H_7	5.3	5.6	3.7	11.1	10.3	8.7
t-C_4H_9	6.1	4.4	3.8	13.2	11.6	13.3

[a] All values are in kJ mol^{-1}.
[b] R components of RH, RCH_3, and RR.
[c] $\delta(\Delta H^0_{20})$ values have been obtained from Table 3.
[d] The required (ZPE + $H_T - H_0$) and E^0_{nb} values have been obtained from refs. 14, 15, 16, and 22.
[e] From Table 8.
[f] The differences in ΔH^0 values have been obtained using $\Delta_f H^0$ values from ref. 24*a*.

It is stressed that, with available data, a definite separation of radical and charge contributions to the stability of an open-shell species is not possible.

At present, Fliszár's method of assessing charge effects on bond strengths cannot be extended to the benzenoid systems. Alternatively, a molecular orbital approach can be used. This will be the topic of the following paper (27).

Acknowledgements

This work was supported by a grant from the Natural Sciences and Engineering Research Council of Canada. We are grateful to R. J. Boyd for his continuing interest in this program. Useful discussions with S. Fliszár (Université de Montréal) are also acknowledged. A. M. N. is grateful for the award of an Izaak Walton Killam Memorial Scholarship.

1. (*a*) A. M. DE P. NICHOLAS and D. R. ARNOLD. Can. J. Chem. **60**, 2165 (1982); (*b*) A. M. DE P. NICHOLAS, R. J. BOYD, and D. R. ARNOLD. Can. J. Chem. **60**, 3011 (1982).
2. D. F. MCMILLEN and D. M. GOLDEN. Ann. Rev. Phys. Chem. **33**, 493 (1982).
3. J. M. DUST and D. R. ARNOLD. J. Am. Chem. Soc. **105**, 1221 (1983); **105**, 6531 (1983).
4. G. LEROY and D. PEETERS. J. Mol. Struct. (Theochem), **85**, 133 (1981).
5. Report of the IUPAC Commission 1.2 on Thermodynamics. J. Chem. Thermodyn. **14**, 805 (1982).
6. W. J. HEHRE, R. DITCHFIELD, L. RADOM, and J. A. POPLE. J. Am. Chem. Soc. **92**, 4796 (1970).
7. M. SZWARC. J. Chem. Phys. **16**, 128 (1948).
8. (*a*) S. W. BENSON. J. Chem. Educ. **42**, 502 (1965); (*b*) Thermochemical kinetics. 2nd ed. Wiley–Interscience, New York. 1976.
9. A. S. RODGERS, M. C. R. WU, and L. KUITU. J. Phys. Chem. **76**, 918 (1972).
10. C. G. SCRETTAS. J. Org. Chem. **45**, 1620 (1980).
11. C. RUECHARDT. Angew. Chem. Int. Ed. Engl. **9**, 830 (1970).
12. S. F. GAINE and F. M. PAIGE. J. Chem. Res. (S), 200 (1980).
13. (*a*) G. LEROY. Int. J. Quantum Chem. **23**, 271 (1983); (*b*) J. Mol. Struct. (Theochem), **93**, 175 (1983).
14. S. FLISZÁR. J. Am. Chem. Soc. **102**, 6946 (1980).
15. S. FLISZÁR and M.-T. BÉRALDIN. Can. J. Chem. **57**, 1772 (1979).
16. H. HENRY, G. KEAN, and S. FLISZÁR. J. Am. Chem. Soc. **99**, 5889 (1977).
17. S. FLISZÁR, M. FOUCRAULT, M.-T. BÉRALDIN, and J. BRIDET. Can. J. Chem. **59**, 1074 (1981).
18. S. FLISZÁR, G. KEAN, and R. MACAULAY. J. Am. Chem. Soc. **96**, 4353 (1974).
19. S. FLISZÁR and M.-T. BÉRALDIN. Can. J. Chem. **60**, 792 (1982).
20. M.-T. BÉRALDIN and S. FLISZÁR. Can. J. Chem. **61**, 197 (1983).
21. S. FLISZÁR, G. CARDINAL, and M.-T. BÉRALDIN. J. Am. Chem. Soc. **104**, 5287 (1982).
22. S. FLISZÁR and J.-L. CANTARA. Can. J. Chem. **59**, 1381 (1981).
23. G. DEL RE. Gazz. Chim. Ital. **102**, 929 (1972).
24. (*a*) J. B. PEDLEY and J. RYLANCE. Sussex-N.P.L. Computer analysed thermochemical data: organic and organometallic compounds. University of Sussex, England. 1977; (*b*) M. Månsson. Pure Appl. Chem. **55**, 417 (1983).
25. K. J. LAIDLER. Can. J. Chem. **34**, 626 (1959).
26. V. M. TATEVSKII, V. A. BENDERSKII, and S. S. YAROVOI. Rules and methods for calculating the physico-chemical properties of paraffinic hydrocarbons. *Translated by* B. P. Mullins. Pergamon Press, Oxford. 1961.
27. A. M. DE P. NICHOLAS and D. R. ARNOLD. Can. J. Chem. **62**, 0000 (1984).
28. Codata Bull. No. 28, ICSU Codata, Paris, 1978. J. Chem. Thermodyn. **10**, 903 (1978).
29. D. M. GRANT and E. G. PAUL. J. Am. Chem. Soc. **86**, 2984 (1964).

Can. J. Chem. Downloaded from www.nrcresearchpress.com by 210.87.254.105 on 09/06/12
For personal use only.

Thermochemical parameters for organic radicals and radical ions. Part 4. The relationship between bond dissociation enthalpy and radical stability in benzenoid systems

A. MARTIN DE P. NICHOLAS AND DONALD R. ARNOLD[1]

Department of Chemistry, Dalhousie University, Halifax, N.S., Canada B3H 4J3

Received December 5, 1983

A. MARTIN DE P. NICHOLAS and DONALD R. ARNOLD. Can. J. Chem. **62**, 1860 (1984).

It is shown that isodesmic reactions used to assess interaction energies between substituents (X and Y) in benzenoid compounds have not been corrected for X/H and Y/H interactions. Excellent linear Mulliken charge – interaction energy relationships are established for *meta*- and *para*-substituted toluenes. These studies illustrate the relative importance of σ- and π-effects on a quantitative basis. The ρ-values obtained show an equal importance of π-effects in *meta*- and *para*-substituted toluenes. The signs of the ρ(π)-values confirm the presence of resonance type π-interactions. The role of ring hydrogens in σ-type interactions cannot be assessed from this study. At present, BDH values in benzenoid systems cannot be corrected such that they can be used to define radical stability. ^{13}C chemical shifts are found not to correlate wih isodesmic interaction energies. The application of ^{13}C chemical shifts is limited by the inability to independently relate these shifts to σ- and π-effects.

A. MARTIN DE P. NICHOLAS et DONALD R. ARNOLD. Can. J. Chem. **62**, 1860 (1984).

On montre que les réactions isodesmiques utilisées pour déterminer les énergies d'interaction entre les substituants (X et Y) dans les composés benzénoïdes ne sont pas corrigées pour les interaction X/H et Y/H. Dans les cas des toluènes *méta* et *para*-substitués, on a établi d'excellentes relations linéaires entre la charge de Mulliken et l'énergie d'interaction. Ces études illustrent l'importance relative des effets σ et π sur une base quantitative. Les valeurs de ρ obtenues montrent que les effets π ont une égale importance dans les toluènes substitués en positions *para* et *méta*. Les signes des valeurs de ρ(π) confirment la présence d'interactions de résonance de type π. A partir de cette étude, on ne peut pas déterminer le rôle des hydrogènes cycliques dans des interactions de type σ. Pour le moment, on ne peut pas corriger les valeurs BDH des systèmes benzénoïdes de façon à pouvoir les utiliser pour définir la stabilité de radicaux. On trouve qu'il n'y a pas de corrélation entre les déplacements chimiques du ^{13}C et les énergies d'interaction isodesmiques. L'application des déplacements chimiques du ^{13}C est limitée par l'incapacité de relier d'une façon indépendante ces déplacements aux effets σ et π.

[Traduit par le journal]

Can. J. Chem. Downloaded from www.nrcresearchpress.com by 210.87.254.105 on 09/06/12
For personal use only.

Introduction

In the preceding paper (1), a study of the relationship between the stability of an alkyl radical R$^{\bullet}$ and BDH(R—X) *g* values enabled us to define the net stabilization energy of a radical R$^{\bullet}$, (SE^0[R$^{\bullet}$, RX]), with reference to the R component of RX. This study has now been extended to benzylic systems. Here we show that the BDH value for the benzylic C—H bond of a toluene is not a true measure of the stability of the corresponding benzyl radical. We also discuss the difficulties of estimating SE^0[R$^{\bullet}$, RX] in benzenoid systems.

The substituent effect on the stability of a benzyl radical will depend on the extent of interaction between a substituent and the $CH_2^{\bullet}$ group. The interaction energy between two substituents X and Y attached to a benzene ring has been estimated (2) using the isodesmic reaction:

[1] $C_6H_5X + C_6H_5Y \rightarrow XC_6H_4Y + C_6H_6$

Applying Y = H to reaction [1] it is evident that interaction energies measured using this reaction are only relative to interactions between X (and Y) and the appropriate ring hydrogens. The X/Y interactions can be understood by considering ΔH^0_{I} values in terms of relative BDH values (1).

[2] $\Delta H^0_{\text{I}} = \delta[\text{BDH}(XC_6H_4—)H] - \delta[\text{BDH}(XC_6H_4—)Y]$

Alternatively, if the X/H interaction ($\Delta H^0_{X/H}$) and the Y/H interaction ($\Delta H^0_{Y/H}$) can be estimated, the interaction enthalpy between X and Y ($\Delta H^0_{X/Y}$) will be given by eqs. [3] and [4]. In eq. [4] the X/Y interaction is represented as a substituent effect.

[3] $\Delta H^0_{X/Y} = \Delta H^0_{\text{I}} + \Delta H^0_{X/H} + \Delta H^0_{Y/H} - \Delta H^0_{H/H}$

[4] $\delta(\Delta H^0_{X/Y}) = \Delta H^0_{\text{I}} + \delta(\Delta H^0_{X/H})$

From eqs. [1]–[4] it is evident that $\Delta H^0_{X/H}$ values must be known before eq. [1] can be used to determine the stability of a benzyl radical.

In this study we demonstrate the presence of substituent effects on X/Y interactions in benzenoid systems using standard heats of formation ($\Delta_f H^0$) of mono- and disubstituted benzenes in the gas phase (3, 4). *Ab initio* MO calculations are used to obtain Mulliken charge – energy relationships in benzenoid systems and to demonstrate the presence of substituent effects on the benzylic C—H bond of substituted toluenes. The toluenes are of special interest, because they have been used as reference states for assessing benzyl radical stability (5).

The toluenes studied represent five groups. Substituents were studied at both the *meta* and *para* positions. These substituents were chosen only to illustrate the presence of charge related interactions between groups attached to a benzene nucleus, and not with a view of establishing an overall picture of such effects.[2]

The following classification was made:

(*i*) H (unsubstituted toluene), representing a σ-donating[3] and π-noninteracting group.

(*ii*) CH_3, representing a π- and σ-donating[3] group.

[1] Author to whom all correspondence should be addressed.

[2] For a recent review of studies on substituent interactions in benzenoid systems using *ab initio* MO calculations and Perturbation MO theory approach, see ref. 2.

[3] The H and CH_3 groups are classified as σ-donors because $q_\sigma(H) < 0$ and $q_\sigma(CH_3) < 0$ (2). This classification is valid within the framework of the Mulliken charge analysis which has been adopted in this work.

TABLE 1. Relative interaction enthalpies, $-\Delta H^0_1$ (kJ mol^{-1}) for the interaction between X and Y (relative to X and H, and Y and H) for the isodesmic reaction [1] in the gas phase at 298.15 K

	Y			
X	*m*-CH_3	*p*-CH_3	*m*-Z	*p*-Z
CH_3	0 ± 0.8[a]	0.7 ± 1.0[a]	1.8 ± 1.3[a,b]	0.4 ± 1.4[a,b]
F	—	1.3 ± 1.9[a]	5.7[c,d]	8.4[c,d]
OMe	−3.3 ± 5.0[a]	—	—	—
CN	—	—	14.2 ± 3.6[d,e,f]	8.6 ± 3.5[d,e,f]
OH	−3.2 ± 1.5[a]	3.8 ± 1.8[a]	3.9 ± 1.9[a,b]	5.9 ± 1.3[a,b]
NO_2	−3.8 ± 4.0[a]	—	—	—
I	4.2 ± 7.5[a]	−7.5 ± 7.5[a]	—	−13.4 ± 7.7[a,g]
Cl	—	—	−16.5 ± 4.1[a,g]	−15.3 ± 3.8[a,g]
NH_2	—	—	7.2 ± 3.7[a,g]	−7.2 ± 4.1[a,g]

[a] Calculated using $\Delta_f H^0$ values given in ref. 3.
[b] Z = C_2H_5.
[c] Z = F.
[d] Reference 4; uncertainty in the data is not given.
[e] Z = CN.
[f] Calculated using $\Delta_f H^0$ values for the dicyano benzenes from ref. 4 and for C_6H_6 and C_6H_5CN from ref. 3.
[g] Z = COOH.

(*iii*) F and OMe,[4] representing π-donating and σ-accepting groups.

(*iv*) CN, exemplifying π- and σ-acceptors.

(*v*) Li, representing a π-accepting and σ-donating group.

Charge effects in benzenoid systems

The charge–energy relationships were studied with two objectives: first, to investigate whether charge and energy were linearly correlated; second, to assess the energetics of the interactions between a substituent and ring hydrogens of monosubstituted benzenes.

Fliszár's method of assessing intrinsic CH bond strengths in terms of charge distributions can be extended in principle to benzenoid systems (6). However, at present the relevant data necessary for such an analysis of these systems is not available.[5] In this paper, the relationship between relative interaction energies (i.e. interaction between substituents and C(ring)—CH_3 group relative to the C(ring)—H group), Mulliken charges on atoms, and ^{13}C chemical shifts in substituted toluenes have been studied. The significance of such a study is that it is a test of the existence of a linear charge–energy or chemical shift – energy relationship in these systems.

The studies of cyclic and acyclic alkanes (6), ethers (7), ethylenes (8), and carbonyl compounds (7) by Fliszár and coworkers have revealed linear ^{13}C nmr chemical shift – calculated atomic charge relationships. They have also shown that these charges are at variance with Mulliken charges derived from *ab initio* MO calculations. The Mulliken population analysis (9) has been found to contain assumptions that can lead to unrealistic results (10).[6] However, Mulliken charges can be used in all cases where carbon forms the same number and type of bonds, because any anticipated error due to an incorrect assignment of overlap populations (e.g. for C—H) cancels in this type of comparison. In fact, linear relationships between STO-3G Mulliken charges (using standard geometries) and ^{13}C chemical shift data have been reported in several benzenoid systems, where the substituent is far removed from the site on which the charge is sampled (11). In this study, the effect of partial geometry optimizations at the STO-3G level on such a charge–shift relationship in monosubstituted benzenes will be investigated.

Satisfactory correlations between Mulliken charges and substituent constants (σ) in benzenoid systems have been reported (11). For reasons that will become clear, we have chosen relative interaction energies rather than σ-values to investigate the presence of linear Mulliken charge – energy and chemical shift – energy relationships.

Results and discussion

The proximity of R and X in a molecule of the type RCH_2X (and the fact that they are bonded to the same atom) is one of the reasons for the large relative interaction energies observed in alkyl systems (1). However, even in *meta*- and *para*-disubstituted benzenes, where the interacting groups are far removed from one another, significant interactions are observed (Table 1).[7] For example, values for the relative interaction between two cyano groups are 14.2 and 8.6 kJ mol^{-1}, respectively, for the *meta* and *para* derivatives. These values clearly show significant interactions between two cyano groups and (or) between a cyano group and hydrogen atoms (CN/H) at these positions. The (CN/H) interaction has to be considered because ΔH^0_1 values in Table 1 are measured relative to X/H and Y/H interactions.

The X/COOH interactions are particularly interesting because the Hammett σ-scale is based on the dissociation of these benzoic acids (12). From Table 1 it is clearly seen that for the benzoic acids, when X = NH_2 and Cl, significant interactions exist both at the *meta* and *para* positions (and when X = I at the *para* position). These are total group effects; at present no separation into contributions from individual bonds in the CO-

[4] It is noted that a σ- and π-separation of charge cannot be made for the methoxy toluenes within the Mulliken framework (2).

[5] S. Fliszár, private communication.

[6] For a discussion on the limitation of the Mulliken scheme see ref. 6 (and ref. 32 therein).

[7] Albeit, the uncertainty in some cases is as large as the corresponding interaction enthalpy.

Can. J. Chem. Downloaded from www.nrcresearchpress.com by 210.87.254.105 on 09/06/12
For personal use only.

TABLE 2. Total energies ($E_{(RHF)}$ (au)) of monosubstituted benzenes and toluenes at STO-3G level

Substituent	Benzene	Toluene	
		meta	*para*
H	−227.89136	−266.47503	
CH_3	−266.47503[a, b]	−305.05875	−305.05849
	−266.47503[b, c]		
F	−325.35104	−363.93508	−363.93452
CN	−318.44427	−357.02832	−357.02873
OCH_3	−340.30661[b, d]	−378.89063[b, d]	−378.88979[b, d]
Li	−234.60178	−273.18506	−273.18499

[a] One of the C—H bonds in the CH_3 group is assumed to be coplanar with the benzenoid ring.
[b] A model CH_3 group (r_{CH} = 1.09 Å and ∠HCH = 109.47 Å) was used.
[c] One of the C—H bonds in the CH_3 group is in a plane perpendicular to the benzenoid ring.
[d] The O—C bond in the OCH_3 group is assumed to be coplanar with the benzenoid ring.

OH group is not possible. The importance of such a separation is that it will indicate the presence (or absence) of a substituent effect in the benzoic acids that may not exist in the ionized state.[8] The interactions are significant even with alkyl groups (X = OH, Z = C_2H_5) and thus can be expected to be general. The significance of these results is that kinetically derived substituent constants reflect interactions in a transition state (or intermediate) relative to a reference state that is also subject to substituent interactions. Undoubtedly the interactions on the reference state will be smaller than on any ionized state or highly polar transition state, but may be large enough (not to be disregarded) when effects on nonionized open or closed shell states are considered. Thus, ΔE^0_I values (rather than σ-values) have been used in this work to investigate the relationship between interaction energies and charges on atoms (or chemical shifts).

Substituent effects on the stability of benzyl radicals is a topic of interest to us (13). In the BDH method, these stabilities are assessed relative to the toluenes. Here we have attempted to study the energetics of the interaction between substituents and the methyl group in toluenes using *ab initio* MO calculations at the STO-3G level (Table 2).[9] These interaction energies (ΔE^0_I) were calculated by considering the appropriate isodesmic reaction (reaction [1]).

In an isodesmic reaction, the formal bond types are conserved on both sides of the equation. This has the advantage that systematic errors inherent in the minimum STO-3G basis set calculations tend to cancel (18). Thus, a fair confidence can be placed in the calculated ΔE^0_I values, although some of the properties of an individual species computed at the STO-3G level may not agree with experiment. For example, while Table 3 shows that, except for the methoxy substituent, the STO-3G equilibrium geometries agree with experiment, Table 4 indicates deviations between STO-3G and experimental dipole moments.

Table 5 clearly shows the presence of significant interactions between substituents (especially the cyano group) and the methyl (and (or) hydrogen atom) group. Similar results have been obtained in the *ab initio* MO study of several series of disubstituted benzenes at the STO-3G level using standard geometries (2). However, at present the dissection of these effects in terms of individual bond contributions of the methyl group is not possible. *Thus, BDH values cannot be corrected to yield substituent effects on the stability of a benzyl radical.*

A major drawback in estimating $SE^0[R^\cdot, RX]$ values (1) has been the inability to determine the charges on atoms in these systems. Table 6 shows that performing partial geometry optimizations does not affect the linear ^{13}C chemical shift – Mulliken charge relationships that have been established previously (11). However, a complete description of charge effects in benzenoid systems requires a separation into σ- and π-contributions. At present, such a dissection of ^{13}C chemical shift values cannot be made. Thus, the usefulness of chemical shift values to establish shift–charge or shift–energy relationships is limited, and it is not surprising that the correlation between ^{13}C chemical shifts and energy is poor (Table 7). In Tables 8–10, the feasibility of using *ab initio* MO calculations, at a minimum STO-3G level, to establish charge–energy relationships is studied.

The Mulliken charges and π-overlap populations given in Tables 8 and 9 show that the donation (or withdrawal) of σ- or π-charges by a substituent to (or from) the ring is changed only slightly in the toluenes compared to the benzenes. Thus, the charge contributions of X to the stability of the toluene relative to the benzene will depend on the different sensitivities of the methyl group and the hydrogen atom to the charge effects of X. If the stabilizing effect of X was independent of Y (including H atoms), $\delta(\Delta E^0_{X/Y})$ would be equal to $\delta(\Delta E^0_{X/H})$ and ΔE^0_I would be zero (eq. [4]). However, ΔE^0_I values in Table 5 show significant interactions between substituents and the *meta*- and *para*-methyl groups (and (or) hydrogen atoms). In Table 10 the importance of charge effects in these interactions is investigated.

In an extensive and incisive study of substituent interactions in substitued benzenes, Pross and Radom (2) outlined factors governing the stability of disubstituted benzenes, and reached qualitative conclusions about σ- and π-interactions. Their study indicated that the dominant σ-effects were the lowering (or raising) of the energy levels of the ring orbitals by a deshielding (or shielding) process caused by σ-acceptors (or donors). It was also found that σ-effects cause changes to π*-energy levels and hence affect π-charges. The π-effects (especially in the *para* position) were found to be dominated by resonance type interactions. In this study the relationship between interaction energies and σ- and π-charges is investigated on a quantitative basis. Results in Table 10 support the above conclusions reached in the study by Pross and Radom (2).

It is clear from Table 10 that a linear Mulliken charge – energy relationship has been established for both *meta*- and *para*-substituted toluenes. However, it must be noted that the linear charge–energy relationship obtained for the disubstituted benzenes does not, in any way, indicate the absence (or presence) of a substituent interaction with the *meta* or *para* hydrogen in the monosubstituted benzene. It can only be con-

[8] If such interactions are present, σ-values will partly reflect stabilization (or destabilization) of the undissociated acid.

[9] Standard single determinant MO theory was used. The *ab initio* MO calculations described were obtained by the use of the GAUSSIAN 76 program (14) on a Control Data CYBER 170-220 system. The closed shell, spin-restricted (RHF) procedure was employed (15) to compute the energies of the mono- and disubstituted benzenes. The minimal STO-3G basis set (16) was used. Partial geometry optimizations, subject to imposed symmetry constraints, were applied. A standard phenyl ring with hexagonal symmetry was assumed in every case (17). r_{CC} = 1.38669 Å and r_{CH} = 1.08258 Å (STO-3G values for benzene, ref. 17).

Can. J. Chem. Downloaded from www.nrcresearchpress.com by 210.87.254.105 on 09/06/12
For personal use only.

Can. J. Chem. Downloaded from www.nrcresearchpress.com by 210.87.254.105 on 09/06/12
For personal use only.

TABLE 3. STO-3G equilibrium geometries of substituents, attached to a standard phenyl ring, in monosubstituted benzenes and toluenes

Substituent	Substituent parameter	Benzene		Toluene STO-3G	
		STO-3G	Expt.	*meta*	*para*
CH_3	r_{CC}	1.533 Å	1.52 ± 0.01 Å[a]	1.533 Å	1.533 Å
F	r_{CF}	1.356	1.354[b]	1.356	1.357
	$r_{CC(\alpha)}$[c]	—	—	1.532	1.533
CN	r_{CN}	1.157	1.1581[b]	1.157	1.157
	$r_{CC(N)}$[d]	1.464	1.4509[b]	1.464	1.463
	$r_{CC(\alpha)}$[d]	—	—	1.532	1.532
OCH_3	r_{CO}	1.432	1.423[b]	1.433	1.432
	$r_{OC(r)}$[e]	1.402	1.361[b]	1.402	1.403
	$r_{CC(\alpha)}$[e]	—	—	1.532	1.533
	∠COC	116.8°	120.0°[b]	116.9°	117.0°
Li	r_{CLi}	1.947	—	1.947	1.944
	$r_{CC(\alpha)}$[c]	—	—	1.534	1.533

[a] Reference 20.
[b] Reference 21.
[c] Carbon of CH_3 group.
[d] Carbon of the CN group.
[e] Carbon of aromatic ring.

TABLE 4. Theoretical STO-3G dipole moments (D) of monosubstituted benzenes and toluenes

Substituent	Benzene			Toluene	
		Exptl.[a]			
	STO-3G	Gas phase	Solution	*meta* (STO-3G)	*para* (STO-3G)
CH_3	0.25	0.37	0.37	0.21	0.04
F	1.02	1.61	1.47	1.17	1.27
CN	3.65	4.39	4.05	3.85	4.02
OMe	1.17	1.35	1.28	0.97	1.22
Li	4.99	—	—	4.93	4.76

[a] Reference 22.

TABLE 5. Relative STO-3G interaction energies, ΔE^0_1 (kJ mol^{-1}), for the interaction between X and CH_3 (relative to X and H, and CH_3 and H) in substituted toluenes

Substituent	Toluene			
	meta		*para*	
	This work	Lit.[a]	This work	Lit.[a]
H	0	—	0	—
CH_3	−0.13	—	+0.54	—
F	−0.96	−1.3	+0.50	+0.8
CN	−5.10	−0.8	−6.19	−2.09
OMe	−0.92	—	+1.30	—
Li	+1.00	0.8	+1.21	1.3

[a] Reference 2.

cluded that, if both types of interactions do exist, they are well correlated. A closer examination of the correlation data in Table 10 enables a better understanding of these interactions.

From Table 10 it is seen that the best correlations are obtained for the three-parameter equations involving $q_\sigma(X)$, $q_\sigma(Y)$, and $q_\pi(X)$ (or $q_\pi(X)\cdot q_\pi(Y)$). Table 9 shows that $q_\pi(Y)$ varies only slightly throughout the series. Thus, we are unable to conclude whether $q_\pi(X)$ or $[q_\pi(X)\cdot q_\pi(Y)]$ is better as one of the parameters describing the linear correlation between charges and energies.

The positive $[\rho_\pi(X)\cdot\rho_\pi(Y)]$ or the negative $\rho_\pi(X)$ values indicate that π-acceptors interact favourably with the π-donating methyl group. This type of π-resonance interaction is found to be equally important with the *meta*-substituents as for the *para*-substituents. There can also be π-type interactions between substituents and the π-electrons of the ring in monosubstituted benzenes. However, such interactions will also be present in the toluenes and will differ from the benzenes due to the π-effect of the methyl group.

A few general conclusions can be made about σ-effects. Table 10 shows $\rho_\sigma(Y) > 0$ and $\rho_\sigma(X) < 0$. A positive $\rho_\sigma(Y)$ value indicates that any substituent that decreases $q_\sigma(Y)$ will stabilize the CH_3/X interaction relative to the H/X interaction. As expected from the shielding–deshielding process described above, σ-acceptors decrease and σ-donors increase $q_\sigma(Y)$. However, π-effects are also found to affect these σ-interactions. Thus, while $q_\sigma(F) > q_\sigma(CN)$, $q_\sigma(CH_3)$ for the cyano toluenes is more negative than that of the corresponding fluoro toluenes. The lithium substituent (with $q_\sigma(X) < 0$) makes $q_\sigma(Y) > 0$. Both $\rho_\sigma(Y)$ and $\rho_\sigma(X)$ values indicate that the Li/CH_3 interaction is destabilizing relative to the Li/H interaction (as is observed in Table 10). This is an unusual case, where the contribution to ΔE^0_1 is positive (destabilizing) for a σ-donor/σ-acceptor pair. A possible explanation for this phenomenon is that lithium forces electrons from the ring to the methyl group and causes a destabilization. Alternatively, it is also possible that the positive ΔE^0_1 values, for X = *m*-Li or *p*-Li, are due to a greater stabilizing Li/H interaction relative to the Li/CH_3 interaction. This would imply that hydrogen is either a weaker σ-donor than methyl or it is a σ-acceptor that will interact favourably with lithium. Such a conclusion is at variance with the Mulliken analysis, which indicates that hydrogen is a fairly strong σ-donor and should not interact favourably with the σ-donating groups like lithium.

Table 10 also shows that the constants in eq. [6] are not zero. These small values may be a reflection of the interaction be-

Can. J. Chem. Downloaded from www.nrcresearchpress.com by 210.87.254.105 on 09/06/12
For personal use only.

TABLE 6. Mulliken STO-3G charges of ring carbons[a] in monosubstituted benzenes and their relationship to the corresponding $\delta^{13}C$ chemical shifts at these positions

Substituent	*meta*-Carbon		*para*-Carbon		*ipso*-Carbon	
	$10^3\Delta q^*_\sigma(m)$	$10^3\Delta q^*_\pi(m)$	$10^3\Delta q^*_\sigma(p)$	$10^3\Delta q^*_\pi(p)$	$10^3\Delta q^*_\sigma(i)$	$10^3\Delta q^*_\pi(i)$
H	0	0	0	0	0	0
CH_3	−4	6	7	−12	50	27
F	−5	15	11	−17	209	−8
CN	2	1	−15	27	133	−55
OMe	−8	17	18	−30	177	13
Li[b]	−3	−8	10	−21	−129	15
ρ values[c]	0.27	0.19	1.04	0.40	0.19	0.49
(Correlation coefficient)[d]	(0.991)[d]		(0.987)[d]		(0.908)[d]	
[No of data points]	[5]		[5]		[5]	

[a] Obtained relative to STO-3G charge for ring carbons of benzene ($q^*_\sigma = -0.063$).
[b] Li is not included in the charge–shift correlation.
[c] ρ values for the correlation of $\delta^{13}C$ values with Δq^*_σ and q^*_π values:
[5] $\delta^{13}C(\gamma) = \rho_\sigma[10^3\Delta q^*_\sigma(\gamma)] + \rho_\pi[q^*_\pi(\gamma)]$
$\delta^{13}C$ values were obtained from ref. 23.
[d] Correlation coefficient for a linear regression analysis of δ values vs. $\Delta q^*_\sigma(\gamma)$ and $q^*_\pi(\gamma)$ (eq. [5]).

TABLE 7. An investigation of the relationship between isodesmic interaction energies (ΔE^0_1) and ^{13}C chemical shifts. Correlation coefficients for the linear regression analysis of ΔE^0_1 values (for *meta*- and *para*-substituted toluenes) versus ^{13}C chemical shifts[a]

Type of substituent (number of data points)	Correlation coefficient [parameters – subscript indicates position]								
	$[C_\alpha]$	$[C_\alpha, C_1]$	$[C_s, C_\alpha]$	$[C_s, C_1]$	$[C_1, C_s, C_\alpha]$	$[C_\alpha]$	$[\Delta C_1]^b$	$[C_\alpha, \Delta C^b_1, \Delta C^b_s]$	$[\Delta C^b_1, C_\alpha]$
meta (5)	0.798	0.817	0.729	0.914	0.835	—	—	0.820	—
para (5)	0.785	0.875	0.676	0.829	0.812	—	—	0.949	—
Δ(*para* − *meta*)[c] (5)	—	—	—	—	—	0.976	0.957	—	0.965

[a] For 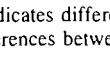 , substituent X attached to C_s ($C_s = C_3$ for *meta*; $C_s = C_4$ for *para*); ^{13}C chemical shifts for the toluenes from ref. 24(*a*), and for the benzenes from ref. 24(*b*).
[b] Δ indicates difference in the chemical shifts between the toluene and the benzene at the indicated positions.
[c] Differences between the *para* and *meta* values were considered for both ΔE^0_1 and $\delta\ ^{13}C$ values.

TABLE 8. Mulliken group charges and overlap populations in monosubstituted benzenes

Substituent (X)	$10^3q_\sigma(m\text{-H})^a$	$10^3q_\sigma(p\text{-H})^a$	$10^3q_\sigma(X)^b$	$10^3q_\pi(X)^b$	$\pi(Ph—X)^c$
H	−62.93	−62.93	−62.93	0	0
CH_3	−61.95[d]	−60.86	−6.93	−7.70	0.009
F	−68.55	−64.28	203.21	−69.58	0.034
CN	−73.13	−73.43	105.72	21.12	0.040
Li	−48.28	−50.22	−282.71	100.78	0.066
OMe	−65.45[d]	−60.36	178.29	−87.68	0.047

[a] $q_\sigma(m\text{-H})$ and $q_\sigma(p\text{-H})$ are the total σ charges donated by the ring hydrogens at the *meta* and *para* positions respectively.
[b] $q_\sigma(X)$ and $q_\pi(X)$ are the total σ and π charges, respectively, donated by the substituent X.
[c] π(Ph—X) is the Mulliken overlap population of the adjacent π-type *p*-orbitals in the bond joining X to the ring.
[d] Average of two values for the different types of *meta* hydrogens.

tween CH_3/H in toluene relative to H/H benzene. However, a definite conclusion cannot be made from this study involving such a limited number of substituents.

It is likely that nonlinear charge effects exist and can be studied using parameters such as $q_\pi(X)/[1 + \epsilon q_\pi(Y)]$ and $q_\sigma(X)/[1 + \epsilon q_\sigma(Y)]$ (19). However, the limited data in this work does not warrant such an attempt.

Conclusions

The present work shows that *ab initio* MO calculations, even at the minimum STO-3G level, can provide a quantitative analysis of interactions in benzenoid systems. Relative interaction energies between a substituent and the methyl group in *meta*- and *para*-substituted toluenes are found to be linearly related to Mulliken σ- and π-charges. Further work needs to be done to

TABLE 9. Mulliken group charges and overlap populations in monosubstituted toluenes

Substituent (X)	$10^3 q_\sigma(Y)^a$	$10^3 q_\sigma(X)^a$	$10^3 q_\pi(Y)^a$	$10^3 q_\pi(X)^a$	π(Ph—Y)^b	π(Ph-X)^b
m-H	−6.93	−61.95	−7.70	—	0.009	0
p-H	−6.93	−60.86	−7.70	—	0.009	0
m-CH_3	−5.66	−5.66	−7.74	−7.74	0.009	0.009
p-CH_3	−4.55	−4.55	−7.17	−7.17	0.008	0.008
m-F	−13.69	204.37	−8.48	−69.87	0.009	0.034
p-F	−8.85	203.58	−7.28	−68.00	0.008	0.033
m-CN	−19.60	107.33	−8.61	20.99	0.009	0.040
p-CN	−19.70	107.54	−9.75	23.25	0.009	0.040
m-Li	11.18	−280.46	−6.21	100.40	0.008	0.065
p-Li	8.29	−279.66	−6.13	105.19	0.008	0.068
m-OMe	[c]	[c]	[c]	[c]	0.009	0.047
p-OMe	[c]	[c]	[c]	[c]	0.008	0.045

[a] $q_\sigma(Y)$, $q_\sigma(X)$, $q_\pi(Y)$, $q_\pi(X)$ are the total σ and π charges, respectively donated by the substituent, Y or X to the ring, Y = CH_3, X = substituent. Negative q values indicate donation and positive q values a withdrawal.
[b] π(Ph—Y) and π(Ph—X) are Mulliken overlap populations of the adjacent π-type *p*-orbitals in the bond joining Y and X, respectively, to the ring. Y = CH_3, X = substituent.
[c] Values not calculable since neither substituent is coplanar with the ring.

TABLE 10. An investigation of the relationship between isodesmic interaction energies (ΔE^0_1) and Mulliken group charges (q). A linear regression analysis of ΔE^0_1 values vs. q_σ and q_π values[a] of *meta*- and *para*-substituted toluenes

	ρ values,[b] correlation coefficients (r), and constants (C) for eq. [6][c]					
Type of substitutent (number of data points)	ρ_1, ρ_3 (r, C_{13})[d]	ρ_1, ρ_4 (r, C_{14})[e]	ρ_2, ρ_3 (r, C_{23})[f]	ρ_2, ρ_4 (r, C_{24})[g]	ρ_1, ρ_2, ρ_3 (r, C_{123})[h]	ρ_1, ρ_2, ρ_4 (r, C_{124})[i]
meta	281, −31	256, 3.7	−26, −61	−24, 8.1	175, −11, −46	91, −16, 6.8
(5)	(0.96, 1.18)	(0.94, 0.85)	(0.92, −0.69)	(0.98, −0.97)	(0.999, 0.50)	(0.995, −0.32)
para	361, −33	335, 4.6	−31, −81	−28, 11	290, −8, −47	239, −10, 7.0
(5)	(0.98, 1.86)	(0.98, 1.64)	(0.78, −0.14)	(0.89, −0.25)	(1.00, 1.51)	(0.999, 1.12)
meta and *para*	318, −32	295, 4.3	−28, −71	−26, 9.5	236, −9.2, −47	194, −10, 6.5
(10)	(0.97, 1.51)	(0.96, 1.25)	(0.88, −0.43)	(0.93, −0.64)	(0.984, 1.05)	(0.979, 0.62)

[a] q_σ and q_π values from Table 9. $q_1 = q_\sigma(Y)$; $q_2 = q_\sigma(X)$; $q_3 = q_\pi(X)$ and $q_4 = q_\pi(X) \cdot q_\pi(Y)$.
[b] $\rho_1 = \rho_\sigma(Y)$; $\rho_2 = \rho_\sigma(X)$; $\rho_3 = \rho_\pi(X)$; and $\rho_4 = \rho_\pi(X) \cdot \rho_\pi(Y)$.
[c] Equation [6]: $Z = \sum_i \rho_i q_i + C_{jk}$ (or C_{jkl}) where $i = j$, k (or j, k, and l) and $Z = \Delta E^0_1$.
[d] Equation [6]: $i = 1, 3$.
[e] Equation [6], $i = 1, 4$.
[f] Equation [6], $i = 2, 3$.
[g] Equation [6], $i = 2, 4$.
[h] Equation [6], $i = 1, 2, 3$.
[i] Equation [6], $i = 1, 2, 4$.

determine whether these linear relationships are generally applicable. We hope that the present approach of analysing ΔE^0_1 values in terms of q_σ and q_π values will stimulate further work in this area. The use of chemical shift values to establish a shift–energy relationship is limited by the inability to separate σ- and π-effects on δ values.

At present, $SE^0_{C^*/X^*}$ values (1) for benzenoid systems cannot be estimated, because the problem of establishing reliable atomic charges has not been overcome. Thus, at present, BDH values or isodesmic interaction energies (ΔE^0_1) cannot be used to estimate the stability of benzyl radicals.

Acknowledgements

This work was supported by a grant from the Natural Sciences and Engineering Research Council of Canada. We are grateful to R. J. Boyd for his continuing interest in this program. Useful discussions with S. Fliszár (Université de Montreal) and W. L. Reynolds (University of Toronto) are also acknowledged. A. M. N. is grateful for the award of an Izaak Walton Killam Memorial Scholarship.

1. A. M. DE P. NICHOLAS and D. R. ARNOLD. Can. J. Chem. **62**, 1850 (1984).
2. A. PROSS and L. RADOM. Prog. Phy. Org. Chem. **13**, 1 (1981).
3. J. B. PEDLEY and J. RYLANCE. Sussex-N.P.L. Computer analysed thermochemical data: organic and organometallic compounds. University of Sussex, England. 1977.
4. M. MÅNSSON. Pure Appl. Chem. **55**, 417 (1983).
5. D. F. MCMILLEN and D. M. GOLDEN. Ann. Rev. Phys. Chem. **33**, 493 (1982).
6. S. FLISZÁR. J. Am. Chem. Soc. **102**, 6946 (1980).
7. S. FLISZÁR and M.-T. BÉRALDIN. Can. J. Chem. **60**, 792 (1982).
8. M.-T. BÉRALDIN and S. FLLISZÁR. Can. J. Chem. **61**, 197 (1983).
9. R. S. MULLIKEN. J. Chem. Phys. **23**, 1833 (1955); **23**, 1841 (1955); **23**, 2338 (1955); **23**, 2343 (1955).
10. (*a*) G. KEAN, D. GRAVEL, and S. FLISZÁR. J. Am. Chem. Soc. **98**, 4749 (1976); (*b*) S. FLISZÁR. Can. J. Chem. **54**, 2839 (1976).

Can. J. Chem. Downloaded from www.nrcresearchpress.com by 210.87.254.105 on 09/06/12
For personal use only.

11. W. J. HEHRE, R. W. TAFT, and R. D. TOPSOM. Prog. Phys. Org. Chem. **12**, 159 (1976).
12. L. P. HAMMETT. J. Am. Chem. Soc. **59**, 96 (1937).
13. J. M. DUST and D. R. ARNOLD. J. Am. Chem. Soc. **105**, 1221 (1983); **105**, 6531 (1983).
14. J. S. BINKLEY, R. A. WHITESIDE, P. C. HARIHARAN, R. SEEGER, J. A. POPLE, W. J. HEHRE, and M. D. NEWTON. QCPE, **11**, 368 (1978).
15. C. C. J. ROOTHAAN. Rev. Mod. Phys. **23**, 69 (1951).
16. W. J. HEHRE, R. F. STEWART, and J. A. POPLE. J. Chem. Phys. **51**, 2657 (1969).
17. R. A. WHITESIDE, J. S. BINKLEY, R. KRISHNAN, D. J. DEFREES, H. B. SCHLEGEL, and J. A. POPLE. Carnegie–Mellon Quantum Chemistry Archive University, Pittsburgh, PA. 1980.
18. W. J. HEHRE, L. RADOM, and J. A. POPLE. J. Am. Chem. Soc. **94**, 1496 (1972).
19. J. BROMILOW, R. T. C. BROWNLEE, D. J. CRAIK, M. SADEK, and R. W. TAFT. J. Org. Chem. **45**, 2429 (1980).
20. L. E. SUTTON. Tables of interatomic distances and configuration in molecules and ions. Supplement 1956–1959. Special Publication no. 18. The Chemical Society, London. 1965.
21. J. H. CALLOMON, E. HIROTA, K. KUCHITSU, W. J. LAFFERTY, A. G. MAKI, and C. S. POTE. Structure data of free polyatomic molecules. Landolt–Bornstein. New Series. Group II. Vol. 7. *Edited by* K.-H. Hellwege and A. M. Hellwege. Springer Verlag, Berlin. 1976.
22. A. J. GORDON and R. A. FORD. The chemicals companion. A handbook of practical data, techniques and references. Wiley, New York. 1972. pp. 124–127.
23. G. L. NELSON, G. C. LEVY, and J. D. CARGIOLI. J. Am. Chem. Soc. **94**, 3089 (1972).
24. (*a*) N. INAMOTO, S. MASUDA, K. TOKUMARU, K. TORI, M. YOSHIDA, and Y. YOSHIMURA. Tetrahedron Lett. 3707 (1976); (*b*) G. L. NELSON, G. C. LEVY, and J. D. CARGIOLI. J. Am. Chem. Soc. **94**, 3089 (1972).

Can. J. Chem. Downloaded from www.nrcresearchpress.com by 210.87.254.105 on 09/06/12
For personal use only.

Limiting low-pressure rate constant for the stepladder model of a thermal unimolecular reaction

H. O. PRITCHARD AND S. R. VATSYA

Centre for Research in Experimental Space Science, York University, Downsview, Ont., Canada M3J 1P3

Received January 4, 1984

H. O. PRITCHARD and S. R. VATSYA. Can. J. Chem. **62**, 1867 (1984).

An explicit formula for the rate constant of a thermal unimolecular reaction with stepladder relaxation probabilities, together with the corresponding eigenvector, are derived; a comment is also made about the limiting behaviour of the incubation time for such a reaction.

H. O. PRITCHARD et S. R. VATSYA. Can. J. Chem. **62**, 1867 (1984).

On a déduit une formule explicite de la constante de vitesse d'une réaction thermique unimoléculaire à probabilités de relaxation par paliers, de même que les vecteurs eigen correspondant; on commente de plus sur le comportement limitant du temps d'incubation d'une telle réaction.

[Traduit par le journal]

Can. J. Chem. Downloaded from www.nrcresearchpress.com by 210.87.254.105 on 09/06/12
For personal use only.

Introduction

Some years ago, Yau derived an analytic formula for the rate constant of a bimolecular reaction in which the internal relaxation consisted of stepladder (i.e. nearest-neighbour) processes, and for which there was only one state which was capable of being transformed into products (1); this formula was applied successfully to semiquantitative discussions of the ionisation of H atoms (2) and of the dissociation of H_2 molecules (3). With trivial modification, this formula can be used to give the rate constant for a thermal unimolecular reaction at its second order limit, provided that the activation processes are nearest-neighbour only, and that there is only one reactive state above the threshold (4). Since the rate of a unimolecular reaction at its low-pressure limit is strictly independent of the decay rate constants for the reactive states (5), it was easily shown by numerical experiment (6) that a minor modification of Yau's formula gave the correct eigenvalue for a stepladder thermal unimolecular reaction at this limit, regardless of the number of reactive states above the threshold. In this paper, we derive an analytic formula for this rate constant — for which hitherto there have only been available a series of steady-state approximations (7) — and also the corresponding eigenvector; the latter is important because it leads directly to the population distribution during the steady phase of the reaction, and also to the incubation time (4).

Preliminaries

Let $\mathbf{Q}$ be the tridiagonal relaxation matrix, with elements $[\mathbf{Q}]_{ji} = q_{ij}$ corresponding to the rate constant for conversion from grain (or state) i to grain (or state) j at unit pressure ($P = 1$); $q_{ij} = 0$ unless $j = i \pm 1$. The thermal unimolecular rate constant is the smallest eigenvalue γ_0 of the matrix $-[p\mathbf{Q} - \mathbf{D}]$, where $\mathbf{D}$ is a diagonal matrix of the decay rate constants d_j for the reactive grains (or states). The matrix $\mathbf{Q}$ is unsymmetric, but may be symmetrised by a similarity transformation constructed from the detailed balancing relationships, to give

$$[1] \quad \mathbf{R} = -\mathbf{E}^{-1/2}\,[p\mathbf{Q} - \mathbf{D}]\,\mathbf{E}^{1/2} = [p\mathbf{A} + \mathbf{D}]$$

where $[\mathbf{E}]_{ij} = \delta_{ij}\tilde{n}_j$, and $\tilde{n}_j$ is the equilibrium population of grain (or state) j at the temperature in question. Let the eigenvector of $\mathbf{A}$ corresponding to its zero eigenvalue be $\mathbf{S}_0$; the elements $(\mathbf{S}_0)_j = \tilde{n}_j^{1/2}$. Also let the notation (,) denote the scalar product of two vectors, and $p_j = \mathbf{S}_j(\mathbf{S}_j, \ )$ are the eigenprojections of $\mathbf{A}$ corresponding to the eigenvalues λ_j. For further details relating to this formulation, see ref. 4.

The limiting low-pressure rate constant

Let the grains (or states) be labelled by the index i, $0 \le i \le n-1$, with i_0 denoting the last one below the reactive threshold. We note that γ_0 is a fixed point of $\chi(x)$ given by (8)

$$[2] \quad \frac{1}{\chi(x)} = (\mathbf{S}_0, [p\mathbf{A} + \mathbf{D} - (1 - p_0)x]^{-1}\mathbf{S}_0)$$

and $\chi(0)$ is an excellent (upper bound) approximation to γ_0 for the entire pressure range. From eq. [4] of ref. 8, $\chi(0)$ is given by

$$[3] \quad \frac{P}{\chi(0)} = -\sum_{i=0}^{n-1}\sum_{j=1}^{n-1}\sum_{k=0}^{j}\frac{\tilde{n}_i^{1/2}\alpha_i\tilde{n}_k^{1/2}\alpha_k}{\alpha_j\alpha_{j+1}A_{j,j+1}} = -\sum_{j=0}^{n-1}\frac{1}{\alpha_j\alpha_{j+1}A_{j,j+1}}\left(\sum_{i=0}^{j}\tilde{n}_i^{1/2}\alpha_i\right)^2$$

where $A_{n-1,n} = A_{n,n-1} = 1/P$, $\alpha_0 = 1$, $\alpha_1 = -A_{00}/A_{01}$, ..., and $\alpha_{i+1} = -[A_{i,i-1}\alpha_{i-1} + (A_{ii} + d_i/P)\alpha_i]/A_{i,i+1}$, $i = 1, 2, \ldots, (n-1)$. (Notice that the elements $A_{n-1,n}$, $A_{n,n-1}$ are not part of the original nth order matrix; they arise from extending the original matrix as described in ref. 8.) It is clear that

$$\alpha_j = \tilde{n}_j^{1/2}/\tilde{n}_0^{1/2},\ j = 0, 1, \ldots, (i_0 + 1)$$

and $\alpha_{i_0+1}/\alpha_{i_0+2} \xrightarrow[P \to 0]{} 0$. Further,

$$\frac{\alpha_j}{\alpha_{j+1}} = \frac{-PA_{j,j+1}}{PA_{jj} + d_j + PA_{j,j-1}\alpha_{j-1}/\alpha_j} \quad \text{for each } j$$

Let $(n-1) \ge j \ge (i_0 + 2)$ if $\alpha_{j-1}/\alpha_j \xrightarrow[P \to 0]{} 0$, then $\alpha_j/\alpha_{j+1} \xrightarrow[P \to 0]{} 0$. Since $\alpha_{i_0+1}/\alpha_{i_0+2} \xrightarrow[P \to 0]{} 0$, it follows that $\alpha_j/\alpha_{j+1} \xrightarrow[P \to 0]{} 0$ for all $(i_0 + 1) \le j \le (n-1)$.

Since

$$\frac{\alpha_i\alpha_k}{\alpha_j\alpha_{j+1}} = \frac{\alpha_j}{\alpha_{j+1}}\prod_{l=1}^{j-i}\frac{\alpha_{i+l-1}}{\alpha_{i+l}}\prod_{m=1}^{j-k}\frac{\alpha_{k+m-1}}{\alpha_{k+m}} \qquad i, k \le j$$

$$\frac{\alpha_i\alpha_k}{\alpha_j\alpha_{j+1}} \xrightarrow[P \to 0]{} 0 \text{ for } (n-1) \ge j \ge i_0 + 1 \text{ and } j \ge i, k$$

It then follows from [3] that

$$[4]\quad \gamma_0 = P\left(\sum_{j=0}^{i_0} t_j\right)^{-1}$$

$$\text{where } t_j = -\left(\sum_{i=0}^{j} \tilde{n}_i\right)^2 \Big/ \tilde{n}_j^{1/2}\tilde{n}_{j+1}^{1/2}A_{j,j+1}$$

The expression for t_j can be simplified a little further, since

$$A_{ij} = -\tilde{n}_i^{-1/2}Q_{ij}\tilde{n}_j^{1/2} = -\tilde{n}_i^{-1/2}q_{ji}\tilde{n}_j^{1/2}, \qquad i \neq j$$

giving finally that

$$t_j = \left(\sum_{i=0}^{j} \tilde{n}_i\right)^2 \Big/ \tilde{n}_j q_{j,j+1}$$

The examination of activation bottlenecks and their effect on the low-pressure unimolecular rate becomes a simple matter with this expression (6); in fact, [4] is quite similar to the earlier steady-state approximations, but the expression for the t_j is different.

The corresponding eigenvector

An eigenvector ψ_0 of $[p\mathbf{A} + \mathbf{D}]$ corresponding to the eigenvalue γ_0 is given by

$$\psi_0 = \gamma_0[p\mathbf{A} + \mathbf{D} - \gamma_0(1 - p_0)]^{-1}\mathbf{S}_0$$

where ψ_0 is normalised so that $(\psi_0, \mathbf{S}_0) = 1$. The vector ψ_0 is approximated by $\bar{\psi} = \chi(0)[p\mathbf{A} + \mathbf{D}]^{-1}\mathbf{S}_0$ to the same degree of accuracy as is γ_0 by $\chi(0)$. Now, from the results in the preceding section, we can write

$$[5]\quad f_i = \lim_{P \to 0} (p[p\mathbf{A} + \mathbf{D}]^{-1}\mathbf{S}_0)_i$$

$$= -\sum_{j=1}^{i_0} \frac{\tilde{n}_i^{1/2} \sum_{k=0}^{j} \tilde{n}_k}{\tilde{n}_j^{1/2}\tilde{n}_{j+1}^{1/2}A_{j,j+1}}, \qquad i \leq i_0$$

$$= 0, \qquad i > i_0$$

where f_i are the elements of the un-normalised vector; the elements of the normalised vector are simply

$$[6]\quad (\bar{\psi}_0)_i = \gamma_0 f_i/P$$

Apart from the different normalisation, this is the same eigenvector as that derived by Brau (9).

Incubation times

It was found recently that for a shock-wave heating process from a low starting temperature, the incubation time (τ_{inc}) for a strong-collision thermal reaction becomes independent of the pressure at the low-pressure limit (10). Intuitively, this is an unphysical result; its existence, however, renders it necessary to prove that in reactions not governed by the strong-collision relaxation rates, the relation $P\tau_{inc}$ = constant still holds, as is usually assumed to be the case in experimental systems. As a beginning, we do this here for the stepladder model of a unimolecular reaction at the low-pressure limit. To the same degree of approximation as γ_0 is approximated by $\chi(0)$, an excellent approximation $\bar{\tau}_{inc}$ to (4, 11)

$$\tau_{inc} = \frac{1}{\gamma_0} \ln [(\mathbf{E}^{-1/2}\mathbf{n}(0),\psi_0)/(\psi_0,\psi_0)]$$

is given by

$$[7]\quad P\bar{\tau}_{inc} = \frac{P}{\chi(0)} \ln \frac{(\mathbf{E}^{-1/2}\mathbf{n}(0),[p\mathbf{A} + \mathbf{D}]^{-1}\mathbf{S}_0)}{\chi(0)(\mathbf{S}_0,[p\mathbf{A} + \mathbf{D}]^{-2}\mathbf{S}_0)}$$

where $\mathbf{n}(0)$ is the starting distribution, taken to be 1, 0, 0, ... for a shock-wave heating from a low starting temperature. Straightforward substitution of [6] into [7] yields

$$[8]\quad \lim_{P \to 0} (P\bar{\tau}_{inc}) = \bar{\gamma}(0)^{-1} \ln (f_0/F\tilde{n}_0^{1/2})$$

where $F = \bar{\gamma}(0) \sum_{i=0}^{i_0} f_i^2$ and $\bar{\gamma}(0) = \lim_{P \to 0} \gamma_0/P$.

This results leads to two conclusions. First, like the limiting rate constant, the incubation time for the stepladder case is also independent of the numerical values of the decay rate constants; this is already known, see e.g. equation (5.2) of ref. 12. Second, since γ_0/P is a constant at the low-pressure limit, the right-hand side of [8] is a constant; hence $P\bar{\tau}_{inc}$ is a constant, as we wished to show.

1. A. W. YAU. Ph.D. Thesis. York University, Toronto. 1978.
2. A. W. YAU and H. O. PRITCHARD. Proc. R. Soc. London Ser. A**362**, 113 (1978).
3. A. W. YAU and H. O. PRITCHARD. J. Phys. Chem. **83**, 134 (1979).
4. H. O. PRITCHARD. Quantum theory of unimolecular reactions. Cambridge University Press. 1984.
5. S. R. VATSYA and H. O. PRITCHARD. Mol. Phys. In press.
6. H. O. PRITCHARD. Can. J. Chem. **62**, 157 (1984).
7. J. KECK and G. CARRIER. J. Chem. Phys. **43**, 2284 (1965).
8. S. R. VATSYA. J. Phys. A, **16**, 201 (1983).
9. C. A. BRAU. J. Chem. Phys. **47**, 3076 (1967).
10. H. O. PRITCHARD. J. Phys. Chem. **87**, 3179 (1983).
11. H. O. PRITCHARD and S. R. VATSYA. Chem. Phys. **72**, 447 (1982).
12. J. TROE. J. Chem. Phys. **73**, 3205 (1980).

Can. J. Chem. Downloaded from www.nrcresearchpress.com by 210.87.254.105 on 09/06/12
For personal use only.

Preparation and crystal and molecular structure of (η^3-nonamethylcyclotetraphosphazanium-*P*,*P*,*P*)tricarbonylmolybdenum(0) iodide – acetonitrile (1:1), $[(\eta^3\text{-Me(MeNPMe)}_4)\text{Mo(CO)}_3]\text{I}\cdot\text{MeCN}$

KEITH D. GALLICANO, NORMAN L. PADDOCK, STEVEN J. RETTIG, AND JAMES TROTTER

Department of Chemistry, University of British Columbia, 2036 Main Mall, Vancouver, B.C., Canada V6T 1Y6

Received January 18, 1984

KEITH D. GALLICANO, NORMAN L. PADDOCK, STEVEN J. RETTIG, and JAMES TROTTER. Can. J. Chem. **62**, 1869 (1984).

The synthesis and physical properties of $[(\eta^3\text{-Me(MeNPMe)}_4)\text{Mo(CO)}_3]\text{I}$ are reported. Crystals of (η^3-nonamethylcyclotetraphosphazanium-*P*,*P*,*P*)tricarbonylmolybdenum(0) iodide – acetonitrile (1:1) are orthorhombic, a = 13.1938(4), b = 13.7847(5), c = 29.281(2) Å, Z = 8, space group *Pcab*. The structure was solved by Patterson and Fourier techniques and was refined by full-matrix least-squares procedures to R = 0.030 and R_w = 0.034 for 2388 reflections with $I \geq 3\sigma(I)$. The structure consists of discrete cations, anions, and solvent molecules. The complex cation has approximate mirror symmetry in the solid state, the Mo atom being coordinated to three phosphazane P atoms and three carbonyl ligands in a distorted octahedral arrangement. Important bond lengths (corrected for libration) are: Mo—P = 2.483(2), 2.439(2), and 2.474(2), mean Mo—C = 1.984(3), mean P—N = 1.710(11) for coordinated P and 1.669(5) Å for quaternized P. The stronger bonding of the cationic ligand to the metal relative to that of the neutral species $(CH_3NPCH_3)_4Mo(CO)_3$, and the strengthening of the ring bonds in both molecules relative to $(CH_3NPCH_3)_4$, are discussed in terms of *d*-orbital contraction.

KEITH D. GALLICANO, NORMAN L. PADDOCK, STEVEN J. RETTIG et JAMES TROTTER. Can. J. Chem. **62**, 1869 (1984).

On rapporte la synthèse et les propriétés physiques du $[(\eta^3\text{-Me(MeNPMe)}_4)\text{Mo(CO)}_3]\text{I}$. Les cristaux de l'iodure-acétonitrile (1:1) du (η^3-nonaméthylcyclotétraphosphazanium-*P*,*P*,*P*)tricarbonylmolybdène(0) sont orthorhombiques, a = 13,1938(4), b = 13,7847(5), c = 29,281(2) Å, Z = 8, groupe d'espace *Pcab*. On a résolu la structure par les techniques de Patterson et Fourier et on l'a affinée par la méthode des moindres carrés (matrices complètes) jusqu'à des valeurs de R = 0,030 et R_w = 0,034 pour 2388 réflexions avec $I \geq 3\sigma(I)$. La structure comporte des cations, des anions et des molécules de solvant qui sont indépendantes. A l'état solide, la symétrie du cation complexe est approximativement celle d'un mirroir alors que l'atome de Mo est coordonné à trois atomes de P des phosphazanes et à trois ligands carbonyles dans un arrangement octaédrique déformé. Les longueurs de liaison importantes (corrigées pour la libration) sont: Mo—P = 2,483(2), 2,439(2) et 2,474(2), Mo—C (moyenne) = 1,984(3), P—N = 1,710(11) (moyenne pour le P coordonné) et 1,669(5) Å (moyenne pour le P quaternaire). C'est à des contractions dues à des orbitales *d* qu'on attribue le fait que la force de la liaison ligand cationique–métal est plus forte que celle impliquant l'espèce neutre $(CH_3NPCH_3)_4Mo(CO)_3$ ainsi que le renforcissement des liaisons du cycle dans chacune de ces deux molécules par rapport au $(CH_3NPCH_3)_4$.

[Traduit par le journal]

Can. J. Chem. Downloaded from www.nrcresearchpress.com by 210.87.254.6 on 09/06/12
For personal use only.

Introduction

An earlier paper (1) described the preparation of the complex $(CH_3NPCH_3)_4Mo(CO)_3$, **1**, and its crystal and molecular structure. Its methiodide can be prepared either from the complex or by reaction of the methiodide of the ligand with molybdenum hexacarbonyl. We have determined its structure to see what effect the positive charge has on the geometry and electron distribution.

Experimental

The compound $[(\eta^3\text{-Me(MeNPMe)}_4)\text{Mo(CO)}_3]\text{I}$, **2** (Fig. 1), was prepared by heating a mixture of **1** and an excess of methyl iodide in tetrahydrofuran under reflux for 4 h. After a further 18 h stirring at room temperature, the pale brown precipitate was filtered off, washed with acetonitrile, and crystallized from hot acetonitrile as pale green–yellow blocks of the monosolvate $[(\eta^3\text{-Me(MeNPMe)}_4)\text{-Mo(CO)}_3]\text{I}\cdot\text{MeCN}$, (**3**). *Anal.* calcd. for $C_{14}H_{30}IMoN_5P_4O_3$: C 25.4, H 4.6, N 10.6, I 19.1; found: C 25.6, H 4.6, N 10.6, I 18.9. The mass spectrum of **2** (70 eV) shows peaks corresponding to the stepwise loss of three CO's, with the characteristic isotopic distribution of Mo, the peak of highest m/e being at 480 (M^+ – MeI). ν_{CO} (cm^{-1}) 1946; 1856, 1836. ^1H nmr spectrum (δ, CD_3OD, int. TMS), 1.76 (3H, doublet, J ~ 6.5 Hz, P(2)), 2.02 (6H, broad, P(1), P(3)), 2.43 (3H, doublet, J ~ 12.5 Hz, P(4)), 2.72 (3H, doublet, J ~ 14.5 Hz, P(4)), 2.96 (6H, quintet, J ~ 4.5 Hz, N(1), N(2)), 3.27 (6H, doublet split into virtual triplets, J ~ 10 Hz, 2Hz, N(3), N(4)).

X-ray crystallographic analysis of **3**

A crystal bounded by the six faces (followed by their distances in mm from a common origin): ±(0 0 1), 0.040, (−1 −1 2), 0.138, (−1 1 2), 0.100, (1 −1 2), 0.100, (1 1 0), 0.153 was mounted in a general orientation. Unit-cell parameters were refined by least-squares on 2 sin θ/λ values for 25 reflections (2θ = 28–40°) measured on a diffractometer with Mo-$K\alpha$ Radiation ($\lambda(K\alpha_1)$ = 0.70930, $\lambda(K\alpha_2)$ = 0.71359 Å). Crystal data at 22°C are:

$C_{14}H_{30}IMoN_5P_4O_3$ fw = 663.16

Orthorhombic, a = 13.1938(4), b = 13.7847(5), c = 29.281(2) Å, V = 5325.4(5) Å^3, Z = 8, ρ_c = 1.654 g cm^{-3}, $F(000)$ = 2624, μ(Mo-$K\alpha$) = 18.9 cm^{-1}. Absent reflections: $0kl$, l odd, $h0l$, h odd, and $hk0$, k odd uniquely indicate the space group *Pcab* (non-standard setting of *Pbca*, D_{2h}^{15}, No. 61, equivalent positions: ±(x, y, z; $-x$, 1/2 − y, 1/2 + z; 1/2 − x, 1/2 + y, $-z$; 1/2 + x, $-y$, 1/2 − z)).

Intensities were measured with graphite-monochromated Mo-$K\alpha$ radiation on an Enraf-Nonius CAD4-F diffractometer. An ω–2θ scan at 1.26–10.06° min^{-1} over a range of (0.65 + 0.35 tan θ) degrees in

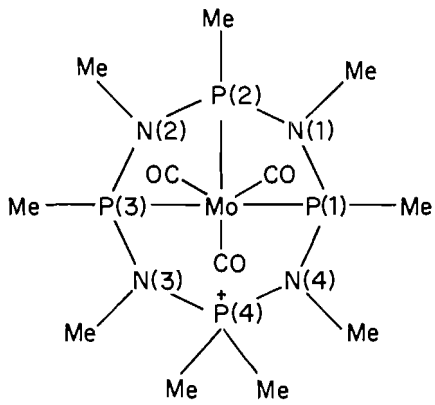

FIG. 1. Bond diagram of the cation **2**.

Can. J. Chem. Downloaded from www.nrcresearchpress.com by 210.87.254.6 on 09/06/12
For personal use only.

ω (extended by 25% on both sides for background measurement) was employed. Data were measured to $2\theta = 55°$. The intensities of three check reflections, measured every 3600 s throughout the data collection, showed uniform decreases of 4.5%, the data being scaled accordingly. After data reduction,[1] an absorption correction was applied using the Gaussian integration method (2, 3). Transmission factors ranged from 0.564 to 0.920 for 98 integration points. Of the 6108 independent reflections measured, 2388 (39.1%) had intensities greater than $3\sigma(I)$ above background where $\sigma^2(I) = S + 2B + (0.04(S - B))^2$ with S = scan count and B = normalized background count. It should be noted that most reflections with 2θ less than 40° were observed but at higher angles most were very weak. The data were collected to 55° in order to maximize the number of observations. Using a 2σ cutoff would have added only 59 reflections.

The coordinates of the I and Mo atoms were determined from the Patterson function and those of the remaining non-hydrogen atoms from a subsequent difference map. After full-matrix least-squares refinement of the non-hydrogen atoms with anisotropic thermal parameters to $R = 0.040$, a difference map revealed the positions of nearly all hydrogen atoms which were included in subsequent cycles of refinement as fixed atoms in idealized positions (based on the observed positions with C—H = 0.98 Å and $U_H = 1.2U_C$), recalculated after each least-squares cycle. The scattering factors of ref. 4 were used for non-hydrogen atoms and those of ref. 5 for hydrogen atoms. Anomalous scattering factors from ref. 6 were used for the I, Mo, and P atoms. The weighting scheme, $w = 1/\sigma^2(F)$ where $\sigma^2(F)$ is derived from the previously defined $\sigma^2(I)$, gave uniform average values of $w(|F_o| - |F_c|)^2$ over ranges of both $|F_o|$ and $\sin\theta/\lambda$ and was employed in the final stages of refinement. Unobserved reflections were not included in the refinement. Convergence was reached at $R = 0.030$ and $R_w = 0.034$ for 2388 reflections with $I \geq 3\sigma(I)$. The function minimized was $\Sigma w(|F_o| - |F_c|)^2$, $R = \Sigma||F_o| - |F_c||/\Sigma|F_o|$ and $R_w = (\Sigma w(|F_o| - |F_c|)^2/\Sigma w|F_o|^2)^{1/2}$.

On the final cycle of refinement the mean and maximum parameter shifts corresponded to 0.015 and 0.09σ respectively. The mean error in an observation of unit weight was 1.340. A final difference map showed no unusual features, the largest residual peak being 0.66 e Å^{-3} near the Mo atom. The final positional and thermal parameters appear in Tables 1 and 6,[2] respectively. Measured and calculated structure factors have been placed in the Depository of Unpublished Data.[2]

The ellipsoids of thermal motion for the non-hydrogen atoms are shown in Fig. 2. The thermal motion has been analysed in terms of the rigid-body modes of translation, libration, and screw motion (7). The rms standard error in the temperature factors σU_{ij} (derived from the least-squares analysis) is 0.0042 Å^2. Analysis of the entire cation (rms $\Delta U_{ij} = 0.0115$ Å^2) indicated significant independent motion of the carbonyl O atoms. A second analysis, excluding the three O atoms, gave rms $\Delta U_{ij} = 0.0051$ Å^2 and physically reasonable derived parameters. The appropriate bond distances have been corrected for libration (7, 8), using shape parameters q^2 of 0.08 for all atoms involved. Corrected bond lengths appear in Table 2 along with the uncorrected values; corrected bond angles do not differ by more than 1σ from the uncorrected values given in Table 3. Intra-annular torsion angles defining the conformations of phosphazane and chelate rings are listed in Table 4. Calculated hydrogen coordinates and thermal parameters (Table 5) are included as supplementary material. A complete list of torsion angles (Table 7) has also been deposited.

[1] The computer programs used include locally written programs for data processing and locally modified versions of the following: ORFLS, full-matrix least-squares, and ORFFE, function and errors, by W. R. Busing, K. O. Martin and H. A. Levy; FORDAP, Patterson and Fourier syntheses, by A. Zalkin; ORTEP II, illustrations, by C. K. Johnson.

[2] The structure factor table, Table 6 (anisotropic thermal parameters), and other material mentioned in the text are available, at a nominal charge, from the Depository of Unpublished Data, CISTI, National Research Council of Canada, Ottawa, Ont., Canada K1A 0S2.

TABLE 1. Final positional (fractional × 10^4; I, Mo, and P × 10^5) and isotropic thermal parameters ($U \times 10^3$ Å^2) with estimated standard deviations in parentheses

Atom	x	y	z	U_{eq}*
I	1506(4)	33191(3)	25620(2)	72
Mo	22593(4)	49177(3)	43274(2)	39
P(1)	39971(12)	47570(10)	40179(6)	40
P(2)	31258(12)	64425(10)	41775(5)	39
P(3)	18767(12)	56565(10)	35794(5)	34
P(4)	32132(13)	42727(11)	31099(6)	43
O(1)	302(5)	5916(5)	4704(2)	114
O(2)	1323(5)	2834(4)	4305(2)	109
O(3)	3050(5)	4556(5)	5318(2)	113
N(1)	4278(4)	5958(3)	4061(2)	40
N(2)	2476(4)	6724(3)	3697(2)	40
N(3)	2418(4)	5213(3)	3092(1)	38
N(4)	4195(4)	4435(3)	3456(2)	44
C(1)	1004(6)	5504(5)	4578(2)	64
C(2)	1663(5)	3603(5)	4304(2)	62
C(3)	2752(5)	4673(5)	4956(3)	63
C(4)	5015(5)	4133(5)	4307(2)	65
C(5)	3386(5)	7592(5)	4446(2)	65
C(6)	624(5)	5977(4)	3388(2)	48
C(7)	2591(6)	3174(4)	3260(2)	62
C(8)	3667(6)	4114(5)	2551(2)	68
C(9)	5197(5)	6451(5)	3893(2)	59
C(10)	2697(5)	7511(4)	3369(2)	56
C(11)	2218(5)	5687(4)	2643(2)	56
C(12)	5247(5)	4374(5)	3266(3)	70
N(5)	2797(7)	5150(7)	1449(3)	119
C(13)	3249(8)	5594(7)	1219(4)	92
C(14)	3849(10)	6180(9)	930(4)	167

* U(eq) = (1/3) trace U(diag).

Results and discussion

The ^{1}H nmr spectrum shows that quaternization strengthens the molecule, in that it is no longer fluxional in solution. It also provides a qualitative proof of the structure. The methyl groups at P(1), P(2), P(3), N(3), and N(4) are deshielded, relative to those in the uncomplexed quaternary iodide (9); those at N(1) and N(2) are unchanged. The two methyl groups at the quaternary centre are now differentiated (a distinction from the uncomplexed quaternary), and their shielding is increased, presumably a diamagnetic effect of the neighboring carbonyl group C(2)—O(2) (Fig. 2). The C≡O stretching frequencies, in comparison with those of the neutral complex (1) show that quaternization leads to a slight strengthening of these bonds.

The detailed geometry of the neutral and cationic complexes is in fact strikingly similar, except in two regions. Both molecules have an approximate plane of symmetry and, for the discussion, the corresponding dimensions are averaged. A large part of the earlier discussion (1) still applies. From the neutral to the quaternary complex, C≡O (mean[3]) decreases insignificantly from 1.154(3) to 1.147(6) Å (though the difference parallels $\delta\nu$ (C≡O)), Mo—C is unchanged at 1.984(3) Å, and the mean C—Mo—C angle increases, again insignificantly, from 90.7(20) to 91.2(17)°. Within the segments P(1)N(1)P(2)N(2)P(3), there is hardly any variation between the two structures. The differences appear near the quaternization centre and in the Mo—P bonds. Electron with-

[3] Here and elsewhere in this report mean values refer to weighted means with rms deviations from the mean in parentheses.

TABLE 2. Bond lengths (Å) with estimated standard deviations in parentheses

Bond	Length		Bond	Length	
	Uncorr.	Corr.		Uncorr.	Corr.
Mo—P(1)	2.475(2)	2.483	P(3)—C(6)	1.800(6)	1.801
Mo—P(2)	2.4326(15)	2.439	P(4)—N(3)	1.669(4)	1.673
Mo—P(3)	2.468(2)	2.474	P(4)—N(4)	1.660(5)	1.664
Mo—C(1)	1.983(8)	1.987	P(4)—C(7)	1.779(6)	1.781
Mo—C(2)	1.976(7)	1.981	P(4)—C(8)	1.757(7)	1.757
Mo—C(3)	1.981(8)	1.985	O(1)—C(1)	1.148(8)	1.148
P(1)—N(1)	1.702(4)	1.707	O(2)—C(2)	1.152(7)	1.152
P(1)—N(4)	1.724(5)	1.729	O(3)—C(3)	1.141(8)	1.141
P(1)—C(4)	1.806(6)	1.807	N(1)—C(9)	1.473(8)	1.474
P(2)—N(1)	1.696(5)	1.701	N(2)—C(10)	1.477(7)	1.479
P(2)—N(2)	1.693(5)	1.697	N(3)—C(11)	1.492(7)	1.493
P(2)—C(5)	1.802(6)	1.802	N(4)—C(12)	1.497(8)	1.497
P(3)—N(2)	1.705(4)	1.710	N(5)—C(13)	1.088(10)	
P(3)—N(3)	1.710(5)	1.715	C(13)—C(14)	1.413(13)	

TABLE 3. Bond angles (deg) with estimated standard deviations in parentheses

Bonds	Angle (deg)	Bonds	Angle (deg)
P(1)—Mo—P(2)	64.91(5)	Mo—P(3)—N(3)	120.5(2)
P(1)—Mo—P(3)	84.35(5)	Mo—P(3)—C(6)	124.4(2)
P(1)—Mo—C(1)	160.9(2)	N(2)—P(3)—N(3)	106.5(2)
P(1)—Mo—C(2)	105.9(2)	N(2)—P(3)—C(6)	106.0(3)
P(1)—Mo—C(3)	91.2(2)	N(3)—P(3)—C(6)	102.2(3)
P(2)—Mo—P(3)	65.13(5)	N(3)—P(4)—N(4)	113.9(2)
P(2)—Mo—C(1)	96.1(2)	N(3)—P(4)—C(7)	112.3(3)
P(2)—Mo—C(2)	166.6(2)	N(3)—P(4)—C(8)	106.3(3)
P(2)—Mo—C(3)	99.2(2)	N(4)—P(4)—C(7)	108.9(3)
P(3)—Mo—C(1)	89.4(2)	N(4)—P(4)—C(8)	108.6(3)
P(3)—Mo—C(2)	105.4(2)	C(7)—P(4)—C(8)	106.4(3)
P(3)—Mo—C(3)	164.2(2)	P(1)—N(1)—P(2)	101.7(2)
C(1)—Mo—C(2)	93.1(3)	P(1)—N(1)—C(9)	127.1(4)
C(1)—Mo—C(3)	90.0(3)	P(2)—N(1)—C(9)	128.6(4)
C(2)—Mo—C(3)	90.4(3)	P(2)—N(2)—P(3)	101.8(2)
Mo—P(1)—N(1)	95.0(2)	P(2)—N(2)—C(10)	127.5(4)
Mo—P(1)—N(4)	120.8(2)	P(3)—N(2)—C(10)	126.5(4)
Mo—P(1)—C(4)	124.1(3)	P(3)—N(3)—P(4)	120.9(3)
N(1)—P(1)—N(4)	106.7(2)	P(3)—N(3)—C(11)	120.4(4)
N(1)—P(1)—C(4)	105.5(3)	P(4)—N(3)—C(11)	118.7(4)
N(4)—P(1)—C(4)	102.2(3)	P(1)—N(4)—P(4)	119.9(3)
Mo—P(2)—N(1)	96.76(15)	P(1)—N(4)—C(12)	120.6(4)
Mo—P(2)—N(2)	96.3(2)	P(4)—N(4)—C(12)	119.2(4)
Mo—P(2)—C(5)	140.4(2)	Mo—C(1)—O(1)	174.1(6)
N(1)—P(2)—N(2)	112.1(2)	Mo—C(2)—O(2)	177.7(6)
N(1)—P(2)—C(5)	105.3(3)	Mo—C(3)—O(3)	178.1(6)
N(2)—P(2)—C(5)	104.9(3)	N(5)—C(13)—C(14)	178.5(14)
Mo—P(3)—N(2)	94.7(2)		

drawal at P(4) increases the ring angles at P(4) from 107.1(1) to 113.9(2)°, at N(3) and N(4) from 111.6(5) to 120.4(5)°, shortens the bonds P(4)—N(3) and P(4)—N(4) from 1.735(7) to 1.669(5) Å, and lengthens slightly the next bonds N(3)—P(3) and N(4)—P(1) from 1.698(8) to 1.722(7) Å. The effect of electron withdrawal is seen also in the sum of the angles at N(3), N(4), which increases from 357.6 to 359.9°. The remaining ring bonds are not changed significantly, but the effective transmission of a partial positive charge to P(1), P(3), and (to a smaller extent) to P(2) is shown by the lengths of the Mo—P(1), Mo—P(3) bonds, reduced from 2.525(12) to 2.479(5) Å, and of Mo—P(2), reduced from 2.467(1) to 2.439(2) Å, the reduction resulting from increased back-donation Mo→P, least at the remote phosphorus atom. Electron release from molybdenum is evidently competitive with that from nitrogen, since the mean sum of angles at N(1), N(2) decreases slightly on quaternization from 358.1 to 356.1°.

Phosphorus can use its *d*-orbitals for bonding if they are sufficiently contracted (10), and, because of the smaller effective nuclear charge, such interactions are expected to be weaker for P(III) than for P(V), for which they are well established. In fact, and as discussed earlier for $(MeNPMe)_4$ (1), nitrogen as a ligand is sufficiently electronegative to induce significant *d*-orbital bonding, even in a neutral molecule. The strength of such bonding is increased by the attachment of acceptor groups, as seen in the variation of mean P—N bond lengths:

Can. J. Chem. Downloaded from www.nrcresearchpress.com by 210.87.254.6 on 09/06/12
For personal use only.

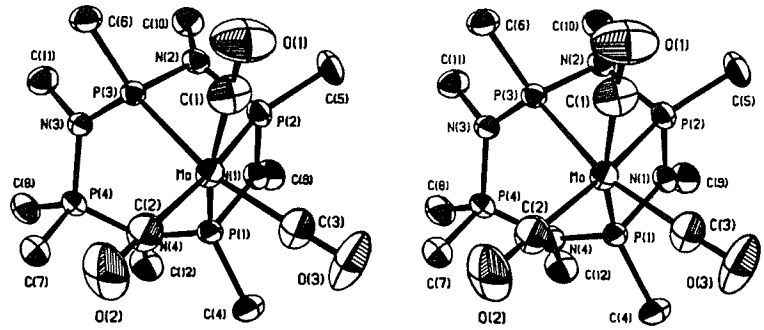

FIG. 2. Stereoscopic view of the $[(CH_3NPCH_3)_4CH_3]Mo(CO)_3$ cation. 50% probability thermal ellipsoids are shown for the non-hydrogen atoms.

TABLE 4. Intra-annular torsion angles (deg) with standard deviations in parentheses

Atoms	Torsion angle (deg)
N(4)—P(1)—N(1)—P(2)	113.3(3)
N(2)—P(2)—N(1)—P(1)	−88.4(3)
N(1)—P(2)—N(2)—P(3)	87.4(3)
N(3)—P(3)—N(2)—P(2)	−111.4(2)
N(2)—P(3)—N(3)—P(4)	106.0(3)
N(4)—P(4)—N(3)—P(3)	−55.8(4)
N(3)—P(4)—N(4)—P(1)	53.8(4)
N(1)—P(1)—N(4)—P(4)	−104.1(3)
P(3)—Mo—P(1)—N(4)	−39.5(2)
Mo—P(1)—N(4)—P(4)	2.5(4)
N(3)—P(4)—N(4)—P(1)	53.8(4)
N(4)—P(4)—N(3)—P(3)	−55.8(4)
Mo—P(3)—N(3)—P(4)	0.1(4)
P(1)—Mo—P(3)—N(3)	38.1(2)
P(2)—Mo—P(1)—N(1)	8.3(2)
Mo—P(1)—N(1)—P(2)	−11.0(2)
Mo—P(2)—N(1)—P(1)	11.2(2)
P(1)—Mo—P(2)—N(1)	−8.3(2)
P(3)—Mo—P(2)—N(2)	9.3(2)
Mo—P(2)—N(2)—P(3)	−12.6(2)
Mo—P(3)—N(2)—P(2)	12.4(2)
P(2)—Mo—P(3)—N(2)	−9.3(2)

$(MeNPMe)_4$, 1.722 Å (11); **1**, 1.711 (1); **3**, 1.699 (this work). The effect of the $Mo(CO)_3$ group is nearly the same as that of Me^+, since in the dication $(MeNPMe)_4Me_2^{2+}$ the mean P—N length is 1.700 Å (9). Similar effects have been found in the pair of structures of $P(NMeNMe)_3P$ (12) and of $OP(NMeNMe)_3PO$ (13), in $P_4(NMe)_6$ and its thioderivatives (14) and its monomethiodide (15), which shows a distinct contraction of the P—N bonds at the quaternized phosphorus atom; the photoelectron spectra of some of these compounds have been interpreted as showing that the formal lone pairs on nitrogen make appreciable contribution to the bonding (16).

A more detailed analysis is possible. Because the angles near P(4) differ in the neutral (**1**) and cationic (**3**) complexes, the differences in bond length cannot be taken as a direct measure of differences in bond strength. The endo- and exo-angles at P(4) are related almost exactly as they would be for hybrids formed from *s*- and *p*-orbitals, and it seems a good approximation to assume that the ring geometry reflects the σ-hybridization state of the ring atoms directly. The method of ref. 17 can then be used to estimate the bond length contractions arising from *d*-orbital interactions; they are arbitrarily classed as π-contractions, even though there is no strict molecular symmetry operation to which they can be referred. We can draw the following conclusions. (*1*) The π-contractions in **3** (mean 0.055 Å) are significant, but small compared to those in phosphazenes (up to 0.16 Å), in which formal π-bonding is required. (*2*) The large reduction in the lengths of the ring bonds from P(4), relative to **1**, results mainly from the change in σ-hybridization, no doubt induced by the d_π-bonding. The π-contraction in these bonds (0.023 Å relative to **1**) is offset by an almost equal π-extension in the adjacent bonds. (*3*) The situation at the phosphorus atoms coordinated to molybdenum is more complex, and strictly requires a deeper analysis. However, it is clear from the shortening of the P—Mo bonds that the effect of the charge on the quaternary centre is relayed at least to P(1), P(3). These bonds are strengthened partly at the expense of the local rings bonds, but, as a result of the increase in the *d*-population at phosphorus by back-donation from molybdenum, the π-contractions in the ring bonds (mean 0.067 Å) are nevertheless greatest in this region. If the *d*-orbitals at phosphorus were not contracted by the charge of the Me^+, then shortening of the P—Mo bonds would be expected to be accompanied by lengthening of the local P—N bonds.

Acknowledgments

We thank the Natural Sciences and Engineering Research Council of Canada for financial support and the University of British Columbia Computing Centre for assistance.

1. K. D. GALLICANO, N. L. PADDOCK, S. J. RETTIG, and J. TROTTER. Can. J. Chem. **60**, 2415 (1982).
2. P. COPPENS, L. LEISEROWITZ, and D. RABINOVICH. Acta Crystallogr. **18**, 1035 (1965).
3. W. R. BUSING and H. A. LEVY. Acta Crystallogr. **22**, 457 (1967).
4. D. T. CROMER and J. B. MANN. Acta Crystallogr. Sect. A, **24**, 321 (1968).
5. R. F. STEWART, E. R. DAVIDSON, and W. T. SIMPSON. J. Chem. Phys. **42**, 3175 (1965).
6. D. T. CROMER and D. LIBERMAN. J. Chem. Phys. **53**, 1891 (1970).
7. V. SCHOMAKER and K. N. TRUEBLOOD. Acta Crystallogr. Sect. B, **24**, 63 (1968).
8. D. W. J. CRUICKSHANK. Acta Crystallogr. **9**, 747 (1956); **9**, 754 (1956); **14**, 896 (1961).
9. W. ZEISS, T. KUHN, D. LUX, W. SCHWARZ, and H. HESS. Z. Naturforsch. **36b**, 561 (1981).
10. D. P. CRAIG, A. MACCOLL, R. S. NYHOLM, L. E. ORGEL, and L. E. SUTTON. J. Chem. Soc. 332 (1954).
11. W. ZEISS, W. SCHWARZ, and H. HESS. Angew. Chem. Int. Ed. Engl. **16**, 407 (1977).

Can. J. Chem. Downloaded from www.nrcresearchpress.com by 210.87.254.6 on 09/06/12
For personal use only.

12. W. VANDOORNE, G. W. HUNT, R. W. PENZ, and A. W. CORDES. Inorg. Chem. **10**, 2591 (1971).
13. J. W. GILJE and K. SEFF. Inorg. Chem. **11**, 1643 (1972).
14. F. A. COTTON, J. G. REISS, C. E. RICE, and B. R. STULTS. Inorg. Chem. **21**, 3123 (1982).
15. G. W. HUNT and A. W. CORDES. Inorg. Chem. **13**, 1688 (1974).
16. F. A. COTTON, J. G. REISS, and B. R. STULTS. Inorg. Chem. **22**, 133 (1983).
17. D. P. CRAIG and N. L. PADDOCK. *In* Non-benzenoid aromatics. Vol. 2. Academic Press, New York. 1971. p. 273.

Can. J. Chem. Downloaded from www.nrcresearchpress.com by 210.87.254.6 on 09/06/12
For personal use only.

COMMUNICATION

Observation of a radical intermediate in the one electron oxidation of 5-methyl-1-thia-5-azacyclooctane by $\cdot Br_2^-$

WARREN KENNETH MUSKER
Department of Chemistry, University of California, Davis, CA 956167, U.S.A.
AND
PARMINDER S. SURDHAR, RIZWAN AHMAD, AND DAVID A. ARMSTRONG[1]
Department of Chemistry, University of Calgary, Calgary, Alta., Canada T2N 1N4

Received February 22, 1984

WARREN KENNETH MUSKER, PARMINDER S. SURDHAR, RIZWAN AHMAD, and DAVID A. ARMSTRONG. Can. J. Chem. **62**, 1874 (1984).

The one electron oxidant $\cdot Br_2^-$ reacts with 5-methyl-1-thia-5-azacyclooctane (**4**) in aqueous solution at high pH with an overall rate constant of $\sim 2 \times 10^8\ M\ s^{-1}$. The radical intermediate produced has a broad maximum at 500 nm with $\epsilon = 2400\ M^{-1}\ cm^{-1}$ and at pH 10 decays with a first order rate constant of $2.3 \pm 0.3 \times 10^4\ s^{-1}$, first half-life of 30 ± 5 μs. Its characteristics do not correspond to those of the >S∴Br or >S∴$^+$S< species reported by Asmus and co-workers. The species appears to be the same as the cation radical reported earlier in the one electron oxidation of **4** in acetonitrile. This species is considered to have an >S∴$^+$N< type structure, which provides transannular stabilization.

WARREN KENNETH MUSKER, PARMINDER S. SURDHAR, RIZWAN AHMAD et DAVID A. ARMSTRONG. Can. J. Chem. **62**, 1874 (1984).

En solution aqueuse et à des pH élevés, l'oxydant à un électron $\cdot Br_2^-$ réagit avec le méthyl-5 thia-1 aza-5 cyclooctane (**4**); la constante globale de la vitesse de la réaction est d'environ $2 \times 10^8\ M\ s^{-1}$. L'intermédiaire radicalaire qui se forme présente une large bande d'absorption autour de 500 nm avec un $\epsilon = 2400\ M^{-1}\ cm^{-1}$; à un pH de 10, il se décompose avec une constante de vitesse du premier ordre de $2{,}3 \pm 0{,}3 \times 10^4\ s^{-1}$ et une première demi-vie de 30 ± 5 μs. Ses caractéristiques ne correspondent pas à celles rapportées par Asmus et ses collaborateurs pour les espèces >S∴Br ou >S∴$^+$S<. Il semble que les espèces impliquées soient les mêmes que celles rapportées antérieurement dans l'oxydation de **4** par un électron dans l'acétonitrile. On considère que cette espèce possède une structure du type >S∴$^+$N< qui permet une stabilisation transannulaire.

[Traduit par le journal]

Mechanisms of oxidation and reduction of sulphur-containing molecules are of importance in many areas of chemistry (1, 2) and biochemistry (3). Previous studies have indicated that intramolecular nucleophilic assistance can facilitate both one (4, 5) and two electron oxidations (1, 6, 7) of compounds, such as disulphides and thioethers. In recent studies of mesocyclic dithia compounds in nonaqueous solvents oxidation has been shown to produce cation radicals (**1**) and dications (**2**), which are stabilized by transannular interactions

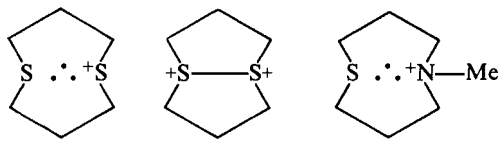

1 **2** **3**

between the sulphur atoms (8, 9). A relatively long-lived N—S bonded cation radical (**3**) and the corresponding dication have also been prepared in nonaqueous media from the mesocyclic aminothioether, 5-methyl-1-thia-5-azacyclooctane (**4**) (10). A N—S interaction similar to that shown in **3** has been considered as a possible step in the mechanism of the one electron oxidation of methionine (4). However, although species similar to **1** have been studied extensively in aqueous media (11–15), direction observation of an >S∴$^+$N< intermediate under those conditions has not thus far been reported. Here we report the characteristics of an intermediate produced in the one electron oxidation of **4** by $\cdot Br_2^-$ in aqueous solution.

The compound **4** was prepared and purified as previously described (10). Required amounts were weighed out on a microbalance and made up in 50-mL volumetric flasks in solutions of phosphate buffer and 0.33 *M* KBr. After thorough purging with N_2O, they were flushed into a 1-cm optical cuvette and subjected to 2-μs pulses of 1.5-MeV electrons. The electron accelerator has already been described (16) and the techniques are well established (17). Experiments were performed at 23 ± 2°C.

Pulse radiolysis of N_2O-saturated solutions of 0.03 *M* KBr produces $6.0 \times 10^{-6}\ M$ $\cdot Br_2^-$ anion complexes per krad of absorbed radiation (17). This species has a strong peak ($\epsilon = 9900 \pm 600\ M^{-1}\ cm^{-1}$) at 360 nm (18). In the absence of a reactant it undergoes second order decay with $2k = 3.6 \times 10^9\ M^{-1}\ s^{-1}$ (19). However, in the presence of 3 to $8 \times 10^{-4}\ M$ **4** at pH 10, the 360-nm peak decayed in a pseudo first order process, with a lifetime which varied inversely with the concentration of **4**. An example of that decay is seen in Figs. 1a and b. In contrast, the absorbance at and above 500 nm, where $\cdot Br_2^-$ absorbs only weakly, exhibited growth over the initial ~10 μs and then decay (Fig. 1c). Spectra 5 μs and 44 μs after

[1] Author to whom correspondence may be addressed.

Can. J. Chem. Downloaded from www.nrcresearchpress.com by 210.87.254.6 on 09/06/12
For personal use only.

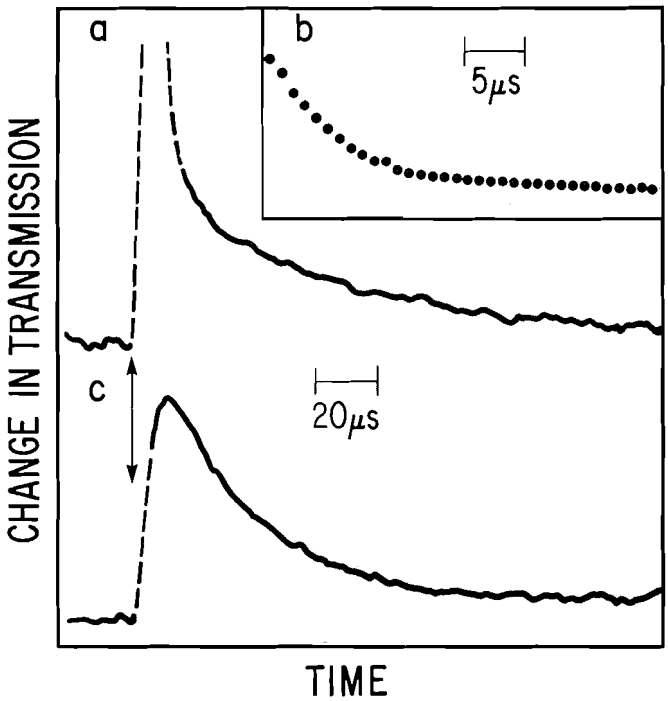

FIG. 1. Changes in transmission as a function of time for 0.8 m*M* 5-methyl-1-thia-5-azacyclooctane (**4**) in 0.03 *M* KBr with 10 m*M* phosphate buffer at pH 10. Wavelength = 360 nm for (a) and (b), and 640 nm for (c). Arrows indicate start of 2-μs electron pulse for (a) and (c). Trace (b) commences 1 μs after pulse ends and the ordinate scale sensitivity is one fifth of that of (a) and (c).

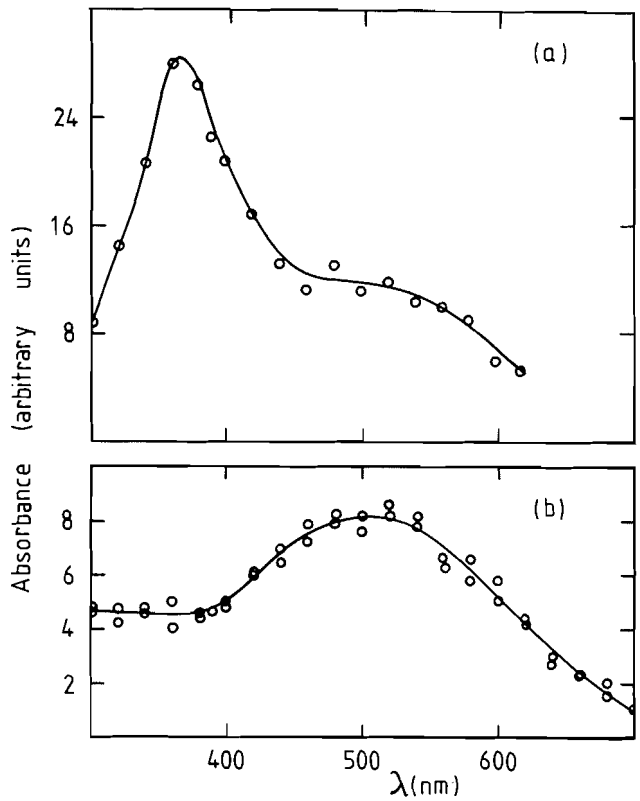

FIG. 2. Absorbance of transient species in buffered (pH 10) solutions of **4** in KBr as a function of wavelength at 5 μs(a) and 44 μs after start of 2-μs pulse. Concentration of **4** was 0.03 m*M* in (a) and 0.4 to 0.8 m*M* in (b).

the start of the electron pulse are shown in Fig. 2.

Beyond three half-lives for the 360-nm decay the spectrum shape above 400 nm was independent of time and corresponded to the line in Fig. 2b. This spectrum, which decayed at pH 10 with a first order rate constant of 2.0 to 2.6 × 10^4 s^{-1}, must correspond to a long-lived transient B formed in the reaction of $\cdot Br_2^-$ and **4**. The intensity of the absorbance due to B and its lifetime were independent of the concentration of **4** over the range 0.4 to 0.8 m*M*. Correction for the first order decay leads to an extinction coefficient of about 2400 M^{-1} cm^{-1} at the 500-nm peak.

Asmus and co-workers (14, 15) have reported the formation of $\rangle S\therefore Br$, three-electron bonded complexes in reactions of thioethers and $\cdot Br_2^-$. These are characterized by absorption maxima at 400 nm and absorbance coefficients of ~7000 M^{-1} cm^{-1}. Also the following equilibria (12–15):

[1] $\rangle S\therefore Br + S\langle \rightleftharpoons \rangle S\therefore {}^+S\langle + Br^-$

[2] $\rangle S\therefore Br \rightleftharpoons \rangle S^{\ddagger} + Br^-$

[3] $\rangle S\therefore {}^+S\langle \rightleftharpoons \rangle S^{\ddagger} + S\langle$

have been observed in a series of thioethers with $K_1 \simeq 1.5$ (14), $K_2 \simeq 1 \times 10^{-3}$ (14), and $K_3 \simeq 1 \times 10^{-3}$ (11, 12). The monomer ($\rangle S\cdot^+$) and dimer ($\rangle S\therefore {}^+S\langle$) cations have $\lambda_{max} \simeq 300$ and $\simeq 480$ nm with $\epsilon_{max} \simeq 1600$ and 6000 M^{-1} cm^{-1} respectively.

Clearly the absorbance maximum of the present transient does not correspond with $\rangle S\therefore Br$ or $\rangle S\cdot^+$. It is closest to that of the dimer cations. However, the absorbance coefficient of 2400 M^{-1} cm^{-1} is much smaller. In addition, with $K_3 = 0.3$ to 1 × 10^{-3} for typical sulphides, the intensity of absorbance should differ by a factor of about two for concentrations of 0.4 and 0.8 m*M* and this was not seen. Thus the species appears to be monomeric. Based on the chemical and esr evidence of the previous study of the oxidation of **4** in acetonitrile solution (10), its structure probably involves transannular stabilization as in **3**. The oxidation of **4** to **3** can be accounted for by the overall reaction:

[4] $\cdot Br_2^- + \mathbf{4} \rightarrow 2Br^- + \mathbf{3}$

which assumes any $\rangle S\therefore Br$ species to be short-lived. The pseudo first order half-lives of $\cdot Br_2^-$ decay correspond to $k_4 \sim 2 \times 10^2$ M^{-1} s^{-1}.

The first order decay of B was found to be enhanced at high pH, a feature which suggests that proton transfer to OH^- or buffer is a dominant mode. This type of decay is also important in cyclic-dithia cation monomers (13). It is interesting to note that the first order half-lives and extinction coefficients of these ions decrease as the wavelength of the maximum absorption increases (13). The half-life and extinction coefficient of B resemble those of 2,5-dithiahexane (ϵ 2500 M^{-1} cm^{-1}, $t_{1/2} \cong 30$ μs), but the value of λ_{max} for that cation system is significantly different (570 nm). Thus the optical properties of B differ significantly from those of species containing sulphur only.

Acknowledgement

This research was supported by NSERCC grant A3571.

Can. J. Chem. Downloaded from www.nrcresearchpress.com by 210.87.254.6 on 09/06/12
For personal use only.

1. J. L. FIELD. *In* Organic chemistry of sulphur. *Edited by* S. Oae. Phenom., New York. 1977 p. 303. See articles by other authors also.
2. J. L. KICE. Acc. Chem. Res. **1**, 58 (1968).
3. (*a*) M. FRIEDMAN. The chemistry and biochemistry of the sulphydryl group in amino acids, peptides and proteins. Pergamon, Oxford. 1973; (*b*) Y. M. TORCHINSKII. Sulphydryl and disulphide groups of proteins. *Translated by* H. B. F. Dixon. Consultants Bureau, New York. 1974.
4. K. O. HILLER and K.-D. ASMUS. J. Phys. Chem. **87**, 3682 (1983).
5. J. R. BOWEN and S. F. YANG. Photochem. Photobiol. **21**, 201 (1975).
6. P. R. YOUNG and L.-S. HSIEH. J. Am. Chem. Soc. **100**, 7121 (1978).
7. J. T. DOI and W. K. MUSKER. To be published.
8. W. K. MUSKER and T. L. WOLFORD. J. Am. Chem. Soc. **98**, 3055 (1976).
9. W. K. MUSKER and P. B. ROUSH. J. Am. Chem. Soc. **98**, 6745 (1976).
10. W. K. MUSKER, A. S. HIRSCHON, and J. T. DOI. J. Am. Chem. Soc. **100**, 7754 (1978).
11. M. BONIFACIĆ, H. MÖCKEL, D. BAHNEMANN, and K.-D. ASMUS. J. Chem. Soc. Chem. Commun. 675 (1975).
12. K.-D. ASMUS, D. BAHNEMANN, M. BONIFACIĆ, and H. A. GILLIS. Faraday Discuss. Chem. Soc. No. 63, 213 (1977).
13. K.-D. ASMUS, D. BAHNEMANN, CH.-H. FISCHER, and D. VELTWISCH. J. Am. Chem. Soc. **101**, 5322 (1979).
14. M. BONIFACIĆ and K.-D. ASMUS. J. Chem. Soc. Perkin Trans. 2, 758 (1980).
15. K.-O. HILLER and K.-D. ASMUS. Int. J. Radiat. Biol. **40**, 583 (1981).
16. A. J. ELLIOT, F. WILKINSON, and D. A. ARMSTRONG. Int. J. Radiat. Biol. **38**, 1 (1980).
17. I. G. DRAGANIĆ and Z. D. DRAGANIĆ. The radiation chemistry of water. Academic Press, New York. 1971.
18. G. L. HUG. Optical spectra of nonmetallic inorganic transient species in aqueous solution. N.S.R.D.S. N.B.S. 69, U.S. Dept. of Commerce, Washington, D.C. 1981.
19. B. CERCEK, M. EBERT, C. W. GILBERT, and A. J. SWALLOW. *In* Pulse radiolysis. Academic Press, London. 1965. p. 83.

Can. J. Chem. Downloaded from www.nrcresearchpress.com by 210.87.254.6 on 09/06/12
For personal use only.

Electrochemical evaluation of electron acceptor materials

R. O. LOUTFY, C. K. HSIAO, B. S. ONG, AND B. KEOSHKERIAN
Xerox Research Centre, 2660 Speakman Drive, Mississauga, Ont., Canada L5K 2L1

Received September 11, 1983[1]

This paper is dedicated to Professor Paul de Mayo on the occasion of his 60th birthday

R. O. LOUTFY, C. K. HSIAO, B. S. ONG, and B. KEOSHKERIAN. Can. J. Chem. **62**, 1877 (1984).

The electrochemical half-wave reduction potential ($E_{1/2}$) of 33 electron acceptor molecules in dry methylene chloride has been measured by cyclic voltammetry (CV) at a mercury electrode. The differences in $E_{1/2}$ values for the reversible reduction to the corresponding anion radicals reflect the electronic influence of the substituent at different ring positions.

The measurements of the half-wave reduction potentials provided a convenient method for determining the conducting energy levels of the electron relay molecules in condensed media. Repetitive potential cycle measurements provided information on the chemical stability and cyclability of the intermediate anion radicals formed during electron transport processes.

R. O. LOUTFY, C. K. HSIAO, B. S. ONG et B. KEOSHKERIAN. Can. J. Chem. **62**, 1877 (1984).

Opérant dans le chlorure de méthylène anhydre et faisant appel à la voltamétrie cyclique au niveau d'une électrode à mercure, on a mesuré le potentiel de réduction électrochimique à demi-vague ($E_{1/2}$) de 33 molécules électroacceptrices. Les différences entre les valeurs de $E_{1/2}$ pour la réduction réversible conduisant aux anions radicalaires correspondants reflètent l'influence électronique des substituants fixés en diverses positions du cycle.

La mesure de potentiels de réduction à demi-onde s'avère donc une méthode convenable de déterminer les niveaux d'énergie de conduction des molécules qui transmettent des électrons en milieu condensé. Des mesures répétitives de cycle de potentiel fournissent de l'information sur la stabilité chimique et la cyclabilité des anions radicalaires intermédiaires formés au cors de processus de transfert d'électron.

[Traduit par le journal]

Can. J. Chem. Downloaded from www.nrcresearchpress.com by 210.87.254.40 on 09/06/12
For personal use only.

Introduction

Electrochemical reduction potential of many aromatic electron acceptor (A) molecules containing one or more nitro (NO_2) or cyano (CN) groups have been reported in the literature (1–6). These reduction potential measurements were performed in order to determine the electron affinity (EA) of these compounds and its dependence on the molecular structure. Recently, considerable interest has been generated in electron acceptor molecules as a means of obtaining one-dimensional conducting charge transfer complexes (7); stabilization of semiconductors (8): electron relays (9), and electron transporting layers for xerographic applications (10–13). The latter, in particular, has stimulated considerable research activity. Attempts were made to correlate the xerographic discharge characteristics of molecularly doped polymer systems and the electron affinity of the acceptor compound (3, 14, 15). It was found that charge carrier mobility and trapping depend on the energy level of the molecular species involved and the electrochemical stability of the intermediate radical ion (3).

In the present work we have examined the electrochemical properties of a large number of electron acceptor compounds to determine their electron conducting level; the stability of the intermediate radical anions, and the rate of electron exchange. In this study we have used the cyclic voltammetric technique, which is capable of rapidly observing the redox behaviour of molecules over a wide potential range. The electrode potential at which the compound undergoes reduction can be rapidly located using the CV method. A very important aspect of cyclic voltammetry is its ability to generate the reduced electron acceptor molecule in the first potential scan:

$$[1] \quad A + e \rightarrow A^{\dot{-}}$$

and then probe the species ($A^{\dot{-}}$) fate on the second and subsequent scans. As such, it is a powerful probe for monitoring stability and cyclability of electron acceptor molecules. In addition, from the dependence of the shape of cyclic voltammogram on potential scan rate it is possible to determine quantitatively the heterogeneous rate of electron transfer (k_s):

$$[2] \quad A + e \overset{k_s}{\rightleftarrows} A^{\dot{-}}$$

The versatility of cyclic voltammetry, combined with its simplicity, makes CV a useful characterization tool for the evaluation of electron acceptor compounds.

Experimental

A. Materials

Synthesis of new electron acceptor compounds are described in ref. 15. Others were commercially available or were synthesized by published techniques. The chemical structure of the electron acceptor materials studied is given in Table 1. Generally, six series of compounds were examined: (*i*) substituted fluoren-9-one derivatives; (*ii*) substituted 9,9-di(alkyl)fluorenes; (*iii*) substituted 9-fluorenylidenemalononitriles; (*iv*) substituted benzylidene malononitriles; (*v*) substituted benzophenone malononitriles; and (*vi*) arylidene-2-indan-1,3-diones. Methylene chloride Caledon Spectral grade was stored over 4A molecular sieves. Tetrabutylammonium perchlorate, TBAP (recrystallized from ethanol/water) was dried in a vacuum oven overnight.

B. Measurements

All measurements were made using PAR 174A polarographic analyzer connected to PAR 175 universal programmer. The current–voltage curves were recorded on a Houston Instruments 2000 X–Y recorder. Experiments were performed using PAR model 303 static mercury drop electrode assembly. The system is equipped with a hanging-mercury-drop working electrode, an aqueous Ag/AgCl, sat. KCl reference electrode, and a platinum wire auxiliary electrode. A 0.1 *M* tetrabutylammonium perchlorate (TBAP) in dry methylene chloride (spectral grade) was used as an indifferent electrolyte. The solutions of 1 m*M* of the electron acceptor compounds were deaerated using dry argon gas and reductions were carried out under a blanket of argon. Methylene chloride was chosen as the solvent for a number of reasons. It is an excellent, yet relatively inert, solvent for a wide variety of organic compounds. It has an exceptionally wide potential

[1] Revision received April 5, 1984.

TABLE 1. The chemical structure of the electron acceptor compounds studied

(*a*) Substituted fluoren-9-ones

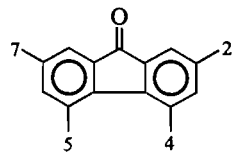

Cpd	Substituent 2	4	5	7	$-E_{1/2}$(I) (V)
1	H	H	H	H	1.3
2	H	CO_2B_u	H	H	1.18
3	NO_2	H	H	NO_2	0.68
4	$(CH_3)_2CPr$	NO_2	H	NO_2	0.76
5	NO_2	NO_2	H	NO_2	0.42
6	$C(CH_3)_3$	NO_2	NO_2	NO_2	0.44
7	NO_2	CO_2B_u	H	NO_2	0.55
8	NO_2	CO_2H	NO_2	NO_2	0.34 (irrev)
9	NO_2	NO_2	NO_2	NO_2	−0.14

(*b*) 9,9-Bis(*n*-butylthio)nitrofluorenes

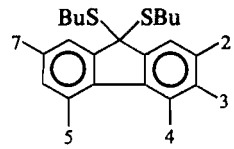

Cpd	Substitution Position 2	3	4	5	7	$-E_{1/2}$(I) (V)
10	H	H	H	H	H	(1.22)
11	H	NO_2	H	H	H	1.02
12	NO_2	H	H	H	NO_2	0.88
13	NO_2	H	NO_2	H	NO_2	0.67
14	NO_2	H	NO_2	NO_2	NO_2	0.33

(*c*) Dialkyl-2,4,5,7-tetranitrofluorene-9,9-dipropionate

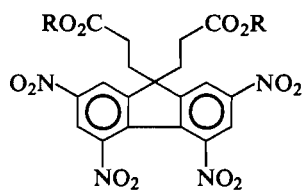

Cpd	R	$-E_{1/2}$(I) (V)
15	Et	0.36
16	Bu	0.36

(*d*) Substituted 9-fluorenylidenemalononitriles

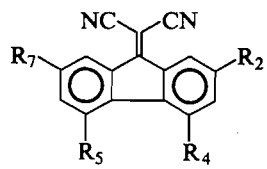

Cpd	R	$-E_{1/2}$(I)
17	H	0.69
18	2,7-diNO_2	0.25
19	2,4,7-triNO_2	0.05
20	2,4,5,7-tetraNO_2	−0.11

(*e*) Benzylidene malononitriles

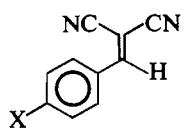

Cpd	X	$E_{1/2}$
23	4-Me_2N	−1.43
24	H	−1.31
25	4-Cl	−1.20
26	4-CN	−0.85
27	4-NO_2	−0.68
28	2,6-diNO_2	−0.51

(*f*) Benzophenone malononitriles

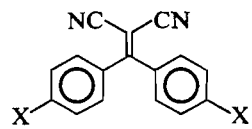

Cpd	X	$E_{1/2}$
21	H	−1.15
22	NO_2	−0.58

Can. J. Chem. Downloaded from www.nrcresearchpress.com by 210.87.254.40 on 09/06/12
For personal use only.

TABLE 1. (*Concluded*)

(*g*) Terphthalylidenemalononitriles

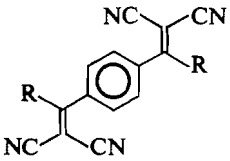

Cpd	R	$E_{1/2}$
29	H	−0.53
30	CH_3	−0.81

(*h*) 2-Arylidene-indan-1,3-diones

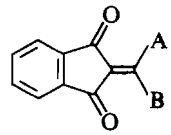

Cpd	A	B	$E_{1/2}$
31	H	Ph	−0.95
32	Ph	Ph	−0.76
33	Fluorenylidene		−0.74

TABLE 2. The electrochemical reduction data for substituted fluoren-9-one

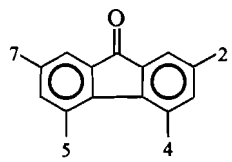

	Substituent									
Cpd	2	4	5	7	$-E_{1/2}$(I)[a]	$-E_{1/2}$(II)[a]	A_g (eV)	$-P_s^-$ (eV)	$-P_c^-$ (eV)	A_C (eV)
1	H	H	H	H	1.3	—	1.05	2.35	2.02	3.07
2	H	CO_2B_u	H	H	1.18	—	1.14	2.37	2.04	3.19
3	NO_2	H	H	NO_2	0.68	0.84	1.55	2.47	2.12	3.67
4	$(CH_3)_2CPr$	NO_2	H	NO_2	0.76	0.89	1.48	2.45	2.11	3.59
5	NO_2	NO_2	H	NO_2	0.42	0.67	1.76	2.52	2.17	3.92
6	$C(CH_3)_3$	NO_2	NO_2	NO_2	0.44	0.73	1.74	2.52	2.16	3.91
7	NO_2	CO_2B_u	H	NO_2	0.55	0.74	1.65	2.49	2.15	3.80
8	NO_2	CO_2H	NO_2	NO_2	0.34	0.51	1.82	2.53	2.18	4.0
9	NO_2	NO_2	NO_2	NO_2	(irrev) −0.14	0.42	1.99	2.57	2.21	4.20

[a] In V, vs. Ag/AgCl.

window for the appropriate redox measurements, it is aprotic, it is the common coating solvent of transport layers, and it has a low dielectric constant. Solvent-induced shifts in $E_{1/2}$ have been discussed by a number of workers (16) and may include contributions from differences in liquid junction potential, ion pairing effects, and interactions of the solvent with the species undergoing the redox reaction. These difficulties can be avoided in principle by referring all measurements to the reversible half-wave potential of a redox couple which does not interact with solvent and is, therefore, unaffected by a change in solvent, 7,7,8,8-tetracyanoquinodimethane (TCNQ) which was shown to have a reduction potential of +0.29 V vs. Ag/AgCl, KCl in methylene chloride was used as internal standard to minimize possible experimental artifacts. Furthermore, it was previously shown (3) that $E_{1/2}$ of fluorenones correlate with Gutmann's donor number (17), which measures the ability of a solvent to donate electrons. Methylene chloride has very low donor number and thus $E_{1/2}$ in that solvent is expected to be free of solvent effect. We also found little difference in $E_{1/2}$'s of 2,4,7-trinitrofluorenone, **5**, measured in methylene chloride or acetonitrile.

Results

Cyclic voltammetry

The compounds studied are shown in Table 1 and their cyclic voltammetric behaviour is discussed below. The compounds are divided into six groups according to their structure.

*Fluoren-9-ones, **1–9***

Many polynitrofluorenones have been prepared before and their electrochemical behaviour has been extensively studied (3). The solubility of these compounds in common organic solvents and in polymers is usually very low. To solve this problem, i.e., to increase the solubility of nitrofluorenones, alkyl and/or *n*-butoxycarbonyl (CO_2Bu) groups were introduced into the fluorenone rings. The electrochemical behaviour of these new compounds was studied and compared with previous data. Table 2 summarizes our electrochemical results on eight fluorenone derivatives. The half-wave reduction potential of the parent compound fluoren-9-one **1** appears at −1.3 V vs. Ag/AgCl in CH_2Cl_2. This value is above the reduction potential of oxygen in the same media and therefore, this material will not be a suitable electron transporter in most applications since the oxygen will act as an electron trap. Substitution of a proton in **1** by a *n*-butoxylcarbonyl (CO_2Bu) group shifts the reduction potential anodically by ~0.12 V, while nitro group substitution shifts $E_{1/2}$ by ~0.28 V for each NO_2 group as

Can. J. Chem. Downloaded from www.nrcresearchpress.com by 210.87.254.40 on 09/06/12
For personal use only.

Can. J. Chem. Downloaded from www.nrcresearchpress.com by 210.87.254.40 on 09/06/12
For personal use only.

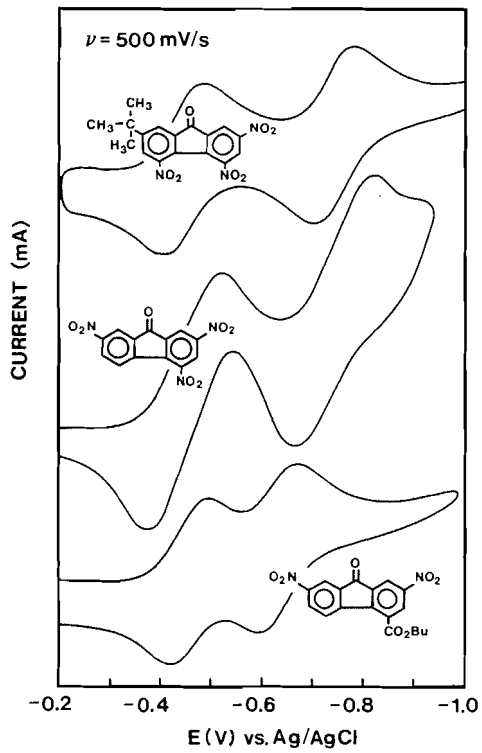

FIG. 1. Cyclic voltammograms of substituted fluorenones in CH_2Cl_2 at Hg electrode vs. Ag/AgCl, KCl.

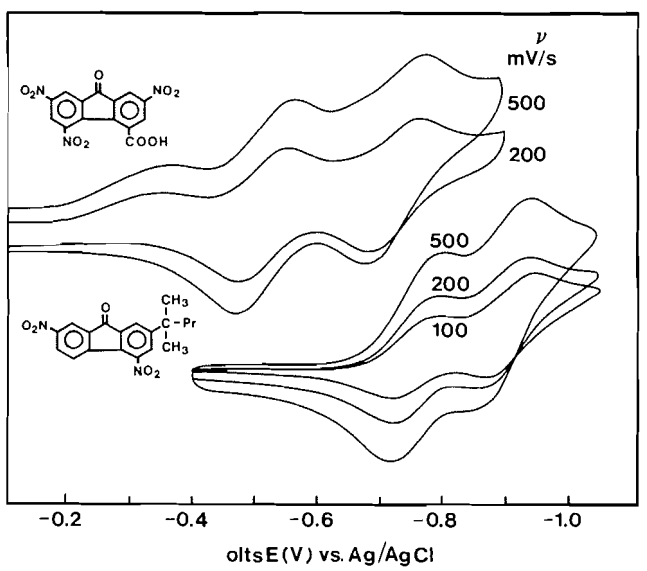

FIG. 2. The CV behavior of tri- and tetra-substituted fluorenones.

indicated in Table 2. Figures 1 and 2 show typical cyclic voltammograms of several of these new compounds along with that of 2,4,7-trinitro fluorenone (TNF), **5** (the best known electron-acceptor compound). Each compound in the series exhibits two reversible one-electron reduction waves separated by ~0.3 V. The reduction potential of the *t*-butyl trinitrofluorenone, **6** (−0.44 V), is identical to that of TNF, **5** (−0.42 V). They also display similar electron mobility. However, **6** is much more soluble than TNF in common solvents. The dinitrobutoxycarbonylfluorenone, **7** is reduced at a slightly more cathodic potential (−0.55 V) than TNF **5** (−0.42 V) reflecting the weaker electronic influence of the CO_2Bu com-

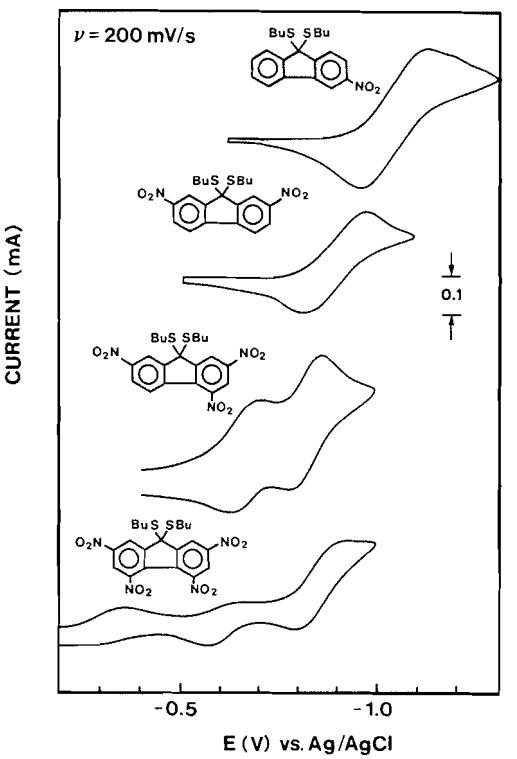

FIG. 3. CV of nitro-9,9-bis(*n*-butylthio)fluorenes.

pared to a NO_2 group. The 2-alkyl 4,7-dinitrofluorenone, **4**, exhibits reversible reduction at −0.76 V, which is 0.34 V cathodic of TNF.

The CV of all fluorenone derivatives show a reversible response, with separation of 70 mV between cathodic and anodic peak potentials, independent of scan rate between 10–200 mV/s, indicating a kinetically uncomplicated diffusion-controlled reduction to the corresponding radicals which are stable within the time scale of the cyclic voltammetric experiment. The only fluorenone derivative which exhibits an irreversible first-reduction wave is 4-carboxyl-2,5,7-trinitrofluorenone, **8**, as shown in Fig. 2. This can be attributed to the protonation of the radical anion by protons of the carboxyl groups.

*9,9-Bis(*n*-butylthio)nitrofluorenones,* ***10–14***

These compounds are derived from the corresponding fluorenone via thioketalization. The compounds exhibit intramolecular charge transfer from the sulfur to the nitrofluorene moiety and display electron mobilities that are higher than that of TNF (15). Figure 3 shows the CV of the mono, di, tri, and tetranitro-9,9-bis(*n*-butylthio)fluoreneone, **11–14**. All exhibit reversible one-electron reduction waves. The reduction potential shifts anodically by ~0.2 V per nitro group. The $E_{1/2}$'s range from −1.02 V for the mononitro to −0.33 V for the tetranitro compound, a shift of approximately 0.70 eV. These materials appear to have good solubility and electrochemical stability; however, xerographically the tetranitro derivative displays high dark decay while the others display heavy bulk trapping of charges. The electron drift mobility (μ_e) measured xerographically (11, 14) for these compounds appears to increase as the electron affinity of the molecule increases. The electrochemical data are summarized in Table 3.

Dialkyl-2,4,5,7-tetranitrofluorene-9,9-dipropionates, ***15–16***

These compounds exhibit four one-electron reversible reduc-

TABLE 3. Summary of electrochemical data for 9,9-bis(*n*-butylthio) nitrofluorene derivatives

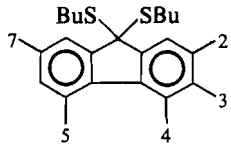

Cpd	Substitution position 2	3	4	5	7	$-E_{1/2}(I)^a$	$-E_{1/2}(II)^a$	A_g (eV)	$-P_s^-$ (eV)	$-P_c^-$ (eV)	A_C (eV)
10	H	H	H	H	H	(1.22)	—	1.11	2.37	2.04	3.15
11	H	NO_2	H	H	H	1.02	—	1.27	2.41	2.07	3.34
12	NO_2	H	H	H	NO_2	0.88	—	1.39	2.43	2.09	3.48
13	NO_2	H	NO_2	H	NO_2	0.67	0.84	1.56	2.47	2.13	3.68
14	NO_2	H	NO_2	NO_2	NO_2	0.33	0.60	1.83	2.54	2.18	4.01

[a] In V, vs. Ag/AgCl.

TABLE 4. Electrochemical data for dialkyl 2,4,5,7-tetranitrofluorene-9,9-dipropionates

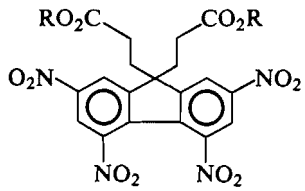

Cpd	R	$-E_{1/2}(I)^a$	$-E_{1/2}(II)^a$	A_g (eV)	$-P_s^-$ (eV)	$-P_c^-$ (eV)	A_C (eV)
15	Et	0.36	0.64	1.81	2.53	2.17	3.99
16	Bu	0.36	0.63	1.81	2.53	2.17	3.99
8	Tetranitrofluorenone	0.14	0.42	1.99	2.54	2.21	4.20

[a] In V, vs. Ag/AgCl.

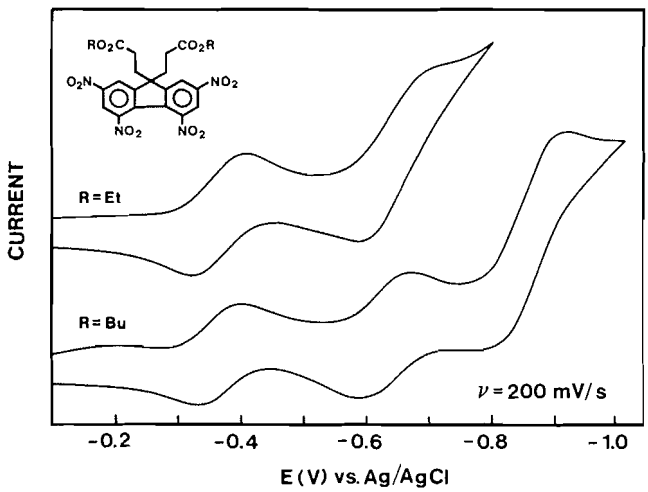

FIG. 4. CV of 9,9-bis (alkylpropionate)-2,4,5,7-tetranitrofluorenes.

tion waves as shown in Fig. 4 and summarized in Table 4.

The first reduction wave occurs at −0.36 V independent of the alkyl group (ethyl **15** or butyl **16**), which is about 0.22 V cathodic of tetranitrofluorenone, **8**, reduction. Although these materials display reasonable solubility in common solvents and polymers, their electron mobility is very low.

9-Fluorenylidenemalononitriles, 17–20

This series of compounds displays a reduction potential ranging from −0.69 V to +0.11 V, i.e., span over a 0.80 eV in potential energy. All exhibit two reversible one-electron reduction waves. The first reduction potential of the parent compound 9-fluorenylidenemalononitrile, **17**, appears at −0.69 V vs. Ag/AgCl and shifts anodically by 0.2 V for each nitro group substitution. Table 5 summarizes the electrochemical results for the polysubstituted fluorenylidene malononitriles. Figure 5 shows a typical cyclic voltammogram of the representative samples of the series. All showed a clean reversible redox couple with peak separations ($E_p^C - E_p^a$) of about 70 mV, indicating a diffusion-controlled reduction to the corresponding radical anion. The radical anion formed at the working electrode has an intense orange–red color. The (nitro-9-fluorenylidene) malononitriles, **18–20**, although better electron acceptors than TNF, **5**, xerographically show high dark decay (in poly vinyl carbazole, PVK matrices).

Benzophenonemalononitriles, 21–22

These compounds are synthesized from the condensation of the benzophenones with malononitrile. The CV of these materials show reversible one-electron reduction. It is interesting to compare the reduction potential of the benzophenone malononitrile, **21** ($E_{1/2} = -1.15$ V), and that of 9-fluorenylidene malononitrile, **17** ($E_{1/2} = -0.69$ V). The CV of both compounds is shown in Fig. 6. Anodic shift of over 0.45 V results from rigidizing the two benzene rings of benzophenone into a fluorene. The 4,4′-dinitrobenzophenone malononitrile, **22**, is quite insoluble in most common solvents and exhibits reduction potential at −0.58 V vs. Ag/AgCl.

Can. J. Chem. Downloaded from www.nrcresearchpress.com by 210.87.254.40 on 09/06/12
For personal use only.

TABLE 5. Electrochemical data for polysubstituted 9-fluorenylidene malononitriles

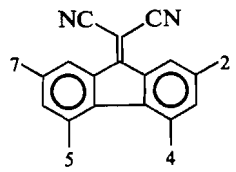

Cpd	Substituent	$-E_{1/2}$(I)	$-E_{1/2}$(II)	A_g (eV)	$-P_s^-$ (eV)	$-P_c^-$ (eV)	A_C (eV)
17	H	0.69	1.30	1.54	2.47	2.12	3.66
18	2,7-diNO_2	0.25	—	1.90	2.55	2.19	4.10
19	2,4,7-triNO_2	0.05	—	2.06	2.59	2.23	4.29
20	2,4,5,7-tetraNO_2	0.11	—	2.19	2.62	2.25	4.44

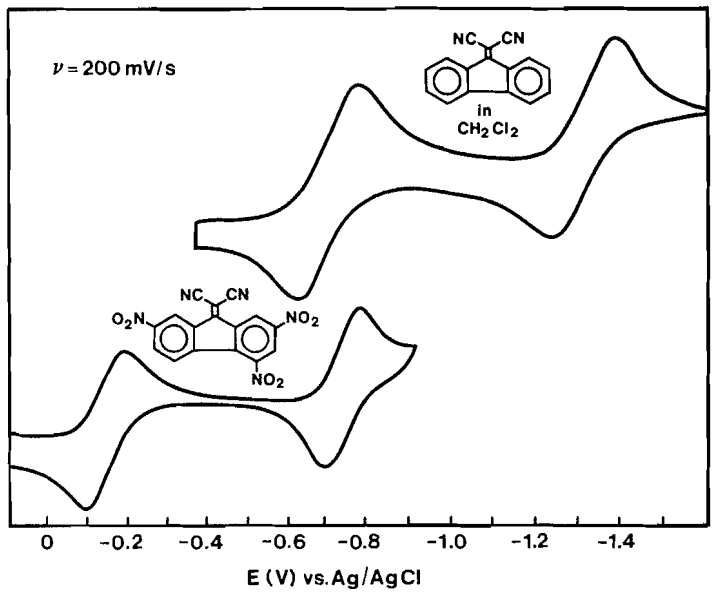

FIG. 5. CV of representative 9-fluorenylidene malononitrile.

Benzylidene malononitriles, 23–30

The synthesis of these compounds involves condensation of the benzaldehyde derivatives with malononitrile. All except the *p-N,N*-dimethyl aminobenzylidene malononitrile, **23**, display irreversible one-electron reduction waves as shown in Fig. 7. The reduction peak potential E_p^c shifts cathodically by 60 mV for a 10-fold increase in scan rate, indicating an irreversible charge transfer involving one-electron and an electron-transfer coefficient, $\beta = 0.5$. The irreversibility can be associated with the presence of the vinylic proton. Displacing the vinylic proton by a phenyl restores reversibility. The terphthalylidene malononitriles, **29** and **30**, show quasi-reversible reduction waves at −0.53 and −0.81 V, respectively. These compounds form very stable radical anions with intense purple color.

2-Arylidene indan-1,3-dione, 31–33

The CV wave of 2-benzylidene indan-1,3-dione, **31**, is a quasi-reversible two-electron reduction, while the CV wave of **32** and **33** is a reversible one-electron reduction as shown in Fig. 7. The electrochemical results for compounds **21** to **33** is shown in Table 6.

Discussion

The electron affinities from electrochemical reduction potential

The energy of the electron conducting level of a molecule in condensed media, A_c, is linked with the gas phase electron affinity A_g via

$$[3] \quad A_c = A_g - P_c^-$$

where P_c^- is the solid medium polarization energy, which can be given by

$$[4] \quad P_c^- = -\left(1 - \frac{1}{n^2}\right)\frac{e^2}{2r}$$

where n^2 is the optical dielectric constant of the medium and r is the effective radius of the radical ion A^-. The gas phase electron affinity, A_g, of a molecule is related to the solution half-wave reduction potential according to

$$[5] \quad A_g = E_{1/2} + P_s^- + E_{RE}$$

Where P_s^- is the differential real solvation energy of the radical anion and E_{RE} is the free energy of electron in the reference electrode vs. an electron in vacuum ($E_{Ag/AgCl} = 4.70$ eV). The solvation energy for a negative ion, P_s^- can be given by:

$$[6] \quad P_s^- = -\frac{e^2}{2r}\left(1 - \frac{1}{\epsilon}\right) - FX_S$$

where ϵ and X_S are the dielectric constant and surface potential of the solvent. Combining eqs. [3] and [5] gives

Can. J. Chem. Downloaded from www.nrcresearchpress.com by 210.87.254.40 on 09/06/12
For personal use only.

Can. J. Chem. Downloaded from www.nrcresearchpress.com by 210.87.254.40 on 09/06/12
For personal use only.

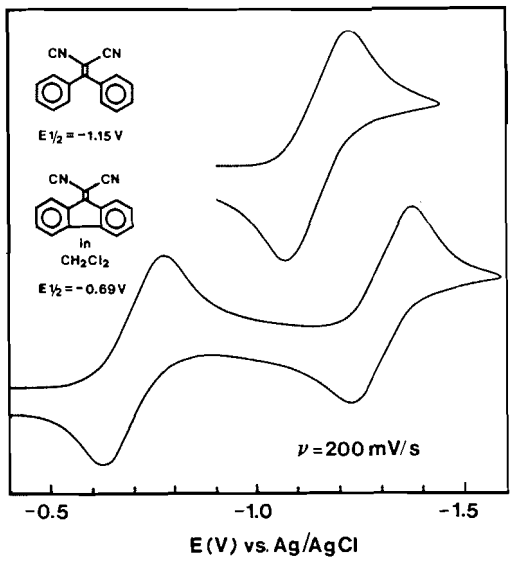

FIG. 6. CV of benzophenone malononitrile and 9-fluorenylidene malononitrile.

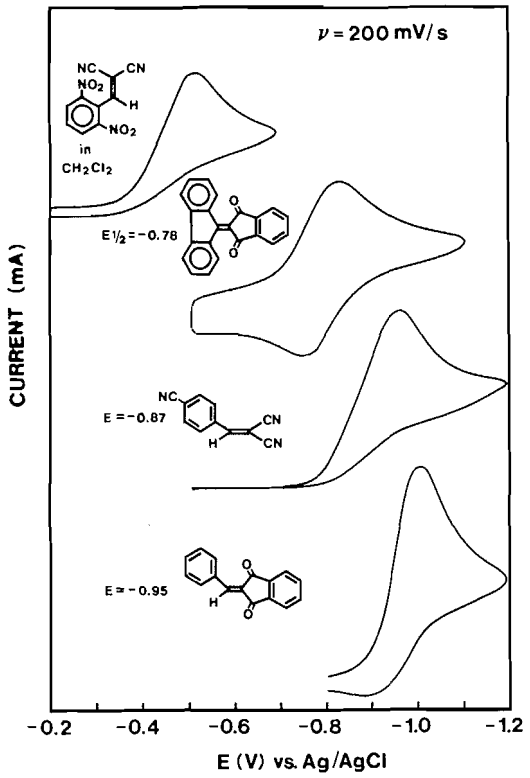

FIG. 7. CV of benzylidene malononitriles and indandiones.

[7] $A_c = E_{1/2} + E_{RE} - (P_c^- - P_s^-)$

The molecular energy levels of electron acceptors in various media are depicted in Fig. 8. Many attempts have been made to correlate A_g and $E_{1/2}$. In most of these correlations the solvation energies of widely different electron acceptors were assumed to be constant. Briegleb (1) found $A_g = E_{1/2} + 1.41$; Chen and Wentworth (5) reported $A_g = E_{1/2} + 2.49 \pm 0.26$; and Lyons and Palmer (6) used $A_g = E_{1/2} + 2.0$. All these linear correlations between A_g and $E_{1/2}$ were obtained in spite of the fact that it is unreasonable to expect that the solvation energy of small molecules such as tetracyanoethylene can be equal to

TABLE 6. Electrochemical reduction data for benzophenone malononitriles, benzylidene malononitriles and arylidine indandiones

Cpd	$E_{1/2}$	A_g	$-P_s^-$	$-P_c^-$	A_C	Remark
21	−1.15	1.17	2.38	2.05	3.21	Reversible
22	−0.58	1.63	2.49	2.14	3.77	Reversible
23	−1.43	0.94	2.32	2.0	2.94	Reversible
24	−1.31	1.04	2.35	2.02	2.94	Reversible
25	−1.20	1.13	2.37	2.04	3.17	Irreversible
26	−0.85	1.41	2.44	2.10	3.51	Irreversible
27	−0.68	1.55	2.47	2.12	3.67	Irreversible
28	−0.51	1.69	2.50	2.15	3.84	Irreversible
29	−0.53	1.67	2.50	2.15	3.82	Quasi-reversible
30	−0.81	1.44	2.45	2.10	3.55	Reversible
31	−0.95	1.33	2.42	2.08	3.41	Irreversible
32	−0.76	1.48	2.45	2.11	3.60	Irreversible
33	−0.74	1.50	2.46	2.11	3.61	Reversible

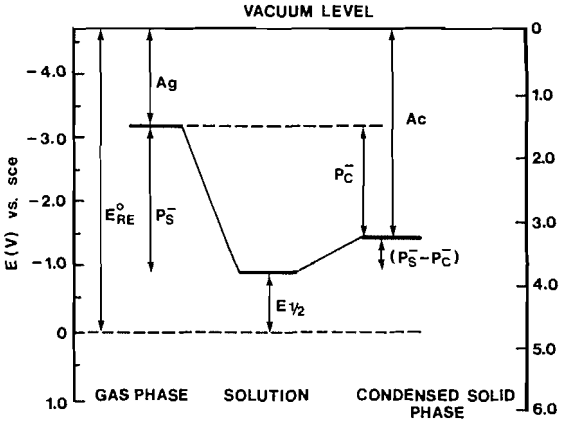

FIG. 8. Molecular energy level scheme for electron conducting level in various media.

that of the relatively larger aromatic hydrocarbons such as anthracene. It is not unreasonable, however, to expect the solvation energy to vary linearly with $E_{1/2}$, i.e., $P_s^- = -(aE_{1/2} + b)$. Thus, A_g can be related to $E_{1/2}$ via

[8] $A_g = (1 - a)E_{1/2} + (4.7 - b)$

where a and b are constants. To determine the value of these constants an empirical correlation between A_g and $E_{1/2}$ was used. The gas phase electron affinity of only a few molecules is known accurately. Recently, Lyons and Palmer (6) accurately measured A_g of tetracyanoethylene by photodetachment experiments to be 2.37 eV. Table 7 lists the best known A_g and $E_{1/2}$ values of a few organic molecules. Figure 9 shows the correlation between A_g and $E_{1/2}$ for the series of molecules listed in Table 7. The least-square fit of the linear correlation shown in Fig. 9 can be given by the eq. [9]:

[9] $A_g = 0.81E_{1/2} + 2.10$

The values of the constants a and b are 0.19 and 2.6 eV, respectively. By using the one-electron reduction potential in Tables 2 to 6, the gas phase electron affinities of the compounds studied here may then be obtained and are listed. Substituting the values of A_g, $E_{1/2}$, and E_{RE} (4.70 eV) into eq. [5], the solvation energies P_s^- can be obtained and are also listed in the tables.

The energy of the electron conducting level of an electron acceptor molecule in polymeric solid-solution can be obtained

TABLE 7. List of gas phase electron affinities and solution reduction potentials of a series of organic molecules[a]

Electron acceptor	$E_{1/2}$[e] (V vs. sce)	A_g[e] (eV)	$-P_s^-$[b] (eV)	$-P_c^-$[c] (eV)	A_C[d] (eV)
Tetracyanoquinodimethane (TCNQ)	+0.35	2.40	2.72	2.33	4.73
Tetracyanoethylene (TCNE)	+0.24	2.30	2.65	2.30	4.58
p-Chloranil (CA)	+0.01	2.13	2.56	2.20	4.33
Anthraquinone (AQ)	−0.97	1.28	2.45	2.10	3.39
Anthracene (A)	−1.97	0.42	2.31	1.99	2.40
1,2-Benzanthracene (BA)	−2.0	0.46	2.24	1.93	2.38
Pyrene (Py)	−2.10	0.39	2.21	1.90	2.29
Chrysene (C)	−2.25	0.33	2.12	1.82	2.15
Phenanthrene (Ph)	−2.45	0.20	2.10	1.80	2.00
Triphenylene (TP)	−2.47	0.14	2.09	1.80	1.94

[a]The correlation between $E_{1/2}$ and A_g gives $A_g = 0.81E_{1/2} + 2.10$.
[b]$P_s^- = A_g - E_{1/2} - 4.70$.
[c]$P_c^- \simeq 0.86P_s^-$.
[d]$A_C = A_g - P_c^- \simeq E_{1/2} + 4.38$; $A_C = 1.2A_g + 1.81$.
[e]References 18–20.

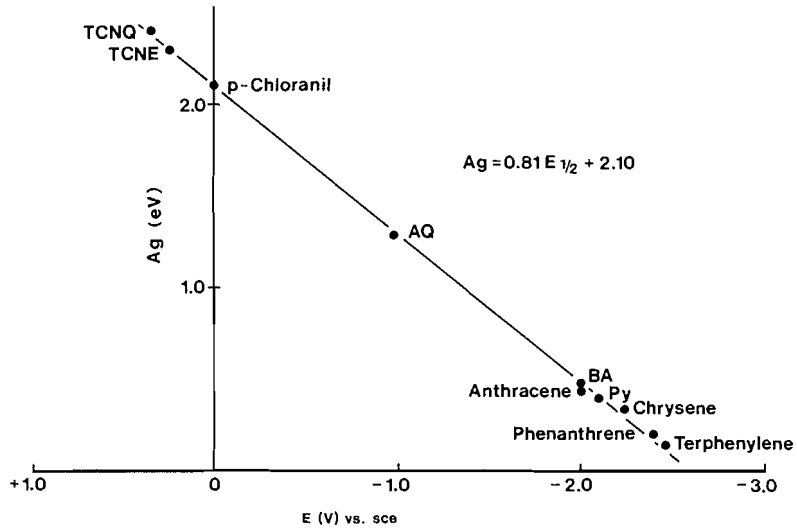

FIG. 9. Correlation between the gas phase electron affinity A_g and the solution half-wave reduction potential of some organic molecules.

using eq. [3], if the value of P_c^- is known. From eqs. [4] and [6], it was found that $P_c^- \simeq 0.86\ P_s^-$. Substituting in eq. [7], using $P_c^- \simeq 0.86\ P_s^-$ and $P_s^- = -(0.19E_{1/2} + 2.6)$ gives

$$[10] \quad A_c \simeq E_{1/2} + 4.38$$

and

$$[11] \quad A_c = 1.2\ A_g + 1.81$$

Using the one-electron reduction potential in Tables 3 to 6, the energy of the electron conducting level of the compounds studied in solid-matrix may thus be obtained and are listed in the tables. The values of A_c of the compound studied varied from 3.0 to 4.44 eV.

Tetracyanoethylene (TCNE) and hexacyanobutadiene has an A_c value of 4.60 and 4.93 eV, respectively. These materials are among the strongest electron-accepting molecules. TNF and **17** has an A_C value of 3.92 and 3.66 eV, which places their accepting level slightly above the conduction band of a −Se (4.0 eV).

The gas phase electron affinity of TNF, **5**, is 1.76 eV, previous estimates have been 2.17 (1), 2.07 (3), 2.1 (5), 1.7 (6), and 1.7 eV (4). The discrepancy is mainly due to the fact that in all previous studies solvation energies of various radical anions were assumed to be constant, while in our study we assumed that P_s^- varies linearly with $E_{1/2}$.

Conclusion

Cyclic voltammetry was used to electrochemically evaluate a series of 33 electron acceptor molecules. The one-electron half-wave reduction potentials were used to determine the electron conducting levels of these materials in various media.

1. G. BRIEGLEB. Angew Chem. **76**, 326 (1964).
2. T. K. MUKHERJEE. Tetrahedron, **24**, 721 (1968).
3. J. E. KUDER, J. M. POCHAN, S. R. TURNER, and D. F. HINMAN. J. Electrochem Soc. **125**, 1750 (1978).
4. A. FULTON. Aust. J. Chem. **21**, 2847 (1968).
5. E. C. M. CHEN and W. E. WENTWORTH. J. Chem. Phys, **63**, 3183 (1975).
6. L. E. LYONS and L. D. PALMER. Aust. J. Chem. **29**, 1919 (1979).
7. P. J. NIGREY. Extended linear chain compounds. Vol. 3. *Edited by* J. S. Miller. Plenum Press. New York. 1983. p. 443.
8. M. S. WRIGHTON, R. G. AUSTIN, A. B. BOCARSLY, J. M. BOLTS, O. HASAS. K. D. LEGG, L. MADJO, and M. C. PALAZZOTTO. J. Am. Chem. Soc. **100**, 1602 (1977).
9. J. B. KERR, L. L. MILLER, and M. R. VAN DE MARK. J. Am.

Can. J. Chem. Downloaded from www.nrcresearchpress.com by 210.87.254.40 on 09/06/12
For personal use only.

Chem. Soc. **102**, 3383 (1980).
10. W. D. GILL. J. Appl. Phys. **43**, 12 (1973); **43**, 5033 (1973); W. D. GILL. Amorphous and liquid semiconductors. *Edited by* J. Stuke and W. Brenig. J. Wiley and Son Inc., New York. 1973. p. 901.
11. G. PFISTER, S. GRAMMATICA, and J. MORT. Phys. Rev. Lett. **37**, 20 (1976); **37**, 1360 (1976).
12. R. M. SCHAFFERT. IBM J. Res. Dev. **15**, 75 (1971).
13. P. J. REGENSBURGER. U.K. Patent No. 1337 227 (1973).
14. J. E. KUDER, W. W. LIMBURG, J. M. POCHAN, and D. WYCHICK. J. Chem. Soc. Perkin Trans. II. 1643 (1977).
15. V. M. VOZZHENNIKOV, Z. V. ZVONKOVA, L. P. SHLYAKHINE, and V. V. BEREZKIN. Russ. J. Phys. Chem. **43**, 1285 (1969).
16. J. N. BUTLER. Advan. Electrochem. Electrochem. Eng. **7**, 77 (1970) and other references therein.
17. V. GUTMANN. Chem. Brit. **7**, 102 (1971).
18. L. E. LYONS and L. D. PALMER. Aust. J. Chem. **29**, 1919 (1979).
19. B. CASE, N. S. HUSH, R. PARSONS, and M. E. PEOVER. J. Electroanal. Chem. **10**, 360 (1965).
20. R. E. BALLARD. Chem. Phys. Lett. **42**, 97 (1976).

Can. J. Chem. Downloaded from www.nrcresearchpress.com by 210.87.254.40 on 09/06/12
For personal use only.

Determination of amphetamine, cocaine, and heroin vapour pressures using a dynamic gas blending system and gas chromatographic analysis[1]

A. H. LAWRENCE,[2] L. ELIAS, AND M. AUTHIER-MARTIN[3]

Unsteady Aerodynamics Laboratory, National Aeronautical Establishment, National Research Council of Canada, Ottawa, Ont., Canada K1A 0R6

Received January 16, 1984

This paper is dedicated to Professor Paul de Mayo on the occasion of his 60th birthday

A. H. LAWRENCE, L. ELIAS, and M. AUTHIER-MARTIN. Can. J. Chem. **62**, 1886 (1984).

A dynamic gas blending system was used to generate controlled vapour concentrations of amphetamine, cocaine, or heroin. An adsorption – thermal desorption – gas chromatographic procedure was developed and used to measure the output vapour concentrations. The vapour pressure of amphetamine at 20°C was determined, and vapour pressures as a function of temperature have been measured for cocaine and heroin.

A. H. LAWRENCE, L. ELIAS et M. AUTHIER-MARTIN. Can. J. Chem. **62**, 1886 (1984).

On a utilisé un système dynamique pour produire des concentrations controlées d'amphétamine, de cocaïne ou d'héroïne en phase gazeuse. On a mis au point une méthode d'adsorption – désorption thermique – chromatographie gazeuse permettant de mesurer la production de concentrations de vapeur. On a déterminé la tension de vapeur de l'amphétamine, à 20°C, et on a mesuré les tensions de vapeur, en fonction de la température, de la cocaïne et de l'héroïne.

[Traduit par le journal]

Introduction

The measurement of the vapour pressure of amphetamine, cocaine, and heroin is an integral part of the continuing effort to develop a highly specific and sensitive technique for the detection of these drugs of abuse. This laboratory has been successful previously in the development of vapour-sensing techniques for the detection of hidden explosives (1).

Amphetamine (**I**), cocaine (**II**), and particularly heroin (**III**), in the free-base form are relatively nonvolatile compounds at ambient conditions, and vapour pressure data for these chemicals have not been determined.

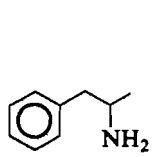

I

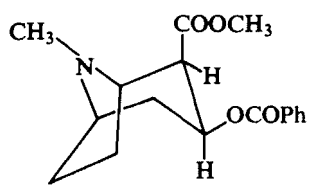

II

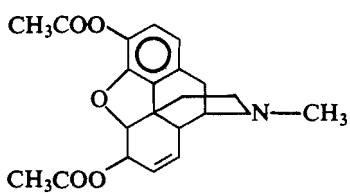

III

The methods of measuring vapour pressure may be classified into two types: static and dynamic, depending on whether the test sample is in a closed system (static), or whether the generated vapour is transported with a carrier stream and the resulting concentration determined (dynamic).

In this work, a dynamic gas-blending system was employed to produce controlled vapour concentrations of amphetamine, cocaine, or heroin. The technique, in brief, is to saturate a flowing gas stream with the narcotic vapour by passage of the stream over the test sample. The vapourized chemical is collected in a solid adsorber sampling tube and then thermally desorbed and analyzed by gas chromatography (gc) using a nitrogen-selective detector. The gc peak area can be related to the amount of compound collected and to the concentration in the flowing stream. A similar procedure was used to measure the vapour pressures of DNT, TNT, and ethylene glycol dinitrate (2).

Experimental

Chemicals

d-Amphetamine sulfate (BDH lot 30603-35403), benzoylmethylecgonine (cocaine) (May & Baker, L64305), and diacetylmorphine (heroin) (T & H Smith EV9022-29) were obtained from Health and Welfare Canada. Amphetamine free base was extracted from the sulfate salt following the procedure described by Predmore and Christian (3). Tenax-GC (35–60 mesh) was obtained from Supelco Inc., Ultra Bond PEGS (80–100 mesh) from Alltech Associates.

Stock solutions ($\sim 10^{-6}$ g/μL) were prepared by dissolving 15 to 25 mg of the drugs in acetone (50 cm^3). Standard hexane solutions were prepared by the appropriate dilution of the stock solutions. The concentration of the standard solutions were amphetamine, 6×10^{-9} g/μL; cocaine, 1.3×10^{-9} g/μL; and heroin, 3×10^{-9} g/μL. All solvents used were distilled-in-glass grade from Caledon.

Solid adsorber sampling tubes

The adsorbent tubes used in this study were constructed of glass tubing 75 mm × 6.3 mm od with a restriction in the middle. For the collection of amphetamine, the tube contained a small amount (ca. 30 mg) of Tenax-GC. The adsorbent was held in place with small plugs of silanized glass wool. For the collection of cocaine and heroin, the tube contained a platinum plug (80 mesh, 7×1.5 cm^2, ~0.5 g) coated with OV-17 (1% in chloroform). All tubes were conditioned for several hours at 250°C in a nitrogen stream at a flow rate of 50 cm^3/min. Before use a chromatogram was recorded to check the purity of each adsorber. Neither peaks nor baseline drift were observed for adsorbers conditioned as above, and stored for up to 2 days. The collection efficiency of the tubes was determined following a previous test procedure (4) and the tubes were found to be 90–95% efficient under the experimental conditions used.

Continuous-flow trace vapour source

A continuous stream of laboratory compressed air containing a

[1]NRCC No. 23399.

[2]To whom all correspondence should be addressed.

[3]Present address: Alcan Analytical Centre, Vaudreuil Works, Arvida, P.Q., Canada G7S 4L2.

Can. J. Chem. Downloaded from www.nrcresearchpress.com by 210.87.254.6 on 09/06/12
For personal use only.

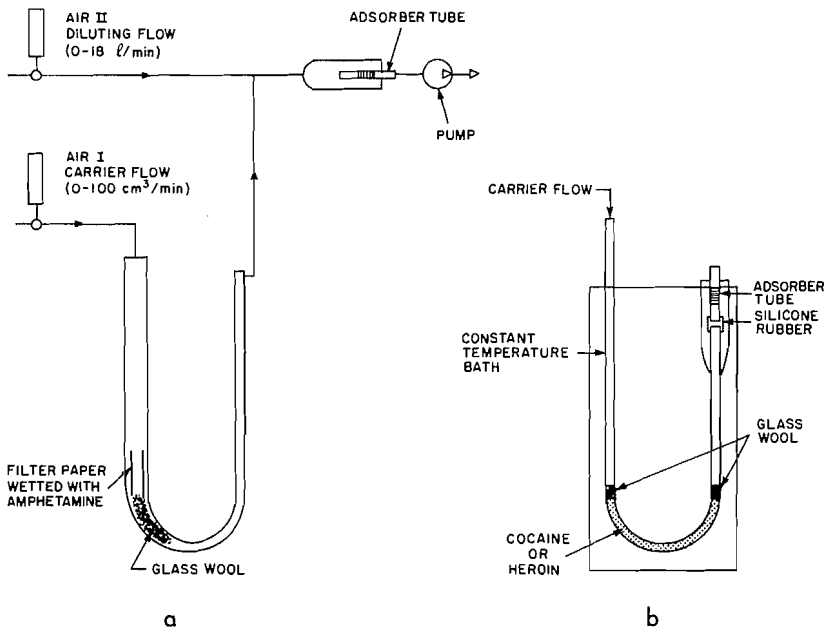

FIG. 1. Continuous-flow trace vapour source.

constant concentration of drug vapour was generated by a continuous-flow trace vapour source developed in this laboratory (5). The trace vapour generator, employing dynamic dilution of vapours of amphetamine, is shown schematically in Fig. 1*a*. For proper sampling, the flow rate of vapour exiting the source was maintained at twice or greater than the sampling rate. A diaphragm pump (Fisher Scientific Instruments) was used for sampling. Amphetamine, which is a liquid at room temperature, was placed in the U-tube on a strip of filter paper wetted with about 200 mg of the substance.

Due to the low vapour pressure of cocaine and heroin, dynamic dilution was not necessary with these compounds (i.e., Air II = 0), and at temperatures above ambient, a much simpler device was used (Fig. 1*b*). Purified air flows at an adjustable rate through the U-tube filled with crystalline cocaine or heroin immersed in a thermostated bath, and carries the vapours directly to the adsorber tube. The connection between the adsorber and the U-tube is also immersed in the temperature-controlled bath. The above design has the advantage of keeping the vapours at the selected temperature until they reach the sorbent material, thus reducing vapour losses. The junction between the source and the adsorber was made with a piece of silicone rubber tubing. After collecting a vapour sample, the adsorber was disconnected from the U-tube and attached to the gas chromatograph for analysis.

Gas chromatographic analysis

A Varian 1400 gas chromatograph equipped with a nitrogen–phosphorus thermionic specific detector (TSD) was used for the experimental work described in this paper. The gc was modified to accommodate a two-stage adsorber system. The second adsorber contained a small amount ca. 30 mg of Ultra Bond PEGS, and is incorporated in the instrument. After sampling, the solid adsorber sampling tube (adsorber I) was connected to the gas chromatograph. The collected vapours were removed by heating, and flushed with a carrier gas stream to the smaller adsorber (adsorber II) from which they were subsequently thermally desorbed for injection into the chromatographic column. A six-port switching valve provided the various functions involved in the analysis as indicated in Fig. 2 and was maintained at 210°C to avoid condensation. The signal from the detector was recorded on a Hewlett Packard 3390A strip chart reporting integrator. The recorded drug peak area was compared with that of a drug standard solution deposited with a syringe directly on adsorber I, and analyzed in the same manner as an air sample. Amphetamine, cocaine, and heroin were successfully chromatographed under the conditions given in Table 1.

Results and discussion

Vapour pressure of amphetamine

The collection efficiency of the Tenax adsorber was tested by measuring the vapour concentration as a function of the sampling flow rate over the range 200 to 500 cm^3/min. The carrier flow and the diluting flow were maintained at 2.1 cm^3/min and 15.7 L/min, respectively. The sampling time was 60 s. The plot of the measured vapour concentration at the sampling port of the vapour source as a function of the sampling rate was found to be linear with a correlation coefficient of 0.996. The vapour source was tested by measuring the equilibrium vapour concentration as a function of the diluting flow. The carrier flow was maintained at a sufficiently low level (2.1 cm^3/min) to permit saturation with the vapour of the amine (deviation from equilibrium conditions was observed at a carrier flow > 7 cm^3/min). The sampling rate was 200 cm^3/min.

Under conditions where the static equilibrium vapour pressure above the sample is nearly maintained, the concentration C in the air stream at the sampling port is simply the equilibrium vapour concentration C_0 of amphetamine reduced by the appropriate dilution ratio according to the equation:

$$[1] \quad C = C_0 \left(\frac{f}{f + F}\right)$$

f is the flow rate of the carrier air and F is the diluting air entering the mixing manifold, the ratio $f/(f + F)$ being the dilution factor. The diluted vapour concentrations were measured experimentally by analyzing the adsorber tubes gas chromatographically as described above. The equilibrium vapour concentrations were calculated from eq. [1]. Measured values of C and the derived values of C_0 are presented in Table 2; the constancy of C_0 indicates a proper vapour generator performance. The vapour pressure of amphetamine at 20°C calculated from the equilibrium concentration data using the ideal gas law was found to be $2.4 \pm 0.2 \times 10^{-1}$ Torr.

Vapour pressures of cocaine and heroin

In a similar procedure, the effect of carrier flow rate on reaching equilibrium conditions was determined by varying the air flow from 50 to 150 cm^3/min through the vapour source

Can. J. Chem. Downloaded from www.nrcresearchpress.com by 210.87.254.6 on 09/06/12
For personal use only.

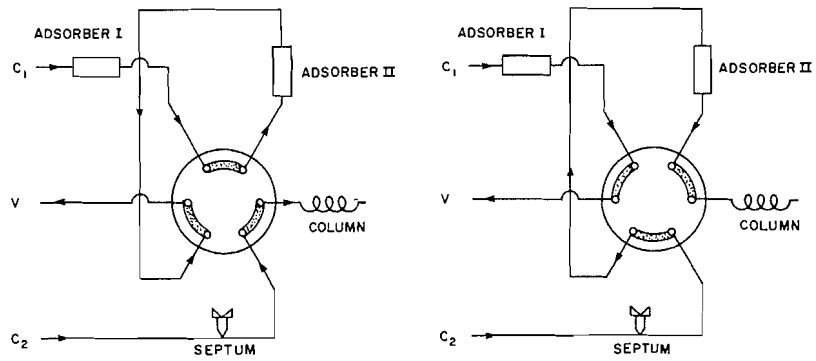

(a) SAMPLE TRANSFER OR SEPTUM INJECTION (b) SAMPLE ANALYSIS OR STANDBY MODE

FIG. 2. Schematic view of the gas chromatograph. C_1, C_2, carrier streams; V, vent to ambient.

TABLE 1. Gas chromatographic conditions

Condition	Amphetamine	Cocaine	Heroin
Column (nickel tubes)	2 m × 3.2 mm od 3% OV-101 on Ultra Bond 20 M 100–120 mesh	0.3 m × 3.2 mm od Ultra Bond 20 M 80–100 mesh	
T (°C)			
Oven	160	155	190
Injector and valve	210	210	210
Detector	250	250	250
Desorption (I and II)	250	250	250
Carrier gas flow rate (cm^3/min)	He; 50	N_2; 40	N_2; 40
TSD conditions			
Air (cm^3/min)	250	150	150
H_2 pressure (psig)	16	18	18
Bead current	7.0	6.0	6.0
Bias voltage	−4	−4	−4
Retention time (min)	1.6	1.2	1.7

(Fig. 1*b*) containing cocaine at 20°C. The measured cocaine concentration was found to be independent of the air carrier flow rate over this range. Measurements made with heroin showed no differences in vapour concentrations when the carrier flow rate was varied from 20 to 95 cm^3/min at 63°C. Accordingly, the air carrier flow rates used for generating cocaine and heroin equilibrium vapour concentrations were 100 cm^3/min and 35 cm^3/min, respectively. Equilibrium vapour concentrations were generated from 21 to 41°C for cocaine and from 51 to 66°C for heroin, and measured chromatographically as described above. Vapour pressure data were calculated using the ideal gas law. Each data set was plotted as log P vs. $1/T$ according to eq. [2] and treated by the weighted least-square method.

$$[2] \quad \log P = A - B/T$$

P is the vapour pressure expressed in Torr, A and B are the intercept and slope, respectively, and T is the temperature in degrees Kelvin. The results obtained are summarized in Table 3.

TABLE 2. Diluted and equilibrium vapour concentrations of amphetamine*

Dilution factor	f (cm^3/min)	F (L/min)	Measured C(g/L)	Calculated C_o(g/L)
0.00021	2.1	9.9	$3.8\pm0.3\times10^{-7}$	1.8×10^{-3}
0.00013	2.1	15.7	$2.5\pm0.2\times10^{-7}$	1.9×10^{-3}

*Temperature, 20°C.

TABLE 3. Vapour pressure constants for cocaine and heroin*

Compound	No. of data pts	A	B	σ_A	σ_B	Correlation coefficient
Cocaine	18	13.02	5884	0.50	147.4	0.995
Heroin	16	16.20	7549	0.62	209.8	0.999

*Log $P = A - B/T$.

In conclusion, the selectivity of the nitrogen/phosphorus detector together with the advantages of the two-stage preconcentration technique (4) renders the dynamic method described above a simple, inexpensive, and sensitive technique for the determination of the vapour pressure of relatively nonvolatile nitrogen-containing compounds.

Acknowledgment

This work was supported in part by funding from the Department of Revenue Canada, Customs and Excise.

1. L. ELIAS. NRC, NAE, LTR-UA-57, National Research Council, Ottawa, Canada. 1981.
2. P. A. PELLA. Anal. Chem. **48**, 1632 (1976).
3. D. B. PREDMORE and G. D. CHRISTIAN. Anal. Chem. **48**, 361 (1976).
4. A. H. LAWRENCE and L. ELIAS. Unpublished results.
5. M. KRZYMIEN and L. ELIAS. J. Phys. (E) Sci. Instrum. **9**, 584 (1976).

Can. J. Chem. Downloaded from www.nrcresearchpress.com by 210.87.254.6 on 09/06/12
For personal use only.

Adsorption characteristics of rhodamine 6G on montmorillonite and laponite, elucidated from electronic absorption and emission spectra

ZVI GRAUER, DAVID AVNIR,[1,2] AND SHMUEL YARIV[1]

Institute of Chemistry, The Hebrew University of Jerusalem, Jerusalem 91904, Israel

Received January 19, 1984

This paper is dedicated to Professor Paul de Mayo on the occasion of his 60th birthday

ZVI GRAUER, DAVID AVNIR, and SHMUEL YARIV. Can. J. Chem. **62**, 1889 (1984).

The adsorption of the cationic dye rhodamine 6G by montmorillonite (Wyoming bentonite) and laponite (synthetic hectorite) was studied by visible and fluorescent spectroscopy and by X-ray diffraction methods. Adsorption of the dye takes place by the mechanism of cation exchange. X-ray data indicate that the adsorbed cationic dye is located in the interlayer spaces of both minerals. It was found that adsorption prevents the dimerization of the dye, and gives rise to red shifts of the principal absorption band of the dye. A study of the effect of varying concentration of dye or clay on the location and intensity of this band proved to be useful in determining the adsorption capacity of the clay. The observed spectral changes are linked to surface polarity and to clay flocculation. At concentrated suspensions of montmorillonite, an additional weak absorption shoulder is obtained at 470–490 nm, which may be attributed to aggregated dye molecules, probably trapped within the cavities of book-house structured flocs. Due to steric hindrance rhodamine 6G does not give π interactions with the oxygen plane of the silicate layer. Therefore the adsorption of the dye by expanding clay minerals does not give rise to metachromasy. Fluorescence of the adsorbed dye is reported: it is red shifted and quenched relative to aqueous solutions. The use of fluorescence spectra to determine the saturation point is described, and aging and ultrasonic effects on spectral features are presented and discussed.

ZVI GRAUER, DAVID AVNIR et SHMUEL YARIV. Can. J. Chem. **62**, 1889 (1984).

Faisant appel à la diffraction des rayons-X et à la spectroscopie visible et de fluorescence, on a étudié l'adsorption du colorant cationique rhodamine 6G par la montmorillonite (bentonite du Wyoming) et par la laponite (hectorite synthétique). L'adsorption du colorant se fait par un mécanisme impliquant un échange de cations. Les données de rayons-X indiquent que, dans le cas de chacun des deux minéraux, le colorant cationique est adsorbé dans les espaces interstitiels. On a trouvé que l'adsorption empêche la dimérisation du colorant. A la suite de l'adsorption, la principale bande d'adsorption du colorant se déplace vers le rouge. Une étude de l'effet d'un changement de concentration du colorant ou de l'argile sur la position et l'intensité de cette bande s'avère un outil utile pour déterminer la capacité d'adsorption de l'argile. Les changements spectraux observés sont liés à la polarité de la surface et à la floculation de l'argile. Pour des suspensions concentrées de montmorillonite, on observe une adsorption supplémentaire faible qui apparaît comme un épaulement à 470–490 nm et que l'on peut attribuer à une aggrégation de molécules de colorant qui sont probablement emprisonnées dans les cavités des flocons. La rhodamine 6G, à cause de l'encombrement stérique, n'a pas d'interactions π avec le plan d'oxygènes de la couche de silicate. Par conséquent, l'adsorption du colorant par la dilatation des minéraux argileux ne provoque pas de métachromasie. On rapporte la fluorescence du colorant adsorbé: par opposition à son comportement en milieux aqueux, il y a déplacement vers le rouge et un piégeage. On décrit une méthode de déterminer le point de saturation qui fait appel à l'utilisation des spectres de fluorescence. On rapporte et on discute des effets ultrasoniques et du vieillissement sur les caractéristiques spectrales.

[Traduit par le journal]

Can. J. Chem. Downloaded from www.nrcresearchpress.com by 210.87.254.105 on 09/06/12
For personal use only.

Introduction

As part of our interest in the use of photoprocess at solid (1, 2) and liquid (3) interfaces as probes for studying these environments, we have investigated the electronic absorption and emission spectra of rhodamine 6G (R6G, **1**) adsorbed on clays in aqueous suspensions. Two smectite minerals were chosen: montmorillonite (Wyoming bentonite) and laponite (synthetic hectorite).

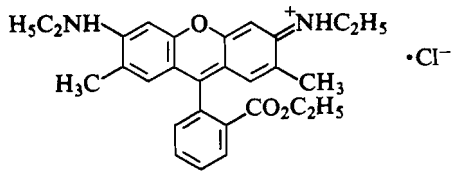

1

The xanthenes comprise a family of fluorescent dyes, with wide applications such as laser dyes (4), photosensitizers (5), and singlet oxygen generators (6). Spectroscopic properties of adsorbed xanthene dyes have been investigated on surfaces of various solid materials such as porous (2*b*, 2*d*, 7) and nonporous (8–11) silica type glasses, semiconductors (10, 12–14), various surface-hydroxylated materials (14), crystals of polycyclic aromatic hydrocarbons (15), silver islands (16), and gold films (8).

Organometallic fluorescent dyes adsorbed on clays have been studied by Van-Damme and co-workers (e.g. ref. 17) and by DellaGuardia and Thomas (e.g. ref. 18) as part of their interest in the applications of photo-redox reactions in organized media.

In previous publications from our laboratory the adsorption of two cationic dyes by montmorillonite was described (1*a*, *b*): methylene blue and acridine orange. The adsorption of these dyes takes place by the mechanism of cation exchange which is reflected by the spectroscopic phenomenon of metachromasy, i.e., the appearance of a new blue shifted band. From those studies it was concluded that metachromasy resulted from π interactions between the oxygen planes of the clay and the aromatic rings of the organic dye. Such π-interaction cannot occur in R6G due to steric hindrance; in this molecule the phenyl ring is sterically constrained to be roughly perpendicular to the planar xanthene group (19). It was therefore expected that if our suggested mechanism of meta-

[1]Authors to whom correspondence should be addressed.
[2] M. Richter Fellow.

chromasy (1) is correct, the adsorption of R6G by smectites should not lead to metachromasy. In the present study we show that this is indeed the case. We also show that the study of electronic absorption and emission spectra of the clay/R6G associates provides information not only on the adsorbed dye itself, but also on saturation ratios, on the structural aspects of the clay suspensions, and on the polarity of the surface.

Experimental

1. Chemicals

R6G (Aldrich) was twice recrystallized from ethanol. The resulting crystals showed a single point on tlc and were fluorescent. Elemental analysis showed the recrystallized material to be of 98.8% purity. Laponite XLG (a synthetic Na-hectorite) was from Laporte Industries Inc., WY. Bentonite (Na-montmorillonite) was supplied by Wards Natural Science Establishment, Inc. It was ground to 80 mesh. Quartz was separated by sedimentation. Clay suspensions of 1% by weight were used as stock suspensions. An aqueous solution of 4.2×10^{-4} *M* R6G was used as a stock solution and kept in the dark in order to avoid photodecomposition.

2. Adsorption and sample preparation

The desired amount of clay was transferred from the concentrated stock suspension into a 25 mL flask, and diluted with triple-distilled water to less than 25 mL. After thorough shaking, the desired amount of dye from the dye stock-solution was added dropwise, and the volume filled to 25 mL. The reverse order of addition is not recommended, since this may cause heavy dye coating on the first added clay particles.

3. Absorption and emission spectra

Absorption and emission spectra were recorded immediately after the preparation of the clay–dye suspension. Absorption spectra were also recorded after aging periods of 1 and 6 days. Some of the aged suspensions were exposed to ultrasonic agitation for 10 min and their visible spectra then recorded. Aliquots of the various aged suspensions were separated by centrifuging on an A. B. Ljungberg spot-test centrifuge and the spectra taken on a Bausch and Lomb spectrophotometer model 2000 and on a Cary 219 (Varian) spectrophotometer. Fluorescence measurements (excitation and emission) were performed on a SLM-Aminco model 4800 Spectrofluorimeter, using 1 mm quartz cells in a front face set up.

4. X-ray diffraction

Oriented samples of R6G treated clay were prepared by drying the suspensions on glass slides. X-ray diffraction patterns were obtained on a Philips Diffractometer using monochromatic CuK_α radiation. Diffractions were also determined after 6 days in an oven at 195°C.

Results

1. Cation exchange

The adsorption of R6G by montmorillonite and laponite takes place largely by a cation exchange mechanism. Exchangeable metallic cations are released into the solution when the clay is equilibrated with R6G. Some representative data are presented in Table 1.

TABLE 1. Metallic cations (in mequiv./100 g clay) released into an equilibrated suspension of montmorillonite and laponite treated with 85 m*M* R6G per 100 g clay

Cation	Montmorillonite	Laponite
Na	97	71
K	4	0.3
Mg	53*	140*

*High values for Mg may be due to the presence of peptized clay in the supernatant.

2. Spectral changes in adsorbed R6G

It is well documented that xanthene dyes tend to dimerize at concentrations as low as 10^{-4} *M* via π interactions. This is usually reflected by the appearance of metachromatic absorption bands (20). For R6G, the monomeric absorption maximum at 525 nm (band α) in dilute solutions (Fig. 1*A*) is accompanied by a blue-shifted new band at 498 nm (band β) at high concentrations (Fig. 2).

The most striking change in the absorption spectrum that R6G undergoes upon adsorption on laponite and montmorillonite is the disappearance of the dimeric band β accompanied by an increase in the intensity of band α, indicating the dissociation of dimers into a monomeric adsorbed species (Fig. 2). Band α is red shifted upon adsorption (Fig. 1). This spectral change is described in detail in the next section.

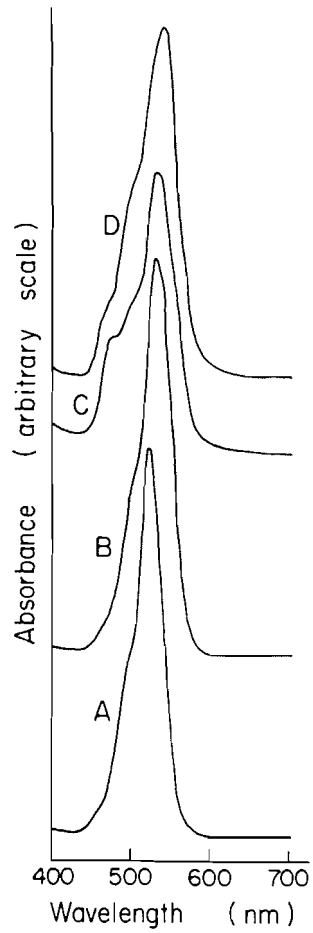

FIG. 1. Absorption spectra of 1.7×10^{-5} *M* R6G in: *A*, aqueous solution; *B*, 0.02% laponite suspension; *C*, 0.02% montmorillonite suspension; *D*, 0.002% montmorillonite suspension.

A new band (band γ) appears as a shoulder at 470–490 nm in the spectrum of R6G adsorbed on montmorillonite (Fig. 1*C*) but not on laponite (Fig. 1*B*). This strongly blue-shifted band appears only for clay concentrations higher than 0.01%, and its intensity increases with dye coverage up to a point which is slightly above the saturation ratio. Beyond this point, the excess dye causes clay peptization. At low clay concentrations, e.g., 0.002%, band γ is not apparent at any dye/clay ratio (Fig. 1*D*).

Can. J. Chem. Downloaded from www.nrcresearchpress.com by 210.87.254.105 on 09/06/12
For personal use only.

Can. J. Chem. Downloaded from www.nrcresearchpress.com by 210.87.254.105 on 09/06/12
For personal use only.

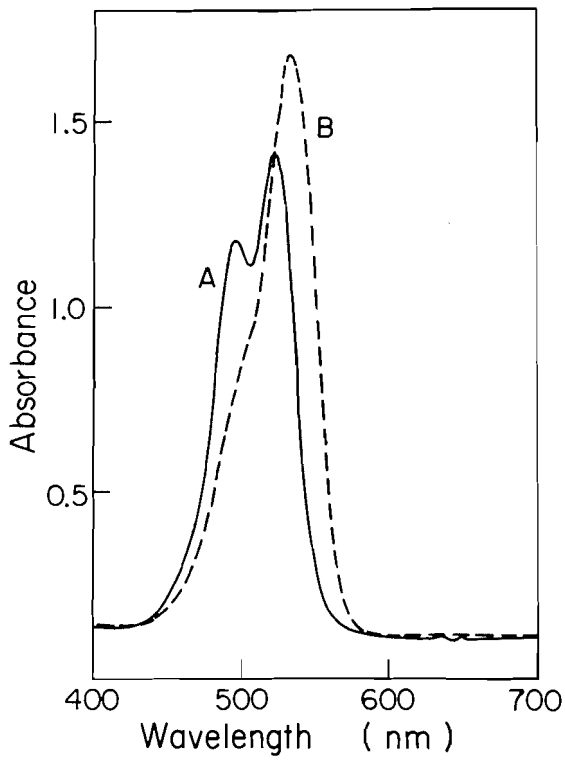

FIG. 2. Absorption spectra of aqueous solutions of R6G: *A*, 2.1×10^{-4} *M*; *B*, 2.1×10^{-4} *M* in the presence of laponite (0.05%). A similar effect is apparent in the case of montmorillonite.

3. Determination of saturation point from analysis of band α

A series of montmorillonite− and laponite−R6G suspensions was prepared using a constant amount of R6G (1.7×10^{-5} *M*) and increasing amounts of clay mineral. Visible and fluorescence spectra of the suspensions were recorded. Figure 3*a* shows the effect of the clay concentration in the suspension on the location of band α in the absorption spectrum of the dye. As indicated in the figure, adsorption on both clays causes a red shift in band α. Maxima are obtained when the ratios between the dye and the clay are equal to 60 and 45 m*M* dye per 100 g montmorillonite and laponite, respectively. At this stage band α is located at 545 and 538 nm in the spectra of montmorillonite− and laponite−R6G suspensions, respectively. The supernatant obtained after the separation of the clay fraction from the suspension by centrifugation shows that up to the stage where maximum wavelength shift is obtained, some of the dye remains in the supernatant, whereas at lower dye/clay ratios the dye is totally adsorbed by the clay. The presence of free R6G in the supernatant is deduced from the location of band α at 525 nm. The saturation point can be also detected in a plot of absorption intensity of a fixed dye amount vs. amount of added clay (Fig. 3*b*). Here the absorption intensities for laponite and montmorillonite are at *minima*, and are slightly shifted with respect to the positions of the maxima in Fig. 3*a*. This shift is significant, and will be discussed below.

The saturation ratios were then cross-checked by changing the dye concentration, and keeping the clay concentration fixed (0.002% and 0.02%). As seen from Fig. 4*a* for the 0.002% case, indeed the same saturation ratios are obtained as in Fig. 3. Similar results were obtained for the 0.02% concentration. A rather complicated curve described the change in absorption maxima as a function of added dye (Fig. 4*b*). This

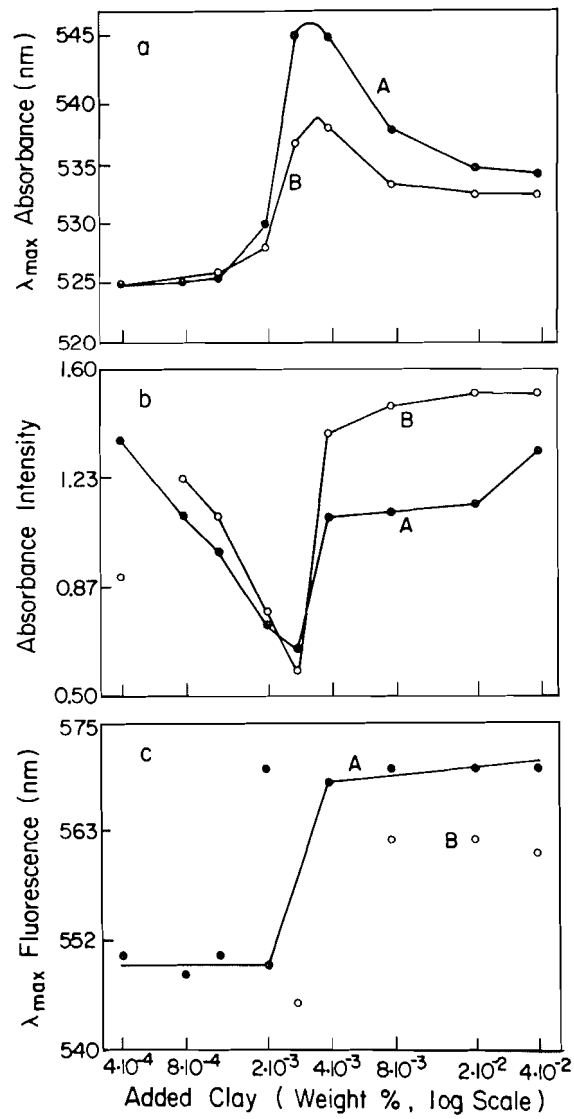

FIG. 3. The effect of added clay mineral on (*a*) the location of band α; (*b*) the absorption intensity of band α; (*c*) the fluorescence maxima, all at a fixed R6G concentration of 1.7×10^{-5} *M*. *A*, montmorillonite; *B*, laponite.

behaviour may reflect (see below) changes in the structure of the colloidal suspension.

4. Determination of saturation point from fluorescence spectra

The effect of clay concentration in the clay−R6G suspension on the fluorescence spectrum was investigated. In solution, the emission band of the dye is quite intense. Upon adsorption of the dye by the clay, the fluorescence intensity decreased substantially. Consequently, as long as there is free R6G in the solution, the recorded spectrum is governed by the features of the aqueous soluble dye molecules (λ_n = 550 nm). When the dye is completely adsorbed by the added clay, so that free dye − molecules do not interfere, a substantial red shift in the emission is revealed; 569 nm and 563 nm for montmorillonite and laponite, respectively (Fig. 5). Excitation spectra of the adsorbed dye are shown in Fig. 5 as well; the maxima of these spectra were close to within 0−2 nm to the absorption maxima. The shoulders in the emission and excitation spectra of R6G−montmorillonite are located at positions of non-adsorbed dye. The abrupt change in fluorescence properties across the saturation point is indicated in Fig. 3*c*.

Can. J. Chem. Downloaded from www.nrcresearchpress.com by 210.87.254.105 on 09/06/12
For personal use only.

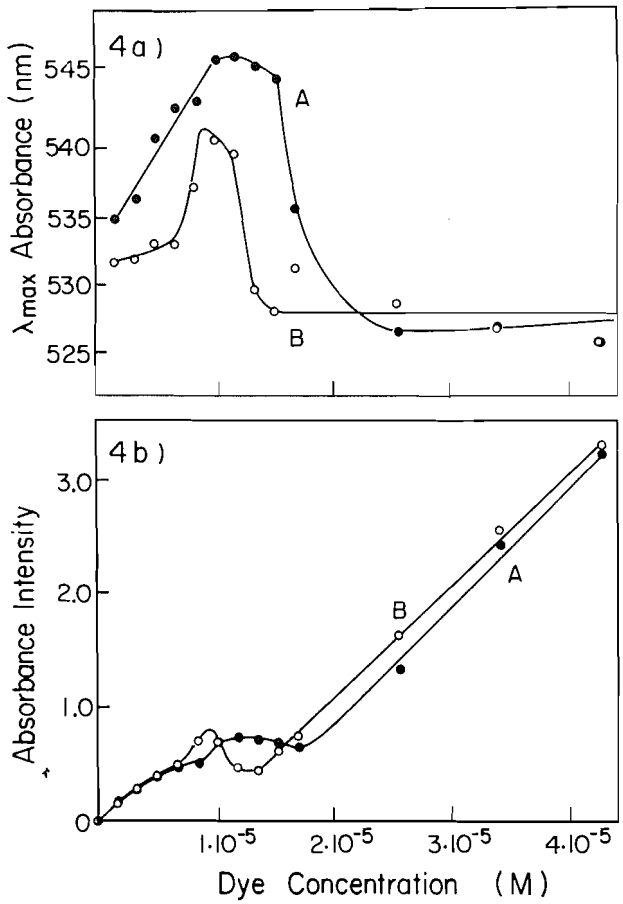

FIG. 4. The effect of R6G concentration on (*a*) the location and (*b*) the absorption intensity of band α at a fixed 0.002% clay. *A*, montmorillonite; *B*, laponite.

5. The effect of aging and ultrasound on flocculation

The above series of clay/R6G suspension with fixed (0.02%) clay concentration and changing amounts of dye was subjected to aging for various periods, and the absorption spectra were then recorded. The results are summarized in Tables 2 and 3. As indicated in the tables, values obtained after the aging periods are lower than those obtained for the fresh systems. The batches which showed lowering in absorbance appeared to be flocculated. During the aging period the suspensions were kept in the dark in order to avoid photodecomposition of the organic dye. It seems therefore that flocculation which occurred during the aging period is the principal reason for the decrease in absorbance.

The aged suspensions were centrifuged for 10 min and the spectra of the supernatants were recorded. The supernatants may contain the soluble dye cation which was not adsorbed by the clay, and peptized clay coloured by the adsorbed dye. The first absorbs at 525 nm, whereas the latter absorbs at higher values (Figs. 3, 4). The difference between the absorbances of the original suspension and of the supernatant can give an indication as to the degree of flocculation of the organo-clay (Tables 2, 3). From the tables it can be seen that flocculation increases with increasing amounts of organic material up to a certain amount, and then decreases. The highest degree of flocculation is obtained when the of R6G in the clay suspension is slightly above the saturation point of the clay.

To examine this assumption, some of the aged suspensions were deflocculated by ultrasonic treatment. The recorded spectra showed a considerable increase in the absorbance of band α (Tables 2 and 3). In some cases the absorbance values recorded after the ultrasonic treatment were even higher than the original values recorded for the fresh suspensions. This increase may reflect better peptization achieved by the ultrasonic treatment.

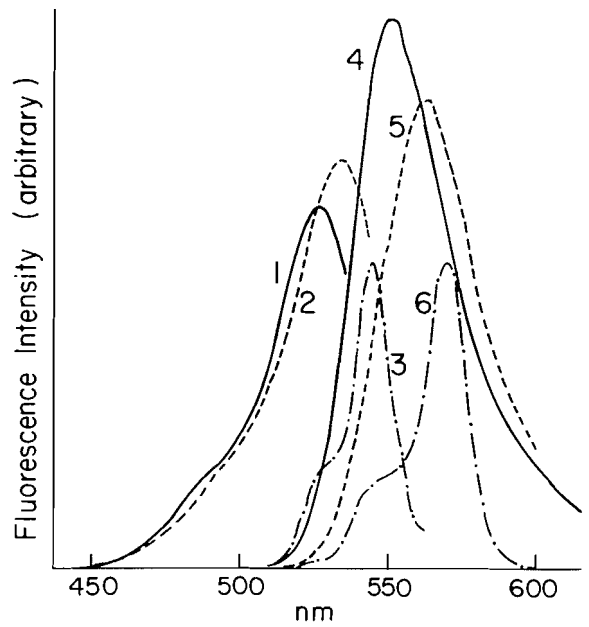

FIG. 5. Excitation and emission spectra of R6G. Excitation in (*1*) water; (*2*) laponite; (*3*) montmorillonite. Emission in (*4*) water; (*5*) laponite; (*6*) montmorillonite. Coverage of laponite: 4 mequiv/100 g; of montmorillonite: 60 mequiv./100 g.

TABLE 2. Absorbance of band α in the spectra of aqueous suspensions of montmorillonite (0.02%) containing different amounts of R6G and of the supernatants separated after an aging period of 6 days

m*M* R6G per 100 g clay	Suspensions‡				Supernatant
	A	B	C	D	
8.4	1.39	1.15	1.30	n.d.	0.27*
16.8	2.42	1.91	1.77	n.d.	0.60*
25.2	3.73	3.58	2.26	n.d.	1.10*
33.6	3.86	3.04	2.38	n.d.	1.50*
42.0	4.72	3.14	2.37	4.92	1.40*
84.0	3.81	2.11	1.52	4.91	0.30†
126.0	9.01	n.d.	10.44	n.d.	2.90†
168.0	11.86	11.53	12.11	n.d.	7.90†

*$\lambda_{max} > 525$.
†$\lambda_{max} = 525$.
‡A, freshly prepared; B, aging period 1 day; C, aging period 6 days; D, ultrasound after 6 days; n.d., not determined.

6. X-ray studies

Oriented specimen of clay samples treated with various amounts of R6G were examined by X-ray diffraction at ambient conditions and after being dried at 195°C for 6 days (Table 4). The thermal treatment of natural Wyoming bentorite or laponite results in a dehydration process, leading to a *c* spacing of 1.0 nm. On the other hand, in the presence of R6G only minor effects of the thermal treatment on the *c* spacing due to dehydration were observed. From these results it may be concluded that the *c* spacing is principally controlled by the presence of the organic dye in the interlayer space.

TABLE 3. Absorbance of band α in the spectra of aqueous suspensions of laponite (0.02%) containing different amounts of R6G and of the supernatants separated after an aging period of 6 days

m*M* R6G per 100 g clay	Suspensions‡				
	A	B	C	D	Supernatant
8.4	1.49	1.41	1.27	n.d.	1.04*
16.8	2.42	2.46	2.38	n.d.	2.30*
25.2	3.86	3.81	3.95	n.d.	0.40*
33.6	5.33	5.49	4.12	n.d.	0.17*
42.0	6.58	6.51	3.24	5.25	0.06*
84.0	6.12	5.36	4.17	7.63	0.66†
126.0	13.35	12.96	12.08	n.d.	2.92†
168.0	18.54	18.33	18.08	n.d.	8.00†

*$\lambda_{max} > 525$.
†$\lambda_{max} = 525$.
‡A, freshly prepared; B, aging period 1 day; C, aging period 6 days; D, ultrasound after 6 days; n.d., not determined.

TABLE 4. Basal spacings (in nm) of montmorillonite and laponite treated with different amounts of R6G*

m*M* R6G per 100 g clay	Montmorillonite		Laponite	
	A	B	A	B
8.4	1.41	1.41 v.br.	1.59 m	1.55–1.70
16.8	1.47	1.50 br	1.70	1.56 v.br.
25.2	1.62	1.62 s	1.70 v.br.	1.70 v.br.
33.5	1.76	1.70 m	1.79 v.br.	1.76 v.br.
42.0	1.82 s	1.75 s	1.84 v.br.	1.76 v.br.
84.0	2.10 s	2.04 s	2.01 v.br.	1.73 v.br.
126.0	1.59 v.w.		2.13	1.79 v.br.
168.0	1.64 v.w.	1.49 v.w.		2.04

*A, before heating; B, after heating at 195°C; s = sharp; v = very; br = broad; m = medium; w = weak.

Discussion

1. The disappearance of band β and its consequences on the question of metachromasy in clay minerals

The metachromatic appearance of band β in R6G aqueous solutions has been studied recently by Arbeloa *et al.* (19). From spectroscopic considerations, and from investigation of molecular models, they proposed a structure for the dimer of R6G which leads to metachromasy. According to the suggested structure, two xanthene moieties form parallel planes held together by π interactions and separated by 0.56 nm, with a twist angle of 76°. This angle is caused by the steric hindrance between the two *ortho* ethyl benzoate substituents, which are roughly perpendicular to the xanthene planes. As described above, upon adsorption on the clays band β disappears, and the monomeric band α increases in intensity. This was interpreted as dimer dissociation upon adsorption.

In contradistinction, metachromasy occurs during adsorption of either methylene blue or acridine orange even when the interlayer spacing of the clay mineral is insufficient for dye aggregation (1). As mentioned in the Introduction, it has been suggested that metachromasy in these systems is due to interactions between the oxygen plane of the aluminosilicate layer and the π electron orbitals of the dye–cation. Whereas a twisting angle in R6G can compensate for the steric hindrance of the benzoic acid substituents in the dimer in solution, such compensation is impossible between the oxygen plane and the xanthene moiety. Therefore, not only is there no metachromasy due to adsorbed aggregates of R6G, there is also no metachromasy due to *monomeric* adsorption, as was the case for methylene blue and acridine orange. It seems to us that these observations strengthen the hypothesis that metachromasy of dyes adsorbed into the interlayers of expandable smectites originate from monomeric adsorption and adsorbate/adsorbant π interactions, and not, as suggested by Bergmann and O'Konski (21), from adsorbed aggregates. According to the adsorbed-aggregates hypothesis, band β should have been seen also in the case of R6G adsorbed on clays.

2. Band γ and the book-house structure of montmorillonite

We do, however, think that there is a very small degree of aggregation on high concentration montmorillonite suspensions as reflected by the weak shoulder at 474 nm (Fig. 1, band γ). This band is located at a wavelength shorter than band β, suggesting that it represents "sandwiched" adsorbed aggregates of more than two R6G molecules. Another possibility is that band γ represents solvated dimers in solutions trapped within "book-house" structures (24). This quasimicellar arrangement may cause a local effect of increase in concentration as reported for micelles (22). Since the intensity of this band is very weak in comparison to that of band α, it seems that only a very small fraction of the R6G molecules undergo this type of aggregation.

In the very dilute suspension the platelets of montmorillonite are initially well dispersed. In the more concentrated suspension the platelets form face-to-face associations (tactoids). When the clay flocculates, as the result of the treatment with R6G, card-house and book-house structures are obtained in dilute and concentrated suspensions, respectively. It seems that the book-house structure is essential for this type of metachromasy, so that dye aggregates form in the vacancies between the tactoids which participate in the floc. Indeed, in laponite, which does not show a tendency to form book-house structures, this type of metachromasy was not detected at any of the concentrations used.

3. Band α as an indicator of surface polarity and of flocculation

Changes in intensity and location of band α as the concentrations of dye or clay vary were described in Figs. 3 and 4. From Fig. 3*a* and 4*a* it is clear that the higher the surface coverage, the larger is the red shift in band α. Even at low degree of coverages the adsorbed molecule is red-shifted relative to R6G in water. The fact that the location of band α changes gradually with change of degree of coverage is an indication to a gradual and even distribution upon adsorption and not to clustered adsorption. A possible sequence of events is first, a gradual coverage of isolated plates, followed by tactoids build up, and then adsorption into the interlayer spacing. We suggest that the gradual change in location is an indication for the gradual change in average local polarity: as more dye molecules are adsorbed, the local environment gradually changes to less polar and becomes more hydrophylic. Indeed, red shifts in R6G were observed when water was substituted by a less polar solvent (23). Consequently, the red shift observed even at low coverages may be interpreted as reflecting surface polarity which is not as high as that of water. This observation is in agreement with the known hydrophobicity of the oxygen plane of the clay (24). Interestingly, in the case of acridine orange, which forms strong π interactions with the oxygen plane, the gradual change in the location of band β is to the *blue* as concentration increases (1*c*). This is a con-

Can. J. Chem. Downloaded from www.nrcresearchpress.com by 210.87.254.105 on 09/06/12
For personal use only.

sequence of gradual water removal from the oxygen plane which enables stronger interaction between the positive π electron cloud of the dye and the clay plane. The opposite trend in spectral shifts for the two dyes is a further indication for the lack of π interactions in R6G.

Figure 4*b* shows clearly local minima of absorption intensities, just after the saturation point is reached. A similar phenomenon is the slight shift in the minima of Fig. 3*b* compared to the maxima of Fig. 3*a*. Supernatant analyses (Tables 2, 3) and simple observation of the samples reveal that flocculation becomes prominent for a certain small range of excess dye beyond the saturation point. The decrease in absorption intensity is therefore very similar to the known effect deviation from Beer–Lambert law upon aggregation. As further indicated in Figs. 3, 4, flocculation ceases above a certain excess of dye. At these higher dye concentrations, the organic material apparently acts as a dispersing agent, causing efficient peptization of the clay. The sensitivity of band α to aging or ultrasonic treatment follows similar lines, i.e., it reflects the clay/dye suspension structures from large flocs down to a fine colloid.

4. Fluorescence quenching and red shift

The quenching of the fluorescence upon adsorption is due to iron impurities in the clays. This well-known phenomenon has been elegantly studied recently by Van-Damme *et al.* (25). Indeed, for laponite which contains less iron (25) the quenching is less severe, as could be judged from relative intensities at the same low concentration coverages. Other possible mechanisms for fluorescence-quenching are intermolecular sequences of energy transfers which act as an energy sink, or simply inner filter-effects within the flocs. In fact, the large difference in fluorescence intensities and maxima between adsorbed and non-adsorbed dye (Fig. 3*c*) suggests the use of this type of spectral analysis for determining the saturation ratios. The red shifts in the fluorescence maxima probably reflect, as discussed above, the reduced polarity of the surface compared to an aqueous hydration shell.

A comparative study of other laser-dyes is in progress, parts of which will be reported soon.

Acknowledgments

This work was sponsored in part by the US–Israel Binational Foundation (to D.A.) and by the Ben-Gurion Foundation (to Z.G.). Laponite was kindly donated by Z. Kurtz of Tambour Dyes, Ltd., Haifa, Israel, and by Laporte Industries, England. D.A. is a member of the F. Haber Research Center for Molecular Dynamics, Jerusalem.

1. (*a*) S. YARIV and D. LURIE. Israel J. Chem. **9**, 537 (1971); (*b*) S. YARIV and D. LURIE. Israel J. Chem. **9**, 553 (1971); (*c*) R. COHEN and S. YARIV. J. Chem. Soc. Faraday I. In press.
2. (*a*) H. MACK, R. REISFELD, and D. AVNIR. Chem. Phys. Lett. **99**, 238 (1983); (*b*) R. REISFELD, N. MANOR, and D. AVNIR. Sol. Energy Mater. **8**, 399 (1983); (*c*) Z. GRAUER, H. DANIEL, and D. AVNIR. J. Coll. Interface Sci. **96**, 411 (1983); (*d*) Z. GRAUER, S. YARIV, L. HELLER-KALLAI, and D. AVNIR. J. Therm. Anal. **26**, 49 (1983).
3. (*a*) D. AVNIR and M. KAGAN. Nature, **307**, 717 (1984); (*b*) M. KAGAN AND D. AVNIR. Origins Life. In press; (*c*) D. AVNIR, M. KAGAN, and A.. LEVI. Naturwissenschaften **70**, 144 (1983); (*d*) M. KAGAN, A. LEVI, and D. AVNIR. Naturwissenschaften, **69**, 548 (1982).
4. P. F. SCHÄFER (*Editor*). Dye lasers. Springer Verlag, Berlin. 1973.
5. D. R. KEARNS. Chem. Rev. **71**, 391 (1975).
6. K. GOLLNICK, T. FRANKEN, M. F. R. FOUDA. Tetrahedron Lett. **22**, 4049 (1982) and references cited therein.
7. (*a*) G. B. ALTSHULER, E. G. DULVENA, I. K. MINKOVSKI, and K. I. DRYLOV. Zh. Prikl. Spektrosk. **36**, 592 (1982); (*b*) V. I. ZEMSKII, I. K. MESHKOVSKII, and A. V. SECHKAREV. Dokl. Akad. Nauk SSSR, **267**, 1357 (1982).
8. H. GERISCHER. Faraday Discuss. Chem. Soc. **58**, 219 (1974).
9. T. F. HEINZ, C. K. CHEN, D. RICARD, and Y. R. SHEN. Phys. Rev. Lett. **48**, 478 (1982).
10. Y. LIANG, A. M. PONTE GONCALVES, and D. K. NEGUS. J. Phys. Chem. **87**, 1 (1983).
11. S. GAROFF, R. B. STEPHENS, C. D. HANSEN, and G. K. SORENSEN. J. Lumin. **24**, 773 (1981).
12. M. SPLITER and M. CALVIN. J. Chem. Phys. **67**, 5193 (1977).
13. W. ARDEN and P. FROMHERZ. J. Am. Chem. Soc. **102**, 6211 (1980).
14. E. LENDRAY. J. Phys. Chem. **69**, 738 (1965).
15. N. NAKASHIMA, K. YOSHIHARA, and F. WILLIG. J. Chem. Phys. **73**, 3553 (1980).
16. (*a*) S. GAROFF, R. B. STEPHENS, C. D. HANSON, and G. K. SORENSEN. Opt. Commun. **41**, 257 (1982); (*b*) S. GAROFF, D. A. WEITZ, and M. S. ALVAREZ. Chem. Phys. Lett. **93**, 283 (1982).
17. H. NIJS, M. I. CRUZ, J. J. FRIPIAT, and H. VAN-DAMME. Nouv. J. Chim. **6**, 551 (1982).
18. R. A. DELLAGUARDIA and J. K. THOMAS. J. Phys. Chem. **87**, 990 (1983).
19. F. L. ARBELOA, I. L. GONZALEZ, P. R. OJEDA, and I. L. ARBELOA. J. Chem. Soc. Faraday Trans. II, **78**, 989 (1982).
20. J. E. SELWYN and J. L. STEINFELD. J. Phys. Chem. **76**, 762 (1972).
21. K. BERGMANN and C. T. O'KONSKI. J. Phys. Chem. **67**, 2169 (1963).
22. H. SATO, M. KAWASAKI, and K. KASATANI. J. Phys. Chem. **87**, 3759 (1983).
23. G. CHU and Z. XINGKANG. Acta Opt. Sinica, **3**, 64 (1983).
24. S. YARIV and H. CROSS. Geochemistry of colloid systems. Springer, Berlin. 1979.
25. A. HABTI, D. KERAVIS, P. LEVITZ, and H. VAN DAMME. J. Chem. Soc. Faraday Trans II. In press.

Can. J. Chem. Downloaded from www.nrcresearchpress.com by 210.87.254.105 on 09/06/12
For personal use only.

Internal rotation in [*p*-(dialkylamino)benzylidene]malononitriles

A. SAFARZADEH-AMIRI

Photochemistry Unit, Department of Chemistry, The University of Western Ontario, London, Ont., Canada N6A 5B7

Received February 10, 1984

This paper is dedicated to Professor Paul de Mayo on the occasion of his 60th birthday

A. SAFARZADEH-AMIRI. Can. J. Chem. **62**, 1895 (1984).

The dynamic structures of [*p*-(dialkylamino)benzylidene]malononitriles have been investigated by ^{1}H nmr, and the kinetic and thermodynamic parameters for the partial rotation of the malononitrile moiety were obtained and those of the dialkylamino group were estimated. The rate of rotation of the above rotors were found to be of the order of $\sim 10^4$ s^{-1} and $\sim 10^7$ s^{-1}, respectively.

A. SAFARZADEH-AMIRI. Can. J. Chem. **62**, 1895 (1984).

Faisant appel à la rmn du ^{1}H, on a étudié les structures dynamiques de [*p*-(dialkylamino)benzylidène]-malonontriles; on a pu déterminer les paramètres thermodynamiques pour la rotation partielle de l'unité malononitrile et l'on a évalué ceux du groupe dialkylamino. On a trouvé que les vitesses de rotation des rotors mentionnés ci-dessus sont respectivement de l'ordre de 10^{-4} s^{-1} et de 10^{-7} s^{-1}.

[Traduit par le journal]

Can. J. Chem. Downloaded from www.nrcresearchpress.com by 210.87.254.6 on 09/06/12
For personal use only.

Introduction

Dynamic nmr spectroscopy is now a standard tool for investigating hindered rotations with activation energies in the range of 20 to 125 kJ/mol. The barrier to rotation is either due to steric hindrance, partial double bond character, or both. Disubstituted benzenes of the type D—Ph—A, where D is an electron donor and A is an electron acceptor moiety (such as *para*-substituted anilines) are examples of molecules where both partial double bond character and steric hindrance could provide an appreciable barrier to rotation around the D—Ph and/or Ph—A bonds (1).

[*p*-*N*,*N*-(Dialkylamino)benzylidene]malononitriles (compounds **1** to **3**) are D—Ph—A type molecules (see Fig. 1) with interesting photophysical properties (2–5). Their absorption and fluorescence emission spectra are solvent polarity dependent and their fluorescence quantum yields are solvent viscosity dependent. These properties make them suitable fluorescent probes to investigate, (*i*) the effective polarity and the microviscosity of micellar environments (5), and (*ii*) the relationship between the limiting conversion and temperature in polymerization processes (4), etc. These molecules, therefore, were of interest to us as possible means of characterizing silica gel surface modification in the presence and absence of additives and as a function of heat treatment.

The fluorescence decay times of compounds **1** to **3** in ordinary solvents were esimated to be 3–10 ps (2), and their fluorescence quantum yields were determined to be ca. (1–3) $\times 10^{-3}$ (2–4). The low quantum yield of emission and fast decay times were attributed to the rotation of the dialkylamino or malononitrile moieties (2–4). Thus, the rotation of the dialkylamino group in compound **1** was estimated to be of the order of 10^{11} s^{-1} in the excited state (2, 3). In order to obtain an estimate of the rate of rotation of both the dialkylamino and the malononitrile moieties, we have investigated the temperature dependence of the dynamic structure of these molecules in the ground state by ^{1}H nmr spectroscopy. The results are presented in this paper. The kinetic parameters of the ground state enable us to draw some conclusions about the excited state dynamics, in so far as the rotation around the partial double bonds D—Ph and Ph—A are concerned. Our conclusion differs from those reached from fluorescence studies.

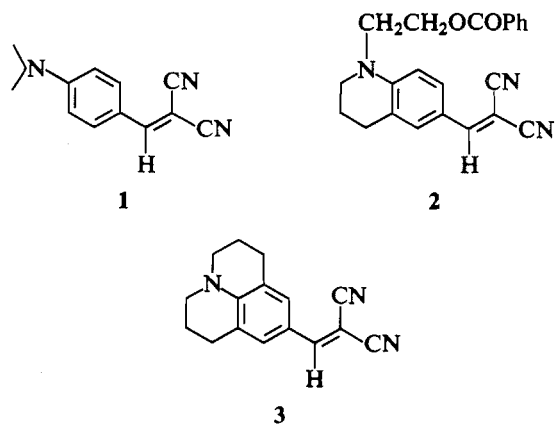

FIG. 1. Structures of [*p*-(dialkylamino)benzylidene]malononitriles.

Experimental

Compounds **1** and **3** were the generous gift of Dr. R. O. Loutfy (Xerox Research Centre, Canada) and were prepared and purified as described before (2). The deuteriated solvents were from Aldrich Chem. Co.

Perdeuteriotetrahydrofuran, THF-d_8, was kept over sodium and was transferred to the nmr tube by distillation and was sealed all in vacuum. Nuclear magnetic resonance spectra were obtained with a Varian XL-100 spectrometer equipped with a variable temperature probe in the pulsed Fourier-transform mode. The temperature was measured with a stationary thermocouple junction which was immersed in toluene in a reference nmr tube. The accuracy of the temperature measurements is estimated to be ca. ±2°C. The kinetic parameters were obtained by line shape analysis using the iterative DNMR 5 program (QCPE No. 365, Indiana University).

Results and discussion

Figure 2 shows the proton nmr spectra at room temperature of compounds **1** and **3** in THF-d_8 and acetone-d_6, respectively. From the signal intensities and by comparison with other systems of similar structure (6), all signals can be readily assigned. The aromatic protons in compound **3** display a single sharp line at room temperature and an AB doublet ($\delta\nu$ = 94 ± 2 Hz) below −66°C. The aromatic protons of compounds **1** are an AB quartet ($\delta\nu$ = 107 ± 2 Hz, J = 9 Hz) at room temperature, each of which splits into a doublet at sufficiently low temperature.

Can. J. Chem. Downloaded from www.nrcresearchpress.com by 210.87.254.6 on 09/06/12
For personal use only.

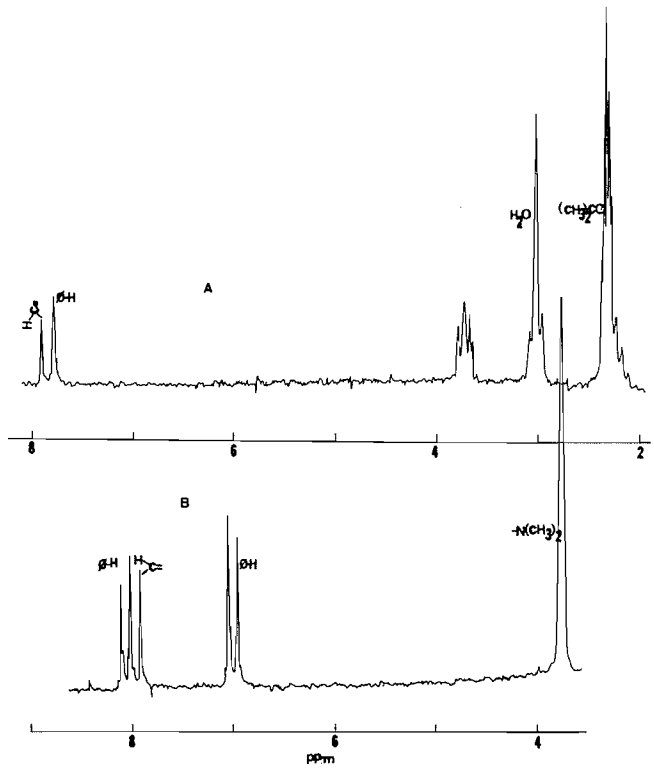

FIG. 2. ^{1}H nmr spectra at room temperature of (*A*) compound **3** in THF-d_8 and (*B*) compound **1** in acetone-d_6.

The protons *ortho* to the amino group become a singlet below ca. −87°C, and then change to a quartet below −90°C, and those *meta* to the amino group become a singlet below about −65°C, an AB doublet below −74°C, and finally become an AB quartet below about −90°C. Figure 3 shows the temperature dependence of the aromatic protons of compounds **1** and **3** in THF-d_8 and acetone-d_6, respectively. Each proton signal becomes narrower as the temperature is decreased. From the temperature dependence of the aromatic proton signals, the rate of rotation of the malononitrile moieties are obtained over a temperature range of 25−30°C. From these rates and the absolute rate theory for internal rotation (7), the enthalpies and the entropies of activation are obtained. These kinetic parameters are given in Table 1 and the plots of ln (k/T) vs. $1/T$, where k is the rate of rotation and T is the absolute temperature, are shown in Fig. 4. Also given in Table 1 are the chemical shifts of the non-equivalent aromatic protons, the coalescence temperatures (T_c), the free energies of activation at T_c, and the rates of rotation at 25°C.

It is appropriate at this point to discuss the nature of the barrier to rotation in these compounds. The conformational energies of compounds **1**−**3** are expected to be dependent on the dihedral angle, θ, between the aromatic ring and the malononitrile moiety. This dependence is due to the steric interaction between the aromatic hydrogens *ortho* to the malononitrile and the nitrile groups, as well as the partial double bond character of the Ph—A bond. Both CNDO/2 MO and *ab initio* calculations performed on (4-hydroxybenzylidene)malononitrile (HBMN) and its anionic form (6) predict that: (*i*) the planar conformation (θ = 0) is quite unstable with a large energy barrier to rotation, (*ii*) the twisted structure (θ = 40−60° depending on the nature of calculation) is the most stable conformation, and (*iii*) there is a small energy barrier for rotating beyond θ = 90° for the malononitrile moiety and that this barrier is higher for anionic HBMN than the neutral molecule. On the basis of these data, it is not unreasonable to assume that compounds **1**−**3** would also have an energy profile similar to HBMN, although with different energy barriers (at θ = 90°) and with a stable twisted conformation. The observed barrier in compounds **1** and **3**, therefore, are due to partial rotation of the malononitrile moiety beyond 90°, because of the partial double bond character of the Ph—A bond.

The ionization potential of the dialkylamino group in compound **1** is greater than that in compound **3** and the ground state dipole moments of compounds **1** and **3** are 8.7 D and 9.4 D (14), respectively. Thus, one would expect that the Ph—A bonds in compound **3** would possess more double bond character as compared with compound **1** and consequently, the barrier to partial rotation in compound **3** should be greater than that in compound **1**. However, the data given in Table 1 show that the enthalpies and free energies (at the coalescence temperature) of activation are the same for both compounds within experimental error. The use of two solvents with different viscosities can not account for the apparent equality of the barriers to partial rotation in the two compounds because the temperature coefficients of the two solvents are very similar (905 K for THF and 935 K for acetone obtained from the variation of viscosity with temperature (8, 9)). Association of solvent−solute molecules could account for the apparent equality of the enthalpies and free energies of activation at T_T (10). This effect is also ruled out on the basis of the following observations. The ($S_1 \leftarrow S_0$) absorption and the ($S_1 \rightarrow S_0$) fluorescence band shapes in benzene do not change with addition of polar solvents (such as methanol). Addition of polar solvents leads only to hypsochromic and bathochromic shifts of the absorption and emissions spectra, respectively, without affecting their band widths (3). The same effect is also observed in solvents of increasing polarity. Lowering the temperature would cause a hypsochromic shift of the fluorescence spectra without affecting the band width (2). The difference in the activation parameters of the two compounds is, therefore, expected to be small and could not be measured by this technique.

Measurements of the barrier to rotation (or rate of rotation) of the dimethylamino group in compound **1** was not possible. However, it is not expected to differ much from that of the malononitrile moiety. A lower limit of this barrier could be established from the available literature data. The barrier to rotation of the dimethylamino group in *p*-dimethylaminobenzonitrile (DMABN) was obtained from the data provided by Mackenzie and MacNicol (11) and is ~30.5 kJ/mol (at 133 K). The rate of rotation of the dimethylamino moiety in DMABN is of the order of $\sim 3 \times 10^7$ s^{-1} at 25°C. The dipole moment of DMABN is 7.6 ± 0.2 D (12), which is 1.1 D smaller than that of compound **1**. Thus the barrier to rotation of the dimethylamino moiety in **1** is expected to be greater than 31 kJ/mol (at 133 K) and its rate of rotation smaller than 3×10^7 s^{-1} at 25°C.

The barrier to partial rotation for the malononitrile moiety of (3,5-di-*tert*-butyl-4-hydroxybenzylidene)malononitrile (DBHBMN) is 31.3 ± 1.0 kJ/mol at T_c (in diethyl-d_{10}-ether) (6*c*) and for the vinyl moiety of styrene in both gas and solution phase is ~7.44 ± 0.08 kJ/mol at room temperature (13). The temperature coefficients of diethylether (834 K) (9) is slightly smaller than those of THF and acetone, and may account for part of the excess activation energies of the hindered rotation in compounds **1** and **3** as compared to their phenolic counterpart. However, the bulk of the energy differences could be ac-

TABLE 1. Kinetic and thermodynamic parameters for internalrotation of the malononitrile and dimethylamino moieties in compounds **1** and **3**

Molecule	Rotating group	$\Delta\nu$/Hz	T_c/K	$\Delta H^{\ddagger}$/ kJ/mol	$\Delta G^{\ddagger}$ (Tc)/ kJ/mol	$\Delta S^{\ddagger}$ J/mol K	$10^{-3}\times k/s^{-1}$
3	Malononitrile	78±1	209±3	20±2	39±5	−110±8	3.2±2.3
	Malononitrile	94±2	203±4	20±1	40±5	−103±8	7.6±5.5
1	Dimethylamino	—	—	—	≃33.0*	—	≃10000*

*Estimated values, see text for details.

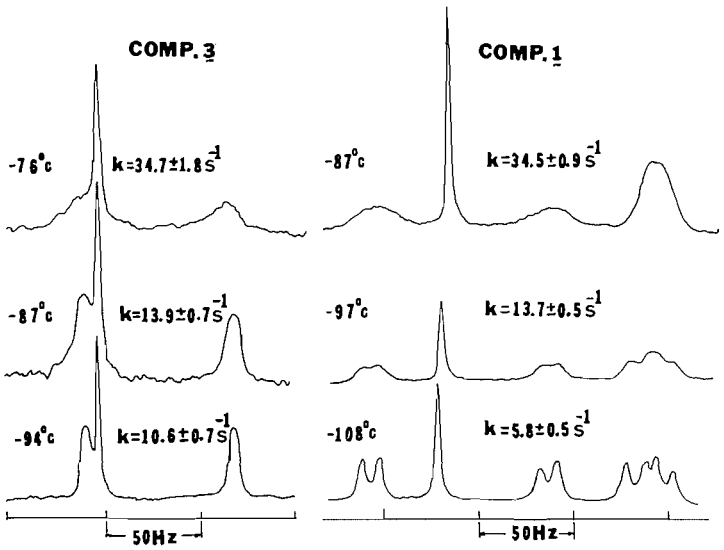

FIG. 3. ^{1}H nmr spectra of compounds **1** and **3** as a function of temperature.

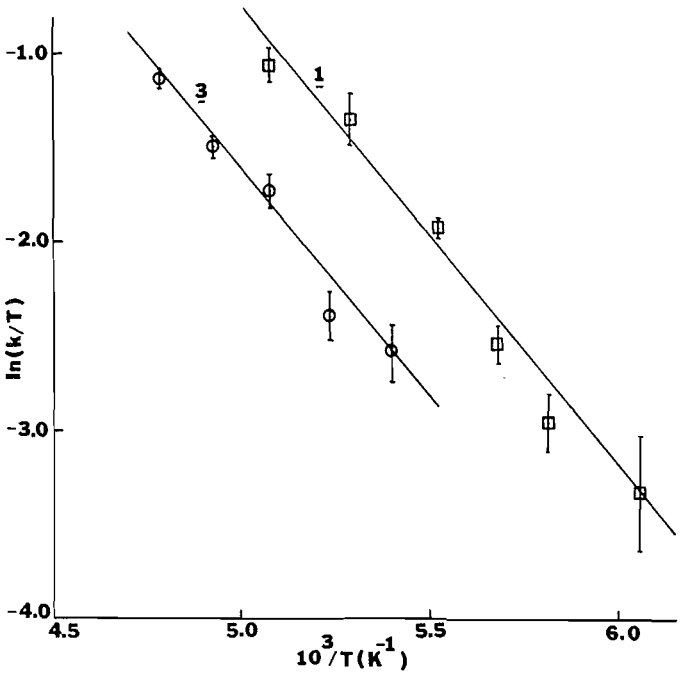

FIG. 4. Eyring plots for the process of internal rotation about the Ph—A bond.

counted for by considering the differences in their dipole moments. The dipole moment of DBHBMN is not known, but it can be estimated from the data provided by Kuder *et al.* (14) and was found to lie in the range of $6.74\ D < \mu_g < 7.54\ D$. This is lower than the corresponding values for compounds **1** and **3** by at least 1.2−1.9 D. Differences of ca. 5 kJ/mol for free energies of activation between the *p*-methoxy- and *p*-dimethylamino-substituent of both benzaldehyde and acetophenone have been reported (10). The much lower barrier to rotation for the vinyl group of styrene as compared to those of the malononitrile moieties in compounds **1** and **3** is due to the negligible dipole moment of styrene (13).

The dipole moments of compounds **1** and **3** in the first excited electronic state are approximately three and two times (2) greater than the ground state values, respectively. The highly polarized excited state was assigned to an intramolecular charge-transfer state (2). This assignment is consistent with the observed spectral properties of these compounds as a function of solvent polarity and electron donating ability of the dialkylamino groups. Further support is obtained by comparison with other systems of similar properties (15). It was pointed out earlier that the barrier to partial rotation around the Ph—A bond is due to the partial double bond character (i.e. resonance structure **II** in Scheme 1) of the Ph—A bond (10). It is also established that the first excited electronic states of compounds **1**−**3** are of intramolecular charge-transfer type. Thus, the resonance form **II** is expected to be the major contributor to the

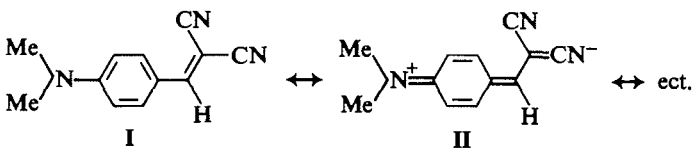

SCHEME 1

Can. J. Chem. Downloaded from www.nrcresearchpress.com by 210.87.254.6 on 09/06/12
For personal use only.

Can. J. Chem. Downloaded from www.nrcresearchpress.com by 210.87.254.6 on 09/06/12
For personal use only.

excited-state electronic charge distribution (16, 17), amongst other possible resonance structures. Other factors being the same, the barrier to rotation is a measure of the double bond character. On the basis of the foregoing discussion, the double bond character of the D—Ph and Ph—A bonds in the first electronic excited state is greater than the ground state in compounds **1** and **3**. Therefore, both the malononitrile and the dimethylamino moieties are expected to have a rate of rotation at room temperature less than ca. 10^4 s^{-1} and $\sim 10^7$ s^{-1}, respectively. These results are in vast disagreement with those estimated from the fluorescences studies (3, 5). The discrepancy lies in the interpretation of the fluorescence data and the mechanism of the excited state relaxation of these compounds. The decay dynamics of these compounds will be the subject of a forthcoming paper.

In conclusion, we have been able to obtain the kinetic and thermodynamic parameters of the malononitrile moiety in compounds **1** and **3** and to estimate the corresponding values for the dimethylamino group in compound **1**. It was shown that the rate of rotation of the dimethylamino and malononitrile moieties are $\leq 10^7$ s^{-1} and $\sim 10^4$ s^{-1} in the ground state, respectively, and should be less than those in the first electronic excited state.

NOTE ADDED IN PROOF: The σ_p^- value for the malononitrile moiety is 1.20 (18). Using this value of σ_p^- and the data provided in ref. 11, we obtain $\Delta G^{\ddagger} \simeq 33.0$ kJ mol^{-1} and $k_r \simeq 10^7$ s^{-1} (at 25°C).

Acknowledgements

The author would like to thank Professor Paul de Mayo for his encouragements, critical and constructive comments and allowing me to carry out this work, Dr. S. K. Wong for helpful discussions, Dr. R. O. Loutfy for samples of the compounds used in this work, and Mr. A. Draper for some of the spectral measurements. Last but not least he thanks Professor W. F. Reynolds for his constructive criticism.

1. L. M. JACKMAN and F. A. COTTON. Dynamic nuclear magnetic resonance spectroscopy. Academic Press, New York. 1975.
2. R. O. LOUTFY and K. Y. LAW. J. Phys. Chem. **84**, 2803 (1980).
3. K. Y. LAW. Chem. Phys. Lett. **75**, 545 (1980).
4. R. O. LOUTFY and K. Y. LAW. Macromolecules, **14**, 587 (1981).
5. K. Y. LAW. Photochem. Photobiol. **33**, 779 (1981).
6. (*a*) K. YOSHIKAWA, N. KUMAZAWA, H. TERADA, and K. AKAGI. Int. J. Quant. Chem. **35**, 539 (1980); (*b*) K. YOSHIKAWA, N. KUMAZAWA, H. TERADA, and M. JU-ICHI. Bull. Chem. Soc. Jpn. **54**, 1108 (1981); (*c*) K. YOSHIKAWA and H. TERADA. J. Am. Chem. Soc. **104**, 7644 (1982).
7. G. GLASSTONE, K. H. LAIDLER, and H. EYRING. The theory of rate processes. McGraw-Hill, New York. 1941.
8. C. CARVAJAL, J. K. TOLLE, J. S. MID, and M. SZWARC. J. Am. Chem. Soc. **87**, 5548 (1965).
9. R. C. WEAST (*Editor*). Handbook of chemistry and physics. 52nd ed. The Chemical Rubber Co., OH. 1971.
10. (*a*) R. E. KLINCK, D. H. MARR, and J. B. STOTHERS. J. Chem. Soc. Chem. Commun. 409 (1967); (*b*) F. A. L. ANET and M. AHMAD. J. AM. CHEM. SOC. **86**, 119 (1964).
11. R. K. MACKENZIE and D. D. MACNICOL. J. Chem. Soc. Chem. Commun. 1299 (1970).
12. H. DECKERS. Ph.D. Thesis, Mainz. 1977.
13. (*a*) L. A. CARREIRA and T. G. TOWNS. J. Chem. Phys. **75**, 5283 (1975); (*b*) T. SCHAEFER and W. J. E. PARR. J. Mol. Spectrosc. **61**, 479 (1976).
14. J. E. KUDER, W. W. LIMBURG, J. M. POCHAN, and D. WYCHICK. J. Chem. Soc. Perkin Trans. II, 1643 (1977).
15. T. P. CARSEY, G. L. FINDLAY, and S. P. MCGLYNN. J. Am. Chem. Soc. **101**, 4502 (1979).
16. R. G. BROWN and G. PORTER. J. Chem. Soc. Faraday Trans. I, **73**, 1569 (1977).
17. N. J. TURRO. Modern molecular photochemistry. The Benjamin/Cummings Publishing Co., Inc., Menlo Park, CA. 1978. Chapt. 10 and references cited therein.
18. O. EXNER. *In* Correlation analysis in chemistry. *Edited by* J. Shorter and N. Chapman.

Stereoselectivity of C(3)-methylation of camphor and derivatives

JOHN H. HUTCHINSON AND THOMAS MONEY
Department of Chemistry, The University of British Columbia, Vancouver, B.C., Canada V6T 1Y6

Received March 2, 1984

This paper is dedicated to Professor Paul de Mayo on the occasion of his 60th birthday

JOHN H. HUTCHINSON and THOMAS MONEY. Can. J. Chem. **62**, 1899 (1984).

Contrary to general expectations, kinetic methylation of camphor, 9-bromocamphor, or 9,10-dibromocamphor produces the 3-*exo*-methyl derivative as the major product.

JOHN H. HUTCHINSON et THOMAS MONEY. Can. J. Chem. **62**, 1899 (1984).

Contrairement à ce qui est généralement attendu, la méthylation cinétique du camphre, du bromo-9 camphre ou dibromo-9,10 camphre conduit principalement au dérivé méthylé en position 3-*exo*.

[Traduit par le journal]

Can. J. Chem. Downloaded from www.nrcresearchpress.com by 210.87.254.5 on 09/06/12
For personal use only.

In connection with our general investigations (1) on the use of (+)-camphor (**1**) or (−)-camphor as chiral starting materials in the enantiospecific synthesis of terpenoids and steroids, we required reaction conditions which would enable us to alkylate camphor and its halogen derivatives stereoselectively at the C(3)-position. Although the literature contains many examples of camphor alkylation the stereochemistry of the C(3)-monoalkyl derivatives is not clearly described (2−6). In our initial investigations we established that addition of (+)-camphor (**1**) to LDA (1 mole equivalent) in THF 0°C followed by treatment with excess methyl iodide for 30 min provided a product (70−85% yield) which was shown by nmr (400 MHz) and capillary glc to be a mixture (~4:1)[1] of 3-*exo*-methylcamphor (**2**) (δ 1.20, d, J = 7.5 Hz)[2] and 3-*endo*-methylcamphor (**3**) (δ 1.06, d, J = 7.5 Hz).[2] Flash chromatography (7) on silica provided pure (+)-3-*exo*-methylcamphor (**2**) as a crystalline solid (mp 50−54°C; δ ($CDCl_3$, 400 MHz), 0.85 (3H, s), 0.90 (3H, s), 0.93 (3H, s), 1.21 (3H, d, J = 7.5 Hz), 1.85 (1H, d, J = 4 Hz), 1.95 (1H, q, J = 7.5 Hz). Treatment of the kinetic mixture (4:1) of 3-*exo*-methylcamphor (**2**) and its C(3)-*endo*-epimer (**3**) with refluxing sodium methoxide in methanol or acetic acid/hydrochloric acid provides a mixture (9:1 by 270 MHz nmr) in which 3-*endo*-methylcamphor (**3**) is the major steroisomer. Subsequent low temperature crystallization of this product from pentane provided pure (+)-3-*endo*-methylcamphor (**3**) as a crystalline solid (mp 37−39°C; δ ($CDCl_3$, 400 MHz), 0.87 (3H, s), 0.90 (3H, s), 1.00 (3H, s), 1.06 (3H, d, J = 7.5 Hz), 1.98 (1H, t, J = 4.5 Hz), 2.48 (1H, pentet[3] J = 4.5 Hz and 7.5 Hz)). The above information leads us to conclude that previous reports (2−6) on the synthesis of (+)-3-methylcamphor (mp 38−39°C) refer to the 3-*endo*-methyl isomer (**3**) prepared under thermodynamic conditions.

C(3)-Methylation of (+)-9-bromocamphor (**4**) (8) can also be accomplished in a similar fashion to provide a product whose nmr spectrum (400 MHz) and capillary glc indicated that it was a mixture of 9-bromo-3-*exo*-methylcamphor (**5**) and 9-bromo-3-*endo*-methylcamphor (**6**)[4] in a ratio of ~1.7:1.

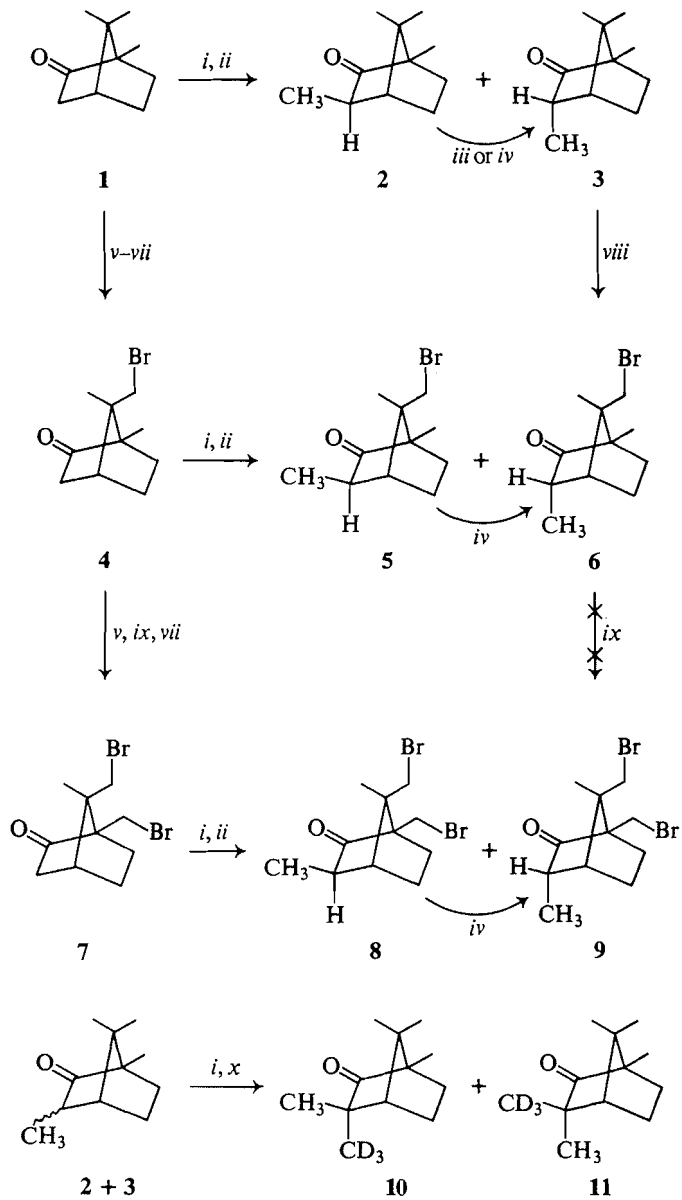

SCHEME 1. *i*, LDA/THF/0°C; *ii*, CH_3I/0°C; *iii*, NaOMe/MeOH/Δ; *iv*, HCl/HOAc/Δ; *v*, Br_2/HOAc; *vi*, Br_2/$ClSO_3H$/4 h; *vii*, Zn/HOAc; *viii*, Br_2/$ClSO_3H$/2 days; *ix*, Br_2/$ClSO_3H$/5 days; *x*, CD_3I/0°C.

[1]Since some equilibration could have occurred during "kinetic methylation" the true kinetic ratio may be greater than observed.

[2]Comparable assignments have been reported for 3-*exo*- and 3-*endo*-methyl groups in norcamphor derivatives (9−11).

[3]Partially coalesced quartet of doublets.

[4]This compound can also be prepared in 50% yield by treating 3-*endo*-methylcamphor (**3**) with bromine in chlorosulfonic acid for 24 hours (13).

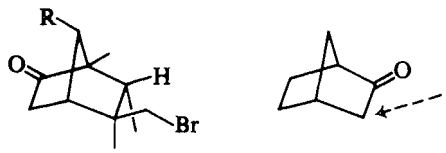

12*a*: R = H
12*b*: R = Br

13

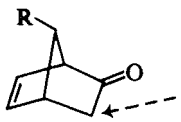

14*a*: R = CH_3
14*b*: R = $CH_2CH_2OCH_2Ph$

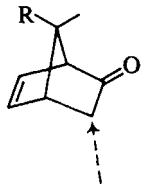

15*a*: R = CH_2OCH_2Ph
15*b*: R = $CH(CH_3)OTHP$
15*c*: R = CH_3
15*d*: R = CH_2OTHP
15*e*: R = $CH_2CH_2CH_2OTHP$

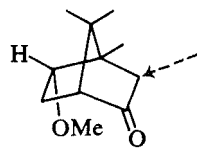

16

SCHEME 2

Subsequent equilibration with HCl/HOAc provided the *endo*-methyl isomer (**6**) as a major component of the mixture (*endo* : *exo* ~10 : 1). When (+)-9,10-dibromocamphor (**7**) was methylated (LDA/MeI) as described, above the product was a mixture (~1.7 : 1) of 9,10-dibromo-3-*exo*-methylcamphor (**8**) and the 3-*endo*-methyl epimer (**9**).[5] Equilibration with acid (HCl/HOAc) provided 9,10-dibromo-3-*endo*-methylcamphor (**9**) as the major product (*endo* : *exo* = ~6 : 1). The latter compound is an important intermediate in our current efforts to develop a stereoselective route from camphor to the steroids.

In contrast to the kinetic *exo*-stereoselectivity described above, C(3)-methylation of 3-methylcamphor displays *endo*-stereoselectivity, i.e., sequential treatment of 3-methylcamphor, (**2**) + (**3**), with LDA in THF at 0°C followed by addition of trideuteromethyl iodide provided a product (~60% yield) which was shown, by ^1H nmr spectroscopy, to be a mixture (~3.4 : 1) of 3-*exo*-methyl-3-*endo*-trideuteromethylcamphor (**10**) and its epimer (**11**).[6]

Other investigations have shown that bicyclo[2,2,1]heptan-2-one (norcamphor) (**13**) (9) and 5,6-dehydroketones (**14***a*,*b*) (10*a*,*b*) undergo kinetic *exo*-methylation while the related 5,6-dehydroketones (**15***a*–*e*) (10*c*–*e*, 11), having a C(7)-*syn*-methyl group, undergo exclusive *endo*-methylation (Scheme 2). In addition, it has been reported that 5-ketobornyl methyl ether (**16**) can be converted exclusively to the corresponding 3-*exo*-allyl derivative (12).

The combined results described above indicate that kinetic *endo*-methylation of bicyclo[2,2,1]heptan-2-ones will occur if (*a*) the compound has a C(7)-*syn* alkyl group and lacks C(5)/C(6)-*endo* hydrogens or (*b*) the compounds has C(7)-*syn* and C(3) alkyl substituents. Correspondingly kinetic C(3)-*exo* alkylation will be preferred if the bicyclic ketone has a C(7)-*syn* alkyl group and C(5)/C(6)-*endo* hydrogens or substituents. When the difference in stereoselectivity between the methylation of camphor (**1**) and the 5,6-dehydro-10-norcamphor derivatives (**15***a*–*e*) (Scheme 2) is considered in conjunction with their structural differences, we are prompted to conclude that the presence or absence of the C(5)-*endo*-hydrogen is a significant factor in determining the stereochemical outcome of reactions of the corresponding enolate ions. The presence of an *endo* methoxy substituent in the epicamphor derivate (**16**) (12) presumably plays a similar but more effective role in directing the electrophilic reagent (in this case allylbromide) to the *exo* position.

While we do not have a convincing explanation for the kinetic stereoselectivity revealed by our investigations it is relevant to note that the reaction of camphor enol trimethylsilyl ether (**17**) with bromine (13), Eschenmoser's salt (15), ozone (16, 17),[7] or diborane (18, 19) provides a considerable proportion of the thermodynamically less stable C(3)-*exo*-product (cf. Scheme 3). The exception is the reaction with singlet oxygen (**17**) which provides a mixture (94 : 6) of 3-*endo*-trimethylsilylperoxycamphor and its C(3)-epimer. It has been suggested (17) that the difference in stereoselectivity between the reactions with ozone and singlet oxygen is due to the fact that O_3 reacts, in a polar fashion, at the end of the enolate double bond while $^1O_2$ adds to the least hindered *endo* face in a [2+2] cycloaddition process.

Experimental

Unless otherwise stated, the following are implied. Melting points (mp) were determined on a Kofler micro heating stage and are uncorrected. The capillary glc analysis was carried out on a Hewlett-Packard 5880A gas chromatograph employing a flame ionization detector and using a W.C.O.T. narrow bore (0.21 mm × 50 m or 12 m) Carbowax 20 M column. Helium was used as the carrier gas. The 270 MHz ^1H nmr spectra were recorded on a 270 MHz instrument constructed from a Bruker console, a Nicolet computer Model 293 A with a Diablo disk and a 270 MHz superconducting magnet supplied by Oxford Instruments. The 400 MHz ^1H spectra were recorded on a Bruker WH-400 instrument. Signal positions are given in delta (δ) with tetramethylsilane (TMS) as internal reference and signal multiplicity and integrated areas are indicated in parentheses. The solvent used was deuteriochloroform. Infrared spectra were recorded on a Perkin-Elmer 137 spectrophotometer and optical rotations were measured using a Perkin-Elmer model 141 polarimeter. Low resolution mass spectra were obtained using a Varian/Mat model CH4B mass spectrometer and high resolution mass spectra using a Kratos MS50 instrument. Microanalysis were performed by Mr. P. Borda, Microanalytical Laboratory, University of British Columbia, Vancouver.

*(+)-3-*Exo-*methylcamphor (2)*

(+)-Camphor (4.0 g, 26 mmol) was added to a freshly prepared solution of lithium diisopropylamide (25 mmol) in dry THF (30 mL) at 0°C under argon and the enolate allowed to form over 0.5 h. Methyl iodide (6.5 mL, 105 mmol) was then added and the reaction stirred for a further 0.5 h before being quenched with 1 *N* hydrochloric acid. The mixture was extracted with ether and the combined ether extracts washed with water three times and dried over anhydrous magnesium sulphate. Removal of the solvent yielded a pale yellow oil (4.28 g) which partially crystallized on standing. Capillary glc analysis of the

[5]By analogy with the reported conversion of 3,9-dibromocamphor to 3,9,10-tribromocamphor (1*a*) we attempted to prepare 9,10-dibromo-3-*endo*-methylcamphor (**9**) by treating 9-bromo-3-*endo*-methylcamphor (**6**) with bromine in chlorosulfonic acid. However, under these reaction conditions, **6** is isomerized to 9-bromo-6-*endo*-methylisofenchone (**12***a*) which undergoes partial bromination to furnish an additional compound, presumably structure **12***b*. Structure **12***a* has been confirmed by X-ray crystallographic analysis (14).

[6]The structural assignments for **10** and **11** were made by comparing the C(3)-methyl chemical shift with that observed for 3-*endo*- and 3-*exo*-methylcamphor.

[7]Reference 16 describes reaction of camphor *tert*-butyldimethylsilyl enol ether with ozone.

Can. J. Chem. Downloaded from www.nrcresearchpress.com by 210.87.254.5 on 09/06/12
For personal use only.

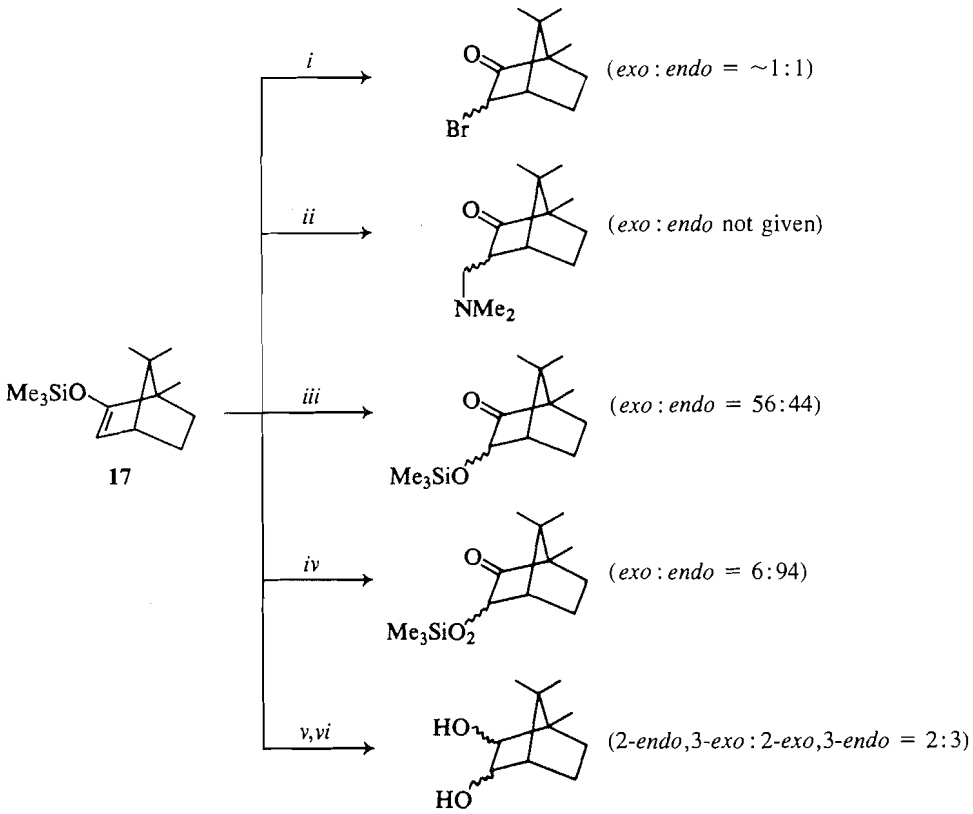

SCHEME 3. *i*, Br_2:dioxane/C_5H_5N; *ii*, $Me_2N^+ = CH_2I^-/CH_2Cl_2$; *iii*, O_3/CH_2Cl_2/MeOH; *iv*, $^1O_2$/CCl_4; *v*, BH_3:THF; *vi*, H_2O_2/HO^-.

crude product indicated the ratio of 3-*exo*- to 3-*endo*-methylcamphor to be in the range 3.4−3.8:1.

Purification by column chromatography (silica gel; petroleum ether) (30−60°C)/(ether 50:1) afforded starting material (0.603 g) and a mixture of 3-*exo*- and 3-*endo*-methylcamphor (3.16 g 72%; 85% yield based on recovered starting material). Nuclear magnetic resonance (400 MHz) and capillary glc analysis showed the ratio of 3-*exo*- to 3-*endo*-methylcamphor to be 3.4−3.8:1.

A sample of pure 3-*exo*-methylcamphor (**2**) was obtained by re-chromatographing the above mixture using the same conditions. The fractions containing pure 3-*exo*-methylcamphor (monitored by capillary glc) were combined and sublimed to provide 3-*exo*-methylcamphor (**2**) as a white crystalline solid, mp 50−54°C: $[\alpha]_D$ +71.4° (*c*, 0.57, MeOH); ν_{max} ($CHCl_3$) 2970, 1740 cm^{-1}; δ ($CDCl_3$, 400 MHz), 0.85 (3H, s), 0.90 (3H, s), 0.93 (3H, s), 1.21 (3H, d, J = 7.5 Hz), 1.85 (1H, d, J = 4 Hz), 1.96 (1H, q, J = 7.5 Hz); *m/e* (relative intensity): 166 (M^+, 32), 123 (40), 108 (51), 95 (100), 83 (83); M.W. calcd. for $C_{11}H_{18}O$: 166.1358; found (high resolution mass spectrometry): 166.1358. *Anal.* calcd. for $C_{11}H_{18}O$: C 79.47, H 10.91; found; C 79.50, H 10.86.

*(+)-3-*Endo-*methylcamphor (3)*

A mixture of 3-*exo*- and 3-*endo*-methylcamphor (239 mg) in glacial acetic acid/conc. hydrochloric acid (2 mL, 9:1) was heated at 80°C for 6 h. The solution was diluted with water, extracted with ether, and the extract washed with sodium bicarbonate solution and then with water. Removal of the dried solvent yielded a white crystalline product (231 mg, 97%). Capillary glc and 270 MHz nmr showed that the ratio of 3-*exo*- to 3-*endo*-methylcamphor was ~1:9.

Low temperature crystallization (CO_2/acetone bath) from pentane provided pure 3-*endo*-methylcamphor (**3**), mp 37−39°C lit. (5) mp 38−39°C; $[\alpha]_D$ +25.4° (*c*, 2.5, MeOH), lit. (5) $[\alpha]_D$ +27.3° (*c*, 10.0, EtOH); ν_{max} ($CHCl_3$): 2975, 1735 cm^{-1} nmr ($CDCl_3$. 400 MHz), δ 0.87 (3H, s), 0.90 (3H, s), 1.00 (3H, s), 1.06 (3H, d, J = 7.5 Hz), 1.98 (1H, t, J = 4.5 Hz), 2.48 (1H, pentet,[3] J = 4.5 Hz and 7.5 Hz); *m/e* (relative intensity): 166 (M^+, 37), 123 (37), 108 (63), 95 (100), 83 (70). M.W. calcd. for $C_{11}H_{18}O$: 166.1358; found (high resolution mass spectrometry): 166.1362. *Anal.* calcd. for $C_{11}H_{18}O$: C 79.47, H 10.91; found: C 79.50, H 10.88.

*(+)-9-Bromo-3-*exo-*methylcamphor (5)*

(+)-9-Bromocamphor (**4**) (2.0 g, 8.7 mmol) was added to a freshly prepared solution of lithium diisopropylamide (8.2 mmol) in dry THF (9.8 mL) at 0°C under argon and the enolate allowed to form over 0.5 h. Methyl iodide (2.2 mL, 34.6 mmol) was then added and the reaction stirred for a further 0.5 h before being quenched with 1 *N* hydrochloric acid. After the normal work up, removal of solvent yielded a pale yellow solid (2.04 g).

Purification by column chromatography (silica gel; petroleum ether) (30−60°C)/(ether 50:1)) afforded starting material (0.471 g) and 9-bromo-3-methylcamphor (1.49 g, 70%; 92% based on recovered starting material) as a mixture of epimers. 400 MHz nmr of this product showed the ratio of the 3-*exo*- to 3-*endo*-methyl epimer to be ~1.7:1. Repeated recrystallization of the mixture of epimers from petroleum ether (30−60°C) afforded pure (+)-9-bromo-3-*exo*-methylcamphor (**5**), mp 115−116°C; $[\alpha]_D$ +158.4°C (*c*, 0.125, CH_2Cl_2); ν_{max} ($CHCl_3$): 2980, 1745 cm^{-1}; δ ($CDCl_3$, 270 MHz), δ 0.96 (3H, s), 1.02 (3H, s), 1.23 (3H, d, J = 8 Hz), 2.04 (1H, q, J = 8 Hz), 2.25 (1H, d, J = 4 Hz), 3.19 (d) and 3.57 (d) (2H, AB quartet, J = 10 Hz); *m/e* (relative intensity); 244/246 (M^+, 15), 186/188 (38), 165 (15), 137 (59), 123 (29), 107 (100), 95 (100); M.W. calcd. for $C_{11}H_{17}OBr$: 246.0442/244.0462; found (high resolution mass spectrometry): 246.0449/244.0456. *Anal.* calcd. for $C_{11}H_{17}OBr$: C 53.89, H 6.99, Br 32.59; found: C 53.87, H 6.98, Br 32.48.

*(+)-9-Bromo-3-*endo-*methylcamphor (6)*

An epimeric mixture of (+)-9-bromo-3-methylcamphor (1.03 g) in glacial acetic acid (19 mL) and conc. hydrochloric acid (1 mL) was heated at 80°C for 16 h. Work up in the usual way provided white solid (1.02 g, 99%) which was shown by nmr (400 MHz) to be a mixture of 3-*exo*- to 3-*endo*-methyl epimers in the ratio ~1:9.5.

The major isomer, (+)-9-bromo-3-*endo*-methylcamphor (identical

Can. J. Chem. Downloaded from www.nrcresearchpress.com by 210.87.254.5 on 09/06/12
For personal use only.

Can. J. Chem. Downloaded from www.nrcresearchpress.com by 210.87.254.5 on 09/06/12
For personal use only.

to an authentic sample[4]) displayed the following characteristics: mp 104–106°C; $[\alpha]_D$ +69.4° (*c*, 0.39, MeOH); ν_{max} ($CHCl_3$): 2975, 1740 cm^{-1}; nmr ($CDCl_3$, 400 MHz), δ 0.92 (3H, s), 1.02 (3H, s), 1.07 (3H, d, *J* = 7.0 Hz), 2.37 (1H, t, *J* = 4 Hz), 2.45 (1H, pentet,[3] *J* = 4.0 and 7.0 Hz), 3.23 (d) and 3.65 (d) (2H, AB quartet, *J* = 10 Hz); *m/e* (relative intensity): 244/246 (M^+, 38), 186/188 (100), 165 (36). M.W. calcd. for $C_{11}H_{17}OBr$: 246.0442/244.0462; found (high resolution mass spectrometry): 246.0444/244.0466. *Anal.* calcd. for $C_{11}H_{17}OBr$: C 53.89, H 6.99, Br 32.59; found: C 53.66, H 7.12, Br 32.38.

*(+)-9,10-Dibromo-3-*exo*-methylcamphor (8)*

(+)-9,10-Dibromocamphor (**7**) (0.908 g, 2.9 mmol) was added to a freshly prepared solution of lithium diisopropylamide (2.78 mmol) in THF (3.3 mL) at 0°C under argon. Methyl iodide (0.72 mL, 11.6 mmol) was added after 15 min and the reaction quenched with 1 *N* hydrochloric acid after a further 0.5 h. Work up in the usual fashion yielded a pale yellow solid (875 mg) which, on column chromatography (silica gel; petroleum ether) (30–60°C)/(ether 50:1), gave starting material (512 mg) and an epimeric mixture of (+)-9,10-dibromo-3-methylcamphor (318 mg, 34%). Capillary glc and 400 MHz nmr showed the ratio of 3-*exo*- to 3-*endo*-methyl epimers to be ~1.7:1. The major isomer, (+)-9,10-dibromo-3-*exo*-methylcamphor (**8**), was obtained after repeated recrystallization from methanol, mp 84–85.5°C; $[\alpha]_D$ +102.0° (*c*, 0.20, CH_2Cl_2); ν_{max} ($CHCl_3$): 2975, 1740 cm^{-1}; δ ($CDCl_3$, 400 MHz), δ 1.11 (3H, s), 1.24 (3H, d, *J* = 8 Hz), 2.09 (1H, q, *J* = 8 Hz), δ 2.34 (1H, d, *J* = 4 Hz), 3.45 (d) and 3.67 (d) (2H, AB quartet, *J* = 12 Hz), 3.49 (d) and 3.63 (d) (2H, AB quartet, *J* = 10 Hz); *m/e* (relative intensity): 243/245 (M^+ – Br, 40), 235/237 (23), 163 (17), 135 (100); M.W. calcd. for $C_{11}H_{16}OBr_2$: 325.9527/323.9547/321.9567; found (high resolution mass spectrometry): 325.9540/323.9572/321.9566. *Anal.* calcd. for $C_{11}H_{16}OBr_2$: C 40.77, H 4.98, Br 49.31; found: C 40.56, H 5.04, Br 49.20.

*(+)-9,10-Dibromo-3-*endo*-methylcamphor (9)*

An epimeric mixture of (+)-9,10-dibromo-3-methylcamphor (1.49 g) in glacial acetic acid (27 mL) and conc. hydrochloric acid (3 mL) was heated at 80°C for 16 h. Work up in the usual way afforded a crystalline product (1.34 g, 90%) which was shown by capillary glc and 400 MHz nmr, to be a mixture of 3-*exo*- to 3-*endo*-methyl epimers in the ratio of ~1:6.

Repeated crystallization from methanol afforded pure (+)-9,10-dibromo-3-*endo*-methylcamphor (**9**), mp 62.5–63°C; $[\alpha]_D$ +46.7° (*c*, 0.30, CH_2Cl_2); ν_{max} ($CHCl_3$) 2980, 1735 cm^{-1}; δ ($CDCl_3$, 400 MHz), δ 1.11 (3H, d, *J* = 8 Hz), 1.15 (3H, s), 2.43–2.54 (2H, m), 4.44 (d) and 4.66 (d) (2H, AB quartet, *J* = 12 Hz), 4.60 (d) and 4.74 (d) (2H, AB quartet, *J* = 10 Hz). *m/e* (relative intensity): 322/324/326 (M^+, 0.8/1.7/0.6), 243/245 (44), 215/217 (24), 163 (19), 135 (100); M.W. calcd. for $C_{11}H_{16}OBr_2$: 325.9527/323.9547/321.9567; found (high resolution mass spectrometry): 325.9512/323.9558/321.9562. *Anal.* calcd. for $C_{11}H_{16}OBr_2$: C 40.77, H 4.98, Br 49.31; found: C 40.65, H 4.92, Br 49.23.

3-Methyl-3-trideuteriomethylcamphor (10 + 11)

(+)-3-Methylcamphor (0.693 g, 4.17 mmol) dissolved in dry THF (9 mL) was added to a freshly prepared solution of lithium diisopropylamide (5.13 mmol) in THF (9 mL) at 0°C under argon. After 45 min d_3-methyl iodide (0.68 mL, 10.7 mmol) was added and the reaction quenched with 1 *N* hydrochloric acid 1 h later. Work up in the usual way afforded a yellow oil (0.737 g) which, on column chromatography (silica gel; petroleum ether (30–60°C)/(ether 50:1)), gave starting material (0.24 g) and 3-methyl-3-trideuteriomethylcamphor, 0.476 g (62%; 95% based on recovered starting material), as a mixture of epimers (**10** + **11**). 400 MHz nmr showed the ratio of the 3-*exo*- (**10**) to 3-*endo*-methyl (**11**) epimers to be ~3.4:1. ν_{max} ($CHCl_3$) 1740 cm^{-1}. M.W. calcd. for $C_{12}H_{17}D_3O$: 183.1703; found (high resolution mass spectrometry): 183.1703; δ ($CDCl_3$, 400 MHz), 0.91 (3H, s), 1.00 (3H, s), 1.03 (0.7H, s, C(3)-*endo*-methyl), 1.19 (2.3H, s, C(3)-*exo*-methyl).

Acknowledgement

We acknowledge financial support for this research from the Natural Sciences and Engineering Research Council of Canada.

1. (*a*) W. M. DADSON, M. LAM, T. MONEY, and S. E. PIPER. Can. J. Chem. **61**, 343 (1983) and references therein; (*b*) J. H. HUTCHINSON, T. MONEY, and S. E. PIPER. J. Chem. Soc. Chem. Commun. 455 (1984).
2. E. JOSEPHY and F. RADT (*Editors*). Elsevier's encyclopaedia for organic chemistry, Vol. 12A. Elsevier Publishing Co., Amsterdam. 1948.
3. J. L. SIMONSEN and L. N. OWEN. The terpenes. Vol. II. Cambridge University Press. 1957.
4. (*a*) A. PELTER and S. H. HARPER. *In* Rodd's chemistry of carbon compounds. Vol. II*c*. *Edited by* S. Coffey. Elsevier, Amsterdam, 1969; (*b*) R. T. BROWN. *In* Rodd's chemistry of carbon compounds. Vol. II*c*. *Edited by* M. F. Ansell. Suppl. Elsevier, Amsterdam. 1974.
5. H. RUPE and M. LENZLINGER. Helv. Chim. Acta, **18**, 255 (1935).
6. K. M. BAKER and B. R. DAVIS. Tetrahedron, **24**, 1655 (1968).
7. W. C. STILL, M. KAHN, and A. MITRA. J. Org. Chem. **43**, 2923 (1978).
8. (*a*) H. NISHIMITSU, M. NISHIKAWA, and M. HAGIWARA. Proc. Jpn. Acad. **27**, 285 (1951); Chem. Abstr. **46**, 6112 (1952); (*b*) E. J. COREY, S. W. CHOW, and R. A. SCHERRER. J. Am. Chem. Soc. **79**, 5773 (1957); (*c*) W. L. MEYER, A. P. LOBO, and R. N. MCCARTY. J. Org. Chem. **32**, 1754 (1967).
9. E. J. COREY, R. HARTMANN, and P. A. VARAKENCHERRY. J. Am. Chem. Soc. **84**, 2611 (1962).
10. (*a*) P. A. GRIECO, Y. OHFUNE, Y. YOKOHAMA, and W. OWENS. J. Am. Chem. Soc. **101**, 4749 (1979); (*b*) P. A. GRIECO, J. INANAGA, N.-H. LIN, and T. YANAMI. J. Am. Chem. Soc. **104**, 5781 (1982); (*c*) P. A. GRIECO, T. TAKIGAWA, and D. R. MOORE. J. Am. Chem. Soc. **101**, 4380 (1979); (*d*) P. A. GRIECO, G. F. MAJETICH, and Y. OHFUNE. J. Am. Chem. Soc. **104**, 4226 (1982); (*e*) P. A. GRIECO, Y. OHFUNE, G. F. MAJETICH, and C.-L. J. WANG. J. Am. Chem. Soc. **104**, 4233 (1982).
11. B. M. TROST, P. R. BERNSTEIN, and P. C. FUNFSCHILLING. J. Am. Chem. Soc. **101**, 4378 (1979).
12. H. SHIBUYA, H. FUJIOKA, A. KAJIWARA, Y. YAMAMOTO, and I. KITIGAWA. Chem. Pharm. Bull. **30**, 1271 (1982).
13. J. H. HUTCHINSON. Unpublished results.
14. S. RETTIG and J. TROTTER. Unpublished results.
15. N. HOLY, R. FOWLER, E. BURNETT, and R. LORENZ. Tetrahedron, **35**, 613 (1979).
16. R. D. CLARK and C. H. HEATHCOCK. J. Org. Chem. **41**, 1396 (1976).
17. C. W. JEFFORD and C. G. RIMBAULT. J. Am. Chem. Soc. **100**, 6437 (1978).
18. M. A. JOHNSON and M. P. FLEMING. Can. J. Chem. **57**, 318 (1979).
19. M. S. ALLEN, J. H. HUTCHINSON, and T. MONEY. Can. J. Chem. In press.

Thermolysis of *gem*-dimethyl-2-cyclohexenones. Evidence for [1,5] sigmatropic methyl shifts

G. L. LANGE,[1] M. J. NYE,[1] V. A. PEREIRA, V. STRATTON, AND T. YURKEVICH
Department of Chemistry, University of Guelph, Guelph, Ont., Canada N1G 2W1

Received July 18, 1983[2]

This paper is dedicated to Professor Paul de Mayo on the occasion of his 60th birthday

G. L. LANGE, M. J. NYE, V. A. PEREIRA, V. STRATTON, and T. YURKEVICH. Can. J. Chem. **62**, 1903 (1984).

The vapour phase thermolyses at 400°C of three *gem*-dimethylated 2-cyclohexenones **1, 2**, and **3** were studied to determine the effect of blocking the direct conversion of these substrates to aromatic systems. In all three reactions it is proposed the major pathway taken was enolization followed by elimination of methane to yield a substituted phenol. This elimination reaction proceeded more readily with **2** than with either **1** or **3**, and HMO calculations which are consistent with this order of reactivity are presented. A general mechanistic scheme is proposed to account for the products formed and it is necessary to include a [1,5] sigmatropic methyl shift to explain the formation of at least one product in each thermolysis.

G. L. LANGE, M. J. NYE, V. A. PEREIRA, V. STRATTON et T. YURKEVICH. Can. J. Chem. **62**, 1903 (1984).

Dans le but de déterminer l'effet de bloquage de la transformation directe de ces substrats en produits aromatiques, on a étudié la thermolyse en phase vapeur à 400°C de trois cyclohexène-2 ones *gem*-diméthylées (**1**, **2**, et **3**). Dans chacune de ces trois réactions, on suggère que la voie de réaction principale est une énolisation suivie par une élimination de méthane qui conduit à un phénol substitué. Cette réaction d'élimination se produit plus facilement avec **2** qu'avec soit **1** ou **3**; on présente des calculs d'orbitales moléculaires suivant Hückel qui sont en accord avec cet ordre de réactivité. On propose un schéma général pour le mécanisme de la réaction qui tient compte des produits formés; il est nécessaire d'introduire une transposition sigmatropique [1,5] du méthyle pour expliquer la formation d'au moins un produit dans chaque thermolyse.

[Traduit par le journal]

Can. J. Chem. Downloaded from www.nrcresearchpress.com by 210.87.254.6 on 09/06/12
For personal use only.

In a previous study we investigated the vapour phase thermolyses at 400°C of a number of mono- and di-alkylated 2-cyclohexenones and showed that the major products were alkylated benzenes and phenols (1). The formation of these products can be explained by enolization of the carbonyl group followed by [1,5] sigmatropic hydrogen shifts and/or loss of a molecule of H_2O, H_2, or RH. We felt it would be of interest to examine the thermolysis of a series of *gem*-dimethylated 2-cyclohexenones where the conversion to the aromatic ring was blocked by these substituents without the involvement of [1,5] sigmatropic methyl shifts or elimination of methane. It was also of interest to discover if the thermolyses of these cyclohexenones bear any resemblance to the thermolysis of 5,5-dimethyl-1,3-cyclohexadiene in which Spangler and Boles (2) observed both [1,5] sigmatropic shifts and eliminations. The three compounds 4,4-dimethyl- (**1**), 3,5,5-trimethyl- (**2**), and 3,6-6-trimethyl-2-cyclohexenone (**3**) were chosen for our study because they have *gem*-dimethyl substitution at the 4-, 5-, and 6-positions, respectively. In this paper we report our results of the thermolysis of these substrates, suggest a general mechanism for the formation of the products, and offer an explanation for the relative reactivities of the three compounds.

Experimental

Instrumentation

Infrared (ir) spectra were recorded on a Beckman Acculab 6 spectrophotometer, proton magnetic resonance (nmr) spectra on a Varian T-60 spectrometer with TMS ($\delta = 0.0$) as internal standard, and mass spectra on a VG Micromass 7070F spectrometer coupled to a gas chromatography unit (gc–ms) equipped with a 6 ft × 0.25 in. 5% Carbowax 20M column.

Gas chromatographic (gc) analyses and collections were performed on an Aerograph Autoprep Model A-700 using the following columns: column A, 8 ft × 0.25 in. 20% Carbowax 20M on Chromosorb W-HP A/W DMCS 80/100 mesh; column B, 6 ft × 0.25 in. 20% DEGS on Chromosorb W 60/80 mesh; column C, 6 ft × 0.25 in. 20% OV-1 on Chromosorb W-HP 80/100 mesh. In the analysis of the products the areas of all peaks on the gc tracings were determined by triangulation and the areas were not corrected for differences in the thermal response of the detector. The values reported are an average of at least two runs for each substrate.

*Preparation of substrates **1**, **2**, and **3** and gas chromatography standards*

4,4-Dimethyl-2-cyclohexenone (**1**) was prepared by acid-catalyzed annelation of isobutyraldehyde and methyl vinyl ketone (3), 3,5,5-trimethyl-2-cyclohexenone (isophorone) (**2**) was commercially available, and 3,6,6-trimethyl-2-cyclohexenone (**3**) was prepared from **1** by reaction with methyllithium followed by oxidation with pyridinium chlorochromate (4).

The following is a list of the compounds which were available in our laboratory and were used for gc comparison with the thermolysis products: benzene; toluene; *o*-, *m*-, and *p*-xylenes; 1,3,5-(mesitylene), 1,2,3- and 1,2,4-trimethylbenzenes; phenol; *o*-, *m*-, and *p*-cresols; 2,3-, 2,4-, 2,5-, 2,6-, 3,4-, and 3,5-dimethylphenols; 2,3,5-, 2,3,6-, and 2,4,6-trimethylphenols.

Thermolyses and product identification

The thermolyses were conducted at 400 ± 2°C for 20 h in an evacuated (<0.02 Torr) 650-mL Pyrex reactor similar to that previously described (5). The substrates **1, 2**, and **3** were purified by vacuum distillation immediately prior to reaction, and the sample size was 0.40 g for each run. The products were distilled into a cold finger cooled in liquid N_2 and then were analyzed by gc. The crude distillation recoveries were always high as very little tar formation was evident in any of the thermolyses. The gc peaks were identified by coincident retentions with known samples on two or three columns, by the peak enhancement method, by gc–ms analysis, and in some instances by preparative gc collection and spectral analysis. No attempt was made to analyze for gaseous products such as methane. Schemes 1, 2, and 3 give a detailed product distribution obtained as described above for thermolysis of the three substrates. In the gc tracings of each of the thermolyses there were a number of small unknown peaks and these have been included in the unidentified products total.

[1]Authors to whom correspondence may be addressed.

[2]Revision received December 6, 1983.

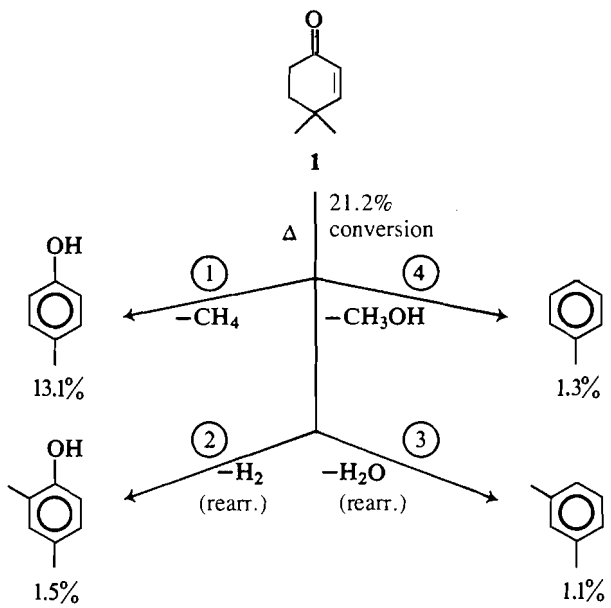

Unidentified products = 4.2%

SCHEME 1

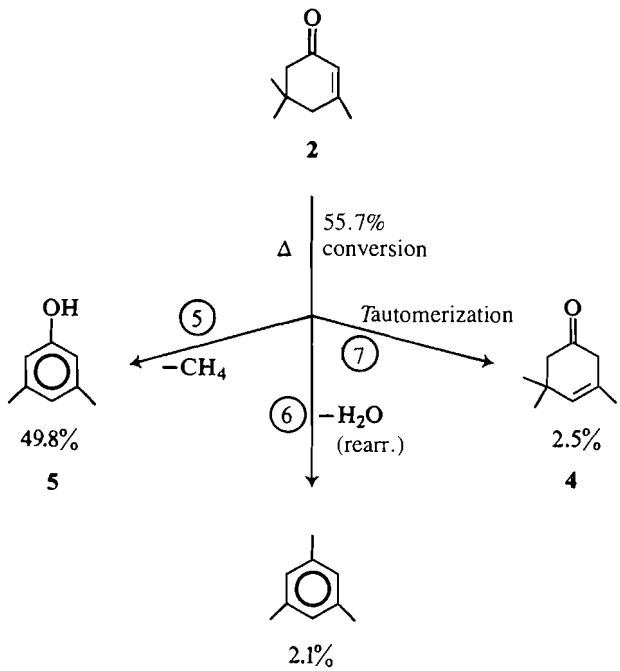

Unidentified products = 1.3%

SCHEME 2

Gas chromatographic collection of peaks

Following is a list of the peaks that were collected by preparative gc (column A) and an indication of how each peak was analyzed.

Thermolysis of 1

The major peak eluted after **1** was collected and its ir and nmr spectra suggested it was a mixture. This peak was resolved into its two components, *p*-cresol and 2,4-dimethylphenol, on column C.

Thermolysis of 2

The peak between mesitylene and **2** was collected and found to have spectral data consistent with 3,5,5-trimethyl-3-cyclohexenone (**4**): ir(CCl_4): 1715 cm^{-1}; nmr was the same as that previously reported (6); mass spectrum *m/e* (rel. int.): 138 (M^+, 64), 123(59), 96(100), 95(66), 71(79). The major peak appearing considerably after **2** was also collected and found to have mp and ir and mass spectra identical to an authentic sample of 3,5-dimethylphenol (**5**).

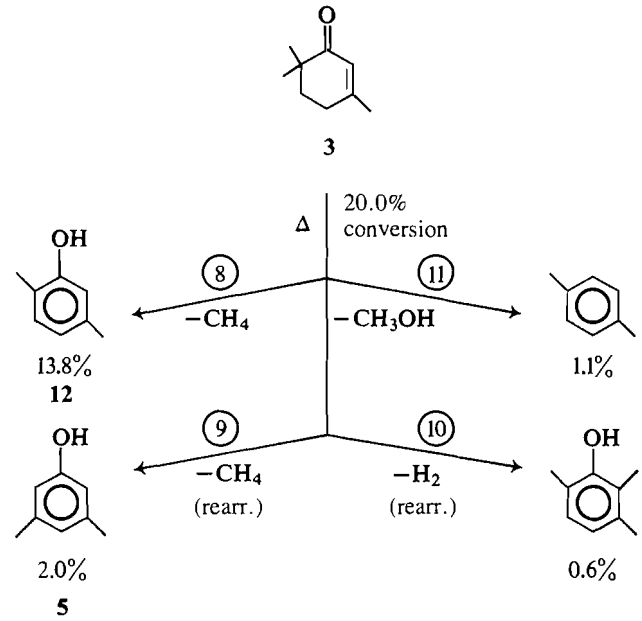

Unidentified products = 2.5%

SCHEME 3

Thermolysis of 3

All three phenolic products had retention times considerably longer than **3** and the major of these was isolated and identified as 2,5-dimethylphenol (**12**) by comparison of its mp and its ir and mass spectra with an authentic sample. A second phenol, which appeared at a longer retention time than **12**, had properties identical to 3,5-dimethylphenol (**5**). A minor peak which appeared as a shoulder on the front side of the peak for **12** was not isolated but its mass spectrum and gc behaviour unambiguously identified it as 2,3,6-trimethylphenol. On polar gc columns such as columns A and B it was found that phenols with methyl substituents at the 2- or 2- and 6-positions were eluted before other isomers, presumably because these alkyl groups reduced or shielded the interaction of the phenolic hydroxyl group with the polar gc phase. This explains why 2,3,6-trimethylphenol elutes before either of the dimethylphenols (**5** or **12**) and also why **12** elutes before **5**. Of course, on a non-polar column such as C, which separates on the basis of boiling points, the trimethylphenols are eluted *after* the dimethylphenols.

Molecular orbital calculations

The standard HMO method with Jacobian optimization by computer (7) was used to calculate the relative energies of the various species. Regarding coulomb integrals, α was used for all carbon atoms and $\alpha + 2$ for OH groups, and the resonance integrals (β') of partial σ or π bonds were calculated from the partial bond order (p) using the very approximate empirical relation $\beta' = \beta\sqrt{p}$. Further explanation is given in the discussion.

Results and discussion

Schemes 1, 2, and 3 summarize the results of the thermolyses of **1**, **2**, and **3** under vapour phase conditions at 400°C for 20 hours. Along with an arrow directed to each product in these schemes is a circled number and an indication of the nature of the reaction involved in the formation of that product. The types of reactions observed in this work and in our previous study (1) are listed below together with examples of each.

Can. J. Chem. Downloaded from www.nrcresearchpress.com by 210.87.254.6 on 09/06/12
For personal use only.

Type of reaction	No. of reaction (or reference)
(*i*) Isomerization	(7), (1)
(*ii*) Loss of H_2	(1)
(*iii*) Loss of H_2 with rearrangement	(2), (3), (10)
(*iv*) Loss of RH	(1), (5), (18), (1)
(*v*) Loss of RH with rearrangement	(9)
(*vi*) Loss of H_2O	(1)
(*vii*) Loss of H_2O with rearrangement	(3), (6)
(viii) Loss of ROH	(11)
(*ix*) Loss of ROH with rearrangement	(4)

These nine reaction types involve only three reaction processes: *isomerization*, *rearrangement*, and *elimination*. In order to arrive at an overall reaction mechanism let us consider each of these processes in turn. *Isomerization* was observed in the conversion of **2** to the unconjugated enone **4** and was also seen in the thermolysis of 3-methyl-2-cyclohexenone (1). The generally accepted mechanism of isomerization of unsaturated ketones involves the formation of enol intermediates in acid or base catalyzed reactions, and the same route may be involved in the thermal isomerizations, with the enolization occurring on the surface of the glass vessel (5). The postulation of surface involvement avoids the objection that Woodward–Hoffmann rules (8) prohibit facile unimolecular enolization, and the observation that addition of glass chips increases the rate of the thermolysis of cyclohexenones (1) lends experimental support to this proposal. Regarding the *rearrangement* process, enolization of substrates **1**, **2**, or **3** leads to a substituted 1,3-cyclohexadiene, a system which is known to undergo [1,5] sigmatropic shifts of hydrogen or alkyl groups below 400°C (2), and hence a mechanism for the rearrangements is apparent. Concerning the *elimination* process, consideration of the Woodward–Hoffmann symmetry rules (8) is a key issue. Although reactions violating these rules cannot be dismissed, we took the view that if Woodward–Hoffmann allowed routes are available they will be of lower energy and hence preferred. Also, we have assumed these transformations to be intramolecular as no products of intermolecular disproportionation (i.e., transfer of H_2, CH_4, H_2O, or CH_3OH) were observed. 1,3-Cyclohexadienes are formally allowed to give benzenes via a Möbius [2 + 2] elimination which involves inversion of one of the two centres being eliminated. As a check of this statement, the Hückel orbital energies were calculated for different points along the reaction coordinate (9) for the [2 + 2] elimination and these are shown in Diagram 1(a) for the mechanism involving one inversion and in 1(b) for no inversions. A high energy process involving crossover of HOMO and LUMO orbitals is clearly seen for 1(b). Hence 1,2-elimination of CH_4, H_2O, or CH_3OH is allowed whereas loss of H_2 by a unimolecular process is prohibited since the *s* orbital of hydrogen is not capable of inversion. In order to explain the observed loss of H_2 without violating the Woodward–Hoffmann rules, it is necessary for the reaction to proceed via 1,4-cyclohexadiene precursors, which can easily arise from observed nonconjugated enones (e.g. **4**) by enolization. This type of reaction has been observed to occur for 1,4-cyclohexadiene itself below 400°C (10), and is presumed to proceed by the allowed Hückel [2 + 4] elimination mechanism.

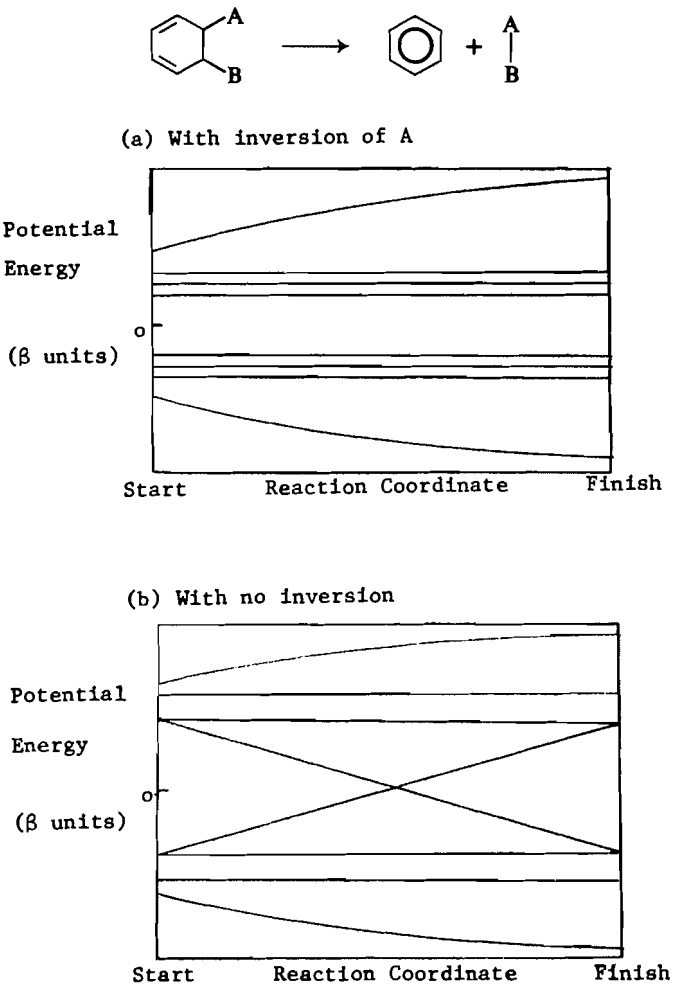

DIAGRAM 1
Orbital following diagram for reaction

Combining the above concepts leads to the general mechanism for thermolysis of cyclohexenones shown in Scheme 4. This mechanistic scheme explains the occurrence of all products reported in this paper (except for the formation of **5** from **3**) and in the previous paper from this laboratory (1), and most of the products predicted using this scheme are actually observed. Furthermore, in most cases the formation of non-observed products involves more steps, particularly methyl shifts, than the observed products involve, and may therefore be formed at lower rates. An illustration of the above argument is the observation of loss of methanol from **3** (three steps with no methyl shifts based on Scheme 4) in contrast to the non-observation of loss of water from **3** (five steps with one methyl shift). In the case of **2**, all of the thermolysis products predicted by the scheme were observed. The product distributions are best explained if the relative rates of reaction are: elimination > hydrogen shifts > methyl shifts (a comparison of hydrogen vs. methyl shifts has been reported (11)).

With respect to alternative mechanisms, a free radical process was ruled out since intermolecular products were not ob-

Can. J. Chem. Downloaded from www.nrcresearchpress.com by 210.87.254.6 on 09/06/12
For personal use only.

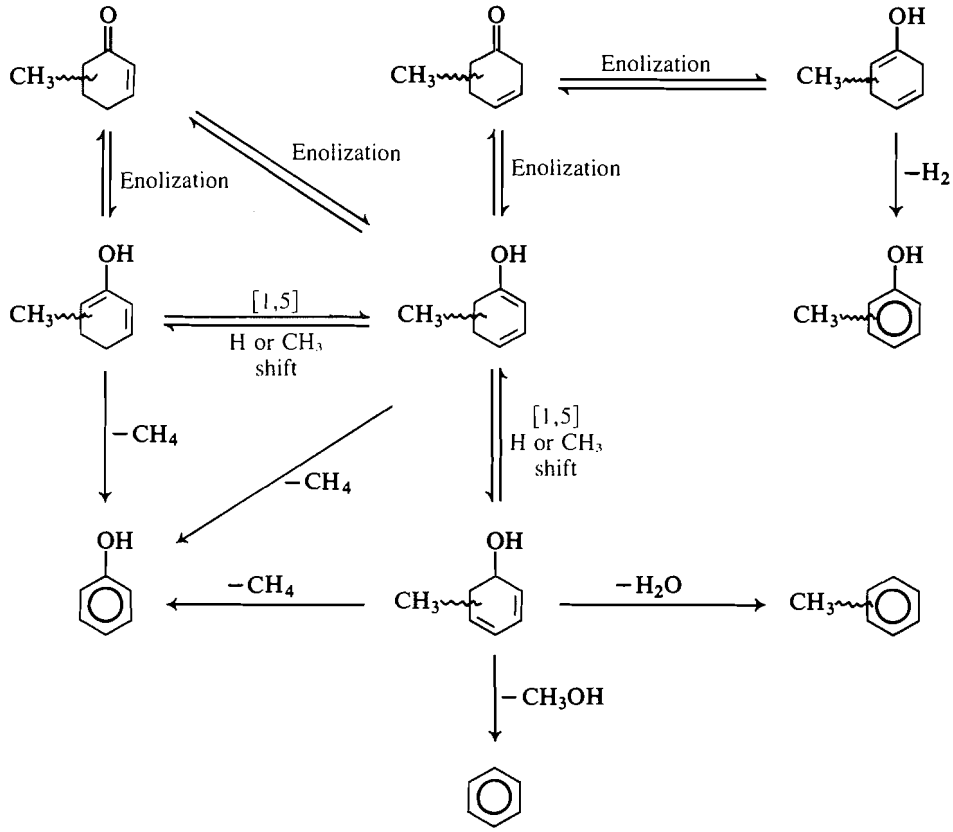

SCHEME 4

served. Schiess and Dinkel (12) have proposed a mechanism involving an electrocyclic ring opening followed by a sigmatropic hydrogen shift and then an electrocyclic ring closing to explain the rearrangements of certain *gem*-disubstituted 1,3-cyclohexadienes, but this mechanism would not explain the formation of many of our products including **5**. Spangler and Boles' paper on *gem*-dialkylated 1,3-cyclohexadienes (2) proposes a mechanism involving [1,5] shifts analogous to ours, and their observed rearrangements and eliminations of CH_4 and H_2 are entirely explicable using Scheme 4.

One distinctive feature of the three thermolyses is the significantly greater conversion of **2** to products (55.7%) as compared with **1** and **3** (21.2 and 20.0%, respectively). Also, in each instance the major product (49.8% for **2** vs. 13.1 and 13.8% for **1** and **3**, respectively) was formed by loss of CH_4, so an explanation was sought for this preferred elimination pathway. The proposed mechanisms for loss of CH_4 based on Scheme 4 are shown in Scheme 5, including two alternatives for the transformation of **2**. The glass chips experiment (1) suggests that enolization of the starting ketones is the rate determining step. If this is entirely true, it would simply be necessary to explain why **2** enolizes faster than **1** or **3**, but it is not apparent why this should be the case. In fact, it would seem more likely that either **2** and **3** would enolize the fastest as they *both* form linearly conjugated dienols (**8** and **9**) or, alternatively, **1** and **2** would enolize the fastest as *both* form cross-conjugated dienols (**6** and **7**). A solution to this problem may be that the second step, the [2 + 2] Möbius elimination, is of similar rate to the enolization and may contribute to the rate determination. In order to test this theory, Hückel Molecular Orbital (HMO) calculations were carried out to estimate the relative energies of the transition states for the elimination reactions of **1**, **2**, and **3**, based on

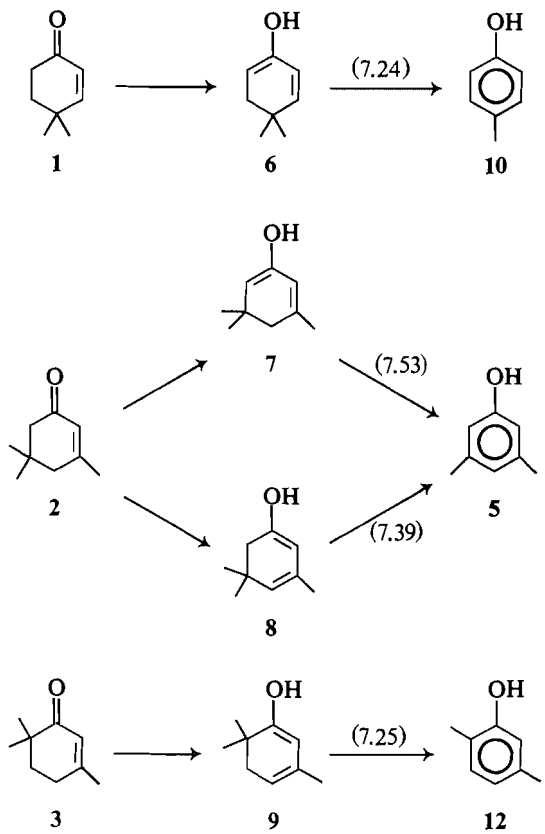

SCHEME 5. Routes for conversion of enones to phenols (relative stabilization energies of transition states in β units for loss of methane are shown in brackets).

Can. J. Chem. Downloaded from www.nrcresearchpress.com by 210.87.254.6 on 09/06/12
For personal use only.

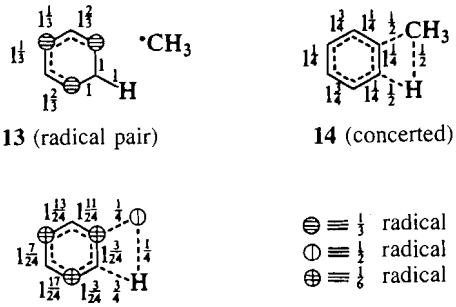

13 (radical pair) **14** (concerted)

15 (1 : 1 blend of **13** and **14**)

SCHEME 6. Transition states for elimination of methane from 5-methyl-1,3-cyclohexadiene showing bond orders.

the reasonable assumption (13) that this step is a blend of a purely free radical mechanism involving the transition state **13** and a purely concerted mechanism involving the transition state **14** (for the calculations a 1 : 1 blend was chosen). Stated in another way, this means that the C—C bond is pictured as breaking ahead of the C—H bond. The resulting transition state is depicted as **15** (Scheme 6), and this is the basic structure for the transition state envisioned during elimination of methane from **6**, **7**, **8**, and **9**, except that the location of the hydroxyl substituents is different for each of these. The relative energies of each of these transition states were calculated, and the results are given in Scheme 5. The larger values indicate higher stabilization, lower energy barrier, and hence faster rate of reaction, so that the relative rates of formation of the products should be **5** > **10** and **12**, which is compatible with our observations. Appreciable alteration of the bond orders in the transition state does not affect the relative calculated energies sufficiently to nullify the argument. An alternative explanation suggested by a referee for the faster thermolysis of **2** relative to **1** and **3** is that reaction of **2** is faster because of the presence of two product-forming enols.

In conclusion, thermolysis of *gem*-dimethylated 2-cyclohexenones **1**, **2**, and **3** at 400°C yields as the major product in each case a phenol, which is formed by loss of methane from the corresponding enol tautomer. The elimination reaction proceeds to a much greater extent with enone **2** than with **1** or **3** and HMO calculations of the relative energies of the transition states in going from the intermediate enols to the phenols predict this order of reactivity. [1,5] Sigmatropic methyl shifts from the enols account for at least one product in each thermolysis. The formation of all products isolated (except for **5** from **3**) may be explained by assuming three processes are operative: enolizations, [1,5] sigmatropic shifts, and eliminations (Scheme 4).

Acknowledgement

The authors acknowledge the financial assistance of the Natural Sciences and Engineering Research Council of Canada.

1. G. L. LANGE, V.A. PEREIRA, and M. WEEDLE. Can. J. Chem. **58**, 1639 (1980).
2. C.W. SPANGLER and D. L. BOLES. J. Org. Chem. **37**, 1020 (1972).
3. M. E. FLAUGH, T. A. CROWELL, and D. S. FARLOW. J. Org. Chem. **45**, 5399 (1980).
4. W. G DAUBEN and D. M. MICHNO. J. Org. Chem. **42**, 682 (1977).
5. J. M. CONIA and P. LEPERCHEC. Synthesis, 1 (1975).
6. J. H. BABLER, N. C. MALEK, and M. J. COGHLAN. J. Org. Chem. **43**, 1821 (1978).
7. H. H. GREENWOOD. Computing methods in quantum organic chemistry. Wiley–Interscience, London. 1972.
8. R. B. WOODWARD and R. HOFFMANN. Convservation of orbital symmetry. Academic Press, New York. 1970.
9. H. E. ZIMMERMAN. Acc. Chem. Res. **5**, 393 (1972).
10. R. J. ELLIS and H. M. FREY. J. Chem. Soc. A, 553 (1966); S. W. ORCHARD and B. A. THRUSH. J. Chem. Soc. Chem. Commun. 14 (1973).
11. L. L. MILLER and R. F. BOYD. J. Am. Chem. Soc. **93**, 650 (1971).
12. P. SCHIESS and R. DINKEL. Tetrahedron Lett. 2503 (1975).
13. J. N. BRADLEY. Proc. Roy. Soc. A, **337**, 199 (1974).

Can. J. Chem. Downloaded from www.nrcresearchpress.com by 210.87.254.6 on 09/06/12
For personal use only.

Carbon atom insertion bicycloannulation: total syntheses of ishwarane and ishwarone

ROBERT M. CORY,[1] LESTER P. J. BURTON, DOMINIC M. T. CHAN, FRED R. MCLAREN, MARY H. RASTALL, AND RICHARD M. RENNEBOOG

Department of Chemistry, University of Western Ontario, London, Ont., Canada N6A 5B7

Received December 16, 1983

This paper is dedicated to Professor Paul de Mayo on the occasion of his 60th birthday

ROBERT M. CORY, LESTER P. J. BURTON, DOMINIC M. T. CHAN, FRED R. MCLAREN, MARY H. RASTALL, and RICHARD M. RENNEBOOG. Can. J. Chem. **62**, 1908 (1984).

Insertion of a carbon atom into a methyl cyclohexene, leading in a single synthetic step to a bicyclo[3.2.1.$0^{2,7}$]octane by carbene addition to the double bond and carbene insertion into a methyl C—H bond, has been accomplished by treating the cyclohexene with carbon tetrabromide and methyllithium at low temperatures. This new bicycloannulation method has been employed in a total synthesis of ishwarane (**1**), the naturally occurring parent hydrocarbon of the ishwarane class of tetracyclic sesquiterpenes. Although this reaction was not successful with various possible precursors of ishwarone (**2**), this natural product was prepared in low yield by a two-step version of the carbon atom insertion bicycloannulation (CAIB) procedure involving addition of bromoform-derived dibromocarbene to the octalone (**5**) followed by treatment of the resulting dibromocyclopropane (**56**) with methyllithium. The same two-step sequence was also successful in the first synthesis of norishwarane (**20**), the hydrocarbon comprising the bare ring system of the ishwarane sesquiterpenoids. The Diels–Alder synthesis used in the preparation of the octalin precursor (**18**) of norishwarane could not be used for the terpenes themselves because of the lack of dienophilic reactivity of the required cyclohexenone (**7**). A regioselective Diels–Alder equivalent sequence was therefore developed, consisting of conjugate addition of lithium di(3-methyl-3-butenyl)cuprate (**42**) to 2,3,4-trimethylcyclohex-2-en-1-one (**7**), epoxidation, base-catalyzed cyclization of the resulting epoxide (**47**) to a mixture of primary and tertiary alcohols (**50** and **49**, respectively), and dehydration of **49** to give **5**. In the case of ishwarane, the octalin precursor (**62**) was synthesized by conjugate addition of lithium dimethylcuprate to octalone **59**, addition of methyl magnesium bromide to the resulting decalone (**60**) to give octalol **61**, and dehydration.

ROBERT M. CORY, LESTER P. J. BURTON, DOMINIC M. T. CHAN, FRED R. MCLAREN, MARY H. RASTALL et RICHARD M. RENNEBOOG. Can. J. Chem. **62**, 1908 (1984).

En faisant réagir le cyclohexène avec le tétrabromure de carbone et le méthyllithium à basse température, on a réalisé l'insertion d'un atome de carbone dans le méthylcyclohexène; on a ainsi obtenu en une seule étape le bicyclo[3.2.1.$0^{2,7}$]octane par l'addition de carbène sur la double liaison et par une insertion de carbène dans une liaison C—H du méthyle. On a utilisée cette nouvelle méthode de bicycloannellation dans une synthèse totale de l'ishwarane (**1**), l'hydrocarbure naturel parent des sesquiterpènes tétracycliques de la classe de l'ishwarane. Bien que cette réaction n'aie pas pu être appliquée avec succès à divers précurseurs possibles de l'ishwarone (**2**), on a préparé ce produit naturel avec un faible rendement en faisant appel à une version en deux étapes de la méthode de bicycloannellation par insertion d'un atome de carbone (BIAC) impliquant une addition d'un dibromocarbène, provenant du bromoforme, sur l'octalone (**5**), puis une réaction du dibromocyclopropane (**56**) qui en résulte avec du méthyllithium. On a aussi utilisé cette méthode avec succès pour réaliser la première synthèse du norishwarane (**20**), l'hydrocarbure comportant le système cyclique de base du sesquiterpène ishwarane. Dû au faible caractère diènophile de la cyclohexènone (**7**) requise, on ne peut pas se servir de la synthèse de Diels–Alder pour la synthèse des terpènes eux-mêmes, même si cette synthèse peut être utilisée pour la préparation de l'octaline (**18**) précurseur du norishwarane. On a donc mis au point une série de réactions régiosélectives équivalentes à la réaction de Diels–Alder qui comprend une addition conjuguée du di(méthyl-3 butényl-3) cuprate de lithium (**42**) sur la triméthyl-2,3,4 cyclohexène-2 one-1 (**7**), une époxydation, une cyclisation, catalysée par les bases, de l'époxyde (**47**) formé qui conduit à un mélange d'alcools primaire et tertiaire (respectivement **50** et **49**) et finalement une déshydratation de l'alcool **49** permet d'aboutir au composé **5**. Dans le cas de l'ishwarane, on a préparé son précurseur, l'octaline (**62**), par une addition conjuguée de diméthylcuprate de lithium sur l'octalone **59**, suivie d'une addition de bromure de méthylmagnésium sur la décalone obtenue (**60**) qui permet d'obtenir l'octalol (**61**) dont la déshydration permet d'accéder au produit désiré.

[Traduit par le journal]

Introduction

Ishwarane (**1**) (1), a tetracyclic sesquiterpene, is found in an interesting variety of tropical plants which seem to have little else in common: *Aristolochia indica* L. (Aristolochiaceae)[2] (2), *Cymbopetalum penduliflorum* (Dunal) Baill. (Annonaceae)[3] (3), and *Bixa orellana* L. (Bixaceae)[4] (7). A small family of

[1]Author to whom correspondence should be addressed.

[2]This is the so-called Indian birthwort, the roots of which have been used for centuries in India as a folk remedy for snake and insect bites and a variety of other complaints. The name ishwarane for the sesquiterpene is derived from the Kanada name for this plant, *ishwari beru* (4). The extract of the roots has recently been found to have potent contraceptive properties, and the active principles have been isolated and characterized (5).

[3]The "ear flower" of the ancient peoples of Mexico, still used as a spice for flavouring food and beverages in Guatemala, is obtained from this tree, which occurs in the mountains of Guatemala and southern Mexico (6).

[4]The lipstick tree, cultivated widely throughout the tropical and subtropical areas of the world, is the source of annatto, an important natural food dye used in the colouration of butter, cheese, and margarine. In ancient times the Aztecs added it (along with the flavouring agent from *C. penduliflorum*) to the world's first chocolate beverage (*xocoatl*) to colour it red (15).

Can. J. Chem. Downloaded from www.nrcresearchpress.com by 210.87.254.105 on 09/06/12
For personal use only.

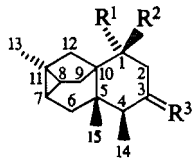

	R^1	R^2	R^3
1	H	H	H_2
2	—O—		H_2
3	H	OH	H_2
4	H	H	O

sesquiterpenoids,[5] of which ishwarane is the parent hydrocarbon, comprises ishwarone (**2**) (8) and ishwarol (**3**) (9) (both congeners of ishwarane in *A. indica*), and 3-oxoishwarane (**4**) (10) (from *A. debillis*). Because of the unusual polycyclic structure of these molecules, they have attracted the attention of a number of synthetic organic chemists, and total syntheses of ishwarane (11–13), ishwarone (13, 14), and ishwarol (13) have been reported. We now wish to describe in detail our own total syntheses of ishwarane and ishwarone.[6]

From a synthetic standpoint, the strategically central structural moiety of the ishwarane terpenes is the tricyclo-[3.2.1.$0^{2,7}$]octane system containing rings B, C, and D.[7] Our plan (Scheme 1) was based on the retrosynthetic removal of a single carbon atom (C-8) from that portion of the ishwarone framework,[8] resulting in a significant simplification of structure and leaving behind an octalone system (**5**), the construction of which would, on the most naive level, be a simple matter using the Diels–Alder strategy. Unfortunately, however, on the basis of the lack of dienophilic reactivity observed (19) for 2,3-dimethylcyclohexenone, cyclohexenone **7** would not be expected to react at all with isoprene.[9] Nonetheless, the ready availability of cyclohexenone **7** led us to propose an *equivalent* of the Diels–Alder synthesis employing a *polarized* isoprene synthon of type **6**, having either an intact or a latent double bond (*vide infra*).[10]

Provided an efficient procedure could be devised for the insertion of the carbon atom into the octalone **5** in the desired fashion, one would have in hand an extremely concise route to a fairly complex terpene structure. In the absence of functional groups other than the olefin and carbonyl in **5** with which to activate this intermediate toward attack by an appropriate reagent, the only viable approach along these lines (Scheme 2) is via a carbon atom equivalent capable of acting as a dicarbene synthon, sequentially adding to the olefin to form the cyclopropane (ring D) and inserting into a C—H bond of a specific methyl group (pro-C-9). In order for this to be of synthetic

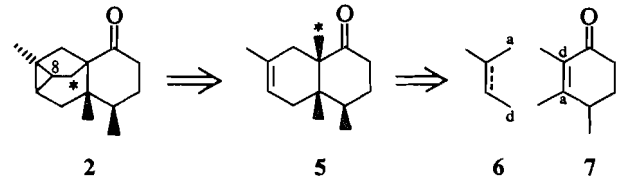

2 **5** **6** **7**

SCHEME 1. Retrosynthetic analysis of ishwarone.

utility, the normal preference for attack on the less hindered convex face of the *cis* octalone (25) must obtain so that the reagent adds stereoselectively to the β side of the olefin, and, equally important, intramolecular insertion of the intermediate cyclopropylidene (**8**) must occur regioselectively, so that little or no insertion into the other angular methyl group or any of the ring C—H bonds takes place. The latter condition was expected to be fulfilled by the fact that conformation **8** should be the preferred one, due to an unfavourable 1,3-diaxial interaction between methyl groups in the other chair conformer (**9**),[11] and by the fact that in conformer **8** the carbene and the

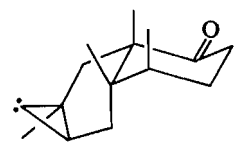

9

methyl into which insertion is desired are within bonding distance of each other.[12] In spite of these encouraging considerations, however, it was apparent from the outset that a source of naked carbon atoms woud not be synthetically useful for this purpose in light of the high reactivity and low selectivity of this simplest of all organic reactive intermediates (29). We therefore sought a less direct means of accomplishing the desired carbon atom insertion.

Results and discussion

Model studies

As we began our work in this area, we were spurred on by the important observation by Paquette *et al.* (30) that applica-

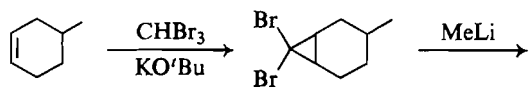

10 **11**

12 **13** **14**

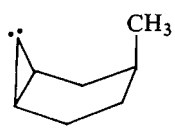

15

[5]For a review of the chemistry of the eremophilane sesquiterpenes, including the ishwarane family, see ref. 16.

[6]For preliminary accounts of portions of this work see refs. 11, 14, and 17. An attempted, but unsuccessful, synthesis of ishwarone has also been reported (18).

[7]This ring system is also present in another sesquiterpene, cycloseychellene (20), and in the trachylobane (21) and helifulvane (22) series of diterpenoids. For an alternative approach to the rapid construction of this system, see our synthesis of trachyloban-19-oic acid (23) and ref. 12*a*.

[8]Since ishwarone has been converted to ishwarane by Wolff–Kishner reduction (8*a*), any synthesis of the former constitutes a formal synthesis of the latter.

[9]We have confirmed this under a variety of conditions.

[10]For annulations via a related conjunctive reagent see ref. 24.

[11]This interaction costs approximately 3.7 kcal mol^{-1} (15.5 kJ mol^{-1}) (26).

[12]Interestingly, this plan would have been rejected by the computer-assisted design program LHASA on the grounds that a bond to a cyclopropane ring is not a strategic one (27). For a related violation of this rule see ref. 28.

Can. J. Chem. Downloaded from www.nrcresearchpress.com by 210.87.254.105 on 09/06/12
For personal use only.

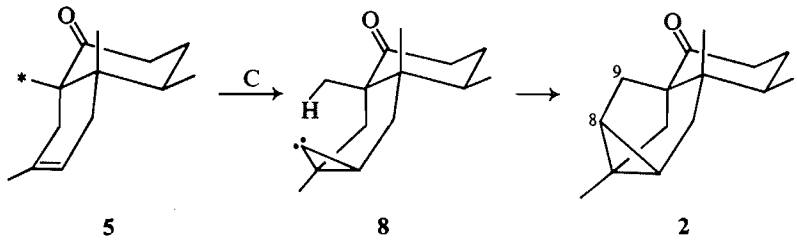

5 8 2

SCHEME 2. Carbon atom insertion.

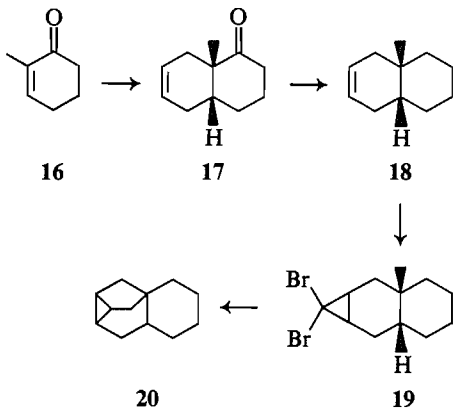

16 17 18 19 20

SCHEME 3. Synthesis of norishwarane.

tion of Moore's bicyclobutane synthesis (31)[13] to 4-methylcyclohexene (**10**) via the dibromocyclopropanes **11** led not only to the expected ring C—H insertion products **12** and **13**, but also to the parent tricyclo[3.2.1.$0^{2,7}$]octane (**14**), resulting from *methyl* C—H insertion, surprisingly, as the major product.[14] Furthermore, it was deduced on the basis of mass balance considerations that this tricyclooctane must have been the *exclusive* product from debromination of *cis*-**11**, while the other two products were derived only from the *trans* dibromide. Methyl insertion was explained by involving kinetic control, in which the *proximity* of the carbenoid[15] and methyl groups in the *cis* axial conformer **15** outweighed all other factors, including the greater nucleophilicity of secondary C—H bonds[16]. Thus, our prediction that ring C—H insertion should not be a problem seemed to be confirmed by this experiment, and carbon atom insertion via a dibromocyclopropane intermediate appeared to be a viable approach to the ishwarane structure.

Accordingly, a model study (Scheme 3) was carried out to test the accommodation of the Moore sequence to the requirement that initial attack on the octalone **5** must be on its β face. In this we followed the plan of Scheme 1, where all structures were simplified by lacking one or more methyl groups. Thus, when the *cis* octalin **18**, prepared by Lewis acid-catalyzed Diels–Alder reaction (19) of 2-methylcyclohex-2-enone (**16**) with 1,3-butadiene followed by Wolff–Kishner reduction of the resulting octalone **17**, was treated with bromoform and aqueous sodium hydroxide under phase-transfer conditions (35), the dibromocarbene adduct **19** was produced in 48% yield. Contrary to expectations, however, this appeared to be a mixture of α and β diastereomers by gas chromatographic analysis, which showed two overlapping peaks in a ratio of about 2:1,[17] in spite of the fact that only one methyl singlet was visible in the ^{1}H nmr spectrum. On reaction of this mixture with methyllithium at −10°C there were obtained three debromination products in a total yield of 77%, of which two could not be separated from each other. Although the latter material could not be completely characterized due to the fact that it was a mixture, the presence of two methyl singlets at δ 0.77 and 0.91 (ca. 2:1 ratio) in its ^{1}H nmr spectrum indicated that *both* of the components had resulted from *ring* C—H insertion rather than methyl C—H insertion. The third product, however, which was produced in 28% yield, lacked a singlet in its ^{1}H nmr spectrum, as expected for methyl insertion, and this compound was therefore assigned the structure of the desired product, norishwarane (**20**), possessing the complete ring system of ishwarane itself (**1**) but divested of the three methyl groups of the natural product.[18] As in the case of the Paquette study (30), mass balance considerations led us to tentatively propose that while the two ring C—H insertion products were derived only from the undesired α dibromocarbene adduct (concave attack on octalin **18**), norishwarane (**20**) was the exclusive product from intramolecular insertion of cyclopropylidene (**21**) (corresponding to **8**). These conclusions, on

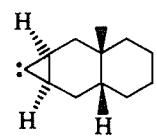

21

the other hand, would appear to imply that the preferred attack of dibromocarbene on octalin **18** is from the (presumably more hindered) concave face of the olefin, a seemingly untenable inference. For this reason, it is believed that at least a portion of one or both of the ring C—H insertion products was derived from the β dibromocyclopropane. Possible factors responsible for this observation, which contradicts Paquette's findings for the simpler 4-methylcyclohexene adduct, are discussed below.

Whatever the causes of the mixed results of this model study, the production of even some of the desired norishwarane was at least encouraging, and a means of inserting the carbon atom in a *single* step, as opposed to the two-step sequence required

[13]For recent applications of this procedure see ref. 32.

[14]Other instances of preferential insertion into primary C—H bonds have been reported (33). This amounts, in this case, to insertion of the cyclopropylidene into a δ C—H bond. For other examples see ref. 34.

[15]For recent work on the elucidation of the nature of this intermediate see ref. 36. For a review of the chemistry of lithium halocarbenoids see ref. 37.

[16]For a recent discussion of the selectivity of the insertion of cyclopropylidenes into C—H bonds see ref. 38.

[17]A 0.2 in × 10 ft copper column packed with 10% SE-30 on Diatoport S was employed at 200°C.

[18]For further proof of this structure by ^{13}C nmr see ref. 39.

Can. J. Chem. Downloaded from www.nrcresearchpress.com by 210.87.254.105 on 09/06/12
For personal use only.

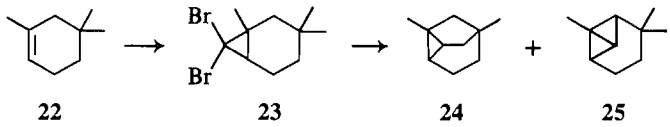

22 23 24 25

SCHEME 4. Carbon atominsertion model study.

by the Moore procedure, was devised to avoid the isolation and purification of the heat sensitive dibromocyclopropane intermediate. Our one-step method is based on the Skattelbøl allene synthesis (40)[19], in which an olefin is converted to the corresponding allene by insertion of a carbon atom between the two carbons of the olefinic double bond. This procedure involves treatment of the olefin with carbon tetrabromide and excess methyllithium at low temperatures, thus generating dibromocarbene by lithium–bromine exchange[20] and converting the resulting dibromocyclopropane *in situ* to the cyclopropylidine, which collapses to the allene. Encouraged by the fact that an excess of cyclohexene had previously been found to give a low yield of the corresponding dibromocyclopropane on reaction with carbon tetrabromide and *n*-butyllithium at −50°C (42), we chose to investigate the use of carbon tetrabromide as a carbon atom equivalent for insertion into cyclohexenes in a single step. In order to allow for the maximum chance of success, a cyclohexene having a methyl substituent on at least one of the olefinic carbons was desirable in view of the higher reactivity toward dichlorocarbene offered by methylcyclohexene over cyclohexene itself (43)[21]. Such a substrate would have the added advantage of having an olefinic group identical in structure to that of the proposed ishwarone precursor, **5**. Furthermore, a cyclohexene having *two* methyl groups at the 4-position, so that *cis* and *trans* dibromocyclopropanes are not possible, would not suffer from any lack of stereoselectivity of the dibromocarbene addition, as do addition to 4-methylcyclohexene and, apparently, octalin **18**.

Accordingly, the substrate chosen for the model study of the one-step carbon atom insertion was 1,5,5-trimethylcyclohexene (**22**), which was obtainable (47) from isophorone as an 85:15 mixture with 1,3,3-trimethylcyclohexene (**26**).[22] Initially, the Moore two-step procedure was tested on this material to serve as a benchmark for comparison with the proposed one-step method (Scheme 4). Thus, treatment of the olefinic mixture of **22** and **26** with bromoform and aqueous base under the same conditions as for octalin **18** (35) gave a 45% yield of dibromocyclopropane **23**, while the more hindered olefin **26** was recovered unchanged. Debromination of **23** with methyllithium at −10°C produced not one product, as expected on the basis of Paquette's earlier report on 4-methylcyclohexene, but *two* tricyclic hydrocarbons: only a 21% yield of the expected tricyclo[3.2.1.$0^{2,7}$]octane **24** and a surprising 33% yield of the

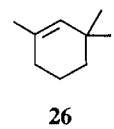

26

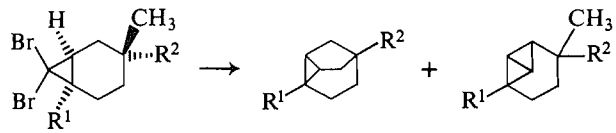

27 28 29

(**a**, R' = Me, R^2 = H; **b**, R' = H, R^2 = Me; **c**, R' = Me, R^2 = Me)

tricyclo[4.1.0.$0^{2,7}$]heptane **25** (yields determined by gas chromatographic analysis).[23] Paquette and Taylor (49) have since found similar behavior for the dibromocyclopropanes **27**, which provide mixtures of tricyclooctane **28** and tricycloheptane **29** on reaction with methyllithium. Both we (50) and these authors have ascribed this increased tendency toward *ring* C—H insertion (vis-à-vis *cis*-**11**) at least partly to a ponderal effect in which additional substituents slow down the rate of conformational interconversion of the intermediate cyclopropylidenes to such an extent that ring C—H insertion becomes competitive with the faster methyl C—H insertion. The latter, however, can only occur when the methyl into which insertion is possible is oriented axially (as in **15**). The behaviour of the dibromocyclopropane (**19**) derived from octalin **18** can be attributed to the same sort of competition between C—H insertion and conformational mobility. In fact, it is the parent 4-methylcyclohexene-derived dibromocyclopropane **11** which is the anomaly, such that ring flipping is apparently *faster* than ring C—H insertion in the intermediate cyclopropylidene (**15**), thus allowing methyl insertion to take over completely. At any rate, these results did not deter us from the pursuit of our goal since, as mentioned above, the conformation shown for the proposed intermediate cyclopropylidene **8** was expected to greatly predominate.

Suitable conditions for the *one*-step conversion of cyclohexene **22** to the carbon atom insertion products **24** and **25** were found after a number of unsuccessful experiments, and it appears on the basis of these results that the reaction is quite sensitive to temperature and concentration. For example, when a solution of cyclohexene **22** and an equimolar amount of carbon tetrabromide in diethyl ether at −78°C was treated with an equimolar amount of methyllithium, and the mixture was stirred at that temperature for 1.5 h and then allowed to warm to 0°C, followed by addition of a *second* equimolar quantity of methyllithium, the tricyclic products **24** and **25** were obtained in 17% and 39% yields (by gas chromatographic analysis), respectively. These yields were, even at this level of development, a significant improvement over the overall yields from the Moore two-step procedure (9% and 15%, respectively), but further increases were observed when a more dilute solution in diethyl ether was used, amounts of carbon tetrabromide and methyllithium were *doubled*, and the second addition of methyllithium was carried out at −30°C instead of 0°C. Under these optimum conditions (17) not only the total yield of carbon atom insertion products, but also the relative proportion of the desired tricyclooctane (**24**) was increased, such that **24** and **25**

[19]For more recent applications of this reaction see ref. 41.

[20]For the determination of the structure of the intermediates in this reaction by ^{13}C nmr see refs. 36 and 44.

[21]Methylcyclohexene is 8.43 times more reactive than cyclohexene toward dichlorocarbene generated from chloroform and potassium *tert*-butoxide, as quoted in ref. 45. Although the sensitivity of dibromocarbene to electronic effects (greater reactivity toward more electron-rich olefins) is somewhat attenuated by steric hindrance, relative to the chlorine analogue, this factor is not so important as to override the electronic one in the cases studied thus far (46).

[22]These olefins, commonly known as α- and β-cyclogeraniolene, occur in the defense secretions of the major soldiers of the African termite *Ancistrotermes cavithorax* (48).

[23]For spectral data establishing the structure of these compounds see refs. 17 and 39.

Can. J. Chem. Downloaded from www.nrcresearchpress.com by 210.87.254.105 on 09/06/12
For personal use only.

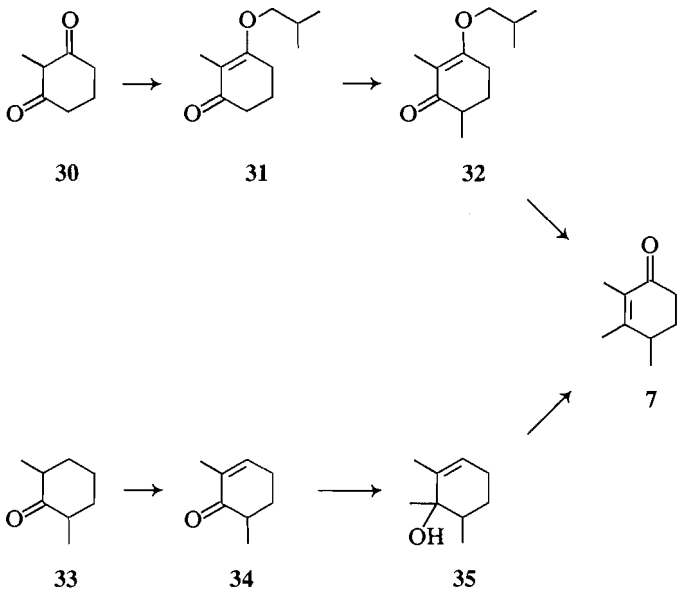

SCHEME 5. Synthesis of 2,3,4-trimethylcyclohexenone.

were obtained in a combined yield of 80%, containing *equal* amounts of the two isomers. Thus our one-step method is, at least in this case, far superior to the Moore two-step sequence, being much more convenient and providing a greater than 300% enhancement in the yield of the ishwarane model compound, **24**. This new synthetic method, which accomplishes the insertion of a single carbon atom into a molecule by addition to a C—C double bond and insertion into a C—H bond in one smooth operation, thereby forming a tricyclic system from a monocyclic one, will hereafter be referred to as *carbon atom insertion bicycloannulation* (CAIB).[24]

Total synthesis of ishwarone

Although cyclohexenone **7** (53) (Scheme 1) had been prepared from Hagemann's ester (54), the low yield of this process (16%) dictated a search for a more efficient route. We therefore explored two relatively new methods which held out the promise of higher yields (Scheme 5). The first of these, based on a sequence suggested by Stork and Danheiser (55), involved kinetically controlled methylation of enol ether **31** to give **32**, which was then converted to cyclohexenone **7** by addition of methyllithium and hydrolysis.[25] The overall yield from the relatively expensive dione, **30**, was a respectable 74%. However, a more economical approach proved to be by way of the allylic oxidation method of Dauben and Michno (56). Thus, chlorination–dehydrochlorination (57) of 2,6-dimethylcyclohexenone (**33**), followed by addition of methyllithium to the resulting cyclohexenone, **34**, provided allylic alcohol **35**, which without purification was directly converted to cyclohexenone **7** by PCC oxidation. In this case the overall yield of **7** from cyclohexenone **33** was 48%, but the greater convenience and less expensive materials used for this sequence made it the method of choice for large scale preparations of **7**.

[24]To the best of our knowledge, only one other type of CAIB has been reported, the Katz-Cheung bicycloannulation of aromatic and other conjugated carbanions (51). For recent applications of this highly useful reaction see ref. 52.

[25]Following our preliminary publication in which this synthesis was described (14), the same route to enol ether **32** was reported by Piers *et al.*, and experimental details have been provided by them (58).

A suitable chemical realization of synthon **6** (Scheme 1) having an intact double bond might be the complex organocuprate **36**, in which the alkoxide moiety is present in the

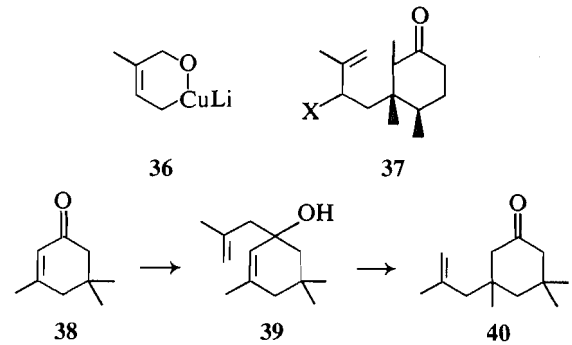

capacity of a latent leaving group (59). Athough it is even conceivable that such a conversion of cyclohexenone **7** to octalone **5** could be carried out in a single pot, where the initial conjugate addition of the organocopper moiety would be followed by addition of a sulfonyl chloride and *in situ* formation of a sulfonate leaving group, our experiments with model compounds did not prove sufficiently promising to justify a full investigation of any version of this plan.

However, a less direct implementation of the protocol embodied in synthon **6** was ultimately successful (Scheme 6).[26] The organocuprate **42** (R = $CH_2CH_2C(CH_3)CH_2$) was prepared without incident from homoallyl iodide **41** (64) by addition of *tert*-butyllithium at −78°C followed by copper(I) iodide at −50°C.[27] Addition of cyclohexenone **7** to the resulting solution in diethyl ether at −45°C and aqueous work-up gave a 45% yield (60% based on consumed **7**) of the keto-olefin, **43**, after chromatography on alumina. Athough this product appeared to be a mixture of epimers by nmr, the major component is believed to have the stereochemistry shown. This assumption is based partly on the previously known preference for attack of organocuprates on 3,4-dimethylcyclohexenone (**44**) to give the

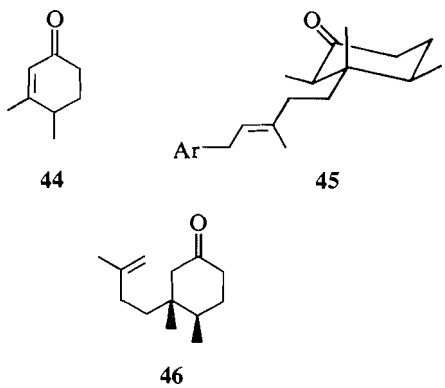

[26]An alternative approach would have involved an allylic precursor, **37**, which was intended to undergo an internal S_N2' ($S_{cN'}$) reaction (60) on treatment with base. Unfortunately, this plan was thwarted at an early stage when it was found in a model study that the anionic oxy-Cope rearrangement (61) of the tertiary allylic alcohol, **39**, prepared from isophorone (**38**) and allyl magnesium chloride, gave mainly isophorone and only a 14% yield of the desired ketone, **40**. The primary pathway of this reaction is thus a β hydroxy olefin cleavage (62) and this has also been observed by Evans *et al.* as a side reaction in some of their anionic oxy-Cope rearrangements with compounds closely related to allylic alcohol **39** (63).

[27]For recent applications employing this same cuprate see ref. 65.

Can. J. Chem. Downloaded from www.nrcresearchpress.com by 210.87.254.105 on 09/06/12
For personal use only.

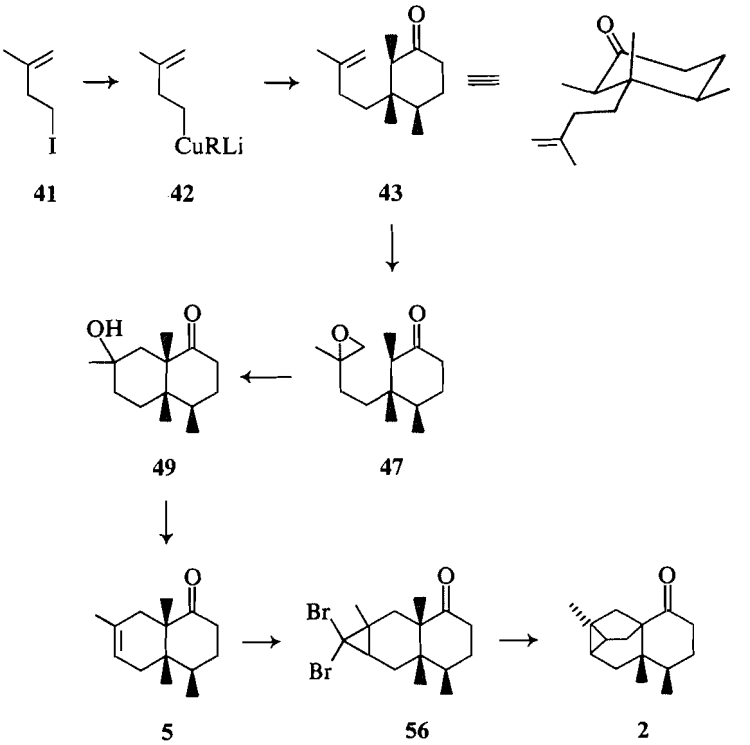

SCHEME 6. Total synthesis of ishwarone.

adduct having *cis* methyl groups with high stereoselectivity (66, 67), and partly on the occurrence of a high field singlet absorption in the nmr at δ 0.57 attributable to an axial methyl at C-3 shielded by the carbonyl group (cf. the microbial metabolite **45**, in which the corresponding absorption appears at δ 0.55 (68)). An attempt to develop a more efficient synthesis of keto-olefin **43** via trapping of the intermediate enolate from addition of **42** to cyclohexenone **44** with methyl iodide (69) produced only the adduct, **46**, none of the desired methylation being observed. Similar lack of success has been obtained in closely related studies by Mori and Fujioka with the same substrate (70).

Epoxidation of keto-olefin **43** with *m*-chloroperbenzoic acid was not accompanied by any detectable amounts of lactones resulting from Baeyer–Villiger oxidation, giving the desired keto-epoxide (**47**) as a mixture of diastereomers.[28] Direct treatment of this mixture, without purification, with potassium *tert*-butoxide in *tert*-butyl alcohol at reflux provided a crude mixture of keto-alcohols which, as a solution in cyclohexane, was subjected to dehydration with 50% aqueous sulfuric acid (25*a*). The major product of these reactions (38% from keto-epoxide **47**) was shown to be a 4.3:1 mixture of the desired octalone, **5**, and its position isomer, **48**, by spectrosopic analysis and ultimate conversion of **5** to ishwarone (**2**). It therefore follows that the major product of the base-catalyzed cyclization was keto-alcohol **49** (presumably as a mixture of diastereomers). However, this compound was accompanied by minor quantities of keto-alcohol **50**, which survived the dehydration conditions used here as a result of its being a primary alcohol. It was therefore convenient to wait until this stage for purification of the intermediates, since octalone **5** was easily separated from keto-alcohol **50** by chromatography on alumina. Although, in the absence of definite information as to the stereochemistry of keto-alcohols **49** and **50** and their precursors, it is not possible to speculate on the factors responsible for the observed low regioselectivity for attack of the enolate moiety of intermediate **51** on the primary carbon of the epoxide moiety, the formation of the five-membered ring of **50** by attack on the tertiary carbon of the epoxide was not surprising in light of previous studies of epoxide – keto-enolate cyclizations (25*a*, 66, 71). However, it is worthy of note that the analogous cyclization of the epoxy-lactam **52** with sodium hydride in benzene has been reported to form exclusively a six-membered ring, giving hydroxy-lactam **53** (72).

With the obtention of octalone **5** the Diels–Alder equivalent

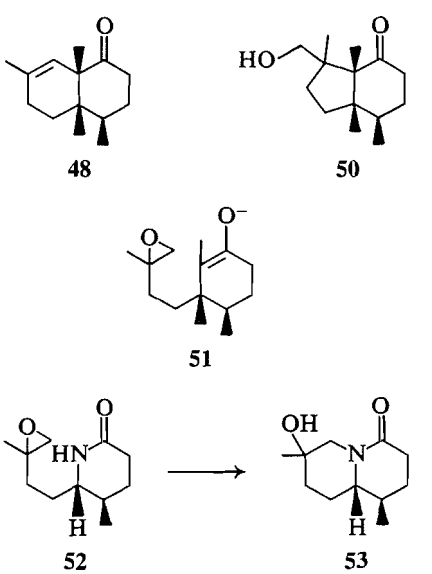

[28]For a more recent, closely related sequence from cyclohexenone **44** see ref. 67.

Can. J. Chem. Downloaded from www.nrcresearchpress.com by 210.87.254.105 on 09/06/12
For personal use only.

Can. J. Chem. Downloaded from www.nrcresearchpress.com by 210.87.254.105 on 09/06/12
For personal use only.

sequence, which represents overall addition of isoprene to cyclohexenone **7** in a specific regiochemical and stereochemical sense, was complete. It remains to be seen how general this process will be in view of the mixture of products obtained in the epoxide cyclization, but the loss of almost half of the material through formation of the side product, **50**, was not so discouraging as to deter us from our goal. Accordingly, the stage was now set for the proposed CAIB of octalone **5**, which was designed to give ishwarone (**2**) in a single step. In spite of the presence of the carbonyl group and the potential for addition of methyllithium or other carbanionic intermediates to it during the application of our new CAIB method, we were led to believe that protection of the ketone function would not be necessary by a report from Sydnes and Skattebøl (73) describing the reaction of methyllithium with dibromocyclopropyl ketones to give exclusively C—H insertion products resulting from bromine–lithium exchange, none of which involved attack at the carbonyl group.[29] Nevertheless, treatment of octalone **5**[30] with carbon tetrabromide and methyllithium under the conditions established in the model studies gave only intractable material.

Accordingly, although the reasons for the failure of the CAIB were not understood, it was decided that the carbonyl group of octalone **5** should be reduced to the alcohol in the hope that the resulting octalol, **54**, would undergo the desired CAIB to give ishwarol (**3**). Reduction of the mixture of octalones **5** and **48** with lithium aluminium hydride gave a mixture of octalols **54** and **55**, the ^{1}H nmr spectrum of which showed a

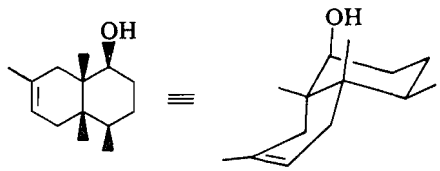

54

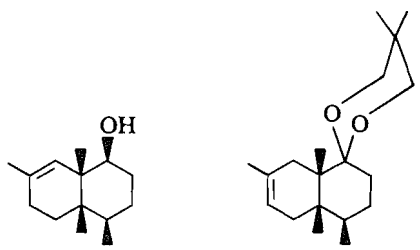

55 **57**

triplet (J = 3Hz) at δ 3.37 for the carbinol C—H, indicating an axial hydroxyl group for the major component, **54**. Since the spectrum of ishwarol (**3**) exhibits a very similar absorption, and it has been obtained by hydride reduction of ishwarone (**2**) (8*a*, 9), it was apparent that attack of the hydride had occurred on the α side of the octalone, away from the hindering methyl groups, as expected. Thus, it can be concluded that **54** has the conformation shown, and, assuming the corresponding intermediate carbenoid in the CAIB adopts an analogous one, intramolecular C—H insertion should occur at the desired methyl group as in Scheme 2. Again, however, attempted CAIB with **54** under our standard conditions failed to produce any identifiable materials.[31]

It would thus appear that our CAIB method is considerably more limited than we had hoped, and that the success or failure of carbon atom insertion with methyllithium – carbon tetrabromide is dependent to a large extent on the structure of the olefinic reactant and other functional groups present. Be that as it may, there was still a chance that the two-step procedure involving bromoform/base followed by lithium–bromine exchange with the resulting dibromocyclopropane could convert our intermediate octalone, **5**, to ishwarone and (or) the corresponding octalol, **54**, to ishwarol. In the latter case, reaction of the octalol with bromoform and aqueous base under the same phase-transfer conditions used for octalin **18** gave a crude tarry product, the nmr of which indicated that the alcohol group was no longer present.[32] Ketones, on the other hand, are generally somewhat less reactive under these conditions than alcohols are (78, 79), and treatment of the mixture of octalones **5** and **48** with bromoform and aqueous sodium hydroxide in the presence of tributylamine (80) gave dibromocyclopropane **56** mixed with unreacted **48**, as expected. When this crude mixture was treated with methyllithium in ether at −10°C, and the crude products were subjected to gas chromatographic analysis, a small amount of material having the same retention time as that of authentic ishwarone (**2**)[33] was collected. This proved to be a mixture, but preparative thick-layer chromatography enabled the separation of a minute amount of material having spectroscopic properties (^{1}H and ^{13}C nmr) identical with those of the authentic ishwarone. Athough the yield of this reaction, and therefore of the overall total synthesis, was very low, the synthesis from the cyclohexanedione, **30**, or the cyclohexenone, **33**, consisted of only nine steps, comparing favourably, in length, at least, with the previously reported synthesis of racemic ishwarone, which required some 19 steps from cyclohexenone **44** (13).

Total synthesis of ishwarane

In spite of the failure of our CAIB method in the synthesis of ishwarone, we were confident that the procedure would be

[29]More recently, mixed results have been obtained with other dibromocyclopropyl ketones (74). For a review of the generation and reactions of carbenes and carbenoids having neighbouring heteroatoms see ref. 75. Adding further complexity to this subject, it has been found that bromolithiocyclopropanes can be induced to add intermolecularly to ketones and aldehydes (76). It thus would appear that the course of reaction which a given substrate takes is dependent to a large extent on its structure and the conditions. In any case the carbonyl group of octalone **5** is a very hindered one, and no interference with the CAIB was expected from it.

[30]The mixture of octalones **5** and **48** was used due to the difficulty in separating these isomers and in the expectation that **48** would be unreactive, as was the analogous olefin, **26**.

[31]Mixed results have been obtained regarding the reactivity of hydroxyl groups under the conditions of alkyllithium-induced bromine–lithium exchange in dibromocyclopropanes (75, 77). Protection of the carbonyl group of octalone **5** as the ketal (**57**) also failed to enable the CAIB.

[32]Although phase transfer catalyzed addition of dibromocarbene to the double bond of olefinic alcohols can usually be accomplished without interference, reaction of dibromocarbene and dichlorocarbene with alcohols is known to give a variety of products, most based on "deoxidation" to carbocations (78). We have also demonstrated that cyclohexanol gives 7,7-dibromonorcarane under the same conditions, presumably by way of cyclohexyl cation and dibromocarbene addition to cyclohexene resulting from loss of a proton from the carbocation.

[33]We are greatly indebted to Dr. P. C. Parthasarathy, C.I.B.A.–Geigy Research Centre, Bombay, for generous samples of ishwarone and ishwarane.

Can. J. Chem. Downloaded from www.nrcresearchpress.com by 210.87.254.105 on 09/06/12
For personal use only.

viable for the corresponding hydrocarbon since it seemed reasonable to assume that the difficulties which prevented us from using it for ishwarone and ishwarol were somehow associated with the presence of the functional groups, and since our model studies, which were carried out on hydrocarbons (e.g. **22**), had already proven the utility of the CAIB methodology. Although the octalin, **62** (Scheme 7), required for a CAIB synthesis of ishwarane (**1**) could conceivably have been prepared from octalone **5** by Wolff–Kishner reduction, the length of the sequence leading to **5** as well as the loss of considerable material at the epoxide cyclization stage dictated a search for more efficient possibilities for the synthesis of the octalin.[34]

The ultimately successful plan (Scheme 7),[35] involved conjugate addition of a methyl group to the octalone, **59**, which has also been employed in two other syntheses of ishwarane (12), followed by addition of a methyl group to the carbonyl of the resulting decalone, and dehydration. When the octalone, **59**, obtainable stereoselectively by the elegant method of Boeckman *et al.* (83)[36] was treated with lithium dimethylcuprate – dimethyl sulfide complex (84), the desired decalone, **60**, was obtained in 77% yield. The assignment of the *cis* stereochemistry to this decalone was based on the eventual success of the total synthesis as well as literature precedent (25*c*, 81*h*). Addition of methyl magnesium iodide gave a mixture of tertiary alcohols, **61**, which, without purification, was dehydrated

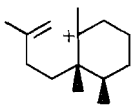

58

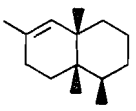

63

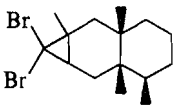

64

as for the analogous ishwarone intermediate, **49**, providing an 87% yield of a 1:1 mixture of octalins **62** and **63**. Although these isomers could not be separated, as was the case with octalone **48**, octalin **63** has the more hindered olefinic group and thus would not be expected to react with dibromocarbene in the next step.

With octalin **62** in hand, the stage was set for the application

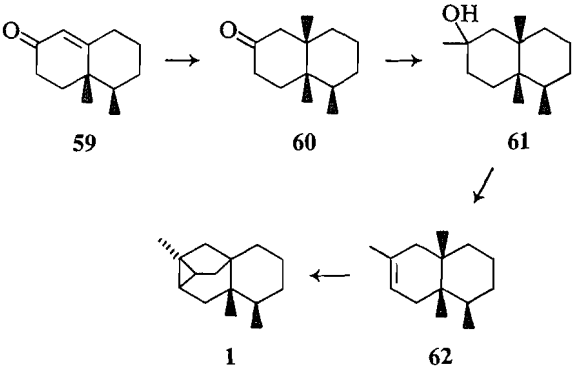

59 **60** **61**

1 **62**

SCHEME 7. Total synthesis of ishwarane.

of our CAIB reaction, and, indeed, treatment of the mixture of octalins **62** and **63** with carbon tetrabromide and methyllithium under the standard conditions gave a mixture of isomeric hydrocarbons from which ishwarane (**1**), identical with an authentic sample,[33] was separated in 20% yield using gas chromatography[37]. Thus, the total synthesis of ishwarane was accomplished in remarkably few steps, namely four from octalone **59**, compared with 12 steps for the Hagiwara synthesis (12*a*) and 10 steps for the Kelly synthesis (12*b*). Unfortunately, the nature of the side products of the CAIB step are not known, since they could not be separated from each other, but it is clear that ishwarane was formed in fairly good yield from octalin **62**, in view of the fact that a 40% yield of octalin **63** was recovered from the reaction.

In summary, the CAIB method that we have developed for the synthesis of the tricyclo[3.2.1.$0^{2,7}$]octane ring system seems to be useful only in cases in which (a) the cyclohexene substrate bears an alkyl substituent on the double bond and (b) there are no interfering functional groups in the substrate, ketone and alcohol groups being the two which we have shown to be detrimental. In the proper cases, limited though they may be, it is clear that CAIB can save a tremendous amount of time and materials over more traditional, multistep procedures.

Experimental

General

All reactions were conducted under a positive pressure of argon. Ethyl ether (when used as a reaction solvent), tetrahydrofuran, and 1,2-dimethoxyethane were distilled from sodium–benzophenone, diisopropylamine and *tert*-butyl alcohol were distilled from calcium hydride, and hexamethylphosphoramide was distilled from 13× molecular sieves. Methyllithium (in ethyl ether), *n*-butyllithium (in hexane), and *tert*-butyllithium (in pentane) were obtained from Ventron. These solutions were titrated (85) with 2-butanol in xylene (bipyridyl indicator) before use.

Preparative thick-layer chromatography was performed on precoated E. Merck silica gel GF (2 mm thick) on glass plates. Ethyl acetate was used to extract the separated components from the silica gel. Gas chromatography was carried out by using 1.5% OV-101 on Chromosorb G (100/120 mesh) in a 0.2 in. × 6 ft stainless-steel column with a helium flow rate of 60 mL/min unless otherwise noted.

[34]Although one could argue that a total synthesis of ishwarane is a redundant exercise at this point,[8] the unsatisfactory yield of the last step in our synthesis of ishwarone and a desire to put our new CAIB method to good use were sufficient reasons to approach ishwarane via octalin **62**.

[35]An alternative approach would have involved a carbocation–olefin cyclization (81) of tertiary carbocation **58** followed by loss of a proton to give **62**. Unfortunately, however, this plan was thwarted at an early stage by the fact that when cyclohexenone **16** was treated with lithium dimethyl cuprate in diethyl ether at 0°C, the solvent was replaced by 1,2-dimethoxyethane, and the resulting solution of enolate was treated with iodo alkene **41**, the major product isolated was that of simple conjugate addition, 2,3-dimethylcyclohexenone, very little alkylation of the enolate having taken place. This undesired result can be attributed at least in part to β elimination from the homoallylic iodide, **41**, (thus providing a source of protons for ketonization of the enolate) under the highly basic conditions of the reaction, although other workers have reported no problems with the same alkylating reagent and related carbanionic substrates (64, 82).

[36]This octalone was prepared, in the early stages of our work, by the method of Kelly and Zamecnik (12*c*), but we later found the more selective Boeckman sequence to be somewhat more satisfactory. We are most grateful to Yousry M. A. Naguib for the preparation of sufficient quantities of octalone **59**.

[37]In one small-scale experiment, probably due to loss of methyllithium during addition, the intermediate dibromocyclopropane, **64**, was isolated and could be completely characterized. It appeared to be a mixture of diastereomers, indicating that the addition of dibromocarbene to the octalin was non-stereoselective (cf. addition to octalin **18**) and presumably accounting for at least some of the side products accompanying the formation of ishwarane in the C—H insertion step.

Can. J. Chem. Downloaded from www.nrcresearchpress.com by 210.87.254.105 on 09/06/12
For personal use only.

Nuclear magnetic resonance (nmr) spectra were recorded on a Varian Model HA-100 or Model XL-100 spectrometer, and proton and carbon-13 chemical shifts are reported in parts per million (δ) downfield from internal tramethylsilane. Infrared (ir) spectra were obtained on a Perkin–Elmer Model 621 spectrophotometer, and mass spectra (ms) were determined on a Varian MAT Model 311A spectrometer employing an ionizing voltage of 70 eV. Melting and boiling points are uncorrected.

Cis-9-Methyl-2-octalin (18)

A solution of 22.3 g (0.136 mmol) of octalone **17** (19) and 150 mL of hydrazine hydrate (99%) in 750 mL of diethylene glycol was heated at 120°C for 11 h. After the resulting solution had been allowed to cool, 94 g of potassium hydroxide was dissolved in it, and the temperature of the oil bath was slowly raised to 210°C over 1 h during which water was removed in a flow of argon and condensed. The mixture was then heated at 210°C for 3 h, cooled, and poured into water. The aqueous phase was extracted with petroleum ether (boiling range 30–60°C) and the combined extracts were washed with water and saturated aqueous sodium chloride and dried over anhydrous sodium sulfate. The aqueous distillate carried over in the initial heating with hydroxide was worked up in the same manner, and the resulting extracts were combined with the others. The solvent was removed by distillation through a Vigreux column, and the residue was distilled to give 12.0 g (59%) of the octalin (**18**); bp 55–58°C/6 Torr (1 Torr = 133.32 Pa) nmr as previously reported (86).

*2,3-(Dibromomethano)-9-methyl-*cis*-decalin (19)*

To a solution of 2.00 g (13.3 mmol) of octalin **18**, 2.33 mL (6.74 g, 26.7 mmol) of bromoform, 27 mg of benzyltriethylammonium chloride, and 0.054 mL of ethanol was added dropwise, with stirring and cooling, 6.7 mL of 50% aqueous sodium hydroxide over 10 min, while the temperature of the mixture was maintained at 40–45°C. The mixture was stirred vigorously for 3 h at 40–45°C, during which 1.5 mL of methylene chloride was added to prevent the emulsion from becoming too thick, and it was then partitioned between 50 mL of water and 25 mL of methylene chloride. The aqueous phase was extracted with methylene chloride (2 × 25 mL), and the combined extracts were washed with 25 mL of water; 25 mL of 5% aqueous hydrochloric acid, another 25 mL of water, and 25 mL of saturated aqueous sodium chloride and dried over anhydrous sodium sulfate. The solvent was evaporated under reduced pressure, and the residue was subjected to bulb-to-bulb distillation to give 2.06 g (48%) of dibromocyclopropane **19** as a colorless oil; bp 75°C/0.05 Torr; ^{1}H nmr (CCl_4) δ: 0.93 (s, 3H); ms *m/e* (relative intensity): 41(51), 55(48), 67(62), 81(100), 95(48), 109(70), 123(40), 135(29), 149(65), 161(37), 210(10), 212(19), 214(9), 305(15), 307(31), 309(15), 320(5, M^+), 322(11, M^+), 324(5, M^+); high resolution ms, *m/e* calcd. for $C_{12}H_{18}Br_{12}$: 321.9755; found: 321.9799.

Norishwarane (20)

To a solution of 1.54 g (4.8 mmol) of dibromocyclopropane **19** in 8.5 mL of ethyl ether at −10°C was added dropwise, with stirring 3.7 mL of 1.5 *M* methyllithium (5.5 mmol) over 2.5 h. After the resulting yellow solution had been stirred at −10°C for an additional 30 min, followed by 1 h of stirring at room temperature, it was recooled to 5°C and 10 mL of water was added dropwise, with stirring. The aqueous phase was extracted with 10 mL of ethyl ether and the combined extracts were washed with 10 mL of saturated aqueous sodium chloride and dried over anhydrous sodium sulfate. The solvent was removed by distillation through a Vigreux column, and bulb-to-bulb distillation of the residue gave 0.60 g (77%) of colorless oil; bp 70°C/5 Torr. This material was then subjected to preparative gas chromatography,[38] which gave two peaks at 32 min and 39 min with relative areas of 64% and 36%, respectively. The first of these appeared to be a 2:1 mixture of two isomers of norishwarane resulting from ring C—H insertion as judged from its nmr and ms data; ^{1}H nmr ($CDCl_3$) δ: 0.77 (s, larger of the two singlets), 0.91 (s), 1.82 (d, J = 12 Hz); ^{13}C nmr ($CDCl_3$) δ: 5.1, 7.0, 11.5, 13.8, 18.6, 19.1, 22.2, 22.4, 22.9, 23.0, 26.3, 27.3, 27.5, 27.6, 27.7, 29.9, 30.4, 30.5, 32.1, 34.9, 37.8, 38.0, 38.8, 41.0, 42.1, 53.6; high resolution, ms, *m/e* calcd. for $C_{12}H_{18}$: 162.1409; found 162.1411. The component with a retention time of 39 min was norishwarane (**20**); ir (CCl_4): 3040 cm^{-1}; ^{1}H nmr ($CDCl_3$) δ: 0.62 (m, 1H), 1.97 (d, J = 11.5 Hz, 1H); ^{13}C nmr ($CDCl_3$) δ: 13.1, 16.7, 17.7, 23.9, 26.4, 26.6, 29.9, 32.1, 37.2, 39.2, 40.2, 41.6; ms *m/e* (relative intensity): 67(25), 79(61), 95(70), 108(25) 120(76), 133(40), 147(18), 162(100, M^+); high resolution ms, *m/e* calcd. for $C_{12}H_{18}$: 162.1409; found: 162.1408.

1,3,3-Trimethyl-7,7-dibromobicyclo[4.1.0]heptane (23)

To a mixture of 4.0 g (32 mmol) of bromoform, 2.0 g (16 mmol) of 1,5,5-trimethylcyclohexene (**22**) (47) (containing 15% of the isomer, 1,3,3-trimethylcyclohexene, **26**), and 0.032 g of benzyltriethylammonium chloride was added dropwise, with stirring, 8 mL of 50% aqueous sodium hydroxide over 10 min, keeping the temperature in the range 40–45°C by means of a cold water bath. Stirring was continued at this temperature for 3 h, and the mixture was then poured into 250 mL of water. The aqueous phase was extracted with methylene chloride and the combined extracts were washed with water, dilute aqueous hydrochloric acid, and more water and dried over anhydrous sodium sulfate. The solvent was removed by distillation, and distillation of the residue gave 1.8 g (45%) of dibromocyclopropane **23**: bp 60°C/0.25 Torr; ir (CCl_4): 1370, 1390 cm^{-1}; ^{1}H nmr ($CDCl_3$) δ: 0.85 (s, 6H), 1.45 (s, 3H); ms *m/e* (relative intensity): 55(65), 69(100), 84(89), 91(50), 107(27), 123(71), 135(65), 147(15), 159(24), 173(24), 199(18), 215(33), 226(18), 281(11), 296(5, M^+).

1,5-Dimethyltricyclo[3.2.1.0^{2,7}]octane (24) and 1,3,3-trimethyltricyclo[4.1.0.0^{2,7}]heptane (25)

To a solution of 1.0 g (3.5 mmol) of dibromocyclopropane **23** in 6 mL of ethyl ether at −10°C was added dropwise, with stirring, 2.6 mL (3.9 mmol) of a 1.5 *M* solution of methyllithium in ethyl ether over 2 h. Stirring was continued for 1 h after the addition was complete, and 6 mL of water was then added. The organic layer was washed with saturated aqueous sodium chloride, dried over anhydrous sodium sulfate, and concentrated by distillation. The residue was subjected to preparative gas chromatography, and yields of 21% for **24** and 33% for **25** were determined using *trans*-decalin as internal standard; spectral data as previously reported (17).

2,3,4-Trimethylcyclohex-2-en-1-one (7)

(a) To a solution of 32.5 g (0.166 mol) of 3-isobutoxy-2,6-dimethylcyclohex-2-en-1-one (**32**) (14, 58) in 300 mL of ethyl ether at 0–4°C was added dropwise, with stirring, 130 mL of 1.5 *M* methyllithium (0.195 mol) over 2 h. After the solution had been allowed to stir at room temperature for 13 h, 1.15 L of 5% aqueous hydrochloric acid was added slowly, and the resulting mixture was stirred vigorously for 3.5 h. The aqueous phase was extracted with petroleum ether (boiling range 30–60°C) and the combined extracts were washed with saturated aqueous sodium bicarbonate and saturated aqueous sodium chloride and dried over anhydrous sodium sulfate. The solvent was evaporated under reduced pressure, and the remaining yellow oil was distilled to give 20.0 g (87%) of enone **7**; bp 103–108°C/15 Torr (lit. (54) bp 93–98°C/8 Torr); ir and nmr as previously reported (53); ms *m/e* (relative intensity): 67(77), 81(55), 96(95), 110(59), 123(23), 138(100, M^+); high resolutions ms, *m/e* calcd. for $C_9H_{14}O$: 138.1045; found: 138.1047.

(b) To a solution of 50.5 g (0.40 mol) of 2,6-dimethylcyclohexanone in 200 mL of carbon tetrachloride was added dropwise, with stirring and cooling with a room temperature water bath, 35.5 mL (59.4 g, 0.44 mol) of sulfuryl chloride in 60 mL of carbon tetrachloride over 75 min, while the evolved hydrogen chloride and sulfur dioxide were removed with an aspirator trap. After the mixture had been stirred for an additional 2 h, it was washed with water (3 × 60

[38]A 0.2 in. × 10 ft copper column packed with 10% SE-30 on Diatoport S was employed at 135°C.

Can. J. Chem. Downloaded from www.nrcresearchpress.com by 210.87.254.105 on 09/06/12
For personal use only.

mL), saturated aqueous sodium bicarbonate (2 × 60 mL), and 60 mL of saturated aqueous sodium chloride and dried over anhydrous sodium sulfate and anhydrous magnesium sulfate. The solvent was distilled off using a Vigreux column, first at atmospheric pressure and then at aspirator pressure, to give the crude chloro ketone which was used directly for the next step. This material was combined with 10.4 g (0.245 mol) of lithium chloride in 100 mL of *N,N*-dimethylformamide, and the mixture was heated at 100°C for 50 min, after which it was cooled to room temperature and added to a mixture of 400 mL of ethyl ether and 400 mL of 2.5% aqueous sulfuric acid. The resulting mixture was stirred vigorously for 4 h, and the aqueous phase was saturated with sodium chloride and extracted with ethyl ether (1 × 100 mL and 3 × 70 mL). The combined extracts were washed with saturated aqueous sodium bicarbonate (2 × 100 mL) and saturated aqueous sodium chloride (2 × 100 mL) and dried over anhydrous sodium sulfate and anhydrous magnesium sulfate. The solvent was removed by distillation through a Vigreux column, and the residue was distilled to give 39.9 g (80%) of 2,6-dimethylcyclohex-2-en-1-one (**34**); bp 71–82°C/15–16 Torr (lit. (87) bp 72–74°C/13 Torr); nmr and ms as reported previously (88).

To this lot of enone **34** in 400 mL of ethyl ether at −78°C was added dropwise, with stirring, 176 mL of 1.95 *M* methyllithium (0.34 mol) over 1.25 h. The mixture was allowed to warm to room temperature and stirred for 4.5 h, after which 200 mL of water was added dropwise, with stirring, and the mixture was allowed to stand overnight. The aqueous phase was extracted with ethyl ether (2 × 200 mL), and the combined extracts were washed with water (2 × 400 mL) and dried over anhydrous sodium sulfate and anhydrous magnesium sulfate. The solvent was evaporated under reduced pressure, and the residual crude alcohol was used without purification for the next step. To a suspension of 77.66 g (0.36 mol) of pyridinium chlorochromate (PCC) in 540 mL of methylene chloride was added, all at once, 25.3 g of the crude alcohol in 180 mL of methylene chloride, and the mixture was stirred for 2 h. The mixture was then diluted with 750 mL of ethyl ether, the solution was decanted, and the black insoluble residue was washed with ethyl ether (1 × 300, 2 × 250, and 1 × 200). The combined extracts were divided into two equal portions, each of which was washed with 5% aqueous sodium hydroxide (2 × 750 mL), 750 mL of 5% aqueous hydrochloric acid, and saturated aqueous sodium bicarbonate (2 × 400 mL) and dried over anhydrous sodium sulfate. The solvent was evaporated under reduced pressure, and the remaining orange oil was distilled to give 15.7 g (60%) of enone **7**.

*2,3,4-Trimethyl-3-(3-methyl-3-butenyl)cyclohexanone (**43**)*

To a solution of 5.32 g (27.1 mmol) of 4-iodo-2-methyl-1-butene (**41**) in 20 mL of ethyl ether at −78°C was added dropwise, with stirring, 25 mL of 1.7 *M tert*-butyllithium (42.5 mmol) over 20 min. After the mixture had been allowed to stir at −78°C for an additional 30 min, the Dry Ice – acetone bath was replaced by a Dry Ice – aqueous calcium chloride bath at −50°C, and 2.71 g (14.7 mmol) of copper(I) iodide was added all at once. The resulting grey suspension was stirred at −40 to −50°C for 3.5 h, after which 1.60 g (11.6 mmol) of 2,3,4-trimethylcyclohex-2-en-1-one (**7**) in 20 mL of ethyl ether was added dropwise, with stirring, over 20 min. After 3 h of stirring at −45°C the mixture was quenched by the addition of 10 mL of saturated aqueous sodium bicarbonate and poured into a mixture of 40 mL of ethyl ether and 60 mL of 10% aqueous ammonium hydroxide. The aqueous phase was extracted with ethyl ether and the combined extracts were washed with 10% aqueous ammonium hydroxide, water, and saturated aqueous sodium chloride, and dried over anhydrous magnesium sulfate. The solvent was evaporated under reduced pressure leaving an oil which was subjected to open column liquid chromatography on activity III neutral alumina. The fractions eluted with 1% ethyl acetate in hexane gave 1.1 g (45% yield) of oily ketone **43**, while 2% ethyl acetate in hexane gave 0.47 g of the starting ketone (**7**). The yield of **43** based on consumed **7** was thus 60%; ir (CCl_4): 1715, 1645, 896 cm^{-1}; ^1H nmr (CCl_4) δ: 0.57 (s, 3H), 0.84 (d, J = 7 Hz, 3H), 0.90 (d, J = 7 Hz, 3H), 1.71 (bs, 3H), 4.63 (bs, 2H); ms *m/e* (relative intensity): 55(68), 69(82), 97(96), 139(100), 163(9), 208(10, M^+); high resolution ms, *m/e* calcd. for $C_{14}H_{24}O$: 208.1827; found: 208.1825.

*3-(3,4-Epoxy-3-methylbutyl)-2,3,4-trimethylcyclohexanone (**47**)*

To a solution 1.04 g (5.0 mmol) of enone **43** in 30 mL of methylene chloride at 0°C was added dropwise, with stirring, 1.12 g (5.5 mmol) of 85% *m*-chloroperbenzoic acid in 25 mL of methylene chloride over 45 min. After the mixture had been allowed to stir for 9 h at room temperature, 75 mL of methylene chloride was added, and the solution was washed with 10% aqueous sodium bisulfite, 5% aqueous sodium hydroxide, water, and saturated aqueous sodium chloride, and dried over anhydrous magnesium sulfate. The solvent was evaporated under reduced pressure to give 1.11 g of a light yellow oil which was a sufficiently pure mixture of diastereomers for use in subsequent reactions; ir (CCl_4): 1715 cm^{-1}; ^1H nmr (CCl_4) δ: 0.58 (s, 3H), four doublets (J = 7 Hz) at 0.85, 0.87, 0.92, and 0.93 (combined 6H), 1.43 (s, 3H), 2.67 (bs, 2H); ms *m/e* (relative intensity): 43(43), 49(81), 55(41), 67(42), 84(100), 96(65), 110(42), 111(42), 123(19), 138(77), 139(88), 154(10), 163(3), 196(2), 208(2), 224(1, M^+); high resolution ms, *m/e* calcd. for $C_{14}H_{24}O_2$: 224.1776; found: 224.1772.

*4,7,9,10-Tetramethyl-6-octal-1-one (**5**), 4,7,9,10-tetramethyl-7-octal-1-one (**48**), and 7-hydroxymethyl-1,2,6,7-tetramethylbicyclo[4.3.0]nonan-5-one (**50**)*

To a solution of 1.11 g (5.0 mmol) of the crude mixture of epoxyketones (**47**) in 6 mL of *tert*-butyl alcohol was added 23 mL of a solution of potassium *tert*-butoxide (26 mmol) freshly prepared by reaction of 1.11 g of potassium with 25 mL of *tert*-butyl alcohol at 50°C. The resulting orange solution was refluxed for 14 h, after which 15 mL of water was added, and the bulk of the solvent was evaporated under reduced pressure. The remaining orange gum was partitioned between 100 mL of water and 80 mL of ethyl ether, and the aqueous phase was extracted with two 50-mL portions of ethyl ether. The combined extracts were washed with water and saturated aqueous sodium chloride, and dried over anhydrous sodium sulfate. The solvent was evaporated under reduced pressure to give 1.3 g of a mixture of keto-alcohols as a crude yellow oil which was used for the next step without purification. To a solution of the above crude product in 20 mL of cyclohexane was added 17 mL of 50% aqueous sulfuric acid, and the mixture was stirred vigorously for 0.5 h. The mixture was then partitioned between ethyl ether and water, and the aqueous phase was neutralized with solid sodium carbonate and extracted with ethyl ether. The combined extracts were washed with saturated aqueous sodium bicarbonate and saturated aqueous sodium chloride, and dried over anhydrous magnesium sulfate, anhydrous sodium sulfate, and potassium carbonate. The solvent was evaporated under reduced pressure, giving a yellow oil which was subjected to open column liquid chromatography on 32 g of activity III alumina, eluting first with hexane, then with 1% ethyl acetate in hexane, and finally with pure ethyl acetate. Fractions eluted with ethyl acetate – hexane gave 0.39 g (38%) of a 4.3:1 mixture (analysis of integration of the olefinic proton signals in the nmr) of octalones **5** and **48** as a light yellow oil; ir (CCl_4): 1708 cm^{-1}; ^1H nmr (CCl_4) δ (relative LIS (for **5** only) with added $Eu(fod)_3$ in brackets): 0.66[2.2] (s, 3H), 0.82[1.0] (d, J = 7 Hz, 3H), 0.92[4.1] (s, 3H), 1.63[0.6] (bs, 3H), 4.99 and 5.28[0.9] (m, width at half-height 4 Hz and 11 Hz, respectively, combined 1H, vinyl protons for **48** and **5**, respectively); ms *m/e* (relative intensity): 55(71), 67(74), 79(68), 91(82), 107(100), 121(87), 163(74), 173(34), 188(11), 191(11), 206(45, M^+); high resolution ms, *m/e* calcd. for $C_{14}H_{22}O$: 206.1670; found 206.1668. A small amount of nearly pure **48** was isolated from an early fraction; ir (CCl_4): 1708 cm^{-1}; ^1H nmr (CCl_4) δ: 0.66 (s, 3H), 0.88 (d, J = 7 Hz, 3H), 0.94 (s, 3H), 1.64 (bs, 3H), 4.99 (m, 1H). Fractions eluted with pure ethyl acetate gave 0.34 g of a yellow oil (ca. 80% pure by ^1H nmr) from which pure keto-alcohol **50** could be isolated as a very light yellow oil by preparative gas chromatography (140°C); ir (CCl_4): 3425, 1687, 1055 cm^{-1}; ^1H nmr (CCl_4) δ: 0.97 (s, 3H), 0.99 (d, J = 7 Hz, 3H) 1.11 (s, 3H), 1.17 (s, 3H), 3.25 (d, J = 12 Hz, 1H), 3.67 (d, J = 12 Hz, 1H); ms *m/e*

Can. J. Chem. Downloaded from www.nrcresearchpress.com by 210.87.254.105 on 09/06/12
For personal use only.

(relative intensity): 55(10), 67(18), 81(14), 95(20), 109(35), 121(20), 139(100), 163(19), 175(7) 191(5), 206(3), 224(1, M^+); high resolution ms, *m/e* calcd. for $C_{14}H_{24}O_2$: 224.1776; found: 224.1776.

*4,7,9,10-Tetramethyl-6-octal-1-ol (**54**) and 4,7,9,10-tetramethyl-7-octal-1-ol (**55**)*

To a suspension of 30 mg (0.79 mmol) of lithium aluminum hydride in 1.0 mL of ethyl ether at 0°C was added dropwise, with stirring, 0.117 g (0.57 mmol) of a 4.3:1 mixture of octalones **5** and **48** in 1.0 mL of ethyl ether, followed by 1.5 mL of ethyl ether. The mixture was allowed to warm to room temperature and stirred for 24 h, after which 0.030 mL of water was added followed by 0.045 mL of 10% aqueous sodium hydroxide and 0.90 mL of water. The resulting suspension was filtered, the solid was washed with ethyl ether, and the filtrate was extracted with ethyl ether. The combined extracts were washed with saturated aqueous sodium chloride and dried over anhydrous sodium sulfate. The solvent was evaporated under reduced pressure to give 0.100 g (85%) of a light yellow oil; ir (CCl_4): 3640, 3510(b) cm^{-1}; ^1H nmr ($CDCl_3$) δ: 1.54 (bs, 3H), 3.37 (t, J = 3 Hz, 1H), 4.80 (small m, 1H, vinyl of **55**), 5.14 (m, 1H, vinyl of **54**); high resolution ms, *m/e* calcd. for $C_{14}H_{24}O$: 208.1827; found: 208.1828.

*Racemic ishwarone (**2**)*

To a solution of 0.104 g (0.50 mmol) of a 4.3:1 mixture of octalones **5** and **48**, 0.060 mL (0.173 g, 0.69 mmol) of bromoform and ca. 3 mg of tributylamine in 0.065 mL of methylene chloride was added dropwise, with stirring, 0.17 mL of 50% aqueous sodium hydroxide. The mixture was stirred vigorously and heated at 40–50°C for 115 h, during which time small amounts of methylene chloride were added occasionally to replace that lost due to evaporation. The cooled mixture was partitioned between ethyl ether and water, and the aqueous phase was neutralized with 50% aqueous sulfuric acid and extracted with ethyl ether. The combined extracts were washed with 5% aqueous hydrochloric acid and saturated aqueous sodium chloride and dried over anhydrous sodium sulfate. The solvent was evaporated under reduced pressure, leaving a brown oil which was subjected to preparative thick-layer chromatography using carbon tetrachloride. The dibromocyclopropane **56** was isolated as a yellow oil containing unreacted octalin **48**; ^1H nmr ($CDCl_3$) δ: 0.80 (s), 0.87 (d, J = 7 Hz), 1.10 (s), 1.52 (s); high resolution ms, *m/e* calcd. for $C_{15}H_{22}Br_2O$: 378.0017; found: 378.0027. To a solution of this mixture of **56** and **48** in 1.5 mL of ethyl ether at −10°C was added dropwise, with stirring, over 2 h, 0.25 mL (0.40 mmol) of 1.6 *M* methyllithium diluted with 1.5 mL of ethyl ether. The mixture was allowed to warm slowly to room temperature and was partitioned between ethyl ether and water. The aqueous phase was extracted with ethyl ether, and the combined extracts were washed with saturated aqueous sodium chloride and dried over anhydrous sodium sulfate. The solvent was evaporated under reduced pressure and the residual oil was subjected to preparative gas chromatography,[39] and the peak having a retention time corresponding to that of authentic ishwarone was collected and subjected to preparative thick-layer chromatography on alumina using 5% ethyl ether in cyclohexane. The band having the same R_f value as that of authentic ishwarone was extracted with ethyl acetate, and the solvent was evaporated under reduced pressure to give 1.5 mg (2%) of an oil, the ^1H and ^{13}C nmr spectra of which were identical to those of authentic ishwarone (**2**); ^1H nmr ($CDCl_3$) δ: 0.56 (m, 1H), 0.73 (s, 3H), 0.87 (d, J = 6.5 Hz, 3H), 1.15 (s, 3H); ^{13}C nmr (CD_2Cl_2) δ: 15.8, 17.9, 19.4, 19.7, 21.7, 22.7, 28.1, 30.7, 34.9, 38.0, 38.9, 39.7 39.8 (the quaternary carbon resonance observed at 58.6 in the spectrum of authentic ishwarone could not be discerned above the noise in the spectrum of the synthetic material due to the small amount available, and the signal due to the carbonyl carbon was not looked for). A 270 MHz ^1H nmr spectrum[40] of natural ishwarone was also obtained, and all resonances could be assigned, partly by decoupling ($CDCl_3$) δ: 0.56 (m, 1H, C-7 cyclopropyl), 0.73 (s, 3H, C-15 tertiary methyl), 0.87 (d, $J_{4,14}$ = 6.5 Hz, 3H, C-14 secondary methyl), 0.94 (dd, $J_{7,8}$ = 7.5 Hz, $J_{8,9\alpha}$ = 3 Hz, 1H, C-8 cyclopropyl), 1.15 (s, 3H, C-13 tertiary methyl), 1.35 (d, $J_{9\alpha,9\beta}$ = 12.5 Hz, 1H, C-9 βH), 1.42 (qd, $J_{2\alpha,3\beta} = J_{3\alpha,3\beta} = J_{3\beta,4}$ = 13.5 Hz, $J_{2\beta,3\beta}$ = 4 Hz, 1H, C-3 βH), 1.59 (dd, $J_{6\alpha,6\beta}$ = 14 Hz, $J_{6\beta,7}$ = 4 Hz, 1H, C-6 βH), 1.73 (dddd, $J_{3\alpha,3\beta}$ = 13.5 Hz, $J_{2\alpha,3\alpha}$ = 6.5 Hz, $J_{2\beta,3\alpha}$ = 4 Hz, $J_{3\alpha,4}$ = 2 Hz, 1H, C-3 αH), 1.86 (d, $J_{12\alpha,12\beta}$ = 12 Hz, 1H, C-12 βH), 1.90 (dd, $J_{6\alpha,6\beta}$ = 14 Hz, $J_{6\alpha,7}$ = 2 Hz, 1H, C-6 αH), 1.99 (dd, $J_{9\alpha,9\beta}$ = 12.5 Hz, $J_{8,9\alpha}$ = 3 Hz, 1H, C-9 αH), 2.13 (dqd, $J_{3\beta,4}$ = 13.5 Hz, $J_{4,14}$ = 6.5 Hz, $J_{3\alpha,4}$ = 2 Hz, 1H, C-4), 2.22 (dt, $J_{2\alpha,2\beta}$ = 13.5 Hz, $J_{2\beta,3\alpha} = J_{2\beta,3\beta}$ = 4Hz, 1H, C-2 βH), 2.25 (d, $J_{12\alpha,12\beta}$ = 12 Hz, 1H, C-12 αH), 2.46 (td, $J_{2\alpha,2\beta} = J_{2\alpha,3\beta}$ = 13.5 Hz, $J_{2\alpha,3\alpha}$ = 6.5 Hz, 1H, C-2 αH).

*5β,9β,10β-Trimethyl-2-decalone (**60**)*

To a solution of 10.7 g (52 mmol)) of the copper(I) bromide – dimethyl sulfide complex (84) and 70 mL of dimethyl sulfide in 70 mL of ethyl ether was added dropwise, with stirring, 64 mL of 1.6 *M* methyllithium (96 mmol), followed by 6.83 g (38 mmol) of octalone **59** (83) in 10 mL of ethyl ether. After the yellow suspension had been stirred for 4 h, the mixture was partitioned between petroleum ether (boiling range 30–60°C) and aqueous ammonium hydroxide (buffered to pH 8 with ammonium chloride). The aqueous phase was extracted with petroleum ether, and the combined extracts were washed with water and saturated aqueous sodium chloride and dried over anhydrous sodium sulfate. The solvent was evaporated under reduced pressure, and the residual oil was distilled to give 5.8 g (77%) of decalone (**60**); bp 80°C/0.02 Torr; ir (CCl_4): 1713 cm^{-1}; ^1H nmr ($CDCl_3$) δ: 0.88 (m, 9H, methyl, not resolved), 3.05 (bd, J = 14 Hz, 1H); ms *m/e* (relative intensity): 55(100), 67(90), 81(60), 95(38), 110(44), 123(44), 179(15), 194(29); high resolution ms, *m/e* calcd. for $C_{13}H_{22}O$: 194.1671; found: 194.1669.

*2,5β,9β,10β-Tetramethyl-2-octalin (**62**) and 2,5β,9β,10β-tetramethyl-1-octalin (**63**)*

To a solution of methylmagnesium bromide (prepared from 0.35 g (14 mmol) of magnesium turnings and 0.95 mL (2.16 g, 15 mmol) of methyl iodide in 4.3 mL of ethyl ether) was added dropwise, with stirring, 1.1 g (5.7 mmol) of decalone **60** in 14.2 mL ethyl ether over 2.5 h. After the mixture had been stirred for 3h, the mixture was quenched with aqueous ammonium chloride, and the aqueous phase was extracted with ethyl ether. The combined extracts were evaporated under reduced pressure to give 1.02 g (85%) of crude gummy decalol **61**, which was used directly for the next step, but which could be purified by preparative thick-layer chromatography on silica gel using 10% ethyl acetate in cyclohexane; ir (CCl_4): 3615, 3490 cm^{-1}; ^1H nmr ($CDCl_3$) δ: 0.76 (s, 3H), 0.76 (d, J = 6.5 Hz, 3H), 1.08 (s, 3H), 1.21 (s, 3H), 2.12 (bd, J = 15 Hz, 1H). To a solution of 0.90 g (4.3 mmol) of the crude decalol in 18 mL of cyclohexane was added 14 mol of 50% aqueous sulfuric acid, and the two-phase mixture was stirred vigorously for 2 h and then partitioned between 25 mL of ethyl ether and 25 mL of water. The aqueous phase was extracted with ethyl ether (3 × 25 mL) and the combined extracts were washed with 50 mL of saturated aqueous sodium bicarbonate, 50 mL of water, and 50 mL of saturated aqueous sodium chloride and dried over anhydrous sodium sulfate. The solvent was evaporated under reduced pressure to give 0.69 g (87%) of a 1:1 mixture of octalins **62** and **63**, which could not be separated; ir (CCl_4): 1670 cm^{-1}; ^1H nmr ($CDCl_3$) δ: 0.77 (s, 3H), 0.80 (d, J = 6.5 Hz, 3H) 0.84 (s, 3H), 1.64 (bs, 3H), 4.98 and 5.21 (broad singlets for **63** and **62**, respectively, 1H); ms *m/e* (relative intensity): 55(29), 67(34), 79(28), 91(30), 109(100), 124(33), 177(9), 192(9, M^+); high resolution, ms, *m/e* calcd. for $C_{14}H_{24}$: 192.1878; found: 192.1880.

*Racemic ishwarane (**1**)*

To a solution of 0.40 g (2.1 mmol) of octalins **62** and **63** and 1.38 g (4.2 mmol) of carbon tetrabromide in 14 mL of ethyl ether at −78°C was added dropwise, with stirring, 2.3 mL of 1.8 *M* methyllithium (4.2 mmol) over 1 h, and the resulting yellow solution was

[39]A 0.2 in. × 6 ft stainless-steel column packed with 5% OV-101 on 80/100 mesh Chromosorb W was employed at 150°C.

[40]Recorded on a Bruker Model WH-270 spectrometer at the University of Wisconsin, Madison.

Can. J. Chem. Downloaded from www.nrcresearchpress.com by 210.87.254.105 on 09/06/12
For personal use only.

stirred at −78°C for 45 min. The mixture was then allowed to warm to −30°C over 1.75 h, during which time the color changed from yellow to black. While the temperature of the mixture was maintained at −30°C, an additional 2.3 mL of 1.8 *M* methyllithium (4.2 mmol) was added dropwise, with stirring, over 45 min, and the black mixture was stirred at −30°C for an additional hour, after which it was allowed to warm to 0°C over 1 h. At this point 10 mL of water was added dropwise, with stirring, and the aqueous phase was extracted with petroleum ether (2 × 25 mL). The combined extracts were washed with 50 mL of water and 50 mL of saturated aqueous sodium chloride and dried over anhydrous sodium sulfate. The solvent was evaporated under reduced pressure, and the residual oil was subjected to preparative thick-layer chromatography on silica gel using hexane, followed by preparative gas chromatography,[41] which gave four peaks: retention time (relative area, amount collected, identity) 20 min (40%, 11 mg, unreacted octalin **63**), 22 min (21%, 4 mg, unreacted octalin **62**), 26 min (19%, 6 mg, unidentified isomer or isomers of ishwarane; high resolution ms, *m/e* calcd. for $C_{15}H_{24}$: 204.1878; found: 204.1879), and 31 min (20%, 10 mg, racemic ishwarane). The latter material was found to have ^1H and ^{13}C nmr spectra which were identical to those of authentic ishwarane (**1**); ^1H nmr ($CDCl_3$) δ: 0.48 (m, 1H), 0.75 (d, J = 6.5 Hz, 3H), 0.80 (s, 3H), 1.14 (s, 3H), 1.88 (bd, J = 12 Hz, 1H), 2.09 (bd, J = 12 Hz, 1 H); ^{13}C nmr ($CDCl_3$) δ: 16.6, 16.7, 19.9, 20.3, 22.4, 23.0, 23.9, 30.9, 33.6, 34.7, 35.7, 35.8, 38.7, 39.3, 44.0; high resolution ms, *m/e* calcd. for $C_{15}H_{24}$: 204.1878; found: 204.1877. A 270 MHz ^1H nmr spectrum[40] of natural ishwarane was also obtained ($CDCl_3$) δ: 0.47 (m, 1H, C-7 cyclopropyl), 0.74 (d, $J_{4,14}$ = 6.4 Hz, 3H, C-14 secondary methyl), 0.79 (s, 3H, C-15 tertiary methyl), 1.00 (d, $J_{9\alpha,9\beta}$ = 11.2 Hz, 1 H, C-9 βH), 1.14 (s, 3H, C-13 tertiary methyl), 1.51 (dd, $J_{6\alpha,6\beta}$ = 14 Hz, $J_{6\beta,7}$ = 4 Hz, 1H, C-6 βH), 1.68 (dd, $J_{6\alpha,6\beta}$ = 14 Hz, $J_{6\alpha,7}$ = 2 Hz, 1H, C-6 αH), 1.87 (d, $J_{12\alpha,12\beta}$ = 12 Hz, 1H, C-12 βH), 2.09 (d, $J_{12\alpha,12\beta}$ = 12 Hz, 1H, C-12 αH).

Acknowledgements

We are grateful to the Research Corporation, Imperial Oil Ltd., and the Natural Sciences and Engineering Research Council of Canada for financial support of this work.

1. T. R. GOVINDACHARI, P. A. MOHAMED, and P. C. PARTHASARATHY. Tetrahedron, **26**, 615 (1970).
2. U. S. K. RAO, B. L. MANJUNATH, and K. N. MENON. J. Indian Chem. Soc. **12**, 494 (1935).
3. L. C. TENG and J. F. DE BARDELEBEN. Experientia, **27**, 14 (1971).
4. R. N. CHOPRA. Indigenous drugs of India. 2nd ed. U. N. Dhur & Sons, Calcutta. 1958. pp. 284−285.
5. C. CHE, G. A. CORDELL, and H. H. S. FONG. Tetrahedron Lett. **24**, 1333 (1983); R. L. FUNK, L. H. M. HORCHER II, J. U. DAGGETT, and M. M. HANSEN. J. Org. Chem. **48**, 2632 (1983); S. C. PAKRASHI, P. P. G. DASTIDAR, S. CHAKRABARTY, and B. ACHARI. J. Org. Chem. **45**, 4765 (1980).
6. P. C. STANDLEY and J. A. STEYERMARK. Flora of Guatemala. Vol. 4. (Fieldiana: Botany. Vol. 24, Part 4). Field Museum of Natural History, Chicago. 1946. p. 282.
7. B. M. LAWRENCE and J. W. HOGG. Phytochemistry, **12**, 2995 (1973); H. K. DESAI, D. H. GAWAD, T. R. GOVINDACHARI, B. S. JOSHI, V. N. KAMAT, J. D. MODI, P. C. PARTHASARATHY, J. RADHAKRISHNAN, M. N. SHANBHAG, A. R. SIDHAYE, and N. VISWANATHAN. Indian J. Chem. **11**, 840 (1973).
8. (*a*) A. K. GANGULY, K. W. GOPINATH, T. R. GOVINDACHARI, K. NAGARAJAN, B. R. PAI, and P. C. PARTHASARATHY. Tetrahedron, **26**, 2371 (1970); (*b*) R. B. KELLY and J. ZAMECNIK. J. Chem. Soc. Chem. Commun. 1102 (1970); (*c*) T. R. GOVINDACHARI, K. NAGARAJAN, and P. C. PARTHASARATHY. J. Chem. Soc. Chem. Commun. 823 (1969); (*d*) H. FUHRER, A. K. GANGULY, K. W. GOPINATH, T. R. GOVINDACHARI, K. NAGARAJAN, B. R. PAI, and P. C. PARTHASARATHY. Tetrahdron Lett. 133 (1969).
9. T. R. GOVINDACHARI and P. C. PARTHASARATHY. Indian J. Chem. **9**, 1310 (1971).
10. R. NISHIDA and Z. KUMAZAWA. Agric. Biol. Chem. **37**, 341 (1973).
11. R. M. CORY and F. R. MCLAREN. J. Chem. Soc. Chem. Commun. 587 (1977).
12. (*a*) H. HAGIWARA, H. UDA, and T. KODAMA. J. Chem Soc. Perkin Trans. 1, 963 (1980); (*b*) R. B. KELLY and S. J. ALWARD. Can. J. Chem. **55**, 1786 (1977); (*c*) R. B. KELLY, J. ZAMECNIK, and B. A. BECKETT. Can. J. Chem. **50**, 3455 (1972); J. Chem. Soc. Chem. Commun. 479 (1971).
13. E. PIERS and T.-W. HALL. Can. J. Chem. **58**, 2613 (1980); Chem. Commun. 880 (1977).
14. R. M. CORY, D. M. T. CHAN, F. R. MCLAREN, M. H. RASMUSSEN, and R. M. RENNEBOOG. Tetrahedron Lett. 4133 (1979).
15. P. C. STANDLEY. Flora of the Panama Canal Zone. J. Cramer, New York. 1968. p. 270.
16. A. R. PINDER. *In* Prog. Chem. Nat. Prod. Vol. 34. *Edited by* W. Herz, H. Grisebach, and G. W. Kirby. Springer Verlag, New York. 1977. pp. 81−186.
17. R. M. CORY, L. P. J. BURTON, and R. G. PECHERLE. Synth. Commun. **9**, 735 (1979).
18. C. J. V. SCANIO and D. L. LICKEI. Abstracts. 166th National Meeting of the American Chemical Society. Chicago. Aug. 1973. No. AGFD 32; D. L. LICKEI. Ph.D. Dissertation. Iowa State University, Ames, Iowa. 1973. S. CAMPBELL, N. PETRAGNANI, T. BROCKSOM, and L. TSUCHIYA. Farmaco Ed. Sci. **33**, 421 (1978).
19. F. FRINGUELLI, F. PIZZO, A.TATICCHI, and E. WENKERT. J. Org. Chem. **48**, 2802 (1983); F. FRINGUELLI, F. PIZZO, A. TATICCHI, T. D. J. HALLS, and E. WENKERT. J. Org. Chem. **47**, 5056 (1982); F. FRINGUELLI, F. PIZZO, A. TATICCHI, and E. WENKERT. Synth. Commun. **9**, 391 (1979); I. NAGAKURA, H. OGATA, M. UENO, and Y. KITAHARA. Bull. Chem. Soc. Jpn. **48**, 2995 (1975).
20. H. NIWA, N. BAN, and K. YAMADA. Tetrahedron Lett. **24**, 937 (1983); M. R. WILLCOTT, P. A. MORRISON, J.-M. ASSERCQ, S. C. WELCH, and R. INNERS. J. Org. Chem. **46**, 4819 (1981).
21. G. FERGUSON, R. MCCRINDLE, S. T. MURPHY, and M. PARVEZ. J. Chem. Res. (S) 200 (1982); B. M. FRAGA, A. G. GONZALEZ, M. G. HERNANDEZ, J. R. HANSON, and P. B. HITCHCOCK. J. Chem. Soc. Chem. Commun. 594 (1982).
22. F. BOHLMANN and W. ROTARD. Ann. Chem. 1220 (1982); F. BOHLMANN, W.-R. ABRAHAM, and W. S. SHELDRICK. Phytochemistry, **19**, 869 (1980); F. BOHLMANN, C. ZDERO, R. ZDERO, R. ZEISBERG, and W. S. SHELDRICK. Phytochemistry, **18**, 1359 (1979).
23. R. M. CORY, D. M. T. CHAN, Y. M. A. NAGUIB, M. H. RASTALL, and R. M. RENNEBOOG. J. Org. Chem. **45**, 1852 (1980); R. M. CORY, Y. M. A. NAGUIB, and M. H. RASMUSSEN. J. Chem. Soc. Chem. Commun. 504 (1979).
24. E. PIERS and V. KARUNARATNE. J. Chem. Soc. Chem. Commun. 935 (1983); E. PIERS and J. M. CHONG. J. Chem. Soc. Chem. Commun. 934 (1983); E. PIERS AND V. KARUNARATNE. J. Org. Chem. **48**, 1774 (1983).
25. (*a*) J. E. MCMURRY and S. J. ISSER. J. Am. Chem. Soc. **94**, 7132 (1972); (*b*) W. L. SCOTT and D. A. EVANS. J. Am. Chem. Soc. **94**, 4779 (1972); (*c*) E. PIERS, W. DE WAAL, and R. W. BRITTON. J. Am. Chem. Soc. **93**, 5113 (1971); (*d*) J. E. MCMURRY. J. Am. Chem. Soc. **90**, 6821 (1968); (*e*) C. H. HEATHCOCK, R. A. BADGER, and J. W. PATTERSON, JR. J. Am. Chem. Soc. **89**, 4133 (1967).
26. D. K. DALLING and D. M. GRANT. J. Am. Chem. Soc. **94**, 5318 (1972); N. L. ALLINGER and M. A. MILLER. J. Am. Chem. Soc.

[41] A 0.2 in. × 10 ft copper column packed with 10% SE-30 on Diatoport S was employed at 165°C.

Can. J. Chem. Downloaded from www.nrcresearchpress.com by 210.87.254.105 on 09/06/12
For personal use only.

83, 2145 (1961).
27. E. J. COREY, W. J. HOWE, H. W. ORF, D. A. PENSAK, and G. PETERSSON. J. Am. Chem. Soc. **97**, 6116 (1975).
28. L. A. LAST, E. R. FRETZ, and R. M. COATES. J. Org. Chem. **47**, 3211 (1982).
29. S. N. AHMED, M. L. MCKEE, and P. B. SHEVLIN. J. Am. Chem. Soc. **105**, 3942 (1983); P. B. SHEVLIN, D. W. MCPHERSON, and P. MELIUS. J. Am. Chem. Soc. **105**, 488 (1983); P. C. MARTINO and P. B. SHEVLIN. Tetrahedron Lett. **23**, 2547 (1982); R. A. FERRIERI, A. P. WOLF, D. A. BALTUSKONIS, and Y.-N. TANG. J. Chem. Soc. Chem. Commun. 1321 (1982); K. A. BIESIADA, C. T. KOCH, and P. B. SHEVLIN. J. Am. Chem. Soc. **102**, 2098 (1980); P. B. SHEVLIN. *In* Reactive intermediates. Vol. 1. *Edited by* R. A. Abramovitch. Plenum, New York. 1980. pp. 1–36; C. MACKAY. *In* Carbenes. Vol. II. *Edited by* R. A. Moss and M. Jones, Jr. Wiley, New York. 1975. pp. 1–42; P. S. SKELL, J. HAVEL, and M. J. MCGLINCHEY. Acc. Chem. Res. **6**, 97 (1973).
30. L. A. PAQUETTE, G. ZON, and R. T. TAYLOR. J. Org. Chem. **39**, 2677 (1974).
31. W. R. MOORE, H. R. WARD, and R. F. MERRITT. J. Am. Chem Soc. **83**, 2019 (1961).
32. U. BURGER and B. BIANCO. Helv. Chim. Acta, **66**, 60 (1983); N. O. NILSEN, L. SKATTEBØL, and L. K. SYDNES. Acta Chem. Scand. Ser. B, **36**, 587 (1982); J. ARCT and L. SKATTEBØL. Acta Chem. Scand. Ser. B, **36**, 593 (1982); H. JENDRALLA and W. PFLAUMBAUM. Chem. Ber. **115**, 210 (1982); P. WARNER, S.-C. CHANG, D. R. POWELL, and R. A. JACOBSON. Tetrahedron Lett. **22**, 533 (1981); D. P. G. HAMON and V. C. TRENERRY, Aust. J. Chem. **33**, 809 (1980); R. T. TAYLOR and D. F. PYTROCZKO. Tetrahedron Lett. **21**, 2471 (1980); L. A. PAQUETTE, A. R. BROWNE, E. CHAMOT, and J. F. BLOUNT. J. Am. Chem. Soc. **102**, 643 (1980).
33. T. SHONO, I. NISHIGUCHI, T. KOMAMURA, and K. FUJITA. Tetrahedron Lett. 4327 (1977); D. P. G. HAMON and V. C. TRENERRY. Tetrahedron Lett. 1371 (1974).
34. A. R. ALLAN and M. S. BAIRD. J. Chem. Research (S) 290 (1982); M. S. BAIRD and A. C. KAURA. J. Chem. Soc. Chem. Commun. 356 (1976); K. G. TAYLOR, J. CHANEY and J. C. DECK. J. Am. Chem. Soc. **98**, 4163 (1976); M. S. BAIRD and C. B. REESE. Tetrahedron, **32**, 2153 (1976); R. F. BOSWELL and R. G. BASS. J. Org. Chem. **40**, 2419 (1975); B. FRASER-REID, R. L. SUN, and J. T. BREWER. Tetrahedron Lett. 2775 (1969); C. G. CARDENAS, B. A. SHOULDERS, and P. D. GARDNER. J. Org. Chem. **32**, 1220 (1967); E. T. MARQUIS and P. D. GARDNER. Tetrahedron Lett. 2793 (1966).
35. M. MAKOSZA and M. FEDORYŃSKI. Synth. Commun. **3**, 305 (1973).
36. D. SEEBACH, R. HÄSSIG, and J. GABRIEL. Helv. Chim. Acta, **66**, 308 (1983); D. SEEBACH, H. SIEGEL, J. GABRIEL, and R. HÄSSIG. Helv. Chim. Acta, **63**, 2046 (1980); D. SEEBACH, H. SIEGEL, K. MÜLLEN, and K. HILTBRUNNER. Angew. Chem. Int. Ed. Engl. **18**, 784 (1979).
37. H. SIEGEL. Top. Curr. Chem. **106**, 55 (1982).
38. J. HATEM, J. P. ZAHRA, and B. WAEGELL. Tetrahedron, **39**, 2175 (1983).
39. R. M. CORY and J. B. STOTHERS. Org. Magn. Reson. **11**, 252 (1978).
40. L. SKATTEBØL. Tetrahedron Lett. 167 (1961).
41. R. VAIDYANATHASWAMY, S. N. MOORTHY, and D. DEVAPRABHAKARA. Indian J. Chem. **15B**, 309 (1977); Synthesis, 194 (1975); K. G. UNTCH, D. J. MARTIN, and N. T. CASTELLUCCI. J. Org. Chem. **30**, 3572 (1965).
42. R. H. FISCHER and G. KÖBRICH. Chem. Ber. **101**, 3230 (1968); W. T. MILLER, JR. and C. S. Y. KIM. J. Am. Chem. Soc. **81**, 5008 (1959).
43. O. M. NEFEDOV, M. N. MANAKOV, and A. A. IVASHENKO. Izv. Akad. Nauk SSSR. Otd. Khim. Nauk, 1242 (1962); O. M. NEFEDOV and R. N. SHAFRAN. Izv. Akad. Nauk SSSR. Ser. Khim. 538 (1965).
44. H. SIEGEL, K. HILTBRUNNER, and D. SEEBACH. Angew. Chem. Int. Ed. Engl. **18**, 785 (1979).
45. R. A. MOSS. *In* Carbenes. Vol. I. *Edited by* M. Jones, Jr. and R. A. Moss. Wiley, New York. 1973. pp. 153–304.
46. R. A. MOSS, C. B. MALLON, and C.-T. HO. J. Am. Chem. Soc. **99**, 4105 (1977).
47. J. KLEIN, E. DUNKELBLUM, and D. AURAHAMI. J. Org. Chem. **32**, 935 (1967).
48. R. BAKER, P. H. BRINER, and D. A. EVANS. J. Chem. Soc. Chem. Commun. 410 (1978).
49. L. A. PAQUETTE and R. T. TAYLOR. J. Am. Chem. Soc. **99**, 5708 (1977).
50. R. M. CORY, L. P. J. BURTON, and F. R. MCLAREN. Abstracts. 172nd National Meeting of the American Chemical Society. San Francisco. Aug. 1976. No. ORGN-11.
51. T. J. KATZ, E. J. WANG, and N. ACTON. J. Am. Chem. Soc. **93**, 3782 (1971); T. J. KATZ, J. J. CHEUNG, and N. ACTON. J. Am. Chem. Soc. **92**, 6643 (1970); K. HOJO, T. T. SEIDNER, and S. MASAMUNE. J. Am. Chem. Soc. **92**, 6641 (1970); T. J. KATZ and J. J. CHEUNG. J. Am. Chem. Soc. **91**, 7772 (1969).
52. U. BURGER and B. BIANCO. Helv. Chim. Acta, **66**, 60 (1983); G. GRANDILLON, B. BIANCO, and U. BURGER. Tetrahedron Lett. **22**, 51 (1981); U. BURGER and F. DREIER. Helv. Chim. Acta, **62**, 540 (1979); U. BURGER and G. GANDILLON. Tetrahedron Lett. 4281 (1979); R. M. PAGNI, M. BURNETT, and A. C. HAZELL. J. Org. Chem. **43**, 2750 (1978); R. M. PAGNI and M. BURNETT. Tetrahedron Lett. 163 (1977); U. BURGER and F. MAZENOD. Tetrahedron Lett. 2881 (1976); I. MURATA, T. TATSUOKA, and Y. SUGIHARA. Tetrahedron Lett. 4261 (1973); R. M. PAGNI and C. R. WATSON, JR. Tetrahedron Lett. 59 (1973); I. MURATA and K. NAKASUJI. Tetrahedron Lett. 53 (1973).
53. B. D. MACKENZIE, M. M. ANGELO, and J. WOLINSKY. J. Org. Chem. **44**, 4042 (1979).
54. K. A. ANANTHANARAYAN and T. S. SORENSEN. Can. J. Chem. **50**, 3550 (1972).
55. G. STORK and R. L. DANHIESER. J. Org. Chem. **38**, 1775 (1973).
56. W. G. DAUBEN and D. M. MICHNO. J. Org. Chem. **42**, 682 (1977).
57. E. W. WARNHOFF, D. G. MARTIN, and W. S. JOHNSON. *In* Org. Synth. Collect. Vol. IV. *Edited by* N. Rabjohn. John Wiley & Sons, New York. 1963. pp. 162–165.
58. E. PIERS, J. R. GRIERSON, C. K. LAU, and I. NAGAKURA. Can. J. Chem. **60**, 212 (1982).
59. G. CAHIEZ, A. ALEXAKIS, and J. F. NORMANT. Tetrahedron Lett. 3013 (1978).
60. G. STORK and A. R. SCHOOFS. J. Am. Chem. Soc. **101**, 5081 (1979); M. BERTRAND, P. TEISSEIRE, AND G. PÉLERIN. Nouv. J. Chim. **7**, 61 (1983).
61. L. A. PAQUETTE, D. R. ANDREWS, and J. P. SPRINGER. J. Org. Chem. **48**, 1147 (1983); M. E. JUNG and G. L. HATFIELD. Tetrahedron Lett. **24**, 2931 (1983); D. A. EVANS and J. V. NELSON. J. Am. Chem. Soc. **102**, 774 (1980), and references therein.
62. R. L. SNOWDEN. Helv. Chim. Acta, **66**, 1031 (1983); R. L. SNOWDEN and K. H. SCHULTE-ELTE. Helv. Chim. Acta, **64**, 2193 (1981), and references therein.
63. D. A. EVANS, D. J. BAILLARGEON, and J. V. NELSON. J. Am. Chem. Soc. **100**, 2242 (1978).
64. B. M. TROST and R. A. KUNZ. J. Am. Chem. Soc. **97**, 7152 (1975).
65. G. PATTENDEN and S. J. TEAGUE. Tetrahedon Lett. **23**, 5471 (1982); B. M. TROST, P. R. BERNSTEIN, and P. C. FUNFSCHILLING. J. Am. Chem. Soc. **101**, 4378 (1979); G. A. LEYES and W. H. OKAMURA. J. Am. Chem. Soc. **104**, 6099 (1982).
66. F. E. ZIEGLER, G. R. REID, W. L. STUDT, and P. A. WENDER. J. Org. Chem. **42**, 1991 (1977); F. E. ZIEGLER and P. A. WENDER. Tetrahedron Lett. 449 (1974); T. A. BLUMENKOPF and C. H. HEATHCOCK. J. Am. Chem. Soc. **105**, 2354 (1983); S.

Can. J. Chem. Downloaded from www.nrcresearchpress.com by 210.87.254.105 on 09/06/12
For personal use only.

DANISHEFSKY, S. CHACKALAMANNIL, M. SILVESTRI, and J. SPRINGER. J. Org. Chem. **48**, 3615 (1983); S. DANISHEFSKY, M. KAHN, and M. SILVESTRI. Tetrahedron Lett. **23**, 1419 (1983); P. M. WEGE, R. D. CLARK, and C. H. HEATHCOCK. J. Org. Chem. **41**, 3144 (1976).

67. S. DANISHEFSKY, M. KAHN, and M. SILVESTRI. Tetrahedron Lett. **23**, 703 (1982).
68. G. A. ELLESTAD, R. H. EVANS, JR., and M. P. KUNSTMANN. Tetrahedron, **25**, 1323 (1969); Y. NAWATA and Y. IITAKA. Bull. Chem. Soc. Jpn. **44**, 2652 (1971).
69. G. H. POSNER. An introduction to synthesis using organocopper reagents. Wiley, New York. 1980. pp. 42–47; G. H. POSNER and C. M. LENTZ. J. Am. Chem. Soc. **101**, 934 (1979); R. M. COATES and L. O. SANDEFUR. J. Org. Chem. **39**, 275 (1974).
70. K. MORI and T. FUJIOKA. Tetrahedron Lett. **23**, 5443 (1982).
71. P. A. COLLINS and D. WEGE. Aust. J. Chem. **32**, 1819 (1979); C. J. M. STIRLING. Chem. Rev. **78**, 517 (1978); E. W. WARNHOFF and V. SRINIVASAN. Can. J. Chem. **55**, 1629 (1977); J. H. BABLER and A. J. TORTORELLO. J. Org. Chem. **41**, 885 (1976); Y. GAONI. Tetrahedron, **28**, 5525 (1972); **28**, 5533 (1972); G. L. HODGSON, D. F. MACSWEENEY, and T. MONEY. Tetrahedron Lett. 3683 (1972); J. E. MCMURRY. J. Org. Chem. **36**, 2826 (1971); A. G. HORTMANN and A. Q. ONG. J. Org. Chem. **35**, 4290 (1970); P. GRAFEN, H. J. KABBE, O. ROOS, G. D. DIANA, T. LI, and R. H. TURNER. J. Am. Chem. Soc. **90**, 6131 (1968); R. B. WOODWARD, T. FUKUNAGA, and R. C. KELLY. J. Am. Chem. Soc. **86**, 3162 (1964); D. H. R. BARTON and A. S. LINDSEY. J. Chem. Soc. 2988 (1951); H. O. HOUSE, P. C. GAA, J. H. C. LEE, and D. VANDERVEER. J. Org. Chem. **48**, 1670 (1983); P. CACHIA, N. DARBY, T. C. W. MAK, T. MONEY, and J. TROTTER. Can. J. Chem. **58**, 1172 (1980).
72. R. T. LALONDE, N. MUHAMMAD, C. F. WONG, and E. R. STURIALE. J. Org. Chem. **45**, 3664 (1980).
73. L. SYDNES and L. SKATTEBØL. Tetrahedron Lett. 4603 (1975).
74. L. SYDNES and L. SKATTEBØL. Acta Chem. Scand. B, **32**, 547 (1978); R. BARLET. Tetrahedron Lett. 4171 (1976).
75. K. G. TAYLOR. Tetrahedron, **38**, 2751 (1982).
76. R. HASSIG, H. SIEGEL, and D. SEEBACH. Chem. Ber. **115**, 1990 (1982); G. SABBIONI, A. WEBER, R. GALLI, and M. NEUENSCHWANDER. Chimia, **35**, 95 (1981); R. DAMMANN and D. SEEBACH. Chem. Ber. **112**, 2167 (1979); R. DAMMANN, M. BRAUN, and D. SEEBACH. Helv. Chim. Acta, **59**, 2821 (1976); M. BRAUN, R. DAMMANN, and D. SEEBACH. Chem. Ber. **108**, 2368 (1975); T. HIYAMA, S. TAKEHARA, K. KITATANI, and N. NOZAKI. Tetrahedron Lett. 3295 (1974); M. BRAUN and D. SEEBACH. Angew. Chem. Int. Ed. Engl. **13**, 277 (1974).
77. N. O. NILSEN, L. SKATTEBØL, and L. K. SYDNES. Acta Chem. Scand. Ser. B, **36**, 587 (1982); D. SEEBACH, H. NEUMANN, and R. DAMMANN. Helv. Chim. Acta, **62**, 1162 (1979); N. O. NILSEN, L. K. SYDNES, and L. SKATTEBØL. J. Chem. Soc. Chem. Commun. 128 (1978); A. R. ALLAN and M. S. BAIRD. J. Chem. Soc. Chem. Commun. 172 (1975); R. MAURIN and M. BERTRAND, Bull. Soc. Chim. Fr. 2349 (1972); L. SYDNES and L. SKATTEBØL. Tetrahedron Lett. 4603 (1975); M. BERTRAND, M. SANTELLI, and R. MAURIN. Bull. Soc. Chim. Fr. 998 (1967); M. BERTRAND and R. MAURIN. C. R. Acad. Sci. Paris, **260**, 6122 (1965).
78. M. MAKOSZA. *In* Survey of progress in chemistry. Vol. 9. *Edited by* A. F. Scott. Academic Press, Toronto. 1980. pp. 1–53; W. P. WEBER and G. W. GOKEL. Phase transfer catalysis in organic synthesis. Springer Verlag, New York. 1977. pp. 18–72; J. T. KEATING and P. S. SKELL. *In* Carbonium ions. Vol. II. *Edited by* G. A. Olah and P. von R. Schleyer. Wiley, New York. 1970. pp. 573–653.
79. A. MERZ and R. TOMAHOGH. Chem. Ber. **110**, 96 (1977); P. KUHL, M. MÜHLSTÄDT, and J. GRAEFE. Synthesis, 825 (1976); Z. HUAN, J. A. LANDGREBE, and K. PETERSON. Tetrahedron Lett. **24**, 2829 (1983).
80. M. MAKOSZA and M. FEDORYNSKI. Rocz. Chem. **50**, 2223 (1976).
81. (*a*) W. S. JOHNSON, Y.-Q. CHEN, and M. S. KELLOGG. J. Am. Chem. Soc. **105**, 6653 (1983); (*b*) E. E. VAN TAMELEN and J. R. HWU. J. Am. Chem. Soc. **105**, 2490 (1983); (*c*) E. E. VAN TAMELEN, S. R. ZAWACKY, R. K. RUSSELL, and J. G. CARLSON. J. Am. Chem. Soc. **105**, 142 (1983); (*d*) J. A. AMUPITAN, E. HUQ, M. MELLOR, E. G. SCOVELL, and J. K. SUTHERLAND. J. Chem. Soc. Perkin Trans. 1, 747 (1983); (*e*) W. S. JOHNSON, D. BERNER, D. J. DUMAS, P. J. R. NEDERLOF, and J. WELCH. J. Am. Chem. Soc. **104**, 3508 (1982); (*f*) W. S. JOHNSON, D. J. DUMAS, and D. BERNER. J. Am. Chem. Soc. **104**, 3510 (1982); (*G*) W. S. JOHNSON. *In* New synthetic methodology and biologically active substrances. *Edited by* Z. Yoshida. Elsevier, New York. 1981. pp. 1–18; (*h*) J. A. MARSHALL, G. L. BUNDY, and W. I. FANTA. J. Org. Chem. **35**, 3913 (1968).
82. D. F. TABER and S. A. SALEH. Tetrahedron Lett. **23**, 2361 (1982).
83. R. K. BOECKMAN, JR., D. M. BLUM, and B. GANEM. *In* Org. Synth. Coll. Vol. 58. *Edited by* W. A. Sheppard. John Wiley & Sons, New York. 1978. pp. 158–163.
84. H. O. HOUSE, C.-Y. CHU. J. M. WILKINS, and M. J. UMEN. J. Org. Chem. **40**, 1460 (1975).
85. S. C. WATSON and J. F. EASTHAM. J. Organomet. Chem. **9**, 165 (1967).
86. C. H. HEATHCOCK, R. RATCLIFFE, and J. VAN. J. Org. Chem. **37**, 1796 (1972).
87. G. M. RUBOTTOM and H. D. JUVE, JR. J. Org. Chem. **48**, 422 (1983).
88. J. P. MARINO and J. C. JAÉN. J. Am. Chem. Soc. **104**, 3165 (1982); B. M. TROST, T. N. SALZMANN, and K. HIROI. J. Am. Chem. Soc. **98**, 4887 (1976).

Synthesis of anthracyclinones. Part 1. Regioselective alkylation of 5-hydroxyquinizarin

LAURENCE M. HARWOOD, LESLIE C. HODGKINSON, JAMES K. SUTHERLAND,[1] AND PATRICK TOWERS
Chemistry Department, The Victoria University of Manchester, Manchester, England M13 9PL

Received November 9, 1983

This paper is dedicated to Professor Paul de Mayo on the occasion of his 60th birthday

LAURENCE M. HARWOOD, LESLIE C. HODGKINSON, JAMES K. SUTHERLAND, and PATRICK TOWERS. Can. J. Chem. **62**, 1922 (1984).

Condensation of *leuco*-5-hydroxyquinizarin with aldehydes under Marschalk conditions (sodium hydroxide − water) gives 2-alkyl-5-hydroxyquinizarins with high regioselectivity, while the 3-alkyl compounds are obtained under Lewis conditions (piperidinium acetate − isopropanol). Reaction of the quinone with nitronate anions in methanol yields 2-alkyl derivatives exclusively.

LAURENCE M. HARWOOD, LESLIE C. HODGKINSON, JAMES K. SUTHERLAND et PATRICK TOWERS. Can. J. Chem. **62**, 1922 (1984).

La condensation de la *leuco* hydroxy-5 quinizarine avec les aldéhydes, en utilisant les conditions de Marschalk (hydroxyde de sodium et eau), conduit aux alkyl-2 hydroxy-5 quinizarines avec une grande régiosélectivité; toutefois, si on utilise les conditions de Lewis (acétate de pipéridinium et isopropanol), on obtient les composés alkylés en position 3. La réaction de la quinone avec les anions nitronates dans le méthanol conduit exclusivement aux dérivés alkylés en position 2.

[Traduit par le journal]

Can. J. Chem. Downloaded from www.nrcresearchpress.com by 210.87.254.4 on 09/06/12
For personal use only.

Our choice of the readily available 5-hydroxyquinizarin (**1**) as a starting point for the synthesis of the aglycones of the anthracycline antibiotics daunomycin and carminomycin (*1*) necessitated the development of methods for the regioselective substitution of **1** at C-2 and (or) C-3. Prior work by Marschalk *et al.* (2) had shown that aldol condensation between *leuco*-quinizarin (**12**) and aldehydes was an effective method for the preparation of 2-alkylquinizarins. Brockmann and Müller (3) carried out Marschalk condensations with *leuco*-5-hydroxy-quinizarin (**13**) and presented evidence for some regioselectivity in favour of C-2.

We first examined the Marschalk condensation of propionaldehyde with the *leuco*-compound **13** and obtained the 2-propyl derivative (**2**). The structure of **2** was established by conversion to the tri-*O*-methyl ether which was cleaved with $KOBu^t-H_2O$ using Hodge's method (4) to give, after methylation of the acidic products with CH_2N_2, *m*-methoxybenzoic acid methyl ester (22%) and the ester **14** (28%). An authentic sample of the ester **14** was synthesized starting with propionylation of 1,4-dimethoxybenzene followed by Clemmensen reduction to 2-*n*-propyl-1,4-dimethoxybenzene; Friedel−Crafts acetylation followed by hypochlorite oxidation and esterification gave material identical with the degradation product. Reaction of the *leuco*-compound **13** with propionaldehyde in isopropanol containing piperidinium acetate (conditions described by Lewis (5)) gave predominantly the 3-propylquinone (**3**). Since we have not found any chromatographic system which will separate the 2- and 3-propyl isomers it is necessary to convert the product to the tri-*O*-methyl ethers to determine isomeric purity; these isomers can be separated by tlc. Degradation of the tri-*O*-methyl ether of **3** by the Hodge procedure was much more complex than in the previous case but did yield *m*-methoxybenzoic acid (9%) and the ester **15** (6%). The tri-*O*-methyl ethers of **2** and **3** show minor differences in their ^1H nmr spectra which we have found to be present in other isomeric pairs. We believe these differences are reliable enough to allow assignment of structures. In the 2-alkyl series the proton resonates at δ_H 7.00 with the methoxyl singlets at 3.94, 3.91, and 3.83 while in the 3-alkyl series the 2-proton absorbs at 6.82 and the methoxyls at 3.94, 3.90, and 3.88. Table 1 summarizes the isomer ratios obtained with a variety of aldehydes using the two alkylation methods.

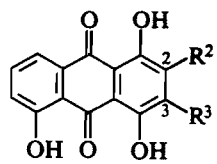

1 $R^2 = R^3 = H$
2 $R^2 = Pr^n$, $R^3 = H$
3 $R^2 = H$, $R^3 = Pr^n$
4 $R^2 = (CH_2)_5OH$, $R^3 = H$
5 $R^2 = (CH_2)_4OH$, $R^3 = H$
6 $R^2 = CH_2CHMe_2$, $R^3 = H$
7 $R^2 = (CH_2)_2OH$, $R^3 = H$
8 $R^2 =$ 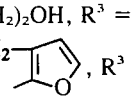 , $R^3 = H$
9 $R^2 = (CH_2)_2C(OCH_2)_2Me$, $R^3 = H$
10 $R^2 = (CH_2)_2COMe$, $R^3 = H$
11 $R^2 = CH(OH)Et$, $R^3 = H$

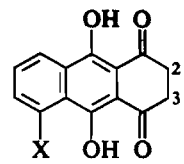

12 X = H
13 X = OH

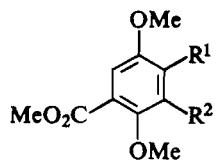

14 $R^1 = Pr^n$, $R^2 = H$
15 $R^1 = H$, $R^2 = Pr^n$

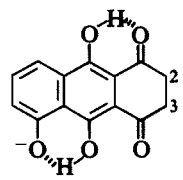

16

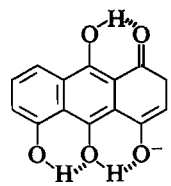

17

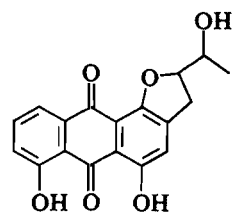

18

We have no definitive experiments pertaining to the origin of the regioselectivity in these reactions; however, titration of *leuco*-5-hydroxyquinizarin indicates that in dilute alkaline

[1]Author to whom correspondence may be addressed.

TABLE 1. Isomer ratios in Marschalk and Lewis condensations

Aldehyde	Conditions[a]	Total yield (%)[b]	Ratio 2-:3-alkylation[c]
EtCHO	A	50	[d]
EtCHO	B	46	1:9
$HO[CH_2]_3CHO$	A	44	7:1
$HO[CH_2]_4CHO$	A	44	9:1
$MeCH(OH)[CH_2]_2CHO$	B	49	1:7
$HOCH_2CHO$	A	50	—

[a]A, Marschalk conditions; B, isopropyl alcohol – piperidinium acetate.
[b]Pure recrystallized material.
[c]Ratios determined after conversion to methylethers.
[d]No 3-alkylation.

solution the bulk species present is a monoanion. This is the likely species present under the conditions of the Marschalk condensation. If the predominant anion present is **16**[2] then the kinetically active species must arise by proton abstraction from position 2 which will generate an enolate stabilized by hydrogen bonding; no such stabilization is available to the enolate arising from proton abstraction from position 3, since the hydrogen bond is stabilizing the oxyanion. Under the Lewis conditions the kinetically reactive species may well be **17**[3] derived from the neutral *leuco*-compound to give, by proton abstraction from position 3, a more stable enolate than that derived from position 2 due to more extensive hydrogen bonding.

With the regioselectivity of the reactions established we turned to the problem of introducing side-chains containing functional groups. Table 1 shows that α-, γ-, and δ-hydroxyaldehydes can be used successfully. Krohn and Radeloff (6) have defined conditions where a wide variety of aldehydes have been successfully condensed with *leuco*-quinizarin and the reaction intercepted at the aldol stage to give 2-(1-hydroxyalkyl)quinizarins after aerial oxidation; we have found this method to be an excellent one using *leuco*-quinizarin but not generally applicable to the 5-hydroxy derivative. However, the protocol described by Shaw and co-workers (7) is an effective method using *leuco*-5-hydroxyquinizarin (**13**). Reaction of 2,3-epoxybutanal with **13** under controlled conditions gave a compound formulated as **18** (ν_{max}: 1665, 1625 cm^{-1}; δ_H: 12.32 (1H, s), 11.93 (1H, s), 7.56 (1H, dd, J = 8.0 and 1.3 Hz), 7.22 (1H, t, J = 8.0 Hz), 7.00 (1H, dd, J = 8.0 and 1.3 Hz), 6.98 (1H, s), 4.93 (1H, td, J = 8.0 and 3.0 Hz), 4.40 (1H, qd, J = 8.0 and 3.0 Hz), 3.72 (1H, bs), 3.17 (2H, m), 1.22 (3H, d, J = 8.0 Hz)). On oxidation with pyridinium chlorochromate a methyl ketone was formed (ν_{max}: 1730, 1660, 1620 cm^{-1}; δ_H: 5.26 (1H, t, J = 7 Hz), 3.45 (2H, d, J = 7 Hz), 2.38 (3H, s)).

The conditions of the Marschalk condensation are not compatible with the presence of certain functionalities in the aldehyde; in particular, leaving groups β to the aldehyde function do not survive. In an effort to define milder conditions for the aldol condensation we attempted to prepare an enamine from *leuco*-quinizarin (**12**); to our surprise, reaction of **12** with pyrrolidine in refluxing toluene gave 1-hydroxyanthraquinone in excellent yield. Application of these conditions to *leuco*-5-hydroxyquinizarin yielded 1,5-dihydroxyanthraquinone. We formulate this reaction as shown in Scheme 1. At lower temperatures amines did not react with *leuco*-quinizarin, but quinizarin (produced by adventitious oxidation) gave amino derivatives. This was confirmed by reaction of quinizarin with pyrrolidine, piperidine, and benzylamine to give the amines of the type **19**. Since a likely mechanism of formation of these compounds is nucleophilic addition followed by aerial oxidation, we investigated the reactions of the quinizarins with carbanions.

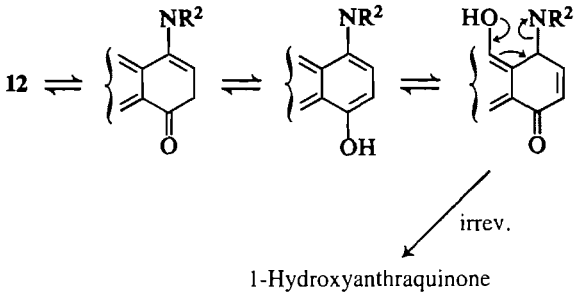

SCHEME 1

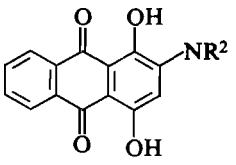

19

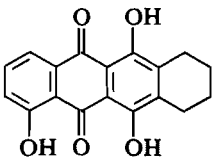

20

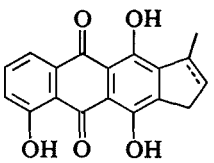

21 (double bond)
22 (without =)

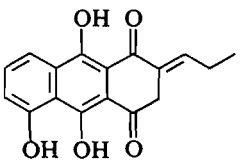

23

Reaction of 5-hydroxyquinizarin with an excess of 1-nitropropane and half that concentration of sodium methoxide in methanol gave the 2-propyl compound **2** in excellent yield. By conversion to the trimethyl ether it was shown, within our detection limits, to be uncontaminated with any of the 3-isomer. 2-Nitropropane and nitromethane gave similar results; in the latter case prolonged reaction gave 2,3-dimethyl-5-hydroxyquinizarin. Reaction with 1,4-dinitrobutane gave the tetracycle **20**, and the ethylene acetal of 4-nitrobutan-2-one produced **9**. We postulate that the regioselectivity is determined in the addition of the nitronate anion to the *unionized* 5-hydroxyquinizarin to give the more stable 3-enolate. In support of this suggestion, no reaction occurs when enough base is present to convert both quinizarin and nitroalkane to their respective anions. Similar arguments can be used to account for regioselectivity in an electron transfer mechanism. When the reaction with 1-nitropropane is carried out in 95% ethanol the likely intermediate **23** can be trapped by water to give, after aerial oxidation, the hydroxypropyl compound **11**.[4]

[2]The huge difference in acidity between 2-acyl-1-naphthols and 2-acyl-1,8-naphthalenediols was established during the structure determination of terramycin (8).

[3]Selective formation of the 3,4-enamine as intermediate instead of **17** was considered but rejected in the expectation that the adduct would undergo aromatization either to the 3-hydroxyalkyl-1,5-dihydroxyanthraquinone (see later) or to the 3-alkyl-1,5-dihydroxy-4-pyrrolidinylanthraquinone. However, the electrophile in the reaction might well be the immonium salt of the aldehyde.

[4]This reaction was discovered by Mr. A. Kumar in these laboratories.

Can. J. Chem. Downloaded from www.nrcresearchpress.com by 210.87.254.4 on 09/06/12
For personal use only.

Can. J. Chem. Downloaded from www.nrcresearchpress.com by 210.87.254.4 on 09/06/12
For personal use only.

In order to test some of the later stages of our proposed synthesis we carried out some model experiments. The alcohol **5** could be oxidized to the aldehyde with pyridinium chlorochromate without oxidation of the quinizarin ring. Dithionite reduction of the aldehyde under Marschalk conditions gave the tetracycle **20**. Hydrolysis of the acetal **9** generated the ketone which, under Marschalk conditions, gave a mixture of **21** and **22**; dithionite reduction of **21** gave **22**.

Experimental

All samples on which accurate mass measurements were determined show a single spot on tlc.

2-n-Propyl-5-hydroxyquinizarin (2)

5-Hydroxyquinizarin (512 mg) was dissolved in 5% NaOH–H_2O and the blue solution adjusted to pH 10 with 10% HCl–H_2O. After warming to 40°C under a N_2 atmosphere a solution of Na_2CO_3 (2 g) and $Na_2S_2O_4$ (1 g) in H_2O (20 mL) was added until the orange *leuco*-anion was formed. Propionaldehyde (348 mg) in H_2O (10 mL) was added over 30 min and the mixture boiled with reflux for 2 h. Heating then ceased and air was passed through the solution for 15 min. After acidification with 10 *M* HCl the precipitate was filtered off, washed with H_2O, dried, and extracted with boiling $CHCl_3$ (4 × 20 mL). The $CHCl_3$ extract was dried and evaporated to give a red solid which on recrystallization from CCl_4 gave the *propyl derivative* (**2**) (300 mg), mp 187–190°C; λ_{max} (EtOH): 233 (40 000), 253 (24 500), 292 (7 800), 466 (9 700), 481 (11 400), 493 (13 000), 514 (9 500), and 527 nm (9 000); δ_H: 1.03 (3H, t, J = 7.5 Hz), 1.73 (2H, m), 2.72 (2H, t, J = 7.5 Hz), 7.09 (1H, s), 7.24 (1H, dd, J = 8 and 1.3 Hz), 7.63 (1H, t, J = 8 Hz), 7.82 (1H, dd, J = 8 and 1.3 Hz), 12.18 (1H, s), 12.25 (1H, s), 13.46 (1H, s). *Anal.* calcd. for $C_{17}H_{14}O_5$: C 68.5, H 4.7%; found: C 68.3, H 4.7%.

The following 2-substituted 5-hydroxyquinizarins were prepared from the aldehydes indicated, in a similar way.

2-(5′-Hydroxypentyl) (**4**) from 5-hydroxypentanal (43%), mp 187–191°C (CCl_4). *Anal.* calcd. for $C_{19}H_{18}O_6$: C 66.7, H 5.3%; found: C 66.4, H 5.4%.

2-(4′-Hydroxybutyl) (**5**) from 4-hydroxybutanal (44%) (CCl_4), mp 195–199°C (CCl_4). *Anal.* calcd. for $C_{18}H_{16}O_6$: C 65.9, H 4.9%; found: C 66.0, H 4.9%.

2-(2′-Hydroxyethyl) (**7**), from hydroxyacetaldehyde (50%) mp >300°C. $C_{16}H_{12}O_6$ requires M^+: 300.0634; found: 300.0629.

2-(2′-Methyl-3′-furyl)methyl (**8**) from 2-methylfuran-3-carboxaldehyde (72%), mp 215–218°C (CCl_4). *Anal.* calcd. for $C_{20}H_{14}O_6$: C 68.6, H 4.0%; found: C 68.6, H 4.0%.

2-Ethyl- from acetaldehyde (67%), mp 125–128°C (Me_2CO). *Anal.* calcd. for $C_{16}H_{12}O_5$: C 67.6, H 4.3%; found: C 67.9, H 4.4%.

2-(2′-Methylpropyl) from 2-methylpropanal (63%), mp 196–199°C (Me_2CO). *Anal.* calcd. for $C_{18}H_{16}O_5$: C 69.2, H 5.2%; found: C 69.6, H 5.6%.

The ether (**18**) from 2,3-epoxybutanal (80%), mp >205°C (dec.) (CCl_4). $C_{18}H_{14}O_6$ requires M^+: 326.0790; found: 326.0785.

Oxidation of **18** with pyridinium chlorochromate gave a ketone, mp >180°C (dec.). ν_{max}: 1720 cm^{-1}; δ_H: 2.40 (3H, s), 3.45 (2H, d, J = 7 Hz), 5.28 (1H, t, J = 7 Hz), 12.11 (1H, s), 12.54 (1H, s).

2-(Cyclopent-3′-enyl)methyl from cyclopent-3-ene carboxaldehyde (42%), mp 199–201°C (sublimation). *Anal.* calcd. for $C_{20}H_{16}O_5$: C 71.4, H 4.8%; M^+: 336.0998; found: C 71.3, H 4.8%; M^+: 336.0991.

2-n-Propyl-1,4,5-trimethoxyanthracene-9,10-dione

2-*n*-Propyl-5-hydroxyquinizarin (**2**) (122 mg) was boiled with reflux in dimethoxyethane (15 mL) containing NaH (400 mg of 50% dispersion in oil) and MeI (1 g) for 12 h. Addition of Et_2O, filtration, and evaporation of solvent gave a brown paste which was washed with pentane, 2 *M* HCl, and extracted with Et_2O. Removal of solvent gave a gum which was purified by plc on silica gel GF254 eluting with EtOAc–Et_2O (5:3) to give the *ether* (58 mg), mp 49–52°C; δ_H: 1.00 (3H, t, J = 7.5 Hz), 1.66 (2H, m), 2.66 (2H, t, J = 7.5 Hz), 3.83 (3H, s), 3.91 (3H, s), 3.94 (3H, s), 6.98 (1H, s), 7.00 (1H, dd, J = 8 and 2 Hz), 7.46 (1H, t, J = 8 Hz), 7.61 (1H, dd, J = 8 and 2 Hz). $C_{20}H_{20}O_5$ requires M^+: 340.1310; found: 340.1304.

Cleavage of 2-n-propyl-1,4,5-trimethoxyanthracene-9,10-dione

The ether (56 mg) in dimethoxyethane (15 mL) containing KOBu′ (250 mg) and H_2O (12 mg) was boiled with reflux under a N_2 atmosphere for 4 h. Brine (20 mL) was added and the solution extracted with Et_2O (2 × 30 mL). Acidification of the aqueous layer, extraction with EtOAc, and concentration of the dried extract gave a gum which was treated with CH_2N_2–Et_2O. Removal of solvent gave a gum which was resolved by plc on silica gel GF254 by eluting with pentane–Et_2O (4:3) into methyl 3-methoxybenzoate (6 mg) (identical to an authentic specimen) and *methyl 2,5-dimethoxy-4-n-propylbenzoate* (11 mg); δ_H: 0.96 (3H, t, J = 7.5 Hz), 1.62 (2H, m), 2.57 (2H, t, J = 7.5 Hz),, 3.69 (3H, s), 3.71 (6H, s), 6.65 (1H, bs), 7.27 (1H, s). $C_{13}H_{18}O_4$ requires M^+: 238.1205; found: 238.1205.

Synthesis of methyl 2,5-dimethoxy-4-n-propylbenzoate

1,4-Dimethoxybenzene (2.76 g) and propionic acid (2.22 g) were dissolved in polyphosphoric acid (120 mL) and the solution stirred at 70°C for 2 h. H_2O (100 mL) was cautiously added and the mixture extracted with Et_2O (2 × 100 mL). The ethereal layer was washed with saturated $NaHCO_3$–H_2O, H_2O, dried, and concentrated to give *2-propionyl-1,4-dimethoxybenzene* (3.69 g) as a low melting (ca. 8°C) solid. *Anal.* calcd. for $C_{11}H_{14}O_3$: C 68.0, H 7.3%; found: C 68.2, H 7.3%. An amalgam was prepared from $HgCl_2$ (150 mg), Zn dust (2 g) in 10 *M* HCl (5 mL) was added to the ketone (970 mg) suspended in H_2O (20 mL), and the mixture boiled with reflux for 5 h. During this time 10 *M* HCl was added in portions (5 × 1 mL). After 18 h at ambient temperature the mixture was extracted with Et_2O (3 × 15 mL), the extract washed with saturated $NaHCO_3$–H_2O, H_2O, dried, and concentrated to give a brown oil which on bulb-to-bulb distillation gave *2,5-dimethoxy-1-n-propylbenzene* (430 mg). *Anal.* calcd. for $C_{11}H_{16}O_2$: C 73.3, H 9.0%; found: C 73.7, H 9.0%. The ether (400 mg) in CS_2 (10 mL) was slowly added to powdered $AlCl_3$ (355 mg) in CS_2 (20 mL) at 0°C. After 17 h the mixture was poured on to ice and 10 *M* HCl (1 mL) added. Extraction with Et_2O (3 × 15 mL) gave, after washing with H_2O, drying, and concentration, an oil which was chromatographed on silica gel; elution with pentane–Et_2O (3:1) gave starting ether (149 mg) and *2,5-dimethoxy-4-n-propylacetophenone*, mp 38–39°C (pentane). *Anal.* calcd. for $C_{13}H_{18}O_3$: C 70.3, H 8.1%; found: C 70.7, H 8.1%. The ketone (30 mg) in dioxan (0.3 mL) was added to 5% NaOCl–H_2O (15 mL) and 10% NaOH–H_2O (1 mL). After heating for 2 h on a steam bath, the cooled solution was extracted with Et_2O and the aqueous layer acidified and extracted with EtOAc (3 × 10 mL). Drying and concentration of the EtOAc extract gave a gum which was treated with CH_2N_2–Et_2O. Preparative layer chromatography of the product on silica GF254 and elution with pentane–Et_2O (4:3) gave methyl 2,5-dimethoxy-4-*n*-propylbenzoate identical with the material obtained from degradation of the ether by nmr, ir, and mass spectroscopy and tlc.

3-n-Propyl-1,4,5-trihydroxyanthraquinone

leuco-5-Hydroxyquinizarin (**13**) (1.087 g) was suspended in EtOH (70 mL) and the mixture warmed to 60°C under a N_2 atmosphere. Propanal (3.6 g) was added, followed by piperidinium acetate (665 mg) in EtOH (5 mL). After boiling with reflux for 3 h, the cooled solution was carefully acidified with 5 *M* HCl. The red precipitate was filtered off, dried (828 mg), and recrystallized from CH_2Cl_2 to give the *3-n-propylquinone* (**3**) (744 mg), mp 193°C. *Anal.* calcd. for $C_{17}H_{14}O_5$: C 68.5, H 4.7%; found: C 67.9, H 4.4%.

1-Hydroxyanthraquinone

leuco-Quinizarin (**12**) (242 mg) in PhMe (150 mL) was refluxed under a N_2 atmosphere in a Dean-Stark apparatus. Pyrrolidine (71 mg) in PhMe (20 mL) was added and the solution boiled with reflux until no more H_2O separated (ca. 4 h). The solid obtained after evaporation of solvent was extracted with hot Me_2CO (3 × 50 mL). Evaporation of the Me_2CO extracts gave a dark yellow solid which was extracted with hot CCl_4 (3 × 50 mL). Evaporation of this extract and recrystallization of the residue from Me_2CO gave the quinone (186 mg),

Can. J. Chem. Downloaded from www.nrcresearchpress.com by 210.87.254.4 on 09/06/12
For personal use only.

mp 194–195°C.

Similar reaction of *leuco*-5-hydroxyquinizarin gave 1,5-dihydroxyanthraquinone.

When Et_2O was substituted for $PhCH_3$ the *amine* **19** was obtained, mp 219–220°C (CCl_4): λ_{max}: 223 (19 000), 235 (16 300), 281 (15 000), 513 (8 700), 545 (15 700), 577 nm (11 500); δ_H: 14.65 (1H, s), 14.28 (1H, s), 8.2 (2H, m), 7.4 (2H, m), 5.93 (1H, s), 3.6 (4H, m), 1.95 (4H, m). $C_{18}H_{15}NO_4$ requires M^+: 309.1001; found: 309.1000. This product was shown to arise from quinizarin produced by oxidation of the *leuco*-compound.

Reactions of 5-hydroxyquinizarin with nitronate anions

5-Hydroxyquinizarin (256 mg) was suspended in EtOH (100 mL) and a NaOEt solution (*ex.* 112 mg Na and 20 mL EtOH) added, forming a blue solution. 1-Nitropropane (890 mg) was added and the solution boiled with reflux until no starting quinone remained (ca. 24 h). The cooled solution was acidified with 10 *M* HCl, extracted with $CHCl_3$, and the dried extract concentrated to give a red solid which, on recrystallization from CCl_4, gave the propyl compound (**2**) (197 mg) identical to that previously prepared and confirmed to be the 2-isomer by conversion to the trimethyl ether.

The following 2-substituted 5-hydroxyquinizarins were prepared in the same manner from the nitro compound indicated.

2-Me (70%), mp 216–218°C (Me_2CO) from $MeNO_2$.

2-Pr^i (53%), mp 187–189°C (Me_2CO) from Pr^iNO_2. $C_{17}H_{14}O_5$ requires M^+: 298.0841; found: 298.0833.

2-$(CH_2)_2C(OCH_2)_2Me$ (66%), mp 194–195°C (CCl_4) from $MeC(OCH_2)_2(CH_2)_2NO_2$. *Anal.* calcd. for $C_{20}H_{18}O_7$: C 64.9, H 4.9%; found: C 64.9, H 4.9%.

2,3-$(CH_2)_4$ (47%), mp sublimes ca. 220°C.

*Preparation of the tetracycle (**20**)*

The alcohol **5** (74 mg) in CH_2Cl_2 (25 mL) was added to a stirred suspension of pyridinium chlorochromate (150 mg) in CH_2Cl_2 (20 mL). After 2 h the mixture was filtered through Celite, after the addition of Et_2O (50 mL). The residues were washed with Et_2O (3 × 15 mL). The combined filtrates were shaken with 5% $NaHCO_3$–H_2O (2 × 30 mL), 1 *M* HCl (30 mL), and then 5% NaOH–H_2O. Acidification of the latter extract and extraction with CH_2Cl_2 (2 × 25 mL) gave the *aldehyde* (44 mg), mp 171–175°C; ν_{max}: 1720 cm^{-1}; δ_H: 9.8 (1H, t, J = 1.5 Hz). *Anal.* calcd. for $C_{18}H_{14}O_6$: C 66.3, H 4.3%; found: C 66.0, H 4.7%.

The aldehyde (31 mg) in 1% NaOH–H_2O (20 mL) was warmed to 90°C and 5% $Na_2S_2O_4$–H_2O added until the blue colour was discharged. After 5 h at 90°C a current of air was passed through the cooled solution for 5 min. Acidification with 1 *M* HCl, extraction with CH_2Cl_2, and drying and concentration of the extract gave the *tetracycle* **20** (24 mg), mp sublimes ca. 220°C. *Anal.* calcd. for $C_{18}H_{14}O_5$: C 69.7, H 4.6%; M^+: 310.0841; found: C 69.5, H 4.7%; M^+: 310.0839.

*2-(1′-Hydroxypropyl)-5-hydroxyquinizarin (**11**)*

5-Hydroxyquinizarin (512 mg) was suspended in 95% EtOH–H_2O (200 mL) and NaOEt in 95% EtOH (*ex.* Na 230 mg and 20 mL solvent) added. After boiling with reflux for 24 h, the cooled solution was acidified with 10% HCl–H_2O and extracted with $CHCl_3$ (3 × 25 mL). Concentration of the dried solution gave the *alcohol* **11** (320 mg), mp 216°C ($CHCl_3$); δ_H: 14.03 (1H, s), 13.46 (1H, s), 13.29 (1H, s), 7.83 (1H, dd, J = 8 and 1.8 Hz), 7.65 (1H, t, J = 8 Hz), 7.41 (1H, t, J = 0.6 Hz), 7.25 (1H, dd, J = 8 and 1.8 Hz), 4.91 (1H, bd, J = 5.6 Hz), 1.78 (2H, m), 0.94 (3H, t, J = 8 Hz). $C_{17}H_{14}O_6$ requires M^+: 314.0790; found: 314.0785.

*Hydrolysis of acetal (**9**)*

The acetal **9** (370 mg) was dissolved in hot Me_2CO (150 mL) and 5% HCl–H_2O (70 mL) added. After 10 h at ambient temperature the Me_2CO was removed *in vacuo* and the solid recrystallized from $CHCl_3$–pentane to give the *ketone* **10** (287 mg), mp 189–190°C; ν_{max}: 1720 cm^{-1}; δ_H: 2.99 (2H, t, J = 8.2 Hz), 2.84 (2H, t, J = 8.2 Hz), 2.18 (3H, s). $C_{18}H_{14}O_6$ requires M^+: 326.0790; found: 326.0781.

*Cyclization of the ketone (**10**)*

The ketone (163 mg) was dissolved in 5% NaOH–H_2O (70 mL) under a N_2 atmosphere and $Na_2S_2O_4$ (500 mg) in H_2O (20 mL) added. After $\frac{1}{2}$ h at 80°C the mixture was acidified and extracted with $CHCl_3$. Concentration of the dried extract gave a solid which on crystallization from $CHCl_3$–pentane gave a fraction rich in **21**, while the mother liquours contained mainly **22**. Complete separation could be effected by sublimation at 150°C/0.01 Torr (1 Torr = 133.32 Pa) when the sublimate was found to be the *cyclopentane* **22** (92 mg), mp 187–189°C; δ_H: 1.04 (3H, d, J = 8.5 Hz). $C_{18}H_{14}O_5$ requires M^+: 310.0841; found: 310.0838. The residue was found to be the *cyclopentene* **21** (54 mg), mp 193–196°C; δ_H: 2.46 (3H, bs), 6.50 (1H, m). $C_{18}H_{12}O_5$ requires M^+: 308.0684; found: 308.0674. Reduction of **21** with $Na_2S_2O_4$ under the reaction conditions formed **22** in quantitative yield.

Acknowledgements

We wish to thank the S.E.R.C. and I.C.I. Organics Division for financial support, I.C.I. for the gift of chemicals, and Dr. C. W. Greenhalgh for most helpful advice and discussion.

1. F. Arcamone, G. Franceschi, P. Orezzi, G. Cassinelli, and R. Mondelli. J. Am. Chem. Soc. **86**, 5335 (1965); V. A. Sharin, V. S. Bashanov, L. A. Averbush, G. N. Lepeshkina, and A. M. Grunschtein. Antibiotiki, **18**, 681 (1973).
2. C. Marschalk, F. Koenig, and N. Ourousoff. Bull. Chim. Soc. Fr. 1545 (1936).
3. H. Brockmann and W. Müller. Chem. Ber. **91**, 1920 (1958).
4. D. G. Davies and P. Hodge. J. Chem. Soc. (C), 3158 (1971).
5. C. E. Lewis. J. Org. Chem. **35**, 2938 (1970).
6. K. Krohn and M. Radeloff. Chem. Ber. **111**, 3823 (1978).
7. D. J. Mincher, G. Shaw, and E. De Clercq. J. Chem. Soc. Perkin Trans. 1, 613 (1983).
8. F. A. Hochstein, C. R. Stephens, L. H. Conover, P. P. Regna, R. Pasternack, P. N. Gordon, F. J. Pilgrim, K. J. Brunings, and R. B. Woodward. J. Am. Chem. Soc. **75**, 5455 (1953).

A new route to the *cis–anti–cis* triquinane ring system. The synthesis of 4,4-dimethyltricyclo[6.3.0.0^{2,6}]undecan-3-one via β-enolate rearrangement[1]

HEMANT A. PATEL AND J. B. STOTHERS
Department of Chemistry, University of Western Ontario, London, Ont., Canada N6A 5B7

Received March 9, 1984

This paper is dedicated to Professor Paul de Mayo on the occasion of his 60th birthday

HEMANT A. PATEL, and J. B. STOTHERS. Can. J. Chem. **62**, 1926 (1984).

A synthesis of *cis*, *anti*, *cis*-4,4-dimethyltricyclo[6.3.0.0^{2,6}]undecan-3-one is described in which the key step is β-enolate rearrangement of 9,9-dimethyltricyclo[5.3.1.0^{1,5}]undecan-10-one proceeding with retention of configuration. The required [5.3.1.0^{1,5}] ketone was prepared in six steps from tricyclo[5.2.1.0^{1,5}]dec-8-ene. This sequence constitutes a new route to the tricyclo[6.3.0.0^{2,6}]undecane ring system characteristic of the hirsutane sesquiterpenes. The ^{13}C data for several tricyclic derivatives are reported.

HEMANT A. PATEL, et J. B. STOTHERS. Can. J. Chem. **62**, 1926 (1984).

On décrit une synthèse de la diméthyl-4,4 tricyclo[6.3.0.0^{2,6}]undécanone-3 *cis*, *anti*, *cis* dans laquelle l'étape déterminante est une transposition β-énolique de la diméthyl-9,9 tricyclo [5.3.1.0^{1,3}]undécanone-10 qui se produit avec une rétention de configuration. On a préparé la cétone [5.3.1.0^{1,5}] requise en six étapes à partir du tricyclo[5.2.1.0^{1,5}]décène-8. Cette série de réaction constitue une nouvelle voie permettant de préparer le système tricyclo[6.3.0.0^{2,6}]undécane qui est caractéristique des sesquiterpènes hirsutanes. On rapporte les données de la rmn du ^{13}C pour plusieurs dérivés tricycliques.

[Traduit par le journal]

The discovery and characterization of several naturally occurring compounds having the linearly fused tricyclopentanoid ring system of *cis*, *anti*, *cis*-tricyclo[6.3.0.0^{2,6}]undecane, such as hirsutene (**1**) and coriolin (**2**), have attracted considerable interest since many of these materials exhibit anti-tumor and (or) antibiotic activity (1). An array of synthetic routes to **1**, **2**, and congeners has been described (2) including, from this laboratory (3), a sequence leading to **1** which utilizes a stereocontrolled β-enolate rearrangement for the generation of the ring system. The key step is the conversion of **3** → **4**[2] via proton abstraction from C-11 in **3** with the stereochemistry of the subsequent rearrangement constrained to give the correct configuration at C-8 in **4**. Through our interest in the potential of homoenolate rearrangement for the generation of less accessible polycyclic carbon skeletons, we have investigated other possible routes to the [6.3.0.0^{2,6}] system. In this report, we wish to describe the formation of 4,4-dimethyltricyclo-[6.3.0.0^{2,6}]undecan-3-one (**5**) in reasonable yield by β-enolization of 9,9-dimethyltricyclo[5.3.1.0^{1,5}]undecan-10-one (**6**).[2]

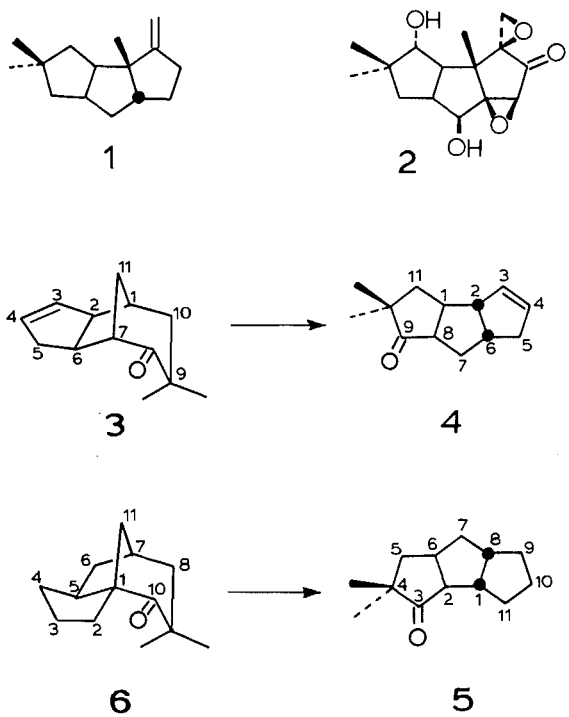

The required tricyclic ketone **6** was prepared from the known epoxide **7** (4) as outlined in Scheme 1. After heating **7** under reflux with lithium triethyl borohydride ("Super Hydride") in THF (5), the product was oxidized with alkaline peroxide to furnish a 85:15 mixture of alcohols **8** and **9** which were separable by flash chromatography (6). Pyridine – chromic acid oxidation (7) of **8** furnished the corresponding ketone **10***a* in high yield. The generation of the homologous ketone **12** via cyclopropanation of the silyl enol ether of **10***a* followed by homoketonization failed, in sharp contrast to the behavior of the isomeric **11***a* which is readily transformed to **14** by this route (8). Each of several attempts, under a variety of conditions, gave a complex mixture of unidentified products. As an alternative, the Tiffeneau–Demjanov ring expansion (9) was examined and found to be satisfactory although less efficient because of the concomitant formation of the unwanted isomer **13**. Treatment of **10***a* with trimethylsilyl cyanide (10) gave the trimethylsilyl cyanohydrin ether **10***b*, which was reduced to the β-aminoalcohol **10***c* with lithium aluminium hydride. Reaction of **10***c* with nitrous acid furnished a 2:1 mixture of ketones **12** and **13** which were separated by flash chromatography. The overall yield for the ring expansion of **10***a* → **12** and **13** was 80%. Ketones **12** and **13** were easily distinguished by their ^{13}Cmr spectra since the quaternary carbon signals appeared at 66.1 and 52.6 ppm, respectively. The 13.5 ppm downfield shift of this signal in **12** is readily attributed to the α-carbonyl group. The identity of these ketones was confirmed by carrying alcohol **9** through the same series of reactions to a 64:36 mixture of two ketones in 74% yield. These two ketones were separated

[1]Part 110 in the series ^{13}Cmr studies; for Part 109 see ref. 8.

[2]With the skeletal rearrangement, a different numbering scheme is required as indicated in the formulas.

Can. J. Chem. Downloaded from www.nrcresearchpress.com by 210.87.254.6 on 09/06/12
For personal use only.

TABLE 1. ^{13}C shielding data[a] for **X–Y**

Compound	C-1	C-2	C-3	C-4	C-5	C-6	C-7	C-8	C-9	C-10	C-11	Other
7	57.2	25.7	26.9	30.9	46.2	34.3	40.4	52.5	54.7	29.2		
10*b*	65.3	24.5	25.9	33.2	38.2	38.9	38.2	46.3	74.6	39.5		123.0 (CN) 1.1 (Me_3Si)
10*c*	62.8	24.1	25.5	32.1	39.7	(39.2)	37.8	42.9	76.9	(39.6)		49.6 (CH_2NH_2)
11*b*	56.3	28.3	25.3	33.3	46.3	31.4	51.7	73.5	50.9	40.0		123.7 (CN) 1.1 (Me_3Si)
11*c*	56.3	29.1	25.8	33.5	(46.9)	32.8	(46.6)	78.7	47.4	41.0		50.7 (CH_2NH_2)
10*a*	67.3	21.8	27.4	32.7	46.0	35.9	36.8	44.5	216.2	40.7		
8,8-Me_2-**10***a*[b]	67.6	22.5	27.5	33.1	46.2	32.4	48.0	47.3	220.5	38.6		23.1 (*exo*-Me) 21.8 (*endo*-Me)
12[b]	66.1	28.1	27.0	35.1	48.7	38.0	38.0	31.6	35.8	213.3	42.9	
6[b]	65.2	29.4	26.7	34.9	47.1	39.8	37.6	45.3	42.4	217.6	39.3	31.7, 31.8 (Me's)
13[b]	52.6	35.1	26.2	36.3	47.1	40.1	37.8	48.7	212.2	55.9	42.2	

[a]In ppm from internal TMS in $CDCl_3$ solutions; assignments for similar values in parentheses may be interchanged.
[b]Assignments obtained from 2D INADEQUATE spectra.

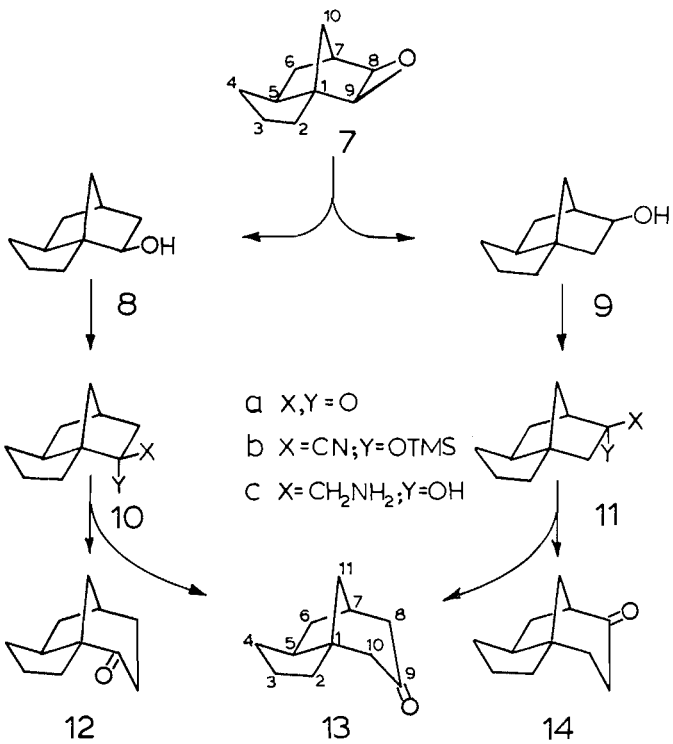

SCHEME 1

by flash chromatography and the major ketone was found to be identical (ir, ^{1}Hmr, ^{13}Cmr, ms) to the known **14** (8). The spectral properties of the minor ketone were the same as those for **13**. Dimethylation of **12** with sodamide – ether – methyl iodide gave the required **6** in 69% yield.

As part of their characterization, the ^{13}Cmr spectra of **6**, **7**, and **10**–**13** were recorded and the shielding data are collected in Table 1. The assignments for the [5.2.1.$0^{1,5}$] derivatives followed from the observed trends throughout the series with due regard for the expected substituent effects and by comparison with the previously reported data for **8**, **9**, and **11***a* (8). In addition, unequivocal assignments for the 8,8-dimethyl derivative of **10***a*, available from another project, were obtained from its two-dimensional, double quantum coherence spectrum (11). Similarly, the 2D INADEQUATE spectra for **6**, **12**, and **13** furnished definitive assignments as listed in Table 1.

Having **6** in hand, we were able to examine its behavior under typical homoenolization conditions. From our earlier study of the simpler 3,3-dimethylbicyclo[3.2.1]octan-2-one under such conditions (12), we could anticipate β-proton abstraction to occur at either, or both, C-5 and -11 to generate, in principle, β-enolates **15** and **16**, respectively. Subsequent cleavage of these β-enolates via mode b (Scheme 2) would lead to the formation of **6** and **5**, respectively. It is significant that, in either case, cleavage b must occur with retention of configuration at the carbon picking up the proton (C-1 in the original skeleton). Although the majority of examples of β-enolate cleavage, for which the stereochemistry has been examined, proceed primarily with inversion of configuration, there are some systems which exhibit a high degree of retention (13). In the present cases of **15** and **16**, inversion of configuration for cleavage via b would lead to a *trans* ring junction in the resulting ketones, each of which is a substituted [3.3.0] system. However, in the parent [3.3.0] system, the *trans* arrangement is disfavored by ca. 6 kcal/mol relative to the *cis* (14). Thus, retention of configuration upon cleavage of **15** and **16** would be expected. It may be noted that for **15** cleavage by either a or b should proceed with retention and that mode b merely constitutes a racemization pathway for **6**. In the case of **16**, cleavage a must proceed with inversion and b with retention.

Treatment of **6** with *t*-BuO^-/*t*-BuOH at 185°C for extended reaction times gave a neutral fraction in 69% yield which was isolated by ether extraction. This fraction consisted of two ketones in a ratio of ca. 1:2; the minor component of the mixture was shown to be **6** after separation by flash chromatography. The major ketonic product was found to be isomeric having the molecular formula $C_{13}H_{20}O$, by precise mass measurement, and to contain a five-membered ring ketone according to its carbonyl absorption (1730 cm^{-1} ($CHCl_3$), δ_c 225.1). Thus the compound could be assigned structure **5** arising by proton abstraction at C-11 in **6** to form **16**, or an equivalent β-enolate, which is cleaved with protonation occurring at C-1 with retention of configuration thereby generating the *cis*-1,8 ring junction in the *cis*, *anti*, *cis* [6.3.0.$0^{2,6}$] skeleton, which is the ring system of the hirsutanes. To confirm this structural assignment, **5** was converted to the corresponding hydrocarbon **17** by Wolff–Kishner reduction (15) in 80% yield. The same hydrocarbon **17** (by ir, ^{1}Hmr, ^{13}Cmr) was found to arise by Wolff–Kishner reduction of a mixture of **18** (1*b*) and its 5-oxo isomer. The latter mixture had been syn-

Can. J. Chem. Downloaded from www.nrcresearchpress.com by 210.87.254.6 on 09/06/12
For personal use only.

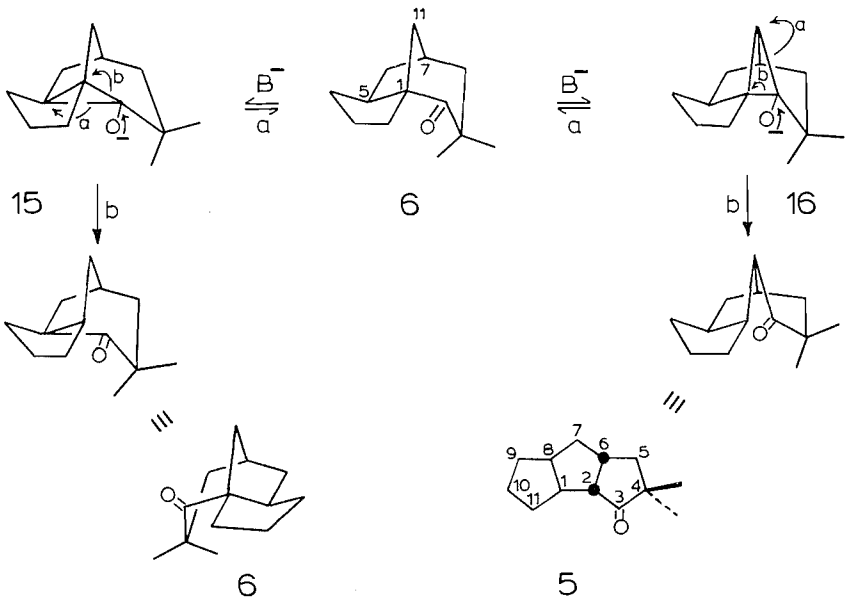

SCHEME 2

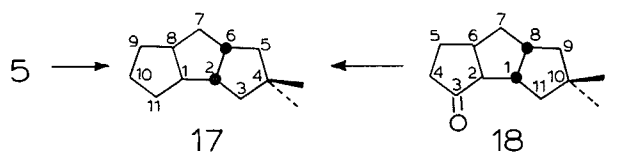

thesized in our sequence leading to hirsutene (**1**) (3).

With the identification of ketone **5** we have established a second route via β-enolate rearrangement to the tricyclo-[6.3.0.$0^{2,6}$]undecane ring system. In this case, the required configuration at C-6 and -8 in **5** is present at the outset (C-5 and -7 in **6**), while the constraints of the ring system govern the stereochemistry at C-1 and -2 leading to the desired *cis*, *anti*, *cis* arrangement of the three cyclopentane rings. It may be noted that, in contrast to the route to the hirsutanes via **4** (3), the rearrangement of **6** → **5** places oxygen at the appropriate carbon in the dimethylated ring of the system for the coriolin family of compounds. Thus this sequence may be capable of adaption for the synthesis of these derivatives and their analogs. Further studies directed toward this goal are in hand.

Experimental

Melting points and boiling points are uncorrected. Thin layer chromatography (tlc) was done on Kiesel gel 60 F_{254} plates and flash chromatography (fc) columns were prepared as described in the literature (6). Tetrahydrofuran (THF) and ether were distilled from Na/benzophenone just before use. Pyridine and *tert*-butyl alcohol were distilled from CaH_2 and stored over 4A molecular sieves. The following compounds were prepared by known methods and gave satisfactory physical and spectral data: pent-4-en-1-ol (16), pent-4-enylcyclopentadienes (4), and **7** (4).

Infrared spectra were recorded with a Beckman 4250 spectrophotometer. Mass spectra were obtained on a Varian MAT-311A system at 70 eV (direct inlet). Routine ^{1}Hmr spectra were recorded on a Varian T-60 instrument while data for pure samples were obtained with a Varian XL-200 spectrometer. The latter instrument was used to record the ^{13}C spectra (50.3 MHz) and comparison of the fully decoupled spectra with those obtained with either the APT (17) or INEPT (18) sequences served to identify the methyl, methylene, methine, and quaternary signals. The 2D INADEQATE spectra (11) were obtained with the CCC2D pulse sequence of the XL software using a 2048 × 128 data point matrix transforming 2048 and 512 points, respectively, with the following sweep widths in both domains: 2000 (**13**), 2200 (**6** and **12**), and 2500 Hz (8,8-Me_2-**10***a*). The ^{13}C data are collected in Table 1.

exo-*Tricyclo[5.2.1.$0^{1,5}$]decan-9-ol (8)*

To a stirred solution of $LiEt_3BH$ in THF (20 mL, 1.0 *M*, 0.02 mol) under N_2 was added **7** (1.5 g, 0.01 mol) in THF (3.0 mL) at room temperature and the solution heated under reflux for 15 h. After cooling, excess reagent was destroyed by the addition of cold water (1 mL) before adding aqueous NaOH (10 mL, 3 *M*). After the cautious slow addition of H_2O_2 (10 mL, 30%) and MeOH (10 mL), the reaction mixture was stirred at room temperature for 24 h. Upon saturation of the mixture with solid NaCl, the THF layer was separated and the aqueous layer extracted with Et_2O (3 × 50 mL). The combined extracts were dried over $MgSO_4$ and then the solvent was evaporated to furnish a mixture of **8** and **9** (1.38 g, 91%) in a 85:15 ratio which was separable by fc (Et_2O – petroleum ether, 30:70). Alcohol **8** (1.5 g): mp 35–36°C; alcohol **9** (0.2 g): mp 47–49°C (lit. (4) mp 45–49°C).

*Tricyclo[5.2.1.$0^{1,5}$]decan-9-one (10*a*)*

Alcohol **8** was added to a stirred solution of CrO_3 (3.0 g, 0.03 mol) in pyridine (4.74 g, 0.06 mol) and methylene chloride (75 mL) at room temperature and the stirring continued for 1.5 h. After decantation of the liquid from the black residue, it was washed sequentially with aqueous NaOH (2 × 50 mL, 10%), aqueous HCl (50 mL, 10%), aqueous $NaHCO_3$, and water, before drying over $MgSO_4$. Upon evaporation of the solvent, the desired ketone (0.67 g, 88%) was isolated, bp 56°C/0.8 Torr (1 Torr = 133.3 Pa).

Tricyclo[5.3.1.$0^{1,5}$]undecan-10-one (12)

Trimethylsilylcyanide (0.73 g, 7.4 mmol) was added to a stirred mixture of **10***a* (1.0 g, 6.7 mmol) and $ZnBr_2$ (10 mg) under N_2 at room temperature and the stirring continued for 24 h. Removal of excess reagents afforded **10***b* (1.6 g, 96%); ir ($CHCl_3$): 2220 cm^{-1}; ^{1}Hmr ($CDCl_3$) δ: 0.25 (s, 9H, Me_3Si), 1.1–2.47 (complex absorption).

Cyanohydrin **10***b* in THF (3 mL) was added to a stirred suspension of LAH (0.54 g, 1.42 mmol) in THF (25 mL) under N_2 and the mixture heated under reflux for 12 h before destruction of the excess LAH by the addition of cold water. The precipitate was removed by filtration, washed with ether, and the washings added to the THF solution before drying over $MgSO_4$. Evpoaration of the solvent afforded aminoalcohol **10***c* (1.12 g, 97%); ir ($CHCl_3$): 3440 cm^{-1}.

The total product **10***c* was dissolved in acetic acid (2.5 mL) and water (14 mL); to this solution was added a solution of $NaNO_2$ (0.87 g, 12.6 mmol) in water (5 mL) at 0°C. After stirring at 0°C for

Can. J. Chem. Downloaded from www.nrcresearchpress.com by 210.87.254.6 on 09/06/12
For personal use only.

Can. J. Chem. Downloaded from www.nrcresearchpress.com by 210.87.254.6 on 09/06/12
For personal use only.

3.5 h, the solution was allowed to stir overnight at room temperature before the product was extracted with ether (3 × 50 mL). The extracts were washed with H_2O, 10% $NaHCO_3$, and H_2O before drying over $MgSO_4$. Evaporation of the solvent gave a yellow oil which was distilled to yield a 2:1 mixture of **12** and **13** as a colorless liquid (0.87 g, 80% overall yield). The ketones were separated by fc (ether − petroleum ether, 10:90). Ketone **12**: bp 64°C/0.2 Torr; ir ($CHCl_3$): 1700 cm^{-1}; ^{1}Hmr ($CDCl_3$) δ: 0.97−2.67 (complex absorption): ms, *m/e* (relative intensity): 164 (M^+, 40), 135 (87), 120 (100), 107 (39), 93 (22), 92 (18), 79 (60). *Exact Mass* calcd. for $C_{11}H_{16}O$: 164.12011; found: 164.12012. Ketone **13**: bp 64°C/0.2 Torr: ir ($CHCl_3$): 1710 cm^{-1}; ^{1}Hmr ($CDCl_3$) δ: 0.97−2.77 (complex absorption); ms, *m/e* (relative intensity): 164 (M^+, 100), 134 (45), 121 (50), 106 (26), 95 (23), 81 (34), 79 (32). *Exact Mass* calcd. for $C_{11}H_{16}O$: 164.12011; found 164.12012.

Tricyclo[5.3.1.0^{1,5}]undecan-9-one (13)

Ketone **11***a* (130 mg, 0.87 mmol), prepared in 86% yield from **9** according to the procedure described above for **10***a*, was converted to the silyloxy cyanohydrin **11***b*, thence to **11***c*, and was treated with nitrous acid in a manner exactly analogous to that described above for **10***a*; **11***b* and *c* were characterized by their ^{13}Cmr spectra (see Table 1). This sequence furnished a 64:36 mixture of two ketones (105 mg, 74% overall yield) which were readily separated by fc; the major component was identical to the previously reported **14** (8) and the minor product was **13**, exhibiting the same properties as those listed above.

9,9-Dimethyltricyclo[5.3.1.0^{1,5}]undecan-10-one (6)

To a stirred suspension of $NaNH_2$ (832 mg, 21.3 mmol) in Et_2O (40 mL) under N_2 was added, over 5 min, **12** (700 mg, 4.27 mmol) in Et_2O (5 mL) at room temperature and the mixture was refluxed for 3.5 h. After cooling, methyl iodide (3.64 g, 25.6 mmol) was added slowly and the mixture refluxed overnight before a second addition of MeI (606 mg, 4.27 mmol). After refluxing for 2.5 h, the mixture was cooled and diluted with water (25 mL). The ether layer was separated and the aqueous layer extracted with ether (4 × 25 mL). The combined extracts were washed with water, dried over $MgSO_4$, and concentrated to provide **6** (560 mg, 69%) as a colorless liquid, bp 2°C/0.1 Torr; ir ($CHCl_3$): 1692 cm^{-1}; ^{1}Hmr ($CDCl_3$) δ: 1.135 (s, 3H, Me), 1.197 (s, 3H, Me), 1.27−2.07 (complex absorption, 11H), 2.36 (m, 2H), 2.50 (m, 1H); ms, *m/e* (relative intensity): 192 (M^+, 46), 177 (20), 135 (100), 121 (33), 120 (42), 107 (98), 96 (21), 79 (55). *Exact Mass* calcd. for $C_{13}H_{20}O$: 192.15141; found: 192.15172.

cis, anti, cis-*4,4-Dimethyltricyclo[6.3.0.0^{2,6}]undecan-3-one (5)*

A solution of **6** (137 mg, 0.713 mmol) in *t*-BuO^-/*t*-BuOH (2.7 mL, H_2O content: 266 μg/mL; prepared from potassium metal (0.111 g) and *t*-BuOH (2.7 mL) was prepared under N_2 and quickly transferred to a predried, thick-walled glass tube (capacity ~30 mL), degassed and sealed under vacuum (~0.1 Torr) before heating to 185°C for 460 h. After cooling, the reaction mixture was diluted with water (10 mL) and the neutral product isolated by ether extraction (3 × 20 mL). The extracts were washed with water, dried over $MgSO_4$, and the solvent evaporated to afford a yellow oil which was subjected to fc (ether − petroleum ether, 5:95) to furnish recovered starting material **6** (29 mg) and the new ketone **5** (61 mg, 56% based on recovered **6**); ir ($CHCl_3$): 1730 cm^{-1}; ^{1}Hmr ($CDCl_3$) δ: 1.027 (s, 3H, Me), 1.090 (s, 3H, Me), 1.25−1.97 (complex absorption, 11H), 2.50 (m, 2H), 2.77 (m, 1H); ^{13}Cmr ($CDCl_3$) δ_c: 225.1 (C=O), 24.9, 25.7 (2 × Me), 25.7, 32.8, 34.1, 39.3, 42.4 (5 × CH_2), 39.5, 43.2, 47.8, 59.4 (4 × CH), 47.0 (quat. C); ms, *m/e* (relative intensity): 192 (M^+, 100), 163 (26), 136 (50), 124 (26), 111 (30), 108 (45), 79 (79), 67 (31). *Exact Mass* calcd. for $C_{13}H_{20}O$: 192.15141; found: 192.15142.

cis, anti, cis-*4,4-Dimethyltricyclo[6.3.0.0^{2,6}]undecane (17)*

A mixture of **5** (27 mg, 0.14 mmol), hydrazine hydrate (70 mg, 1.4 mmol), KOH (118 mg, 2.11 mmol), and diethylene glycol (0.6 mL) was placed in a thick-walled glass tube; the tube was sealed and heated at 182°C for 60 h. After cooling and dilution with H_2O (5 mL), the reaction mixture was extracted with ether (3 × 10 mL) and the extracts washed with H_2O before drying over $MgSO_4$. Evaporation of the ether gave an oil which was passed through a short column (1 × 5 cm) of SiO_2 (eluent: *n*-pentane, 30 mL) to furnish **17** (20 mg, 80%) as a colorless liquid; ^{1}Hmr ($CDCl_3$) δ: 0.85 (s, 3H, Me), 1.00 (s, 3H, Me), 1.0−2.8 (complex absorption, 16H); ^{13}Cmr ($CDCl_3$) δ_c: 28.1, 29.9 (2 × CH_3), 25.8, 32.0, 33.3, 39.8, 48.1, 49.0 (6 × CH_2), 44.0, 44.2, 50.9, 52.1 (4 × CH), 41.2 (quat. C); ms, *m/e* (relative intensity): 178 (M^+, 10), 163 (42), 122 (100), 95 (26), 93 (31), 81 (49), 67 (33). *Exact Mass* calcd. for $C_{13}H_{22}$: 178.17215; found: 178.17227.

Repetition of the preceding procedure with a mixture (21 mg, 0.109 mmol) of **18** (1*b*) and its 5-oxo isomer (8) gave hydrocarbon **17** (13 mg, 65%).

Acknowledgements

We wish to thank the Natural Sciences and Engineering Research Council of Canada for financial support.

1. (*a*) W. A. AYER and L. M. BROWNE. Tetrahedron, **37**, 2199 (1981); (*b*) R. D. LITTLE and G. W. MULLER. J. Am. Chem. Soc. **101**, 7129 (1979).
2. A. E. GREENE, M.-J. LUCHE, and J.-P. DEPRES. J. Am. Chem. Soc. **105**, 2435 (1983); E. EXON and P. MAGNUS. J. Am. Chem. Soc. **105**, 2477 (1983); S. V. LEY and P. J. MURRAY. J. Chem. Soc. Chem. Commun. 1252 (1982); P. F. SCHUDA, H. L. AMMON, M. R. HEIMAN, and S. BHATTACHARJEE. J. Org. Chem. **47**, 3434 (1982), and references therein.
3. B. A. DAWSON, A. K. GHOSH, J. L. JURLINA, and J. B. STOTHERS. J. Chem. Soc. Chem. Commun. 204 (1983).
4. E. J. COREY and R. S. GLASS. J. Am. Chem. Soc. **89**, 2600 (1967).
5. S. KRISHNAMURTHY, R. M. SCHUBERT, and H. C. BROWN. J. Am. Chem. Soc. **95**, 8486 (1973).
6. W. C. STILL, M. KAHN, and A. MITRA. J. Org. Chem. **43**, 2923 (1978).
7. R. RATCLIFFE and R. RODEHORST. J. Org. Chem. **35**, 4000 (1970).
8. J. L. JURLINA, H. A. PATEL, and J. B. STOTHERS. Can. J. Chem. **62**, 1159 (1984).
9. R. K. MURRAY and T. M. FORD. J. Org. Chem. **44**, 3504 (1979); E. G. BREITHOLLE and A. G. FALLIS. J. Org. Chem. **43**, 1964 (1978).
10. D. A. EVANS, G. L. CARROLL, and L. K. TRUESDALE. J. Org. Chem. **39**, 914 (1974).
11. A. BAX, R. FREEMAN, T. A. FRENKIEL, and M. H. LEVITT. J. Magn. Reson. **43**, 478 (1981).
12. A. L. JOHNSON, N. O. PETERSEN, M. B. RAMPERSAD, and J. B. STOTHERS. Can. J. Chem. **52**, 4143 (1974).
13. N. H. WERSTIUK. Tetrahedron, **39**, 205 (1983).
14. E. L. ELIEL, N. A. ALLINGER, S. J. ANGYAL, and G. A. MORRISON. *In* Conformational analysis. Interscience, New York. 1965. p. 227.
15. D. TODD. Org. React. **4**, 378 (1948).
16. L. A. BROOKS and H. R. SNYDER. Org. Synth. Coll. Vol. III. Wiley, New York. 1955. p. 698.
17. S. L. PATT and J. N. SHOOLERY. J. Magn. Reson. **46**, 535 (1982).
18. G. A. MORRIS and R. FREEMAN. J. Am. Chem. Soc. **107**, 760 (1979).

A synthesis of (+)-aphidicol-15-ene

RONALD B. KELLY, G. SANKAR LAL, GOPALA GOWDA, AND RABINDRA N. REJ
Department of Chemistry, University of New Brunswick, P.O. Box 5050, Saint John, N.B., Canada E2L 4L5

Received March 14, 1984

This paper is dedicated to Professor Paul de Mayo on the occasion of his 60th birthday

RONALD B. KELLY, G. SANKAR LAL, GOPALA GOWDA, and RABINDRA N. REJ. Can. J. Chem. **62**, 1930 (1984).

A stereospecific synthesis of (+)-aphidicol-15-ene is described. Pursuing a concept successfully applied to our total synthesis of stemarin and the stemodane diterpenoids, the C/D ring system was elaborated by functional group manipulation and rearrangement of a 6-hydroxybicyclo[2.2.2]octan-2-one system.

RONALD B. KELLY, G. SANKAR LAL, GOPALA GOWDA et RABINDRA N. REJ. Can. J. Chem. **62**, 1930 (1984).

On décrit une synthèse stéréospecifique du (+)-aphidicolène-15. Faisant appel à un concept utilisé avec succès lors de nos synthèses totales des diterpénoïdes stémarine et stémodane, on a élaboré le système cyclique C/D grâce à la manipulation des groupes fonctionnels et à une transposition du système hydroxy-6 bicyclo[2.2.2] octanone-2.

[Traduit par le journal]

Can. J. Chem. Downloaded from www.nrcresearchpress.com by 210.87.254.105 on 09/06/12
For personal use only.

More than four years ago (ref. 1, see also ref. 2) we conceived the possibility of constructing the C/D ring systems of stemarin (**1**), the stemodane diterpenoids (e.g. **2**), and aphidicolin (**3**) by stereospecific rearrangement of a common 6-hydroxybicyclo[2.2.2]octan-2-one system represented by **4**. This concept was an efficient feature of total syntheses of stemarin (**1**)(1), and of 2-desoxystemodinone (**2***a*) and stemodinol (**2***b*)(2,3); we now wish to describe its application to a stereospecific synthesis of (+)-aphidicol-15-ene (**5**), a derivative of aphidicolin (**3**)(4).[1] This synthesis was undertaken as a model, relative to a projected total synthesis of aphidicolin.

The keto alcohol **6**, formerly encountered as an intermediate in our synthesis of (+)-2-desoxystemodinone (**2***a*)(3), served also as an intermediate in the present synthesis. This intermediate, prepared from podocarpic acid (3), is the enantiomer represented by **6** and leads to the enantiomer **5** derived from aphidicolin (4).

In preparation for the rearrangement of the bicyclic system of **6** to that of **5**, it was necessary to reduce the secondary hydroxyl group to a methylene group and convert the keto

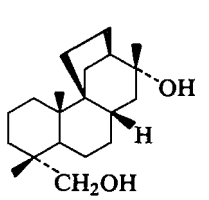

1

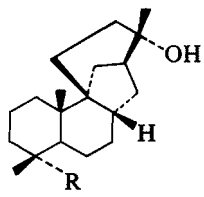

2*a* R = CH_3
2*b* R = CH_2OH

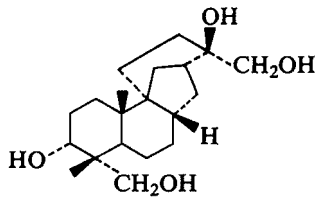

3

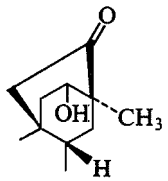

4

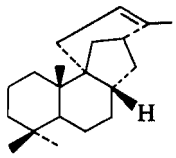

5

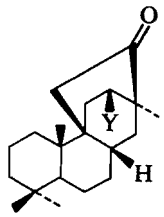

6 Y = OH
7 Y = $OCSSCH_3$

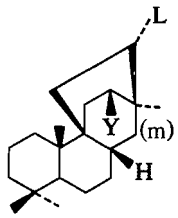

8 Y = $OCSSCH_3$; L = OH
9 Y = $OCSSCH_3$; L = OBz
10 Y = H; L = OBz
11 Y = H; L = OH
12 Y = H; L = OTs

[1]For synthesis of aphidicolin by routes different from that implied in this paper see ref. 5.

Can. J. Chem. Downloaded from www.nrcresearchpress.com by 210.87.254.105 on 09/06/12
For personal use only.

group to an appropriate leaving group. The former task was accomplished efficiently by Barton's procedure (6). Thus, the keto alcohol was converted in 87% yield into the *S*-methyldithiocarbonate **7**. Reduction of **7** with $NaBH_4$ afforded, in 90% yield, the alcohol **8**. The stereospecific reduction of the keto group of **7** to the required epimer **8** is attributable to the "propeller" effect of the bulky dithiocarbonate group. The alcohol **8** was converted in 97% yield into the benzoate **9**. Reduction of the latter with tri-n-butyltin (6) followed by hydrolysis of the benzoate **10** afforded (75% from **9**) the alcohol **11**.

The alcohol **11** was converted into the tosylate **12** in which the tosylate group, serving as a leaving group, has the correct stereo-alignment for rearrangement via migration of bond (m) and elimination of a proton (Y). The tosylate **12**, on heating for 2 h at 60°C in DMSO containing methyl sulfinyl carbanion, underwent the anticipated rearrangement to give (+)-aphidicol-15-ene (**5**) (4) in 60% yield (cf. refs. 1–3). The synthetic diterpene had properties (mp, ir and nmr spectra) identical with (+)-aphidicol-15-ene derived from aphidicolin (4).

Experimental

Instrumentation, methods, and materials

Proton nmr were recorded in $CDCl_3$ on a Varian T-60 instrument; chemical shifts are expressed in ppm (δ values) relative to TMS as an internal standard. Unless otherwise stated, ir spectra were recorded as $CHCl_3$ solutions with a Perkin–Elmer 297 instrument. The ms were recorded on a Vacuum Generator UG-ZAB-1F instrument. Melting points were determined on a Fisher–Johns apparatus and are uncorrected.

Silica gel G-60 was used for column chromatography and silica gel GF-240 for tlc (E. Merck, Darmstadt). Petroleum ether refers to the fraction with boiling point range 30–60°C. Brine refers to a saturated solution of NaCl.

Keto S-methyldithiocarbonate 7

The following reaction sequence was carried out under a nitrogen atmosphere.

A solution of 155 mg of the keto alcohol **6** in 5 mL of THF was treated with 37 mg of NaH and 2 mg of imidazole, then refluxed for 3 h. After cooling, 0.20 mL of CS_2 was added to the reaction solution and refluxing was continued for 30 min. The reaction solution was again cooled and, after the addition of 0.10 mL of CH_3I, refluxing was continued for a further 30 min. The cooled reaction solution was treated with 0.05 mL of acetic acid, then diluted with 25 mL of water. The aqueous mixture was extracted with three 50-mL portions of CH_2Cl_2. The extracts were washed with 25 mL of 0.05 *M* HCl, 25 mL of saturates $NaHCO_3$, and, finally, with 25 mL of water. The aqueous washings were extracted with two 50-mL portions of CH_2Cl_2 and the extracts were combined, dried over $MgSO_4$, and evaporated *in vacuo*. Chromatography of the residue on 20 g of silica gel in petroleum ether-ether afforded 175 mg (87%) of **7**, mp 128°C; ir (Nujol): 1715 (ketone) cm^{-1}; nmr δ: 0.88 and 0.92 (3-proton singlets, tertiary methyls), 1.01 (s, 6H, superimposed signals for two tertiary methyls), 2.51 (s, 3H, SCH_3), and 5.70 (dd, 1H, *H*COCSSCH$_3$). *Anal.* calcd. for $C_{22}H_{34}S_2O_2$: C 66.96, H 8.68; found: C 67.03, H, 8.52%.

Reduction of keto S-methyldithiocarbonate 7 to 8

A solution of 130 mg of **7** in 5 mL each of ether and methanol was cooled to −10°C, treated with 50 mg of $NaBH_4$, and stirred at −10°C for 1 h. The reaction solution was diluted with 25 mL of brine and the aqueous mixture was extracted with two 50-mL portions of ether. Evaporation of the combined, dried ($MgSO_4$) extracts and chromatography of the residue on 10 g of silica gel in petroleum ether – ether afforded 118 mg (90%) of **8** as an oil; ir: 3580 (OH) cm^{-1}; nmr δ: 0.85 (s, 6H, superimposed signals for two tertiary methyls), 0.91 and 0.98 (3-proton singlets, tertiary methyls), 2.55 (s, 3H, SCH_3), 3.60 (m, 1H, *H*COH), and 5.51 (m, 1H, *H*COCSSCH$_3$).

This compound was further characterized as the benzoate (*vide infra*).

Benzoate 9

A solution of 100 mg of **8** and 0.3 mL of benzoyl chloride in 1 mL of pyridine was kept at −5°C for 4 h. The reaction mixture was diluted with 50 mL of ether and the resulting solution was washed with 25 mL of saturated $NaHCO_3$, 25 mL of 0.05 *M* HCl, and 25 mL of water. The aqueous washings were extracted with two 50 mL portions of ether. The combined ether extracts were dried ($MgSO_4$) and evaporated *in vacuo*. Chromatography of the residue on 40 g of silica gel in petroleum ether – ether afforded 122 mg (97%) of the benzoate **9**, mp 194°C; ir: 1710 (ester) cm^{-1}; nmr δ: 0.85 and 0.88 (3-proton singlets, tertiary methyls), 0.97 (br s, 6H, superimposed signals for two tertiary methyls), 2.61 (s, 3H, SCH_3), 4.98 (m, 1H, *H*OBz), 5.67 (m, 1H, *H*COCSSCH$_3$), and 7.45 and 8.12 (br m, 5H, aromatic protons). *Anal.* calcd. for $C_{29}H_{40}S_2O_3$: C 69.56, H 8.05; found: C 68.99, H 8.19%.

Alcohol 11

The following reaction sequence was carried out under a nitrogen atmosphere.

A solution of 342 mg of the benzoate **9** in 11 mL of toluene was added over 1 h to a refluxing solution of 0.56 mL of tri-n-butyltin hydride in 17 mL of toluene. Refluxing was continued for 33 h during which time 0.20-mL portions of tri-n-butyltin hydride were added after 10, 22, and 25 h. The solvent was evaporated *in vacuo* and the residue was filtered through a column of 50 g of silica gel in petroleum ether – ether (1:1). Evaporation of the eluant afforded a crude product (**10**) which was refluxed in 58 mL of 1 *M* ethanolic KOH for 1 h. The solvent was evaporated *in vacuo* and 50 mL of water was added to the residue. The product was extracted from the aqueous mixture into three 50-mL portions of CH_2CL_2. The extracts were dried over $MgSO_4$ and evaporated *in vacuo*. Chromatography of the residue over 40 g of silica gel in petroleum ether – ether afforded 148 mg (75%) of **11** as an oil; ir: 3620 (OH) cm^{-1}; nmr δ: 0.78 and 0.90 (3-proton singlets, tertiary methyls), 0.84 (s, 6H, superimposed signals for two tertiary methyls), and 3.56 (br m, 1H, *H*COH).

(+)-aphidicolin-15-ene

A solution of 55 mg of the alcohol **11** in 1.1 mL of pyridine was treated with 134 mg of *p*-toluenesulfonyl chloride and left at 3°C for 72 h. The solution was diluted with 5 mL of ice water and extracted with three 50-mL portions of ether. The ether extracts were washed with 50 mL each of cold 2 *M* HCl and cold water. The combined extracts were dried (K_2CO_3) and evaporated *in vacuo* to give 86 mg of tosylate **12**, which was used immediately for the next reaction.

A solution of 86 mg of the tosylate **12** in 12 mL of DMSO was treated with 0.6 mL of a 0.5 *M* DMSO solution of methyl sulfinyl carbanion (7). The resulting solution was stirred under nitrogen for 2 h at 60°C, cooled, treated with 1 mL of water and diluted with 50 mL of ether. The ether solution was washed with three 30-mL portions of brine, followed by two 30-mL portions of water, and the aqueous washings were extracted with five 50-mL portions of ether. Evaporation of the combined, dried ($MgSO_4$) extracts and chromatography of the residue on 10 g of silica gel in pentane afforded 31 mg (60%) of aphidicol-15-ene **5**, mp 101–103°C (lit. (4) mp 101–105°C). *Mol. Wt.* calcd. for $C_{20}H_{32}$: 272.2504; found (ms): 272.2514. The spectral properties (ir and nmr) of the synthetic diterpene **5** were identical to spectra for aphidicol-15-ene derived from aphidicolin.

Acknowledgements

We are grateful to the Natural Sciences and Engineering Research Council of Canada for a grant to R. B. K., to Dr. Percy S. Manchand, Hoffmann-La Roche, Nutley, New Jersey, for a mass spectrum, and to Dr. A. H. Ratcliffe, Imperial Chemical Industries, Macclesfield, England, for ir and nmr spectra of the title compound.

1. (*a*) M. L. HARLEY. PhD Thesis, University of New Brunswick. February 1980; (*b*) R. B. KELLY, M. L. HARLEY, and S. J. ALWARD. Can. J. Chem. **58**, 755(1980).
2. R. B. KELLY, M. L. HARLEY, S. J. ALWARD, and P. S. MANCHAND. Can. J. Chem. **60**, 675(1982).
3. R. B. KELLY, M. L. HARLEY, S. J. ALWARD, R. N. REJ, G. GOWDA, A. MUKHOPADHYAY, and P. S. MANCHAND. Can. J. Chem. **61**, 269(1983).
4. W. DALZIEL, B. HESP, K. STEVENSON, and J. A. J. JARVIS. J. Chem. Soc. Perkin Trans. 1, 2841(1973).
5. (*a*) B. M. TROST, Y. NISHIMURA, K. YAMAMOTO, and S. S. MCELVAIN. J. Am. Chem. Soc. **101**, 1328(1979); (*b*) J. E. MCMURRY, A. ANDRUS, G. M. KSANDER, J. H. MUSSER, and M. A. JOHNSON, Tetrahedron, **37**, 319(1981); (*c*) E. J. COREY, M. A. TITUS, and J. DAS. J. Am. Chem. Soc. **102**, 1742(1980); (*d*) R. E. IRELAND, J. D. GODFREY, and S. THAISRIVONGS. J. Am. Chem. Soc. **103**, 2446(1981); (*e*) E. E. VAN TAMELEN, S. R. ZAWACKY, R. K. RUSSELL, and J. G. CARLSON. J. Am. Chem. Soc. **105**, 142(1983); (*f*) R. MARINI BETTOLO, P. TAGLIATESTA, A. LUPI and D. BRAVETTI. Helv. Chim. Acta, **66**, 1922(1983).
6. D. H. R. BARTON and S. W. MCCOMBIE. J. Chem. Soc. Perkin Trans 1, 1574(1975).
7. E. J. COREY and M. CHAYKOVSKY. J. Am. Chem. Soc. **87**, 1345(1965).

Can. J. Chem. Downloaded from www.nrcresearchpress.com by 210.87.254.105 on 09/06/12
For personal use only.

Base catalysis as an alternative explanation for an apparent deuterium solvent isotope effect in the photochemical reactions of α,β-unsaturated esters[1]

ALAN C. WEEDON

Photochemistry Unit, Department of Chemistry, The University of Western Ontario, London, Ont., Canada N6A 5B7

Received January 19, 1984

This paper is dedicated to Professor Paul de Mayo on the occasion of his 60th birthday

ALAN C. WEEDON. Can. J. Chem. **62**, 1933 (1984).

An apparent deuterium solvent isotope effect upon the photochemical reactions of the α,β-unsaturated esters ethyl 3,4,4-trimethyl-2-pentenoate, **1**, and ethyl 3,4-dimethyl-2-pentenoate, **4**, is re-examined; it is concluded that the changes in reaction rate can be attributed to interception of the reaction intermediates (photochemically produced dienols) by basic impurities present in the solvent used. This conclusion is used to explain the apparently anomalous photochemistry of esters **1** and **5** in non-deuterated solvents. The results described also exemplify the use of a base to enhance the efficiency and to alter the direction of deconjugation in the photochemical conversion of α,β-unsaturated esters to their β,γ-unsaturated isomers.

ALAN C. WEEDON. Can. J. Chem. **62**, 1933 (1984).

On a réétudié un effet isotopique apparent de solvants deutérés sur les réactions photochimiques des esters α,β-non saturés, triméthyl-3,4,4 pentène-2 oate de méthyle (**1**) et diméthyl-3,4 pentène-2 oate de méthyle (**4**); on en conclut que les changements dans les vitesses de réactions peuvent être attribués à l'interception des intermédiaires réactionnels (des diénols produits photochimiquement) par des impuretés basiques présentes dans le solvant utilisé. On utilise cette conclusion pour expliquer la photochimie apparemment anormale des esters **1** et **5** dans des solvants qui ne sont pas deutérés. Les résultats décrits servent aussi d'exemples pour démontrer l'utilité d'une base pour augmenter l'efficacité et pour modifier la direction de la déconjugaison lors de la transformation photochimique d'esters α,β-non saturés en leurs isomères β,γ-non saturés.

[Traduit par le journal]

Introduction

Direct irradiation of α,β-unsaturated esters with ultraviolet light results in *E*–*Z* isomerization around the double bond with a quantum efficiency of the order of 5–10% (1). If the ester possesses hydrogen substituents at the 4-position oriented *syn* with respect to the ester function, then these can be abstracted in competition with *E*–*Z* isomerization to yield a dienol intermediate which can reketonize by protonation at the 2-position to give a β,γ-unsaturated ester (Scheme 1). This photoenolization reaction has been shown to proceed via the singlet excited state (2), and may be regarded as a photochemically allowed antarafacial 1,5-sigmatropic hydrogen shift. The formation of β,γ-unsaturated esters by this pathway has frequently been observed (3–8) and has been proposed as a synthetic route to these compounds (9).

One of the earliest reports concerning this reaction described an exception (10); ultraviolet light irradiation of ethyl 3,4,4-trimethyl-2-pentenoate, **1**, in diethyl ether resulted in formation of the cyclopropane derivative **2** rather than the expected product, the β,γ-unsaturated ester **3**, which would be formed following photoenolization. This result is especially surprising in view of the relative bond energies of the C—H bonds undergoing cleavage and because formation of **2** proceeds via δ rather than the normally preferred γ-hydrogen abstraction. A later report from the same laboratory (11) described the irradiation of **1** in methanol, and in this solvent the products were the cyclopropane derivative **2** along with the β,γ-unsaturated ester **3**. The chemical yield of the latter was, however, found to be erratic, varying from 2% to 30–40%. Subsequent work (12) revealed that when the reaction was performed in methanol-O-*d* the product ratio was dramatically altered with the β,γ-unsaturated ester **3** being formed in 90–95% yield. A remarkable deuterium solvent isotope effect was also found with the esters **4**, **5**, and **6** (12): when **4** was irradiated in methanol, **7** was the major product along with small amounts of the alternative deconjugated isomer **8**; however, when the reaction was carried out in methanol-O-*d* the two β,γ-unsaturated esters were found to be formed in comparable amounts. In contrast to the results obtained with **1**, the use of a deuterated solvent with **4** resulted in an enhanced chemical yield of the product obtained from cleavage of the

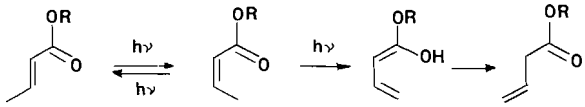

SCHEME 1

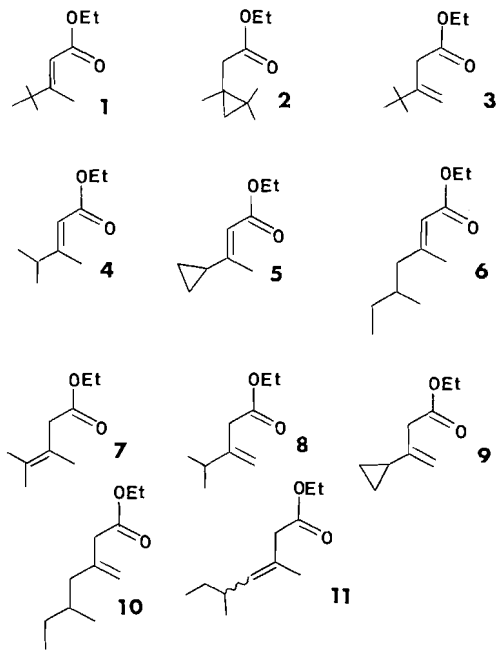

[1] Contribution number 322 from the Photochemistry Unit, Department of Chemistry, The University of Western Ontario, London.

Can. J. Chem. Downloaded from www.nrcresearchpress.com by 210.87.254.105 on 09/06/12
For personal use only.

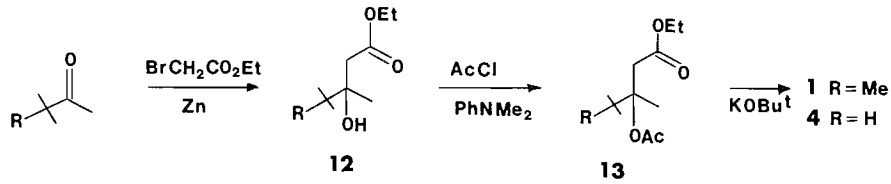

SCHEME 2

stronger C—H bond, rather than the weaker as was observed with **1**. In the case of ester **5**, irradiation in methanol-O-*d* enhanced the chemical yield of the β,γ-unsaturated ester **9** and with ester **6** the yield of **10** was enhanced relative to **11**.

Recently in this laboratory the photoenolization and photodeconjugation reaction has been investigated for α,β-unsaturated ketones and esters in the presence of weak organic bases (13–15), and the results of these studies suggest that the photochemically formed dienol can reketonize by two competing pathways; the dienol can isomerize back to the α,β-unsaturated carbonyl compound, by way of a thermally allowed suprafacial 1,5-sigmatropic hydrogen shift, or it can be intercepted by a base to give the β,γ-unsaturated isomer. In view of these results it seemed that the apparent deuterium solvent isotope effects described above could be a result of the presence in the solvents of species capable of intercepting the photochemically produced dienols and catalysing their conversion to the β,γ-unsaturated products. Described here are the results of a study designed to investigate this possibility.

Results

The esters **1** and **4** were prepared as shown in Scheme 2 by base catalysed elimination of the acetates prepared from the Reformatsky hydroxy esters **12**. This procedure has been developed by Fung *et al.* (16) and readily yields large quantities of the α,β-unsaturated esters, predominantly in the thermodynamically more stable *E*-geometry, and with minimal contamination by the β,γ-unsaturated isomers.

The esters **1** and **4** were irradiated with ultraviolet light of wavelength 254 nm as 0.1 *M* solutions in diethyl ether, methanol, and methanol-O-*d* in both the presence and absence of a weak organic base, under conditions such that the esters adsorbed all of the incident light. The base used, 1,2-dimethylimidazole, was chosen because it is soluble in the solvents used, adsorbs very weakly at 254 nm, and is insufficiently strong to catalyse reconjugation of the β,γ-unsaturated ester products or attack the ester functions as a nucleophile. The quantum yields measured in each reaction are shown in Tables 1 and 2, and the progress of typical reactions in Figs. 1 and 2.

Irradiation of ester **1** in diethyl ether resulted in relatively rapid (ϕ = ca. 0.1) *E*–*Z* isomerization to give a photostationary state with *E*–**1** and *Z*–**1** present in the ratio 74:26, respectively. Continued irradiation resulted in slow loss of **1** (ϕ = 0.0084), with the cyclopropane **2** being formed as the major product (10). Also formed, but at a ten-fold slower rate, was the β,γ-unsaturated isomer of the starting material, ester **3**. At complete conversion the esters **2** and **3** were present in 76% and 8% yields, respectively, along with small amounts of two further products which were isolated and identified as the *d,l* and *meso* forms of 1,2-diethoxybutane from ^{1}H nmr and mass spectroscopic evidence. These last products, which account for the missing 16% of the starting material, are presumed to arise from inefficient abstraction of hydrogen from the solvent by either photo-excited esters, or by radicals formed from photolysis of the esters.[2]

TABLE 1. Quantum yields[a] for conversion of **1** to **2** and **3**

Solvent	ϕ**1**[b]	ϕ**2**[c]	ϕ**3**[d]	Photostationary state composition (% *Z*–**1**)
Et_2O	0.0084	0.0066	0.00065	26
MeOH	0.012	0.0043	0.0021	27.5
MeOD	0.011	0.0035	0.0031	27.5
Et_2O + base[e]	0.053	0.0068	0.046	29.5
MeOH + base[f]	0.056	0.0055	0.048	33
MeOD + base[g]	0.049	0.0043	0.040	33

[a]Quantum yields were measured close to the photostationary state and are accurate to ±10%.
[b]Quantum yield of disappearance of *E* + *Z*–**1**.
[c]Quantum yield of appearance of **2**.
[d]Quantum yield of appearance of **3**.
[e][1,2-Dimethylimidazole] = 1.73 × 10^{-2} *M*.
[f][1,2-Dimethylimidazole] = 1.78 × 10^{-2} *M*.
[g][1,2-Dimethylimidazole] = 1.75 × 10^{-2} *M*.

TABLE 2. Quantum yields[a] for conversion of **4** to **7** and **8**

Solvent	ϕ**4**[b]	ϕ**8**[c]	ϕ**7**[d]	Photostationary state composition (% *Z*–**1**)
MeOH	0.047	0.0028	0.032	46.5
MeOH + base[e]	0.083	0.027	0.038	53.5
MeOD	0.050	0.0028	0.031	46.5
MeOD + base[f]	0.071	0.031	0.035	53.5

[a]Measured close to the photostationary state and are accurate to ±10%.
[b]Quantum yield of disappearance of *E* + *Z* **4**.
[c]Quantum yield of appearance of **7**.
[d]Quantum yield of appearance of **8**.
[e]Base = 1,2-dimethylimidazole, conc. = 7.0 × 10^{-3} *M*.
[f]Base = 1,2-dimethylimidazole, conc. = 9.6 × 10^{-3} *M*.

Irradiation of ester **1** in methanol also resulted in the rapid formation of a photostationary state (27.5% *Z*–**1**) followed by subsequent production of the cyclopropane **2** at a rate similar to that in diethyl ether (Table 1); however, the chemical yield of **2** was suppressed to 36% at complete conversion due to competitive formation of the deconjugated ester **3**, which was produced at a three-fold faster rate in this solvent, resulting in a chemical yield of 25% at complete conversion.

Very similar results were obtained when methanol-O-*d* was used as solvent; the quantum yield of formation of **2** was found to be the same as in methanol within the experimental error of

[2] When esters **1** and **4** were irradiated in methanol, or methanol-O-*d*, similar losses of material were observed, but the extra products were not isolated or identified. The losses by this route in the faster reactions did not exceed ca. 3%, but in the slower reactions (i.e., in absence of added base) were as high as 30%. In all reactions, the quantum yield of disappearance of ester to unidentified products by this route was approximately constant at 0.005.

Can. J. Chem. Downloaded from www.nrcresearchpress.com by 210.87.254.105 on 09/06/12
For personal use only.

Can. J. Chem. Downloaded from www.nrcresearchpress.com by 210.87.254.105 on 09/06/12
For personal use only.

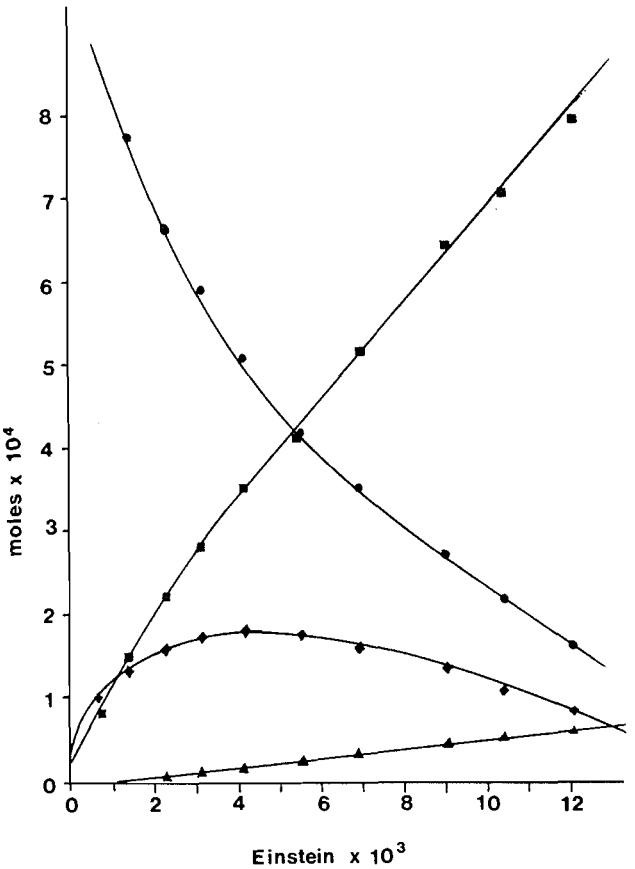

FIG. 1. Plot of reaction mixture composition against amount of light absorbed for the irradiation of 10.00 mL of a 0.100 *M* solution of ester **1** in methanol containing 1,2-dimethylimidazole (1.73×10^{-2} *M*). ●, *E*–**1**; ◆, *Z*–**1**; ■, **3**; ▲, **2**.

the determination, while the quantum yield of formation of **3** was slightly increased in deuterated solvent (Table 1).

Addition of catalytic amounts of 1,2-dimethylimidazole to solutions of **1** in diethyl ether, methanol, or methanol-O-*d* resulted in a large increase in the rate of formation of **3**, while the rate of formation of **2** increased only slightly (Table 1). The course of a typical reaction in methanol is shown in Fig. 1; very similar results were observed in methanol-O-*d* and diethyl ether. As can be seen in Fig. 1, irradiation produces fast *E*–*Z* isomerization of **1**, as was observed in the absence of base, but now deconjugation to **3** also occurs at a comparable rate with the result that the position of the photostationary state between *E*–**1** and *Z*–**1** is shifted from 27.5% *Z*–**1** in the absence of base to 33% with base present. Subsequent to attainment of the photostationary state, the rate of formation of **2** and **3** becomes zero order and the quantum yield of formation of **3** at this point is an order of magnitude greater than the yield when base was absent. When diethyl ether was used as solvent, the increase in rate of formation of **3** following addition of base was even greater, with the quantum yield of formation of **3** rising by a factor of 70. In both methanol and methanol-O-*d* the addition of base resulted in chemical yields at complete conversion of 7% for **2** and 92% for **3**.

The photochemistry of ester **4** followed a parallel course and Fig. 2 shows the progress of a reaction in methanol; initial rapid *E*–*Z* isomerization and formation of a photostationary state are followed by formation of ethyl 3,4-dimethyl-3-pentenoate, **7**. Production of *Z*–**4** and **7** was accompanied by slower formation of ethyl 3-methylene-4-methylpentanoate, **8**. The quantum yields are shown in Table 2, and the chemical yields at complete conversion were 6% for **8** and 58% for **7**. When a catalytic quantity of 1,2-dimethylimidazole was added to the irradiation mixture, the rate of formation of **7** was increased slightly, the position of the photostationary state was perturbed, and the rate of formation of **8** was increased by a factor of ten to a rate similar to that for the formation of **7**. In constrast to the previously reported work (12), *identical* results were obtained when the irradiations were performed in methanol-O-*d*.

Discussion

The previously published work on the photochemistry of the esters **1** and **4** found that use of a deuterated solvent exerted a large effect upon the rate of deconjugation (12). In the study reported here this effect was not found; in the case of ester **4** identical results were obtained in methanol-O-*d* and methanol, while with **1** a slight increase in the quantum efficiency of deconjugation was noted when methanol-O-*d* was used. However, the previously observed behaviour could be obtained if a weak base was added to the solvents.

In the previously published work, the possibility that impurities could cause the observed apparent isotope effect was considered, but discounted on the grounds that methanol-O-*d* prepared by different routes gave the same results, and deliberate addition of acid did not produce a rate change (12). In the work described here the methanol-O-*d* was prepared by additon of deuterium oxide to excess sodium methoxide followed by distillation. Two batches were prepared; one was used for the experiments with ester **1** and the other for experiments with ester **4**. The slight rate enhancement observed in this work for ester **1** but not for ester **4** may reflect the relative purities of the two samples of deuterated solvent.

The effect of addition of base can be understood in terms of the mechanism of the photoenolization and deconjugation reaction proposed in a previous publication from this laboratory (15) and outlined in Schemes 3 and 4 for esters **1** and **4**.

For ester **1** irradiation of *E*–**1** produces *Z*–**1** which when present in sufficient quantity can itself absorb light and either isomerize back to *E*–**1** or undergo intramolecular hydrogen abstraction from the δ-position to yield the biradical **16**.[3] This in turn can couple to give enol **17** whose only fate can be acid or base catalysed reketonization to **2**. In competition with isomerization around the double bond, photo-excited *E*–**1** can undergo intramolecular hydrogen abstraction to yield dienol **14**. As this is a singlet excited state process (2, 11), a biradical need not be an intermediate on the reaction pathway and the formation of **14** may be regarded as a photochemical 1,5-sigmatropic hydrogen shift proceeding antarafacially. In the absence of a base **14** reverses rapidly to *E*–**1**, by a thermal 1,5-sigmatropic hydrogen shift, this time proceeding suprafacially; if base is present, either as an impurity or deliberately added, **14** can be intercepted and converted to the dienolate **15** which on C-protonation can yield **1** and **3**. In the absence of added base the formation of **3** is inefficient, but is faster in methanol; this

[3] A referee has suggested that *E*–**1** and *Z*–**1** may react from a common excited state. However, if this were the case no induction period would be observed prior to the formation of products derived from *Z*–**1**. Such an induction period was observed, as shown in Fig. 1, and has been observed in the photochemistry of other esters (see refs. 2 and 11), suggesting that the *singlet* excited states of *E* and *Z* α,β-unsaturated esters are distinct.

Can. J. Chem. Downloaded from www.nrcresearchpress.com by 210.87.254.105 on 09/06/12
For personal use only.

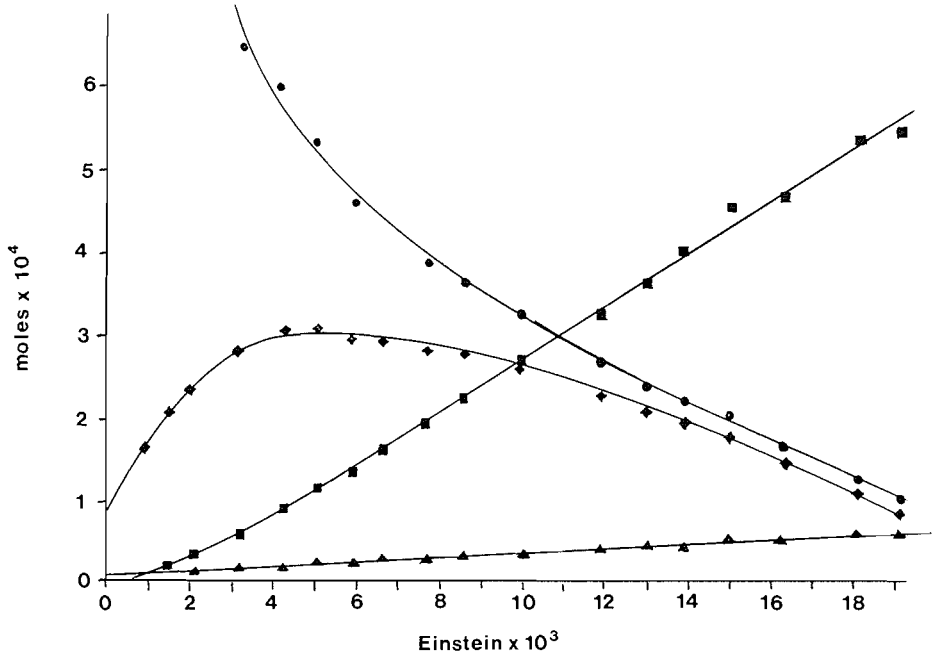

FIG. 2. Plot of reaction mixture composition against amount of light absorbed for the irradiation of 10.00 mL of a 0.100 *M* solution of ester **4** in methanol. ●, *E*–**4**; ◆, *Z*–**4**; ■, **7**; ▲, **8**.

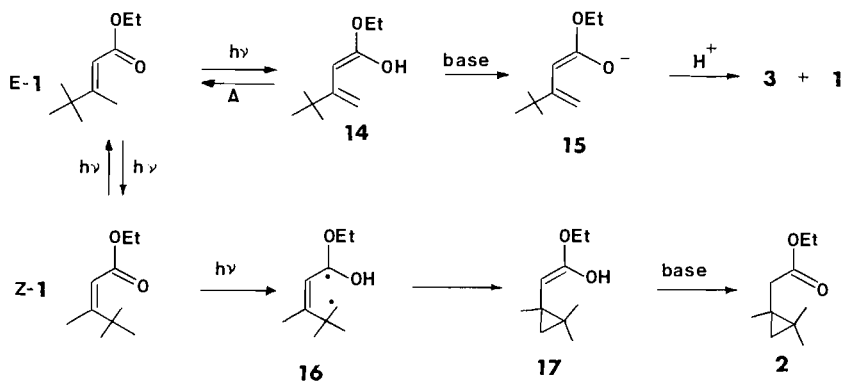

SCHEME 3

may reflect the relative purities of these solvents or the relative basicities of ether and methanol if the solvent is acting as the base, or it may reflect the lower solvating power of ether which would destabilize **15** and decrease its rate of formation relative to the rate of thermal reversal of **14** to *E*–**1**.[4]

This mechanism suggests that the quantum yield of formation of **2** from *Z*–**1** should not be affected by the addition of base. As can be seen in Table 1, this appears not to be the case as the quantum yield of formation of **2** is increased slightly by the presence of base; this can be understood in terms of a shift in the position of the photostationary state towards *Z*–**1** when base is present, which increases the rate of light absorption by *Z*–**1**. The change in photostationary state composition is caused by removal of *E*–**1** to give **3** at a rate comparable to *E*–*Z* isomerization.

For ester **4** the quantum yield of deconjugation is increased greatly by addition of base for the β,γ-unsaturated ester **8**, but only slightly for **7**. The mechanism which accounts for this is shown in Scheme 3. Irradiation of *E*–**4** yields *Z*–**4** which, after an induction period during which its concentration builds up to a level at which it can absorb light, undergoes photoenolization to give dienol **20** in the *cis* conformation of the diene. Bond rotation allows adoption of the more stable *trans* conformation by relieving the unfavorable steric interaction between the hydroxyl and isoproylidene functions. Adoption of the *trans* conformation slows reversion of **20** to *Z*–**4** and allows base impurities or weakly basic solvent to compete effectively by catalysing reketonization of **20** to give **7** via dienolate **21**. The very small effect of addition of base upon the quantum yield of formation of **7** suggests that the rate of conversion of **20** to **7** via **21** is fast compared to thermal reversion of **20** to **4**; it is possible that all of **20** undergoes base catalysed reketonization with no reversion to **4**, and that the observed rate enhancement with base is derived from a shift in the photostationary state towards *Z*–**4** caused by depletion of *E*–**4** to give **8**, as was described for **2**.

In competition with double bond isomerization, *E*–**4** can photoenolize to **18** which is fixed in the *cis* conformation be-

[4] A referee has suggested that the greater efficiency of deconjugation in polar solvents may reflect hydrogen bonding of the dienol which would inhibit the thermal reversion of **14** to *E*–**1**.

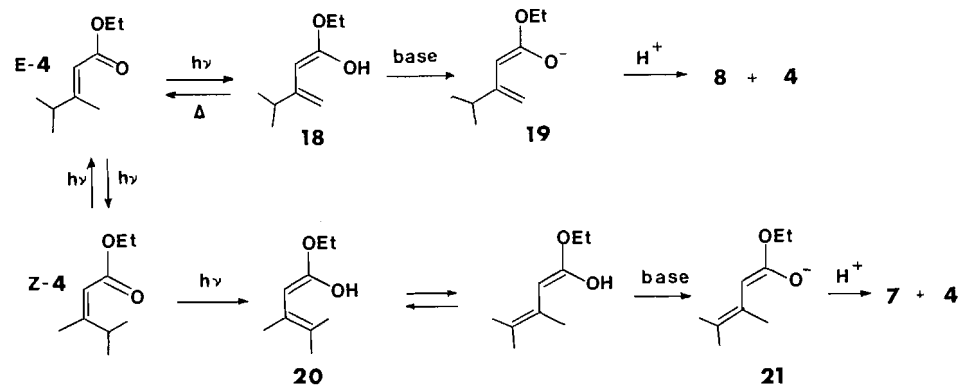

SCHEME 4

cause of destabilization of the *trans* conformation by the bulky isopropyl substituent. This being the case, thermal reversion of **18** to *E*–**4** via a 1,5-sigmatropic hydrogen shift is fast relative to conversion to **8** via **19** unless a high enough concentration of base is present to intercept **18** and convert it to **19**. Thus the yield of **8** is low unless sufficient base is present.

The reported photochemistry of ester **6** can be explained in an identical manner. It was observed (12) that irradiation of **6** in methanol gave **11** only, but that in methanol-O-*d* the yield of **10** was enhanced. This is reasonable if the dienol produced by irradiation of *E*–**6** reverts to *E*–**6**, while the dienol from *Z*–**6** is forced into a *trans* conformation by the bulky γ-substituent and undergoes base catalysed reketonization to **11**. In methanol-O-*d* higher levels of basic impurities can intercept the dienol from *E*–**6** prior to reversion and so the yield of **10** is enhanced.

Conclusions

The effect of a deuterated solvent upon the efficiencies of the photochemical reactions of esters **1** and **4** can be accounted for in terms of basic impurities present in the methanol-O-*d* used and is not due to the presence of deuterium. The observations described also explain the anomalous behaviour of esters **1** and **5** in non-deuterated solvents. In the case of **1**, δ-hydrogen abstraction in *Z*–**1** of a non-allylic hydrogen appears to proceed with similar efficiency to γ-hydrogen abstraction of an allylic hydrogen in *E*–**1**, as indicated by the relative chemical yields of **2** and **3**. However, addition of base demonstrates that the true rate of γ-hydrogen abstraction in *E*–**1** is greater than the rate of δ-hydrogen abstraction in *Z*–**1**. In the case of **5**, irradiation in methanol leads to products derived from fragmentation following abstraction of the cyclopropyl methine and not to the deconjugated ester **9**, apparently indicating a faster rate of abstraction for a hydrogen bound to a cyclopropyl ring than a primary allylic C—H (12). This would be the expected result if the dienol formed from *E*–**5** reverts efficiently to **5** rather than undergoing base catalysed reketonization to yield **9**, and leads to the prediction that **9** would be a major product if base were present. In fact, when **5** was irradiated in methanol-O-*d* (12) the yield of **9** was increased, and in view of the results described here this can be ascribed to basic impurities in the deuterated solvent.

The observations reported here support the previously proposed (15) mechanism for base catalysed deconjugation of α,β-unsaturated carbonyl compounds. They also extend the synthetic utility of photochemical deconjugation as a useful procedure for the preparation of β,γ-unsaturated carbonyl compounds by demonstrating how the efficiency and yield of deconjugation, and the direction of deconjugation in non-symmetrically β,β-disubstituted α,β-unsaturated carbonyl compounds can be modified by addition of base.

Experimental

Preparation of E*-ethyl 3,4,4-trimethyl-2-pentenoate,* **1**

Ethyl 3-hydroxy-3,4,4-trimethylpentanoate (**12**, R = Me) was prepared in 36% yield by the Reformatsky reaction between pinacolone and ethyl bromoacetate (17, 18). Compound **12** (R = Me) (10 g, 0.053 mol), N,N-dimethylaniline (7 g, 0.058 mol), and acetyl chloride (4.4 g, 0.056 mol) were dissolved together in chloroform (30 mL) and the solution was refluxed for 9 h after which time gc (5% SE 30, 120°C) of a worked-up sample indicated complete reaction. The reaction mixture was poured into excess dilute sulphuric acid (100 mL) and extracted with two portions of ether (75 mL, 25 mL). The organic extracts were dried ($MgSO_4$ + Na_2CO_3) and evaporated to yield an oil which on distillation gave the acetate **13** (R = Me), 7.74 g (63%), bp 80–82°C/0.6 Torr (1Torr = 133.3 Pa); ^{1}H nmr ($CDCl_3$, 60 MHz): 1.01 (9H, s), 1.21 (3H, t, *J* = 7 Hz), 1.59 (3H, s), 2.01 (3H, s), 2.9 (2H, m), 4.02 (2H, q, *J* = 7 Hz) ppm.

The acetate **13** (R = Me) (7.74 g, 0.0337 mol) was dissolved in dry *tert*-butanol (15 mL) and added over 5 min to a stirred solution of potassium *tert*-butoxide in *tert*-butanol (50 mL of a 1.03 *M* solution). The solution became warm during the addition and a white gelatinous precipitate began to form when half of the acetate had been added. At completion of the addition the mixture was stirred for 15 min, poured into water (200 mL), and extracted with ether (100 mL, 2 × 50 mL). The organic phases were combined, dried ($MgSO_4$), and evaporated to give an oil which was distilled to give 3.58 g (63%) of **1**, bp 97°C/19 Torr (lit. (18) 65°C/6 Torr; ^{1}H nmr ($CDCl_3$, 60 MHz): 1.12 (9H, s), 1.31 (3H, t, *J* = 7 Hz), 2.20 (3H, d, *J* = 1 Hz), 4.15 (2H, q, *J* = 7 Hz), 5.72 (1H, q, *J* = 1 Hz). From the gc (10% OV101, 100°C) the prepared sample was 96% *E*–**1**, 3% *Z*–**1**, and 1% deconjugated isomer **3**.

Preparation of Z*-ethyl 3,4,4-trimethyl-2-pentenoate,* **1**

A sample of the *Z* isomer was prepared for gc calibration as follows.

E-ethyl 3,4,4-trimethyl-2-pentenoate, **1** (0.2265 g), was irradiated in pentane (10 mL) using a low pressure mercury lamp for 2 h after which time gc (5% SE30, 110°C) indicated that the mixture consisted of 26% *Z*–**1** and 74% *E*–**1**. The pentane was evaporated and the residue was separated by gc (10% OV101, 100°C) to give *Z*–**1** (30 mg) which had ^{1}H nmr ($CDCl_3$, 60 MHz): 1.19 (9H, s), 1.28 (3H, t, *J* = 7 Hz), 1.81 (3H, d, *J* = 1 Hz), 4.10 (2H, q, *J* = 7 Hz), 5.58 (1H, q, *J* = 1 Hz) ppm.

Preparation of ethyl 2-(1′,2′,2′-trimethylcyclopropyl)acetate, **2**

A sample of **2** was prepared for gc calibration as follows.

Ester **1** (0.194 g) was dissolved in ether (10 mL) and irradiated in quartz to complete conversion (gc; 5% SE30, 100°C) using a low pressure mercury lamp. The ether was distilled off through a short

Can. J. Chem. Downloaded from www.nrcresearchpress.com by 210.87.254.105 on 09/06/12
For personal use only.

Can. J. Chem. Downloaded from www.nrcresearchpress.com by 210.87.254.105 on 09/06/12
For personal use only.

Vigreux column and the residue was separated by gc (10% OV101, 100°C) to give 2,3-diethoxybutane (12 mg) as the more volatile component and the cyclopropane ester **2** (67 mg). The 2,3-diethoxybutane was isolated as a mixture, presumed to be the *d,l* and *meso* isomers and had ^{1}H nmr ($CDCl_3$): 1.0–1.3 (12H, m), 3.2–3.7 (6H, m) ppm; *m/e*: 146, 73, 45. *Mol. Wt.* calcd. for $C_8H_{18}O_2$: 146.1307; found: 146.1300. For the cyclopropane ester **2**, ^{1}H nmr ($CDCl_3$, 100 MHz): 0.22 (1H, d, J = 4.5 Hz), 0.32 (1H, d, J = 4.5 Hz), 1.11 (6H, s), 1.15 (3H, s), 1.26 (3H, t, J = 7 Hz), 2.24 (1H, d, J = 15.5 Hz), 2.49 (1H, d, J = 15.5 Hz), 4.16 (2H, q, J = 7 Hz) ppm.

Preparation of ethyl 4,4-dimethyl-3-methylenepentanoate, 3

A sample of **3** was prepared for gc calibration as follows.

Ester **1** (0.198 g) and 1,2-dimethylimidazole (0.016 g) were dissolved in ether (10 mL) and irradiated in quartz to complete conversion (gc; 5% SE30, 100°C) using a low pressure mercury lamp. The ether was evaporated and the residue separated by gc (10% OV101, 100°C) to give **3** (0.092 g); ^{1}H nmr ($CDCl_3$, 100 MHz): 1.07 (9H, s), 1.26 (3H, t, J = 7 Hz), 3.06 (2H, d, J = 1 Hz), 4.16 (2H, q, J = 7 Hz), 4.90 (1H, d, J = 1 Hz), 5.07 (1H, s) ppm.

Preparation of E*-ethyl 3,4-dimethyl-2-pentanoate, 4*

Ethyl 3,4-dimethyl-3-hydroxypentanoate, **12** (R = H), was prepared by the Reformatsky reaction between 3-methyl-2-butanone and ethyl bromoacetate in 72% yield and had bp 120°C/50 Torr; ^{1}H nmr ($CDCl_3$, 100 MHz): 0.90 (3H, d, J = 6.5 Hz), 0.94 (3H, d, J = 6.5 Hz), 1.16 (3H, s), 1.28 (3H, t, J = 7 Hz), 1.77 (1H, septet, J = 6.5 Hz), 2.37 (1H, d, J = 15 Hz), 2.55 (1H, d, J = 15 Hz), 3.60 (1H, exchanges with D_2O), 4.18 (2H, q, J = 7 Hz) ppm.

The hydroxy ester **12** (R = H) was converted to the acetoxy ester **13** (R = H) as follows.

Compound **12** (R = H) (31.2 g, 0.179 mol), N,N-dimethylaniline (25.0 g, 0.207 mol), and acetyl chloride (15.0 g, 0.191 mol) were refluxed together in chloroform (50 mL) for 2.5 h after which time gc (5% SE30, 120°C) of a worked-up sample indicated that the reaction was complete. The reaction mixture was washed with excess dilute sulphuric acid and dried (Na_2CO_3 + K_2CO_3). The chloroform was evaporated and the residual oil distilled through a 12-in Vigreux column to yield acetate **13** (R = H), 34 g (88%), bp 80°C/1.2 Torr which had ^{1}H nmr ($CDCl_3$, 100 MHz): 0.93 (6H, d, J = 7 Hz), 1.25 (3H, t, J = 7 Hz), 1.43 (3H, s), 1.99 (3H, s), 2.40 (1H, septet, J = 7 Hz), 2.86 (1H, d, J = 14 Hz), 3.05 (1H, d, J = 14 Hz), 4.13 (2H, q, J = 7 Hz) ppm.

The acetate **13** (R = H) (20 g, 0.093 mol) was dissolved in *tert*-butanol (15 mL) and added over 5 min to a stirred solution of potassium *tert*-butoxide in *tert*-butanol (prepared from 4.6 g, 0.12 mol K and 100 mL *tert*-butanol). Following completion of the addition the solution, which had become warm and precipitated a gelatinous white solid, was stirred for 15 min, poured into water (250 mL), and extracted with ether (200 mL, 2 × 100 mL). The extracts were combined, dried ($MgSO_4$), and evaporated, and the residual oil was distilled through a 12-in Vigreux column to give **4**, 7.7 g (53%), bp 100°C/37 Torr (lit. (20) bp 80°C/20 Torr). The gc analysis (10% OV101, 100°C) of the sample of **4** prepared indicated that it consisted of 90% *E*–**4**, 9% *Z*–**4**, 0.7% ethyl 4-methyl-3-methylenepentanoate, **8**, and 0.3% ethyl 3,4-dimethyl-3-pentenoate, **7**. For *E*–**4**, ^{1}H nmr ($CDCl_3$, 60 MHz): 1.1 (6H, d, J = 7 Hz), 1.3 (3H, t, J = 7 Hz), 2.1 (3H, d, J = 1 Hz), 2.4 (1H, septet, J = 7 Hz), 4.2 (2H, q, J = 7 Hz), 5.73 (1H, broad, s) ppm.

Preparation of ethyl 3,4-dimethyl-3-pentanoate, 7

A sample of **7** was prepared for gc calibration as follows.

Ethyl 3,4-dimethyl-2-pentenoate, **4** (0.167 g), was dissolved in diethyl ether (10 mL) and irradiated using light of wavelength 254 nm until gc (10% OV101, 100°C) indicated no starting material remained. The ether was evaporated and the residual oil was purified by gc (20% Carbowax 20 M, 110°C) to give **7**, 0.100 g as a colourless oil; ^{1}H nmr ($CDCl_3$, 60 MHz): 1.23 (3H, t, J = 7 Hz), 1.77 (9H, s), 3.05 (2H, s), 4.10 (2H, q, J = 7 Hz) ppm.

Preparation of ethyl 3-methylene-4-methylpentanoate, 8

A sample of **8** was prepared for gc calibration as follows.

Ethyl 3,4-dimethyl-2-pentenoate, **4** (0.165 g), and 1,2-dimethylimidazole (0.018 g) were dissolved in diethyl ether (10 mL) and irradiated using light of wavelength 254 nm until gc (10% OV101, 100°C) indicated no starting material remained. The ether was evaporated and the residual oil was purified by gc (10% UCON LB 550X, 100°C) to give **7**, 0.070 g, and **8**, 0.041 g, as colourless oils. For **8**, ^{1}H nmr ($CDCl_3$, 60 MHz): 1.04 (6H, d, J = 8 Hz), 1.24 (3H, t, J = 7 Hz), 2.0–2.6 (1H, m), 3.04 (2H, s), 4.01 (2H, q, J = 7 Hz), 4.86 (1H, s), 4.93 (1H, s) ppm.

Irradiations

Irradiations were performed using a low pressure mercury lamp housed in a quartz tube which was immersed into the solution to be irradiated in such a manner that all of the emitted light entered the solution. Since the lamp became warm during operation (ca. 40°C) the solution being irradiated was placed in a bath maintained at 21° ± 0.5°C.

Quantum yields were determined by performing the irradiations on solutions containing a non-light-absorbing, inert internal standard and monitoring the progress of the reactions with time by gas chromatography using 10% OV101 on Chromosorb at 100°C for **4** and 120°C for **1**. Internal standards used were dimethylsuccinate for **1** and n-pentylacetate for **4**.

The light source was calibrated following each irradiation using azoxybenzene as an actinometer according to the procedure developed by Bunce *et al.* (21).[5] Solutions of azoxybenzene (0.035 *M*) in 95% ethanol were irradiated to 5% conversion; 1.00-mL aliquots were withdrawn periodically during the irradiations and diluted to 10.00 mL with 5% KOH in 95% ethanol. The amount of O-hydroxy azoxybenzene formed was determined from the absorbance of these solutions at 454 nm assuming an extinction coefficient of 7600, and the light intensity was calculated assuming a quantum yield of 0.017 for the conversion of azoxybenzene to O-hydroxyazobenzene. The lamp output in all irradiations performed in this work was (1.16 ± 0.06) × 10^{-6} Einsteins s^{-1}.

Acknowledgements

Financial support from the Natural Sciences and Engineering Research Council of Canada, and Imperial Oil Ltd. is gratefully acknowledged.

1. P. BORRELL and J. D. HOLMES. J. Photochem. **1**, 433 (1972/3).
2. J. A. BARLTROP and J. WILLS. Tetrahedron Lett. 4987 (1968).
3. M. MOUSSERON. Pure Appl. Chem. **9**, 481 (1964).
4. P. J. KROPP and H. J. KRAUSS. J. Org. Chem. **32**, 3222 (1967).
5. G. BÜCHI and S. H. FEAIRHELLER. J. Org. Chem. **34**, 609 (1969).
6. J. K. CRANDALL and C. F. MAYER. J. Org. Chem. **35**, 3049 (1970).
7. J. R. SCHEFFER and B. A. BOIRE. J. Am. Chem. Soc. **93**, 5490 (1971).
8. M. ITOH, M. TOKUDA, M. HATAYA, and A. SUZUKI. Hokkaido Daigaku Kogakubu Kenkuy Hokoku, **60**, 37 (1971).
9. R. R. RANDO and W. E. DOERING. J. Org. Chem. **33**, 1671 (1968).
10. M. J. JORGENSON. J. Chem. Soc. Chem. Commun. 137 (1965).
11. M. J. JORGENSON and L. GUNDEL. Tetrahedron Lett. 4991 (1968).
12. M. J. JORGENSON. J. Am. Chem. Soc. **91**, 198 (1969); **91**, 6432 (1969).
13. C. S. K. WAN and A. C. WEEDON. J. Chem. Soc. Chem. Commun. 1235 (1981).
14. S. L. ENG, R. RICARD, C. S. K. WAN, and A. C. WEEDON.

[5] The author thanks Professor Bunce for a preprint describing this procedure.

J. Chem. Soc. Chem. Commun. 236 (1983).
15. I. A. SKINNER and A. C. WEEDON. Tetrahedron Lett. 4299 (1983).
16. K. H. FUNG, K. J. SCHMALZL, and R. N. MIRRINGTON. Tetrahedron Lett. 5017 (1969).
17. R. HEILMANN and R. GLENAT. Bull. Soc. Chim. Fr. 1586 (1955).
18. A. DEBOER and J. A. HUNTER. J. Org. Chem. **38**, 144 (1973).
19. L. I. SMITH, W. L. KOHLHASE, and R. J. BROTHERTON. J. Am. Chem. Soc. **78**, 2532 (1956).
20. M. J. JORGENSON and T. LEUNG. J. Am. Chem. Soc. **90**, 3769 (1968).
21. N. J. BUNCE, J. LAMARRE, and S. P. VAISH. Photochem. Photobiol. In press.

Can. J. Chem. Downloaded from www.nrcresearchpress.com by 210.87.254.105 on 09/06/12
For personal use only.

Synthesis of 3-isoxazolols revisited. Diketene and β-ketoesters as starting materials

NIELS JACOBSEN, HANS KOLIND-ANDERSEN, AND JENS CHRISTENSEN

Research and Development Departments, Cheminova Ltd., P.O. Box 9, DK-7620 Lemvig, Denmark

Received January 24, 1984

This paper is dedicated to Professor Paul de Mayo on the occasion of his 60th birthday

NIELS JACOBSEN, HANS KOLIND-ANDERSEN, and JENS CHRISTENSEN. Can. J. Chem. **62**, 1940 (1984).

3-Isoxazolols can be made in good yields from β-ketoesters or diketene and hydroxylamine, provided that pH is kept at about 10 throughout the reaction, and that the reaction mixture is quenched with an excess of strong mineral acid. This suppresses the formation of 5-isoxazolones, which are otherwise normally the main products of the reaction.

NIELS JACOBSEN, HANS KOLIND-ANDERSEN et JENS CHRISTENSEN. Can. J. Chem. **62**, 1940 (1984).

On peut préparer les isoxazolols-3 avec de bons rendements en utilisant de l'hydroxylamine et des β-cétoesters ou dicétènes comme produits de départ à condition de maintenir le pH à environ 10 pendant toute la réaction et de piéger le mélange réactionnel avec un excès d'acide minéral fort. Cette précaution supprime la possibilité de formation des isoxazolones-5, qui sont autrement les produits principaux de la réaction.

[Traduit par le journal]

Can. J. Chem. Downloaded from www.nrcresearchpress.com by 210.87.254.5 on 09/06/12
For personal use only.

Introduction

In recent years much interest has been given to the 3-isoxazolol moiety, which is contained in a variety of physiologically active compounds. Thus the naturally occurring alkaloid muscimol **1** is an in vivo active mimetic of the neurotransmitter γ-aminobutyric acid (GABA) (1).

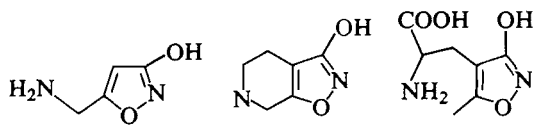

1 **2** **3**

The synthetic analogue THIP, **2**, is a very potent GABA receptor agonist and, as it is relatively nontoxic, it is of considerable pharmacological interest (1). The compound AMPA, **3**, has been pointed out as an agonist of glutamic acid, and has powerful pharmacological effects after local injection into various brain areas of the rat (2). A rather simple molecule, 5-methyl-3-isoxazolol **4**, has been commercialized under the names Tachigaren or Hymexazol. It is a soil fungicide and a growth promoter (3). Also the contact insecticide Karphos **5**

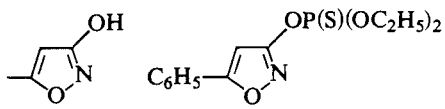

4 **5**

contains the 3-isoxazolol moiety (4). A general and economical synthetic method for this interesting class of compounds is therefore desirable.

Although one of the most direct routes to 3-isoxazolols would appear to be the reaction of a β-ketoester (or diketene) with hydroxylamine, this method is unsuitable in most cases, largely because of preferential formation of 5-isoxazolones. This is particularly the case when 2-unsubstituted β-ketoesters are employed (5–8). Thus, it has been claimed that **4** cannot be prepared by direct condensation of hydroxylamine with acetoacetic esters or diketene (ref. 9, and references therein). As a consequence, these compounds are usually prepared from protected β-ketoesters or by entirely different methods (3, 9–11). Some 2-substituted β-ketoesters (e.g. ethyl 2-methylacetoacetate, **6**) have, however, been shown to yield 3-isoxazolols (5), although these were originally described as 5-isoxazolones (8). Jacquier *et al.* (12–14) made a detailed investigation of the reaction of β-ketoesters and hydroxylamine under alkaline conditions. They demonstrated that in the few cases where 3-isoxazolols were formed in substantial amounts (5, 15), their formation depended on rapid acidification of the reaction mixture with a large excess of concentrated hydrochloric acid, whereas only 5-isoxazolones were formed upon slow acidification to pH 3–5. These authors suggested hydroxamic acids **7** and oximes **8** as discrete intermediates for 3-isoxazolols and 5-isoxazolones, respectively.

7 **8**

It seemed likely that the ratio of **7** to **8** and hence the total outcome of the reaction would be greatly influenced by the pH of the reaction mixture. The subject of the present paper is an investigation of the pH dependence of this reaction, which, combined with the "acidification brusque" of Jacquier *et al.*, ultimately led to a practical synthesis of 3-isoxazolols from β-ketoesters or diketene.

Results and discussion

Due to the economic importance of **4** and the availability and low price of methyl acetoacetate **9***a*, reaction of the latter with hydroxylamine was first investigated in detail. Addition of **9***a* to an aqueous solution of one equivalent of hydroxylamine hydrochloride, neutralized with 0.5 molar equivalents of sodium carbonate, and quenching the reaction mixture with a tenfold molar excess of concentrated hydrochloric acid gave 3-methyl-5-isoxazolone **10** as the main product. Only traces of **4** were detected.

When, however, the hydroxylamine hydrochloride solution was buffered with a twofold excess of sodium carbonate (ph 10–11) prior to the addition of **9***a* an approximately equimolar mixture of **4** and **10** resulted, whereas substituting the carbonate with bicarbonate (pH ~8) led to the formation of **10** only.

We therefore investigated the dependence on pH of the for-

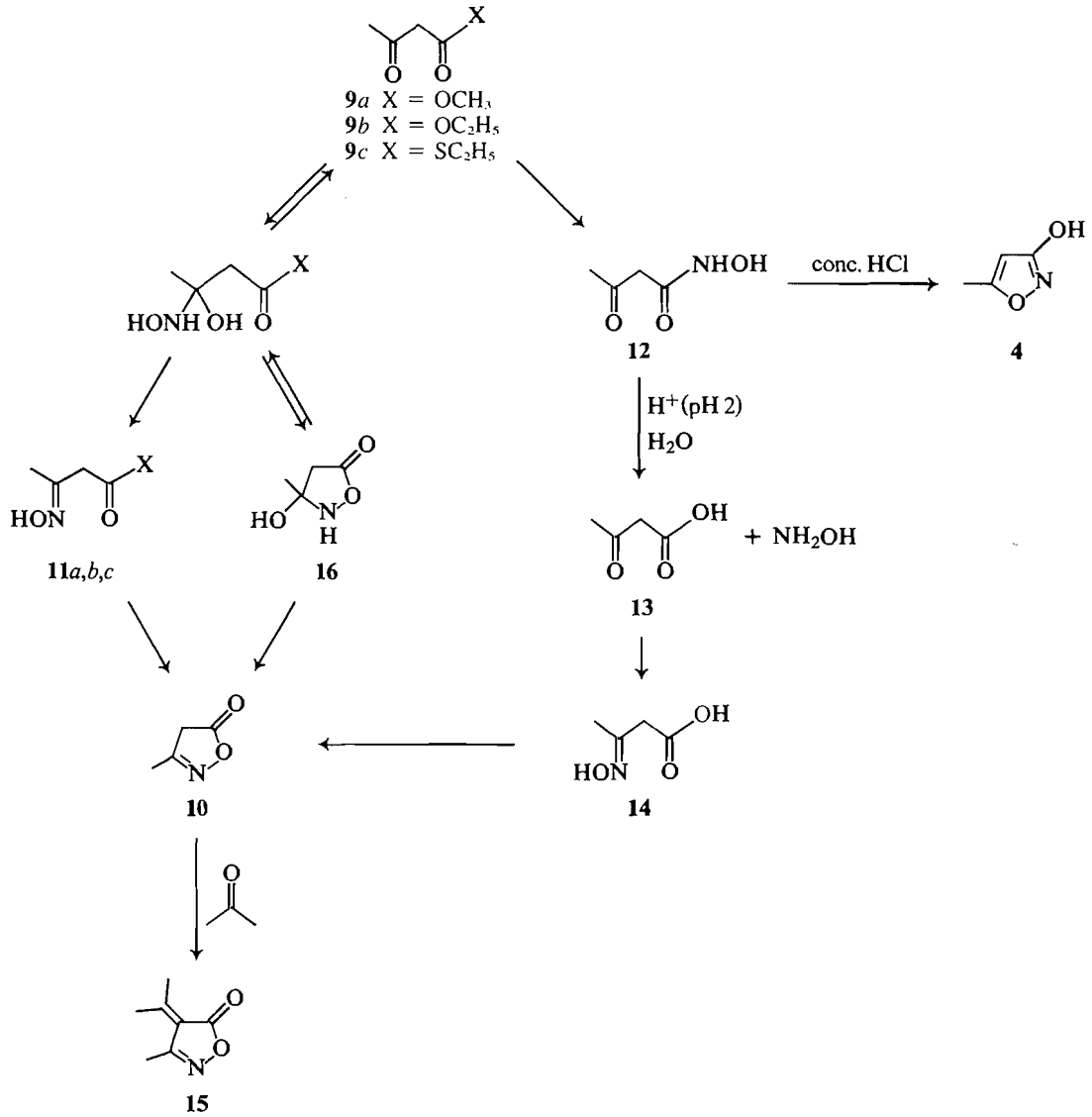

SCHEME 1

mation of **4** by running the reaction at constant pH values using a pH-stat with 2 *N* sodium hydroxide as the modifying reagent. In each case the reaction mixture was poured into a large excess of concentrated hydrochloric acid and the yield of **4** determined by hplc after continuous extraction with methylene chloride. The optimum pH for the formation of **4** was found to be 9–10, giving a yield of 70%. At pH 8.5 or 10.5 the yield is already reduced, at pH 8 it is below 40%, and at pH 11 it is below 50%.

At pH = 10, which is intermediate between the pK_a value of the hydroxylammonium ion (5.9) (10, 16) and hydroxylamine (13.7) (10) respectively, the dominant species is the neutral hydroxylamine molecule. This species has its nucleophilicity centered on the nitrogen atom (10), whose attack on **9***a* could lead to either the oxime **11***a* or the hydroxamic acid **12**. Formation in alkaline solution of **10** via **11***b* is well documented (17, 18), and **11***a* could be isolated from the reaction buffered by bicarbonate upon extraction with methylene chloride prior to the acidification. When treated with concentrated hydrochloric acid **11***a* was transformed into **10** exclusively. Thus **11***a* cannot be an intermediate in the formation of **4**. Lowering the pH from 10, it therefore seems likely that enhanced oxime formation can account for the decrease in yield of **4**. Around pH 10 the hydroxamic acid **12** could be suggested as the main intermediate, leading upon very rapid acidification to **4**, whereas moving towards higher pH would cause an increasing participation of deprotonated hydroxylamine (NH_2O^-). This species has its nucleophilicity located mainly on the oxygen atom (10), which could lead to the formation of different intermediates incapable of forming **4**. Our attempts to isolate the hydroxamic acid **12** have remained unsuccessful and, to our knowledge, only one hydroxamic acid of this type has been described (**7**, R = Ph, R′ = CH_3 (14)).

Quenching of the reaction mixture with excess strong acid is crucial for obtaining high yields of **4**. Diminution of the amounts of acid led to a decrease in the yield of **4** accompanied by an increase in the yield of **10**. When the mixture from the reaction at pH 10 was brought to pH 2 by dropwise addition of concentrated hydrochloric acid, only approximately 1% **4** could be detected. Instead, a 85% yield of **10** was obtained, compared to the 70% yield of **4** obtained by rapid acidification.

Since the sum of these yields exceeds 100%, at least part of the mass of **4** and **10** must be derived from a common precursor. Our data do not allow definite assignment of a structure to this precursor, but if it were the hydroxamic acid **12**, formation of **10** requires breaking of the C—N bond in **12**. Thus hydrolysis of **12** would lead to acetoacetic acid **13**, which under the

Can. J. Chem. Downloaded from www.nrcresearchpress.com by 210.87.254.5 on 09/06/12
For personal use only.

Can. J. Chem. Downloaded from www.nrcresearchpress.com by 210.87.254.5 on 09/06/12
For personal use only.

weakly acidic conditions could react with the liberated hydroxylamine to form an oxime **14** and, subsequently, **10**. It is known that hydroxamic acids can be hydrolysed (19). The results of the different modes of acidification would thus reflect perturbations of the balance between cyclization and hydrolysis of **12**.

The condensation product **15** (18, 20) between **10** and acetone is formed as a minor by-product in all the reactions. The acetone required for the formation of **15** can originate from several sources, e.g. via decarboxylation of **13**. The reaction pathways discussed are depicted in Scheme 1. When ethyl acetoacetate **9***b* or diketene were used instead of **9***a* under optimum conditions for the formation of **4**, almost identical yields were obtained (Table 1), whereas ethyl thiolacetoacetate **9***c* gave a mixture of **4** (15%) and **10** (40%), probably reflecting formation of **10** via the carbinolamine intermediate **16** (16), a pathway which is not operative for **9***b* (17). The reaction of **9***b* and ketene had similar pH profiles to that of **9***a*, with an optimum around pH 10.

Using the same reaction conditions, several β-ketoesters were reacted with hydroxylamine, and the results are found in Table 1. In several examples (**4**, **23**, **26**, **28**, **38**, and, presumably, **20**) 3-isoxazolols, which were not previously accessible by this method, have been obtained, whereas in other examples (**17**, **34**) substantial increases in the yield of 3-isoxazolols were obtained compared to those reported in the literature. Most of the 5-isoxazolones are unstable under our reaction and work-up conditions, so the yields given for these compounds must be interpreted with care.

Using 2-carbethoxycyclopentanone **40** as substrate, the reaction failed completely, and cyclopentanone oxime was the only product isolated. In spite of the apparent formation of **20** from 2-carbethoxycyclohexanone **19**, all attempts to transform the structural analogue **41** into **42**, a precursor of THIP **2** (22), failed. Only the 5-isoxazolone **43** was isolated. The previously unknown compound **28** seems well suited as a starting material for the synthesis of AMPA **3**.

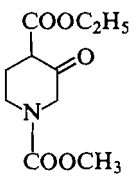

41

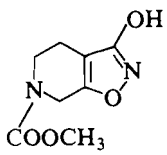

42

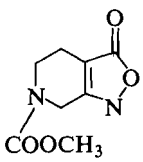

43

Experimental

Melting points were obtained with a Büchi 510 Melting Point Determinator and are uncorrected. The ir spectra were recorded on a Perkin–Elmer 177 grating spectrophotometer. The 60 mHz ^{1}Hmr spectra were obtained with a JEOL JNM-PMX 60 spectrometer. Peak positions are δ values in ppm downfield from TMS. The uv spectra were recorded on a Shimadzu UV-240 spectrophotometer. The pH-stat consisted of a Radiometer PHM 82 standard pH meter equipped with a titrator TTT 80 loaded with 2 *N* sodium hydroxide, a magnetic valve Type MNV I D, and a GK 2403 C electrode. The gc and hplc equipment was Hewlett–Packard 5840A and 1084B, respectively.

Reaction of β-ketoesters or diketene with hydroxylamine. General procedure

Hydroxylammonium chloride (0.20 mol) was dissolved in approximately 100 mL of 2 *N* sodium hydroxide to achieve a solution of pH 10.0. This solution was cooled to 0–5°C (20°C in the case of **30** and **33**) and vigorously stirred while the β-ketoester (0.20 mol) was added during 30 min, keeping pH at 10.0 ± 0.2 by means of the pH-stat. Stirring was continued for about 30 min at pH 10. At this point approximately 100 mL of 2 *N* sodium hydroxide had been added. The mixture was then poured into 150 mL ice-cooled concentrated hydrochloric acid and the mixture left overnight at room temperature. In some cases the 3-isoxazolols crystallized from this mixture, but in most cases the products were isolated by continuous extraction with methylene chloride.

In the case of **9***a*, *b* or diketene as substrates, the pH dependence was determined using the general procedure, only varying the pH.

*Methyl acetoacetate oxime **11**a*

To a solution of sodium bicarbonate (40 g) in 300 mL of water was added hydroxylammonium chloride (16 g, 0.23 mol) followed by methyl acetoacetate **9***a* (23 g, 0.20 mol). After 80 min the mixture was extracted with three 150-mL portions of methylene chloride. After drying and evaporation of the methylene chloride, the residue was bulb-to-bulb distilled at 150°C/0.05 Torr (1 Torr = 133.3 Pa) to give **11***a* (8.5 g) as a colourless oil; ^{1}Hmr ($CDCl_3$) δ: 1.97 (s, 3H), 3.27 (s, 2H), 3.72 (s, 3H), 9.6 (broad s, 1H). *Anal.* calcd. for $C_5H_9NO_3$: C 45.80, H 6.92, N 10.68; found: C 45.96, H 6.78, N 10.86.

*4,5,6,7-Tetrahydro-1,2-benz-3-isoxazolol, **20** and 4,5,6,7-tetrahydro-2,1-benzisoxazolin-3-one, **21***

The product from the standard procedure using 2-carbethoxycyclohexanone **19** as substrate was a crystalline solid (25.4 g), whose mp (90.5–93°C) did not change significantly after repeated recrystallization from MeOAc. From spectroscopic data, a 2:1 mixture of **20** and **21** may be proposed; uv (EtOH) λ_{max}: 218 and 256 nm; ^{1}Hmr ($CDCl_3$) δ: 1.3–3.0 (m, 8H), 3.1 (dd, 1H, **21**), 11.3 (s, 1H, **20**). *Anal.* calcd. for $C_7H_9NO_2$: C 60.42, H 6.52, N 10.07, O 22.99; found: C 59.74, H 6.49, N 10.21, O 23.00.

*5-Isopropyl-3-isoxazolol, **23** and 3-isopropyl-5-isoxazolone, **24***

The compound **23** crystallized spontaneously from the reaction mixture after acidification, yield 46%, mp (heptane) 45–46°C. Extraction of the filtrate gave a mixture of **23** and **24** in 21 and 16% yield, respectively (gc).

*5-Propyl-3-isoxazolol, **26***

The crude methylene chloride extract contained **26**, corresponding to a yield of 59% (gc). Crystallization from H_2O and heptane, successively, gave **26**, mp 43–44°C.

*4-(2-Hydroxyethyl)-5-methyl-3-isoxazolol, **28***

The general procedure was followed, using 2-acetylbutyrolactone **27** as substrate, and, upon cooling the methylene chloride extract to 0°C, **28** crystallized in 48% yield, mp (MeOH) 167–169°C. The mother liquor contained **27**, 24% yield, and 5-hydroxy-2-pentanone, 24% yield (gc). Data of **28**: uv (EtOH) λ_{max} (log ε): 225 (3.1) nm; ir (KBr) ν_{max}: 3180, 2940, 2810, 1660, 1520, 1390, 1350, 1330, 1245, and 1050 cm^{-1}; ^{1}Hmr ($CDCl_3$ + DMSO-d_6) δ: 2.33 (s, 3H), 2.53 (t, J = 7.0 cps, 2H), 3.77 (t, J = 7.0 cps, 2H), 7–9 (broad signal, 2 × OH). *Anal.* calcd. for $C_6H_9NO_3$: C 50.34, H 6.34, N 9.79; found: C 50.26, H 6.41, N 9.76.

*5-tert-Butyl-3-isoxazolol, **38** and 3-tert-butyl-5-isoxazolone, **39***

The crude product from the general procedure contained **38** and **39**, corresponding to yields of 73 and 22%, respectively, (nmr). Separation by fractional crystallization from aqueous methanol gave the pure compounds: **38**, mp 99–101°C; uv (EtOH) λ_{max} (log ε): 207 (3.8) nm; ir (KBr) ν_{max}: 3400, 2960, 1615, 1530, 1455, 1365, 1345, and 1270 cm^{-1}; ^{1}Hmr (DMSO-d_6) δ: 1.25 (s, 9H), 5.65 (s, 1H), 10.5

Can. J. Chem. Downloaded from www.nrcresearchpress.com by 210.87.254.5 on 09/06/12
For personal use only.

TABLE 1. 3-Isoxazololes and 5-isoxazolones from β-ketoesters

β-Ketoesters	RCOCHR′ COOR″			3-Isoxazololes 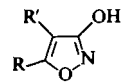					5-Isoxazolones 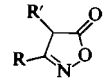				
					Yield (%)		Melting point (°C)			Yield (%)		Melting point (°C)	
Compound	R	R′	R″	Compound	Found	(lit.)	Found	(lit.)	Compound	Found	(lit.)	Found	(lit.)
9*a*	CH_3	H	CH_3	**4**	70[a]		85.5–86	86–87 (3)	**10**			Oil	
9*b*	CH_3	H	C_2H_5	**4**	61[a]	0 (13)			**10**		65 (13)	Oil	
6	CH_3	CH_3	C_2H_5	**17**	80[c]	40 (13)	122–124 (H_2O)	123–124 (11)	**18**		55 (13)		49–51 (15)
19	—C_4H_8— (ring)		C_2H_5	**20**	See experimental	0 (13)		130 (11)	**21**	See experimental	85 (13)		66 (13)
22	*iso*-C_3H_7	H	C_2H_5	**23**	67[c]	0 (13)	45–46	41–42 (11)	**24**	16[c]	50 (13)		Oil
25	*n*-C_3H_7	H	C_2H_5	**26**	59[c]		43–44	41–41.5 (3)					
27	CH_3	—C_2H_4— (ring)		**28**	48[d]		167–169		**29**		70 (21)		113–114 (21)
30	CH_3	C_2H_5	C_2H_5	**31**	32[c]	35 (13)			**32**	56[c]	50 (13)		
33	Ph	H	C_2H_5	**34**	Trace[a]	0 (13)			**35**	88[a]	75 (13)		
36	Ph	H	CH_3	**34**	49[a]				**35**	40[a]			
37	*tert*-C_4H_9	H	CH_3	**38**	73[b]	0 (5)	99–101		**39**	22[b]		106–107	107–108 (5)
40	—C_3H_6— (ring)		C_2H_5		0					0			
9*c*	$CH_3COCH_2COSC_2H_5$			**4**	15[c]				**10**	40[c]			
	Diketene			**4**	71[a]								

[a] By hplc.
[b] By nmr.
[c] By gc.
[d] Isolated yield.

(broad singlet, 1H). *Anal.* calcd. for $C_7H_{11}NO_2$: C 59.56, H 7.86, N 9.92; found: C 59.17, H 7.83, N 9.83. Compound **39**, mp 106–107°C (lit. (5) mp 107–108°C); ^{1}Hmr ($CDCl_3$) δ: 1.28 (s, 9H), 3.57 (s, 2H).

Methyl 3-hydroxy-4,5,6,7-tetrahydroisoxazolol[3,4-c]pyridine-6-carboxylate, 43

Reaction of ethyl 1-methoxycarbonyl-3-oxopiperidine-4-carboxylate, **41**, with hydroxylamine by the standard procedure yielded 76% of **43** in which traces of methyl 3-hydroxy-4,5,6,7-tetrahydroisoxazolol[5,4-*c*]pyridine-6-carboxylate, **42** (22) was detected by tlc. The compound **43** was identical (tlc, ir, uv, mp and mixture mp) with an authentic sample generously supplied by P. Krogsgaard-Larsen; mp (MeOH) 140–142°C (dec.); uv (EtOH) λ_{max} (log ε): 260 (3.9) nm; ir (KBr) ν_{max}: 3090, 1725, 1685, 1625, 1615 (sh), 1475, 1440, 1410, and 1425 cm^{-1}; ^{1}Hmr ($CDCl_3$ + DMSO-d_6) δ: 2.46 (dt, J = 6.0 and 2.0 cps, 2H), 3.76 (t, J = 6.0 cps, 2H), 3.85 (s, 3H), 4.56 (broadened s, 2H), 8–10 (broad and flat signal, 1H). The *tert*-butylester corresponding to **43** has been described (1). Compounds **42** (22) and **43**: mixture mp 122–124°C (dec.).

Acknowledgement

We thank Dr. P. Krogsgaard-Larsen, Royal Danish School of Pharmacy, Copenhagen, for fruitful discussions and for a sample of compound **43**.

1. P. KROGSGAARD-LARSEN and T. ROLDSKOV-CHRISTIANSEN. Eur. J. Med. Chem. **14**, 157 (1979).
2. T. HONORÉ, J. LAURIDSEN, and P. KROGSGAARD-LARSEN. J. Neurochem. **38**, 173 (1982).
3. Ann. Sankyo Res. Lab. **25**, 1 (1973); Chem. Abstr. **80**, 120808 (1974); **80**, 141703 (1974).
4. Ann. Sankyo Res. Lab. **22**, 221 (1970); Chem. Abstr. **75**, 20257 (1971).
5. A. R. KATRITZKY and S. ØKSNE. Proc. Chem. Soc. 387 (1961).
6. L. CLAISEN and W. ZEDEL. Ber. **24**, 140 (1891).
7. A. HANTZSCH. Ber. **24**, 495 (1891).
8. R. UHLENHUTH. Ann., **296**, 33 (1897).
9. T. A. OSTER and T. M. HARRIS. J. Org. Chem. **48**, 4307 (1983).
10. C. KASHIMA, Y. KONNO, N. YOSHIWARA, and T. TAJIMA. J. Heterocycl. Chem. **19**, 1535 (1982).
11. R. JACQUIER, C. PETRUS, F. PETRUS, and J. VERDUCCI. Bull. Soc. Chim. Fr. 1978 (1970).
12. R. JACQUIER, C. PETRUS, F. PETRUS, and J. VERDUCCI. Bull. Soc. Chim. Fr. 3003 (1967).
13. R. JACQUIER, C. PETRUS, F. PETRUS, and J. VERDUCCI. Bull. Soc. Chim. Fr. 2685 (1970).
14. R. JACQUIER, F. PETRUS, J. VERDUCCI, and Y. VIDAL. Bull. Soc. Chim. Fr. 3664 (1971).
15. F. DE SARLO. Tetrahedron, **23**, 831 (1967).
16. M. COCIVERA, S. BASU, L. COPP, and V. MALATESTA. Can. J. Chem. **59**, 629 (1981).
17. M. COCIVERA, A. EFFIO, H. E. CHEN, and S. VAISH. J. Am. Chem. Soc. **98**, 7362 (1976).
18. H. SCHULZ and S. J. WAKIL. Anal. Biochem. **37**, 457 (1970).
19. D. C. BERNDT and J. K. SHARP. J. Org. Chem. **38**, 396 (1973).
20. T. KATO, N. KATAGIRI, and N. MINAMI. Chem. Pharm. Bull. **20**, 1368 (1972).
21. H. WAMHOFF and F. KORTE. Chem. Ber. **99**, 2962 (1966).
22. P. KROGSGAARD-LARSEN. Acta Chem. Scand. Ser. B, **31**, 584 (1977).

Can. J. Chem. Downloaded from www.nrcresearchpress.com by 210.87.254.5 on 09/06/12
For personal use only.

An efficient synthesis of pterosin C and other pterosins

KAM-MUI EVA NG AND TREVOR C. MCMORRIS
Department of Chemistry, University of California, San Diego, La Jolla, CA 92093, U.S.A.

Received January 13, 1984

This paper is dedicated to Professor Paul de Mayo on the occasion of his 60th birthday

KAM-MUI EVA NG and TREVOR C. MCMORRIS. Can. J. Chem. **62**, 1945 (1984).

A versatile synthetic route to pterosins, sesquiterpenoid indanones present in bracken, *Pteridium aquilinum*, has been developed. The route is exemplified by the synthesis of (2*S*,3*S*)-pterosin C by Friedel–Crafts bisacylation of the methyl ether of 2-(2,6-dimethylphenyl)ethanol with methylmalonyl chloride. Demethylation of the resulting 1,3-indandione and reduction with zinc and acetic acid in the presence of acetic anhydride and sodium acetate afforded a mixture of racemic *cis* and *trans* isomers of pterosin C diacetate, which was hydrolysed to the corresponding pterosins. Separation and resolution via the *S*-(+)-α-phenylbutyric esters gave (2*S*,3*S*)-pterosin C and (2*R*,3*R*)-pterosin C. Other pterosins were prepared as racemates from the 1,3-indandione.

KAM-MUI EVA NG et TREVOR C. MCMORRIS. Can. J. Chem. **62**, 1945 (1984).

On a développé une voie de synthèse versatile conduisant aux ptérosines, les indanones sesquiterpéniques présentes dans le *Pteridium aquilinum*. Un exemple de cette nouvelle voie est la synthèse de la ptérosine C (2*S*,3*S*) en faisant appel à une bis acylation suivant Friedel et Crafts de l'éther méthylique du (diméthyl-2,6 phényl)-2 éthanol avec le chlorure de méthylmalonyle. La déméthylation de l'indanedione-1,3 qui en résulte et sa réduction par le zinc et l'acide acétique en présence d'anhydride acétique et d'acétate de sodium conduit à un mélange racémique des isomères *cis* et *trans* du diacétate de ptérosine C, qui peut être hydrolysé en ptérosines correspondantes. La séparation et la résolution grâce aux esters de l'acide *S*-(+)-α-phénylbutyrique conduit aux ptérosines C (2*S*,3*S*) et (2*R*,3*R*). Partant de l'indanedione-1,3, on a préparé d'autres ptérosines sous forme de racémiques.

[Traduit par le journal]

The pterosins are a large group of sesquiterpenes and norsesquiterpenes first isolated from bracken fern, *Pteridium aquilinum*, in Japan (1). These compounds have since been found to occur widely in ferns (2) and they are also present in certain fungi of the class Basidiomycetes, e.g., *Fomes annosus*, *Fomitopsis insularis*, and *Cyathus bulleri* (3).

The structures of the pterosins indicate that they are derived from farnesyl pyrophosphate via the same protoilludane precursor which was proposed for the basidiomycete metabolites illudin-S and illudol nearly twenty years ago (Scheme 1) (4). It is interesting to note that pterosins sometimes occur together with compounds closely related to illudin-S or to illudol. An unstable norsesquiterpene glucoside, ptaquiloside, was recently isolated from bracken and it was readily converted to pterosin B by mild acid or base treatment (3, 5). This suggests that some of the pterosins may actually be formed from unstable precursors during isolation.

We first encountered the pterosins during our investigation of the male reproductive organ inducing substance antheridiogen A, in cultures of gametophytes of bracken fern (6). Chromatography of ethyl acetate extracts of the culture filtrates gave fractions which had high activity in the biological assay for antheridiogen A. These fractions contained ponasterone A, ecdysterone, and perhaps other ecdysones as well as a number of pterosins, two of which were tentatively identified as pterosin C and pterosin L (7). However, the antheridiogen has not yet been characterized.

During the past ten years there have been several reports on the biological properties of various pterosins. Natori and coworkers (2*a*, *b*) isolated these compounds in their search for carcinogens present in bracken. None of the pterosins was found to be carcinogenic although some did show cytotoxicity to HeLa cells (2*a*). Kobayashi and Koshimizu reported that several of the pterosins produce cytotoxic effects on the ciliate, *Paramecium caudatum*, and also induced abnormal development of the urchin embryos (8). Pterosins B and O have been

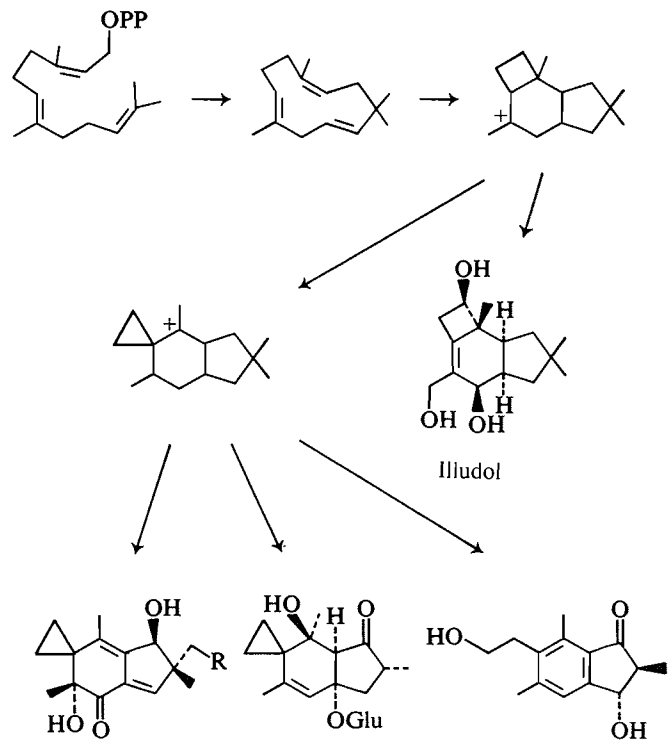

SCHEME 1

isolated from the fern *Pteris inequalis* and shown to be active against *Bacillus subtilis* (9). The 3β-D-glucoside of (2*S*,3*S*)-pterosin C, "wallichoside", has been isolated from *Pteris wallichiana* which grows in the Himalayas. It is reported to be active against *Staphylococcus aureus* (2*d*). Pterosin Z and related sesquiterpene, calomelanolactone, have been isolated

Can. J. Chem. Downloaded from www.nrcresearchpress.com by 210.87.254.5 on 09/06/12
For personal use only.

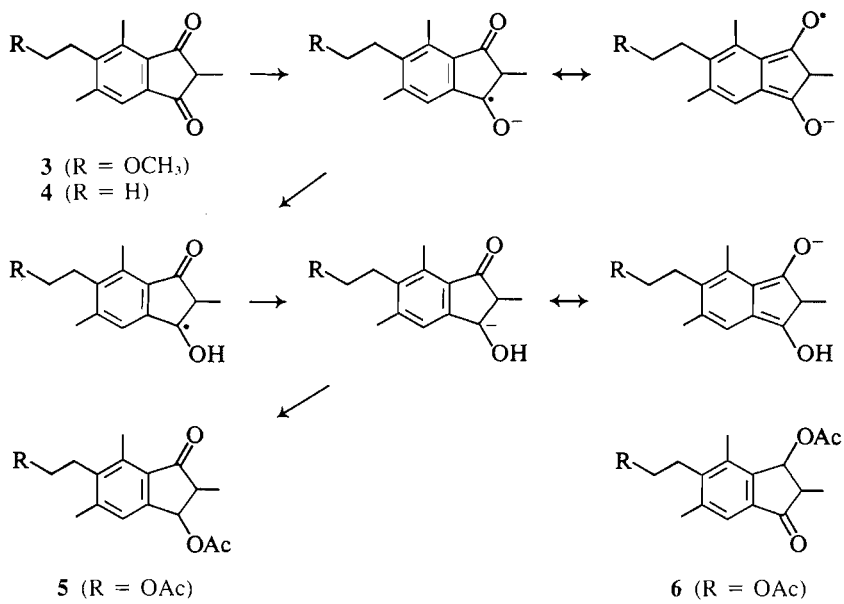

SCHEME 2

from "silver fern" *Pityrogramma calomelanos* L. which is used in Guyana for treatment of venereal diseases (2*e*).

Bracken itself is widely distributed throughout the temperate zone. It has been known from the end of the last century that the fern contains a toxin which is capable of producing a fatal hemorrhagic syndrome in cattle when they feed on the plant. Evans *et al.* (10) were the first to describe the fundamental lesions leading to the condition, severe damage of the bone marrow with consequent loss of cellular elements in the blood, together with aplasia of the intestinal mucosa resulting in loss of function and ulceration. The toxin, which can be extracted from the fronds with hot ethanol or water, has not yet been identified. However, the purified toxin extract contained a number of known organic compounds including pterosin B and its glucoside pteroside B.

Because of the possible link between bracken toxin and the pterosins, we were encouraged a few years ago to develop an efficient method for making these compounds. This would provide enough material for a thorough evaluation of their biological properties. Pterosins are present only in minute amounts in ferns and their isolation is tedious. The syntheses of pterosins E (11), B, D, H (12), Z, I, and F (7) have been reported but none of the methods appeared to be readily adaptable to large scale preparation of all the pterosins.

In this paper we describe a new method which is simple and efficient and has been employed for the preparation of many pterosins. The key step is Friedel–Crafts bisacylation of the methyl ether of 2-(2,6-dimethylphenyl)ethanol (**1**) with methylmalonyl chloride (**2**) to form the pure 1,3-indandione (**3**) in a yield of 73%.

Optimum conditions were as follows. Aluminum chloride was added gradually during 3 h to a solution of the acid chloride and benzene derivative (1.5:1 molar ratio) in refluxing carbon disulfide. Three moles of catalyst to every one mole of acid chloride were used, the third mole, presumably, being necessary because of complex formation of the catalyst with the ether oxygen. Total reaction time was about 7 h. This bisacylation reaction was developed many years ago by Freund and Fleischer and has proved to be a valuable method for introducing 3-carbon units as new rings (13).

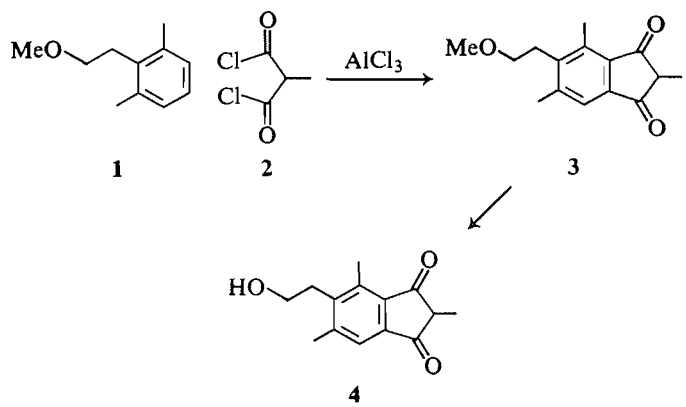

Cleavage of the methyl ether in **3** to give the corresponding alcohol (**4**) was achieved in 91% yield by treatment with 48% hydrobromic acid in acetic acid.

Another unusual reaction employed in our synthesis was the selective reduction of the 1,3-indandione (**4**) to the diacetoxyindanone (**5**) by means of zinc and acetic acid in the presence of acetic anhydride and sodium acetate (14). The product contained the *cis* and *trans* isomers of **5** (64%, ratio of *cis* to *trans*, 1:2) and the regioisomer **6** (16%). The latter was readily separated from **5** by chromatography.

Two features of this reaction deserve comment. One is that the indanone carbonyl is not reduced by zinc and acetic acid. The reduction of the indandione may well proceed via the radical anion shown (Scheme 2) for which an isoindene resonance structure is possible. Protonation and further reduction followed by protonation gives, after acetylation, the observed product. The second feature is the regioselectivity which is probably the result of steric hindrance of one of the carbonyl groups by the *peri* methyl group.

Acid hydrolysis (5% sulfuric acid, dioxane 1:4, 45°C) of the diacetate **5** gave pterosin C (**7**) as a mixture of *cis* and *trans* isomers (1:2). Mild base treatment (sodium bicarbonate in water–tetrahydrofuran) of **5** caused elimination of the secondary acetoxy group, giving the bright yellow indenone (**8**). The indenone was also obtained by acid hydrolysis at higher tem-

Can. J. Chem. Downloaded from www.nrcresearchpress.com by 210.87.254.5 on 09/06/12
For personal use only.

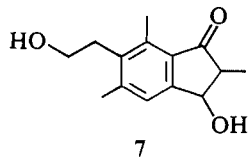

7

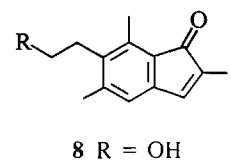

8 R = OH
14 R = OCH_3

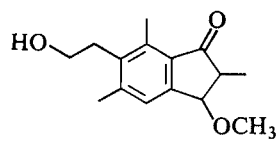

9

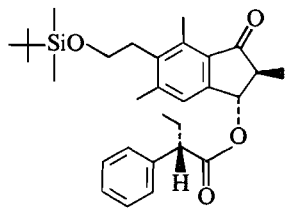

10

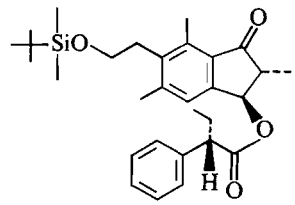

11

peratures (>45°C). When the diacetate **5** was treated with aqueous sodium bicarbonate in excess methanol the methoxy derivative (**9**) was formed in high yield. Presumably, elimination of the acetoxy group occurred, followed by Michael reaction of the resulting indenone with methanol. The high reactivity of indenone to nucleophiles has been noted previously by Lacy and Smith (14).

All four pterosin C isomers have been isolated from bracken, the 2*R*,3*R* isomer and 2*S*,3*R* isomer (as its glucoside at the primary hydroxyl) from rhizomes, and the 2*R*,3*S* and 2*S*,3*S* isomers from fronds (15). The *cis* and *trans* isomers can be readily distinguished by their nmr spectra. In the spectrum of the *cis* isomers (2*S*,3*R* and 2*R*,3*S*). The C2 methyl appears as a doublet at δ 1.17 (J = 7 Hz) and the C3 proton as a doublet at δ 5.09 (J = 7 Hz). In the spectrum of the *trans* isomers the corresponding signals are δ 1.29 (J = 7 Hz) and δ 4.70 (J = 3 Hz). The ratio of *cis* to *trans* isomers varied from one isolate to another. This may have been due partly to the ready epimerization at C2. Thus treatment of 2*S*,3*R*-pterosin C with 2% sodium hydroxide in methanol gave a mixture containing mainly the *trans* isomer (2*R*,3*R*).

The cd (circular dichroism) curves of mixtures of *cis* and *trans* isomers exhibited nearly the same ellipticity values irrespective of the ratio of *cis* to *trans* (16). A mixture with ratio of 2*R*,3*S*:2*S*,3*S* = 1:2 had $[\theta]_{326}$ +20 688 and for the ratio 1:4, $[\theta]_{326}$ +22 939. A sample of pterosin C isolated from rhizomes was a mixture of the 2*S*,3*R* and 2*R*,3*R* isomers (ratio 1:4) and had $[\theta]_{330}$ −12 320. Thus the sign of the cd curves is apparently determined by the configuration at C3 regardless of the configuration at C2.

Our synthetic mixture of *cis* and *trans* pterosin C could be separated only by hplc using a reverse phase column. In order to resolve the enantiomers, the mixture (*cis* and *trans*) was first treated with *tert*-butyldimethylsilyl chloride, dimethylaminopyridine, and triethylamine to form the monosilylether. Treatment of this compound with *S*-(+)-α-phenylbutyric acid, dimethylaminopyridine, and dicyclohexylcarbodiimide gave the corresponding ester which was mainly *trans* isomer (**10** and **11**). Apparently, during these reactions epimerization occurred at C2, leading to the more stable product. Separation of the diastereomeric esters was accomplished by hplc. The cd curve of isomer **10** showed $[\theta]_{331.5}$ +26 496 while that of isomer **11** showed $[\theta]_{330.5}$ −24 812. The isomers could also be distinguished by their 360-MHz nmr spectra. Thus the signal for the C4 aromatic proton in **10** appeared at δ 6.68 while that for the C4 proton in **11** appeared at δ 7.02, indicating a preferred conformation for **10** in which the C4 proton is shielded by the aromatic ring of the *S*-(+)-α-phenylbutyric ester. The absolute configuration assigned to isomer **10** followed from its conversion to 2*S*,3*S* pterosin C by treatment with acetic acid – water–tetrahydrofuran (2:1:1) followed by 5% aqueous sulfuric acid – dioxane (2:5) at 80°C.

TABLE 1. Structures of some pterosins

Compound		R^1	R^2
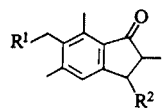	(±)-Pterosin O	CH_2OCH_3	H
	(2*R*)-Pterosin B	CH_2OH	H
	(2*R*)-Pterosin F	CH_2Cl	H
	(2*R*)-Pterosin E	COOH	H
	(2*R*)-Palmitylpterosin B	CH_2Opalmityl	H
	(2*R*)-Pteroside B	CH_2OGlu	H
	(2*S*,3*S*)-Pterosin C	CH_2OH	OH
	(2*S*,3*S*)-Pterosin J	CH_2Cl	OH
	(2*S*,3*S*)-Acetylpterosin C	CH_2OAc	OH
	(2*R*,3*R*)-Pteroside C	CH_2OGlu	OH
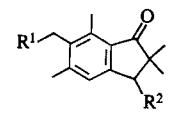	Pterosin I	CH_2OCH_3	H
	Pterosin Z	CH_2OH	H
	Pterosin H	CH_2Cl	H
	(3*R*)-Pterosin D	CH_2OH	OH
	(3*S*)-Pteroside D	CH_2OGlu	OH
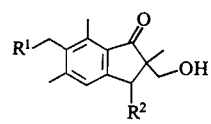	(2*S*)-Pterosin A	CH_2OH	H
	(2*S*)-Pterosin K	CH_2Cl	H
	(2*R*,3*R*)-Pterosin L	CH_2OH	OH
	Pterosin V	CH_2OCH_3	H

Glu = 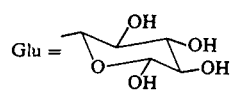

The synthesis of other pterosins as racemates from the key intermediate indandione (**3**) was readily achieved by means of well-known reactions. In the following discussion the pterosins are arranged in three groups: (1) norsesquiterpenoid skeleton; (2) sesquiterpenes containing a *gem* dimethyl group; and (3) sesquiterpenes containing a hydroxymethyl at C2.

Pterosin O. Reduction of indandione (**3**) in a similar way to reduction of (**4**) described earlier gave the 3-acetoxy indanone derivative which, on treatment with base, afforded the corresponding indenone. Catalytic hydrogenation with 5% Pd on

Can. J. Chem. Downloaded from www.nrcresearchpress.com by 210.87.254.5 on 09/06/12
For personal use only.

Can. J. Chem. Downloaded from www.nrcresearchpress.com by 210.87.254.5 on 09/06/12
For personal use only.

carbon in ethyl acetate then gave pterosin O (mp 45–46°C) (17).

Pterosin B. This compound (mp 109–110°C) (8, 17) was obtained from pterosin O by demethylation with 48% hydrobromic acid in acetic acid.

Pterosin F. A mixture of pterosin B and triphenylphosphine in carbon tetrachoride was refluxed for 3 h. Work-up of the reaction yielded pterosin F in 79% yield (mp 69–70°C) (8, 17).

Pterosin E. This compound (mp 149–150°C) (11, 17) was obtained by oxidation of pterosin B wih Jones reagent.

Pterosin J. Treatment of the indandione (4) with triphenylphosphine in carbon tetrachloride afforded the corresponding chloro analogue (87%) which, on reduction similar to that of **4**, gave pterosin J acetate and isopterosin J acetate (4:1, overall yield 86%). Separation of the isomers by chromatography followed by gentle acid hydrolysis of the major isomer gave pterosin J, mp 120–121°C (17) (85%).

Pterosin I. Methylation of pterosin O with methyl iodide and potassium *tert*-butoxide in *tert*-butanol gave an 89% yield of pterosin I (mp 59–60°C) (8, 12).

Pterosin Z. Demethylation of pterosin I with hydrobromic acid in acetic acid afforded pterosin Z (mp 89–90°C) (8, 12, 17).

Pterosin H. Displacement of the hydroxyl of pterosin Z by chloride gave pterosin H (mp 87–88°C). (8, 12).

Pterosin D. Methylation of indandione (**3**) with methyl iodide and sodium hydride in benzene gave 5-(β-methoxy)ethyl-2,2,4,6-tetramethyl-1,3-indandione in 89% yield. Treatment of this compound with 48% hydrobromic acid in acetic acid yielded the corresponding alcohol which was reduced in a similar way to the reduction of **4**. Pterosin D diacetate and isopterosin D diacetate were obtained in the ratio of 7:3 (overall yield 86%). Acid hydrolysis of the diacetate furnished pterosin D (mp 183–184°C) (17).

Pterosins V, A, and *K.* These compounds were obtained by hydroxymethylation of pterosins O, B, and F respectively. Only pterosin K was obtained crystalline (mp 85–86°C) (17).

Pterosin L. Hydroxymethylation of indandione **4** followed by reduction as for **4** gave a mixture of pterosin L triacetate and isopterosin L triacetate in a ratio of 4:1. Acid hydrolysis of the major triacetate yielded pterosin L (70%, mp 147–149°C) (17) and *epi* pterosin L (21%, mp 80–81°C) (17).

Biological studies on some of the pterosins and related indandiones and indenones will be reported in another paper.

Experimental

Melting points were determined on a Kofler hot stage apparatus and are uncorrected. Spectra were obtained on the following instruments: JEOL CFT-100, ^{13}C nmr, 25.34 MHz; Pye–Unicam SP 3-200 and Perkin–Elmer PE 281B, ir; Finnigan 4021, gc–ms DS; Perkin–Elmer 550, uv; Varian EM 390, ^{1}H nmr, 90 MHz. In cases where indicated, a 360-MHz nmr spectrometer with highly modified Varian HR-220 console, an Oxford magnet, and a Nicolet 1180-E computer system were used. The nmr (^{1}H) spectra were taken in $CDCl_3$ (except where indicated) with Me_4Si as internal standard. For ^{13}C nmr spectra, peak positions were assigned relative to the $CHCl_3$ resonances at 78.16, 76.90, and 75.62 ppm as well as the DMSO resonances at 42.12, 41.28, 40.43, 39.60, 38.77, 37.92, and 37.07 ppm. The uv spectra were taken in methanol. Elemental analysis were performed by Galbraith Laboratories, Knoxville, Tennessee.

Column chromatography was carried out with silica gel (230–400 mesh) and thin layer chromatography with silica gel 60 F-245 plates (E. Merck Laboratories).

Dry tetrahydrofuran (THF) was prepared by heating the reagent grade liquid at reflux over potassium in a circulating still. Benzene, methylene chloride, and carbon disulfide were distilled from powdered calcium hydride.

In the work-up of reactions, the solutions containing the products were dried over anhydrous magnesium sulfate, filtered, and concentrated under reduced pressure prior to chromatography.

2,6-Dimethylbromobenzene

To a magnetically stirred suspension of 2,6-dimethylaniline (50 mL, 0.41 mol) in 140 mL of 48% HBr, was added a solution of $NaNO_2$ (30 g, 0.43 mol) in 100 mL water. The temperature was kept below 10°C during the addition. When the diazotization was complete (KI–starch paper test positive), copper bronze (2 g) was added and the mixture was warmed on a steam bath until evolution of N_2 began. The flask containing the mixture was removed from the bath to moderate the reaction. When the evolution of N_2 slowed, the flask was warmed again until evolution of N_2 ceased. The mixture was then steam distilled. The organic layer was washed with 10% NaOH solution, brine, and then dried. Distillation of the organic liquid gave 35 g (47% yield) of 2,6-dimethylbromobenzene (bp 40°C/0.5 Torr) (1 Torr = 133.3 Pa). It was further purified by filtering the hexane solution through a column of alumina; nmr (^{1}H, CCl_4) δ: 2.30 (s, 6), 6.97 (s, 3); nmr (^{13}C) δ: 138.0 (s), 127.9 (d), 127.4 (s), 126.4 (d), 23.7 (q); ms *m/z* (relative intensity): 186 (M^+ + 2, 26), 184 (M^+, 29), 105 (100).

2-(2,6-Dimethylphenyl)ethanol

To a three-necked 1-L flask equipped with a reflux condenser, a dropping funnel, and a sealed stirrer was added 2,6-dimethylbromobenzene (25 g, 0.14 mol) in 140 mL dry THF followed by magnesium turnings (3.62 g, 0.15 mol). When the spontaneous reaction had ceased the mixture was refluxed for 30 min. The water condenser was replaced by a Dry Ice condenser. A well-cooled solution of ethylene oxide (20 mL) in dry THF (50 mL) was added during 5 min, then the mixture was refluxed for 3 h. After cooling, the dark colored oil was added to ice water and concentrated HCl (10 mL). The two layers were separated and the aqueous phase was extracted with ether (twice). The combined organic phases were washed with brine, then dried. 2-(2,6-Dimethylphenyl)ethanol was isolated by distillation (bp 95°C/0.6 Torr). The liquid product (17.52 g, 87%) crystallized on cooling. Recrystallization from hexane gave colorless needles, mp 59–60°C (lit. (18) mp 62.5–63°C); ir (film): 3300, 1470, 1035 cm^{-1}; nmr (^{1}H, CCl_4) δ: 2.27 (s, 6), 2.80 (t, J = 7 Hz, 2), 3.57 (t, J = 7 Hz, 2), 6.87 (s, 3); nmr (^{13}C) δ: 136.3 (s), 134.4 (s), 127.8 (d), 125.8 (d), 60.8 (t), 32.6 (t), 19.6 (q); ms *m/z*: 150 (M^+, 51), 132 (3), 119 (100).

Methyl 2-(2,6-dimethylphenyl)ethyl ether (1)

A mixture of the above alcohol (17.52 g, 0.12 mol), tetrabutylammonium iodide (3 g, 8.12 mmol), 50% NaOH solution (40 mL), and hexane (250 mL) was stirred at room temperature for 0.5 h. Dimethylsulfate (60 mL) was added during 0.5 h and the mixture was refluxed for 15 h. It was acidified with saturated NH_4Cl solution and extracted with ether (three times). The extract was washed with brine, dried, and distilled to give methyl 2-(2,6-dimethylphenyl)ethyl ether (**1**), 18 g, bp 55°C/0.6 Torr, (94% yield); ir (film): 2880, 1100 cm^{-1}; nmr (^{1}H) δ: 2.23 (s, 6), 2.80 (t, J = 7 Hz, 2), 3.20 (s, 3), 3.33 (t, J = 7 Hz, 2), 6.83 (s, 3); nmr (^{13}C) δ: 136.5 (s), 134.7 (s), 127.9 (d), 125.9 (d), 71.1 (t), 58.3 (q), 29.9 (t), 19.7 (q); ms *m/z*: 164 (M^+, 19), 150 (9), 132 (18), 119 (100).

Methylmalonyl chloride (2)

To a solution of diethyl methylmalonate (50 g, 0.29 mol) in absolute ethanol (200 mL) was added a solution of KOH in absolute ethanol (38 g in 200 mL) with stirring during 1 h. Stirring was continued at room temperature overnight. The salt was filtered off, washed with anhydrous ether, and dried *in vacuo*. To the cooled solution of the salt (ice bath) in water (50 mL) was added gradually concentrated HCl solution (40 mL). It was extracted three times with ether and the extract was washed with brine, dried, and the solvent was removed, leaving 33.4 g methylmalonic acid (99% yield), mp 132–132.5°C; nmr (^{1}H, CD_3OD) δ: 1.40 (d, J = 7 Hz, 3), 3.41 (q,

Can. J. Chem. Downloaded from www.nrcresearchpress.com by 210.87.254.5 on 09/06/12
For personal use only.

J = 7 Hz, 1), 5.73 (br s, disappeared on adding D_2O, 2).

A mixture of diacid (30 g, 0.25 mol) and thionylchloride (100 mL) was warmed at 55–60°C for 4 h. Distillation then yielded methylmalonyl chloride (**2**) (31.5 g, 81%), bp 45°C/0.5 Torr; nmr (^{1}H, CCl_4) δ: 1.63 (d, J = 7 Hz, 3), 4.25 (q, J = 7 Hz, 1).

5-(β-Methoxy)ethyl-2,4,6-trimethyl-1,3-indandione (3)

To a solution of methyl 2-(2,6-dimethylphenyl)ethyl ether **1** (14.1 g, 0.09 mol) and methylmalonyl chloride (21.4 g, 0.14 mol) in carbon disulfide (50 mL) was added portionwise $AlCl_3$ (55 g, 0.41 mol) during a period of about 3 h. The mixture was refluxed for 4 h more, then added to crushed ice and the whole extracted three times with chloroform. The combined extract was washed with brine, dried, and the solvent removed, leaving a residue which on chromatography with 5% ethyl acetate in benzene gave the indandione **3**, 15.5 g (73% yield), mp 86.5–87.5°C (from ether–hexane); uv λ_{max} nm (log ε): 203 (4.66), 235 (5.06), 256 (4.59), 266 (4.59), 315 (3.66); ir (KBr): 1740, 1700, 1590 cm^{-1}; nmr (^{1}H) δ: 1.32 (d, J = 7 Hz, 3), 2.50 (s, 3), 2.73 (s, 3), 2.93 (q, J = 7 Hz, 1), 3.07 (t, J = 7 Hz, 2), 3.33 (s, 3), 3.48 (t, J = 7 Hz, 2), 7.57 (s, 1); nmr (^{13}C) δ: 201.6 (s), 200.6 (s), 145.2 (s), 144.9 (s), 140.2 (s), 137.1 (s), 121.4 (d), 70.4 (t), 58.3 (q), 48.8 (d), 29.5 (t), 21.0 (q), 13.9 (q), 10.1 (q); ms m/z: 246 (M$^+$, 60), 231 (11), 201 (100).

5-(β-Hydroxy)ethyl-2,4,6-trimethyl-1,3-indandione (4)

A solution of indandione **3** (8.8 g, 0.04 mol) in glacial acetic acid (80 mL) and 48% hydrobromic acid (40 mL) was heated at 100°C for 4 h. The solution was concentrated under reduced pressure, then extracted three times with chloroform. The extract was washed with saturated $NaHCO_3$ solution (twice), brine, and dried. Removal of solvent and chromatography with 30% ethyl acetate in benzene gave the alcohol **4**, 7.51 g (91%), mp 103–106°C (from ether–hexane); ir (KBr): 3360, 1740, 1700, 1590, 1050 cm^{-1}; nmr (^{1}H) δ: 1.32 (d, J = 7 Hz, 3), 2.55 (s, 3), 2.77 (s, 3), 2.97 (q, J = 7 Hz, 1), 3.17 (t, J = 7 Hz, 2), 3.87 (t, J = 7 Hz, 2), 7.67 (br s, 1); nmr (^{13}C) δ: 202.1 (s), 201.3 (s), 145.6 (s), 145.1 (s), 140.4 (s), 137.5 (s), 137.3 (s), 121.8 (d), 60.8 (t), 49.0 (d), 32.4 (t), 21.3 (q), 14.3 (q), 10.4 (q); ms m/z: 232 (M$^+$, 77), 217 (34), 201 (100).

Pterosin C diacetate (5) and isopterosin C diacetate (6)

To a stirred mixture of indandione **4** (513 mg, 2.21 mmol), acetic acid (20 mL), acetic anhydride (20 mL), and anhydrous sodium acetate (1.74 g) was added zinc dust (3.02 g) during 15 min. Stirring was continued for 24 h at 45°C, after which the mixture was filtered. Acetic acid was added to the solid and the combined filtrate and washings were concentrated under reduced pressure. The semi-solid product was dissolved in a mixture of ethyl acetate (50 mL) and brine (50 mL). The organic layer was washed with brine, then the solvent was removed and the residue was chromatographed with 5% ethyl acetate in benzene to give pterosin C diacetate **5** (400 mg, oil), a mixture of **5** and **6** (80 mg), and **6** (88 mg). Total yield was 80%. Spectral data for **5** (mixture of *cis* and *trans* isomers 1:1) were as follows: ir (film): 1735, 1710, 1600, 1240, 1220 cm^{-1}; nmr (^{1}H) *trans* isomer, δ: 1.28 (d, J = 8 Hz, 3), 2.00 (s, 3), 2.08 (s, 3), 2.47 (s, 3), 2.67 (s, 3), 2.50–2.80 (m, 1), 3.00 (t, J = 8 Hz, 2), 4.07 (t, J = 8 Hz, 2), 5.73 (d, J = 3 Hz, 1), 7.17 (s, 1); *cis* isomer, δ: 1.07 (d, J = 8 Hz, 3), 2.00 (s, 3), 2.03 (s, 3), 2.47 (s, 3), 2.67 (s, 3), 2.50–2.80 (m, 1), 3.00 (t, J = 8 Hz, 2), 4.07 (t, J = 8 Hz, 2), 6.17 (d, J = 7 Hz, 1), 7.23 (s, 1); ms m/z: 318 (M$^+$, 3), 258 (15), 216 (100), 198 (67), 185 (31). Spectral data for **6** (mixture of *cis* and *trans* isomers 3:7) included: ir ($CHCl_3$): 1720, 1710, 1600, 1240 cm^{-1}; nmr (^{1}H) *trans* isomer, δ: 1.28 (d, J = 8 Hz, 3), 1.97 (s, 3), 2.05 (s, 3), 2.30 (s, 3), 2.43 (s, 3), 2.50–2.90 (m, 1), 3.00 (t, J = 8 Hz, 2), 4.10 (t, J = 8 Hz, 2), 5.87 (br s, 1), 7.33 (s, 1); *cis* isomer, δ: 1.05 (d, J = 8 Hz, 3), 1.97 (s, 3), 2.05 (s, 3), 2.30 (s, 3), 2.43 (s, 3), 2.50–2.90 (m, 1), 3.00 (t, J = 8 Hz, 2), 4.10 (t, J = 8 Hz, 2), 6.45 (d, J = 7 Hz, 1), 7.33 (s, 1); ms m/z: 318 (M$^+$, 1), 276 (28), 258 (67), 216 (100), 201 (64), 198 (55).

Pterosin C 7

A solution of pterosin C diacetate **5** (352 mg, 1.11 mmol) in dioxane (20 mL) and dilute sulfuric acid (5%, 5 mL) was warmed at 45°C for 10 h. The cooled solution was extracted with chloroform (three times) and the extract was washed with brine and dried. Removal of the solvent and chromatography of the residue with 5% methanol in chloroform gave pterosin C **7** as a mixture of *cis* and *trans* isomers 1:2 (234 mg, 90%). Recrystallization from ethyl acetate gave white needles, mp 160–162°C (lit. (17) mp 153–156°C, lit. (15) mp 162–164°C, lit. (3*c*) mp 160–162°C); uv λ_{max} nm (log ε): 212 (4.78), 255 (4.45), 297 (3.60); ir (KBr): 3400, 1670, 1590, 1020 cm^{-1}; nmr (^{1}H, 360 mHz) *trans* isomer, δ: 1.29 (d, J = 7 Hz, 3), 2.47 (s, 3), 2.64 (s, 3), 2.50–2.90 (m, 1), 3.00 (t, J = 7 Hz, 2), 3.63 (t, J = 7 Hz, 2), 4.70 (d, J = 3 Hz, 1), 7.37 (s, 1); *cis* isomer, δ: 1.17 (d, J = 7 Hz, 3), 2.47 (s, 3), 2.64 (s, 3), 2.50–2.90 (m, 1), 3.00 (t, J = 7 Hz, 2), 3.63 (t, J = 7 Hz, 2), 5.09 (d, J = 7 Hz, 1), 7.37 (s, 1); nmr (^{13}C, DMSO) *trans* isomer, δ: 2.05.0 (s), 153.5 (s, 144.0 (s), 136.9 (s), 135.4 (s), 130.7 (s), 124.3 (d), 73.7 (d), 59.8 (t), 53.2 (d), 32.1 (t), 20.9 (q), 13.3 (q), 12.7 (q); *cis* isomer, δ: 207.9 (s), 154.1 (s), 144.0 (s), 137.2 (s), 136.8 (s), 130.6 (s), 125.4 (d), 67.9 (d), 59.8 (t), 47.8 (d), 32.1 (t), 20.9 (q), 13.4 (q), 10.4 (q); ms m/z: 234 (M$^+$, 46), 219 (10), 203 (100). *Anal.* calcd. for $C_{14}H_{18}O_3$: C 71.77, H 7.74; found: C 71.60, H 7.74.

6-(β-Hydroxy)ethyl-2,5,7-trimethyl-3-methoxy-1-indanone

A solution of pterosin C diacetate **5** (94 mg, 0.4 mmol) in methanol (5 mL) and saturated $NaHCO_3$ solution (1 mL) was stirred at room temperature for 20 h. It was extracted with ether (three times), and the extract was washed with brine and dried. Removal of the solvent yielded crude product (63 mg) which was 15% 6-(β-hydroxy)ethyl-2,5,7-trimethyl-1-indenone **8**: nmr (^{1}H) δ: 1.77 (d, J = 1.5 Hz, 3), 2.30 (s, 3), 2.50 (s, 3), 3.00 (t, J = 7 Hz, 2), 3.73 (t, J = 7 Hz, 2), 6.60 (s, 1), 6.93 (q, J = 1.5 Hz, 1) and 85% 6-(β-hydroxy)ethyl-2,5,7-trimethyl-3-methoxy-1-indanone **9** (mixture of *cis* and *trans* isomers 1:3): nmr (^{1}H) *trans* isomer, δ: 1.33 (d, J = 7 Hz, 3), 2.45 (s, 3), 2.67 (s, 3), 3.00 (t, J = 7 Hz, 2), 3.53 (s, 3), 4.43 (d, J = 3 Hz, 1), 7.33 (s, 1); *cis* isomer, δ: 1.27 (d, J = 7 Hz,, 3), 2.45 (s, 3), 2.67 (s, 3), 3.00 (t, J = 7 Hz, 2), 3.47 (s, 3), 4.73 (d, J = 7 Hz, 1), 7.33 (s, 1).

6-(β-tert-Butyldimethylsilyloxy)ethyl-3-hydroxy-2,5,7-trimethyl-1-indanone

A mixture of pterosin C **7** (1.18 g, 5.0 mmol), *tert*-butyldimethylsilylchloride (2.19 g, 10 mmol), 4-dimethylaminopyridine (98 mg, 0.8 mmol), triethylamine (1 mL), and dichloromethane (30 mL) was stirred at room temperature for 4 h, saturated NH_4Cl solution was added, and the mixture was extracted with chloroform (three times). Chromatography of the product with 25% ethyl acetate in hexane gave the bis-*tert*-butyldimethylsilyl ether (322 mg, 17%), and the desired mono-*tert*-butyldimethylsilyl ether (1.15 g, 83%) as an oil. (The reaction was 79% complete.) Spectral properties for the mono-*tert*-butyldimethylsilyl ether (mixture of *cis* and *trans* isomers 1:1) were as follows: ir (film): 3400, 1710, 1600 cm^{-1}; nmr (^{1}H) *trans* isomer, δ: 0.00 (s, 6), 0.85 (s, 9), 1.30 (d, J = 7 Hz, 3), 2.43 (s, 3), 2.63 (s, 3), 2.40–2.80 (m, 1), 2.97 (t, J = 7 Hz, 2), 3.70 (t, J = 7 Hz, 2), 4.77 (d, J = 3 Hz, 1), 7.33 (s, 1); *cis* isomer, δ: 0.00 (s, 6), 0.85 (s, 9), 1.20 (d, J = 7 Hz, 3), 2.43 (s, 3), 2.63 (s, 3), 2.40–2.80 (m, 1), 2.97 (t, J = 7 Hz, 2), 3.70 (t, J = 7 Hz, 2), 5.20 (d, J = 6 Hz, 1), 7.33 (s, 1); ms m/z: 291 (M$^+$ − C_4H_9, 100), 261 (60), 243 (2), 217 (4), 199 (4). Spectral data for the bis-*tert*-butyldimethylsilyl ether included: ir (film): 1700, 1590 cm^{-1}; nmr (^{1}H) δ: 0.00 (s, 6), 0.06 (s, 6), 0.70 (s, 9), 0.78 (s, 9), 1.13 (d, J = 7 Hz, 3), 2.26 (s, 3), 2.52 (s, 3), 2.30–2.70 (m, 1), 2.86 (t, J = 7 Hz, 2), 3.50 (t, J = 7 Hz, 2), 4.60 (d, J = 3 Hz, 1), 7.00 (s, 1); ms m/z: 463 (M$^+$, 3), 447 (5), 405 (96), 349 (17), 331 (12), 289 (28), 215 (31), 199 (60).

Esterification of pterosin C tert*-butyldimethylsilyl ether with S-(+)-α-phenylbutyric acid*

A mixture of the *tert*-butyldimethylsilyl ether of pterosin C (568 mg, 1.63 mmol), *S*-(+)-α-phenylbutyric acid (282 mg, 1.72 mmol), and 4-dimethylaminopyridine (20 mg, 0.16 mmol) in dichloromethane (10 mL) was stirred under N_2 at 0°C. Dicyclohexyl-

Can. J. Chem. Downloaded from www.nrcresearchpress.com by 210.87.254.5 on 09/06/12
For personal use only.

carbodiimide (382 mg, 1.85 mmol) was added to the mixture, which was stirred at 0°C for 30 min, then at room temperature for 8 h. It was filtered and the filtrate was washed with saturated $NaHCO_3$ solution, 1% $KHCO_3$ solution, and finally with brine. Removal of the solvent and chromatography of the residue with 2.5% ethyl acetate in hexane gave the *trans* isomer of the desired ester (366 mg), a mixture of *trans* and *cis* isomers (283 mg), and the *cis* isomer (93 mg) for a total yield of 95% (ratio of *trans* to *cis*, 4:1). The *trans* isomer was actually a mixture of two diastereomers **10** and **11**. They were only partially separated by hplc on a μ Porasil column with 2% ether in hexane. However, on recycling the effluent from the column six times, complete separation of the diastereomers was achieved. The more polar isomer **10** gave a positive cd curve, $[\theta]_{331.5}$ +26 496; ir (film): 1710, 1700 cm^{-1}; nmr (^1H, 360 MHz) δ: 0.00 (s, 6), 0.79 (s, 9), 0.88 (t, J = 7 Hz, 3), 1.30 (d, J = 7 Hz, 3), 1.79 (m, 1), 2.06 (m, 1), 2.25 (s, 3), 2.40–2.60 (m, 1), 2.59 (s, 3), 2.88 (t, J = 7 Hz, 2), 3.46 (t, J = 7 Hz, 1), 3.60 (t, J = 7 Hz, 2), 5.80 (d, J = 3 Hz, 1), 6.68 (s, 1), 7.28 (br s, 5); ms m/z: 437 ($M^+ - C_4H_9$, 10), 273 (20), 199 (100). The less polar isomer **11** had $[\theta]_{330.5}$ −24 812; nmr (^1H, 360 MHz) δ: 0.00 (s, 6), 0.79 (s, 9), 0.87 (t, J = 7 Hz, 3), 1.20 (d, J = 7 Hz, 3), 1.79 (m, 1), 2.06 (m, 1), 2.35 (s, 3), 2.30–2.50 (m, 1), 2.59 (s, 3), 2.90 (t, J = 7 Hz, 2), 3.44 (t, J = 7 Hz, 1), 3.61 (t, J = 7 Hz, 2), 5.80 (d, J = 3 Hz, 1), 7.02 (s, 1), 7.23 (br s, 5).

Pterosin C-3-(+)-α-phenylbutyrate

A solution of the *trans* isomer of the ester **10** (14.5 mg, 0.03 mmol) in acetic acid – THF–water (3:1:1, 10 mL) was stirred at room temperature for 12 h. It was extracted with ether (three times). The extract was washed with brine, the solvent was removed, and the residue was chromatographed with 30% ethyl acetate in hexane to give 2*S*,3*S*-pterosin C-3-(+)-α-phenylbutyrate (10.6 mg, 97%). Spectral properties included: ir (film): 3400, 1730, 1700, 1600 cm^{-1}; nmr (^1H, 360 MHz) δ: 0.93 (t, J = 7 Hz, 3), 1.34 (d, J = 7 Hz, 3), 1.82 (m, 1), 1.85 (m, 1), 2.29 (s, 3), 2.40–2.60 (m, 1), 2.64 (s, 3), 3.00 (t, J = 7 Hz, 2), 3.51 (t, J = 7 Hz, 1), 3.72 (t, J = 7 Hz, 2), 5.84 (d, J = 3 Hz, 1), 6.73 (s, 1), 7.31 (br s, 5); ms m/z: 380 (M^+, 2), 234 (12), 217 (83), 185 (25). The other diastereomer **11** was treated as above and gave the 2*R*,3*R* alcohol; nmr (^1H, 360 MHz) δ: 0.93 (t, J = 7 Hz, 3), 1.25 (d, J = 7 Hz, 3), 1.82 (m, 1), 1.85 (m, 1), 2.40 (s, 3), 2.30–2.50 (m, 1), 2.64 (s, 3), 3.00 (t, J = 7 Hz, 2), 3.51 (t, J = 7 Hz, 1), 3.72 (t, J = 7 Hz, 2), 5.84 (d, J = 3 Hz, 1), 7.08 (s, 1), 7.27 (br s, 5).

(2S,3S)-Pterosin C and (2R,3R)-pterosin C

Separate solutions of the α-phenylbutyrate esters (10.6 mg, 0.027 mmol) in 5% aqueous sulfuric acid – dioxane (2:5, 14 mL) were stirred at 80°C for 48 h. They were extracted with chloroform (three times), and the extracts were washed with brine and dried. Removal of the solvent and chromatography of the residue with 5% methanol in chloroform gave optically active 2*S*,3*S*-pterosin C and 2*R*,3*R*-pterosin C (5 mg, 71% for each isomer). The cd curves showed $[\theta]_{323.5}$ +23 070 and $[\theta]_{329.5}$ −16 692 respectively.

3-Acetoxy-6-(β-methoxy)ethyl-2,5,7-trimethyl-1-indanone and its regioisomer 3-acetoxy-5-(β-methoxy)ethyl-2,4,6-trimethyl-1-indanone

Zinc dust (50 g, 0.77 mol) was added to a solution of indandione **3** (9.2 g, 0.04 mol) and sodium acetate (30 g, 0.37 mol) in acetic acid (150 mL) and acetic anhydride (150 mL). The mixture was stirred at 50°C for 12 h and then filtered. The solids were washed with acetic acid and the combined filtrate and washings were concentrated under reduced pressure to give a sticky solid. It was dissolved in a mixture of ethyl acetate (150 mL) and brine (150 mL), the organic phase was separated, washed with brine, and dried. Removal of solvent and chromatography of the residue with 5% ethyl acetate in benzene gave the desired indanone (6.06 g, oil), the regioisomer (1.51 g), and a mixture of the two (1.10 g). Total yield was 80%. The indanone was a 1:1 mixture of the *cis* and *trans* isomers: ir (film): 1730, 1700, 1590, 1200, 1100 cm^{-1}; nmr (^1H) *trans* isomer, δ: 1.27 (d, J = 7 Hz, 3), 2.05 (s, 3), 2.37 (s, 3), 2.57 (s, 3), 2.93 (t, J = 7 Hz, 2), 3.23 (s, 3), 3.37 (t, J = 7 Hz, 2), 5.70 (d, J = 3 Hz, 1), 7.15 (s, 1); *cis* isomer, δ: 1.06 (d, J = 7 Hz, 3), 2.00 (s, 3), 2.37 (s, 3), 2.57 (s, 3), 2.93 (t, J = 7 Hz, 2), 3.23 (s, 3), 3.37 (t, J = 7 Hz, 2), 6.12 (d, J = 7 Hz, 1), 7.17 (s, 1); ms m/z: 290 (M^+, 22), 248 (32), 230 (95), 215 (31), 203 (87), 185 (100). The regioisomer was a 1:4 mixture of *cis* and *trans* isomers: ir (film): 1730, 1700, 1600, 1230, 1100 cm^{-1}; nmr (^1H) *trans* isomer, δ: 1.37 (d, J = 7 Hz, 3), 2.17 (s, 3), 2.35 (s, 3), 2.43 (s, 3), 3.05 (t, J = 7 Hz, 2), 3.37 (s, 3), 3.52 (t, J = 7 Hz, 2), 5.97 (br s, 1), 7.43 (br s, 1); *cis* isomer, δ: 1.13 (d, J = 7 Hz, 3), 2.17 (s, 3), 2.35 (s, 3), 2.43 (s, 3), 3.05 (t, J = 7 Hz, 2), 3.37 (s, 3), 3.52 (t, J = 7 Hz, 2), 6.57 (d, J = 7 Hz, 1), 7.43 (br s, 1); ms m/z: 290 (M^+, 2), 248 (30), 230 (100), 215 (31), 203 (22).

6-(β-Methoxy)ethyl-2,5,7-trimethyl-1-indenone

A solution of the acetoxy indanone from above (1.60 g, 5.5 mmol) in 10% potassium hydroxide solution (10 mL) and tetrahydrofuran (20 mL) was refluxed for 2 h. It was cooled and extracted with ether (three times). The combined ether extracts were washed with brine, dried, and the solvent removed, leaving a residue which was chromatographed with 2% ethyl acetate in benzene to give 968 mg of the indenone (76%), a bright yellow compound, mp 72–73°C; uv λ_{max} nm (log ε): 206 (4.32), 246 (4.92), 328 (3.72); ir (film): 1680, 1590, 1100 cm^{-1}; nmr (^1H) δ: 1.80 (d, J = 1.5 Hz, 3), 2.27 (s, 3), 2.50 (s, 3), 2.87 (t, J = 7 Hz, 2), 3.33 (s, 3), 3.40 (t, J = 7 Hz, 2), 6.53 (s, 1), 6.90 (q, J = 1.5 Hz, 1); nmr (^{13}C) δ: 199.7 (s), 143.3 (s), 142.0 (s), 141.3 (d), 137.1 (s), 135.8 (s), 135.7 (s), 125.6 (s), 121.6 (d), 71.1 (t), 58.5 (q), 28.9 (t), 20.6 (q), 12.9 (q), 9.9 (q); ms m/z: 230 (M^+, 20), 215 (1), 201 (27), 185 (100).

Pterosin O

A solution of the above indenone (1.72 g, 7.48 mmol) in ethyl acetate (50 mL) was shaken in an atmosphere of hydrogen with 5% palladium/charcoal (~500 mg) until there was no further uptake of hydrogen (~1 h). The mixture was filtered through Celite. The Celite was eluted with ethyl acetate and the combined filtrates on removal of solvent gave a quantitative yield of pterosin O (1.74 g), mp 45–46°C (from hexane; lit. (17) mp 45–46°C); ir (film): 1690, 1595, 1100 cm^{-1}; nmr (^1H, CCl_4) δ: 1.17 (d, J = 7 Hz, 3), 2.33 (s, 3), 2.30–2.70 (m, 1), 2.60 (s, 3), 2.80–3.60 (m, 2), 2.93 (t, J = 7 Hz, 2), 3.27 (s, 3), 3.37 (t, J = 7 Hz, 2), 7.07 (br s, 1); nmr (^{13}C) δ: 209.1 (s) 151.7 (s), 143.5 (s), 136.9 (s), 134.6 (s), 131.5 (s), 125.1 (d), 70.8 (t), 58.0 (q), 41.9 (d), 33.2 (t), 28.5 (t), 20.6 (q), 16.0 (q), 12.9 (q); ms m/z: 232 (M^+, 27), 217 (40), 187 (100).

Pterosin B

A solution of pterosin O (1.07 g, 4.6 mmol) in 48% hydrobromic acid (30 mL) and acetic acid (60 mL) was warmed at 100°C for 4 h. The solution was concentrated under reduced pressure and then extracted with ether (three times). The combined extracts were washed with brine, dried, and chromatographed with 30% ethyl acetate in benzene to give pterosin B (879 mg, 88%), mp 109–110°C (from chloroform–hexane; lit. (8) mp 107–109°C, lit. (17) mp 109–110°C, lit. (2*d*) mp 89–91°C); ir (film): 3420, 1670, 1590, 1040 cm^{-1}; nmr (^1H) δ: 1.27 (d, J = 7 Hz, 3), 2.17 (br s, exchangeable, 1), 2.44 (s, 3), 2.68 (s, 3), 2.50–2.70 (m, 2), 3.00 (t, J = 7 Hz, 2), 3.24 (dd, J = 7.5, 16.5 Hz, 1), 3.75 (t, J = 7 Hz, 2), 7.10 (s, 1); nmr (^{13}C) δ: 210.3 (s), 152.3 (s), 144.2 (s), 137.6 (s), 134.7 (s), 131.8 (s), 125.4 (d), 61.2 (t), 42.3 (d), 33.6 (t), 31.7 (t), 21.1 (q), 16.3 (q), 13.5 (q); ms m/z: 218 (M^+, 39), 203 (81), 187 (100).

Pterosin F

A mixture of pterosin B (879 mg, 4.0 mmol), carbon tetrachloride (20 mL), and triphenylphosphine (1.56 g, 5.96 mmol) was heated and the resulting solution was refluxed for 3 h. It was cooled, hexane (50 mL) was added, and the mixture was stirred for 15 min. The precipitate of triphenylphosphine oxide was filtered off and washed with hexane (50 mL). The combined filtrate and washings were combined, the solvent removed, and the residue chromatographed with 2.5% ethyl acetate in hexane to give 753 mg (79%) of pterosin F, mp 69–70°C (from hexane, lit. (17) mp 66–67°C, lit. (8) mp 65–68°C); ir (film): 1690, 1595 cm^{-1}; nmr (^1H, CCl_4) δ: 1.20 (d, J = 7 Hz, 3),

Can. J. Chem. Downloaded from www.nrcresearchpress.com by 210.87.254.5 on 09/06/12
For personal use only.

2.40 (s, 3), 2.30–2.70 (m, 2), 2.60 (s, 3), 3.13 (m, 3), 3.47 (m, 2), 7.00 (br s, 1); nmr (^{13}C) δ: 209.6 (s), 152.7 (s), 143.6 (s), 137.4 (s), 134.3 (s), 132.0 (s), 125.6 (d), 42.3 (d), 41.8 (t), 33.6 (t), 32.0 (t), 20.9 (q), 16.3 (q), 13.3 (q); ms *m/z*: 238 (M^+ + 2, 13), 236 (M^+, 43), 221 (9), 201 (100), 187 (97).

Pterosin E

An excess of Jones reagent was added dropwise to a solution of pterosin B (314 mg, 1.44 mmol) in acetone cooled in ice water. It was diluted with ether and filtered through Celite. Removal of the solvent from the filtrate gave pterosin E which was recrystallized from carbon tetrachloride, yield 300 mg (90%), mp 149–150°C (lit. (17) mp 160–162°C, lit. (11) mp 151–153°C); ir (film): 3500–2400, 1710, 1690, 1590 cm^{-1}; nmr (^{1}H) δ: 1.27 (d, J = 7 Hz, 3), 2.39 (s, 3), 2.30–2.70 (m, 2), 2.65 (s, 3), 3.25 (dd, J = 7.5, 16.5 Hz, 1), 3.78 (s, 2), 7.13 (s, 1); nmr (^{13}C) δ: 210.1 (s), 176.6 (s), 153.4 (s), 144.2 (s), 138.1 (s), 131.9 (s), 131.0 (s), 125.5 (d), 42.3 (d), 33.9 (t), 33.7 (t), 21.2 (q), 16.3 (q), 13.6 (q); ms *m/z*: 232 (M^+, 64), 217 (46), 187 (100).

5-(β-Chloro)ethyl-2,4,6-trimethyl-1,3-indandione

This compound was prepared from indandione **4** (1.51 g, 6.49 mmol) in the same way as the preparation of pterosin F from pterosin B. Yield 1.28 g (87%), mp 114–115°C (from hexane); ir (film): 1725, 1690, 1590 cm^{-1}; nmr (^{1}H, CCl_4) δ: 1.27 (d, J = 7 Hz, 3), 2.50 (s, 3), 2.70 (s, 3), 2.95 (q, J = 7 Hz, 1), 3.20 (m, 2), 3.50 (m, 2), 7.53 (br s, 1); nmr (^{13}C) δ: 201.9 (s), 201.0 (s), 145.3 (s), 143.9 (s), 140.9 (s), 137.5 (s), 122.1 (d), 49.1 (d), 41.3 (t), 32.5 (t), 21.2 (q), 14.3 (q), 10.5 (q); ms *m/z*: 252 (M^+ + 2, 15), 250 (M^+, 49), 215 (66), 201 (100).

Pterosin J acetate and isopterosin J acetate

Reduction of the above indandione (990 mg, 3.94 mmol) in the same way as for the reduction of **4** gave, after chromatography with 2% ethyl acetate in benzene, 540 mg of pterosin J acetate (a 1:1 mixture of *cis* and *trans* isomers), 150 mg of the regioisomer (a 1:4 mixture of *cis* and *trans* isomers), and 310 mg of a mixture of all the four isomers (total yield 86%). Spectral properties for pterosin J acetate included: ir (film): 1730, 1710, 1700, 1590, 1220 cm^{-1}; nmr (^{1}H, CCl_4) *trans* isomer, δ: 1.37 (d, J = 7 Hz, 3), 2.17 (s, 3), 2.47 (s, 3), 2.70 (s, 3), 2.40–3.00 (m, 1), 3.23 (m, 2), 3.60 (m, 2), 5.91 (d, J = 3 Hz, 1), 7.33 (br s, 1); *cis* isomer, δ: 1.17 (d, J = 7 Hz, 3), 2.13 (s, 3), 2.47 (s, 3), 2.70 (s, 3), 2.40–3.00 (m, 1), 3.23 (m, 2), 3.60 (m, 2), 6.35 (d, J = 6 Hz, 1), 7.37 (br s, 1); ms *m/z*: 296 (M^+ + 2, 6), 294 (M^+, 18), 252 (77), 237 (57), 234 (83), 203 (94), 199 (71), 185 (100). Spectral properties for isopterosin J acetate included: ir (film): 1730, 1720, 1710, 1600, 1230 cm^{-1}; nmr (^{1}H, CCl_4) *trans* isomer, δ: 1.37 (d, J = 7 Hz, 3), 2.12 (s, 3), 2.35 (s, 3), 2.45 (s, 3), 2.30–3.00 (m, 1), 3.25 (m, 2), 3.62 (m, 2), 5.98 (br s, 1), 7.50 (br s, 1); *cis* isomer, δ: 1.13 (d, J = 7 Hz, 3), 2.12 (s, 3), 2.35 (s, 3), 2.45 (s, 3), 2.30–3.00 (m, 1), 3.25 (m, 2), 3.62 (m, 2), 6.57 (d, J = 7 Hz, 1), 7.50 (br s, 1); ms *m/z*: 254 (M^+ + 2 − CH_2CO, 16), 252 (M^+ − CH_2CO, 53), 237 (75), 234 (100), 219 (25), 217 (34), 203 (15), 199 (81), 185 (59).

Pterosin J

Acid hydrolysis of pterosin J acetate (200 mg, 0.69 mmol) was carried out in the same way as that for pterosin C diacetate. The yield of pterosin J after chromatography with 30% ethyl acetate in benzene was 147 mg (85%), a 2:3 mixture of *cis* and *trans* isomers, mp 120–121°C (from benzene–hexane; lit. (17) mp 136–137°C); ir (film): 3400, 1690, 1595 cm^{-1}; nmr (^{1}H) *trans* isomer, δ: 1.30 (d, J = 8 Hz, 3), 2.43 (s, 3), 2.63 (s, 3), 2.40–2.80 (m, 1), 3.17 (m, 2), 3.53 (m, 2), 4.73 (d, J = 3 Hz, 1), 7.37 (s, 1); *cis* isomer, δ: 1.20 (d, J = 8 Hz, 3), 2.43 (s, 3), 2.63 (s, 3), 2.40–2.80 (m, 1), 3.17 (m, 2), 3.53 (m, 2), 5.20 (d, J = 6 Hz, 1), 7.37 (s, 1); nmr (^{13}C) *cis* isomer, δ: 207.5 (s), 153.3 (s), 144.5 (s), 137.2 (s), 136.8 (s), 131.2 (s), 125.4 (d), 69.5 (d), 48.1 (d), 41.8 (t), 32.1 (t), 21.1 (q), 13.8 (q), 10.1 (q); *trans* isomer, δ: 205.1 (s), 152.7 (s), 144.4 (s), 136.9 (s), 136.4 (s), 131.5 (s), 124.4 (d), 75.2 (d), 53.6 (d), 41.8 (t), 32.1 (t), 21.1 (q), 13.8 (q), 12.9 (q); ms *m/z*: 254 (M^+ + 2, 13), 252 (M^+, 40), 237 (29), 203 (100).

Pterosin I

A solution of pterosin O (1.16 g, 5.0 mmol) in *tert*-butanol (10 mL) was added dropwise to potassium *tert*-butoxide (3.26 g, 30 mmol) in *tert*-butanol (2 mL). The mixture was stirred at room temperature for 15 min, then methyl iodide (10 mL) was added and the mixture was kept overnight. It was acidified (diluted hydrochloric acid) and extracted with ether. The extract was dried, the solvent removed, and the residue chromatographed with 10% ethyl acetate in hexane to give pterosin I (1.1 g, 89%), mp 59–60°C (from hexane, lit. (12) mp 61–62°C, lit. (8) mp 60–63°C, lit. (17) mp 56–57°C); ir (film): 1690, 1600 cm^{-1}; nmr (^{1}H, CCl_4) δ: 1.17 (s, 6), 2.30 (s, 3), 2.63 (s, 3), 2.80 (s, 2), 2.93 (t, J = 7 Hz, 2), 3.27 (s, 3), 3.40 (t, J = 7 Hz, 2), 7.03 (br s, 1); nmr (^{13}C) δ: 211.2 (s), 150.5 (s), 143.7 (s), 137.5 (s), 134.7 (s), 130.4 (s), 125.3 (d), 70.8 (t), 58.1 (q), 44.9 (s), 41.2 (t), 28.5 (t), 25.1 (q), 20.7 (q), 13.0 (q); ms *m/z*: 246 (M^+, 25), 231 (45), 201 (100).

Pterosin Z

This compound was prepared by demethylation of pterosin I (576 mg, 2.34 mmol) in the same way as described for preparation of pterosin B. Purification by chromatography with 30% ethyl acetate in benzene gave a (493 mg) 90% yield of pterosin Z, mp 89–90°C (from ether–hexane; lit. (17) mp 86–88°C, lit. (12) mp 93–93.5°C, lit. (8) mp 87–89°C); ir (film): 3400, 1680, 1590, 1040 cm^{-1}; nmr (^{1}H) δ: 1.10 (s, 6), 2.37 (s, 3), 2.60 (s, 3), 2.73 (s, 2), 2.93 (t, J = 7 Hz, 2), 3.63 (t, J = 7 Hz, 2), 4.07 (br s, exchangeable, 1), 6.97 (br s, 1); nmr (^{13}C) δ: 212.3 (s), 151.1 (s), 144.3 (s), 138.0 (s), 134.8 (s), 130.7 (s), 125.6 (d), 61.2 (t), 45.4 (s), 41.5 (t), 31.7 (t), 25.3 (q), 21.1 (q), 13.5 (q); ms *m/z*: 232 (M^+, 35), 217 (96), 201 (100).

Pterosin H

This compound was prepared from pterosin Z (294 mg, 1.27 mmol) in a similar way to that for pterosin F, though the reflux time was 17 h. It was purified by chromatography with 2.5% ethyl acetate in hexane, yielding pterosin H 195 mg, 74% (83% conversion), mp 87–88°C (from hexane; lit. (8) mp 87–88°C, lit. (12) mp 87.5–88°C); ir (film): 1690, 1590 cm^{-1}; nmr (^{1}H) δ: 1.17 (s, 6), 2.40 (s, 3), 2.67 (s, 3), 2.80 (s, 2), 3.13 (m, 2), 3.50 (m, 2), 7.05 (br, s, 1); nmr (^{13}C) δ: 211.8 (s), 151.6 (s), 143.8 (s), 138.0 (s), 134.5 (s), 128.5 (s), 125.9 (d), 45.5 (s), 41.9 (t), 41.6 (t), 32.1 (t), 25.4 (q), 21.0 (q), 13.5 (q); ms *m/z*: 252 (M^+ + 2, 18), 250 (M^+, 56), 235 (91), 215 (100), 201 (71).

5-(β-Methoxy)ethyl-2,2,4,6-tetramethyl-1,3-indandione

A solution of indandione **3** (250 mg, 1.0 mmol) in benzene (10 mL) was added dropwise to a stirred suspension of 50% sodium hydride (135 mg, 2.8 mmol) in benzene (2 mL). After a further 30 min, excess methyl iodide (10 mL, 0.16 mol) was added dropwise and the mixture was refluxed for 24 h. Water was added and the mixture was extracted with chloroform (three times). The combined extracts were dried, the solvent was removed, and the residue was chromatographed with 5% ethyl acetate in benzene, yielding the product as an oil (235 mg, 89%); ir (film): 1720, 1690, 1580, 1100 cm^{-1}; nmr (^{1}H) δ: 1.25 (s, 6), 2.50 (s, 3), 2.77 (s, 3), 3.10 (t, J = 7 Hz, 2), 3.33 (s, 3), 3.50 (t, J = 7 Hz, 2), 7.63 (br s, 1); nmr (^{13}C) δ: 205.5 (s), 204.6 (s), 145.7 (s), 145.4 (s), 138.9 (s), 137.8 (s), 135.7 (s), 122.2 (d), 70.7 (t), 58.6 (q), 49.8 (s), 29.8 (t), 21.3 (q), 20.3 (q), 14.3 (q); ms *m/z*: 260 (M^+, 56), 245 (11), 230 (13), 215 (100).

5-(β-Hydroxy)ethyl-2,2,4,6-tetramethyl-1,3-indandione

This compound was prepared by demethylation of the preceding methyl ether (235 mg, 0.90 mmol) in the same way as for pterosin B. Purification by chromatography with 30% ethyl acetate in benzene gave a (206 mg) 93% yield of the product, mp 108–109°C (from ether; lit. (17) mp 111°C); ir (film): 3400, 1720, 1690, 1580, 1030 cm^{-1}; nmr (^{1}H) δ: 1.25 (s, 6), 1.70 (br s, exchangeable, 1), 2.53 (s, 3), 2.77 (s, 3), 3.13 (t, J = 7 Hz, 2), 3.83 (t, J = 7 Hz, 2), 7.67 (br s, 1); nmr (^{13}C) δ: 205.4 (s), 204.7 (s), 145.8 (s), 138.7 (s), 137.9 (s),

Can. J. Chem. Downloaded from www.nrcresearchpress.com by 210.87.254.5 on 09/06/12
For personal use only.

135.6 (s), 122.2 (d), 60.6 (t), 49.7 (s), 32.5 (t), 21.3 (q), 20.4 (q), 14.2 (q); ms *m/z*: 246 (M^+, 58), 231 (22), 215 (100).

Pterosin D diacetate and isopterosin D diacetate

The above indandione (206 mg, 0.84 mmol) was reduced in a similar way to that used in the preparation of pterosin C diacetate, but the reaction temperature was 75°C and the time was 40 h. Purification of the product by chromatography with 5% ethyl acetate in benzene gave pterosin D diacetate (179 mg, oil), isopterosin D diacetate (51 mg), and a mixture of the two compounds (8 mg). Total yield was 86%. Spectral properties for pterosin D diacetate included: ir (film): 1720, 1700, 1590, 1230 cm^{-1}; nmr (^1H, CCl_4) δ: 1.00 (s, 3), 1.20 (s, 3), 1.97 (s, 3), 2.07 (s, 3), 2.43 (s, 3), 2.63 (s, 3), 3.00 (t, J = 7 Hz, 2), 4.07 (t, J = 7 Hz, 2), 5.80 (s, 1), 7.17 (br s, 1); nmr (^{13}C) δ: 207.9 (s), 170.7 (s), 170.6 (s), 148.3 (s), 144.8 (s), 137.9 (s), 136.7 (s), 130.5 (s), 125.5 (d), 77.5 (d), 62.3 (t), 49.6 (s), 27.9 (t), 24.1 (q), 21.0 (q), 20.7 (q), 19.5 (q), 13.6 (q); ms *m/z*: 332 (M^+, 12), 290 (54), 272 (2), 230 (100). Spectral properties for isopterosin D diacetate included: ir (film): 1730, 1710, 1700, 1600, 1240, 1220 cm^{-1}; nmr (^1H, CCl_4) δ: 1.00 (s, 3), 1.20 (s, 3), 1.97 (s, 3), 2.03 (s, 3), 2.30 (s, 3), 2.43 (s, 3), 3.03 (t, J = 7 Hz, 2), 4.10 (t, J = 7 Hz, 2), 6.00 (s, 1), 7.37 (s, 1); nmr (^{13}C) δ: 207.8 (s), 170.5 (s), 170.4 (s), 145.2 (s), 142.3 (s), 139.8 (s), 135.7 (s), 133.6 (s), 122.7 (d), 77.8 (d), 62.0 (t), 49.2 (s), 29.1 (t), 24.8 (q), 20.6 (q), 20.3 (q), 18.3 (q), 14.4 (q); ms *m/z*: 332 (M^+, 1), 290 (43), 272 (26), 230 (31), 215 (42).

Pterosin D

Acid hydrolysis of pterosin D diacetate (119 mg, 0.36 mmol) in the same way as for pterosin C diacetate gave, after chromatography with 5% methanol in chloroform, an 88% yield of pterosin D (78 mg), mp 183–184°C (from chloroform–methanol; lit. (17) mp 189–190°C); ir (film): 3300, 1670, 1580, 1090 cm^{-1}; nmr (^1H, CD_3OD) δ: 1.07 (s, 3), 1.20 (s, 3), 2.47 (s, 3), 2.63 (s, 3), 2.98 (t, J = 7 Hz, 2), 3.63 (t, J = 7 Hz, 2), 4.73 (s, 1), 7.37 (br s, 1); nmr (^{13}C, DMSO) δ: 209.0 (s), 152.7 (s), 144.2 (s), 137.2 (s), 136.1 (s), 129.4 (s), 124.9 (d), 75.3 (d), 59.8 (t), 50.9 (s), 32.2 (t), 23.0 (q), 21.0 (q), 20.6 (q), 13.5 (q); ms *m/z*: 248 (M^+, 77), 233 (69), 217 (100), 199 (79).

Pterosin A

A solution of pterosin B (594 mg, 2.7 mmol) in THF (10 mL) was added dropwise to a suspension of sodium hydride (50% dispersion, 270 mg, 5.6 mmol) in THF and the mixture was stirred at room temperature for 30 min. Formaldehyde solution (37%, 10 mL) was added and the mixture was then refluxed for 12 h. Work-up included addition of water, extraction with chloroform, and chromatography with 5% methanol in chloroform. The yield of pterosin A was quantitative (673 mg). Attempts at crystallization were not successful; ir (film): 3400, 1680, 1590, 1020 cm^{-1}; nmr (^1H, 360 MHz) δ: 1.21 (s, 3), 1.76 (br s, exchangeable, 1), 2.43 (s, 3), 2.66 (s, 3), 2.74 (d, J = 17 Hz, 1), 3.00 (t, J = 7 Hz, 2), 3.05 (d, J = 17 Hz, 1), 3.59 (d, J = 10 Hz, 1), 3.74 (t, J = 7 Hz, 2), 3.77 (d, J = 10 Hz, 1), 7.11 (s, 1); nmr (^{13}C, DMSO) δ: 218.5 (s), 152.2 (s), 144.2 (s), 136.7 (s), 135.6 (s), 131.8 (s), 125.7 (d), 66.8 (t), 60.1 (t), 51.2 (s), 36.2 (t), 32.2 (t), 21.0 (q), 13.4 (q); ms *m/z*: 248 (M^+, 51), 233 (43), 217 (70), 203 (52), 199 (60), 187 (100).

Pterosin K

A solution of pterosin F (474 mg, 2 mmol) in 10% potassium hydroxide in methanol (50 mL) was stirred at room temperature for 30 min, then aqueous formaldehyde (37%, 20 mL) was added and the solution was refluxed for 90 min. It was then cooled and extracted with chloroform (three times) and the combined extracts washed with brine. Removal of solvent and chromatography of the residue with 15% ethyl acetate in benzene gave pterosin K (497 mg, 93%), mp 85–86°C (from hexane; lit. (17) mp 85–87°C); ir (film): 3400, 1680, 1590 cm^{-1}; nmr (^1H) δ: 1.13 (s, 3), 2.40 (s, 3), 2.61 (s, 3), 2.66 (d, J = 17 Hz, 1), 3.11 (d, J = 17 Hz, 1), 3.23 (m, 2), 3.43 (m, 2), 3.53 (d, J = 11 Hz, 1), 3.76 (d, J = 11 Hz, 1), 7.11 (br s, 1); nmr (^{13}C) δ: 211.1 (s), 152.6 (s), 144.0 (s), 137.4 (s), 134.2 (s), 131.4 (s), 125.7 (d), 67.2 (t), 50.7 (s), 41.6 (t), 36.3 (t), 31.7 (t), 20.7 (q), 20.6 (q), 13.3 (q); ms *m/z*: 268 (M^+ + 2, 27), 266 (M^+, 76), 251 (18), 248 (10), 235 (100), 231 (19).

Pterosin V

A solution of pterosin O (354 mg, 1.5 mmol) in methanolic potassium hydroxide was treated with formaldehyde solution in the same way as in the preparation of pterosin K. Purification by chromatography with 15% ethyl acetate in benzene gave pure pterosin V (374 mg, 93%); ir (film): 3420, 1670, 1590, 1100 cm^{-1}; nmr (^1H) δ: 1.15 (s, 3), 2.40 (s, 3), 2.63 (s, 3), 2.66 (d, J = 17 Hz, 1), 2.97 (t, J = 7 Hz, 2), 3.15 (d, J = 17 Hz, 1), 3.35 (s, 3), 3.43 (t, J = 7 Hz, 2), 3.53 (d, J = 11 Hz, 1), 3.78 (d, J = 11 Hz, 1), 7.10 (s, 1); nmr (^{13}C) δ: 211.1 (s), 152.0 (s), 144.2 (s), 137.4 (s), 134.6 (s), 131.2 (s), 125.4 (d), 70.8 (t), 67.2 (t), 58.1 (q), 50.6 (s), 36.2 (t), 28.4 (t), 20.7 (q), 20.5 (q), 13.2 (q); ms *m/z*: 262 (M^+, 82), 247 (77), 231 (55), 217 (35), 200 (57), 199 (100).

5-(β-Hydroxy)ethyl-2-hydroxymethyl-2,4,6-trimethyl-1,3-indandione

A solution of indandione **4** (1.71 g, 7.4 mmol) in 10% potassium hydroxide in methanol (100 mL) was stirred at room temperature for 30 min, then aqueous formaldehyde (37%, 50 mL) was added and the solution was refluxed for 90 min. It was neutralized with 10% hydrochloric acid and the solution was then extracted with chloroform (three times). The extract on work-up, which included chromatography with 5% methanol in chloroform, gave 1.22 g (63%) of the desired hydroxymethyl compound, mp 150–152°C (from ethyl acetate); ir (KBr): 3400, 1740, 1700, 1590, 1050 cm^{-1}; nmr (^1H, CD_3OD) δ: 1.00 (s, 3), 2.43 (s, 3), 2.62 (s, 3), 2.96 (t, J = 7 Hz, 2), 3.67 (t, J = 7 Hz, 2), 3.90 (s, 2), 7.37 (s, 1); nmr (^{13}C, DMSO) δ: 207.6 (s), 144.2 (s), 137.2 (s), 135.8 (s), 131.2 (s), 124.6 (d), 65.6 (t), 60.0 (t), 55.8 (s), 32.3 (t), 21.1 (q), 18.7 (q), 13.7 (q); ms *m/z*: 264 (M^+, 19), 246 (68), 233 (79), 231 (44), 218 (65), 215 (99), 202 (30), 201 (57), 187 (100).

Pterosin L triacetate and isopterosin L triacetate

The above indandione (1.22 g, 4.7 mmol), acetic acid (50 mL), acetic anhydride (50 mL), sodium acetate (3.8 g), and zinc dust (6.1 g) was stirred at 75°C for 40 h. Work-up in a similar way to that for the preparation of pterosin C diacetate gave pterosin L triacetate (865 mg), a mixture of pterosin L triacetate and isopterosin L triacetate (84 mg), and isopterosin L triacetate (419 mg), The total yield was 75%. Spectral properties for pterosin L triacetate (oil, a 7:3 mixture of *cis* and *trans* isomers) included: ir (film): 1730, 1720, 1700, 1590, 1220, 1210, 1030 cm^{-1}; nmr (^1H) *trans* isomer, δ: 1.00 (s, 3), 2.00 (s, 3), 2.07 (s, 3), 2.11 (s, 3), 2.47 (s, 3), 2.67 (s, 3), 3.03 (t, J = 7 Hz, 2), 4.00–4.40 (m, 4), 6.17 (s, 1), 7.20 (br s, 1); *cis* isomer, δ: 1.27 (s, 3), 1.83 (s, 3), 2.00 (s, 3), 2.07 (s, 3), 2.47 (s, 3), 2.67 (s, 3), 3.03 (t, J = 7 Hz, 2), 4.00–4.40 (m, 4), 5.97 (s, 1), 7.20 (br s, 1): ms *m/z*: 390 (M^+, 12), 348 (10), 347 (7), 288 (66), 287 (30), 228 (100). Spectral properties for isopterosin L triacetate (a mixture of isomers *cis/trans* 1:2) included: ir (film): 1730, 1710, 1700, 1590, 1240, 1220, 1020 cm^{-1}; nmr (^1H) *trans* isomer, δ: 1.10 (s, 3), 1.82 (s, 3) 1.93 (s, 3), 2.03 (s, 3), 2.22 (s, 3), 2.27 (s, 3), 3.03 (t, J = 7 Hz, 2), 4.00–4.40 (m, 4), 6.20 (s, 1), 7.40 (br s, 1); *cis* isomer, δ: 0.93 (s, 3), 1.82 (s, 3), 1.93 (s, 3), 2.00 (s, 3), 2.22 (s, 3), 2.27 (s, 3), 3.03 (t, J = 7 Hz, 2), 4.00–4.40 (m, 4), 6.32 (s, 1), 7.40 (br s, 1); ms *m/z*: 390 (M^+, 4), 348 (16), 347 (7), 330 (7), 288 (34), 287 (39).

Pterosin L and epi *pterosin L*

A solution of pterosin L triacetate (153 mg, 0.39 mmol), a mixture of two isomers, was hydrolysed in a similar way to that of pterosin C diacetate (but at 50°C for 15 h). Work-up, which included chromatography with 10% methanol in chloroform, gave pterosin L, the *cis* isomer, (72 mg, 70%) and *epi* pterosin L, the *trans* isomer, (22 mg, 21%). Properties of pterosin L included: mp 147–149°C (from benzene; lit. (17) mp 139–141°C); ir (KBr): 3350, 1670, 1590 cm^{-1}; nmr (^1H, $CDCl_3$ and CD_3OD) δ: 1.17 (s, 3), 2.47 (s, 3), 2.67 (s, 3), 3.00 (t, J = 7 Hz, 2), 3.63 (t, J = 7 Hz, 2), 3.78 (s, 2), 4.87 (s, 1), 7.37 (br s, 1); nmr (^{13}C, DMSO) δ: 207.5 (s), 153.4 (s), 144.1 (s), 137.1 (s), 135.6 (s), 131.1 (s), 124.5 (d), 75.4 (d), 65.3 (t), 59.8 (t), 55.7 (s), 32.2 (t), 21.0 (q), 18.5 (q), 13.5 (q); ms *m/z*: 264 (M^+, 14), 246

(9), 233 (43), 215 (53), 203 (75), 185 (100). Properties of *epi* pterosin L included: mp 80–81°C (from benzene; lit. (17) mp 86–89°C); ir (KBr): 3400, 1695, 1685, 1600 cm^{-1}; nmr (^1H, $CDCl_3$ and CD_3OD) δ: 1.00 (s, 3), 2.48 (s, 3), 2.67 (s, 3), 3.00 (t, J = 7 Hz, 2), 3.60 (d, J = 10 Hz, 1), 3.67 (t, J = 7 Hz, 2), 3.85 (d, J = 10 Hz, 1), 5.20 (s, 1), 7.41 (br s, 1); nmr (^{13}C, DMSO) δ: 208.4 (s), 154.3 (s), 144.3 (s), 137.1 (s), 135.9 (s), 130.7 (s), 125.1 (d), 70.0 (d), 64.9 (t), 60.0 (t), 56.4 (s), 32.3 (t), 21.0 (q), 16.0 (q), 13.7 (q).

Acknowledgements

The interest of Professor W. Charles Evans, University College of North Wales, is gratefully acknowledged. This investigation was supported in part with funds from the Academic Senate, University of California.

1. K. YOSHIHIRA, M. FUKUOKA, M. KUROYANAGI, and S. NATORI. Chem. Pharm. Bull. **19**, 1491 (1971).
2. (*a*) K. YOSHIHIRA, M. FUKUOKA, M. KUROYANAGI, S. NATORI, M. UMEDA, T. MOROHOSHI, M. ENOMOTO, and M. SAITO. Chem. Pharm. Bull. **26**, 2346 (1978); (*b*) M. KUROYANAGI, M. FUKUOKA, K. YOSHIHIRA, and S. NATORI. Chem. Pharm. Bull. **27**, 592 (1979); (*c*) H. HIKINO, T. TAKAHASHI, and T. TAKEMOTO. Chem. Pharm. Bull. **20**, 210 (1972); (*d*) P. SENGUPTA, M. SEN, S. K. NIYOGI, S. C. PAKRASHI, and E. ALI. Phytochemistry, **15**, 995 (1976); (*e*) V. BARDOUILLE, B. S. MOOTOO, K. HIROTSU, and J. CLARDY. Phytochemistry, **17**, 275 (1978); (*f*) T. MURAKAMI, N. TANAKA, and C. CHEN. Chem. Pharm. Bull. **23**, 1890 (1975); (*g*) T. MURAKAMI, H. WADA, N. TANAKA, Y. SAIKI, and C. CHEN. Chem. Pharm. Bull. **28**, 1869 (1980).
3. (*a*) D. M. X. DONELLY, J. O'REILLY, J. POLONSKY, and M. H. SHERIDAN. J. Chem. Soc. Chem. Commun. 615 (1983); (*b*) S. NOZOE, H. KOBAYASHI, S. URANO, and J. FURUKAWA. Tetrahedron Lett. 1381 (1977); (*c*) W. A. AYER and R. H. MCCASKILL. Can. J. Chem. **59**, 2150 (1981).
4. (*a*) T. C. MCMORRIS and M. ANCHEL. J. Am. Chem. Soc. **87**, 1594 (1965); (*b*) T. C. MCMORRIS, M. S. R. NAIR, and M. ANCHEL. J. Am. Chem. Soc. **89**, 4562 (1967); (*c*) J. J. DUGAN, P. DEMAYO, M. NISBET, J. R. ROBINSON, and M. ANCHEL. J. Am. Chem. Soc. **88**, 2838 (1966); (*d*) K. NAKANISHI, M. OHASHI, M. TADA, and Y. YAMADA. Tetrahedron, **21**, 1231 (1965); (*e*) T. MATSUMOTO, H. SHIRAHEMA, A. ICHIHARA, Y. FUKUOKA, Y. TAKAHASHI, Y. MORI, and M. WATANABE. Tetrahedron, **21**, 2671 (1965).
5. H. NIWA, M. OJIKA, K. WAKAMATSU, K. YAMADA, S. OHBA, Y. SAITO, I. HIRONO, and K. MATSUSHITA. Tetrahedron Lett. 5371 (1983); Y. HAYASHI, M. NISHIZAWA, and T. SAKAN. Chem. Lett. 63 (1973).
6. T. C. MCMORRIS and B. VOELLER. Phytochemistry, **10**, 3253 (1971).
7. T. C. MCMORRIS, M. LIU, and R. H. WHITE. Lloydia, **40**, 221 (1977).
8. A. KOBAYASHI and K. KOSHIMIZU. Agric. Biol. Chem. **44**, 393 (1980).
9. A. KOBAYASHI, H. EGAWA, K. KOSHIMIZU, and T. MITSUI. Agric. Biol. Chem. **39**, 1851 (1975).
10. E. T. R. EVANS, W. C. EVANS, and L. E. HUGHES. Vet. Rec. **63**, 444 (1951); W. C. EVANS, M. C. PATEL, and Y. KOOHY. Proc. R. Soc. Edinburgh, Sect. B, **81**, 29 (1982).
11. M. E. N. NAMBUDIRY and G. S. K. RAO. J. Chem. Soc. Perkin Trans. 1, 317 (1974).
12. Y. HAYASHI, M. NISHIZAWA, S. HARITA, and T. SAKAN. Chem. Lett. 375 (1972).
13. M. FREUND and K. FLEISCHER. Justus Liebigs Ann. Chem. **411**, 14 (1916); PETER H. GORE. *In* Friedel–Crafts and related reactions. Vol. III. *Edited by* G. Olah. Interscience, New York. 1964. Part I. p. 28.
14. P. H. LACY and D. C. C. SMITH. J. Chem. Soc. C, 41 (1971).
15. M. KUROYANAGI, M. FUKUOKA, K. YOSHIHIRA, and S. NATORI. Chem. Pharm. Bull. **27**, 592 (1979).
16. M. KUROYANAGI, M. FUKUOKA, K. YOSHIHIRA, and S. NATORI. Chem. Pharm. Bull. **27**, 731 (1979).
17. M. FUKUOKA, M. KUROYANAGI, K. YOSHIHIRA, and S. NATORI. Chem. Pharm. Bull. **26**, 2365 (1978).
18. N. LÖFGREN, V. RAGNARSSON, and K. SJOBERG. Acta Chem. Scand. **17**, 1252 (1963).

Can. J. Chem. Downloaded from www.nrcresearchpress.com by 210.87.254.5 on 09/06/12
For personal use only.

Preparation and evaluation of a perhydroazulene intermediate for lactarane sesquiterpene synthesis

JOEL R. CHRISTENSEN AND WILLIAM REUSCH

Department of Chemistry, Michigan State University, East Lansing, MI 48824-1322, U.S.A.

Received February 2, 1984

This article is dedicated to Professor Paul de Mayo on the occasion of his 60th birthday

JOEL R. CHRISTENSEN and WILLIAM REUSCH. Can. J. Chem. **62**, 1954 (1984).

A facile preparation of 6,9,9-trimethylbicyclo[5.3.0]deca-1,6-dien-3-one (**6**) from 2,5,5-trimethylcyclohexane-1,3-dione is described. Enolate reactions of **6** do not yield norcaradiene products, but proceed in the conventional manner (e.g., α-methylation and O-silylation). Nucleophilic addition reactions at the carbonyl function, and epoxidation of the γ,δ double bond are also observed. Under a variety of conditions, singlet oxygen reacts with the diene moiety in **6** to give both endoperoxide (**13**) and ene reaction (**14**) products in roughly equal amounts. The endoperoxide rearranges to cyclic hemiketal (**15**) on treatment with base.

JOEL R. CHRISTENSEN et WILLIAM REUSCH. Can. J. Chem. **62**, 1954 (1984).

On décrit une préparation simple de la triméthyl-6,9,9 bicyclo[5,3,0] décadiène-1,6 one-3 (**6**) à partir de la triméthyl-2,5,5 cyclohexanedione-1,3. Les réactions énoliques du composé **6** ne conduisent pas à des dérivés du norcaradiène; elles donnent plutôt les produits conventionnels (soit l'α-méthylation et la O-sylilation). On a aussi observé des réactions d'addition nucléophile sur la fonction carbonyle et une époxydation de la double liaison γ,δ. L'oxygène singulet réagit, sous diverses conditions, avec la portion diénique du composé **6** pour donner des quantités à peu près égales de l'endoperoxyde **13** et du produit **14** qui provient d'une réaction ene. Sous l'influence des bases, l'endoperoxyde se transpose en un hémicétal cyclique (**15**).

[Traduit par le journal]

Can. J. Chem. Downloaded from www.nrcresearchpress.com by 210.87.254.105 on 09/06/12
For personal use only.

Introduction

Sesquiterpenes belonging to the lactarane family, such as velleral (**1*a***), vellerolactone (**1*b***), and lactaroruffin A (**2**), represent an interesting variation of the perhydroazulene skeleton in natural products (cf. guaianolides and pseudo-guaianolides). Over a dozen such compounds have been isolated from Basidomycetes fungi, and the chemistry of these humulene-derived terpenes has been reviewed (1).

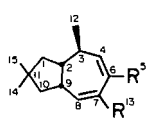

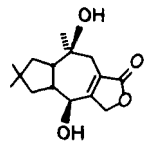

2

1a $R^5 = R^{13} = CHO$

1b $R^5 = CO$, $R^{13} = CH_2O$ (γ-lactone)

Total syntheses of velleral, vellerolactone, and pyrovellerolactone (an isomer of **1*b***) have been reported by Magnusson's group in Lund, Sweden (2). Their construction of the perhydrozaulene skeleton was accomplished by a [2+2] cycloaddition of dimethyl acetylenedicarboxylate to an enamine derivative of 2,7,7-trimethylbicyclo[3.3.0]octan-3-one, followed by electrocyclic opening of the resulting fused-cyclobutene ring. In this paper we describe an efficient synthesis of the 5,13-bisnorlactarane **6**, which we believe offers an alternative approach for the total synthesis of lactarane sesquiterpenes. We also present a survey of reactions which bear on the potential usefulness of **6** as a synthetic intermediate.

Results and discussion

Robinson annulation of methyldimedone gave the bicyclic enedione **3** in good yield (3). Dissolving metal reduction of **3** proceeded smoothly to a fused cyclopropanol (4) which was converted to a mesylate derivative **5** without purification. Solvolysis of **5** in trifluroacetic acid yielded dienone **6**, our lactarane precursor, in greater than 60% overall yield from **3**.

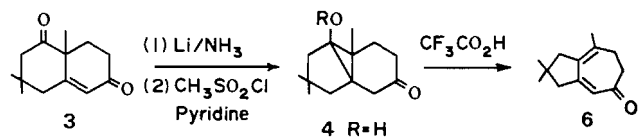

3 4 R=H 5 R=SO_2CH_3 6

Although the disposition of functional groups in **6** is such that structural elaboration should be possible, certain questions concerning the chemical behavior of this intermediate needed to be answered. Foremost among these addressed was the potential valence bond isomerism that might perturb reactions of enolate derivatives of **6**, as in the case of eucarvone (5). In the event, treatment of **6** with lithium diisopropylamide (LDA) generated a lithium enolate, which reacted rapidly with trimethylsilyl chloride to give the O-silylated product **7**, and sluggishly with methyl iodide to give the α-methylation product **8** (Scheme 1). The corresponding sodium enolate (from the action of sodium hydride on **6**) proved to be more reactive than the lithium enolate with weak electrophiles such as ethyl formate, but the resulting **6**-hydroxymethylene product was obtained only in poor yield. Fortunately, the corresponding dimethyl acetal **9** could be prepared in good yield by Lewis-acid promoted alkylation of **7** with trimethyl orthoformate (6). In light of these findings, we conclude that enolate reactions of **6**, unlike those of eucarvone, show no tendency to give norcaradiene products.

In other experiments with **6** (Scheme 1) we determined that the carbonyl function gave 1,2-addition reactions with methyllithium and cerium(III)-doped borohydride (7), and that the γ,δ double bond was epoxidized selectively on treatment with peracid. Acid-catalyzed reaction of **6** with ethylene glycol gave a mixture of diene–ketal derivatives, which were hydrolyzed back to **6**. This mixture of unsaturated ketals was not separated

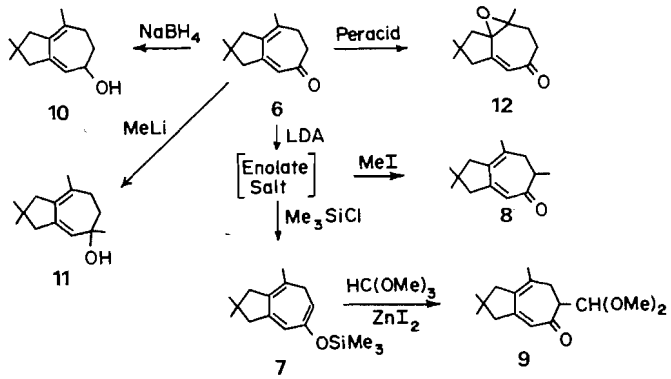

SCHEME 1

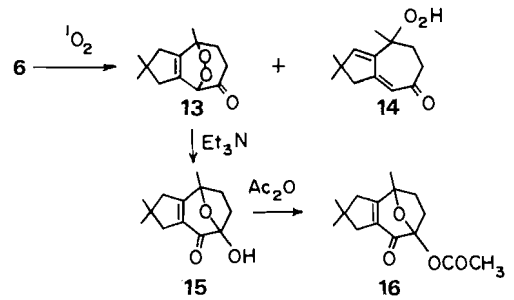

SCHEME 2

or characterized in an unambiguous fashion.

The last aspect of the chemical behavior of **6** that we chose to study in this survey concerned its reactions with singlet oxygen. Lactaroruffin A (**2**) and several other lactarane sesquiterpenes have *cis*-hydroxyl groups at C-3 and C-8, and an endoperoxide derivative of **6** seemed to be an ideal intermediate for the construction of such compounds (8). The desired endoperoxide, **13**, should result from a [4+2] cycloaddition of singlet oxygen to the diene moiety of **6**; however, competing ene reactions often occur at highly-substituted double bonds, and may be a problem in this case. In the event, hematoporphyrin-sensitized photooxidation of **6** in acetone solution gave a 1.2:1 mixture of **13** and a single ene product **14** in over 90% yield (Scheme 2). A similar photooxidation of dienols **10** and **11** gave complex mixtures of ene products and very little endoperoxide, indicating that the electron-withdrawing influence of the carbonyl function in **6** not only facilitates the cycloaddition reaction, but also favors one of the four possible ene products (that involving the most nucleophilic double bond). All our efforts to increase the **13**/**14** ratio by changing the sensitizer, the solvent, or the reaction temperature resulted in small to moderate decreases in this ratio. In particular, the 0.67 ratio observed for hematoporphyrin or tetraphenylporphine-sensitized reactions in carbon tetrachloride solution was surprising, since recent work by Matsumoto and Kuroda indicated that endoperoxide formation should be enhanced in this solvent (9). When the temperature of the reaction mixture was lowered to 0°C, this ratio decreased further to 0.44.

A number of reductive transformations of endoperoxides that might be useful in transforming **13** to a saturated *cis*-diol have been described (8,10). Unfortunately, our attempts to react **13** with diimide or palladium and hydrogen resulted in complex mixtures of unidentified products. These failures were counterbalanced, however, by a facile base-catalyzed rearrangement of **13** to the bridged hemiketal **15**. This compound and its acetate derivative (**16**) appear to offer good opportunities for selective reduction reactions but, except for their lack of reaction with diimide, these possibilities have not been tested. Obviously, the usefulness of such a study is diminished by our inability to suppress the ene reaction during singlet oxygen addition to **6**. If the selectivity of this reaction cannot be improved, or if alternative routes to intermediates such as **15** cannot be devised (possibly via epoxide **12**), applications of **6** to lactarane sesquiterpene sysnthesis will be limited.

Experimental

The ir spectra were recorded on a Perkin–Elmer 237B grating spectrophotometer. The ^{1}H nmr spectra were taken in $CDCl_3$ solution on either a Varian T-60 or a Bruker 250-MHz spectrometer and are calibrated in ppm downfield from Me_4Si as an internal standard. The ^{13}C nmr spectra were obtained with a Varian CFT-20 spectrometer or with the Bruker 250-MHz instrument. Mass spectra were taken with a Finnigan 4000 gc/ms spectrometer. The uv spectra were recorded on a Unicam SP-800 spectrophotometer. Melting points were measured on either a Hoover–Thomas apparatus (capillary tube) or on a Reichert hot-stage microscope and are uncorrected.

Microanalyses of C and H were performed by Spang Microanalytical Laboratories, Eagle Harbor, MI.

With the exception of the singlet oxygen reactions, all reactions were conducted under nitrogen or argon with solvents purified by distillation from suitable drying agents.

Preparation of mesylate **5**

Ammonia (1 L) was condensed in a dry, 2 L, three-neck, round bottom flask containing 75 mL of tetrahydrofuran (THF), and equipped with a mechanical stirrer, an addition funnel, and a Dry Ice condenser. Lithium wire (1.02 g, 147 mmol) was dissolved in the ammonia, followed by dropwise addition of a solution of 12.0 g (59.3 mmol) of **3** (3) in 150 mL THF. This solution was stirred for 0.5 h, and was then quenched by careful addition of approximately 3 g of ammonium chloride. After the cooling bath was removed, the ammonia was evaporated under nitrogen and the residue was diluted with 500 mL ether, washed with water, and dried over sodium sulfate. Evaporation of the ether gave 11.9 g of a yellow oil, which by ^{1}H nmr analysis still contained ca. 6% of enedione **3**. This crude cyclopropanol (**4**) was dissolved in 35 mL of cold pyridine and added to a solution of 7.0 mL (90 mmol) of freshly-distilled methanesulfonyl chloride in 35 mL of pyridine, containing 0.5 g of 4-(*N*,*N*-dimethylamino) pyridine. After being stirred overnight, this mixture was poured into 400 mL of ice water, and extracted twice with 500-mL portions of ether. The combined ether layers were washed successively with 2% hydrochloric acid, saturated sodium bicarbonate solution, and then dried. Evaporation of the solvent gave a solid, which was triturated with cold ether and filtered, yielding 11.0 g of **5**, mp 101 – 103°C (dec.) Characteristic properties of **5** are: infrared $\bar{\nu}_{max}$ ($CHCl_3$): 1715 cm^{-1}; ^{1}H nmr methyl signals at δ: 1.0 (3H,s), 1.16(6H,s), 3.08(3H,s) ppm; ^{13}C nmr ($CDCl_3$) δ: 14.2, 25.9, 27.2, 30.8, 33.1, 35.5, 35.6, 39.4, 40.5, 45.1, 45.2, 46.9, 81.0, 211.5 ppm; mass spectrum (70 eV) *m/e* (rel. intens.): 286(5), 271(5), 207(55), 189(100), 175(20), 165(92), 147(54), 123(40). *Anal.* calcd. for $C_{14}H_{22}O_4S$: C 58.71, H 7.74; found C 58.54, H 7.75.

6.9.9-Trimethylbicyclo[5.3.0]deca-1,6-dien-3-one (**6**)

A solution of 2.0 g (7.0 mmol) of **5** in 20 mL of trifluroacetic acid was stirred for 0.5 h at room temperature, poured into 100 mL of water, and extracted with 100 mL of ether. The ether extract was washed with 100-mL portions of aqueous sodium bicarbonate until gas evolution ceased, and was then dried. Evaporation of the solvent, followed by chromatography of the residue (silica gel, 25% ethyl acetate/hexane) gave 1.18 g (91%) of **6**, a light yellow oil. Characteristic properties of **6** are: infrared $\bar{\nu}_{max}$ ($CHCl_3$): 1630, 1590 cm^{-1}; λ_{max} (95% EtOH): 315 nm (ε = 6250); ^{1}H nmr ($CDCl_3$) δ: 1.05 (6H,s),

Can. J. Chem. Downloaded from www.nrcresearchpress.com by 210.87.254.105 on 09/06/12
For personal use only.

Can. J. Chem. Downloaded from www.nrcresearchpress.com by 210.87.254.105 on 09/06/12
For personal use only.

1.92 (3H,s), 2.2 – 2.7 (8H,m), 6.0 (1H, br s) ppm; ^{13}C nmr ($CDCl_3$) δ: 22.4, 27.0 $(CH_3)_2$, 29.3, 35.4, 39.4, 46.3, 51.4, 122.8, 134.4, 142.5, 158.0, 198.5 ppm; mass spectrum (70eV) *m/e* (rel. intens.): 190(96), 175(26), 162(49), 147(95), 119(33), 106(96), 105(56), 91(100), 77(24). *Anal.* calcd. for $C_{13}H_{18}O$: C 82.06, H 9.54; found: C 81.92, H 9.47.

3-Trimethylsilyloxy-6,9,9-trimethylbicyclo[5.3.0]deca-1,3,6-triene (7)

A solution of LDA in THF was prepared by first reacting diisopropyl amine (2.6 mmol) with n-butyllithium (2.4 mmol) in 5 mL of hexane, removing the solvent and excess amine at reduced pressure, and finally dissolving the resulting white solid in 2.5 mL of THF. The LDA solution was cooled to 0°C and a solution of **6** (418 mg, 2.2 mmol) in 1 mL THF was then added. After a 10-min reaction period, 0.32 mL (2.4 mmol) of trimethylsilyl chloride was introduced, the reaction mixture was stirred for 5 min. and the solvent was removed. The residue was dissolved in 20 mL of pentane, filtered, and then evaporated to give 536 mg (93%) of pure **7** as a volatile yellow oil. Characteristic properties of **7** are: infrared $\bar{\nu}_{max}$: 1620, 1250 cm^{-1}; ^{1}H nmr ($CDCl_3$) δ: 0.16 (9H,s), 1.03 (6H,s), 1.85 (3H,br s), 2.2 – 2.4 (6H,m), 4.58 (1H,br t, J = 4 Hz), 5.95 (1H,br s) ppm; ^{13}C nmr ($CDCl_3$) δ: 0.7, 21.9, 29.1 $(CH_3)_2$, 31.7, 37.8, 46.1, 50.7, 98.3, 121.7, 127.9, 135.6, 148.3, 150.8 ppm; mass spectrum (70 eV) *m/e* (rel. intens.): 262(87), 261(55), 247(100), 73(51). Parent ion isotope ions calcd. for $C_{16}H_{26}OSi$: P + 1, 22.88; P + 2, 5.03; found: (corrected for P – 1 contributions): P + 1, 23.89; P + 2, 5.57.[1]

4,6,9,9-Tetra methylbicyclo[5.3.0]deca-1,6-dien-3-one (8)

A solution of 0.13 g (0.7 mmol) of **6** in 1 mL THF was added to a cold solution of LDA (0.8 mmol) in 2.2 mL THF (prepared as above). After stirring this mixture for 10 min, 140 mg (1.0 mmol) of methyl iodide was added and this solution was refluxed for 30 min. The cooled reaction mixture was then diluted with ether (30 mL), washed successively with water and brine, and dried. Evaporation of the solvent followed by chromatography of the residue (silica gel, 20% ethyl acetate/hexane) gave 120 mg (82%) of **8** as a yellow oil. Characteristic properties of **8** are: infrared $\bar{\nu}_{max}$ ($CHCl_3$): 1630, 1590 cm^{-1}; λ_{max} (95% EtOh): 315 nm (ε = 6100); ^{1}H nmr ($CDCl_3$) δ: 1.04 (6H,s) 1.06 (3H,d, J = 7.5 Hz), 1.91 (3H,s), 2.2 – 2.7 (7H,m), 5.98 (1H, br s) ppm; mass spectrum (70 eV) *m/e* (rel. intens.): 204(4), 189(3), 176(7), 161(8), 149(15), 147(27), 129(100), 119(11), 112(34), 105(15). *Anal.* calcd. for $C_{14}H_{20}O$: C 82.30, H 9.87; found: C 82.15, H 9.76.

4-Dimethoxymethyl-6,9,9-trimethylbicyclo[5.3.0]deca-1,6-dien-3-one (9)

To a solution of 0.97 g (3.67 mmol) of **7** in 20 mL of dry trimethylorthoformate was added 1.28 g (4.0 mmol) of zinc iodide. This mixture was stirred for 1 h, diluted with 100 mL of ether, washed with 100-mL portions of water and brine, and dried. Evaporation of the solvent followed by chromatography (silica gel, 25% ethyl acetate/hexane) gave 0.86 g (85%) of **9** as a yellow oil. Characteristic properties of **9** are: infrared $\bar{\nu}_{max}$ ($CHCl_3$): 1645, 1585 cm^{-1}; ^{1}H nmr ($CDCl_3$) δ: 1.03 (3H,s), 1.05 (3H,s), 1.92 (3H,s), 2.2 – 2.9 (7H,m), 3.35 (3H,s), 3.38 (3H,s), 4.80 (1H,d, J = 7 Hz), 6.0 (1H,br s) ppm; ^{13}C nmr ($CDCl_3$) δ: 23.6, 27.8, 27.9, 31.3, 36.5, 47.1, 50.8, 52.2, 54.1, 54.3, 102.6, 123.2, 135.5, 141.5, 158.6, 198.0 ppm; mass spectrum (70 eV) *m/e* (rel. intens.): 264(3), 249(3), 232(11), 217(4), 189(5), 115(15), 75(100).

6,9,9-Trimethylbicyclo[5.3.0]deca-1,6-dien-3-ol (10)

To 4.6 mL (1.84 mmol) of a 0.4 *M* solution of cerium(III) chloride in methanol was added 0.35 g (1.84 mmol) of **6** followed by 69.3 mg (1.8 mmol) of sodium borohydride. After stirring the reaction mixture for 5 min, it was treated with ice water and extracted with ether. The washed and dried ether extracts were evaporated, and chromatography (silica gel, 40% ethyl acetate/hexane) yielded 280 mg (80%) of **10** as a colorless oil. Characteristic properties of **10** are: infrared $\bar{\nu}_{max}$ (neat): 3350 (broad), 1625 cm^{-1}; ^{1}H nmr ($CDCl_3$) δ: 0.97 (3H,s), 1.00 (3H,s), 1.78 (3H,s), 1.5 – 2.4 (9H,m), 4.32 (1H,m), 5.65 (1H,br d, J = 4 Hz) ppm; ^{13}C nmr ($CDCl_3$) δ: 23.2, 27.8, 28.0, 30.9, 33.4, 35.8, 48.3, 51.8, 69.1, 123.9, 133.2, 136.5, 142.3 ppm; mass spectrum (70 eV) *m/e* (rel. intens.): 192(33), 177(57), 174(34), 159(67), 149(20), 105(16), 91(100), 79(64), 77(86).

3,6,9,9-Tetramethylbicyclo[5.3.0]deca-1,6-dien-3-ol (11)

A stirred solution of **6** (90 mg, 0.47 mmol) in 1.5 mL of ether was cooled to −78°C, and to this was added 0.34 mL (0.51 mmol) of a 1.5 *M* solution of methyl lithium in ether. The reaction mixture was then warmed to room temperature, stirred 1 h, and quenched with saturated ammonium chloride solution. The ether layer was washed with brine, dried (Na_2SO_4), and evaporated. Chromatography (silica gel, 25% ethyl acetate/hexane) gave 75 mg (77%) of **11** as a pale yellow oil. Characteristic properties of **11** are: ^{1}H nmr ($CDCl_3$) δ: 0.96 (3H,s), 0.98 (3H,s), 1.30 (3H,s), 1.76 (3H,s), 1.5 – 2.5 (9H,m), 5.54 (1H,br s) ppm; mass spectrum (70 eV) *m/e* (rel. intens.): 206(16), 191(30), 188(72), 173(100), 163(45), 107(23). *Anal.* calcd. for $C_{14}H_{22}O$: C 81.50; H 10.75; found: C 81.23, H 10.70.

6,7-Epoxy-6,9,9-trimethylbicyclo[5.3.0]deca-1-en-3-one (12)

A solution of 4.8 g (25 mmol) of **6** in 100 mL chloroform was treated with 10.1 g (50 mmol) of 85% *m*-chloroperoxybenzoic acid. This solution was stirred for 1 h and then washed successively with aqueous sodium sulfite, sodium bicarbonate, and brine. Evaporation of the dried chloroform solution followed by chromatography of the residue (silica gel, 25% ethyl acetate/hexane) gave 4.1 g (80%) of **12** as a clear oil. Characteristic properties of **12** are: infrared $\bar{\nu}_{max}$ ($CHCl_3$): 1660, 1200 cm^{-1}; ^{1}H nmr ($CDCl_3$) δ: 1.08 (3H,s), 1.15 (3H,s), 1.44 (3H,s), 1.6 – 2.9 (8H,m), 6.03 (1H,br s) ppm; ^{13}C nmr ($CDCl_3$) δ: 21.4, 27.4, 27.6, 28.1, 36.2, 36.8, 46.9, 51.1, 65.6, 69.2, 127.6, 159.7, 200.9 ppm; mass spectrum (70 eV) *m/e* (rel. intens.): 206(62), 191(27), 163(30), 150(97), 149(100), 135(65), 121(13), 107(30). *Anal.* calcd. for $C_{13}H_{18}O_2$: C 75.69, H 8.79; found: C 75.51, H 8.74.

Reaction of 6 with singlet oxygen

A solution of 190 mg (1.0 mmol) of **6** and 10 mg of hematoporphyrin in 15 mL of acetone was irradiated by a 200-W incandescent light while oxygen was slowly bubbled through the solution. From time to time acetone was added to the reaction solution to replace that lost by evaporation. After 10 h the irradiation was stopped and the reaction solution was evaporated, leaving 230 mg of a solid residue. Chromatography of this residue (silica gel, 50% ethyl acetate/hexane) gave 110 mg (49%) of **13**, mp 67.5 – 68°C, and 93 mg (42%) of **14**, mp 133.5 – 134.5°C.

Characteristic properties of **13**: infrared $\bar{\nu}_{max}$ ($CHCl_3$): 1716 cm^{-1}; ^{1}H nmr ($CDCl_3$) δ: 1.08 (3H,s), 1.18 (3H,s), 1.33 (3H,s), 1.9 – 3.3 (8H,m), 4.78 (1H,s) ppm; ^{13}C nmr ($CDCl_3$) δ: 22.3, 29.4, 29.9, 36.7, 37.3, 38.9, 46.8, 47.9, 82.7, 85.6, 131.1, 145.0, 202.9 ppm; mass spectrum (70 eV) *m/e* (re. intens.): 223(M + 1, 15), 222(1.3), 207(10), 206(28), 205(50), 195(8), 179(29), 178(79), 177(71), 164(100), 163(75), 149(25), 145(23), 135(93), 121(79), 107(57). *Anal.* calcd. for $C_{13}H_{18}O_3$: C 70.24, H 8.16; found: C 70.31, H 8.22.

Characteristic properties of **14**: infrared $\bar{\nu}_{max}$ ($CHCl_3$): 3535 (sharp), 3250 (broad), 1610 (broad) cm^{-1}; ^{1}H nmr ($CDCl_3$) δ: 1.15 (3H,s), 1.17 (3H,s), 1.52 (3H,s), 1.9 – 3.0 (7H,m), 5.88 (1H,br s), 6.63 (1H,s) ppm; ^{13}C nmr ($CDCl_3$) δ: 24.7, 28.0 (overlapping signals), 31.2, 37.1, 42.4, 49.7, 81.6, 120.6, 143.2, 158.5, 161.3, 201.2 ppm; mass spectrum (70 eV) *m/e* (rel. intens.): 223(M + 1, 7), 222(14), 207(11), 206(16), 205(8), 189(91), 177(43), 163(34), 161(100), 149(30), 147(64), 145(32), 133(35), 121(27), 119(62), 107(34), 105(59). *Anal.* calcd. for $C_{13}H_{18}O_3$: C 70.24, H 8.16; found: C 70.34, H 8.21.

[1]Because of its volatility, conventional microanalysis of **7** was not attempted. Although high-resolution mass spectrometry was not available to us, we believe the characteristic isotope distribution of natural silicon makes the P + 1 and P + 2 measurement particularly informative.

*1-Hydroxy-5,5,8-trimethyl-11-oxatricyclo[6.2.1.0^{3,7}]undec-3(7)-en-2-one (**15**)*

To a solution of 100 mg (0.45 mmol) of **13** in 5 mL of methylene chloride was added 4.5 mg of triethylamine. This solution was stirred for 1 h and the solvent and amine were removed under vacuum. The resulting solid (100 mg) was crystallized from ethyl acetate/hexane to give pure **15**, mp 106 − 108°C (>90% yield). Characteristic properties of **15** are: infrared $\bar{\nu}_{max}$ ($CHCl_3$): 3500, 1685, 1620, 1200 cm^{-1}; ^1H nmr ($CDCl_3$) δ: 1.08 (3H,s), 1.18 (3H,s), 1.52 (3H,s), 1.8 − 2.7 (8H,m), 4.55 (1H,br s, exchange D_2O); ^{13}C nmr ($CDCl_3$) δ: 21.5, 29.0, 29.4, 32.1, 33.7, 39.2, 42.9, 47.5, 80.9, 103.7, 132.5, 171.3, 195.0 ppm; mass spectrum (70 eV) *m/e* (rel. intens.): 222(28), 207(2), 189(1), 178(20), 163(100), 136(21), 135(50), 121(33), 119(13), 107(34). *Anal.* calcd. for $C_{13}H_{18}O_3$: C 70.24, H 8.16; found: C 69.92, H 8.16.

An acetate derivative **16** was prepared from **15** by treatment with acetic anhydride in pyridine containing DMAP. This derivative, mp 112−113°C, exhibited the following properties: infrared $\bar{\nu}_{max}$ ($CHCl_3$): 1750, 1690, 1620, 1210 cm^{-1}; ^1H nmr ($CDCl_3$) δ: 1.06 (3H,s), 1.19 (3H,s), 1.56 (3H,s), 2.18 (3H,s), 1.6 − 2.7 (8H,m) ppm; ^{13}C nmr ($CDCl_3$): fifteen peaks; mass spectrum (70 eV): molecular ion at *m/e* 264 amu. *Anal.* calcd. for $C_{15}H_{20}O_4$: C 68.16, H 7.62; found: C 68.23, H 7.66.

1. W. A. AYER and L. M. BROWNE. Tetrahedron, **37**, 2199 (1981).
2. (*a*) J. FROBORG, G. MAGNUSSON, and S. THOREN. J. Org. Chem. **40**, 1595 (1975); (*b*) T. FEX, J. FROBORG, G. MAGNUSSON, and S. THOREN. J. Org. Chem. **41**, 3518 (1976); (*c*) J. FROBORG and G. MAGNUSSON. J. Am. Chem. Soc. **100**, 6728 (1978).
3. J. E. ELLIS, J. DUTCHER, and C. H. HEATHCOCK. J. Org. Chem. **41**, 2670 (1976).
4. W. REUSCH, K. GRIMM, J. KAROGLAN, J. MARTIN, K. P. SUBRAHAMANIAN, Y.-C. TOONG, P. S. VENKATARAMANI, J. YORDY, and P. ZOUTENDAM. J. Am. Chem. Soc. **99**, 1953 (1977).
5. E. J. COREY and H. J. BURKE. J. Am. Chem. Soc. **78**, 174 (1956).
6. (*a*) T. MUKAIYAMA and M. HAYASHI. Chem. Lett. 15 (1974); (*b*) I. FLEMING, J. GOLDHILL, and I. PATERSON. Tetrahedron Lett. 3209 (1979).
7. J.-L. LUCHE. J. Am. Chem. Soc. **100**, 2226 (1978).
8. M. BALCI. Chem. Rev. **81**, 91 (1981).
9. M. MATSUMOTO and K. KURODA. Synth. Commun. **11**, 987 (1981).
10. W. ADAM and A. J. BLOODWORTH. Top. Curr. Chem. **97**, 121 (1981).

Can. J. Chem. Downloaded from www.nrcresearchpress.com by 210.87.254.105 on 09/06/12
For personal use only.

The formation and hydrolytic cleavage of substituted benzalacetones

J. PETER GUTHRIE,[1] JOHN COSSAR, AND KATHLEEN F. TAYLOR
Department of Chemistry, University of Western Ontario, London, Ont., Canada N6A 5B7

Received January 24, 1984

This paper is dedicated to Professor Paul de Mayo on the occasion of his 60th birthday

J. PETER GUTHRIE, JOHN COSSAR, and KATHLEEN F. TAYLOR. Can. J. Chem. **62**, 1958 (1984).

The base catalyzed aldol condensation of acetone and benzaldehyde, as well as two substituted benzaldehydes, has been reinvestigated in both the formation and cleavage directions. Microscopic rate and equilibrium constants have been deduced from the experimental data in a fashion consistent with the rigorously correct integrated rate law. The values so obtained are as follows: (substituent, rate constants, equilibrium constants); H: $k'_{12} = 3.2 \times 10^{-4}\ M^{-1}\ s^{-1}$, $k'_{21} = 7.5 \times 10^{-3}\ M^{-1}\ s^{-1}$, $k'_{23} = 1.4 \times 10^{-2}\ M^{-1}\ s^{-1}$, $k''_{32} = 0.17\ M^{-2}\ s^{-1}$; $K_{12} = 0.042$, $K_{32} = 12.\ M^{-1}$, $K_{overall} = 286.$; *p*-MeO: $k'_{12} = 1.6 \times 10^{-4}\ M^{-1}\ s^{-1}$, $k'_{21} = 1.3 \times 10^{-2}\ M^{-1}\ s^{-1}$, $k'_{23} = 3 \times 10^{-2}\ M^{-1}\ s^{-1}$, $k''_{32} = 0.047\ M^{-2}\ s^{-1}$; $K_{12} = 0.012$, $K_{32} = 1.6\ M^{-1}$, $K_{overall} = 131.$; *p*-NO_2: $k'_{12} = 1.8 \times 10^{-3}\ M^{-1}\ s^{-1}$, $k'_{21} = 1.3 \times 10^{-2}\ M^{-1}\ s^{-1}$, $k'_{23} = 1.6 \times 10^{-2}\ M^{-1}\ s^{-1}$, $k''_{32} = 3.8\ M^{-2}\ s^{-1}$; $K_{12} = 0.14$, $K_{32} = 235.\ M^{-1}$, $K_{overall} = 1730.$

J. PETER GUTHRIE, JOHN COSSAR et KATHLEEN F. TAYLOR. Can. J. Chem. **62**, 1958 (1984).

On a étudié de nouveau la condensation aldolique, catalysée par les bases, de l'acétone, du benzaldéhyde ainsi que de deux benzaldéhydes substitués, tant du point de vue de la condensation que du point de vue du clivage des produits. Pour obtenir les constantes d'équilibre et de vitesse microscopique à partir des donnés expérimentales, on a utilisé une méthode qui est en accord avec la loi intégrée de vitesse qui est rigoureusement correcte. On a ainsi obtenu les valeurs suivantes: (substituant, constantes de vitesse, constante d'équilibre); H: $k'_{12} = 3{,}2 \times 10^{-4}\ M^{-1}\ s^{-1}$, $k'_{21} = 7{,}5 \times 10^{-3}\ M^{-1}\ s^{-1}$, $k'_{23} = 1{,}4 \times 10^{-2}\ M^{-1}\ s^{-1}$, $k''_{32} = 0{,}17\ M^{-2}\ s^{-1}$; $K_{12} = 0{,}042$, $K_{32} = 12\ M^{-1}$, $K_{global} = 286$; *p*-MeO: $k'_{12} = 1{,}6 \times 10^{-4}\ M^{-1}\ s^{-1}$, $k'_{21} = 1{,}3 \times 10^{-2}\ M^{-1}\ s^{-1}$, $k'_{23} = 3{,}0 \times 10^{-2}\ M^{-1}\ s^{-1}$, $k''_{32} = 0{,}047\ M^{-2}\ s^{-1}$; $K_{12} = 0{,}012$, $K_{32} = 1{,}6\ M^{-1}$, $K_{global} = 131$; *p*-NO_2: $k'_{12} = 1{,}8 \times 10^{-3}\ M^{-1}\ s^{-1}$, $k'_{21} = 1{,}3 \times 10^{-2}\ M^{-1}\ s^{-1}$, $k'_{23} = 1{,}6 \times 10^{-2}\ M^{-1}\ s^{-1}$, $k''_{32} = 3{,}8\ M^{-2}\ s^{-1}$; $K_{12} = 0{,}14$, $K_{32} = 235\ M^{-1}$, $K_{global} = 1730$.

[Traduit par le journal]

Introduction

We have reported a study (1) of the equilibrium constants for aldol condensation reactions. One of the few cases for which a full kinetic analysis had been reported was that of benzalacetone (4-phenyl-3-buten-2-one), which had been studied by Noyce and Reed (2). On further examination of their paper it was realized that the analysis was flawed, among other things involving a violation of microscopic reversibility. Since we consider it important to have a reliable set of rate and equilibrium constants for a set of simple aldol reactions and need such data for an examination of rate equilibrium correlations for the aldol reaction, we have reinvestigated the retroaldol reactions of some simple benzalacetones.

Results and discussion

The retroaldol reaction of benzalacetone can be followed spectrophotometrically; when benzalacetone, as a solution in acetonitrile, is injected into aqueous sodium hydroxide solution there is a smooth disappearance of the absorbance at 291 nm, which follows a simple first-order rate law. Thus one can see no sign of the two stages which are believed to be essential for this reaction; eq. [1]

[1] $$\mathrm{Ph{-}CH{=}CH{-}CO{-}CH_3} \underset{k_{21}}{\overset{k_{12}}{\rightleftarrows}} \mathrm{Ph{-}CHOH{-}CH_2{-}CO{-}CH_3}$$

$$\mathrm{Ph{-}CHOH{-}CH_2{-}CO{-}CH_3} \underset{k_{32}}{\overset{k_{23}}{\rightleftarrows}} \mathrm{Ph{-}CHO + CH_3{-}CO{-}CH_3}$$

The two phases of the reaction are quite apparent when the ketol, 4-phenyl-4-hydroxy-2-butanone, is injected into aqueous sodium hydroxide solution; the absorbance at 291 nm first rises and then, about 100 times more slowly, falls again: see Fig. 1. The rate of the slow fall in absorbance is essentially identical to the rate of disappearance of the absorbance of benzalacetone when the latter is used to initiate reaction. Analysis of the two-phase kinetics data permits evaluation of the rate constants. For the cleavage reactions of benzalacetones or ketols, where a low concentration of aldol product undergoes retroaldol cleavage, the rate of the second-order aldol formation process, k_{32}, is negligible. A rigorous solution of the kinetics equations is possible following the procedure described in Moore and Pearson (3), and leads to eq. [2] which gives the absorbance as a function of time.

[2] $$A = A_\infty + \alpha \exp(-\lambda_2 t) + \beta \exp(-\lambda_3 t)$$

where A = absorbance; $\lambda_{2,3} = (p \pm q)/2$; $p = k_{12} + k_{21} + k_{23}$; $q = (p^2 - k_{12}k_{23})^{1/2}$. When kinetics of benzalacetone formation are studied, all four rate constants are necessary, but the rigorously correct rate law still follows eq. [2], although now $p = k_{12} + k_{21} + k_{23} + k_{32}$ and $q = (p^2 - (k_{12}k_{23} + k_{32}k_{12} + k_{32}k_{21}))^{1/2}$. The initial rapid phase of the reaction is observed as a lag before the absorbance begins to rise: see Fig. 2.

When reaction starts with benzalacetone,

$$\alpha = C_1^0 k_{12}\epsilon_1(\lambda_2 - k_{23})\{1 - \epsilon_2\lambda_2/\epsilon_1(\lambda_2 - k_{23}) + \epsilon_3 k_{23}/\epsilon_1(\lambda_2 - k_{23})\}/\lambda_2(\lambda_2 - \lambda_3)$$

[1]Author to whom correspondence may be addressed.

Can. J. Chem. Downloaded from www.nrcresearchpress.com by 210.87.254.42 on 09/06/12
For personal use only.

Can. J. Chem. Downloaded from www.nrcresearchpress.com by 210.87.254.42 on 09/06/12
For personal use only.

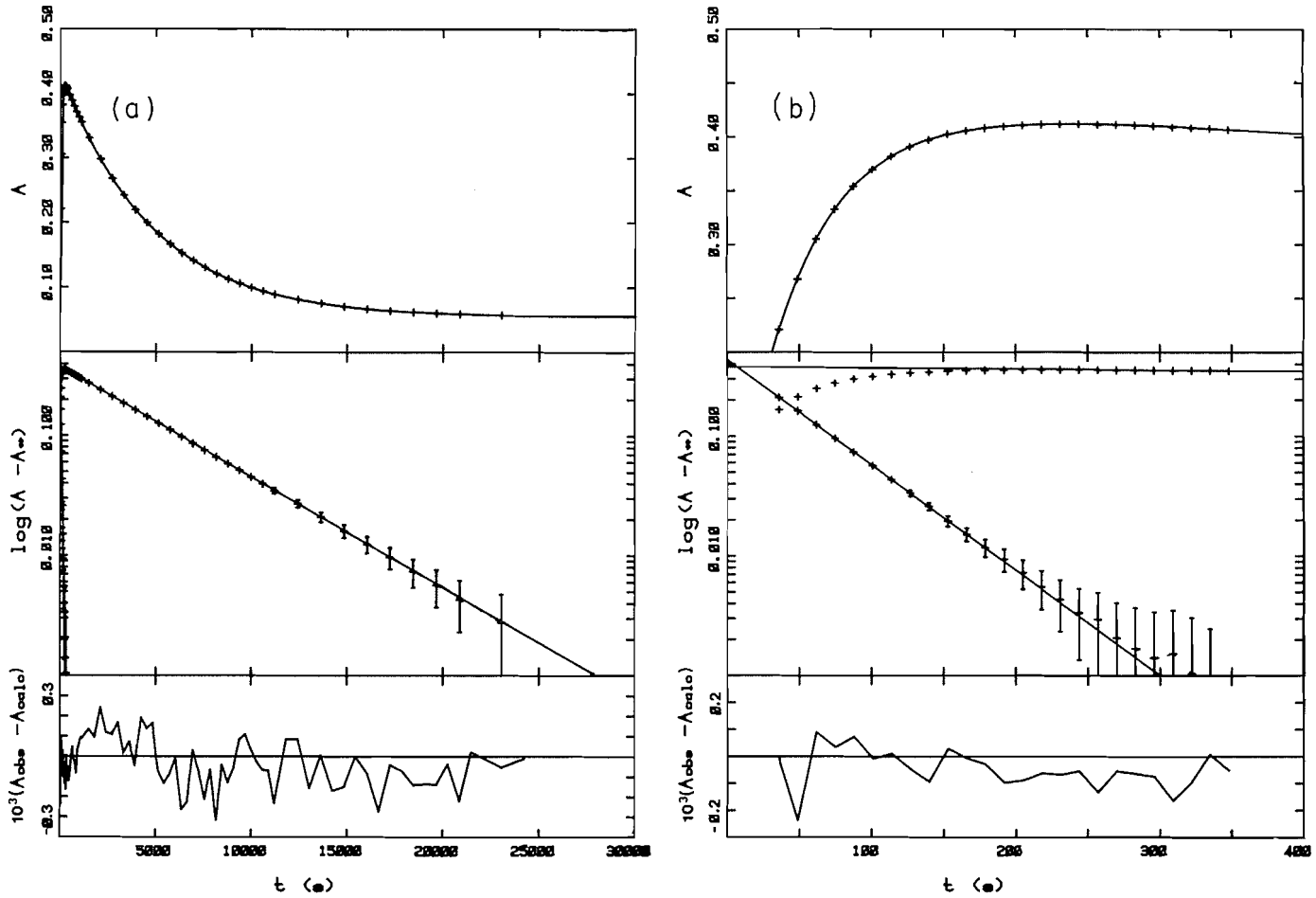

FIG. 1. Retroaldol reaction of 4-hydroxy-4-phenyl-2-butanone. Absorbance as a function of time for the reaction of 6.3×10^{-6} *M* ketol in 1 *M* NaOH.

$$\beta = C_1^0 k_{12}\epsilon_1(k_{23} - \lambda_3)\{1 - \epsilon_2\lambda_2/\epsilon_1(k_{23} - \lambda_3) - \epsilon_3 k_{23}/\epsilon_1(k_{23} - \lambda_3)\}/\lambda_3(\lambda_2 - \lambda_3)$$

When reaction starts with the ketol,

$$\alpha = C_2^0 k_{21}\epsilon_1\{-1 + \epsilon_2(\lambda_2 - k_{12})/\epsilon_1 k_{21} - \epsilon_3 k_{23}(\lambda_2 - k_{12})/\epsilon_1 k_{21}\lambda_2\}/(\lambda_2 - \lambda_3)$$

$$\beta = C_2^0 k_{21}\epsilon_1\{1 - \epsilon_2(\lambda_3 - k_{12})/\epsilon_1 k_{21} + \epsilon_3 k_{23}(\lambda_3 - k_{12})/\epsilon_1 k_{21}\lambda_3\}/(\lambda_2 - \lambda_3)$$

where, in either case, ϵ_1 = extinction coefficient for benzalacetone; ϵ_2 = extinction coefficient for the ketol; ϵ_3 = extinction coefficient for the products (benzaldehyde plus acetone); and C_i^0 = initial concentration of benzalacetone ($i = 1$) or ketol ($i = 2$). When reaction starts with benzaldehyde plus acetone (acetone in excess),

$$\alpha = C_3^0 k_{32}\{\epsilon_3(\lambda_2 - k_{12} - k_{21}) + \epsilon_2(k_{12} - \lambda_2) + \epsilon_1 k_{21}\}/\lambda_2(\lambda_2 - \lambda_3)$$

$$\beta = C_3^0 k_{32}\{\epsilon_3(k_{21} + k_{12} - \lambda_3) + \epsilon_2(\lambda_3 - k_{12}) - \epsilon_1 k_{21}\}/\lambda_3(\lambda_2 - \lambda_3)$$

where C_3^0 = initial concentration of benzaldehyde, and the concentration of acetone has been absorbed into k_{32}, now a pseudo first-order rate constant.

These equations can be usefully simplified by noting that ϵ_1, $\epsilon_3 \gg \epsilon_2$, so that for reaction starting with benzalacetone:

$$\alpha \cong C_1^0 k_{12}\{\epsilon_1\lambda_2 - k_{23}(\epsilon_1 - \epsilon_3)\}/\lambda_2(\lambda_2 - \lambda_3)$$

$$\beta \cong C_1^0 k_{12}\{(\epsilon_1 - \epsilon_3)k_{23} - \epsilon_3\lambda_3\}/\lambda_3(\lambda_2 - \lambda_3)$$

for reaction starting with the ketol:

$$\alpha \cong C_2^0\{-\lambda_2(k_{21}\epsilon_1 + k_{23}\epsilon_3) + k_{12}k_{23}\epsilon_3\}/\lambda_2(\lambda_2 - \lambda_3)$$

$$\beta \cong C_2^0\{\lambda_3(k_{21}\epsilon_1 + k_{23}\epsilon_3) - k_{12}k_{23}\epsilon_3\}/\lambda_3(\lambda_2 - \lambda_3)$$

and for reactions starting with benzaldehyde and excess acetone:

$$\alpha \cong C_3^0 k_{32}\{\epsilon_3(\lambda_2 - k_{12}) - (\epsilon_3 - \epsilon_1)k_{21})\}/\lambda_2(\lambda_2 - \lambda_3)$$

$$\beta = C_3^0 k_{32}\{\epsilon_3(k_{12} - \lambda_3) + (\epsilon_3 - \epsilon_1)k_{21}\}/\lambda_3(\lambda_2 - \lambda_3)$$

For reactions starting with the ketol the individual rate constants may now be calculated using:

$$k_{23} = (\epsilon_1(\lambda_2 + \lambda_3) - \lambda_2\epsilon_3 - ((\lambda_2 - \lambda_3)\beta/C_2^0) \pm((\epsilon_1(\lambda_2 + \lambda_3) - \lambda_2\epsilon_3 - (\lambda_2 - \lambda_3)\beta/C_2^0)^2 - 4(\epsilon_1 - \epsilon_3)\epsilon_1\lambda_2\lambda_3)^{\frac{1}{2}})/2(\epsilon_1 - \epsilon_3)$$

$$k_{21} = \lambda_2 + \lambda_3 - k_{23} - \lambda_2\lambda_3/k_{23}$$

$$k_{12} = \lambda_2\lambda_3/k_{23}$$

λ_3 can also be expressed by the steady state rate equation,

[3] $\lambda_3 \cong k_{12}k_{23}/(k_{21} + k_{23})$

which can also be derived from the above rigorous solution

Can. J. Chem. Downloaded from www.nrcresearchpress.com by 210.87.254.42 on 09/06/12
For personal use only.

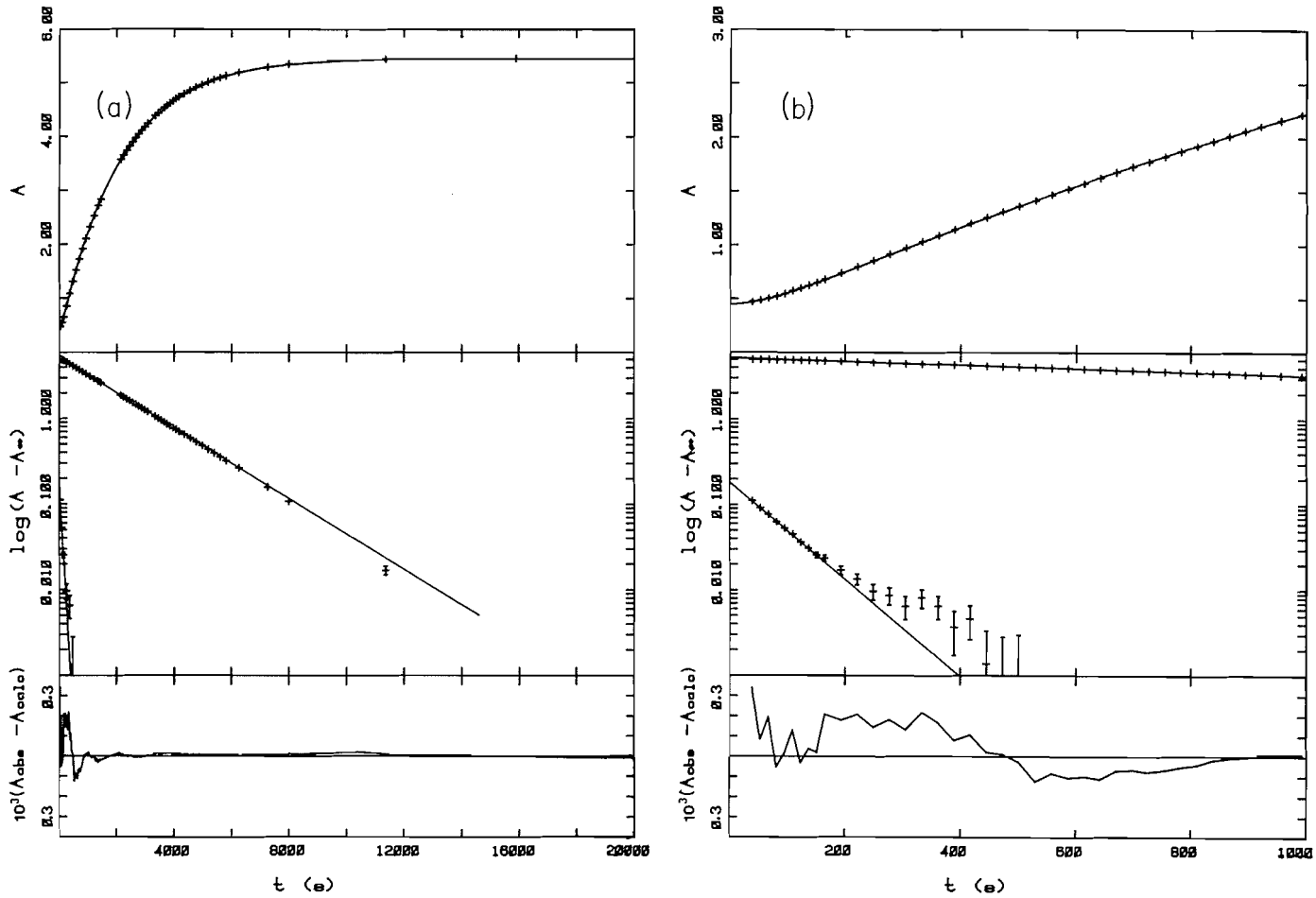

FIG. 2. Formation of 4-(*p*-methoxyphenyl)-3-buten-2-one, starting with 0.107 *M* acetone and 6.75×10^{-6} *M* *p*-methoxybenzaldehyde in 0.3 *M* NaOH.

when $k_{12} \ll k_{21}$, k_{23} (as it is for the present reaction). There is an ambiguity as to which of the quadratic solutions is the physically meaningful one. In the present case the ambiguity is easily resolved by comparison with the results of the unambiguous analysis of the kinetics of the benzalacetone formation kinetics discussed below. Alternatively we could carry out a first approximation solution, making the further simplifying assumption that $\epsilon_1 \gg \epsilon_3$ (which is not really correct in the present case) and apply the reasoning used for 3-methyl-2-butenal (4).

For kinetics where only the second phase was studied, we used the steady state expression for λ_3, eq. [3], and the ratio k_{21}/k_{23} derived from the analysis of biphasic kinetics to calculate k_{12}. For kinetics where only the first phase was studied, we used the approximate equation for α given above with the further simplifications, justified by the results from the analysis of biphasic kinetics, that $k_{23} \gg \lambda_3$ and $\lambda_2 \gg \lambda_3$ to obtain:

$$|\alpha| \cong C_2^0(\epsilon_3 k_{23} + \epsilon_1 k_{21})/\lambda_2$$

$$\lambda_2 \cong k_{21} + \lambda_{23}$$

These can easily be solved for k_{21} and k_{23}. For kinetics at high NaOH concentrations, where the reactions are faster, we felt that β was the better defined parameter.

Table 1 shows the results of applying this analysis to the experimental data for benzalacetone and the corresponding ketol. The individual rate constants show the expected first-order dependence upon the hydroxide concentration. The equilibrium constant for addition of water to the enone, K_{12}, may be showing a slight dependence upon $[OH^-]$. There is a corresponding slight dependence upon $[OH^-]$ for the second-order rate constants, k'_{12}. This effect is small, amounting to as much as 12% in k'_{12} or 25% in K_{12}. There is no obvious mechanistic path by which k_{12} could show a second-order dependence upon $[OH^-]$, and it seems unlikely that Na^+ ion is exerting a catalytic effect. We suspect that this behavior represents an artifact, and have taken average values for the rate and equilibrium constants. The rate constant ratio k_{23}/k_{21} describing the partitioning of the ketol intermediate is independent of the concentration of hydroxide; the weighted average value is 1.18 ± 0.28. It should be noted that the value of this ratio corresponds to nearly equal amounts of ketol undergoing cleavage or loss of water. Errors reported for the microscopic rate constants are based on propagation of error calculations (5) carried out using simple BASIC programs.

The final rate constant needed to describe the system, k_{32}, is obtained by studying the formation reaction, starting with solutions of benzaldehyde plus acetone. In this case the reaction remains simple because the condensation of acetone with benzaldehyde is much more favorable than the condensation of acetone with acetone. The reaction is carried out with low and limiting concentrations of benzaldehyde. The apparent rate constants determined in these experiments are found in Table 2.

Can. J. Chem. Downloaded from www.nrcresearchpress.com by 210.87.254.42 on 09/06/12
For personal use only.

TABLE 1. Kinetic results for the retroaldol reactions of benzalacetone and *p*-methoxybenzalacetone[a]

[NaOH]	α	$10^2 \times \lambda_2$	β	$10^4 \times \lambda_3$	$10^3 \times k_{21}$	$10^2 \times k_{23}$	$10^4 \times k_{12}$	K_{12}^{app}
a. Starting with benzalacetone								
0.1[b,c]			1.415±0.003	0.1993±0.0001			0.368±0.039	
1.0[c]			1.420±0.002	2.104±0.0005			3.89±0.42	
1.0[d]			0.145±0.00004	2.089±0.0013			3.86±0.41	
b. Starting with 4-hydroxy-4-phenyl-2-butanone								
0.1[b,e]	−1.119±0.0001	0.2741±0.0076			0.552±0.032	0.219±0.007		
0.1[e]	−1.094±0.0001	0.2529±0.0069			0.488±0.029	0.204±0.006		
0.1[f]	−0.109±0.0001	0.262±0.0007			0.502±0.026	0.212±0.003		
0.3[g]	−1.675±0.0007	0.764±0.0006			2.77±0.11	0.487±0.011		
0.3[g]	−1.724±0.004	0.755±0.0029	1.468±0.0005	0.560±0.0003	3.56±0.12	0.394±0.012	1.07±0.023	0.030±0.0001
0.3[h]	−1.392±0.0005	0.713±0.0006	1.203±0.0003	0.551±0.0002	3.29±0.11	0.379±0.011	1.04±0.030	0.032±0.0001
0.6[g]	−1.700±0.015	1.427±0.013	1.467±0.001	1.174±0.0011	6.72±0.24	0.745±0.024	2.25±0.070	0.034±0.0003
0.6[i]	−1.576±0.011	1.435±0.015	1.458±0.002	1.173±0.002	7.14±0.25	0.708±0.026	2.23±0.082	0.033±0.0004
1.0[i]	−1.719±0.012	2.308±0.024	1.340±0.003	2.130±0.004	10.6±0.37	1.23±0.038	3.98±0.116	0.038±0.0005
1.0[j]	−0.436±0.0007	2.024±0.004	0.379±0.0001	2.122±0.0008	6.46±0.21	1.37±0.022	3.14±0.050	0.049±0.0009
1.0[h]	−1.433±0.009	2.084±0.015	1.206±0.001	2.066±0.003	9.62±0.33	1.10±0.034	3.90±0.116	0.041±0.0003
c. Starting with 4-hydroxy-4-(*p*-methoxyphenyl)-2-butanone								
0.01[k,l]	−1.486±0.0003	0.0501±0.0016			0.224±0.009	0.0277±0.0011		
0.01[k,m]	−0.148±0.0001	0.0506±0.0001			0.226±0.006	0.0280±0.0006		
0.01[l]	−1.472±0.002	0.0449±0.00008			0.199±0.005	0.0250±0.0005		
0.3[l]	−1.521±0.002	1.282±0.002	1.392±0.0003	0.340±0.0001	5.53±0.15	0.727±0.015	0.600±0.013	0.011±0.0001
0.6[l]	−1.871±0.024	2.929±0.035	1.415±0.002	0.716±0.0009	12.8±0.38	1.64±0.040	1.28±0.028	0.010±0.001
1.0[l]	−0.153±0.002	4.23±0.028	0.138±0.0001	1.320±0.001	18.1±1.8	2.41±0.19	2.32±0.18	0.013±0.003
1.0[l]			1.364±0.0007	1.307±0.0006				

[a]All in aqueous solution, 1% acetonitrile, v/v, ionic strength 1.0 (KCl) unless otherwise noted.
[b]Ionic strength 0.1.
[c]Initial benzalacetone concentration was 6.64×10^{-6} *M*.
[d]Initial benzalacetone concentration was 6.64×10^{-7} *M*.
[e]Initial ketol concentration was 1.58×10^{-5} *M*.
[f]Initial ketol concentration was 1.58×10^{-6} *M*.
[g]Initial ketol concentration was 1.66×10^{-5} *M*.
[h]Initial ketol concentration was 1.39×10^{-5} *M*.
[i]Initial ketol concentration was 1.56×10^{-5} *M*.
[j]Initial ketol concentration was 6.31×10^{-6} *M*.
[k]Ionic strength 0.01.
[l]Initial ketol concentration was 1.40×10^{-5} *M*.
[m]Initial ketol concentration was 1.40×10^{-6} *M*.

Can. J. Chem. Downloaded from www.nrcresearchpress.com by 210.87.254.42 on 09/06/12
For personal use only.

TABLE 2. Kinetics of substituted benzalacetone formation[a]

[Acetone]	α	$10^2 \times \lambda_2$	β	$10^4 \times \lambda_3$
a. Benzaldehyde[b]				
0.005[c]	0.0430±0.0006	0.188±0.008	−1.894±0.0006	0.447±0.0004
0.01[c]	0.0852±0.0007	0.233±0.005	−2.258±0.0005	0.778±0.0006
0.02[d]	0.0687±0.0006	0.222±0.004	−1.260±0.0004	1.182±0.0009
0.04[d]	0.1438±0.0011	0.261±0.004	−1.470±0.001	2.176±0.0004
b. *p*-Methoxybenzaldehyde[e]				
0.0107[f]	0.0062±0.0003	0.618±0.051	−2.938±0.001	0.819±0.0009
0.0213[f]	0.0427±0.0015	1.15±0.04	−3.936±0.001	1.248±0.001
0.0428[f]	0.0906±0.0012	1.35±0.03	−4.732±0.002	2.166±0.002
0.107[f]	0.183±0.002	1.31±0.03	−5.198±0.002	4.746±0.005
1.03[g]	0.0266±0.0003	2.55±0.06	−0.233±0.0002	26.7±0.047
c. *p*-Nitrobenzaldehyde[h]				
0.00225[i]	0.072±0.0003	0.316±0.003	−0.916±0.0003	2.548±0.002
0.00449[i]	0.135±0.0006	0.344±0.003	−1.102±0.0006	4.016±0.003
0.00931[i]	0.165±0.0005	0.463±0.003	−1.233±0.0006	6.126±0.004
0.00931[i]	0.194±0.002	0.393±0.005	−1.239±0.002	6.126±0.010

[a]In aqueous solution, 25°C, 1% acetonitrile, v/v, ionic strength 1.0 unless otherwise specified.
[b]0.1 *N* NaOH.
[c]Initial benzaldehyde concentration, 1.47×10^{-5} *M*.
[d]Initial benzaldehyde concentration, 7.26×10^{-6} *M*.
[e]0.305 *N* NaOH.
[f]Initial *p*-methoxybenzaldehyde concentration, 8.1×10^{-6} *M*.
[g]Initial *p*-methoxybenzaldehyde concentration, 8.2×10^{-6} *M*.
[h]0.1 *N* NaOH, ionic strength 0.1 *M*.
[i]Initial *p*-nitrobenzaldehyde cncentration, 6.75×10^{-6} *M*.

TABLE 3. Microscopic rate and equilibrium constants for formation and hydrolysis of substituted benzalacetones[a]

Substituent	$10^4 k'_{12}$	$10^3 k'_{21}$	$10^3 k'_{23}$	k''_{32}	K_{12}	K_{32}	$K_{overall}$
H	3.16±0.55	7.50±2.14	13.8±2.4	0.165±0.044	0.042±0.014	12. ±3.8	286.±131.
							365.±53., 499.±147.
	3.45±0.11	8.15±0.88	14.3±1.1		0.033±0.004		
p-MeO	1.61±0.26	12.8±4.7	30.0±4.8	0.047±0.017	0.012±0.005	1.57±0.62	131.±75.
							93.±10., 93.±20.
	2.07±0.06	19.6±0.7	25.2±0.7		0.011±0.0007		
p-NO_2	17.6±4.1	12.9±1.7	16.1±1.8	1.61±0.15	0.136±0.036	101. ±15.	742.±225.
							1160.±10., 1800.±1000.
				3.75±0.35		235. ±35.	1729.±524.

[a]In aqueous solution at 25°C; μ = 1.0 for H and *p*-MeO, 0.1 for *p*-NO_2.

For these kinetics there was a slight lag before the absorbance began to increase, which allowed least-squares fitting to a double exponential expression. It is possible to carry out the analysis to obtain microscopic rate constants using only the directly measured rate constants by taking advantage of the concentration dependence of the pseudo first-order rate constant k_{32}, which is a function of acetone concentration. One plots $\lambda_2 + \lambda_3$ and $\lambda_2\lambda_3$ vs. the acetone concentration and obtains from the plot of $\lambda_2 + \lambda_3$: slope = k'_{32} and intercept = $k_{23} + k_{12} + k_{21}$, and from the plot of $\lambda_2\lambda_3$: slope = $k'_{32}(k_{21} + k_{12})$ and intercept = $k_{23}k_{12}$, where k_{32} is the pseudo first-order rate constant and k'_{32} is the corresponding second-order rate constant, k_{32}/[acetone]. From these four equations, the four rate constants can be determined. This is the preferred method whenever the formation kinetics show both phases of the reaction so that the two apparent rate constants can be determined with satisfactory precision. The rate constants so obtained are found in Table 3.

The total change in absorbance, (α + β), as a function of acetone concentration depends upon the change in extinction coefficient from benzaldehyde to benzalacetone, and the equilibrium constant. These parameters can be extracted by fitting to the equation:

$$\epsilon_{app} = \Delta\epsilon/(1 + 1/K[\text{acetone}])$$

When this is done we obtain $\Delta\epsilon = 1.90 \times 10^4$ (expected 1.88×10^4), and $K = 460. \pm 63$. Examination of a plot of the data shows that our experiments were done at acetone concentrations leading to extensive conversion, so that Δε is expected to be precise, but K is not.

For *p*-methoxybenzalacetone, we studied the kinetics of the retroaldol reaction of 4-hydroxy-4-(*p*-methoxyphenyl)-2-butanone, and also of the formation reaction starting with *p*-methoxybenzaldehyde and acetone. In the cleavage reaction the two kinetic phases were well marked, but in the formation kinetics it was necessary to go to relatively high acetone concentrations to make the fast phase significant and to have k_{32} make a significant contribution to λ_2. The kinetics of the cleavage reaction were analyzed as described above, leading to the microscopic rate constants in Tables 1 and 3. The kinetics of

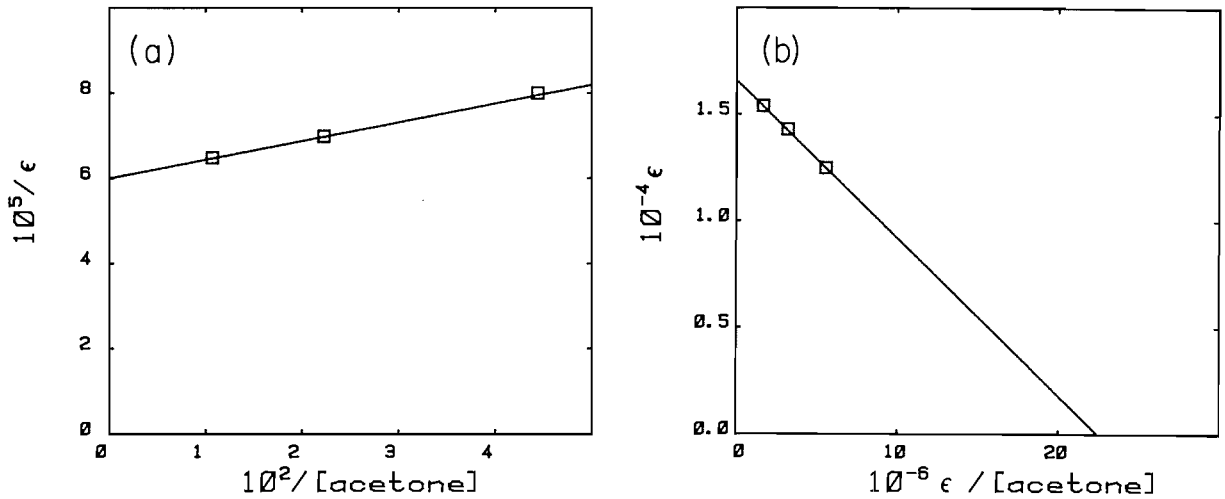

FIG. 3. Plots allowing evaluation of $\Delta\epsilon$ and K for formation of 4-(*p*-nitrophenyl)-3-buten-2-one. (a) Plot of $1/\epsilon_{app}$ vs. 1/(acetone). (b) ϵ_{app} vs. ϵ_{app}/[acetone].

the formation reactions, Table 2, were analyzed as for benzalacetone, leading to the rate constants in Table 3. Although the runs at lower acetone concentrations led to stable infinity points, the experiment at 1.07 M acetone showed a slow upward drift in the infinity value. We attribute this to self condensation of the acetone. The least-squares fit used a double exponential equation with an extra term linear in time to allow for this drift. The dependence of the total absorbance change upon acetone concentration leads to $\Delta\epsilon = (2.38 \pm 0.06) \times 10^4$ (expected 2.30×10^4) and $K = 93 \pm 10\ M^{-1}$.

For the cleavage reactions of 4-phenyl-3-buten-2-one, 4-hydroxy-4-phenyl-2-butanone, and 4-hydroxy-4-(*p*-methoxyphenyl)-2-butanone, we studied some reactions at lower ionic strength (0.01 or 0.1 M) as well as at 1.0 M. Although the observed rate constants did vary, by about 10%, clearly the reaction is not very sensitive to ionic strength.

For *p*-nitrobenzaldehyde we studied only the formation kinetics; the two phases were well marked, so the analysis was straightforward. The apparent rate constants are found in Table 2 and the derived microcopic rate constants are found in Table 3. From the dependence of the apparent extinction coefficient upon acetone concentration we obtained $\Delta\epsilon = (1.67 \pm 0.001) \times 10^4$ and $K = 1160. \pm 10.$

The value of the equilibrium constant derived from the dependence of the final absorbance upon the acetone concentration is quite different from that deduced from the kinetics, and the errors calculated by least squares are impressively small. However, it should be borne in mind that there were only three points so that a statistical method can give a spuriously low standard deviation if the points happen to fall on a line. More important is the question of why the two values differ so much. Since the analysis involved (frequently carried out using double reciprocal plots) is of some generality, arising in equilibrium studies, enzyme kinetics, and photochemistry, it is perhaps worthwhile to point out some things which have been learned in enzymology (6). The normal double reciprocal plot, see Fig. 3(a), where $1/\epsilon_{app}$ is plotted against 1/[acetone], because the ordinate and abscissa are defined from zero to infinity, can easily look better than it deserves. Seeing the three points falling on a line one could think that slope and intercept are both well defined, although careful examination would show that if the true errors in the *y*-values were 10% the slope would be almost indistinguishable from zero. It is harder to fool oneself using a plot such as Fig. 3(b), where ϵ_{app} is plotted against ϵ_{app}/[acetone], because now the coordinates are only defined between the *x*- and *y*-intercepts of the line, all larger or smaller abscissa values having no physical significance. (Such a plot is analogous to the Eadie plot (7, 8) used in enzymology.) Since the entire allowed range of the plot is shown, it is easier to see how well the data cover this range. The *y*-intercept is $\Delta\epsilon$ and the slope is $-1/K$; the *x*-intercept is $K\Delta\epsilon$. It is more apparent from Fig. 3(b) than from Fig. 3(a) that the data define $\Delta\epsilon$ well but do not define K. In fact the experiments were designed to evaluate K from the kinetics and not from the equilibrium absorbance.

TABLE 4. Comparison of rate constants for benzalacetone with literature results[a]

Rate constant	Value: Ref. 2	Value: This work[b]
a. Benzalacetone cleavage		
$10^4 \times \lambda_3/[OH^-]$	2.26±0.03	2.00±0.12
$10^2 \times \lambda_2/[OH^-]$	2.87±0.21	2.64±0.10
$10^4 \times k_{12}/[OH^-]$	2.26±0.03	3.37±0.12
$10^2 \times k_{21}/[OH^-]$	1.14±0.08	0.90±0.09
$10^2 \times k_{23}/[OH^-]$	1.72±0.12	1.31±0.35
b. Benzalacetone formation		
$10^2 \times k_{32}/[OH^-][acetone]$	5.93±0.15	16.5±4.4
c. *p*-Methoxybenzalacetone cleavage		
$10^2 \times \lambda_2/[OH^-]$	5.44±0.38	4.46±0.36 5.40[c]
$10^2 \times k_{23}/[OH^-]$	2.98±0.19	2.53±0.01
$10^2 \times k_{21}/[OH^-]$	2.44±0.17	1.95±0.10

[a] In aqueous solution at 25°C.
[b] All at ionic strength 1.0 M unless noted.
[c] Ionic strength 0.01.

Table 4 shows the second-order rate constants for the individual steps evaluated in this work and the corresponding values reported by Noyce and Reed. Although we reproduce their experimental results within about 5−10%, we do not obtain the same values for the individual rate constants, nor for the derived equilibrium constants for the individual steps. The

Can. J. Chem. Downloaded from www.nrcresearchpress.com by 210.87.254.42 on 09/06/12
For personal use only.

TABLE 5. Hammett slopes for rate and equilibrium constants

Rate constant	ρ	Equilibrium constant	ρ
k'_{12}	0.98±0.02	K_{12}	0.86±0.23
k'_{21}	0.14±0.17	K_{32}	1.88±0.22
k'_{23}	−0.15±0.22	$K_{overall}$	1.03±0.04
k''_{32}	1.76±0.03		

principal source of the discrepancy is the assumption in ref. 2 that the rate of the retroaldol reaction is given by k_{12} (k_4 in the notation of ref. 2) rather than by the steady state expression given above.

The aromatic aldehydes are partially converted to their hydroxide adducts in NaOH solutions. The equilibrium constants are: H, 0.18 M^{-1}; p-NO_2, 13.3 M^{-1} (9). For benzaldehyde (and even more so for p-methoxybenzaldehyde, for which the equilibrium constants will be even smaller) the correction is trivial except at high [OH^-], and would only be 20% at 1 N NaOH. For p-nitrobenzaldehyde the correction is more serious, amounting to a factor of 2.33 at 0.1 N NaOH. This correction was made to the values in Table 4, and the corrected data were used for Hammett correlations.

The dependence of the rate and equilibrium constants upon Hammett σ can be examined: see Table 5.

The rate-determining step for the condensation reaction, k_{32}, is the carbon−carbon bond-forming step, and not proton abstraction from acetone, because the observed reaction rate is slower than the known rate of enolate formation. The post equilibrium for this addition is a proton transfer from solvent to the alkoxide ion corresponding to the ketol, and should be very fast.

In marked contrast, there is a possible ambiguity as to the rate-determining step for the k_{12} process, because the immediate product is an enolate ion which must either protonate on carbon or expel hydroxide ion. If the carbon protonation rate constant is the same as for acetone, then it is probably fast relative to expulsion of hydroxide ion, but if there is steric hindrance leading to a slower rate of reprotonation, then the two paths could occur at competitive rates. This can be seen by estimating the equilibrium constant for the actual addition step:

$$Ph—CH=CH—CO—CH_3 + OH^- \rightleftharpoons Ph—CHOH—CH=C(O^-)—CH_3$$

so that the rate constant for expulsion of hydroxide can be calculated from the known rate of the overall addition reaction. We assume that the basicity of the ketone is similar to that of acetone ($pK_a \cong 19$ (10)); from the value of K_{12} we deduce that for the actual addition step, $K = 4 \times 10^{-7}$, and the rate constant for the expulsion of hydroxide is 750 s^{-1}. If the rate of protonation is even ten-fold slower than that for acetone, it would be ca. 10^3 s^{-1}, and both steps would be partly rate determining.

Experimental

Materials

Benzaldehyde and p-methoxybenzaldehyde were redistilled before use. p-Methoxybenzaldehyde was stored as the crystalline solid (lit. (11) mp 2.5°C) in a refrigerator. p-Nitrobenzaldehyde was recrystallized from diethyl ether; mp 105−106°C (lit. (11) mp 106°C). Benzalacetone was prepared following Drake and Allen (12); mp 39.2−40.5°C (lit. (12) mp 40−42°C). 4-Hydroxy-4-phenyl-2-butanone was prepared following Noyce and Reed (13); mp 37.0−37.2°C (lit. (13) mp 34−36°C; (14) mp 38°C. 4-Hydroxy-4-(p-methoxyphenyl)-2-butanone was made following the procedure of Noyce and Reed (13) except that purification of the initial crude distillate was by two-fold bulb-to-bulb distillation in vacuum followed by crystallization from ether − petroleum ether; mp 42.5−43°C (lit. (13) mp 40°C). 4-(p-Methoxyphenyl)-3-buten-2-one was prepared by the procedure of Drake and Allen (12); mp 72.5−73.6°C (lit. (12) mp 72−74°C). Acetone and acetonitrile were spectrophotometric grade.

Extinction coefficients were determined for the wavelengths used for kinetics. Benzalacetone: 2.2×10^4 at 291 nm. 4-Hydroxy-4-phenyl-2-butanone: 36 at 291 nm. Benzaldehyde: 3320 at 291 nm. 4-(p-Methoxyphenyl)-3-buten-2-one: 2.37×10^4 at 320 nm. 4-Hydroxy-4-(p-methoxyphenyl)-2-butanone: 38 at 320 nm. p-Methoxybenzaldehyde: 735 at 320 nm. Acetone: 0.12 at 320 nm. p-Nitrobenzaldehyde: 3200 at 308 nm. Acetone: 0.72 at 308 nm.

Methods

The procedure for kinetics was as previously described (15, 4). Reactions were followed at λ_{max} for the substituted benzalacetone. Most kinetics were carried out in 10-cm cells, so that low concentrations, assuring complete solubility, could be employed.

Calculations

Least-squares calculations were carried out using a Xitan microcomputer and FORTRAN or BASIC programs written for the purpose. Plots similar to Figs. 1 and 2 were prepared for each run. The residual plots were frequently not the random scatter about the zero line which should be seen for a good fit. The absolute values of the weighted residuals were in all cases small, being less than 0.001 absorbance. In the case of Fig. 2 it was clear that the fit was imperfect, but the worst deviation corresponds to an unweighted error of 0.004 at an overall absorbance of 1.2 for a relative error of 0.5%. Thus the fit can be considered satisfactory, as is shown by the plot of absorbance vs. time.

Acknowledgments

We thank the Natural Sciences and Engineering Research Council of Canada for financial support of this work.

1. J. P. GUTHRIE. Can. J. Chem. **56**, 962 (1978).
2. D. S. NOYCE and W. L. REED. J. Am. Chem. Soc. **81**, 624 (1959).
3. J. W. MOORE and R. G. PEARSON. Kinetics and mechanism, 3rd ed. Wiley, New York. 1981. p. 296.
4. J. P. GUTHRIE and A. B. DAWSON. Can. J. Chem. **61**, 171 (1983).
5. P. R. BEVINGTON. Data reduction and error analysis for the physical sciences. McGraw−Hill, New York. 1969.
6. A. R. FERSHT. Enzyme structure and mechanism. Freeman, San Francisco. 1977. p. 91.
7. G. S. EADIE. J. Biol. Chem. **146**, 85 (1942).
8. B. H. J. HOFSTEE. Nature, **184**, 1296 (1959).
9. P. GREENZAID. J. Org. Chem. **38**, 3164 (1973).
10. J. P. GUTHRIE, J. COSSAR, and A. KLYM. J. Am. Chem. Soc. **104**, 895 (1982).
11. R. C. WEAST (*Editor*). Handbook of chemistry and physics. 48th ed. Chemical Rubber Co., Cleveland, OH. 1967.
12. N. L. DRAKE and P. ALLEN. Org. Synth. Coll. Vol. 1, Wiley, New York. 1941. p. 77.
13. D. S. NOYCE and W. L. REED. J. Am. Chem. Soc. **80**, 5539 (1958).
14. C. SCHOPF and K. THIERFELDER. Ann., **518**, 127 (1935).
15. J. P. GUTHRIE. Can. J. Chem. **59**, 45 (1981).

Can. J. Chem. Downloaded from www.nrcresearchpress.com by 210.87.254.42 on 09/06/12
For personal use only.

Conformational and steric effects on regioselectivity in the Baeyer–Villiger reaction

VINOD DAVE, J. B. STOTHERS, and E. W. WARNHOFF
Department of Chemistry, University of Western Ontario, London, Ont., Canada N6A 5B7

Received February 27, 1984

This paper is dedicated to Professor Paul de Mayo on the occasion of his 60th birthday

VINOD DAVE, J. B. STOTHERS, and E. W. WARNHOFF. Can. J. Chem. **62**, 1965 (1984).

The Baeyer–Villiger oxidation of six β,β,γ-trisubstituted cyclopentanones and cyclohexanones leads to preferential migration of the α-carbon relative to the α′-carbon by a factor of 1.5–4:1. The origin of the preference is suggested to be steric and is ascribed to the greater relief of non-bonded interactions as the α—β bond lengthens in going to the transition state. Thus, in the carbonyl addition intermediate the 1,3-diaxial-like interaction between the hydroxyl and the closest γ-carbon is diminished to a greater extent when the α-carbon migrates relative to the α′-carbon.

VINOD DAVE, J. B. STOTHERS et E. W. WARNHOFF. Can. J. Chem. **62**, 1965 (1984).

L'oxydation selon Baeyer–Villiger de six cyclopentanones et cyclohexanones β,β,γ-substituées conduit d'une façon préférentielle (rapport de 1,5–4:1) à la migration du carbone α par rapport au carbone α′. On croit que cette préférence est d'origine stérique et on l'attribue à une plus grande réduction d'interactions non-liées lorsque la liaison α—β s'allonge au moment de passer à l'état de transition. Lors de l'addition intermédiaire sur le carbonyle, il se développe une interaction de type 1,3-diaxial entre l'hydroxyle et le carbone en γ le plus rapproché; cette interaction diminuerait plus lors de la migration du carbone α que lorsque le carbone α′ migre.

[Traduit par le journal]

Can. J. Chem. Downloaded from www.nrcresearchpress.com by 210.87.254.40 on 09/06/12
For personal use only.

Recently there has been renewed interest in the migratory selectivity exhibited in Baeyer–Villiger reactions of cyclic ketones (1–16). This revival is due partly to new attempts to separate and understand further the factors that influence the regioselectivity of the reaction, and partly to the discovery of "naturally occurring Baeyer–Villiger products", the plant growth regulating brassino steroids (17–30).

The earlier general conclusion that the α-carbon better able to stabilize positive charge migrates preferentially has long been known to be an oversimplification (31). While recent work (1, 4, 9, 17) has provided complementary evidence for the operation of an electronic effect, in that nearby electron-withdrawing groups retard the migration of an α-carbon, nevertheless in a number of cases the electronic effect has been overridden by other factors. In fact, merely changing the peroxyacid/solvent combination can affect the lactone product ratio drastically (5, 6, 15, 31). Steric or conformational effects on the relative energies of the transition states for the two possible migrations to oxygen can also dictate the lactone ratio, as is apparently the case under some conditions for 7-*syn* substituted norbornanones in which the enforced *endo* addition of peroxyacid (→**1**, e.g. camphor) allows a chair-like transition state for CH_2 migration to be of lower energy than the boat-like transition state for migration of the electronically favored tertiary or quaternary bridgehead (6, 16). However, even here other factors may intervene since the effect is reversed if the 7-*syn*-substituent is COOMe as in **2** (2).

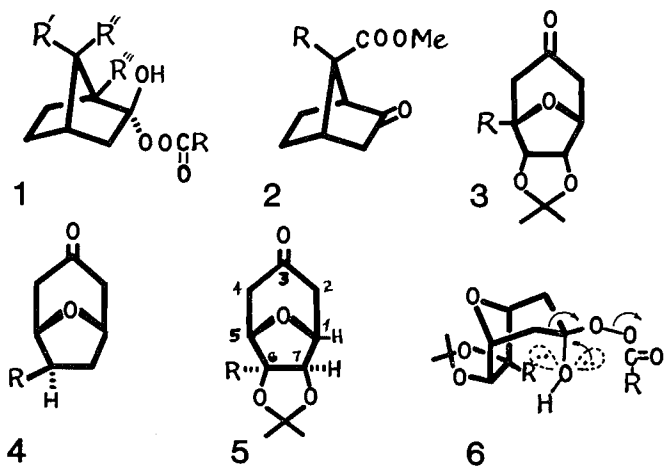

Noyori *et al.* (1, 9, 10) have used three series of highly oxygenated C-nucleoside structures **3**, **4**, and **5** to probe electronic and steric effects systematically, **3** and **4** presumably responding only to electronic effects and **5** only to γ-steric effects. In seven differently substituted examples of **5**, the carbonyl α-CH_2 more remote from R was found to migrate preferentially by a factor of 2–3:1. A complex rationalization for the observation was offered (see **6**) involving *exo* addition of peroxyacid, antiperiplanar orientation of the migrating α-carbon and the peroxide bond, the necessity of a stereoelectronic push by an *anti*-aligned non-bonding electron pair on the OH, and repulsion between the hydroxyl hydrogen and the R group (1, 32). We now present several Baeyer–Villiger reactions for which the last part of this rationale is irrelevant, and in which the product ratio is apparently determined by differential relief of conformational crowding in going to the two possible migratory transition states.

Our interest in Baeyer–Villiger regioselectivity began some time ago with examination of how remote a substituent could be and still affect the migration ratio in rearrangements of 3-keto 5α- and 5β-steroid derivatives (11, 14). With the most convenient and reliable analytical method – integration of appropriate ^{13}Cmr signals – it was found that only when polar substituents got as close as C-6 or C-5, i.e. γ or β with respect to the carbonyl group, was the migratory ratio much different from ~1:1. Not surprisingly, with such a high degree of symmetry in the vicinity of the chair cyclohexanone carbonyl group, the migratory potential of both α-CH_2 groups is essentially the same in the absence of nearby perturbing groups.

In the light of this work, the reported reactions of several *A*-nor-5α- and 5β-steroid 2-ketones seemed anomalous (33–35). For example, both 5α- and 5β-*A*-norcholestan-2-one were reported to give only the 2-oxa-3-one lactones **13** and **14** with peroxybenzoic or trifluoroperoxyacetic acids (33, 34). Whilst these ketones are not so symmetrical near the carbonyl group as the cholestan-3-ones, there is no obvious structural

Can. J. Chem. Downloaded from www.nrcresearchpress.com by 210.87.254.40 on 09/06/12
For personal use only.

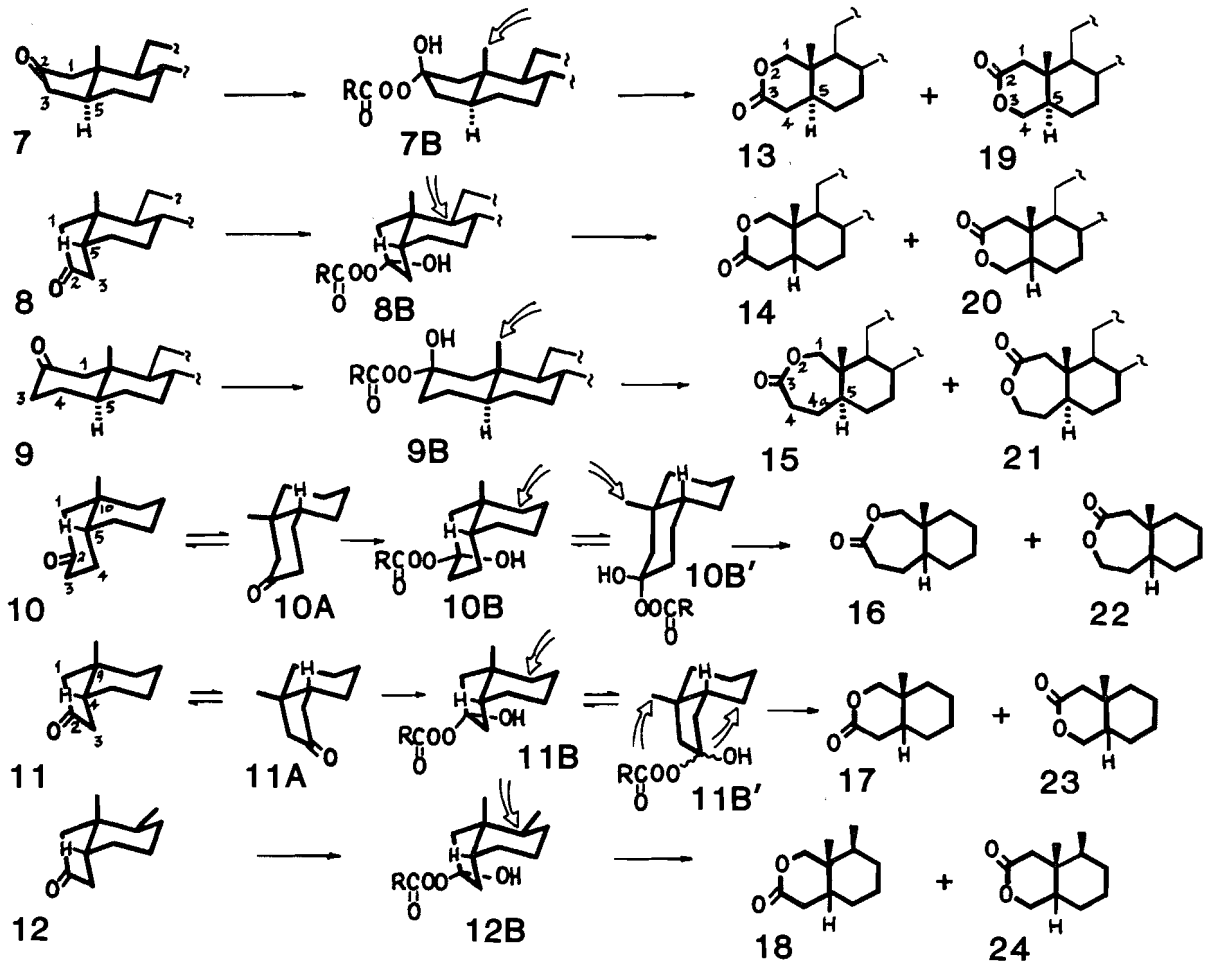

Ketones **7**, **8**, and **9** are cholestane derivatives

TABLE 1. ^{13}C shieldings of **7**–**9** and the corresponding lactones[a]

Compound	C-1	C-2	C-3	C-4	C-5	C-6	C-7	C-8	C-9	C-10	C-11	C-12	C-13	C-14	C-19
7	54.0	218.9	41.2	—	47.7	24.7	31.7	35.6	54.2	42.1	23.6	39.7	42.9	56.2	13.7
13	81.1	—	170.6	33.8	40.4	27.2	31.0	34.7	49.6	34.6	21.3	39.4	42.4	56.0	10.1
19	44.6	171.0	—	71.0	41.4	28.0	30.7	34.9	52.8	42.4	20.5	39.5	42.4	56.0	12.6
Desoxo-**8**[b]	38.5	23.8	27.5	—	(47.3)	22.3	26.2	36.0	(43.6)	42.8	23.8	40.4	42.7	56.6	21.3
8	53.3	219.5	40.0	—	(44.6)	22.8	25.4	35.8	(43.7)	40.8	22.2	40.0	42.8	56.3	20.8
14	75.3	—	172.5	31.2	38.2	(25.2)	(25.4)	34.9	39.5	34.4	21.1	39.5	42.6	56.0	17.3
20	42.5	172.5	—	70.0	45.1	22.4	26.2	35.4	39.5	34.4	21.5	40.1	42.7	56.1	22.7
9	54.1	211.7	41.4	28.3	45.4	29.3	31.8	35.0	54.1	40.6	21.0	39.9	42.6	56.4	12.6
15	76.0	—	175.8	33.9 26.5 (4a)	48.3	29.2	31.6	35.3	50.7	40.0	21.7	39.9	42.3	56.6	9.8
21	44.7	174.9	—	68.6 33.3 (4a)	51.4	29.3	31.7	35.6	52.1	37.3	21.8	40.0	42.4	56.7	12.2

[a] In ppm from internal TMS for $CDCl_3$ solutions, similar values in parentheses may be interchanged. In these compounds C-15 to C-18 and C-20 to C-27 absorb at 24.2, 28.2, 56.3, 12.1, 35.7, 18.7, 36.1, 23.8, 39.5, 28.0, 22.6, 22.8 ppm, respectively.
[b] *A*-Nor-5β-cholestane.

feature which would tip the balance completely in favor of migration of C-1. Therefore these reactions were reinvestigated. Pure specimens of the two *A*-nor-2-ketones **7** and **8** were prepared (see Experimental) and their Baeyer–Villiger oxidations carried out with *m*-chloroperoxybenzoic acid (MCPBA) in chloroform. The product from the 5α-ketone **7** gave a single tlc spot, whereas that from the 5β-ketone **8** gave two overlapping tlc spots. Contrary to previous reports (33–35) it was evident from both the ^{1}Hmr and ^{13}Cmr spectra that both products were mixtures, but in each mixture the ratio of lactones was distinctly different from 1 : 1. Structural assignment to the pairs of lactones was obvious from the ^{1}Hmr signals of the O—CH_2 group. The C-1 methylene of the major products **13** and **14** was a sharp AB pattern while the C-4 methylene of the minor products **19** and **20** was broadened by coupling with the C-5 hydrogen (see Fig. 1).

The ^{13}Cmr spectra confirmed these assignments and permitted analysis by integration of appropriate signals (see Experimental). The major lactones **13** and **14** had the lower field O—CH_2 signals at δ 81.1 and 75.3, respectively, while the

Can. J. Chem. Downloaded from www.nrcresearchpress.com by 210.87.254.40 on 09/06/12
For personal use only.

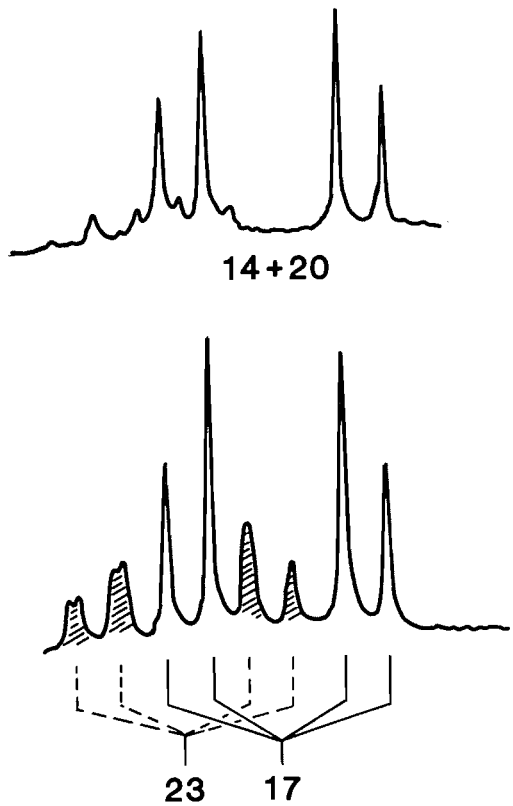

FIG. 1. The O—CH_2 region of the ^{1}Hmr spectra of the Baeyer–Villiger oxidation products of 5β-*A*-norcholestan-2-one (**8**) (upper trace) and *cis*-9-methyl-2-hydrindanone (**11**) (lower trace).

minor lactones had the O—CH_2 absorption at higher field δ 71.0 and 70.0, respectively.[1] Integration gave a lactone ratio **13**:**19** of 80:20 from the 5α-*A*-nor-2-ketone **7** and a ratio **14**:**20** of 79:21 from the 5β-*A*-nor-2-ketone **8**. With trifluoroperoxyacetic acid the 5α-ketone **7** gave a **13**:**19** ratio of 70:30, only slightly different from the *m*-chloroperoxybenzoic acid result. Thus C-1 had migrated preferentially by a substantial amount in each case.

Such regioselectivity seemed likely to originate in a conformational or steric effect, and additional ketones were rearranged in hope of defining the cause. It was not necessary to have a cyclopentanone to observe the effect. Oxidation of 5α-cholestan-2-one (**9**) with MCPBA/$CHCl_3$ gave a 75:25 mixture of two lactones which could be separated by thick layer chromatography. The less polar major component had a sharply defined four-line O—CH_2 ^{1}Hmr pattern at δ 3.87 and δ 4.23 (J = 13 Hz) while the minor component had an ill-defined multiplet centered at δ 4.20. In the ^{13}C spectrum the major lactone had the lower field O—CH_2 signal at δ 76.0 compared to the minor lactone O—CH_2 peak at δ 68.8. Therefore, the major lactone was again the product **15** of C-1 migration.

Finally, two bicyclic analogs of the preceding ketones were oxidized to test further the generality of the regioselectivity. *cis*-10-Methyl-2-decalone **10** ⇄ **10A** on treatment with MCPBA/$CHCl_3$ afforded two lactones separated on tlc. The major lactone **16** again had the sharper O—CH_2 ^{1}Hmr pattern superimposed on the more lumpy pattern of the minor isomer **22**. In the ^{13}Cmr spectrum only the O—CH_2 from the major lactone **16** was visible as a broadened (by conformational averaging?) peak at δ 74.1 (cf. 76.0 in **15**). Integration of the well-separated CH_3 signals in the ^{1}Hmr spectrum gave a **16**:**22** ratio of 81:19.

cis-9-Methyl-2-hydrindanone **11** ⇄ **11A** on reaction with MCPBA/$CHCl_3$ also produced two lactones separable by tlc. The major lactone **17** had the sharper O—CH_2 ^{1}Hmr pattern (see Fig. 1) separated from the broader pattern of the minor isomer. In the ^{13}Cmr spectrum the O—CH_2 from the major isomer **17** was at δ 75.6 and at 71.9 from the minor isomer **23**. The lactone ratio (60:40) from comparison of the intensity of these ^{13}Cmr signals agreed well with that (62:38) obtained by integration of the O—CH_2 peaks in the ^{1}Hmr spectrum. The regioselectivity had been somewhat reduced, but the major lactone was still the product of C-1 migration.

To the above five examples may be added a sixth from the literature, the dimethylhydrindanone **12**, which on Baeyer–Villiger oxidation with MCPBA/CH_2Cl_2 gave a lactone ratio **18**:**24** of 77:23 (8).

The consistent pattern of all these results suggests a common basis for the observed regioselectivity favoring migration of C-1. The only structural difference to distinguish the α- from the α′-CH_2 of each ketone is the methyl group which is closer to C-1 in each compound. Its *electronic* effect on the migratory ratio would be negligible, as shown by the 53:47 ratio of lactones from example **3**(R=CH_3) of Noyori *et al.* (1, 9). However, the *steric* effect of this methyl group is not symmetrically disposed toward both the α- and the α′-CH_2, and this fact can account for the regioselectivity.

For the two A/B *trans*-fused ketones the preferred conformations will be those shown in **7** and **9**. For two of the four A/B *cis*-fused ketones there is a single preferred conformation **8** and **12**, but for the other two *cis*-fused ketones there are two conformations of comparable energy **10** ⇄ **10A** and **11** ⇄ **11A**.[2] On the usual assumption that the lowest energy transition states for rearrangement will result from the peroxyacid adding to the less hindered carbonyl face, the tetrahedral addition intermediates which undergo rearrangement will be **7B** – **12B** plus **10B′** and **11B′**.[3] These would be expected to rearrange with the *anti* orientation of an α- or α′-CH_2 and the peroxide bond. Inspection of Dreiding models reveals that for either potential migration in each of the ketones it is possible to have a hydroxyl lone pair of electrons aligned *anti* to the migrating CH_2 for a "stereoelectronic push" *without* the hydroxyl H being crowded into the CH_3, CH_2, or CH marked in the **B** series of formulas. Consequently, the final postulate of Noyori *et al.* (1, 32) (repulsion between hydroxyl H and the nearby group prevents oxygen lone pair alignment for one migration) does not apply to the present cases.[4] Nor can it be suggested for the four cyclopentanones **7**, **8**, **11**, and **12** that migration of the CH_2 leading to a chair-like transition state is the preferred path (6, 16), because for all four the preferred C-1 migration leads to a twist boat-like transition state.

[1] This order of signals is expected since C-1 is bonded to a tertiary center while C-4 is adjacent to a secondary carbon.

[2] The B-ring methyl group in **12** would be axial in a conformation corresponding to **11A** and therefore would be about 1.7 kcal/mol higher in energy relative to **12**.

[3] For **11B′** both sides of the molecule have an encumbering group, and the two addition intermediates are probably of about the same energy.

[4] The stereochemistry of **6** forces the OH and substituent R closer together in Noyori's series of rigid molecules than in the present six examples.

Can. J. Chem. Downloaded from www.nrcresearchpress.com by 210.87.254.40 on 09/06/12
For personal use only.

A consistent explanation for all six of these reactions is simply that that CH_2 migrates preferentially which leads to a greater relief of repulsive steric interactions at the transition state. Migration of C-1 in each case will lead (by lengthening the C-1—C-2 bond) to the greater reduction of the 1,3-diaxial-like crowding of the OH with the indicated CH_3, CH_2, or CH in structures **7B**–**12B**, **10B'**, **11B'**.[5] In this view, it would not be surprising that the hydrindanone **11** ⇄ **11A** with the ambiguous intermediate **11B'** would show the least regioselectivity. It remains to be seen whether this pronounced selectivity will be found with even simpler monocyclic ketones.

Finally it should be emphasized that the regioselectivity observed with ketones **7**–**12** is in just the opposite sense from that reported by Noyori *et al.* for ketones **5**. This reversal is apparently caused by the closer approach of OH and R in **6** which, according to Noyori *et al.*, would affect differently (by hydroxyl H—R repulsion) the ability of the hydroxyl O to offer stereoelectronic help to the two potential migrating groups.[6]

Experimental

General

Melting points were determined on a Reichert–Kofler microscope hotstage and are corrected. The ir spectra were recorded on a Beckman Acculab 4 instrument with $CHCl_3$ solutions. The ^{1}Hmr spectra were recorded on Varian T-60 and XL-100 spectrometers with $CDCl_3$ solutions containing Me_4Si. The ^{13}Cmr spectra were taken with $CDCl_3$ solutions on a Varian XL-200 instrument. Exact masses were determined on a MAT 311A mass spectrometer. Optical rotations were determined with $CHCl_3$ solutions on a Rudolph Model 80 polarimeter.

Unless otherwise stated, peroxyacid reactions were worked up by evaporating the $CHCl_3$, dissolving he residue in ether, and then washing the solution successively with 5% aqueous KI, 5% aqueous $Na_2S_2O_3$, saturated aqueous $NaHCO_3$, and saturated aqueous NaCl before drying with anhydrous $MgSO_4$ and evaporation of solvent at aspirator vacuum on a rotating evaporator. Camag DF-5 silica gel was used for thick and thin layer chromatography. Unless otherwise specified, preparative thick plates were 20 × 20 cm and held 20 g of silica gel. The MCPBA was from the Aldrich Co.

Oxidation of A-*nor*-5α-*cholestan*-2-*one* (**7**)

(a) Ketone **7** was prepared by the pyrolysis of 2,3-seco-5α-cholestane-2,3-dioic acid (36) and was shown to be pure by its ^{13}Cmr spectrum. A solution of 50 mg (0.134 mmol) of ketone **7** and 111 mg (0.48 mmol) of MCPBA (75%) in 1.5 mL of $CHCl_3$ was allowed to stand at room temperature for 2 days. Work-up gave 50 mg (96%) of colorless solid which gave a single tlc spot more polar than **7**. The ^{1}Hmr and ^{13}Cmr spectra were taken. The reaction was repeated on a 25-mg scale with the same results.

(b) To a stirred (magnetic bar) solution of 15 mg (0.26 mmol) of 60% H_2O_2 and 55 mg of trifluoroacetic anhydride in 0.5 mL of $CHCl_3$ was added 15 mg of Na_2HPO_4 followed by a solution of 25 mg (0.067 mmol) of ketone **7** in 0.5 mL of $CHCl_3$. The reaction mixture was stirred at room temperature for 24 h. Work-up afforded 23 mg (88%) of colorless solid which gave a single tlc spot more polar than **7**. The ^{1}Hmr and ^{13}Cmr spectra were taken (cf. the oxidation of **7** in ref. 33).

The lactone mixtures from the above three preparations were combined and recrystallized thrice from CH_3OH to give 35 mg of pure major lactone **2-oxa-5α-cholestan-3-one** (**13**) as colorless plates, mp 125–133°C, mp 130–132°C (capillary); $[\alpha]_D^{24}$ +14.7° (*c*, 1.93 in $CHCl_3$) (lit. (34) mp 134–136°C, lit. (33) mp 134–135°C, $[\alpha]_D$ +20° (*c*, 1.1 in $CHCl_3$)); ir: 1720 cm^{-1}; ^{1}Hmr δ: 3.92 and 4.22 (2H, AB, J = 11 Hz, OCH_2); M^+ calcd. for $C_{26}H_{44}O_2$: 388.3341; found: 388.3340. The ^{13}Cmr spectrum contained 24 peaks with the 28.0 and 39.5 ppm absorptions corresponding to two carbons each. The ^{13}Cmr spectrum of the minor lactone **19** was obtained by subtracting the peaks of the major isomer from the ^{13}Cmr spectrum of the lactone mixture. For determination of the lactone ratio the following ^{13}Cmr peaks were integrated (14): C-18, C-19, C-1 (**13**), C-4 (**19**), C-9.

A-*Nor*-5β-*cholestan*-2-*one* (**8**)

To a mixture of 7 mg of PtO_2 (Johnson and Matthey) and 1.0 mL of glacial HOAc saturated with hydrogen was added a solution of 43 mg of *A*-nor-5β-cholest-3-en-2-onc (37, 38) in 1.0 mL of glacial HOAc. The reaction was stirred (magnetic bar) at room temperature for 12 h. The catalyst was removed by filtration, and the filtrate was concentrated to leave 43 mg of viscous oil. Thin layer chromatography (hexanes–EtOAc, 90:10) indicated some overreduction to alcohol. The product was dissolved in 2.0 mL of CH_2Cl_2 and oxidized with 20 mg of $PyH^+ClCrO_3^-$ for 2 h. The CH_2Cl_2 soluble material was chromatographed on a 10-g plate developed with hexanes–EtOAc (90:10). The band at R_f 0.37 yielded 26 mg of colorless granules of **A-nor-5β-cholestan-2-one** (**8**), mp 99–103°C (lit. (37) mp 102–103°C); ir: 1740 cm^{-1}; ^{1}Hmr: no absorption between δ 2.5–8; M^+ calcd. for $C_{26}H_{44}O$: 372.3392; found: 372.3390. The ^{13}Cmr spectrum contained 26 peaks with no trace of any absorption from the 5α-epimer **7**.

The tlc band moving with the solvent front gave 7 mg of crystalline **A-nor-5β-cholestane**, mp 48–50°C; M^+ calcd. for $C_{26}H_{46}$: 358.3599; found: 358.3595.

Oxidation of A-*nor*-5β-*cholestan*-2-*one* (**8**)

A solution of 25 mg (0.067 mmol) of ketone **8** and 55 mg (0.24 mmol) of MCPBA (75% peroxyacid) in 1.0 mL of $CHCl_3$ was allowed to stand at room temperature for 43 h. Work-up gave 25 mg (96%) of oily solid whose tlc (hexanes–EtOAc, 80:20) revealed two overlapping spots more polar than **8** in a ratio of ~85:15; ir: 1725 cm^{-1}; ^{1}Hmr: see Fig. 1. For determination of the lactone ratio the following ^{13}Cmr peaks were integrated (14): C-1, C-4, and C-5 of each lactone.

The lactone mixture was chromatographed on a 10-g plate developed four times in hexanes–EtOAc (80:20). The lower band at R_f 0.59 yielded 9.5 mg of pure **2-oxa-5β-cholestan-3-one** (**14**), mp 123–125°C after recrystallization from MeOH (lit. (34) mp 125–128°C); ir: 1725 cm^{-1}; ^{1}Hmr δ: 3.76 and 4.22 (2H, AB, J = 12 Hz, O—H_2C-1); M^+ calcd. for $C_{26}H_{44}O_2$: 388.3341; found: 388.3336. The ^{13}Cmr spectrum contained 24 peaks with the absorption at δ 39.5 corresponding to three carbons.

Oxidation of 5α-*cholestan*-2-*one* (**9**)

A solution of 25 mg (0.065 mmol) of ketone **9** (39) and 55 mg (0.24 mmol) of MCPBA (75%) in 1.2 mL of $CHCl_3$ was allowed to stand at room temperature for 5 days. Since tlc still indicated some unreacted **9**, 21 mg (0.095 mmol) more of MCPBA was added, and the reaction was allowed to proceed for 2 days more. Work-up gave 24 mg (92%) of colorless solid whose tlc (hexanes–EtOAc, 90:10) showed two spots more polar than **9**. For determination of the lactone ratio the following ^{13}Cmr peaks were integrated: C-1 (**21**), C-5, C-9, C-18, and C-19. C-1 in **15** was too close to $CDCl_3$ absorption to be used for integration.

The above reaction was repeated on 72 mg more of the ketone **9**, and the combined product (98 mg) from the two reactions was chromatographed on a thick plate developed four times in hexanes–EtOAc (80:20).

[5] In ref. 8 it was suggested that preferential migration of C-1 in **12B** was "presumably due to a relief of eclipsing interactions involving the substituents at C-9, C-1, C-2" (C-2, C-3, and C-3a according to the numbering in ref. 8). Actually, each of the two bonds involved is more staggered than eclipsed. Also C-1 migration leads to a twist boat conformation whose "partially-eclipsed" bonds would be of higher energy than the staggered bonds of the chair conformation that would result from migration of C-3.

[6] The basis for structural assignment to the pairs of lactones from compound **5** was the Δδ (0.20–0.44) for H—C-7 in the ^{1}Hmr spectra (1), the isomer absorbing at lower field being assigned the structure with H—C-7 in the *deshielding* region of the nearby ether oxygen in the chair conformation of the lactone ring, while the isomer absorbing at higher field has H—C-7 in the *shielding* zone of the carbonyl π-bond in the chair conformation of the lactone ring.

Can. J. Chem. Downloaded from www.nrcresearchpress.com by 210.87.254.40 on 09/06/12
For personal use only.

The upper band at R_f 0.60 afforded 39 mg of solid major lactone. Three recrystallizations from MeOH gave 33.8 mg of colorless plates of **2-oxa-A-homo-5α-cholestan-3-one** (**15**), mp 133–135°C; $[\alpha]_D^{23}$ −19.3° (*c*, 1.87 in $CHCl_3$); ir: 1725 cm^{-1}; ^{1}Hmr δ: 2.62 (2H, m, O=C—H_2C-4), 3.87 and 4.23 (2H, AB, J = 13 Hz, O—H_2C-1); M^+ calcd. for $C_{27}H_{46}O_2$: 402.3497; found: 402.3480.

The lower band at R_f 0.55 yielded 15.8 mg of colorless solid minor lactone. Three recrystallizations from MeOH gave 10 mg of colorless plates of **3-oxa-A-homo-5α-cholestan-2-one** (**21**), mp 136–141°C; ir: 1720 cm^{-1}; ^{1}Hmr δ: 2.37 and 2.86 (2H, AB, J = 13 Hz, O=C—H_2C-1) and 4.20 (2H, m, O—H_2C-4); M^+ calcd. for $C_{27}H_{46}O_2$: 402.3497; found: 402.3491.

Oxidation of cis-*10-methyl-2-decalone* (***10***)

The starting ketone **10**, ir: 1700 cm^{-1}, was prepared by the CuBr - catalyzed addition of CH_3MgI to $\Delta^{1,9}$-2-octalone (40, 41) and was shown to be pure by its ^{13}Cmr spectrum δ: 28.4 (CH_3), 22.2, 25.1, 27.1, 28.2, 37.8, 38.0, 49.1 (7 × CH_2), 40.4 (CH), 38.6 (quat. C), 213.1 (C=O). A solution of 35 mg (0.21 mmol) of **10** and 96 mg (0.42 mmol) of MCPBA (75%) in 1.5 mL of $CHCl_3$ was allowed to stand at room temperature for 2 days. Work-up afforded 35 mg (91%) of colorless oil; ir: 1725 cm^{-1}; ^{1}Hmr δ: 1.01 (s, CH_3 of major lactone), 1.11 (s, CH_3 of minor lactone), 3.87 and 4.19 (AB, J = 13 Hz, O—H_2C-1 of major lactone); ^{13}Cmr δ: 21.9, 22.1, 24.0, 25.2 (CH_3), 27.4, 27.7, 27.9, 30.7 (b), 31.6, 33.9 (quat. C), 36.5, 42.3 (b), 74.1 (b), 175.8 (C=O). Thin layer chromatography in benzene–ether (85:15) with three developments revealed two spots more polar than **10** in the ratio of ~70:30. M^+ of the mixture calcd. for $C_{11}H_{18}O_2$: 182.1307; found: 182.1306.

Oxidation of cis-*9-methyl-2-hydrindanone* (***11***)

The ketone **11**, ir: 1745 cm^{-1}, was prepared by the method of Lansbury and Nienhouse (42) and was shown to be pure by its ^{13}Cmr spectrum δ: 26.6 (CH_3), 21.8, 22.0, 26.4, 34.1, 42.6, 51.6 (6 × CH_2), 41.3 (CH), 37.8 (quat. C), 219.8 (C=O). A solution of 30 mg (0.20 mmol) of **11** and 138 mg (0.60 mmol) of MCPBA (75%) in 1.5 mL of $CHCl_3$ was allowed to stand at room temperature for 2.5 days. Work-up gave 25 mg (74%) of pale yellow oil whose tlc (benzene–ether, 95:5) showed a single spot more polar than **11**; ir: 1720 cm^{-1}; ^{1}Hmr (see Fig. 1) δ: 3.89 and 4.35 (AB, J = 11.5 Hz, O—H_2C-1 of major lactone), 4.15 and 4.59 (AB part of ABX, J_{AB} = 11.5 Hz, O—H_2C-4 of minor lactone); M^+ calcd. for $C_{10}H_{16}O_2$: 168.1150; found: 168.1150; ^{13}Cmr δ (major lactone): 24.3 (CH_3), 75.6 (O—H_2C-1), 21.3, 23.1, 28.4, 32.4, 33.0 (5 × CH_2), 37.3 (CH), 31.4 (quat. C), 171.3 (C=O); (minor lactone): 28.6 (CH_3), 71.9 (O—H_2C-4), 21.5, 24.8, 25.8, 37.2, 37.8 (5 × CH_2), 39.2 (CH), 32.2 (quat. C), 171.3 (C=O).

^{13}C Nuclear magnetic resonance spectra

The ^{13}Cmr spectra were recorded at 50.3 MHz and comparison of the fully decoupled spectra with those obtained with either the APT (43) or INEPT (44) sequences served to identify the methyl, methylene, methine, and quaternary signals. Unequivocal assignments for **7** were obtained from its 2D INADEQUATE spectrum (45) using the CCC2D pulse sequence of the XL software with a 2048 × 128 data point matrix transforming 2048 and 512 points, respectively, with a 2400-Hz sweep width in both domains. The ^{13}C data are collected in Table 1. It has been demonstrated previously (see ref. 14, pp. 1558 and 1563) that integration of proton-decoupled ^{13}Cmr signals is accurate and reproducible with the large rigid steroid molecules under non-saturating conditions.

Acknowledgements

We would like to thank the Natural Sciences and Engineering Research Council of Canada for financial support, Susan Wilson for the 100 MHz ^{1}Hmr spectra, and Doug Hairsine for the mass spectra.

1. R. NOYORI, T. SATO, and H. KOBAYASHI. Bull. Chem. Soc. Jpn. **56**, 2661 (1983).
2. T. L. HO and S. H. LIU. Synth. Commun. **12**, 501 (1982).
3. B. M. TROST, P. BUHLMAYER, and M. MAO. Tetrahedron Lett. **23**, 1443 (1982).
4. H. DUDDECK and M. KAISER. Z. Naturforsch. Teil B, **37**, 1672 (1982).
5. G. R. KROW, C. A. JOHNSON, J. P. GUARE, D. KUBRAK, K. J. HENZ, D. A. SHAW, S. W. SZCZEPANSKI, and J. T. CAREY. J. Org. Chem. **47**, 5239 (1982).
6. G. R. KROW. Tetrahedron, **37**, 2697 (1981).
7. E. WISTUBA and C. RUCHARDT. Tetrahedron Lett. **22**, 3389 (1981).
8. P. A. JACOBI and D. G. WALKER. J. Am. Chem. Soc. **103**, 4611 (1981).
9. R. NOYORI, T. SATO, and H. KOBAYASHI. Tetrahedron Lett. **21**, 2569 (1980).
10. R. NOYORI, H. KOBAYASHI, and T. SATO. Tetrahedron Lett. **21**, 2573 (1980).
11. V. DAVE, J. B. STOTHERS, and E. W. WARNHOFF. Can. J. Chem. **58**, 2666 (1980).
12. P. F. HUDRLIK, A. M. HUDRLIK, G. NAGENDRAPPA, T. YIMENU, E. T. ZELLERS, and E. CHIN. J. Am. Chem. Soc. **102**, 6894 (1980).
13. R. POZAS, R. CETINA, and L. J. REYES. Rev. Soc. Quim. Mex. **24**, 342 (1980).
14. V. DAVE, J. B. STOTHERS, and E. W. WARNHOFF. Can. J. Chem. **57**, 1557 (1979).
15. Z. GRUDZINSKI, S. M. ROBERTS, C. HOWARD, and R. F. NEWTON. J. Chem. Soc. Perkin Trans. 1, 1182 (1978).
16. P. A. GRIECO, C. S. POGONOWSKI, S. D. BURKE, M. NISHIZAWA, M. MIYASHITA, Y. MASAKI, C. L. J. WANG, and G. MAJETICH. J. Am. Chem. Soc. **99**, 4113 (1977).
17. S. TAKATSUTO and N. IKEKAWA. Tetrahedron Lett. **24**, 917 (1983).
18. S. TAKATSUTO and N. IKEKAWA. Tetrahedron Lett. **24**, 773 (1983).
19. M. SAKAKIBARA and K. MORI. Agric. Biol. Chem. **47**, 1407 (1983).
20. M. SAKAKIBARA and K. MORI. Agric. Biol. Chem. **47**, 663 (1983).
21. M. KONDO and K. MORI. Agric. Biol. Chem. **47**, 97 (1983).
22. K. OKADA and K. MORI. Agric. Biol. Chem. **47**, 89 (1983).
23. A. A. AKHREM, F. A. LAKHVICH, V. A. KHRIPACH, and N. V. KOVGANKO. Dokl. Akad. Nauk USSR, **269**, 366 (1983); Engl. Transl. **269**, 87 (1983).
24. S. C. CHEN. Chem. Can. 13, September (1983).
25. M. ANASTASIA, P. CIUFFREDA, M. DEL PUPPO, and A. FIECCHI. J. Chem. Soc. Perkin Trans. 1, 383 (1983).
26. M. SAKAKIBARA and K. MORI. Agric. Biol. Chem. **46**, 2769 (1982).
27. K. WADA and S. MARUMO. Agric. Biol. Chem. **45**, 2579 (1981).
28. M. ISHIGURO, S. TAKATSUTO, M. MORISAKI, and N. IKEKAWA. J. Chem. Soc. Chem. Commun. 962 (1980).
29. S. FUNG and J. B. SIDDALL. J. Am. Chem. Soc. **102**, 6580 (1980).
30. M. J. THOMPSON, N. MANDAVA, J. L. FLIPPEN-ANDERSON, J. F. WORLEY, S. R. DUTKY, W. E. ROBBINS, and W. LUSBY. J. Org. Chem. **44**, 5002 (1979).
31. P. A. S. SMITH. *In* Molecular rearrangements *Edited by* P. de Mayo. Interscience Publishers, New York. 1963. Chapt. 8. pp. 577–589.
32. P. DESLONGCHAMPS. Stereoelectronic effects in organic chemistry. Pergamon Press, Oxford. 1983. pp. 313–314.
33. J. E. BOLLIGER and J. L. COURTNEY. Aust. J. Chem. **17**, 440 (1964).
34. S. HARA. Chem. Pharm. Bull. **12**, 1531 (1964).
35. S. HARA. Jpn. Patent 70 05,773, 1970; Chem. Abstr. **72**, 111706r (1970).
36. C. W. SHOPPEE and J. C. P. SLY. J. Chem. Soc. 353 (1959).
37. T. L. JACOBS and N. TAKAHASHI. J. Am. Chem. Soc. **80**, 4865

(1958).
38. W. G. DAUBEN, G. A. BOSWELL, and W. H. TEMPLETON. J. Am. Chem. Soc. **83**, 5006 (1961).
39. D. H. R. BARTON and G. H. ALT. J. Chem. Soc. 4284 (1954).
40. G. STORK and J. BENAIM. Org. Synth. **57**, 69 (Note 2) (1977).
41. A. J. BIRCH and R. ROBINSON. J. Chem. Soc. 501 (1943).
42. P. T. LANSBURY and E. J. NIENHOUSE. J. Am. Chem. Soc. **88**, 4290 (1966).
43. S. L. PATT and J. N. SHOOLERY. J. Magn. Reson. **46**, 535 (1982).
44. G. A. MORRIS and R. FREEMAN. J. Am. Chem. Soc. **107**, 760 (1979).
45. A. BAX, R. FREEMAN, T. A. FRENKIEL, and M. H. LEVITT. J. Magn. Reson. **43**, 478 (1981).

Can. J. Chem. Downloaded from www.nrcresearchpress.com by 210.87.254.40 on 09/06/12
For personal use only.

The marticins: confirmation of structure, elucidation of biosynthetic origin by ^{13}Cmr studies, and revision of stereochemical assignments[1]

JÜRG E. HOLENSTEIN[2] AND ALBERT STOESSL[3]
Research Centre, Agriculture Canada, University Sub Post Office, London, Ont., Canada N6A 5B7

HEINZ KERN
Institut für Phytomedizin, Eidgenössische Technische Hochschule, ETH Zentrum/LFW, CH-8092 Zurich, Switzerland

AND

J. B. STOTHERS[3]
The Chemistry Department, University of Western Ontario, London, Ont., Canada N6A 5B7

Received January 23, 1984

This paper is dedicated to Professor Paul de Mayo on the occasion of his 60th birthday

JÜRG E. HOLENSTEIN, ALBERT STOESSL, HEINZ KERN, and J. B. STOTHERS. Can. J. Chem. **62**, 1971 (1984).

The structure of the phytotoxin marticin **7***a* has been confirmed on the basis of ^{1}H and ^{13}Cmr data for the methyl ester **7***c*, but these and other considerations have led to a revision of the stereochemistry assignable to the isomeric isomarticin from **7***b* to **13**. Incorporation of [1,2-$^{13}C_2$]- and [2-$^{13}C_1$]-acetates into **7***a*, isolated as **7***c*, has established a heptaketide origin for its fusarubin (**1**) moiety, and the tricarboxylic acid cycle as the biogenetic source of the remaining C_3 fragment, only the first three turns of the cycle making significant contributions.

JÜRG E. HOLENSTEIN, ALBERT STOESSL, HEINZ KERN et J. B. STOTHERS. Can. J. Chem. **62**, 1971 (1984).

Faisant appel à la rmn du ^{1}H et du ^{13}C de l'ester méthylique **7***c*, on a confirmé la structure de la phytotoxine marticine, **7***a*; toutefois, ces données et d'autres considérations nous ont amené à reviser la stéréochimie que l'ont doit attribuer à l'isomarticine isomère, de **7***b* à **13**. Des unités acétates, marquées au [1,2-$^{13}C_2$]- et au [2-$^{13}C_1$], ont été incorporées au **7***a*, qui a été isolé sous forme de **7***c*, et ont permis d'établir que l'origine de sa portion fusarubine (**1**) est un heptacétide alors que la source biogénétique du fragment résiduel en C_3 est le cycle de l'acide tricarboxylique; toutefois, seuls les trois premiers tours du cycle contribuent d'une façon importante.

[Traduit par le journal]

Species of the fungal genus *Fusarium* produce naphthazirinoid pigments, several of which have received much attention because of their antibiotic, insecticidal, and phototoxic properties (1–5) and non-host-specific phytotoxicity (2, 6–10). Biogenetically, some eighteen of these compounds, exemplified by fusarubin (**1**) and javanicin (**2**), are heptaketides; at least one, norjavanicin (**3**), is a non-exceptional norheptaketide; another, novarubin (**4**) (2, 5) is either a rearranged heptaketide or a norheptaketide with an extra, C_1-pool derived hydroxymethyl group. Bikaverin (**5***a*) and its 0-demethyl derivative norbikaverin (**5***b*) are probably nonaketides (11). Excellent experimental evidence for an acetate–polymalonate origin has been adduced for **2** by Gatenbeck and Bentley (12) and similarly, for **1** and **3**, by Kurobane *et al.* (13) and McCulloch *et al.* (5). The two latter studies demonstrated that **1** and **3** are formed non-enzymically from the congeneric dihydrofusarubins (**6***a*, *b*) which must, therefore, be regarded as the true fungal metabolites.[4] Two further naphthazirins, marticin and isomarticin, for which structures **7***a* and *b* have been assigned (15) are congeneric with **1**–**4**, **6***a* and *b* in certain *Fusarium* strains (2, 6, 10, 14) but differ in the presence of an additional C_3 chain, attached to C-14 of **1**. This feature may be significant for structure–activity and virulence relations, because the two compounds appear to be the most phytotoxic of the group (2, 6, 10), and, clearly, is also of considerable biogenetic interest. Early time–sequence studies (16) had suggested that **7***a* and *b* might be precursors of their congeners, which would accordingly be derived by degradative reactions. If this is correct, the marticins would presumably be derived from nonaketides by the loss of one carbon. It is therefore relevant that nonaketides, while relatively rare as fungal products (17; see also ref. 18), are, in fact, well known as metabolites of *Fusarium* species; viz., zearalenone (**8**) and several derivatives from *F. roseum*, and the more immediately pertinent bikaverin (**5***a*) and norbikaverin (**5***b*) from *F. oxysporum* and the related *Gibberella fujikuroi* (18). Despite this, a nonaketide origin of the marticins is difficult to reconcile with the "rule" that "the uncyclized residues from the methyl ends of polyketide chains are never shorter than residues from the carboxyl end of the chain" (17), and also with the proven intermediacy of the dihydrofusarubins in the formation of **1** and **3** (5, 13). For these reasons, an alternative hypothesis was suggested (7), according to which the marticins would be biosynthesized by addition of a C_3 unit to a heptaketide precursor.

To distinguish between these two, mutually exclusive possibilities, we have studied the incorporation of [1,2-$^{13}C_2$]- and [2-$^{13}C_1$]-acetate into the marticins. The results, as briefly reported in a preliminary communication (19), unambiguously demonstrate a heptaketide origin for the marticins and, in addition, implicate the tricarboxylic acid (Krebs) cycle as the source of the extra C_3 fragment. These results are discussed here in greater detail, with, in addition, comments on the structures and stereochemistries of the marticins.

The marticins were first examined in detail by Hardegger and Pfiffner and the results of their extensive chemical and spectroscopic studies, published only in thesis form (15), led to the assignment of structures **7***a* and *b* to marticin and isomarticin,

[1] Part 111 of ^{13}Cmr studies; for Part 110 see ref. 26.

[2] Present address: Stauffer Chemicals, Europe Division, Geneva, Switzerland.

[3] Authors to whom correspondence may be addressed.

[4] Tatum and Baker (14) have reported **1** to be a true metabolite rather than an artifact, from their *F. solani* strain.

Can. J. Chem. Downloaded from www.nrcresearchpress.com by 84.22.46.98 on 09/08/12
For personal use only.

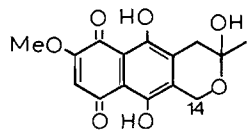

1

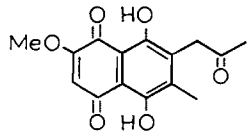

2

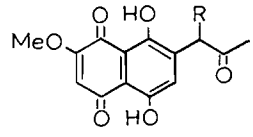

3 R = H
R = CH_2OH

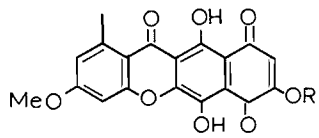

5a R = Me
b R = H

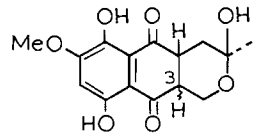

6a 3β-H
b 3α-H

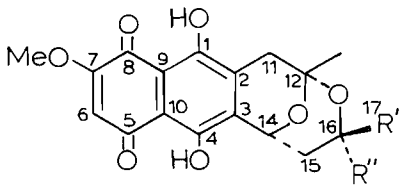

7a R′ = CO_2H R″ = H
b R′ = H R″ = CO_2H
c R′ = CO_2Me R″ = H

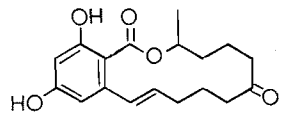

8

respectively. The two compounds are obtained from the acid portion of the fungal extract as a difficultly separable mixture in which the thermodynamically less stable isomarticin predominates. Treatment of either marticin or isomarticin with methanolic HCl, however, gives marticin methyl ester as the major (>90%) product (15). Since only relatively small quantities of material were available in the present work, the crude acidic product was esterified to render marticin methyl ester **7***c* isolable by crystallization. This material was found to be identical (ir, mp, ^{1}Hmr) with that reported by Pfiffner (15).

The ^{13}Cmr spectrum of **7***c* contained signals consistent with the previously assigned structure. In the sp^2 region, the following signals appeared (δ_C): two quinonoid carbonyls, 180.3, 186.7; a carboxyl, 170.9; three aryl carbons bearing oxygen, 154.3, 156.9, 160.8; a single aryl C—H, 110.1; and four fully substituted aryl carbons, 108.4, 110.1, 135.1, 137.7. The coincidence of the two signals at 110.1 was confirmed by examination of the proton-coupled spectrum. In the sp^3 region, the spectrum contained signals for a quaternary carbon, 96.3; two methoxyls, 52.4, 56.9; two carbinyl carbons, 65.3, 67.2; two methylenes, 30.7, 32.5; and one methyl carbon, 29.0.

Comparison of the ^{13}Cmr spectrum of **7***c*-$^{13}C_x$, obtained from the incorporation experiments with [1,2-$^{13}C_2$]-acetate, with that for natural **7***c* readily revealed that seventeen of the nineteen carbons were enriched, the exceptions being the two methoxyl carbons, as expected. Each of the signals for the labelled carbons was accompanied by ^{13}C satellites arising from spin coupling between adjacent labelled centres demonstrating the pairwise incorporation of carbons in intact acetate units for C-1 through C-14. Since each of these seven coupling constants is different, the pairwise assignments were straightforward as set out in **9**, in which the heavy bonds indicate intact acetate incorporation, with the *J* values given in parentheses. The absorption patterns for C-15, -16, and the carboxyl carbon also contained ^{13}C satellites. With the exception of the methyl and carboxyl absorptions, the patterns for all labelled centres exhibited detectable ^{13}C satellites of the satellites, undoubtedly owing to the relatively high probability of incorporation of enriched acetate units into adjacent sites during the limited period of active uptake of exogenous acetate (13). The intensities of the satellite signals relative to that of the central signal for C-1 through C-14 indicated a ^{13}C enrichment level of ca. 2%. For C-15, -16, and the carboxyl carbon the enrichment level was distinctly lower, ca. 1%. Prominent satellites with J = 68 Hz for C-16 and the carboxyl carbon indicated that incorporation of an intact acetate unit occurred. The C-16 pattern also contained less intense satellites with J = 35 Hz due to coupling with C-15, confirming its enrichment. Although C-16 and the carboxyl carbon thus arise largely from an intact acetate unit, the C_3 cannot be part of an initially formed nonaketide chain without a somewhat improbable rearrangement involving the extrusion of one carbon atom. If no rearrangement is involved, the results are compatible with the derivation of **7***c* from a fusarubin (or precursor) skeleton which gains a C_3 unit derived, most probably, from a metabolite of the tricarboxylic acid cycle into which acetate readily enters in the required manner. In particular, it was predictable for this case that the incorporation of [2-$^{13}C_1$]-acetate via citrate would result in a high probability of labelling of both C-15 and C-16, which would be revealed by readily observable coupling of these two nuclei.

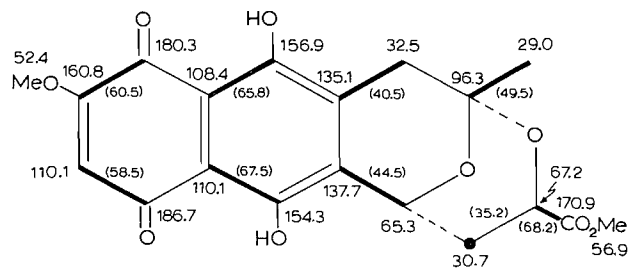

9

Can. J. Chem. Downloaded from www.nrcresearchpress.com by 84.22.46.98 on 09/08/12
For personal use only.

Can. J. Chem. Downloaded from www.nrcresearchpress.com by 84.22.46.98 on 09/08/12
For personal use only.

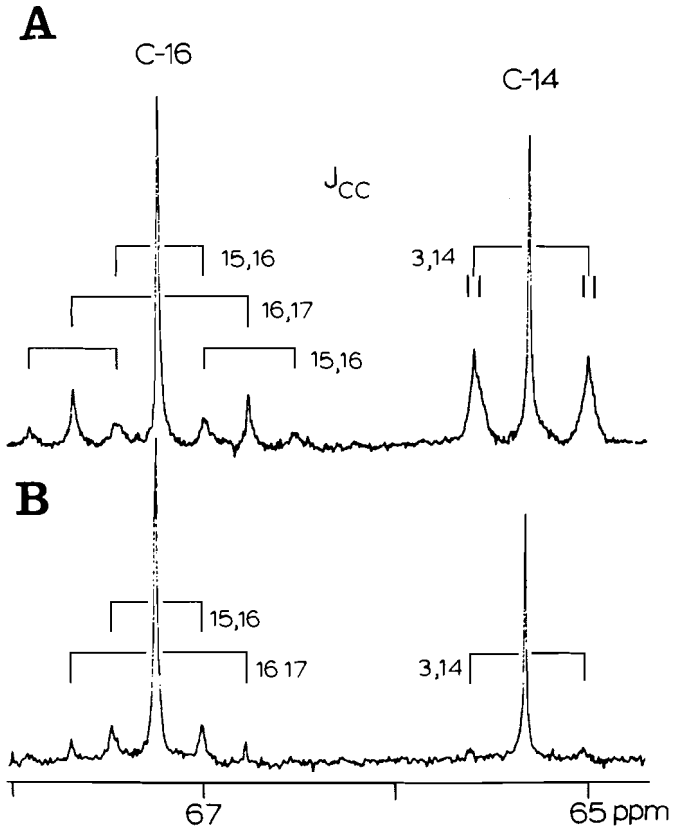

FIG. 1. The carbinyl carbon (C-14 and -16) absorptions in the 75.4-MHz spectra of (A) 7*c*-$^{13}C_x$ and (B) 7*c*-$^{13}C_y$ (see text). The origins of the one-bond, $^{13}C—^{13}C$ couplings are indicated; $J_{15,16}$ = 35.2 Hz, $J_{16,17}$ = 68.2 Hz, $J_{3,14}$ = 44.5 Hz. The broadening of these satellites for C-14 in (A) arises from geminal $^{13}C—^{13}C$ coupling with C-2, -4, and -12 in the variously labelled moieties of this enriched sample.

Setting out from this consideration, cultures of the fungus were supplemented with [2-$^{13}C_1$]-acetate and the ^{13}Cmr spectrum of the isolated 7*c*-$^{13}C_y$ was recorded. The intensities of the signals for the alternate carbons in the fusarubin portion of the molecule were significantly enhanced as were those for C-15, -16, and the carboxyl carbon. These data confirm the assignments shown in **9**, clearly distinguishing between C-1 and -4 and between C-5 and -8. Thus, the original structural assignment by Pfiffner was confirmed. It may be noted that in the thesis (15) there was some doubt regarding the placement of the aryl methoxyl group but the spectra of the labelled metabolites establish its bonding to C-7. Most importantly for our purpose, however, the absorption for both C-15 and C-16 in 7*c*-$^{13}C_y$ contained prominent ^{13}C satellites, J = 35 Hz, indicating a high level of incorporation of acetate into a Krebs cycle precursor in which the methyl carbons of two acetate units are directly bonded. In addition, the C-16 pattern has less intense satellites, with J = 68 Hz, which match those found for the carboxyl carbon, C-17. To illustrate the differences in the C-16 patterns for the two labelled metabolites, 7*c*-$^{13}C_x$ and 7*c*-$^{13}C_y$, the carbinyl regions of the spectra are shown in Fig. 1. Weak satellites (J = 44 Hz) were also apparent for C-14 in the spectrum of 7*c*-$^{13}C_y$; in fact each of the signals for the enriched centres in 7*c*-$^{13}C_y$ exhibited similar weak satellite peaks and each of the patterns for the protonated carbons contained a closely spaced pair of satellites, $J \sim 4$ Hz, arising from geminal $^{13}C—^{13}C$ coupling. As noted above, this is undoubtedly owing to the relatively high probability of incorporation of enriched acetate units into adjacent sites during the limited period of active uptake.

We turn now to a more detailed consideration of the argument that C-15 through C-17 are derived from acetate via one to several turns of the Krebs cycle. Such incorporations have been observed previously in ^{13}Cmr biosynthetic studies (20). A detailed mathematical analysis of the flux of [2-$^{13}C_1$]-acetate into primary Krebs cycle metabolites in perfused rat hearts was published very recently (21), after our work had been completed. In another, similar but mathematically less explicit study, also published very recently (22), the incorporation of [2-$^{13}C_1$]-acetate into citrate and glutamate by *Saccharomyces cerevisiae* was followed on a time basis; a particularly interesting feature which emerged from this is that after the relatively brief interval of ca. 4 h, a steady state is reached. in which glutamate is markedly labelled in the 2,3,4- and the 1,2,3,4-positions whereas 4-, 2,4-, 3,4-, and 1,3,4-labelled glutamate decreases from initially modest to very low concentrations.

With respect to the results for 7*c*, it is salient to recall, in addition, that the 2- and 3-positions of succinate are equivalent in the operation of the Krebs cycle (16, 23). Thus, unlabelled, pool-derived oxaloacetate will condense with [**1**,**2**-$^{13}C_2$]-acetate to give citrate, which will furnish in succession [**4**,**5**-$^{13}C_2$]-oxoglutarate, [**1**,**2**-$^{13}C_2$]-succinate, and, hence, equal amounts of [**1**,**2**-$^{13}C_2$]- and [**3**,**4**-$^{13}C_2$]-oxaloacetate in the first turn of the cycle. The bold face numbers indicate paired labels arising through uptake of an intact doubly labelled acetate unit. Degradative condensation of these or other intermediates of the cycle (but most probably that of oxaloacetate) with a heptaketide precursor will lead to two different labelled species of marticin, one labelled at C-15 and one with paired labels at C-**16**, -**17**. On the second turn of the cycle, condensation of [**1**,**2**-$^{13}C_2$]- and [**3**,**4**-$^{13}C_2$]-oxaloacetate with [**1**,**2**-$^{13}C_2$]-acetate will furnish [3,**4**,**5**-$^{13}C_3$]- and [**1**,**2**,**4**,**5**-$^{13}C_4$]-2-oxoglutarate and, hence, [**1**,**2**,3-$^{13}C_3$]- and [**1**,**2**,4-$^{13}C_3$]-succinate, respectively. This would lead to marticin labelled at C-15 and -16, C-15 and -17, C-**16**, -**17**, and C-15, -**16**, -**17** with the four species accruing in a 1 : 1 : 1 : 1 ratio. However, the second turn of the cycle will also involve natural acetate. Thus [2-$^{13}C_1$]- and [3-$^{13}C_1$]-2-oxoglutarate will be produced, leading to [1-$^{13}C_1$]- and [2-$^{13}C_1$]-succinate which will give rise to one unlabelled and three monolabelled species (C-15, C-16, and C-17) of marticin. A third turn of the cycle, with [**1**,**2**-$^{13}C_2$]-acetate as well as with natural acetate, can give rise to nine different labelled species, allowing for the distinction between C-**16**, -**17** and C-16, -17 and between C-15, -**16**, -**17** and C-15, -16, -17, by 32 possible routes. Thus, labelled acetate will lead by two routes each to the labelling patterns C-15, C-15, -16, C-15, -17, and C-15, -16, -17, and by four routes each to C-**16**, -**17** and C-15, -**16**, -**17**. Unlabelled acetate will lead by two routes each to the patterns C-16, C-17, C-16, -17 and by four to C-15. The relative magnitudes of the contributions from the various turns of the cycle, and those from unlabelled acetate in the second and third turns, cannot be readily predicted nor quantitated from the available experimental data. However, the intensities of the observed satellites (Fig. 1A) indicate that the 16, 17-doubly labelled species are about four times as abundant as their 15, 16-labelled counterparts and this indicates that the contributions from the first turn were predominant.

The incorporation of [2-$^{13}C_1$]-acetate into the C-15, -16, -17

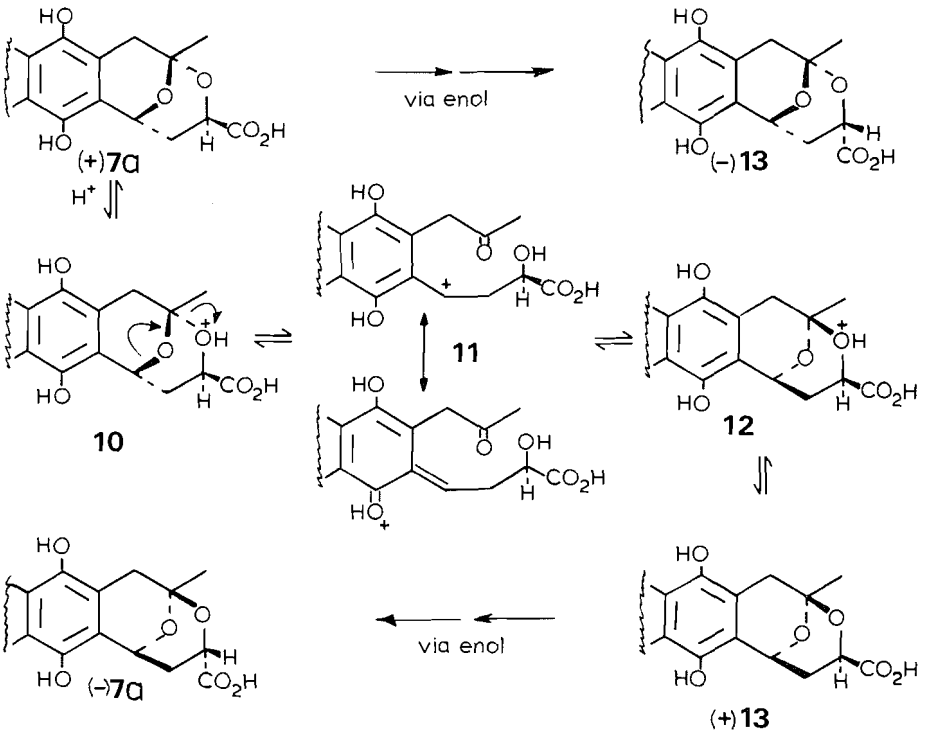

SCHEME 1

fragment of marticin will proceed via the Krebs cycle in a manner analogous to that described by Dickinson *et al.* (22)[5] with the important difference that intermediates of the cycle are withdrawn for marticin formation before a steady state is attained. The first turn through the tricarboxylic acid cycle with [2-$^{13}C_1$]-acetate will produce [2-$^{13}C_1$]-succinate and, consequently, marticin monolabelled at C-15 and at C-16 in a 1:1 ratio. The second turn with [2-$^{13}C_1$]-acetate will provide marticin labelled at C-16, at C-15, -17, and at C-15, -16 in a ratio of 1:1:2, while the second turn utilizing natural acetate will produce unlabelled and the three possible monolabelled species in a ratio of 1:1:1. The third turn of the cycle with both [2-$^{13}C_1$]-acetate and natural acetate leads to all seven possible labelling combinations for the three pertinent carbons. Of the thirty-two routes via oxaloacetate, there are six which lead to each of the following species: unlabelled, monolabelled at C-15 and at C-16, and dilabelled at C-15, -16, while there are two routes to each of the C-15, -17 and C-16, -17 dilabelled species and the trilabelled material. Clearly the enrichment of C-15 and C-16 will be expected to exceed that for C-17. This is the situation observed; for the C-16 pattern in Fig. 1B the intensity of the satellites with $J = 35$ Hz is about three times greater than that for the satellites with $J = 68$ Hz. As mentioned previously, the immediate precursor for marticin production is probably a C_4 Krebs cycle metabolite, oxaloacetate being the most favored mechanistically but its prior decarboxylation to pyruvate cannot be excluded.

While the ^{13}C results confirm the original structural assignment for marticin methyl ester as **7***c* and thereby **7***a* for marticin itself, these data do not provide definitive information on the stereochemistry of these compounds and the original stereochemical assignments appear open to question. Pfiffner (15) established that marticin ($[\alpha]_D$ +132°), isomarticin ($[\alpha]_D$ +26°), and their methyl esters are optically active; furthermore, the ord curves for marticin and its methyl ester are essentially superimposable and in an approximate mirror-image relationship with those for all isomarticin derivatives, even though all $[\alpha]_D$ values are positive. The mixture of marticin and isomarticin isolated from the fungal extract contains predominantly the less stable isomarticin, but on brief heating with methanolic HCl, the mixture is converted largely to marticin methyl ester. In one experiment Pfiffner heated 1.5 g of pure isomarticin with MeOH/HCl and obtained 1.3 g of marticin methyl ester after recrystallization, while fractional crystallization of the mother liquors gave 39 mg of pure isomarticin methyl ester. The isomerization of isomarticin was ascribed, without explanation, to epimerization at C-16, presumably by enolization. Tatum and Baker (14) have accepted this assignment and in fact ascribe the 16-*S* and 16-*R* configurations to marticin and isomarticin, respectively, with no additional evidence but merely noting that isomarticin is converted to marticin "when cleaning up on tlc". Both groups have apparently overlooked the fact that an acetal is much more labile under acidic conditions than a hydrogen α to a carboxy group. Consideration of the behavior of the marticin system under acidic conditions must take account of the consequences of simple acid catalyzed cleavage and reclosure of the acetal function.

To examine the situation in detail, Scheme 1 has been constructed in which we have arbitrarily labelled one of the marticin enantiomers as (+)-**7***a*. Its protonation will lead to **10** which will readily ketonize to give **11** in which the carbonium ion centre is not only benzylic but *o*-hydroxybenzylic! Reclosure on the opposite face of the carbonyl group will furnish **12**, deprotonation of which gives (+)-**13** as in the scheme. The sequence (+)-**7***a* → (+)-**13** inverts the configuration at C-12 and -14 while the configuration at C-16 is unchanged. It is to

[5] It should be noted that their flow chart for ^{13}C isotopomer distribution for incorporation of [2-^{13}C]-acetate on sequential terms of the cycle does not include condensation with natural abundance acetate.

Can. J. Chem. Downloaded from www.nrcresearchpress.com by 84.22.46.98 on 09/08/12
For personal use only.

Can. J. Chem. Downloaded from www.nrcresearchpress.com by 84.22.46.98 on 09/08/12
For personal use only.

be noted that in the scheme, enolization at C-16 transforms (+)-**7***a* to (−)-**13**, the enantiomer of **13** produced by acetal cleavage and reclosure, while enolization of (+)-**13** will produce (−)-**7***a*. The much greater probability of acetal cleavage under acidic conditions than enolization necessitates the conclusion that the facile isomerization of isomarticin to marticin involves inversion at C-12 and -14 with no change in configuration at C-16, contrary to the earlier suggestion (15).

With regard to the stereochemical assignments for marticin, an examination of the ^{1}Hmr data should be informative and, to this end, the proton spectrum of **7***c* was recorded. Although Pfiffner utilized proton spectroscopy extensively throughout the original investigation (15), he did not provide a complete ^{1}H data set for marticin methyl ester. The proton spectra of marticin and isomarticin were reported by Tatum and Baker (14) very recently, while our own studies were in progress. Unfortunately, however, the latter authors did not provide all of the coupling constant data. Furthermore, data *tabulated* for their "more stable" isomer agree better with those for Pfiffner's less stable material and their results for their "less stable" acid agree closely with our data for the more stable ester. In addition, their assignments for the carbinyl protons in each isomer require reversal.

Nevertheless the proton data provide a clear distinction between the two isomers on the following grounds. The carbinyl protons give rise to doublets of doublets owing to vicinal coupling to the 15-methylene protons. For H-14, δ 5.44, the couplings are 1.7 and 5.2 Hz, while for H-16, δ 4.376, J = 3.0 and 12.2 Hz; the absorptions for H-14 and H-16 were conclusively identified by a heteronuclear correlation spectrum since the signals for C-14 and -16 were unequivocally distinguished by the spectra of the labelled samples described earlier. The eight-line patterns for each of the 15-protons were at δ 2.387 (axial H-15), J = 5.2, 12.2, 13.4 Hz and δ 1.956, J = 1.7, 3.0, 13.4 Hz (equatorial H-15). These coupling constants agree remarkably well with those found for a series of 2-alkyl-1,3-dioxanes (24) in which the vicinal interactions ($J_{4,5}$) were found to be 12.4–12.5 (4_{ax}, 5_{ax}), 2.6 (4_{ax}, 5_{eq}), 5.0 (4_{eq}, 5_{ax}), 1.3 Hz (4_{eq}, 5_{eq}) and the geminal coupling $J_{5_{ax},5_{eq}}$ = 13.3 Hz. Since the 2-alkyl-1,3-dioxanes undoubtedly adopt chair conformations, it follows that the ketal ring of marticin and its methyl ester is

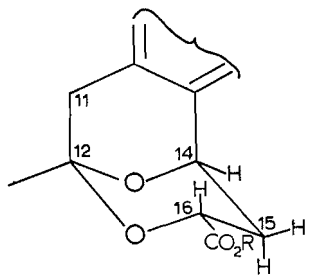

14

also a chair as in **14**, corresponding to **7***a* (Scheme 1). Isomarticin is, therefore, **13** and its methyl ester **15**, for which the

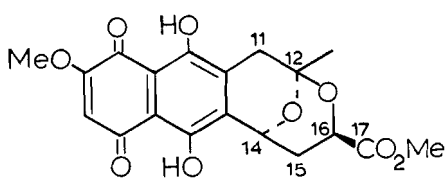

15

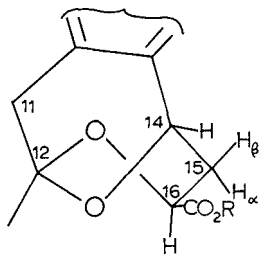

16

favored conformation can be represented as the twist-boat **16**. Fortunately, Pfiffner (15) reported the following data for isomarticin methyl ester: H-14, δ 5.33, J = 2.0, 9.0 Hz; H-15, δ 2.14, J = 2.0, 8.5, 13.5 Hz; H-15, δ 2.71, J = 6.0, 9.0, 13.5 Hz; H-16, δ 4.53, J = 6.0, 8.5 Hz. The results are entirely compatible with structure **15** existing in conformation **16**. It can be mentioned that the proton spectra of the O-methyl derivatives of the marticin and isomarticin methyl esters were fully described in Pfiffner's thesis and the data accord very well with the results for the esters themselves. The 11-methylene proton patterns found for the marticin and isomarticin series offer a clear distinction between the two since δ_{AB} for these patterns is $\leq$ 0.15 ppm for marticin and derivatives while $\delta_{AB} \geq$ 0.4 ppm for the isomarticin series. For example, **7***c* has δ_A 3.097, δ_B 2.992, J_{AB} = 20 Hz and **15**, δ_A 3.13, δ_B 2.68, J_{AB} = 18.5 Hz (15).

We conclude from all of these data that marticin methyl ester is **7***c* (or enantiomer) and isomarticin methyl ester is **15** (or enantiomer) rather than **7***b* as had been previously claimed.

Experimental

Reference samples of isomarticin, fusarubin, javanicin, and novarubin were available from earlier work (2, 10). Sodium [1,2-$^{13}C_2$]- and [2-$^{13}C_1$]-acetate, as well as $CDCl_3$ were purchased from MSD Isotopes, Pointe Claire – Dorval. The ^{1}H spectra were determined on a Varian XL-200 spectrometer with solutions of 5–10 mg/0.4 mL of $CDCl_3$. The ^{13}C spectra were obtained with a Varian XL-300 instrument at 75.4 MHz (28° pulses, 3-s rep rate with 18-kHz sweep widths and 60 000 points with 64K transforms) using the same solutions as those employed for the proton spectra; comparison of the decoupled spectra with those obtained by the INEPT sequence identified the methyl, methylene, methine, and quaternary carbons. A coupled spectrum of **7***c* was obtained with gated decoupling (17% duty cycle) to aid the initial assignments. A ^{13}C—^{1}H correlation experiment was done using the HETCOR sequence of the XL software (25) to permit definitive assignments for the two methylene and the two carbinyl absorptions. For this purpose, a 2048 × 256 data matrix with a 4800-Hz spectral width for ^{13}C and 1200-Hz width for ^{1}H, transforming 2048 and 512 points, respectively, was employed.

The fungal organism used was *Fusarium martii* App. et Wr. var. *pisi* F.R. Jones, strain F1.1 from the collection at the Institut für Phytomedizin, ETH, Zurich, and was routinely maintained on malt agar (10). Shake cultures on Raulin medium (80 mL/200 mL Delong flask) were grown at 27°C (the temperature requirement being critical) and harvested by filtration, usually after 5–7 days, when the culture media were dark purple. The mixture of metabolites extracted from the acidified filtrates (a few drops of concentrated HCl to pH 3) by EtOAc (2 × 1 vol) was separated into acidic and neutral fractions by distribution between $NaHCO_3$ (1 *M*, 3 × 100 mL) and EtOAc (4 × 100 mL), essentially as described by Pfiffner (15). The $NaHCO_3$ extracts were acidified (concentrated HCl) and reextracted with EtOAc (2 × 1 vol) to give a product containing isomarticin (**7***b*) as major component, together with smaller quantities of marticin (**7***a*) and fusarubin (**1**) (tlc). The crude acidic product was methylated by brief boiling with methanolic HCl (15), crude crystalline marticin methyl ester separating on standing at room temperature for 1–2 days. The pure

component was obtained by repeated recrystallizations with MeOH/$CHCl_3$.

Incorporation of [1,2-$^{13}C_2$]-acetate

Fifteen cultures of the fungus were injected with [1,2-$^{13}C_2$]-acetate (99% ^{13}C; 0.093 *M*, 4 mL/culture) when the culture media had turned orange-yellow (66 h after inoculation). The addition was repeated after a further 24 h and the cultures were harvested another 24 h thereafter. Methylation of the acidic product gave 20 mg of crude **7***c*, mp 150–210°C, which afforded 10 mg of pure compound, mp 236–238°C, after two recrystallizations. This sample was enriched by ca. 2% according to ^{13}Cmr analysis.

Incorporation of [2-$^{13}C_1$]-acetate

Twelve fungal cultures were treated analogously with [2-$^{13}C_1$]-acetate (99% $^{13}C_1$; 0.096 *M*, 4 mL/culture) 67 h and, again, 91 h after inoculation, and harvested 24 h thereafter. Methylation of the acidic metabolic product and recrystallization of the crude methyl ester (17 mg) gave pure **7***c* (7.8 mg), mp 238–240°C.

1. H. R. V. ARNSTEIN, A. H. COOK, and M. S. LACEY. Nature (London), **157**, 333 (1946).
2. H. KERN and S. NAEF-ROTH. Phytopathol. Z. **60**, 316 (1967).
3. N. CLAYDON, J. F. GROVE, and M. POPLE. J. Invert. Pathol. **30**, 216 (1977).
4. M. S. AMMAR, N. N. GERBER, and L. E. MCDANIEL. J. Antibiot. **32**, 679 (1979).
5. A. W. MCCULLOCH, A. G. MCINNES, D. G. SMITH, I. KUROBANE, and L. C. VINING. Can. J. Chem. **60**, 2943 (1982).
6. H. KERN. Ann. Phytopathol. **10**, 327 (1978).
7. A. STOESSL. *In* Toxins in plant disease. *Edited by* R. D. Durbin. Academic Press, New York. 1981. pp. 109–219.
8. Y. KIMURA, T. HAMASAKI, and H. NAKAJIMA. Agric. Biol. Chem. **45**, 2653 (1981).
9. J. MARCINKOWSKA, J. M. KRAFT, and L. Y. MARQUIS. Can. J. Plant Sci. **62**, 1027 (1982).
10. J. HOLENSTEIN and G. DÉFAGO. J. Expt. Bot. **34**, 927 (1983).
11. A. G. MCINNES, D. G. SMITH, J. A. WALTER, L. C. VINING, and J. L. C. WRIGHT. J. Chem. Soc. Chem. Commun. 66 (1975).
12. S. GATENBECK and R. BENTLEY. Biochem. J. **94**, 478 (1965).
13. I. KUROBANE, L. C. VINING, A. G. MCINNES, and J. A. WALTER. Can. J. Chem. **58**, 1380 (1980).
14. J. H. TATUM and R. A. BAKER. Phytochemistry, **22**, 543 (1983).
15. A. PFIFFNER. Isolierung und Konstitutionermittlung von Marticin und Isomarticin, zwei neuen Welketoxinen aus Fusarium Martii. Dissert. No. 3361, ETH, Zurich, 1963.
16. H. KERN and S. NAEF-ROTH. Phytopathol. Z. **53**, 45 (1965).
17. W. B. TURNER. Fungal metabolites. Academic Press, London and New York. 1971. p. 176.
18. W. B. TURNER and D. C. ALDRIDGE. Fungal metabolites II. Academic Press, London and New York. 1983.
19. J. E. HOLENSTEIN, H. KERN, A. STOESSL, and J. B. STOTHERS. Tetrahedron Lett. **24**, 4059 (1983).
20. C. P. GORST-ALLMANN, P. S. STEYN, and R. VLEGGARR. J. Chem. Soc. Chem. Commun. 652 (1982); J. Chem. Soc. Perkin Trans. **1**, 1357 (1983); A. E. DE JESUS, W. E. HULL, P. S. STEYN, F. R. VAN HEERDEN, R. VLEGGAAR, and P. L. WESSELS. J. Chem. Soc. Chem. Commun. 837 (1982).
21. E. M. CHANCE, S. H. SEEHOLZER, K. KOBAYASHI, and J. R. WILLIAMSON. J. Biol. Chem. **258**, 13785 (1983).
22. J. R. DICKINSON, I. W. DAWES, A. S. F. BOYD, and R. L. BAXTER. Proc. Nat. Acad. Sci. USA, **80**, 5847 (1983).
23. H. BEEVERS, M. L. STILLER, and V. S. BUTT. *In* Plant physiology. Vol. IVB: Metabolism: Intermediary Metabolism and Pathology. *Edited by* F. C. Steward. Academic Press, New York and London. 1966. pp. 119–243; D. R. BUHLER, E. HANSEN, B. E. CHRISTENSEN, and C. H. WANG. Plant Physiol. **31**, 192 (1956).
24. H. R. BUYS and E. L. ELIEL. Tetrahedron Lett. 2779 (1970).
25. A. BAX and G. A. MORRIS. J. Magn. Res. **42**, 501 (1981).
26. H. A. PATEL and J. B. STOTHERS. Can. J. Chem. **62**, 1926 (1984).

Can. J. Chem. Downloaded from www.nrcresearchpress.com by 84.22.46.98 on 09/08/12
For personal use only.

Vinylogous nucleophilic catalysis. Tertiary amine promoted hydrolysis of 1-alkene-1-sulfonyl chlorides[1]

JAMES FREDERICK KING, JOHN HENRY HILLHOUSE, AND STANISŁAW SKONIECZNY[2]
Department of Chemistry, University of Western Ontario, London, Ont., Canada N6A 5B7

Received February 2, 1984

This paper is dedicated to Professor Paul de Mayo on the occasion of his 60th birthday

JAMES FREDERICK KING, JOHN HENRY HILLHOUSE, and STANISŁAW SKONIECZNY. Can. J. Chem. **62**, 1977 (1984).

We present evidence that the reactions of ethenesulfonyl chloride (**1**) and *trans*-1-propene-1-sulfonyl chloride (**3**) with water in the presence of pyridine, trimethylamine, and a number of other tertiary amines proceed primarily by way of an initial vinylogous substitution reaction to form the cationic sulfene, $R_3^+NCHRCH{=}SO_2$, which subsequently reacts with water either by addition (and deprotonation) to form the betaine $R_3^+NCHRCH_2SO_3^-$, or by vinylogous substitution (and deprotonation) to give the alkenesulfonate anion, $CHR{=}CHSO_3^-$ (R = H or CH_3). Formation of the latter represents the first well-supported example of vinylogous nucleophilic catalysis. These conclusions are drawn from kinetic and product composition observations, including (*a*) α-monodeuteration in the betaine and lack of deuteration of the ethenesulfonate ($CH_2{=}CHSO_3^-$) from the reaction in D_2O, (*b*) rate lowerings of up to 2000-fold for 2- (and 6-) substituted pyridines from those expected from Brønsted-type relationships shown by "unhindered" pyridine bases, (*c*) lack of a kinetic solvent isotope effect in the reaction of **1** with 3-cyanopyridine, (*d*) a lower rate of reaction of **3** vs. **1** not directly correlated with product composition, and (*e*) formation of similar product mixtures from either **1** or $Pyr^+CH_2CH_2SO_2Cl\ Cl^-$ (**18***a*) with aqueous pyridine. For the initial formation of the sulfene, $R_3^+NCH_2CH{=}SO_2$, the available evidence does not distinguish between a two-step mechanism via an intermediate zwitterion and a closely related concerted reaction, but for the further reaction of the sulfene a process involving a zwitterionic intermediate common to both products is favoured. For the reaction of **1** or **3** in the absence of tertiary amines evidence is presented for a direct displacement on sulfur mechanism leading to the alkenesulfonate anion, plus a small proportion (up to 15%) of formation of the 2-hydroxy-1-alkanesulfonate anion by way of the sulfene $HOCHRCH{=}SO_2$ (R = H or CH_3).

JAMES FREDERICK KING, JOHN HENRY HILLHOUSE et STANISŁAW SKONIECZNY. Can. J. Chem. **62**, 1977 (1984).

On rapporte des données qui suggèrent que la réaction du chlorure d'éthènesulfonyle (**1**) et du chlorure de propène-1 sulfonyle-1 *trans* (**3**) avec de l'eau, en présence de pyridine, de triméthylamine et d'un certain nombre d'autres amines tertiaires, se produit principalement par le biais d'une réaction initiale de substitution vinylogue conduisant à la formation du sulfène cationique $R_3^+NCHRCH{=}SO_2$, qui réagit ensuite avec de l'eau soit par une addition (et une déprotonation) pour former la bétaïne $R_3^+NCHRCH_2SO_3^-$ soit par une substitution vinylogue (et une déprotonation) pour donner l'anion alcènesulfonate, $CHR{=}CHSO_3^-$ (R = H ou CH_3). La formation de ce dernier composé représente le premier exemple bien documenté d'une catalyse nucléophile vinylogue. On tire ces conclusions en se basant sur les données cinétiques et sur des observations relatives à la composition du produit; en particulier sur le fait que (*a*) si on effectue la réaction dans le D_2O, il y a α-monodeutération de la bétaïne alors qu'il n'y a pas de deutération de l'éthènesulfonate ($CH_2{=}CHSO_3^-$) dans les mêmes conditions; (*b*) pour les pyridines substituées en position 2 (et 6), les vitesses de réaction sont jusqu'à 2000 fois plus faibles que celles prévues, par des relations de type Brønsted, pour des pyridines "non encombrées"; (*c*) il n'y a pas d'effet isotopique cinétique du solvant lors de la réaction du composé **1** avec la cyano-3 pyridine; (*d*) la différence dans les vitesses de réactions des composés **3** vs. **1** n'est pas reliée avec la composition du produit; et (*e*) dans un milieu de pyridine aqueuse, il y a formation du même mélange réactionnel que le produit de départ soit le composé **1** ou **18***a* ($Pyr^+CH_2CH_2SO_2Cl\ Cl^-$). Dans le cas de la formation initiale du sulfène, $R_3^+NCH_2CH{=}SO_2$, les données disponibles ne permettent pas de faire la distinction entre un mécanisme en deux étapes impliquant un zwitterion intermédiaire et une réaction concertée qui lui est très semblable; toutefois pour tenir compte de la réaction subséquente du sulfène, on favorise un processus qui implique un zwitterion intermédiaire commun aux deux produits. Dans le cas de la réaction des composés **1** ou **3**, en l'absence d'amines tertiaires, on présente des données suggérant l'existence d'un mécanisme par déplacement direct au niveau du soufre qui conduit à l'anion alcènesulfonate aux côtés d'une faible quantité (jusqu'à 15%) de l'anion hydroxy-2 alcanesulfonate-1, qui se forme par l'intermédiaire du sulfène $HOCHRCH{=}SO_2$ (R = H ou CH_3).

[Traduit par le journal]

Introduction

There are two accepted general mechanisms for hydrolysis of alkanesulfonyl chlorides, or, more generally, for reactions of the following type

$$RSO_2Z + Nu^{(-)} \rightarrow RSO_2Nu + Z^{(-)}$$

wherein Z is a leaving group (nucleofuge), and $Nu^{(-)}$ a nucleophile: (*i*) a direct displacement on the sulfur atom (DDS mechanism) (2–11, and refs. cited), and (*ii*) an elimination–addition process going by way of an intermediate sulfene ($R'R''C{=}SO_2$) (12–16). Direct displacement, which may be a single reaction or involve two consecutive direct displacements in a nucleophilic catalysis mechanism, is observed in reactions of arenesulfonyl chlorides (2–7) and related species (10, 11), and presumably with derivatives of alkanesulfonic acids lacking an α-hydrogen. Elimination–addition, on the other hand, is the usual pathway for reactions of alkanesulfonyl chlorides and the like that have an α-hydrogen, in such common preparative reactions as the formation of alkanesulfonate esters by reaction of the alkanesulfonyl chloride with an alcohol and a tertiary amine (12–14); the direct displacement is observed, however, in the simple uncatalyzed hydrolysis and alcoholysis

[1] Part 26 in the series Organic Sulfur Mechanisms; for Part 25 see ref. 1.

[2] On leave from the Technical University of Gdańsk, Poland.

Can. J. Chem. Downloaded from www.nrcresearchpress.com by 210.87.254.6 on 09/06/12
For personal use only.

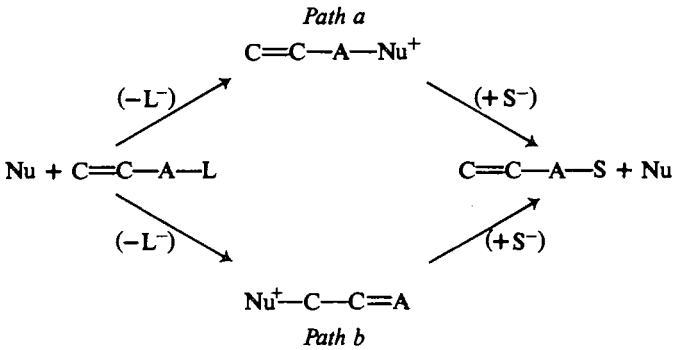

SCHEME 1

of alkanesulfonyl chlorides and other reactions as well (6, 8, 12–14, 16).

Upon considering the reactions of ethenesulfonyl chloride (**1**) it became evident that previous knowledge was not sufficient to predict its mode of reaction with any confidence. Two mechanistic questions in particular appeared to have especial mechanistic interest; (*i*) is the cumulated sulfene (**2**) formed from **1** and, if so, how does it react, or, alternatively, (*ii*) if **1**

$CH_2{=}CHSO_2Cl$ $CH_2{=}C{=}SO_2$

1 **2**

is subject to nucleophilic attack, does the reaction occur at the sulfur or vinylogously at C-2? The two possible pathways considered in question (*ii*) are illustrated in Scheme 1 for the simplest form of the general substitution without rearrangement. As we show in this paper, the simple tertiary amine-promoted hydrolysis of ethenesulfonyl chloride does, in fact, proceed by a "*path b*" mechanism. In preliminary communications (17, 18) we have already outlined this and a related study of the corresponding reaction with alcohols in a nonpolar medium, and used the terms "S_N2' catalysis" and "vinylogous nucleophilic catalysis" for the "*path b*" process. The former description, though brief, appears to convey an unintended implication that the reaction is necessarily concerted, and we therefore now use the less connotative term "vinylogous nucleophilic catalysis". Our first experiments and communication (17) investigated esterification in nonpolar media, but subsequent work on the hydrolysis has provided a system which, because it is simpler in its chemistry and easier to study kinetically, now appears to be the logical starting point for a detailed presentation of the mechanism of the reaction; the esterification reactions will be discussed in a subsequent paper.

Prior to the present study comparatively little work had been published on the reactions of hydroxylic reagents with ethenesulfonyl chloride (**1**) and its companion in our work, *trans*-1-propene-1-sulfonyl chloride (**3**). Most previous reports

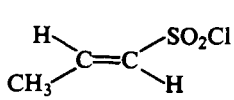

3

(19–22) described essentially synthetic investigations of **1**, including a valuable study (21) of the formation of betaines by reaction with tertiary amines in glacial acetic acid and certain other media. Two kinetic studies have been reported (8*b*, 23); the former concluded that the cation $CH_2{=}CHSO_2^+$ was probably not an intermediate in the ethanolysis of **1** and ascribed the ten-fold increase in its rate of ethanolysis (relative to saturated analogues) to inductive withdrawal by unsaturation, while the latter investigation tentatively pointed to the possibility of conjugation in the transition state for the solvolysis of **3** in aqueous dioxan. Truce and Campbell (13) noted that reaction of **3** with triethylamine and methyl and ethyl alcohols gave both the rearranged and unrearranged esters and suggested that the former arose from vinylsulfene ($CH_2{=}CHCH{=}SO_2$) and the latter from the sulfonylammonium ion ($CH_3CH{=}CHSO_2N^+Et_3$). Remarkably, however, the products of simple hydrolysis of neither **1** nor **3** seem to have been described.

Results and discussion

Hydrolysis of 1 and 3 without amines. Products and kinetics

At pH 4.0 (pH-stat) **1** gave the expected ethenesulfonic acid (**4**) in 90% yield, along with a 10% yield of a second product identified as 2-hydroxyethanesulfonic acid (**5**). At pH 10.5 and 10.8 there seemed to be slightly more **5** (15% and 13%, as the

$CH_2{=}CHSO_2Cl + H_2O \rightarrow CH_2{=}CHSO_3H$

1 **4**

$+ HOCH_2CH_2SO_3H$

5

salt). The presence of potassium chloride up to 0.5 *M* had no effect on the composition of the reaction product at pH 4.0. Similar reaction of **3** gave at high pH (11.5 and 12.7) the salt of the propenesulfonic acid (**6**) with a small amount of that of the hydroxyacid (**7**) (5%), but there was not sign of **7** (<2%) visible in the ^{1}Hmr spectrum of the product of reaction at pH 4.0.

$CH_3CH{=}CHSO_2Cl + H_2O \rightarrow CH_3CH{=}CHSO_3H$

3 **6**

$CH_3CHOHCH_2SO_3H$

7

The rates of hydrolysis of **1** and **3** at 25.0°C were determined by the pH-stat technique over the pH range 3.0 to 10.75 or 11.0 (in 0.1 *M* KCl containing 0.2% of 1,2-dimethoxyethane (DME)). Plots of log k_ψ (where k_ψ is the pseudo-first-order rate constant for hydrolysis) vs. pH showed the familiar hockey-stick pattern (Fig. 1) corresponding to the equation $k_\psi = k_1 + k_{OH}[OH^-]$; k_1 and k_{OH} values for the reactions of **1** and **3** are listed in Table 1.[3]

In D_2O at apparent pH's (i.e. meter readings) of 3.4 and 5.0 we observed k_1 values for **1** of 8.48×10^{-4} s^{-1} and 8.68×10^{-4} s^{-1}, and so obtained a kinetic solvent isotope effect, $(k_1)_H/(k_1)_D$, of 1.54 at 25°C. The ^{1}Hmr spectrum of the product at the kinetic concentrations showed mostly undeuterated **4** (90% yield, <5% deuterated) plus a little monodeuterated **5**, $HOCH_2CHDSO_3H$ (10% yield, >90% mono D).

[3] Complete set of tables giving observed first-order rate constants, product composition, and reaction conditions (5 tables) is available, at a nominal charge, from the Depository of Unpublished Data, CISTI, National Research Council of Canada, Ottawa, Canada, K1A 0R6.

Can. J. Chem. Downloaded from www.nrcresearchpress.com by 210.87.254.6 on 09/06/12
For personal use only.

TABLE 1. Rate constants[a] for the reaction of some alkene- and arene-sulfonyl chlorides with water and hydroxide at 25.0°C[b]

R	10^3k_1 (s^{-1})	10^3k_{1S} (s^{-1})	10^3k_{1C} (s^{-1})	k_{OH} (M^{-1} s^{-1})	$k_{(OH)S}$ (M^{-1} s^{-1})	$k_{(OH)C}$ (M^{-1} s^{-1})
CH_2=CH (**1**)	1.32 ± 0.07[c]	1.2	0.1	124 ± 10	107	17
CH_3CH=CH (**3**)	1.22 ± 0.08[d]	1.2	<0.02	37 ± 4	35	~2
C_6H_5[e]	3.06	(3.06)	—	40.4	(40.4)	—
p-$CH_3C_6H_4$[e]	3.00	(3.00)	—	16.1	(16.1)	—

[a] k_1 and k_{OH} are the experimental first- and second-order rate constants for reaction with H_2O and OH^-, respectively; k_{1S} and k_{1C} are calculated from $k_1 = k_{1S} + k_{1C}$ and k_{1S}/k_{1C} = the ratio of **4** to **5** (or of **6** to **7**) in the product at pH 4.0; similarly $k_{(OH)S}$ and $k_{(OH)C}$ are from $k_{OH} = k_{(OH)S} + k_{(OH)C}$ and $k_{(OH)S}/k_{(OH)C}$ = the ratio of **4** to **5** (or of **6** to **7**) in the product at pH 10.5 to 12.7 (see discussion in text).

[b] In 0.1 M aqueous KCl (plus 0.2% 1,2-dimethoxyethane) for **1** and **3**, 0.05 M KCl for $C_6H_5SO_2Cl$ and p-$MeC_6H_4SO_2Cl$.

[c] Values of k_1 for **1** at other temperatures are 8.86×10^{-5} at 1.0, 5.14×10^{-4} at 17.3, 2.91×10^{-3} at 35.0, 7.18×10^{-3} at 45.0, and 3.47×10^{-2} s^{-1} at 60.0°C (see also Table S1); these, after conversion to second-order rate constants (by dividing by 55.5 M), gave $\Delta H^{\ddagger} = 17.5 \pm 2$ kcal mol^{-1} and $\Delta S^{\ddagger} = -21 \pm 8$ cal K^{-1} mol^{-1} (maximum errors as estimated by Wiberg's method (24)).

[d] At 1.0°C k_1 for **3** is 8.1×10^{-5} s^{-1}; $\Delta H^{\ddagger} = 17.5 \pm 3$ kcal mol^{-1} and $\Delta S^{\ddagger} = -21 \pm 10$ cal K^{-1} mol^{-1} (also from second-order rate constants).

[e] Reference 3.

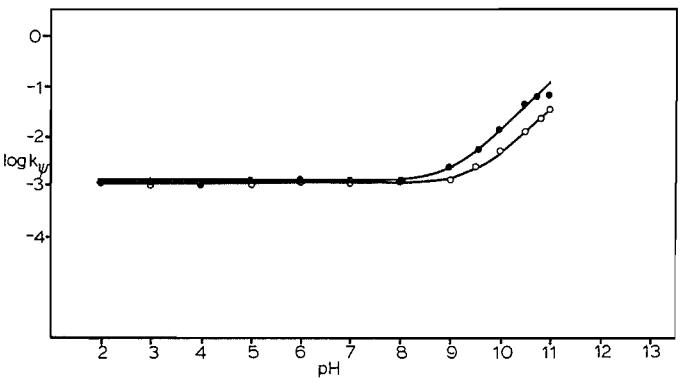

FIG. 1. pH–rate profile for the hydrolysis (in 0.1 M KCl containing 0.2% DME at 25.0°C) of ethenesulfonyl chloride (**1**) (closed circles) and *trans*-1-propene-1-sulfonyl chloride (**3**) (open circles). The points are experimental and the lines calculated from $\log k_\psi = \log (1.32 \times 10^{-3} + 124[OH^-])$ for **1** and $\log k_\psi = \log (1.22 \times 10^{-3} + 37[OH^-])$ for **3**.

TABLE 2. Product composition: reaction of ethenesulfonyl chloride (**1**) with pyridine in 0.1 M aqueous KCl at 25.0°C[a]

			Betaine fraction[c]	
pH	B_T (M)[b]	10^3[B] (M)	q	q'
3.0	0.23	1.0	0.80	0.84
3.0	1.19	5.3	0.77	0.78
4.0	0.23	10	0.80	0.80
4.0	0.23	10	0.83[d]	0.83
4.0	0.13	5.5	0.79[d]	0.80
5.0	0.16	5.0	0.85	0.85

[a] Initial concentration of **1**, 1.6×10^{-2} M.

[b] B_T = [B] + [BH^+].

[c] Betaine fractions: experimental betaine fraction, q = (yield of betaine)/(yield of betaine plus alkenesulfonate anion); yields were determined by ^{1}Hmr integration, except as otherwise noted; corrected betaine fraction, q', refers to the fraction of betaine produced in the amine-induced reaction only; $q' = q\,(1 + k_1/k_B[B])$.

[d] Determined by weighing betaine obtained after isolation via the deionization procedure.

*Reactions of **1** and **3** with pyridine bases in aqueous 0.1 M KCl*

In the presence of pyridine, reaction of **1** in 0.1 M KCl is much accelerated and gives mostly the betaine (**9**, X = H) along with the salt (**10**, X = H) (and the pyridinium chloride).

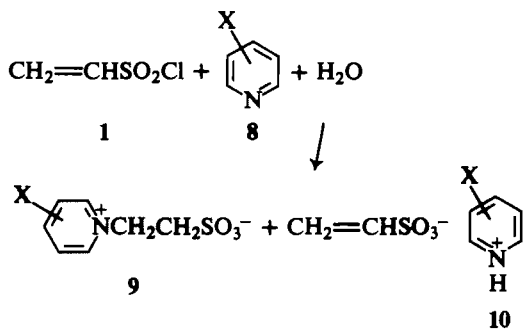

Passage of the reaction product through a deionizing resin removed the salts and the product so obtained was identified as **9** (X = H) by comparing with an authentic specimen (21). The fraction of betaine (**9**, X = H) in the reaction product was determined either by ^{1}Hmr integration or by weighing the product obtained after deionization, and the results given as "betaine fraction", q, in Table 2. Within the experimental uncertainty of these procedures (about ± 0.05) q is unaffected by change in pH or in the concentration of either the pyridine or the pyridinium ion; control experiments showed that the products are stable to the conditions of reaction and work-up. Similar treatment of *trans*-1-propene-1-sulfonyl chloride (**3**) gave the betaine (**11**, X = H) (56%) and the propenesulfonate salt (**12**, X = H) (44%). In D_2O at apparent pH 3.4, **1** gave the

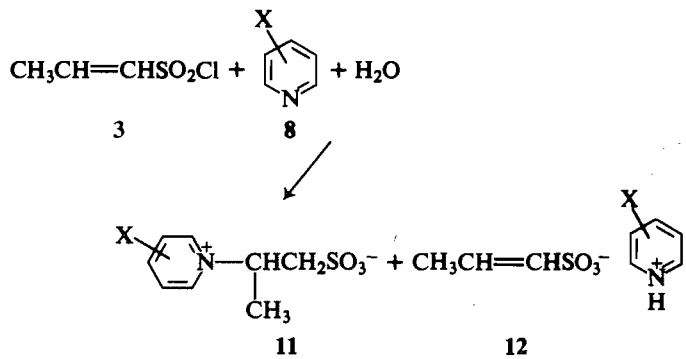

monodeuterated betaine, $Pyr^+CH_2CHDSO_3^-$ (75% yield, >95% monodeuterated) and undeuterated ethenesulfonate anion, CH_2=$CHSO_3^-$ (25% yield).

As shown in Fig. 2, the pseudo-first-order rate constants for

Can. J. Chem. Downloaded from www.nrcresearchpress.com by 210.87.254.6 on 09/06/12
For personal use only.

Can. J. Chem. Downloaded from www.nrcresearchpress.com by 210.87.254.6 on 09/06/12
For personal use only.

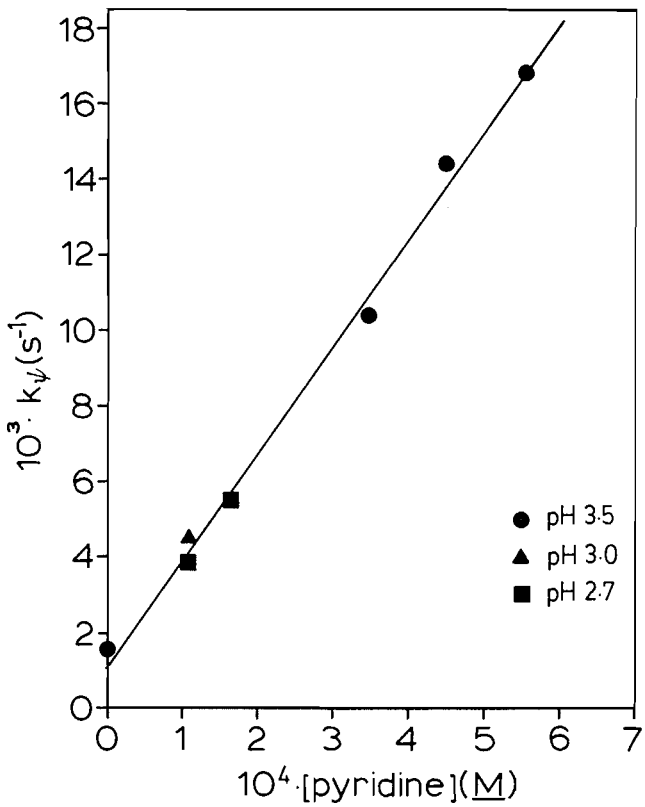

FIG. 2. Dependence of the observed pseudo-first-order rate constant on pyridine concentration in the reaction of **1** with pyridine in aqueous 0.1 *M* KCl (plus 0.2% DME) at 25.0°C; the points are experimental, the line that obtained from least squares: $k_\psi = 1.03 \times 10^{-3} + 28[B]$.

reaction **1** with pyridine in the pH range 2.7–3.5 obey the simple expression,

$$k_\psi = k_l + k_B[B]$$

with k_B, the second-order rate constant for the reaction of **1** with pyridine, equal to $28 \pm 3\ M^{-1}\ s^{-1}$; **3** behaved similarly with $k_B = 1.5 \pm 0.2\ M^{-1}\ s^{-1}$.

The rate constants were determined for an array of substituted pyridine bases (see Table 3). As may be seen from Fig. 3, a Brønsted plot (k_B vs. pK_a') for the reaction of **1** at 25.0°C with the "unhindered" bases – i.e. those with substituents in only the 3 or 4 positions – gave a good straight line ($r = 0.993$), corresponding to the equation $\log k_B = 0.32\ pK_a' - 0.22$. The same pattern was found with **3** at 25.0°C and **1** at 45.0°C: the values of β_{nuc}, the slope of the line for the "unhindered" bases, were respectively 0.31 for **1** at 45.0°C and 0.30 for **3** at 25.0°C. The "hindered" bases (those with 2- or both 2- and 6-substitution) invariably showed a lower value of k_B than predicted by this expression. It would seem reasonable to ascribe this deviation to the steric effect of the substituent(s) in the 2 (and 6) position(s)[4] and, with the aim of enabling a quantitative discussion of this effect, we define for the "hindered" bases a steric factor $SF = k/k_{predicted}$, in which k is

[4] The specific rates of the Menschutkin reaction of methyl iodide with 2- (and 6-) substituted pyridines show similar deviations from the Brønsted correlation of "unhindered" bases; this deviation has been assigned to steric effects (26, 27) and quantitatively correlated with steric parameters (28).

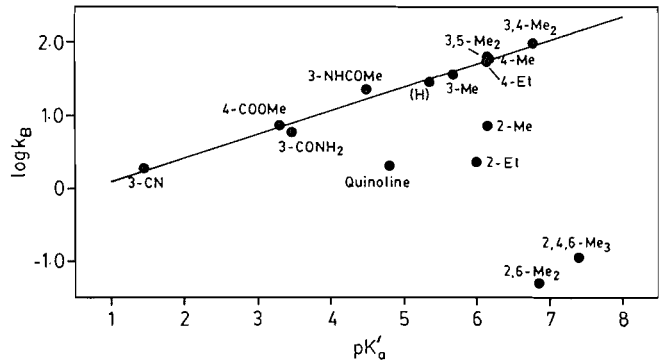

FIG. 3. Brønsted plot of the reaction of pyridine bases with ethenesulfonyl chloride (**1**). The points are experimental, the line is that of the expression, $\log k_B = 0.322\ pK_a' - 0.219$, obtained by linear regression ($r = 0.994$) from the k_B values for the "unhindered" bases, i.e. those lacking substituents in the 2 or 6 positions.

simply the experimental value of the rate constant for the particular "hindered" base, and $k_{predicted}$ is given by $\log k_{predicted} = \beta pK_a' + C$, where pK_a' refers to the same "hindered" base and β and C are obtained from the Brønsted plot of $\log k$ vs. pK_a' for the "unhindered" bases; SF is thus conveniently given by

$$\log SF = \log k - \beta pK_a' - C$$

In this form steric retardation is indicated by $SF < 1$, steric acceleration by $SF > 1$, and no steric effect at all (as, by definition, with the "unhindered" bases) by $SF = 1.0$. These steric factors are specific to both the particular base and the particular reaction; their function here is simply to separate steric and electronic factors as an aid in assessing the reasonableness of different possible mechanisms. Since we mention more than one kind of steric factor in this paper we attach a subscript that distinguishes the origin of each, e.g. SF_B is the steric factor for the reaction of hindered tertiary amines with **1** and **3**, as determined from k_B's. It should be noted specifically that SF_B does not give an absolute measure of the total steric effect in a reaction but rather the *difference* between the steric effect in the transition state for the reaction of the amine with **1** (or **3**) and the steric effect in the comparison species, i.e. the hydrated ammonium cation, on the assumption that electronic effects are not changed by the difference in steric effects.

The steric factors listed in Table 3 for reaction of **1** (at 25.0°C) point to steric retardations varying from eight-fold for 2-picoline to about two thousand-fold for 2,6-lutidine, while for the reaction of **3** the steric factors follow a similar pattern with invariably somewhat greater retardations.

For the reaction of **1** with 3-cyanopyridine in D_2O at 25.0°C (apparent pH 4.0) k_B was found to be $1.95\ M^{-1}\ s^{-1}$, giving a kinetic solvent isotope effect (KSIE), $(k_B)_H/(k_B)_D$, of 1.0.

The fraction of betaine in the reaction product (q in Tables 2 and 4) varied considerably with substitution. Where possible, the product composition was determined under conditions in which $k_B[B]/k_l > 20$, i.e. in which >95% of the product was formed in the base-induced reaction. With slow reacting or poorly soluble amines, however, this was not always feasible and with these reactions in particular the value of q describes a product from both the base-promoted and simple hydrolysis processes. To enable comparison of betaine fractions only from the amine-induced reactions, a "corrected" betaine fraction, q', and a product ratio, p, were calculated (see footnote *a*, Table 2). Again, to separate steric and electronic effects, we define

Can. J. Chem. Downloaded from www.nrcresearchpress.com by 210.87.254.6 on 09/06/12
For personal use only.

TABLE 3. Reaction of ethenesulfonyl and *trans*-1-propene-1-sulfonyl chlorides (**1** and **3**) with pyridine bases in 0.1 *M* aqueous potassium chloride: kinetic results

			Ethenesulfonyl chloride (**1**)						*trans*-1-Propene-1-sulfonyl chloride (**3**) (25.0°C)	
	pK'_a of base[a]		k_B (M^{-1} s^{-1})[b]		$\Delta H^{\ddagger}$	$\Delta S^{\ddagger}$	Steric factor, SF_B[c]		k_B	
Substituent(s)	25.0°C	45.0°C	25.0°C[c]	45.0°C[c]	(kcal mol^{-1})	(cal K^{-1} mol^{-1})	25.0°C	45.0°C	(M^{-1} s^{-1})[b]	Steric factor, SF_B[c]
"Unhindered" bases										
3,4-Dimethyl	6.68	6.46	95	277	9.5	−17.7			5.5	
3,5-Dimethyl	6.13	—	62	—	—	—			3.8	
4-Methyl	6.17	6.03	58	197	10.9	−14.0			2.9	
4-Ethyl	6.15	—	53	—	—	—			—	
3-Methyl	5.68	5.68	38	151	12.4	−10.0			2.0	
(None)	5.35	5.28	28	81	9.4	−20.4			1.5	
3-Ethanamido	4.50	4.55	22	86	12.2	−11.3			1.2	
3-Carbamoyl	3.47	3.55	6.2	24	12.1	−14.0			0.57	
4-Methoxycarbonyl	3.30	—	7.2	—	—	—			0.44	
3-Cyano	(1.45)[d]	(1.45)[d]	1.9	6.4	10.8	−21.0			0.12	
"Hindered" bases										
2-Methyl	6.15	6.00	6.9	31	13.5	−9.2	0.12	7.3×10^{-2}	0.16	4.9×10^{-2}
2-Ethyl	6.00	—	2.3	—	—	—	4.4×10^{-2}	—	0.10	3.4×10^{-2}
2,6-Dimethyl	6.87	6.67	0.05	0.15	9.7	−31.8	5.1×10^{-4}	4.9×10^{-4}	<0.002[e]	$<3.7 \times 10^{-4}$
2,4,6-Trimethyl	7.40	—	0.11	—	—	—	7.5×10^{-4}	—	—	—
Benzo[b]	4.80	—	2.0	—	—	—	9.4×10^{-2}	—	0.074	5.8×10^{-2}

[a] Titrimetric pK_a values determined in 0.1 *M* aqueous KCl.

[b] For the "unhindered bases", $\log k_B = 0.322\ pK'_a - 0.219$ for **1** at 25.0°C ($r = 0.994$); at 45.0°C $\log k_B = 0.327\ pK'_a + 0.307$ ($r = 0.989$), and for **3** at 25.0°C $\log k_B = 0.302\ pK'_a - 1.344$ ($r = 0.992$). For some of the "hindered" amines, e.g. 2-picoline and especially 2,6-lutidine, the values of k_B are substantially lower than those reported in our communication (18); this arises because these amines, though originally judged pure (by ^{1}Hmr and vpc), were found on inspection of the betaines produced under kinetic conditions to contain significant amounts of much faster reacting impurities. We therefore adopted the careful purification and stringent purity tests described in the Experimental.

[c] The "steric factor", SF_B, for the "hindered" bases is given by: $\log SF_B = \log k_B - \beta_{nuc} pK'_a - C$; β_{nuc} and C are given in footnote *b* for the appropriate reaction, and k_B and pK'_a are listed in the table. SF_B is assigned as 1.0 for the "unhindered" bases (see text).

[d] Estimated from a literature value (25) for pure water by adding a small (estimated) correction (0.06) for the change to 0.1 *M* KCl.

[e] No detectable catalytic effect ($k_\psi = 1.0 \times 10^{-3}$ s^{-1}) at pH 8.0, total base 5.16×10^{-2} *M* ([B] = 4.8×10^{-2} *M*).

TABLE 4. Reaction of ethenesulfonyl and *trans*-1-propene-1-sulfonyl chlorides (**1** and **3**) with pyridine bases in 0.1 *M* aqueous KCl at 25.0°C: product composition and derived steric factors

	Ethenesulfonyl chloride (**1**)				*trans*-1-Propene-1-sulfonyl chloride (**3**)			
	Betaine fraction[a]		Product ratio,[b,c]	Steric factor,[c]	Betaine fraction[a]		Product ratio,[b,c]	Steric factor,[d]
Substituent(s), (pK_a')	q	q'	p	SF_p	q	q'	p	SF_p
"Unhindered" bases								
3,4-Dimethyl (6.68)	0.87	0.89	0.12		0.74	0.76	0.32	
3,5-Dimethyl (6.13)	0.83	0.84	0.19		0.69	0.71	0.41	
4-Methyl (6.17)	0.87	0.88	0.14		0.74	0.75	0.33	
4-Ethyl (6.15)	0.83	0.84	0.19		—	—	—	
3-Methyl (5.68)	0.86	0.87	0.15		0.65	0.71	0.41	
(None) (5.35)	[e]	0.82[f]	0.22		0.56	0.59	0.69	
3-Ethanamido (4.50)	0.65	0.66	0.52		0.43	0.45	1.22	
3-Carbamoyl (3.47)	0.52	0.52	0.92		—	—	—	
4-Methoxycarbonyl (3.30)	0.5	0.5	1		0.26	0.27	2.7	
3-Cyano (1.45)	0.17	0.17	4.9		0.08	0.09	10	
"Hindered" bases								
2-Methyl (6.15)	0.55	0.60	0.67	4.4	0.39	0.40	1.5	4.0
2-Ethyl (6.00)	0.61[g]	0.63	0.59	3.5	0.24	0.39	1.6	3.8
2,6-Dimethyl (6.87)	0.66	0.76	0.32	3.5	—	—	—	—
2,4,6-Trimethyl (7.40)	0.65	0.67	0.49	7.7	—	—	—	—
Benzo[b] (4.80)	0.51	0.52	0.92	2.3	0.35	0.45	1.2	1.2

[a] As defined in Table 2, footnote *c*; q values from ^{1}Hmr integration unless otherwise noted.
[b] The product ratio, p, is the ratio of **10** to **9** (or **12** to **11**) and is given by $(1 - q')/q'$.
[c] For the "unhindered" bases and **1** $\log p = 1.056 - 0.305\ pK_a'$ ($r = 0.987$); SF_p values are from $\log SF_p = \log p - 1.056 + 0.305\ pK_a'$.
[d] For the "unhindered" bases and **3**, $\log p = 1.422 - 0.300\ pK_a'$ ($r = 0.994$); SF_p values are from $\log SF_p = \log p - 1.422 + 0.300\ pK_a'$.
[e] For q and individual q' values see Table 2.
[f] Mean value of those in Table 2.
[g] Determined from weight of product after deionization.

another steric factor, SF_p, from the product ratio, p, following the pattern detailed above. The values of SF_p are listed in Table 4 and are notably limited in range compared to SF_B's. As may also be seen from Table 4, both greater steric "bulk" and a low pK_a' of the amine favour a larger value of p, i.e. the greater proportion of the alkenesulfonate salt (**10** or **12**) in the product of the amine-induced reaction.

The reaction of 1 and 3 with tertiary alkylamines

We have also looked at the reaction of **1** and **3** with some simple saturated tertiary amines in the same medium (0.1 *M* aqueous KCl containing 0.2% DME), and found the rates to be measurable at 1.0°C when very low concentrations of the free amine were used. As is shown in Table 5, the reaction product is a mixture of the betaine (**13**) and the tertiary ammonium alkenesulfonate (**14**), plus the chloride salt as well:

$$R_3N + R'CH{=}CHSO_2Cl$$

1 R′ = H
3 R′ = CH_3

$$R_3\overset{+}{N}CHCH_2SO_3^- + R_3\overset{+}{N}H\ R'CH{=}CHSO_3^- + R_3\overset{+}{N}H\ Cl^-$$

$$\begin{matrix} & & \\ & R' & \end{matrix}$$

13 **14**

a R′ = H
b R′ = CH_3

As with the pyridine bases, the essentially constant values of q' with each base (Table 5) show that change in pH, or the concentration of the base or the conjugate acid of the base does not alter the composition of the product from the reaction of the aqueous amines with **1** or **3**.

Table 6 gives the k_B, average q', and p values for these reactions at 1.0°C. The k_B's show two effects: (*i*) the 30-fold greater rate for quinuclidine vs. trimethylamine indicates that in the absence of significant steric differences a stronger base reacts faster than a weaker, and (*ii*) the successive lowering of k_B as methyl groups are replaced by ethyl or isopropyl, even though accompanied by increasing base strength, points to significant steric effects in these reactions as well. In order to separate steric from electronic factors, we follow the method already described for the pyridine bases by making the reasonable assumption that trimethylamine and quinuclidine show very similar steric effects, and that these may be expected to be the smallest possible such effects for tertiary alkylamines, i.e. that among such amines these two are the "unhindered" members of the class. The specific rates for these two bases therefore provide the basis for a Brønsted-type expression for "unhindered" tertiary alkylamines, which makes it possible to calculate steric factors, SF_B, for the other tertiary amines; these are listed in Table 6 along with the analogously obtained values for SF_p, the steric factor derived from the product ratio, p. Although any Brønsted expression based on only two points must be regarded as very approximate, the basic validity of this procedure is supported not only by the arguments given above but also by the consistency of the parameters so obtained. The Brønsted exponents from the k_B's are 0.37 for **1** and 0.41 for **3**, values in accord with each other and in the general range found for the corresponding reactions of the pyridine bases

Can. J. Chem. Downloaded from www.nrcresearchpress.com by 210.87.254.6 on 09/06/12
For personal use only.

TABLE 5. Product composition: reaction of ethenesulfonyl and *trans*-1-propene-1-sulfonyl chlorides (**1** and **3**) with saturated tertiary amines in 0.1 *M* aqueous KCl at 1.0°C

		Ethenesulfonyl chloride (**1**)				*trans*-1-Propene-1-sulfonyl chloride (**3**)			
				Betaine fraction[c]				Betaine fraction[c]	
Amine	pK_a'	pH	B_T $(M)^b$	q	q'	pH	B_T $(M)^b$	q	q'
Me_3N	10.30	3.5	0.32	0.52	0.78	6.5	0.32	0.20	0.21
		4.0	0.32	0.64	0.77	7.0	0.32	0.19	0.19
		4.5	0.32	0.68	0.71				
		4.5	0.32	0.67[d]	0.70				
		4.0	0.064	0.41	0.74				
		5.0	0.064	0.69	0.75				
Me_2NEt	10.42	5.0	0.08	0.53	0.58	—	—	—	—
		5.5	0.08	0.55	0.57				
$MeNEt_2$	10.85	6.0	0.08	0.47	0.51	—	—	—	—
		6.5	0.08	0.50	0.52				
Et_3N	11.29	7.0	0.08	0.40	0.47	8.0	0.08	<0.004[e]	<0.05
		7.5	0.08	0.46	0.48				
		7.5	0.08	0.46[d]	0.48				
$EtNPr^i_2$	11.51	9.0	0.08	(<0.04)[f]	(<0.04)[f]	—	—	—	—
Quinuclidine	11.70	5.3	0.10	0.77	0.92	7.0	0.08	0.26	0.41
		6.0	0.10	0.90	0.93	8.0	0.008	0.36	0.38

[a] Titrimetric pK_a values determined in 0.1 *M* aqueous KCl at 1.0°C.
[b] $B_T = [B] + [BH^+]$.
[c] Terms defined in Table 2, footnote *c*; q values were determined by weighing the betaine obtained after deionization, except as otherwise noted.
[d] Determined by ^{1}Hmr integration.
[e] No sign of any betaine after deionization.
[f] Peaks tentatively ascribable to the betaine (~3% yield) were observed in the product of deionization; no authentic sample of the betaine has been prepared and its stability to the work-up not proved; the values of q, q', and also p and SF_p (Table 6) are therefore tentative.

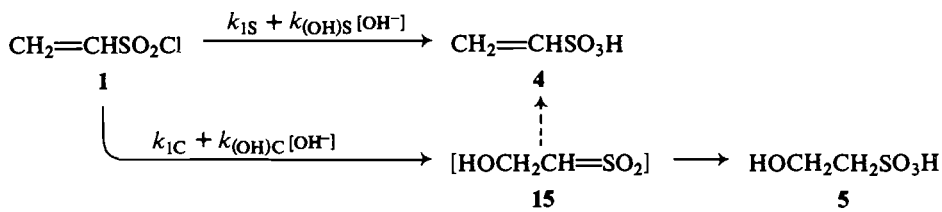

SCHEME 2

(0.32 and 0.30, respectively). The greater difference in Brønsted exponents from p values, i.e. 0.5 for **1** vs. 0.3 for **3** (footnotes *d* and *e*, Table 6) is due at least in part to experimental uncertainty; the former value in particular, because it derives from p for the reaction of **1** with quinuclidine in which the small amount of the salt (**14**) is difficult to determine accurately, is only a rough number (±0.2). The SF_B values, as might be expected, show a progression from a very small steric effect (SF_B = 0.77) with dimethylethylamine to the 900-fold steric effect with diisopropylethylamine. As was noted already with the pyridine bases, (*i*) the steric effect of a particular base (triethylamine in this case) is more pronounced in its reaction with **3** than with **1**, and (*ii*) the steric effects for the attack of the amine (shown by SF_B) are larger than in product formation (as shown by SF_p).

In D_2O at apparent pH 10.0, trimethylamine gave the monodeuterated betaine, $Me_3\overset{+}{N}CH_2CHDSO_3^-$ (>90% mono D), and undeuterated ethenesulfonate salt (<5% deuteration on the anion); similarly, diisopropylethylamine in D_2O–DME (80:20) at pH (meter reading) 9.0 (under conditions in which the presence of the amine increased the pseudo-first-order rate constant by a factor of 2.9) also gave the ethenesulfonate salt with no sign of deuteration on the anion.

Mechanisms. First considerations

For the reaction of **1** or **3** with water in the absence of amines, our observations are nicely consistent with a direct displacement on sulfur (DDS) mechanism in which most of the reactions occur by attack of water or hydroxide ion on the sulfonyl sulfur to produce **4** (or **6**).[5]

The small amount of 2-hydroxyethanesulfonic acid (**5**) formed by reaction of **1** at both high and low pH points to the hydroxysulfene (**15**) as an intermediate as indicated in Scheme 2; **15** is presumably formed in acidic medium by attack of water, with attack of hydroxide ion becoming important above pH ~9. Postulation of the intermediacy of **15** raises the possibility that at least some of the ethenesulfonic acid (**4**) may arise from **15** (as shown by the broken arrow in Scheme 2); this, of course, would be a form of vinylogous nucleophilic catalysis. As we have described elsewhere (31), however, we have pre-

[5] The present study is not primarily concerned with the detailed mechanism of the DDS process, but if, as has been suggested by Williams and co-workers (29, 30), hydroxide ion reacts with aryl sulfonic esters with concerted extrusion of aryloxide anion, then it would seem likely that expulsion of the relatively nucleofugal chloride ion from **1** or **3** is also concerted.

Can. J. Chem. Downloaded from www.nrcresearchpress.com by 210.87.254.6 on 09/06/12
For personal use only.

Can. J. Chem. Downloaded from www.nrcresearchpress.com by 210.87.254.6 on 09/06/12
For personal use only.

TABLE 6. Reaction of saturated tertiary alkylamines with ethenesulfonyl and *trans*-1-propene-1-sulfonyl chlorides (**1** and **3**) in aqueous 0.1 *M* KCl at 1.0°C: kinetic results, summary of product composition, and estimated steric factors

	Ethenesulfonyl chloride (**1**)					*trans*-1-Propene-1-sulfonyl chloride (**3**)				
Amine (pK'_a)	k_B (M^{-1} s^{-1})	Steric factor, SF_B[a]	q[b]	p[c]	Steric factor, SF_p[d]	k_B (M^{-1} s^{-1})	Steric factor, SF_B	q[b]	p[c]	Steric factor, SF_p[e]
Me_3N (10.30)	3.48×10^3	(1.0)	0.74	0.35	(1.0)	23	(1.0)	0.20	4.0	(1.0)
Me_2NEt (10.42)	2.96×10^3	0.77	0.58	0.72	2	—	—	—	—	—
Me_2NPr^i (10.80)	1.78×10^3	0.33	—	—	—	—	—	—	—	—
$MeNEt_2$ (10.85)	6.93×10^2	0.12	0.52	0.92	5	—	—	—	—	—
Et_3N (11.29)	1.10×10^2	1.4×10^{-2}	0.48	1.08	10	~0.2[f]	$\sim 3 \times 10^{-3}$	<0.05	>20	>10
$EtNPr^i_2$ (11.51)	11	1.1×10^{-3}	(<0.04)[g]	(>24)[g]	(>200)[g]					
Quinuclidine (11.70)	1.14×10^4	(1.0)	0.93	0.075	(1.0)	86	(1.0)	0.39	1.56	(1.0)

[a] As defined in Table 3, footnote *c*; the Brønsted-type expressions from the reactions of the "unhindered" bases Me_3N and quinuclidine are, for **1**, $\log k_B = 0.368\ pK'_a - 0.250$, and for **3**, $0.409\ pK'_a - 2.852$.
[b] Average of those in Table 5.
[c] The product ratio, p, is the ratio of **14** to **13**, and is given by $(1 - q')/q'$.
[d] From $\log SF_p = \log p - 4.47 + 0.48\ pK'_a$ (cf. Table 4, footnote *d*).
[e] From $\log SF_p = \log p - 3.61 + 0.29\ pK'_a$.
[f] Approximate value only, owing to small catalytic effect (7% and 17% increases in k_ψ for reactions at pH 8.0 and 8.5, $B_T = 0.08\ M$).
[g] See footnote *f*, Table 5.

pared 2-hydroxyethanesulfonyl chloride ($HOCH_2CH_2SO_2Cl$) and seen clear signs of the formation of **15** therefrom, and concluded that **15** gives **5** with little or no **4**, thereby excluding the route **1** → **15** → **4**.

It is therefore reasonable to infer that **4** (and also **6**) arises by the DDS mechanism and **5** (and **7**) by way of the sulfene resulting from attack on C-2, in each case by reaction with either water or hydroxide ion. On this basis, by simply taking the proportions of **4** and **5** (or **6** and **7**) we may factor the experimental rate constants k_I and k_{OH} into k_{IS} and k_{IC}, and $k_{(OH)S}$ and $k_{(OH)C}$ values,[6] as defined in Scheme 2 and listed in Table 1. Note that k_{IS} is the same for **1** and **3** within experimental uncertainty (1.2×10^{-3} s^{-1}), whereas $k_{(OH)S}$ for **1** is about three times that for **3**. A similar effect of methyl substitution in reaction with water and hydroxide ion (in a presumed DDS reaction) is seen by comparing the k_I and k_{OH} values for benzenesulfonyl and *p*-toluenesulfonyl chlorides reported by Rogne (3) and listed in Table 1.

In contrast with those reactions which involve attack of water on the sulfur atom, those in which water bonds to C-2 with ultimate formation of the sulfene (e.g. **15**) are evidently sensitive to the presence of the methyl group, with k_{IC} being at least five times greater for **1** than for **3**. This result is consistent with modest steric interference by the methyl group to attack at C-2; a similar effect is probably influencing attack of hydroxide as well, though here the steric and electronic effects are hard to sort out.

Also in full accord with this mechanistic picture are the results of the experiments carried out in deuterium oxide. The absence of deuterium in the ethenesulfonate (**4**) clearly shows that it cannot have been formed by way of the cumulated sulfene (**2**), while the presence of one (and only one) deuterium in the 2-hydroxyethanesulfonate is fully consistent with its formation from **15**. The kinetic solvent isotope effect (KSIE), k_H/k_D, of 1.54 is close to those reported by Robertson and Laughton for the hydrolyses of methanesulfonyl chloride (1.58 at 20.0°C) and benzenesulfonyl chloride (1.58 at 10.0°C) (32).

Tertiary amine bases completely alter the reaction, the major product with pyridine bases in most cases being the betaine (**9** or **11**). As initially suggested by Le Berre *et al.* (21) the simplest route to the betaine (**9**) is via the sulfene (**16**) (Scheme 3); the formation in D_2O of monodeuterated betaine, $Pyr^+CH_2CHDSO_3^-$, accords with this picture. The origin of the ethenesulfonate salt (**10**), however, is not as easily settled, with three possible pathways shown in Scheme 3. The first of these, **1** → **16** → **10** is a vinylogous nucleophilic catalysis (VNC) mechanism, the second, **1** → **10**, is a general base-catalyzed DDS reaction, and the third, **1** → **17** → **10**, is a conventional nucleophilic catalysis (CNC) process. A further possible route, that via the cumulated sulfene (**2**), is readily dismissed by the observation of undeuterated ethenesulfonate anion $CH_2{=}CHSO_3^-$ from the reaction in D_2O.

Two pieces of evidence combine to provide a convincing case against the general base-catalyzed DDS mechanism. First is the observation that the presence of a 2-substituent in the pyridine base consistently retards the reaction. This effect is quantitatively characterized by the steric factor, SF_B, (see Table 3), which for the "hindered" bases is always less than one and in some cases less than 10^{-3}, corresponding to retardations

[6] The additional subscripts S and C indicate the site of nucleophilic attack, sulfur or carbon, respectively.

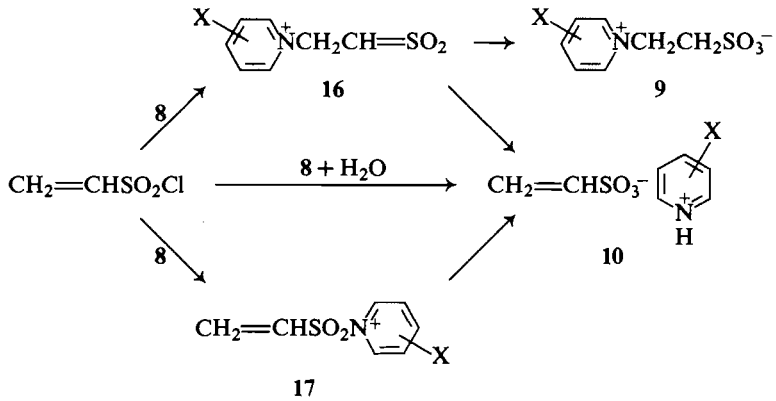

SCHEME 3

of more than a thousand times. Such a sizeable deviation from the Brønsted-type expression obeyed by the "unhindered" bases is much more readily accommodated by a nucleophilic catalysis mechanism than a general-base process (33). Second, the lack of a KSIE in the reaction of **1** with 3-cyanopyridine is also more easily reconciled with nucleophilic catalysis than general base promotion (33). 3-Cyanopyridine was chosen as the base for investigation of the KSIE primarily because it gives the largest proportion of **10** (~80%) of any of the "unhindered" bases and hence any KSIE in the formation of **10** would be readily apparent from the simple measurement of the KSIE for the overall transformation to a mixture of **9** and **10**.[7]

Distinguishing rigorously between vinylogous and conventional nucleophilic catalysis is, however, a little more difficult. It is perhaps helpful to consider separately the two extreme mechanisms for formation of the alkenesulfonate salt **10** (or **12**); i.e. (*i*) the salt is formed exclusively by VNC, or (*ii*) **10** (or **12**) is produced entirely by CNC. The two limiting pictures may thus be summarized for the overall reaction of **1** as follows:

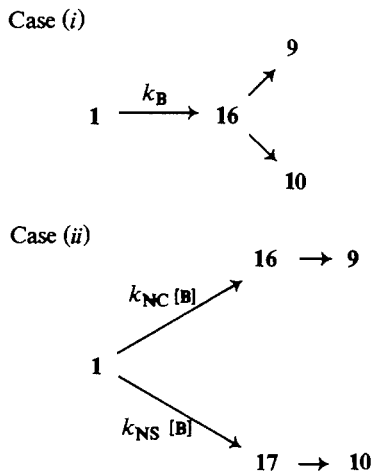

With case (*i*) the measured k_B is simply the rate constant for the rate-determining attack of the amine on **1** with formation of **16**, while *p* provides information about the subsequent fate of **16**, being simply the ratio of the rate of formation of the betaine **9** (or **11**) to that of the salt **10** (or **12**). With the case (*ii*) mechanism, however, k_B is the sum of two rate constants, $k_{NC} + k_{NS}$, where k_{NC} refers to attack on carbon to form the sulfene (e.g. **16**) and k_{NS} to formation of the sulfonylammonium salt[6] (e.g. **17**); q' then describes the fraction of attack at carbon and $(1 - q')$ the fraction of attack on sulfur. On this basis, then

$$k_{NC} = q'k_B \text{ and } k_{NS} = (1 - q')k_B$$

and one may easily assemble an array of k_{NC} and k_{NS} values from those for k_B and q' given in Table 4. At this point we may examine the trends and variations in the respective sets of parameters for case (*i*) and for case (*ii*), to see if we can decide which is the more reasonable mechanism.

The values of k_{NC} and k_{NS} for **1** and **3** with the "unhindered" bases show good to mediocre correlations with pK_a', with linear regression giving the following: for **1**, $\log k_{NC} = 0.45\ pK_a' - 0.49$ and $\log k_{NS} = 0.14\ pK_a' + 0.04$ ($r = 0.996$ and 0.91, respectively), while for **3**, $\log k_{NC} = 0.49\ pK_a' - 2.63$ and $\log k_{NC} = 0.18\ pK_a' - 1.16$ ($r = 0.995$ and 0.96). Following the established procedure we can also calculate steric factors for the "hindered" bases from the k_{NC} and k_{NS} values for attack on C-2 and on the sulfur. This analysis reveals three points. (*a*) We note that k_{NS} for **1** is always greater than that for **3** by factors varying from 7.3 to 29 and averaging 12.4; this contrasts with the corresponding reaction with water (also a neutral nucleophile), in which **1** and **3** react at the *same* rate ($k_{1S} = 1.2 \times 10^{-3}$ s^{-1} for each, see Table 1). (*b*) On comparing the reactions of the only "hindered" bases for which we have results for reaction with both **1** and **3**, viz. 2-picoline and quinoline, we note that the steric factors determined from the k_{NS} values for reaction with **1** differ from those with **3**; for 2-picoline the steric factor is 0.4 with **1** and 0.1 with **3**, and for quinoline it is 0.2 with **1** and 0.08 with **3**. By way of comparison, k_{NC} values give steric factors of 0.08 and 0.03 for 2-picoline with **1** and **3**, respectively, and 0.08 and 0.06 for the corresponding quinoline reactions. Interpretation of these results in terms of the case (*ii*) mechanism presents the following odd situation: we have two substrates which differ only in that the differentiating group is attached directly to one reaction centre (C-2) and well removed from the other (the sulfur atom), and yet not only do we see a change in steric factor for the reaction at the remote centre on changing substrates, but also this change in steric factor is actually greater than that for the reaction at C-2, the substituent-bearing site. (*c*) Further, we note an anomaly of a different kind. The Brønsted exponent, β_{nuc}, for the putative DDS reaction (from k_{NS} values) is respectively 0.14 and 0.18. This contrasts with $\beta_{nuc} = 0.45$ reported by Rogne (34) for the reaction of benzenesulfonyl chloride (34) with pyridine bases under fairly similar conditions (0.05 *M* aqueous KCl, 25.0°C). If, as we have reason to believe, the benzenesulfonyl chloride

[7] The general base-catalyzed reaction is not necessarily excluded for *all* of the reactions in this study, see footnote 9.

Can. J. Chem. Downloaded from www.nrcresearchpress.com by 210.87.254.6 on 09/06/12
For personal use only.

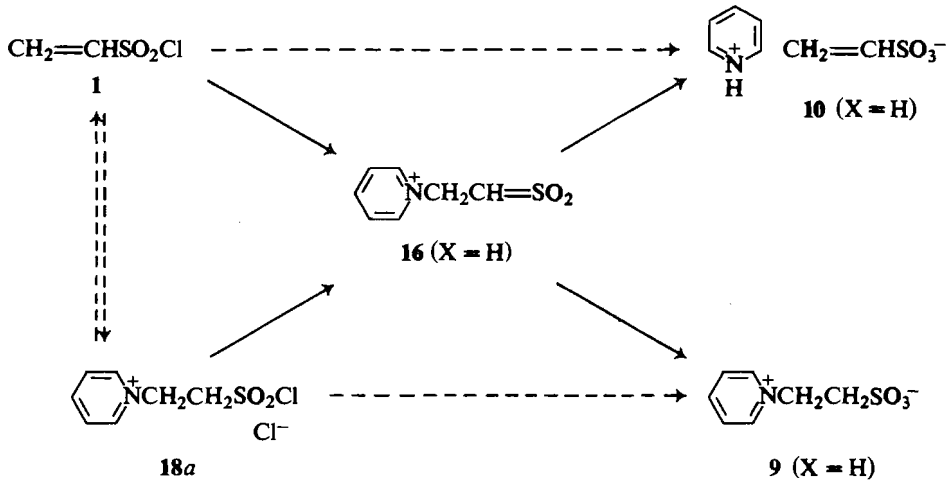

SCHEME 4

reaction is indeed a CNC process, then it is difficult to see how such different β_{nuc} values are compatible with such similar reactions. When taken with the two additional points above, it is clear that the case (*ii*) mechanism presents serious difficulties.

Similarly we find that our results for the reactions of saturated tertiary alkylamines with **1** and **3** also lead to difficulties when interpreted in terms of the case (*ii*) mechanism. From the k_{NS} values, particularly, we note the following. (*a*) For the reaction of **1** with quinuclidine k_{NS} is about the same (or, if anything, smaller) than that with trimethylamine, implying a Brønsted exponent of zero (or possibly lower) for the attack of these amines at a sulfonyl sulfur; this, of course, is quite different from $\beta_{nuc} = 0.45$, already mentioned, for the attack of pyridine bases on arenesulfonyl chlorides (34). (*b*) The k_{NS} values for **1** are substantially greater than those for **3**, by factors of 49, >285, and 15 for Me_3N, Et_3N, and quinuclidine, respectively.[8] We can remove the somewhat remote possibility that these differences reflect significant electronic effects by extracting steric factors, SF_{NS}, (from k_{NS} values for the three amines as already described); the SF_{NS} so obtained are 0.07 for the reaction of triethylamine with **1** and <0.005 for that with **3**. Such an increase in steric retardation of the reaction at sulfur of more than 14-fold on going from **1** to **3** seems difficult to explain and begs an alternative explanation.

Analysis of the kinetic and product composition data on the basis of the case (*i*) mechanism, on the other hand, gives apparently reasonable values both for the Brønsted exponents (0.30 and 0.32 for the pyridine bases and 0.37 and 0.41 for the saturated amines, as given above) and also for the rate constant ratios deduced from *p* discussed later in this paper. We were thus led to conclude that the above results argued strongly against the CNC process and in favour of the VNC mechanism for formation of **10** (and **12** and **14** also). But, since the latter was an unprecedented mechanism, we felt that further evidence would be desirable, and to this end we turned to one of the classic arguments of chemistry, viz., that a postulated intermediate, however generated, must give the same products under the same conditions. As our source of **16**, the presumed intermediate from **1**, we turned to the chlorosulfonylammonium salt **18***a*, which had already been prepared by Dr. Sheena Loosmore in these laboratories.

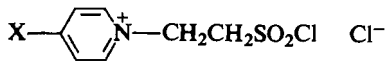

18
a **X = H**
b **X = Me**

Preparation and reactions of N-*(2-chlorosulfonylethyl)pyridinium chloride (18*a)

The salt (**18***a*) was prepared simply by adding a methylene chloride solution of **1** to a solution of pyridinium chloride and collecting the crystals. The mode of synthesis, taken with (*i*) satisfactory elemental analyses and (*ii*) appropriate ^{1}Hmr and infrared spectra (see Experimental), suffices to identify this material as **18***a*. Similar reaction of **1** and 4-picolinium chloride gave crystalline **18***b*.

Reaction of **18***a* with pyridine in 0.1 *M* aqueous KCl at pH 4.0 gave an 83:17 ratio of the betaine (**9**, X = H) and the ethenesulfonate salt (**10**, X = H). The concentration of pyridine in this reaction ($B_T = 0.5$ *M*, [B] = 0.021 *M*) was such that virtually all (99%) of the product would be expected to arise from the amine-induced reaction, and hence to a fair approximation $q = q' = 0.83$. On comparison with q' values given in Table 2 it is clear that the value from **18***a* is indistinguishable from those from **1**. In D_2O (0.1 *M* in KCl) at apparent pH 4.0, **18***a* and pyridine ($B_T = 2.5$ *M*) gave a mixture containing monodeuterated betaine (>95% $PyrCH_2CHDSO_3^-$) and undeuterated ethenesulfonate salt, corresponding to $q = 0.76$. Ethenesulfonyl chloride (**1**) in 0.1 *M* KCl in D_2O at apparent pH 3.4 ($B_T = 0.5$ *M*) gave similarly monodeuterated betaine and undeuterated salt with $q = 0.70$. With the 4-picoline analogue (**18***b*), similar reaction with 4-picoline ($B_T = 0.62$ *M*) gave the betaine (**9**, X = 4-Me) and the ethenesulfonate salt (**10**, X = 4-Me) in a 92:8 ratio: q' for 4-picoline (Table 2) is 0.88. Scheme 4 summarizes pathways consistent with these observations. To the extent that the products from **18** and **1** differ at all, the former appear to show more betaine (**9**) and the latter more of the salt (**10**), as would be expected from incursion of a small proportion of the DDS

[8] For comparison we note, in addition to those in Table 1, the following rate constants: (*a*) for solvolysis at 25.0°C in H_2O–dioxane (20:80) $MeSO_2Cl$ 14.8×10^{-6}, $EtSO_2Cl$ 13.0×10^{-6}, $PrSO_2Cl$ 11.2×10^{-6}, and Bu^iSO_2Cl 7.49×10^{-6} s^{-1} (35); (*b*) for reaction in methanol of $PhSO_2Cl$ and *p*-$MeC_6H_4SO_2Cl$, respectively, with pyridine (at 25.0°C) 2.51×10^{-2} and 2.06×10^{-2} M^{-1} s^{-1} (36), and with aniline (at 35.0°C) 10.6×10^{-2} and 7.85×10^{-2} M^{-1} s^{-1} (9). The effect of replacing a hydrogen by a methyl group is small in each case.

Can. J. Chem. Downloaded from www.nrcresearchpress.com by 210.87.254.6 on 09/06/12
For personal use only.

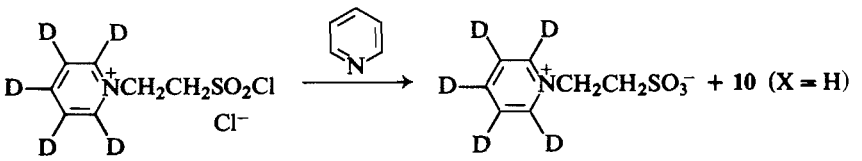

20 **21**

reaction (either uncatalyzed or general base catalyzed) shown by the horizontal dotted arrows in Scheme 4, but in the light of similarity of the products from **1** and **18** we conclude that the reactions shown by the horizontal dotted arrows are at most only minor contributors (<3%) to the reactions of **1** or **18** with aqueous pyridine bases under our conditions.

The two vertical dotted arrows in Scheme 4 describe the conversion of **1** to **18** and vice versa, two essentially trivial processes which could also, however, lead to common products from **1** and **18**. The first of these, **1** → **18***a*, is easily excluded by the results already described for the reaction in D_2O, the products of which were undeuterated ethenesulfonate salt (**10**) and the monodeuterated betaine. If **1** were indeed to form **18***a*, then in D_2O it would have to be largely monodeuterated, i.e. $Pyr^+CH_2CHDSO_2Cl\ Cl^-$ (**19**), which in turn would be expected to give some α-dideuterated betaine. We have, in fact, prepared a sample of **19** and found that it does give such products; their absence in the product of the reaction of **1** in D_2O therefore excludes the reaction **1** → **18** in the conversion to **9** and **10**.

The alternative possibility, **18***a* → **1**, was excluded by preparing **20**, by using pyridinium-d_5 chloride in place of ordinary pyridinium chloride. Reaction of **20** with ordinary pyridine (>200-fold excess) in water gave the betaine-d_5 (**21**) and **10** (81% and 19%, respectively). Any conversion of **18** to **1** would simply mix a little pyridine-d_5 with a much larger amount of ordinary pyridine and further reaction of the **1** so obtained would give almost entirely **9** (X = H) rather than **21**. Since even a small amount (<5%) of **9** (X = H) would have been readily seen by ^{1}Hmr, we conclude that there is no significant formation of **1** from **18** either, and hence that none of the reactions indicated by dotted arrows in Scheme 4 are important in the reaction of **1** or **18** with aqueous pyridines. We conclude that the hitherto unrecognized vinylogous nucleophilic catalysis mechanism must be regarded as the only important pathway consistent with our observations on the conversion of **1** to **10** and **3** to **12**. In the light of the evident similarity of these reactions to those of the saturated tertiary amines, it seems highly likely that the latter reactions leading to **14** also proceed by way of the VNC route.[9]

Further mechanistic points

(a) The sulfene formation

More detailed consideration raises the two additional questions of the mechanisms of formation and trapping of the sulfene (**16**). Extensive study of the generation of sulfenes by way of elimination reactions from alkanesulfonyl chlorides, aryl alkanesulfonates, and alkyl α-disulfones (12–16, 37, 38), has shown some of these reactions to proceed via α-sulfonyl carbanions (E1cB reactions, both reversible and irreversible) and some also very likely by a concerted elimination process in which there is a sizeable buildup of negative charge on the α-carbon in the transition state (E1cB-like E2). With this in mind it would appear likely that reaction of **1** with tertiary amines might also take place either by way of the analogue of the discrete carbanion, namely the zwitterion **22** (Z = Cl), or

$$R_3\overset{+}{N}CH_2\bar{C}HSO_2Z$$

22

in a one-step concerted but nonsynchronous displacement in which there is a considerable accumulation of negative charge on C-1. It should be noted that the conformation of the putative zwitterionic intermediate (**22**, Z = Cl) in which the chlorine and nitrogen atoms are *syn* to each other has a particularly favourable arrangement leading to stabilization of the lone pair of electrons by the anomeric effect (39–42).[10] This conformation is very close to that expected for the transition state of a concerted (but not necessarily fully synchronous) *syn* S_N2' displacement and, in the light of the extensive studies on allylic systems which have concluded that the favoured stereochemistry with uncharged nucleophiles is also *syn* (44–47, and refs. cited), we find it particularly easy to imagine, for the formation of **16** from **1**, a family of closely related mechanisms with very similar geometry and differing only in the extent by which C—N bond formation precedes S—Cl bond breakage. From the evidence for considerable buildup of negative charge on the α-carbon in sulfene formation from phenylmethanesulfonyl chloride (48), we are inclined to expect a considerable negative charge on C-1 in the **1** → **16** conversion, but whether or not this actually leads to formation of **22** (Z = Cl) as a discrete intermediate, we are unable to determine at this stage.

(b) Trapping of the sulfene

In contrast to formation of the sulfene (**16**), however, trapping of **16** shows features which incline us in favour of a stepwise mechanism as shown in Scheme 5. Formation of two

[9] The value of SF_p for the reaction of **1** with diisopropylethylamine is tentative (see Table 5, footnote *f*) but, if real, would seem sufficiently different from the other SF_p values listed in Tables 4 and 6 as to suggest that the observed weakly catalytic effect of the base may not derive from VNC at all but rather from another process, e.g. general base catalysis, a process in which steric factors are less important than nucleophilic catalysis (33); reaction in D_2O–DME (80:20) showed no sign of deuterium uptake in the ethenesulfonate anion, showing that the cumulated sulfene (**2**) could not be an intermediate even with this highly hindered amine.

[10] The influence of the ammonio group in stabilizing the negative charge in **22**, though smaller than that of the sulfonyl function, would appear to be considerable. Thomas and Stirling (43) estimate that hydrogen exchange in sulfones of the type $PhSO_2CH_2CH_2Z$ proceeds about 10^8 times faster when Z = Me_3N^+ than when Z = H (with EtONa in EtOH at 25°C). Although we know of no experimental demonstration of the geometrical requirements of this stabilization of negative charge, it seems highly likely from the obvious similarity of the $\bar{C}—CN^+R_3$ system to those that show the anomeric effect that an effect of this magnitude should have similar origins and the corresponding preferred periplanar orientation of the free electron pair and the C—N bond.

Can. J. Chem. Downloaded from www.nrcresearchpress.com by 210.87.254.6 on 09/06/12
For personal use only.

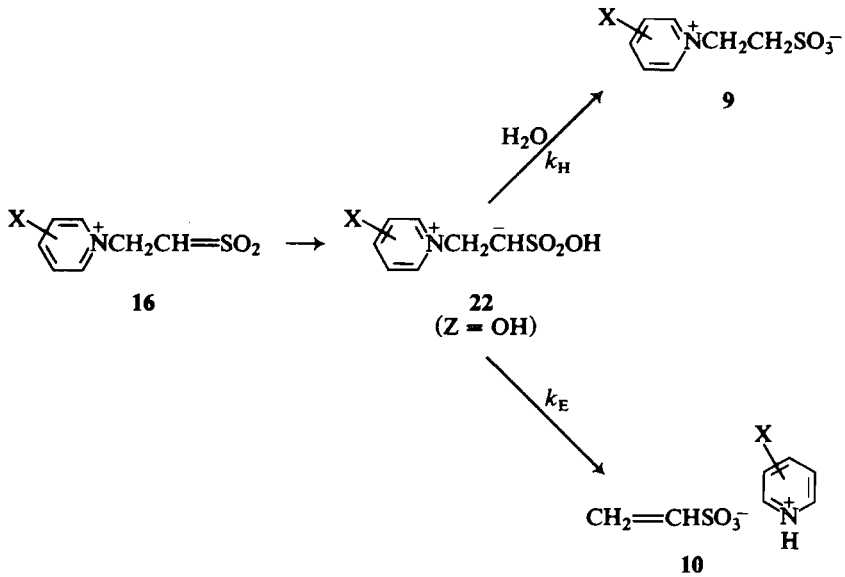

SCHEME 5

products (e.g. **9** and **10**) from a common species requires that that species (**22**, Z = OH, in this case) be a discrete intermediate and the product ratio (**10**/**9** = p, see Table 4) therefore reflect the relative rates of the unimolecular elimination to form **10** and proton uptake to give **9**. From our observation that the product ratio is insensitive to change in either pH or the concentration of pyridine or pyridinium ion (see Table 2, compare also Table 5), it would appear that the proton required to form **9** comes from neither H_3O^+ nor the pyridinium ion and so must be provided by the water, as shown. The ratio of the two rate constants is simply given by the product ratio, i.e. $p = k_E/k_H$. A plot of log p for the reaction of **1** vs. the pK_a of the unhindered pyridine bases gives a fair straight line corresponding to the expression $-0.31\ pK_a' + 1.05$, while for the corresponding reaction of **3** we obtain, similarly, $-0.31\ pK_a' + 1.42$ (with $r = 0.984$ and 0.994, respectively). The similarity of the slopes of these lines points to very similar charge development in the transition states for trapping of **16** and the sulfene from **3**. The difference in product ratios from **1** and **3** is therefore evidently associated with the vertical displacement of these parallel lines, which is reasonably assigned to a two- to three-fold steric acceleration of elimination by the methyl group. The deviations of p for the "hindered" bases from the pattern of the "unhindered" bases are given in Table 4 by the SB_p values, which, in full accord with this steric acceleration picture, are all greater than 1.0.

The mechanism in Scheme 5 is also consistent with the lower proportion of betaine (73 ± 3%) formed in D_2O than in H_2O (82 ± 2%). If we make the reasonable assumption that the kinetic solvent isotope effect for formation of **10** from **22** (Z = OH) is negligible, then this difference can be ascribed largely to a primary kinetic isotope effect in the trapping of **22** (Z = OH) to form the betaine (**9**). The kinetic isotope effect so obtained (1.7 ± 0.5) agrees with the value (1.9 ± 0.1) observed in these laboratories for the competitive trapping of sulfene (from methanesulfonyl chloride and triethylamine) with a mixture of H_2O and D_2O (J. D. Lock, unpublished observations). We note, on the basis of the mechanism in Scheme 5, that these observations define a rather narrow range for the rate of the protonation of **22** (Z = OH) by water and hence of the elimination to form **10** as well. This may be seen as follows. The specific rate of protonation of $(PhSO_2)_2CH^-$ with H_3O^+ (at 25°C, in 0.1 M aqueous HCl) is reported to be $2.1 \times 10^{10}\ M^{-1}\ s^{-1}$ (49), and it is likely that for the same reaction of **22** (Z = OH), which must be a stronger base, the rate constant will also be $>10^{10}\ M^{-1}\ s^{-1}$; at pH 3.0 the pseudo-first-order rate constant will thus be $>10^7\ s^{-1}$ and, since this reaction is not in evidence, the postulated reaction with water must be faster yet, i.e. have a rate constant $>10^8\ s^{-1}$. At the same time, however, both the protonation and the elimination, though very fast, show (*a*) a hydrogen isotope effect, and (*b*) normal β and SF_p values, thereby indicating that these processes are not in general occurring at the maximum rates, which are controlled by vibration or solvent-relaxation limits and at which such selectivity would be expected to disappear.

Instead of the mechanism in Scheme 5, however, it is also possible to imagine a pathway in which the two products **9** and **10** are formed from **16** by two quite separate processes. For example, attack on the sulfene (**16**) in a conformation in which the ammonio group and the attacking molecule of water are more or less *syn* to each other might permit a concerted displacement to form **10**, whereas reaction of the sulfene **16** in another conformation might well lead to the betaine (**9**). A concerted *trans* elimination is also conceivable but, to the extent that the S_N2' displacement on **16** would be expected to follow the pattern of the S_N2' reaction of neutral nucleophiles with simple allylic systems (as mentioned above), the *syn* process is the more likely. Inspection of molecular models suggests that such a *syn* orientation of nucleophile and nucleofuge will lead to increasing nonbonding repulsions with increase in the number and size of the 2- (and 6-) substituents, and hence, if the nucleophilic displacement step determines the rate of formation of **10** relative to **9**, then this picture predicts that p will decrease as the "size" of the amine increases. It is evident from Table 4, however, that this is contrary to experiment, with the "larger" bases giving *larger* values of p. The discussion in this paragraph has assumed that interconversion of the conformations of **16** is fast relative to their further reaction; the alternative possibility in which the conformational interconversion is relatively slow is also conceivable, but would appear unlikely since it does not readily account for the kinetic isotope effect (1.7 ± 0.5) noted above.

Can. J. Chem. Downloaded from www.nrcresearchpress.com by 210.87.254.6 on 09/06/12
For personal use only.

Can. J. Chem. Downloaded from www.nrcresearchpress.com by 210.87.254.6 on 09/06/12
For personal use only.

We therefore conclude that the simplest mechanism consistent with our observations on both the pyridine bases and the saturated tertiary amines is that shown in Scheme 5, in which trapping of the cationic sulfene (e.g. **16**) proceeds in a two-step process via a discrete zwitterionic intermediate (**22**). It is tempting to extend this picture and to suggest that trapping of neutral sulfenes in hydroxylic media to form sulfonic acids or esters takes place analogously, i.e. by way of the corresponding discrete intermediate carbanion.

(c) Related work and comments

Finally, we recall that in our communications (17, 18) we pointed to the likelihood that vinylogous nucleophilic catalysis would show up in other systems, and we are gratified to note that this prediction would appear to have been fulfilled for the α,β-unsaturated carbonyl system by the reports of Inoue and Bruice (50, 51) describing their work on what they term an "extended E1cB mechanism" in the hydrolysis of *p*-nitrophenyl 2-cyano-3-(*p*-methoxyphenyl)propenoate.[11] These authors, in addition to reporting their own studies, comment on the mechanism of the formation of the sulfene (**16**), stating that they "believe that this reaction also proceeds by the stepwise mechanism as is shown in this paper (i.e. nucleophilic attack of pyridine on the double bond to yield a carbanion (betaine) followed by departure of the leaving group (chloride))" (51). Inoue and Bruice do not detail the basis of this comment but if, as seems possible, it is influenced by their experience with their own system in which the leaving group is *p*-nitrophenoxide, than it may be appropriate to recall the differences that have been noted in sulfene formation by elimination when the leaving group, Z, in $PhCH_2SO_2Z$ is changed. With Z = *p*-nitrophenoxy the reaction is $(E1cB)_R$ or $(E1cB)_I$ depending on reaction conditions and with Z = 2-chloro-4-nitrophenoxy the mechanism was found to be clearly $(E1cB)_I$ (37, 38); but with Z = Cl the situation is less clear (53), though published evidence favours an E1cB-like E2 process (48). As we have already noted, we feel that the question of stepwise vs. concerted formation of **16** cannot be settled with the evidence at hand, and the belief announced by Inoue and Bruice (51), though possibly correct, is at present without visible scientific basis.

Experimental

Proton magnetic resonance (^{1}Hmr) spectra were recorded using Varian T-60, HA-100, and XL-100 spectrometers; unless otherwise stated, all δ values reported were recorded from spectra obtained on the XL-100 or HA-100 spectrometers; ^{13}Cmr spectra were determined on a Varian XL-200 instrument. Spectra of deuterochloroform (Merck, Sharp and Dohme Ltd.) and nitromethane-d_3 (Aldrich, 99 at.% D) solutions were calibrated with tetramethylsilane (TMS, Merck, Sharp and Dohme), those in deuterium oxide (D_2O, Merck, Sharp and Dohme) with either sodium 3-(trimethylsilyl)propionate (TSP, Aldrich) or sodium 3-(trimethylsilyl)propanesulfonate (DSS, Aldrich). Infrared (ir) spectra were recorded on Perkin–Elmer 621 or Beckman 4250 spectrometers using sodium chloride or potassium bromide cells; all ir spectra were calibrated with a polystyrene reference film. All melting points were obtained on a Gallenkamp melting point apparatus, and are uncorrected. Refractive indices were determined on a thermostatically controlled Bausch and Lomb Abbé refractometer.

1,2-Dimethoxyethane (DME) (Eastman) and methylene chloride (Fisher) were dried by distillation from calcium hydride (Fisher) and stored over molecular sieves (3 Å grade 564, 8–12 mesh). All other solvents and reagents used were reagent grade and used as supplied unless otherwise specified. Rexyn 300 (H-OH) deionizing resin (Fisher) was used as supplied, usually in excess. Standard sodium hydroxide and hydrochloric acid solutions were prepared volumetrically from sodium hydroxide solution concentrate, *N*/1 or *N*/10 (Fisher). For a few kinetic determinations the titrant used was prepared from sodium hydroxide electrolytic pellets (Fisher); identical rate constants were obtained from titrant solutions prepared by either method.

Methylene chloride and ether extracts were dried over anhydrous magnesium sulfate (Fisher, certified grade) prior to evaporation. The spinning band distillation apparatus was a Nester/Faust model NFT50 (Nester/Faust Manufacturing Corp., Newark, Delaware) equipped with a 24-in. Teflon spinning band.

Ethenesulfonyl chloride (**1**) was prepared from 2-chloroethanesulfonyl chloride and triethylamine (54) and further purified by fractional distillation under reduced pressure (1.5 Torr, bp 25°C; (1 Torr = 133.3 Pa)) using the spinning band apparatus. The ^{1}Hmr ($CDCl_3$) spectrum showed an ABC multiplet which was reproduced within experimental uncertainty on computer simulation with the following parameters: δ_A 6.25 (H *trans* to SO_2Cl), δ_B 6.54 (H *cis* to SO_2Cl), δ_C 7.04 (CH); J_{AB} = −1.4 Hz, J_{AC} = 9.3 Hz, J_{BC} = 16.1 Hz); ir (CH_2Cl_2) ν_{max}: 3115 (w), 3075 (m), 1380 (vs), 1170 (vs), 980 (s), 940 (m), 650 (s) cm^{-1}; n_D^{20} 1.4681 (lit. (19), n_D^{20} 1.4686). *trans*-1-Propene-1-sulfonyl chloride (**3**) prepared from 2-chloropropane-1-sulfonyl chloride (55) by the method of Rondestvedt and Chang (56) consistently showed in the ^{1}Hmr spectrum (*a*) an ABX_3 pattern consistent (computer simulation) with δ_A 7.14, δ_B 6.80, δ_X 2.05, J_{AB} 14.9, J_{AX} 7.1, and J_{BX} −1.7 Hz, the *trans* stereochemistry being assigned from the large J_{AB}, and (*b*) the presence of a second set of signals at (T-60) 2.2 ("d", 3H), 6.0 (m, 1H), and 6.3 ppm ("s", 1H), J_{XY} = 2 Hz, attributed to the presence of a small amount (about 3 to 10% in different preparations) of 1-propene-2-sulfonyl chloride. Spinning band distillation (15 Torr, bp ~70°C) gave a clean material showing only the above signals assigned to **3** in the ^{1}Hmr spectrum and the following peaks in the ir (CH_2Cl_2), ν_{max}: 3060 (w), 1635 (m), 1435 (m), 1375 (vs), 1295 (w), 1170 (s), 945 (s), 805 (s) cm^{-1}.

3,4-Dimethylpyridine, 3,5-dimethylpyridine, 4-methylpyridine, 4-ethylpyridine, 3-methylpyridine, methyl 4-pyridinecarboxylate, and pyridine were obtained commercially and were all fractionally distilled at atmospheric pressure before use. 3-Carbamoylpyridine (nicotinamide) was recrystallized from benzene (mp 128–129°C, lit. (57) mp 128°C). Commercial samples of 2-ethylpyridine, 2-methylpyridine, and quinoline were purified through their picrate salts and fractionally distilled (57–59). 2,6-Dimethylpyridine and 2,4,6-trimethylpyridine were treated with 5 mol% of dimethyl sulfate overnight; the mixture was filtered and fractionally distilled. 3-Ethanamidopyridine was prepared from 3-aminopyridine and acetic anhydride (60) and recrystallized (benzene), mp 133–134.5°C; lit. (60) mp 133°C. 3-Cyanopyridine was made from nicotinamide with P_2O_5 and purified by vacuum distillation; mp 49.5–51°C, lit. (61) mp 50–51°C.

The purity of the hindered pyridines was checked by performing a reaction with the base and ethenesulfonyl chloride (**1**), using initial sulfonyl chloride concentrations at or near those employed in the kinetic runs. The ^{1}Hmr spectra of the crude reaction products (occasionally the crude products were treated with Rexyn 300 (H-OH) deionizing resin to remove all ions except the betaine) were then compared with ^{1}Hmr spectra of authentic samples of the pyridine betaines; the base was deemed sufficiently pure when no signals due to betaines other than the one corresponding to the pyridine employed were visible.

[11] We are, however, surprised by Inoue and Bruice's suggestion that conversion of the enolate to the ketene requires that the enolate assume an "energetically unfavorable conformation... wherein the delocalization energy of the enolate anion system is lost" (51). Such a twisting of the carbon–carbon double bond of the enolate would seem to us to be so "unfavorable" as to be impossible, and it is puzzling that the authors do not indicate why they prefer this unlikely process to the straightforward extrusion of aryloxide with the assistance of the appropriately oriented electron pair on the enolate (charged) oxygen as described by Farrar and Williams (52).

Can. J. Chem. Downloaded from www.nrcresearchpress.com by 210.87.254.6 on 09/06/12
For personal use only.

Quinuclidine (Aldrich) was recrystallized from petroleum ether and stored under nitrogen. Trimethylamine was used as supplied by Eastman Kodak Company. All other aliphatic tertiary amines were dried over CaH_2 and freshly distilled.

*Preparation of substituted pyridine betaines from ethenesulfonyl chloride (**1**) and* trans-*1-propene-1-sulfonyl chloride (**3**)*

The substituted pyridine betaines were prepared according to the method of Le Berre *et al.* (62) in glacial acetic acid. The reactions of **1** were worked up after 2–3 h at room temperature, the last traces of acetic acid being removed by azeotroping with toluene. The residue was recrystallized from 95% alcohol unless otherwise specified. The yields of betaines (**9**) obtained in this manner were in the range 50–90%, depending upon the nucleophilicity of the base employed (hindered pyridines generally gave lower yields, sometimes <50%). For the reaction with **3**, the reactions were usually allowed to stand at room temperature overnight before work-up. The elemental analyses (where the compound was previously unknown) and the physical properties of these compounds are given in Tables 7 and 8.

Preparation of the betaines of the aliphatic amines

To a mixture of triethylamine (5 g, 50 mmol) and water (15 mL) stirred in an ice bath, 2-hydroxyethanesulfonyl chloride (31) (1.735 g, 12 mmol) was added dropwise slowly and the contents stirred for 0.5 h at room temperature. The solution was then extracted four times with methylene chloride (25-mL portions), and the aqueous phase was concentrated to ~5 mL under reduced pressure and passed through a column of deionization resin (Rexyn 300 (H-OH), Fisher). 2-(*N,N,N*-Triethylammonio)ethanesulfonate was obtained as a colorless crystalline solid (341 mg, 13.5%) and recrystallized from 95% ethanol, mp 294–296°C (dec.). All spectroscopic data were identical with those reported earlier (31).

Reactions of 2-hydroxyethanesulfonyl chloride with diethylmethylamine, dimethylethylamine, trimethylamine, and quinuclidine were carried out in the same manner with yields of 19, 23, 28.5, and 34%, respectively. Similarly, 1-propene-1-sulfonyl chloride (**3**) gave betaines with trimethylamine and quinuclidine in 8.5% and 17.5% yields, respectively. Analytical and spectroscopic data for these betaines are summarized in Table 9.

*Procedure for determining the products of the uncatalysed solvolyses of ethenesulfonyl chloride (**1**) and* trans-*1-propene-1-sulfonyl chloride (**3**) at 25.0°C*

A solution of the sulfonyl chloride in ~0.5 mL DME (sufficient to give an initial concentration of the sulfonyl chloride in the range $1.6 \times 10^{-3} - 2.9 \times 10^{-2}$ *M*) was injected into a stirred solution of potassium chloride in water or D_2O (50 mL) at 25.0°C at the desired pH. The pH was maintained until the addition of titrant had stopped. For those reactions performed above pH 7, the reaction was then neutralized to pH 7 with dilute HCl solution. The solvent was then evaporated to dryness, and the composition of the residue determined by integration of the peaks corresponding to the methylene protons of the hydroxyalkanesulfonate anion and the characteristic vinyl protons of the alkenesulfonate anion. The product from one run (at pH 4.0; starting with 0.20 g, 1.6 mmol, of ethenesulfonyl chloride) was dissolved in hot water (5 mL) and *S*-benzylthiuronium chloride (0.32 g, 1.6 mmol) in water (5 mL) added. The crystalline precipitate was recrystallized from 95% alcohol, mp 145–146.5°C; reported (64) for benzylthiuronium ethenesulfonate, mp 145–146°C.

*General procedure for determining the product composition for reactions of **1** and **3** with substituted pyridines in water containing 0.1* M *potassium chloride*

The reaction products (and their relative proportions) for the reactions at 25°C of **1** and **3** with substituted pyridines were determined using initial concentrations of sulfonyl chloride in the range $1.0 - 16 \times 10^{-3}$ *M*. Where possible, a sufficient amount of the substituted pyridine base was employed in these reactions to ensure pseudo-first-order conditions, and to exceed the uncatalysed hydrolysis reaction of **1** or **3** by a factor of at least 50 (so that the relative proportions of the products would not be subject to large corrections for the presence of any alkenesulfonate anion derived from the uncatalysed hydrolysis reaction). After completion of the reaction, the pH was normally raised to at least one pH unit above the apparent pK_a of the substituted pyridine, and the solution extracted with ether. Evaporation of the aqueous layer gave a residue the ^{1}Hmr spectrum (D_2O) of which was compared with authentic spectra of the pyridine betaines **9** and **11** and alkenesulfonate anions **10** and **12**. Integration of the methylene protons of the betaine and the olefinic protons of the alkenesulfonate anion gave the relative proportions of the products expressed as the "betaine fraction", or q value (q = % betaine/(% betaine + %alkenesulfonate anion)) (see Tables 2 and 4); these were also corrected for the generation of any alkenesulfonate anion derived from any uncatalysed hydrolysis reaction and listed as the q' values.

For the specific case of the reaction of **1** with pyridine the betaine was isolated and identified as follows. Ethenesulfonyl chloride (**1**) (0.065 g, 0.52 mmol) was allowed to react with a solution of pyridine (1.0 mL, 125 mmol) in water (50 mL) containing potassium chloride (0.400 g, 5.36 mmol) at 25.0°C and pH 4.0. After the reaction was judged to be complete, the pH was raised to 7.0 and the aqueous solution extracted several times with ether. The aqueous layer was then evaporated to dryness, dissolved in 1–2 mL of water, and passed down a column containing Rexyn 300 (H-OH) deionizing resin. Evaporation of the eluant gave **9** (X = H) as a colorless residue (80 mg) which was recrystallized from 95% alcohol. The mp, mixture mp (255–257°C), and the ^{1}Hmr spectrum (D_2O) of this material were identical with those of an authentic specimen of **9** (X = H) (21).

Kinetic determinations

The pH-stat apparatus has been described (31). A typical rate measurement was carried out by injecting (from a 100-μL syringe) a 100-μL aliquot of a solution of **1** or **3** in dry DME into the reaction solution (50 mL of water containing 0.40 g of KCl, plus amine where appropriate) previously brought to the desired pH and temperature; initial concentrations of the sulfonyl chloride were in the range $4 \times 10^{-4} - 3 \times 10^{-3}$ *M*. The rate of reaction was followed by recording the volume of sodium hydroxide solution with time. Due care was taken to avoid very low pH's and buffered solutions. Half-lives varied from 0.25 min to several hours, with most in the range 0.5 – 10 min. The slopes of the best straight line fit for a plot of log $(V_\infty - V_t)$ vs. time gave the (pseudo) first-order rate constant. The concentrations of free base used to obtain k_B from k_ψ from the amine reactions were calculated from the apparent pK_a' values of the amines obtained from the half-neutralization point from a titration of the base with 1.0 *M* HCl in 0.1 *M* KCl, with appropriate correction for hydrolysis for bases with pK_a's below 4.0.

*Composition of the products of the reaction of the saturated tertiary amines with **1** and **3** in 0.1* M *aqueous KCl*

(a) ^{1}H magnetic resonance identification

Ethenesulfonyl chloride (**1**) (55 mg, 0.435 mmol) was dissolved in dry DME (0.5 mL) and 30 μL of the solution was injected into a triethylamine solution (50 mL, 0.08 *M* triethylamine, 0.1 *M* KCL in H_2O, 1°C). The pH was maintained constant (pH = 7.5) in a pH-stat apparatus with 0.1 *M* sodium hydroxide titrant. About every 20 min (roughly 3–4 half-lives) another 30 μL of the ethenesulfonyl chloride solution was added till the addition was completed. Reaction was judged complete when no further addition of titrant was observed during 10 min (total 8.70 mL of titrant was used; calculated for 2 equiv of the substrate, 8.70 mL). The pH then was raised to ca. 11.3 and the aqueous solution extracted three times with ether (100-mL portions), neutralized with 1 *M* HCl, and water evaporated. The solid residue was dissolved in D_2O; the ^{1}Hmr spectrum indicated that the reaction products consist of only two compounds: the ethenesulfonate salt (**14**, R = Et, R′ = H) and the triethyl betaine (**13**, R = Et, R′ = H) (54% and 46% as judged from integration of the peaks at 5.80–6.90 ppm and 1.25–1.35 ppm, respectively).

(b) Isolation of the betaines

Ethenesulfonyl chloride (**1**) (70.5 mg, 0.557 mmol) dissolved in dry DME (0.8 mL) was hydrolyzed in the presence of triethylamine as

Can. J. Chem. Downloaded from www.nrcresearchpress.com by 210.87.254.6 on 09/06/12
For personal use only.

TABLE 7. Characterization of the 2-(*N*-pyridinio)ethanesulfonates (**9**)

X	Melting point (°C)		Analysis	Infrared (ν_{max} cm^{-1}, Nujol)	^1H magnetic resonance (D_2O) δ
3,4-$(CH_3)_2$	315–316	Calcd. for $C_9H_{13}NO_3S$: Found:	C 50.21, H 6.09, N 6.51, S 14.89 C 50.13, H 6.20, N 6.38, S 14.67	3045(m), 1641(m), 1515(m), 1488(m), 1272(m), 1251(s), 1210(vs), 1183(vs), 1153(s), 1052(s), 1035(vs), 665(m)	2.49(s,3H), 2.61(s,3H), 3.59(t,2H), 4.94 (t,2H), 7.85(d,1H), 8.61(d,2H)
3,5-$(CH_3)_2$	370	Calcd. for $C_9H_{13}NO_3S$: Found:	C 50.21, H 6.09, N 6.51, S 14.09 C 50.28, H 6.20, N 6.42, S 14.76	3062(m), 1600(m), 1268(m), 1210(vs), 1183(s), 1158(m), 1045(m), 1035(m), 687(m), 663(m)	2.46(s,6H), 3.55(t,2H), 4.90(t,2H), 8.22 (s,1H), 8.58(s,2H)
4-CH_3	322–324	Calcd. for $C_8H_{11}NO_3S$: Found:	C 47.75, H 5.51, N 6.96, S 15.93 C 47.91, H 5.67, N 6.78, S 16.02	1645(m), 1488(m), 1208(vs), 1179(vs), 1034(s), 843(m)	2.68(s,3H), 3.59(t,2H), 4.86(t,2H), 7.92 (d,2H), 8.76(d,2H)
4-CH_2CH_3	350–352 (dec.)	Calcd. for $C_9H_{13}NO_3S$: Found:	C 50.21, H 6.09, N 6.51, S 14.89 C 50.45, H 6.14, N 6.41, S 14.92	1642(m), 1515(w), 1205(vs), 1182(vs), 1031(s), 860(s), 730(s)	1.32(t,3H), 2.98(q,2H), 3.59(t,2H), 4.97 (t,2H), 7.96(d,2H), 8.77(d,2H)
3-CH_3	279–280	Calcd. for $C_8H_{11}NO_3S$: Found:	C 47.75, H 5.51, N 6.96, S 15.93 C 47.63, H 5.57, N 6.81, S 15.79	3063(m), 1508(m), 1267(m), 1204(vs), 1171(s), 1050(s), 1034(s), 683(m), 663(m), 630(s)	2.60(s,3H), 3.52(t,2H), 5.00(t,2H), 7.98 (t,1H), 8.25(d,1H), 8.78(m,1H)
3-$CONH_2$	303–304 (dec.)	Calcd. for $C_8H_{10}N_2O_4S$: Found:	C 41.73, H 4.38, N 12.17, S 13.93 C 41.59, H 4.51, N 12.01, S 13.76	3310(m), 3155(m), 3080(m), 3065(m), 1697(s), 1628(m), 1410(s), 1280(s), 1248(s), 1230(s), 1040(s), 1027(m), 740(m)	3.72(t,2H), 5.20(t,2H), 8.34(m,2H), 9.0–9.36(m,3H), 9.50(s,1H)
3-$NHCOCH_3$	291–292	Calcd. for $C_9H_{12}H_2O_4S$: Found:	C 46.56, H 5.21, N 12.07, S 13.81 C 46.41, H 5.13, N 11.78, S 13.58	3401(w), 3226(w), 1515(m), 1212(s), 1171(s), 1042(s), 739(m), 728(m)	3.55(t,2H), 4.76(s,3H), 4.83(t,2H), 7.71 (m,2H), 8.16(m,3H)
3-CN	302–303 (dec.)	Calcd. for $C_8H_8N_2O_3S$: Found:	C 45.27, H 3.80, N 13.20, S 15.10 C 45.21, H 3.96, N 13.06, S 15.01	1632(w), 1495(m), 1273(m), 1220(vs), 1205(vs), 1175(s), 1150(m), 1057(m), 1043(s), 680(s)	3.68(t,2H), 5.20(t,2H), 8.38(t,1H), 9.05 (m,1H), 9.39(m,1H), 9.62(m,1H)
4-CO_2CH_3	255–257	Calcd. for $C_9H_{11}NO_5S$: Found:	C 44.08, H 4.52, N 5.71, S 13.07 C 44.10, H 4.60, N 5.65, S 12.89	3060(s), 1718(s), 1205(vs), 1280(s), 1180(vs), 1110(s), 1030(vs), 728(s), 635(s)	3.64(t,2H), 4.07(s,3H), 5.12(t,2H), 8.56 (d,2H), 9.16(d,2H)
2-CH_2CH_3	254–256 (dec.)	Calcd. for $C_9H_{13}NO_3S$: Found:	C 50.21, H 6.09, N 6.51, S 14.89 C 50.07, H 6.17, N 6.37, S 14.68	3090(m), 3060(m), 1630(s), 1580(m), 1515(s), 1255(vs), 1200(vs), 1162(vs), 1048(vs), 1033(vs), 795(m), 781(m), 630(s)	1.44(t,3H), 3.24(q,2H), 3.56(t,2H), 5.01 (t,2H), 7.95(m,2H), 8.52(t,1H), 8.86(d,1H)
$^2H_5$	255–256	Calcd. for $C_7{}^1H_4{}^2H_5NO_3S$: Found:	55.56% excess ^2H 53.50% excess ^2H		3.64(t,2H), 5.07(t,2H)
$^1H_5$[a]	255–256				3.62(t,2H), 5.05(t,2H), 8.11(t,2H), 8.62 (t,1H), 8.97(d,2H)
2-CH_3[a]	224–225			3090(m), 3060(m), 1615(s), 1565(m), 1490(s), 1470(s), 1300(m), 1230(vs), 1210–1180(br,vs), 1150(vs), 1035(vs), 775(s)	2.93(s,3H), 3.57(t,2H), 5.01(t,2H), 7.82–8.05(m,2H), 8.45(t,1H), 8.85(t,1H)
2,6$(CH_3)_2$	dec. >340	Calcd. for $C_9H_{13}NO_3S$: Found:	C 50.21, H 6.09, N 6.51, S 14.89 C 50.11, H 5.92, N 6.46, S 14.71	1620(m), 1588(m), 1495(m), 1250(m), 1213(s), 1175(s), 1035(s), 823(m), 725(m)	2.94(s,6H), 3.50(m,2H), 4.92(m,2H), 7.78 (d,2H), 8.25(t,1H)
Benzo[b][a,b]	285–286				3.70(t,2H), 5.50(t,2H), 8.90–9.52(m,5H), 9.15(d,1H), 9.36(d,1H)
2,4,6-$(CH_3)_3$	dec. >335	Calcd. for $C_{10}H_{15}NO_3S$: Found:	C 52.28, H 6.59, N 6.11, S 13.98 C 52.21, H 6.63, N 6.21, S 13.68	1640(m), 1575(w), 1308(m), 1245(s), 1198 (b,vs), 1140(s), 1033(s), 1023(s), 745(m)	2.52(s,3H), 2.86(s,6H), 3.47(m,2H), 4.84 (m,2H), 7.62(s,2H)

[a] Reference 21.
[b] i.e., 2-(*N*-quinolinio)ethanesulfonate.

Can. J. Chem. Downloaded from www.nrcresearchpress.com by 210.87.254.6 on 09/06/12
For personal use only.

TABLE 8. Characterization of the 2-(*N*-pyridinio)-1-propanesulfonates (**11**)

X	Melting point (°C)		Analysis	Infrared (ν_{max} cm^{-1}, Nujol)	^1H magnetic resonance (D_2O) δ
3,4-$(CH_3)_2$	258 (subl.)	Calcd. for $C_{10}H_{15}NO_3S$: Found:	C 52.38, H 6.59, N 6.11, S 13.98 C 52.53, H 6.65, N 6.04, S 13.77	1639(m), 1511(m), 1230(vs), 1208(vs), 1183(vs), 1166(vs), 1145(s), 1035(vs), 1000(m), 878(m)	1.76(d,3H), 2.45(s,3H), 2.57(s,3H), 3.59(m,2H), 5.16(m,1H), 7.85(d,1H), 8.65(m,2H)
3,5-$(CH_3)_2$	344–345 (dec.)	Calcd. for $C_{10}H_{15}NO_3S$: Found:	C 52.38, H 6.59, N 6.11, S 13.98 C 52.53, H 6.65, N 5.99, S 13.77	1508(m), 1274(m), 1220(vs), 1182(vs), 1130(m), 1040(s), 895(m), 779(m), 695(m)	1.82(d,3H), 2.55(s,6H), 3.62(m,2H), 5.16 (m,1H), 8.24(s,1H), 8.65(s,2H)
4-CH_3	293–294 (dec.)	Calcd. for $C_9H_{13}NO_3S$: Found:	C 50.21, H 6.09, N 6.51, S 14.89 C 50.01, H 6.09, N 6.62, S 14.63	1647(s), 1272(s), 1202(vs), 1175(vs), 1031(s), 838(m), 775(s)	1.80(d,3H), 2.69(s,3H), 3.62(m,2H), 5.22 (m,1H), 8.04(d,2H), 8.91(d,2H)
H	307–308	Calcd. for $C_8H_{11}NO_3S$: Found:	C 47.75, H 5.51, N 6.96, S 15.93 C 47.97, H 5.44, N 6.83, S 15.88	1637(m), 1495(s), 1264(m), 1205(s), 1183(s), 1163(s), 1122(m), 1036(s), 797(m)	1.86(d,3H), 3.66(m,2H), 5.31(m,2H), 8.18 (t,2H), 8.54(t,1H), 9.05(d,2H)
4-CO_2CH_3	268–269 (dec.)	Calcd. for $C_{10}H_{13}NO_5S$: Found:	C 46.32, H 5.05, N 5.40, S 12.37 C 46.21, H 5.15, N 5.36, S 12.31	1739(s), 1642(m), 1333(m), 1299(vs), 1264(vs), 1235(vs), 1212(vs), 1202(vs), 1172(vs), 1122(s), 1093(vs), 781(m), 773(m)	1.84(d,3H), 3.66(m,2H), 4.08(s,3H), 5.39 (m,1H), 8.58(d,2H), 9.12(d,2H)
3-CN	268–269 (dec.)	Calcd. for $C_9H_{10}N_2O_3S$: Found:	C 47.78, H 4.46, N 12.38, S 14.17 C 47.59, H 4.60, N 12.19, S 13.95	1639(w), 1499(m), 1261(m), 1224(s), 1198(s), 1170(s), 1156(m), 1036(s), 783(m)	1.84(d,3H), 3.65(m,2H), 5.41(m,1H), 8.34 (t,1H), 9.01(d,1H), 9.32(d,1H), 9.67(s,1H)
2-CH_3	288–289	Calcd. for $C_9H_{13}NO_3S$: Found:	C 50.21, H 6.09, N 6.51, S 14.89 C 50.05, H 6.09, N 6.37, S 14.88	1629(m), 1578(w), 1175(vs), 1150(vs), 1030(vs), 780(s)	1.73(d,3H), 2.97(s,3H), 3.64(m,2H), 5.58 (m,1H), 7.98(t,2H), 8.42(t,1H), 8.96(d,1H)
Benzo[b][a]	267–269 (dec.)	Calcd. for $C_{12}H_{13}NO_3S$: Found:	C 57.35, H 5.21, N 5.57, S 12.76 C 57.18, H 5.42, N 5.50, S 12.92	3090(w), 1622(w), 1588(w), 1230(m), 1200(m), 1043(m), 783(m)	2.04(d,3H), 3.87(m,2H), 6.31(m,1H), 7.89–8.54(m,4H), 8.72(d,1H), 9.14(d,1H), 9.53(d,1H)
3-$NHCOCH_3$	325–327	Calcd. for $C_{10}H_{14}N_2O_4S$: Found:	C 46.50, H 5.46, N 10.85, S 12.41 C 46.40, H 5.47, N 10.72, S 12.03	3390(m), 3226(m), 3077(m), 1631(m), 1513(m), 1342(m), 1302(m), 1212(s), 1176(s), 1036(s), 1017(m), 783(m)	1.80(m,6H), 2.27(s,1H), 3.64(m,2H), 5.08 (m,1H), 7.74(m,2H), 8.27(m,2H)
3-CH_3	297–298 (dec.)	Calcd. for $C_9H_{13}NO_3S$: Found:	C 50.21, H 6.09, N 6.51, S 14.89 C 50.09, H 6.12, N 6.45, S 14.72	1511(m), 1263(m), 1214(vs), 1188(vs), 1172(s), 1152(s), 1032(vs), 778(s), 691(m)	1.84(d,3H), 2.62(s,3H), 5.27(m,1H), 8.03 (m,1H), 8.45(d,1H), 8.85(d,2H)
2-CH_2CH_3	280–282	Calcd. for $C_{10}H_{15}NO_3S$: Found:	C 52.38, H 6.59, N 6.11, S 13.98 C 52.28, H 6.68, N 6.17, S 13.93	3035(s), 1635(s), 1240(s), 1225(s), 1200(vs), 1175(vs), 1155(s), 1035(vs), 805(m), 782(s)	1.46(t,3H), 1.90(d,3H), 3.35(q,2H), 3.68 (m,2H), 5.64(m,1H), 8.00(m,2H), 8.46 (t,1H), 8.96(m,1H)

[a]i.e. 2-(*N*-quinolinio)-1-propanesulfonate.

Can. J. Chem. Downloaded from www.nrcresearchpress.com by 210.87.254.6 on 09/06/12
For personal use only.

TABLE 9. Characterization of the betaines of the tertiary aliphatic amines (**13**)

R_3N	R′	Melting point[a] (°C)	Infrared (KBr) ν_{max} (cm^{-1})	^1H magnetic resonance (D_2O) δ	^{13}C magnetic resonance (D_2O) δ	Further characterization
Me_3N	H	350–352 (dec.)	3020(m), 2980(w), 1480(s), 1205(vs), 1195(vs), 1090–1080(vs), 1030(vs), 910(m)	3.22(s,9H), 3.57–3.79(m,4H)	47.3, 56.0(t, *J* 3.7 Hz), 64.3(t, *J* 3.1 Hz)	Melting point and ^1Hmr spectrum identical to those of sample prepared by the literature procedure[b]
Me_2EtN	H	330–332 (dec.)	3025(w), 2985(m), 1490(m), 1460(m), 1235(s), 1215–1205(vs), 1200(vs), 1195–1190(vs), 1055(s), 1035(vs)	1.38(t,3H), 3.11(s,6H), 3.45 (quartet, *J* 7.5 Hz superimposed on a multiplet 3.34–3.71, total 6H).	10.2, 46.8, 53.0, 61.2, 62.9	Melting point and ^1Hmr spectrum similar to reported values[c]
$MeEt_2N$	H	309–310 (dec.)	3030(w), 2980(w), 1485(m), 1240(s), 1210–1200(vs), 1195–1190(vs), 1055(m), 1035(vs)	1.35(t,6H), 3.03(s,3H), 3.41 (quartet, *J* 7.3 Hz superimposed on a multiplet 3.26–3.72, total 8H).	9.8, 46.5, 49.9, 58.0, 59.8	Melting point and ^1Hmr spectrum similar to reported values[c]
Et_3N	H	294–296 (dec.)	2990–2970(m), 1475(m), 1265(s), 1235(s), 1225(s), 1200(vs), 1190–1180(vs), 1175(vs), 1045(s), 1030(vs)	1.30(t,9H), 3.34(quartet, *J* 7.4 Hz superimposed on a multiplet 3.23–3.62 total 10H)	9.5, 46.1, 54.5, 55.9	Melting point, ^1Hmr and ir spectra identical to those reported earlier[d]
Quinuclidine	H	Above 350 (dec.)	2960(m), 1280(m), 1200(vs), 1190(vs), 1040(vs)	1.82–2.35(m,7H), 3.20–3.70 (m,10H)	21.6, 25.3, 46.8, 49.6, 58.0	Melting point, ^1Hmr and ir spectra identical to those reported earlier[d]
Me_3N	CH_3	295–299 (dec.)	3020(m), 1490(m), 1480(m), 1290(m), 1245(m), 1230(s), 1220–1205(vs), 1200–1180(vs,br), 1040(vs), 955(w), 945(m)	1.66(d, *J* 6.2 Hz,3H), 3.14(s, superimposed on a multiplet 3.01–3.9, total 12H)	17.6, 53.7(t, *J* 4 Hz), 65.4(t, *J* 2.5 Hz), 70.8	Calcd. for $C_6H_{15}NSO_3$: C 39.76, H 8.34, N 7.72, S 17.85; found: C 39.77, H 8.60, N 7.58, S 17.85
Quinuclidine	CH_3	294–298 (dec.)	2960–2950(m), 2880(w), 1465(m), 1400(w), 1265–1250(s), 1235–1205 (vs,br), 1200–1180(vs,br), 1140(s), 1040(vs), 950(w), 925(w)	1.59(d, *J* 3.5 Hz,3H), 1.93–2.35 (m,7H), 2.92–3.89(m,9H)	17.3, 26.1, 53.6, 54.8, 60.8, 68.7	Calcd. for $C_{10}H_{19}NSO_3$: C 51.47, H 8.21, N 6.00, S 13.74; found: C 51.29, H 8.49, N 5.97, S 13.65

[a] Samples were put into a preheated melting point apparatus at temperatures about 10° below the observed decomposition temperature range.
[b] Reference 63.
[c] Reference 62.
[d] Reference 31.

Can. J. Chem. Downloaded from www.nrcresearchpress.com by 210.87.254.6 on 09/06/12
For personal use only.

described above. The aqueous solution containing hydrolysis product was concentrated and passed through the Rexyn 300 (H-OH). A crystalline product, 53.5 mg, was isolated, the mp and ^{1}Hmr and ^{13}Cmr spectra of which were identical with those of authentic *N,N,N*-triethylammonium-2-ethanesulfonate (**13**, R = Et, R′ = H). The yield of the betaine (46%) was identical to that determined by ^{1}Hmr integration.

All other betaines obtained in the hydrolysis reactions were isolated and identified in the same manner and the yields (expressed as *q* values) are summarized in Tables 5 and S4). In the case of the reaction of **1** in the presence of *N,N*-diisopropylethylamine and of **3** in the presence of triethylamine no betaines were isolated by this procedure, even with the total amounts of starting material doubled.

Preparation and reactions of N-*(2-chlorosulfonylethyl)pyridinium chloride (**18**a)*

Ethenesulfonyl chloride (**1**) (1.7 g, 13.4 mmol) was added dropwise over 1 min to freshly prepared pyridine hydrochloride (1.6 g, 14 mmol) dissolved in dry methylene chloride (20 mL). The immediately formed colorless precipitate was filtered in the cold and washed with pentane, yield 2.4 g (72%); mp 103–105°C; ir (Nujol) ν_{max}: 1640 (m), 1495 (m), 1376 (s), 1168 (s), 835 (w), 775 (m), 667 (s) cm^{-1}; ^{1}Hmr (CD_3NO_2) δ: 5.02 (t, 2H), 5.57 (t, 2H), 8.26 (m, 2H), 8.76 (t, 1H), 9.40 (d, 2H). *Anal.* calcd. for $C_7H_9Cl_2NO_2S$: C 34.72, H 3.75, Cl 29.28, N 5.79, S 13.22; found: C 34.97, H 4.03, Cl 29.32, N 5.71, S 13.09.

The sulfonyl chloride (**18***a*) (90 mg, 0.37 mmol) was added to an aqueous solution (50 mL) of KCl (0.400 g, 5.36 mmol) at pH 4.0 (pH-stat, 1.0 *M* NaOH) and 25.0°C. After 1 h the solvent was evaporated and the residue investigated by ^{1}Hmr spectroscopy, which indicated the presence of **9** (X = H) (88%) and **10** (X = H) (12%). Under the same conditions **18***a* (X = H) (0.15 g, 5.6 mmol) with pyridine (2.0 mL, 24.8 mmol) as above gave, after acidification to pH 7.5 and washing with ether and evaporation of the water, a product shown by ^{1}Hmr to contain **9** (X = H) (83%) and **10** (X = H) (17%).

In D_2O (50 mL, 0.1 *M* KCl, no pyridine) **18***a* (X = H) (38 mg, 0.16 mmol) similarly gave pyridine betaine **9** (X = H) (86%) (~80% $Pyr^+CH_2CHDSO_3^-$, ~20% $Pyr^+CH_2CH_2SO_3^-$) and **10** (X = H) (14%, undeuterated). In the presence of pyridine (10 μL) in D_2O (50 mL, with KCl, 0.400 g) as before, the ^{1}Hmr of the product showed **9** (X = H) (75%, >95% $Pyr^+CH_2CHDSO_3^-$) and **10** (X = H) (25%, undeuterated).

Preparation and reactions of deuterated N-*(2-chlorosulfonylethyl)-pyridinium chlorides **19** and **20***

Pyridine deuterochloride (400 mg, 3.4 mmol), prepared by bubbling DCl gas (generated by addition of oxalyl chloride to D_2O) into a solution of pyridine in benzene, was dissolved in dry CH_2Cl_2 (10 mL) and **1** (0.5 mL, 5.4 mmol) was added dropwise over 1 min. The immediately formed colorless precipitate of **19** was collected by filtration in the cold, washed with CH_2Cl_2, and used as such (500 mg, 60%); the ^{1}Hmr spectrum (DMSO-d_6) indicated >64% α-monodeuteration (—$CHDSO_2Cl$). Sulfonyl chloride **19** (150 mg, 0.62 mmol) was added to a stirred solution of pyridine (1.0 mL, 12.5 mmol) and KCl (400 mg, 5.36 mmol) in D_2O (50 mL) at pH (meter reading) 3.4 and 25.0°C in the pH-stat, with the pH maintained constant with 2.5 *M* NaOD in D_2O. After 1 h the pH was adjusted to 7.0 and the mixture worked up as before. The ^{1}Hmr spectrum (D_2O) of the residue showed the presence of partially deuterated pyridinoethanesulfonate and ethenesulfonate anion (product ratio 75:25), with the relative areas of the ^{1}Hmr signals due to the protons on C-1 and C-2 being, respectively, 0.5:2.0 and 0.6:2.0.

Pyridine-d_5 hydrochloride (550 mg, 4.58 mmol), freshly prepared as above from pyridine-d_5 (Merck, Sharp and Dohme) and gaseous HCl in CH_2Cl_2 (15 mL), with **1** (575 mg, 4.54 mmol) as above except that the precipitate was washed with pentane, gave **20** (470 mg, 42%); ^{1}Hmr (T-60, CD_3NO_2) δ: 5.0 (m, 2H) and 5.3 (m, 2H) with no signals in the range 8–10 ppm. This material (**20**, 160 mg, 0.65 mmol) was added to a stirred solution of pyridine (2.0 mL, 24.9 mmol) and KCl (400 mg, 5.36 mmol) in water (50 mL) at pH 4.0 and 25.0°C in the pH-stat with 0.1 *M* NaOH as titrant. After 2 h the pH was adjusted to 7.5 and worked up as above; the ^{1}Hmr spectrum (D_2O) showed the presence of the betaine (**21**) and ethenesulfonate salt (**10**) (relative proportions 81:19), plus peaks in the range 8–10 ppm ascribable to the pyridinium cation ($C_5H_5\overset{+}{N}H$). Further washing with ether (×5) removed all signs of this ion, leaving the characteristic peaks due to **21** and **10** with no absorption at all in the range (8.0–10.5) expected for the aromatic hydrogens in **9** (R = H); passage through a deionizing resin removed the olefinic signals due to **10**, leaving only the strong upfield triplets of **21** with no sign of aromatic hydrogens.

*Preparation and reactions of 4-methyl-*N-*(2-chlorosulfonylethyl)-pyridinium chloride (**18**b)*

Freshly prepared 4-picoline hydrochloride (1.0 g, 7.7 mmol) in dry CH_2Cl_2 (20 mL) and **1** (1.0 g, 7.9 mmol) as with preparation of **20**, gave **18***b* (1.5 g, 76%), mp 80–85°C (sealed tube); ir (CH_2Cl_2) ν_{max}: 3025 (w), 2940 (w), 2860 (w), 1640 (m), 1560 (w), 1475 (w), 1380 (s), 1168 (s), 1035 (w), 820 (w) cm^{-1}; ^{1}Hmr (T-60, CD_3NO_2) δ: 2.7 (s, 3H), 5.0 (t, 2H), 5.5 (t, 2H), 8.0 (d, 2H), 9.1 (d, 2H). A solution of **18***b* in D_2O after standing for 1 h at room temperature showed peaks in the ^{1}Hmr appropriate to the betaine (**9**, X = 4-Me) (>95%) plus a small amount of ethenesulfonate; no sign of deuteration of either product was evident. Sulfonyl chloride **18***b* (100 mg, 3.9 mmol) was added to a solution of 4-picoline (3.0 mL, 31 mmol) and KCl (400 mg, 5.36 mmol) in water (50 mL) at pH 4.0 and 25.0°C, in the pH-stat as above. Work-up after 15 min gave a product shown by ^{1}Hmr to consist of **9** (X = 4-Me) and **10** (X = 4-Me) in the ratio 92:8.

*Ethenesulfonyl chloride (**1**) with tertiary amines in D_2O: reaction products*

(a) Pyridine

A solution of **1** (29 mg, 0.23 mmol) in dry DME (0.5 mL) was injected into a stirred solution of pyridine (2.0 mL, 24.8 mmol) and KCl (400 mg) in D_2O (50 mL) at 25.0°C and pH (meter reading) 3.4, maintained in the pH-stat with 1.2 *M* NaOD in D_2O. After 15 min the pH (reading) was adjusted to 7.0 and the mixture worked up as above. The ^{1}Hmr spectrum (D_2O) of the material so obtained showed the presence of the betaine and ethenesulfonate anion with the ratio ~70:30; the latter showed no sign of deuterium incorporation, whereas the betaine was estimated (by comparison of the integrals of the peaks at 3.5 and 5.0 ppm) to be >90% $Pyr^+CH_2CHDSO_3^-$ (with a small amount of **9**, R = H).

(b) Trimethylamine

The hydrolysis of ethenesulfonyl chloride (**1**) (27 mg, 0.21 mmol) in D_2O was carried out using a solution in DME (1.0 mL, dried) under similar conditions as those for kinetic measurements: 1°C, pH-stat, pH reading = 10.0, ~0.1 *M* NaOD as a titrant, with 30-μL portions of the DME solution injected to ~0.2 *M* NMe_3 solution in D_2O (40 mL, maximum substrate concentration ~1.6×10^{-4} mol/L) at 5-min intervals. The excess of NMe_3 was then extracted with ether, the solvents evaporated to dryness, and the residue dissolved in D_2O. The ^{1}Hmr spectrum showed that the characteristic A_2B_2 pattern of the undeuterated betaine with its two multiplets of equal area at 3.4–3.6 ppm and 3.7–3.9 ppm was distinctly altered, as expected for conversion largely to $Me_3\overset{+}{N}CH_2CHDSO_3^-$, with the integral of the high field component reduced in area to approximately half of the low field part of the signal; the characteristic peaks of $CH_2{=}CHSO_3^-$ were observed from 5.8–6.9 ppm; we also noted two small 1:1:1 triplets centred around 5.9 and 6.1 ppm, indicating that a small part (~5%) of the ethenesulfonate anion was α-deuterated ($CH_2CDSO_3^-$).

Control experiments

Experiments were carried out showing that: (*a*) sodium ethenesulfonate give no H–D exchange in D_2O at pH (meter readings) 3.4 for 100 min or pH 10.5 for 30 min at 25.0°C followed by work-up, (*b*) the ratio of **9** to **10** is unchanged on standing for 2 h at pH 4.0 followed by work-up, (*c*) the ratio of **9** to **10** in the product obtained on carrying out the reaction of **1** in the presence of added sodium ethenesulfonate corresponds to that of the reaction plus the added ethenesulfonate (and hence the product mixture is not an equilibrium

mixture), and (*d*) sodium hydroxyethanesulfonate gives no H–D exchange on carbon in 0.08 *M* NaOD in D_2O at room temperature for 2 h followed by work-up. Further details may be found elsewhere (65).

Reaction of ethenesulfonyl chloride (1) in D_2O–DME (80:20) without and with diisopropylethylamine

Ethenesulfonyl chloride (50 mg, 0.4 mmol) was dissolved in DME (4.5 mL, dried) and 50 μL of this solution was injected into aqueous DME (25 mL, DME/D_2O 20:80 v/v) at pH (meter reading) 9.0 and maintained at constant pH in the pH-stat apparatus with ~0.1 *M* NaOD in D_2O at 25°C. About every 15 min (ca. 4 half-lives) another 50 μL of the solution was added till the hydrolysis was completed (the concentration of starting material never exceed 1.8×10^{-4} *M*). The solution was then neutralized, and solvent evaporated and the residue dissolved in D_2O. The ^{1}Hmr spectrum did not show any incorporation of deuterium (i.e. <5%) into the ethenesulfonate. (In other experiments, however, where concentration of free **1** exceeded 5×10^{-4} *M*, the presence of deuterium in ethenesulfonate was observed (at 5.86 and 6.07 ppm); it seemed to increase with the increase of concentration of the substrate.)

In a similarly carried out experiment, except for the presence of *N*,*N*-diisopropylethylamine in the D_2O solution ($B_T = 0.265$ *M*, conditions in which k_ψ was 2.9 times that without the amine) did not produce any incorporation of deuterium.

Can. J. Chem. Downloaded from www.nrcresearchpress.com by 210.87.254.6 on 09/06/12
For personal use only.

1. M. M. ABDEL-MALIK, P. A. W. DEAN, and J. F. KING. Can. J. Chem. **62**, 69 (1984).
2. R. V. VIZGERT. Usp. Khim. 3 (1963).
3. O. ROGNE. J. Chem. Soc. B, 1294 (1968).
4. O. ROGNE. J. Chem. Soc. Perkin Trans. 2, 472 (1972).
5. E. TOMMILA and P. HIRSJÄRVI. Acta Chim. Scand. **5**, 659 (1951).
6. H. K. HALL. J. Am. Chem. Soc. **78**, 1450 (1956).
7. F. E. JENKINS and A. N. HAMBLY. Aust. J. Chem. **14**, 190 (1961).
8. R. FOON and A. N. HAMBLY. Aust. J. Chem. (*a*) **15**, 668 (1962); (*b*) **15**, 684 (1962).
9. I. LEE and I. S. KOO. Tetrahedron, **39**, 1803 (1983).
10. N. H. CHRISTENSEN. Acta Chem. Scand. **20**, 1955 (1966).
11. J. L. KICE and G. J. KASPEREK. J. Am. Chem. Soc. **91**, 5510 (1969).
12. J. F. KING and T. DURST. J. Am. Chem. Soc. **87**, 5684 (1965).
13. W. E. TRUCE and R. W. CAMPBELL. J. Am. Chem. Soc. **88**, 3599 (1966).
14. J. F. KING. Acc. Chem. Res. **8**, 10 (1975).
15. A. WILLIAMS and K. T. DOUGLAS. Chem. Rev. **75**, 627 (1975).
16. L. O. FARNG and J. L. KICE. J. Am. Chem. Soc. **103**, 1137 (1981).
17. J. F. KING and S. M. LOOSMORE. J. Chem. Soc. Chem. Commun. 1011 (1976).
18. J. F. KING and J. H. HILLHOUSE. J. Chem. Soc. Chem. Commun. 454 (1979).
19. C. RONDESTVEDT, JR. J. Am. Chem. Soc. **76**, 1926 (1954).
20. H. DISTLER. Angew. Chem. Int. Ed. Engl. **4**, 300 (1965).
21. A. LE BERRE, A. ÉTIENNE, and B. DUMAITRE. Bull. Soc. Chim. Fr. 954 (1970).
22. A. ÉTIENNE, A. LE BERRE, and J.-P. GIORGETTI. Bull. Soc. Chim. Fr. 985 (1973).
23. J. PRESTON and R. B. SCOTT, JR. J. Org. Chem. **33**, 4343 (1968).
24. K. B. WIBERG. Physical organic chemistry. John Wiley & Sons, New York. 1964. p. 378.
25. D. D. PERRIN. Dissociation constants of organic basis in aqueous solution. Butterworths, London. 1965. p. 153.
26. U. BERG, R. GALLO, J. METZGER. J. Org. Chem. **41**, 2621 (1976).
27. L. W. DEADY, W. L. FINLAYSON, and O. L. KORYTSKY. Aust. J. Chem. **32**, 1735 (1979).
28. K.-J. SCHAPER. Arch. Pharm. **311**, 641, 650 (1978).
29. T. DEACON, C. R. FARRAR, B. J. SIKKEL, and A. WILLIAMS. J. Am. Chem. Soc. **100**, 2525 (1978).
30. S. THEA and A. WILLIAMS. J. Chem. Soc. Perkin Trans. 2, 72 (1981).
31. J. F. KING and J. H. HILLHOUSE. Can. J. Chem. **61**, 1583 (1983).
32. R. E. ROBERTSON and P. M. LAUGHTON. Can. J. Chem. **35**, 1319 (1957).
33. S. L. JOHNSON. Adv. Phys. Org. Chem. **5**, 237 (1967).
34. O. ROGNE. J. Chem. Soc. (B), 727 (1970).
35. G. GEISELER and F. ASINGER. Chem. Ber. **89**, 1100 (1956).
36. O. ROGNE. J. Chem. Soc. (B), 1334 (1971).
37. M. B. DAVY, K. T. DOUGLAS, J. S. LORAN, A. STELTNER, and A. WILLIAMS. J. Am. Chem. Soc. **99**, 1196 (1977).
38. J. F. KING and R. P. BEATSON. Tetrahedron Lett. 973 (1975).
39. C. ROMERS, C. ALTONA, H. R. BUYS, and E. HAVINGA. Top. Stereochem. **4**, 39 (1969).
40. S. DAVID, O. EISENSTEIN, W. J. HEHRE, L. SALEM, and R. HOFFMANN. J. Am. Chem. Soc. **95**, 3806 (1973).
41. S. WOLFE, M.-H. WHANGBO, and D. J. MITCHELL. Carbohydr. Res. **69**, 1 (1979).
42. S. WOLFE, A. STOLOW, and L. A. LAJOHN. Tetrahedron Lett. **24**, 4071 (1983).
43. P. J. THOMAS and C. J. M. STIRLING. J. Chem. Soc. Perkin Trans. 2, 1909 (1977).
44. G. STORK and W. N. WHITE. J. Am. Chem. Soc. **78**, 4609 (1956).
45. R. L. YATES, N. D. EPIOTIS, and F. BERNARDI. J. Am. Chem. Soc. **97**, 6615 (1975).
46. R. M. MAGID. Tetrahedron, **36**, 1901 (1980).
47. W.-D. STOHRER. Angew. Chem. Int. Ed. Engl. **22**, 613 (1983).
48. J. F. KING and T. W. S. LEE. J. Am. Chem. Soc. **91**, 6524 (1969).
49. F. HIBBERT. J. Chem. Soc. Perkin Trans. 2, 1289 (1973).
50. M. INOUE and T. C. BRUICE. J. Chem. Soc. Chem. Commun. 884 (1981).
51. M. INOUE and T. C. BRUICE. J. Am. Chem. Soc. **104**, 1644 (1982).
52. C. R. FARRAR and A. WILLIAMS. J. Chem. Soc. Perkin Trans. 2, 1758 (1979).
53. R. P. BEATSON. Ph. D. Thesis, University of Western Ontario, 1975. pp. 92–94.
54. A. ÉTIENNE, G. LONCHAMBON, and C. BENARD. Bull Soc. Chim. Fr. 483 (1976).
55. J. M. STEWART and H. P. CORDTS. J. Am. Chem. Soc. **74**, 5880 (1952).
56. C. RONDESTVEDT, JR. and P. K. CHANG. J. Am. Chem. Soc. **77**, 6532 (1955).
57. H. H. G. JELLINEK and M. G. WAYNE. J. Phys. Chem. **55**, 173 (1951).
58. H. C. BROWN and W. A. MURPHEY. J. Am. Chem. Soc. **73**, 3308 (1951).
59. A. C. BRATTON and J. R. BAILEY. J. Am. Chem. Soc. **59**, 175 (1937).
60. R. CAMPS. Arch. Pharm. **240**, 355 (1902).
61. F. B. LAFORGE. J. Am. Chem. Soc. **50**, 2477 (1928).
62. A. LE BERRE, A. ÉTIENNE, and B. DUMAITRE. Bull. Soc. Chim. Fr. 946 (1970).
63. J. D. BARNHURST. J. Org. Chem. **26**, 4520 (1961).
64. W. F. WHITMORE and E. F. LANDAU. J. Am. Chem. Soc. **68**, 1797 (1946).
65. J. H. HILLHOUSE. Ph.D. Thesis, University of Western Ontario, 1982. pp. 115–117.

Photochemical and mass spectrometric transformation of gibberellenic acid to 9-epiallogibberic acid

HUSSAIN K. AL-EKABI AND GHAZI A. W. DERWISH
Chemistry Department, College of Science, University of Baghdad, Adamyia, Baghdad, Iraq

Received February 6, 1984

This paper is dedicated to Professor Paul de Mayo on the occasion of his 60th birthday

HUSSAIN K. AL-EKABI and GHAZI A. W. DERWISH. Can. J. Chem. **62**, 1996 (1984).

Gibberellenic acid (**2**) reacted thermally in a modified immersion photochemical reactor, to give an intermediate triene (**3**). This triene then isomerized photochemically, via suprafacial [1,3]-hydrogen migration, to 9-epiallogibberic acid (**5**). On the other hand, comparison of the positive mass spectra of gibberellenic acid (**2**), allogibberic acid (**4**), and 9-epiallogibberic acid (**5**) showed that gibberellenic acid underwent electron impact fragmentation to the triene **3** cation. This cation then rearranged through suprafacial [1,3]-hydrogen migration to the 9-epiallogibberic acid (**5**) cation.

HUSSAIN K. AL-EKABI et GHAZI A. W. DERWISH. Can. J. Chem. **62**, 1996 (1984).

L'acide gibbérellènique (**2**), traité dans un réacteur photochimique à immersion modifié, subit une réaction thermique conduisant à l'intermédiaire triène (**3**) qui s'isomérise alors par un processus photochimique, via une migration [1,3] suprafaciale d'hydrogène, pour conduire à l'acide 9-épiallogibbérique (**5**). Par ailleurs, une comparaison des spectres de masse positives des acides gibbérellènique (**2**), allogibbérique (**4**) et 9-épiallogibbérique (**5**) a permis de montrer que l'acide gibbérellènique subit une fragmentation, sous impact électronique, conduisant au cation triénique **3**. Ce cation se transpose alors, par le biais d'une migration [1,3] suprafaciale d'hydrogène, pour conduire au cation de l'acide 9-épiallogibbérique (**5**).
[Traduit par le journal]

Can. J. Chem. Downloaded from www.nrcresearchpress.com by 210.87.254.105 on 09/06/12
For personal use only.

Gibberellic acid (**1**) is known to be the most biologically active in most circumstances among the gibberellins (1). It decomposes thermally in aqueous solutions to gibberellenic acid (**2**) (2–4), which is also thermally unstable in aqueous solution, giving allogibberic acid (**4**) in 80% yield and 10% of 9-epiallogibberic acid (**5**) (2–4). Pryce (4) proposed a mechanism (Scheme 1) in which **2** decomposes thermally to the intermediate triene **3**, which then rearranges, through a solvent exchange process, to **4**. Neither a photochemical nor an electron impact fragmentation study of **2** has been carried out. We wish to report now on (a) the thermal and subsequent photochemical rearrangement of **2** to 9-epiallogibberic acid (**5**), and (b) electron impact fragmentation of **2** to the **5** cation. Furthermore, the work is also aimed at presenting evidence that **2** is the first step in the fragmentation of **1**.

Results and discussion

(a) *Thermal and subsequent photochemical rearrangement of 2 to 5*

An aqueous solution of **2** (λ_{max} = 253 nm) at 25–30°C is fairly stable, and irradiation at this temperature under argon in Pyrex produced no reaction. However, according to Pryce (4), an aqueous solution of **2** is thermally reactive at about 100°C, giving the intermediate triene **3** (λ_{max} = 326 nm). An experiment was therefore designed to follow the subsequent photochemical behaviour of the thermally formed triene. An immersion photochemical reactor (Applied Photophysics Ltd., Model RQ 100) was used with some modifications, which led to simultaneous heating and irradiation (above 300 nm) of the sample (see Experimental). After 30 min irradiation in water the starting material was consumed and a product identified as 9-epiallogibberic acid (**5**) precipitated in good yield. When the reaction was repeated in D_2O (Merck 99.7^{2}H) as the solvent, **5** was formed which, in contrast to the experiment described by Pryce (4), contained no deuterium at C-9, as indicated by nmr (experimental error ±10%).

In both experiments (thermal (4) and thermal–photochemical) the first step should be the formation of the intermediate triene (**3**). The fate of this triene then depends on the conditions, reflecting the different symmetry properties of a triene in its ground and first excited state. Thus, in accordance with orbital symmetry rules, a mechanism is proposed (Scheme 2) in which the triene undergoes photochemically suprafacial

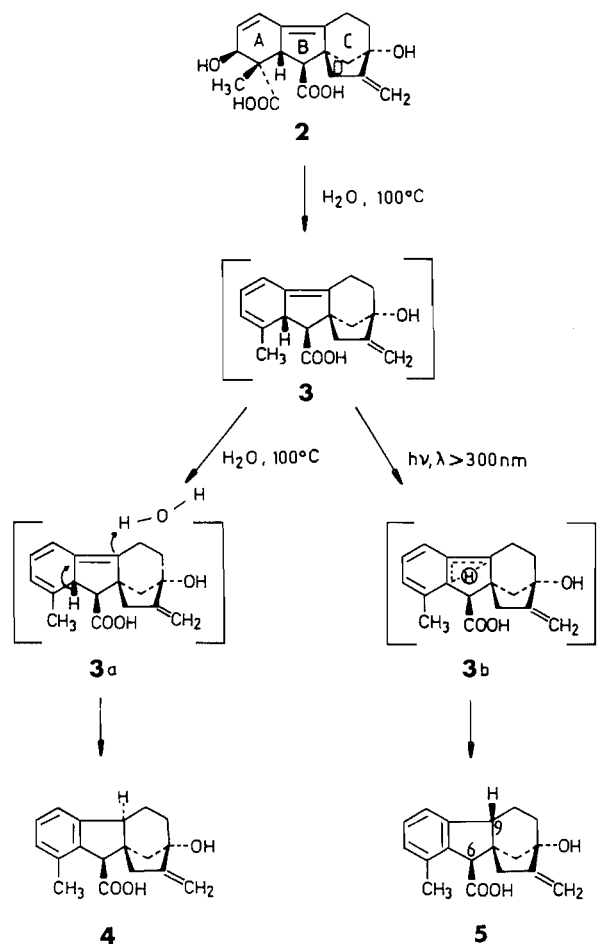

SCHEME 1

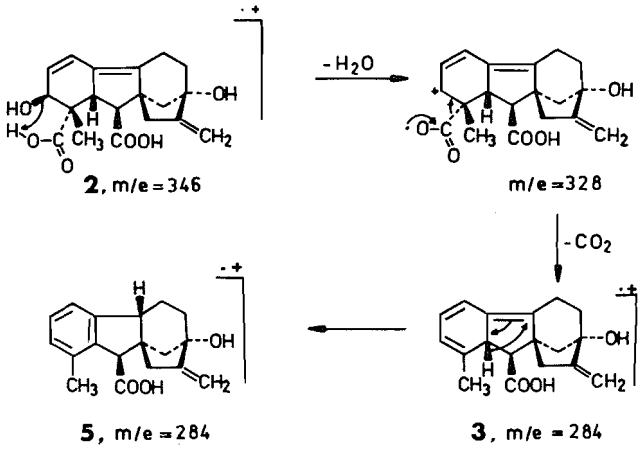

SCHEME 2

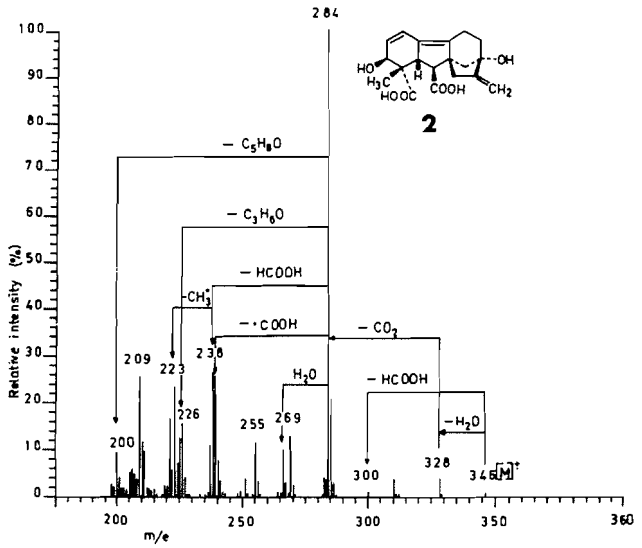

FIG. 1. 70-eV Mass spectrum of gibberellenic acid **2**.

[1,3]-hydrogen migration to give 9-epiallogibberic acid (**5**) in a high yield (90%).

(b) *Electron impact fragmentation of* ***1*** *to the* ***5*** *cation*

The positive ion mass spectrum of **2** showed the expected molecular ion peak at *m/e* 346 (Fig. 1). The base peak at *m/e* 284 indicates that aromatization of ring A is favoured.

In order to identify the origin of the base peak, the positive ion mass spectra of **4** and **5**, which are the expected aromatic derivatives of **2**, were measured (Figs. 2 and 3). They showed indeed the base peaks at *m/e* 284.

Although the three spectra have much the same fragmentation pattern below *m/e* 284, the ion peak of *m/e* 226 exhibits significant differences. While it is the second most intense peak of **4**, it is much less intense in **2** and **5**. It can be considered as a key peak in distinguishing between **4** and **5** by mass spectroscopy.

Voigt *et al.* (5) attributed the 226 peak to the loss of a C_3H_6O

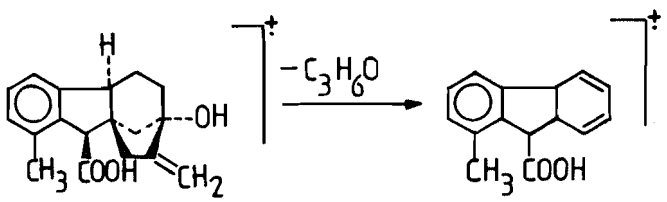

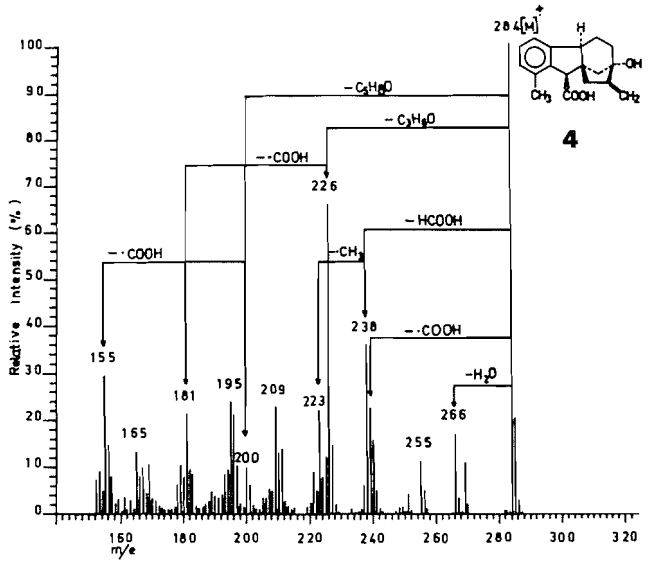

FIG. 2. 70-eV Mass spectrum of allogibberic acid **4**.

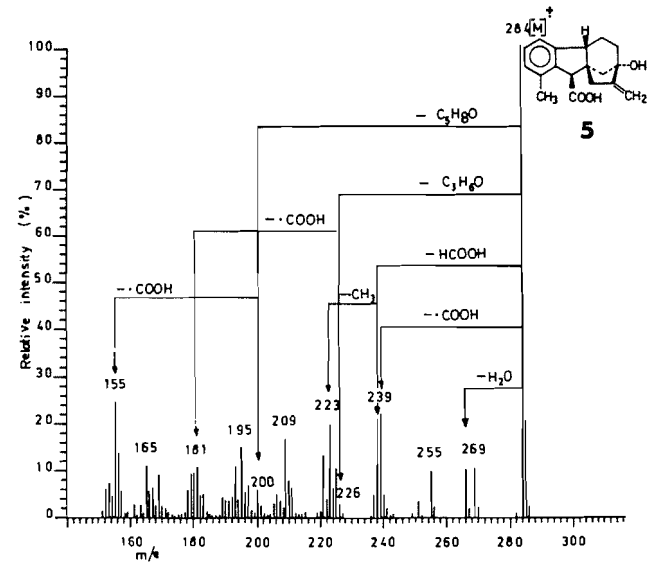

FIG. 3. 70-eV Mass spectrum of epiallogibberic acid **5**.

unit from the molecular ion peak *m/e* 284 of **4** as follows:

The extremely low intensity of the peak in **5** may be explained by stereochemical considerations of **4** and **5**. According to the stereomodel, ring D should have a normal envelope conformation in **5** but a much more twisted envelope in **4**. The latter conformation may facilitate the loss of a C_3H_6O unit and thus produce another π-system contributing to the stability of the proposed cation.

In view of the similarity of the mass spectra of **2** and **5** below *m/e* 284, it seems reasonable to conclude that the base peak in **2** originates from the fragmentation of **2** to the **5** cation. Thus, the aromatization of ring A involves the loss of water to give an ion peak at *m/e* 328. This is followed by elimination of carbon dioxide to yield the triene ion, which then rearranges (as in the photochemical reaction) to the corresponding aromatic ion of *m/e* 284 (9-epiallogibberic acid cation **5**; Scheme 2). If this were not the case, a highly intense peak at *m/e* 226 would appear in the spectrum of **2**. The results led us to reinvestigate the positive ion mass spectrum of gibberellic acid

Can. J. Chem. Downloaded from www.nrcresearchpress.com by 210.87.254.105 on 09/06/12
For personal use only.

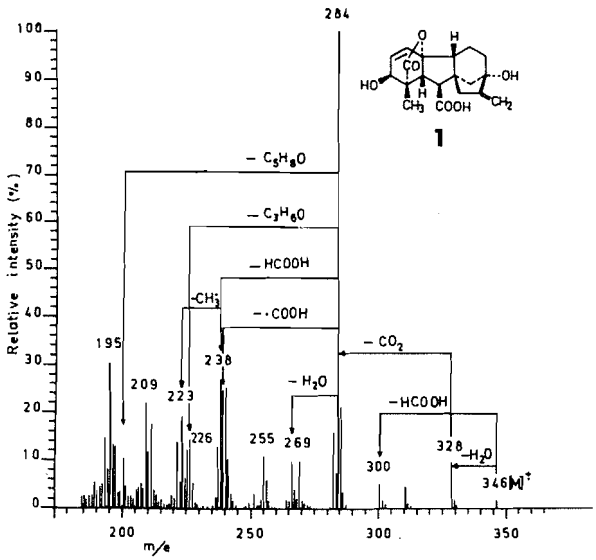

FIG. 4. 70-eV Mass spectrum of gibberellic acid **1**.

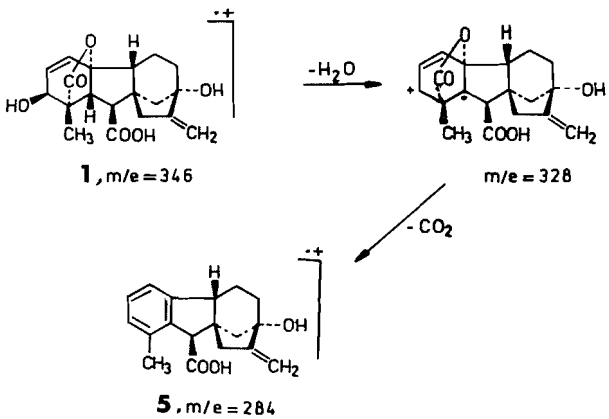

SCHEME 3

(Fig. 4), which again shows, as in **2**, the expected molecular ion peak at *m/e* 346. However, its intensity is about three times higher than that of **2**. The base peak at *m/e* 284 indicates that aromatization of ring A is favoured.

The close similarity of the mass spectra of **1** and **2** and the higher intensity of the molecular ion peak of **1** may suggest that **2** is the first step in the fragmentation of **1**. Incidentally, **2** is the first aqueous decomposition product of **1** (2–4). Alternatively, a fragmentation pathway of **1** to **5** without passing through the intermediate **2** is also possible (Scheme 3).

Experimental

Ultraviolet (uv) spectra were run in MeOH and infrared (ir) spectra were taken in Nujol. Varian A-60 and Bruker WH 200 spectrometers were used to record the ^{1}H nmr spectra. The spectra were run in pyridine-d_5 solution, with HMDS as an internal standard. Mass spectra were taken on a Varian CH5 instrument (70 eV) (source temperature 150–200°C).

The photolysis was carried out on a modified immersion photochemical reactor (Applied Photophysics, Ltd. Model RQ 100). Thus, a single-wall Pyrex immersion well instead of the double-wall quartz was used to hold the medium pressure mercury lamp (125 W). The lamps could thus act as a convenient heat source as well as a light source ($\lambda > 300$ nm). Practically, the solution started to boil 5 min after switching on the lamp. Thus a solution of 500 mg of **2** in 100 mL of doubly distilled water was irradiated under argon and reflux conditions. After about 30 min the starting material was consumed, as indicated by tlc, and a product precipitated. The latter was separated (450 mg), recrystallized from methanol–water as prisms, mp 245°C, and was identified, on the basis of the physical constants, as 9-epiallogibberic acid (**5**) (4); uv λ_{max}: 266 nm, ϵ_{max} = 350 L mol^{-1} cm^{-1}; ir: aromatic band at 1600 cm^{-1} instead of the original conjugated C=C band at 1655 cm^{-1}; nmr (pyridine-d_5): no olefinic ring A protons, 3 adjacent aromatic protons at δ: 7.26 (1H, t, J = 7.3 Hz), 7.15 (1H, d, J = 7.4 Hz) and 7.06 (1H, d, J = 7.4 Hz), 4.02 (H-6, s), and 3.88 (H-9, d, J = 5 Hz); ms: molecular ion peak at *m/e* 284.

Gibberellic acid **1** (Fluka) was used after several recrystallizations from MeOH–H_2O. Gibberellenic acid **2** was prepared from **1** according to the procedures of Moffat (6).

1. R. L. WAIN. Chem. Soc. Rev. **6**, 261 (1977).
2. R. J. PRYCE. Phytochemistry, **12**, 507 (1973).
3. R. J. PRYCE. Phytochemistry, **12**, 1745 (1973).
4. R. J. PRYCE. J. Chem. Soc. 1179 (1974).
5. D. VOIGT, G. ADAM, and J. SCHMIDT. Org. Mass. Spectrom. **13**, 599 (1978).
6. J. S. MOFFAT. J. Chem. Soc. 3045 (1960).

Can. J. Chem. Downloaded from www.nrcresearchpress.com by 210.87.254.105 on 09/06/12
For personal use only.

Surface photochemistry: ^{13}C enrichment by photolysis on silica gel[1]

LINDA J. JOHNSTON AND S. KING WONG

Photochemistry Unit, Department of Chemistry, The University of Western Ontario, London, Ont., Canada N6A 5B7

Received February 10, 1984

This paper is dedicated to Professor Paul de Mayo on the occasion of his 60th birthday

LINDA J. JOHNSTON and S. KING WONG. Can. J. Chem. **62**, 1999 (1984).

The enrichment of the ^{13}C isotope by partial photolysis of dibenzyl ketone on silica gel has been demonstrated. The ^{13}C enrichment is substantial and is parallel to the increase in the probability of geminate radical recombination on a silica surface as compared with that in solution. A substantial ^{13}C enrichment was also observed for the rearranged starting material, 1-phenyl-4′-methylacetophenone. The single-stage isotope separation factors are different for the two ketones although both are isomers derived from the same benzyl–phenylacetyl radical pairs.

LINDA J. JOHNSTON et S. KING WONG. Can. J. Chem. **62**, 1999 (1984).

On a démontré qu'il se produit un enrichissement de l'isotope ^{13}C lors de la photolyse partielle de la dibenzylcétone sur du gel de silice. L'enrichissement en ^{13}C est important et il augmente avec l'augmentation de la probabilité de recominaison du radical geminé sur la surface de la silice par opposition à la probabilité en solution. On a aussi observé un enrichissement important en ^{13}C dans le produit de départ transposé, la phényl-1 méthyl-4′ acétophénone. Même si les deux cétones sont des isomères dérivés de la même paire de radicaux benzyl–phénylacétyles, les facteurs de séparation isotopique pour une étape sont différents.

[Traduit par le journal]

Can. J. Chem. Downloaded from www.nrcresearchpress.com by 210.87.254.105 on 09/06/12
For personal use only.

Virtually all methods of isotope enrichment are based upon differences in mass or related properties. However, in 1971, Lawler and Evans (1) predicted that, according to the radical pair theory for magnetic polarization (2, 3), the separation of isotopes based upon differences in their magnetic moments rather than their masses should be possible. In 1976 the observation of Buchachenko *et al.* (4*a*) of ^{13}C enrichment during the photolysis of dibenzyl ketone confirmed that magnetic effects could lead to isotope separation. Since then there have been a number of investigations of the influence of magnetic isotope and magnetic field effects on radical reactions (4–8).

A geminate radical pair in solution may undergo a number of processes: intersystem crossing (isc), diffusional separation, recombination to produce products or regenerate starting materials, or transformation to a new radical pair. A basic premise of the radical pair theory is the postulate that the chemical behaviour of a radical pair may be influenced by the spin of magnetic nuclei through the electron-nuclear hyperfine coupling (hfc) isc interaction. Since the hfc interaction is one of the major mechanisms for isc in radical pairs containing magnetic nuclei, the presence of such nuclei will increase the isc rate, particularly when the hfc constants are large. For example, a triplet radical pair containing a magnetic isotope with a large hfc constant (e.g., ^{13}C) will undergo more rapid isc than will the same triplet pair containing a nonmagnetic isotope (^{12}C). If isc to a singlet radical pair followed by cage recombination competes with diffusional separation and nongeminate reaction of the radicals, then the cage products are expected to be enriched in the magnetic isotope while the escape products will be impoverished.

The ^{13}C enrichment which occurs during the photolysis of dibenzyl ketone, **1**, (4, 6, 7) can be explained in terms of Scheme 1. Excitation followed by rapid isc produces a short-lived triplet which undergoes α cleavage to generate a triplet phenylacetyl–benzyl radical pair (9, 10). In solution this radical pair decays by either recombination to generate starting material or diffusional separation (10). Decarbonylation of the free phenylacetyl radicals occurs and the benzyl radicals combine to yield dibenzyl. The original acyl–benzyl radical pairs containing ^{13}C nuclei will undergo more rapid isc to a singlet pair than will those containing ^{12}C nuclei, while more of the radicals containing ^{12}C will escape from their original partners. Therefore, the cage products, regenerated **1** (and its isomer, 1-phenyl-4′-methylacetophenone, **2**, when formed (6)) will be enriched in ^{13}C. The free radical products will, on the other hand, contain more ^{12}C than did the original starting material.

Small amounts of ^{13}C enrichment have been observed in **1** recovered after partial photolysis in solution (4, 6, 7); the value for α, the single-stage enrichment parameter, was ~1.04 in benzene (6*a*). Pines and co-workers (7) concluded from their investigations of temperature and solvent viscosity effects that the enrichment efficiency was strongly dependent on viscosity with maximum effects at intermediate viscosities. Turro and co-workers (6) have reported substantial increases in enrichment for photolysis of **1** in aqueous micellar solutions: α_{CO} (**1**) ≃ 1.35, α_{CH} (**1**) ≃ 1.18, and α'_{CO} (**2**) ≃ 1.26, where α′ refers to the single stage enrichment parameter for **2** and the subscripts refer to the position of the ^{13}C enrichment. The larger enrichment at the carbonyl rather than the methylene carbon was consistent with the hfc constants (6*d*) for ^{13}C at the various positions. The efficient ^{13}C enrichment in micelles has been attributed to the restricted space in which the radical pair finds itself (6); the micelle is thought to provide a boundary which prevents the radical pair from diffusing apart and allows more time for hfc-induced isc to occur. Decarbonylation, rather than diffusion (as in solution), was proposed as the competing escape mechanism for the triplet radical pair in a micelle.

Substantial enrichment (α = 1.66) was also reported for **1** photolysed on a surface prepared by chemically bonding a hydrocarbon layer to the surface of silica gel (11). The authors suggested that the synthetic monolayer surface was analogous to a micelle in providing an artificial "reflecting boundary" which led to an enhanced magnetic isotope effect. However, it appeared more likely that the above results were a reflection of the silica gel surface properties rather than the micelle-like properties of the synthetic monolayer surface, since a number of studies have indicated that radical mobility is restricted on

[1] Publication No. 317 from the Photochemistry Unit, Department of Chemistry, The University of Western Ontario.

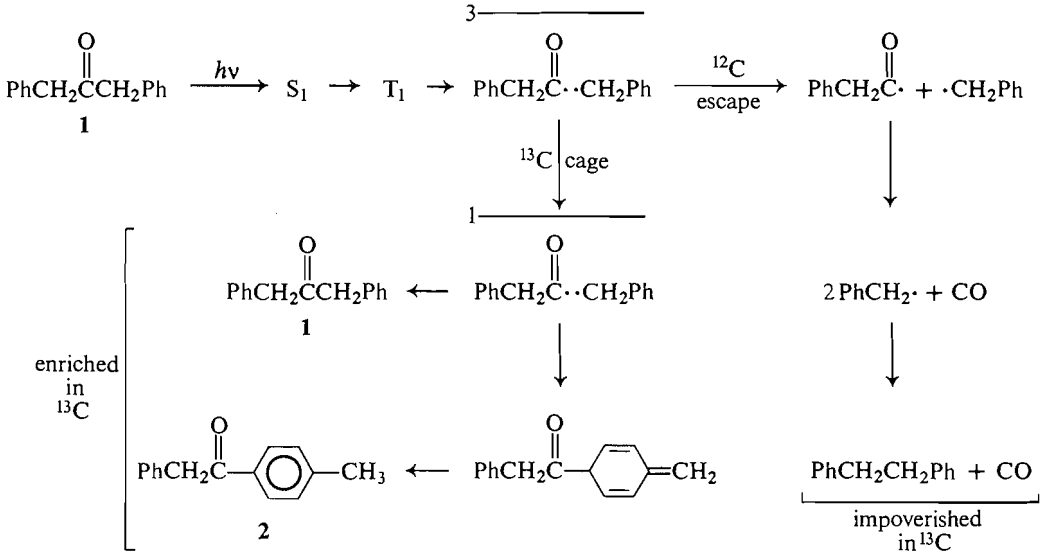

SCHEME 1

silica surfaces (12–16). For example, limited translational motion has been shown to precede recombination of a singlet radical pair generated on silica gel by the photo-Fries rearrangement (12). A greater amount of movement has been reported for both benzyl (13) and cyanopropyl (14) radical pairs on silica gel. Similarly, some surface mobility has been observed for radical pairs generated by photolysis of azocumene (15*a*) and diacyl peroxides (15*b*) on silica gel. Evidence for restriction of the mobility of adsorbed radicals has been provided by the observation of previously undetected reaction pathways in the photolysis of benzoin methyl ether on silica gel (16).

Efficient ^{13}C enrichment requires that diffusional separation of the radical pair be sufficiently slow that hfc-induced isc can compete, but not so slow that the rates of isc of all radical pairs are the same, regardless of whether or not they contain ^{13}C or ^{12}C. The slower escape of a radical from its original geminate partner on silica gel, as compared to solution, suggested that the silica gel surface should provide a suitable environment for the observation of substantial amounts of ^{13}C enrichment. The present study of ^{13}C enrichment on silica gel was, therefore, undertaken with the intention of searching for conditions for optimization of ^{13}C enrichment and of obtaining further information concerning the mechanism of the magnetic isotope effect in restricted environments and the diffusional motion of radicals on a surface.

Data analysis

Since the amount of enrichment depends on the extent of conversion, it is useful to express the results in terms of a single-stage isotope separation factor, α, (17) which is independent of conversion and thus allows comparison of isotope separation efficiencies for different experiments. Bernstein (17) has shown that, for competitive, first-order reactions of isotopically different species, the residual unreacted starting material becomes exponentially enriched in the slower reacting isotope. This may be applied to the competitive $^{12}C/^{13}C$ reactions in the photolysis of dibenzyl ketone, as shown by Turro *et al.* (6*a*). Since molecules containing ^{13}C proceed to products at a slower rate (i.e., more geminate recombination to regenerate starting material occurs for ^{13}C radical pairs) than do those containing ^{12}C, the residual unreacted ketone will become enriched in ^{13}C.

The parameter α is defined as the single-stage separation (17) and may be computed from the measured quantities, S, the overall separation factor, and f, the fractional conversion. These are defined for carbon isotopes in eqs. [1] and [2], where the subscripts 0 and f refer to concentrations in the initial and recovered material.

$$[1] \quad S = \frac{[^{12}C]_0[^{13}C]_f}{[^{12}C]_f[^{13}C]_0}$$

$$[2] \quad f = 1 - \frac{[^{12}C]_f + [^{13}C]_f}{[^{12}C]_0 + [^{13}C]_0}$$

The magnitude of α is then obtained from eq. [3] which can, for most purposes, be approximated by eq. [5].

$$[3] \quad \log S = \frac{\alpha - 1}{\alpha}\left[\log\left(\frac{1 + SR_0}{1 + R_0}\right) - \log(1 - f)\right]$$

$$[4] \quad R_0 = \frac{[^{13}C]_0}{[^{12}C]_0}$$

$$[5] \quad \log S = \frac{\alpha - 1}{\alpha}[-\log(1 - f)]$$

In practice, α can be evaluated directly from [3] or [5] for each experiment or can be computed from the slope ($(\alpha - 1)/\alpha$) of a plot of $\log S$ versus $-\log(1 - f)$.

The above method for obtaining enrichment efficiencies cannot be used to express isotope separation efficiencies for products formed in the reaction. When dibenzyl ketone is photolysed in either micelles (6) or on silica gel (18), an isomeric product, 1-phenyl-4′-methylacetophenone, **2**, is produced. This isomer is formed by geminate recombination of the initial radical pair and is thus expected to be formed more often from ^{13}C ketone molecules than from ^{12}C molecules. Any isomer formed is not diluted by a large pool of unreacted, unenriched material, as is the case for regenerated dibenzyl ketone. As a result, the ^{13}C enrichment, as measured by S, is much higher for **2** than for **1** at low conversions but increases more slowly with increasing conversion. The increase in S for **2** with conversion

Can. J. Chem. Downloaded from www.nrcresearchpress.com by 210.87.254.105 on 09/06/12
For personal use only.

occurs because the ketone from which **2** is formed is being constantly enriched in ^{13}C as the reaction progresses.

In principle, measurement of S for **2** at very low conversions for which the ^{13}C enrichment for **1** is negligible can yield directly the single-stage enrichment parameter, α', for **2**. Kraeutler and Turro (*6d*) obtained α' by plotting log S against $-\log(1-f)$ for **2** and extrapolating to zero conversion. The physical meaning of the plot is not clear and a considerable number of points at low conversion are required to obtain α' in this way. Therefore, a method based upon the overall separation factor, S, for **1** (i.e., the variation in $^{13}C/^{12}C$ ratios for **1** throughout the photolysis was developed for the calculation of α' for **2** in the present experiments.

The single-stage enrichment parameter α' for **2** may be defined as shown in eq. [6] where k_{13} and k_{12} are the rate constants

$$[6] \quad \alpha' = \frac{k_{13}}{k_{12}}$$

for the formation of ^{13}C and ^{12}C **2**, respectively. The rate of formation of **2** depends on the concentration of **1**; integration

$$[7] \quad \frac{d[^{13}C_2]}{dt} = k_{13}[^{13}C_1]$$

of both sides of eq. [7], followed by a change of variable (from time to conversion, f) and substitution for $[^{13}C_1]$, as outlined in the Appendix, yields the following expression:

$$[8] \quad [^{13}C_2]_{total} = k_{13}C_0 \int_0^f \left(\frac{SR_0}{1+SR_0}\right)(1-f)\,df$$

A similar expression is obtained for $[^{12}C_2]_{total}$:

$$[9] \quad [^{12}C_2]_{total} = k_{12}C_0 \int_0^f \left(\frac{1}{1+SR_0}\right)(1-f)\,df$$

After evaluation of the integrals in eqs. [8] and [9], the relative amounts of $^{13}C/^{12}C$ for **2** may be used to evaluate k_{13}/k_{12} which, from [6], is equivalent to α'. The integration is done numerically using the known values of α and f to obtain S.

Results and discussion

Carbon 13 enriched ketone was used as the starting material for all measurements of ^{13}C enrichment resulting from photolysis of dibenzyl ketone, **1**. Analysis of the $^{13}C/^{12}C$ ratios was more accurate if enriched material was used; several preliminary experiments had indicated that there was considerable error in the mass spectral analysis if unenriched ketone was used. Dibenzyl ketone was prepared (19) from ^{13}C-labelled phenylacetic acid (90% ^{13}C in the carbonyl) and was mixed with an appropriate amount of natural abundance **1** to give ketone which contained 25% ^{13}C in the carbonyl position. All reported α values, therefore, refer to enrichment at the carbonyl and have been corrected for the natural abundance ^{13}C content at other positions.

^{13}C enrichment on silica gel

Substantial ^{13}C enrichment was observed in both **1** and its isomer, **2**, recovered after partial photolysis of **1** on silica gel. The mass spectral results obtained for an experiment at 84.3% conversion are shown in Fig. 1: the intensity at m/e 211 relative to that at 210 was greater for recovered **1** than for the starting material. The ^{13}C contents of recovered **1** and **2** were 30.4% and 35.6%, respectively, from the mass spectral intensities. These results were confirmed by nmr analysis of the two ketones. The methylene protons of both show signals that

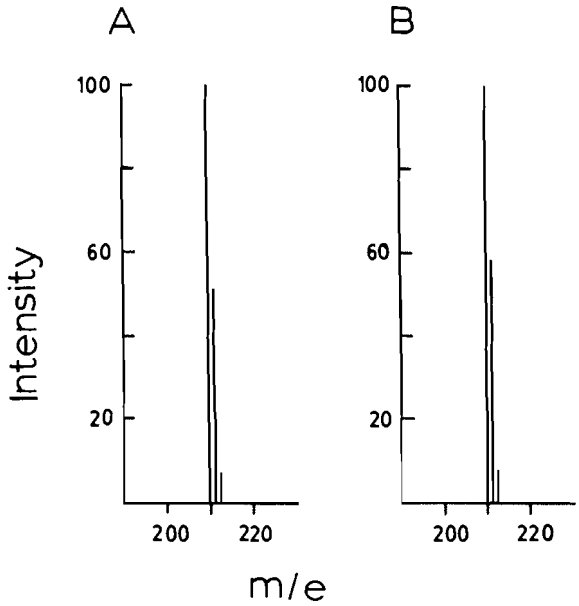

FIG. 1. Mass spectral intensities for **1** (25% $^{13}C{=}O$) before photolysis (A) and after photolysis to 84.3% conversion (B).

are a combination of a singlet due to a ^{12}C carbonyl and a doublet centred at the same chemical shift, the latter arising from the ^{13}C carbonyl. Integration of the singlet and the two satellites allowed determination of the ^{13}C content at the carbonyl; values determined by nmr integration agreed well with those determined mass spectrally.

The ^{13}C contents in **1** and **2** recovered after photolysis on silica gel at 20°C are listed in Table 1. As expected, the ^{13}C content of ketone **1** increased steadily with conversion. The calculated values for α, the single-stage enrichment factor, ranged from 1.12 to 1.18; the average was 1.14. The lower α values obtained at higher conversions may result from the over-irradiation of enriched ketone caused by inhomogeneous photolysis on the silica gel surface. This explanation is substantiated by the fact that lower α values ($\alpha < 1.04$) were obtained for experiments carried out to >98% conversion. The α values of ~1.18 for the lower conversion appear, therefore, to provide a more reliable measure of the ^{13}C enrichment efficiency on the silica gel surface. An α value of 1.13 was calculated from the slope of a plot of log S versus $-\log(1-f)$ (Fig. 2) for the data in Table 1 (20°C experiments).

Comparison of the results obtained under various experimental conditions (Table 1) showed that the ^{13}C enrichment was not affected by the water content of the silica gel or by the method of sample mixing. Lowering the photolysis temperature had little effect on α; at −55°C the observed enrichments (Table 1) were similar to those obtained at 20°C, although the α values were slightly higher for dry silica gel than for undried silica.

For isomer **2** the ^{13}C content was, as expected, already quite high at low conversion and did not increase very rapidly thereafter. For example, at 20°C the 33.0% ^{13}C content at 29.9% conversion increased to only 35.6 at 84.3% conversion (Table 1). Values of α' were all ~1.5 for **2** recovered after photolysis of **1** at 20°C on silica gel. As for ketone **1**, the enrichment for **2** at room temperature was not affected by either the dryness of the silical gel or the method of sample mixing. However, in contrast to results obtained for **1**, changing the photolysis temperature from 20°C to −55°C substantially decreased the en-

Can. J. Chem. Downloaded from www.nrcresearchpress.com by 210.87.254.105 on 09/06/12
For personal use only.

TABLE 1. ^{13}C enrichment for **1** and **2** recovered after photolysis of **1** on silica gel

Reaction conditions[a]	Temperature (°C)	Conversion %	% ^{13}C at C=O[b]			
			1	**2**	α	α′
A	20	84.3	30.4	35.6	1.12	1.58
A	20	70.9	27.7	34.6	1.11	1.52
A	20	69.8	28.1	34.1	1.14	1.48
A	20	43.8	26.8	33.8	1.18	1.48
A	20	29.9	26.1	33.0	1.17	1.44
A	−55	66.8	26.9	28.2	1.09	1.14
A	−55	28.7	25.5	25.8	1.07	1.03
B, C	20	91.6	30.7	35.4	1.12	1.56
B, C	20	73.6	28.3	34.3	1.14	1.49
B	20	27.4	25.4	[c]	1.08	—
B	−55	74.0	28.9	30.1	1.22	1.20
B	−55	50.2	27.3	28.1	1.18	1.12

[a] A: silica gel used without drying; B: silica gel dried at 200°C; C: sample rotated in an ultrasonic bath to aid in sample mixing.
[b] The reported % ^{13}C values are approximately ±0.9 (3%); these yield α values of approximately ±0.03.
[c] Yields of **2** insufficient for isolation and analysis.

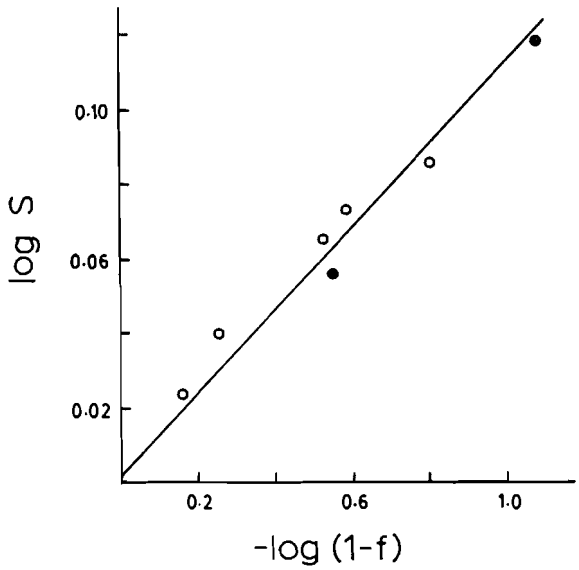

FIG. 2. Log S versus $-\log(1-f)$ for **1** recovered after photolysis at 20°C on dried (●) and undried (○) silica gel.

richment efficiency for **2** ($\alpha' \sim 1.1$ at −55°C).

The above results indicate that, as predicted, photolysis of **1** on dry silica gel does yield substantial ^{13}C enrichments in recovered ketones **1** and **2**. The observed α values for **1** are larger than those in solution ($\alpha \sim 1.04$ (6*a*)) but enrichment occurs less efficiently on the surface than it does in a micellar environment ($\alpha \sim 1.3$ (6) and the present work reported below). The α′ values for **2** on the surface are, however, larger than those in micelles.

^{13}C enrichment on other surfaces

Ketone **1** was photolysed on several other types of surfaces to determine their effect upon ^{13}C enrichment. The results are summarized in Table 2. First, **1** recovered after photolysis on a smaller particle size (6 μm rather than 0.2–0.5 mm) silica gel showed an enrichment ($\alpha \sim 1.13$) similar to that already observed. Second, photolysis of **1** on neutral alumina also gave a similar α value (~1.1); however, the situation on alumina may

TABLE 2. ^{13}C enrichment for **1** and **2** recovered after photolysis of **1** on various surfaces at 20°C

Surface	Conversion (%)	% ^{13}C at C=O		α	α′
		1	**2**		
6 μm silica gel	67.1	27.6	[a]	1.13	—
Silica gel + decanol[b]	43.6	27.0	33.0	1.20	1.42
Silica gel + decanol[c]	74.9	27.7	34.2	1.11	1.50
Silica gel + decanol[c,d]	54.1	27.1	27.9	1.15	1.12
Alumina	27.3	25.4	[a]	1.08	—
Alumina	22.6	25.6	[a]	1.12	—

[a] Compound **2** not detected by gc (<0.2%).
[b] 4.77×10^{-4} mol **1**/g silica gel; 7.8×10^{-4} mol decanol/g.
[c] 1.03×10^{-4} mol **1**/g silica gel; 7.5×10^{-4} mol decanol/g.
[d] −55°C.

be more complex than that on silica gel since the product recovery as dibenzyl was only ~20% for the former. Isomer **2** was not detected among the reaction products when **1** was photolysed on either 6-μm silica or on alumina. This suggests that a particular surface site may be instrumental in permitting the formation of **2** during the photolysis on silica gel.

Third, **1** was photolysed on silica gel on which decanol had been coadsorbed at ~55% monolayer coverage, based upon calculated molecular areas. The values obtained for both α and α′ at 20°C and at −55°C were not appreciably different from those for silica gel in the absence of decanol. Comparison of the present results for silica gel and silica gel plus decanol with those of Epling and Florio (11) suggest that it is the silica gel surface, not the bound hydrocarbon layer, which is responsible for the enhanced ^{13}C enrichment efficiency. It seems unlikely that the hydrocarbon layer makes the surface "micelle-like" as has been suggested (11). Radicals on a hydrocarbon layer would be expected to be more mobile than those attached directly to silica gel and would be less likely to produce ^{13}C enriched material via the geminate recombination pathway. Although a higher α value was obtained in the previous study (11), it should be noted that this reflects the total enrichment at all carbons and is, consequently, expected to be higher than the present α values for carbonyl enrichment.

Can. J. Chem. Downloaded from www.nrcresearchpress.com by 210.87.254.105 on 09/06/12
For personal use only.

TABLE 3. ^{13}C enrichment for **1** and **2** recovered after photolysis of **1** in aqueous potassium dodecanoate

$\bar{N}$	Conversion	α	α′
0.34[a]	98.0	1.19	1.73
0.43[a]	34.7	1.28	1.20
0.43[a]	39.2	1.19	1.23
1.17[b]	94.4	1.24	1.67
1.24[b]	54.7	1.37	1.20

[a][Surfactant] = 0.16 *M*.
[b][Surfactant] = 0.08 *M*.

^{13}C enrichment in micelles

For comparison with earlier work in micelles (6) and for correlation with our work on cage recombination (13), ^{13}C enriched dibenzyl ketone was photolysed in aqueous potassium dodecanoate. Our previous experimental results on the photolysis of an unsymmetrically substituted dibenzyl ketone in micelles showed that there is a strong dependence of geminate formation of dibenzyl on the average number of molecules per micelle $\bar{N}$ (13). The probability of geminate combination decreases from 92% to 51% when $\bar{N}$ is changed from 0.35 to 0.85. The present work was, therefore, designed to investigate the effect of variations in $\bar{N}$ on the ^{13}C enrichment efficiency. It might be expected that the ^{13}C enrichment efficiency would decrease with an increase of $\bar{N}$ since the rapid escape of radicals from their geminate partners is thought to be responsible for the low α values in solution. The results shown in Table 3 indicate that α and α′ values for the recovered ketones are not particularly sensitive to $\bar{N}$. The high α′ values at high conversion could be due to photolysis of **2** and its further enrichment by recombination to regenerate itself; the lower yields of **2** obtained at >80% conversion support this hypothesis. The observed enrichments are comparable to those reported by Turro and co-workers in other micelle systems (6).

The insensitivity of ^{13}C enrichment to changes in $\bar{N}$ was unexpected. In fact there may be a slight trend opposite to the expected one of more free radical combination products when $\bar{N}$ is increased. It seems obvious now that the behaviour of the benzyl–benzyl radical pair is not directly correlated to that of the benzyl–phenylacetyl radical pair, which is the reaction intermediate responsible for the magnetic isotope enrichments of **1** and **2**. For instance, one expects that the average initial interradical separation for the two radical pairs will be different; this separation is crucial for both radical escape by diffusion and for ^{13}C enrichment by recombination.

Further discussions

Consideration of α values for **1** on a variety of surfaces and in micelles indicates that both environments are effective in enhancing the ^{13}C enrichment. Since restrictions on the diffusion of the initial radical pair appear to be important in the enrichment process, the results suggest that the silica gel surface provides a slightly less restricted environment than does a micelle. The dibenzyl ratios obtained upon photolysis of unsymmetrical dibenzyl ketones also indicate more restriction of radical motion by micelles than by the silica surface. However, the differences are much greater in the latter case. This is reasonable if the lifetimes of the radical pairs are considered. The acyl–benzyl radical pair involved in the ^{13}C enrichment process has a shorter lifetime than the benzyl radical pair and the surface will be much more effective in localizing this shorter-lived radical pair. On the other hand, since radical exit from a micelle is relatively slow (10^5–10^6 s^{-1} (20)), the micelles can effectively localize both radical pairs until recombination occurs.

Substantially higher enrichments were observed for isomer **2** than for **1** at 20°C on silica gel. Different efficiencies had also been observed for the two ketones in micelles (6). Both **1** and **2** are derived from the same initial radical pair and one would expect α and α′ values to be the same. The differences in enrichment must be a reflection of differences in the rates of processes leading to each ketone. While the initial state of the primary radical pair must be identical, the final states leading to products **1** and **2** must be different. The developing singlet character and the geometric positions of the radicals within the radical pair before coupling are the deciding factors. The present theories of CIDNP have only considered radicals as hard spheres without structures. Apparently the structure of the individual components of the radical pair and their relative positions can affect the ^{13}C enrichment efficiency, and rotation should also be considered.

The different temperature dependence of α and α′ may be understood within this context. While α values for **1** are much less sensitive to temperature variations, α′ values for **2** decreased considerably at lower temperature on silica gel. Turro has also obtained different temperature dependences for α and α′ in micelles (6). The precise nature of the structure of the radical pair and its dynamics of motion as related to the electron-nuclear hfc induced intersystem crossing is at present unclear. More detailed studies of the ^{13}C enrichment of **1** and **2** are required for better understanding.

Experimental

Apparatus

Proton nmr spectra were recorded on either a Varian T-60 (60 MHz) or an XL-100 (100 MHz) spectrometer. Gas chromatography – mass spectrometry was done on a Varian 1400 gas chromatograph interfaced with a Varian MAT 311 A mass spectrometer and data system. Gas chromatography was done on a Varian 2400 instrument equipped with a flame ionization detector, a temperature programmer, and a 5 ft × 1/4 in. glass column packed with 10% SE 30 on Chromosorb W. Operating conditions were as follows: carrier gas, helium, 40 mL/min; injector, 225°C; column, 170°C; detector, 250°C. Irradiations were carried out with either a 1000-W XBO high pressure xenon lamp in a Photochemical Research Associates lamp housing or a 450-W Hanovia medium pressure mercury lamp.

Materials

Silical gel (35–70 mesh, Merck, cat. no. 7733) was used as received or dried as outlined below. Silica gel, 6-μm particle size, was used as received. Alumina, neutral (Fisher, Brockmann Activity 1) was dried for 12 h at 200°C, 0.1 Torr (1 Torr = 133.3 Pa), and was stored in a desiccator until used. Methylene chloride (Fisher spectrograde) was refluxed over P_2O_5 and distilled directly before use for adsorption of compounds onto dry silica gel, but was used as received for adsorption of compounds onto undried silica or other surfaces. Water for micelle solutions was triply distilled (second distillation from potassium permanganate). All other solvents were reagent grade and were used as received. Decanol was distilled before use. Potassium dodecanoate was prepared form dodecanoic acid and potassium hydroxide and purified by recrystallization from methanol. Dibenzyl ketone (ICN Pharmaceutical) was recrystallized from ether (at −78°C) or petroleum ether (40–60°C), mp 30.5–32°C. ^{13}C labelled dibenzyl ketone was prepared by the method of Coan and Becker (19) from phenylacetic acid (90% $^{13}C{=}O$, Merck, Sharp and Dohme), and was purified by bulb-to-bulb distillation followed by crystallization from 40–60°C petroleum ether, mp 32.5–33.5°C.

Can. J. Chem. Downloaded from www.nrcresearchpress.com by 210.87.254.105 on 09/06/12
For personal use only.

Can. J. Chem. Downloaded from www.nrcresearchpress.com by 210.87.254.105 on 09/06/12
For personal use only.

Photolysis of 1 on silica gel

Dibenzyl ketone was adsorbed on silica gel (4.77×10^{-4} mol/g) from a methylene chloride solution. When the ketone was to be adsorbed on silica gel dried at 200°C at $\leq$ 1 Torr for $\geq$ 5 h, the previously described method and apparatus were used (18). For samples on silica gel which had not been predried, a methylene chloride solution of **1** was added to a preweighed silica sample in a round bottom flask. After solvent removal by evacuation, the sample was transferred to an irradiation cell and evacuated for ~15 min at 1 Torr. All samples were then degassed to 10^{-5} Torr by 3 or more freeze–thaw cycles at liquid nitrogen temperatures. Dry, deoxygenated nitrogen was then added to the sample tube before it was sealed. The samples were rotated and irradiated with a 1000-W xenon lamp. The light was focused on one end of a 16-mm quartz light pipe and the sample was rotated under the other end. During irradiation the samples were cooled with either cold running water (20°C) or by immersion in a methanol – Dry Ice bath (−78°C).

The adsorbed materials were removed from the silica gel by extraction with 100 mL of diethyl ether. The ether solution was concentrated and analyzed by gc after the addition of a known amount of eicosane as an internal standard. Calibration curves were constructed for **1**, **2**, and **3**; the average of three or more injections was used for each determination. Dibenzyl always accounted for ≥90% of the photolysed ketone. Yields of **2** were typically from 2–4%.

For samples containing coadsorbed decanol, the decanol was adsorbed first, followed by **1**. The samples were prepared as described above using undried silica gel.

Photolysis of 1 in micelles

An appropriate amount of **1** was added to a solution of potassium dodecanoate in triply distilled water and the mixture was sonicated for 1–2 h to dissolve the ketone completely. The solution was then transferred to an irradiation vessel and degassed by purging with nitrogen for 30 min. All samples were stirred and irradiated through Pyrex with a 450-W Hanovia medium pressure mercury lamp. After photolysis, the sample was diluted to <0.02 *M* (i.e., below the cmc) and was extracted three times with ether. The formation of emulsions during the extraction procedure was minimized by the addition of sodium chloride to the aqueous phase. The combined ether layers were washed once with 10% Na_2CO_3 and once with water and were dried over anhydrous $MgSO_4$. The extract was concentrated and analyzed by gc as previously described. Dibenzyl accounted for ~90% of the photolysed ketone. Yields of **2** were from 6–10% for most experiments but decreased to 1–2% at >90% conversion.

^{13}C analyses

1 and **2** were separated from the photolysis mixtures by preparative chromatography on silica gel plates using 10% ethyl acetate in petroleum ether as eluent. The ^{13}C content in the recovered ketones was then determined by gc/ms. A Varian 1400 gas chromatograph interfaced with a Varian MAT311A mass spectrometer and a Varian data system was used. A standard sample of **1** (25% $^{13}C{=}O$) was always analyzed before samples of recovered **1** were run. Comparison of the ^{13}C calculated for the standard with that determined mass spectrally allowed correction of the data for instrumental variations. For **1** the relative intensities of the molecular ion peaks at *m/e* 210 and 211 were used. Since **2** gave a very weak molecular ion, the ^{13}C content was determined from the mass fragment peaks at *m/e* 119 and 120. The mass spectral intensities for both ketones were corrected for the natural abundance distributions of ^{13}C at other than the carbonyl, ^{2}H, and ^{17}O. Separation factors, *S*, were then calculated from the corrected intensities and used to evaluate α and α' values.

Acknowledgements

We thank the Natural Sciencies and Engineering Research Council of Canada for financial support. We are very grateful for Professor Paul de Mayo's initiation and constant encouragement of the project.

1. (*a*) R. G. LAWLER and G. T. EVANS. Ind. Chem. Belg. **36**, 1087 (1971); (*b*) G. T. EVANS and R. G. LAWLER. Mol. Phys. **30**, 1085 (1975).
2. F. J. ADRIAN. *In* Chemically induced magnetic polarization. *Edited by* L. T. Muus, P. W. Atkin, K. A. McLauchlan, and J. B. Pedersen. D. Reidel Publishing Co., Dordrecht, Holland. 1977. p. 77.
3. R. KAPTEIN. Adv. Free Radical Chem. **5**, 381 (1975).
4. (*a*) A. L. BUCHACHENKO, E. M. GALIMOV, V. V. ERSHOWV, G. A. NIKIFOROV, and A. D. PERSHIN. Dokl. Akad. Nauk SSSR, **228**, 379 (1976); (*b*) A. L. BUCHACHENKO. Russ. J. Phys. Chem. **51**, 1445 (1977).
5. N. J. TURRO. Proc. Natl. Acad. Sci. U. S. A. **80**, 609 (1983).
6. (*a*) N. J. TURRO, M. F. CHOW, C. J. CHUNG, and B. KRAEUTLER. J. Am. Chem. Soc. **103**, 3886 (1981); (*b*) N. J. TURRO, D. R. ANDERSON, M. F. CHOW, C. J. CHUNG, and B. KRAEUTLER. J. Am. Chem. Soc. **103**, 3892 (1981); (*c*) N. J. TURRO, M. F. CHOW, and B. KRAEUTLER. Chem. Phys. Lett. **73**, 545 (1980); (*d*) B. KRAEUTLER and N. J. TURRO. Chem. Phys. Lett. **70**, 266 (1980).
7. L. STERNA, D. RONIS, S. WOLFE, and A. PINES. J. Chem. Phys. **73**, 5493 (1980).
8. (*a*) R. Z. SAGDEEV, T. V. LESHINA, M. KAMHA, A. RESVUKHIN, and YU. M. MOLIN. Chem. Phys. Lett. **48**, 89 (1977); (*b*) A. V. PODOPLELOV, T. V. LESHINA, R. Z. SAGDEEV, YU. M. MOLIN, and V. I. GOLDANSKII. JETP Lett. **29**, 419 (1979).
9. (*a*) P. S. ENGEL. J. Am. Chem. Soc. **92**, 6074 (1970); (*b*) W. K. ROBBINS and R. H. EASTMAN. J. Am. Chem. Soc. **92**, 6076, 6077 (1970).
10. (*a*) B. BLANK, P. G. MENNITT, and H. FISCHER. Spec. Lect. 23rd Cong. Pure Appl. Chem. **4**, 1 (1971); (*b*) H. LANGHALS and H. FISCHER. Chem. Ber. **111**, 543 (1978); (*c*) M. LEHNI, H. SCHUH, and H. FISCHER. Int. J. Chem. Kinet. **11**, 705 (1979).
11. G. A. EPLING and E. FLORIO. J. Am. Chem. Soc. **103**, 1237 (1981).
12. D. AVNIR, P. DE MAYO, and I. ONO. J. Chem. Soc. Chem. Commun. 1109 (1978).
13. D. AVNIR, L. J. JOHNSTON, P. DE MAYO, and S. K. WONG. J. Chem. Soc. Chem. Commun. 958 (1981).
14. L. J. JOHNSTON, P. DE MAYO, and S. K. WONG. J. Chem. Soc. Chem. Commun. 1106 (1982).
15. (*a*) J. E. LEFFLER and J. J. ZUPANCIC. J. Am. Chem. Soc. **102**, 259 (1980); (*b*) J. E. LEFFLER and J. T. BARBAS. J. Am. Chem. Soc. **103**, 7768 (1981).
16. P. DE MAYO, A. NAKAMURA, P. W. K. TSANG, and S. K. WONG. J. Am. Chem. Soc. **104**, 6824 (1982).
17. R. B. BERNSTEIN. J. Phys. Chem. **56**, 893 (1952).
18. B. FREDERICK, L. J. JOHNSTON, P. DE MAYO, and S. K. WONG. Can. J. Chem. **62**, 403 (1984).
19. S. B. COAN and E. I. BECKER. *In* Org. Synth. Collect. Vol. **IV**. John Wiley and Sons, Inc., New York. 1968. pp. 174, 176.
20. (*a*) N. J. TURRO, M. F. CHOW, C. J. CHUNG, Y. TANIMOTO, and G. C. WEED. J. Am. Chem. Soc. **103**, 4574 (1981); (*b*) J. C. SCAIANO, E. B. ABUIN, and L. C. STEWART. J. Am. Chem. Soc. **104**, 5673 (1982).

Appendix

Integration of [7] yields [10], which may be rewritten as

$$[10] \quad [^{13}C_2]_{total} = k_{13} \int_0^t [^{13}C_1]\, dt$$

[11] after the appropriate change of variable from time to conversion, *f*. The $[^{13}C_1]$ at a particular conversion, *f*, may be

$$[11] \quad [^{13}C_2]_{total} = k_{13} \int_0^f [^{13}C_1]\, df$$

expressed as shown in [12] where C_0 is the initial total [**1**] and the fraction $^{13}C_1$ is determined as shown below:

$$[12] \quad [^{13}C_1]_f = (\text{fraction } ^{13}C_1)_f\,(1 - f)C_0$$

$$[13] \quad (\text{fraction } ^{13}C_1)_f = \frac{^{13}C_f}{^{13}C_f + {}^{12}C_f}$$

$$[14] \quad = \frac{SR_0}{1 + SR_0}$$

$$[15] \quad [^{13}C_1]_f = \frac{SR_0}{1 + SR_0}\,(1 - f)C_0$$

substitution of [15] in [11] yields

$$[16] \quad [^{13}C_2]_{total} = k_{13}\int_0^f \frac{SR_0}{1 + SR_0}\,(1 - f)C_0\,df$$

A similar set of operations gives $[^{12}C_2]_{total}$ as expressed in eq. [9].

Can. J. Chem. Downloaded from www.nrcresearchpress.com by 210.87.254.105 on 09/06/12
For personal use only.

Coumarin–nucleotide base pairs. Ultraviolet absorption, fluorescence, and photochemical study

GRAŻYNA WENSKA AND STEFAN PASZYC
Faculty of Chemistry, A. Mickiewicz University, Poznań, Poland

Received January 6, 1984

This paper is dedicated to Professor Paul de Mayo on the occasion of his 60th birthday

GRAŻYNA WENSKA and STEFAN PASZYC. Can. J. Chem. **62**, 2006 (1984).

Bichromophoric compounds containing a nucleotide base and coumarin linked with a polymethylene chain have been synthesized. A hypochromic effect was observed for adenine–coumarin pairs in contrast to the thymine containing compound. The fluorescence intensity of coumarin when bound into these systems was found to be significantly reduced. It has also been demonstrated that excitation energy is transferred from adenine or thymine to the coumarin moiety. Intermolecular dimerization of coumarin residues was observed upon irradiation of an adenine–coumarin pair.

GRAŻYNA WENSKA et STEFAN PASZYC. Can. J. Chem. **62**, 2006 (1984).

On a synthétisé des composés à deux chromophores contenant un nucléotide et une coumarine reliés par une chaîne polyméthylène. Par opposition à ce qui est observé avec le composé semblable contenant de la thymine, on a observé un effet hypsochrome avec les paires adénine–coumarine. On a observé que l'intensité de la fluorescence de la coumarine liée à ces systèmes est considérablement réduite. On a aussi démontré que l'énergie d'excitation est transféré de l'adénine ou de la thymine vers la portion coumarine. Lors de l'irradiation d'une paire adénine–coumarine, on a observé une dimérisation intermoléculaire des résidus de la coumarine.

[Traduit par le journal]

Can. J. Chem. Downloaded from www.nrcresearchpress.com by 210.87.254.105 on 09/06/12
For personal use only.

Introduction

Furocoumarins (psoralens) and some simple coumarins form weak complexes with nucleic acids in the ground state by intercalation of planar furocoumarin chromophores between the base pairs of nucleic acids. It has been suggested that aromatic ring stacking, hydrogen bonding, and hydrophobic and van der Waals forces are involved in the interaction of furocoumarins and nucleic acids. The intercalated molecule can form a covalent bond with a nucleic acid base upon irradiation with ultraviolet (uv) light and photomodifications of nucleic acids appear to be responsible for observed biological effects (1, 2).

In order to get more insight into an interaction process and a photoreaction between respective chromophores, synthesis of bichromophoric compounds which serve as spectroscopic models may be carried out. This approach has been used recently to study the ring–ring stacking interaction and photocycloaddition of psoralen and thymine (3, 4).

We have prepared bichromophoric compounds containing adenine or thymine linked by a polymethylene chain with 7-oxycoumarin. The aim of this work is to study the ring–ring interactions between pyrimidine (thymine) or purine (adenine) bases and coumarin in the absence of the complicating factors present in the nucleic acid – furocoumarin complex (eg. hydrogen bonding). The intramolecular interactions could be detected in these systems by both absorption and emission spectroscopy. The results of such studies can be useful in the explanation of the origin of spectral changes resulting from complexation of coumarin in biological systems.

In this paper we present our results of uv absorption and fluorescence studies. The photochemistry of an adenine–coumarin pair was also of interest. Although it has been generally accepted that coumaryl compounds react mainly with thymine, there is experimental evidence that 8-methoxypsoralen can photochemically add to adenine (1).

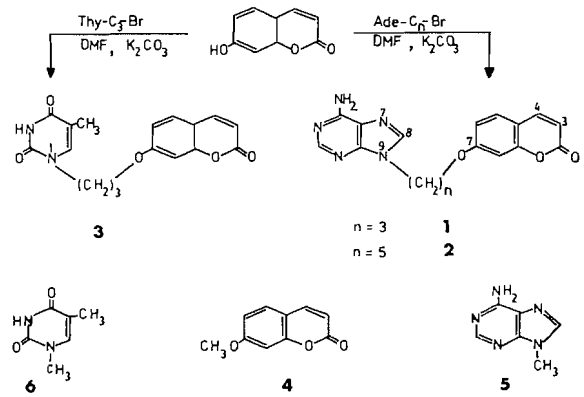

SCHEME 1

Results and discussion

The compounds CouO-C_3-Ade (**1**),[1] CouO-C_5-Ade (**2**), and CouO-C_3-Thy (**3**) were synthesized according to Scheme 1. Thus 7-hydroxycoumarin was treated with 9-(3-bromopropyl)-adenine (Ade-C_3-Br) or 9-(5-bromopentyl)adenine (Ade-C_5-Br) in DMF solution in the presence of anhydrous K_2CO_3 to afford **1** and **2** respectively. Similar reaction of 1-(3-bromopropyl)thymine (Thy-C_3-Br) led to compound **3**. The ω-bromoalkyl derivatives of adenine and thymine were prepared as described previously (5, 6). We attempted the synthesis of **1**, **2**, and **3** starting from α-(7-oxycoumarinyl)ω-bromoalkane as a common intermediate, but difficulties occurred in the purification of this precursor, probably because of its lability. The reference compounds CouO-CH_3 (**4**), Ade-CH_3 (**5**), and Thy-CH_3 (**6**) were also prepared.

The compounds **1**, **2**, and **3** were examined by uv absorption

[1]Abbrevations used: Ade – aden-9-yl; Thy – thym-1-yl; CouO – 7-oxycoumarinyl; C_3, C_5 – n-propyl, n-pentyl.

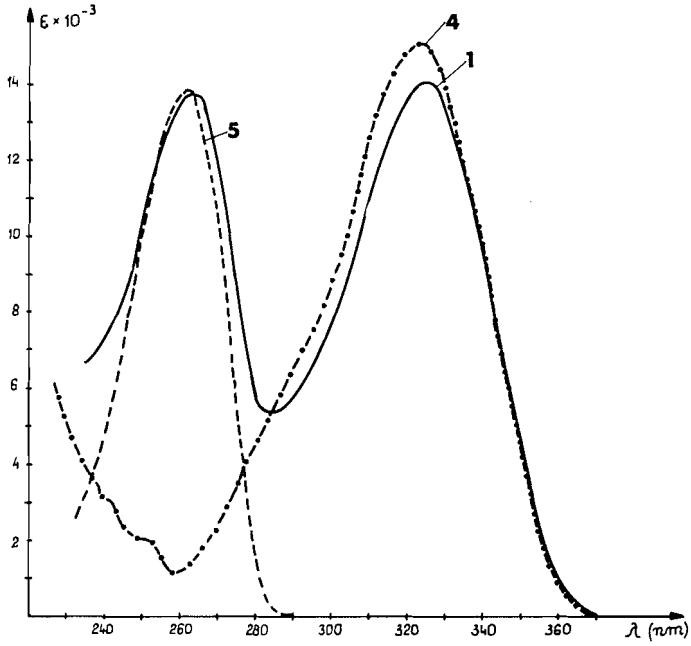

FIG. 1. Ultraviolet absorption spectra of **1** (———), **4** (–·–·–), and **5** (– – –) in water.

spectroscopy. This technique has been used to detect ground state complex formation of coumarins and psoralens with DNA (2). A bathochromic shift and a decrease in uv absorption had been observed in the spectrum of 5,7-dimethoxycoumarin as a result of intercalation into DNA (7). Similar but much smaller effects were observed for the coumarin chromophore in the synthesized compounds **1**, **2**, and **3**. Quanitatively, the spectral shape of the uv absorption bands of each compound closely resembles an equimolar mixture of its constituent monomers (Fig. 1).

Linking of the 7-oxycoumarin moiety to a nucleic acid base through the polymethylene chain caused only a small red shift (ca. 3 mm) of the near uv band of the former. Quantitatively, a reduction in band intensities compared to the sum of the absorption intensities of the component monomers was observed for aqueous solutions of the synthesized bichromophoric compounds. This loss of intensity is usually described by percent hypochromism (*%H*) and Table 1 shows the values calculated for the nucleotide base (adenine or thymine) and coumarin absorption bands of **1**, **2**, and **3**. The uv spectra were determined at a concentration low enough to avoid any intermolecular association (see Experimental). Hypochromism is common for systems which are stacked with chromophores one on the top of the other and has been widely used to assess intramolecular stacking in various bichromophoric systems (3, 4, 8, 9).

The appreciable hypochromism exhibited by CouO-C_3-Ade (**1**) in water indicates that at least a fraction of the molecules were in a stacked (folded) conformation in the ground state. CouO-C_5-Ade (**2**) is stacked to a lesser degree. Lengthening of a chain linking two chromophores reduces the *%H* value, as has been found previously for other systems (8, 10). The very weak hypochromic effect exhibited by CouO-C_3-Thy (**3**) in water probably indicates that the interactions between coumarin and thymine are weaker than those between coumarin and adenine. Water plays an important role in the interaction process because a reduced hypochromism or even hyperchromism was observed in methanol (Table 1). Methanol has been shown to destroy the stacking of bases in nucleic acids (11).

TABLE 1. Computed percent hypochromism (*%H*)

Compound	Water		Methanol
	238–300 nm[a]	300–370 nm[b]	300–370 nm[b]
CouO-C_3-Ade (**1**)	9.8±0.8[c]	7.0±1.0	1.7±1.0
CouO-C_5-Ade (**2**)	7.3±0.2	4.4±0.2	−5.3±1.0
CouO-C_3-Thy (**3**)	2.0±0.5	−0.1±0.4	−0.6±0.4

[a]Absorption is mainly due to adenine or thymine.
[b]Coumarin is the sole absorbing chromophore.
[c]The values calculated from three determinations were in this range.

In addition, CouO-C_3-Ade (**1**) showed essentially no hypochromism in dimethylsulfoxide which is known to disfavour stacking between intercalating molecules and nucleic acid base pairs (12). Whereas thymine and adenine display only a very weak fluorescence at room temperature ($\Phi_n \sim 10^{-4}$) (13), 7-methoxycoumarin does emit under these conditions (14). Fluorescence emission spectra of CouO-C_3-Ade (**1**), CouO-C_5-Ade (**2**), CouO-C_3-Thy (**3**), and CouO-CH_3 (**4**) were recorded in water and in methanol. Figure 2 shows the emission spectra in water measured for samples of equal optical density. The excitation wavelength was 324 nm, i.e. only the coumarin moiety was excited.

The fluorescence spectra of **1**, **2**, and **3** showed the same shape as that of **4** in the same solvent. The fluorescence quantum efficiencies for **4** in water and in methanol, relative quantum efficiencies (see Experimental), and maximum emission wavelengths are given in Table 2. In water, the fluorescence intensity of coumarin bound into the CouO-C_3-Ade (**1**), CouO-C_5-Ade (**2**), and CouO-C_3-Thy (**3**) systems was found to be sensitive to the environment (attached nucleotide base) and considerably less than that of CouO-CH_3 (**4**) itself. This reduction in intensity is certainly due to intramolecular quenching of the coumarin fluorescence by the neighbouring nucleotide base. The fluorescence quenching is consistent with the existence of a portion of the molecules **1**, **2**, **3** in folded or stacked conformations which are nonfluorescent. In the ground state the presence of such folded forms in aqueous solution follows from the calculated *%H* values, at least in the case of **1** and **2**. Although *%H* calculated for CouO-C_3-Thy (**3**) in aqueous solution is near zero, the fluorescence quantum yield for **3** is only 30% of the value found for CouO-CH_3 (**4**). It should be pointed out, however, that hypochromism is dependent both on π-orbital overlap and the relative orientation of transition moments and, as has been shown previously (10), zero hypochromism does not necessarily mean that there are no ground state stacked conformations. Moreover, in molecules like **1**, **2**, and **3**, in which intramolecularly complexed forms are in dynamic equilibrium with open forms, the observed quenching of the fuorescence may arise not only from a ground state complexation (static quenching), but also from a quenching occurring during the excited state lifetime (dynamic quenching) (8). Better understanding of the role of static quenching in observed fluorescence quenching must await fluorescence lifetime determinations. The relative fluorescence quantum yields for **1**, **2**, and **3** are much higher in methanol, indicating very little or no quenching. The fluorescence intensity of 5,7-dimethoxycoumarin in the presence of DNA has been shown to be significantly diminished by static quenching, i.e. the fluorescence lifetime remained unchanged (7, 15).

Can. J. Chem. Downloaded from www.nrcresearchpress.com by 210.87.254.105 on 09/06/12
For personal use only.

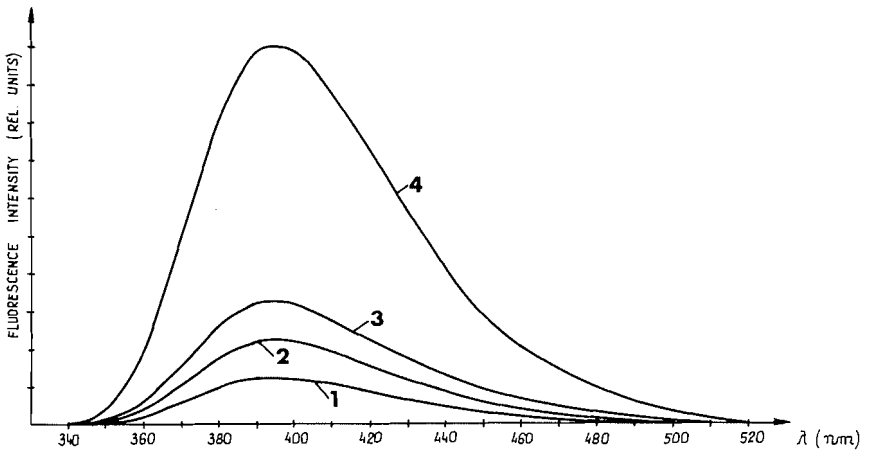

FIG. 2. Fluorescence spectra of **1**, **2**, **3**, and **4** in water; λ_{ex} = 324 nm.

TABLE 2. Relative quantum efficiencies[a,b]

Compound	Water[c]	Methanol[d]
CouO-C_3-Ade (**1**)	0.12	0.81
CouO-C_5-Ade (**2**)	0.22	1.44
CouO-C_3-Thy (**3**)	0.32	1.01

[a]The values had a reproducibility of ±10%.
[b]Excitation 324 nm.
[c]Relative to 7-methoxycoumarin (**4**) in water, fluorescence max 393 nm (corr). Φ_n = 0.16 (quinine sulfate as a standard).
[d]Relative to **4** in methanol, fluorescence max 388 nm (corr). Φ_n = 0.02 (quinine sulfate as a standard).

Fluorescence studies of **1**, **2**, and **3** have also revealed that light energy absorbed in the adenine or thymine part of the molecules is transferred to the fluorescent coumarin moiety. Excitation energy transfer was demonstrated by a comparison of corrected fluorescence excitation and absorption spectra (Figs. 3 and 4). The absorption spectrum of CouO-C_3-Thy (**3**) is almost identical to that of an equimolar mixture of the single chromophores (negligible $\%H$, Table 1) but their fluorescence excitation spectra differ considerably (Fig. 3).

The excitation spectrum of the mixture of Thy-CH_3 (**6**) and CouO-CH_3 (**4**) is superimposable upon that of **4**, indicating no energy transfer. However, an additional peak in the region where thymine absorbs appears in the excitation spectrum of **3**. Energy transfer, although less efficient, was demonstrated also for CouO-C_3-Ade (**1**) and CouO-C_5-Ade (**2**), (Fig. 4). This energy transfer process was further indicated by the observed dependency of the relative fluorescence quantum efficiencies of **1**, **2**, and **3** on excitation wavelength. These values are constant at $\lambda_{ex} > 300$ nm, where only coumarin absorbs the light, and are presented in Table 2 for λ_{ex} = 324 nm. At $\lambda <$ 300 nm, where nucleotide base and coumarin were simultaneously excited, the relative fluorescence efficiencies (determined as described in the experimental section) increased. The respective values are 1.43, 1.07, and 0.65 for **3** at λ_{ex} = 260, 270, and 280 nm and 0.42 for **1** and 0.44 for **2** at λ_{ex} = 260 nm.

The energy transfer efficiency T can be determined from these measurements using the equation derived by A. Kawski and co-workers (16) for systems in which the absorption of the macromolecule is a sum of the absorption of single chromophores. Thus the energy transfer efficiency for CouO-C_3-Thy

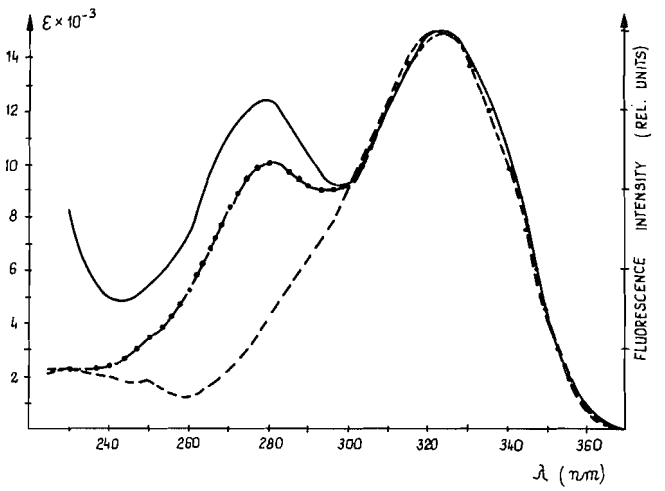

FIG. 3. Absorption spectrum of **3** (——); corrected excitation spectrum of **3** (–·–·–); corrected excitation spectrum of **4** + **6** (– – –). Solvent: water; fluorescence at 393 nm was monitored.

(**3**) (negligible $\%H$, Table 1) was calculated, e.g. for λ_{ex} = 260 nm;

$$T = \left[\frac{\text{rel.fluoresc. efficiency for } \mathbf{3}\ (\lambda_{ex} = 260\text{ nm})}{\text{rel.fluoresc. efficiency for } \mathbf{3}\ (\lambda_{ex} = 324\text{ nm})} - 1\right] \times \frac{A_{260\,nm} \text{ of } \mathbf{4}}{A_{260\,nm} \text{ of } \mathbf{6}}$$

where A is the absorbance. The value of T for **3** calculated for λ_{ex} = 260, 270, 280 nm was found to be 0.60.

Photochemistry of CouO-C_5-Ade (**2**) was also investigated. This compound was chosen because a chain with at least five methylene units is necessary to allow the superposition of the $C^3{=}C^4$ coumarin and $N^7{=}C^8$ adenine reactive bonds. This imidazole part of adenine has been shown to be involved in formation of a photocycloadduct with thymine (17). Since **2** was only sparingly soluble in water, a solution in methanol ($c = 3 \times 10^{-4}$ M) was used. Analysis of the product mixture showed, however, that intermolecular photodimerization of coumarin residues was dominant. The major product was isolated and assigned the dihydroxy diester structure, **7** (Scheme 2). Analysis of uv absorption and ^{1}H nmr spectra of the photoproduct and starting CouO-C_5-Ade (**2**) led to the conclusion that adenine remained intact in **7**.

Can. J. Chem. Downloaded from www.nrcresearchpress.com by 210.87.254.105 on 09/06/12
For personal use only.

Can. J. Chem. Downloaded from www.nrcresearchpress.com by 210.87.254.105 on 09/06/12
For personal use only.

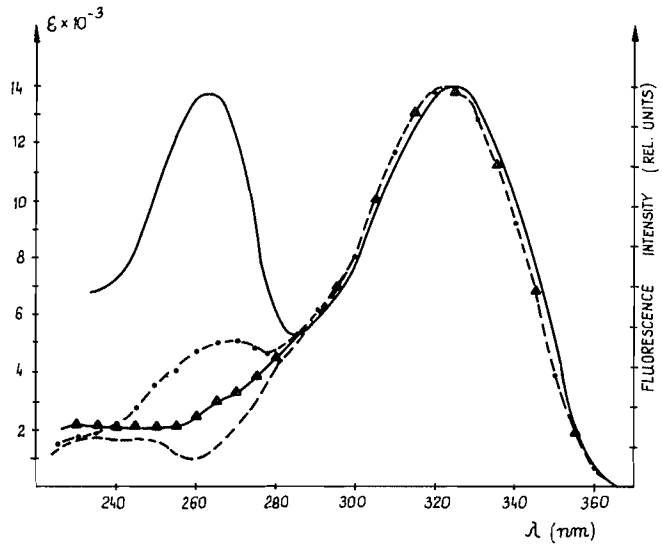

FIG. 4. Absorption spectrum of **1** (——); corrected excitation spectra of **1** (–·–·–), **2** (–▲–▲–), and **4** + **5** (– – –). Solvent: water; fluorescence at 393 nm was monitored.

The ^{1}H nmr spectrum of **7** shows no pyrone double bond protons but instead new signals are observed in a spectral region typical for cyclobutane protons. It was not possible to establish the configuration of **7** on the basis of the ^{1}H nmr spectrum because of overlapping cyclobutane and pentamethylene bridge proton signals. However, a comparison of the low field part of the absorption of cyclobutane protons with that of the four possible coumarinic acid photodimers suggests the *anti* head-to-head configuration for **7** (18). This assignment is in accord with literature data. Dependence of the photodimer distribution on the solvent polarity and coumarin concentration has been observed (19). Photolysis of a dilute methanolic solution of coumarin (10^{-2} *M*) has been reported to give *anti* head-to-head and *syn* head-to-head dimers in the ratio of 13:1. However, only the dihydropyrone ring of the former opened easily in methanol (20). One of the minor photoproducts was tentatively assigned as the cyclobutane photodimer **8** on the basis of its properties. It converts to **7** in the presence of methanol and splits to give back CouO-C_5-Ade (**2**) after reirradiation with λ = 254 nm. On the other hand, **2** was not recovered from **7** although the irradiation with λ = 254 nm is accompanied by appearance of a low intensity band at λ > 300 nm.

Experimental

All melting points are uncorrected. The ir spectra were run on a Perkin-Elmer 580 and uv absorption spectra were recorded on a Zeiss Specord M-40 spectrophotometer. The ^{1}H nmr spectra were determined on Varian A-60 (60 MHz) and JEOL FX 90 Q (90 MHz) spectrometers using tetramethylsilane as internal standard. The mass spectra were determined using a JEOL D-100 spectrometer at an ionization potential of 70 eV. Microanalyses were performed using a Perkin–Elmer Elemental Analyzer 240. Doubly distilled water, methanol, and dimethylsulfoxide (spectroscopic grade, Merck) were used as solvents.

Electronic absorption

Quantitative measurements were made using 6×10^{-5} *M* solutions of bichromophoric compounds **1**, **2**, and **3** and constituent monomers (reference compounds) **4**, **5** and **6** in water, methanol, and dimethylsulfoxide. Spectra were determined in 10-mm cells. In the case of

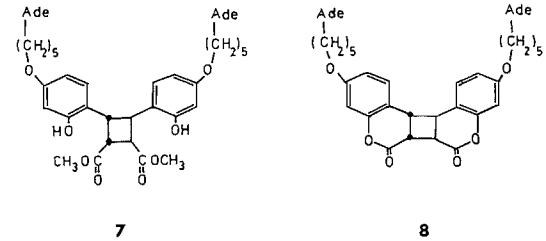

SCHEME 2

CouO-C_5-Ade (**2**) in water, because of solubility limitation, a 9×10^{-6} *M* solution was used and absorption measured in 50-mm cells. Percentages of hypochromism (%*H*) were determined by quantitative comparison of absorption spectra of bichromophoric compounds with the summation of the spectra of reference compounds as described earlier (6). Oscillator strengths $f = 4.32 \times 10^{-9} \times \int \epsilon(\tilde{\nu}) d\tilde{\nu}$ were computed from absorption spectra using Simpson's rule.

Fluorescence measurements

Uncorrected emission spectra were recorded on a Perkin–Elmer MPF-3 spectrofluorometer. Relative fluorescence quantum efficiencies were determined by integration and comparison of uncorrected emission spectra of the compounds **1**, **2**, and **3** with that of **4** when exciting at λ > 300 nm (coumarin solely absorbs) or an equimolar mixture of reference compounds: **4** + **5** or **4** + **6** at λ_{ex} < 300 nm. Both the solution of bichromophoric compound and the mixture of reference compounds had equal optical density at the exciting wavelength. Fluorescence spectra used for these determinations were not corrected for photomultiplier response and monochromator efficiency because only coumarin fluorescence was observed. Corrected fluorescence emission and excitation spectra were recorded on a Perkin–Elmer MPF-44 spectrofluorometer. Fluorescence quantum efficiencies for **4** in water (pH 6.5) and in methanol were measured from corrected spectra using quinine sulfate as a standard (0.1 *N* H_2SO_4, Φ_{fl} = 0.55 (21)). Optical densities of the samples (10-mm cells) for fluorescence studies were ≤ 0.05, i.e. concentrations of the solutions were in the range of $2.2-6.8 \times 10^{-6}$ *M*.

Materials

The following compounds had been described previously: 9-(3-bromopropyl)adenine, 9-(5-bromopentyl)adenine (5), 1-methylthymine (22), 9-methyladenine (23), 7-methoxycoumarin (24). All these materials have been synthesized in this work by alkylation of a heterocycle with an appropriate 1,ω-dibromoalkane or methyl iodide in DMF solution in the presence of K_2CO_3. 1-(3-Bromopropyl)thymine has been synthesized by the method described in ref. 6.

Synthesis of CouO-C_3-Ade (1), CouO-C_5-Ade (2) and CouO-C_3-Thy (3)

All the compounds were synthesized following the same general procedure. In a typical experiment a solution of 256 mg (1 mmol) of 9-(3-bromopropyl)adenine in 30 mL of dry dimethylformamide was added dropwise to a suspension of 162 mg (1 mmol) of 7-hydroxycoumarin and 152 mg (1.1 mmol) of anhydrous potassium carbonate in 10 mL of dimethylformamide. The mixture was stirred overnight at room temperature. After filtration, solvent was removed from the filtrate *in vacuo* and the yellow residue treated with methanol–isopentane mixture. The resulting suspension was filtered to collect the crude **1**. Crude products were chromatographed on silica gel (ethyl acetate – methanol, 3:1) and finally crystallized from aqueous methanol.

7-[3-(Aden-9-yl)propyloxy]coumarin (1)

Yield: 55%; mp 200°C; uv (H_2O): 263 nm (13 700), 325 nm (13 800); ^{1}H nmr (DMSO-d_6)δ: 8.1 (s, 2, Ade^{2}H and Ade C^{8}H), 7.9 (d, *J* = 10 Hz, 1, CouC=C^{4}H), 7.7–7.4 (m, 1, phenyl H), 7.2 (br s, 2, NH_2), 7.0–6.8 (m, 2, phenyl H), 6.2 (d, *J* = 10 Hz, 1, CouC=C^{3}H), 4.5–3.9 (m, 4, NCH_2 and OCH_2), 3.3–3.1 (m, 2, CCH_2C); ms *m/e* (rel int %): M^+ 337 (34), 192 (14), 176 (100), 175

(6), 162 (8), 149 (92), 135 (42), 134 (14). *Anal.* calcd. for $C_{17}H_{15}N_5O_3$: C 60.5, H 4.5, N 20.8; found: C 60.2, H 4.5, N 20.9.

7-[5-(Aden-9-yl)pentyloxy]coumarin (2)

Yield: 67%; mp 223°C; uv (H_2O): 264 nm (14 400), 325 nm (14 100); ^{1}H nmr (TFA)δ: 8.7 (s, 2, Ade C^2H and Ade C^8H), 8.1 (d, 1, CouC=C^4H), 7.7–7.4 (m, 1, phenyl H), 7.2–6.9 (m, 2, phenyl H), 6.5 (d, 1, CouC=C^3H), 4.9–4.5 and 4.4–4.0 (2t, 4, NCH_2 and OCH_2), 1.7–2.4 (m, 6, $C(CH_2)_3C$); ms *m/e* (rel int %): M^+ 365 (10), 337 (3), 220 (6), 204 (52), 191 (100), 190 (59), 176 (27), 175 (9), 162 (27), 149 (77), 135 (42), 134 (9). *Anal.* calcd. for $C_{19}H_{19}N_5O_3$: C 62.4, H 5.2, N 19.2; found: C 62.6, H 5.4, N 19.0.

7-[3-(Thym-1-yl)propyloxy]coumarin (3)

Yield: 30%; mp 228–229°C; uv (H_2O): 278 nm (12 300), 324 nm (15 000); ^{1}H nmr (TFA)δ: 8.0 (d, 1, CouC=C^4H), 7.7–7.4 (m, 2, ThyC^6H and phenyl H), 7.2–6.9 (m, 2, phenyl H), 6.6 (d, 1, CouC=C^3H), 4.5–4.0 (m, 4, NCH_2 and OCH_2), 2.6–2.2 (m, 2, CCH_2C), 2.0 (s, 3, CH_3); ms *m/e* (rel int %): M^+ 328 (6), 189 (1), 175 (1), 167 (100), 139 (12), 134 (3). *Anal.* calcd. for $C_{17}H_{16}N_2O_5$: C 62.2, H 4.9, N 8.5; found: C 61.9, H 5.0, N 8.4.

Irradiation of 2

A high-pressure mercury lamp TQ 150 (Original Hanau) cooled with water was used as a light source. This was immersed in a Pyrex reactor provided with an additional jacket filled with a 2-mm layer of the filter solution. A 1-mm layer of the filter solution (sodium bromide and lead acetate (24)) had optical densities >3, 1.0, 0.40, and 0.18 at 313, 324, 330, and 335 nm respectively. Compound **2** (427 mg) was dissolved in 3.5 L of methanol ($c = 3 \times 10^{-4} M$). A portion (130 mL) of the solution was placed in the reactor and deoxygenated by bubbling nitrogen 1 h before and during the irradiation. Irradiation was performed until 60% of starting material reacted (2 h) as judged from the uv spectrum. Chromatography over silica gel (ethyl acetate – methanol, 5:1) gave 189 mg of the mixture of dimers **7** and **8** and unidentified material. The products were further separated on a silical gel column. Elution with chloroform–methanol – acetic acid (140:7.5:2.5) gave 136 mg of **7** (50% yield based on **2** reacted); 25 mg of homogeneous material (free of **7**), which yielded the mixture of **7** and the other product upon standing in methanol, was also obtained.

Photoproduct 7

Ultraviolet (CH_3OH): 237 nm (21 000), 263 nm (28 000), shoulder 285 nm (7000); ir (KBr): 3430, 3340, 3180, 2950, 2870, 1725, 1640, 1615, 1600, 1520, 1475, 1435, 1415, 1290, 1250, 1170, 1030, 835, 800 cm^{-1}; ^{1}H nmr (DMSO-d_6)δ: 8.2 (s, 4, Ade C^2H and Ade C^8H), 7.2 (br s, 4, NH_2), 6.3–7.0 (m, 6, phenyl H), 6.2 (br s, 2, OH), 4.8–4.4 (m, 2, cyclobutyl H), 4.3–3.3 (m, 10, cyclobutyl H and OCH_2, NCH_2), 3.3 (s, 6, OCH_3), 2.0–1.3 (m, 12, $C(CH_2)_3C$); ms *m/e* (rel int %): 204 (4), 191 (73), 190 (46), 176 (11), 162 (18), 149 (60), 148 (100), 145 (5), 135 (51), 134 (54), 133 (16). *Anal.* calcd. for $C_{40}H_{46}N_{10}O_8$: C 60.4, H 5.8, N 17.6; found: C 60.1, H 5.7, N 17.4.

1. P. S. Song and K. J. Tapley, Jr. Photochem. Photobiol. **29**, 1177 (1979), and references cited therein.
2. B. J. Parsons. Photochem. Photobiol. **32**, 813 (1980), and references cited therein.
3. A. Castellan and J. P. Desvergne. Photochem. Photobiol. **34**, 183 (1981).
4. J. L. Decout and J. Lhomme. Tetrahedron Lett. **22**, 1247 (1981).
5. I. Gryczyński, A. Kawski, S. Paszyc, M. Rafalska, and B. Skalski. Bull. Acad. Polon. Sci. Ser. Sci. Phys. Astronom. **27**, 271 (1979).
6. D. T. Browne, J. Eisinger, and N. J. Leonard. J. Am. Chem. Soc. **90**, 7302 (1968).
7. C. N. Ou, P. S. Song, M. L. Harter, and I. C. Felkner. Photochem. Photobiol. **24**, 487 (1977).
8. N. J. Leonard. Acc. Chem. Res. **12**, 423 (1979), and references cited therein.
9. P. O. Ts'o. Basic principles in nucleic acid chemistry. Vol. 2. Academic Press, New York. 1974. p. 332.
10. K. Mutai, B. A. Gruber, and N. J. Leonard. J. Am. Chem. Soc. **97**, 4095 (1975).
11. T. T. Herskovits, S. J. Singer, and E. P. Geiduschek. Arch. Biochem. Biophys. **94**, 99 (1961).
12. W. Müller, D. M. Crothers, and M. Waring. Eur. J. Biochem. **39**, 223 (1973).
13. P. Vigny and M. Duquesne. *In* Excited states of biological molecules. *Edited by* J. B. Birks. Wiley–Interscience, New York. 1976. p. 166.
14. G. F. Fedorin and V. P. Georgievskii. Zh. Prikl. Spektrosk. **21**, 165 (1974).
15. C. N. Ou, C. H. Tsai, K. J. Tapley, and P. S. Song. Biochemistry, **17**, 1047 (1978).
16. M. Kupryszewska, I. Gryczyński, and A. Kawski. Photochem. Photobiol. **36**, 499 (1982).
17. S. Paszyc, B. Skalski, and G. Wenska. Tetrahedron Lett. 449 (1976).
18. C. H. Krauch, S. Farid, and G. O. Schenck. Chem. Ber. **99**, 625 (1966).
19. D. O. Cowan and R. L. Drisko. Elements of organic photochemistry. Plenum Press, New York. 1976. p. 465.
20. H. Morrison, H. Curtis, and T. McDowell. J. Am. Chem. Soc. **88**, 5415 (1966).
21. W. H. Melhuish. J. Phys. Chem. **65**, 229 (1961).
22. H. Bredereck, G. Müller, and E. Berger. Ber. Dtsch. Chem. Ges. B, **73**, 1058 (1940).
23. R. K. Robins. J. Am. Chem. Soc. **79**, 490 (1957).
24. L. H. Leenders, E. Schouteden, and F. C. de Schryver. J. Org. Chem. **38**, 957 (1973).

Can. J. Chem. Downloaded from www.nrcresearchpress.com by 210.87.254.105 on 09/06/12
For personal use only.

Structures of rengyol, rengyoxide, and rengyolone, new cyclohexylethane derivatives from *Forsythia suspensa* fruits

KATSUYA ENDO AND HIROSHI HIKINO
Pharmaceutical Institute, Tohoku University, Aoba-yama, Sendai, Japan

Received January 23, 1984

This paper is dedicated to Professor Paul De Mayo on the occasion of his 60th birthday

KATSUYA ENDO and HIROSHI HIKINO. 1984. Can. J. Chem. **62**, 2011 (1984).

Three new C_6-C_2 natural alcohols, rengyol (**1**), rengyoxide (**2**), and rengyolone (**3**), have been isolated from *Forsythia suspensa* fruits, along with a novel glycoside, forsythoside E (**4**), a new sugar ester, 4-caffeoylrutinose, and a known quinol glucoside, cornoside (**5**). Chemical and spectroscopic studies have established the structures of these new constituents.

KATSUYA ENDO et HIROSHI HIKINO. 1984. Can. J. Chem. **62**, 2011 (1984).

On a isolé trois nouveaux alcools naturels en C_6—C_2 des fruits de la *Forsythia suspensa*, soit le rengyol (**1**), le rengyoxide (**2**) et la rengyolone (**3**); on a aussi isolé de la même source un nouveau glycoside, le forsythoside E (**4**), un nouvel ester d'un sucre, le caféoyl-4 rutinose, et un glucoside connu du quinol, le cornoside (**5**). Des études chimiques et spectroscopiques ont permis d'établir les structures de ces nouveaux constituants.

[Traduit par le journal]

Can. J. Chem. Downloaded from www.nrcresearchpress.com by 210.87.254.6 on 09/06/12
For personal use only.

Forsythia suspensa Vahl (Oleaceae) is an important original plant of the crude drug "rengyo" (Forsythiae Fructus) which has been used for antiinflammatory, diuretic, drainage, and antidotal purposes in Oriental medicine. The crude drug has also been known to exhibit antibacterial activity, and we have recently disclosed that the principal antibacterial constituent of the crude drug originating from the fruits of *F. suspensa* is the glycoside, forsythoside A (**6**), which occurs also in the leaves of the same plant (1). We have also revealed that the fruits of *F. suspensa* contain other antibacterial glycosides, forsythoside C (**7**) and forsythoside D (**8**), in addition to D-glucose, L-rhamnose, and rutinose (2).

In a continuation of our chemical and pharmacological study of this crude drug, the fruits of *F. suspensa*, we have now isolated three new natural alcohols, rengyol (**1**), rengyoxide (**2**), and rengyolone (**3**), having an unusual nonaromatic C_6—C_2 carbon skeleton presumably derived from phenylpropanoids, together with a new glycoside, forsythoside E (**4**), a new sugar ester, 4-caffeoylrutinose, and a known glucoside, cornoside (**5**). This report deals with the structure determination of these new constituents.

Rengyol (**1**), mp 124°C, $[\alpha]_D$ +0.08°, analyzed for $C_8H_{16}O_3$ and displayed ion peaks at *m/e* 161.1206 ($C_8H_{17}O_3$: 161.1203) and 142.0992 ($C_8H_{14}O_2$: 142.0992) in its high resolution mass spectrum. The ^{13}C nmr spectrum of rengyol exhibited three signals (δ 58.7, 69.7, 69.9) assignable to the carbon substituted with an oxygen. Since the number of these carbon atoms was the same as that of the oxygen atoms present in the molecule, all oxygen atoms were expected to constitute hydroxyl groups. In fact, rengyol yielded the diacetate (**1***a*) on acetylation with acetic anhydride in pyridine and the dibenzoate (**1***b*) on benzoylation with benzoyl chloride in pyridine. The former was acetylated further to the triacetate (**1***c*) by acetic anhydride and 4-dimethylaminopyridine in triethylamine, while on controlled reaction with acetic anhydride in ethanolic pyridine, rengyol yielded the monoacetate (**1***d*). These results substantiated that three hydroxyl groups existed in rengyol (**1**) and they suffered from different degrees of steric hindrance. The ^1H nmr spectra of the diacetate (**1***a*) and the dibenzoate (**1***b*) revealed the presence of a primary acyloxyl group (δ 4.24, 2H triplet, *J* 7 Hz for **1***a*; δ 4.54, 2H triplet, *J* 7 Hz for **1***b*), adjacent to a methylene group, and a secondary acyloxyl group (δ 4.66, 1H quintet, *J* 6.5 Hz for **1***a*; δ 4.98, 1H quintet, *J* 6.5 Hz for **1***b*). The corresponding signals for rengyol (**1**) were observed at δ 3.74 (2H triplet, *J* 7 Hz) and 3.53 (1H broad quintet, *J* 6.5 Hz), while those for the triacetate (**1***c*) and the monoacetate (**1***d*) appeared at δ 4.10 (2H triplet, *J* 7 Hz), 4.69 (1H m), and δ 4.27 (2H triplet, *J* 7 Hz), 3.61 (1H multiplet), respectively.

The ^{13}C nmr spectrum of rengyol exhibited only six carbon signals, indicating the presence of two pairs of equivalent methylene groups (δ 31.6, 2C triplet; 36.0, 2C triplet) (Table 1). The absence of optical activity as well as the structural features described above suggested that three hydroxyl groups were situated in a plane of symmetry. Hence, the presence of a cyclohexane system substituted with a β-hydroxyethyl group and two hydroxyl groups at the C-1 and C-4 positions was deduced. The configuration of the secondary hydroxyl group at the C-4 position was assigned to be equatorial, based on the half-height width, $W_{1/2}$ 20 Hz, of the multiplet signals for the axially oriented C-4 methine hydrogen of the

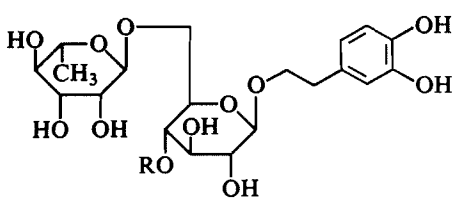

4: R=H
6: R=Caffeoyl

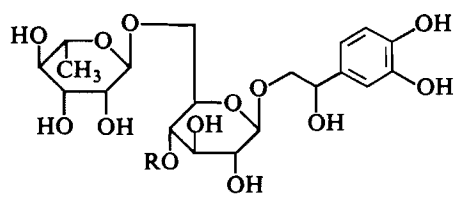

7: R=Caffeoyl
8: R=H

TABLE 1. Carbon-13 shieldings of the C_6—C_2 parts of *Forsythia suspensa* constituents*

Compound	C-1	C-2	C-3	C-4	C-5	C-6	C-7	C-8
Rengyol (**1**)	69.9 s	36.0 t	31.6 t	69.7 d	31.6 t	36.0 t	45.1 t	58.7 t
Rengyoxide (**2**)	70.3 s	28.6 t	34.7 t	100.2 s	34.7 t	28.6 t	44.4 t	58.8 t
Rengyolone (**3**)	74.7 s	81.7 d	40.3 t	196.8 s	127.9 d	150.0 d	40.2 t	66.2 t
Cornoside (**5**)	68.2 s	153.6 d	127.0 d	185.8 s	127.0 d	153.6 d	40.9 t	65.1 t

*Chemical shifts from internal TMS in pyridine-d_5.

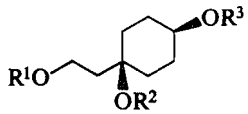

1 : $R^1=R^2=R^3=H$

1*a*: $R^1=R^3=Ac$, $R^2=H$

1*b*: $R^1=R^3=$Benzoyl, $R^2=H$

1*c*: $R^1=R^2=R^3=Ac$

1*d*: $R^1=Ac$, $R^2=R^3=H$

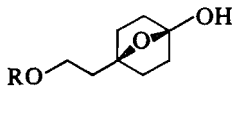

2 : R=H

2*a*: R=Ac

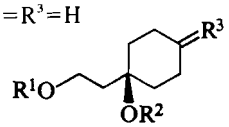

2*b*: $R^1=R^2=Ac$, $R^3=O$

2*c*: $R^1=R^2=H$, $R^3=(OCH_3)_2$

2*d*: $R^1=R^2=Ac$, $R^3=(OCH_3)_2$

triacetate (**1***c*, δ 4.69) and the monoacetate (**1***d*, δ 3.61), although the coupling constants and the half-height width of the corresponding methine signals in rengyol (**1**) and its diesters (**1***a* and **1***b*) were not informative because of the virtual coupling. This assignment was supported further by the result of an empirical calculation of the carbon-13 shielding. Thus the observed resonance at δ 69.7 for the C-4 carbon of rengyol was in good accordance with the calculated value, δ 69.4, for 1-alkyl substituted *cis*-1,4-cyclohexanediol, but clearly different from the value, δ 64.0, for the *trans* isomer (3). Consequently, the stereostructure of rengyol has been concluded to be **1**, provided that the substituent with a higher conformational energy, the β-hydroxyethyl group, assumes the more stable equatorial configuration.

Rengyoxide (**2**), $[\alpha]_D$ +0.16°, exhibited ion peaks at *m/e* 158 (M) in its mass spectrum, corresponding to the molecular formula, $C_8H_{14}O_3$. The ^1H nmr spectrum of rengyoxide resembled that of rengyol (**1**) and displayed the signal compatible with a primary hydroxyl group (δ 3.77, 2H triplet, *J* 7 Hz) that was next to a methylene group (δ 1.80, 2H triplet), but lacked the signal assignable to a secondary hydroxyl group. The ^{13}C nmr spectrum of rengyoxide was also similar to that of rengyol (**1**) and showed only six carbon signals, suggesting the presence of two pairs of equivalent methylene groups (δ 28.6, 2C triplet; 34.7, 2C triplet) in addition to one primary and one tertiary carbon-oxygen bond (δ 58.8, 1C triplet; 70.3, 1C singlet) (Table 1). Elemental composition of rengyoxide indicated the presence of two degrees of unsaturation in the structure. Since infrared and ^{13}C nmr spectra of rengyoxide did not exhibit any signal assignable to an olefinic group or a carbonyl group, it was expected to contain one oxide ring in a cyclohexyl group. The resonance signal at δ 100.2 (singlet) in the ^{13}C nmr spectrum was thus assigned to a geminally dioxygenated carbon. The absence of optical activity as well as the structural features described above suggested that the structure of rengyoxide corresponded to the 4-dehydro derivative of rengyol existing almost exclusively in the hemiketal form by intramolecular interaction with a hydroxyl group.

In coincidence with this view, reaction of rengyoxide (**2**) with acetic anhydride in pyridine at room temperature yielded, as a sole product, the monoacetate (**2***a*), which, however, was esterified further by acetic anhydride in triethylamine with the aid of 4-dimethylaminopyridine affording the diacetate (**2***b*). On the other hand, treatment of rengyoxide with methanolic hydrogen chloride at room temperature produced the dimethyl ketal (**2***c*), which in turn was transformed into the corresponding diacetate (**2***d*) by acetic anhydride and 4-dimethylaminopyridine in triethylamine. Moreover, the reaction of rengyoxide with sodium borohydride in aqueous methanol resulted in almost exclusive formation of only one epimeric alcohol, which was identified as rengyol (**1**) itself. Reversibly, Collins oxidation of the rengyol monoacetate (**1***d*) yielded the corresponding dehydro derivative (**2***a*), identical to the rengyoxide monoacetate, which on alkaline hydrolysis generated rengyoxide (**2**). These reactions, as well as the interconversions of rengyol (**1**) and rengyoxide (**2**), rigorously established the nature and location of the oxygen functions in the molecule, and consequently the structure of rengyoxide has been established as represented by the formula **2**.

Rengyolone (**3**), $[\alpha]_D$ +0.26°, exhibited ion peaks at *m/e* 154 (M) corresponding to the molecular formula $C_8H_{10}O_3$. The ultraviolet and ^1H nmr spectra of rengyolone revealed the presence of an oxymethylene group (δ 4.02, 2H triplet, *J* 7 Hz) adjacent to a methylene group (δ 2.27, 2H multiplet), an oxymethine group (δ 4.24, 1H double doublet with doubling, *J* 6, 5, and 1.5 Hz) next to another methylene group (δ 2.64, 1H double doublet, *J* 17 and 6 Hz; 2.73, 1H double doublet, *J* 17 and 5 Hz), and an α,β-unsaturated carbonyl group (λ_{max} 227 nm; δ 5.95, 1H doublet, *J* 10 Hz; 6.74, 1H double doublet, *J* 10 and 1.5 Hz). The existence of a long-range coupling (*J* 1.5 Hz) between the signals at δ 6.74 and 4.24 indicated that the corresponding hydrogens were situated in quasi equatorial orientation. Although rengyolone exhibited a broad absorption at 3420 cm^{-1} in its infrared spectrum, it was recovered unchanged from a reaction with acetic anhydride in pyridine at room temperature overnight, showing the presence of a hydroxyl group which was in a hindered position. This structural information, as well as the carbon-13 shieldings (Table 1), led to the stereostructure **3** for rengyolone, and the spectral data of rengyolone were in good agreement with those of the substance derived from *p*-hydroxyphenylethanol by photosensitized oxygenation (4). Since rengyolone (**3**) shows no cd (circular dichroism) absorption, it is regarded as a racemic mixture.

Forsythoside E (**4**), $[\alpha]_D$ −35.3°, showed ion peaks at *m/e* 501 (M+K), 485 (M+Na), and 463 (M+H) in its field desorption mass spectrum, corresponding to the molecular formula $C_{20}H_{30}O_{12}$. The ultraviolet and ^1H nmr spectra of forsythoside

Can. J. Chem. Downloaded from www.nrcresearchpress.com by 210.87.254.6 on 09/06/12
For personal use only.

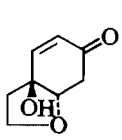

3

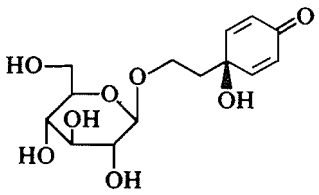

5

E indicated the presence of a secondary methyl group (δ 1.25, 3H doublet, *J* 6 Hz), a benzylic methylene group (δ 2.77, 2H triplet, *J* 7 Hz), two anomeric methine groups (δ 4.27, 1H doublet, *J* 8 Hz; 4.74, 1H doublet, *J* 1.5 Hz), and a trisubstituted phenyl group (λ_{max} 282 nm; δ 6.4−6.9, 3H multiplet). From this information, forsythoside E was regarded as the decaffeoyl derivative of forsythoside A (**6**). In fact, on mild alkaline hydrolysis with sodium hydroxide in aqueous methanol, forsythoside A (**6**) yielded methyl caffeoate (2) and decaffeoylforsythoside A (**4**), $[\alpha]_D$ −39.9°, which was found identical to forsythoside E.

4-Caffeoylrutinose, $[\alpha]_D$ −8.0°, displayed an ion peak at 512 (M+Na+1) in its field desorption mass spectrum, reflecting the molecular formula $C_{21}H_{28}O_{13}$. The ultraviolet and ^{1}H nmr spectra of this substance revealed the presence of a secondary methyl group (δ 1.19, 3H doublet, *J* 6.5 Hz), an anomeric methine group (δ 4.59, 1H doublet, *J* 1.5 Hz) and a caffeoyl group (λ_{max} 328 nm; δ 6.7−7.1, 3H multiplet; 6.26, 1H doublet, *J* 16 Hz; 7.56, 1H doublet, *J* 16 Hz). Further, the presence of another anomeric methine group in equilibrium was indicated by a pair of signals at δ 4.52 (doublet, *J* 8 Hz) and 5.08 (broad singlet), totalling one hydrogen equivalent. Alkaline hydrolysis of this substance with sodium hydroxide as above yielded methyl caffeoate and rutinose (2), proving that this substance was a caffeoyl ester of rutinose. The acyl group was allocated to the C-4 position of the glucosyl group based on a detailed analysis of the ^{13}C nmr spectrum (2,3). Thus the new sugar ester has been characterized as 4-caffeoylrutinose.

Cornoside (**5**), $[\alpha]_D$ −10.5°, exhibited ion peaks at *m/e* 316 (M) in its field desorption mass spectrum, corresponding to the molecular formula $C_{14}H_{20}O_8$. The ultraviolet and ^{1}H nmr spectra of this substance disclosed the presence of a methylene group (δ 2.05, 2H triplet, *J* 7 Hz), an anomeric methine group (δ 4.23, 1H doublet, *J* 7 Hz), and an α,β-unsaturated carbonyl group (λ_{max} 224 nm; δ 6.11, 2H doublet, *J* 10 Hz; 7.01, 2H doublet, *J* 10 Hz). The characteristic chemical shift of the carbonyl resonance (δ 185.8, singlet) in its ^{13}C nmr spectrum, in addition to the presence of two equivalent olefinic groups (δ 127.0, 2C doublet; 153.6, 2C doublet) and a quaternary carbon (δ 68.2, singlet) (Table 1), demonstrated that this substance had a *para*-quinol type partial structure (5). The ^{13}C nmr spectrum also indicated the presence of a β-glucosyl group. Consequently, the sugar derivative was considered to be cornoside (**5**) (6), and in fact, the physicochemical data presented above agreed well with the reported values (6).

Experimental

Melting points are uncorrected. The nmr spectra were run at 100 MHz (^{1}H) and 25 MHz (^{13}C). Chemical shifts (δ) are reported in ppm from internal TMS and coupling constants (*J*) given in Hz. Abbreviations: s = singlet, d = doublet, t = triplet, q = quartet, m = multiplet.

Isolation of the constituents

The methanol extract (109 g) of *F. suspensa* fruits (1.0 kg) was extracted successively with AcOEt and BuOH in the presence of water, yielding the AcOEt soluble fraction (45 g), BuOH soluble fraction (21 g), and water soluble fraction (25 g), respectively.

The BuOH fraction (16 g) was then placed on a column of polyamide (Wako Polyamide C-200, 300 g) and eluted with 20% water−MeOH (800−1200 mL) to give a fraction (3.26 g) that was further fractionated on Sephadex LH-20 (Pharmacia, 350 mL) with MeOH, yielding a crystalline substance, rengyol (**1**, 1.1 g): colourless prisms (MeOH), mp 123−124°C, $[\alpha]_D$ +0.08° (*c* 1.21, MeOH); ^{1}H nmr (CD_3OD) δ: 3.53 (1H broad quintet, *J* 6.5), 3.74 (2H t, *J* 7); ms *m/e*: 142 (M − H_2O), 115 (M − C_2H_4OH). *Anal.* calcd. for $C_8H_{16}O_3$: C 59.97, H 10.07; found: C 59.34, H 10.08.

The mother liquid (850 mg) of recrystallization of **1** was chromatographed on silica gel (Merck Kiesel gel 60, 30 g) and eluted with 3% MeOH−$CHCl_3$ to afford the crude rengyoxide fraction (60 mg) that was purified by repeated chromatography to give rengyoxide (**2**): colourless oil, $[\alpha]_D$ +0.16° (*c* 1.66, MeOH); ^{1}H nmr (CD_3OD) δ: 1.80 (2H t, *J* 7), 3.77 (2H t, *J* 7); ms *m/e*: 158 (M), 140 (M − H_2O), 130 (M − CO).

The crude rengyol fraction (1.65 g) of the Sephadex LH-20 chromatography mentioned above was again applied on a Sephadex LH-20 column and eluted with MeOH to yield the following constituents.

Rengyolone (**3**, 120 mg): colourless oil, $[\alpha]_D$ +0.26° (*c* 1.14, MeOH); uv λ_{max} (MeOH) nm: 227; ir ($CHCl_3$) cm^{-1}: 3420, 1680; ^{1}H nmr ($CDCl_3$) δ: 2.27 (2H m), 2.64 (1H dd, *J* 6, 17), 2.73 (1H dd, *J* 5, 17), 4.02 (2H t, *J* 7), 4.24 (1H ddd, *J* 1.5, 5, 6), 5.95 (1H d, *J* 10), 6.74 (1H dd, *J* 1.5, 10) ms *m/e*: 154 (M), 137 (M − OH), 110 (M − C_2H_4OH).

Cornoside (**5**, 26 mg): colourless oil, $[\alpha]_D$ −10.5° (*c* 0.26, MeOH); uv λ_{max} (MeOH) nm: 224; ^{1}H nmr (CD_3OD) δ: 2.05 (2H t, *J* 7), 4.23 (1H d, *J* 7), 6.11 (2H d, *J* 10), 7.01 (2H d, *J* 10); ^{13}C nmr (pyridine-d_5) δ: 104.5 (d, C-1′), 75.0 (d, C-2′), 78.3 (d, C-3′), 71.5 (d, C-4′), 78.3 (d, C-5′), 62.6 (t, C-6′) for the β-glucosyl group. Data for the aglycone part is given in the Table 1.

Continued elution of the above polyamide column, for the BuOH-solubles of the crude drug extract, with 20% water − MeOH (1200−2400 mL) yielded, after purification by repeated chromatography (Sephadex LH-20/MeOH), the following constituents.

Forsythoside E (**4**, 35 mg): a pale yellow amorphous solid, $[\alpha]_D$ −35.3° (*c* 0.41, MeOH); uv λ_{max} (MeOH) nm: 282; ^{1}H nmr (CD_3OD) δ: 1.25 (1H d, *J* 6), 2.77 (2H t, *J* 7), 4.27 (1H d, *J* 8), 4.74 (1H d, *J* 1.5), 6.4−6.9 (3H m); ^{13}C nmr (pyridine-d_5) δ: 130.3 (s, C-1), 117.2 (d, C-2), 146.7 (s, C-3), 145.2 (s, C-4), 116.4 (d, C-5), 120.4 (d, C-6), 36.2 (t, C-7), 71.2 (t, C-8) for the aglycone; 104.4 (d, C-1′), 74.8 (d, C-2′), 78.3 (d, C-3′), 71.6 (d, C-4′), 76.8 (d, C-5′), 68.0 (t, C-6′) for the glucosyl group; and 102.2 (d, C-1″), 72.5 (d, C-2″), 72.0 (d, C-3″), 73.7 (d, C-4″), 69.6 (d, C-5″), 18.5 (q, C-6″) for the rhamnosyl group; fd−ms *m/e*: 501 (M+K), 485 (M+Na), 463 (M+H).

4-Caffeoylrutinose (28 mg): a pale yellow amorphous solid, $[\alpha]_D$ −8.0° (*c* 0.20, MeOH); uv λ_{max} (MeOH) nm: 245, 295, 328; ^{1}H nmr (CD_3OD) δ: 1.19 (3H d, *J* 6.5), 4.59 (1H d, *J* 1.5), 4.52 (d, *J* 8) and 5.08 (broad s) totalling 1H, 6.26 (1H d, *J* 16), 6.7−7.1 (3H m), 7.56 (1H d, *J* 16); ^{13}C nmr (pyridine-d_5) δ: 126.6 (s, C-1″), 115.6 (d, C-2″), 147.4 (s, C-3″), 151.7 (s, C-4″), 116.5 (d, C-5″), 122.0 (d, C-6″), 146.1 (d, C-7″), 114.6 (d, C-8″), 167.0 (s, C-9″) for the caffeoyl group; 93.8 (d, C-1), 74.0 (d, C-2), 72.6 (d, C-3), 73.1 (d, C-4), 70.0 (d, C-5), 67.5 (t, C-6) for the α-glucosyl group; 98.7 (d, C-1), 76.6 (d, C-2), 74.6 (d, C-3), 72.6 (d, C-4), 75.7 (d, C-5), 67.4 (t, C-6) for the β-glucosyl group; 102.1 (d, C-1′), 72.6 (d, C-2′), 71.9 (d, C-3′), 73.9 (d, C-4′), 69.6 (d, C-5′), 18.4 (q, C-6′) for the rhamnosyl group; fd−ms *m/e*: 512 (M+Na+1).

*Rengyol diacetate (**1**a)*

Rengyol (**1**, 80 mg) was treated with acetic anhydride (1 mL) in pyridine (5 mL) at room temperature overnight. The mixture was then worked up as usual and the product purified by column chromatography (silica gel/5% MeOH − $CHCl_3$) to afford the diacetate (**1***a*, 92 mg): colourless oil; ir ($CHCl_3$) cm^{-1}: 3530, 1725; ^{1}H nmr

Can. J. Chem. Downloaded from www.nrcresearchpress.com by 210.87.254.6 on 09/06/12
For personal use only.

Can. J. Chem. Downloaded from www.nrcresearchpress.com by 210.87.254.6 on 09/06/12
For personal use only.

($CDCl_3$) δ: 1.81 (2H t, *J* 7), 2.03 (3H s), 2.04 (3H s), 4.24 (2H t, *J* 7), 4.66 (1H quintet, *J* 6.5); ms *m/e*: 245 (M+1), 227 (M − OH), 184 (M − AcOH), 157 (M − C_2H_4OAc).

*Rengyol dibenzoate (**1**b)*

Rengyol (**1**, 50 mg) was allowed to react with benzoyl chloride (1.0 mL) in pyridine (10 mL) at room temperature overnight. Usual work-up of the reaction mixture followed by chromatographic purification (silica gel/$CHCl_3$) afforded the dibenzoate (**1***b*, 105 mg): colourless prisms (ether), mp 113°C; ir (KBr) cm^{-1}: 3590, 1715, 1698; ^1H nmr ($CDCl_3$) δ: 2.00 (2H t, *J* 7), 4.54 (2H t, *J* 7), 4.98 (1H quintet, *J* 6.5), 7.3−8.1 (10H m); ms *m/e*: 369 (M+1), 351 (M − OH), 245 (M − C_6H_5COOH), 219 (M − $C_2H_4OCOC_6H_5$).

*Rengyol triacetate (**1**c)*

Rengyol diacetate (**1***a*, 50 mg) was treated with acetic anhydride (0.5 mL) and 4-dimethylaminopyridine (50 mg) in triethylamine (2 mL) at room temperature overnight. The reaction mixture was concentrated under vacuum, and the residue was subjected to column chromatography (silica gel/$CHCl_3$ and silica gel/ether) to yield the triacetate (**1***c*, 45 mg): colourless oil; ir ($CHCl_3$) cm^{-1}: 1725; ^1H nmr ($CDCl_3$) δ: 2.02 (3H s), 2.03 (3H s), 2.05 (3H s), 2.25 (2H t, *J* 7), 4.10 (2H t, *J* 7), 4.69 (1H m); ms *m/e*: 227 (M − OAc), 199 (M − C_2H_4OAc).

*Rengyol monoacetate (**1**d)*

Rengyol (**1**, 200 mg) was dissolved in EtOH (2 mL) and pyridine (10 mL). Acetic anhydride (4 mL) was added to the solution in small portions for two days under stirring at room temperature. The reaction mixture was then worked up as usual, followed by column chromatography (silica gel/5% MeOH − $CHCl_3$) to give the starting compound **1** (53 mg), the diacetate (**1***a*, 40 mg), and the monoacetate (**1***d*, 171 mg): ^1H nmr ($CDCl_3$) δ: 2.06 (3H s), 3.61 (1H m), 4.27 (2H t, *J* 7); ms *m/e*: 142 (M − AcOH), 124 (M − AcOH − H_2O).

*Rengyoxide monoacetate (**2**a)*

Rengyoxide (**2**, 20 mg) was esterified with acetic anhydride (0.5 mL) in pyridine (5 mL) at room temperature overnight followed by work-up as above to give the monoacetate (**2***a*, 20 mg): colourless oil; ir ($CHCl_3$) cm^{-1}: 3480, 1710; ^1H nmr ($CDCl_3$) δ: 1.93 (2H t, *J* 7), 2.07 (3H s), 4.31 (2H t, *J* 7); ms *m/e*: 201 (M+1), 183 (M − OH), 140 (M − AcOH), 122 (M − AcOH − H_2O).

*Rengyoxide diacetate (**2**b)*

Rengyoxide monoacetate (**2***a*, 6 mg) was treated with acetic anhydride (0.3 mL) and 4-dimethylaminopyridine (5 mg) in triethylamine (2 mL) at room temperature overnight. The reaction mixture was worked up as before to yield the diacetate (**2***b*, 4 mg): colourless oil; ir ($CHCl_3$) cm^{-1}: 1735, 1720; ^1H nmr ($CDCl_3$) δ: 2.03 (3H s), 2.05 (3H s), 2.35 (2H t, *J* 7), 4.16 (2H t, *J* 7); ms *m/e*: 183 (M − OAc), 155 (M − C_2H_4OAc).

*Rengyoxide dimethyl ketal (**2**c)*

Rengyoxide (**2**, 20 mg) was treated with 5% HCl − MeOH (5 mL) at room temperature overnight. The reaction mixture was then neutralized with $NaHCO_3$, followed by concentration, to yield a residue that was purified by column chromatography (silica gel/10% MeOH − $CHCl_3$) to afford the dimethyl ketal (**2***c*, 15 mg): colourless oil; ^1H nmr ($CDCl_3$) δ: 1.74 (2H t, *J* 7), 3.13 (3H s), 3.19 (3H s), 3.88 (2H t, *J* 7); ms *m/e*: 205 (M+1), 173 (M − OCH_3).

*Rengyoxide dimethyl ketal diacetate (**2**d)*

Rengyoxide dimethyl ketal (**2***c*, 10 mg) was treated with acetic anhydride (0.5 mL) and 4-dimethylaminopyridine (5 mg) in triethylamine (2 mL) at room temperature overnight, followed by the usual work-up as before, to afford the diacetate (**2***d*, 7 mg): colourless oil; ^1H nmr ($CDCl_3$) δ: 2.02 (6H s), 2.27 (2H t, *J* 7), 3.14 (3H s), 3.19 (3H s), 4.10 (2H t, *J* 7); ms *m/e*: 257 (M − OCH_3), 228 (M − AcOH).

*Sodium borohydride reduction of rengyoxide (**2**)*

Rengyoxide (**2**, 5 mg) was dissolved in 50% water − MeOH (10 mL) and was treated with $NaBH_4$ (large excess) at room temperature for 3 h. The reaction mixture was then acidified with Amberlite IR-120 (Rohm and Haas, H^+ form) and concentrated to dryness. The residue was redissolved, followed by repeated concentration with water and methanol to give the crystalline product (5 mg): mp 122°C; ^1H nmr (CD_3OD) δ: 3.51 (1H m), 3.72 (2H t, *J* 7), which was identical to rengyol (**1**) in spectroscopic and chromatographic behaviour.

*Transformation of rengyol (**1**) into rengyoxide (**2**)*

Rengyol monoacetate (**1***d*, 50 mg) was oxidized with Collins reagent (excess) in CH_2Cl_2 (30 mL) overnight at room temperature. The reaction mixture was then worked up as usual and the product purified by column chromatography (silica gel/AcOEt) to afford the dehydro derivative (**2***a*, 39 mg): ^1H nmr ($CDCl_3$) δ: 1.93 (2H t, *J* 7), 2.07 (3H s), 4.31 (2H t, *J* 7), which was found identical chromatographically as well as spectroscopically to rengyoxide monoacetate. The oxidation product was then hydrolysed with 5% NaOH in 50% water − MeOH (10 mL) to give its deacetyl product (**2**): ^1H nmr (CD_3OD) δ: 1.81 (2H t, *J* 7), 3.79 (2H t, *J* 7), which was identified as rengyoxide.

*Transformation of forsythoside A (**6**) into forsythoside E (**4**)*

Forsythoside A (**6**, 100 mg) was hydrolysed with 5% NaOH in 50% water − MeOH (20 mL) overnight at room temperature under a nitrogen atmosphere. The mixture was neutralized with Amberlite IR 120 (H^+ form) and concentrated to dryness. The residue was partitioned with water and AcOEt. The organic layer yielded methyl caffeoate (18 mg): mp 150°C; ^1H nmr (CD_3OD) δ: 3.74 (3H s), 6.23 (1H d, *J* 16), 6.6−7.1 (3H m), 7.52 (1H d, *J* 16), while the aqueous layer afforded the decaffeoylforsythoside A (**4**, 25 mg): $[\alpha]_D$ −39.9° (*c* 0.14, MeOH); ^1H nmr (CD_3OD) δ: 1.26 (3H d, *J* 6), 2.79 (2H t, *J* 7), 4.28 (1H d, *J* 8), 4.78 (1H d, *J* 1.5), 6.4−6.8 (3H m), which was found identical to forsythoside E in chromatographic and spectroscopic characteristics.

Alkaline hydrolysis of 4-caffeoylrutinose

4-Caffeoylrutinose (9 mg) was dissolved in MeOH (10 mL) and treated with 2% NaOH in 50% water − MeOH (2 mL) under a nitrogen atmosphere overnight at room temperature. The reaction mixture was then neutralized with Amberlite IR 120 (H^+ form), followed by partitioning with water and AcOEt to give, as the organic extract, methyl caffeoate: ^1H nmr (CD_3OD) δ: 3.75 (3H s), 6.22 (1H d, *J* 16), 6.6−7.1 (3H m), 7.52 (1H d, *J* 16), and, from the aqueous fraction, rutinose: ^1H nmr (CD_3OD) δ: 1.26 (3H broad d, *J* 6), 4.46 (d, *J* 8) and 5.15 (broad s) 1H in total, 4.46 (1H, broad s).

1. K. ENDO, K. TAKAHASHI, T. ABE, and H. HIKINO. Heterocycles, **16**, 1311 (1981).
2. K. ENDO and H. HIKINO. Heterocycles, **19**, 2033 (1982).
3. J. D. ROBERTS, F. J. WEIGERT, J. I. KROSCHWITZ, and H. J. REICH. J. Am. Chem. Soc. **92**, 1338 (1970); E. BREITMAIR and W. VOELTER. ^{13}C NMR Spectroscopy. 2nd ed. Verlag Chemie, New York. 1978. p. 210.
4. I. SAITO, Y. CHUJO, H. SHIMAZU, M. YAMANE, T. MATSUURA, and H. J. CHANMANN. J. Am. Chem. Soc. **97**, 5272 (1975); J. SCHWEIZER, R. LATTRELL, and E. HECKER. Experientia, **31**, 1267 (1975).
5. R. HOLLENSTEIN and W. VON PHILIPSBORN. Helv. Chim. Acta, **55**, 2030 (1972); K. A. PARKER and S. KONG. J. Org. Chem. **45**, 1218 (1980).
6. S. R. JENSEN, A. KJOER, and B. J. NIELSEN. Acta Chem. Scand. **27**, 367 (1973); H. SASAKI, H. TAGUCHI, T. ENDO, I. YOSIOKA, K. HIGASHIYAMA, and H. OTOMASU. Chem. Pharm. Bull. **26**, 2111 (1978).

4-Iodophenylcholine: a potential myocardial imaging agent

DUNCAN H. HUNTER AND YOLANDA ZEA PONCE
Department of Chemistry, University of Western Ontario, London, Ont., Canada N6A 5A5
G. WILLIAM BROWN AND MICHAEL J. CHAMBERLAIN
Department of Nuclear Medicine, University Hospital, University of Western Ontario, London, Ont., Canada N6A 5B7
AND
ALBERT A. DRIEDGER AND GARY MORRISSEY
Department of Nuclear Medicine, Victoria Hospital, University of Western Ontario, London, Ont., Canada N6A 4G5

Received February 1, 1984

This paper is dedicated to Professor Paul de Mayo on the occasion of his 60th birthday

DUNCAN H. HUNTER, YOLANDA ZEA PONCE, G. WILLIAM BROWN, MICHAEL J. CHAMBERLAIN, ALBERT A. DRIEDGER, and GARY MORRISSEY. Can. J. Chem. **62**, 2015 (1984).

The compound O-(4-iodophenyl)choline iodide has been synthesized using iodine-125, iodine-127, and iodine-131 by diazonium salt and melt exchange procedures. Radiochemical yields of approximately 2% and 56%, respectively, were obtained. The biodistribution of this compound in mice was analyzed in order to determine its potential as a myocardial imaging agent. Selective myocardial concentration was observed at 5 min post-injection, with a heart-to-blood ratio of 18:1.

DUNCAN H. HUNTER, YOLANDA ZEA PONCE, G. WILLIAM BROWN, MICHAEL J. CHAMBERLAIN, ALBERT A. DRIEDGER et GARY MORRISSEY. Can. J. Chem. **62**, 2015 (1984).

On a synthétisé l'iodure de la O-(iodo-4 phényl) choline marquée à l'iode-125, à l'iode-127 et à l'iode-131 en faisant appel soit à un processus impliquant un sel de diazonium soit à des échanges à l'état fondu. Pour chacune de ces méthodes, les rendements radiochimiques sont respectivement de 2% et 56%. Afin de déterminer le potentiel de ce composé comme agent pouvant créer des images du myocarde, on a analysé la biodistribution de ce composé dans les souris. On a déterminé les concentrations sélectives au niveau du myocarde 5 min après les injections et avec un rapport coeur/sang de 18:1.
[Traduit par le journal]

Can. J. Chem. Downloaded from www.nrcresearchpress.com by 210.87.254.42 on 09/06/12
For personal use only.

Introduction

Variations in regional myocardial blood flow can be detected by external imaging of radiotracer distributions in the myocardium, after intravenous injection. Thallous-201 ion is the current radionuclide of choice (1), but it has the disadvantages of being costly, of having suboptimal energy emmissions, and of requiring long study times during which the distribution may change. In tracer studies the initial distribution is blood flow limited and therefore a number of compounds may be considered as myocardial perfusion agents regardless of the mechanism of their concentration in the tissue.

Since iodine-123 is less expensive than thallous-201 ion, the development of an iodine-labelled myocardial imaging agent seemed attractive. Bioactive quaternary ammonium compounds are taken up by heart tissue by mechanisms which may or may not be receptor specific (2) and, when radiolabelled, are potentially useful as heart imaging agents. In pursuit of such agents, we were attracted to certain choline derivatives.

Benzoyl choline derivatives have been recently investigated (3) as myocardial imaging agents and have proven somewhat successful. While the ester **1** hydrolyzes too readily to permit accumulation, this is not the case for the amide **2**. An ether analog **3** should also be resistant to hydrolysis.

The 4-iodophenyl derivative **3** of choline can be labelled by a diazonium salt procedure. Alternatively, a direct exchange of iodide ion for aromatic iodide is another route to the labelled compound, provided that the specific activity is not critical.

The position of the radioiodide within the molecule may affect both the labelling procedure and the biological distribution. From considerations of receptor specificity, an *ortho* halogen may produce undesirable steric effects. Further, it has been noted that nicotinic activity is more pronounced with *meta* halogen substitution than with the *para* analog (4). With the hope of minimizing such activity, the 4-iodo compound was prepared.

Results and discussion

As illustrated in the preparative scheme, several independent routes to the iodine-labelled quaternary ammonium salt **3** were investigated. The final step in each case involved reaction of the amine **6** with excess methyl iodide. Even with radioiodine-labelled **6**, this methylation requires only a few minutes and yields directly a saline solution of **3**. Using [^{125}I]-**6**, a sample of [^{125}I]-**3** was obtained in about 95% radiochemical yield and showed only one radioactive spot on tlc with an R_f corresponding to **3**.

As shown, the preparation of the radioiodine-labelled amine **6** was attempted both by a diazonium salt procedure (5) and by the direct exchange of **6**. The diazonium salt procedure using [^{125}I]-NaI gave very low radiochemical yields even with added carrier ([^{127}I]-NaI) to increase the overall iodide ion concentration. For example, with a 10,000-fold excess of [^{127}I]-NaI, a radiochemical yield of 2% was obtained. Consequently, the direct exchange of **6** with radioiodide in molten benzoic acid (6) was investigated. Treatment of 1 mg of **6** with [^{131}I]-NaI at 165°C for 1 h resulted in a 56% radiochemical yield. The **6** prepared in both these ways showed the same chromatographic behaviour as **6** that had been characterized by spectroscopic techniques.

This surprisingly facile and efficient exchange between iodide ion and aryl iodide seems to be fairly general and does not require a ring activated to nucleophilic substitution. A variety of solvents and conditions have been reported for iodide ion – aryl iodide exchange; neat liquid at 100–185°C (3, 7); acetamide at 140–180°C (8); benzoic acid at 170°C (6); and water at 100–150°C (9). We have found that, for **6**, thorough re-

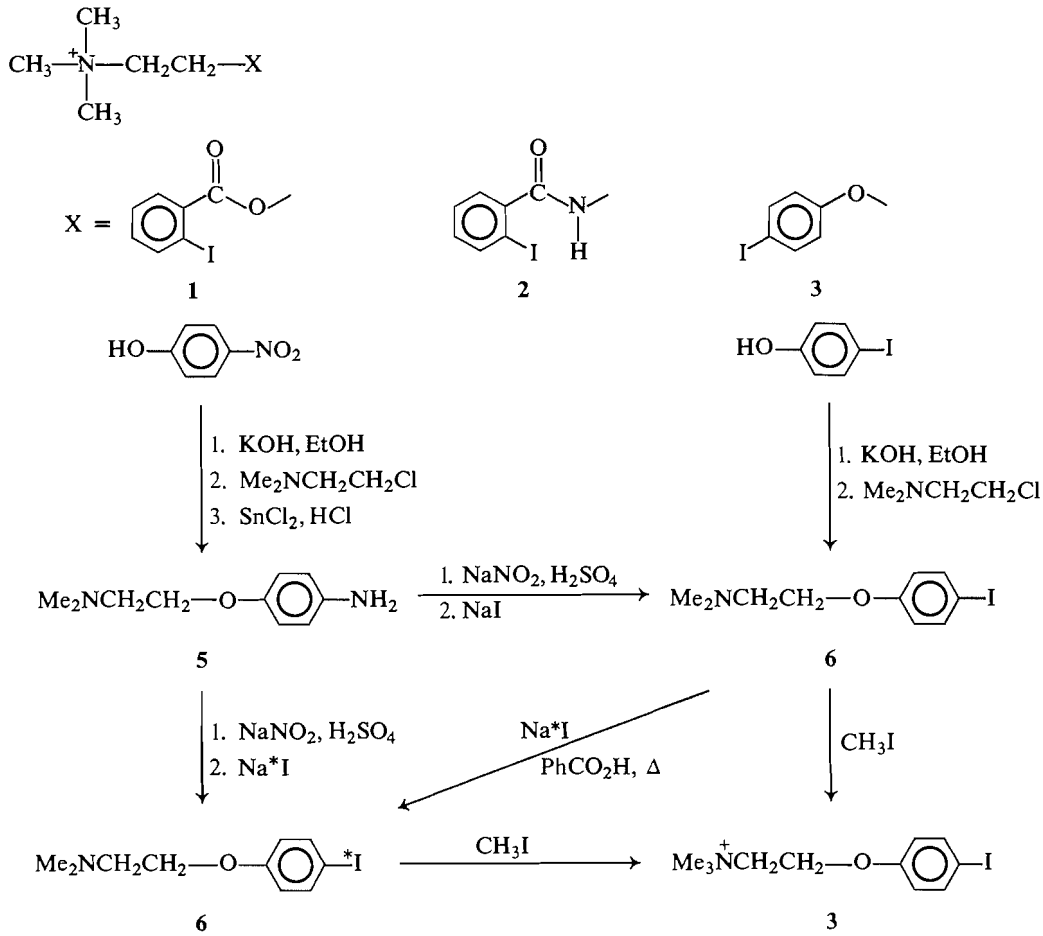

moval of water is essential for efficient exchange using benzoic acid. While the mechanism of this process is in doubt ($S_{RN}1$?) (10), it is worth noting that there seems to be no production of the *ortho* or *meta* iodo analogues during the exchange process. A simple equilibration does not seem to be involved, since the exchange stops short of the anticipated equilibrium value and further heating does not lead to further exchange.

The time needed to convert the amino compound **5** into the ammonium salt **3** or to exchange **6** and convert it to **3** is about 2 h, which should be short enough to extend its use to iodine-123, which has a half-life of 13.3 h.

Biodistribution studies (Table 1) in mice showed rapid uptake in the myocardial tissue, with a maximum value of 20% of the injected dose per gram of tissue at 5 min post-injection. This percentage decreased continually from 5 min onward, dropping substantially in the heart between 15 and 30 min post injection. The only other organs showing significant amounts of radioactivity were the liver (21%) and the lungs (13%). Liver radioactivity decreased more slowly, as did the radioactivity in the other organs sampled. Blood radioactivity was always very low and increased somwhat as the study progressed, contrasting with the drop of radioactivity in the other organs.

From Table 2 it can be seen that the optimal time for imaging in mice as judged by heart/lung and heart/liver ratios would be within 5 to 15 min post-injection. In contrast, the amide **2** showed optimal ratios nearer to 30 min post-injection (3).

In considering the application of this to human imaging, interspecies variation must be borne in mind together with the shorter time scale often seen for physiological processes in smaller animals (11).

TABLE 1. Biodistribution of [^{125}I]-O-(4-iodophenyl)choline in mice

	% Uptake per gram of tissue: average of 4 mice ± S.D.			
Organ	5 min	15 min	30 min	60 min
Blood	1.1 ± 0.3	1.2 ± 0.2	1.4 ± 0.3	1.5 ± 0.2
Heart	19.9 ± 2.1	17.9 ± 1.6	6.0 ± 3.0	4.6 ± 1.0
Lung	13.1 ± 3.7	10.0 ± 0.4	4.1 ± 0.5	3.8 ± 1.0
Liver	20.6 ± 1.9	13.9 ± 1.4	11.1 ± 1.5	9.6 ± 3.0
Spleen	6.6 ± 1.9	6.4 ± 0.2	4.6 ± 0.6	5.8 ± 0.9
Muscle	1.9 ± 1.0	1.8 ± 0.3	1.2 ± 0.1	1.2 ± 0.4
Bone	3.0 ± 0.9	2.5 ± 0.3	1.6 ± 0.1	1.6 ± 0.5

Although in vitro protein binding experiments showed relatively high plasma protein binding (65%), very little of the compound was present in the blood at any time during the study. Since significant amounts of radioactivity resided in the heart, it would appear that the affinity of [^{125}I]-**3** for the heart tissue was much greater than that for the plasma protein component of the blood.

The present work involving radiolabelling with [^{125}I]-NaI and [^{131}I]-NaI has led to **3**, with specific activities of about 7.4 GBq/mmol (0.2 Ci/mmol) from the diazonium salt procedure and 148 MBq/mmol (4 mCi/mmol) for the melt exchange technique. Work is in progress to augment the specific activities from both these procedures in order to obtain material for experiments in receptor localization.

Biodistribution studies using the 4-iodo compound have shown significant uptake in the myocardium of mice at 5–15

Can. J. Chem. Downloaded from www.nrcresearchpress.com by 210.87.254.42 on 09/06/12
For personal use only.

Can. J. Chem. Downloaded from www.nrcresearchpress.com by 210.87.254.42 on 09/06/12
For personal use only.

TABLE 2. Selected organ ratios

Time (min)	Heart/blood ratio	Heart/lung ratio	Heart/liver ratio
5	18	1.5	1.0
15	15	1.8	1.3
30	4.3	1.5	0.5
60	3	1.2	0.5

min post-injection, with favourable heart/lung and heart/blood ratios at these times. At present the *meta* and *ortho* iodinated phenyl analogs are being investigated to improve labelling yield, specific activity, and biodistribution.

Experimental

Materials and methods

Melting points reported are uncorrected, elemental analyses were performed commercially (Guelph Chem. Labs. Ltd., Guelph, Ontario), and gas chromatography separations were accomplished with a 6-ft stainless steel column packed with 10% Carbowax-20M on Chromosorb P. The iodide-125 and iodide-131 were obtained commercially (C.E. Frosst and Co., Kirkland, P.Q.) as aqueous solutions of sodium iodide with concentrations of about 1.85 GBq/mL (50 mCi/mL). Radioactivity was assayed in a dose calibrator and in an automatic γ counter.

*1-Dimethylamino-2-(4-nitrophenoxy)ethane (**4**)*

A solution of potassium hydroxide (5.16 g, 0.1 mol) in 30 mL absolute ethanol was added to a solution of 4-nitrophenol (14 g, 0.1 mol) in 20 mL absolute ethanol. The orange-yellow potassium 4-nitrophenoxide salt was filtered, washed with a few milliliters of cold absolute ethanol, and air dried. Yield, 14.3 g (81%).

To a cooled solution of 2-dimethylamino ethylchloride hydrochloride (12.6 g, 0.09 mol) in 40 mL water, a solution of sodium hydroxide (4.2 g, 0.1 mol) in 20 mL water was added. The reaction mixture was saturated with solid sodium chloride and extracted with five 30-mL portions of toluene. The toluene fractions were combined and dried over potassium hydroxide pellets. The dried toluene solution was added to a suspension of potassium 4-nitrophenoxide (14 g, 0.08 mol) in 80 mL toluene and refluxed overnight.

After cooling, the reaction mixture was filtered and the filtrate concentrated on a rotary evaporator. A brown oily residue was obtained (13.1 g, 78%). Proton nmr (chloroform-*d*) δ: 2.25 (s, 6H, CH_3), 2.65 (t, 2H, CH_2), 4.10 (t, 2H, CH_2), 6.9 (d, 2H, aromatic H), 8.10 (d, 2H, aromatic H).

About 1 g of the crude product was purified as its hydrochloride salt by recrystallization from 2-propanol (mp 166–167°C). Infrared (ir) (Nujol): 1510 cm^{-1} (s, NO_2), 1330 cm^{-1} (s, NO_2), 1300 cm^{-1} (m, C—O—C). The proton nmr spectrum (DMSO-d_6) was consistent with its structure; δ: 2.80 ppm (s, 6H, CH_3), 3.50 (t, 2H, CH_2), 4.50 (t, 2H, CH_2), 7.10 (d, 2H, aromatic H), 8.10 (d, 2H, aromatic H).

*1-Dimethylamino-2-(4-aminophenoxy)ethane (**5**)*

Compound **4** (11 g, 0.052 mol) was added slowly, with stirring, to a solution of concentrated hydrochloric acid (80 mL) and stannous chloride dihydrate (47.2 g, 0.2 mol). After stirring at 0°C for 30 min, and then at room temperature overnight, the reaction mixture was made basic by addition of a very concentrated sodium hydroxide solution until all stannous hydroxide redissolved.

The resulting mixture was extracted with dichloromethane (4 × 100 mL). After washing with water (100 mL), drying, and solvent evaporation, a dark brown oil was left as residue. Recrystallization from petroleum ether (30–55° bp) gave pale yellowish needles, mp 51–52°C; yield: 7.72 g, 82%; ^{1}Hmr (chloroform-*d*) δ: 2.25 (s, 6H, CH_3), 2.60 (t, 2H, CH_2), 3.37 (s, 2H, NH_2), 3.90 (t, 2H, CH_2), 6.50 (m, 4H, aromatic H). *Exact Mass* determination calcd. for $C_{10}H_{16}N_2O$: 180.126; found (ms): 180.126.

*1-Dimethylamino-2-(4-iodophenoxy)ethane (**6**)*

(a) From 4-iodophenol

Reaction of potassium hydroxide (13 g, 22.7 mmol) with 4-iodophenol (5 g, 22.7 mmol) in 20 mL of absolute ethanol at room temperature left the 4-iodophenoxide salt as a yellowish oil after solvent evaporation. This salt was refluxed overnight with a 50-mL toluene solution of 2-dimethylaminoethylchloride prepared from the hydrochloride (3.3 g, 22.7 mmol) as described above.

After cooling and filtration, solvent removal on a rotary evaporator yielded 6.4 g of a crude oil which was converted to its hydrochloride by bubbling dry hydrochloric acid into an ether solution. Yield: 5.88 g, 79%; mp 186–187°C; ^{1}Hmr (dimethylsulfoxide-d_6) δ: 2.8 (s, 6H, CH_3), 3.42 (t, 2H, CH_2), 4.34 (t, 2H, CH_2), 6.76 (d, 2H, aromatic H), 7.52 (d, 2H, aromatic H).

(b) *From **5** using the diazonium salt method*

*(i) [^{127}I]-**6***

A 1.02-g (5.7 mmol) sample of **5** in 25 mL of 50% sulfuric acid at 0°C was reacted with a 1.17-g (17 mmol) solution of sodium nitrite in 3 mL of water. After about 10 min at 0°C, urea (0.7 g, 12 mmol) was added to destroy any excess nitrite. After bubbling had ceased (~10 min), a solution of sodium iodide (8.5 g, 57 mmol) and sodium sulfite (2.9 g, 23 mmol) in 30 mL of water was added. After 10 min at 0°C, 10 min at ambient temperature, and about 6 min heating at 80°C, the reaction was worked up by first making basic with sodium hydroxide.

Extraction with methylene chloride followed by a water wash, drying with sodium sulfate, and solvent evaporation left a dark solid residue. Filtration of an ether solution of this residue through a short column of neutral alumina yielded 0.21 g of a red oily product. This was further purified by tlc on alumina using ether as the eluent to yield 0.18 g (11%) of a material showing identical tlc and gc behaviour, as well as identical ^{1}Hmr and ir spectra, to the material from *p*-iodophenol. *Anal.* calcd. for $C_{10}H_{14}NOI$: C 41.25, H 4.85, N 4.81, I 43.59; found: C 41.29, H 4.85, N 5.0, I 43.01. *Exact Mass* determination: calcd. for $C_{10}H_{14}NOI$: 291.011; found (ms): 291.011. A mp of the hydrochloride of this material and a mixture mp with the hydrochloride of **6** from *p*-iodophenol were identical.

*(ii) [^{125}I]-**6***

Following the procedure described above, 2 mg (11 μmol) of **5** in 100 μL of 50% sulfuric acid was reacted with sodium nitrite (2.3 mg in 40 μL, 33 μmol). Urea (1.5 mg, 25 μmol) was added after 10 min at 0°C and, when bubbling had ceased, sodium iodide-125, 92.5 MBq (2.5 mCi in 50 μL) was added, followed by 40 μL of a solution of sodium iodide-127 (3.0 mg, 20 μmol) and sodium sulfite (1.0 mg, 8 μmol). After the usual extractive work-up, a material showing the same R_f on tlc as the authentic sample prepared above, with an activity of 50 μCi (2% yield), was isolated. This material was used without further purification for the synthesis of O-(4-iodophenyl)choline iodide.

(c) *[^{131}I]-**6** from **6** using a melt exchange method*

In a typical experiment, 1 mg of [^{127}I]-**6** and 3 mg of benzoic acid were dissolved in 0.2 mL of absolute ethanol in a 1-mL multi-dose vial. Approximately 80 μL (192 μCi) of [^{131}I]-NaI solution, 92.5 MBq (2.5 mCi/mL); was added and, after cooling in a Dry Ice – acetone mixture, the solvents were removed on a rotary evaporator.

The vial was then sealed with a rubber septum and aluminum cap and the solid mixture heated in an oil bath at 165°C for 60 min. After alkalinization and extraction with portions of methylene chloride, and washing and drying of the combined extracts, the radioactivity in the CH_2Cl_2 layer was 5.18 MBq (140 μCi) (73%). The CH_2Cl_2 was reduced in volume and used for tlc purification on alumina/ether against [^{127}I]-**6**.

The [^{131}I]-**6** was recovered from the tlc plate by extraction with methanol, filtered, and the solvent evaporated to yield purified[^{131}I]-**6**, 3.96 MBq, (107 μCi; 56% incorporation).

*O-(4-iodophenyl)choline iodide (**3**)*

(a) *From [^{127}I]-**6***

To 44 mg (0.15 mmol) of **6** dissolved in 3 mL chloroform, at room temperature, was added a solution of 440 mg (3.1 mmol) methyl

iodide in 2 mL chloroform. The reaction mixture was stirred for 30 min at room temperature. The excess methyl iodide and chloroform were evaporated and the white crystals left were washed with three portions (3–5 mL each) of chloroform and air dried.

The crystals were redissolved in methanol, filtered, and the solvent evaporated, yielding 62 mg of **3** as white crystals (95%), mp (dec.) 246°C; ^{1}Hmr (dimethylsulfoxide-d_6) δ: 3.2 (s, 9H, $^+$N $(CH_3)_3$), 3.8 (t (br), 2H, CH_2), 4.45 (t (br), 2H, CH_2), 6.84 (d, 2H, aromatic H), 7.60 (d, 2H, aromatic H). *Anal.* calcd. for $C_{11}H_{17}NOI_2$: C 30.51, H 3.96, N 3.23, I 58.61; found: C 30.66, H 3.98, N 3.25, I 58.32.

(b) *From [^{125}I]-6 or [^{131}I]-6*

The 1.85-MBq (50 μCi) sample of [^{125}I]-**6** prepared as previously described was dissolved in 2 mL chloroform and excess methyl iodide (20–30 mg) was added. The mixture was refluxed for 30 min (65–70°C). After cooling, the chloroform layer was transferred to a 12-mL centrifuge tube and the reaction flask washed twice with 0.5 mL saline solution. The saline portions were added to the chloroform and thoroughly mixed. After separation of the two layers had occurred, the saline was carefully recovered and transferred to a 3-mL screw cap vial and its radioactivity assayed: 1.81 MBq (about 49 μCi).

The saline solution of [^{125}I]-**3** was later diluted, filtered through a millipore filter, and used for the biodistribution studies.

This material showed tlc (alumina; CH_3CN/H_2O 9:1) behaviour identical to the [^{127}I]-**3** material characterized above.

Biodistribution studies

White Swiss mice were initially anaesthetized with an intraperitoneal injection of sodium pentobarbital (80 mg/kg body weight) and then received a 0.1-mL intravenous tail injection of 93 MBq (2.5 μCi) of [^{125}I]-**3**. Four mice were sacrificed by cardiac puncture/exsanguination at each post-injection period of 5, 15, 30, and 60 min. Selected organs were washed, patted dry, and weighed, along with the blood samples. Tissues and injection standards were subsequently assayed for radioactivity. Results were expressed as percent uptake per gram of wet tissue.

Protein binding

The in vitro binding of **3** to human serum proteins was determined by adding 100-μL aliquots of [^{125}I]-**3** to 1 mL of plasma in each of four centrifuge tubes. At 5, 15, 30, and 60 min, 100 μL of the plasma – [^{125}I]-**3** mixture was added to duplicate tubes containing 1 mL of 10% trichloroacetic acid, followed by centrifugation.

The supernatant was removed and, after washing the pellet with normal saline, the combined supernatant washings and the pellets were assayed for radioactivity. 66% of [^{125}I]-**3** was found bound at 5 and 15 min, 65% at 30 and 60 min.

Acknowledgements

We wish to thank Peter D. Corcoran for his technical assistance with the biodistribution studies and Susan Wilson and Doug Hairsine for obtaining spectra. We wish to thank NSERC for financial support.

1. R. A. VOGEL. Semin. Nucl. Med. **10**, 146 (1980).
2. (*a*) B. FRANCIS, W. C. EIKELMAN, M. P. GRISSOM, R. E. GIBSON, and R. C. REBA. Int. J. Nucl. Med. Biol. **9**, 173 (1982); (*b*) H. D. BURNS, L. E. MARZILLI, R. F. DANNALS, T. E. DANNALS, T. C. TRAGESER, P. CONTI, and H. N. WAGNER. J. Nucl. Med. **21**, 875 (1980).
3. R. F. DANNALS, H. D. BURNS, L. G. MARZILLI, T. C. TRAGESER, and H. N. WAGNER. J. Pharm. Sci. **70**, 439 (1981).
4. P. HEY. Br. J. Pharmacol. **7**, 117 (1952).
5. G. J. MEYER, K. ROSSLER, and G. STOCKLIN. J. Am. Chem. Soc. **101**, 3121 (1979).
6. M. EISENHUT. Int. J. Appl. Radiat. Isot. **33**, 499 (1982).
7. R. N. HANSON, B. L. HOLMAN, and M. A. DAVIS. J. Med. Chem. **21**, 830 (1978).
8. H. ELIAS and H. F. LOTTERHOS. Chem. Ber. **109**, 1580 (1976).
9. (*a*) D. E. KUHL, J. R. BARRIO, S.-C. HUANG, R. F. ACKERMANN, J. L. LEAR, J. L. WU, T. H. LIN, and M. E. PHELPS. J. Nucl. Med. **23**, 196 (1982); (*b*) H. F. KUNG, K. M. TRAMPOSCH, and M. BLAU. J. Nucl. Med. **24**, 66 (1983); (*c*) K. M. TRAMPOSCH, H. F. KUNG, and M. BLAU. J. Med. Chem. **26**, 121 (1983).
10. M. CHANON and M. L. TOBE. Angew. Chem. Int. Ed. Engl. **21**, 1 (1982).
11. J. F. MCAFEE and G. SUBRAMANIAN. Third Internat. Radiopharmaceut. Dosimetry Symp., Oakridge, Tennessee. 1980 p. 292.

Can. J. Chem. Downloaded from www.nrcresearchpress.com by 210.87.254.42 on 09/06/12
For personal use only.

Une synthèse hautement stéréosélective de dienes conjugués (*E*)

R. Bloch, J. Abecassis et D. Hassan

Laboratoire des Carbocycles, ERA 316, Bâtiment 420, Université de Paris-Sud, 91405 Orsay Cedex, France

Reçu le 3 janvier 1984

Cet article est dédié au Professeur Paul de Mayo à l'occasion de son 60ème anniversaire

R. Bloch, J. Abecassis et D. Hassan. Can. J. Chem. **62**, 2019 (1984).

Une méthode générale de préparation de dienes conjugués terminaux de stéréochimie (*E*) a été développée par thermolyse éclair de dihydro-2,5 thiophènedioxides-1,1 monosubstitués, eux-mêmes engendrés par réaction de rétro Diels–Alder. Ce procédé permet d'obtenir des dienes conjugués fonctionnels (alcools, esters. . .) ou non avec une excellente pureté stéréochimique (en général supérieure à 98%). L'application à la synthèse du dodécadiène-9,11 yl-1 acétate (*E*), le composant principal de la phéromone sexuelle de *Diparopsis castanea* montre l'intérêt et l'efficacité de cette méthode.

R. Bloch, J. Abecassis, and D. Hassan. Can. J. Chem. **62**, 2019 (1984).

A general method for the preparation of (*E*) terminal conjugated dienes was developed by the flash thermolysis of 2-substituted 2,5-dihydrothiophene-1,1-dioxides generated by a retro Diels–Alder reaction. This process allows the obtention of conjugated dienes, bearing or not a functionality (alcohols, esters), with an excellent stereoisomeric purity (in general higher than 98%). An application to the synthesis of (*E*)-9,11-dodecadien-1-yl acetate, the major component of the sex pheromone of *Diparopsis castanea*, shows the generality and the efficacy of this method.

Can. J. Chem. Downloaded from www.nrcresearchpress.com by 210.87.254.40 on 09/06/12
For personal use only.

Introduction

La préparation stéréosélective de dienes conjugués a pris une importance croissante durant ces quelques dernières années. Deux raisons principales semblent être à l'origine de ce regain d'intérêt: (*i*) la présence d'un enchaînement diénique conjugué de stéréochimie bien précise dans de nombreux composés naturels et en particulier dans les phéromones sexuelles d'insectes (pour une revue voir la référence 1); (*ii*) l'utilisation croissante des réactions de Diels–Alder intra- ou intermoléculaires pour la synthèse totale de molécules complexes (2).

Plusieurs méthodes de synthèse stéréosélective des dienes-1,3 ont été récemment décrites soit par réactions de Wittig modifiées (3), soit par couplage croisé d'un dérivé organométallique vinylique et d'un halogénure vinylique de stéréochimies bien définies (4), soit encore par ouverture thermique concertée de cyclobutènes substitués (5). Ces différentes méthodes sont en général difficilement applicables à la préparation de dienes fonctionnels. Dans ce mémoire est exposée la mise au point d'une méthode générale de préparation hautement stéréosélective de dienes conjugués (*E*) par extrusion thermique de SO_2 à partir de dioxides de dihydro-2,5 thiofènes (ou sulfolènes) **1**, eux-mêmes engendrés par une réaction de rétro Diels–Alder.

Il a été en effet montré il y a quelques années (6) que la thermolyse des sulfolènes monosubstitués **1** conduit, par extrusion de SO_2 selon un processus concerté disrotatoire, à des dienes conjugués **2** de stéréochimie *E* d'excellente pureté stéréoisomérique et avec d'excellents rendements:

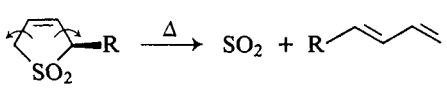

1 **2** (*E*) > 99,5%

Pourtant ce procédé très simple n'a pas été développé, probablement en raison de la difficulté d'obtention des sulfolènes convenablement substitués **1**. En particulier, la substitution directe du sulfolène parent **3** est rendue délicate[1] par l'ouverture facile du cycle en milieu basique (7):

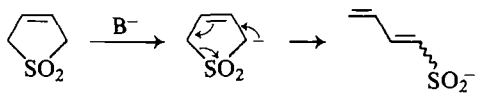

3

Cependant, après protection de la double liaison, il devrait être possible d'engendrer un anion stable qui, après réaction avec des électrophiles variés suivie de la régénération de la double liaison conduirait aux sulfolènes **1** puis aux dienes **2**. La sulfone tricyclique **4** paraît être un synthon intéressant dans un tel processus pour les raisons suivantes. (*i*) Le groupe protecteur étant thermiquement labile, son élimination par une réaction de rétro Diels–Alder ainsi que l'extrusion de SO_2 peuvent s'effectuer en une seule étape. (*ii*) En raison de la structure tricyclique rigide de la molécule, la face *endo* du cycle hétéroatomique à cinq chaînons est très encombrée: une attaque sélective des électrophiles par la face *exo* devrait conduire à l'introduction stéréocontrolée des substituants. (*iii*) Enfin l'anion de la sulfone **4** peut entrer en réaction non seulement avec des halogènures d'alkyle mais aussi avec différents électrophiles (aldéhydes, cétones, esters . . .) pour donner des précurseurs de dienes conjugués fonctionnels de stéréochimie *E*.

La méthode que nous avons développée est donc décrite par le schéma suivant:[2]

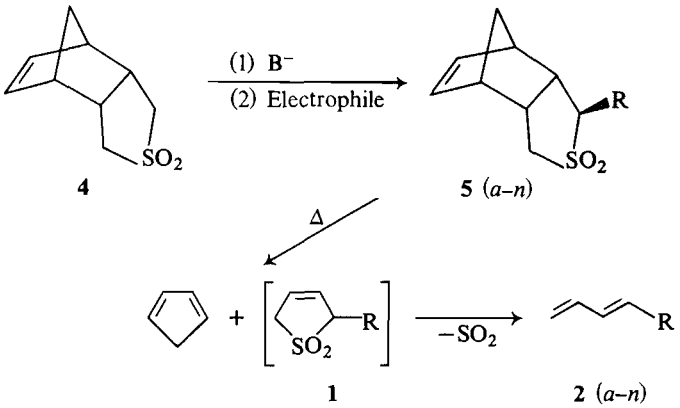

4 **5** (*a–n*) **1** **2** (*a–n*)

[1] Cependant, par utilisation de conditions opératoires très précises, l'alkylation directe du sulfolène **3** a pu être effectuée avec des rendements de 15 à 33% par rapport au sulfolène mis en réaction: voir les références 8 et 9.

[2] Une partie de ce travail a fait l'objet de notes préliminaires: voir la référence 10.

Can. J. Chem. Downloaded from www.nrcresearchpress.com by 210.87.254.40 on 09/06/12
For personal use only.

Résultats et discussion

(a) *Préparation de la sulfone tricyclique 4*

Une méthode simple et à haut rendement de préparation de cette sulfone était nécessaire. La réaction directe de Diels–Alder entre le cyclopentadiène et le sulfolène **3** n'a pu être effectuée même en présence de catalyseurs (acides de Lewis, SiO_2). La sulfone **4** a donc été synthétisée par modifications d'une méthode décrite par Photis et Paquette (11) selon le schéma suivant:

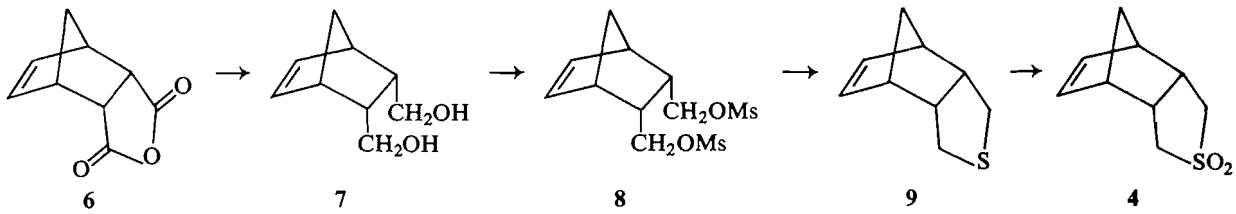

6 **7** **8** **9** **4**

L'adduit **6** du cyclopentadiène et de l'anhydride maléique est réduit en diol **7** par l'hydrure de lithium-aluminium dans le THF à reflux. Ce diol est ensuite transformé en dimésylate **8** par action de deux équivalents de chlorure de méthane sulfonyle en présence de pyridine. Le sulfure **9** est obtenu avec d'excellents rendements par réaction du dimésylate **8** avec une solution aqueuse de sulfure de sodium dans les conditions de transfert de phase en utilisant l'aliquat 336 comme agent de transfert (12). Finalement le sulfure est oxydé en sulfone par action d'une solution aqueuse méthanolique d'oxone ($2KHSO_5$, K_2SO_4, $KHSO_4$). Contrairement à ce qui avait été décrit sur d'autres substrats (13) nous avons obtenu à température ambiante une proportion non négligeable d'époxydation de la double liaison. Cette époxydation est supprimée en effectuant la réaction à une température inférieure à 0°C. La sulfone **4** a pu ainsi être obtenue avec un rendement global de 50–55% par rapport à l'adduit **6**.

(b) *Action des électrophiles sur la sulfone 4*

Le traitement de la sulfone **4** en solution dans le THF anhydre avec un équivalent de nBuLi à −78°C, suivi de l'addition de 1,1 équivalent de réactif électrophile et hydrolyse après retour à la température ambiante fournit les sulfones monosubstituées **5**(*a–n*) avec les rendements reportés dans le tableau 1.

Dans de nombreux cas (**5***b–e*, **5***i* et **5***j*) les sulfones monosubstituées sont accompagnées de la sulfone de départ et de sulfones α,α′-disubstituées. Il faut noter que les rendements et les proportions relatives de ces trois produits ne sont pas affectés par la présence de HMPT dans le milieu ou par la nature de l'halogène ($C_5H_{11}I$ ou $C_5H_{11}Br$), mais par contre dépendent de l'encombrement stérique des substituants introduits. Ainsi, la proportion de sulfone dialkylée est très faible lors de l'alkylation avec un halogénure secondaire tel que l'iodure d'isopropyle. La réaction de la sulfone **4** avec le chloroformiate d'éthyle est limitée par la formation d'un anion en α du groupe ester et si le rendement en **5***f* est excellent par rapport à l'électrophile, il ne peut dépasser 50% par rapport à la sulfone **4** mise en réaction, alors que l'action des esters avec la sulfone **4** conduit aux cétones **5** (*l–n*) avec d'excellents rendements.

Dans tous les cas, la rmn du proton et la chromatographie en phase gazeuse sur colonne capillaire couplée à la spectrométrie de masse montrent qu'un seul stéréoisomère **5** est formé. Il s'agit très probablement de l'isomère où le groupe R est en position *exo*, provenant d'une attaque de l'électrophile par la face la moins encombrée.

(c) *Thermolyse des sulfones 5*

Les thermolyses ont été effectuées en phase vapeur avec un temps de contact dans la zone chaude de l'ordre de 10 à 50 ms (pour une description de l'appareillage voir la référence 14). Il a été nécessaire de chauffer à 650°C pour obtenir une conversion totale des sulfones **5**. Dans ces conditions, les sulfolènes **1** intermédiaires perdent spontanément SO_2 pour conduire directement aux dienes conjugués **2** en général avec d'excellents rendements. Les dienes conjugués terminaux n'étant pas séparables en chromatographie en phase vapeur conventionnelle même sur colonne capillaire,[3] leur pureté stéréoisomérique a été déterminée par résonance magnétique nucléaire soit du proton, soit du carbone 13. Dans la grande majorité des cas (voir tableau 1) un seul stéréoisomère a pu être décelé dans les spectres de rmn ^{13}C des dienes obtenus et leur pureté stéréoisomérique a donc été estimée supérieure à 98% (limite de précision de l'appareillage). La stéréochimie *E* des dienes **2** qui découle directement de leur mode de formation (6) a pu être vérifiée: dans le cas du pentadiène-1,3 **2***a* par comparaison de son spectre de rmn ^1H avec celui d'un échantillon authentique; dans le cas du nonadiène-1,3 **2***b* par comparaison de son spectre de rmn ^{13}C avec celui d'un mélange de nonadiène-1,3 *E* + *Z* obtenu par réaction de Wittig, en particulier par comparaison des déplacements chimiques des carbones allyliques (16): 32,7 ppm pour l'isomère *E* et 27,9 ppm pour l'isomère *Z*; enfin dans le cas du méthyl-5 hexadiène-1,3 **2***k* par une analyse de son spectre de rmn ^1H à 400 MHz et en particulier par la détermination des constantes de couplage:

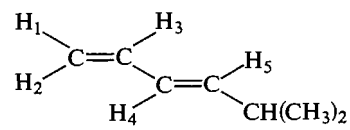

$J_{H_1H_2}$ = 2 Hz
$J_{H_1H_3}$ = 10,5 Hz
$J_{H_2H_3}$ = 17 Hz
$J_{H_3H_4}$ = 10,5 Hz
$J_{H_4H_5}$ = 15 Hz

La moins bonne stéréosélectivité observée lors de l'obtention des dienes **2***d* (R = $SiMe_3$) et **2***e* (R = $SnMe_3$) peut être expliquée par les plus grandes longueurs de liaison C—Si et

[3] Les dienes conjugués terminaux peuvent être cependant séparés en chromatographie en phase vapeur sur des supports enrobés d'une phase stationnaire de cristaux liquides nématiques (15). Nous avons cependant observé que les stéréoisomères des cétones dièniques sont facilement séparables tant par chromatographie en phase vapeur que par chromatographie sur colonne.

TABLEAU 1. Synthèse stéréosélective de diènes conjugués (*E*)

Préparation des sulfones **5**			Thermolyse		
Electrophile	Produit obtenu	Rendement(%)[a]	Diènes obtenus	Rendemen(%)[a]	Pureté stéréoisomérique[b]
ICH_3	**5***a*	85	**2***a* 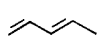	85	>95
IC_5H_{11}	**5***b*	65	**2***b* 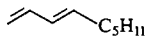	90	>98
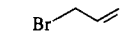	**5***c*	67	**2***c* 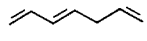	71	>98
$ClSiMe_3$	**5***d*	84	**2***d* 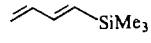	89	96
$ClSnMe_3$	**5***e*	76	**2***e* 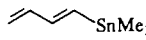	25	85
$ClCO_2Et$	**5***f*	47	**2***f* 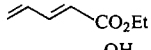	80	>98
$CH_3COCH_2CH_2CH_3$	**5***g*	95	**2***g* 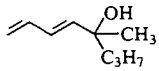	73	>98
	5*h*	77	**2***h* 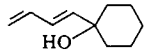	78	>98
CH_3CH_2CHO	**5***i*	56	**2***i* 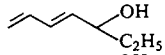	77	>98
C_4H_9CHO	**5***j*	52	**2***j* 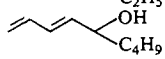	73	>98
$ICH(CH_3)_2$	**5***k*	72	**2***k* 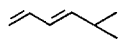	80	>98
CH_3CO_2Et	**5***l*	72	**2***l* 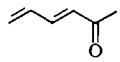	85	>98
$CH_3(CH_2)_3CO_2Et$	**5***m*	77	**2***m* 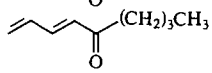	91	>98
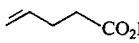	**5***n*	76	**2***n* 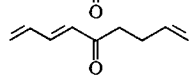	45	>98

[a] Les rendements et les puretés stéréoisomériques sont données pour des produits purs isolés par distillation ou par chromatographie sur colonne.
[b] Déterminée par rmn ^{13}C ou rmn ^1H.

C—Sn qui permettent un deuxième mode d'ouverture disrotatoire des sulfolènes **1**.[4]

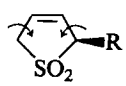

1 R = $SiMe_3$, $SnMe_3$

Le diène **2***e* (R = $SnMe_3$) est un diène particulièrement intéressant car c'est un précurseur d'un anion butadiènyl-1,3 de stéréochimie *E* (17):

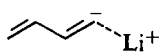

Ce diène n'a pu être obtenu jusqu'à présent qu'avec de faibles rendements (même par thermolyse à 600°C) en raison de la fragilité des liaisons allyliques C—Sn.

Les cétones diéniques **2**(*l*–*n*) sont obtenues chimiquement et stéréoisomériquement pures après chromatographie sur colonne de silice. (La stéréochimie *E* est facilement déterminée par le couplage *trans* (J = 15–17 Hz) observé entre le proton vinylique situé en α du carbonyle et le proton vinylique voisin.) Cependant dans le produit brut de thermolyse, la spectrométrie de masse couplée à la chromatographie en phase vapeur montre la présence d'une faible quantité (3 à 6%) d'un isomère. Dans le cas de la nonadiène-6,8 one-5 **2***m*, cet isomère minoritaire a été séparé et purifié. Le spectre de rmn ^1H montre qu'il s'agit de l'isomère *Z* (couplage *cis* J = 10 Hz entre le proton vinylique en α du carbonyle et le proton vinylique voisin). La cétone triénique **2***n* semblait être un synthon intéressant pour la préparation d'hydrindanones par réaction de Diels–Alder intramoléculaire. Cependant la cyclisation n'a pu être effectuée ni en phase vapeur ni par chauffage en tube scellé en solution dans le toluène. Jusqu'à 150°C la cétone **2***n* est récupérée inchangée; à 250°C seuls des polymères sont formés:

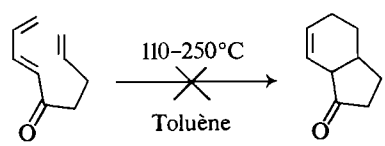

(d) *Synthèse du dodécadiène-9,11 yl-1 acétate* (E)

Le lépidoptère *Diparopsis castanea* est un fléau majeur des plantations de coton du sud-ouest de l'Afrique. Nesbitt *et al.* (18) ont montré que la phéromone sexuelle la plus efficace produite par le femelle de cet insecte est le dodécadiène-9,11 yl-1 acétate **12** de stéréochimie *E*. La méthode décrite ci-dessus a été appliquée à une synthèse simple et efficace de cette phéromone sexuelle **12** selon le schéma suivant (pour les synthèses antérieures voir la référence 19):

[4] On pourrait aussi invoquer un processus de rupture radicalaire et de recombinaison de la liaison C—$SnMe_3$; cependant une recombinaison efficace paraît difficile dans les conditions de la réaction (pression de 10^{-2} Torr; 1 Torr = 133.3 Pa).

Can. J. Chem. Downloaded from www.nrcresearchpress.com by 210.87.254.40 on 09/06/12
For personal use only.

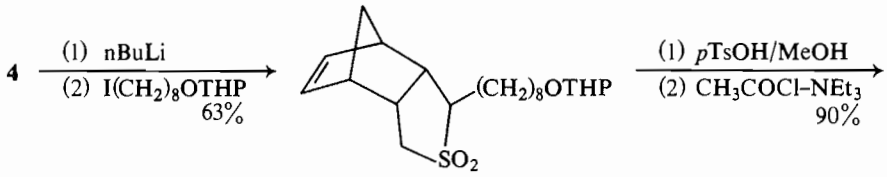

10

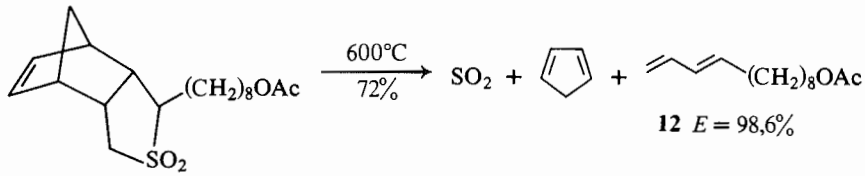

11 **12** $E = 98{,}6\%$

L'anion de sulfone **4** réagit facilement avec l'éther tétrahydropyrannylique de l'iodo-8 octanol (20) pour donner la sulfone alkylée **10** sous forme d'un seul isomère. La régénération de l'alcool par l'acide *p*-toluènesulfonique suivie d'une acétylation par le chlorure d'acétyle en présence de triéthylamine conduit à l'acétate **11** avec un excellent rendement. La thermolyse à 600°C de **11**[5] fournit directement la phéromone **12**.

Une analyse de l'acétate **12** obtenu par chromatographie gazeuse sur phase nématique[6] montre que la pureté stéréoisomérique de cette phéromone est de 98,6%. La stéréosélectivité observée ainsi que le rendement (~40–45% à partir de la sulfone **4**) font de cette méthode une des plus efficaces pour l'obtention de cette phéromone sexuelle d'insecte.

Partie expérimentale

Les spectres de rmn ont été enregistrés avec un spectromètre Perkin–Elmer R-12A (60 MHz) ou/et un spectromètre Perkin–Elmer R-32 (90 MHz). Le tétraméthylsilane est utilisé comme référence interne et la position des pics est donnée dans l'échelle δ (en ppm) (δ = 0 pour le TMS).

Les spectres infrarouges ont été enregistrés avec un spectrophotomètre Perkin–Elmer 682. Les positions des bandes d'absorption caractéristiques sont données en cm^{-1}.

Les spectres de masse ont été enregistrés avec un spectromètre GC/MS Hewlett-Packard 5992A ou un spectromètre GC/MS Ribermag R10-10 (colonne capillaire CPSIL 5 de 25 m). Les intensités relatives sont indiquées entre parenthèses, le chiffre 100 étant attribué au pic de base.

Thia-4 tricyclo[5.2.1.$0^{2,6}$] décène-8 **9**

Dans un tricol de 100 mL muni d'un thermomètre, d'un réfrigérant et d'une agitation mécanique on place 77,5 g (0.25 mol) de dimésylate **8** (11) dissout dans 250 mL de toluène, 108 g (0,45 mol) de Na_2S9H_2O dissout dans 250 mL d'eau et 10,1 g (0,025 mol) d'aliquat 336. Le mélange réactionnel est violemment agité à 90°C pendant 6 h. Après refroidissement, la phase organique est décantée et la phase aqueuse extraite 2 fois avec 100 mL d'éther. Les phases organiques sont séchées sur $MgSO_4$, le solvant est éliminé au rotavapor et le résidu donne par distillation 30,5 g (81%) de sulfure **9**; Eb/0,05 Torr 54–55°C; rmn (CCl_4) δ: 6,4 (m, 2H); 3,4 (m, 2H), 3,0 (s élargi, 4H), 2,6 (m, 2H), 2,0 (m, 2H) ppm. Masse: 152 (M^+, 49), 86 (78), 85 (100), 66 (74).

Dioxo-4,4 thia-4 tricyclo[5.2.1.$0^{2,6}$] décène-8 **4**

Dans un tricol de 2000 mL muni d'un thermomètre, d'une agitation mécanique et d'une ampoule à brome on place 30,4 g (0,2 mol) de sulfure **9** dissout dans 750 mL de méthanol. La solution est refroidie à −20°C et on ajoute lentement une solution de 184 g (0,6 mol de $KHSO_5$) d'oxone dans 750 mL d'eau de façon à ce que la température ne dépasse pas −10°C. On agite pendant 15 h à −20°C après addition puis reprend par 1000 mL d'eau. Après 3 extractions avec 300 mL de chlorure de méthylène, les phases organiques sont séchées et le solvant éliminé au rotavapor. On obtient 36,7 g (98%) de sulfone **4** de pureté supérieure à 95% (rmn). Après chromatographie sur colonne de silice (éluant: CH_2Cl_2 90, acétate d'éthyle 10) on obtient 31 g de sulfone **4** pure + 4 g de sulfone **4** contenant quelques pour cent d'un produit provenant d'une époxydation de la double liaison.

Sulfone **4**. *F* 129°C; ir ($CDCl_3$): 3060 (f), 1310 (F), 1150 (F); rmn ($CDCl_3$) δ: 6,3 (s élargi, 2H), 3,05 (m, 4H), 2,3 (m, 4H), 1,6 (m, 2H) ppm. Masse: 184 (M^+, 0,3), 66 (100). *Anal.* calc. pour $C_9H_{12}O_2S$: C 58,67, H 6,56, S 17,40; trouvé: C 58,82, H 6,68, S 17,24.

Méthode générale de préparation des sulfones **5**

Dans un bicol de 25 mL muni de bouchons à jupe rabattable et maintenu sous atmosphère d'azote, on place 920 mg (5 mmol) de sulfone **4** en solution dans 10 mL de THF anhydre. On refroidit la solution à −78°C (acétone–Carboglace) et on ajoute lentement au moyen d'une seringue 5 mmol d'une solution de nBuLi dans l'hexane. On agite pendant 15 min puis ajoute 6 mmol de l'électrophile par l'intermédiaire d'une seringue. Après 1/2 h d'agitation à −78°C, on laisse le mélange réactionnel revenir à température ambiante, hydrolyse par addition de 10 mL H_2O et extrait 3 fois avec 10 mL d'éther. La phase organique séchée est évaporée au rotavapor et le résidu est purifié par chromatographie sur colonne de silice (éluant: hexane 70, acétate d'éthyle 30). Les sulfones **5** ainsi préparées ont les caractéristiques suivantes.

5*a*: ir ($CDCl_3$): 3040 (f), 1300 (F), 1140 (F); rmn ($CDCl_3$) δ: 6,3 (m, 2H), 3,05 (s élargi, 3H), 2,3 (m, 4H), 1,7 (m, 2H), 1,35 (d, J = 7 Hz, 3H) ppm. Masse: 198 (M^+: 1,4), 66 (100).

5*b*: ir ($CDCl_3$): 3060 (f), 1300 (F), 1130 (F); rmn ($CDCl_3$) δ: 6,2 (m, 2H), 3 (m, 3H), 2,3 (m, 4H), 1,4 (m, 12H), 0.9 (t déformé, 3H) ppm. Masse: 254 (M^+: 0,4), 66 (100).

5*c*: ir ($CDCl_3$): 3040 (m), 1640 (f); rmn ($CDCl_3$) δ: 6,3 (m, 2H), 5,25 (m, 3H), 3 (m, 3H), 2,5 (m, 4H), 1,2–1,9 (m, 4H) ppm. Masse: 224 (M^+: 0,2), 66 (100).

5*d*: *F* 131°C; ir ($CDCl_3$): 3040 (f), 1310 (F), 1220 (F), 1130 (F); rmn ($CDCl_3$) δ: 6,25 (s élargi, 2H), 2,95 (m, 3H), 2,1 (m, 4H), 1,7 (m, 2H), 0,3 (s, 9H) ppm. Masse: 256 (M^+: 0,9), 241 (28), 73 (71), 66 (100). *Anal.* calc. pour $C_{12}H_{20}O_2SSi$: C 56,20, H 7,86, S 12,50; trouvé: C 56,24, H 7,96, S 12,47.

[5] A cette température la conversion de **11** n'est que de 95%. Mais à 650°C, où la conversion de **11** est totale, le rendement en diène **12** est limité par une décomposition partielle de l'acétate avec élimination d'acide acétique.

[6] Cette analyse a été effectuée au Tropical Products Institute à Londres dans le laboratoire du Docteur D. R. Hall que nous remercions pour son aimable assistance.

Can. J. Chem. Downloaded from www.nrcresearchpress.com by 210.87.254.40 on 09/06/12
For personal use only.

Can. J. Chem. Downloaded from www.nrcresearchpress.com by 210.87.254.40 on 09/06/12
For personal use only.

5*e*: *F* 118°C; rmn ($CDCl_3$) δ: 6,3 (m, 2H), 3 (m, 3H), 2,2 (m, 4H), 1,7 (m, 2H), 0,4 (s, 9H) ppm. Masse (avec ^{120}Sn): 333 (58), 282 (65), 165 (100). *Anal.* calc. pour $C_{12}H_{20}O_2SSn$: C 41,53, H 5,81, S 9,24; trouvé: C 41,77, H 5,91, S 9,29.

5*f*: ir ($CDCl_3$): 3040 (m), 1740 (FF); rmn ($CDCl_3$) δ: 6,31 (s élargi, 2H), 4,34 (q, J = 7 Hz, 2H), 2,7–3,5 (m, 7H), 1,65 (m, 2H), 1,34 (t, J = 7 Hz, 3H) ppm. Masse: 105 (7), 91 (7), 66 (100). *Anal.* calc. pour $C_{12}H_{16}O_4S$: C 56,23, H 6,29, S 12,51; Trouvé: C 56,22, H 6,34, S 12,28.

5*g*: ir ($CDCl_3$): 3540 (F), 3080 (f); rmn ($CDCl_3$) δ: 6,35 (m, 2H), 3,3 (s, 1H), 2,8–3,2 (m, 5H), 2,2–2,4 (m, 2H), 1,3–1,8 (m, 7H), 0,9 (t déformé, 3H) ppm.

5*h*: *F* 139°C; ir ($CDCl_3$): 3520 (F), 3080 (f); rmn ($CDCl_3$) δ: 6,3 (2H), 3,3 (s, 1H), 3 (m, 7H), 1,6 (m, 12H) ppm. Masse: 282 (M^+: 8), 151 (100), 66 (97). *Anal.* calc. pour $C_{15}H_{22}O_3S$: C 63,80, H 7,85, S 11,35; trouvé: C 63,63, H 7,82, S 11,35.

5*i*: ir ($CDCl_3$): 3700 (m), 3560 (m), 3080 (m); rmn ($CDCl_3$) δ: 6,35 (m, 2H), 3,8 (m, 2H), 3,1 (m, 7H), 1,5–2 (m, 4H), 1,2 (t déformé, 3H) ppm. Masse: 242 (M^+: 14), 191 (37), 111 (32), 73 (100), 59 (44), 45 (42).

5*j*: ir ($CDCl_3$): 3500 (m), 3080 (m); rmn ($CDCl_3$) δ: 6,25 (m, 2H), 4,2 (m, 1H), 2,5–3,35 (massif, 8H), 1,2–2,4 (m, 8H), 0,95 (t déformé, 3H) ppm.

5*k*: *F* 102°C; ir ($CDCl_3$): 3060 (f); rmn ($CDCl_3$) δ: 6,25 (m, 2H), 3,05 (m, 3H), 1,8–2,9 (massif, 5H), 1,55 (m, 1H), 1,15 (2d, J = 7 Hz, 6H) ppm. *Anal.* calc. pour $C_{12}H_{18}O_2S$: C 63,68, H 8,02, S 14,17; trouvé: C 63,64, H 8,10, S 14,08.

5*l*: *F* 115°C; ir ($CDCl_3$): 3060 (f), 1730 (F); rmn ($CDCl_3$) δ: 6,3 (m, 2H), 3,5–3,1 (massif, 3H), 3 (massif, 4H), 2,4 (s, 3H), 1,5–1,8 (m, 2H) ppm. Masse: 66 (100). *Anal.* calc. pour $C_{11}H_{14}O_3S$: C 58,38, H 6,24, S 14,17; trouvé: C 58,54, H 6,38, S 14,12.

5*m*: *F* 86°C; ir ($CDCl_3$): 1725 (F); rmn ($CDCl_3$) δ: 6,3 (m, 2H), 2,4–3,4 (massif, 9H), 1,1–1,5 (massif, 6H), 0,9 (t déformé, 3H) ppm. Masse: 268 (M^+: 0,2), 66 (100). *Anal.* calc. pour $C_{14}H_{20}O_3S$: C 62,66, H 7,51, S 11,95; trouvé: C 62,67, H 7,59, S 11,83.

5*n*: *F* 80°C; ir ($CDCl_3$): 3080 (m), 3060 (f), 1725 (F), 1640 (m); rmn ($CDCl_3$) δ: 6,30 (m, 2H), 5,6–6,1 (m, 1H), 4,9–5,2 (m, 2H), 2,3–3,5 (massif, 11H), 1,55 (m, 2H) ppm. Masse: 135 (18), 66 (100). *Anal.* calc. pour $C_{14}H_{18}O_3S$: C 63,13, H 6,81, S 12,04; trouvé: C 63,40, H 6,87, S 11,98.

*Thermolyse des sulfones **4**: méthode générale d'obtention des diènes **2***

Des échantillons de 200 mg à 1 g de sulfones **5** sont évaporés sous 0,01 Torr dans un tube en mullite horizontal (diamètre intérieur 10 mm) chauffé à 650°C sur une longueur de 10 cm (14). Les produits formés sont recueillis à la sortie du four sur la paroi froide d'un Dewar rempli d'azote liquide. Les diènes formés sont isolés de deux manières différentes selon leur volatilité: les diènes volatils (à l'exception de **2***a*) sont distillés directement à température ambiante sous 10^{-2} Torr dans un piège refroidi à −78°C, le cyclopentadiène n'étant pas piégé dans ces conditions. Les diènes moins volatils sont isolés par lavage du Dewar avec 20 mL d'éther et élimination de l'éther et du cyclopentadiène au rotavapor puis purifiés par chromatographie sur silice.

Le pentadiène-1,3 **2***a*, obtenu sous forme d'un mélange avec le cyclopentadiène, a été identifié par comparaison de son spectre de rmn avec celui d'un échantillon authentique. Les caractéristiques des autres diènes sont les suivantes.

Nonadiène-1,3 **2***b*: rmn ^1H ($CDCl_3$) δ: 4,8–6,6 (m, 5H), 2,1 (m, 2H), 1,35 (m, 6H), 0,95 (t déformé, 3H) ppm. rmn ^{13}C ($CDCl_3$) δ: 137,6; 135,7; 131,2; 114,7; 32,7; 31,7; 29,1; 22,7; 14,2. Masse: 124 (M^+: 19), 67 (68), 54 (100).

Heptatriène-1,3,6 **2***c*: rmn ^1H ($CDCl_3$) δ: 5,5–6,5 (m, 5H), 4,9–5,25 (m, 3H), 2,3 (m, 2H) ppm; rmn ^{13}C ($CDCl_3$) δ: 137,3, 136,5, 132,5, 132,2, 115,8, 115,6, 35,8. Masse: 94 (M^+: 22), 79 (100).

Triméthylsilyl-1 butadiène-1,3 **2***d*: Les spectres de rmn ^1H et ir sont en accord avec ceux déjà décrits (21); rmn ^{13}C ($CDCl_3$) δ: 146,2, 141,1, 137,2, 119,6, −1,1.

Triméthylstannyl-1 butadiène-1,3 **2***e*: ir (film): 3100 (m), 3020 (f), 1570 (F); rmn ^1H ($CDCl_3$) δ: 5,2–7,2 (5H), 0,4 (s, 9H) ppm; rmn ^{13}C ($CDCl_3$) δ: 147,2, 140,1, 135,4, 116,6, −9.6. Masse (avec ^{120}Sn): 218 (M^+: 1,3), 203 (100), 165 (14).

Pentadiène-2,4 oate d'éthyle **2***f*: ir (film): 1720 (FF), 1650 (F), 1610 (F); rmn ^1H ($CDCl_3$) δ: 7,3 (m, 1H), 6,3–6,6 (m, 1H), 3,95 (d, J = 15 Hz, 1H), 5,4–5,7 (m, 2H), 4,25 (q, J = 7 Hz, 2H), 1,3 (t, J = 7 Hz, 3H) ppm; rmn ^{13}C ($CDCl_3$) δ: 144,8, 135, 125,6, 122,5, 60,5, 14,3.

Méthyl-5 octadiène-1,3 ol-4 **2***g*: ir (film): 3400 (F), 3100 (m), 1610 (F); rmn ^1H ($CDCl_3$) δ: 4,9–6,5 (m, 5H), 1,4–1,7 (m, 5H), 1,2 (s, 3H), 0,95 (t déformé, 3H) ppm; rmn ^{13}C ($CDCl_3$) δ: 141,2, 136,9, 128,6, 116,9, 73,1, 45,03, 28,1, 17,4, 14,7. Masse: 140 (M^+: 1,6), 97 (43), 43 (100).

Cyclohexyl-1 pentadiène-2,4 ol-1 **2***h*: ir (film): 3400 (F), 3100 (m), 1610 (F); rmn ^1H ($CDCl_3$) δ: 5–6,6 (massif, 5H), 2,05 (s, 1H), 1,6 (m, 10H) ppm; rmn ^{13}C ($CDCl_3$) δ: 144, 139, 130, 119, 73, 39, 26, 23.

Heptadiène-4,6 ol-3 **2***i*: ir (film): 3400 (F), 3100 (m), 1610 (F); rmn ^1H ($CDCl_3$) δ: 4,9–6,6 (m, 5H), 3,95 (m, 1H), 3,14 (s, 1H), 1,45 (m, 2H), 0,9 (t, J = 7 Hz, 3H) ppm. rmn ^{13}C ($CDCl_3$) δ: 136,6, 131,3, 117,5, 74,0, 30,3, 9,8. Masse: 112 (M^+: 7), 83 (79), 57 (100), 55 (68).

Nonadiène-1,3 ol-5 **2***j*: ir (film): 3400 (F), 3100 (f), 1610 (F); rmn ^1H ($CDCl_3$) δ: 5–6,5 (m, 5H), 4,15 (m, 1H), 2,12 (s, 1H), 1,38 (m, 6H), 0,89 (t déformé, 3H) ppm; rmn ^{13}C ($CDCl_3$) δ: 136,9, 136,6, 131,2, 117,6, 72,7, 37,1, 27,7, 22,8, 14,1. Masse: 86 (70), 84 (100).

Méthyl-5 hexadiène-1,3 **2***k*: rmn ^1H ($CDCl_3$) δ: 6,42 (2dd, J = 10,5 Hz, 17 Hz, 10,5 Hz, 1H), 6,11 (dd, J = 15 Hz, 10,5, 1H), 5,75 (dd, J = 15 Hz, 7 Hz, 1H), 5,14 (dd, J = 2 Hz, 17 Hz, 1H), 5,00 (dd, J = 2 Hz, 10,5 Hz, 1H), 2,23 (septuplet, J = 4,5 Hz, 1H), 0,83 (d, J = 4,5 Hz, 6H) ppm. Masse: 96 (M^+: 34), 81 (100), 53 (36).

Hexadiène-3,5 one-2 **2***l*: ir ($CDCl_3$): 3100 (f), 3040 (f), 1690 (m), 1670 (F), 1630 (m), 1595 (F); rmn ^1H ($CDCl_3$) δ: 7,12 (dd, J = 17 Hz, 10 Hz, 1H), 6,5 (m, 1H), 6,16 (d, J = 17 Hz, 1H), 5,4–5,8 (m, 2H), 2,23 (s, 3H) ppm; rmn ^{13}C ($CDCl_3$) δ: 198,5, 143,5, 135,5, 131,5, 126,3, 27,4. Masse: 96 (M^+: 26), 95 (23), 81 (19), 53 (100), 43 (50).

Nonadiène-6,8 one-5 **2***m*: ir (film): 3100 (f), 3040 (f), 1690 (F), 1670 (F), 1625 (F), 1595 (F); rmn ^1H ($CDCl_3$) δ: 7,2 (dd, J = 17 Hz, 10 Hz, 1H), 6,55 (m, 1H), 6,22 (d, J = 17 Hz, 1H), 5,5–5,8 (m, 2H), 2,6 (t, J = 8 Hz, 2H), 1,2–1,8 (massif, 4H), 0,93 (t, J = 6 Hz, 3H) ppm; rmn ^{13}C ($CDCl_3$) δ: 201, 142,5, 135,6, 130,6, 126,3, 40,5, 26,6, 22,6, 14,02. Masse: 138 (M^+: 2,2), 96 (24), 81 (66), 53 (100).

Nonatriène-1,3,8 one-5 **2***n*: ir (film): 3080 (m), 3040 (f), 1690 (F), 1670 (F), 1620 (F), 1590 (F); rmn ^1H ($CDCl_3$) δ: 7,08 (dd, J = 17 Hz, 10 Hz, 1H), 6,5 (m, 1H), 6,12 (d, J = 17 Hz, 1H), 5,4–5,9 (massif, 3H), 5,0 (m, 2H), 2,25–2,70 (m, 4H) ppm. Masse: 136 (M^+: 3), 94 (14), 81 (100), 53 (60).

*Préparation de la sulfone **10***

Dans un bicol muni d'une ampoule à brome et d'une entrée d'azote, on place 1,38 g (7,5 mmol) de sulfone **4** dissout dans 30 mL de THF anhydre. On ajoute lentement à la solution refroidie à −78°C 4,8 mL de nBuLi 1,55 *M* en solution dans l'hexane (7,5 mmol). On laisse agiter 10 min puis on ajoute 2,72 g (8 mmol) de l'éther tétrahydropyrannylique de l'iodo-8 octanol (20). On laisse agiter 1 h 30 à −78°C puis laisse revenir à température ambiante. On ajoute alors 80 mL d'eau + 50 mL d'éther, décante, extrait la phase aqueuse 2 fois avec 35 mL d'éther, sèche la phase éthérée sur $MgSO_4$ puis élimine les solvants au rotavapor. Le résidu (3,20 g) est chromatographié sur silicagel (éluant: hexane 75, acétate d'éthyle 25). On obtient par ordre d'élution: la sulfone dialkylée (630 mg), la sulfone **10** (1,87 g, 63%), la sulfone **4** de départ (175 mg).

*Sulfone **10***: ir ($CDCl_3$): 3070 (f), 1300 (F), 1140 (F); rmn ($CDCl_3$) δ: 6,19 (m, 2H), 4,55 (s élargi, 1H), 3,1–4,1 (m, 4H), 2,8–3,1 (m, 3H), 1,3–2,7 (massifs, 26H) ppm.

*Préparation de la sulfone **11***

Un mélange de 1,78 g (4,5 mmol) de sulfone **10**, 25 mL de méth-

anol, 1,2 mL d'eau et 40 mg d'acide paratoluène sulfonique est agité à 40°C pendant 2 h (disparition totale de **10**). Après évaporation du méthanol, le résidu est repris par 10 mL H_2O et extrait 3 fois avec 10 mL d'éther. La phase éthérée est séchée puis l'éther éliminé au rotavapor. On obtient 1,34 g d'alcool qui sont dissout dans 15 mL de CH_2Cl_2 anhydre. On ajoute à la solution en agitant 630 mg de triéthylamine puis 504 mg de chlorure d'acétyle. La réaction es terminée en 15 min (ccm). Après addition de 15 mL d'eau, décantation et extraction avec 2 fois 10 mL de CH_2Cl_2, les phases organiques sont séchées sur $MgSO_4$ puis le solvant éliminé au rotavapor. On obtient ainsi 1,42 g (90%) d';acétate **11**: ir ($CDCl_3$): 3070 (f), 1735 (F), 1300 (F), 1140 (F); rmn ($CDCl_3$) δ: 6,25 (m, 2H), 4,08 (t, J = 7 Hz, 2H), 1,2–3,4 (massifs, 26H avec 1 singulet à 2,07 ppm) ppm.

Dodécadiène-9,11 yl-1 acétate ***12***

La sulfone **11** (531 mg, 1,5 mmol) est thermolysée à 600°C (durée 1 h) et le produit de thermolyse est piégé sur la paroi d'un Dewar refroidie à −196°C. Après réchauffement à température ambiante, la paroi du Dewar est rincée avec 10 mL d'acétone, l'acétone évaporée et le résidu est chromatographié (30 g silice, éluant: hexane 90, éther 10). On obtient 242 mg (72%) d'acétate diénique **12** dont les caractéristiques spectrales (ir, rmn, masse) sont identiques à celles déjà rapportées (22). Sa pureté stéréoisomérique a été déterminée par chromatographie en phase vapeur sur cristaux liquides. Colonne en verre de 1,8 m × 2 mm de diamètre intérieur remplie de Gazchrom Q enrobé de 5% de (*p*-méthoxycinnamyloxy)-4 méthoxy-4′ azobenzène; température programmée à 4°/min à partir de 110°C. L'échantillon ainsi analysé contient au moins 98,5% d'isomère *E*.

1. K. MORI. The total synthesis of natural products. Vol. 4 John Wiley and Sons, New York. 1981. p. 1.
2. G. BRIEGER et J. N. BENNETT. Chem. Rev. **80**, 63 (1980).
3. H. J. BESTMANN, J. SÜB et O. VOSTROWSKY. Justus Liebigs Ann. Chem. 2117 (1981).
4. J. F. NORMANT et A. ALEXAKIS. Current trends in organic synthesis. Pergamon Press, Oxford. 1983. p. 291.
5. B. M. TROST, S. A. GODLESKI et J. IPPEN. J. Org. Chem. **43**, 4559 (1978).
6. (*a*) W. MOCK. J. Am. Chem. Soc. **88**, 2857 (1966); (*b*) S. D. MCGREGOR et D. M. LEMAL. J. Am. Chem. Soc. **88**, 2858 (1966).
7. R. L. CRUMBIE et D. D. RIDLEY. Aust. J. Chem. **34**, 1017 (1981).
8. D. D. NARAGON. Thèse, Case Western University, Cleveland, Ohio, U.S.A., 1971; Diss. Abstr. Int. B, **32**, 1458 (1971).
9. S. YAMADA, H. OSHAWA, T. SUZUKI et H. TAKAYAMA. Chem. Lett. 1003 (1983).
10. (*a*) R. BLOCH et J. ABECASSIS. Tetrahedron Lett. **23**, 3277 (1982); (*b*) R. BLOCH, D. HASSAN et X. MANDARD. Tetrahedron Lett. **24**, 4691 (1983).
11. J. M. PHOTIS et L. A. PAQUETTE. J. Am. Chem. Soc. **96**, 4715 (1974).
12. D. LANDINI et F. ROLLA. Synthesis, 565 (1974).
13. B. M. TROST et D. P. CURRAN. Tetrahedron Lett. 1287 (1981).
14. J. F. KING, P. DE MAYO, C. L. MCINTOSH, K. PIERS et D. J. H. SMITH. Can. J. Chem. **48**, 3704 (1970).
15. R. LESTER et D. R. HALL. J. Chromatogr. **190**, 35 (1980).
16. R. ROSSI, A. CARPITA, M. G. QUIRICI et C. A. VERACINI. Tetrahedron, **38**, 639 (1982).
17. P. A. WENDER, S. MCN. SIEBURTH, J. J. PETRAITIS ET S. K. SINGH. Tetrahedron, **37**, 3967 (1981).
18. B. F. NESBITT, P. S. BEEVOR, R. A. COLE, R. LESTER et R. G. POPPI. J. Insect Physiol. **21**, 1091 (1975).
19. (*a*) R. ROSSI, A. CARPITA et M. G. QUIRICI. Tetrahedron, **37**, 2617 (1981) et références citées; (*b*) G. R. KNOX et I. G. THOM. J. Chem. Soc. Chem. Commun. 373 (1981); (*c*) S. RANGANATHAN, R. KUMAR et V. MANIKTALA. Synth. Commun. **12**, 921 (1982); (*d*) B. B. SNIDER et G. B. PHILLIPS. J. Org. Chem. **48**, 464 (1983); (*e*) T. HAYASHI, M. YANAGIDA, Y. MATSUDA et T. OISHI. Tetrahedron Lett. **24**, 2665 (1983).
20. D. SAVOIA, C. TROMBINI et A. UMANI-RONCHI. J. Org. Chem. **47**, 564 (1982).
21. M. J. CARTER, I. FLEMING et A. PERCIVAL. J. Chem. Soc. Perkin Trans. 1, 2415 (1981).
22. K. MORI. Tetrahedron, **30**, 3807 (1974).

Can. J. Chem. Downloaded from www.nrcresearchpress.com by 210.87.254.40 on 09/06/12
For personal use only.

Structure-reactivity correlation in inclusion complexes: deoxycholic acid di-*tert*-butyl thioketone

K. PADMANABHAN, K. VENKATESAN, AND V. RAMAMURTHY

Department of Organic Chemistry, Indian Institute of Science, Bangalore 560 012, India

Received January 12, 1984

This paper is dedicated to Professor Paul de Mayo on the occasion of his 60th birthday

K. PADMANABHAN, K. VENKATESAN, and V. RAMAMURTHY. Can. J. Chem. **62**, 2025 (1984).

Ultraviolet irradiation of crystalline molecular inclusion complexes of deoxycholic acid with di-*tert*-butyl thioketone results in no reaction. The structure of the above complex has been determined via X-ray diffraction. The absence of expected photoreactions, namely, photoreduction and photooxidation, is rationalized on the basis of the X-ray structure analysis of the complex.

K. PADMANABHAN, K. VENKATESAN et V. RAMAMURTHY. Can. J. Chem. **62**, 2025 (1984).

Lors de l'irradiation, par de la lumière uv, de complexes cristallins d'inclusion moléculaire d'acide déoxycholique en présence de la di-*tert*-butyl thiocétone il ne se produit aucune réaction. Faisant appel à la diffraction des rayons-X, on a déterminé la structure du complexe décrit plus haut. C'est en se basant sur une analyse de la structure du complexe, telle que déterminée par diffraction des rayons-X, que l'on rationalise le fait que les photoréactions attendues, soit une photoréduction et une photo-oxydation, ne se produisent pas.

[Traduit par le journal]

Can. J. Chem. Downloaded from www.nrcresearchpress.com by 210.87.254.40 on 09/06/12
For personal use only.

The control and modification of reactivity through incorporation of molecules into organized assemblies, functionalized polymers, and interfacial sites remain an area of considerable interest (1). Molecular inclusion complexes can serve as matrices for the performance of clean stereo and regiospecific reactions. The advantages of utilization of inclusion complexes (2) and host-controlled guest reactions (3) have been demonstrated quite recently. In this regard, we have initiated a programme utilizing thioketones as the guest molecules and deoxycholic acid (DCA, **1**) as the host with the view to bring about selective

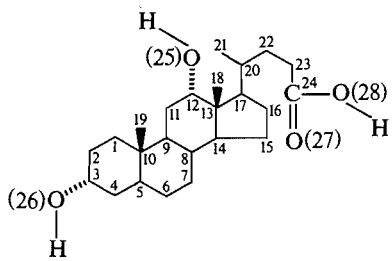

1, DCA

functionalization of the host molecules or to achieve selectivity in the unimolecular photoprocesses of the guest thioketones. In our attempt to obtain crystals of complexes of DCA with thioketones **2**–**8**, only **2**–**4** gave good crystals with DCA. Photochemical and crystallographic results obtained with the inclusion complex of DCA and di-*tert*-butyl thioketone (**2**) are presented here.

Light red-coloured single crystals of the inclusion complex of DCA and **2** were powdered and irradiated using a low pressure mercury arc lamp. The progress of the photolysis was followed by the variation in the mp and the ir and ^{1}H-nmr spectra. Surprisingly, no change was observed even after 50 days of continuous exposure to uv radiation. Oxidation of **2** to the corresponding ketone and sulfine is a well-established reaction in solution (4). Further, facile photoreduction from S_2 of di-*tert*-butyl thioketone is known (5). Therefore the absence of the above reactions of **2** in the DCA matrix is unexpected. A systematic crystallographic study of the inclusion complex was thus undertaken in order to understand the non-reactivity of the

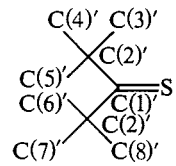

2

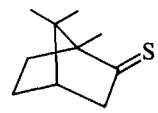

3

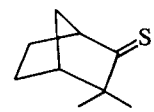

4

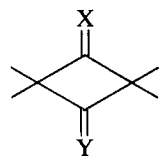

5

a, X = O; Y = S
b, X = Y = S

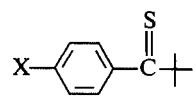

6

X = H, —Cl, —F, —OMe

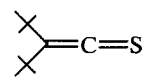

7

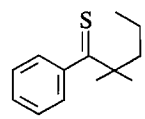

8

complex in terms of the three-dimensional arrangement.

Figure 1 shows the three-dimensional packing arrangement of the DCA–**2** complex in a unit cell. As mentioned in the Experimental section there are two guest molecules in the crystal lattice. The space group being $P_{2_12_12}$, it was expected that the molecular symmetry of the guest molecule would be a two-fold axis, the C=S bond being coincident with the crystallographic two-fold axis. However, it was found from a careful analysis of the crystal structure that the guest molecule exhibited an orientational disorder, as shown in Fig. 2, with the disordered arrangement exhibiting a two-fold axis of symmetry.

The two halves of the bilayer are related by a 2_1 axis at $b = 1/4$ and are parallel to the a axis. The bilayers are stacked along the b direction and are related by the two-fold rotation axis. The DCA molecules in the bilayer are held together by a helical system of intermolecular hydrogen bonds about the c-axis. (O(26)—H···O(27): 2.755(14) Å; O(28)—H···O(25): 2.644(10) Å; O(25)—H···O(26): 2.705(10) Å.) The

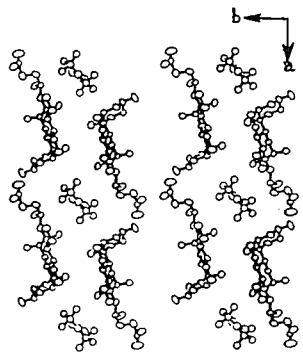

FIG. 1. Packing arangement of deoxycholic acid di-*tert*-butyl thioketone complex.

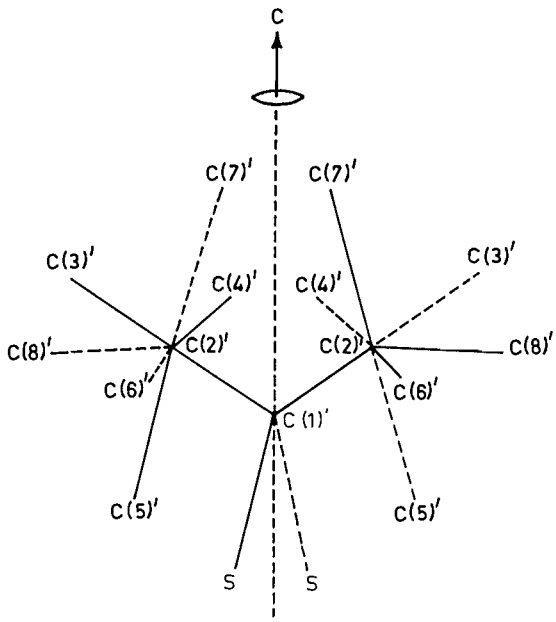

FIG. 2. Projection on the *XOZ* plane showing the two position of the disordered guest di-*tert*-butyl thioketone molecule (related by a two-fold axis).

overall packing of the DCA molecules in our crystal is the same as in DCA–camphor complex (2:1) (6*a*) which also crystallizes in $P_{2_12_12}$ with a = 27.353(3), b = 13.814(2), c = 7.233(1) Å. In both these complexes, the DCA channel walls are directly opposite, the molecules being related by the two-fold rotation axis. It may be noted again that the packing in the DCA:acetic acid complex (6*b*) is similar to the structure discussed in this paper. However, as the DCA:acetic acid complex crystallizes in $P_{2_12_12_1}$ with a = 25.55, b = 13.81, c = 7.109 Å, the opposite walls of DCA channel are staggered. Between the hydrophobic surfaces of adjacent DCA bilayers there are channels with cross sectional area of 4 × 7 Å^2 centered on the two-fold axis, and the void in the channel is sufficient to accommodate the guest thioketones. The interaction between the host and guest molecules is mainly of the van der Waals type.

The absence of an intermolecular addition reaction between the guest **2** and the host **1** is most unexpected for the reason that the thiocarbonyl chromophore has been established to undergo inter and intramolecular hydrogen abstraction reactions from both S_2 ($\pi\pi^*$) and T_1 ($n\pi^*$) states (7). Further, intermolecular topochemical photoaddition of aliphatic and aromatic ketones

TABLE 1. Intermolecular contacts (<5 Å) of importance for reactivity between host and guest atoms

(*a*) S(thione)···H(steroid) contacts (Å)

Atom pair	Distance	Atom pair	Distance
S···H(3)	4.92	S···1H(16)	3.60
S···1H(4)	4.49	S···1H(18)	4.22
S···H(5)	4.11	S···3H(18)	4.69
S···1H(6)	4.84	S···H(20)	3.32
S···2H(6)	4.48	S···1H(22)	3.91
S···1H(15)	4.87	S···2H(22)	3.59

(*b*) C_{sp^2}(thione)···H(steroid) contacts (Å)

Atom pair	Distance
C(1)'···1H(15)	4.80
C(1)'···1H(16)	3.89
C(1)'···1H(18)	4.86
C(1)'···1H(20)	4.67
C(1)'···2H(22)	4.28

(*c*) C_{sp^2}(thione)···C(steroid) contacts (Å)

Atom pair	Distance
C(16)···C(1)'	4.702

to deoxycholic acid in the crystalline phase is known (2). However, the absence of such reactions in the present system may be rationalized on the basis of unfavourable intermolecular contacts in the crystal. Distances between the carbon and sulfur atoms of the thiocarbonyl chromophore and the host hydrogens (<5 Å) and those between the thiocarbonyl carbon and the steroid carbon (<5 Å) are listed in Table 1. Initial hydrogen abstraction by the thiocarbonyl chromophore can occur either by carbon or by sulfur. However, none of the hydrogens of DCA are within the sum of the van der Waals radii of hydrogen and either the carbon or sulfur of the thiocarbonyl group. Therefore, the first requirement for efficient hydrogen abstraction in the crystalline medium, namely, that the atoms involved are to be within the sum of the van der Waals radii (8) is not obeyed. However, violations especially in DCA–ketone complexes are known (2). In the ketone complexes investigated (2), the distance between O′(ketone) and H(steroid) range from 2.9 to 3.9 Å. Based on these results, one could expect thiocarbonyl sulfur to abstract any one of the following hydrogens: H(5), 1H(16), H(20), 1H(22), or 2H(22). But the distance between the steroid carbon and C′(thione) is too large to allow the resulting diradicals from the hydrogen abstraction to interact and form a C—C σ bond. The distance C(16)···C(1)′ alone is less than 5 Å, but even this is too large to allow the resulting diradicals from the abstraction of 1H(16) by sulfur to interact and eventually form the C(16)—C(1)′ bond. Thus in our case, hydrogen abstraction by sulfur and eventual carbon–carbon bond formation is not expected as all C′(thioketone) and C(steroid) distances are beyond these limits. Similarly, hydrogen abstraction by thiocarbonyl carbon may not occur due to the large distance between the reactive atoms as seen in Table 1.

The possible occurrence of photooxidation of the guest molecule in these crystals was also considered. It has been established that the photooxidation (to the corresponding carbonyls)

Can. J. Chem. Downloaded from www.nrcresearchpress.com by 210.87.254.40 on 09/06/12
For personal use only.

Can. J. Chem. Downloaded from www.nrcresearchpress.com by 210.87.254.40 on 09/06/12
For personal use only.

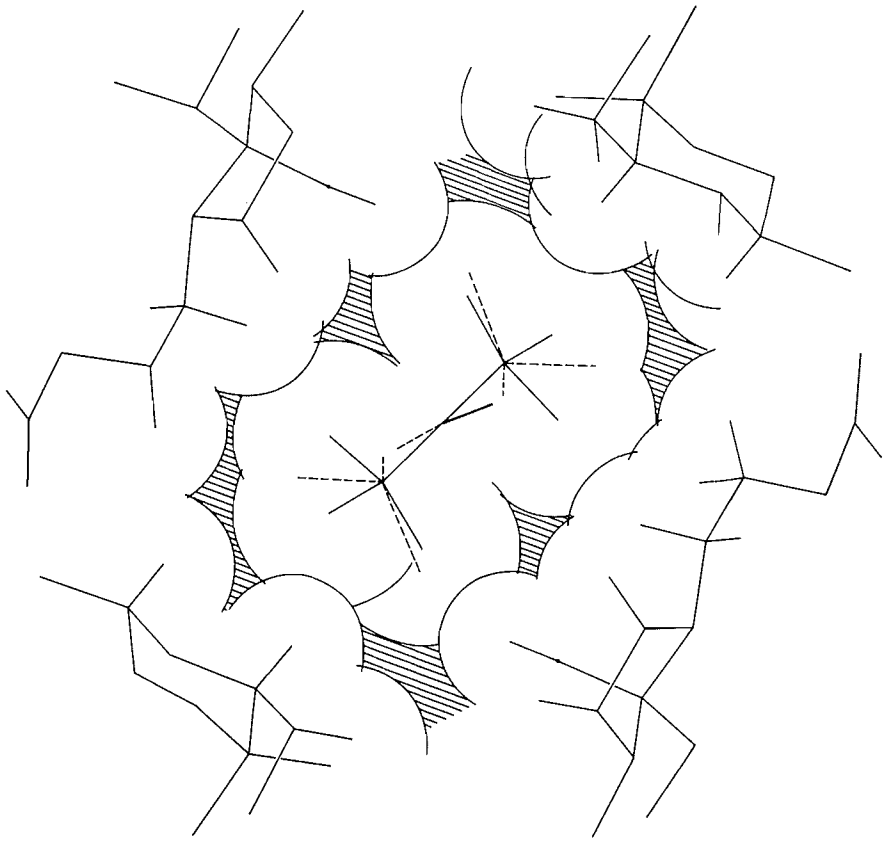

FIG. 3. Projection of the crystal packing down the *c*-axis showing a cross-section of the channel.

of a few thioketones occurs in the solid state if the molecular packing is such that there is enough void for the oxygen molecule to diffuse into the crystal lattice (9). It has been reported from our laboratory that di-*tert*-butyl thioketone is readily oxidized in solution to the corresponding ketone and *S*-oxides upon exposure to uv/visible light (4). In this connection, the inertness of **2** in the DCA matrix is quite remarkable. The modification of the reactivity of **2** by the DCA matrix can be understood on the basis of the X-ray crystal structure. the projection of the crystal packing down the channel axis (*c* axis) is shown in Fig. 3. It is quite obvious from this figure that, with the guest molecule occupying the void, there is no space for the molecular oxygen to diffuse into the crystal to effect oxidation of the guest molecules. At the most there can only be surface oxidation.

In conclusion, the absence of expected reactions of di-*tert*-butyl thioketone in the deoxycholic acid matrix has been understood on the basis of the molecular arrangement in the crystals.

Experimental

Di-*tert*-butyl thioketone was prepared by the reported procedure (10). Deoxycholic acid (Sigma) was used as received. Single crystals of the inclusion complex of DCA with di-*tert*-butyl thioketone were grown by slow evaporation of methanol from an ice cold solution containing a 2:1 molecular ratio of DCA and thione. The above crystals were light red and did not have a sharp melting point (mp 135–155°C). Formation of the inclusion complex was identified by its spectral properties both in solution and the solid state. An ethanol solution of these well grown crystals had the following spectral characteristics indicating the inclusion of the thione. uv (EtOH) λ_{max}: 536; 237 nm; ^{1}H nmr ($CDCl_3$): δ1.1 (s, 18H) in addition to DCA hydrogen signals. Confirmatory evidence for the inclusion of the thioketone in DCA came from the solid state ir and solid state ^{13}C-nmr spectra: ir (KBr): 1115 cm^{-1} (C=S); ^{13}C-nmr: δ 275.0 (C=S), 54.1 C(*t*Bu), 33.1 $(CH_3)_3$ in addition to the DCA carbon signals.

Photolysis

Powdered single crystals of the complex were irradiated using a low pressure mercury arc lamp (254 nm) in a petri dish. Samples were turned around periodically to provide uniform exposure. The progress of the irradiation was monitored by the variation in mp, ^{1}H-nmr and ir spectra. However, no change was observed even after 50 days of irradiation.

X-ray structural analysis

Unit cell dimensions were determined from the least-squares analysis of diffractometer measurements for 20 centered reflections: a = 13.933(1), b = 27.294(3), c = 7.285(2) Å, V = 2770.3 Å^3, Z = 4 ($C_{24}H_{40}O_4 \cdot \frac{1}{2}C_9H_{18}S$) and d = 1.130 g cm^{-3} (floatation in aqueous KI).

Intensity data were collected on an Enraf-Nonius CAD-4 diffractometer using monochromated MoKα radiation (λ = 0.71073 Å) in $\omega/2\theta$ scan mode for a crystal of dimensions 0.06 × 0.25 × 0.44 mm^3. A total of 2830 reflections were collected, out of which 1364 were considered significant $|F_o| \geq 3\sigma(|F_o|)$. Lorentz and polarization corrections were applied but the absorption correction was not considered important (μ = 0.75 cm^{-1}). The structure was solved by the direct methods program "MULTAN-80" (11). From the E map with 300 reflections ($E \geq 1.331$), 26 out of 28 non-hydrogen atoms of the host molecule were identified. The remaining two atoms were fixed after a Karle recycling (12) operation using these 26 atoms.

A difference electron density map calculated at this stage showed clearly that the guest molecule is disordered, with the two orientations of the molecule related by the two-fold axis on which the atom C(1)′ lies (Fig. 2). The difference map calculated at R = 0.132 revealed further disorder for the *tert*-butyl methyl groups corresponding to hindered rotation about the C(1)′—C(2)′$(CH_3)_3$ bond. The full-matrix least-squares refinement (SHELX 76) (13) of the positional and anisotropic thermal parameters of 28 non-hydrogen atoms of the DCA

molecule and the positional and isotropic thermal parameters of 40 hydrogens (kept fixed in the penultimate cycles) of the DCA and the positional and isotropic termperature factors of the non-hydrogen atoms of di-*tert*-butyl thioketone with an occupancy value of 0.5 using the weighting scheme $w = 1/\sigma^2(|F|) + 0.0058\,|F|^2$ has led to a final R-value of 0.101 for the significant reflections. The function minimized was $\Sigma w(|F_o| - |F_c|)^2$.[1]

Acknowledgements

We thank the University Grants Commission for financial support and Dr. J. A. Ripmeester for obtaining the solid state ^{13}C-nmr spectra of the inclusion complex.

1. D. G. WHITTEN, R. C. RUSSELL, and R. H. SCHMEHL. Tetrahedron, **38**, 2455 (1982); N. J. TURRO, M. GRATZEL, and A. N. BRAUN. Angew. Chem. Int. Ed. Engl. **19**, 675 (1980).
2. R. POPOVITZ-BIRO, H. C. CHANG, C. P. TANG, N. R. SHOCHET, M. LAHAV, and L. LEISEROWITZ. Pure Appl. Chem. **52**, 2693 (1980); H. C. CHANG, R. POPOVITZ-BIRO, M. LAHAV, and L. LEISEROWITZ. J. Am. Chem. Soc. **104**, 614 (1982) and other papers in this series.

[1]Complete set of data, which included the atomic co-ordinates and thermal parameter tables for the complex, is available upon request, from the Depository of Unpublished Data, CISTI, National Research Council of Canada, Ottawa, Ont., Canada K1A 0S2.

3. H. AOYAMA, K. MIYAZAKI, M. SAKAMOTO, and Y. OMOTE. J. CHEM. SOC. CHEM. COMMUN. 333 (1983); H. L. Casal, P. de Mayo, J. F. Miranda, and J. C. SCAIANO. J. Am. Chem. Soc. **105**, 5155 (1983).
4. V. JAYATHIRTHA RAO, K. MUTHURAMU, and V. RAMAMURTHY. J. Org. Chem. **47**, 127 (1982).
5. R. RAJEE, and V. RAMAMURTHY. Tetrahedron Lett. 3463 (1978); V. JAYATHIRTHA RAO, and V. RAMAMURTHY. Indian J. Chem. **18**B, 265 (1979).
6. (*a*) J. G. JONES, S. SCHWARZBAUN, L. LESSINGER, and B. W. LOW. Acta Crystallogr. B**38**, 1207 (1982); (*b*) B. M. CRAVEN and G. T. DETITTA. J. Chem. Soc. Chem. Commun. 530 (1972).
7. K. W. HO and P. DE MAYO. J. Am. Chem. Soc. **101**, 5725 (1979); A. COUTURE, K. W. HO, M. HOSHINO, P. DE MAYO, R. SUAU, and W. R. WARE. J. Am. Chem. Soc. **98**, 6218 (1976).
8. W. K. APPEL, Z. Q. JIANG, J. R. SCHEFFER, and L. WALSH. J. Am. Chem. Soc. **105**, 5354 (1983).
9. P. ARJUNAN, V. RAMAMURTHY, and K. VENKATESAN. J. Org. Chem. **49**, 1765 (1984).
10. A. OHNO, K. NAKAMURA, Y. NAKAZIMA, and S. OKA. Bull. Chem. Soc. Jpn. **48**, 2403 (1975).
11. P. MAIN, S. J. FISKE, S. E. HULL, L. LESSINGER, G. GERMAIN, J. P. DECLERCQ, and M. M. WOOLFSON. MULTAN-80 System of Computer Programs. University of York, York, England. 1980.
12. J. KARLE. Acta Crystallogr. B**24**, 182 (1968).
13. G. M. SHELDRICK. "SHELX-76". A program for crystal structure determination. University of Cambridge, England. 1976.

Can. J. Chem. Downloaded from www.nrcresearchpress.com by 210.87.254.40 on 09/06/12
For personal use only.

Photochemistry of methyl(hydrido)diplatinum(II) complexes, including examples of C—H and C—C bond formation by intramolecular reductive elimination[1]

KAZI A. AZAM, ROSS H. HILL, AND RICHARD J. PUDDEPHATT[2]

Department of Chemistry, University of Western Ontario, London, Ont., Canada N6A 5B7

Received January 16, 1984

This paper is dedicated to Professor Paul de Mayo on the occasion of his 60th birthday

KAZI A. AZAM, ROSS H. HILL, and RICHARD J. PUDDEPHATT. Can. J. Chem. **62**, 2029 (1984).

Photolyses of the complex cations $[Pt_2H(\mu\text{-}H)Me(\mu\text{-}dppm)_2]^+$, $[Pt_2(\mu\text{-}H)Me_2(\mu\text{-}dppm)_2]^+$, and $[Pt_2Me_3(\mu\text{-}dppm)_2]^+$ lead to reductive elimination of H_2, CH_4, and C_2H_6, respectively. However, photolysis of $[Pt_2Me_3(\mu\text{-}dppm)_2]^+$ in pyridine gives $[PtMe_2(dppm)]$ and $[PtMe(C_5H_5N)(dppm)]^+$. The reductive eliminations of CH_4 and C_2H_6 are shown to be primarily intramolecular reactions by isotopic labelling. Quantum yields are reported and the mechanisms of reaction discussed.

KAZI A. AZAM, ROSS H. HILL et RICHARD J. PUDDEPHATT. Can. J. Chem. **62**, 2029 (1984).

Les photolyses des complexes cationiques $[Pt_2H(\mu\text{-}H)Me(\mu\text{-}dppm)_2]^+$, $[Pt_2(\mu\text{-}H)Me_2(\mu\text{-}dppm)_2]^+$ et $[Pt_2Me_3(\mu\text{-}dppm)_2]^+$ conduisent respectivement à des éliminations réductrices de H_2, CH_4 et C_2H_6. Toutefois, la photolyse de $[Pt_2Me_3(\mu\text{-}dppm)_2]^+$ dans la pyridine fournit du $[PtMe_2(dppm)]$ et du $[PtMe(C_5H_5N)(dppm)]^+$. Faisant appel à des marquages isotopiques, on démontre que les éliminations réductrices de CH_4 et C_2H_6 sont principalement des réactions intramoléculaires. On rapporte les rendements quantiques et on discute des mécanismes réactionnels.

[Traduit par le journal]

Introduction

In previous papers we have reported the synthesis and reactions of the complexes ions $[Pt_2H_nMe_{3-n}(\mu\text{-}dppm)_2]^+$, n = 0–3, dppm = $Ph_2PCH_2PPh_2$, **1**–**4** (1–6).

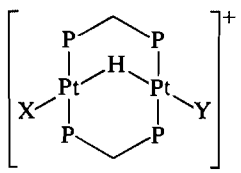

1, X = Y = H
2, X = H, Y = Me
3, X = Y = Me

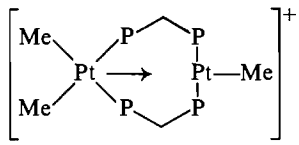

4

The thermal and photochemical reductive elimination of H_2 from complex **1** was been well studied (3, 7–13) but the properties of **2**–**4** have not been investigated in detail. Complex **2** undergoes reductive elimination of methane on treatment with the alkyne $CF_3C{\equiv}CCF_3$, but hydrogen is eliminated on reaction with tertiary phosphines (5, 6). Complex **3** undergoes reductive elimination of methane on reaction with $CF_3C{\equiv}CCF_3$, but reacts only very slowly with phosphines (4, 6), while **4** is stable to thermal reductive elimination (2). All complexes **1**–**4** have been shown to be photosensitive, but only for **1** has the reaction been studied in detail (reaction [1], L = C_5H_5N, MeCN, or tetrahydrofuran) (7–9).

[1] $1 + L \xrightarrow{h\nu}$ 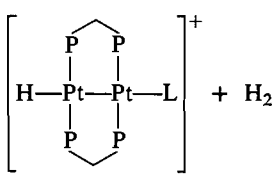 $+ H_2$

5*a*, L = C_5H_5N
5*b*, L = MeCN

The photochemical reactions of **2**–**4** are of considerable interest because, potentially, they can lead to binuclear coupling of C—H or C—C bonds and such reductive eliminations (or the reverse oxidative additions) are significant in catalysis involving formation or activation of alkanes at transition metal centres (14–20). There have been no detailed studies of photochemical reductive eliminations leading to C—H or C—C bond formation even in mononuclear systems, and there are only a few qualitative reports of such reactions (4, 14, 21–25). This article reports a study of the photochemistry of complexes **2**–**4**, with particular emphasis on **3** and **4** which can give reductive elimination of methane and ethane, respectively. A preliminary account of parts of this work has been published (26).

Results

Photochemistry of the methyl(hydrido)diplatinum complexes 2 and 3

Photolysis of complexes **2** and **3** in pyridine or acetonitrile solution occurred according to eqs. [2] and [3], giving in each case the methyldiplatinum(II) complex.

[2] 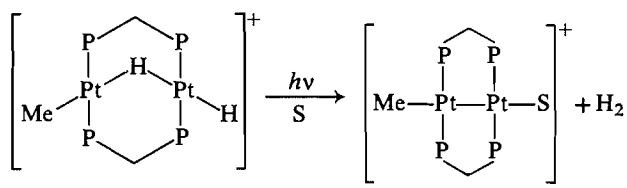

6*a*, S = C_5H_5N
6*b*, S = MeCN
6*c*, S = Me_2CO

[3] 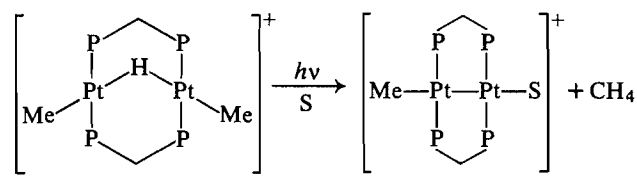

The gaseous products, H_2 or CH_4, were detected using gas chromatography. In reaction [3] no ethane was detected, while in reaction [2] only a trace of the alternative product methane was detected. The complexes **6***a* and **6***b* were formed without

[1]Publication 309 from the Photochemistry Unit, University of Western Ontario.

[2]To whom all correspondence should be addressed.

Can. J. Chem. Downloaded from www.nrcresearchpress.com by 210.87.254.6 on 09/06/12
For personal use only.

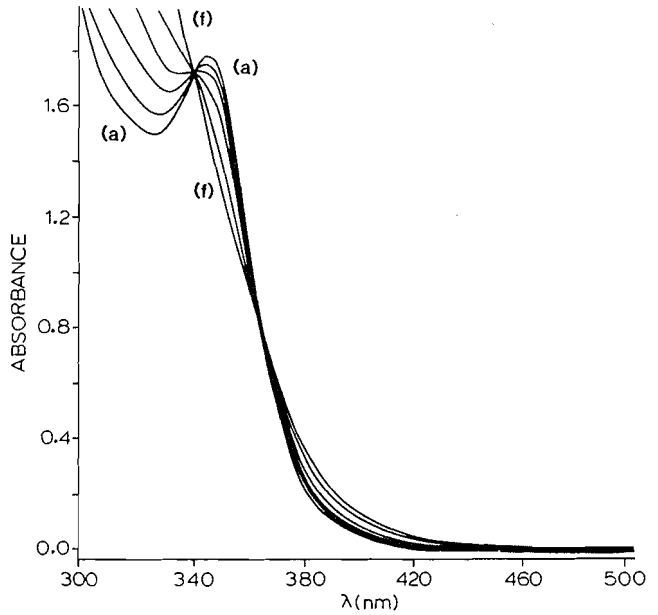

FIG. 1. Changes in the uv–visible absorption spectrum on irradiation of **2** in MeCN, with the following numbers of Einsteins of incident light (362 ± 7 nm): (*a*) 0, (*b*) 4.0×10^{-7}, (*c*) 8.0×10^{-7}, (*d*) 14.4×10^{-7}, (*e*) 26.4×10^{-7}, (*f*) extended irradiation.

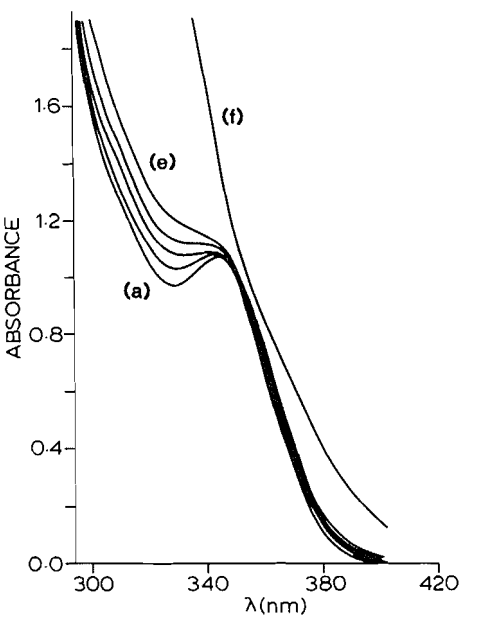

FIG. 2. Changes in the uv–visible absorption spectrum on irradiation of **3** in MeCN, with the following numbers of Einsteins of incident light (362 ± 7 nm): (*a*) 0, (*b*) 3.6×10^{-7}, (*c*) 6.0×10^{-7}, (*d*) 8.4×10^{-7}, (*e*) 11.2×10^{-7}, (*f*) extended irradiation.

detectable impurities (^{1}H and ^{31}P nmr spectra) of the alternative products **5***a* and **5***b*, respectively, indicating that the reactions are very selective.

Complex **6***a*, as the $[SbF_6]^-$ salt, is a yellow solid, which is stable in air at room temperature. It was characterized by elemental analysis and by the ^{1}H and $^{31}P\{^1H\}$ nmr spectra. The spectra are very characteristic and the parameters (Experimental section) are very similar to those for other methyldiplatinum(I) complexes $[Pt_2MeL(\mu\text{-dppm})_2]^+$, with L = tertiary phosphine, which have been discussed in detail elsewhere (5, 27). Complexes **6***b* and **6***c*, with the weakly co-ordinated MeCN or Me_2CO ligands, were not sufficiently stable to be isolated but were positively characterized by comparison of the ^{1}H nmr data with those for **6***a*, and by conversion to **6***a* on addition of pyridine.

Reaction [2] involving reductive elimination of H_2 is analogous to reaction [1] studied previously (7–9), but reaction [3] is of a new and significant type and so a labelling experiment was carried out to determine if reductive elimination of methane is an intramolecular or intermolecular process. A mixture of $[Pt_2(\mu\text{-H})Me_2(\mu\text{-dppm})_2][PF_6]$ and $[Pt_2(\mu\text{-D})(CD_3)_2(\mu\text{-dppm})_2][PF_6]$ gave CH_4 and CD_4, with only traces of CH_3D or CD_3H, on photolysis. It is thus proved that intramolecular reduction elimination occurs. When photolysis was not complete, the yield of CH_4 was greater than that of CD_4. This suggests that, as in the photolysis of **1**, there is a significant primary isotope effect on the rate of reaction (9).

Quantum yields for photolysis of **2** or **3** in pyridine or acetonitrile were determined by irradiation of rigorously degassed solutions in quartz cuvettes with 362 ± 7 nm light from a Jasco Spectroirradiator, previously calibrated using ferrioxalate actinometry. Typical sets of uv–visible absorption spectra obtained during irradiation of **2** and **3** are shown in Figs. 1 and 2. For photolysis of **2** good isosbestic points were observed (Fig. 1) but for photolysis of **3** there were no crossover points in the uv–visible spectra (Fig. 2). In each case, the extent of reaction was determined by monitoring the optical density at suitable points, and good linear plots of quanta absorbed by **2** or **3** vs. extent of conversion were then obtained. From these data, the quantum yields were determined and their values are given in Table 1.

TABLE 1. Quantum yields (362 ± 7 nm) for photolysis of diplatinum complexes

Complex	Quantum yield[a] py	MeCN	Reference
$[Pt_2H_2(\mu\text{-H})(\mu\text{-dppm})_2][PF_6]$	0.57	0.81[b]	9
$[Pt_2H(\mu\text{-H})Me(\mu\text{-dppm})_2][SbF_6]$	0.21	0.37	This work
$[Pt_2(\mu\text{-H})Me_2(\mu\text{-dppm})_2][PF_6]$	0.30	0.34	This work
$[Pt_2Me_3(\mu\text{-dppm})_2][PF_6]$[c]	0.6	0.1	This work

[a]In all cases, these are Φ for photodecomposition of reagent.
[b]Geoffroy *et al.* quote Φ = 0.62 for photolysis using 366 nm light (7).
[c]Φ = 0.6 in C_6H_6, 1.2 ± 0.3 in acetone, 2.0 ± 0.1 in CH_2Cl_2.

It can be seen from Table 1 that the quantum yields for photolysis of **1**–**3** are all high, with Φ for **1** > **2** ≈ **3**, and the quantum yields are in all cases slightly higher in acetonitrile than in pyridine.

Photochemistry of the trimethyldiplatinum(II) complex, 4

Photolysis of complex **4** in pyridine gave no gas evolution, and monitoring by ^{1}H and $^{31}P\{^1H\}$ nmr indicated that the products were mononuclear complexes as shown in reaction [4].

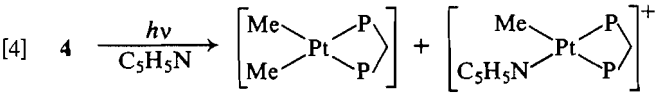

These complexes could not be separated, but were positively identified by the ^{1}H and $^{31}P\{^1H\}$ nmr spectra. $[PtMe_2(dppm)]$ is a known complex and was characterized by comparison of the nmr parameters with those for an authentic sample (28, 29). A sample containing the cation $[PtMe(C_5H_5N)(dppm)]^+$ was pre-

Can. J. Chem. Downloaded from www.nrcresearchpress.com by 210.87.254.6 on 09/06/12
For personal use only.

Can. J. Chem. Downloaded from www.nrcresearchpress.com by 210.87.254.6 on 09/06/12
For personal use only.

pared independently by reaction of [PtClMe(dppm)] with 1 mol-equiv. of silver nitrate followed by excess pyridine. The ^1H and $^{31}P\{^1H\}$ nmr spectra, which are very characteristic (Experimental section), were identical with those of the second photolysis product of reaction [4].

Extended photolysis of the above mixture did lead to some ethane formation and an uncharacterized symmetrical diplatinum complex was also formed. The quantum yield of the primary photochemical reaction of reaction [4] was high (Table 1) but the secondary photolysis was very inefficient and has not been studied in detail.

Photolysis of **4** in acetonitrile occurred cleanly in the initial stages to give ethane and complex **6***b*, identified by its ^1H and $^{31}P\{^1H\}$ nmr and uv–visible absorption spectra. However, the quantum yield was low (Table 1), and, as a result, further photolysis of product **6***b* became competitive in the later stages and the isosbestic points were lost. This reaction gave the first indication of a photochemical reductive elimination with C—C bond formation, and so the photolysis was studied in several other solvents.

Efficient reductive elimination of ethane occurred on photolysis of **4** in benzene, acetone, or dichloromethane as solvents. In benzene, the product of photolysis was very insoluble and precipitated during photolysis so that an accurate quantum yield could not be obtained. In acetone, the primary products were C_2H_6 and complex **6***c* and the stoichiometry was clean until the late stages, when photolysis of **6***c* became a problem. In this reaction 1.0 ± 0.1 mol of ethane was formed for each mol of **4** decomposed and the quantum yield (362 ± 7 nm) was 1.2 ± 0.3. The large uncertainty in the quantum yield arose due to problems with the secondary photolysis of **6***c*. The quantum yield is within experimental error of 1.0, and is an order of magnitude greater than that in acetonitrile solvent.

In dichloromethane solution, the stoichiometry of reaction was different and only 0.5 mol of C_2H_6 was formed for each mole of **4** decomposed (reaction [5]).

$$[5]\quad 2[Pt_2Me_3(\mu\text{-dppm})_2]^+ \xrightarrow[CH_2Cl_2]{h\nu} 2[Pt_2Me_2(\mu\text{-Cl})(\mu\text{-dppm})_2]^+ + C_2H_6$$

The product **7** has been characterized previously (29) and was isolated in quantitative yield. It is clear that a chlorine atom abstraction from solvent dichloromethane occurs during this reaction. The quantum yield for disappearance of **4** was 2.0 ± 0.1.

Because this clean photochemical C—C coupling reaction has no precedents, attempts were made to determine if the elimination is an intramolecular process. Photolysis of an equimolar amount of $[Pt_2Me_3(\mu\text{-dppm})_2][PF_6]$ and $[Pt_2(CD_3)_3(\mu\text{-dppm})_2][PF_6]$ in CH_2Cl_2 or acetone gave a product ratio of C_2D_6:CH_3CD_3 of 1:0.4 and 1:1.0, respectively (C_2H_6 yields could not be determined accurately due to high background at m/e 30, under the conditions used, with analysis by mass spectrometry). An intramolecular reaction should give C_2D_6:CH_3CD_3 = 1:0, while an intermolecular coupling reaction should give a ratio of 1:2. The experiment thus proves that at least 50% of the reaction occurs by intramolecular coupling in acetone and at least 80% in dichloromethane.

An effort was made to determine which two methyl groups in **4** were eliminated. However, an attempt to synthesize the unsymmetrical labelled complex ion $[(CD_3)_2Pt(\mu\text{-dppm})_2Pt\text{-}CH_3]^+$ by reaction of $[Pt(CD_3)_2(dppm)]$ with [PtClMe(dppm)] gave a sample of **4** in which complete scrambling of CD_3 and CH_3 groups had occurred, as determined by ^1H nmr spectroscopy. Thus it was not possible to solve this important problem. We suspect that the alkyl-for-alkyl exchange reactions which lead to this scrambling, and which have also been observed in other diplatinum complexes (30), may also account for the apparent intermolecular component of the reductive elimination reaction noted above.

Discussion

The photolyses of the family of complex cations, **1**–**3**, in each case leads to an overall binuclear reductive elimination in which the formal oxidation state of each platinum centre decreases from +II to +I. The reactions are very selective. Thus complex **2** gives hydrogen rather than CH_4 and complex **3** gives CH_4 rather than C_2H_6, and so it can be concluded that bond formation is favoured in the sequence H—H > CH_3—H > CH_3—CH_3 in these complexes. However, it should be noted that, in **1**–**3**, hydride occupies the bridging position and, since it is possible that the reaction always involve loss of the bridging ligand, only for **2** is there positive evidence that H—H bond formation is preferred rather than CH_3—H bond formation. The same selectivity is observed in thermal reductive eliminations induced by tertiary phosphine ligands (4, 5, 27), but hexafluorobut-2-yne induces selective reductive elimination of methane from **2** (6). In the thermal reactions, the rates of reaction follow the sequence **1** > **2** ≫ **3** (4, 13, 27), but there are only small differences in the rates of the photochemical reactions (Table 1). In particular, the quantum yields for photolysis of **2** (which gives H_2) and **3** (which gives CH_4) are very similar.

It has been proved that the reductive eliminations from **1** and **3** are intramolecular, but the detailed mechanisms of reaction cannot be determined unequivocally. For photolysis of **1**, a mechanism involving reductive elimination of H_2 from a single metal centre was proposed (9), but a subsequent study of the thermal reductive elimination suggested a true binuclear reductive elimination in which hydride ligands coupled across two platinum centres (13). The results from the present study can be interpreted in terms of either mechanism (see refs. 13, 18, 30, 32–35 for related discussions of mechanisms in binuclear and cluster complexes), but the primary photochemical step in all cases is probably the cleavage of the $Pt_2(\mu\text{-H})$ linkage by excitation of an electron to a σ^*(PtPt) orbital (9, 31).

The photochemically-induced reductive elimination of ethane from **4** appears to be a unique reaction. Photolysis of alkyl transition metal complexes usually gives homolysis of the M—C bond to give alkyl radicals (36, 37), though β-elimination, isomerization, loss of other ligands with no reaction of the M—R bond, and other reactions can also occur (22–25, 38–40). Photolysis of mononuclear alkyl platinum(II) or alkylplatinum(IV) complexes leads primarily to the formation of alkyl radicals (41–43), though reductive elimination may be oberved with platina(IV)cycloalkanes (22, 23, 44, 45). There are two properties of **4** which might lead to its unique reactivity. Firstly, the primary photochemical process almost certainly will involve cleavage of the Pt—Pt bond by excitation of an electron to the σ^*(PtPt) orbital, and this excited state is not possible with mononuclear complexes. However, it is not obvious why this excited state should cause reductive elimination from the dimethylplatinum centre (46). Secondly, since **4** is binuclear, new mechanisms, such as a coupling of methyl groups across two platinum centres, become available. The experimental data cannot distinguish between these

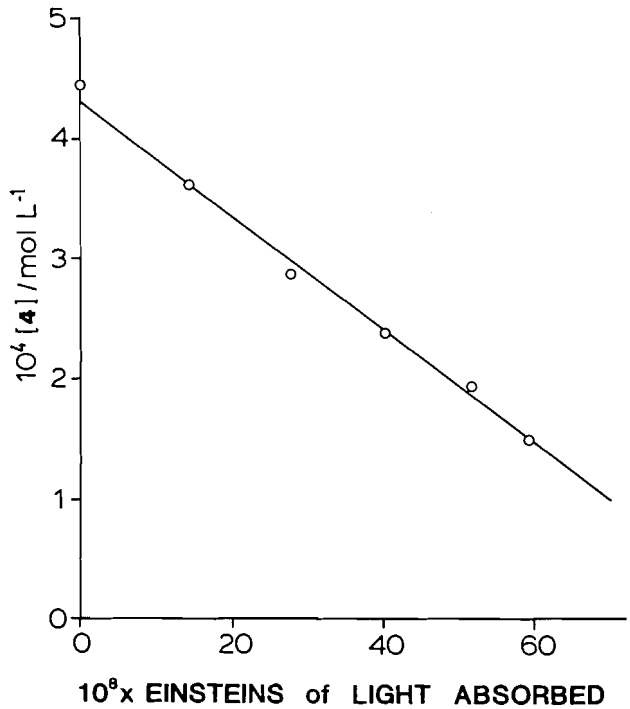

FIG. 3. Plot of concentration of **4** (mol L^{-1}) vs. light (362 ± 7 nm) absorbed by **4** (E), showing that the quantum yield is independent of concentration of **4**.

possibilities.

We have shown that the reductive elimination of ethane is at least partially intramolecular by a labelling experiment, and we believe that this reaction is almost entirely intramolecular. In order to give the observed quantum yields (Table 1) for an intermolecular elimination, the lifetime of the excited state would need to exceed 10^{-5} s to allow complete quenching by a second molecule of **4** (assuming $k_q \sim 10^{10}$ s^{-1} and ~99% efficiency of quenching) at the concentrations used. Few lifetimes of organometallic excited states have been measured but most such lifetimes are $<10^{-6}$ s at 298 K (47). In addition, an intermolecular process should give a concentration-dependent quantum yield which was not observed (Fig. 3).

Finally, a comment is needed on the solvent dependence of the quantum yields and reaction products. The good donor pyridine can presumably co-ordinate to the monomethylplatinum centre of **4** after photochemical cleavage of the PtPt bond, and cleavage of the dimer to mononuclear fragments (reaction [4]) follows. In the poor donor solvent acetone, the excited state gives intramolecular loss of C_2H_6 with a quantum yield of ~1. The lower quantum yield in acetonitrile may be explained if this is a good enough ligand for platinum to co-ordinate reversibly and hence deactivate the excited state but not good enough to cause breakdown to mononuclear fragments. Finally, in dichloromethane intramolecular loss of ethane from **4** gives $[Pt_2Me(\mu\text{-dppm})_2]^+$, which must then accept a methyl group from a second molecule of **4** in a rapid thermal reaction and abstraction of Cl radicals from CH_2Cl_2 solvent gives the observed product (reaction [5]). The true quantum yield for the reductive elimination is therefore 1.0.

Experimental

^1H and $^{31}P\{^1H\}$ nmr spectra were recorded using Varian XL100 or XL200 NMR spectrometers, and chemical shifts are quoted with respect to TMS or trimethylphosphate, respectively. Gas analysis (H_2, CH_4, and C_2H_6) was carried out by injection of a standard volume of gas formed in the photochemical reaction into a Varian Series 1400 gas chromatograph. Calibration was carried out by injection of known volumes of the pure gases into the reaction vessel containing only solvent, then allowing to equilibrate and sampling as above. The columns used were 6′ × 1/8″ packed with Molecular Sieve 5A or Porapak Q.

[Pt(CD$_3$)$_2$(dppm)]

A solution of CD_3Li (24 mL, 1.7 *M*), freshly prepared from Li and CD_3I in ether, was added dropwise to a suspension of $[PtCl_2(dppm)]$ (1.52 g) in ether (30 mL) cooled to 0°C. The solution was allowed to warm to room temperature. After 1 h, the mixture was hydrolysed with cold saturated aqueous NH_4Cl solution (5 mL). The layers were separated, and the aqueous layer was further extracted with CH_2Cl_2. The organic extracts were dried over $MgSO_4$ and evaporated to yield the product (0.62 g).

[Pt$_2$(CD$_3$)$_3$(μ-dppm)$_2$][PF$_6$]

A mixture of $[Pt(CD_3)_2(dppm)]$ (0.19 g) and $[PtCl_2(dppm)]$ (0.066 g) in methanol (15 mL) was heated under reflux for 1 h. $[NH_4][PF_6]$ (0.12 g) was then added, heating was continued for 5 min, the solution was cooled, and water was added dropwise to precipitate the product as a yellow solid. This was purified by precipitation from CH_2Cl_2 solution by slow addition of hexane, and was identified by the ^1H and $^{31}P\{^1H\}$ nmr spectra (2).

[Pt$_2$(μ-D)(CD$_3$)$_2$(μ-dppm)$_2$][PF$_6$]

This was prepared by the literature method for the synthesis of **3** (4), but using $[Pt(CD_3)_3(\mu\text{-dppm})_2][PF_6]$ (0.09 g), $NH_4[PF_6]$ (0.06 g) in CH_3OD (10 mL) with $Na[BD_4]$ (0.1 g) in CH_3OD (3 mL). The yield was 0.06 g (70%) and the complex was characterised by the ^1H and $^{31}P\{^1H\}$ nmr spectra (4).

[Pt$_2$Me(C$_5$H$_5$N)(μ-dppm)$_2$][SbF$_6$]

A solution of $[Pt_2H(\mu\text{-H})Me(\mu\text{-dppm})_2][SbF_6]$ (0.05 g) in dry pyridine (20 mL) was deoxygenated by passing nitrogen through the solution for 45 min. The reaction vessel was a flat-sided Pyrex flask, with a sidearm fitted with a 1 mm quartz cuvette to allow monitoring of the reaction by uv–visible absorption spectroscopy. The solution was irradiated for 2h, using a medium pressure Hg lamp 12 cm from the sample and using a water filter, after which no further change in absorption spectrum occurred. A sample of the gas phase was analysed by gc, and showed hydrogen and a trace of methane to be present. The solvent was then removed under high vacuum to give the product as a yellow solid in quantitative yield. *Anal.* calcd. for $C_{56}H_{52}NF_6P_4Pt_2Sb$: C 45.2, H 3.5; found: C 44.7, H 3.6. ^{1}Hmr (C_5D_5N)δ: 0.53[*m*, ^2J(PtH) 72.5, ^3J(PH) 11, *Me*Pt], 5.29[*m*, CH_2P_2]. ^{31}Pmr (C_5D_5N)δ: 8.4[*m*, $^1J(PtP^A)$ 2930], −4.7[*m*, $^1J(PtP^B)$ 2850, $^2J(P^AP^B)$ 37.5, $^3J(P^AP^{B'})$ 57.5].

This same product was formed by the similar photolysis of $[Pt_2(\mu\text{-H})Me_2(\mu\text{-dppm})_2][SbF_6]$ (0.03 g) in pyridine (5 mL), but in this case the only gaseous product was CH_4. The product was identified by the ^1H and $^{31}P\{^1H\}$ nmr spectra.

[Pt$_2$Me(Me$_2$CO)(μ-dppm)$_2$][PF$_6$]

A solution of $[Pt_2Me_3(\mu\text{-dppm})_2][PF_6]$ (0.05 g, 3.9×10^{-5} mol) in dry acetone (5 mL), in an apparatus with a sidearm fitted with a 1 mm quartz cuvette, was degassed by several freeze–pump–thaw cycles and then photolysed using a 150 W xenon lamp with water and Corning 0-52 filters. The reaction was monitored by uv–visible spectroscopy, and when complete the gaseous phase was analysed by gc. Ethane ($4.0 \pm 0.2 \times 10^{-5}$ mol) was the only gas formed.

The product was isolated as a yellow solid by evaporation of the solvent under high vacuum, and was identified by the ^1H nmr spectrum in $(CD_3)_2CO$ [δ: 0.29, ^2J(PtH)70, ^3J(PH)7.5, *Me*Pt] and by conversion to $[Pt_2Me(C_5H_5N)(\mu\text{-dppm})][PF_6]$ on addition of pyridine. The acetone complex decomposed over a period of several hours to an unidentified product having δ 0.24 [*m*, ^2J(PtH)82, ^3J(PH)7].

This product **6***c*, as the SbF_6^- salt, was also prepared by similar

Can. J. Chem. Downloaded from www.nrcresearchpress.com by 210.87.254.6 on 09/06/12
For personal use only.

photolysis of a degassed solution of $[Pt_2H(\mu\text{-}H)Me(\mu\text{-}dppm)_2][SbF_6]$ (0.10 g) in $(CD_3)_2CO$ (0.7 mL) and was identified as above.

$[Pt_2Me(CD_3CN)(\mu\text{-}dppm)_2][SbF_6]$

This was obtained and identified by photolysis of $[Pt_2H(\mu\text{-}H)Me(\mu\text{-}dppm)_2][SbF_6]$ in CD_3CN as described above. ^{1}Hmr (CD_3CN)δ: 0.80[m, ^2J(PtH)60, ^3J(PH)6.5 Hz]. This complex was stable in CD_3CN solution in the absence of oxygen, but decomposed on evaporation of the solvent. The same product was formed by similar photolysis of $[Pt_2(\mu\text{-}H)Me_2(\mu\text{-}dppm)_2][SbF_6]$ or, as the PF_6^- salt, by photolysis of $[Pt_2Me_3(\mu\text{-}dppm)_2][PF_6]$.

Photolysis of $[Pt_2Me_3(\mu\text{-}dppm)_2][PF_6]$ in CD_2Cl_2

$[Pt_2Me_3(\mu\text{-}dppm)_2][PF_6]$ (0.0843 g) was dissolved in CD_2Cl_2 (1 mL) in a 5 mm nmr tube. The solution was then degassed, flame sealed, and then irradiated using a 150 W xenon lamp source filtered through Corning 0-52 and H_2O filters. Photolysis was continued for 30 min. The ^{1}H and ^{31}P{^{1}H} nmr spectra showed the product to be $[Pt_2Me_2(\mu\text{-}Cl)(\mu\text{-}dppm)_2][PF_6]$ (29).

The nmr tube was then opened and the gas product analysed by gc. The gases C_2H_6, CH_4, and C_2H_4 were observed in a ratio of 1:0.08:0.02. The absolute yield of C_2H_6 was 45% mol/mol **4** decomposed.

$[PtMe(C_5H_5N)(dppm)][NO_3]$

A solution of $AgNO_3$ (0.060 g) in methanol (12 mL) was added dropwise to a solution of [PtClMe(dppm)] (0.20 g) (29) in CH_2Cl_2 (50 mL). The mixture was then filtered to remove AgCl and pyridine (0.5 mL) was added. After 10 min, the solvent was evaporated under vacuum to give the product. This was characterised by the nmr spectra in C_5D_5N. ^{31}Pmr, δ: −26.6[*m*, $^2J(P^AP^B)$38, $^1J(PtP^A)$-3388, P^A *trans* to C_5H_5N], −42.3[*m*, $^2J(P^AP^B)$38, $^1J(PtP^B)$1270, P^B *trans* to Me]. ^{1}Hmr, δ: 1.02 [*m*, $^3J(P^BH)$8, $^3J(P^AH)$3, ^2J(PtH)61, *Me*Pt]. These assignments were confirmed by selective ^{31}P decoupling experiments.

When the photolysis of $[Pt_2Me_3(\mu\text{-}dppm)_2][PF_6]$ was carried out in C_5D_5N with monitoring by ^{1}H and ^{31}P{^{1}H} nmr, an equimolar mixture of [$PtMe_2$(dppm)] (29) and $[PtMe(C_5D_5N)(dppm)]^+$ was formed. The parameters for the latter complex were identical with those of the sample prepared above.

Quantum yield determinations

Irradiations were performed with a Jasco CRM-FA Spectro-irradiator equipped with a counter. The light flux and counter were calibrated by using ferrioxalate actinometry at 362 ± 7 nm.

In a typical experiment, a solution of $[Pt_2Me_3(\mu\text{-}dppm)_2][PF_6]$ in CH_2Cl_2 (4.0 mL, 4.45×10^{-4} *M*) was degassed by three freeze−pump−thaw cycles, each time pumping to a residual pressure of 5×10^{-5} mbar at 77 K. The solution was then flame sealed in a 1 cm quartz cuvette. The reaction was monitored by following the change in optical density at 440 nm. The data were then analysed by calculating the concentration of $[Pt_2Me_3(\mu\text{-}dppm)_2]^+$ after each irradiation. From this an average concentration over each irradiation interval, and hence the percent light absorbed was calculated. Linear plots of $[Pt_2Me_3(\mu\text{-}dppm)_2]^+$ concentration vs. quanta of light absorbed by $[Pt_2Me_3(\mu\text{-}dppm)_2]^+$ were obtained (correlation coefficient > 0.99). The quantum yields were then calculated from the slopes of these lines.

The quantum yield measurement in benzene was complicated by precipitation of a white microcrystalline material after ~40% reaction at which stage an isosbestic point at 360 nm was lost. The final absorption was estimated and the quantum yield calculated as 0.6. The error due to this estimation is difficult to assess.

Proof of intramolecular reaction

A mixture of $[Pt_2(\mu\text{-}D)(CD_3)_2(\mu\text{-}dppm)_2][PF_6]$ (0.025 g) and $[Pt_2(\mu\text{-}H)(CH_3)_2(\mu\text{-}dppm)_2][PF_6]$ (0.025 g) in pyridine (5 mL) was degassed and photolysed to partial conversion. The gaseous products were analysed using a Varian MAT 311A mass spectrometer. For comparison, photolysis of the pure labelled materials were also carried out and the gases analysed in the same way. The above system gave $CD_4:CD_3H:CH_3D:CH_4$ = 1:0.04:0.02:1.6.

Experiments using $[Pt_2(CD_3)_3(\mu\text{-}dppm)_2][PF_6]$ and $[Pt_2(CH_3)_3(\mu\text{-}dppm)_2][PF_6]$ were carried out in a similar way.

Acknowledgments

We thank the Natural Sciences and Engineering Research Council of Canada for financial support and Professor P. de Mayo for access to the Jasco Spectroirradiator used in the quantum yield determinations and for valuable discussions.

1. M. P. Brown, R. J. Puddephatt, M. Rashidi, and K. R. Seddon. J. Chem. Soc. Dalton Trans. 516 (1978).
2. M. P. Brown, S. J. Cooper, A. A. Frew, Lj. Manojlović-Muir, K. W. Muir, R. J. Puddephatt, K. R. Seddon, and M. A. Thomson. Inorg. Chem. **20**, 1500 (1981).
3. M. P. Brown, J. R. Fisher, R. H. Hill, R. J. Puddephatt, and K. R. Seddon. Inorg. Chem. **20**, 3516 (1981).
4. M. P. Brown, S. J. Cooper, A. A. Frew, Lj. Manojlović-Muir, K. W. Muir, R. J. Puddephatt, and M. A. Thomson. J. Chem. Soc. Dalton Trans. 299 (1982).
5. K. A. Azam, R. J. Puddephatt, M. P. Brown, and A. Yavari. J. Organomet. Chem. **234**, C31 (1982).
6. K. A. Azam and R. J. Puddephatt. Organometallics, **2**, 1396 (1983).
7. H. C. Foley, R. H. Morris, T. S. Targos, and G. L. Geoffroy. J. Am. Chem. Soc. **103**, 7337 (1981).
8. R. H. Hill and R. J. Puddephatt. Inorg. Chim. Acta, **54**, L277 (1981).
9. R. H. Hill, P. de Mayo, and R. J. Puddephatt. Inorg. Chem. **21**, 3642 (1982).
10. R. J. Puddephatt and M. A. Thomson. Inorg. Chem. **21**, 725 (1982).
11. A. A. Frew, R. H. Hill, Lj. Manojlović-Muir, K. W. Muir, and R. J. Puddephatt. J. Chem. Soc. Chem. Commun. 198 (1982).
12. J. R. Fisher, A. J. Mills, S. Sumner, M. P. Brown, M. A. Thomson, R. J. Puddephatt, A. A. Frew, Lj. Manojlović-Muir, and K. W. Muir. Organometallics, **1**, 1421 (1982).
13. R. H. Hill and R. J. Puddephatt. J. Am. Chem. Soc. **105**, 5797 (1983).
14. A. H. Janowicz and R. G. Bergman. J. Am. Chem. Soc. **105**, 3929 (1983).
15. J. K. Hoyano and W. A. G. Graham. J. Am. Chem. Soc. **104**, 3723 (1982).
16. W. D. Jones and F. J. Feher. Organometallics, **2**, 562 (1983).
17. D. Milstein. J. Am. Chem. Soc. **104**, 5227 (1982).
18. J. Halpern. Acc. Chem. Res. **15**, 332 (1982).
19. G. W. Parshall, T. Herskovitz, F. N. Tebbe, A. D. English, and J. V. Zeile. Fundam. Res. Homogen. Catal. **3**, 95 (1979).
20. R. H. Crabtree, P. C. Demou, D. Eden, J. M. Mihelcic, C. A. Parnell, J. M. Quirk, and G. E. Morris. J. Am. Chem. Soc. **104**, 6994 (1982).
21. G. Erker. J. Organomet. Chem. **134**, 189 (1977).
22. G. Phillips, R. J. Puddephatt, and C. F. H. Tipper. J. Organomet. Chem. **131**, 467 (1977).
23. D. C. L. Perkins, R. J. Puddephatt, and C. F. H. Tipper. J. Organomet Chem. **186**, 419 (1980).
24. F. Ozawa, A. Yamamoto, T. Ikariya, and R. H. Grubbs. Organometallics, **1**, 1481 (1982).
25. G. L. Geoffroy and M. S. Wrighton. Organometallic photochemistry. Academic, New York. 1979.
26. R. H. Hill and R. J. Puddephatt. Organometallics, **2**, 1472 (1983).
27. K. A. Azam, M. P. Brown, R. H. Hill, R. J. Puddephatt, and A. Yavari. Organometallics. **3**, 697 (1984).
28. T. G. Appleton, M. A. Bennett, and I. B. Tomkins. J. Chem. Soc. Dalton Trans. 439 (1976).
29. S. J. Cooper, M. P. Brown, and R. J. Puddephatt. Inorg.

Can. J. Chem. Downloaded from www.nrcresearchpress.com by 210.87.254.6 on 09/06/12
For personal use only.

Chem. **20**, 1374 (1981).
30. K. A. AZAM, M. P. BROWN, S. J. COOPER, and R. J. PUDDEPHATT. Organometallics, **1**, 1183 (1982).
31. D. M. HOFFMAN and R. HOFFMANN. Inorg. Chem. **20**, 3543 (1981).
32. W. H. HERSH and R. G. BERGMAN. J. Am. Chem. Soc. **105**, 5846 (1983).
33. L. M. BAVARO, P. MONTANGERO, and J. B. KEISTER. J. Am. Chem. Soc. **105**, 4977 (1983).
34. M. H. CHISHOLM, J. C. HUFFMAN, and R. J. TATZ. J. Am. Chem. Soc. **105**, 2075 (1983).
35. C. B. KNOBLER, H. D. KAESZ, G. MINGHETTI, A. L. BANDINI, G. BANDITELLI, and F. BONATI. Inorg. Chem. **22**, 2324 (1983).
36. H. B. ABRAHAMSON and M. E. MARTIN. J. Organomet. Chem. **238**, C58 (1982).
37. H. B. ABRAHAMSON and E. DENNIS. J. Organomet. Chem. **201**, C19 (1980).
38. J. W. BRUNO, D. G. KALINA, E. A. MINTZ, and T. J. MARKS. J. Am. Chem. Soc. **104**, 1860 (1982).
39. R. J. KAZLAUSKAS and M. S. WRIGHTON. J. Am. Chem. Soc. **102**, 1727 (1980).
40. R. SEVERSON and A. WOJCICKI. J. Organomet. Chem. **157**, 173 (1978),
41. P. W. N. M. VAN LEEUWEN, C. F. ROOBEEK, and R. HUIS. J. Organomet. Chem. **142**, 233 (1977).
42. R. PIERANTOZZI, C. MCLAREN, and G. L. GEOFFROY. Unpublished work quoted in ref. 25.
43. D. C. L. PERKINS, R. J. PUDDEPHATT, and C. F. H. TIPPER. J. Organomet. Chem. **166**, 261 (1979).
44. D. C. L. PERKINS, R. J. PUDDEPHATT, and C. F. H. TIPPER. J. Organomet. Chem. **191**, 481 (1980).
45. C. BARTOCCI, A. MALDOTTI, S. SOSTERO, and O. TRAVERSO. J. Organomet. Chem. **253**, 253 (1983).
46. J. Y. CHEN and J. K. KOCHI. J. Am. Chem. Soc. **99**, 1450 (1977).
47. D. L. MORSE and M. S. WRIGHTON. J. Am. Chem. Soc. **98**, 3931 (1976); J. C. LUONG, R. A. FALTYNEK, and M. S. WRIGHTON. J. Am. Chem. Soc. **101**, 1597 (1979); **102**, 7892 (1980); J. J. MILDER, R. A. GOLDBECK, D. S. KLIGER, and H. B. GRAY. J. Am. Chem. Soc. **102**, 6761 (1980).

Can. J. Chem. Downloaded from www.nrcresearchpress.com by 210.87.254.6 on 09/06/12
For personal use only.

Stereospecific *trans*-elimination of 2-alkoxy- and 2-cycloalkoxytropones to alkenes and cycloalkenes[1]

HITOSHI TAKESHITA AND HIROAKI MAMETSUKA

Research Institute of Industrial Science, 86, Kyushu University, Sakamoto, Kasuga, Fukuoka 816, Japan

Received February 2, 1984

This paper is dedicated to Professor Paul de Mayo on the occasion of his 60th birthday

HITOSHI TAKESHITA and HIROAKI MAMETSUKA. Can. J. Chem. **62**, 2035 (1984).

The title compounds undergo thermal fragmentation to tropolones and alkenes and cycloalkenes. Product distribution and kinetic analyses of specifically labelled deuterio compounds establish the process to be a concerted $[s8\pi + a2\sigma + s2\sigma]$ electrocyclic reaction.

HITOSHI TAKESHITA et HIROAKI MAMETSUKA. Can. J. Chem. **62**, 2035 (1984).

Les composés mentionnés dans le titre subissent une fragmentation thermique conduisant à des tropolones, à des alcènes et à des cycloalcènes. Faisant appel à des analyses de la cinétique et de la distribution de produits marqués spécifiquement par du deutérium, on a établi que le processus est une réaction électrocyclique concertée du type $[s8\pi + a2\sigma + s2\sigma]$.

[Traduit par le journal]

Can. J. Chem. Downloaded from www.nrcresearchpress.com by 210.87.254.105 on 09/06/12
For personal use only.

Introduction

Recently, we have observed terminal diene formation by heating 2-(2-alkenyloxy)tropones (1), and on this basis have explained the low yields in the previous syntheses of nootkatin from hinokitiol (2) and procerin from β-dolabrin (3). We now wish to report a new thermal reaction of troponoid ethers, namely the electrocyclic fragmentation of 2-alkoxytropones to alkenes.

Results and discussion

When 2-(cyclopentyloxy)tropone (**1***d*) (4) was heated in DMSO at 180°C in a sealed tube for 2 h, in the hope of obtaining cyclopentanone (5), unexpected formation of cyclopentene (**2***d*) and tropolone (**3**) occurred as shown by nmr spectroscopy. This contrasted with our earlier work; i.e., heating of 2-isopropoxytropone (**4***a*) in that solvent gave acetone (**5***a*) and **3**, and prompted us to investigate similar reactions with other alkoxy- and cycloalkoxytropones. The treatment of alkoxytropones (**4**) indeed formed mixtures of alkenes (**6**) and alkanones (**5**); heating 2-(2-butyloxy)tropone (**4***b*) in DMSO at 180°C for 30 min gave *Z*- and *E*-2-butenes (*Z*-**6***b* and *E*-**6***b*, 1:1) and 2-butanone (**5***b*). Similar treatment of 2-(3-pentyloxy)tropone (**4***c*) gave *Z*- and *E*-2-pentenes (*Z*-**6***c* and *E*-**6***c*, 1:2) and 3-pentanone (**5***c*). Conversely, all the cycloalkoxytropones examined, including 2-(cyclododecyloxy)tropone (**1***h*), a macrocyclic derivative, gave only the corresponding cycloalkenes (**2**) in good yields.

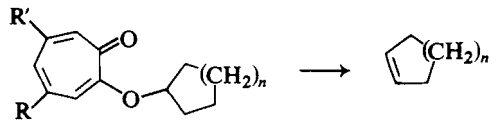

1*d* R = R′ = H, *n* = 1 — **2***d* *n* = 1
1*e* R = R′ = H, *n* = 2 — **2***e* *n* = 2
1*f* R = R′ = H, *n* = 3 — **2***f* *n* = 3
1*g* R = R′ = H, *n* = 4 — **2***g* *n* = 4
1*h* R = R′ = H, *n* = 8 — **2***h* *n* = 8
8*d* R = $CHMe_2$, R′ = H, *n* = 1
8*g* R = $CHMe_2$, R′ = H, *n* = 1
9*d* R = H, R′ = $CHMe_2$, *n* = 4
9*g* R = H, R′ = $CHMe_2$, *n* = 4

4*a* R^1 = Me, R^2 = H — **6***b* R^1 = R^2 = Me — **5***a* R^1 = Me, R^2 = H — **3**
4*b* R^1 = R^2 = Me — **6***c* R^1 = Me, R^2 = Et — **5***b* R^1 = R^2 = Me
4*c* R^1 = Et, R^2 = Me — **5***c* R^1 = Et, R^2 = Me

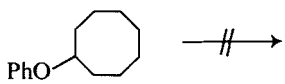

7

SCHEME 1

[1] A part of these results has been published in a preliminary form. See ref. 4.

TABLE 1. Preparation of alkoxy- and cycloalkoxythropones

Compounds (forms)	Conditions	Yields (%)	*Anal.* found (calcd. C, H, or M^+, for)
4*b* (c.l.)[a]	55°C, 22 h → 85°C, 23 h	87	178.0993 (178.0993, $C_{11}H_{14}O_2$)
4*c* (c. needles, mp 49–50°C)	50°C, 23 h → 80°C, 23 h	48	74.97, 8.28 (74.97, 8.39, $C_{12}H_{16}O_2$)
1*d* (c. l.)	50°C, 22 h → 75°C, 24 h	90	190.0995 (190.0993, $C_{12}H_{14}O_2$)
1*e* (c. l.)	55°C, 24 h → 80°C, 20 h	15	204.1150 (204.1149, $C_{13}H_{18}O_2$)
1*f* (c. l.)	[b]	8	218.1292 (218.1306, $C_{14}H_{18}O_2$)
1*g* (c. needles, mp 54–55°C)	55°C, 23 h → 85°C, 21 h	82	77.45, 8.44 (77.55, 8.68, $C_{15}H_{20}O_2$)
1*h* (c. l.)	55°C, 23 h → 80°C, 20 h	11	288.2098 (288.2088, $C_{19}H_{28}O_2$)
8*d* (c. l.)	55°C, 23 h → 90°C, 3 h	23	76.25, 9.00 (76.32, 9.15, $C_{15}H_{20}O_2$)
8*g* (c. l.)		39	76.17, 9.0 (76.32, 9.15, $C_{15}H_{20}O_2$)
9*d* (c. l.)	55°C, 23 h → 90°C, 3 h	26	78.78, 9.42 (78.79, 9.55, $C_{18}H_{26}O_2$)
9*g* (c. l.)		37	78.54, 9.33 (78.79, 9.55, $C_{18}H_{26}O_2$)

[a] Colorless liquid.
[b] Due to unavailability of **11***f*, this was prepared from cycloheptyl bromide and **3** in HMPA at 125°C for 8 h.

TABLE 2. The ^{13}C nuclear magnetic resonance characterizations of alkoxy- and cycloalkoxytropones

Compounds	C-1	C-2	C-3	C-4	C-5	C-6	C-7	Others
4*b*	180.9	164.4	115.1	132.7	127.6	136.1	136.7	9.8, 18.8, 28.8, 76.7
4*c*	180.8	164.9	115.1	132.7	127.6	136.1	136.8	9.6, 25.9, 81.9
1*d*	180.7	164.3	114.6	132.7	127.3	136.1	136.6	24.2, 32.6, 80.8
1*e*	181.0	164.0	115.5	132.6	127.8	136.1	136.9	23.9, 25.4, 31.3, 77.1
1*f*	181.1	164.1	115.3	132.6	127.6	136.1	136.9	23.1, 28.2, 33.4, 79.8
1*g*	180.9	163.9	115.4	132.8	127.6	136.1	136.6	23.2, 25.7, 26.8, 31.6, 79.5
1*h*	180.9	164.6	115.1	132.6	127.6	136.0	136.9	20.8, 23.1, 24.2, 24.5, 28.4, 77.1
8*d*	180.4	163.6	116.4	153.9	124.4	136.5	134.9	23.4, 24.3, 32.7, 38.9, 80.5
8*g*	180.7	163.2	117.7	153.9	124.7	136.4	135.1	23.4, 23.5, 26.0, 26.8, 31.9, 38.9, 79.5
9*d*	180.5	163.8	113.8	131.7	128.6	157.1	134.2	23.1, 24.3, 32.6, 38.3, 80.6
9*g*	180.8	163.3	114.4	131.6	128.8	156.9	134.2	23.0, 23.4, 25.8, 26.8, 31.8, 38.8, 79.5

Heating, as above, of the cyclooctyl phenyl ether (**7**) had no effect and, therefore, the presence of an adjacent carbonyl group is essential for the elimination to occur.

The ethers (**8***d*, **8***g*, **9***d*, and **9***g*) derived from hinokitiol (4-isopropyltropolone, **10**) gave products similar to those from ethers of **3**; this suggests the generality of this elimination in tropolonyl ethers.

To provide information about mechanism, several deuterium-labelling experiments were carried out using appropriately labelled **1***g*, which could be prepared from **3** and deuterated cyclooctanols (**11**). The first feature observed was that the mass spectrometric and ^1H and ^{13}C nmr analyses of the purified **3** generated by heating 2-(*Z*-2-deuteriocyclooctyloxy)tropone (*Z*-D-**1***g*), 2-(*E*-2-deuteriocyclooctyloxy)tropone (*E*-D-**1***g*), and 2-(2,2,8,8-tetradeuteriocyclooctyloxy)tropone (D_4-**1***g*) in decalin showed it to contain no deuterium. In this solvent, the hydrogen exchange of the aromatic ring of **3** does not occur, although substantial exchange was observed in dimethyl-d_6 sulfoxide. Thus, a possible $[2\pi + 2\sigma + 2\sigma]$ process may be rejected. In addition, the mass spectrometric analysis of the deuteriodibromocyclooctanes, **12***a* obtained from thermolysis of *E*-D-**1***g* in decalin and **12***b* obtained from *Z*-D−**1***g* in decalin, showed the process to be a *trans*-elimination; i.e., according to mass spectral analysis of deuterium distributions, **12***a* contains the deuterium-free **12**, while **12***b* retains all the deuterium, as shown in Fig. 1.

The ^{13}C nmr spectrum of **12***b* showed signals attributable to a mixture of *E*-3-deuterio (*E*-D-**12**) and *Z*-3-deuterio (*Z*-D-**12**) derivatives together with 1-deuterio **12** (1-D-**12**) in a ratio of 1:1:2, while the ^{13}C nmr of **12***a* showed signals attributable to *E*-D-**12** and *Z*-D-**12** derivatives and the deuterium-free **12** in a ratio of 1:1:1.[2]

TABLE 3. Thermolysis of 2-cycloalkoxytropones in decalin at 180°C

Reactants	Time (h)	Products	Yields (%)
1*d*	4	Cyclopentene (**2***d*)	70[a]
1*e*	4	Cyclohexene (**2***e*)	85[a]
1*f*	2	Cycloheptene (**2***f*)	95[a]
1*g*	2	Cyclooctene (**2***g*)	95[a]
1*h*	3	Cyclododecene (**2***h*)	95[a]
8*d*	4	Cyclopentene (**2***d*)	95[b]
8*g*	3	Cyclooctene (**2***g*)	95[b]
8*d*	4	Cyclopentene (**2***d*)	95[b]
9*g*	3	Cyclooctene (**2***g*)	95[b]

[a] Determined after isolation as dibromo derivatives.
[b] Determined by nmr spectrometry.

These isotopic distributions led to the conclusion that H-abstraction is twice as fast as D-abstraction. Indeed, this has been verified by measurement of reaction rates for the thermol-

[2] Locations of the deuterium in the compounds were conveniently determined by the gated decoupling ^{13}C nmr spectra (irradiation time = 2 s, pulse interval = 90 s) δ: 30.7 (t, J = 19 Hz) and 31.7 (t, J = 19 Hz) for *E*- or *Z*-D-**12** and 61.1 (t, J = 24 Hz) for 1-D-**12**.

Can. J. Chem. Downloaded from www.nrcresearchpress.com by 210.87.254.105 on 09/06/12
For personal use only.

Can. J. Chem. Downloaded from www.nrcresearchpress.com by 210.87.254.105 on 09/06/12
For personal use only.

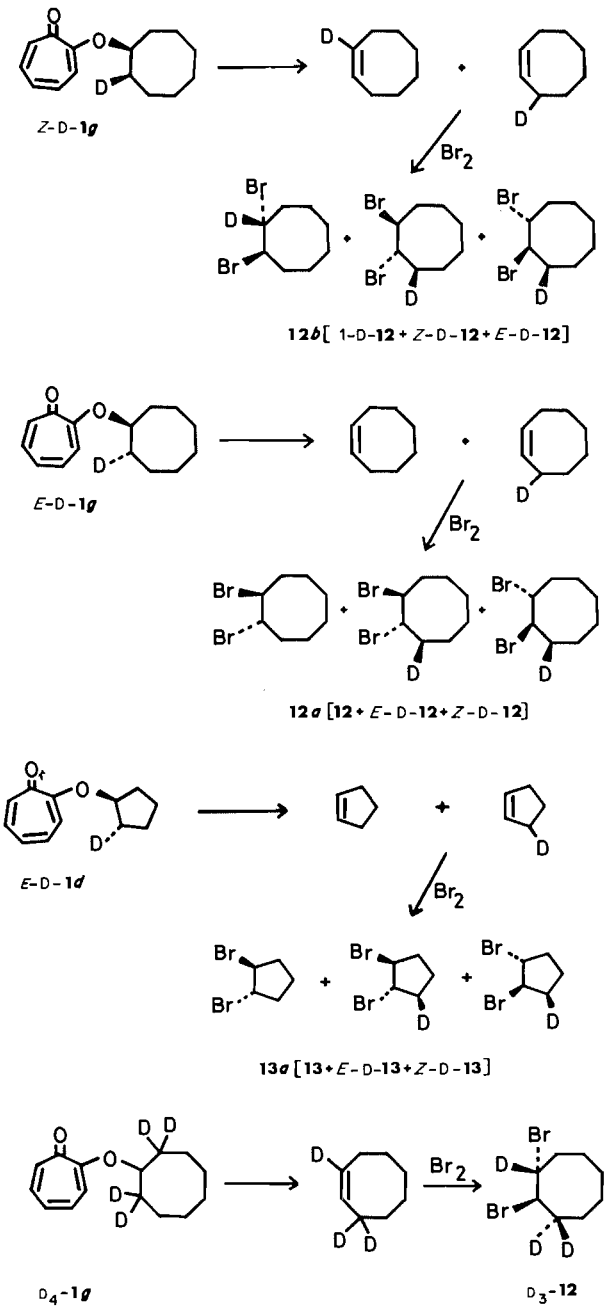

SCHEME 2

ysis of tetradeuterio and deuterium-free *g* to be k_H(453.7 K) = 3.2×10^{-5} s^{-1} and k_D(453.7 K) = 1.3×10^{-5} s^{-1}; thus, the relative rate was calculated as 1:2.5, a reasonable value for a primary isotope effect. The isotopic composition, which is crucial for the rate analysis, of the brominated thermolysates 1,3,3-trideuterio **12** (D_3-**12**) was $d_3:d_2:d_1:d_0$ = 95:4:1:0. Therefore, these two observations (*i*) the stereospecific *trans*-elimination and the recognition of this primary isotope effect, and (*ii*) a rate-determining nature for the C—H(D) bond-breaking step, have proven the reaction to be concerted. Furthermore, the exclusive formation of the trideuterio derivative from D_4-**1***g* ruled out a possible transannular hydrogen shift; this may be regarded as additional evidence for the electrocyclic mechanism.

In addition to the stereospecific feature, *trans*-elimination, a kinetic study provided supporting evidence; i.e., the rates of

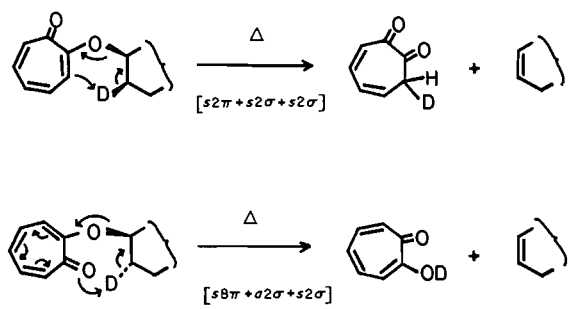

SCHEME 3

the reaction of **1***g* at various temperatures have been measured; in addition to k(453.7 K), the following rate constants k(447.2 K) = 1.6×10^{-5} s^{-1}, k(441.2 K) = 1.1×10^{-5} s^{-1}, k(435.2 K) = 6.3×10^{-6} s^{-1}, and k(426.2 K) = 2.6×10^{-6} s^{-1}, led us to obtain E_a = +140 kJ mol^{-1}, and $\Delta S^{\neq}$ = −21 J mol^{-1} K^{-1} at 180.5°C. This negative $\Delta S^{\neq}$ value was in the range of those observed for typical electrocyclic reactions, Cope rearrangement (6–8). Should the twelve-electron system be the concerted process, there should be an *antara* mode, which is in accord with the observed *trans* relationship; thus, the elimination may be designated as the [$s8\pi + a2\sigma + s2\sigma$] process.

Because formation of *trans*-cyclooctene is known, it might be suggested that the olefin (*cis*-**2***g*) isolated from **1***g* is the thermodynamically stable secondary product formed via the all-*supra* mode. However, this is unlikely since (*i*) assumption of primary formation of *trans*-**2***g* with the observed deuterium distributions via a thermally-forbidden [$s8\pi + a2\sigma + s2\sigma$] reaction requires a folded conformation of **1***g* having severe I-strain, and (*ii*) it is difficult to explain the unreactivity of the unstrained conformer of **1***g*. Nevertheless, this possibility can be eliminated by looking at a deuterated cyclopentyl ether. When *E*-D-**1***d* in decalin was refluxed at 180°C with the nitrogen stream, the volatile product collected as the dibromides (**13***a*) was found to contain the deuterium-free **13**, *E*-D-**13**, and *Z*-D-**13** in the ratio of 1:1:1. Consequently, no ambiguity has been left on this point.

The thermal *cis*-elimination of alkyl carboxylates to alkenes and carboxylic acids, which may be designated as the [$s2\pi + s2\sigma + s2\sigma$] process, generally needs more severe conditions: 1,3-di(acetoxymethyl)cyclohexane yielded 1,3-bis-methylenecyclohexane by heating at 555°C (9) and 4-(2-acetoxyethyl)-imidazole could be converted to 4-vinylimidazole at 500°C (10). The mildness of the pyrolysis of tropolonyl ethers, together with the reversal of the usual selectivity of the acid-induced dehydration of alcohols, makes this simple procedure valuable as a new method in organic syntheses for preparing or masking alkenes.

Experimental

The elemental analyses were performed by Miss M. Yamaguchi, this Institute. The nmr spectra were measured by an FX 100 Model spectrometer, JEOL, in $CDCl_3$ solutions unless otherwise stated, and the chemical shifts expressed in δ units were those from the internal $SiMe_4$. The mass spectra were measured by an 01SG Model spectrometer, JEOL.

*General procedure for preparation of 2-alkoxy- (**4**) and 2-cycloalkoxytropones (**1**) (ref. 11)*

A mixture of alkanol or cycloalkanol (**11**, ca. 2.3 mmol), *N*,*N*′-dicyclohexylcarbodiimide (DCC, 2.2 mmol), and CuCl (10 mg) in benzene (1 mL) was kept under a N_2 atmosphere with stirring for

Can. J. Chem. Downloaded from www.nrcresearchpress.com by 210.87.254.105 on 09/06/12
For personal use only.

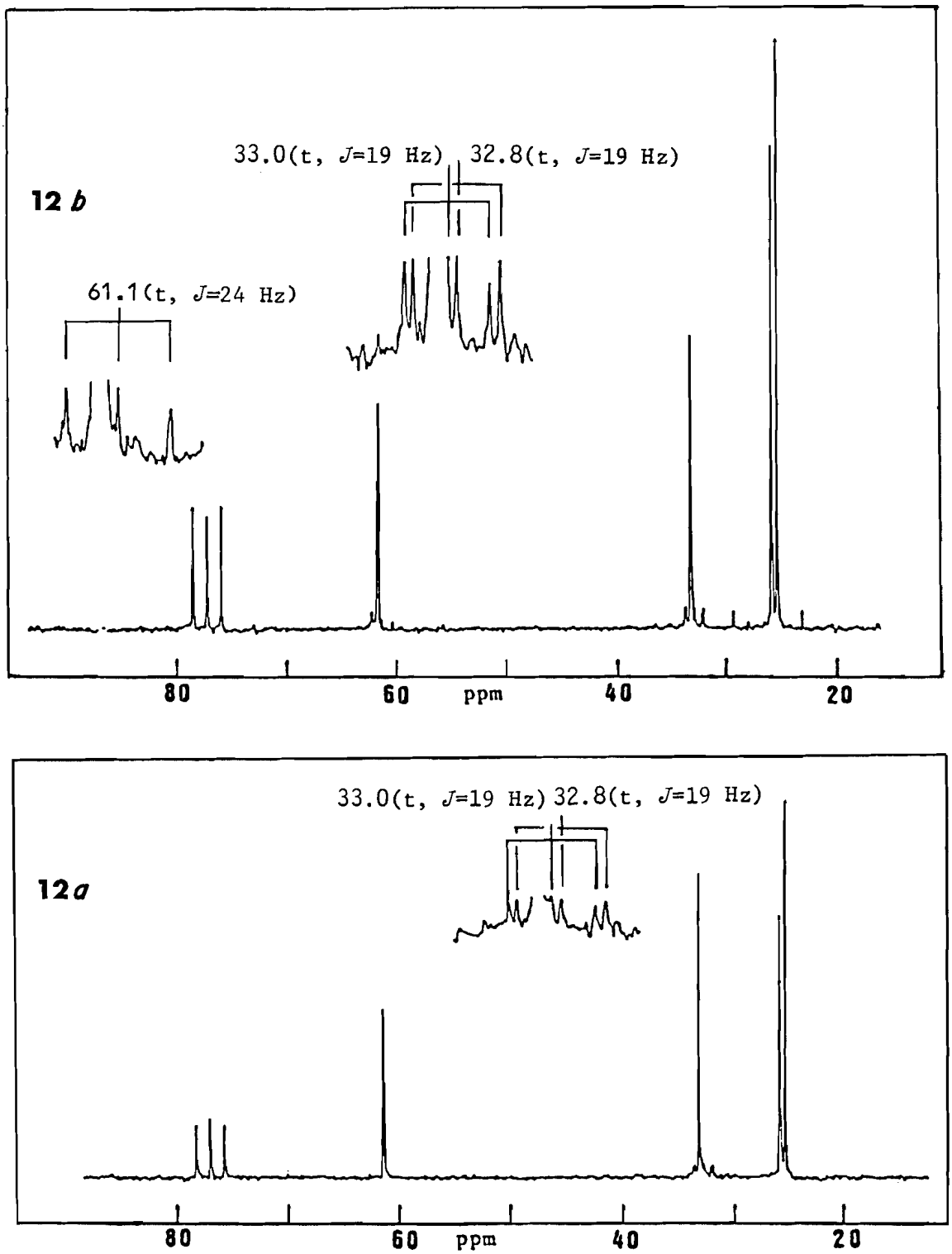

FIG. 1. The ^{13}C nmr spectra (expanded in part) of **12***a* and **12***b*.

10 to 24 h at 55°C depending on the progress of the reaction (tlc). A benzene solution (1 mL) of **3** or **10** (ca. 2.0 mmol) was added to the mixture, and heating at 80°C continued for another 24 h. After cooling, ethyl acetate (2 mL) was added to the mixture, and the resultant *N,N'*-dicyclohexylurea filtered. The organic layer was diluted with ether, and washed with aqueous KOH to remove the unreacted **3** or **10**. A residual oil obtained by distillation of ether *in vacuo* was chromatographed on a silica gel column; fractions eluted with benzene – ethyl acetate (9:1 to 8:2) afforded the desired **4** and **1**. The yields of the ethers were satisfactory in most cases. Characterizations of the ethers are summarized in Tables 1 and 2.[3]

[3] The ^1H nmr spectra of these alkoxy and cycloalkoxytropones are similar, and we wish to record the spectrum of **9***g* as representative: δ: 1.21 (6H, d, J = 7 Hz), 1.3–2.1 (14H, m), 2.75 (1H, sept, J = 7 Hz), 4.50 (1H, m), 6.57 (1H, dd, J = 9.5, 1.5 Hz), 6.72 (1H, dt, J = 11, 1.5 Hz), 6.95 (1H, dd, J = 11, 9.5 Hz), and 7.11 (1H, d, J = 1.5 Hz).

Can. J. Chem. Downloaded from www.nrcresearchpress.com by 210.87.254.105 on 09/06/12
For personal use only.

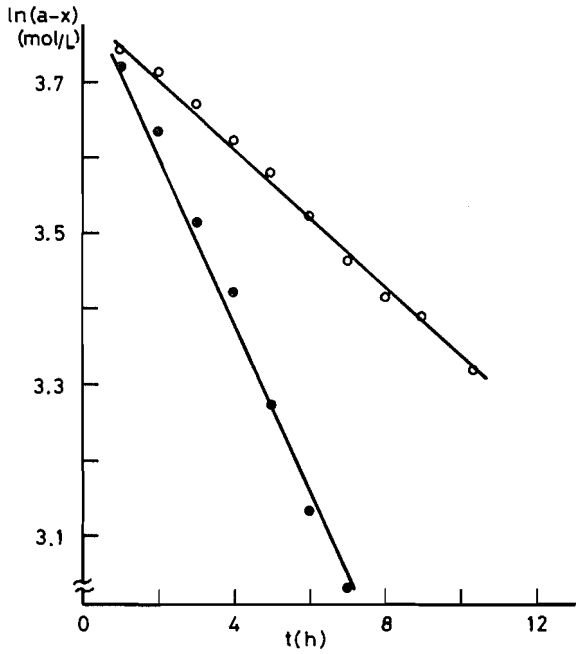

FIG. 2. The reaction rates for **1***g* (●) and D-**1***g* (○) at 180.5°C.

*Thermolysis of 2-(cyclopentyloxy)tropone (**1**d) in DMSO*

An anhydrous DMSO solution (0.5 mL) of **1***d* (45 mg) was heated at 180°C in a sealed tube for 8 h. Liberation of **3** was confirmed by $FeCl_3$ coloration, but absence of dimethyl sulfide eliminated the occurrence of the oxidation. The mixture was diluted with H_2O, and bubbled with a N_2 stream to collect the volatile material into a $CDCl_3$ solution. The nmr spectrum confirmed the formation of **2***d*.

*Thermolysis of 2-(2-butyloxy)tropone (**4**b) in DMSO*

An anhydrous DMSO solution (0.5 mL) of **4***b* (45 mg) was heated in a top-sealed glass ampule at 180°C for 8 h. Liberation of **3** was recognized ($FeCl_3$). After opening the vessel, the mixture was bubbled with a N_2 stream and volatile material was collected into a $CDCl_3$ solution. The nmr spectrum showed a formation of *Z*-**6***b* (δ: 1.50 (6H, d, J = 6 Hz) and 5.28 (2H, m)); *E*-**6***b* (δ: 1.53 (6H, d, J = 6 Hz) and 5.35 (2H, m)[4]); and **5***b* in 5%, 7%, and 7% yields, respectively.[5]

*Thermolysis of 2-(3-pentyloxy)tropone (**4**c) in DMSO*

An anhydrous DMSO solution (0.5 mL) of **4***c* (45 mg) was heated in a sealed glass ampule at 180°C for 8 h. The volatile material in the reaction mixture was similarly collected into a $CDCl_3$ solution with a N_2 stream. Its nmr spectrum showed a formation of *Z*-**6***c* (δ(C): 12.3, 14.1, 20.1, 122.8, and 132.3), 4%; *E*-**6***c* (δ(C): 13.9, 17.8, 25.5, 123.4, and 133.0),[6] 8%; and **5***c*, 20%.

*Thermolysis of **4**c in dioxane-d_8*

A dioxane-d_8 solution (0.3 mL) of **4***c* (45 mg) was heated at 180°C in a top-sealed nmr tube for 20 h. The ^{13}C nmr spectrometry revealed a formation of only *E*- and *Z*-**6***c* in a 1:2 ratio.

*Thermolysis of 2-cycloalkoxytropones (**1**, **8**, or **9**) in decalin. General procedure*

A decalin solution (0.5 mL) of **1**, **8**, or **9** (ca. 50–70 mg, 0.2 to 0.3 mmol) was sealed in a glass ampule, and heated at 180°C for 2 to 8 h. After cooling, the mixture was diluted with CCl_4 and extracted with 2 *N* KOH to recover **3** or **10**. The organic layer was washed with H_2O and dried on $MgSO_4$. Bromination of the CCl_4 solution at 0°C for 2 h, distillation of the solvent *in vacuo*, and purification through a silica gel column gave dibromoalkanes. The results of the thermolysis can be found in Table 2.

*Preparation of 2-(2-E-deuteriocyclooctyloxy)tropone (E-D-**1**g)*

To an anhydrous THF solution (50 mL) of $LiAlD_4$ (600 mg, 15 mmol), 1,2-epoxycyclooctane (3.6 g, 28 mmol) in THF (50 mL) was added drop by drop at 0°C. After 1 h, the mixture was refluxed for 17 h, and treated with ice and 1 *N* NaOH. An ether extract of the mixture was dried on $MgSO_4$, and removal of the solvent left an oil, 3.1 g, which was purified by distillation *in vacuo* (bath temperature 80–88°C/6 Torr (1 Torr = 133.3 Pa)) to give *E*-D-**11**, 2.05 g, 57%.

Similarly to deuterio-free **11**, *E*-D-**11** (967 mg, 7.5 mmol) and **3** (810 mg, 6.6 mmol) were condensed by DCC (1.51 g, 6.6 mmol) and CuCl (15 mg) to give *E*-D-**1***g*, 871 mg (75%) (δ: 1.3–2.0 (13H, m), 4.50 (1H, m), and 6.6–7.2 (5H, m); δ(C): 23.2, 23.3, 25.7, 26.8 (2C), 31.3 (t, $J_{C\text{-}D}$ = 19.6 Hz), 31.6, 79.5, 115.3, 127.5, 132.7, 136.1, 136.7, 164.0, and 181.0; *m/e*: 232 (5), 233 (100), 234 (22); d_0:d_1 = 5:95).

*Preparation of 2-(2-Z-deuteriocyclooctyloxy)tropone (Z-D-**1**g)*

To an anhydrous THF solution (25 mL) of $NaBD_4$ (1.08 g, 26 mmol) and **2***g* (3.85 g, 35 mmol), BF_3 etherate (2.4 mL, 20 mmol) in THF (10 mL) was added dropwise under the N_2 atmosphere, and kept at 20–25°C for 2 h with stirring. The mixtue was then diluted with H_2O, basified with 3 *N* NaOH (7.5 mL), and oxidized with 30% H_2O_2 (7.5 mmol) at 50°C for 75 min. After cooling, the solution was fractionated with aqueous NaCl and ether, then dried over $MgSO_4$ and heated to remove the solvent. A colorless oily residue, 3.2 g, was distilled *in vacuo* (bath temperature 80–88°C/6 Torr) to give a colorless liquid, *Z*-D-**11**, 2.3 g, 51%.

Similarly, from *Z*-D-**11** (983 mg, 7.6 mmol), **3** (806 mg, 6.6 mmol), DCC (1.54 g, 6.6 mmol), and CuCl (15 mg), *Z*-D-**11** was obtained as colorless needles, 917 mg (89%) (δ: 1.3–2.0 (13H, m), 4.50 (1H, m), and 6.6–7.2 (5H, m); δ(C): 23.2, 23.3, 25.8, 26.8 (2C), 31.4 (t, $J_{C\text{-}D}$ = 18.5 Hz), 31.7, 79.6, 115.4, 127.5, 132.7, 136.1, 136.7, 164.0, and 181.0; *m/e*: 232 (14), 233 (100), 234 (25); d_0:d_1 = 12:88).

*Preparation of 2-(2,2,8,8-tetradeuteriocyclooctyloxy)tropone (D_4-**1**g)*

Cyclooctanone (2.5 g, 20 mmol) was treated wih a mixture of dioxane (1.5 mL) and D_2O (6 mL) with K_2CO_3 (60 mg) at 145°C in a sealed tube for 46 h. From the mixture, the solvent was removed *in vacuo*, and the residue was fractionated with ether and H_2O. Ether extracts afforded a colorless oily deuteriocyclooctanone, 2.4 g, which was then dissolved in methanol (25 mL) and reduced with $NaBH_4$ (700 mg, 19 mmol) at 0°C to colorless oily D_4-**11**, 1.55 g, 59%.

As above, D_4-**11** (660 mg, 5 mmol) was treated with **3** (660 mg, 5.4 mmol), DCC (1 g, 5 mmol), and CuCl (10 mg) to give colorless crystalline D_4-**1***g*, 538 mg, 53% (δ: 1.4–2.0 (10H, m), 4.53 (1H, br s), and 6.6–7.2 (5H, m); δ(C): 23.1 (2C), 25.7, 26.7 (2C), 31.3 (2C, m), 79.4, 115.3, 127.5, 132.7, 136.1, 136.6, 163.9, and 181.0; *m/e*: 234 (2), 235 (4), 235 (100), 237 (26); d_2:d_3:d_4 = 2:3:95).

*Preparation of 2-(2-E-deuteriocyclopentyloxy)tropone (E-D-**1**d)*

To a mixture of benzene and 2-*E*-D-cyclopentanol (710 mg), prepared from **2***d* by MCPBA oxidation and following $LiAlD_4$ reduction, DCC (1.375 g) and CuCl (20 mg) were added and kept at 55°C for 21 h. Then **3** (1.040 g) was added and kept at 80°C for a further 5 h. The product, *E*-D-**1***d*, obtained in 86.5%, was characterized by the nmr (δ: 1.4–2.1 (7H, m), 4.80 (1H, qm, J = 6 Hz), and 6.6–7.3 (5H, m); δ(C): 24.1, 24.2, 32.3 (t, J = 19.5 Hz), 32.6, 80.7, 114.6, 127.3, 132.8, 136.1, 136.5, 164.3, and 180.7) and mass spectrum (*m/e*: 191 and 190 (M^+); d_1:d_0 = 98:2).

Thermolysis of E-D-**1**g *in decalin*

E-D-**1***g* (151 mg, 0.7 mmol) in decalin (1 mL) was heated at 180°C

[4] In the literature (12) are reported ^1H nmr values measured for neat liquid: δ: 1.54 (6H, d, J = 7 Hz) and 5.37 (2H, m) for *Z*-**6***b* and δ: 1.58 (6H, d, J = 6 Hz) for *E*-**6***b*.

[5] Low yields after the work-up are due to the volatility of the products. The nmr spectrometry of the whole mixture indeed disclosed no signals other than for the described rpoducts.

[6] The ^1H nmr spectra of *E*-**6***c* and *Z*-**6***c* are mutually indistinguishable. These ^{13}C nmr values were obtained by determination with the authentic samples prepared independently.

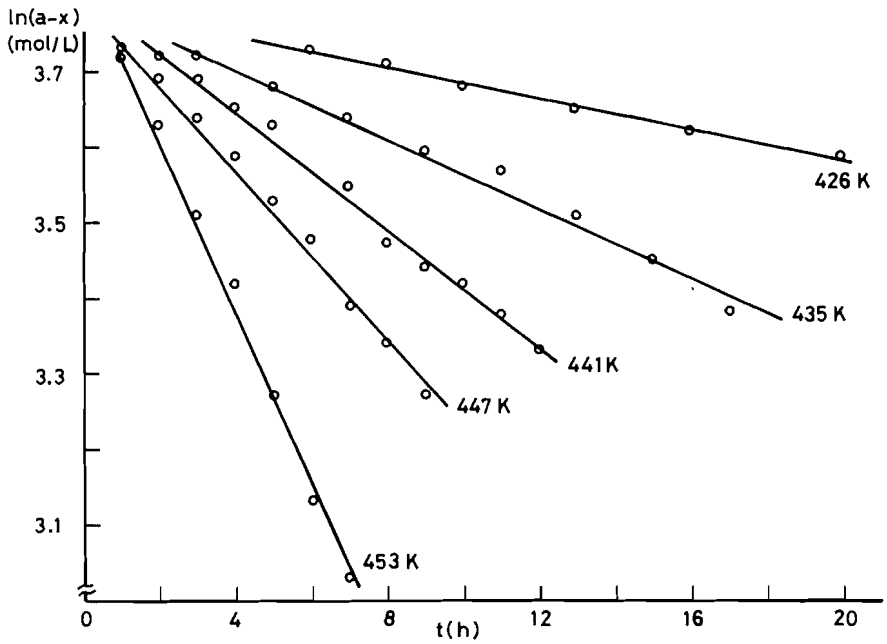

FIG. 3. The reaction rates for **1***g* at various temperatures.

for 14 h. The mixture was then diluted with CCl_4 and washed with 3 *N* KOH. The organic layer was treated with Br_2 in CCl_4, and the solvent was removed by distillation *in vacuo*. The residue was chromatographed on a silica gel column to give a colorless oil, **12***a*, 145 mg (77%).

Thermolysis of Z-D-**1***g in decalin*

Similarly, Z-D-**1***g* (209 mg, 0.96 mmol) in decalin (1 mL) was heated at 180°C for 14 h. After similar work-up, the thermolysates were characterized as the dibromide, a colorless oil, **12***b*, 190 mg (73%).

Thermolysis of D_4-**1***g in decalin*

Similarly, D_4-**1***g* (90 mg, 0.41 mmol) in decalin (0.5 mL) was heated at 180°C for 14 h. After the bromination as above, the deuterio **2***d* was obtained as a colorless liquid, 82 mg (73%), whose mass spectrum showed it to be solely the trideuterio derivative.

Thermolysis of E-*D*-**1***d in decalin*

E-D-**1***d* (322 mg) in decalin (5 mL) was refluxed for 14 h with a continuous bubbling of the N_2 stream to collect a volatile thermolysate into a cold Br_2-containing CCl_4 solution. Subsequently, the solution was evaporated *in vacuo* to leave a colorless oil, **13***a*, 90 mg (24%). The ^{13}C nmr (δ(C): 21.0 (C-4 of d_0) and 21.1 (C-4 of d_1) with a ratio of 2:1, 33.6 (t, J = 20 Hz, C-3 of d_1)[7] and 33.9 (C-3 bearing no *d*), and 57.2 (C-1 and C-2 of d_0) and 57.3 (C-1 and C-2 of d_1) with a ratio of 1:2) indicated the product to be a mixture of the deuterium-free **13**, *E*-D-**13**, and Z-D-**13** in a ratio of 1:1:1.

Kinetic experiments of deuterated 2-(cyclooctyloxy)tropones

Dioxane-d_8 solutions (0.3 mL) containing the deuterio **1***g* (ca. 35 mg) were placed in top-sealed nmr tubes, and heated on a constant temperature bath for appropriate periods. The reaction was monitored by ^1H nmr spectrometry in respect to signals at δ 4.5 due to the carbinyl proton of **1***g* and δ 5.7 due to the resultant olefinic protons of **2***g*.

Preparation of cyclooctyl phenyl ether (7) and its attempted thermolysis

A mixture of **11** (610 mg, 4.7 mmol), DCC (1.1 g, 5.5 mmol), and CuCl (10 mg) was heated at 55°C for 22 h under the N_2 atmosphere. To the mixture, phenol (580 mg, 6.2 mmol) was added, and heated again at 100°C for 23 h. A work-up in the usual manner gave 210 mg (19%) of **7**, a colorless liquid (δ: 1.2–2.0 (14H, m), 4.28 (1H, m), 6.87 (3H, m), and 7.23 (2H, m); δ(C): 23.2 (2C), 25.8, 27.1 (2C), 31.7 (2C), 77.6, 115.9 (2C), 120.2, 129.3 (2C), and 157.7. *Anal.* calcd. for $C_{14}H_{20}O$: C 82.30, H 9.87; found: C 82.35, H 9.60).

A dioxane-d_8 solution (0.3 mL) containing **7** (50 mg) was placed in a top-sealed nmr tube and heated at 180°C for 28 h. The nmr spectrum revealed no reaction. Removal of the solvent by evaporation left 45 mg of the starting **7**.

[7] In the case of **13**, the δ of C-3 was the same for both *E*- and Z-D-**13**.

Acknowledgement

The authors thank the Ministry of Education, Science, and Culture of Japan for the operating grant (No. 58740235) to H. M.

1. H. TAKESHITA, H. MAMETSUKA, and K. UCHIDA. Chem. Lett. 1071 (1982).
2. Y. KITAHARA and M. FUNAMIZU. Bull. Chem. Soc. Jpn. **31**, 782 (1958).
3. Y. KITAHARA and T. KATO. Bull. Chem. Soc. Jpn. **37**, 895 (1964).
4. H. TAKESHITA and H. MAMETSUKA. J. Chem. Soc. Chem. Commun. 483 (1983).
5. H. TAKESHITA, H. MAMETSUKA, and N. MATSUO. Bull. Chem. Soc. Jpn. **55**, 1137 (1982).
6. B. W. BYCROFT and W. LANDEN. Chem. Commun. 168 (1970).
7. P. MESTNER, T. N. PHAM, and J. VIALLE. J. Chem. Res. (S), 478 (1978).
8. M. J. S. DEWAR and L. E. WADE, JR. J. Am. Chem. Soc. **99**, 4417 (1977).
9. W. G. BAILEY and J. ECONOMY. J. Org. Chem. **23**, 1002 (1958).
10. C. G. OVERBERGER and N. VORCKHEIMER. J. Am. Chem. Soc. **85**, 951 (1963).
11. E. VOWINKEL Chem. Ber. **99**, 1479 (1966).
12. W. BRUGEL. Handbook of NMR spectral parameters. Vol. 1. Heiden and Son Ltd., London. 1979. p. 161.

Can. J. Chem. Downloaded from www.nrcresearchpress.com by 210.87.254.105 on 09/06/12
For personal use only.

Acid–base properties in the triplet state of aromatic ketones studied by nanosecond laser flash photolysis[1]

HARUO SHIZUKA AND EHICHI KIMURA
Department of Chemistry, Gunma University, Kiryu, Gunma 376, Japan

Received January 26, 1984

This paper is dedicated to Professor Paul de Mayo on the occasion of his 60th birthday

HARUO SHIZUKA and EHICHI KIMURA. Can. J. Chem. **62**, 2041 (1984).

Acid–base properties in the triplet state of aromatic ketones in H_2O-CH_3CN (4:1) mixtures have been studied by means of nanosecond laser flash photolysis. The acidity constants $pK_a(T)$ in the triplet state were determined by the $T_n \leftarrow T_1$ absorbance titration curve, the Ware plot, and the Rayner–Wyatt plot. Good agreement among them shows that the acid–base equilibrium in the T_1 state of aromatic ketones is established during the triplet lifetime. A linear relation between $pK_a(T)$ and the Taft σ^* values was obtained for phenyl alkyl ketones.

HARUO SHIZUKA et EHICHI KIMURA. Can. J. Chem. **62**, 2041 (1984).

Opérant dans des mélanges H_2O-CH_3CN (4:1) et faisant appel à la photolyse flash au laser à l'échelle de la nanoseconde, on a étudié les propriétés acide–base dans l'état triplet de cétones aromatiques. On a déterminé les constantes d'acidité, $pK_a(T)$, dans l'état triplet en se basant sur les courbes de titration d'absorbance $T_n \leftarrow T_1$, sur les courbes de Ware et sur les courbes de Rayner–Watt. L'existence d'une bonne concordance entre les diverses valeurs démontre que l'équilibre acide–base dans l'état T_1 des cétones aromatiques s'établit au cours de la durée de vie du triplet. Dans le cas des phényl alkyl cétones, on a obtenu une corrélation linéaire entre les $pK_a(T)$ et les valeurs σ^* de Taft.

[Traduit par le journal]

Can. J. Chem. Downloaded from www.nrcresearchpress.com by 210.87.254.6 on 09/06/12
For personal use only.

Introduction

Proton transfer reactions in the excited states of aromatic compounds are elementary processes not only in photochemistry but also in biochemistry. The acid–base properties of aromatic compounds in the excited state are closely related to the corresponding electronic structure, which is considerably different from that in the ground state.

Since the original work of Förster (1950) (1) and Weller (1952) (2) showing that the acidity constant pK_a^* in the excited state is markedly different from that in the ground state, a number of studies on pK_a^* have been reported (3–9). It is known that the pK_a^* values can be estimated by means of the Förster cycle (1–3, 10), the fluorescence titration curve (2, 3), and the $T_n \leftarrow T_1$ absorbance titration curve (11). These methods involve the assumptions that proton transfer in the excited state is very fast and that the acid–base equilibrium may be attained during the lifetime of the excited state. Establishment of prototropic equilibrium in the excited singlet state has been reported in the cases of 2-naphthol-6,8-disulfonate (12), 2-naphthol (13), and 1-isoquinoline (14).

However, the prototropic equilibrium in the S_1 state of aromatic compounds having an electron-donating group (e.g., an amino or hydroxy group), where protonation or dissociation occurs, is not to be the case. Proton-induced fluorescence quenching takes place effectively due to electrophilic protonation at a carbon atom of the aromatic ring in the S_1 state of such species, leading to hydrogen exchange (or isotope exchange) (15). Electron migration from the electron donating substituent to the aromatic ring (i.e., intramolecular charge transfer) occurs in the S_1 state in polar media, and the CT state is responsible for the proton-induced quenching (15, 16). In fact, it has been shown that the proton-induced quenching is competitive with proton transfer reactions in the excited state of neutral naphthylamines (that is, the simple acid–base equilibrium cannot be established in the excited state of aromatic amines) and dynamic analyses taking into account the proton-induced quenching are, therefore, needed in order to obtain the correct pK_a^* values (17). The dynamic analyses by means of nanosecond time-resolved spectroscopy with fluorimetry were applied to the other aromatic amines (18–20) and naphthols (13). The Stuttgart group (21) has supported our method to determine the pK_a^* values of naphthylamines. Similar experiments for excited naphthols have been reported by Harris and Selinger (22).

As for the triplet state, a laser study of the prototropic equilibrium of triplet benzophenone has been reported by Rayner and Wyatt (23). Recently, the acid–base equilibrium in the triplet acridinium ion has been investigated by Nishida *et al.* (24). Establishment of the prototropic equilibrium in the triplet state of phenyl alkyl ketones has not yet been given. A study of the acid–base equilibrium in the triplet state of aromatic ketones was needed in the course of our investigation of proton-transfer reactions in the excited state of aromatic compounds. In addition, the variation of acid–base properties in the triplet state of aromatic ketones as a function of their electronic structures was of interest. This paper reports an examination of the acid–base properties in the T_1 state of aromatic ketones studied by means of nanosecond laser flash photolysis. The $pK_a(T)$ values were determined by the $T_n \leftarrow T_1$ absorbance titration curve (11), the Ware plot (25), and the Rayner–Wyatt plot (23).

Experimental

Materials

Benzophenone, acetophenone, propiophenone, and benzyl phenyl ketone were G.R. grade products from Tokyo Kasei. Benzophenone was purified by repeated recrystallization from H_2O–EtOH mixtures. Sulfuric acid (97%, Wako), D_2SO_4 (96–98%, isotope purity 99%, Merck), and D_2O (99.7% Merck) were used. Distilled water and acetonitrile (G.R. grade, Wako) were used as a H_2O-CH_3CN mixture (4:1 in volume). The concentrations of benzophenone and the other ketones were 3×10^{-3} *M* and ca. 1×10^{-2} *M*, respectively. The pH values of samples were recorded with a pH meter (Corning M-125). The samples were thoroughly degassed by freeze–pump–thaw cycles on a high vacuum line. All experiments were carried out at 20°C.

[1] This paper was supported by a Scientific Research Grant-in-Aid from the Ministry of Education of Japan (No. 58470001).

Absorption spectra were recorded of the ketones at the high acidities used; no changes were observed indicating that they are stable with respect to ground state condensation reactions.

Laser flash photolysis

Nanosecond laser flash photolysis at 347 nm was carried out using a Q-switched ruby laser (JEOL JLS-R34A, 23-ns half-width). The output energy of the 347 nm pulse was recorded digitally on a peak-hold meter calibrated with a thermopile (TRG Model 107) and a pulse generator (Anritsu MG 411B). The output energy for excitation was attenuated to less than 15 mJ/pulse by glass plates in order to avoid triplet–triplet annihilation. The transient absorbances for a series of experiments at different acidities were corrected to the same laser intensity. A xenon flash (~600-μs half-width) from a stroboscope (Sunpack Model 107) was used as an analytic flash for the detection of the transients. The monitoring light was passed through a grating monochrometer (Hitachi Model 139) and was analyzed by a detection system consisting of a photomultiplier tube (HTV R636) and a 200 MHz oscilloscope (Iwatsu SS-6200). The triplet transients of benzophenone, acetophenone, propiophenone, and benzyl phenyl ketone were monitored at 525, 370, 360, and 350 nm, respectively.

Photochemical isotope-exchange reaction

The photochemical isotope-exchange reactions were carried out with 2×10^{-2} *M* acetophenone (or propiophenone) in D_2O–CH_3CN (4:1) with $[D_2SO_4] = 0.05$ *M*. A medium-pressure mercury lamp with an interference glass filter was used as the 313-nm radiation source. The isotope-exchange reaction in the dark was also performed at room temperature as a blank test. Actinometry was carried out with a ferric oxalate solution (26, 27). After a definite irradiation, the sample solution was neutralized wih sodium carbonate solution. The sample was then extracted with benzene several times, followed by evaporation under reduced pressure. The resulting residue was purified by passing it through a silica gel column with benzene as a developing solvent. The H–D isotope-exchange positions of acetophenone or propiophenone were determined by means of ^1H nmr spectroscopy (Varian EM-360 60 MHz) and quantitative analyses of the exchange reaction were carried out by means of mass spectroscopy (JEOL JMS6).

Results and discussion

Nanosecond laser flash photolyses of aromatic ketones

The transient absorption spectra of aromatic ketones at the delay time 200 ns after the pulse, in the absence of protons, are shown in Fig. 1 (28).

It is well known that triplet formation or decay through intersystem crossing of carbonyl compounds is very rapid, according to El-Sayed's rule (29). For benzophenone (BP), a strong absorption band with a maximum at 525 nm was observed just after pulsing, which decayed by first-order kinetics with the decay rate $(\tau_0)^{-1} = 2.3_8 \times 10^5\ s^{-1}$. This band corresponds to that of the $T_n \leftarrow T_1$ absorption in water (30). The absorption bands at longer wavelengths (600 nm), which decayed very slowly in comparison with the decay rate of the $T_n \leftarrow T_1$ band at 525 nm, may be due to those of the ketyl radical (545 nm) and the radical anion (600 nm) (31). These long-lived transients are also produced by flash photolysis of BP in water (30, 32). Fortunately, the triplet lifetime τ_0 was relatively short, and its decay rate could be measured at 525 nm without interference from the longer-lived transients (28).

Laser flash photolysis of a 5 *M* H_2SO_4 solution of benzophenone produced a weak transient with $\lambda_{max} = 505$ nm. The transient spectrum with a lifetime of 17 ns was similar to that observed by conventional flash photolysis (33) as shown in Fig. 2. The transient spectrum is, therefore, believed to be protonated benzophenone triplet. This transient absorption was weak, and the decay rate of benzophenone triplet could be measured at 525 nm. The $T_n \leftarrow T_1$ absorption of acetophenone (34) and the other phenyl alkyl ketones are also shown in Fig. 1. The decay rate of the triplet state of aromatic ketones were monitored at 370 nm (acetophenone), 360 nm (propiophenone), and 350 nm (benzyl phenyl ketone), where the $T_n \leftarrow T_1$ absorption of the corresponding protonated ketone was very weak as shown in Fig. 2. There was no ketyl radical (or anion radical) formation in laser flash photolysis of phenyl alkyl ketones in neutral H_2O–CH_3CN (4:1), in contrast to that of BP. This is due to the fact that the lowest triplet state of the phenyl alkyl ketones is not $^3(n,\pi^*)$ but $^3(\pi,\pi^*)$ in polar media (34, 35), whereas the lowest triplet state of BP is $^3(n,\pi^*)$.

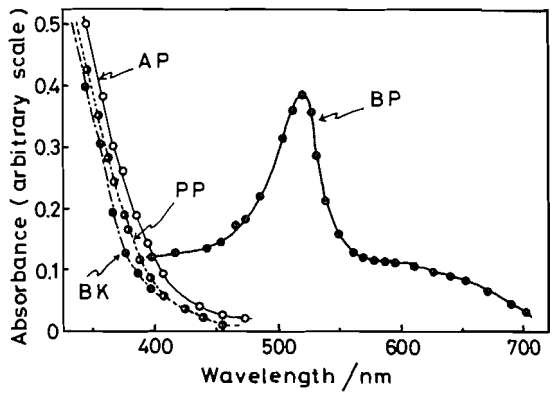

FIG. 1. Transient absorption spectra of benzophenone (BP) acetophenone (AP), propiophenone (PP), and benzyl phenyl ketone (BK) in H_2O–CH_3CN (4:1) mixtures at 200 ns after pulsing at room temperature. The spectra were taken from ref. 28, except for BK.

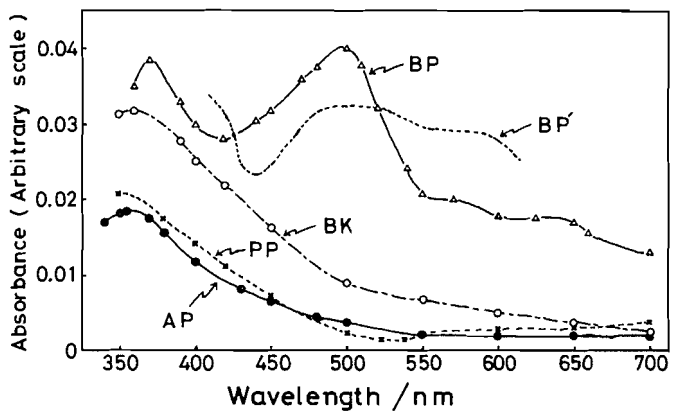

FIG. 2. Transient absorption spectra of aromatic ketones in H_2O–CH_3CN (4:1) mixtures in the presence of 5M H_2SO_4 just after pulsing at 20°C, where BP′ denotes the transient observed by conventional flash photolysis (33).

It is known that the triplet lifetime of BP depends upon its concentration (self-quenching) (30). However, if the same concentration of the ketone is used throughout the experiments with and without acids, this problem may be excluded. There is little or no quenching of triplet ketones by the counter anion SO_4^{2-} under the experimental conditions (28).

Triplet–Triplet absorbance titration curve

The $T_n \leftarrow T_1$ absorbance titration curves of benzophenone (BP), acetophenone (AP), propiophenone (PP), and benzyl phenyl ketone (BK) at various acidities are shown in Fig. 3 (a)–(d), respectively. The absorbance was the value of the initial absorbance. From the midpoint of the titration curve

Can. J. Chem. Downloaded from www.nrcresearchpress.com by 210.87.254.6 on 09/06/12
For personal use only.

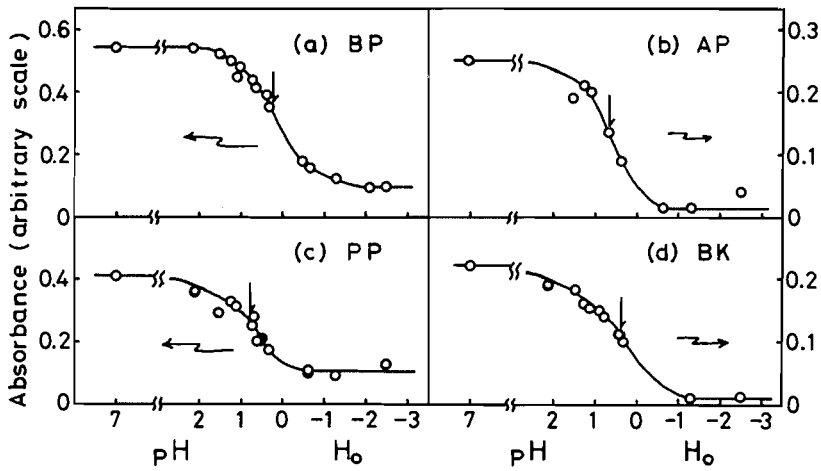

FIG. 3. The $T_n \leftarrow T_1$ titration curves of aromatic ketones in H_2O–CH_3CN (4:1) at 20°C.

(11), the acidity constant $pK_a(T)$ of the triplet state of aromatic ketones can be simply determined to be 0.20 ± 0.02 (BP), 0.63 ± 0.07 (AP), 0.75 ± 0.05 (PP), and 0.35 ± 0.05 (BK).

Kinetic analyses: Ware and Rayner–Wyatt plots

The oscillogram trace of the $T_n \leftarrow T_1$ absorption of each of the aromatic ketones showed a single exponential decay with and without protons. The observed triplet lifetimes τ of BP, AP, PP, and BK are listed in Table 1. The τ values decreased quickly with increasing proton concentration. The acid–base reaction in the triplet state of aromatic ketones (^3A) can be accounted for by the scheme in reaction [1]:

[1]
$$\begin{array}{ccccc} {}^1A & \xrightarrow{k_{isc}} & {}^3A + H^+ & \underset{k_2}{\overset{k_1}{\rightleftharpoons}} & {}^3A^+H \\ \uparrow h\nu & & \downarrow (\tau_0)^{-1} & & \downarrow (\tau_0')^{-1} \\ A & & + H^+ & \underset{k_2^0}{\overset{k_1^0}{\rightleftharpoons}} & A^+H \end{array}$$

where τ_0 and τ_0' denote the lifetimes of ^3A (in the absence of protons) and $^3A^+H$ respectively, k_1 and k_2 the protonation and dissociation rate constants in the triplet state, respectively, and A^+H protonated aromatic ketones. At the highest acidities used the ground state ketones are unprotonated (6). If we assume that the rates of the proton transfer reactions ($k_1[H^+]$ and k_2) in the triplet state are very fast in comparison with the triplet decay rates ($(\tau_0)^{-1}$ and $(\tau_0')^{-1}$), respectively (that is, an acid–base equilibrium is established within the triplet lifetime), the following equations proposed by Ware (25) and Rayner–Wyatt (23) may be applied to the present system. The Ware equation reads

$$[2] \quad \{\tau^{-1} - \tau_0^{-1}\}^{-1} = \{(\tau_0')^{-1} - \tau_0^{-1}\}^{-1}\left\{1 + \frac{K_a}{[H^+]}\right\}$$

The Rayner–Wyatt equation reads

$$[3] \quad \frac{1}{[H^+]}\{\tau^{-1} - \tau_0^{-1}\} = \frac{(\tau_0')^{-1}}{K_a} - \frac{\tau^{-1}}{K_a}$$

where τ denotes the observed triplet lifetime and K_a the equilibrium constant in the triplet state, which is equal to k_2/k_1. Both equations are derived on the assumptions that $k_1[H^+] \gg \tau_0^{-1}$ and $k_2 \gg (\tau_0')^{-1}$, as described above. In fact, if eq. [4] (23) is substituted into eq. [3] one can derive the Ware equation (eq. [2]).

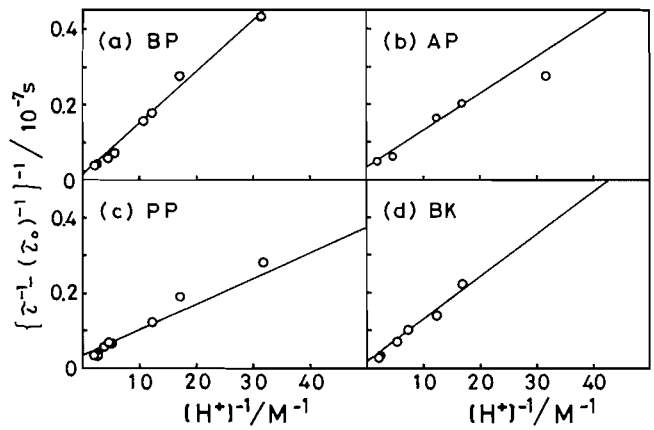

FIG. 4. The Ware plot of aromatic ketones. For details see text.

$$[4] \quad \tau^{-1} = \frac{k_1[H^+]}{k_2 + k_1[H^+]}(\tau_0')^{-1} + \frac{k_2}{k_2 + k_1[H^+]}\tau_0^{-1}$$

The Rayner–Wyatt equation is very sensitive to the τ value which appears on both sides in eq. [3]. The Ware equation is sensitive to $[H^+]$, since the difference between τ^{-1} and τ_0^{-1} becomes small at lower concentrations of protons. The Ware plot of $(\tau^{-1} - \tau_0^{-1})^{-1}$ as a function of $[H^+]^{-1}$ is shown in Fig. 4, and a straight line is obtained, demonstrating that the experimental results agree with eq. [2]. From the slope and intercept, the K_a value can be determined. The $pK_a(T)$ values of aromatic ketones obtained by the Ware plot are 0.13 ± 0.02 (BP), 0.60 ± 0.10 (AP), 0.70 ± 0.10 (PP), and 0.30 ± 0.05 (BK). These data are listed in Table 2.

The Rayner–Wyatt plot of $(\tau^{-1} - \tau_0^{-1})[H^+]^{-1}$ vs. τ^{-1} is depicted in Fig. 5. Although the deviation from linearity in the case of PP (*c*) and simple scatter in the cases of BP (*a*) and AP (*b*) exist in Fig. 5, the experimental results are approximately fitted to eq. [3], except for BK. From Rayner–Wyatt plot, the $pK_a(T)$ values are estimated to be 0.1 ± 0.1 (BP), 0.60 ± 0.15 (AP), and 0.78 ± 0.20 (PP). For BK, the laser flash experiments were repeated four times independently. However, similar results were obtained as shown in Fig. 5(*d*). The reason why no slope was obtained in the case of BK is unknown at the present time. Judging from the Ware and Rayner–Wyatt plots, in Figs. 4 and 5, the former is obviously superior to the latter in yielding the K_a values, though both eqs. [2] and [3] are essentially the same.

Can. J. Chem. Downloaded from www.nrcresearchpress.com by 210.87.254.6 on 09/06/12
For personal use only.

TABLE 1. Initial absorbance (A_b), first order decay constant (τ^{-1}) and lifetime (τ) of the transient observed in H_2O–CH_3CN (4:1) at 20°C at different acidities

Compound	pH or H_0	wt. % H_2SO_4	A_b[a]	$\tau^{-1}/10^6\ s^{-1}$	τ/ns
BP	7.00		0.545	0.238	4200[b]
	2.13		0.545	0.685	1460
	1.50		0.525	2.54	394
	1.23		0.500	3.85	260
	1.09		0.446	5.81	172
	1.04		0.480	6.58	152
	0.73		0.440	14.0	71.6
	0.67		0.413	15.6	64.0
	0.37		0.390	24.1	41.5
	0.31		0.352	24.3	41.1
	−0.50	10.8	0.175	27.9	35.9
	−0.67	13.0	0.160	32.1	31.2
	−1.3	23.2	0.123	37.0	27.0
	−2.1	30.1	0.093	36.9	27.1
	−2.5	36.8	0.095	37.0	27.0
AP	7.00		0.250	0.980	1020[b]
	1.50		0.190	4.61	217
	1.23		0.211	5.88	170
	1.09		0.200	7.04	142
	0.67		0.135	17.3	57.6
	0.31		0.093	21.7	46.1
	−0.67	13.0	0.015	28.2	35.4
	−1.3	23.2	0.015	34.7	28.8
	−2.5	36.8	0.040	13.2	76.0
PP	7.00		0.410	0.877	1140[b]
	2.09		0.361	2.04	490
	1.50		0.293	4.44	225
	1.23		0.328	6.21	161
	1.09		0.311	9.10	110
	0.73		0.252	16.1	62.1
	0.67		0.280	15.4	65.0
	0.59		0.202	18.7	53.6
	0.50		0.201	28.6	35.0
	0.46		0.212	31.5	32.0
	0.31		0.172	31.3	32.0
	−0.66	12.9	0.110	38.5	26.0
	−0.67	13.0	0.090	43.5	23.0
	−1.3	23.2	0.091	41.7	24.0
	−2.5	36.8	0.130	24.3	41.2
BK	7.00		0.222	2.21	453[b]
	2.09		0.190	2.81	356
	1.50		0.182	4.17	240
	1.23		0.158	6.67	150
	1.09		0.154	9.35	107
	0.88		0.150	11.6	86.5
	0.73		0.140	16.7	60.0
	0.40		0.110	33.3	30.0
	0.31		0.098	38.5	26.0
	−1.3	23.2	0.001	[c]	
	−2.5	36.8	0.001	[c]	

[a] Arbitrary scale.
[b] $\tau = \tau_0$ at pH = 7.0.
[c] Transient absorption is too weak for kinetic analysis.

It is noteworthy that the $pK_a(T)$ values determined by the $T_n \leftarrow T_1$ absorbance titration curve are in good agreement with those by the kinetic analyses (Ware and Rayner–Wyatt plots) as shown in Table 2. This means that for aromatic ketones the acid–base equilibrium in the T_1 state is attained during its lifetime. Equation [2], which is derived on the assumptions that

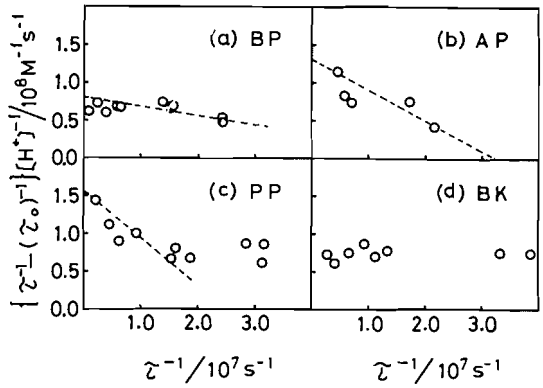

FIG. 5. The Rayner–Wyatt plot of aromatic ketones. See text.

$k_1[H^+] \gg \tau_0^{-1}$ and $k_2 \gg (\tau_0')^{-1}$, fairly holds in the present system. The establishment of prototropic equilibria in the triplet states of BP (23) and acridine (24) has been reported. Therefore it can be said that the prototropic equilibrium in the T_1 state of aromatic compounds is generally accomplished during the excited-state lifetime. The establishment is due to the fact that the forbidden $T_1 \rightarrow S_0$ decay is slow compared with the rate of proton transfer reaction.

Isotope-exchange reactions in the T_1 *state and proton-induced quenching*

It has been reported that the triplet state of acetone is quenched by water and the quenching is caused by the hydrogen (or isotope) exchange reaction in the triplet state (36). In the present work, a similar isotope-exchange reaction was observed. For example, the isotope-exchange reaction occurred effectively in the triplet state of AP (or PP) as shown in eq. [5] (or eq. [6]):

[5] 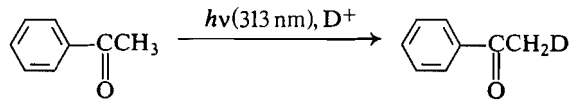

[6] 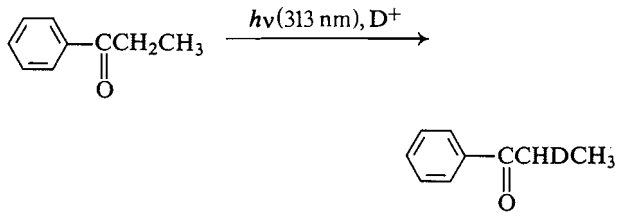

These reactions were detected by nmr and ms methods. The isotope-exchanged position (the methyl or methylene group adjacent to the carbonyl group) of AP or PP was determined by nmr spectroscopy (AP: methyl protons 2.59 ppm; PP: methylene protons 2.70–3.07 ppm). For BP having no methyl or methylene group, no isotope-exchange reaction in the T_1 state was observed under the experimental conditions. The reaction quantum yield for AP was ca. 0.2 in D_2O:CH_3CN (4:1) in the presence of 0.05 *M* D_2SO_4 at 313 nm. The value was determined by ms measurements at m/e = 120 and m/e = 121, calibrating naturally abundant ^{13}C in acetophenone. Unfortunately, the quantitative work for the photochemical isotope-exchange reaction was very difficult since it took place in the dark, even at room temperature. The isotope-exchange reaction of AP may proceed via enol formation (reaction [7]).

Can. J. Chem. Downloaded from www.nrcresearchpress.com by 210.87.254.6 on 09/06/12
For personal use only.

TABLE 2. The Taft σ* values (σ*), $pK_a(T)$ values, the triplet lifetimes (τ_0) of aromatic ketones, and the triplet lifetimes of protonated aromatic ketones (τ_0')

Compound	R^a	σ*[b]	$pK_a(T)$ Titration	$pK_a(T)$ Ware	$pK_a(T)$ Rayner–Wyatt	τ_0/μs[c]	τ_0'/ns[d]
BP	Ph	+0.600	0.20 ± 0.02	0.13 ± 0.02	0.1 ± 0.1	4.2_0	17
AP	CH_3	0.000	0.63 ± 0.07	0.60 ± 0.10	0.60 ± 0.15	1.0_2	30
PP	CH_2CH_3	−0.100	0.75 ± 0.05	0.70 ± 0.10	0.78 ± 0.20	1.1_4	38
BK	CH_2Ph	+0.215	0.35 ± 0.05	0.30 ± 0.05	[e]	0.45_3	25

[a] The substituent of aromatic ketones (PhCOR).
[b] Taken from ref. 38.
[c] Experimental errors within ±5%.
[d] Experimental errors within ±20%.
[e] The $pK_a(T)$ value of BK could not be determined by the Rayner–Wyatt plot.

[7]

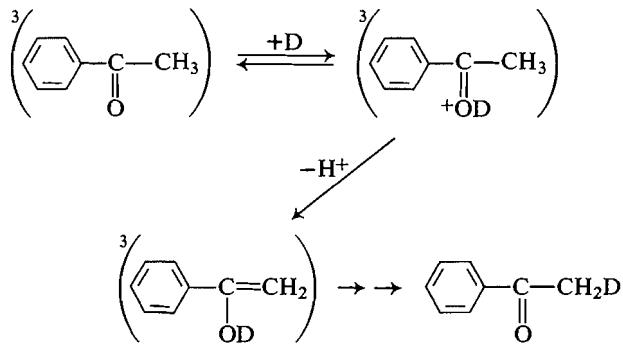

The radiationless decay due to deuterium (or proton) exchange does not exceed the proton dissociation rate k_2 in eq. [1], whereas the radiationless decay due to isotope (or proton) exchange is competitive with the protonation rate in the excited singlet state of aromatic compounds (15, 17–22).

There may be two reasons why the proton-induced quenching is not so effective in the triplet state. First, the excited state properties reflect the rates of the proton-induced quenching; the ionic reaction is dominant in the S_1 state and in contrast little or no proton-induced quenching in the T_1 state occurs (15). For 2-naphthylammonium ion, the proton transfer reaction occurs effectively in the S_1 state while the hydrogen atom transfer from triplet naphthylammonium ion to the ground aromatic ketones takes place (37). This is another example of the triplet state being more favourable for the radical reaction rather than the ionic reaction. Secondly, the prototropic position in an excited molecule is important for proton-induced quenching (15). When the prototropic reaction takes place at the electron-donating substituent (amino or hydroxy group) of aromatic compounds, proton-induced quenching occurs effectively by electrophilic attack at one of the carbon atoms of the aromatic ring (13, 15, 18–20). That is, effective proton-induced quenching is caused in the case that the electrophilic protonation occurs at a different position from that of the prototropic reaction. However, when the prototropic position (e.g., the oxygen atom of carbonyl group) having a relatively high charge density produced by intramolecular charge transfer is just the same as that of the electrophilic attack by protons, there is little or no proton-induced quenching and only the pK_a value may increase significantly in the excited state. The prototropic feature in the T_1 state of aromatic ketones is of the latter case, as discussed later.

Relationship between $pK_a(T)$ *and Taft* σ* *values*

Substituents attached to aromatic ketones may affect the basic properties in the triplet state, leading to a change in the $pK_a(T)$ values. We examined, therefore, the plot of $pK_a(T)$ as a function of Taft σ* values (38), as shown in Fig. 6. The plot suggests that there is a linear relation between $pK_a(T)$ and σ* values, except for BP. The σ-electron donating power of the alkyl group (R) increases the $pK_a(T)$ value; the +I effect of the group is in the order $CH_2CH_3 > CH_3 > CH_2Ph$. From Fig. 6, eq. [8] is obtained:

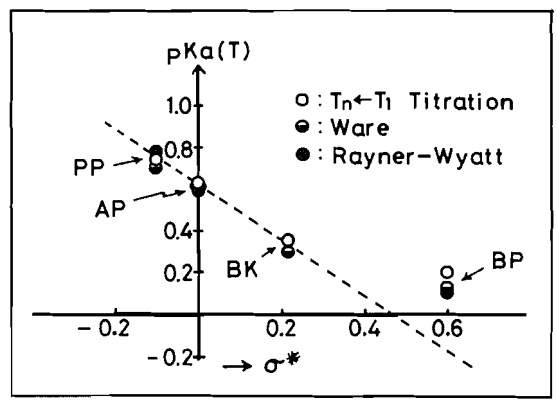

FIG. 6. The relation between $pK_a(T)$ and Taft σ* values.

[8] $pK_a(T) = \rho^*\sigma^* + pK_a(T)_0$

where the slope $\rho^* = -1.33$ and $pK_a(T)_0$ denotes the $pK_a(T)$ value of AP (0.60). The +I effect of R increases the charge density (i.e., basicity) at the oxygen atom of the carbonyl group, resulting in an increase of the $pK_a(T)$ value. For BP, a positive deviation from the line can be seen in Fig. 6. The $pK_a(T)$ of BP has a greater value than that (−0.2) expected from its σ* value. This fact cannot be explained by the difference in the T_1 character between $^3(n,\pi^*)$ (BP) and $^3(\pi,\pi^*)$ (phenyl alkyl ketones) in polar media. The electron density at the carbonyl group in the $^3(n,\pi^*)$ state should be smaller than that in the $^3(\pi,\pi^*)$ state, since the $^3(n,\pi^*)$ state involves back charge-transfer (from the carbonyl group to the phenyl ring). Actually the $^3(n,\pi^*)$ and $^3(\pi,\pi^*)$ states are perturbed by one another since the energy separation between them is very small in polar media (as discussed previously (28)). The reason why the basicity in the T_1 state of BP is relatively high may be due to a positive mesomeric effect (+M) from the phenyl group. That is, the $pK_a(T)$ value of BP becomes large compared to that estimated from eq. [8]. Electron migration from the phenyl group to the carbonyl group may occur in the T_1 state of BP resulting in an increase in the charge density at the carbonyl

Can. J. Chem. Downloaded from www.nrcresearchpress.com by 210.87.254.6 on 09/06/12
For personal use only.

group in ^{3}BP. The electronic structure in the T_1 state of BP in polar media has an intramolecular CT structure to some extent.

The experimental value (0.20 ± 0.1) of $pK_a(T)$ of BP obtained in a 20% acetonitrile solution is close to that (0.5 ± 0.3) in a 20% ethanol solution reported by Rayner and Wyatt (23). The $pK_a(T)$ value of BP in aqueous solution is known to be 1.5 ± 0.2 (23). The solvent effect on $pK_a(T)$ may be caused by the intramolecular CT character in ^{3}BP, which is dominant in aqueous solution compared to that in mixtures. The pK_a values in the T_1 state of aromatic ketones having an electron-withdrawing group (carbonyl group) are greatly increased in comparison with those in the ground state (BP: $pK_a(S_0) = -5.7$ (39); AP: $pK_a(S_0) = -6.1$ (6)).

The determination of $pK_a(T)$ value of BP by means of the Förster cycle is more difficult than by laser flash photolysis because the measurement of the correct value of $pK_a(S_0)$ in the ground state of BP is not easy. The $pK_a(S_0)$ value of BP is negatively large ($-6.09 \sim -6.25$ on the H_0 scale (40); -5.70 on the H_B scale (39)). At higher concentrations of H_2SO_4, the $pK_a(S_0)$ value depends upon the H_0 or H_B scale as discussed by Rayner and Wyatt (23). A similar situation may exist for other aromatic ketones. Therefore, it can be said that the determination of $pK_a(T)$ values of aromatic ketones by means of the $T_n \leftarrow T_1$ absorbance titration method (11) has the advantage of greater simplicity. The kinetic analysis by the Ware plot (25) is also available for the determination of $pK_a(T)$ values.

Conclusion

The results reported are consistent with the scheme shown in reaction [1] and allow the following conclusions to be drawn: (*1*) The $pK_a(T)$ values determined by the $T_n \leftarrow T_1$ absorbance titration curve, the Ware plot, and the Rayner–Wyatt plot show the same values within experimental errors. (*2*) The acid–base equilibrium in the triplet state of aromatic ketones is established during the lifetime of triplet aromatic ketones. The triplet lifetime is long enough to produce the prototropic equilibrium. (*3*) A linear relation between $pK_a(T)$ and the Taft σ^* values is obtained, except for benzophenone. (*4*) Proton-induced quenching in the T_1 state is small compared to the rates of proton transfer reactions.

1. TH. FÖRSTER. Z. Elektrochem. Angew. Phys. Chem. **54**, 42 (1950); **54**, 531 (1950).
2. A. WELLER. Ber. Bunsenges. Phys. Chem. **56**, 662 (1952); **66**, 1144 (1956).
3. A. WELLER. Prog. React. Kinet. **5**, 273 (1970).
4. H. BEENS, K. H. GRELLMAN, M. GURR, and A. WELLER. Discuss. Faraday Soc. **39**, 183 (1965).
5. E. V. DONCKT. Prog. React. Kinet. **5**, 273 (1970).
6. J. F. IRELAND and P. A. H. WYATT. Adv. Phys. Org. Chem. **12**, 131 (1976).
7. E. L. WEHRY and L. B. ROGERS. *In* Fluorescence and phosphorescence analyses. *Edited by* D. M. Hercules. Wiley-Interscience, New York. 1966. p. 125.
8. S. G. SCHULMAN. *In* Modern fluorescence spectroscopy. Vol. 2. *Edited by* E. L. Wehry. Plenum, New York. 1976.
9. W. KLOPFFER. Adv. Photochem. **10**, 311 (1977).
10. Z. R. GRABOWSKI and A. GRABOWSKA. Z. Phys. Chem. Wiesbaden, **101**, 197 (1976).
11. G. JACKSON and G. PORTER. Proc. R. Soc. London, Ser. A, **260**, 13 (1961).
12. S. G. SCHULMAN, L. S. ROSENBERG, and W. R. VINCENT, JR. J. Am. Chem. Soc. **101**, 139 (1979).
13. K. TSUTSUMI and H. SHIZUKA. Z. Phys. Chem. Wiesbaden, **122**, 129 (1980).
14. B. S. VOGT and S. G. SCHULMAN. Chem. Phys. Lett. **95**, 159 (1983).
15. H. SHIZUKA and S. TOBITA. J. Am. Chem. Soc. **104**, 6919 (1982); S. TOBITA and H. SHIZUKA. Chem. Phys. Lett. **75**, 140 (1980).
16. H. SHIZUKA and K. TSUTSUMI. Bull. Chem. Soc. Jpn. **56**, 629 (1983).
17. K. TSUTSUMI and H. SHIZUKA. Chem. Phys. Lett. **52**, 485 (1977); Z. Phys. Chem. Wiesbaden, **111**, 129 (1978).
18. H. SHIZUKA, K. TSUTSUMI, H. TAKEUCHI, and I. TANAKA. Chem. Phys. Lett. **62**, 409 (1979); Chem. Phys. **59**, 183 (1981).
19. H. SHIZUKA and K. TSUTSUMI. J. Photochem. **9**, 334 (1978).
20. K. TSUTSUMI, S. SEKIGUCHI, and H. SHIZUKA. J. Chem. Soc. Faraday Trans. 1, **78**, 1087 (1982).
21. F. HAFNER, J. WORNER, U. STEINER, and M. HAUSER. Chem. Phys. Lett. **72**, 139 (1980).
22. C. M. HARRIS and B. K. SELINGER. J. Phys. Chem. **84**, 891 (1980); **84**, 1366 (1980).
23. D. M. RAYNER and P. A. H. WYATT. J. Chem. Soc. Faraday Trans. 2, **70**, 945 (1974).
24. Y. NISHIDA, K. KIKUCHI, and H. KOKUBUN. J. Photochem. **13**, 75 (1980).
25. W. R. WARE, D. WATT, and J. D. HOLMES. J. Am. Chem. Soc. **96**, 7853 (1974).
26. C. G. HATCHARD and C. A. PARKER. Proc. R. Soc. London, Ser. A, **235**, 518 (1956).
27. P. DE MAYO and H. SHIZUKA. *In* Creation and detection of the excited state. Vol. 4. *Edited by* W. R. Ware. Marcel Dekker, New York. Chapt. 4.
28. H. SHIZUKA and H. OBUCHI. J. Phys. Chem. **86**, 1297 (1982).
29. M. A. EL-SAYED. J. Chem. Phys. **36**, 573 (1962); **38**, 2834 (1963); **41**, 2462 (1964).
30. M. B. LEDGER and G. PORTER. J. Chem. Soc. Faraday Trans. 1, **68**, 539 (1972).
31. G. E. ADAMS and K. L. WILLSON. J. Chem. Soc. Faraday Trans. 1, **68**, 719 (1973).
32. R. V. BENSASSON and J.-C. GRAMAN. J. Chem. Soc. Faraday Trans. 1, **76**, 1801 (1980).
33. J. F. IRELAND and P. A. H. WYATT. J. Chem. Soc. Faraday Trans. 1, **69**, 161 (1973).
34. H. LUTZ, E. BRÉKÉRET, and L. LINDQUIST. J. Phys. Chem. **77**, 1758 (1973).
35. A. A. LAMOLA. J. Chem. Phys. **47**, 4810 (1967).
36. G. PORTER, S. K. DOGRA, R. O. LOUTFY, S. E. SUGAMORI, and R. W. YIP. J. Chem. Soc. Faraday Trans. 1, **69**, 1462 (1973).
37. H. SHIZUKA and M. FUKUSHIMA. Chem. Phys. Lett. **101**, 598 (1983).
38. R. W. TAFT, JR. *In* Steric effects in organic chemistry. *Edited by* M. S. Newman. John Wiley and Sons, New York. 1956. p. 619.
39. T. G. BONNER and J. PHILLIPS. J. Chem. Soc. B, 650 (1966).
40. A. FISHER, B. A. GRIGOR, J. PACKER, and J. VAUGHAN. J. Am. Chem. Soc. **83**, 4208 (1961).

Can. J. Chem. Downloaded from www.nrcresearchpress.com by 210.87.254.6 on 09/06/12
For personal use only.

The effect of heavy-atom solvents on the photooxidation of anthracene

NAOKI TOSHIMA, TOSHIHIKO SUGANO, AND HIDEFUMI HIRAI

Department of Industrial Chemistry, Faculty of Engineering, The University of Tokyo, Hongo, Bunkyo-ku, Tokyo 113, Japan

Received January 30, 1984

This paper is dedicated to Professor Paul de Mayo on the occasion of his 60th birthday

NAOKI TOSHIMA, TOSHIHIKO SUGANO, and HIDEFUMI HIRAI. Can. J. Chem. **62**, 2047 (1984).

Photoirradiation of anthracene in benzene in the presence of oxygen gave predominantly a photodimer of anthracene, and very little oxidation product. Similar irradiation of anthracene in bromobenzene, however, produced 9,10-anthraquinone in high yield. The yield of anthraquinone increased in the presence of a heavy-atom solvent such as bromobenzene, *p*-dibromobenzene, 1,3,5-tribromobenzene, 1-bromopropane, and dibromomethane in proportion to the sum of squares of the spin–orbit coupling parameter ζ of the solvent molecule. This relationship indicates an external heavy-atom effect on the photooxidation of anthracene. The mechanistic investigations suggest the involvement of singlet oxygen, anthracene peroxide, and a radical intermediate in the formation of anthraquinone.

NAOKI TOSHIMA, TOSHIHIKO SUGANO et HIDEFUMI HIRAI. Can. J. Chem. **62**, 2047 (1984).

La photoirradiation de l'anthracène dans le benzène, en présence d'oxygène, conduit principalement au photodimère de l'anthracène et à très peu de produits d'oxydation. Toutefois, une irradiation analogue de l'anthracène dans le bromobenzène conduit à l'anthraquinone-9,10 avec un rendement élevé. Le rendement en anthraquinone augmente lorsqu'on opère la réaction dans des solvants comme le bromobenzène, le *p*-dibromobenzène, le tribromo-1,3,5-benzène, le bromo-1 propane et le dibromométhane qui portent des atomes lourds; d'un point de vue quantitatif, le rendement en anthraquinone est proportionnel à la somme du carré du paramètre de couplage spin–orbite (ζ) de la molécule de solvant. Cette relation suggère l'existence d'un effet extérieur des atomes lourds sur la photoxydation de l'anthracène. Les recherches sur le mécanisme réactionnel suggèrent l'implication d'oxygène singulet, de peroxyde d'anthracène et d'un intermédiaire radicalaire dans la formation de l'anthraquinone.

[Traduit par le journal]

Can. J. Chem. Downloaded from www.nrcresearchpress.com by 210.87.254.42 on 09/06/12
For personal use only.

Introduction

Heavy-atom enhanced $S_1 \rightarrow T_1$ intersystem crossing has proven quite useful in synthetic and mechanistic photochemistry. The heavy-atom effect is synthetically useful for increasing quantum yield, product yield, and product selectivity. For example, Cowan and Drisko (1–3) have detected an increase in the yield of *trans*-photodimer due to a heavy-atom effect in photodimerization of acenaphthylene. We have found that heavy-atom solvents are effective for accelerating the photoaddition (4) and photoreduction (5) of *N*-acetyldiphenylketimine in spite of the molecule having a carbonyl group.

Photodimerization of anthracene is known as one of the oldest organic photoreactions. Fluorescence of anthracene can be quenched by the addition of a heavy-atom solvent, which has been explained in terms of a heavy-atom effect (6, 7). Since the photodimerization of anthracene and its derivatives proceeds through a singlet excimer (8), the photodimerization should be quenched by a heavy-atom effect. The same heavy-atom effect has been also discovered in photoreactions in micelles recently. Thus, the heavy-atom effect of the bromide counter-ions of cetyltrimethylammonium micelles reduces the photodimerization quantum yield (9) as well as the fluorescence quantum yield (10) of 9-methylanthracene.

In this paper we present confirmation of the decrease of photodimerization yields of anthracene by the addition of heavy-atom solvents such as bromobenzenes, and then extend the effect to the reaction of anthracene and its derivatives through triplet states with a resulting increase in their photooxidation yields.

Experimental

Chemicals

Commercial anthracene of an extra pure grade was purified by recrystallization from benzene and chloroform. Commercial anthracene derivatives of an extra pure grade were used as received. Benzene was purified by distillation through a Vigreux column from sodium metal. Bromobenzene was distilled before use. Other solvents were used as received. Commercial pure solvents (Luminasol) for fluorescence spectra were used for the fluorescence measurements. Anthracene peroxide was prepared according to the method of Foote (11) by using methylene blue as a sensitizer and a tungsten–halogen lamp as a light source.

Instruments

Photoirradiations were carried out in Pyrex tubes fixed in a Rikōkagaku irradiation apparatus of a merry-go-round type using an Eikōsha 500 W high pressure mercury lamp. The rotating Pyrex tubes were held in a constant temperature water bath with a turntable device, which also rotated around the lamp housed in a water-cooled quartz immersion well. A Rikōkagaku 300 W tungsten–halogen lamp was used as a light source for the preparation of anthracene peroxide. Reaction products were analyzed with a Tōyōsōda HPLC apparatus equipped with an LS-410K reverse column by using a mixed solvent of water and methanol (1:9) as a carrier. Fluorescence and phosphorescence spectra were measured with a Hitachi MPF-4 fluorescence spectrometer. Ultraviolet and visibile spectra were recorded with a Hitachi 340 recording spectrophotometer. Infrared spectra were measured with a JASCO A-3 spectrometer. A Hitachi M-52 mass spectrometer was used for mass spectrum analyses. Nuclear magnetic resonance spectra were observed with a JEOL JNM-PS-100 spectrometer.

Photodimerization of anthracene

A solution of anthracene (3 mmol dm^{-3}) in a mixed solvent of benzene and bromobenzenes in a Pyrex tube was degassed in three successive freeze–pump–thaw cycles, and then irradiated under argon with a 500 W high pressure mercury lamp in a 30°C water bath for 60 min through Pyrex glass ($\lambda_{max} > 300$ nm). The conversion yield (%) of anthracene was measured by hplc using dibenzyl as an internal standard.

Photooxidation of anthracene and its derivatives

The same solution of anthracene used for photodimerization was

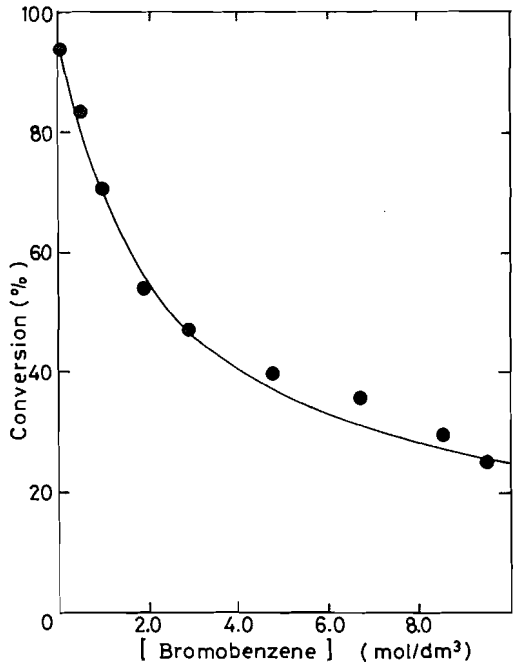

FIG. 1. Dependence of the photodimerization rate of anthracene upon the concentration of bromobenzene on irradiation of 3 mmol dm^{-3} anthracene in benzene under argon at 30°C for 60 min.

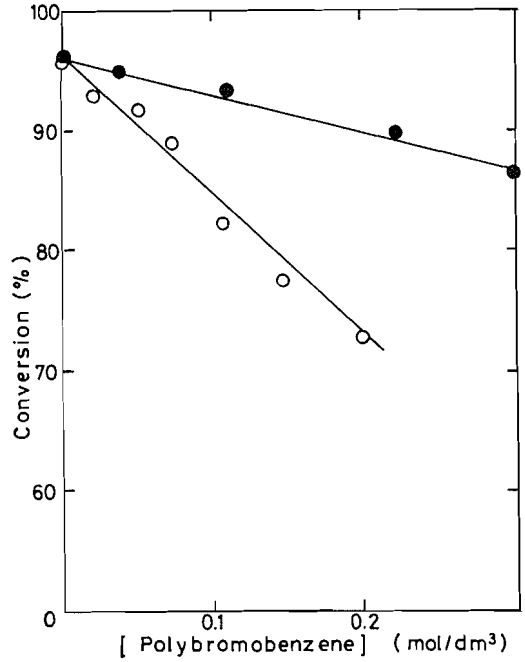

FIG. 2. Dependence of the photodimerization rate of anthracene upon the concentration of *p*-dibromobenzene (●) and 1,3,5-tribromobenzene (○) under the same conditions as Fig. 1.

oxygenated by passing a stream of oxygen through it for 2 min. Photoirradiation of the solution was carried out in the same way as that for photodimerization, but under oxygen, for 60 min or 120 min. The product was isolated by preparative thin layer chromatography using chloroform as the developing solvent. The isolated yellow crystalline compound was identified as 9,10-anthraquinone by comparing the uv, ir, and nmr spectra with those of the authentic sample. The product yields were determined by measuring the peak area of the hplc traces using dibenzyl as an internal standard.

Similar conditions were also employed in the presence of the additives described in the Discussion section.

Results

Effect of bromobenzenes on photodimerization of anthracene

Irradiation of anthracene (3 mmol dm^{-3}) in benzene in the absence of oxygen produced the photodimer of anthracene as a precipitate. Addition of bromobenzene to the solution decreased the conversion of anthracene as shown in Fig. 1. The presence of about 3 mol dm^{-3} of bromobenzene reduced the conversion to half, but the effect of further addition of bromobenzene, however, was less marked (see Fig. 1). Similar reduction of the conversion rate was observed by the addition of smaller amounts of *p*-dibromobenzene or 1,3,5-tribromobenzene as shown in Fig. 2. The bromobenzenes were recovered from these photoreactions without change.

Effect of bromo compounds on photooxidation of anthracene

Irradiation of a dilute solution of anthracene (3 mmol dm^{-3}) in benzene under oxygen still gave the photodimer of anthracene and a small amount of 9,10-anthraquinone. Addition of bromobenzene to the solution decreased the yield of the photodimer and increased the yield of anthraquinone. The effect of the concentration of bromobenzene on the yield of anthraquinone is shown in Fig. 3. The yield of anthraquinone increased with the increase of the concentration of bromobenzene until about 4 mol dm^{-3}, then started to decrease slowly. This trend was observed whether the irradiation time was 60 min or

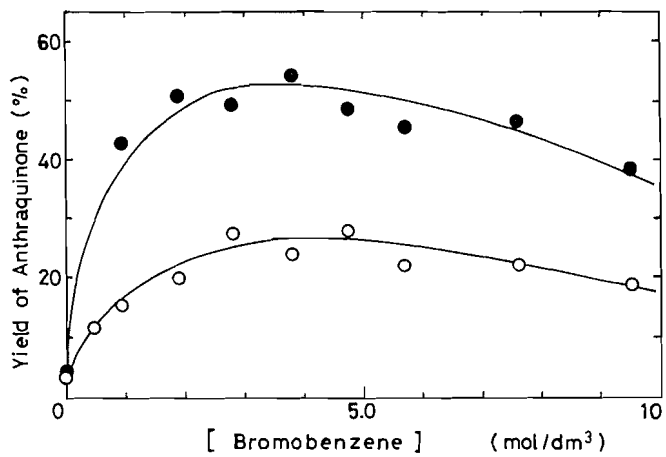

FIG. 3. Effect of the concentration of bromobenzene upon the yield of 9,10-anthraquinone on irradiation of 3 mmol dm^{-3} anthracene in benzene under oxygen at 60°C for 30 min (○) or 120 min (●).

120 min. When other bromocompounds were used instead of bromobenzene, similar increases in the yields of anthraquinone were observed as shown in Fig. 4. The effect of the concentration of bromo compounds depends on the number of bromine atoms per molecule, i.e., the effect increases in the order of bromobenzene, *p*-dibromobenzene, and 1,3,5-tribromobenzene. No products other than anthraquinone and the photodimer were detected in these photoreactions.

Chlorobenzene, iodomethane, and nitrobenzene were used as co-solvents instead of bromo compounds in the photoreaction. Chlorobenzene showed a small effect on the yield of anthraquinone. In the case of iodomethane, most of the photoenergy was consumed in the cleavage of the C—I bond and the anthraquinone yield increased modestly. No effect was detected by addition of nitrobenzene.

Can. J. Chem. Downloaded from www.nrcresearchpress.com by 210.87.254.42 on 09/06/12
For personal use only.

TABLE 1. Formation of anthraquinone by photooxidation of anthracene derivatives in the presence and absence of 1,3,5-tribromobenzene (TBB)[a]

Anthracene		Anthraquinone yield (%)					
9-Substituent	10-Substituent	Without TBB (ϕ^0)	With TBB (ϕ)	ϕ/ϕ^0	ϕ_{isc}[b]	E_T[b] (kcal mol^{-1})	Photo-dimerization
H	H	4.5	22.5	5.00	0.31 0.75	42.0	Yes
Me	H	9.5	19.2	2.02	0.72 0.65	40.6	Yes
Me	Me	11.6	11.6	1.00	0.19	~40	No
Ph	H	4.1	3.4	0.83	0.37	~40	No
Cl	Cl	28.1	23.9	0.85	0.45	40.4	No
Br	H	31.1	52.0	1.67	0.95	~40	Yes
Br	Br	36.5	33.1	0.91	0.99	~40	No

[a]Irradiations were carried out for 60 min in Pyrex tubes under oxygen at constant concentration of anthracene derivative (3 mmol dm^{-3}) and TBB (0.2 mol dm^{-3}).
[b]The quantum yield of the intersystem crossing (ϕ_{isc}) and the triplet energy (E_T) were taken form ref. 25.

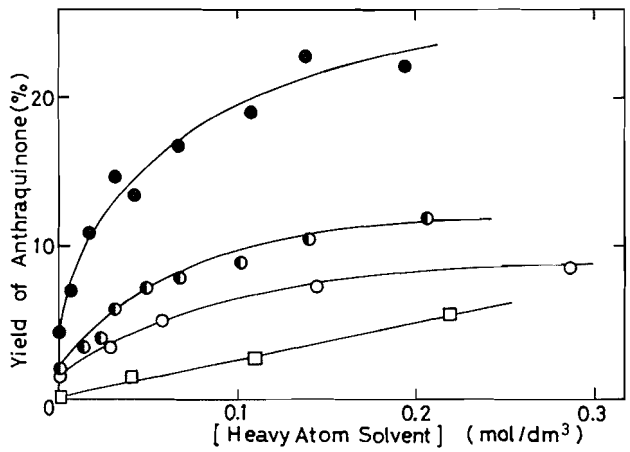

FIG. 4. Effect of the concentrations of 1,3,5-tribromobenzene (●), *p*-dibromobenzene (◐), dibromomethane (○), and 1-bromopropane (□) upon the yield of 9,10-anthraquinone on irradiation of 3 mmol dm^{-3} anthracene in benzene under oxygen at 30°C for 60 min.

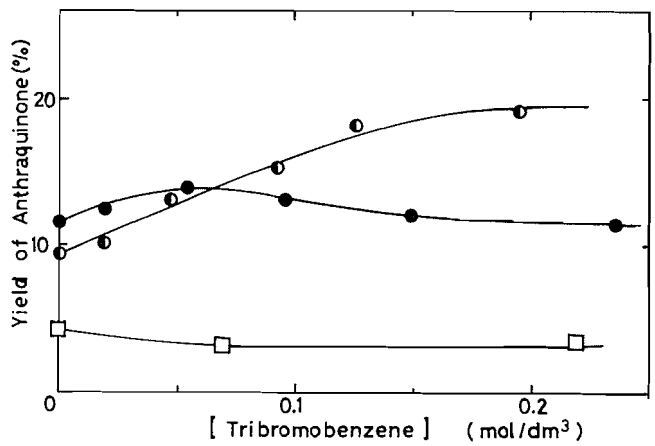

FIG. 5. Effect of the concentration of tribromobenzene upon the yield of 9,10-anthraquinone on irradiation of 3 mmol dm^{-3} 9-methylanthracene (◐), 9,10-dimethylanthracene (●), and 9-phenylanthracene (□) in benzene under oxygen for 60 min.

Photooxidation of anthracene derivatives in the presence of tribromobenzene

The effect of tribromobenzene on the photooxidation was examined for 9- and 9,10-substituted anthracene. Dependence of anthraquinone yield on the concentration of tribromobenzene is illustrated in Fig. 5 for 9-methylanthracene, 9,10-dimethylanthracene, and 9-phenylanthracene. In the irradiation of 9-methylanthracene, addition of tribromobenzene increased the yield of anthraquinone. By way of contrast, little effect of the addition of tribromobenzene was observed in the case of 9,10-dimethylanthracene and 9-phenylanthracene. Other products detected were methane, identified by ir and mass spectra of the gaseous product in the photooxidation of 9,10-dimethylanthracene, and 9-phenylanthrone, identified by ir spectra in the photooxidation of 9-phenylanthracene.

Photooxidation of chloro- or bromo-substituted anthracene was carried out in the absence and presence of 1,3,5-tribromobenzene. The results of other substituted anthracenes mentioned above are summarized in Table 1. Effects of the presence of tribromobenzene (TBB) are indicated by the ratio of the yields of anthraquinone in the presence and absence of TBB (ϕ/ϕ^0).

Effect of additives on the photooxidation of anthracene

A benzene solution of anthracene was irradiated in oxygen with the addition of benzil using a VY-42 filter ($\lambda > 400$ nm), also producing anthraquinone, although no light was absorbed by anthracene. In contrast, the addition of piperylene to a benzene–bromobenzene (3.81 mol dm^{-3}) solution of anthracene (3 mmol dm^{-3}) quenched the photooxidation of anthracene under oxygen, as shown in Fig. 6. These results indicate the contribution of the excited triplet state of anthracene to the photooxidation (see Discussion section).

Anthraquinone was also obtained in moderate yield by the irradiation of anthracene with a VY-42 filter under oxygen in the presence of rose bengal or methylene blue instead of bromo compounds. In contrast, addition of tetramethylethylene (2,3-dimethyl-2-butene, 3 to 40 mmol dm^{-3}) to benzene–bromobenzene or benzene–dibromobenzene solution of anthracene rapidly decreased the yield of anthraquinone when irradiated in oxygen. Reduction of mixtures of the photoproducts with sodium borohydride gave 2,3-dimethylbut-3-en-2-ol, which was identified by comparing the mass spectrum of the corresponding peak in the gas chromatograph of the products with that of the authentic sample prepared separately. Addition of

Can. J. Chem. Downloaded from www.nrcresearchpress.com by 210.87.254.42 on 09/06/12
For personal use only.

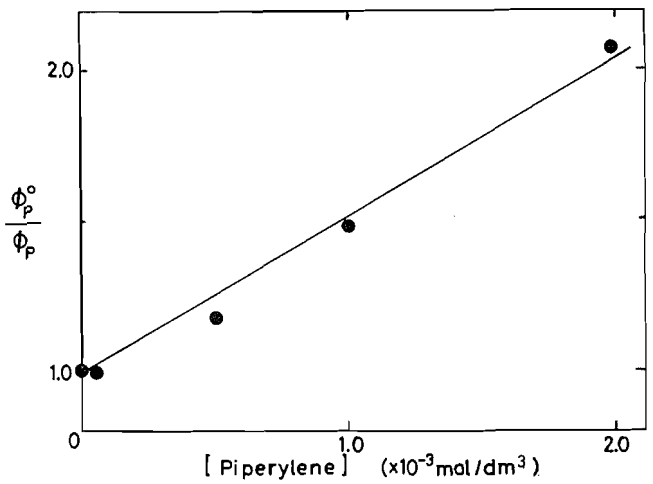

FIG. 6. Stern–Volmer plot for the quenching of 9,10-anthraquinone yield by piperylene (1,3-pentadiene) on irradiation of 3 mmol dm^{-3} anthracene in benzene with addition of 3.81 mol dm^{-3} bromobenzene under oxygen at 30°C for 60 min.

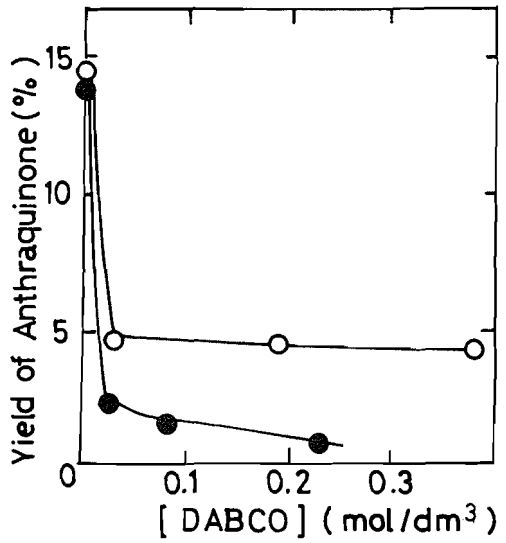

FIG. 7. Effect of the concentration of 1,4-diazabicyclo[2.2.2]-octane (DABCO) upon the yield of 9,10-anthraquinone on irradiation under oxygen for 60 min of 3 mmol dm^{-3} anthracene (○) in benzene with addition of 1.9 mol dm^{-3} bromobenzene, and of 3 mmol dm^{-3} 9-methylanthracene (●) in benzene with addition of 0.11 mol dm^{-3} 1,3,5-tribromobenzene.

1,4-diazabicyclo[2.2.2]octane (DABCO) to a solution of anthracene in bromobenzene, or 9-methylanthracene in tribromobenzene caused a large decrease in the yield of anthraquinone on irradiation as shown in Fig. 7. The inhibiting effect of DABCO on the formation of anthraquinone was also observed in other anthracene derivatives as summarized in Table 2. These results suggest the contribution of singlet oxygen in the photooxidation of anthracene in the presence of a heavy-atom solvent (see Discussion section).

Effect of *p*-hydroquinone as a radical scavenger was examined. Since hydroquinone is not soluble in benzene, mixed benzene–methanol (6:4) instead of benzene was used as a solvent in the photooxidation of anthracene. Irradiation of anthracene in benzene–methanol with the addition of *p*-dibromobenzene (0.13 mol dm^{-3}) under oxygen for 60 min gave anthraquinone in 15.3% yield. By way of contrast, the presence of hydroquinone (6 mmol dm^{-3}) inhibited the formation of anthraquinone and reduced the yield to 0.69%.

TABLE 2. Effect of 1,4-diazabicyclo[2.2.2]octane (DABCO) upon the anthraquinone yield in the photooxidation of anthracene derivatives[a]

Anthracene		Yield of anthraquinone (%)	
9-Substituent	10-Substituent	Without DABCO	With DABCO[b]
H	H	14.2	4.3
Me	H	16.8	2.4
Me	Me	12.8	0.42
Ph	H	4.05	0.56
Cl	Cl[c]	28.1	0.42
Br	H[c]	41.1	5.45
Br	Br[c]	36.5	2.72

[a]The benzene solutions were irradiated under oxygen at 30°C for 60 min in the presence of bromobenzene (1.9 mol dm^{-3}).
[b][DABCO] = 0.027 mol dm^{-3}.
[c]Irradiations were carried out without bromobenzene in these cases.

Reactions of anthracene peroxide

The reactions of singlet oxygen and anthracene derivatives are known to produce anthracene peroxide derivatives (12–15). In the present photooxidation of anthracene it seemed possible that anthracene peroxide might exist as an intermediate in the formation of anthraquinone from anthracene. Attempts to isolate anthracene peroxide, however, failed even at low temperature.

Heating the endoperoxide of 9,10-diphenylanthracene has been reported to produce anthracene and singlet oxygen (16, 17). Heating a dilute solution of anthracene peroxide gave isomerized products, plus anthracene and anthraquinone in minor amounts (18). The reactions of anthracene peroxide were examined under the same conditions employed in the photooxidation of anthracene in the present investigations. When a benzene solution of anthracene peroxide was first kept at 30°C under oxygen for 60 min, no change was detected. However, photoirradiation of anthracene peroxide in benzene under oxygen in a Pyrex tube gave anthraquinone in about 15% yield. Addition of tribromobenzene (0.1 mol dm^{-3}) to this system decreased the yield of anthraquinone to about 10%. The same results were obtained in the case of 9,10-dimethylanthracene peroxide.

Discussion

Heavy-atom effect in the photoreaction of anthracene

It is well known that anthracene readily dimerizes on irradiation, producing the photodimer. A 3 mol dm^{-3} benzene solution of anthracene produced the dimer in 94% yield on irradiation with 500 W high-pressure mercury lamp for 60 min. Addition of bromobenzene to this system reduced the yield of the photodimer as shown in Fig. 1. The effect of bromobenzene can be explained in terms of an external heavy-atom effect. The singlet excited state of anthracene gives the photodimer via an excimer which is formed from singlet excited anthracene and ground state anthracene (8). A solvent molecule containing one or more heavy-atom can promote a forbidden singlet–triplet transition in an aromatic molecule by an external heavy-atom effect. Therefore, the bromobenzene-induced reduction in the yield of anthracene photodimer should be proportional to the quenching effect of bromobenzene upon the fluorescence of anthracene. This relationship has been confirmed by experi-

Can. J. Chem. Downloaded from www.nrcresearchpress.com by 210.87.254.42 on 09/06/12
For personal use only.

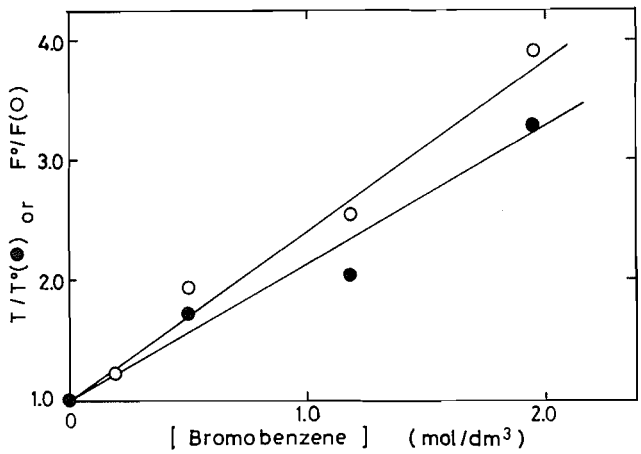

FIG. 8. Stern–Volmer plots for the quenching of anthracene fluorescence by bromobenzene (F^0/F, ○), and for the quenching of 35% anthracene conversion in time (T/T^0, ●). See text for detail.

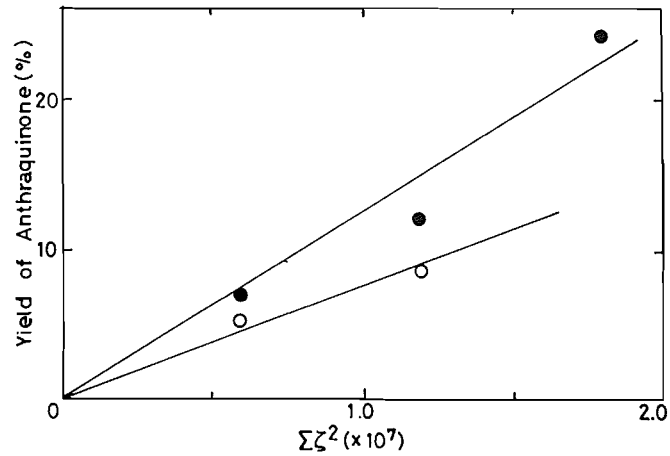

FIG. 9. Relationships between the 9,10-anthraquinone yields and the sum of the square of the spin–orbit coupling parameter (ζ) of heavy-atom solvents. Data were taken from Figs. 1 and 2 at 0.2 mol dm^{-3} concentration of each heavy-atom solvent. See text for detail.

ments with 0.1 mmol dm^{-3} anthracene in benzene. The black circles in Fig. 8 show the ratio of the time for 35% photoconversion of anthracene in the presence of the prescribed amount of bromobenzene to that in the absence of bromobenzene. The open circles indicate a Stern–Volmer plot for the quenching of anthracene fluorescence by bromobenzene. The slopes in the two plots are nearly the same. This consistency supports the idea that the bromobenzene-derived reduction in the photodimer yield and the fluorescence quenching have the same origin, namely, the external heavy-atom effect. Larger effects were observed with dibromobenzene and tribromobenzene (Fig. 2).

The heavy-atom effect in the photooxidation of anthracene and its derivatives

The photolysis products from air-saturated anthracene solutions are known to be strongly dependent on the anthracene concentration and the type of solvent used (8, 19, 20). The important effect of solvent has been demonstrated by Aspler *et al.* Thus, in isooctane, photolysis of a dilute solution of anthracene gives a high yield of the photodimer, whereas in Freon 113, roughly equimolar yields of endoperoxide, anthraquinone, and anthracene dimer are formed (20).

The present results concerning the effect of bromo compounds suggest that the photooxidation proceeds through a triplet excited state of anthracene, the formation of which is promoted by an external heavy-atom effect. This suggestion is supported by the plot of the anthraquinone yields in the presence of a 0.2 mol dm^{-3} brominated solvent against the square of the spin–orbit coupling parameters of the solvent molecules as shown in Fig. 9 (21). Here, the spin–orbit coupling parameter was estimated by summing up the spin–orbit coupling parameter(s) of the heavy atom(s) (bromine) present in the solvent molecule. The linear relationships indicate that the heavy-atom effect plays an important role in the reaction and implicates the triplet state of anthracene. Two lines in Fig. 9 show the relationship in the series of aromatic solvents (black circles: bromobenzene, *p*-dibromobenzene, and 1,3,5-tribromobenzene) and that in aliphatic solvents (open circles: 1-bromopropane and dibromomethane). The difference between the two lines can be explained in terms of the charge-transfer interaction between anthracene and the aromatic solvents. The small effects of chlorobenzene and nitrobenzene can be understood in the same way. The yield of anthraquinone decreased when the concentration of bromobenzene was increased beyond 4 mol dm^{-3} (Fig. 3). Similar reasoning may be used to explain the photodimerization results of acenaphthylene in the presence of iodoethane (22). Thus, highly concentrated bromobenzene could be effective for enhancing intersystem crossing from the triplet excited state to the singlet ground state whereas diluted bromobenzene is effective for enhancing intersystem crossing from the singlet excited state to the triplet excited state.

The above considerations indicate that although photoirradiation of anthracene in usual solvents predominantly gives the photodimer and does not produce anthraquinone under oxygen, the presence of a heavy-atom solvent inhibits the photodimerization by promoting the intersystem crossing, resulting in the formation of anthraquinone on irradiation under oxygen.

In a series of 9- or 9,10-substituted anthracenes, the increases of the anthraquinone yields by the addition of tribromobenzene (ϕ/ϕ^0), the reported quantum yields of the intersystem crossing (ϕ_{isc}), the triplet energies (E_T), and the probabilities of photodimerization have been reported in Table 1. The increase (ϕ/ϕ^0) is not directly related to either ϕ_{isc} or to E_T, but rather appears to be connected to the probability of photodimerization. Thus, the derivative which can dimerize on irradiation also gives the increase in the anthraquinone yield ($\phi/\phi^0 > 1$), as shown in Table 1. This result agrees with the proposal that the presence of a heavy-atom solvent inhibits photodimerization by promoting intersystem crossing, resulting in an increase in the anthraquinone yield upon irradiation under oxygen. Considerably higher yields of anthraquinone in the photooxidation of 9- or 9,10-halosubstituted anthracenes in the absence of tribromobenzene might be partially due to the internal heavy-atom effect.

Photooxidation mechanism

It has been proposed (20, 23) that anthracene photooxidation proceeds via oxygen quenching of the triplet excited state of anthracene molecules and reaction of the resulting singlet oxygen with an anthracene molecule in its ground state. An alternative possibility has been suggested involving electron transfer from triplet anthracene to an oxygen molecule (24).

In the present photooxidation, the presence of the triplet intermediate is supported by the sensitization by benzil, a sensitizer, and the quenching effect of piperylene, a triplet

Can. J. Chem. Downloaded from www.nrcresearchpress.com by 210.87.254.42 on 09/06/12
For personal use only.

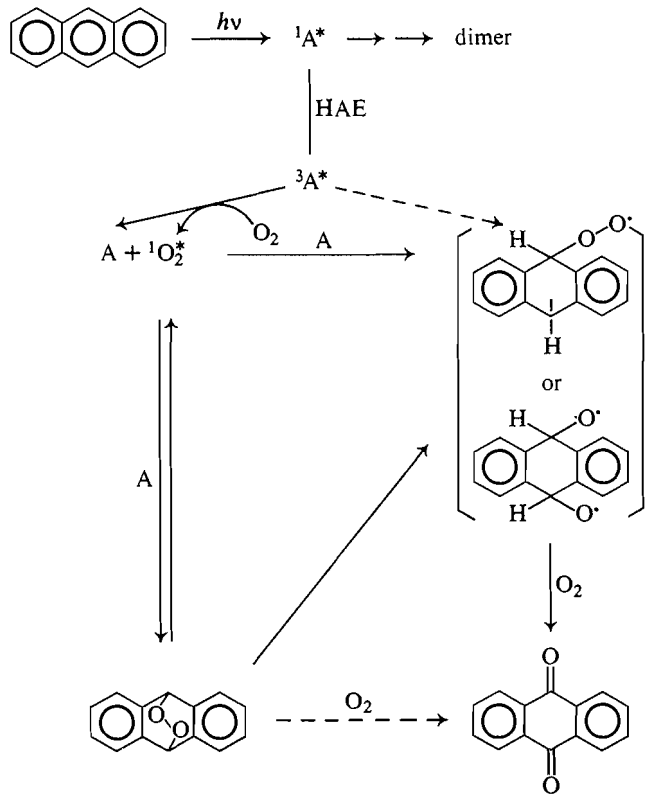

SCHEME 1. Proposed paths for the photooxidation of anthracene (A) in the presence of heavy-atom solvents.

quencher, as well as the heavy atom effect. The quenching of the excited state of anthracene by piperylene is surprising since the triplet energy of piperylene is 59.2 kcal mol^{-1} for the *trans*-isomer or 58.3 kcal mol^{-1} for the *cis*-isomer (25), and anthracene has a first excited triplet energy of 42.0 kcal mol^{-1}. However, the quenching by piperylene may possibly occur from the second excited triplet state (T_2) of anthracene (74.5 kcal mol^{-1}), because the T_2 state of anthracene is known to have a long enough lifetime for energy transfer (26–28).

Photooxidation takes place mostly through the singlet excited state of oxygen (29), and the excitation of oxygen molecules from their triplet ground state ($^3O_2$) to the excited singlet state ($^1O_2^*$) is known to take place by energy transfer from the triplet excited state of anthracene and other aromatic molecules (30). The involvement of the singlet oxygen in the present system was examined by the addition of tetramethylethylene (TME) and DABCO, both singlet oxygen quenchers (31, 32). These results indicate that at least part of the present photooxidation of anthracene in the presence of a heavy-atom solvent involves the singlet oxygen.[1]

There are two possible paths in the reaction of singlet oxygen with anthracene to form anthraquinone. One path involves anthracene peroxide (20, 23), although it could not be isolated from the reaction mixtures in this work.

The other possible path involves a photoperoxidation process where the singlet excited oxygen molecule interacts with the ground state aromatic hydrocarbon (^1M) to form the peroxide $MO_2\cdot$ (33). Inhibition of anthraquinone formation by hydroquinone, a radical scavenger, suggests the involvement of a radical intermediate in the present photooxidation. Hydroquinone also acted partially as an inhibitor in the formation of anthraquinone during the irradiation of anthracene peroxide. Therefore, it cannot be decided whether the radical intermediate is produced directly or via anthracene peroxide.

In summary, the most probable paths of photooxidation of anthracene in the presence of a heavy-atom solvent are shown in Scheme 1. An anthracene molecule absorbs the light leading to a singlet excited state and then to a triplet state. The efficiency of the latter process is enhanced by an external heavy-atom effect. Interaction of triplet excited anthracene with an oxygen molecule in the ground state produces singlet excited oxygen. Reaction of singlet excited oxygen with anthracene in the ground state forms the peroxide radical intermediate, either directly or through anthracene peroxide, which then yields anthraquinone.

[1]A referee has suggested the involvement of an electron transfer step from triplet anthracene to an oxygen molecule (24). According to this mechanism, anthracene radical cation, a product of the above electron transfer, should be quenched by TME or DABCO through electron transfer.

1. D. O. COWAN and R. L. DRISKO. Tetrahedron Lett. 1255 (1967).
2. D. O. COWAN and R. L. DRISKO. J. Am. Chem. Soc. **92**, 6282 (1970).
3. D. O. COWAN and R. L. DRISKO. J. Am. Chem. Soc. **98**, 1001 (1976) and references cited therein.
4. S. ASAO, N. TOSHIMA, and H. HIRAI. Bull. Chem. Soc. Jpn. **49**, 224 (1976).
5. N. TOSHIMA, S. ASAO, and H. HIRAI. Bull. Chem. Soc. Jpn. **51**, 578 (1978).
6. T. MEDINGER and F. WILKINSON. Trans. Faraday Soc. **61**, 620 (1965).
7. A. R. HORROCKS, A. KEARVELL, K. TICKLE, and F. WILKINSON. Trans. Faraday Soc. **62**, 3393 (1966).
8. E. J. BOWEN. Adv. Photochem. **1**, 23 (1963).
9. T. WOLFF, N. MÜLLER, and G. VON BÜNAU. J. Photochem. **22**, 61 (1983).
10. T. WOLFF. Ber. Bunsenges. Phys. Chem. **86**, 1132 (1982).
11. C. S. FOOTE, S. WEXLER, W. ANDO, and R. HIGGINS. J. Am. Chem. Soc. **90**, 975 (1968).
12. K. GOLLNICK and G. O. SCHENCK. Pure Appl. Chem. **9**, 507 (1964).
13. B. STEVENS and B. E. ALGAR. Ann. N.Y. Acad. Sci. **171**, 50 (1970).
14. O. L. J. GIJZEMAN, F. KAUFMAN, and G. PORTER. J. Chem. Soc. Faraday Trans. 2, **69**, 708 (1973).
15. E. WASSERMAN, V. J. KUCK, W. M. DELAVAN, and W. A. YAGER. J. Am. Chem. Soc. **91**, 104 (1969).
16. H. H. WASSERMAN and J. R. SCHEFFER. J. Am. Chem. Soc. **89**, 3073 (1967).
17. H. H. WASSERMAN, J. R. SCHEFFER, and J. L. COOPER. J. Am. Chem. Soc. **94**, 4991 (1972).
18. J. RIGAUDY, J. BARANNE-LAFONT, A. DEFOIN, and N. K. CUONG. Tetrahedron, **34**, 73 (1978).
19. K. GOLLNICK. Adv. Photochem. **6**, 1 (1968).
20. J. ASPLER, D. J. CARLSSON, and D. M. WILES. Macromolecules, **9**, 691 (1976).
21. N. J. TURRO. Molecular photochemistry. W. A. Benjamin, New York. 1965.
22. D. O. COWAN and J. C. KOZIAR. J. Am. Chem. Soc. **97**, 249 (1975).
23. M. NOWAKOWSKA. Makromol. Chem. **179**, 2953 (1978).
24. I. SHEVCHUK and V. P CHEKULAEV. Eesti NSV Tead. Akad. Toim. Keem. **31**, 117 (1982); Chem. Abstr. **97**, 91431*h* (1982).
25. S. L. MUROV. Handbook of photochemistry. Marcel Dekker, New York. 1973.
26. R. S. H. LIU and R. E. KELLOOG. J. Am. Chem. Soc. **91**, 250 (1969).

Can. J. Chem. Downloaded from www.nrcresearchpress.com by 210.87.254.42 on 09/06/12
For personal use only.

27. R. S. H. LIU and R. EDMAN. J. Am. Chem. Soc. **91**, 1492 (1969).
28. G. D. GILLISPDE and E. L. LIM. J. Chem. Phys. **65**, 2022 (1976).
29. H. H. WASSERMAN and R. W. MURRAY. Singlet oxygen. Academic Press, New York. 1979.
30. B. STEVENS, S. R. PEREZ, and J. A. ORS. J. Am. Chem. Soc. **90**, 6846 (1974).
31. C. OUANNES and T. WILSON. J. Am. Chem. Soc. **90**, 6527 (1968).
32. B. M. MONROE. J. Phys. Chem. **81**, 1861 (1977).
33. B. STEVENS and B. E. ALGAR. Chem. Phys. Lett. **1**, 58 (1967).

Can. J. Chem. Downloaded from www.nrcresearchpress.com by 210.87.254.42 on 09/06/12
For personal use only.

Synthèse de méso-α,γ bis(diamino-2,6 phényl) porphyrines

ALEXANDRA LECAS-NAWROCKA, JACQUES LEVISALLES, CLAIRE MARIACHER, ZAFIARISOA RENKO ET ERIC ROSE[1]

Laboratoire de Chimie Organique (UA 408), Université Pierre et Marie Curie, 4 Place Jussieu, 75230 Paris, Cedex 05, France

Reçu le 17 janvier 1984

Cet article est dédié au Professeur Paul de Mayo à l'occasion de son 60e anniversaire

ALEXANDRA LECAS-NAWROCKA, JACQUES LEVISALLES, CLAIRE MARIACHER, ZAFIARISOA RENKO et ERIC ROSE. Can. J. Chem. **62**, 2054 (1984).

Les synthèses de méso-α,γ bis(diamino-2,6 phényl) octaalkyl-porphyrines ont été réalisées à partir de diacétamido-2,6 phényl bis(benzyloxycarbonyl-2′ dialkyl-3′,4′ pyrryl-5′) méthanes. La synthèse de telles porphyrines à double piquet permet la fonctionnalisation des quatre groupes amino de manière à protéger les deux faces de la porphyrine.

ALEXANDRA LECAS-NAWROCKA, JACQUES LEVISALLES, CLAIRE MARIACHER, ZAFIARISOA RENKO, and ERIC ROSE. Can. J. Chem. **62**, 2054 (1984).

The syntheses of α,γ-meso-bis(2,6 diaminophenyl) octaalkyl-porphyrins are described starting from 2,6-diacetamidophenyl-bis(2′-benzyloxycarbonyl, 3′,4′-dialkyl, 5′-pyrryl) methanes. The synthesis of such double-picket-fence porphyrins enables the four amino groups to function in such a way as to protect both faces of these porphyrins.

Can. J. Chem. Downloaded from www.nrcresearchpress.com by 210.87.254.5 on 09/06/12
For personal use only.

La recherche de modèles de l'hémoglobine a conduit divers groupes à synthétiser des porphyrines à piquets (1) ou des porphyrines à anses (2). Les porphyrines à anses déjà synthétisées ne comportent qu'une seule anse, ou deux anses indépendantes (une sur chaque face du squelette porphyrinique). Cet arrangement confère à ces molécules une mobilité conformationnelle notablement supérieure à celle de l'hémoglobine, donc en fait des modèles imparfaits. S'il était possible de coupler mécaniquement le mouvement des deux anses, la mobilité conformationnelle devrait être diminuée, et les modèles ainsi synthétisés devraient être meilleurs. Ce couplage mécanique peut en principe être obtenu en greffant les deux anses sur des groupes phényles, fixés sur des positions *méso* opposées (α et γ) du squelette porphyrinique et disubstitués en positions 2 et 6, par des groupements fonctionnels permettant la greffe (3).

La préparation de porphyrines méso (α,γ) disubstituées par des groupes phényles 2,6 disubstitués fait l'objet du présent mémoire.

Résultats

Trois pyrroles ont été employés dans la réaction de synthèse: le diméthyl-3,4 pyrrole carboxylate de benzyle **1***c*, à cause de la simplicité de sa préparation, est un candidat évident, mais les octaméthyl porphyrines sont notoirement insolubles, ce qui peut poser des problèmes pour le greffage des anses. C'est pourquoi les butyl-3 méthyl-4 pyrrole carboxylates d'éthyle **1***a* et de benzyle **1***b* ont été également préparés avec l'espoir que les tétraméthyl-tétrabutyl-porphyrines obtenues auraient des solubilités satisfaisantes.

Les pyrroles **1***a* et **1***b* sont synthétisés par la méthode employée pour le pyrrole **1***d* (4). L'éthoxycarbonyl-2 diméthyl-3,5 butyl-4 pyrrole **2***a* est préparé selon la méthode de Kleinspehn (5) par condensation de l'oximinomalonate de diéthyle (6) sur l'acétyl-3 heptanone-2 (7).

La transestérification (5) de l'ester éthylique **2***a* livre l'ester benzylique **2***b*. Le pyrrole **2***b* est transformé en pyrrole **1***a* selon la méthode de McDonald *et al.* (8): l'oxydation du pyrrole **2***b* par 3 équivalents de chlorure de sulfuryle, suivie d'un traitement à l'éthanol conduit au diester **2***c* dont l'hydrogénolyse fournit l'acide **2***d*. La décarboxylation de l'acide **2***d* selon la méthode de Battersby *et al.* (9) conduit au pyrrole **1***a* qui est transestérifié en pyrrole **1***b*. Le rendement global du pyrrole **1***b* à partir du malonate d'éthyle est de 18%.

La réactivité du pyrrole **1***b* a été testée sur le diéthoxy-3,3 propionate d'éthyle selon le mode opératoire classique (10) en présence de *p*-TsOH. Le dipyrrylméthane correspondant **3***a* se forme avec un rendement de 70%.

Dans les conditions habituelles (EtOH, HCl) (10) utilisées lors de la condensation d'un pyrrole avec un aldéhyde, les pyrroles **1***a* et **1***b* ne réagissent pas en présence de dinitro-2,6 benzaldéhyde, mais sont récupérés intacts. Lorsque la condensation est effectuée en présence de *p*-TsOH, les produits qui se

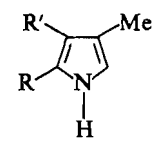

1*a* R′ = Bu R = COOEt
b R′ = Bu R = $COOCH_2Ph$
c R′ = Me R = $COOCH_2Ph$
d R′ = Et R = $COOCH_2Ph$

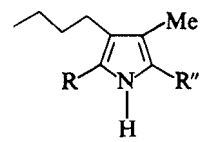

2*a* R = Me R″ = COOEt
b R = Me R″ = $COOCH_2Ph$
c R = COOEt R″ = $COOCH_2Ph$
d R = COOEt R″ = COOH
e R = COOEt R″ = I

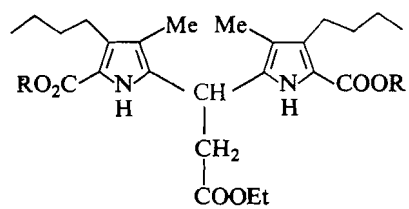

3*a* R = $PhCH_2$
b R = H
c R = Et

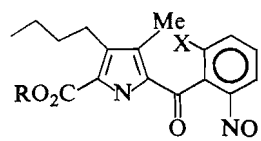

4*a* X = NO R = Et
b X = NHOH R = Et
c X = NO R = CH_2Ph

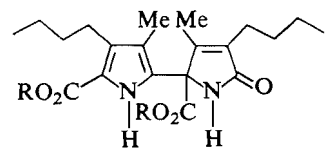

5*a* R = Et
b R = CH_2Ph

[1] Auteur à qui toute correspondance doit être adressée.

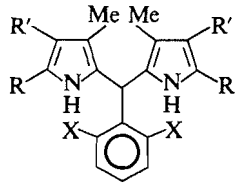

6*a*	R = COOEt	R′ = Bu	X = NO_2
b	R = $COOCH_2Ph$	R′ = Bu	X = NO_2
c	R = $COOCH_2Ph$	R′ = Me	X = NHAc
d	R = $COOCH_2Ph$	R′ = Bu	X = NHAc
e	R = COOH	R′ = Bu	X = NO_2
f	R = COOH	R′ = Me	X = NHAc
g	R = COOH	R′ = Bu	X = NHAc
h	R = COOH	R′ = Bu	X = NH_2
i	R = CO_2CH_2Ph	R′ = Me	X = NO_2

forment ne sont pas des phényl-dipyrrylméthanes. Leurs structures **4** et **5** et leur mode de formation sont décrits dans le mémoire suivant (11).

En revanche, lorsque la condensation est effectuée en présence de quantités catalytiques de CF_3CO_3H dans le benzène, les dipyrrylméthanes attendus **6***a* et **6***b* sont obtenus à côté de faibles quantités des produits **4** et **5**. Le choix des conditions expérimentales est assez limité, car le dipyrrylméthane **6***a* est obtenu avec un rendement de 63% si l'on opère dans le benzène à température ordinaire, de 34% si l'on opère au reflux du benzène pendant 1 h, et de 8% si l'on opère dans le chloroforme.

Si on emploie le diacétamido-2,6 benzaldéhyde (12)[2] dans le benzène, en présence de *p*-TsOH, les pyrroles **1***c* et **1***b* conduisent respectivement aux dipyrrylméthanes **6***c* et **6***d*. Ce passage par le diacétamido benzaldéhyde est rendu nécessaire par le fait que l'hydrolyse (acide ou basique) du dipyrrylméthane **6***b* ne conduit qu'à des polymères, que l'hydrogénolyse de **6***b* conduit apparement au diacide **6***e*, mais que celui-ci n'est pas transformable en porphyrine et que la réduction des groupes NO_2 ne conduit à aucun produit renfermant le squelette du dipyrrylméthane.

L'hydrogénolyse des dipyrrylméthanes **3***a*, **6***c* et **6***d* conduit aux diacides **3***b*, **6***f* et **6***q* respectivement.

Afin de vérifier que les groupes n-butyles ne gênent pas la formation de porphyrines, le diacide **3***b* a été traité par $HC(OEt)_3$ et CCl_3CO_2H ou CF_3CO_2H, ce qui conduit après déshydrogénation par la dichlorodicyanoquinone (DDQ), à la porphyrine **7***a*. De même les diacides **6***f* et **6***g* conduisent respectivement aux porphyrines **7***c* et **7***b*.

La désacétylation de **7***c* en **7***d* et la transformation en dérivé triméthylacetylé de **7***d* en **7***e* ont également pu être effectuées.

En conclusion, la synthèse de porphyrines méso-disubstituées en α et γ par des groupes phényles *ortho* disubstitués est possible. La synthèse et les propriétés des porphyrines à deux anses couplées, qui en dérivent, seront décrites dans des mémoires ultérieurs.

Partie expérimentale

Les spectres rmn ont été enregistrés sur un appareil JEOL C 60 HL (60 MHz). Les spectres d'absorption ir ont été enregistrés sur un spectrophotomètre Beckman 4240. Les spectres uv sont réalisés avec un appareil Beckman DK 2A. Les spectres de masse ont été réalisés sur un appareil Crantos MS 30 MS 50. Les spectres de rmn ^{13}C et

[2] La synthèse du diacétamido-2,6 benzaldéhyde a été réalisée au laboratoire par une autre méthode qui sera décrite dans une autre publication.

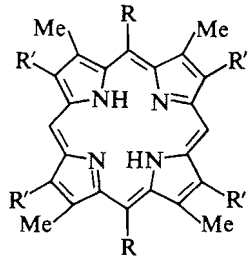

7*a* R = CH_2—CO_2Et R′ = Bu

b R = 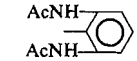 R′ = Bu

c R = 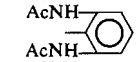 R′ = Me

d R = 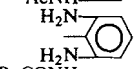 R′ = Me

e R = 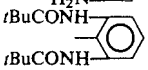 R′ = Me

certains spectres rmn ^1H ont été effectués sur un appareil JEOL FX 90Q. Les microanalyses ont été effectuées au service de microanalyse de l'Université Pierre et Marie Curie.

Lorsque la méthode d'isolement des produits réactionnels comporte une dilution éventuelle du milieu par l'eau, une extraction par solvant organique par l'eau et éventuellement une solution diluée d'acide ou de bicarbonate, un séchage sur Na_2SO_4 et l'évaporation du solvant, l'expression "traitement habituel" sera utilisée.

La chromatographie sur gel de silice se fait avec un éluant qui consiste en un mélange en quantité variable d'éther de pétrole (EP) (fraction Eb = 35–60°C) et d'éther (Et_2O).

1. *Synthèse de pyrroles*

Ethoxycarbonyl-2 diméthyl-3,5 butyl-4 pyrrole **2**a

L'acétyl-3 heptanone-2 (1 mol, 156 g) dans l'acide acétique (716 mL) est chauffée à 80°C avec agitation. On y additionne dans un premier temps le mélange de zinc (3,3 mol, 218 g) et d'acétate de sodium (3,1 mol, 260 g) puis durant 40 min une solution d'oximino malonate de diéthyle (191 g) dans le mélange acide acétique (376 g), eau (155 mL). Le milieu réactionnel est maintenu encore 20 min entre 95 et 105°C, puis versé dans un mélange eau–glace. Le pyrrole **2***a* est recristallisé dans l'éthanol et obtenu sous forme d'un solide blanc nacré; *m* = 155 g, Rdt 70%; *F* = 102°C; *M*, $C_{13}H_{21}NO_2$ = 223; ir ($CHCl_3$): 3460, 1670 cm^{-1}; rmn (CCl_4): 0,9–2,5 (m, 10H), 2,2 (s large, 8H), 4,2 (q, *J* = 6,5 Hz, 2H); rmn ^{13}C ($CDCl_3$): 162,20 (C=O), 129,99, 126,92, 122,21, 116,76 (C pyrroliques), 59,49 (CO_2CH_2), 33,09, 23,73, 22,45, 14,53, 13,93, 11,25, 10,63 (nBu, 2 pyrroles Me, CO_2—CH_3); sm (*M* = 223): pics à 223, 180, 134.

Benzyloxycarbonyl-2 diméthyl-3,5 butyl-4 pyrrole **2**b

Le pyrrole **2***a* (89 g, 0,4 mol) en solution dans l'alcool benzylique (300 mL) contenant du sodium (5 g) est chauffé vers 80°C sous une pression de 15 Torr (1 Torr = 133.3 Pa) durant 4 h. L'éthanol formé est distillé, puis sous pression de 2 Torr l'alcool benzylique est distillé. Après extraction de façon habituelle, le pyrrole **2***b* est recristallisé dans l'hexane; *m* = 72 g, Rdt 67%; *F* = 75–76°C *M*, $C_{18}H_{23}NO_2$ = 285; ir (CCl_4): 3430, 1675 cm^{-1}; rmn (CCl_4): 0,9–1,5 (m, 7H), 2,1 (s, 3H), 2,2 (s, 3H), 2–2,4 (m, 2H), 5,1 (s, 2H), 7,1 (s large, 5H), 10,0 (s, 1H). *Anal.* calc.: C 75,76, H 8,12, N 4,91; tr.: C 75,62, H 8,26, N 5,01.

Benzyloxycarbonyl-2 méthyl-3 butyl-4 éthoxycarbonyl-5 pyrrole **2**c

A une solution de pyrrole **2***b* (0,23 mol) dans l'éther anhydre (500 mL) est ajouté le chlorure du sulfuryle (89 g, 0,66 mol). Le mélange est agité 18 h en maintenant la température entre 10 et 15°C. L'éther est évaporé, puis on ajoute sous la hotte goutte à goutte l'éthanol (325 mL) puis l'eau (455 mL). Le milieu réactionnel est traité de la façon habituelle comprenant en plus un lavage avec une solution de bisulfite de sodium. Le pyrrole **2***c* est recristallisé dans l'hexane; *m* = 67 g, Rdt 85%; *F* = 74°C; *M*, $C_{20}H_{25}NO_4$ = 343; ir (CCl_4): 3430, 1712, 1700

Can. J. Chem. Downloaded from www.nrcresearchpress.com by 210.87.254.5 on 09/06/12
For personal use only.

Can. J. Chem. Downloaded from www.nrcresearchpress.com by 210.87.254.5 on 09/06/12
For personal use only.

TABLEAU 1. Formules moléculaires, points de fusion, rendements, analyses A et (ou) spectres de masse

Composés	Formule moléculaire	Analyses et (ou) spectres de masse	Point de fusion (°C)	Rendements (%)
2*a*	$C_{13}H_{21}NO_2$	223	102	70/acetyl-3 heptanone-2
2*b*	$C_{18}H_{23}NO_2$	A*	75–76	67/**2***a*
2*c*	$C_{20}H_{25}NO_4$	343	74	85/**2***b*
2*d*	$C_{13}H_{19}NO_4$	A, 253	216	70/**2***c*
2*e*	$C_{12}H_{18}NO_2I$	A, 335	103	85/**2***d*
1*a*	$C_{12}H_{19}NO_2$	A, 209	46	88/**2***e*
1*b*	$C_{17}H_{21}NO_2$	A, 271	64–65	70/**1***a*
3*b*	$C_{25}H_{36}N_2O_6$		Huile instable	99/**3***a*
3*c*	$C_{29}H_{44}N_2O_6$	A	Huile rose	70/**1***a*
6*a*	$C_{31}H_{40}N_4O_8$	596	Huile rouge	63/**1***a*
6*b*	$C_{41}H_{44}N_4O$	A, 720	F_{dec} = 58	57/**1***b*
6*c*	$C_{39}H_{40}N_4O_6$	660	128	78/**1***c*
6*d*	$C_{45}H_{52}N_4O_6$	A, 744	149	60/**1***b*
6*i*	$C_{35}H_{32}N_4O_8$	A, 636	166–167	70/**1***c*
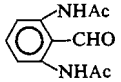	$C_{11}H_{12}N_2O_3$	220	179–181	(12)
7*a*	$C_{48}H_{66}N_4O_4$	762		2,6/**3***a*
7*b*	$C_{60}H_{74}N_8O_4$	970		10/**6***d*
7*c*	$C_{48}H_{50}N_8O_4$	802		11/**6***c*
7*e*	$C_{60}H_{74}N_8O_4$	970		60/**7***c*

* A = Analyses: cf. partie expérimentale.

cm^{-1}; rmn ($CDCl_3$): 0,9–1,5 (m, 10H), 2,2 (s, 3H), 2,5–2,8 (m, 2H), 4,1 (q, 2H), 5,2 (s, 2H), 7,2 (s large, 5H), 9,6 (s, 1H).

Ethoxycarbonyl-2 butyl-3 méthyl-4 carboxyl-5 pyrrole **2**d

Le pyrrole **2***c* (10 g, 0,03 mol) est mis en solution dans le THF anhydre (100 mL) contenant du palladium sur charbon à 10% (100 mg) et une goutte de triéthylamine. Le ballon est relié à un système de burettes contenant de l'hydrogène. Une forte agitation est maintenue. Il y a absorption de 500 mL d'H_2. Le mélange réactionnel est filtré à chaud sur Célite. Après évaporation est obtenu un solide blanc insoluble dans H_2O, C_6H_6, CH_2Cl_2, $CHCl_3$, CH_3COCH_3, m = 5,1 g, Rdt 70%; F = 216°C; M, $C_{13}H_{19}NO_4$ = 253; ir (KBr): 3210, 1695, 1660 cm^{-1}; rmn (DMSO): 0,9–1,5 (m, 10H), 2,2 (s, 3H), 2,6 (m, 2H), 4,2 (q, J = 7 Hz, 2H), 5,8 (m, 1H): s'échange avec D_2O; 11,5 (s, 1H): s'échange avec D_2O; sm (M = 253): pics à 253, 210, 192, 182, 138, 120. *Anal.* calc.: C 61,64, H 7,56, N 5,53; tr.: C 61,47, H 7,81, N 5,63.

Ethoxycarbonyl-2 butyl-3 méthyl-4 iodo-5 pyrrole **2**e

Le mélange bicarbonate de sodium (32×10^{-3} mol, 2,7 g) dans l'eau (11,3 mL) et le dichloro-1,2 éthane (13,2 mL) est chauffé à 50°C. On y ajoute successivement le pyrrole **2***d* (2,1 g, 9×10^{-3} mol), puis durant 5 min la solution d'iodure de sodium (3,5 g, 23×10^{-3} mol) et d'iode (2,8 g, 11×10^{-3} mol) dans l'eau (11,3 mL). Le reflux est maintenu 1 h, puis une solution saturée de thiosulfate est additionnée, la solution est traitée de façon habituelle. Le pyrrole obtenu est recristallisé dans l'hexane: il se présente sous forme de cristaux blancs rosés; m = 2,6 g, Rdt 85%; F = 103°C; M, $C_{12}H_{18}NO_2I$ = 335; ir (KBr): 3280, 1670 cm^{-1}; ($CHCl_3$): 3260, 1705, 1680 cm^{-1}; rmn ($CDCl_3$): 0,9–1,8 (s, 10H), 2,0 (s, 3H), 2,7 (m, 2H), 4,4 (q, J = 7 Hz, 2H), 9,5 (m, 1H); rmn ^{13}C ($CDCl_3$): 161,06 (C=O), 131,95, 127,8, 125,61, 123,40 (C pyrroliques), 60,32 (CO_2CH_2), 32,91, 25,52, 22,69, 14,50, 14,00, 11,98 (nBu, CO_2—CH_2—CH_3, pyrrole —CH_3); sm (M = 335): pics à 335, 293, 264, 246, 220. *Anal.* calc.: C 43,00, H 5,41, N 4,18, I 37,86; tr.: C 42,66, H 5,63, N 4,49, I 37,47.

Ethoxycarbonyl-2 butyl-3 méthyl-4 pyrrole **1**a

A une solution du pyrrole précédent **2***e* (41 g, 0,13 mol) dans l'éthanol bouillant est additionné goutte à goutte tout d'abord l'iodure de sodium (31,1 g, 0,21 mol) dans l'eau (250 mL), puis l'acide chlorhydrique (0,19 mol), le reflux est maintenu 1 h. Après addition d'une solution de bisulfite de sodium à 37% (55 mL, soit 0,2 mol $NaHSO_3$) le milieu réactionnel est refroidi doucement, puis extrait de la façon habituelle (CH_2Cl_2). Le pyrrole recristallisé dans l'hexane est obtenu sous forme de cristaux blancs rosés; m = 24 g, Rdt 88%; F = 46°C; M, $C_{12}H_{19}NO_2$ = 209; ir ($CHCl_3$): 3470, 1665 large (épaulement 1720 et 1655) cm^{-1}; rmn ($CDCl_3$): 0,8–1,6 (m, 10H), 1,9 (s, 3H), 2,5–3,0 (m, 2H), 4,2 (q, J = 7 Hz, 2H), 6,5 (d, 1H), 9,3 (m, 1H); sm (M = 209): pics à 94, 138, 166, 167, 180. *Anal.* calc.: C 68,86, H 9,15, N 6,69; tr.: C 68,86, H 9,07, N 6,88.

Benzyloxycarbonyl-2 butyl-3 méthyl-4 pyrrole **1**b

On opère par transestérification de la même façon que précédemment lors de la formation de **2***b*. Le pyrrole **1***b* se présente sous la forme d'un solide blanc qui est recristallisé dans l'hexane; m = 5,2 g, Rdt 70%; F = 64–65°C; M, $C_{17}H_{21}NO_2$ = 271; ir ($CDCl_3$): 3465, 1700, 1680 cm^{-1}; uv (EtOH): 205 (35 000), 275 (17 000); rmn ($CDCl_3$): 0,8–1,5 (m, 7H), 1,9 (s, 3H), 2,5–2,9 (m, 2H), 5,1 (s, 2H), 6,4 (d, J = 3 Hz, 1H), 7,2 (s, 5H), 9,3 (s large, 1H); rmn ^{13}C ($CDCl_3$): 161,42 (C=O), 136,51, 132,28, 120,21, 118,66 (C pyrroliques), 128,53, 128,23, 128,11 et 120,78 (Ar), 65,75 (CO_2CH_2), 33,12, 24,84, 22,81, 13,99 et 9,88 (n-Bu, pyrrole —Me); (C_6D_6): 161,64 (C=O), 137,03, 132,26, 119,89 et 119,03 (C pyrroliques), 128,54, 128,15 et 121,24 (Ar), 65,82 (CO_2CH_2), 33,58, 25,23, 23,09, 14,18 et 9,98 (n-Bu et pyrrole —Me); sm (M = 271): pics à 91, 138, 180, 229. *Anal.* calc.: C 75,25, N 7,80, N 5,16; tr.: C 75.03, H 7,79, N 5,08.

2. *Synthèse de dipyrrylméthanes*

Bis(benzyloxycarbonyl-5, butyl-4, méthyl-3, pyrryl-2)-3,3 propionate d'éthyle **3**a

A une solution de pyrrole **1***b* (15×10^{-4} mol, 0,136 g) dans le benzène (1,5 mL) est ajouté l'acide paratoluène sulfonique (2 mg). La solution est portée à reflux sous azote et on y ajoute le diéthoxypropionate d'éthyle (9×10^{-4} mol, 0,171 g). Le reflux est maintenu 24 h sous azote. Après traitement habituel et filtration sur colonne de silice, une huile jaune est obtenue (0,11 g); Rdt = 70%; ir ($CHCl_3$): 3450, 3360, 1685 (large) cm^{-1}; rmn (CCl_4): 0,8–1,5 (m, 17H), 2,0 (s, 6H), 2,4–2,8 (m, 4H), 3,1 (d, J = 8 Hz, 2H), 3,8 (q, J = 7 Hz, 2H), 4,7 (t, J = 8 Hz, 1H), 5,1 (s, 4H), 7,1 (s, 10H), 10,2 (s large, 2H); rmn ($CDCl_3$): 0,7–1,4 (m, 17H), 1,90 (s, 6H), 2,62 (m, 4H),

Can. J. Chem. Downloaded from www.nrcresearchpress.com by 210.87.254.5 on 09/06/12
For personal use only.

3,06 (d, J = 8 Hz, 2H), 4,00 (q, J = 7 Hz, 2H), 4,70 (t, J = 8 Hz, 1H), 5,20 (s, 4H), 7,25 (s, 10H), 9,60 (s, 2H). De la même manière est obtenu le bis(éthoxycarbonyl-5, butyl-4, méthyl-3 pyrryl-2)-3,3 propionate d'éthyle **3***c*. Rdt 70%; M, $C_{29}H_{44}N_2O_6$ = 516. *Anal.* calc.: C 67,35, H 8,51, N 5,42; tr.: C 67,31, H 8,52, N 5,59.

Bis(carboxy-5, butyl-4, méthyl-3, pyrryl-2)-3,3 propionate d'éthyle **3**b

Une solution de dipyrrylméthane **3***a* ($1,7 \times 10^{-4}$ mol, 0,11 g) dans le THF (3 mL) contenant du palladium sur charbon à 10% (10 mg) et une goutte de triéthylamine est mise en contact d'hydrogène pendant 4 h sous forte agitation. Le contenu du ballon est filtré sur Célite, lavé au THF et le solvant évaporé sous vide à température ambiante. Le solide jaune clair obtenu (0,08 g) est utilisé tel quel pour la synthèse de la porphyrine **7***a*; ir ($CHCl_3$): 3330, 3250, 1728, 1665 cm^{-1}; rmn (CCl_4): 0,8–1,5 (m, 17H), 2,00 (s, 3H), 2,03 (s, 3H), 2,4–2,8 (m, 4H), 3,16 (d, J = 8 Hz, 2H), 3,80 (q, J = 7 Hz, 2H), 4,73 (t, J = 8 Hz, 1H), 5,13 (s, 4H), 7,10 (s, 10H), 10,20 (s large, 2H).

Dinitro-2,6 phényl-bis(méthyl-3', butyl-4', éthoxycarbonyl-5', pyrryl-2') méthane **6**a

Dans un ballon surmonté d'un Dean–Stark le pyrrole **1***a* (5×10^{-4} mol, 0,105 g) et le dinitro-2,6 benzaldéhyde ($2,7 \times 10^{-4}$ mol, 0,053 g) sont mis en solution dans le toluène contenant l'acide trifluorométhane sulfonique (1×10^{-4} mol). Le mélange est porté à reflux 2 h sous azote. Après traitement habituel comprenant en plus un lavage avec une solution de bisulfite de sodium pour éliminer l'aldéhyde n'ayant pas réagi et un traitement au noir animal dans le THF, les différents constituants sont séparés par chromatographie sur silice. Un premier produit **4***a* (11) (5 mg) moins polaire que le pyrrole de départ est élué avec le mélange éther–EP (20:80).[3] Ce produit a été obtenu dans une autre réaction (11). Le dipyrrylméthane **6***a* (60 mg) est alors élué avec un mélange éther–EP (35:65), Rdt 40%, huile rouge, M, $C_{31}H_{40}N_4O_8$ = 596. Deux autres produits **4***b* et **5***a* caractérisés par ailleurs (11) sont alors élués: 10 mg **4***b* avec un mélange éther–EP (60:40); puis 10 mg **5***a* avec un mélange éther–EP (65:35). **6***a*, ir ($CHCl_3$): 3440, 1700–1680, 1500, 1360 cm^{-1}; rmn ($CDCl_3$): 0,8–1,6 (m, 20H), 1,76 (s, 6H), 2,5–2,9 (m, 4H), 4,23 (q, J = 7 Hz, 4H), 6,16 (s, 1H), 7,5–7,9 (m, 3H), 8,8 (s large, 2H).

Dinitro-2,6 phényl bis(méthyl-3', butyl-4', benzyloxycarbonyl-5', pyrryl-2) méthane **6**b

Dans un ballon surmonté d'un Dean–Stark, le mélange constitué du pyrrole **1***b* ($9,68 \times 10^{-3}$ mol), de dinitro-2,6 benzaldéhyde ($4,84 \times 10^{-3}$ mol) et d'acide trifluorométhane sulfonique (2×10^{-3} mol) dans le benzène (10 mL) est laissé avec agitation 1 h à température ambiante, puis porté à reflux 10 min. En traitant comme précédemment 15 mg de **4***c* (11), 1,2 g de **6***b* (Rdt = 34%) et 0,25 g de **5***b* (11) sont obtenus.

En effectuant la réaction à température ordinaire le mélange constitué du pyrrole **1***b* (30×10^{-3} mol, 8,1 g), de dinitro-2,6 benzaldéhyde (15×10^{-3} mol) et d'acide trifluorométhane sulfonique (6×10^{-3} mol) dans le benzène (30 mL) est agité 3 h; après traitement habituel, une chromatographie sur colonne de silice fournit les quatre produits suivants: l'élution avec le mélange éther–EP (10:90)[3] fournit le pyrrole de départ **1***b* (0,8 g), puis le produit **4***c*, caractérisé par ailleurs (11) (0,1 g) avec le mélange éther–EP (40:60), puis le dipyrrylméthane **6***b* (6,2 g, Rdt 57%, F déc. = 58°C, M, $C_{41}H_{44}N_4O_8$ = 720) avec le mélange éther–EP (45:55), puis le produit **5***b* (1,4 g) caractérisé par ailleurs (11) avec le mélange éther–EP (50:50). **6***b*, ir ($CHCl_3$): 3420, 1700–1680, 1540, 1355 cm^{-1}; uv (EtOH): 280 (31 900), 240 (31 500), 209 (74 600); rmn ($CDCl_3$): 0,8–1,6 (m, 14H), 1,8 (s, 6H), 2,5–2,9 (m, 4H), 5,1 (s, 4H), 6,2 (s, 1H), 7,9 (m, 13H), 9,1 (s large, 2H). *Anal.* calc.: C 68,33, H 6,15, N 7,77; tr.: C 68,26, H 5,93, N 7,98.

De la même manière est obtenu le dipyrrylméthane **6***i* à partir du pyrrole **1***c* et du dinitro-2,6 benzaldéhyde. **6***i*,Rdt 70%; F = 166–167°C; M, $C_{35}H_{32}N_4O_8$ = 636. ir ($CHCl_3$): 3440, 1690, 1540, 1360 cm^{-1}; rmn ^1H ($CDCl_3$): 1,7 (s, 6H), 2,2 (s, 6H), 5,2 (s, 4H), 6,2 (s, 1H), 7,2–7,8 (m, 13H), 8,8 (s large, 2H). *Anal.* calc.: C 66,02, H 5,06, N 8,80; tr.: C 66,28, H 5,06, N 8,96.

Diamino-2,6 phényl bis(méthyl-3', butyl-4', carboxy-5', pyrryl-2) méthane **6**h

Le dipyrrylméthane **6***b* (3×10^{-3} mol, 2,16 g) en solution dans le THF (75 mL) est introduit dans le THF (20 mL) contenant la triéthylamine (6 gouttes) et le palladium sur charbon à 10% (0,3 g). Le ballon est relié à un système de burettes contenant de l'hydrogène, en 10 h il y a absorption de 24×10^{-3} mol d'hydrogène.

Le contenu du ballon est filtré sur Célite, lavé au THF, on opère sous atmosphère d'azote dans une boîte à gants du fait de l'instabilité du diacide botenu. Le solvant est évaporé sous vide à température ordinaire et l'on obtient une huile jaune, m = 1,5 g (composé instable que l'on utilise tel quel et que l'on suppose être **6***h*); ir ($CHCl_3$): 3440, large bande 3000, 1660 cm^{-1}; rmn (DMSO): 0,8–1,5 (m, 14H), 1,63 (s, 6H), 2,4–2,7 (m, 4H), 4,5 (s large (s'échange avec D_2O), 1H), 5,8 (s, 1H), 6,7–7,4 (m, 3H), 9,8 et 10,0 (deux massifs qui s'échangent avec D_2O).

3. *Synthèse de porphyrines*

Bis(éthoxycarbonyl)-5,15 tétrabutyl-2,8,12,18 tétraméthyl-3,7,13,17 porphyrine **7**a

Le mélange constitué de diacide **3***b* (0,1 mmol), d'acide trichloroacétique (0,23 mL d'une solution 5,2 M CCl_3COOH/CH_2Cl_2 soit 0,12 mol) et d'orthoformiate de triméthyle (0,8 mmol) est porté à reflux 18 h. Du DDQ[3] (0,1 mmol) est alors ajouté et le reflux est continué 90 min. La solution est lavée avec une solution de bicarbonate à 20%, puis à l'eau, séchée puis évaporée. Après filtration sur colonne de silice, la porphyrine **7***a* éluée au CH_2Cl_2 est obtenue (2 mg) (Rdt 2,6%), M, $C_{48}H_{66}N_4O_4$ = 762; uv (CH_2Cl_2 + 1 goutte $N(Et)_3$): bande de Soret 408 et bandes I, II, III, IV à 630, 577, 545, 510 nm; (CH_2Cl_2 + 1 goutte HCl): bande de Soret 435 et bandes ép 537, 570 et 620 nm; ir ($CHCl_3$): 1720 (large) cm^{-1}; rmn ($CDCl_3$): 10,07 (s, 2H), 5,91 (s, 4H), 4,40 (q, J = 8 Hz, 4H), 4,00 (t, J = 8 Hz, 8H), 3,40 (s, 12H), 1,8–1,1 (m, 28H); sm: 762.

Bis(diacétamido-2,6 phényl)-5,15 tétrabutyl-2,8,12,18 tétraméthyl-3,7,13,17 porphyrine **7**b

Dans un ballon surmonté d'un Dean–Stark, le pyrrole **1***b* (0,3 mmol, 81,6 mg) et le diacétamido-2,6 benzaldéhyde (12) (0,15 mmol, 33 mg) sont mis en solution dans le benzène en présence d'acide paratoluène sulfonique (2 mg). Le mélange est porté à reflux pendant 48 h sous azote. Après traitement habituel, l'huile obtenue est chromatographiée sur silice. Le dipyrrylméthane **6***d* est élué avec le mélange acétone–éther (15:85) (Rdt 60%). Le dipyrrylméthane **6***d* (22 mg) est traité en solution dans le THF (5 mL) et la triéthylamine (1 goutte) en présence de Pd/C sous hydrogène pendant 100 min. Après filtration et évaporation du solvent, le produit obtenu **6***g* utilisé sans autre purification (produit instable) est dissout dans CH_2Cl_2 (15 mL), puis traité avec CCl_3CO_2H (1 mmol, 163 mg) et $HC(OMe)_3$ (0,15 mmol, 16 mg). La solution est agitée 4 jours puis traitée au DDQ. Après traitement habituel, le brut est chromatographié sur colonne de silice, la porphyrine **7***b* est éluée au chloroforme: m = 4 mg, Rdt 10%.

Diacétamido-2,6 benzaldéhyde (12): M, $C_{11}H_{12}N_2O_3$ = 220; ir ($CHCl_3$): 1700, 1670, 1617, 1597 cm^{-1}; (KBr): 3300–3285, 1700, 1685, 1645, 1620, 1600 cm^{-1}; rmn ($CDCl_3$): 9,86 (s, 1H), 7,53 (m, 3H), 2,15 (s, 6H); rmn (Me_2CO): 10,3 (s large s'échange avec D_2O), 9,8 (s, 1H), 7,6 (m, 3H), 2,06 (s, 6H); sm: 220, 192 (—CO), 177 (—CH_3), 150 (—CH_2CO), 108 (—CH_2CO). *Anal.* calc.: C 59,99, H 5,49, N 12,72; tr.: C 60,32, H 5,79, N 12,93.

Dipyrrylméthane **6**d: $F \approx$ 149°C; M, $C_{45}H_{52}N_4O_6$ = 744; ir ($CHCl_3$): 1710, 1645 cm^{-1}; rmn ($CDCl_3$): 9,27 (s large, 1H), 7,28 (m, 13H), 6,70 (s large, 2H), 5,17 (s, 4H), 2,69 (m, 4H), 1,74 (s, 6H), 1,30 (m, 14H). *Anal.* calc.: C 72,55, H 7,04, N 7,52; tr.: C 72,79, H 7,20, N 7,78.

Porphyrine **7**b: M, $C_{60}H_{74}N_8O_4$ = 970; ir ($CHCl_3$): 1695 (large) cm^{-1}; uv (CH_2Cl_2): 405, 504, 531, 567, 617; ($CHCl_3$): 407, 505, 537, 568, 618; uv ($CHCl_3$ + HCl): ép 400–451, ép 540–583, 629; rmn ($CDCl_3$): 10,4 (s, 2H), 8,5 (m, 4H), 7,9 (m, 2H), 6,3 (s, 4H), 4,0 (m,

[3] DDQ: dichloro, dicyano, parabenzoquinone; EP: éther de pétrole fraction Eb = 35–60°C; *p*-TsOH: acide paratoluène sulfonique.

8H), 2,6 (s, 12H), 1,2 (s, 12H); sm: 970.

Bis(diacétamido-2,6 phényl)-5,15 octaméthyl-2,3,7,8,12,13,17,18 porphyrine 7c

Dans un ballon surmonté d'un Dean–Stark, le pyrrole **1***c*[3] (10 mmol) et le diacétamido-2,6 benzaldéhyde (5,5 mmol) sont mis en solution dans le benzène en présence de quantité catalytique de *p*-TsOH. Le mélange est porté à reflux sous azote pendant 17 h. Après traitement habituel, l'huile obtenue est chromatographiée sur colonne de silice. Le dipyrrylméthane **6***c* est élué avec le mélange acétone–éther (15:85) (3,9 mmol; Rdt 78%), F = 128°C; M, $C_{39}H_{40}N_4O_6$ = 660; ir (KBr): 3450, 1710, 1645 cm^{-1}; rmn ($CDCl_3$): 9,47 (s, 2H, NH), 7,66 (s, 13H, ArH), 5,73 (s, 1H, CH-Pyr), 5,20 (s, 4H, CH_2Ar), 2,25 (s, 6H, $COCH_3$), 1,83 (s, 6H, Me), 1,75 (s, 6H, Me). *Anal.* calc.: C 70,88, H 6,10, N 8,48; tr.: C 70,53, H 6,17, N 8,43.

Le dipyrrylméthane **6***c* (1 mmol) est dissout dans le THF (30 mL) en présence de NEt_3 (3 gouttes) et de Pd/C sous pression atmosphérique d'H_2 jusqu'à ce que la quantité d'H_2 devant être absorbée corresponde à 2 mmol (44,8 mL). Après filtration et évaporation du solvant, le produit obtenu **6***f* est dissout sans autre purification dans CH_2Cl_2 sec. A cette solution est ajouté CCl_3CO_2H (1,89 g) dissout dans 25 mL de CH_2Cl_2 puis $HC(OMe)_3$ (0,9 mL) à l'abri de la lumière, à température ambiante. La solution est agitée pendant 4 jours, puis traitée au DDQ[3] (220 mg) pendant 2 jours. Après traitement habituel, le brut est filtré sur colonne de silice: la tétraacétamido-porphyrine **7***c* est éluée avec le mélange CH_2Cl_2/acétone (85:15) (88 mg; Rdt 11%; M, $C_{48}H_{50}N_8O_4$ = 802); uv ($CHCl_3$): 401, 504, 538, 571, 624; ir ($CHCl_3$): 1690–1670 cm^{-1}; rmn ($CDCl_3$): 10,4 (s, 2H meso), 8,5 (d, J = 8 Hz, 2H, ArH), 7,9 (t, J = 9 Hz, 2H, ArH), 6,4 (s large, 2H, NH), 3,6 (s, 12H, CH_3), 2,6 (s, 12H, CH_3), 1,20 (s, 12H, $COCH_3$); ($CDCl_3$ + CF_3CO_2H): 9,37 (s, 2H meso), 8,2 et 8,0 (ArH); Me (3,3); Me (2,45); NHAC (1,35); sm m/e: 802.

Bis(dipivalamido-2,6 phényl)-5,15 octamethyl-2,3,7,8,12,13,17,18 porphyrine 7e

L'hydrolyse de la porphyrine **7***c* par HCl 6 *N* (13) sous azote, à l'abri de la lumière à reflux pendant 2 h fournit une solution verte qui est traitée par NaOH 10%. Le précipité rouge **7***d* formé est filtré, puis lavé à l'eau (Rdt 94%), M, $C_{40}H_{42}N_8$ = 634; uv (CH_2Cl_2): 408, 506, 538, 571, 625; rmn (CF_3CO_2D): 8,35 (m, ArH), 3,5 (s, Me), 2,7 (s, Me). La tétraamino-porphyrine **7***d* dissoute dans une solution de CH_2Cl_2 et de CF_3CO_2H est traitée à température ordinaire pendant 8 h avec un excès de chlorure de pivaloyle dissout dans du chlorure de méthylène et de la pyridine (13). La réaction fournit après lavage à l'eau une huile qui est chromatographiée sur colonne de silice. L'éluant 50% Et_2O/EP livre la tétrapivalamido porphyrine **7***e* qui est recristallisée dans le mélange éther–cyclohexane; Rdt 60% (solide rouge violet); M, $C_{60}H_{74}N_8O_4$ = 970; uv (CH_2Cl_2): 405, 505, 537, 572, 637; ir (KBr): 3430, 1690 cm^{-1}; ($CHCl_3$): 3425, 1690 cm^{-1}; rmn ($CDCl_3$): 10,22 (s, CH meso), 8,48 (d, J = 8 Hz, 4H, ArH), 7,81 (t, J = 8 Hz, 2H, ArH), 6,83 (s, 4H, NH), 3,5 (s, 12H, CH_3), 2,55 (s, 12H, CH_3), 0,04 (s, 36H, *t*Bu); sm m/e: 970.

1. (*a*) J. P. COLLMAN. Acc. Chem. Res. **10**, 265 (1977); (*b*) J. P. COLLMAN, J. P. BRAUMAN, T. J. COLLINS, B. IVERSON et J. L. SESSLER. J. Am. Chem. Soc. **103**, 2450 (1981); (*c*) G. B. JAMESON, F. S. MOLINARO, J. A. IBERS, J. P. COLLMAN, J. I. BRAUMAN, E. ROSE et K. S. SUSLICK. J. Am. Chem. Soc. **102**, 3224 (1980).
2. (*a*) A. R. BATTERSBY, S. G. HARTLEY et M. D. TURNBULL. Tetrahedron Lett. 3169 (1978); (*b*) A. R. BATTERSBY et A. D. HAMILTON. J. Chem. Soc. Chem. Commun. 117 (1980); (*c*) M. MOMENTEAU, J. MISDELTER, B. LOOCK et E. BISAGNI. J. Chem. Soc. Perkin Trans. 1, 189 (1983); (*d*) M. MOMENTEAU et B. LOOCK. J. Mol. Catal. **7**, 315 (1980); (*e*) J. E. BALDWIN, T. KLOSE et M. PETERS. J. Chem. Soc. Chem. Commun. 881 (1976); (*f*) J. R. BUDGE, P. E. ELLIS, JR., R. D. JONES, I. E. LINARD, T. SZYNANSKI, F. BASOLO, J. E. BALDWIN et R. H. DYER. J. Am. Chem. Soc. **101**, 4762 (1979); (*g*) A. R. BATTERSBY, S. A. J. BARTHOLOMEW et T. NITTA. J. Chem. Soc. Chem. Commun. 1291 (1983); (*h*) J. E. BALDWIN et P. PERLMUTTER. Top. Curr. Chem. **121**, 181 (1984), et références citées; (*i*) T. G. TRAYLOR, M. J. MITCHELL, S. TSUCHIYA, S. CAMPBELL, D. H. STYNES et D. V. KOGA. J. Am. Chem. Soc. **103**, 5234 (1981); (*j*) C. K. CHANG. J. Am. Chem. Soc. **99**, 2819 (1977).
3. A. LECAS, J. LEVISALLES, Z. RENKO et E. ROSE. Tetrahedron Lett. **25**, 1563 (1984).
4. (*a*) G. M. BADGER, R. A. JONES et R. L. LASLETT. Aust. J. Chem. **17**, 1157 (1964); (*b*) E. R. SCHMITTOU. Thèse 1979, Université de Stanford, U.S.A.
5. G. G. KLEINSPEHN. J. Am. Chem. Soc. **77**, 1546 (1955).
6. A. J. ZAMBITO et E. E. HOWE. Org. Synth. Coll. Vol. **5**, 373 (1973).
7. A. W. JOHNSON, E. MARHAM et A. PRICE. Org. Synth. **42**, 75 (1962).
8. J. L. ARCHIBALD, D. M. WALKER, K. B. SHAW, A. MARKOVAC et J. F. MCDONALD. Can. J. Chem. **44**, 345 (1966).
9. A. R. BATTERSBY, E. HUNT, E. MCDONALD, J. B. PAINE et J. SAUNDERS. J. Chem. Soc. Perkin Trans. 1, 1008 (1976).
10. F. DOLPHIN. The porphyrins. Vol. I. Academic Press, New York. 1978.
11. A. LECAS, J. LEVISALLES, C. MARIACHER et E. ROSE. Can. J. Chem. **62**, 2059 (1984).
12. B. D. ANDREWS et I. D. RAE. Aust. J. Chem. **24**, 413 (1971).
13. M. J. GUNTER et L. N. MANDER. J. Org. Chem. **46**, 4792 (1981).

Can. J. Chem. Downloaded from www.nrcresearchpress.com by 210.87.254.5 on 09/06/12
For personal use only.

Condensation inhabituelle d'un pyrrole et d'un benzaldéhyde encombré

ALEXANDRA LECAS-NAWROCKA, JACQUES LEVISALLES, CLAIRE MARIACHER ET ERIC ROSE[1]

Laboratoire de Chimie Organique (UA 408), Université Pierre et Marie Curie, 4 Place Jussieu, 75230 Paris Cedex 05, France

Reçu le 17 janvier 1984

Cet article est dédié au Professeur Paul de Mayo à l'occasion de son 60e anniversaire

ALEXANDRA LECAS-NAWROCKA, JACQUES LEVISALLES, CLAIRE MARIACHER et ERIC ROSE. Can. J. Chem. **62**, 2059 (1984).

La condensation du dinitro-2,6 benzaldéhyde et d'un pyrrole ne conduit pas à un dipyrrylméthane, mais à des produits résultant soit d'un doublement des molécules de pyrrole de départ, soit de réactions d'oxydo-réduction de l'intermédiaire **9** correspondant à un début de condensation entre une molécule de pyrrole et une molécule d'aldéhyde. Les groupes nitro du dinitro-2,6 benzaldéhyde jouent un rôle important dans ces réactions inattendues.

ALEXANDRA LECAS-NAWROCKA, JACQUES LEVISALLES, CLAIRE MARIACHER, and ERIC ROSE. Can. J. Chem. **62**, 2059 (1984).

The condensation between 2,6-dinitrobenzaldehyde and a pyrrole does not afford a dipyrrylmethane but products which result from a duplication of the starting pyrrole or from oxydo-reduction reactions of the pyrryl-arylcarbinol **9** which arise from the condensation between one molecule of pyrrole and one molecule of aldehyde. The nitro groups of the benzaldehyde play a crucial role in these reactions.

Il est bien connu que la condensation d'un aldéhyde avec un pyrrole dans le rapport 1:2 conduit à un dipyrrylméthane, précurseur de porphyrines (1, 2) (éq. [1]). Le présent mémoire décrit le cours anormal de la condensation du dinitro-2,6 benzaldéhyde avec les pyrroles **1***a* et **1***b*, qui a été observé dans le cadre des études de porphyrines du laboratoire (3, 4).

[1] 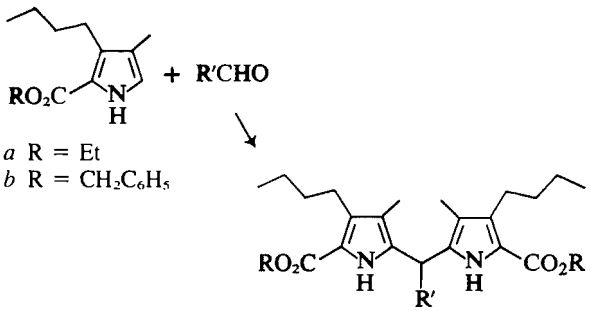

1*a* R = Et
b R = $CH_2C_6H_5$

Au lieu des dipyrrylméthanes attendus, on observe la formation des trois produits **2***a*, **3***a* et **4***a* à partir de **1***a*, et de deux produits **2***b* et **4***b* à partir de **1***b* (éq. [2]). Les structures de ces composés résultent des observations spectroscopiques suivantes.

[2] 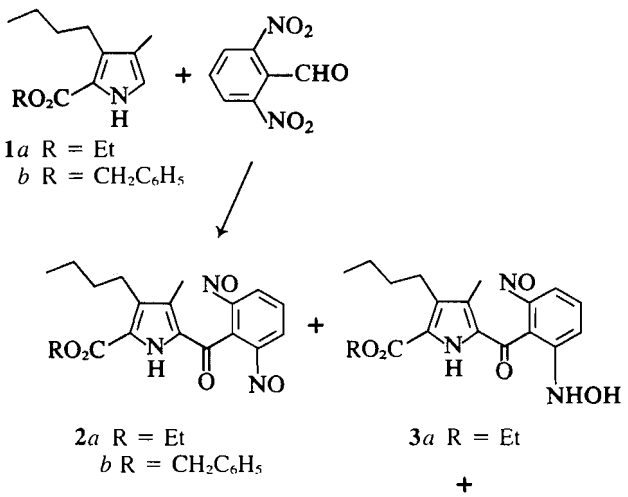

1*a* R = Et
b R = $CH_2C_6H_5$

2*a* R = Et
b R = $CH_2C_6H_5$

3*a* R = Et

+

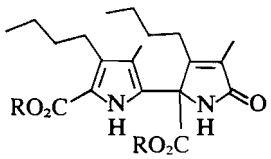

4*a* R = Et
b R = CH_2Ph

Composés 2 et 3

Les spectres de rmn ^1H des composés **2** et **3** montrent qu'il n'y a qu'un seul motif pyrrolique par motif dinitrobenzénique (tableau 1). Le composés **3***a* possède deux protons de plus que le composé **2***a* (ce que confirment les spectres de masse), et l'un de ces protons est échangeable par traitement par D_2O, mais le reste du spectre de rmn est très semblable à celui de **2***a*. Les protons arèniques des composés **2***a*, **2***b* et **3***a* présentent des signaux caractéristiques dont l'empreinte est analogue à celle des protons arèniques du dinitro-2,6 benzaldéhyde.

Les fréquences d'élongation observées dans les spectres ir pour les vibrateurs NH, CO et NO sont rassemblées dans le tableau 1. Les bandes à 1710−1720 cm^{-1} peuvent être attribuées aux groupes carbonyles libres des alcoxycarbonyl-2 pyrroles, et les bandes à 1690−1685 cm^{-1} aux mêmes groupes liés par pont hydrogène au groupe NH pyrrolique (5−7). Quant aux groupes carbonyles cétoniques, on peut leur attribuer les bandes situées entre 1650 et 1590 cm^{-1}, par analogie avec celle que le benzoyl-2 triméthyl-3,4,5 pyrrole présente à 1608 cm^{-1} (8). Outre les bandes NH vers 3450−3280 cm^{-1} on notera dans le tableau 1 la bande présentée par **3***a* vers 3500 cm^{-1}, probablement due au groupe OH. Enfin la présence de groupe NO est visible dans les spectres ir vers 1530−1540 cm^{-1} (tableau 1) et dans les spectres de masse (perte de 30 unités de masse = NO) (9).

Composés 4

Les spectres de rmn montrent l'absence de groupement dinitrophényle (notamment pour **4***a* où il n'y a aucun signal au delà de 4,2 ppm). En revanche, l'existence de deux singulets (1,76 et 1,88 ppm pour **4***a*, 1,80 et 1,86 ppm pour **4***b*) révèle la présence de deux groupes méthyles *différents*, de même que l'existence de deux quadruplets presque superposés pour **4***a* (—COO—CH_2—CH_3) et de deux singulets pour **4***b* (—COO—CH_2—C_6H_5) révèle la présence de deux groupes

[1]Auteur á qui toute correspondance doit être adressée.

Can. J. Chem. Downloaded from www.nrcresearchpress.com by 210.87.254.40 on 09/06/12
For personal use only.

Can. J. Chem. Downloaded from www.nrcresearchpress.com by 210.87.254.40 on 09/06/12
For personal use only.

TABLEAU 1. Spectroscopies de résonance magnétique nucléaire et infrarouges des composés **2**, **3** et **4***

	Résonance magnétique nucléaire		Infrarouge		
Composé	(a)	Région ArH (d)	Région 3600−3200	Région 1750−1600	Région 1580−1300
2*a*	3H à 2,0 CH_3 (s) 3ArH à 7,2−8	7,65 dd, J = 9,1 et 9,0 (1H) 8,10 d, J = 8,6 (1H) 8,14 dd, J = 7,2 et 2,3 (1H)	3450 NH (c) 3280 3450, 3270 (b)	1710 CO_2Et libre (b) 1685 CO_2Et lié 1650−1625−1595 (C═O)	1530 large (b) 1535 (c)
2*b*	3H à 2,0 CH_3 (s) 8ArH à 7,3−8,1	7,40 m (5H) 7,63 deux d, J = 9,0 et 7,0 (1H) 8,09 d, J = 8,9 (1H) 8,13 d, J = 6,9 (1H)	3457 NH (b)	1717 ép 1702, 1690 CO_2Et (b) 1655, 1620, 1590 (C═O)	1540 large NO (b)
3*a*	3H à 1,7 CH_3 (s) 7,01 dd, J = 7,5 et 2,2 (1H) 7,20 d, J = 7,5 (1H) 7,41 d de d, J = 7,5 et 2,2 (1H)	3H à 7,1−7,5 m	3500−3435 (b) 3500−3450−3410 (c) 3280 (c)	1712−1700 (b) 1627−1600 (b) 1725−1710 (c) 1636−1605 (c)	1530 (c)
4*a*	3H à 1,80 CH_3 (s) 3H à 1,86 CH_3 (s) 2H à 4,2 q déformé 2H à 4,2 q déformé		3440 (b)	1700 ép 1740 et 1660 (b)	
4*b*	3H à 1,80 CH_3 (s) 3H à 1,86 CH_3 (s) 2H à 5,20 $CH_2C_6H_5$ (s) 2H à 5,26 $CH_2C_6H_5$ (s)	7,35 m (10H)	3445 (b) 3450 (c)	1710 ép 1745 et 1680 (b) 1700 ép 1730 et 1670 (c)	

*En ppm/TMS (a) $CDCl_3$; (b) $CHCl_3$; (c) CCl_4); (d) Me_2CO-d_6.

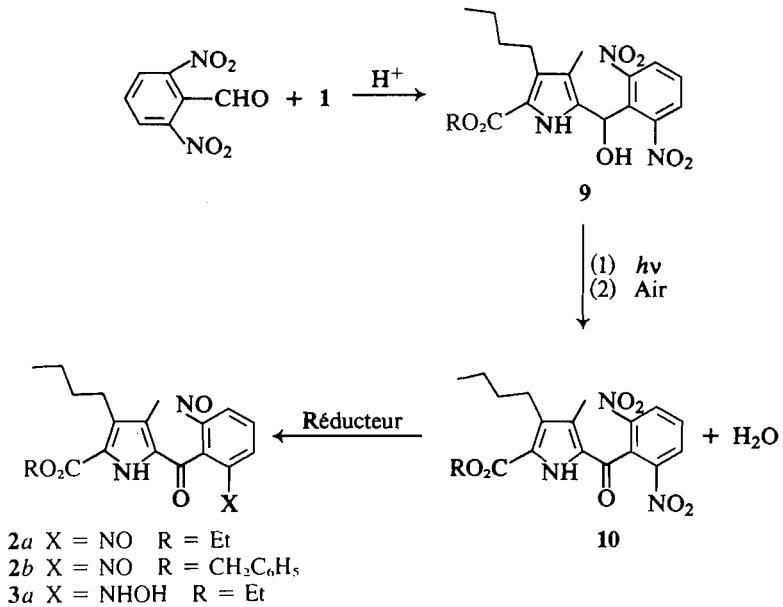

SCHÉMA 1

esters *différents* (tableau 1). Ces données suggèrent la superposition dans **4** de deux motifs différents dérivés de **1**.

Dans la région des fréquences d'élongation des vibrateurs C=O, les spectres ir présentent de larges bandes centrées vers 1700 cm^{-1} pour **4***a* et 1710 cm^{-1} pour **4***b*. Par analogie avec les fréquences observées pour les composés modèles **5** (10), **6** (11), **7** (12) et **8** (13), qui sont de l'ordre de 1680 cm^{-1} pour le groupe CONH et de 1740 cm^{-1} pour le groupe ester de **5**, et par analogie avec les fréquences observées pour les fonctions esters de **1***a* (1700, 1675, 1655 cm^{-1}) et de **1***b* (1700, 1680, 1655 cm^{-1}) on peut considérer que les larges bandes observées pour **4***a* et **4***b* résultent du recouvrement des bandes dûes aux groupes amide conjugué, ester conjugué et ester non conjugué.

Enfin dans les spectres de masse la perte du groupe ester non conjugué—CO_2R donne lieu à un pic intense (m/e = 359 = M—$CO_2CH_2CH_3$ pour **4***a*, m/e = 421 = M − $CO_2CH_2C_6H_5$ pour **4***b*), accompagné d'un autre pic à m/e = 313, correspondant à M − CO_2R − ROH, et commun aux spectres de masse de **4***a* et de **4***b*.

L'ensemble des données précédentes est en accord avec les structures de benzoyl-pyrroles substitués pour **2** et **3** et de pyrryl-pyrrolidones pour **4**.

Discussion

Le tableau 2 donne les rendements en produits **2**, **3** et **4** obtenus lors des essais de préparation des dipyrrylméthanes, en présence d'acide *p*-toluène sulfonique (TsOH). On voit que le rapport **2** + **3**/**4** varie de 1,7 à 3,2. On notera que par rapport au composé primaire attendu de la condensation, l'alcool **9**, les composés **2** et **3** sont plus oxydés d'un côté (l'alcool est devenu cétone), moins oxydés de l'autre (les groupes NO_2 sont devenus NO ou NHOH). Cette anomalie s'explique aisément par le comportement photochimique de l'alcool *ortho*-nitrobenzylique et de l'aldéhyde *ortho*-nitrobenzoïque qui se transforment en aldéhyde et en acide *ortho*-nitrosobenzoïque respectivement (14). En présence de lumière l'alcool **9** peut donner la cétone **10**, qui peut être réduite en composé **2** ou **3** si un réducteur est présent dans le milieu (schéma 1).

La présence d'un réducteur dans le milieu est plausible. Il est

TABLEAU 2. Rendements des produits obtenus lors de la condensation du pyrrole **1***a* ou **1***b* avec le dinitro-2,6 benzaldéhyde DNB

			Composé					
Pyrrole	1/DNB	Solvant	**2***a*	**3***a*	**4***a*	**2***b*	**4***b*	Catalyseur
1*a* ou **1***b*	1/0,55	Éthanol	Aucune réaction					HCl
1*a*	1/0,55	Toluène	27	11	18			*p*TsOH (a)*
1*a*	1/0,55	Toluène	0	16	13			*p*TsOH (b)
1*b*	1/1,8	Benzène				36	20	*p*TsOH (a)
1*b*	1/1,8	Xylène				40	24	*p*TsOH (a)
1*b*	1/1,8	Xylène				39	12	*p*TsOH (a)

*(a) Quantité catalytique; (b) *p*TsOH/pyrrole **1***a* = 2.

en effet bien connu qu'en milieu acide, un pyrrole tel que **1** peut se condenser sur lui-même pour donner une pyrryl-pyrroline (1) telle que **11** qui peut se transformer en composé **4**, en présence des oxydants que sont les groupes NO_2 de la cétone **10** et du dinitro-2,6 benzaldéhyde. On sait par exemple que le nitrobenzène peut oxyder photochimiquement l'isopropanol en donnant la phénylhydroxylamine en l'absence d'oxygène, ou le nitrosobenzène en présence d'oxygène (les arylhydroxylamines s'oxydent spontanément en nitrosoarènes en présence d'air) (15, 16). Comme la formation de la pyrroline **11** en milieu acide est réversible, c'est son oxydation par les groupes NO_2 de la cétone **10** ou du dinitrobenzaldéhyde, qui provoque la formation irreversible du composé **4**. Ceci peut être vérifié par le traitement des pyrroles **1**, qui, placés dans les conditions de la formation de **4**, mais *sans* aldéhyde, sont récupérés inchangés après 48 h, même en présence d'air, ou de nitrobenzène, alors que l'autoxydation à 50°C du *N*-méthyl pyrrole et du triméthyl-2,3,4 pyrrole conduit respectivement aux composés **12** (17) et **13** (18).

On peut se demander pourquoi un tel comportement n'a pas été observé avec l'*ortho*-nitrobenzaldéhyde. Il est vraisemblable que ce dernier, moins encombré que le dinitro-2,6 benzaldéhyde, réagit rapidement avec une deuxième molécule de pyrrole pour conduire au dipyrrylméthane; en revanche le dini-

Can. J. Chem. Downloaded from www.nrcresearchpress.com by 210.87.254.40 on 09/06/12
For personal use only.

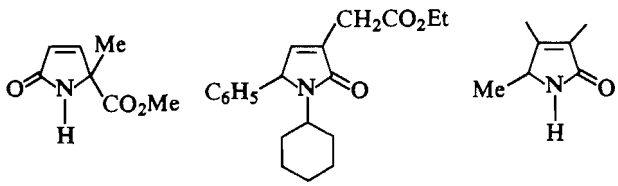

5 6 7

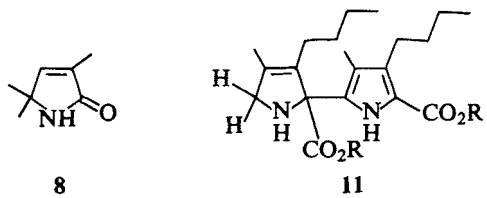

8 11

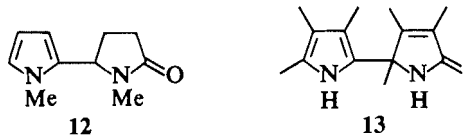

12 13

trobenzaldéhyde, très encombré, donne l'alcool **9** qui, trop encombré pour se condenser une deuxième fois, subit les réactions photochimiques secondaires conduisant à **2**, **3** et **4**.

En conclusion, les essais de synthèse de dipyrrylméthane, infructueux à partir du dinitro-2,6 benzaldéhyde, mettent en évidence les produits qui résultent d'un début de condensation et qui par leur nature oxydante facilitent la formation de produits de doublement des molécules de pyrrole de départ.

Partie expérimentale

L'action du pyrrole **1***a* ou **1***b* à reflux pendant 24 h ou plus en présence d'un demi équivalent de dinitro-2,6 benzaldéhyde et d'acide chlorhydrique en quantité catalytique dans l'éthanol ne conduit à aucun produit nouveau. Les produits de départ sont récupérés.

Dans un ballon surmonté d'un Dean–Stark le pyrrole **1***a* ou **1***b* et le dinitro-2,6 benzaldéhyde DNB sont mis en solution dans le solvant (tableau 2) en présence de quantité catalytique d'acide *para*-toluène sulfonique *p*-TsOH. Le mélange est porté à reflux 48 h. Après "traitement habituel" (3) comportant en plus un lavage avec une solution de bisulfite de sodium pour éliminer l'aldéhyde qui n'a pas réagi, les différents prduits sont chromatographiés sur colonne de silice. Les rendements en produits formés sont donnés au tableau 2.

Dans le cas du pyrrole **1***a*, la chromatographie sur colonne de silice fournit un premier produit **2***a* légèrement moins polaire que le pyrrole de départ **1***a* qui est élué avec le mélange éther – éther de pétrole EP 20:80, puis un deuxième produit **3***a* plus polaire que le pyrrole de départ **1***a* élué avec un mélange éther–EP 60:40 et enfin un troisième produit **4***a* élué avec un mélange éther–EP 65:35.

Dans le cas du pyrrole **1***b*, les produits **2***b* et **4***b* sont élués avec les mélanges Et_2O–EP 40:60 et 50:50.

2*a*, poudre jaune, F = 142°C; ir ($CHCl_3$): 3450, 3270 (large), 1710–1685, 1650–1625, 1595, 1530 et 1335 cm^{-1}; (CCl_4): 3450, 3290 (large), 1720, 1700, 1652, 1612, 1585, 1535 et 1340 cm^{-1}; rmn ^1H (60 MHz, $CDCl_3$): 0,8–1,6 (m, 10H), 2,0 (s, 3H), 2,5–2,9 (m, 2H), 4,2 (q, J = 7 Hz, 2H), 7,2–8,0 (m, 3H), 9,5 (s large, 1H); rmn ^1H (90 MHz, Me_2CO): région des aromatiques: 7,65 (d de d, 1H (doublet à 7,69, J = 9,1 Hz et doublet à 7,62, J = 9,0 Hz)), 8,10 (d, J = 8,6 Hz, 1H *ortho* à NO), 8,14 (d de d, J = 7,2 et 2,3 Hz, 1H *ortho* à NO); sm: 371, 267, 233, 180 (M, $C_{19}H_{21}N_3O_5$ = 371). *Anal.* calc.: C 61,44, H 5,70; tr.: C 61,16, H 5,97.

3*a*, huile jaune; ir ($CHCl_3$): 3435, 1712, 1700, 1627, 1600, 1350 cm^{-1}; (CCl_4): 3500, 3450, 3410, 3280 (large), 1725, 1710, 1636, 1605, 1530, 1350 cm^{-1}; rmn ^1H (60 MHz, $CDCl_3$): 0,8–1,5 (m, 10H), 1,70 (s, 3H), 2,5–2,8 (m, 2H), 4,4–4,5 (q déformé, J = 7 Hz; si $+D_2O$ q, J = 7 Hz), 7,01 (d de d, J = 7,5 et 2,2 Hz, 1H, ArH *meta* par rapport au groupe NO), 7,20 (d, J = 7,5 Hz, 1H, ArH), 7,41 (d de d, J = 7,5 et 2,2 Hz, 1H, ArH), 9,5 (s large, 1H s'échange avec D_2O); rmn ^1H (90 MHz, Me_2CO): 0,8–1,40 (10H dont un triplet à 1,33, J = 7,1 Hz), 1,88 (s, 3H), 2,6–2,9 (m, 2H), 4,30 (q, J = 7,1), 7,1–7,5 (m, 3H); sm: 373, 343, 341, 328 (M, $C_{19}H_{23}N_3O_5$ = 373).

4*a*, huile rouge; ir ($CHCl_3$): 3440, 1700 (large) (ép 1740, 1660) cm^{-1}; rmn ^1H (60 MHz, $CDCl_3$): 0,8–1,5 (m, 20H), 1,80 (s, 3H), 1,86 (s, 3H), 2,1–2,8 (m, 4H), 4,2 (q, 4H), 6,56 (s, 1H), 9,5 (s large, 1H); rmn ^1H (90 MHz, Me_2CO): 0,70–1,5 (m, 30H dont deux triplets à 1,27 (t, J = 7,1 Hz) et 1,31 (t, J = 7,1 Hz), 1,79 (s, 3H), 1,82 (s, 3H), 2,1 à 2,9 (m, 4H), 4,26 (q, J = 7,1 Hz, 3H), 4,27 (q, J = 7,1 Hz, 3H), 7,80 (s, 1H), 10,38 (s large, 1H); sm: 432, 359, 313 (M, $C_{24}H_{36}N_2O_5$ = 432). *Anal.* calc.: C 66,64, H 8,39, N 6,48; tr.: C 66,80, H 8,41, N 6,23.

2*b*, cristaux jaunes, F = 137°C; ir ($CHCl_3$): 3457, 1717 ép, 1702 ép, 1690, 1655, 1620, 1590, 1540, 1355 cm^{-1}; rmn ^1H (60 MHz, $CDCl_3$): 0,8–1,6 (m, 7H), 2,0 (s, 3H), 2,5–2,9 (m, 2H), 5,1 (s, 2H), 7,3–8,1 (m, 8H), 9,5 (s large, 1H); rmn ^1H (90 MHz, Me_2CO): 0,8–1,5 (m, 7H), 2,10 (s, 3H), 2,84 (t, J = 8,6 Hz, 2H), 5,19 (s, 2H), 7,40 (m, 5H), 7,63 (d de d, J = 9,0 et 7,0 Hz, 1H *méta* à Ar-NO), 8,09 (d, J = 8,9 Hz, 1H *ortho* à Ar-No), 8,13 (d, J = 6,9 Hz, 1H *ortho* à Ar-NO), 11,15 (s large, 1H); sm: 433, 403 (M, $C_{24}H_{23}N_3O_5$ = 433). *Anal.* calc.: C 66,50, H 5,35, N 9,69; tr.: C 66,44, H 5,56, N 9,77.

4*b*, huile visqueuse rouge; uv (EtOH): 280 (14 300), 235 (12 600), 207 (20 000); ir ($CHCl_3$): 3445, 1710 (large) (ép 1745, 1680) cm^{-1}; (CCl_4): 3450, 1700 (large) (ép 1730, 1670) cm^{-1}; rmn ^1H (60 MHz, $CDCl_3$): 0,8–1,5 (m, 14H), 1,80 (s, 3H), 1,86 (s, 3H), 2,1–2,8 (m, 4H), 5,20 (s, 2H), 5,26 (s, 2H), 6,73 (s, 1H), 7,3 (s large, 10H); rmn ^1H (90 MHz, Me_2CO): 0,70–1,35 (m, 14H), 1,77 (s, 3H), 1,80 (s, 3H), 2,27 (t, J = 7,1 Hz, 2H), 2,69 (t, J = 7,0 Hz, 2H), 5,26 (s, 2H), 5,28 (s, 2H), 7,35 (m, 10H), 7,98 (s large, 1H); sm: 556, 421, 313 (M, $C_{34}H_{40}N_2O_5$ = 556).

1. D. DOLPHIN (*Editeur*). The porphyrins. Vol. 1 et 2. Academic Press, New York. 1978.
2. J. P. COLLMAN, A. O. CHONG, G. B. JAMESON, R. T. OAKLEY, E. ROSE, E. R. SCHMITTOU et J. A. IBERS. J. Am. Chem. Soc. **103**, 516 (1981).
3. A. LECAS, J. LEVISALLES, C. MARIACHER, D. RENKO et E. ROSE. Can. J. Chem. **62**, 2054 (1984).
4. A. LECAS, J. LEVISALLES, D. RENKO et E. ROSE. Tetrahedron Lett. **25**, 1563 (1984).
5. M. P. SAMNES and A. R. KATRITZKY. Adv. Heterocycl. Chem. **32**, 268 (1982).
6. L. J. BELLAMY. The infrared spectra of complex molecules. Methuen, London et John Wiley, New York. 1960.
7. A. R. KATRITZKY. Physical methods in heterocyclic chemistry. Vol. IV. 1971. p. 302.
8. W. R. GUY et R. A. JONES. Austr. J. Chem. **19**, 107 (1966).
9. G. SCHROLL, R. G. COOKS, P. KLEHNENSEN et S. O. LAWESON. Arkiv Kemi, **28**, 413 (1968).
10. P. BEY et J. P. VEVERT. J. Org. Chem. **45**, 3249 (1980).
11. J. BARLUENGA, F. PALACIOS, S. FUSTERO et V. GOTOR. Synthesis, 200 (1981).
12. D. SEEBACH. Chem. Ber. **96**, 2723 (1963).
13. H. BREDERECK, R. GOMPPER et H. SEIZ. Justus Liebigs Ann. Chem. **504**, 178 (1957).
14. (*a*) E. BAMBERGER. Chem. Ber. **51**, 606 (1918); (*b*) I. TANASESCU. Bull. Soc. Chim. Fr. 1718 (1926); 1443 (1926); (*c*) P. DE MAYO et S. T. REID. Q. Rev. **15**, 393 (1961).
15. R. HURLEY et A. TESTA. J. Am. Chem. Soc. **88**, 4330 (1966).
16. C. KANEKO, S. YAMADA et I. YOKOE. Tetrahedron Lett. 4729 (1966).
17. E. B. SMITH et H. B. JENSEN. J. Org. Chem. **32**, 3330 (1967).
18. E. HÖFT, A. R. KATRITSKY et M. R. NESBIT. Tetrahedron Lett. 2028 (1968); 3041 (1967).

Can. J. Chem. Downloaded from www.nrcresearchpress.com by 210.87.254.40 on 09/06/12
For personal use only.

Action des métaux sur les esters carboxyliques en présence d'hexaméthylphosphortriamide: une méthode simple et efficace de réduction des alcools en alcanes

HENRI DESHAYES ET JEAN-PIERRE PETE[1]

Laboratoire de Photochimie, Equipe de Recherche Associée au CNRS n° 688, U.E.R. Sciences, 51062 Reims Cedex, France

Reçu le 7 février 1984

Cet article est dédié au Professeur Paul de Mayo à l'occasion de son 60e anniversaire

HENRI DESHAYES et JEAN-PIERRE PETE. Can. J. Chem. **62**, 2063 (1984).

Lorsqu'on traite un ester carboxylique (R—C(=O)—OR') par une solution de sodium dans l'hexaméthylphosphortriamide (HMPA), on observe essentiellement la formation de l'acide carboxylique, d'un mélange de l'alcool R'OH et de l'alcane R'H correspondant. La proportion d'alcane est très importante pour les esters d'alcools encombrés et diminue lorsque l'encombrement au niveau du groupe carboxyle baisse. Le taux d'alcane augmente aussi en présence de *tert*-butanol. La discussion de ces résultats et leur comparaison avec la réduction des esters dans les amines primaires indiquent que l'alcane provient essentiellement de la décomposition d'un radical anion solvaté ou non alors que l'alcool résulte de processus bimoléculaires de décomposition de l'ester. L'acide carboxylique est dû à la fois à une réaction de fragmentation du radical anion et à des réactions bimoléculaires.

HENRI DESHAYES and JEAN-PIERRE PETE. Can. J. Chem. **62**, 2063 (1984).

Carboxylic acids, alcohols (R'OH), and alkanes (R'H) are the main products of the reduction of carboxylic esters (RCO_2R') by sodium in hexamethylphosphoric triamide (HMPA). Alkanes are preferentially formed from the carboxylic esters of hindered alcohols. The alkane content, however, is lowered when there is less steric hindrance on the carboxylic group, and increased when *tert*-butanol is introduced into the reaction mixture. The reduction of esters in HMPA has been compared to the reduction in alkylamines. The alkane is produced mainly by the decomposition of a radical anion intermediate which can be solvated by HMPA. The alcohol is the result of several possible bimolecular nucleophilic reactions; however, unimolecular and bimolecular processes are involved in the production of the carboxylic acid.

Depuis l'observation à la fin du siècle dernier de la réduction des amides par l'amalgame de sodium en solution aqueuse et depuis la mise en évidence par Bouveault et Blanc de la transformation des esters en alcools par action réductrice du sodium dans les alcools éthylique ou amylique anhydre (1), de nombreux travaux ont été consacrés à l'action des métaux sur les dérivés d'acide et plus particulièrement sur les esters carboxyliques (2). Ainsi, il a pu être montré qu'en solvant protique, la réaction de Bouveault et Blanc présentait une grande généralité et un certain intérêt pour la transformation de la fonction acide en fonction alcool. En solvant aprotique par contre, une nouvelle réaction réductrice nommée condensation acyloïne est observée préférentiellement (3). Bien que l'intérêt synthétique de ces réductions ait été rapidement exploré, l'étude mécanistique et la caractérisation d'intermédiaires n'est intervenue que beaucoup plus tard (4). Si la formation intermédiaire d'un radical anion par action du sodium sur un ester carboxylique ne fait aucun doute, les processus de formation des produits de réaction à partir de cet intermédiaire sont encore mal connus.

Ainsi, le mécanisme de la condensation acyloïne a pu être récemment remis en question (5); de même, l'isolement d'acides carboxyliques par action des métaux alcalins sur les esters carboxyliques dans l'ammoniac liquide (6)[2] ou dans l'hexaméthylphosphortriamide (HMPA) (7) a conduit divers auteurs à proposer une nouvelle voie de décomposition (éq. [1]) pour le radical anion qui ferait intervenir la réduction du groupe alcoxy de l'ester.

[1] 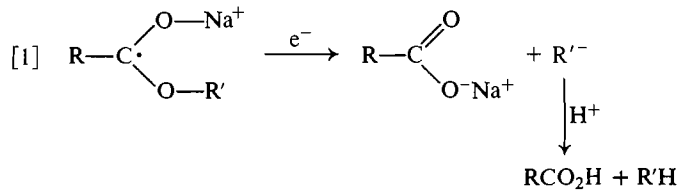

Cependant, si la formation d'hydrocarbures était bien observée au cours de la réduction d'esters benzyliques (7), il n'existait pas d'exemple clair d'une telle réduction en absence de groupes allyliques ou benzyliques, au moment où nous avons entrepris notre étude.[3]

Par ailleurs, au cours de travaux sur la photolyse, des esters carboxyliques dans un mélange HMPA–eau, il a été proposé qu'un complexe de transfert de charge pouvait être responsable de la réduction des groupes alcoxy d'esters carboxyliques (9) (éq. [2]). Il était donc envisageable si le mécanisme proposé

[2] 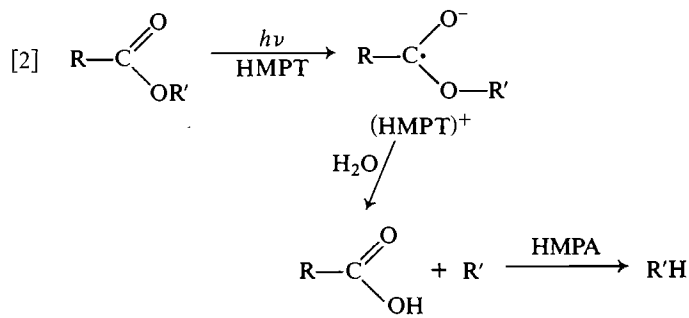

[1] Auteur à qui toute correspondance doit être adressée.

[2] La formation d'acide pourrait, dans ce cas, résulter aussi d'une attaque nucléophile d'amidure sur le groupe méthyle de l'ester.

[3] Il en est de même au cours des réductions cathodiques; la réduction du groupe alcoxy de l'ester n'est observée que pour des dérivés d'alcools benzyliques ou allyliques. cf. réf. 8.

Can. J. Chem. Downloaded from www.nrcresearchpress.com by 210.87.254.40 on 09/06/12
For personal use only.

Can. J. Chem. Downloaded from www.nrcresearchpress.com by 210.87.254.40 on 09/06/12
For personal use only.

TABLEAU 1. Réduction d'acétates d'alkyle CH_3CO_2—R'[a]

Essai	R'	R'H (%)	R'OH (%)
1	n-C_9H_{19}	42[b]	28
2	n-C_7H_{15}	56[b]	30
3	Cyclohexyl	43[b]	43[b]
4	Bornyl	>32[b]	37[b]
5	Menthyl	57	35
6	5α-Cholestanyl-3β	69	20
7	Cholestène-5 yl-3β	68	29
8	Diméthyl-4,4 5α-cholestanyl-3β	50	50
9	Méthyl-3β 5α-cholestanyl-3α	>95[c]	—
10	Méthyl-3α 5α-cholestanyl-3β	>95[c]	—
11	Triméthyl-3α,4,4 5α-cholestanyl-3β	>95[c]	—
12	Triméthyl-3β,4,4 5α-cholestanyl-3α	>95[c]	—

[a] On arrête la réaction 5 min après la fin de l'addition de l'ester (cf. partie expérimentale).
[b] Déterminé par cpv.
[c] Le même isomère est obtenu à partir des deux épimères avec un rendement de 85% environ après recristallisation.

pour la réaction photochimique était fondé, de rendre préparative la réduction du groupe alcoxy d'esters carboxyliques par action du sodium ou d'autres métaux alcalins dans le HMPA en présence d'un donneur de protons.[4] Le HMPA, bon solvant des métaux alcalins et du sodium en particulier (11), donne des solutions bleues paramagnétiques caractéristiques de la présence d'électrons solvatés dans le milieu (11, 12) et douées d'un fort pouvoir réducteur. Le potentiel développé entre une électrode saturée au calomel (SCE) en contact électrique avec une solution de Na-HMPA et mesuré à 28°C est de −2,96 V (13), alors que des valeurs de −2,2 et −2,3 V (vs. SCE) ont été décrites pour des solutions de sodium dans l'ammoniac liquide à −33°C (14).

La réduction des alcools en hydrocarbures par action du sodium dissous dans le HMPA sur les esters carboxyliques correspondants est une réaction efficace; nous rapportons dans ce mémoire la généralité de la réaction, ses limites et nous comparons nos résultats avec ceux décrits récemment pour l'action sur les esters des métaux alcalins dissous dans l'éthylamine et la *tert*-butylamine (15).

Résultats

1. *Aspect préparatif*

Lorsqu'on ajoute une solution diluée d'ester dans l'éther – *t*-BuOH (1 : 1) à une suspension de sodium dans le HMPA à une vitesse telle que le milieu restement constamment coloré, les résultats de la réduction observée (tableau 1) peuvent être résumés dans l'éq. [3]:

[3]

$$R'H + R'OH + RCO_2H + RCH_2OH$$

Dans les réactions utilisées, les alcools primaires, secondaires ou tertiaires sont transformés en hydrocarbures par réduction des acétates correspondants. Les rendements en alcanes augmentent avec l'encombrement au niveau du groupe alcoxy et la réduction devient même quantitative lorsque l'on soumet au sodium-HMPA les esters d'alcools tertiaires. On

[4] Une partie de ce travail a fait l'objet d'une note préliminaire (10).

TABLEAU 2. Influence de la nature du groupe carboxyle sur la réduction d'esters de cholestanyle

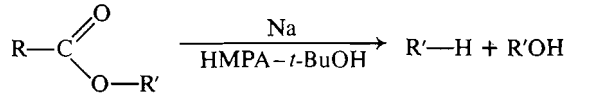

Essais	R—CO_2—	R'H (%)[a]	R'OH (%)[b]
1	Formiate	30	70
2	Acétate	69	20
3	Heptanoate	52	48[c]
4	Pivalate	67	33
5	Méthyl-1 cyclohexane carboxylate	67	31
6	Cyclohexane carboxylate	65	35
7	Phényl-2 acétate	52	47
8	Benzoate	45	50
9	Stéarate	56	38[d]

[a] 5α-Cholestane.
[b] 5α-Cholestanol-3β.
[c] Acide heptanoïque 83%.
[d] Acide stéarique 77%.

note qu'une quantité notable d'alcool est obtenue dans le mélange réactionnel lorsqu'on réduit dans le mélange HMPA – *tert*-butanol des esters d'alcools primaires et secondaires.

La nature de l'ester carboxylique influe également sur le cours de la réaction sans en modifier la généralité. Le tableau 2 montre que l'augmentation de l'encombrement au niveau du groupe carboxyle a aussi pour effet d'augmenter la part du processus de réduction, puisque la production d'alcool, très majoritaire dans le cas des formiates, est fortement diminuée pour les autres esters de cholestanyle. Cependant, l'effet d'encombrement est plus limité que lors du passage des dérivés d'alcools primaires à des dérivés d'alcools tertiaires puisque le passage de l'acétate au pivalate et au méthyl-1 cyclohexène carboxylate de cholestanyle n'améliore plus le rendement de la désoxygénation.

Une des applications intéressantes de la réaction de photoréduction du groupe alcoxy d'esters concernait la préparation de déoxysucres. Nous avons essayé d'obtenir ces mêmes déoxysucres par action du sodium dans le HMPA. Malheureusement, la libération d'alcool s'est révélée plus efficace et nous n'avons pu isoler le dérivé désoxy attendu par traitement par le sodium de l'acétate suivant:

[4] 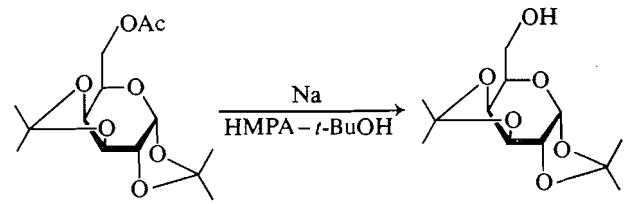

Les raisons de l'échec de cette réaction de réduction par le sodium dans le HMPA ne sont pas connues. Nous pouvons toutefois remarquer que la présence des deux groupes acétonides dans la molécule peut modifier la chélation aussi bien du cation sodium que du *tert*-butanol. Le même échec est rencontré lorsque la réduction est conduite en absence de *tert*-butanol.

2. *Aspect mécanistique*

(a) *Rôle du* tert-*butanol*

Les études de la photoréduction des esters carboxyliques en

TABLEAU 3. Rôle du *tert*-butanol sur la réduction des esters par le sodium dans le HMPA

Essai	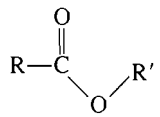	R′—H (%)		R′OH (%)	
		Sans *t*-BuOH	En présence de *t*-BuOH[a]	Sans *t*-BuOH	En présence de *t*-BuOH[a]
1	CH_3CO_2—C_9H_{19}	27	42	54	28
2	CH_3CO_2—C_7H_{15}	33	56	60	30
3	Acétoxy-3β 5α-cholestane	35	69	58	20
4	Acétoxy-3β cholestène-5	60	68	36	29
5	Formyloxy-3β 5α-cholestane	7	30	87	70
6	Acétoxy-3β méthyl-3α 5α-cholestane	84	>95	14	—
7	Acétoxy-3α méthyl-3β 5α-cholestane	84	[b]	8	[b]

[a] HMPA/*t*-BuOH 90:10.
[b] Non déterminé.

TABLEAU 4. Essai d'incorporation de deutérium sur un intermédiaire carbanionique

$$RCO_2—R' + R''OD \xrightarrow[HMPA]{Na} R'H + R'D + R'OH$$

Ester	R″OD	Hydrocarbure (%)	Teneur en deutérium	R′OH (%)
Acétoxy-3β 5α-cholestane	*t*-BuOD	68	0,87 d_1	29
	t-BuOD[a]	42	0,65 d_1	58
	t-BuOD[a]	40	0,76 d_1	50
	CH_3OD	21	0,83 d_1	74
Méthyl-1 cyclohexane carboxy-3β 5α-cholestane	*t*-BuOD	87	0,60 d_1	[b]

[a] Addition inverse: la solution de sodium dans le HMPA est ajoutée à la solution d'ester.
[b] Non dosé.

présence de HMPA ayant montré la nécessité de la présence d'un agent protique dans le milieu, nous avons examiné si la réduction de ces esters en alcanes par action du sodium dans le HMPA était sensible à la présence de protons. Nous avons, pour cela, effectué la réaction de réduction d'esters en absence de source de protons et comparé les résultats à ceux de témoins réalisés en présence de *tert*-butanol (tableau 3).

La présence de *tert*-butanol dans le milieu favorise la formation d'alcanes aux dépens de la formation d'alcools dans le cas des esters peu encombrés d'alcools primaires ou secondaires. Dans le cas d'esters encombrés, la présence de protons dans le milieu ne semble pas améliorer sensiblement le rendement en produit de réduction du groupe alcoxy.

(b) *Nature des intermédiaires réactionnels*

L'examen des essais 9 et 10 ou 11 et 12 décrits dans le tableau 1 montre que le même hydrocarbure est obtenu au cours de la réduction de deux esters épimères.

Afin de déterminer la nature de l'intermédiaire commun qui rend compte de la formation de l'épimère le plus stable au cours de la réaction, nous avons procédé à deux séries d'expériences permettant de déterminer si un radical $R^{\cdot}$ était ou non sur le chemin réactionnel.

Le remplacement du *tert*-butanol par un alcool deutérié (R—OD) permet de deutérier les carbanions suceptibles de se former dans le milieu. Le dosage de la teneur en deutérium dans les hydrocarbures isolés indique dans quelle mesure l'arrachement d'hydrogène au HMPA par un radical intermédiaire est susceptible d'entrer en compétition avec la protonation d'un anion par l'alcool deutérié.

Le tableau 4 fait apparaître que la nature du donneur de protons influe considérablement sur la proportion des produits obtenus puisque le méthanol plus acide que le *tert*-butanol favorise la libération de cholestanol. D'autre part, le dosage du deutérium dans le cholestane isolé montre dans chaque cas une incorporation importante de deutérium. Un intermédiaire carbanionique est donc sur le chemin privilégié qui conduit à l'alcane. Cependant, la teneur en deutérium inférieure à l'unité indique qu'une partie de l'alcane pourrait provenir d'un intermédiaire radicalaire après arrachement d'un atome d'hydrogène au solvant. La réduction d'un ester de cyclopropylcarbinyle est susceptible de nous apprendre si l'intermédiaire formé initialement par rupture de la liaison C—O du groupe alcoxy possède une structure radicalaire ou anionique. En effet, il a pu être montré dans l'action de radicaux anions dans le glyme sur le chloro-6β cyclo-3α, 5α-cholestane que le radical

[5] 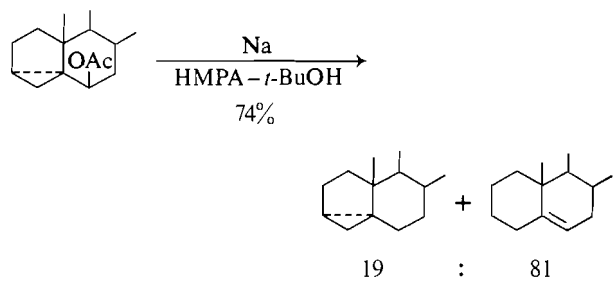

intermédiaire conduisait à 25°C à un dérivé du cholestène-5, alors que l'anion du système cyclopropylcarbinyle conduisait, de préférence, aux dérivés cyclopropaniques (16). La forte proportion de cholestène-5 observé semble indiquer qu'un radical intermédiaire est initialement formé lorsque la rupture C—O du groupe alcoxy intervient.

Can. J. Chem. Downloaded from www.nrcresearchpress.com by 210.87.254.40 on 09/06/12
For personal use only.

TABLEAU 5. Influence de la température sur la réduction de l'acétoxy-3β 5α-cholestane

°C	Additif	5α-Cholestane	5α-Cholestanol-3β	CH_3CO_2R
−20	*t*-BuOH	36	40	24
+20	—	35	58	
	t-BuOH	69	20	
+40	—	51	46	
+60	*t*-BuOH	18	69	

(c) *Influence des conditions réactionnelles*

Les divers produits observés, lorsqu'on fait réagir un métal sur un ester, résultent de processus compétitifs au niveau du radical anion initialement peuplé. Nous avons donc cherché à déterminer l'influence de la température, de la durée de réaction et de la nature du métal sur le cours de la réduction de l'acétate de cholestanyle en cholestane. Bien que la réduction des esters par les métaux dans les amines primaires soit sensible à la température, nous n'avons pu mettre en évidence une augmentation conséquente du taux d'alcane lorsqu'il y a augmentation de la température, surtout lorsque la réaction est réalisée en présence de *tert*-butanol.

La vitesse d'addition de l'ester dans la solution d'électrons solvatés à 25°C étant effectuée de manière à éviter que la couleur bleue ne disparaisse au cours de l'addition, nous avons procédé à l'isolement des produits de réaction dès la fin de l'introduction de l'ester dans le milieu réducteur. Le rendement en alcane isolé est alors optimum. Ceci nous permet de conclure que la transformation du radical anion intermédiaire est rapide à température ambiante.

Le pouvoir réducteur élevé des solutions de sodium dans le HMPA permet la réduction des liaisons multiples (11) y compris les liaisons éthyléniques (17). Il est néanmoins possible de contrôler le cours de la réduction d'un ester insaturé en contrôlant le temps de contact de l'ester avec la solution réductrice. Ainsi, nous pouvons orienter la réduction de l'acétate de cholestéryle vers la formation de dérivés du cholestène-5 ou du 5α-cholestane.

[6] 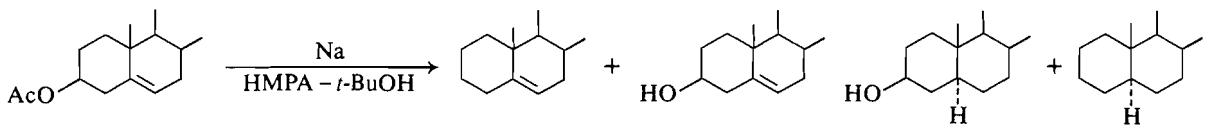

5 min 68% 29%

24 h 28% 64%

L'étude de l'influence de la nature du métal sur la réduction est rendue difficile par la grande instabilité des solutions de lithium et de potassium dans le HMPA (7). Il a en effet été montré que les solutions de métal alcalin-HMPA voient rapidement leur conductibilité baisser pour le lithium ou le potassium, contrairement au cas des solutions de sodium pour lesquelles la conductibilité reste constante durant des périodes assez longues (18). La baisse de conductibilité semblerait liée à une décomposition du HMPA.

Un essai de réduction d'acétate de cholestanyle par une solution de Li-HMPA conduit à une formation prépondérante d'alcool (cholestanol 81%, cholestane 9%). Nous constatons en outre que la dissolution du lithium dans le HMPA est bien plus rapide que celle du sodium et que l'hydrolyse du brut de réduction par Li-HMPA conduit à la formation de produits gazeux à odeur de phosphine. De plus, la libération d'ions diméthylamidure susceptibles de réagir sur les esters (7) a déjà été notée. Des travaux récents ayant montré que des esters encombrés pouvaient être réduits sélectivement par le lithium dans une amine primaire (15, 19, 20), nous avons comparé le cours de la réduction de l'acétate de cholestanyle pris comme modèle d'un acétate d'alcool secondaire dans différents milieux et nous avons rassemblé les résultats dans le tableau 6.

Ces divers essais montrent d'une part que le taux d'alcane est plus élevé lorsque le HMPA est utilisé comme solvant, d'autre part que la présence de *tert*-butanol dans le milieu accroît la formation d'alcane aux dépens de la réduction en alcool, aussi bien dans l'éthylamine que dans le HMPA.

L'introduction d'une solution de sodium-HMPA préalablement titrée (13) à une solution d'ester dans un mélange HMPA–éther permet de déterminer le nombre d'électrons nécessaires à la réduction. On constate en effet, et à la précision des déterminations près (tableau 7), qu'en absence de *tert*-butanol, il y a consommation de moins de deux équivalents de sodium et donc de moins de deux électrons par mole d'ester au moment où la solution maintient une couleur bleue persistante. Un tel résultat est donc en accord à la fois avec la formation rapide du radical anion dérivé de l'ester et avec la non compétitivité d'autres processus de réduction en absence de *tert*-butanol.

En présence de *tert*-butanol, on observe non seulement que plusieurs équivalents "électrons solvatés" sont nécessaires avant l'observation du maintien d'une couleur bleue persistante, mais aussi une grande instabilité de ces colutions colorées même pour un nombre d'équivalents très supérieur à 2. Des processus de réduction successifs semblent devoir être retenus dans la mesure où nous avons vérifié que le *tert*-butanol ne décolore pratiquement pas la solution de sodium dans le HMPA.

Les proportions d'alcane et d'alcool obtenus au cours de ces expériences de titrage sont conformes aux résultats préparatifs décrits dans les tableaux 3 et 7. On vérifie ainsi qu'il y a davantage de produits de réduction en présence de *t*-BuOH et qu'il y a dans chaque cas formation d'une quantité importante d'alcool.

Discussion

La réduction des esters carboxyliques, par les métaux dissous, conduit à un mélange d'alcanes, d'alcools et d'acide carboxylique. Le degré de substitution du groupe alcoxy de l'ester, la nature du dérivé acide, les conditions de réaction et, plus particulièrement, la nature du milieu réactionnel, influencent les rendements respectifs dans les divers produits. Dans tous les milieux cependant, on peut considérer que la première étape réalise la fixation d'un électron sur l'ester et fournit un radical anion d'où découleront les divers produits de réaction.

L'alcane issu de la réduction du groupe alcoxy et les alcools peuvent, a priori, découler d'une décomposition du radical

Can. J. Chem. Downloaded from www.nrcresearchpress.com by 210.87.254.40 on 09/06/12
For personal use only.

TABLEAU 6. Influence de la nature du milieu sur la réduction de l'acétoxy-3β 5α-cholestane

Essai	M	Solvant	5α-Cholestane (%)	5α-Cholestanol-3β (%)
1	Na	HMPA	35	58
2	Na	HMPA – *t*-BuOH 90:10	69	20
3	Na	NH_3	0	92
4	Li	HMPA – *t*-BuOH 90:10	9	81
5	Li	$PrNH_2$	0	>95
6	Li	$EtNH_2$ + *t*-BuOH 90:10	10	77
7	Li	$EtNH_2$	<1	91

TABLEAU 7. Réduction d'ester par une solution titrée de sodium-HMPA

R—CO_2R′	Quantité $\times10^{-4}$ mol	Na-HMPA	Conditions	Quantité Na intr. $\times10^{-4}$ mol	RH (%)	ROH (%)
Acétoxy-3β	1,88	0,119 *M*	HMPA–éther	1,84	30	70
5α-cholestane	1,23	0,119 *M*	HMPA–éther	1,12	17	83
Cyclohexane carboxy-3β	2,65	0,088 *M*	HMPA–éther	5,2	16	84
5α-cholestane	2,65	0,088 *M*	HMPA–éther	2,34	5	85
	2,96	0,088 *M*	HMPA + *t*-BuOH (90:10)	15	67	33

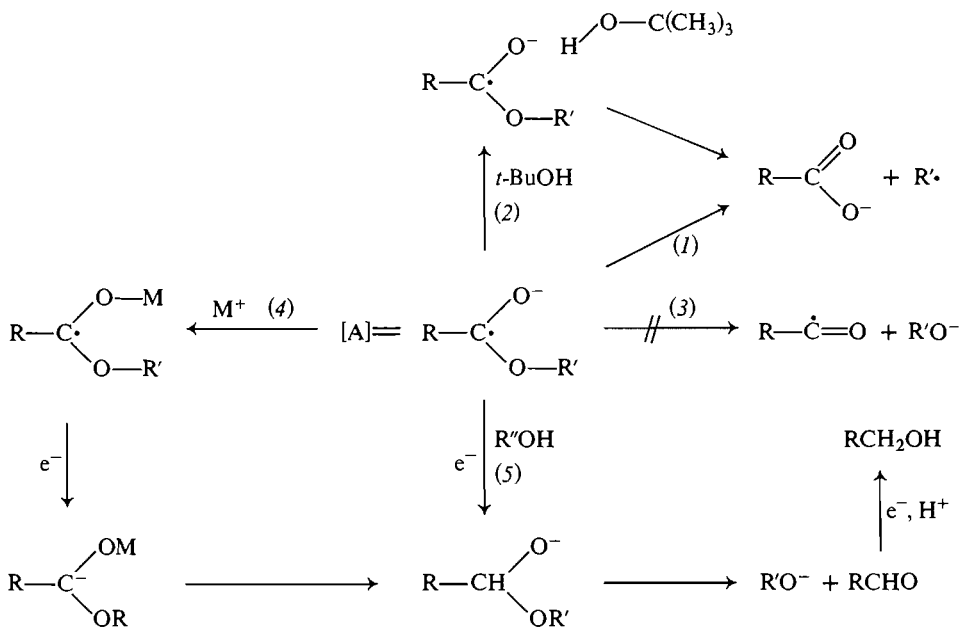

SCHÉMA 1

anion selon les divers processus regroupés dans le schéma 1.

En milieu dilué, on peut négliger, dans le HMPA, la duplication du radical anion conduisant aux α-cétols et considérer que la décomposition de cette espèce [A] va dépendre essentiellement des conditions du milieu: présence ou non de protons, solvatation spécifique des cations, température . . .

La grande stabilité de l'anion carboxylate permet la fragmentation selon la voie (*1*). Le radical R$^{\bullet}$ ainsi formé, par arrachement d'un atome d'hydrogène au HMPA ou capture d'un électron puis d'un proton, fournit l'alcane observé. Une telle décomposition unimoléculaire est sensible à la variation de contraintes stériques. Le passage d'un ester d'alcool primaire à un ester d'alcool tertiaire provoque une augmentation considérable de l'encombrement. Il est probable que les contraintes stériques sont modifiées au niveau du radical anion qui tend à adopter une structure tétraédrique aplatie (24). La relaxation stérique sera donc d'autant plus importante que le radical anion [A] sera encombré. Il en résulte que plus l'encombrement est important, plus la vitesse de fragmentation est élevée, et moins les réactions parasites ont la possibilité d'apparaître. On observe effectivement que l'encombrement au niveau des groupes alcoxy ou groupe carboxy (10, 22) augmente la proportion d'alcane.

Le rôle du *tert*-butanol est sans doute complexe. On peut cependant considérer qu'il est capable de solvater le radical anion [A] dans le HMPA, voie (*2*), augmenter ainsi les contraintes stériques à ce niveau et accélérer sa décomposition. En effet, il est connu que les alcools sont susceptibles de solvater

Can. J. Chem. Downloaded from www.nrcresearchpress.com by 210.87.254.40 on 09/06/12
For personal use only.

Can. J. Chem. Downloaded from www.nrcresearchpress.com by 210.87.254.40 on 09/06/12
For personal use only.

les radicaux anions dans le HMPA et de provoquer ainsi une modification notable du spectre rpe de cet intermédiaire (25). De plus, nous avons pu montrer que la libération d'acide carboxylique à partir d'un radical 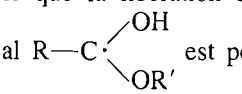 est possible lors de la photolyse des esters dans le HMPA, bien que celle-ci soit sans doute moins favorable que la fragmentation de [A] en ion carboxylate correspondant.

Le radical anion peut aussi fournir l'alcool $R'O^-$ selon divers processus. La décomposition unimoléculaire de [A] en radical acyle et $R'O^-$, voie (*3*), semble devoir être exclue. En effet, des calculs *ab initio* effectués sur le radical anion dérivé du formiate de méthyle indiquent que la fragmentation en radical méthyle et anion formiate est, de loin, plus favorable que la fragmentation en radical acyle et anion méthylate (ΔE = 263 kJ) (26). La capture d'un second électron par le radical anion ne semble pas possible, ni dans le HMPA, ni dans une amine en présence d'éthers couronnes. En effet, la répulsion électronique au niveau du dianion ainsi formé est trop importante et les processus compétitifs sont prépondérants. C'est ainsi que l'alcool RCH_2OH attendu après la capture d'un second électron n'est pas observé, ou reste un produit trés minoritaire aussi bien dans le HMPA que dans un mélange de *tert*-butylamine et de tétrahydrofuranne en présence d'éther couronne (cf. réfs. 22, 23, tableau 2, entrées 1–5 et 12). La réduction du radical anion devient possible si l'anion reste lié au cation métallique ou, éventuellement, de manière concertée avec la fixation d'un proton (21, 22) dans les conditions de Bouveault et Blanc. L'absence d'un taux élevé de réduction en présence de *tert*-butanol indique que la protonation concertée avec la fixation d'un second électron par le radical anion est sans doute considérablement ralentie pour des raisons stériques.

La formation d'alcool R'OH peut résulter également d'un déplacement de $R'O^-$ dans l'ester par une base présente dans le milieu. La mise en évidence d'amides au cours de réductions par le lithium dans l'éthylamine (22) ou le lithium dans le HMPA (7), montrent que le lithium est capable de produire dans ces deux milieux des ions amidures susceptibles de libérer $R'O^-$ de l'ester correspondant. Cependant, les solutions de sodium dans le HMPA sont stables sur de longues périodes dans nos conditions de réduction et ne conduisent donc pas à la formation d'amides.

Les pK_a relatifs des amines primaires et secondaires ($41 < pK_a < 44$) sont plus élevés que ceux du *tert*-butanol (pK_a = 32,2) (27). En présence d'un large excès de *tert*-butanol, nous pouvons considérer que les ions amidures ou diméthyl amidures sont entièrement et rapidement neutralisés, aussi bien dans les amines primaires que dans le HMPA. La formation d'alcool R'OH par action d'un ion amidure sur l'ester devrait donc être totalement inhibée par le *tert*-butanol, dès lors que la décomposition de ce même ester par le *tert*-butylate de potassium, et selon le processus de Bouveault et Blanc, est exclue. Or, il n'en est rien! Le tableau 6, entrées 6 et 7, montre qu'en présence d'un grand excès de *tert*-butanol, on obtient une augmentation de 10% du rendement en cholestane et une diminution de 10% de l'alcool correspondant.

Une autre base, l'hydroxyde de sodium, aurait pu résulter de la présence d'une certaine quantité d'eau dans le HMPA utilisé. Nous pouvons exclure cette possibilité pour plusieurs raisons: (a) la coloration bleue caractéristique de la présence d'électrons solvatés dans le milieu, est obtenue dès que l'on ajoute du sodium au HMPA anhydre utilisé, sans qu'aucun dégagement gazeux puisse être detecté; (b) pour une même quantité de solvant HMPA–ether, la proportion d'alcool, si celui-ci résultait au moins en partie d'une saponification de l'ester, devrait diminuer lorsque la quantité d'ester introduit est elle-même augmentée. Lorsqu'on réduit, dans la même quantité de solvant 0,232 mmol ou 0,88 mmol d'acétoxy-3β cholestane, on obtient la même proportion de cholestane et de cholestanol.

Une *trans* estérification de l'ester par le *tert*-butanol ou le *tert*-butoxyde de sodium est peu probable en raison de l'encombrement de l'ion *tert*-butoxyde et de la rapidité des réductions. Une *trans* estérification ayant été détectée lors de la réduction des esters dans les amines primaires (22) mais pas dans nos conditions de réduction, nous avons aussi examiné le rôle du cholestanol sur la réduction de l'heptanoate de méthyle par le sodium dans le HMPA. Contrairement aux résultats obtenus dans les amines, nous n'avons pu détecter que des traces (~1%) de cholestane provenant de l'heptanoate de cholestanyle intermédiairement formé par *trans* estérification. Le milieu réactionnel étant très basique, la formation d'énolate suivie d'une condensation de Claisen, pouvait être responsable d'une partie de l'alcool R'OH libéré. Un tel processus a effectivement été détecté lors d'une addition d'une solution d'électrons solvatés dans une solution d'ester (addition inverse). Cependant, la quantité d'acétylacétoxy-3β cholestane (10%) à partir d'acétoxy-3β cholestane reste très faible tout comme la proportion de produits issus de la condensation acyloïne.

Lors de la réduction des esters dans les différents milieux, on peut considérer que la formation d'une molécule d'alcane fournit nécessairement un équivalent d'acide carboxylique. Cependant, le rendement en RCO_2H est bien supérieur à celui de R'H (tableau 8). Ce rendement sensiblement égal à la somme des rendements en R'H et R'OH est voisin de 100%. Il existe donc une ou plusieurs voies susceptibles de conduire à la fois à RCO_2H et R'OH.[5] La discussion précédente met en évidence que, dans le HMPA, ni l'anion diméthylamidure ou l'ion hydroxyle, ni l'ion *tert*-butoxyde ou l'ion énolate, ne peuvent être considérés comme responsables de la formation d'une quantité importante d'alcool. Une autre observation méritant d'être soulignée est que, pour 1 à 1,8 équivalent de sodium introduit dans une solution d'acétate de cholestanyle dans le HMPA, on ne récupère pas d'ester non transformé d'une part, et la proportion de cholestane et de cholestanol (25:75) est équivalente à celle obtenue en présence d'un grand excès de réducteur d'autre part.

Le tableau 8 montre que le même problème de la formation simultanée d'alcool (R'OH) et d'acide carboxylique (RCO_2H) est rencontré dans des milieux extrêmement différents. Une interprétation commune pourrait impliquer, quel que soit le milieu, la formation d'intermédiaires semblables et suffisamment instables pour être hydrolysés rapidement au moment de l'isolement. Une telle possibilité représentée dans le schéma 2 mérite d'être considérée. L'addition nucléophile de radicaux anions sur des dérivés carbonylés a déja été envisagée pour rendre compte de la réaction de dismutation de Cannizzaro et de certaines anomalies rencontrées dans la réaction de condensation acyloïne (5). Cette addition de [A] sur une molécule d'ester fournirait [B] susceptible de se fragmenter en R'· et [C]

[5] Le processus de Bouveault et Blanc conduisant à la fois à R'OH et RCH_2OH est négligeable dans les exemples retenus. Dans les résultats obtenus par Barrett *et al.* (réf. 22), la formation de *tert*-butyl amidure intervient peu ou pas dans le milieu réactionnel de même que la réaction de Bouveault et Blanc.

TABLEAU 8. Rôle des conditions sur la formation simultanée d'alcool et d'acide carboxylique

Ester R—C(=O)—OR′	Conditions	°C	RCO_2H	RCH_2OH	R′OH	R′H	Réf.
Adamantane-1 carboxy-3β cholestane-5α	K-*t*-$BuNH_2$ – THF (30:10) 18-crown 6	46	96	2	57	43	22
		20	86		43	53	22
	K-DME – CH_3I (55:2) 18-crown 6	20	92		57	30	22
	K-*t*-$BuNH_2$ – THF (30:20) 18-crown 6	−45	77	5	66	27	22
	K–Na (28:8,7) *t*-$BuNH_2$ – THF (10:3), 18-crown 6	46	95	0	20	78	22
Heptanoate de 5α-cholestanyl-3β	Na-HMPA-*t*-BuOH	20	83	—	48	52	[a]
Stéarate de 5α-cholestanyl-3β	Na-HMPA – *t*-BuOH	20	77	—	38	56	[a]

[a] Ce travail.

TABLEAU 9. Influence de la concentration en acétoxy-3β 5α-cholestane sur la proportion cholestane/cholestanol en présence de sodium dans le HMPA

Acétoxy-3β 5α-cholestane	Conditions	Cholestane (%)	Cholestanol (%)
$2{,}5 \times 10^{-3}\ M\ L^{-1}$	HMPA	43	54
$2{,}4 \times 10^{-2}\ M\ L^{-1}$	HMPA	35	58
$1{,}2 \times 10^{-3}\ M\ L^{-1}$	HMPA – *t*-BuOH (20:1)	64	33
$7{,}7 \times 10^{-2}\ M\ L^{-1}$	HMPA – *t*-BuOH (20:6)	69	20

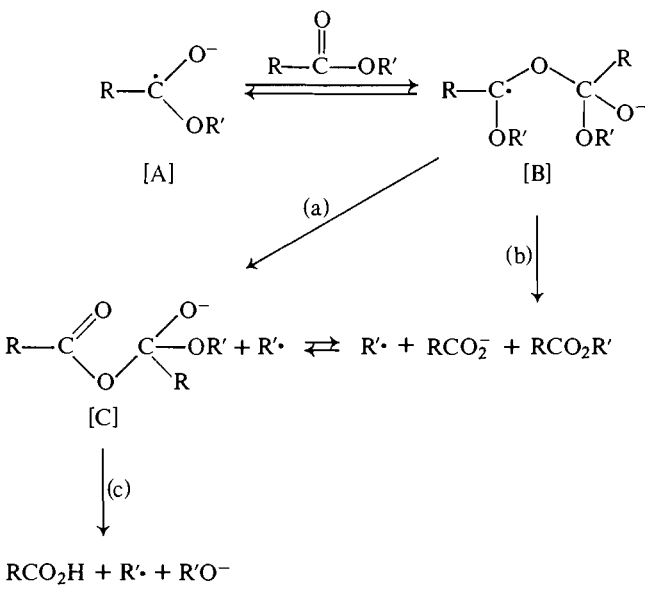

SCHÉMA 2

selon la voie (a) ou en R′·, RCO_2R' et RCO_2^- selon la voie (b).

Si l'addition du radical anion sur une molécule d'ester intervient, l'alcane peut provenir, en partie, de la fragmentation de l'intermédiaire [B] selon les voies (a) et (b) du schéma 2. De même, la formation d'alcool pourrait résulter de la fragmentation, soit dans le milieu réactionnel, soit au moment de l'isolement d'un intermédiaire tel que [C] formé au cours de la réaction. Le bilan de cette suite de réactions indique qu'une molécule d'alcane, une molécule d'alcool et deux molécules d'acide carboxylique sont susceptibles d'être produites pour chaque électron piégé par l'ester. Tous les autres processus bimoléculaires envisagés précédemment conduiraient à une molécule d'alcool et une molécule d'un dérivé d'acide suffisamment stable dans le milieu pour être isolé. En fait, nous constatons (essai 9, tableau 2) que le rapport acide carboxylique – alcane est supérieur à l'unité. La quantité d'alcool formé devrait dépendre de la concentration et nous avons testé l'influence de la concentration sur le cours de la réaction dans le HMPA. L'alcool, qui résulte uniquement d'une réaction bimoléculaire, devrait voir son rendement diminuer alors que l'alcane, qui provient surtout d'une fragmentation intramoléculaire, devrait voir son rendement augmenter pour une diminution de la concentration. Or, les résultats du tableau 9 indiquent que la dilution du milieu ne modifie pas sensiblement la proportion d'alcool et d'alcane, et qu'un dérivé du HMPA pourrait être impliqué dans la formation à la fois d'alcool et d'acide.

En conclusion, la réduction des esters par le sodium dans le HMPA est une réaction générale qui est d'autant plus efficace que les esters sont encombrés. Le rendement en alcane, à partir d'un ester donné, augmente en présence du *tert*-butanol qui peut à la fois neutraliser le diméthylamidure de lithium susceptible de se former et accroître, par solvatation, l'encombrement au niveau du radical intermédiaire.

De même, l'utilisation d'une faible concentration en ester carboxylique permet d'éviter la réaction bimoléculaire de condensation acyloïne et favorise la formation d'alcane. L'alcane provient essentiellement de la fragmentation du radical anion formé après capture d'un électron par l'ester. La formation d'alcool est due à plusieurs réactions bimoléculaires compétitives impliquant le diméthylamidure, la *tert*-butylate de sodium et, éventuellement, un dérivé du HMPA comme nucléophile.

Can. J. Chem. Downloaded from www.nrcresearchpress.com by 210.87.254.40 on 09/06/12
For personal use only.

TABLEAU 10. Réduction d'esters en présence de *tert*-butanol monodeutérié[a]

Ester	R″OD	Rendement RH (%) (RD)	M^+	$M^+ + 1$	$M^+ + 2$	Teneur en deutérium	R′OH
Acétoxy-3β 5α-cholestane	*t*-BuOH	69	100	31	3,4	0	20
	t-BuOD	68	100	760	23,7	0,87	29
	CH_3OD	21	100	590	193	0,83	74
Méthyl-1 cyclo hexanecarboxy-3β 5α-cholestane	*t*-BuOD	87	100	180	40	0,60	
Acétoxy-3β 5α-cholestane[b]	*t*-BuOD	42	100	185	60	0,65	58
	t-BuOH	40	100	350	100	0,76	50

[a]La technique opératoire est la même que dans le cas général.
[b]Addition inverse.

Partie expérimentale

Les spectres ir ont été enregistrés sur un appareil Philips SP2000, rmn sur Varian A60. Les points de fusion sont déterminés sur banc Kofler.

Produits de départ

Formoxy-3β 5α-cholestane préparé par action de l'acide formique à 98% sur le cholestanol-3β en présence de quantité catalytique d'acide perchlorique (28).

Acétoxy-6β cyclo-3α, 5α-cholestane obtenu par traitement du tosyloxy-3β cholestène-5 par l'acétate de potassium anhydre dans l'acide acétique (29).

Dans les autres cas: les esters sont obtenus par action du chlorure d'acide sur l'alcool dans le HMPA (30). Le HMPA a été séché plusieurs jours sur CaH_2 puis distillé sur CaH_2. Les points de fusion et analyses sont donnés dans le tableau 11.

Identification des produits

Les produits ont été identifiés par chromatographie sur couche mince, point de fusion, spectroscopie ir et rmn.

Réduction par le sodium

Une solution d'ester (1 g) dans un mélange éther – *t*-BuOH (1:1) (5 mL) est ajoutée à une solution de sodium (1 g) dans un mélange solvant (10 mL) – éther (5 mL) à une vitesse telle que la solution bleue obtenue ne se décolore pas quand l'addition est terminée, l'excès de sodium est éliminé. La solution versée dans l'éthanol est ensuite hydrolysée.

Méthode générale décrite pour la réduction d'ester carboxylique par la solution Na-HMPT

Du sodium finement divisé (1 g) est introduit dans le HMPA (10 cm^3). A la solution bleue, une solution d'acétoxy-3β cholestane (0,760 g) dans un mélange d'éther (10 cm^3) et de *tert*-butanol (3 cm^3), est ajoutée goutte à goutte à une vitesse telle que la solution n'est jamais décolorée. Dix minutes après la fin de l'addition, l'excès de sodium est filtré puis la solution est hydrolysée en milieu acide et extraite à l'éther (3 × 50 cm^3). Une chromatographie sur silice permet de séparer le cholestane (recristallisé dans l'acétone, 454 mg, 69%) et le cholestanol-3β (134 mg, 20%).

Réduction d'esters carboxyliques par la solution Li-ethylamine

Du lithium finement divisé (0,106 g) est introduit dans l'éthylamine (10cm^3). A la solution bleue, on ajoute goutte à goutte un mélange d'acétoxy-3β cholestane (0,098 g) avec du *tert*-butanol (2 cm^3) et de l'éthylamine (5 cm^3), de façon à éviter la décoloration. Ce mélange est alors laissé 1 h à reflux de l'éthylamine, puis l'éthylamine est distillée. Une hydrolyse acide puis extraction avec de l'éther et une chromatographie sur silice permettent d'isoler le cholestane (9 mg, 10%) et le cholestanol-3β (68 mg, 77%).

Réduction de l'acétoxy-3β cholestène-5

Dans une solution bleue de HMPA (10 cm^3) sodium (0,5 g), est ajouté goutte à goutte l'acétoxy-3β cholestène-5 (100 mg) en solution dans l'éther (5 cm^3) et le *tert*-butanol (2 cm^3). Cette addition dure 5 min en évitant la décoloration de la solution. Le sodium restant est immédiatement filtré, la solution hydrolysée en milieu acide puis extraite à l'éther (3 × 50 cm^3). Une chromatographie sur colonne de silice permet de séparer le cholestène-5 (59 mg, 68%) du cholestérol (26 mg, 29%). Le cholestène-5 est contrôlé par ccm sur silice imprégnée de $AgNO_3$ puis par rmn.

Si le temps de contact est de 24 h, le cholestane pur est isolé (58 mg, 64%) ainsi que le 5α-cholestanol-3β (21 mg, 28%). Le cholestane a été contrôlé par ccm sur silice imprégnée de $AgNO_3$ et par rmn, le cholestanol par rmn.

Dosage d'une solution de HMPA-Na

La solution bleue obtenue à partir de sodium (2 g) en suspension dans le HMPA (40 cm^3) est versée à l'aide d'une microburette dans une solution (1 cm^3) de n-butanol 0,214 *M* dans l'éther jusqu'à persistance de la coloration bleue (1,68 cm^3 versé; c = 0,119 *M*).

Réduction de l'acétoxy-3β 5α-cholestane par la solution de HMPA-Na 0,119 M

La solution bleue de HMPA-Na 0,119 *M* est versée goutte à goutte dans l'acétoxy-3β 5α-cholestane (81 mg) mis en solution dans l'éther (10 cm^3) jusqu'à persistance de la coloration (1,54 cm^3). Après hydrolyse, extraction et chromatographie, le cholestane (21 mg, 30%) et le cholestanol (51 mg, 70%) sont isolés.

Action de la solution bleue de HMPA-Na sur le tert*-butanol*

Une solution bleue de HMPA-Na (c = 0,0366 *M*) est ajoutée goutte à goutte au *tert*-butanol (191 mg) dilué dans l'éther (10 cm^3) jusqu'à persistance de la coloration. La persistance de la couleur bleue est obtenue après que 0,524 cm^3 de solution ait été ajoutée.

Réduction de l'acétoxy-3β 5α-cholestane pur par la solution bleue de HMPA-Na

Une solution bleue de HMPA-Na (4,13 cm^3, c = 0,049 *M*) est ajoutée rapidement sur l'acétoxy-3β 5α-cholestane pur (152 mg, 3,45 × 10^{-4} mol). Le mélange obtenu est laissé 10 min à la température ambiante puis hydrolysé en milieu acide. Une chromatographie sur silice permet d'isoler le cholestane (58 mg, 44%), l'acétylacétoxy-3β 5α-cholestane (17 mg, 10%) et le cholestanol-3β (54 mg, 39%).

Action de $NaNH_2$ sur l'acétoxy-3β 5α-cholestane en milieu HMPA

De l'amidure de sodium (253 mg) est mis en suspension dans le HMPA (10 cm^3) puis l'acétoxy-3β 5α-cholestane (552 mg) est mis en présence de ce mélange pendant 30 min. On ajoute alors rapidement de l'alcool puis de l'acide chlorhydrique 3 *M* avant d'extraire à l'éther. La chromatographie sur silice permet d'isoler de l'ester non transformé (477 mg, 86%) et le 5α-cholestanol-3β (75 mg, 14%).

Action de $NaNH_2$ sur l'ester en milieu HMPA-Na

De l'amidure de sodium (325 mg) est mis en suspension dans le HMPA (10 cm^3) en présence de sodium (solution bleue). L'acétoxy-

Can. J. Chem. Downloaded from www.nrcresearchpress.com by 210.87.254.40 on 09/06/12
For personal use only.

TABLEAU 11. Caractérisation des esters d'alkyle

Ester	F (°C)	Analyse Trouvé C	Analyse Trouvé H	Analyse Calculé C	Analyse Calculé H
Acétate de triméthyl-3β,4,4 5α-cholestanyle-3	128–129	80,88	11,65	81,28	11,94
Pivalate de 5α-cholestanyle-3β	160–161	81,34	11,77	81,28	11,94
Cyclohexane carboxylate de 5α-cholestanyle-3β	158–159	81,79	11,73	81,86	11,72
Heptanoate de 5α-cholestanyle-3β	78–79	81,29	11,90	81,53	12,68
Méthyl-1 cyclohexane carboxylate de 5α-cholestanyle-3β	136–137	81,46	11,80	81,97	11,80

Ester	F (°C)	F (litt.)	Réf.
Acétate de 5α-cholestanyle-3β	107	91–111	31
Acétate de cholesten-5 yl-3β	114	111–116	32
Acétate de diméthyl-4,4 5α-cholestanyl-3β	138	138–139	33
Benzoate de 5α-cholestanyl-3β	131	136–137	34
Phényl-2 acétate de 5α-cholestanyl-3β	90	91–92	35
Acétate de méthyl-3β 5α-cholestanyl-3α	87	—	36
Acétate de méthyl-3α 5α-cholestanyl-3β	114	—	36

3β 5α-cholestane (567 mg) en solution dans l'éther est ajouté et laissé en présence de cette solution pendant 30 min. Après élimination du sodium, hydrolyse et chromatographie sur silice, le cholestane est isolé (152 mg, 31%) ainsi que le cholestanol-3β (309 mg, 60%) et l'acétoxy-3β 5α-cholestane non transformé (12 mg, 2%).

Action de $NaNH_2$ sur l'ester en milieu HMPA en présence de tert-*butanol*

De l'amidure de sodium (150 mg) est mis en suspension dans le HMPA (10 cm^3) puis de l'acétoxy-3β 5α-cholestane (860 mg) en solution dans un mélange éther – *tert*-butanol (9:1) (10 cm^3) pendant 30 min. On ajoute alors de l'alcool puis de l'acide chlorhydrique 3 *M* avant d'extraire à l'éther. La chromatographie sur silice permet de séparer de l'ester (150 mg, 22%) et du cholestanol-3β (423 mg, 69%).

Action de $NaNH_2$ sur l'ester en milieu HMPA-Na en présence de tert-*butanol*

De l'amidure de sodium (330 mg) est mis en suspension dans la solution bleue HMPA-Na. L'acétoxy-3β 5α-cholestane (703 mg) en solution dans un mélange éther – *tert*-butanol (9:1) (10 cm^3) est alors additionné et laissé à la température ambiante pendant 30 min. Après traitement identique au précédent, le cholestane (317 mg, 52%), le cholestanol-3β (280 mg, 44%) et l'ester de départ (4 mg, 0,5%) sont isolés.

1. L. BOUVEAULT et G. BLANC. Bull. Soc. Chim. Fr. **29**, 787 (1903); **31**, 666 (1904); **31**, 672 (1904).
2. (*a*) C. A. BUEHLER and D. E. PEARSON. Survey of organic syntheses. J. Wiley, New York. 1970. p. 199; (*b*) E. CHABLAY. Ann. Chim. **8**, 205 (1917); (*c*) Org. Synth. Coll. Vol. **II**, 372 (1943).
3. (*a*) L. BOUVEAULT et R. LOCQUIN. C. R. Acad. Sci. Paris, **140**, 1593 (1905); (*b*) L. BOUVEAULT et R. LOCQUIN. Bull. Soc. Chim. Fr. **35**, 629 (1906); **35**, 633 (1906); **35**, 637 (1906); (*c*) S. M. MCELVAIN. Org. React. **4**, 256 (1948); (*d*) J. J. BLOOMFIELD, D. C. OWSLEY et J. M. NELKE. Org. React. **23**, 259 (1976).
4. (*a*) F. F. BLICKE. J. Am. Chem. Soc. **47**, 229 (1925); (*b*) M. S. KHARASH, E. STERNFELD et F. R. MAYO. J. Org. Chem. **5**, 362 (1940).
5. J. J. BLOOMFIELD, D. C. OWSLEY, C. AINSWORTH et R. E. ROBERTSON. J. Org. Chem. **40**, 393 (1975).
6. E. WENKERT et B. G. JACKSON. J. Am. Chem. Soc. **80**, 217 (1958).
7. T. CUVIGNY et M. LARCHEVÊQUE. C.R. Acad. Sc. Paris (C), **275**, 241 (1972).
8. J. G. GOUREY, M. HODLER, B. TEREIN et J. H. P. UTLEY. J. Chem. Soc. Chem. Commun. 779 (1976).
9. (*a*) H. DESHAYES, J. P. PETE, C. PORTELLA et D. SCHOLLER. J. Chem. Soc. Chem. Commun. 439 (1975); (*b*) H. DESHAYES, J. P. PETE et C. PORTELLA. Tetrahedron Lett. 2019 (1976); (*c*) J. P. PETE, C. PORTELLA, C. MONNERET, J. C. FLORENT et Q. KHUONG HUU. Synthesis, 774 (1977).
10. H. DESHAYES et J. P. PETE. J. Chem. Soc. Chem. Commun. 568 (1978).
11. H. NORMANT. Bull. Soc. Chim. Fr. 791 (1968); Angew. Chem. Int. Ed. Engl. **6**, 1046 (1967).
12. N. GREMMO et I. RANDLES. J. Chem. Soc. Faraday Trans. 1, 1480 (1974).
13. K. W. BOWERS, R. W. GIESE, J. GRIMSHAW, H. O. HOUSE, N. H. KOLODNY, K. KRONBERGER et D. K. ROC. J. Am. Chem. Soc. **92**, 2783 (1970).
14. J. L. DYE, G. E. SMITH et R. F. SANKNER. J. Am. Chem. Soc. **82**, 4803 (1960).
15. R. B. BOAR, L. JOUKHADAR, J. F. MCGHIE, S. C. MISRA, A. G. M. BARRETT, D. H. R. BARTON et P. A. PROKOPIOU. J. Chem. Soc. Chem. Commun. 68 (1978).
16. S. J. CRISTOL et R. V. BARBOUR. J. Am. Chem. Soc. **88**, 4262 (1966); **90**, 2832 (1968).
17. G. WHITESIDES ET W. EHMANN. J. Org. Chem. **35**, 3565 (1970).
18. H. NORMANT, T. CUVIGNY, J. NORMANT et B. ANGELO. Bull. Soc. Chim. Fr. 3441 (1965); N. GREMMO et J. E. B. RANDLES. J. Chem. Soc. Faraday Trans. 1, 1480 (1974).
19. A. G. M. BARRETT, P. A. PROKOPIOU et D. H. R. BARTON. J. Chem. Soc. Chem. Commun. 1175 (1979).
20. D. H. R. BARTON et W. B. MOTHERWELL. Pure Appl. Chem. **53**, 15 (1981).
21. M. BAIZER. Organic electrochemistry. Marcel Dekker, Inc., New York. 1973. p. 419.
22. A. G. M. BARRETT, C. R. A. GODFREY, D. M. HOLLINSHEAD, P. A. PROKOPIOU, D. H. R. BARTON, R. B. BOAR, L. JOUKHADAR, J. F. MCGHIE et S. C. MISRA. J. Chem. Soc. Perkin Trans. 1, 1501 (1981).
23. A. G. M. BARRETT, P. A. PROKOPIOU, D. H. R. BARTON, R. B. BOAR et J. F. MCGHIE. J. Chem. Soc. Chem. Commun 1173 (1979).

Can. J. Chem. Downloaded from www.nrcresearchpress.com by 210.87.254.40 on 09/06/12
For personal use only.

24. D. SURYANARAYANA et M. D. SEVILLA. J. Phys. Chem. **84**, 3045 (1980).
25. G. R. STEVENSON et C. A. CASTILLO. S. J. Am. Chem. Soc. **98**, 7950 (1976).
26. P. CREMASCHI, G. MOROSI et M. SIMONETTA. Angew. Chem. **93**, 712 (1981); Angew. Chem. Int. Ed. Engl. **20**, 673 (1981).
27. R. B. BATES et C. A. OGLE. Carbanion chemistry, reactivity and structure concepts in organic chemistry. Vol. XVII. Springer Verlag, Berlin. 1983. p. 17.
28. I. W. HUGUES, F. SMITH et M. WEBB. J. Chem. Soc. 3437 (1949).
29. E. S. WALLIS. J. Am. Chem. Soc. **59**, 137 (1937).
30. J. F. NORMANT et H. DESHAYES. Bull. Soc. Chim. Fr. 2854 (1972).
31. F. SONDHEIMER et R. MECHOULAM. J. Am. Chem. Soc. **80**, 3087 (1958).
32. E. D. BERGMANN, M. RABINOVITZ et Z. H. LEVINSON. J. Am. Chem. Soc. **81**, 1239 (1959).
33. (*a*) Y. MAZUR et F. SONDHEIMER. J. Am. Chem. Soc. **80**, 5220 (1958); (*b*) A. LABLACHE-COMBIER, J. LEVISALLES, J. P. PETE et H. RUDLER. Bull. Soc. Chim. Fr. 1689 (1963); (*c*) F. HEMMER, A. LABLACHE-COMBIER, B. LACOUME et J. LEVISALLES. Bull. Soc. Chim. Fr. 982 (1966).
34. W. BERGMANN, M. KITA et D. J. GIANCOLA. J. Am. Chem. Soc. **76**, 4974 (1954).
35. J. ELLIS et R. SCHIBECI. Aust. J. Chem. **27**, 429 (1974).
36. C. R. NARAYANAN et A. K. KULKARNI. Indian J. Chem. **12**, 677 (1974).

Can. J. Chem. Downloaded from www.nrcresearchpress.com by 210.87.254.40 on 09/06/12
For personal use only.

Reactions of 2,2-dibromocyclopropyl carboxylic acids with methyllithium

LEIV K. SYDNES[1] AND SØLVI SKARE
Department of Chemistry, University of Tromsø, P.O. Box 953, N-9001 Tromsø, Norway

Received Janaury 3, 1984

This paper is dedicated to Professor Paul de Mayo on the occasion of his 60th birthday

LEIV K. SYDNES and SØLVI SKARE. Can. J. Chem. **62**, 2073 (1984).

For reactions of 2,2-dibromocyclopropyl carboxylic acids with methyllithium, the course of reaction depends mainly on the position of the carboxyl group. When the COOH group is directly attached to the *gem*-dibromocyclopropane ring MeLi generally attacks the *gem*-dibromo moiety and gives the corresponding monobromocyclopropane as the principal product. When the reaction is performed above −80°C the monobromides are formed stereospecifically in the *trans* configuration. The highest yields, as high as 80−90%, are obtained at 0°C. When the carboxyl group is not directly attached to the cyclopropane ring most of the MeLi is consumed in an acid−base reaction with the COOH group.

LEIV K. SYDNES et SØLVI SKARE. Can. J. Chem. **62**, 2073 (1984).

L'orientation de la réaction dépend principalement de la position du groupe carboxylique. Lorsque le groupe COOH est attaché directement au cycle *gem*-dibromocyclopropane, le MeLi attaque généralement la portion *gem*-dibromo et conduit principalement au produit monobromocyclopropane correspondant. Lorsqu'on effectue la réaction à des températures supérieures à −80°C, les monobromures se forment stéréospécifiquement en configuration *trans*. C'est à 0°C que l'on obtient les rendements les plus élevés, qui peuvent aller jusqu'à 80−90%. Lorsque le groupe carboxyle n'est pas attaché directement au cyclopropane, la majorité du MeLi est utilisé dans une réaction acide−base avec le groupe COOH.

[Traduit par le journal]

Introduction

Reactions of *gem*-dibromocyclopropanes with methyllithium generally occur with initial lithium−bromine exchange, resulting in formation of the corresponding bromolithio derivatives (**1**, **2**). The subsequent reaction of such derivatives is significantly influenced by the nature of the substituents attached to the ring. When the substituents are nonpolar, like alkyl and aryl groups, the organometallic intermediates usually collapse by elimination of lithium bromide to yield allene and (or) bicyclobutane derivatives (**1**−**10**). On the other hand, a variety of polar groups, e.g. the carbonyl, alkoxy, and silyloxy moieties, may stabilize the lithio-bromocyclopropane by intramolecular coordination and thus prevent LiBr elimination (**9**−**13**). In such cases the major product is generally the corresponding monobromocyclopropane, which is formed by hydrolysis of the lithium derivative during aqueous work-up.

An exception to this general pattern is 2,2-dibromo-1-methylcyclopropanecarboxylic acid (**1***b*). When this compound was treated with methyllithium at 0°C, a stereospecific formation of *trans*-2-bromo-1-methylcyclopropanecarboxylic acid (**2***b*) was observed (14). According to Stein and Morton

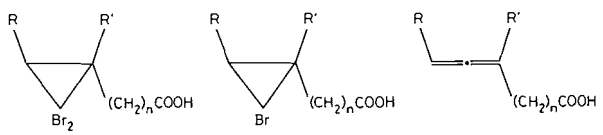

1 **2** **3**

a R = R′ = H, *n* = 0
b R = H, R = CH_3, *n* = 0
c R = R′ = CH_3, *n* = 0
d R = H, R′ = Ph, *n* = 0
e R = H, R′ = CH_3, *n* = 1

this product resulted from an intramolecular quenching of a cyclopropyl anion *prior to* hydrolysis (14). It is thus conceivable that a COOH group attached to a *gem*-dibromocyclopropane can function as a general directing group and act as a vehicle for stereoselective preparation of a variety of monobromocyclopropanes. It was therefore of interest to study the reactions between methyllithium and various *gem*-dibromocyclopropanecarboxylic acids; the results of this investigation are reported here.

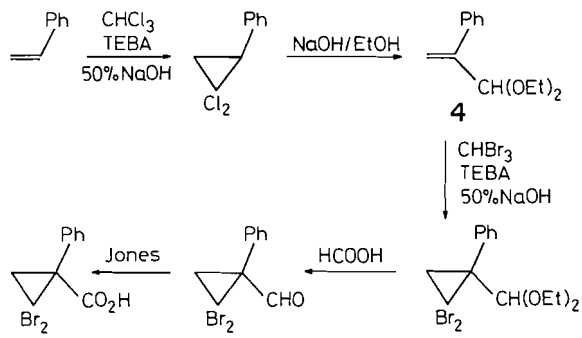

SCHEME 1

Results and discussion

Most of the acids employed were prepared in good yields by literature procedures. 2,2-Dibromo-1-phenylcyclopropanecarboxylic acid (**1***d*), however, was obtained from styrene as outlined in Scheme 1. The low overall yield (23%) results from inefficient addition of dibromocarbene to the carbon−carbon double bond of atropaldehyde diethylacetal (**4**); this is not surprising since dichlorocarbene addition to similar acetals is fairly ineffective (15). 2-(2,2-Dibromo-1-methylcyclopropyl)-ethanoic acid (**1***e*) was prepared by Jones oxidation of the corresponding primary alcohol, which was obtained by dibromocarbene addition to 3-methyl-3-buten-1-ol under phase-transfer conditions.The cyclopropyl alcohol formed in the latter reaction was contaminated with a minor product tentatively identified as 2,2-dibromo-1-methyl-1-(2-dibromomethoxyethyl)cyclopropane (**5**) on the basis of analogy with earlier work (16); **5** is probably produced by dibromocarbene insertion into the O—H bond (Scheme 2) (16).

The *gem*-dibromocyclopropane acids were reacted with

[1]Author to whom correspondence should be addressed.

Can. J. Chem. Downloaded from www.nrcresearchpress.com by 210.87.254.40 on 09/06/12
For personal use only.

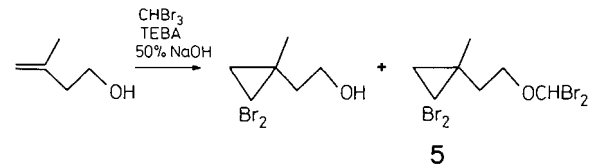

5

SCHEME 2

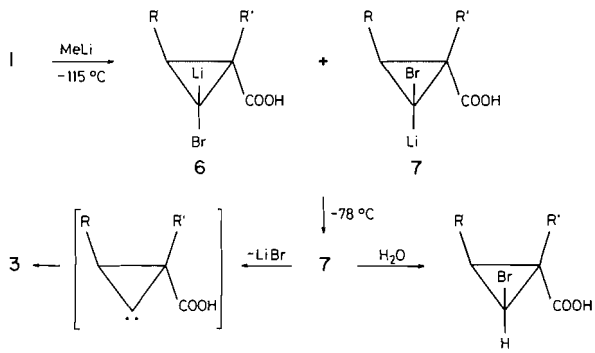

SCHEME 3

methyllithium at −115 to 25°C using, in most cases, 1.2 molar equivalents of the lithium reagent. The reaction mixtures were analyzed by gas−liquid chromatography (glc) before the products were isolated by distillation or column chromatography and identified by spectroscopic means. Most of the results are summarized in Table 1, which reveals several interesting features.

With the exception of **1***e*, the acids generally react to give the corresponding monobromocyclopropanes **2** as the main products. When the reactions were carried out below −80°C the monobromides were formed as isomeric mixtures. However, above −80°C the monobromo derivatives were formed as single isomers with the bromine and carboxyl groups *trans* to each other. The stereochemistry is assigned by ^{1}H nmr spectroscopy on the basis of two assumptions. Firstly, it is assumed that in a cyclopropane ring the *cis* coupling constant is larger than the *trans*, which is in accordance with calculations as well as experimental data (17). Secondly, the assumption is that for a pair of isomers the hydrogen atom geminal to the bromine atom gives rise to signals at a lower field for the *trans* than for the *cis* isomer, because of the anisotropy of the carbonyl group (12, 13, 17).

Treatment of acid **1***e* with methyllithium, on the other hand, gave no monobromocyclopropane at all; the predominant product was 3-methyl-3,4-pentadienoic acid (**3***e*) which was isolated in low yield when the reaction was carried out above −5°C. An allene, 2-methyl-2,3-pentadienoic acid (**3***c*), was also formed when **1***c* was treated with MeLi at and above 0°C, but in this case the monobromide was the major product.

The products isolated can be accounted for as outlined in Scheme 3. The first step involves an exchange of bromine with lithium, which has been reported to be a faster reaction than proton abstraction from the carboxyl and hydroxyl groups of various bromosubstituted acids and alcohols (14, 18−20). The organolithium intermediate is not formed stereospecifically since reactions performed at −115°C result in formation of mixtures of isomeric monobromocyclopropane acids. Consequently, at −115°C the stereoisomeric organolithium derivatives **6** and **7** equilibriate very slowly. However, at −78°C and above, the only isomer present is **7**, which is the more

TABLE 1. Product distribution in reactions of 2,2-dibromocyclopropyl acids (**1**) with 1.2 equivalents of methyllithium

Acid (% unreacted)[a]	Reaction temperature (°C)	Products (% yield)[a] *cis*-**2**	*trans*-**2**	**3**	Unknown
1*a* (90)	−115	5	5		
(77)	−78		23		
(1)	0		99		
(67)	25		33		
1*b* (74)	−115	13	13		
(61)	−78		39		
(36)	0		64		
(50)	25		45		5
1*c* (84)	−78		16		
(47)	0		38	15	
(55)	25		30	15	
1*d* (75)	−78		25		
(18)	0		82		
(28)	25		72		
1*e* (100)	−115				
(100)	−78				
(84)	0			10[b]	6
(88)	25			8[b]	4

[a]% of reaction mixture as determined by glc and ^{1}H nmr analyses; for isolated yields, see Experimental.
[b]Identified by spectra only.

TABLE 2. pK_a values of various cyclopropanecarboxylic acids in water at 25°C

Acid	pK_a
Cyclopropanecarboxylic acid	4.83[a]
2-Bromocyclopropanecarboxylic acid	4.09[a]
2,2-Dibromocyclopropanecarboxylic acid (**1***a*)	3.27
2,2-Dibromo-1-methylcyclopropanecarboxylic acid (**1***b*)	3.12
trans-1,2-Dimethylcyclopropanecarboxylic acid	5.17[b]
trans-2,2-Dibromo-1,3-dimethylcyclopropanecarboxylic acid (**1***c*)	3.81
2,2-Dibromo-1-phenylcyclopropanecarboxylic acid (**1***d*)	3.10
2-(2,2-Dibromo-1-methylcyclopropyl)ethanoic acid (**1***e*)	4.56

[a]From ref. 23.
[b]From res. 22.

stable due to lithium−oxygen coordination. Stabilization of organolithium intermediates by adjacent oxygen functions has been extensively reported in the literature (9, 11−13). The final products result from two competing reactions following the formation of the lithio-bromocyclopropanes, viz. quenching of the cyclopropyl anion and allene formation via a cyclopropylidene intermediate. When the carboxyl group is directly attached to the ring, the former alternative is generally the predominant reaction; α-elimination of lithium bromide and subsequent allene production are only observed when steric interactions increase the internal energy of **7** and render opening of the ring a more favourable process.

The amount of recovered starting material depends, in addition to the relative amount of methyllithium employed, mainly on two factors. More important is obviously the position of the carboxyl group relative to the *gem*-dibromocyclopropane ring. When the COOH group is directly attached to the ring, as in **1***a*−**1***d*, the dibromo moiety and the carboxyl group will mutually interact; this is convincingly borne out by comparing the pK_a values of the acids with those of similar cyclopropane-

Can. J. Chem. Downloaded from www.nrcresearchpress.com by 210.87.254.40 on 09/06/12
For personal use only.

TABLE 3. The ratio between the acids before and after treatment of the **1***b*/**1***e* and **1***b*/1,1-dibromo-2,2,3-trimethylcyclopropane (DTC) mixtures with MeLi

Mixtures	Before MeLi	After MeLi	Yield of *trans*-**2***b* (%)
1*b*/**1***e*	51:49	42:58	9
1*b*/DTC	48:52	36:59	12

carboxylic acids (Table 2) (21–23). As a result of this interaction the bromine atoms become more positive and compounds **1***a*–**1***d* are therefore more prone to undergo lithium–bromine exchange than proton abstraction from the carboxyl group when treated with MeLi. On the other hand, in **1***e* such interactions are impossible, and proton abstraction is therefore the predominant reaction when this compound is treated with methyllithium; consequently, most of the acid is recovered unchanged during the work-up.

The reaction temperature also influences considerably the amount of recovered starting material. At and below −70°C the irreversible consumption of acid is generally very low, primarily because most of the methyllithium is consumed in reaction with the carboxyl group. When the temperature increases, however, the relative importance of the lithium–bromine exchange reaction increases and reaches, for no obvious reason, its maximum at 0°C. The attack on the *gem*-dibromo moiety is therefore a more temperature sensitive process than the abstraction of a proton from the carboxyl group.

If the rationale above correctly describes the course of reaction between methyllithium and acids **1***a*–**1***e*, then 2,2-dibromo-1-methylcyclopropanecarboxylic acid (**1***b*) should be more reactive toward MeLi than either acid **1***e* or alkyl-substituted *gem*-dibromocyclopropanes. Experimentally, this was found to be the case; when acid **1***b* was mixed with **1***e* and 1,1-dibromo-2,2,3-trimethylcyclopropane and treated with MeLi, **1***b* was selectively attacked by the lithium reagent. This is borne out by a decrease in the relative amount of **1***b* in the mixtures and by a simultaneous formation of *trans*-**2***b* as the main reaction product (Table 3).

From acids **1***a*–**1***d* the monobromocyclopropanes are formed by an acid–base reaction between the lithiocyclopropyl moiety and a proton source. From experiments performed with deuterated reactants at 0°C (Scheme 4) Stein and Morton concluded that the proton was supplied by the carboxyl group in an intramolecular process. This conclusion would have been correct if the lithium intermediates corresponding to **6** and **7** both had been present at 0°C. This is, however, not the case; the only cyclopropyl lithium derivative present at this temperature is **8**, which will yield the *trans* monobromides **9**

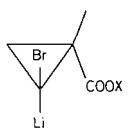

8

and **10** as the only products whether **8** is quenched intramolecularly or intermolecularly. In order to shed more light on this problem, acid **1***b* was treated with MeLi at −115°C and subsequently hydrolyzed, first with DCl/D_2O and then with H_2O. By comparing glc and ^1H nmr analyses of the reaction

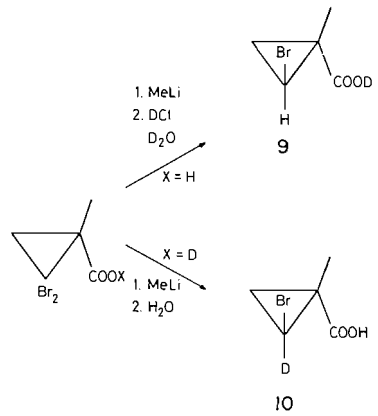

SCHEME 4

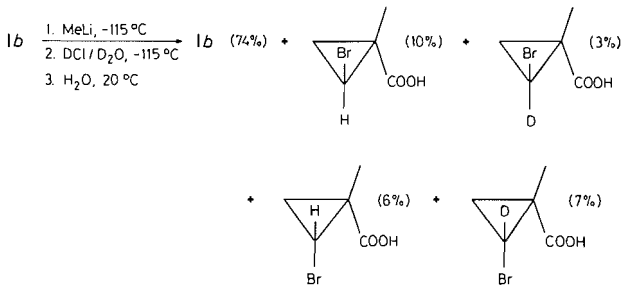

SCHEME 5

mixture the results summarized in Scheme 5 emerge. Most striking is the fact that *trans*-**2***b* and a second product which from the similarity of its ^1H nmr signals is almost certainly the *cis* isomer, were both formed as a mixture of 2-bromo-1-methylcyclopropanecarboxylic acid and 2-bromo-1-methylcyclopropanecarboxylic-2-*d* acid. This clearly shows that the cyclopropyl anions abstract protons both prior to *and* during the hydrolysis and, consequently, that the organolithium intermediates live long enough to permit intermolecular quenching. In fact, studies of models of the *anti* cyclopropyl anion **11** clearly indicate that only intermolecular quenching is conceivable for this and other intermediates with the same configuration.

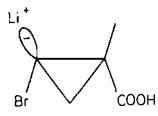

11

From the results outlined above it is evident that one can influence the course of reaction by employing a salt of the acids instead of the acids themselves. Such salts, prepared quantitatively by treating the acids with 1 equivalent of sodium hydride, were therefore treated with methyllithium in the usual way. When the reaction mixtures were worked up it turned out that the reduced loss of methyllithium did not increase the yield of *trans*-2-bromocyclopropanecarboxylic acids but rather the yield of other products. Typical examples are shown in Scheme 6: 2-acetyl-1,1-dibromo-2-methylcyclopropane was formed as a minor product from the sodium salt of **1***b* at 0°C (24), whereas the yield of allene **3***c* tripled when sodium 2,2-dibromo-1,3-dimethylcyclopropanecarboxylate was reacted under the same conditions. Consequently, the sodium salts react less selec-

Can. J. Chem. Downloaded from www.nrcresearchpress.com by 210.87.254.40 on 09/06/12
For personal use only.

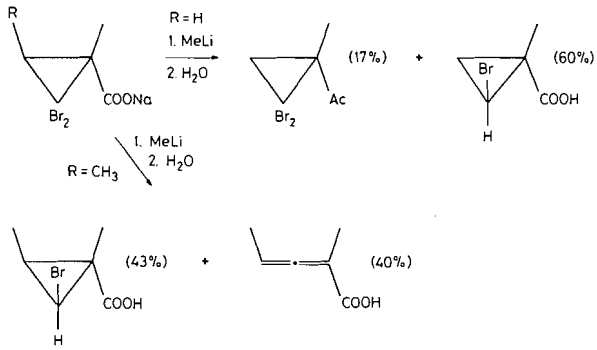

SCHEME 6

tively with methyllithium than the corresponding acids, but it is interesting to note that the monobromocyclopropanecarboxylic acids are formed exclusively in the *trans* configuration, i.e from cyclopropyllithium intermediates in which lithium coordinates with the sodium carboxylate moiety.

Experimental

Gas chromatographic analyses were carried out on a Varian 3700 gas chromatograph equipped with thermal conductivity and flame ionization detectors. The columns were 2 m long and were packed with 3% OV17 on Chromosorb W-HP, 80/100. The ir spectra were recorded on a Shimadzu IR 420 spectrophotometer. The nmr spectra were obtained on JEOL PMX 60 SI and JEOL FX 90Q spectrometers, using tetramethylsilane as internal standard. Mass spectra were run on a Micromass 7070 H spectrometer, operated in the EI mode with an ionization potential of 70 eV. Boiling points and melting points are uncorrected. Melting points were determined on a Mettler FP61 apparatus. Elemental analyses were performed by Ilse Betz Microanalytical Laboratory, Kronach, West Germany. A PHM 62 pH-meter with a Radiometer SK2401 C glass electrode was used to determine the pK_a values of carboxylic acids.

Preparation of starting materials

2,2-Dibromocyclopropanecarboxylic acid (**1***b*), 2,2-dibromo-1-methylcyclopropanecarboxylic acid (**1***b*), and 2,2-dibromo-1,3-dimethylcyclopropanecarboxylic acid (**1***c*) were prepared as described in the literature (13, 25).

2,2-Dibromo-1-phenylcyclopropanecarboxylic acid (**1***d*) was made in the following way. Dibromocarbene, from bromoform (43.0 g, 0.17 mol) and 50% aqueous NaOH (10.0 g, 0.225 mol), was added to atropaldehyde diethylacetal (**4**) (15.0 g, 0.07 mol) under phase-transfer conditions using TEBA (0.50 g, 0.002 mol) as catalyst (26, 27) to give 2,2-dibromo-1-phenylcyclopropanecarbaldehyde diethylacetal (10.6 g, 40%), bp 122–125°C/0.2 Torr (1 Torr = 133.3 Pa); ir (film): 1602, 1500, 1450, 1370, 1300, 1240, 1200–1000, 695 cm^{-1}; ^1H nmr (90 MHz, $CDCl_3$) δ: 1.13 (3H, t, *J* 7 Hz), 1.22 (3H, t, *J* 7 Hz), 2.10 (2H, s), 3.57 (2H, q, *J* 7 Hz), 3.65 (2H, q, *J* 7 Hz), 4.49 (1H, s), 7.34 (5H, br s) ppm; the compound isolated was not pure enough for elemental analysis. A solution of the cyclopropanecarbaldehyde diethylacetal (4.6 g, 0.012 mol) in 80% formic acid (50 mL) was then refluxed for 3 h; after extraction (diethyl ether), washing (aqueous $NaHCO_3$), and drying ($MgSO_4$), work-up in the usual way left a residue which was essentially pure 2,2-dibromo-1-phenylcyclopropanecarbaldehyde (3.4 g, 97%) (25). Jones oxidation (17) of this aldehyde (3.4 g, 0.012 mol) gave 2,2-dibromo-1-phenylcyclopropanecarboxylic acid (**1***d*) (3.5 g, 97%), mp 121–122°C (from water) (lit. (25) mp 118–120°C (sublimed)).

2-(2,2-Dibromo-1-methylcyclopropyl)ethanoic acid (**1***e*) was prepared as follows. Dibromocarbene, from bromoform (116.0 g, 0.46 mol) and 50% aqueous NaOH (56.0 g, 0.70 mol), was added to 3-methyl-3-buten-1-ol (20.0 g, 0.23 mol) in the presence of TEBA (0.70 g, 0.003 mol) (27) to give 2-(2,2-dibromo-1-methylcyclopropyl)ethanol (34.3 g, 58%) by distillation, bp 95–98°C/0.2 Torr; ir (film): 3300, 1730, 1460, 1390, 1180, 1050, 700 cm^{-1}; ^1H nmr (90 MHz, $CDCl_3$) δ: 1.41 (3H, s), 1.44 (1H, d, *J* 8 Hz), 1.52 (1H, d, *J* 8 Hz), 1.90 (1H, br s), 1.95 (2H, 2t, *J* 7 Hz), 3.87 (2H, 2t, *J* 7 Hz), 4.38 (weak signal, t, *J* 7.5 Hz), 8.07 (weak signal, s) ppm; the compound gave no molecular ion in ms and was not obtained pure enough for elemental analysis; the ir absorption at 1730 cm^{-1} and the nmr signals at 4.38 and 8.07 ppm are tentatively ascribed to cyclopropane **5**. Jones oxidation (17) of the dibromocyclopropylethanol (34.0 g, 0.13 mol) afforded acid **1***e* (18.0 g, 51%) by recrystallization from water, mp 94–96°C; ir (CCl_4): 3500–2300, 1710, 1410, 1260, 1220, 1115, 1020, 695 cm^{-1}; ^1H nmr (90 MHz, $CDCl_3$) δ: 1.52 (3H, s), 1.54 (1H, d, *J* 8 Hz), 1.59 (1H, d, *J* 8 Hz), 2.78 (2H, s), 9.66 (1H, s) ppm; ^{13}C nmr (22.5 MHz, $CDCl_3$) δ: 23.1 (CCH_3), 26.9(CCH_3), 34.4 (CH_2), 36.8 (Br*C*Br), 43.0 (CH_2COOH), 176.9(CH_2COOH) ppm; ms *m/e*: 215(8), 213(14), 211(7), 193(19), 191(19), 151(27), 149(29), 133(12), 131(11), 111(100), 82(73), 81(28), 80(77), 79(29). *Anal.* calcd. for $C_6H_8Br_2O_2$: C 26.50, H 2.94; found: C 26.09, H 3.25.

Treatment of gem*-dibromocyclopropyl acids with methyllithium; general procedure*

The reaction was carried out under pure nitrogen.

An etheral solution (1.4 *M*) of MeLi, containing lithium bromide, was added dropwise to a stirred solution of acid in dry ether (15 mL ether/10 mmol acid) at and above −78°C and in a 11:3:6 mixture of tetrahydrofuran, ether, and petroleum ether (5 mL/mmol acid) at −115°C. The mixture was stirred for another 1.5 h at bath temperature and was then hydrolyzed with 1.0 *M* HCl and extracted with ether. The combined organic fractions were dried ($MgSO_4$). Evaporation of ether left a residue which was analyzed by glc prior to purification by distillation or recrystallization.

Reactions of **1**a

The acid was treated with MeLi (1.2 equivalents) at temperatures from −115 to 25°C. The glc (column temperature 60–180°C, 6°/min) and ^1H nmr analyses gave the results included in Table 1.

The products formed at −115°C were, according to ^1H nmr spectra of the reaction mixture, the *cis* and *trans* isomers of 2-bromocyclopropanecarboxylic acid (**2***a*) (23, 29).

At and above −78°C the only product formed was *trans*-**2***a*, bp 105°C/1.5 Torr; mp 64.5–65°C (sublimed); ir (film): 3600–2200, 1700, 1440, 1260, 1215, 1020, 945 cm^{-1}; ^1H nmr (60 MHz, $CDCl_3$) δ: 1.15–2.30 (3H, very complex m), 3.20–3.55 (1H, m), 9.65 (1H, br s).

When the reaction was carried out at −78, 0, and 25°C with 0.98 g (4.0 mmol) of **1***a*, *trans*-**2***a* was isolated by sublimation in 20, 90, and 30% yield, respectively.

Reactions of **1**b

The acid was reacted with MeLi (1.2 equivalents) at temperatures from −115 to 25°C; The glc analyses (column temperature 80–180°C, 10°/min) gave the results compiled in Table 1.

When the acid (2.58 g, 0.010 mol) was treated with MeLi at −115°C a 1:1 mixture (0.35 g, 20%) of the *trans* and (evidently) *cis* isomers of 2-bromo-1-methylcyclopropanecarboxylic acid (**2***b*) was formed, bp 64–65°C/10 Torr; ir (film): 3500–2500, 1690, 1460, 1405, 1310, 1185, 1040, 690 cm^{-1}; ^1H nmr (90 MHz, $CDCl_3$) δ: 0.92–1.99 (2H, m, *cis* and *trans*), 1.40 and 1.47 (3H, 2s, due to *cis* and *trans*, respectively), 3.05 and 3.57 (1H, 2dd, due to *cis* and *trans*, respectively, *J* 6 and 7.5 Hz), 10.75 (1H, s).

When reacted at −78 and 0°C, *trans*-**2***b* was the only product formed. The boiling point and spectroscopic data were in accordance with literature data (14). At −78°C 2.58 g (10 mmol) of **1***b* gave 0.54 g (30%) of *trans*-**2***b* by distillation. At 0°C 2.28 g (8.8 mmol) of **1***b* afforded 1.21 g (81%) of the same product by distillation.

When the acid (1.29 g, 5 mmol) was reacted at 25°C, 0.31 g (35%) of *trans*-**2***b* was isolated by Kugelrohr distillation. In addition, glc analyses (column temperature 80–180°C, 10°/min) showed that 5 additional products had been formed in approximately 5% yield; these

Can. J. Chem. Downloaded from www.nrcresearchpress.com by 210.87.254.40 on 09/06/12
For personal use only.

products were not identified.

Reactions of **1**c

This acid was reacted with MeLi (1.2 equivalents) at temperatures ranging from −78 to 25°C. The glc analyses (column temperature 80−180°C, 10°/min) of the reaction mixture prior to work-up gave the results presented in Table 1.

At −78°C, treatment of 1.36 g (5.0 mmol) of **1***c* gave a reaction mixture from which 0.14 g (15%) of the *trans* isomer of 2-bromo-1,3-dimethylcyclopropanecarboxylic acid (**2***c*) was isolated by Kugelrohr distillation at 90°C/0.5 Torr. The product crystallized during the distillation, mp 98−99°C; ir (CCl_4): 3400−2400, 1690, 1420, 1290, 1180, 600 cm^{-1}; ^1H nmr (90 MHz, $CDCl_3$) δ: 1.12 (3H, d, *J* 6.5 Hz), 1.27 (3H, s), 1.55−1.94 (1H, m), 3.73 (1H, d, *J* 8 Hz), 12.28 (1H, s) ppm; ^{13}C nmr (22.5 MHz, $CDCl_3$) δ: 10.00 ($CHCH_3$), 10.54 (CCH_3), 24.78 (CH_3CH), 25.76 (CCH_3), 36.51 (*H*C*B*r), 180.33 (*C*OOH) ppm; ms *m/e*: 194(2, M^+), 192(2, M^+), 179(2), 177(2), 149(2), 113(100), 95(31), 82(6), 80(6), 67(66). *Anal.* calcd. for $C_6H_9BrO_2$: C 37.34, H 4.66; found: C 37.27, H 5.13.

When **1***c* (2.72 g, 10 mmol) was treated with MeLi at 0°C distillation afforded *trans*-**2***c* (0.56 g, 29%), bp 94°C/0.4 Torr, and 2-methyl-2,3-pentadienoic acid (**3***c*) (0.15 g, 13%), bp 85°C/0.4 Torr (lit. (28) bp 74°C/0.03 Torr).

When **1***c* (2.72 g, 10 mmol) reacted with MeLi at 25°C, the yield of isolated *trans*-**2***c* and **3***c* dropped to 25% and 12%, respectively.

Reactions of **1**d

Reactions between this acid and MeLi (1.2 equivalents) were performed at temperatures ranging from −78°C to 25°C. The glc analyses (column temperature 100−200°C, 20°/min) of the reaction mixture, after quenching with water but prior to work-up, gave the results given in Table 1.

Reactions on a preparative scale were only performed at 0 and 25°C. At 0°C acid **1***d* (3.20 g, 10 mmol) gave *trans*-2-bromo-1-phenylcyclopropanecarboxylic acid (*trans*-**2***d*), which was isolated in 70% yield (1.69 g) when recrystallized from water, mp 136.5−137.5°C; ir (CCl_4): 3350−2200, 1690, 1420, 1300, 1180, 1055, 695, 650, 600 cm^{-1}; ^1H nmr (90 MHz, $CDCl_3$) δ: 1.75 (2H, t, *J* 6 Hz), 2.24 (2H, dd, *J* 6 and 8 Hz), 3.80 (2H, dd, *J* 6 and 8 Hz), 7.33 (5H, br s), 11.60 (1H, br s) ppm; ^{13}C nmr (22.5 MHz, $CDCl_3$) δ: 24.87 (H*C*H), 27.76 (H*C*Br), 34.16 (*C*Ph), 128.10 (*C*H), 128.20 (*C*), 131.45 (*C*H), 134.24 (*C*), 178.37 (*C*OOH) ppm; ms *m/e*: 242(9, M^+), 240(9, M^+), 224(0.5), 222(0.5), 197(0.5), 195(0.6), 161(6), 160(7), 133(20), 117(13), 116(20), 115(100), 103(21), 91(8). *Anal.* calcd. for $C_{10}H_9BrO_2$: C 49.83%, H 3.73; found: C 50.19%, H 3.45%.

When the same reaction was carried out at 25°C the isolated yield of *trans*-**2***d* dropped to 58%.

Reactions of **1**e

The acid was treated with 1.2 equivalents of MeLi at temperatures between −115 and 25°C. The glc analyses (column temperature 80−180°C, 10°/min) gave the results compiled in Table 1. Three products, formed in 6 and 4% yield at 0 and 25°C, respectively, could not be identified although there are indications that one of the compounds is 3-(2,2-dibromo-1-methylcyclopropyl)-2-propanone.

The reactions performed at −115 and −78°C gave no product except recovered starting material.

When the acid (2.70 g, 10 mmol) was reacted with MeLi at 0°C, a product believed to be 3-methyl-3,4-pentadienoic acid (**3***e*) (0.09 g, 8%) was obtained by distillation, bp 100°C/0.5 Torr; ir (film): 3500−2500, 1970, 1740, 850 cm^{-1}; ^1H nmr (90 MHz, $CDCl_3$) δ: 1.79 (3H, t, *J* 3.2 Hz), 3.03 (2H, t, *J* 2.3 Hz), 4.70 (2H, m), 10.05 (1H, s); the compound was not obtained pure enough for elemental analysis.

An identical reaction carried out at 25°C gave **3***e* in 6% yield.

pK_a *measurements*

The measurements were carried out by titration of aqueous solutions (25.0 mL) of the acids with 0.100 *M* aqueous NaOH. The pK_a values were determined graphically from plots of pH as a function of added base. The results are presented in Table 2.

Reactions of methyllithium with **1**b/**1**e *and* **1**b/*1,1-dibromo-2,2,3-trimethylcyclopropane mixtures*

Both reactions were performed in the following way. An etheral solution (5 mL), containing approximately 1.00 mmol of each acid, was stirred at 0°C and treated with 1.0 mL of a 1.0 *M* etheral solution of MeLi. The reaction was quenched and worked up in the usual way after 40 min. The composition of the reaction mixture was determined by glc (column temperature 80−180°C, 10°/min). The results are summarized in Table 3.

Treatment of **1**b *with MeLi and DCl/*D_2O *at −115°C*

Acid **1***b* (0.51 g, 2.0 mmol), dissolved in a dry mixture (10 mL) of THF, ether, and petroleum ether, was stirred at −115°C and treated with 2.0 mL of a 1.2 *M* solution of MeLi. The mixture was kept at bath temperature for 30 min and was then hydrolyzed at the same temperature with DCl/D_2O (5 mL, 2.0 *M*). The hydrolysate was allowed to reach room temperature before 20 mL H_2O was added. The reaction mixture was then worked up in the usual way and analyzed. The glc analysis (column temperature 60−180°C, 8°/min) indicated that a 1.0:1.0 mixture of the *cis* and *trans* isomers of deuterated and nondeuterated **2***b* had been formed in 26% yield. The ^1H nmr (90 MHz, $CDCl_3$) analysis showed, by comparing the integral of the double doublet at 3.57 ppm (*H*CBr due to *trans*-**2***b*), the double doublet at 3.05 ppm (*H*CBr due to *cis*-**2***b*), and the doublet at 2.44 ppm (*H*CH due to **1***b*), that the reaction mixture contained 16% of nondeuterated **2***b* in a *trans*/*cis* ratio of 5.0:3.0.

Preparation of etheral solutions of sodium salts of 2,2-dibromocyclopropanecarboxylic acids

The sodium salts were prepared by treating a 0.20 *M* etheral solution of the acids at 0°C with an equivalent amount of sodium hydride, which was obtained from a NaH dispersion by removing the mineral oil with pentane. The mixture was stirred for 45 min at ambient temperature to complete the reaction.

Hydrolysis and adjustment of pH to 1 followed by standard work-up gave recovered acids in quantitative yields (30).

Reactions of the sodium salts of **1**b *and* **1**c *with methyllithium*

The reactions were carried out according to the general procedure for treatment of the corresponding acids with methyllithium. A 20% excess of MeLi was used. The glc analyses of the reaction mixtures (column temperature 80−180°C, 10°/min) gave the results presented in Scheme 6.

When the sodium salt of **1***b* was reacted with 1.2 equivalents of MeLi, 2-acetyl-1,1-dibromo-2-methylcyclopropane was isolated in 15% yield, bp 33°C/0.2 Torr (lit. (31) bp 38°C/0.6).

1. W. R. MOORE and H. R. WARD. J. Org. Chem. **27**, 4179 (1962).
2. L. SKATTEBØL. Acta Chem. Scand. **17**, 1683 (1963).
3. W. R. MOORE and J. B. HILL. Tetrahedron Lett. 4553 (1970).
4. M. S. BAIRD. J. Chem. Soc. Chem. Commun. 1145 (1971).
5. D. W. BROWN, M. E. HENDRICK, and M. JONES, JR. Tetrahedron Lett. 3951 (1973).
6. D. P. G. HAMON and V. C. TRENERRY. Tetrahedron Lett. 1371 (1974).
7. M. S. BAIRD and A. C. KAURA. J. Chem. Soc. Chem. Comun. 356 (1976).
8. M. S. BAIRD. J. Chem. Soc. Chem. Commun. 776 (1979).
9. N. O. NILSEN, L. SKATTEBØL, and L. K. SYDNES. Acta Chem. Scand. B, **36**, 587 (1982).
10. J. ARCT and L. SKATTEBØL. Acta Chem. Scand. B, **36**, 593 (1982).
11. K. G. TAYLOR, W. E. HOBBS, and M. SAQUET. J. Org. Chem. **36**, 369 (1971).
12. L. K. SYDNES and L. SKATTEBØL. Acta Chem. Scand. B, **32**, 547 (1978).
13. M. S. BAIRD and A. G. W. BAXTER. J. Chem. Soc. Perkin Trans. 1, 2317 (1979).
14. C. A. STEIN and T. H. MORTON. Tetrahedron Lett. 4933 (1973).
15. A. K. KHUSID, G. V. KRYSHTAL, V. A. DOMBROVSKY, V. F.

Can. J. Chem. Downloaded from www.nrcresearchpress.com by 210.87.254.40 on 09/06/12
For personal use only.

KUCHEROV, L. A. YANOVSKAYA, V. I. KADENTSEV, and O. S. CHIZHOV. Tetrahedron, **33**, 77 (1977).
16. K. KLEVELAND, L. SKATTEBØL, and L. K. SYDNES. Acta Chem. Scand. B, **31**, 463 (1977).
17. L. K. SYDNES. Acta Chem. Scand. B, **32**, 47 (1978).
18. A. R. ALLAN and M. S. BAIRD. J. Chem. Soc. Chem. Commun. 172 (1975).
19. R. J. BOATMAN, B. J. WHITLOCK, and H. W. WHITLOCK, JR. J. Am. Chem. Soc. **99**, 4822 (1977).
20. D. SEEBACH, H. NEUMANN, and R. DAMMANN. Helv. Chim. Acta, **62**, 1162 (1979).
21. Y. KUSUYAMA and Y. IKEDA. Bull. Chem. Soc. Jpn. **49**, 724 (1976).
22. R. N. MCDONALD and R. R. REITZ. J. Am. Chem. Soc. **98**, 8144 (1976).
23. Y. KUSUYAMA. Bull. Chem. Soc. Jpn. **52**, 1944 (1979).
24. C. TEGNER. Acta Chem. Scand. **6**, 782 (1952).
25. K. H. HOLM, D. G. LEE, and L. SKATTEBØL. Acta Chem. Scand. B, **32**, 693 (1978).
26. I. CROSSLAND. Org. Synth. **60**, 6 (1981).
27. M. MAKOSZA and M. WAWRZYNIEWICS. Tetrahedron Lett. 4659 (1969).
28. W. RUNGE, G. KRESZE, and E. RUCH. Justus Liebigs Ann. Chem. **1975**, 1361 (1975).
29. K. B. WIBERG, R. K. BARNES, and J. ALBIN. J. Am. Chem. Soc. **79**, 4994 (1957).
30. C. MARCAILLOU, G. FONTAINE, and P. MAITTE. C. R. Acad. Sci. Ser. C, **267**, 846 (1968).
31. R. BARLET. C. R. Acad. Sci. Ser. C, **278**, 621 (1974).

Can. J. Chem. Downloaded from www.nrcresearchpress.com by 210.87.254.40 on 09/06/12
For personal use only.

Biosynthesis of γ-bisabolene in tissue cultures of *Andrographis paniculata*

PANAYIOTIS ANASTASIS, ISABEL FREER, CHRISTOPHER GILMORE, HUGH MACKIE, KARL OVERTON,[1] AND DOUGLAS PICKEN

Plant Tissue Culture Unit, Department of Chemistry, University of Glasgow, Glasgow G12 8QQ, Scotland

AND

STEPHEN SWANSON

Department of Chemistry, Brown University, Providence, RI 02912, U.S.A.

Received March 14, 1984

This article is dedicated to Professor Paul de Mayo on the occasion of his 60th birthday

PANAYIOTIS ANASTASIS, ISABEL FREER, CHRISTOPHER GILMORE, HUGH MACKIE, KARL OVERTON, DOUGLAS PICKEN, and STEPHEN SWANSON. Can. J. Chem. **62**, 2079 (1984).

Experiments with intact callus cultures of *Andrographis paniculata* and a derived cell-free system have established that: (1) the biosynthesised γ-bisabolene has the *Z*-configuration **6**; (2) the biosynthetic intermediate is a 6-*trans*-**13** and not a 6-*cis*-**15** farnesyl pyrophosphate; (3) in paniculide B **17**, and probably also in γ-bisabolene **14**, the ring carbon derived from C-2 of mevalonate is *anti* to the side chain; (4) mevalonolactone and *trans,trans*-farnesyl pyrophosphate are incorporated into γ-bisabolene without hydrogen loss respectively from C-5 and C-1; cyclisation to the bisabolenyl cation therefore does not involve prior *trans* to *cis* isomerisation of the terminal double bond of farnesol by a redox mechanism; (5) taken together with our previous findings, it is established that *Andrographis* cultures contain two independently functioning enzymes: (*i*) a *trans,trans*- to *cis,trans*-farnesol isomerase, and (*ii*) a *trans,trans*-farnesyl pyrophosphate isomerase-cyclase. The absolute configuration of paniculide B has been established by an X-ray crystallographic analysis of its bis-*p*-bromobenzoate.

PANAYIOTIS ANASTASIS, ISABEL FREER, CHRISTOPHER GILMORE, HUGH MACKIE, KARL OVERTON, DOUGLAS PICKEN et STEPHEN SWANSON. Can. J. Chem. **62**, 2079 (1984).

En se basant sur des expériences réalisées avec des cultures intactes de *Andrographis paniculata* ainsi qu'avec un système dérivé sans cellules, on a établi que: (1) le γ-bisabolène biosynthétisé possède la configuration *Z*, **6**; (2) l'intermédiaire biosynthétique est un pyrophosphate de farnésyle *trans*-6 (**13**) et non pas *cis*-6 (**15**); (3) le carbone cyclique de la paniculide B (**17**) ainsi que celui du γ-bisabolène (**14**), dérivée de C-2 de la mévalonate, est *anti* par rapport à la chaîne latérale; (4) la mévalonolactone et le pyrophosphate de farnésyle-*trans,trans* sont incorporés dans le γ-bisabolène sans perte d'hydrogène respectivement des positions C-5 et C-1; la cyclisation conduisant au cation bisabolènyle n'implique vraisemblablement pas une isomérisation préliminaire, *trans* en *cis* de la double liaison terminale du farnésol par un mécanisme rédox; (5) si l'on considère ces résultats avec ceux que nous avons obtenus antérieurement, on peut considérer qu'il a été établi que les cultures d'*Andrographis* contiennent deux systèmes indépendants d'enzymes qui sont opérationnels: (*i*) une isomérase *trans,trans* à *cis,trans* du farnésol et (*ii*) une isomérase-cyclase du pyrophosphate du farnésyle *trans,trans*. On a établi la configuration absolue de la paniculide B en se basant sur la diffraction par les rayons-X de son bis-*p*-bromobenzoate.

[Traduit par le journal]

At a notional level, γ-bisabolene (or cations derived from it) are early intermediates in the biosynthesis of a whole range of sesquiterpenoids that manifest remarkable structural variety (1). The stratagems that Nature uses to construct the carbon skeleton of γ-bisabolene therefore merit detailed attention.

The two basic questions to be addressed are: (*i*) is γ-bisabolene formed by cyclisation of 2-*trans*,6-*trans* (*trans,trans*)- **2** or 2-*trans*,6-*cis* (*trans,cis*)-farnesyl pyrophosphate **3**, and (*ii*) how is the terminal *trans* double bond of farnesyl pyrophosphate cyclised to a cyclohexenyl cation?

We have studied both problems using callus cultures of *Andrographis paniculata*. When grown in suspension in presence of oxygen and light, these cultures produce the sesquiterpene lactones, paniculides A **7**, B **8**, and C **9**, which we have described previously (2). The structure of paniculide A has recently been confirmed by total synthesis (3) and that of paniculide B by X-ray analysis (this paper) which also confirms the absolute configuration. A cell-free system obtained from the callus cultures, grown under anaerobic conditions, accumulates γ-bisabolene **6** as well as *trans,trans*-**10** and *cis,trans*-farnesol **11** (5). A plausible biosynthetic relationship between these substances that is fully supported by the sequel is indicated in Scheme 1.

We deal first with the question "Is γ-bisabolene formed by cyclisation of *trans,trans*-**2** or *trans,cis*-farnesyl pyrophosphate **3**?". The question was formulated by Ruzicka in 1962 (6), but had not been subjected to experimental scrutiny prior to our studies (7). In essence, Ruzicka's analysis leads to the conclusion that *Z*-γ-bisabolene **14** could be formed from *cis,trans*-farnesyl pyrophosphate **13** or *E*-γ-bisabolene **16** from *cis,cis*-farnesyl pyrophosphate **15** directly (Scheme 2). Alternatively, a cross-over pathway via bridged cations could lead from **13** to **16** or from **15** to **14**. The *cis*-allylic pyrophosphates (**13** = **4** or **15** = **5**) were tacitly assumed to be the substrates required for cyclisation without any suggestion as to how they might be formed from the (presumably) initially biosynthesised *trans*-allylic pyrophosphates (**2** or **3**) (see below). We decided that a choice between the several alternatives posed by Ruzicka's analysis might be made by devising experiments to answer the following questions: (*i*) in γ-bisabolene, is the ring carbon atom derived from C-2 of mevalonate **12** *anti* (as **14**) or *syn* (as **16**) to the side chain; (*ii*) is natural γ-bisabolene the *Z*-**14** or *E*-isomer **16**; (*iii*) is *cis,trans*-**13** or *cis,cis*-farnesyl pyrophosphate **15** the intermediate to γ-bisabolene?

An answer to question (*i*) can in principle be obtained by examining the ^{13}C nmr spectrum of γ-bisabolene (**14** or **16**)

[1] Author to whom correspondence should be addressed.

Can. J. Chem. Downloaded from www.nrcresearchpress.com by 210.87.254.105 on 09/06/12
For personal use only.

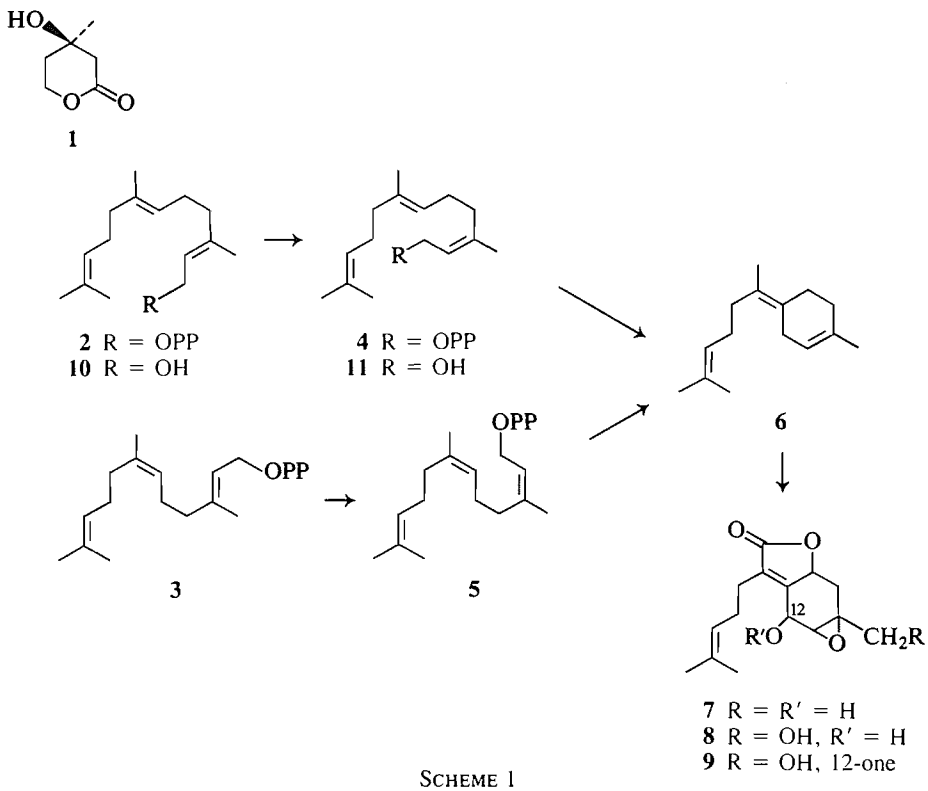

SCHEME 1

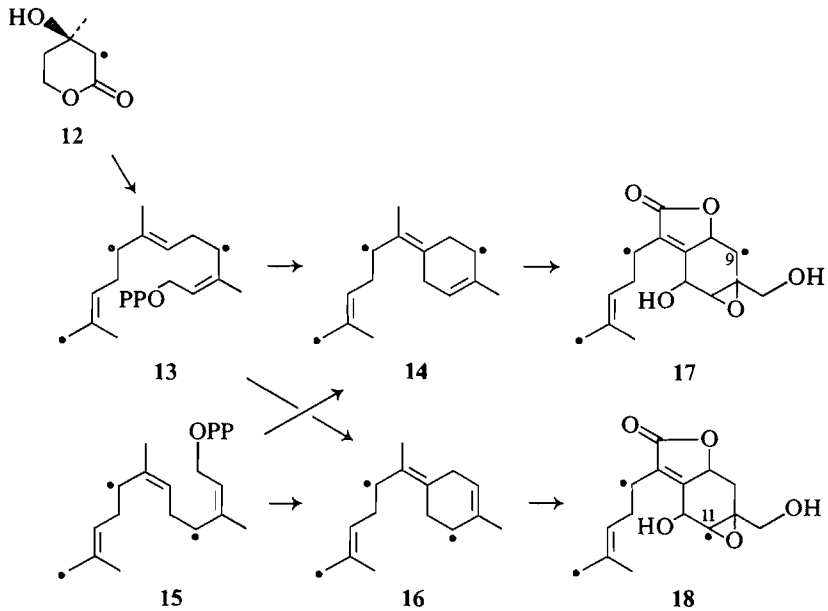

SCHEME 2

produced by incubating [2-^{13}C]mevalonate with the cell-free system from *Andrographis* cultures. It would be difficult to make a distinction between the alternative labelling patterns as in **14** or **16** ^{13}C nmr. If, however, one assumes the reasonable direct biosynthetic relationship between **14** and **17** on the one hand and between **16** and **18** on the other, then the experimental problem is immediately simplified, since a distinction in the ^{13}C nmr spectrum between C-9 and C-11 in paniculide B (**17** or **18**) is vastly simpler than it is in γ-bisabolene. The experiment was further simplified by using not [2-^{13}C]mevalonate but [1,2-$^{13}C_2$]acetate as the labelled precursor. It is well known (8) that carbon atoms derived from C-2 of mevalonate will then appear as enriched singlets, whereas those derived from C-3, C-3′, C-4, and C-5 of mevalonate appear as triplets (natural abundance singlet + doublet from vicinally doubly labelled molecules). The natural abundance ^{13}C nmr spectrum of paniculide B **8** was assigned from chemical shift data and off-resonance decoupling experiments and by examining the spectrum of paniculide B enriched from [1-^{13}C]acetate. Table 1 and Fig. 1 record the ^{13}C nmr spectrum of paniculide B enriched from [1,2-$^{13}C_2$]acetate. It is immediately evident that the signals corresponding to C-1, C-5, and *C-9* (deriving from C-2 of mevalonate) are *singlets*, but that the signal for *C-11* is a triplet. *It follows that in paniculide B (as 17) and therefore probably*

Can. J. Chem. Downloaded from www.nrcresearchpress.com by 210.87.254.105 on 09/06/12
For personal use only.

TABLE 1. ^{13}C chemical shifts of paniculide B and coupling constants ($^1J(^{13}C—^{13}C)$) of [1,2-$^{13}C_2$]acetate-enriched paniculide B

Carbon	δ (ppm)[a]	$^1J(^{13}C—^{13}C)$ (Hz)	Carbon	δ (ppm)[a]	$^1J(^{13}C—^{13}C)$ (Hz)
1	25.3	—	9	32.7	—
2	131.3	42	10	60.1	49
3	123.5	43	11	61.8	46
4	27.1	44	12	67.2	46
5	22.8	—	13	17.4	42
6	126.4	62	14	173.3	63
7	161.0	35	15	63.6	49
8	75.2	35			

[a]Relative to internal Me_4Si.

*also in γ-bisabolene (as **14**) the ring carbon atom derived from C-2 of mevalonic acid is* anti *to the side chain.*

(*ii*) The conclusion in (*i*) above implies, on the simplest basis, that natural γ-bisabolene is the *Z*-**14** rather than the *E*-isomer **16**. However, the point had not at the time been established for any sample of γ-bisabolene of natural provenance and therefore required experimental support. This was obtained in the following way. *Z*- and *E*-γ-bisabolenes had recently been synthesised (9) and their configurations established by X-ray analysis (9) of an intermediate in the synthesis. γ-Bisabolene, biosynthesised from [2-^{14}C]mevalonate by the *Andrographis* cell-free system, was purified by preparative tlc after adding carrier and then co-injected with the synthetic *Z*/*E*-γ-bisabolene mixture (kindly made available by Dr. D.J. Faulkner, La Jolla) on a gas–liquid chromatograph equipped with radioactivity detector (see Experimental). Radioactivity appeared in the peak corresponding to *Z*-γ-bisabolene **14** (*I* = 1500) but not in that corresponding to *E*-γ-bisabolene **16** (*I* = 1515). *Natural γ-bisabolene biosynthesised by* Andrographis *cultures is therefore the Z-isomer **14**.* It is interesting to note that Faulkner and co-workers (9) subsequently identified γ-bisabolene from plant sources (Oil of Myrrh and Oil of Lime) as the Z-isomer, but a sample from a species of seaweed (Laurencia) as the *E*-isomer.

(*iii*) A decision as to whether *cis,trans*-**13** or *cis,cis*-farnesyl pyrophosphate **15** is the intermediate was reached as follows: [2-^{14}C]*cis,cis*-farnesol **19** was prepared by lithium aluminium hydride reduction of the Wittig reaction product from neryl acetone with ^{14}C-labelled diethylmethoxycarbonyl methylphosphonate, itself prepared by Michaelis–Arbuzov reaction

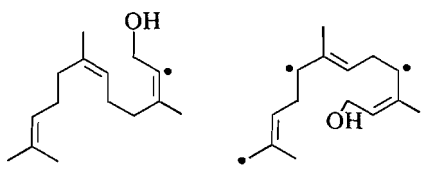

19 **20**

of triethyl phosphite with methyl [2-^{14}C]bromoacetate (10). [4,8,12-$^{14}C_3$]*cis,trans*-farnesol **20** was prepared biosynthetically from [2-^{14}C]mevalonate, using the cell-free system from *Andrographis* cultures (5*a*). Each of the labelled farnesols[2] was incubated with the *Andrographis* cell-free system and the bisabolene fractions isolated by preparative tlc after addition of carrier. Each was converted into crystalline trihydrochloride and crystallised to constant activity. Incorporation from [2-^{14}C]*cis,cis*-farnesol was 0.02%, while from [4,8,12-$^{14}C_3$]*cis,trans*-farnesol it was 1.2%. *Thus,* cis,trans- *and not* cis,cis-*farnesyl pyrophosphate is the intermediate to Z-γ-bisabolene biosynthesised by* Andrographis *cultures.*

We now turn to the second question: "How is the terminal *trans* double bond of farnesyl pyrophosphate cyclised to a cyclohexenyl cation?" (11). As noted above, the point was glossed over in Ruzicka's analysis of the possible modes of formation of γ-bisabolenes from farnesyl pyrophosphates. Yet the problem posed by this particular cyclisation is a general one that arises in the formation of six-membered rings from allylic pyrophosphates throughout terpene biosynthesis: a terminal *cis* double bond is required in the acyclic precursor to avoid formation of a *trans*-cyclohexene. Cane has provided a penetrating discussion of the problem (12, see also ref. 1*c*), which has three possible solutions: (*i*) condensation of geranyl- and isopentenyl-pyrophosphate to form *cis,trans*-farnesol directly; (*ii*) isomerisation of initially formed *trans,trans*-farnesol to *cis,trans*-farnesol by a redox mechanism; (*iii*) isomerisation of *trans,trans*- to *cis,trans*-farnesyl pyrophosphate via nerolidyl pyrophosphate.

We had previously found that the cell-free system from *Andrographis* cultures formed *trans,trans*- and *cis,trans*-farnesols with total loss of tritium from (3*RS*)-[2-^{14}C, (4*S*)-$^3H_1$]mevalonate and total retention from the (4*R*)-isomer (5*a*). At the time this strongly suggested to us that *cis,trans*-farnesyl pyrophosphate was not formed directly. This supposition indeed turns out to be correct, as demonstrated by the experiments reported below. Recent reports (13) of *Z*-double bond formation in plant polyprenols with loss of the (4*S*)-hydrogen of mevalonate would have made the prediction less secure. We had also found previously (5*a*) that the *Andrographis* cell-free preparation contains a redox system that isomerises *trans,trans*- to *cis,trans*-farnesol with loss of 1-H_{si} and *cis,trans*- to *trans,trans*-farnesol with loss of 1-H_{re}. It was tempting to suppose that this same enzyme mediates the required *trans,trans*- to *cis,trans*-farnesol isomerisation in preparation for cyclisation to γ-bisabolene. However, it should be noted that intervention of such a redox system requires pyrophosphate hydrolysis and rephosphorylation prior to cyclisation, an uneconomical diversion of the metabolic pathway that turns out to be unnecessary. In any event, a clear experimental distinction is available between, on the one hand, *trans,cis*-isomerisation at the alcochol level and, on the other, *trans,cis*-isomerisation via nerolidyl pyrophosphate **24**: *the*

[2]The cell-free system evidently contains the necessary phosphokinases to transform the free alcohols into their pyrophosphates, since the evidence reported below clearly indicates that pyrophosphate rather than free alcohol is cyclised to γ-bisabolene.

Can. J. Chem. Downloaded from www.nrcresearchpress.com by 210.87.254.105 on 09/06/12
For personal use only.

Can. J. Chem. Downloaded from www.nrcresearchpress.com by 210.87.254.105 on 09/06/12
For personal use only.

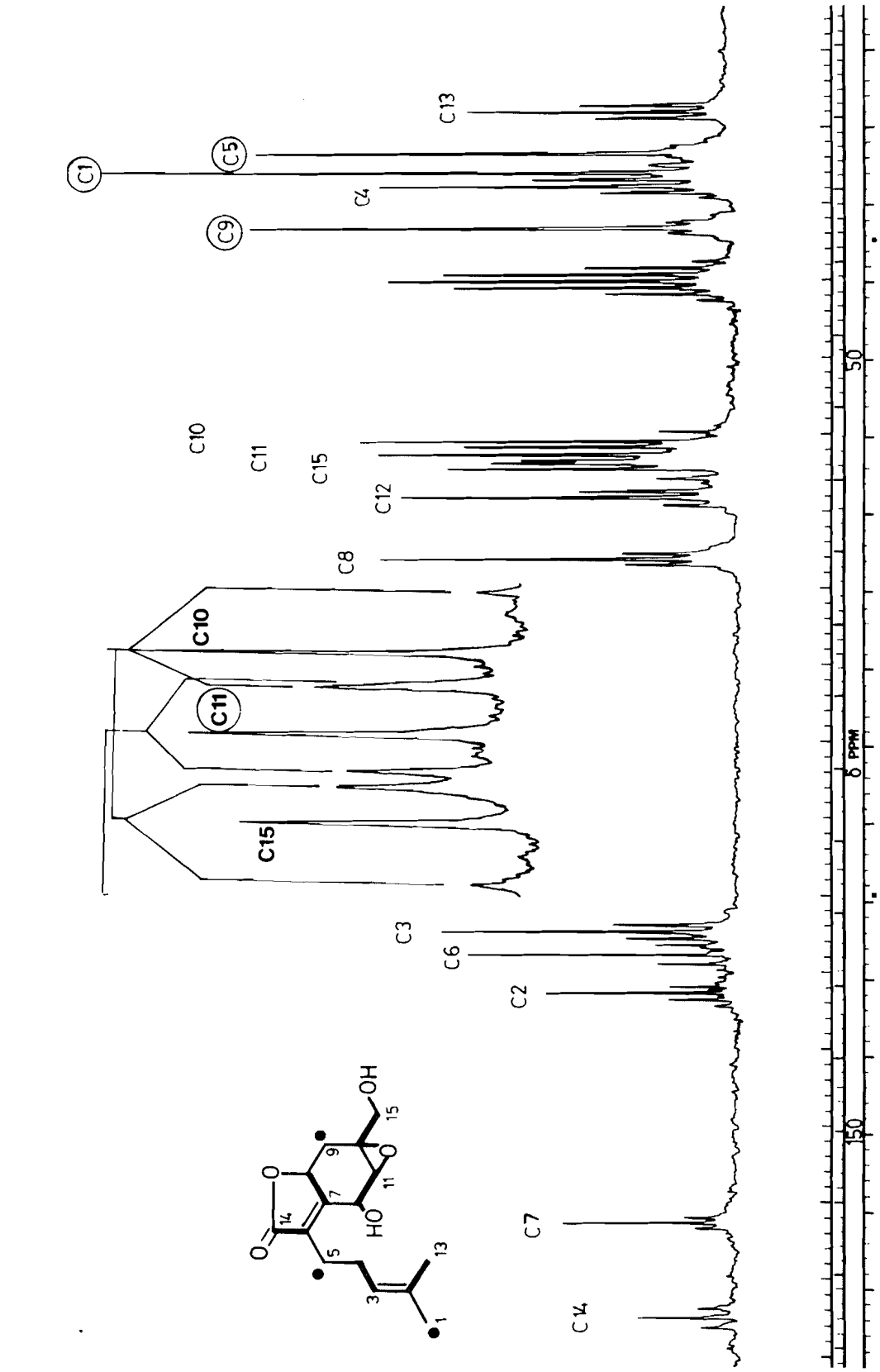

FIG. 1. The ^{13}C nmr spectrum (at 25.2 MHz; proton noise-decoupled) of paniculide B biosynthesised from [1,2-$^{13}C_2$]acetate.

Can. J. Chem. Downloaded from www.nrcresearchpress.com by 210.87.254.105 on 09/06/12
For personal use only.

former must result in loss of one hydrogen from C-1 of farnesol; the latter does not.

Accordingly, *trans,trans*-[1-$^3H_2$, 12,13-$^{14}C_2$]farnesyl pyrophosphate (14) (**22**; X = Y = ^3H; $^3H/^{14}C$ of diphenyl urethane crystallised to constant activity 3.26 ± 0.07) was incubated with the 75 000 g supernatant from *Andrographis* cultures. Labelled γ-bisabolene was recovered after addition of carrier, separated by preparative tlc, converted to trihydrochloride, and crystallised to constant isotopic ratio ($^3H/^{14}C$ 3.44 ± 0.28). The total retention of tritium label here observed parallels recent results concerning the in vivo formation of trichodiene from *trans,trans*-[1-$^3H_2$, 12,13-$^{14}C_2$]farnesyl pyrophosphate by a cell-free preparation from *Trichothecium roseum* (14) and of coccinol from [5-$^3H_2$, 2-^{14}C]mevalonate by whole cells of *Fusidium coccineum* (15). In both cases the initial cyclisation of *trans,trans*-farnesyl pyrophosphate to the γ-bisabolenyl cation occurs with complete retention of the tritium label. Analogous results in the monoterpene series have recently been reported by Croteau and co-workers (16, 17).

The incorporation of *both* C-1 hydrogen atoms of *trans,trans*-farnesyl pyrophosphate into γ-bisabolene is at variance with our previous findings (5*b*, 7) that one-sixth of the tritium activity was apparently lost when the same cell-free system converted [5-$^3H_2$, 2-^{14}C]mevalonate into γ-bisabolene. These misleading results may be attributable to the low, albeit consistent, counts obtained in these experiments; furthermore, the apparent loss of one in six tritium atoms corresponds to an error of only 2.78% per labelled site. This discrepancy has now been resolved beyond doubt and further insight gained into the detailed mechanism of the cyclisation by the following additional experiments with (5*S*)- and (5*R*)-[5-^{3}H]mevalonates.

A doubly labelled specimen obtained by mixing (3*R*, 5*R*)-[5-^{3}H]- (18) (**21**; X = ^1H, Y = ^3H) and (3*RS*)-[2-^{14}C]mevalonolactones ($^3H/^{14}C$ for the recrystallised diphenylmethylamides 1.05 ± 0.02) was incubated as the potassium salt with the cell-free system. The γ-bisabolene (incorporation 0.1%), recovered as before, had (as the crystalline trihydrochloride) a $^3H/^{14}C$ ratio of 2.09 ± 0.03 (only (3*R*)-mevalonate metabolised), corresponding to 99.7% tritium retention. Similar incubation of (3*R*,5*S*)-[5-^{3}H]- (19) (**21**; X = ^3H, Y = ^1H) + (3*RS*)-[2-^{14}C]mevalonates ($^3H/^{14}C$ 7.01) gave recovered γ-bisabolene (incoporation 0.18%) whose trihydrochloride had a constant $^3H/^{14}C$ ratio of 13.49, corresponding to 96.3% retention of tritium. *Clearly, then, both hydrogens at C-5 of mevalonate, which become the C-1 hydrogens of farnesol, are retained on incorporation into γ-bisabolene. trans,cis*-Isomerisation of the terminal double bond in farnesol cannot, therefore, involve a redox system at the alcohol level and so most probably proceeds at the pyrophosphate level via the tertiary nerolidyl pyrophosphate **24**, by a mechanism previously discussed by Arigoni and others (20). Whether such a mechanism operates here can be further checked by establishing the configuration of the hydrogens at C-12 in γ-bisabolene **25**. Again, this is more easily done in practice by examining the stereochemistry at C-12 of the derived paniculides A **26**, B **27**, and C **28**. Thus, the specimen of (3*R*,5*S*)-[5-^{3}H]- (**21**; X = ^3H, Y = ^1H) + (3*RS*)-[2-^{14}C]mevalonates above was incubated with callus tissue, grown in suspension for 21 days after transfer from solid medium, and the paniculides A, B, and C were harvested after six days, purified by preparative tlc, and crystallised to constant isotopic ratio (for paniculides A and B). Obtained in this way, paniculide A (**26**; X = ^3H, Y = ^1H) had a $^3H/^{14}C$ atomic ratio of 1.92^3:3, paniculide B (**27**; X = ^3H, Y = ^1H) had a ratio of 1.16^3:3, and paniculide C (**28**; X = ^3H, Y = ^1H) had a ratio 0.93^3:3. Oxidation of the biosynthesised paniculide B wth manganese dioxide afforded paniculide C ($^3H/^{14}C$ atomic ratio 1.01^3:3). The shortfall of tritium label in paniculide B ($^3H/^{14}C$ 1.16^3:3 instead of 2:3) is unexplained, but consistent. Thus, with [5-$^3H_2$, 2-^{14}C]mevalonate as precursor, the biosynthesised paniculide B (**27**; X = Y = ^3H) had $^3H/^{14}C$ 2.38:^{3}:3 (instead of 3:3) and the paniculide C (**28**; X = Y = ^3H) obtained from it with MnO_2 had $^3H/^{14}C$ 2.06^3:3.

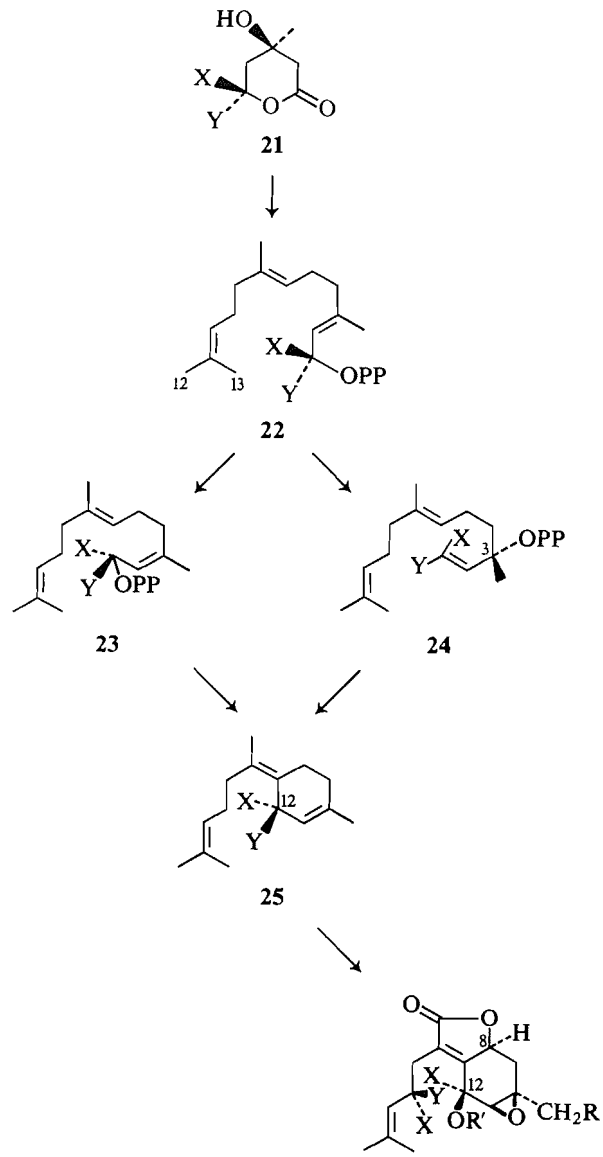

26 R = R′ = H
27 R = OH; R′ = H
28 R = OH; 12-one
29 R = $OCOC_6H_4Br$; R′ = COC_6H_4Br
30 R = $OCOC_6H_4Br$; R′ = H

SCHEME 3

As illustrated in Scheme 3, (3*R*,5*S*)-[5-^{3}H]mevalonate (**21**; X = ^3H, Y = ^1H)[4] will lead (21) to *trans,trans*-(1*S*)-[1,5,9-$^3H_3$]farnesyl pyrophosphate (**22**; X = ^3H, Y = ^1H).[4]

[3] Both hydrogens at C-8 of γ-bisabolene are apparently lost on lactone formation.

[4] Only the isotopic labels relevant to the discussion are shown in Scheme 3.

Can. J. Chem. Downloaded from www.nrcresearchpress.com by 210.87.254.105 on 09/06/12
For personal use only.

This will isomerise, without hydrogen loss, to *cis,trans*-(1*R*)-[1,5,9-$^3H_3$]farnesyl pyrophosphate (**23**; X = ^{3}H, Y = ^{1}H).[4] Epimerisation at C-1 is a predictable consequence of the isomerisation mechanism (20*a*).

Cyclisation with inversion at C-1 then affords (12*S*)-[4,8,12-$^3H_3$]-γ-bisabolene (**25**; X = ^{3}H, Y = ^{1}H).[4] Alternatively, the nerolidyl pyrophosphate (**24**; X = ^{3}H, Y = ^{1}H)[4] (or its C-3 epimer with ^{3}H and ^{1}H interchanged), which is an intermediate in the above *cis,trans*-isomersation, cyclises by an *anti*-S_N1' process to the *same* (12*S*)-[4,8,12-$^3H_3$]-γ-bisabolene (**25**; X = ^{3}H, Y = ^{1}H).[4] There are indeed several recorded examples of the in vivo formation of six-membered rings by (formal) *anti*-S_N1' displacement of allylic pyrophosphates by a suitably located double bond (12). The distinction made above between S_N displacement of the primary pyrophosphate **23** and S_N1' displacement of the tertiary pyrophosphate **24** is convenient as a heuristic device but probably not meaningful, since the biosynthetic intermediate will approximate to the delocalised ion pair accessible from **22**, **23**, or **24**. In this connection it is relevant to recall that in our earlier experiments [4,8,12-$^{14}C_3$]*cis,trans*-farnesol **20** was efficiently (1.2%) incorporated into γ-bisabolene.

Hydroxylation at C-12 of the γ-bisabolene (**25**; X = ^{3}H, Y = ^{1}H) should lead, with expected retention (22), to paniculides A (**26**; X = ^{3}H, Y = ^{1}H) and B (**27**; X = ^{3}H, Y = ^{1}H), having the (12*S*)-configuration as shown, and in which tritium is retained. Tritium was indeed retained (see above) and the predicted absolute configuration (as **27**) of natural paniculide B, previously inferred (2) from the circular dichroism of the corresponding ketone, has been confirmed by an X-ray structure determination of its bis-*p*-bromobenzoate **29**.

The results of the single-crystal X-ray analysis are summarised in Table 2, which lists the coordinates of the non-hydrogen atoms with their equivalent isotropic temperature factors. Other material has been deposited in the Depository of Unpublished Data.[5] A perspective drawing of the molecule is given in Fig. 2. This analysis was primarily concerned with the establishment of the absolute configuration, and this has been achieved with a confidence level well in excess of 99.5%. The structure itself has, crystallographically, no unusual or unexpected features.

Our experiments demonstrate that the *Andrographis* cell-free system contains two independent enzymes: (*i*) a farnesol *trans,cis*-isomerase that operates by stereospecific hydrogen removal from C-1 in either direction and (*ii*) a *trans,trans*-farnesyl pyrophosphate isomerase-cyclase that transforms its substrate into γ-bisabolene without hydrogen loss from C-1.

TABLE 2. Fractional atomic coordinates and equivalent isotropic temperature factors (Å^2) for the non-hydrogen atoms in paniculide B bis-*p*-bromobenzoate. The equivalent isotropic temperature factor is defined as $(U_{11} + U_{22} + U_{33})/3$. The standard deviations in the last significant digits are in parentheses

Atom	*X/A*	*Y/B*	*Z/C*	*U*
Br(20)	0.68241(5)	1.20306(31)	0.49085(3)	0.0607(5)
Br(27)	0.66767(7)	0.72700	1.34939(4)	0.852(7)
C(1)	0.9668(8)	0.4308(32)	0.5859(5)	0.11(1)
C(2)	1.0431(5)	0.5421(20)	0.6427(4)	0.068(5)
C(3)	1.0533(5)	0.4782(18)	0.7079(4)	0.065(5)
C(4)	1.0007(5)	0.2728(18)	0.7412(4)	0.067(6)
C(5)	0.9719(4)	0.3984(16)	0.8047(3)	0.049(4)
C(6)	0.9391(4)	0.1841(16)	0.8485(3)	0.038(3)
C(7)	0.8545(4)	0.0823(14)	0.8546(3)	0.038(3)
C(8)	0.7541(4)	0.1234(15)	0.8152(3)	0.042(4)
C(9)	0.6872(4)	0.1622(13)	0.8640(3)	0.039(4)
C(10)	0.7158(5)	0.0960(15)	0.9361(3)	0.040(4)
C(11)	0.8168(4)	0.0016(16)	0.9682(3)	0.046(4)
C(12)	0.8652(4)	−0.1117(16)	0.9122(3)	0.044(4)
C(13)	1.1076(7)	0.7496(29)	0.6175(5)	0.104(8)
C(14)	1.0119(4)	0.0381(15)	0.9015(3)	0.046(4)
C(15)	0.6379(4)	0.0182(16)	0.9730(3)	0.046(4)
C(16)	0.6696(4)	0.3571(16)	0.7166(3)	0.043(4)
C(17)	0.6750(4)	0.5724(16)	0.6652(3)	0.045(4)
C(18)	0.5918(4)	0.6397(15)	0.6180(3)	0.048(5)
C(19)	0.5929(4)	0.8290(16)	0.5681(3)	0.051(4)
C(20)	0.6786(5)	0.9516(15)	0.5627(3)	0.048(4)
C(21)	0.7610(5)	0.8866(18)	0.6087(4)	0.058(5)
C(22)	0.7600(4)	0.6956(22)	0.6601(3)	0.051(4)
C(23)	0.5971(4)	0.1045(22)	1.0779(3)	0.050(4)
C(24)	0.6180(4)	0.2528(17)	1.1420(3)	0.051(5)
C(25)	0.6963(5)	0.4350(19)	1.1606(4)	0.062(5)
C(26)	0.7093(5)	0.5727(23)	1.2225(4)	0.073(6)
C(27)	0.6485(6)	0.5348(18)	1.2644(3)	0.060(5)
C(28)	0.5728(6)	0.3586(20)	1.2483(4)	0.069(5)
C(29)	0.5567(5)	0.2209(23)	1.1868(3)	0.065(4)
O(8)	0.7501(3)	0.3499(10)	0.7680(2)	0.043(3)
O(9)	0.7107(3)	0.3794(10)	0.9114(2)	0.048(3)
O(12)	0.9673(3)	−0.1318(11)	0.9392(2)	0.049(3)
O(14)	1.0970(3)	0.0546(13)	0.9108(2)	0.059(4)
O(15)	0.6610(3)	0.1460(10)	1.0385(2)	0.051(4)
O(16)	0.6035(3)	0.2041(15)	0.7148(2)	0.056(3)
O(23)	0.5296(4)	−0.0498(14)	1.0607(3)	0.080(4)

Experimental

Radioactivity was determined by liquid scintillation counting in a Philips model PW-4530 liquid-scintillation analyser, with 2,5-diphenyloxazole (5 g/L) and 1,4-bis-(5-phenyloxazol-2-yl)benzene (0.1 g/L) in toluene as scintillant. Counting efficiencies were typically 90% for ^{14}C alone and 75% and 32% respectively for ^{14}C and ^{3}H in experiments using both nuclides. Corrections for counting efficiency and quenching were automatically computed, using a channels-ratio mode of operation with ^{137}Cs as external standard. Chromatograms were scanned for radioactive components using a Panax thin layer scanner RTLS 1A. Radiogas–liquid chromatography was performed on a Pye 104/Panax Radiogas detector system operated in either the ^{14}C only or ^{3}H mode. Counting efficiencies were ~40% for ^{3}H and 90% for ^{14}C. Analytical glc was performed on a Perkin–Elmer F11 gas chromatograph with a flame ionisation detector using nitrogen as carrier gas.

The ^{1}H nmr spectra were recorded at 60 MHz on a Varian spectrometer. The ^{13}C nmr spectra were obtained on a Varian XL 100 spectrometer at 25.2 MHz operated in the Fourier transform mode using deuterium internal lock. All chemical shifts are reported as parts per million downfield of internal tetramethylsilane reference. Mass spectra were recorded on EMI MS 12 spectrometer. High speed centrifugation was carried out in a MSE High Speed 25 centrifuge.

Culture techniques

Procedures for establishing and maintaining stock cultures of *A. paniculata* have been described (23). Hypocotyl isolates were grown as callus cultures on a modified White's medium (24), solidified with 0.7% agar (Oxoid No. 3) and containing Fe-EDTA as the iron source. Callus cultures were grown on agar for 21 days after subculture and then inoculated into liquid medium (composition as solid medium

[5] The structure factor table, a table of hydrogen atom coordinates, a table of anisotropic thermal parameters, a table of bond lengths and angles, and a table of torsion angles are available from the Depository of Unpublished Data, CISTI, National Research Council of Canada, Ottawa, Canada K1A 0S2.

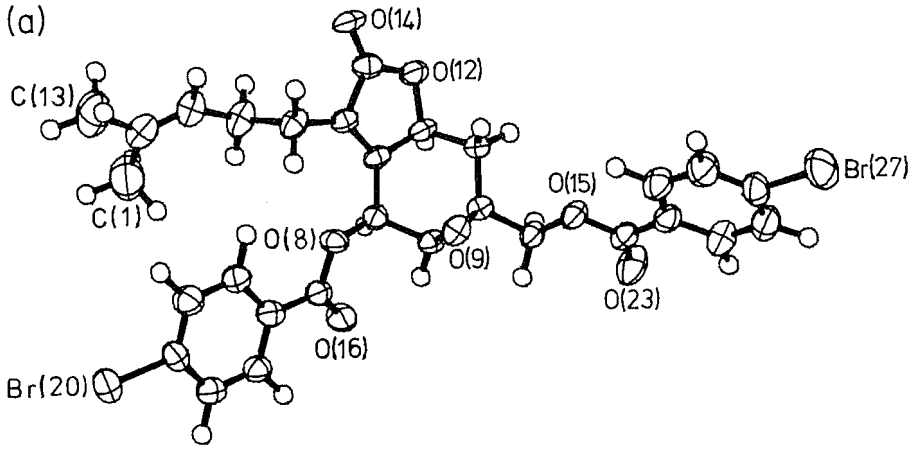

FIG. 2. (a) A perspective view of paniculide B bis-*p*-bromobenzoate. The ellipsoids are 50% ellipsoids; the hydrogen atoms have been drawn with an arbitary radius of 0.15 Å. For clarity, only the Br, O, and terminal methyl atoms have been labelled.

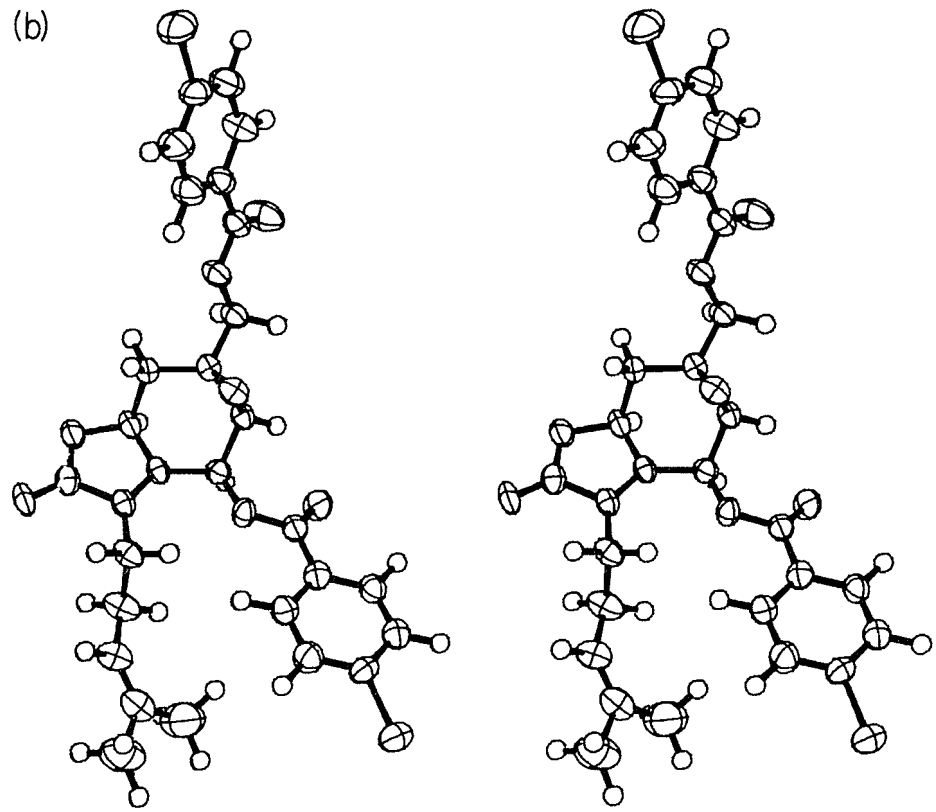

FIG. 2. (b) A stereo view of paniculide B bis-*p*-bromobenzoate. The ellipsoids are 50% ellipsoids; the hydrogen atoms have been given an arbitary radius of 0.15 Å.

without agar; 0.5 g fresh callus/100 mL medium) contained in 250-mL modified Erlenmeyer flasks having four vertical glass ridges running up the inside of each flask to aid agitation. Flasks were kept on a horizontal rotary shaker (140 rev/min) for 21 days at 25 ± 1°C with illumination (approx. 3200 lx).

Preparation of cell-free extracts

Hypocotyl tissues that had grown in suspension culture for 21 days were collected by filtration and homogenized in a precooled tissue homogenizer (Kontes Glass Co., Vineland, N.J., U.S.A.) for 2 min at 0°C in sodium phosphate buffer (0.1 *M*, pH 7.6; 1 mL buffer per g of fresh cells) containing sucrose (0.35 *M*), GSH (5 m*M*), nicotinamide (5 m*M*), and soluble polyvinylpyrrolidone (mol. wt. 24 500; 1%, w/v). The homogenate was centrifuged at 75 000 g/min for 1 h at 4°C and the supernatant used direct for incubation.

Biosynthesis of paniculide B ***17*** *from [1,2-$^{13}C_2$]acetate*

A filter-sterilized solution of [1,2-$^{13}C_2$]acetate (Merck and Co. Inc., Rahway, N.J.; 150.8 mg, 91.7 at.%) was administered to cultures of *A. paniculata* (15 flasks, 2.55 g dry callus tissue), that had been grown in suspension for 21 days following transfer from solid medium. After a further 10 days' growth, the tissue was removed by filtration and the medium was concentrated *in vacuo* at below 40°C to one-quarter its original volume. The concentrate was extracted three times with an equal volume of ethyl acetate. Drying of the combined extracts over anhydrous Na_2SO_4 and solvent removal *in vacuo* afforded a residue from which pure paniculide B (117 mg; mp 145–146°C) was isolated by preparative tlc over silica gel ($CHCl_3$–CH_3OH, 94:6 v/v) and

Can. J. Chem. Downloaded from www.nrcresearchpress.com by 210.87.254.105 on 09/06/12
For personal use only.

Can. J. Chem. Downloaded from www.nrcresearchpress.com by 210.87.254.105 on 09/06/12
For personal use only.

crystallisation from chloroform. The ^{13}C nmr spectrum of the paniculide B obtained in this experiment is reproduced in Fig. 1. Table 1 records the observed chemical shifts (δ) and coupling constants ($^1J(^{13}C—^{13}C)$).

Biosynthesis of paniculide B from [1-^{13}C]acetate

[1-^{13}C]Acetate (Merck; 149.7 mg, 90.0 at.%) incubated in the same manner and on the same scale afforded paniculide B (86.5 mg; mp 144–146°C). The ^{13}C nmr spectrum of this material showed enhancement (approx. 150%) of the signals corresponding to C-2, C-4, C-6, C-8, C-10, and C-12.

*Incorporation of 3*RS-*[2-^{14}C]mevalonate **12** into γ-bisabolene; comparison of the product with synthetic* Z- *and* E-γ-bisabolene

(3*RS*)-[2-^{14}C]Mevalonic acid lactone (radiochemical Centre, Amersham; 5 μCi, 0.28 μmol) was converted into its K-salt by treating it with KOH–H_2O (1 *M*, 100 μL) at 37°C for 1 h. The solution was neutralized with NaH_2PO_4 (1 *M*, 100 μL) and incubated at 27°C for 16 h with the cell-free system (3 mL) containing NADH (0.5 m*M*), NADPH (0.5 m*M*), ATP (1 m*M*), and NaF (1 m*M*) (final volume 4 mL) in a 15-mL Warburg flask. The flask was evacuated and filled with Ar six times before mixing substrate and medium. The incubation was terminated by adding ice-cold EtOH (8 mL) and the suspension kept at 0°C for 30 min more. Denatured protein was removed by centrifugation (17 000 rpm, 30 min) and the supernatant extracted with hexane (3 × 10 mL). The combined extracts were dried over anhydrous Na_2SO_4, concentrated *in vacuo* to a small volume, carrier bisabolene (200 μg, commerical mixture) added, and the mixture subjected to preparative tlc (Merck Kieselgel G, 20 × 20 cm; ethyl acetate – hexane, 1:3, v/v). Radio scanning showed activity in the bands corresponding to farnesol (R_f 0.23) and γ-bisabolene (R_f 0.8); incorporations were approximately 1.2% and 0.4% respectively.

The γ-bisabolene recovered from the plate with hexane was examined by radio-glc (1% SE 30 at 110°C) on a Pye 104/Panax Radiogas detector system operating in the "^{14}C only" mode. Co-injection of an aliquot of the γ-bisabolene fraction, purified as above, with a mixture of synthetic Z- and E-γ-bisabolene (9) (kindly furnished by Dr. D.J. Faulkner, La Jolla) demonstrated that Z-γ-bisabolene (I = 1500) was labelled but that E-γ-bisabolene (I = 1515) was not.

*Biosynthesis of [4,8,12-$^{14}C_3$]*cis,trans-*farnesol **20***

[4,8,12-$^{14}C_3$]*cis,trans*-Farnesol was biosynthesised from 3*RS*-[2-^{14}C]mevalonate (50 μCi) as the potassium salt, by the cell-free preparation from *Andrographis* callus tissues, by the method previously described (5*a*).

*Synthesis of [2-^{14}C]*cis,cis-*farnesol **19** (ref. 10)*

Nerylacetone (Z-6,10-dimethyl-2-keto-5,9-diene) was obtained from a mixture containing the E- and Z-isomers by preparative glc on 5% SE 30 at 135°C. The Z-isomer has a retention index of 1340, the E-isomer has I = 1380.

Triethylphosphite (15 mg, 0.09 mmol) was heated at 120–130°C for 5 h with [2-^{14}C]methyl bromoacetate (Radiochemical Centre, Amersham; 50 μCi, 12 mg, 0.08 mmol) under an air condenser. Volatile material was then removed by very gentle heating of the resulting [^{14}C]diethylphosphonoacetate *in vacuo*. The residue (15 mg, 0.076 mmol) was dissolved in dry tetrahydrofuran (25 μL) and added slowly to a stirred suspension of sodium hydride (7.3 mg, 50% dispersion, 0.155 mmol) in the same solvent (200 μL) under nitrogen. Stirring was continued at room temperature for a further 45 min before addition of a solution of nerylacetone (14.8 mg, 0.076 mmol) in tetrahydrofuran (25 μL). After stirring for a further two days at room temperature, water (1 mL) was added, and the mixture extracted with ether (3 × 5 mL). The dried solution was then evaporated to ~5 mL and added over a period of 30 min to a stirred suspension of lithium aluminium hydride (7.5 mg, 0.156 mmol) in dry ether (1 mL) at 0°C. The reaction mixture was stirred 30 min more and then saturated aqueous NH_4Cl solution (5 mL) was cautiously added, followed by water (10 mL). The organic layer was separated, and the aqueous layer extracted with ether (3 × 5 mL). Farnesol was purified by preparative tlc over silica (ethyl acetate – hexane, 1:3, v/v) and *cis,cis*-farnesol was separated from the *trans,cis*-isomer by preparative tlc over silver nitrate – silica (ethyl acetate – acetic acid, 499:1, v/v). Analytical glc on 1% SE 30 at 150°C showed that the material was >95% *cis,cis*-isomer. The radiochemical yield of [2-^{14}C]*cis,cis*-farnesol **19** was 9%.

*Incorporation of [4,8,12-$^{14}C_3$]*cis,trans-*farnesol **20** and [2-^{14}C]-*cis,cis-*farnesol **19** into γ-bisabolene by Andrographis cell-free system*

[4,8,12-$^{14}C_3$]*cis,trans*-Farnesol (6.2 × 10^5 dpm), prepared as above from 3*RS*-[2-^{14}C]mevalonate by the *Andrographis* cell-free system, was ultrasonically dispersed in 0.2 mL sodium phosphate buffer (0.1 *M*, pH 7.6) with Tween 80 (1 mg). The suspension was incubated anaerobically overnight with the cell-free system and added co-factors and then worked up as previously described. Carrier γ-bisabolene (1 mg, commercial material) was added before preparative tlc. The radioactive γ-bisabolene which was isolated was dissolved in dry ether (2 mL) and the crystalline trihydrochloride derivative was prepared by passing dry hydrogen chloride gas through the solution for 15 min at 0°C. The solution was then allowed to stand at room temperature overnight before addition of carrier bisabolene trihydrochloride (6 mg). The ether was then evaporated and the solid residue was recrystallised from a small quantity of methanol. After five recrystallisations, the specific acitivity was constant at 1062 dpm/mg. This represents an incorporation of 1.2%.

In a parallel experiment, [2-^{14}C]*cis,cis*-farnesol (7.7 × 10^5 dpm), prepared as above, was incubated with the cell-free system under identical conditions. After the second recrystallisation, the bisabolene trihydrochloride obtained in the experiment was found to have a very low level of ^{14}C activity, representing an incorporation of 0.02%.

Incorporation of trans,trans*[1-$^3H_2$, 12,13-$^{14}C_2$]farnesyl pyrophosphate (**22**; X = Y = ^3H) into γ-bisabolene*

trans,trans--[1-$^3H_2$, 12,13-$^{14}C_2$]Farnesyl pyrophosphate (14*a*, *b*) (2.63 μmol, 2.43 μCi, ^{14}C μmol^{-1}; $^3H/^{14}C$ of diphenyl urethane crystallised to constant activity 3.26 ± 0.07, atomic ratio 2:2) was incubated with the 75 000 g supernatant (3 mL; 7.5 mg protein) from *Andrographis* cultures. The incubation was terminated after 17 h by adding ethanol and then kept at 0°C for 30 min. The denatured protein was removed by centrifugation and the supernatant extracted with hexane (3 × 10 mL). Labelled γ-bisabolene was recovered from the extract after adding carrier bisabolene (9 mg, regenerated from the trihydrochloride, mp 78–79°C, with Li_2CO_3–LiBr in DMF at 100°C; 2 major peaks (after HCl/MeOH–$CHCl_3$ treatment at 20°C) ratio 3:2 on OV-1 at 100°C) by preparative tlc (ethyl acetate – hexane, 1:3, R_f 0.8, incorporation 0.23%) and converted into the trihydrochloride (dissolution in dry ether, HCl gas for 1 h at 0°C). This was mixed with carrier (18 mg, mp 78–80°C) and crystallised (3×) from methanol to constant isotopic ratio ($^3H/^{14}C$ 3.44 ± 0.28). The crystalline hydrochloride (mp 78–80°C) from the combined mother liquors had $^3H/^{14}C$ 3.61 ± 0.10.

*Incorporation of (3*R,5R*)-[5-^3H]- (ref. 18) + (3*RS*)-[2-^{14}C]-mevalonolactones into γ-bisabolene*

The compounds in the title were mixed ($^3H/^{14}C$ 1.08 ± 0.02; atomic ratio 1:1) and a portion was converted into the diphenylmethylamide (4), which after three crystallisations from benzene–hexane had mp 98–99°C, $^3H/^{14}C$ 1.05 ± 0.02. The doubly labelled lactone (3 μCi ^{14}C) was converted to the K-salt and then incubated with the cell-free system (4 mL) and added co-factors and the γ-bisabolene recovered (incorporation 0.1%), derivatised, and the trihydrochloride crystallised to constant ratio as above: $^3H/^{14}C$ 2.09 ± 0.03 (only (3*R*)-mevalonolactone metabolised); atomic ratio 2.99:3, corresponding to 99.7% retention of tritium label.

*Incorporation of (3*R,5S*)-[5-^3H]- (ref. 19) + (3*RS*)-[2-^{14}C]-mevalonolactones into γ-bisabolene and paniculides*

The mixture of (3*R*,5*S*)-[5-^3H]- + (3*RS*)-[2-^{14}C]mevalonate (K-salts; 0.6 μCi ^{14}C, $^3H/^{14}C$ 7.01; atomic ratio 1:1) was divided into two equal portions. One was incubated with the cell-free system as for the (3*R*,5*R*)-isomer above. The recovered γ-bisabolene (incorporation

Can. J. Chem. Downloaded from www.nrcresearchpress.com by 210.87.254.105 on 09/06/12
For personal use only.

0.18%) afforded the trihydrochloride of constant isotope ratio $^3H/^{14}C$ 13.49, atomic ratio 2.89:3, corresponding to 96.3% retention of the tritium label.

The other portion was incubated with callus tissue (dry weight 5.0 g) grown in suspension for 21 days following transfer from solid agar, and the paniculides A **26**, B **27**, and C **28** were harvested after 6 days by solvent extraction and purified by preparative tlc (5% MeOH–$CHCl_3$) (see above). Crystallisation to constant isotopic ratio afforded paniculide A **26**, mp 118–120°C, $^3H/^{14}C$ 1.92:3, incorporation of ^{14}C 0.05%; paniculide B **27**, mp 146–148°C, $^3H/^{14}C$ 1.16:3, incorporation of ^{14}C 2.26%; paniculide C **28** (oil), purified by preparative tlc (5% MeOH–$CHCl_3$) $^3H/^{14}C$ 0.93:3, incorporation of ^{14}C 0.15%. Oxidation of one half of the above paniculide B with MnO_2 in benzene afforded the oily paniculide C which, after purification by preparative tlc, had ^1H nmr and mass spectra identical with those of the natural material, and $^3H/^{14}C$ 1.01:3.

*Formation of the mono- **30** and bis-*p*-bromobenzoate **29** of paniculide B*

To paniculide B (200 mg; 0.71 mmol) dissolved in dry THF (20 mL) containing 4-dimethylaminopyridine (2 crystals) was added *p*-bromobenzoylchloride (250 mg; 1.14 mmol) and then dry triethylamine (1 mL) under Ar. The resulting cloudy solution was heated under reflux for 2 h, cooled, poured into ice-water (200 mL), and extracted with ethyl acetate (3 × 25 mL). Evaporation of the washed and dried ($MgSO_4$) organic extracts afforded a solid residue (365 mg) consisting of two major compounds (tlc). Chromatography over silica gel (ethyl acetate – chloroform mixtures, 4:1 to 1:1) afforded first the *bis*-p-*bromobenzoate* **29**, 120 mg, mp 142–143°C (from chloroform – light petroleum); ir ν_{max} (KBr disc): 1760, 1727, 1694, 1591 and 1485 cm^{-1}; nmr δ ($CDCl_3$): 1.43 and 1.58 (3H, each, br s's), 1.75–2.55 (4H, m), 2.87 (2H, dd, J = 17, 9 Hz), 3.65 (1H, d, J = 3 Hz), 4.42 (2H, q, J = 22 Hz), 4.88 (2H, m), 6.52 (1H, br s), 7.52–8.12 (8H, m). *Anal.* calcd. for $C_{29}H_{26}Br_2O_7$: C 53.9, H 4.0, Br 24.75%; found: C 53.6, H 4.05, Br 24.6; and then the *mono*-p-*bromobenzoate* **30** 122 mg, mp 178–180°C (from ethyl acetate – hexane); ir ν_{max} (KBr disc): 3500, 1763, 1730, 1705, 1590 and 1485 cm^{-1}; nmr δ ($CHCl_3$): 1.57 and 1.73 (3H each, br s's), 1.80–2.63 (5H, m), 2.80 (2H, dd, J = 18, 9 Hz), 3.52 (1H, d, J = 3 Hz), 4.38 (2H, q), 4.60–5.35 (3H, m), 7.56, and 7.87 (4H). *Anal.* calcd. for $C_{22}H_{23}O_6Br$: C 57.0, H 4.95, Br 17.25%; M^+ 462.0672; found: C 57.0, H 4.7, Br 17.2; M^+ 462.0687.

X-ray crystallography studies

A crystal ca. 0.13 × 0.25 × 0.54 mm was used. Unit cell parameters were determined from 25 reflections having θ > 12° mounted on an Enraf–Nonius CAD-4 diffractometer with MoKα radiation (λ = 0.71069 Å). Crystal data are:

$C_{29}H_{26}Br_2O_7$ fw = 646.3

Monoclinic, $P2_1$, a = 14.326(6), b = 4.826(2), c = 19.974(9) Å, β = 102.27(3)°, V = 1349.4 $Å^3$, ρ_c = 1.59 g cm^{-3}, Z = 2, $F(000)$ = 652, μ(MoKα) = 29.94 cm^{-1}. Data collection was carried out at room temperature (16 ± 3°C). An ω–2θ scan was used with an ω scan width of 0.66 ± 0.3 tan θ degrees in ω and a maximum ω scan speed of 10° min^{-1}. The maximum scan time was 180 s with the background counted for one quarter of the scan time at each end of the scan. Two standard reflections were measured every 2 h, and the orientation checked every 200 measured reflections. Only minor variations were noted. The quadrant having h 0–17, k 0–5, and l −24–24 was measured with a θ limit of 26 degrees. Of the 3285 reflections measured, 2101 had $I > 2.0\sigma(I)$ and were classified as observed. The data were corrected for absorption via an analytical method. The maximum and minimum transmission factors were 0.65 and 0.30 respectively.

The structure was solved by direct methods (25) and completed via weighted Fourier methods. The hydrogen atoms were included in their calculated positions; the orientation of hydrogen atoms on the terminal methyl atoms was derived from peaks on a difference electron density map. The hydrogen atoms were given a single, overall isotropic temperature factor; all other atoms had individual anisotropic thermal parameters. The scattering factors from the International Tables for X-ray Crystallography were used (26). The function minimised was $\Sigma\omega\Delta^2$ where $\omega = (\sigma^2|F_o| + 0.0008|F_o|^2)^{-1}$. Refinement converged at R = 0.041, R_w = 0.044.

At this point anomalous scattering factors were introduced for the first time, and a structure factor calculation performed, without scale factor refinement, for each enantiomeric form of the molecule. The weighted R-factors were 0.0522 and 0.0552 respectively, giving an R-factor ratio of 1.057 (27), thus establishing the preferred enantiomer with a confidence level in excess of 99.5%. The final R factor was 0.039 (R_w = 0.042). The corresponding factors for the enantiomer were 0.044 and 0.047. The final difference map had no features larger than 0.58 e $Å^{-3}$. The maximum parameter shifts in the final cycle of refinement were 0.3σ. Full-matrix refinement was used throughout the analysis.

Acknowledgments

We thank Professor D. Arigoni, ETH Zurich, for samples of (3*R*,5*R*)- and (3*R*,5*S*)-mevalonolactones; Professor D. Cane, Brown University, Rhode Island, for *trans,trans*-[1-$^3H_2$, 12,13-$^{14}C_2$]farnesyl pyrophosphate; and the Science Research Council, London, for pre- (D.P.) and post- (P.A. and H.M.) doctoral support.

1. (*a*) W. PARKER, J. S. ROBERTS, and R. RAMAGE. Q. Rev. **21**, 331 (1967); (*b*) G. A. CORDELL. Chem. Rev. **76**, 425 (1976); (*c*) D. E. CANE. *In* Biosynthesis of isoprenoid compounds. Vol. 1. *Edited by* J. W. Porter and S. L. Spurgeon. Wiley, New York. 1981. Chapt. 6.
2. A. J. ALLISON, D. N. BUTCHER, J. D. CONNOLLY, and K. H. OVERTON. J. Chem. Soc. Chem. Commun. 1493 (1968).
3. A. B. SMITH and R. E. RICHMOND. J. Org. Chem. **46**, 4814 (1981).
4. R. H. CORNFORTH, J. W. CORNFORTH, and G. POPJAK. Tetrahedron, **18**, 1354 (1962).
5. (*a*) K. H. OVERTON and F. M. ROBERTS. Biochem. J. **144**, 585 (1974); (*b*) H. MACKIE and K. H. OVERTON. Eur. J. Biochem. **77**, 101 (1977).
6. L. RUZICKA. Pure Appl. Chem. **6**, 493 (1963).
7. K. H. OVERTON and D. PICKEN. J. Chem. Soc. Chem. Commun. 105 (1976).
8. (*a*) H. SETO, T. SATO, and H. YONEHARA. J. Am. Chem. Soc. **95**, 8461 (1973); (*b*) H. SETO, L. W. CARY, and M. TANABE. J. Chem. Soc. Chem. Commun. 867 (1973); (*c*) A. G. MCINNES, D. G. SMITH, J. A. WALTER, J. C. VINING, and J. L. C. WRIGHT. J. Chem. Soc. Chem. Commun. 282 (1974); (*d*) T. J. SIMPSON. Chem. Soc. Rev. **14**, 497 (1975).
9. J. E. WOLINSKY, D. J. FAULKNER, J. FINER, and J. CLARDY. J. Org. Chem. **41**, 697 (1976).
10. R. H. CORNFORTH and G. POPJAK. *In* Methods in enzymology. Vol. 15. *Edited by* R. B. Clayton. Academic Press. 1969. p. 378.
11. P. ANASTASIS, I. FREER, C. GILMORE, H. MACKIE, K. OVERTON, and S. SWANSON. J. Chem. Soc. Chem. Commun. 268 (1982).
12. D. E. CANE. Tetrahedron, **36**, 1109 (1980).
13. T. SUGA, T. HIRATA, T. AOKI, and T. SHISHIBORI. J. Am. Chem. Soc. **105**, 6178 (1983).
14. (*a*) D. E. CANE, S. SWANSON, and P. P. N. MURTHY. J. Am. Chem. Soc. **103**, 2136 (1981); (*b*) D. E. CANE, R. IYENGAR, and M.-S. SHIAO. J. Am. Chem. Soc. **103**, 914 (1981).
15. S. E. GOTFREDSEN. Dissertation, ETH Zürich. No. 6243 (1978).
16. R. CROTEAU and M. FELTON. Arch. Biochem. Biophys. **207**, 460 (1981).
17. (*a*) H. GAMBLIEL and R. CROTEAU. J. Biol. Chem. **257**, 2335 (1982); (*b*) R. CROTEAU. *In* Biosynthesis of isoprenoid compounds. Vol. 1. *Edited by* J. W. Porter and S. L. Spurgeon. Wiley, New York. 1981 Chapt. 5.
18. C. DONNINGER and G. POPJAK. Proc. R. Soc. London, Ser. B, **163**, 465 (1966).
19. P. BLATTMAN and J. RETEY. J. Chem. Soc. Chem. Commun.

1394 (1970); P. BLATTMAN and J. RETEY. Z. Physiol. Chem. **352**, 369 (1971).
20. (*a*) D. ARIGONI. Pure Appl. Chem. **41**, 219 (1975); (*b*) S. GOTFREDSEN, J. P. OBRECHT, and D. ARIGONI. Chimia, **31**, 62 (1977); (*c*) N. H. ANDERSEN, Y. OHTA, and D. D. SYVDAL. *In* Bio-organic Chemistry. Vol. 2. *Edited by* E. E. van Tamelen. Academic Press, New York. 1977. p. 1; (*d*) D. V. BANTHORPE, V. V. CHARLWOOD, and M. J. O. FRANCIS. Chem. Rev. **72**, 115 (1972).
21. (*a*) J. W. CORNFORTH. Tetrahedron, **30**, 1515 (1974); (*b*) G. POPJAK and J. W. CORNFORTH. Biochem. J. **101**, 553 (1966).
22. R. BENTLEY. Molecular asymmetry in biology. Vol. 2. Academic Press, New York. 1970. p. 259.
23. D. N. BUTCHER and B. G. BOWES. Z. Pflanzenphysiol. **58**, 86 (1969).
24. H. E. STREET. *In* Cells and tissue culture. Vol. 3. *Edited by* E. N. Willmer. Academic Press, New York. 1965. p. 533.
25. C. J. GILMORE. J. Appl. Crystallogr. **17**, 42 (1984).
26. International Tables for X-Ray Crystallography. Vol. IV. The Kynoch Press, Birmingham. 1974.
27. W. C. HAMILTON. Acta Crystallogr. Sect. A, **18**, 502 (1965).

Can. J. Chem. Downloaded from www.nrcresearchpress.com by 210.87.254.105 on 09/06/12
For personal use only.

Dihydrothiophenes.10. The preparation and Diels–Alder reactions of some sulfur and phosphorus-substituted dienophiles and 2-aza-substituted 1,3-dienes[1]

JOHN M. MCINTOSH AND LILIANNA Z. PILLON
Department of Chemistry, University of Windsor, Windsor, Ont., Canada, N9B 3P4

Received January 6, 1984

JOHN M. MCINTOSH and LILIANNA Z. PILLON. Can. J. Chem. **62**, 2089 (1984).

The use of 3-carboxylated 2,5-dihydrothiophenes as the dienophilic component of the Diels–Alder reaction has been investigated. The yields are generally quite low. The formation of conjugated dienes that are aminated at an interior position of the conjugated chain by formation and thermal decomposition of 3-acetamido-2,5-dihydrothiophenes appears to be a viable route to these useful compounds. One example of the Diels–Alder reaction of 2-carboxylated diethyl vinylphosphonates is reported.

JOHN M. MCINTOSH et LILIANNA Z. PILLON. Can. J. Chem. **62**, 2089 (1984).

On a évalué les possibilités d'utiliser les dihydro-2,5 thiophènes portant des groupes carboxyliques en position 3 comme dièns dans des réactions de Diels–Alder. Les rendements sont généralement assez bas. Il semble que la formation de dièns conjugués et aminés sur une position intérieure de la chaîne conjugée par la formation et par la décomposition thermique d'acétamido-3 dihydro-2,5 thiophènes est une route viable pour obtenir ces composés utiles. On rapporte un exemple de réaction de Diels–Alder de diéthyl vinyl phosphonates carboxylés en position 2.

[Traduit par le journal]

In recent years, we have developed a remarkably facile approach to the preparation of 2,5-dihydrothiophenes and noted their use as sources of regiospecifically generated conjugated dienes and other useful derivatives (1). In this report we draw attention to the use of certain of these compounds as sources of the dienophilic component of the Diels–Alder reaction and to the preparation and use of some interesting nitrogen-substituted dienes and one unusual phosphorus-substituted dienophile.

The possibility of using the same molecular type as the source of either the diene or dienophilic component of the Diels–Alder reaction is predicated on the different properties of two easily interconverted forms of sulfur (Scheme 1). Compounds **1**, easily assembled from 2-mercaptoaldehydes or ketones and vinyl phosphonium salts (X = H) (1*a*–1*d*) or vinyl phosphonates (X = *E*lectron-*W*ithdrawing *G*roup) (1*e*–1*f*) are oxidized to **2** with peracid in quantitative yield. Mild thermal decomposition of **2** affords dienes in a regiospecific and stereospecific manner. These in turn provide substituted cyclohexenes on reaction with dienophiles. The limitations to the predictability of regio- and stereoselectivity in such processes are well known. On the other hand, **1** (X = EWG) are potential dienophiles. Annelation of a cyclohexene ring via a Diels–Alder reaction followed by desulfurization should provide regiospecifically and stereospecifically substituted cyclohexenes. Such a process was exploited by Stork and Stotter (2) in an intriguing apporach to the *trans*-C/D ring fusion of steroids. Stork's work has appeared only as a communication and no yields were stated. To further expand the knowledge in this area, we have briefly investigated some additional examples of this reaction.

Reaction of **1***a* (R = R′ = H, X = COOMe) (1*e*) or **1***b* (R = H, R′ = Ph, X = COOMe) (1*e*) with either butadiene or isoprene at 180°C led to the formation of the Diels–Alder products in only modest yields (Scheme 1). Attempts to improve the yields and (or) reduce the severity of the reaction conditions by employing catalysis ($AlCl_3$, $SnCl_4$) failed. Extensive polymerization of the diene was the major result of such modifications. While both the gc and the ^1H nmr of **3**–**6** indicated the presence of only one isomer, the ^{13}C nmr of **4** clearly indicated the presence of **4***a* and **4***b* in a 3:2 ratio. Compounds **5** and **6** showed only one set of signals in their ^{13}C nmr spectra. It is clear from these results that, while the approach appears viable, practical application in synthesis must await a significant improvement in yields.

An attractive addition to the use of **1** in synthesis is represented by **8**. Such compounds should lead to dienes and thence to cyclohexenes which possess a regiospecifically-generated enamine-type functionality which, in turn, could be alkylated, reduced, or hydrolyzed. Formation of 1,3-dienamines or dienamides in which the nitrogen atom is at the end of the conjugated chain is straightforward, and such compounds have been used extensively in Diels–Alder reactions by Oppolzer *et al.* (3). However, generation of such systems which possess the nitrogen function at an interior position is a problem fraught with difficulties. Perhaps the most useful method is the thermal rearrangement of trichloroacetimidates pioneered by Overman *et al.* (4). However, even this method affords 2-substituted diene systems only when the 1-substituted isomers cannot form (4*c*). Evidence is available that compounds **8** function efficiently in Diels–Alder reactions with reactive dienophiles (4*a*). In 1979, Field (5) reported the serendipitous formation of two examples of **8** from the cyclization in refluxing acetic anhydride of the condensation products of 2-haloketones and *N*-acetylcysteine (**7**) (Scheme 2). Detailed below are our observations on some of the limitations to Field's method and the efficacy of the conversion of **8** to aminated dienes.

Reaction of 2-chlorocyclohexanone (**9**) or chloroacetone (**15**) with **7** followed by treatment with acetic anhydride afforded **11** (5) and **17** in 52 and 50% yields respectively. The reasons for the incorporation of the extra acetyl unit in **17** is obscure at this time. A minor by-product (**19**) was also isolated from the chloroacetone reaction. Oxidation of **11** and **17** with MCPBA gave **12** and **18** in quantitative yields. Heating these compounds in refluxing toluene in the presence of maleic anhydride, followed by hydrolysis in the case of **12**, gave the products **14** and **20** in 42 and 70% yields, respectively.

When haloketone **21** was alkylated with **7**, **22** was formed. Acetic anhydride treatment of **22** led mainly to decomposition products. From this mixture a compound to which we assign

[1]Taken in part from the Ph.D. dissertation of L. Z. Pillon, University of Windsor, September, 1983.

Can. J. Chem. Downloaded from www.nrcresearchpress.com by 210.87.254.105 on 09/06/12
For personal use only.

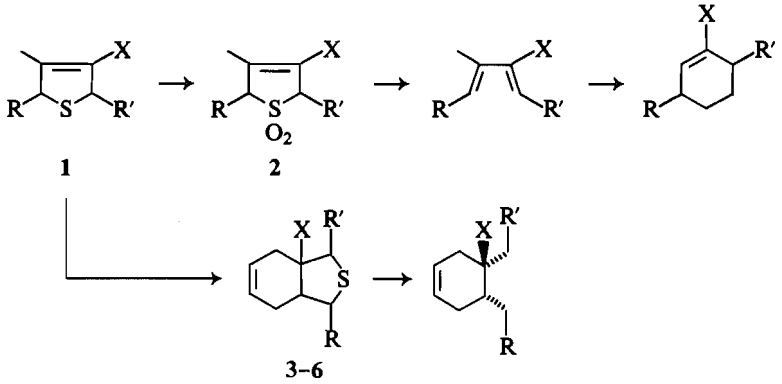

1 **2** **3–6**

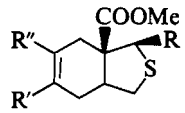

3 R = R′ = R″ = H (38%)
4*a* R = R″ = H R′ = Me } (16%)
4*b* R = R′ = H R″ = Me }
5 R′ = R″ = H R = Ph (55%)
6 R″ = H R = Ph R′ = Me (29%)

SCHEME 1

the structure **23** could be isolated. We have been unable to effect the double elimination reaction required to form the desired substitution dihydrothiophene under either acidic or basic conditions.

Inter alia it should be noted that an exactly analogous result was obtained using *N*-acetylhomocysteine (generated *in situ* from the commercially available acetylated thiolactone of homocysteine). In this way **15** or **21** afforded **24** or **26** respectively. Again we have been unable to effect the decarboxylative elimination of **26** and the reason for the formation of the diacetylated derivative **24** is unclear. Oxidation of **24** afforded **25** in 45% overall yield.

It seems apparent from these results and those of Field that, in the absence of steric congestion around the carbonyl group, acceptable yields of 3-acetamido-2,5-dihydrothiophenes can be realized and that sulfone formation and decomposition lead to a viable synthesis of conjugated dienes that are regiospecifically aminated at an interior position.

Several phosphonate-type dienophiles have been used in Diels–Alder reactions (6). The nmr of the crude product from reaction of diethyl vinylphosphonate with isoprene indicated the formation of a mixture of isomeric products in a 4:1 ratio (6*c*). Vinyl phosphonates bearing a 2-carboalkoxy group might be expected to be more reactive dienophiles than their unsubstituted analogs and orientational specificity might also be expected to be more pronounced. Since we had available some of the vinylphosphonates **27**, we decided to examine an example of their Diels–Alder reactions. When **27***a* was treated with isoprene, a product which was homogeneous to all tests used (including ^{13}C nmr) was obtained in 95% yield, to which we assign the structure **28**. Hydrolysis and decarboxylation of **28** gave phosphonate **29**. Unfortunately phosphonate **27***b* could not be induced to undergo Diels–Alder addition with isoprene or butadiene.

It is well known that phosphonates like **29** will not undergo olefination reactions (7). However, the corresponding phosphonamides do (8). Therefore, we made several attempts to prepare the bis(dimethylamide) derivative of **27***a* or **27***b* by

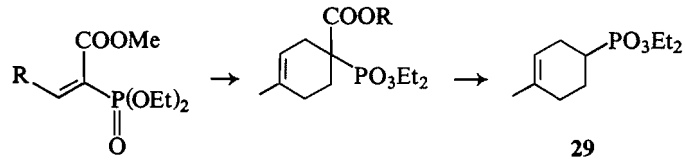

27*a* R = H **28***a* R = Me
27*b* R = Ph **28***b* R = H

29

methods analogous to those used for the preparation of **27**. As of this time, these efforts have been uniformly unsuccessful. However, in the experimental section, we report a simplified preparation of the useful (8) methylphosphonic acid bis(dimethylamide) **30** which avoids the necessity of using gaseous dimethyl amine.

Experimental

Infrared spectra were run on a Beckman IR-12 instrument as neat liquids or in $CHCl_3$ unless otherwise noted. The ^1H nmr spectra were usually run at 60 MHz in $CDCl_3$ solution and ^{13}C nmr spectra were run in the same solvent at 22.64 MHz in the FT mode using a flip angle of 45°. The nmr spectra are reported in ppm relative to TMS as internal standard. Mass spectra were run on a Varian MAT CH-5 DF instrument equipped with electron impact (EI), field ionization (FI), and field desorption (FD) sources. Gas chromatographic analyses were performed using 20% SE-30 on Chromosorb W columns. Preparative tlc was performed using 2 mm thick plates of silica gel GF (Analtech). Solvents were removed at reduced pressure and the drying agent was anhydrous $MgSO_4$. Microanalyses were done by Guelph Microanalytical Laboratories and Canadian Microanalytical Services, Vancouver, B.C.

General procedure for the Diels–Alder reactions of **1**a *and* **1**b

A solution of **1***a* or **1***b* (2 mmol), hydroquinone (0.01 g), and either butadiene or isoprene (20 mmol) in 5 mL of xylene was heated (sealed tube) at 180°C for 20 h. The cooled solution was concentrated and the product was separated from the hydrocarbon polymer using thick layer chromatography (1:9 ether/petroleum ether). The physical data on the products follows. Addition of catalytic amounts of $AlCl_3$ or $SnCl_4$ reduced the yields considerably.

Can. J. Chem. Downloaded from www.nrcresearchpress.com by 210.87.254.105 on 09/06/12
For personal use only.

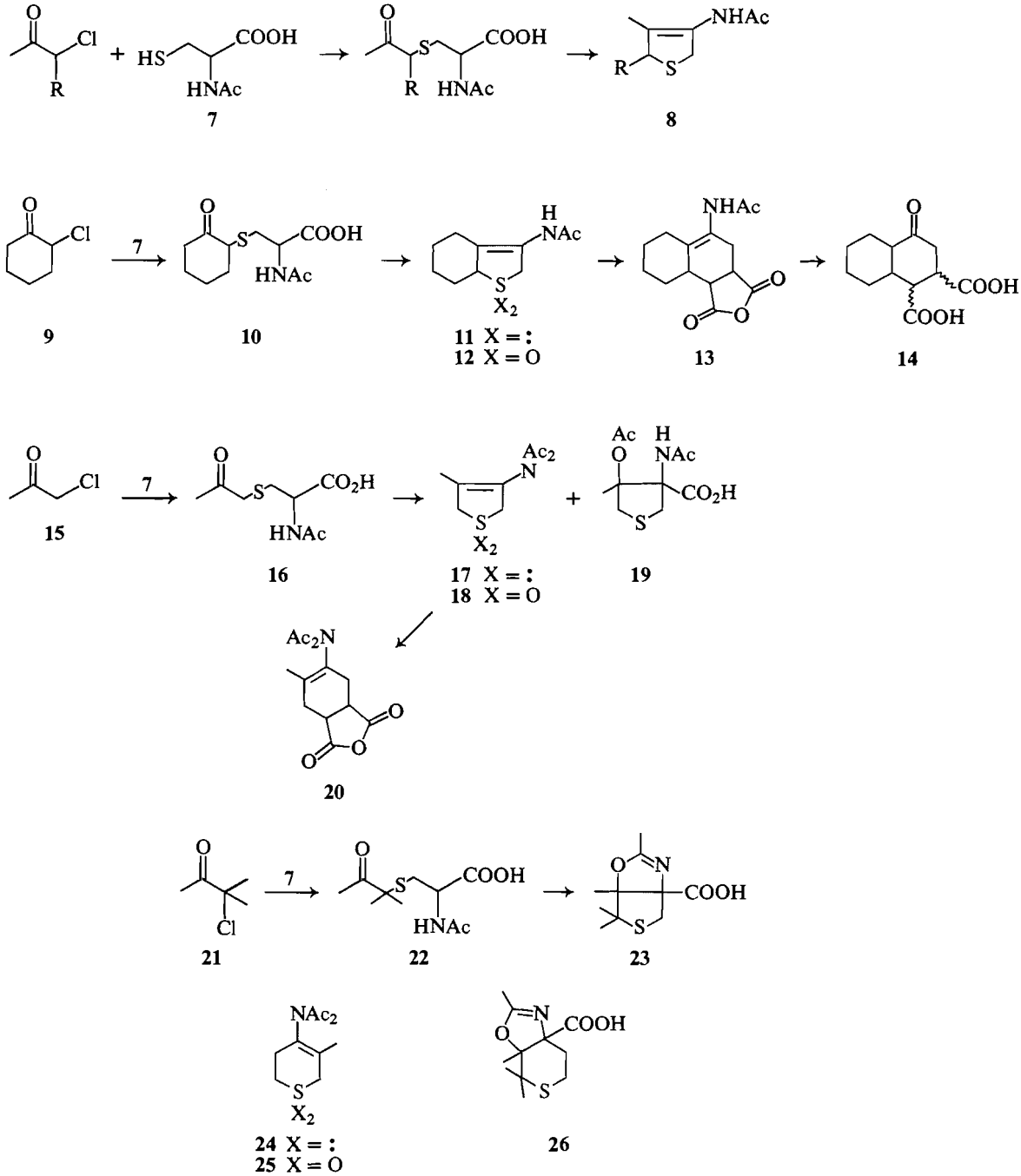

SCHEME 2

Compound 3: colorless oil, 159 mg (38%); ir ($CHCl_3$): 1710, 1640, 1180 cm^{-1}; ^1H nmr: 5.6 (bs, 2H), 3.7 (s, 3H), 3.3–1.95 (m, 9H). *Anal.* calcd. ($C_{10}H_{14}O_2S$): C 60.61, H 7.06; found' C 60.85, H 7.10.

*Compounds 4*a *and 4*b: yellowish oil, 68 mg, (16%); ir ($CHCl_3$): 1730, 1615, 1225 cm^{-1}; ^1H nmr: 5.3 (bs, 1H), 3.75 (s, 3H), 3.35–1.90 (m, 9H), 1.65 (s, 3H): ^{13}C nmr: 175.3, 175.2, 134.8, 131.0, 130.4, 124.2, 53.9, 53.1, 52.1, 42.3, 41.6, 39.5, 39.2, 38.7, 35.2, 32.7, 30.8, 28.6, 26.5, 26.2. *Anal.* calcd. ($C_{11}H_{16}O_2S$): C 62.27, H 7.54; found: C 62.62, H 7.13.

Compound 5: colorless oil, 300 mg (55%); ir ($CHCl_3$): 1720, 1650, 1590, 1520, 1490, 1210 cm^{-1}; ^1H nmr: 7.4 (m, 5H), 5.65 (bs, 2H), 4.31 (s, 1H), 3.65–2.0 (m, 10H); ^{13}C nmr: 172.6, 141.1, 129.1, 127.7, 127.5, 124.9, 123.9, 60.9, 59.2, 51.4, 39.3, 35.1, 30.3, 26.1; *m/z* (FI) = 274 (M^+), 183, 138, 135, 91. *Anal.* calcd. ($C_{16}H_{18}O_2S$): C 70.08, H 6.57; found: C 70.43, H 6.57.

Compound 6: colorless oil, 160 mg (29%); ir ($CHCl_3$): 3020, 1720, 1640, 1595, 1580, 1490, 1200 cm^{-1}; ^1H nmr: 7.3 (m, 5H), 5.20 (bs, 1H), 4.23 (s, 1H), 3.55–1.6 (m, 13H); ^{13}C nmr: 172.7, 141.2, 131.8, 130.1, 129.1, 127.7, 127.5, 60.6, 59.2, 51.4, 39.8, 38.8, 35.2, 30.7, 26.3. *Anal.* calcd. ($C_{17}H_{20}O_2S$): C 70.84, H 6.93; found: C 70.40, H 7.14.

Alkylation of N-*acetylcysteine*

The alkylations of **7** with 2-haloketones were carried out by the method reported by Field (5). The following products were obtained.

N-*acetyl*-S-*(2-oxocyclohexyl)cysteine* ***(10)***, 60%, mp 117–120°C (lit. (5) 124–128°C).

N-*acetyl*-S-*acetonylcysteine* ***(16)***, 68%, yellowish oil; ir (neat): 3600–2600, 1720, 1650, 1565, 1425, 1380, 1250 cm^{-1}; ^1H nmr (DMSO): 8.15 (bd, 1H), 4.40 (nm, 1H), 3.45 (s, 2H), 2.82 (m, 2H), 2.20 (s, 3H), 1.85 (s, 3H); *m/z* (FI) = 219 (M^+), 201, 165, 159.

N-*acetyl*-S-*(1,1-dimethylacetonyl)cysteine* ***(21)***, white crystals

Can. J. Chem. Downloaded from www.nrcresearchpress.com by 210.87.254.105 on 09/06/12
For personal use only.

Can. J. Chem. Downloaded from www.nrcresearchpress.com by 210.87.254.105 on 09/06/12
For personal use only.

(74%), mp 131–133°C; ir (KBr): 3300–2600, 1715, 1695, 1620, 1545, 1460, 1380, 1260 cm^{-1}; ^1H nmr (DMSO): 8.3 (bd, 1H), 4.32 (m, 1H), 2.52 (m, 2H), 2.20 (s, 3H), 1.85 (s, 3H), 1.35 (s, 6H); ^{13}C nmr (DMSO): 205.3, 171.6, 169.2, 52.2, 51.8, 30.3, 23.9, 23.6, 22.2; *m/z* (FI) = 247 (M^+), 248, 202. *Anal.* calcd. ($C_{10}H_{17}NO_4S$): C 48.59, H 6.87; found: C 48.45, H 6.63.

Alkylations of N-*acetylhomocysteine*

These were carried out in the same way as the alkylations of **7**, except that the solvent was 2-propanol and the starting material was *N*-acetylhomocysteine thiolactone. The following products were obtained.

N-*acetyl*-S-*acetonylhomocysteine* (84%), yellowish oil; ir (neat): 3500–2500, 1710, 1660, 1605, 1555, 1440, 1325, 1300, 1240 cm^{-1}; ^1H nmr (DMSO): 8.05 (bd, 1H), 4.30 (m, 1H), 3.52 (s, 2H), 2.25 (s, 3H), 1.85 (s, 3H), 2.4–1.7 (m, 4H); ^{13}C nmr (DMSO): 203.8, 173.1, 169.4, 58.1, 50.8, 41.3. 30.7, 27.8, 22.2. *Anal.* calcd. ($C_9H_{15}NO_4S$): C 46.36, H 6.43; N 6.00; found: C 46.56, H 6.80, N 6.02.

N-*acetyl*-S-*(1,1-dimethylacetonyl)homocysteine (22)*: 50%, mp 151–152°C (from EtOAc); ir (KBr): 3600–3200, 1710, 1655, 1560, 1450, 1385, 1245 cm^{-1}; ^1H nmr (DMSO): 8.15 (bd, 1H), 4.25 (m, 1H), 2.4–1.55 (m, 4H), 2.25 (s, 3H), 1.80 (s, 3H), 1.35 (s, 3H); ^{13}C nmr (DMSO): 205.5, 173.1, 169.5, 52.4, 51.0, 31.0, 25.3, 24.1, 23.7, 22.4; *m/z* (FI) = 261 (M^+), 218, 156, 143. *Anal.* calcd. ($C_{11}H_{19}NO_4S$): C 50.58, H 7.27; found: C 50.31, H 7.04.

Cyclizations of S-*alkylated cysteine and homocysteine*

The cyclizations were carried out essentially using Field's procedure (5). The following procedure is representative. Compound **22** (1.48 g, 6 mmol) was mixed with 1.3 mL of acetic anhydride and stirred at 130–135°C for 5 h. The cooled mixture was diluted with 5 mL of water which caused **23** to precipitate as a heavy yellow oil which was separated. An analytical sample of **23** was purified using preparative tlc (ether). In this way the following products were isolated.

From **10**, after heating 1 h, amide **11**, yellow solid (52%), mp 135–138°C (lit. (5) 139–144°C) was obtained.

From **16**, after heating for 1 h, was obtained a mixture of a yellow oil and white crystals which were separated by filtration. The filtrate (amide **17**) was not purified but converted directly to sulfone **18** (*vide infra*). The residue gave, after recrystallization from EtOH, acid **19**, white crystals (15%), mp 211–213°C; ir (KBr): 3400–2600, 1760, 1740, 1660, 1570, 1260 cm^{-1}; ^1H nmr (DMSO): 8.05 (s, 1H), 3.6–2.9 (m, 4H), 2.05 (s, 3H), 1.91 (s, 3H), 1.53 (s, 3H); ^{13}C nmr (DMSO): 169.9, 169,6, 169,4, 87,1, 71.4, 36.1, 32.7, 25.5, 21.8, 18.9; *m/z* (FI) = 261 (M^+), 157, 60. *Anal.* calcd. ($C_{10}H_{15}NO_5S$): C 45.99, H 5.74, N 5.36; found: C 45.65, H 5.77, N 5.49.

From **22**, acid **23**, yellow oil (25%); ir ($CHCl_3$): 3600–2700, 2990, 1715, 1465, 1440, 1375, 1270, 1110 cm^{-1}; ^1H nmr ($CDCl_3$): 2.35 (s, 3H), 2.31 (dd, 2H, J = 2, 2 Hz), 1.50 (s, 6H), 1.45 (s, 3H); *m/z* (FI) = 229 (M^+), 227, 185. *Anal.* calcd. ($C_{10}H_{15}NO_3S$): C 52.42, H 6.53; found: C 52.92, H 6.53. Heating **23** with NaH in toluene or with 10% aqueous HCl failed to produce any dihydrothiophene.

From *N*-acetyl-*S*-acetonylhomocysteine, after heating for 1 h, was obtained amide **24**, which was not purified, but oxidized directly to sulfone **25**.

From *N*-acetyl-*S*-(1,1-dimethylacetonyl)homocysteine, after heating for 5 h, acid **26**, yellow oil (35%); ir ($CHCl_3$): 3500–2500, 1720, 1670, 1605, 1575, 1440, 1375, 1270 cm^{-1}; ^1H nmr ($CDCl_3$): 2.65–2.05 (m, 4H), 2.35 (s, 3H), 2.30 (s, 3H), 1.45 (s, 6H); *m/z* (FI) = 243 (M^+), 199, 185, 159. *Anal.* calcd. $C_{11}H_{17}NO_3S$): C 54.33, H 6.99; found: C 54.24, H 6.82.

Oxidations of sulfides to sulfones

The previously reported procedure (1*b*) was followed. Products obtained were as follows.

From **11**, sulfone **12**, yellowish crystals (68%), mp 157–159°C; ir ($CHCl_3$): 3420, 1700, 1670, 1500, 1310, 1115 cm^{-1}; ^1H nmr ($CDCl_3$): 7.58 (bs, 1H), 4.20–3.55 (m, 3H), 2.35 (s, 3H), 2.30–1.00 (m, 8H); *m/z* (FI) = 229 (M^+), 165. *Anal.* calcd. ($C_{10}H_{15}NO_3S$): C 52.40, H 6.55, N 6.11; found: C 51.96, H 6.36, N 6.31.

From **17**, sulfone **18**, white crystals (42%), mp 151–152°C; ir ($CHCl_3$): 1720, 1330, 1260, 1130, 1010 cm^{-1}; ^1H nmr ($CDCl_3$): 3.9 (bs, 4H), 2.40 (s, 6H), 1.75 (s, 3H); ^{13}C nmr (DMSO): 171.4, 135.0, 128.6, 59.3, 55.6, 25.3, 13.2; *m/z* (FI) = 231 (M^+), 188. *Anal.* calcd. ($C_9H_{13}NO_4S$): C 46.76, H 5.62, N 6.06; found: C 46.38, H 5.82, N 6.52.

From **24**, sulfone **25**, white crystals (45%), mp 181–182°C; ir ($CHCl_3$): 1710, 1580, 1420, 1370, 1325, 1295 cm^{-1}; ^1H nmr ($CDCl_3$): 3.65 (s, 2H), 3.35–2.50 (m, 4H), 2.35 (s, 6H), 1.60 (s, 3H); ^{13}C nmr ($CDCl_3$): 171.9, 151.7, 127.8, 67.1, 53.7, 47.3, 29.1, 25.5; *m/z* (FI) = 245 (M^+), 202, 186. *Anal.* calcd. ($C_{10}H_{15}NO_4S$): C 48.99, H 6.12, N 5.71; found: C 48.94, H 6.48, N 5.89.

Diels–Alder reactions of **12** *and* **18**

To a solution of sulfone **15** or **18** (0.01 mol) in 50 mL of xylene was added 0.01 mol of maleic anhydride and a small amount of hydroquinone. The reaction was heated at reflux overnight under a nitrogen atmosphere. The solution was cooled and the crystalline product was isolated by filtration. Since **13** was very prone to hydrolysis, it was converted to **14** before analysis. Data on the products follows.

Compound **13**, yellow crystals (62%), mp 213–215°C; ir ($CHCl_3$): 3280, 1860, 1780, 1675, 1660, 1550, 1455, 1375 cm^{-1}; ^1H nmr (DMSO): 8.95 (bs, 1H), 4.0–3.15 (m, 5H), 2.35–1.00 (m, 11H); ^{13}C nmr (DMSO): 173.3, 135.6, 110.2, 67.5, 45.4, 43.0, 42.4, 40.8, 39.9, 38.7, 31.5, 29.5, 26.3; *m/z* (FI) = 263 (M^+), 261, 245, 222, 197.

Hydrolysis to **14** was achieved by refluxing **13** (1.5 g, 6 mmol) with 40 mL of 15% HCl overnight. Filtration of the cooled mixture gave **14**, white crystals (54%), mp 111–113°C; ir (KBr): 3200–2600, 1715, 1700, 1445, 1345, 1250 cm^{-1}; ^1H nmr (DMSO): 3.15–2.81 (m, 3H), 2.35–0.8 (m, 11H); ^{13}C nmr (DMSO): 182.2, 181.3, 173.1, 47.7, 45.3, 43.2, 42.3, 36.7, 31.1, 25.4, 25.1, 24.8. *Anal.* calcd. ($C_{12}H_{16}O_5 \cdot H_2O$): C 55.87, H 6.97; found: C 56.06, H 7.22.

Compound **20**, white crystals (70%), mp 162–163°C; ir ($CHCl_3$): 1860, 1790, 1720, 1445, 1430, 1375, 1270 cm^{-1}; ^1H nmr ($CDCl_3$): 3.52 (m, 2H), 2.63 (m, 4H), 2.30 (s, 6H), 1.71 (s, 3H); ^{13}C nmr ($CDCl_3$): 178.6, 178.2, 172.8, 172.5, 132.6, 128.8, 40.2, 39.8, 31.2, 29.6, 28.8, 26.7, 25.7; *m/z* (FI) = 265 (M^+), 223, 183. *Anal.* calcd. ($C_{13}H_{15}NO_5$): C 58.86, H 5.66, N 5.28; found: C 58.52, H 5.56, N 5.68.

*Methyl 4-methyl-1-(diethylphosphono)-3-cyclohexenecarboxyate (28*a*)*

A mixture of **27** (1*e*) (0.22 g, 1 mmol), 0.1 g (1.5 mmol) of isoprene, and a small quantity of hydroquinone was dissolved in 25 mL of toluene and heated at reflux for 3 h. Evaporation and tlc purification (ether) gave **28***a* as a yellow oil (0.27 g, 95%); ir ($CHCl_3$): 1730, 1650, 1460, 1380, 1270 cm^{-1}; ^1H nmr ($CDCl_3$): 5.32 (bs, 1H); 4.15 (qq, 4H, J = 7, 7 Hz), 3.71 (s, 3H), 2.85–1.80 (m, 6H), 1.65 (s, 3H), 1.35 (t, 6H, J = 7 Hz); ^{13}C nmr ($CDCl_3$): 171.2, 133.3, 118.7 (J_{P-C} = 13 Hz), 63.1, 62.8, 52.5, 47.8 (J_{P-C} = 134 Hz), 28.4, 27.4 (J_{P-C} = 13 Hz), 25.8, 23.5, 16.6. *Anal.* calcd. ($C_{13}H_{23}PO_5$): C 53.82, H 7.92; found: C 53.86, H 7.66.

*4-Methyl-1-(diethylphosphono)-3-cyclohexenecarboxylate (28*b*)*

To a solution of 0.05 g (1.25 mmol) of NaOH in 5 mL of absolute ethanol was added 0.28 g (1 mmol) of **28***a*. The mixture was refluxed for 3 h and the solvent was removed. The residue was dissolved in water, acidified, and extracted with ether. The ether extracts were dried and evaporated to yield **28***b*, white crystals (0.24 g, 90%), mp 134–135°C; ir ($CHCl_3$): 3500–2700, 1740, 1670, 1475, 1415, 1280, 1210 cm^{-1}; ^1H nmr ($CDCl_3$): 10.25 (bs, 1H), 5.25 (bs, 1H), 4.10 (qq, 4H, J = 7, 7 Hz), 2.7–1.85 (m, 6H), 1.6 (s, 3H), 1.33 (tt, 6H, J = 7, 7 Hz); ^{13}C nmr ($CDCl_3$) (100 MHz): 172.7, 133.5, 118.1 (J_{P-C} = 14 Hz), 63.5 (J_{P-C} = 7.5 Hz), 63.4 (J_{P-C} = 6.2 Hz), 47.5 (J_{P-C} = 133 Hz), 28.2, 26.8 (J_{P-C} = 12.5 Hz), 25.3, 23.4, 16.4. *Anal.* calcd. ($C_{12}H_{21}PO_5$): C 52.20, H 7.60; found: C 52.16, H 7.57.

Diethyl 4-methyl-3-cyclohexen-1-ylphosphonate (29)

Acid **28***b* (2.7 g, 10 mmol) was heated at 200°C for 30 min at normal pressure. The reaction mixture was cooled and purified using

preparative tlc (ether) to give **29**, yellowish oil (1.59 g, 70%); ir ($CHCl_3$): 3000, 1660, 1460, 1390, 1270, 1050 cm^{-1}; ^1H nmr ($CDCl_3$): 5.35 (bs, 1H), 4.15 (qq, 4H, J = 6, 6 Hz), 3.50 (m, 1H), 2.72–1.85 (m, 6H), 1.59 (s, 3H), 1.25 (tt, 6H, J = 6, 6 Hz). *Anal.* calcd. ($C_{11}H_{21}PO_3$): C 56.93, H 9.04; found: C 57.09, H 9.23.

*Improved preparation of methylphosphonic acid bis(dimethylamide) **30***

To a cooled suspension of 32.6 g (0.4 mol) of dimethylamine hydrochloride in 125 mL of ether was added 32 g of 50% aqueous NaOH and the mixture was stirred vigorously overnight under nitrogen. The layers were separated, the ether layer dried for 15 min over $MgSO_4$, cooled to 0°C and 10 g (0.075 mol) of methylphosphonic acid dichloride (Aldrich) was added. The mixture was stirred at 0°C for 1 h and at ambient temperature for 3 h. The reaction mixture was filtered, the filtrate evaporated, and the residue distilled to give 9.6 g (85%) of methylphosphonic acid bis(dimethylamide), bp 85–88°C (2.5 Torr (1 Torr = 133.3 Pa)) (lit. (9) bp 138°C (32 Torr)).

Acknowledgements

The financial assistance of the Natural Sciences and Engineering Research Council of Canada made this work possible. The assistance of the Southwestern Ontario NMR Centre in obtaining the 100 MHz ^{13}C nmr spectra is gratefully acknowledged.

1. (*a*) J. M. McINTOSH, H. B. GOODBRAND, and G. M. MASSE. J. Org. chem. **39**, 202 (1974); (*b*) J. M. McINTOSH and G. M. MASSE. J. Org. Chem. **40**, 1294 (1975); (*c*) J. M. McINTOSH and R. S. STEEVENSZ. Can. J. Chem. **52**, 1934 (1974); (*d*) J. M. McINTOSH and H. KHALIL. Can. J. Chem. **53**, 209 (1975); (*e*) J. M. McINTOSH and R. A. SIELER. Can. J. Chem. **56**, 226 (1978); (*f*) J. M. McINTOSH and R. A. SIELER. J. Org. Chem. **43**; 4431 (1978).
2. G. STORK and P. L. STOTTER. J. Am. Chem. Soc. **91**, 7780 (1969).
3. W. OPPOLZER and W. FROSTL. Helv. Chim. Acta, **58**, 587 (1975); W. OPPOLZER, L. BIEBER, and E. FRANCOTTE. Tetrahedron Lett. 981 (1979).
4. (*a*) L. E. OVERMAN and L. A. CLIZBE. J. Am. Chem. Soc. **98**, 2352 (1976); (*b*) L. E. OVERMAN. J. Am. Chem. Soc. **98**, 2901 (1976); (*c*) L. E. OVERMAN, L. A. CLIZBE, R. L. FRANKS, and C. K. MARLOVE. J. Am. Chem. Soc. **103**, 2807 (1981).
5. G. F. FIELD. J. Org. Chem. **44**, 825 (1979).
6. (*a*) A. N. PUDOVIK and M. G. IMAEV. Otdel. Khim. Nauk, 916 (1952); (*b*) S. D. DARLING and N. SUBRAMANIAN. Tetrahedron Lett. 1413 (1975); (*c*) W. M. DANIEWSKI and C. E. GRIFFIN. J. Org. Chem. **31**, 3236 (1966).
7. W. S. WADSWORTH. Synthetic applications of phosphoryl-stabilized anions. Org. Reactions. Vol. 25. *Edited by* W. G. Dauben. Wiley, New York. 1977. p. 73ff.
8. E. J. COREY and G. T. KWIATKOWSKI. J. Am. Chem. Soc. **90**, 6816 (1968), and references therein.
9. G. M. KOSOLAPOFF and L. B. PAYNE. J. Org. Chem. **21**, 4131 (1956).

Can. J. Chem. Downloaded from www.nrcresearchpress.com by 210.87.254.105 on 09/06/12
For personal use only.

Complexes of tungsten(VI) with thiomalic acid studied by ^1H and ^{13}C nuclear magnetic resonance spectroscopy

M. MADALENA CALDEIRA AND VICTOR M. S. GIL
Department of Chemistry, University of Coimbra, 3000 Coimbra, Portugal

Received September 27, 1983[1]

M. MADALENA CALDEIRA and VICTOR M. S. GIL. Can. J. Chem. **62**, 2094 (1984).

Proton and carbon-13 nmr evidence is presented on the number, stoichiometry, geometry, and stability of the complexes which form when sodium tungstate and (D,L)-thiomalic acid are mixed in aqueous solution at pH values in the range 2–7. In particular, three (or four) complexes are detected having a 1:2 composition (metal–ligand), as well as a less stable complex which seems to be a 1:1 species. Preliminary data are also given on the exchange of bound ligand in these complexes.

M. MADALENA CALDEIRA et VICTOR M. S. GIL. Can. J. Chem. **62**, 2094 (1984).

Faisant appel à la rmn du ^1H et du ^{13}C, on a étudié le nombre, la stoichiométrie, la géométrie et la stabilité des complexes qui se forment lorsqu'on mélange du tungstate de sodium et de l'acide (D,L)-thiomalique en solutions aqueuses, à des pH allant de 2 à 7. En particulier, on a pu détecter trois (ou quatre) complexes de composition 1:2 (métal–ligand) ainsi qu'un autre complexe moins stable qui semble être une espèce 1:1. On présente aussi des données préliminaires sur l'échange des ligands qui sont liés dans ces complexes.

[Traduit par le journal]

Can. J. Chem. Downloaded from www.nrcresearchpress.com by 210.87.254.40 on 09/06/12
For personal use only.

Introduction

Complexes of tungsten(VI) with hydroxycarboxylic acids and complexes of other transition metals with thiomalic acid have been studied since about 1900, using various techniques. In more recent years, there has been a renewed interest in the metal complexes of thiomalic acid, partly because of their relevance in medicine, biology, and industry. Also, complexes of W(VI) with ligands containing oxygen, nitrogen, or sulphur have drawn increased attention, especially in view of their importance in studies of enzymatic activity.

The only study of the the W(VI) – thiomalic acid system of which we are aware is a preliminary work done in our laboratory some years ago (1). This was carried out in aqueous solution at pH ≅ 3 using visible spectroscopy and 100-MHz proton nmr. Evidence for 1:2 (metal–ligand) complexation was found and a discussion on the conformation of the bound ligand was presented.

The work now reported is a more thorough investigation of this system using 200- and 300-MHz proton nmr as well as ^{13}C nmr spectroscopy, with extension to pH values up to 7 and to more dilute solutions.

The approach is essentially the same as that used in previous papers of ours (2). Information on the number of complexes formed, their relative stabilities, and their structures is obtained; also, preliminary evidence is given on ligand exchange phenomena.

Experimental

Analytical grade sodium tungstate and commercially available (D,L)-thiomalic acid were used (unavailability of the optically active forms and failure in attempts to resolve the racemic mixture preclude us from also using one of the optical isomers, at this stage). In order to reduce the intensity of the OH nmr signal, the former was dried at 120°C, the latter was lyophilized from a solution in deuterium oxide, and D_2O solutions were used throughout. The concentrations of the tungstate solutions were established by weight and the acid solutions were standardized by potentiometry. The pH was adjusted by addition of solutions of DCl and NaOD; the pH* values quoted are the direct pH-meter readings (room temperature) after standardization with aqueous (H_2O) buffers. Whenever necessary, the ionic strength was kept approximately constant by making the solutions 1 *M* in KNO_3. In order to minimize air oxidation of the thiomalic acid, N_2 was run through the solutions during preparation and the nmr tubes were sealed under nitrogen atmosphere. The ^1H spectra were obtained on Varian XL-200 and Bruker CXP-300 spectrometers. The ^{13}C spectra were recorded on the Varian XL-200 instrument (50.3 MHz for ^{13}C) using gated decoupling techniques with suppression of the nuclear Overhauser effect; in this manner, temperature fluctuations were reduced to ca. ±1°C. Typically, spectral widths of 10 000 Hz, acquisition times of 1.5 s, pulse delays of 8–12 s, and 2000 pulses were used.

Results and discussion

1. *Spectral parameters and stoichiometry of complexes*

Figure 1(A) shows the 300-MHz proton nmr spectrum of a 0.017 *M*:0.033 *M* (metal–ligand) solution of sodium tungstate and (D,L)-thiomalic acid in D_2O (pH* 5.5, temperature 278 K). Six ABX spectra can be identified (although the AB subspectra are in part superposed) corresponding to the methylene and methyne protons of bound (five spectra) and free ligand: CO_2H—CH(SH)—CH_2—CO_2H. No further spectra are observed for higher concentrations (up to 2 *M*) for other metal–ligand ratios (4:1 to 1:4 was the range covered) and other pH values; the range of pH studied was 2–7. Free ligand is always detected and its relative concentration increases with dilution; for pH above ca. 7 almost all ligand occurs as free species for dilute solutions. For pH < 2, the signals become very broad, presumably due to extensive polymerization.

The presence of a small amount of the disulphide due to partial oxidation of thiomalic acid is also revealed by the spectra (Fig. 1(A)). It increases with time but can be greatly diminished by running N_2 through the solutions and keeping them under an atmosphere of N_2. As a matter of fact, without these precautions, practically all free and bound thiomalic acid is oxidized to the disulphide in about 3–4 months time, all spectral evidence for complexation with W(VI) having disappeared by then.

The fact that different spectra are observed for ligand molecules in different situations means that, at room and low temperatures, these are undergoing exchange processes that are slow in the nmr time scale. Most proton nmr spectra were obtained not at room temperature but at 278 K to ensure both sharper signals and smaller interference of the residual OH

[1]Revision received March 29, 1984.

Can. J. Chem. Downloaded from www.nrcresearchpress.com by 210.87.254.40 on 09/06/12
For personal use only.

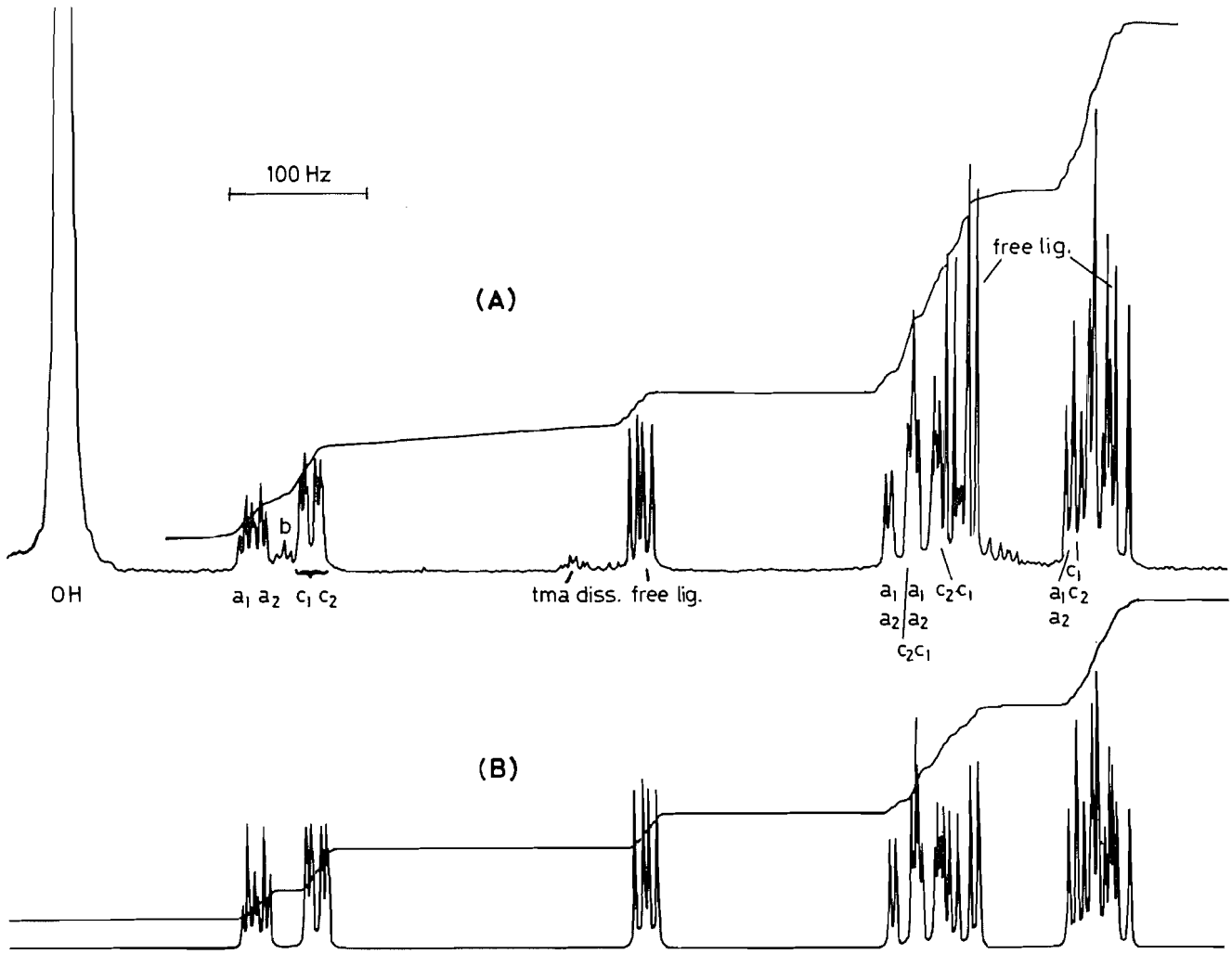

FIG. 1. Observed (A) and simulated (B) (only a_1, a_2, c_1, c_2, and free ligand) 300-MHz proton nmr spectrum of a 0.017 M:0.033 M (metal−ligand) solution of sodium tungstate and (D,L)-thiomalic acid in D_2O, at pH* 5.5 and at 278 K.

signal; however, since no noticeable changes in the position and intensities of the various signals were observed, the results can be taken as valid for room temperature. Some preliminary high temperature results are also presented below.

Whereas the weak X-spectrum denoted by b in Fig. 1(A) can be directly assigned to a less abundant complex, the close X-multiplets a_1 and a_2 and c_1 and c_2 can either be due to distinct complexes or else to a smaller number of complexes possessing two (or more) magnetically nonequivalent ligand molecules.

The assignment of the a_1 and a_2 X-peaks in Fig. 1(A) was done by comparison with the corresponding signals at different spectrometer frequencies (100 and 200 MHz) in conjunction with the analysis of the AB subspectra. The A and B signals were assigned on the basis of intensity considerations and proton spin decoupling experiments.

It is noted that, whereas the AB signals of thiomalic acid undergo only a small low-field shift upon complexation (0−0.15 ppm), the X peaks are much more shifted: 0.7−0.9 ppm to low field. The various chemical shifts relative to free ligand in the same conditions were obtained from ABX analysis of the spectra and are shown in Table 1 for three typical pH values. The results for free thiomalic acid agree with those of ref. 3, except in the case of $\nu_B - \nu_A$ for pH $\cong$ 3 which is given as 0.27 ppm in that paper. The remaining spectral parameters are also given in the table. We have assumed that the relative position of the A and B resonances is retained on complexation, the only hypothesis which is fully supported by the whole set of results (see below). For complex b only ν_X and the sum $J_{AX} + J_{BX}$ could be obtained.

Figure 1(B) shows the simulated spectrum corresponding to bound ligands a_1, a_2, c_1, and c_2 present as well as free ligand, with concentrations given by the integrated X-multiplets. The differences observed in the AB part when comparing the real and the simulated spectra are due to superposed spectra arising from the remaining species, namely complex b and the thiomalic acid disulphide.

The existence of five types of magnetically nonequivalent bound ligand molecules contrasts with the observation of only two ^{13}C sets of signals due to complexation. One reason is that complex b is practically absent for higher concentrations, as is proved by the proton nmr spectrum in the same conditions. Figure 2 shows the ^{13}C 50.3-MHz proton decoupled spectrum of a 0.25 M:0.50 M (metal−ligand) solution of WO_4^{2-} and (D,L)-thiomalic acid in H_2O (with 20% D_2O), pH 4.7, obtained at room temperature. Three sets of peaks are observed, one due to free ligand and the other two to bound ligand. These two are likely to correspond to the close a_1,a_2 and c_1,c_2 proton spectra, respectively. This hypothesis is supported by the relative in-

TABLE 1. Proton magnetic resonance spectral parameters (coupling constants in Hz and shifts in ppm) for WO_4^{2-} + thiomalic acid (tma) (temperature 278 K)

Solution	Ligand	$\|J_{AB}\|$	J_{AX}	J_{BX}	$\nu_B - \nu_A$	$\nu_X - \nu_{X,tma}$	$\nu_B - \nu_{B,tma}$	$\nu_A - \nu_{A,tma}$
pH* = 3.1	Free ligand	16.9	6.6	8.2	0.093	—	—	—
(a)†	a_1	16.2	9.0	4.3	0.169	0.816	0.076	0.00
	a_2	16.2	9.0	4.3	0.169	0.799	0.076	0.00
	b*							
	c_1,c_2	16.2	8.3	4.3	0.112	0.665	0.019	0.00
pH* = 5.5	Free ligand	15.5	9.6	5.9	0.360	—	—	—
(b)†	a_1	15.4	11.1	4.3	0.441	0.951	0.146	0.065
	a_2	15.4	11.1	4.3	0.441	0.936	0.146	0.065
	b		$J_{AX} + J_{BX} = 8.1$			0.864		
	c_1	15.4	11.4	4.0	0.396	0.799	0.082	0.046
	c_2	15.4	11.4	4.0	0.403	0.794	0.089	0.046
pH* = 7.0	Free ligand	15.3	8.8	6.6	0.340	—	—	—
(c)†	a_1	15.6	10.4	4.3	0.438	0.919	0.144	0.046
	a_2	15.6	10.4	4.3	0.438	0.902	0.144	0.046
	b		$J_{AX} + J_{BX} = 9.0$			0.814		
	c_1,c_2	15.9	11.1	3.6	0.399	0.778	0.091	0.032

*Not observed.

†(a) 0.025 M:0.025 M solution; (b) 0.017 M:0.033 M solution; (c) 0.20 M:0.20 M solution.

Can. J. Chem. Downloaded from www.nrcresearchpress.com by 210.87.254.40 on 09/06/12
For personal use only.

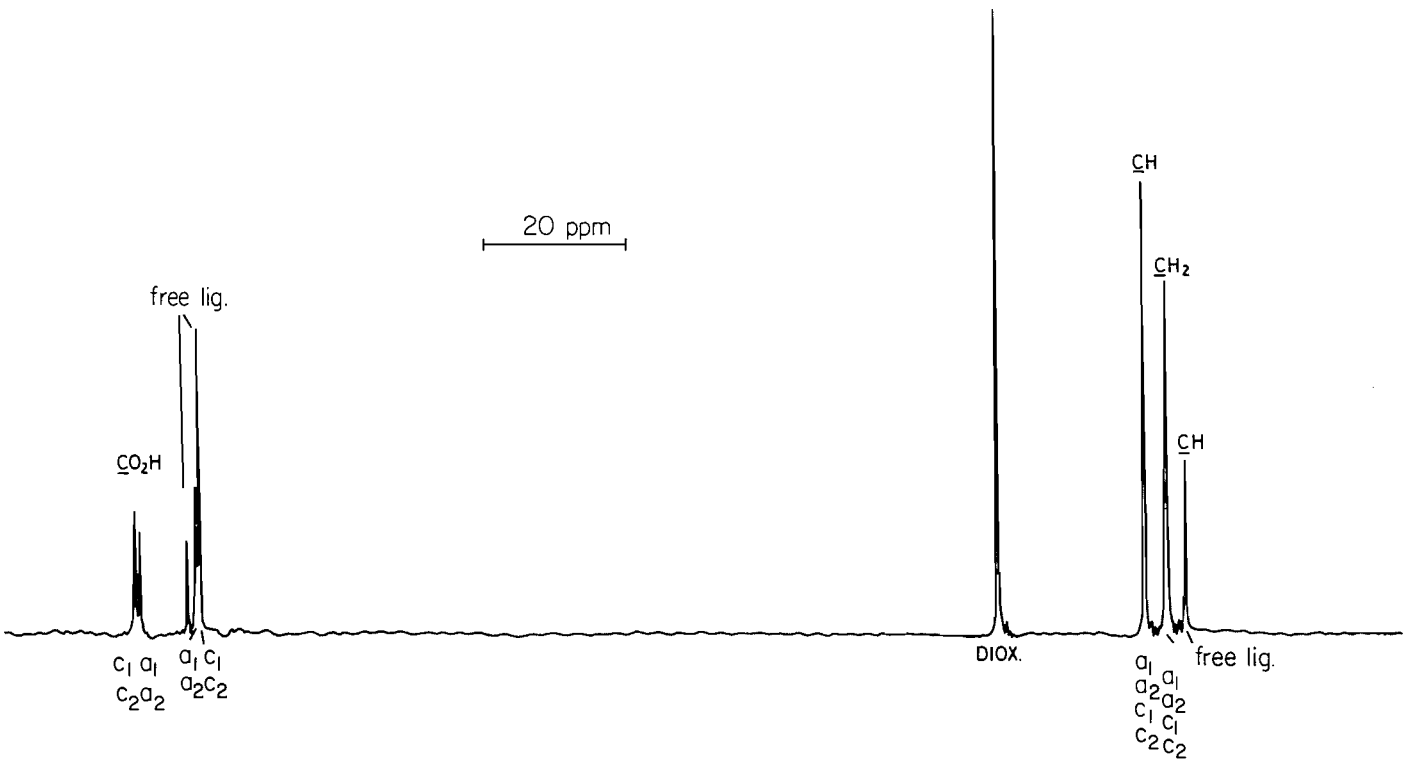

FIG. 2. 50.3-MHz ^{13}C proton decoupled spectrum of a 0.25 M:0.50 M solution of sodium tungstate and (D,L)-thiomalic acid in H_2O/D_2O (pH 4.7, 296 K).

tensities of the ^{13}C signals as compared to the ^1H spectra. The chemical shifts of free ligand relative to dioxane (see also ref. 4) and those of bound ligand relative to free thiomalic acid in the same conditions are given in Table 2. The assignment of the carboxyl signals of each complex has been made on the basis of the observation that only one is appreciably shifted by the formation of complex (shift to low field) and assuming that this corresponds to the carboxyl group next to the sulfhydryl group; since S is also involved in complexation (see below), this assumption means chelation with formation of 5-membered rings. It is noted that the ordering of the C(H) and C(H_2) signals changes on complexation.

From the relative intensities of the X signals in the proton nmr spectra, the amount of bound ligand a_1, a_2, b, $c_1 + c_2$ (due to broadening effects in some solutions, the c_1 and c_2 signals could not always be integrated separately) was determined as a function of metal−ligand molar ratio. The Job's plots thus obtained are given in Fig. 3, for a total concentration of metal + ligand of 0.050 M and pH* 5.0 throughout; the ionic strength was kept approximately constant from solution to solution by

TABLE 2. ^{13}C chemical shifts (in ppm) for WO_4^{2-} + thiomalic acid (0.25 *M*:0.50 *M*; pH 4.7; temperature 296 K)

	HO_2C —	CH(SH) —	CH_2 —	CO_2H
Free ligand (relative to dioxane)	114.4	−26.2	−24.0	112.8
a_1,a_2 (relative to free ligand)	6.4	5.6	0.0	0.4
c_1,c_2 (relative to free ligand)	7.2	5.6	0.4	0.0

making them 1 *M* in KNO_3. For more concentrated conditions (total concentration of metal + ligand = 1.0 *M*, pH* 5.0) the maxima at the 1:2 ratio are again well defined for the ligands *a* and *c*; however, as already mentioned, complex *b* is not detected in those conditions.

In view of the neat maximum at 1:2 for $c_1 + c_2$, and because the intensity ratio for c_1 and c_2 always remains practically constant whenever separate signals can be detected, we conclude that both bound ligands c_1 and c_2 show maximal concentration for a metal−ligand molar ratio of 1:2.

In spite of the limitations of Job's method when there is more than one complex, Fig. 3 is a firm indication that the complexes with spectra a_1, a_2, c_1, and c_2 in Fig. 1 are 1:2 (metal−ligand) species. As for the much less abundant complex *b*, the occurrence of a (less well-defined) maximum at the molar ratio 1:1 can only be taken as a hint of its stoichiometry; this is because there is always a large excess of the other complexes present and, in such circumstances, a maximum in a Job's plot is not necessarily a proof of a certain stoichiometry. We note that evidence for a 1:1 and two 1:2 complexes has previously been found by us for the system tungstate − malic acid (8).

The different intensities of the a_1 and a_2 signals show that they do not arise from two (slightly magnetically nonequivalent) ligand molecules in a 1:2 complex. The same is true of the c_1 and c_2 peaks. The hypothesis of a_1 and c_2 (less intense signals) belonging to one 1:2 complex and, simultaneously, a_2 and c_1 to another can also be ruled out, because then the total intensity of $a_1 + a_2$ should be equal to that of $c_1 + c_2$; this is not the case. Careful analysis of the intensities in those few cases when c_1 and c_2 could be resolved shows that the only hypothesis left is that of a_2 and c_2 corresponding to one 1:2 complex.

2. *The geometry of the complexes*

The large low-field shifts of the methyne proton (X) and of the S-bonded carbon nucleus of thiomalic acid upon complexation indicate that the sulfhydryl group is involved in complexation to W(VI). This is in line with the fact that the disulphide does not complex and with evidence from solid state studies in related complexes (5).

The large low-field shift of one of the carboxyl ^{13}C nuclei of the bound ligands a_1, a_2, c_1, c_2, which we have attributed to the carboxyl group next to SH, is consistent with chelation through the formation of 5-membered rings, as is the case with complexes of malic acid[2] and of α-mercaptocarboxylic acids studied in the solid state (5).

Support for this conclusion comes also from the fact that

[2]The hypothesis of formation of 6-membered rings in complexes of thiomalic acid with Mo(VI) and of malic acid with Mo(VI) and W(VI), considered for some of the complexes in our previous studies (2, 8, 9), must be revised in view of this and other data (5).

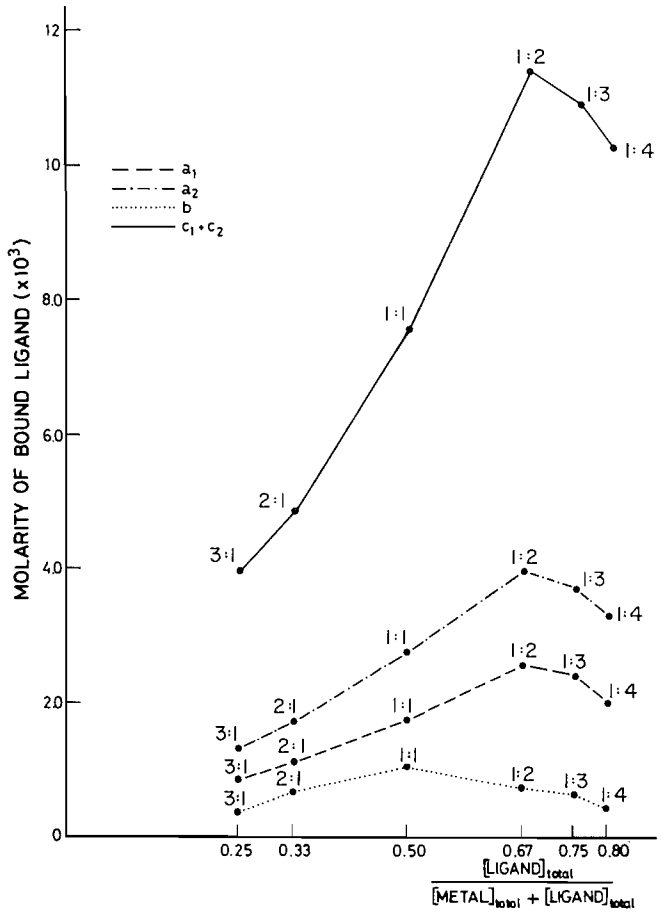

FIG. 3. Job's curves based on proton nmr spectral intensitites. Total concentration of complexing species: 0.050 *M* (solvent D_2O, pH* 5.0, 278 K).

2-mercaptopropionic acid (thiolactic acid), CH_3—CH(SH)—CO_2H, undergoes similar shifts on complexation with W(VI), whereas complexation with the 3-mercapto isomer, CH_2(SH)—CH_2—CO_2H, is almost nonexistent. In fact, the ^1H and ^{13}C nmr spectra of a solution of 3-mercaptopropionic acid are practically not affected by the presence of WO_4^{2-}. On the contrary, important changes occur in the case of the 2-mercapto isomer. For a 1:2 (metal−ligand) solution, at pH* 7, two CH patterns in the proton spectrum occur 0.797 and 0.677 ppm to low field of the corresponding signal of free ligand and having different intensities; the ^{13}C shift for the same group is 4.4 ppm, also to low field relative to free ligand, and those for the carboxyl group are 6.8 ppm and 7.6 ppm (two types of bound ligand). These and other preliminary results point to the presence of two 1:2 complexes.

Further evidence for the involvement of sulfhydryl and carboxyl groups in chelation arises also from Raman spectroscopy. In particular, the band at 1870 cm^{-1} due to the stretching vibration of the deuterated sulfhydryl group markedly decreases in intensity upon complexation, which is indicative of ionization of this group as a result of bonding to the metal; simultaneously, the band at ca. 1200 cm^{-1} becomes stronger, suggesting an enhanced contribution of the C—O stretching vibration upon complexation (6).

The H—H vicinal coupling constants observed for bound ligands *a* and *c* are of similar magnitude. This shows that the conformation of the ligand is approximately the same in all the

Can. J. Chem. Downloaded from www.nrcresearchpress.com by 210.87.254.40 on 09/06/12
For personal use only.

1:2 complexes. More precisely, with the $—CH_2—CO_2H$ moiety still rotating around the central C—C axis, we conclude that the potential energy functions for internal rotation most likely have similar features in those complexes. For about pH 5 and above, comparison with the J_{AX} and J_{BX} values for the free ligand in the same conditions shows that the most stable conformation of the acid for these pH values (3, 4), which is conformation **I** below, is further stabilized relative to the others on complexation. The pronounced decrease of J_{AX} for the 1:2 complexes on going from pH 5 to pH 3, accompanied by only a slight change of J_{BX} in ligands c_1, c_2 and no change in a_1, a_2 suggests that conformation **I** loses stability (especially in favour of **III**), as is the case with the free ligand itself (3, 4). However, contrary to free thiomalic acid at this low pH, conformation **I** is still the most stable in the complexes ($J_{AX} > J_{BX}$).

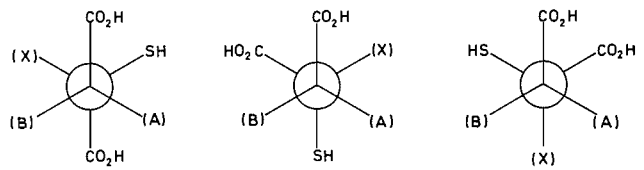

I **II** **III**

Regarding complex *b*, only $J_{AX} + J_{BX}$ could be obtained from the spectrum. The small value for this sum (ca. 8 Hz) suggests that the main conformation of the ligand now is **III**. This is in accordance with a terdentate function of the ligand in this presumably 1:1 complex.

The tungstyl group $—WO_2$ in the 1:2 complexes is expected to have *cis* configuration (5). The occurrence of two Raman bands observed at 930 cm^{-1} and 880 cm^{-1} (room temperature, pH 4, various metal−ligand molar ratios) supports this hypothesis (6, 7).

Thus, one possible structure for a 1:2 complex is

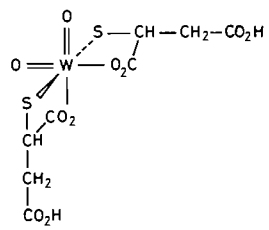

where the S atoms are *trans* to each other (and are assumed nonprotonated). Other possibilities do of course exist. In addition, the use of racemic thiomalic acid increases the number of isomers. Depending on the configuration at the tungsten centre and on the optically active forms of acid involved being the same or not, 12 magnetically nonequivalent 1:2 complexes can in principle form, four of which would have C_2 symmetry (with two magnetically equivalent ligands). The use of one of the optical isomers of thiomalic acid as ligand would reduce the number of possible complexes and would help to clarify the characterization of this system. Unfortunately, difficulties related to the resolution of (D,L)-thiomalic acid force us to postpone such a study.

On the basis of molecular models, it is found that the CH group of bound ligand lies either almost parallel to one of the W=O bonds or away. This may be the main reason for the observation of the two groups of X signals a_1,a_2 and c_1,c_2. The former would then be associated with a parallel orientation for which the CH proton shielding constant is decreased by the magnetic anisotropy and the electric field effects of the W=O group.

It is also found that when the bound ligand adopts the most stable conformation − conformation **I** − proton B of CH_2 (which is then *trans* to the S atom) lies approximately in the plane of the bonded carboxyl group and parallel to the C=O axis

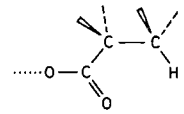

thus experiencing a deshielding effect due to the C=O group. This is in accordance with the shift of proton B to low field relative to proton A on complexation; for instance, for pH* 5.5, $\nu_B - \nu_A$ is 0.360 for free ligand, 0.441 for bound ligands a_1, a_2, and 0.396 and 0.403 for ligands c_1 and c_2. This chemical shift decreases as pH changes from 5 to 3, in agreement with a decrease of the contribution of conformation **I**.

3. *The effect of pH and the stability of the complexes*

The effect of pH on the concentrations of bound ligands a_1, a_2, *b*, and $c_1 + c_2$ is shown in Fig. 4 for various metal−ligand molar ratios. The behaviour of the curves is quite similar, with maxima occurring for pH* in the region 4−4.5 for *b* and $c_1 + c_2$ and in the region 3−4 for a_1, a_2. The results, especially for a_1 and a_2, enable us to rule out the hypothesis of the corresponding complexes differing just on the degree of ligand protonation.

The complexes of W(VI) with thiomalic acid are found to be less stable than the complexes between W(VI) and malic acid; in fact, in the first case free ligand is detected by nmr even for a 4:1 metal−ligand molar ratio, whereas the same only happens for 1:*n* ratios of metal and malic acid with $n \geqq 1.5$ (8). The difference is especially marked for complex *b*, which is always less abundant than the 1:2 complexes.

The fact that separate ^1H nmr signals are observed for bound and free ligand in the various complexes naturally prompted us to make an estimate of their formation constants from the spectral intensities. It must, however, be recognized that we are dealing with a very complex system in which the metal oxoions are involved in various polymerization equilibria depending on concentration, pH, and ionic strength (10) besides being involved in complexation equilibria. This can lead to errors. Additional uncertainties arise from the fact that the ionizations of thiomalic acid (the microscopic constants of which we are determining in a separate study) are affected by complexation, especially in the case of the SH group; also, we are using D_2O and not H_2O solutions. Therefore, the conditions for which any determination is done can be very critical.

We have performed calculations at pH* 4.0, for 2:1 (0.033 *M*:0.017 *M*; 0.050 *M*:0.025 *M*), 1:1 (0.017 *M*:0.017 *M*; 0.025 *M*:0.025 *M*), 1:2 (0.017 *M*:0.033 *M*; 0.025 *M*:0.050 *M*), and 1:3 (0.017 *M*:0.050 *M*) solutions; the ionic strength was held approximately constant with 1 *M* KNO_3. For these conditions, the main species of W(VI) present is believed to be the polyanion $W_{12}O_{39}^{6-}$ (10). On the other hand, from the published values (11) of pK_1 (3.1) and pK_2 (4.6) for aqueous solution at 298 K, we conclude that the main species of thiomalic acid (here represented by D_3Y) present at pH* 4.0 is D_2Y^- (one carboxyl group ionized). Thus the main equilibrium for 1:2 complexation at this pH* is

Can. J. Chem. Downloaded from www.nrcresearchpress.com by 210.87.254.40 on 09/06/12
For personal use only.

Can. J. Chem. Downloaded from www.nrcresearchpress.com by 210.87.254.40 on 09/06/12
For personal use only.

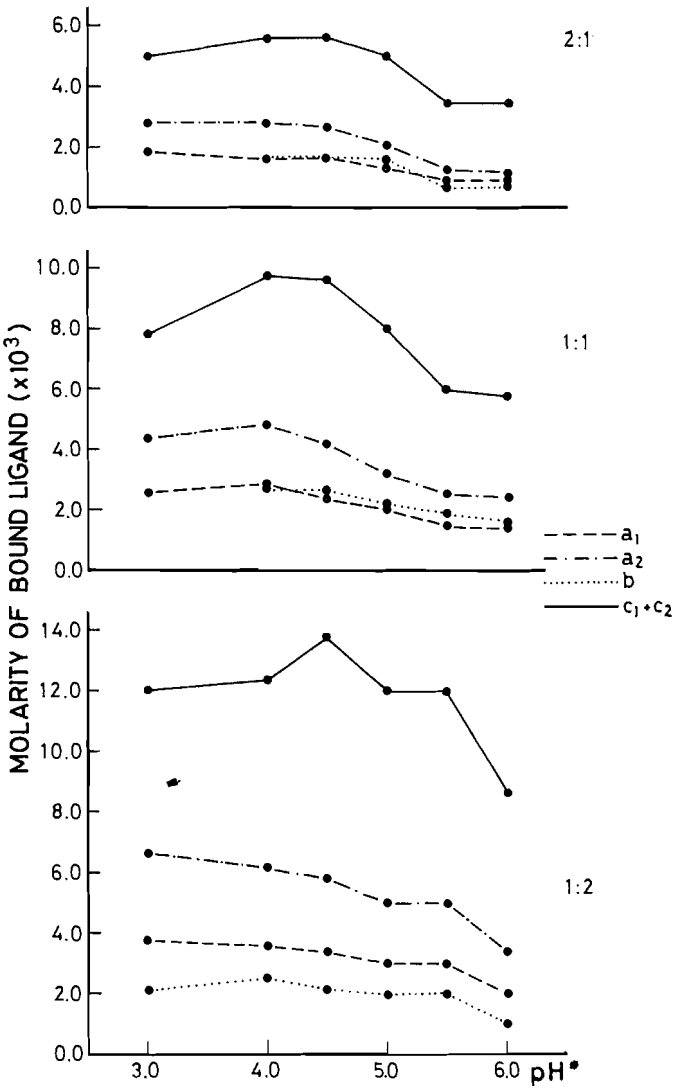

FIG. 4. Effect of pH on concentration of bound ligands for various metal–ligand molar ratios (0.033 *M*:0.017 *M*; 0.025 *M*:0.025 *M*; 0.017 *M*:0.033 *M*).

$$W_{12}O_{39}^{6-} + 24D_2Y^- + 6D^+ \rightleftarrows 12WO_2(DY)_2^{2-} + 15D_2O$$

use being made of the previous conclusion that the sulfhydryl group is ionized in the complexes.

From the concentrations of free and bound ligand obtained from the spectral intensities for each solution, and ignoring other equilibria, we obtained pK values of formation for the 1:2 complexes, according to the equation above, which range from −47.5 to −49 in the case of a 1:2 a_1 complex, and from −50 to −51.5 for a 1:2 a_2 complex; the corresponding values for c_1 and c_2 complexes are lower by about −1 to −2 relative to a_2 and a_1, respectively. If a_2 corresponds to just one of the ligands in a 1:2 complex, the other ligand being responsible for c_2, then the calculated pK value for such a complex is from −54 to −55.

In spite of the limited dispersion of values obtained, they should be taken with caution. We note, in particular, that if the free ligand is only 70% in the form D_2Y^-, then all pK values go up by almost 4 units.

Similar determinations at lower pH* values, at which the dominant form of thiomalic acid is D_3Y, were not feasible, owing to excessive broadening of the nmr signals. On the other hand, identical calculations at higher pH* values become increasingly unwarranted because of the presence of various polymerization equilibria of WO_4^{2-} (10).

4. *Ligand exchange*

The proton nmr spectrum shown in Fig. 1 was obtained at 278 K. At room and higher temperatures some of the signals due to the complexes become broader and eventually coalesce into groups of smaller numbers of lines. This is an indication of ligand exchange at these temperatures. As the chemical shifts between the A protons for the various complexes are different from those for B or X protons, coalescence of the corresponding signals occurs at different temperatures.

Thus, for a 1:2 solution at pH* 5.0, the A signals due to bound ligands a_1,a_2 and c_1,c_2 are only 0.019 ppm apart and coalesce into one group of four lines at 294 K. This points to a rate of ligand exchange for these complexes of about 8 s^{-1} at room temperature.

The B signals, which have an internal chemical shift of ca. 0.060 ppm, only coalesce at 315 K; at this temperature the rate of ligand exchange will then be about 26 s^{-1}.

The X multiples due to a_1,a_2 and c_1,c_2, which are 0.15 ppm apart, turn into a broad peak at ca. 333 K; the rate of ligand exchange will then be about 65 s^{-1}.

From these preliminary rates of ligand exchange obtained for the 1:2 complexes, a value of about 40 kJ mol^{-1} is estimated for the corresponding free energy of activation. A more complete study is in progress.

Conclusions

When thiomalic acid and sodium tungstate are mixed in aqueous solution, at pH ranging from 2 to 7, four (or five) complexes form, especially at pH 3–4.5, as follows.

(*a*) Three (or four) are comparatively strong and they have a 1:2 (metal–ligand) stoichiometry; the ligand acts as bidentate, involving the (deprotonated) sulfhydryl group and the (ionized) adjacent carboxyl group, the two carboxyl groups being approximately *trans* to each other; ligand exchange is slow at room temperature (rate about 8 s^{-1}) with a free energy of activation of the order of 40 kJ mol^{-1}; evidence exists for the presence of a *cis* tungstyl group in these complexes.

(*b*) One weaker complex, less well characterized, is probably of 1:1 stoichiometry; the bound ligand has a conformation where the sulfhydryl group and the adjacent carboxyl group are both approximately *gauche* to the other carboxyl group, a conformation which is appropriate to a tridentate function of the ligand.

(*c*) By ignoring secondary equilibria, a crude nmr estimation was made of the formation constants of the 1:2 complexes, but the results must be taken with caution owing to the great complexity of the system. Nevertheless, clear evidence exists for weaker complexes of W(VI) with thiomalic acid than with malic acid.

Acknowledgements

Thanks are due to I.N.I.C. (of the Portuguese Ministry of Education) for financial support and to Prof. A. Xavier and his NMR laboratory in Lisbon for the 300-MHz spectra. The authors also thank the referees for several helpful comments.

1. A. M. D. PEREIRA and V. M. S. GIL. J. Inorg. Nucl. Chem. **39**, 857 (1977).
2. M. M. CALDEIRA, M. E. SARAIVA, and V. M. S. GIL. Inorg.

Nucl. Chem. Lett. **17**, 295 (1981) and references therein.
3. D. E. LEYDEN and D. B. WALTERS. Spectrochim Acta Part A, **25**, 1869 (1969).
4. V. M. S. GIL. Org. Magn. Res. **15**, 96 (1981).
5. R. E. TAPSCOTT. *In* Transition metal chemistry. Vol. 8. *Edited by* G. A. Melson and B. N. Figgis. Marcel Dekker Inc., New York. 1982. p. 253, and references therein.
6. M. M. CALDEIRA and J. J. C. TEIXEIRA DIAS. Spectrochim. Acta, Part A, **40**, 265 (1984).
7. W. P. GRIFFITH. J. Chem. Soc. (A), 211 (1969).
8. V. M. S. GIL, M. E. SARAIVA, M. M. CALDEIRA, and A. M. D. PEREIRA. J. Inorg. Nucl. Chem. **42**, 389 (1980).
9. V. M. S. GIL, M. M. CALDEIRA, and M. E. SARAIVA. Inorg. Nucl. Chem. Lett. **16**, 65 (1980).
10. C. F. BAES, JR. and R. E. MESMER. The hydrolysis of cations. J. Wiley, New York. 1976.
11. R. S. REID and D. L. RABENSTEIN. Can. J. Chem. **59**, 1505 (1981).

Can. J. Chem. Downloaded from www.nrcresearchpress.com by 210.87.254.40 on 09/06/12
For personal use only.

Pyrones. X.[1] Lateropyrone, a new antibiotic from the fungus *Fusarium lateritium* Nees

GORDON WILLIAM BUSHNELL, YUN-LONG LI,[2] AND GERALD ARTHUR POULTON
Department of Chemistry, University of Victoria, Victoria, B.C., Canada V8W 2Y2

Received February 7, 1984

GORDON WILLIAM BUSHNELL, YUN-LONG LI, and GERALD ARTHUR POULTON. Can. J. Chem. **62**, 2101 (1984).

Lateropyrone, 5-hydroxy-9-methoxy-2-methyl-4*H*,6*H*-pyrano[3,4-*g*]-1-benzopyran-4,6-dione-8-carboxylic acid, **1**, has been isolated from cultures of the fungus *Fusarium lateritium* Nees, and shown to have inhibitory activity against the growth of a gram-positive bacterium and a yeast. A crystal structure of the dimethyl derivative of lateropyrone, **2**, was determined. The crystals are monoclinic, space group $P2_1/c$, with a = 9.663(4), b = 22.317(9), c = 7.747(5) Å, β = 113.03(4)°, D_c = 1.496 g cm^{-3}, V = 1538(1) Å^3, T = 25°C, $C_{17}H_{14}O_8$. The structure was refined to R = 0.0543 by least squares using 2100 observed, independent reflections measured on a 4-circle diffractometer, to obtain 241 parameters. The linearly fused tricyclic ring system is only approximately planar. In- and out-of-plane distortions are rationalized in terms of molecular overcrowding.

GORDON WILLIAM BUSHNELL, YUN-LONG LI et GERALD ARTHUR POULTON. Can. J. Chem. **62**, 2101 (1984).

On a isolé la latéropyrone, l'acide hydroxy-5 méthoxy-9 méthyl-2 4*H*,6*H*-pyranno[3,4-*g*] benzopyranne-1 dione-4,6 carboxylique-8, **1**, de cultures du champignon *Fusarium lateritium* Nees et on montre qu'elle a une activité inhibitrice vis-à-vis la croissance d'une bactérie gramme-positive et d'une levure. On a déterminé la structure cristalline du dérivé diméthylé, **2**, de la latéropyrone. Les cristaux sont monocliniques et appartiennent au groupe d'espace $P2_1/c$ avec a = 9,663(4), b = 22,317(9), c = 7,747(5) Å, β = 113,03(4)°, D_c = 1,496 g cm^{-3}, V = 1538(1) Å^3, T = 25°C, $C_{17}H_{14}O_8$. On a affiné la structure par la méthode des moindres carrés jusqu'à une valeur de R = 0,0543 pour 2100 réflexions indépendantes observées et mesurées à l'aide d'un diffractomètre à 4 cercles pour obtenir 241 paramètres. Le système tricyclique condensé linéaire n'est qu'approximativement planaire. On rationalise les distortions dans le plan et hors du plan en fonction d'un encombrement moléculaire.

[Traduit par le journal]

Can. J. Chem. Downloaded from www.nrcresearchpress.com by 210.87.254.105 on 09/06/12
For personal use only.

The *Fusaria* fungi are well known as contaminants in cereal grains (1), as the causative agents of stem and branch cankers in trees (2), and as an insect pathogen (3). Many investigations of the metabolites of *Fusaria* species have been carried out, with toxins causing fusariotoxicoses in animals (4, 5), and metabolites possessing insecticidal activity (3) or antibiotic activity (6, 7) having been identified. A recent review has appeared (8).

Fusarium lateritium Nees has been isolated[3] from *Tsuga heterophylla* (Raf.) Sarg. trees suffering from dieback, and produces visible quantities of crystals when cultured on malt extract at room temperature. Extraction of the culture plates with dichloromethane allowed the isolation of a crystalline metabolite which showed significant antimicrobial activity; this communication details the structural elucidation of this metabolite, hereafter called lateropyrone. The identical metabolite was also isolated from an unidentified contaminant fungus.

Results and discussion

Lateropyrone has the molecular formula $C_{15}H_{10}O_8$, as indicated by accurate mass measurement, and contains a carboxylic acid function (deuterium exchangeable signal at 14.7 ppm, ir absorption at 3200−2500 and 1750 cm^{-1}) and a hydrogen-bonded phenol (deuterium exchangeable signal at 10.4 ppm, ir absorption at 3450 cm^{-1}). The presence of these functional groups was confirmed by pK* measurements,[4] which gave values of 6.70 ± 0.05 (acid) and 10.9 ± 0.2 (phenol), and by the formation of a monoacetate (acid peak at 14.68 ppm, ir absorption at 3100−2300, 1750 cm^{-1}, acetate at 2.44 ppm, carbonyl absorption at 1727 cm^{-1}) and a dimethyl ether methyl ester (three 3H singlets at 4.08, 3.99, and 3.97 ppm). The latter compound was chosen for X-ray analysis, as suitable crystals of the natural product could not be obtained.

Figure 1 is an ORTEP drawing of this derivative, giving the atomic labelling scheme, and a display of the thermal motion ellipsoids scaled to enclose 50% probability. The fractional atomic coordinates are presented in Table 1 together with isotropic temperature parameters derived from the deposited anisotropic temperature parameters. The interatomic distances are given in Table 2. The central ring is aromatic and the mean bond length is 1.398 Å, but the rings on either side are of the α- and γ-pyrone types and are not aromatic. The olefinic double bonds are similar, but not identical in length, as they are situated differently with respect to the oxygen atoms and the aromatic ring. Considering the error limits, the C—O single bonds in the pyrone rings are of the same length, as are the exocyclic C—C bonds, and all three CH_3—O bonds. However, the carbonyl bond C(1)=O(1) is longer than the other two in the structure. The difference of 0.031(4) Å is significant and may possibly be ascribed to the close intramolecular approach of H(132) to O(1) of 2.43(1) Å (the sum of the van der Waals radii = 2.60 Å) in contrast to the other oxygen atoms of carbonyl groups whose shorter contacts with hydrogen atoms are greater than 2.585 Å. Such a lengthening of a carbonyl bond may be regarded as a very weak hydrogen bonding. In comparison, hydrogen bonding in 2,6-dimethyl-γ-pyrone·HBr·H_2O lengthens the carbonyl group to 1.32 Å (11). The central aromatic ring has normal bond lengths. The positions of the double bonds in the pyrone rings are indicated by C—C lengths in the 1.32−1.35 Å range, by the detection of H(2), and by the approximate planarity of O(10), C(9), C(91), C(8), O(8), and C(7).

The bond angles are given in Table 3 and the mean plane and

[1]For part IX in this series, see ref. 9.

[2]On leave from the Guangzhou Institute of Chemistry, Academy of Science of China, People's Republic of China.

[3]A. Funk. Private communication.

[4]pH-metric titrations were performed as described by Dietrich *et al.* (10*a*); measurements were made in DMF/water (85:15), and have been corrected (10*b*). These values may be compared to those obtained under similar conditions for *m*-hydroxybenzoic acid (7.08, acid, and >12.6, phenol).

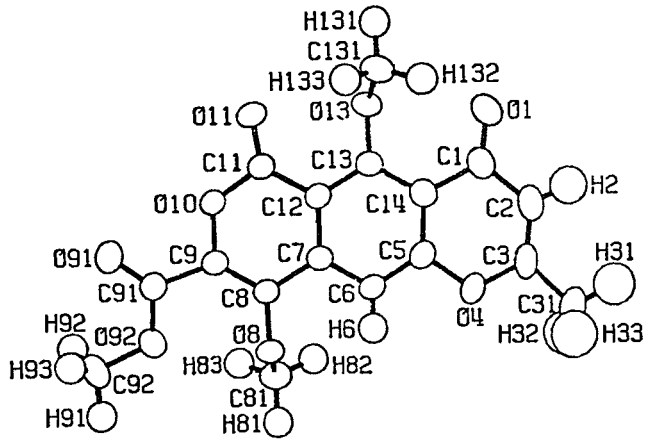

FIG. 1.

TABLE 1. Fractional atomic coordinates and temperature parameters*

Atom	x/a	y/b	z/c	U_{eq}
O(1)	8189(2)	5217(1)	6057(3)	578(9)
O(4)	4080(2)	5779(1)	2394(3)	486(8)
O(8)	1250(2)	4156(1)	−1698(3)	453(7)
O(10)	4366(2)	3113(1)	−46(3)	479(8)
O(11)	6716(2)	3175(1)	1845(4)	715(10)
O(13)	7578(2)	4128(1)	4198(3)	460(7)
O(91)	2450(3)	2398(1)	−2493(4)	916(13)
O(92)	556(2)	3029(1)	−3022(3)	595(9)
C(1)	6973(3)	5377(1)	4888(4)	442(11)
C(2)	6406(4)	5982(1)	4868(5)	523(13)
C(3)	5044(3)	6156(1)	3719(4)	483(12)
C(5)	4526(3)	5205(1)	2248(4)	381(10)
C(6)	3440(3)	4865(1)	911(4)	386(10)
C(7)	3753(3)	4276(1)	641(3)	351(9)
C(8)	2609(3)	3902(1)	−687(3)	365(9)
C(9)	2944(3)	3334(1)	−959(4)	403(10)
C(11)	5533(3)	3427(1)	1249(4)	437(10)
C(12)	5189(3)	4034(1)	1694(3)	361(9)
C(13)	6259(3)	4383(1)	3080(4)	377(9)
C(14)	5944(3)	4983(1)	3389(4)	392(10)
C(31)	4324(4)	6748(1)	3655(6)	649(15)
C(81)	162(3)	4125(1)	−856(5)	592(13)
C(91)	1985(3)	2869(1)	−2232(4)	471(11)
C(92)	−486(4)	2611(2)	−4305(5)	698(14)
C(131)	8846(3)	4262(2)	3734(4)	544(12)
H(2)	707(4)	626(2)	578(5)	76(10)′
H(6)	249(3)	502(1)	23(4)	48(8)′

*Estimated standard deviations are given in parentheses. Coordinates $\times 10^n$ where n = 4,4,3 for O, C, H. Temperature parameters $\times 10^n$ where n = 4,4,3 for O, C, and H. U_{eq} = the equivalent isotropic temperature parameter. $U_{eq} = 1/3\ \Sigma_i\Sigma_j U_{ij} a_i^* a_j^* (a_i \cdot a_j)$ Primed values indicate that U_{iso} is given. $T = \exp -(8\pi^2 U_{iso} \sin^2\theta/\lambda^2)$.

TABLE 2. Interatomic distances (Å)*

Atoms	Distance	Atoms	Distance
C(2)—C(1)	1.455(4)	C(9)—C(8)	1.346(4)
C(1)—O(1)	1.223(3)	C(91)—C(9)	1.480(4)
C(3)—C(2)	1.326(4)	C(91)—O(91)	1.191(3)
H(2)—C(2)	0.96(4)	C(91)—O(92)	1.322(3)
C(31)—C(3)	1.484(4)	C(92)—O(92)	1.445(4)
C(3)—O(4)	1.373(3)	C(9)—O(10)	1.369(3)
C(5)—O(4)	1.369(3)	C(11)—O(10)	1.374(3)
C(14)—C(5)	1.399(4)	C(11)—O(11)	1.193(3)
C(6)—C(5)	1.378(4)	C(12)—C(11)	1.466(4)
H(6)—C(6)	0.93(3)	C(13)—C(12)	1.400(4)
C(7)—C(6)	1.384(4)	C(13)—O(13)	1.355(3)
C(12)—C(7)	1.413(3)	C(131)—O(13)	1.437(3)
C(8)—C(7)	1.444(3)	C(14)—C(13)	1.414(4)
C(8)—O(8)	1.362(3)	C(14)—C(1)	1.487(4)
C(81)—O(8)	1.440(4)		

*Estimated standard deviations are given in parentheses.

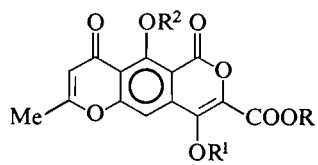

1 R = R² = H, R¹ = Me
2 R = R¹ = R² = Me
3 R = R¹ = H, R² = Me
4 R = H, R¹ = Me, R² = OAc

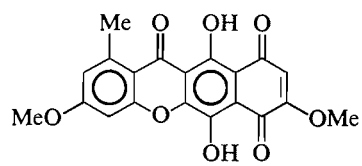

5 Bikaverin

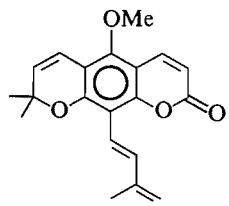

6 Avicennin

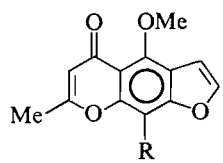

7 R = H
8 R = OMe

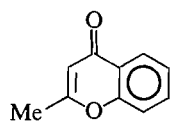

9

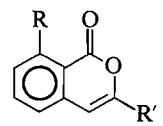

11 R = H, R′ = Ph
12 R = OMe, R′ = C_5H_{11}

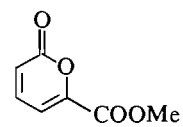

10

torsion angles in Table 4. The most striking feature is the lateral displacement of O(1) and O(11) away from the O(13) methoxy group. The angles bout C(13) are very close to 120° because the steric repulsion, which we shall discuss further, between O(13) and O(1),O(11) comes from both sides. The bond angles around the ethylenic bonds in the α- and γ-pyrone rings are remarkably similar to each other. The angles at the methoxy oxygen atoms on the ring system are essentially identical, with a mean value of 115.6°. The conformation of the methoxy groups on ring systems of this kind is of some interest. In *p*-dimethoxybenzene (12) the MeO groups are approximately in-plane and *trans* for electronic reasons. For the bikaverin molecule **5**, in which there is little possibility of the methoxy groups being crowded, the conformation is again approximately planar (13). On the other hand, the methoxy group in avicennin **6** is crowded by two adjacent ethylenic hydrogen atoms, and adopts a conformation with the C—O—C plane approximately perpendicular to the ring system (14). In the title compound the O(13) methoxy group is inescapably restricted in its rotation by O(1) and O(11), and the O(8) methoxy group is confined by H(6) and also by O(92) in the observed conformation of the methyl ester. The methoxy groups project on opposite sides of the molecular plane.

The weighted least-squares plane and torsion angle results are given in Table 4. The least-squares plane of the central aromatic ring was chosen as the best reference plane. The molecule is significantly non-planar, and even the six atoms of the central ring do not form a planar set. The non-planarity is

Can. J. Chem. Downloaded from www.nrcresearchpress.com by 210.87.254.105 on 09/06/12
For personal use only.

TABLE 3. Bond angles (°)*

Atoms	Angle	Atoms	Angles
C(14)—C(1)—O(1)	124.1(3)	C(8)—C(9)—O(10)	120.9(2)
C(2)—C(1)—O(1)	121.9(3)	C(91)—C(9)—O(10)	109.4(2)
C(14)—C(1)—C(2)	114.1(3)	C(91)—C(9)—C(8)	129.7(2)
H(2)—C(2)—C(1)	116.3(20)	C(11)—O(10)—C(9)	124.4(2)
H(2)—C(2)—C(3)	120.3(20)	C(12)—C(11)—O(11)	128.0(3)
C(3)—C(2)—C(1)	123.4(3)	O(11)—C(11)—O(10)	115.5(2)
C(2)—C(3)—O(4)	121.8(3)	C(12)—C(11)—O(10)	116.5(2)
C(31)—C(3)—O(4)	110.5(3)	C(13)—C(12)—C(11)	121.8(2)
C(31)—C(3)—C(2)	127.8(3)	C(11)—C(12)—C(7)	118.6(2)
C(5)—O(4)—C(3)	119.5(2)	C(13)—C(12)—C(7)	119.6(2)
C(6)—C(5)—O(4)	113.9(2)	C(14)—C(13)—C(12)	120.9(2)
C(14)—C(5)—O(4)	122.9(2)	C(12)—C(13)—O(13)	119.0(2)
C(14)—C(5)—C(6)	123.3(2)	C(14)—C(13)—O(13)	120.0(2)
C(7)—C(6)—C(5)	119.4(2)	C(131)—O(13)—C(13)	115.7(2)
C(8)—C(7)—C(6)	120.4(2)	C(5)—C(14)—C(1)	118.2(2)
C(12)—C(7)—C(8)	119.7(2)	C(13)—C(14)—C(5)	116.9(2)
C(12)—C(7)—C(6)	119.9(2)	C(13)—C(14)—C(1)	124.8(2)
C(7)—C(8)—O(8)	117.8(2)	O(92)—C(91)—O(91)	123.6(3)
C(9)—C(8)—O(8)	122.6(2)	C(9)—C(91)—O(91)	123.5(3)
C(9)—C(8)—C(7)	119.5(2)	C(9)—C(91)—O(92)	112.8(2)
C(81)—O(8)—C(8)	115.5(2)	C(92)—O(92)—C(91)	117.7(2)

*Estimated standard deviations are given in parentheses.

TABLE 4. Weighted least-squares plane and torsion angle results

(a) Equation of the plane for the central aromatic ring

Coefficients of $Ax + By + Cz = D$ (Å)*

A	*B*	*C*	*D*	χ^2
0.6656	0.3066	−0.6804	4.916	138

(b) Perpendicular distances from the least-squares plane (Å)

Atoms defining the plane:

C(5), 0.014(3); C(6), 0.001(3); C(7), −0.016(3); C(12), 0.019(3); C(13), −0.006(3); C(14), −0.010(3).

Other atoms:

O(1), −0.239(2); O(4), 0.019(2); O(8), −0.101(2); O(10), 0.055(2); O(11), 0.310(3); O(13), −0.100(2); O(91), 0.013(3); O(92), −0.410(2); C(1), −0.108(3); C(2), −0.045(4); C(3), −0.013(3); C(8), −0.096(3); C(9), −0.082(3); C(11), 0.131(3); C(31), −0.027(4); C(91), −0.142(3); C(92), −0.485(4); H(2), −0.05(4); H(6), −0.04(3).

(c) Torsion angles

For the methoxy groups:	
C(12)—C(13)—O(13)—C(131)	+101.7(3)
C(7)—C(8)—O(8)—C(81)	−89.7(3)
For the ester group:	
C(8)—C(9)—C(91)—O(92)	−9.0(5)
C(9)—C(91)—O(92)—C(92)	+179.6(3)
C(8)—C(9)—C(91)—O(91)	+172.1(4)
O(91)—C(91)—O(92)—C(92)	−1.5(5)
O(10)—C(9)—C(91)—O(91)	−5.3(5)
For the ketone groups:	
C(13)—C(14)—C(1)—O(1)	−2.5(5)
C(13)—C(12)—C(11)—O(11)	−6.1(5)

*The coordinate system used has *x* along *a*, *y* along *b*, and *z* along *c**. $\chi^2 = \sum_i (P_i^2/\sigma^2(P_i))$, the summation being over all atoms in the plane.

largely a consequence of overcrowding between the peripheral C—O bonds, which in an idealized molecule of this kind would be parallel and about 2 × 1.4 × cos 30° = 2.4 Å apart. As the van der Waals radius of oxygen is 1.4 Å (15), the molecule is deformed. The deformation can be analyzed into in-plane and out-of-plane components. The former have been dealt with in discussing the bond angles. For the ester group, out-of-plane deformation is particularly easy, and O(92) is more out-of-plane than O(8), and in the opposite direction. The set of atoms C(9), C(91), O(91), O(92) maintains planarity (χ^2 = 5.5), and is at 11.6° to the plane of the aromatic ring. On the other side of the molecule O(1) and O(11) move out of the plane in opposite directions. O(13) is −0.100(2) from the plane in the same direction as O(1), whereas C(131) is at +1.126(3) Å on the same side as O(11). The torsion angle for this MeO group shows that it is 11.7° away from orthogonality with the aromatic ring, in the direction to be expected from the O(1),O(11) out-of-plane distortions. The twisting of the molecule, arising from the overcrowding of O(1), O(13), and O(11), is transmitted to the aromatic ring (through C(1) to C(14), and through C(11) to C(12)) and largely accounts for its non-planarity.

In seeking analogous structural effects, bikaverin **5** is the closest natural product whose crystal structure is available (14). It contains four linearly fused six-membered rings, in the order aromatic, γ-pyrone, hydroquinone, quinone. An hydroxyl group therefore lies between, and parallel to, two ketone groups. Unfortunately for the comparison, this hydroxyl group is not methylated and can hydrogen bond with one of the adjacent O atoms, thus countering the repulsive effect on that side. We cannot say with certainty on which side this occurs, since the hydrogen atoms were not found in this structure. However, the adjacent quinone oxygen has a slight lengthening of the C=O bond 1.25(2) Å combined with a closing of the external angle at C facing the OH group (117.8(15)°), suggesting that the H-bonding occurs here. The adjacent oxygen atom on the other side (γ-pyrone), has a C=O bond length of 1.22(2) Å, an external angle facing OH of 123.7(15)°, and out-of-plane distortion of 0.17(1) Å suggesting repulsion, and so reinforcing the assignment already given. Thus bikaverin does provide an example of overcrowding between adjacent oxygen atoms along the edge of a linearly fused system.

Similar structural effects have been observed further afield in

Can. J. Chem. Downloaded from www.nrcresearchpress.com by 210.87.254.105 on 09/06/12
For personal use only.

Can. J. Chem. Downloaded from www.nrcresearchpress.com by 210.87.254.105 on 09/06/12
For personal use only.

the Russion crystallographic work on 1,8-dihaloanthraquinones (hal = Cl and I) (16, 17). This work confirms that out-of-plane deformations do occur in response to overcrowding of this kind. The dichloro compound distorts to put the central ring in the boat form, whereas the diiodo compound distorts the quinone ring into shallow chair form. Surprisingly, the dichloro compound shows the greater deviation from planarity. The steric repulsion between chlorine and oxygen atoms thus placed in a linear tricyclic system is also well exemplified by a pair of crystal structures in which central γ-pyrone and pyran rings respectively are flanked by 1,2,4-trichlorobenzene rings (18). The Cl---Cl distances (between 1,8 type positions) are 5.61 Å, 5.28 Å, and 4.26 or 4.37 Å as the intervening group is ketone, methylene, and ether. When the central ring is γ-pyrone, the out-of-plane distortions show the molecule to be twisted. The van der Waals radius for Cl is 1.80 Å (15), so that it is to be expected that the overcrowding effects will be greater for these halo compounds than for ours.

With the structure **2** confirmed for the dimethyl derivative of lateropyrone, the natural product is either the 5-methoxy-9-hydroxy compound **3** or the 5-hydroxy-9-methoxy compound **1**; we prefer the latter choice, as **3** is a β-ketoacid and, as such, should be susceptible to decarboxylation. Lateropyrone is therefore assigned the structure 5-hydroxy-9-methoxy-2-methyl-4*H*,6*H*-pyrano[3,4-*g*]-1-benzopyran-4,6-dione-8-carboxylic acid, **1**.

Lateropyrone shows significant inhibitory activity towards the growth of the gram-positive bacterium *S. aureus* and the yeast *C. albicans*, but did not affect the gram-negative bacterium *E. coli*. The dimethyl derivative **2** showed no effect on all three test organisms.

Experimental

General

Melting points were determined on a Kofler hot stage and are uncorrected. Proton nmr spectra were determined on a Perkin–Elmer R32 spectrometer at 90 MHz or on a Bruker WM250 spectrometer at 250 MHz with reference to TMS. Infrared spectra were obtained on a Perkin–Elmer 283 spectrometer, and ultraviolet spectra on the Beckman DU-8 spectrophotometer. Microanalyses were conducted by Canadian Microanalytical Service Ltd., Vancouver, Canada. Accurate mass measurements were kindly provided by the University of British Columbia Mass Spectrometry Centre using the Kratos MS-50 instrument.

Cultures

F. lateritium was cultured on 3% malt extract (DIFCO) in Petri dishes at room temperature in the dark for 5 weeks. Test organisms were obtained from the Department of Biochemistry and Microbiology, and were grown on 3% malt extract (DIFCO) at 37°C; filter paper discs of compounds to be tested and of standard antibiotics were placed on the surface of the agar and covered with a coating of soft agar. Test organisms used were *Escherichia coli* W3110, *Staphylococcus aureus* 3538P, and *Candida albicans* 10231. Antibiotic activity was monitored by the inhibition of growth of the microorganism after approximately 24 h.

Extraction

Mycelium and agar from 40 dishes were extracted by stirring with dichloromethane at room temperature (3 × 800 mL). The crude extract was concentrated, and the product recrystallized from acetone–dichloromethane (5:1). Lateropyrone (50 mg) was isolated as pale yellow needles, mp 257–259°C.

Lateropyrone 1

Showed ν_{max} (KBr): 3450, 3200–2500 (br), 1750, 1650, 1610 cm^{-1}; λ_{max} (CH_2Cl_2): 370 (log ε = 4.16), 351 (4.16), 282 (4.19), 272 (4.15), and 244 nm (4.23); ^{1}Hmr (CD_2Cl_2): 14.7 (1H, s, COOH, D_2O exchangeable), 10.4 (1H, s, OH, D_2O exchangeable), 7.44 (1H, s, 10-H), 6.26 (1H, s, 3-H), 4.01 (3H, s, OMe), 2.45 (3H, s, 2-Me); ms, *m/z* (relative intensity): 318.0369 (M^+, 19, calculated for $C_{15}H_{10}O_8$: 318.0376), 231 (6), 230 (21), 203 (14), 202 (100), 175 (16), 174 (33), 134 (16). *Anal.* calcd. for $C_{15}H_{10}O_8$: C 56.61, H 3.17%; found: C 56.36, H 2.88%.

Lateropyrone dimethyl derivative 2

Lateropyrone (100 mg) in dichloromethane (110 mL) was added to excess ethereal diazomethane at room temperature. After 2 h, a few drops of acetic acid were added, and the resulting solution washed (water, saturated aqueous NaCl). The combined aqueous layers were extracted with dichloromethane (2 × 30 mL). The organic phases were dried and evaporated, and the residue chromatographed on silica gel; elution with dichloromethane–acetone (92:8) gave the crude product, which was recrystallized from dichloromethane–acetone to yield colourless needles of the dimethyl ether, 45 mg (41%), mp 250–252°C; ν_{max} (KBr): 1745, 1718, 1650, 1600 cm^{-1}; λ_{max} (CH_2Cl_2): 320 (4.06), 292 (4.16), 276 (4.29), 234 nm (4.04); ^{1}Hmr ($CDCl_3$): 7.59 (1H, s, 10-H), 6.14 (1H, s, 3-H), 4.08 (3H, s, OMe), 3.99 (3H, s, OMe), 3.97 (3H, s, OMe), 2.37 (3H, s, Me); ^{13}Cmr, see Table 5; ms, *m/z* (relative intensity): 346 (M^+, 39), 328 (60), 275 (100), 243 (94), 216 (40), 188 (90), 158 (39), 117 (30). *Anal.* calcd. for $C_{17}H_{14}O_8$: C 58.96, H 4.08%; found: C 58.71, H 3.97%.

Lateropyrone acetate 4

Lateropyrone (30 mg) in acetic anhydride (30 mL) was treated with 70% perchloric acid (3 drops) and left until dissolution was complete. Ice was added and the mixture boiled to decompose excess anhydride. The solution was extracted with dichloromethane, the extracts dried and evaporated. The residue was triturated with water, and the resulting acetate recrystallized from dichloromethane–hexane, mp 271–273°C; ν_{max} (KBr): 3100–2300 (br), 1770, 1750, 1727, 1650, 1610 cm^{-1}; λ_{max} (CH_2Cl_2): 352 (4.02), 328 (4.16), 313 (4.04), and 274 nm (4.43); ^{1}Hmr ($CDCl_3$): 14.68 (1H, s, COOH), 6.96 (1H, s, 10-H), 6.24 (1H, s, 3-H), 3.91 (3H, s, OMe), 2.44 (6H, s, 2-Me and OAc); ms, *m/z* (relative intensity): 360 (M^+, 2), 318 (74), 259 (56), 202 (100), 174 (37), and 134 (28).

Microbiological screening

	Lateropyrone **1**	Dimethyl derivative **2**	Ampicillin
E. coli W3110	×	×	√
S. aureus 3538P	√	×	√
C. albicans 10231	√	×	×

X-ray

The colourless needle-shaped crystal was mounted on a glass fibre in the direction of its greatest length, and photographed using Weissenberg and precession cameras with CuK_α radiation. The symmetry was found to be monoclinic and an approximate unit cell was established. The crystal was then transferred to a Picker 4-circle diffractometer using MoK_α radiation and automated with a PDP-11/10 computer, on which all further work was done. The unit cell was refined by least squares from 12 pairs of reflections (at ±2θ) in the range 2θ = 11–39°. The crystal data are:

$C_{17}H_{14}O_8$ Mol. wt. 346.29

Space group $P2_1/c$ (No. 14), a = 9.663(4), b = 22.317(9), c = 7.747(5) Å, β = 113.03(4)°, V = 1538(1) Å^3, T = 25°C, Z = 4 molecules per cell, D_{meas} = 1.477 g cm^{-3} (flotation in CCl_4/*m*-xylene), D_{calc} = 1.496 g cm^{-3}, λ = 0.71069 Å, μ = 1.299 cm^{-1}, needle length 0.98 mm, cross section 0.086 × 0.090 mm, no absorption correction applied. Intensity measurements were done for 1 quadrant ($k,l \geq 0$) in the range 2θ = 0–50°, using a stepped scan of 120 steps of 0.01° in 2θ counting for 0.40 s per step. Background counting was for 24 s at each end of the scan. A set of standards 300;

Can. J. Chem. Downloaded from www.nrcresearchpress.com by 210.87.254.105 on 09/06/12
For personal use only.

TABLE 5. ^{13}C magnetic resonance data for lateropyrone, selected chromone and isocoumarin compounds

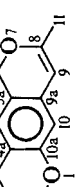

Compound	Carbon number (see formula*)												OMe	Reference
	2	3	4	4a	5	5a	6	8	9	9a	10	10a	11		
2	161.4	112.7	175.7	112.9	164.4	119.7	165.6†	143.5‡	138.8‡	137.1‡	107.7	154.3†	159.6†	52.8, 63.3, 63.4	
5	166	113	182	113	180	105	175			114	169	159		59, 58	19
7	163.5	110.4	177.6	112.1	157.4	116.7				153.1	94.7	155.5		61.3	20
8	164.0	110.5	178.1	113.6	148.7	119.3				147.0	129.8	147.2		61.4, 62.3	21
9	165.3	109.5	176.8	122.6	124.5	123.9				132.4	116.9	155.4			22
10						121.0	159.7	149.6	110.0	141.9			159.9	53.0	23
11				97.1	161.6	101.9	158.2	157.7	101.9	141.0	98.4	163.7			24
12				129.4	125.8	120.4	162.0	153.4	101.7	137.3	127.9	134.7		55.0, 55.7	25

*In all cases, the numbering used conforms to that used for the same carbons as in the lateropyrone nucleus.
†Assignments may be reversed.
‡Assignments may be reversed.

0,10,0; 002 were measured before each batch of 50 reflections. 3222 measurements consisting of 195 standards and 3027 reflections were obtained. Lorentz and polarisation corrections were applied and equivalent measurements were averaged to obtain a final file with 2177 entries. 611 reflections having $I < 2.5\sigma(I)$ were suppressed in the subsequent calculations.

Structure solution and refinement

The programs used were SHELX-76 by G. M. Sheldrick (26), and ORTEP (27). The atomic scattering factors were those given in the SHELX-76 program (26, 28). The structure was solved using direct methods, and refined by standard Fourier synthesis techniques and by least squares minimizing $\Sigma w\Delta^2$ (where w is a weight derived from the counting statistics, $w = 1/(\sigma^2(F) + 0.001F^2)$, and $\Delta = ||F_o| - |F_c||$). Initially carbon atomic scattering factors were used for all the ring atoms. O(4) and O(10) were identified as the oxygen atoms by abnormally low temperature parameters and by the clear detection of hydrogen atoms H(2) and H(6). The hydrogen atoms of the methoxy and ester groups were placed at their calculated positions (C—H = 1.08 Å). The hydrogen atoms of the C(31) methyl group were first calculated, and then the group as a whole was refined as a rigid body. The hydrogen atoms were treated as isotropic scatterers, and the heavier atoms were allowed the freedom of anisotropic thermal motion. U_{iso} was refined for those hydrogen atoms whose positional coordinates were refined. The hydrogen atoms fixed at calculated positions were assigned U_{iso} values of 0.05 Å^2. H(2) and H(6) were relatively well determined. The final residuals were $R = 0.0543$, $R_g = \sqrt{(\Sigma w\Delta^2/\Sigma wF_o^2)} = 0.0835$. The convergence was good with the final maximum (shift/esd) = 0.10. The final difference map had no important features, maximum 0.27 e Å^{-3}, minimum -0.33 e Å^{-3}. The number of measurements, 2100, was sufficient to determine the 241 parameters well. Supplementary Tables containing hydrogen atom parameters, anisotropic thermal parameters, bond angles involving hydrogen atoms, selected intermolecular distances, and observed and calculated structure amplitudes have been deposited.[5]

Acknowledgements

We would like to acknowledge the continued financial support of the University of Victoria and the Natural Sciences and Engineering Research Council of Canada. We thank Dr. T. M. Fyles for measuring the pK* values, and Dr. Günter Eigendorf and the University of British Columbia Mass Spectrometry Centre for their assistance.

1. R. ILUS, M.-L. NIKU-PAAVOLA, and T.-M. ENARI. Eur. J. Appl. Microbiol. Biotech. **11**, 244 (1981).
2. A. FUNK. Parasitic microfungi of western trees. Environment Canada, Ottawa. 1981. p. 64.
3. J. F. GROVE and M. POPLE. J. Chem. Soc. Perkin Trans. 1, 2048 (1979).
4. C. SZATHMARY, J. GALACZ, L. VIDA, and G. ALEXANDER. J. Chromatogr. **191**, 327 (1980).
5. R. SCHOENTAL. Biochem. Soc. Trans. **8**, 147 (1980).
6. G. C. BISHOP and A. H. ILSLEY. Aust. J. Biol. Sci. **31**, 93 (1978).
7. The Merck Index. 9th ed. Merck & So., Inc., Rahway, NJ. 1976. 4167, 3525.
8. H. MEYER and H. K. FRANK. BFE-Ber. 1979; Chem. Abstr. **92**, 209649n (1980).
9. G. A. POULTON and T. D. CYR. Can. J. Chem. **60**, 2821 (1982).
10. (*a*) B. DIETRICH, D. L. FYLES, T. M. FYLES, and J. M. LEHN. Helv. Chim. Acta, **62**, 2763 (1979); (*b*) D. D. PERRIN and B. DEMPSEY. Buffers for pH and metal ion control. Chapman & Hall, London. 1974.

[5]Copies may be obtained, at a nominal charge, from the Depository of Unpublished Data, CISTI, National Research Council of Canada, Ottawa, Ont., Canada, K1A 0S2.

11. H. HOPE. Acta Chem. Scand. **19**, 217 (1965).
12. T. H. GOODWIN, M. PRZYBYLSKA, and J. M. ROBERTSON. Acta Crystallogr. **3**, 279 (1950).
13. J. J. DE BOER, D. BRIGHT, G. DALLINGA, and T. G. HEWITT. J. Chem. Soc. (C), 2788 (1971).
14. T. F. LAI and R. E. MARSH. Acta Crystallogr. Sect. B, **30**, 1570 (1974).
15. F. A. COTTON and G. WILKINSON. Advanced inorganic chemistry. 2nd ed. Interscience Publishers, New York. 1966. p. 115.
16. O. A. MIKHNO, Z. I. EZHKOVA, B. N. KOLOKOLOV, and G. S. ZHDANOV. Sov. Phys. Crystallogr. **17**, 1013 (1973).
17. O. A. MIKHNO, Z. I. EZHKOVA, and B. N. KOLOKOLOV. Sov. Phys. Crystallogr. **17**, 580 (1972).
18. M. SÖDERHOLM, U. SONNERSTAM, R. NORRESTAM, and T.-B. PALM. Acta Crystallogr. Sect. B, **32**, 3013 (1976).
19. A. G. MCINNES, D. G. SMITH, J. A. WALTER, L. C. VINING, and J. L. C. WRIGHT. J. Chem. Soc. Chem. Commun. 66 (1975).
20. M. H. A. ELGAMAL, N. H. ELEWA, E. A. M. ELKHRISY, and H. DUDDECK. Phytochemistry, **18**, 139 (1979).
21. T. N. HUCKERBY and G. SUNMAN. J. Mol. Struct. **56**, 87 (1979).
22. R. BEUGELMANS and C. MORIN. J. Org. Chem. **42**, 1356 (1977).
23. T. IMAGAWA, A. HANEDA, and M. KAWANISI. Org. Magn. Reson. **13**, 244 (1980).
24. A. PELTER, R. S. WARD, and T. I. GRAY. J. Chem. Soc. Perkin Trans. 1, 2475 (1976).
25. A. J. JONES, J. A. ELIX, and U. ENGKANINAN. Aust. J. Chem. **29**, 1947 (1976).
26. G. M. SHELDRICK. SHELX-76, a program for crystal structure determination. Anorganisch-Chemisches Institut der Universität Göttingen. 1976.
27. C. K. JOHNSON. ORTEP: a Fortran thermal ellipsoid plot program for crystal structure illustrations. ORNL-3794, Revised. Oak Ridge National Laboratory, Oak Ridge, Tennessee. 1965.
28. D. T. CROMER and J. T. WABER. International Tables for X-ray Crystallography. Vol. 4. Kynoch Press, Birmingham, England. 1974. pp. 99 and 149.

Can. J. Chem. Downloaded from www.nrcresearchpress.com by 210.87.254.105 on 09/06/12
For personal use only.

Synthesis of ^{18}F-labelled 2-fluoroethyl-nitrosoureas[1]

SIMIN FARROKHZAD, MIRKO DIKSIC,[2] LUCAS Y. YAMAMOTO, AND WILLIAM FEINDEL
Montreal Neurological Institute and Department of Neurology and Neurosurgery, McGill University, Montreal, P.Q., Canada H3A 2B4

Received January 25, 1984

SIMIN FARROKHZAD, MIRKO DIKSIC, LUCAS Y. YAMAMOTO, and WILLIAM FEINDEL. Can. J. Chem. **62**, 2107 (1984).

^{18}F-labelled 1,3-bis-(2-fluoroethyl) nitrosourea (^{18}F-BFNU) (**9**) and 1-(2-chloroethyl)-3-(2-fluoroethyl) nitrosourea (^{18}F-CFNU) (isomeric mixture, **11**,**12**) were synthesized by nucleophilic attack of ^{18}F-labelled tetra-n-butylammonium fluoride on the aziridine ring of 1,3-substituted ureas. Diethyleneurea (DEU) (**5**), 1-(2-fluoroethyl)-3-ethyleneurea (FEU) (**7**), and 1-(2-chloroethyl)-3-ethyleneurea (CEU) (**14**) were used as starting materials in the synthesis. Nitrosation of ^{18}F-labelled 1,3-bis-(2-fluoroethyl) urea (^{18}F-BFU) (**6**) produced ^{18}F-BFNU with a radiochemical yield of 5–10%. Nitrosation of ^{18}F-labelled 1-(2-chloroethyl)-3-(2-fluoroethyl) urea (^{18}F-CFU) (**15**) gave ^{18}F-CFNU as a mixture of two isomers. Geometrical isomers of CFNU were separated by hplc, and the radiochemical yield of the two isomers ranged from 8% to 15%, with a radiochemical purity exceeding 96%. Syntheses, which took about 60 min, yielded products with specific activity of 680 mCi/mmol when n-$Bu_4N^+F^-$ was used, or 300 mCi/mmol when HF was used to complete the opening of the aziridine ring.

SIMIN FARROKHZAD, MIRKO DIKSIC, LUCAS Y. YAMAMOTO et WILLIAM FEINDEL. Can. J. Chem. **62**, 2107 (1984).

On a réalisé la synthèse des bis(fluoro-2 éthyl)-1,3 (^{18}F-BFNU) (**9**) et (chloro-2 éthyl)-1 (fluoro-2 éthyl)-3 (^{18}F-CFNU) (mélange d'isomères, **11**,**12**) nitrosourées marquées au ^{18}F en faisant appel à une attaque nucléophile du fluorure de tétra n-butylammonium, marqué au ^{18}F, sur le cycle aziridine d'urées substituées en 1,3. On a utilisé les diéthylène (DEU), (**5**), (fluoro-2 éthyl)-1 éthylène-3 (FEU), (**7**) et (chloro-2 éthyl)-1 éthylène-3 urées (CEU), (**14**) comme produits de départ pour ces synthèses. La nitrosation de la bis(fluoro-2 éthyl)-1,3 urée marquée au ^{18}F (^{18}F-BFU), (**6**) conduit au ^{18}F-BFNU avec un rendement radiochimique de 5 à 10%. La nitrosation de la (chloro-2'éthyl)-1 (fluoro-2 éthyl)-3 urée marqué au ^{18}F (^{18}F-CFU), (**15**) conduit au ^{18}F-CFNU sous forme de mélange de deux isomères. On a séparé les isomères géométriques du CFNU par clhp et le rendement radiochimique des deux isomères varie de 8 à 15% alors que leur pureté radiochimique dépasse 96%. Les synthèses, qui prennent environ 60 min, fournissent des produits dont l'activité spécifique est respectivement de 680 ou 300 mCi/mmol suivant que l'on utilise du n-$Bu_4N^+F^-$ ou du HF pour compléter l'ouverture de l'aziridine.

[Traduit par le journal]

Introduction

Nitrosoureas such as 3-cyclohexyl-1-(2-chloroethyl)-1-nitrosourea (CCNU), 1,3-bis-(2-chloroethyl) nitrosourea (BCNU), and 3-(4-methylcyclohexyl)-1-(2-chloroethyl)-1-nitrosourea (MeCCNU) are used to treat patients with malignant brain tumors, including brain gliomas (1–4). Even after numerous studies, however, the pharmacokinetics and mode of action of these drugs remain unknown (5–7). The distribution of these 2-chloroethylnitrosoureas and their breakdown products is of particular importance if we are to understand their oncologenic activity.

The Sloan–Kettering group labelled several nitrosoureas with ^{13}N (8) and then studied their in vivo decomposition and the radioactivity tissue distribution after intravenous injection (9). In an attempt to determine the in vivo distribution of BCNU we recently labelled BCNU with ^{11}C in the carbonyl group (10) and with ^{13}N in the nitroso group (11), and studied their metabolic decomposition. We also studied their behaviour in human brain tumors using positron emission tomography (PET) (28) and in the animal brain tumor model by tissue sampling (29).

However, since it was difficult to evaluate the complete pharmacokinetics of BCNU using only these two compounds (^{13}N- and ^{11}C-labelled BCNU), we synthesized the analog of BCNU, 1,3-bis-(2-fluoroethyl)nitrosourea (BFNU) (**9**), and 1-(2-chloroethyl)-3-(2-fluoroethyl) nitrosourea (CFNU) (isomers **11** and **12**), both labelled with positron-emitting fluorine-18. Because of the longer half-life of fluorine-18 ($t_{1/2}$ = 110 min) as compared to the other positron emitting radionuclides (^{11}C $t_{1/2}$ = 20 min and ^{13}N $t_{1/2}$ = 10 min), we believed it would be more convenient to study the decomposition of these BCNU analogs into 2-haloethyldiazonium hydroxide and 2-haloethylisocyanate, and try to correlate the results with the decomposition of BCNU into 2-chloroethyldiazonium hydroxide and 2-chloroethylisocyanate (12, 13). The mixture of ^{18}F-CFNU isomers is particularly interesting, since one part of each molecule is identical with BCNU, and the other with BFNU. Since the nitroso group is present on different sides of the CFNU molecule, after decomposition it would give two different fragments carrying the ^{18}F-label, therefore providing information about both fragments of nitrosourea molecules. By using labelled fluorine attached to the ethylene group, we might also obtain information on the interstrand crosslinking of related nitrosoureas with DNA (14, 15). Since these BCNU analogs themselves have antitumor properties (16, 17) their pharmacokinetics is also of interest to us.

This report describes the synthesis of ^{18}F-labelled 1,3-bis-(2-fluoroethyl) nitrosourea (**9**) (Fig. 2) and 1-(2-chloroethyl)-3-(2-fluoroethyl) nitrosourea (geometrical isomers **11** and **12**) (Fig. 3) via nucleophilic attack of fluoride on the aziridine ring of 1,3-substituted ureas as well as through heterogenous exchange of chloride with fluoride. The synthesis described here represents a new approach to the preparation of these nitrosoureas. Since the synthesis for "cold" material described in the literature does not allow introduction of an ^{18}F-label into the molecule (16), a new technique was definitely needed.

Materials and methods

Research purity chemicals used in this work were obtained from regular suppliers. Dimethyl sulfoxide (DMSO) was dried by distillation over calcium hydride and stored over 4 Å molecular sieves

[1] Part of this paper was presented at the 30th Annual Meeting of the Society of Nuclear Medicine, June 7, 1983, St-Louis, Missouri; see ref. 27.

[2] Address correspondence to: Mirko Diksic, Ph.D., Medical Cyclotron Unit, Montreal Neurological Institute, 3801 University St., Montreal, P.Q., Canada H3A 2B4.

Can. J. Chem. Downloaded from www.nrcresearchpress.com by 210.87.254.6 on 09/06/12
For personal use only.

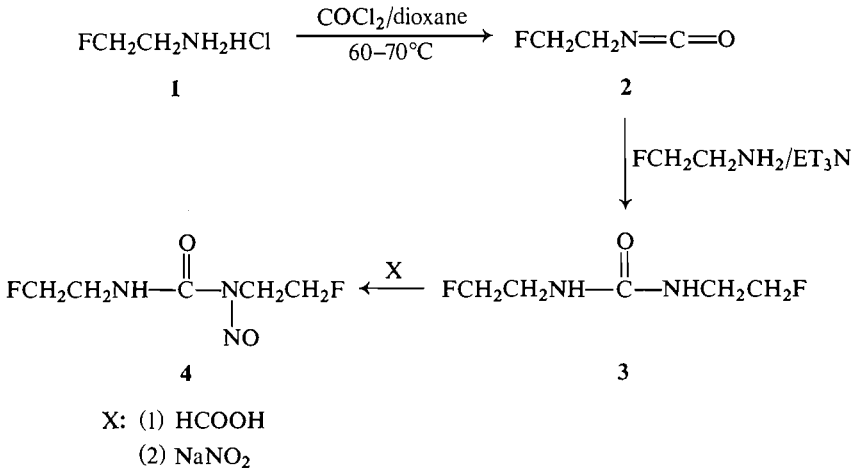

FIG. 1. Synthesis of unlabelled 1,3-bis-(2-fluoroethyl) nitrosourea (BFNU) (**4**).

activated at 110°C. Melting points were determined in a conventional melting apparatus and are reported uncorrected.

The infrared spectra (ir) were recorded in chloroform or film (oil) on a Perkin–Elmer 297 spectrophotometer. Proton nuclear magnetic resonance spectra (^{1}H nmr) were obtained in acetone-d_6 or chloroform-d on a Varian XL-200 or a Varian-60A spectrometer at 200 MHz and 60 MHz respectively, using tetramethylsilane as an internal standard. The ^{19}F nmr spectra were recorded on a Bruker WP-80SY spectrometer at 75.386 MHz. These spectra were also obtained in chloroform-d by using trichlorotrifluoroethane (with a chemical shift of −82.204 ppm) as an external standard. The notation used for the identification of nmr spectra is: s = singlet, d = doublet, t = triplet, dt = doublet of triplet, m = multiplet, dm = doublet of multiplets, bs = broad singlet. Mass spectra (ms) were determined on an HP 5980A mass spectrometer at 70 eV.

Thin-layer chromatograms (tlc) and thin-layer radiochromatograms (tlrc) were developed on hard layer silica gel plates with a fluorescent indicator (254 nm) by using appropriate solvent mixtures. A chloroform–acetone mixture was used for ureas, and an ether–hexane mixture for nitrosoureas. Ureas were detected by examining plates under ultraviolet light after spraying them with sodium nitrite and formic acid (99%), and then heating to 90°C (18). The nitrosoureas were visualized by spraying with Griess reagent,[3] which is specific for nitroso compounds. The hplc separations were performed on a Partisil-10 PAC-column.[4] The silica gel (mesh 40–140)[5] was used for flash chromatography instead of 230–400 mesh used in the original method (19). In the work-up procedures for various syntheses, unless otherwise noted, the solvents were removed with a rotary evaporator under reduced pressure (0.3 Torr; 1 Torr = 133.3 Pa) at a bath temperature of 80°C.

1,3-Diethyleneurea prepared by a procedure described in the literature (20) from ethylenimine (aziridine) (21) and phosgene in the presence of triethylamine was identified by nmr, ir, and ms spectroscopy; ir (Nujol), ν: 1680 (C=O), 1350, 1255, (C—N) cm^{-1}; ^{1}H nmr ($CDCl_3$), δ: 2.01 (s, 8H) ppm; ms, *m/e* (relative intensity); 112 (2.8, M^+), 70 (23.1).

The specific activity of the final radiopharmaceuticals was determined by measuring the radioactivity in an isotope calibrator and dividing it by the absolute amount of BFNU. The absolute amount of BFNU was measured by hplc, by comparing the responses of the uv detector at λ = 236 nm to standards of known concentration and BFNU samples. In the synthesis where no HF was added, the specific activity of ^{18}F-F_2 was measured as described earlier (23).

Since the data published on proton nmr is inadequate and no data has been published on fluorine nmr, we have provided this information for the ureas and nitrosoureas described here.

(a) *Synthesis of 2-fluoroethylisocyanate (2) (Fig. 1)*

A suspension of 2-fluoroethylamine hydrochloride (**1**) (400 mg, 4 mmol) in 15 mL dioxane was heated to 60°C, and phosgene gas was slowly bubbled through the suspension for 15 min. (A similiar procedure was reported for the synthesis of 2-chloroethylisocyanate (22).) The reaction mixture was stirred at 65°C for an additional 30 min. The excess of phosgene was removed by flushing it with nitrogen, and unreacted fluoroethylamine hydrochloride was filtered off. The 2-fluoroethylisocyanate was used without further purification in the subsequent step. The presence of isocyanate was confirmed by ir (ν: 2275 cm^{-1}) as well as by the reaction performed in the subsequent step.

(b) *Synthesis of 1-(2-fluoroethyl)-3-ethylene urea (FEU) (7)*

A solution of aziridine (344 mg, 8 mmol) in dioxane (1 mL) containing triethylamine (2.1 g, 21 mmol) was added dropwise to a stirred solution of 2-fluoroethylisocyanate (**2**) in dioxane, prepared as described above, and kept in a 0°C bath for 20 min. The insoluble white precipitate of triethylammonium hydrochloride was filtered off. (Since 2-fluoroethylisocyanate from the previous step was not purified, the HCl produced in this step precipitated as triethyleneammonium hydrochloride.) After evaporation of the solvent, a mixture of FEU (**7**) and 1-(2-fluoroethyl)-3-(2-chloroethyl) urea (CFU) (**8**) in a ratio of 9:1 was obtained as a colorless oil. This was used without further purification for the preparation of BFU (**3**). The ^{1}H nmr ($CDCl_3$) of FEU (**7**), δ: 2.13 (s, 4H, aziridine group), 3.47 (dm, 2H, —CH_2—NH, $^3J_{HF}$ = 27.6 Hz), 4.47 (dt, 2H, —CH_2—F, $^2J_{HF}$ = 47.6 Hz, $^3J_{HH}$ = 4.8 Hz), 6.74 (bs, 1H, N—H) ppm; ms, *m/e* (relative intensity); 132 (0.5, M^+), 113 (0.8), 99 (1.8), 90 (4.7).

(c) *Synthesis of 1-(2-chloroethyl)-3-(2-fluoroethyl) urea (CFU) (8)*

2-Chloroethylisocyanate (**13**) (211 mg, 2 mmol) in dioxane (0.5 mL) was added dropwise to a mixture of 2-fluoroethylamine hydrochloride (**1**) (199 mg, 2 mmol) and triethylamine (303 mg, 3 mmol) in dioxane (4 mL), and kept in a 0°C bath. The reaction mixture was stirred at 50–60°C for 30 min, then at room temperature for an additional 3 h. After removal of triethylamine hydrochloride by filtration and evaporation of the solvent under reduced pressure, pale yellow crystals were obtained, which were recrystallized from chloroform–hexane (1:12) in a 50% yield; mp 94–95°C (lit. (16) mp 94–96°C); ^{1}H nmr ($CDCl_3$), δ: 3.51 (m, 6H, —CH_2 groups), 4.45 (dt, 2H, —CH_2F, $^2J_{HF}$ = 47.6 Hz, $^3J_{HH}$ = 4.7 Hz), 5.89 (bs, 2H, for

[3] Griess reagent: a mixture of 1% solution of sulfanilic acid in 30% acetic acid and 1% solution of naphthylamine in 30% acetic acid with the ratio 1:1.

[4] Alltech Associates, Inc., Cat. No. C-6000.

[5] J.T. Baker Chemical Co., Cat. No. 1-3404.

Can. J. Chem. Downloaded from www.nrcresearchpress.com by 210.87.254.6 on 09/06/12
For personal use only.

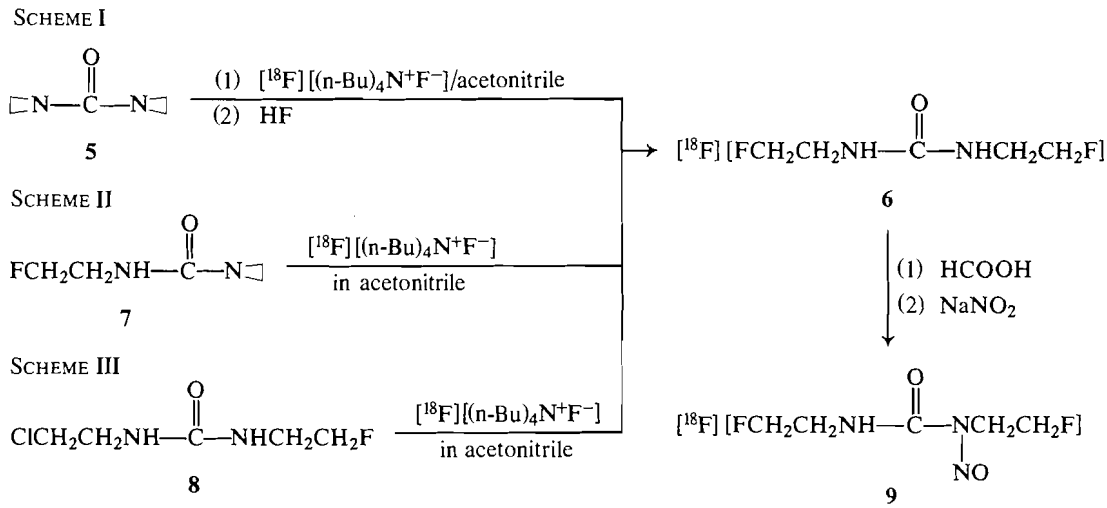

FIG. 2. Synthesis of ^{18}F-labelled 1,3-bis-(2-fluoroethyl) urea (^{18}F-BFU) (**6**) and ^{18}F-labelled 1,3-bis-(2-fluoroethyl) nitrosourea (^{18}F-BFNU) (**9**).

two NH groups) ppm; ms, *m/e* (relative intensity); 169 (0.5, M^+), 136 (0.3), 133 (0.9), 106 (1.3), 63 (22.4).

(d) *Synthesis of ^{18}F-BFU (6) (Fig. 2)*

^{18}F-F_2 was produced through a (d, α) reaction on ^{20}Ne in a nickel target containing a mixture of 0.5% F_2 in research purity neon (23). At the end of the irradiation, gas was bubbled through the reaction mixture, which contained tetra-n-butylammonium hydroxide (19.6 mg, 0.07 mmol) in water (6 mL) where F_2 reacted with water and /(or) hydroxide anion and water yielding $[^{18}F]F^-$. Evaporation of the solvent under reduced pressure (0.3 Torr) at 60°C gave a white solid residue that was dried by using acetonitrile (3 mL) (twice) and benzene (3 mL). The dry ^{18}F-labelled tetra-n-butylammonium fluoride was then dissolved in acetonitrile (2 mL) and added to DEU (**5**), FEU (**7**), or CFU (**8**) (0.1–0.2 mmol) in the presence of catalytic amounts of 18-crown-6 ether, a compound known to influence the nucleophilic activity of fluoride (24). The reaction vial was closed and heated in an oil bath at 145°C for 20 min. Evaporation of the solvent under reduced pressure gave white crystals that were treated with chloroform and washed with a potassium fluoride solution (0.1 *M*) and water. After drying the chloroform layer with sodium sulphate it was evaporated to dryness under reduced pressure.

When DEU (**5**) was used as the aziridine-containing compound, after evaporation of chloroform it was stirred with 0.5 mL HF (14 *M*) for 6 min to complete the opening of the aziridine ring. Partial opening of the aziridine ring was confirmed by tlc. After removing the acid solution, a sample of the product was examined by thin-layer radiochromatography (silica gel, solvent acetone–chloroform (1:2)). The major radioactivity present in the reaction mixture had the same R_f value (0.45) as that of authentic BFU (**3**). The product was used without further purification in the subsequent step. The yield of BFNU was not changed when nucleophilic substitution was made in acetonitrile without any crown ether, but by-products were detected on tlc. This complicated the purification of ^{18}F-BFNU.

(e) *Synthesis of BFU (3) (Fig. 1)*

Unlabelled BFU (**3**) (Fig. 1) was prepared from 2-fluoroethylisocyanate (**2**) as follows: to a stirred solution of 2-fluoroethylisocyanate (**2**) (prepared as described earlier) and 2-fluoroethylamine hydrochloride (**1**) in dioxane kept at 0°C, 8 mL of water and 2 mL of triethylamine were added dropwise. The reaction mixture was maintained at room temperature for 1 h. Triethylamine hydrochloride formed during the reaction was removed by filtration. After evaporation of the solvent under reduced pressure, the colorless oil was purified by flash chromatography (chloroform–acetone, 4:1). The white solid residue was then further purified by recrystallization from ethanol. The yield of BFU (**3**) as white needles was 200 mg (65%), mp 139–141°C (lit. (16) mp 141°C). The product was identified by ^{1}H nmr and ms spectroscopy; ^{1}H nmr (acetone-d_6), δ: 3.42 (dm, 4H, CH_2—NH, $^3J_{HF}$ = 26.61 Hz), 4.43 (dt, 4H, CH_2F, $^2J_{HF}$ = 47.66 Hz, $^3J_{HH}$ = 5.1 Hz) ppm; ms, *m/e* (relative intensity): 152 (14.6, M^+), 119 (24.6), 86 (4.7), 47 (100).

Unlabelled BFU was also prepared from DEU (**5**) by the method described earlier for preparing ^{18}F-labelled BFU (**6**). For this synthesis we used DEU (**5**) (55 mg, 0.5 mmol), dry tetra-n-butylammonium fluoride (379 mg, 1.2 mmol), and a catalytic amount of 18-crown-6 ether in acetonitrile (1.5 mL). The product was identified by ^{1}H nmr. Thin-layer chromatography on silica gel in acetone–chloroform (1:2) as a developing solvent gave R_f 0.45. The ^{1}H nmr spectra and the R_f value of the product were identical with those of a sample prepared from 2-fluoroethylamine hydrochloride (**1**) and 2-fluoroethylisocyanate (**2**). The product was used without further purification in the nitrosation reaction.

(f) *Synthesis of ^{18}F-BFNU (9) (Fig. 2)*

^{18}F-BFU (**6**) prepared in a previous reaction was dissolved in 99% formic acid (1 mL) at 0°C. Sodium nitrite (69 mg, 1 mmol) dissolved in water (0.2 mL) was added dropwise to this solution and stirred for 5 min. The final product (BFNU) (**9**) was extracted with chloroform, and the chloroform layer washed with water and dried over sodium sulphate. The ^{18}F-BFNU was purified by hplc using an ether–hexane mixture (1:1) as the solvent on a Partisil-10 PAC-column. ^{18}F-BFNU was eluted after 4 min, with an elution volume of 8 mL. The R_f 0.6 of ^{18}F-labelled BFNU, using tlc on silica gel with ether–hexane (7:3), was identical to the BFNU (**4**) sample prepared from 2-fluoroethylamine hydrochloride (**1**), as explained later in this paper. Both values were identical to those of an authentic sample of BFNU. The synthesis time was about 40 min after the end of the fluorine collection, and the radiochemical yield for the total synthesis of BFNU was between 5% and 10%.

The unlabelled BFNU (**4**) (Fig. 1) was prepared as follows: a solution of sodium nitrite (69 mg, 1 mmol) in water (0.2 mL) was added dropwise to a cold (0°C) stirred solution of BFU (**3**) (16 mg, 0.5 mmol) in 99% formic acid (1.5 mL) (16). The reaction was stirred at 0°C for 40 min. The work-up procedure was the same as that described for ^{18}F-BFNU. Evaporation of the solvent yielded BFNU, which was purified by hplc (ether–hexane, 1:1). Yield 63 mg (70%), mp 30–34°C (lit. (16) mp 30–34°C); ir (film), *v*: 1725 (C=O) and 1532 (C—NH) cm^{-1}; ^{1}H nmr ($CDCl_3$), δ: 3.82 (dm, 2H, CH_2F—CH_2—NH, $^3J_{HF}$ = 27.37 Hz), 4.21 (dm, 2H, —CH_2—N—NO, $^3J_{HF}$ = 22.7 Hz, $^3J_{HH}$ = 5.11 Hz), 4.43 (d of semi t, 2H, CH_2F—CH_2—N—NO—, $^2J_{HF}$ = 46.85 Hz, $^3J_{HH}$ = 5.10 Hz), 4.63 (dt, 2H, CH_2F—CH_2—NH, $^2J_{HF}$ = 47.12 Hz, $^3J_{HH}$ = 4.8 Hz)

Can. J. Chem. Downloaded from www.nrcresearchpress.com by 210.87.254.6 on 09/06/12
For personal use only.

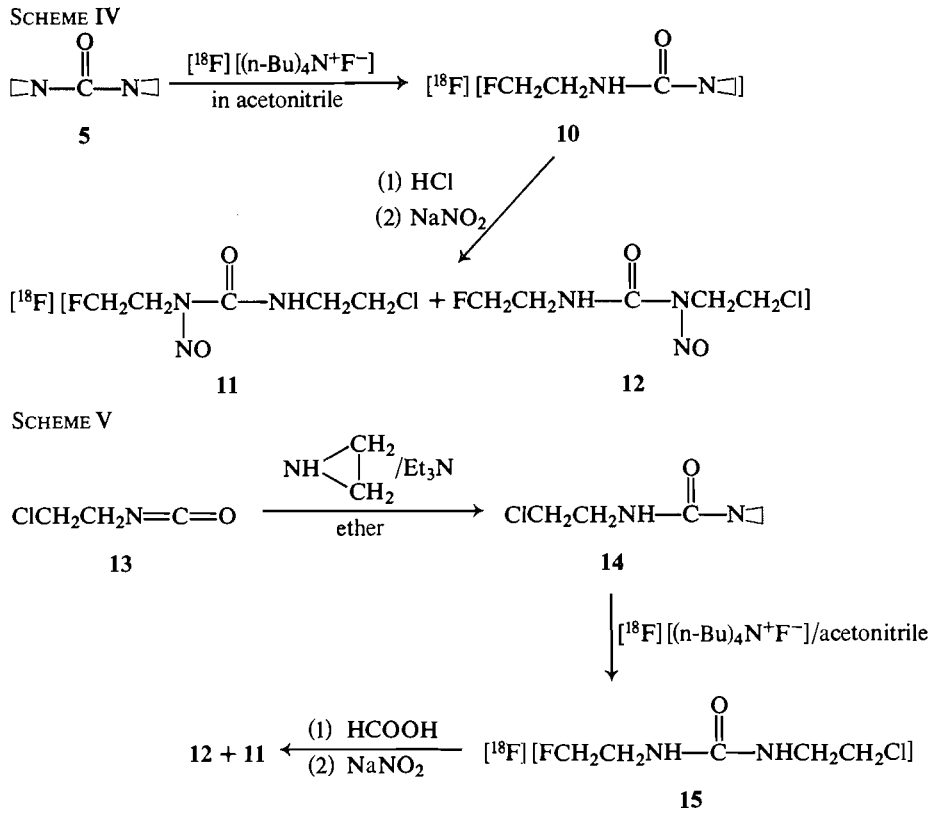

FIG. 3. Synthesis of ^{18}F-labelled 1-(2-chloroethyl)-3-(2-fluoroethyl) nitrosoureas (^{18}F-CFNU) (isomer mixtures **11** and **12**).

ppm; ^{19}F nmr ($CDCl_3$), ϕ: −230.47 (s, 1F, FCH_2CH_2NH), ϕ: −230.65 (s, 1F, F—CH_2CH_2—N—NO) ppm.

(g) *Synthesis of ^{18}F-CFNU mixtures (**11** and **12**), from DEU (**5**)*

Anhydrous ^{18}F-labelled tetra-n-butylammonium fluoride was prepared as described earlier and dissolved in 2 mL dry acetonitrile. After DEU (**5**) (11 mg, 0.1 mmol) and a crystal of crown-ether were added, the vial was closed and heated to 100°C for 15 min. Evaporation of the solvent under reduced pressure (60°C, 0.3 Torr) left a solid residue, which was dissolved in hydrochloric acid (12 *M*). The mixture was stirred at room temperature for 5 min. Sodium nitrite (69 mg, 1 mmol) was added to this solution at 0°C and stirred for an additional 5 min. The final product was extracted with chloroform, and the chloroform layer was washed with water and dried over sodium sulfate. After removing the chloroform under reduced pressure, the residue was redissolved in ether (0.4 mL) and injected on hplc (solvent: ether–hexane (1:9), column: Partisil 10-PAC). An elution volume of about 32 mL was obtained for isomer **11**. The 3:1 ratio between **11** and **12** was established by hplc for these two isomers by means of ^{18}F-labelled compounds using radioactivity and uv detectors. However, from ^{1}H nmr the 2:1 ratio for isomers **11** and **12** was obtained; tlrc R_f values of purified isomers, obtained on silica gel in ether–hexane (2:3) as a solvent, were 0.30 for **11** and 0.29 for **12**. The radiochemical yield for isomer **11** ranged from 10% to 15%, and for isomer **12** was 4%–8%.

(h) *Synthesis of CEU (**14**) (Fig. 3)*

To a stirred solution of 2-chloroethylisocyanate (**13**) (1.0 g, 10 mmol) in ether (3 mL) was added dropwise a solution of aziridine (473 mg, 11 mmol) in ether (2 mL). The mixture was kept in a 0°C bath for 30 min. Evaporation of the solvent under reduced pressure gave an 82% yield of CEU (**14**), which was used without further purification in the subsequent step; ^{1}H nmr (acetone-d_6), δ: 3.1 (s, 4H, aziridine group), 3.5 (m, 4H, —CH_2—CH_2—), 6.1 (bs, 1H, —N—H) ppm.

(i) *Synthesis of ^{18}F-CFNU (isomers mixture) from CEU (**14**)*

Dry ^{18}F-labelled tetra-n-butylammonium fluoride prepared as described earlier in this paper was added to CEU (**14**) (14.9 mg, 0.1 mmol) and a crystal of crown ether dissolved in acetonitrile (2 mL). The reaction was carried out in a closed vial at 120°C for 15 min. After removing the solvent under reduced pressure, the residue was dissolved in 99% formic acid (1 mL). A solution of sodium nitrite (69 mg, 1 mmol) in water (0.2 mL) was added to this mixture at 0°C and stirred for 5 min. The procedure, purification of the final product (CFNU isomer mixtures **11** and **12**), and the radiochemical yield of isomers were the same as described for preparation of ^{18}F-CFNU in paragraph (g). An example of hplc radiochromatogram of ^{18}F-CFNU isomers mixture is shown in Fig. 4.

Results and discussion

For the first time, a nucleophilic attack of ^{18}F-labelled tetra-n-butylammonium fluoride on an aziridine ring (Scheme I and II, Fig. 2), or nucleophilic displacement of chloride in CFU (**8**, Scheme III, Fig. 2) in acetonitrile (an aprotic solvent), has been used in the synthesis of ^{18}F-labelled ureas/nitrosoureas. The reactions reported here were done in the presence of 18-crown-6 ether (24). In the experiments reported here the use of crown ether did not significantly increase the yield in any of the reactions. However, it should be noted that absence of crown ether resulted in side products in the synthesis of ^{18}F-BFU, complicating purification of ^{18}F-BFNU. Since the nucleophilic substitution investigated in this work was done on ureas and $(n\text{-}Bu)_4N^+F^-$ was used, our observations on the usefulness of crown ether in the nucleophilic reactions may not be conclusive. All three reactions (Fig. 2) examined in this work had approximately the same radiochemical yield, purification procedure, and complexity of synthesis. Because of the HF used in the synthesis, ^{18}F-BFNU derived from DEU (**5**) (Scheme I, Fig. 2) had the lowest specific activity. However, if a high specific activity is not required, this is the method of choice, since the starting material has great shelf stability and

Can. J. Chem. Downloaded from www.nrcresearchpress.com by 210.87.254.6 on 09/06/12
For personal use only.

Can. J. Chem. Downloaded from www.nrcresearchpress.com by 210.87.254.6 on 09/06/12
For personal use only.

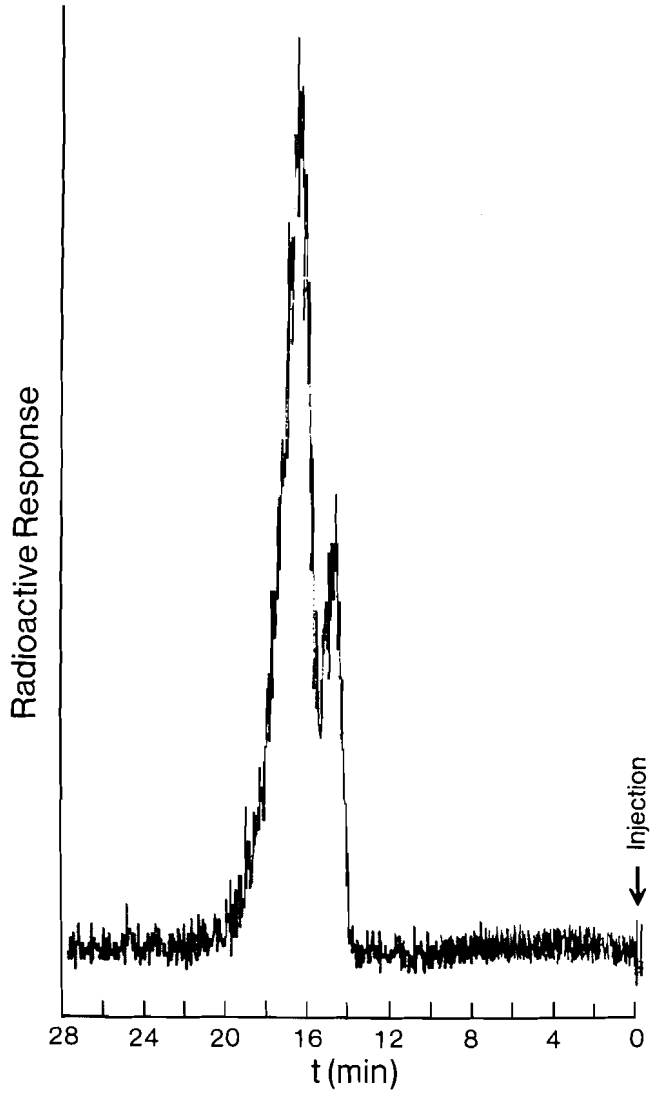

FIG. 4. The hplc chromatogram of ^{18}F-labelled 1-(2-chloroethyl)-3-(2-fluoroethyl) nitrosourea (^{18}F-CFNU) (isomers **11** and **12**) on a Partisil 10-PAC column with ether–hexane (1:9) as solvent.

the radiochemical yield is always slightly higher than that of the other two syntheses.

The synthesis of BFU (**3**) as described in the literature (16) uses a reaction of 2-fluoroethylamine hydrochloride with 3-(2-fluoroethyl)-1-methyl-1-nitrosourea in water in the presence of 50% aqueous sodium hydroxide. The nitrosation with solid sodium nitrite in hydrochloric acid gave BFNU in an overall chemical yield of about 33% (16). Although this reaction has a higher chemical yield than the one we used, it cannot be used in the synthesis of an ^{18}F-labelled compound because it does not allow introduction of the ^{18}F-label into the molecule of BFU.

Radiochemical yields are marginally better in the syntheses of CFU/CFNU (Schemes IV and V, Fig. 3) than in the synthesis of ^{18}F-BFU/BFNU. The only difference between the two syntheses (CFU/CFNU and BFU/BFNU) is the presence of chlorine in the compound used for introduction of ^{18}F into the molecule, which indicates that fluoride opens the aziridine ring more easily when chlorine is already present in the molecule (comparison of Scheme II, Fig. 2 and Scheme V, Fig. 3). It also seems that the introduction of chloride into compound **10** (Scheme IV, Fig. 3) results in a better yield than does nucleophilic opening of the aziridine ring with fluoride (Scheme II, Fig. 2).

The ^{1}H and ^{19}F nmr spectra of alkylureas had narrow line widths; it was therefore relatively easy to explain and identify the chemical shifts as well as to obtain all the coupling constants. However, the introduction of the nitroso group complicates both types of spectra with many coupling constants. It is only through computer simulation[6] that chemical shifts have been explained and coupling constants deduced for all nitrosoureas. This complexity is probably one of the reasons why the nmr spectra of BFNU have not been described in the literature. The methylene group adjacent to fluorine on the nitroso side resonates at a higher field than does the same group on the NH side. The geminal H—F coupling constant on the side of the nitroso group is slightly lower than on the NH side, indicating the influence of the electron-withdrawing nitroso group. The influence of the nitroso group is clearly evident in the magnitude of the vicinal H—F coupling constants (see Materials and methods), where the constant on the side of the nitroso group is smaller. It was possible to simulate ^{1}H- and ^{18}F-spectra by computer,[6] with identical coupling constants and chemical shifts. Infrared spectroscopy of BFNU in Nujol oil shows absorption at 1725 cm^{-1}, for C=O stretch. This agrees with results reported earlier (16). Mass spectra gave M^+ with the relative intensity of 0.1%.

The ^{1}H and ^{19}F nmr spectra of CFU were also identifiable because they contained those resonances found in the spectra of BCU and BFU. The nmr spectra of the mixture of nitroso isomers **11** and **12** are complex, because they contain all resonances of BCNU and BFNU. Fortunately there was little overlap of the peaks, allowing us to identify corresponding chemical shifts and coupling constants. Chemical shifts and coupling constants for the part of the molecule identical to that of BCNU are given in ref. 25, and those for the part of the molecule identical to that of BFNU are given in this paper. From ^{1}H and ^{19}F nmr spectra we concluded that neither side of the CFNU molecule, respective to the carbonyl group, influences the chemical shift and coupling constants on the other side. Both geminal and vicinal coupling constants for all nitrosoureas described here agree well with the published values for such constants (26).

The ratio between isomers **11** and **12** is different when determined from hplc chromatograms and ^{1}H nmr spectra. Reasons for this discrepancy might be found in the complexity of the ^{1}H nmr spectra as well as in the partial separation obtained by hplc. Our ratio for isomers **11** and **12** differs from the 1:1 ratio reported by Johnston *et al.* (16), who did not describe how they measured this ratio. However, they nitrosated in concentrated hydrochloric acid with solid sodium nitrite, which might influence the ratio of the two isomers.

^{18}F-labelled CFNU isomers, when used in in vivo studies, could give us valuable information about the fate of the decomposition fragments. One side of the molecule might behave like the BCNU molecule, while the other side would carry the ^{18}F-label and behave as BFNU, giving us information about both drugs. The latter fragment might be easier to follow than the same fragment carrying the ^{11}C-label, which is partially lost through the formation of carbamic acid (17). Using ^{18}F-labelled

[6] Computer simulation of the nmr spectra was done by Professor L.D. Colebrooke, Chemistry Department, Concordia University, Montreal, Quebec.

CFNU isomers we should also be able to correlate the amounts of 2-fluoroethanol, 2-fluoroethylamine, and part of the compound decomposing through the isocyanate, and to compare these with the fragments obtained during decomposition of ^{11}C-labelled BCNU, the compound synthesized (10) and used by us in in vivo studies (28, 29).

Conclusion

This paper describes for the first time the synthesis of ^{18}F-labelled BFNU and CFNU, analogs of the chemotherapeutic drug BCNU. Although both syntheses give a rather low yield, a 60-min irradiation with a small medical cyclotron can produce enough ^{18}F-labelled radiopharmaceutical for a human PET study.

These BCNU analogs will be used to study the in vivo pharmacokinetics, and the results obtained with these analogs will be compared to those obtained for BCNU. The yield of the synthesis is around 10%, taking the amount of ^{18}F-F_2 as 100%. Except in the synthesis with HF, where the specific activity was 300 mCi/mmol, the specific activity of nitrosoureas was 680 mCi/mmol, the same as that of ^{18}F-F_2 determined by titration (23).

Acknowledgements

This investigation was supported in part by the National Cancer Institute of Canada, the Medical Research Council of Canada, a Killam Scholarship to Dr. Mirko Diksic, and the Cone Memorial Research Fund of the Montreal Neurological Institute. We are specially grateful to Dr. Victoria Lees for editing several versions of this manuscript. We thank Mr. Stephen Irwin for operation of the medical cyclotron and Mr. Dean Jolly, radiochemist, for his assistance in one stage of the work reported here. The Faculty for Graduate Studies and Research, McGill University, provided financial support toward the purchase of an hplc system.

1. S. B. GREEN, D. P. BYAR, M. D. WALKER, *et al.* Cancer Treat. Rep. **67**, 121 (1983), and references therein.
2. M. D. WALKER, S. B. GREEN, D. P. BYAR, *et al.* N. Engl. J. Med. **303**, 1323 (1980), and references therein.
3. W. R. SHAPIRO. Ann. Neurol. **12**, 231 (1982), and references therein.
4. V. A. LEVIN and N. S. EDWARDS. *In* Brain tumors, scientific basis, clinical investigation and current therapy. *Edited by* D. G. T. Thomas and D. I. Graham. Butterworth, London. 1980. p. 344.
5. G. A. DIGENIS and C. H. ISSIDORIDES. Bioorg. Chem. **8**, 97 (1979), and references therein.
6. J. W. LOWN and S. M. S. CHAUHAN. J. Org. Chem. **46**, 5309 (1981).
7. R. J. WEINKAM and H.-S. LIN. J. Med. Chem. **22**, 1193 (1979), and references therein.
8. W. A. PETTIT, R. S. TILBURY, G. A. DIGENIS, and R. H. MORTARA. J. Labelled Comp. Radiopharm. **13**, 119 (1976).
9. B. R. FREED, R. L. MCQUINN, R. S. TILBURY, and G. A. DIGENIS. Cancer Chemother. Pharmacol. **10**, 16 (1982).
10. M. DIKSIC, S. FARROKHZAD, Y. L. YAMAMOTO, and W. FEINDEL. J. Nucl. Med. **23**, 895 (1982).
11. M. DIKSIC, S. FARROKHZAD, Y. L. YAMAMOTO, and W. FEINDEL. 4th International Symp. Radiopharm. Chem. Jülich, August 23–27, 1982. p. 124.
12. J. A. MONTGOMERY, R. JAMES, G. S. MCCALEB, and T. P. JOHNSTON. J. Med. Chem. **10**, 668 (1967).
13. M. COLVIN, R. B. BRUNDRETT, W. COWERS, I. JARDINE, and D. B. LUDLUM. Biochem. Pharmacol. **25**, 695 (1976).
14. K. W. KOHN, C. L. SPEARS, and P. DOTY. J. Mol. Biol. **19**, 266 (1966).
15. P. D. LAWLEY and P. D. BROOKES. J. Mol. Biol. **25**, 143 (1967).
16. T. P. JOHNSTON, G. S. MCCALEB, P. S. OPLIGER, and J. A. MONTGOMERY. J. Med. Chem. **9**, 892 (1966).
17. J. W. LOWN, L. W. MCLAUGHLIN, and Y.-M. CHANG. Bioorg. Chem. **7**, 97 (1978), and references therein.
18. M. DIKSIC and S. FARROKHZAD. Chromatographia, **15**, 665 (1982).
19. B. LOEV and K. M. SNADER. Chem. Ind. 15 (1965).
20. H. BESTIAN. Ann. Chem. **566**, 210 (1950).
21. C. F. H. ALLEN, F. W. SPANGLER, and E. R. WEBSTER. *In* Org. Synth. Coll. Vol. **4**, 433 (1963).
22. R. NARAYAN and C.-J. CHANG. J. Labelled Comp. Radiopharm. **19**, 129 (1982).
23. M. DIKSIC and Y. TODA. Can J. Chem. **61**, 661 (1983).
24. C. L. LIOTTA and H. P. HARRIS. J. Am. Chem. Soc. **96**, 2251 (1974).
25. M. DIKSIC, S. FARROKHZAD, Y. L. YAMAMOTO, and W. FEINDEL. J. Radioanal. Chem. In press.
26. W. W. PAUDLER. Nuclear magnetic resonance. Allyn and Bacon, Inc., Boston. 1971. p. 53.
27. S. FARROKHZAD, M. DIKSIC, L. Y. YAMAMOTO, and W. FEINDEL. J. Nucl. Med. **24**, P119 (1983).
28. M. DIKSIC, K. SAKO, W. FEINDEL, A. KATO, Y. L. YAMAMOTO, S. FARROKHZAD, and C. THOMPSON. Cancer Res. **44**, 3120 (1984).
29. K. SAKO, M. DIKSIC, S. FARROKHZAD, Y. L. YAMAMOTO, and W. FEINDEL. J. Neurosurg. Submitted.

Can. J. Chem. Downloaded from www.nrcresearchpress.com by 210.87.254.6 on 09/06/12
For personal use only.

Heterogeneous permanganate oxidations. 4. The oxidation of sulfides and selenides[1]

N. A. Noureldin, W. B. McConnell, and Donald G. Lee
Department of Chemistry, University of Regina, Regina, Sask., Canada S4S 0A2

Received October 3, 1983

N. A. Noureldin, W. B. McConnell, and Donald G. Lee. Can. J. Chem. **62**, 2113 (1984).

The heterogeneous oxidation of sulfides and selenides by copper(II) permanganate octahydrate or a mixture of potassium permanganate and copper(II) sulfate pentahydrate has been studied. Conditions under which quantitative conversions of the sulfides and selenides to the corresponding sulfones and selenones take place have been determined and an attempt has been made to visualize a mechanism for the reaction.

N. A. Noureldin, W. B. McConnell et Donald G. Lee. Can. J. Chem. **62**, 2113 (1984).

On a étudié l'oxydation hétérogène de sulfures et de sélénures par l'octahydrate du permanganate de cuivre(II) ou par un mélange de permanganate de potassium et du pentahydrate du sulfate de cuivre(II). On a déterminé les conditions qui permettent de transformer quantitativement les sulfures et les sélénures en sulfones et en sélénones et on a essayé de visualiser une mécanisme pour la réaction.

[Traduit par le journal]

Can. J. Chem. Downloaded from www.nrcresearchpress.com by 210.87.254.5 on 09/06/12
For personal use only.

Introduction

The use of heterogeneous reagents in organic synthesis has dramatically increased during the last decade. It has been found that a large number of substitution, elimination, addition, oxidation, and reduction reactions can be achieved by use of insoluble or polymer supported reagents (1, 2). For example, recent publications have described the heterogeneous oxidation of organic compounds by chromyl chloride chemisorbed on silica/alumina (3), pyridinium chlorochromate or dichromate on molecular sieve (4), chromium trioxide on graphite, Celite, or silica gel (5), alumina or silica supported sodium metaperiodate (6), clay supported iron(III) nitrate (7), silver carbonate on Celite (8), polymer supported iodate, periodate, pyridinium dichromate, or hypochlorite (9), and permanganate on a variety of solid supports including molecular sieve (10), alumina (11), silica (12), or bentonite (13).

It has also been observed that permanganate can be used effectively as a heterogeneous oxidant in nonaqueous solvents if it is associated with a hydrated metal cation. For example, copper(II) permanganate octahydrate is an excellent oxidant (14), as are sodium, zinc, and magnesium permanganates (15). Mixtures of potassium permanganate and copper sulfate pentahydrate (16) or other hydrated salts[2] also serve as good, inexpensive heterogeneous oxidants. One of the functions of these added supports is to provide moisture to the system; when the reagents and solvents are carefully dried, reaction takes place very slowly, if at all (17).

The use of permanganate as a heterogeneous oxidant in organic solvents such as hexane or methylene chloride dramatically modifies its selectivity. Whereas it readily attacks carbon–carbon double bonds when used homogeneously (18), permanganate reacts very slowly with alkenes under the conditions described above (15). This property has led to its use as an oxidant for unsaturated alcohols (13, 14).

In a recent mechanism study it was found that although alkenes are not oxidized heterogeneously by permanganate their presence inhibits the oxidation of alcohols (19), presumably by the formation of π-complexes at the reactive sites on the reagent (eq. [1]). Furthermore, the evidence indicates that the oxidation of allylic alcohols is initiated by complexation of the double bond followed by a rearrangement in which

[1] 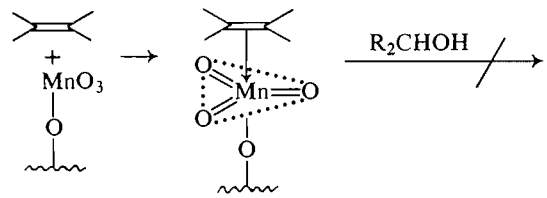

the alcohol oxygen also becomes a ligand of the central manganese atom (eq. [2]).

It has also been briefly mentioned in the literature that sulfides can be oxidized heterogeneously to the corresponding sulfones (14, 15). In this paper we wish to describe more fully the oxidation of sulfides and attempt to expose the synthetic potential of the reaction as well as to expand our understanding of the reaction mechanism.

[2] 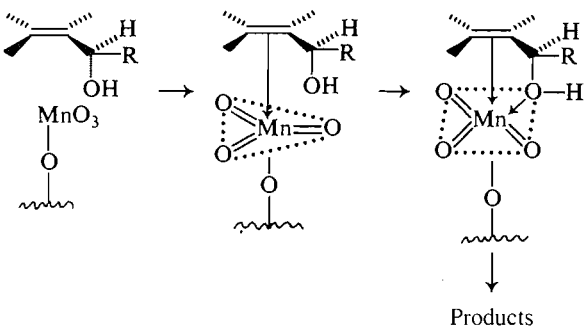

Experimental

Materials

Commercial methylene chloride was found to contain impurities which interfered with the reaction. Purification was achieved by treatment with potassium permanganate (along with a small amount of phase transfer agent) for 24 h, followed by distillation. *n*-Hexane (BDH) was used without further purification except that it was treated with sodium metal when anhydrous conditions were required. Hydrated copper permanganate and potassium permanganate were obtained from the Carus Chemical Co. Copper sulfate pentahydrate was obtained from the Fisher Scientific Co. These reagents were dried over phosphorus pentoxide at 0.1 Torr (1 Torr = 133.3 Pa) before use in those experiments requiring anhydrous conditions. The sulfides were obtained commercially and purified by distillation before use. Diphenyl selenide (K&K) was purified by distillation, followed by column chromatography on silica gel using hexane–ether (20:1) as the eluant.

[1] For part 3 of this series see ref. 19.
[2] C. F. Sebastian. Unpublished results.

Yields were calculated as isolated and (or) from gas chromatograms after application of predetermined response factors. Diethylene glycol or Apiezon L on Chromosorb W were used as column packings.

*Oxidation of di-*n*-butyl sulfide*

A mixture of potassium permanganate (1.0 g) and copper sulfate pentahydrate (0.5 g) was added to di-*n*-butyl sulfide (0.36 g, 2.5 mmol), dissolved in 20 mL of *n*-hexane. The reaction mixture was stirred under reflux for 25 h, cooled to room temperature, diluted by addition of 20 mL of ether, and then stirred for another 10 min. This mixture was filtered through Celite and concentrated by flash evaporation. After partial removal of the solvent a sample was withdrawn and injected into the gas chromatograph. Only one product (with a retention time identical to that of authentic di-*n*-butyl sulfone) was detected. Evaporation to dryness gave a solid product (0.43 g, 2.4 mmol, 96%), mp 43–45°C (lit. (20) mp 46°C).

When the experiment was repeated under identical conditions except for the addition of cyclohexene (0.2 g, 2.4 mmol) to the initial mixture the yield was reduced to 7%. When the reaction was completed under anhydrous conditions the yield was reduced to 22%.

Oxidation of diphenyl selenide

A mixture of potassium permanganate (3 g) and copper sulfate pentahydrate (1 g) was added to freshly purified diphenyl selenide (0.5 g, 2.4 mmol), dissolved in 20 mL of *n*-hexane. The reaction mixture was refluxed for 22 h and then filtered through Celite, the inorganic residue being washed thoroughly with ether. The combined filtrates were dried and concentrated, slowly, using a rotary evaporator to give crude diphenyl selenone (0.32 g, 1.2 mmol, 56%) mp 147–149°C. Recrystallization from cold ether gave 0.25 g (0.94 mmol, 44%) of colorless crystals, mp 154–155°C (lit. (21) mp 154.9°C). The inorganic residue was washed with dilute hydrochloric acid and the filtrate, extracted with ether, was in turn washed with water until neutral. After drying, the solvent was evaporated to give 0.16 g of a semi-solid, colorless product with a sharp odour. When analyzed by tlc this residue exhibited several unidentified spots.

Oxidation of pentamethylene sulfide (tetrahydrothiopyran)

Copper permanganate octahydrate (2.0 g) was added to a stirred solution of pentamethylene sulfide (0.25 g, 2.5 mmol) in 15 mL of hexane. The reaction mixture was stirred at room temperature for 1 h and filtered through Celite. The inorganic residue was washed with ether (3 × 10 mL) and the combined organic layers were dried over anhydrous magnesium sulfate, filtered, and evaporated, leaving very pure pentamethylene sulfone (0.31 g, 2.31 mmol, 94%), mp 101.0–101.5°C (lit. (22) mp 98–99°C).

Results and discussion

Alkyl and aryl sulfides and selenides are very easily converted into the corresponding sulfones or selenones when treated with either copper(II) permanganate octahydrate or a mixture of potassium permanganate and copper(II) sulfate pentahydrate. The yields obtained for a number of representative sulfides are summarized in Table 1.

Since it is known that the oxidation of alcohols is inhibited by the complexation of alkenes on the surface of the heterogeneous oxidant (16, 19), it was of interest to also examine their effect on the oxidation of sulfides. The possibility existed that sulfides would compete more effectively with alkenes for attachment at the active sites on the oxidant. However, the experimental results demonstrated that the oxidation of sulfides is also inhibited by the presence of an alkene in the solution. It may therefore be concluded that the equilibrium depicted in eq. [3] must lie to the left. The formation of π-complexes with d^0 transition metals has been described by Sharpless *et al.* (23).

The mode of transfer of oxygen from the oxidant to the substrate, while open to considerable speculation, may be visualized as proceeding by way of the mechanism outlined in

[3] 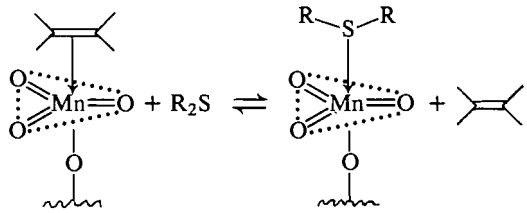

Scheme 1. Following the suggestion of Sharpless *et al.* (23), it is assumed that the reaction will be initiated by formation of a coordinate covalent bond between the sulfur and the manganese (step a). The sulfur would thereby acquire a partial positive charge and thus be attracted to an oppositely charged oxygen ligand leading to the formation of a new bond (step b). The intermediate, **1**, is directly analogous to the metallocyclooxetanes, **3**, that are formed during the oxidation of alkenes by permanganate (eq. [4]), the major difference being that a three- rather than a four-membered ring is formed (24, 25). Conversion of **1** into **2** involves migration of the sulfur from manganese to an oxo group, a transformation which is analogous to the migration of carbon from manganese to oxygen during the oxidation of alkenes (step d, eq. [4]). The

[4] 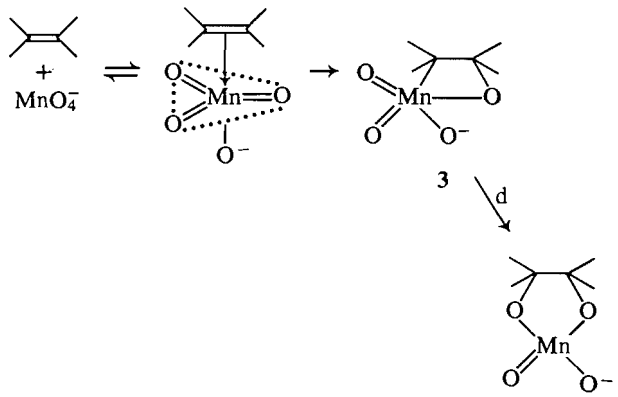

intermediate **2** is similar to the one which has been proposed by Block to occur during the oxidation of sulfoxides by permanganate (26). It would also be stabilized by the presence of a spectator oxo which has been shown to have a major influence on the course of oxidations by transition metal oxides (24).

This mechanism envisages the conversion of sulfides directly into sulfones without formation of intermediate sulfoxides. Although traces of compounds with retention times identical to those of the corresponding sulfoxides were occasionally noted during analysis of the products by glc, it is not clear if they are intermediates or by-products. However, it was noted that sulfoxides are also readily oxidized under these conditions and it is possible that they could be formed as intermediates and rapidly converted into sulfones, thus preventing their accumulation in the final products. In such a case the reaction could be considered to proceed by way of path c in Scheme 1.

Although the oxidation of selenides was less completely studied, it was found that they are also easily converted into the corresponding selenones, presumably by way of a similar reaction mechanism. The major product obtained from diphenyl selenide was the corresponding selenone. The oxidation of phenyl methyl selenide under these conditions produced a foul smelling product mixture that appeared to be quite toxic.[3] Be-

[3] The products obtained from the oxidation of methyl phenyl selenide had an offensive odour that caused violent retching.

Can. J. Chem. Downloaded from www.nrcresearchpress.com by 210.87.254.5 on 09/06/12
For personal use only.

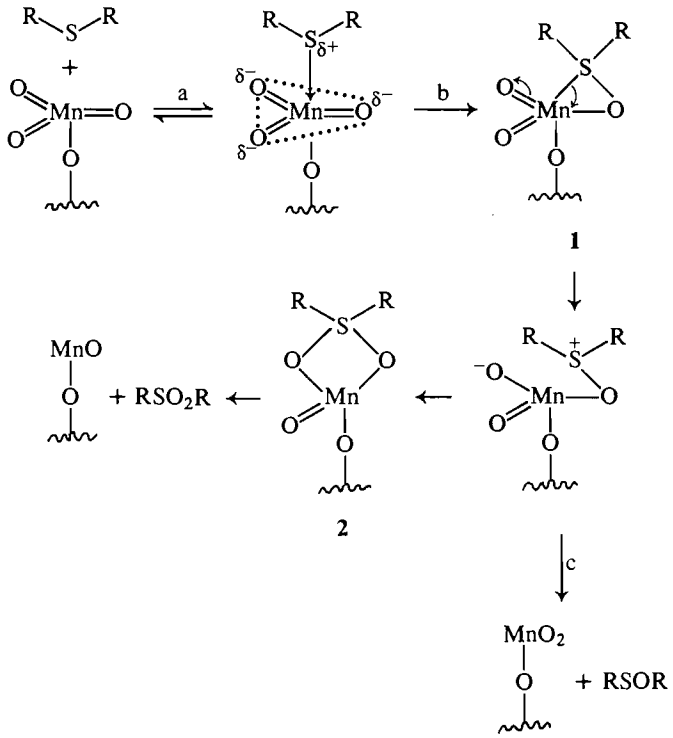

SCHEME 1

TABLE 1. Heterogeneous oxidation of sulfides and selenides

Substrate	Conditions	Products (yield, %)[g]
Di-*n*-butyl sulfide	[a]	Di-*n*-butyl sulfone (100)
Di-*n*-butyl sulfide	[b]	Di-*n*-butyl sulfone (98)[h]
Di-*n*-butyl sulfide	[c]	Di-*n*-butyl sulfone (100)
Di-*n*-butyl sulfide	[d]	Di-*n*-butyl sulfone (22)
Di-*n*-butyl sulfide	[e]	Di-*n*-butyl sulfone (11)
Di-*n*-butyl sulfide	[f]	Di-*n*-butyl sulfone (7)
Di-*sec*-butyl sulfide	[a]	Di-*sec*-butyl sulfone (100)
Di-*tert*-butyl sulfide	[a]	Di-*tert*-butyl sulfone (98)
Di-*tert*-butyl sulfide	[b]	Di-*tert*-butyl sulfone (100)[h]
Di-*n*-octyl sulfide	[a]	Di-*n*-octyl sulfone (92)
Pentamethylene sulfide	[a]	Pentamethylene sulfone (94)[h]
Pentamethylene sulfide	[b]	Pentamethylene sulfone (96)[h]
Tetramethylene sulfide	[a]	Tetramethylene sulfone (95)
Diphenyl sulfide	[a]	Diphenyl sulfone (98)[h]
Di-*n*-butyl sulfoxide	[a]	Di-*n*-butyl sulfone (100)
Diphenyl selenide	[b]	Diphenyl selenone (50)[h]
Methyl phenyl selenide	[b]	Unidentified (toxic)

[a] Substrate (2.5 mmol) was dissolved in 15 mL of *n*-hexane and stirred over 2.5 g of $Cu(MnO_4)_2 \cdot 8H_2O$ for 1.0 h at room temperature.

[b] Substrate (2.5 mmol) was dissolved in 20 mL of methylene chloride over 1.0 g of $KMnO_4$ and 0.5 g $CuSO_4 \cdot 5H_2O$ and refluxed for 25 h.

[c] Substrate (2.5 mmol) was dissolved in 20 mL of *n*-hexane over 1.0 g of $KMnO_4$ and 0.5 g $CuSO_4 \cdot 5H_2O$ and refluxed for 25 h.

[d] As in *c* with anhydrous conditions maintained.

[e] As in *b* with 2.5 mmol of cyclohexene added.

[f] As in *c* with 2.5 mmol of cyclohexene added.

[g] Unless otherwise indicated, yields were determined by glc.

[h] Isolated yield.

cause the analytical facilities available to us are not equipped to handle toxic substances we were unable to thoroughly characterize this product. However, three compounds were detected by use of thin layer chromatography. These may have been formed by partial rearrangement of the expected product, phenyl methyl selenone, to the corresponding ester, methyl benzeneselenonate (**4**), followed by incomplete hydrolysis to benzeneselenonic acid (**5**) as in eq. [5]. Such rearrangement and hydrolysis reactions have previously been observed for these compounds.[4]

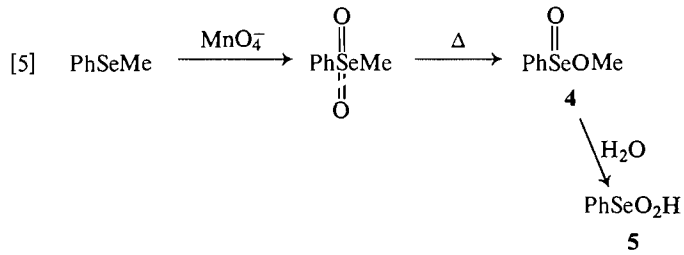

Finally, it should be noted that this procedure for the oxidation of sulfides and selenides is of potential value in organic synthesis. The reaction is fairly selective and, since it is heterogeneous, the isolation of products is easily achieved by filtration and flash evaporation of the solvent.

Acknowledgements

The authors are grateful to the Natural Sciences and Engineering Research Council of Canada and the Alberta Oil Sands Technology and Research Authority for financial support.

1. N. K. MATHUR, C. K. NARANG, and R. E. WILLIAMS. Polymers as aids in organic chemistry. Academic Press, New York. 1980.
2. P. HODGE and D. C. SHERRINGTON. Polymer supported reactions. Wiley, New York. 1980.
3. J. S. FILIPPO, JR. and C.-I. CHERN. J. Org. Chem. **42**, 2182 (1977).
4. J. HERSCOVICI, M.-J. EGRON, and K. ANTONAKIS. J. Chem. Soc. Perkin Trans. 1, 1967 (1982); J. HERSCOVICI and K. ANTONAKIS. J. Chem. Soc. Chem. Commun. 561 (1980).
5. W. METZ and H. MEYER-SPASCHE. Synth. Met. **1**, 63 (1979); S. J. FLATT, G. W. J. FLEET, and B. J. TAYLOR. Synthesis, 815 (1979); E. SANTANIELLO, F. PONTI, and A. MANZOCCHI. Synthesis, 534 (1978).
6. D. N. GUPTA, P. HODGE, and J. E. DAVIS. J. Chem. Soc. Perkin Trans. 1, 2970 (1981); K.-T. LIU and Y.-C. TONG. J. Org. Chem. **43**, 2717 (1978).
7. A. CORNELIS and P. LASZLO. Synthesis, 849 (1980); A. CORNELIS, P.-Y. HERZE, and P. LASZLO. Tetrahedron Lett. **23**, 5035 (1982).
8. M. FETIZON, M. GOLFIER, and J.-M. LOUIS. Tetrahedron, **31**, 171 (1975).
9. C. R. HARRISON and P. HODGE. J. Chem. Soc. Perkin Trans. 1, 509 (1982); M. SCHNEIDER, J.-V. WEBER, and P. FALLER. J. Org. Chem. **47**, 364 (1982); J. M. J. FRECHET, P. DARLING, and M. J. FARRALL. J. Org. Chem. **46**, 1728 (1981).
10. S. L. REGEN and C. KOTEEL. J. Am. Chem. Soc. **99**, 3837 (1977).
11. S. QUICI and S. L. REGEN. J. Org. Chem. **44**, 3436 (1979).
12. A. A. JAZZAA, J. H. CLARK, and M. ROBERTSON. Chem. Lett. 405 (1982).
13. N. A. NOURELDIN and D. G. LEE. Tetrahedron Lett. **22**, 4889 (1981).
14. N. A. NOURELDIN and D. G. LEE. J. Org. Chem. **47**, 2790 (1982).
15. F. M. MENGER and C. LEE. Tetrahedron Lett. **22**, 1655 (1981); S. WOLFE and C. F. INGOLD. J. Am. Chem. Soc. **105**, 7755 (1983).

[4] H. J. Reich. Private communication.

Can. J. Chem. Downloaded from www.nrcresearchpress.com by 210.87.254.5 on 09/06/12
For personal use only.

16. F. M. MENGER and C. LEE. J. Org. Chem. **44**, 3446 (1979).
17. F. M. MENGER. *In* Organic reactions in organized media. *Edited by* S. L. Holt. ACS Symposium Series, No. 177. 1982. p. 213.
18. R. STEWART. Oxidation in organic chemistry, Part A. *Edited by* K. B. Wiberg. Academic Press, New York. 1965, p. 1; D. G. LEE. Oxidation in organic chemistry, Part D. *Edited by* W. S. Tranhanovsky. Academic Press, New York. 1982. p. 147.
19. D. G. LEE and N. A. NOURELDIN. J. Am. Chem. Soc. **105**, 3188 (1983).
20. ROBERT C. WEAST (*Editor*). Handbook of chemistry and physics, 62nd ed. CRC Press, Boca Ration, FL. 1982–1983.
21. H. RHEINBOLDT and E. GIESBRECHT. J. Am. Chem. Soc. **68**, 2671 (1946).
22. J. G. GRASSELLI (*Editor*). Atlas of spectral data nd physical constants for organic compounds. The Chemical Rubber Company, Cleveland. 1973. pp. 3–920.
23. K. B. SHARPLESS, A. Y. TERANISHI, and J. E. BACKVALL. J. Am. Chem. Soc. **99**, 3120 (1977).
24. A. K. RAPPÉ and W. A. GODDARD III. J. Am. Chem. Soc. **104**, 448 (1982); **104**, 3287 (1982).
25. D. G. LEE and K. C. BROWN. J. Am. Chem. Soc. **104**, 5076 (1982).
26. E. BLOCK. Reactions of organosulfur compounds. Academic Press, New York. 1978. p. 15.

Can. J. Chem. Downloaded from www.nrcresearchpress.com by 210.87.254.5 on 09/06/12
For personal use only.

Electrogenerated luminescence in the Kolbe reactions of pyruvic and phenylglyoxylic acids

J. DE LA FUENTE, E. A. LISSI, AND R. ROZAS
Departamento de Química, Facultad de Ciencias, USACH, Santiago, Chile

Received October 11, 1983

J. DE LA FUENTE, E. A. LISSI, and R. ROZAS. Can. J. Chem. **62**, 2117 (1984).

The Kolbe reaction of pyruvic and phenylglyoxylic acids in acetonitrile takes place with high yields of biacetyl and benzil, respectively. Electroluminescence is produced during the electrolysis. This luminescence can be attributed to phosphorescence following the generation of excited triplets of the α-diketones in the acyl radical recombination. The efficiencies of the triplet production, relative to ground state formation, were evaluated to be of the order of 8×10^{-3} and 10^{-4} for the recombination leading to benzil and biacetyl, respectively.

J. DE LA FUENTE, E. A. LISSI et R. ROZAS. Can. J. Chem. **62**, 2117 (1984).

Les réactions de Kolbe, dans l'acétonitrile, des acides pyruvique et phénylglyoxylique conduisent respectivement aux biacétyle et au benzile, avec d'excellents rendements. Il se produit de l'électroluminescence au cours de l'électrolyse. On peut attribuer cette luminescence à une phosphorescence qui suit la génération des triplets excités des α-dicétones lors de la recombinaison des radicaux acyles. On a évalué que les efficacités de production de triplets, relatives à la formation de l'état fondamental, sont de l'ordre de 8×10^{-3} et 10^{-4} pour les recombinaisons conduisant respectivement au benzile et au biacétyle.
[Traduit par le journal]

Can. J. Chem. Downloaded from www.nrcresearchpress.com by 210.87.254.105 on 09/06/12
For personal use only.

The electrogeneration of ion-radicals leads frequently to luminescence (1, 2). On the other hand, there are no reported data on luminescence arising from the recombination of neutral free radicals. The probability of excited state formation in the recombination of free radicals has been evaluated for several radicals pairs (3). These calculations show that this probability is relatively high for those recombinations whose exothermicity is larger than the energies of the product excited states. This situation is found, for example, in the recombination of acyl radicals. In the present work we report results obtained in the electrogeneration of acyl free radicals by the Kolbe reaction. In this process, an electroluminescence that can be interpreted in terms of the following reaction scheme is observed:

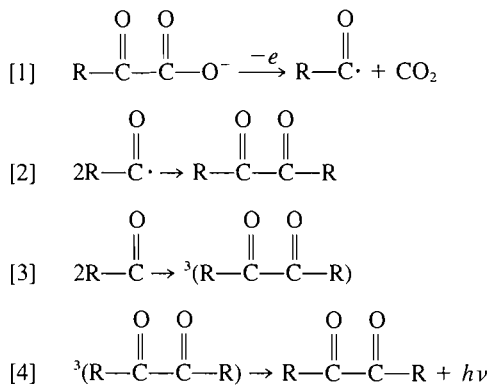

Experimental

Pyruvic acid (PA) and triethylamine were Fluka products. They were purified by distillation. Acetonitrile (Aldrich gold label) was employed as received. Phenylglyoxylic acid (PhGA) was prepared from mandelic acid (Fluka) (4). The melting point of the product obtained was 64−65°C.

$Ru(bpy)_3(ClO_4)_2$ was prepared by melting $RuCl_3$ with 3 equiv. of 2,2′-dipyridyl. The product obtained was dissolved in ethanol:water (1:1) and reduced on a Pt electrode at −0.85 V vs. sce. The reduced product was treated with an excess of $NaClO_4$ in a perchloric acid solution at pH = 4. The resulting complex was characterized by cyclic voltammetry and by its emission spectrum (5).

The electrochemical equipment employed comprised a Princeton Applied Research model 173 Potentiostat, a model 175 Universal Programmer, and a model 179 Integrator. The electrochemical cell designed for this work is shown in Fig. 1. The anodic and cathodic compartments were separated by a glass frit. The anode was made of Pt grill, with a geometric area of 4.5 cm^2. An sce was employed as reference. A Pyrex glass flat window was placed in front of the anode and near the front window of an EMI 9502-S photomultiplier. The photocurrent was measured with a KEITHLEY 414 A picoammeter. Glass filters and absorbing solutions were placed between the cell and the photomultiplier in order to characterize the emitted spectra. The reactions were carried out under nitrogen in a temperature-controlled bath at 20 ± 1°C.

The electrochemical reaction was made either potentiostatic or galvanostatic. The potentiostatic electrolysis was carried out between 2.0 and 2.3 V vs. sce. The galvanostatic experiments were carried out in the same range of potentials. All measurements were carried out employing a 10% solution of tetrabutylammonium bisulphate in the cathodic compartment.

The number of electrons transferred in the electrochemical oxidations (n) was determined by coulometry at 30 mV more positive than the peak determined by cyclic voltammetry (see Fig. 2).

Detection and determination of the α-diketones produced during the electrolysis were done by gas−liquid chromatography, thin layer chromatography, and fluorescence spectroscopy. The emission yield was evaluated employing the electro-oxidation of $Ru(bpy)_3^{2+}$ in the presence of $C_2O_4^{2-}$ as reference. For this reaction an electroluminescence efficiency of 2% has been reported (6).

Integrated emission spectra were obtained employing solutions of picric acid or potassium dichromate of different concentrations. The cut-off of the filter was assumed to be at the wavelength at which the absorbance of the solution was 0.5. The spectra obtained in the electroreactions were compared to those obtained from benzil and biacetyl triplets. These triplets were generated by decomposing dioxetane in the presence of biacetyl or benzil in acetonitrile solution. The dioxetane was kindly supplied by Dr. E. Bechara, University of Sao Paulo, Brazil.

Luminescence measurements were carried out in a Hitachi-Perkin Elmer 204-S spectrofluorimeter. 2,5-Dimethyl-2,4-hexadiene (Aldrich) and anthracene (Hopkins and Williams, sublimed) were employed as selective triplet quenchers in the electroluminescence experiments and in the luminescence measurements. Sodium pyruvate (Merck), triethylamine (Fluka, bidistilled), and pyruvic acid (Aldrich) were employed in the luminescence quenching experiments. Biacetyl triplet lifetimes were measured in a Perkin-Elmer LS-5 spectrofluorimeter.

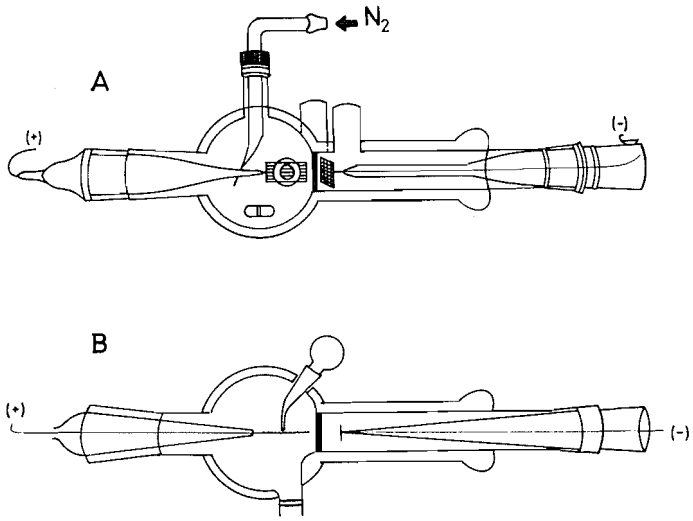

FIG. 1. Electrochemical cell: (*A*) front view; (*B*) top view, anodic compartment capacity = 100 mL and cathodic compartment capacity = 30 mL.

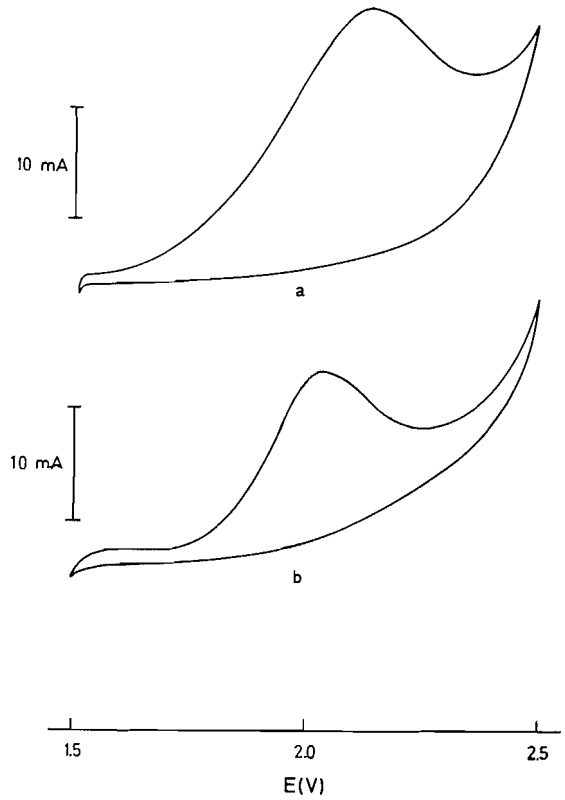

FIG. 2. Typical cyclic voltammograms — *E* in V against sce; sweep rate, 100 mV/s; (*a*) pyruvic acid, 0.5 *M* and (*b*) phenylglyoxylic acid, 0.5 *M*.

Results

Electrochemical processes

The Kolbe electro-oxidation of aliphatic α-ketoacids has been previously studied in aqueous and methanolic solutions (7, 8). As a result of the nucleophilic media the dimers comprise less than 20% of the observed products. In our work several experimental conditions were tested in order to improve the yield of the α-diketones. The highest electrochemical yields

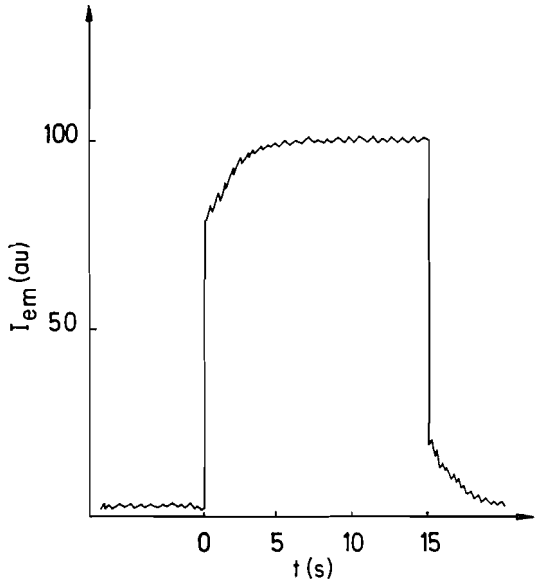

FIG. 3. Measured luminescence from a pyruvic acid solution as a function of time in a galvanostatic step.

were obtained with the α-ketoacids partially (25%) neutralized with triethylamine in acetonitrile solution (75% yield of biacetyl and more than 90% yield of benzil).

The fact that no other products than biacetyl and benzil were observed by glc and tlc at low α-ketoacids conversion, as well as the large electrochemical yields already mentioned, indicate that the electro-oxidation can be described by

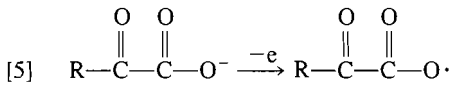

followed almost quantitatively by

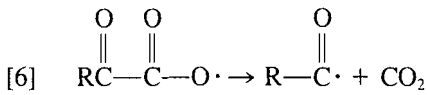

This conclusion is in agreement with the known instability of these types of radicals (9). Nevertheless, the possibility that decarboxylation is concerted with the electron transfer step is also compatible with the present results (10):

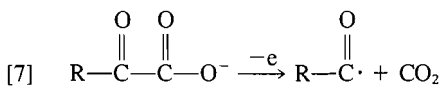

The number of electrons transferred per acid molecule reacted obtained by coulometry were 0.91 and 0.95 for PA and PhGA, respectively. All the results are then in agreement with a single electrochemical process that can be represented by reaction [1], followed mainly by the dimerization of the electrogenerated acyl radicals.

Electroluminescence

During the electrolysis a significant luminescence is observed (signal-to-noise ratio from 20 to 200). The luminescence observed as a function of time is shown in Fig. 3 for a galvanostatic pulsed electrolysis. The steady state electroluminescence is reached approximately 7 s after applying the current. The luminescence drops to the background level immediately after turning-off the applied current. Similar behaviours were observed with PA and PhGA. The delay time to

Can. J. Chem. Downloaded from www.nrcresearchpress.com by 210.87.254.105 on 09/06/12
For personal use only.

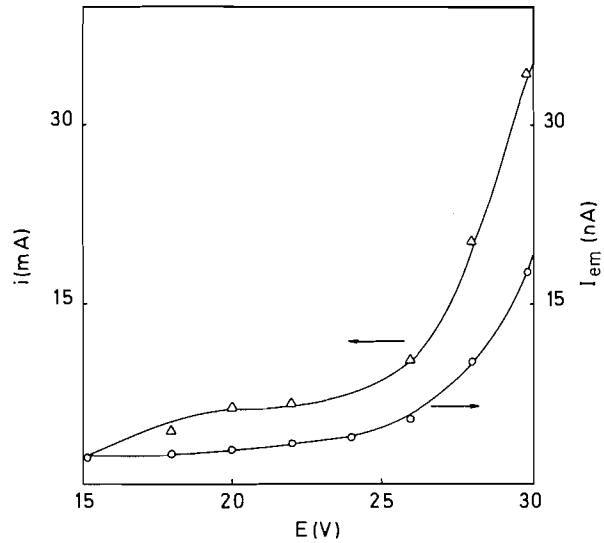

FIG. 4. Current intensity and luminescence intensity as a function of applied potential in the electrolysis of pyruvic acid (E in V against sce). △, current intensity; ○, luminescence intensity.

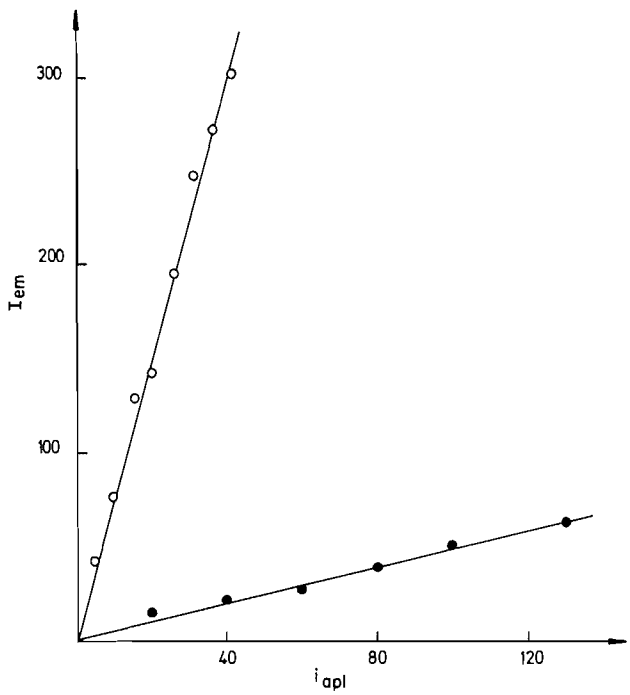

FIG. 5. Luminescence intensity as a function of applied current intensity; ●, pyruvic acid, 0.1 M; ○, phenylglyoxylic acid, 0.05 M.

reach the steady state emission is not due to the necessity of product accumulation since addition of biacetyl or benzil do not change either the delay time or the steady state emission intensity observed. The delay time could be related to the time required to deplete traces of oxygen in the surroundings of the anode. In fact, it was observed that oxygen is an efficient luminescence quencher.

Figure 4 shows the current intensity and luminescence intensity (in the plateau region) as a function of the operating potentials in the Kolbe region. Figure 5 shows the relationship between applied current and measured intensities in the steady state region in galvanostatic experiments. A linear relationship between current and light intensity is observed for PA and

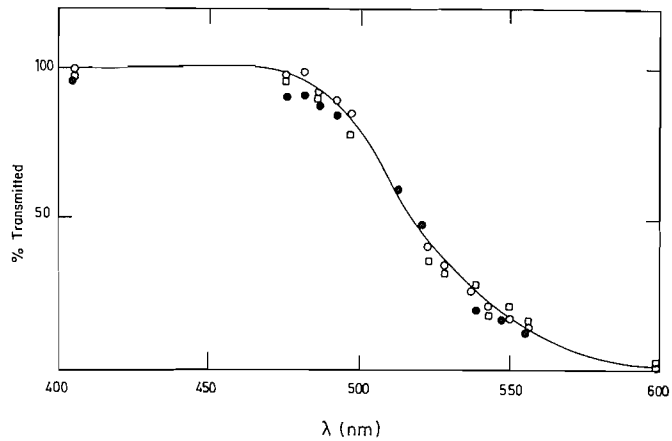

FIG. 6. Integrated spectra in the electrolysis of pyruvic acid; □, electrolysis of pyruvic acid; ●, electrolysis of pyruvic acid in the presence of 10^{-4} M 2,5-dimethyl-2,4-hexadiene; ○, spectra obtained in the pyrolysis of tetramethyldioxetane in the presence of 5×10^{-2} M biacetyl.

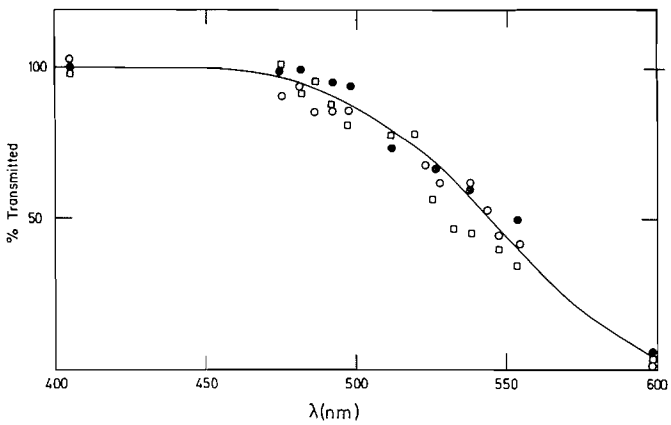

FIG. 7. Integrated spectra in the electrolysis of phenylglyoxylic acid; □, electrolysis of phenylglyoxylic acid; ●, electrolysis of phenylglyoxylic acid in the presence of 10^{-4} M 2,5-dimethyl-2,4-hexadiene; ○, spectra obtained in the pyrolysis of tetramethyldioxetane in the presence of 5×10^{-2} M benzil.

PhGA. The slopes of these plots are 0.47 and 7.65 nA of photocurrent per mA of applied current for PA and PhGA, respectively. Change in the substrate concentration between 5×10^{-2} and 0.1 M does not modify significantly the luminescence efficiency. With the same experimental set up, the $Ru(bpy)_3^{2+}/C_2O_4^{2-}$ system gives 1.2×10^4 nA of photocurrent per mA of applied current.

The integrated emission spectra obtained in the electrolysis of PA and PhGA are given in Figs. 6 and 7. These spectra were obtained employing cut-off filters since the signal-to-noise ratio was not enough to allow the use of a monochromator. In these figures are also included the results obtained when biacetyl and benzil triplets were directly sensitized by dioxetane thermolysis at 60°C in the presence of the corresponding diketones.

Addition of anthracene or 2,5-dimethyl-2,4-hexadiene decreases the electroluminescence intensity without affecting the current intensity. The ratio between the measured intensity in the presence of 2,5-dimethyl-2,4-hexadiene and that measured in the absence of additive are given in Figs. 8 and 9. In these figures are also included data obtained in the quenching of

Can. J. Chem. Downloaded from www.nrcresearchpress.com by 210.87.254.105 on 09/06/12
For personal use only.

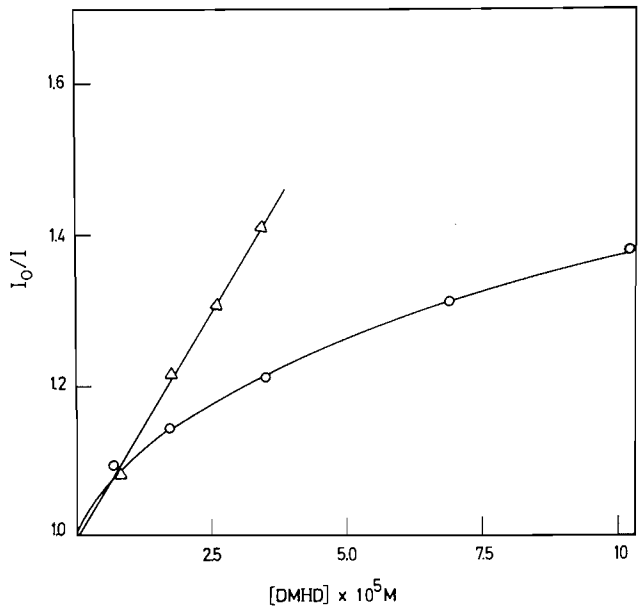

FIG. 8. Quenching of the luminescence produced in the electrolysis of pyruvic acid by 2,4-dimethyl-2,4-hexadiene; ○, electroluminescence; △, quenching of biacetyl phosphorescence in the same medium (irradiation wavelength 410 nm).

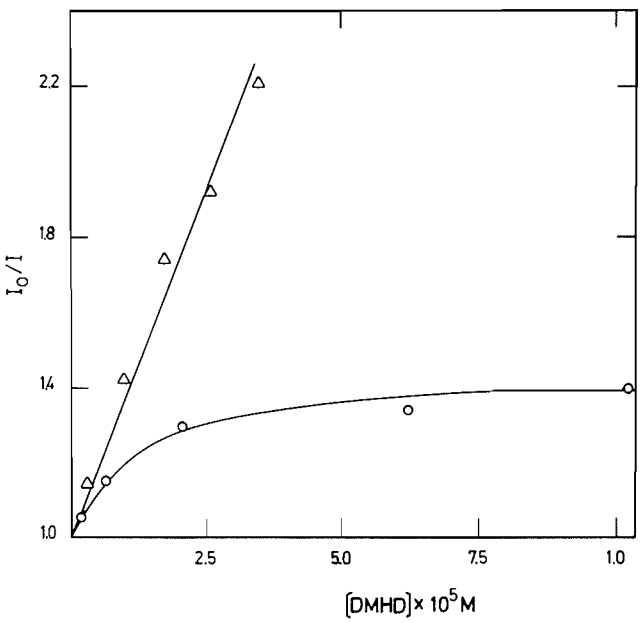

FIG. 9. Quenching of the luminescence produced in the electrolysis of phenylglyoxylic acid by 2,5-dimethyl-2,4-hexadiene; ○, electroluminescence; △, quenching of benzil phosphorescence in the same medium (irradiation wavelength 440 nm).

biacetyl and benzil phosphorescence. These data were obtained by irradiating benzil and biacetyl at 440 and 410 nm, respectively, in the reaction media employed in the electroluminescence experiments.

Biacetyl phosphorescence yields in the electrolysis mixture were determined by relating the phosphorescence yield in the working solution to that measured in benzene. This latter value was obtained from the triplet lifetime (7.5×10^{-4} s) and the phosphorescence rate constant (1×10^2 s (11)). By this procedure, a value of 2.1×10^{-3} was obtained for the phosphorescence yield of biacetyl in 10^{-1} *M* pyruvic acid partially

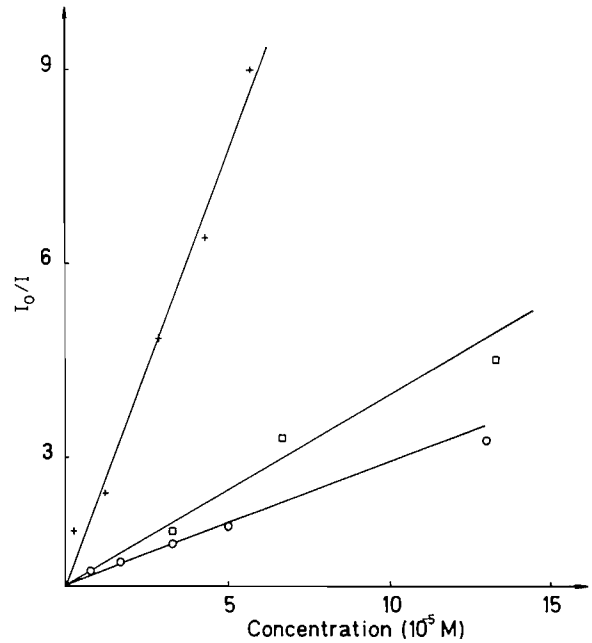

FIG. 10. Quenching of biacetyl phosphorescence by the components of the anodic solution; +, triethylamine; □, pyruvate anion (solvent acetonitrile plus 20% of water) added as sodium pyruvate; ○, pyruvic acid (concentrations has to be multiplied by 10^3); irradiation wavelength, 410 nm.

neutralized with triethylamine. A similar value was obtained by a comparison of the phosphorescence yield in this solvent and the fluorescence yield in benzene (12, 13).

Benzil phosphorescence yields in the working mixture were evaluated by relating the phosphorescence yield to the fluorescence yield measured in benzene (12). From this procedure, a value of 5×10^{-4} was obtained for the phosphorescence yield in 5×10^{-2} *M* phenylglyoxylic acid partially neutralized by triethylamine. The low phosphorescence yields measured in the working solutions are due to quenching of the excited carbonyl triplets by the parent acid, the acid anion, and the free triethylamine. Figure 10 shows the data obtained measuring the biacetyl phosphorescence yield as a function of added triethylamine, pyruvic acid, and the pyruvate anion (added as sodium salt). These data show that the quenching capacity of the additives follows the order amine > pyruvate ⩾ pyruvic acid. Figure 11 shows the Stern–Volmer plot obtained when a mixture of pyruvic acid and triethylamine (4:1) is added to biacetyl up to the concentrations employed in the electrolysis. The downward curvature observed is compatible with the partial neutralization of the pyruvic acid and the larger quenching capacity of the amine (whose free fraction decreases when the added concentration increases). Similar results were obtained by measuring the benzil phosphorescence yield as a function of the added concentration of partially neutralized phenylglyoxylic acid.

Discussion

The results given in Figs. 6 and 7 would indicate that most of the observed luminescence can be assigned to biacetyl and benzil phosphorescence. This phosphorescence imply direct triplet production since the sequence

[8] $2R-\overset{O}{\overset{\|}{C}}\cdot \rightarrow {}^1(R-\overset{O}{\overset{\|}{C}}-\overset{O}{\overset{\|}{C}}-R)$

Can. J. Chem. Downloaded from www.nrcresearchpress.com by 210.87.254.105 on 09/06/12
For personal use only.

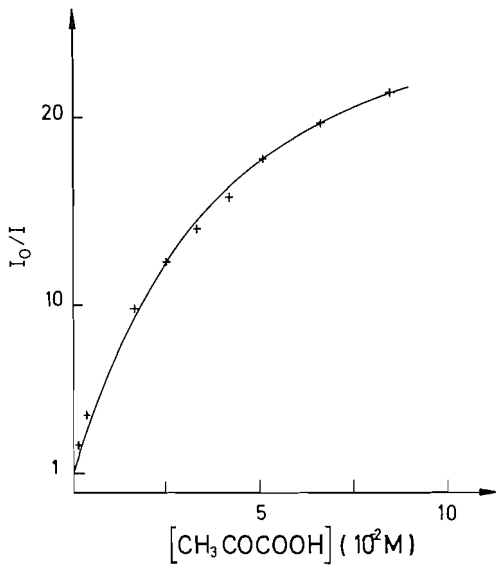

FIG. 11. Quenching of biacetyl phosphorescence by addition of a mixture of pyruvic acid and triethylamine (4:1); irradiation wavelength, 410 nm.

[9] $$^1(R{-}\overset{O}{\overset{\|}{C}}{-}\overset{O}{\overset{\|}{C}}{-}R) \rightarrow {}^3(R{-}\overset{O}{\overset{\|}{C}}{-}\overset{O}{\overset{\|}{C}}{-}R)$$

followed by triplet emission, would lead mainly to biacetyl fluorescence due to significant triplet quenching in the reaction media employed.

Significant emission from biacetyl and benzil triplets is also in agreement with the quenching effect of oxygen, anthracene, and 2,5-dimethyl-2,4-hexadiene. Furthermore, it is interesting to note that anthracene is more effective than 2,5-dimethyl-2,4-hexadiene (as observed in the quenching of diketone triplets) and that the initial slopes are similar in the luminescence quenching and electroluminescence quenching experiments. Nevertheless, the data given in Figs. 8 and 9 show that Stern–Volmer type plots obtained employing 2,5-dimethyl-2,4-hexadiene as quencher present a strong downward curvature (a similar behaviour was observed with anthracene).

This behaviour could be due to the presence of more than an emitting species, or to different triplet lifetimes in different reaction zones. In order to test the first possibility, we have measured the emitted light distribution in the absence and in the presence of 2,5-dimethyl-2,4-hexadiene. These data have been included in Figs. 6 and 7 and show that the presence of the quencher do not significantly modify the spectral distribution of the electroluminescence. We consider then that the most likely explanation of the curvature in the Stern–Volmer plots is a shorter lifetime of the triplet in the neighbourhood of the electrodes as a consequence of electrode deactivation and/or impurity quenching.

The possibility of having a gradient in excited biacetyl lifetimes in the neighbourhood of the electrode, as well as the decreased concentration of the anion that could take place in their surroundings, could explain the apparent contradiction observed between the data of Fig. 10 (that shows a dependence in phosphorescence yield with salt concentration in the working region) and the stated independence of the measured photocurrent per mA of applied current with the substrate concentration. Nevertheless, it must be noted that the reproducibility of the electroluminescence measurements is rather low (±15%) and that the range of working concentrations that can be employed is small. This, together with the rather small slope of the Stern–Volmer plot obtained in the quenching experiments at large salt concentrations (see Fig. 11), makes it difficult to quantitatively compare both sets of data.

We consider then that all the experimental results are compatible with and suggestive of a reaction scheme such as that comprising reactions [1] and [4]. The triplet yield in the electrolysis can be obtained from the electroluminescence yield and the phosphorescence yield measured when the diketone is directly excited in the same reaction medium. The electroluminescence yield was obtained employing $Ru(bpy)_3^{2+}/C_2O_4^{2-}$ as reference (6). This method has the advantage that, since both electroprocesses take place on the same electrode, all geometrical factors cancel out. On the other hand, it has the disadvantage that it is necessary to introduce a correction for spectral sensitivity of the detection system. The electroluminescence yield will be given by

[10] $$\phi_{ECL} = f(I/I_{ref})(\phi_{ECL})_{ref}$$

where I and I_{ref} are the photocurrents of the sample and the reference reaction per mA of applied current, $(\phi_{ECL})_{ref}$ is the number of photons emitted by transferred electron in the reference reaction, and f is the factor that takes into account differences in the photomultiplier response. Taking $(\phi_{ECL})_{ref}$ as 0.02 Einstein/Faraday (6), we obtain yields of 1.3×10^{-7} and 2.1×10^{-6} Einstein/Faraday for the electrolysis of PA and PhGA, respectively.

Triplet yields can be obtained from

[11] $$\phi_T = \phi_{ECL}/\phi_{Ph}$$

where ϕ_{Ph} is the phosphorescence efficiency of a triplet under the conditions employed. These values were estimated as 2.7×10^{-3} and 5×10^{-4} for PA and PhGA in the luminescence experiments. If these values are considered to apply to the triplets produced in the electrochemical process, we obtain ϕ_T of 6.2×10^{-5} and 4×10^{-3} for PA and PhGA, respectively.

These values are bound to be large errors, mainly due to the difficulty in evaluating the phosphorescence efficiency of the electrogenerated triplet. They must then be considered only as an indication of the order of magnitude of the triplet yield.

Combining these values with the biacetyl and benzil electrochemical yields, we obtain

[12] $$(k_3/k_2)_{biacetyl} \approx 10^{-4}$$

and

[13] $$(k_3/k_2)_{benzil} \approx 8 \times 10^{-3}$$

The excited recombination of acetyl radical has been proposed as a possible source of the chemiluminescence observed in the thermal reaction between ethylhyponitrite and acetaldehyde (14). Abuin and Lissi (3) have estimated, from thermochemical considerations and the rate of triplet photocleavage, a rate constant of $3 \times 10^3\ M^{-1}\ s^{-1}$ for the recombination of acetyl radicals leading to the excited biacetyl triplet. Furthermore, from the luminescence observed in the photolysis of 3,3-dimethyl-2-butanone they concluded that $k(CH_3COCOCH_3)^3/k(CH_3COCOCH_3)$ must be lower than 2×10^{-3}. This estimation is in agreement with the presently reported value. Furthermore, if a diffusion controlled rate is assumed for the $CH_3CO\cdot$ radical recombination ($5 \times 10^9\ M^{-1}\ s^{-1}$), we conclude from the present data that

Can. J. Chem. Downloaded from www.nrcresearchpress.com by 210.87.254.105 on 09/06/12
For personal use only.

$$k(CH_3COCOCH_3)^3 \approx 5 \times 10^5\ M^{-1}\ s^{-1}$$

This value, although considerably larger than that estimated by Abuin and Lissi (3), seems reasonable if it is considered that the energy barrier imposed on the triplet state decomposition of biacetyl is, at least in the gas phase, nearly equal to the endothermicity of the process (15).

The possibility of luminescence emission in the recombination of PhCO radicals has been considered by Huggenberger *et al.* (16) and Abuin and Lissi (3). The former authors concluded that less than 3% of the recombination leads to the excited triplet. Abuin and Lissi estimated that the fraction of triplet could be as large as 0.05, a value bound to large errors (3). The value found in the present work is then not incompatible with these previous estimates. Benzoyl recombination is a diffusionally controlled process (16) and its rate constant can be taken as $5 \times 10^9\ M^{-1}$ in acetonitrile. This leads to $k_3 \approx 4 \times 10^7\ M^{-1}\ s^{-1}$. For the benzil triplet photocleavage at room temperature, a value of $\sim 3 \times 10^3$ has been obtained in dodecane by extrapolation of high temperature data (17), leading to a ΔG^0 of ≈ 6.5 kcal/mol for benzoyl radicals formation from the excited benzil triplet. This value, although larger than that evaluated from thermochemical methods, is inside the indetermination of the estimates (16).

Conclusions

In the present work it is shown that the Kolbe reaction of pyruvic and phenylglyoxylic acids can be carried out with high yields in acetonitrile solution. The luminescence observed in the electrolysis can be related to the formation of the excited α-diketone in the combination of the corresponding acyl radicals. The data provide the first experimental values of the efficiency of these processes.

1. F. PRAGST, R. ZIEBIG, and E. BOCHE. J. Luminescence, **21**, 21 (1979).
2. S. M. PARK and A. J. BARD. J. Am. Chem. Soc. **97**, 2978 (1975).
3. E. ABUIN and E. LISSI. Photochem. Photobiol. **30**, 59 (1979).
4. B. B. CORSON, R. A. DODGE, S. A. HARRIS, and R. K. HAZEN. Org. Syntheses Coll. Vol. I. Wiley, New York. 1941. p. 241.
5. F. A. COTTON and G. WILKINSON. Química Inorgánica Avanzada. Limusa-Wiley. 1971. 1026.
6. I. RUBINSTEIN and A. J. BARD. J. Am. Chem. Soc. **103**, 512 (1981).
7. W. WLADISLAW and J. P. ZIMMERMAN. J. Chem. Soc. B, 290 (1970).
8. V. FR. FICHTER and S. LURIE. Helv. Chim. Acta, **16**, 885 (1933).
9. (*a*) S. W. BENSON. Thermochemical kinetics. Wiley. 1976; (*b*) Y. SAWAKI and Y. OGATA. J. Am. Chem. Soc. **103**, 6455 (1981).
10. (*a*) L. EBERSON and K. NYBERG. Adv. Phys. Org. Chem. **12**, 104 (1976); (*b*) L. EBERSON and G. RYDE-PETTERSON. Acta Chem. Scand. **27**, 1159 (1973).
11. J. T. DUBOIS and F. WILKINSON. J. Chem. Phys. **39**, 899 (1963); R. S. BECKER. Theory and interpretation of fluorescence and phosphorescence. Wiley Interscience, New York. 1969. p. 162.
12. S. L. MUROV. Handbook of photochemistry. Marcel Dekker Inc., New York. 1973. p. 4.
13. K. SANDROS and M. ALMGREN. Acta Chem. Scand. **17**, 552 (1963).
14. H. W. HOLDEN and K. O. KUTSCHE. Can. J. Chem. **39**, 1552 (1961).
15. A. HOROWITZ and J. C. CALVERT. Int. J. Chem. Kinet. **4**, 207 (1972).
16. C. H. HUGGENBERGER, J. LIPSCHER, and H. FISCHER. J. Phys. Chem. **84**, 3467 (1980).
17. T. CÁCERES, M. V. ENCINA, and E. A. LISSI. J. Photochem. To be published.

Can. J. Chem. Downloaded from www.nrcresearchpress.com by 210.87.254.105 on 09/06/12
For personal use only.

Studies of the initial steps in the polymerization of C_2N_2 induced by Xe^+

ASIT BARAN RAKSIT AND DIETHARD KURT BOHME
Department of Chemistry and Centre for Research in Experimental Space Science, York University, Downsview, Ont., Canada M3J 1P3

Received December 12, 1983

ASIT BARAN RAKSIT and DIETHARD KURT BOHME. Can. J. Chem. **62**, 2123 (1984).

A Selected-Ion Flow Tube (SIFT) apparatus has been used to produce Xe^+ by electron impact and to study its reactions with C_2N_2. The $^2P_{3/2}$ and $^2P_{1/2}$ spin states of Xe^+ were observed to react differently: by C_2N_2 addition to form $Xe^+ \cdot C_2N_2$ and by charge transfer to form $C_2N_2^+$, respectively. Further ion–molecule reactions with C_2N_2 were observed to establish polymeric ions of the type $(C_2N_2)_x^+$. The results indicate that the simple charge transfer model may be sufficient to account for the rate enhancement observed in the radiolytic polymerization of C_2N_2/Xe mixtures.

ASIT BARAN RAKSIT et DIETHARD KURT BOHME. Can. J. Chem. **62**, 2123 (1984).

On a utilisé un tube à écoulement sélecteur d'ions (TESI) pour produire des ions Xe^+ par impact électronique et pour étudier leurs réactions avec le C_2N_2. On a observé que les états de spin $^2P_{3/2}$ et $^2P_{1/2}$ du Xe^+ réagissent différemment alors qu'ils donnent respectivement une addition du C_2N_2 pour former l'ion $Xe^+ \cdot C_2N_2$ et un transfert de charge qui conduit à l'ion $C_2N_2^+$. On a observé que d'autres réactions ion–molécule avec le C_2N_2 conduisent à des ions polymères de type $(C_2N_2)_x^+$. Les résultats indiquent que le modèle simple de transfert de charge peut être suffisant pour expliquer l'augmentation de la vitesse réaction observée lors de la polymérisation par radiolyse de mélanges de C_2N_2/Xe.

[Traduit par le journal]

Introduction

The rate of radiolytic polymerization of C_2N_2 is known to be enhanced by noble gases approximately in proportion to the stopping power of the noble gas (1). This increase in rate has been explained in terms of an initial charge transfer reaction involving the rare gas ion for those noble gases which have a higher ionization energy than C_2N_2 (2). Xenon has been viewed as an exception because of its relatively low ionization energy and it has been argued that the simple charge transfer theory cannot explain the observations with xenon additive (3). An alternative mechanism has been proposed in which a complex of the type $[XeC_2N_2]^+$ is invoked as an intermediate in a sequence of steps [1] to [3]

$$[1] \quad Xe \rightarrow Xe^+ + e^-$$

$$[2] \quad Xe^+ + C_2N_2 \rightarrow [XeC_2N_2^*]^+$$

$$[3] \quad [XeC_2N_2^*]^+ + C_2N_2 \rightarrow (C_nN_m)^+ + \cdot C_pN_q + Xe$$

where n and m equal 1 to 4 but n is not necessarily equal to m, $p = 4 - n$ and $q = 4 - m$ (1, 3). Neutral cyanogen can continue to react with the ionic species produced in step [3] to form polymeric ions which ultimately can lead to neutral products by ion–ion or ion–electron recombination. The addition complex $[XeC_2N_2]^+$ has actually been observed with a mass spectrometer to be formed in a 3.5:1 mixture of cyanogen and xenon at a total pressure of 1 Torr (1). Its observation has provided support for this mechanism which has become known as the "cluster theory".

We report here laboratory measurements directed towards elucidating the nature and kinetics of the initial steps in the Xe^+-induced polymerization of C_2N_2. The reaction of Xe^+ with C_2N_2 is studied in complete "isolation" in helium carrier gas at room temperature. The primary ionic products are identified along with ionic products from ensuing secondary reactions. The results provide evidence for the direct formation of the adduct $Xe^+ \cdot C_2N_2$ from Xe^+ and C_2N_2 but they also suggest that the simple charge transfer model may be entirely adequate to account for the Xe/C_2N_2 radiolysis results.

Experimental

The measurements were performed with the Selected-Ion Flow Tube (SIFT) apparatus in the Ion Chemistry Laboratory (4, 5). For the measurements reported here the instrument was fitted with an axial electron impact ionizer (Extranuclear, Model 041-3). Xe^+ and He^+ were derived from their parent gases at an electron energy of ca. 26 eV and an ion injection energy of ca. 13 V. Helium was used as the carrier gas in all experiments. The cyanogen was of a commercial grade (Matheson, 98.5% minimum by volume in the liquid phase). Separate measurements using H_3^+ as a chemical ionization reagent indicated a purity for the gas of more than 99%. All measurements were made at an ambient temperature of 296 ± 2 K.

Results and discussion

Figure 1 displays observations recorded with the addition of cyanogen into the reaction region of the SIFT apparatus in which the m/z 129 isotope of Xe^+ was established as the dominant ion. The loss curve for Xe^+ shows initial curvature followed by only a gradual decay. There is a sharp concomitant growth and decay in $C_2N_2^+$ and further reactions with C_2N_2 to form polymeric ions of the type $(C_2N_2)_x^+$. Also the cluster ion $Xe^+ \cdot C_2N_2$ is observed to be formed as a product ion.

Overall the observations shown in Fig. 1 show a complicated behaviour. However, the behaviour may be understood if one recognizes the existence of the spin states of Xe^+ with configurations $^2P_{3/2}$ (lowest energy) and $^2P_{1/2}$ formed initially by electron impact, and if one allows for a possible difference in the reactivity of these two spin states (6). A difference in reactivity can be expected simply from a consideration of energetics. The recombination energies of $Xe^+(^2P_{3/2}) = 12.13$ eV and $Xe^+(^2P_{1/2}) = 13.44$ eV are such that charge transfer with C_2N_2, IE = 13.374 ± 0.008 eV (7), is endothermic for the $^2P_{3/2}$ state and slightly exothermic for the $^2P_{1/2}$ state.

The decay of Xe^+ shown in Fig. 1 contains contributions from both Xe^+ spin states and may be analysed in the manner described by Adams *et al.* for the analogous reactions of the spin states of Xe^+ with CH_4 (6). The decay in Xe^+ at small C_2N_2 additions may be attributed to reaction of the 1/2 spin state. The sharp rise in $C_2N_2^+$ at these additions indicates that this state reacts by charge transfer and Fig. 1 shows that $C_2N_2^+$ reacts further with C_2N_2 by addition to form $(C_2N_2)_2^+$ and then $(C_2N_2)_3^+$. Small amounts of $C_3N_3^+$ appear to be produced in a biomolecular reaction of $(C_2N_2)_2^+$ with C_2N_2. The much more gradual decay in Xe^+ at higher C_2N_2 additions may be attribut-

Can. J. Chem. Downloaded from www.nrcresearchpress.com by 210.87.254.105 on 09/06/12
For personal use only.

Can. J. Chem. Downloaded from www.nrcresearchpress.com by 210.87.254.105 on 09/06/12
For personal use only.

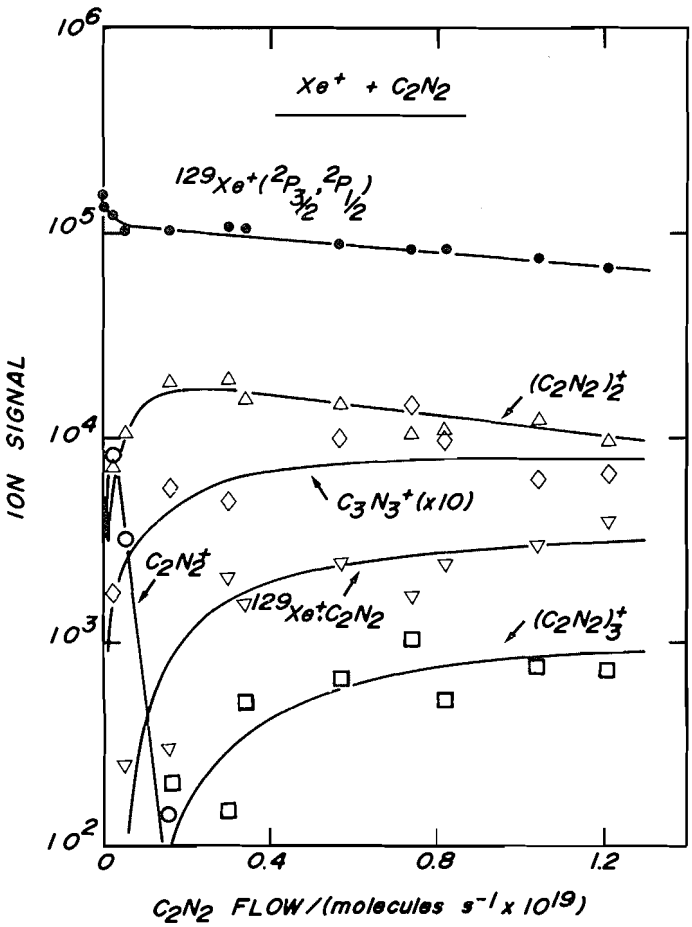

FIG. 1. The observed variation in ion signals for the addition of cyanogen into the reaction region where $^{129}Xe^+$ has been established by injection upstream into helium buffer gas. P = 0.296 Torr, $\bar{v}$ = 7.2 × 10^3 cm s^{-1}, L = 46 cm, T = 295 K. No correction has been made for mass discrimination in the mass spectrometer.

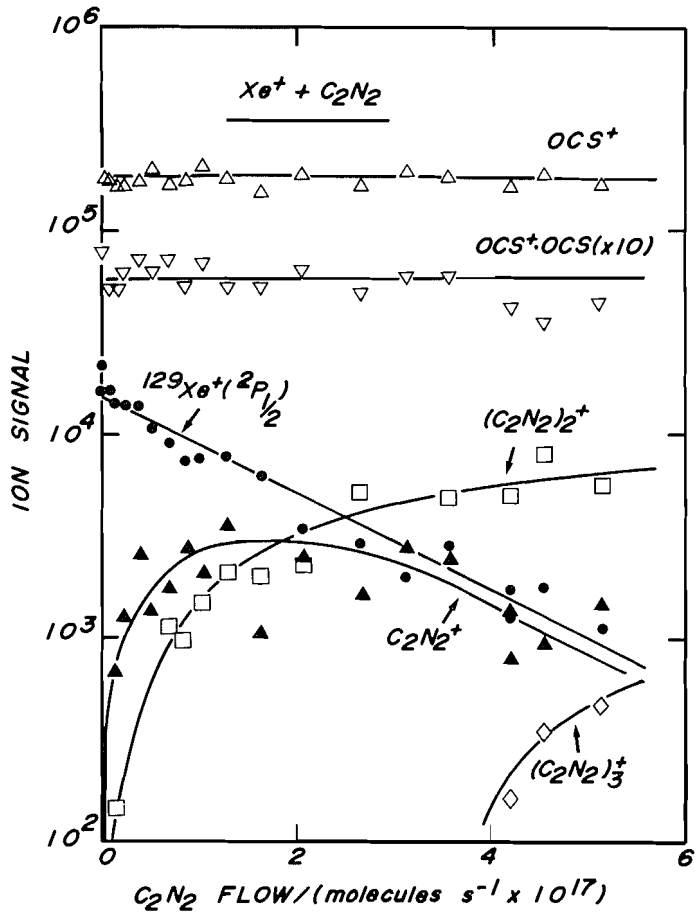

FIG. 2. The observed variation in ion signals for the addition of cyanogen into the reaction region where the 1/2 spin state of Xe^+ has been established by injection of Xe^+ and addition of 6 × 10^{17} molecules s^{-1} of OCS "filter gas" upstream into helium buffer gas. P = 0.298 Torr, $\bar{v}$ = 7.1 × 10^3 cm s^{-1}, L = 46 cm, T = 295 K. No correction has been made for mass discrimination in the mass spectrometer.

ed to the reaction of the 3/2 spin state and it is matched by the appearance of $Xe^+ \cdot C_2N_2$ due presumably to the thermolecular reaction [4]. The slope of this decay corresponds to an effective second-order rate constant of 4 × 10^{-12} cm^3 $molecule^{-1}$ s^{-1}

[4] $Xe^+(^2P_{3/2}) + C_2N_2 + He \rightarrow Xe^+(^2P_{3/2}) \cdot C_2N_2 + He$

at a helium density of 9.7 × 10^{15} atoms cm^{-3} or a third-order rate constant of 4 × 10^{-28} cm^6 $molecule^{-2}$ s^{-1}. The $Xe^+(^2P_{3/2}) \cdot C_2N_2$ may add a second C_2N_2 molecule but there was no evidence for measurable amounts of $Xe^+ \cdot (C_2N_2)_2$ up to the largest flow of C_2N_2 indicated in Fig. 1. A bimolecular reaction between $Xe^+(^2P_{3/2}) \cdot C_2N_2$ and C_2N_2 is much less likely. Certainly charge transfer to produce $C_2N_2^+$ is endothermic. Also formation of $(C_2N_2)_2^+$ is exothermic only if the difference in the ionization energies of C_2N_2 and Xe (1.24 eV) is exceeded by the relative binding energies of $C_2N_2^+$ and Xe^+ (which are not known). However, the occurrence or non-occurrence of such a reaction cannot be resolved with the data in Fig. 1. The loss of $Xe^+(^2P_{3/2}) \cdot C_2N_2$ may be determined by its slow rate of formation and any $(C_2N_2)_2^+$ which might be produced is indistinguishable from the $(C_2N_2)_2^+$ produced concomitantly in large amounts from the reaction sequence initiated by the charge transfer reaction with the 1/2 spin state of Xe^+.

The 1/2 and 3/2 spin states are expected to be produced in the ion source in the ratio of 1 to 2 from statistical considerations (6). The initial reduction in the Xe^+ signal is about 25% which is sufficiently close to the statistical weight prediction (≈33%) that we may conclude that collisional quenching is not a significant loss process for the 1/2 spin state (6). This was corroborated with additional experiments in which OCS was added as a "filter gas" to study separately the reaction of the 1/2 spin state of Xe^+. Adams *et al.* (6) have shown that OCS reacts about 40 times more rapidly with the 3/2 spin state than with the 1/2 spin state. We have reproduced this result in our SIFT apparatus and added OCS upstream in a separate study of the reaction of Xe^+ with C_2N_2. Figure 2 shows observations made under these conditions. OCS^+ and $OCS^+ \cdot OCS$ are the primary and secondary products, respectively, of the charge transfer reaction of the 3/2 spin state of Xe^+ with OCS. With addition of C_2N_2 the remaining Xe^+, which is now predominantly in the 1/2 spin state, decays rapidly with a rate constant of 6.5 × 10^{-10} cm^3 $molecule^{-1}$ s^{-1}. The primary charge transfer product, $C_2N_2^+$, appears and, as before, adds C_2N_2 in two sequential reactions. The Xe^+ decay is not strongly curved so that collisional quenching by C_2N_2 to form the much less reactive 3/2 spin state is not proceeding efficiently. Also $Xe^+ \cdot C_2N_2$ is observed *not* to be present in the product spectrum under these operating conditions from which we may conclude that the 1/2 spin state reacts predominantly by charge transfer.

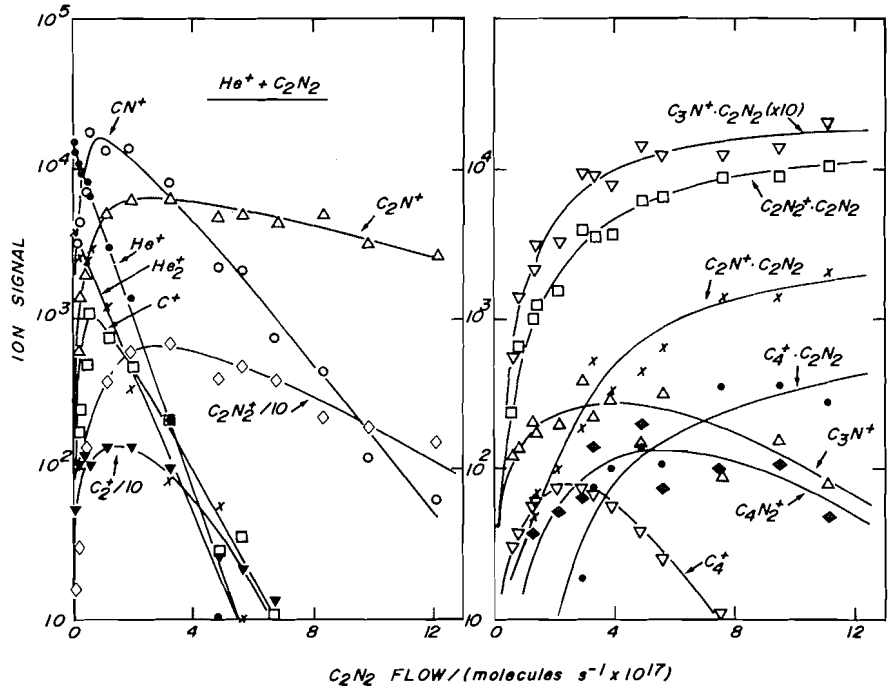

FIG. 3. The observed variation in ion signals for the addition of cyanogen into the reaction region where He^+ and He_2^+ have been established by injection of He^+ upstream into helium buffer gas. $P = 0.335$ Torr, $\bar{v} = 7.4 \times 10^3$ cm s^{-1}, $L = 46$ cm, $T = 297$ K. Left diagram: reactant ions and possible primary ions. Right diagram: secondary product ions.

To contrast the behaviour of Xe^+ towards C_2N_2 with that of another rare gas ion we have included in Fig. 3 results obtained for the reaction of He^+ which has a recombination energy of 24.6 eV which is well above the ionization energy of C_2N_2. Since helium was used as the buffer gas He_2^+ was established in the reaction region by reaction [5]. Both He^+ and He_2^+

[5] $He^+ + He + He \rightarrow He_2^+ + He$

appear to react rapidly with C_2N_2 primarily by dissociative charge transfer. The decay in the He^+ signal corresponds to a rate constant of 1.6×10^{-9} cm^3 molecule^{-1} s^{-1}. The decay in the He_2^+ is influenced in part by the depletion of the He^+ ion in the reaction region. The ions CN^+, C_2N^+, C_2^+, and C^+ were observed to be the principal primary product ions. There was no evidence for the formation of the cluster ion $He^+ \cdot C_2N_2$. The product analysis indicated that $C_2N_2^+$ was largely produced in a secondary reaction. In separate studies we have shown and characterized the occurrence of reactions [6] to [9] (8). All these reactions are seen to operate as secondary reactions in

[6] $CN^+ + C_2N_2 \rightarrow C_2N_2^+ + CN$
$\rightarrow C_3N^+ + N_2$
$\rightarrow C_2N^+ + CN_2$

[7] $C_2N^+ + C_2N_2 + He \rightarrow C_2N^+ \cdot C_2N_2 + He$

[8] $C_2^+ + C_2N_2 \rightarrow C_2N^+ + C_2N$
$\rightarrow C_3N^+ + CN$
$\rightarrow C_4^+ + N_2$

[9] $C^+ + C_2N_2 \rightarrow C_2N^+ + CN$

Fig. 3. Further C_2N_2 addition reactions establish $C_2N_2^+ \cdot C_2N_2$, $C_3N^+ \cdot C_2N_2$, $C_2N^+ \cdot C_2N_2$, and $C_4^+ \cdot C_2N_2$ already at relatively low flows of cyanogen.

The much larger variety of ion chemistry observed with He^+ in contrast to that observed with Xe^+ clearly is to be attributed to the much higher recombination energy of He^+. The high recombination energy results in charge transfer which is almost entirely dissociative so that fragment ions of $C_2N_2^+$ initiate the secondary ion chemistry. Dissociative charge transfer is endothermic with Xe^+ and the observed secondary ion chemistry appears to be initiated exclusively by $C_2N_2^+$.

Conclusions

(*1*) The two spin states of Xe^+ ($^2P_{3/2}$, $^2P_{1/2}$) react differently with C_2N_2. The $^2P_{1/2}$ state which has a recombination energy *higher* than IE(C_2N_2) reacts predominantly by charge transfer while the $^2P_{3/2}$ state which has a recombination energy *lower* than IE(C_2N_2) reacts to form the adduct $Xe^+ \cdot C_2N_2$.

(*2*) The $C_2N_2^+$ charge transfer product of the reaction with Xe^+ ($^2P_{1/2}$) reacts sequentially to add C_2N_2. The addition of two molecules of C_2N_2 was observed under the operating conditions adopted for the measurements reported here. The nature of the further reaction of $Xe^+ \cdot C_2N_2$ remains uncertain but we expect fast bimolecular reactions with C_2N_2 to be unlikely on thermodynamic grounds.

(*3*) If the two spin states of Xe^+ are produced in the ratio expected from statistical considerations, the ionization of Xe in a Xe/C_2N_2 mixture will result in rapid charge transfer with Xe^+ ($^2P_{1/2}$) to produce $C_2N_2^+$ which quickly establishes polymeric ions of the type $(C_2N_2)_x^+$ in sequential addition reactions. Consequently the charge transfer mechanism will make a substantial contribution to the enhanced rate of polymerization of C_2N_2 observed in the radiolysis of such mixtures. Formation of the cluster ion $Xe^+ \cdot C_2N_2$ will also proceed initially but the $Xe^+ \cdot C_2N_2$ is not expected to react rapidly with C_2N_2 in a bimolecular fashion. Consequently the 3/2 spin state of Xe^+ is expected to have a relatively minor effect on cyanogen polymerization.

Can. J. Chem. Downloaded from www.nrcresearchpress.com by 210.87.254.105 on 09/06/12
For personal use only.

Acknowledgement

We thank the Natural Sciences and Engineering Research Council of Canada for financial support.

1. C. E. MELTON and P. S. RUDOLPH. J. Chem. Phys. **33**, 1594 (1960).
2. S. C. LIND and D. C. BARDWELL. Science, **62**, 593 (1925).
3. P. S. RUDOLPH, S. C. LIND, and C. E. MELTON. J. Chem. Phys. **36**, 1031 (1962).
4. G. I. MACKAY, G. D. VLACHOS, D. K. BOHME, and H. I. SCHIFF. Int. J. Mass Spectrom. Ion Phys. **36**, 259 (1980).
5. A. B. RAKSIT and D. K. BOHME. Int. J. Mass Spectrom. Ion Proc. **55**, 69 (1984).
6. N. G. ADAMS, D. SMITH, and E. ALGE. J. Phys. B: Atom. Molec. Phys. **13**, 3235 (1980).
7. V. H. DIBELER and S. K. LISTON. J. Chem. Phys. **47**, 4548 (1967).
8. A. B. RAKSIT and D. K. BOHME. Int. J. Mass Spectrom. Ion Proc. To be published.

Can. J. Chem. Downloaded from www.nrcresearchpress.com by 210.87.254.105 on 09/06/12
For personal use only.

The dependence of the rates of reduction of cobalt(III)-μ-peroxo complexes on isomeric structure

STEVE C. F. AU-YEUNG AND DONALD R. EATON[1]
Department of Chemistry, McMaster University, Hamilton, Ont., Canada L8S 4M1

Received October 27, 1983

STEVE C. F. AU-YEUNG and DONALD R. EATON. Can. J. Chem. **62**, 2127 (1984).

The reaction of μ-peroxybis(ethylenediamine)bis(diethylenetriamine)cobalt(III) with ferrous ions has been studied by stopped flow spectrophotometry and by ^{59}Co nmr. Two separate initial reduction steps with second order rate constants of 1.07 and 3.04 M^{-1} s^{-1}, respectively, can be discerned in the stopped flow experiments. These two rate constants are assigned to inner sphere reduction of the aef,cd,b and edf,ac,b isomers of the peroxy cobalt complex, respectively. The different isomers can be distinguished by ^{59}Co nmr. If there is insufficient Fe^{2+} present to completely reduce the complex to Co(II) and water, the change in the relative intensities of the ^{59}Co resonances after partial reduction shows that one isomer has reacted faster than the other. The ^{59}Co resonances can be assigned to the different isomers on the basis of a point charge model for the chemical shifts and line widths. Based on this model it is concluded that the isomer with the central NH of the diethylenetriamine *trans* to the peroxy ligand reacts faster. This result is compared to literature reports on the relative rates of substitution of isomers of Co(III) complexes with ethylenediamine and diethylenetriamine ligands.

STEVE C. F. AU-YEUNG et DONALD R. EATON. Can. J. Chem. **62**, 2127 (1984).

Faisant appel à la spectrométrie par flux stoppé et à la rmn du ^{59}Co, on a étudié la réaction du μ-peroxy bis(éthylènediamine) bis(diétylènetriamine)cobalt(III) avec les ions ferreux. Dans les expériences à flux stoppé, on peut distinguer deux étapes initiales distinctes pour la réduction et leurs constantes de vitesses d'ordre deux sont respectivement 1,07 et 3,04 M^{-1} s^{-1}. On attribue ces deux constantes de vitesse aux réductions respectives, dans la sphère intérieure, des isomères aef,cd,b et edf,ac,b du complexe de peroxy cobalt. On peut distinguer les différents isomères grâce à la rmn du ^{59}Co. Si la quantité de Fe^{2+} présente n'est pas suffisante pour réduire complètement le complexe en Co(II) et en eau, le changement des intensités relatives de la résonance du ^{59}Co, après la réduction partielle, montre qu'un isomère réagit plus vite que l'autre. On peut attribuer les résonances du ^{59}Co aux différents isomères en se basant sur un modèle de charge ponctuelle pour les déplacements chimiques et les largeurs des pics. En se basant sur ce modèle, on conclut que l'isomère qui réagit le plus rapidement est celui qui porte le NH central de la diéthylènetriamine en position *trans* par rapport aux ligand époxy. On compare ce résultat à ceux répertoriés dans la littérature pour les vitesses relatives de substitution des isomères des complexes du Co(III) avec des ligands d'éthylènediamine et de diéthylènetriamine.

[Traduit par le journal]

Introduction

A series of compounds formed by the reaction of molecular oxygen with solutions containing Co(II) ions has been extensively studied (1−3). The complexes with the stoichiometry of two Co atoms to one oxygen molecule are correctly formulated as peroxy compounds containing Co in the 3+ oxidation state. One electron oxidation of these compounds leads to the corresponding superoxy complexes. Complete reduction of the peroxo compounds to Co(II) and water requires four equivalents of a one electron reducing agent. There have been a number of studies of the mechanisms of these reductions motivated by the analogies with reactions of biological importance (4−6). It seems well established (4) that the first step in the reduction of the superoxo complexes is an outer sphere electron transfer and that reduction of the peroxy compounds is initiated by an inner sphere electron transfer. Subsequent steps are less well understood.

McLendon and Martell (5) have examined the reduction of several of these compounds with ferrous ions. They found that the rate of the inner sphere electron transfer varied by two orders of magnitude for complexes with different amine ligands. In the present paper we show that this rate is also affected by different isomeric arrangements of the same amine ligands.

Experimental

Kinetic measurements were carried out on a Durrum D110 Stopped Flow spectrophotometer. Temperature was controlled with a thermostatted water bath. Data were collected on a Nicolet-1170 Signal Averager. The reaction was followed at 420 nm which is a wavelength corresponding to absorption of the product Fe^{3+}. Most measurements were carried out at pH 4.5 using potassium hydrogen phthalate buffer but some runs were made at pH's of 3.5 and 4.0. No significant difference in rates was found at the different pH values. The reactions were examined at 24°C and at a total ionic strength of 1.2 *M* ($NaClO_4$). The concentration of Co complex used was 0.78 m*M* and that of Fe^{2+} varied from 4 m*M* to 50 m*M*. It was apparent that two distinct reactions were occurring. The difference in rates (a factor of approximately 3) is sufficient to allow reasonably good separation of the two processes using the dual time base provided on the Nicolet-1170 signal averaging system. Good exponential formation curves were obtained indicating pseudo first order reactions. We estimate the errors in the rate constants to be ±10%.

^{59}Co nmr spectra were obtained using a Bruker WH90 FT spectrometer operating at 21 MHz. A few spectra were also run on WM250 and WM400 high field instruments to obtain optimum resolution of the isomers. Relative intensities of the different ^{59}Co resonances were obtained by computer fitting to the sum of the three Lorentzian lines centred at the chemical shifts of the three isomers. $Coen_3^{3+}$ was used as an internal intensity standard (concentration 8 m*M*). The peroxo complex was prepared as a perchlorate salt by the procedure of Duffy, House, and Weil (7). Its optical and nmr spectra agreed with those reported in the literature. Other chemicals were of reagent grade and used without further purification.

Results and discussion

Both of the reactions observed by stopped-flow spectrophotometry have rates which are first order with the Fe concentration. In agreement with the findings of McLendon and Martell (5), there is no significant change of rate with pH.

[1]To whom all correspondence should be addressed.

Can. J. Chem. Downloaded from www.nrcresearchpress.com by 210.87.254.5 on 09/06/12
For personal use only.

TABLE 1. Kinetic data* for the reduction of $[Co(en)(dien)]_2O_2^{4+}$ by $FeSO_4 \cdot 7H_2O$

		First reaction		Second reaction	
$[FeSO_4 \cdot 7H_2O]$ (mM)	pH	k_{obs} (s^{-1})	$k_{obs}/[FeSO_4 \cdot 7H_2O]$ (M^{-1} s^{-1})	k_{obs} (s^{-1})	$k_{obs}/[FeSO_4 \cdot 7H_2O]$ (M^{-1} s^{-1})
3.91	4.5	0.0108±0.0021	2.7621	—	—
7.81	4.5	0.0265±0.0015	3.3931	0.0103±0.0039	1.3188
15.62	4.5	0.0396±0.0015	2.5352	0.0175±0.0025	1.1204
23.43	4.5	0.0817±0.0007	3.4869	0.0232±0.0011	0.9902
31.24	4.5	0.0910±0.008	2.9129	0.0338±0.0016	1.0819
39.05	4.5	0.1077±0.0019	2.7580	0.0418±0.0013	1.0704
47.31	4.5	0.1506±0.0013	3.1828	0.0523±0.0021	1.1055
			Ave. (3.0044±0.3568)		Ave. (1.1145±0.1098)
			Least square (3.0403±0.0496)		Least square (1.0655±0.0158)
39.05	3.46†	0.1033±0.015	2.6451	0.0403±0.0012	1.0322
39.05	3.89	0.100±0.021	2.5653	0.0420±0.0008	1.0755
39.05	4.22	0.094±0.010	2.4072	0.0365±0.0010	0.9347
39.05	4.42	0.113±0.008	2.8948	0.0405±0.0009	1.0627
39.05	4.55	0.103±0.018	2.6385	0.0385±0.0009	0.9859
			Ave. (2.6302±0.1762)		Ave. (1.0186±0.0572)

*$[(Co(en)(dien))_2O_2(ClO_4)_4]$ = 0.781 mM; μ = 1.2 M ($NaClO_4$); buffer = 0.2 M NaOAc − 0.2 M HOAc.
†Buffer = 0.1 M KH phthalate − 0.1 M NaOH.

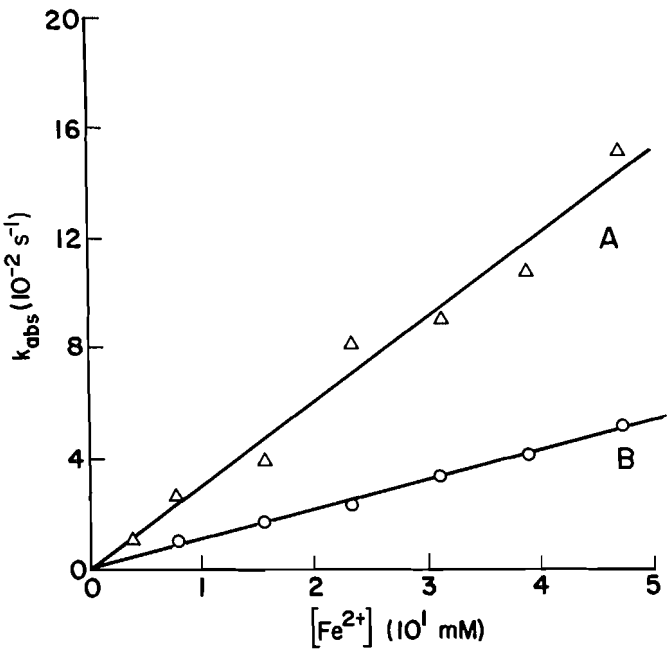

FIG. 1. Plots of k_{obs} versus $[Fe^{2+}]$: (*A*) *sym*-edf,ac,b-$[Co(en)(dien)]_2O_2^{4+}$, (*B*) *sym*-aef,cd,b-$[Co(en)(dien)]_2O_2^{4+}$. Solid line is the linear least-squares fit. *T*, 24°C; pH, 4.5; Co complex, 0.78 mM; ionic strength 1.2 M.

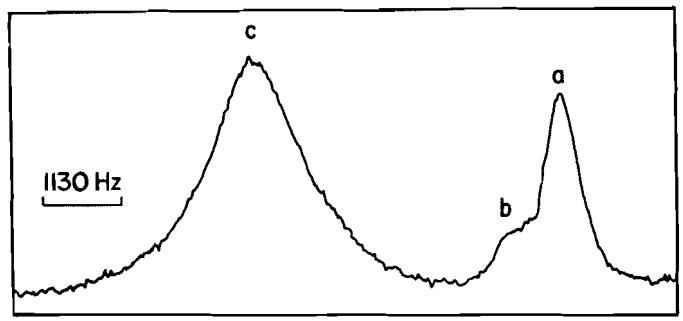

FIG. 2. ^{59}Co nmr spectra (94 MHz) of (*a*) sym-edf,ac,b-$[Co(en)(dien)]_2O_2^{4+}$, (*b*) sym-def,ac,b-$[Co(en)(dien)]_2O_2^{4+}$, (*c*) sym-aef,cd,b-$[Co(en)(dien)]_2O_2^{4+}$. *T*, 24°C; pH, 4.5.

Measured pseudo first order rate constants are given in Table 1 and plots against Fe concentration are shown in Fig. 1. The second order rate constants obtained from these plots are 1.07 and 3.04 M^{-1} s^{-1} for the slower and the faster reaction, respectively. These may be compared with the value of 3.0 M^{-1} s^{-1} given by McLendon and Martell for the inner sphere reduction of the corresponding tetraethylene−pentamine complex with Fe^{2+}. Other complexes studied by these authors were dibridged and react significantly faster. It is clear that both the rate constants are best assigned to inner sphere reduction steps and it is suggested that they correspond to the reduction of different isomers. The change in optical absorption for the two reactions correspond reasonably well to the fractions of each isomer indicated by nmr.

This conclusion is supported by ^{59}Co nmr measurements. Figure 2 shows a ^{59}Co nmr spectrum of $[Co(dien)(en)]_2O_2^{4+}$ obtained at 94.5 MHz on a Bruker WH400 spectrometer (8). Separate resonances corresponding to the three possible isomeric arrangements of the dien and en ligands are clearly observed. The time dependence of the nmr spectrum of a reaction mixture equimolar in Co and Fe was examined. The amount of Fe present is insufficient to complete the reduction process. Reaction schemes have been suggested by Sykes (4) and McLendon and Martell (5). They differ in detail but agree that the first one electron reduction liberates one Co^{2+} ion and that the second electron reduces the other Co, leaving the oxygen moiety in the peroxide oxidation state. Two further electrons are required to reduce peroxide to water. In the case of strong reducing agents such as Cr^{2+} this may occur by direct reaction with the metal ion (6). In the case of Fe^{2+} a more likely sequence is decomposition of the peroxide to molecular oxygen and water (probably catalyzed by the metal ions present), followed by reaction of the oxygen with the Co^{2+} and amine to reform the Co/oxygen complex. It should be noted that at the end of this sequence half of the Co^{3+} has been reduced to Co^{2+} and half of the peroxide has been reduced to water. Reaction with more Fe^{2+} will eventually complete the reduction. The results of the nmr kinetic experiment shown in Fig. 3 are

Can. J. Chem. Downloaded from www.nrcresearchpress.com by 210.87.254.5 on 09/06/12
For personal use only.

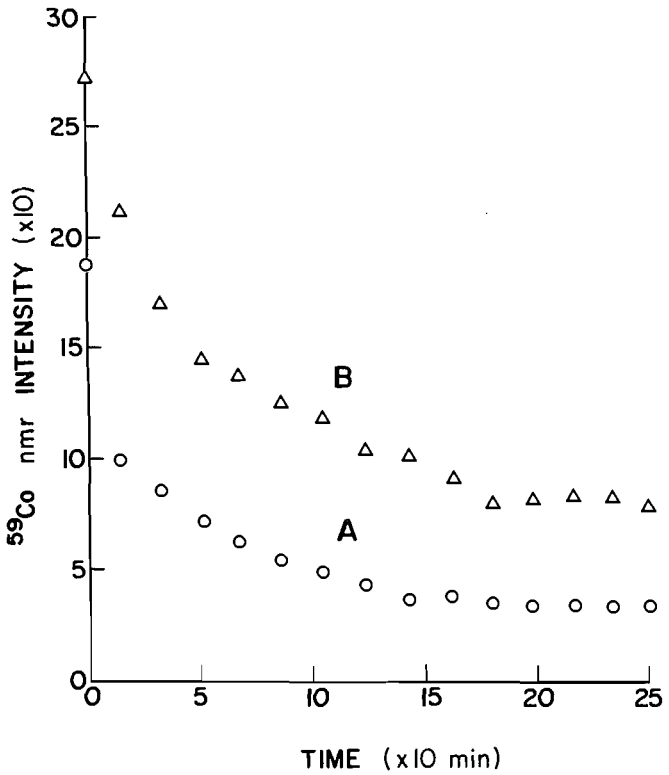

FIG. 3. ^{59}Co nmr intensity versus time plot of the reduction reaction of $[Co(en)(dien)]_2O_2^{4+}$ by $FeSO_4 \cdot 7H_2O$: (*A*) sym-edf,-ac,b-$[Co(en)(dien)]_2O_2^{4+}$; (*B*) sym-aef,cd,b-$[Co(en)(dien)]_2O_2^{4+}$. $[(Co(en)(dien))_2O_2^{4+}]_{tot}$, 20 m*M*. *T*, 6°C; pH, 4.5; $[FeSO_4 \cdot 7H_2O]$, 40 m*M*.

consistent with this scheme. The reactions studied by stopped-flow spectrophotometry are complete before the first nmr spectrum has been acquired. There is therefore a sharp initial decrease in ^{59}Co intensity followed by a much slower decay. The intensity does not fall to zero even after several hours, showing that some of the Fe has been used to reduce peroxide rather than Co. This experiment was performed at 6°C in the hope of identifying intermediates of the type postulated by Sykes and McLendon and Martell. There is no indication of other species other than the starting complexes and we infer that all the reactions in these schemes are fast compared to the time taken to obtain the nmr spectra. The important observation is that the relative intensities of the resonances arising from the different isomers is significantly different after the initial stage of the reaction is finished. Thus the ratio of the intensity of the high field line (*a* in Fig. 2) to that of the low field line (*c*) is 0.68 initially and 0.47 on the first nmr spectrum obtained on the reacting solution. Clearly one isomer is consumed faster than the other, confirming the interpretation of the stopped-flow data. Similar nmr experiments have been carried out using 1, 3, 4, and 5 mol of iron for each mole of dimeric cobalt complex. Rather more than 4 mol of reducing reagent are required to completely eliminate the ^{59}Co nmr signal. The ratio of the isomeric nmr signals after addition of Fe^{2+} differs in every case from the ratio before the addition of Fe^{2+} as described above for the 2:1 reaction mixture.

We have previously suggested the use of a point charge model for assigning ^{59}Co resonances (9). This model assumes the predominant influence of the paramagnetic term in determining the chemical shifts and uses simple crystal field theory

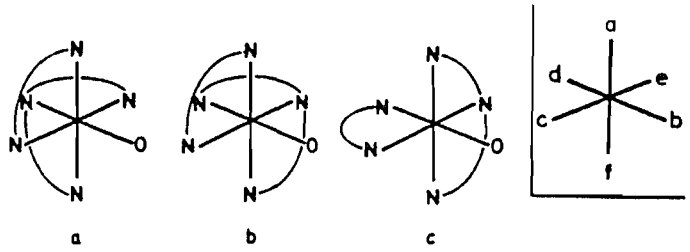

FIG. 4. Isomers of $[Co(dien)(en)]_2O_2^{4+}$: (*a*) edf,ac,b isomer, (*b*) def,ac,b isomer, (*c*) aef,cd,b isomer.

to obtain the energy differences required in the calculations. One parameter is required for each different kind of ligand and it was shown that the relative chemical shifts of isomeric compounds can be predicted to within a few ppm. The necessary parameters for the ligands of the present complexes have been reported previously (9). Figure 4 shows the isomeric structures. The calculated chemical shifts for the def,cd,b, the edf,ac,b and the def,ac,b isomers are 7795, 7681, and 7718 ppm compared with the experimental values of 7652, 7555, and 7572 ppm. There is an absolute discrepancy of about 140 ppm between the experimental and calculated values but the relative shifts allow assignment of the different isomers. This assignment can be confirmed by a further calculation of the expected line widths based on a point charge quadrupolar approximation. This leads to the prediction that the edf,ac,b isomer will have a linewidth approximately half of that of the other isomers as is apparent in Fig. 2. This result confirms the assignment given above. Thus the edf,ac,b isomer reacts faster than the aef,cd,b isomer. The third isomer is present in low abundance and is not well resolved at 21 MHz but appears to react slower than either of the others. It is interesting that the most reactive isomer has the central NH of the dien ligand, which is the ligand with the highest point charge (or crystal field splitting) parameter, *trans* to the peroxy group.

There have been a number of previous studies of the relative rates of reaction of isomeric Co(III) complexes. This area has been reviewed by House (10). The results most pertinent to the present findings are measurements of the rates of aquation, of base hydrolysis, and of Hg^{2+} assisted aquation of isomers of $Co(en)(dien)X^{2+}$ where X^- is a halide ion (10). For all three reactions a difference in rate of around three was found for the two isomers corresponding to the peroxy complexes discussed above. This ratio is very similar to that found in the present study. However, the direction of the effect is opposite since the aef,cd,b isomer reacts faster than the edf,ac,b isomer. This result is reasonable considering the nature of the reactions involved. In the peroxy reactions with Fe^{2+}, electrons must be donated from the peroxy ligand to the Co. Consistent with this π electron withdrawing ligands such as CN^- increase the rate of decomposition (11, 12). The initial step of a hydration reaction on the other hand is likely to be dissociation of the halide ion which removes electrons from the Co. The reverse dependence of the rate on structure is therefore to be anticipated.

Acknowledgements

We are indebted to the Natural Science and Engineering Research Council of Canada for financial support of this research and to the S.W. Ontario High Field NMR Centre for 94 MHz ^{59}Co nmr spectra.

Can. J. Chem. Downloaded from www.nrcresearchpress.com by 210.87.254.5 on 09/06/12
For personal use only.

1. G. MCLENDON and A. E. MARTELL. Coord. Chem. Rev. **19**, 3 (1976).
2. A. E. MARTELL. Acc. Chem. Res. **15**, 155 (1982).
3. R. D. JONES, D. A. SUMMERVILLE, and F. BASOLO. Chem. Rev. **79**, 144 (1979).
4. M. R. HYDE and A. G. SYKES. J. Chem. Soc. Dalton Trans. 1550 (1974).
5. G. MCLENDON and A. E. MARTELL. Inorg. Chem. **15**, 2662 (1976).
6. A. HOFFMAN and H. TAUBE. Inorg. Chem. **7**, 1971 (1968).
7. D. L. DUFFY, D. HOUSE, and J. A. WEIL. J. Inorg. Nucl. Chem. **31**, 2053 (1969).
8. S. C. F. AU-YEUNG and D. R. EATON. Inorg. Chim. Acta, **76**, L141 (1983).
9. S. C. F. AU-YEUNG and D. R. EATON. Can. J. Chem. **61**, 2431 (1983).
10. D. A. HOUSE. Coord. Chem. Rev. **23**, 223 (1977).
11. R. S. GALL, J. F. ROGERS, W. P. SCHAEFER, and G. C. CHRISTOPH. J. Am. Chem. Soc. **98**, 5135 (1976).
12. M. J. CARTER, D. P. RILLEMA, and F. BASOLO. J. Am. Chem. Soc. **96**, 392 (1974).

Can. J. Chem. Downloaded from www.nrcresearchpress.com by 210.87.254.5 on 09/06/12
For personal use only.

Nuclear magnetic resonance study of conformation and dynamics in solution of *p*-(*o*-propyloxybenzamido)benzoate diethyl(2-hydroxyethyl)methylammonium bromide: a smooth muscle relaxant agent

GIANNI VALENSIN AND LIONELLO POGLIANI
Department of Chemistry, University of Siena, Pian dei Mantellini 44, 53100 Siena, Italy
MARIO GHELARDONI
Istituto di Chimica Farmaceutica e Tossicologica, Via Gino Capponi 9, Firenze, Italy
VITTORIO PESTELLINI
Laboratori Chimico Farmaceutici A. Menarini, Via Sette Santi 3, Firenze, Italy
AND
ALESSANDRO SEGA
Institute of Organic Chemistry, University of Siena, Pian dei Mantellini 44, 53100 Siena, Italy

Received November 25, 1983

GIANNI VALENSIN, LIONELLO POGLIANI, MARIO GHELARDONI, VITTORIO PESTELLINI, and ALESSANDRO SEGA. Can. J. Chem. **62**, 2131 (1984).

The relative conformation of the aromatic rings and the amide bridge as well as important details of the two side chains of the title compound in a DMSO-d_6 solution have been established by use of non-selective and selective proton spin-lattice relaxation times coupled with nOe experiments. The complete analysis of ^{13}C spin-lattice relaxation times has shown the main features of the dynamic behavior of the title compound.

GIANNI VALENSIN, LIONELLO POGLIANI, MARIO GHELARDONI, VITTORIO PESTELLINI et ALESSANDRO SEGA. Can. J. Chem. **62**, 2131 (1984).

En se basant sur des déterminations sélectives et non-sélectives de temps de relaxation spin-réseau du proton couplées à des expériences d'effet Overhauser nucléaire, on a établi les configurations relatives des cycles aromatiques et du pont amide ainsi que des détails importants de deux chaînes latérales du composé mentionné dans le titre en solution dans le DMSO-d_6. L'analyse complète des temps de relaxation spin-réseau ^{13}C a permis de mettre en évidence les caractéristiques principales du comportement dynamique du composé mentionné dans le titre.

[Traduit par le journal]

Can. J. Chem. Downloaded from www.nrcresearchpress.com by 210.87.254.42 on 09/06/12
For personal use only.

Introduction

When dealing with pharmacological and biological molecules one important step is the elucidation of conformational features in solution in order to find out the relationship with biological activity.

For this purpose nmr investigations are well suited, since several parameters can be pursued from which dynamic and conformational information can be obtained at the molecular level.

Here we present a study of the structure and dynamics of the title compound **1** (see Fig. 1), which is the first in a series of synthesized drugs which show smooth muscle relaxing activity (1). The combined discussion of (1) ^1H and ^{13}C chemical shifts, (2) ^1H and ^{13}C spin-lattice relaxation rates, (3) ^1H single-selective and double-selective spin-lattice relaxation rates, (4) nuclear Overhauser enhancement experiments, gave us the opportunity of measuring the $^{13}C—^1H$ and $^1H—^1H$ dipole–dipole interactions from which motional and structural features could be inferred. Namely, the dipolar interaction gives the function τ_c/r^6 and measuring τ_c from dipolar contributions to ^{13}C spin-lattice relaxation rates from directly bonded protons allows the evaluation of interproton distances, provided $^1H—^1H$ dipole–dipole mechanism dominates proton relaxation.

Results

The measured proton spin-lattice relaxation rates (R_1) of **1** are reported in Table 1 together with the chemical shift data. The R_1 values of the carbon nuclei of **1** are reported in Table 2 together with the chemical shift data. The assignments in the ^{13}C nmr spectrum were determined by observing selective decoupling of resonances on irradiation of single proton frequencies in the normal proton coupled spectrum. The non-selective and double-selective proton spin-lattice relaxation rates were measured for some protons relevant for conformational analysis (see below). The relaxation data, calculated in the initial slope approximation (2), were previously used to point out the main configurational features of the title compound (3). A typical nOe difference spectrum, showing positive nOe enhancements for H_5, H_3, H_{18}, and NH resonances with saturating irradiation of the H_6 resonance, is illustrated in Fig. 2. The full intensity perturbation pattern is summarized in Table 3, where the significant nOe enhancements are reported to be discussed for conformational purposes.

Discussion

^1H nuclear magnetic resonance chemical shift data

It is important for the following discussion to establish the stereochemistry of the amide group. The configuration around the nitrogen is planar or nearly planar as a consequence of the reduction of electronic density caused by electron withdrawing substituents (4). The configuration about the C—N amide bond must be *cis* with the carbonylic group and ring B on the same side, as *trans* configuration is forbidden by steric hindrance between the two aromatic rings (5).

The high value of the chemical shift of the $H_{10,10'}$ protons can be taken to indicate coplanarity between ring B and the carbonylic group, since it has been demonstrated (6) that whenever the carbonyl group is forced outside the plane of the benzene

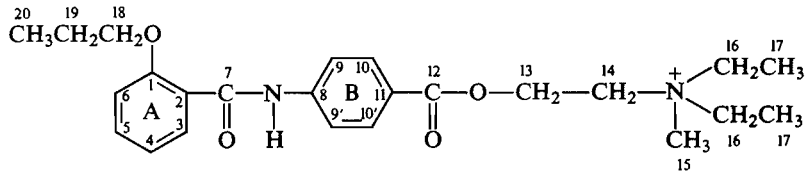

FIG. 1. Title compound.

TABLE 1. ^1H chemical shifts[a] and spin-lattice relaxation rates[b] for compound **1** (0.2 mol dm^{-3} in DMSO-d_6, T = 298 K)

	Chemical shift (ppm)	R_1 (s^{-1})
H_{20}	0.97	2.38 ± 0.10
H_{17}	1.27	3.33 ± 0.17
H_{19}	1.79	2.33 ± 0.10
H_{15}	3.12	5.56 ± 0.27
H_{16}	3.51	5.56 ± 0.28
H_{14}	3.82	5.88 ± 0.30
H_{18}	4.08	3.03 ± 0.15
H_{13}	4.70	5.26 ± 0.26
H_4	7.08	1.52 ± 0.07
H_6	7.19	2.33 ± 0.12
H_5	7.51	1.52 ± 0.07
H_3	7.66	1.08 ± 0.04
$H_{9,9'}$	7.91	1.54 ± 0.08
$H_{10,10'}$	8.00	1.25 ± 0.05
NH	10.44	2.67 ± 0.14

[a]Measured downfield from internal TMS.
[b](±) Figures denote approximate 95% confidence limits of the exponential regression analysis.

TABLE 2. ^{13}C chemical shifts[a] and spin-lattice relaxation rates for compound **1** (0.2 mol dm^{-3} in DMSO-d_6, T = 298 K)

	Chemical shift (ppm)	R_1 (s^{-1})
C_{17}	7.5	0.81 ± 0.05
C_{20}	10.1	0.38 ± 0.03
C_{19}	22.0	1.13 ± 0.04
C_{15}	47.1	2.69 ± 0.25
C_{16}	56.3	3.73 ± 0.19
C_{14}	57.9	4.63 ± 0.25
C_{13}	58.7	5.92 ± 0.48
C_{18}	70.0	2.62 ± 0.26
C_6	112.8	3.11 ± 0.30
$C_{9,9'}$	118.7	2.86 ± 0.13
C_4	120.2	2.77 ± 0.19
C_{11}	123.3	0.20 ± 0.04
C_2	124.4	0.14 ± 0.02
C_3	129.7	3.00 ± 0.19
$C_{10,10'}$	130.4	2.73 ± 0.05
C_5	132.6	4.93 ± 0.43
C_8	143.6	0.30 ± 0.02
C_1	155.9	0.18 ± 0.02
C_{12}	164.5	0.16 ± 0.01
C_7	164.9	0.17 ± 0.02

[a]Measured downfield from internal TMS.
[b](±) Figures denote approximate 95% confidence limits of the exponential regression analysis.

ring the usual downfield shift of the protons *ortho* to this group is greatly reduced. On the other hand, the chemical shift of the H_3 proton and its small difference with respect to the chemical shift of the H_5 *para* proton could indicate a possible deviation from coplanarity between ring A and the amide carbonyl; however, in this case, a qualitative analysis of the chemical shifts is complicated by the presence of two *ortho* substituents.

The equivalence of the two ethyl groups at the quaternary nitrogen can be ascribed to rapid rotation around the C_{14}—N bond accompanied, but not necessarily, by fast free internal rotations (see discussion on relaxation times).

The unresolved lineshape of H_{13} and H_{14} may, on the contrary, be due to hindrance of fast internal motions with resulting incomplete averaging of electronic environments. In fact the quadrupolar interaction with the nitrogen atom is expected to give only a small contribution.

^{13}C nuclear magnetic resonance chemical shift data

The ^{13}C nmr spectrum, obtained at 50.309 MHz, ratifies the suggestion that the two ethyl groups at the quaternary nitrogen are equivalent due to fast rotation around the C_{14}—N bond. In a similar way the magnetic equivalence of the two C_9 and the two C_{10} carbons is pointing to fast rotation of the ring B around the C_8—C_{11} molecular axis. The chemical shifts found for ring B carbons are in perfect agreement with those reported for derivatives of benzanilide (7).

The most interesting result is the chemical shift for C_{13} and C_{14}. In **1**, C_{14} is found upfield with respect to C_{13} and their chemical shift difference is very small. On the contrary, in the ^{13}C nmr study of a series of benzocaine hydrochloride anesthetics (8) it has been found that C_{14} is downfield independently of the substituent in position 8. Similar results are also reported for acetylcholine (9). A downfield shift of the same order of magnitude is also observed for C_{16} with respect to benzocaine hydrochloride anesthetics, while, on the contrary, C_{15} is shifted 7 ppm upfield with respect to acetylcholine. The best explanation for these results is a change in the conformation of the N^+—C_{14}—C_{13}—O backbone and (to a lesser extent) an alteration of the electric field gradient at the nearby carbon atoms (10).

^1H and ^{13}C spin-lattice relaxation data

The relaxation of protons is mostly determined by mutual dipolar interaction of proton pairs. In dilute solutions intramolecular interactions are expected to yield the major contribution.

The measured proton spin-lattice relaxation rates (Table 1) do not allow any quantitative calculation of conformational and motional molecular features, but the following spectulations are nonetheless possible. The fast relaxation rates of H_{13}, H_{14}, H_{15}, and H_{16} suggest a restriction of free segmental motion and, as a consequence, a certain rigidity of this part of the chain; in fact the dipolar and/(or) scalar interaction with the nitrogen atom are not expected to be large enough to provide efficient relaxation pathways. The difference in relaxation rate between H_9 and H_{10} is due to an additional contribution to the relaxation of H_9 from the NH group and such difference may be taken as an aid in proton resonance assignments. The slowest relaxation rate of H_3 is consistent with the environment of that proton,

Can. J. Chem. Downloaded from www.nrcresearchpress.com by 210.87.254.42 on 09/06/12
For personal use only.

TABLE 3. Nuclear Overhauser enhancements for selected proton resonances of compound **1** (0.2 mol dm^{-3} in DMSO-d_6, T = 298 K)

	Proton observed									
Proton irradiated	NH	H_{20}	H_{18}	H_{17}	H_9	H_{10}	H_3	H_4	H_5	H_6
NH					0.094	0.029	0.016			
H_{19}		0.034	0.027							
H_{18}	0.043									0.202
H_{14}				0.025						
H_9, H_{10}	0.117									
H_3	0.002							0.064		
H_4			0.023				0.060			
H_6			0.072				0.034		0.088	

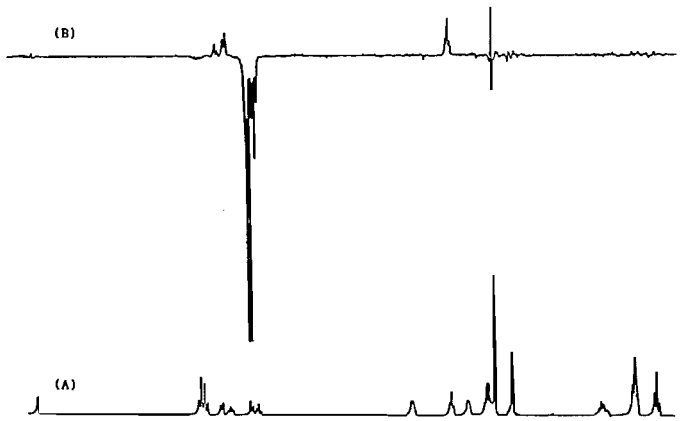

FIG. 2. Result of the difference nOe experiment performed at 200 MHz and 298 K upon saturation fo teh H_6 proton resonance of compound **1** (spectrum B). The normal spectrum is seen in A.

TABLE 4. Correlation times for internal motions of selected carbons of compound **1** (0.2 mol dm^{-3} in DMSO-d_6 at 298 K) with respect to a rotational molecular correlation time $\tau_R = 1.97 \times 10^{-10}$ s

Carbons	τ_G (s)
C_6, C_4, C_3	5.50×10^{-11}
C_9, C_{10}	5.50×10^{-11}
C_{13}	5.48×10^{-11}
C_{14}	2.95×10^{-11}
C_{16}	1.80×10^{-11}
C_{18}	1.00×10^{-11}

which has the dipolar interaction with H_4 as a unique relaxation pathway. On the contrary, H_6, which apparently experiences a molecular environment similar to that of H_3, displays a relatively fast R_1, suggesting the existence of additional proton–proton interactions leading to efficient relaxation.

Since the ^{13}C spin-lattice relaxation rates are almost exclusively determined by dipolar interaction with directly bonded protons (11, 12), the data reported in Table 2 can be suitably used to speculate about the molecular dynamics of compound **1**.

First of all, it is worth noting that all the protonated aromatic carbons display the same spin-lattice relaxation rates, with the exception of C_5 which relaxes with a faster kinetic constant. As already stated in other cases (11, 12), these findings can be accounted for in terms of a main molecular rotation axis which passes through C_5 and C_2 such that the C_5—H_5 vector undergoes slower tumbling motions as compared to the other C—H vectors. Since the relaxation rates of C_9 and C_{10} are very similar to those of C_3, C_4, and C_6, the same dynamic features can be inferred for ring B where the main molecular axis (C_8—C_{11}) can be suggested to be tumbling at the same reorientational rate as the C_5—C_2 axis. As a consequence, an anisotropic model made by rotational reorientation around the two molecular axes with some degree of internal motion (13) was used. Such a model can also be suitably applied to the other carbons in the molecule: the data shown in Table 4 were obtained where τ_R^{-1} represents the reorientational rate of the C_5—C_2 and C_8—C_{11} axes and τ_G^{-1} the rate of internal motions.

It can be seen that the degree of internal motion is increasing with the distance from the aromatic rings. It is worth noting that C_{13} does not show internal motions faster than those of the aromatic rings, but rather it looks as if it is reorientating jointly with the rings, in agreement with inferences from proton relaxation data.

The relaxation rates of C_{18}, C_{19}, and C_{20} show segmental motion through the aliphatic chain. Since C_{20} relaxes more slowly than C_{19}, as usually expected for segmental motion, any attractive interaction from the oxygen atom can be excluded, with consequent stabilization of a *gauche* conformation through the C_{18}—C_{19} bond. In fact such an attractive interaction has been shown to yield reduced T_1 values for terminal methyl groups in three carbon chains (14).

Selective proton relaxation data

Measuring non-selective (R_{ns}), single-selective (R_s), and double-selective proton spin-lattice relaxation rates has been suggested as a suitable aid to conformational studies in solution (15–17). In fact the ratio (R^i_{ns}/R^i_s) for any proton i allows evaluation of the extent to which pairwise dipole–dipole interactions provide the relaxation mechanism (the ratio is 1.5 for a purely dipolar mechanism).

The non-selective and single-selective relaxation rates of some protons of compound **1** were found (3) to yield R^i_{ns}/R^i_s ratios which are in fairly good agreement with the 1.5 value of the aromatic protons, while H_{20} and NH displayed ratios much lower than 1.5. Since it is not possible to avoid partial irradiation of proton resonances occurring in the neighborhood of the selectively irradiated proton, it could be suggested that mechanisms other than the dipolar interaction are not effective. Ratios lower than 1.5 can be ascribed to one or more of the following causes: (a) effectiveness of other relaxation mech-

Can. J. Chem. Downloaded from www.nrcresearchpress.com by 210.87.254.42 on 09/06/12
For personal use only.

Can. J. Chem. Downloaded from www.nrcresearchpress.com by 210.87.254.42 on 09/06/12
For personal use only.

anisms, such as spin-rotation, scalar relaxation, or, seldom, chemical shift anisotropy; (b) scalar and (or) dipolar coupling with rapidly relaxing nuclear species, mostly nitrogen atoms; (c) reorientational correlation times much longer than the inverse of the nuclear Larmor frequency; (d) occurrence of more than one proton species at the same value of chemical shift: in this case, e.g., for a CH_3 or a CH_2 group, the selective relaxation rate contains also the cross-relaxation terms of the intermethyl or intermethylene proton dipolar interaction.

The ratio found for NH ($R_{ns}/R_s = 1.14$) could be suitably accounted for by cause (b), as has been shown by calculating the dipolar contribution from ^{14}N to protons at small internuclear distances (18), whereas the ratio found for methyl H_{20} ($R_{ns}/R_s = 0.98$) could be justified by cause (d) and, likely, by (a), i.e., an actual contribution from spin-rotation. In fact the slowest correlation time measured by ^{13}C nmr relaxation data excludes the possibility that the extreme narrowing limit does not hold.

The non-selective proton relaxation rate of H_9 ($R^9_{ns} = 1.538$) is faster than that of H_{10} ($R^{10}_{ns} = 1.250$), suggesting that, besides the dipolar H_9—H_{10} interaction, other protons, which means the NH proton, are yielding valuable contributions to the relaxation of H_9. In this case the double-selective irradiation of the two proton resonances allows the evaluation of structural parameters. The following equations can be, in fact, written:

$$[1] \quad R^9_{ns} = \rho_{9,10} + \rho_{9,NH} + \sigma_{9,10} + \sigma_{9,NH}$$

$$[2] \quad R^9_{9,10} = \rho_{9,10} + \rho_{9,NH} + \sigma_{9,10}$$

$$[3] \quad R^9_{ns} - R^9_{9,10} = \sigma_{9,NH}$$

where $R^9_{9,10}$ is the measured initial rate of recovery of the longitudinal magnetization of H_9 when H_9 and H_{10} are simultaneously inverted by a double-selective pulse. The ρ's are direct relaxation terms (20) and the σ's are cross-relaxation terms (20), which for a dipolarly coupled proton pair are given by (20):

$$[4] \quad \sigma_{ij} = \frac{1}{10}\frac{\hbar^2\gamma_H^2}{r_{ij}^6}\left\{\frac{6\tau_c}{1+4\omega_0^2\tau_c^2} - \tau_c\right\}$$

where r_{ij} is the interproton distance, ω_0 is the Larmor frequency, and τ_c is the motional correlation time.

By inspection of the single-selective relaxation rates of H_5 and H_4, which are found 2.45 Å apart as determined by neutron scattering data (19), theoretical values for R^4_s and R^5_s were calculated (3) which fit the experimental ones when using $\tau_c = (1.97 \pm 0.09) \times 10^{-10}$ s, which represents the molecular reorientational time. Using this value of τ_c, a distance of 2.52 ± 0.05 Å was calculated between the NH proton and H_9. This distance is in very good agreement with that calculated from a Dreiding molecular model of **1** on the basis of coplanarity between the amide unit and ring B (2.41 Å) (see Fig. 3). The difference between the two values can be accounted for in terms of an angle of ±10° between the two moieties.

Since the difference $R^{NH}_{ns} - R^{NH}_s$ should be expected to yield the same value as the difference $R^9_{ns} - R^9_{9,10}$, if the NH was interacting with H_9 only, and since this was not the case, the following equations can be given:

$$[5] \quad R^{NH}_{ns} - R^{NH}_s = \sigma_{9,NH} + \sigma_{3,NH}$$

$$[6] \quad \sigma_{3,NH} = (R^{NH}_{ns} - R^{NH}_s) - (R^9_{ns} - R^9_{9,10})$$

Using the value of $\sigma_{3,NH} = 0.12 \pm 0.03$ s^{-1} and $\tau_c = (1.97 \pm 0.09) \times 10^{-10}$ s it was possible to evaluate $r_{3,NH} = 2.81 \pm 0.06$ Å. This distance is consistent with an angle of ±55° between the plane of ring A and the plane defined by the amide unit and ring B (3).

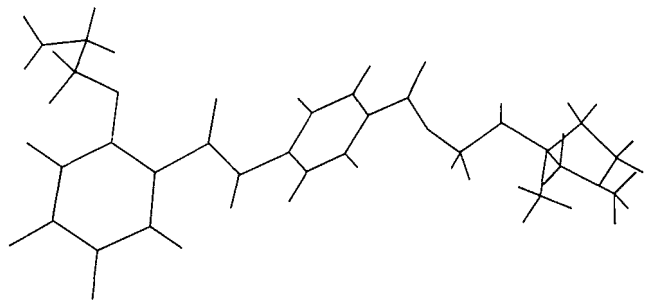

FIG. 3. Main conformation of **1** (0.2 mol dm^{-3}) in DMSO-d_6 solution.

The relatively fast non-selective and single-selective proton relaxation rates of H_6 ($R^6_{ns} = 2.33 \pm 0.11$ s^{-1}, $R^6_s = 1.61 \pm 0.07$ s^{-1}) (3) cannot be accounted for by considering only dipolar interactions with nearby aromatic protons, since the long distance between two protons in the *meta* position ($r = 4.30$ Å) is expected to give small contributions to the proton relaxation rate ($\rho = 0.02$ s^{-1}, $\sigma = 0.01$ s^{-1}). As a consequence, a dipolar interaction with protons within the propyloxy chain may be suggested. In this case, by applying the same equations as before, it was possible to calculate an average distance between H_6 and dipolarly coupled protons in the side chain of 2.42 ± 0.04 Å, which gives a strong contribution to proton relaxation.

The non-selective and double-selective proton relaxation rates of H_{10} are nearly equal, being the difference of the same order of magnitude of experimental error. In any case the small difference ($\sigma_{10,others} = 0.06 \pm 0.02$ s^{-1}) could be taken as a dipolar contribution from protons far away in the molecule. Since the NH is too far to exert any influence on dipolar relaxation of H_{10} ($r_{10,NH} = 4.74$ Å), a certain contribution from the H_{13} protons may be suggested. These findings might point to a configuration such that the C_{13} methylene is forced outside the plane defined by ring B and the carboxylic group.

The magnitude of dipolar contribution, however, excludes dramatic folding of the moiety around the quaternary nitrogen toward ring B: no protons at distances less than 3.15 Å can be found, according to calculations based on the previous analysis.

$^1H\{^1H\}$ nuclear Overhauser enhancement data

The origins of $^1H\{^1H\}$ nOe have been extensively investigated and a comprehensive review published (20). The fractional nOe enhancement of an observed spin d when spin s is saturated ($f_d(s)$) is given by:

$$[7] \quad f_d(s) = 0.5\ \rho_{ds}/R_d - 0.5 \sum_{n \neq d,s} \rho_{dn} f_n(s)/R_d$$

where:

$$[8] \quad R_i = \sum_{i \neq j} \rho_{ij} + \rho^*_i$$

$$[9] \quad \rho_{ij} = \gamma^2_i\gamma^2_j\hbar^2\ \tau_c(ij)/r^6_{ij}$$

$\tau_c(ij)$ is the correlation time of the vector r_{ij} between spin i and j, and ρ^*_i is the relaxation rate of spin i due to other relaxation mechanisms (see the discussion of ^{13}C and ^1H relaxation data). The R_i's correspond to the selective relaxation rate of proton i

Can. J. Chem. Downloaded from www.nrcresearchpress.com by 210.87.254.42 on 09/06/12
For personal use only.

($R_i = R_s^i$) provided other relaxation mechanisms are not relevant. The expression [7] is valid only at low concentration, where intermolecular dipole–dipole interactions can be neglected, and for loosely coupled spin $\frac{1}{2}$ systems.

A qualitative exploiting of nOe data (see Table 3), based on the relative nOe values, confirms the relative proximity of H_{18} protons to H_6. The absence of $f_{NH}(H_{19})$, $f_{NH}(H_{20})$, and $f_{H_{19}}(H_6)$ indicates that only the C_{18} methylene is somehow folded toward H_6, while the terminal part of the chain folds back and away from ring A and the amide unit.

It must be stressed that the relative distance is not the only parameter affecting the nOe enhancement. Cross-correlation and (or) cross-saturation terms, as stated in eq. [7], can make quantitative analysis a complicated matter, especially in cases where the loose coupling approximation breaks down.

In one case only was it worth running nOe analysis, namely, when presaturation of two different protons, *s* and *m*, produces nOe's at the same proton *d*. Then from eq. [7] the following relationship can be drawn, provided cross-saturation terms are irrelevant:

$$[10] \quad f_d(s)/f_d(m) = r^6_{dm}/r^6_{ds}$$

By applying this equation to the nOe's produced at H_3, upon presaturation of H_4 and NH, the distance $r_{3,NH}$ can be evaluated taking the fixed distance $r_{3,4} = 2.45$ Å. Such calculation gives $r_{3,NH} = 3.05$ Å, to be compared with the value $r_{3,NH} = 2.81$ Å calculated from single-selective measurements. Since, in theory, cross-saturation can affect the observed nOe's, the calculated distance can be thought to be in satisfactory agreement with the more accurate measurement from selective relaxation data.

Conclusions

The analysis of all the nmr parameters allows the delineation of the main conformational features of compound **1** (see Fig. 3). The amide unit, ring B, and the carboxylic group are nearly coplanar, while ring A forms an angle of ±55° with that plane. The angles of rings A and B with the amide unit can be measured by means of a clockwise or anti-clockwise rotation around the C_2—C_5 and C_8—C_{11} axes respectively; moreover, the librations of the two rings around the molecular axes can be paired or unpaired: namely ring B can be rotated +10°, with ring A rotated ±55°, or −10° with ring B rotated ±55°. The conformation sketched in Fig. 3 is only one of the possible preferred conformations.

The C_{18} methylene is brought near H_6 (mean distance 2.42 Å) while the terminal part of the chain folds back and away from ring A and the amide function. The C_{13} methylene could be forced outside the plane of ring B while the quaternary nitrogen moiety is stretched away from ring B.

The dynamic features of the two aromatic moieties keep a large part of the molecule in a fixed structure although some degrees of librational motion are allowed. Even the C_{13} methylene is somehow involved in the reorientational dynamics of the rings such that the motion of the C_{13}—H_{13} vectors is joined to the motion of ring B.

Experimental

The title compound was synthesized as already described (1). Solutions were made in 99.96% DMSO-d_6 and were carefully deoxygenated. The nmr spectra were taken on a Varian XL-200 spectrometer in the pulse-FT mode at probe temperatures of 25 ± 1°C; chemical shifts were referenced to the ^1H and ^{13}C resonances of internal TMS.

The ^1H and ^{13}C nmr spectra were measured with 5-mm and 10-mm od sample tubes respectively. Non-selective spin-lattice relaxation rates were measured with the inversion recovery pulse sequence $(t-\pi-\tau-\pi/2)_n$; 4 and 100 FIDs were collected for ^1H and ^{13}C T_1 experiments respectively; the $1/T_1 (= R_1)$ values were calculated from exponential regression analysis of the recovery curves of longitudinal magnetization components by using the computer of the spectrometer.

Single-selective and double-selective proton spin-lattice relaxation rates were measured with inversion recovery pulse sequences where the π pulse was given by the proton decoupler at the selected frequency for relatively long times at low power. The $\pi/2$ pulse was, on the contrary, the usual non-selective $\pi/2$ pulse given by the proton transmitter. The R_s values were measured in the initial slope approximation (2).

The nOes were determined by applying a 10-s low power saturating pulse at the appropriate peak position, followed immediately by a high power $\pi/2$ observing pulse. Since the maximum T_1 observed is of 1.09 s, the presaturating pulse is long enough to allow Overhauser equilibrium to establish. Off-resonance control spectra were measured with the presaturating pulse offset 1000 Hz to low field. Difference spectra were obtained by subtracting 40 on-resonance FIDs from 40 off-resonance FIDs followed by Fourier transformation.

1. M. GHELARDONI, V. PESTELLINI, N. PISANTI, and G. VOLTERRA. J. Med. Chem. **16**, 1063 (1973).
2. R. FREEMAN, H. D. W. HILL, B. L. TOMLINSON, and L. D. HALL. J. Chem. Phys. **61**, 4466 (1974).
3. A. SEGA, M. GHELARDONI, V. PESTELLINI, L. POGLIANI, and G. VALENSIN. Org. Magn. Reson. In press.
4. C. C. CONSTAIN and J. M. DOWLING. J. Chem. Phys. **32**, 158 (1960); J. C. BRAND, D. R. WILLIAMS, and T. J. COOK. J. Mol. Spectrosc. **20**, 193 (1966); F. A. L. ANET and J. M. OSYANY. J. Am. Chem. Soc. **89**, 352 (1967); J. KARLE and I. L. KARLE. J. Am. Chem. Soc. **89**, 804 (1967).
5. R. F. C. BROWN, L. RADOM, S. STERNHELL, and I. D. RAE. Can. J. Chem. **46**, 2577 (1968).
6. B. M. LYNCH and Y. Y. HUNG. Can. J. Chem. **42**, 1605 (1964); I. CROSSLAND. Acta Chem. Scand. **20**, 258 (1966); L. G. TENSMEYER and C. AINSWORTH. J. Org. Chem. **31**, 1878 (1966); V. I. STENBERG, S. P. SINGH, and N. K. NARAIN. J. Org. Chem. **42**, 2244 (1977).
7. S. GOULD and D. A. LAUFER. J. Magn. Reson. **34**, 37 (1979).
8. O. A. GANSOW, W. M. BECKENBAUGH, and R. L. SASS. Tetrahedron, **28**, 2691 (1972).
9. L. SIMERAL and G. E. MACIEL. Org. Magn. Reson. **6**, 226 (1974).
10. F. W. WEHRLI and T. WIRTHLIN. Interpretation of carbon-13 NMR spectra. Heyden and Sons, London. 1980. pp. 29–30.
11. J. R. LYERLA, JR. and G. C. LEVY. *In* Topics in carbon-13 NMR spectroscopy. Vol. 1. *Edited by* G. C. Levy. John Wiley and Sons, New York, NY. 1974. pp. 79–148.
12. F. W. WEHRLI. *In* Topics in carbon-13 NMR spectroscopy. Vol. 2. *Edited by* G. C. Levy. John Wiley and Sons, New York, NY. 1976. pp. 343–399.
13. A. ALLERHAND, D. DODDRELL, and R. KOMOROSKI. J. Chem. Phys. **55**, 189 (1971).
14. SOON NG. Org. Magn. Reson. **21**, 50 (1983).
15. C. W. M. GRANT, L. D. HALL, and C. M. PRESTON. J. Am. Chem. Soc. **95**, 7742 (1972).
16. L. D. HALL. Chem. Soc. Rev. **4**, 401 (1975).
17. L. D. HALL, K. F. WONG, and H. D. W. HILL. J. Chem. Soc. Chem. Commun. 951 (1979).
18. H. E. BLEICH, K. R. K. EASWARAN, and J. A. GLASEL. J. Magn. Reson. **31**, 517 (1978).
19. M. N. FREY, T. F. KOETZLE, M. S. LEHMANN, and W. C. HAMILTON. J. Chem. Phys. **58**, 2547 (1973).
20. J. H. NOGGLE and R. E. SCHIRMER. The nuclear Overhauser effect. Academic Press, New York. 1971.

S-Adenosylcoenzyme *M* and (±) *S*-methyl adenosylcoenzyme *M*. Preparation and role in methane biosynthesis

WILLIAM R. CULLEN,[1] DAVID DOLPHIN,[1] DALE HOFFMAN, AND EVERARD TRIP
Chemistry Department, University of British Columbia, Vancouver, B.C., Canada V6T 1Y6

Received December 22, 1983

WILLIAM R. CULLEN, DAVID DOLPHIN, DALE HOFFMAN, and EVERARD TRIP. Can. J. Chem. **62**, 2136 (1984).

5′-*S*-(2-Sulphoethyl)-5′-deoxy-5′-thioadenosine (*S*-adenosylcoenzyme M), **5**, was prepared from adenosine by reacting its 2′,3′-isopropylidine tosylate with the disodium salt of coenzyme M ($NaSCH_2CH_2SO_3Na$) followed by removal of the protecting group. Methylation of **5** to give methylsulphonium (±) *S*-adenosylcoenzyme M, **6**, was achieved with methyl iodide in acetic acid. Neither **5** nor **6** stimulated methane production from cell free preparations of *M. thermoautotrophicum*, negating the possibility of a biochemical analogy between **6** and *S*-adenosylmethionine (SAM).

WILLIAM R. CULLEN, DAVID DOLPHIN, DALE HOFFMAN et EVERARD TRIP. Can. J. Chem. **62**, 2136 (1984).

On a préparé la *S*-(sulfo-2 éthyl)-5′ déoxy-5′ thio-5′ adénosine (*S*-adénosylcoenzyme M), **5**, en faisant réagir l'isopropilidène-2′,3′ tosylate de l'adénosine avec le sel de disodium du coenzyme M ($NaSCH_2CH_2SO_3Na$), puis en éliminant le groupe protecteur. Grâce à sa réaction avec l'iodure de méthyle dans l'acide acétique, on a réussi à méthyler le composé **5**, pour obtenir le méthylsulfonium (±) *S*-adénosylcoenzyme M, **6**. Ni le composé **5** ni le composé **6** ne provoquent la production de méthane sous l'influence de préparations de *M. thermoautotrophicum* qui ne contiennent pas de cellules; d'après ce résultat, il ne peut y avoir d'analogie biochimique entre le composé **6** et le *S*-adénosylméthionine (SAM).

[Traduit par le journal]

Can. J. Chem. Downloaded from www.nrcresearchpress.com by 210.87.254.5 on 09/06/12
For personal use only.

Introduction

It is estimated that more methane is produced biochemically than any other single organic compound. Despite this, details on the mechanisms by which methane is produced, or metabolised, are still far from complete.

Methane producing bacteria – the methanogens – represent an unusual and evolutionary primitive group of microorganisms which perform some unique biochemistry employing equally unique coenzymes and cofactors (1). A variety of carbon sources at all oxidation levels act as sources of methane (eqs. [1]–[4]).

[1] $4CH_3OH \rightarrow 3CH_4 + CO_2 + 2H_2O$

[2] $CH_3CO_2H \rightarrow CH_4 + CO_2$

[3] $4CO + 2H_2O \rightarrow CH_4 + CO_2$

[4] $CO_2 + 4H_2 \rightarrow CH_4 + 3CO_2$

The methyl groups of both methanol and acetic acid are incorporated "directly" into methane (eqs. [1], [2]) and methylcobalamin appears to be a cofactor in these reactions (2). However, although cobamide derivatives stimulate methane production from hydrogen and carbon dioxide (eq. [4]) this is thought to be an artifact and at the present time there is no definitive role for B_{12} derivatives in this reaction.[2] A 5′-deazaflavin (F_{420}) (3, 4) and a nickel tetrapyrrole (F_{430}) (5) are found only in the methanogens but, as with most biochemistry involving one-carbon fragments, a pterin, methanopterin (6), is probably involved as a carrier.

The transport and activation of methyl groups in most procaryotic and eucaryotic biochemistry is achieved via *S*-adenosyl methionine (SAM). Such is not the case with the methanogens, where the lowest molecular weight coenzyme so far reported, coenzyme M, 2-mercaptoethanesulfonic acid, serves in methyl transfer reactions, once again exemplifying the uniqueness of these microorganisms (7). Methyl coenzyme M, 2-(methylthio)ethanesulfonic acid (**2**), is the direct precursor of methane (8) and it has been variously reported (9, 10) that catalytic amounts of adenosine triphosphate (ATP) are required to activate the reduction of **2** to methane. We speculated that if the biochemistry of coenzyme M parallels that of SAM, then either *S*-adenosylcoenzyme M (**5**) or *S*-methyladenosylcoenzyme M (**6**) might be involved in methane production. We report here the synthesis of **5** and **6** and some results pertaining to their involvement in methane biosynthesis.

$HSCH_2CH_2SO_3H$ **1** $CH_3—S—CH_2CH_2SO_3H$ **2**

Experimental

All reactions were carried out under a nitrogen or argon atmosphere. The nmr spectra were run on a Varian XL-100 or Bruker WH-400 MHz spectrometer. Microanalyses were performed by Mr. Peter Borda (U.B.C).

2′,3′-O-Isopropylidene adenosine

The preparation parallels that reported previously (11) on a 1-mmol scale. The following procedure represents a direct scale-up (× 46) and includes some modifications, particularly in the isolation.

To a magnetically stirred suspension of adenosine (12.25 g, 46.2 mmol) in acetone (462 mL) was added 2,2-dimethoxypropane (38.7 g (46 mL), 0.37 mol). Di-*p*-nitrophenyl hydrogen phosphate 18.85 g (55.5 mmol, mp 173.5°C, was added and the solution stirred under N_2. After 2 h some solids remained and additional 2,2-dimethoxypropane (23 mL) was added. After stirring for a further 3 h the solution became homogeneous. The mixture was stirred overnight and then a solution of $NaHCO_3$ (9.33 g, 0.111 mol) in water (111 mL) was added. The mixture was taken to dryness by rotary evaporation (bath 50°C) and the yellow solid residue was pulverized and dried for 1 h at 70°C under high vacuum. The solid was then extracted five times with 200-mL portions of boiling $CHCl_3$. The chloroform extracts were combined, filtered, and taken down to dryness (bath 50°C) to give 14.78 g of crude product which was crystallized from boiling water (200 mL) to give, after air drying, 11.85 g (83%), mp 219–220°C, lit. (11) mp 216–217°C.

2′,3′-O-Isopropylidene-5′-O-toluene-p-sulfonyladenosine (3)

The procedure follows that previously reported (12), with these additional modifications. Reagent grade pyridine was distilled from

[1] Authors to whom all correspondence should be addressed.

[2] R. S. Wolfe, personal communication.

Can. J. Chem. Downloaded from www.nrcresearchpress.com by 210.87.254.5 on 09/06/12
For personal use only.

CaH_2 and the tosyl chloride purified by the method of Pelletier (13). Pyridine was removed by washing with 1 *N* H_2SO_4 until the last aqueous wash had a pH of 1. The chloroform was dried over sodium sulfate, filtered, and reduced in volume to 50 mL. This solution was then slowly added with stirring to petroleum ether (1.5 L). The amorphous solid was collected by filtration and dried over P_2O_5 under high vacuum to give 9.94 g (57%).

2′,3′-O-Isopropylidene-5′-S-(2-sulphoethyl)-5′-deoxy-5′-thioadenosine (4)

To a magnetically stirred solution of sodium coenzyme-M (2.07 g, 12.6 mmol, Pierce Chemical Co.) in liquid ammonia (125 mL), kept at −73°C under dry nitrogen, was added approximately 0.3 g (13 mmol) of sodium metal. The sodium was added in small chips until a light blue color persisted for a few minutes. To the resulting solution was added 2′,3′-*O*-isopropylidene-5′-*p*-toluenesulphonyladenosine, 4.61 g (10.0 mmol). The blue coloration was immediately discharged and, after 5 min, a clear, light-orange solution was produced. This solution was stirred for 3 h while the temperature was gradually increased to −40°C and then for a further 1 h in the temperature range −40 to −30°C. The cold bath was removed, the flask was wrapped in cotton, and the ammonia was allowed to evaporate over 4 h. After storage overnight at 4°C, the flask was put under high vacuum for 0.5 h to remove excess ammonia. The yellow residue was dissolved in 50 mL of H_2O and the aqueous phase was washed with one 50-mL and two 25-mL portions of $CHCl_3$ to remove small amounts of 2′,3′-*O*-isopropylideneadenosine and unreacted starting material. Thin-layer chromatography (in *n*-PrOH/concentrated NH_3/H_2O; 70:3:7 (v/v/v); Eastman silica gel) of the aqueous phase showed a single product spot at $R_f \sim 0.45$.

The aqueous phase was evaporated and the residual orange syrup dissolved in H_2O to a final volume of 60 mL. This solution was stirred and 1.0 *M* HCl was added dropwise to cause precipitation of **2** (final pH 1.5). The precipitate was filtered and dried under high vacuum, over frequent changes of P_2O_5 for 18 h, to give 3.69 g (85.5%) of colorless, amorphous product.

Attempted recrystallization of this material from boiling H_2O gave extensive hydrolysis to *S*-adenosylcoenzyme M.

5′-S-(2-Sulphoethyl)-5′-deoxy-5′-thioadenosine (S-adenosylcoenzyme M) (5)

To a magnetically stirred suspension of crude 2′,3′-*O*-isopropylidene-5′-*S*-(2-sulphoethyl)-5′-deoxy-5′-thioadenosine (1.73 g, 4.0 mmol) in 80 mL of H_2O heated at 55–60°C, was added 8.0 mL of a 20% (w/v) suspension of AG 50W-X2 (H^+) in H_2O (capacity of stock resin suspension ~1 mequiv./mL). Thin-layer chromatography (*n*-PrOH/concentrated NH_3/H_2O; 70:3:7; Eastman silica gel), after stirring 2 h, showed quantitative conversion of the starting material ($R_f \sim 0.45$) to product ($R_f \sim 0.25$). After 2.5 h the resin was filtered and washed well on the filter with H_2O. The filtrate was evaporated and the residual yellow syrup was dissolved in 4.0 mL of H_2O and then treated with 20 mL of warm MeOH. Crystallization was rapid and, after standing 1 h at room temperature and 3 h at 4°C, fine colorless needles were filtered and washed well with MeOH. Drying overnight under high vacuum over Drierite gave 1.45 g (88%) as the monohydrate; mp 152–156°C (dec.). *Anal.* calcd. for $C_{12}H_{17}N_5O_6S_2 \cdot H_2O$: C 35.20, H 4.68, N 17.10, S 15.66; found: C 35.16, H 4.60, N 16.87, S 15.44.

Methylsulphonium (±) S-Adenosyl Coenzyme M (6)

A suspension of *S*-adenosylcoenzyme M (328 mg, 0.8 mmol), in 30 mL of glacial acetic acid and 6.0 mL of H_2O, was warmed and swirled to dissolve the major part of the suspension. After cooling, 6.0 mL (96 mmol) of methyl iodide was added and the resulting mixture was magnetically stirred in the dark. After 4-1/2 days, tlc (*n*-PrOH/AcOH/H_2O; 85:5:10; Eastman silica gel) showed quantitative conversion of starting material ($R_f \sim 0.4$) to product ($R_f \sim 0.16$). The resulting deep red/orange solution was partitioned between 350 mL of H_2O and 150 mL of ether. The ether layer was discarded and the aqueous phase was washed with a further 3 × 50 mL of ether. The colorless aqueous phase was filtered and the filtrate was evaporated. The residual pale yellow syrup was dissolved in, and coevaporated three times with, 30-mL portions of H_2O to remove acetic acid. The residue was dried under high vacuum to give an almost colorless glass. Trituration of this glass with MeOH caused partial solidification. The MeOH was evaporated from the resulting suspension and the trituration was repeated. Evaporation then yielded 342 mg (77%) of very pale yellow amorphous product which was dried under high vacuum. Thin-layer chromatography (as above) of an aqueous solution of this product, when spotted heavily, showed only trace impurities at the origin and at $R_f \sim 0.35$. The microanalytical (found: C 33.25, H 4.66, N 14.27, I 8.90) data indicate an empirical formula of $C_{13}H_{20}N_5O_6S_2 \cdot 0.3HI$. Thus 2/3 of the product was the neutral zwitterion and 1/3 the hydriodic salt.

Results and discussion

Adenosylcoenzyme M was prepared by a route analogous to that developed for the synthesis of *S*-adenosyl methionine (14) as modified in the syntheses of other 5′-*S*-adenosine derivatives (12, 15). Condensation of 2,3′*O*-isopropylidene-5′-*O*-toluenesulfonyl adenosine (**3**) (16), Scheme 1, with the disodium salt of coenzyme M in liquid ammonia, gave an essentially quantitative conversion to 2′,3′-*O*-isopropylidene-5′-*S*-(2-sulphoethyl)-5′-deoxy-5′-thioadenosine (**4**) which was isolated as the zwitterion by precipitation at low pH. Quantitative removal of the isopropylidene protecting group was readily effected using a strongly acid ion exchanging resin (AG 50W-X2) at 50–60°C and **5** was isolated crystalline and in high yield.

The structure of **5** was confirmed by nmr spectroscopy (Table 1). The sugar proton resonances were assigned with the aid of spin decoupling experiments. The ribofuranoside ring protons have chemical shifts similar to those of **3** while the two diastereotopic 5′ hydrogens are shifted approximately 0.8 ppm upfield, consistent with the substitution at 5′ by the sulfur of coenzyme M. A singlet at 2.72 ppm contained the four ethanic protons of the coenzyme M moiety.

Previous workers (14, 17, 18) have successfully methylated 5′-alkylthio derivatives of adenosine, giving the 5′-alkylsulfonium derivatives, using methyl iodide in formic or acetic acids. Attempted methylation of **5** by similar reactions in formic or formic/acetic acid mixtures lead to extensive degradation. In glacial acetic acid little reaction was observed; however, in 83% acetic acid a quantitative conversion to **6** occurred over a period of 4 to 5 days. The product was isolated pure chromatographically, as a homogeneous amorphous solid. However, attempts at crystallization or other manipulations invariably led to the gradual breakdown of the product. SAM is similarly unstable, due in part to the nucleophilic attack of iodide at the activated methyl group. The structure of **6** was again confirmed by nmr spectroscopy. Methylation of the sulfur atom will produce a chiral sulphonium residue and give two diastereomeric products. The two methyl sulfonium groups exhibited slightly different chemical shifts at 3.09 and 3.10, shifted downfield by 0.8 ppm with respect to the methyl group of 2-(methylthio)ethane-sulfonic acid. The positively charged sulfur causes similar downfield shifts of the 5′ protons and a methylene group of the coenzyme M fragment.

Methyl transfers via SAM involve *inter alia* the transfer of a methyl group from N^5-methyltetrahydrofolic acid (a pterin) to homocystysteine to give methionine. Methionine is then adenylated using ATP to SAM. After transfer of a methyl group, the adenosylhomocysteine is cleaved to adenine and homocysteine such that methyl transfer under these conditions is not catalytic, but rather stoichiometric in ATP. Nevertheless, the

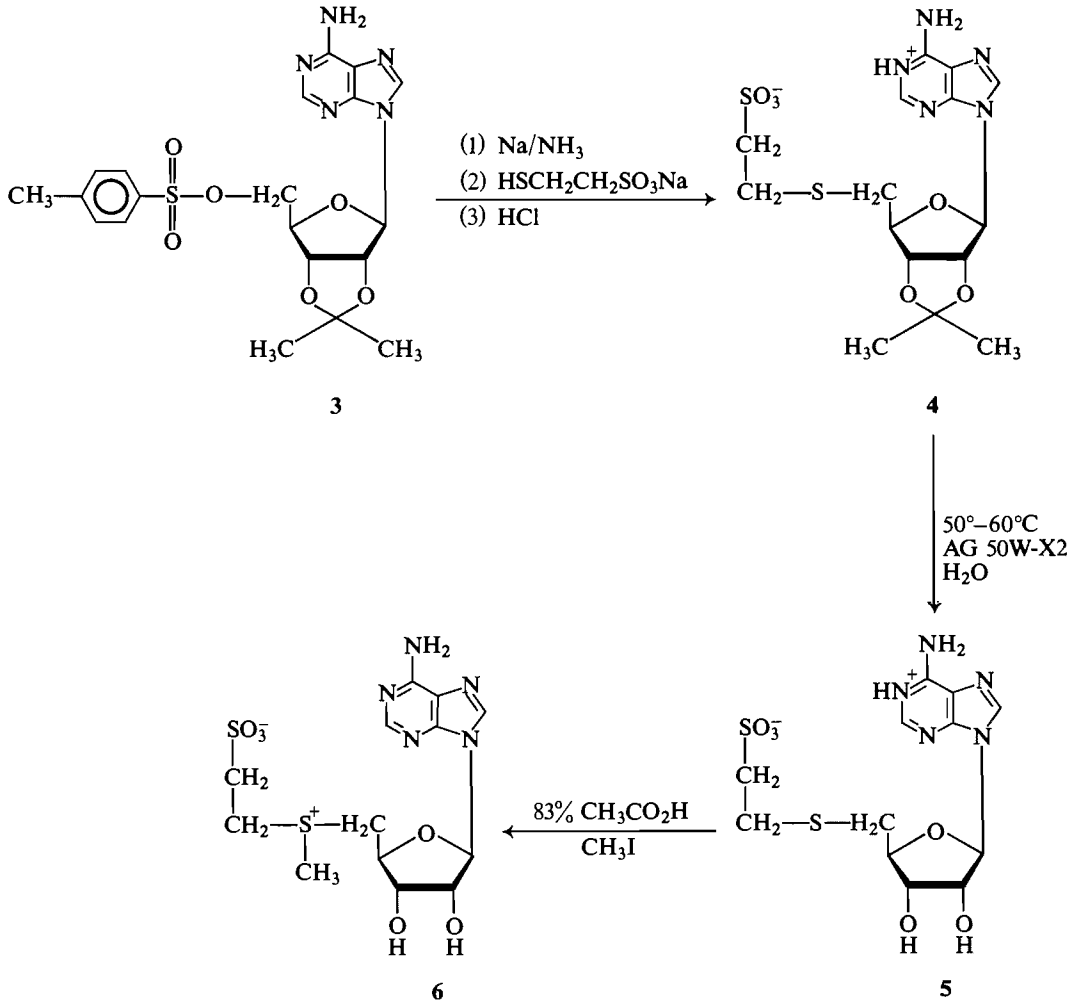

3 4 5 6

SCHEME 1

TABLE 1. Correlation of ^1H nuclear magnetic resonance chemical shifts[a]

	D_2O[b]			DMSO-d_6[c]		
	4	**5**	**6**	Adenosine	**5**	**6**[d]
H_2	8.05	8.40	8.42	8.2	8.48	8.53 (d, J = 8 Hz)
H_8	8.11	8.48	8.45	8.4	8.70	8.32 (s)
$H_{1'}$	6.04	6.11	6.20	5.95	5.94	6.03 (d, J = 6 Hz)
$H_{2'}$	5.35	4.91	4.99	4.68	4.66	4.68 (d, d)
$H_{3'}$	4.97	4.45	4.7[e]	4.2	4.0–4.2[e]	4.3–4.4[e]
$H_{4'}$	4.36	4.37		4.05		
$H_{5',5''}$			4.08	3.68	2.88	3.77, 4.1 (d, m)
S—CH_2	2.7–3.2[e]	2.7–3.1[e]	3.81	—	2.72[e]	2.95 (t, J = 8 Hz)
$^-O_3SCH_2$			3.40	—		3.5, 3.7[e]
$\overset{+}{S}$—CH_3	—	—	3.09, 3.10	—	—	2.94, 2.89
CH_3	1.38					
C		—	—	—	—	—
CH_3	1.60					

[a] Spectra measured at 100 MHz unless noted otherwise.
[b] DSS as internal standard.
[c] TMS as internal standard.
[d] Recorded at 400 MHz.
[e] Complex multiplet.

Can. J. Chem. Downloaded from www.nrcresearchpress.com by 210.87.254.5 on 09/06/12
For personal use only.

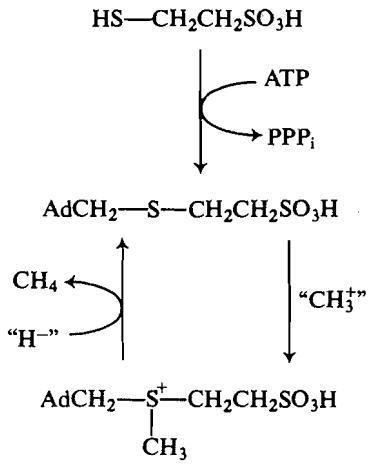

SCHEME 2

TABLE 2. Effect of *S*-adenosylcoenzyme M **6** on methane production[a]

No.	Addition to cell extract[b] (mmol)	Methylreductase[b] activity (mmol/h)
1	200 **2**	1070
2	200 **6**	0
3	200 **2** + 200 **6**	720

[a]These data were collected in Professor R. S. Wolfe's laboratory.

[b]Cell free preparations of *Methanobacterium thermoautotrophium* were used.

catalytic role of ATP in methane formation using coenzyme M could be envisaged as outlined in Scheme 2. This would require that adenosylcoenzyme M (**5**) should replace the need for the catalytic ATP and then **6** should give methane. Neither reaction is observed. Adenosylcoenzyme M (**5**) prepared as described here and separately by Romesser and Wolfe (19) did not replace the ATP requirement and no methane was generated (Table 2) upon the addition of **6**. Since these experiments were carried out on viable cell-free preparations, one can only conclude that neither **5** or **6** play a role in methane biosynthesis and that the catalytic role of ATP is not involved in sulfur alkylation but in some other, as yet to be elucidated, reaction.

Acknowledgements

The authors are grateful to the Natural Sciences and Engineering Research Council of Canada for financial support and to Professor R.S. Wolfe for comments and the results presented in Table 2.

1. W. E. BALCH, G. E. FOX, L. J. MARGRUM, C. R. WOESE, and R. S. WOLFE. Microbiol. Rev. **43**, 260 (1979).
2. G. T. VOGELS. Arch. Microbiol. **134**, 238 (1983).
3. W. L. ELLEFSON and R. S. WOLFE. J. Biol. Chem. **255**, 8388 (1980).
4. L. D. EIRCH, G. T. Vogels, and R. S. WOLFE. Biochemistry, **17**, 4583 (1978).
5. W. E. ELLEFSON, W. B. WHITMAN, and R. S. WOLFE. Proc. Natl. Acad. Sci. USA, **79**, 3707 (1982).
6. J. T. KELTJENS and G. T. VOGELS. *In* Microbial growth on C_1 compounds. *Edited by* G. Dalton. Heyden Publishers, London. 1981. pp. 152–158.
7. B. C. MCBRIDE and R. S. WOLFE. Biochemistry, **10**, 2317 (1971).
8. C. D. TAYLOR and R. S. WOLFE. J. Biol. Chem. **249**, 4879 (1974).
9. R. P. GUNSALUS and R. S. WOLFE. J. Bacteriol. **135**, 8516 (1978).
10. S. SHAPIRO and R. S. WOLFE. J. Bacteriol. **141**, 728 (1980).
11. A. HAMPTON. J. Am. Chem. Soc. **83**, 3640 (1961).
12. W. SAKAMI. Biochem. Prep. **8**, 5 (1961).
13. S. W. PELLETIER. Chem. Ind. 1034 (1953).
14. J. BADDILEY and G. A. JAMIESON. J. Chem. Soc. 1085 (1955).
15. G. A. JAMIESON. J. Org. Chem. **28**, 2397 (1963); G. A. JAMIESON. *In* Synthetic procedures in nucleic acid chemistry. Vol. 1. *Edited by* W. W. Zorbach and R. S. Tipson. John Wiley and Sons, Inc., New York, NY. 1968. p. 176.
16. V. M. CLARK, A. R. TODD, and J. ZUSSMAN. J. Chem. Soc. 2952 (1951); W. SAKAMI. Biochem. Prep. **8**, 5 (1961).
17. J. BADDILEY, W. FRANK, N. A. HUGHES, and J. WIECZORKOWSKI. J. Chem. Soc. 1999 (1962).
18. G. DE LA HABA, G. A. JAMIESON, S. H. MUDD, and H. H. RICHARDS. J. Am. Chem. Soc. **81**, 3975 (1959); G. A. JAMIESON. *In* Synthetic procedures in nucleic acid chemistry. Vol. 1. *Edited by* W. W. Zorbach and R. S. Tipson. John Wiley and Sons, Inc., New York, NY. 1968. p. 215.
19. J. A. ROMESSER and R. S. WOLFE. J. Bacteriol. **152**, 840 (1982).

Can. J. Chem. Downloaded from www.nrcresearchpress.com by 210.87.254.5 on 09/06/12
For personal use only.

Comparative analysis of hazardous compounds on fly-ash from municipal waste incineration by gas chromatography/mass spectrometry

A. C. VIAU, S. M. STUDAK, AND F. W. KARASEK[1]

The Guelph–Waterloo Centre for Graduate Work in Chemistry, Department of Chemistry, University of Waterloo, Waterloo, Ont., Canada N2L 3G1

Received November 17, 1983

A. C. VIAU, S. M. STUDAK, and F. W. KARASEK. Can. J. Chem. **62**, 2140 (1984).

Fly-ash samples from municipal incinerators in Canada and Norway were analyzed for polychlorinated dibenzo-*p*-dioxins using gas chromatography/mass spectrometry preceded by fractionation on column chromatography. Qualitative and quantitative differences in the organic compounds identified were found between the two samples. Many of the same dioxin congeners were present in both samples; however, tetrachlorodibenzo-*p*-dioxins were only detected in the Canadian sample.

A. C. VIAU, S. M. STUDAK et F. W. KARASEK. Can. J. Chem. **62**, 2140 (1984).

Faisant appel à une méthode impliquant un examen par chromatographie en phase gazeuse couplée à la spectrométrie de masse d'échantillons pré-fractionnés par chromatographie sur colonne, on a analysé des échantillons de suie provenant d'incinérateurs municipaux du Canada et de la Norvège afin de déterminer leur teneur en dibenzo *p*-dioxines polychlorées. On a trouvé des différences qualitative et quantitative dans les composés organiques identifiés dans les deux échantillons. Les deux échantillons contiennent sensiblement les mêmes congénères de la dioxine; toutefois, ce n'est que dans l'échantillon canadien que l'on a pu détecter les tétrachlorodibenzo *p*-dioxines.

[Traduit par le journal]

Introduction

Electrostatically precipitated fly-ash from municipal incinerators is known to contain hundreds of compounds, many being toxic in low concentrations (1). Classes of compounds found include hydrocarbons, polycyclic aromatic hydrocarbons (PAH), polychlorinated benzenes, polychlorinated biphenyls (PCB), polychlorinated dibenzo-*p*-dioxins (PCDD), and polychlorinated dibenzofurans (PCDF).

PCDD and PCDF have been found to be extremely toxic and have been the subject of numerous studies (1–4). Recent research has demonstrated that these compounds still occur after incineration above 1200°C (5). However, other chlorinated compounds have been identified in waterwall incinerators, while PAH and hydrocarbons are not found (6). The source of PCDD and PCDF has been suggested to be polyvinyl chloride (PVC) incineration, but no change in the level of these compounds was found in fly-ash samples obtained in a planned experiment in which additional PVC was added to the incinerator waste feed (6).

Organic compounds found on fly-ash samples from municipal incinerators in Norway and Canada are extracted and preseparated using pressurized liquid chromatography. The differences in the concentrations of hazardous compounds for these two samples are compared. Although these are single samples, it has been found that under normal operating conditions, the concentration of chlorinated species do not vary more than 70% relative, as compared to near 200% relative for alkanes (7). The analyses performed in this study can be considered representative of the differences in the emissions of harzardous compounds from municipal waste incineration, based on previous analyses of fly-ash from both countries.

It is found that fly-ash from Norway contained more PAH, thio-PAH, and chlorinated biphenyls than the Canada fly-ash. Canada fly-ash was found to have a greater concentration of PCDD, PCDF, chlorobenzenes, and chlorophenols. A comparison of individual compounds within a class shows that there is also a difference in the components. The levels of PCDD for both samples are also compared and observations are made.

[1]To whom all correspondence should be addressed.

Experimental

Sampling

Samples of fly-ash were received from two separate municipal incinerators. One was from Ontario, Canada, and the other from Oslo, Norway. These were collected from the hoppers of electrostatic precipitators.

Sample extraction and fractionation

The samples underwent a 16-h soxhlet extraction of 15–20 g of fly-ash with 200 mL of distilled-in-glass benzene and concentrated to 100 μL by rotary evaporation under aspirator vacuum (1). A column of 6 g 44% sulfuric acid/silica gel was washed with 50 mL of hexane. The concentrate was introduced and eluted with 75 mL of hexane and quantitatively concentrated to 100 μL. A 1 g alumina gel (Woelm Neutral) column 2 mm id was prepared by 10 mL sequential washings of methylene chloride, 10% carbon tetrachloride in hexane and hexane. It was then utilized for separation of the concentrate into three fractions; 20 mL each of hexane, 10% carbon tetrachloride in hexane and methylene chloride. The two adsorbents, alumina and silica gel, were kept in a 200°C oven previous to use. To enable a more rapid elution, 10 psig of air pressure was applied directly to the alumina column. Each of the three fractions were concentrated to 100 μL and analyzed for polychlorinated dibenzo-*p*-dioxins and other organic compounds by gc/ms. The clean-up and analysis was performed twice for PCDD on the Canada fly-ash to test the reproducibility of this method. An average relative standard deviation of 17% was observed; this is within variations previously published for this analytical system (8).

Gas chromatographic analysis

A Hewlett-Packard 5830A Gas Chromatograph was used with a 2 m × 2 mm id column with Aue packing and flame ionization detector for prescreening of extracts prior to gc/ms analysis (9). A temperature program of 90°C initial temperature to 250°C final temperature at 4°C per min was employed for all extracts. The He carrier gas flow rate was about 32 mL/min.

Gas chromatographic/mass spectrometry analysis

The extracts were analyzed with a Hewlett-Packard 5992A gc/ms/computer in the selected ion monitoring (SIM) mode for PCDD determination. This instrument was equipped with a cool-on-column injection port, 30 m × 0.32 mm id fused silica capillary columns with cross-linked DB-5 stationary phase (J&W Scientific, Rancho Cardova, CA), capillary glass restrictor inlet, $x-y$ plotter, and dual floppy disk system. The He carrier gas flow rate was 3 mL/min.

Can. J. Chem. Downloaded from www.nrcresearchpress.com by 210.87.254.40 on 09/06/12
For personal use only.

Can. J. Chem. Downloaded from www.nrcresearchpress.com by 210.87.254.40 on 09/06/12
For personal use only.

The ions monitored for tetrachlorodibenzo-*p*-dioxin (TCDD) were 319.9 and 321.9. Other ions selected for penta- through octachlorodibenzo-*p*-dioxin were 355.9 (P5CDD), 389.8 (H6CDD), 425.8 (H7CDD), and 459.7 (OCDD). A dwell time of 50 ms was used for each ion. SIM areas were used for quantification. PCDD congeners were quantified using a standard mixture of 1,2,3,4-TCDD, 1,2,3,4,7,8-H6CDD, 1,2,3,4,6,7,8-H7CDD, and OCDD. P5CDD was quantified using a response factor intermediate to TCDD and H6CDD standards (8).

Chromatographic conditions were as follows: initial oven temperature 180°C to 300°C final temperature at 4°C/min and the injection port temperature was 70°C.

Mass spectra were obtained by scanning from 500 to 50 amu at 330 amu/s. Spectra taken at the top of the eluting gc peaks were saved on floppy disk, in addition to those at the lowest valley between peaks for later background subtraction. A user-developed program called Dual Mode was employed which allowed storage of total ion abundances and mass chromatograms in addition to mass spectra.

Before operation, the mass spectrometer was tuned daily by the manufacturer-supplied program AUTOTUNE using a perfluorotributylamine calibration standard. Identification of compounds was based on their mass spectra by using Eight Peak Index of Mass Spectra and EPA/NIH Mass Spectral Data Base. The mass spectra search systems, Probability Based Matching (PBM) and Self-Training Interpretive Retreval system (STIRS) were accessed by telephone hook-up to Cornell University. This procedure provides an identification with varying degrees of certainty. The only way to provide a more certain identification is to directly obtain the mass spectrum and retention time of pure standards for each compound. The mass spectra of the compounds identified were well matched to their reference spectra. In cases where only the type of compound was indicated, mass spectra characteristic of that type were clearly obtained. If no identification resulted from this procedure, the compound was labelled unidentified. Not having the standards of the many isomers of the PCDD and PCDF compounds it was not possible to indicate these separately.

Further identification was done using the PAH retention index system (10). Retention data from other sources were also used (11, 12). It has been found that the retention index can vary for some compounds (12). Consequently, a window of two retention index units was used.

Compounds were quantified using response factors of standards and the peak height method. PAH compounds and thio-PAH compounds were quantitated using the response factor for fluorene, anthracene, fluoranthene, and pyrene. Chlorobenzenes and chlorophenols concentrations were calculated using the response factors of 1,2,3,4-tetrachlorobenzene, pentachlorobenzene, and hexachlorobenzene. The response factors of tetrachlorodibenzofuran (TCDF) and octachlorodibenzofuran (OCDF) were used in the estimation of the concentrations of PCDF and PCB. Since pure PCB isomers were not available at the time of the study, this method was used to closely approximate their concentrations.

Results and discussion

The extracted compounds for the two fly-ash samples were identified by gc/ms. These compounds are listed in Table 1 with their corresponding retention indices and labeled in Figs. 1 and 2. The majority of compounds were identified by both mass spectra and retention index. Compounds which were only identified by their mass spectra are marked. Saturated and unsaturated hydrocarbons were not identified or quantified because of their relative non-toxic nature. There were 36 individual compounds found in the sample from Canada and 46 compounds found in the sample from Norway.

Many organic compounds such as alkyl substituted benzenes and various polycyclic aromatic compounds (PAC) were found to occur. Also present were numerous chlorinated compounds such as chlorinated benzenes, chlorinated phenols, chlorinated

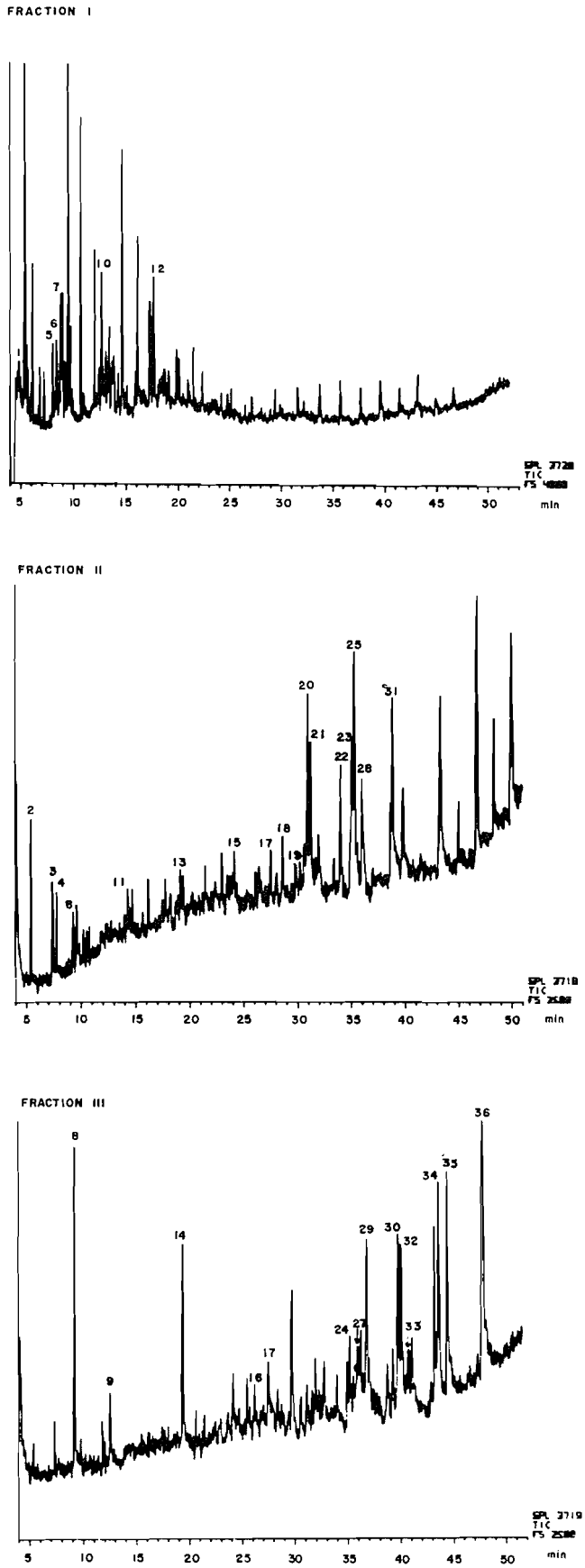

FIG. 1. Comparison of the total ion currents (TIC) from Canada fly-ash extract divided into three fractions. The numbered peaks correspond to the compounds identified in Table 1.

Can. J. Chem. Downloaded from www.nrcresearchpress.com by 210.87.254.40 on 09/06/12
For personal use only.

TABLE 1. List of compounds identified in Canada and Norway fly-ash; peak numbers correspond to those in Figs. 1 and 2

Compound	Molecular weight	Retention index	Peak number		Compound	Molecular weight	Retention index	Peak number	
			Canada	Norway				Canada	Norway
Tetramethylbenzene	134	191.7	1	—	Tetrachlorobiphenyl*	290	338.7	—	30
Trichlorobenzene	180	195.6	—	1	Fluoranthene	202	344.7	16	—
Naphthalene	128	200.0	2	2	Tetrachlorobiphenyl*	290	352.0	—	31
2-Methylnaphthalene	142	216.6	3	3	Trichlorodibenzo-*p*-dioxin	285	352.6	17	—
1-Methylnaphthalene	142	219.1	4	4	C2-Alkyl-9,10-anthracenedione*	236	354.9	—	32
1,2,3,4-Tetrachlorobenzene*	214	219.2	5	5	2,5-Bis(*p*-chlorophenyl)1,4-diithin†	334	360.9	18	—
1,2,3,5-Tetrachlorobenzene	214	221.3	6	6	C2-Alkyl-9,10-anthracenedione*	236	362.3	—	33
1,2,4,5-Tetrachlorobenzene*	214	228.3	7	7	Tetrachlorodibenzofuran	304	367.5	19	—
Biphenyl	154	229.8	8	8	C2-Alkyl-9,10-anthracenedione*	238	370.4	—	34
2,6- or 2,7-dimethylnaphthalene	156	233.9	—	9	Pentachlorobiphenyl*	324	374.8	—	35
1,3- or 1,7- or 1,6-dimethylnaphthalene	156	236.0	—	10	Tetrachlorodibenzo-*p*-dioxin	320	375.1	20	—
2,3- or 1,4- or 1,5-dimethylnaphthalene	156	239.0	—	11	Tetrachlorodibenzo-*p*-dioxin	320	377.1	21	—
Methylbiphenyl isomer	168	247.8	—	12	C4-Alkyl phenanthrene(anthracene)*	234	377.7	—	36
3- or 4-methylbiphenyl	168	251.4	—	13	Hexachlorobiphenyl*	358	382.9	—	37
Dibenzofuran	168	252.5	9	14	Pentachlorodibenzofuran	338	395.5	22	—
Pentachlorobenzene	248	254.8	10	15	Hexachlorobiphenyl*	358	398.5	—	38
C3-Alkylnaphthalene	170	258.9	—	16	Pentachlorodibenzofuran	338	401.9	23	—
Fluorene	166	266.2	—	17	Pentachlorodibenzofuran	338	402.7	24	—
2,4,6-Trichlorophenol	196	266.6	11	—	Pentachlorodibenzofuran	338	403.5	25	—
C2-Alkyl(phenylmethyl)benzene isomer*	196	275.0	—	18	Pentachlorodibenzo-*p*-dioxin	354	404.2	26	—
C2-Alkyl(phenylmethyl)benzene isomer*	196	280.2	—	19	Pentachlorodibenzo-*p*-dioxin	354	404.9	27	—
Hexachlorobenzene	282	287.1	12	—	Pentachlorodibenzo-*p*-dioxin	354	409.4	28	—
1,1′-(C6-Alkyl)bisbenzene*	236	291.9	—	20	Dioctylphthalate	390	416.1	29	—
C2-Alkyl(phenylmethyl)benzene isomer*	196	297.8	—	21	10*b*,10*c*-dihydro-10*b*,10*c*-dipropyltranspyrene*	288	422.7	—	39
2,3,4,6-Tetrachlorophenol	230	298.6	13	—	Hexachlorodibenzofuran	372	430.1	30	—
Phenanthrene	178	300.0	14	22	Hexachlorodibenzofuran	372	436.1	31	40
4-Methyldibenzothiophene	198	315.2	—	23	Hexachlorodibenzo-*p*-dioxin	388	437.5	32	—
Trichlorobiphenyl*	256	319.6	—	24	Hexachlorodibenzo-*p*-dioxin	388	441.7	33	41
Trichlorobiphenyl*	256	322.5	—	25	Unidentified	330	457.6	—	42
1-Methylanthracene (methylphenanthrene)	192	327.7	—	26	Unidentified	330	462.6	—	43
Pentachlorophenol*	264	331.1	15	—	1,2,3,4,6,7,9-Heptachlorodibenzo-*p*-dioxin	424	465.8	34	44
Tetrachlorobiphenyl	290	332.1	—	27	1,2,3,4,6,8,9-Heptachlorodibenzo-*p*-dioxin	424	471.7	35	45
4,6-Dimethyldibenzothiophene	212	333.6	—	28	Methyldiphenylhexahydrocyclopentaindene†	326	471.8	—	46
2,6-Dimethyldibenzothiophene	212	336.5	—	29	Octachlorodibenzo-*p*-dioxin	456	494.8	36	47

*Identified by mass spectra only.
†Identified by STIRS.

Can. J. Chem. Downloaded from www.nrcresearchpress.com by 210.87.254.40 on 09/06/12
For personal use only.

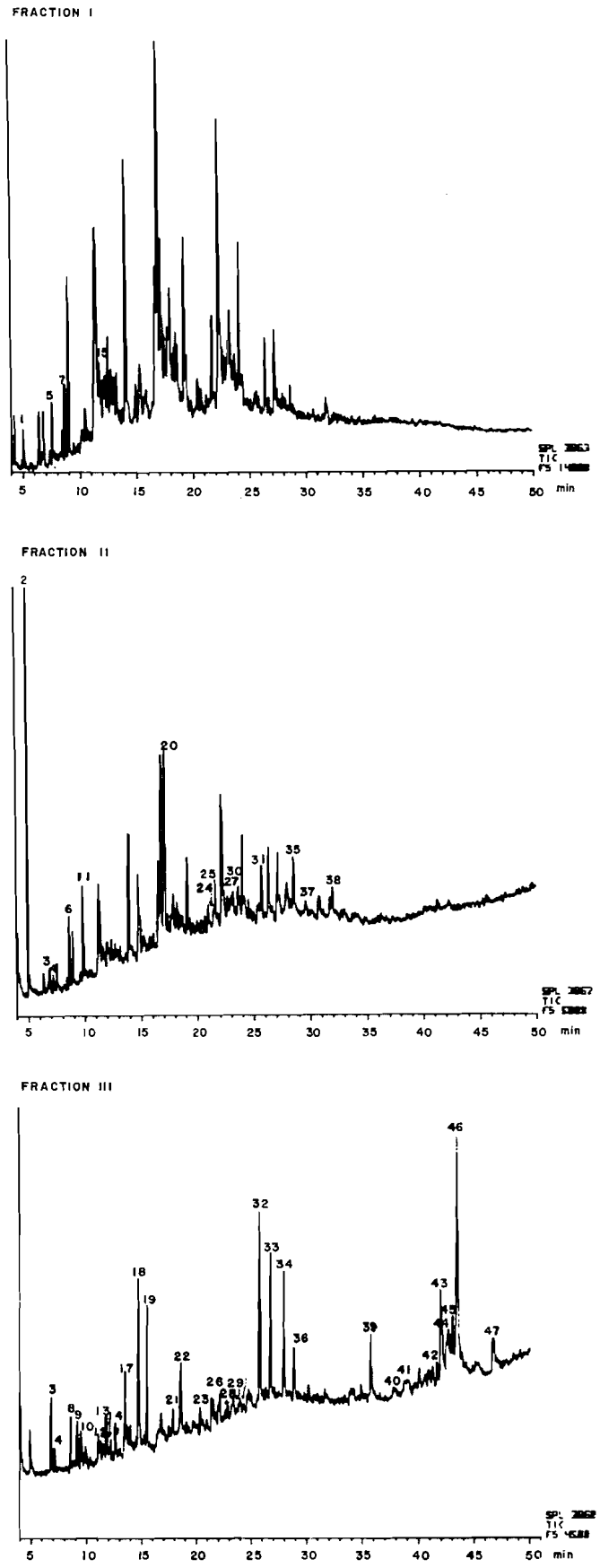

FIG. 2. Comparison of the total ion currents (TIC) from Norway fly-ash extract divided into three fractions. The numbered peaks correspond to the compounds identified in Table 2.

TABLE 2. Comparison of specific compounds from Canada and Norway fly-ash extracts in ng/g concentration

Compound		Concentration Norway	Canada
Polycyclic aromatic hydrocarbons	**Total**	**2125**	**735**
Naphthalene		760	130
Alkyl-substituted naphthalene		470	180
Biphenyl		70	190
Alkyl-substituted biphenyl		520	—
Phenanthrene		130	140
Fluoranthene		—	95
Fluorene		115	—
Methyldiphenylhexahydrocyclopentaindene		60	—
Polychlorinated biphenyls	**Total**	**360**	**—**
Trichloro-		110	—
Tetrachloro-		140	—
Pentachloro-		60	—
Hexachloro-		50	—
Polychlorinated benzenes	**Total**	**685**	**1130**
Trichloro-		235	—
Tetrachloro-		400	590
Pentachloro-		50	270
Hexachloro-		—	270
Polychlorinated phenols	**Total**	**11**	**94**
Trichloro-		11	35
Tetrachloro-		—	32
Pentachloro-		—	27
Polychlorinated dibenzofurans	**Total**	**20**	**830**
Tetrachloro-		—	20
Pentachloro-		—	350
Hexachloro-		20	260
Heptachloro-		—	200
Thio-PAH	**Total**	**75**	**50**
Alkyl-substituted dibenzothiophene		75	—
2,5-Bis(*p*-Chlorophenyl)1,4-diithin		—	50

biphenyls, chlorinated dioxins, and furans. More uncommon compounds such as alkyl-substituted dibenzothiophenes and chlorophenyl diithin were also identified.

Each fraction from the adsorption column contained groups of compounds. Fraction I had a high abundance of hydrocarbons, alkyl-substituted benzenes, and polychlorinated benzenes. Fraction II contained mainly PCB and chlorophenols. PAH, thiophenes, and indenes were present in both Fractions II and III. The PCDD and PCDF were present mainly in Fraction III.

Comparison of the two fractions was done by calculating the concentrations of selected hazardous compounds. Table 2 lists specific compounds classes and the corresponding concentrations (ng/g) for both Norway and Canada fly-ash extracts, seen in Figs. 1 and 2 calculated by the peak height method. The relative amounts of a component per weight of fly-ash for each sample can be compared.

From Table 2, the Norway extract is seen to contain more PAH and in greater concentration than in the Canada sample. Napthalene and alkyl-substituted naphthalene were present in both samples but were more abundant in the Norway fly-ash. The Canada extract did contain more biphenyl, phenanthrene, and fluoranthene than the Norway sample. Alkyl-substituted

Can. J. Chem. Downloaded from www.nrcresearchpress.com by 210.87.254.40 on 09/06/12
For personal use only.

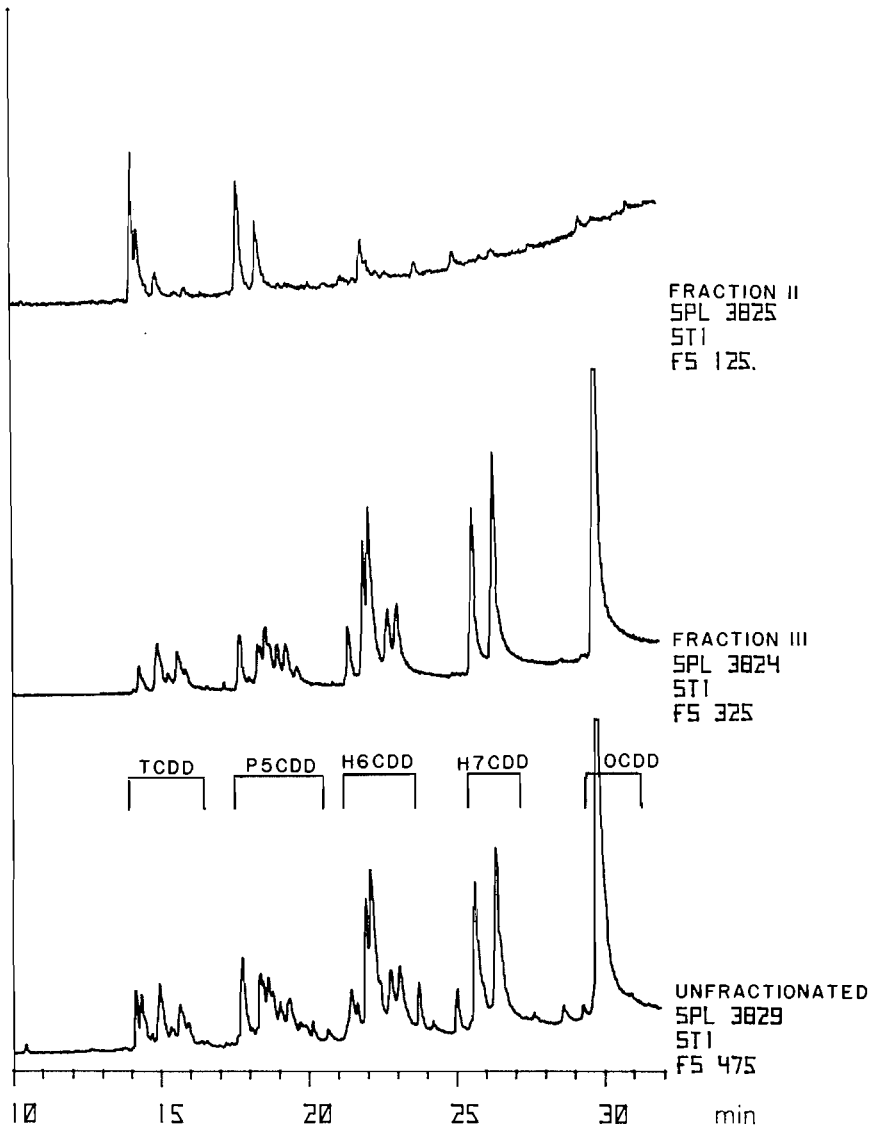

FIG. 3. Comparison of sim total ions (STI) for PCDD from Canada fly-ash unfractionated and Fractions II and III. Brackets indicate the elution retention times for the PCDD congeners.

biphenyl compounds were found only in the Norway sample and they were second in abundance to naphthalene, the most abundant of the PAH. Other substituted PAH were found to occur only in the Norway extract.

Chlorinated benzenes present in both extracts were more prominent in the Canada fly-ash, as seen in Table 2. The Canada extract contained tetrachlorobenzene as the most abundant compound with pentachlorobenzene and hexachlorobenzene occurring in equal amounts. In contrast, the Norway extract contained only trichloro-, tetrachloro- and pentachlorobenzene with tetrachlorobenzene being the most abundant compound of this class.

The Canada fly-ash also contained more chlorinated phenols than the Norway fly-ash. There was an equal amount of trichloro-, tetrachloro- and pentachloro-phenol in the Canada extract but only a small quantity of trichlorophenol was found in the Norway sample.

Polychlorinated biphenyls, trichloro- through to hexachloro-biphenyls were detected only in the Norway extract. Tetrachlorobiphenyl was the most abundant of the four isomeric classes.

In contrast, polychlorinated dibenzofurans (PCDF) were found mostly in the Canada sample. The Norway fly-ash contained only hexachlorodibenzofuran while the Canada fly-ash had the congeners from tetra- to octachlorodibenzofuran.

Thio-PAH were found in both samples. The compound 2,5-bis(*p*-chlorophenyl)1,4-diithin, identified by STIRS, was present only in the Canada fly-ash. Norway fly-ash contained a wide variety of alkyl-substituted dibenzothiophenes.

Compounds found specifically in the Norway extract but not in the Canada extract were 10*b*,10*c*-dihydro-10*b*,10*c*-dipropyltranspyrene, C2-akyl-9,10-anthracenedione, methyldiphenylhexahydrocyclopentaindene, and C2-alkyl(phenylmethyl)benzene isomers.

Table 3 lists concentrations (ng PCDD/g fly-ash) calculated using SIM areas of PCDD present in each extract, and Fig. 3 shows the SIM total ion (STI) which sums all SIM ions into one trace for the Canada fly-ash (13). It can be seen that PCDD are separated mostly in Fraction III. Some TCDD and P5CDD are present in Fraction II. The percentage recovery of PCDD from the Canada fly-ash was calculated by summing the calculated concentrations from Fractions II and III and comparing these

TABLE 3. Concentrations of PCDD on fly-ash from Canada and Norway

(*a*) Canada

Compound	Concentration (ng/g) Trial 1	Trial 2	Mean	Unfractionated	Recovery
TCDD	160	177	168	330	51%
P5CDD	226	183	204	390	52%
H6CDD	237	187	212	610	34%
H7CDD	190	148	169	460	37%
OCDD	380	275	328	470	35%

(*b*) Norway

Compound	Concentration (ng/g)	Corrected for recovery
TCDD	Not detected	—
P5CDD	15	29
H6CDD	38	112
H7CDD	62	167
OCDD	92	263

additions to the unfractionated sample. This percentage recovery was used for correction of the PCDD concentration in the Norway extracts. No PCDD were detected by SIM for the Norway unfractionated extract because of the high content of organic compounds.

The large amount of quantitative data now available on PCDD from municipal incinerators has revealed that the emission pattern of PCDD can be divided into two groups. Some incinerators emit PCDD on fly-ash so that H6CDD is among the highest congener found and TCDD is almost one-half the amount of OCDD present (14). The Canada fly-ash studied fits into this category.

The second group is characterized by having OCDD as the most concentrated PCDD congener and all other congeners in decreasing quantity, so that TCDD is approximately 3% of the OCDD concentration (15). This pattern has been found in France, Germany, and now Norway (5, 15, 16). The differences between these two groups have not been explained. Some suggest that burning efficiency and/or chlorine content of the fuel may have some effect (7, 16).

The uncorrected concentrations of organic compounds present on the Norway and Canada fly-ash from Table 3 can be summarized as follows:

Norway

PAH > chlorobenzenes > PCB > PCDD > thio-PAH > PCDF > chlorophenols

Canada

Chlorobenzenes > PCDD > PCDF > PAH > chlorophenols > Thio-PAH > PCB

It can be seen that there are more chlorobenzenes than any other chlorinated species present in either samples. This has been previously observed in a study of chlorinated compounds emitted from municipal incineration (16). It becomes evident that the Canada fly-ash is more concentrated in chlorinated organic compounds than the Norway fly-ash. Conversely, the Norway fly-ash is more concentrated in PAH and thio-PAH compounds than the Canada fly-ash. This indicates that the Canada municipal waste combustion must contain more chlorine than the Norway municipal waste combustion, strictly from mass balance. However, the primary source of chlorine need not be from PVC (6). It has been suggested that HCl in the furnace can be the reactant chlorine source (16). The greater concentration of thio-PAH compounds in the Norway fly-ash could be related to a substantial sulphur content in the furnace. Consequently, mass balance would dictate a higher content of thio-PAH. In both samples, the concentration of compounds are from reaction of an abundant reactant, chlorine or sulphur, to a PAH nucleus. This implies that dynamic radical molecular reactions could be occurring so that an incinerator furnace would be governed by mass balance. Consequently, reduction of PCDD emissions on fly-ash could be accomplished by alterations in the mass balance relationship.

1. G. A. EICEMAN, R. E. CLEMENT, and F. W. KARASEK. Anal. Chem. **51**, 2343 (1979).
2. K. OLIE, P. L. VERMENLEN, and O. HUTZINGER. Chemosphere, **6**, 165 (1977).
3. H. R. BUSER, H. P. BOSSHANDT, and C. RAPPE. Chemosphere, **7**, 165 (1978).
4. L. L. LAMPARSKI and T. J. NESTRICK. Anal. Chem. **52**, 2045 (1980).
5. F. W. KARASEK and A. C. VIAU. J. Chromatogr. **265**, 79 (1983).
6. F. W. KARASEK, A. C. VIAU, G. GUIOCHON, and M. F. GONNORD. J. Chromatogr. **270**, 227 (1983).
7. R. E. CLEMENT, A. C. VIAU, and F. W. KARASEK. Int. J. Environ. Anal. Chem. To be published.
8. A. C. VIAU and F. W. KARASEK. J. Chromatogr. **270**, 235 (1983).
9. W. A. AUE, C. R. HASTINGS, and S. KAPILA. Anal. Chem. **45**, 725 (1973).
10. M. L. LEE, D. L. VASSILAROS, C. M. WHITE, and M. NOVOTNY. Anal. Chem. **51**, 768 (1979).
11. D. L. VASSILAROS, R. C. KONG, D. W. LATER, and M. L. LEE. J. Chromatogr. **252**, 1 (1982).
12. H. Y. TONG, D. L. SHORE, F. W. KARASEK, P. HELLAND, and E. JELLUM. J. Chromatogr. **285**, 423 (1984).
13. L. C. DICKSON, F. W. KARASEK, and R. E. CLEMENT. J. Chromatogr. **280**, 23 (1983).
14. K. OLIE, J. W. A. LUSTENHOUWER, and O. HUTZINGER. Pergamon series on environmental science. Vol. 5. Pergamon Press, Oxford. 1982. p. 227.
15. F. W. KARASEK, A. C. VIAU, G. GUIOCHON, and M. F. GONNORD. To be published.
16. K. BALLSCHMITER, W. ZOLLER, CH. SCHOLZ, and A. NOTTRODT. Chemosphere, **12**, 585 (1983).

Can. J. Chem. Downloaded from www.nrcresearchpress.com by 210.87.254.40 on 09/06/12
For personal use only.

Facile access to (*S*)-1,2,4-butanetriol and its derivatives

STEPHEN HANESSIAN, ANTONIO UGOLINI,[1] DANIEL DUBÉ AND ANI GLAMYAN
Department of Chemistry, Université de Montréal, Montreal, P.Q., Canada H3C 3V1

Received February 21, 1984

STEPHEN HANESSIAN, ANTONIO UGOLINI, DANIEL DUBÉ, and ANI GLAMYAN. Can. J. Chem. **62**, 2146 (1984).

The synthesis of (*S*)-1,2,4-butanetriol from the readily available (*S*)-malic acid in one step using borane – dimethyl sulfide is described.

STEPHEN HANESSIAN, ANTONIO UGOLINI, DANIEL DUBÉ et ANI GLAMYAN. Can. J. Chem. **62**, 2146 (1984).

On décrit la synthèse en une seule étape du (*S*)-butanetriol-1,2,4 à partir de l'acide (*S*)-malique facilement obtenu en utilisant le complexe de borane – sulfur de diméthyl.

[Traduit par le journal]

Can. J. Chem. Downloaded from www.nrcresearchpress.com by 210.87.254.105 on 09/06/12
For personal use only.

Optically active acetal derivatives of 1,2,4-butanetriol **1***a* and the corresponding aldehyde **3** are frequently used as starting materials for natural product synthesis (1,2). In the course of a program aimed at the total synthesis of avermectin Bla aglycon (3), we required substantial quantities of **3**, which can be readily obtained from a modified (4) pyridinium chlorochromate oxidation (5) of **2***a*. In a recent report,[2] Meyers and Lawson (6) have shown that all reported preparations of **2***a*

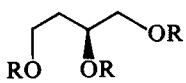

1*a* R = H
1*b* R = Ac
1*c* R = 3,5-dinitrobenzoyl

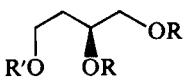

2*a* R,R = , R′ = H

2*b* R,R = , R′ = 3,5-dinitrobenzoyl

2*c* R,R = , R′ = H

2*d* R,R = , R′ = 3,5-dinitrobenzoyl

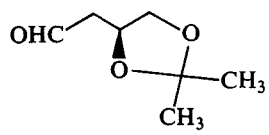

contain 10% of the isomeric 6-membered acetal and separation of the corresponding 3,5-dinitrobenzoate esters by fractional crystallization has been found necessary. The reported procedures for the preparation of **1***a* involve reduction of derivatives of malic acid (2). In some cases, prior O-protection of malic acid esters has been necessary (2*a*–*c*, *e*). However, these reductions using lithium aluminum hydride have proven to be somewhat tedious and low yielding at times in our hands. We wish to report on a facile and efficient preparation of (*S*)-1,2,4-butanetriol from (*S*)-malic acid using borane – dimethyl sulfide as reducing agent.

Borane reductions of carboxylic acids proceed rapidly, quantitatively, and under remarkably mild conditions (7). Thus, treatment of (*S*)-malic acid with borane – dimethyl sulfide in THF gave (*S*)-1,2,4-butanetriol **1***a* in quantitative yield. Acetylation with acetic anhydride afforded triacetate **1***b* in 93% yield. Esterification with 3,5-dinitrobenzoyl chloride afforded the solid derivative **1***c* in 97% yield. Alternatively, the crude triol **1***a* could be converted directly into **2***a* as a ~9:1 mixture of 5- and 6-membered acetals (92% overall yield from malic acid). The corresponding cyclohexylidene acetal **2***c* was prepared in 85% yield, in this case, containing only 5% of the isomeric 6-membered cyclohexylidene acetal. Unlike the case of the isopropylidene derivative, the 3,5-dinitrobenzoate **2***d* was prepared and purified by a single recrystallization. Pure **2***c* could thus be obtained from **2***d* by methanolysis. This simple access to (*S*)-1,2,4-butanetriol from the readily available (*S*)-malic acid should find many applications in natural products synthesis based on the chiral precursor (chiron) approach (8). A number of recent syntheses have relied on (*S*)-malic acid and its derivatives as chiral building blocks (1, 9) and in the confirmation of absolute configuration of natural products (10).

Experimental

Melting points are uncorrected. Optical rotations were measured on a Perkin–Elmer automatic spectropolarimeter, model 141. The ^{1}H nmr spectra were recorded on Bruker WH-90 (90 MHz) and WH-400 (400 MHz) spectrometers with tetramethylsilane as internal standard, in deuterochloroform as solvent, unless otherwise specified. Mass spectra were recorded on a VG-1212 mass spectrometer at low resolution. Column chromatography was done by the flash technique.

(S)-*1,2,4-Butanetriol*, *1*a

To a stirred solution of 2 *M* BMS·THF complex (11) (120 mL, 0.24 mol) and trimethylborate (12) (25 mL) at 0°C was added dropwise (*S*)-malic acid (10 g, 0.75 mol) in THF (50 mL). After stirring the homogeneous solution for an additional 5 min at 0°C, the cooling bath was removed. A white precipitate appeared and redissolved within 20 min. After stirring overnight, methanol (60 mL) was carefully added dropwise over 1 h and the resulting solution evaporated to dryness. A further three co-evaporations with methanol (50 mL) afforded 11.8 g of (*S*)-1,2,4-butanetriol containing residual boron by-products. Flash chromatography (CH_2Cl_2–MeOH; 9:1) of the crude triol yielded pure (*S*)-1,2,4-butanetriol **1***a* (quantitative), $[\alpha]_D$ −28° (*c* 1.07, MeOH), lit. (13) $[\alpha]_D$ −29° (*c* 1.03, MeOH)).

(S)-*1,2,4-triacetoxybutane*, *1*b

A solution of (*S*)-1,2,4-butanetriol (110 mg, 1.04 mmol) in dichloromethane (1 mL), containing acetic anhydride (340 mg, 3.3 mmol),

[1]NSERCC Postdoctorate Fellow, 1982–1983.

[2]Meyers and Lawson have found all reported preparations of **1***a* invariably lead to the formation of about 10% of the isomeric 6-membered acetonide.

Can. J. Chem. Downloaded from www.nrcresearchpress.com by 210.87.254.105 on 09/06/12
For personal use only.

pyridine (0.3 mL), and DMAP (12 mg), was stirred for 2 h at room temperature. The solution was diluted with EtOAc (20 mL) and washed successively with saturated $NaHCO_3$, water, and brine, then dried ($MgSO_4$) and evaporated to give (*S*)-1,2,4-triacetoxybutane, (225 mg, 93%),$[\alpha]_D$ −16.5° (*c* 1.43, acetone), as a colorless oil after flash chromatography (4.5:7 hexane−EtOAc); ir ν_{max}: 1740 cm^{-1} (OAc); ^1H nmr 400 MHz (benzene-d_6) δ: 5.2 (dddd, 1H, *J* = 3.4, 5.9, 5.9, 7.5 Hz, H-2), 4.17 (dd, 1H, *J* = 3.4, 12 Hz, H-1), 4.02 (ddd, 1H, *J* = 6.3, 7.4, 11.3 Hz, H-4), 3.93 (ddd, 1H, *J* = 5.7, 5.7, 11.4 Hz, H-4′), 3.85 (dd, 1H, *J* = 6.1, 12.4 Hz, H-1′), 1.69 (s, 6H, 2 OAc), 1.67 (s, 3H, OAc), 1.57−1.62 (m, 2H, H−3,3′); CI-ms *m/z* (%): 173 (100, MH^+ −HOAc), 113 (11.9, MH^+ −2HOAc).

(S)-*1,2,4-tris-(3,5-dinitrobenzoyloxy)butane,* **1**c

To a solution of (*S*)-1,2,4-butanetriol (125.6 mg, 1.18 mmol) in dichloromethane (2 mL) containing Et_3N (0.5 mL) and DMAP (11 mg) was added 3,5-dinitrobenzoyl chloride (873 mg, 3.79 mmol) in portions at 0°C. The suspension was allowed to warm to room temperature. After 3 h ether (25 mL) was added and the mixture washed successively with aqueous KH_2PO_4, saturated aqueous $NaHCO_3$, water, and brine. The organic phase was dried ($MgSO_4$) and evaporated and the residue eluted through a small SiO_2 plug to give (*S*)-1,2,4-tris-(3,5-dinitrobenzoyloxy)butane (791 mg, 97%), $[\alpha]_D$ −40.7° (*c* 1.0, pyridine), mp 172−174°C, after recrystallization from THF−hexane; ir ν_{max} (KBr pellet): 1730 (ester), 1550, 1350 cm^{-1} ($ArNO_2$); ^1H nmr (pyridine-d_5) δ: 9.2−9.0 (m, 9H, Ar), 6.1 (m, 1H, H-2), 5.1−4.7 (m, 4H, H-1, 1′, 4, 4′), 2.6−2.4 (m, 2H, H-3, 3′); CI-ms, *m/z* (%): 477 (11.5, $MH^+ - HO_2CC_6H_3(NO_2)_2$), 265 (15.8, $MH^+ - 2HO_2CC_6H_3(NO_2)_2$).

(S)*1,2*-O-*isopropylidenebutane-1,2,4-triol,* **2**a

The crude triol **1***a* (11.8 g) was dissolved in acetone (600 mL) containing *p*-TsOH (0.65 g) and stirred at room temperature overnight. Following the addition of Et_3N (0.5 mL), the solution was evaporated to near dryness, and filtered through a plug of SiO_2 with 30% acetone in hexane to give **2***a* (10 g, 92% from malic acid) containing about 10% of the corresponding 2,4-*O*-isopropylidene derivative (6). Transformation into the 3,5-dinitrobenzoate derivative and fractional recrystallization gave the crystalline ester **2***b*, mp 63−64°C (lit. (6) mp 62.5−63°C). Methanolysis as described by Meyers and Lawson (6) gave the pure title compound as a syrup.

(S)-*1,2,*-O-*cyclohexylidene-1,2,4-butanetriol,* **2**c

To (*S*)-1,2,4-butanetriol, obtained from the reduction of (*S*)-malic acid (10 g, 74.6 mmol), dissolved in cyclohexanone (400 mL) was added *p*-TsOH (1.4 g, 7.4 mmol) and the solution was stirred overnight. Triethylamine (5 mL) was added and the solution evaporated. The residue was flash chromatographed (3:7 EtOAc−hexanes) to give *O*-cyclohexylidene-1,2,4-butanetriol (11.8 g, 85%), consisting of a mixture of the 1,2- and 2,4-acetals (95:5 ratio). This mixture was dissolved in dichloromethane (100 mL) containing 10.6 mL (76 mmol) of triethylamine and 775 mg (6.3 mmol) of DMAP; then 17.5 g (75.9 mmol) of 3,5-dinitrobenzoyl chloride was added. After stirring at room temperature for 4 h, the solution was washed successively with aqueous KH_2PO_4, aqueous $NaHCO_3$, and brine, dried ($MgSO_4$) and evaporated to give the dinitrobenzoate **2***d*, (15.1 g, 65%); after recrystallization (Et_2O−hexane), mp 67−68°C; $[\alpha]_D$ −15.4° (*c* 1.2, acetone); ^1H nmr δ: 9.3−9.2 (m, 3H, Ar), 4.67 (t, 2H, *J* = 6.4 Hz, CH_2CH_2O), 4.3−4.1 (m, 2H, $CHCH_2O$), 3.77−3.57 (m, 1H, $CHCH_2O$), 2.14 (dt, 2H, *J* = 6.4, 6.7 Hz, CH_2CH_2O), 1.84−1.44 (bs, 10H, cyclohexylidene).

To dinitrobenzoate **2***d* (15.1 g, 38.3 mmol) in MeOH (400 mL) was added K_2CO_3 (8.2 g, 59.3 mmol) and the mixture stirred for 4 h at room temperature. The mixture was neutralized with Dowex 50W-X8, filtered, and evaporated. The pink residue was flash chromatographed (7:3 hexanes−EtOAc) to give pure alcohol **2***c*, (6.95 g, 94%), $[\alpha]_D$ −10.55 (*c* 1.1, MeOH); ir ν_{max}: 3400 cm^{-1}(OH); ^1H nmr (60 MHz) δ: 4.4−3.5 (m, 5H, OCH_2CH and CH_2OH), 3.0 (bs, 1H, OH), 1,85 (dt, 2H, CH_2CH_2OH).

Acknowledgements

We wish to thank the Natural Sciences and Engineering Research Council of Canada and Le Ministère de l'éducation du Québec for financial assistance. We also thank Dr. P. V. Tan for high field nmr spectra and Michael Evans for mass spectra.

1. D. SEEBACH. Modern synthetic methods 1980. *Edited by* R. Scheffold. Otto Salle and Sauerlander, Frankfurt-am-Main, Germany. 1980.
2. (*a*) P. W. FEIT and O. T. NIELSEN. J. Med. Chem. **9**, 416 (1966); (*b*) E. J. COREY, H. SHIRAHAMA, H. YAMAMOTO, S. TERASHIMA, A. VENKATESWARLU, and T. K. SCHAFF. J. Am. Chem. Soc. **93**, 1490 (1971); (*c*) E. J. COREY, H. NIWA, and J. KNOLLE. J. Am. Chem. Soc. **100**, 1942 (1978); (*d*) H. HAYASHI, K. NAKANISHI, C. BRANDON, and J. MARMUR. J. Am. Chem. Soc. **95**, 8749 (1973); (*e*) K. MORI, T. TAKIGAWA, and T. MATSUO. Tetrahedron, **35**, 933 (1979); (*f*) A. HOLY. Collect Czech. Chem. Commun. **40**, 187 (1975); (*g*) P. MA, V. S. MARTIN, S. MASAMUNE, K. B. SHARPLESS, and S. M. VITI. J. Org. Chem. **47**, 1378 (1982); (*h*) K.-C. TANG, B. E. TROPP, and R. E. ENGEL. Tetrahedron, **34**, 2873 (1978); (*i*) K. ISSAC and P. KOCIENSKI. J. Chem. Soc. Chem. Commun. 460 (1982); (*j*) V. K. TANDON, A. M. VANLEUSEN, and H. WYNBERG. J. Org. Chem. **48**, 2767 (1983).
3. S. HANESSIAN, A. UGOLINI, and M. THERIEN. J. Org. Chem. **48**, 4427 (1983).
4. J. HERSCOVICI and K. ANTONAKIS. J. Chem. Soc. Chem. Commun. 561 (1980).
5. E. J. COREY and J. W. SUGGS. Tetrahedron Lett. 2647 (1975).
6. A. I. MEYERS and J. P. LAWSON. Tetrahedron Lett. **23**, 4483 (1982).
7. H. C. BROWN. Boranes in organic chemistry. Cornell Univ. Press, Ithaca, NY. 1972; H. C. BROWN, P. HEIM, and N. M. YOON. J. Am. Chem. Soc. **92**, 1637 (1970); N.M. YOON, C. S. PAK, H. C. BROWN, S. KIRSHAMURTHY, and T. P. STOCKY. J. Org. Chem. **38**, 2786 (1973).
8. S. HANESSIAN. Total synthesis of natural products: the 'chiron' approach. *Edited by* J. E. Baldwin. Pergamon Press, Oxford. 1983.
9. K. MORI. *In* The total synthesis of natural products. Vol. 4. *Edited by* J. ApSimon. Wiley-Interscience, New York, NY 1981. p. 1, and references cited therein.
10. H. H. MEYER. Justus Liebigs Ann. Chem. 484 (1978).
11. C. F. LANE. Aldrichimica Acta, **8**, 20 (1975); R. O. HUTCHINS and F. CISTONE. Org. Prep. Proced. Int. **13**, 227 (1981).
12. C. F. LANE, H. L. MYATT, J. DANIELS, and H. B. HOPPS. J. Org. Chem. **39**, 3052 (1974).
13. E. HUNGERBUHLER, D. SEEBACH, and D. WASMUTH. Helv. Chim. Acta, **64**, 1467 (1981).

Facile synthesis of the enantiomers of frontalin[1,2]

B. D. JOHNSTON AND A. C. OEHLSCHLAGER
Department of Chemistry, Simon Fraser University, Burnaby, B. C., Canada V5A 1S6

Received February 20, 1984

B. D. JOHNSTON AND A. C. OEHLSCHLAGER. Can. J. Chem. **62**, 2148 (1984).

S-(−)- and *R*-(+)-frontalin (1,5-dimethyl-6,8-dioxabicyclo[3.2.1]octane) were prepared from (*E*)-2-methyl-2,6-heptadiene-1-ol utilizing the Sharpless asymmetric epoxidation reaction to induce chirality. The six-step synthetic sequence proceeded in approximately 50% overall yield and was found to be suitable for the preparation of multi-gram quantities of either enantiomer with ≥ 90% ee.

B. D. JOHNSTON AND A. C. OEHLSCHLAGER. Can. J. Chem. **62**, 2148 (1984).

Faisant appel à la réaction d'époxydation asymétrique de Sharpless pour induire la chiralité, on a préparé les *S*-(−)- et *R*-(+)-frontalines (diméthyl-1,5 dioxo-6,8 bicyclo[3.2.1] octanes) à partir du (*E*)-méthyl-2 hetadiène-2,6 ol-1. La synthèse implique six étapes et procède avec un rendement global de 50%; on a trouvé qu'elle est appropriée pour la préparation de plusieurs grammes de chacun des énantiomères avec des ee ≥ 90%.

[Traduit par le journal]

Can. J. Chem. Downloaded from www.nrcresearchpress.com by 210.87.254.42 on 09/06/12
For personal use only.

Our recent synthesis of both enantiomers of brevicomin (1) which utilized the Sharpless asymmetric epoxidation (2) in the key chiral induction step has led us to investigate the use of this reaction in the asymmetric synthesis of other natural products, particularly other chiral insect pheromones. Immediately obvious as synthetic targets were the chiral isomers of frontalin **1** which contain the 6,8-dioxabicyclooctane nucleus in common with brevicomin **2**.

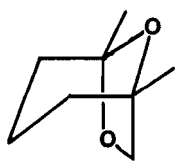

1

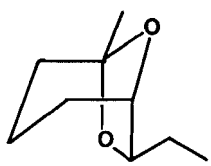

2

Frontalin has been shown to possess aggregation pheromone activity in several species of *Dendroctonus* bark beetles (3). As part of a collaborative multidisciplinary project involving the detection, monitoring, and control of bark beetle populations using pheromone baited traps, we required 3 − 5-g amounts of each chiral isomer of frontalin in order to determine if different *Dendroctonus* species would respond with chiral recognition to the enantiomers.

Frontalin has been a popular target for synthetic chemists and there have been a number of racemic (4) and chiral (5) syntheses of the molecule. An examination of the published chiral synthetic routes, however, reveals that several did not appear amenable to scale-up for the amounts we required and the others seemed only directly applicable to production of one of the two possible enantiomers.

Our initial synthetic plan was to utilize the Sharpless method in a short sequence, beginning with commercially available 6-methyl- 5-hepten-2-one, **3** (Scheme 1). The ketone was protected as the ethylene ketal. Subsequent allylic oxidation (6), followed by reduction of the mixture of aldehyde **5** and alcohol **6** with $NaBH_4$, gave an acceptable yield of the *E* allylic alcohol **6**. Unfortunately, Sharpless epoxidation (2) of **6** did not yield the expected epoxide **7** but rather the interesting dioxabicyclo

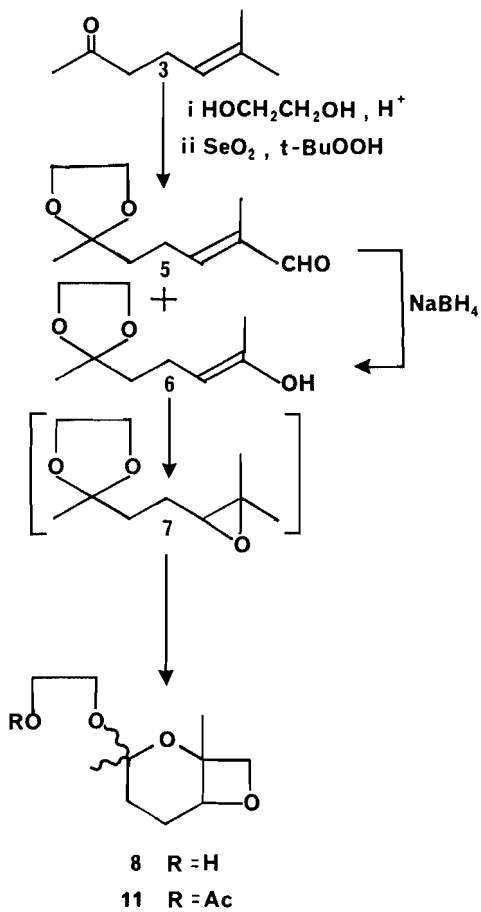

SCHEME 1

compound **8**. Evidently Sharpless epoxidation conditions promote opening of both the ketal and the epoxide. After completion of this work, Sharpless et al. (7) reported that the 4,4-dimethyl-2,6-dioxolane analog of **7** does not undergo this rearrangement and this epoxide can be efficiently (≈74% overall) converted to frontalin.

Structure **8** was assigned on the basis of spectroscopic analysis. The mass spectrum indicated a molecular ion of 202, which corresponded to the expected epoxide product, but the ^1H nmr spectrum in several solvents (DMSO-d_6, benzene-d_6, $CDCl_3$)

[1]Research supported by the Natural Sciences and Engineering Research Council of Canada, Operating Grant No. A3881.

[2]Preliminary Communication, 66th Canadian Chemical Conference, Calgary, Alberta, June, 1983.

Can. J. Chem. Downloaded from www.nrcresearchpress.com by 210.87.254.42 on 09/06/12
For personal use only.

could not be reconciled with structure **7**. In particular, an AB pattern characteristic of an isolated methylene with diastereotopic hydrogens was apparent, but, under conditions where OH coupling was observed (DMSO-d_6, triplet, J = 6 Hz), no extra coupling was observed in the AB pattern. This indicated that, although a primary alcohol was present, the product could not be the expected epoxide, **7**.

Secondary and tertiary alcohol structures **9** and **10**, which were initially considered as possibilities, were also eliminated by this result. Comparison of the ^{1}H nmr of the acetate of **8** with that of the parent alcohol indicated that the AB pattern was still present but that a downfield shift of ≈0.5 ppm had occurred for a second highly coupled methylene group. A partial structure of $-OCH_2CH_2OH$ which must contain methylenes with diastereotopic hydrogens was therefore deduced. A choice between structures **8** and **11** was made on the basis of ^{13}C nmr. The chemical shifts of the carbons involved in the ether linkages of **8** were indicative of an oxetane rather than an epoxide (8). As further confirmation, attempted reduction of **8** with excess lithium tetrahydridoaluminate in ether at room

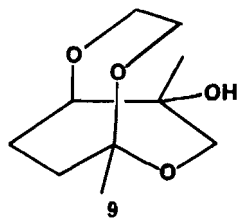

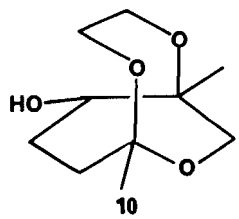

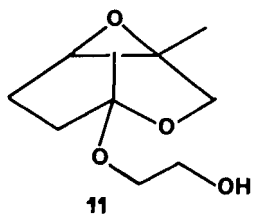

temperature resulted in recovery of starting material, a result which would not be expected if an epoxide had been present.

Reasoning that protection of the ketone as outlined in Scheme 1 might not be required, we undertook the alternate synthesis outlined in Scheme 2. The ethylene ketal protecting group was removed from allylic alcohol **6** to yield **13** which was subjected to Sharpless epoxidation. Again, the expected epoxide **14** could not be isolated due to epoxide hydrolysis and intramolecular ketal formation during the work-up. In order to determine if **14** was a stable, isolable compound, the epoxidation was performed racemically using *meta*-chloroperoxybenzoic acid. The epoxide (±)−**14** could be obtained in satisfactory yield with a nonaqueous work-up (9) but proved to be unstable and slowly cyclized to **15** (the same structure as obtained from Sharpless epoxidation) over a period of several days. The tendency of γ-keto epoxides to undergo thermal rearrangement to intramolecular ketals is well documented (10, 11).

The dioxabicyclo alcohol **15** corresponds to frontalin if the alcohol function was to be replaced with hydride. Towards this end, racemic **15** was converted to mesylate **16**. Unfortunately, reduction of this hindered, *neo*-pentyl-like mesylate was unsuccessful using either $LiAlH_4$ in Et_2O (no reaction) or $LiBHEt_3$ in refluxing THF (complex mixture of ring-opened products).

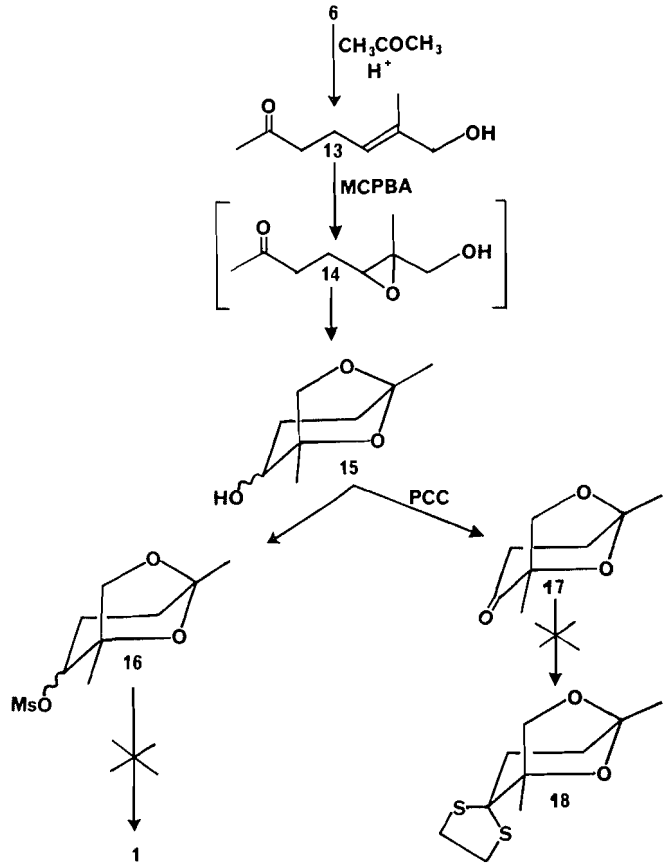

SCHEME 2

A further attempt to convert **15** to frontalin was also made. With the aim of deoxygenation through reduction of the dithiolane **18**, racemic **15** was oxidized with pyridinium chlorochromate to ketone **17**. Conversion of **17** to the dithiolane derivative **18** using 1,2-ethanedithiol and BF_3/Et_2O was, however, unsuccessful, leading to a complex mixture of sulfur-containing products.

The problems encountered in Schemes 1 and 2 appear to center around the presence of a ketone in either its free or protected form in the substrate during Sharpless epoxidation. We therefore decided to postpone introduction of the ketone to a later stage. Reasoning that a terminal alkene is synthetically equivalent to a methyl ketone, the diene alcohol **20** was prepared by the literature method (12). Sharpless epoxidation of **20** gave good yields of the expected chiral epoxides **21**. The enantiomeric excess of each chiral isomer was determined by integration of the diastereotopic hydrogens of the $-OCH_2-$ group in the (+)-α-methoxy-α-trifluoromethylphenyl acetate derivatives to be 95% ee for (−)-**21** and 96% ee for (+)-**21** (ee: enantiomeric excess).

Lithium tetrahydridoaluminate reduction of the chiral isomers of **21** using a nonacidic work-up and limited amounts of water gave excellent yields of the chiral diols **22**. Two different methods for completion of the synthesis were investigated. Initially, we employed a Wacker-type oxidation to obtain frontalin directly from diol **22**. This method has been employed by Grigg and co-workers (13), albeit in low yield, in a racemic synthesis of brevicomin. In an attempt to improve upon the original Wacker conditions ($CuCl$, O_2, Pd^{2+}) used by Grigg, we chose the modified conditons (H_2O_2, Pd^{2+}) developed by Roussel and Mimoun (14). Several attempts at this method

Can. J. Chem. Downloaded from www.nrcresearchpress.com by 210.87.254.42 on 09/06/12
For personal use only.

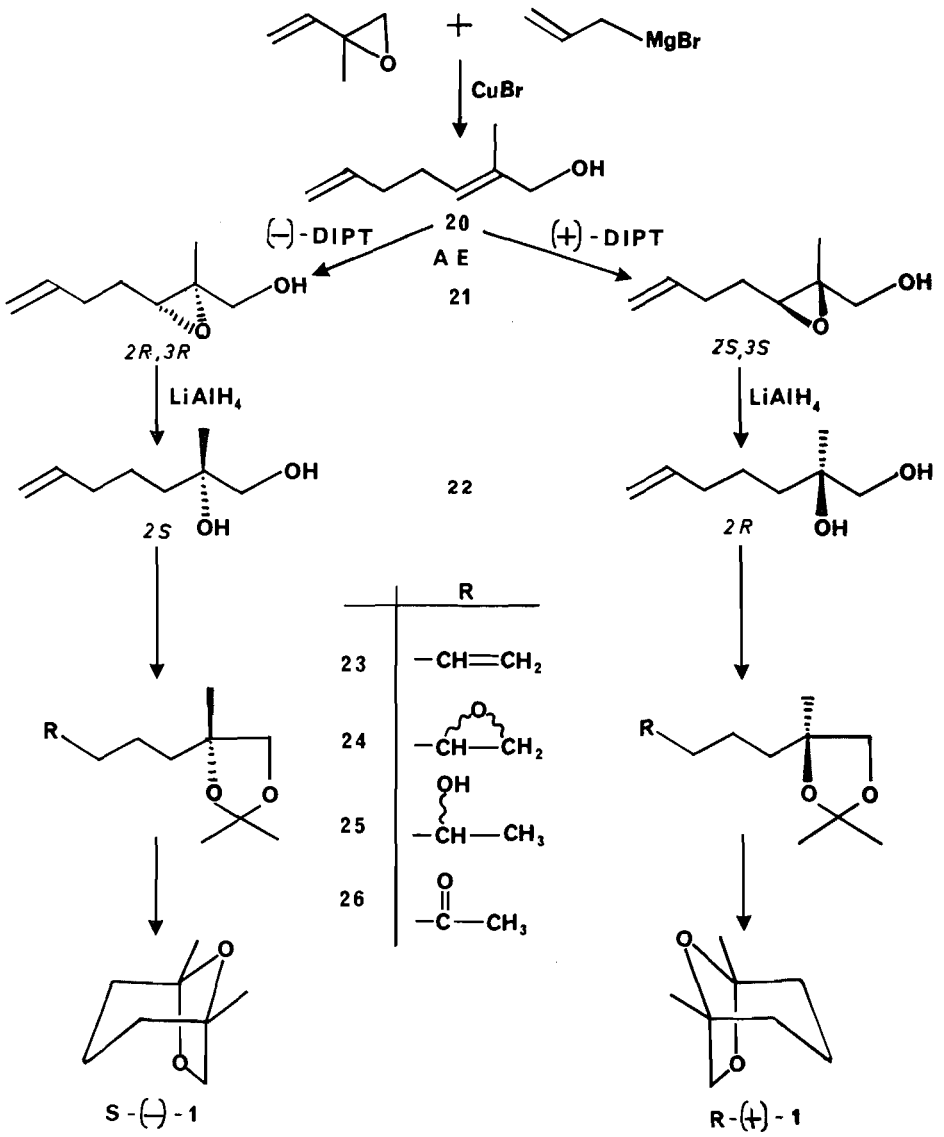

SCHEME 3

using various reaction conditions and work-up procedures gave dismally low yields of frontalin (10−12%) and the chemical purity of the final product could not be improved above 85% by simple fractional distillation.

The synthesis was completed in a satisfactory manner using the route from **22** outlined in Scheme 3. This relatively lengthy but nevertheless high yield sequence began by protection of the diol **22** containing the sensitive chiral tertiary alcohol function as the acetone ketal **23**. Peracid oxidation of the terminal double bond gave epoxide **24** as a mixture of diastereomers. Lithium tetrahydridoaluminate reduction of **24** afforded excellent yields of secondary alcohol **25**, again as a mixture of diastereomers. Sodium hypochlorite oxidation in acetic acid gave the methyl ketone **26** which, although it could be detected by gc analysis of the crude reaction mixture, was not isolated due to slow *in situ* hydrolysis of the ketal and spontaneous cyclization to cleanly give frontalin **1** in 75% yield.

The optical purity of the frontalin enantiomers as determined by a combination of optical rotation measurements and nmr integration in the presence of the chiral shift reagent tris[3-(trifluoromethylhydroxymethylene)-*d*-camphorato]europium(III) indicated 89−93% ee for (+)-frontalin and 97% ee for (−)-frontalin. In the case of (+)-frontalin, we speculate that the decrease in optical purity from the initial Sharpless epoxidation product may be due to a small amount of acid-catalyzed racemization of one of the tertiary alcohol intermediates.

In summary, the application of the Sharpless asymmetric epoxidation reaction to an appropriate acyclic allylic alcohol precursor has been shown to afford both chiral (≥90% ee) frontalin enantiomers in overall chemical yields of ≈50% (from **20**). The synthetic sequence is suitable for the production of multi-gram quantities of the frontalin enantiomers and proceeds entirely without the necessity for chromatographic purification of intermediates.

Experimental

The ^{1}H nmr (400 MHz) and ^{13}C nmr (100 MHz) spectra were recorded using $CDCl_3$ solutions on a Bruker WM 400 spectrometer unless otherwise noted. Infrared spectra were recorded using neat films between NaCl plates on a Perkin Elmer 599B spectrophotometer unless otherwise noted. Mass spectra were obtained on a Hewlett−Packard 5985B gc−ms spectrometer. Optical rotations were measured with a Perkin Elmer P_{22} spectropolarimeter using a 0.5 dm × 5-mm id sample cell. Concentrations are reported in g/100 mL of solvent.

Can. J. Chem. Downloaded from www.nrcresearchpress.com by 210.87.254.42 on 09/06/12
For personal use only.

Elemental analyses were performed by Mr. M. Yang of the Department of Biological Sciences, Simon Fraser University using a Perkin Elmer Model 240 elemental analyzer. Gas chromatographic analysis utilized a Hewlett–Packard 5880A operated with a J+W fused silica DB-1 capillary column (15 m × 0.25 mm), a flame ionization detector, and a suitable linear oven temperature program.

Solvents and reagents were used as supplied from commercial sources with the following exceptions. Anhydrous CH_2Cl_2 was obtained by distillation from P_2O_5. Anhydrous solutions of *tert*-butylhydroperoxide in CH_2Cl_2 were prepared from 90% *t*-BuOOH (Aldrich) using the azeotropic distillation method described by Sharpless et al. (7). Chromatography solvents were distilled before use and anhydrous ether was obtained only from freshly opened cans (Fisher Scientific).

*2-Methyl-2-(4-methyl-3-pentenyl)-1,3-dioxolane, **4***

This compound was prepared by the literature method using the acid catalyzed reaction of 6-methyl-5-heptene-2-one with ethylene glycol; yield 89%, bp 86–87°C/12 Torr (1 Torr = 133.3 Pa); lit. (15) bp 58°C/1.5 Torr.

*2-Methyl-2-(4-methyl-5-hydroxy-3-pentenyl)-1,3-dioxolane, **6***

To a solution of **4** (85 g, 0.50 mol) in CH_2Cl_2 (400 mL) was added *tert*-butylhydroperoxide (90%, 110 mL, 0.99 mol) and SeO_2 (5.5 g, 50 mmol). The mixture was refluxed with stirring for 9 h and then poured into a 2:1 mixture of saturated aqueous $NaHCO_3$ and 10% aqueous $Na_2S_2O_3$ solutions (300 mL). The organic phase was separated and the aqueous phase extracted with ether (3 × 200 mL). The combined organics were washed with saturated brine (100 mL), dried ($MgSO_4$), and concentrated to a syrup. Gas chromatographic analysis of this crude material indicated ≈3% starting alkene, ≈78% aldehyde **5**, and ≈14% alcohol **6**. The mixture was taken up in methanol (150 mL) and cooled with an ice bath while $NaBH_4$ (8g, 0.2 mol) was added in small portions over 0.5 h. After a further 0.5 h, the ice bath was removed and stirring continued for a further 0.5 h at ambient temperature. Water (600 mL) was then added and the reaction mixture extracted with ether (3 × 200 mL). The aqueous phase was saturated with NaCl and further extracted with ether (3 × 100 mL). The combined ether extracts were dried ($MgSO_4$) and concentrated *in vacuo*. Distillation (bp 102–110°C/0.5 Torr) yielded **6** (53.6 g, 58%). Spectral data were in accord with those reported in the literature (16).

This procedure, utilizing catalytic amounts of SeO_2, was found to be preferable to the reported procedure involving stoichiometric amounts of SeO_2 (16).

*Attempted Sharpless asymmetric epoxidation of **6***

*Preparation of 1,3-dimethyl-3-(2-hydroxyethoxy)-7-oxabicyclo [4.2.0]octane, **8***

To a solution of titanium tetraisopropoxide (28.4 g, 100 mmol) in dry methylene chloride (700 mL) was added (+)-diisopropyltartrate (DIPT) (25.7 g, 110 mmol) with the temperature maintained at −30°C with a CCl_4 slush. After 10 min, allyl alcohol **6** (18.6 g, 100 mmol) was added in one portion followed in 5 min by an anhydrous 5 *M* solution of *tert*-butylhydroperoxide in methylene chloride (50 mL, 0.25 mol). The reaction was kept in a freezer for 18 h (≈−30°C), quenched by the addition of water (10 mL, 0.56 mol), and stirred while warming to room temperature over 2.5 h. The CH_2Cl_2 was removed *in vacuo* and to the residue was added ether (700 mL) and saturated aqueous NaF solution (1 L). After stirring for 20 h at room temperature, the mixture was filtered through Celite and the filter cake washed with ether (4 × 150 mL). The DIPT was hydrolyzed by the addition of NaOH (8 g, 0.25 mol) followed by rapid stirring at room temperature for 2 h. The aqueous phase was separated, saturated with NaCl, and extracted with ether (4 × 150 mL). The combined ether extracts were dried ($MgSO_4$) and concentrated *in vacuo* to yield an almost colorless oil. Excess *tert*-butylhydroperoxide was removed over 4 h on high vacuum (0.1 Torr); yield 16.2 g (80%), >97% pure by gc. An analytical sample was purified by preparative tlc (hexane – ethyl acetate, 1:5); ir: 3460(s), 2940(s), 2885(s), 1645(w), 1450(m), 1390(s), 1380(s), 1358(m), 1270(m), 1245(s), 1210(s), 1130(s), 1105(s), 940(m), 843(s), 826(m) cm^{-1} ^1H nmr δ: 1.40 (3H, CH_3, s), 1.45 (3H, CH_3, s), 1.56 (1H, C(4)H, m), 1.80 (1H, C(4)H,m), 1.86 (2H, C(3)H, m), 2.29 (1H, OH, br s), 3.13 (1H, C(6)H, t, J = 2.5 Hz), 3.49 (1H, C(8)H, d, J = 7.5 Hz), 3.50 (1H, OCH, m), 3.72 (1H, OCH, m), 3.74 (2H, CH_2O, m), 3.76 (1H, C(8)H, d, J = 7.5 Hz); ^{13}C nmr δ: 18.9(q), 21.5 (t), 24.2(q), 31.1(t), 61.9(t), 71.0(t), 73.1(t), 76.4(d), 81.9(s), 108.2(s); ms: 202(5), 173(10), 145(56), 114(100), 99(72), 84(35), 71(48), 43(72). *Anal.* calcd. for $C_{10}H_{18}O_4$: C 59.35, H 8.99; found: C 59.19, H 9.09.

*1,3-Dimethyl-3-(2-acetoxyethoxy)-7-oxabicyclo[4.2.0]octane, **11***

Alcohol **8** (200 mg, 0.99 mmol) was dissolved in CH_2Cl_2 (5 mL). After addition of pyridine (350 mg, 4.4 mmol) and acetic anhydride (300 mg, 2.9 mmol), the mixture was stirred for 16 h at room temperature. The CH_2Cl_2 solution was washed with saturated $NaHCO_3$ solution (2 mL) and water (2 mL), dried ($MgSO_4$), and concentrated to a yellow syrup. Purification by preparative tlc (ethyl acetate – hexane, 3:1) yielded **11** (186 mg, 76%) as a colorless oil; ir 2990(m), 2945(m), 2890(m), 1744(s), 1450(m), 1392(m), 1382(m), 1256(s), 1213(m), 1113(m), 1050(m), 1033(m), 943(w), 890(w), 857(m), 830(w) cm^{-1} ^1H nmr δ: 1.38 (3H, CH_3, s), 1.45 (3H, CH_3, s), 1.55 (1H, C(4, 5)H, m), 2.06(3H, C(4,5)H, m), 3.48 (1H, C(8)H, d, J = 7.5 Hz), 3.61 (1H, −OCH−, m), 3.79 (1H, C(8)H,, d, J = 7.5 Hz), 3.83 (1H, −OCH−, m), 4.22 (2H, $-CH_2O-$, m). *Anal.* calcd. for $C_{12}H_{20}O_5$: C 59.00, H 8.25; found: C 59.16, H 8.41.

*2-Methyl-2-hepten-6-one-1-ol, **13***

Ethylene ketal **6** (53 g, 0.28 mol) was dissolved in acetone (150 mL) to which was added concentrated H_2SO_4 (5 drops) and the reaction stirred at room temperature for 2 h. Anhydrous K_2CO_3 (2 g) was then added and stirring continued for a further 0.5 h. Filtration, concentration, and distillation (bp 98–102°C/ 0.2 Torr) yielded **13** (30.5 g, 75%, >94% pure by gc); ir 3400 (m) 2910(m), 2860(m), 1715(s), 1410(m), 1360(m), 1165(m), 1070(m), 1015(m) cm^{-1}; ^1H nmr δ: 1.66 (3H, C(7)H_3, s), 2.13 (3H, C(2) methyl, br s), 2.29 (2H, C(4)H, q, J = 7 Hz), 2.48 (2H, C(5)H_2, t, J = 7Hz), 3.96 (2H, C(1)H_2, s), 4.32 (1H, C(3)H, triplet of quartets, J = 7, 1.25 Hz). *Anal.* calcd. for $C_8H_{14}O_2$: C 67.57, H 9.92; found: C 67.38, H10.04.

*(±)-2-Hydroxy-1,5-dimethyl-6,8-dioxabicyclo[3.2.1]octane, **15***

Alkene **13** (14.2 g, 100 mmol) was dissolved in anhydrous CH_2Cl_2 (200 mL) *meta*-Chloroperoxybenzoic acid (21.5 g of purity ≈85%, 106 mmol) was then added in small portions over a period of 15 min with ice-bath cooling. After stirring at ambient temperature for 0.5 h, anhydrous KF (24 g, 0.5 mol) was added and stirring continued for 1 h. Filtration and removal of the solvent yielded crude epoxide **14**; ^1H nmr (100 MHz, $CDCl_3$) δ: 1.17 (3H, C(2) methyl, s), 1.6–2.1 (2H, C(4)H_2, m) 2.26 (3H, C(7)H_3, s), 2.30 (1H, OH, br s), 2.68 (2H, C(5)H_2, t, J = 7 Hz), 3.05 (1H, C(3)H, dd, J = 8, 6 Hz), 3.59, 3.72 (2H, C(2)H_2, dd, J_{AB} = 15 Hz). This sample underwent slow, spontaneous rearrangement to bicyclo alcohol **15** over a period of several days.

The bulk of the crude material was dissolved in methanol (150 mL) and treated with $SOCl_2$ (5 drops). After 1 h, gc analysis showed the absence of epoxide **14** and the formation of two products in a ratio of ≈60:40. Equilibration of the acidic alcohol solution for 18 h at room temperature gave a 15:1 ratio of the two diastereomeric bicyclo alcohols **15** with the isomer of shorter retention time predominating. Removal of the solvent *in vacuo* and distillation of the residue yielded **15** (12.8 g, 81%), bp 80–95°C/0.05 Torr; ir: 3440(s), 2980(s), 2930(s), 2875(s), 1710(w), 1640(w), 1485(w), 1450(m), 1387(s), 1255(s), 1207(s), 1105(s), 1067(s), 1030(s), 972(m), 952(m), 938(m), 910(w), 887(w), 851(s), 811(m), 774(w), 707(m) cm^{-1}; nmr analysis of the initially formed mixture of diastereomers as well as the equilibrium mixture allowed the ^1H nmr of each isomer to be assigned as follows. Major isomer δ: 1.37 (3H, CH_3, s), 1.43 (3H, CH_3,s), 1.58 (1H, C(3,4)H, m), 1.75 (2H, C(3,4)H, m), 2.00 (1H, C(3,4)H,m), 2.28 (1H, OH, d, J = 9 Hz), 3.42 (1H, C(2)H, br d, J = 9 Hz), 3.52 (1H, C(7)H, d, J = 12 Hz), 3.84 (1H, C(7)H, d, J = 12 Hz). Minor isomer δ: 1.02 (3H, CH_3, s), 1.51 (3H, CH_3,s), 1.80 (2H, C(3,4)H, m), 2.08 (2H, C(3,4)H, m), 3.51 (1H, C(7)H, dd,

Can. J. Chem. Downloaded from www.nrcresearchpress.com by 210.87.254.42 on 09/06/12
For personal use only.

J = 12, 2 Hz), 3.65 (1H, OH, br s), 3.67 (1H, C(7)H, J = 12 Hz), 4.07 (1H, C(2)H, dd, J = 7, 2 Hz); ms (major isomer): 158(M^+,2), 129(30), 114(66), 101(100), 99(52), 98(38), 84(94), 71(58), 70(76), 69(43), 61(45), 43(44); ms (minor isomer): 158(M^+,1.4), 127(10), 101(100), 98(13), 95(10), 85(43), 84(44), 83(61), 71(28), 58(41), 55(15), 43(46). *Anal.* calcd. for $C_8H_{14}O_3$: C 60.74, H 8.92; found: C 60.51, H 8.93.

Attempted Sharpless epoxidation of ***13***

Titanium tetraisopropoxide (3.0 mL, 2.9 g, 10 mmol) was dissolved in anhydrous CH_2Cl_2 (50 mL) and the solution cooled to < -30°C with a Dry Ice − acetone bath while successive additions of (+)-DIPT (2.6 g, 11 mmol), alkene **13** (1.0 g, 0.7 mmol), and *t*-BuOOH (20 mL of a 1 *M* anhydrous CH_2Cl_2 solution) were made at 10-min intervals. The reaction was kept at −30°C for 3.5 h and then poured into a rapidly stirred mixture of ether (300 mL) and 10% aqueous tartaric acid (50 mL). After stirring for 4.5 h at room temperature, the organic phase was washed with saturated aqueous $NaHCO_3$ (50 mL) and saturated NaCl (50mL). Drying ($MgSO_4$) and removal of the solvent yielded a mixture of crude **15**, excess *t*-BuOOH, and (+)-DIPT. Coevaporation with toluene (2 × 100 mL) removed most of the *t*-BuOOH and the residue was purified by column chromatography on silica gel (hexane − ethyl acetate, 1:2) to yield 0.82 g (74%) of **15** as a mixture (≈9:1) of alcohols with identical spectral and gc characteristics to those observed for the racemic material.

(±)-1,5-Dimethyl-2-methanesulfonyloxy-6,8-dioxabicyclo[3.2.1] octane, ***16***

Alcohol **15** (1.58 g, 10 mmol) was dissolved in pyridine (10 mL). Methanesulfonyl chloride (2.0 mL, 2.9 g, 26 mmol) was added and the reaction warmed to 50°C for 1.5 h. After cooling to room temperature, CH_2Cl_2 (100 mL) was added and the solution washed with saturated aqueous $NaHCO_3$ (2 × 50 mL) and water (2 × 50 mL). Drying ($MgSO_4$) and removal of the solvent *in vacuo* yielded an orange syrup which crystallized upon cooling. Recrystallization (hexane−$CHCl_3$, 50:1) gave **16** as light yellow crystals (1.32 g, 56%, mp 110−112°C); ir (KBr pellet): 3010(m), 2970(m), 2935(m), 2910(m), 1393(m), 1384(m), 1360(m), 1350(s), 1343(s), 1335(s), 1260(m), 1252(s), 1208(m), 1183(s), 1116(s), 1024(m), 1012(s), 991(m), 954(s), 938(s), 917(m), 900(m), 880(s), 854(s), 774(m), 750(m) cm^{-1}; ^1H nmr δ: 1.42 (3H, CH_3, s), 1.49(3H, CH_3,s), 1.66 (1H, C(4)H, ddd, J = 13.3, 6.0, 1.5 Hz), 1.90 (1H, C(4)H, td, J = 13.3, 5.7 Hz), 2.06 (1H, C(3)H, ddt, J = 15.5, 5.7, 1.5 Hz), 2.17 (1H, C(3)H, m), 3.10 (3H, $-SO_2CH_3$, s), 3.54 (1H, C(7)H, d, J = 7.9 Hz), 3.86 (1H, C(7)H, d, J = 7.9 Hz), 4.54 (1H, C(2)H, dd, J = 3.8, 1.9 Hz); ^{13}C nmr δ: 19.0(q), 24.0(q), 24.5(t), 30.7(t), 38.7(q), 72.6(t), 76.6(d), 80.8(s), 108.3(s); ms: 236(M^+,0.4), 140(11), 129(30), 114(13), 99(11), 98(15), 97(19), 87(18), 83(20), 71(12), 69(12), 57(13), 55(10), 43(100). *Anal.* calcd. for $C_9H_{18}O_5S$: C 45.75, H 6.82; found: C 45.75, H 7.00.

(±)-1,5-Dimethyl-6,8-dioxabicyclo[3.2.1]octan-2-one, ***17***

Alcohol **15** (110 mg, 0.69 mmol) was dissolved in CH_2Cl_2 (5 mL) and stirred while pyridinium chlorochromate (1.0 g, 4.6 mmol) was added in two portions at 2-h intervals. After 18 h at room temperature, the reaction mixture was passed through a short silica gel column using CH_2Cl_2 as the eluant. The solvent was removed and the residue subjected to bulb-to-bulb distillation to yield ketone **17** (72 mg, 67%); bp 80−100°C (bath temperature)/15 Torr. The purified material slowly crystallized (mp 50−52°C). An analytical sample was prepared by recrystallization from hexane; ir: 2991(w), 2940(s), 2881(s), 1729(s), 1480(w), 1449(s), 1417(m), 1388(s), 1379(s), 1261(m), 1214(s), 1184(s), 1168(m), 1135(s), 1106(s), 1079(s), 1036(s), 1011(m), 935(m), 907(m), 879(m), 855(s), 799(m) cm^{-1}; ^1H nmr (100 MHz, $CDCl_3$) δ: 1.40 (3H, CH_3,s), 1.58 (3H, CH_3, s), 2.34 (4H, C(3,4)H, m), 3.60 (1H, C(7)H, d, J = 8 Hz), 3.97 (1H, C(7)H, d, J = 8 Hz); ms: 156(M^+,2), 114(15), 99(100), 85(16), 71(22), 69(18), 58(17), 55(27), 43(58). *Anal.* calcd. for $C_8H_{12}O_3$: C 61.15, H 7.74; found: C 61.10, H 7.70.

2-Methyl-2-vinyloxirane, ***19***

The method of Reist *et al.* (17) for the preparation of this epoxide from isoprene was modified with a resulting increase in yield. Freshly distilled isoprene (125 g, 1.8 mol) was added to water (350 mL) and vigorously stirred with ice-bath cooling. *N*-bromosuccinimide (200 g, 1.1 mol) was then added in small portions over a period of 1 h with the temperature of the reaction maintained at 10−15°C. The cooling bath was removed and the reaction stirred at ambient temperature for 2 h, after which a test for an oxidizing agent with starch iodide paper proved negative. The lower organic phase was separated and the aqueous phase extracted with ether (3 × 125 mL). The combined organics were dried ($MgSO_4$), filtered, and concentrated on a rotary evaporator to ≈250 mL.

The resulting solution of isoprene bromohydrin was then added dropwise to a warm (50−55°C) aqueous 30% NaOH solution (300 mL) under aspirator vacuum (≈15 Torr). Volatile material which distilled was collected in a Dry Ice − acetone cooled trap placed in the line between the reaction flask and the water aspirator. The aqueous phase of this distillate was separated and discarded and the remainder dried over $MgSO_4$. Filtration and distillation (bp 75−82°C, 750 Torr) yielded 54.5 g (59%) of a 10:1 mixture of the desired product **19** and its isomer, isopropenyloxirane. Distillation of the mixture on a 30-cm spinning band column allowed separation of the isomers to yield pure **19**, bp 81−82°C/760 Torr, lit. (17) bp 78−82°C.

2-Methyl-2,6-heptadien-1-ol, ***20***

This compound was prepared by the coupling of allyl magnesium bromide with 2-methyl-2-vinyloxirane, essentially by the procedure briefly oulined in ref. 12. Thus, magnesium turnings (24.0 g, 1.0 mol) in dry ether (100 mL) were stirred rapidly under argon while a solution of freshly distilled allyl bromide (28.0 g, 232 mmol) in dry ether (150 mL) was added dropwise over 3 h. After cooling to room temperature over 0.5 h, the black solution was decanted from the excess magnesium into a dry, argon filled dropping funnel. The excess magnesium was rinsed with an additional portion of dry ether (50 mL) which was also decanted into the dropping funnel.

This solution, which was estimated to contain between 185 and 200 mmol of allyl magnesium bromide (18), was added dropwise over 1 h to a stirred solution of **19** (16.8 g, 200 mmol) in dry THF (250 mL) containing a catalytic amount of $CuBr/S(CH_3)_2$ (1 g, 5 mmol). The temperature during this addition was maintained at ≤ -30°C with a Dry Ice − acetone bath. The yellow color of allyl copper could be observed momentarily as each drop of Grignard solution entered this reaction mixture. After a further 0.5 h at −20° to −30°C, the reaction was quenched by the addition of saturated aqueous NH_4Cl solution (250 mL) and allowed to warm to ≈10°C. The aqueous phase was separated and further extracted with ether (3 × 200 mL). The combined ethereal extracts were washed with 14% NH_4OH solution (100 mL), water (100 mL), and dried over $MgSO_4$. Concentration of the extracts by distillation of the solvents at atmospheric pressure through a 30-cm Vigreux column followed by vacuum distillation of the residue yielded **20** (15.2 g, 73%; bp 88−92°C/12 Torr, lit. (12) bp 93°C/15 Torr). Analysis by gc indicated a purity of 93% with ≈4% of the 2-Z isomer and ≈3% of an unidentified more volatile impurity. The spectral data (^1H nmr, ir) were in accord with those reported (12).

*2,3-(−)-2,3-Epoxy-2-methyl-6-hepten-1-ol, (−)-****21***

A dry round-bottom flask (1 L) was charged with anhydrous CH_2Cl_2 (700 mL) and stirred in a Dry Ice − acetone bath until the temperature reached −30°C. Titanium tetraisopropoxide (30 mL, 28.6 g, 100 mmol) was then added, followed by (+)-diisopropyl tartrate (25 g, 107 mmol). After 10 min at −20 to −30°C, dienol **20** (12.6 g, 100 mmol) was added and, after a further 5 min, a 4 *M* anhydrous CH_2Cl_2 solution of *t*-BuOOH (50 mL, 200 mmol). After 2.5 h (−30°C freezer) gc analysis showed the absence of starting material. The cold reaction mixture was then poured in a thin stream into an ice-bath-cooled, rapidly stirred mixture of ether (750 mL) and 10% aqueous tartaric acid (250 mL). After stirring for 15 min in the ice bath, a clean separation into two clear layers could be achieved. The aqueous phase was further extracted with ether (2 × 100 mL) and the combined

Can. J. Chem. Downloaded from www.nrcresearchpress.com by 210.87.254.42 on 09/06/12
For personal use only.

organics washed with saturated $NaHCO_3$ solution (100 mL) and saturated NaCl solution (100 mL). After drying ($MgSO_4$), the solvents were removed on a rotary evaporator and the residue subjected to two successive vacuum distillations. In the first distillation, separation of most of the excess *t*-BuOOH and (+)-DIPT was achieved and the fraction containing the epoxide (bp 50−80°C/0.5 Torr) was redistilled to yield (−)-**21** (12.2 g, 86%; bp 52−54°C/0.2 Torr); $[\alpha]_D^{25}$ −4.4° (*c* 2.0, EtOH); ir (film): 3430(s), 3080(w), 3000(m), 2970(m), 2930(s), 2875(m), 1645(m), 1450(m), 1387(m), 1040(s), 917(m), 870(m) cm^{-1}; ^1H nmr δ: 1.29 (3H, C(2) methyl, s), 1.68(2H, C(4)H, m), 1.86 (1H, OH, br s), 2.25 (2H, C(5)H, m), 3.05 (1H, C(3)H, t, J = 6.25 Hz), 3.56 (1H, C(1)H, br dd, J = 12, 6 Hz), 3.69 (1H, C(1)H, d, J = 12 Hz), 5.00 (1H, C(7)H, d, J = 10.5 Hz), 5.06 (1H, C(7)H, d of q, J = 17, 2 Hz), 5.82 (1H, C(6)H, m, J_{trans} = 17 Hz, J_{cis} = 10.5 Hz, J_{vic} = 6 Hz); ms (EI): 67(35), 58(100), 57(85), 55(30), 43(71), 41(42); ms (isobutane CI): 143(47) (M^+ + 1). *Anal.* calcd. for $C_8H_{14}O_2$: C 67.57, H 9.92; found: C 67.39, H 10.05.

Preparation of the (+)-α-methoxytrifluoromethylphenyl acetate ((+)-MTPA ester) of (−)-**21** and of racemic **21** by the published method (19) and analysis of the differentially shifted diastereotopic C(1) methylene hydrogens by 400-MHz ^1H nmr gave 95 ± 1% ee for (−)-**21**.

2,3-(+)-2,3-Epoxy-2-methyl-6-hepten-1-ol, (+)-21

This material was described for (−)-**21** with the exception that (−)-DIPT was used in the asymmetric epoxidation to yield 84%, $[\alpha]_D^{25}$ +4.3 (*c* 2.2, EtOH) and 96 ± 1% ee by integration of the ^1H nmr of the (+)-MTPA ester as described above.

4-Methyl-4-(4-pentenyl)-2,2-dimethyl-1,3-dioxolane, 23

Lithium tetrahydridoaluminate (5.0 g, 130 mmol) was dissolved in anhydrous ether (300 mL) and the solution cooled with an ice bath while epoxide (−)-**21** (20.6 g, 145 mmol) dissolved in anhydrous ether (100 mL) was added dropwise over 1 h. The reaction was quenched by cautious sequential addition of water (5 mL), 15% aqueous NaOH (5 mL), and, finally, water (15 mL). Filtration and thorough extraction of the aluminum salts with additional ether (3 × 200 mL) followed by removal of the solvent provided diol *R*-**22** which was essentially pure by ^1H nmr δ: 1.17 (3H, C(2) methyl, s), 1.47 (4H, C(2)H, C(3)H, m), 2.05 (2H, C(5)H, q, J = 7 Hz), 2.13 (1H, C(2)OH, s), 2.37 (1H, C(1)OH, t, J = 6.5 Hz), 3.40 (1H, C(1)H, dd, J_{AB} = 11 Hz, J_{OH} = 6.5 Hz), 3.46 (1H, C(1)H, dd, J_{AB} = 11 Hz, J_{OH} = 6.5 Hz), 4.95 (1H, C(7)H, d of m, J_{cis} = 10 Hz), 5.01 (1H, C(7)H, d of q, J_{trans} = 17 Hz, $J_{gem,allylic}$ = 2 Hz), 5.78 (1H, C(6)H, 10 line multiplet, J_{trans} = 17 Hz, J_{cis} = 10 Hz, J_{vic} = 7 Hz).

The above diol was dissolved in 2,2-dimethoxypropane (50 mL) and stirred while *p*-toluenesulfonic acid (100 mg) was added. After 4 h at ambient temperature, the reaction mixture was diluted with ether (300 mL) and washed with saturated $NaHCO_3$ solution (50 mL). After drying with $MgSO_4$, filtration, and concentration *in vacuo*, the residue was distilled to yield *R*-**23** (23.9 g, 86% from **21**, bp 48−50°C/0.2 Torr); $[\alpha]_D^{25}$ ≈0 (*c* 5.4, EtOH); ir (film): 3070(w), 2980(s), 2930(s), 2860(s), 1640(m), 1455(m), 1375(s), 1370(s), 1245(s), 1210(s), 1115(m), 1060(s), 990(m), 910(s), 860(m), 805(m) cm^{-1}; ^1H nmr δ: 1.28 (3H, C(2) methyl, s), 1.39 (3H, CH_3, s), 1.41 (3H, CH_3, s), 1.53 (4H, C(3)C(4)H, m), 2.07 (2H, C(5)H, q, J = 6.5 Hz), 3.71 (1H, C(1)H, d, J_{AB} = 8.1 Hz), 3.79 (1H, C(1)H, d, J_{AB} = 8.1 Hz), 4.97 (1H, C(7)H, doublet of multiplets, J_{cis} = 10 Hz), 5.02 (1H, C(7)H, doublet of quartets, J_{trans} = 17 Hz, $J_{gem,allylic}$ = 2 Hz), 5.82 (1H,C(6)H, ten line multiplet, J_{cis} = 10 Hz, J_{trans} = 17 Hz, J_{vic} = 7 Hz); ms (EI): 169(100), 115(100), 109(97), 72(89), 67(54), 43(58); ms (isobutane CI): 185(100) (M^+ + 1). *Anal.* calcd. for $C_{11}H_{20}O_2$: C 71.69, H 10.94; found: C 71.98, H 11.25.

Preparation of S-23

Reduction of epoxide (+)-**21** and protection of the diol as the acetone ketal using the procedure described for the preparation of *R*-**23** yielded *S*-**23** in 85% yield; $[\alpha]_D^{25}$ −0.6 (*c* 5.7, EtOH). Spectral data for *S*-**23** were identical with those of *R*-**23**.

(2R)-4-Methyl-4-(3,4-epoxypentyl)-2,2-dimethyl-1,3-dioxolane, 24

Alkene *R*-**23** (23.0 g, 125 mmol) was dissolved in dry CH_2Cl_2 (300 mL) and stirred at ambient temperature while *meta*-chloroperoxybenzoic acid (28.0 g, 85% pure, 138 mmol) was added in small portions over 0.5 h. After 5 h, anhydrous KF (30 g, 0.52 mol) was added and stirring continued for a further 6 h (9). Insoluble material was removed by suction filtration and the filter cake washed with additional CH_2Cl_2 (3 × 100 mL). The combined CH_2Cl_2 solutions were concentrated to yield a 1:1 diastereomeric mixture of *R*-**24** as a colorless oil (24.8 g, 99%). An analytical sample was purified by bulb-to-bulb distillation (bath temperature 90−110°C/0.2 Torr); ir (film): 3043(w), 1458(m), 1380(s), 1370(s), 1250(s), 1213(5), 1120(m), 1060(s), 985(m), 915(m), 852(m), ms (EI) 185(72), 125(22), 115(93), 97(25), 81(41), 79(22), 72(100), 67(31), 57(38), 55(49), 43(90) cm^{-1}; ^1H nmr δ: 1.28 (3H, C(2) methyl, s), 1.38, 1.39 (6H, $2CH_3$, 2s), 1.56 (6H, C(3)C(4)C(5)H, m), 2.47 (1H, C(6)H, m), 2.75 (1H, C(7)H, t, J = 4.5 Hz), 2.92 (1H, C(7)H, br s), 3.70 (1H, C(1)H, d, J_{AB} = 8.3 Hz), 3.78, 3.79 (1H, C(1)H diastereomers, dd, J_{AB} = 8.3 Hz); ms (CI isobutane): 201 (M^+ + 1) (10). *Anal.* calcd. for $C_{11}H_{20}O_3$: C 69.97, H 10.07; found: 65.73, 9.85.

Preparation of 24

Epoxidation of *S*-**23**, as described above, yielded *S*-**24** quantitatively as a 1:1 diastereomeric mixture. Spectral data for *S*-**24** were identical with those of *R*-**24**.

(2R)-4-Methyl-4-(4-hydroxypentyl)-2,2-dimethyl-1,3-dioxolane, 25

Lithium tetrahydridoaluminate (4.5 g, 118 mmol) was added to dry ether (300 mL). With ice-bath cooling, a solution of *R*-**24** (23.8 g, 119 mmol) in dry Et_2O (100 mL) was added dropwise over 45 min. The cooling bath was removed and after 1 h at ambient temperature the reaction was quenched by the successive dropwise addition of water (4.5 mL), 15% NaOH (4.5 mL), and water (13.5 mL). Insoluble material was removed by suction filtration and the filter cake washed with additional ether (3 × 100 mL). Removal of the solvent *in vacuo* yielded a 50:50 diastereomeric mixture of *R*-**25** (24.0 g, 100%). An analytical sample was distilled (bulb-to-bulb, bath temperature 100−120°C/0.2 Torr); ir (film): 3420(m), 2980(s), 2870(m), 1457(m), 1375(s), 1245(m), 1215(s), 1125(m), 1060(s), 987(w); ^1H nmr δ: 1.18 (3H, C(2) methyl, d, J = 6.2 Hz), 1.26 (3H, CH_3, s), 1.36 (3H, CH_3, s), 1.44 (4H, C(3)C(4)H, m), 1.54 (2H, C(5)H, m), 1.70 (1H, OH, s), 3.69 (1H, C(1)H diastereomers, 2 doublets separated by 1.6 Hz, J = 8.3 Hz), 3.77 (1H, C(1)H diastereomers, 2 doublets separated by 1.6 Hz, J = 8.3 Hz), 3.81 (1H, C(6)H, m); ms (EI): 187(53), 127(32), 115(98), 109(100), 72(99), 47(35), 43(93); ms (CI isobutane): 203(8) (M^+ + 1). *Anal.* calcd. for $C_{11}H_{22}O_3$: C 65.31, H 10.96; found: C 65.20, H 11.20.

Preparation of 25

Lithium tetrahydridoaluminate reduction of *S*-**24** yielded *S*-**25** as a 1:1 diastereomeric mixture in 98% yield. Spectral data for *S*-**25** were identical with those of *R*-**25**.

(+)-Frontalin, 1

Alcohol *R*-**25** (23.0 g, 114 mmol) was dissolved in glacial acetic acid (100 mL). The solution was cooled in an ice bath and 5% aqueous NaOCl solution (160 mL, ≈130 mmol) was added dropwise over 0.5 h. After 18 h at ambient temperature and 5 h at 50°C, the reaction was diluted with water (400 mL) and extracted with ether (4 × 100 mL). The ether was washed with 5% aqueous NaOH solution until the washings were basic (4 × 80 mL), then with water (100 mL) and saturated NaCl solution (100 mL). After drying ($MgSO_4$), the extracts were concentrated to ≈50 mL by distillation of the solvent through a 30-cm Vigreux column at atmospheric pressure. The residue was fractionally distilled to yield *R*-**1** (12.4 g, 77%); bp 65−67°C/30 Torr; >98% pure by gc; $[\alpha]_D^{23}$ +50.7 (*c* 4.6, Et_2O). Infrared and ^1H nmr were in accord with the literature (5). The optical purity on the basis of the rotation, compared with the highest reported value (54.4°, reference (5)), was 93%. As confirmation, the nmr spectra of (±)-**1** and (+)-**1** were recorded in the presence of tris[3-trifluoromethylhydroxymethylene-*d*-camphorato]europium(III) shift re-

agent as described by Mori *et al.* (4). Inspection of the low field C(7) hydrogen showed a near baseline separation of the enantiomeric signals if the higher field C(7) hydrogen was simultaneously decoupled. Integration (cut and weigh) gave an estimated 89% ee.

Preparation of (−)-frontalin, 1

Alcohol *S*-**25** was oxidized and cyclized as described above to yield 74% of *S*-**1**; bp 66−67°C/30 Torr, $[\alpha]_D^{23}$ −52.9° (*c* 4.7, Et_2O). The optical purity of this material was estimated to be 97% ee by comparison of the observed rotation to that reported by Ohrui and Emoto (5).

1. B. D. JOHNSTON and A. C. OEHLSCHLAGER. J. Org. Chem. **47**, 5384 (1982).
2. T. KATSUKI and K. B. SHARPLESS. J. Am. Chem. Soc. **102**, 5974 (1980); V. S. MARTIN, S. S. WOODWARD, T. KATSUKI, Y. YAMADA, M. IKEDA, and K. B. SHARPLESS. J. Am. Chem. Soc. **103**, 6237 (1981).
3. *D. adjunctus*, P. R. HUGHES, J. A. A. RENWICK, and J. P. VITÉ. Environ. Entomol. **5**, 1165 (1976); *D. brevicomis*, D. L. WOOD, L. E. BROWNE, B. EWING, K. LINDAHL, W. D. BEDARD, P. E. TILDEN, K. MORI, G. B. PITMAN, and P. R. HUGHES. Science, **192**, 896 (1976); *D. frontalis*, J. A. A. RENWICK and J. P. VITÉ. Nature, **224**, 1222 (1969); *D. pseusotsugae*, G. B. PITMAN and J. P. VITÉ. Ann. Entomol. Soc. Am. **63**, 661 (1970); *D. rufipennis*, E. D. A. DYER. Can. Entomol. **107**, 979 (1975); *D. vitei*, J. A. A. RENWICK, P. R. HUGHES, and J. P. VITÉ. J. Insect Physiol. **21**, 1097 (1975).
4. G. W. KINZER, A. F. FENTIMAN, JR, T. F. PAGE, JR., R. L. FOLTZ, J. P. VITÉ, and G. B. PITMAN. Nature, **221**, 477 (1969); B. P. MUNDY, R. D. OTZENBERGER, and A. R. DE BERNARDIS. J. Org. Chem. **36**, 2390 (1971); T. D. D'SILVA and D. W. PECK. J. Org. Chem. **37**, 1828 (1972); K. MORI, S. KOBAYASHI, and M. MATSUI. Agric. Biol. Chem. **39**, 1889 (1975); J. KNOLLE and H. J. SCHÄFER. Angew. Chem. Int. Ed. Eng. **14**, 758 (1975); P. E. SUM and L. WEILER. Can. J. Chem. **57**, 1475 (1979); T. SATO, H. KANEKO, and S. YAMAGUCHI. J. Org. Chem. **45**, 3778 (1980); R. M. WILSON and J. W. REKERS. J. Am. Chem. Soc. **103**, 206 (1981).
5. K. MORI. Tetrahedron, **31**, 1381 (1975); H. OHURI and S. EMOTO. Agric. Biol. Chem. **40**, 2267 (1976); T. TADASHI, S. YAMAGUCHI, and H. KANEKO. Tetrahedron Lett. 1863 (1979); Y. SAKITO and T. MUKAIYAMA. Chem. Lett. 1027 (1979); F. COOKE, G. ROY, and P. MAGNUS. Organometallics, **1**, 893 (1982); S. JAROSZ, D. R. HICKS, and B. FRASER-REID. J. Org. Chem. **47**, 935 (1982); C. FUGANTI, P. GRASSELLI, and S. SERVI. J. Chem. Soc. Perkin Trans. I, 241 (1983); R. BARNER and J. HUBSCHER. Helv. Chim. Acta, **66**, 880 (1983); R. NAEF and D. SEEBACH. Justus Liebigs Ann. Chem. 1930 (1983).
6. M. A. UMBREIT and K. B. SHARPLESS. J. Am. Chem. Soc. **99**, 5526 (1977).
7. K. B. SHARPLESS, C. H. BEHRENS, T. KATSUKI, A. W. M. LEE, V. S. MARTIN, M. TAKATANI, S. M. VITI, F. J. WALKER, and S. S. WOODWARD. Pure Appl. Chem. **55**, 589 (1983); A. W. M. LEE. J. Chem. Soc. Chem. Commun. 578 (1984).
8. R. M. SILVERSTEIN, G. C. BASSLER, and T. C. MORRILL. Spectroscopic identification of organic compounds. 4th ed. J. Wiley and Sons, New York. 1981.
9. F. CAMPS, J. COLL, A. MESSEGUER, and M. A. PERICÀS. Tetrahedron Lett. **22**, 3895 (1981).
10. W. K. ANDERSON and T. VEYSOGLU. J. Org. Chem. **38**, 2267 (1973).
11. H. H. WASSERMAN and E. H. BARBER. J. Am. Chem. Soc. **91**, 3674 (1969).
12. C. CAHIEZ, A. ALEXAKIS, and J. F. NORMANT. Synthesis, 528 (1978).
13. N. T. BYROM, R. GRIGG, and B. KONG-RATHIP. J. Chem. Soc. Chem. Commun. 216 (1976).
14. M. ROUSSEL and H. MIMOUN. J. Org. Chem. **45**, 5387 (1980).
15. U. T. BHALERAO and H. RAPOPORT. J. Am. Chem. Soc. **93**, 4835 (1971).
16. W. G. TAYLOR. J. Org. Chem. **44**, 1020 (1979).
17. E. J. REIST, I. G. JUNGA, and B. R. BAKER. J. Org. Chem. **25**, 1673 (1960).
18. J. J. EISCH. Organometallic syntheses. Vol. 2. Non-transition-metal compounds. Academic Press, New York. 1981. p. 105.
19. J. A. DALE, D. L. DULL, and H. S. MOSHER. J. Org. Chem. **34**, 2543 (1969).

Can. J. Chem. Downloaded from www.nrcresearchpress.com by 210.87.254.42 on 09/06/12
For personal use only.

Thermodynamics of protonation of weak bases in H_2SO_4-H_2O media, determined using the excess acidity method

ROBIN A. COX AND KEITH YATES

Department of Chemistry, University of Toronto, 80 St. George St., Toronto, Ont., Canada M5S 1A1

Received June 20, 1983[1]

ROBIN A. COX and KEITH YATES. Can. J. Chem. **62**, 2155 (1984).

The excess acidity method has been used to investigate the thermodynamics of the protonation process for those weak bases for which the ionization ratios (or optical densities) at several temperatures have been measured in aqueous sulfuric acid. Standard enthalpies and entropies, at 25°C in the aqueous reference state, are given for thirteen primary, one secondary, and two tertiary nitroanilines, three cyanocompounds, thirteen triphenylmethanols, three other carbocation precursors, two ketones, nine pyridines, and nine azine *N*-oxides. Guidelines for estimating pK_{BH^+} at any temperature for other weak bases are discussed.

ROBIN A. COX et KEITH YATES. Can. J. Chem. **62**, 2155 (1984).

On a utilisé la méthode des acidités en excès pour étudier la thermodynamique du processus de protonation des bases faibles pour lesquelles les rapports d'ionisation (ou les densités optiques) ont été mesurés dans l'acide sulfurique aqueux, à diverses températures. On rapporte les enthalpies et les entropies standards, à 25°C et dans l'état de référence aqueux, de nitroanilines primaires (13), secondaire (1) et tertiaires (2), de cétones (2), de pyridines (9), de *N*-oxydes d'azines (9), de composés cyanés (3), de triphénylméthanols (13) et de trois autres précurseurs de carbocations. On discute des normes qu'il faut appliquer pour évaluer, à n'importe quelle température, les pK_{BH^+} d'autres bases faibles.

[Traduit par le journal]

Can. J. Chem. Downloaded from www.nrcresearchpress.com by 210.87.254.5 on 09/06/12
For personal use only.

Introduction

The excess acidity method for equilibria, reaction [1], involves the use of eq. [2] (1). Ionization ratios I of a weak base B are measured as a function of acid concentration, and these, with the proton concentration C_{H^+} and the excess acidity X (2, 3), give the intercept protonation acidity constant pK_{BH^+} defined for reaction [1].

$$[1]\quad B + H^+ \overset{K_{BH^+}}{\rightleftharpoons} BH^+$$

$$[2]\quad \log I - \log C_{H^+} = pK_{BH^+} + m^*X$$

$$[3]\quad ROH + H^+ \overset{K_{R^+}}{\rightleftharpoons} R^+ + H_2O$$

$$[4]\quad \log I - \log (C_{H^+}/C_{H_2O}) - 1.743 = pK_{R^+} + m^*X$$

The slope parameters m^* describe the protonation behaviour of B relative to the hypothetical standard base B* used in defining X (2), with values in sulfuric acid of 1.0 for primary aromatic amines, 1.4 for tertiary amines, 0.6 for amides, and so on (2). For the protonation–dehydration reaction [3] (H_R compounds (1)) the corresponding equation is eq. [4]. Here I is C_{R^+}/C_{ROH} and the 1.743 is included because definitions of K_{R^+} customarily do not include the water concentration (3); values of m^* of about 1.8 have been found for triarylcarbinols in aqueous HCl (3). The method has found widespread use for these equilibria, as has the corresponding method applied to reaction rates; many references are collected in ref. 1.

Often pK_{BH^+} values are needed at temperatures different from those at which they have been measured, for instance for kinetic studies. Common practice has been to use the same pK_{BH^+} regardless of temperature. Our more recent practice has been to assume that $\Delta S^0 = 0$ and to calculate $\Delta H^0/RT \ln 10 = \Delta G^0/RT \ln 10 = pK_{BH^+}$ at absolute temperature T (4–6), after finding experimentally that this worked well for methyl benzoate (4) (R is the gas constant). The purpose of this paper is to see if this practice is justified in general, and to calculate enthalpies and entropies of protonation in the aqueous standard state, by extrapolation, from existing ionization ratio data obtained as a function of temperature. Many of these data are provided by major studies of the variation of the H_0 (7, 8), H_R (9, 10), and H_A (11) acidity functions with temperature. The excess acidity X is easily corrected to different temperatures by taking advantage of its definition as a combination of transfer activity coefficients as discussed previously (4), by multiplying by the absolute temperature ratio: $X_T = 298.15X/T$. Thus X can be used at any temperature. This means that the hypothetical base B* used to define X (1) is now also defined as having $\Delta S^0 = 0$, and that the m^* slopes are temperature independent.

Experimental

In order to use eqs. [2] and [4], X was corrected to the measurement temperature as described above, and the existing log C_{H^+} values (1) were corrected using listed densities (12) and the method of Young *et al.* (13), which gives HSO_4^- concentrations in sulfuric acid at 0, 25, and 50°C. Unfortunately, this 1959 study is the only one available, but the correction is very small and could have been reasonably neglected (i.e., by using only the densities) without affecting the results. Water concentrations required for eq. [4] were also calculated from the solution densities (12).

$$[5]\quad pK_{BH^+} \text{ or } pK_{R^+} = \Delta G^0_{25°}/R\theta \ln 10 + \Delta H^0_{25°}/R\theta \ln 10 \times (\theta - T)/T$$

The method of Clarke and Glew (14) was used to express pK in terms of ΔG^0 and ΔH^0 as shown in eq. [5], as before (5). This has the advantage over the conventional expression in terms of ΔH^0 and ΔS^0 in that ΔG^0 and ΔH^0 are more easily and reliably separated (14); the values obtained are valid at the standard temperature θ of 298.15 K, or 25°C. ΔS^0 was calculated using $\Delta G^0 = \Delta H^0 - \theta\Delta S^0$. Equation [5] can be easily expanded to provide ΔC_p^0 and its derivatives (14), but this was found not to be justified by the data in the present work. Substitution of eq. [5] into eqs. [2] and [4] gives a double linear regression with variables X and $(\theta - T)/T$, which was solved by a suitably modified multiple linear regression program (15) on a Commodore PET microcomputer.

Log I data for the compounds studied came from the following sources. Major studies of many of the primary nitroanilines are by Johnson *et al.* at 25, 40, 60, 80, and 90°C (7), by Tickle, Briggs, and Wilson at 15, 25, 35, 45, and 55°C (8), and by Gel'bshtein and

[1] Revision received January 18, 1984.

Can. J. Chem. Downloaded from www.nrcresearchpress.com by 210.87.254.5 on 09/06/12
For personal use only.

co-workers at 20, 40, 60, and 80°C (16). Marcus' group report data at 25 and 60°C (17), and Boyd and Wang have studied 4-nitroaniline at 1, 10, 20, 25, 30, 40, and 50°C (18). Additional data at 25°C (19–24), 17°C (25), and "room temperature", taken as 22°C (26–28), are also available. The cyanocompounds have been studied by Boyd and Wang at −5, 1, 10, 20, 25, 40, and 50°C (18), and by Boyd at 25°C (29). Data for the pyridines and azine *N*-oxides at 25, 40, 60, 80, and 90°C have been reported by Dassanayake, of Johnson's group (11).

Optical density (D) measurements at 0, 15, 30, and 45°C are given by Arnett and Bushick (10) for nine triarylmethanols, two benzhydrols, hexamethylbenzene, xanthone, 4,4′-dimethoxybenzophenone, *N*-methyl-2-nitro-4-chloroaniline, and *N*,*N*-dimethyl-2,4,6-trinitroaniline. These data were curve fitted as described elsewhere (30) to give optimum values of D_B and D_{BH^+}, and ionization ratios calculated using $I = (D - D_B)/(D_{BH^+} - D)$. Interpolated log I values for thirteen triarylmethanols are given by Toone (9) at 25, 40, 60, 80, and 90°C; nine of these compounds were also studied by Arnett and Bushick (10). Bonner and Phillips (31) give log I values for 4,4′-dimethoxybenzophenone at 23°C, and Arnett and Mach (32) studied *N*,*N*-dimethyl-2,4,6-trinitroaniline at 26°C. Extensive optical density data provided by Vinnik's group (33) yielded log I values for *N*,*N*-dimethyl-2,4-dinitroaniline at 25, 40, 50, and 60°C; this compound was also studied at 25°C by Bascombe and Bell (19).

All of the log I data from the various sources, for each base, were amalgamated and treated together. The data were weighted using an error function given by Kresge and Chen (34), which ensured that log I values between ±1 received higher weighting, in accord with the sigmoid shapes of the original titration curves (34). Otherwise each data source was given equal priority. The computer program used rejected points which, to a 95% confidence level, did not belong in the data set (points in parentheses in Table 1 and Figs 1 and 2); this refers to any point falling more than about two standard deviations away from the best regression line, depending on the weighting. Less than 7.5% of the data points were rejected in this way. Full statistical information is given in Table 1.

Results

Table 1 lists all 55 compounds in the study, with their derived $\Delta G^0_{25°}$, $\Delta H^0_{25°}$, and $\Delta S^0_{25°}$ values. Also given are pK_{BH^+} at 25°C, and the m^* slopes. The experimental error of each of these is given as the standard deviation. Also listed are the number of data points per compound, together with the number rejected by the computer program (see Experimental), the multiple correlation coefficient and the root-mean-square error of the fit.

As an example chosen at random, the experimental data for 2,5-dichloro-4-nitroaniline (7, 8, 17, 26) are illustrated in Fig. 1. In this figure the lines for the different temperatures are separated for clarity; the intercepts range from −1.74 at 15°C to −1.70 at 90°C. As can be seen, the data (101 points in all) are fitted very well by the parameters in Table 1. No systematic departure from linearity is evident, and the same slope applies at all temperatures, as discussed above. Results obtained by the different groups agree quite well, on the whole (e.g. at 25°C), although the measurements by Marcus' group at 60°C (17) are somewhat divergent, as are the lowest points at the higher temperatures by Tickle *et al.* (8). In general divergent points tend to cancel out, as can be seen in Fig. 1 (six rejected points above the line, and six below).

Of the various possible linear correlations, perhaps the most useful is that of ΔG^0 against ΔH^0 (9, 11, 35), and one of these is given in Fig. 2, for the anilines. In addition to the Table 1 data, Fig. 2 includes results obtained in the pH region for 25 variously substituted anilines by Bolton and Hall (36–39), and by Liotta *et al.* (40). The data are represented by the line ΔH^0

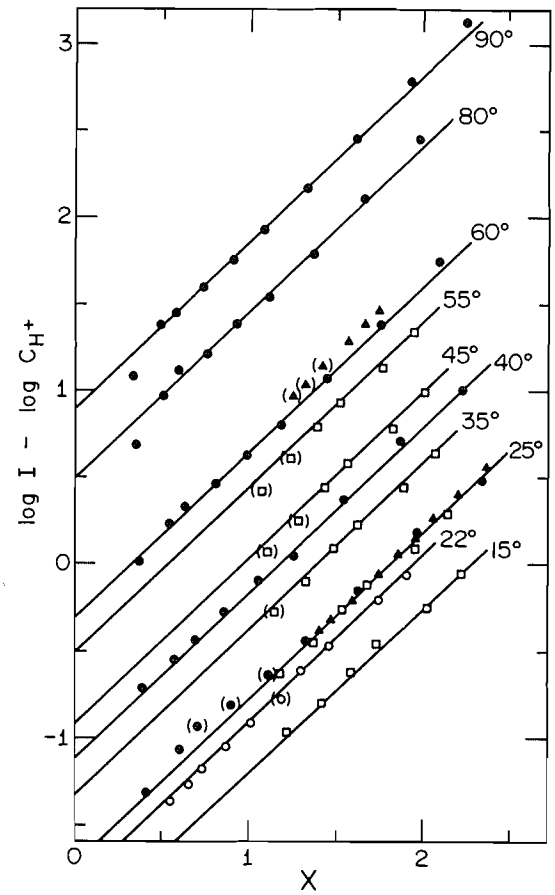

FIG. 1. Plots according to eq. [2] for 2,5-dichloro-4-nitroaniline. ●, ref. 7 (25, 40, 60, 80, and 90°C); □, ref. 8 (15, 25, 35, 45, and 55°C); ▲, ref. 17 (25 and 60°C); ○, ref. 26 (measurements at room temperature). The y-axis numbers refer to 25°C; all other lines are offset up or down, by amounts proportional to the measurement temperature, in order to avoid superimposition.

= (0.89 ± 0.01) ΔG^0 + (2.03 ± 0.06), with a root-mean-square error of 0.37 kcal/mol and a correlation coefficient of 0.997 over 38 points, one of which (that for 2,4,6-trinitroaniline) was rejected as being off the line. A similar plot for the triphenylmethanols, excluding those with the $^+NMe_3$ substituents, is ΔH^0 = (0.97 ± 0.07) ΔG^0 − (3.4 ± 0.6), σ_y = 1.05 kcal/mol, r = 0.979 (11 points). Plots for the other series of compounds were too scattered to be useful, particularly if literature data obtained for similar compounds in the pH region were included.

Discussion

The criterion for the rejection of anomalous data points used in this work is quite impartial. This is useful when measurements made by many different groups are combined, as is done here; each group naturally assumes that their results are accurate, and we should accept this and treat each measurement impartially. It was found, in fact, that very seldom were the results of one group systematically discarded because of disagreement with other workers, rejected points being scattered more or less at random. The example shown in Fig. 1 is typical. The primary data, i.e. the ionization ratios (or, better still, the original optical density data) as a function of acidity, are what can best be compared between the different groups. Agreement is, in general, excellent. However, because the pK_{BH^+} values

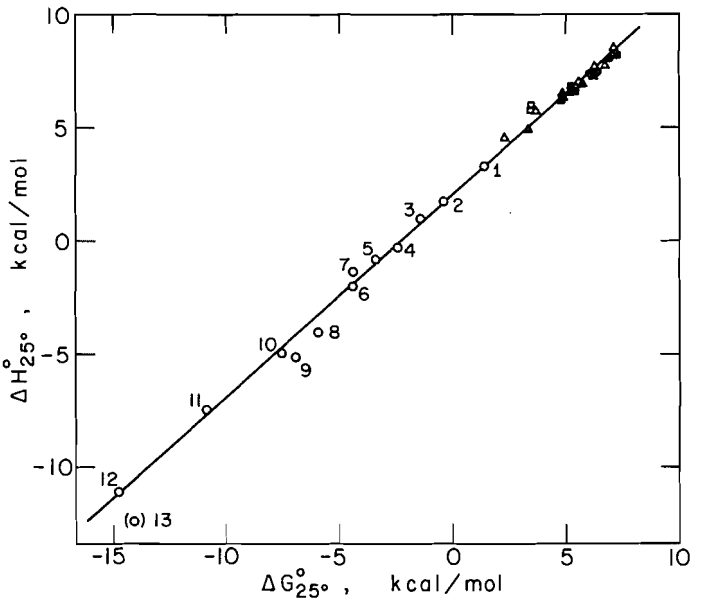

FIG. 2. Free energy/enthalpy plot for the protonation of substituted anilines. ○, this work (the numbers referring to Table 1); ●, aniline and *o*-, *m*-, and *p*-toluidine (36); ▲, *m*-OMe, Cl, Br, I, and NO_2 (37); ■, *p*-OMe, Cl, Br, and I (38); □, *o*-OMe, Cl, Br, and I (39); △, *m*- and *p*-Et, *m*- and *p*-OEt, *m*- and *p*-CN, and *m*- and *p*-F substituents (40).

obtained from this primary data are usually derived using different acidity functions, when ΔH^0 and ΔS^0 are in turn derived from pK_{BH^+} at different temperatures the numbers obtained by different groups are sometimes startlingly different. Arnett and Scorrano (41) have discussed this problem; a good example is the disagreement between refs. 9 and 10, discussed in ref. 9.

To illustrate that this is not a problem in this work, a "worst case" will be discussed. Combining the results obtained by Arnett and Bushick (10) and by Toone and co-workers (9) on the ionization of triarylmethanols could have presented problems; Bushick's data consist of optical density measurements with quite high random errors, and the log *I* values quoted by Toone and co-workers are interpolated to rounded sulfuric acid concentrations, meaning that much of the error information originally present is lost. As an example, after treatment as described here Toone's results for 4-methyltriphenylmethanol, taken alone, give $\Delta H^0 = -8.15 \pm 0.23$ kcal/mol and $\Delta S^0 = -4.1 \pm 0.8$ eu, $\sigma_y = \pm 0.052$, and $r = 0.992$ over 45 points, of which one was rejected. Bushick's data give $\Delta H^0 = -8.72 \pm 0.44$ and $\Delta S^0 = -6.8 \pm 1.6$; $\sigma_y = \pm 0.077$, and $r = 0.984$ over 32 points, five are rejected. The agreement is excellent and treatment of all of the data together gives the values in Table 1. In general, data for all nine compounds in both studies, when taken alone as described, gave results within two standard deviations of one another, and combination was possible in all but two cases. Thus the disagreement between the ΔG^0 and ΔH^0 values originally obtained by the two groups, discussed in ref. 9, is an artefact of the methods by which they were obtained. There is no disagreement.

Using the excess acidity method, and combining all of the data as described, means that the values in Table 1 should be much more reliable than those quoted by any one group of workers. They are in accord with reasonable expectations. For instance it is reasonable that the pK_{BH^+} of 2,4,6-trinitroaniline should be less than that of the 3-methyl derivative (electron donor) but more than that of the 3-bromo (electron acceptor). This is the order in which the excess acidity method gives them (ref. 2, Table 1), but not that given by the H_0 acidity function (7). It is also reasonable that ΔS^0 for the triphenylmethanols should be negative, since the reaction is bimolecular attack of water on a carbocation (reaction [3] in reverse), and that for the anilines should be positive, since the reaction is an acid dissociation (reaction [1] in reverse). Previous work gives positive ΔS^0 values in the latter case (35), but also mostly positive values for the former (9, 10). The data in Table 1 should refer only to the compounds themselves, since we have gone to some trouble to remove possible contributions caused by the changes of *X* and the H^+ and H_2O concentrations with temperature (see Experimental).

The numbers in Table 1 support the contention that the nitroanilines are a very "well-behaved" series of acidity indicators in sulfuric acid (2). The average m^* value is 1.01 ± 0.09 over 13 compounds. In contrast the other series of compounds have a much larger scatter, 1.86 ± 0.49 for twelve triarylmethanols (excluding the 4,4′,4″-trimethoxy compound, also found to be anomalous previously (3)), 0.96 ± 0.25 for seven pyridines, and 0.69 ± 0.14 for eight azine *N*-oxides (excluding pyridine 1-oxide).

By most criteria the free energy/enthalpy plot in Fig. 2 would be regarded as very good. The root-mean-square error of the fit, however, at 0.37 kcal/mol, is much larger than any of the errors in ΔH^0 found for these compounds (Table 1), and far larger still than the errors in the literature data (36–40). What this means is that these values should not be correlated by a line in the first place; the individual measurements are more accurate than the values predicted by the correlation. Thus, for the best results, thermodynamic parameters for compounds of interest should really be measured individually. Often this is not practical, however, and relationships such as Fig. 2 have been, are, and will be often used for estimates of thermodynamic parameters.

Figure 2 is a useful predictor for anilines, with the exception of 2,4,6-trinitroaniline. The reason for this exception is not clear, but it is interesting that the next weakest H_0 bases of the series used in really strong acids (27) are nitro-compounds, which presumably protonate on the nitro-group in media not that different from those in which trinitroaniline is assumed to protonate at NH_2. The slope of the line is significantly different from unity, which means that the agreement among the ΔS^0 values in Table 1, which average 8.3 ± 2.2 eu over the 13 anilines, is illusory rather than real.

The equation given for the triphenylmethanols, on the other hand, has a slope of unity within experimental error. Thus a reasonable estimate of ΔH^0 for these compounds could be obtained from ΔG^0 by assuming that a constant value of ΔS^0 applies to all of them. This value is -10.4 ± 3.3 eu, excluding the $^+NMe_3$-substituted compounds, clearly anomalous at -0.9 and $+6.4$ eu.

The pyridines and azine *N*-oxides show no clearly established trend. The slopes of free energy/enthalpy plots do not really differ from unity, and the ΔS^0 values do not really differ from zero ($+0.6 \pm 3.7$ and $+0.8 \pm 4.5$, respectively). It is clear from Table 1 that the term $T\Delta S^0$ becomes progressively less important the weaker the base, making the $\Delta S^0 = 0$ estimate more reasonable in stronger acids. For instance, for the nitroanilines $-T\Delta S^0$ is -2.47 ± 0.66 kcal/mol at 25°C, which makes only a small percentage contribution to ΔG^0 for the trinitroanilines, and for the triphenylmethanols it is +3.10

Can. J. Chem. Downloaded from www.nrcresearchpress.com by 210.87.254.5 on 09/06/12
For personal use only.

Can. J. Chem. Downloaded from www.nrcresearchpress.com by 210.87.254.5 on 09/06/12
For personal use only.

TABLE 1. Thermodynamic data for the protonation of some weak bases in sulfuric acid

Compound	No.[a]	r^b	$\pm\sigma_v{}^c$	m^*	pK_{BH^+}, 25°C	$\Delta G^0{}_{25°}{}^d$	$\Delta H^0{}_{25°}{}^d$	$\Delta S^0{}_{25°}{}^e$
Primary nitroanilines								
1, 4-NO_2-aniline (An)	290(25)	0.992	0.020	1.13 ± 0.02	1.023 ± 0.002	1.3956 ± 0.0023	3.374 ± 0.028	6.63 ± 0.09
2, 2-NO_2-An	194(12)	0.989	0.026	0.96 ± 0.01	−0.253 ± 0.004	−0.3447 ± 0.0054	1.804 ± 0.040	7.21 ± 0.14
3, 4-Cl-2-NO_2-An	135(18)	0.997	0.020	1.033 ± 0.007	−1.039 ± 0.006	−1.4178 ± 0.0082	1.019 ± 0.039	8.17 ± 0.14
4, 2,5-Di-Cl-4-NO_2-An	101(12)	0.997	0.029	0.953 ± 0.009	−1.73 ± 0.01	−2.365 ± 0.017	−0.252 ± 0.062	7.09 ± 0.22
5, 2-Cl-6-NO_2-An	47(3)	0.995	0.038	1.40 ± 0.02	−2.48 ± 0.03	−3.390 ± 0.037	−0.83 ± 0.11	8.60 ± 0.38
6, 2,4-Di-Cl-6-NO_2-An	99(7)	0.992	0.043	1.05 ± 0.01	−3.21 ± 0.03	−4.378 ± 0.044	−2.05 ± 0.11	7.81 ± 0.40
7, 2,6-Di-Cl-4-NO_2-An	87(5)	0.992	0.049	1.00 ± 0.01	−3.21 ± 0.03	−4.384 ± 0.047	1.33 ± 0.10	10.24 ± 0.38
8, 2,4-Di-NO_2-An	141(14)	0.993	0.048	1.03 ± 0.01	−4.33 ± 0.04	−5.912 ± 0.050	−3.980 ± 0.095	6.48 ± 0.36
9, 2,6-Di-NO_2-An	105(4)	0.986	0.069	0.95 ± 0.02	−5.05 ± 0.07	−6.889 ± 0.093	−5.11 ± 0.16	5.97 ± 0.63
10, 2-Br-4,6-di-NO_2-An	136(14)	0.988	0.066	0.82 ± 0.01	−5.52 ± 0.07	−7.534 ± 0.090	−4.88 ± 0.14	8.89 ± 0.57
11, 3-Me-2,4,6-tri-NO_2-An	111(7)	0.996	0.049	0.985 ± 0.009	−8.20 ± 0.07	−11.183 ± 0.091	−7.40 ± 0.13	12.70 ± 0.52
12, 3-Br-2,4,6-tri-NO_2-An	61(3)	0.993	0.078	1.18 ± 0.02	−10.82 ± 0.17	−14.76 ± 0.23	−11.14 ± 0.26	12.1 ± 1.2
13, 2,4,6-Tri-NO_2-An	145(8)	0.991	0.101	1.04 ± 0.01	−10.35 ± 0.11	−14.12 ± 0.15	−12.33 ± 0.23	5.99 ± 0.92
Other nitroanilines								
14, *N*-Me-4-Cl-2-NO_2-An	18(1)	0.994	0.033	1.32 ± 0.04	−1.51 ± 0.03	−2.066 ± 0.044	−1.44 ± 0.23	2.11 ± 0.79
15, *N*,*N*-Di-Me-2,4-di-NO_2-An	91(3)	0.998	0.020	1.39 ± 0.01	−1.225 ± 0.007	−1.6708 ± 0.0095	−0.175 ± 0.069	5.02 ± 0.24
16, *N*,*N*-Di-Me-2,4,6-tri-NO_2-An	28(4)	0.987	0.082	1.32 ± 0.05	−5.84 ± 0.17	−7.97 ± 0.23	−9.17 ± 0.70	−4.0 ± 2.5
Cyanocompounds								
17, 4-(Tricyanovinyl)phenyldicyanomethane	102(13)	0.978	0.024	1.30 ± 0.03	0.320 ± 0.004	0.4366 ± 0.0058	−0.881 ± 0.053	−4.42 ± 0.18
18, Methyl dicyanoacetate	40(2)	0.998	0.026	1.23 ± 0.01	−2.83 ± 0.02	−3.867 ± 0.028	−4.03 ± 0.11	−0.56 ± 0.39
19, Bis(tricyanovinyl)amine	40(3)	0.997	0.036	0.79 ± 0.01	−4.44 ± 0.05	−6.052 ± 0.064	−6.26 ± 0.16	−0.69 ± 0.58
Triphenylmethanols								
20, 4,4′,4″-Tri-OMe-TPM	92(4)	0.909	0.064	0.63 ± 0.17	0.78 ± 0.01	1.605 ± 0.015	−2.44 ± 0.12	−11.74 ± 0.41
21, 4,4′-Di-OMe-TPM	116(11)	0.986	0.057	2.17 ± 0.04	−1.16 ± 0.02	−1.584 ± 0.024	−6.20 ± 0.11	−15.48 ± 0.38
22, 4-OMe-TPM	96(10)	0.990	0.060	1.96 ± 0.03	−3.11 ± 0.04	−4.239 ± 0.052	−6.22 ± 0.16	−6.65 ± 0.57
23, 4,4′Di-Me-TPM	69(4)	0.995	0.033	2.24 ± 0.03	−4.60 ± 0.05	−6.275 ± 0.064	−9.29 ± 0.13	−10.10 ± 0.47
24, 4-Me-TPM	77(7)	0.990	0.060	2.09 ± 0.04	−5.02 ± 0.07	−6.848 ± 0.099	−8.12 ± 0.20	−4.25 ± 0.73
25, Triphenylmethanol (TPM)	41(1)	0.983	0.078	2.04 ± 0.06	−6.47 ± 0.17	−8.83 ± 0.23	−11.54 ± 0.44	−9.1 ± 1.7
26, 4,4′-Di-NO_2-TPM	69(6)	0.940	0.152	1.09 ± 0.05	−7.18 ± 0.28	−9.80 ± 0.39	−13.31 ± 0.64	−11.8 ± 2.5
27, 4,4′-Di-($^+NMe_3$)-TPM	35(2)	0.992	0.059	1.30 ± 0.03	−7.70 ± 0.15	−10.50 ± 0.20	−10.78 ± 0.40	−0.9 ± 1.5
28, 4-NO_2-TPM	80(8)	0.966	0.125	2.11 ± 0.07	−8.49 ± 0.23	−11.59 ± 0.32	−15.60 ± 0.53	−13.5 ± 2.1
29, 3,3′,3″-Tri-Cl-TPM	38(0)	0.994	0.045	1.72 ± 0.03	−8.70 ± 0.13	−11.86 ± 0.18	−14.44 ± 0.29	−8.7 ± 1.2
30, 4,4′,4″-Tri-Cl-TPM	36(0)	0.996	0.038	2.77 ± 0.05	−9.35 ± 0.13	−12.76 ± 0.18	−16.82 ± 0.30	−13.6 ± 1.2
31, 4,4′,4″-Tri-NO_2-TPM	59(5)	0.961	0.124	1.15 ± 0.05	−10.56 ± 0.35	−14.40 ± 0.48	−17.11 ± 0.75	−9.1 ± 3.0
32, 4,4,4″-Tri-($^+NMe_3$)-TPM	35(4)	0.997	0.033	1.68 ± 0.03	−13.38 ± 0.18	−18.25 ± 0.25	−16.34 ± 0.29	6.4 ± 1.3

Can. J. Chem. Downloaded from www.nrcresearchpress.com by 210.87.254.5 on 09/06/12
For personal use only.

TABLE 1. (*Concluded*)

Compound	No.[a]	r[b]	$\pm\sigma_y$[c]	m*	pK_{BH^+}, 25°C	$\Delta G^0_{25°}$[d]	$\Delta H^0_{25°}$[d]	$\Delta S^0_{25°}$[e]
Other carbocation precursors								
33, Xanthydrol	32(4)	0.998	0.013	1.94 ± 0.03	−0.805 ± 0.009	−1.098 ± 0.012	−3.642 ± 0.062	−8.53 ± 0.21
34, 4,4′-Di-OMe-benzhydrol	32(2)	0.992	0.054	1.86 ± 0.05	−4.91 ± 0.10	−6.70 ± 0.13	−6.82 ± 0.27	−0.4 ± 1.0
35, Hexamethylbenzene	12(1)	0.993	0.089	1.71 ± 0.07	−14.65 ± 0.60	−19.98 ± 0.81	−19.8 ± 1.3	0.7 ± 5.0
Ketones								
36, Xanthone	39(3)	0.942	0.133	0.61 ± 0.04	−3.24 ± 0.13	−4.42 ± 0.18	−3.58 ± 0.54	2.8 ± 1.9
37, 4,4′-Di-OMe-benzophenone	44(3)	0.963	0.112	0.72 ± 0.03	−3.45 ± 0.11	−4.70 ± 0.15	−3.56 ± 0.46	3.85 ± 0.59
Pyridines								
38, 3-Cl-pyridine (Py)	30(1)	0.970	0.032	1[f]	2.84 ± 0.01	3.872 ± 0.014	2.56 ± 0.12	−4.41 ± 0.41
39, 2-Cl-Py	30(3)	0.382	0.103	1[f]	1.25 ± 0.03	1.711 ± 0.045	0.84 ± 0.38	−2.9 ± 1.3
40, 2,4-Di-Cl-Py	20(1)	0.972	0.070	0.94 ± 0.06	−1.21 ± 0.05	−1.653 ± 0.070	−2.68 ± 0.33	−3.5 ± 1.1
41, 2,6-Di-Cl-Py	20(2)	0.994	0.043	1.45 ± 0.04	−3.36 ± 0.08	−4.58 ± 0.10	−3.66 ± 0.22	3.10 ± 0.83
42, 2-NO_2-Py	30(2)	0.941	0.135	0.70 ± 0.05	−2.07 ± 0.11	−2.82 ± 0.14	−1.37 ± 0.51	4.9 ± 1.8
43, 2,3,4,5-Tetra-Cl-Py	35(3)	0.991	0.054	1.06 ± 0.03	−3.28 ± 0.06	−4.470 ± 0.081	−3.34 ± 0.20	3.79 ± 0.72
44, 2-F-6-Cl-Py	30(3)	0.984	0.074	0.97 ± 0.04	−3.70 ± 0.10	−5.05 ± 0.13	−5.21 ± 0.33	−0.5 ± 1.2
45, Penta-Cl-Py	35(1)	0.970	0.113	0.85 ± 0.04	−5.13 ± 0.19	−7.00 ± 0.25	−5.55 ± 0.48	4.9 ± 1.8
46, 2,3,4,5-Tetra-Cl-6-F-Py	45(4)	0.984	0.093	0.78 ± 0.02	−6.26 ± 0.15	−8.54 ± 0.21	−8.44 ± 0.39	0.3 ± 1.5
Azine N-oxides								
47, Pyridine 1-oxide (Py 1-Ox)	55(3)	0.979	0.019	1.77 ± 0.09	0.691 ± 0.006	0.9433 ± 0.0082	−1.705 ± 0.057	−8.88 ± 0.19
48, 3,5-Di-Me-4-NO_2-Py 1-Ox	85(4)	0.984	0.028	0.69 ± 0.01	−0.514 ± 0.008	−0.701 ± 0.011	−1.119 ± 0.064	−1.40 ± 0.22
49, 3,5-Di-Cl-Py 1-Ox	85(3)	0.997	0.015	0.668 ± 0.006	−0.807 ± 0.005	−1.1009 ± 0.0071	−1.135 ± 0.036	−0.11 ± 0.12
50, 3,5-Di-OMe-2-NO_2-Py 1-Ox	55(3)	0.970	0.070	0.70 ± 0.03	−1.61 ± 0.03	−2.196 ± 0.048	−1.71 ± 0.21	1.64 ± 0.73
51, 2,6-Di-Cl-Py 1-Ox	55(4)	0.997	0.025	0.536 ± 0.006	−1.90 ± 0.01	−2.599 ± 0.019	−2.585 ± 0.076	0.05 ± 0.26
52, Penta-Cl-Py 1-Ox	45(3)	0.984	0.058	0.48 ± 0.01	−2.20 ± 0.04	−3.002 ± 0.054	−2.72 ± 0.19	0.96 ± 0.67
53, 4-Methylquinazoline 3-oxide	40(4)	0.992	0.056	0.93 ± 0.02	−5.06 ± 0.09	−6.90 ± 0.12	−5.13 ± 0.23	5.93 ± 0.87
54, 2,3,5,6-Tetra-Me-pyrazine 1,4-dioxide	40(1)	0.986	0.049	0.76 ± 0.02	−5.02 ± 0.11	−6.85 ± 0.15	−4.90 ± 0.21	6.54 ± 0.87
55, Phenazine 5-oxide	45(2)	0.971	0.095	0.73 ± 0.03	−5.22 ± 0.16	−7.12 ± 0.22	−6.27 ± 0.36	2.9 ± 1.4

[a] Total number of experimental values; the number of these rejected as not being part of the data set, to 95% confidence, is in parentheses.
[b] Multiple correlation coefficient.
[c] Root-mean-square error of the fit.
[d] In kcal/mol.
[e] In entropy units.
[f] m = 1 because the acidity range covered is in the pH region.

± 0.98, also a small percentage contribution.

It must be concluded, however, that there is no substitute for the experimental determination of the thermodynamic behaviour of individual compounds. In cases where this is impossible or impractical, the results quoted in Table 1 and the free energy/enthalpy correlations may prove useful. It appears in general that the assumption that $\Delta G^0 = \Delta H^0$ is no better and no worse than other common assumptions, but that it does become a better one as the base becomes weaker.

Acknowledgements

We would like to thank Professors E. M. Arnett, C. D. Johnson, and A. J. Kresge for helpful discussions, and for providing unpublished ionization ratio data from theses. Financial support by the Natural Sciences and Engineering Research Council of Canada is gratefully acknowledged.

1. R. A. Cox and K. Yates. Can. J. Chem. **61**, 2225 (1983).
2. R. A. Cox and K. Yates. J. Am. Chem. Soc. **100**, 3861 (1978).
3. R. A. Cox and K. Yates. Can. J. Chem. **59**, 2116 (1981).
4. R. A. Cox, M. F. Goldman, and K. Yates. Can. J. Chem. **57**, 2960 (1979).
5. R. A. Cox and K. Yates. Can. J. Chem. **59**, 2853 (1981).
6. R. A. Cox and K. Yates. Can. J. Chem. **60**, 3061 (1982).
7. C. D. Johnson, A. R. Katritzky, and S. A. Shapiro. J. Am. Chem. Soc. **91**, 6654 (1969).
8. P. Tickle, A. G. Briggs, and J. M. Wilson. J. Chem. Soc. B, 65 (1970).
9. M. J. Cook, N. L. Dassanayake, C. D. Johnson, A. R. Katritzky, and T. W. Toone. J. Am. Chem. Soc. **97**, 760 (1975); T. W. Toone. Ph. D. Thesis, University of East Anglia. 1972.
10. E. M. Arnett and R. D. Bushick. J. Am. Chem. Soc. **86**, 1564 (1964); R. D. Bushick. Ph.D. Thesis, University of Pittsburgh. 1961.
11. M. J. Cook, N. L. Dassanayake, C. D. Johnson, A. R. Katritzky, and T. W. Toone. J. Chem. Soc. Perkin Trans. II, 1069 (1974); N. L. Dassanayake. Ph.D. Thesis, University of East Anglia. 1973.
12. International critical tables. Vol. 3. McGraw-Hill, New York. 1930. p. 35.
13. T. F. Young, L. F. Maranville, and H. M. Smith. *In* The structure of electrolytic solutions. *Edited by* W. J. Hamer. Wiley, New York. 1959. p. 35.
14. E. C. W. Clarke and D. N. Glew. Trans. Faraday Soc. **62**, 539 (1966).
15. P. R. Bevington. Data reduction and error analysis for the physical sciences. McGraw-Hill, New York. 1969. pp. 171–176.
16. A. I. Gel'bshtein, G. G. Shcheglova, and M. I. Temkin. Zh. Neorg. Khim. **1**, 506 (1956); Russ. J. Inorg. Chem. **1**(3), 167 (1956).
17. Y. Marcus, E. Pross, and N. Soffer. J. Phys. Chem. **84**, 1725 (1980).
18. R. H. Boyd and C.-H. Wang. J. Am. Chem. Soc. **87**, 430 (1965).
19. K. N. Bascombe and R. P. Bell. J. Chem. Soc. 1096 (1959).
20. R. H. Boyd. J. Am. Chem. Soc. **85**, 1555 (1963).
21. R. S. Ryabova, I. M. Medvetskaya, and M. I. Vinnik. Zh. Fiz. Khim. **40**, 339 (1966); Russ. J. Phys. Chem. **40**, 182 (1966).
22. A. J. Kresge, H. J. Chen, G. L. Capen, and M. F. Powell. Can. J. Chem. **61**, 249 (1983); A. J. Kresge, H. J. Chen, and Y. Chiang. J. Chem. Soc. Chem. Commun. 969 (1972); H. J. Chen. Ph.D. Thesis, Illinois Institute of Technology. 1970.
23. M. I. Vinnik and N. B. Librovich. Tetrahedron, **22**, 2945 (1966).
24. M. I. Vinnik and R. S. Ryabova. Zh. Fiz. Khim. **38**, 606 (1964); Russ. J. Phys. Chem. **38**, 320 (1964).
25. N. M. Milyaeva. Zh. Neorg. Khim. **3**, 2011 (1958); Russ. J. Inorg. Chem. **3**(9), 27 (1958).
26. M. J. Jorgenson and D. R. Hartter. J. Am. Chem. Soc. **85**, 878 (1963).
27. R. J. Gillespie, T. E. Peel, and E. A. Robinson. J. Am. Chem. Soc. **93**, 5083 (1971).
28. B. Torck, M. Hellin, and F. Coussemant. Bull. Soc. Chim. Fr. 1657 (1962).
29. R. H. Boyd. J. Phys. Chem. **67**, 737 (1963).
30. R. A. Cox and K. Yates. Can. J. Chem. **59**, 1560 (1981).
31. T. G. Bonner and J. Phillips. J. Chem. Soc. B, 650 (1966).
32. E. M. Arnett and G. W. Mach. J. Am. Chem. Soc. **86**, 2671 (1964).
33. I. S. Kislina, N. B. Librovich, and M. I. Vinnik. Zh. Fiz. Khim. **53**, 1523 (1979); Russ. J. Phys. Chem. **53**, 858 (1979); N. B. Librovich, Yu. K. Karasevich, and M. I. Vinnik. Zh. Fiz. Khim. **46**, 2343 (1972); Russ. J. Phys. Chem. **46**, 1336 (1972).
34. A. J. Kresge and H. J. Chen. Anal. Chem. **41**, 74 (1969).
35. P. D. Bolton, C. D. Johnson, A. R. Katritzky, and S. A. Shapiro. J. Am. Chem. Soc. **92**, 1567 (1970).
36. P. D. Bolton and F. M. Hall. Aust. J. Chem. **20**, 1797 (1967).
37. P. D. Bolton and F. M. Hall. Aust. J. Chem. **21**, 939 (1968).
38. P. D. Bolton and F. M. Hall. J. Chem. Soc. B, 259 (1969).
39. P. D. Bolton and F. M. Hall. J. Chem. Soc. B, 1047 (1969).
40. C. L. Liotta, E. M. Perdue, and H. P. Hopkins. J. Am. Chem. Soc. **95**, 2439 (1973).
41. E. M. Arnett and G. Scorrano. Adv. Phys. Org. Chem. **13**, 83 (1976).

Can. J. Chem. Downloaded from www.nrcresearchpress.com by 210.87.254.5 on 09/06/12
For personal use only.

The interactions of the chloride and bromide ions in nematic lyotropic liquid crystalline solution

ALAN S. TRACEY

Department of Chemistry, Simon Fraser University, Burnaby, B.C., Canada V5A 1S6

Received February 22, 1984

ALAN S. TRACEY. Can. J. Chem. **62**, 2161 (1984).

The binding interactions of chloride and bromide ions have been studied in nematic lyotropic liquid crystalline materials prepared using the mixed detergent system of potassium dodecanoate/dodecylpyridinium chloride. The results from this study show that a three-site model of binding is sufficient to describe the behaviour of the observed quadrupole splittings. The results clearly reveal that the selectivity of ion binding is a function not only of the counterion but also of the detergent ion to which it is bound. In the cationic mesophase prepared from decylpyridinium, Cl^- binds simultaneously to two and Br^- to three headgroups. This contrasts with the alkyltrimethylammonium bromide system, where Cl^- binds to three cationic amphiphiles while Br^- binds to two. Sodium ion appears indifferent to the type of cationic detergent present, a result in accordance with the expectation that its binding is determined only by the headgroup of the anionic detergent. Extension of the three-site theory to take into account the effect of surface charge on ion binding provides information concerning relative strengths of binding. In the dodecylpyridinium system Cl^- binds only weakly compared to Br^- whereas in the alkyltrimethylammonium system Cl^- binds more strongly than Br^-. K^+ binds most strongly to dodecanoate anion, Cs^+ least strongly, and the other alkali metal ions occupy intermediate positions.

ALAN S. TRACEY. Can. J. Chem. **62**, 2161 (1984).

On a étudié les interactions de liaison des ions chlorure et bromure dans des cristaux liquides lyotropes nématiques préparés en utilisant un système de détergent mixte à base de dodécanoate de potassium et de chlorure de dodécylpyridinium. Les résultats de cette étude montrent qu'un modèle de liaison par trois sites suffit pour décrire le comportement des couplages quadrupolaires observés. Les résultats révèlent clairement que la sélectivité de la liaison de l'ion dépend non seulement de l'ion opposé mais aussi de l'ion du détergent auquel il est lié. Dans la mésophase cationique préparée à partir du décylpyridinium, l'ion Cl^- se lie simultanément à deux groupes de tête alors que l'ion Br^- se lie à trois groupes de tête. Ce comportement est en opposition ave celui observé avec le système du bromure d'alkylméthylammonium dans lequel les ions Cl^- se lient à trois amphiphiles cationiques tandis que les ions Br^- se lient à deux amphiphiles cationiques. Les ions sodium semblent être indifférents au type de détergent cationique présent; c'est un résultat qui s'accorde avec l'hypothèse d'après l'aquelle sa liaison ne serait déterminée que par le groupe de tête du détergent anionique. L'extension de la théorie à trois sites, pour tenir compte de l'effet de la charge de surface sur la liaison de l'ion, fournit des informations concernant les forces relatives de liaison. Par opposition à l'ion Br^-, l'ion Cl^- ne se lie que faiblement dans le système dodécylpyridinium alors que c'est le contraire dans le système alkyltriméthylammonium. Vis-à-vis l'anion dodécanoate, le cation K^+ est celui qui se lie le plus fortement alors que l'ion Cs^+ est celui qui se lie le plus faiblement; les ions des autres métaux alcalins occupent des positions intermédiaires.

[Traduit par le journal]

Introduction

The binding of ions to the polar groups of amphiphilic compounds is a subject of continuing interest and of great importance in various areas of chemistry and biochemistry (1–12). Unfortunately, as is often the case with biological systems, studies are hampered by the extreme complexity of the system being studied. For the particular case of ion binding a further impediment often encountered is that the details of the stereochemical requirements which are imposed on a substrate by the ion during binding interactions are not known. A study of simple systems can often provide the background information necessary for understanding the more complex systems.

A particularly suitable medium for studying ion interactions is that of lyotropic liquid crystals. Of these materials, those which have the property of spontaneously aligning in the magnetic field of a nuclear magnetic resonance spectrometer provide distinct advantages, the most important one being "sharp" nmr transitions, which result from the fact that the mesophase directors are aligned homogeneously by the magnetic field of the spectrometer (13).

Of particular utility in the study of ion binding is the mixed detergent system prepared from potassium dodecanoate (potassium laurate) and alkyltrimethylammonium bromide. This system has the advantage in that, under the appropriate conditions, the potassium dodecanoate can be replaced in a stepwise fashion by alkyltrimethylammonium bromide, thus progressing from the extreme of an anionic mesophase to that of a cationic mesophase (14, 15). Using this liquid crystalline system, in conjunction with the appropriate ions as additives, it was possible to show that there were distinct differences in the binding behaviour of the alkali ions to the dodecanoate ion throughout the series lithium to cesium. It was also possible to develop a picture of the binding sites specific to each ion. Similarly, a description of the binding of the halide ions, Cl^- and Br^-, to the trimethylammonium group was obtained (16).

It was found that the chloride ion binds differently from bromide, with the former ion simultaneously binding to three trimethylammonium headgroups while bromide binds simultaneously to only two. It was suggested that this occurred because of the interplay between electrostatic and steric forces. The trimethylammonium group is very bulky with the major charge-carrying species, the nitrogen, well shielded by the four alkyl groups. Since binding in such circumstances is probably significantly different from, say, nitrogen in an aromatic heterocyclic system it was decided to look at halide binding to the pyridinium group of the dodecylpyridinium detergent.

Unfortunately, because of the mesophase instability problems often encountered when anionic detergents are replaced with cationic detergents in a stepwise procedure, one is highly restricted to the systems which can be used. Undoubtedly, the list will be expanded from the two systems now known, potassium dodecanoate/*n*-alkyltrimethylammonium bromide (alkyl:

Can. J. Chem. Downloaded from www.nrcresearchpress.com by 210.87.254.40 on 09/06/12
For personal use only.

Can. J. Chem. Downloaded from www.nrcresearchpress.com by 210.87.254.40 on 09/06/12
For personal use only.

C_{10}, C_{12}, C_{14}, C_{16}) (14) and the present potassium dodecanoate/dodecylpyridinium chloride. The advantage of these mixed systems is that, by progressively changing the surface charge carried by the hydrocarbon superstructure, sites of one kind or another are being created or destroyed. From the binding model adopted, the behaviour of various physical parameters as a function of surface charge (mole fraction of either amphiphile in total amphiphile) can be predicted. With the adoption of a reasonable model of ion binding, the experimental results can be used both to support the model and to suggest refinements to it.

The physical parameter of interest in this study is the quadrupole splittings from the $^{35}Cl^-$ and $^{81}Br^-$ nuclei. This splitting is determined by the nuclear electric quadrupole moment of the nucleus and the alignment of electric field gradients, with which the quadrupole moment interacts, in the magnetic field of the nmr spectrometer.

The quadrupole splitting, $\Delta\nu$, is given by eq. [1],

$$[1] \qquad \Delta\nu = \frac{3QS}{2I(2I-1)}$$

where Q is the quadrupole coupling constant and S is the order parameter. I is the nuclear spin angular momentum, equal to 3/2 for both $^{35}Cl^-$ and $^{81}Br^-$. In the circumstance that the ion is undergoing rapid exchange between various binding sites, the observed splitting, $\Delta\nu$, is a weighted average of the splitting from the various sites; that is, the splitting is given by eq. [2],

$$[2] \qquad \Delta\nu = \sum_i \Delta\nu_i X_i$$

where X_i is the mole fraction of nuclei in site i and $\Delta\nu_i$ is the splitting characteristic for that site. In the previous study of ion binding it was found that consideration of averaging of the quadrupolar nucleus between three sites was sufficient to provide good agreement between calculated and observed quadrupole splittings and to account well for the bulk of experimental results. The present results show that some refinements to this model of ion binding are required.

In this three-site model of binding, the first site, site I, is taken to correspond to the counterion being bound, presumably through its hydration sphere, to n amphiphiles, where n ranges from 2 to 4. With partial replacement of this amphiphile by ones of opposite charge, sites of type I are destroyed and sites for binding of a second type, site II, in which the counterion binds to only one amphiphile, are created. The third site, site III, corresponds to counterions not bound to amphiphiles, although long range interactions with the micellar surface are occurring. This last site may correspond to free ions in the water located between the micellar elements which cause the formation of the liquid crystalline material. This interstitial water is expected to be essentially isotropic in nature.

Experimental

Potassium dodecanoate was prepared from dodecanoic acid by neutralization with KOH followed by recrystallization several times from ethanol (95%). Dodecylpyridinium chloride was prepared similarly to that previously described for hexadecylpyridinium chloride (17).

The lyotropic mesophases used in this study had the general molar composition: total detergent/salt/D_2O/decanol, 1.00/0.39/28.3–33.3/0.0–0.32. The percentage of potassium dodecanoate in total detergent was varied from 10 to 100% on a molar basis. With the above general composition, dodecylpyridinium chloride did not form the desired mesophase when it was used without at least 10 mol% of the potassium dodecanoate combined with it. The mesophase could be obtained with other compositions. A mesophase formation problem was also encountered at 60% dodecanoate. This problem, which is typical, derives from the strong positive interactions between the oppositely charged headgroups as found for the *n*-alkyltrimethylammonium system (14). No attempt to obtain the missing data point by using decyl- instead of dodecyl-pyridinium chloride was made.

The nematic materials were prepared by direct weighing of the components followed by alternate stirring and centrifuging until a homogeneous anisotropic fluid was obtained.

Nuclear magnetic resonance spectra were obtained from samples contained in 5 mm sample tubes using a 10 mm broadband probe of a 400 MHz spectrometer. All spectra were obtained at 25°C. The signs of quadrupole splittings given in the tables and displayed in the figures are relative signs only.

Results and discussion

From a three-site model of ion binding and under the condition that chemical exchange between all sites is fast on the nmr time-scale, the observed quadrupole splitting, $\Delta\nu$, is given by expression [3] which follows directly from eq. [2].

$$[3] \qquad \Delta\nu = \Delta\nu_I X_I + \Delta\nu_{II} X_{II} + \Delta\nu_{III} X_{III}$$

Under the condition that an insignificant number of the available binding sites are not occupied, a condition aided by the large proportion of added salt, eq. [4] can be obtained. A further assumption implicit in this equation is that sites of type I are occupied, if available, at the expense of occupancy in sites II or III and, correspondingly, site II is occupied at the expense of site III. In eq. [4],

$$[4A] \quad 1 \geq x \geq (1 - 1/n)$$
$$\Delta\nu = [\Delta\nu_I C_D(nx - (n-1)) + (n-1)\,\Delta\nu_{II} C_D(1-x) + \Delta\nu_{III} C_E]/[xC_D + C_E]$$

$$[4B] \quad (1 - 1/n) \geq x \geq 0$$
$$\Delta\nu = [\Delta\nu_{II} x C_D + \Delta\nu_{III} C_E]/[xC_D + C_E]$$

x is the mole fraction of potassium dodecanoate in total detergent, while n specifies the number of amphiphiles required by the counterion occupying a site I. This equation provides a description of alkali metal ions binding to the carboxylate headgroup of dodecanoate. C_D and C_E are the relative number of moles of detergent and electrolyte, respectively, in the liquid crystalline system. In practice, the parameter, n, varies from two to four for the alkali metal ions; 2 for Li^+, 3 for Na^+, and 4 for K^+, Rb^+, and Cs^+ (16).

For halide ion binding, x in the above expression, is replaced by $1 - x$. This replacement simply reflects the fact that halides are binding to the cationic amphiphiles, which mole fraction is given by $1 - x$ rather than x.

$$[5A] \quad 1 \geq x \geq 1/n$$
$$\Delta\nu = [\Delta\nu_{II}(1-x)C_D + \Delta\nu_{III} C_E]/[(1-x)C_D + C_E]$$

$$[5B] \quad 1/n \geq x \geq 0$$
$$\Delta\nu = [\Delta\nu_I(-nx+1)C_D + (n-1)\,\Delta\nu_{II} x C_D + \Delta\nu_{III} C_E]/[(1-x)C_D + C_E]$$

From this three-site model for ion binding to amphiphiles it is expected that the binding of an alkali metal ion, say Na^+, to carboxylate should be described by eq. [4], independent of which cationic amphiphile is used as the second component. Under these same circumstances, the halide ion which binds to the cationic amphiphile could show significantly different be-

TABLE 1. Mesophase compositions and observed quadrupole splittings

	Composition of mesophases[a]					Quadrupole splittings[b]			
X	KDodec	DDPyrCl	Decanol	D_2O	NaBr	^2H	^{23}Na	^{35}Cl	^{81}Br
1.00	238	—	33	600	40	0.295	6.75	1.00[c]	5.9
0.90	214	28	17	590	40	0.289	3.75	1.63	11.6
0.80	190	56	5	585	40	0.308	1.63	2.70	20.3
0.75	178	70	—	585	40	0.282	0.38	3.10	23.5
0.55	131	128	—	580	40	0.195	−2.04	6.78	37.1
0.50	119	141	2	550	40	0.167	−1.88	6.72	30.3
0.40	95	170	10	540	40	0.105	−1.37	5.69	7.0[d]
0.30	72	198	20	530	40	0.065	−0.641	3.41	−12.2
0.20	48	227	35	520	40	0.046	−0.138	1.00	−48.5
0.10	24	255	55	510	40	0.062	0.357	−1.91	−110.0

[a] Weights are given in mg.
[b] Quadrupole splittings are given in kHz, signs are relative.
[c] Value obtained from the data in ref. 16.
[d] Quadrupole splitting is comparable to line width.

haviour as this latter detergent is replaced by another.

Table 1 gives the mesophase compositions and the ^2H, $^{23}Na^+$, $^{35}Cl^-$, and $^{81}Br^-$ quadrupole splittings which were observed for the various mesophases studied. Unfortunately, under the limitation adopted here that the ratio of total amphiphile to electrolyte is a constant, a mesophase containing only dodecylpyridinium chloride could not be prepared. The corresponding lack of information is not a serious one since the observed curve is readily extrapolated to $x = 0$.

From these results one main point must be established. This is that the Na^+ quadrupole splittings behave according to eq. [4] with $n = 3$, as has been shown for the case when the cationic amphiphile is dodecyltrimethylammonium bromide (16) rather than the dodecylpyridinium chloride employed here. A curve calculated from the characteristic splittings $\Delta\nu_I$, $\Delta\nu_{II}$, and $\Delta\nu_{III}$, equal to 8.55, −4.1, and 1.0 kHz, respectively, fits the experimental results very well as shown in Fig. 1. The major region of discrepancy, which occurs also in the trimethylammonium case, is in the region for x equal to from 0.0 to 0.5.

Also of interest in this study is the behaviour of the deuterium quadrupole splitting of the deuterium in the deuterated water. As can be seen from Table 1, this splitting has a plateau-like region from $x = 1$ to $x \approx 0.75$, then a transition zone followed by a second fairly constant region from $x \approx 0.3$. Similar behaviour has previously been observed (15). This result may indicate that a fairly stable water structure is built around the carboxylate headgroups. This water structure appears to be stable until about 30% of the carboxylate is replaced by pyridinium or trimethylammonium, at which point it becomes unstable and, with continued replacement of carboxylate, eventually disappears. With about 70% replacement of dodecanoate apparently a second type of water structure appears, this one built around the pyridinium headgroups. Since the structures presumably are different, the quadrupole splittings also will be different. It should be noted that, because of rapid exchange, the observed splittings are on average of those from the near isotropic water in the interstitial regions and the water in the more organized areas of the mesophase. Since there is no apparent correlation between the behaviour of water quadrupole splitting and of the counterion quadrupole splittings, these two types of splittings probably arise by different mechanisms.

The bromide ion quadrupole splittings given in Table 1 are reproduced from eq. [5] with $n = 3$ when the characteristic values $\Delta\nu_I = -185.0$, $\Delta\nu_{II} = 51.5$, and $\Delta\nu_{III} = 5.9$ kHz, respectively, describe the calculated curve. As seen in Fig. 1 the agreement between calculated and observed curves is reasonable, with the major discrepancy occurring in the transition region as might be expected. This result is consistent with binding of Br^- to three pyridinium headgroups in the dodecylpyridinium mesophase. The results here are in contrast to those of the alkyltrimethylammonium case, where bromide binds to two headgroups (16). This result clearly establishes that the binding of counterions is a function not only of the properties of the counterion itself but also of the amphiphile to which it is bound.

Figure 1 also shows the observed chloride quadrupole splittings and dashed curves calculated according to $n = 2$ and $n = 3$. In this case, the agreement between the calculated and observed points is not particularly good for either calculated curve. It is necessary to provide an explanation of the deviation between the calculated and observed curves. This behaviour is typical but highly exaggerated here. The discrepancy is ion dependent and generally very much less than that exhibited by the Cl^- ion, as can been seen here for the Na^+ and Br^- ions.

In the cationic mesophase, Cl^- or Br^- is bound by the pyridinium headgroups. As the cationic amphiphile is replaced by the anionic amphiphile, sites of type I are destroyed and those of type II created but, simultaneously to this, the surface charge is being changed from positive to negative in a stepwise fashion. When binding is sufficiently strong the binding forces are able to compete successfully with the developing repulsive electrostatic forces and close agreement between observed and calculated curves is obtained. If binding is weak, then with the buildup of negative charge on the micellar surface the ion undergoing the binding interaction is progressively displaced into the interstitial water. This means that the various relevant quantities in eq. [4] and [5] may not properly represent the proportions of free and bound ions. In this regard, it should be noted that $\Delta\nu$ of eq. [5A] becomes nearly linear in x when C_E is much larger than $(1 - x)C_D$.

For the chloride ion through the range $x = 1$ to 0.5 an approximately linearity is observed for the quadrupole splitting which indicates that the concentration of ions in site III is effectively very large compared to $(1 - x)C_D$. This behaviour is probably related to the development of negative surface charge. It might then be expected that in conjunction with the

Can. J. Chem. Downloaded from www.nrcresearchpress.com by 210.87.254.40 on 09/06/12
For personal use only.

Can. J. Chem. Downloaded from www.nrcresearchpress.com by 210.87.254.40 on 09/06/12
For personal use only.

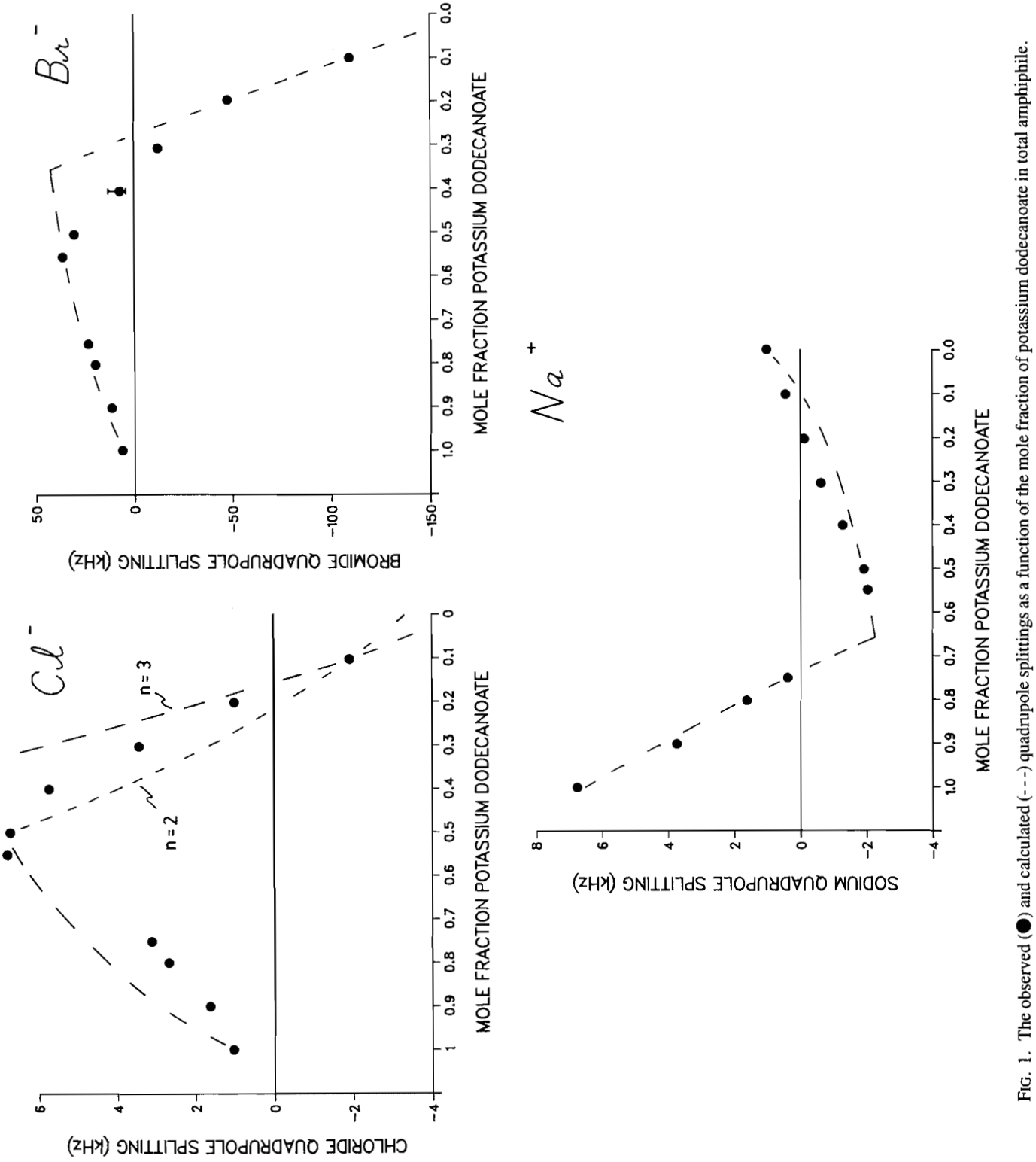

FIG. 1. The observed (●) and calculated (- - -) quadrupole splittings as a function of the mole fraction of potassium dodecanoate in total amphiphile.

TABLE 2. Physical parameters describing the variation of the quadrupole splittings from various halide and alkali metal ions

Ion	Amphiphile	n	k_I	$\Delta\nu_I$[a]	$\Delta\nu_{II}$[a]	$\Delta\nu_{III}$[a]	Reference
$^{35}Cl^-$	*n*-Alkylpyridinium	2	0.96	−6.86	21.7	1.00	—
$^{35}Cl^-$	*n*-Alkyltrimethylammonium	3	0.11	−4.58	8.68	1.08	16
$^{81}Br^-$	*n*-Alkylpyridinium	3	0.55	−241.0	79.0	5.90	—
$^{81}Br^-$	*n*-Alkyltrimethylammonium	2	0.40	−211.0	71.6	6.53	16
$^{7}Li^+$	Dodecanoate	2	0.36	1.98	−0.267	0.033	16
$^{23}Na^+$	Dodecanoate[b]	3	0.50	8.79	−5.28	1.00	—
$^{23}Na^+$	Dodecanoate	3	0.41	9.00	−6.43	0.688	16
$^{23}Na^+$	Dodecanoate	3	0.46	9.69	−6.59	0.672	16
$^{39}K^+$	Dodecanoate	4	0.25	6.67	−5.20	0.820	16
$^{39}K^+$	Dodecanoate	4	0.18	8.23	−5.62	0.961	16
$^{87}Rb^+$	Dodecanoate	4	0.39	36.6	−26.5	3.80	16
$^{133}Cs^+$	Dodecanoate	4	0.69	0.382	−0.193	0.021	16

[a] Quadrupole splittings are in kHz, signs of splittings within each data set are relative signs only.
[b] Second component of this system is *n*-alkylpyridinium; for the remaining alkali metal ions it is *n*-alkyltrimethylammonium.

Can. J. Chem. Downloaded from www.nrcresearchpress.com by 210.87.254.40 on 09/06/12
For personal use only.

binding behaviour as described in eqs. [4] and [5] there is a systematic displacement of ions into the interstitial water as the surface charge is varied. In a first approximation this displacement may be assumed to be linear so that eq. [6] is obtained from eq. [4].

$$[6A] \quad 1 \geq x \geq (1 - 1/n)$$
$$\Delta\nu = [A(B + C] + \Delta\nu_{III}(xC_D(1 - A) + C_E)]/[xC_D + C_E]$$

$$[6B] \quad (1 - 1/n) \geq x \geq 0$$
$$\Delta\nu = [A\Delta\nu_{II}xC_D + \Delta\nu_{III}(xC_D(1 - A) + C_E)]/[xC_D + C_E]$$

In this expression, $A = k_0 - k_I(1 - xC_D)$, $B = \Delta\nu_I C_D(nx - (n - 1))$ and $C = (n - 1)\Delta\nu_{II}C_D(1 - x)$. A similar expression is readily written from eq. [5].

Within the limits of the approximation adopted here k_I is a measure of how tightly ions are being bound in the interface. A k_I equals to 1 means a minimum of sites are occupied while a k_I of 0 means all sites are occupied. When k_I takes values near 1 the basic assumption that $k_0 = 1$ is probably no longer valid. Beyond this, these results can provide little information concerning k_0. It is worth noting that within this approximation $k_I = 0.5$ means that with $x = 0.5$, 75% of all binding sites are occupied. Decreasing the value of k_0 from 1.0 to another value simply results in a scaling of the characteristic splittings $\Delta\nu_I$ and $\Delta\nu_{II}$ and has negligible effect on the calculated curve.

Figure 2 shows the best fit curves calculated using eq. [6] with $n = 2$ for Cl^- and $n = 3$ for Br^- and Na^+. The agreement is excellent in these three cases and similarly as good when the data of ref. 16 is utilized. Figure 1 tends to suggest that Cl^- in site I might be in an equilibrium situation, binding at one time to 2 headgroups and at another time to 3. Testing of such an assumption gives a much improved correlation between calculated and observed quadrupole splittings over that displayed in Fig. 1. The agreement, however, continually improves with decreasing admixture of the second component and clearly is maximized with 100% of the $n = 2$ component.

It is of interest to compare the various k_I values obtained from eq. [6]. Table 2 collects together the values obtained in this study and those calculated from the data in ref. 16. Particularly interesting are the values of k_I for the chloride ion. For the binding of chloride to the pyridinium headgroup this value is 0.96, indicating that binding is weak. This compares dramatically with the binding to the trimethylammonium headgroup where $k_I = 0.11$, indicative of very strong binding. Bromide ion has corresponding values of 0.55 and 0.40 again indicating a stronger binding to the trimethylammonium group. However, in this case the difference is much smaller.

The values of k_I for the binding of the alkali metal cations to the dodecanoate anion also show an interesting behaviour. The value of $k_I = 0.36$ for Li^+ rises to ≈0.44 for Na^+ then drops to ≈0.21 for K^+ then rises through 0.39 for Rb^+ to 0.69 for Cs^+. These values indicate that potassium is bound most tightly by the carboxylate anion and cesium least tightly while the others have intermediate strengths of binding. It is interesting to note that k_I for the first sodium entry in Table 2 is not very different from the other two entries, showing that the sodium cation is not very sensitive to the cationic detergent present. It should be mentioned that the dominating influence on the value obtained for k_I comes from experimental points in the region corresponding to ion binding to only one amphiphile, i.e. site II, so that k_I gives essentially no information concerning relative strengths of binding of ions in site I.

There does, however, appear to be a correlation between k_I and the strength of binding in site I. Turning to Fig. 2 it is seen that the remaining region of major discrepancy between calculated and observed curves lies in a more or less restricted transition zone between site I and site II. This discrepancy is small when binding is weak, as indicated by k_I (i.e. Cl^-), and increasingly large as binding is stronger as for Br^- and Na^+. Similar conclusions can be drawn from the information in ref. 16 and Table 2. This indicates that dispersive forces generated by changes in detergent ratios are, to an extent, overridden by the strength of binding in site I. The consequence of this is that in the transition region there will in general be more ions in site I than predicted by eq. [6]. In the future systems may be found where the opposite is true, this is to say that ions will move into site II faster than predicted by eq. [6], in fact Cl^- binding to pyridinium may be showing a slight tendency in this regard.

It is clear that considerably more study of these systems is

Can. J. Chem. Downloaded from www.nrcresearchpress.com by 210.87.254.40 on 09/06/12
For personal use only.

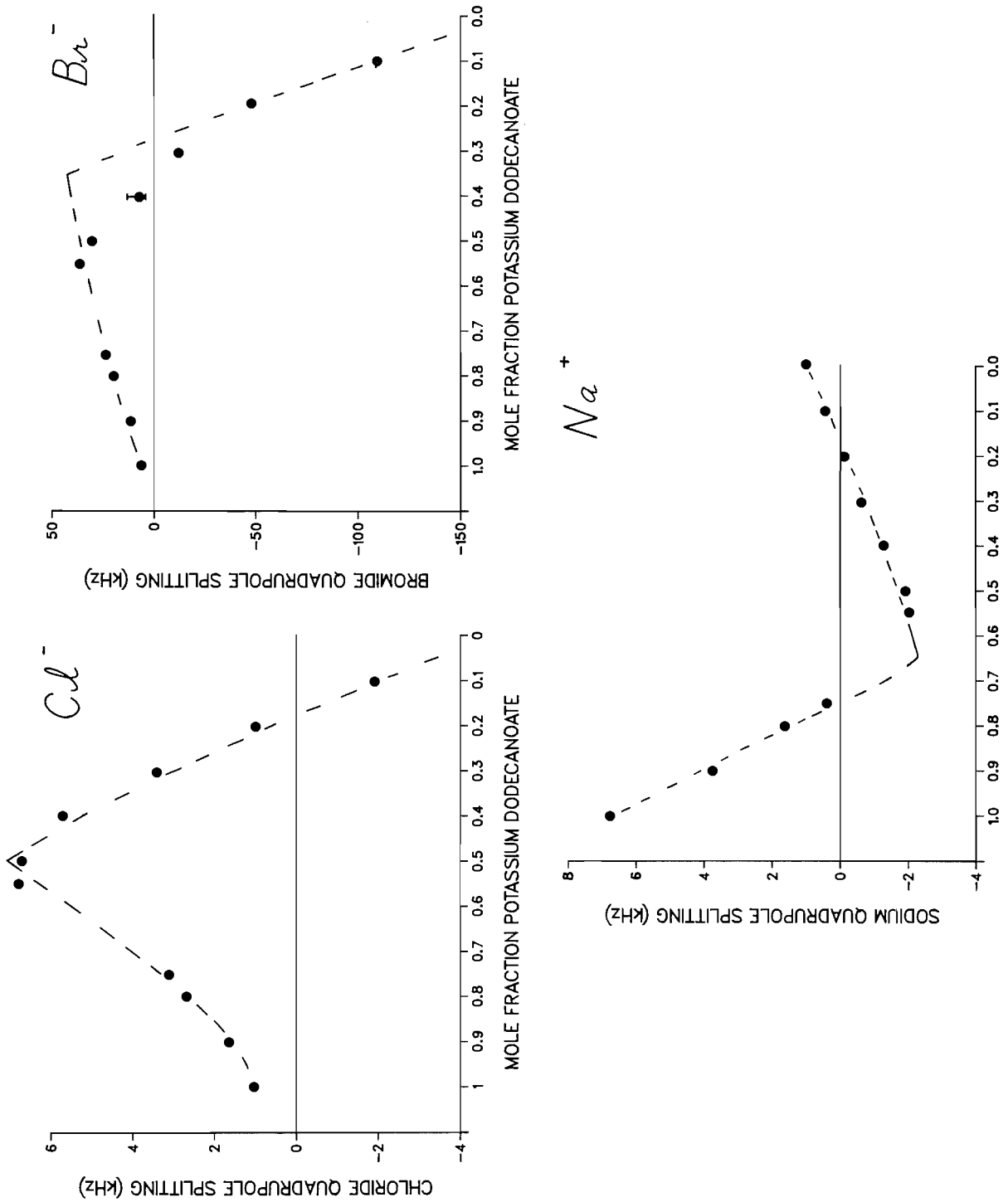

FIG. 2. The observed (●) and calculated (- - -) quadrupole splittings taking into account the development of charge on the bilayer interface.

required. In particular one must be concerned with effects of temperature and of changes in electrolyte concentration. The details of ion competition in these systems have not been properly addressed nor indeed the effects of changes in pH on binding. The problem of diffuse binding of ions in site III has not been examined in this study and this aspect of ion binding could be of importance. Extension of ion binding studies into these areas will enable development of this model of ion binding to proceed. Ultimately, of course, it may be superceded by an alternative description of the binding of ions in these amphiphilic systems.

Acknowledgement

Thanks are extended to the Natural Sciences and Engineering Research Council of Canada for its financial support of this work, in the form of an operating grant, Number A1558.

1. T. SHIMUZU, M. HATANO, S. NAGAO, and Y. NOZAWA. Biochem. Biophys. Res. Commun. **106**, 1112 (1982).
2. B. JOENSSON and H. WENNERSTROM. J. Colloid Interface Sci. **80**, 482 (1981).
3. D. CHAPMAN. Liquid crystals and biological membranes, Liq. Cryst.: Fourth State of Matter, 1979, *Edited by* F. D. D. Saeva, New York, N.Y.
4. G. J. T. TIDDY, G. LINDBLOM, and B. LINDMAN. J. Chem. Soc. Faraday Trans. 1, **74**, 1290 (1978).
5. J. H. HAPPE and R. L. WARD. J. Am. Chem. Soc. **91**, 4906 (1969).
6. I. M. ARMITAGE, R. T. PAIER, A. J. M. SCHOOT UITERKAMP, J. F. CHLEBOWSKI, and J. E. COLEMAN. J. Am. Chem. Soc. **98**, 5710 (1976).
7. J. L. SUDMEIER and S. J. BELL. J. Am. Chem. Soc. **99**, 99 (1977).
8. E. O. MARTINS and T. DRAKENBERG. Inorg. Chim. Acta, **67**, 71 (1952).
9. T. ANDERSSON, T. DRAKENBERG, S. FORSÉN, and E. THULIN. Eur. J. Biochem. **126**, 501 (1982).
10. T. L. JAMES and J. H. NOGGLE. Anal. Biochem. **49**, 208 (1972).
11. J. A. BEUNEN and E. RUCKENSTEIN. J. Colloid Interface Sci. **96**, 469 (1983).
12. A. DELVILLE and P. LASZLO. Biophys. Chem. **17**, 119 (1983).
13. C. L. KHETRAPAL, A. C. KUNWAR, A. S. TRACEY, and P. DIEHL. NMR. Basic Principles and Progress **9** (1975).
14. L. HECKER, L. W. REEVES, and A. S. TRACEY. Mol. Cryst. Liq. Cryst. **53**, 77 (1979).
15. Y. LEE, L. W. REEVES, and A. S. TRACEY. Can. J. Chem. **58**, 110 (1980).
16. A. S. TRACEY and T. L. BOIVIN. J. Phys. Chem. **88**, 1017 (1984).
17. L. W. REEVES, A. S. TRACEY, and M. M. TRACEY. Can. J. Chem. **57**, 749 (1979).

Can. J. Chem. Downloaded from www.nrcresearchpress.com by 210.87.254.40 on 09/06/12
For personal use only.

A five-coordinate dicarbonyl rhodium(I) complex containing monohapto-2-diphenylphosphinothiophene: $[RhCl(CO)_2(DPT)_2]$

ALAN R. SANGER
Alberta Research Council, 11315-87 Avenue, Edmonton, Alta., Canada T6G 2C2

Received March 1, 1984

ALAN R. SANGER. Can. J. Chem. **62**, 2168 (1984).

Facile reversible addition of CO to *trans*-$[RhCl(CO)(Ph_2PC_4H_3S)_2]$ gives the five-coordinate complex $[RhCl(CO)_2(Ph_2PC_4H_3S)_2]$, which represents the first complex of the type $[RhCl(CO)_2(PR_3)_2]$ to be identified, and which is trigonal bipyramidal with axial carbonyls and equatorial phosphine ligands.

ALAN R. SANGER. Can. J. Chem. **62**, 2168 (1984).

Une addition réversible facile de CO au $[RhCl(CO)(Ph_2PC_4H_3S)_2]$-*trans* conduit au complexe penta-coordonné $[RhCl\text{-}(CO)_2(Ph_2PC_4H_3S)_2]$ qui correspond au premier complexe du type $[RhCl(CO)_2(PR_3)]$ à être identifié; sa géométrie est trigonale bipyramidale et il porte les ligands carbonyles en position axiale et les ligands phosphines en position équatoriale.
[Traduit par le journal]

Can. J. Chem. Downloaded from www.nrcresearchpress.com by 210.87.254.42 on 09/06/12
For personal use only.

Introduction

The reactions of tertiary phosphines (PR_3; R = alkyl or aryl) with either $[Rh_2Cl_2(CO)_4]$, or with $[Rh_2Cl_2(cod)_2]$ (cod is 1,5-cyclooctadiene) under an atmosphere of CO, have been well studied (1). In all cases previously reported, when PR_3/Rh is two or more the ultimate product is *trans*-$[RhCl(CO)(PR_3)_2]$. Decarbonylation of aroyl chlorides using $[RhCl(PPh_3)_3]$ was reported to give both the *cis* and *trans* isomers of $[RhCl(CO)(PPh_3)_2]$ (2). Similarly, attempted synthesis of $[RhI(CO)(PPh_3)_2]$ by halogen exchange under various conditions gave different products which, on the basis of their ir spectra, were assigned *cis* and *trans* structures (3). No isolated complex of the form $[RhCl(CO)_2(PR_3)_2]$ has previously been reported. However, the pentacoordinate rhodium complexes $RHg[Rh(CO)_2(PPh_3)_2]$ and $Hg[Rh(CO)_2(PPh_3)_2]_2$ can be prepared by the reduction of *trans*-$[RhCl(CO)(PPh_3)_2]$ with sodium amalgam under an atmosphere of CO (4). The dicarbonyl complex $[RhH(CO)_2(PPh_3)_2]$ is formed from $[RhH(CO)(PPh_3)_3]$ and CO, and is of high hydroformylation catalytic activity due to facile ligand dissociation (5). Further, the complex $[IrCl(CO)_2(PPh_3)_2]$ is known, and is trigonal bipyramidal with axial triphenylphosphine ligands (6).

Experimental

Under an atmosphere of CO, $[Rh_2Cl_2(cod)_2]$ (0.597 g, 1.21 mmol) (or equivalent amount of $[Rh_2Cl_2(CO)_4]$) was added to a solution of 2-diphenylphosphinothiophene ("DPT") (1.59 g, 5.93 mmol) (7, 8) in dichloromethane (30 mL) to form an orange–yellow solution. Slowly, under a stream of CO, yellow crystals (1.11 g, 63%) of $[RhCl(CO)_2(DPT)_2]$, **1**, contaminated with a trace of *trans*-$[RhCl(CO)(DPT)_2]$, **2**, were formed. The remaining solution was diluted with ethanol, and then evaporation of dichloromethane gave pure **1** (0.73 g, 37%) as yellow needles.

Under an atmosphere of nitrogen a portion of **1** was dissolved in dichloromethane and then a layer of ethanol was added. The solvents mixed to form a yellow solution. Slow evaporation of dichloromethane gave light yellow crystals of *trans*-$[RhCl(CO)(DPT)_2]$, **2**.

Similarly, a sample of **2** was dissolved in dichloromethane, ethanol was added, and the solvents slowly evaporated under a stream of CO to give crystals of **1**.

Solutions of **1** or **2** in acetone under an atmosphere of CO, N_2, or air were each non-conducting. Spectra (Table 1) were obtained using the following instruments: ir, Perkin-Elmer 283; ^{13}C and ^{31}P nmr, Brüker WP80; gc-ms, Finnigan 4000/4500.

Results and discussion

The reaction of DPT (7, 8) with either $[Rh_2Cl_2(CO)_4]$ or $[Rh_2Cl_2(cod)_2]$ under an atmosphere of CO gave yellow crystals of a complex, **1**, which is assigned the formula $[RhCl(CO)_2(DPT)_2]$ and the structure shown in Fig. 1, based on elemental analyses and for the following reasons. Complex **1** is not an electrolyte. The phosphine ligands are equivalent (^{31}P nmr). The ^{13}CO (90% enriched) complex exhibits broader ^{31}P resonances, but $^2J(^{13}C—^{31}P)$ is not clearly resolved to −80°C. The increased breadth may be due to a reduction in the rate of exchange of ^{13}CO liquids at −80°C. The ^{13}C nmr spectrum (30°C) exhibited a single resonance (δ_C 187 ppm) in the carbonyl-^{13}C region. No coupling was evident at this temperature. The ir spectrum exhibits one very strong carbonyl band and one weak Rh—Cl band. When a solution of **1** is flushed with nitrogen the monocarbonyl complex **2** is formed, and **2** reacts with CO to reform **1**. Complex **1** therefore represents the first reported five-coordinate complex of the formula $[RhCl(CO)_2(PR_3)_2]$. The proposed structure differs from that of $[Rh(HgPh)(CO)_2(PPh_3)_2]$, which has inequivalent phosphine ligands (4), or $[IrCl(CO)_2(PPh_3)_2]$, which has axial phosphine ligands (6). For each of these complexes two carbonyl bands are observed in the ir spectrum, whereas for **1** there is only one.

Attempted recrystallization of **1** from dichloromethane/ethanol under an atmosphere of nitrogen gave exclusively the monocarbonyl complex **2**. This complex also contains equivalent phosphine ligands, is a non-electrolyte, and exhibits one carbonyl stretching band and one Rh—Cl band in the ir spectrum. The ^{31}P nmr spectrum of the ^{13}CO complex exhibits coupling to a single ^{13}C nucleus ($^2J(CP) = 16.5$ Hz). At −50°C coupling of ^{13}C to two ^{31}P was also observed (δ_C 187 ppm; $^1J(RhC)$ 74.5 Hz; $^2J(PC)$ 16.5 Hz). On the basis of the above data, and by comparison of the spectroscopic parameters with those known complexes of the form *trans*-$[RhCl(CO)(PR_3)_2]$ (1), complex **2** is assigned the structure *trans*-$[RhCl(CO)(DPT)_2]$. Reaction of **2** with CO regenerates **1**. The value of $^1J(Rh—P)$ for **1** is lower than for **2**, as is appropriate for a complex in which there are more competing σ-donor π-acceptor ligands about rhodium. It is noteworthy that for both **1** and **2** the phosphine ligands are equivalent to −50°C, therefore neither complex can have the structure *cis*-$[RhCl(CO)(PR_3)_2]$. As assignments of such a *cis* structure have been on the basis of ir spectra only, a reassessment of the nature of such materials is probably in order.

Addition of $NaBPh_4$ to a solution of **1** or **2** in ethanol caused no colour change, and no formation of an ionic complex of rhodium was detected. In contrast to complexes of

TABLE 1. Spectral data of monohapto-2-diphenylphosphinothiophene

	Analysis[a]				Infrared[b]		^{31}P nmr[c]		
	C	H	Cl[d]	S	ν(CO)	ν(RhCl)	δP	^{1}J(RhP)	^{2}J(CP)
$Ph_2PC_4H_3S$ (DPT)[e]					—	—	−20.8	—	
$[RhCl(CO)_2(DPT)_2]$	56.0	3.7	5.9	9.1	1990	303	20.0	117	See,
	(55.9)	(3.6)	(4.9)	(8.9)	(1944)				text
$[RhCl(CO)(DPT)_2]$	56.3	3.7	5.2	9.1	1974	308	18.6	126	16.5
	(56.4)	(3.7)	(5.0)	(9.1)	(1925)				
$[Rh(HgPh)(CO)_2(PPh_3)_2]$[f]					1975, 1920	—	—	—	
$[IrCl(CO)_2(PPh_3)_2]$[g]					1976, 1923	—	—	—	

[a]Analyses were performed by the Microanalytical Laboratory, Department of Chemistry, University of Alberta. Calculated values in parentheses.

[b]Nujol mulls; values in wavenumbers. Values for ^{13}CO are in parentheses.

[c]Dichloromethane-d_2 solutions, −50°C, ^{1}H-decoupled; chemical shifts are in ppm relative to 85% H_3PO_4, and coupling constants are in Hz. ^{13}C nmr parameters are discussed in the text.

[d]Determination of Cl is complicated by interference due to the presence of P and Rh. Consequently values for Cl are less accurate than other values reported.

[e]Prepared as in ref. 7, by Schallig. The material is very air-sensitive and difficult to manipulate and so was characterized by its ir, nmr, and mass spectra (M^+ found 268, calculated 268) (see also ref. 8).

[f]Reference 4.

[g]Reference 6.

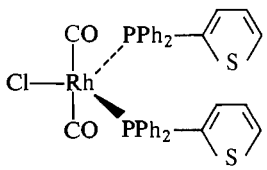

FIG. 1. Structure of complex **1**.

Ph_2PCH_2SPh (7), chelation of rhodium by coordination of the thioether function of DPT is not facile, probably due to the greater rigidity of DPT. Similar nonchelating behaviour of DPT was observed for complexes of cobalt(III) or nickel(II) (8).

Complexes of Rh^{I} similar to **2** are effective catalysts for hydrogenation, hydroformylation, carbonylation, or decarbonylation. Structures similar to **1** must now be considered as possible intermediates in such reactions; experiments to investigate the existence of complexes $[RhX(CO)_2(PPh_3)_2]$ (X = Cl, Br, I) will be described separately.

Acknowledgements

Thanks are due to L. R. Schallig for the preparation of DPT, and M. D. Rawluk, C. M. Goulet, and W. Wade for the gc-ms and ^{31}P nmr spectra.

1. C. A. MCAULIFFE and W. LEVASON. Phosphine, arsine, and stibine complexes of the transition elements. Elsevier, Amsterdam. 1979.
2. J. BLUM, E. OPPENHEIMER, and E. D. BERGMANN. J. Am. Chem. Soc. **89**, 2338 (1967).
3. F. R. HARTLEY, S. G. MURRAY, and D. M. POTTER. J. Organomet. Chem. **254**, 119 (1983).
4. G. M. INTILLE and M. J. BRAITHWAITE. J. Chem. Soc. Dalton, 645 (1972).
5. G. YAGUPSKY, C. K. BROWN, and G. WILKINSON. J. Chem. Soc. A, 1392 (1970); C. K. BROWN and G. WILKINSON. J. Chem. Soc. A, 2753 (1970).
6. N. C. PAYNE and J. A. IBERS. Inorg. Chem. **8**, 2714 (1969); L. VASKA, Science, **152**, 769 (1966).
7. A. R. SANGER. Can. J. Chem. **61**, 2214 (1983).
8. D. W. ALLEN and D. F. ASHFORD. J. Inorg. Nucl. Chem. **38**, 1953 (1976).

Can. J. Chem. Downloaded from www.nrcresearchpress.com by 210.87.254.42 on 09/06/12
For personal use only.

Acidité de Brønsted des phosphoranes à liaison P—H; identification de leurs bases conjuguées; détermination de leur pK_a

B. GARRIGUES, D. BOYER ET A. MUNOZ

E.R.A. C.N.R.S. N° 926, Université Paul Sabatier, 118 route de Narbonne, 31062 Toulouse Cedex, France

Reçu le 19 octobre 1983

B. GARRIGUES, D. BOYER et A. MUNOZ. Can. J. Chem. **62**, 2170 (1984).

Le proton P—H de phosphoranes contenant le ligand α hydroxyacide ou acide iminodiacétique, est suffisamment mobile pour être arraché à la température ambiante, par des bases moyennes comme la triéthylamine. Les entités phosphorées résultant de cette déprotonation, identifiées par rmn de ^{31}P, sont: (a) le phosphoranure pour le composé bicyclique préparé à partir de l'acide iminodiacétique, (b) le phosphite anionique isomère du phosphoranure, dans le cas d'un phosphorane contenant un ligand α hydroxyacide, (c) le phosphite et le phosphoranure en équilibre, pour les phosphoranes contenant deux ligands α hydroxyacide. Les pK_a, déterminés en solution dans le DMF par potentiométrie, en titrant les phosphoranes par la triéthylamine, correspondent à des acides moyens ou faibles. Cependant, les phosphoranes étudiés sont, dans le DMF, plus acides que les autres composés phosphorés à liaison P—H connus. Ils sont également plus dissociés, dans ce solvant, que les acides carboxyliques.

B. GARRIGUES, D. BOYER, and A. MUNOZ. Can. J. Chem. **62**, 2170 (1984).

The P—H proton of phosphoranes containing an α-hydroxy acid or iminodiacetic acid ligand is sufficiently mobile to be removed at room temperature by medium strength bases such as triethylamine. The deprotonation products identified by ^{31}P nmr are (a) the phosphoranide for the bicyclic compound prepared from iminodiacetic acid, (b) the anionic phosphite isomeric to the above, for phosphoranes containing the α-hydroxy acid ligand, (c) the phosphite and the phosphoramide in equilibrium, for phosphoranes containing two α-hydroxy ligands. The pK_a values potentiometrically determined in DMF solution by titration of the phosphoranes with triethylamine correspond to weak or mild acids. However, the phosphoranes studied are more acid in DMF than other known compounds containing the P—H bond. They are also more dissociated in this solvent than carboxylic acids.

[Journal translation]

I. Introduction

Si la liaison P—H, dans la coordinence V du phosphore a donné lieu à de nombreuses études physicochimiques, notamment par rmn et ir, les données quantitatives concernant sa dissociation sont beaucoup plus rares. On sait que dans les composés tri et tétracoordonnés, à l'exception des sels de phosphonium, cette dissociation est peu importante (1–4). Par exemple, le pK_a du diéthylphosphite est de 13, en solution dans l'eau (4).

Les résultats décrits en ce qui concerne les phosphoranes à liaison P—H, dans lesquels l'atome de phosphore est relié à plusieurs atomes de carbone, montrent que ces composés ne se singularisent pas des dérivés appartenant aux coordinences inférieures (5): le pK_a a été estimé pour l'un d'eux à 11,7, en solution dans l'eau (5*c*). Ce sont donc des acides faibles. La base conjuguée présente en rmn de ^{31}P, un singulet situé dans un champ de résonance proche de celui du phosphorane (5*b*, 5*c*). Il s'agit donc d'un composé du phosphore tétracoordonne dans lequel cet élément conserve dix électrons dans sa sphère de coordinence. Il a été désigné par le terme de "phosphoranure" (5*b*).

Les phosphoranes à liaison P—H, où l'atome de phosphore est relié à des atomes d'oxygène sont nettement plus réactifs vis-à-vis des bases que les composés homologues à liaison P—C. Ils sont susceptibles de réagir avec des bases moyennes comme la pyridine ou la triéthylamine (6). Suivant leur structure, ils peuvent donner lieu à deux types de phénomènes: formation d'un composé d'addition à phosphore hexacoordonné (6), et déplacement de l'équilibre phosphorane ⇌ phosphite vers la forme à phosphore tricoordonné (6). Dans le cas des phosphoranes contenant un reste α hydroxyacide, les amines aliphatiques, comme la diéthylamine conduisent au sel du phosphite isomère (6) (schéma 1).

[1] 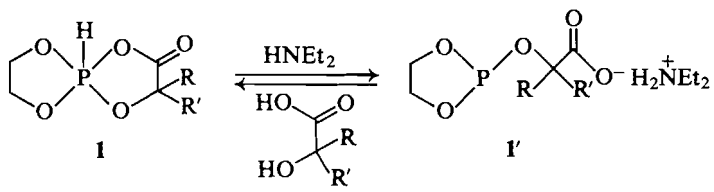

1 **1′**

SCHÉMA 1

Il est important de préciser que les composés **1** existent, pour les termes substitués, uniquement, en l'absence de base et au regard de la rmn, sous la forme phosphorane (6). Le résultat représenté par le schéma 1 peut s'interpréter par la déprotonation du phosphorane, conduisant au phosphoranure, lequel, peu stable, se transformerait finalement en phsophite **1′** (schéma 2).

Can. J. Chem. Downloaded from www.nrcresearchpress.com by 210.87.254.6 on 09/06/12
For personal use only.

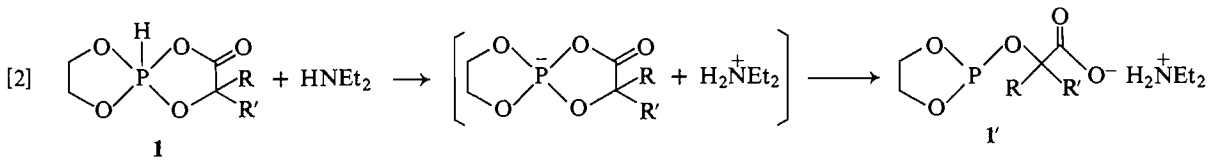

SCHÉMA 2

Afin d'identifier le phosphoranure dans ce type de composés, les auteurs ont traité par les bases les tétraoxyspirophosphoranes les plus stables. C'est ainsi qu'en faisant réagir l'amidure de sodium sur le spirophosphorane contenant deux restes pinacol, Savignac *et al.* (7) ont observé des processus comparables à ceux du schéma 1. Là encore, le composé obtenu est le sel du phosphite isomère (7). Cependant, l'action, *in situ*, d'halogénures d'alcoyle sur le mélange phosphorane + base conduit au remplacement du proton P—H par le reste alcoyle, ce qui a été considéré par les auteurs comme une preuve de la formation préliminaire du phosphoranure (7).

Pour notre part, nous avons essayé de stabiliser le phosphoranure, en introduisant dans les composés **1** le maximum de facteurs favorables: c'est ainsi que nous avons envisagé les composés **2** contenant deux ligands α hydroxyacide. On sait que pour les termes substitués, l'équilibre phosphite ⇌ phosphorane n'a pas été mis en évidence par rmn, même à +120°C.

En revanche, cet équilibre a été décelé récemment, pour le terme non substitué (**2***a*) à des températures supérieures à +40°C (9).

Des résultats préliminaires observés en faisant réagir la pyridine et la triéthylamine sur le composé **2***e* ont permis de mettre en évidence un équilibre entre le phosphorane, le phosphite et le phosphoranure isomères, auxquels il convient d'ajouter des complexes d'addition à phosphore hexacoordonné (schéma 3) (10). Cependant ce dernier phénomène, seulement visible à basse température, est nettement minoritaire et peut être négligé.

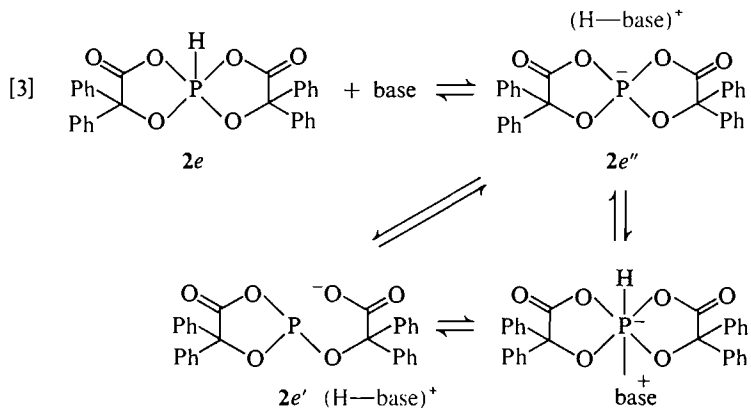

SCHÉMA 3

Des phénomènes analogues ont été observés avec le phosphorane dimère **2***f* (11).

Tout récemment, Schombourg *et al* (12) ont étudié l'action de la triéthylamine sur un phosphorane à liaison P—H homologue et ont déterminé la structure du phosphoranure correspondant par diffraction des rayons X. Le phosphoranure a été enfin stabilisé dans le cas du phosphorane bicylique **3**, (schéma 4) (13).

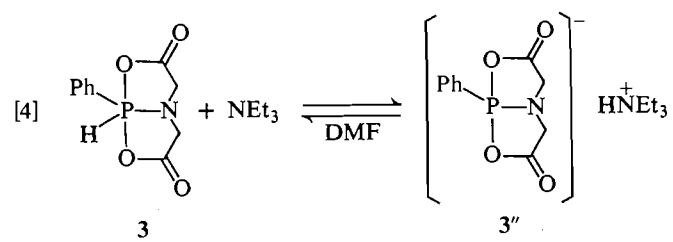

SCHÉMA 4

Nous avons montré que l'équilibre [4] était fortement déplacé vers le phosphoranure, dès la température ordinaire (13).

Remarquons que si les phosphoranures formés par déprotonation de phosphoranes à liaison P—H ont été identifiés seulement dans quelques cas, des phosphoranures halogénés ont été décrits, la structure cristalline de certains d'entre eux ayant même été déterminée (13). Cependant, à l'inverse des précédents, c'est l'acide conjugué, le phosphorane, qui n'est pas connu (14). Ces phosphoranures s'obtiennent, en effet, par addition d'un ion halogénure (ou cyanogène) sur l'atome de phosphore électrophile d'un trihalogénure (ou pseudo-halogénure) de phosphore (14). Signalons, en plus, l'existence de complexes métalliques où l'ion phosphoranure joue le rôle de ligand (15). Ces composés peuvent être considérés, également, comme des phosphoranes à liaison phosphore–métal.

La réactivité des composés **1**, **2** et **3** vis-à-vis de bases moyennes, comme la triéthylamine, ou même faibles, comme la pyridine, laisse présager, pour ces composés, d'une acidité de Brønsted relativement forte que nous avons entrepris de mesurer. Pour celà, nous avons titré les composés **1***d*, **2***b*–**2***f* et **3**, par la triéthylamine dans des solvants aprotiques polaires (DMF, DMSO), les phosphoranes réagissant avec les solvants protiques (eau, alcools). Le titrage a été suivi par potentiométrie. Afin de bien connaitre les entités qui participent aux

Can. J. Chem. Downloaded from www.nrcresearchpress.com by 210.87.254.6 on 09/06/12
For personal use only.

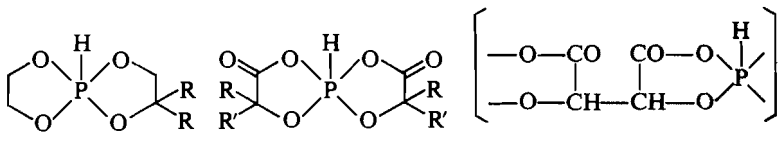

1 **2** **2*f***

1*d*: R = CH_3

2*a*: R = R′ = H
2*b*: R = H, R′ = iPr
2*c*: R = H, R′ = Ph
2*d*: R = R′ = CH_3
2*e*: R = R′ = Ph

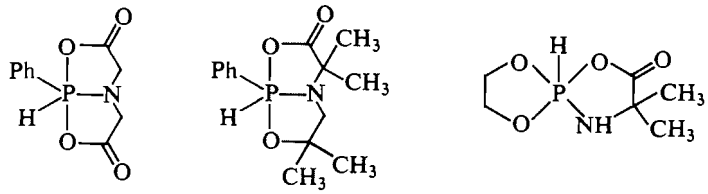

3 **4** **5**

équilibres acido-basiques, nous avons étudié par rmn de ^{31}P, à différentes températures, les mélanges de ces phosphoranes avec la même base et, dans quelques cas particuliers avec le diazabicycloundécane (DBU) ou la pyridine.

Nous avons étudié également les composés **4** et **5**. Le premier, de structure comparable à celle de **3**, en diffère par le remplacement d'un groupement carbonyle par un reste méthylène, alors que le second est isologue du phosphorane **1*d***, le reste α hydroxyacide étant remplacé par le reste α aminoacide.

II. Action de la triéthylamine sur les phosphoranes *1*d–*5*

1. *Etude par résonance magnétique nucléaire de ^{31}P*

Nous avons étudié systématiquement, par rmn de ^{31}P à température variable, l'action de la triéthylamine sur les phosphoranes **1*d*–5**, généralement en solution dans le DMF. D'après ce qui précède, nous pouvons nous attendre à la déprotonation du phosphorane, avec formation de phosphoranure (schèma 4), de phosphite isomère salifié (schéma 1), d'un équilibre entre ces deux dérivés (schéma 3), ou efin à l'addition de la base sur le phosphorane pour donner un composé à phosphore hexacoordonné (schéma 3).

A la température ambiante, pour une quantité de triéthylamine inférieure ou égale à la quantité stoechiométrique, on observe la disparition de tout signal dans le spectre de rmn ^{31}P, des composés **1*d***, **2*b***, **2*c***, **2*e***, **2*f*** et **3**. Dans le cas du phosphorane **2*d***, le doublet P—H est remplacé par un singulet large dont le $\delta^{31}P$ varie avec la quantité de base: −14 (pour 1/2 équivalent), +51 (pour 1 équivalent). Quant aux phosphoranes **4** et **5** le doublet P—H reste inaltéré quelle que soit la quantité d'amine ajoutée.

Aux basses températures, des signaux apparaissent. D'une manière générale, pour des proportions de bases inférieures à la stoechiométrie, on observe la réapparition du doublet du phosphorane, accompagné de signaux à champ faible (tableau 1(a)). Ce doublet disparaît définitivement dès que la quantité d'amine atteint ou dépasse un équivalent (tableau 1(b)).

Ce phénomène montre que la base arrache le proton de l'atome de phosphore. L'absence de doublets P—H situés dans le domaine de résonance des composés à phosphore hexacoordonné permet d'exclure une réaction d'addition entre le phosphorane et la triéthylamine. Il s'agit bien d'un équilibre acido-basique: au fur et à mesure de son addition, la triéthylamine déprotone le phosphorane, l'évolution du spectre de rmn ^{31}P à basse température montrant la disparition progressive de l'acide à liaison P—H et l'apparition concomitante des signaux des formes déprotonées. Le fait qu'aucun signal ne soit observable à la température ambiante, indique que la vitesse d'échange du proton entre les espèces déprontonées, la triéthylamine et le phosphorane (pour des quantités de base inférieures à la stoechiométrie 1 : 1), est du même ordre de grandeur que l'échelle de temps de la rmn, qui, en conséquence ne distingue aucun signal. Remarquons que les signaux des formes déprotonées apparaissent nettement, à la température ambiante, avec une base plus forte comme le DBU (diazabicycloundecane). Par exemple, l'addition d'un équivalent de DBU à une solution de **2*d***, dans CH_2Cl_2, provoque la disparition du doublet P—H et l'apparition d'un singulet fin et intense à δ = +88,7. Le même résultat ne peut être atteint, avec la triéthylamine, qu'aux basses températures.

Les signaux des bases conjuguées sont situés, d'une manière générale, à champ faible. Ils se déplacent légèrement à champ fort quand on diminue encore la température. De ce fait, ils ne correspondent pas aux anions phosphoranure qui doivent résonner à champ fort: on sait, effectivement que ces composés présentent en rmn de ^{31}P un singulet dans le domaine des phosphoranes correspondants (**5*b***, **5*c***, 13).

D'autre part, si le singulet observé à la place du doublet P—H peut être attribué avec certitude au phosphite isomère dans le cas du composé **1*d*** (6), il n'en est pas de même pour les composés **2*b*–2*f***. En effet pour ces derniers, la forme phosphite **2′** a été mise en évidence, en ce qui concerne le terme non substitué **2*a***, à partir de 40°C (schéma 5).

[5] 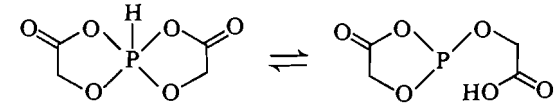

2*a* **2′*a***

$\delta^{31}P = -35$, $J_{P-H} = 950$ Hz $\delta^{31}P = +142$

SCHÉMA 5

Son $\delta^{31}P$ (+142) peut être retenu comme paramètre pour les autres formes **2′*b*–2′*f***′, les substituants fixés sur le cycle oxo-4 dioxaphospholane-1,3,2 ayant peu d'incidence sur la position

Can. J. Chem. Downloaded from www.nrcresearchpress.com by 210.87.254.6 on 09/06/12
For personal use only.

TABLEAU 1. (a) $\delta^{31}P$ à différentes températures des signaux des spectres de résonance magnétique nucléaire ^{31}P des mélanges (**1***d*, **2***b*–**2***f*) + 1/2 Et_3N

T (°C)	**1***d* (CH_2Cl_2)	**2***b* (DMF)	**2***d* (CH_2Cl_2)	**2***e* (DMF)
	−34[c]		−14[b]	
+30	J_{P-H} = 800 Hz	Pas de signaux	−93[c]	Pas de signaux
	+131[c]		−50[c]	
−20	−36[a]		J_{P-H} = 930 Hz	
	J_{P-H} = 887 Hz		−96[a]	
		+109[a]		
−30		−44,1[c]		
		J_{P-H} = 960 Hz		
−40				
	+130,4[a]		−51[a]	+79,4[a]
−50	−36,7[a]		J_{P-H} = 930 Hz	−47[a]
	J_{P-H} = 887 Hz		−96[a]	J_{P-H} = 980 Hz
				−134[c]
				J_{P-H} = 920 Hz
		+106[a]		
−60		+103[a]		
		−44[c]		
		J_{P-H} = 980 Hz		
−80		+104[a]		
		+101[a]		
		−42[c]		
		J_{P-H} = 1000 Hz		

[a] Signaux fins et intenses.
[b] Signaux larges.
[c] Très larges presque confondus avec le bruit de fond.

TABLEAU 1. (b) $\delta^{31}P$ à différentes températures des signaux des spectres de résonance magnétique nucléaire ^{31}P des mélanges spirophosphoranes (**1***d*, **2***b*–**2***f*) + 1 à 1,3 Et_3N

T (°C)	**1***d* (CH_2Cl_2)	**2***b* (DMF)	**2***c* (DMF)	**2***d* (CH_2Cl_2)	**2***e* (DMF)	**2***f* (DMF)
	Pas de		Pas de	+51[b]	Pas de	Pas de
+30	signaux	−88[c]	signaux	−93,6[d]	signaux	signaux
−10		+108[c]				
		−88[c]				
				+92,5[b]		
−20				−95,4[a]		+84,1[b]
				−99[d]		
		+119[a]	+101[a]			
−30		+116[a]	+96[a]			
				+100,4[a]		
−40				−95,2[a]		+79,9[a]
				−99[b]		
		+109[a]				
−50		+106[a]			+79,4[a]	
		−89[c]				
			+98[a]	+103,1[a]		
−60			+93[a]	−96,2[a]		
				−99[d]		
		+108[a]	+100[a]			
−70		+106[a]	+95[a]			
		−89[b]				
				+103,8[a]		
−80				−96,5[b]		

[a] Signaux intenses.
[b] Signaux larges d'intensité moyenne.
[c] Signaux larges et peu intenses.
[d] Signaux fins et peu intenses.

Can. J. Chem. Downloaded from www.nrcresearchpress.com by 210.87.254.6 on 09/06/12
For personal use only.

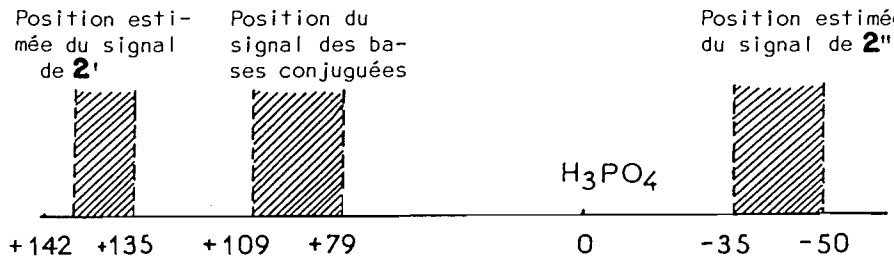

FIG. 1. Position des signaux des bases conjuguées des phosphoranes **2***b*–**2***f*.

du signal, comme on peut le constater sur la série des phosphites isologues **6**.

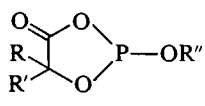

6

	$\delta^{31}P$
R = R′ = H, R″ = Pr	+135
R = Ph, R′ = H, R″ = iPr	+140, +137
R = R′ = CH_3, R″ = iPr	+137
R = R′ = CH_3, R″ = Ph	+127 (réf. 15)
R = R′ = Ph, R″ = Ph	+127 (réf. 15)

Cette valeur est très éloignée des $\delta^{31}P$ des produits de déprotonation des composés **2***b*–**2***f* (tableaux 1 et fig. 1). En fait, les pics observés sont situés entre le domaine des phosphoranures **2″** et celui des phosphites **2′** (fig. 1).

Nous retrouvons les phénomènes mis en évidence lors de l'action de la triéthylamine sur les phosphoranes **2***e* (10) (schéma 3) et **2***f* (11). Les résultats observés généralisent l'équilibre [3] aux phosphoranes **1***d*, **2***b*, **2***c*, **2***d*, **2***f* et **3**, les composés **1***d* et **3** constituant les cas extrêmes: pour le premier, au regard de la rmn, l'équilibre phosphite **1′***d* ⇌ phosphoranure **1″***d* est entièrement déplacé vers la forme à phosphore tricoordonné. A l'opposé, la déprotonation du phosphorane bicyclique **3** conduit exclusivement au phosphoranure **3″** (13) (schéma 4). Les composés **2***b*–**2***f* se situent entre ces deux limites (schéma 6).

[6]

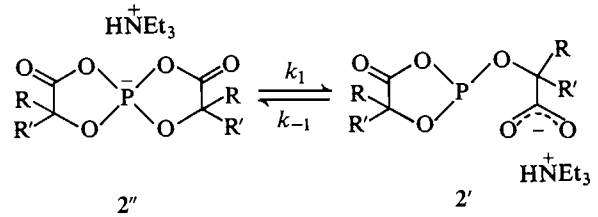

2″ **2′**

SCHÉMA 6

Les constantes de vitesse k_1 et k_{-1}, même à basse température, sont grandes par rapport à l'échelle de temps de la rmn de ^{31}P, qui, de ce fait, distingue seulement un signal composite pour les deux espèces **2′** et **2″**. Pour appuyer l'existence de cet équilibre, les signaux se déplacent vers les champs forts aux basses températures à l'exception du composé **2***d* (voir ci-après) (tableaux 1). En outre, ils sont d'autant plus blindés (donc l'équilibre est d'autant plus favorable au phosphoranure **2″**) que les restes α hydroxyacide sont substitués (tableaux 1). On retrouve l'influence de la température et des substituants sur les équilibres chaîne ⇌ cycle (16).

Cas particuliers

Les phosphoranes **2***b*, et surtout **2***d*, posent un problème supplémentaire, par rapport à leurs homologues **2***c*–**2***e*, **2***f*. Les spectres de leurs mélanges avec la triéthylamine et notamment pour des quantités de base inférieures à un équivalent, présentent un singulet fin situé dans le domaine des composés du phosphore hexacoordonné (tableaux 1). Il ne correspond ni à un composé d'addition (**2***b*, Et_3N), (**2***d*, Et_3N), pour lequel on attend un doublet P—H à champ fort, ni à un dérivé du phosphore hexacoordonné formé à partir de 3 ligands bidentés α hydroxyacide, dont le signal est plus blindé (travail en cours). Son $\delta^{31}P$ varie légèrement avec la température: −88 à +30°C, −92 à −80°C, pour **2***b*, −93,4 à +30°C et −96,5 à −80°C pour **2***d*. Dans le cas de **2***d*, il est possible d'orienter la réaction de déprotonation vers la présence exclusive dans le spectre du pic à δ −95, en remplaçant la triéthylamine par un équivalent de HNa. Lorsque la quantité d'hydrure est supérieure, le spectre présente le singulet à δ +88 et non plus le pic à champ fort. Dans les deux cas, l'addition d'un excès d'iodure de méthyle conduit au phosphorane à liaison P—CH_3 correspondant, la réaction étant nettement plus lente dans le premier cas. Cependant, ces résultats montrent que le phosphoranure se forme avec les deux stoechiométries adoptées (10).

Nous étant assuré de la reproductibilité des résultats, des travaux sont en cours pour essayer d'attribuer le signal à champ fort.

Le spectre des mélanges (phosphorane **2***b* + Et_3N) et (phosphorane **2***c* + Et_3N) présente deux signaux attribuables à l'existence possible de 3 diastéréoisomères, aussi bien pour les phosphites que pour les phosphoranures. Ces derniers offrent, en effet, les mêmes possibilités d'isomérie que les phosphoranes correspondants (8). (*i*) Le composé **2***a*, non substitué sur le reste α hydroxyacide, réagit sur la triéthylamine pour conduire à des mélanges complexes de composés à phosphore tétracoordonné. Ses bases conjuguées **2′***a* et **2″***a*, instables, n'ont pu être identifiées. (*ii*) Les phosphoranes **4** et **5** ne réagissent pas sur la triéthylamine. Ce résultat négatif met bien en évidence la finesse des phénomènes étudiés: le simple remplacement d'un groupement carbonyle dans le squelette du phosphorane **3** ou d'un atome d'oxygène par un groupement NH, dans celui de **1***d*, abaisse l'acidité du proton P—H au point, de le rendre inerte vis-à-vis de bases moyennes. Les composés **4** et **5** sont, toutefois déprontonés par les bases fortes, comme les hydrures alcalins.

Proportions des formes phosphite et phosphoranure en équilibre

L'existence d'un seul pic composite pour les deux espèces **2′** et **2″** ne nous permet pas de connaître directement les taux respectifs de ces entités. Nous pouvons, cependant, les estimer à partir de leur $\delta^{31}P$. Pour la première, ce paramètre est compris entre +135 et +142, alors que pour la seconde, il convient de prendre en compte un $\delta^{31}P$ proche de celui du phosphorane correspondant (5*b*, 13) ($-50 < \delta^{31}P < -35$).

Dans le cas des composés **2***b*–**2***f*, on trouve, même à basse température, des pourcentages de phosphoranure **2″** nettement plus faibles que ceux du phosphite **2′** (tableau 2). Rappelons

Can. J. Chem. Downloaded from www.nrcresearchpress.com by 210.87.254.6 on 09/06/12
For personal use only.

TABLEAU 2. Pourcentages respectifs des formes phosphite et phosphoranure dans les équilibres [1], [4] et [6] à −50°, −60°C et en solution dans le DMF

Composés	$\delta^{31}P$ phosphorane	$\delta^{31}P$ de la forme **2′**	$\delta^{31}P$ de la forme **2″**	$\delta^{31}P$ du signal composite	**2′** (%)	**2″** (%)
2*b* + NEt_3	−42 (réf. 8) J_{P-H} = 920 Hz	+135 à +142	−37 à −42	+109 +106	83 ± 2	17 ± 1
2*c* + NEt_3	−42 (réf. 8) J_{P-H} = 970 Hz	+135 à +142	−37 à −42	+106 +103	81 ± 2	19 ± 1
2*e* + NEt_3	−50 (réf. 8) J_{P-H} = 940 Hz	+135 à +142	−45 à −50	+79,4 (réf. 10)	68 ± 1	32 ± 1
2*f* + NEt_3	−38 J_{P-H} = 980 Hz	+135 à +142	−35 à −40	+79,9	67 ± 1	33 ± 1
1*d* + NEt_3 (CH_2Cl_2)	−36 J_{P-H} = 890 Hz	+132	−30 à −36	+131	100	0
3 + $2NEt_3$	−47 (réf. 19) J_{P-H} = 780 Hz		−46	−46 (réf. 12)	0	100

que pour le phosphorane **3** le spectre de rmn ^1H montre que l'équilibre est déplacé vers le phosphoranure (13).

En conclusion, l'action de la triéthylamine sur les phosphoranes **1***d*, **2***b*–**2***f* et **3** se traduit par la salification de la forme tricooordonnée en équilibre avec le phosphoranure, cet équilibre étant entièrement déplacé vers la première (composé **1***d*) ou vers la seconde (composé **3**) ou nettement favorable à la première (composés **2***b*–**2***f*). Ces résultats montrent que les phosphites **1′** et **2′** sont des acides de Brønsted plus forts que les phosphoranes **1** et **2**. Cependant, dans le cas des composés **2**, la présence dans les mélanges phosphorane + Et_3N, des deux bases conjuguées montre que la différence d'acidité entre le phosphorane et le phosphite isomères, n'est pas très importante.

Le phosphorane bicyclique **3** serait plus acide que la forme à phosphore tricoordonné tautomère. Nous pouvons envisager, pour ces dernières les composés **3′***a* et **3′***b*.

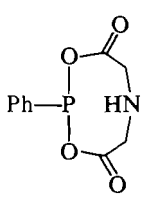

3′*a*

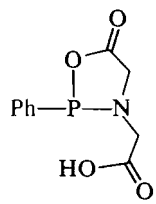

3′*b*

La première permet d'expliquer facilement pourquoi le phosphorane **3** serait plus acide, la fonction NH étant basique.

L'existence de la seconde signifierait que le composé **3** est plus acide que la fonction carboxylique de **3′***b*, ce qui est en contradiction avec les résultats observés pour le composé **1***d*.

Précisons que la seule forme à phosphore tricoordonné, tautomère de phosphoranes bicycliques analogues à **3**, mise en évidence par complexation avec des métaux de transition, a la structure **3′***a* et non **3′***b* (17).

2. *Etude potentiométrique: acidité de Brønsted des phosphoranes* **1**d, **2**b–**2**f *et* **3**

Les composés étudiés étant peu stables dans les solvants protiques, nous les avons titrés par la triéthylamine en solution dans le DMF. Le DMSO qui les oxyde en esters phosphoriques (composé **1***d*) ou en hydroxyphosphoranes (composés **2***b*–**2***f*) (18) n'a été utilisé que pour le phosphorane **3**, moins réactif dans ce solvant que les autres phosphoranes. La réaction de neutralisation a été suivie par potentiométrie. L'échelle électrique, en millivolts, a été étalonnée en unités de pH par titrage de deux acides étalons: les acides picrique et dichloroacétique (19).

D'après ce qui précède, la triéthylamine neutralise le phosphorane **3**. La valeur de pK_a tirée de la courbe de titrage correspondra effectivement à ce composé. En revanche, la même base sera protonée par la fonction acide carboxylique du phosphite **1′***d* plutôt que par le phosphorane **1***d*. Le pK_a sera attribué au premier et non au second. Enfin ce paramètre caractérisera l'acidité des phosphoranes **2** et de leur forme tricoordonnée tautomère **2′**, les bases conjuguées correspondantes étant en équilibre à la neutralisation. Nous aurons affaire à une valeur apparente.

Les courbes de neutralisation des phosphoranes **2** correspondent à des acides moyen-faibles, avec un point d'inflexion bien marqué, alors que les courbes des composés **1***d* et **3**, plus faibles, ne présentent pas de point d'inflexion. Pour les premiers, nous avons tiré les valeurs de pK_a par lecture de pH à demi-neutralisation, alors que pour les seconds nous avons adopté la valeur du pH à la demi-neutralisation théorique. L'indétermination est de 0,3 à 0,6 unités de pK_a (tableau 3).

Les pK_a ainsi déterminés, tout en étant élevés, correspondent à une acidité nettement plus forte que celle des autres composés organophosphorés à liaison P—H (tableau 4). Ils sont même inférieurs aux pK_a des acides carboxyliques, dans le même solvant (pK_a de l'acide benzoïque en solution dans le DMF: 12,3; dans le DMSO: 11) (20).

Il existe une différence remarquable entre les valeurs des composés **2**, d'une part, et de **1***d* et **3**, de l'autre. L'équilibre entre les deux acides, phosphorane **2** et phosphite **2′**, a pour résultat d'exalter considérablement l'acidité par rapport aux systèmes où l'acide neutralisé est univoque (phosphite **1′***d*, pour **1***d* et phosphorane **3**, pour **3**).

La labilité anormale du proton P—H, dans tous ces composés, s'explique par le caractère électrophile de l'atome de phosphore dont la densité électronique se trouve amoindrie par l'effet de conjugaison des groupements carbonyle intracycliques (19). Un seul groupement C=O n'est pas suffisant pour que ce phénomène soit sensible: ainsi, le composé **4** ne

Can. J. Chem. Downloaded from www.nrcresearchpress.com by 210.87.254.6 on 09/06/12
For personal use only.

TABLEAU 3. pK_a des composés **1***d*, **2***b*–**2***f* et **3** en solution dans le DMF et le DMSO (**3** seulement)

	Composés								
	Acide picrique	Acide dichloroacétique	**1***d*	**2***b*	**2***c*	**2***d*	**2***e*	**2***f*	**3**
pK_a (DMF)	1,2	7,2	7,0	4,1	4,1	4,0	4,2	3,8	8,7
pK_a (DMSO)	−0,3	5,9							6,8

TABLEAU 4. pK_a de quelques composés à liaison P—H décrits

	Composés			
	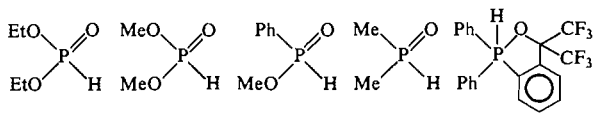			
pK_a (DMSO)		19,9	21,4	27,1	
pK_a (H_2O)	13				11,6
Références		3*a*	3*a*	3*a*	5*c*

réagit plus sur la triéthylamine. Par ailleurs, le remplacement du cycle oxo-4 dioxaphospholane-1,3,2 par un cycle oxo-4 oxazaphospholane (composé **5**) suffit également à anhiler la réactivité vis-à-vis de cette base.

III. Conclusion

Notre travail se démarque, à notre sens, de l'ensemble important de résultats observés dans le domaine des phosphoranes préparés à partir de molécules α hydroxylées ou α hydroxyaminées (α diols, α hydroxyacides, éthanolamines, ortho-aminophénols, α aminoacides . . .). Pour la première fois leur base conjuguée phosphoranure a été identifiée et des sels correspondants isolés. Grâce à un effet de délocalisation dans les hétérocycles formés à partir de restes α hydroxyacide ou acide iminodiacétique, l'acidité du phosphorane a été suffisamment exaltée pour que le pK_a soit déterminé par titration directe.

Les valeurs de pK_a ainsi déterminées, correspondent à des acides beaucoup plus dissociés que les composés organophosphorés à liaison P—H connus. Ils sont même plus forts, dans le DMF que les acides carboxyliques, comme l'acide benzoïque. Ces résultats éclairent d'un jour nouveau la réactivité des phosphoranes et notamment leurs propriétés nucléophiles. L'existence fréquente de l'équilibre phosphorane, phosphite (ou amidophosphite) a masqué pendant longtemps celle de l'équilibre phosphorane, phosphoranure. Aussi les auteurs ont-ils inteprété de façon systématique, les réactions des phosphoranes sur les électrophiles, par l'intervention exclusive de la forme à phosphore tricoordiné comme entité réactive. Nos résultats observés sur des phosphoranes ne présentant pas, d'après la rmn, l'équilibre phosphorane, phosphite, montrent que, pour ces composés, il convient de prendre en compte le phosphoranure. Désormais, toute approche rigoureuse de la connaissance du mécanisme des réactions entre les phosphoranes et les électrophiles devra envisager, *à priori*, les formes phosphite et phosphoranure, en tant qu'entités réactives. L'élimination de l'une des deux ne pourra être décidée qu'à l'issue d'observations d'ordre cinétique.

Partie expérimentale

Les analyses élementaires ont été effectuées par le service Central d'Analyse du CNRS (BP 22 69390 Vernaison).

Dans les dosages du carbone, lorsque cet élément est particulièrement abondant (50–70%) nous avons quelquefois observé des erreurs absolues dépassant le 1% par défaut. Ce fait est fréquent dans les composés organophosphorés. Ainsi, nous avons observé des erreurs absolues comprises entre 1,7 et 2 (relevées pour plusieurs échantillons provenant de préparations différentes) pour le phosphorane ci-après, dont la structure cristalline a été déterminée par diffraction des rayons-X (18, 19).

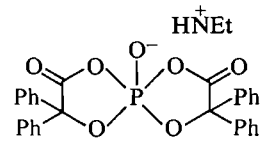

Nous avons également remarqué des écarts de cet ordre pour des composés à phosphore hexacoordonné dont la pureté a été démontrée, soit par diffraction des rayons X (20) soit par une bonne rmn (21).

Les spectres de rmn ^{31}P ont été enregistrés sur un appareil Perkin–Elmer R32 à transformée de Fourier (36,433 MHz). Les déplacements chimiques ont été comptés négativement à champ fort par rapport au signal de l'acide phosphorique pris comme référence. Les spectres de rmn ^1H ont été enregistrés sur un appareil Varian T 60 (60 MHz).

I. *Action des bases sur les phosphoranes* ***1***, ***2***, ***3*** *et* ***5***

Les mélanges (phosphorane + base) étudiés par rmn de ^{31}P à température variable, ont été préparés par pesée sous atmosphère d'argon. Sans cette précaution, on observe la formation de composés parasites à phosphore tétracoordiné. Les spectres ont été enregistrés sur un spectrographe Perkin–Elmer R32 à transformée de Fourier (26,433 MHz).

Préparation des phosphites ***6***

Ces composés ont été synthétisés en faisant réagir les chlorures d'acide: PrO—PCl_2 (composé **6***a*), iPrO—PCl_2 (composés **6***b*, **6***c*) ou PhO—PCl_2 (composés **6***d* et **6***e*), mole à mole avec les α hydroxyacides correspondants, en présence de deux équivalents de triéthylamine, suivant le mode opératoire décrit dans un travail antérieur (22). Les phosphites **6***a*, **6***b* et **6***c*, moins stables que leurs homologues **6***d* et **6***e*, déjà décrits (15), ont été isolés sous forme de liquides, accompagnés de faibles quantités (environ 10%) du spirophosphorane correspondant **2**. Leur $\delta^{31}P$ (voir la partie théorique) est caractéristique des composés de cette famille.

Isolement des phosphoranures de triéthylammonium

Le phosphoranure de triéthylammonium correspondant au dimère

Can. J. Chem. Downloaded from www.nrcresearchpress.com by 210.87.254.6 on 09/06/12
For personal use only.

TABLEAU 5. Valeurs aux points de demi-équivalence en mV et pK_a des composés **1***d*, **2**(*b*–*f*) et **4**

Composés	Titre $Et_3N \times 10^2$ *M*	Titre composés $\times 10^2$ *M*	Descente burette théo.	Obs.	Point de demi-équivalence (mV)	pK_a
Acide picrique	0,959[c]	1,137	2,40	3,00	449[a] 428[b] 480[c]	1,2
Acide chloroacétique	0,959[c]	2,987[c]	6,2		156[a] 150[b] 180[c]	7,2
1*d*	0,957[c]	0,976[c]	2,00[c]	Pas de point d'inflex.	255[c]	6,9
2*b*	0,900	1,683	3,75	3,8	307[a]	4,1[a]
2*c*	0,900	0,980	2,15	2,15	306[a]	4,1[a]
2*d*	0,900	1,229	2,95	3,00	310[a]	4,00[a]
2*e*	0,973	0,945	1,95	1,55	287[b]	4,2[b]
2*f*	0,900	0,797	1,8	2,2	320[a]	3,8[a]
3	0,935	1,095	2,3	Pas de point d'inflex.	87[a]	8,7[a]

[a] Echelle moyenne établie sur plusieurs titrages des acides étalon, effectués sur 5 jours à $+23°C < T < 30°C$.
[b] Echelle établie sur des titrages effectués dans le même jour à +21°C.
[c] Echelle établie sur un jour à +28°C.

2*f*, préparé à partir de l'acide tartrique, a été déjà décrit (11).

*Sel du phosphoranure 2″*e

A 4,54 g de phosphorane **2***e* (0,01 mol) dissous dans 5 mL de DMF, on ajoute 4,04 g de triéthylamine (0,0025 mol). Il se produit un échauffement léger. On ajoute 20 mL d'éther: un précipité blanc se forme qui est décanté, lavé plusieurs fois à l'éther: un précipité blanc se forme qui est décanté, lavé plusieurs fois à l'éther, en atmosphère d'argon rigoureusement anhydre, puis séché; Rdt: supérieur à 90%; rmn ^1H ($CDCl_3$, TMS, 60 MHz): 10,48 (1H, s, *H*NEt_3), 7,33 (20H, m, C_6H_5), 2,76 (6H, q, $J_{H-C-C-H}$ = 7 Hz, N—CH_2), 1,06 (9H, t, $J_{H-C-C-H}$ = 7 Hz, N—CH_2—CH_3). *Anal.* calc. pour $C_{34}H_{36}NO_6P$: C 69,80, H 6,20, N 2,39, P 5,30; tr.: C 68,32, H 6,15, N 2,50, P 5,31%.

Sel du phosphoranure 3″: préparation du phosphorane 3

On disperse 2,6 g d'acide iminodiacétique (0,005 mol) dans 30 mL de DMF; 3,6 g de phényldichlorophosphine (0,005 mol) sont ajoutés en refroidissant dans un mélange alcool–Carboglace. Il se produit un échauffement. L'acide se dissout progressivement. On laisse pendant une demi-heure. Spectre rmn de $\delta^{31}P$ δ: −48, J_{P-H} = 780 Hz. On reprend par 20 à 30 mL d'eau froide: il se forme un précipité pâteux qui est lavé à l'eau (30 mL), filtré puis lavé à l'éther et séché. Une poudre blanche est finalement obtenue. Elle est dissoute dans CH_2Cl_2. Un peu d'insoluble est éliminé par filtration. Le filtrat, repris par l'éther laisse déposer une précipité blanc qui est filtré, lavé à l'éther et séché; Rdt: 80%. Soluble dans CH_2Cl_2, THF, CH_3CN et DMF; rmn de ^{31}P (CH_2Cl_2) δ: −51,4, J_{P-H} = 780 Hz; rmn ^1H ($CDCl_3$, TMS, 60 MHz): 7,5 (1H, d, J_{H-P} = 766 Hz, P—*H*), 7,1 (5H, m, C_6H_5), 3,22 (4H, m, CH_2). *Anal.* calc. pour $C_{10}H_{10}NO_4P$: C 50,20, H 4,18, N 5,85, P 12,97; tr.: C 49,59, H 4,21, N 5,83, P 12,97%.

Action de la triéthylamine: isolement du sel du phosphoranure 3″

On dissout 2,4 g de phosphorane **3** (0,01 mol) dans 20 mL de DMF; 2,02 g de triéthylamine (0,005 mol) sont ajoutés. La solution est reprise par 30 mL d'éther: un précipité se forme qui est décanté, lavé à l'éther et séché; Rdt: supérieur à 90%; rmn ^1H (DMSO-d_6, TMS, 60 MHz): 11,5 (1H, s, *H*NEt_3), 7,5 (5H, m, C_6H_5), 3,8 (4H, m, CH_2), 2,9 (6H, q, $J_{H-C-C-H}$ = 7 Hz, N—CH_2), 1,1 (9H, t, $J_{H-C-C-H}$ = 7 Hz, N—CH_2—CH_3).

Phosphorane 4

Ce composé a été préparé en faisant réagir la phényldichlorophosphine sur l'hydroxyaminoacide ci-après, en présence de triéthylamine, en solution dans le THF (travail en cours).

HO—CO—$C(CH_3)_2$—NH—CH_2—$C(CH_3)_2$—OH

II. *Mésures potentiométriques*

Les solvants, DMF et DMSO Aldrich, ont été distillés sous 12 Torr et conservés sur tamis moléculaires 4 Å pendant 2 jours avant d'être utilisés. Le point de fusion du DMSO ainsi obtenu est de 18°, 515°C: l'acide picrique a été recristallisé dans le benzène et utilisé dans le semaine suivant la recristallisation. La triéthylamine a été distillée sous la pession atmosphérique et conservée sur de la soude en paillettes.

Les titrages ont été effectués dans le laboratoire de Génie chimique associé au CNRS N° 192, sous la responsabilité du Professeur Comtat. Nous avons utilisé un titreur automatique Metrohm E536 muni d'électrodes de marque Tacussel. L'électrode de référence est au calomel dans le cas du DMF et au chlorure d'argent dans celui du DMSO. Les concentrations des solutions, préparées par pesée au 0,01 mg, sont voisines de 10^{-2} *M*. Les dosages ont été effectués sur 2 à 4 mL de solution. Les volumes de solution de triéthylamine utilisés pour les neutralisations diffèrent de 1 à 10% des volumes théoriques. L'erreur commise est liée au temps d'introduction du volume de titrant; elle est maximale pour les vitesses d'introduction rapides (5 et 10 min), ce qui indique une réponse lente de l'électrode de verre à la modification du pH de la solution. Pour des temps d'introduction de l'ordre de 2 h, on observe un décalage des courbes de neutralisation vers les pH faibles, vraisemblablement dû à l'absorption de la vapeur d'eau par le solvant. Ces observations nous ont conduit à choisir un temps d'introduction intermédiaire (30 min pour 3.5 cm^3 de triéthylamine) et à effectuer les prises d'essai et les titrages dans des récipients conservés en atmosphère d'argon. La forte densité de ce gaz par rapport à l'air protège le récipient de mesure de l'humidité ambiante pour des temps inférieurs à 40 min. Les valeurs en millivolts, lues sur l'appareil, varient avec la température et également dans le temps. Nous avons renoncé à thermostater les solutions, cette opération ayant pour résultat de prolonger la durée du titrage au-delà des conditions précédentes de sécurité vis-à-vis de l'humidité. Nous avons adopté deux stratégies: (*i*) etablissement d'une échelle moyenne basée sur plusieurs titrages des acides picrique et dichloroacétique, effectués dans une période ne dépassant pas 5 jours, pendant laquelle la température ambiante est restée située aux alentours de +23°C. (*ii*) Utilisation d'une échelle "du jour" établie sur des titrages des acides étalon effectués le même jour que ceux des phosphoranes. Nous avons considéré que les variations de pK_a dues à des différences de température étaient négligeables

Can. J. Chem. Downloaded from www.nrcresearchpress.com by 210.87.254.6 on 09/06/12
For personal use only.

devant la précision des titrages (0,3 unités de pK_a pour les phosphoranes **2** et 0,5 unités pour **3** et **1***d*).

Le tableau 5 rassemble l'ensemble des résultats observés.

Remerciement

Nous remercions MM. Tran et Dall'ava pour leur collaboration technique.

1. L. A. HAMILTON et P. S. LANDIS. Organic phosphorus compounds. Vol. 4. *Edité par* G. M. Kosolapoff et L. Maier. Wiley–Interscience, New York. 1972. p. 463.
2. S. O. GRIM et L. C. SATEK. J. Inorg. Nucl. Chem. **39**, 499 (1977) et références incluses.
3. (*a*) E. N. ISVETKOV, M. I. TEREKHOVA, E. S. PETROV, R. A. MALENVANNAYA, S. P. MESYATS, A. I. SHATENSHTEIN et M. I. KABACHNIK. Izv. Akad. Nauk. SSSR Ser. Khim. 1981 (1978); traduc. Engl. 1743 (1979); (*b*) E. S. PETROV, M. I. TEREKHOVA, I. G. MALAKHOVA, E. N. TSVETKOV, A. I. SHATENSHTEIN et M. I. KABACHNIK. Zh. Obshch. Khim. **49**, 2410 (1979); traduc. Engl. J. Gen. Chem. **49**, 2127 (1979); (*c*) M. I. TEREKHOVA, N. A. BONDARINKO, I. G. MALAKHOVA, E. N. TSVETKOVA, E. S. PETROV et A. I. SHATENSHTEIN. Zh. Obsch. Khim. **52**, 516 (1982) et références incluses.
4. J. P. GUTHRIE. Can. J. Chem. **57**, 236 (1979).
5. (*a*) D. HELLWINKELL. Chem. Ber. **102**, 528 (1966); (*b*) I. GRANOTH et J. C. MARTIN. J. Am. Chem. Soc. **100**, 7434 (1978); **101**, 4626 (1979); (*c*) M. R. ROSS et J. C. MARTIN. J. Am. Chem. Soc. **103**, 1234 (1981).
6. A. MUNOZ, M. SANCHEZ, M. KOENIG et R. WOLF. Bull. Soc. Chim. Fr. 2193 (1974) et références incluses.
7. P. SAVIGNAC, B. RICHARD, Y. LEROUX et R. BURGADA. J. Organometal. Chem. **93**, 331 (1975).
8. M. KOENIG, A. MUNOZ, B. GARRIGUES et R. WOLF. Phosphorus Sulfur, **6**, 435 (1979).
9. D. Boyer. Thèse n° 2763, Toulouse (1983).
10. B. GARRIGUES, M. KOENIG et A. MUNOZ. Tetrahedron Lett. 4205 (1979).
11. A. MUNOZ, L. LAMANDÉ, M. KOENIG et R. WOLF. Phosphorus Sulfur, **11**, 71 (1981).
12. D. SCHOMBURG, W. STORZER, R. BOHLEN, W. KUHN et G. V. RÖSCHENTHALER. Chem. Ber. **116**, 3301 (1983).
13. B. GARRIGUES et A. MUNOZ. C.R. Acad. Sci. Paris, **293**, 677 (1981).
14. W. S. SHELDRICK, A. SCHMIDPETER, F. Z. WASCHKA, K. B. DILLON, A. G. W. PLATT et T. C. WADDINGTON. J. Chem. Soc. Dalton Trans. 413 (1981) et références incluses.
15. (*a*) J. WACHTER, B. F. MENTZEN et J. RIESS. Angew. Chem. Int. Ed. Engl. **20**, 284 (1981); (*b*) J. M. DUPART, A. GRAND, S. PACE et J. RIESS. J. Am. Chem. Soc. **104**, 2316 (1982).
16. R. ESCALE et J. VERDUCCI. Bull. Soc. Chim. Fr. 1203 (1974).
17. D. BONDOUX, I. TKATCHENKO, D. HOUALLA, R. WOLF, C. PRADAT, J. G. RIESS et B. F. MENTZEN. J. Chem. Soc. Chem. Commun. 1022 (1978); C. PRADAT, J. G. RIESS, D. BONDOUX, B. F. MENTZEN, I. TKACHENKO et D. HOUALLA. J. Am. Chem. Soc. **101**, 2234 (1979); J. WACHTER, F. J. JEANNEAUX et J. G. RIESS. Inorg. Chem. **19**, 2169 (1980).
18. A. MUNOZ, B. GARRIGUES et M. KOENIG. Tetrahedron, **36**, 2467 (1980).
19. A. DUBOURG, R. ROQUES, G. GERMAIN, J. P. DECLERCQ, B. GARRIGUES, D. BOYER, A. MUNOZ, A. KLAÉBÉ et M. COMTAT. J. Chem. Res. (S) 180 (1982); (M) 1901 (1982).
20. K. P. JOHN, R. SCHMUTZLER et W. S. SHELDRICK. J. Chem. Soc. Dalton Trans. 1841 (1974).
21. C. BUI CONG, G. GENCE, B. GARRIGUES, M. KOENIG et A. MUNOZ. Tetrahedron, **35**, 1825 (1979).
22. A. MUNOZ, B. GARRIGUES et R. WOLF. Phosphorus Sulfur, **4**, 47 (1978).

Can. J. Chem. Downloaded from www.nrcresearchpress.com by 210.87.254.6 on 09/06/12
For personal use only.

Propriétés nucléophiles des phosphoranures[1]

B. GARRIGUES ET A. MUNOZ
E.R.A. N° 926, Université Paul Sabatier, 118 route de Narbonne, 31062 Toulouse Cédex, France

Reçu le 19 octobre 1983

B. GARRIGUES et A MUNOZ. Can. J. Chem. **62**, 2179 (1984).

Les phosphoranures formés par action des bases sur des phosphoranes à liaison P—H contenant les ligands α hydroxyacide, α aminoacide ou acide iminodiacétique, réagissent avec des électrophiles comme les halogénures d'alcoyle, l'azoture de phényle, le disulfure de carbone, les orthoquinones ou les cétoacides. Ces réactions ont permis de préparer des phosphoranes et des composés à phosphore hexacoordonné nouveaux.

B. GARRIGUES and A MUNOZ. Can. J. Chem. **62**, 2179 (1984).

The reaction of various bases with P—H bond-containing phosphoranes bearing α-hydroxy acid, α-aminoacid, or iminodiacetic acid ligands leads to the formation of phosphoronates which react with electrophiles such as alkyl halides, phenyl azide, carbon disulfide, orthoquinones, or keto-acids. New phosphoranes and hexacoordinated phosphorus compounds could thus be prepared.

[Journal translation]

Can. J. Chem. Downloaded from www.nrcresearchpress.com by 210.87.254.6 on 09/06/12
For personal use only.

I. Introduction

Dans un travail précédent (1), nous avons identifié par rmn, la base conjuguée des phosphoranes **1**, **2** et **3**, en traitant ces composés par la triéthylamine. Leur déprotonation conduit au phosphite **1′** seul dans le cas des premiers, à un équilibre entre le phosphoranure **2″** et le phosphite **2′** dans celui des seconds et au phosphoranure **3″** seul en ce qui concerne le troisième. Quant au phosphorane **4**, il ne réagit pas avec la triéthylamine.

Il est important de souligner que les composés **1**–**4** ne présentent pas, en solution, et au regard de la rmn, l'équilibre tautomère phosphite ⇌ phosphorane à l'exception des premiers termes non substitués **1***a* et **2***a* (R = R′ = H) (1, 2). Ces résultats nous inclinent à prendre en considération, pour les composés **2** et **3**, le phosphoranure **2″** et **3″** comme entité réactive vis-à-vis des électrophiles, plutôt que les formes phosphites tautomères. Ce choix parait d'autant plus justifié que les phosphites contenant le motif dioxaphospholane sont peu nucléophiles et manifestent même des propriétés d'électrophiles (3). Nous montrerons, d'ailleurs, sur quelques exemples de réactions entre des phosphoranes et des électrophiles que l'espèce réactive est bien le phosphoranure et non les phosphite.

Déjà en 1975, P. Savignac *et al.* (4) ont postulé l'intervention du phosphoranure et non du phosphite lors de la réaction d'iodures d'alcoyle sur un spirophosphorane, traité au préalable par des bases fortes.

Nous avons entrepris une étude systématique de la réactivité des phosphoranures, bases conjuguées des phosphoranes **2** et **3**, vis-à-vis d'électrophiles variés: halogénures d'alcoyle, azoture de phényle, disulfure de carbone, orthoquinones et cétoacides. Les phosphoranures ont été formés en traitant par la tri-

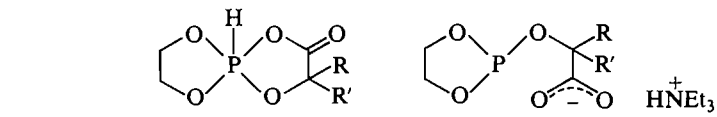

1 **1′**

a R = R′ = H
d R = R′ = CH_3

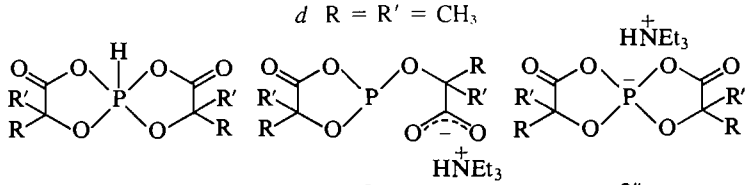

2 **2′** **2″**

a R = R′ = H
b R = H, R′ = iPr
c R = H, R′ = C_6H_5
d R = R′ = CH_3
e R = R′ = C_6H_5

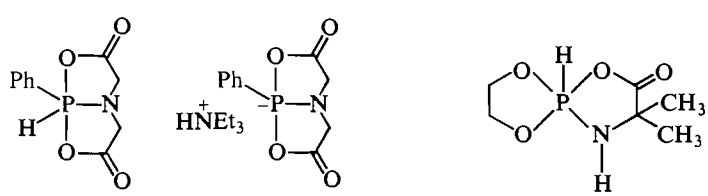

3 **3″** **4**

[1] Ce travail a fait l'objet de deux notes préliminaires (22, 23).

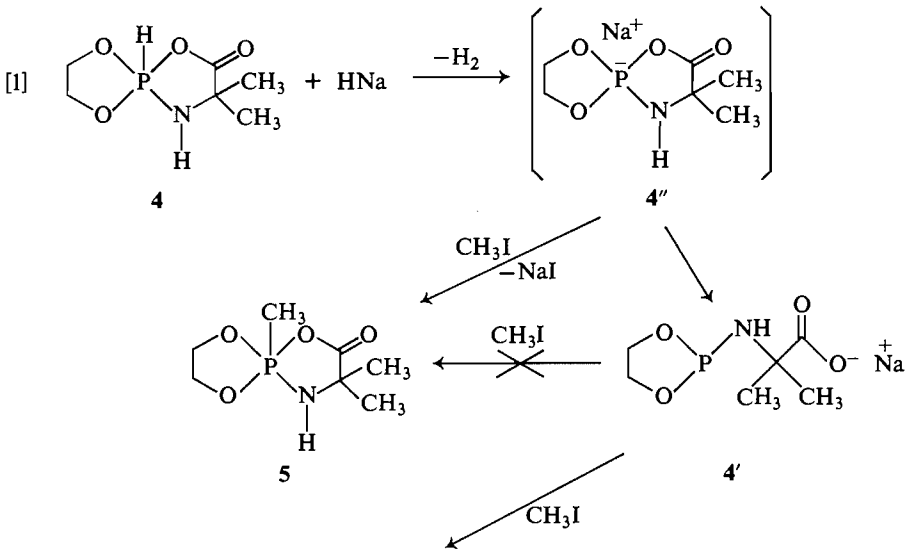

SCHÉMA 1

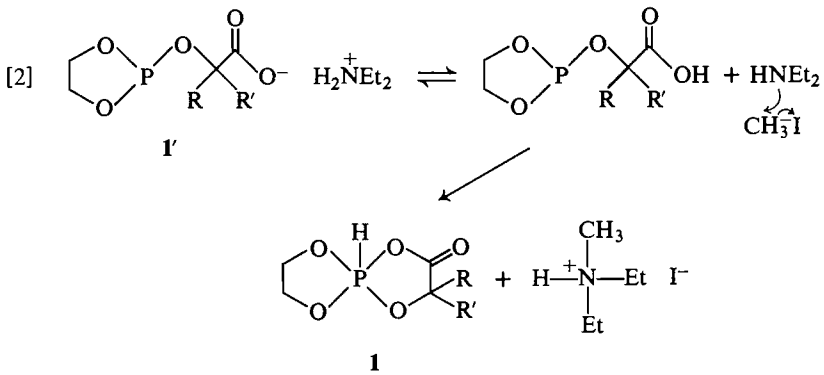

SCHÉMA 2

éthylamine les phosphoranes. Nous avons mené des essais parallèles en metant en contact ces derniers avec les électrophiles, en l'absence de base. Nous avons également étudié l'action de l'iodure de méthyle en présence de bases, sur les spirophosphoranes **1** et **4**, dont les phosphoranures n'on pas été identifiés (1).

II. Résultats et discussion

1. *Action des phosphoranures sur les halogénures d'alcoyle*

(a) *Réaction du phosphorane 4 avec l'iodure de méthyle en présence d'hydrure de sodium*

Nous avons opéré de trois façons différentes: (*i*) addition simultanée, à une solution de phosphorane **4** dans le DMF, de l'iodure de méthyle et de l'hydrure de sodium. Le spectre de rmn de ^{31}P montre la disparition du doublet P—H du composé **4** et l'apparition d'un quadruplet correspondant à un phosphorane à liaison P—CH_3. (*ii*) Addition de l'iodure de méthyle seul au spirophosphorane **4**: aucune réaction n'est observée au bout de 24 h. En ajoutant alors l'hydrure, on obtient quantitativement le même phosphorane à liaison P—CH_3. (*iii*) Si on inverse l'ordre d'introduction des réactifs, le résultat est différent: l'action de HNa sur le composé **4** conduit à l'amidosphosphite **4′** qui a été isolé (Schéma 1). Un résultat comparable a déjà été décrit pour un phosphorane contenant deux restes pinacol (4). Le composé **4′** réagit avec l'iodure de méthyle en donnant un mélange complexe de composés du phosphore tétracoordonné.

Le phosphorane à liaison P—CH_3 **5** a été isolé complexé à 0,4 molécules d'iodure de sodium. Ce dernier a été éliminé par passage sur de l'alumine activée (voir partie expérimentale).

Les résultats précédents excluent l'amidophosphite **4′** comme entité réactive dans la formation du phosphorane **5**. En fait, le produit cinétique de la réaction de HNa sur le phosphorane **4** doit être le phosphoranure **4″**, qui, en présence d'iodure de méthyle, conduit au composé **5**. En l'absence de ce réactif, il se transforme en amidophosphite **4′** qui est l'entité thermodynamiquement stable (Schéma 1).

(b) *Action des phosphoranes 1–3 sur les halogénures d'alcoyle en présence de triéthylamine*

La réaction de l'iodure de méthyle sur le sel de diéthylammonium des phosphites **1′** régénère les phosphoranes **1**. Le même résultat est observé quand on ajoute un excès d'iodure au mélange **1***d* (R = CH_3) + Et_3N ou **1***e* (R = C_6H_5) + Et_3N. Ces réactions confirment le faible caractère nucléophile de l'atome de phosphore des phosphites **1′**, possédant le motif dioxaphospholane, préalablement souligné par Hudson et Brown (3). En fait, c'est l'atome d'azote de la base, en équilibre avec son cation ammonium, qui attaque le groupement méthyle (schéma 2).

Can. J. Chem. Downloaded from www.nrcresearchpress.com by 210.87.254.6 on 09/06/12
For personal use only.

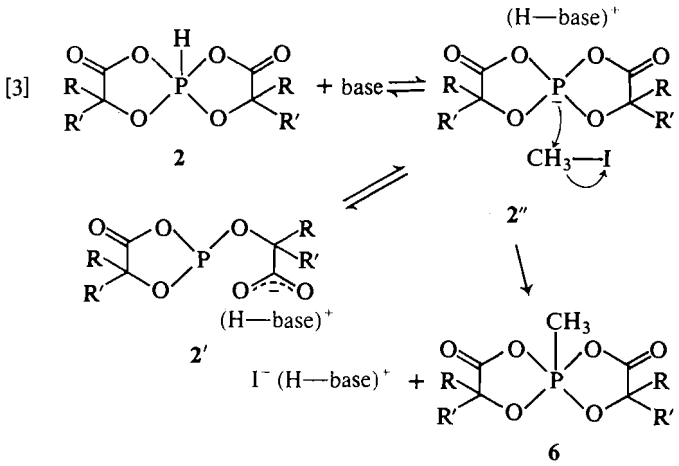

SCHÉMA 3

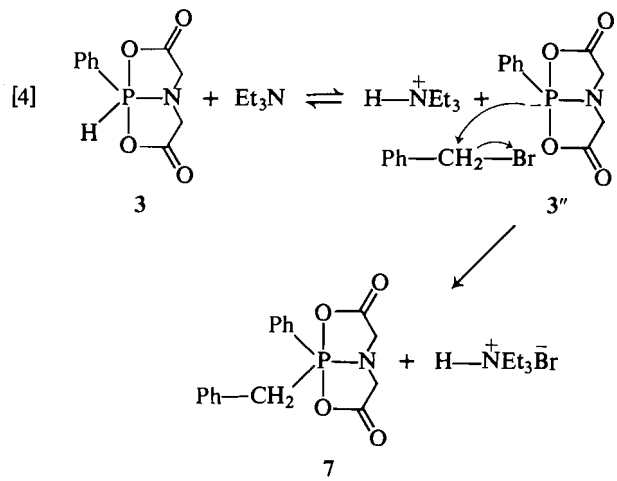

SCHÉMA 4

L'action d'un excès d'iodure de méthyle sur les mélanges phosphoranes **2** + base (Et_3N, DBU, HNa) ne régénère pas, comme précédemment, le phosphorane **2**. Dans tous les cas essayés, nous avons observé la formation du phosphorane à liaison P—CH_3 **6** que nous avons isolé en partant du phosphorane **2***e* (R = R′ = C_6H_5). Ce résultat montre encore que l'entité réactive est l'ion phosphoranure **2″** et non le phosphite **2′** (schéma 3).

Le phosphoranure **3″** est moins réactif que ses homologues **2″**: la formation du phosphorane à liaison P—CH_3 n'est pas observée, comme dans le cas des composés **2**, immédiatement après l'addition de CH_3—I. Cependant, en remplaçant ce dernier par le bromure de benzyle, nous avons préparé, avec un bond rendement, le phosphorane **7** (schéma 4).

2. *Action des phosphoranures sur l'azoture de phényle*

On sait que les phosphoranes réagissent sur les azotures organiques pour conduire, après élimination d'azote, à des aminophosphoranes. Cette réaction est facile quand le phosphorane est en équilibre avec sa forme à phosphore tricoordonné tautomère (5). Dans le cas où cette dernière n'est pas décelable à la température ambiante, la réaction n'a lieu qu'à température élevée (5).

Les phosphoranes **2***d* ou **3** ne réagissent pas sur l'azoture de phényle, à la température ambiante. En revanche, avec leurs phosphoranures de triéthylammonium, il se produit un dégagement immédiat d'azote. Le spectre de rmn de ^{31}P du mélange réactionnel montre que les phosphoranes **2***d* et **3** ont été transformés quantitativement en composés du phosphore pentacoordonné dépourvus de liaison P—H, **8** et **9**, que nous avons isolés (schéma 5).

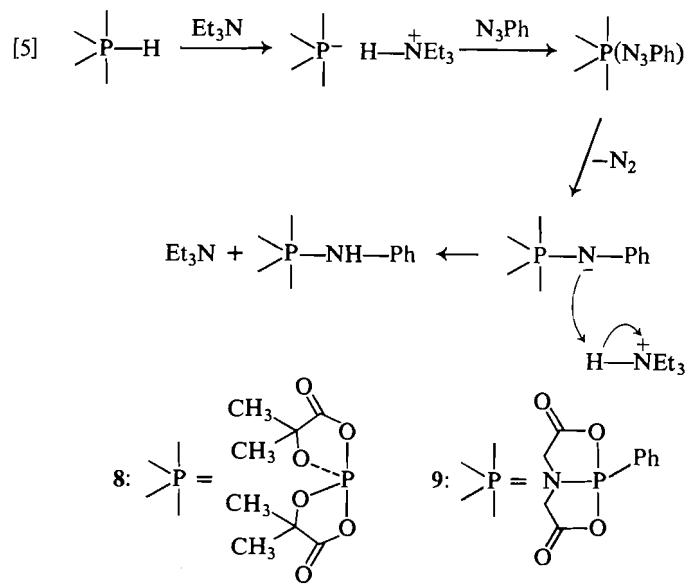

SCHÉMA 5

Nous pouvons proposer l'attaque du site déficient en électrons de l'azoture par le phosphoranure, suivie de la décomposition du produit intermédiaire, avec élimination d'azote, et de la formation d'un anion amidure, lequel, protoné donne finalement l'aminophosphorane **8** ou **9** (schéma 5).

3. *Action des phosphoranures sur le disulfure de carbone*

Le disulfure de carbone réagit avec de nombreux composés à phosphore tricoordonné pour donner, soit des composés d'addition (6), soit d'insertion, lorsque les substrats phosphorés contiennent des liaisons P—N (7). Des réactions d'insertion sont également connues, dans le cas de phosphoranes à liaison P—N. Dans ces derniers composés l'atome de phosphore atteint l'hexacoordination par retour d'un atome de soufre (8). Cependant, aucune réaction d'addition entre un phosphorane et le disulfure de carbone n'a encore été décrite, à notre connaissance.

Les phosphoranures de triéthylammonium **2″***d* (R = R′ = CH_3) et **3″** réagissent immédiatement et à la température ambiante, sur le disulfure de carbone. Nous avons isolé des substances cristallines fortement colorées. Dans le cas du phosphoranure **2″***d* (R = R′ = CH_3) nous en avons déterminé la structure par diffraction de rayons X. Nous avons affaire au sel de triéthylammonium d'un dithiophosphorane **10** (9). Cette structure est confirmée en solution, par les spectres de rmn (^{31}P et ^{1}H). A partir du phosphoranure **3″**, nous avons obtenu le phosphorane homologue **11** (schéma 6).

Comme dans le cas de l'azoture de phényle, aucune réaction n'est observée entre les phosphoranes **2***d*, **3** et le disulfure de carbone. Nous pouvons encore postuler une attaque du site électrophile, en l'occurrence l'atome de carbone du disulfure, par le doublet du phosphoranure (schéma 6).

4. *Action des phosphoranures 2″ sur les composés carbonylés: ditertiobutylorthoquinone et acide benzoylformique*

Les réactions des α dicétones ou orthoquinones et des cé-

Can. J. Chem. Downloaded from www.nrcresearchpress.com by 210.87.254.6 on 09/06/12
For personal use only.

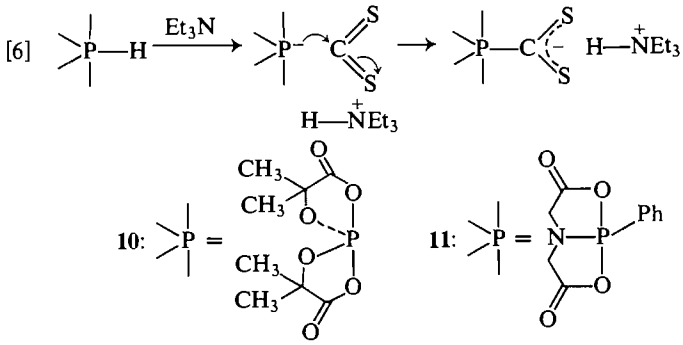

SCHÉMA 6

toacides avec les composés du phosphore tricoordonné, ont été abondamment étudiées (10, 11). La formation de phosphoranes qui en découle a été expliquée par des processus ayant comme point de départ l'attaque du doublet de l'atome de phosphore tricoordonné sur l'atome de carbone électrophile d'un groupement carbonylé (10, 11). La forme phosphite tautomère des phosphoranes à liaison P—H, peut également réagir avec les α dicétones pour donner un γ hydroxyphosphorane, capable de se transformer en présence de bases, en composé du phosphore hexacoordonné (12). Cependant, de telles réactions peuvent également se produire même quand l'équilibre phosphite ⇌ phosphorane n'est pas décelable à température relativement élevée. Ainsi le phosphorane **2***d* et la ditertiobutylorthoquinone réagissent, au bout de 12 h pour donner naissance au γ hydroxyphosphorane **12** (schéma 7). Sa structure est bien démontrée par son $\delta^{31}P$ (−44), très proche de celui de composé isologue **14** (13). En milieu basique (DMF, DMSO, solvant neutre + un équivalent de Et_3N), le composé 12 se transforme quantitativement d'après la rmn de ^{31}P, en composé du phosphore hexacoordonné **13**.

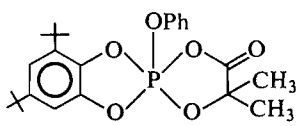

14 $\delta^{31}P = -46$ (réf. 13)

Ce dernier peut être obtenu directement et de façon instantanée, en mélangeant le phosphorane et la quinone en présence de triéthylamine.

Ces résultats peuvent s'interpréter par des schémas classiques à partir de la forme à phosphore tricoordonné **2′***d*, aussi bien par voie ionique (mécanisme proposé par Ogata et Yamashita (10)) que par voie radicalaire (Boekenstein *et al.* (14)). Cependant, nous pouvons également proposer un processus inspiré des schémas ioniques d'Ogata, faisant intervenir le phosphoranure (schéma 7), sans oublier toutefois que des entités radicalaires peuvent également jouer un rôle.

L'action des cétoacides sur les spirophosphoranes à liaison P—H, contrairement aux réactions avec les orthoquinones, n'a pas encore été décrite, à notre connaissance. Nous exposons, dans ce travail, des résultats préliminaires observés lors de la réaction entre le phosphorane **2***d* et l'acide benzoylformique.

On sait que les composés à phosphore tricoordonné (phosphites, phosphonites) contenant le motif dioxaphospholane réagissent avec les cétoacides. Le composé principal de la réaction est un spirophosphorane contenant le ligand α hydroxyacide résultant de la réduction de la fonction cétone en fonction alcool (11).

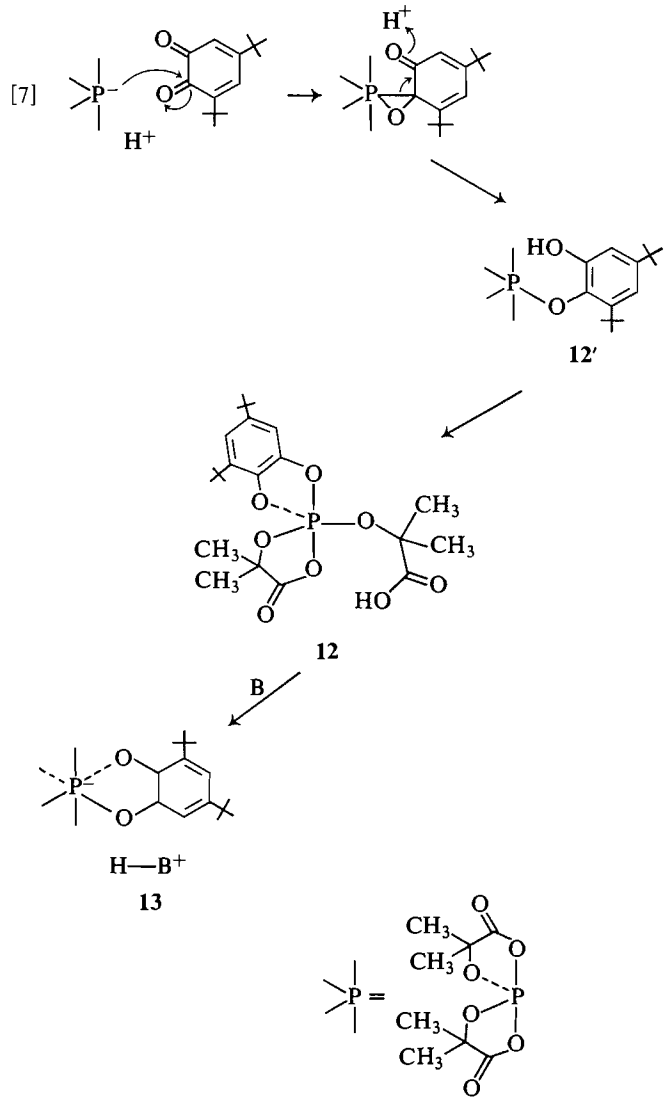

SCHÉMA 7

Les spirophosphoranes **2** ne réagissent pas à la température ambiante et sur une durée de plusieurs heures, sur l'acide benzoylformique. Cependant, en présence de triéthylamine qui entraîne la formation du phosphoranure **2″** on observe une réaction légèrement exothermique. Ainsi, avec le phosphoranure **2″***d*, R = R′ = CH_3, on observe la formation de composés dont le $\delta^{31}P$ correspond à des entités du phosphore hexacoordonné ($-108 < \delta^{31}P < -102$). Stables en solution (le spectre de rmn ^{31}P reste inchangé pendant plusieurs jours), ils se dégradent dès qu'ils sont isolés. Leur spectre de rmn de ^1H présente un multiplet à δ = 5,4 attribuable à des protons CH—C_6H_5.

La présence de ces signaux montre que la fonction cétonique a été réduite en fonction alcool et que le ligand cétoacide a été transformé en reste acide mandélique. Compte tenu de la valeur absolue élevée des $\delta^{31}P$, nous pouvons alors proposer la structure **15** (schéma 8), qui est confirmée par les intensités relatives des différents signaux de rmn ^1H. La multiplicité des signaux de rmn ^{31}P ainsi que celle des pics des protons CH—C_6H_5 et C—CH_3, s'explique par l'existence possible de nombreux diastéréoisomères.

La formation des composés **15** peut encore s'expliquer par l'attaque de l'atome de carbone électrophile de la fonction

Can. J. Chem. Downloaded from www.nrcresearchpress.com by 210.87.254.6 on 09/06/12
For personal use only.

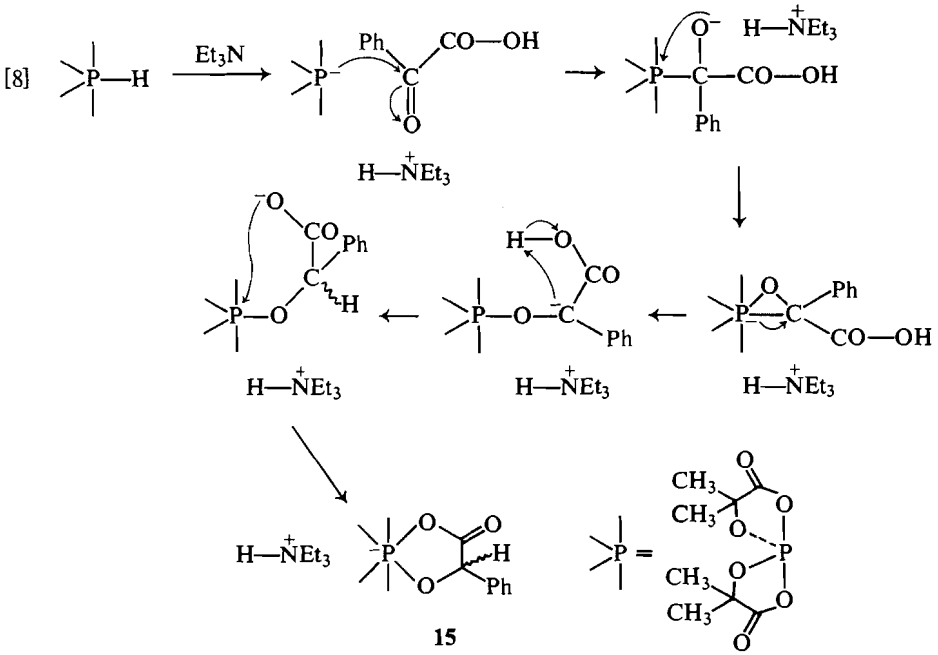

SCHÉMA 8

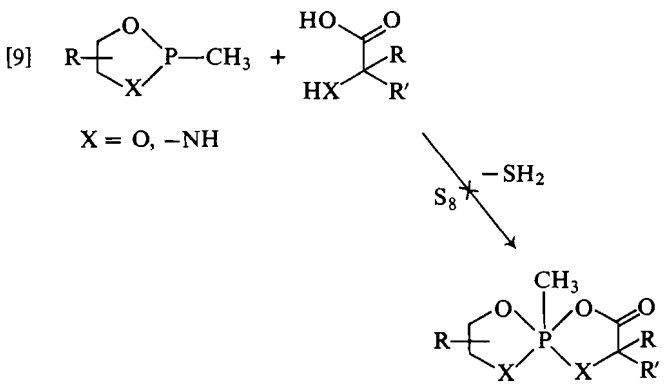

SCHÉMA 9

cétone de l'acide benzoylformique par le phosphoranure, suivie de réactions de réarrangement aboutissant finalement à la création de la fonction ester phosphorique P—O—CH—Ph (schéma 8). On peut remarquer que dans le benzène, la triéthylamine et l'ion benzoylformate ont une basicité comparable. Par conséquent le proton lié au phosphore peut être arraché par l'une ou l'autre des deux bases, d'où le schéma 8.

III. Conclusion

Jusqu'à ce jour, la réactivité des phosphoranes à liaison P—H a été envisagée, d'une façon générale, uniquement à travers l'intervention des formes à phosphore tricoordonné tautomères. Les résultats exposés dans ce travail montrent qu'il convient de prendre également en considération les phosphoranures.

Nous avons démontré que dans les réactions entre les phosphoranes **2**–**4** et les halogénures d'alcoyle, en présence de bases, les phosphoranures correspondants étaient les seules entités phosphorées réactives. Dans tous les autres cas étudiés nous pouvons affirmer que l'intervention exclusive de ces derniers est très probable.

Les réactions ainsi étudiées nous ont permis d'accéder à des phosphoranes originaux difficiles à préparer par des méthodes plus classiques. C'est le cas, notamment des phosphoranes **5** et **6** qui n'ont pas été obtenus à partir des réactions mises au point pour les pyrocatéchols, les diols et les éthanolamines (schéma 9) (15).

De même, les composés à phosphore hexacoordonné **15** n'ont pas été isolés par réaction directe d'α hydroxyacides sur le pentacholorure de phosphore alors que la condensation de pyrocatéchols (12*b*) ou d'acides benzhydroxamiques (16) sur le même substrat conduit assez facilement aux composés à phosphore hexacoordonné correspondants.

Quant aux phosphoranes isolés à partir du disulfure de carbone, ils représentent des exemples intéressants d'activation de ce dernier par les phosphoranures.

Ces résultats laissent entrevoir une utilisation systématique de ces composés comparable à celle des phosphines dont ils se rapprochent par leurs propriétés nucléophiles.

Partie expérimentale

Les analyses élémentaires ont été effectuées dans le service central d'analyse du CNRS (BP 22 69390 Vernaison).

Les spectres de rmn ^{31}P ont été enregistrés sur un appareil Perkin–Elmer R32 à transformée de Fourier (36, 433 MHz). Les déplacements chimiques ont été comptés négativement à champ fort par rapport au signal de l'acide phosphorique pris comme référence.

Les spectres de rmn ^{1}H ont été enregistrés sur un appareil Varian T60 (60 MHz) ou Perkin–Elmer R24 (60 MHz).

I. *Action des phosphoranes 1–4 sur CH_3I et $PhCH_2Br$ en présence de bases*

1. *Action de HNa sur le phosphorane 4: préparation du composé 4'*

La préparation du phosphorane **4** a été décrite (17); 1,93 g de phosphorane **4** (0,01 mol) sont dissous dans 5 mL de DMF; 1,2 g de HNa (0,05 mol) sont ajoutés en une seule fois: un fort dégagement gazeux est observé. Le volume de gaz recueilli, 220 mL, correspond environ à 0,01 mol d'hydrogène. On maintient sous agitation pendant 30 min. L'excès d'hydrure est filtré. Le filtrat présente en rmn de ^{31}P un seul pic à δ +135. Il est repris par 50 mL d'éther: un précipité blanc laiteux se forme que l'on centrifuge, lave à l'éther et sèche sous 10^{-2}

Can. J. Chem. Downloaded from www.nrcresearchpress.com by 210.87.254.6 on 09/06/12
For personal use only.

Can. J. Chem. Downloaded from www.nrcresearchpress.com by 210.87.254.6 on 09/06/12
For personal use only.

Torr (1 Torr = 133.3 Pa). On obtient une poudre blanche soluble seulement dans le DMSO. *Anal.* calc. pour $C_6H_{11}N\,NaO_4P$: C 33,52, H 5,16, N 6,52, Na 10,69, P 14,43; tr.: C 33,04, H 5,20, N 6,50, Na 10,70, P 14,07%.

2. *Action de CH_3I sur le phosphorane* **2**e *(R = R′ = Ph) en présence de triéthylamine*

A 0,01 mol (4,54 g) du phosphorane **2***e* (R = R′ = C_6H_5) on ajoute dans 10 cm^3 de DMF à la température ambiante, 0,04 mol (4,04 g) de triéthylamine. La réaction est instantanée. Un large excès d'éther entraîne la formation d'un précipité blanc qui est lavé plusieurs fois à l'éther. Le rendement est quantitatif.

A 5,85 g (0,01 mol) de sel de triéthylammonium du mélange **2′***e*, **2″***e* (R = R′ = C_6H_5) en équilibre, dispersés dans 20 mL de THF, on ajoute 4,26 g de CH_3I (0,03 mol). Un précipité d'iodure de triéthylammonium se forme qui est filtré. Le filtrat, repris par 20 mL d'hexane laisse déposer un precipité qui est filtré, redissous dans le THF, puis passé à travers une couche de silice. L'éluant, débarrassé du solvant sous 12 Torr abandonne une poudre blanche qui est le composé **6** pur; rmn de ^{31}P δ: −24 (sol. THF); rmn ^1H (DMSO-d_6, TMS, 60 MHz): 2,1 (3H, d, $^2J_{H-C-P}$ = 18 Hz, CH_3—P). *Anal.* calc. pour $C_{29}H_{23}O_6P$: C 69,94, H 4,66, P 6,23; tr.: C 70,8, H 5,28, P 6,19%.

3. *Action de Ph—CH_2—Br sur le phosphorane* **3** *en présence de Et_3N*

Préparation du composé **7**: 1,2 g de composé **3** (0,005 mol) sont dissous dans 5 mL de DMF; 1,01 g de Et_3N (0,01 mol) sont ajoutés, puis 1,4 g de bromure de benzyle (0,005 mol). Il se forme un précipité blanc de bromure de triéthylammonium. On filtre, lave à l'éther. Le filtrat est repris par 20 mL d'eau froide: un précipité se forme que l'on filtre, lave à l'eau puis à l'éther et sèche sous 10^{-2} Torr; Rdt: 80%; rmn ^{31}P δ: −31 (sol. DMF); rmn ^1H ($CDCl_3$, TMS, 60 MHz): 8 et 7,3 (10H, m, C_6H_5), 3,7 (d, $^2J_{H-C-P}$ = 11 Hz, CH_2—P), 3,3 (2q, parties AB d'un système ABX, X étant l'atome de phosphore, formé par les protons CH_2—N—P, J_{AB} = 15 Hz). L'ensemble de l'intensité des protons CH_2 représente 6 protons conformément à la structure **7**. *Anal.* calc. pour $C_{17}H_{16}NO_4P$: C 62,00, H 4,86, N 4,25, P 9,42; tr.: C 61,98, H 4,91, N 4,22, P 9,36%.

4. *Action de CH_3I sur le phosphorane* **4** *en présence de HNa*

Préparation du phosphorane **5**: 1,93 g de composé **4** (0,01 mol) sont dissous dans 10 mL de THF; 7,1 g d'iodure de méthyle (0,05 mol) sont introduits, suivis de 1,2 g d'hydrure de sodium (0,05 mol). Un fort dégagement gazeux se produit. Le volume de gaz, recueilli dans une éprouvette est de 220 mL. La solution est maintenue sous agitation pendant 1 h. L'iodure de sodium formé et l'excès d'hydrure sont éliminés par centrifugation. Le filtrat est concentré sous pression réduite; rmn de ^{31}P (sol. THF) δ: −24. On reprend par 50 mL d'hexane: une poudre précipite qui est filtrée, lavée à l'hexane et séchée; rmn ^1H (DMSO-d_6, TMS, 60 MHz): 5,33 (1H, d, $^2J_{H-N-P}$ = 19,5 Hz, P—N*H*—), 3,3 (4H, m, CH_2—O—), 1,63 (3H, d, $^2J_{H-C-P}$ = 18 Hz, CH_3—P), 1,27 (6H, s, C—CH_3). Ce spectre correspond bien au composé **6**. Cependant des quantités non négligeables d'iodure de sodium restent retenues (test de détection de l'ion iodure largement positif). L'analyse élémentaire correspond à **6** + 0,4 NaI.

La spectrographie de masse par désorption de champ permet de mettre en évidence les cations M^+, M + Na^+, 2M + Na^+. Ces résultats peuvent s'expliquer par la complexation du phosphorane et de l'iodure probablement au niveau du groupement carbonyle ou au niveau de l'atome de phosphore. Des phénomènes comparables ont été observés pour les adduits NaI, 3 DMF (18) et entre l'ion Al^{3+} et des composés organophosphorés (19). La poudre est soluble dans CH_2Cl_2. L'iodure a été éliminé par passage de la solution à travers une colonne d'alumine Merck 1077 activée par chauffage à +149°C, pendant 3 h. L'éluant, débarrassé du solvant sous pression réduite fournit directement le composé **5** pur sous la forme de cristaux blancs. *Anal.* calc. pour $C_7H_{14}NO_4P$: C 40,61, H 6,82, N 6,77, P 14,99; tr.: C 40,33, H 6,75, N 6,76, P 14,09%.

II. *Action de l'azoture de phényle sur les composés* **2**d *et* **3**

Les composés **2***d* ou **3** (0,0025 mol) sont dissous dans 10 mL de CH_2Cl_2; 0,25 g d'azoture de phényle (0,0025 mol) sont ajoutés. Aucun échauffement ni dégagement gazeux n'est observé. Le spectre de rmn de ^{31}P des solutions, 2 h plus tard présente seulement les signaux des phosphoranes **2***d* et **3**. On ajoute alors 0,25 g de Et_3N (0,0025 mol). Il se produit un dégagement gazeux abondant et un léger échauffement. On concentre sous pression réduite; rmn de ^{31}P (CH_2Cl_2) δ: −50,2 (peu intense), −58,3 (très intense), pour **2***d* et δ: +35,7, +17,6, +4,2 (très peu intenses) et −50,8 (très intense), pour **3**.

Isolement du composé **8**

On porte le volume de la solution à 10 mL de CH_2Cl_2, puis on ajoute 10 mL d'hexane: il se forme un trouble. On laisse à −20°C pendant 4 h. Des menus cristaux sont décantés, lavés à l'hexane et séchés; Rdt: 30%; rmn de ^{31}P ($CDCl_3$) δ: −57,6; rmn ^1H ($CDCl_3$, TMS, 60 MHz): 7,3 (5H, m, C_6H_5), 5,4 (1H, d, $^3J_{H-N-P}$ = 13 Hz, P—N*H*), 1,6 (12H, d, *J* = 4 Hz, C—CH_3). *Anal.* calc. pour $C_{14}H_{18}NO_6P$: C 51,37, H 5,50, N 4,28, P 9,44; tr.: C 50,77, H 5,46, N 4,28, P 9,51%.

Isolement du composé **9**

Le volume de la solution est porté à 20 mL. On ajoute 30 mL d'éther. Une huile dorée précipite. On laisse à −20°C pendant 16 h. On décante, lave à l'éther et sèche. Un solide jaune-clair est obtenu, qui, séché sous 10^{-2} Torr, se transforme en une poudre ocre clair. Celle-ci est dissoute dans 10 mL de CH_2Cl_2 et reprise par 1 mL d'éther: une huile orangée précipite qui est décantée immédiatement. On rajoute 2 mL d'éther au filtrat: un peu d'huile précipite encore que l'on décante. Le filtrat est laissé à −20°C pendant 4 h. Des microcristaux se forment que l'on décante, lave à l'éther et sèche; Rdt: 40%; rmn de ^{31}P ($CDCl_3$) δ: −50,8; rmn ^1H ($CDCl_3$, TMS, 60 MHz): 7,7, 7,4, 7,2 (10H, m, C_6H_5), 5,3 (1H, d, $^3J_{H-N-P}$ = 14 Hz, N*H*—P), 3,9 (4H, d, $J_{H-C-N-P}$ = 12 Hz, CH_2—CO—). *Anal.* calc. pour $C_{16}H_{15}NO_4P$: C 58,18, H 4,54, N 8,48, P 9,39; tr.: C 58,30, H 4,70, N 8,20, P 8,82%.

III. *Action du disulfure de carbone sur les phosphoranes* **2**d *et* **3**

Préparation des composés **10** *et* **11**

La préparation du composé d'addition **10** entre **2***d* et CS_2, en présence de Et_3N a été décrite (9).

Isolement du composé **11**

Phosphorane **3** (0,6 g; 0,0025 mol) est dissous dans 4 mL de CH_2Cl_2; 0,8 g de disulfure de carbone (0,01 mol) sont ajoutés. Le spectre de rmn de ^{31}P de la solution enregistré 3 h plus tard présente uniquement le doublet P—H du composé **3**; 0,25 g de Et_3N (0,0025 mol) sont alors ajoutés. Un léger échauffement se produit. La solution se colore rapidement en orangé intense; rmn de ^{31}P δ: −21, +11, +3,4 (très peu intense), −45,8 (très intense). On reprend par 30 mL d'éther: une huile orangée précipite qu'on laisse à −20°C pendant 2 h. On décante, lave à l'éther et sèche. On obtient une masse orangée visqueuse qui est redissoute dans 10 mL de CH_2Cl_2 puis reprise par 10 mL d'éther. Une huile orangée précipite. On laisse pendant quelques heures à la température ambiante. On décante, lave à l'éther et sèche. Une poudre orangée et hygroscopique est finalement obtenue; Rdt: 50%; rmn de ^{31}P δ: −46 (sol. CH_2Cl_2); rmn ^1H ($CDCl_3$, TMS, 60 MHz): 8 et 7,6 (5H, m, C_6H_5), 3,8 (4H, 5 raies, N—CH_2—CO—), 3,1 (6H, q, $J_{H-C-C-H}$ = 7 Hz, N—CH_2—), 1,2 (9H, t, $J_{H-C-C-H}$ = 7 Hz, N—CH_2—CH_3).

IV. *Action de la ditertiobutylorthoquinone sur le phosphorane* **2**d

Préparation du composé **12**

On dissout 2,4 g de phosphorane **2***d* dans 10 mL de THF; 2,2 g de ditertiobutylorthoquinone (0,01 mol), dissous dans 10 mL de THF sont ajoutés, à la température ambiante; rmn de ^{31}P après 12 h, δ: −45. La solution est reprise par 20 mL d'hexane: une huile brune précipite qu'on laisse déposer pendant 12 h à −20°C. Elle est ensuite décantée, lavée à l'hexane et séchée. Une poudre brune est ainsi finalement obtenue; PF: 128°C; ir (pastille KBr), $\nu_{C=O}$: 1725 et 1795 cm^{-1}; rmn de ^{31}P (CH_2Cl_2) δ: −45; rmn de ^1H ($CDCl_3$, TMS, 60

Can. J. Chem. Downloaded from www.nrcresearchpress.com by 210.87.254.6 on 09/06/12
For personal use only.

MHz): 9,7 (1H, s, O*H*), 7 (2H, s, C_6H_2), 1,4–1,7 (30H, m, *t*Bu et $C(CH_3)_2$).

Masse moléculaire: nous l'avons déterminée par cryoscopie dans le DMSO. Dans ce solvant, il faut prendre en compte les deux espèces chimiques anion hexacoordonné et H^+... DMSO qui constituent le composé à phosphore hexacoordonné **13**. La valeur trouvée est, dans ces conditions, apparente et il est nécessaire de la multiplier par deux pour avoir la masse réelle. PF, DMSO: 18,45°C; $K = 4{,}4$ K Kg mol^{-1}. Cette constante a été déterminée en étalonnant le solvant avec la triphénylphosphine et l'acide phénylphosphinique. Celle est conforme aux valeurs de la littérature (20, 21). Poids de **12**: 80,45 mg. Poids de DMSO: 4985 mg. $\Delta T = 0{,}36$°C. *M* apparente: 200; *M* réelle: 400; théorique pour **12**: 456. *Anal.* calc. pour $C_{22}H_{33}O_8P$: C 57,89, H 7,28, P 6,78; tr.: C 55,82, H 7,41, P 6,78%.

Isolement de 13 (HB = $HNEt_3^+$)

La réaction est conduite comme pour la préparation du phosphorane **12**. A la solution brute de ce composé dans le THF, on ajoute 1,01 g de Et_3N (0,01 mol). Il se produit un léger échauffement; rmn de ^{31}P δ: −98 (60%) et −100 (40%). Les deux pics correspondent à deux des huit diastéréoisomères possibles du composé **13**. On reprend par 20 mL d'hexane: un précipité brun se forme qu'on laisse déposer quelques heures à la température ambiante. On filtre, lave à l'hexane et sèche. Une poudre brune est finalement obtenue; Rdt: 80%; rmn de ^{31}P (THF) δ: −98 (60%), −100 (40%); rmn ^1H ($CDCl_3$, TMS, 60 MHz): 6,7 (2H, m, C_6H_2), 3,0 (6H, q, $J_{H-C-C-H} = 7$ Hz, N—CH_2—), 1,7 (39H, m, N—CH_2—CH_3 + C—CH_3 + $C(CH_3)_3$). *Anal.* calc. pour $C_{28}H_{49}NO_8P$: C 60,32, H 8,61, N 2,51, P 5,56; tr.: C 60,34, H 8,79, N 2,56, P 5,39%.

V. *Action de l'acide benzoylformique sur le spirophosphorane* **2**d *(R = R' = CH_3)*

Deux solutions sont préparées en dissolvant 1,18 g de phosphorane **2***d* (0,005 mol) et 0,75 g de Ph—CO—COOH (0,005 mol) dans 10 mL de benzène. A l'une des deux, on ajoute 0,5 g de Et_3N (0,005 mol). Un échauffement sensible se produit. On refroidit dans la glace. On laisse pendant 20 h à la température ambiante; rmn ^{31}P δ: −2, J_{P-H} = 630 Hz, −1 (10%), −104,3 (20%), −105,4 (45%), −107,2 (15%), −108 (10%). Le benzène est chassé sous 10^{-2} Torr. Il reste une substance résineuse légérement ambrée; rmn ^1H (60 MHz, C_6D_6, TMS): 8,7 (s, 1H, N*H*$^+$), 7 et 7,5 (m, 5H, C_6H_5), 5,4 (m, 1H, C*H*—C_6H_5), 2,6 (q, 6H, N—CH_2, *J* = 7 Hz), 1,6 (m, 12H, C—CH_3), 0,85 (t, 9H, N—CH_2CH_3, *J* = 7 Hz). Ce spectre correspond aux composés **15**.

Essai de purification: la substance précédente est dissoute dans 10 mL de CH_2Cl_2 puis reprécipitée par 20 mL d'éther. Une huile précipite que l'on décante. Le filtrat, débarrassé du solvant, abandonne une huile épaisse. Les spectres rmn ^{31}P des deux fractions ainsi obtenues sont à peu près les mêmes que celui du produit de départ. Cependant, la quantité de phosphonate à liaison P—H est plus importante (entre 10 et 30%). Les composés **15** se détériorent. Le spectre du produit brut en solution dans le benzène demeure inchangé pendant plusieurs jours. Spectre rmn ^{31}P de l'essai en l'absence de triéthylamine: δ −48, J_{P-H} = 934 Hz (phosphorane **2***d* de départ). Il reste inchangé après une semaine à la température ambiante.

Deux autres essais ont été effectués avec les mêmes quantités de réactifs, en remplacant le benzène par le chlorure de méthylène; rmn de ^{31}P (après 20 h de réaction) δ: +2, −0,5, −6, −8 (10%), −48, J_{P-H} = 934 Hz (15%), −101,7 (15%) −102,6 (45%), −103,5 (7%), −106,2 (8%).

Un fractionnement par redissolution dans CH_2Cl_2 et reprécipitation par l'éther ou l'hexane conduit à deux fractions dont les spectres de rmn ^{31}P sont comparables à celui du produit brut. Ce dernier reste stable en solution et s'altère assez rapidement une fois isolé (augmentation sensible du taux des phosphonates à liaison P—H).

Le spectre de rmn de ^{31}P des mélanges (**2***d* + PhCOCOOH) dans CH_2Cl_2 présente le doublet P—H du phosphorane de départ ($\delta^{31}P$: −48, J_{P-H} = 934 Hz). Vingt jours plus tard, ce doublet reste majoritaire. On note la présence de signaux larges à δ + 7, J_{P-H} = 727 Hz.

Remerciement

Nous remercions MM. Tran et Dall'ava pour leur collaboration technique.

1. B. GARRIGUES, D. BOYER et A. MUNOZ. Can. J. Chem. **62**, 2170 (1984).
2. A. MUNOZ, M. SANCHEZ, M. KOENIG et R. WOLF. Bull. Soc. Chim. Fr. 2193 (1974).
3. R. F. HUDSON et C. BROWN. Acc. Chem. Res. **5**, 204 (1972).
4. P. SAVIGNAC, B. RICHARD, Y. LEROUX et R. BURGADA. J. Organometal. Chem. **93**, 331 (1975).
5. M. SANCHEZ, J. F. BRAZIER, D. HOUALLA et R. WOLF. Nouv. J. Chim. **3**, 775 (1979).
6. A. W. HOFMANN. Justus Liebigs Ann. Chem. Suppl. 1, 1 (1861); K. A. JENSEN. J. Prakt. Chem. **148**, 101 (1937); T. N. MARGULIS et D. H. TEMPLETON. J. Chem. Phys. **36**, 2311 (1962); M. A. PUDOVIK, L. K. KIBARDINA, I. A. ALEKSANDROVA, V. K. KHAIRULLEN et A. N. PUDOVICK. Zh. Obshch. Khim. Traduc. Angl. **51**, 23 (1981); O. DAHL. Acta. Chem. Scand. **25**, 3163 (1971) et références incluses; E. NIECKE et R. RÜGER. Angew. Chem. Int. Ed. Engl. **21**, 62 (1982).
7. G. OERTEL, M. MALZ et H. HOLTSCHMIDT. Ber. **97**, 891 (1964); K. A. JENSEN et O. DAHL. Acta. Chem. Scand. **24**, 1179 (1970); H. J. VETTER et H. NÖTH. Chem. Ber. **96**, 1308 (1963); H. BOUDJEBEL, H. GONÇALVES et F. MATHIS. Bull. Soc. Chim. Fr. 1671 (1974).
8. R. G. CAVELL, K. I. THE et L. VANDEGRIEND. Inorg. Chem. **20**, 3813 (1981).
9. A. DUBOURG, R. ROQUES, G. GERMAIN, J. P. DECLERCQ, A. MUNOZ, A. KLAÉBÉ, B. GARRIGUES et R. WOLF. Phosphorus Sulfur, **14**, 121 (1982).
10. Y. OGATA et M. J. YAMASHITA. J. Am. Chem. Soc. **92**, 4670 (1970); J. Org. Chem. **38**, 3423 (1973) et références incluses.
11. T. SAEGUSA, S. KOBAYASHI, Y. KIMURA et T. YOKOYAMA. J. Am. Chem. Soc. **98**, 7843 (1976).
12. (*a*) M. KOENIG, A. MUNOZ, D. HOUALLA et R. WOLF. J. Chem. Soc. Chem. Commun. 182 (1974); (*b*) M. KOENIG, A. KLAÉBÉ, A. MUNOZ et R. WOLF. J. Chem. Soc. Perkin Trans. 2, 40 (1979).
13. A. MUNOZ, B. GARRIGUES et R. WOLF. Phosphorus Sulfur, **4**, 47, (1978).
14. G. BOEKESTEIN, W. G. VONCKEN, E. H. JANSEN et H. M. BUCK. Recl. Trav. Chim. Pays-Bas, **23**, 69 (1974).
15. (*a*) M. WIEBER et K. FOROUGHI. Angew. Chem. Int. Ed. Engl. **12**, 419 (1973); (*b*) C. MALAVAUD, Y. CHARBONNEL et J. BARRANS. Tetrahedron Lett. 497 (1975).
16. E. FLUCK et M. VARGAS. Z. Anorg. Allg. Chem. **437**, 53 (1977); E. V. HINRICHS et I. UGI. J. Chem. Res. (S), 338 (1978).
17. B. GARRIGUES, A. MUNOZ, M. KOENIG, M. SANCHEZ et R. WOLF. Tetrahedron, **33**, 635 (1977).
18. P. PIRET, Y. GOBILLON et M. VAN MURSSCHE. Bull. Soc. Chim. Fr. 205 (1963).
19. J. DELPUECH, M. KHADDAR, A. PEGUY et P. RUBINI. J. Am. Chem. Soc. **97**, 3373 (1975).
20. A. MUNOZ, L. LAMANDÉ, M. KOENIG. R. WOLF et J. BROSSAS. Phosphorus Sulfur, **11**, 71 (1981).
21. R. GARNSEY et J. E. PRUE. Trans. Faraday. Soc. **64**, 1206 (1968).
22. B. GARRIGUES, M. KOENIG et A. MUNOZ. Tetrahedron Lett. 4205 (1979).
23. B. GARRIGUES et A. MUNOZ. C. R. Acad. Sci. Paris, **293**, 677 (1981).

Les liaisons phosphore–azote via l'étude cristalline et moléculaire d'un iminodiazaphospholane

MARIE-ROSE MARRE, MICHEL SANCHEZ[1] ET ROBERT WOLF

Synthèse, structure et réactivité de molécules phosphorées, ERA 926 associée à l'Université Paul Sabatier, 31062 Toulouse Cédex, France

ET

JOËL JAUD ET JEAN GALY

GITER, Laboratoire de chimie de coordination du C.N.R.S., 205 route de Narbonne, 31400 Toulouse, France

Reçue le 11 octobre 1983

MARIE-ROSE MARRE, MICHEL SANCHEZ, ROBERT WOLF, JOËL JAUD et JEAN GALY. Can. J. Chem. **62**, 2186 (1984).

L'iminodiazaphospholane **1** cristallise dans le système monoclinique, groupe spatial $P2_1/c$ avec a = 10,243(9), b = 17,236(5), c = 11,992(9) Å et Z = 4. La structure a été déterminée par des méthodes de diffraction de rayons X sur monocristal et affinée jusqu'à R = 0,056 pour 1342 réflexions. La géométrie est celle d'un tétraèdre déformé. Les angles ∠NPN

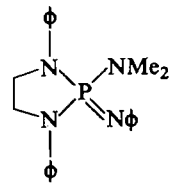

varient de 91,8° (angle du cycle) à 121,7° $\angle N_1P_2N_6\phi$. Le cycle diazaphospholane a une conformation enveloppe, dont la pointe est représentée par l'un des 2 atomes de carbone. Les 3 atomes d'azote tricoordonné ont une structure planaire; les directions des doublets des deux atomes du cycle sont parallèles et toutes deux orthogonales au doublet de l'atome d'azote exocyclique (N_7). Les longueurs de liaison P—N sont relativement courtes, comprises entre 1,620 Å et 1,669 Å alors que la liaison $P_2{=}N_6$ de 1,539 Å est parmi les plus faibles valeurs de la littérature. A partir d'une méthode empirique la multiplicité des liaisons P—N a été évaluée: 0,10 pour les deux P—N cycliques, 0,25 pour P—N exocyclique et 0,60 pour P=Nϕ.

MARIE-ROSE MARRE, MICHEL SANCHEZ, ROBERT WOLF, JOËL JAUD et JEAN GALY. Can. J. Chem. **62**, 2186 (1984).

Iminodiazophospholane **1** was obtained as monoclinic crystals, space group $P2_1/c$ with a = 10.243(9), b = 17.236(5), c = 11.992(9) Å, and Z = 4. The structure was determined by single-crystal X-ray diffraction and was refined up to R = 0.056

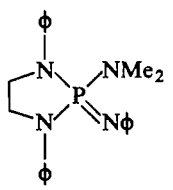

for 1342 reflections. The geometry of the molecule is that of a distorted tetrahedron with ∠NPN angles varying from 91.8° (ring angle) to 121.7° for $\angle N_1P_2N_6\phi$. The diazophospholane ring has an envelope conformation where one of the 2 carbon atoms is at the tip. The three tricoordinated nitrogen atoms have a planar structure; the lone pairs on the two ring nitrogens have parallel orientation and both are orthogonal to the lone pair of the exocyclic nitrogen atom (N_7). The P—N bond lengths are relatively short, falling between 1.620 Å and 1.669 Å, while the $P_2{=}N_6$ bond of 1.539 Å is among the smallest values ever reported. The multiplicities of the P—N bonds were assigned on the basis of an empirical method: 0.10 for the two cyclic P—N, 0.25 for the exocyclic P—N, and 0.60 for P=Nϕ.

[Journal translation]

Introduction

L'étude cristallographique que nous présentons entre dans le cadre d'un travail concernant la liaison formellement double phosphore–azote d'iminophospholanes (>P=N—), et fait suite à un article paru dans cette même revue (1) sur quelques propriétés chimiques des iminophospholanes. La diversité du comportement réactionnel de la liaison phosphazène caractérisée par: (a) une réaction d'addition de la fonction X—H (X = —O, —N) sur >P=NR conduisant à des entités pentacoordonnées (>P(X)NHR) ou à des sels de phosphonium (>P⁺—NHR X^-) (1–3); (b) une aptitude à la dimérisation dépendante de la nature des substituants sur l'atome de phosphore et d'azote (4); (c) le caractère donneur de l'atome d'azote imino (1, 5), nous astreint à mieux connaître des structures

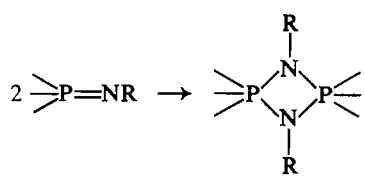

[1] Auteur à qui la correspondance doit être adressée.

Can. J. Chem. Downloaded from www.nrcresearchpress.com by 210.87.254.105 on 09/06/12
For personal use only.

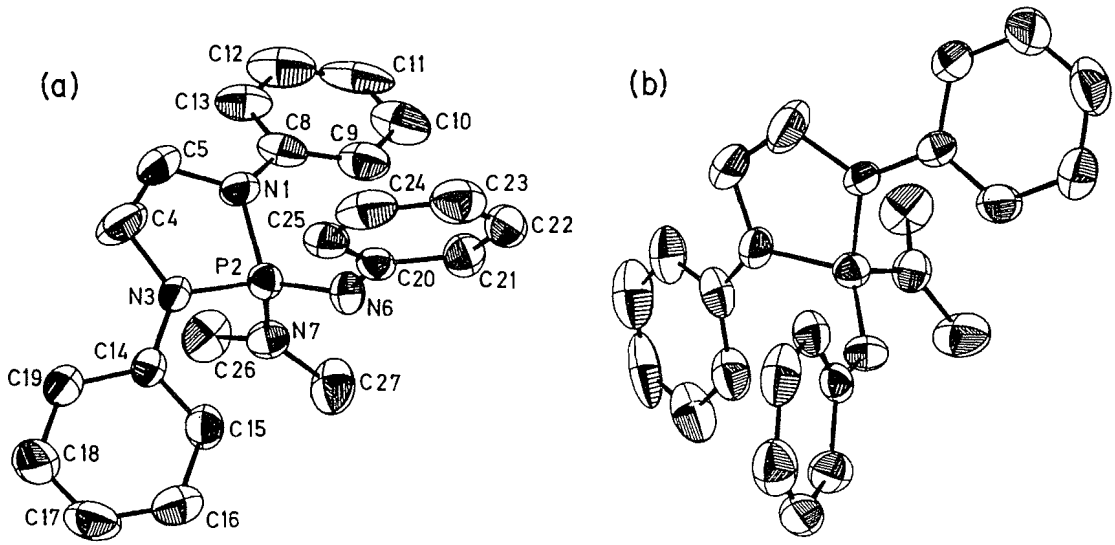

FIG. 1. (a) Vue perspective de la molécule et label des différents atomes. (b) Vue perspective (programme ORTEP).

moléculaires contenant le motif $\rangle P{=}N$. S'il existe quelques déterminations de structures d'iminophosphanes acycliques (voir tableau VI), l'étude cristallographique de l'iminodiazaphospholane **1** est le premier exemple original de cette famille, comportant quatre liaisons phosphore–azote:

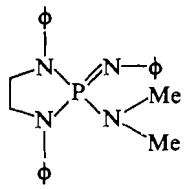

1

Au cours de ce travail nous nous proposons de préciser les points suivants: (*i*) configuration tétraédrique autour de l'atome de phosphore et conformation du cycle diazaphospholane; (*ii*) conformation planaire ou pyramidale des trois types d'atomes d'azote ce qui permet d'estimer les dispositions relatives des paires libres; (*iii*) longueurs comparées des liaisons phosphore–azote à caractère double (P=N—R) ou simple ($P{-}N\langle$) et utilisation de ce modèle moléculaire pour tester les formules empiriques concernant la multiplicité des liaisons P—N; (*iv*) relation entre la longueur de la liaison phosphazène et sa réactivité.

Résultats expérimentaux

Le composé **1** ($C_{22}H_{25}N_4P$)[2] cristallise dans le système cristallin monoclinique, groupe spatial $P2_1/c$ avec les paramètres: a = 10,243(9) Å, b = 17,236(5) Å, c = 11,992(9) Å, V: 2028(2) Å^3, Z = 4, D_{exp} = 1,22 g cm^{-3}, D_X = 1,23, μ (MoK$_\alpha$) = 1,0 cm^{-1}.

Les conditions d'enregistrement sont celles définies dans une précédente publication (6). Précisons quelques points: température ambiante; radiation utilisant une lame de graphite orientée MoK$_\alpha$ (λ = 0,7106 Å). Un total de 1443 réflexions indépendantes ont été enregistrées avec un angle de Bragg maximum de 24°; 1342 réflexions ont été utilisées.

La structure cristalline résolue par les méthodes directes a été affinée par moindres carrées (programme MULTAN). Le facteur de fiabilité final est R = 0,056 pour 1342 réflexions et 245 variables. La détermination de la structure et son affinement ont été conduits de la manière suivante: affinement isotrope de l'ensemble des atomes (hydrogènes exclus) dont les positions ont été déterminées par utilisation du programme MULTAN (R = 0,12); affinement des mêmes atomes avec agitation thermique anisotrope (R = 0,08); localisation des atomes d'hydrogène par fonction différence et vérification des positions repérées par calcul théorique; lors du calcul final les atomes d'hydrogène sont introduits avec une agitation thermique isotrope (B_H = 1,2 B_A où B_A est l'agitation thermique équivalente de l'atome auquel l'hydrogène est lié) et une position fixe. L'extinction secondaire a été également affinée et sa valeur est de 0,555 × 10^{-6}.

Le label des différents atomes est précisé sur la vue perspective de la molécule (programme ORTEP) (Fig. 1).

Les distances interatomiques et les angles avec leur écart type sont regroupés dans les tableaux 1 et 2. Le tableau 3 présente par ailleurs une étude comparative des paramètres les plus significatifs entre quatre composés (**1** à **4**) de formule générale $(R_2N)_3P{=}X$

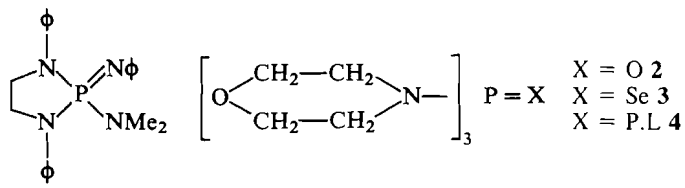

1

Les structures des dérivés **2**, **3** et **4** ont été résolues par Romming et Songstad (7, 8). Enfin le tableau 4 présente une

[2] La synthèse, les données spectroscopiques et les propriétés chimiques de **1** ont été décrites dans la réf. 1.

[3] Les tableaux rassemblant d'une part les coordonnées atomiques de tous les atomes et les facteurs d'agitation thermique et d'autre part les distances des principaux atomes aux plans moyens $P_2N_1C_3C_5$ et $P_2N_6N_7$ sont disponibles. On peut les obtenir en s'adressant au Dépôt de données non publiées, ICIST, Conseil national de recherches du Canada, Ottawa (Ont.), Canada K1A 0S2.

Can. J. Chem. Downloaded from www.nrcresearchpress.com by 210.87.254.105 on 09/06/12
For personal use only.

TABLEAU 1. Distances interatomiques (Å) et écart type ( )*

Atomes	Distances (Å)	Atomes	Distances (Å)
P(2)—N(1)	1,663(6)	P(2)—N(3)	1,669(7)
P(2)—N(6)	1,539(6)	P(2)—N(7)	1,620(7)
N(1)—C(5)	1,442(10)	N(1)—C(8)	1,406(9)
N(3)—C(4)	1,437(10)	N(3)—C(14)	1,414(10)
N(6)—C(20)	1,368(9)	N(7)—C(26)	1,452(11)
N(7)—C(27)	1,433(11)	C(4)—C(5)	1,470(12)
C(8)—C(9)	1,392(11)	C(9)—C(10)	1,382(13)
C(10)—C(11)	1,357(14)	C(11)—C(12)	1,355(13)
C(12)—C(13)	1,390(12)	C(13)—C(8)	1,365(10)
C(20)—C(21)	1,381(10)	C(21)—C(22)	1,389(11)
C(22)—C(23)	1,376(13)	C(23)—C(24)	1,374(13)
C(24)—C(25)	1,387(12)	C(25)—C(20)	1,397(10)
C(14)—C(15)	1,393(12)	C(15)—C(16)	1,388(14)
C(16)—C(17)	1,349(17)	C(17)—C(18)	1,369(16)
C(18)—C(19)	1,402(13)	C(19)—C(14)	1,388(12)

* Les longueurs C—H ont été déterminées, elles sont comprises entre 0,97 et 1,00 Å.

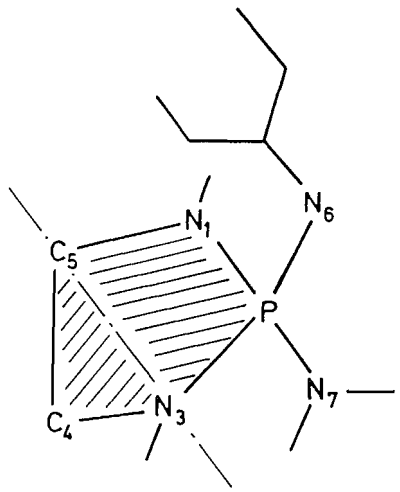

FIG. 2. Conformation enveloppe du cycle diazaphospholane.

compilation des longueurs de liaison P=N et des angles ∠P=N—R de treize iminophosphanes.

Description et discussion de la structure

L'examen des paramètres structuraux obtenus et des données comparatives (tableaux 1 a 4) nous permet d'apporter une réponse aux différentes questions que nous avons évoquées.

1. *Angles des liaisons autour de P*

La molécule est monomère à l'état cristallin; la rmn de ^{31}P du composé en solution dans le toluène ($\delta^{31}P$ = 1,5) constituait déjà une forte présomption pour trouver également une structure monomère à l'état solide.

L'atome de phosphore est au centre d'un tétraèdre déformé dont les longueurs des six arêtes N . . . N sont comprises entre 2,79 (6) pour N_1—N_6 et 2,39(2) Å pour N_3—N_1. Ces distances interatomiques s'harmonisent avec les valeurs des angles autour de P qui varient entre 121,7° (3) pour $\angle N_1P_2N_6$ et 91,8° (3) pour $\angle N_3P_2N_1$; cette dernière valeur est due à la contrainte du cycle pentagonal. La déformation angulaire la plus évidente concerne les angles $\angle N_1P_2N_6$ (121,7°) et $\angle N_3P_2N_6$ (118,1°). Celle-ci plus importante dans notre composé **1** que dans les dérivés **2** (moyenne des ∠NPO: 113°) et **3** (moyenne des ∠NPSe: 112°) (voir tableau 3).

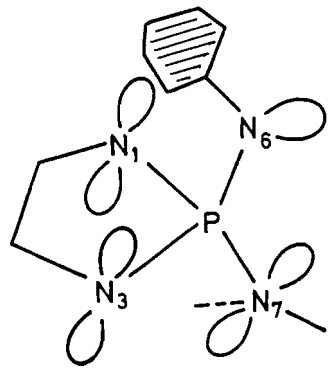

FIG. 3. Positions des doublets libres des atomes d'azote.

L'ouverture des angles ∠N—P=Nϕ montre en accord avec les règles de Gillespie (9) que la liaison P_2—N_6 se situe au plus loin des deux liaisons P_2—N_1 (N_1N_6 = 2,79 Å) et P_2N_3(N_3N_6 = 2,75 Å) afin de diminuer les interactions fortes entre les doublets libres des atomes d'azote N_1 et N_3 et les électrons de la liaison phosphazène P_2=N_6.

2. *Conformation du cycle*

Le cycle diazaphospholane défini par les cinq atomes N_1, P_2, N_3, C_4 et C_5 a une conformation enveloppe (Fig. 2). Le plan du rabat constitué par les atomes N_3, C_4, C_5 est dans la direction de l'espace opposé au groupe phényl imino (=Nϕ) et forme un angle de 10,7° avec le plan 1 moyen contenant les quatre atomes $N_1P_2N_3C_5$. Cette particularité mise à part le plan 2 ($P_2N_6N_7$) est pratiquement bissecteur du cycle à cinq chainons et des cycles benzéniques qui lui sont associés.

3. *Angles des liaisons autour de N et considérations conformationnelles*

La configuration des trois atomes d'azote tricoordonné (N_1, N_3, N_7) est pratiquement planaire puisque la somme des angles autour de N est respectivement de 360,0, 357,3 et 359,4° soit une valeur moyenne de 358,9°. Il est intéressant de comparer cette valeur à celle des dérivés **2** (352,9°) et **3** (348,2°) (tableau 3). Cette planéité presque parfaite des atomes d'azote dans **1** confirme les observations de Romming et Songstad (7) selon lesquelles l'accroissement de la polarité de la liaison P=Nϕ par rapport à >P=O ou >P=Se augmente le transfert électronique des atomes d'azote vers P et par suite accroît la structure plane de ces atomes d'azote. Corrélativement à la configuration des atomes d'azote nous avons cherché à préciser l'arrangement relatif des quatre doublets libres dans l'espace. La figure 3 en donne une représentation schématique; la direction de la paire libre d'un azote tricoordonné étant perpendiculaire au plan moyen des trois liaisons de cet atome, nous avons évalué les angles entre les directions des paires libres entre les atomes N_1, N_3 et N_7 (tableau 3). On constate que les doublets libres sur N_1 et N_3 sont presque parallèles (5, 7°) et tous deux orthogonaux aux doublets libres de N_7 (91,5°). Ce dernier doublet libre n'est pas en position *anti* par rapport à la liaison N=ϕ contrairement à **2** et **3** mais orthogonal au doublet libre de l'azote imino N_6 (Fig. 3).

4. *Longueur et multiplicité des liaisons P—N*

Il est couramment admis lorsqu'un atome d'azote est directement lié à un atome de phosphore qu'une structure planaire trigonale de l'azote favorise l'interaction $p\Pi$–$d\Pi$ entre la paire

Can. J. Chem. Downloaded from www.nrcresearchpress.com by 210.87.254.105 on 09/06/12
For personal use only.

Can. J. Chem. Downloaded from www.nrcresearchpress.com by 210.87.254.105 on 09/06/12
For personal use only.

TABLEAU 2. Angles entres liaisons (°) et écart type ( )*

Liaisons	Angles (°)	Liaisons	Angles (°)
N(1)—P(2)—N(3)	91,8(3)	N(1)—P(2)—N(6)	121,7(3)
N(1)—P(2)—N(7)	108.1(3)	N(3)—P(2)—N(6)	118.1(4)
N(3)—P(2)—N(7)	110.4(4)	N(6)—P(2)—N(7)	105.9(4)
P(2)—N(1)—C(5)	115.0(6)	P(2)—N(1)—C(8)	124.8(5)
C(5)—N(1)—C(8)	120.2(7)	P(2)—N(3)—C(4)	115.1(5)
P(2)—N(3)—C(14)	112.5(6)	C(4)—N(3)—C(14)	119.7(7)
P(2)—N(6)—C(20)	131.3(6)	P(2)—N(7)—C(26)	119.5(6)
P(2)—N(7)—C(27)	125.0(6)	C(26)—N(7)—C(27)	114.9(8)
N(3)—C(4)—C(5)	108.2(8)	N(1)—C(5)—C(4)	108.4(8)
N(1)—C(8)—C(9)	120.2(7)	N(1)—C(8)—C(13)	121.4(7)
C(9)—C(8)—C(13)	118.4(8)	C(8)—C(9)—C(10)	119.2(9)
C(9)—C(10)—C(11)	121.7(9)	C(10)—C(11)—C(12)	119.3(9)
C(11)—C(12)—C(13)	120.0(9)	C(12)—C(13)—C(8)	121.3(8)
N(3)—C(14)—C(15)	120.9(9)	N(3)—C(14)—C(19)	120.3(9)
C(15)—C(14)—C(19)	118.8(9)	C(14)—C(15)—C(16)	120.4(1.1)
C(15)—C(16)—C(17)	120.7(1.2)	C(16)—C(17)—C(18)	120.1(1.2)
C(17)—C(18)—C(19)	120.8(1.1)	C(18)—C(19)—C(14)	119.2(1.0)
N(6)—C(20)—C(21)	125.3(7)	N(6)—C(20)—C(25)	117.8(7)
C(21)—C(20)—C(25)	116.8(7)	C(20)—C(21)—C(22)	121.1(8)
C(21)—C(22)—C(23)	121.5(9)	C(22)—C(23)—C(24)	118.2(9)
C(23)—C(24)—C(25)	120.6(8)	C(24)—C(25)—C(20)	121.7(8)

TABLEAU 3. Comparaison entre les paramètres structuraux du composé **1** et 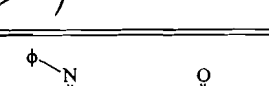 $_3$P=X (X = O **2**, X = Se **3**, X = P.L **4**)

Paramètres	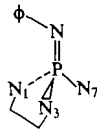 **1**	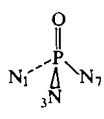 **2**	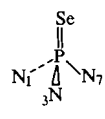 **3**	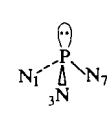 **4**
Longueur de liaison (Å)				
P—N_1	1,663	1,616	1,659	1,691
P—N_3	1,669	1,701	1,668	1,696
P—N_7	1,620	1,665	1,681	1,726
P=X	1,539	1,483	2,106	
Angles (°)				
N_1PN_3	91,8	114,4	114,1	110,7
N_1PN_7	108,1	98,9	101,2	98,0
N_3PN_7	110,4	101,3	102,4	97,9
ΣN_1	360	349,1	354,9	337,6
ΣN_3	357,3	352,1	349,7	353,2
ΣN_7	359,4	351,6	340,1	350,5
Angles des directions des P.L.				
N_1—N_3	5,7		80	83,4
N_1—N_7	91,9		107	114,9
N_3—N_7	91,2		115	109,1
P=X.N_7	84,8*	167,5	170	170,6

* N_7 désigne l'atome d'azote tricoordonné exocyclique dans **1** et celui de conformation *anti* par rapport à P=X dans **2** à **4**.

libre de N et les orbitales *d* vacantes du phosphore (10). En conséquence un raccourcissement de la liaison simple P—N doit être observé. Si l'on adopte comme longueur de liaison P—N simple 1,77 Å valeur déterminée par Cruikshank (11*a*) pour H_3N^+—PO_3^{2-} Na^+ ou 1,80 Å valeur déterminée par Cameron *et al.* (11*b*) pour H_3N^+—PO_3^{2-} K^+, les valeurs obtenues pour P_2—N_1 = 1,663 Å, P_2—N_3 = 1,669 Å, P_2—N_7 = 1,620 Å indiquent que ces liaisons présentent un caractère significatif de liaison multiple.

Les distances P_2—N_1 et P_2—N_3 sont équivalentes alors que P_2—N_7 est nettement plus courte, ce qui laisserait envisager une délocalisation des doublets Π, sur N_7, P_2 et N_6. Cette remarque serait confirmée par la longueur N_6—C_{20} = 1,368 Å plus petite que N_1—C_8 = 1,406 Å et N_3—C_{14} = 1,414 Å. Le résultat le plus important est la distance P_2—N_6 = 1,539 Å, la plus courte des quatre liaisons P—N, ce qui confirme son caractère de *double liaison*. Dans le tableau 4 nous avons classé par ordre croissant treize longueurs de liaison phosphazène P=N. On constate que la valeur trouvée pour **1** est une des plus courtes. De plus on peut observer un recouvrement entre la longueur de la liaison simple acyclique P_2—N_7 (1,620 Å) et celle formellement double à partir du composé ϕ_3P=N—C_3N_3ClNMe (20).

Il est intéressant d'avoir une idée plus quantitative de cette multiplicité. Pour cela, nous avons choisi d'appliquer la méthode des "valences de liaison" développée par Brown (12), basée sur les mesures des longueurs de liaison (R . X) qui permettent de calculer "les valences pondérées" autour d'un atome donné. Pour calculer la valence de liaison *s*, Brown propose l'équation générale:

$$s = \left(\frac{R}{R_0}\right)^{-n}$$

où *R*: longueur de liaison, R_0: longueur prise comme référence. Pour les composés phosphorés tétracoordonnés pentavalents, les paramètres sont les suivants: $N = 4{,}8$ et $R_0 = 1{,}70$ Å.

Nous avons appliqué cette équation au dérivé **1** et obtenu les valeurs suivantes:

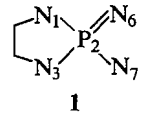
1

s(P—N_1) = 1,09
s(P—N_3) = 1,11
s(P—N_7) = 1,26
s(P—N_6) = 1,61
Σs = 5,07

Ce résultat est tout à fait remarquable car d'une part la somme des valences de liaison est de 5,07, soit à 1,5% près la

TABLEAU 4. Longueurs de liaison P=N et angles P=N—R dans 13 iminophosphanes

Molécules	Longueur P=N	Angle P=N—R	Références
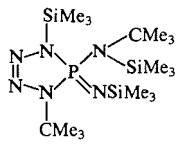	1,47		*
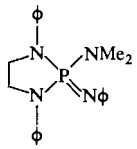	1,539*	131,3	Ce travail
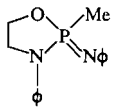	1,543	126,4	13
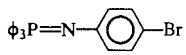	1,567	124,2	14
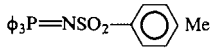	1,579	126,4	15
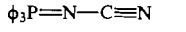	1,595	123,0	16
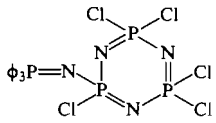	1,597	134,8	17
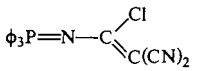	1,608	131,0	18
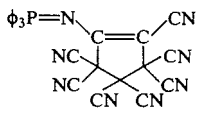	1,615	130,0	19
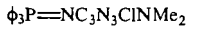	1,622	121	20
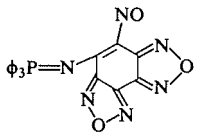	1,630	130	21
$F\phi_2P{=}NMe$	1,641	119,1	22
$\phi_3P{=}NS_3N_3$	1,645	121,0	23

* H. G. Schäfer et E. Niecke, communication personnelle (1983).

valeur théorique 5, et d'autre part, il montre que le caractère de double liaison $P_2{=}N_6$ est de 61%, alors que les liaisons P—N simples dans le cycle (P_2N_1 et P_2N_3) et exocyclique P_2N_7 ont un caractère de multiplicité de 10% et de 25%. Cet accroissement de l'indice de valence pour les liaisons "simples" se fait donc au détriment de la liaison formellement double P=N.

5. *Relation entre réactivité et structure*

Le composé **1** est très peu réactif, en particulier lors de l'addition des alcools, nous n'avons pas observé de réaction d'addition sur la liaison phosphazène, mais une simple interaction de type pont hydrogène due à la basicité de l'atome d'azote imino (1). Il est généralement admis d'interpréter la réactivité de la liaison phosphazène en terme de polarisation $P^{\delta+}—N^{\delta+}$, celle-ci étant très liée à la nature des substituants sur l'atome de phosphore et d'azote. Dans le composé **1** la faible valeur de la longueur P_2N_6 = 1,539 Å confirme donc son caractère de double liaison et sa faible polarisation; par suite elle peut expliquer la grande stabilité chimique manifestée par ce composé.

En conclusion l'étude de la structure du diphényl-1,3 diméthylamino-2, phénylimino-2 diazaphospholane-1,3,2 nous a permis de déterminer sur un même modèle moléculaire trois types de liaison phosphore–azote. Ces liaisons de longueur comprise entre 1,539 (6) Å et 1,669 (7) Å présentent toutes un caractère de multiplicité que nous avons évalué grâce au modèle empirique de Brown (12). La liaison phosphazène $P_2{=}N_6$ est comme attendue la plus petite (1,539 Å); parmi les longueurs P=N relevées dans la littérature cette distance est une des plus courtes. Les trois atomes d'azote tricoordonné sont plans, les orientations relatives des doublets libres ont été précisées. La comparaison avec trois autres dérivés acycliques de type ($\diagdown$N)$_3$PX (X = O, Se, D.L) montrent une disposition originale des quatre doublets libres dans le dérivé que nous avons étudié.

Remerciements

Le C.N.R.S., la D.G.R.S. et la D.E.S.R. ont apporté leur aide matérielle à la réalisation de ce travail; nous les en remerçions.

1. M. R. MARRE, M. SANCHEZ, J. F. BRAZIER, R. WOLF et J. BELLAN. Can. J. Chem. **60**, 456 (1982).
2. M. SANCHEZ, J. F. BRAZIER, D. HOUALLA et R. WOLF. Nouv. J. Chem. **3**, 775 (1979).
3. M. R. MARRE. Thèse de l'Université Paul Sabatier de Toulouse, n° 1084, 1983.
4. A. F. GRAPOV, L. V. RAZVODOVSKAYA et N. N. MEL'NIKOV. Russ. Chem. Rev. **50**, 324 (1981).
5. W. BUDER et A. SCHMIDT. Spectrochim. Acta, Part A, **32**, 457 (1976); R. MATHIS, N. ZENATI, N. AYED et M. SANCHEZ. Spectrochim. Acta, Part A, **38**, 1181 (1982).
6. A. MOSSET, J. J. BONNET et J. GALY. Acta Crystallogr. Sect. B, **33**, 2639 (1977).
7. C. ROMMING et J. SONGSTAD. Acta Chem. Scand. Ser. A, **36**, 665 (1982); **33**, 187 (1979).
8. C. ROMMING et J. SONGSTAD. Acta Chem. Scand. Ser. A, **32**, 689 (1978).
9. R. J. GILLESPIE. Molecular geometry. Van Nostrand Reinhold C^{ie}, London. 1972.
10. J. EMSLEY et D. HALL. The chemistry of phosphorus. Harper Row, London. 1976. Chap. 10.
11. (*a*) D. W. J. CRUIKSHANK. Acta Crystallogr. **17**, 671 (1964); (*b*) T. S. CAMERON, C. CHAN et W. J. CHUTE. Acta Crystallogr. Sect. B, **36**, 2391 (1980).
12. I. D. BROWN. Struct. Bonding, **11**, 1, (1981).
13. M. YU. ANTIPIN, YU. T. STRUCHKOV, N. A. TIKHONINA, V. A. GILYAROV et M. I. KABACHNIK. Zh. Strukt. Khim., **22**, 93 (russe), 220 (traduction anglaise) (1981).
14. M. J. E. HEWLINS. J. Chem. Soc. (B), 942 (1971).
15. A. F. CAMERON, N. J. HAIR et D. G. MORRIS. Acta Crystallogr. Sect. B, **30**, 221 (1974).
16. J. KAISER, H. HARTUNG et R. RICHTER. Z. Anorg. Allg. Chem. **469**, 188 (1980).
17. Y. S. BABU, T. S. CAMERON, S. S. KRISHNAMURTHY, H. MANOHAR et R. A. SHAW. Z. Naturforsch. Teil. B, **31**, 999 (1976).

Can. J. Chem. Downloaded from www.nrcresearchpress.com by 210.87.254.105 on 09/06/12
For personal use only.

18. M. YU. ANTIPIN, A. E. KALININ, YU. T. STRUCHKOV et YU. P. EGOROV. Zh. Strukt. Khim. **20**, 868 (1979).
19. P. J. BUTTERFIELD et J. C. TEBBY. J. Chem. Soc. Perkin Trans. 1, 1237 (1978).
20. T. S. CAMERON, K. MANNAN, M. BIDDLESTONE et R. A. SHAW. Z. Naturforsch. Teil B, **30**, 973 (1975).
21. T. S. CAMERON et C. K. PROUT. J. Chem. Soc. (C), 2285 (1969).
22. G. W. ADAMSON et J. C. J. BART. J. Chem. Soc. (A), 1452 (1970).
23. E. M. HOLT et S. L. HOLT. J. Chem. Soc. Dalton Trans. 1990 (1974).

Can. J. Chem. Downloaded from www.nrcresearchpress.com by 210.87.254.105 on 09/06/12
For personal use only.

Induced S_A-mesophases in binary, ternary, and quaternary mixtures of nematic α,α′-dimethylbenzalazine derivatives

MERCEDES MARCOS, ENRIQUE MELENDEZ, AND JOSE LUIS SERRANO
Departamento de Química Orgánica, Facultad de Ciencias, Universidad de Zaragoza, Spain

AND

DIDIER MATHIEU AND ROGER PHAN TAN LUU
Laboratoire de Prospective Réactionnelle et d'Analyse de l'Information, I.U.T., Avenue Gaston Berger, 13625 Aix-en-Provence, France

Received January 26, 1984

MERCEDES MARCOS, ENRIQUE MELENDEZ, JOSE LUIS SERRANO, DIDIER MATHIEU, and ROGER PHAN TAN LUU. Can. J. Chem. **62**, 2192 (1984).

Binary, ternary, and quaternary mixtures of four nematogenic compounds, 2-hydroxy-4,4′-dihexoxy-α,α′-dimethylbenzalazine, 4′-butyl-2-hydroxy-4-octoxy-α,α′-dimethylbenzalazine, *S*-4′-butoxy-2-hydroxy-4-(2-methylbutoxy)-α,α′-dimethylbenzalazine, and 2-hydroxy-4′-nitro-4-octoxy-α,α′-dimethylbenzalazine, were studied. In the mixtures with a nitro group a S_A-induced phase appeared.

These systems of mixtures were studied using the Scheffé algorithm. A comparative study of the prediction methods of the eutectic points was made.

MERCEDES MARCOS, ENRIQUE MELENDEZ, JOSE LUIS SERRANO, DIDIER MATHIEU et ROGER PHAN TAN LUU. Can. J. Chem. **62**, 2192 (1984).

On a étudié des mélanges binaires, tertiaires et quaternaires de quatre composés nématogènes: hydroxy-2 dihexoxy-4,4′ α,α′-diméthylbenzalazine, butyl-4′ hydroxy-2 octoxy-4 α,α′-diméthylbenzalazine, *S*-butoxy-4′ hydroxy-2 (méthyl-2 butoxy)-4 α,α′-diméthylbenzalazine et hydroxy-2 nitro-4′ octoxy-4 α,α′-diméthylbenzalazine. Dans les cas des mélanges contenant le composé nitré, il apparait une phase induite S_A.

On a étudié ces systèmes de mélanges en utilisant un algorithme de Scheffé. On a fait une étude comparative des méthodes de prédiction des points eutectiques.

[Traduit par le journal]

Introduction

In this paper we report on our study of the binary, ternary, and quaternary mixtures of four synthesized nematogenic compounds.

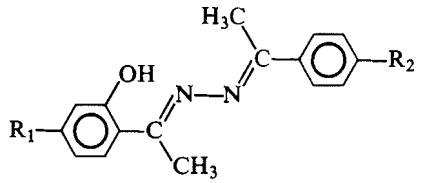

A: $R_1 = R_2 =$ O-*n*-C_6H_{13} (ref. 1)
B: R_1 = O-*n*-C_8H_{17} R_2 = *n*-C_4H_9 (ref. 2)
C: R_1 = O-CH_2—*CH(CH$_3$)—C_2H_5 R_2 = O-*n*-C_4H_9 (ref. 3)
D: R_1 = O-*n*-C_8H_{17} $R_2 = NO_2$ (ref. 4)

It was observed that when the compound **D** (2-hydroxy-4-octoxy-4′-nitro-α,α′-dimethylbenzalazine) was one component of the mixture a S_A-induced mesophase appeared. This behaviour, which occurs in some mixtures containing compounds with a nitro or cyano group as a terminal chain, has already been described by other researchers. However, the —C≡N group has been more frequently studied (5–7) than the nitro group (8).

In this paper we report a detailed investigation of the induced mesophase in the binary, ternary, and quaternary mixtures. While binary mixtures are relatively easy to study, the more complex mixtures present some problems. We have recently published two papers on the study of mesogenic compounds by a mathematical method using Scheffé algorithm (9, 10).

We have compared the results of the thermal properties and the eutectic composition of the mixtures using the above-mentioned mathematical method and those using thermodynamic equations (11, 12).

Experimental

In the study of mixtures the Scheffé algorithm is applied sequentially, starting with the most simple models, which require the least number of experiments, and continuing with the more complicated models if satisfactory results are not obtained.

The evaluation of each model used is carried out by test points.

In our previous paper (10), it was observed that in the study of mixtures of four components the full cubic model gave satisfactory results. With this model only 20 experiments are required to obtain the coefficients of the equation and 6 additional experiments to give test points. It is therefore only necessary to make 26 mixtures, four of which correspond to the pure compounds (Fig. 1).

For each mixture the following properties were measured: Y_1 (melting point, in K), Y_2 (clearing point, in K), Y_3 (S_A-mesophase range), Y_4 (*N*-mesophase range), Y_5 (total mesophase range), and Y_6 (ΔH total transition-crystal mesophase, in cal/g).

In mixtures of nematic compounds, two transitions usually appear during the melting process (11). The first one corresponds to the eutectic mixture (crystal → crystal + mesophase) whereas the second corresponds to the transition of the entire mixture to the corresponding mesophase (crystal + mesophase → mesophase).

The data used for the Y_1 response (melting point) correspond to the transition crystal + mesophase → mesophase.

All the properties were studied using the full cubic model with the exception of the Y_3, induced S_A-mesophase range, which was studied by means of the quadratic model.

The composition of the prepared mixtures as well as their respective measured properties are shown in Table 1.

We have expanded on the experimental studies of the binary mixtures in order to study the induced S_A-phase and to compare the various predictions of the eutectic.

Can. J. Chem. Downloaded from www.nrcresearchpress.com by 210.87.254.42 on 09/06/12
For personal use only.

TABLE 1. Mixture composition and experimental results

No.	Matrix A	B	C	D	% Components A	B	C	D	Y_1	Y_2	Y_3	Y_4	Y_5	Y_6
1	1	0	0	0	100	0	0	0	387.6	424.6	0	37.0	37.0	16.31
2	0	1	0	0	0	100	0	0	338.2	393.0	0	54.8	54.8	11.08
3	0	0	1	0	0	0	100	0	379.0	403.7	0	24.7	24.7	17.43
4	0	0	0	1	0	0	0	100	372.2	420.2	0	48.0	48.0	17.91
5	1/2	1/2	0	0	50.2	49.8	0	0	354.7	407.5	0	52.8	52.8	8.44
6	1/2	0	1/2	0	54.9	0	45.1	0	368.4	416.6	0	48.2	48.2	15.56
7	1/2	0	0	1/2	49.9	0	0	50.1	360.0	427.4	53.9	13.5	67.4	13.76
8	0	1/2	1/2	0	0	51.5	48.5	0	344.2	395.7	0	51.5	51.5	11.09
9	0	1/2	0	1/2	0	51.7	0	48.3	344.4	411.3	51.7	15.2	66.9	12.12
10	0	0	1/2	1/2	0	0	49.2	50.8	352.3	416.5	38.0	26.2	64.2	9.98
11	1/3	1/3	1/3	0	37.0	32.9	30.1	0	352.5	408.1	0	55.6	55.6	8.94
12	1/3	1/3	0	1/3	32.7	32.9	0	34.4	349.2	416.8	57.4	10.1	67.5	8.26
13	1/3	0	1/3	1/3	32.1	0	36.0	31.9	362.2	419.6	43.3	14.1	57.4	9.96
14	0	1/3	1/3	1/3	0	29.3	36.3	34.4	348.8	410.0	46.8	14.4	61.2	8.43
15	1/3	2/3	0	0	33.3	66.7	0	0	349.2	402.1	0	52.9	52.9	8.09
16	2/3	1/3	0	0	67.7	32.3	0	0	365.9	411.6	0	45.7	45.7	15.44
17	1/3	0	2/3	0	31.2	0	68.8	0	362.0	411.9	0	49.9	49.9	14.22
18	2/3	0	1/3	0	64.9	0	35.1	0	370.7	419.1	0	48.4	48.4	14.23
19	1/3	0	0	2/3	30.7	0	0	69.3	358.7	435.0	17.6	48.7	66.3	16.52
20	2/3	0	0	1/3	66.0	0	0	34.0	367.5	427.9	50.8	9.6	60.4	13.35
21	0	1/3	2/3	0	0	32.3	67.7	0	360.7	401.2	0	40.5	40.5	10.59
22	0	2/3	1/3	0	0	67.1	32.9	0	329.0	395.9	0	66.9	66.9	9.89
23	0	1/3	0	2/3	0	33.5	0	66.5	357.5	413.9	18.9	37.5	56.4	12.61
24	0	2/3	0	1/3	0	68.6	0	31.4	341.1	406.1	52.7	12.3	65.0	8.30
25	0	0	1/3	2/3	0	0	31.8	68.2	356.9	416.7	2.3	57.5	59.8	11.53
26	0	0	2/3	1/3	0	0	66.2	33.8	360.0	412.0	36.2	15.8	52.0	11.82

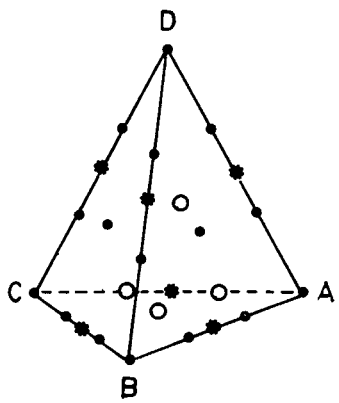

FIG. 1. Experimental domain: ●, experimental points; *, test points.

Table 2 shows the observed transitions and the thermal and thermodynamic data.

The mixtures were prepared by melting the compounds in a glass tube, stirring with a thin glass rod for 1 min, then cooling rapidly.

Transition temperatures and enthalpies were measured by differential scanning calorimetry (Perkin-Elmer DSC-2) operated at a scanning rate of 4 K/min on heating. The apparatus was calibrated by taking the known melting point and the known melting heat of indium (429.6 K, 6.8 cal/g).

Phase textures were identified using a polarizing microscope with a hot-stage (Reichert-Thermovar HT-1 B11).

Results and discussion

Studies were made with different orders of mathematical models. The best results for Y_1, Y_2, Y_4, Y_5, and Y_6 were obtained with the full cubic model. For Y_3, with an elevated number of zeros, the quadratic model gave a better approximation.

The equations for both models and the coefficients calculated using matrix algebra are shown in Table 3.

Data in an analytical form can be obtained for any mixture using the Scheffé algorithm as a starting point. Nevertheless, for the study of binary, ternary, and quaternary mixtures a graphic representation of the results, easily done using a computer, is much more effective.

Figures 3 to 8 show the isoresponse curves of the mixtures for the six parameters studied.

Quaternary mixtures corresponding to the inside of the tetrahedron can be studied easily by making regular sections parallel to one of the surfaces (Fig. 2). In this particular case the regular arrangement of the isoresponse curves on the surface of the tetrahedron provide fairly exact information about their distribution inside and thus we give only the interior sections for two properties, melting point (Y_1) (Fig. 9) and induced S_A-mesophase range (Y_3) (Fig. 10), as examples.

Figure 3 shows the calculated isoresponse surfaces of the melting points. The lowest melting points are to be found in an area very near component **B** and correspond to the binary mixtures of compounds **B** and **C**, where the first component is in greater quantity, and a small surface of the ternary and quaternary mixtures where the percentage of the other two components is very small.

Study of the quaternary mixture does not show any modification of the results found with the ternary mixtures (Fig. 9). The lowest melting points are found in very limited areas around the binary mixtures (see ruled zone in Fig. 3).

Figure 4 shows the calculated isoresponse curves for the clearing temperature. As expected, the variation of the curves is much smoother than that of the melting points. The highest

Can. J. Chem. Downloaded from www.nrcresearchpress.com by 210.87.254.42 on 09/06/12
For personal use only.

TABLE 2. Thermal and thermodynamic data for binary mixtures

System	Composition (mol%)		C——C + M——S_A——N(or CH)I					ΔH* (cal/g)
A−B	67.7	32.3	. 326.4	.	---------	365.9 .	411.6 .	15.4
	50.2	49.8	. 323.9	.	---------	354.7 .	407.2 .	8.4
	33.3	66.7	. 325.1	.	---------	349.2 .	402.1 .	8.1
	18.6	81.4	. ----------			327.9 .	399.1 .	8.0
A−C	80.2	19.8	. 371.8	.	---------	377.7 .	422.3 .	15.8
	64.9	35.1	. ----------			370.7 .	419.1 .	14.2
	54.9	45.1	. 361.7	.	---------	368.4 .	416.6 .	15.6
	38.0	62.0	. 361.8	.	---------	364.2 .	413.2 .	14.0
	31.2	68.8	. ----------			362.0 .	411.9 .	14.2
	18.8	81.2	. 361.1	.	---------	369.6 .	408.2 .	12.9
A−D	90.7	9.3	. 354.6	.	383.4 .	404.9 .	427.1 .	12.7
	80.6	19.4	. 350.2	.	377.1 .	414.3 .	427.8 .	12.7
	66.0	34.0	. 352.5	.	367.5 .	418.3 .	427.9 .	13.4
	49.9	50.1	. 353.9	.	360.0 .	413.9 .	427.4 .	13.8
	30.7	69.3	. 354.2	.	358.7 .	376.3 .	425.0 .	16.5
	19.9	80.1	. 352.0	.	---------	362.4 .	424.2 .	15.8
B−C	76.9	23.1	. 328.0	.	---------	332.9 .	395.0 .	10.0
	67.1	32.9	. ----------			329.0 .	395.9 .	9.9
	51.5	48.5	. 327.8	.	---------	344.2 .	398.7 .	11.1
	32.3	67.7	. 329.7	.	---------	360.7 .	401.2 .	10.6
B−D	95.1	4.5	. ----------		336.7 .	346.0 .	396.0 .	11.3
	89.8	10.2	. ----------		337.7 .	360.5 .	398.0 .	9.6
	80.0	20.0	. ----------		340.1 .	384.1 .	402.6 .	7.9
	68.6	31.4	. ----------		341.1 .	393.8 .	406.1 .	8.3
	51.7	48.3	. 338.3	.	344.4 .	396.1 .	411.3 .	12.1
	33.5	66.5	. 337.5	.	357.5 .	376.4 .	413.9 .	12.6
	19.9	80.1	. 336.2	.	---------	366.4 .	417.7 .	19.1
C−D	94.2	5.8	. 360.1	.	---------	376.1 .	404.7 .	16.4
	90.2	9.8	. 361.4	.	372.0 .	373.9 .	406.2 .	13.6
	77.0	23.0	. 361.9	.	366.1 .	390.8 .	409.4 .	10.8
	66.2	33.8	. ----------		360.0 .	396.2 .	412.0 .	11.8
	49.2	50.8	. 350.8	.	352.3 .	390.3 .	416.5 .	10.0
	31.8	68.2	. 350.6	.	356.9 .	359.2 .	416.7 .	11.5
	19.9	80.1	. 348.9	.	---------	362.5 .	418.6 .	16.0

*Total ΔH of melting.

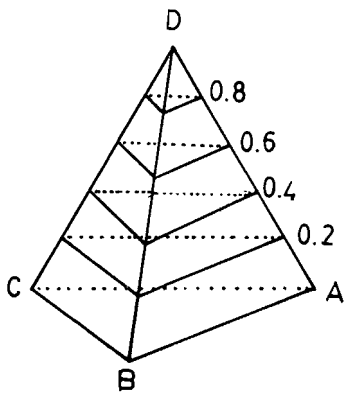

FIG. 2. Sections of a tetrahedron parallel to one surface.

clearing points are obtained in the area corresponding to the **A−D** binary mixture. This was expected because both compounds have the highest clearing temperatures.

Figure 5 corresponds to the calculated isoresponse curves for Y_3, the induced S_A-mesophase range.

The induced S_A-mesophase appears when compound **D** is present in the mixture. The highest value (approx. 60°) is obtained with a ternary mixture of compounds **A**, **B**, and **D** (**A**, ~30.2%; **B**, ~29.0%; **D**, ~40.8%).

The induced mesophase appears when a small concentration of compound **D** (approximately 10%) is present in the mixture but does not appear when its concentration is above 70%.

In quaternary mixtures the isoresponse surfaces are planes almost parallel to the plane defined by the **A−B−C** mixture, which does not show induced S_A-mesophase.

As can be seen in Fig. 10 the planes are slightly inclined towards the edge **CD**, which always shows the lowest values for this parameter. This can be explained by that compound **C**, with a chiral terminal chain, is the one that shows the greatest hindrance to the regular arrangement. Consequently, none of the quaternary mixtures has a greater induced S_A-mesophase range than that found in the **A−B−D** ternary mixture.

The calculated isoresponse curves for Y_4, the nematic mesophase range, are shown in Fig. 6.

As expected they show variation opposite to that shown by Y_3. The widest nematic mesophase ranges are found in areas next to the vertex of pures compounds **B** and **D** and correspond to binary and ternary mixtures where these compounds are

Can. J. Chem. Downloaded from www.nrcresearchpress.com by 210.87.254.42 on 09/06/12
For personal use only.

Can. J. Chem. Downloaded from www.nrcresearchpress.com by 210.87.254.42 on 09/06/12
For personal use only.

TABLE 3. Equations and coefficients of the mathematical models

$$\text{Quadratic model: } \eta = \sum_{i=1}^{4}\beta_i x_i + \sum_{1\le i<j\le 4}\beta_{ij}x_i x_j|I|$$

$$\text{Cubic model: } \eta = |I| + \sum_{1\le i<j\le 4}\nu_{ij}x_i x_j(x_i - x_j) + \sum_{1\le i<j\le 4}\beta_{ijk}x_i x_j x_k$$

Coefficients	Y_1	Y_2	Y_3	Y_4	Y_5	Y_6
β_1	388	425	1.11	37.4	36.9	16.4
β_2	338	393	1.76	55.1	54.7	11.0
β_3	379	404	1.73	25.4	24.8	17.4
β_4	373	420	−19.3	49.2	47.5	17.9
β_{12}	−28.8	−7.9	0.3	18.9	20.9	14.0
β_{13}	−71.5	7.1	−2.4	76.1	78.6	−9.6
β_{14}	−7.8	19.8	233	−90.3	97.5	−11.8
β_{23}	−59.2	−3.5	−2.3	53.4	55.7	−15.8
β_{24}	−31.8	18.3	230	−130	50.1	−14.1
β_{34}	−84.2	13.3	164	−23.5	97.5	−28.4
ν_{12}	−2.4	−9.1	—	−7.0	−6.8	36.1
ν_{13}	48.5	−0.3	—	−48.3	−48.8	5.7
ν_{14}	28.1	7.1	—	−224	−21.0	−16.5
ν_{23}	−113	−11.3	—	102	101	10.7
ν_{24}	−31.0	12.1	—	−185	43.1	−12.5
ν_{34}	9.8	5.4	—	−220	−4.4	1.4
β_{123}	26.7	21.1	—	0.7	−5.5	52.1
β_{124}	−42.9	20.1	—	−408	60.3	−67.7
β_{134}	231	−12.0	—	−508	−243	−45.7
β_{234}	80.4	16.5	—	−470	−63.9	−16.6
R^2	0.99	0.99	0.85	0.98	0.98	0.95
Standard error	2.2	1.1	1.1	5.8	3.2	1.4

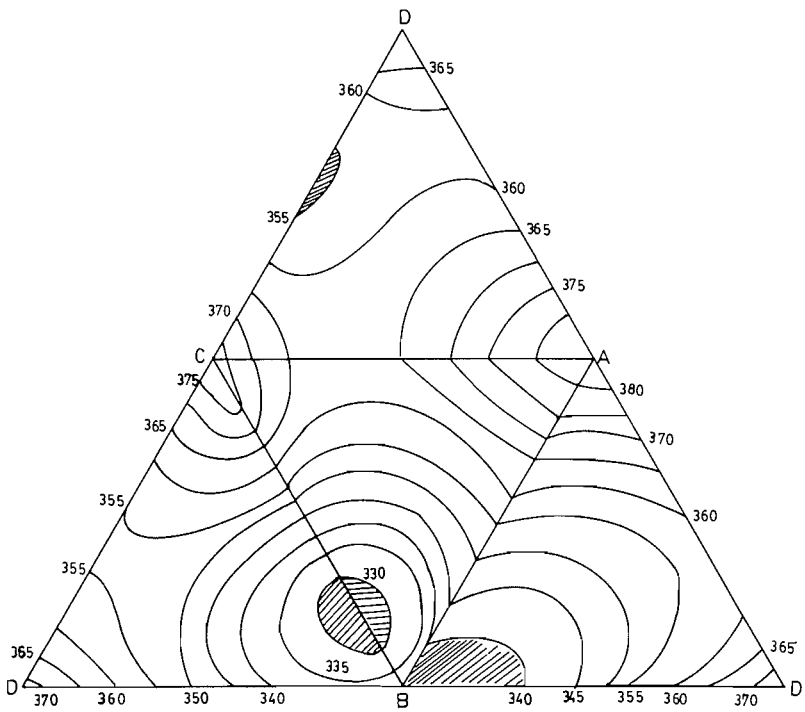

FIG. 3. Isoresponse curves for Y_1; cubic model.

present in greater proportion. And the smallest ranges are in the regions where the induced S_A-mesophase exists.

Figure 7 shows the isoresponse curves for Y_5, the total mesophase range.

It is a combination of the two preceding parameters that a much smoother variation of the isoresponse curves can be seen. On the surface **A**−**B**−**C** the modifications with respect to Y_4 are practically void, although in this case they are more accurate.

It can be seen that wide mesophase ranges in the three types

Can. J. Chem. Downloaded from www.nrcresearchpress.com by 210.87.254.42 on 09/06/12
For personal use only.

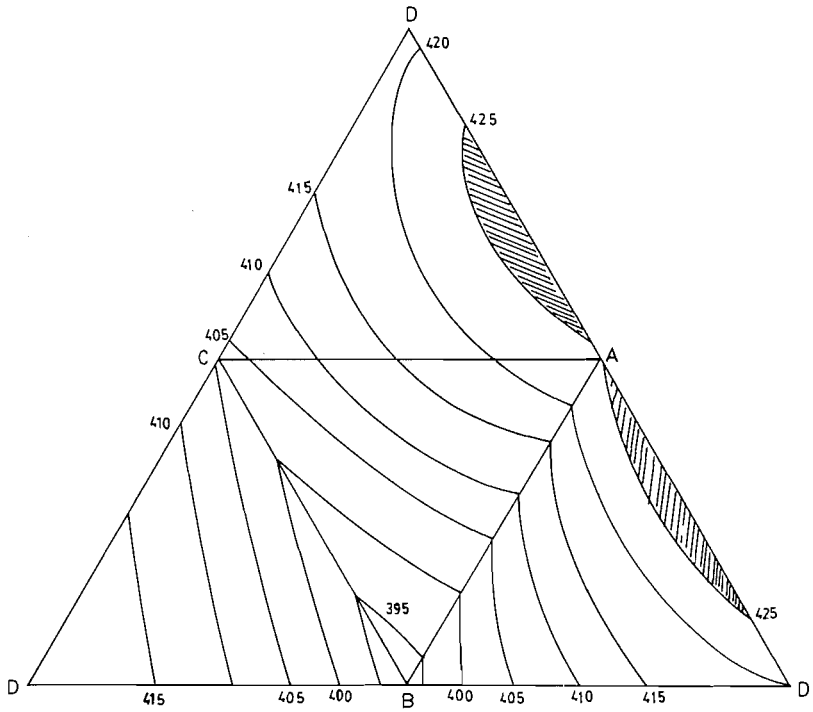

FIG. 4. Isoresponse curves for Y_2; cubic model.

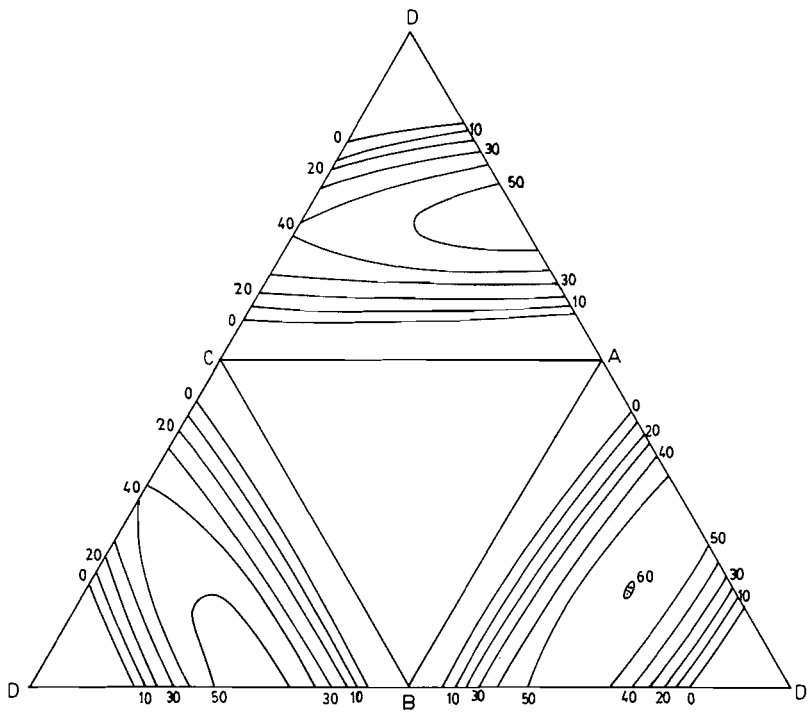

FIG. 5. Isoresponse curves for Y_3; quadratic model.

of mixture studied, binary, ternary, and quaternary, can generally be obtained. For ternary and quaternary mixtures of similarly-structured compounds, their mesophase ranges do not improve significantly over those of binary mixtures.

Y_6 represents the total ΔH of melting in cal/g. The calculated isoresponse curves are in Fig. 8. The highest values for Y_6 correspond to the pure compounds and they decrease gradually when the proportion of one or more of the other compounds in mixture increases. The lowest values of ΔH are obtained for a mixture zone near the vertex of component **B**, which shows a melting enthalpy much lower than that of the other three compounds.

It is notable that no change is observed in the data of the melting enthalpies in areas where the induced S_A-mesophase appears, and a regular variation of the isoresponse curves can be seen in the mixtures where compound **D** is present.

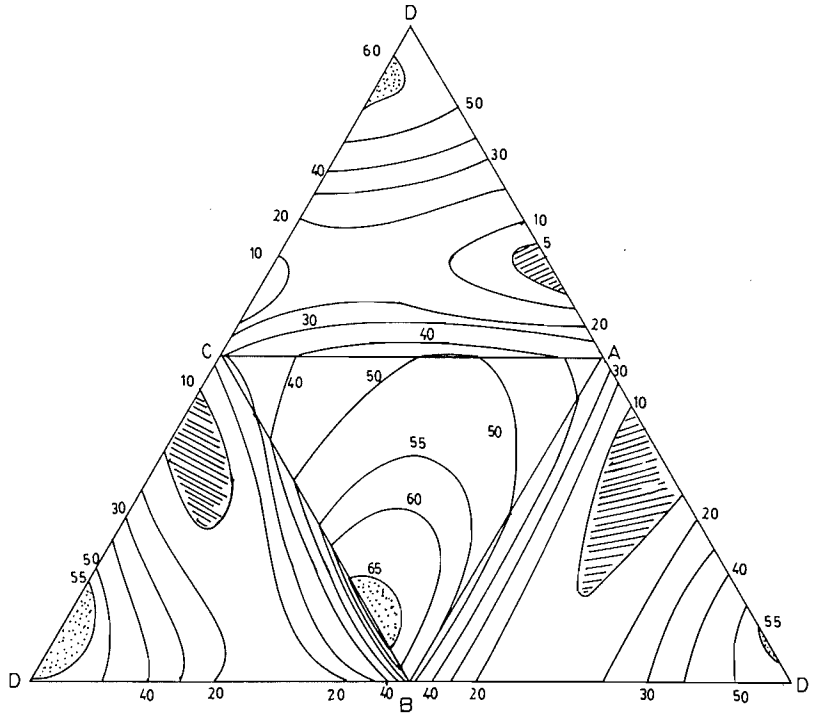

FIG. 6. Isoresponse curves for Y_4; cubic model.

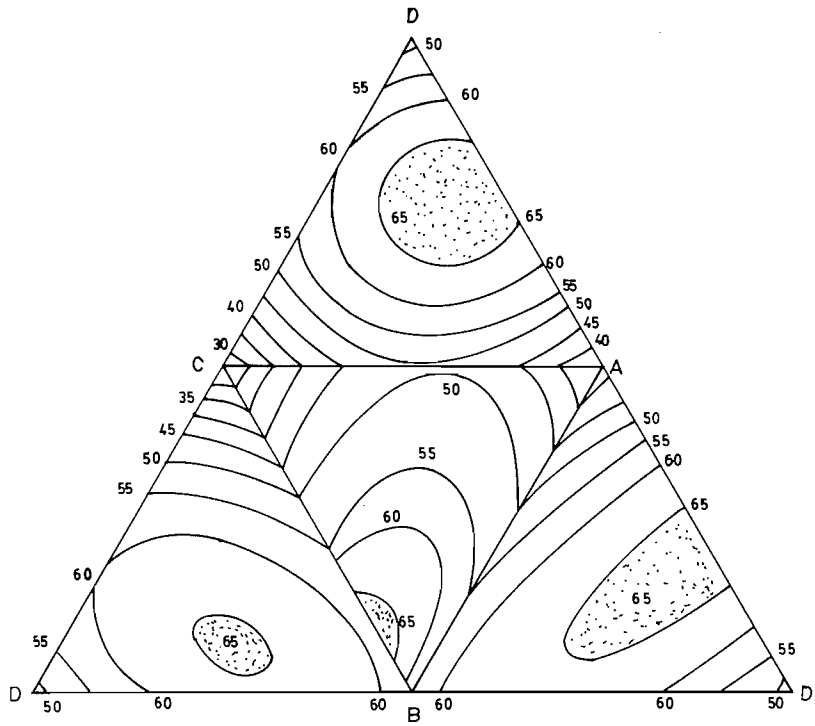

FIG. 7. Isoresponse curves for Y_5; cubic model.

Eutectic point study for binary, ternary, and quaternary mixtures

Binary mixtures

Experimental results obtained for binary mixtures are shown in Figs. 11 to 16.

The eutectic temperature was determined experimentally as the average temperatures of the crystal + mesophase → mesophase transition.

With the exception of **A**−**C** (2 points) and **C**−**D** (4 points) mixtures, this transition agrees with all the experiments carried out for each mixture.

With regard to the mixture **C**−**D** it could be thought that two eutectic points exist, and their form is similar to that described by Yu and Labes (7) in mixtures showing an induced S_A-mesophase for compounds with the cyano group. However, in this case the experimental data do not confirm that

Can. J. Chem. Downloaded from www.nrcresearchpress.com by 210.87.254.42 on 09/06/12
For personal use only.

Can. J. Chem. Downloaded from www.nrcresearchpress.com by 210.87.254.42 on 09/06/12
For personal use only.

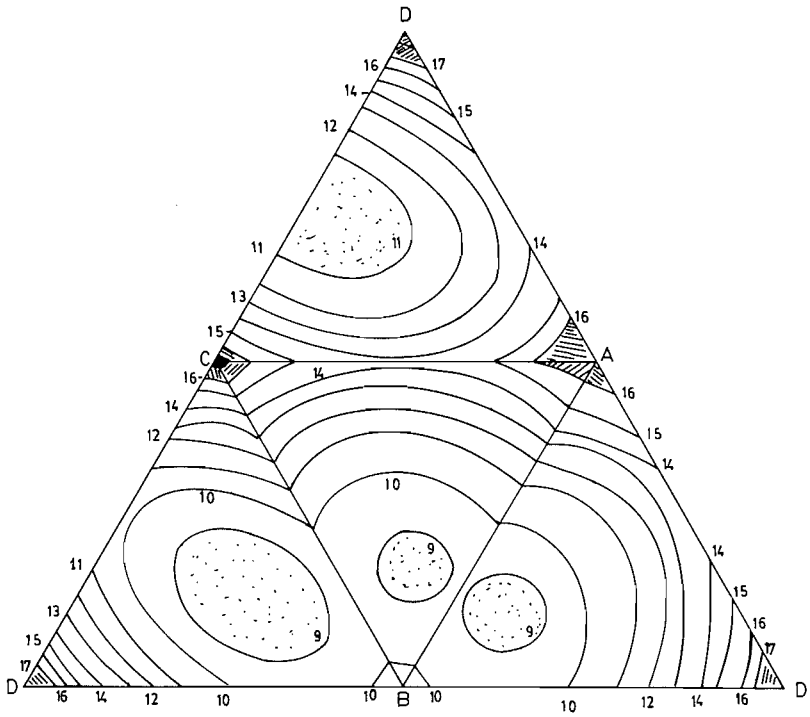

FIG. 8. Isoresponse curves for Y_6; cubic model.

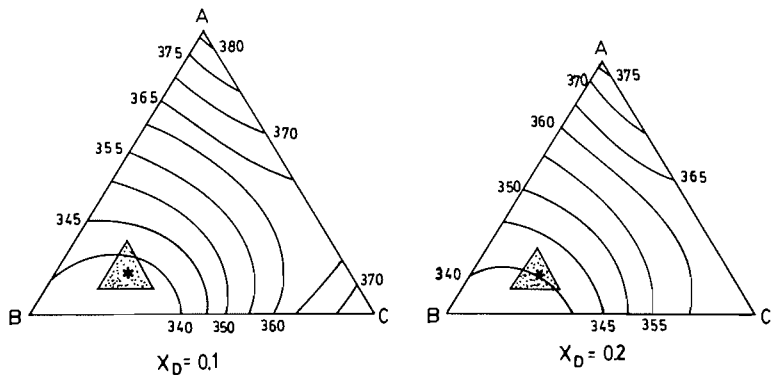

FIG. 9. Isoresponse curves for Y_1; sections parallel to **A**—**B**—**C** surface, where $x_D = 0.1$ and $x_D = 0.2$.

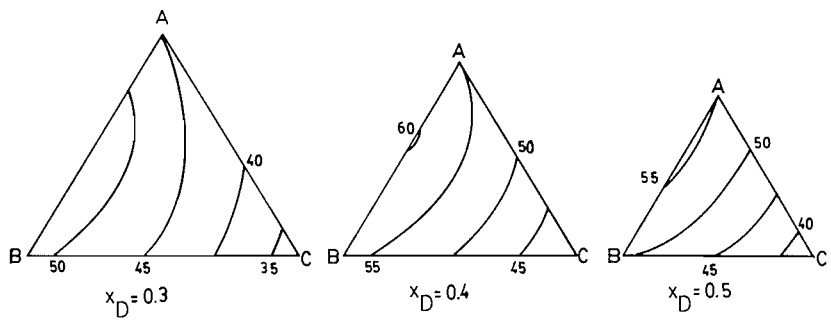

FIG. 10. Isoresponse curves for Y_3; sections parallel to **A**—**B**—**C** surface, where $x_D = 0.3$, $x_D = 0.4$, and $x_D = 0.5$.

phenomenon.

In mixtures where compounds **D** (**A**−**B**, **A**−**C**, **B**−**C**) is not present only one mesophase appears. In the three cases the eutectic point is well established and the N−I or Ch−I transition gives a practically linear variation.

In mixtures where compound **D** with the nitro group as a terminal chain participates, the appearance of an induced S_A-mesophase was observed (Figs. 13, 15, and 16).

The fact that in the mixtures **A**−**D** and **C**−**D**, the appearance of an induced S_A-mesophase does not have an effect on the temperature of the transition crystal + mesophase → mesophase and they are shown to be ideal mixtures is worth drawing

Can. J. Chem. Downloaded from www.nrcresearchpress.com by 210.87.254.42 on 09/06/12
For personal use only.

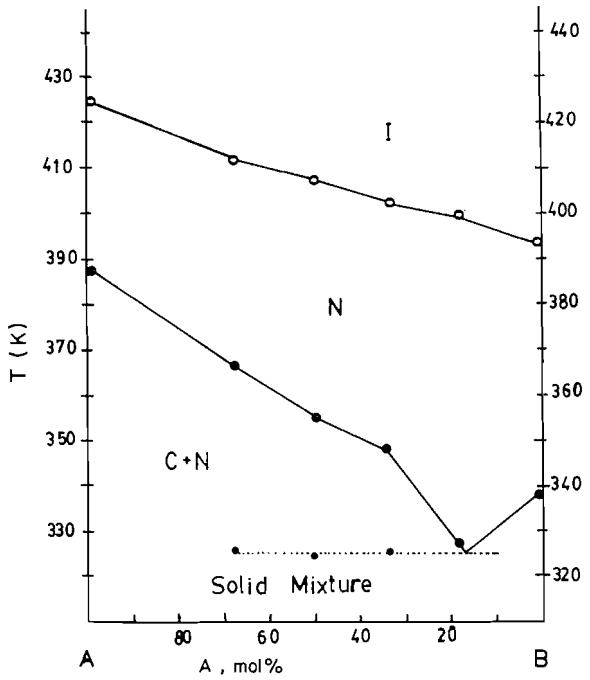

FIG. 11. Binary phase diagram of 4,4′-dihexoxy-2-hydroxy-α,α′-dimethylbenzalazine/2-hydroxy-4′-butyl-4-octoxy-α,α′-dimethylbenzalazine system.

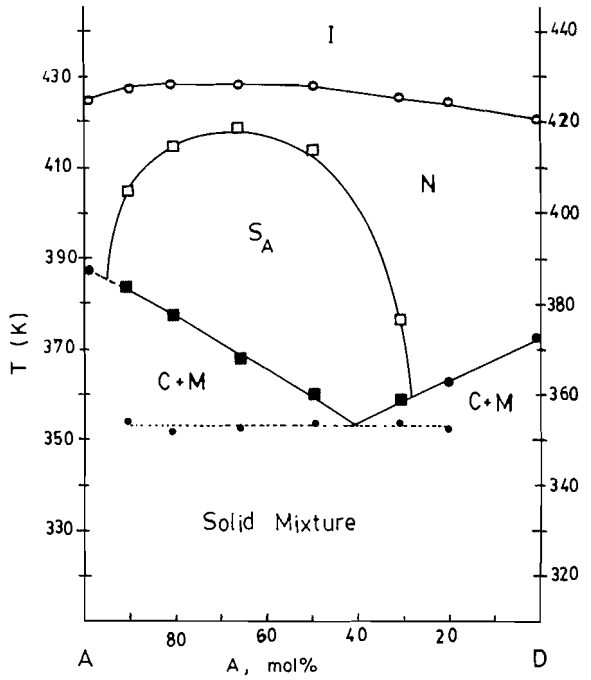

FIG. 13. Binary phase diagram of 4,4′-dihexoxy-2-hydroxy-α,α′-dimethylbenzalazine/2-hydroxy-4′-nitro-4-octoxy-α,α′-dimethylbenzalazine system.

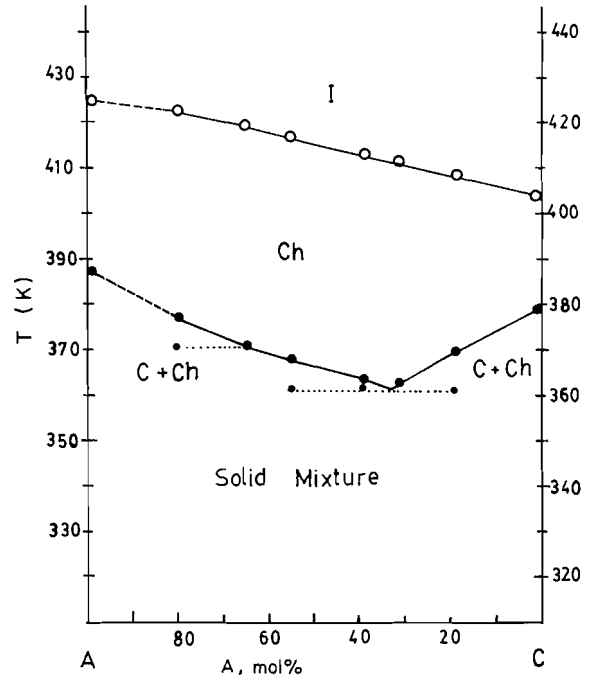

FIG. 12. Binary phase diagram of 4,4′-dihexoxy-2-hydroxy-α,α′-dimethylbenzalazine/4′-butoxy-2-hydroxy-4-(2-methylbutoxy)-α,α′--dimethylbenzalazine system.

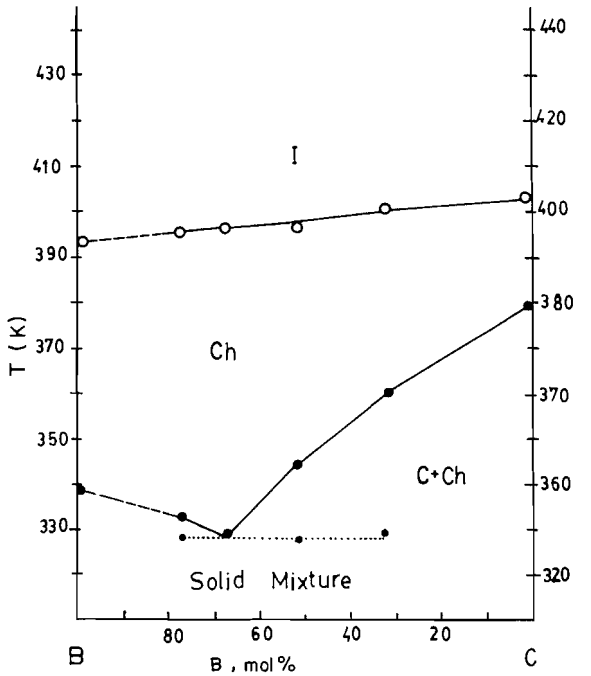

FIG. 14. Binary phase diagram of 4′-butyl-2-hydroxy-4-octoxy-α,α′-dimethylbenzalazine/4′-butoxy-2-hydroxy-4-(2-methylbutoxy)-α,α′-dimethylbenzalazine system.

attention to. However, judging by its behaviour, mixture **B−D** (Fig. 15) is obviously not an ideal mixture, and a strong inflexion in the long line of the transition crystal + mesophase → mesophase in the binary diagram can be observed.

In the three mixtures a slight convex shape forms in the line of transition to isotropic liquid, caused by the induced S_A-mesophase, can be observed.

Table 4 shows the thermal data and the composition of the eutectic mixtures obtained experimentally for each of the binary mixtures, as well as the results obtained using the Scheffé algorithm and the Schröder − van Laar's equations (11) for melting points and $T_{cl} = \Sigma T_{cli} x_i$ (12) for clearing points.

In general none of the methods used is better in all cases. In melting temperatures of eutectic compositions either prediction method is quite good for five of the six mixtures studied. However, there are discrepancies observed in the **A−B** and

TABLE 4. Experimental and calculated eutectic composition and temperatures for binary mixtures

System	Eutectic composition (mol%) component 1			Eutectic melting point (K)			Eutectic clearing point (K)		
	Exp.	SvL*	Scheffé†	Exp.	SvL*	Scheffé†	Exp.	Theor.‡	Scheffé†
A–B	17.0	18.3	0	325.8	328.9	338.9	398.7	398.7	393.0
A–C	34.0	43.6	32.9	361.6	356.5	362.4	413.0	410.8	412.5
A–D	41.0	41.2	34.0	352.9	354.5	358.2	426.0	422.0	425.6
B–C	68.0	76.7	80.0	328.6	326.1	326.2	396.0	396.4	393.6
B–D	95.1	76.5	87.4	336.7	326.0	336.6	396.3	394.3	399.4
C–D	45.0	47.9	43.4	350.1	350.5	354.3	417.0	412.7	416.2

*Calculated values using Schröder – van Laar's equations.
†Calculated values using Scheffé algorithm (cubic model).
‡Calculated values using $T_{cl} = \Sigma x_i T_{cli}$ equation.

Can. J. Chem. Downloaded from www.nrcresearchpress.com by 210.87.254.42 on 09/06/12
For personal use only.

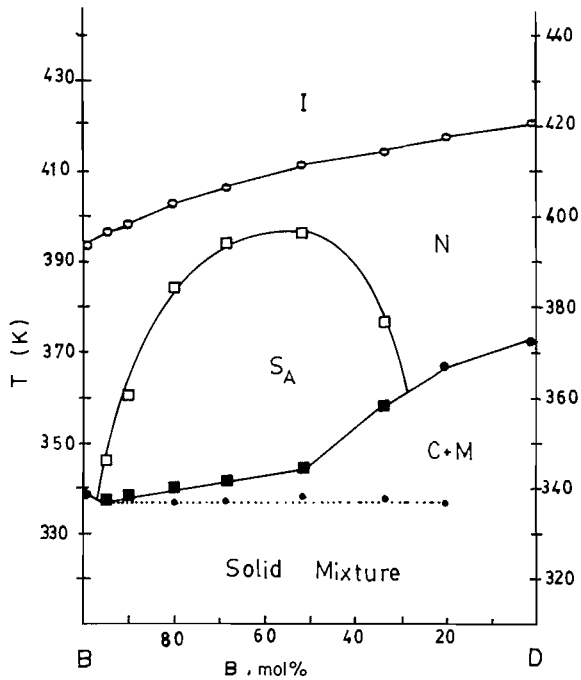

FIG. 15. Binary phase diagram of 4′-butyl-2-hydroxy-4-octoxy-α,α′-dimethylbenzalazine/2-hydroxy-4′-nitro-4-octoxy-α,α′-dimethylbenzalazine system.

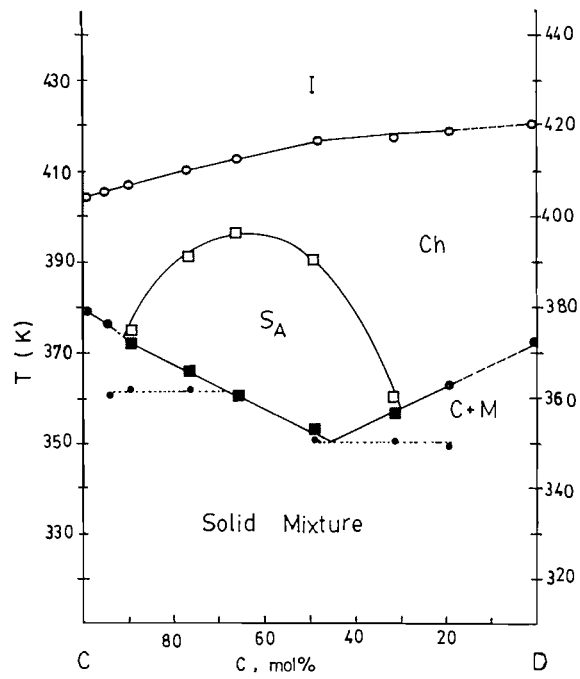

FIG. 16. Binary phase diagram of 4′-butoxy-2-hydroxy-4-(2-methylbutoxy)-α,α′-dimethylbenzalazine/2-hydroxy-4′-nitro-4-octoxy-α,α′-dimethylbenzalazine system.

B–D mixtures.

With regard to the former (Fig. 11), it is clear that the three experiments using the Scheffé algorithm are not sufficient. The curve obtained by the equation of the full-cubic model is not appropriate in that zone. The minimum predicted temperature in this case corresponds to the data of the pure component **B**.

On the other hand, with mixture **B–D** (Fig. 15) which is quite different from ideal, the data obtained by the mathematical model are much better.

As expected, something similar happens with the composition of the eutectic mixture, where, with the exception of the mixtures already referred to, the results obtained using the various methods are not too different and each method is successful in certain respects.

The same is true for the eutectic clearing temperature. In this case though, the experimental value is closer to the predicted values.

Ternary and quaternary mixtures

Here the eutectic point was studied in a manner different from that of the binary mixture.

The theoretical eutectic temperature and composition were calculated using the Schröder – van Laar's equation, and the eutectic temperature again calculated using Scheffé's algorithm.

Experiments were then performed to check the validity of the predictions. The results are gathered in Table 5.

It can be observed that in every case, a step closer to reality is obtained with the application of the mathematical method. This justifies its use in the study of complex mixtures whose behaviour is generally different from ideal.

Conclusions

The 2-hydroxy-4′-nitro-4-octoxy-α,α′-dimethylbenzalazine only shows a nematic mesophase, but as a component in mixtures with other nematogenic compounds induces the appearance of a S_A-mesophase.

In the binary, ternary, and quaternary mixtures studied, this mesophase already appears with a low concentration of this

TABLE 5. Calculated and experimental eutectic composition and temperatures for ternary and quaternary systems

System	Composition (mol%)		Melting temperature (K)		
			Calculated		Measured
	SvL*	Experimental	SvL*	Scheffé	DSC
A–B–C	13.6; 67.3; 19.1	13.5; 67.6; 18.9	320.4	332.5	329.1
A–B–D	13.6; 67.3; 19.1	12.9; 68.0; 19.1	320.4	340.0	340.6
A–C–D	27.1; 36.2; 36.7	26.7; 37.3; 36.0	340.8	360.6	360.9
B–C–D	64.1; 18.1; 17.8	64.1; 18.2; 17.7	318.4	333.0	342.8
A–B–C–D	11.0; 58.0; 16.0; 16.0	10.4; 58.4; 15.6; 15.6	314.6	339.3	344.4

*Composition and temperature for eutectic point calculated using the Schröder – van Laar's equations.

compound (~10%) but not when its concentration is higher than 70%.

The principal modification caused by the induced S_A-mesophase can be seen in its change in the clearing temperatures. However, in general neither temperature nor enthalpy of transition from crystal to mesophase undergo marked changes.

The use of the Scheffé algorithm to study mixtures of mesogenic compounds gives excellent results, especially in the study of complex mixtures. It proves to be very valuable in the study of mixtures of liquid crystals, including the infrequent cases of the induced S_A-mesophase.

1. M. MARCOS, E. MELÉNDEZ, and J. L. SERRANO. Mol. Cryst. Liq. Cryst. **91**, 157 (1983).
2. J. BARBERÁ, M. MARCOS, E. MELÉNDEZ, and J. L. SERRANO. Mol. Cryst. Liq. Cryst. **94**, 367 (1983).
3. J. L. ALABART, M. MARCOS, E. MELÉNDEZ, and J. L. SERRANO. Ferroelectrics. In press.
4. M. MARCOS, E. MELÉNDEZ, B. ROS, and J. L. SERRANO. To be published.
5. J. W. PARK, C. S. BAK, and M. M. LABES. J. Am. Chem. Soc. **97**, 4398 (1975).
6. C. S. OH. Mol. Cryst. Liq. Cryst. **42**, 1 (1977).
7. L. J. YU and M. M. LABES. Mol. Cryst. Liq. Cryst. **54**, 1 (1979).
8. J. S. DAVE, P. R. PATEL, and K. L. VASANTH. Ind. J. Chem. **4**, 505 (1966).
9. M. MARCOS, E. MELÉNDEZ, J. L. SERRANO, D. MATHIEU, R. PHAN TAN LUU, and J. ELGUERO. Bull. Soc. Chim. Bel. **92** (5), 429 (1983).
10. M. MARCOS, E. MELÉNDEZ, J. L. SERRANO, J. ELGUERO, D. MATHIEU, and R. PHAN THAN LUU. Anal. Quím. Ser. C, **79**, 664 (1983).
11. E. C. H. HSU and J. F. JOHNSON. Mol. Cryst. Liq. Cryst. **20**, 177 (1973).
12. R. L. HUMPHRIES, R. G. JAMES, and G. R. LUCKHURST. Symp. Faraday. Soc. **5**, 107 (1971).

Can. J. Chem. Downloaded from www.nrcresearchpress.com by 210.87.254.42 on 09/06/12
For personal use only.

Reactions of α-aryl carbonyl compounds with lithium ester enolates

REINHOUT H. VAN DER VEEN, JAN A. J. GEENEVASEN, AND HANS CERFONTAIN[1]

Laboratory for Organic Chemistry, University of Amsterdam, Nieuwe Achtergracht 129, 1018 WS Amsterdam, The Netherlands

Received December 9, 1983

REINOUT H. VAN DER VEEN, JAN A. J. GEENEVASEN, and HANS. CERFONTAIN. Can. J. Chem. **62**, 2202 (1984).

This report describes the synthesis of β-hydroxy esters in good yields by reaction of α-aryl substituted ketones and phenylethanal with lithium methyl acetate and derivatives as anionoid reagents. The incomplete substrate conversion is ascribed to the enolate formation of the α-aryl carbonyl compounds, which concurrent reaction is negligibly small with aliphatic carbonyl compounds. The conversion of β-tetralone with lithium methyl acetate has been examined in some detail.

REINOUT H. VAN DER VEEN, JAN A. J. GEENEVASEN, et HANS. CERFONTAIN. Can. J. Chem. **62**, 2202 (1984).

La réaction, en présence d'acétate de méthyl lithium ou de ses dérivés qui agissent comme réactifs anionoïdes, du phényléthanal avec des cétones portant des groupes aryles en position α correspond à une synthèse efficace des β-hydroxy esters qui sont obtenus avec de bons rendements. Le fait que la conversion du substrat n'est pas complète est probablement dû à la formation de l'énolate des composés carbonylés substitués en α par des groupes aryles; la réactivité de ces énolates vis-à-vis les composés carbonylés aliphatiques est faible. On a étudié plus en détail la conversion de la β-tétralone avec l'acétate de méthyl lithium.

[Traduit par le journal]

Can. J. Chem. Downloaded from www.nrcresearchpress.com by 210.87.254.6 on 09/06/12
For personal use only.

Introduction

Lithiated enolates and dienolates are currently investigated by virtue of their applicability in organic synthesis, as appears from recent reports (1, 2). The broad accessibility of lithiated anions and dianions by proton abstraction from active methylene compounds such as nitriles (3, 4), esters (4), and acids (5) using lithium diisopropylamide (LiDIPA) as base is advantageous. Also the high yield in which α-haloalkyllithium reagents are formed on reaction of α,α-dihalogenoalkanes with butyllithium deserves attention (6). Recently, Freeman and Hutchinson and Bogdanović and Wermeckes developed a special route in which alkyl halogenides are converted into alkyllithium reagents in excellent yields (7).

The use of lithium methyl acetate (LiMA) as a synthon to convert aliphatic ketones into β-hydroxy esters was already described by Hauser and Dunnavant (8) and Rathke (9) as an improvement on the usual Reformatski procedure (10). With the latter method excellent yields of β-hydroxy esters are obtained within minutes on using ultrasonic irradiation (11). The use of the Reformatski reagent on a large synthetic scale is troublesome in view of the high exothermicity of the addition reaction.

Application of the addition of lithium enolates to aldehydes or ketones opens a route to α-vinylation.[2] Rathke and Sullivan (14) examined the addition of acetone to the lithium enolate of ethyl crotonate which afforded 78% of the β-hydroxy ester. However, several attempts to dehydrate the formed adduct in acidic or basic medium unexpectedly failed.[2] Also, various methods using *in situ* formed intermediates derived from methyl 2-(1′-hydroxy-1′-methyl)ethylbut-3-enoate with (*i*) methanesulfonyl chloride, (ii) thionyl chloride and pyridine, (iii) phenol, or (iv) trifluoromethanesulfonyl chloride and pyridine did not show the desired elimination, and frequently the starting β-hydroxy ester was recovered unchanged.[3]

A promising route leading to α-vinylation of β,γ-unsaturated carbonyl compounds would be the one-step joining reaction of activated olefins with thiolate anions and aldehydes or ketones (15), but the dehydration of the resulting β-hydroxy ester afforded the lactone rather than the desired diene ester. A successful route for α-vinylation proved to be the Michael addition of phenyl vinyl sulfoxide to β,γ-unsaturated esters and ketones (16).

Results and discussion

The conversion of a number of α-aryl ketones into the corresponding β-hydroxy esters has been carried out under the conditions described by Rathke (9) in satisfactory yields (Table 1). In the crude reaction mixtures there remained starting material. If the isolated yields are corrected for the amounts of (recovered) starting material then the converison is quantitative. This agrees with the observation that the ^{1}H nmr spectra of the crude reaction mixture residues only contained absorptions of the β-hydroxy ester and the starting ketone. Based on these observations and those of Kikkawa and Tadahiko (17), the incomplete substrate conversion is ascribed to the acidity of the α-hydrogen(s) of the α-aryl ketones and aldehyde (lithium methyl acetate enol is not only a reactive nucleophile but also a strong base), which leads to an unprofitable storage of these carbonyl compounds as their enol anions.[4] It should be realized that the acidity of the α-hydrogens is very much higher with the presently studied α-aryl ketones than aliphatic ketones which give higher yields of the β-hydroxy ester than the former (cf. entry XII with, for example, entry V).

The conversion of β-tetralone has been examined under different reaction conditions in order to obtain information as to

[1]Author to whom correspondence may be addressed.

[2]A useful synthetic application in this field developed by Clive et al. (12) and Kowalski and Dung (13) is the reaction of (phenylseleno)ethanal with lithium- and zinc-enolates prepared from ketones; PhSeOH elimination from the resulting addition product affords β,γ-enones. In a similar way Hudrlik and Kulkarni effected electrophilic α-vinylation by addition of α-(*tert*-butyldimethylsilyl)-aldehydes to lithium enolates of ketones or esters and subsequent elimination using $BF_3 \cdot Et_2O$ (13).

[3]P. M. N. Nossin and W. N. Speckamp, unpublished results.

[4]Profitable use of storage of a ketone as enolate is made in the well-known reaction of esters with Grignard reagents using an excess of triethylamine (17, 18). The intermediate ketone is then converted rapidly into its enolate, thus preventing subsequent addition of the Grignard reagent to the ketone which would yield the corresponding tertiary alcohol.

TABLE 1. Reaction of $CR^1R^2{=}C(OCH_3)OLi$ in the presence of an amine in THF at −78°C with α-aryl ketones and an aldehyde

Entry	Substrate	Enolate ester		Amine		β-Hydroxy ester	Unreacted substrate[c]	β,γ-Unsaturated ester[d]
		Structure	Equiv.	Type[a]	Equiv.[b]	%	%	%
I	Phenylethanal	$Li(CH_3)CH{=}CO_2CH_3$	1.0	DIPA	1.0	**1** 75 (80)	8 (20)	**1***a* 0
II	2-Phenylcyclopentanone	$Li(CH_3)_2C{=}CO_2CH_3$	1.0	N-IPCHA	1.0	**2** 34 (39)	45 (61)	**2***a* 89
III	2-Phenylcyclopentanone	$LiCH_2{=}CO_2CH_3$	1.0	DTSA	1.0	**3** 80 (87)	8 (13)	**3***a* 52
IV	2-Indanone	$LiCH_2{=}CO_2CH_3$	1.0	DIPA	1.0	**4** 75 (82)	6 (18)	
V	β-Tetralone	$LiCH_2{=}CO_2CH_3$	1.0	DIPA	1.0	**5** (58)	(42)	
VI	β-Tetralone	$LiCH_2{=}CO_2CH_3$	2.0	DIPA	2.0	**5** 68 (75)	20 (25)	**5***a* 75
VII	β-Tetralone	$LiCH_2{=}CO_2CH_3$	1.0	DIPA	10.0	**5** (32)	(68)	
VIII	β-Tetralone	$Li(CH_3)CH{=}CO_2CH_3$	1.0	DIPA	1.0	**6** (25)	(75)	
IX	β-Tetralone	$LiCH_2{=}CO_2CH_3$ at −30°C	2.0	DIPA	2.0	**5** (66)	(34)	
X	β-Tetralone	$LiCH_2{=}CO_2CH_3$	1.0	DTSA	1.0	**5** (45)	(55)	
XI[e]	β-Tetralone	$BrZnCH_2{=}CO_2CH_3$	3.0	—	—	**5** 35[e]	<5	**5***a* 80[e]
XII[f]	Cyclohexanone	$LiCH_2{=}CO_2CH_3$	1.0	DTSA	1.0	**7** 91		

[a]DIPA, N-IPCHA, and DTSA stand for diisopropylamine, *N*-isopropylcyclohexylamine, and di(trimethylsilyl)amine respectively.
[b]Number of equivalents relative to the amount of substrate.
[c]Yields without parentheses refer to isolated products, those within parentheses to yields estimated from ^1H nmr spectra of the reaction mixture residue.
[d]Some of the β,γ-unsaturated esters obtained by dehydration of the corresponding β-hydroxy ester contained up to 10% of the corresponding α,β-isomer.
[e]The reaction was performed as described before with reported yields of 50 and 83% for **5** and **5***a* respectively; see ref. 22.
[f]See ref. 9.

the origin of the incomplete substrate conversion. β-Tetralone on reaction with 1.0 equiv. LiMA, prepared using 1.0 equiv. LiDIPA, affords the addition product in 58% (entry V). Upon reaction with 2.0 equiv. LiMA (prepared using 2.0 equiv. of LiDIPA, entry VI), higher yields are obtained (75%), whereas an excess of diisopropyl amine (DIPA, 10 equiv., entry VII) reduces the yield of the β-hydroxy ester to 32%. The effect of the excess of amine implies a decrease in the ratio of the effective nucleophilicity to basicity of the LiMA, which may be the result of the change in the solvent composition or of coordination of the amine to the lithium of the LiMA. Attempts to suppress the substrate enolization by increasing the temperature up to −30°C, which was thought to accelerate the nucleophilic attack (19), had no effect (entry IX). Above −30°C the DIPA solution coloured due to self condensation as already described by Rathke (9). Also the use of a more sterically hindered amine such as di(trimethylsilyl)amine, chosen with the aim of decreasing the degree of enolate formation of the α-aryl ketones, was not successful (cf. entries III and X).

The nucleophilic attack of ester enolates on α-aryl carbonyl compounds is very susceptible to steric hindrance. This may be concluded from the lower yield of β-hydroxy ester on coupling of 2-phenylcyclopentanone with lithium methyl isobutyrate (39%, entry II) as compared with lithium methyl acetate (87%, entry III). In a similar way the low yield of β-hydroxy ester from β-tetralone and lithium methyl propionate (25%, entry VIII) as compared with lithium methyl acetate (58%, entry V) may be explained. The yield of coupling LiMA to 2-indanone is higher (80%, entry IV) as compared with its addition to β-tetralone (58%, entry V). This may be explained in terms of a lower degree of steric hindrance for the addition to 2-indanone, but also in terms of a reduction in the strain of the five-membered ring upon forming the addition intermediate.

Some of the prepared β-hydroxy esters have been dehydrated with thionyl chloride and pyridine in benzene (see Table 1) to yield the corresponding β,γ-unsaturated esters.

Experimental

The ^1H nmr spectra were recorded in $CDCl_3$ or CCl_4 as solvent on a Varian A 60-D or a Varian XL-100 FT spectrometer, using TMS as internal reference. The ir spectra were recorded on a Perkin Elmer 257 grating infrared spectrometer or a Perkin Elmer 298 instrument, using a neat film of purified oils or $CHCl_3$ solutions. Microanalyses were performed by the Institute for Organic Chemistry, TNO, Utrecht. The glc analyses were carried out on a Varian Model-3700 chromatograph and the semi-preparative glc separations were conducted using a Varian Model-2700 chromatograph.

THF was freshly distilled prior to use from sodium wire using benzophenone as indicator under nitrogen. $SOCl_2$ and pyridine were purified as described (20).

General procedure for the conversion of α-aryl ketones

To a solution of 30.4 g (300 mmol) diisopropylamine in 200 mL THF, 200 mL (300 mmol) n-BuLi in hexane (1.50 mmol/mL) were added dropwise over 45 min at −78°C, followed by slow addition of 300 mmol of the ester (30 min). The solution was stirred for 30 min and remained colourless. Then 1.0 equiv. (150 mmol) of the ketone was added rapidly at the desired temperature. The solution coloured immediately and the solution was stirred for another 30 min. Then the mixture was allowed to warm to −30°C and quenched with 100 mL aqueous THF (THF−H_2O, 1:1 v/v). Subsequently 100 mL 10% aqueous NH_4Cl was added and the solution acidified with 5% aqueous HCl to pH 4. The β-hydroxy ester was extracted with ether and the organic layer washed with 5% aqueous HCl (twice), water, brine, and then dried with anhydrous $MgSO_4$. The solvents were removed under reduced pressure, leaving a yellow oil which was distilled *in vacuo*.

Methyl 2-methyl-3-hydroxy-4-phenylbutanoate ***1***

Purified phenylethanal (2.45 g, 20.4 mmol) distilled from a mixture (1:1 v/v) with diethyl phthalate) was reacted with 40.8 mmol of lithium methyl propionate prepared from 4.14 g (40.9 mmol) diisopropylamine, 3.60 g (40.8 mmol) methyl propionate, and 28.5 mL (1.44 mmol/mL hexane) n-BuLi in 100 mL THF to afford a crude residual oil (4.60 g). Distillation at 105−107°C/1 Torr (1 Torr = 133.3 Pa) yielded 0.2 g of the aldehyde and 3.2 g of **1**, ir (liq. cap.; cm^{-1}): 3510, 3425 br (OH); 2980 (CH aliph.); 1735 (C=O); 1270, 1140 (O—CH_3); 700 (C_6H_5); ^1H nmr (CCl_4), 60 MHz (δ in ppm): 7.1 (s, 5H, arom.), 4.3−3.6 (m, C*H*—OH), 3.6 (s, 3H, OCH_3), 2.7 (br s, 1H, OH), 2.6 (d, J = 6 Hz, 2H, CH_2), 2.7−2.2 (m, 1H, CH—CO), 1.2 (d, J = 7 Hz, 3H, CH_3). *Anal.* calcd. for $C_{12}H_{16}O_3$: C 69.21, H 7.74; found C, 69.31, H 7.70.

Dehydration of **1** with thionyl chloride and pyridine failed and so did the reaction of **1** with concentrated hydrochloric acid in ethanol

Can. J. Chem. Downloaded from www.nrcresearchpress.com by 210.87.254.6 on 09/06/12
For personal use only.

Can. J. Chem. Downloaded from www.nrcresearchpress.com by 210.87.254.6 on 09/06/12
For personal use only.

and with a catalytic amount of diethylamine in ethanol. In all cases only the starting material was recovered.

Methyl 2-(1'-hydroxy-2'-phenylcyclopentyl)-2-methylpropanoate **2**

2-Phenylcyclopentanone (21) was treated with lithium methyl isobutyrate, and afforded 42 g of the crude mixture which contained 61% of the ketone and 39% of the β-hydroxy ester. In this case lithium *N*-isopropylcyclohexylamide was used for the preparation of lithium methyl isobutyrate. Distillation *in vacuo* at 73−75°C/0.05 Torr yielded 11.7 g (45%) of the ketone and 14.8 g (34%) of the β-hydroxy ester **2**; ir ($CHCl_3$, cm^{-1}): 3550, 2960 br (OH); 3000, 2960 (CH, aliph.); 1725 (C═O); 1280, 1150 (O—CH_3); 700 (C_6H_5); ^1H nmr (CCl_4), 60 MHz (δ in ppm): 7.2 (m, 5H, arom.), 3.5 (s, 1H, OH) 3.1 (s, 3H, OCH_3), 2.9 (t, J = 9 Hz, 1H, methine-H), 2.2−1.6 (m, 6H, $CH_2CH_2CH_2$), 1.2^2 + 1.1^9 (ds, 6H, $C(CH_3)_2$). *Anal.* calcd. for $C_{16}H_{22}O_3$: C 73.25, H 8.45; found: C 73.20, H 8.42.

Methyl 2-(2'-phenylcyclopent-1'-enyl)-2-methylpropanoate **2***a*

Dehydration of the β-hydroxy ester **2** (14.8 g) with thionyl chloride and pyridine afforded upon distillation (97−101°C/0.08 Torr), 12.3 g (89%) of a mixture containing the β,γ-unsaturated ester **2***a* and its β,γ-unsaturated isomer in a ratio of 4:1. Renewed distillation (bp 85−90°C/0.05 Torr) yielded 10.2 g of a colourless oil which was further purified by preparative glc (copper column, l = 3 m, ϕ = 1/4 in., 12% SE-30 on Chromosorb WAW 60−80 mesh, 180°C, helium flow rate 20 mL/min); ir ($CHCl_3$, cm^{-1}): 2960, 2850 (CH, aliph.); 1720 (C═O); 1280, 1165 (O—CH_3); 700 (C_6H_5); ^1H nmr ($CDCl_3$), 100 MHz (δ in ppm): 7.2−6.9 (m, 5H, arom.), 3.07 (s, 3H, OCH_3), 2.75−2.40 (m, 4H, CH_2—CH_2—CH_2), 2.05 (m, 2H, CH_2—CH_2—CH_2), 1.2 (s, 6H, $C(CH_3)_2$). *Anal.* calcd. for $C_{16}H_{20}O_2$: C 78.65, H 8.25; found: C 78.61, H 8.27.

Methyl 2-(1'-hydroxy-2'-phenylcyclopentyl)ethanoate **3**

2-Phenylcyclopentanone (21) (23.5 g, 147 mmol) was converted with 147 mmol lithium methyl acetate, prepared from 10.9 g (147 mmol) methyl acetate, 25.3 g di(trimethylsilyl)amine, and 100 mL n-BuLi in hexane (1.50 mmol/mL). The residue (31.4 g) was distilled *in vacuo* (125−127°C/1 Torr) and yielded 1.9 g (11.9 mmol), i.e. 8%, recovered ketone (bp 94−100°C/0.1 Torr) and 27.6 g (80%) of the 3-hydroxy ester **3** (bp 100−102°C/0.07 Torr); (ir liq. cap., cm^{-1}): 3550 (OH); 2970 (CH, aliph.); 1740, 1730 (C═O); 700 (C_6H_5); ^1H nmr (CCl_4), 60 MHz (δ in ppm): 7.2−7.1 (m, 5H, arom.), 3.5 (s, 3H, OCH_3), 2.7 (br s, 1 H, OH), 2.4 (s, 2H, CH_2CO), 2.4−1.8 (m, 7H, aliph.). *Anal.* calcd. for $C_{14}H_{18}O_3$: C 71.77, H 7.74; found: C 71.69, H 7.77.

Methyl 2-(2'-phenylcyclopent-1'-enyl)ethanoate **3**a

Dehydration of the β-hydroxy ester **3** (27.3 g) with thionyl chloride and pyridine afforded after distillation (88−90°C/0.1 Torr) 21.5 g of a mixture of the β,γ-unsaturated ester **3***a* and the α,β- and β,γ'-unsaturated ester isomers in a ratio of 6:3:1. Compound **3***a* was isolated and purified by preparative glc (copper column, l = 3 m, ϕ = 1/4 in., 12% SE-30 on Chromosorb WAW 60−80 mesh, 190°C, helium flow rate 20 mL/min.); ir ($CHCl_3$, cm^{-1}): 2970 (CH, aliph.); 1710 (C═O); 1600, 700 (C_6H_5); ^1H nmr (CCl_4), 60 MHz (δ in ppm): 7.3−7.0 (m, 5H, arom.), 3.6 (s, 3H, OCH_3), 3.1 (s, 2H, CH_2CO), 2.9−2.3 (m, 4H, aliph.), 2.1−1.6 (m, 2H, aliph.). *Anal.* calcd. for $C_{14}H_{16}O_2$: C 77.75, H 7.46; found: C 77.77, H 7.44.

Methyl 2-(2'-hydroxy-2'-indenyl)ethanoate **4**

2-Indanone (5 g, 37.8 mmol) was converted with 37.8 mmol lithium methyl acetate, prepared from 37.8 mmol lithium diisopropylamine in 100 mL THF, as described in the general procedure. The residue (7.5 g) contained 18% 2-indanone and 82% β-hydroxy ester. Distillation *in vacuo* (101°C/0.02 Torr) afforded 5 g (75%) of pure **4**; ir (liq. cap., cm^{-1}): 3545, 3440 br (OH); 2980 (CH, aliph.); 1740 (C═O); 1265, 1150 (O—CH_3); 705 (C_6H_4); ^1H nmr ($CDCl_3$), 60 MHz (δ in ppm): 7.1 (s, 4H, arom.), 3.6 (s, 4H, OCH_3 and OH), 3.0 (s, 4H, benzylic CH_2's), 2.6 (s, 2H, CH_2CO). *Anal.* calcd. for $C_{12}H_{14}O_3$: C 69.88, H 6.84; found: C 69.74, H 6.87.

Methyl 2-(2'-hydroxy-1',2',3'4'-tetrahydro-2'-naphthyl)ethanoate **5**

β-Tetralone (10.0 g, 68 mmol) was reacted with 136 mmol lithium methyl acetate prepared from 136 mmol lithium diisopropylamide in 300 mL THF to yield eventually a residue of 14.2 g. Based on the 1H nmr spectrum, it contained 25% unreacted ketone and 75% of the β-hydroxy ester. Distillation afforded 2.2 g β-tetralone (22%) and 10.4 g (69%) of the β-hydroxy ester **5** (bp 115°C/0.01 Torr); ir (liq. cap., cm^{-1}): 3540, 3440 br (OH); 2980 (CH, aliph.); 1735 (C═O), 1270, 1140 (O—CH_3); 700 (C_6H_4); ^1H nmr ($CDCl_3$), 60 MHz (δ in ppm): 6.90 (s, 4H, arom.), 3.60 (s, 3H, OCH_3), 3.40 (s, 1H, OH), 2.75 (br s, 2H, CH_2CO), 3.0−2.4 (m, 2H, C_{ar}—CH_2—CH_2), 2.45 (s, 2H, C_{ar}—CH_2—C_q), 2.01−1.5 (m, C_{ar}—CH_2—CH_2). *Anal.* calcd. for $C_{13}H_{16}O_3$: C 70.89, H 7.32; found: C 70.52, H 7.34.

Methyl 2'-(3',4'-dihydro-2'-naphthyl)ethanoate **5**a

The β-hydroxy ester **5** was dehydrated with thionyl chloride and pyridine in benzene to yield 75% of **5***a*. After distillation (115°C/0.015 Torr) the β,γ-unsaturated ester proved to be admixed with ca. 20% of the α,β-unsaturated isomer; an analytical sample was obtained by preparative glc (copper column, l = 5 m, ϕ = 1/4 in., 15% SE-30 on Chromosorb WAW 60−80 mesh, 240°C, helium flow rate 60 mL/min); ir (liq. cap., cm^{-1}): 2960, 2940 (CH, aliph.); 1740 (C═O); 1260, 1160 (O—CH_3); 770, 765 (C_6H_4); ^1H nmr (CCl_4), 60 MHz (δ in ppm): 7.2−7.0 (m, 4H, arom.), 6.30 (br s, 1H, olef.), 3.70 (s, 3H, OCH_3), 3.20 (br s, 2H, CH_2CO), 3.5−2.0 (m, 4H, CH_2−CH_2). *Anal.* calcd. for $C_{13}H_{14}O_2$: C 77.20, H 6.98; found: C 77.21, H 7.00.

Methyl 2-(2'-hydroxy-1',2',3',4'-tetrahydro-2'-naphtyl)propanoate **6**

This compound was prepared as described for **5** using lithium methyl propanoate instead of lithium methyl acetate. Based on the ^1H nmr spectrum, the residue contained 25% of the β-hydroxy ester and 75% unreacted ketone; ^1H nmr ($CDCl_3$), 60 MHz (δ in ppm): 6.90 (m, 4H, arom.), 4.1−3.8 (m, 1H, C_tH), 3.6 (s, 3H, OCH_3), 3.30 (br s, 1H, OH), 3.2−2.7 (m, 2H, C_{ar}—CH_2—CH_2), 2.7 (br s, 2H, C_{ar}—CH_2—C_q), 1.9−1.6 (m, 2H, C_{ar}—CH_2—CH_2), 1.3 + 1.1 (dd, J = 7 Hz, 3H, C_tCH_3).

Acknowledgement

This work was carried out in part under the auspices of the Netherlands Foundation for Chemical Research (S.O.N.) with financial support from the Netherlands Organization for Advancement of Pure Research (Z.W.O.).

1. D. IVANOV, G. VASSILEV, and I. PANAYOTOV. Synthesis, 83 (1975).
2. E. M. KAISER, J. D. PETTY, and P. L. A. KNUTSON. Synthesis, 509 (1977).
3. V. REUTRAKUL, P. RATANANUKUL, and S. NIMGIRAWATH. Chem. Lett. 71 (1980).
4. K. TAKAKI, K. NEGORO, and T. AGAWA. J. Chem. Soc. Perkin Trans. 1, 1490 (1979).
5. C. R. JOHNSON and T. R. BADE. J. Org. Chem. **47**, 1205 (1982).
6. J. VILLIERAS, M. RAMBAUD, R. TARHOUNI, and B. KIRSCHLEGER. Synthesis, 68 (1981).
7. P. K. FREEMAN and L. L. HUTCHINSON. J. Org. Chem. **45**, 1924 (1980); B. BOGDANOVIĆ and B. WERMECKES. Angew. Chem. **93**, 691 (1981).
8. C. R. HAUSER and W. R. DUNNAVANT. J. Org. Chem. **25**, 503 (1960).
9. M. W. RATHKE. J. Am. Chem. Soc. **92**, 3222 (1970).
10. J. W. FRANKENFELD and J. J. WERNER. J. Org. Chem. **34**, 3689 (1969); M. BOGAVAC, L. ARSENYEVIC, and V. ARSENYEVIC. Bull. Soc. Chim. Fr. 145 (1980); D. A. CORNFORTH, A. E. OPARA, and G. READ. J. Chem. Soc. (C), 2799 (1969).
11. B. H. HAN and P. BOUDJOUK. J. Org. Chem. **47**, 5030 (1982).
12. D. L. J. CLIVE and C. G. RUSSELL. J. Chem. Soc. Chem. Commun. 434 (1981); D. L. J. CLIVE, C. G. RUSSELL, and S. C. SURI. J. Org. Chem. **47**, 1632 (1982).

13. C. J. KOWALSKI and J. S. DUNG. J. Am. Chem. Soc. **102**, 7950 (1980); P. F. HUDRLIK and A. K. KULKARNI. J. Am. Chem. Soc. **103**, 6251 (1981).
14. M. W. RATHKE and D. SULLIVAN. Tetrahedron Lett. 4249 (1972).
15. T. SHONO, Y. MATSUMURA, S. KASHIMURA, and K. HATANAKA. J. Am. Chem. Soc. **101**, 4752 (1979).
16. R. H. VAN DER VEEN, C. KRUK, and H. CERFONTAIN. J. Am. Chem. Soc. **105**, 4367 (1983); R. H. VAN DER VEEN and H. CERFONTAIN. J. Chem. Soc. Perkin Trans. 1. Submitted.
17. I. KIKKAWA and T. TADAHIKO. Synthesis, 877 (1980).
18. A. G. PINKERS and A. SABESAN. J. Chem. Soc. Perkin Trans. 2, 473 (1981), and references cited therein.
19. N. AWATER. J. Am. Chem. Soc. **82**, 2847 (1960); H. J. RINGOLD and S. K. MALHOTRA. J. Am. Chem. Soc. **84**, 3402 (1962).
20. A. I. VOGEL. Textbook of practical organic chemistry. 3rd ed. Longman, London and New York. 1967. p. 19.
21. R. T. ARNOLDS, J. S. BUCKLEY, and R. M. DODSON. J. Am. Chem. Soc. **72**, 3153 (1950).
22. W. G. DAUBEN and R. TERANISHI. J. Org. Chem. **16**, 550 (1951).

Can. J. Chem. Downloaded from www.nrcresearchpress.com by 210.87.254.6 on 09/06/12
For personal use only.

Studies on γ-irradiated aqueous solutions of tripeptides composed of glycine and L-alanine by the spin-trap high-performance liquid chromatography – electron spin resonance method

FUMIO MORIYA,[1] NAOHISA IGUCHI, KEISUKE MAKINO,[2] SOUJI ROKUSHIKA, AND HIROYUKI HATANO
Department of Chemistry, Faculty of Science, Kyoto University, Sakyo-ku, Kyoto, 606 Japan

Received November 3, 1983

FUMIO MORIYA, NAOHISA IGUCHI, KEISUKE MAKINO, SOUJI ROKUSHIKA, and HIROYUKI HATANO. Can. J. Chem. **62**, 2206 (1984).

The γ-irradiated aqueous solutions of four tripeptides were studied by the spin-trap hplc–esr method with 2-methyl-2-nitrosopropane. Four types of spin adducts were separated and identified as follows: (a) deamino adducts derived from short-lived radicals produced by reductive deaminations from the addition of hydrated electrons to the N-terminal peptide carbonyl groups, (b) C-terminal backbone adducts, (c) internal backbone adducts, and (d) side-chain adducts derived from short-lived radicals produced by hydrogen abstractions by hydroxyl radicals, mainly from so-called α-carbons in the C-terminal and internal main-chains and a carbon in an aliphatic side-chain, respectively. For polyglycine, internal backbone radicals produced by hydrogen abstraction were spin-trapped and detected.

FUMIO MORIYA, NAOHISA IGUCHI, KEISUKE MAKINO, SOUJI ROKUSHIKA et HIROYUKI HATANO. Can. J. Chem. **62**, 2206 (1984).

Faisant appel à la méthode rpe–clhp des pièges à spin et opérant dans des solutions aqueuses, on a étudié les réactions du méthyl-2 nitroso-2 propane avec quatre tripeptides irradiés aux rayons-γ. On a isolé quatre types d'adduits de spin et on les a identifiés comme suit: (a) les adduits désaminés provenant de radicaux à faibles temps de vie produits par la désamination réductrice causée par l'addition d'électrons hydratés sur les groupes carbonyles des peptides en position N-terminale, (b) les adduits sur le squelette carboné en position C-terminale, (c) les aduits en position interne du squelette carboné et (d) les adduits sur les chaines latérales qui proviennent de radicaux de faibles temps de vie qui ont été produits respectivement (pour les trois dernières catégories) par l'élimination d'hydrogènes, par des radicaux hydroxyles, des soit-disants carbones en α soit des chaînes principales en position C-terminale (cas b) ou interne (cas c) soit d'un carbone dans la chaîne latérale aliphatique (cas d). Dans le cas de la polyglycine, on a piégé les spin et détecté les radicaux formés par une abstraction d'hydrogène en position interne du squelette carboné.

[Traduit par le journal]

Can. J. Chem. Downloaded from www.nrcresearchpress.com by 210.87.254.42 on 09/06/12
For personal use only.

Introduction

In order to understand the radiation chemistry of aqueous solutions of proteins, several workers have done numerous studies concerning such systems as amino acids and peptides (1–3, and refs. therein). Transient free radicals produced in proteins by active radiolytic species of water, hydrated electrons (e^-_{aq}), hydroxyl radicals (·OH), hydrogen atoms (·H), etc., are quite conceivably the primary species responsible for the radiation effects on proteins (2, 3).

For the elucidation of primary processes in the radiation chemistry of biomolecules, the analysis of unstable transient species has been introduced and has rapidly become important (2, 4). The spin-trapping method (5–7, and refs. therein) is one of several valuable techniques for detecting and identifying transient short-lived radicals in various reaction systems by means of which short-lived radicals are converted into relatively stable aminoxyl radicals[3] (spin adducts) through reactions with spin traps such as nitroso and nitrone compounds. When 2-methyl-2-nitrosopropane (MNP) is used as a spin trap, its reaction with a short-lived radical (R·) is represented by eq. [1].

The spin-trapping method with MNP has been applied to γ- and uv-irradiated aqueous solutions of amino acids and peptides (3, 9–13). Because of the complexity of the esr spectra arising from the overlapping of signals of several spin adducts present, however, few of the components could be identified. To better analyze such spectra, high-performance liquid chromatography (hplc) has been combined with spin trapping (the spin-trap hplc–esr method), and been applied to studies on γ-irradiated aqueous systems of several amino acids (14–20). The main general mechanisms found for aliphatic amino acids were reductive deamination reactions induced by e^-_{aq} addition to carboxyl carbons (eq. [2]) (2) and hydrogen abstraction

[1] $$t\text{-Bu}-N{=}O + R\cdot \longrightarrow t\text{-Bu}-\underset{\underset{O\cdot}{|}}{N}-R \leftrightarrow t\text{-Bu}-\overset{+}{\underset{\underset{O^-}{|}}{N}}\cdot-R$$

[2] $$NH_3^+-\underset{\underset{R}{|}}{CH}-\underset{\underset{O}{\|}}{C}-O^- + e^-_{aq} \longrightarrow NH_3^+-\underset{\underset{R}{|}}{CH}-\underset{\underset{O^-}{|}}{\dot{C}}-O^- \longrightarrow NH_3 + \cdot\underset{\underset{R}{|}}{CH}-\underset{\underset{O}{\|}}{C}-O^-$$

[3] $$\rangle C-H + \cdot OH \longrightarrow \rangle C\cdot + H_2O$$

reactions from most of the saturated alkyl carbons mainly by ·OH (eq. [3]). Especially in the case of L-isoleucine, spin adducts derived from the H abstractions from all of the C—H bonds were separated and detected (16).

When one wants to obtain basic information concerning the radiation damage of the main-chain structures in proteins, the use of peptides composed of glycine and L-alanine seems to simplify this subject. In previous papers (21, 22) we have

[1] Present address: Department of Chemistry, Kobe University of Commerce, Tarumi-ku, Kobe, 655 Japan.

[2] Present address: Department of Textile Chemistry, Faculty of Textile Science, Kyoto Institute of Technology, Sakyo-ku, Kyoto, 606 Japan.

[3] The term "aminoxyl" was introduced during the International Symposium on Spin Trapping and Nitroxyl Radical Chemistry (at the University of Guelph, Guelph, Ont., Canada, July 12–18, 1981) and was deemed more appropriate than "nitroxyl"; see ref. 8.

Can. J. Chem. Downloaded from www.nrcresearchpress.com by 210.87.254.42 on 09/06/12
For personal use only.

demonstrated that spin adducts produced in γ-irradiated aqueous solutions of dipeptides (Gly-Gly, Gly-L-Ala, L-Ala-Gly, and L-Ala-L-Ala) with MNP could be identified by this technique. These studies indicated that most of the short-lived radicals found in aqueous solutions of the dipeptides by other methods (23, 24) were spin-trapped. Consequently, γ-radiolytic and spin-trapping mechanisms shown in eqs. [4]–[6] for dipeptides have been proposed,

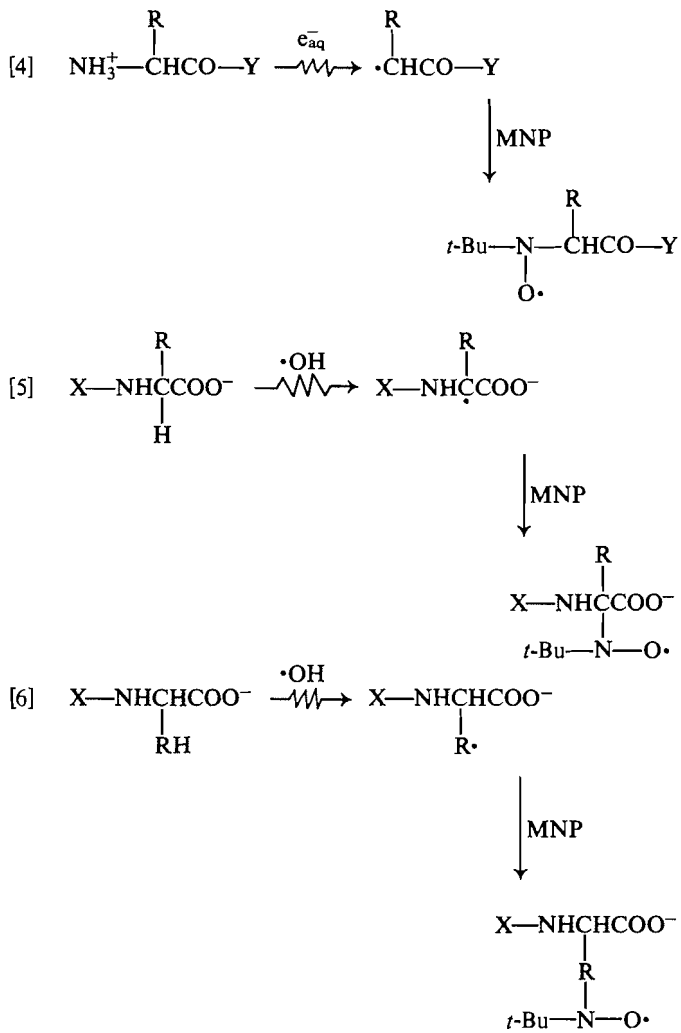

where X and Y represent amino acid residues, R is H or a side-chain, RH is an aliphatic side-chain, and the left, central, and right members of each equation are a dipeptide, a short-lived radical, and a spin adduct, respectively. The spin adduct in eq. [4] is derived from a deaminated radical resulting from the addition of e^-_{aq} to the peptide carbonyl group (2, 25). The spin adducts in eqs. [5] and [6] are produced from radicals generated by hydrogen abstractions from a so-called α-carbon in the C-terminal main-chain and a carbon in an aliphatic side-chain, respectively, mainly by ·OH. The spin adducts in eqs. [4]–[6] have been called a deamino adduct, a C-terminal backbone adduct, and a side-chain adduct, respectively.

This information about the amino acids and dipeptides (14–22) can be a good guide for understanding the radiation damage of N- and C-terminals and aliphatic side-chains in proteins. However, it gives no evidence of the radiation damage of inner parts of the main-chains in proteins. In the present work, in order to explore the primary radiation-chemical processes of inner parts of the main-chains, γ-irradiated aqueous solutions of tripeptides (Gly-Gly-Gly, Gly-Gly-L-Ala, Gly-L-Ala-Gly, and L-Ala-Gly-Gly) have been studied by the spin-trap hplc–esr method with MNP. Most of the spin adducts expected from eqs. [4]–[6] were found and characterized. Internal backbone adducts derived in analogy with C-terminal backbone adducts were newly found. We have also studied spin-trapping of γ-irradiated aqueous solutions of polyglycine and detected its internal backbone adduct.

Experimental

MNP was synthesized and purified according to the method of Stowell (26). Gly-Gly-Gly, Gly-Gly-L-Ala, L-Ala-Gly-Gly, and polyglycine (approximate molecular weight was 6000) were purchased from Sigma Chemical Co., Saint Louis, MO, USA. Gly-L-Ala-Gly was supplied from Prof. Haruaki Yajima, Kyoto University. Potassium nitrosodisulfonate (Fremy's salt, $\cdot ON(SO_3K)_2$) was synthesized and purified according to the method of Moser and Howie (27). All other chemicals were of reagent grade.

The tripeptides (0.1 *M*) were dissolved in 5 mg/mL of MNP aqueous solutions (28). Each of the sample solutions was cooled by ice and irradiated with ^{60}Co γ-rays at a dose rate of ca. 75 Gy/min to a total dose of 3 kGy (unless otherwise specified) without deaeration. The concentration of phosphoric ion in the irradiated solution was adjusted to that in the starting eluent by 2 *M* sodium phosphate, and 1.0 mL of the solution was added to a 0.75 × 60 cm cation-exchange column (IEX-210SC of Toyo Soda Manufacturing Co., Tokyo, Japan). The hplc was a Toyo Soda HLC-803. The eluate was passed through uv and esr detectors and collected into fraction tubes. The uv detector was a JASCO UVIDEC 100 (10-mm light path), which was tuned to 240 nm. The esr spectrometer was a JEOL PE-3X, which was operated at 100-kHz modulation frequency in the X-band. For detection of the radicals during chromatography, the magnetic field was fixed at the position where the esr signals were expected. The magnetic field modulation was used at a high amplitude of 1 mT to cover a wide range. A quartz flow cell (the practical part being 0.6 mm id and 5 cm long) was fixed in the esr cavity. Each of the parts in the chromatographic system was connected with 0.25-mm id PTFE tubing.

The esr spectra were recorded at ca. 25°C in the dark. The hyperfine splitting constants (hfsc's) were measured with Mn^{2+} in MgO as a reference. The concentration of the radicals was estimated by double integration of the first-derivative esr signal with a JEOL JEC-980A mini-computer, which was compared with Fremy's salt of known concentrations. Ninhydrin-positive fractions were analyzed by an amino acid analyzer (KLA-3B of Hitachi Corporation, Hitachi, Japan).

For other experimental details previous publications can be consulted (21).

Results and discussion

Glycylglycylglycine

Figure 1(a) shows the esr spectrum of a γ-irradiated aqueous Gly-Gly-Gly solution with MNP. The esr signals asterisked in Fig. 1(a) decayed relatively quickly and disappeared within 1 h. The chromatogram of the solution by uv and esr detections is shown in Fig. 1(b). The esr chromatogram exhibited three peaks (A–C) as shown by the solid line. Typical esr spectra for the fractions of peaks A–C are depicted in parts (a), (b) and (e) of Fig. 2, respectively. Most of the spin adducts produced by the self-trapping of MNP (29) were adsorbed on the column and eluted very slowly. In the uv chromatogram shown by the broken line in Fig. 1(b), peak D′ was due to intact Gly-Gly-Gly and peak E′ was mainly due to *tert*-butylnitrosohydroxylamine (*t*-BuN(OH)N=O) (28).

Figure 2(a) shows the esr spectrum (0.05 mT modulation amplitude) obtained for the peak A fraction, which can be

Can. J. Chem. Downloaded from www.nrcresearchpress.com by 210.87.254.42 on 09/06/12
For personal use only.

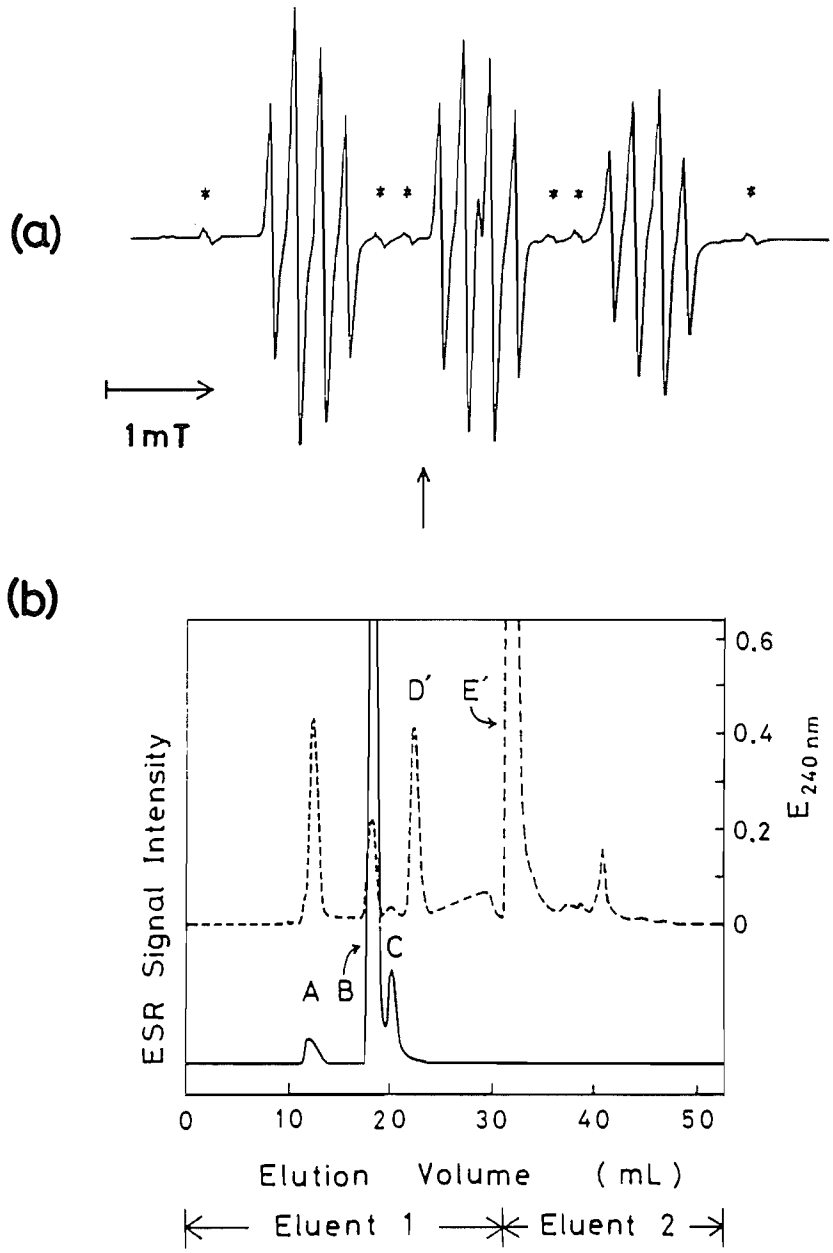

FIG. 1. (a) The esr spectrum of an aqueous solution of Gly-Gly-Gly with MNP observed just after γ-irradiation (at pH 5.7). During chromatography the magnetic field was fixed at the position indicated by the vertical arrow. (b) Chromatogram of the solution drawn by uv (broken line) and esr (solid line) detections: flow rate, ca. 0.3 mL/min; eluent 1, 0.25 *M* sodium phosphate buffer, pH 6.0; eluent 2, 0.2 *M* Na_2HPO_4–NaOH buffer, pH 11.5.

analyzed as a triplet-triplet. The primary triplet of 1.58 mT splitting is due to the nitrogen nucleus in the aminoxyl group. The secondary triplet of 0.92 mT splitting with an intensity ratio of 1:2:1 is assigned to two equivalent β-hydrogens. The spin adduct was assigned to structure **1**, the deamino adduct from Gly-Gly-Gly, on the basis of its hyperfine structure (hfs)

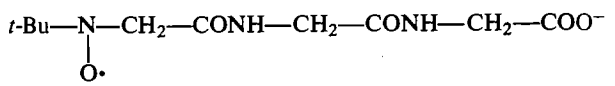

1

and elution position. In addition, a 0.03-mT triplet due to a γ-nitrogen in the peptide bond was observed by esr measurement with 0.02 mT modulation amplitude. Parts of the esr signals in Fig. 2(a) coincided with the asterisked signals in Fig. 1. The separated spin adduct **1** in the fraction of peak A was fairly stable in contrast to the unseparated one in the irradiated solution.

Parts (b) and (e) of Fig. 2 show the esr spectra for the fractions of peaks B and C, respectively, which are similar to each other. Each of them can be analyzed as a triplet of four lines with an apparent intensity ratio of 1:2:2:1. Around pH 6 the primary N-hfsc's (a_N) are 1.56 and 1.51 mT for peaks B and C, respectively. The difference between the N-hfsc's is significant. The secondary hfs is due to a β-hydrogen and a β-nitrogen ($a_{\beta H}$ = 0.20 mT and $a_{\beta N}$ = 0.24 mT for both peaks). This esr signal pattern suggests a spin adduct which has a

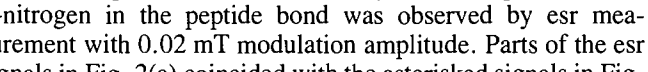

component part, *t*-BuN(O·)—CH—N<, that is, structure **2**, **3**, or **4**.

Can. J. Chem. Downloaded from www.nrcresearchpress.com by 210.87.254.42 on 09/06/12
For personal use only.

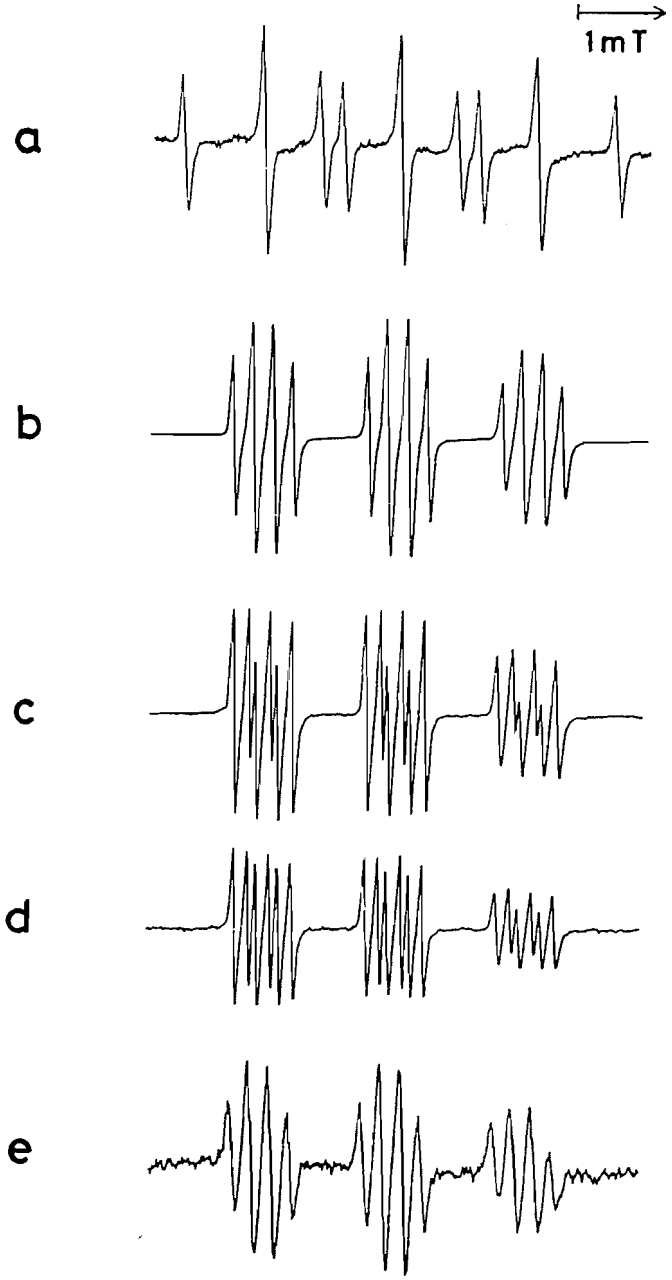

FIG. 2. The esr spectra of the separated spin adducts. (a), (b)–(d), and (e) represent the spectra obtained from the fractions giving peaks A–C in Fig. 1(b), respectively. (a) and (b), pH 6.0; (c), pH 1.8; (d), pH 0.6; (e), pH 6.3.

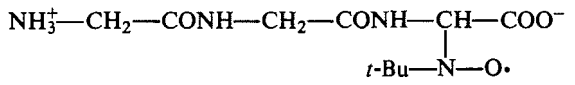

2

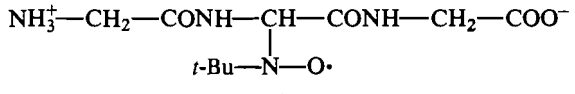

3

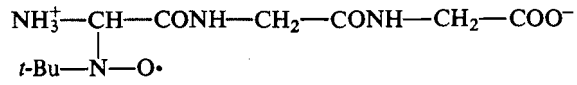

4

These spin adducts are derived from the hydrogen abstraction from one of three methylene groups in Gly-Gly-Gly.

In the neutral and alkaline solutions the esr spectral pattern of the peak B fractions was almost pH-independent (a_N = 1.59 mT, $a_{\beta H}$ = 0.20 mT, and $a_{\beta N}$ = 0.26 mT at pH 11.1), which suggests the absence of an amino group near the aminoxyl group. In contrast, in the acidic pH range (around pH 2) the spin adduct exhibited reversible pH-dependent shifts of the signals as shown in parts (c) and (d) of Fig. 2. At pH 0.6, the hfsc's a_N, $a_{\beta H}$, and $a_{\beta H}$ are 1.52, 0.16, and 0.255 mT, respectively. The remarkable spectral changes are mainly due to the increase in difference of the β-hfsc's and do not derive from new hyperfine splittings. Consequently, this acid dissociation property is ascribed to the protonation of a carboxyl group near the aminoxyl center, not to the protonation of the aminoxyl group itself which should give an additional H-hfsc of several gauss (30, 31). Therefore the spin adduct was assigned to the structure **2** (neither to **3** nor to **4**), the C-terminal backbone adduct from Gly-Gly-Gly. In the acid-dissociation equilibrium of the carboxyl group of adduct **2**, the observed hfsc's represented the weighted average of the acid form and the base form because of rapid interchange between the two forms (32).

The esr spectral pattern for the peak C fraction changed little in the acidic, neutral, and alkaline pH ranges (a_N = 1.50 mT, $a_{\beta H}$ = 0.21 mT, and $a_{\beta N}$ = 0.235 mT at pH 0.7; a_N = 1.53 mT, $a_{\beta H}$ = 0.20 mT, and $a_{\beta N}$ = 0.23 mT at pH 11.2). This fact shows that neither a carboxyl group nor an amino group is close to the aminoxyl group. Therefore, the spin adduct was assigned to structure **3**, the internal backbone adduct from Gly-Gly-Gly.

The spectral pattern of spin adducts **2** and **3** near pH 6, a triplet of 1:2:2:1 quartet, is apparently a major component of the esr signals in Fig. 1(a). The signal component in the γ-irradiated solution exhibited reversible pH-dependent changes in the acidic pH range and changed little in the neutral and alkaline ranges. The pH effect on the spectral pattern was almost consistent with that of adduct **2**, not **3**. Therefore spin adduct **2**, which gives peak B, seems to be a major component of stable adducts from Gly-Gly-Gly. This inference is also supported by rough estimates of relative amounts of radicals in the fractions of the individual peaks.

Glycylglycyl-L-alanine

Figure 3 shows the esr spectrum and chromatogram of a γ-irradiated aqueous Gly-Gly-L-Ala solution with MNP, respectively. The esr signals asterisked in Fig. 3(a) decayed relatively quickly. The signal intensity at 33 min after the irradiation was one eighth that at 5.5 min. The time-dependent decay curve of the signal indicated that the kinetic order is larger than one. The esr chromatogram exhibited four peaks (A–D) as shown by the solid line in Fig. 3(b). Typical esr spectra for the fractions of peaks A–D are depicted in parts (a)–(d) of Fig. 4, respectively. In the uv chromatogram shown by the broken line in Fig. 3(b), peak E′ was due to intact Gly-Gly-L-Ala and peak F′ was mainly due to *t*-BuN(OH)NO (28).

Figure 4(a) shows the esr spectrum (0.05 mT modulation amplitude) obtained for the peak A fraction. The hfsc's are given in Table 1. The spin adduct was assigned to structure **5**,

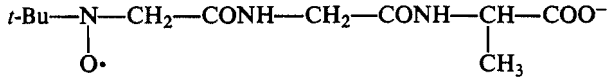

5

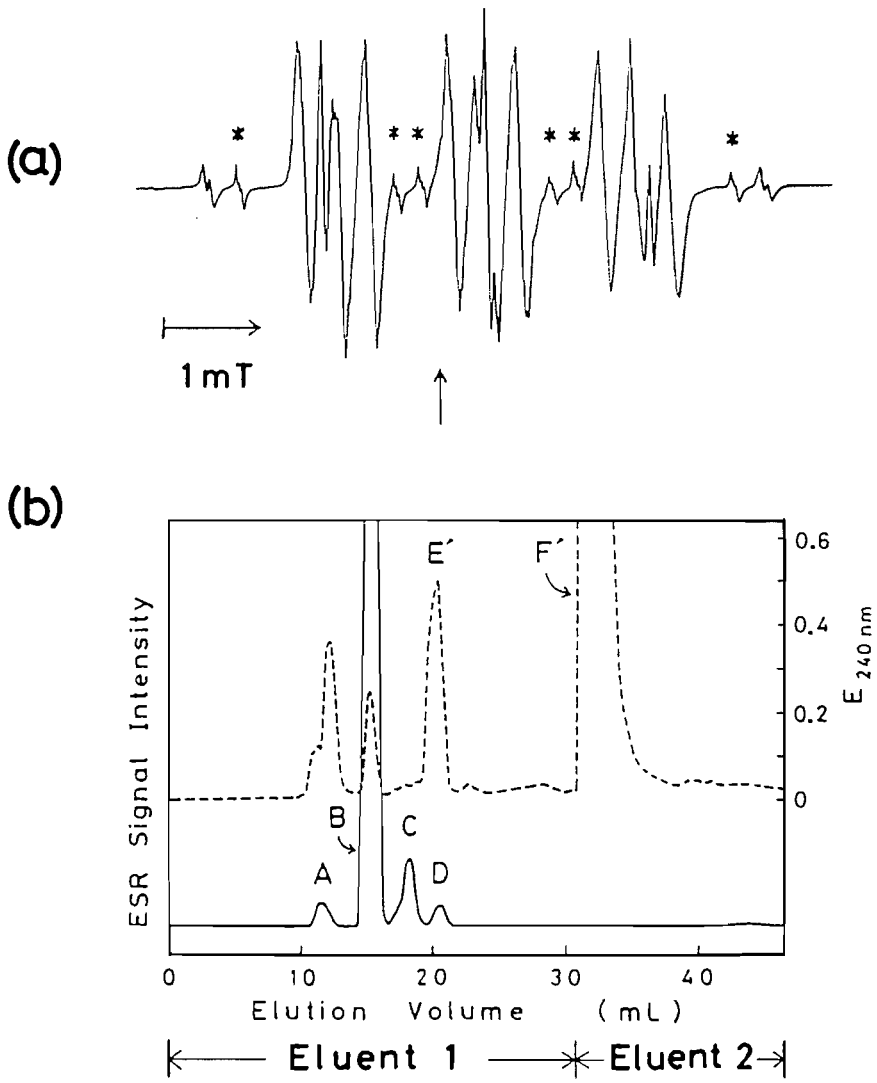

FIG. 3. (a) The esr spectrum of an aqueous solution of Gly-Gly-L-Ala with MNP observed just after γ-irradiation (at pH 5.7). During chromatography the magnetic field was fixed at the position indicated by the vertical arrow. (b) Chromatogram of the solution drawn by uv (broken line) and esr (solid line) detections: flow rate, ca. 0.2 mL/min; eluent 1, 0.25 *M* sodium phosphate buffer, pH 6.0; eluent 2, 0.2 *M* Na_2HPO_4–NaOH buffer, pH 11.5.

the deamino adduct from Gly-Gly-L-Ala. Parts of the esr signals in Fig. 4(a) coincided with the asterisked signals in Fig. 3(a). The separated spin adduct **5** in the peak A fraction was fairly stable.

Figure 4(b) shows the esr spectrum for the peak B fraction, which can be analyzed as a triplet-triplet, and which is apparently a major component of esr signals in Fig. 3(a). The primary hfsc of a nitrogen nucleus is 1.52 mT, and the secondary 0.33 mT triplet with equal intensities was assigned to a β-nitrogen. This esr signal pattern was assigned to structure **6**, the C-terminal backbone adduct from Gly-Gly-L-Ala.

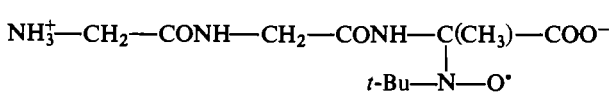

6

Figure 4(c) shows the esr spectrum for the peak C. The secondary hfs consists of a β-hydrogen and a β-nitrogen. The spectral pattern was almost pH-independent. The hfsc's at pH 1.0, 6.0, and 12.0 are given in Table 1. The spin adduct was assigned to structure **7**, the internal backbone adduct from

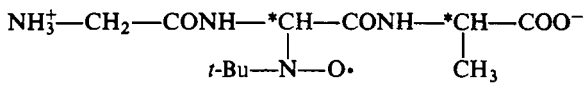

7

Gly-Gly-L-Ala. Slight distortions observed in the esr spectra suggest the coexistence of a pair of diastereomeric adducts (15, 22, 33), *S-S* and *R-S* forms, by the primary asymmetric center of the L-alanyl residue and the new asymmetric center formed by the addition of MNP to the short-lived radical.

Figure 4(d) shows the esr spectrum for the peak D fraction, which apparently exhibits a mixture of six narrow and six broad lines. Each of the narrow lines further splits into a small doublet. Since the narrow set and the broad set gave the same *g* value and N-hfsc, the spectrum was inferred to be due to only one kind of spin adduct with line-width alternation (LWA). It can be analyzed as three groups of a 1:1:1:1 quartet whose internal pair is selectively broad. The hfsc's at pH 5.9 are as follows: a_N = 1.63 mT, $a_{\beta H}(2H)$ = 1.36 and 1.02 mT, and $a_{\gamma H}$ = 0.07 mT. Such a spectrum as shown in Fig. 4(d) is a typical pattern of an aminoxyl radical, *t*-BuN(O•)—CH_2—*CXYZ

Can. J. Chem. Downloaded from www.nrcresearchpress.com by 210.87.254.42 on 09/06/12
For personal use only.

Can. J. Chem. Downloaded from www.nrcresearchpress.com by 210.87.254.42 on 09/06/12
For personal use only.

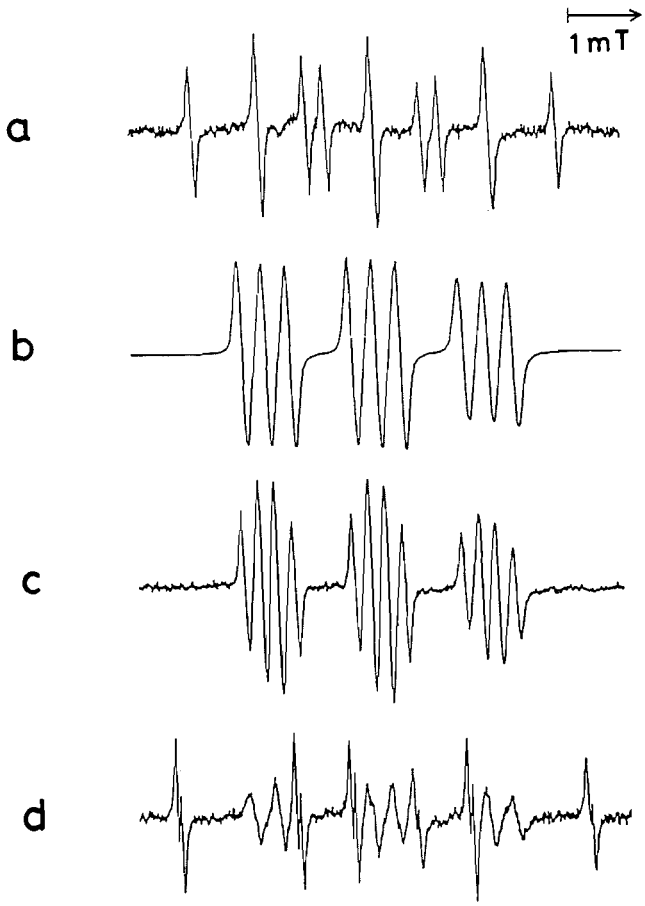

FIG. 4. The esr spectra of the separated spin adducts. (a)–(d) represent the spectra obtained from the fractions giving peaks A–D in Fig. 3(b), respectively. (a) and (d), pH 5.9; (b) and (c), pH 6.0.

(34). The nonequivalence with LWA is interpreted by assuming, for instance, insufficiently rapid interconversion between two rotamers which have mutually different sets of β-H hfsc's. The mechanism of such hfs patterns has been discussed in detail by Gilbert and Trenwith (34). The spin adduct was assigned to structure **8**, the side-chain adduct from Gly-Gly-L-Ala.

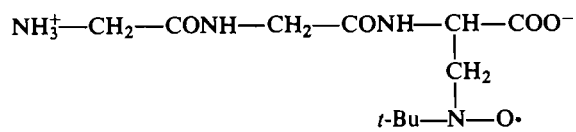

8

The total concentration of stable spin adducts produced in the γ-irradiated aqueous solution of Gly-Gly-L-Ala (0.1 *M*) with MNP (5 mg/mL) was plotted against the total dose as shown in Fig. 5. Each of the concentrations was calculated from the esr spectrum obtained 3 h after the irradiation. The *G* value was estimated to be about 0.9 from the linearly increased range in Fig. 5. Although the *G* value of spin adducts does not always reflect that of short-lived radicals directly, the obtained spin adduct mixtures consist of adducts originating predominantly from Gly-Gly-L-Ala, particularly the backbone adducts. Therefore, the short-lived peptide radicals converted into the spin adducts seem never to be negligible during consideration of the primary processes of radiolysis of peptides.

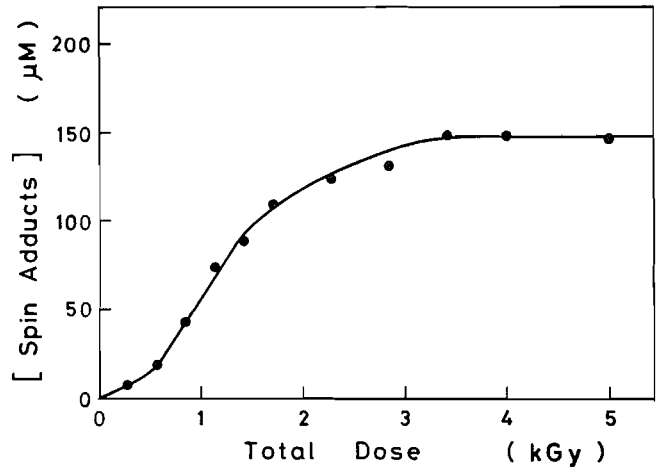

FIG. 5. Dose dependence of the concentration of stable spin adducts produced in γ-irradiated aqueous solutions of Gly-Gly-L-Ala with MNP. Each estimation of the concentration was carried out 3 h after the irradiation.

Figure 6 shows the dose dependence of the esr spectral patterns obtained from the γ-irradiated aqueous system of Gly-Gly-L-Ala with MNP. Most of the spin adducts which formed these spectra have already been separated individually by hplc and analyzed spectroscopically by esr. That is to say, spin adducts **5**–**8** from Gly-Gly-L-Ala were found in the present work, and the adducts by the self-trapping of MNP were reported in the previous paper (29). The observed spectral changes suggest transitions of concentration ratios of the individual spin adducts. For the complicated spectra shown in Fig. 6 it is very difficult to achieve computer simulations, even using the known esr parameters of these adducts, since there are too many parameters. Satisfactory simulated spectra have not been obtained so far.

Glycyl-L-alanylglycine

Figure 7 shows the chromatogram of a γ-irradiated aqueous Gly-L-Ala-Gly solution with MNP. The esr chromatogram exhibited four peaks (A–D) as shown by the solid line. Typical esr spectra for the fractions of peaks A–C are depicted in parts (a)–(c) of Fig. 8, respectively. In the uv chromatogram shown by the broken line in Fig. 7, peaks E′ and F′ were due to intact Gly-L-Ala-Gly and *t*-BuN(OH)NO (28).

Figure 8(a) shows the esr spectrum (0.05 mT modulation amplitude) obtained for the peak A fraction, and the hfsc's are given in Table 1. The spin adduct was assigned to structure **9**, the deamino adduct from Gly-L-Ala-Gly.

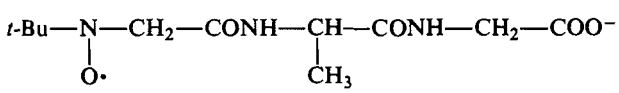

9

Parts (b) and (c) of Fig. 8 show the esr spectra for the fractions of peaks B and C, respectively, which are similar to each other. Both spin adducts exhibited little spectral change in the neutral and alkaline pH range, while in the acidic pH range they exhibited reversible pH-dependent shifts of their signals which resemble the behavior of adduct **2**. Their hfsc's at various pH's are given in Table 1. Both spin adducts were assigned to a pair of the diastereomeric C-terminal backbone adducts (*S*-*S* and *S*-*R* forms), that is

Can. J. Chem. Downloaded from www.nrcresearchpress.com by 210.87.254.42 on 09/06/12
For personal use only.

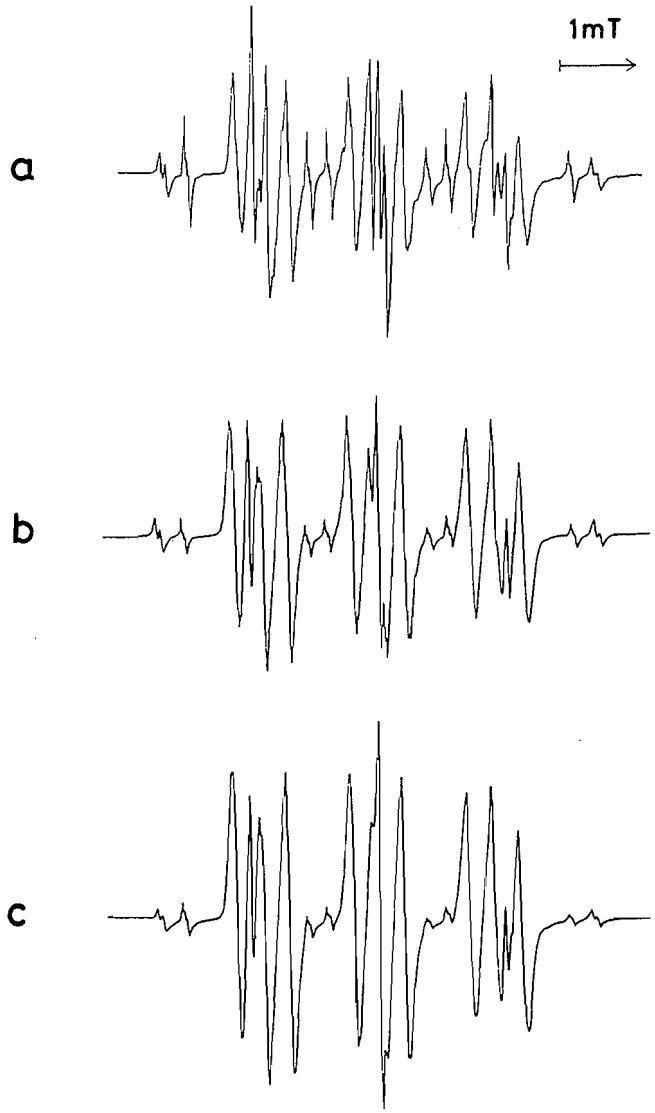

FIG. 6. Dose dependence of the esr spectral pattern of an aqueous Gly-Gly-L-Ala solution with MNP observed just after γ-irradiation. (a), 0.7 kGy; (b), 3 kGy; (c), 9 kGy.

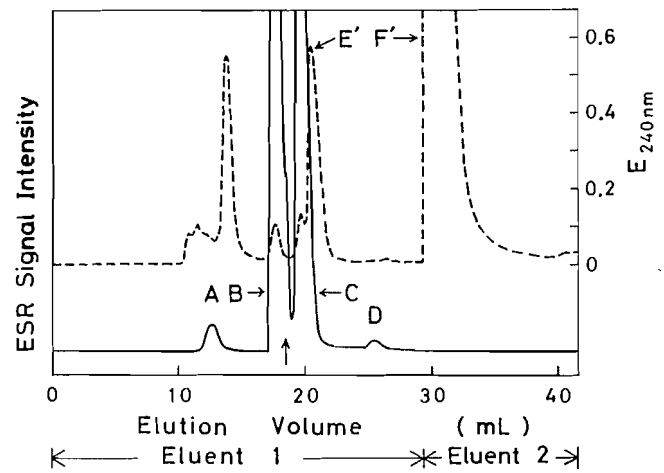

FIG. 7. Chromatogram of a γ-irradiated aqueous solution of a Gly-L-Ala-Gly with MNP drawn by uv (broken line) and esr (solid line) detections: flow rate, ca. 0.2 mL/min; eluent 1, 0.35 *M* sodium phosphate buffer, pH 6.0; eluent 2, 0.2 *M* Na_2HPO_4–NaOH buffer, pH 11.5. The magnetic field fixed for the esr detection was 4.03 mT higher than the $g = 2.034$ signal of Mn^{2+} in MgO.

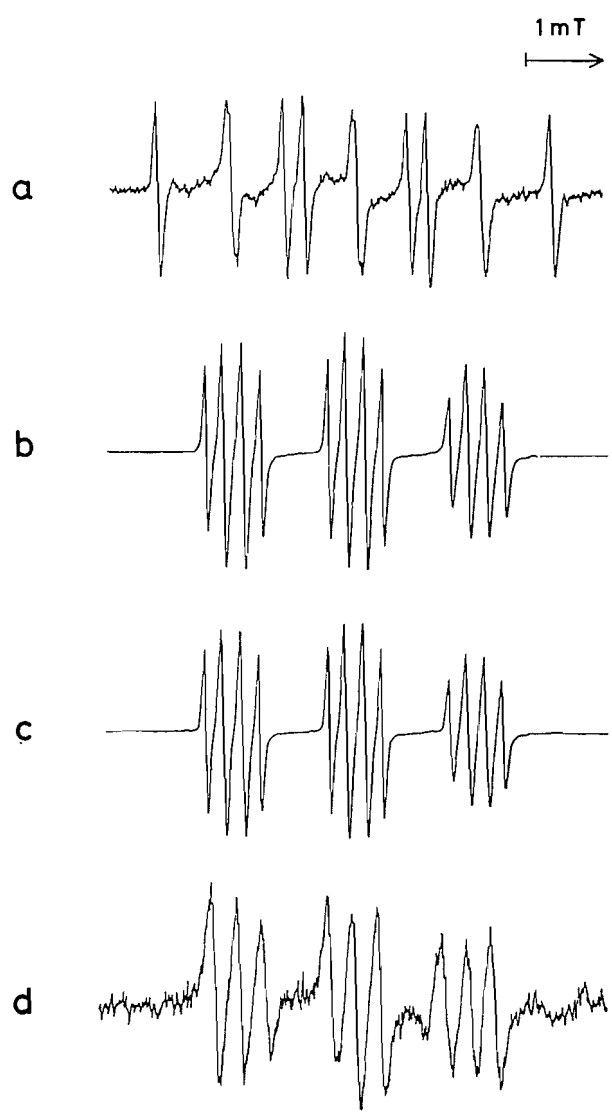

FIG. 8. The esr spectra of the separated spin adducts. (a)–(c) represent the spectra obtained from the fractions (pH 6.0) giving peaks A–C in Fig. 7(b), respectively. (d) The spectrum for the fraction at the position indicated by the vertical arrow in Fig. 7. It was measured more than 1 h after the adjustment of pH to 0.4.

$$NH_3^+—CH_2—CONH—*CH(CH_3)—CONH—*CH(N(t\text{-Bu})—O\cdot)—COO^-$$

10

The adduct of peak B refers to structure **10***a* and that of peak C to **10***b*.

In the esr chromatogram, a slight shoulder of peak B was found at the position indicated by the vertical arrow in Fig. 7. The esr spectrum for the fraction at this position exhibited a fairly asymmetric triplet-quartet pattern with distortions, which suggested that the fraction contained new radicals other than spin adduct **10***a*. Since the C-terminal backbone adducts derived from peptides whose C-terminal residues are glycines are unstable and decay relatively quickly at strong acidic pH, spin adduct **10***a* was eliminated by lowering the pH of the fraction. Figure 8(d) shows the esr spectrum for the fraction measured more than 1 h after the adjustment of pH to 0.4. In the spectrum a triplet-triplet pattern was newly observed ($a_N = 1.46$ mT, $a_{\beta N}$

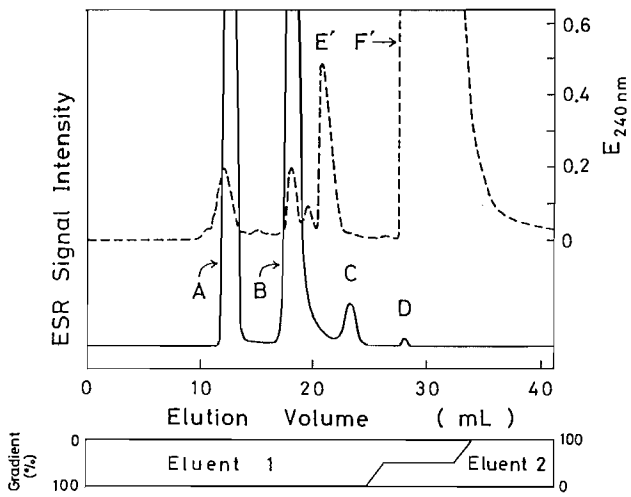

FIG. 9. Chromatogram of a γ-irradiated aqueous solution of L-Ala-Gly-Gly with MNP drawn by uv (broken line) and esr (solid line) detections: flow rate, ca. 0.2 mL/min; eluent 1, 0.35 *M* sodium phosphate buffer, pH 6.0; eluent 2, 0.2 *M* Na_2HPO_4–NaOH buffer, pH 11.5. The magnetic field fixed for the esr detection was 2.67 mT higher than the $g = 2.034$ signal of Mn^{2+} in MgO.

= 0.31 mT). The spin adduct was assigned to structure **11**, the internal backbone adduct from Gly-L-Ala-Gly.

$$NH_3^+—CH_2—CONH—C(CH_3)(t\text{-Bu}—N(O\cdot))—CONH—CH_2—COO^-$$

11

The esr spectrum for the peak D fraction contained two kinds of radicals. One was spin adduct **10***b* due to the tailing of peak C, and the other was a new spin adduct whose hfs was analyzed as follows: $a_{\gamma H} = 0.06$ mT and $2a_N + a_{\beta H1} + a_{\beta H2} = 5.78$ mT at pH 6.1. At pH ~ 6, the $2a_N + a_{\beta H1} + a_{\beta H2}$ values of the side-chain adducts, *t*-BuN(O·)—CH_2CH(NH—)CO—, give values between 5.64 and 6.04 mT (17, 21, 22). No other spin adducts can give these values. Accordingly, the new adduct was plausibly assigned to structure **12**, the side-chain adduct from Gly-L-Ala-Gly.

$$NH_3^+—CH_2—CONH—CH(CH_2(t\text{-Bu}—N(O\cdot)))—CONH—CH_2—COO^-$$

12

L-Alanylglycylglycine

Figure 9 shows the chromatogram of a γ-irradiated aqueous L-Ala-Gly-Gly solution with MNP. The esr chromatogram exhibited four peaks (A–D) as shown by the solid line. Typical esr spectra for the fractions of peaks A–C are depicted in parts (a)–(c) of Fig. 10, respectively. In the uv chromatogram shown by the broken line in Fig. 9, peaks E′ and F′ were due to intact L-Ala-Gly-Gly and *t*-BuN(OH)NO (28).

The spin adducts of peaks A–C were assigned to the deamino adduct (structure **13**), the C-terminal backbone adduct (**14**), and the internal backbone adduct (**15**) from L-Ala-Gly-Gly, respectively, and their hfsc's are given in Table 1.

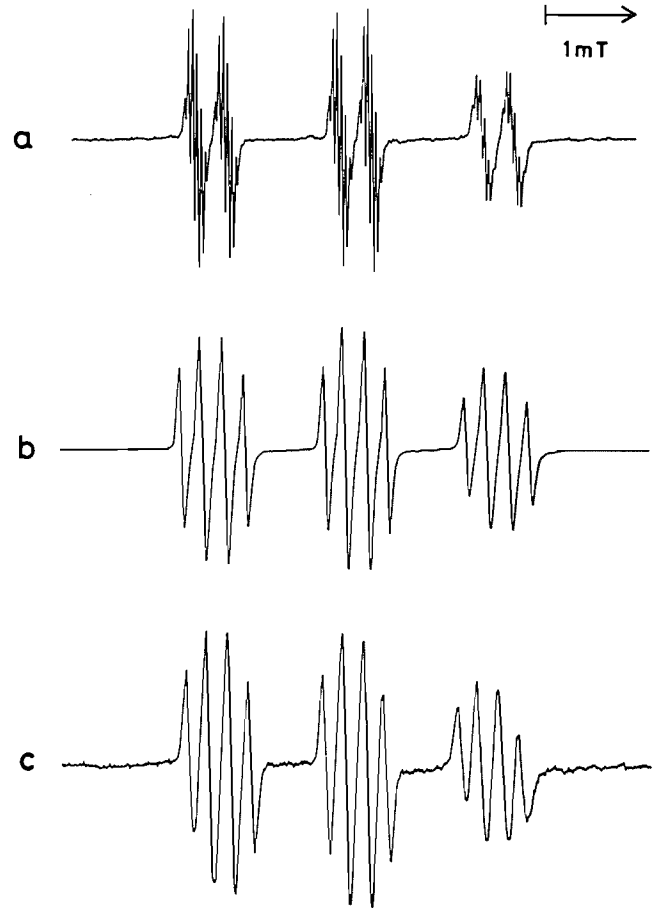

FIG. 10. The esr spectra of the separated spin adducts. (a)–(c) represent the spectra obtained from the fractions giving peaks A–C in Fig. 9, respectively. (a), pH 5.7; (b) and (c), pH 6.0.

$$t\text{-Bu}—N(O\cdot)—CH(CH_3)—CONH—CH_2—CONH—CH_2—COO^-$$

13

$$NH_3^+—CH(CH_3)—CONH—CH_2—CONH—CH(t\text{-Bu}—N(O\cdot))—COO^-$$

14

$$NH_3^+—CH(CH_3)—CONH—CH(t\text{-Bu}—N(O\cdot))—CONH—CH_2—COO^-$$

15

The esr spectrum for the peak D fraction was analyzed as a mixture of the side-chain adduct (structure **16**) from L-Ala-Gly-Gly and spin adduct **17** from *t*-BuN(OH)NO (29).

$$NH_3^+—CH(CH_2(t\text{-Bu}—N(O\cdot)))—CONH—CH_2—CONH—CH_2—COO^-$$

16

$$t\text{-Bu}—N(O\cdot)—CH_2—C(CH_3)_2—N(O^-)—N{=}O$$

17

Can. J. Chem. Downloaded from www.nrcresearchpress.com by 210.87.254.42 on 09/06/12
For personal use only.

Can. J. Chem. Downloaded from www.nrcresearchpress.com by 210.87.254.42 on 09/06/12
For personal use only.

TABLE 1. Hyperfine splitting constants (mT) of spin adducts from tripeptides

Substrate	Spin adduct	pH	a_N	$a_{\beta H}$	$a_{\beta N}$	$a_{\gamma H}$	$a_{\gamma N}$
Gly-Gly-Gly	**1**	6.0	1.58	0.92[a]			0.03
	2	11.1	1.59	0.20	0.26		
		6.0	1.56	0.20	0.24		
		0.6	1.52	0.16	0.255		
	3	11.2	1.53	0.20	0.23		
		6.3	1.51	0.20	0.24		
		0.7	1.50	0.21	0.235		
Gly-Gly-L-Ala	**5**	5.9	1.59	0.92[a]			0.03
	6	6.0	1.52		0.33		
	7[b]	12.0	1.53	0.25	0.22		
		6.0	1.51	0.25	0.22		
		1.0	1.51	0.27	0.22		
	8	5.9	1.63	1.36, 1.02		0.07	
Gly-L-Ala-Gly	**9**	6.0	1.59	0.95, 0.89			0.03
	10*a*[c]	11.3	1.56	0.21	0.245		
		6.0	1.54	0.20	0.24		
		0.6	1.52	0.16	0.265		
	10*b*[c]	11.1	1.56	0.21	0.24		
		6.0	1.55	0.20	0.24		
		0.6	1.52	0.155	0.255		
	11	0.4	1.46		0.31		
	12	6.1	[d]	[d]		0.06	
L-Ala-Gly-Gly	**13**	5.7	1.56	0.33		0.045[e]	0.045
	14[b]	11.5	1.56	0.205	0.245		
		6.0	1.55	0.21	0.24		
		0.4	1.52	0.15	0.255		
	15[b]	11.7	1.52	0.20	0.23		
		6.0	1.51	0.19	0.24		
		0.5	1.50	0.22	0.24		
	16	6.6	1.64	1.33[f]		0.06	

[a] Two equivalent hydrogens.
[b] All hfsc's are the average values of two diastereoisomers.
[c] **10***a* and **10***b* are a pair of diastereomeric adducts separated individually.
[d] $2a_N + a_{\beta H1} + a_{\beta H2} = 5.78$ mT.
[e] Three equivalent hydrogens.
[f] Average value of two hydrogens.

Polyglycine

An aqueous solution of polyglycine (ca. 1 m*M*, approximate molecular weight 6000) with 5 mg/mL MNP was cooled by ice and γ-irradiated at a dose rate of ca. 75 Gy/min to a total dose of 0.2 kGy without deaeration. Figure 11 shows the esr spectra of the irradiated solution. The spectrum observed immediately after irradiation obviously contains more than two kinds of radicals, as shown in Fig. 11(a). The triplet signals asterisked in Fig. 11(a) (a_N = 1.72 mT) are due to di-*tert*-butyl nitroxide (29). These triplet signals decayed slowly at room temperature and became the extent of trace after ca. 11.5 h, as shown in Fig. 11(b). Almost pure esr signals in Fig. 11(b) are interpreted as a triplet of quartet with approximate intensity ratio of 1:2:2:1. The hfsc's at pH 4.7 are as follows: a_N = 1.50 mT, $a_{\beta H}$ = 0.25 mT, and $a_{\beta N}$ = 0.27 mT. The spectral pattern is ascribed to the basic structure of a backbone adduct from a glycyl residue, *t*-Bu—N(O·)—CH—N<. The results from γ-radiolytic aqueous systems of dipeptides (21, 22) and tripeptides suggest two possibilities for this polyglycine system: C-terminal and internal spin adducts. Considering that the backbone adduct from polyglycine seems to exist as a zwitterion form under the conditions of the esr measurements, the hfsc's obtained from the polyglycine adduct were compared with those of the backbone adducts (the *t*-BuN(O·)CH—N< type) from dipeptides (21, 22) and tripeptides at pH ~ 6. The hfsc of the aminoxyl nitrogen is 1.55 ± 0.01 mT for the C-terminal backbone adduct, while it is 1.51 mT for the internal backbone adduct. Therefore the observed polyglycine adduct (a_N = 1.50 mT) was assigned to structure **18**, the internal backbone adduct from polyglycine.

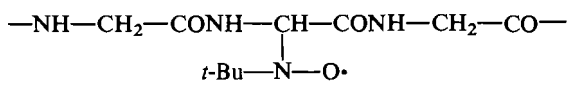

18

Conclusions

Many kinds of spin adducts in the γ-irradiated aqueous solutions of four tripeptides with MNP as a spin trap were separated and identified by the spin-trap hplc–esr method. Their hfsc's are summarized in Table 1. Spin adducts **1**, **5**, **9**, and **13** are deamino adducts derived from the reductive deaminations induced by the e_{aq}^- addition to the carbonyl group of the N-terminal peptide bond (2, 25). Spin adducts **2**, **6**, **10***a*, **10***b*, and **14** are C-terminal backbone adducts derived from the short-lived radicals produced by the hydrogen abstraction from a so-called α-carbon in the C-terminal main-chain, mainly by ·OH. Spin adducts **3**, **7**, **11**, and **15**, which are newly classified as a type characteristic of tripeptides, are internal backbone

adducts originating from the H abstraction from an α-carbon in the internal main-chain. Spin adducts **8**, **12**, and **16** are side-chain adducts originating from the H abstraction from the methyl group of the L-alanyl residue. From these results on tripeptide systems, proposed γ-radiolytic and spin-trapping mechanisms to produce spin adducts from the tripeptides are summarized as follows:

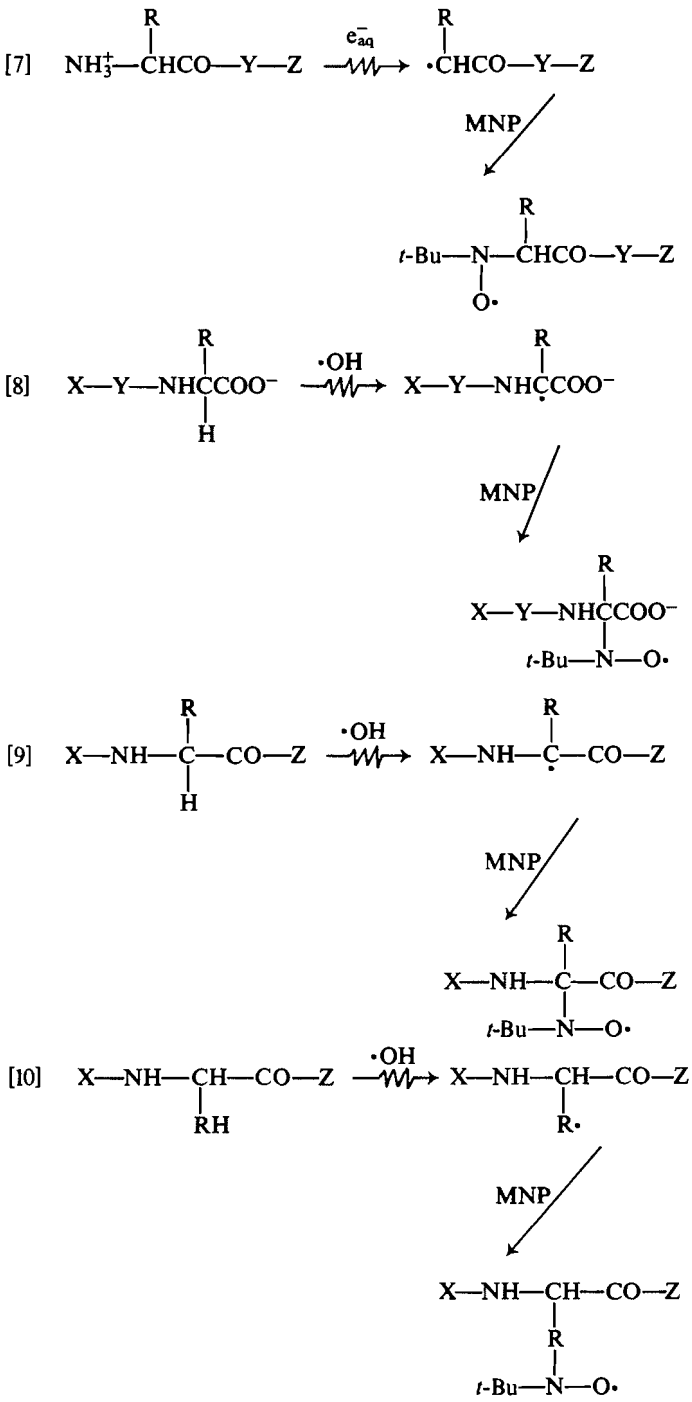

where X, Y, and Z represent amino acid residues, R is H or a side-chain, RH is a saturated aliphatic side-chain (16, 20), and the left, central, and right members of each equation are a tripeptide, a short-lived radical, and a spin adduct, respectively. The spin adducts in eqs. [7]–[10] are a deamino adduct, a C-terminal backbone adduct, an internal backbone adduct, and a side-chain adduct from a tripeptide, respectively.

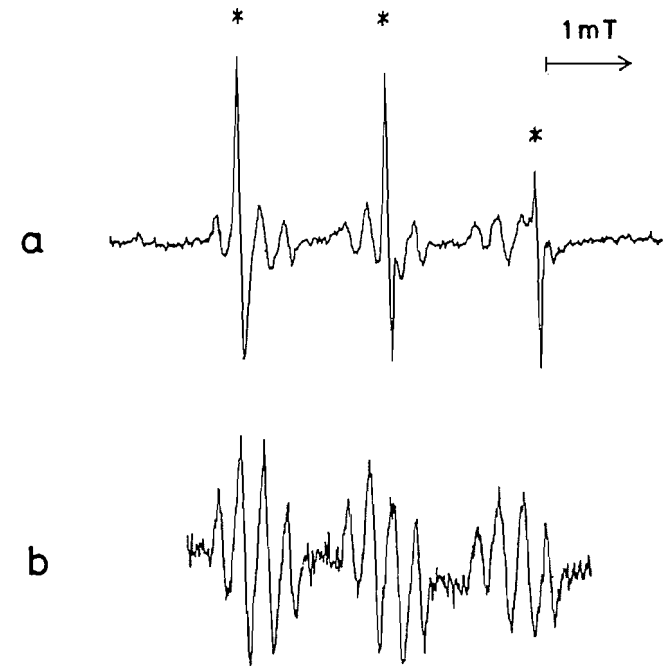

FIG. 11. (a) The esr spectrum of an aqueous solution of polyglycine with MNP observed just after γ-irradiation (at pH 4.7). (b) The esr spectrum of the solution ca. 11.5 h after irradiation.

It was reported that a hydroxyl radical attacks Gly-Gly at the α-position to the peptide nitrogen and not to the NH_3^+ group (1, 25). Hydrogen abstraction by ·OH at the α-position to the peptide nitrogen of dipeptides was observed by uv photolysis with H_2O_2 (24), and the $Ti^{3+}-H_2O_2$ method (35). It was confirmed that, for alphatic oligopeptides, the enhancement of reactivity of internal and C-terminal α-carbons toward ·OH is due to the disappearance of suppression by NH_3^+ groups (36). It is compatible with these previous conclusions that C-terminal and internal backbone adducts from tripeptides were detected and N-terminal backbone adducts such as *t*-BuN(O·)—$CH(NH_3^+)CONHCH_2CONHCH(CH_3)COO^-$ from Gly-Gly-L-Ala were not ascertained in the present work.

The second-order rate constants for reactions between e_{aq}^- and amino acids or peptides were determined by pulse radiolysis (2, 37). The results suggested that an e_{aq}^- attack on a peptide carbonyl group is much faster than on a carboxyl group. Therefore it is reasonable that "tertiary deamino adducts" originating from attacks of e_{aq}^- on carboxyl groups such as *t*-Bu—N(O·)—$CH(CH_3)COO^-$ from Gly-Gly-L-Ala were not found in our present work. "Secondary deamino adducts" such as *t*-BuN(O·)—$CH_2CONHCH(CH_3)COO^-$ from Gly-Gly-L-Ala were not ascertained in this study, which is consistent with previous results indicating that cleavage next to an internal peptide bond does not occur (2, 38, 39).

In the γ-irradiated aqueous polyglycine solution, spin adduct **18**, the internal backbone adduct from polyglycine, was found by the spin-trapping method with MNP. The backbone adduct for polyalanine was also reported previously (11). Consequently, these results on radiolysis of the tripeptides and polypeptides suggest that, in general, short-lived backbone radicals, —CONH—ĊR—CONH—, are produced in γ-irradiated aqueous solutions by hydrogen abstraction from an internal so-called α-carbon in main-chains of proteins, mainly by ·OH (eq. [11]).

Can. J. Chem. Downloaded from www.nrcresearchpress.com by 210.87.254.42 on 09/06/12
For personal use only.

[11] —CONH—CHR—CONH— + ·OH ⟶

—CONH—ĊR—CONH— + H_2O

Conclusions from the present and previous works (14–22) will be utilized for a general discussion on radiolysis of proteins in aqueous solutions, with conclusions on amino acids and peptides with functional or aromatic groups in side-chains, which will be presented in the future.

Acknowledgment

The authors express their sincere gratitude to Prof. Dr. Haruaki Yajima, Kyoto University, for supplying Gly-L-Ala-Gly.

1. W. M. GARRISON. Radiat. Res. Rev. **3**, 305, (1972).
2. M. H. KLAPPER and M. FARAGGI. Q. Rev. Biophys. **12**, 465 (1979).
3. P. RIESZ and S. RUSTGI. Radiat. Phys. Chem. **13**, 21 (1979).
4. J. HÜTTERMANN, W. KÖHNLEIN, R. TÉOULE, and A. J. BERTINCHAMPS (*Editors*). Effects of ionizing radiation on DNA. Springer Verlag, Berlin. 1978.
5. E. G. JANZEN. Acc. Chem. Res. **4**, 31 (1971).
6. C. A. EVANS. Aldrichimica Acta, **12**, 23 (1979).
7. M. J. PERKINS. Adv. Phys. Org. Chem. **17**, 1 (1980).
8. D. L. HAIRE and E. G. JANZEN. Can. J. Chem. **60**, 1514 (1982).
9. S. RUSTGI, A. JOSHI, H. MOSS, and P. RIESZ. Int. J. Radiat. Biol. **31**, 415 (1977).
10. S. RUSTGI, A. JOSHI, P. RIESZ, and F. FRIEDBERG. Int. J. Radiat. Biol. **32**, 533 (1977).
11. A. JOSHI, S. RUSTGI, H. MOSS, and P. RIESZ. Int. J. Radiat. Biol. **33**, 205 (1978).
12. S. RUSTGI and P. RIESZ. Int. J. Radiat. Biol. **34**, 127 (1978).
13. S. RUSTGI and P. RIESZ. Int. J. Radiat. Biol. **34**, 449 (1978).
14. K. MAKINO and H. HATANO. Chem. Lett. 119 (1979); K. MAKINO. J. Phys. Chem. **83**, 2520 (1979).
15. K. MAKINO, N. SUZUKI, F. MORIYA, S. ROKUSHIKA, and H. HATANO. Anal. Lett. **13**, 301 (1980); K. MAKINO. J. Phys. Chem. **84**, 1016 (1980).
16. K. MAKINO. J. Phys. Chem. **84**, 1968 (1980).
17. F. MORIYA, K. MAKINO, N. SUZUKI, S. ROKUSHIKA, and H. HATANO. J. Phys. Chem. **84**, 3085 (1980).
18. N. SUZUKI, K. MAKINO, F. MORIYA, S. ROKUSHIKA, and H. HATANO. J. Phys. Chem. **85**, 263 (1981).
19. F. MORIYA, K. MAKINO, N. IGUCHI, N. SUZUKI, S. ROKUSHIKA, and H. HATANO. J. Phys. Chem. **88**, 2373(1984).
20. K. MAKINO, F. MORIYA, and H. HATANO. Radiat. Phys. Chem. **23**, 217 (1984).
21. F. MORIYA, K. MAKINO, N. SUZUKI, S. ROKUSHIKA, and H. HATANO. J. Phys. Chem. **84**, 3614 (1980).
22. F. MORIYA, K. MAKINO, N. SUZUKI, S. ROKUSHIKA, and H. HATANO. J. Am. Chem. Soc. **104**, 830 (1982).
23. P. NETA and R. W. FESSENDEN. J. Phys. Chem. **74**, 2263 (1970).
24. R. LIVINGSTON, D. G. DOHERTY, and H. ZELDES. J. Am. Chem. Soc. **97**, 3198 (1975).
25. R. L. S. WILLIX and W. M. GARRISON. Radiat. Res. **32**, 452 (1967).
26. J. C. STOWELL. J. Org. Chem. **36**, 3055 (1971).
27. W. MOSER and R. A. HOWIE. J. Chem. Soc. (A), 3039 (1968).
28. K. MAKINO, N. SUZUKI, F. MORIYA, S. ROKUSHIKA, and H. HATANO. Anal. Lett. **13**, 311 (1980); Radiat. Res. **86**, 294 (1981).
29. K. MAKINO, N. SUZUKI, F. MORIYA, S. ROKUSHIKA, and H. HATANO. Chem. Lett. 675 (1979); K. MAKINO. J. Phys. Chem. **84**, 1012 (1980).
30. H. HOGEVEEN, H. R. GERSMANN, and A. P. PRAAT. Recl. Trav. Chim. Pays-Bas, **86**, 1063 (1967).
31. B. M. HOFFMAN and T. B. EAMES. J. Am. Chem. Soc. **91**, 2169 (1969).
32. Y. KIRINO. J. Phys. Chem. **79**, 1296 (1975).
33. L. JONKMAN, H. MULLER, and J. KOMMANDEUR. J. Am. Chem. Soc. **93**, 5833 (1971).
34. B. C. GILBERT and M. TRENWITH. J. Chem. Soc. Perkin Trans. 2, 1834 (1973).
35. H. TANIGUCHI, H. HATANO, H. HASEGAWA, and T. MARUYAMA. J. Phys. Chem. **74**, 3063 (1970).
36. T. MASUDA, K. YOSHIHARA, H. SHINOHARA, and M. KONDO. J. Radiat. Res. **17**, 106 (1976).
37. P. S. RAO and E. HAYON. J. Phys. Chem. **78**, 1193 (1974).
38. M. SIMIC and E. HAYON. Radiat. Res. **48**, 244 (1971).
39. M. FARAGGI and Y. TAL. Radiat. Res. **62**, 347 (1975).

Can. J. Chem. Downloaded from www.nrcresearchpress.com by 210.87.254.42 on 09/06/12
For personal use only.

Electron behavior in mixed solvents: optical spectra and reactivities in water/alkane diols[1]

K. M. IDRISS-ALI AND GORDON R. FREEMAN
Chemistry Department, University of Alberta, Edmonton, Alta., Canada T6G 2G2

Received February 8, 1984

K. M. IDRISS-ALI and GORDON R. FREEMAN. Can. J. Chem. **62**, 2217 (1984).

Investigation of the effect of solvent structure on the optical absorption spectrum and reactivity of solvated electrons has been extended to diol/water mixed solvents, using 1,2-ethanediol (12ED) and 1,4-butanediol (14BD). The large effects that had been found in mono-ol/water mixed solvents did not occur in diol/water. Although addition of 3 mol% of a diol to water increased the optical absorption energies of e^-_s by 0.06 eV, similar to the shift caused by addition of 3 mol% of a mono-ol, the variation of the spectrum over the rest of the composition range was nearly ideal in diol/water, in contrast to the very non-ideal variation in mono-ol/water. Reaction rate constants k_S at 298 K in the diol/water mixed solvents vary approximately as the inverse viscosity, $\eta^{-1.0}$, in the diffusion-controlled limit. However, when reactions are two or three orders of magnitude slower than diffusion controlled, k_S at 298 K is independent of η. Toluene reacts with e^-_s at a 10^{-3}-fold smaller rate than does nitrobenzene; the difference is nearly completely due to a ~50 J/mol K lower entropy of activation of the former reaction.

Viscosities and their temperature coefficients are reported for the diol/water mixtures.

K. M. IDRISS-ALI et GORDON R. FREEMAN. Can. J. Chem. **62**, 2217 (1984).

On a étendu nos études sur la relation qui existe entre la structure du solvant et les spectres d'absorption optique ainsi que la réactivité des électrons solvatés dans le but d'inclure des solvants mixtes eau/diols comprenant l'éthanediol-1,2 et le butanediol-1,4. Dans ces cas, on ne retrouve pas les grands effets que l'on avait observé avec les solvants mixtes eau/mono-ols. Même si l'addition de 3 mol% de diol à l'eau augmente les énergies d'absorption optique des e^-_s par 0,06 eV et que ces résultats sont semblables à ceux causés par l'addition de 3 mol% de mono-ol, la variation du spectre sur le reste des compositions est pratiquement idéal par rapport aux diols/eau et ceci est en opposition avec la variation observée avec les mono-ols/eau alors que l'on observait une déviation importante par rapport à l'idéalité. A 298 K et dans la zone controlée par la diffusion, les constantes de vitesse des réactions, k_S, dans les solvants mixtes eau/diol, sont reliées d'une façon pratiquement inverse avec la viscosité, $\eta^{-1.0}$. Toutefois, lorsque les réactions ont des vitesses qui sont de cent à mille fois plus lentes que celles qui sont controlées par la diffusion, les valeurs de k_S à 298 K sont indépendantes de η. La vitesse de la réaction du toluène avec les e^-_s est mille fois plus lente que celle du nitrobenzène; cette différence est pratiquement complètement due à une entropie d'activation plus faible (environ 50 J/mol K) pour la première réaction.

On rapporte les viscosités ainsi que les coefficients de température des mélanges eau/diols.

[Traduit par le journal]

Introduction

The localization energy (1–9) and reactivity (10–16) of solvated electrons are strongly dependent upon the nature of the solvent. The internal structure of the liquid, reflected by the Kirkwood correlation parameter g_K, has a greater influence upon the energy levels of solvated electrons than does the magnitude of the dielectric constant or of the molecular dipole moment (6).

Optical absorption spectra of solvated electrons in mixed alcohol/water solvents have revealed unexpected effects that are attributed to changes in the internal structure of the liquid (7). The structure changes occur because of the interplay between nonpolar and hydrogen-bonding groups, and are reflected in physical properties such as heat of mixing (17, 18) and viscosity (19, 20). Allied reactivity studies have been reported for electrons in 2-propanol/water mixed solvents (16). The present article reports spectral and reactivity changes in water/diol solutions.

Reactivities in pure diol solvents are significantly different from those in mono-ol solvents when normalized for viscosity or electron trap depth (21). Two diols that have different distances between the hydroxy groups were chosen for study of aqueous mixtures: 1,2-ethanediol (12ED) and 1,4-butanediol (14BD). In the latter neat liquid the viscosity is larger but the solvated electron excitation (solvation) energy is smaller than

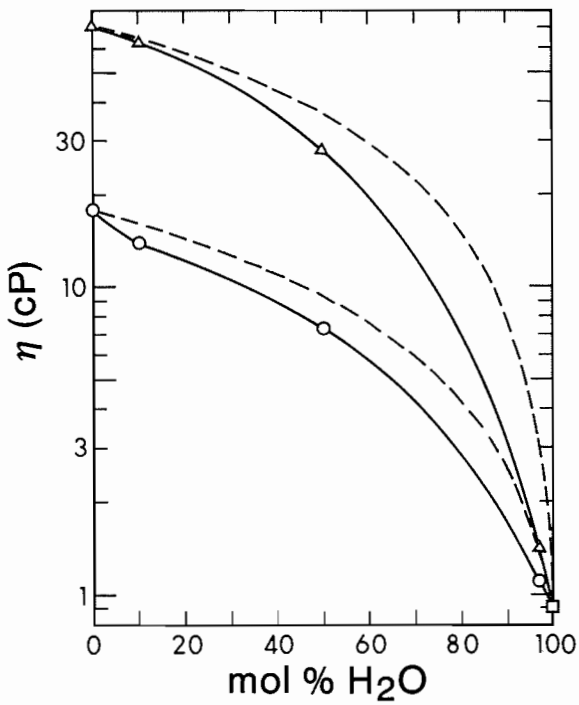

FIG. 1. Solvent dynamic viscosities η (Poise) at 298 K, against mol% water. △, 14BD; ○, 12ED; □, water. The dashed lines represent $\eta = X_W\eta_W + X_D\eta_D$, where X_W and X_D are the mole fractions of water and diol, respectively.

[1] Financially assisted by the Natural Sciences and Engineering Research Council of Canada.

Can. J. Chem. Downloaded from www.nrcresearchpress.com by 210.87.254.6 on 09/06/12
For personal use only.

Can. J. Chem. Downloaded from www.nrcresearchpress.com by 210.87.254.6 on 09/06/12
For personal use only.

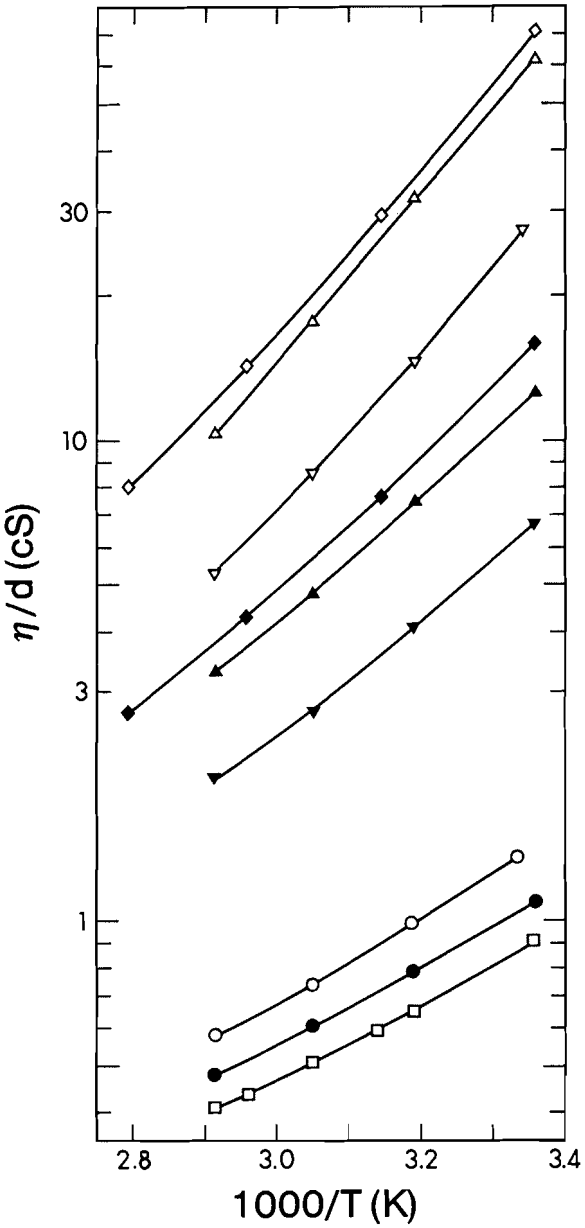

FIG. 2. Arrhenius plots of solvent kinematic viscosities η/D (Stokes). Mol% water: ◇, ◆, zero; △, ▲, 10; ▽, ▼, 50; ○, ●, 97; □, 100. Filled points, 12ED; open points 14BD and water.

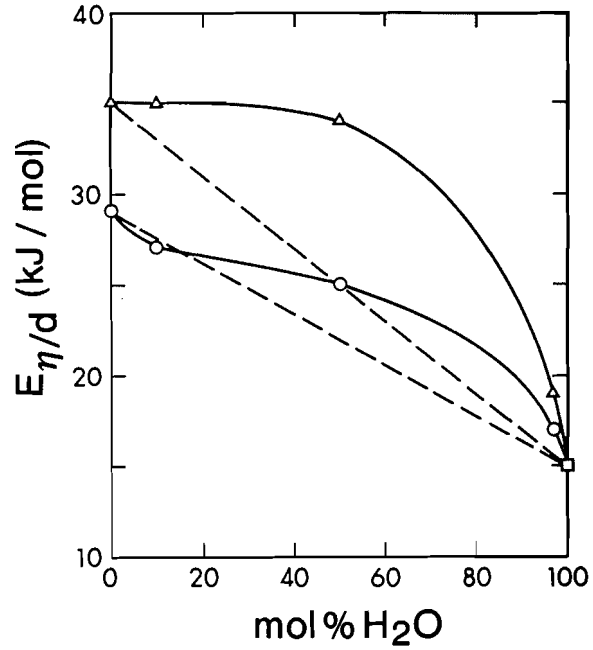

FIG. 3. Composition dependence of viscosity temperature coefficients in diol/water. △, 14BD; ○, 12ED; □, water. $E_{\eta/d}$ was measured near 306 K.

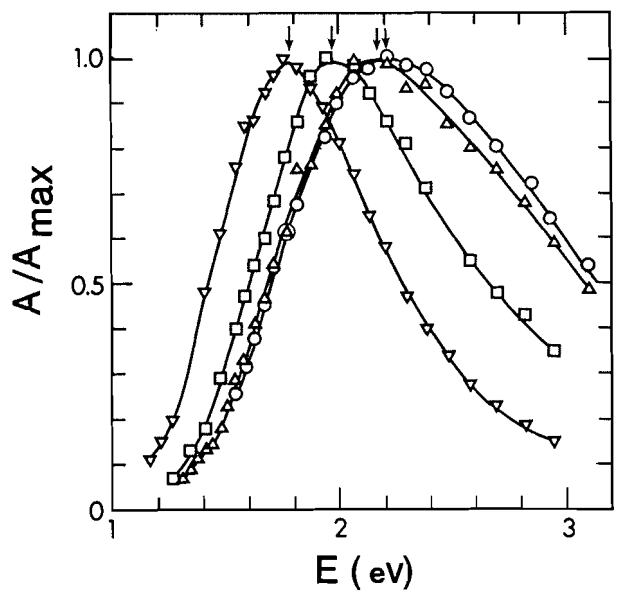

FIG. 4. Normalized absorption spectra of solvated electrons in 12ED/water mixed solvents at 297 K. Mol% water: ○, zero; △, 10; □, 50; ▽, 97.

those in the former (22). The viscosities of the mixed solvents were measured, along with the optical and reactive properties of the solvated electrons.

Experimental

All chemicals were obtained from Aldrich Chemical Co. Purification of solvents and solutes and preparation of solutions were as described earlier (21). The methods of cell filling (23), temperature control, irradiation, dosimetry, and spectroscopy (24) were nearly the same as that reported in the references indicated. The main difference was in the optical system; the light beam was split into two parts, one passing below the optical cell and serving as a reference, the other passing through the sample solution. The two parts of the beam were adjusted to an appropriate ratio for subtraction, before they fell onto the monochromator (Bausch and Lomb 33-86-25, grating type 33-86-02) and dual detector (SGD-444-2). The oscilloscope traces were recorded with a series 1200 Zeta plotter (Zeta Research Inc.) interfaced with a Texas Instrument 980 minicomputer.

The temperature was controlled to within ±0.1 K. A 100 ns pulse of 1.9 MeV electrons delivered a dose of 2×10^{16} eV/g to the sample. Solvated electron decay rates were measured at the maximum of the optical absorption band at each temperature.

The compositions of the water/diol mixed solvents were 0, 10, 50, 97, and 100 mol% water. Concentrations of solute were in the range 0.028–0.21 m*M* (nitrobenzene), 0.37–2.2 m*M* (acetone), 19–113 m*M* (toluene), and 1.7–5.7 m*M* (allyl alcohol).

Viscosities and densities of the water/diol mixed solvents were measured in the manner described elsewhere (21). The results are listed in Table 1. Values for pure 12ED and water agreed with those in ref. 25 within 0.5% in density and 2% in viscosity.

Can. J. Chem. Downloaded from www.nrcresearchpress.com by 210.87.254.6 on 09/06/12
For personal use only.

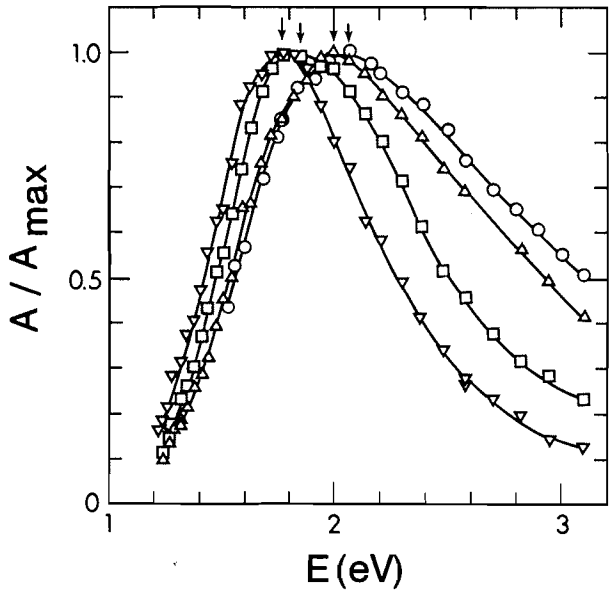

FIG. 5. Normalized absorption spectra of solvated electrons in 14BD/water mixed solvents at 296 K. Mol% water: ○, zero; △, 10; □, 50; ▽, 97.

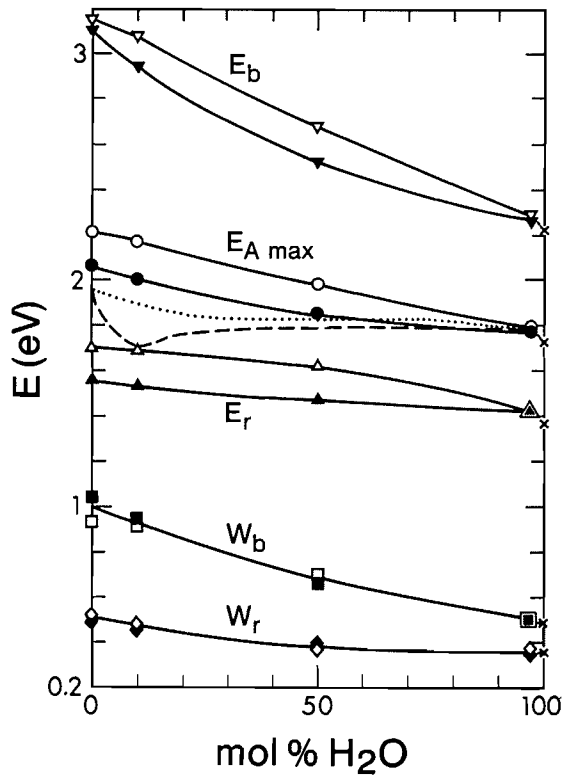

FIG. 6. Composition dependence of spectrum parameters in diol/water mixed solvents at ~296 K. 12ED, open points; 14BD, filled points; water, X. The E_{Amax} curves for aqueous methanol, ····, and 1-propanol, - - -, are shown for comparison (7). $W_r = E_{Amax} - E_r$; $W_b = E_b - E_{Amax}$; E_r and E_b are the energies at $A/A_{max} = 0.5$ on the red and blue sides of the band, respectively.

Results and discussion

Solvent viscosities

The viscosities of the mixed solvents display nonideal behavior. They are lower than if they were directly proportional to the mole fractions of the components (Fig. 1). The Arrhenius temperature coefficients decrease slightly with increasing temperature (Fig. 2). For example, in pure 14BD the coefficient is 35 kJ/mol at 308 K and 29 kJ/mol at 348 K. The coefficients are larger than if they varied linearly with mol% composition, except when up to 15 mol% water is added to 12ED (Fig. 3). These temperature coefficients indicate that the liquid structures in 12ED and 14BD change in different fashions when up to 50 mol% water is added.

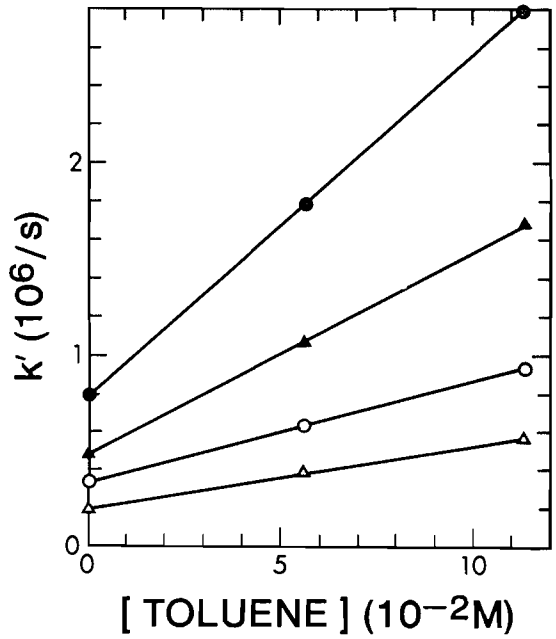

FIG. 7. First order decay constants of e^-_s in 10 mol% water in 14BD, as functions of toluene concentration and temperature. △, 283 K; ○, 296 K; ▲, 313 K; ●, 329 K.

Optical absorption spectra of e^-_s

The spectrum was measured in each solvent at ~296 K. The energy at the absorption maximum, E_{Amax}, decreases as the water content increases in each diol (Figs. 4 and 5). The values of E_{Amax} in aqueous solutions of the primary alcohols ethanol and 1-propanol have a minimum at 10 mol% water (7), but this does not occur in the aqueous diols (Fig. 6). The shapes of the curves of E_{Amax} against mol% water follow a sequence in which the minimum disappears and the curve becomes more nearly linear: primary alcohols RCH_2OH, methanol, 14BD, 12ED (Fig. 6). The liquid structures of the diols are less easily perturbed by water than is that of a primary alcohol. However, addition of 3 mol% of a diol to water causes the same blue shift in the absorption band as does 3 mol% of a mono-ol (Fig. 6). The water liquid structure is perturbed in a similar way by the addition of 3 mol% of either a mono- or di-ol.

The widths of the bands at half height on the red, W_r, and blue, W_b, sides of E_{Amax} are nearly independent of the diol molecular structure (Fig. 6). The band asymmetry factor W_b/W_r equals 1.9 ± 0.1 in both diols containing up to 50 mol% water, then decreases gradually and reaches 1.4 in pure water.

The temperature coefficients in 50 mol% water/12ED are similar to those in pure 12ED; $dE_{Amax}/dT \approx -3$ meV/K, and W_r is independent of temperature.

Reactivities of e^-_s with solutes

Rate constants were measured for four solutes that differ

TABLE 1. Viscosities and densities of water/diol mixtures

Diol	mol% water	T (K)	η/d^a (10^{-7} m^2/s)	d (kg/m^3)	$E_{\eta/d}{}^b$ (kJ/mol)	η^c (10^{-4} Pa s)
12ED	0	298	160	1109	29	177
		318	76	1094		83
		338	43	1080		46
		358	27	1065		29
	10	298	126	1105	27	139
		313	75			
		328	48			
		343	33			
	50	298	67	1096	25	73
		313	41			
		328	29			
		343	20			
	97	298	11	1018	17	11
		313	7.9			
		328	6.0			
		343	4.8			
14BD	0	298	709	1009	35	716
		318	295			
		338	142			
		358	80			
	10	298	620	1011	35	626
		313	325			
		328	177			
		343	103			
	50	299	275	1016	34	279
		313	146			
		328	85			
		343	53			
	97	300	14	1001	19	14
		313	9.8			
		328	7.3			
		343	5.8			
	100	298	9.1	997	16	9.1
		313	6.5	992		6.5
		328	5.1	986		5.1
		343	4.1	978		4.0

[a] Stokes = 10^{-4} m^2/s.
[b] Measured near 306 K.
[c] Poise = Stokes × density = 0.1 Pa s. Values for 12ED and water agree with those in ref. 25 within 2%.

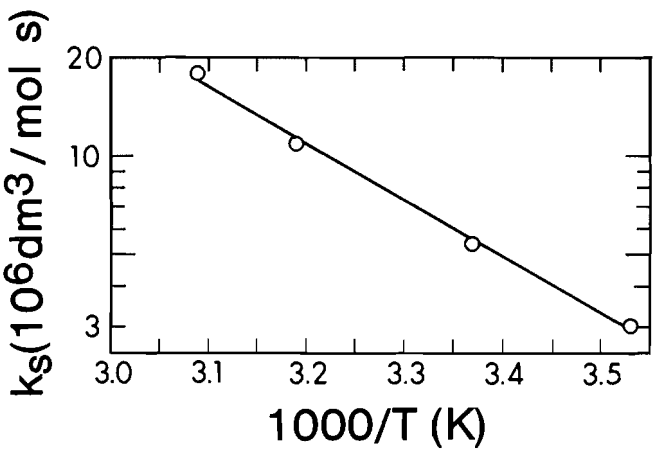

FIG. 8. Arrhenius plot of k_S (e^-_s + toluene) in 10 mol% water in 14BD. Data from Fig. 7.

widely in reactivity: nitrobenzene, acetone, allyl alcohol, and toluene. Figure 7 shows example plots of the first order decay rates of e^-_s as a function of toluene concentration in 10 mol% water/14BD. The values of the second order rate constants were obtained from the slopes and are displayed as an Arrhenius plot in Fig. 8. The reactivity parameters from eqs. [1] and [2] (15), corresponding to the data in Fig. 8, are $A_S = 2.1 \times 10^{12}$ dm^3/mol s, $E_S = 32$ kJ/mol and $\Delta S_S^{\ddagger} = -9$ J/mol K.

$$[1] \qquad k_S = A_S \exp(-E_S/RT)\ \text{dm}^3/\text{mol s}$$

$$[2] \qquad \Delta S_S^{\dagger} = 19\ (\log A_S - 12.8)\ \text{J/mol K at 298 K}$$

The values of log k_S at 298 K, log A_S, E_S, and $\Delta S_S^{\ddagger}$ for each of the solutes in each of the solvents are listed in Table 2.

The reaction of e^-_s with nitrobenzene is nearly diffusion controlled. The rate constants in water, 12ED, 14BD, and the water/diol mixtures at 298 K vary approximately as $\eta^{-0.9}$ (Fig.

Can. J. Chem. Downloaded from www.nrcresearchpress.com by 210.87.254.6 on 09/06/12
For personal use only.

Can. J. Chem. Downloaded from www.nrcresearchpress.com by 210.87.254.6 on 09/06/12
For personal use only.

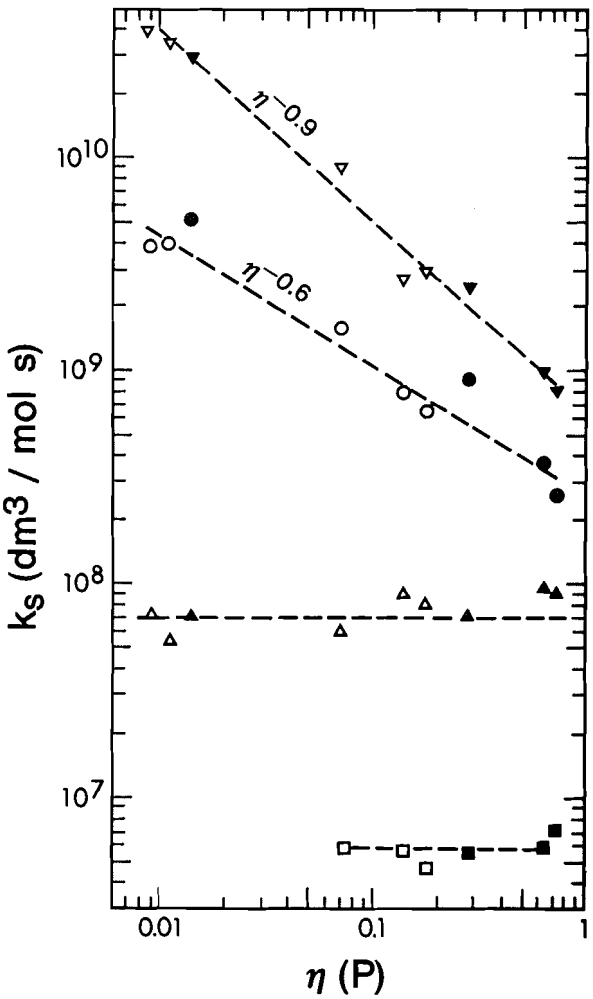

FIG. 9. Effect of solvent viscosity on k_S at 298 K. Open points, water and 12ED solutions; filled points, 14BD solutions. ▽, ▼, nitrobenzene; ○, ●, acetone; △, ▲, allyl alcohol; □, ■, toluene. The dashed lines are guides for the eye.

9). This reflects mainly the viscosity dependence of the diffusion coefficients of e^-_s and nitrobenzene. Reactions with other solutes that are progressively farther below the diffusion-controlled limit are progressively less dependent on the solvent viscosity. Thus, k_S at 298 K for acetone in the diol/water systems varies roughly as $\eta^{-0.6}$, while those for allyl alcohol and toluene are nearly independent of viscosity (Fig. 9).

The above result also means that at 298 K the values of k_S for allyl alcohol and toluene are nearly independent of the composition of the diol/water solvent. The temperature coefficient E_S for the least reactive solute, toluene, is nearly the same as that for the most reactive solute, nitrobenzene, in a given solvent (Table 2). The thousand-fold decrease of k_S on going from nitrobenzene to toluene is due mainly to a large decrease, 50 ± 10 J/mol K, in the entropy of activation (Table 2).

Electron capture by toluene, and probably by allyl alcohol, is stabilized by protonation (26, 27):

[3, -3] $e^-_s + S \rightleftarrows S^-_s$

[4] $S^-_s + ROH \rightarrow \dot{S}H + RO^-_s$

Reaction [4] involves the rotation of solvent dipoles adjacent to the reaction site as the charge center changes from S^- to RO^-; the reaction rate should correlate with the dielectric relaxation

TABLE 2. Solvated electron reaction rate parameters and E_r in diol/water solvents

Solvent		Solute = nitrobenzene				Solute = acetone				Solute = allyl alcohol				Solute = toluene				
diol	mol% water	log k_S[a]	log A_S	E_S[b]	$\Delta S_S^{\ddagger}$[c]	log k_S[a]	log A_S	E_S[b]	$\Delta S_S^{\ddagger}$[c]	log k_S[a]	log A_S	E_S[b]	$\Delta S_S^{\ddagger}$[c]	log k_S[a]	log A_S	E_S[b]	$\Delta S_S^{\ddagger}$[c]	E_r[b] (298 K)
12ED	0	9.47	14.80	30	38	8.81	13.30	26	10	7.91	11.90	23	−17	6.66	11.60	28	−22	164
	10	9.43	14.06	26	24	8.89	12.57	21	−4	7.95	11.53	20	−24	6.75	11.97	30	−16	163
	50	9.95	14.85	28	39	9.20	13.58	25	15	7.78	12.51	27	−6	6.76	11.14	25	−32	155
	97	10.53	14.03	20	23	9.59	13.00	20	4	7.73	11.30	20	−28		Insoluble			137
14BD	0	8.91	14.10	30	25	8.42	13.60	30	16	7.96	12.70	27	−3	6.85	12.00	30	−15	151
	10	9.00	14.39	31	30	8.57	12.57	23	−4	8.00	12.10	23	−13	6.76	12.33	32	−9	148
	50	9.40	14.65	30	35	8.96	13.23	24	8	7.86	11.96	23	−16	6.75	11.37	26	−27	142
	97	10.47	13.90	20	21	9.71	13.17	20	7	7.85	12.59	27	−4		Insoluble			137
	100	10.59	13.87	19	20	9.76[d]	12.70[d]	17[d]	−2[d]	7.86	11.84	24	−18		Insoluble			132

[a] At 298 K, in dm^3/mol s.
[b] In kJ/mol.
[c] In J/mol K.
[d] Data of C. Senanayake (unpublished results).

time τ. The values of the Arrhenius temperature coefficients E_τ would probably be significantly different from those of E_η in the mixed solvents. A comparison of E_τ with E_S would be of great interest. Measurements of τ at different temperatures are needed.

There is no correlation of k_S with the optical absorption energy E_τ in diol/water solvents, as there is for inefficient scavengers in mono-ol solvents (14, 15).

Acknowledgement

We thank the personnel of the Radiation Research Center for aid with the electronics.

1. T. SHIDA, S. IWATA, and T. WATANABE. J. Phys. Chem. **76**, 3683 (1972).
2. L. M. PERKEY, FARHATAZIZ, and R. R. HENTZ. Chem. Phys. Lett. **27**, 531 (1974).
3. H. Y. WANG and J. E. WILLARD. J. Chem. Phys. **69**, 2964 (1978).
4. K. OKAZAKI and G. R. FREEMAN. Can. J. Chem. **56**, 2305 (1978).
5. F.-Y. JOU and G. R. FREEMAN. Can. J. Chem. **57**, 591 (1979).
6. F.-Y. JOU and G. R. FREEMAN. Can. J. Chem. **60**, 1809 (1982).
7. A.-D. LEU, K. N. JHA, and G. R. FREEMAN. Can. J. Chem. **60**, 2342 (1982).
8. Z. WU, N. V. KLASSEN, H. A. GILLIS, and G. G. TEATHER. Can. J. Chem. **61**, 189 (1983).
9. N. V. KLASSEN and G. G. TEATHER. J. Phys. Chem. **87**, 3894 (1983).
10. A. HENGLEIN. Ber. Buns. Ges. Phys. Chem. **79**, 129 (1975).
11. K. FUNABASHI and J. L. MAGEE. J. Chem. Phys. **62**, 4428 (1975).
12. G. L. BOLTON and G. R. FREEMAN. J. Am. Chem. Soc. **98**, 6825 (1976).
13. G. BAKALE, U. SOWADA, and W. F. SCHMIDT. J. Phys. Chem. **86**, 2556 (1976).
14. A. M. AFANASSIEV, K. OKAZAKI, and G. R. FREEMAN. J. Phys. Chem. **83**, 1244 (1979).
15. A. M. AFANASSIEV, K. OKAZAKI, and G. R. FREEMAN. Can. J. Chem. **57**, 839 (1979).
16. J. CYGLER and G. R. FREEMAN. Can. J. Chem. In press.
17. F. FRANKS. Physico-chemical processes in mixed aqueous solvents. Elsevier Publishers, New York. 1967. p. 54.
18. C. H. CHIEN, R. A. GREENKORN, and K. C. CHAO. AIChE J. **27**, 303 (1981).
19. J. TIMMERMANS. Physico-chemical constants of binary systems. Vol. 4. Interscience, New York. 1960. pp. 163–236.
20. J. A. RIDDICK and W. B. BUNGER. Techniques of chemistry. Vol. II. Organic solvents, physical properties and methods of purification. 3rd ed. Wiley Interscience, New York. 1970. p. 145.
21. K. M. IDRISS-ALI and G. R. FREEMAN. Radiat. Phys. Chem. **23**, 89 (1984).
22. K. OKAZAKI, K. M. IDRISS-ALI, and G. R. FREEMAN. Can. J. Chem. To be published.
23. K. N. JHA, G. L. BOLTON, and G. R. FREEMAN. J. Phys. Chem. **76**, 3876 (1972).
24. F.-Y. JOU and G. R. FREEMAN. Can. J. Chem. **54**, 3693 (1976).
25. R. W. GALLANT. Physical properties of hydrocarbons. Vols. 1 and 2. Gulf Publishing Co., Houston, TX. 1968.
26. T. SHIDA and W. H. HAMILL. J. Am. Chem. Soc. **88**, 3689 (1966).
27. G. L. BOLTON, M. G. ROBINSON, and G. R. FREEMAN. Can. J. Chem. **54**, 1177 (1976).

Can. J. Chem. Downloaded from www.nrcresearchpress.com by 210.87.254.6 on 09/06/12
For personal use only.

Temperature and molecular structure dependences of optical spectra of electrons in liquid diols[1]

KIYOSHI OKAZAKI, K. M. IDRISS-ALI, AND GORDON R. FREEMAN
Department of Chemistry, University of Alberta, Edmonton, Alta., Canada T6G 2G2

Received January 23, 1984

KIYOSHI OKAZAKI, K. M. IDRISS-ALI, and GORDON R. FREEMAN. Can. J. Chem. **62**, 2223 (1984).

In 1,2-propanediol (12PD) at 215 K the optical spectrum of e^-_s shifted unsymmetrically towards higher energy the first 500 ns. Approximating the decay of the low energy side and the growth of the high energy side of the band as first order, the mean decay time at $0.5E_{Amax}$ (e^-_s) was $\tau_d \approx 160$ ns and the mean growth time at $E > E_{Amax}$ (e^-_s) was $\tau_g \approx 40$ ns. The behavior in 1,3-butanediol (13BD) at 225 K was similar, with $\tau_d \approx 170$ ns at $0.5E_{Amax}$ and $\tau_g \approx 40$ ns at $E > E_{Amax}$. The solvation time constant τ_s is only slightly greater than τ_g. The larger value of τ_d is caused by replenishment of the state at $0.5E_{Amax}$ by relaxation from lower energy states. In all diols at $T \gtrsim 240$ K ($\geq$298 K for 14BD) the spectra reached their equilibrium shape within 150 ns after the start of the 100 ns radiation pulse. The value of E_{Amax} of e^-_s in the 1,2-diols is ~0.1 eV greater than those in the other diols and 0.2−0.3 eV greater than that in a primary alcohol at the same temperature. In the secondary−secondary diol 23BD at 296 K, E_{Amax} is 0.6 eV greater than that in 2-propanol. The vicinal diol part of the molecule dominates the intermolecular solvation site of the electron. The temperature coefficient ($-dE_{Amax}/dT$) increases from 2.6 meV/K in 12 ED to 3.6 meV/K in 23BD. The asymmetry factors W_b/W_r of the e^-_s bands in the diols are 1.6−2.1, somewhat lower than those in the analogous alcohols, 1.9−2.4. The values of W_r are similar, 0.54 ± 0.04 eV, in all the diols, independent of T, with $W_r/E_{Amax} = 0.24 \pm 0.02$; $dW_b/dT < 1.0$ meV/K. The value of $(G\epsilon)_{max}$ has an upper limit of ~2.5×10^4 e^-_s/100 eV M cm in the low temperature liquid diols. The value of $G_{fi}\epsilon_{max}$ is 1.2×10^4 in all diols except 23BD, in which it is 1.3×10^4, independent of T.

KIYOSHI OKAZAKI, K. M. IDRISS-ALI et GORDON R. FREEMAN. Can. J. Chem. **62**, 2223 (1984).

Dans le propanediol-1,2 (PD12), à 215 K, le spectre optique des e^-_s glisse d'une façon non symétrique vers les hautes énergies pendant les 500 premières nanosecondes. En faisant l'hypothèse que la décroissement du côté de faible énergie et que la croissance du côté de haute énergie de la bande sont d'ordre un, le temps moyen de décroissement à $0{,}5E_{Amax}$ (e^-_s) est $\tau_d = 160$ ns et le temps moyen de croissance à $E > E_{Amax}$ (e^-_s) est de $\tau_g = 40$ ns. A 225 K, le butanediol-1,3 (BD13) se comporte de la même façon et $\tau_d = 170$ ns à $0{,}5E_{Amax}$ et $\tau_g = 40$ ns à $E > E_{Amax}$. La constante de temps de solvatation τ_s n'est que légèrement supérieure à τ_g. La valeur plus élevée de τ_g est due au remplissage de l'état à $0{,}5E_{Amax}$ par une relaxation des états de plus faible énergie. Dans tous les diols, à des $T \geq 240$ K ($\geq$298 K pour le BD14), les spectres atteignent leur forme d'équilibre en moins de 150 ns après le début de la radiation pulsée de 100 ns. A des températures constantes, la valeur de E_{Amax} des e^-_s, dans les diols-1,2, est supérieure d'environ 0,1 eV à celles observées avec d'autres diols et de 0,2 à 0,3 eV supérieure à celle observée dans un alcool primaire. Dans le diol secondaire−secondaire (BD23), à 296 K, la valeur de E_{Amax} est de 0,6 eV supérieure à celle observée dans le propanol-2. La portion viccinale de la molécule de diol domine le site de solvatation intermoléculaire de l'électron. Le coefficient de température ($-dE_{Amax}/dT$) passe de 2,6 meV/K dans le ED12 jusqu'à 3,6 meV/K dans le BD23. Les facteurs d'asymétrie des bandes des e^-_s dans les diols, W_b/W_r, varient de 1,6 à 2,1; ces valeurs sont un peu plus faibles que celles observées avec les alcools analogues qui varient de 1,9 à 2,4. Les valeurs de W_r sont identiques (0,54 ± 0,04 eV) dans tous les diols, elles ne dépendent pas de T, et $W_r/E_{Amax} = 0{,}24 \pm 0{,}02$; $dW_b/dT < 1{,}0$ meV/K. Dans les diols liquides à basse température, la limite supérieure de la valeur de $(G\epsilon)_{max}$ est d'environ $2{,}5 \times 10^4$ e^-_s/100 eV M cm. Quelle que soit la température, la valeur de $G_{fi}\epsilon_{max}$ est de $1{,}2 \times 10^4$ dans tous les diols, à l'exception du BD23 pour lequel cette valeur est $1{,}3 \times 10^4$.

[Traduit par le journal]

Introduction

The influence of solvent structure on the optical absorption spectra of solvated electrons continues to grow in interest. Alcohols (1−5) and alcohol/water mixtures (6,7) have been particularly informative about the sensitivity of the spectrum to changes of internal structure of the liquid. In these liquids, structure changes occur because of the interplay between nonpolar and hydrogen-bonding groups. The electron spectral shifts are a source of information, although it has not yet been possible to quantify the structure changes.

A series of diols (dihydroxyalkanes), with different distances between the hydroxy groups and placed at different positions along the chain, offers another approach to the interplay between nonpolar and hydrogen bonding groups. Half the number of diol molecules could provide the multihydroxyl group configuration required to solvate the electron, compared to the number of monohydroxy alcohols. Solvated electron spectra have therefore been measured in a series of seven diols as functions of temperature.

Experimental

Materials

Diols obtained from Aldrich Chemical Co. were 1,2 ethanediol (12ED), 99+%; 1,2-propanediol (12PD), analyzed U.S.P. grade; 1,3-propanediol (13PD), 98%; 1,2-butanediol (12BD), analyzed 98%; 1,3-butanediol (13BD), 99+%; 1,4-butanediol (14BD), analyzed 99+%; 2,3 butanediol (23BD).

The diols were purified as described earlier (8).

Techniques

Five cm^3 of diol was transferred into a Spectrosil optical cell with a syringe, then bubbled with UHP argon (~5 cm^3/min for 40 min). The cell was then sealed with a flame by a technique that prevented diol vapor from contacting the hot glass (9).

The methods of irradiation, dosimetry, and temperature control (10, 15) were described earlier. Briefly, a 100 ns pulse of 1.9 MeV electrons delivered a dose of 2×10^{16} eV/g to the sample.

The optical system had a 0−97% rise time of 100 ± 10 ns (3).

[1]Assisted financially by the Natural Sciences and Engineering Research Council of Canada.

Can. J. Chem. Downloaded from www.nrcresearchpress.com by 210.87.254.42 on 09/06/12
For personal use only.

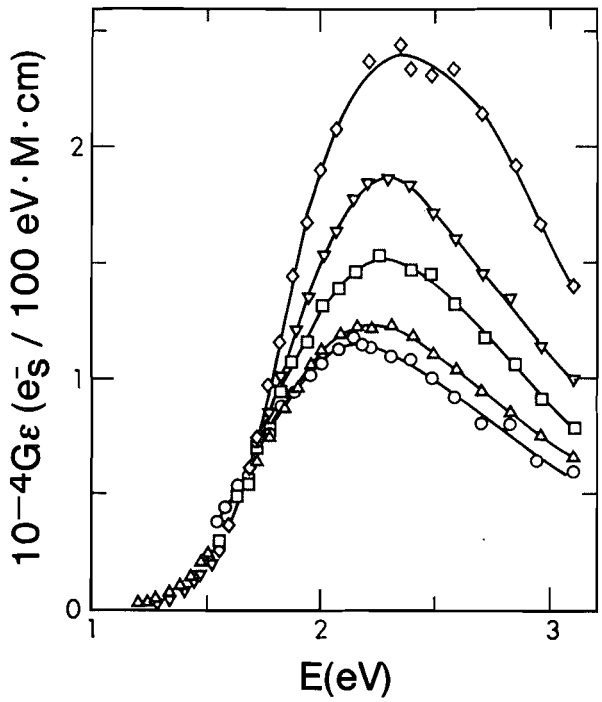

FIG. 1. Optical absorption spectra of e^-_s in 1,2-ethanediol at 314 K, ○; 298 K, △; 276 K, □; 262 K, ▽; 235 K, ◇. Time = 150 ns after the start of a 100 ns pulse.

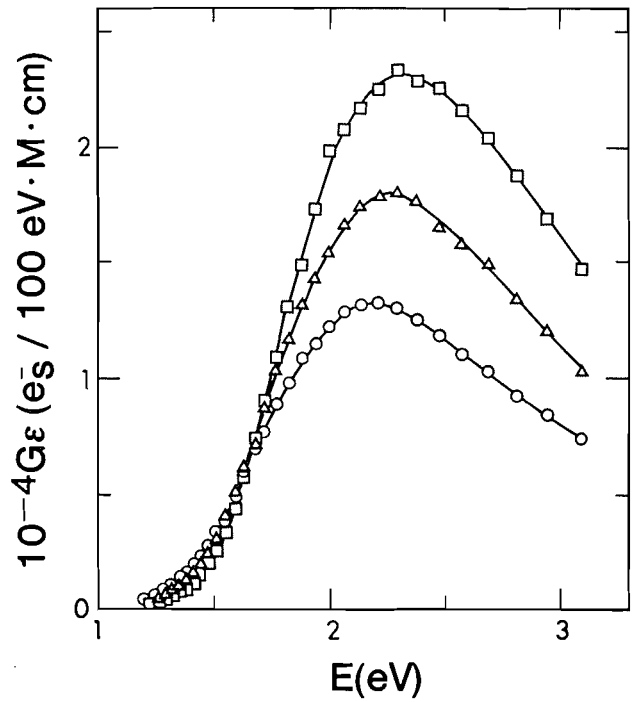

FIG. 2. Optical absorption spectra of e^-_s in 1,2-propanediol at 298 K, ○; 270 K, △; and 242 K, □. Time = 150 ns.

Results and discussion

The response characteristics of the measuring circuit were such that the optical absorption signal reached a maximum ~140 ns after the start of the 100 ns pulse, when decay after the pulse was fast (say 10% in 50 ns due to geminate reaction). The shortest time at which spectra were recorded was therefore 150 ns after the start of the pulse.

In most instances the shape of the optical spectrum in a given liquid at a given temperature was independent of time. The constant shape indicates that the electrons had relaxed into the equilibrium solvated state at $t \lesssim 100$ ns. However, the rate of decay of the signal had an initial fast portion corresponding to geminate reaction, followed by a slower part corresponding to the reaction of the free ions $(e^-_s)_{fi}$.

At the lowest temperatures in 12PD and 13BD spectral relaxation from lower to higher energies occurred over periods of ~500 ns. This corresponds to the final stages of relaxation of the localized electron and adjacent solvent molecules into the equilibrium solvated state.

In the figures the product $G\epsilon$ is plotted against photon energy, where G is the number of localized electrons formed/100 eV of energy absorbed and ϵ is the decadic molar absorbance M^{-1} cm^{-1}.

12ED

Spectra taken 150 ns after the start of a 100 ns pulse are shown in Fig. 1 for temperatures ranging from 235 to 314 K. At all temperatures the spectra decayed uniformly at all energies, indicating that the electrons had relaxed to the equilibrium solvated state e^-_s within the resolution time of the measurement. The energy at the absorption maximum, E_{Amax}, and the value of $(G\epsilon)_{max}$ increase with decreasing temperature.

12PD

Spectra taken at 242–298 K are shown in Fig. 2. The behavior is similar to that in 12ED. However, at 215 K for the first 500 ns the spectrum shape changed and shifted nonuniformly towards higher energies (Fig. 3). Approximating the decay of the absorbance in the low energy tail at 1.24 eV ($0.53E_{Amax}$ of e^-_s) as exponential, $\exp(-t/\tau_d)$, the mean decay time is $\tau_d \approx 160$ ns at 215 K. By comparison, the exponential growth

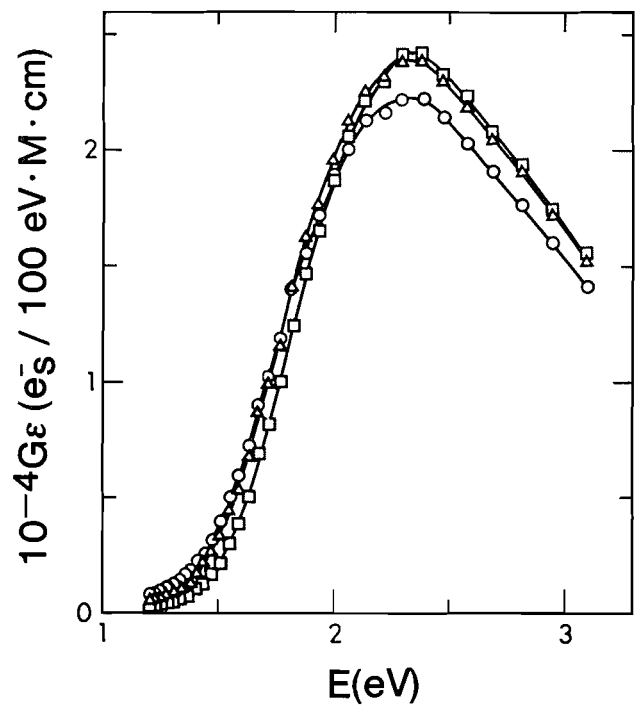

FIG. 3. Absorption spectra of localized electrons in 1,2-propanediol at 215 K at several times after the start of a 100 ns pulse. 150 ns, ○; 200 ns, △; 500 ns, □.

Can. J. Chem. Downloaded from www.nrcresearchpress.com by 210.87.254.42 on 09/06/12
For personal use only.

Can. J. Chem. Downloaded from www.nrcresearchpress.com by 210.87.254.42 on 09/06/12
For personal use only.

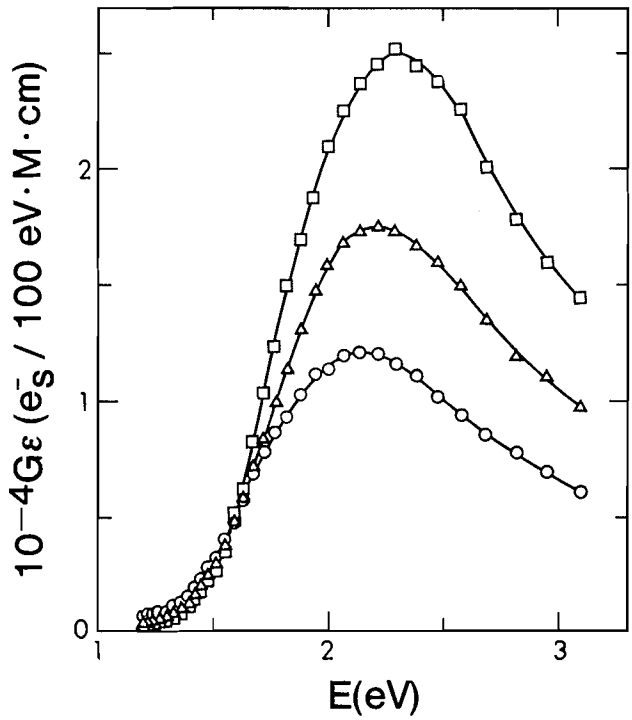

FIG. 4. Optical absorption spectra of e^-_s in 1,3-propanediol at 298 K, ○; 272 K, △; 248 K, □. Time = 150 ns.

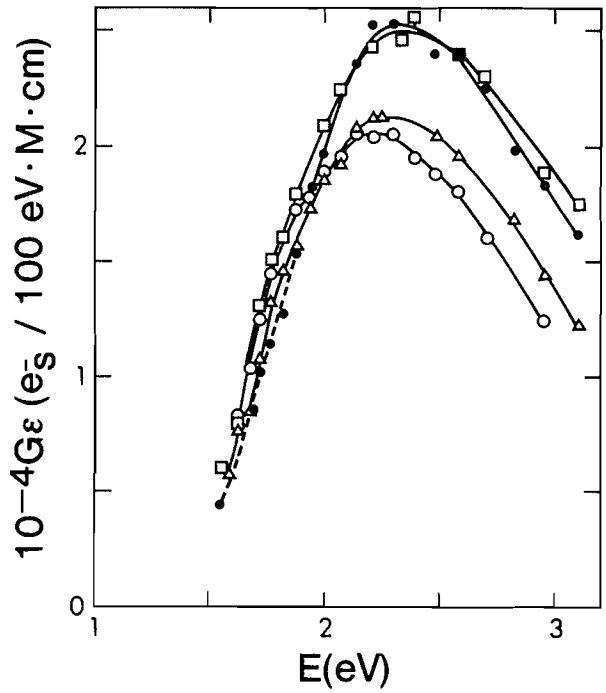

FIG. 5. Optical absorption spectra of e^-_s in 1,2-butanediol at 296 K, ○; 275 K, △; 257 K, □; 235 K, ●. Time = 150 ns.

time τ_g at $E > E_{Amax}$ of e^-_s is $\tau_g \approx 40$ ns at this temperature. Thus for the final stages of the spectrum shift, the value of τ_d at $E = 0.53E_{Amax}$ is about quadruple that of τ_g at $E > E_{Amax}$. Similar behavior was noted in 2-butanol at 171 K, where $\tau_d \approx 2\tau_g$ (3). In ref. 3 the symbol τ_s was used for τ_g, and the actual solvation time constant τ_s is probably similar to τ_g (see below).

13PD, 12BD, 13BD, 14BD, and 23BD

Similar observations were made with the other diols (Figs. 4–9).

In 12BD the spectrum at 150 ns shifted to higher absorbancies and higher energies as the temperature decreased from 295 to 257 K, as usual. However, at 235 K the spectrum became narrower and had approximately the same value of $(G\epsilon)_{max}$ as at 257 K (Fig. 5). The cause is probably that 12BD was a glass at 235 K. Solvated electron spectra tend to be narrower in a glass than in a liquid of the same material (11).

The behavior in 23BD (Fig. 9) was similar to that in 12BD.

The spectrum in 13BD at 225 K shifted slightly to higher energies during the period 150–500 ns (Fig. 7). The value of τ_d at 1.24 eV ($0.54E_{Amax}$) is ~170 ns, while $\tau_g \approx 40$ ns at $E > E_{Amax}$ of the equilibrium state. The times are similar to those in 12PD at 215 K.

Characteristic energies

The energy E_{Amax} at the absorption maximum, $(G\epsilon)_{max}$ in Figs. 1–9, varies little with the structure of the *n*-alkane-diols. The value of E_{Amax} in the 1,2-diols is 0.1 eV greater than those in the other diols (Fig. 10). The terminal —CH_2OH group is analogous to that in a primary alcohol. The —OH group on the adjacent carbon apparently provides a liquid phase structure that enhances electron solvation to the extent that E_{Amax} in a 1,2-diol at 298 K is 0.2–0.3 eV (10–15%) greater than that in a primary alcohol at the same temperature (Table 1 and refs. 12 and 13).

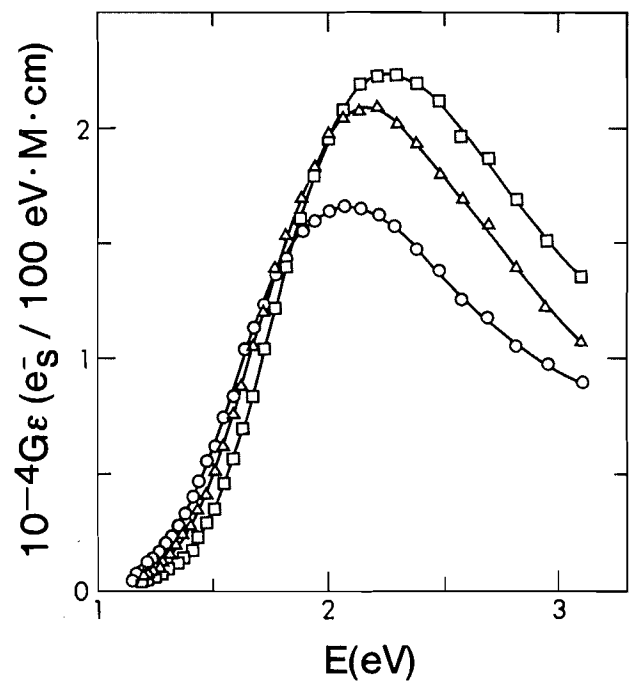

FIG. 6. Optical absorption spectra of e^-_s in 1,3-butanediol at 298 K, ○; 272 K, △; 248 K, □. Time = 150 ns.

The —OH groups in 23BD are both secondary, but the value of E_{Amax} in this diol at 296 K is 0.6 eV greater than that in 2-propanol at the same temperature (Table 1). Although E_{Amax} in a secondary alcohol is 0.4 eV lower than that in a similar primary alcohol (12), the value in 23BD is 0.1–0.2 eV higher than that in a primary alcohol at the same temperature. The vicinal diol part of the molecule dominates the intermolecular solvation site of the electron. Two vicinal diol molecules can readily provide the four —OH groups in close proximity that

Can. J. Chem. Downloaded from www.nrcresearchpress.com by 210.87.254.42 on 09/06/12
For personal use only.

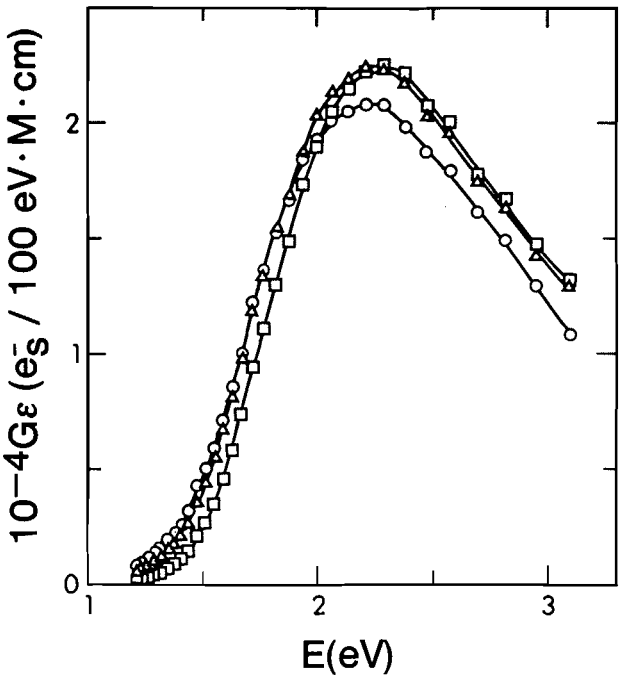

FIG. 7. Absorption spectra of localized electrons in 1,3-butanediol at 225 K at several times after the start of a 100 ns pulse. The times in ns are: 150, ○; 200, △; 500, □.

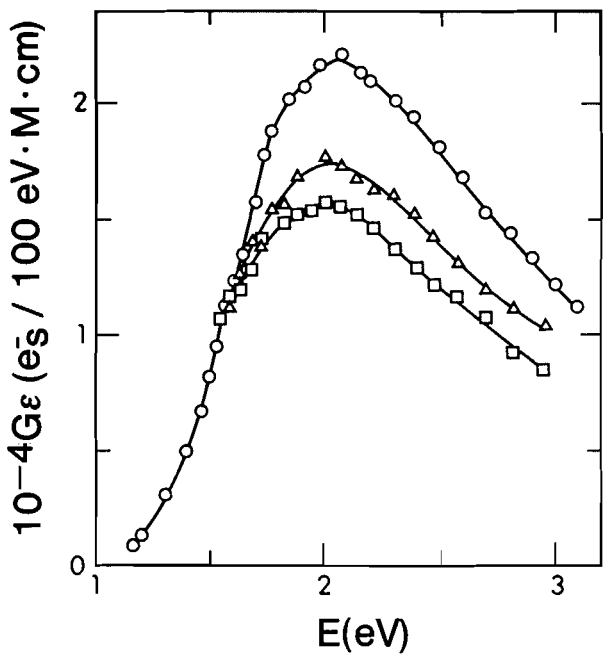

FIG. 8. Optical absorption spectra of e^-_s in 1,4-butanediol at 333 K, □; 314 K, △; 298 K, ○. Time = 150 ns.

constitute the solvated electron site in an alcohol (14).

The negative temperature coefficient ($-dE_{Amax}/dT$) in the liquid diols increases in magnitude from 2.5 meV/K in 12ED to 3.6 meV/K in 23BD (Table 1). The low value obtained for 14BD is uncertain due to the small temperature range accessible to measurement above the high freezing point. The relatively large coefficient in 23BD reflects its secondary alcohol structure. For comparison, the temperature coefficient in 2-propanol, −4.4 meV/K, is greater than that in 1-propanol, −3.3 meV/K (Table 1). The coefficient in 12ED is similar to

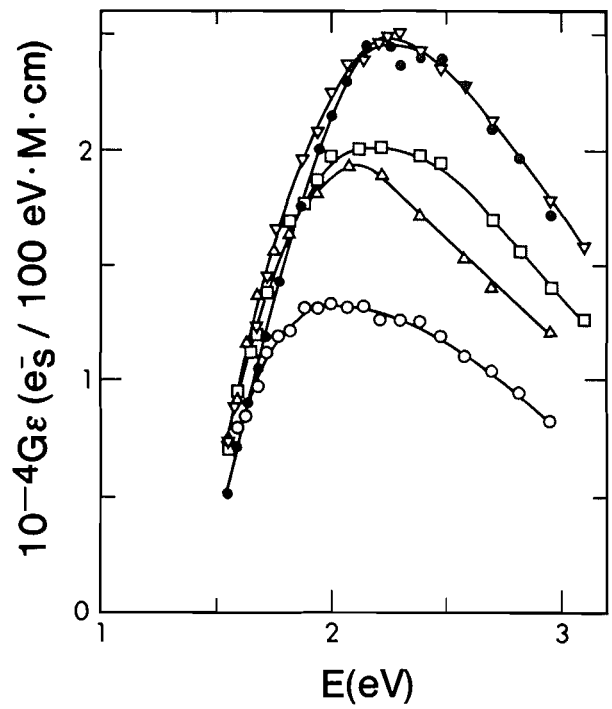

FIG. 9. Optical absorption spectra of e^-_s in 2,3-butanediol at 314 K, ○; 296 K, △; 276 K, □; 257 K, ▽; 236 K, ●. Time = 150 ns.

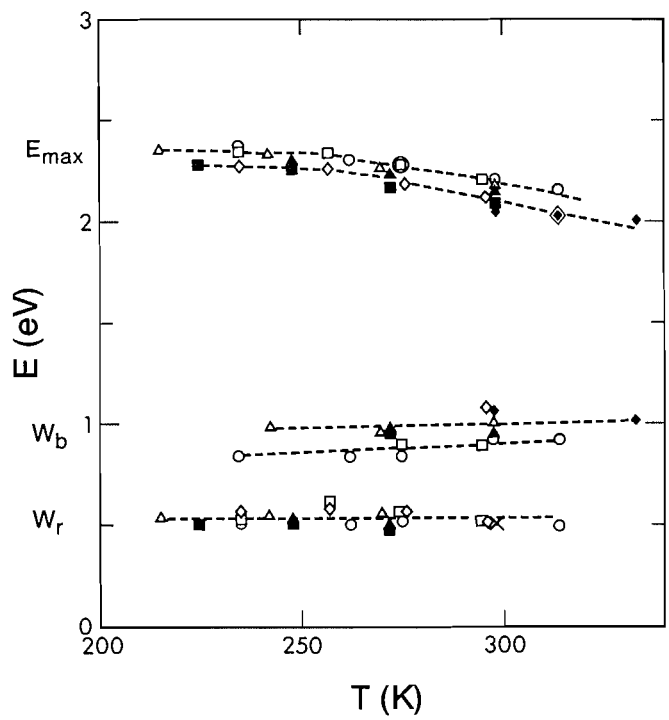

FIG. 10. Temperature dependences of optical spectrum parameters. ○, 12ED; △, 12PD; ▲, 13PD; □, 12BD; ■, 13BD; ◆, 14BD; ◇, 23BD. $X = 0.51 \pm 0.01$ eV for 12ED, 12PD, 13PD, 13BD, and 14BD. The dashed lines are merely guides for the eye.

that in water (Table 1); there are no alkyl groups in 12ED that are not anchored by an —OH in the liquid structure.

In the low temperature glasses (dE_{Amax}/dT) for the equilibrium solvated electrons is approximately zero, as witnessed by the behavior between the lowest two temperatures in 12BD

TABLE 1. Solvated electron optical spectrum parameters

Solvent	fp (K)	T (K)	E_{Amax} (eV)	$\frac{-dE_{Amax}}{dT}$ (meV/K)	W_r (eV)	W_b (eV)	W_b/W_r	W_r/E_{Amax}	$G_{fi}\epsilon_{max} \times 10^{-4}$
12ED	260	314	2.16	2.5	0.50	0.92	1.8	0.23	1.15
		298	2.21		0.51	0.92	1.8	0.23	1.10
		275	2.28		0.52	0.84	1.6	0.23	1.21
		262	2.30		0.50	0.84	1.7	0.22	1.15
		235[a]	2.36		0.53	0.84	1.6	0.22	1.24
12PD	213	298	2.18	2.7	0.52	1.00	1.9	0.24	1.11
		270	2.26		0.55	0.96	1.7	0.24	1.10
		242	2.33		0.55	—	—	0.24	1.14
		215	2.35		0.53	—	—	0.23	—
13PD	246	298	2.16	3.0	0.52	0.94	1.8	0.24	1.12
		272	2.22		0.49	0.98	2.0	0.22	1.15
		248	2.30		0.53	—	—	0.23	—
12BD	—	295	2.21	3.2	0.53	0.89	1.7	0.24	—
		275	2.28		0.56	0.90	1.6	0.25	—
		257	2.34		0.61	—	—	0.26	—
		235	2.34[b]		0.54[b]	—	—	0.23[b]	—
13BD	<223	298	2.08	3.3	0.49	—	—	0.24	1.14
		272	2.16		0.48	0.97	2.0	0.22	1.17
		248	2.26		0.52	—	—	0.23	1.16
		225	2.28		0.50	—	—	0.22	—
14BD	292	333	2.00	2	—	1.02	—	—	1.25
		314	2.03		—	—	—	—	1.20
		298	2.06		0.50	1.04	2.1	0.24	—
23BD	—	314	2.03	3.6	—	—	—	—	1.32
		296	2.12		0.52	1.08	2.1	0.25	1.35
		275	2.18		0.57	—	—	0.26	1.28
		257	2.26		0.58	—	—	0.26	—
		235	2.28[b]		0.56[b]	—	—	0.25[b]	—
H_2O[c]	273	298	1.73	2.4	0.36	0.49	1.4	0.21	5.0[d]
MeOH[c]	176	298	1.98	2.7	0.50	0.93	1.9	0.25	1.8[d]
EtOH[c]	159	298	1.82	3.1	0.48	1.12	2.3	0.26	1.5[d]
1PrOH[c]	146	298	1.95	3.3	0.53	1.10	2.1	0.27	1.4[d]
2PrOH[c]	187	298	1.52	4.4	0.44	1.01	2.3	0.29	1.4[d]

[a]Supercooled Liquid.
[b]Probably a glass.
[c]Reference 13.
[d]Reference 18.

and 23BD (Table 1). Similar behavior has been observed in dipropyl ether glass (15).

The width of the band at half height is divided into the portions W_b on the high energy side of E_{Amax} and W_r on the low energy side. The ratio W_b/W_r is the asymmetry factor of the band. The asymmetry factor is always greater than unity and has values 1.3 ± 0.1 in liquids of the symmetrical compounds water (16) and ammonia (17), and 1.9−2.4 in methanol, ethanol, and 2-propanaol (12, 13). The values in the diols are in the range 1.6−2.1 (Table 1), somewhat lower than those in analogous alcohols. Lower values of the asymmetry ratio might indicate somewhat less disorder in the solvation sites.

The values of W_b in 12ED and 12BD are ~0.1 eV lower than those in the other diols (Fig. 10). The temperature coefficient is small, $dW_b/dT < 1.0$ meV/K.

The widths of the low energy side of the bands are similar, $W_r = 0.54 \pm 0.04$ eV, in all the diols, independent of temperature (Fig. 10). The values are similar to those in primary alcohols (compare 1-propanol in Table 1). The ratio W_r/E_{Amax} equals 0.23 ± 0.01 in all of the liquid diols except 12BD and 23BD, in which it equals 0.25 ± 0.01 (Table 1). The ratio in diols is slightly larger than in water, and slightly smaller than in analogous mono-alcohols (13, 18). It seems to be another indicator of the degree of disorder in the solvation sites.

Solvation time of e^-_{loc}

The change of optical absorbance A at $E \approx 0.5E_{Amax}$ (e^-_s) at short times is attributed to two processes: (*a*) dipolar reorientation of solvent molecules near e^-_{loc} due to the field of the electron, and (*b*) migration of e^-_{loc}. The first process tends to increase A by relaxation of sites at $E < 0.5E_{Amax}$ (e^-_s) to $E = 0.5E_{Amax}$ (e^-_s), but also to decrease A by relaxation of the latter sites to $E > 0.5E_{Amax}$ (e^-_s). Migration of e^-_{loc} to geminate ions decreases the absorbance, while migration to deeper traps

Can. J. Chem. Downloaded from www.nrcresearchpress.com by 210.87.254.42 on 09/06/12
For personal use only.

Can. J. Chem. Downloaded from www.nrcresearchpress.com by 210.87.254.42 on 09/06/12
For personal use only.

has the same double effect as (*a*). The observed mean decay time τ_d is governed by the balance between growth and decay at $0.5E_{Amax}$ (e^-_s), and is therefore longer than the actual mean time of the decay processes alone.

The growth of absorbance at $E > E_{Amax}$ (e^-_s) at short times is attributed to the above process (*a*) without loss by relaxation to still higher energy states, and to the portion of (*b*) that terminates in traps that have nearly the final equilibrium depths. Geminate neutralization of electrons that absorb at $E > E_{Amax}$ (e^-_s) reduces the net growth in absorbance at early times; at intermediate times it matches the growth so that the net is zero; at later times it causes the net absorbance to decay (see Fig. 7 in ref. 3). The observed net growth to the equilibrium spectrum may be crudely approximated as a sum of roughly first order processes (relaxation plus migration to deeper traps minus migration to geminate ions). By analogy with the approach of reversible first order reactions to equilibrium (19), one may write the mean net growth rate constant τ_g^{-1} for approach to maximum absorbance at $E > E_{Amax}$ (e^-_s) as:

$$[1]\quad \tau_g^{-1} \approx \tau_r^{-1} + \tau_m^{-1} + \tau_{gn}^{-1}$$

where τ_r is the mean relaxation time of the dielectric near e^-_{loc}, τ_m is the mean migration time of a localized electron into a deeper trap of nearly the equilibrium depth, and τ_{gn} is the geminate neutralization time crudely approximated as that of a first order process.[2]

The mean solvation time τ_s is related to the times in eq. [1] by:

$$[2]\quad \tau_s^{-1} \approx \tau_r^{-1} + \tau_m^{-1} \approx \tau_g^{-1} - \tau_{gn}^{-1}$$

The values of τ_{gn} for the geminate decay that occurs after the equilibrium spectrum has been attained, in low temperature alcohols, are an order of magnitude greater than τ_g (estimated from Figs. 7, 8, and 12 in ref. 3). Hence $\tau_{gn} >> \tau_g$, and from eq. [2] $\tau_s \approx \tau_g$.

The values of τ_d at 1.24 eV are larger than those of τ_g at 2.4 eV in glycols and alcohols (Table 2). The time τ_d is extended by replenishment of the 1.24 eV level by relaxation from lower energy states.

The τ_s = 5 ps reported for 12ED at 296 K (20) is a τ_g.

$(G\epsilon)_{max}$ and $G_{fi}\epsilon_{max}$ of e^-_s

The diffusion rates of the ions and solvated electrons decrease with decreasing temperature, so the time required for geminate reaction increases. When the time required to complete geminate reaction is greater than the response time of the system (100 ns), the value of $(G\epsilon)_{max}$ increases. In the present work $(G\epsilon)_{max}$ increased with decreasing temperature below 320 K in 12ED and the two PD's (Fig. 11). The increase occurred below 340 K in 14BD.

The value of $(G\epsilon)_{max}$ in the diols tends to have an upper limit of $\sim 2.5 \times 10^4$ e^-_s/100 eV *M* cm, where the low temperature liquid becomes glassy (Fig. 10). By analogy with behaviour in other polar systems (3, 15, 21–23), the value of $(G\epsilon)_{max}$ would probably decrease as the temperature of the glass was lowered farther. A greater fraction of electrons undergoes geminate reaction before relaxation to the solvated state is complete in the low temperature glasses.

The value of $G_{fi}\epsilon_{max}$ is 1.2×10^4 e^-_s/100 eV *M* cm in all of the diols except 23BD, in which it is 1.3×10^4, essentially independent of temperature (Fig. 11).

Decay of e^-_s free ions in purified solvents

The free ion e^-_s decayed by a first order reaction. The decay rate was measured after the geminate reaction was complete.

The decay rate at a given temperature was greatest in the vicinal diols and slowest in 14BD and 13BD (Fig. 12). The

TABLE 2. Decay and growth times of the shifting optical spectrum of e^-_{loc}

Solvent	*T* (K)	τ_d (ns)[a]	τ_g (ns)[b]	Reference
12ED	296		0.005	*c*
12PD	215	160	40	*d*
13BD	225	170	40	*d*
*i*BOH	167	170	120	*e*
	169	150	100	*e*
2BOH	162	1500	730	*e*
	171	530	250	*e*
	183	200	100	*e*

[a]Mean decay time at 1.24 eV $\approx 0.5\ E_{Amax}$ (e^-_s).
[b]Mean growth time at $E \geq 2.4$ eV $> E_{Amax}$ (e^-_s).
[c]Reference 20.
[d]Present work.
[e]Reference 3, butanols.

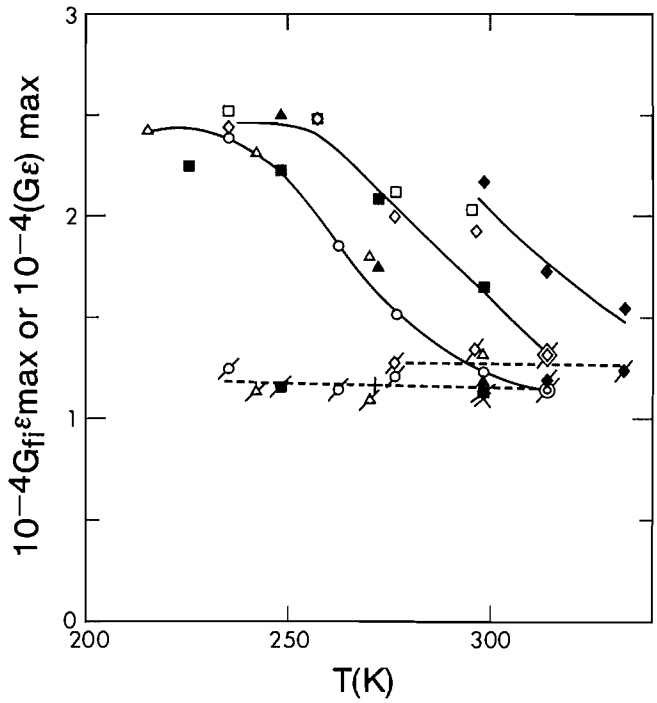

FIG. 11. Variation of $(G\epsilon)_{max}$ of e^-_s and $G_{fi}\epsilon_{max}$ (crossed points) with temperature. The values of $(G\epsilon)_{max}$ were measured 150 ns after the beginning of a 100 ns pulse, or at the time when relaxation to e^-_s was just complete, whichever was the longer. ○, 12ED; △, 12PD; ▲, 13PD; □, 12BD; ■, 13BD; ◆, 14BD; ◇, 23BD. + = 1.16 ± 0.01 = ▲ and ■; × = 1.11 ± 0.01 = ○, △ and ▲.

[2]Geminate neutralization is a nonrandom process, so the concept of order does not apply to it. However, the concept of order is familiar and is sometimes used to make crude comparisons and quick estimates. The *rate* of geminate neutralization decreases relatively faster than does a first order reaction, which means that the effective order is greater than unity. The appropriate value of τ_{gn} in eq. [1] is therefore smaller than the value of τ for the total geminate neutralization process.

TABLE 3. Solvent and solvated electron properties

Solvent	η^a (mP)	$E_\eta{}^b$	τ^a (ps)	$E_\tau{}^b$	$E_r{}^{b,c}$	$k_1{}^a$ (10^5 s^{-1})	log A_1	$E_1{}^b$	$E_{Ac}{}^{b,d}$
				Monohydric alcohols					
M	5.4[e]	11	48[f]	16	144	2.0[g]	8.35[g]	17[g]	11
E	10.8[e]	14	130[f]	18	129	1.4[g]	8.80[g]	21[g]	12
				Dihydric alcohols[h]					
12ED	177[e]	29	120[f]	29	164	11.3	9.76	21.2	26
12PD	450[e]	40	—	—	160	9.5	9.83	22.0	30
13PD	420[d]	32	—	—	158	6.2	9.73	22.5	29
12BD	526[d]	44	—	—	162	22	11.04	26.7	34
13BD	1010[d]	46	—	—	153	3.0	10.12	26.4	29
14BD	716[d]	36	—	—	151	2.8	9.41	22.6	30
23BD	400[d]	46	—	—	154	10.0	10.18	23.8	31
15PeD[i]	1100	40	1050	28	—	—	—	—	—
24PeD[i]	1400	70	900	25	—	—	—	—	—

[a]298 K.
[b]kJ/mol; measured near 298 K.
[c]Optical absorption energy of solvated electrons at 0.5 A_{max} on the low energy (red) side of the band. Reference 10 and present work.
[d]Reference 8.
[e]Reference 24.
[f]References 26–28.
[g]Reference 25.
[h]The e^-_s data supercede the preliminary data in Table 2 of ref. 8.
[i]Reference 30, pentanediols.

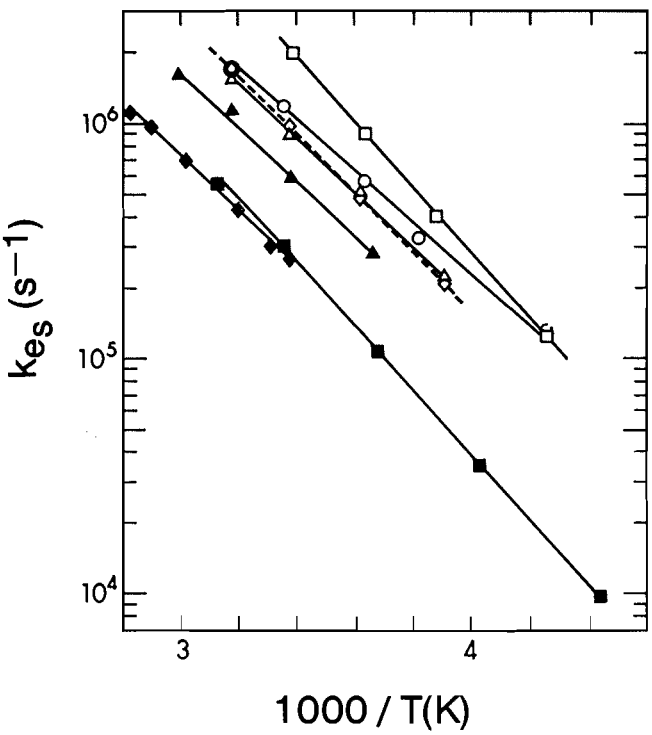

FIG. 12. First order decay constants of e^-_s in diols; Arrhenius plot. ○, 12ED; △, 12PD; ▲, 13PD; □, 12BD; ■, 13BD; ◆14BD; ◇, 23BD.

vicinal diols are the most easily oxidized, and therefore the most difficult to purify; they also appear to be the most reactive with solvated electrons. Repeated treatment of the diols with sodium borohydride under UHP argon and distillation under reduced argon pressure at temperatures below 100°C gave e^-_s decay that was at least partly due to reaction with the diol. Purification of a diol reduced not only the rate of e^-_s decay but also the activation energy of decay E_1, where

$$[3]\quad k_1(s^{-1}) = A_1 \exp(-E_1/RT)$$

For example, purification of 13PD reduced the apparent value of k_1 at 298 K from 3.1×10^6 s^{-1} to 0.6×10^6 s^{-1}, and E_1 from 32 to 22 kJ/mol. The most probable impurities are carbonyl compounds. The values of E_1 in the purified diols were much smaller than the activation energies E_{Ac} for reaction with acetone (Table 3). The values of E_1 listed in Table 3 are therefore upper limits.

The values of E_1 in the diols are about 2/3 the magnitude of E_η (refs. 8, 24, and Table 3). By contrast, the values of E_1 in the monohydric alcohols methanol and ethanol (25) were larger than E_η by about 1.5-fold, and were similar to E_τ for dielectric relaxation (refs. 26–28 and Table 3). Molecular rotational rearrangements are probably involved in the rate limiting step of the reaction of the electron with the solvent,

$$[4]\quad e^-_s \rightarrow RO^-_s + H$$

because the reaction is driven by the large difference between the solvation energies of RO^- and e^-, the former being larger (29). With the exception of 12ED, which has no unsubstituted alkyl group, the values of E_1 probably correlate with those of E_τ in the diols as well. For example, the viscous behaviour of 13BD is similar to that of 15PeD (30)[3] and E_1 in 13BD is similar to E_τ in 15PeD, where PeD is pentanediol (Table 3).

Acknowledgement

We are grateful to the personnel of the Radiation Research Center for aid with the electronics.

[3]The τ_2 determined by low frequency depolarized light scattering is similar to the τ_1 measured by microwave dispersion (molecular reorientation relatively unperturbed by fields).

Can. J. Chem. Downloaded from www.nrcresearchpress.com by 210.87.254.42 on 09/06/12
For personal use only.

1. J. H. BAXENDALE and P. WARDMAN. J. Chem Soc. Faraday Trans. I, **69**, 584 (1973).
2. J. H. BAXENDALE and P. H. G. SHARPE. Chem. Phys. Lett. **39**, 401 (1976).
3. K. OKAZAKI and G. R. FREEMAN. Can. J. Chem. **56**, 2305 (1978).
4. H. MIYASAKA, H. MASUHARA, and N. MATAGA. Chem. Phys. Lett. **98**, 277 (1983).
5. N. V. KLASSEN and G. G. TEATHER. J. Phys. Chem. **87**, 3894 (1983).
6. A.-D. LEU. K. N. JHA, and G. R. FREEMAN. Can. J. Chem. **60**, 2342 (1982).
7. Z. WU, N. V. KLASSEN, H. A. GILLIS, and G. G. TEATHER. Can. J. Chem. **61**, 189 (1983).
8. K. M. IDRISS-ALI and G. R. FREEMAN. Radiat. Phys. Chem. ***23***, 96 (1984).
9. K. N. JHA, G. L. BOLTON, and G. R. FREEMAN. J. Phys. Chem. **76**, 3876 (1972).
10. F.-Y. JOU and G. R. FREEEMAN. J. Phys. Chem. **81**, 909 (1977).
11. G. R. FREEMAN. Radiation chemistry of ethanol. NSRDS-NBS 48, U.S. Dept. of Commerce, Washington, DC. 1974. pp. 25–30.
12. A.-D. LEU, K. N. JHA, and G. R. FREEMAN. Can. J. Chem. **61**, 1115 (1983).
13. A.-D. LEU and G. R. FREEMAN. To be published.
14. M. NARAYANA and L. KEVAN. J. Chem. Phys. **72**, 2891 (1980).
15. F.-Y. JOU and G. R. FREEMAN. Can. J. Chem. **54**, 3693 (1976).
16. F.-Y. JOU and G. R. FREEMAN. J. Phys. Chem. **83**, 2383 (1979).
17. F.-Y. JOU and G. R. FREEMAN. J. Phys. Chem. **85**, 629 (1981).
18. F.-Y. JOU and G. R. FREEMAN. Can. J. Chem. **57**, 591 (1979).
19. A. A. FROST and R. G. PEARSON. Kinetics and mechanism. 2nd ed. Wiley, New York. 1961, p. 186.
20. J. W. HUNT and W. J. CHASE. Can. J. Chem. **55**, 2080 (1977).
21. G. V. BUXTON, F. C. R. CATTELL, and F. S. DAINTON. Trans. Faraday Soc. **67**, 687 (1971).
22. R. S. DIXON and V. J. LOPATA. J. Chem. Phys. **62**, 4573 (1975); **63**, 5149 (1975).
23. J. H. BAXENDALE and P. H. G. SHARPE. Int. J. Radiat. Phys. Chem. **8**, 621 (1976).
24. R. W. GALLANT. Physical properties of hydrocarbons. Vol. 1. Gulf Publishing Co., Houston, TX. 1968.
25. G. L. BOLTON, K. N. JHA, and G. R. FREEMAN. Can. J. Chem. **54**, 1497 (1976).
26. F. BUCKLEY and A. A. MARYOTT. Natl. Bur. Stand. Circular 589, U.S. Dept. of Commerce, Washington, DC. 1958.
27. S. K. GARG and C. P. SMYTH. J. Phys. Chem. **69**, 1294 (1965).
28. B. P. JORDAN, R. J. SHEPPARD, and S. SZWARNOWSKI. J. Phys. **D11**, 695 (1978).
29. K. N. JHA and G. R. FREEMAN. J. Chem. Phys. **51**, 2846 (1969).
30. G. FYTAS and TH. DORMÜLLER. J. Chem. Phys. **75**, 5232 (1981).

Can. J. Chem. Downloaded from www.nrcresearchpress.com by 210.87.254.42 on 09/06/12
For personal use only.

Mécanisme des réactions du chlorite et du dioxyde de chlore. 2. Cinétique des réactions du chlorite en présence d'*ortho*-tolidine

GUY SCHMITZ ET HENRI ROOZE

Faculté des Sciences Appliquées, Université Libre de Bruxelles, 50 avenue F. Roosevelt, 1050 Bruxelles, Belgique

Reçu le 17 octobre 1983

GUY SCHMITZ et HENRI ROOZE. Can. J. Chem. **62**, 2231 (1984).

En présence d'*ortho*-tolidine (NH_2RNH_2), utilisée pour éliminer les complications dues aux réactions des produits intermédiaires de la dismutation du chlorite, la stoechiométrie est $HClO_2 + 2NH_2RNH_2 \rightarrow Cl^- + H^+ + 2NHRNH + 2H_2O$. On ne forme pas de chlorate. La loi cinétique, en l'absence de chlorure, est

$$-\,d[HClO_2]/dt = k\,[ClO_2^-]\,[Fe^{3+}]$$

$k = 269\ M^{-1}\ s^{-1}$ à 25°C et une force ionique de 1 *M*. Sans fer ajouté, la vitesse observée est due uniquement aux traces de fer toujours présentes comme impureté des réactifs. La réaction $2HClO_2 \rightarrow HClO + ClO_3^- + H^+$ n'est donc pas une réaction élémentaire.

GUY SCHMITZ and HENRI ROOZE. Can. J. Chem. **62**, 2231 (1984).

With added *ortho*-tolidine (NH_2RNH_2) in order to eliminate complicating side reactions of the intermediate products of the disproportionation of chlorite, the stoichiometry is $HClO_2 + 2NH_2RNH_2 \rightarrow Cl^- + H^+ + 2NHRNH + 2H_2O$. No chlorate is formed. The rate law, in the absence of chloride ions, is

$$-\,d[HClO_2]/dt = k\,[ClO_2^-]\,[Fe^{3+}]$$

$k = 269\ M^{-1}\ s^{-1}$ at 25°C and 1 *M* ionic strength. Without added iron, the observed rate is only due to the small amount of iron always present as an impurity in the reactants. Thus the reaction $2HClO_2 \rightarrow HClO + ClO_3^- + H^+$ is not an elementary reaction.

Introduction

Conservées à l'abri de la lumière, les solutions de chlorite sont stables en milieux alcalins. En milieux neutres elles se décomposent lentement suivant l'éq. [1]. La vitesse n'est notable que dans les solutions chaudes (1, 2).

[1] $3ClO_2^- = 2ClO_3^- + Cl^-$

En milieux acides elles se décomposent dès la température ordinaire, d'autant plus vite que l'acidité est grande. En absence de chlorure l'éq. [2] est la plus fréquemment citée mais des écarts importants ont été observés (réfs. 1 à 8).

[2] $4HClO_2 = 2ClO_2 + ClO_3^- + Cl^- + 2H^+ + H_2O$

Les ions chlorures augmentent la vitesse de décomposition et modifient la stoechiométrie. En milieux très acides et très riches en chlorures elle tend vers [3].

[3] $5HClO_2 = 4ClO_2 + Cl^- + H^+ + 2H_2O$

Dans notre article précédent (9), nous avons montré qu'une des causes de la variation des rapports stoechiométriques est l'existence d'une bifurcation dans le mécanisme, que l'on peut schématiser comme suit:

$$HClO_2 \rightarrow \rightarrow HClO \xrightarrow{HClO_2} Cl_2O_2 \begin{cases} \nearrow ClO_3^- \\ \searrow ClO_2 \end{cases}$$

En absence de chlorure la loi cinétique [4] proposée par Barnett (10) est généralement admise, avec éventuellement un effet de l'acidité sur la constante k_4 (réfs. 4 à 8, 11, 12).

[4] $-\,d[HClO_2]/dt = k_4\,[HClO_2]^2$

Kieffer et Gordon ont vérifié la loi [4] en milieux 2 et 1.2 molaires en $HClO_4$ mais ont constaté qu'elle n'est pas satisfaite en milieux 0.2 molaires. Ils n'on pas trouvé de loi satisfaisante dans ces conditions.

Nous avons étudié l'effet accélérateur des ions chlorures (9) et obtenu l'éq. [5] en bon accord avec les travaux précédents; $k_{II} = 9.1 \times 10^{-3}\ M^{-1}\ s^{-1}$ à 25°C et $I = 1\ M$; v_I représente la vitesse en l'absence de chlorure, objet de notre étude actuelle.

[5] $-\,d[HClO_2]/dt = v_I + k_{II}\,[HClO_2][Cl^-][H^+]$

Cherchant l'explication des écarts à la loi [4] observés par Kieffer et Gordon (8) nous avons fait une observation qui remet en cause les conclusions de plusieurs travaux antérieurs. La dismutation du chlorite est catalysée par des traces de fer, de l'ordre de celles que l'on trouve couramment comme impureté des réactifs. La figure 1 en donne un exemple. Pour étudier la cinétique de cette catalyse nous avons mis à profit les propriétés de l'*ortho*-tolidine, comme nous l'avions fait pour la catalyse par les ions chlorures.

Téchnique expérimentale

Nous avons vu (9) que l'*ortho*-tolidine ne réagit pas directement avec le chlorite mais est oxydée extrêmement rapidement par le dioxyde de chlore, le chlore et l'acide hypochloreux. Elle permet ainsi d'étudier la cinétique de la dismutation du chlorite en évitant les complications dues à la réaction entre le chlorite et le chlore ou l'acide hypochloreux. Toutes les vitesses indiquées dans cet article sont des vitesses initiales obtenues dans des conditions telles que l'effet des ions chlorures soit négligeable. Elles ont été mesurées en suivant l'absorbance des solutions due au dérivé oxydé de l'*ortho*-tolidine. Son absorbance molaire étant élevée ($\epsilon = 59\,750$) on obtient aisément des valeurs précises des vitesses initiales. Pour plus de détails, cf. la réf. 9. Les symboles suivants seront utilisés: NH_2RNH_2 et NHRNH, formules abrégées de l'*ortho*-tolidine et de son dérivé oxydé; $[NaClO_2]$, concentration totale du chlorite, c'est-à-dire $[HClO_2] + [ClO_2^-]$; [Fe] concentration totale du fer ajouté.

Résultats en présence de fer ajouté

Stoechiométrie

On ajoute le chlorite à un mélange d'acide perchlorique (0.1 *M*), d'*ortho*-tolidine en excès et de fer. Lorsque la réaction est terminée on mesure le pouvoir oxydant de la solution

Can. J. Chem. Downloaded from www.nrcresearchpress.com by 210.87.254.5 on 09/06/12
For personal use only.

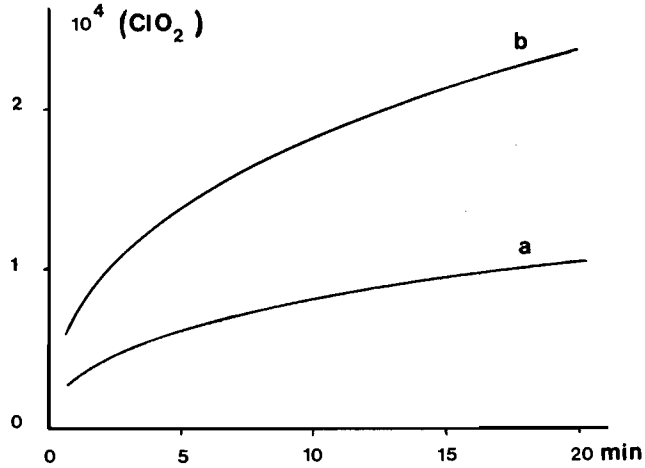

FIG. 1. Effet catalytique du fer sur la production de ClO_2. $[NaClO_2] = 2{,}5 \times 10^{-3}$ *M*, $[HClO_4] = 0{,}1$ *M*. (a) Sans addition de fer. (b) Addition de 5×10^{-6} *M* de fer.

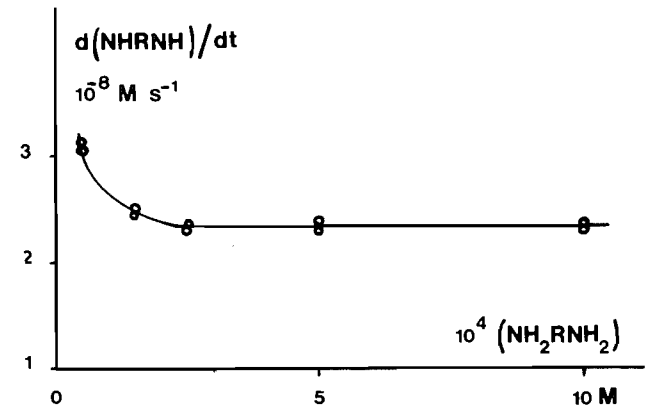

FIG. 2. Effet de l'*ortho*-tolidine sur la vitesse de [6]. $[HClO_4] = 0{,}105$ *M*, $[NaClO_2] = 1{,}97 \times 10^{-4}$ *M*, $[Fe] = 1{,}0 \times 10^{-6}$ *M*.

par iodométrie et l'*ortho*-tolidine oxydée par absorptiométrie. On constate que le pouvoir oxydant est conservé, normalité finale = 4.0 ± 0.2 $[NaClO_2]_0$, et que le rapport [NHRNH]/$[NaClO_2]_0$ vaut en moyenne 2.08 ± 0.15. L'*ortho*-tolidine supprime donc la formation de chlorate et le système évolue conformément à [6].

[6] $HClO_2 + 2NH_2RNH_2 = Cl^- + H^+ + 2H_2O + 2NHRNH$

Cinétique

L'effet de la force ionique *I* entre 0.2 et 1 *M* est faible. Elle a été fixée à 1 *M* avec du $NaClO_4$. La figure 2 montre que la vitesse de [6] est indépendante de la concentration de l'*ortho*-tolidine, à condition que celle-ci soit suffisamment grande. La valeur minimale de la concentration à utiliser augmente avec l'acidité et avec la concentration du chlorite. La raison de l'augmentation de la vitesse aux faibles concentrations apparaîtra lorsque nous discuterons la figure 5.

Les figures 3 et 4 montrent que la vitesse de [6] est proportionnelle à la concentration du fer. Nous ne considérons ici que les pentes des droites, les ordonnées à l'origine seront discutées dans le paragraphe suivant. Les résultats ne dépendent pas de la nature du sel de fer utilisé, nitrate de Fe(III), sulfate de Fe(III) ou sel de Mohr. Les pentes des droites de la figure 3 étant proportionnelles à $[NaClO_2]$ posons

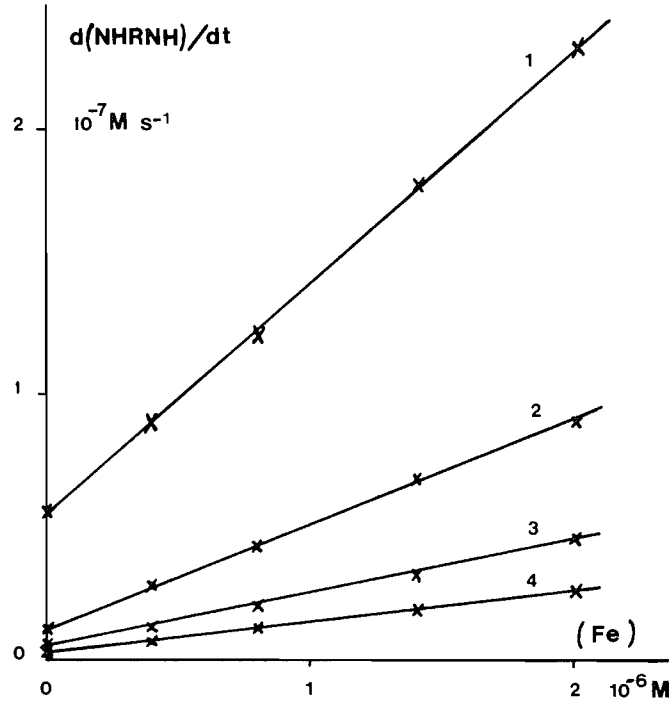

FIG. 3. Vitesses en présence d'*ortho*-tolidine. $[HClO_4] = 0{,}107$ *M*; $[NaClO_2] = 8{,}66 \times 10^{-4}$ *M* (1), $3{,}98 \times 10^{-4}$ *M* (2), $1{,}99 \times 10^{-4}$ *M* (3), $1{,}19 \times 10^{-4}$ *M* (4).

[7] $d[NHRNH]/dt = k' [NaClO_2][Fe]$

L'effet de l'acidité sur k' est donné dans le tableau 1. On constate que $1/k'$ est proportionnel à $1 + [H^+]/K_a$ avec $K_a = 2.4 \times 10^{-2}$, valeur obtenue par Hong et Rapson (7) pour la constante d'acidité de $HClO_2$ si $T = 25°C$ et $I = 1$ *M*. L'écart à la valeur thermodynamique $K_a = 1.1 \times 10^{-2}$ (9) correspond à une valeur vraisemblable du coefficient d'activité, $\gamma_\pm = 0.66$. On en déduit la loi cinétique [8].

[8] $d[NHRNH]/dt = k_8 [ClO_2^-][Fe^{3+}]$

$$k_8 = k' \left(1 + \frac{[H^+]}{K_a}\right)$$

Lors de la discussion du modèle cinétique nous montrerons qu'au cours de nos expériences la quasi-totalité du fer est maintenue sous forme de Fe(III). D'autre part la constante de première hydrolyse du Fe(III) vaut 9×10^{-4} (13, 14). Aux acidités considérées on a donc $[FeOH^{++}] \ll [Fe^{3+}]$ et $[Fe^{3+}] \simeq [Fe]$. Les valeurs du tableau 1 donnent $k_8 = 538 \pm 18$ M^{-1} s^{-1}.

Effet de la température

Nous avons vérifié la proportionnalité entre la vitesse de [6] et la concentration du fer à trois autres températures. Si $[HClO_4] = 0.41$ *M* on obtient $k' = 7.0$ (15.1°C), 110 (35.6°C), 267 (44.2°C) et une énergie d'activation apparente de 95 kJ/mol. Pour obtenir l'énergie d'activation relative à k_8 il faudrait connaître la variation de K_a en fonction de la température.

Résultats sans addition de fer

Dans la zone de pH étudiée le chlorite se dismute en absence de fer introduit intentionnellement, mais cela ne signifie pas qu'il existe un chemin réactionnel indépendant du fer. Les ordonnées à l'origine des figures 3 et 4 résultent des traces de fer inévitablement présentes dans les réactifs. Cette affirmation

Can. J. Chem. Downloaded from www.nrcresearchpress.com by 210.87.254.5 on 09/06/12
For personal use only.

Can. J. Chem. Downloaded from www.nrcresearchpress.com by 210.87.254.5 on 09/06/12
For personal use only.

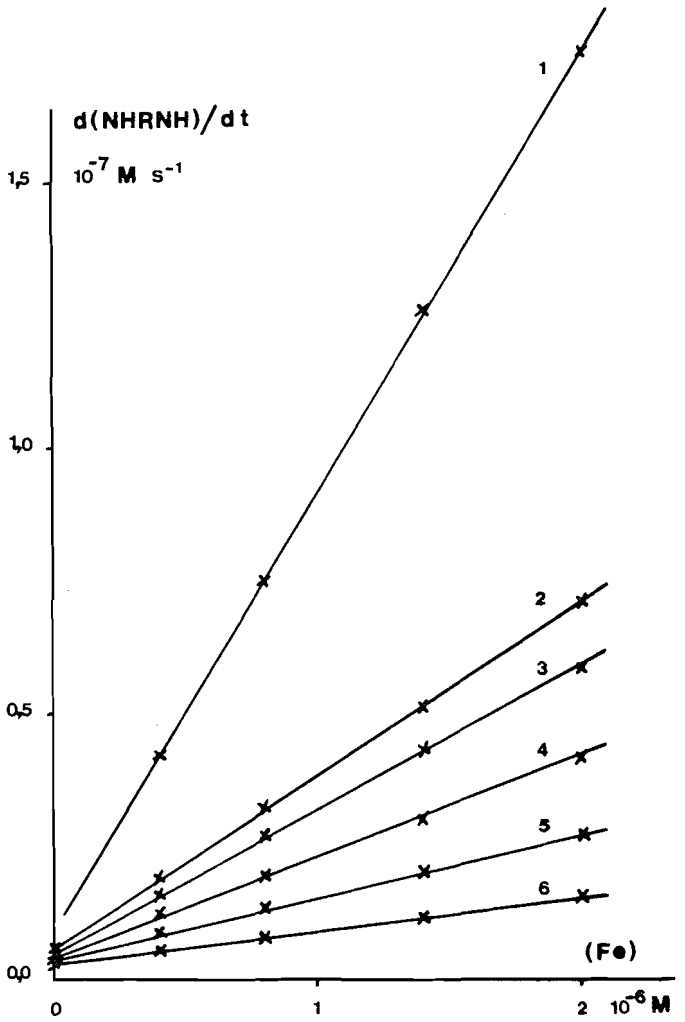

FIG. 4. Vitesses en présence d'*ortho*-tolidine. $[NaClO_2] = 2{,}13 \times 10^{-4}$ *M*; $[HClO_4]$ = 0,0087 *M* (1), 0,055 *M* (2), 0,075 *M* (3), 0,107 *M* (4), 0,208 *M* (5), 0,416 *M* (6).

remettant en cause un aspect important du mécanisme de la dismutation du chlorite nous détaillerons quelque peu nos observations.

Si l'on purifie davantage les réactifs les vitesses diminuent. On ne peut cependant les rendre négligeables à cause de la grande sensiblité de la réaction et de l'impossibilité d'éliminer suffisamment le fer des réactifs. L'acide perchlorique Merck "Suprapur" et le chlorite recristallisé plusieurs fois contiennent assez de fer pour catalyser la réaction. L'un de nous a montré (15) que les ordonnées à l'origine de droites telles que celles des figures 3 et 4 correspondent bien aux vitesses calculées par [7] en utilisant les valeurs des teneurs en fer des réactifs déterminées par spectroscopie d'émission de plasma.

En milieux perchloriques 1 *M* et en absence d'*ortho*-tolidine la dismutation du chlorite obéit à une loi d'ordre deux. La figure 5 montre nos résultats en présence d'*ortho*-tolidine. Si la concentration de celle-ci est faible on obtient une somme de deux termes, l'un d'ordre un, l'autre d'ordre deux. Si on l'augmente, on supprime le terme d'ordre deux. Les analyses par spectroscopie d'émission de plasma ont montré que lors des expériences de la figure 5 le fer provenait principalement de l'acide perchlorique, pour le reste de la solution d'*ortho*-tolidine et que la concentration totale du fer était quasi-indépendante du chlorite. Le terme d'ordre un est ainsi conforme à la loi [7].

TABLEAU 1. Constantes cinétiques; 25°C, I = 1 *M*

$[HClO_4]$ (*M*)	$[NaClO_2]$ (10^{-4} *M*)	k' (M^{-1} s^{-1})	k_8 (M^{-1} s^{-1})
0,107	1,19	98,9	539
0,107	1,99	103,6	564
0,107	3,98	101,3	552
0,107	8,66	102,2	557
0,0087	2,13	392	534
0,055	2,13	154,5	506
0,075	2,13	124,4	515
0,208	2,13	55,4	536
0,416	2,13	30,0	551
0,305	1,64	38,2	524
1,02	1,64	12,5	544

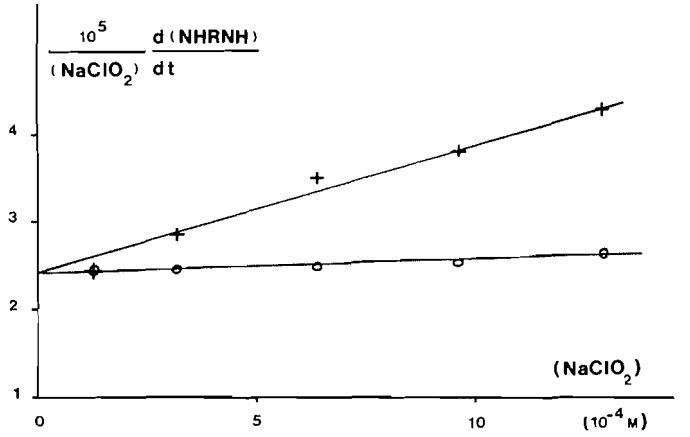

FIG. 5. Suppression par l'*ortho*-tolidine de la réaction d'ordre deux. $[HClO_4]$ = 1 *M*, $[NH_2RNH_2] = 2{,}5 \times 10^{-4}$ *M* (+), $2{,}5 \times 10^{-3}$ *M* (○).

La réaction d'ordre un étant catalysée par le fer on prévoit qu'un agent complexant tel que l'EDTA réduise sa vitesse, ce que nous avons vérifié. Par exemple si $[HClO_4] = 0.1$ *M*, $[NaClO_2] = 8.7 \times 10^{-4}$ *M* et $[NH_2RNH_2] = 2.5 \times 10^{-4}$ *M* nous avons obtenu $d[NHRNH]/dt = 5.48\ 10^{-8}$ *M* s^{-1} sans EDTA et 0.33×10^{-8} *M* s^{-1} avec 5×10^{-3} mol/L d'EDTA. Par contre, dans nos conditions expérimentales, il n'y a pas lieu de considérer de complexe avec l'*ortho*-tolidine, la vitesse de la réaction d'ordre un étant indépendante de sa concentration.

Discussion

La loi [8] peut être interprétée[1] en admettant l'étape déterminante [9].

[9] $ClO_2^- + Fe^{3+} \rightarrow ClO_2 + Fe^{2+}$

Nous savons (9) que le dioxyde de chlore oxyde très rapidement l'*ortho*-tolidine suivant [10].

[10] $2ClO_2 + NH_2RNH_2 \rightarrow 2HClO_2 + NHRNH$

Pour compléter le mécanisme nous nous basons sur les résultats d'Ondrus et Gordon (16). Ils ont étudié l'oxydation du Fe(II)

[1] Remarquons que nos résultats pourraient également être interprétés par $HClO_2 + FeOH^{2+} \rightarrow ClO_2 + Fe^{2+} + H_2O$, sans que cela change nos conclusions.

par le chlorite, en présence de phénol pour capter le HClO, et ont obtenu

$$-d[Fe^{2+}]/dt = k_{obs}\,[NaClO_2][Fe^{2+}]$$

k_{obs} est une fonction décroissante de l'acidité. Ils ont montré que l'étape déterminante correspond à l'échange d'un seul électron et ont admis le mécanisme suivant.

$$HClO_2 + Fe^{2+} \rightarrow Fe^{3+} + Cl(II)$$

$$ClO_2^- + Fe^{2+} \rightarrow Fe^{3+} + Cl(II)$$

$$Cl(II) + Fe^{2+} \rightarrow Fe^{3+} + HOCl$$

En considérant que l'intermédiaire qu'ils désignent par Cl(II) est le radical ClO leur mécanisme s'écrit:

[11] $HClO_2 + Fe^{2+} \rightarrow ClO + FeOH^{++}$

[12] $ClO_2^- + Fe^{2+} + H_2O \rightarrow ClO + Fe(OH)_2^+$

[13] $ClO + Fe^{2+} + H^+ \rightarrow HClO + Fe^{3+}$

$$Fe(OH)_2^+ + H^+ \rightleftharpoons FeOH^{++} + H_2O$$

$$FeOH^{++} + H^+ \rightleftharpoons Fe^{3+} + H_2O$$

Dans le domaine d'acidité étudié les concentrations des formes hydroxylées du Fe(III) sont négligeables. En présence d'*ortho*-tolidine, il est probable que le ClO est réduit directement, la réaction globale [14] remplaçant [13].

[14] $2ClO + 3NH_2RNH_2 \rightarrow 2Cl^- + 2H^+ + 3NHRNH + 2H_2O$

On obtient la stoechiométrie [6] en faisant la somme [9] + 1/2 [10] + [11] ou [12] + 1/2 [14].

En vitesse initiale, l'effet des ions Cl^- est négligeable et la vitesse est déterminée par [9]. On retrouve ainsi la loi expérimentale.

$$d[NHRNH]/dt = 2k_9\,[ClO_2^-][Fe^{3+}]$$

$$k_9 = 269 \pm 9\ M^{-1}\ s^{-1} \qquad K_a = 2.4 \times 10^{-2}$$

Pour obtenir les valeurs de k_{11} et k_{12} nous avons recalculé les valeurs de k_{obs} données par Ondrus et Gordon (16).

$$k_{11} + \frac{K_a}{[H^+]}\,k_{12} = \frac{1}{2}\left(1 + \frac{K_a}{[H^+]}\right)k_{obs}$$

Ayant $[HClO_4] = 0.05$ à 1 M le second nombre de cette relation dépend peu de K_a. Nous l'avons calculé en prenant $K_a = 2.4 \times 10^{-2}$. Un ajustement par la méthode des moindres carrés donne

$$k_{11} = 930; \qquad K_a k_{12} = 64 \quad (25°C,\ I = 2\ M)$$

Ces valeurs nous permettent de vérifier que nous pouvions interpréter [7] en admettant $[Fe^{3+}] \gg [Fe^{2+}]$. L'approximation de la stationnarité donne

$$\frac{[Fe^{3+}]}{[Fe^{2+}]} = \frac{2}{K_a k_9}\,(k_{11}\,[H^+] + K_a k_{12})$$

$$= 290\,[H^+] + 20 \gg 1$$

Conclusions

En présence d'assez d'*ortho*-tolidine on obtient uniquement la réaction [6], sans formation de chlorate, obéissant à la loi [7]. Il n'y a pas de réaction directe entre le chlorite et l'*ortho*-tolidine mais uniquement une décomposition du chlorite catalysée par le fer et l'oxydation de l'*ortho*-tolidine par les produits de cette décomposition.

Les vitesses observées en absence de fer ajouté sont dues aux traces de fer présentes dans les réactifs. La réaction $2HClO_2 \rightarrow HClO + ClO_3^- + H^+$ d'ordre deux obtenue en absence d'*ortho*-tolidine n'est pas une réaction simple, car si elle l'était, elle subsisterait en sa présence. Le mécanisme proposé pour la réaction [6] nous fournit les premiers éléments du mécanisme de la dismutation du chlorite en absence d'*ortho*-tolidine, objet de notre prochain article.

1. M. C. Taylor, J. F. White, G. P. Vincent et G. L. Cunningham. Ind. Eng. Chem. **32**, 899 (1940).
2. J. F. White, M. C. Taylor et G. P. Vincent. Ind. Eng. Chem. **34**, 783 (1942).
3. W. Busser et H. Hanisch. Helv. Chim. Acta, **35**, 2547 (1952).
4. F. Stitt, S. Frielander, H. J. Lewis et F. E. Young. Anal. Chem. **26**, 1479 (1954).
5. F. Boemlander. Von Wasser, **29**, 78 (1962); Gas Wasserfach. **104**, 518 (1963).
6. G. M. Nabar, V. A. Shenai et S. Sundaram. Indian J. Technol. **2**, 7 (1964).
7. C. C. Hong et W. H. Rapson. Can. J. Chem. **46**, 2053 (1968).
8. R. G. Kieffer et G. Gordon. Inorg. Chem. **7**, 235 (1968); **7**, 239 (1968).
9. G. Schmitz et H. Rooze. Can. J. Chem. **59**, 1177 (1981).
10. B. Barnett. Dissertation, University of California, 1935.
11. H. F. Launer, W. K. Wilson et J. H. Flynn. J. Res. Natl. Bur. Stand. **51**, 237 (1953).
12. H. F. Launer et Y. Tomatsu. J. Am. Chem. Soc. **76**, 2591 (1954).
13. B. O. Hedstrom. Ark. Kemi, **6**, 1 (1953).
14. R. Arnek et K. Schlyter. Acta Chem. Scand. **22**, 1327 (1968).
15. H. Rooze. Anal. Chem. **56**, 601 (1984).
16. M. G. Ondrus et G. Gordon. Inorg. Chem. **11**, 985 (1972).

Can. J. Chem. Downloaded from www.nrcresearchpress.com by 210.87.254.5 on 09/06/12
For personal use only.

Strained heterocyclic systems. 12.[1] The crystal structure of 1,8-diazabiphenylene

BETTY R. DEROSKI AND JOHN S. RICCI, JR
Chemistry Department, Brookhaven National Laboratory, Upton, NY 11973, U.S.A.

J. A. HUGH MACBRIDE
Chemistry Division, The Polytechnic, Chester Road, Sunderland SR1 3SD, U.K.

AND

J. HODGE MARKGRAF[2]
Department of Chemistry, Williams College, Williamstown, MA 01267, U.S.A.

Received March 9, 1984

BETTY R. DEROSKI, JOHN S. RICCI, JR., J. A. HUGH MACBRIDE, and J. HODGE MARKGRAF. Can. J. Chem. **62**, 2235 (1984).

The structure of 1,8-diazabiphenylene (**5**) has been determined by X-ray methods. Crystals of **5** are monoclinic, space group $P2_1/n$, with a = 3.786(2), b = 8.532(1), c = 11.218 (2) Å, β = 92.24(2)°, and two molecules per unit cell. The planar molecule contains distorted aromatic rings with the smallest angle (112.9°) adjacent to the fused strained ring.

BETTY R. DEROSKI, JOHN S. RICCI, JR., J. A. HUGH MACBRIDE et J. HODGE MARKGRAF. Can. J. Chem. **62**, 2235 (1984).

Faisant appel à la diffraction des rayons-X, on a déterminé la structure du diaza-1,8 biphénylène (**5**). Les cristaux de **5** sont monocliniques, groupe d'espace $P2_1/n$, avec a = 3,786(2), b = 8,532(1), c = 11,218(2) Å, β = 92,24(2)° et contiennent deux molécules par maille. La molécule plane comporte des cycles aromatiques déformés dans lesquels l'angle le plus petit (112,9°) est adjacent au cycle condensé qui est tendu.

[Traduit par le journal]

Can. J. Chem. Downloaded from www.nrcresearchpress.com by 210.87.254.5 on 09/06/12
For personal use only.

Introduction

The incorporation of strained rings into organic molecules is known to influence the physical properties and the chemical reactivity of such compounds. For the past two decades these effects have been studied extensively in aromatic systems containing fused, four-membered rings. The definitive work on the crystal structure of biphenylene **1** was reported by Trotter and co-workers, who noted that the internal angles of the six-membered rings differed significantly from 120° (1). The site of maximum distortion in the aromatic ring was the C(8b)—C(1)—C(2) angle, which averaged 115.2°; the same value was reported later by others (2). From structural studies on unsymmetrical systems (e.g. **2**) it is clear that the smallest angle of the benzene ring is always adjacent to the site of the fused four-membered ring (3–8).

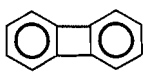

1

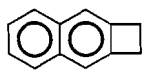

2

In contrast to the variety of carbocyclic systems, crystal structures have been determined for only two heterocyclic analogs: a quaternized derivative of 2,7-diazabiphenylene **3** (9) and 1,2-dihydrocyclobuta[*b*]quinoline **4** (10). In each case the position of the most acute angle of the six-membered rings was the

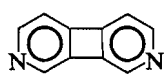

3

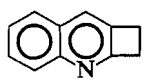

4

same as that in **1** and **2**. The C(3a)—N(3)—C(2a) angle of **4** (112.5°) was the smallest reported to date for such ring systems. In **3**, containing N(2) quaternized with an allyl substituent, the pyridinium ring exhibited a C(8b)—C(1)—N(2) angle of 114.4°, while the comparable angle in the pyridine ring was 119.2°. The availability of 1,8-diazabiphenylene **5** afforded a novel heterocyclic framework which combined features of both **1** (all carbons of the four-membered ring nominally sp^2) and **4** (nitrogen atom adjacent to the strained ring). Accordingly, we undertook an X-ray diffraction study of **5** to determine the extent of CNC bond angle distortion.

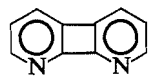

5

TABLE 1. Summary of data collection and processing parameters

Parameter	Value
Space group[a]	$P2_1/n$
Cell constants	a = 3.786(2) Å
	b = 8.532(1)
	c = 11.218(2)
	β = 92.24(2)°
	V = 362 Å^3
Molecular formula	$C_{10}H_6N_2$
Molecular weight	154.17
Molecules per cell	Z = 2
Density (calcd.)	ρ = 1.41 g cm^{-3}
Absorption coefficient (CuK_α)	μ = 7.02 g cm^{-1}
Total data collected	1685
Unique data	823
Data with $I \geq 3\sigma(I)$	614
Total variables	67
$R = \Sigma\|\|F_o\| - \|F_c\|\|/\Sigma\|F_o\|$	0.059
$R_w = (\Sigma_w(\|F_o\| - \|F_c\|)^2/\Sigma_w\|F_o\|^2)^{1/2}$	0.076

[a]Equivalent positions: $1/2 + x, y, z$; $1/2 - x, \bar{y}, \bar{z}$; $1/2 - x, 1/2 + y, 1/2 - z$; $1/2 + x, 1/2 - y, 1/2 + z$.

Experimental

Synthesis

1,8-Diazabiphenylene was prepared by flash vacuum pyrolysis of 4,5,9,10-tetra-azaphenanthrene (9, 11), mp 156.5–158.5°C.

[1]For Part 11, see ref. 10.

[2]Author to whom correspondence should be addressed.

TABLE 2. Positional parameters ($\times 10^4$) and anisotropic thermal parameters ($\times 10^4$) with estimated standard deviation in parentheses[a]

Atom	x	y	z	β_{11}	β_{22}	β_{33}	β_{12}	β_{13}	β_{23}
N(1)	−1972(5)	2575(3)	285(2)	740(16)	171(4)	68(2)	21(7)	59(3)	−23(2)
C(2)	−1871(6)	3388(3)	−802(2)	701(15)	131(4)	97(2)	13(7)	22(4)	−18(2)
C(3)	−789(6)	2710(3)	−1831(2)	762(17)	131(3)	70(2)	−9(7)	32(4)	17(2)
C(4)	358(5)	1170(2)	−1897(1)	788(16)	130(3)	56(1)	−8(6)	53(3)	2(2)
C(4a)	222(5)	415(3)	−861(2)	563(12)	124(4)	60(1)	−38(6)	23(3)	−2(2)
C(8b)	−901(5)	1118(3)	204(1)	559(14)	134(4)	56(1)	−23(6)	28(3)	2(2)
H(2)[b]	−2734(72)	4467(37)	−797(20)						
H(3)	−722(74)	3383(30)	−2583(23)						
H(4)	1333(147)	806(60)	−2682(45)						
H(5)	2802(158)	−3200(62)	−954(47)						

[a]Anisotropic thermal parameters in the form $\exp[-(\beta_{11}h^2 + \beta_{22}k^2 + \beta_{33}l^2 + \beta_{12}hk + 2\beta_{13}hl + 2\beta_{23}hl)]$.
[b]Hydrogens were assigned the isotropic thermal parameter of 5.5 Å^2.

Data collection

Precession photographs and cell reduction calculations revealed the crystal to be monoclinic. The cell dimensions were determined by a least-squares fit of the observed 2θ angles for 24 reflections centered automatically. Reflections for $0k0$, $k \neq 2n$ and $h0l$, $(h + l) \neq 2n$ were absent.

Three dimensional intensity data were measured on a computer-controlled Enraf–Nonius CAD-4 diffractometer, using CuK_α (λ = 1.5418 Å) radiation monochromatized by reflection from a highly ordered graphite monochromator. The data crystal (ca. 0.1 × 0.1 × 0.2 mm), which was clear, yellow, and air stable, was coated with epoxy resin. Data were collected at 18°C by $\theta-2\theta$ scans to 2θ (CuK_α) = 154° ($\sin\theta/\lambda$ = 0.63). Peak backgrounds were measured as one-tenth of the total scan width on each side. Normal scans which did not result in sufficiently high precision on net intensity measurements were repeated at a slower scan speed. The take-off angle was 3.2° and the diffracted beam was automatically corrected for coincidence losses. Two complete independent sets of data were collected, yielding 1685 reflections. The intensities of three monitor reflections were measured periodically and showed no significant variation over the course of data collection. No correction for absorption was made. The data were averaged to yield 823 unique reflections.

Solutions and refinement of the structure

From space group consideration the molecule appeared to contain a center of inversion and thus to be disordered. The structure was solved by direct methods using MULTAN (12), which revealed all six nonhydrogen atoms of the asymmetric unit.

All six atoms located by direct methods were initially refined as carbon atoms by differential synthesis refinement,[3] and the hydrogen atoms were located as the first four peaks in a difference Fourier synthesis. The first two peaks corresponded to the ordered hydrogens and the next two peaks to the disordered hydrogens. The location of four independent hydrogen atoms confirmed a disordered structure with nitrogen and carbon atoms randomly occupying the same position. Atomic scattering factors were taken from a standard source (13), while that for hydrogen was the best spherically averaged value of Stewart *et al.* (14). The accommodate the disorder, N(1) and C(4) were refined using an atomic scattering factor based on an average of those for nitrogen and carbon. The hydrogens involved in the disorder, H(4) and H(5), were given an occupancy factor of 0.50. In the full-matrix least-squares calculations the function minimized was $\Sigma w\Delta^2$, where $\Delta = |F_o - F_c|$ with weights $w = 4F_o^2/\sigma^2(F_o^2)$ and $\sigma^2(F_o^2) = \sigma^2_{count}(I) + (0.02F^2)^2$. Using a three-sigma rejection, 614 reflections were included in the refinement of 67 parameters. In the final refinement all nonhydrogen atoms were allowed to vary anisotropically and hydrogen atoms were assigned an isotropic thermal parameter of 5.5 Å^2. The error in an observation of unit weight was 2.77. The maximum density in a final difference Fourier was 0.26 e Å^{-3}, which was 3.2% of the largest peak in a final observed Fourier. The data collection and processing parameters are summarized in Table 1. Positional and thermal parameters are listed in Table 2. Bond lengths and bond angles are given in Tables 3 and 4, respectively. The list of structure factors has been placed in the Depository of Unpublished Data.[4]

TABLE 3. Interatomic distances with estimated standard deviation in parentheses[a]

Bond	Length (Å)
N(1)—C(2)	1.404(3)
N(1)—C(8b)	1.311(2)
C(2)—C(3)	1.368(3)
C(3)—C(4)	1.386(3)
C(4)—C(4a)	1.331(2)
C(4a)—C(8b)	1.417(2)
C(4a)—C(4b)	1.518(3)
C(2)—H(2)	0.98 (3)
C(3)—H(3)	1.02 (3)
C(4)—H(4)	1.02 (5)
C(5)—H(5)	0.98 (5)

[a]Due to the disorder and the inversion center contained in the molecule the following atoms are related: N(1) = C(5), C(2) = C(6), C(3) = C(7), C(4) = N(8), C(4a) = C(8a), C(8b) = C(4b), and the corresponding hydrogens.

Results and discussion

The structure of 1,8-dizabiphenylene is shown in Fig. 1 together with atom labelling. The molecule is planar with a maximum deviation from planarity of 0.09(5) Å for a hydrogen atom and 0.006(2) Å for any other atom. A drawing of the packing in the unit cell is presented in Fig. 2. The distance between planes is 3.52 Å; the shortest intermolecular contacts are C(4)···H(5) of 2.593 Å and H(3)···H(5) of 2.425 Å.

A significant feature of **5** is the CNC bond angle of 112.9(2)°; the value is an average for (C8b)—N(1)—C(2) and C(3)—C(4)—C(4a), resulting from the inversion center and the disorder. This value compares favorably with that of the

[3]DIFSYN, a differential synthesis crystal structure refinement program. R. R. McMullan. 1979. Unpublished.

[4]Available, at a nominal charge, from the Depository of Unpublished Data, CISTI, National Research Council, Ottawa, Ont., Canada K1A 0S2.

Can. J. Chem. Downloaded from www.nrcresearchpress.com by 210.87.254.5 on 09/06/12
For personal use only.

TABLE 4. Bond angles with estimated standard deviations in parentheses[a]

Bond	Angle (°)
C(8b)—N(1)—C(2)	112.9(2)
N(1)—C(2)—C(3)	122.9(2)
N(1)—C(2)—H(2)	116.1(14)
C(3)—C(2)—H(2)	120.9(14)
C(2)—C(3)—C(4)	123.4(2)
C(2)—C(3)—H(3)	118.5(14)
C(4)—C(3)—H(3)	118.0(14)
C(3)—C(4)—C(4a)	112.9(2)
C(3)—C(4)—H(4)	117.4(29)
C(4a)—C(4)—H(4)	129.5(30)
C(4)—C(4a)—C(8b)	123.7(2)
C(4)—C(4a)—C(4b)	146.0(2)
C(8b)—C(4a)—C(4b)	90.4(2)
C(4a)—C(8b)—N(1)	124.2(2)
N(1)—C(8b)—C(8a)	146.1(2)
C(4a)—C(8b)—C(8a)	89.6(2)
C(4b)—C(5)—H(5)	132.6(31)
C(6)—C(5)—H(5)	114.5(31)

[a]Due to disorder and the inversion centers contained in the molecule the following atoms are related: N(1) = C(5), C(2) = C(6), C(3) = C(7), C(4) = N(8), C(4a) = C(8a), C(8b) = C(4b), and the corresponding hydrogens.

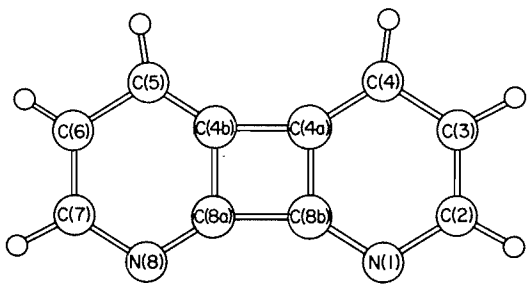

FIG. 1. Molecular structure of **5** with atom labelling.

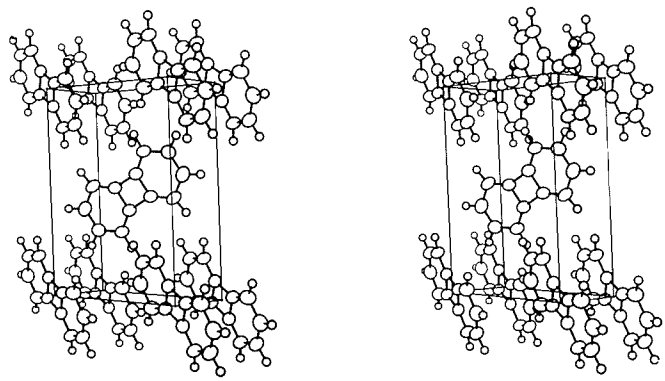

FIG. 2. The unit cell. Due to disorder, hydrogens occur with 50% occupancy at N(1) or C(5) and at N(8) or C(4) and are included to illustrate all possible modes of packing.

comparable angle in **4**, whose structure was determined recently (10) as a result of prior molecular orbital calculations which predicted a CNC angle of 112.1° (15). The observed angle was 112.5°, considerably smaller than the 117.3° reported for the corresponding angle in **2** (3*b*). Thus the present work on **5** represents only the second system in which an abnormally acute CNC angle adjacent to a fused strained ring has been confirmed.

Earlier papers in this series (16), as well as work by others (17), established that the fusion of a strained, four-membered ring across the [*b*] face of an aza-aromatic system causes a reduction in basicity. Compound **5**, with a pK_a of 1.92, affords a dramatic example of this effect (18); for comparison 2,2′-bipyridine has a pK_a of 4.33 (19).

Acknowledgements

We thank Mr. Max Muir for preparative assistance. Research at Brookhaven National Laboratory was performed under contract with the U.S. Department of Energy and was supported by its Office of Basic Energy Sciences. J.H.M. thanks the Department of Chemistry, Duke University, for its hospitality during a leave in 1983–1984.

1. (*a*) T. C. W. MAK and J. TROTTER. J. Chem. Soc. 1 (1962); (*b*) J. K. FAWCETT and J. TROTTER. Acta Crystallogr. **20**, 87 (1966).
2. A. YOKOZEKI, C. F. WILCOX, JR., and S. H. BAUER. J. Am. Chem. Soc. **96**, 1026 (1974).
3. (*a*) T. C. W. MAK and J. TROTTER. Acta Crystallogr. **17**, 610 (1964); (*b*) J. L. CRAWFORD and R. E. MARSH. Acta Crystallogr. Sect. B, **29**, 1238 (1973).
4. J. D. KORP, R. P. THUMMEL, and I. BERNAL. Tetrahedron, **33**, 3069 (1977).
5. (*a*) R. P. THUMMEL and W. NUTAKUL. J. Am. Chem. Soc. **100**, 6171 (1978); (*b*) J. D. KORP and I. BERNAL. J. Am. Chem. Soc. **101**, 4273 (1979).
6. (*a*) H. HART, M. JEFFARES, A. TEUERSTEIN, and D. L. WARD. J. Am. Chem. Soc. **100**, 8012 (1978); (*b*) D. L. WARD. Acta Crystallogr. Sect. B, **36**, 963 (1980).
7. H. HART, A. TEUERSTEIN, M. JEFFARES, W.-J. H. KUNG, and D. L. WARD. J. Org. Chem. **45**, 3731 (1980).
8. N. P. HACKER, J. F. W. MCOMIE, J. MEUNIER-PIRET, and M. VAN MEERSSCHE. J. Chem. Soc. Perkin Trans. 1, 19 (1982).
9. S. KANOKTANAPORN, J. A. H. MACBRIDE, and T. J. KING. J. Chem. Res. (M) 2911 (1980).
10. B. R. DEROSKI, J. H. MARKGRAF, and J. S. RICCI, JR. J. Heterocycl. Chem. **20**, 1155 (1983).
11. J. W. BARTON and R. B. WALKER. Tetrahedron Lett. 569 (1975).
12. G. GERMAIN, P. MAIN, and M. M. WOOLFSON. Acta Crystallogr. Sect. B, **26**, 274 (1970).
13. International tables for X-ray crystallography. Vol. 3. Kynoch Press, Birmingham. 1962. Table 3.3.1 A.
14. R. F. STEWART, E. R. DAVIDSON, and W. T. SIMPSON. J. Chem. Phys. **42**, 3175 (1965).
15. W. R. MOOMAW, D. A. KLEIER, J. H. MARKGRAF, J. W. THOMAN, JR., and J. N. A. RIDYARD. Manuscript in preparation.
16. (*a*) J. H. MARKGRAF and W. L. SCOTT. J. Chem. Soc. Chem. Commun. 296 (1967); (*b*) J. H. MARKGRAF and R. J. KATT. Tetrahedron Lett. 6067 (1968); (*c*) J. H. MARKGRAF and R. J. KATT. J. Org. Chem. **37**, 717 (1972).
17. (*a*) R. P. THUMMEL and D. K. KOHLI. J. Org. Chem. **43**, 4882 (1978); (*b*) R. P. THUMMEL and D. K. KOHLI. Tetrahedron Lett. 143 (1979).
18. R. HULL, J. A. H. MACBRIDE, and P. M. WRIGHT. Manuscript in preparation.
19. W. A. E. MCBRYDE. Can. J. Chem. **45**, 2093 (1967).

Can. J. Chem. Downloaded from www.nrcresearchpress.com by 210.87.254.5 on 09/06/12
For personal use only.

Vibrational spectra of substituted toluenes — 4-amino-3-bromotoluene and 5-amino-2-bromotoluene

N. SYAM SUNDAR[1]

Molecular Spectroscopy Laboratories, Department of Physics, Andhra University, Visakhapatnam 530 003, India

Received October 12, 1983[2]

N. SYAM SUNDAR. Can. J. Chem. **62**, 2238 (1984).

The infrared absorption and laser Raman spectra of 4-amino-3-bromotoluene and 5-amino-2-bromotoluene have been recorded. The vibrational analysis is presented assuming C_s symmetry for the molecules.

N. SYAM SUNDAR. Can. J. Chem. **62**, 2238 (1984).

On a enregistré les spectres d'absorbtion infrarouge et laser Raman de l'amino-4 bromo-3 toluène et de l'amino-5 bromo-2 toluène. On présente une analyse vibrationelle en faisant l'hypothèse que la symétrie des molécules C_s.

[Traduit par le journal]

Can. J. Chem. Downloaded from www.nrcresearchpress.com by 210.87.254.6 on 09/06/12
For personal use only.

Introduction

The vibrational spectra of toluene, aniline, and bromobenzene were extensively studied and analysed (1–3). Similar spectral investigations on isomers of toluidine, bromotoluene, and bromoaniline were reported by earlier workers (1, 4–7). The vibrational spectra of certain isomers of aminofluorotoluene (8, 9) and aminochlorotoluene (10) were already reported while those of aminobromotoluene were, so far, not reported and analysed. The present paper deals with the recording and analysis of the infrared absorption and laser Raman spectra of 4-amino-3-bromotoluene and 5-amino-2-bromotoluene.

Experimental

4-Amino-3-bromotoluene (2-bromo-4-methylbenzenamine) and 5-amino-2-bromotoluene (4-bromo-3-methylbenzenamine), hereafter referred to as molecules **A** and **B** respectively, were obtained from M/s. Fluka A. G., Switzerland. Both **A** and **B** are "purum" grade, the purity of **A** being greater than 98% and that of **B** greater than 99%. **A** is in liquid form and **B** is in solid form at room temperature. The infrared absorption spectra were recorded in the region 400–4000 cm^{-1} on a Zeiss UR-10 spectrophotometer using a 0.029 mm path length cell with KBr windows for **A**, and KBr pellet technique for **B**. The infrared spectrum of **B** was also obtained as a dilute solution in CCl_4 in the regions 800–1800 cm^{-1} and 2800–3600 cm^{-1}. The infrared spectrophotometer was calibrated using a thin film of polystyrene. The absorption spectrum of **B** in the far-infrared region was recorded on a Polytec FIR30 Fourier far-infrared spectrophotometer using polyethylene pellet technique. The laser Raman spectra of **A** (liquid form) and **B** (powder form) were obtained on Jobin Yvon Ramanor HG 2S and Cary 82 spectrophotometers, respectively. The polarization characteristics could be studied for some of the Raman lines of **A**. The infrared frequencies are accurate within ±2 cm^{-1} in the region 100–700 cm^{-1} and ±4 cm^{-1} in the region 700–4000 cm^{-1}. The Raman shifts are accurate within ±4 cm^{-1}. The traces of the spectra recorded are shown in Figs. 1–6.

Results and discussion

Assuming the substituents as single mass points, both **A** and **B** may be considered to belong to the C_s point group. Each of these molecules has 17 atoms and is expected to give rise to 45 vibrations — 30, characteristic of the phenyl ring and 15, characteristic of the substituent groups. These 45 vibrations, in C_s point group, are classified among the symmetry species as $31a' + 14a''$ and all are allowed both in the infrared and Raman spectra.

The vibrational spectra could be analysed in terms of the fundamental characteristic of the molecules, overtones, and combinations on the basis of Varsanyi's (1, 11) classification of the benzene derivatives, the frequency ranges suggested by him for each mode of vibration, and a comparison with the vibrational spectra of related molecules. **A** and **B** come under "1,4-dilight-2-heavy" and "1-heavy-2,4-dilight" classes, respectively (1). The frequencies obtained from the infrared and Raman spectra together with their visual intensities and probable assignments are shown in Table 1.

C—H and C—X (X = substituent) stretching vibrations

Benzene modes 2, 20*a*, 20*b* remain as C—H stretching modes while modes 7*a*, 7*b*, 13 transform into C—X stretching modes in both molecules studied.

The aromatic C—H stretching frequencies generally lie in the region 3000–3100 cm^{-1} and this is also the case in the present study.

The C—CH_3 stretching mode in a number of methylbenzenes was observed at around 1200 cm^{-1} (1, 4, 8–10, 12). The frequencies 1187 cm^{-1} (1185 cm^{-1})[3] in **A** and 1186 cm^{-1} in **B** are identified as due to C—CH_3 stretching vibrations and are attributed to mode 13. Primary aromatic amines absorb strongly in the region 1250–1340 cm^{-1}, due to stretching of the phenyl carbon–nitrogen bond (13). The medium intense absorption at 1270 cm^{-1} (1266 cm^{-1}) in **A** is taken to represent the C—NH_2 stretching mode in conformity with a similar vibration reported at 1278 cm^{-1} in aniline (1), 1265 cm^{-1}, 1265 cm^{-1}, 1273 cm^{-1} in bromoanilines (7), 1275 cm^{-1}, 1260 cm^{-1}, 1289 cm^{-1} in dibromoanilines (14), 1273 cm^{-1} in *p*-toluidine (4) and also in a number of other substituted anilines (1). In **B**, where the two "light" substituents NH_2 and CH_3 are vibrating out-of-phase in the *meta* position, the C—X stretching vibration, mode 7*b*, corresponding to one of the substituents will be observed below 1000 cm^{-1} (1, 11). The absorption at 950 cm^{-1} (940 cm^{-1}) in this molecule is assigned to C—NH_2 stretching vibration corresponding to mode 7*b*.

The C—X stretching vibration, mode 7*a*, of the "heavy" substituent lies in the low frequency region 200–480 cm^{-1}. The frequencies (345 cm^{-1}) in **A** and 320 cm^{-1} (328 cm^{-1}) in **B** are associated with the C—Br stretching mode by way of

[1]On leave from: Physics Department, Mrs. A.V.N. College, Visakhapatnam 530 001, India.

[2]Revision received April 12, 1984.

[3]Frequencies shown in parentheses are those obtained from Raman data.

Can. J. Chem. Downloaded from www.nrcresearchpress.com by 210.87.254.6 on 09/06/12
For personal use only.

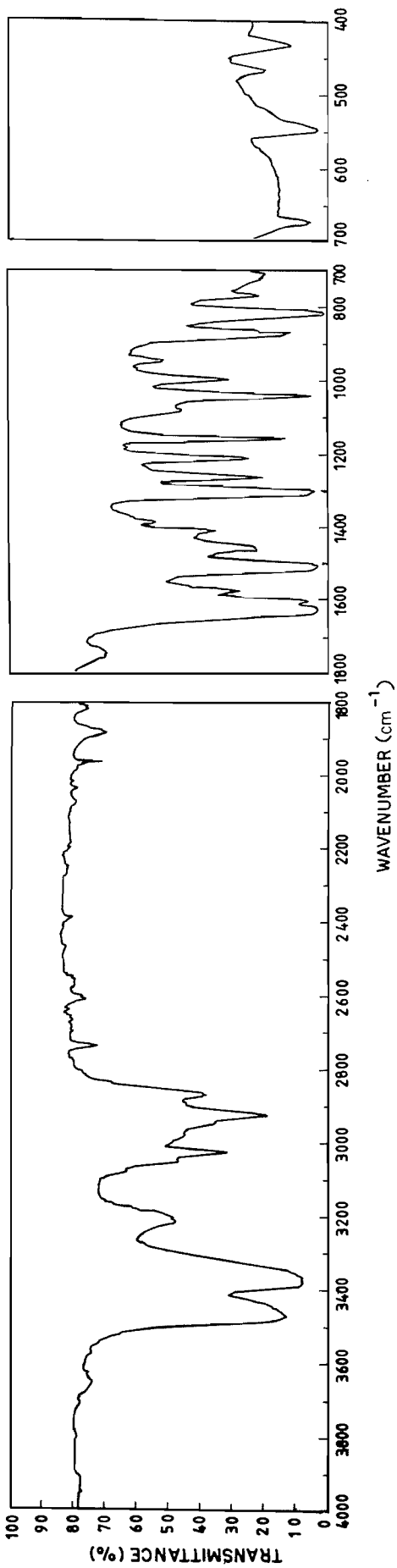

FIG. 1. Infrared absorption spectrum of 4-amino-3-bromotoluene (liquid).

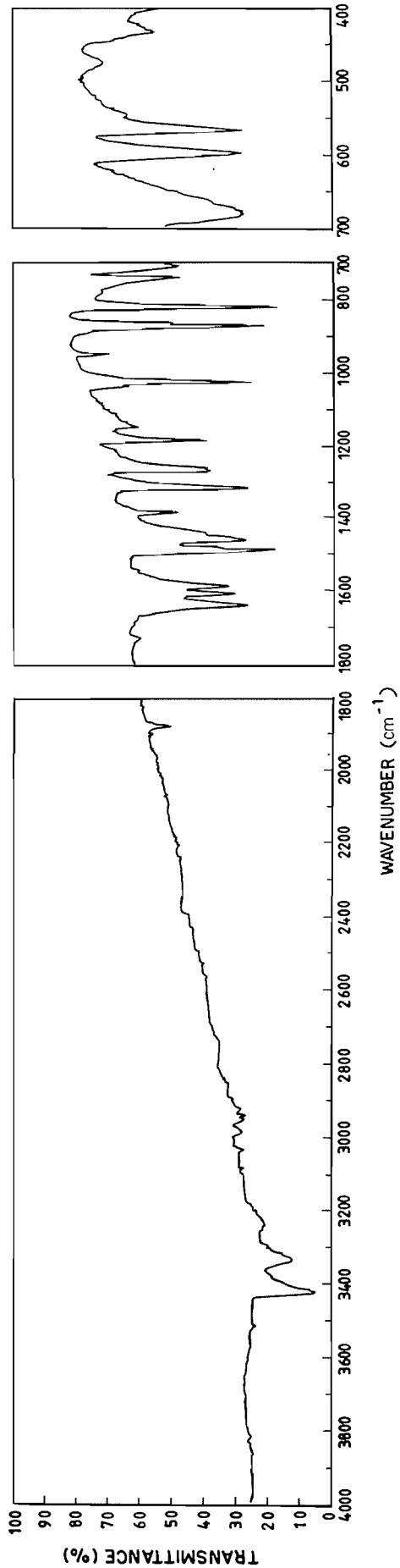

FIG. 2. Infrared absorption spectrum of 5-amino-2-bromotoluene (in KBr).

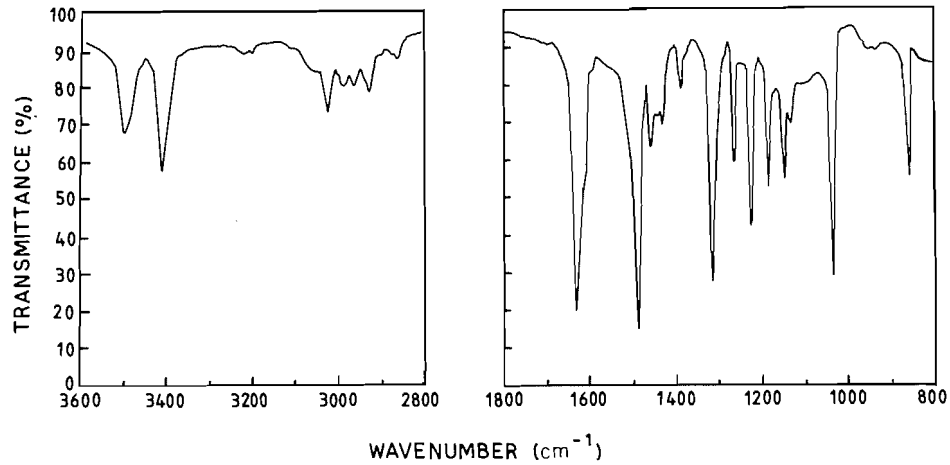

FIG. 3. Infrared absorption spectrum of 5-amino-2-bromotoluene (in CCl_4).

comparison with the C—Br stretching frequencies reported in a number of bromobenzenes (1).

C—C stretching vibrations

The degeneracy of the C—C stretching modes 8*a*, 8*b*, and 19*a*, 19*b* of benzene is removed on reduction of symmetry. In the present class of molecules modes 8*a*, 8*b* are observable in the region 1555−1635 cm^{-1} while modes 19*a*, 19*b* lie in the region 1380−1515 cm^{-1}. Mode 8*b* appears at a higher frequency than mode 8*a* while mode 19*b* is found at a higher magnitude than mode 19*a*. The non-degenerate mode 14, the Kekule vibration, lies in the region 1220−1270 cm^{-1}. The asymmetric and symmetric deformation vibrations of the methyl group also give rise to absorptions in the vicinity of the C—C stretching modes 19*a*, 19*b*. The scissoring mode of the amino group appears in the neighbourhood of modes 8*a* and 8*b*. Assignments for all these vibrations are shown in Table 1.

The totally symmetric ring breathing vibration, mode 1, is very sensitive to substitution. In **A** this mode strongly couples with the C—X stretching vibration of a "light" substituent, resulting in a decrease in frequency when compared to benzene, the suggested frequency range being 600−700 cm^{-1} (1). However, in **B** mode 1 weakly couples with the C—X stretching mode of the "heavy" substituent; as a consequence of which the frequency is slightly increased when compared to benzene, the expected frequency interval being 1020−1060 cm^{-1} (1). The medium intense band at 674 cm^{-1} (680 cm^{-1}, polarized) in **A** and the strong band at 1026 cm^{-1} in **B** are attributed to the ring breathing mode and are in good agreement with those reported in similar class of molecules (1).

C—H and C—X (X = substituent) in-plane bending vibrations

The normal modes 3, 18*a*, 18*b* remain as C—H in-plane bending modes whereas modes 9*a*, 9*b*, 15 represent C—X in-plane bending vibrations in both molecules in the present study.

The non-degenerate C—H in-plane bending vibration, mode 3, appears generally as a weak band in the region 1270−1310 cm^{-1} in the present class of molecules (1). However, in *o*- and *m*-bromoanilines, this mode was identified with strong bands at 1316 cm^{-1}, 1320 cm^{-1} based on normal co-ordinate analysis (7). The absorption bands at 1304 cm^{-1} (1305 cm^{-1}) in **A** and 1315 cm^{-1} (1324 cm^{-1}) in **B** are assigned to the C—H in-plane bending mode 3. The degenerate C—H in-plane bending modes 18*a*, 18*b* are observable in the region 1045−1170 cm^{-1}, the former being at a higher frequency than the latter. The

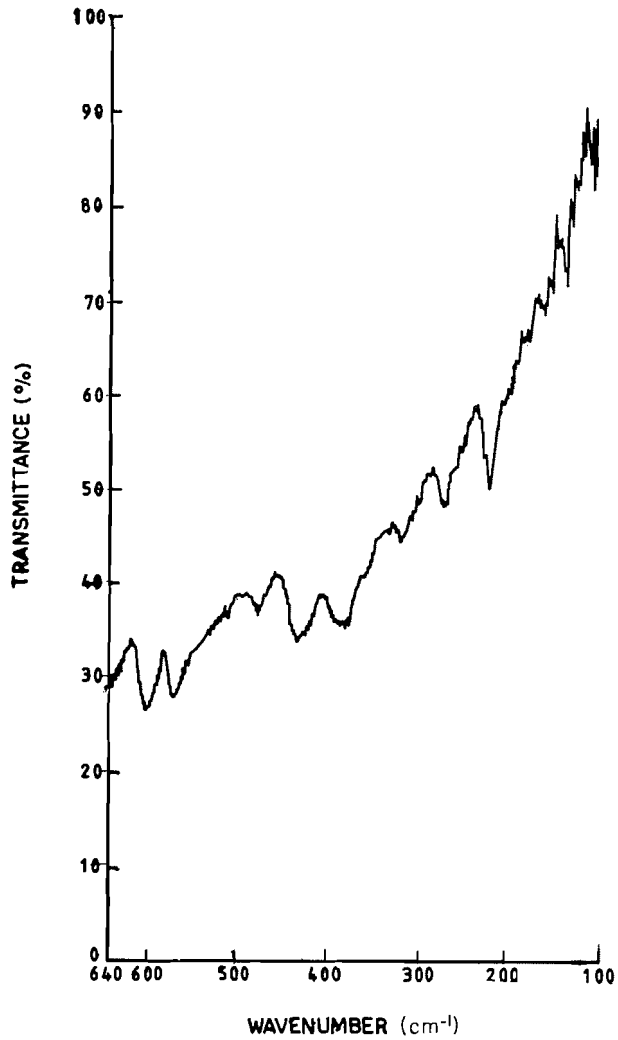

FIG. 4. Far-infrared spectrum of 5-amino-2-bromotoluene.

mode 18*a* could be identified in both molecules **A** and **B** whereas mode 18*b* is observed only in molecule **B**.

The C—X in-plane bending modes lie in the low frequency region below 440 cm^{-1}. The assignments made for these vibrations in the present study are shown in Table 1 and are in agreement with those reported in a number of related molecules (1, 4, 12, 15−19).

Can. J. Chem. Downloaded from www.nrcresearchpress.com by 210.87.254.6 on 09/06/12
For personal use only.

C—H and C—X (X = substituent) out-of-plane bending vibrations

The benzene modes 5, 11, 17*b* remain as C—H out-of-plane bending modes while the modes 10*a*, 10*b*, 17*a* correspond to C—X out-of-plane bending vibrations in **A** and **B**.

The above C—H out-of-plane bending modes lie in the region 800–990 cm^{-1}, the umbrella vibration, mode 11, appearing as a strong band with least frequency, and mode 17*b* occurring at a higher value than mode 5. The frequency due to the umbrella vibration can be well correlated with the number of unsubstituted vicinal hydrogen atoms on the aromatic ring. The present molecules have two unsubstituted vicinal hydrogen atoms on the ring, in which case there will be a strong band at 817 ± 13 cm^{-1} due to the C—H out-of-plane bending mode (13). The strong bands at 817 cm^{-1} in **A** and 824 cm^{-1} in **B** are accordingly identified with the umbrella vibration. The other C—H out-of-plane bending modes 5, 17*b* could be identified in **A** whereas only mode 5 is observed in **B**.

The C—X out-of-plane bending vibrations lie in the low frequency region below 350 cm^{-1}. The Raman frequencies 203 cm^{-1} (depolarized), 155 cm^{-1} in **A** and 216 cm^{-1} (225 cm^{-1} in the infrared), 138 cm^{-1} in **B** are taken to represent the C—NH_2 and C—Br out-of-plane bending modes, respectively, and are in good agreement with those reported in related molecules (1, 9, 10, 16).

C—C—C in-plane bending vibrations

Modes 6*a*, 6*b*, 12 are the C—C—C in-plane bending modes.

In the present class of molecules, vibration 6*a* appears at a higher frequency than that of benzene due to its coupling with the C—X stretching mode of the "heavy" substituent whereas mode 6*b* lies in the region 350–550 cm^{-1} (1). The frequencies (880 cm^{-1}), 467 cm^{-1} (475 cm^{-1}, polarized) in **A** and 874 cm^{-1}, 476 cm^{-1} in **B** are associated with the vibrational modes 6*a* and 6*b*, respectively. In both **A** and **B**, the normal mode 12 will be observed at a lower value than that of benzene as a result of its coupling with the C—X stretching vibration of a "light" substituent (1). The frequencies 772 cm^{-1} (773 cm^{-1}, polarized) in **A** and 743 cm^{-1} (732 cm^{-1}) in **B** are attributed to vibration 12.

C—C—C out-of-plane bending vibrations

The C—C—C out-of-plane bending vibrations are represented by modes 4, 16*a*, 16*b*.

Vibration 4, the C—C—C puckering mode, which was observed at 707 cm^{-1} in benzene, is rather insensitive to substitution. The absorptions at 713 cm^{-1} and 709 cm^{-1} in **A** and **B**, respectively, are assigned to this mode. The frequency of the vibrational components 16 rises on substitution as a result of coupling with out-of-plane C—X vibrations of lower frequencies, and mode 16*a* occurs at a higher frequency than mode 16*b* (1). Further, in 1,2,4-trisubstituted benzene derivatives, a medium intense or strong band appears in the region 428–476 cm^{-1} due to an out-of-plane ring deformation (15). The absorption bands at 550 cm^{-1}, 435 cm^{-1} in **A** and 567 cm^{-1}, 434 cm^{-1} in **B** are identified with the vibrations 16*a* and 16*b*, respectively.

Internal vibrations of the substituent groups

(*a*) CH_3 group: The methyl group gives rise to nine characteristic vibrations — two asymmetric stretchings, one symmetric stretching, two asymmetric deformations, one symmetric deformation, two rocking modes, and one torsion mode.

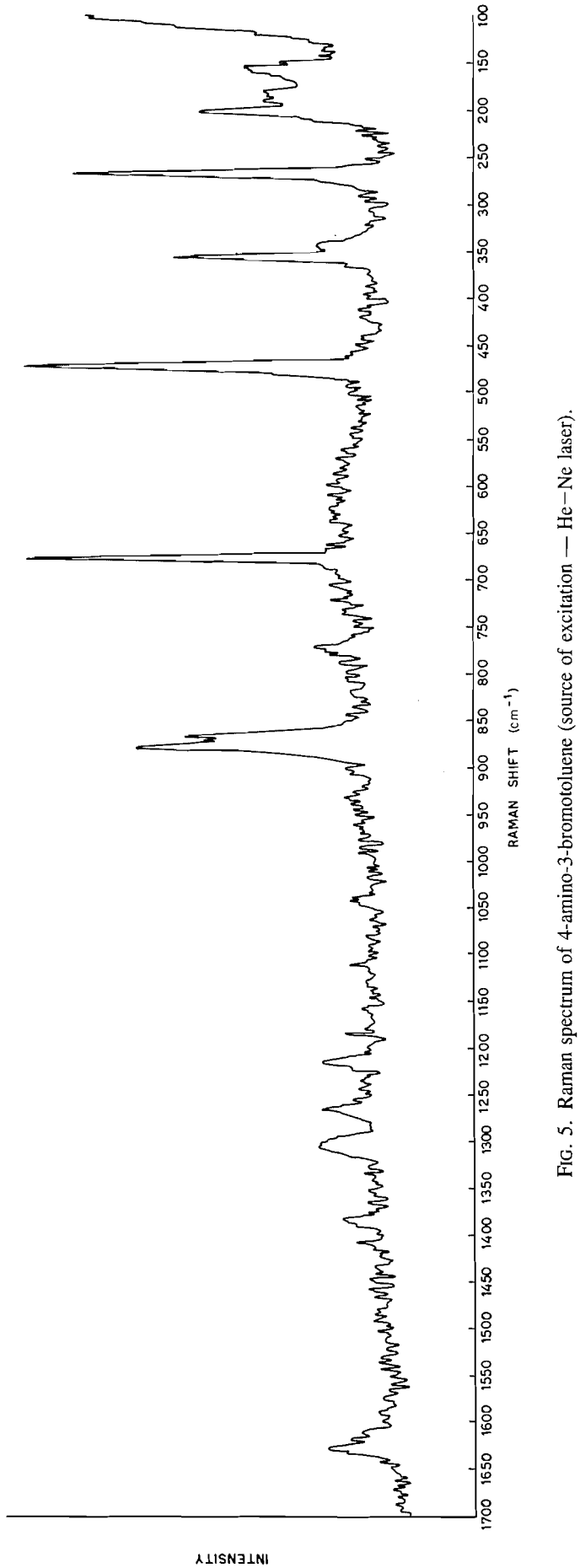

FIG. 5. Raman spectrum of 4-amino-3-bromotoluene (source of excitation — He–Ne laser).

Can. J. Chem. Downloaded from www.nrcresearchpress.com by 210.87.254.6 on 09/06/12
For personal use only.

TABLE 1. Vibrational frequencies and their probable assignments for 4-amino-3-bromotoluene and 5-amino-2-bromotoluene*

4-Amino-3-bromotoluene		5-Amino-2-bromotoluene			Probable assignments	
		Infrared (cm^{-1})				
Infrared (cm^{-1})	Raman (cm^{-1})	Solid	Solution	Raman (cm^{-1})	Mode No. (Wilson) notation)	Description
3652 vw	—	—	—	—	—	2926 + 713
3474 vs	—	3420 m	3496 m	—	—	Asymmetric stretching of NH_2
3378 vvs	—	3335 w	3409 m	—	—	Symmetric stretching of NH_2
3217 m	—	3235 vw	3213 vw, br	—	—	2 × scissoring of NH_2
3083 w	—	3083 vw	—	—	20*a*	C—H stretching
3052 m	—	3035 vw	—	—	2	C—H stretching
3026 m	—	—	3019 w	—	20*b*	C—H stretching
2978 m	—	2987 vw	2987 w	—	—	Asymmetric stretching of CH_3
2952 m	—	2952 vw	2961 w	—	—	Asymmetric stretching of CH_3
2926 s	—	2917 vw	2926 w	—	—	Symmetric stretching of CH_3
2870 m	—	—	2861 vw	—	—	2 × asymmetric deformation of CH_3
2739 vw	—	—	—	—	—	1579 + 1161
2611 vw	—	—	—	—	—	2 × 1304
2565 vw	—	—	—	—	—	1511 + 1046
2387 vw	—	—	—	—	—	1511 + 872
1963 vw	—	—	—	—	—	1411 + 550
1887 vw	—	—	—	—	—	1217 + 674
—	—	1879 vw	1872 vw	—	—	1315 + 567
1813 vw	—	—	—	—	—	1046 + 772 or 1000 + 817
1748 vw	—	—	—	—	—	2 × 872
—	—	1726 vw	—	—	—	1026 + 709
1630 vs	1628 m	1635 m	1626 vs	1646 vw	—	Scissoring of NH_2
1607 s	—	1604 m	—	1590 vw	8*b*	C—C stretching
1579 m	—	1587 m	—	1570 vw	8*a*	C—C stretching
1511 s	—	1487 m	1487 vs	—	19*b*	C—C stretching
1461 m	—	1459 m	1461 m	—	—	Asymmetric deformation of CH_3
—	—	1443 sh	1443 w	—	—	Asymmetric deformation of CH_3
1411 m	1408 vw	—	1437 w	—	19*a*	C—C stretching
1387 vw	1383 w	1383 w	1383 w	—	—	Symmetric deformation of CH_3
1304 vs	1305 m	1315 m	1313 vs	1324 vw	3	C—H in-plane bending
1270 m	1266 m	950 w	—	940 vw	7*b*	C—NH_2 stretching
1217 m	1215 m	1270 m	1265 m	—	14	C—C stretching
—	—	1261 sh	—	—	—	824 + 434
—	—	1213 vw	1222 m	—	—	743 + 476
1187 vw	1185 w	1186 m	1187 m	—	13	C—CH_3 stretching
1161 s	—	1148 w	1148 m	—	18*a*	C—H in-plane bending
—	—	—	1133 w	—	18*b*	C—H in-plane bending
1084 w	—	—	1089 vw	—	—	Rocking of NH_2
1046 s	1045 vw	1039 sh	1035 vs	—	—	Rocking of CH_3
—	1040 vw	—	—	—	—	680 + 358
1000 m	—	—	—	—	—	Rocking of CH_3
948 w	—	—	—	—	17*b*	C—H out-of-plane bending
—	880 s	874 s	—	—	6*a*	C—C—C in-plane bending
—	873 m	—	—	—	—	680 + 203
872 m	870 s	865 sh	860 m	—	5	C—H out-of-plane bending
817 s	—	824 vs	—	—	11	C—H out-of-plane bending
—	—	783 vw	—	—	—	567 + 225
772 w	773 w, p	743 m	—	732 w	12	C—C—C in-plane bending
713 w	—	709 w	—	—	4	C—C—C out-of-plane bending
674 m	680 vs, p	1026 s	—	—	1	Ring breathing
~629 w, d	—	680 m, br	—	—	—	Wagging of NH_2
—	—	599 m †600 vw	—	—	—	380 + 225
550 m	—	567 m †570 vw	—	—	16*a*	C—C—C out-of-plane bending
—	—	548 w	—	544 w	—	2 × 275
467 vw	475 vs, p	476 vw †477 vw	—	—	6*b*	C—C—C in-plane bending
435 w	—	434 w †435 vw	—	—	16*b*	C—C—C out-of-plane bending

Can. J. Chem. Downloaded from www.nrcresearchpress.com by 210.87.254.6 on 09/06/12
For personal use only.

TABLE 1. (*Concluded*)

4-Amino-3-bromotoluene		5-Amino-2-bromotoluene			Probable assignments	
		Infrared (cm^{-1})				
Infrared (cm^{-1})	Raman (cm^{-1})	Solid	Solution	Raman (cm^{-1})	Mode No. (Wilson) notation)	Description
—	365 sh	†380 vw, br	—	—	9*b*	C—NH_2 in-plane bending
—	358 s, p	—	—	—	9*a*	C—CH_3 in-plane bending
—	345 sh	†320 vw	—	328 w	7*a*	C—Br stretching
—	270 vs, p	†275 vw	—	270 w	15	C—Br in-plane bending
—	203 s, dp	†225 w	—	216 w	10*b*	C—NH_2 out-of-plane bending
—	155 m	—	—	138 w	17*a*	C—Br out-of-plane bending
—	—	—	—	84 s	—	Lattice
—	—	—	—	52 s	—	Lattice
—	—	—	—	40 vs	—	Lattice
—	—	—	—	34 s	—	Lattice
—	—	—	—	24 m	—	Lattice

*v, very; s, strong; m, medium; w, weak; sh, shoulder; br, broad; d, diffuse; p, polarized; dp, depolarized.
†Bands observed in the far-infrared spectrum.

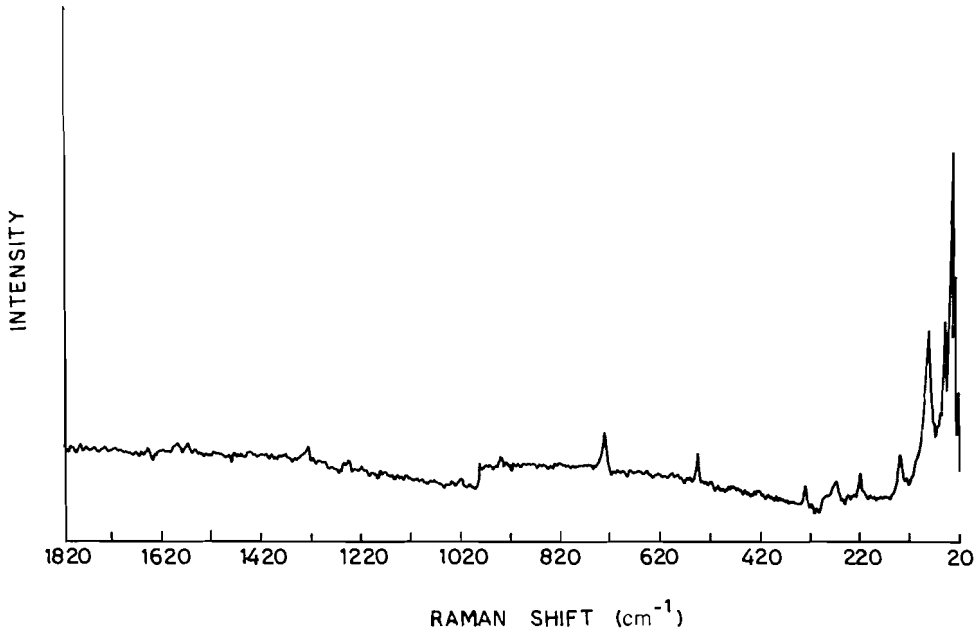

FIG. 6. Raman spectrum of 5-amino-2-bromotoluene (source of excitation — argon-ion laser).

The assignments made for these vibrations in these molecules are in very good agreement with those reported in a number of methylbenzenes (1, 6). The torsion mode could not be identified in either **A** or **B**.

(*b*) NH_2 group: The amino group gives rise to six characteristic vibrations — asymmetric and symmetric stretchings, scissoring, rocking, wagging, and twisting modes. Primary aromatic amines show absorptions in the region 3250–3550 cm^{-1} due to the asymmetric and symmetric stretching modes, the former mode being always at a higher frequency (20). The absorptions at 3474 cm^{-1}, 3378 cm^{-1} in **A** and 3420 cm^{-1}, 3335 cm^{-1} in **B** are associated with the asymmetric and symmetric stretching modes, respectively. The bands at 3217 cm^{-1} in **A** and 3235 cm^{-1} in **B** may involve a considerable contribution from an overtone of the scissoring mode intensified by Fermi resonance due to their proximity to the stretching fundamentals. A large frequency shift to a higher magnitude is observed in the NH_2 stretching frequencies of **B** in solution phase, indicating the likelihood of an association in the molecule through hydrogen bonds. The scissoring mode of the amino group in general lies in the region 1610–1640 cm^{-1} (1) where the C—C stretching modes 8*a* and 8*b* also give rise to absorptions. However, in almost all aniline derivatives, the scissoring mode is found at a higher frequency than the C—C stretching modes 8*a* or 8*b* (1). Further, Kumpawat *et al.* (7) calculated the HNH bending mode of the NH_2 group in isomers of chloroaniline, bromoaniline, and anisidine. They obtained a value of 1629 cm^{-1} for the *para* and *meta* isomers, and 1628 cm^{-1} for the *ortho* isomers. The frequencies 1630 cm^{-1} (1628 cm^{-1}) in molecule **A** and 1635 cm^{-1} (1646 cm^{-1}) in molecule **B** are attributed to the scissoring vibration of the amino group. This assignment is in excellent agreement with those reported in isomers of fluoromethylaniline (9) and chloromethylaniline (10). The assignments for the rocking and wagging modes in

Can. J. Chem. Downloaded from www.nrcresearchpress.com by 210.87.254.6 on 09/06/12
For personal use only.

the present study are shown in Table 1 and are in good comparison with those reported in a number of anilines (1). The twisting mode could not be identified in either **A** or **B**.

Acknowledgements

The author thanks to Drs. J. Ramakrishna and A. Selvarajan of Indian Institute of Science, Bangalore, and the Heads of the Regional Sophisticated Instrumentation Centres, Madras and Bombay, for extending facilities to record the various spectra. Financial assistance from the University Grants Commission, New Delhi, is gratefully acknowledged. The author is much indebted to his research director Professor (Mrs.) C. Santhamma for her valuable guidance.

1. G. VARSANYI. Assignments for vibrational spectra of seven hundred benzene derivatives. Vols. 1 and 2. Adam Hilger, England. 1974.
2. N. FUSON, C. GARRIGOU-LAGRANGE, and M. L. JOSIEN. Spectrochim. Acta, **16**, 106 (1960).
3. J. C. EVANS. Spectrochim. Acta, **16**, 428 (1960).
4. N. ABASBEGOVIC, L. COLOMBO, and P. BLECKMANN. J. Raman Spectrosc. **6**, 92 (1977).
5. A. K. ANSARI and P. K. VERMA. Indian J. Pure Appl. Phys. **16**, 454 (1978).
6. J. H. S. GREEN. Spectrochim. Acta, **26**A, 1503 (1970); **26**A, 1523 (1970); **26**A, 1913 (1970).
7. M. P. KUMPAWAT, A. OJHA, and N. D. PATEL. Can. J. Spectrosc. **25**, 1 (1980).
8. S. J. SINGH and S. M. PANDEY. Indian J. Pure Appl. Phys. **12**, 300 (1974).
9. S. N. SHARMA and C. P. D. DWIVEDI. Indian J. Pure Appl. Phys. **13**, 570 (1975).
10. S. N. SHARMA and C. P. D. DWIVEDI. Indian J. Phys. **50**, 25 (1976).
11. G. VARSANYI. Vibrational spectra of benzene derivatives. Academic Press, New York. 1969.
12. R. B. SINGH. Ph.D. Thesis. Bhagalpur University, India. 1980.
13. L. J. BELLAMY. The infra-red spectra of complex molecules. Chapmann and Hall, London. 1975.
14. V. N. VERMA, K. P. R. NAIR, and D. K. RAI. J. Indian Chem. Soc. **47**, 1169 (1970).
15. F. F. BENTLEY, L. D. SMITHSON, and A. L. ROZEK. Infrared spectra and characteristic frequencies ~700–300 cm^{-1}. Interscience Publishers, New York. 1968.
16. R. K. GOEL and S. K. GUPTA. Indian J. Pure Appl. Phys. **18**, 223 (1980).
17. NITISH K. SANYAL and R. K. GOEL. Indian J. Pure Appl. Phys. **18**, 299 (1980).
18. L. N. TRIPATHI. Indian J. Pure Appl. Phys. **8**, 730 (1970).
19. S. R. TRIPATHI and G. N. R. TRIPATHI. Indian J. Pure Appl. Phys. **18**, 143 (1980).
20. N. B. COLTHUP, L. H. DALY, and S. E. WIBERLY. Introduction to infrared and Raman spectroscopy. Academic Press, New York. 1964.

Can. J. Chem. Downloaded from www.nrcresearchpress.com by 210.87.254.6 on 09/06/12
For personal use only.

Solvent effect on the dissociation of *p*-nitroanilinium ion in glycerol–water media at 25°C

AMRITA LAL DE[1] AND TAPAS KUMAR DE
Department of Chemistry, Presidency College, Calcutta-700073, India

Received January 16, 1984

AMRITA LAL DE and TAPAS KUMAR DE. Can. J. Chem. **62**, 2245 (1984).

Thermodynamic dissociation constants ($_sK$) of *p*-nitroanilinium ion (BH^+) have been determined at 25°C in aqueous mixtures of 10, 30, 50, 70, and 90 wt.% of glycerol (GL) by spectrophotometric measurements. Standard free energies, ΔG_t^0(B), of *p*-nitroaniline (B) from water to mixed solvents have been evaluated from the measurement of solubilities at 25°C. $p(_sK)$ values decrease with increase in mol% of GL and pass through a minimum and then increase very slowly. The solvent effect on the dissociation, $\delta(\Delta G^0) = 2.303RT[p(_sK)_N - p(_wK)_N]$ has been discussed in terms of the standard free energies of transfer ΔG_t^0 from water to aqueous mixtures of GL of the uncharged base (B), the hydrochloride of the base (BHCl), hydrochloric acid (HCl), and also in terms of the individual species involved in the dissociation process. The solvent effect in trihydric alcohol – water (GL + H_2O) system has been compared with those in dihydric alcohol – water (ethylene glycol + water) and monohydric alcohol – water (ethanol + water) systems available from literature. The much less solvent effect in GL + H_2O has been primarily attributed to the contrasting nature of interaction of H^+ and of partially charged H atoms of $—NH_3^+$ group in BH^+ compared to those in other two solvent systems.

AMRITA LAL DE et TAPAS KUMAR DE. Can. J. Chem. **62**, 2245 (1984).

Opérant à 25°C, dans des mélanges aqueux contenant 10, 30, 50, 70 et 90% en poids de glycérol (GL), et faisant appel à des mesures spectroscopiques, on a déterminé les constantes de dissociation thermodynamique ($_sK$) de l'ion *p*-nitroanilinium (BH^+). En se basant sur des mesures de solubilité à 25°C, on a évalué les énergies libres standard, ΔG_t^0(B), pour le passage de la *p*-nitroaniline (B) de l'eau à des solvants mixtes. La valeur du $p(_sK)$ diminue lorsqu'on augmente la teneur en GL; elle passe par un minimum puis augmente très lentement. On discute de l'effet du solvant sur la dissociation: $\delta(\Delta G^0) = 2{,}303RT[p(_sK)_N - p(_wK)_N]$, en fonction des énergies libres standard de transfer ΔG_t^0 pour le transfert de la base neutre (B), de son chlorhydrate (BHCl) et de l'acide chlorhydrique (HCl) de l'eau vers des mélanges aqueux de GL; on en discute également en fonction des espèces individuelles impliquées dans le processus de dissociation. On a comparé le rôle de l'effet du solvant dans le système glycérol–eau à ceux qui avaient été antérieurement observés avec les systèmes éthylèneglycol–eau et éthanol–eau et qui ont été rapportés dans la littérature. On attribue le fait que l'effet de solvant soit moins prononcé pour le système GL–eau à la nature contrastante de l'interaction de l'ion H^+ et des atomes d'hydrogène partiellement chargés du groupe NH_3^+ de l'ion BH^+ par comparaison à ceux des deux autres systèmes de solvants.

[Traduit par le journal]

Introduction

Dissociation constants of *p*-nitroanilinium ion (BH^+) were reported earlier in aqueous mixtures of monohydric (1) and dihydric (2) alcohols. This paper reports a study of the dissociation constants of *p*-nitroanilinium ion in aqueous mixtures of glycerol, a trihydric alcohol. Since the solvent effect involves $\Delta G_t^0(H^+)$ (2–5), the standard free energy of transfer of H^+ from water to other solvents concerned, a quantity giving a measure of the basicity of the solvent relative to that of reference solvent, water (5), and since $\Delta G_t^0(H^+)$ has been found to be of contrasting nature (positive magnitude) in glycerol–water (GL + H_2O) (6, 7) system compared to other solvent systems (2, 8–10), it would be interesting to study proton transfer process in this particular solvent system. In order to see the contribution of the uncharged base (2, 3, 11), *p*-nitroaniline (B), ΔG_t^0(B) values have been determined from the measurement of solubilities of B in water as well as in GL + H_2O mixtures.

Experimental

Glycerol (GR Merck) and water were purified as described (12). Preparation of solvents as well as HCl solutions and purification of *p*-nitroaniline were similar to those described earlier (2). The dissociation constant $(_sK)_m$ of *p*-nitroanilinium ion (BH^+) on the molal scale in aqueous mixtures of glycerol was determined spectrophotometrically using unbuffered solutions of HCl at different concentrations in a manner essentially similar to that described earlier (2, 3, 13, 14). The $p(_sK)_m$ values were obtained by linear extrapolation of the plots of $p(_sK)'_m$ of eq. [1] against μ to $\mu = 0$

$$[1] \quad p(_sK)'_m = -\log m_{SH_2^+} - \log \frac{\alpha}{1-\alpha} = p(_sK)_m + \log \frac{\gamma_{SH_2^+}\gamma_B}{\gamma_{BH^+}} = p(_sK)_m + f(\mu)$$

where α and $1 - \alpha$ are the fractions of the indicator species present in the neutral form B and the ionic form BH^+, respectively, and $m_{SH_2^+}$ is the effective molality of H^+ in the solution. A series of solutions were prepared by adding weighed amounts of HCl solutions and the solvent to weighed amounts of the *p*-nitroaniline solutions. The spectral absorbances were determined at 25 ± 0.2°C with a UNICAM SP 500 model spectrophotometer (England) with 1 cm quartz cells at 380 nm where the absorbance shows a maximum for the base form (13). The limiting absorbances of the acidic form at 380 nm, though small, were taken into account, and the absorbance readings were corrected, where necessary, for the identical total concentration of the indicator (*p*-nitroaniline). The limiting absorbances (2, 13) of the acidic and basic forms of *p*-nitroaniline were measured in very concentrated HCl solutions (6 *M*) and in very dilute sodium hydroxide solutions (0.001 *M*). The values of $\alpha/(1-\alpha) = (D - D_1)/(D_2 - D)$ were obtained from the optical densities D_1, D_2, and D of the completely acid form (BH^+), completely base form (B), and the mixture of the two forms measured at an identical concentration of the indicator in the same cell. The molality of the *p*-nitroanilinium ion at equilibrium was negligibly small with respect to the molality of HCl, so that $-\log m_{SH_2^+}$ was virtually the same as that of $-\log m_{HCl}$ in most cases. The values of μ were taken to be equal to $m_{HCl}d_s$, where d_s is the density of the solvent (12).

The standard free energies of transfer of the uncharged base, *p*-

[1] To whom all correspondence should be addressed.

Can. J. Chem. Downloaded from www.nrcresearchpress.com by 210.87.254.5 on 09/06/12
For personal use only.

Can. J. Chem. Downloaded from www.nrcresearchpress.com by 210.87.254.5 on 09/06/12
For personal use only.

nitroaniline (B) from water to mixed-solvents were computed by the method described earlier (2, 3, 11, 15) using the relation $\Delta G_t^0(B) = RT \ln ({}_wX_B/{}_sX_B)$ where ${}_wX_B$ and ${}_sX_B$ are the solubilities of the base in water and respective solvents (SH) on the mole fraction scale. As for uncharged solutes such as benzoic acid (16), tris(hydroxymethyl)aminomethane (2, 11), and nitroanilines (2, 3) in different aquo-organic solvents, the validity of this relation depends on the assumption that the ratio of activity coefficients of the uncharged base in the saturated solutions in the mixed solvent and in water is unity. Solubilities of B were determined at 25°C by the same method described earlier (2).

Results

The values of $p({}_sK)'_m$ corresponding to different molalities of HCl are shown in Table 1. The $p({}_sK)_m$ values obtained in the different solvent mixtures are also recorded in Table 1. The uncertainties in the $p({}_sK)_m$ values are of the order of ±0.005 unit. The solubilities of B and the $\Delta G_t^0(B)$ values at 25°C are recorded in Table 2. The maximum uncertainties in the $\Delta G_t^0(B)$ values are ±0.04 kJ mol^{-1}.

Discussion

For the sake of comparison (17) of the results in different solvent mixtures, the $p({}_sK)_m$ values have been converted into the mole fraction scale, $p({}_sK)_N$, by the usual relation (18) and are recorded in Table 1. In order to have a better understanding of the solvent effect, the changes of standard free energy accompanying the ionization of the acid BH^+ in any solvent, ${}_s\Delta G^0$, relative to that in pure water, ${}_w\Delta G^0$, have been computed at 25°C on the mole fraction scale using eq. [2].

$$[2] \quad \text{Solvent effect} = \delta(\Delta G^0) = {}_s\Delta G^0 - {}_w\Delta G^0 = 2.303RT\,[p({}_sK)_N - p({}_wK)_N]$$

Figure 1 illustrates the variations of $\delta(\Delta G^0)$ with mol% of glycerol (GL). For comparison, the corresponding profiles for the ethanol–water (EtOH + H_2O) (1) and ethylene glycol – water (EG + H_2O) (2) are also shown. For EtOH + H_2O system the dissociation constants were reported on the molal scale and the values were converted to the mole fraction scale for computation of $\delta(\Delta G^0)$ values. In GL + H_2O system $\delta(\Delta G^0)$ decreases with increase in mol% of GL and passes through a shallow minimum and then increases very slowly showing a small solvent effect on the dissociation of BH^+ ion. In contrast much larger solvent effect is observed in EtOH + H_2O and EG + H_2O systems showing a distinct minimum, the effect being greater in EtOH + H_2O. The characteristic minimum in the $\delta(\Delta G^0)$ curve for a BH^+-type acid has been observed in aqueous mixtures of many other organic solvents (1, 19, 20) but the solvent effect in the present case of study is less compared to those found in all other solvent systems.

The solvent effect on the dissociation of BH^+ is the resultant of free energy transfer values of the individual species involved in the ionization and is given by (2, 3, 15)

$$[3a] \quad \delta(\Delta G^0) = \Delta G_t^0(H^+) + \Delta G_t^0(B) - \Delta G_t^0(BH^+)$$

$$[3b] \quad = \Delta G_t^0(HCl) + \Delta G_t^0(B) - \Delta G_t^0(BHCl)$$

where $\Delta G_t^0(i)$ represents the free energy change accompanying the transfer of one mole of species i from the standard state in water to the standard state in the solvent concerned, both on the mole fraction scale. Variations of $\Delta G_t^0(B)$ in three alcohol–water systems are shown in Fig. 2. $\Delta G_t^0(B)$ values in EtOH + H_2O (21) and EG + H_2O (2) are taken from literature. The

TABLE 1. Data for determination of $p({}_sK)_m$ for *p*-nitroanilinium ion in glycerol–water solvents at 25°C[a]

m_{HCl}	$p({}_sK)'_m$	m_{HCl}	$p({}_sK)'_m$
10 wt.% glycerol		70 wt.% glycerol	
[Indicator] = 4.4 × 10^{-5} *M*		[Indicator] = 3.07 × 10^{-5} *M*	
0.1523	0.961	0.1216	1.180
0.1194	0.955	0.08927	1.171
0.1067	0.942	0.07214	1.173
0.08224	0.946	0.06139	1.164
0.05970	0.941	0.03845	1.147
0.03829	0.927	0.02127	1.149
0.01653	0.922		
	$p({}_sK)_m$ = 0.92		$p({}_sK)_m$ = 1.14
30 wt.% glycerol		90 wt.% glycerol	
[Indicator] = 3.03 × 10^{-5} *M*		[Indicator] = 3.25 × 10^{-5} *M*	
0.1403	0.933	0.1181	1.432
0.1117	0.920	0.9144	1.430
0.07405	0.917	0.08123	1.412
0.05113	0.922	0.06612	1.420
0.03217	0.902	0.04610	1.415
0.01552	0.891	0.02426	1.411
		0.01007	1.398
	$p({}_sK)_m$ = 0.89		$p({}_sK)_m$ = 1.40
50 wt.% glycerol			
[Indicator] = 3.46 × 10^{-5} *M*			
0.1517	1.021		
0.1340	1.015		
0.09823	1.005		
0.06617	0.995		
0.05424	1.003		
0.02927	0.992		
0.01329	0.979		
	$p({}_sK)_m$ = 0.98		

[a] $(pK)_N$ values (mole fraction scale) are 2.744 (ref. 2), 2.628, 2.515, 2.501, 2.525, and 2.585 in 0, 10, 30, 50, 70, and 90% by weight of glycerol, respectively.

TABLE 2. Solubilities and $\Delta G_t^0(B)$ of *p*-nitroaniline in water–glycerol solvents at 25°C (ΔG^0 values in kJ mol^{-1} (mole fraction scale))

Wt.% glycerol	$10^3\, m_B$[a]	$10^5\, X_B$[b]	$\Delta G_t^0(B)$
0	4.267[c]	7.686[c]	0
10	5.083	9.949	−0.640
30	7.387	17.530	−2.100
50	12.81	38.58	−3.998
70	18.56	76.43	−5.694
90	37.72	245.60	−8.583

[a] m_B = solubility in mol per kg of GL + H_2O solvent.
[b] X_B = mole fraction of the base in the saturated solution.
[c] Reference 2.

increasing negative magnitudes of $\Delta G_t^0(B)$ with increase in mol% of EG has been primarily attributed (2) to the dispersion interaction of the benzene nucleus with the organic component of the solvent mixtures. Solvation through H-bond formation between —NH_2 and —NO_2 groups of the base and the solvent appears to contribute little to overall $\Delta G_t^0(B)$ values. GL (containing more —OH groups) has more associated structures than EG (bp of GL = 290°C; bp of EG = 197°C). It is also expected that GL + H_2O mixture is more associated than EG + H_2O. Consequently, it can be expected that less energy will be re-

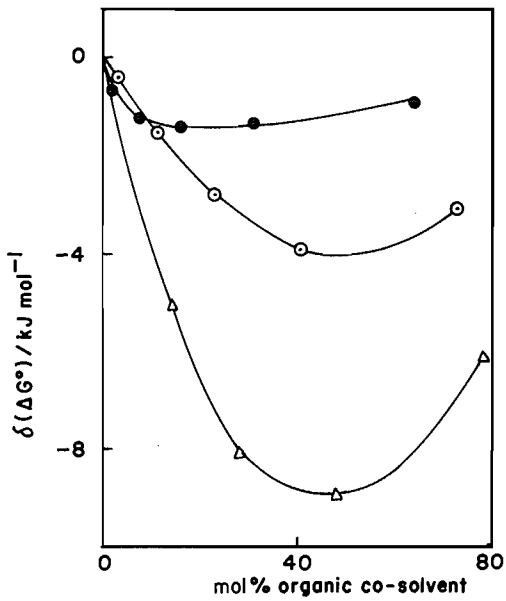

FIG. 1. Variation of $\delta(\Delta G^0)$ for *p*-nitroanilinium ion in GL + H_2O [●], EG + H_2O [⊙] and EtOH + H_2O [△] mixture at 25°C.

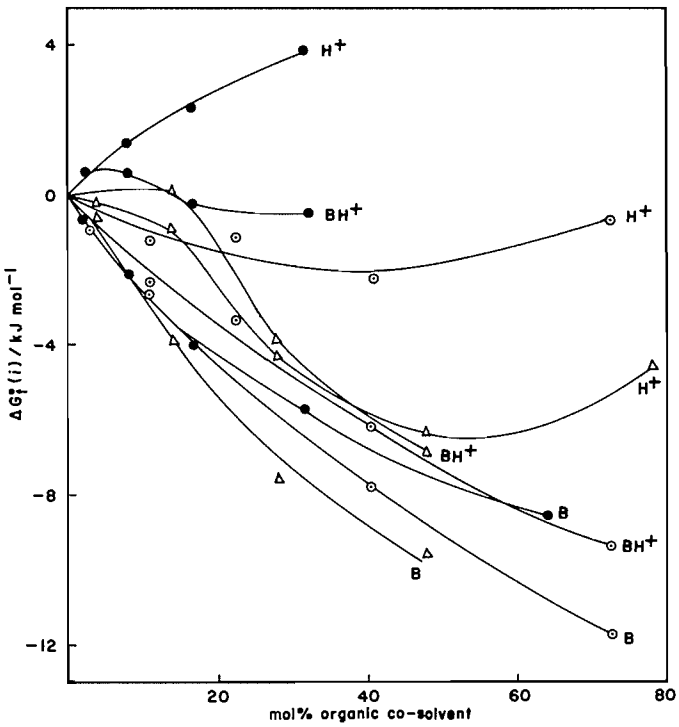

FIG. 2. Variation of $\Delta G_t^0(i)$ of some species in GL + H_2O [●], EG + H_2O [⊙], and EtOH + H_2O [△] mixture at 25°C; B = *p*-nitroaniline; BH^+ = *p*-nitroanilinium ion.

quired to create a cavity for the accommodation of B in EG + H_2O compared to that in GL + H_2O, thus making the cavity formation contribution to the total $\Delta G_t^0(B)$ for B more negative in the EG + H_2O solvent system. This may explain the observed relative order of $\Delta G_t^0(B)$ in EG + H_2O and GL + H_2O. The number of —CH_2— groups relative to that of hydrophilic —OH groups being greater in EtOH, a greater dispersion effect is expected in EtOH + H_2O and this may be largely responsible for the greater stability of B (more negative $\Delta G_t^0(B)$) in EtOH + H_2O as observed.

TABLE 3. Values of $\Delta G_t^0(HCl)$, $\Delta G_t^0(BHCl)$, and $\Delta G_t^0(B) - \Delta G_t^0(BHCl)$ in water–glycerol solvents at 25°C on mole fraction scale, B = *p*-nitroaniline

Wt.% glycerol	$\Delta G_t^0(HCl)^a$ (kJ mol^{-1})	$\Delta G_t^0(BHCl)$ (kJ mol^{-1})	$\Delta G_t^0(B) - \Delta G_t^0(BHCl)$ (kJ mol^{-1})
10	0.16	0.182	−0.822
30	0.55	−0.243	−1.857
50	1.21	−1.401	−2.597
70	2.40	−2.044	−3.650

[a] Reference 12.

$\Delta G_t^0(HCl)$ values (mole fraction scale) in GL + H_2O are available in literature (12) up to 70 wt.% GL (Table 3) and this permits the calculation of $\Delta G_t^0(BHCl)$ through eq. [3*b*]. It is noted from Table 3 that $\Delta G_t^0(HCl)$ increases progressively with increase in GL content of the solvent whereas $\Delta G_t^0(BHCl) - \Delta G_t^0(B)$ decreases simultaneously and the resultant of these two opposing factors is reflected in the variation of $\delta(\Delta G^0)$. Similar nature has been observed with other solvent systems (1–3, 20). But, in order to understand the solvent effect in various solvent systems, it is necessary to obtain the ΔG_t^0 values of all the individual species involved in the ionization equilibrium. $\Delta G_t^0(H^+)$ values for all the three alcohol–water solvent systems based on different extra-thermodynamic assumptions are available in literature (6–9) but, since the method using the reference electrolyte (RE = Ph_4AsBPh_4) (Ph = phenyl) assumption: $\Delta G_t^0(Ph_4As^+) = \Delta G_t^0(Ph_4B^-) = \frac{1}{2}\Delta G_t^0(Ph_4AsBPh_4)$ has been proved to be most sound, reasonable, and consistent (22, 23) and is widely used (8, 24), we have utilized $\Delta G_t^0(H^+)$ values based on RE assumption available from literature for EG + H_2O (9*a*) and GL + H_2O (6) to compute the $\Delta G_t^0(BH^+)$ values. For EtOH + H_2O, however, the reported values based on the average of Ph_4AsBPh_4 and Ph_4PBPh_4 assumptions (8*a*) have been used (results calculated via the two assumptions, however, differ by small amount which is within the range of experimental error (8*a*, *c*). Variations of $\Delta G_t^0(H^+)$ and $\Delta G_t^0(BH^+)$ on the mole fraction scale with mol% nonaqueous component are shown in Fig. 2. The relative positions of the $\Delta G_t^0(H^+)$ curve indicate a different nature of interaction of H^+ in GL + H_2O. The basicity of GL + H_2O mixture continuously decreases with increase in mol% of GL but, for the other two mixtures, it first decreases and then begins to rise and the more detailed interpretation of the behaviour in respective cases have been presented (6, 8).

It is observed from Fig. 2 that $\Delta G_t^0(BH^+)$ values are always less than those of $\Delta G_t^0(H^+)$ in each solvent system reflecting the dispersion interaction between the benzene ring of BH^+ and the organic component of the solvent mixture which is absent for H^+. Again, $\Delta G_t^0(BH^+)$ values are always greater as compared with $\Delta G_t^0(B)$ values and reflect the electrostatic interaction effect on charged BH^+ which is absent for uncharged base B. Figure 2 shows that $\Delta G_t^0(BH^+)$ values in EtOH + H_2O are almost constant at the initial composition and then a continuous decrease is observed but, in EG + H_2O, the values decrease continuously with increase in mol% EG. It is also noted from Fig. 2 that, though $\Delta G_t^0(B)$ values in EtOH + H_2O are somewhat more negative than those in EG + H_2O, the reverse is the case for $\Delta G_t^0(BH^+)$. The dielectric constant values for EtOH + H_2O mixtures being less (25) than those for EG + H_2O mixtures of similar compositions (mol%) a greater electrostatic interaction is expected in EtOH + H_2O and this

Can. J. Chem. Downloaded from www.nrcresearchpress.com by 210.87.254.5 on 09/06/12
For personal use only.

may explain qualitatively the observed behaviour. $\Delta G_t^0(BH^+)$ values in GL + H_2O comparatively shows a somewhat different behaviour. Values first increase, pass through a maximum, and then decrease slowly to small negative values. Dielectric constant values of GL + H_2O mixture being only slightly less (25) than that of EG + H_2O mixture of similar mol% composition, the Born-type electrostatic interaction should be almost the same in both GL + H_2O and EG + H_2O systems. Since BH^+ is a positively charged ion, interaction will also take place predominantly through positively charged hydrogen centres of $—NH_3^+$ group (3) (interaction of BH^+ through $—NO_2$ group will be hindered (3)). Now, so far as interaction of H^+ is concerned, it has been mentioned earlier that the GL + H_2O system shows a difference in behaviour; $\Delta G_t^0(H^+)$ values unlike those in EG + H_2O and EtOH + H_2O, being increasingly positive with increase in mol% nonaqueous component. Similarly, the interaction of the three partially charged H atoms of NH_3^+ group in BH^+ is likely to make a positive contribution to the total free energy of transfer of BH^+ in GL + H_2O system and probably this can account for the observed behaviour of BH^+ in GL + H_2O relative to those found in other two solvent systems. The maximum in $\Delta G_t^0(BH^+)$ curve in GL + H_2O results from the combined effect of the opposing free energy transfer values, viz., the positive contribution due to electrostatic interaction and interaction with $—NH_3^+$ and the negative contribution due to other reasons as for the neutral base B. It appears that the large difference of solvent effect in GL + H_2O system is primarily ascribable to the different nature of interaction of H^+ and BH^+ with the GL + H_2O mixed solvents as compared with aqueous mixture of EtOH or EG.

1. R. G. BATES. J. electroanal. Chem. **29**, 6 (1971).
2. K. K. KUNDU, A. L. DE, and M. N. DAS. J. Chem. Soc. Perkin II, 2063 (1972).
3. A. L. DE. Electrochim. Acta, **28**, 1643 (1983).
4. A. L. DE. Indian J. Chem. **22**A, 932 (1983).
5. R. G. BATES. *In* Hydrogen-bonded solvent systems. *Edited by* A. K. Covington and P. Jones. Taylor and Francis, London. 1968.
6. I. N. BASUMULLICK and K. K. KUNDU. Indian J. Chem. **18**A, 1 (1979).
7. C. F. WELLS. J. Chem. Soc. Faraday-I, **70**, 695 (1974).
8. (*a*) O. POPOVYCH, A. GIBOLSKY, and D. H. BERNE. Anal. Chem. **44**, 811 (1972); (*b*) O. POPOVYCH. Crit. Rev. Anal. Chem. **I**, 73 (1970); (*c*) O. POPOVYCH. Anal. Chem. **46**, 2009 (1974).
9. (*a*) A. K. DAS and K. K. KUNDU. Indian J. Chem. **16**A, 467 (1978); (*b*) K. K. KUNDU, A. K. RAKSHIT, and M. N. DAS. Electrochim. Acta, **17**, 1921 (1972); (*c*) K. DAS, K. BOSE, and K. K. KUNDU. Electrochim. Acta, **26**, 479 (1981); (*d*) K. DAS, A. K. DAS, and K. K. KUNDU. Electrochim. Acta, **26**, 471 (1981); (*e*) J. DATTA and K. K. KUNDU. Can. J. Chem. **59**, 3141 (1981).
10. D. FEAKINS. *In* Physico-chemical processes in mixed solvents. *Edited by* F. Franks. Heinemann, London. 1967.
11. P. SCHINDLER, R. A. ROBINSON, and R. G. BATES. J. Res. Natl. Bur. Stand. **72**A, 141 (1968).
12. I. N. BASUMULLICK and K. K. KUNDU. Can. J. Chem. **57**, 961 (1979).
13. D. ROSENTHAL, H. B. HETZER, and R. G. BATES. J. Am. Chem. Soc. **86**, 549 (1964).
14. K. K. KUNDU, A. L. DE, and M. N. DAS. J. Chem. Soc. Dalton, 386 (1972).
15. A. L. DE. Electrochim. Acta, **29**, 683 (1984).
16. K. DAS, A. K. DAS, K. BASU, and K. K. KUNDU. J. Phys. Chem. **82**, 1242 (1978).
17. R. A. ROBINSON and R. H. STOKES. Electrolyte solutions. Butterworths, London. 2nd ed. 1965.
18. H. S. HARNED and B. B. OWEN. The physical chemistry of electrolyte solutions. 3rd ed. Reinhold, New York. 1958.
19. C. KALIDAS. Indian J. Chem. **22**A, 17 (1983).
20. A. L. DE and T. K. DE. Can. J. Chem. In press.
21. K. BOSE and K. K. KUNDU. Can. J. Chem. **55**, 3961 (1977).
22. J. I. KIM. J. Phys. Chem. **82**, 191 (1978).
23. M. H. ABRAHAM and N. NASEHZADEH. Can. J. Chem. **57**, 71 (1979); **57**, 2004 (1979).
24. B. G. COX, G. R. HEDWIG, A. J. PARKAR, and D. W. WATTS. Aust. J. Chem. **27**, 477 (1974).
25. G. AKERLOF. J. Am. Chem. Soc. **54**, 4125 (1932).

Can. J. Chem. Downloaded from www.nrcresearchpress.com by 210.87.254.5 on 09/06/12
For personal use only.

Reactions of the methylmercury cation with xanthine and crystal structures of μ-(xanthinato-*N*3,*N*7,*N*9)tris(methylmercury(II)) nitrate and μ-(xanthinato-*N*1,*N*3,*N*7,*N*9)tetrakis(methylmercury(II)) nitrate

FRANÇOIS ALLAIRE AND ANDRÉ L. BEAUCHAMP[1]

Département de Chimie, Université de Montréal, C.P. 6210, Succ. A, Montréal, Qué., Canada H3C 3V1

Received February 16, 1984

FRANÇOIS ALLAIRE and ANDRÉ L. BEAUCHAMP. Can. J. Chem. **62**, 2249 (1984).

Compounds of the types $[(CH_3Hg)_3X]$, $[(CH_3Hg)_4X]Z$, and $[(CH_3Hg)_3(HX)]Z$ (where $Z = NO_3^-$, ClO_4^-) were obtained by reacting the methylmercury cation with xanthine (H_3X) in aqueous media. The three acidic protons of H_3X at N(1), N(3), and N(7) are substituted by CH_3Hg^+ groups in $[(CH_3Hg)_3X].2H_2O$. Crystals of $[(CH_3Hg)_3(HX)]NO_3.H_2O$ belong to the triclinic $P\bar{1}$ space group, with $a = 7.319(3)$, $b = 9.466(8)$, $c = 12.004(3)$ Å, $\alpha = 96{,}06(5)$, $\beta = 95.00(3)$, $\gamma = 97.69(5)°$, and $Z = 2$. The structure was refined on 1610 nonzero reflections to an R factor of 0.038. The CH_3Hg^+ groups are linearly coordinated to N(3), N(7), and N(9) of a dianionic xanthine retaining its N(1)—H proton (mean Hg—N = 2.07(3) Å). The $[(CH_3Hg)_4X]NO_3$ compound is monoclinic, space group $C2/c$, $a = 24.55(2)$, $b = 17.016(4)$, $c = 19.108(9)$ Å, $\beta = 110.26(5)°$, $Z = 16$. The structure was refined on 1418 nonzero reflections to $R = 0.046$. The two independent $[(CH_3Hg)_4X]^+$ ions possess methylmercury groups linearly coordinated to the four nitrogen atoms of the X^{3-} anion (mean Hg—N = 2.07(5) Å). The compounds prepared were characterized by ir spectroscopy, and by ^1H and ^{13}C nmr. The $[(CH_3Hg)_3X].2H_2O$ and $[(CH_3Hg)_4X]Z$ compounds were found to remain undissociated in DMSO solution. The $[(CH_3Hg)_3(HX)]^+$ salts disproportionated to some extent into $[(CH_3Hg)_4X]^+$ and a lower complex which was identified as the N(7),N(9)-bonded $[(CH_3Hg)_2(H_2X)]^+$ ion.

FRANÇOIS ALLAIRE et ANDRÉ L. BEAUCHAMP. Can. J. Chem. **62**, 2249 (1984).

Des composés de types $[(CH_3Hg)_3X]$, $[(CH_3Hg)_4X]Z$ et $[(CH_3Hg)_3(HX)]Z$ (où $Z = NO_3^-$, ClO_4^-) ont été préparés par réaction du cation méthylmercure avec la xanthine (H_3X) en milieu aqueux. Les trois protons acides de H_3X liés à N(1), N(3) et N(7) sont substitués par des groupes CH_3Hg^+ dans $[(CH_3Hg)_3X].2H_2O$. Les cristaux de $[(CH_3Hg)_3(HX)]NO_3.H_2O$ appartiennent au groupe triclinique $P\bar{1}$, $a = 7{,}319(3)$, $b = 9{,}466(8)$, $c = 12{,}004(3)$ Å, $\alpha = 96{,}06(5)$, $\beta = 95{,}00(3)$, $\gamma = 97{,}69(5)°$, $Z = 2$. La structure a été affinée au moyen 1610 réflexions significativement observées jusqu'à un facteur R de 0,038. Les groupes CH_3Hg^+ sont linéairement coordonnées aux azotes N(3), N(7) et N(9) de la xanthine dianionique qui a conservé son proton N(1)—H (Hg—N = 2.07(3) Å, moyenne). Le composé $[(CH_3Hg)_4X]NO_3$ est monoclinique, groupe spatial $C2/c$, $a = 24{,}55(2)$, $b = 17{,}016(4)$, $c = 19{,}108(9)$ Å, $\beta = 110{,}26(5)°$, $Z = 16$. La structure a été affinée au moyen de 1418 réflexions significativement observées jusqu'à $R = 0{,}046$. Les deux ions $[(CH_3Hg)_4X]^+$ indépendants possèdent des groupes CH_3Hg^+ linéairement liées aux quatre atomes d'azote de l'ion X^{3-} (Hg—N = 2.07(5) Å, moyenne). Les composés préparés ont été caractérisés par spectroscopie infrarouge et par rmn ^1H et ^{13}C. $[(CH_3Hg)_3X].2H_2O$ et $[(CH_3Hg)_4X]Z$ ne sont pas dissociés en solution dans le DMSO. Par contre, les sels de $[(CH_3Hg)_3(HX)]^+$ se dismutent partiellement dans le DMSO, pour donner $[(CH_3Hg)_4X]^+$ et un complexe de stoëchiométrie inférieure, qui s'est avéré être l'ion $[(CH_3Hg)_2(H_2X)]^+$, dans lequel les groupes CH_3Hg^+ sont liés à N(7) et N(9).

Introduction

As part of our continuing studies on the use of CH_3Hg^+ to probe the affinity of the basic sites of DNA constituents and related molecules for heavy metal ions (1), we are reporting on the reactivity of xanthine **1** in aqueous media. Complexes of the corresponding nucleoside xanthosine, in which the xanthine ring bears a ribose moiety at position N(9), have been recently prepared and characterized (2).

The present paper describes the preparation of various CH_3Hg/xanthine complexes and the crystal structures of two of these compounds. Their infrared spectra were studied in detail with the aim of identifying diagnostic bands which would be characteristic for each pattern of site occupancy. The behavior of these compounds in DMSO was examined by means of ^1H and ^{13}C nmr.

Experimental section

Xanthine (Aldrich) and CH_3HgOH (Alfa, 1 *M* aqueous solution) were used without further purification. Solutions of CH_3HgNO_3 and CH_3HgClO_4 were prepared as described elsewhere (3). Their concentrations were determined by mixing 1.00 mL of solution with 100 mL of 100% ethanol and titrating with standard 0.05 *M* aqueous KCl. The endpoint corresponding to complete formation of undissociated CH_3HgCl was detected with a Ag/AgCl electrode (4). Mercury in the complexes was determined by the same method. The sample (50−100 mg) was attacked with a few drops of concentrated HNO_3 before dilution in ethanol.

The infrared spectra were recorded on KBr pellets with a Digilab FTS-15 C/D Fourier transform spectrometer equipped with a Globar source and a wideband Hg/Cd/Te detector (Infrared Associates, New Brunswick, NJ). Typically, 100 interferograms of 4096 points recorded with an optical velocity of 1.2 cm s^{-1} and maximum optical retardation of 0.5 cm were co-added, apodized with a boxcar function and Fourier transformed with four levels of zero filling resulting in a spectral resolution of 2 cm^{-1}. The apparatus was purged with nitrogen during the experiment.

The ^1H nmr spectra were obtained with a Bruker WH-90 instrument and the ^{13}C spectra with a WH-80 instrument operating at 20.11 MHz. In all cases, the solvent used was DMSO-d_6 (Merck, Sharp and Dohme Canada) and the chemical shifts were referenced to TMS. Solutions of ~100 mg per mL were used whenever possible; otherwise, solutions saturated at room temperature were used.

Preparations

$[(CH_3Hg)_3X].2H_2O$ (2). Xanthine (0.15 g, 1.0 mmol) was suspended in a mixture of 75 mL of concentrated NH_4OH and 5.0 mL of 1 *M* CH_3HgOH (5.0 mmol). The suspension was refluxed for 4 days and allowed to cool to room temperature. Two days later, the white solid was filtered and dried *in vacuo* (0.69 g, 83%). *Anal.* calcd. for $C_8H_{14}Hg_3N_4O_4$: Hg 72.3; found, 72.0. The presence of three CH_3Hg^+ groups per xanthine was deduced from the integrated intensities of the

[1]To whom all correspondence should be addressed.

Can. J. Chem. Downloaded from www.nrcresearchpress.com by 210.87.254.105 on 09/06/12
For personal use only.

Can. J. Chem. Downloaded from www.nrcresearchpress.com by 210.87.254.105 on 09/06/12
For personal use only.

^{1}H resonances for H(8) and the methyl protons. The ν(OH) region of the infrared spectrum was consistent with the presence of water.

[(CH$_3$Hg)$_3$(HX)]NO$_3$.H$_2$O (3a). Xanthine (0.30 g, 2.0 mmol) was dissolved in a boiling mixture of 4.0 mL of 1 *M* CH_3HgOH (4.0 mmol), 4.6 mL of 0.44 *M* CH_3HgNO_3 (2.0 mmol), and 50 mL of water. The clear hot solution was stirred for 1 h and allowed to cool. After 3 days, the white crystalline solid was filtered, washed with ethanol, and dried *in vacuo* (1.51 g, 86%). The structure of this solid was determined by X-ray diffraction (*vide infra*). The ^{1}H spectrum showed the expected intensity ratio for the H(8) and methyl proton signals. *Anal.* calcd. for $C_8H_{13}Hg_3N_5O_6$: Hg 68.62, C 10.96, H 1.49, N 7.99; found: Hg 69.04, C 10.63, H 1.60, N 7.89.

[(CH$_3$Hg)$_3$(HX)]ClO$_4$.H$_2$O (3b). Same method as **3a**, after replacing CH_3HgNO_3 by CH_3HgClO_4. White powder, 1.51 g, 83%. *Anal.* calcd. for $C_8H_{13}Hg_3N_4O_7Cl$: Hg 65.8; found 66.1. The ^{1}H and ^{13}C nmr spectra were identical with those of **3a**.

[(CH$_3$Hg)$_4$X]NO$_3$ (4a). Xanthine (0.30 g, 2.0 mmol) was dissolved in a boiling mixture of 6.0 mL of 1 *M* CH_3HgOH (6.0 mmol), 4.6 mL of 0.44 *M* CH_3HgNO_3 (2.0 mmol), and 50 mL of H_2O, and stirred for 1 h. After 3 days, the white crystalline solid was filtered, washed with ethanol, and dried *in vacuo* (1.81 g, 83%). Its structure was determined
by X-ray diffraction (*vide infra*). *Anal.* calcd. for $C_9H_{13}Hg_4N_5O_5$: Hg 74.7; found 74.4. The 4:1 CH_3Hg:xanthine ratio was clearly indicated by ^{1}H nmr spectroscopy.

[(CH$_3$Hg)$_4$X]ClO$_4$.2H$_2$O (4b). Same method as **4a**, with CH_3HgClO_4 replacing the nitrate. Flaky white solid, 1.60 g, 70%. *Anal.* calcd. for $C_9H_{17}Hg_4N_4O_8Cl$: Hg 69.9; found 69.6. The ^{1}H and ^{13}C nmr spectra were identical with those of **4a**.

Structure of [(CH$_3$Hg)$_3$(HX)]NO$_3$.H$_2$O (3a)

Crystal data

$C_8H_{13}Hg_3N_5O_6$ fw = 876.99

Triclinic, $P\bar{1}$, a = 7.319(3), b = 9.466(8), c = 12.004(3) Å, α = 96.06(5), β = 95.00 (3), γ = 97.69(5)°, V = 815.2 Å^3, D_{calcd} = 3.572 g cm^{-3}, Z = 2, λ(MoK$\bar{\alpha}$) = 0.71067 Å (graphite monochromator), T = 293 K, μ(MoKα) = 280.8 cm^{-1}. Crystal dimensions: 0.72 mm (010−0$\bar{1}$0) × 0.22 mm (100−$\bar{1}$00) × 0.11 mm (001−00$\bar{1}$), transmission range: 0.014−0.120 (Gaussian integration, grid 8 × 8 × 8).

Crystallographic measurements and structure resolution. The crystals were grown by slow recrystallization from hot water. The precession and cone-axis photographs were consistent with space groups $P1$ and $P\bar{1}$. The $P\bar{1}$ space group was assumed and this choice was confirmed by successful refinement. The accurate cell parameters and the intensity data were obtained with an Enraf-Nonius CAD4 diffractometer, following a procedure described elsewhere (5). A set 2119 independent hkl, $h\bar{k}l$, $hk\bar{l}$, and $h\bar{k}\bar{l}$ MoKα reflections were collected within a sphere limited by $2\theta = 45°$. A total of 1610 reflections were retained ($I/\sigma(I) > 3.0$) for structure determination. These data were corrected for the effect of Lorentz, polarization and absorption.

The structure was solved by the heavy-atom method and refined on $|F|$ by full-matrix least-squares in the early stages. The three Hg atoms were located from a Patterson map and the remaining nonhydrogen atoms were found from a difference Fourier (ΔF) map. Isotropic refinement converged to $R = \Sigma||F_o| - |F_c||/\Sigma|F_o| = 0.098$ and $R_w = [\Sigma_w(|F_o| - |F_c|)^2/\Sigma_w|F_o|^2]^{1/2} = 0.113$. Refinement was terminated by block-diagonal least-squares. The hydrogen atoms H(1) and H(8) were fixed at ideal positions (B = 4.0 Å^2). Their parameters were not refined, but the coordinates were recalculated after each cycle. The hydrogens of the methyl groups were neglected. Anisotropic refinement of all nonhydrogen atoms converged to R = 0.038 and R_w = 0.052. The goodness-of-fit ratio was 2.02. The highest residuals on the final ΔF map (± (0.9−1.8) e Å^{-3}) were all around Hg atoms. The general background was below ±0.8 e Å^{-3}.

Structure of [(CH$_3$Hg)$_4$X]NO$_3$ (4a)

Crystal data

$C_9H_{13}Hg_4N_5O_5$ fw = 1073.59

Monoclinic, $C2/c$, a = 24.55(2), b = 17.016(4), c = 19.108(9) Å, β = 110.26(5)°, V = 7489 Å^3, D_{calcd} = 3.808 g cm^{-3}, Z = 16, λ(MoK$\bar{\alpha}$) = 0.71067 Å (graphite monochromator), T = 293 K, μ(MoKα) = 326.7 cm^{-1}, crystal dimensions: 0.44 × 0.06 × 0.06 mm^3, transmission range = 0.090−0.160 (Gaussian integration, grid 8 × 8 × 8).

Crystallographic measurements and structure resolution

Crystals suitable for X-ray work were grown by recrystallization from hot water. Cell dimensions and space group were determined from precession and cone-axis films. In space group $C2/c$, there are two molecules per asymmetric unit. The corresponding noncentric space group Cc would require four molecules per asymmetric unit. Structure resolution was attempted in $C2/c$ first and this choice was subsequently confirmed by successful refinement.

A total of 5187 independent hkl and $hk\bar{l}$ reflections ($h + k = 2n$) within a sphere limited by $2\theta = 46°$ was collected (MoK$\bar{\alpha}$ radiation). Only 1418 of these reflections were significantly above background ($I/\sigma(I) > 3.0$). They were corrected for the effect of Lorentz, polarization and absorption.

The structure was solved by direct methods, using the MULTAN80 package, which provided one solution with a combined FOM of 3.0. The eight strongest peaks corresponding to the nonequivalent Hg atoms were used to calculate a ΔF map and locate the remaining nonhydrogen atoms. The Hg atoms were refined anisotropically, the other nonhydrogen atoms isotropically. The H(8) hydrogens were fixed at the calculated positions and repositioned after each least-squares cycle. Those of the methyl groups were neglected. No attempts were made to refine the light atoms anisotropically because of the low proportion of observed reflections. The final residuals were R = 0.046 and R_w = 0.048. The goodness-of-fit ratio was 1.43. The residual background in the final ΔF map was below ± 0.45 e Å^{-3}, with several peaks (±(0.45−0.60) e Å^{-3}) near Hg.

The coordinates for both structures are listed in Table 1. The temperature factors and structure factor amplitudes are part of the supplementary material.[2] The scattering curves used were from standard sources (6). The real and imaginary contributions to anomalous dispersion of Hg was taken from Cromer (7). The programs used are listed elsewhere (8).

Results and discussion

Reactions and nmr spectroscopy

Xanthine **1** (H_3X) contains three acidic protons, two of which are attached to N(1) and N(3) in the pyrimidine ring (Scheme 1). From nmr studies in DMSO and DMSO/D_2O solutions, it was concluded that the third proton is bound to N(7) (9, 10). The N(7)—H tautomer was also observed in crystals of 3-hydroxyxanthine (11) and theophylline (1,3-dimethylxanthine) (12).

In strongly acidic media, the free imidazolic nitrogen of xanthine can accept a proton to form the H_4X^+ ion (pk_a = 1.2) (10). The dissociation equilibria H_3X/H_2X^- and H_2X^-/HX^{2-} are characterized by pk_a values of 7.7 and 11.9, respectively (13). Ionisation of HX^{2-} takes place only in very basic media, and the proton involved in this last dissociation step is definitely N(1)—H. On the other hand, it is not clear whether the proton lost by H_3X at pH 7.7 originates from N(7)—H, N(3)—H, or in part from both positions. Indeed, the most acidic proton of H_2X^- is probably involved in a tautomeric

[2]The supplementary material includes tables of temperature factors, structure factor amplitudes, and hydrogen coordinates, details on the least-squares planes, and lists of distances and angles related to intermolecular interactions for both structures. Figures of the Fourier-transform infrared spectra of the methylmercury complexes are also included. Copies can be obtained at a nominal charge from the Depository of Unpublished Data, CISTI, National Research Council of Canada, Ottawa, Ont., Canada K1A 0S2.

TABLE 1

(*a*) Refined parameters for $[(CH_3Hg)_3(HX)]NO_3.H_2O$ (coordinates $\times 10^3$, Hg $\times 10^5$; $U_{eq} \times 10^3$, Hg $\times 10^4$)

Atom	*X*	*Y*	*Z*	U_{eq}	Atom	*X*	*Y*	*Z*	U_{eq}
Hg(3)	18793(12)	68462(9)	21112(8)	456	O(6)	154(2)	596(2)	712(1)	55
Hg(7)	−24242(12)	73153(9)	74175(8)	448	N(7)	−122(2)	760(2)	591(2)	44
Hg(9)	−13139(11)	90655(9)	27082(8)	436	C(7)	−363(4)	701(3)	893(2)	78
N(1)	285(2)	584(2)	545(1)	35	C(8)	−187(3)	824(2)	507(2)	43
C(2)	300(3)	608(2)	438(2)	47	N(9)	−88(2)	809(2)	418(2)	49
O(2)	416(2)	555(1)	380(1)	42	C(9)	−162(4)	1020(3)	138(2)	71
N(3)	174(2)	682(2)	379(1)	34	N(10)	449(2)	982(2)	320(2)	58
C(3)	198(4)	672(3)	40(2)	85	O(10)	288(2)	984(2)	278(2)	75
C(4)	47(2)	732(2)	453(2)	48	O(11)	513(2)	867(2)	310(2)	76
C(5)	29(3)	700(2)	555(2)	39	O(12)	546(2)	1090(2)	367(2)	102
C(6)	156(2)	624(2)	616(2)	32	O(20)	306(3)	376(2)	809(2)	87

(*b*) Refined parameters for $[(CH_3Hg)_4X]NO_3$ (coordinates $\times 10^3$, Hg $\times 10^4$; $U_{eq} \times 10^2$, Hg $\times 10^3$)

Atom	*X*	*Y*	*Z*	U_{eq}	Atom	*X*	*Y*	*Z*	U_{eq}
Hg(11)	838(1)	3445(1)	2336(1)	68	C(15)	43(2)	158(2)	354(2)	3
Hg(13)	1618(1)	192(1)	2740(1)	60	C(16)	51(2)	232(2)	330(2)	3
Hg(17)	−425(1)	2003(1)	4326(1)	61	O(16)	32(1)	294(2)	354(2)	6
Hg(19)	727(1)	−928(1)	3560(1)	62	N(17)	14(1)	125(2)	402(2)	5
Hg(21)	2476(1)	2298(2)	2805(1)	79	C(17)	−97(3)	279(4)	468(4)	12
Hg(23)	1213(1)	3904(1)	4482(2)	79	C(18)	26(2)	52(3)	405(3)	5
Hg(27)	2405(1)	−104(2)	5155(2)	111	N(19)	59(2)	22(3)	365(2)	7
Hg(29)	990(1)	2690(2)	5738(2)	80	C(19)	84(2)	−206(3)	341(3)	5
N(1)	136(2)	61(3)	63(3)	10	N(21)	227(2)	237(2)	377(2)	6
O(1)	179(2)	43(3)	115(3)	13	C(21)	268(3)	212(4)	185(4)	13
O(2)	93(2)	45(3)	89(3)	16	C(22)	189(2)	298(4)	387(3)	9
O(3)	135(3)	86(4)	4(3)	22	O(22)	191(1)	354(2)	355(2)	8
N(2)	437(2)	376(3)	346(2)	7	N(23)	166(2)	291(3)	440(2)	7
O(4)	446(2)	423(2)	303(2)	9	C(23)	82(3)	495(5)	460(4)	14
O(5)	386(2)	347(2)	325(2)	9	C(24)	172(2)	222(3)	474(3)	7
O(6)	471(2)	363(2)	410(2)	11	C(25)	201(2)	156(3)	468(3)	7
N(11)	77(1)	233(2)	276(2)	5	C(26)	230(2)	167(3)	410(3)	4
C(11)	91(3)	451(4)	190(3)	10	O(26)	258(1)	106(2)	398(2)	7
C(12)	108(2)	166(3)	264(3)	5	N(27)	197(2)	92(3)	506(2)	7
O(12)	130(1)	188(2)	217(2)	7	C(27)	279(3)	−114(4)	509(4)	13
N(13)	98(1)	98(2)	290(2)	4	C(28)	162(2)	126(3)	543(3)	7
C(13)	229(2)	−50(3)	272(3)	8	N(29)	143(2)	197(2)	527(2)	7
C(14)	65(2)	90(4)	336(3)	9	C(29)	51(3)	354(5)	604(4)	16

equilibrium, whereby N(7), N(3), and even N(9), could act as acceptors. From nmr and uv studies (10), it was concluded that H_2X^- has N(1)—H and N(3)—H protons. However, the solid-state structure of $Na[H_2X]$ shows a xanthine moiety lacking a proton at N(3), whereas the imidazolic proton is attached to N(9) instead of N(7) (14). The only metal complex of xanthine for which crystallographic results are available, contains a H_2X^- anion as the above N(1)—H/N(3)—H tautomer, bonded to cobalt via N(9) (15). In the latter structure, H-bonding between H(3) and oxygen atoms in other ligands coordinated to cobalt might promote N(9)-coordination.

From the bulk of information available on complexes of guanosine, inosine, 9-methylhypoxanthine, xanthosine, and theophylline (11, 16), it can be anticipated that the carbonyl groups of xanthine will show only low affinity, if any, for mercury. Firstly, these hard sites are less suited than the softer nitrogen atoms to bind the soft CH_3Hg^+ cation. Secondly, coordination to the carbonyl group has been found to be favored by bulky ligands in the metal coordination sphere (17). These ligand render the endocyclic nitrogens inaccessible for the metal, while keeping the less hindered exocyclic carbonyl oxygens still accessible. As the CH_3Hg^+ ion has no other ligands in the plane perpendicular to the Hg—C bond, steric effects are minimized. Therefore, mercury binding to oxygen is unlikely. Even if only the nitrogen sites are considered, various types of CH_3Hg^+ complexes of xanthine can be anticipated. Neutral compounds could be obtained by displacement of one, two, or three acidic protons by CH_3Hg^+. These molecules could then accept an extra CH_3Hg^+ ion on the imidazolic nitrogen lone pair to produce cationic species. Among the possible species, those found in the present study are shown in Scheme 1. In some cases, different occupancy patterns for H^+ and CH_3Hg^+ ions are in principle possible, leading to different isomers possibly involved in tautomeric exchanges. Compounds in which H(8) is substituted by CH_3Hg^+ can probably be prepared (2), but no attempts have been made to obtain them in the present study.

Reacting xanthine **1** with excess CH_3HgOH yields the neutral 3:1 complex **2**, in which the three acidic protons are displaced. The low-field signals for these protons are absent from the ^1H nmr spectrum of the complex (Table 2) and the ir spectrum shows no ν(N—H) bands at ~3000 cm^{-1} (*vide in-*

Can. J. Chem. Downloaded from www.nrcresearchpress.com by 210.87.254.105 on 09/06/12
For personal use only.

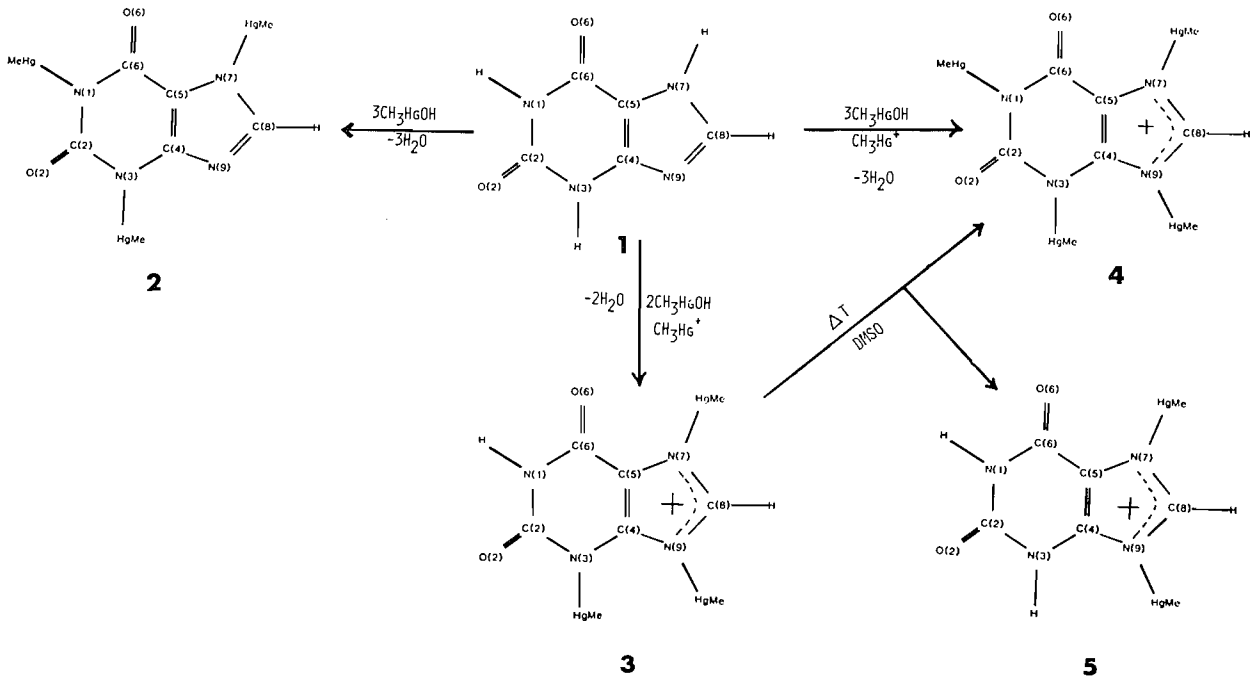

SCHEME 1

TABLE 2. ^{1}H nmr data for the CH_3Hg–xanthine compounds[a]

Compound	H(1)	H(3)	H(7)	H(8)	$CH_3(Hg)$	$^2J(^{199}Hg—^1H)$
H_3X[b]	10.85	11.53	13.3	7.93	—	—
$[(CH_3Hg)_3X].2H_2O$ (**2**)	—	—	—	7.38	0.78	197
$[(CH_3Hg)_4X]NO_3$ (**4***a*)	—	—	—	7.92	0.82	208
$[(CH_3Hg)_4X]ClO_4.2H_2O$ (**4***b*)	—	—	—	7.89	0.82	210
$[(CH_3Hg)_3(HX)]NO_3.H_2O$ (**3***a*)	11.10	—	—	8.03	0.83	214
$[(CH_3Hg)_3(HX)]ClO_4.H_2O$ (**3***b*)	11.10	—	—	8.00	0.82	215
$[(CH_3Hg)_2(H_2X)]NO_3$ (**5**)	11.2	12.0	—	—	—	—

[a]δ in ppm vs. TMS; ^2J in Hz.
[b]Assignments from refs. 9, 10.

fra). The upfield shift of 0.55 ppm on H(8) is similar to that observed for the theophylline (HTh) complex $[(CH_3Hg)Th].H_2O$ (0.42 ppm), in which the imidazolic N—H proton had been similarly substituted (18). X-ray work indicated (19) methylmercury binding to the theophylline N(7) position, which was the site formerly occupied by the displaced proton. This site was also favored over N(9) in theophylline, on the ground of steric hindrance from the N(3)—CH_3 group. Binding of the imidazolic CH_3Hg^+ group at N(7) in compound **2** is proposed by analogy, although coordination to N(9) or tautomeric exchange between N(7) and N(9) in solution cannot be ruled out, since position N(3) is occupied by a CH_3Hg^+ unit in this case, and simultaneous CH_3Hg^+ binding to N(3) and N(9) has been observed (ref. 20, and X-ray work below). ^{13}C nmr could provide more information, but the spectrum could not be obtained because of the low solubility of the complex in DMSO.

When xanthine is boiled in a solution containing 3 equiv. of CH_3HgOH and 1 equiv. of CH_3HgZ (Z = NO_3^- or ClO_4^-), compounds **4** are isolated (crystal structure described below). All acidic protons are absent from the ^{1}H nmr spectra and the H(8) signals, displaced upfield in the previous compound, return to the original position in xanthine after both imidazolic nitrogens have been occupied. A similar effect has been noted for the CH_3Hg/theophylline system (18). The ^{13}C nmr spectrum is given in Table 3. All xanthine signals are shifted downfield in **4**. Buncel, Norris, and co-workers (2) recently reported the spectrum of a 2:1 N(1)/N(3)-bonded xanthosine compound in which the six-membered ring is similar to ours. They observed for this compound the following displacement (Δδ) of the ^{13}C resonances with respect to xanthosine: C(2), 7.8; C(4), 7.2; C(5), 1.8; C(6), 4.0; C(8), −2.9 ppm. On the other hand, our five-membered ring is similar to that of $[(CH_3Hg)_2Th]NO_3$, for which the following Δδ values were found: C(2), −0.2; C(4), −1.2; C(5), 7.2; C(6), 2.3; C(8), 5.5 ppm (18). Our Δδ results for compound **4** are of the same sign and of roughly the same magnitude (except for C(4)) as the sum of the above effects: C(2), 8.8; C(4), 2.6; C(5), 9.5; C(6), 5.4; C(8), 4.5 ppm.

If xanthine is allowed to react with 1 equiv. of CH_3HgZ and only 2 equiv. of CH_3HgOH, the 3:1 cationic compounds **3** precipitate. The presence of H(1) is detected from the low-field signals at 11.1 ppm in the ^{1}H spectra. The H(8) resonances occur at a slightly lower field than those of **4**. The ^{13}C resonances of C(2) and C(5) are shifted by −2.8 and −2.3 ppm, respectively, with respect to **4**. The remaining signals are essentially unmoved.

When solutions of **3** (NO_3^- or ClO_4^-) are prepared by heat-

Can. J. Chem. Downloaded from www.nrcresearchpress.com by 210.87.254.105 on 09/06/12
For personal use only.

TABLE 3. ^{13}C nmr data for the CH_3Hg–xanthine compounds[a]

Compound	C(2)	C(4)	C(5)	C(6)	C(8)	$CH_3(Hg)$
H_3X[b]	151.3	148.8	106.5	155.4	140.4	—
$[(CH_3Hg)_4X]NO_3$ (**4***a*)	160.1	151.4	116.0	160.8	144.9	1.0
$[(CH_3Hg)_4X]ClO_4.2H_2O$ (**4***b*)	160.2	151.5	116.1	160.9	145.0	1.2
$[(CH_3Hg)_3(HX)]NO_3.H_2O$ (**3***a*)	157.3	150.9	113.4	160.7	145.0	0.8
$[(CH_3Hg)_3(HX)]ClO_4.H_2O$ (**3***b*)	157.4	151.3	113.8	160.8	145.7	1.1
$[(CH_3Hg)_2(H_2X)]NO_3$ (**5**)[c]	(151)	(148)	(114)	155	(146)	—

[a]δ in ppm vs. TMS.
[b]Assignments from ref. 21.
[c]Minor components in warmed DMSO solutions of **3***a*. Similar signals in the corresponding perchlorate solutions **3***b*. The C(6) resonance was found in the spectra. The values in brackets were calculated assuming that the xanthine resonances would undergo the same shifts as in the analogous $[(CH_3Hg)_2Th].H_2O$ compound of theophylline (18).

ing the solid in DMSO, additional weak signals, not all resolved, appear in both the ^1H and ^{13}C spectra. Some of these signals correspond to the $[(CH_3Hg)_4X]Z$ salts. As a confirmation, ^1H spectra of solutions were recorded after adding increasing amounts of the pure 4:1 compound. The set of weaker signals initially assigned to the 4:1 compound were indeed found to gain intensity. At this point, it was suspected that the original samples of **3***a* and **3***b* could be impure. As a check, complete elemental analysis was carried out on **3***a* and it was found to be consistent with the proposed formula. The ir spectra and X-ray powder patterns of **3***a* and **3***b* were carefully examined and compared with those of **4***a* and **4***b*, respectively. In no case was it possible to gain evidence for significant amounts of 4:1 impurity in the 3:1 solid samples. Therefore, it was concluded that heating compounds **3** in DMSO induced some reaction. The presence of other peaks, in addition to those of **3** and **4**, suggested that the following disproportionation reaction was taking place:

$$2[(CH_3Hg)_3(HX)]^+ \rightleftharpoons [(CH_3Hg)_4X]^+ + [(CH_3Hg)_2(H_2X)]^+$$

According to the integration of the ^1H nmr peaks, 20% of the 3:1 compound had disproportionated. Evidence for the 2:1 species as the second product comes mainly from the presence of two low-field signals in the ^1H spectra at 12.0 and 11.2 ppm for H(3) and H(1), respectively. The H(8) signal cannot be distinguished from that of the 3:1 species. In the ^{13}C spectra, a resolved signal at 155 ppm, not found for the 3:1 and 4:1 ions, is assigned to C(6) of the 2:1 species. This resonance cannot be due to unreacted xanthine (which also exhibits a resonance at this position), since xanthine should also show well-defined peak for C(8) at 140 ppm. No such signal is present in the spectra. The positions of the other ^{13}C signals of $[(CH_3Hg)_2(H_2X)]^+$ were predicted by comparison with the Δδ values obtained for the analogous 2:1 theophylline complex (18). The contributions for C(2), C(5), and C(8) would be overlapping with those of the other two components. As to the C(4) signal predicted to occur at 148 ppm, it is normally weak in the spectrum of xanthine and its complexes, and no significant peak could be detected.

The nonequivalent CH_3Hg^+ groups produce only single resonances in the ^1H and ^{13}C spectra, indicating fast exchange of these groups on the nmr time scale. The chemical shifts in both types of spectra are not very informative of the complexation sites. The methyl protons signals show only one pair of satellites due to coupling between ^{199}Hg (17% abundance) and the methyl protons. The values of $^2J(^{199}Hg—^1H)$ are listed in Table 2. Other authors (22) have noticed that the ^2J constant is smoothly related in an inverse manner to the nucleophilic character of the site of attachement of mercury. Our results are in good qualitative agreement with these observations. As the order of increasing basic character is presumably N(9) < N(7) < N(3) < N(1), the ^2J value should be lowest for $[(CH_3Hg)_3X]$ and highest for $[(CH_3Hg)_3(HX)]Z$. This is indeed the observed order.

The present study in aqueous media led to compounds containing high CH_3Hg:xanthine ratios. We tried to prepare lower compounds, such as $[(CH_3Hg)_2(HX)]$ or $[(CH_3Hg)(H_2X)]$, by reacting xanthine with 2 or 1 equiv. of CH_3HgOH. The solid material so obtained invariably consisted of $[(CH_3Hg)_3X].2H_2O$ **2** and unreacted xanthine. However, the nmr spectra show that some reaction occurs when these solids are heated in DMSO to make solutions. So far we have been unable to determine the number of species formed and to identify them, because rapid equilibria between these complexes and even tautomeric exchanges between species of the same stoichiometries seem to be taking place. This problem is being further investigated.

*Crystal structure of $[(CH_3Hg)_3(HX)]NO_3.H_2O$ (**3**a)*

The $[(CH_3Hg)_3(HX)]^+$ cation is shown schematically in Fig. 1 with the bond lengths and some bond angles. The angles in the xanthine unit are listed in Table 4. Three CH_3Hg^+ ions having displaced altogether two acidic protons are found to occupy positions N(3), N(7), and N(9) of xanthine. An acidic proton still remains at N(1).

The Hg—C and Hg—N distances (ave. 2.07(3) Å in both cases) are normal (1, 20) and the linear two-coordination commonly found for Hg(II) is again found. In one case, significant departure from linearity is observed (N(9)—Hg(9)—C(9) = 174.2(8)°), but distortions of this magnitude are often noted, presumably in response to packing constraints. The presence of two CH_3Hg^+ groups on adjacent N(3) and N(9) sites has previously been found for several adenine complexes, namely the nitrate and perchlorate salts of $[(CH_3Hg)_3(Ade—H)]^{2+}$, a cation showing the CH_3Hg^+ similarly distributed on N(3), N(7), and N(9) of the purine (20). The C—N—Hg angles at both N(3) and N(9) are unequal (117(1)° vs. 131(1)° at N(3), 124(1)° vs. 131(1)° at N(9)) and the two CH_3Hg groups have slipped away from the xanthine plane in opposite directions. These indications suggest repulsive interactions between the neighboring Hg atoms, but the distance observed here (3.429(1) Å) is much greater than those found in the analogous adenine compounds (3.270(2) to 3.310(2) Å) (20), or in a methylcytosine compound (3.150(2) Å) (23). Therefore, un-

Can. J. Chem. Downloaded from www.nrcresearchpress.com by 210.87.254.105 on 09/06/12
For personal use only.

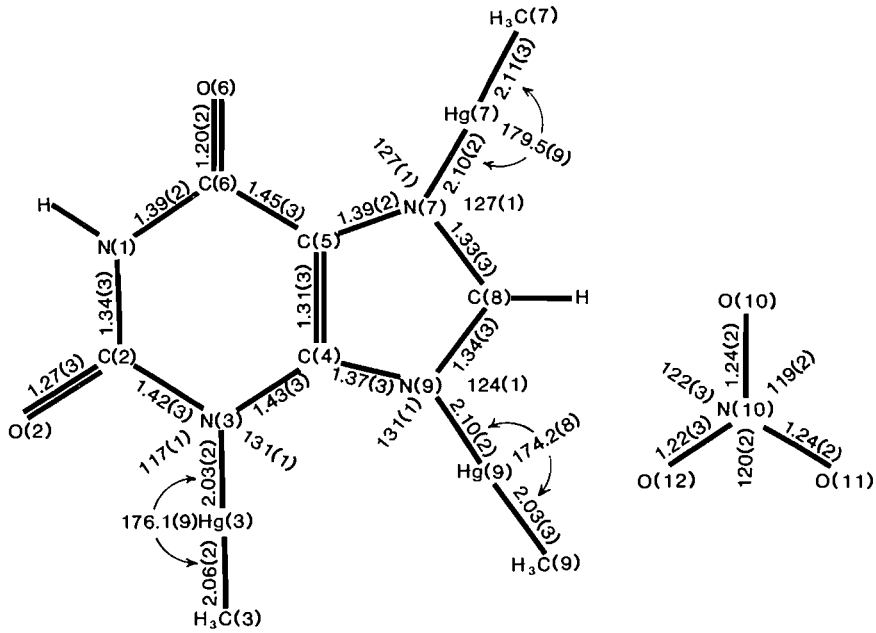

FIG. 1. Schematic representation of the $[(CH_3Hg)_3(HX)]^+$ cation with bond lengths and some bond angles.

TABLE 4. Bond angles in various xanthine compounds

Bonds	Angle					
	$[(CH_3Hg)_3(HX)]NO_3.H_2O$ (this work)	$[(CH_3Hg)_4X]NO_3$ (this work)		Xanthosine (23)	NaH_2X (14)	Co-xanthine complex[a] (15)
C(2)—N(1)—C(6)	129(2)	121(4)	120(4)	128.1(4)	125.7(7)	128.3(4)
N(1)—C(2)—N(3)	122(2)	117(4)	120(5)	116.5(4)	120.5(8)	115.2(4)
N(1)—C(2)—O(2)	122(2)	105(4)	112(5)	121.6(4)	116.5(8)	122.6(4)
N(3)—C(2)—O(2)	116(2)	136(4)	126(6)	121.8(4)	122.9(8)	122.2(4)
C(2)—N(3)—C(4)	110(2)	123(4)	117(5)	118.3(3)	114.7(7)	120.7(4)
N(3)—C(4)—C(5)	126(2)	116(5)	132(5)	124.4(4)	127.7(7)	122.6(4)
N(9)—C(4)—C(5)	111(2)	122(5)	122(3)	106.3(3)	105.5(7)	109.3(4)
N(3)—C(4)—N(9)	122(2)	122(5)	126(5)	129.2(4)	126.8(7)	128.1(4)
C(4)—C(5)—C(6)	124(2)	125(4)	110(5)	120.3(4)	118.2(7)	119.8(4)
C(4)—C(5)—N(7)	107(2)	99(4)	119(5)	110.6(4)	111.7(7)	109.8(4)
C(6)—C(5)—N(7)	129(2)	136(4)	130(5)	129.0(4)	130.0(7)	130.4(4)
N(1)—C(6)—C(5)	108(2)	114(4)	119(4)	112.1(4)	113.0(7)	113.4(4)
N(1)—C(6)—O(6)	124(2)	124(4)	125(4)	121.1(4)	119.7(8)	119.7(4)
C(5)—C(6)—O(6)	127(2)	121(4)	116(4)	126.7(4)	127.3(8)	126.9(4)
C(5)—N(7)—C(8)	106(2)	104(4)	96(4)	104.7(3)	101.9(7)	103.4(4)
N(7)—C(8)—N(9)	112(2)	120(4)	120(5)	112.8(4)	115.0(9)	115.0(4)
C(4)—N(9)—C(8)	104(2)	95(4)	102(4)	105.5(3)	106.0(7)	102.5(4)

[a][Bis(dimethylglyoximato)(xanthinato)(tri-*n*-butylphosphine)cobalt(III)].

symmetrical coordination at N(3) and N(9) seems to result from molecular packing.

The distances in xanthine do not significantly differ from those reported for other compounds containing the same ring (14, 15, 23). The angles will be discussed later. The ring is planar within 2σ (0.04 Å). This plane also contains O(6), but O(2) is 0.09(1) Å from the plane. All three CH_3Hg^+ groups are significantly distant from this plane: Hg(3), 0.351(1); C(3), 0.79(3); Hg(7), 0.316(1); C(7), 0.61(3); Hg(9), −0.255(1); C(9), −0.66(3) Å. These distortions probably result from optimization of packing interactions.

A packing diagram is shown in Fig. 2. Planar complex cations oriented ~45° from the ***ac*** plane are stacked in columns along ***b***. The pyrimidine ring of one cation overlaps the imidazole ring of the adjacent cations, and *vice versa*. Water molecule O(20) contributes to cohesion in the column by forming a weak bond with Hg(9) of one ion and a H-bond with O(6) of the next ion (Table 5). Centrosymmetrically related cations in adjacent columns are linked by a pair of complementary N(1)—H(1)···O(2) hydrogen bonds. Space between the columns is filled with NO_3^- ions acting as multiple bridges between Hg atoms. The Hg···O distances are listed in Table 5 (more details are provided in Table 11, supplementary material). The NO_3^- ion is involved in a chelating interaction with Hg(3) through O(10) and O(11). At the same time, O(10) interacts with Hg(7) of a second cation and O(11) forms a very short contact (2.67(1) Å) with Hg(9) of a third cation. In all cases the Hg···O contacts lie close to the equatorial plane

Can. J. Chem. Downloaded from www.nrcresearchpress.com by 210.87.254.105 on 09/06/12
For personal use only.

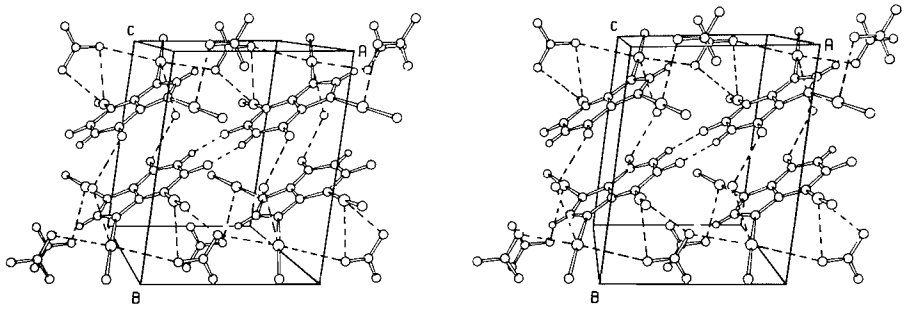

FIG. 2. Unit-cell content of $[(CH_3Hg)_3(HX)]NO_3.H_2O$ (**3***a*). The atoms are represented by spheres of arbitrary sizes, the largest corresponding to Hg atoms. Dashed lines correspond to H-bonds or Hg—O contacts.

TABLE 5. Distances (Å) involved in hydrogen bonds and Hg···O contacts

(*a*) $[(CH_3Hg)_3(HX)]NO_3.H_2O$

Atoms	Distance	Atoms	Distance
N(1)—O(2)[a]	2.83(2)	Hg(7)—O(10)[b]	2.80(2)
O(6)—O(20)	2.81(2)	Hg(9)—O(10)	3.06(1)
Hg(3)—O(10)	2.85(2)	Hg(9)—O(11)[c]	2.67(1)
Hg(3)—O(11)	2.83(2)	Hg(9)—O(20)[d]	2.84(2)

(*b*) $[(CH_3Hg)_4X]NO_3$

Atoms	Distance	Atoms	Distance
Hg(11)—O(12)	2.96(4)	Hg(19)—O(10)[f]	2.92(4)
Hg(11)—O(22)	2.85(4)	Hg(19)—O(30)[i]	3.11(4)
Hg(11)—O(16)[e]	2.88(3)	Hg(21)—O(12)	2.81(4)
Hg(13)—O(12)	3.08(3)	Hg(21)—O(26)	3.02(3)
Hg(13)—O(26)	3.08(4)	Hg(23)—O(16)	2.83(3)
Hg(13)—O(10)[f]	3.02(4)	Hg(23)—O(22)	2.93(4)
Hg(17)—O(12)[e]	2.93(3)	Hg(27)—O(1)[h]	2.86(5)
Hg(17)—O(2)[e]	2.89(5)	Hg(27)—O(3)[h]	2.83(7)
Hg(17)—O(30)[g]	3.10(4)	Hg(29)—O(20)[g]	2.70(4)
Hg(19)—O(3)[h]	2.71(6)	Hg(29)—O(30)[g]	2.91(4)
Hg(19)—O(10)[i]	2.93(4)		

[a] $1-x, 1-y, 1-z$.
[b] $\bar{x}, 2-y, 1-z$.
[c] $-1+x, y, z$.
[d] $\bar{x}, 1-y, 1-z$.
[e] $\bar{x}, y, \frac{1}{2}-z$.
[f] $\frac{1}{2}-x, -\frac{1}{2}+y, \frac{1}{2}-z$.
[g] $\frac{1}{2}-x, \frac{1}{2}-y, 1-z$.
[h] $x, \bar{y}, \frac{1}{2}+z$.
[i] $x-\frac{1}{2}, y-\frac{1}{2}, z$.

(assuming that the H_3C—Hg—N direction is axial), the C—Hg—O and N—Hg—O angles being all within 90 ± 15°. The third nitrate oxygen, which shows much higher thermal motion than the other two, does not participate in H-bonding or Hg···O contacts.

*Crystal structure of $[(CH_3Hg)_4X]NO_3$ (**4**a)*

This crystal contains two symmetry-independent $[(CH_3Hg)_4X]^+$ cations (Fig. 3), which both contain CH_3Hg^+ ions bonded to the four N atoms available on xanthine, after displacement of the three acidic protons. None of the carbonyl oxygens is used to form strong coordination bonds to Hg. The distances and angles around Hg are given in Fig. 3. The bond angles in the xanthine ring are listed in Table 2. Distances in the ring have very high esd's and a complete list is provided only in the supplementary material.

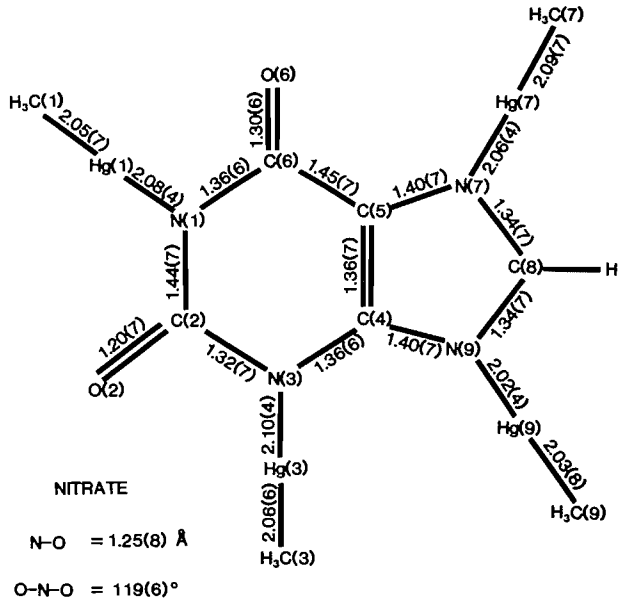

FIG. 3. Schematic representation of the $[(CH_3Hg)_4X]^+$ cation (**4***a*). The bond length values are averages for the two nonequivalent molecules in the unit cell. Individual values are given in the supplementary material.

The Hg—N and Hg—C distances (ave. 2.07, 2.06 Å, σ = 0.05 Å, respectively) as well as the N—Hg—C angles compare well with those of the previous structure (Tables 4 and 6). Again, two CH_3Hg^+ groups occupy nearby positions on N(3) and N(9), but the relatively large Hg···Hg separation (Hg(13)—Hg(19) = 3.639(4); Hg(23)—Hg(29) = 3.353(4) Å) is well above the low value of 3.15 Å mentioned earlier (3). Thus, there seems to be no significant repulsive interactions between these two groups. The xanthine rings are planar within 2σ (0.08 Å). The deviation of the CH_3Hg^+ groups from these planes is generally highly significant, and especially marked for Hg(13) and Hg(21). The atom-to-plane distances are Hg(11), 0.124(3); C(11), 0.18(6); Hg(13), −0.567(2); C(13), −1.35(6); Hg(17), 0.330(2); C(17), 0.56(7); Hg(19), 0.200(2); C(19), 0.49(5); Hg(21), 0.620(2); C(21), 1.31(7); Hg(23), −0.008(3); C(23), −0.13(7); Hg(27), −0.128(3); C(27), −0.05(7); Hg(29), −0.179(3); C(29), −0.24(8) Å.

The packing pattern shown in Fig. 4 is rather complex. It shows two columns of $[(CH_3Hg)_4X]^+$ cations. This time, the plane of the cation is roughly perpendicular to the direction of stacking. These columns are rigorously ordered and contain equal numbers of type #1 and of type #2 cations, according to a −1−2−2−1−1−2−2−1− pattern. The contacts between a

Can. J. Chem. Downloaded from www.nrcresearchpress.com by 210.87.254.105 on 09/06/12
For personal use only.

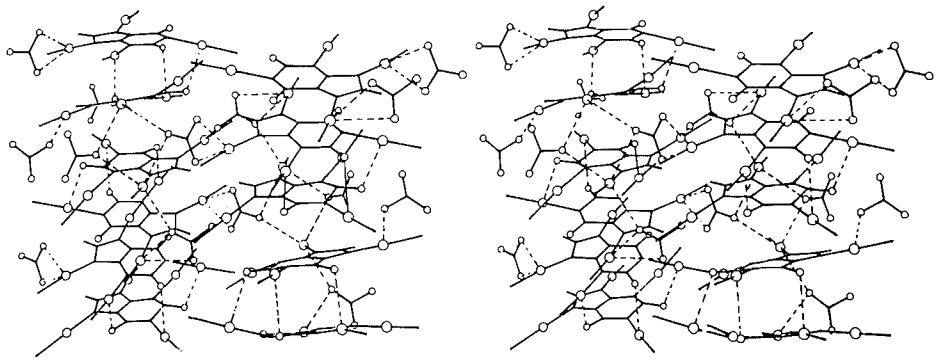

FIG. 4. Part of the unit cell of $[(CH_3Hg)_4X]NO_3$ (**4***a*), showing two columns of stacked $[(CH_3Hg)_4X]^+$ cations. The small circles correspond to oxygens atoms, the large ones to Hg atoms. Dashed lines represent Hg...O contacts.

TABLE 6. Angles involving mercury in $[(CH_3Hg)_4X]NO_3$

Bonds	Angle	Bonds	Angle
C(11)—Hg(11)—N(11)	178(2)	C(21)—Hg(21)—N(21)	175(2)
C(12)—N(11)—Hg(11)	123(3)	C(22)—N(21)—Hg(21)	122(3)
C(16)—N(11)—Hg(11)	115(3)	C(26)—N(21)—Hg(21)	112(3)
C(13)—Hg(13)—N(13)	172(2)	C(23)—Hg(23)—N(23)	176(2)
C(12)—N(13)—Hg(13)	105(3)	C(22)—N(23)—Hg(23)	111(4)
C(14)—N(13)—Hg(13)	130(3)	C(24)—N(23)—Hg(23)	132(4)
C(17)—Hg(17)—N(17)	177(2)	C(27)—Hg(27)—N(27)	172(2)
C(15)—N(17)—Hg(17)	117(3)	C(25)—N(27)—Hg(27)	128(4)
C(18)—N(17)—Hg(17)	138(3)	C(28)—N(27)—Hg(27)	135(4)
C(19)—Hg(19)—N(19)	177(2)	C(29)—Hg(29)—N(29)	170(2)
C(18)—N(19)—Hg(19)	124(3)	C(28)—N(29)—Hg(29)	131(4)
C(14)—N(19)—Hg(19)	141(4)	C(24)—N(29)—Hg(29)	125(3)

type #1 and a type #2 cations are particularly interesting. The six- and the five-membered ring of one cation are, respectively, overlapping the same rings in the other cation, but the latter is rotated with respect to the former by 180° about the direction through C(8) and the middle of the N(1)—C(2) bond. This brings Hg(11), O(12), Hg(13), and O(16) roughly below O(22), Hg(21), O(26), and Hg(23), respectively. These four Hg···O contacts vary between 2.81(4) and 3.08(4) Å. At the 1−1 or 2−2 interfaces, the xanthine units are in contact through opposite rings. The nitrate ions filling space between the columns are involved in an intricate network of Hg···O interactions (Table 6).

The high standard deviations on distances preclude any discussion concerning bond length changes in the xanthine moiety upon complexation. Angles generally respond to a more significant degree. Taylor and Kennard (24) have noticed that removing an N-H proton in purines increases the C—N—C angles by ~5°. In general, alkylated nitrogens behave like if they were protonated, whereas metal coordination does not drastically change the geometry of the nitrogen with free lone pair. The data in Table 4 follow these trends. For instance, $[(CH_3Hg)_4X]NO_3$ is the only compound lacking the N(1)-H proton and its C(2)—N(1)—C(6) angle is the smallest. Similarly, the highest values of C(4)—N(9)—C(8) are found for $Na[H_2X]$ and xanthosine, which have a proton and a ribosyl group, respectively, attached to N(9). Xanthosine and the Co-xanthine complex, which have retained their N(3)—H proton, show C(2)—N(3)—C(4) angles of 118.3(3)° and 120.7(4)°, respectively, whereas the same angles reduce to 114.7(7)° in $Na[H_2X]$ and 110(2)° in $[(CH_3Hg)_3(HX)]NO_3.H_2O$, which both have lost it. However, the $[(CH_3Hg)_4X]NO_3$ complex does not fit into this pattern. Simultaneous loss of N(1)-H seems to produce long range perturbations extending as far as N(3) and balancing the effect of N(3) deprotonation.

Infrared spectroscopy

The spectra of the complex salts contain the bands associated to the anion (25) Table 7. In addition to a strong absorption at ~1380 cm^{-1}, the NO_3^- ion produces weak features at ~820 cm^{-1}, a region where the ligand also absorbs. The ClO_4^- ion generates a very strong band ~1100 cm^{-1}, as well as a weaker, but well-defined, absorption at ~625 cm^{-1}.

The presence of the CH_3Hg^+ group in the complexes can be identified from characteristic infrared bands (26). A sharp absorption at ~2920 cm^{-1}, especially clear when the broad underlying ν(N—H) modes have been removed in $[(CH_3Hg)_3X].2H_2O$ and the $[(CH_3Hg)_4X]^+$ salts, originates in the $\nu_s(CH_3)$ mode. The corresponding antisymmetric mode is expected to show weakly at ~3000 cm^{-1} and the spectra indeed contain small features at 2994 cm^{-1}. The rocking motion produces a characteristic broad peak at ~800 cm^{-1}. Of the two expected deformation bands, only the symmetric mode leads to observable absorption at ~1200 cm^{-1} in infrared, although assignment is made difficult by the presence of ligand bands in the same region. The δ_a mode should appear very weakly at ~1400 cm^{-1}, but it is usually unobserved and the bands found in this region for our compounds probably have a different origin. All complexes show a broad, generally weak, absorption due to the ν(Hg—C) vibration at ~560 cm^{-1}.

The spectrum of xanthine is considerably modified by complexation. The most obvious changes take place between 1700 and 1550 cm^{-1}, where bands due to the C=O groups are

Can. J. Chem. Downloaded from www.nrcresearchpress.com by 210.87.254.105 on 09/06/12
For personal use only.

TABLE 7. Infrared wavenumbers (cm^{-1}) for the methylmercury–xanthine complexes

	H_3X	$[(CH_3Hg)_3(HX)]NO_3 .H_2O$	$[(CH_3Hg)_3(HX)]ClO_4 .H_2O$	$[(CH_3Hg)_3X] .2H_2O$	$[(CH_3Hg)_4X]NO_3$	$[(CH_3Hg)_4X]ClO_4 .2H_2O$
$\nu(H_2O)$	—	3406 m	3456 m	3400 w, br		3430 m
ν(C(8)—H(8))	3132 vw	3130 m	3130 m	3120 vw	3138 w	3125 w
ν(N-H)	3006 s	—	—	—	—	—
$\nu_a(CH_3(Hg))$	—	—	2993 w, sh	—	2994 vw	2994 vw
ν(N—H)	2881 s	2968 m, br	2964 m	—	—	—
$\nu_s(CH_3(Hg))$	—	2919 m	2923 m	2919 w	2922 m	2919 m
ν(N—H)	2828 m	—	—	—	—	—
	2795 m					
		2803 w	2804 w	2803 w	2803 w	2803 w
ν(C(6)=O(6))	1702 s	1688 s	1694 s		1632 s	
		1681 m, sh	1680 m, sh	1625 s		1625 s
ν(C(2)=O(2))	1672 s	1625 s	1625 s		1614 s	
		1605 s	1618 s, sh			
ν(C(4)=C(5))	1569 m	1584 w, sh	1573 m	1579 m	1582 m	1584 s
					1573 m	
	—	1552 w	1551 w	1541 vw, sh	1556 m	1561 w, sh
				1537 vw		1556 m
	—	1524 s	1523 s	1501 s	1508 s	1506 s
	1465 m	1458 w	1467 vw	—	—	—
	1459 m, sh					
	1438 w	1447 m	1446 m	—	1444 m	1442 m
	1420 m	—	1417 m	1420 m	1414 w, sh	1416 w
						1410 w
NO_3^-	—	1384 vs	—	—	1384 vs	—
	1391 w		1389 m	1374 m	1368 s	1375 w
	1336 m	1319 s	1321 w	—	1335 m	—
			1311 w			
	1328 m	1302 m	1302 w, sh	1302 m	1314 m	1314 w
	1260 w	—	—	1288 w, sh	1284 m	1286 m
	1234 vw	1248 w	1242 w	1247 w	1249 w, sh	1247 w
	1206 m	1195 m, sh	1197 w, sh	1202 w, sh	1203 m	1196 m
	1199 m	1185 m	1189 m	1186 s	1188 m	1190 m
	1161 w			1161 w	1167 m	1170 m
	1153 w	1153 w	1150 m, sh			
	1122 w	—	1122 s	—	—	1121 s
	—	—	—	1087 w	1089 w	—
			1109 vs			1108 vs
ClO_4^-	—	—	1091 vs	—	—	1091 vs
			1063 vs			
	1031 w	1030 w	1025 w, sh	—	1030 vw	—
	959 w	912 w	912 w	—	—	—
γ(N-H)	895 w, br	880 w	887 w	—	—	—
	854 m	866 w	—	—	—	—
$\rho(CH_3(Hg))$	—	798 m, br	800 m, br	794 m, br	794 m, br	798 m, br
	767 m	772 m	774 m	775 m	774 m	775 m
	—	758 m	758 m	761 m	761 m	764 m
	723 m	722 w	730 w	—	—	—
		716 w				
	—	665 w	662 w	670 w	667 w	667 w
	—	632 w	635 w	635 w	628 w	636 w
ClO_4	—	—	622 w	—	—	625 m
	614 w	602 m	602 m	—	—	—
ν(C—Hg)	—	560 w, sh	561 w, sh	561 w	560 w	561 w
	538 m	—	—	534 w	534 w	534 w
	500 m	—	—	—	—	—

observed at 1702 and 1672 cm^{-1} (27). When the N—H proton is substituted by a CH_3Hg^+ ion, electron distribution in the —N—C=O region approximates that of the corresponding anion, leading to a reduction of the C=O bond orders and an increase of the C—N bond orders. When the two N—H protons of the six-membered ring are substituted (Scheme 2), both bands are shifted to lower wavenumbers (~1625 cm^{-1}). On the other hand, in the monosubstituted six-membered ring (Scheme 3), only one of the carbonyl groups is shifted. Since X-ray diffraction shows that the N(1)—H(1) bond is intact in these compounds, the higher wavenumber must correspond mainly to ν(C(6)=O(6)), whereas the other is due to ν(C(2)=O(2)).

Can. J. Chem. Downloaded from www.nrcresearchpress.com by 210.87.254.105 on 09/06/12
For personal use only.

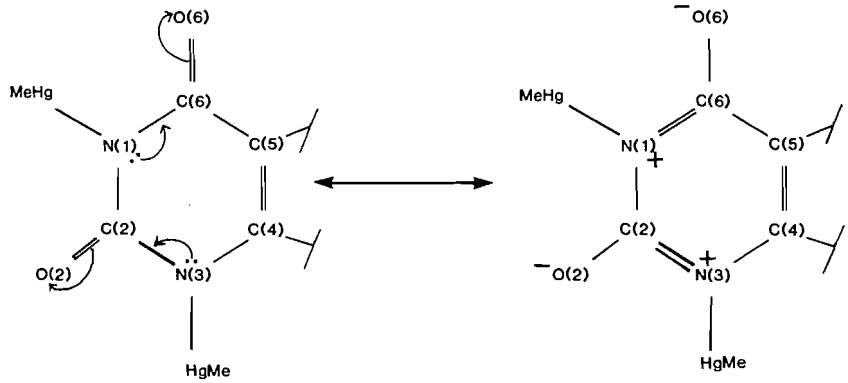

SCHEME 2

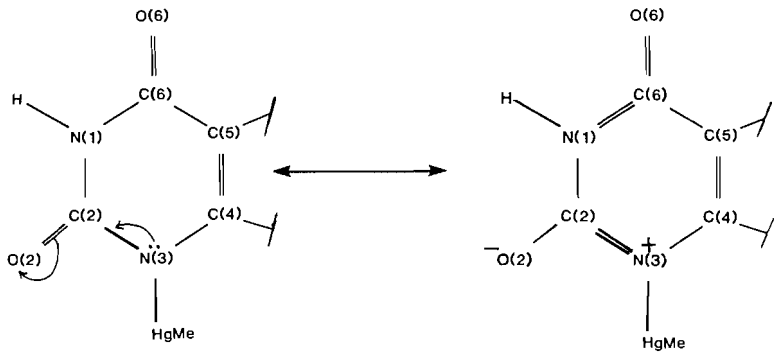

SCHEME 3

The C(4)=C(5) bond produces a band around 1570 cm^{-1} in all compounds, which is not very sensitive to the substitution pattern.

Other major changes are associated with the disappearance of the N—H vibrator. The stretching (2700–3200 cm^{-1}) and out-of-plane modes (850–900 cm^{-1}) are relatively pure (27). Their intensities are considerably reduced in the $[(CH_3Hg)_3(HX)]^+$ salts and washed out when all three N—H bonds are substituted in $[(CH_3Hg)_3X].2H_2O$ and the $[(CH_3Hg)_4X]^+$ compounds. In the high wavenumber region, the ν(C(8)—H(8)) mode at 3130 cm^{-1}, as well as a weak band at 2800 cm^{-1}, probably due to a combination mode, are clearly detected.

Extensive coupling with ring modes is anticipated for the three N—H bonds. Spectral changes resulting from complexation can arise both from the loss of this N—H coupling and from bond order changes in the ring. Detailed assignment is beyond the scope of this work. However, attempts have been made to empirically identify diagnostic bands which could be used to distinguish between the three complexation patterns observed here. Some modifications have been found to take place uniformly for all complex types. For instance, the bands at 1122 and 538 cm^{-1} lose most of their intensities in all cases, the former appearing as a small feature superimposed on the strong anion band for the ClO_4^- compounds. Other changes are more characteristic. The $[(CH_3Hg)_3(HX)]Z$ compounds possess a strong band at 1524 cm^{-1}, which is absent from the spectrum of xanthine and shifted to 1505 cm^{-1} in $[(CH_3Hg)_3X].2H_2O$ and $[(CH_3Hg)_4X]Z$. A very weak xanthine band at 1391 cm^{-1}, gaining intensity for $[(CH_3Hg)_3(HX)]Z$, is shifted to 1375 cm^{-1} for both other types of complexes. A similar distinction can be made from several other spectral regions. For instance, a weak ligand absorption at 1260 cm^{-1} disappears for $[(CH_3Hg)_3(HX)]Z$, but reappears at 1287 cm^{-1} for the remaining compounds. Similarly, weak ligand bands at 959, 895, 854, and 614 cm^{-1} are displaced to 912, 880, 866, and 602 cm^{-1}, respectively, in the spectra of the $[(CH_3Hg)_3(HX)]Z$ compounds, but absent in the other cases.

Distinction between the two types of N(1)-substituted compounds is more difficult. The best diagnostic feature is probably the 1336/1328 cm^{-1} doublet of xanthine. It is observed at 1320/1310 cm^{-1} for the $[(CH_3Hg)_3(HX)]Z$ salts, but gives rise to single bands at 1302 cm^{-1} for $[(CH_3Hg)_3X].2H_2O$ and at 1314 cm^{-1} for $[(CH_3Hg)_4X]Z$. A weak ligand doublet at 1161/1153 cm^{-1} is replaced by a single peak at 1153 cm^{-1} for $[(CH_3Hg)_3(HX)]Z$, at 1161 cm^{-1} for $[(CH_3Hg)_3X].2H_2O$ and 1168 cm^{-1} for the $[(CH_3Hg)_4X]Z$ compounds.

Concluding remarks

Reaction of methylmercury with xanthine in aqueous solution yields pure solid compounds only for high CH_3Hg:xanthine ratios. In the 4:1 cationic complex, saturation of all available nitrogens of xanthine is taking place, whereas in the 3:1 neutral compound, the N(9)-bound CH_3Hg^+ groups is removed. These materials are both stable when dissolved in DMSO. In contrast, the 3:1 cationic compounds, in which the N(1)—H(1) bond is retained, are found to disproportionate in warm DMSO into the 4:1 cationic compound and a lower species identified as $[(CH_3Hg)_2(H_2X)]^+$. Attempts to prepare compounds with a low CH_3Hg:xanthine ratio invariably led to mixtures of $[(CH_3Hg)_3X].2H_2O$ and unreacted xanthine. However, when these mixtures are warmed in DMSO, equilibration produces complex species of intermediate stoichiometries, which have not been unambiguously identified so far. Thus, reaction of xanthine in water appears to be limited by its very

Can. J. Chem. Downloaded from www.nrcresearchpress.com by 210.87.254.105 on 09/06/12
For personal use only.

low solubility. The presence of three H-bond donors and three H-bond acceptors in relative orientations favorable to form complementary H-bond pairs, imparts to xanthine an insoluble character analogous to that of guanine. Pure compounds are isolated when H-bonding opportunity is reduced after substituting most of the N—H groups in the CH_3Hg-rich compounds. Compounds of lower stoichiometries are likely to exist in non-aqueous solvents having good H-bonding capabilities, which would improve xanthine solubility. This is being currently examined.

Acknowledgments

We wish to thank M. J. Olivier (X-ray), R. Mayer (nmr), and J. C. Bolduc (ir) for technical assistance. We are grateful to the Natural Science and Engineering Council of Canada and the Ministère de l'Education du Québec for financial support.

1. L. PRIZANT, M. J. OLIVIER, R. RIVEST, and A. L. BEAUCHAMP. Can. J. Chem. **59**, 1311 (1981); F. GUAY and A. L. BEAUCHAMP. Inorg. Chim. Acta, **66**, 57 (1982); J. P. CHARLAND, M. SIMARD, and A. L. BEAUCHAMP. Inorg. Chim. Acta, **80**, L57 (1983).
2. E. BUNCEL, B. K. HUNTER, R. KUMAR, and A. R. NORRIS. J. Inorg. Biochem. **20**, 171 (1984).
3. L. PRIZANT, R. RIVEST, and A. L. BEAUCHAMP. Can. J. Chem. **59**, 2290 (1981).
4. F. BÉLANGER-GARIÉPY. Mémoire de Maîtrise, Université de Montréal. 1981.
5. F. BÉLANGER-GARIÉPY and A. L. BEAUCHAMP. J. Am. Chem. Soc. **102**, 3461 (1980).
6. D. T. CROMER and J. T. WABER. Acta Crystallogr. **18**, 104 (1965); R. F. STEWART, E. R. DAVIDSON, and W. T. SIMPSON. J. Chem. Phys. **42**, 3175 (1965).
7. D. T. CROMER. Acta Crystallogr. **18**, 17 (1965).
8. M. AUTHIER-MARTIN and A. L. BEAUCHAMP. Can. J. Chem. **55**, 1213 (1977).
9. L. M. TWANMOH, H. B. WOOD, JR., and J. S. DRISCOLL. J. Heterocycl. Chem. **10**, 187 (1973).
10. D. LICHTENBERG, F. BERGMANN, and Z. NEIMAN. J. Chem. Soc. C, 1676 (1971).
11. D. J. HODGSON. Prog. Inorg. Chem. **23**, 211 (1977).
12. E. SHEFTER. J. Pharm. Sci. **58**, 710 (1969).
13. W. PFLEIDERER and G. NUBEL. Ann. **647**, 155 (1961); A. ALBERT. Synthetic procedures in nucleic acids chemistry. Vol. 2. *Edited by* Z. Zorbach and Z. Tipson. New York. 1973. p. 106.
14. H. MIZUNO, T. FUJIWARA, and K. TOMITA. Bull. Chem. Soc. Jpn. **42**, 3099 (1969).
15. L. G. MARZILLI, L. A. EPPS, T. SORRELL, and T. J. KISTENMACHER. J. Am. Chem. Soc. **97**, 3351 (1975).
16. L. G. MARZILLI, T. J. KISTENMACHER, and G. L. EICHHORN. Nucleic acid – metal ion interactions. Metal ions in biology series. Vol. 1. 1980. p. 179; D. V. SWAMINATHAN and M. SUNDARALINGAM. CRC Crit. Rev. Biochem. **6**, 245 (1979).
17. D. W. ABBOTT and C. WOODS. Inorg. Chem. **22**, 597 (1983).
18. A. R. NORRIS, R. KUMAR, E. BUNCEL, and A. L. BEAUCHAMP. J. Inorg. Biochem. In press.
19. A. R. NORRIS, S. E. TAYLOR, E. BUNCEL, F. BÉLANGER-GARIÉPY, and A. L. BEAUCHAMP. Inorg. Chim. Acta. In press.
20. J. HUBERT and A. L. BEAUCHAMP. Acta Crystallogr. Sect. B, **36**, 2613 (1980); Can. J. Chem. **58**, 1439 (1980).
21. B. COXON, A. J. FATIADI, L. T. SNEIGOSKI, H. S. HERTZ, and R. SCHAFFER. J. Org. Chem. **42**, 3132 (1977).
22. D. L. RABENSTEIN. Acc. Chem. Res. **11**, 100 (1978); A. R. NORRIS, E. BUNCEL, and S. E. TAYLOR. J. Inorg. Biochem. **16**, 279 (1982); A. J. CANTY and A. MARKER. Inorg. Chem. **15**, 425 (1976).
23. G. KOYAMA, H. NAKAMURA, H. UMEZAWA, and Y. IITAKA. Acta Crystallogr. Sect. B, **32**, 969 (1976).
24. R. TAYLOR and O. KENNARD. J. Mol. Struct. **78**, 1 (1982).
25. K. NAKAMOTO. Infrared spectra of inorganic and coordination compounds. Interscience, New York. 1970 pp. 98 and 111.
26. J. H. S. GREEN. Spectrochim. Acta, A**24**, 863 (1968).
27. M. TSUBOI, S. TAKAHASHI and I. HARADA. Physico-chemical properties of nucleic acids. Vol. 2. *Edited by* J. Duchesne. Academic Press, London. 1973. p. 91.

Can. J. Chem. Downloaded from www.nrcresearchpress.com by 210.87.254.105 on 09/06/12
For personal use only.

Experiments with a cyclic closed-loop gas chromatograph[1]

ROBERTA BACK[2] AND R. A. BACK
Division of Chemistry, National Research Council of Canada, 100 Sussex Drive, Ottawa, Ont., Canada K1A 0R6

Received March 24, 1984

R. BACK and R. A. BACK. Can. J. Chem. **62**, 2260 (1984).

A cyclic closed-loop gas chromatrograph, comprising a column, a thermal conductivity detector, and a peristaltic circulating pump, together with valves for sample pick-up and carrier gas admission, is described. Injected samples could be recycled many times, providing very long effective column lengths, and separations were markedly better than on a single-pass column of equivalent length. Separation of two components, and peak broadening with single components, were measured over many successive cycles for a variety of samples, carrier gases, and conditions. The use of the cyclic chromatograph for testing columns and for studying basic processes in gas chromatography is demonstrated and discussed.

R. BACK et R. A. BACK. Can. J. Chem. **62**, 2260 (1984).

On décrit un appareil à chromatographie en phase gazeuse munie d'une boucle fermée cyclique et comprenant une colonne, un détecteur à conductivité thermique, une pompe à circulation péristaltique ainsi que des valves pour l'injection des échantillons et l'entrée du gaz porteur. Les échantillons injectés peuvent être recyclés plusieurs fois, la longueur effective des colonnes devient très grande et les séparations sont bien meilleures que celles obtenues à l'aide de colonnes à passage unique de longueur équivalente. Opérant avec plusieurs cycles successifs et avec une variété d'échantillons, de gaz porteurs et de conditions expérimentales, on a mesuré la séparation des deux composants et l'élargissement des pics avec des composants uniques. On démontre l'utilité du chromatographe cyclique pour vérifier des colonnes et pour étudier les procédés de base de la chromatographie en phase gazeuse et on en discute.

[Traduit par le journal]

Can. J. Chem. Downloaded from www.nrcresearchpress.com by 210.87.254.105 on 09/06/12
For personal use only.

Introduction

About 25 years ago, a brief note was published (1) describing a circular closed-loop gas chromatograph in which the exit gases were recirculated through the column and detector by a peristaltic pump. About ten years later a very similar system was developed independently in this laboratory (2). Samples of air were separated into N_2 and O_2 on a Porapak T column, and comparison with a single pass through a column of equivalent length showed that the cyclic closed-loop was much more efficient. There appear to be no other published accounts of similar cyclic chromatographs. These earlier experiments (1, 2) suggested some interesting possible uses for such a chromatograph, and the present paper describes a belated exploration of some of these.

Experimental

The chromatograph in its final form is shown schematically in Fig. 1, which is largely self-explanatory. The column used in all experiments was 3 ft. of 3/16th-in. od stainless-steel tubing packed with 80–100 mesh Porapak T, divided into two equal parts, as shown. This arrangement was found to give better performance than a single column of the same total length on one side or other of the pump; peaks were narrower, separations were better, and small pressure fluctuations caused by the circulating pump, which induced a ripple in the detector signal at low pump speeds, were damped out. All connecting tubing was 1/8th-in. od copper, and in all connections dead space was minimized. The detector was one side of a Carle model-100 thermistor microdetector, balanced against a Helipot variable resistor, operated at room temperature with only enough current to give a sensitivity which permitted easy measurement on a chart recorder with good signal-to-noise ratio. The sample loop, of 1/8th-in. copper tubing, had a volume of 0.2 cm^3. The circulatory pump was a Cole-Parmer Masterflex #1014 3-roller peristaltic pump, fitted with thick-walled, 5 mm od, 1.5 mm id silicone rubber tubing. It was run at settings of the speed control which gave volume flowrates of air from about 10 to 110 cm^3/min, measured with air at 1 atm. with zero pressure difference across the pump.

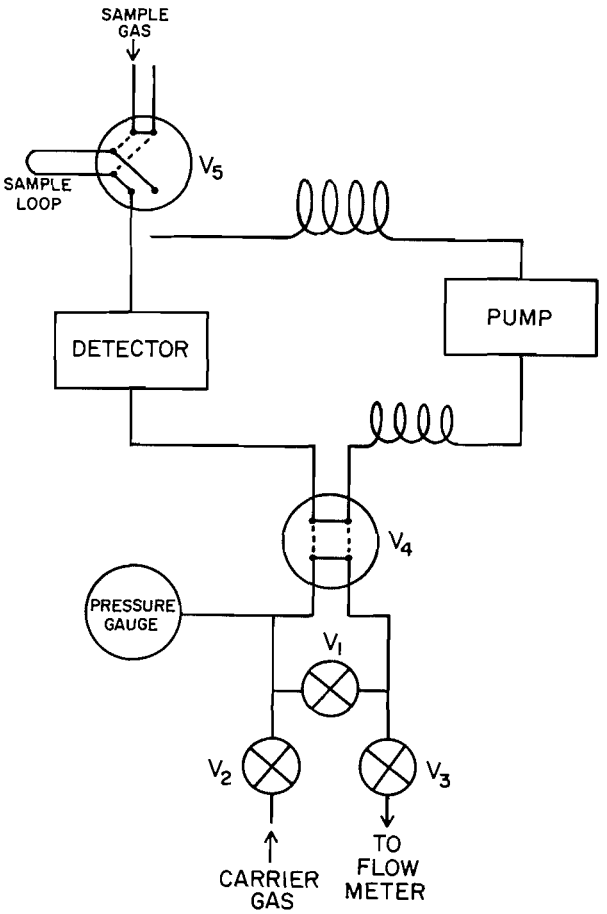

FIG. 1. Schematic diagram of cyclic chromatograph. V_1, V_2, and V_3 are simple on–off metal valves (Nupro #4J); V_4 and V_5 are 4- and 6-port, stainless-steel-and-Teflon switching valves (Valco).

In an experiment, the system was first pressurized and flushed with carrier gas through V_4, with V_1 closed and V_2 and V_3 open, with the pump and detector operating. When the baseline signal was steady and the pressure at the desired value, V_2 and V_3 were closed and V_1

[1]NRCC No. 23573.
[2]Summer assistant.

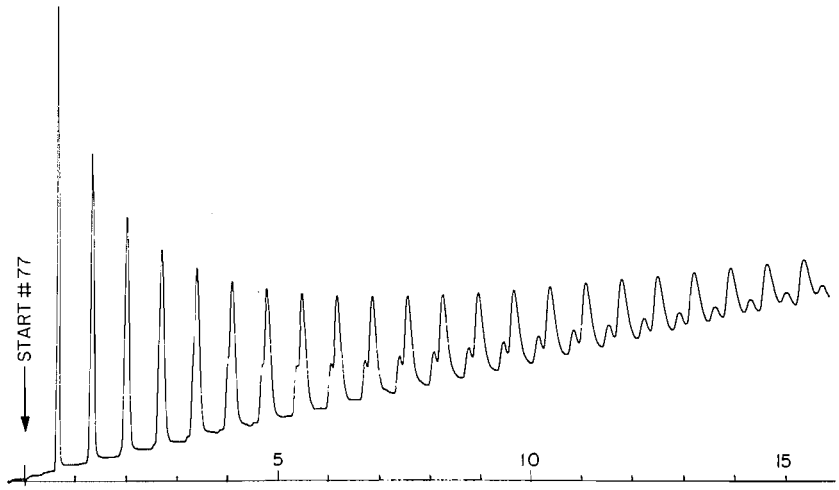

FIG. 2. Chromatogram of O_2–Ar sample in He carrier; O_2 has the shorter retention time. Peak height is plotted against retention time in minutes.

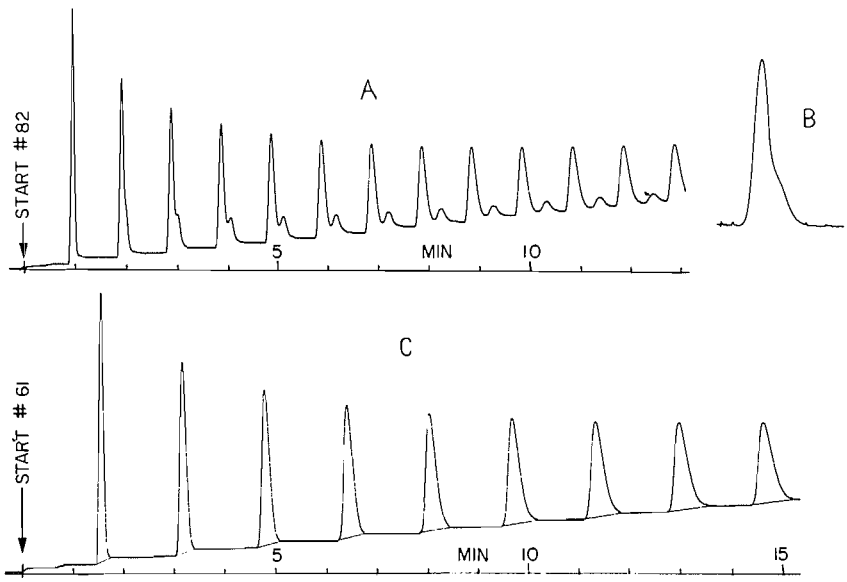

FIG. 3. *A*, chromatogram of air sample in He carrier, N_2 has the shorter retention time; *B*, chromatogram of air sample in He carrier from single pass through 50-ft. column; *C*, chromatogram of N_2 in He carrier, showing broadening of a single peak.

opened, so that the carrier gas continued to circulate through V_1. Pressure was recorded and could be monitored for a few minutes to test for leakage. V_4 was then switched to bypass the carrier gas supply, and finally V_5 was switched to pick up the sample gas which had been flushing through the sample loop.

Results and discussion

Figure 2 shows a typical chromatogram for a sample of O_2 and Ar in He carrier gas. The two components are first resolved on the ninth cycle and completely separated after 19 cycles, corresponding to 57 ft. of column. Faster separation is shown for a sample of air in He (Fig. 3*A*) where N_2 and O_2 are resolved after four cycles and separated after eight, corresponding to 24 ft. of column. For comparison an air peak is shown after a single pass through a 50-ft. column of Porapak T under comparable conditions (Fig. 3*B*) and it is seen that O_2 is only slightly resolved as a shoulder on the nitrogen peak. The improvement of the separation in the cyclic system is striking, probably reflecting the well-known loss of efficiency in the single-pass system due to the high pressure drop across the column and consequent non-uniform volume flowrate.

From the data in Figs. 2 and 3*A*, peak separations were measured and are plotted in Fig. 4 vs. the number of cycles. The separation of N_2 and O_2 increases linearly from zero, whereas that of O_2 and Ar shows some deviation. Lateral displacement of overlapping peaks,[3] and non-Gaussian peak shapes may have contributed to the different behaviour, and these measurements show how the cyclic system could be used to study factors affecting peak separation. The data in Figs. 2 and 3*A* also demonstrate a very practical use for the system for testing a particular column for a desired separation. Thus a short inexpensive column could be prepared and tested to determine whether a much longer column would be useful in a conventional single-pass chromatograph. We tested, for example, H_2–D_2 mixtures on the Porapak T column, and found no

[3]The position of the true maximum of a peak on a sloping baseline is not at the top of the peak, but rather is at the point at which the slope of the curve equals the slope of the baseline. For two overlapping peaks, this has the effect of pulling the apparent maxima closer together than the true maxima. For unequal peaks, the smaller is displaced more than the larger.

Can. J. Chem. Downloaded from www.nrcresearchpress.com by 210.87.254.105 on 09/06/12
For personal use only.

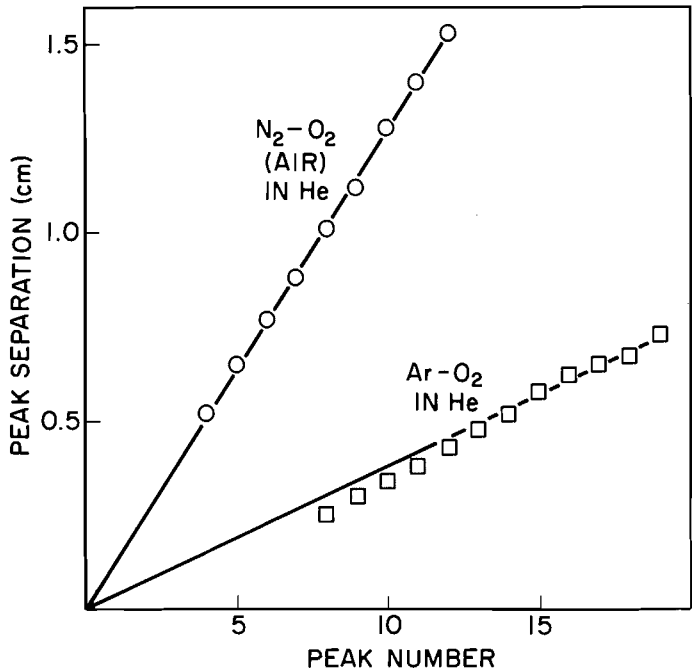

FIG. 4. Peak separation vs. peak number, from chromatograms in Figs. 2 and 3*A*.

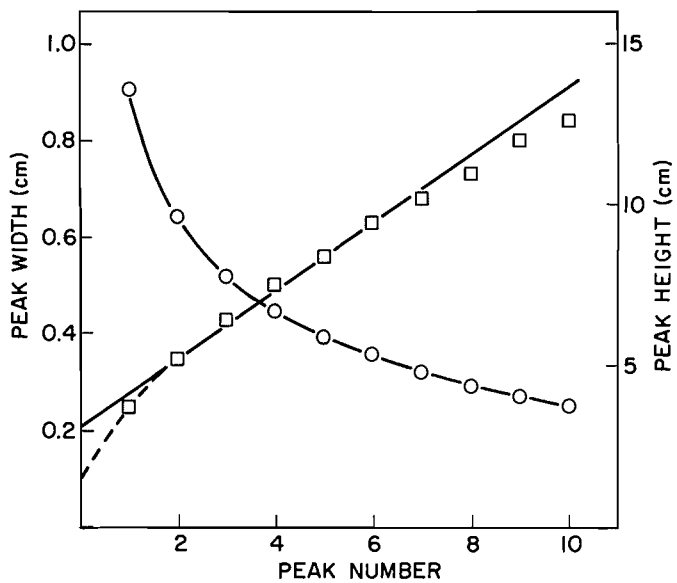

FIG. 5. Peak heights (○) and peak widths (□) from chromatogram in Fig. 3*C*.

separation after 51 cycles (153 ft. of column), although the sample peak was still well defined; there is clearly no point in trying a single column of this length for this separation.

The cyclic column could also be used itself for analysis of suitable two-component systems, but with more than two components overlap of peaks from successive cycles would probably cause problems. A second limitation is the need for a non-destructive detector such as a katharometer, which may lack the required sensitivity.

The cyclic chromatograph is also well suited to study the mechanism of peak broadening, which is of fundamental interest in gas chromatography. Figure 3*C* shows a fairly typical

TABLE 1. Peak broadening measurements

Carrier gas	Sample gas	Nominal* pump speed (cm^3/min)	Rate of broadening (min/cycle)	Time between peaks (min/cycle)
He	Ar	13	0.030	1.812
		28	0.020	1.062
		73	0.014	0.688
Ar	He	13	0.030	1.438
		28	0.014	0.859
		73	0.008	0.562
He	N_2	13	0.028	1.625
		28	0.020	1.000
		73	0.009	0.625
Ar	N_2	13	0.030	1.750
		28	0.015	1.062
		73	0.011	0.688
He	CH_4	13	0.066	2.625
		28	0.033	1.562
		73	0.021	1.000
Ar	CH_4	13	0.063	2.750
		28	0.046	1.625
		73	0.018	1.094

*Nominal pump speeds were measured in air at 1 atm. and zero pressure drop across the pump. True carrier gas flows were less because of pressure drop on inlet side of pump, which in turn depends on the flow rate and the viscosity of carrier. Rate of broadening was measured from linear portions of plots of peak width as in Fig. 5.

chromatogram from a sample of N_2 in He carrier gas. In Fig. 5 are plotted peak heights and peak widths at half maximum against the number of cycles. For four or five cyles, beginning usually with the second peak, the increase in peak width was approximately linear, falling off with subsequent cycles. The first peak often fell below this straight line as in Fig. 5. The major cause of peak broadening in gas chromatography is the simple statistical effect of the adsorption and desorption of the sample as it moves along the column. As treated simply by Phillips (3), for example, first-order adsorption and desorption will lead to a Gaussian peak for which it can be shown that for a given sample species and column, the width at half maximum should increase linearly with increasing retention time. This corresponds in the present system to a linear increase with the number of cycles, as seen in Fig. 5. The intercept of the linear plot should ideally correspond to the initial width of the peak as it is injected on the column. In fact it is about twice the value which can be estimated from the pickup volume of 0.2 cm^3 plus a small contribution from the detector volume (0.058 cm^3). The true behaviour of the system probably follows approximately the dashed curve in Fig. 5, with an initial more-rapid peak broadening, perhaps due to saturation of the solid adsorbent at the high initial concentration injected, and perhaps also an effect involving the change from the initial square shape of the injected sample into a Gaussian form. These effects were not further investigated. Peak area, as esimated by the product of peak height and peak width at half maximum, was almost constant in these experiments (Fig. 5), indicating that peak tails were not overlapping appreciably; this could be a problem at larger numbers of cycles.

Measurements of the linear rate of peak broadening were made from plots like Fig. 5 for a variety of samples and carrier gases, for different pump speeds, and results are summarized in Table 1. Each combination of sample and carrier was mea-

Can. J. Chem. Downloaded from www.nrcresearchpress.com by 210.87.254.105 on 09/06/12
For personal use only.

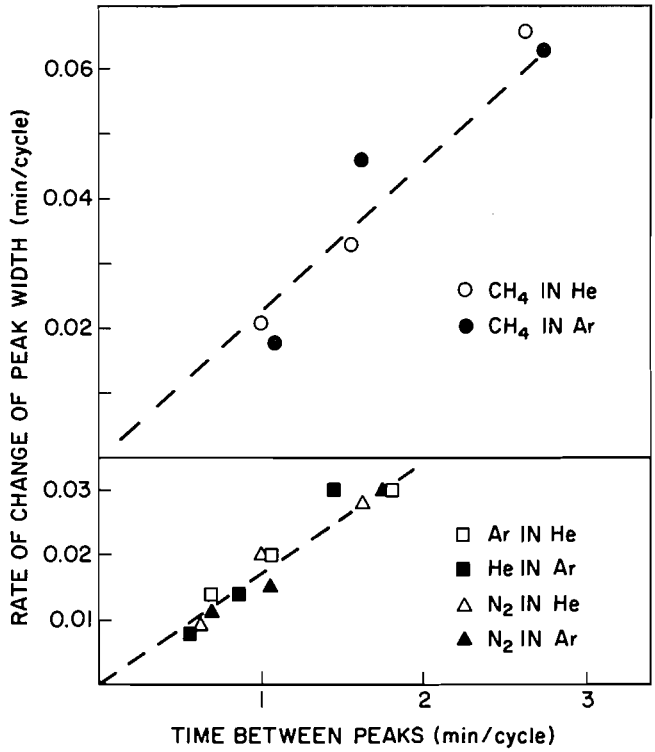

FIG. 6. Rate of peak broadening for a variety of sample and carrier gases.

sured at three different flowrates, and simple theory indicates that the peak broadening per cycle should increase linearly with the cycle period. Figure 6 shows that this is approximately true, and in fact the data from all the systems except those with methane samples fall around a single line. Two conclusions can be drawn from these data. First, there is little if any peak broadening due to circulation of the sample through the pump, valves, connections, detector, etc., i.e., the components in the loop other than the columns. If this occurred, peak broadening would be relatively faster at faster pump speeds, and the data in Fig. 6 would curve upwards. The absence of such broadening is not unexpected, as minimum-volume components were used throughout, but it is encouraging in as much as more fundamental causes of broadening can be examined without interference. Second, diffusion apparently contributes little to peak broadening in these experiments, as shown by the approximate similarity between systems such as He in Ar, N_2 in Ar, and Ar in He, in which the much faster diffusion of helium would have led to faster broadening if diffusion were an important factor. There are some minor but probably real trends evident in the data in Table 1 and Fig. 6 which will not be discussed further at the present time. The slopes of plots such as those in Figs. 5 and 6 are related to the number of theoretical plates for each system, and to the partition coefficient of the sample gas between the adsorbed phase and the gas phase, and such parameters could be obtained from these or similar measurements.

We have not attempted in this brief article to investigate and analyse rigorously factos affecting separation and broadening of peaks in gas chromatography. Liquid stationary phases would be better suited to this than the solid Porapak T employed, and results with the latter could doubtless be improved by more careful preparation and conditioning. We have instead tried to show how a simple cyclic closed-loop chromatograph can be operated, and to explore some of the ways it can be used to test columns and to study fundamental processes in gas chromatography.

1. R. S. PORTER and J. F. JOHNSON. Nature, **183**, 391 (1959).
2. R. A. BACK and J. M. PARSONS. Unpublished results.
3. C. PHILLIPS. Gas chromatography. Butterworths, London. 1956.

Can. J. Chem. Downloaded from www.nrcresearchpress.com by 210.87.254.105 on 09/06/12
For personal use only.

Thermostable sites of palladium phthalocyanine in Shpol'skii matrices of mixed solvents

WEN-HSIUNG CHEN, KLAUS E. RIECKHOFF, AND EVA-MARIA VOIGT
Departments of Physics and Chemistry, Simon Fraser University, Burnaby, B.C., Canada V5A 1S6

Received March 26, 1984

WEN-HSIUNG CHEN, KLAUS E. RIECKHOFF, and EVA-MARIA VOIGT. Can. J. Chem. **62**, 2264 (1984).

A study was made of the effects of three different mixed solvent Shpol'skii matrices at 4.2 K on site formation and on vibronic progressions of palladium phthalocyanine. It is found that only a limited number of thermostable sites are formed and these sites are common to all three matrices, but vary in their statistical weights. However, in all solvents the statistical weights of the first few most important sites are similar, with the predominant site at least eight or nine times stronger than the next. As well, the vibrational features of both the ground state and the first excited states of a few of the most populated sites examined are practically the same for the different mixed solvents. The absence of any significant differences in site splitting implies the absence of any dipolar interaction effects on these splittings.

The above findings provide a better insight into the interaction between phthalocyanine, intermediate solvent, and basic solvent (*n*-octane) in the three-component solutions and give a clear guideline for choosing convenient solvents and for using Shpol'skii matrices as a simple effective mechanism for producing quasi-line vibronic spectra of phthalocyanines and other related large molecules insoluble in the alkanes.

WEN-HSIUNG CHEN, KLAUS E. RIECKHOFF et EVA-MARIA VOIGT. Can. J. Chem. **62**, 2264 (1984).

Opérant à 4,2 K, on a étudié les effets de trois matrices, de type Shpol'skii et comportant trois solvants mixtes différents, sur le site de formation et sur les progressions vibroniques de la phtalocyanine de palladium. On a trouvé qu'il se forme un nombre restreint de sites thermostables, que ces sites sont communs à toutes les matrices, mais qu'ils varient dans leurs pondérations statistiques. Dans tous les solvants, les pondérations statistiques des quelques sites les plus importants sont toutefois toutes semblables et le poids statistique du site prédominant est au moins huit ou neuf fois plus important que celui du suivant. De la même manière, les caractéristiques vibrationnelles de l'état fondamental ainsi que du premier état excité, de quelques-uns des sites examinés les plus populeux, sont pratiquement les mêmes pour les différents solvants mixtes. L'absence de différences importantes dans le dédoublement des sites implique l'absence de tout effet d'interaction dipolaire sur ces dédoublements.

Ces observations fournissent une meilleure connaissance des interactions entre la phtalocyanine, le solvant intermédiaire et le solvant de base (*n*-octane) dans des solutions à trois composantes et elles fournissent des règles directrices claires dans le but de choisir des solvants convenables et pour utiliser des matrices de type Shpol'skii comme mécanisme efficace et simple de produire des spectres vibroniques quasi-lignes des phtalocyanines et d'autres molécules apparentées qui sont insolubles dans les alcanes.

[Traduit par le journal]

I. Introduction

The achievement of well-resolved vibronic spectra of phthalocyanine (Pc) complexes thus far has depended on the gas-phase supersonic jet-cooling (1) and low temperature matrix isolation of normal alkane (Shpol'skii) (2–4) and inert gas (5, 6) techniques. The technique of doping by substitution of suitable molecules in a condensed phase solution or crystal, although being successful in some smaller organic molecules (7, 8), is not applicable to the case of Pc due to the lack of substitutable molecules in the host. All the above techniques are capable of freezing the rotational degrees of freedom and producing resolved vibronic bands with width of several cm^{-1} or better, but the matrix isolation of Shpol'skii appears to be the simplest one for obtaining the desired effect. However, in this type of matrix one always encounters more than one possible site of symmetry for the Pc molecules and thus a number of different electronic potential curves result. This situation complicates the resulting overall vibronic structures. Therefore, it is useful to examine how many of these sites can actually be created by a specific host matrix under a fixed condition, what their statistical weights are, and how a slight change of host solvent can affect the site formation as well as the vibrational characteristics associated with each of the sites.

Since, in general, Pc complexes are not soluble in alkanes, intermediate solvents (inter-sols) can be used to incorporate them into the alkanes to achieve the Shpol'skii effect. The inter-sols used in this report included α-chloronaphthalene (α-ClN), tetrahydrofuran (THF), and benzene. These structurally different molecules are all mixed with the same alkane: *n*-octane $C_8H_{18}(C_8)$. When these mixed solvent Pc solutions are cooled quickly, one finds great inhomogeneity both in site formation (increasing the number of possible sites) and in the electronic potential curves of a site (broadening the band width of an individual site). Accordingly, these solutions must be frozen slowly to obtain a thermostable site distribution as well as to optimize the spectral band resolution.

Among the many metallophthalocyanines (M—Pcs) studied in our laboratory (3, 4, 9, 10), PdPc was found to be one of the best for experimental study of such complexes. The existing data (9, 10) show that it has fairly strong emissions in both fluorescence and phosphorescence, with a Q-band absorption that can be easily reached by a tunable laser using DCM dye. It exhibits several detectable sites of symmetry when incorporated into an alkane base mixed solvent. Aside from the well studied predominant site, represented by the set of origins {15286, 15355 cm^{-1}}, there is at least one more site whose vibrational features are strong enough to be adduced for comparison. The presence of two origins in the 0–0 fluorescence of a site comes from the lifting of the excited states E_u double degeneracy in a matrix environment as was reported in the cases of metalloporphyrins (M—Ps) (11, 12). We shall designate the upper origin, the zero-point high energy component of the first excited singlet state, S_y, and the lower origin, the vibrationless lower energy component, S_x. Counterparts of S_y

Can. J. Chem. Downloaded from www.nrcresearchpress.com by 210.87.254.105 on 09/06/12
For personal use only.

Can. J. Chem. Downloaded from www.nrcresearchpress.com by 210.87.254.105 on 09/06/12
For personal use only.

and S_x in the triplet state shall respectively be called T_y and T_x. At the experimental temperature, 4.2 K, in the fluorescence region, both the low and the high energy components (S_y and S_x) of the doublets of some strong sites are discernable. However, in the phosphorescence region this is not the case: one sees only the low energy component (T_x) of these sites. The doublet splitting detected either in the fluorescence region or from the emission−excitations varies from site to site between 60 to 90 cm^{-1}. The site−site separations normally are from a few to several tens of cm^{-1}. Therefore it is often possible to select an individual site for study by preferential excitation.

II. Experimental

The apparatus and techniques used in this report have been described previously (3, 4, 10). PdPc was obtained from K & K commercially and, without further purification, was dissolved in an inter-sol before being incorporated into C_8. The concentrations were about 10^{-5} *M* Pc or less in the mixed final solutions, which were cooled in a small glass cell inside a dewar. The emissions of the sample at liquid helium temperature were excited by a dye laser using DCM pumped by an Ar^+ laser and detected after dispersion by a Spex Industries 3/4 m (single grating) or a 1/2 m (double grating) spectrometer by a Philips 150 CVP (S1) or an ITT FW130 (S20) photomultiplier. The output signal was processed by either photon counters (PAR SSR 1105, SSR 1110) or lock-in-amplifiers (PAR model 124, HR 8). The total uncertainty in spectral band position is less than ±2.0 cm^{-1}.

III. Results and discussion

Although Pc complexes are difficult to separate, complexes have their own "finger-print" emissions and absorptions (or rather emission-excitations in our case) and hence can be identified. In the general 0−0 fluorescence region (15250−15450 cm^{-1}) of PdPc in the Shpol'skii matrices, there is no overlapping with other impurity Pc's 0−0 bands, especially the ubiquitous metal-free Pc. However, active vibrations of the first excited singlet states of most Pcs do fall into this region, but can be suppressed by the careful choice of monitoring positions during emission excitation study. Consequently, spurious excitation bands appearing in this region are distinguishable from the genuine ones, and all emission bands reported can be unambiguously assigned to the 0−0 fluorescence of the multiple sites of PdPc in the matrices. In the phosphorescence region (10070−9970 cm^{-1}) two impurity bands of non-Pc origin, 10037 and 9992 cm^{-1}, with intensities comparable to those of the minor site 0−0 phosphorescences, were found and not included in the discussion. In total, eight sites appeared consistently in both fluorescence and phosphorescence regions. The single band 0−0 phosphorescence positions represent, in order of decreasing energy (cm^{-1}), site A to site H. Detectable vibronic progressions normally cover a range of less than 1500 cm^{-1} above the origins. However, not all of the progressions belonging to the eight sites are detectable or suitable for recording.

(A) Symmetry-species in the α-ClN + C_8 Shpol'skii matrix

The general 0−0 fluorescences of the multiple sites of PdPc in Shpol'skii matrices spanned some 200 cm^{-1} in range, as was previously stated. This can be most easily seen in Fig. 8 (N) discussed later in III(*C*), where sharp band multiple site 0−0 fluorescences in α-ClN + C_8 are shown. Although the intensities of these emissions vary by orders of magnitude, we first of all enumerated in detail all of them; followed by pairwise grouping to determine the number of sites, since each pair

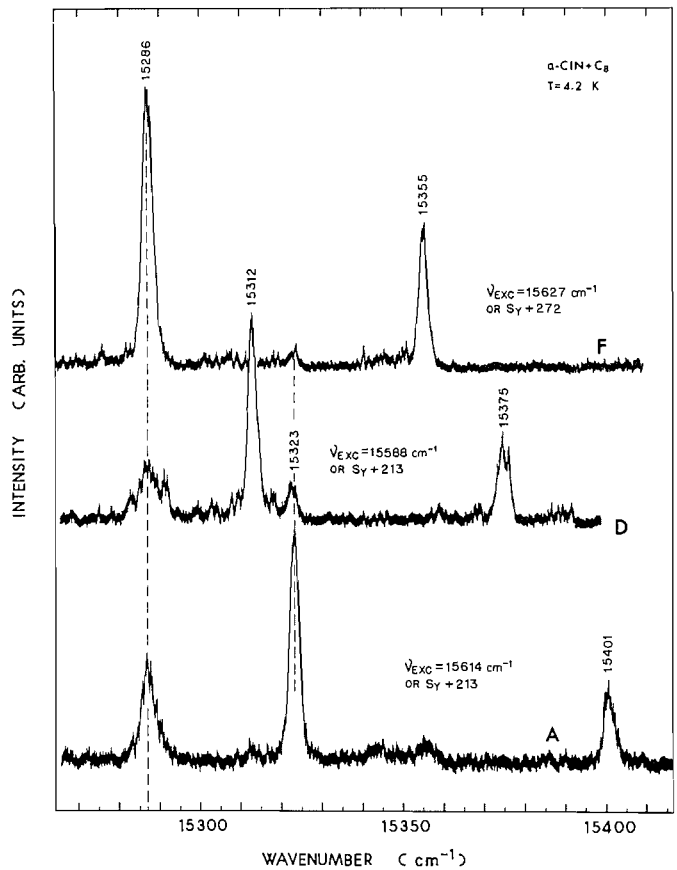

FIG. 1. 0−0 fluorescences of some of the most populated sites of PdPc in α-ClN + C_8 obtained by exciting the fundamentals of the S_y components of the sites, using ν_{exc} = 15627 (S_y(F) + 272), 15588 (S_y(D) + 213), and 15614 (S_y(A) + 213) cm^{-1}, respectively for (F), (D), and (A). The numbered bands represent the doublets of the sites. It is seen that the 15286 cm^{-1} band appeared also in the other two cases (D) and (A).

belongs to a single site of symmetry in the matrix and the number of pairs represents the number of sites. Figure 1 illustrates the doublet feature of some of the most populated sites of PdPc in α-ClN + C_8, obtained by exciting their S_y fundamentals. Since the high energy (S_y) components of the less populated sites are too weak to be excited in this manner, the doublet feature of these sites does not appear in this figure. However, the doublet can be easily seen in the excitation spectra that we shall discuss later.

The 0−0 phosphorescences of these thermostable sites were subsequently observed in the ir region of 10070−9970 cm^{-1} using the previously found 0−0 fluorescence frequencies as excitation. At 4.2 K only one band was observed for each site because of much faster relaxation from the T_y component into the lower energy T_x component than the radiative phosphorescent rate of the T_y component. Figure 2 shows the phosphorescences of these multiple sites in the matrix. These phosphorescence bands were shown to be genuine by their respective excitation spectra which have the doublet structures in the same positions as the 0−0 fluorescences of these sites. Figure 3 shows this correspondence in all of the eight sites. To conclude the present sub-section we list all the possible sites (from A to H) of PdPc in α-ClN + C_8 in Table 1 where the sites are represented by the doublet positions and the statistical weights by the intensity ratios with respect to the predominant

TABLE 1. Positions of 0−0 fluorescences (or phosphorescence-excitations) and 0−0 phosphorescences of the multiple site PdPc in α-ClN + C_8 at 4.2 K

Symmetry species	Phosphorescence position (cm^{-1}) $\{T_x, T_y\}$	Fluorescence or excitation position (cm^{-1}) $\{S_x, S_y\}$	Splitting ($S_y - S_x$) $\Delta \pm 2$ cm^{-1}	Approximate intensity ratio
A	10054, —	15322, 15401	79	5
B	10052, —	15321, 15407	86	5
C	10049, —	15311, 15374	63	10
D	10047, —	15311, 15376	65	10
E	10024, —	15291, 15369	78	5
F	10017, —	15286, 15355	69	100
G	09988, —	15336, 15426	90	1
H	09974, —	15255, 15343	88	1

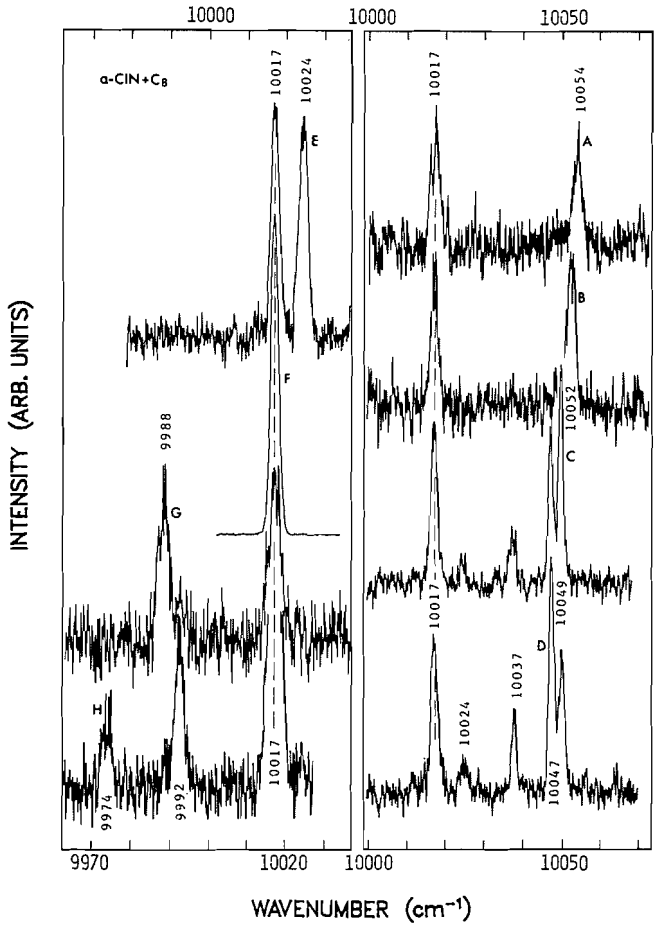

FIG. 2. 0−0 phosphorescences of the multiple site PdPc in α-ClN + C_8 at 4.2 K. From sites A to H, they are peaked at 10054, 10052, 10049, 10047, 10024, 10017, 9988, and 9974 cm^{-1}, respectively. Note that the 10017 cm^{-1} band of the prominent site F appears in all of the cases. The excitation frequencies used were the S_y components of the sites, except the one used for the F site, where S_x was used instead. Consecutively for site A to H, they are 15401, 15407, 15373, 15375, 15369, 15286, 15426, and 15344 cm^{-1}. Two impurity bands, 10037 and 9992 cm^{-1}, alongside of some PdPc phosphorescence bands are also shown.

site F (taken as 100).

PdPc aggregation species are not strong enough to compete with the symmetry species, and they do not emit or absorb in the same general region as the monomeric symmetry species. This is clear from the following. First, the concentrations of PdPc in the mixed solvents are low; second, the divalent Pd does not aggregate readily; and third, the size of the Davydov splitting of Pc complexes due to dimerization is known to be of the order of 1000 cm^{-1} or more (13), suggesting dimeric contributions be found at least 500 cm^{-1} away from the present region.

(B) Vibronic progressions of different site symmetries in different Shpol'skii matrices

The vibronic progressions for PdPc in matrices, just like most of the M—Pc complexes studied (3, 4, 14), show very strong 0−0, weak 0−1 (4% of the 0−0 or less), and even weaker 0−2 (usually undetectable) bands, characterizing a very small Stokes loss for the normal vibrations or very weak vibronic and electron−phonon interactions (15). Most of the fundamental vibrations that are found in the emissions can also be found in the excitations, which implies that the molecular symmetry is roughly preserved in the excited state. However, intensity mirror symmetry of these fundamentals between emission and excitation is not observed usually. Furthermore, these vibronic progressions are quite short and most of the important fundamentals are found in a range of less than 1000 cm^{-1} above their respective origins. Therefore it is sufficient to compare the fundamentals of the different sites in this spectral range.

1. Excitation spectra of sites in the α-ClN + C_8 matrix

Details of the fluorescence-excitation spectra on the predominant site F {15286, 15355 cm^{-1}} covering 1500 cm^{-1} above the doublet origins (S_x and S_y) have been reported elsewhere (10). The vibronic progressions of the next important site C {15311, 15374 cm^{-1}} show very much the same general features as those found in the predominant site reflecting an extremely weak effect of the local environment on the π-electron resonance of Pc. This can be clearly seen in Fig. 4 (NC and NF), illustrating the 0−0 fluorescence-excitations of the low energy S_x components of the C and F sites in α-ClN + C_8. The numbers marked on the progressive bands represent the vibrational energies with respect to the specific origins. Progressive bands that are not numbered belong to the S_y components. As there is a difference in crystal field splitting of the C and F sites ~(63 vs. 69 cm^{-1}), the relative spacings between the numbered and the unnumbered bands in these sites are not the same. Therefore, in order to show the correspondence of the numbered bands in the different sites of the matrices, we have employed a relative scale on the abscissa which puts all origins at zero. This scheme is used in Fig. 4 as well as in the next three figures. Figure 5 (NC and NF) displays the 0−0 fluorescence

Can. J. Chem. Downloaded from www.nrcresearchpress.com by 210.87.254.105 on 09/06/12
For personal use only.

Can. J. Chem. Downloaded from www.nrcresearchpress.com by 210.87.254.105 on 09/06/12
For personal use only.

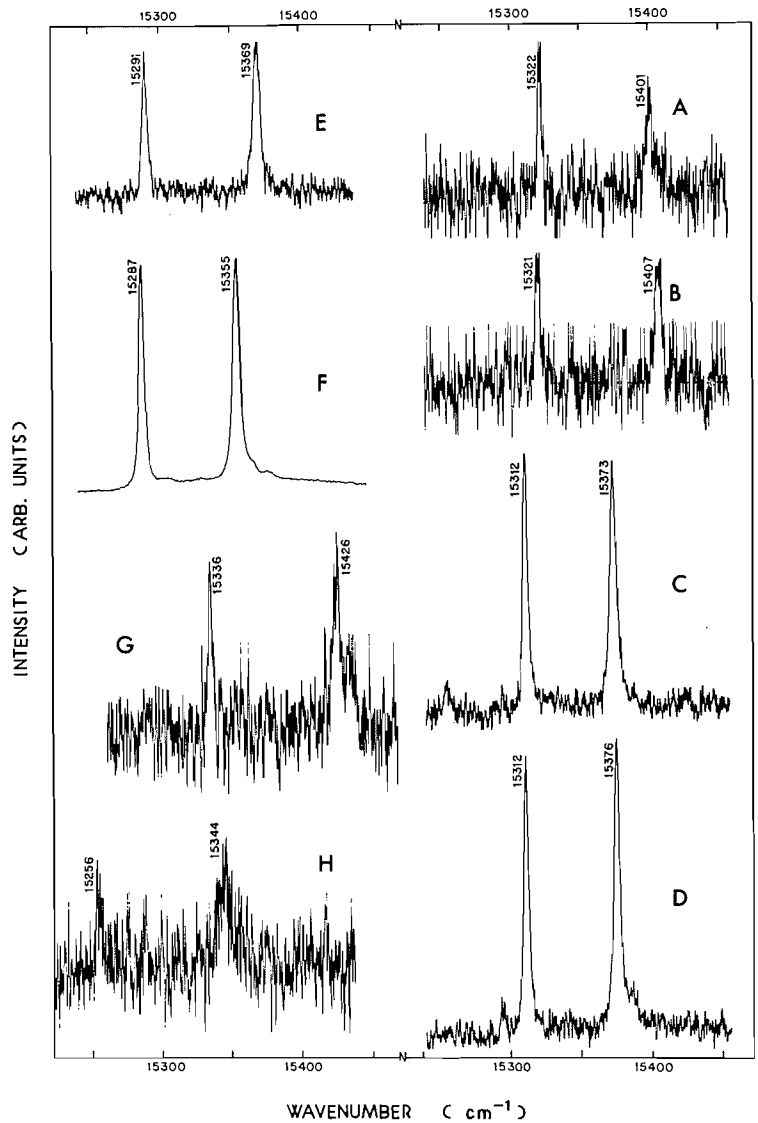

FIG. 3. Phosphorescence excitation spectra of the multiple site PdPc in α-ClN + C_8. Each shows a doublet feature corresponding to the two zero-point components of the first excited singlet state (S_x and S_y) of the sites. They are obtained by monitoring the intensities of the 0−0 phosphorescence (T_x) of the sites, from A to H, at 10054, 10052, 10049, 10047, 10024, 10017, 9988, and 9974 cm^{-1}, respectively.

excitations of the high energy S_y components of the sites in the matrix where, since the progressive bands are numbered with respect to these origins, the alignment of the vibrational bands in the C and F sites is seen to be restored. The effect of the crystal field is now on the weaker unnumbered bands of the S_x components and therefore not clearly perceptible.

2. Fluorescence/Raman spectra of sites in the α-ClN + C_8 matrix

While the fluorescence-excitation spectra of the vibronics of PdPc multiple sites are not interfered with by Pc impurity emissions from different centers, the fluorescence/Raman spectra, in contrast, are often masked or overlapped by contributions from impurities, especially the strong H_2Pc fluorescences. These Raman/fluorescence spectra on the whole cover a spectral region from 13400 to 15300 cm^{-1}, and those of the predominant site F in α-ClN + C_8 have been reported in detail and analyzed by us in another paper (10). These spectra can be obtained by exciting either the high energy S_y components or the low energy S_x components of the doublets. When excitation is made to S_x the progressions appear in Raman, whereas if excitation is made to S_y both progressions appear in Raman and fluorescence, causing overall weaker and messier spectra due to energy sharing and band overlapping. The concurrence of Raman and fluorescence bands with a single excitation frequency in PdPc (and in RuPc)[1] is an interesting case which is rare in the Pc complexes and deserves attention (10). The vibronic transitions from S_x of the B {15321, 15407 cm^{-1}}, C {15311, 15374 cm^{-1}}, and F {15286, 15355 cm^{-1}} sites in α-ClN + C_8 are presented in Fig. 6 (NB, NC, and NF). It is seen that the fundamentals of all three sites are the same when the origins are shifted to a common point. This is particularly clear for those vibrations with energies lower than the 0−0 fluorescences of H_2Pc (14410 and 14474 cm^{-1}). For those with energies higher than those 0−0's of H_2Pc, the same correspondence can be exemplified by the 1533±2 cm^{-1} fundamental. The combined Raman/fluorescence vibronic spectra obtained

[1]Unpublished results.

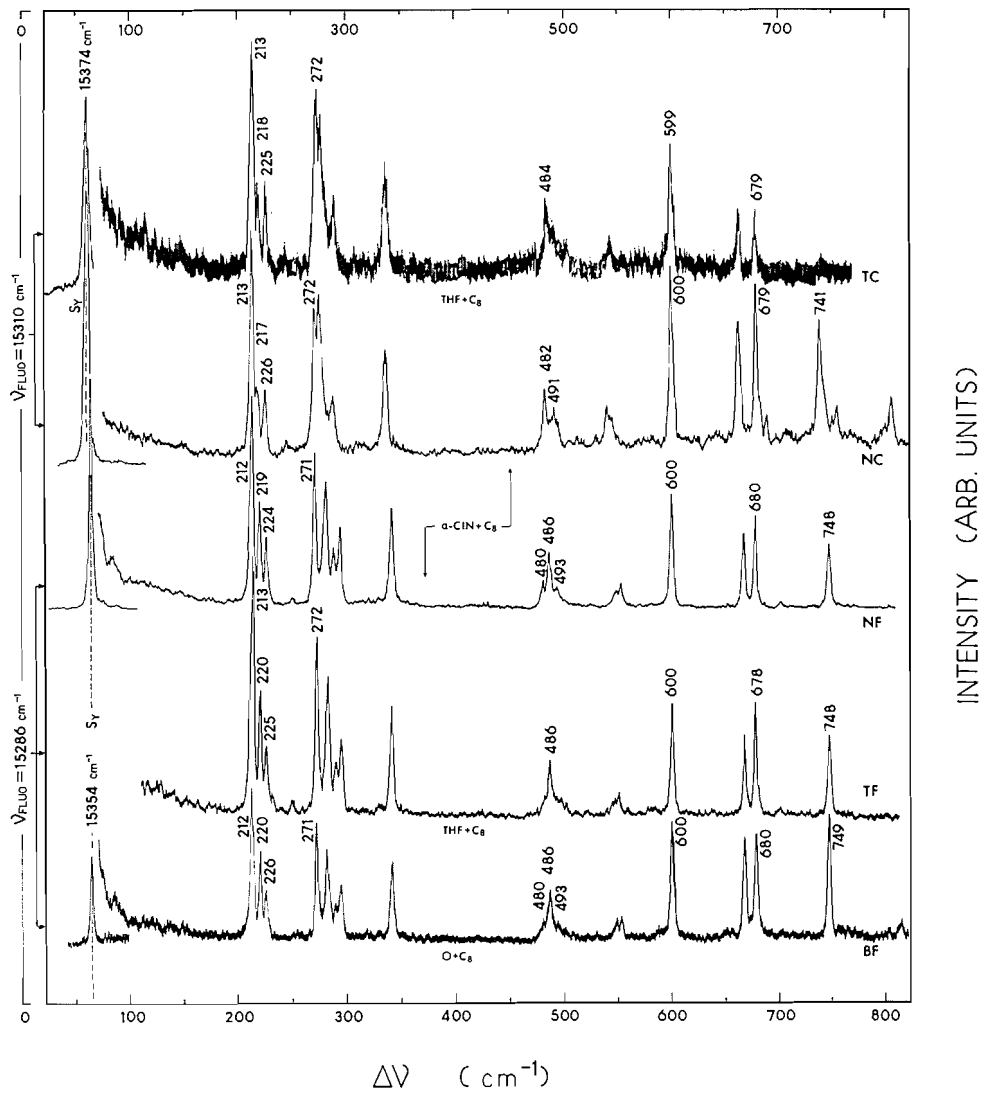

FIG. 4. 0−0 fluorescence excitation spectra of the C and F sites in both α-ClN + C_8 (NC and NF) and THF + C_8 (TC and TF), and the F site in benzene + C_8 (BF), using $\nu_{fluo} = S_x$. The abscissa measures the vibrational energies of S_x of the sites in the matrices. Absolute progressive band positions can be obtained by simply adding the vibrational numbers to their respective origins in cm^{-1}. Unnumbered bands are the vibronics of S_y components and are labeled in Fig. 5.

by exciting S_y of the C and F sites in α-ClN + C_8 are given in Fig. 7 (NC and NF). Although weaker and more complicated, the correspondence is recognizable in most of the low frequency vibrations. Here the correspondence was made in the fluorescence (F) bands, leaving the Raman (R) bands of the site C to shift a few cm^{-1} away from those of the site F due to unequal crystal field splittings mentioned previously in these two sites. From these results it is clear that the site effect on the molecular fundamental vibrations in the ground state is minimal or negligible, as well.

3. Vibronic progressions in the two other matrices

Fluorescence-excitation spectra of the C and F sites in THF + C_8 using $\nu_{fluo} = S_x$ and S_y are presented in Figs. 4 (TC and TF) and 5 (TC and TF), respectively. Those of the predominant F site in benzene + C_8 are given in Figs. 4 (BF) and 5 (BF), respectively. The emission spectra of the F site in THF + C_8 using $\nu_{exc} = S_x$ and S_y are shown in Figs. 6 (TF) and 7 (TF), respectively. The same spectrum of the F site in benzene + C_8 excited with S_x is presented in Fig. 6 (BF). The spectrum excited with S_y appeared too weak to provide any meaningful information and therefore is not included in Fig. 7. All of the spectra that belong to a particular site presented in Figs. 4−7 are found to be practically identical in all three matrices. The only difference among the same type of spectra in different matrices is the solvent-related overall intensity response and spectral quality. Therefore we conclude that the intermediate solvents (inter-sols) show no effect on the molecular symmetry in both the ground and the first excited states.

In general, we have found that for the best overall intensity response and spectral quality when using a good inter-sol, one can afford to increase the mixing ratio of C_8 to inter-sol and still get a good signal-to-noise ratio. Meanwhile, the high mixing ratio isolates the doublet components and prevents site/site communications more effectively, resulting in better intensity-balanced spectra originating from the doublet components of a site. The mixing ratio also appears to affect the weight distribution of the sites in different matrices.

(C) Comparison of symmetry-species in different matrices

PdPc in an α-ClN + C_8 matrix when excited with 15425

Can. J. Chem. Downloaded from www.nrcresearchpress.com by 210.87.254.105 on 09/06/12
For personal use only.

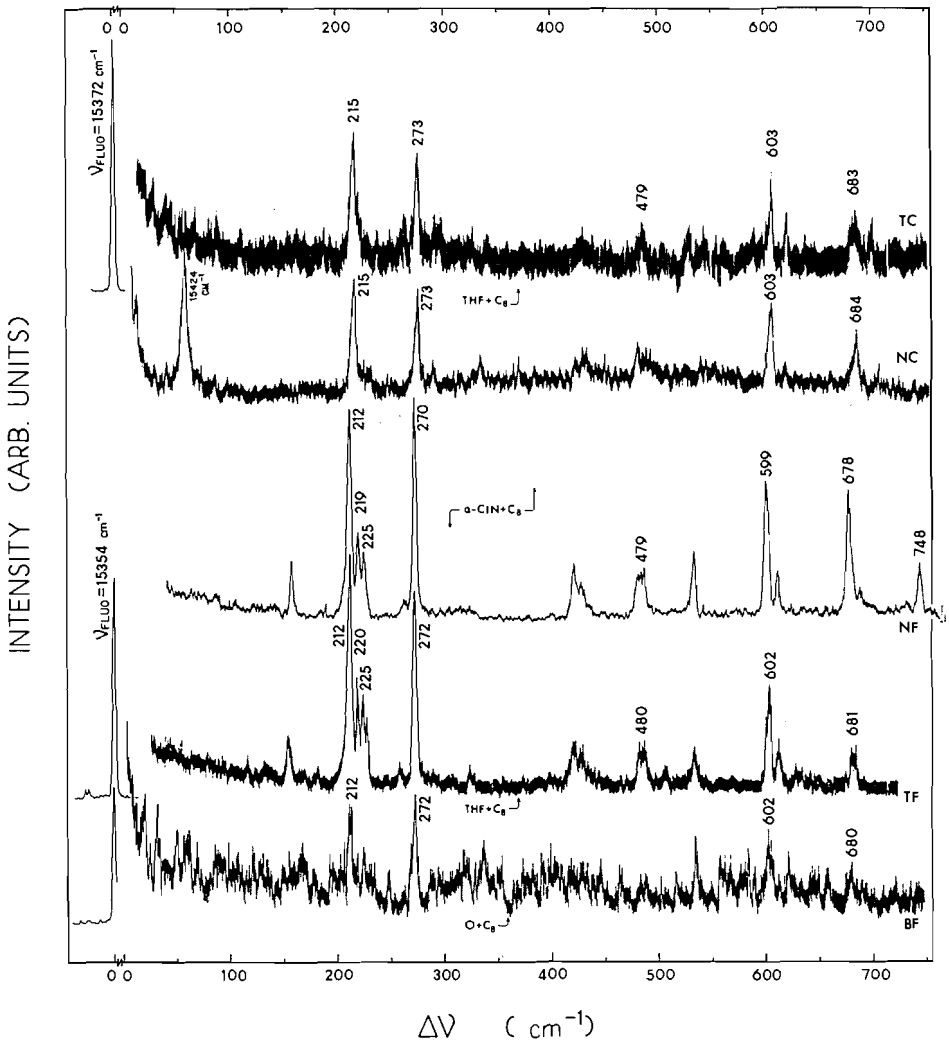

FIG. 5. 0−0 fluorescence excitation spectra of the C and F sites in both α-ClN + C_8 (NC and NF) and THF + C_8 (TC and TF), and the F site in benzene + C_8 (BF), using $\nu_{fluo} = S_y$. The horizontal axis scales the vibrational energies associated with their respective origins in cm^{-1}. A few unnumbered S_x fundamentals also showed up in the spectra which are labeled in Fig. 4 previously. The 15424 cm^{-1} band in (NC) may be assigned to the G site S_y.

cm^{-1} showed seven bands: Fig. 8 (N). These bands in fact depict all eight sites that are known to us: the 15256 and 15342 cm^{-1} (not resolved from the 15336 cm^{-1} band) stand for site H. The 15287 and 15356 cm^{-1} represent site F. The 15291 cm^{-1} band, residing on the high-energy shoulder of the prominant 15287 cm^{-1} band and masked by it, is the low energy (S_x) component of site E. The 15311 and 15373 cm^{-1} bands stand for the two unresolved sites of C and D, which are only 1−2 cm^{-1} apart; and the 15321 cm^{-1} band stands for the S_x components of two other unresolved sites A and B. Finally, the 15336 cm^{-1} band is the S_x component of site G. The unresolved sites in the figure resulted from the selection of excitation and slit width, which were chosen to display as many sites as possible with one single frequency. The same excitation frequency of 15425 cm^{-1} was subsequently used for the other two matrices: THF + C_8 and benzene + C_8. The results are illustrated in Fig. 8 (T) and (B). It is seen that some of the bands that showed up in Fig. 8 (N) are no longer discernable in (T) or (B). For example, the 15321 cm^{-1} band is not clearly seen in (T) and (B), and the 15256 cm^{-1} band is missing in (B). However, these missing bands can be made to reappear if their S_y counterparts are chosen as excitation reflecting the existence of these sites but with an overall variation of the statistical weight distribution of sites in the different matrices. The weight distribution of sites was found to vary with the concentration of PdPc, the sample freezing rate, and annealing process, the slight variation (uncertainty) in excitation frequencies (±1 cm^{-1}), the type of intermediate and basic solvents, and, possibly, the mixing ratio of the two solvents. Reproduction of the identical weight distribution of sites in one matrix can be obtained only when those variables are fully controlled. In our experimental situation, the Pc concentrations in the three different matrices were roughly the same and the freezing rate was also kept about the same (2 to 3 h to solidify the samples from room temperature). After solidification, the samples were subsequently chilled to 4.2 K and were not annealed at any higher temperatures. The mixing ratios of α-ClN, THF, and benzene to C_8 were approximately 1:5−6, 1:2, and 1:2, respectively. Under those conditions we have the weight distribution, represented by the intensity ratios, for each matrix as listed in Table 2. Even though there is a variation in the statistical weights of the minor sites, in these matrices there is a unique site that is dominant and constitutes at least 70% of the total site population.

Can. J. Chem. Downloaded from www.nrcresearchpress.com by 210.87.254.105 on 09/06/12
For personal use only.

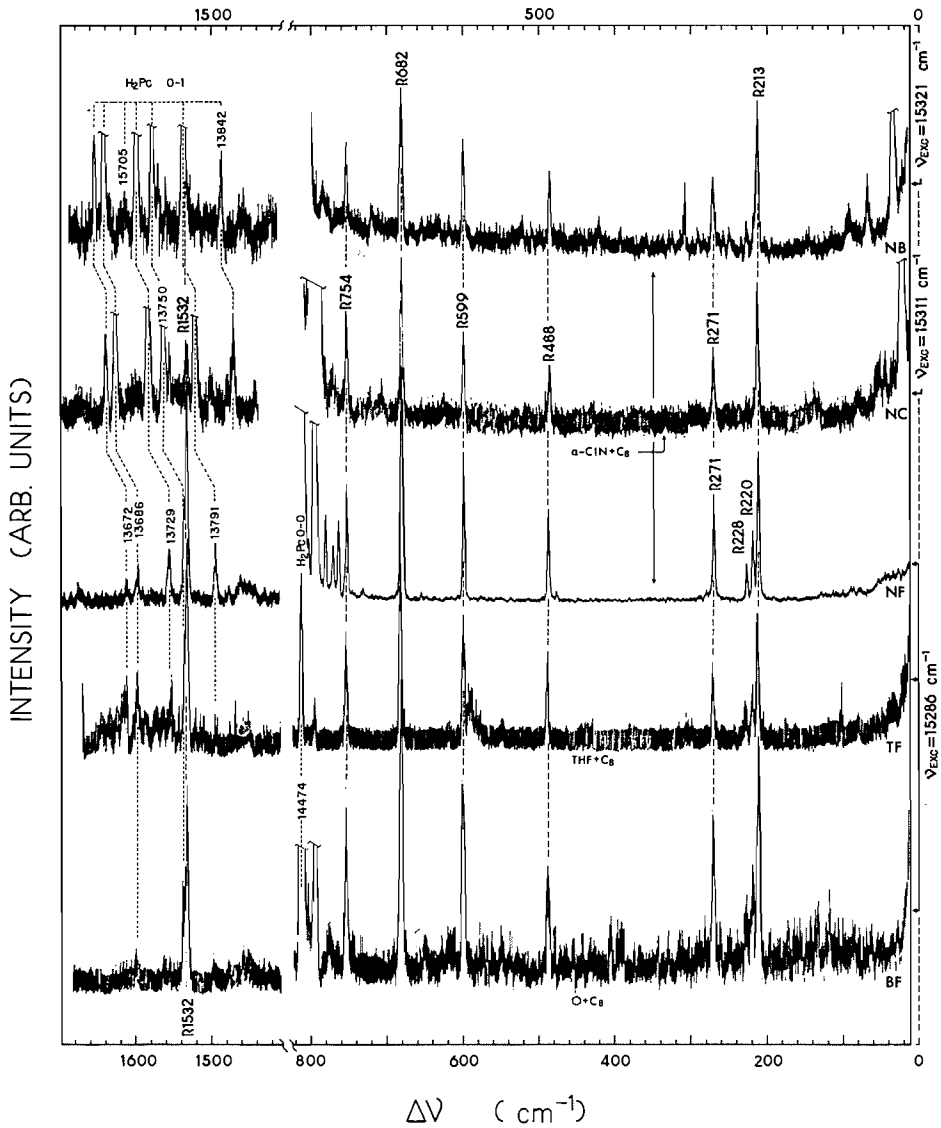

FIG. 6. Resonance Raman spectra of the B, C, and F sites in α-ClN + C_8 (NB, NC, and NF), and the F site in both THF + C_8 (TF) and benzene + C_8 (BF). The excitation frequencies used were the S_x components of the sites. The abscissa measures the vibrational energies of the ground state from zero and hence is relative. The letter R is used to emphasize the bands are Raman in nature. Their absolute positions can be calculated by subtracting the R numbers from their excitation frequencies. The five digit H_2Pc band positions in cm^{-1} are absolute.

Further examples which generalize the study of similar symmetry sites in different matrices are found in the site splittings of PtPc and ZnPc in α-ClN + C_8 and benzene + C_8 matrices, where, incidentally, the samples were frozen rapidly.[1] Since PtPc does not fluoresce, the investigation of the distinct sites was made in the phosphorescence region (10530−10580 cm^{-1}) with the 0−0 emission bands. We have found that all ten sites that the benzene + C_8 matrix can support are also to be found in the α-ClN + C_8 matrix. On the other hand, the site splittings of ZnPc were studied with the 0−0 fluorescence bands in the spectral range 14930−14800 cm^{-1}. Again, it is found that the site splittings in both matrices were the same. α-ClN is a molecule with a permanent electric dipole moment, whereas benzene is not. Therefore the above findings clearly indicate that the electric dipole moment associated with an inter-sol molecule has no effect on the site splitting. Such an absence of dipolar interaction effects on the spectral features sheds additional light on the relationship between Pc and the inter-sol molecules and that between the inter-sol and C_8 as is discussed below.

Porphyrin (P) and other structurally related molecules also exhibit multiple sites in the Shpol'skii matrices. A theoretical study of P in a C_8 matrix (16) has elucidated the nature of the particular defects corresponding to the observed sites in this system. It was shown that the C_8 lattice was capable of supporting two or three molecule vacancy cages which do not collapse and could accommodate a P molecule in such a way that its π-orbital system was less perturbed than is usual in typical solid environments. However, this work does not completely fit our study in two different aspects. First, in our case the host was not a pure C_8 crystalline matrix but rather a matrix obtained from the mixture of an inter-sol with C_8 whose crystalline condition is not yet explored. Second, the number of distinct sites found in our case is greater than those theoretically predicted for pure C_8. As was mentioned, to incorporate the PdPc into C_8 requires the aid of an inter-sol, thus two different views concerning the close association of the inter-sol molecule and the PdPc can be hypothesized: one is that the close association

Can. J. Chem. Downloaded from www.nrcresearchpress.com by 210.87.254.105 on 09/06/12
For personal use only.

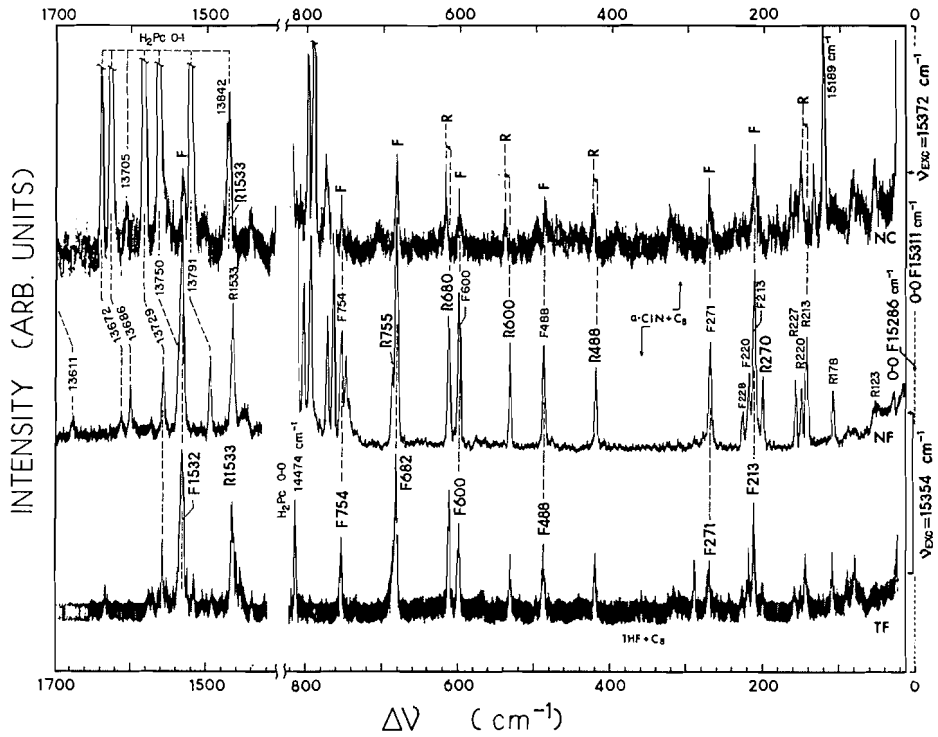

FIG. 7. Resonance Raman (R) and fluorescence (F) spectra of the C and F sites in α-ClN + C_8 (NC and NF) and the F site in THF + C_8 (TF). The excitation frequencies used were of the S_y components of the sites. The abscissa applies only to the F numbers which represent the fundamentals of the ground state of the system. The absolute positions of R and F bands can be obtained by subtracting the numbers from their excitation frequencies and 0−0 fluorescences, respectively. Bands labeled in five digit numbers are absolute and are contributions of impurities. In (NC) the 15189 cm^{-1} impurity band is related to the 10037 cm^{-1} band in Fig. 2, and R1533 is masked by the metal free 13842 cm^{-1} band and is not clearly seen.

TABLE 2. Statistical weights of the symmetry species of PdPc in Shpol'skii matrices

Site $\{S_x, S_y\ cm^{-1}\}^a$	Intensity ratios in matrices[b,c] α-ClN + C_8 (1:5−6)	THF + C_8 (1:2)	Benzene + C_8 (1:2)
A {15322, 15401}	5	3	4
B {15321, 15407}	6	4	5
C {15311, 15374}	8	11	9
D {15311, 15376}	12	9	12
E {15291, 15369}	5	3	5
F {15286, 15355}	100	100	100
G {15336, 15426}	2	1	4
H {15255, 15343}	1	1	3

[a]Position uncertainty ±2 cm^{-1}.
[b]Ratio uncertainties on the A, B, E, G, and H sites are about 20−30%; those on the C and D sites, 5−15%.
[c]Estimated under site selection excitations.

of the inter-sol molecule and PdPc is maintained in the two component matrix, i.e., both inter-sol and Pc are found in the cage; the other is that this close association breaks down and only Pc is found in the cage. If the first view prevailed, we would anticipate no drastic reduction of the band-width when the spectra of Pc in inter-sol are compared with those in inter-sol + C_8. Furthermore, we would expect a more sensitive inter-sol dependency on the overall spectral response. Since we have found well defined spectral bands of only several cm^{-1} in width and we have demonstrated that site formation and vibronic features are hardly affected by a change of inter-sol, we are led to the second view that the "bare" PdPc is isolated in a matrix of mixed solvent. Such a mixed solvent matrix of unspecified crystalline state would provide more variety in vacancy defects into which a PdPc molecule could be accommodated than the theory described for P in a pure C matrix. Furthermore, the inter-sols in the mixed solvent matrices would have less direct influence on the π-orbital system of the PdPc than would the pure inter-sols in their own matrices. This interpretation is supported by a dynamic study in which it was found that the phosphorescence lifetime of PdPc remains the same when α-ClN in the mixed solvent matrix is replaced by α-IN (α-iodonaphthalene) (10).

IV. Conclusion

It was concluded that two component mixed solvents, such as α-ClN + C_8, THF + C_8, and benzene + C_8, form Shpol'skii matrices which have a limited number of vacancy defects in various weight distributions, comparable to the case described for pure C_8 (16, 17). As shown here in detail for PdPc and further confirmed by our analogous studies of ZnPc and PtPc,[1] any Pc molecule in a particular vacancy will interact weakly with its environmental "cage"; and depending on the cage size and relative orientation, it will have a different energy of doublet splitting. This interpretation explains why for matrices composed of C_8 plus different inter-sols of approximately the same size but of different electric dipolar nature:

we always find the same number of symmetry sites; the sizes of the doublet splitting vary; there is no discernable dipolar interaction effect on the details of the spectra; and there is no perceptible difference in the vibronic characteristics associ-

Can. J. Chem. Downloaded from www.nrcresearchpress.com by 210.87.254.105 on 09/06/12
For personal use only.

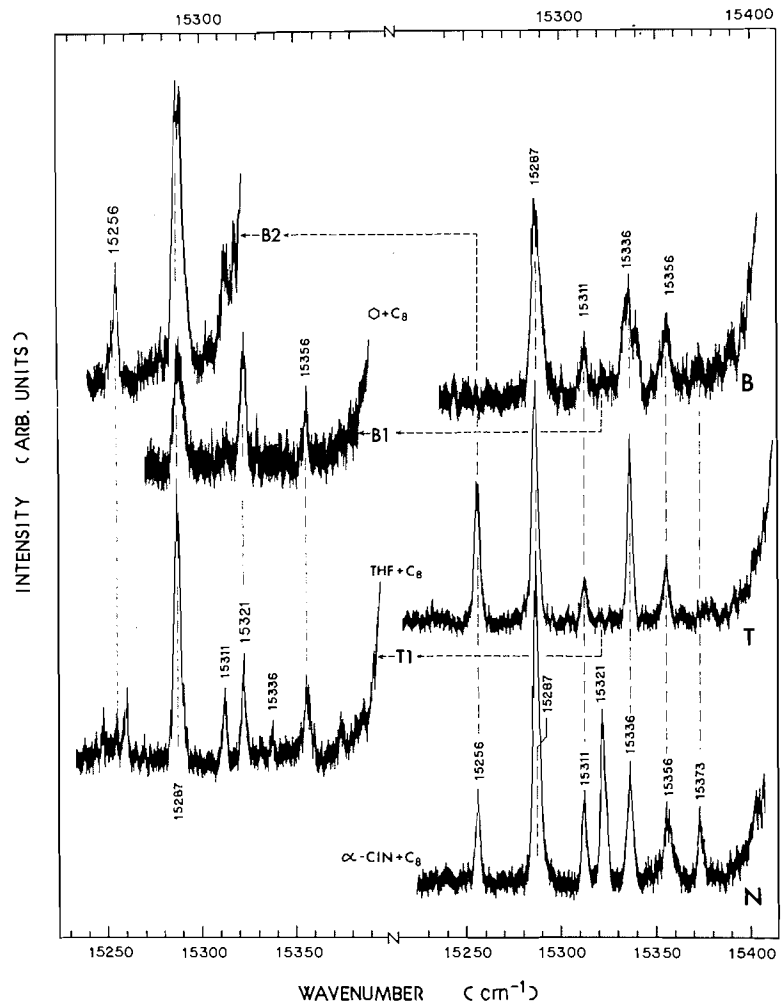

FIG. 8. 0−0 fluorescences of the multiple site PdPc in α-ClN + C_8 (N), THF + C_8 (T and T1), and benzene + C_8 (B, B1, and B2). The first three spectra on the right-hand side of the figure, (B), (N), and (T), were obtained by exciting with the same frequency of 15425 cm^{-1}. The 15321 cm^{-1} band not clearly seen in (T) and (B) is shown to reappear in (T1) and (B1) by utilizing ν_{exc} = 15408 cm^{-1}; and the 15256 cm^{-1} band, missing in (B), is shown to restore in (B2) by employing ν_{exc} = 15342 cm^{-1}.

ated with a given site among the different types of the two component matrices.

In all matrices examined there was always a unique thermodynamically most stable site which was weighted overwhelmingly in the distribution. This unique site is by its very nature an excellent representative for the study of the system and thus the analysis and interpretation of the complex vibronic features and other fundamental aspects of the multisite systems is greatly simplified.

Because the spectra detail is practically unaffected by the different inter-sol applied, one is free to select virtually any solvent that dissolves enough Pc and is also miscible with *n*-alkanes.

Acknowledgement

This research was supported by operating and equipment grants from the Natural Sciences and Engineering Research Council of Canada to K.E.R. and E.M.V.

1. P. S. H. FITCH, C. A. HAYNAM, and D. H. LEVY. J. Chem. Phys. **73**(3), 1064 (1968).
2. A. A. GOROKHOVSKII. Opt. Spectrosc. **40**(3), 272 (1976).
3. T.-H. HUANG, K. E. RIECKHOFF, and E. M. VOIGT. Chem. Phys. **36**(3), 423 (1979).
4. T.-H. HUANG, K. E. RIECKHOFF, and E. M. VOIGT. J. Chem. Phys. **77**(7), 3424 (1982).
5. E. BAJEMA, M. GOUTERMAN, and B. MEYER. J. Mol. Spectrosc. **27**, 225 (1968).
6. V. E. BANDYBEY and J. H. ENGLISH. Am. Chem. Soc. **101**(13), 3446 (1979).
7. D. S. MCCLURE. J. Chem. Phys. **22**(10), 1668 (1954).
8. R. OSTERTAG and H. C. WOLF. Phys. Stat. Sol. **31**, 139 (1969).
9. P. S. VINCETT, E. M. VOIGT, and K. E. RIECKHOFF. J. Chem. Phys. **55**(8), 4132 (1971).
10. T.-H. HUANG, W.-H. CHEN, K. E. RIECKHOFF, and E. M. VOIGT. J. Chem. Phys. **80**(9), 4051 (1984).
11. I. Y. CHAN, W. G. VAN DORP, T. J. SCHAAFSMA, and J. H. VAN DER WAALS. Mol. Phys. **22**(5), 741 (1971).
12. G. W. CANTERS, G. JANSEN, M. NOORT, and J. H. VAN DER WAALS. J. Phys. Chem. **80**(20), 2253 (1976).
13. A. R. MONAHAN, J. A. BRADO, and A. F. DELUCA. J. Phys. Chem. **76**(14), 1994 (1972).
14. T.-H. HUANG, K. E. RIECKHOFF, and E. M. VOIGT. Can. J. Chem. **56**(7), 976 (1978).
15. K. K. REBANE. Impurity spectra of solids. Plenum, New York. 1970. p. 71.
16. T. R. KOEHLER. J. Chem. Phys. **72**(5), 3389 (1980).
17. T. A. WEBER and E. HELFAND. J. Chem. Phys. **72**(7), 4014 (1980).

Can. J. Chem. Downloaded from www.nrcresearchpress.com by 210.87.254.105 on 09/06/12
For personal use only.

Gas phase chemistry of α-thio carbanions

STEEN INGEMANN AND NICO M. M. NIBBERING[1]

Laboratory of Organic Chemistry, University of Amsterdam, Nieuwe Achtergracht 129, 1018 WS Amsterdam, The Netherlands

Received January 9, 1984

STEEN INGEMANN and NICO M. M. NIBBERING. Can. J. Chem. **62**, 2273 (1984.

Proton abstraction from CH_3SCH_3 and $C_6H_5SCH_3$ in the gas phase has been studied by the use of Fourier Transform Ion Cyclotron Resonance (FT-ICR) mass spectrometry. The gas phase acidity of CH_3SCH_3 is reported to be $\Delta G^0_{acid} = 1615 \pm 8$ kJ/mol. The methyl group in $C_6H_5SCH_3$ is observed to be the most acidic position. The gas phase acidity of this group is determined to be $\Delta G^0_{acid} = 1560 \pm 8$ kJ/mol. The structure and reactivity of the $[M - H]^-$ ions from CH_3SCH_3 and $C_6H_5SCH_3$ are probed by studying their reactions with various molecules. Rate constants are reported for the reactions of $CH_3SCH_2^-$ – and several other nucleophiles – with CH_3Cl, CH_3Br, and HCO_2CH_3.

STEEN INGEMANN et NICO M. M. NIBBERING. Can. J. Chem. **62**, 2273 (1984).

Opérant en phase gazeuse et faisant appel à la spectrométrie de masse par résonance cylotronique des ions combinée à la transformation de Fourier (RCI-TF), on a étudié l'abstraction de protons du CH_3SCH_3 et du $C_6H_5SCH_3$. L'acidité en phase gazeuse du CH_3SCH_3 est $\Delta G^0_{acide} = 1615 \pm 8$ kJ/mol. On observe que le groupe méthyle du $C_6H_5SCH_3$ est la position la plus acide. On a déterminé que l'acidité en phase gazeuse de ce groupe est $\Delta G^0_{acide} = 1560 \pm 8$ kJ/mol. On a évalué la structure et la réactivité des ions $[M - H]^-$ obtenus à partir du CH_3SCH_3 et du $C_6H_5SCH_3$ en étudiant leurs réactions avec diverses molécules. On rapporte les constantes de vitesse des réactions du $CH_3SCH_2^-$ – et de plusieurs autres nucléophiles – avec le CH_3Cl, le CH_3Br et le HCO_2CH_3.

[Traduit par le journal]

Introduction

The influence of a heteroatom on an adjacent carbanionic center has received considerable attention (1–9). The fact that the acidity of C—H bonds α to a heteroatom can be enhanced has led to the development of synthetically important organometallic compounds (1–3). The mechanism of the stabilization of the negative charge on a carbon atom adjacent to second row elements – especially sulfur – has been a matter of debate. Overlap between the carbanionic lone pair with a vacant 3*d* orbital on the sulfur atom has been used to explain the higher acidity of the α C—H bonds in sulfides compared to the α C—H bonds in ethers (1, 2). Earlier MO calculations indicated that the 3*d* orbitals on the sulfur atom had no effect on the proton affinity of α-thio carbanions (4, 5, 6*b*, 8). Recent calculations on geometry optimized ions predict, however, that the 3*d* orbitals are essential for a proper description of α-thio carbanions (10). On the basis of the PMO theory, interaction between the carbanionic lone pair and the anti bonding σ* orbital of the X—R (X = O, S) group was proposed to contribute to the stabilization of the carbanionic site (5, 7, 10). This interaction was argued to be stronger in the α-thio carbanions than in the α-oxy carbanions and to be more effective when the carbanionic lone pair is antiperiplanar to the X—R bond, thus providing a possible explanation for the preferential equatorial lithiation of 1,3-dithiane (11). Qualitatively, the lower proton affinity of α-thio carbanions compared to that of α-oxy carbanions has been ascribed to the larger polarizability of the sulfur atom compared to that of the oxygen atom (4, 6, 8).[2]

The experimentally obtained information on the properties of α-thio carbanions has been derived nearly exclusively from solution studies. Simple α-thio carbanions do not exist, however, as free ions in solution; only the corresponding organometallic compounds are known. In order to determine the stability and reactivity of simple α-thio carbanions free from solvent and counterion effects, it is necessary to generate them in the gas phase.[3] Proton removal from 1,3-dithiane and 1,3-dithiolane in the gas phase has been studied by Bartmess *et al.* (13), but no quantitative data on the gas phase acidity of these compounds could be obtained due to dominant elimination reactions and fragmentation of the formed carbanions. The present paper reports the gas phase acidity of CH_3SCH_3 and the methyl group in $C_6H_5SCH_3$. The reactivity of α-thio carbanions in the gas phase is probed by studying the reactions between $CH_3SCH_2^-$ and varius molecules. The results have been obtained by the use of Fourier Transform Ion Cyclotron Resonance (FT-ICR) mass spectrometry (14).

Experimental

All experiments were performed with a homemade Fourier Transform Ion Cyclotron Resonance (FT-ICR) mass spectrometer. The basic hardware (15), software (16), and the general operation procedure (17, 18) of the instrument have been described previously. The total pressure was normally $0{,}5-1{,}0 \times 10^{-4}$ Pa. The ratio of the partial pressures of $RSCH_3$, NH_3, and HA (conjugate acid of the anion of interest) was typically 1/0,5–1/0,5–1. The pressures were measured on an ionization gauge placed in a side arm of the main pumping line. The ionization gauge was calibrated against a MKS Baratron (type 170 M, head type 94 AH-1) placed in the same side arm using N_2 as calibrant.

General procedure

The primary reactant ions NH_2^-, OH^-, F^- and Cl^- were generated by dissociative resonance capture of electrons (electron energy in brackets) by NH_3 (5 eV), H_2O (6 eV; HO^- is formed via H^-), CF_4 (6 eV), and CCl_4 (0 eV) respectively. Dissociative resonance capture of electrons by NH_3 leads also to formation of H^- ions. The H^- ions were ejected from the cell by applying a radio frequency (rf) pulse with a frequency of 180 kHz to the trapping plates of the cell. This pulse was

[1]Author to whom correspondence may be addressed.

[2]NOTE ADDED IN PROOF: Very recent *ab initio* calculations by P. v. R. Schleyer, T. Clark, A. J. Kos, G. W. Spitznagel, C. Rohde, D. Arad, K. N. Houk, and N. G. Rondan have shown that the stabilization of carbanions by second row substituents is due chiefly to polarization and to negative hyperconjugation, but not to *d*-orbital effects as suggested in ref. 10. We thank Professor Schleyer for communicating these results to us prior to publication.

[3]Mechanistic aspects of gas phase anion–molecule reactions are reviewed in ref. 12.

Can. J. Chem. Downloaded from www.nrcresearchpress.com by 210.87.254.40 on 09/06/12
For personal use only.

Can. J. Chem. Downloaded from www.nrcresearchpress.com by 210.87.254.40 on 09/06/12
For personal use only.

generated with the oscillator normally used for ejection of electrons (18). The pulse started simultaneously with the quench pulse (18) and ended shortly after the electron beam pulse. The other reactant ions used were generated by exothermic proton transfer to NH_2^-. The H^- ions formed from NH_3 were ejected in the cases of anions having a larger proton affinity than CH_3O^-. In the cases of anions having a lower proton affinity than no ejection of H^- was applied.

To observe the reactions of a given ion all other ions present in the cell were ejected by applying an rf pulse to the excitation plates. At the frequency corresponding to the m/z ratio of the ion of interest, the phase of this pulse was shifted 180 degrees. This causes a notch in the wave form of the ejection pulse at that frequency (16*b*). The relationship between a reactant ion and its product ion(s) was established in all cases by ejecting the reactant ion with an rf pulse starting just after the "notch ejection" pulse.

Rate and equilibrium constants

Rate and equilibrium constants were measured by monitoring the abundances of the ions present in the cell as a function of reaction time. In the kinetic experiments exponential decrease of the abundance of the reactant ion was observed in all cases. Correction for variation of the total ion current expressed as the sum of the ion abundances was achieved by normalizing this sum of ion abundances. The total ion current varied on an average less than 30% over the time interval studied. The pressures used to calculate the rate and equilibrium constants were measured with the ionization gauge. These pressures were used because oversaturation of the ionization gauge at pressures larger than 10^{-2} Pa led to a non-linear correlation with the Baratron readings in most of the cases.

Materials

The majority of the chemicals used were commercially available. The CH_3SCD_3 and $C_6H_5SCD_3$ (both about 99% d_3) compounds were prepared by reaction between RSK and CD_3I. The compounds were purified by preparative gc before use; CH_3SCD_3: OV 17, temperature 30–40°C; $C_6H_5SCD_3$: OV 17, temperature 100°C.

Results

CH_3SCH_3

Reaction of NH_2^-, $C_2H_5NH^-$, and $(CH_3)_2N^-$ with CH_3SCH_3 proceeds exclusively by proton transfer. The rate constants and reaction efficiencies are given in Table 1 (19).

The intramolecular kinetic deuterium isotope effects associated with the reaction between the amide ions and CH_3SCD_3 are given in Table 2. The values in Table 2 have been determined by monitoring the relative abundance of the $[M - H]^-$ and $[M - D]^-$ ions as a function of reaction time and then extrapolating to zero reaction time. This procedure proved necessary because hydrogen–deuterium exchange reactions between the ions and $C_2H_5NH_2$ or $(CH_3)_2NH$ caused a rather fast change in the relative abundance of the $[M - H]^-$ and $[M - D]^-$ ions with increasing reaction time (see ion structures).

In the OH^-/H_2O system equilibrium [1] is observed (see Fig. 1).

$$[1]\quad \underset{m/z\ 17}{HO^-} + CH_3SCH_3 \rightleftharpoons H_2O + \underset{m/z\ 61}{[M - H]^-}$$

The equilibrium constant for reaction [1] is determined to be $K = 0.058 \pm 0.012$. This value is the average of 7 experiments using different partial pressures of the acids. Moreover, the system has been allowed to reach equilibrium starting with either OH^- and CH_3SCH_3 or the $[M - H]^-$ ion and H_2O. Although propene has a gas phase acidity very close to that of H_2O (20), reaction [2] could not be observed.

$$[2]\quad \underset{m/z\ 41}{CH_2{=}CH{-}CH_2^-} + CH_3SCH_3 \not\rightleftharpoons CH_2{=}CH{-}CH_3 + \underset{m/z\ 61}{[M - H]^-}$$

TABLE 1. Rate constants for proton abstraction from CH_3SCH_3 by amide ions

A^-	k_{exp}[a]	k_{ADO}[b]	Efficiency[c]	ΔH_r^d (kJ/mol)
NH_2^-	2.7±0.4	2.60	1.04	−44
$C_2H_5NH^-$	0.8±0.1	1.82	0.44	−26
$(CH_3)_2N^-$	0.7±0.1	1.82	0.38	−14

[a]In units of 10^{-9} cm^3 molecule^{-1} s^{-1}. The error given is the standard deviation. Temperature assumed to be 298 K.
[b]In units of 10^{-9} cm^3 molecule^{-1} s^{-1}. Calculated using the Average Dipole Orientation Theory by Su and Bowers (19).
[c]The reaction efficiency is k_{exp}/k_{ADO}.
[d]Calculated using ΔH_f^0 data given in ref. 22 and Table 8.

TABLE 2. Intramolecular kinetic isotope effects associated with the reaction between CD_3SCH_3 and the amide ions

A^-	$PA(A^-)$ (kJ/mol)[a]	k_H/k_D[b]	No. of experiments
NH_2^-	1689	2.43±0.07	5
$C_2H_5NH^-$	1671	3.29±0.18	6
$(CH_3)_2N^-$	1658	2.92±0.03	4

[a]Values taken from ref. 20.
[b]Values obtained by extrapolation to zero reaction time and corrected for ^{13}C and ^{33}S contributions. The error given is the standard deviation. The actual error might be ~10%.

The weaker gas phase base CH_3O^- does not react with CH_3SCH_3 under the experimental conditions even though S_N2 substitution is exothermic.[4]

$$[3]\quad \underset{m/z\ 31}{CH_3O^-} + CH_3SCH_3 \not\rightarrow CH_3OCH_3 + \underset{m/z\ 47}{CH_3S^-}$$
$$\Delta H_r^0 = -53.6\ \text{kJ/mol}$$

In accord with this, no S_N2 substitution is observed in any of the other anion/CH_3SCH_3 systems studied.

The gas phase nucleophilicity of the $[M - H]^-$ ion from CH_3SCH_3 has been probed by studying its reactions with CH_3Cl, CH_3Br, and HCO_2CH_3. Rate constants for the displacement of Cl^- and Br^- from CH_3Cl and CH_3Br respectively have been measured for several nucleophiles in order to provide a basis for comparison. Furthermore these measurements have verified whether the rate constants for S_N2 substitutions previously measured with either the Ion Cyclotron Resonance (ICR) or the Flowing Afterglow (FA) method could be reproduced with our FT-ICR instrument (21, 23, 24). The data have been collected in Tables 3 and 4. The rate constants for the reaction of the $[M - H]^-$ ion from CH_3SCH_3 and the allyl anion with HCO_2CH_3 are given in Table 5.

The rate constants given in the tables have been obtained as outlined in the experimental section. The values are an average of 3–6 measurements using different partial pressures of the substrates. The error on the absolute values might be quite large (~50%), basically due to the uncertainty in the measurement of the exact pressure of the substrate. For a given substrate the relative values can be considered more accurate (~20%). The rate constants measured with our FT-ICR instrument agree

[4]Local energy barriers towards gas phase S_N2 substitutions have been discussed in ref. 21 and heat of formation data have been taken from refs. 20 and 22.

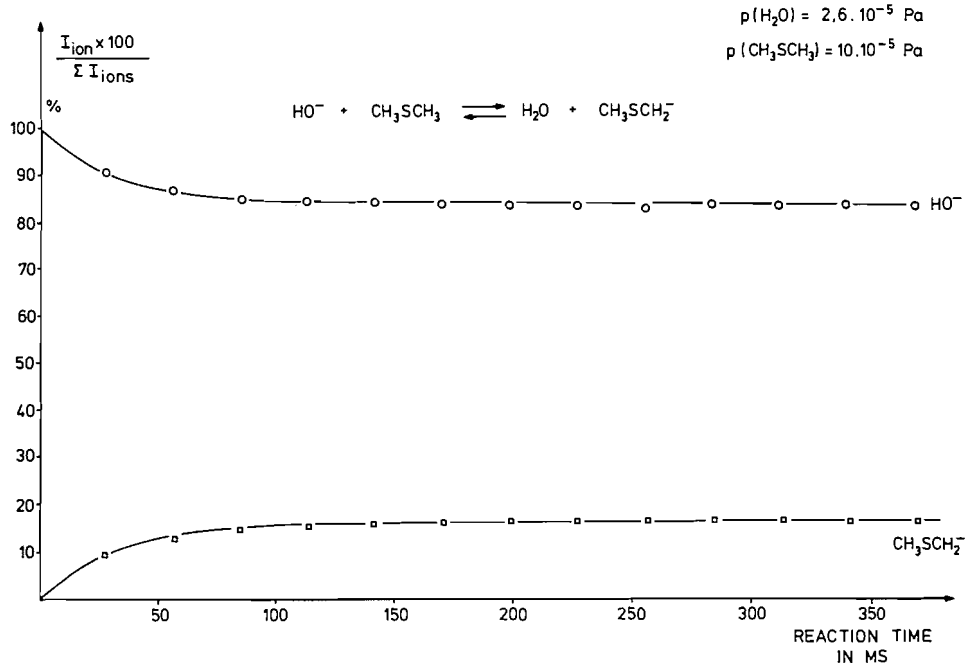

FIG. 1. Relative intensities of the HO^- and $CH_3SCH_2^-$ ions in the $HO^-/H_2O/CH_3SCH_3$ system followed as a function of reaction time.

TABLE 3. Rate constants for reaction between anions and CH_3Cl

A^-	k_{exp}[a] FT-ICR	k_{exp}[a] ICR[b]	k_{exp}[a] FA[c]	k_{ADO}[d]	Efficiency[d]	ΔH_r (kJ/mol)[e]
$CH_3SCH_2^-$	0.30±0.03	—	—	1.60	0.19	−383
$CH_2{=}CH{-}CH_2^-$	0.26±0.04	—	0.29[f]	1.79	0.15	−271
$HC{\equiv}C^-$	0.087±0.003	0.052	0.13	2.11	0.041	−228
HO^-	1.7±0.1	1.6	1.5	2.44	0.70	−210
CH_3O^-	0.80±0.06	0.49	1.3	1.96	0.41	−185
$C_2H_5O^-$	0.78±0.03	—	—	1.74	0.45	−169
CH_3S^-	0.064±0.004	0.078	0.11	1.72	0.037	−132
$C_2H_5S^-$	0.026±0.004	—	—	1.60	0.016	−124
F^-	0.83±0.05	0.8	1.9	2.34	0.35	−129

[a]In units of 10^{-9} cm^3 $molecule^{-1}$ s^{-1}. The error on the FT-ICR results is the standard deviation. Temperature assumed to be 298 K.
[b]Values taken from ref. 21.
[c]Values taken from ref. 23.
[d]See notes *b* and *c* for Table 1. Calculated using values from ref. 22 and Table 8.
[f]Value taken from ref. 24.

quite well with the values obtained by other experimental methods (see Tables 3 and 4).

$C_6H_5SCH_3$

$C_6H_5SCH_3$ contains several acidic sites. To determine whether the phenyl or the methyl hydrogen atoms are the more acidic, reactions of a series of anions with $C_6H_5SCD_3$ have been investigated. The competition between proton and deuteron abstraction in each system has been determined by monitoring the relative abundances of the $[M - H]^-$ and $[M - D]^-$ ions as a function of reaction time and extrapolating to zero reaction time (see Fig. 2 for an example). The results are given in Table 6. In the $CH_3O^-/C_6H_5SCH_3$ system equilibrium [4] is observed (Fig. 3).

[4] $CH_3O^- + C_6H_5SCH_3 \rightleftharpoons CH_3OH + [M - H]^-$
m/z 31 m/z 123

The equilibrium constant for reaction [4] is $K = 0.774 \pm 0.064$ as an average of 6 experiments. Different partial pressures of the acids have been used and the reaction has been studied from either side of eq. [4].

No reaction could be observed between the $[M - H]^-$ ion from $C_6H_5SCH_3$ and *p*-xylene or toluene although the latter compounds have gas phase acidities close to the value for CH_3OH (20). Similarly, no reaction between the $[M - H]^-$ ions from *p*-xylene or toluene and $C_6H_5SCH_3$ has been observed.

To gain more insight into the relative acidity of the different positions in $C_6H_5SCH_3$, hydrogen–deuterium exchange between the $[M - H]^-$ ion and D_2O has been studied (Fig. 4) (25). The corresponding results for the $C_6H_5SCD_3/OD^-/D_2O$ systems are shown in Fig. 5.

In the amide ion systems no S_N2 substitution is observed which would produce $C_6H_5S^-$ ions. In the OH^-/H_2O system a very minor amount of $C_6H_5S^-$ ions is formed after completion of proton transfer to OH^-. In the OD^-/D_2O system up to four

Can. J. Chem. Downloaded from www.nrcresearchpress.com by 210.87.254.40 on 09/06/12
For personal use only.

TABLE 4. Rate constants for reaction between anions and CH_3Br

A^-	k_{exp}[a] FT-ICR	ICR[b]	FA[c]	k_{ADO}[d]	Efficiency[d]	ΔH_r (kJ/mol)[e]
$CH_3SCH_2^-$	0.93±0.03		—	1.53	0.63	−310
$CH_2{=}CH{-}CH_2^-$	1.1±0.1	—	0.77[f]	1.75	0.63	−298
$HC{\equiv}C^-$	0.43±0.02	0.31	0.52	2.10	0.20	−255
HO^-	2.2±0.1	1.9	0.99	2.46	0.89	−237
CH_3O^-	1.3±0.1	0.72	1.1	1.93	0.67	−212
$C_2H_5O^-$	1.1±0.1	—	—	1.69	0.65	−197
CH_3S^-	0.40±0.04	0.14	0.52	1.67	0.24	−159
$C_2H_5S^-$	0.36±0.01	—	—	1.53	0.24	−151
F^-	1.2±0.1	0.6	1.2	2.35	0.51	−156
$^{35}Cl^-$	0.026±0.002	0.012	0.021	1.85	0.014	−27

[a]In units of 10^{-9} cm^3 $molecule^{-1}$ s^{-1}. The error given for FT-ICR results is the standard deviation. Temperature assumed to be 298 K.
[b]Values taken from ref. 21.
[c]Values taken from ref. 23.
[d]See notes *b* and *c* for Table 1.
[e]Calculated using values from ref. 22 and Table 8.
[f]Value taken from ref. 24.

TABLE 5. Data for reaction of $CH_3SCH_2^-$ and $CH_2{=}CH{-}CH_2^-$ with HCO_2CH_3

A^-	Products[a]	% [b]	k_{exp}[c]	k_{ADO}[d]	Efficiency[d]
$CH_3SCH_2^-$	CH_3O^- + C_3H_6SO	48	0.28±0.01	1.64	0.17
	$HCO\bar{C}HSCH_3$ + CH_3OH	52			
$CH_2{=}CH{-}CH_2^-$	CH_3O^- + C_4H_6O	5	0.38±0.01	1.83	0.21
	$HCO\bar{C}H{-}CH{=}CH_2$ + CH_3OH	95			

[a]Neutral products assumed.
[b]Obtained by extrapolation to zero reaction time. Error on the percentages ~ 10%.
[c]In units of 10^{-9} cm^3 $molecule^{-1}$ s^{-1}. Temperature assumed to be 298 K.
[d]See notes *c* and *d* for Table 1.

TABLE 6. Competition between proton and deuteron abstraction from $C_6H_5SCD_3$[a]

A^-	PA(A^-) (kJ/mol)[b]	$[M - H]^-$ *m/z* 126 (%)	$[M - D]^-$ *m/z* 125 (%)	$[M - 2D + H]^-$ *m/z* 124 (%)	$[M - 2H + D]^-$ *m/z* 127 (%)
NH_2^-	1689	49	51	—	—
$C_2H_5NH^-$	1671	48	52	—	—
$(CH_3)_2N^-$	1658	39	61	—	—
HO^-	1635	15	55	30[c]	—
DO^-	—	20	77		3[c]
CH_3O^-	1587	—	100	—	—

[a]Values obtained by extrapolation to zero reaction time and corrected for ^{13}C and ^{33}S contributions. Error on the percentages ~10%.
[b]Values taken from ref. 20.
[c]Caused by multiple hydrogen−deuterium exchange in the collision complex composed of HO^- or DO^- and $C_6H_5SCD_3$, see ref. 25.

deuterium atoms are incorporated in the thiophenolate ions. These observations are analogous to those previously reported for reactions of anions with 2-, 3-, 4-fluoranisole, and anisole itself (26). The mechanistic interpretation is given in eq. [5].

[5] $C_6H_5SCH_3 + HO^- \underset{}{\overset{}{\rightleftharpoons}} [M - H]^- + H_2O$
m/z 17 *m/z* 123

$[M - H]^- + H_2O \rightleftharpoons [[M - H]^- \cdot H_2O]^* \rightleftharpoons [C_6H_5SCH_3 \cdot {}^-OH]^*$
m/z 123

$\rightarrow C_6H_5S^- + CH_3OH$
m/z 109

S_N2 substitution becomes significant in the CH_3O^-/CH_3OH system at longer reaction times (>1000 ms). This does not interfere, however, with the determination of the equilibrium constant for reaction [4] (see Fig. 3).

Discussion

Ion structures

In order to ascertain that the $[M - H]^-$ ion from CH_3SCH_3 has the structure of a primary carbanion, reactions of this ion with N_2O, CF_2O, and C_6F_6 have been studied. The product ions observed are listed in Table 7. All the observed reactions point to the primary carbanion structure **1**:

$CH_3SCH_2^-$ **1**

Can. J. Chem. Downloaded from www.nrcresearchpress.com by 210.87.254.40 on 09/06/12
For personal use only.

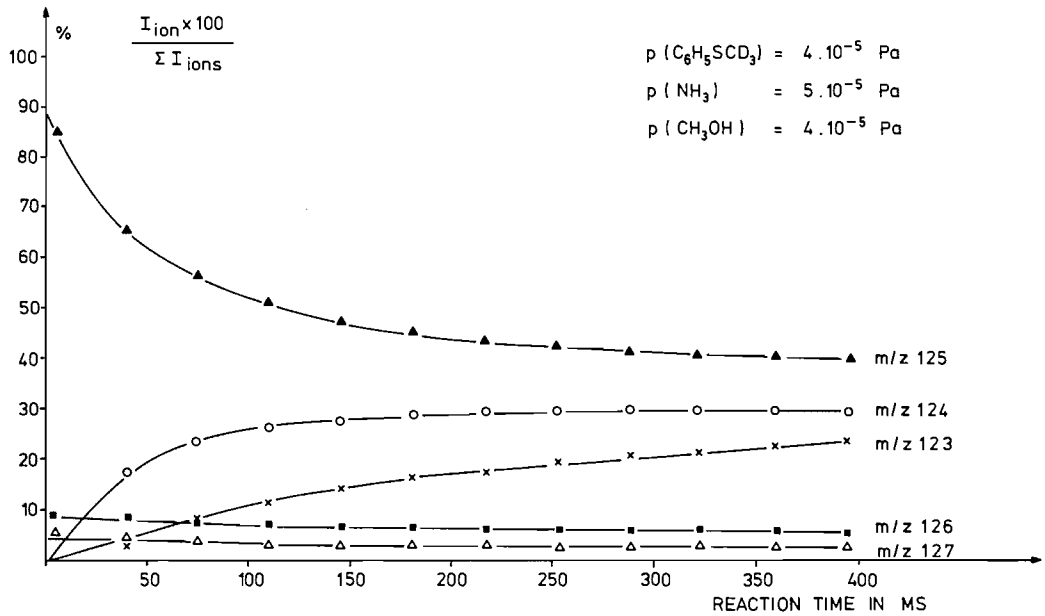

FIG. 2. Variation of the relative intensities of the m/z 123–127 ions formed in the $CH_3O^-/CH_3OH/C_6H_5SCD_3$ system with reaction time. The m/z 125 ion is the $[M - D]^-$ ion from $C_6H_5SCD_3$. The m/z 126 and 127 ions are the $^{13}C/^{33}S$ and ^{34}S isotopic species of the $[M - D]^-$ ions, respectively. The m/z 124 and 123 ions are formed by hydrogen–deuterium exchange reactions between the $[M - D]^-$ ions and CH_3OH.

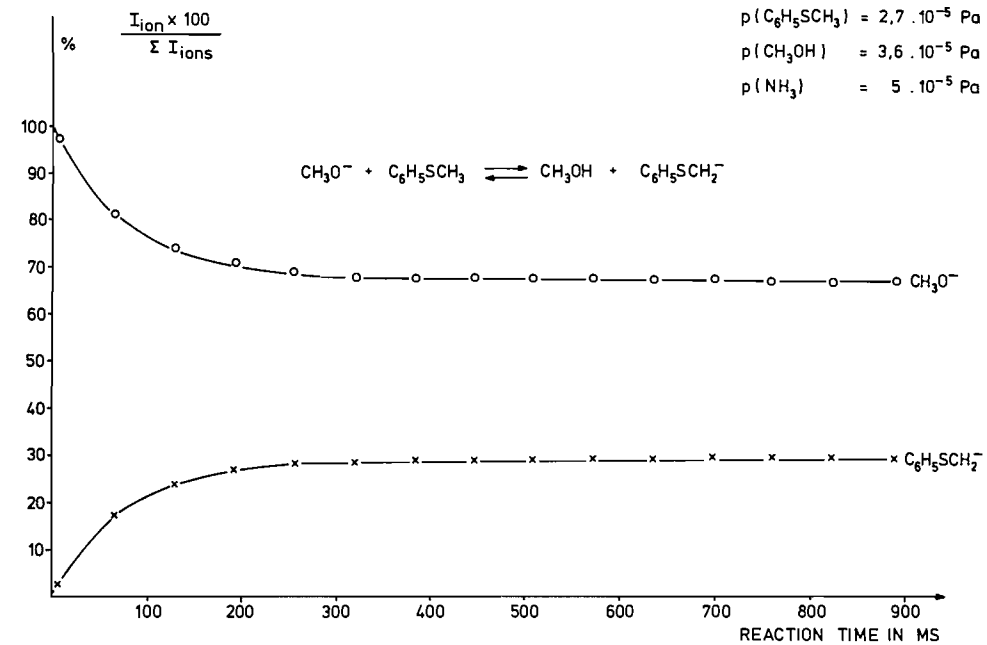

FIG. 3. Relative intensities of the CH_3O^- and $C_6H_5SCH_2^-$ ions in the $CH_3O^-/CH_3OH/C_6H_5SCH_3$ system followed as a function of reaction time.

The mechanisms of the reactions with N_2O and CF_2O have been reported previously in detail (27, 28). The reaction with C_6F_6 is rationalized in eq. [6].

$$[6]\quad \underset{m/z\ 61}{CH_3SCH_2^-} + C_6F_6 \xrightarrow{S_NAr} [C_6F_5CH_2SCH_3 \cdot F^-]^* \xrightarrow{-HF} [C_6F_5CHSCH_3]^* \rightarrow \underset{m/z\ 212}{C_6F_5CHS^{-\cdot}} + {}^{\cdot}CH_3$$

This reaction type has been discussed in previous articles (see refs. 18, 26, 29) and provides in general for a good probe as to the structure and reactivity of anions in the gas phase.

The $[M - H]^-$ and $[M - D]^-$ ions from CD_3SCH_3 react with CF_2O as shown in eqs. [7] and [8].[5]

$$[7]\quad \underset{m/z\ 64}{CD_3SCH_2^-} + CF_2O \rightarrow \underset{m/z\ 90}{CD_3S\bar{C}{=}C{=}O} + 2HF$$

$$[8]\quad \underset{m/z\ 63}{CH_3SCD_2^-} + CF_2O \rightarrow \underset{m/z\ 87}{CH_3S\bar{C}{=}C{=}O} + 2DF$$

[5]The ion formed by loss of 2 HF molecules from the collision complex reacts further with CF_2O. For example, the CD_3—S—$\bar{C}$=C=O ions react to give $C_3FO_2^-$ (m/z 87) and $C_3F_2SO_2^{-\cdot}$ (m/z 138) ions.

Can. J. Chem. Downloaded from www.nrcresearchpress.com by 210.87.254.40 on 09/06/12
For personal use only.

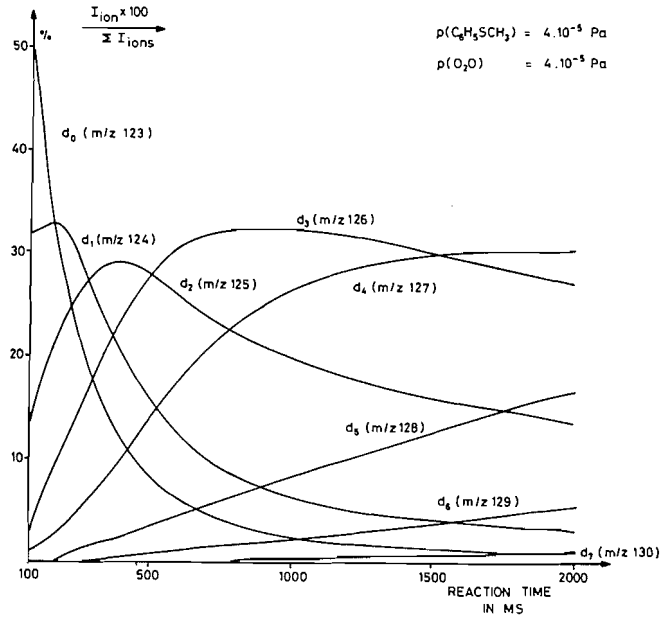

FIG. 4. The hydrogen–deuterium exchange reaction between the conjugate base of $C_6H_5SCH_3$ and D_2O followed as a function of reaction time. The time was increased linearly from 100 to 2000 ms in 24 steps. The relative intensities have not been corrected for isotopic contributions.

The clean occurrence of reactions [7] and [8] indicates that no 1,3-proton or deuteron shifts take place within the carbanion.

[9] $CH_3SCD_2^- \not\rightarrow {}^-CH_2SCD_2H$

The structure of the $[M - H]^-$ ion from CH_3SCH_3 has been probed further by studying hydrogen–deuterium exchange reactions between the ion and an exchange reagent (25). Under the experimental conditions no exchange could be observed if ND_3 was used as exchange reagent. In a system composed of $ND_3/(CH_3)_2NH/CH_3SCH_3$, however, exchange could be observed. In that case the exchange reagent is $(CH_3)_2ND$, which is prepared *in situ* from reaction between ND_3 and $(CH_3)_2NH$. Up to four hydrogen atoms in the $[M - H]^-$ ion could be exchanged with deuterium atoms in this system, supporting the conclusion that proton abstraction from CH_3SCH_3 leads to a primary carbanion. In the case of $C_6H_5SCH_3$, proton abstraction can lead in principle to a primary carbanion (ion **2**) and (or) a substituted phenide in (ion **3**) where the charge can be in the *ortho*, *meta*, or *para* position with respect to the CH_3S— group.

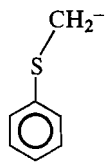

Ion **2**

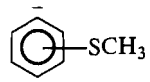

Ion **3**

The results from reactions between the $[M - H]^-$ ion from $C_6H_5SCH_3$ (generated by hydroxide ions, see also Table 6) and N_2O, CF_2O, and HCO_2CH_3 are collected in Table 7. The reaction with CF_2O points to ion **2**[6] whereas the reactions with HCO_2CH_3 can be explained on the basis of both ions **2** and **3**. These results and the results from the hydrogen–deuterium exchange reactions (see Figs. 4 and 5) indicate that isomerization of the $[M - H]^-$ ion from $C_6H_5SCH_3$ to other structures than **2** or **3** is not occurring. The possibility exists, however, that ion **3** rearranges via an intramolecular proton shift to ion **2** when the negative charge is located in the *ortho* position. Such a rearrangement has been verified for carbanions derived from 2-, 3-, 4-fluoroanisole and anisole (26). For the $[M - H]^-$ ion from $C_6H_5SCH_3$ we have been unable to clarify whether such intramolecular proton shifts take place. An isomerization of ion **3** to the more stable ion **2** (see Acidities) can occur, of course, via reaction with molecules such as NH_3 or H_2O.

Acidities

Proton abstraction from CH_3SCH_3 by NH_2^- occurs with the collision rate (Table 1). The $C_2H_5NH^-$ and $(CH_3)_2N^-$ ions, which have lower proton affinities, abstract a proton from CH_3SCH_3 with lower efficiency. The intramolecular primary kinetic isotope effect associated with this process is observed to change when the proton affinity of the amide ions is changed (Table 2). The maximum in isotope effect observed for the $C_2H_5NH^-$ ion could mean that the transition state is more symmetric in this case than in the other two. The occurrence of these isotope effects indicates that there is a significant local energy barrier towards proton removal from CH_3SCH_3.[7] This is also reflected in the fact that reaction [10] is not observed to occur to any appreciable extent.

[10] $\underset{m/z\ 63}{CH_3SCD_2^-} + CH_3SCD_3 \not\rightarrow \underset{m/z\ 64}{CH_3SCD_2H} + CD_3SCH_2^-$

The thermochemical gas phase acidity ΔG^0_{acid} of CH_3SCH_3 can be obtained from eqs. [11] and [12] using the measured equilibrium constant for reaction [1].

[11] $\delta\Delta G^0_{acid} = -RT \ln K$

[12] $\delta\Delta G^0_{acid} = \Delta G^0_{acid}(CH_3SCH_3) - \Delta G^0_{acid}(H_2O)$

The temperature T in our system is not known, but is simply assumed to be 298 K. This gives $\delta\Delta G^0_{acid} = 7.1 \pm 0.5$ kJ/mol and $\Delta G^0_{acid}(CH_3SCH_3) = 1615 \pm 8$ kJ/mol with the use of $\Delta G^0_{acid}(H_2O) = 1608 \pm 4$ kJ/mol.[8] The error in the obtained gas phase acidity of CH_3SCH_3 might be somewhat larger due to the uncertainties in the measurement of the pressures and the temperature not being known accurately. The $\Delta H^0_{acid}(CH_3SCH_3) = PA(CH_3SCH_2^-)$ given in Table 8 has been obtained with the use of an estimated $\Delta S^0_{acid}(CH_3SCH_3)$ values.[9] No $[M - H]^-$ ion from CH_3OCH_3 has been observed, indicating that the ΔG^0_{acid} and the ΔH^0_{acid} of this compound is above those for NH_3 ($\Delta G^0_{acid} = 1657$ kJ/mol; $\Delta H^0_{acid} = 1689$ kJ/mol) (20). This indicates that substitution of the oxygen atom in CH_3OCH_3 by a sulfur atom increases the gas phase acidity of the methyl group by more than 42 kJ/mol. The decrease in proton affinity when going from $CH_3OCH_2^-$ to $CH_3SCH_2^-$ can be expected to be more than 44 kJ/mol with the use of the value for the $PA(CH_3SCH_2^-)$ given in Table 8. This can be compared with the result from *ab initio* calculations which indicate a

[6]The C_6H_5—S—$\bar{C}$=C=O ions added slowly to CF_2O leading to $C_9H_5F_2SO_2^-$ (m/z 215) ions.

[7]Energy barriers towards proton transfer in gas phase ion–molecule reactions have been discussed in ref. 30.

[8]Calculated using data from refs. 20, 22, and 31.

[9]The entropy change for the reaction $RSCH_3 \rightarrow RSCH_2^- + H^+$ has been estimated using the general approach given in ref. 32.

Can. J. Chem. Downloaded from www.nrcresearchpress.com by 210.87.254.40 on 09/06/12
For personal use only.

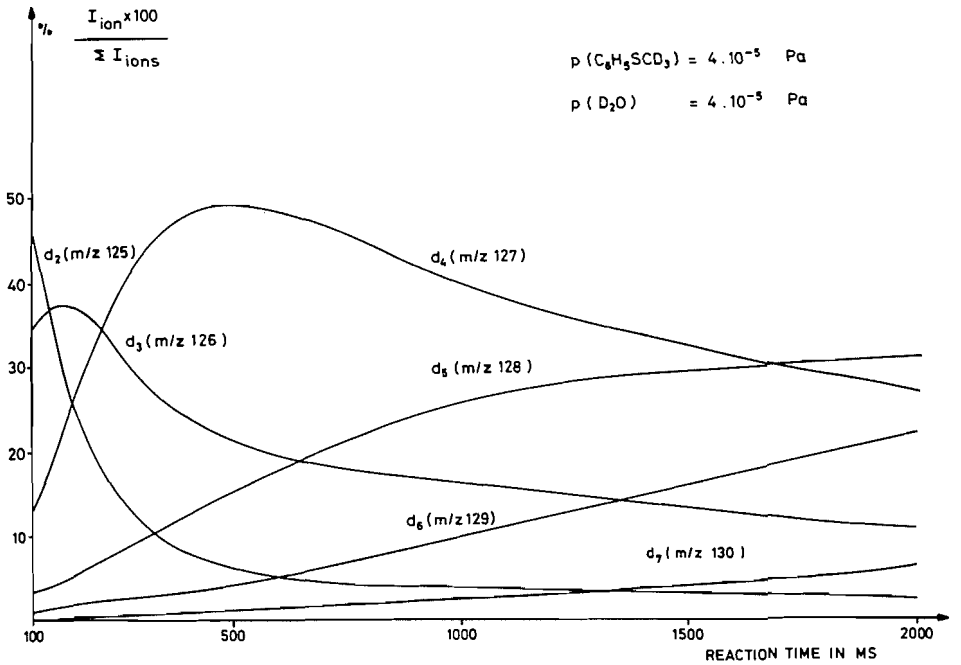

FIG. 5. The hydrogen–deuterium exchange reaction between the conjugate base of $C_6H_5SCD_3$ and D_2O followed as a function of reaction time. The time was increased linearly from 100 ms to 2000 ms in 18 steps. The m/z 125 and 126 ions are formally the $[M - H]^-$ and $[M - D]^-$ ions from $C_6H_5SCD_3$ (see also Table 6). The relative intensities have not been corrected for isotopic contributions.

TABLE 7. Product ions formed in the reactions of the $[M - H]^-$ ions from CH_3SCH_3 and $C_6H_5SCH_3$ with various molecules

Substrate	Products[a]	% [b]	Conversion into products at the given reaction time[c]
CH_3SCH_3			
N_2O	$CH_3S\bar{C}=\overset{+}{N}=\bar{N} + H_2O$	100	39% at 2000 ms
CF_2O	$CH_3S\bar{C}=C=O + 2HF$	100	97% at 1000 ms[d]
C_6F_6	$C_6F_5CHS^{-\cdot} + HF + CH_3^{\cdot}$	100	100% at 1000 ms
$C_6H_5SCH_3$			
N_2O	No reaction		
CF_2O	$C_6H_5S\bar{C}=C=O + 2HF$	100	100% at 2500 ms[e]
HCO_2CH_3	$CH_3O^- + C_8H_8SO$	<20	
	$C_8H_7SO^- + CH_3OH$	>80	86% at 2500 ms[f]

[a]Structure of ionic product assumed. Neutral product assumed.
[b]Obtained by extrapolation to zero reaction time.
[c]Conversion into products at the pressures used. In the case of N_2O the partial pressure of this compound was a factor of 3 higher than the partial pressure of the sulfide (see also experimental section).
[d]See footnote 4.
[e]See footnote 5.
[f]See text.

decrease in proton affinity of ~33 kJ/mol (8). Relative to CH_3^- (PA = 1743 kJ/mol) (20), the CH_3S— group decreases the proton affinity by around 98 kJ/mol. This is comparable to the proton affinity decrease observed when going from CH_3^- to $CH_2{=}CH{-}CH_2^-$ (20).

The present experiments do not reveal anything directly about the mechanism(s) of the stabilization of the negative charge in the $CH_3SCH_2^-$ ion. The acidity order of CH_3OCH_3 and CH_3SCH_3 is observed, however, to follow the polarizability order of the heteroatoms. It can further be mentioned here that experiments carried out in our laboratory indicate that the acidity increases continuously down the series CH_3F, CH_3Cl, CH_3Br, CH_3I.[10]

Based upon the results in Table 6 it can be concluded that the most acidic position in $C_6H_5SCH_3$ is the methyl group and that only this position is involved in equilibrium [4]. The measured equilibrium gives $\delta\Delta G^0_{acid} = 0.6 \pm 0.2$ kJ/mol. With ΔG^0_{acid} (CH_3OH) = 1559 ± 8 kJ/mol,[11] the gas phase acidity of

[10]S. Ingemann and N. M. M. Nibbering, in preparation (see also ref. 23).

[11]This value is the one obtained using the ICR method (ref. 20). It should be noted that a value for ΔG^0_{acid} (CH_3OH) = 1667 ± 8 kJ/mol has been recommended in ref. 33.

Can. J. Chem. Downloaded from www.nrcresearchpress.com by 210.87.254.40 on 09/06/12
For personal use only.

TABLE 8. Estimated thermochemical data for CH_3SCH_3 and $C_6H_5SCH_3$

Compound	ΔG^0_{acid} [a] (kJ/mol)	ΔS^0_{acid} [b] (J/mol K)	ΔH^0_{acid} = PA($RSCH_2^-$) [c] (kJ/mol)	ΔH^0_f ($RSCH_2^-$) [c] (kJ/mol)
CH_3SCH_3	1615±8 [d]	101±8	1645±8	71±8
$C_6H_5SCH_3$	1560±8 [e]	103±8	1591±8	153±8

[a] Temperature assumed to be 298 K, see text.
[b] Estimated using the general approach in ref. 32.
[c] Appropriate ΔH^0_f data from ref. 22.
[d] Measured relative to H_2O (ΔG^0_{acid} = 1608 ± 4 kJ/mol) (see text and ref. 20).
[e] Measured relative to CH_3OH (ΔG^0_{acid} = 1559 ± 8 kJ/mol) (see text and ref. 20).

the methyl group becomes ΔG^0_{acid} ($C_6H_5SCH_3$) = 1560 ± 8 kJ/mol. The estimated PA($C_6H_5SCH_2^-$) and the ΔH^0_f ($C_6H_5SCH_2^-$) are given in Table 8.

The failure to observe proton abstraction from $C_6H_5CH_3$ (ΔG^0_{acid} = 1558 kJ/mol) (20) or *p*-$CH_3C_6H_4CH_3$ (ΔG^0_{acid} = 1562 kJ/mol) (20) by the $C_6H_5SCH_2^-$ ion indicates a kinetic barrier which apparently renders the reaction too slow to be observed. The fact that the $[M - H]^-$ ions from $C_6H_5CH_3$ or *p*-$CH_3C_6H_4CH_3$ do not react with $C_6H_5SCH_3$ even though proton transfer is thermochemically feasible can be accounted for similarly. Substitution of a methyl group in CH_3SCH_3 by a phenyl group can be seen to enhance the acidity by ~55 kJ/mol. This effect is somewhat larger than the one observed when going from CH_3OH to $C_6H_5CH_2OH$ where the acidity increases by ~40 kJ/mol (20). Relative to CH_3^- the $C_6H_5S^-$ group decreases the proton affinity with ~152 kJ/mol (see ref. 20 and Table 8). This effect is close to the decrease in proton affinity when going from CH_3^- to $C_6H_5CH_2^-$.

The relative order of the acidity of the different positions within $C_6H_5SCH_3$ is probed by the hydrogen–deuterium exchange reactions. In Fig. 4 it can be seen that the first four hydrogen atoms are exchanged somewhat faster than the rest. At the time (~750 ms) where the fifth exchange is rather unimportant there are only 2 deuterium atoms incorporated in the thiophenolate ions arising through the minor reaction [5]. In the $C_6H_5SCD_3/OH^-/H_2O$ system the hydrogen–deuterium exchange is relatively fast and in the $C_6H_5SCD_3/OD^-/D_2O$ system (see Figs. 4 and 5) 2 hydrogen atoms are relatively easily exchanged whereas the rest exchange more slowly. Combination of these results indicates that the methyl and the *ortho* hydrogen atoms are exchanged faster than the *meta* and *para* hydrogen atoms within the conjugate base of $C_6H_5SCH_3$ in the OD^-/D_2O system (see Ion structures). This can be interpreted as the relative gas phase acidity being methyl > *ortho* > *meta*, *para* (see also Table 6). It can here be mentioned that lithiation of $C_6H_5SCH_3$ initially yields a mixture of $C_6H_5SCH_2Li$ and 2- or 3-$LiC_6H_4SCH_3$ which after a prolonged reaction time converts nearly exclusively into $C_6H_5SCH_2Li$ (34).

Reactivity

The variation in reaction efficiencies for the S_N2 substitutions studied is observed to be somewhat larger for CH_3Cl than for CH_3Br (see Tables 3 and 4). The data for CH_3Cl provide, therefore, a better basis for comparison although the overall trend is the same for both substrates.

The reaction rates and efficiencies for displacement of Cl^- from CH_3Cl are observed to be similar for $CH_3SCH_2^-$ and $CH_2{=}CH{-}CH_2^-$. The exothermicity of these S_N2 substitutions is also similar. There is, however, in general no correlation between exothermicity and reaction efficiency for gas phase S_N2 substitutions (see also Tables 3 and 4) (21, 23). The similar reaction efficiency therefore points to a similar local energy barrier towards the displacement of Cl^- from CH_3Cl by $CH_3SCH_2^-$ and $CH_2{=}CH{-}CH_2^-$.

Compared to the other carbon nucleophile studied, i.e. $HC{\equiv}C^-$, the $CH_3SCH_2^-$ ion is 5 times as effective in displacing Cl^- from CH_3Cl. The oxygen nucleophile $C_2H_5O^-$ reacts with a higher efficiency, whereas the $C_2H_5S^-$ ion reacts with an efficiency 12 times lower than the isomeric $CH_3SCH_2^-$ ion. The data in Tabe 5 show that the $CH_3SCH_2^-$ ion reacts with HCO_2CH_3 with an efficiency similar to that of the $CH_2{=}CH{-}CH_2^-$ ion. The reaction proceeds, in both cases, most likely exclusively through the $B_{AC}2$ pathway:

$$[13]\quad RCH_2^- + HCO_2CH_3 \xrightarrow{B_{AC}2} [RCH_2CHO\cdot CH_3O^-]^* \begin{cases} \rightarrow CH_3O^- + RCH_2CHO \\ \rightarrow RCH{=}CHO^- + CH_3OH \end{cases}$$

R = $CH_2{=}CH$, CH_3S

The larger amount of CH_3O^- ions produced in the reaction of $CH_3SCH_2^-$ can be explained if it is assumed that the methylene hydrogen atoms in the RCH_2CHO molecule formed are somewhat less acidic for R = CH_3S— than for R = $CH_2{=}CH$—.

Conclusions

Proton abstraction from CH_3SCH_3 in the gas phase leads to a primary carbanion. The gas phase acidity of CH_3SCH_3 is determined to be ΔG^0_{acid} = 1615 ± 8 kJ/mol. The CH_3S— group stabilizes the carbanionic site by ~43 kJ/mol relative to a CH_3O— group.

The most acidic position within $C_6H_5SCH_3$ is the methyl group. The gas phase acidity of this position is found to be ΔG^0_{acid} = 1560 ± 8 kJ/mol. On the basis of this observation and the results from hydrogen–deuterium exchange reactions between the $[M - H]^-$ ion from $C_6H_5SCH_3$ and D_2O, the relative acidity of the different positions is established to be *methyl* > *ortho* > *meta*, *para*.

The reactivity of $CH_3SCH_2^-$ and $CH_2{=}CHCH_2^-$ ions in gas phase reactions with CH_3Cl, CH_3Br, and HCO_2CH_3 is observed to be similar.

Acknowledgements

We thank Dr. G. H. Wegdam (Laboratory of Physical Chemistry, University of Amsterdam) for valuable discussions on the estimation of the ΔS^0_{acid} values and The Netherlands Organization for Pure Research (SON/ZWO) for financial support.

1. D. J. PETERSON. Organomet. Chem. Rev. A, **7**, 295 (1972).
2. E. BLOCK. Reactions of organosulfur compounds. Academic Press, New York. 1978. Chapt. 2. pp. 36–90.

Can. J. Chem. Downloaded from www.nrcresearchpress.com by 210.87.254.40 on 09/06/12
For personal use only.

3. H. W. GSCHWEND and H. R. RODRIGUES. Org. React. **26**, 1 (1979).
4. F. BERNARDI, I. G. CSIZMADIA, A. MANGINI, H. B. SCHLEGEL, M. H. WHANGBO, and S. WOLFE. J. Am. Chem. Soc. **97**, 2209 (1975).
5. N. D. EPIOTIS, R. L. YATES, F. BERNARDI, and S. WOLFE. J. Am. Chem. Soc. **98**, 5435 (1976).
6. (*a*) A. STREITWIESER, JR. and S. P. EWING. J. Am. Chem. Soc. **97**, 190 (1975); (*b*) A. STREITWIESER, JR. and J. E. WILLIAMS. J. Am. Chem. Soc. **97**, 191 (1975).
7. J. M. LEHN and G. WIPFF. J. Am. Chem. Soc. **98**, 7498 (1976).
8. A. PROSS, D. J. DEFREES, B. A. LEVI, S. K. POLLACK, L. RADOM, and W. J. HEHRE. J. Org. Chem. **46**, 1693 (1981).
9. G. W. SPITZNAGEL, T. CLARK, J. CHANDRASEKHAR, and P. VON R. SCHLEYER. J. Comput. Chem. **3**, 363 (1982).
10. S. WOLFE, L. A. LA JOHN, F. BERNARDI, A. MANGINI, and C. TONACHINI. Tetrahedron Lett. **24**, 3789 (1983).
11. E. L. ELIEL, A. A. HARTMANN, and A. G. ABATJOGLOU. J. Am. Chem. Soc. **96**, 1807 (1974).
12. (*a*) C. H. DEPUY, J. J. GRABOWSKI, and V. M. BIERBAUM. Science, **218**, 955 (1982); (*b*) C. H. DEPUY and V. M. BIERBAUM. Acc. Chem. Res. **14**, 146 (1981); (*c*) S. INGEMANN, J. C. KLEINGELD, and N. M. M. NIBBERING. *In* Ionic processes in the gas phase. *Edited by* A. M. Almoster Ferreira. Reidel, Dordrecht. 1984. pp. 87–110; (*d*) N. M. M. NIBBERING. Recl. Trav. Chim. Pays-Bas, **100**, 297 (1981).
13. J. E. BARTMESS, R. L. HAYS, H. N. KHATRI, R. N. MISRA, and S. R. WILSON. J. Am. Chem. Soc. **103**, 4746 (1981).
14. (*a*) M. B. COMISAROW. *In* Transform techniques in chemistry. *Edited by* P. R. Griffits. Plenum Press, New York. 1978. Chapt. 10. pp. 257–284; (*b*) C. L. WILKINS and M. L. GROSS. Anal. Chem. **53**, 1661A (1981).
15. J. H. J. DAWSON. Lect. Notes Chem. **31**, 331 (1982).
16. (*a*) A. J. NOEST and C. W. F. KORT. Comput. Chem. **6**, 111 (1982); **6** 115 (1982); (*b*) Comput. Chem. **7**, 81 (1983).
17. J. C. KLEINGELD and N. M. M. NIBBERING. Org. Mass Spectrom. **17**, 136 (1982).
18. S. INGEMANN, N. M. M. NIBBERING, S. A. SULLIVAN, and C. H. DEPUY. J. Am. Chem. Soc. **104**, 6520 (1982).
19. T. SU and M. T. BOWERS. *In* Gas phase ion chemistry. Vol. 1. *Edited by* M. T. Bowers. Academic Press, New York. 1979. Chapt 3. pp. 83–118, and references cited therein.
20. J. E. BARTMESS and R. T. MCIVER, JR. *In* Gas phase ion chemistry. Vol. 2. *Edited by* M. T. Bowers. Academic Press, New York. 1979. Chapt. 11. pp. 87–121.
21. (*a*) W. N. OLMSTEAD and J. I. BRAUMAN. J. Am. Chem. Soc. **99**, 4219 (1977); (*b*) M. J. PELLERITE and J. I. BRAUMAN. J. Am. Chem. Soc. **102**, 5993 (1980); (*c*) M. J. PELLERITE and J. I. BRAUMAN. J. Am. Chem. Soc. **105**, 2672 (1983).
22. S. W. BENSON. Thermochemical kinetics. 2nd ed. Wiley (Interscience), New York. 1976.
23. K. TANAKA, G. I. MACKAY, J. D. PAYZANT, and D. K. BOHME. Can. J. Chem. **54**, 1643 (1976).
24. R. N. MCDONALD and A. K. CHOWDHURY. J. Am. Chem. Soc. **105**, 2194 (1983).
25. (*a*) R. R. SQUIRES, C. H. DEPUY, and V. M. BIERBAUM. J. Am. Chem. Soc. **103**, 4256 (1981); (*b*) J. J. GRABOWSKI, C. H. DEPUY, and V. M. BIERBAUM. J. Am. Chem. Soc. **105**, 2565 (1983); (*c*) R. R. SQUIRES, V. M. BIERBAUM, J. J. GRABOWSKI, and C. H. DEPUY. J. Am. Chem. Soc. **105**, 5185 (1983).
26. (*a*) S. INGEMANN and N. M. M. NIBBERING. J. Org. Chem. **48**, 183 (1983); (*b*) J. C. KLEINGELD and N. M. M. NIBBERING. Tetrahedron, **39**, 4193 (1983).
27. V. M. BIERBAUM, C. H. DEPUY, and R. H. SHAPIRO. J. Am. Chem. Soc. **99**, 5800 (1977).
28. J. H. J. DAWSON, A. J. NOEST, and N. M. M. NIBBERING. Int. J. Mass Spectrom. Ion Phys. **29**, 205 (1979).
29. S. INGEMANN and N. M. M. NIBBERING. Nouv. J. Chim. **8**, 299 (1984).
30. (*a*) W. F. FARNETH and J. I. BRAUMAN. J. Am. Chem. Soc. **98**, 7891 (1976); (*b*) J. M. JASINSKI and J. I. BRAUMAN. J. Am. Chem. Soc. **102**, 2906 (1980).
31. D. R. STULL and H. PROPHET. JANAF thermochemical tables. NSRDS-NBS 37, U.S. Government Printing Office, Washington, DC. 1971.
32. J. B. CUMMING and P. KEBARLE. Can. J. Chem. **56**, 1 (1978).
33. G. I. MACKAY, A. S. RASHIT, and D. K. BOHME. Can. J. Chem. **60**, 2594 (1982).
34. D. A. SHIRLEY and B. J. REEVES. J. Organomet. Chem. **16**, 1 (1969).

Can. J. Chem. Downloaded from www.nrcresearchpress.com by 210.87.254.40 on 09/06/12
For personal use only.

Nuclear analogs of β-lactam antibiotics. XX.[1] Synthesis and X-ray structure determination of exocyclic penems: sulfur analogs of clavulanic acid

JAMES L. DOUGLAS, ALAIN MARTEL, GILLES CARON, AND MARCEL MÉNARD
Bristol Laboratories of Canada, 100 Industrial Blvd., Candiac (Qué.), Canada J5R 1J1

AND

LINDA SILVEIRA AND JON CLARDY
Department of Chemistry, Baker Laboratory, Cornell University, Ithaca, NY 14853, U.S.A.

Received October 21, 1983

JAMES L. DOUGLAS, ALAIN MARTEL, GILLES CARON, MARCEL MÉNARD, LINDA SILVEIRA, and JON CLARDY. Can. J. Chem. **62**, 2282 (1984).

Penems **5** were converted to exocyclic analogs **6** and **10**. These served as substrates for conversion to the sulfone **11** and oxopenam **12**. None of the products showed any activity as antibiotics or as β-lactamase inhibitors. A single cyrstal X-ray diffraction analysis of compound **6***a* verified the exocyclic penem structure.

JAMES L. DOUGLAS, ALAIN MARTEL, GILLES CARON, MARCEL MÉNARD, LINDA SILVEIRA et JON CLARDY. Can. J. Chem. **62**, 2282 (1984).

On a transformé des pénèmes **5** en analogues exocycliques **6** et **10** qui servent de substrats pour leur conversion en sulfone **11** et oxopéname **12**. Aucun de ces produits ne présente d'activité comme antibiotique ou comme inhibiteur de β-lactamase. Faisant appel à une analyse par diffraction de rayons-X sur un cristal unique, on a vérifié la structure pénème exocyclique du composé **6***a*.

[Traduit par le journal]

Introduction

The synthesis of simple penem structures **1** (R = H, Me) by Woodward and co-workers (1) and the modification by various groups (2–4) of their synthetic methodology to give generalized 2-substituted[2] penems **1** have made such compounds readily available as substrates for conversion to other novel β-lactams. Furthermore, the observation of β-lactamase inhibitory properties for clavulanic acid (5) provides incentive for generating structures such as **2** in which the 5-membered ring has an exocyclic double bond. One can then envisage ozonolysis of the double bond to oxopenam **3** which could be used as a substrate for further transformation.

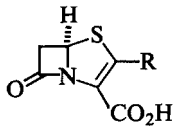

1

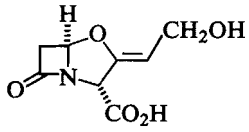

Clavulanic acid

As part of our ongoing program aimed at the discovery of β-lactam antibiotics (and (or) β-lactamase inhibitors) we set out to synthesize compounds of types **2** and **3** (and readily available) derivatives thereof).

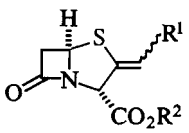

2

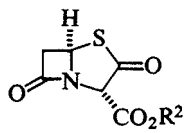

3

[1]For Part XIX, see ref. 16.

[2]The common penem numbers system as follows will be used, except in the Experimental titles.

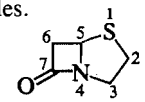

Since the inception of our work in this area, several research groups have published findings on the same or related compounds. A group at Sankyo has described the synthesis of oxopenam **3** (R^2 = H) and substituted derivatives from cephalosporins (6). Penicillin G has been converted to a 6-amido-oxopenam (7). The Glaxo research group has converted clavulanic acid into the exocyclic penem *Z*-**2** (R^1 = CH_2SAc, R^2 = H) but report it to have reduced antibacterial and β-lactamase inhibitory activity (3). Workers at Farmitalia have used a variation on the Woodward route (1) to prepare exocyclic penem **2** (R^1 = CO_2Et, R^2 = benzyl) (4). Beecham (8) and Pfizer (9) research groups have both prepared exocyclic penems **4** (lacking the important 3-carboxyl substituent) and report them to be devoid of antibacterial or β-lactamase inhibitory activity.

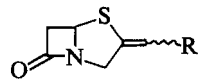

4

Results and discussion

The Beecham group have described the base catalyzed isomerization of the endocyclic double bond of oxapenems to the exocyclic (clavulanic acid type) position (10). Using their reaction conditions (organic base in an organic solvent) we have converted the 2-arylmethylpenems **5** (2) into the exocyclic penems **6**. In the case of R = phenyl, an equilibrium mixture of 80% **6** and 20% **5** was formed; for R = furyl or thienyl,

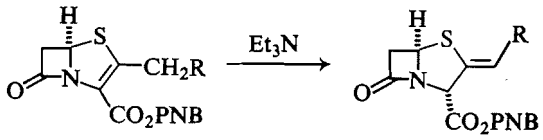

5 **6**

a R = phenyl *b* R = 2-furyl *c* R = 2-thienyl

Can. J. Chem. Downloaded from www.nrcresearchpress.com by 210.87.254.40 on 09/06/12
For personal use only.

TABLE 1. Nuclear magnetic resonance spectra[a]

Compound	Vinyl	H-3	H-5	H-6α	H-6β	Other
2[b] (R^1 = CO_2Et; R^2 = benzyl)	6.14 (d, J = 1.2)	5.53 (d, J = 1.2)	5.36 (q)	3.70 (dd, J = 16 and 14)	3.20 (dd, J = 16 and 2)	1.28 (t), 4.22 (q)
6*a*	6.70 (d, J = 1)	5.58 (d, J = 1)	5.52 (q)	3.77 (dd, J = 16 and 4)	3.23 (dd, J = 16 and 2)	7.35 (s, Ph)
6*b*	6.57 (d, J = 1)	5.53 (d, J = 1)	5.50 (q)	3.77 (dd, J = 16 and 4)	3.25 (dd, J = 16 and 1.5)	7.43 and 6.4 (furyl)
6*c*	ca. 6.9	5.5–5.7	5.5–5.7	3.76 (dd, J = 16 and 5)	3.22 (dd, J = 16 and 1.8)	6.8–7.5 (thienyl)
6*d*	6.10 (d, J = 1)	5.58 (d, J = 1)	5.38 (q)	3.75 (dd, J = 16 and 4)	3.20 (dd, J = 16 and 2)	1.28 (t, J = 7, Et) 4.22 (q, J = 7, Et)
8	7.17 (d, J = 2)	5.37 (overlap with PNB)	4.68 (m)	3.6 (m)	3.6 (m)	7.4 (m, Ph)
9	—	5.17 (s)	5.57 (q)	3.97 (dd, J = 16.5 and 4)	3.45 (dd, J = 16.5 and 2)	—
10*a*	6.83 (d, J = 1)	5.48 (d, J = 1)	5.57 (q)	3.85 (dd, J = 16 and 4)	3.20 (dd, J = 16 and 1.5)	7.4 (m, Ph)
10*b*	6.75 (s)	5.53 (s)	5.55 (q)	3.87 (dd, J = 16 and 4)	3.20 (dd, J = 16 and 1.5)	7.61 and 6.5 (furyl)
10*c*	ca. 7.1	5.6–5.7	5.6–5.7	3.97 (dd, J = 16 and 4)	3.35 (dd, J = 16 and 1.5)	7.1–7.3 (thienyl)
10*d*	6.00 (s)	4.87 (s)	5.17 (m)	3.0–3.5 (m)	3.0–3.5 (m)	1.28 (t, J = 7, Et) 4.22 (q, J = 7, Et)
11	ca. 7.4	5.50 (d, J = 2)	4.83 (q)	3.82 (dd, J = 16 and 4)	3.46 (dd, J = 16 and 2)	7.35–8.0 (Ph)
12	—	5.10 (s)	5.72 (q)	4.10 (dd, J = 17 and 4)	3.47 (dd, J = 17 and 2)	—

[a]Spectra were recorded at 60 MHz and are reported in ppm downfield from TMS. All esters were in $CDCl_3$; free acids in acetone-d_6 except **10***c* in DMSO-d_6 and salt **10***d* in D_2O. Coupling constants are in Hz. All PNB esters showed doublets at δ 8.15–8.27 and 7.47–7.58 (J = 8.5) and a singlet at 5.29–5.37.
[b]Reference 4.

virtually complete conversion to the exocyclic form occurred. Minor changes in the *exo*/*endo* ratio (when R = Ph) were made by varying the reaction solvent. That the reaction only occurs when R contains a function that can conjugate with the exocyclic double bond is shown by the example of **5** (R = CH_2CO_2PNB): no isomerization was observed after prolonged treatment with base. The relative stereochemistry[3] shown for **6** (3 and 5 positions) follows from analogy to that found for **2** (R^1 = CO_2Et, R^2 = benzyl) by the Farmitalia group (4) since nmr spectra of the vinyl, H-3, and H-5 protons show a very close match between **2** and **6** both in chemical shift and coupling constants (see Table 1). The Beecham group have evidence that their isomerization product **7** (R = Me) is the *Z* isomer shown; the vinyl proton has a chemical shift of 5.57 ppm (10). If one adds a shift value of 0.6 to 0.7 ppm for going from an oxygen ring to sulfur ring (11), then one would predict a vinyl proton shift of 6.2 to 6.3 ppm for the *Z* isomer **6***a*. In fact, a vinyl proton shift of 6.70 ppm was observed (see Table 1), thus supporting the *E* assignment. However, these minor differences in chemical shift values do not provide very compelling evidence without having both isomers on hand. Molecular models of structure **6** show marked steric crowding between the aromatic ring in the *E* isomer and the ester at the 3-position, whereas the *Z* isomer shows no steric congestion. Thus, while ^1H nmr arguments favor the *E* geometry for compounds **6**, steric arguments favor the *Z* geometry.

A single crystal X-ray diffraction analysis of **6***a* conclusively verified the nmr based stereochemical assignments for the 3,5-relationship, while the double bond was shown to have the *Z* geometry. The phenyl ring, at least in the solid state conformation, is twisted slightly out of the plane of the double bond (~11°) presumably to relieve steric congestion. The molecular parameters[4] were unsurprising for a penem and the bridgehead nitrogen was 0.43 Å out of the plane of its nearest

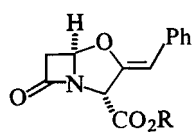

7

[3]All compounds described are racemates; for convenience, just one enantiomer is shown.

[4]Fractional coordinates and thermal parameters, bond distances, bond angles, and observed and calculated structure factors for structure **6***a* are available, at a nominal charge, from the Depository of Unpublished Data, CISTI, National Research Council of Canada, Ottawa, Ont., Canada K1A 0S2.

Can. J. Chem. Downloaded from www.nrcresearchpress.com by 210.87.254.40 on 09/06/12
For personal use only.

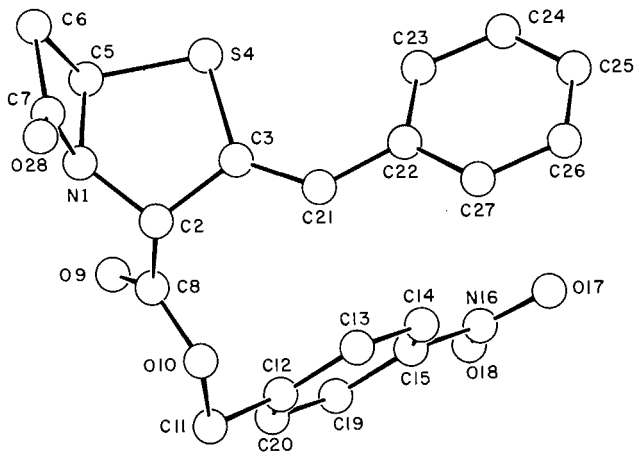

FIG. 1. A computer generated perspective drawing of the final X-ray model of **6***a*. Hydrogens are omitted.

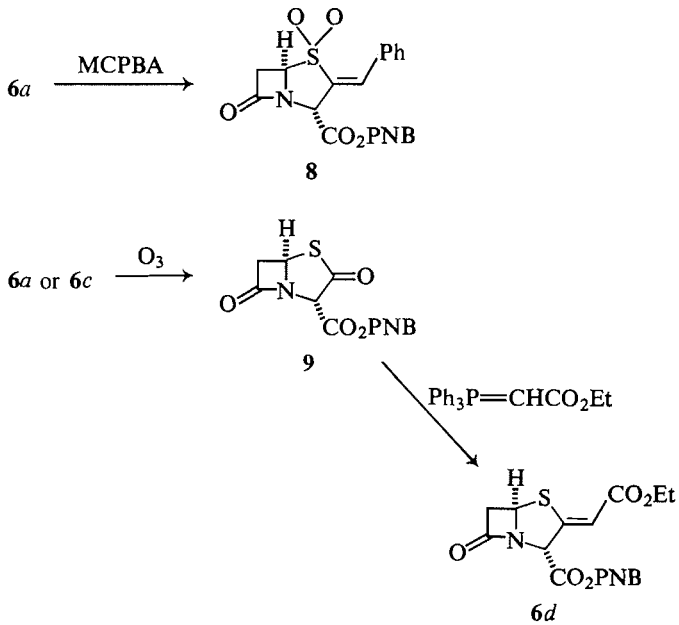

SCHEME 1

neighbors. A drawing of the final X-ray model is given in Fig. 1.

The sulfone **8** was prepared by the action of *m*-chloroperbenzoic acid on penem **6***a* (analogous to sulfone formation in the isocephems (12)) (see Scheme 1). The infrared spectrum of **8** shows strong peaks at 1320 and 1135 cm^{-1} (which do not appear in the spectrum of **6***a*), indicating the formation of the sulfone rather than the sulfoxide (ν(S=O) for sulfoxide: 1035–1070 cm^{-1}). Ozonolysis of the exocyclic double bond of **6***a* or **6***c* gave oxopenam **9**. Numerous attempts were made to carry out reactions between oxopenam **9** and Wittig reagents. All failed except for (carboxymethylene)triphenylphosphorane. This reagent gave penem **6***d* in low yield. Infrared and ^1H nmr spectra of **6***d* closely matched those reported for **2** (R^1 = CO_2Et, R^2 = benzyl) (4) (allowing for the difference between the *p*-nitrobenzyl and benzyl esters). The double bond geometry in **6***d* is uncertain but is probably *Z* in analogy with compound **6***a*.

Deprotection of the esters **6** proceeded by the usual hydrogenolysis conditions (although in low yield for some) to give

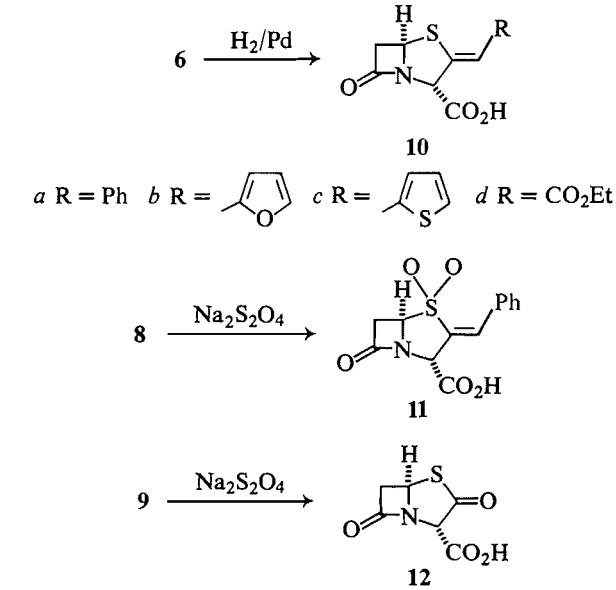

SCHEME 2

acids **10** (see Scheme 2). However, compounds **8** and **9** could not be hydrogenolyzed to their free acids due to the instability of the latter under these reaction conditions. Use of sodium dithionite (13) did give the acids **11** and **12** in good yield. The ^1H nmr spectrum of **12** was the same (allowing for the different solvents used) as the spectrum for **12** reported by the Sankyo group (6).

All of the free acids were insufficiently stable to be purified enough to give an acceptable elemental analysis (see, for example, compound **10***c* in the Experimental). However, it was felt that their level of purity (as determined by ^1H nmr) was such that microbiological evaluation would provide reliable qualitative data. In fact, none of the compounds showed any microbiological activity, either as antibacterials or as β-lactamase inhibitors. Because of concerns over stability affecting microbiological results, the chemical integrity of oxopenam **12** was determined under conditions of the β-lactamase inhibition tests: a solution of compound **12** in pH 7 buffer maintained at room temperature for 45 min showed continued presence of intact **12** (although some decomposition did occur). The lack of activity cannot be ascribed to chemical decomposition. Since oxopenem **7** (R = Na) is described as a potent β-lactamase inhibitor (10), the lack of activity in the sulfur analogs **10** must be ascribed to the replacement of oxygen by sulfur. It is interesting to note that the close analog of **12**, cephem **13**, is described as being "only marginally active against Staphylococcus aureus" (14) while the oxopenam **14** is claimed in a patent (15) as a β-lactamase inhibitor.

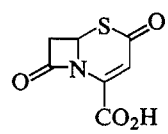

13

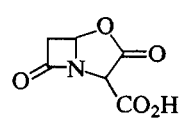

14

Experimental

Conversion of penems 5 to exocyclic penems 6

A solution of compound **5** (*a*, *b*, or *c*, 1.0 mmol), triethylamine (100 mg, 1.0 mmol), and tetrahydrofuran (4 mL) was stirred at 23°C for 15 min. The solution was concentrated *in vacuo* (40°C), the residue

Can. J. Chem. Downloaded from www.nrcresearchpress.com by 210.87.254.40 on 09/06/12
For personal use only.

Can. J. Chem. Downloaded from www.nrcresearchpress.com by 210.87.254.40 on 09/06/12
For personal use only.

was redissolved in dichloromethane (20 mL), and the solution was washed with 0.1 *M* hydrochloric acid, then water (10 mL each). The organic layer was dried and the solvent was evaporated *in vacuo* to give **6***a*, *b*, or *c*.

4-Nitrobenzyl 3-benzylidene-7-oxo-4-thia-1-azabicyclo[3.2.0]heptane-2-carboxylate **6**a

With penem **5***a* (R = Ph) the reaction product consisted of an 80:20 mixture of **6***a* and **5***a* (as determined by ^{1}H nmr). Purification was achieved by column chromatography on silica gel: elution with ether/hexane, then with ether. The appropriate fractions were concentrated *in vacuo* to give compound **6***a* (ca. 95% pure), 65% yield; mp 110−113°C; ir (amorphous film) *ν*: 1785, 1745 cm^{-1}. A portion was recrystallized several times from benzene, the last time by very slow evaporation of solvent to give crystals suitable for X-ray diffraction analysis (see below).

4-Nitrobenzyl 3-(2-furylidene)-7-oxo-4-thia-1-azabicyclo[3.2.0]heptane-2-carboxylate **6**b

With R = 2-furyl the reaction product consisted of almost pure **6***b* (97% yield); ir (amorphous film) *ν*: 1785, 1750 cm^{-1}.

4-Nitrobenzyl 3-(2-thienylidene)-7-oxo-4-thia-1-azabicyclo[3.2.0]heptane-2-carboxylate **6**c

With R = 2-thienyl the reaction product consisted of pure **6***c* (99% yield); mp 103−104°C; ir ($CHCl_3$) *ν*: 1790, 1750 cm^{-1}; uv (EtOH) λ_{max}: 267 (ϵ = 15 700), 304 (ϵ = 18 300) nm. *Anal.* calcd. for $C_{18}H_{14}N_2O_5S_2$: C 53.72, H 3.51, N 6.96, S 15.93; found: C 53.77, N 3.50, N 6.90, S 16.15.

4-Nitrobenzyl 3-benzylidene-4,4,7-trioxo-4-thia-1-azabicyclo-[3.2.0]heptane-2-carboxylate **8**

A solution of compund **6***a* (198 mg, 0.50 mmol), *m*-chloroperbenzoic acid (220 mg, containing ca. 1.1 mmol), and dichloromethane (20 mL) was stirred at 23°C for 17 h. The solution was washed with 1% sodium bicarbonate (2 × 20 mL), dried, and concentrated *in vacuo*. The product was purified by chromatography on silica gel: elution with ether. Evaporation of solvent from the appropriate fractions gave the sulfone **8** as an oil; 95 mg (44% yield), in about 90% purity; ir (film) *ν*: 1800, 1750, 1320, 1135 cm^{-1}.

Ozonolysis of **6**a *and* **6**c

4-Nitrobenzyl 3,7-dioxo-4-thia-1-azabicyclo[3.2.0]heptane-2-carboxylate **9**

A solution of compound **6***a* (396 mg, 1.0 mmol) or compound **6***c* (402 mg, 1.0 mmol) in ethyl acetate (20 mL) was ozonized at −78°C until a blue color persisted. The excess ozone was purged with oxygen and the solution was allowed to warm gradually to 23°C. The solution was washed with dilute aqueous sodium bicarbonate, then saturated sodium chloride, dried, and the solvent was evaporated *in vacuo* to give a yellow gum, 340 mg. The product was purified by column chromatography on silica gel: elution with hexane/ether 9:1 followed by ether. Evaporation of solvent from the appropriate fractions gave oxopenam **9**, 230 mg (70% yield), in greater than 90% purity. Recrystallization from benzene gave **9**; mp 114−117°C; ir (solid film) *ν*: 1790, 1750, 1710 cm^{-1}. *Anal.* calcd. for $C_{13}H_{10}N_2O_6S$: C 48.45, H 3.13, N 8.69, S 9.95; found: C 48.37, H 3.23, N 8.78, S 9.91.

4-Nitrobenzyl 3-carbethoxymethylene-7-oxo-4-thia-1-azabicyclo-[3.2.0]heptane-2-carboxylate **6**d

A solution of oxopenam **9** (97 mg, 0.30 mmol) and (carbethoxymethylene)triphenylphosphorane (111 mg, 0.32 mmol) in benzene (10 mL) was heated under reflux for 2 h. The solvent was evaporated *in vacuo* and the residue was purified by chromatography on silica gel (elution with ether) to give compound **6***d* as an oil, 30 mg (23% yield); ir ($CHCl_3$) *ν*: 1785, 1755, 1700 cm^{-1}.

Hydrogenolysis of p-*nitrobenzyl esters*

Compounds **6** were hydrogenated on a Parr apparatus (details for each compound below) at 30 to 50 psi (1 psi = 6.89 kPa) and 23°C. The catalyst was removed by filtration and the phases were separated. In the case of **6***a* and **6***b*, the aqueous phase was acidified with dilute hydrochloric acid and extracted with ethyl acetate. The organic extract was washed with saturated sodium chloride, dried, and the solvent was evaporated *in vacuo* to give the title compounds. In the case of **6***c* and **6***d*, work-up was as given below.

3-Benzylidene-7-oxo-4-thia-1-azabicyclo[3.2.0]heptane-2-carboxylic acid **10**a

Hydrogenolysis mixture: compound **6***a* (198 mg, 0.50 mmol), sodium bicarbonate (42 mg, 0.5 mmol), palladium on Celite (30%, 200 mg), tetrahydrofuran (30 mL), ether (30 mL), and water (30 mL) for 6 h. The product was obtained in 98% yield and recrystallized from ethyl acetate to give acid **10***a*; mp 153−154°C; ir (Nujol mull) *ν*: 1775, 1760, 1730 cm^{-1}; uv (EtOH) λ_{max}: 286 (ϵ = 18 100) nm.

3-(2-Furylidene)-7-oxo-4-thia-1-azabicyclo[3.2.0]heptane-2-carboxylic acid **10**b

Hydrogenolysis mixture as for preparation of **10***a* except: compound **6***b* (193 mg, 0.50 mmol). The product was obtained as a brown solid, 98% yield, in about 90% purity (by nmr); ir (Nujol mull) *ν*: 1755 (very broad) cm^{-1}; uv (EtOH) λ_{max}: 296 (ϵ = 20 400), 308 (ϵ = 17 600) nm.

3-(2-Thienylidene)-7-oxo-4-thia-1-azabicyclo[3.2.0]heptane-2-carboxylic acid **10**c

Hydrogenolysis mixture: compound **6***c* (344 mg, 0.855 mmol), palladium hydroxide (345 mg), tetrahydrofuran (60 mL), and water (30 mL) for 18 h. Dilute hydrochloric acid and ether were added, mixed, and the organic layer was separated and washed with water and saturated sodium chloride. The solvent was evaporated *in vacuo* and the residue was crystallized with benzene to give acid **10***c*, 100 mg (44% yield); mp 115°C (dec.); ir (Nujol) *ν*: 1775, 1765, 1730 cm^{-1}; uv (EtOH) λ_{max}: 304 (ϵ = 17 700), 315 (ϵ = 15 400) nm. *Anal.* calcd. for $C_{11}H_9NO_3S_2$: C 49.42, H 3.39, N 5.24, S 23.99; found: C 50.20, H 3.57, N 5.09, S 23.06.

Sodium 3-carbethoxymethylene-7-oxo-4-thia-1-azabicyclo[3.2.0]heptane-2-carboxylate **10**d

Hydrogenolysis mixture: compound **6***d* (60 mg, 0.153 mmol), sodium bicarbonate (13 mg, 0.153 mmol), palladium on Celite (30%, 60 mg), tetrahydrofuran (8 mL), and water (8 mL) for 2 h. Ether was added, mixed, and the phases were separated. The aqueous phase was washed with ether, then lyophilized to give compound **10***d*, 6 mg (14% yield); ir (KBr) *ν*: 1772, 1698, 1660, 1630 cm^{-1}.

Ester cleavage by sodium dithionite

A solution of sodium dithionite (195 mg, 1.12 mmol for **8**; 260 mg, 1.5 mmol for **9**) in water (10 mL) was added to a solution of sulfone **8** (80 mg, 0.187 mmol) or oxopenam **9** (80 mg, 0.25 mmol) in tetrahydrofuran (10 mL) at 0°C. Dilute sodium bicarbonate was added until the solution was pH 7, it was stirred at 0°C for 30 min, and then it was washed with ether. The aqueous phase was acidified with dilute hydrochloric acid (0°C) to pH 2−2.5 and extracted with ethyl acetate (2 × 25 mL). The organic extracts were washed with saturated sodium chloride, dried, and the solvent was evaporated *in vacuo* to give the products as amorphous solids.

3-Benzylidene-4,4,7-trioxo-4-thia-1-azabicyclo[3.2.0]heptane-2-carboxylic acid **11**

Sulfone **11**: 45 mg (82% yield); 80−90% pure (by nmr); ir (solid film) *ν*: 1800, 1750 cm^{-1}.

3,7-Dioxo-4-thia-1-azabicyclo[3.2.0]heptane-2-carboxylic acid **12**

Oxopenam **12**: 39 mg (83% yield); ir (solid film) *ν*: 1790, 1730, 1718 cm^{-1}.

Stability of oxopenam **12**

The conditions of the chemical stability test were the same as those of the β-lactamase inhibition experiment with the exception of the following. Compound **12** was used in higher concentration (20 mg/mL vs. 0.1 mg/mL in the inhibition test), no bacteria were present (*Staphylococcus aureus* or *Klebsiella pneumoniae*), and no chromogenic cephalosporin indicator was present.

A solution of 5 mg of oxapenam **12** in 0.05 mL of acetonitrile plus 0.25 mL of phosphate buffer (pH 7) was maintained at 23°C for 45 min. Reversed phase thin-layer chromatography (Analtech RPSF

250-micron plates; developed with pH 7 buffer/acetonitrile 95:5; visualized with iodine; compound **12** at R_f 0.57) showed the presence of intact oxopenam **12** and some decomposition products.

Single crystal X-ray analysis of ***6***a

$C_{20}H_{16}N_2O_5S$ fw = 396.4

Triclinic, a = 5.529(2), b = 18.665(5), c = 13.481(4) Å, α = 129.04(3), β = 113.69(3), γ = 89.31(3)°, V = 931 Å^3, Z = 2, ρ_c = 1.41 g/cc, space group = $P\bar{1}$, (22°C, CuK$\bar{\alpha}$).

Preliminary X-ray photographs displayed only triclinic symmetry and accurate lattice constants, determined from a least-squares fit of fifteen diffractometer measured 2θ-values, were as above. A crystal of roughly cubic shape was used, 0.25 mm on a side. An estimated density indicated two molecules formed the unit cell and space group $P\bar{1}$ was assumed. All unique diffraction maxima with $2\theta \leq 114°$ were collected on a computer controlled four-circle diffractometer using a variable speed, 1° ω-scan and graphite monochromated CuK$\bar{\alpha}$ radiation. After correction for Lorentz, polarization, and background effects, 1715 (74%) of the 2357 reflections were judged observed. A phasing model was readily achieved using a multisolution sign determining procedure.[5] Block diagonal least-squares refinement with anisotropic nonhydrogen atoms and isotropic hydrogens have converged to a standard crystallographic agreement factor of 0.056 for the observed data. (Quantity minimized: $\Sigma w \| F_o | - | F_c \|^2$.) Fractional coordinates and thermal parameters, bond distances, bond angles, and observed and calculated structure factors are listed in Tables 2 to 5 respectively.[4]

[5]All crystallographic calculations were done on a Prime 850 computer, operated by the Cornell Chemistry Computing Facility. Principal programs employed were as follows. REDUCE and UNIQUE, data reduction programs: M. E. Lewonowicz. Cornell University, 1978. MULTAN 78, "A System of Computer Programs for the Automatic Solution of Crystal Structures from X-ray Diffraction Data", direct methods programs and fast Fourier transformation routine (locally modified to perform all Fourier calculations including Patterson syntheses): P. Main, S. E. Hull, L. Lessinger, G. Germain, J.-P. Declercq, and M. M. Woolfson. University of York, England, 1978. NQEST, CYBER 173 version negative quartets figure of merit calculation: C. M. Weeks. Medical Foundation of Buffalo, Inc., August 1976. BLS78A, anisotropic block-diagonal least-squares refinement: K. Hirotsu and E. Arnold. Cornell University, 1980. ORTEP, crystallographic illustration program: C. K. Johnson. Oak Ridge, TN. ORNL3794, June, 1965. Scattering factors were from ref. 17.

Acknowledgements

We would like to thank Dr. B. Belleau of McGill University for advice during the course of this work. We also thank Dr. M. Misiek of the microbiological department, Bristol Laboratories, Syracuse, N.Y., for the antibacterial and β-lactamase inhibitory tests.

1. M. LANG, K. PRASAD, W. HOLICK, J. GOSTELI, I. ERNEST, and R. B. WOODWARD. J. Am. Chem. Soc. **101**, 6296 (1979).
2. M. MÉNARD and A. MARTEL. U. S. Patent 4 272 437 (1981); Chem. Abstr. **95**, 203 941 (1981); A. MARTEL, P. DEXTRAZE, J. P. DARIS, R. SAINTONGE, P. LAPOINTE, T. CONWAY, I. MONKOVIC, G. KAVADIAS, Y. UEDA, P. ELIE, S. PATIL, G. CARON, J. DOUGLAS, M. MÉNARD, and B. BELLEAU. Can. J. Chem. **60**, 942 (1982).
3. P. CHERRY, D. EVANS, C. NEWALL, and N. WATSON. Tetrahedron Lett. 561 (1980).
4. P. LOMBARDI, G. FRANCESCHI, and F. ARCAMONE. Tetrahedron Lett. 3777 (1979).
5. T. HOWARTH, A. BROWN, and T. KING. J. Chem. Soc. Chem. Commun. 266 (1976).
6. F. SHIMIZU, A. SAITO, T. NISHIMURA, and M. NAKAHARA. Japan Kokai, 79-66695 (1979); Chem. Abstr. **91**, 193 300 (1979).
7. J. MARCHAND-BRYNAEST and L. GHOSEZ. Tetrahedron Lett. 3085 (1980).
8. E. BRAIN, N. BROWN, and R. HICKLING. J. Chem. Soc. Perkin Trans. 1, 892 (1981).
9. J. ARROWSMITH and G. GREENGRASS. Tetrahedron Lett. 357 (1982).
10. P. BENTLEY, G. BROOKS, M. GILPIN, and E. HUNT. J. Chem. Soc. Chem. Commun. 905 (1977).
11. T. BRYSON. J. Org. Chem. **38**, 3428 (1973).
12. T. DOYLE, J. L. DOUGLAS, B. BELLEAU, J. MEUNIER, and B. LUH. Can. J. Chem. **55**, 2873 (1977).
13. B. JACKSON. U. S. Patent 3 799 924 (1974); Chem. Abstr. **81**, 3957 (1974); E. GUIBE-JAMPEL and M. WAKSELMAN. Synth. Commun. **12**, 219 (1982).
14. I. ERNEST, A. MAIN, and R. WOODWARD. Helv. Chim. Acta, **64**, 1303 (1981).
15. T. HOWARTH and I. STIRLING. Ger. Offen. 2 655 675 (1977); Chem. Abstr. **87**, 102 313 (1977).
16. Y. UEDA, C. E. DAMAS, and V. VINET. Can. J. Chem. **61**, 2257 (1983).
17. D. T. CROMER and J. B. MANN. Acta Crystallogr. Sect. A, **24**, 321 (1968).

Can. J. Chem. Downloaded from www.nrcresearchpress.com by 210.87.254.40 on 09/06/12
For personal use only.

A vectorial model of photon–molecule interactions and the development of an Octupole Rule of vibrational excitation

B. R. HOLLEBONE

Department of Chemistry, Carleton University, Ottawa, Ont., Canada K1S 5B6

Received January 4, 1984

B. R. HOLLEBONE. Can. J. Chem. **62**, 2287 (1984).

An alternative approach to the assignment of molecular vibrations is suggested in which both the molecule and the photon are taken as coincident quantum mechanical entities at the instant of impulse. This model permits the description of the excitation in a simple vectorial form. Using subduction techniques, complete and orthonormal basis vectors for both particles can be defined and the probabilities of excitation are directly related to the overlap of these basis vectors at the instant of space and time coincidence. The model obeys fully the requirements of the $3n - 6$ degrees of freedom rule and is found to express the motions of atoms in terms of their overlap with available multipole fields of the photon. To first order the photon–molecule interaction is taken as the Coulomb potential between the electric fields of the photon and those of the shielded atomic nuclei. The relatively low valence electron density is ignored but becomes important in second order. With this assumption, molecular translational motion correlates to, and exhausts, the dipolar photon field, rotation corresponds to three of the five components of the photon quadrupole and ungerade internal modes are first permitted by overlap with the photon octupole. Some of the consequences of this Octupole Rule are discussed with particular reference to octahedral molecules from which molecules of lower symmetry can be algebraically subduced.

B. R. HOLLEBONE. Can. J. Chem. **62**, 2287 (1984).

On suggère une approche de rechange pour attribuer les vibrations moléculaires; dans cette approche, la molécule et le photon sont considérés comme des entités de mécanique quantique qui sont coincidentes au moment de l'impulsion. Ce modèle permet de décrire l'excitation sous une forme vectorielle simple. En utilisant des techniques de subduction, chacune des particules peut être définie à l'aide de vecteurs complets et orthonormaux et les probabilités d'excitation sont directement reliées au recouvrement de ces vecteurs de base au moment de la coincidence de l'espace et du temps. Le modèle obéit pleinement aux exigences de la loi des $3n - 6$ degrés de liberté et on trouve qu'il exprime le mouvement des atomes en fonction de leur recouvrement avec les champs multipolaires disponibles du photon. En première approximation, on considère l'interaction photon–molécule comme le potentiel de Coulomb entre les champs électriques du photon et ceux des noyaux atomiques blindés. On ne tient pas compte de la faible densité des électrons de valence, mais celle-ci devient importante au deuxième ordre. Sur la base de cette hypothèse, (*a*) on peut établir une corrélation entre le mouvement moléculaire de translation et le champ dipolaire du photon et épuiser ce dernier; (*b*) la rotation correspond à trois des cinq composantes du quadrupole du photon et (*c*) les modes internes d'ungerade sont permis en premier par un recouvrement avec l'octupole du photon. On discute de quelques conséquences de cette règle de l'Octupole en se référant particulièrement aux molécules octaédriques à partir desquelles on peut subduire algébriquement des molécules de plus faible symétrie.

[Traduit par le journal]

Can. J. Chem. Downloaded from www.nrcresearchpress.com by 210.87.254.40 on 09/06/12
For personal use only.

Introduction

Group theoretical analysis of selection rules of molecular vibrations has for many years provided useful insight into molecular structure. This utility is essentially due to the separation of radial and angular terms in the molecular basis functions imposed by the nature of the point groups. In molecules of more than three atoms, however, different internal modes may require identical representations in the finite group of the molecule. Since these assignments are not unique, the algebra of the point group cannot support the actual orthonormality of these different modes and hence is an incomplete description of the system.

This problem applies not only to the molecule itself but also to the exciting particle and to the description of the physical two body complex at the time of energy transfer. As a result, the excitation process is often described in a semiclassical model without identifying the covering symmetry and its accompanying selection rules. A description involving the covering symmetry is possible if some of the parameters of the process are restated. This restatement may provide an alternative approach to the description and calculation of energies and intensities of fundamental vibrations, particularly in molecules of moderate to high symmetry where the numbers of purely radial theoretical parameters is less than the number of available experimental observations.

Theory

Phenomenology of excitation of bound states

Most models of time dependent excitation processes involve a molecule of fixed mass in a fixed position with respect to a set of reference coordinates. Under these conservation conditions for both mass and position, $3n - 6$ degrees of internal freedom remain as fundamental bound excited states. The excitation process is then considered as a time-dependent disturbance of this fixed system by a second body, often in a semiclassical description (1).

In order to avoid the approximations of semiclassical theories which may obscure important features, the complete model of a mass body can be made fully quantum mechanical. Thus, all transitions involving all types of change are made to occur between bound states of the total potential. These transitions can include changes in mass and position. The potential appropriate to this situation is infinitely deep. The classical continuance representing translation or rotation of semiclassical models is avoided in this description.

The simplest infinitely deep potential is that representing simple harmonic motion. Any other more complex, infinitely deep potential, can be resolved into sums of SHM potentials so that the following considerations are readily extended if necessary to coupled systems of higher complexities. The SHM potential is characterized by rigid angular and radial symmetry.

Can. J. Chem. Downloaded from www.nrcresearchpress.com by 210.87.254.40 on 09/06/12
For personal use only.

In particular there is no radial anharmonicity to introduce any dependence of energy difference between states on the total energy of the system.

However, the identification of states of individual molecules requires a series of specializations of this model. In the full potential, mass is a variable. A change in mass has full angular symmetry in the overall Hamiltonian and corresponds to the scalar operation within the infinite potential. Conservation of mass in a finite isolated mass system removes this degree of freedom and exhausts the scalar operation. Removal of the scalar operation coincides with removal of the scalar contribution to the infinitely deep potential. This removal of the scalar potential term reduces the radial symmetry of the body and must result in an anharmonic radial part of the potential (2). The descent in radial symmetry is from the U(3) group of SHM potentials to the C_0 (3) conservation group of the fixed mass. The resulting anharmonic potential must be finite in depth and resembles a Morse curve.

Conservation of position of a mass array which obeys Bose statistics corresponds to elimination of two further types of operation and hence two further terms from the Hamiltonian. The first is translation, which in three-dimensional mass systems is a triply degenerate dipolar operation. The dipolar movement of mass from one position to another leaves nothing behind. For a finite mass this is an unbound operation which completely exhausts the dipolar operations which may be performed on the body. The second operation is rotation about three independent axes and is again triply degenerate. In terms of the formal static potential it is an unbound operation and its removal from the potential exhausts three of the five components of the quadrupole operation.

Removal of the entire mass dipole and part of the mass quadrupole operations by considering systems in which translational and rotational motion are forbidden corresponds to removal of six additional vector components from the system potential. This further reduction in radial and angular symmetry beyond the loss of the scalar imposes increased anharmonicity on the remaining potential of the fully constrained system and results in the final shape of the three dimensional Morse potential for the chosen mass body.

The remaining degrees of freedom, identified by the $3n - 6$ rule, can only be excited by a symmetry change corresponding to the remaining two components of the quarupole or the components of any higher multipole tensorial operators. The exhaustion of the scalar, dipole, and part of the quadrupole operations by conserving the conditions which these operators could alter means that these operators, representing the possible influences of second bodies, cannot participate in altering the internal vibrational states of the mass body in any way.

Coupling of a mass body to a photon

No direct coupling of a pure mass body with a massless photon can occur. Indirect coupling can arise through an interaction of the electrical multipoles of the photon with the distributed electric field on the mass body. The details of this coupling will be determined by two overlap conditions. The first is the correspondence of the molecular electric field to the molecular mass array and the second is the overlap of the molecular mass-change field with the photon as a function of relative positions.

The coupling of the molecular mass and electric fields can be described using the descent in symmetry approximation just discussed. Considering only the mass field, internal fundamental excited states correspond to quadrupolar or higher perturbations of the initial body. Conversely, considering only the electric field in which the fundamental particles obey Fermi statistics, internal excited states may correspond to dipolar perturbations since this centre of charge is not displaced during a dipolar separation of charge. Hence the mass and electron arrays exist in *different effective potentials*, each with its characteristic depth, anharmonicity, separation energy between excited states, and selection rules. Indeed, since the restrictions on Bosons are more severe than on Fermions, the mass potential must be more anharmonic than the electron potential. This conclusion is borne out by experiment for in most molecules, bond breaking energies are 5 to 10 times lower than first ionization energies in the gas phase. These vectorial differences, reflected in the selection rules and the radial differences, are displayed in a mismatch of excitation energies mitigating strongly against any significant first order coupling of valence electrons with the mass field. Given this situation, the behaviour of valence electrons during excitation by external fields may be ignored to first order. A much more important electronic feature of the mass array is the coincident array of sharp cusps of positive charge representing the unshielded nuclear charge on each atom in the array. These cusps are well established by recent calculations (3) and are orders of magnitude more intense than the surrounding diffuse background of valence electron density. This array of positive cusps is strongly coupled to the mass array, remains coincident in first order during vibrational excitations, and is the relevant part of the molecular electric field for the excitation of the mass field.

The second stage of coupling involves the overlap of this array of positive cusps with the field of the photon. Under normal circumstances the wave length of the exciting photons is two orders of magnitude greater than the dimensions of the molecule (or the chromophore) being excited. Experimentally, it is almost always the normal modes localized at the centre of highest symmetry that are involved, for which the Brillouin displacement vector $\boldsymbol{K} = 0$ (5). This suggests that, to first order, the model needs only consider a photon with origin coincident with that of the molecule and no integration over time or space is necessary to identify the initial impulse. The most important consideration in describing the detailed overlap of the molecular positive cusp array and the photon at the point of coincidence of origins is the description of the structure of the photon itself. The conventional model of this particle defines the radiation field in terms of a vector potential $\boldsymbol{A}$ and a scalar potential, σ, the latter may be ignored by appropriate gauge selection. To first order, $\boldsymbol{A}$ may be considered a tensor of order 1 with three orthonormal vector components. In this form it is known as the electric dipole approximation (5, 6). It carries with it the implication that, because of the relative sizes of the photon and molecule, the field is constant across the molecule.

Superimposing this simplified photon on the molecule with mutually coincident origins, the effect of the photon tensor field gradient on the molecule is clear. All the positive cusps representing each atom will be accelerated in the same negative direction of the field for each of the three field components. This corresponds directly to the three translation degrees of freedom of the molecule. It does *not* correspond to an overlap of the photon and molecular fields which could initiate nuclear motion in opposite directions and hence preserve the centre of mass in an internal mode. This dipole field overlap is therefore *exhausted in inducing translation*.

Can. J. Chem. Downloaded from www.nrcresearchpress.com by 210.87.254.40 on 09/06/12
For personal use only.

More detailed models of photon structure have been used, usually involving an electric multipolar expansion about the origin (7). The overlap of these higher pole field distributions with the molecular mass charge array shows that three quadrupole components lead directly to molecular rotation but that all other tensorial components of the higher poles may induce internal modes.

Transition probabilities

The quantitative description of this model again involves three stages, the quantum mechanical derivation of the coupled mass charge system, of the radiation field and of their mutual interaction.

(a) The molecular model

The quantum mechanical description of the mass charge array has been derived in earlier work. Essentially, the internal density harmonics of a spherical continuous mass are derived in momentum space. The imposition of conservation of monopole and dipole properties results in an anharmonic potential whose solutions arise from a non-linear second order differential equation of parametric form

$$-\frac{d^2\psi}{dr^2} - \frac{2(\lambda + 1)}{r}\frac{d\psi}{dr} + b\psi^2 - E\psi = 0$$

When $\lambda = 0$ the Lane–Ender equation for radial spherical systems results and this also corresponds to conservation of position in a one-dimensional space (4). The general form of this equation can be applied to the spherical mass body with conservation group symmetry C_1 (3), using an approximation based on the Poschl–Teller potential;

$$V_m = K(K - 1)k^2 \operatorname{cosech}^2(kx) - \lambda(\lambda - 1)k^2 \operatorname{sech}^2(kx)$$

The potential occurs in two parts, a positive term related to K representing a repulsive potential and a negative term related to λ representing the attractive potential. After conversion to spherical coordinates, the states related to the two potentials can be linearly combined to create two subspaces of states, those bound in an anharmonic well and those unbound above the well. The depth of the well is determined by the values of K and λ, which are related to the fixed amount of mass in the system.

The normal mode angular momenta of lower symmetry molecules are readily identified by subduction in a physically significant chain from the conservation group $C_1(3)$. By direct application of Racah's Lemma, the components of the angular parts of representations in $C_1(3)$, which are the spherical harmonics, may be linearly combined to mimic the states of any Hamiltonian in any array which may be derived by reduction in symmetry from the generative sphere (2). Thus, basic functions retain their generative group representations while being further specified by those of the subgroup used to label the recombined components (8).

(b) The photon model

The quantum mechanical description of the radiation field relies upon the demonstration that the classical radiation field may be regarded as a set of independent harmonic oscillators, each with its own Hamiltonian. From the vector potential

$$A = \sum_\alpha (q_\alpha A_\alpha + \bar{q}_\alpha \bar{A}_\alpha)$$

$$H_F = H_\alpha = 2D^2 \bar{q}_\alpha \cdot q_\alpha$$

where

$$q_\alpha = |q_\alpha| \exp(-iv_\alpha t)$$

Under this Hamiltonian a change of state occurs only when there is a gain or loss of one independent oscillator or photon by the field.

(c) The interaction model

The fully quantum mechanical description of interaction of the coupled mass – nuclear charge array with the field involves a Hamiltonian with three terms

$$H = H_M + H_F + H_I = H_0 + H_I$$

where H_I is the interaction term. The interaction operator is readily constructed for the P.T. potential in a Coulomb gauge which permits the scalar potential to be set to zero. Then, for the absorption of energy from the radiation field, the extinction coefficient becomes (6)

$$M_k = \sum_\alpha \frac{e}{mc} \left\langle a \left| \sum_{j=1}^{n} p_j A_{j\alpha} \right| a_0 \right\rangle \left\langle F |q_\alpha| F_0 \right\rangle$$

This element vanishes unless at least one of the photons is removed from the radiation field, when the matrix element is non-zero. The magnitude of M_k is determined by the sum of all interaction contributions for each harmonic oscillator of the field labelled and by the magnitude of the potential A_j at the position of each of the j charged particles in the coupled mass-charge array.

In the simplest approximation, a single photon event is considered. Then, the further approximation is made that all A_j are equal, that is, the field is constant. Then (6)

$$M_k = \frac{e}{mc} |\boldsymbol{A}| \sum_j \langle a | p_j | a_0 \rangle$$

The limitations due to these approximations have recently been examined (9). They are not determined for the excitation processes of electrons in atoms (9) but for the excitations of mass charge arrays they are clearly inappropriate. The extended array is large enough to encounter variations in direction and magnitude of $\boldsymbol{A}$ and vectorial properties must be retained in the dynamic Hamiltonian. Moreover, with all the $3n - 6$ degrees of freedom available it is inevitable that the lower poles of the harmonic oscillating photon will be exhausted and the higher poles needed for correct overlap to excite the remaining modes. This is not the case with excitation of electrons since only the dipole and occasionally the quadrupole is involved.

The expression of both p and $\boldsymbol{A}$ in conventional descriptions is clumsy in that it is evaluated at all points separately. Both are readily converted to spherical descriptions, the momenta as eigenvectors of the subduced molecular point group G descended from O(3) (8) and the field as the representations and components of the group R_3. This is particularly appropriate since under the $K = 0$ approximation both vectorial properties have the same origin.

Multiplication of the two tensor operators is equivalent to taking the direct product of the representations of allowed molecular momenta with available field tensors in the photon. Each of these two bodies is described in its own three dimensional space. The only phenomenon relevant to both is the coupling of electric fields in the molecule with those of the photon. Assuming strong coupling of the molecular charge array to the mass array, the direct product becomes equivalent to coupling the nuclear mass momenta with the photon. When strong coupling is lost this equivalence is lost. In each space the bodies are described by a dynamic point group. The photon is

Can. J. Chem. Downloaded from www.nrcresearchpress.com by 210.87.254.40 on 09/06/12
For personal use only.

adequately described by R_3 and all molecular properties can be subduced from the $U(3)$ group representing the angular subgroup of $C_1(3)$ (10). The direct product must be restricted to three dimensions and this is achieved by collapsing the outer direct product down to the diagonal subgroup of the system. Within this diagonal subgroup, which is isomorphous with $SU(3)$, the representations can be equally applied to molecular momenta and photon fields because of the common electric field metric. However, the direct products are limited to the scalar result (6) and the complete formation for these coupled operators has the form

$$\sum_j |p_j A_j| \equiv \sum_{V=0}^{\infty} \sum_{L=0}^{\infty} |R_{LV}(r) \hat{V} \hat{L} \hat{C} c|$$

where $R_{LV}(r)$ is the radial overlap integral between the molecular and photon fields, V is the molecular momentum operator, L is the photon field operator, and C is the resultant coupled operator with its component c. For scalar coupling, $|\hat{C} c| = |00|$ and

$$\hat{V} = \hat{L}$$

by vector coupling rules (11) for all values. Thus, for all multipoles the matrix elements all have the form

$$R_{LV}(r) \langle V'L'C'c' | \hat{V}\hat{L}00 | VLCc \rangle$$

where V and V' characterize the molecular momenta in ground and excited states, L and L' characterize the initial and final photon states and C and C' the states of the coupled system. Since C is scalar, $C = C'$ and $c = c'$. As well, V is usually the ground molecular state with no momentum, so the matrix element is specialized to

$$R_{LV}(r) \langle V'0Cc | \hat{V}\hat{V}00 | 0V'Cc \rangle$$

The creation of a state V' is accompanied by the destruction of a photon field of the same symmetry without changing the net description C of the complete system. In physical terms, the photon is absorbed without exchange of energy with a third body.

Coupling of V and L by vector multiplication would represent an event in which the photon either completely (Rayleigh) or with partial absorption (Raman) leaving a polarized resultant photon. This will be discussed in further work.

Since the photon is fully absorbed by the change of state in the molecule with no exchange of energy to the medium, the excitation of any molecular momentum corresponds exactly with the photon field operator represented by L. Thus each of the $3n$ degrees of freedom of coupled mass charge array can be associated with one and only one component of one representation L. The scalar field $L = 0$ cannot change any angular momentum but can correspond to any change in $R_{00}(r)$ which describes the total mass charge of the system. (The radial operator could be derived from $E = mc^2$ and represents a change in mass.) The dipole field $\hat{L} = 1$ can initiate motion of all positively charged particles in the x, y or z orthonormal directions but is completely exhausted by this assignment since the photon is completely annihilated by this interaction. The quadrupole can initiate rotation xz, yz, or xy or internal gerade modes associated with z^2 or $x^2 - y^2$ displacements. The higher multipoles in $\hat{L}$ may all initiate changes in internal angular momenta.

As discussed qualitatively, the first three moments of $\hat{L}$ clearly represent excitation processes of change of mass content, centre of mass or rotation of mass respectively which are irrelevant to the excitation of internal normal modes. In molecules which are centro-symmetric derivatives from $U(3)$, all gerade normal modes are forbidden since in the operator $|\hat{V}\hat{L}\hat{C}c|$, $\hat{L}$ is ungerade for odd values. Thus, the first internal modes which permit absorption of photons are those subduced from the octupolar modes in $U(3)$ labelled $|3\Gamma_v\gamma_v\rangle$ for subgroup S of $U(3)$. This behaviour can be identified as an "*Octupole Rule*" for infrared spectroscopy (2, 10).

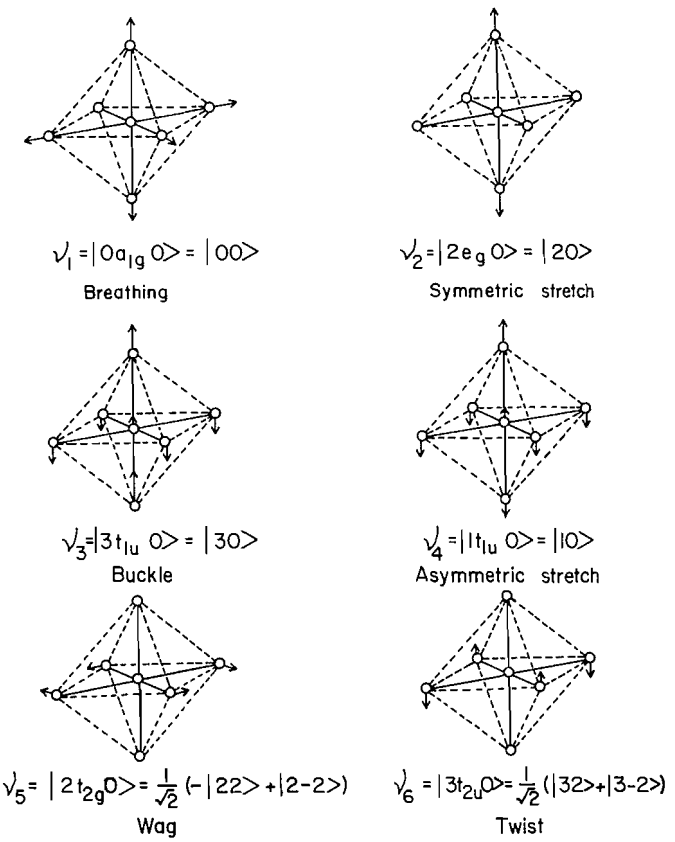

FIG. 1. Vibrational modes of an octahedral molecule.

Orders of transition moments

In all finite point groups the octupole is split into several different representations, for example in O_h it becomes A_2T_1 and T_2. In the T_1 representation it is coincident with the dipole and the orthonormality of these two basis vectors can only be specified by retention of the $U(3)$ labels in kets $|V_{vv}\rangle$.

In molecules with sufficient numbers of atoms to occupy the different available field regions of components of the octupole photon the overlap of these components with normal modes of vibration becomes obvious. In octahedra the acceleration acting on the positive points representing the seven atoms from both the $|3T_{1u}\gamma|$ and $|3T_{2u}\gamma|$ photon fields are readily identified (Fig. 1). Both are clearly "bending modes", the first being a buckling motion and the second a twist of the octahedral framework. The intensities of these modes may be identified with a "*first order octupole mechanism*".

There is a second type of T_1 mode corresponding to the antisymmetric stretch which is experimentally orthonormal to the $|3T_{1u}\rangle$ mode. It cannot be assigned as an octupole for this field is already exhausted. It has the appearance of a dipolar mode but is in fact subduced from $V' = 5$. However, under the fourfold symmetry of the octahedron $V' = 5$ is degenerate with

Can. J. Chem. Downloaded from www.nrcresearchpress.com by 210.87.254.40 on 09/06/12
For personal use only.

$V' = 1$ and the mode has been labelled $|1T_{1u}\gamma\rangle$. Clearly, it is not a simple dipole which would not preserve the position of the centre of mass. Moreover, a first order dipole mode would be expected to have intensity 10^8 stronger than the first order octupole just identified, while in fact the two modes $|3T_{1u}\gamma\rangle$ and $|1T_{1u}\gamma\rangle$ show approximately equal intensities. This low intensity implies that the $|1T_{1u}\gamma\rangle$ is a *second order dipole* mode which obeys the Octupole Rule but gains intensity by weak coupling (10^{-8} of the first order) to other angular momenta in the molecule.

The most obvious coupling is to the valence electrons through a breakdown of the adiabatic assumption of the Born–Oppenheimer principle (1). Physically, the nature of the coupling seems straightforward. Antisymmetric stretching reduces valence electron density in the stretched area while it increases the density in the compressed area. For conventionally bonded systems, this is an oscillation of inter electron repulsion (IER) in the bond region which is directly coupled to the major nuclear motion. The IER phenomenon requires a two electron description and the strongest term arises from the quadrupolar product of two coupled dipolar intensity mechanisms. In other words, the dipolar nuclear motion is coupled to quadrupolar two-electron transitions of the molecule. The resulting intensity of the dipolar nuclear motion will be small for two reasons; quadrupolar intensities are 10^{-4} times less intense than dipolar transitions and the coupled, two-electron states are usually at 10^5 cm^{-1} while vibrational modes are at 10^3 cm^{-1}. In formal terms the second order intensity will be approximately $10^{-4}/10^5 \simeq 10^{-9}$ as strong as an allowed dipole and fall close to the expected intensities of allowed octupole transitions.

This distinction between first order octupole bending modes and second order dipolar antisymmetric stretching modes is carried down through physically significant chains to all molecules of lower symmetry. It means in practice that there are two distinct mechanisms in most molecules whose intensities cannot be solved with the one basis set and one absorption operator (usually a dipole) used in conventional normal mode analysis. This conclusion is corroborated by the well known instability of basis function solutions as functions of force constant choice (12).

Radial integrals and parameters

At a sufficiently high level of symmetry, all mechanical properties of matter can be described by quantum models. Considered in a four dimensional space, the structure of electron orbitals in atoms involves quantum behaviour of radial as well as angular properties and N, L, M_L, and M_s are all valid quantum numbers. The hydrogen atom retains this structure in the lower symmetry of three dimensions because there are no two-electron interactions. Proceeding to even higher symmetries in higher dimensional spaces the atomic charge Z may also be quantized. The work of Wulfman (13) suggests that the periodic table in the long form is isomorphous with the $SO(7)$ group in which each long period is one representation of this group. At this point, all mechanical properties are represented by quantized angular momenta.

This ascent in symmetry is neither trivial nor irrelevant to the problems of spectroscopic analysis in three dimensions. Rather, the choice of a generative group of high symmetry which can represent all mechanical features in quantized form provides a basis for deductive rather than conventional inductive methods for assignment of molecular states and the calculation of the fitting parameters. As the descent in symmetry from the generative group to the detectable point group takes place, angular nodes get converted into radial nodes (2). Through stepwise symmetry descent, the number of radial nodes in each molecular basis function remain well defined. As this process of conversion continues, progressively more of the mechanical information about the molecule is converted into scalar magnitudes of radial matrix elements which become mixed together in the magnitudes of spectroscopic fitting parameters. At the same time, the increasing complexity of the radial basis functions requires expression as linear combinations of discrete radial functions of different quantum numbers n (from 1 to ∞). Thus the effective value of n in each of the final molecular radial basis function is non-integer and is a variable function of bond lengths and charge distributions in ground and excited states (14).

The same formal concepts can be applied to the structure of the "one-vibration" (by analogy to the one-electron) mass-charge array. Indeed, the model has been extensively used to describe the very similar problem of fundamental vibrations of atomic nuclei (15).

This procedure can be applied to finding expansions of the experimental parameters under any operator. Under the Hamiltonian of the static molecule, radial parameters representing the energies of fundamental vibrations and overtones can be calculated. For small molecules possessing some symmetry this parametrization of the energies has some important advantages over conventional force field analysis. The first advantage is that the subduction process which identifies the radial parameter *guarantees* that the number of such parameters is the minimum required. Since the number of experimental measurements is often limited, it is a *practical advantage* to reduce the number of theoretical parameters to its minimum for this reduces the requirement for approximations of unknown quantities in the model. The second major advantage is that this procedure also guarantees that molecular data are completely *scalar* and can be compared directly with data in compounds of different symmetries. In conventional force field analysis the force constants at multiple centres are almost invariably vectorial entities unique to the molecule being analysed. Comparison of parameter magnitudes between molecules is then meaningless because these vectorial attributes vary, often in a complicated manner, from one compound to the next.

The advantages of a symmetry decent model are equally applicable to the dynamic Hamiltonian for the calculation of transient linear momenta, $R_{LV}(r)$, which evolve from the definition of transition probabilities. These radial integrals are a minimum set of truly scalar parameters and represent a sum of integrals characterized by a principal quantum number in the generative point group describing the overlapped particles, $U(3)$;

$$R_{LV}(r) = \sum_{N=1}^{\infty} C_{NM} R_{NM}(r)$$

where the C_{NM} are the mixing coefficients for each of the radial basis functions in the generative group (M represents the allowed coupling of L and V). The range of N is limited to the minimum value necessary for L and V to exist and to a maximum practical value beyond which the $R_{NM}(r)$ values become insignificant. Each of the $R_{NM}(r)$ is readily expanded, by means of coupling coefficients in the generative group, into overlap integrals of the fields in the two particles described in terms of angular momenta. Thus,

$$R_{NM} = \sum_{PQ} \int_0^\infty R_{N'M'}\, a_p \hat{R}_{Pa} R_{NM}\, \mathrm{d}r$$

$$= \sum_{PQ} a_P \langle R_{N'M'} | \hat{R}_{PQ} | R_{NM} \rangle$$

$$= \sum_{\substack{PQ \\ KU \\ LV}} a_P \sum_{\substack{KL \\ UV \\ K'L' \\ U'V'}} \begin{pmatrix} K'U'N' \\ L'V'M' \end{pmatrix} \begin{pmatrix} \hat{K}\hat{U}\hat{P} \\ LVQ \end{pmatrix} \begin{pmatrix} KUN \\ LVM \end{pmatrix}$$

$$\cdot (-1)^x [D] \langle R_{K'U'} \| \hat{R}_{\hat{K}\hat{U}} \| R_{KU} \rangle$$

in which the principal quantum numbers K and K' in the generative group of the molecule $U(3)$ and U and U' of the generative group R_3 of the photon are identified by the uncoupling calculation. The parameter x is the phase factor which is unity if chosen by analogy with earlier work, $[D]$ is a degeneracy term also set to unity (10) and $\langle R_{K'U'} \| \hat{R}_{\hat{K}\hat{U}} \| R_{KU} \rangle$ is the reduced matrix element describing the overlap of radial bases of the molecule and the photon. The remaining parameter a_p is a product of the effective charges generating the molecular and photon fields, Z_M and Z_p. The charge Z_M can be derived from single centre molecular orbital calculations (16). The "effective central charge" of the photon Z_p is the instantaneous charge when $\boldsymbol{K} = 0$ is valid; this would produce the electric field gradient of the $|00\rangle$ component of the photon. This is clearly an inverse function of wave length

$$Z_p \propto \frac{1}{\lambda} \propto \nu$$

since the larger Z_p the more sharply $|00\rangle$ falls off with r.

This expansion of the radial integral emphasizes several features of intensity calculation. One of them is that the radial wave functions of both the molecule and the photon involved in the overlap may have high principal quantum numbers. In the octupole transitions resulting in excitation of internal modes, both L' and V equal 3, thus K' and U must equal at least 4 and could be larger depending on the magnitudes of central charges. Thus, one or more radial nodes could appear within the molecular framework, causing a reversal of phase from the simple angular momentum assignment of normal mode motions. This is particularly important for the apparent dipolar asymmetric stretch where K' must be 6. Then up to 3 radial nodes could be involved in the vibrational excited mode.

Secondly, in order for resonance to occur between molecule and photon, there must be constructive overlap of the two sets of radial functions, that is, $R_{LV}(r)$ must reach a maximum value. Since molecules are usually one to two orders of magnitude smaller than the wave length of the photon it is not obvious that overlap could be maximized. However, the radial wave function of the molecule could constructively interfere with the photon in that region between the origin and the first radial node of the photon. If the principal quantum number of the photon is higher than the minimum value identified earlier, this distance could readily conform to the molecular dimensions in spite of the fact that the classical wavelength is long.

Finally, the expansion of both the angular and radial parts make it clear that a vibration, allowed by selection rules, may be inactive if no atoms in the molecule are sited on the available field gradients. Typical of this is the $|3T_{2u}\gamma\rangle$ mode of the octahedral molecule. While allowed by angular symmetry, there are no atoms at the sites of maximum field gradient which occurs in the middle of each edge of the octahedral array. The vibration is observed in crystal lattices, frozen solutions, and films (12) when ligands from a second coordination layer occupy these positions. In gas phase molecules such as MoF_6, TcF_6, and RuF_6, the transition is inactive because the F atoms remain on the angular nodes of the $|3T_{2u}\gamma\rangle$ distribution.

Phenomenology of coupled systems

This model of vibrational excitation can be incorporated into descriptions of other forms of vibronic coupling, Raman and resonance Raman, double photon Raman, circular and magnetic circular dichroism (10), and photochemistry (17). The essential feature is the retention of the overall octupole rule. In the current development, first and second order fundamentals were identified which both obeyed this rule. The vibrational octupole allowed transitions which attribute the entire change in angular momentum to the change in vibrational momentum. The vibrational dipole required, in contrast, an accompanying quadrupolar charge in the electronic structure. This can be generalized for coupling systems to the rule (10, 17).

$$|\Delta J| + |\Delta V| = |\Delta T| = 3$$

where ΔJ incorporates both orbital and spin moment changes.

Based on this rule, the selection rules for coupled systems can be derived and predictions are readily made of the specific vibrations to accompany specific electronic transitions allowed or forbidden. Some examples of vibronic coupling in absorption and MCD spectroscopy have already been analysed with this formalism (10) and a method of predicting the course of fast photochemical reactions of six coordinate transition metal complexes has been proposed (17). Various aspects of light scattering spectroscopy will be discussed in future work.

1. W. KAUZMANN. Quantum chemistry. Academic Press, New York. 1957. Chapt. 14.
2. A. CEULEMANS and B. R. HOLLEBONE. Theoret. Chim. Acta, Berl. **61**, 403 (1982).
3. R. F. W. BADER, Y. TAL, S. G. ANDERSON, and T. T. NGUGEN-DANG. Isr. J. Chem. **19**, 8 (1980).
4. G. HERZBERG. Molecular spectra and molecular structure. II. Infrared and Raman spectra of polyatomic molecules. D. Van Nostrad Co. Inc., New York. 1950.
5. H. POULET and J. P. MATHIEU. Vibration spectra and symmetry of crystals. Gordon and Breach, New York. 1976. Chapt. 9.
6. J. S. GRIFFITH. The theory of transition metal ions. Cambridge University Press, London. 1961. Chapt. 3.
7. P. R. BUNKER. Molecular symmetry and spectroscopy. Academic Press, New York. 1979. Chapt. 11.
8. J. C. DONINI and B. R. HOLLEBONE. Theoret. Chim. Acta, Berl. **42**, 97 (1976); **42**, 111 (1976).
9. D. H. KOBE. Am. J. Phys. **50**, 128 (1982).
10. B. R. HOLLEBONE. Theoret. Chim. Acta, Berl. **56**, 45 (1980).
11. B. R. JUDD. Operator techniques in atomic spectroscopy. McGraw Hill, New York. 1963.
12. C. D. FLINT and A. G. PAULUSZ. Inorg. Chem. **20**, 1768 (1980).
13. C. E. WULFMAN. Dynamical groups in atomic and molecular physics. *In* Recent advances in group theory and their application to spectroscopy. *Edited by* J. C. Donini. NATO ASI B43, Plenum Press, New York. 1979.
14. B. R. HOLLEBONE and M. J. STILLMAN. Inorg. Chim. Acta, **42**, 169 (1980).
15. F. E. CLOSE. An introduction to quarks and partons. Academic Press, New York. 1979. Chapts. 7 and 8.
16. H. H. CLAASSEN, H. SELIG, and J. G. MALM. J. Chem. Phys. **36**, 2888 (1962).
17. B. R. HOLLEBONE, C. H. LANGFORD, and N. SERPONE. Coord. Chem. Rev. **39**, 181 (1981).

Can. J. Chem. Downloaded from www.nrcresearchpress.com by 210.87.254.40 on 09/06/12
For personal use only.

New complexes of the hydronium ion with crown ethers: synthesis and vibrational spectra

ROBERT CHÊNEVERT,[1] ANDRÉ RODRIGUE, PIERRE BEAUCHESNE, AND RODRIGUE SAVOIE[1]

Département de chimie et Centre de recherches sur les atomes et les molécules, Université Laval, Québec (Qué.), Canada G1K 7P4

Received February 14, 1984

ROBERT CHÊNEVERT, ANDRÉ RODRIGUE, PIERRE BEAUCHESNE, and RODRIGUE SAVOIE. Can. J. Chem. **62**, 2293 (1984).

The charged-component complexes H_3O^+.18-crown-6.$CF_3SO_3^-$, H_3O^+.18-crown-6.SbF_6^-, and $(H_3O^+.18\text{-crown-6})_2.PtCl_6^{2-}$ have been isolated and studied by infrared and Raman spectroscopy, along with the previously reported H_3O^+.18-crown-6.ClO_4^- and H_3O^+.18-crown-6.PF_6^- adducts. Also synthesized were the corresponding derivatives with BF_4^- and $PtCl_6^{2-}$ anions, using dicyclohexano-18-crown-6 as the host for the hydronium ion.

ROBERT CHÊNEVERT, ANDRÉ RODRIGUE, PIERRE BEAUCHESNE et RODRIGUE SAVOIE. Can. J. Chem. **62**, 2293 (1984).

Nous avons préparé les complexes H_3O^+.18-couronne-6.$CF_3SO_3^-$, H_3O^+.18-couronne-6.SbF_6^- et $(H_3O^+.18\text{-couronne-6})_2.PtCl_6^{2-}$, que nous avons étudié par spectroscopie infrarouge et Raman, de même que les dérivés H_3O^+.18-couronne-6.ClO_4^- et H_3O^+.18-couronne-6.PF_6^-, dont l'existence a déjà été rapportée. Nous avons également obtenu des dérivés analogues, dans lesquels l'éther dicyclohexano-18-couronne-6 sert d'hôte à l'ion hydronium.

Can. J. Chem. Downloaded from www.nrcresearchpress.com by 210.87.254.42 on 09/06/12
For personal use only.

Introduction

The first stoichiometric hydronium – crown ether complexes were obtained by Izatt *et al.* (1, 2); they consisted of H_3O^+.dicyclohexano-18-crown-6 adducts associated with the ClO_4^- and PF_6^- counterions. Cram *et al.* (3), in their exhaustive study on host–guest complexation using macrocyclic polyethers, later obtained similar complexes using hydronium *p*-toluenesulfonate and a 18-crown-6 ether in which a CH_2—CH_2 group was replaced by a 1,1′-dinaphthyl unit bound in the 2,2′ position. In recent years, it has been shown that 18-crown-6 (hereafter referred to as 18C6) is a good complexing agent for the hydronium ion, and H_3O^+.18C6 complexes of 1:1 stoichiometry have been obtained with associated BF_4^- (4, 5) and ClO_4^-, PF_6^-, I^-, Br_3^- (5) ions.

In these studies, it was generally assumed that the H_3O^+ ion in the adduct is located at, or near, the center of the macrocyclic ether cavity, as this would maximize the electrostatic interactions between the two units. This was also expected on the basis of the strong hydrogen bonds revealed from the infrared spectra, as these bonds presumably involve the H_3O^+ ion and the oxygen atoms lining the interior of the ether cavity. This hypothesis has recently been confirmed by an X-ray diffraction study on a similar complex, formed by a tetracarboxylic 18C6 ligand and H_3O^+ (6). Preliminary X-ray data on H_3O^+.18C6.BF_4^- also suggest a similar attachment of the hydronium to the crown ether (7).

In the present study, we report the synthesis of several new stoichiometric complexes of the hydronium ion with 18C6 and dicyclohexano-18C6. Raman and infrared spectroscopic measurements have been made on these systems, in order to determine the structure of the H_3O^+.crown adducts and to detect conformational changes which occur in some of these compounds at low temperature. Some other similar complexes with no definite composition are also discussed.

Experimental

The complexes were generally obtained by precipitation from a solution of 18C6 after addition of the acid. The precipitate was filtered, washed with diethyl ether, and dried under vacuum. All the complexes obtained were colorless, except for the orange colored $PtCl_6^{2-}$ derivative. The stoichiometry of the complexes was determined from the integrated intensity of the ^1H nmr peaks (Bruker HX-90 instrument) and, more accurately, by titration with 0.1 *N* NaOH after dissolution of the samples in water or methanol. The measured H_3O^+/crown ether ratio agreed with that calculated within ± 0.5% in all cases. Details pertaining to the individual complexes are given below:

H_3O^+.18C6.ClO_4^-

Concentrated (70%) $HClO_4$ (0.25 mL) is slowly added to a solution of 18C6 (2 mmol) in tetrahydrofuran (20 mL). The complex precipitates. Yield: 85%; mp: 163–164°C (dec.) (168–169°C reported by Heo and Bartsch (5)); ^1H nmr (CD_2Cl_2): δ 10.86 (H_3O^+) and 3.77 (18C6).

H_3O^+.18C6.$CF_3SO_3^-$

Trifluoromethanesulfonic acid (0.25 mL) is slowly added to a solution of 18C6 (2 mmol) in benzene (20 mL). After a few minutes, diethyl ether is added to the resulting solution until the complex precipitates. Yield: 76%; mp: 142–143°C; ^1H nmr ($CDCl_3$): δ 11.15 (H_3O^+) and 3.78 (18C6).

H_3O^+.18C6.PF_6^-

Concentrated hexafluorophosphoric acid (0.25 mL) is slowly added to a solution of 18C6 (2 mmol) in tetrahydrofuran (40 mL). After a few minutes the complex precipitates as colorless needles. Yield: 98%; mp: 141–142°C (Heo and Bartsch (5) have reported a mp of 131–132°C and a yield of 71% for this complex); ^1H nmr (CD_2Cl_2): δ 11.70 (H_3O^+) and 3.70 (18C6).

H_3O^+.18C6.SbF_6^-

A solution of hexahydrated hexafluoroantimonic acid (10 mL) dissolved in 10 mL tetrahydrofuran is added to a solution of 18C6 (2 mmol) in the same solvent (30 mL). The complex precipitates immediately. Yield: 78%; mp: 200°C (dec.); ^1H nmr (CD_2Cl_2): δ 11.20 (H_3O^+) and 3.77 (18C6).

$(H_3O^+.18C6)_2.PtCl_6^{2-}$

The method of preparation is identical to that for the SbF_6^- complex. Yield: 97%; mp: 161–162°C (decomp.); ^1H nmr (CD_3NO_2): δ 6.20 (H_3O^+) and 3.82 (18C6). *Anal.* cacld. for $(H_3O^+.18C6)_2.PtCl_6^{2-}$: C 29.58, H 5.64; found: C 29.19, H 5.58.

H_3O^+.DCy-18C6.BF_4^-

To a solution of 2 m*M* dicyclohexano-18-crown-6 (DCy-18C6) in 20 mL CH_2Cl_2 is added 2 mL of tetrafluoroboric acid (40%). After shaking the mixture for 15 to 30 min, the two phases are allowed to separate and the aqueous phase is washed with two portions of CH_2Cl_2 (10 mL). The organic phases are evaporated and the residue is recrystallized from a tetrahydrofuran/petroleum ether (110–165°C)

[1]To whom correspondence should be addressed.

solution (yield, 70%). Alternatively, the crown (1 m*M*) is dissolved in H_2O (20 mL) and the concentrated acid (2 mL) is added to the solution. After a few days the complex precipitates as large crystals (yield, 75%); mp: 110–120°C. *Anal.* calcd. for H_3O^+.DCy-18C6.BF_4^-: C 50.21, H 8.15, F 15.88; found: C 50.20, H 8.31, F 15.71. ^{1}H nmr ($CDCl_3$): δ 11.60 (H_3O^+), 3.78 (crown), and 1.2–2.3 (CH_2 from cyclohexano-).

$(H_3O^+.DCy\text{-}18C6)_2.PtCl_6^{2-}$

Prepared as by the first method given above for the BF_4^- complex, using solid hexahydrated hexachloroplatinic acid dissolved in 1 mL H_2O. The complex is orange colored. Yield: 68%; mp: 143–150°C; ^{1}H nmr (CD_3NO_2): δ 10.16 (H_3O^+), 3.83 (crown), and 1.0–2.3 (cyclohexano-).

Vibrational spectra

The infrared spectra were obtained from Nujol, hexachlorobutadiene, and Fluorolube mulls contained between Irtran-4 (ZnSe) or silver chloride windows. The low-temperature measurements were made on these same samples fixed in a conventional liquid nitrogen cryostat. The spectra were recorded on a Beckman IR 4250 spectrophotometer or on a Perkin Elmer Model 621 instrument linked to a North Star microcomputer.

For the Raman measurements, the solid samples were contained in sealed capillary cells. These were generally mounted on a motor shaft and rotated at high speed in order to prevent sample decomposition in the laser beam. For the low-temperature measurements, the cell was fixed inside a cavity in the copper tail section of a liquid nitrogen cryostat. The spectra were recorded on a microcomputer-controlled Spex Model 1400 spectrometer (8), using the 514.5 nm exciting line from a Spectra Physics Model 165 argon ion laser. Typical operating conditions were as follows: laser power at sample, 300 mW; spectral slit width, 2 cm^{-1}; integration time, 2 s per data point; frequency increment, 1 cm^{-1}. The orange colored $PtCl_6^{2-}$ complex could only be studied (at room temperature) in a rotating cell and with laser power at 40 mW or less.

Results and discussion

Although the structure of the H_3O^+.18C6 moiety need not be exactly the same in all the complexes discussed here, some general comments can be made about this adduct. First, the orientations of the lone pairs on the oxygen atoms of the crown, assuming sp^3 hybridization, are such that the H_3O^+ ion is expected to form hydrogen bonds with the three oxygen atoms located on the opposite side of the crown (see Fig. 1). This also helps to stabilize the adduct through electrostatic interactions by allowing the hydronium ion to penetrate farther into the ether cavity. Secondly, the H_3O^+ ion fits very loosely into this cavity, and both the spectroscopic (4) and X-ray data (6, 7) point to hydrogen bond lengths (O···O = 2.65–2.80 Å) which are appreciably shorter than expected for the crown ether in its highly symmetrical structure of D_{3d} symmetry (O···O = 2.95 Å (9)). The crown is therefore distorted to a lower symmetry in the H_3O^+.18C6 adduct, and this can be easily determined from the splitting of some of the infrared bands (e.g. 820/840, 950/970 cm^{-1} ...) which occur as singlets (835, 960 cm^{-1} ...) in the spectra of complexes such as K^+.18C6.Br^- (10) where the crown retains its full D_{3d} conformation. Particulars pertaining to specific complexes will now be discussed.

$H_3O^+.18C6.ClO_4^-$

The synthesis of this complex has already been reported by Heo and Bartsch (5). The infrared spectrum of the solid in the high-frequency region (Fig. 2*A*) is clearly indicative of the presence of the H_3O^+ ion (11). The stretching modes of this species are responsible for the very broad band at ~2950 cm^{-1}, which overlaps the sharper maximum arising from the C—H stretching motions of the crown ether in the 2900 cm^{-1} region. Also characteristic are the bands at 1680 and 2200 cm^{-1}, attributable to the ν_4 bending mode and to the first harmonic of ν_2 (symmetric bending mode) respectively. The ν_2 mode itself is of little use here, as it occurs in a region of strong absorption by the crown ether. The Raman bands of the H_3O^+ ion are normally extremely weak, and they were not detected in this study.

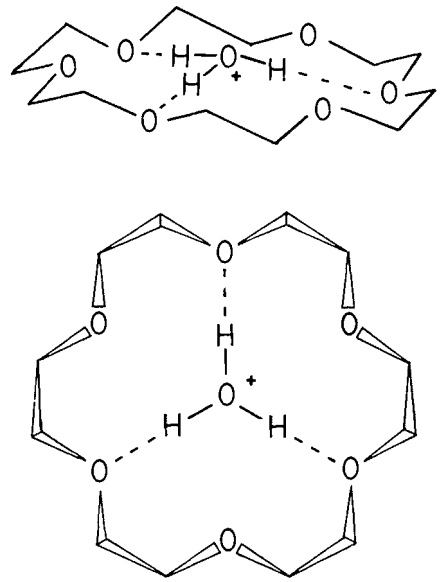

FIG. 1. Schematic representation of the H_3O^+.18-crown-6 adduct.

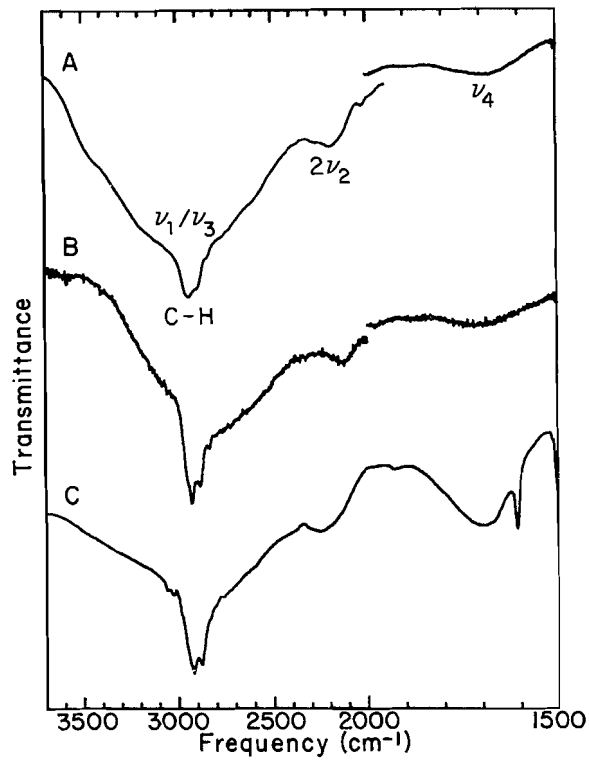

FIG. 2. High-frequency region of the infrared spectra of (*A*) H_3O^+.18C6.ClO_4^- (hexachlorobutadiene mull), (*B*) H_3O^+.18C6.-SbF_6^- (hexachlorobutadiene mull), and (*C*) oily liquid with approximate composition 18C6/*p*-toluenesulfonic acid/1.3 hydronium *p*-toluenesulfonate.

Can. J. Chem. Downloaded from www.nrcresearchpress.com by 210.87.254.42 on 09/06/12
For personal use only.

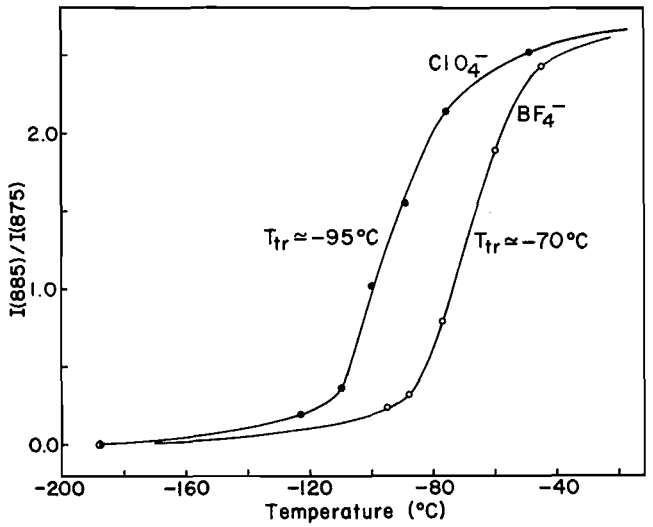

FIG. 3. Variation of the intensity ratio of the 885/875 cm^{-1} bands in the Raman spectra of $H_3O^+.18C6.ClO_4^-$ (full circles) and $H_3O^+.18C6.BF_4^-$ (open circles).

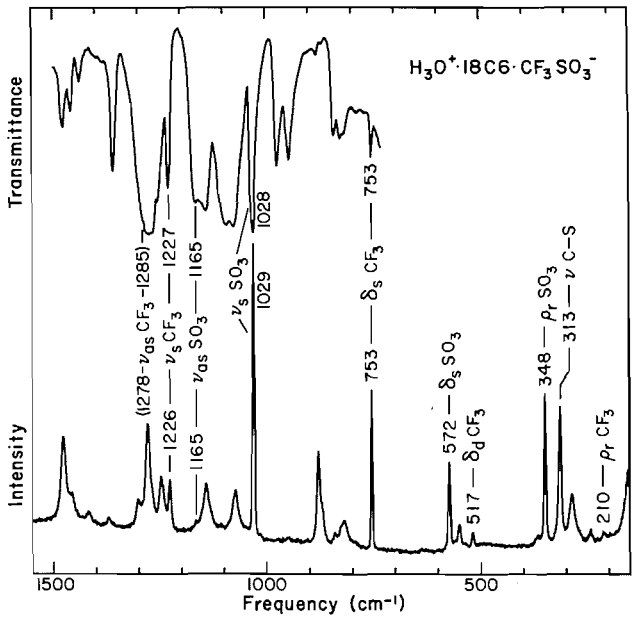

FIG. 4. Infrared (Nujol and hexachlorobutadiene mulls) and Raman spectra of the $H_3O^+.18C6.CF_3SO_3^-$ complex.

The complete ionization of $HClO_4$ in the complex is readily established from the absence in the Raman spectrum (not shown) of the characteristic bands of this acid (12–14), in particular at ~740 cm^{-1} (ν_{Cl-OH}). Instead, sharp peaks due to the ClO_4^- ions are observed at 932 cm^{-1} (ν_1), 458 cm^{-1} (ν_2), and 624 cm^{-1} (ν_4). These frequencies are comparable to those measured in the Raman spectrum of the high-temperature crystalline form of $H_3O^+.ClO_4^-$ (15, 16). In the infrared spectrum of the complex with 18C6 (not shown), the ν_4 mode gives a sharp peak at 626 cm^{-1}, whereas the ν_3 vibration gives a very strong absorption band near 1100 cm^{-1}.

The main difference between the ir spectrum of the $H_3O^+.18C6.ClO_4^-$ complex and that of the corresponding $H_3O^+.ClO_4^-$ salt at room temperature, besides the presence in the former of characteristic bands of the ether, comes from the vibrational bands of the H_3O^+ ion. The ν_3 band of this ion, centered at ~3250 cm^{-1} in $H_3O^+.ClO_4^-$ (15, 17), is shifted appreciably in the crown ether complex, where it merges with ν_1 to give the broad band at ~2950 cm^{-1} (Fig. 2*A*). This shift is indicative of widely different hydrogen bond lengths and energies in the two compounds. The $OH^+\cdots O$ ($O\cdots O$) distances in the hydronium salt are 2.9 Å on the average (18), whereas empirical relations between the ν_{OH} frequency and the $O\cdots O$ distance (11, 19) yield ~2.65 Å for the 18C6 complex. This is a good indication that the H_3O^+ ion in this complex is located within the macrocyclic cavity, and H-bonded to the oxygen atom of the ether. The situation is therefore similar to that encountered in the $18C6.H_3O^+.BF_4^-$ complex (4), for which preliminary X-ray diffraction data give $OH^+\cdots O$ distances of 2.66–2.81 Å (7), and in the complex formed by a tetracarboxylic 18C6 ligand with H_3O^+, and three $OH^+\cdots O$ hydrogen bonds of length 2.67–2.74 Å (6). One can also draw a parallel between the increase in H-bond energy in the $H_3O^+.18C6.ClO_4^-$ complex and the high melting point of this compound (dec. 163–164°C) relative to the $H_3O^+.ClO_4^-$ salt (50°C).

Except for the bands of the anions, the vibrational spectra of the $H_3O^+.18C6.ClO_4^-$ and $H_3O^+.18C6.BF_4^-$ (4) are identical, suggesting that they are structurally isomorphous. Furthermore, the conformational change which was found to take place in the tetrafluoroborate complex at ~−70°C (4) also occurs in the perchlorate complex, although at a somewhat lower temperature (−95°C). The progression of this conformational change, as followed by the intensity reversal of the 885/875 cm^{-1} Raman peaks, is illustrated in Fig. 3. This transition in the BF_4^- complex was explained by a gradual folding of the crown ether around the hydronium ion, which is too small to effectively fill the macrocyclic cavity. In the ClO_4^- complex, the pulling effect of the $OH^+\cdots O$ bonds appears to be slightly less than in the BF_4^- complex, as evidenced by the higher ν_{OH} frequency (2950 cm^{-1} in the ClO_4^- complex as compared to 2850 cm^{-1} in $H_3O^+.18C6.BF_4^-$), and the transition takes place at a lower temperature. The change appears to involve mainly the 18C6 molecules in the complex, and the ClO_4^- ions probably retain a high degree of symmetry at all temperatures, as no apparent site splitting of the degenerate vibrational modes of these ions is observed in the Raman spectrum of the complex.

$H_3O^+.18C6.CF_3SO_3^-$

The monohydrate of trifluorosulfonic acid has been shown by X-ray diffraction to exist as an ionic solid, $H_3O^+.CF_3SO_3^-$ (20). The corresponding complex with 18C6 also contains this basic unit, as evidenced by the presence in the infrared spectrum of the characteristic bands of this ion (2880, 2140, and 1725 cm^{-1}) and the absence of the undissociated acid bands (Fig. 4), particularly at 930 cm^{-1} (ν_{S-OH}) and 1400 cm^{-1} ($\nu_{as}SO_2$) (13). However, the high melting point of $H_3O^+.18C6.CF_3SO_3^-$ (141–142°C) with respect to that of the hydronium salt (35°C) strongly suggests that the H_3O^+ ion in this complex is H-bonded to the crown ether, as is the case in the BF_4^- complex. This conclusion is further substantiated by the splitting of some of the ether vibrational modes, namely, in the 840 and 960 cm^{-1} regions, which characterizes the $18C6.H_3O^+$ intra-cavity adduct.

The infrared and Raman spectra of the $H_3O^+.18C6.CF_3SO_3^-$ complex in the region below 1500 cm^{-1} (Fig. 4) are dominated by the strong bands of the anion, whose frequencies are slightly lower than in solid $NaCF_3SO_3$ and $Ba(CF_3SO_3)_2$, and in a concentrated aqueous solution of the $CF_3SO_3^-$ ion (21). In the

Can. J. Chem. Downloaded from www.nrcresearchpress.com by 210.87.254.42 on 09/06/12
For personal use only.

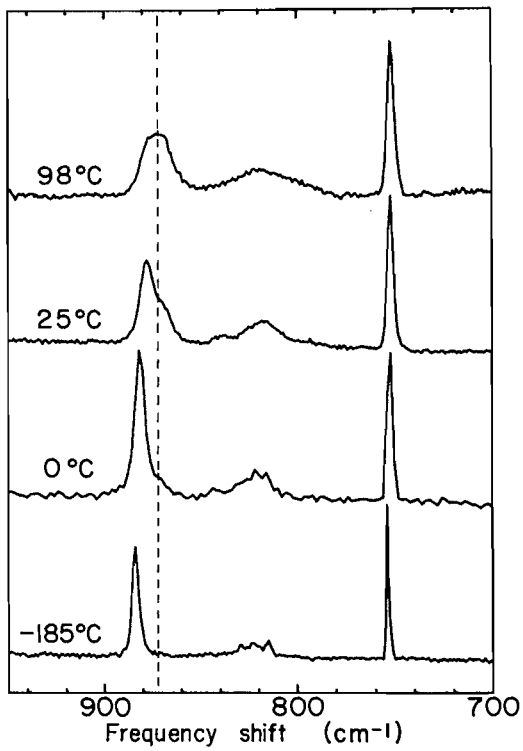

FIG. 5. Temperature-dependent spectral changes in the Raman spectrum of the $H_3O^+.18C6.CF_3SO_3^-$ complex.

regions of the spectra which are free of the bands of the anions, the vibrational bands of the crown ether are very similar to those in the BF_4^- and ClO_4^- complexes, which suggests that the $18C6.H_3O^+$ adduct has the same overall geometry in all three cases.

The vibrational spectra of $H_3O^+.18C6.CF_3SO_3^-$ do not indicate the occurrence of a conformational change in this complex at low temperature. However, spectral changes are observed upon raising the temperature to 100°C, and it appears that a conformational change, apparently different from that which occurs in the BF_4^- and ClO_4^- complexes at low temperature, does take place in the $CF_3SO_3^-$ complex in the temperature range 0–80°C. As shown in Fig. 5, the sharp peak at 883 cm^{-1} in the Raman spectrum progressively transfers its intensity to a broad band centered at 872 cm^{-1} over this temperature range. This band is due to the ring breathing mode of the ether, and the observed spectral changes suggest that conformational disorder sets in the crystal at high temperature. This disordering process, which seems to involve mainly the $H_3O^+.18C6$ adduct, probably takes place in most complexes of this type, as a similar trend was observed in the BF_4^- and ClO_4^- compounds, although in these cases the transition was not complete at 80°C. One can speculate that this disordering process involves a tunneling motion of the $H_3O^+.18C6$ pyramidal adducts between their two opposite mirror-image structures in the solid. Preliminary X-ray data on the $H_3O^+.18C6.BF_4^-$ complex (7) would be consistent with this interpretation, as they indicate that one half of the H_3O^+ ion is located on each side of the crown in this particular compound at room temperature.

$H_3O^+.18C6.SbF_6^-$

The $H_3O^+.SbF_6^-$ salt, first isolated and studied by vibrational spectroscopy by Criste *et al.* (22), along with the corresponding AsF_6^- derivative, is an extremely stable hydronium compound (dec. 357°C). Although this stability suggests strong anion–cation interactions, the relatively high values for the O—H stretching vibrations (3150/3300 cm^{-1}) indicate that the "H-bonds" are rather weak in this solid. These characteristics contrast sharply with those of the $H_3O^+.18C6.SbF_6^-$ complex (dec. 200°C), whose ir spectrum (Fig. 2*B*) reveals a low ν_{O-H} band (2850 cm^{-1}) characteristic of strong hydrogen bonds. These are certainly of the $^+O—H\cdots O$ type, and there seems to be no doubt that an intra-cavity $H_3O^+.18C6$ adduct is present in this complex. No attempt has been made in this study to prepare the $H_3O^+.18C6.AsF_6^-$ complex, but we have obtained the $H_3O^+.18C6.PF_6^-$ derivative already reported by Heo and Bartsch (5). Except for the bands of the anion, the spectrum of the latter is identical to that of the SbF_6^- complex.

The vibrational spectra of $H_3O^+.18C6.SbF_6^-$ (not shown) are easily interpreted, as they contain but few bands of the anion. In the Raman spectrum only the totally symmetric mode, $\nu_1(A_g)$, and the triply degenerate $\nu_5(F_g)$ mode give strong peaks, at 645 and 279 cm^{-1}, respectively, whereas in the infrared spectrum only the $\nu_3(F_{1u})$ mode falls in the region studied, giving an intense absorption band at 654 cm^{-1}. The corresponding bands in the $H_3O^+.18C6.PF_6^-$ complex are easily identified after comparison with salts such as KPF_6 (23) and $NaPF_6.H_2O$ (24); they are found at 739 cm^{-1} (ν_1) and 466 cm^{-1} (ν_5) in the Raman and at 837 cm^{-1} (ν_3) and 561 cm^{-1} (ν_4) in the infrared spectrum.

There are basic differences between the vibrational spectra of the $H_3O^+.SbF_6^-$ adduct in the free hydronium salt (22) and the corresponding unit in the 18C6 complex. Splitting of the SbF_6^- ion vibrational modes clearly occurs in the free hydronium salt. For example, the ν_1 vibration gives a well-resolved doublet at 640/674 cm^{-1} in the Raman spectrum at −120°C. This splitting, which is probably too large to be accounted for by an intermolecular vibrational effect, is likely caused by a distortion of the SbF_6^- ions from their basic octahedral conformation. No such effect is detected in the SbF_6^- and PF_6^- complexes with 18C6, for which the Raman spectra at both room and liquid-nitrogen temperatures show only one sharp peak for the ν_1 and ν_5 vibrations. This suggests that the AB_6^- ions in these complexes are isolated from one another and that they are little distorted from their ideal O_h symmetry. It should also be pointed out that the spectra of these two complexes give no evidence of a conformational change of the $18C6.H_3O^+$ adduct at low-temperature, as was observed in the BF_4^- and ClO_4^- complexes.

$(H_3O^+.18C6)_2.PtCl_6^{2-}$

The compound usually referred to as "chloroplatinic acid dihydrate" is in fact a hydronium salt: $(H_3O^+)_2.PtCl_6^{2-}$. This solid, which is stable up to 400°C, is extremely deliquescent. This probably explains why several different versions of its infrared spectrum have been published (25–27). The corresponding complex with 18C6 (dec. 161–162°C) retains much of the orange coloration of the starting hydronium salt, making it very difficult to study by Raman spectroscopy. It was nevertheless possible to obtain its spectrum in the low-frequency region (below 500 cm^{-1}) by using a rotating cell, at very low laser power excitation. The two main peaks detected at 335 and 310 cm^{-1} in this spectrum are readily assigned to the $\nu_1(A_g)$ and $\nu_2(E_g)$ modes of the $PtCl_6^{2-}$ ion (28), which proves the ionic nature of the complex. This is further substantiated by the high-frequency region of the ir spectrum, which shows the characteristic absorption pattern of the H_3O^+ ion.

Can. J. Chem. Downloaded from www.nrcresearchpress.com by 210.87.254.42 on 09/06/12
For personal use only.

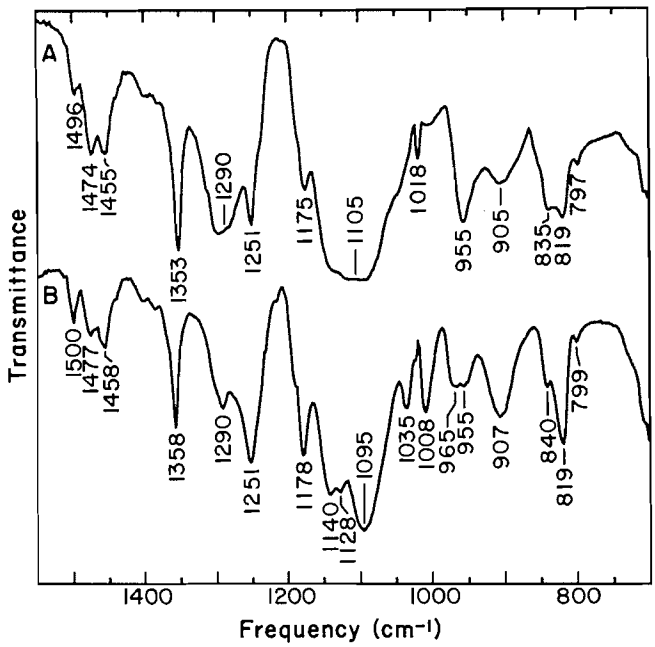

FIG. 6. Infrared spectra of mixtures of 18C6 and hydronium *p*-toluenesulfonate: (*A*) starting composition 18C6 + ($H_3O^+.CH_3-C_6H_4-SO_3^-$) and (*B*) composition as in Fig. 2*C*.

The 2:2:1 ratio of the H_3O^+:18C6:$PtCl_6^{2-}$ constituents in this complex is by itself indicative of the formation of a 18C6.H_3O^+ adduct; that is, the formula of the complex should be $(H_3O^+.18C6)_2.PtCl_6^{2-}$. The infrared spectrum of this complex, which is free of bands from the anion in the region studied, is quite similar to that of the SbF_6^- complex, and it is likely that the nature of the complexation is the same in both cases. However, the 2:1 anion/cation ratio in the $PtCl_6^{2-}$ complex probably makes it more difficult for these units to be packed into a highly symmetrical arrangement in the crystal, and this in turn could explain the relatively higher complexity of its ir spectrum, particularly at liquid-nitrogen temperature. As in the case of the PF_6^- and SbF_6^- complexes, no low-temperature conformational change of the 18C6 moiety in the $PtCl_6^{2-}$ derivative is indicated by its ir spectrum.

18C6 + ($H_3O^+.CH_3-C_6H_4-SO_3^-$)

Although a 1:1 complex between hydronium *p*-toluenesulfonate ($H_3O^+.PTS^-$) and 18C6 containing one 1,1′-dinaphtyl unit bound to adjacent oxygen atoms of the polyether host has been reported (3), attempts to form such a complex with unsubstituted 18C6 have failed (5). However, there is no doubt that some sort of association does take place between $H_3O^+.PTS^-$ and 18C6, as the latter makes soluble this hydronium salt in solvents such as CH_2Cl_2 and $CHCl_3$, in which it is normally quite insoluble.

We have used infrared and ^1H nmr spectroscopy to determine what happens when $H_3O^+.PTS^-$ is added to a solution of 18C6 in CH_2Cl_2 (1% w/w), in an attempt to form a 18C6.H_3O^+ complex through a solid-liquid phase transfer process. When an excess of the hydronium salt is used (4 acid:1 crown), typically 2.7 molecules of the "hydrated" acid dissolve for each 18C6 molecule in the solution. This process, however, occurs with a variable loss of "hydration" water. After evaporation of the solvent from the organic phase, one is left with an oily liquid containing non stoichiometric amounts of 18C6, PTSH, PTS^-, and H_3O^+. The H_3O^+/18C6 ratio in this mixture is larger than one (typically 1.4), most likely because of the presence of uncomplexed $H_3O^+.PTS^-$ in the CH_2Cl_2 medium used for the preparation. When one tries to impose a 1:1 H_3O^+/18C6 stoichiometry to the system in the preparation procedure, an oily liquid is obtained, which sometimes crystallizes (mp: 50–51°C, ^1H nmr ($CDCl_3$): δ 10.85 and 3.72). The solid thus obtained also contains nonstoichiometric amounts of PTSH and PTS^-.

Although the high-frequency region of the infrared spectra (Fig. 2*C*) indicates the presence of H_3O^+ in the mixtures obtained, it is probable that most of these ions are not linked to the ether molecules in the usual way: the lack of appreciable splitting of the crown vibrational mode at 958 cm^{-1} (Fig. 6) is characteristic of an undistorted, and most likely uncomplexed, molecule of D_{3d} symmetry (10). By comparison, the H_3O^+.-18C6 moiety in $H_3O^+.18C6.SbF_6^-$ gives a well-resolved infrared doublet with components at 947 and 972 cm^{-1}. Also present in the infrared spectrum is a band of variable intensity at 910 cm^{-1}, which is not present in the spectrum of the hydronium salt (19), but characterizes the free acid (29). Extra absorption at ~2400 cm^{-1} further suggests that the free acid molecules in the mixture are associated into dimeric units. The high stability of these H-bonded dimers (29) and their solubility in the solvent used could explain their presence in the 18C6 mixture obtained. This would also partly explain our failure to obtain a complex of definite $H_3O^+.18C6.PTS^-$ composition in this case.

Other complexes

Izatt *et al.* (1, 2) have shown that the *cis–syn–cis* isomer of dicyclohexano-18C6 (DCy-18C6) can form complexes with $H_3O^+.ClO_4^-$ and $H_3O^+.PF_6^-$. Due to the added rigidity of this crown, the complexes are not quite as stable as those with unsubstituted 18C6, whose melting points are higher by ~20°C. Nevertheless, the complexing ability of this ether towards the hydronium ion is quite high, and we were able to synthesize the complexes H_3O^+.DCy-18C6.BF_4^- and $(H_3O^+.DCy\text{-}18C6)_2.PtCl_6^{2-}$ (see Experimental section). No detailed spectroscopic investigation of these complexes was performed.

Attempts to form H_3O^+.15-crown-5 and H_3O^+.12-crown-4 complexes were not successful, inasmuch as no well defined stoichiometric compounds were obtained. Using a method of preparation similar to that for the H_3O^+.DCy-18C6 complexes, we have obtained an ill-defined solid complex $H_3O^+.BF_4^-.(15C5)_X$ (X = 1 to 2) (mp 118–119°C; ^1H nmr: 9.80 (H_3O^+) and 3.73 (15C5)). This result is very similar to that previously obtained with HPF_6 by Heo and Bartsch (5). These authors also obtained the $H_3O^+.(12C4)_2.PF_6^-$ complex. Our attempts to isolate the corresponding derivative with BF_4^- led to a colorless oily liquid of approximate stoichiometry $(H_3O^+.BF_4^-)_2.(12C4)_3$. The hypothesis put forward by Heo and Bartsch regarding the formation of sandwich type complexes of 12C4 and 15C5 with H_3O^+, each hydronium ion being H-bonded to two adjacent ether molecules, offers a good explanation for the present results.

We have found that carboxylic acids are readily complexed by 18C6, although in an unionized form. Among the complexes formed are the stoichiometric compounds $(CH_3COOH)_2.18C6$ and $(HCOOH)_3.(18C6)_2$. Halogenated derivatives of acetic acid are also complexed, yielding well-characterized solids of the type $(acid.H_2O)_x.18C6$ (with x = 1 or 2). Finally, some "inorganic" acids can form similar complexes: besides the $(HNO_3.H_2O)_2.18C6$ compound already reported

Can. J. Chem. Downloaded from www.nrcresearchpress.com by 210.87.254.42 on 09/06/12
For personal use only.

(5), we have found that hydrated H_2TiF_6 can also associate with 18C6. These neutral-component complexes will be the subject of a later publication.

Acknowledgements

Financial support of this work by the Natural Sciences and Engineering Research Council of Canada and by the Ministère de l'éducation du Québec is gratefully acknowledged.

1. R. M. IZATT, B. L. HAYMORE, and J. J. CHRISTENSEN. J. Chem. Soc. Chem. Commun. 1308 (1972).
2. R. M. IZATT, B. L. HAYMORE, J. S. BRADSHAW, and J. J. CHRISTENSEN. Inorg. Chem. **14**, 3132 (1975).
3. D. J. CRAM, R. C. HELGESON, K. KOGA, E. P. KYBA, K. MADAN, L. R. SOUSA, M. G. SIEGEL, P. MOREAU, G. W. GOKEL, J. M. TIMKO, and G. D. Y. SOGAH. J. Org. Chem. **43**, 2758 (1978).
4. R. CHÊNEVERT, A. RODRIGUE, M. PIGEON-GOSSELIN, and R. SAVOIE. Can. J. Chem. **60**, 853 (1982).
5. G. S. HEO and R. A. BARTSCH. J. Org. Chem. **47**, 3557 (1982).
6. J.-P. BEHR, P. DUMAS, and D. MORAS. J. Am. Chem. Soc. **104**, 4540 (1982).
7. J.-F. BRISSE. Personal communication.
8. R. SAVOIE, B. BOULÉ, G. GENEST, and M. PÉZOLET. Can. J. Spectrosc. **24**, 112 (1979).
9. J. D. DUNITZ, M. DOBLER, P. SEILER, and R. P. PHIZACKERLEY. Acta Crystallogr. **30B**, 2733 (1974).
10. M. FOUASSIER and J.-C. LASSEGUES. J. Chim. Phys. **75**, 865 (1978).
11. B. DESBAT and P. V. HUONG. Spectrochim. Acta, **31A**, 1109 (1975).
12. M. P. THI, M.-H. HERZOG-CANCE, A. POTIER, and J. POTIER. J. Raman Spectrosc. **12**, 238 (1982).
13. M. LEUCHS and G. ZUNDEL. J. Chem. Soc. Faraday Trans. *II*, **74**, 2256 (1978).
14. P. A. GIGUÈRE and R. SAVOIE. Can. J. Chem. **40**, 495 (1962).
15. R. C. TAYLOR and G. L. VIDALE. J. Am. Chem. Soc. **78**, 5999 (1956).
16. R. SAVOIE and P. A. GIGUÈRE. J. Chem. Phys. **41**, 2698 (1964).
17. J. ROZIÈRE. Thèse de 3e cycle, Université de Montpellier. 1970.
18. F. S. LEE and G. B. CARPENTER. J. Phys. Chem. **63**, 279 (1959).
19. L. J. BASILE, P. LABONVILLE, J. R. FERRARO, and J. M. WILLIAMS. J. Chem. Phys. **60**, 1981 (1974).
20. J. B. SPENCER and J.-O. LUNDGREN. Acta Crystallogr. **29B**, 1923 (1973).
21. M. G. MILES, G. DOYLE, R. P. COONEY, and R. S. TOBIAS. Spectrochim. Acta, **25A**, 1515 (1969).
22. K. O. CRISTE, C. J. SCHACK, and R. D. WILSON. Inorg. Chem. **14**, 2224 (1975).
23. G. M. BEGUN and A. C. RUTENBERGER. Inorg. Chem. **6**, 2212 (1967).
24. A. M. HEYNS. J. Raman Spectrosc. **7**, 137 (1978).
25. R. D. GILLARD and G. WILKINSON. J. Chem. Soc. 1640 (1964).
26. VON U. GREHER and A. SCHMIDT. Z. Anorg. Allg. Chem. **444**, 97 (1978).
27. M.-H. HERZOG-CANCE, J. POTIER, and A. POTIER. Adv. Mol. Relax. Inter. Processes, **14**, 245 (1979).
28. M. DEBEAU and H. POULET. Spectrochim. Acta, **25A**, 1553 (1969).
29. G. ZUNDEL. Hydration and intermolecular interactions. Academic Press, New York. 1969. pp. 128–131.

Can. J. Chem. Downloaded from www.nrcresearchpress.com by 210.87.254.42 on 09/06/12
For personal use only.

Stability constants and spectral studies of complexes of 2-hydroxy-5-methylazobenzene-2′-carboxylic acid with some divalent metal ions

C. MAHALINGAM, J. K. STHAPAK,[1] D. D. SHARMA, R. L. TIWARI, AND SMITA STHAPAK
Department of Applied Chemistry, Government Engineering College, Jabalpur, India
Received March 29, 1983[2]

C. MAHALINGAM, J. K. STHAPAK, D. D. SHARMA, R. L. TIWARI, and SMITA STHAPAK. Can. J. Chem. **62**, 2299 (1984).

The stability constants of metal complexes of 2-hydroxy-5-methylazobenzene-2′-carboxylic acid have been determined spectrophotometrically. These follow the Irving–Williams sequence: log K_{OH}(H) = 10.67, log K_1(Co) = 9.02, log K_1(Ni) = 9.68, log K_1(Cu) =13.37, log K_1(Zn) = 7.58, and log $K_1(UO_2^{2+})$ = 11.63

The chelates of Mn(II), Fe(II), Co(II), Ni(II), Cu(II), Zn(II), and UO_2^{2+} with the dye have been prepared and characterized on the basis of their ir and reflectance spectra.

C. MAHALINGAM, J. K. STHAPAK, D. D. SHARMA, R. L. TIWARI et SMITA STHAPAK. Can. J. Chem. **62**, 2299 (1984).

On a déterminé spectrophotométriquement, les constantes de stabilité des complexes métalliques de l'acide hydroxy-2 méthyl-5 azobenzènecarboxylique-2′. Ces constantes obéissent à la séquence de Irwing–Williams: log K_{OH}(H) = 10,67, log K_1(Co) = 9,02, log K_1(Ni) = 9,68, log K_1(Cu) =13,37, log K_1(Zn) = 7,58, and log $K_1(UO_2^{2+})$ = 11,63.

Les spectres ir et les spectres de pouvoir réflecteur ont permis de caractérisér les chélates du Mn(II), du Fe(II), du Co(II), du Ni(II), du Cu(II), du Zn(II) et du UO_2^{2+} préparés à partir de ce colorant.

[Traduit par le journal]

Introduction

The formation of metal derivatives by those azo dyes which contain hydroxy, carboxyl, amino, etc., groups in one or more of the *ortho* positions has been studied in detail (2). Such compounds have found many applications in the dyeing of fabrics and in the preparation of organic pigments (3). The study of the stabilities of the complexes of such mordant azo dyes would be interesting because of their importance as a factor in the fastness of such dyes towards washing (4). This paper deals with the study of the stability constants of the complexes formed by metal ions Co(II), Ni(II), Cu(II), Zn(II), and UO_2^{2+} with 2-hydroxy-5-methylazobenzene-2′-carboxylic acid. The proton stability constants of the dye have been explained on the basis of hydrogen bonding as evidenced from the ir spectra of the dye obtained. The azo dye studied herein has the structure:

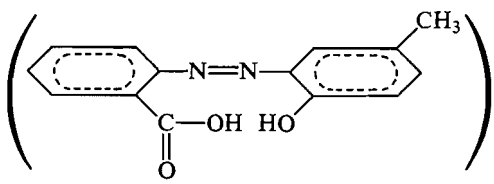

FIG. 1.

Experimental

The azo dye studied is not available commercially. It was, therefore, synthesized.

(A) *5-Methyl dye*

The dye was synthesized and stock solutions of metal ions and dye were prepared using AR grade salts, HCl, and NaOH. *Anal.* calc. for $C_{14}H_{12}N_2O_3$: C 65.63, H 4.68, N 10.94; found: C 65.53, H 4.71, N 10.70.

(B) *Synthesis of metal complexes of 2-hydroxy-5-methylazobenzene-2′-carboxylic acid*

The calculated quantities of the sodium salt of the dye solution and the metal salts were mixed in alcohol (100 mL) and were stirred at room temperature for one hour. The solid started precipitating, and was filtered and recrystallized to give the desired product.

(C) *Instruments*

A digital pH meter (Systronics) reading to 0.01 unit was used for pH reading after standardization at two points with suitable buffers in the region of the pH of the solution under study. Buffers used were potassium hydrogen phthalate (AR) and borax (AR). Absorbances were measured on a Beckman DU Grating Spectrophotometer with a tungsten lamp.

The absorption spectra of the ligand and metal complexes were measured in dimethylformamide solution. Silica cuvettes having 10-mm optical path-length, supplied with the instrument, were used. A Beckman DU spectrophotometer was used for diffuse reflectance spectra with spectroscopically pure magnesium carbonate as a reference. The structures of the ligand and their complexes were checked by ir spectra which were recorded on a Beckman IR-20 instrument in KBr. Conductivity measurements were made in dimethylformamide solution using a Metrohm conductivity bridge at 25°C ± 0.1°C.

Proton stability constant

In the case of the azo dye studied, only the log K_{OH}(H) value has been determined spectrophotometrically. The log K_{COOH}(H) value could not be determined for reasons offered in the discussion. The absorption spectra of the unionized species (OH group completely unionized at pH 6.50), and those of the ionized species (OH group completely ionized at pH ~ 14.00) were recorded and then the extinction coefficients at the chosen analytical wavelength were determined accurately; Beer's law was found to be obeyed.

Calculations

The proton stability constant log K_{OH}(H) was then determined by the relation (6):

$$\log K_{OH}(H) = pH + \log \frac{E_l - E}{E - E_u}$$

where the terms have their usual meanings (5). The values of E_u, E_l, and log K_{OH}(H) obtained at a wavelength of 470 nm, pH 10.00, temp. 25°C ± 0.1°, and ionic strength 8×10^{-5} *M* are 1740, 8450, and 10.67 ± 0.02, respectively.

Metal stability constants

Metal stability constants were determined by Janssen's spectrophotometric method (7) and the log K_1(M) values have been calculated from the equation

[1]Author to whom correspondence may be addressed. Present address: Govt. Engineering College, Sagar, 470005, India.

[2]Revision received July 26, 1983.

Can. J. Chem. Downloaded from www.nrcresearchpress.com by 210.87.254.5 on 09/06/12
For personal use only.

TABLE 1.

Metal ion	Ionic strength (M)	λ (nm)	pH	E_L	E_I	Log K_I(M)
Co^{2+}	2.8×10^{-4}	470	9.00	1740.0	5742	9.02 ± 0.08
Ni^{2+}	3.2×10^{-4}	490	10.00	978.8	8750	9.68 ± 0.02
Cu^{2+}	2.5×10^{-4}	500	13.00	694.0	9033	13.37 ± 0.10
Zn^{2+}	3.3×10^{-4}	480	7.00	1240.0	7415	7.58 ± 0.02
UO_2^{2+}	2.1×10^{-4}	450	11.00	3308.3	5191	11.63 ± 0.06

*Temperature: 25°C ± 0.1°.

$$K_I(M) = \frac{(A - E_L T_L)(E_I - E_L)F}{\{(E_I - E_L)T_M + E_L T_L - A\}(E_I T_L - A)}$$

where A, E_I, E_L, T_M, T_L, and F have their usual meanings described elsewhere (5).

Table 1 gives the wavelength chosen, E_L, E_I, and log K(M) values obtained for the various metal ions.

Discussion

(A) *Proton stability constant*

No change in the absorption spectra of the dye was observed in the whole recorded spectral region at pH 1 to 8 (below pH 1, the dye was too insoluble for any studies to be made and hence such values were unapproachable). Literature survey confirmed that Dieh and Ellingbde (8) had also found the same with their dyes (5-methyl dye and its naphthalene analogue). Presence of the COOH group was confirmed by elemental analysis and ir spectra of the ligand which show bands at 1680−1700 cm^{-1} due to —C=O asymmetric stretching of an aromatic carboxylic group. The band around 1590 cm^{-1} is due to —N=N— and those at 1250 cm^{-1} and between 1440−1395 cm^{-1} are due to C—O of phenol and COO^- symmetric stretching, respectively. The bands around 900−950 cm^{-1} could be assigned to —OH of the carboxylic group. Hence the presence of the —COOH group is confirmed. The spectrum also shows evidence for a strongly hydrogen-bonded hydroxyl group, as seen by a very broad absorption band extending from 3000 cm^{-1} to as low as 2300 cm^{-1}. The presence of a phenolic OH group in close proximity to a COOH group favours strong hydrogen bonding, which is known to stabilize the carboxyl ionized species as well as the phenolic unionized species quite considerably, the carboxylic group thus becoming more acidic and the phenolic less acidic than expected. The log K_{OH}(H) value of the dye (10.67) is comparable with that of *para*-cresol (10.26) (6), from which the dye is obtained by substituting the azo group in the *ortho* position. Normally, the effect of the azo group is electron withdrawing, being comparable to that of the nitro group. Therefore, the log K_{OH}(H) value of the dye may be expected to be about 2 units lower than that of *p*-cresol. The reason for the value actually being higher, instead of lower, is obviously the strong hydrogen-bonded character of the phenolic group.

(B) *Metal stability constants*

The data obtained in the present work are in full conformity with the Irving−Williams order (1) for the stability sequence of bivalent metal ions. UO_2^{2+} does not belong to the Irving−Williams series. The value for UO_2^{2+} obtained is lower than that of Cu(II) (see Table 1). This is in agreement with what has been reported in the literature for other ligands (9, 10).The lowest value of the metal stability constant has been obtained for Zn^{2+}, which is due to lack of bonding through the azo group of the dye. This has been confirmed from the ir spectrum of the solid complex. The spectrophotometric study, reported herein, shows no evidence at all for the formation of any 1:2 complexes in solution. Moreover, when a large excess of ligand is added to the solution of any of these metal ions, the absorbance throughout the recorded range is exactly the same as that calculated by the additivity rule, on the basis of the formation of 1:1 complex and the excess ligand remaining uncombined. Hence, only 1:1 complexes exist in solution. This has also been confirmed from conductance studies by Job's method of continuous variations (11). Infrared ir spectral studies provide evidence for the participation of the —N=N— group in complexation and hence the lack of formation of 1:2 species in solution due to steric factors.

Conductance and infrared spectral studies

The solid complexes of 2-hydroxy-5-methylazobenzene-2′-carboxylic acid with the metal ions reported herein are coloured, and are insoluble in organic solvents, viz., carbon tetrachloride, chloroform, benzene, and alcohol, but soluble in dimethylformamide and sodium hydroxide. Their molar conductances in dimethylformamide solution are low, indicating them to be nonelectrolytes.

The infrared spectra of Mn(II), Fe(II), Co(II), Ni(II), Cu(II), and UO_2^{2+} complexes show the disappearance of the band in the region 950 cm^{-1}, suggesting removal of proton from the ligand. The ν(C=N) shifts to the low-frequency region in all but the Zn(II) complexes, indicating coordination through the nitrogen atom of the azo group. Mn(II) and Co(II) complexes show a very broad band in the region 3000−3400 cm^{-1}, indicating the presence of water molecules in the complexes. In order to complete the octahedral stereochemistry of the complexes, one or two water molecules have to be coordinated to the metal ions. The UO_2^{2+} complex shows a strong but broad band at 900 cm^{-1}, which may be assigned to ν(asy. O—U—O) (12−16).

Absorbance and diffuse reflectance spectra

The absorption spectrum of the dye was recorded using dimethylformamide as the solvent. Two bands near 30 kK and 20 kK were observed which may be assigned to $\pi \rightarrow \pi^*$ and $n \rightarrow \pi^*$ transitions, respectively, and are characteristic of the azo group (17).

The diffuse reflectance spectrum of the Co(II) − 5-methyl dye complex having bands in the region 10−10.65 kK (ν_1) may be assigned to the transition $4T_{1g}(F) \rightarrow 4T_{2g}(F)$. The band at 21−24 kK is due to $4T_{1g}(F) \rightarrow 4T_{1g}(P)$ (ν_3 transition). It is difficult to assign for the transition (ν_2) $4T_{1g}(F) \rightarrow 4A_{2g}(F)$ since this band and the ligand $n \rightarrow \pi^*$ transitions are expected in the same region.

Can. J. Chem. Downloaded from www.nrcresearchpress.com by 210.87.254.5 on 09/06/12
For personal use only.

Crystal field parameters Dq, B, and β have been calculated with the help of secular determinant (20) and are 1175 cm^{-1}, 909 cm^{-1}, and 0.812, respectively. The value of B in the free ion has been taken to be 1120 cm^{-1} from the literature (18). These values of crystal field parameters for the Co(II) complex with the 5-methyl dye can be compared with the values reported by Pappalarado and Seminora (19) for the high-spin octahedral Co(II) complexes.

The diffuse reflectance spectrum of the Ni(II) complex with the 5-methyl dye was studied in the range 265–1200 nm. Three bands in the region 9–30 kK were obtained. A lower energy band obtained near 10 kK can be assigned to the (ν_1) $3A_{2g}(F) \rightarrow 3T_{1g}(F)$ transition (ν_2). The ratio ν_2/ν_1 lies between 1.6 and 1.8. A third band near 19 kK may be assigned to the $3A_{2g}(F) \rightarrow 3T_{1g}(P)$ transition (ν_3) for an octahedral Ni(II) complex (21).

The complex of the 5-methyl dye with Fe(II) shows bands around 11.10 kK which may be assigned to $5T_{2g} \rightarrow 5E_g$ transitions. Other bands may be assigned to $n \rightarrow \pi^*$ or charge-transfer transitions of the ligand. A comparison of the spectrum of the 5-methyl dye and its complex with Fe(II) indicates that, after complexation, λ_{max} of the ligand shifts to the longer wavelength region.

The spectrum of the UO_2^{2+} complex generally shows well-defined vibronic structure between 21 280 and 30 300 cm^{-1} (19). In the present study, the complex shows two bands at 27 030 and 20 410 cm^{-1}. The latter band might be due to a ligand → metal charge-transfer transition. The Mn(II) complex exhibits bands around 29.41 and 19.23 kK. The Zn(II) complex is diamagnetic. The solution spectra of these complexes in dimethylformamide are similar to their diffuse reflectance spectra and so these complexes may have octahedral geometry.

Magnetic susceptibility measurements

The magnetic susceptibility measurements at room temperature were carried out by Gouy's method (see refs. 18 and 22). Magnetic data of the complexes of the azo dye with bivalent metal ions, viz. Mn(II), Fe(II), Co(II), and Ni(II) are 5.75 BM, 5.45 BM, 5.25 BM, and 3.20 BM, respectively. These magnetic moment values suggest octahedral geometry for the complexes of these bivalent metal ions.

[3]J. K. Sthapak, Smita Sthapak, and R. L. Tiwari; unpublished work.

Applications of the 5-methyl dye

This dye has been used as a metal-ion indicator in titrimetric determinations of various metal ions and also in the spectrophotometric determination of Th(IV).[3]

Acknowledgements

One of the authors (J. K. S.) is grateful to the University Grants Commission, New Delhi for the award of a National Associateship during the tenure of which the spectral studies of solid complexes and magnetic susceptibility measurements could be completed.

1. H. IRVING and R. J. P. WILLIAMS. Nature (London), **162**, 746, (1948), J. Chem. Soc. 3192 (1952).
2. F. A. SAVELY, W. C. FERNELIUS, and B. E. DOUGLAS. J. Soc. Dyers Colour. 73 (1957).
3. L. S. PRATT. Chemistry and physics of organic pigments. Wiley, New York. 1947. p. 75.
4. F. A. SAVELY and W. C. FERNELIUS. Science, **117**, 15 (1953).
5. V. P. GUPTA, J. K. STHAPAK, and D. D. SHARMA. J. Inorg. Nucl. Chem. **43**, 3019 (1981).
6. A. ALBERT and E. P. SERJEANT. The determination of ionization constants. 2nd ed. Chapman & Hall Ltd., London. 1971. pp. 44, 45, 87.
7. M. J. JANSSEN. Recl. Trav. Chim. Pays-Bas, **75**, 1397 (1956).
8. H. DIEH and J. ELLINGBDE. Anal. Chem. **32**, 1120 (1960).
9. R. L. MARTIN. Nature, **166**, 474 (1950).
10. D. G. VARTAK and N. G. MENON. J. Inorg. Nucl. Chem. **28**, 2911 (1966).
11. P. JOB. Ann. Chim. **10**, 9 (1928); **10**, 113 (1928).
12. R. CRZESKOWIAK and M. GOLDSTEIN. Inorg. Chim. Acta Lett. **33**, 453 (1979).
13. L. H. JONES. Spectrochim. Acta, **10**, 395 (1958).
14. S. P. MCGLYNN, J. K. SMITH, and W. C. NEELY. J. Chem. Phys. **35**, 105 (1961).
15. J. I. BULLOCK and F. W. PARRET. Can. J. Chem. **48**, 3095 (1970).
16. H. D. BIST. J. Mol. Spectrosc. **27**, 542 (1968).
17. H. RAVI. Angew Chem. **85**, 248 (1973).
18. B. N. FIGGIS. Introduction to ligand fields. Wiley Eastern Ltd., New Delhi. 1976.
19. G. C. PAPPALARDO and A. SEMINORA. J. Inorg. Nucl. Chem. **38**, 1993 (1976).
20. C. J. BALLHAUSEN. Introduction to ligand field theory. McGraw Hill Series, New York. 1962. pp. 251, 255, 271.
21. A. B. P. LEVER. Inorganic electronic spectroscopy. Elsevier Pub. Co., 1968.
22. A. E. MARTELL and M. CALVIN. Chemistry of metal chelates. McGraw–Hill Pub. Co. Ltd., New York. 1966.

Can. J. Chem. Downloaded from www.nrcresearchpress.com by 210.87.254.5 on 09/06/12
For personal use only.

Laser-induced addition of hydrogen fluoride to unsaturated molecules: the HF + CH_2CF_2 system

WALTER H. BECK[1] AND GEORGE BURNS

Lash-Miller Chemical Laboratories, University of Toronto, Toronto, Ont., Canada M5S 1A1

Received January 27, 1984

WALTER H. BECK AND GEORGE BURNS. Can. J. Chem. **62**, 2302 (1984).

Although certain classes of reactions are known to occur via 4-centre transition states, there has been no irrefutable proof that in the gas phase addition reactions also proceed via a 4-centre concerted process. Results of recent information theory calculations on the HF(v) + CH_2CF_2 system indicate that it should be possible to observe reaction products for HF(v = 5). Results are presented here on experiments attempting to achieve laser-induced 4-centre addition of HF to several unsaturated molecules (C_2H_2, C_2H_4, C_4H_6, CH_2CF_2, and CF_2CClF). A mixture of HF and co-reactant was irradiated by a dye-laser tuned photo-acoustically to the fifth vibrational level of HF, and the resulting mixture was analysed by gas chromatography and mass spectrometry. There was no evidence of any laser-induced products. An upper bound was deduced for the HF + CH_2CF_2 addition rate constant at 610 K: $k_r^{610} < 1 \times 10^8$ L mol^{-1} s^{-1}.

WALTER H. BECK et GEORGE BURNS. Can. J. Chem. **62**, 2302 (1984).

Même si on sait que certaines réactions se produisent par l'intermédiaire d'un état de transition à 4 centres, il n'existe aucune preuve irréfutable que les réactions d'addition en phase gazeuse se produisent également par l'intermédiaire d'un processus concerté à 4 centres. Des résultats récents, obtenus par des calculs basés sur la théorie de l'information et réalisés sur le système HF(v) + CH_2CF_2, indiquent qu'il devrait être possible d'observer des produits de réaction pour HF(v = 5). On rapporte les résultats d'expériences effectuées en vue de réaliser une addition à 4 centres, induite au laser, du HF sur diverses molécules insaturées (C_2H_2, C_2H_4, C_4H_6, CH_2CF_2 et CF_2CClF). On a irradié les mélanges de HF et de ses co-réactifs à l'aide d'un laser ajusté d'une façon photoaccoustique jusqu'au cinquième niveau vibrationnel du HF et on analysé les mélanges réactionnels obtenus en faisant appel à la chromatographie en phase gazeuse et à la spectrométrie de masse. On n'a pas pu mettre en évidence la présence de produits provenant d'une réaction induite au laser. On a déduit une limite supérieure pour la constante de vitesse d'addition de la réaction HF + CH_2CF_2, à 610 K: $k_r^{610} < 1 \times 10^8$ L mol^{-1} s^{-1}.

[Traduit par le journal]

Introduction

There is still much conjecture regarding the mechanism of the addition of hydrogen halides HX to unsaturated molecules in the gas phase (1). The reaction can be either a single-step, concerted process, proceeding through a 4-centre transition state, or can proceed via a chain mechanism made up of many separate steps, each of which is a bimolecular reaction involving atoms and radicals as intermediates (2, 3). The former process obviously leads to just one end-product, whereas the latter can produce several, depending on the complexity of the reactants. Determination of the addition reaction product/s would therefore be useful in determining the mechanism of reaction.

The existence of 4-centre reactions has been clearly demonstrated for certain classes of reactions: exchange reactions between alkali halides (4) and between isotopically labelled nitrogen oxides (5), ion/molecule reactions (6), and certain free radical reactions (7). On the other hand, what was once considered the classic example of a 4-centre concerted process, the H_2/I_2 reaction (2), has been shown by Sullivan (8) to be made up of a series of bimolecular atom/radical reactions.

Since the pioneering work of Farkas and Farkas (9) on the H_2 + H_2 exchange reaction, there has been a continual refinement in experimental (mainly shock tube) methods to attempt to elucidate the analogous D_2 + H_2 reaction. Measured activation energies (around 40 kcal mol^{-1} (10)) have typically been well below the expected value of 88 kcal mol^{-1} (11) for dissociation of H_2 by Ar, and even smaller than H—H bond energy (103.4 kcal mol^{-1}). This finding was taken to indicate that the reaction must proceed by some mechanism (such as 4-centre concerted) other than H_2 bond rupture as the first step. By monitoring H atom concentrations in shock-heated H_2/D_2 mixtures, Lifschitz and Frenklach (12) found that only a small proportion of their HD yield arose from H atom reactions, and that the remainder originated from a 4-centre bimolecular reaction with an activation energy of 38 ± 5 kcal mol^{-1}. However, since then, the experiments have been repeated in an ultra-clean shock tube (13) and the results have disproved the 4-centre mechanism. It was shown that the previous spurious results were due to minute impurities (probably hydrocarbons) leading to false interpretations of the role of H atoms in the mechanism.

Based on simple geometric considerations, it does not seem unreasonable for hydrogen halides to add to unsaturated molecules via a 4-centre transition state. Experimental addition reaction studies have so far been largely restricted to HI, since HF, HCl, and HBr in general require very high temperatures and pressures for reaction to occur. HI was found to add to several olefins (14, 15), butadiene (15), and other conjugated dienes (14, 16). Benson and Egger (14) found that the activation energy E_a for addition of HI to dienes was lower than that to olefins, and explained this result using the Benson and Bose model (17) of a 4-centre transition state. Kubota (15) obtained the same trend, but by invoking Woodward–Hoffmann symmetry rules (18), decided against a 4-centre transition state for addition of HI to butadiene. This conclusion is also backed by Gorton and Walsh (16), who favour a 6- over a 4-centre transition state.

Elimination of HX (the reverse reaction to addition) has been extensively studied using various techniques. Tschuikow-Roux co-workers (19) and Trotman-Dickenson and co-workers (20) have used the shock tube techniques to determine E_a for elimination of HF from various alkyl and ethylene fluorides. E_a values were found to be higher than those for elimination of HCl, HBr, HI from their corresponding alkyl halides, which is in agreement with the findings mentioned above on the HI

[1]Present address: Weapons Systems Research Laboratory, Defence Research Centre, Salisbury, South Australia.

Can. J. Chem. Downloaded from www.nrcresearchpress.com by 210.87.254.105 on 09/06/12
For personal use only.

addition reactions.

In a classic paper on HF elimination, Clough *et al.* (21) used the combination–elimination reaction

$$CH_3 + CF_3^{\ddagger} \rightarrow CH_3CF_3 \rightarrow CH_2CF_2 + HF\dagger$$

and the mercury-sensitized reaction

$$CH_2CF_2 + Hg^* \rightarrow CHCF + HF + Hg$$

to show that HF is produced rotationally and vibrationally (up to $v = 4$) excited. This effect was first observed by Berry and Pimentel (22), who monitored HF laser emission following uv photo-elimination of HF from CH_2CFH. Since then, Pimentel and co-workers (23) have succeeded in producing HF rotational chemical lasers via a similar flash-induced dissociation of CH_3CF_3 and CH_2CF_2.

The above uv photolytic methods are totally non-selective in that it is not even certain which alkyl halide transition is being excited to produce the reaction. The advent and development over the last 5–10 years of the ir multi-photon absorption (IRMPA) technique (24) has made it possible to gain higher selectivity in choosing which transition of the alkyl halide is excited. Moore and co-workers (25) used an optical parametric oscillator (3.3 μm) and a CO_2 laser (10 μm) to excite the CH stretching modes of ethyl chloride, bringing about the HCl photo-elimination reaction. Dissociation yields were measured as a function of laser fluence and wavelength. Jang and Setser (26) further studied the effect of added inert gas on dissociation yields from IRMPA of CH_3CH_2F and CH_3CF_3. They also observed only a single product (apart from HF) from the elimination reaction, indicating that it occurs via a concerted process. The same conclusion was reached by Steinfeld and co-workers (27) in their study of IRMPA of vinyl chloride using a CO_2 laser, followed by the elimination reaction.

In a molecular beam experiment, Lee and co-workers (28) studied the 4-centre unimolecular elimination of HCl from CH_3CCl_3, CH_3CF_2Cl, and $CHClCF_2$ using the IRMPA technique, and found that the combined energy of the two resulting species was only 20% of the barrier for the back (addition) reaction, suggesting that the energy deficit must be contained as internal (vibrational/rotational) energy of the species.

There is, of course, still a problem of non-selectivity using the IRMPA approach. Specifically, it is unclear what is the internal energy distribution of the reacting molecules when excited by the laser. Moore and co-workers (25) and Steinfeld and co-workers (27) were able to explain their results using a statistical approach, the molecular internal energy distribution being represented by a non-specific-mode model, and the reaction rates being calculated by RRKM approach which assumes a rapid attainment of microcanonical internal equilibrium of the molecule prior to reaction. More rigorous master equation calculations (29) for IRMPA confirm the above; Steinfeld and co-workers (27) based their statistical model on these approaches.

The production of vibrationally and rotationally excited HX from elimination reactions strongly suggests on the basis of the principle of microscopic reversibility that the excitation of HX (or the olefin?) may help accelerate the reverse addition reaction. Intuitively this seems logical, since it is the HX bond which will need to be broken, and more energy put selectively into this bond should accelerate the reaction.

The effect of vibrational excitation on reaction rate has been clearly shown. Very large enhancements have been determined for the atom/molecule reactions

$$D + H_2 \xrightarrow{k_v} HD + H, \text{ where } k(v = 1)/k(v = 0) > 10^4 \quad (30)$$

and for

$$H + HF(v) \xrightarrow{k_v} H_2 + F, \; k(v = 1)/k(v = 0) \simeq 5 \times 10^8 \quad (31)$$

Although no enhancement was found for the $HF(v)/D_2$ exchange reaction (1), presumably because the $HF(v)$ relaxation rate is too large relative to the reaction rate, a 4-centre concerted process could still not be ruled out.

Indirect evidence for vibrational enhancement for a molecule/molecule reaction came from the results of Horiguchi and Tsuchiya (32), who irradiated HI and HI/CO_2 mixtures with a CO_2 laser, and found an increased rate for the reaction

$$HI + HI \rightarrow H_2 + I_2$$

when CO_2 was present. This was said to be due to the near-resonant energy transfer from the excited CO_2 to the HI,

$$CO_2(001) + HI(v = 0) \rightarrow CO_2(000) + HI(v = 1)$$

followed by reaction between $HI(v = 1)$ and $HI(v = 0)$. An earlier molecular beam study on the HI + DI reaction made use of a seeded HI beam to raise the centre-of-mass (viz. translational) energy to as high as 110 kcal mol^{-1} (which lies well above the expected 4-centre concerted process activation energy of 44 kcal mol^{-1}), but still no reactive HD was detected (33). The relative importance of vibrational as against translational energy in the HI/DI system was thus clearly demonstrated.

The possibility of laser-induced, specific-mode reactions between HX and an olefin has been discussed by Marling *et al.* (34), and has been tested experimentally by several groups (35–38). Bauer (35) attempted to react vibrationally excited HF ($v = 1$, using a HF laser) with various substituted olefins and acetylene, while Herman and Marling (36) excited the $v = 5$ or 6 overtone of HCl and also the fourth overtone of the C_2H_2 asymmetric CH stretch in an attempt to obtain an addition reaction: both studies failed to show any laser-induced reaction. Berry (37) claimed to have found reaction between 2-methylpropene and HCl ($v = 5$, intra-cavity laser study), but there were no subsequent reports confirming this. Hager *et al.* (38) studied the deactivation by HBr of vibrationally excited C_2H_2 (01000), and concluded that the low collision number obtained for its relaxation could be interpreted as incipient chemical reaction.

The dominant process in all the above studies was the far greater rate of the inter- and intra-molecular relaxation of the laser-excited species compared to its reaction rate. If these relaxation processes could be slowed down, such as in a solid gas matrix where the rotational and translational modes are frozen out, then the reaction may be able to compete favourably with relaxation. In a very recent study, Frei and Pimentel (39) irradiated frozen mixtures of F_2, C_2H_4, and an inert gas over the range 1000–4000 cm^{-1}, and used FTIR spectroscopy to monitor the appearance of products. They described their results in terms of a 4-centre addition of F_2 to C_2H_4. Although the nature of their irradiation does not strictly correspond to single mode excitation, they claim that small peaks in their quantum yield versus wave number plots occurring at certain vibration combination modes indicate that excitation of these modes must lead to enhancement of reaction.

Assuming that the addition and elimination reactions do occur via a 4-centre transition state, it is possible to relate their

Can. J. Chem. Downloaded from www.nrcresearchpress.com by 210.87.254.105 on 09/06/12
For personal use only.

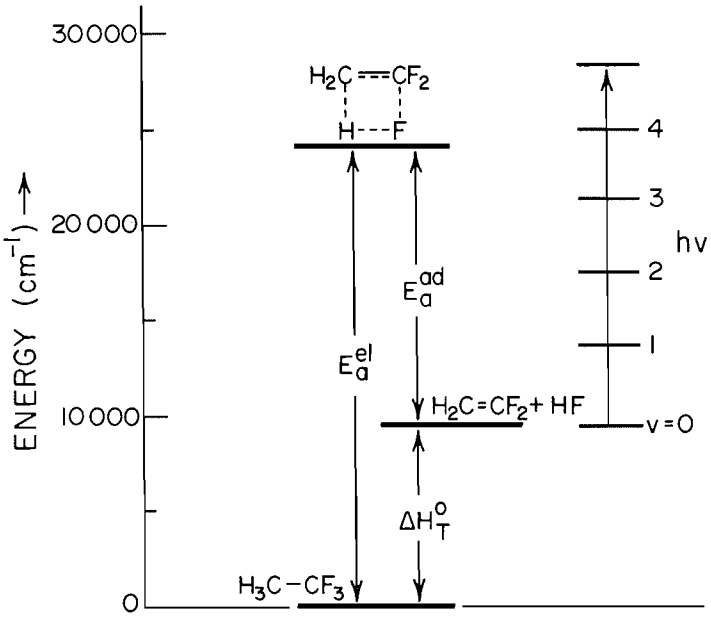

FIG. 1. Energy level diagram for the HF + CH_2CF_2 system. E_a^{el} = 69 kcal mol^{-1}, E_a^{ad} = 42 kcal mol^{-1}, ΔH_T^0 = 27 kcal mol^{-1}.

TABLE 1. Activation energies* for addition of hydrogen halides to unsaturated molecules HX (X = F, Cl, Br, I) + A

	E_a^{ad}/(kcal mol^{-1}) for HX + A when X =			
A	F	Cl	Br	I
CH_2:CH_2	51 (20)	40	34	28.5
CH:CH	50	42 (41)		—
CH_3CH:CH_2	45	34 39.4 (42)	28.5	23.5
CH_2:CHCH:CH_2	—		24 (est) (34)	18.7 (15)
Me	—	34 (43)	—	—
CX_2:CX_2	45.2	35.5	—	—
CH_2:CX_2	37.2 35.5 (20)	38.8	—	—
CH_2:CHX	36.6	36.3	—	—

*All values are taken from ref. 45, unless otherwise shown, the number of the references are in parentheses.

activation energies E_a via the reaction enthalpy change ΔH_T^0 as shown in Fig. 1. E_a^{el} for elimination of HX from several halogenated olefins has been measured by several workers (19, 40), enabling E_a^{ad} for the reverse addition reaction to be estimated (34). Direct measurements of E_a^{ad} for HI (14–16) and HCl (41–43) additions are also available. Several attempts have also been made to calculate theoretically E_a^{ad} for a 4-centre concerted process using a semi-empirical model based on bond order conservation (17, 44, 45). Some typical experimental and theoretical values of E_a^{ad} are presented in Table 1. Note that there is a general trend of E_a^{ad} decreasing down and across the table; this explains why most experimental studies on (non-mode-specific) addition reactions have been carried out with HI.

In the case of HF additions, even the reaction HF + CH_2CF_2 with the lowest value of E_a^{ad} (35.5 kcal mol^{-1}) still has a vanishingly small thermal rate. Figure 1 shows that if HF can be excited to a sufficiently high vibrational level, then its energy will be above the activation barrier E_a^{ad}. At this stage it is still not known how effective the HF vibrational excitation is in overcoming this barrier, although results on vibrational distribution in HF elimination reactions may provide a clue.

Berry (46) has concluded that of the total energy E_{tot} (= E_a^{el} = E_a^{ad} + ΔH_T^0; Fig. 1) available to the elimination reaction products, only about 15–40% ends up in HF vibration. This is confirmed in the detailed dynamical calculations of Kato and Morokuma (47), who examined the mechanism of energy disposal along the reaction pathway for the elimination reaction

$$CH_3CH_2F \rightarrow CH_2CH_2 + HF$$

~30% of E_{tot} ended up in HF vibration. One further important dynamical aspect arises from their calculations; at short distances (along their reaction coordinate) from the transition state, most E_{tot} is in the HF stretching mode, but as the distance increases, energy is lost very rapidly from this mode, being transferred largely to the HF – CH_2CH_2 relative translation "mode". These results suggest that for the reverse addition reaction, vibrational excitation alone is not sufficient to overcome the reaction barrier, but relative translational energy may also be important. This idea has been discussed before (36). On the other hand, the results of Clough *et al.* (21) on the CH_3CF_3 elimination reaction showed that most of E_{tot} ended up in HF *and* CH_2CF_2 internal energies, suggesting that excitation of *both* HF and CH_2CF_3 may be necessary to accelerate the reverse addition reaction. The question is still an open one.

Levine and co-workers (48) have used an information theoretic approach to predict the energy disposal for several elimination reactions, and using detailed balance have calculated vibrational enhancement factors for the reverse addition reactions. Their results for HF at 600 K are summarized in Table 2. When one considers that typical frequency factors for addition reactions are about 10^8 L mol^{-1} s^{-1} (34), then even with enhancement factors as large as $2 \times 10^{10} - 7 \times 10^{13}$, it is clear from the table that there is only one reaction system with an appreciable rate—CH_2CF_2 + HF. (Note from Table 1 that this reaction also has one of the lowest activation energies.)

Can. J. Chem. Downloaded from www.nrcresearchpress.com by 210.87.254.105 on 09/06/12
For personal use only.

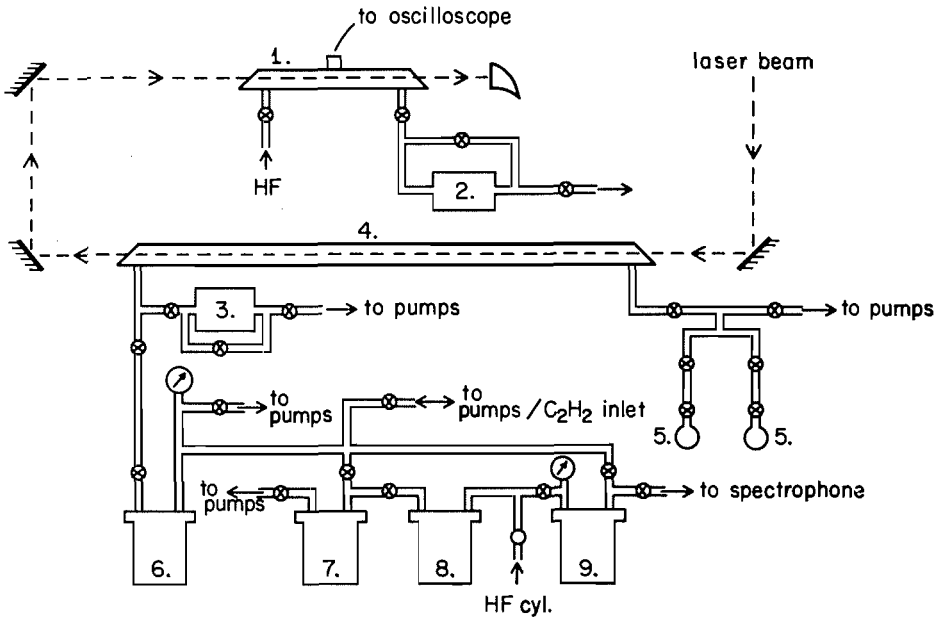

FIG. 2. Schematic diagram of the experimental apparatus. (*1*), Spectrophone; (*2*), (*3*), bar cel capacitance manometers; (*4*), reaction vessel; (*5*) sample flasks; (*6*), mixing vessel; (*7*), trap (77 K); (*8*), (*9*), preparation vessels.

TABLE 2. Rate constants for the addition reaction HF(v) + A for v = 0, 3, 4, 5*

A	$k_r^{600}(v)/(\text{L mol}^{-1}\text{ s}^{-1})$			
	$k_r^{600}(0)$	$k_r^{600}(3)$	$k_r^{600}(4)$	$k_r^{600}(5)$
CH:CH	2.3×10^{-9}	350	4600	4600
CH:CF	7.4×10^{-14}	0.0031	0.5	0.38
CH_2:CH_2	4×10^{-11}	1.4	76	2600
CH_2:CF_2	5.6×10^{-6}	1.2×10^{5}	7.3×10^{6}	3.0×10^{8}
HCl + CH:CH	1.5×10^{-6}	7.7	1.1×10^{4}	8.3×10^{4}

*All data taken from ref. 48, Table 1, p. 2685.

The results of the above two theoretical approaches were published after Bauer's and Marling's first attempts to obtain a laser-enhanced reaction. Marling *et al.* (34, 36) studied HCl(v = 5, 6) + various olefins (but not CH_2CCl_2), and Bauer (35) attempted HF(v = 1) + CH_2CF_2, but neither has studied the system HX(v = 5) + CH_2CX_2 (X = F or Cl).

The aim of this report is to present results of experimental studies on this reaction, and also on the related HF(v = 5) + C_2H_2, C_2H_4, C_4H_6 (1,3-butadiene), and CF_2CClF systems. Assuming the reaction to be a 4-centred concerted process, the results also present a useful test of the predictive ability of information theory as applied to HX/olefin addition reactions.

Experimental method

The schematic of the experimental apparatus is shown in Fig. 2. The laser output was passed through the reaction cell containing the test gas mixture (HF + co-reactant) and then through a spectrophone cell used to tune the laser to the required HF transition.

The P(2) line of the HF(v = 5 ← v = 0) transition (563.6 nm) was excited using a Rhodamine-6G dye pumped by a Nd:YAG laser (Quanta Ray PDL-1 Dye Laser System). Laser pulses were typically 5 ns wide at an energy of 25–30 mJ, and by means of an intra-cavity high-finesse pressure-tuned etalon attained a linewidth of 0.15 cm^{-1}.

The reaction vessel was a 1.5 m length of 1.3 cm id SS316 tubing fitted at both ends with sapphire windows set at Brewster's angle. The whole gas handling system which came into contact with the test gases was also constructed of stainless steel. The cell could be heated by means of two heating coils wrapped around it — the temperature was estimated to be constant (up to 350°C) over at least 80% of its length by direct measurement at its centre using a thermocouple. The cell and remaining gas system were pumped down to 10^{-4} Torr for at least a day before each new experiment.

The spectrophone was constructed from a 25 cm length aluminium block with a 1.3 cm hole bored lengthways through it, and was again fitted with sapphire windows at Brewster's angle. A Bruel and Kjaar 4144 Microphone was mounted vertically so that it was just recessed from the bore. The output from the microphone was magnified by about a factor of 10 using a high-impedance low-capacitance amplifier, and then displayed on an oscilloscope. Typical signals were 10 mV at a HF pressure of 30 Torr, and with a laser pulse energy of 6 mJ.

The HF gas was frozen into vessel 8 at 77 K, and was pumped on for 15–20 min to remove any non-condensable gasses (e.g. H_2) present. After thawing, the gas was re-frozen in the same vessel with a dry ice/acetone mixture (195 K), and was further pumped for 1 min through another trap (vessel 7) at 77 K. Vessel 8 was then opened to a further vessel 9 at 77 K, and allowed to distil over a period of 30–40 min. After further pumping down of the distillation vessel 9 while still at 77 K, the gas was allowed to thaw slowly. This fractional distillation procedure gave good separation of HF and H_2O vapour (at 195 K, the equilibrium vapour pressures of HF and H_2O are 1–5 Torr and $4 - 10^{-4}$ Torr, respectively, so that a separation of at least 10^4:1 was possible). Other gasses (C_2H_2, purified, 99.6% min; C_2H_4, research purity, 99.99% min; C_4H_6, also research purity, 99.9% min; CH_2CF_2 and CF_2CClF, both research purity) were taken directly from their container (lecture bottle) without further purification. It was assumed that the purity of the gasses is sufficiently high and that any residual gasses are present in too low concentration to affect the course of the reaction. These impurities could not be detected in our gas chromatographic and mass spectrometric experiments.

A summary of the experimental procedure is as follows:

(*1*) HF gas distilled;

(*2*) HF added to spectrophone cell, laser tuned to HF transition (without any gas in the reaction vessel) by adjusting pressure in the pressure-tuned etalon;

(*3*) HF and co-reactant gas added to mixing vessel with HF added first, and left to mix for 15 min;

(*4*) laser warmed up (maximum energy and stability were obtained after a warm-up period of 5–10 min), tuning re-checked, gas mixture

Can. J. Chem. Downloaded from www.nrcresearchpress.com by 210.87.254.105 on 09/06/12
For personal use only.

TABLE 3. Experimental results from laser-irradiation of HF(v = 5) + A mixtures

Run	A	[HF]/[A]	T (K)	P (Torr)	Time* (min)	With or w/o laser†	Mass spec results‡	Gas chrom. results‡
I	C_2H_2	0.1	295	180	10	×	No product	—
II	C_2H_2	0.5	295	110	10	✓	No product	—
IV	C_2H_2	0.1	295	680	10	✓	No product	—
V	C_2H_2	0.1	295	25	10	✓	No product	—
VI	C_2H_4	1.0	295	110	10	×	No product	—
VII	C_2H_4	0.1	295	110	15	✓	No product	—
VIII	C_2H_2	0.1	480	175	15	×	No product	—
	C_2H_4	0.1	480	175	15	×	No product	—
IX	C_4H_6	0.1	510	150	15	✓	No product	—
X	C_4H_6	0.1	510	150	18	✓	No product	—
XI	CH_2CF_2	0.15	520	450	40	✓	No product	—
XII	CH_2CF_2	0.11	620	680	40	✓	Peak at 69 m/e (no blank)	—
XIV	CH_2CF_2	0.16	600	900	30	×	—	No product
XV	CH_2CF_2	0.5	610	450	30	×	—	12% (see text)
	CH_2CF_2	0.5	610	200	30	×	—	6% (see text)
	CH_2CF_2	0.2	610	300	30	×	—	6% (see text)
	CH_2CF_2	0.2	610	240	30	×	—	4% (see text)
XVI	CH_2CF_2	0.5	630	50	20	✓	—	Tuned/detuned 2:1
XVII	CH_2CF_2	0.5	610	50	20	✓	—	No product
XVIII	CH_2CF_2	0.4	600	100	20	✓	—	Tuned/detuned 2:1
XIX	CH_2CF_2	0.4	610	100	20	✓	—	No product
XX	CH_2CF_2	1.0	610	25	20	✓	—	No product
XXI	CH_2CF_2	1.0	610	25	20	✓	—	No product
XXII	C_4H_6	1.0	610	20	20	✓	No product	—
XXIII	CF_2CClF	1.0	610	20	20	✓	No product	—
XXIV	CF_2CClF	1.0	610	40	20	✓	No product	—

*Duration of laser irradiation.
†×, without laser irradiation; ✓, with laser irradiation.
‡"No product", no product detected within stated sensitivity of technique; —, technique not used.

Can. J. Chem. Downloaded from www.nrcresearchpress.com by 210.87.254.105 on 09/06/12
For personal use only.

added to pre-heated reaction cell and irradiated for appropriate time period;

(*5*) gas mixture frozen out directly from reaction vessel to Pyrex sample flasks cooled to 77 K;

(*6*) blank run carried out with freshly-prepared gas mixture, procedure as above repeated except laser de-tuned off HF transition by lowering pressure in the pressure-tuned etalon. (This procedure differs from that of Herman and Marling (36), who did not irradiate their blank);

(*7*) laser retuned, and experiment repeated;

(*8*) contents of flasks analysed by gas chromatography (Varian V1700 Gas Chromatograph with Porapak-Q column and flame ionization detector) and/or mass spectrometry. The sensitivity of both methods was tested with a series of dilutions of CH_2CF_2 in C_2H_2 — gas chromatography provided semi-quantitative separation down to 0.1%, while mass spectrometry could detect 0.01% dilutions.

Mixtures of HF + co-reactant in proportions ranging from 1:1 to 1:5, at pressures of 25−900 Torr and temperatures 295−630 K were irradiated for periods from 10−40 min.

Results

The experimental results are summarized in Table 3. Note that most runs involved the HF + CH_2CF_2 systems, and that most but not all runs were at 610 K.

Although reaction products were observed in several experiments, there was no evidence for any laser-induced reaction product. Run XII did produce a mass spectrometric signal at 69 m/e (the expected product of the HF + CH_2CF_2 addition reaction is CH_3CF_3, whose cracking pattern shows the largest peak at 69 m/e due to the CH_3 radical), but no blank run was available for comparison. Under other similar (or even more conducive) conditions (e.g. run XVIII), there was no product. Several runs (XV) at high temperature and pressure did yield significant product yields (up to 12%), but these were shown by gas chromatographic separation not to be the desired product, but rather longer chain species most likely due to wall or thermal chain reactions. They were not further identified, but experimental conditions after these runs were controlled to prevent these reactions from occurring. There were two cases (XVI and XVIII) where there did appear to be a laser-enhanced effect: gas chromatographic analysis of products showed a doubling of relative product yield for the laser-tuned case. These results could not be further reproduced (see run XIX, or even runs XX and XXI).

Discussion

In order to explain the apparent lack of any detectable laser-enhanced effect, it is necessary to examine in more detail the processes occurring in the irradiated gas mixture. Since most attention has been given to the HF + CH_2CF_2 system, it will be used as the example in the following model calculation. The procedure adopted will be as follows: calculate the proportion

Can. J. Chem. Downloaded from www.nrcresearchpress.com by 210.87.254.105 on 09/06/12
For personal use only.

of HF(v = 5); set up a model describing the fate of these HF; develop an expression for the yield of product (i.e. CH_3CF_3); using available data on HF relaxation rates, estimate an upper bound for the HF + CH_2CF_2 reaction rate constant.

Proportion of HF (v = 5)

Although the calculation for the HF(v = 5) level has been given elsewhere (49), it will be repeated here since some experimental conditions may be different.

HF transition: $\nu_0 = 17743\ cm^{-1}$ (= 5.3192×10^{14} Hz)
Laser bandwidth: $\Delta\nu_0 = 0.15\ cm^{-1}$ (= 4.5×10^9 Hz)
Laser power: $P = 5.4$ MW
Laser pulselength: $\Delta t = 5 \times 10^{-9}$ s
Laser beam area: $A_c = 3.3 \times 10^{-5}\ m^2$
Reaction vessel length: $l_c = 1.5$ m
Reaction volume: $V_c = 2.00 \times 10^{-4}\ m^3$
HF pressure: $P_{HF} = 25$ Torr

From the above, one calculates:

Total HF concentration:
$$[HF]_{tot} = P_{HF}/RT = 3.96 \times 10^{20}\ m^{-3} \text{ (at 610 K)}$$
Total number of HF: $HF_{tot} = [HF]_{tot} V_C = 7.92 \times 10^{16}$
Concentration of $HF^{J=2}_{v=0}$: $[HF]_0^2 = 0.25[HF]_{tot} = 9.90 \times 10^{19}\ m^{-3}$

Laser flux per unit bandwidth is given by:

$$\frac{\phi}{\Delta\nu_o} = P/h\nu_0 \cdot 1/A_C \cdot 1/\nu_0 = 1.026 \times 10^{26} \text{ photons } m^{-2}$$

The absorbed flux is then:

$$-\Delta\phi = \frac{\phi}{\Delta\nu_0} \cdot l_C \cdot [HF]_0^2 \cdot A_{0\leftrightarrow 5} \cdot (2J' + 1)/(2J'' + 1) \times c^2/(8\nu^2_0)$$

where $A_{0\leftrightarrow 5} = 7.697 \times 10^{-3}\ s^{-1}$ is the Einstein coefficient for the transition (50).

Hence

$$-\Delta\phi = 2.078 \times 10^{24} \text{ photons } s^{-1}\ m^{-2}$$

The number of HF(v = 5) produced is

$$HF(v = 5) = -\Delta\phi \cdot \Delta t \cdot A_C = 3.447 \times 10^{11}$$

Lastly, the proportion of HF(v = 5) is

$$HF(v = 5)/HF_{tot} = 5.66 \times 10^{-6}$$

The model

Once formed, HF(v = 5) can either react with CH_2CF_2 to form products, or be relaxed by CH_2CF_2 or HF(v = 0) to lower vibrational levels:

Reaction

[I] $HF(v = 5) + CH_2CF_2 \xrightarrow{k_r^T} CH_3CF_3$

Relaxation ([II] + [III])

[II] $HF(v = 5) + CH_2CF_2 \xrightarrow{k_v^T} HF(v < 5) + CH_2CF_2$

[III] $HF(v = 5) + HF(v = 0) \xrightarrow{k_s^T} HF(v = 4) + HF(v = 1)$

Relaxation by radiative means has been neglected. Note that step [III] is not meant to imply a resonant energy transfer process (the energy deficit is about 662 cm^{-1} (51), but rather a generalized self-relaxation of HF. Further, although HF(v = 4) in step [III] could in principle also react with CH_2CF_2, its rate is predicted to be 100 times slower than with HF(v = 5) (48) — for this reason, only HF(v = 5) reactions are considered.

Product yield calculation

For the reaction steps above, it is possible to write two rate expressions, one for relaxation, one for reaction:

$$\text{Relaxation rate} = \{k_v^T \cdot [CH_2CF_2] + k_s^T \cdot [HF]_{tot}\} \times [HF(v = 5)]$$

$$\text{Reaction rate} = k_r^T \cdot [CH_2CF_2] \cdot [HF(v = 5)]$$

The relative rate is then:

[1] $$R = \frac{k_r^T}{k_v^T + k_s^T \cdot [HF_{tot}/[CH_2CF_2]}$$

Now let $\alpha = [HF(v = 5)]/[HF]_{tot}$, m = number of laser flashes, $\beta = [HF]_{tot}/[CH_2CF_2]$; then it is straightforward to derive an expression for the yield Y of product, expressed as a percentage of $[CH_2CF_2]$:

$$Y = 100mR\alpha\beta \qquad (\%)$$

Inserting typical values for an experimental run:

$m = 12000$
$\alpha = 5.66 \times 10^{-6}$ (see previous calculation)
$\beta = 0.5$

and taking $Y = 0.01\%$ as the experimental limitation on sensitivity (see experimental section), we get

[2] $$R \Leftarrow 0.00294$$

Hence, even if reaction rate [I] is a factor of 340 (i.e. 1/0.00294) slower than the combined relaxation rate ([II] + [III]), it should still be possible to detect the reaction product. Since no product was detected, the above expression can be used to set an upper bound to k_r^T, providing the relaxation rate constant k_v^T and k_s^T can be reasonably accurately estimated. This will now be considered.

HF relaxation studies

The self-relaxation of HF for v = 3, 4, 5, has recently been measured directly by a laser-excited vibrational-overtone fluorescence study in the temperature range 295–670 K (52). A value for HF(v = 5) relaxation, $k_s^{610} = 4.5 \times 10^{10}$ L mol^{-1} s^{-1} was obtained. This is about a factor of 10 faster than a value obtained by Kwok and Wilkins (53) of 5.2×10^9 L mol^{-1} s^{-1} at 298 K. Relaxation of HF(v = 5) by CH_2CF_2 has not been measured yet, although work on HF relaxation continues in this laboratory. Poole and Smith (40) measured the relaxation rate of HF(v = 5) by CH_4 to be 1.8×10^{10} L mol^{-1} s^{-1} (at 298 K), while relaxation of HF(v = 4) by isobutene was measured by Moore (54) to have an extremely fast rate, 9×10^{10} L mol^{-1} s^{-1}. In view of the above, values of $k_s^{610} = 1 \times 10^{10}$ L mol^{-1} s^{-1} and $k_v^{610} = 5 \times 10^{10}$ L mol^{-1} s^{-1} were adopted.

Reaction rate constant k_r^{610}

Using the above values, an upper limit for k_r^{610} can be calculated from [1] and [2]:

$$R = \frac{k_r^{610}}{k_v^{610} + k_s^{610} \cdot \beta} \Leftarrow 0.00294$$

Hence

$$k_r^{610} \Leftarrow 1 \times 10^8 \text{ L mol}^{-1} \text{ s}^{-1}$$

The gas kinetic collision rate for HF:HF is about 5×10^{11} L mol^{-1} s^{-1} (55), so that less than one in every 5000 collisions can lead to reaction — on the other hand, one in every 10 collisions leads to relaxation. Herman and Marling (36) also arrived at a similar conclusion for the addition reactions of HCl($v = 6$) + olefin, the rate constants being $10^{-1}-10^{-3}$ of the pre-exponential factor (i.e. collision number) for the corresponding thermal reaction.

Levine (48) arrived at a value of $k_r^{610} = 7.3 \times 10^6$ L mol^{-1} s^{-1} (see Table 2), so if a correction factor is applied to allow for the difference in temperature, $k_r^{610} = 1.5 \times 10^7$ L mol^{-1} s^{-1}. This value is in substantial agreement with the trend for k_r^{610} obtained here experimentally, there being approximately an order of magnitude difference between them. Although the results can neither confirm nor disprove the information theory predictions, they do indicate that if a factor of 10 increase in reaction rate, product yield, or product detection sensitivity could be attained, then according to the theory it should be possible to observe a laser-enhanced effect. By exciting HF($v = 6$ 480.4 nm), the addition reaction rate enhancement is 40 times larger, which more than offsets the factor of 10 lost in the term $A_{0\leftrightarrow 6}/\nu_0^2$ for the laser-excited transition (see Discussion). The further possibility of exciting both HF and CH_2CF_2 also remains, but this is not feasible in a bulk experiment if only such low proportions (1 in 10^5 for HF($v = 5$)) of the species are excited.

Conclusion

The present study on the addition reactions of HF to various unsaturated species was unable to detect any laser-induced 4-centre reaction. It was possible to deduce from these results an upper limit for the rate constant for the reaction HF($v = 5$) + CH_2CF_2, a value which supports (without confirming) information theory calculations of this system. The results also show that the failure to observe any reaction is almost certainly due to the very rapid relaxation rate of HF($v = 5$) compared to its reaction rate, and until these rates can be made more comparable, it is unlikely any reaction will be observed. This can be achieved either by increasing the reaction rate (such as by using HF($v = 6$), or by decreasing the relaxation rate (such as using cold gas matrices, or by "freezing" the HF in a combination laser/supersonic molecular beam experiment).

Acknowledgements

We would like to acknowledge the support of the Air Force Office of Scientific Research, under Grant A81-0028, the Natural Sciences and Engineering Council of Canada, and the Ontario Hydro.

1. S. H. BAUER. Ann. Rev. Phys. Chem. **30**, 271 (1979).
2. M. BODENSTEIN. Z. Phys. Chem. **13**, 56 (1894); **22**, 1 (1897); **29**, 295 (1899).
3. J. H. SULLIVAN. J. Chem. Phys. **36**, 1925 (1962).
4. D. L. KING and D. R. HERSCHBACH. Faraday Discuss. Chem. Soc. **55**, 331 (1973).
5. H. D. SHARMA, R. E. JERVIS, and K. Y. WONG. J. Phys. Chem. **74**, 923 (1970).
6. A. COHEN and F. S. KLEIN. J. Chem. Phys. **55**, 2600 (1971).
7. W. SHAUB and S. H. BAUER. Combust. Flame, **32**, 35 (1978).
8. J. H. SULLIVAN. J. Chem. Phys. **46**, 73 (1967).
9. A. FARKAS and L. FARKAS. Proc. R. Soc. London Ser. A**152**, 124 (1935).
10. R. D. KERN and G. G. NIKA. J. Phys. Chem. **75**, 1615 (1971); **75**, 2541 (1971).
11. W. D. BRESHEARS and P. F. BIRD. 14th Int. Symp. Combust. 211 (1973).
12. A. LIFSCHITZ and M. FRENKLACH. J. Chem. Phys. **67**, 2803 (1977).
13. A. LIFSCHITZ, M. BIDANI, and H. F. CARROLL. J. Chem. Phys. **79**, 2742 (1983).
14. K. W. EGGER and S. W. BENSON. J. Phys. Chem. **71**, 1933 (1967).
15. H. KUBOTA. Rev. Phys. Chem. Jpn. **37**, 25 (1967); **37**, 32 (1967).
16. P. J. GORTON and R. WALSH. J. Chem. Soc. Chem. Commun. 782 (1972).
17. S. W. BENSON and A. N. BOSE. J. Chem. Phys. **39**, 3463 (1963).
18. R. HOFFMAN and R. B. WOODWARD. J. Am. Chem. Soc. **87**, 2046 (1965).
19. J. M. SIMMIE, W. J. QUIRING, and E. TSCHUIKOW-ROUX. J. Phys. Chem. **74**, 992 (1970); J. M. SIMMIE and E. TSCHUIKOW-ROUX. J. Phys. Chem. **74**, 4075 (1970).
20. P. CADMAN, M. DAY, A. W. KIRK, and A. F. TROTMAN-DICKENSON. J. Chem. Soc. Chem. Commun. 203 (1970).
21. P. N. CLOUGH, J. C. POLANYI, and R. T. TAGUCHI. Can. J. Chem. **48**, 2929 (1970).
22. M. J. BERRY and G. C. PIMENTEL. J. Chem. Phys. **49**, 5190 (1968); **51**, 2274 (1969).
23. E. CUELLAR, J. H. PARKER, and G. C. PIMENTEL. J. Chem. Phys. **61**, 442 (1974).
24. N. R. ISENOR and M. C. RICHARDSON. Appl. Phys. Chem. **18**, 225 (1971).
25. H. L. DAI, A. H. KUNG, and C. B. MOORE. J. Chem. Phys. **73**, 6124 (1980).
26. J. C. JANG and D. W. SETSER. J. Phys. Chem. **83**, 2809 (1979).
27. C. REISER, F. M. LUSSIER, C. C. JENSEN, and J. I. STEINFELD. J. Am. Chem. Soc. **101**, 350 (1979).
28. A. S. SUDBO, P. A. SCHULZ, Y. R. SHEN, and Y. T. LEE. J. Chem. Phys. **69**, 2312 (1978).
29. J. L. LYMAN. J. Chem. Phys. **67**, 1868 (1977).
30. M. KNEBA, U. WELLHAUSEN, and J. WOLFRUM. Ber. Bunsenges. Phys. Chem. **83**, 940 (1979).
31. M. J. BERRY. J. Chem. Phys. **59**, 6229 (1973).
32. H. HORIGUCHI and S. TSUCHIYA. Int. J. Chem. Kinet. **13**, 1085 (1981).
33. S. B. JAFFE and J. B. ANDERSON. J. Chem. Phys. **51**, 1057 (1969).
34. J. B. MARLING, J. R. SIMPSON, and M. M. MILLER. Am. Chem. Soc. Symp. Ser. **68**, 134 (1976).
35. S. H. BAUER. Am. Chem. Soc. Symp. Ser. **68**, 152 (1976).
36. I. P. HERMAN and J. B. MARLING. J. Chem. Phys. **71**, 643 (1979).
37. M. J. BERRY. Ref. 38 in ref. 33.
38. J. HAGER, W. KRIEGER, and J. PFAB. J. Chem. Soc. Faraday II, **77**, 469 (1981).
39. H. FREI and G. PIMENTEL. J. Chem. Phys. **78**, 3698 (1983).
40. P. R. POOLE and I. W. M. SMITH. J. Chem. Soc. Faraday II, **73**, 1447 (1977).
41. F. ZABEL. Int. J. Chem. Kinet. **9**, 65 (1977).
42. A. MCCOL and P. J. THOMAS. Prog. React. Kinet. **4**, 119 (1967).
43. B. E. HOMES and D. W. SETSER. J. Phys. Chem. **82**, 2450 (1978).
44. R. M. NOYES. J. Am. Chem. Soc. **88**, 4311 (1966); **88**, 4318 (1966).
45. K. R. MALTMAN, E. TSCHUIKOW-ROUX, and K. H. JUNG. J. Phys. Chem. **78**, 1035 (1974); E. TSCHUIKOW-ROUX and K. R. MALTMAN. Int. J. Chem. Kinet. **7**, 363 (1975).
46. M. J. BERRY. J. Chem. Phys. **61**, 3114 (1974).
47. S. KATO and K. MOROKUMA. J. Chem. Phys. **73**, 3900 (1980);

Can. J. Chem. Downloaded from www.nrcresearchpress.com by 210.87.254.105 on 09/06/12
For personal use only.

74, 6285 (1981).
48. E. ZAMIR, Y. HAAS, and R. D. LEVINE. J. Chem. Phys. **73**, 2680 (1980); E. ZAMIR and R. D. LEVINE. Chem. Phys. Lett. **67**, 237 (1979); Chem. Phys. **52**, 253 (1980).
49. G. BURNS. Research proposal "Reaction dynamics" Jan. 1980. p. 7.
50. J. M. HERBELIN and G. EMANUEL. J. Chem. Phys. **60**, 689 (1974).
51. D. PROCH and J. WANNER. Tables of vibrational and rotational transitions in diatomic molecules pertinent to chemical lasers. MPI Plasmaphysik, Report IPP IV/17. 1971.
52. G. M. JURSICH and F. F. CRIM. J. Chem. Phys. **75**, 3871 (1981).
53. M. A. KWOK and R. L. WILKINS. J. Chem. Phys. **63**, 2453 (1975).
54. C. B. MOORE. *In* Laser induced processes in molecules. *Edited by* K. Kompa and S. Smith. 1979. p. 337.
55. E. H. KENNARD. Kinetic theory of gases. McGraw-Hill. p. 138.

Can. J. Chem. Downloaded from www.nrcresearchpress.com by 210.87.254.105 on 09/06/12
For personal use only.

A reinvestigation of the vapor phase bromination of 2-bromobutane

DENNIS D. TANNER, TOMOKI C. S. RUO,[1] YOSHIO KOSUGI,[2] AND ALAN POTTER[3]
Department of Chemistry, University of Alberta, Edmonton, Alta., Canada T6G 2G2

Received July 15, 1983[4]

DENNIS D. TANNER, TOMOKO C. S. RUO, YOSHIO KOSUGI, and ALAN POTTER. Can. J. Chem. **62**, 2310 (1984).

The solution phase photobromination of 2-bromobutane yields 2,2-dibromobutane, *meso*-2,3-dibromobutane, *dl*-2,3-dibromobutane, small amounts of 1,2-dibromobutane, and 2,2,3-tribromobutane. However, in the corresponding vapor phase bromination these products appear along with other polybrominated products. The yield of these polybromides increases with temperature. The increase in yield of the polyhalogenated materials is rationalized by considering the thermal instability of the β-bromoalkyl radical, which eliminates a bromine atom to form the corresponding alkene. It is demonstrated that in the vapor phase allylic bromination competes successfully with bromine addition. Reaction schemes are suggested to explain the formation of polybromides. An explanation is also offered for the discrepancy between these results and those of previously reported vapor phase work.

DENNIS D. TANNER, TOMOKO C. S. RUO, YOSHIO KOSUGI et ALAN POTTER. Can. J. Chem. **62**, 2310 (1984).

La photobromation en solution du bromo-2 butane conduit au dibromo-2,2 butane, au *méso*-dibromo-2,3 butane, au *dl*-dibromo-2,3 butane et à de petites quantités du dibromo-1,2 butane et du tribromo-2,2,3 butane. Cependant, lors de la bromation correspondante en phase gazeuse, ces produits sont accompagnés d'autres produits polybromés. Le rendement en produits polybromés augmente avec une augmentation de la température. On rationalise ce dernier résultat en faisant intervenir l'instabilité thermique du radical β-bromoalkyle qui élimine un atome de brome pour conduire à l'alcène correspondant. On démontre qu'en phase gazeuse la bromation allylique entre en compétition avec l'addition du brome. On suggère des mécanismes réactionnels pour expliquer la formation des dérivés polybromés. On avance aussi quelques suggestions pour expliquer les différences qui existent entre nos résultats et ceux rapportés antérieurement pour des bromations en phase gazeuse.
[Traduit par le journal]

Can. J. Chem. Downloaded from www.nrcresearchpress.com by 210.87.254.5 on 09/06/12
For personal use only.

Introduction

The bromination of 2-bromobutane has been quite extensively studied.

The reaction was first investigated by Kharasch *et al.* (1) who used a "loop" reactor system which recycled the reactants; the products were separated by fractional distillation. The reaction was carried out at 100°C with a 2.5:1 ratio of 2-bromobutane/bromine. Although nominally a vapor phase reaction, the authors concede that this may have been a "wall reaction" and there may have been a fine mist of reactants in the reaction chamber. Five fractions were detected and attributed to: 2,2-dibromobutane (19%), *meso*-2,3-dibromobutane (22%), *dl*-2,3-dibromobutane (10%), a mixture of tribromides, mainly 1,2,3-tribromobutane (34%), and a mixture of tetrabromides (6%).

With the advent of gas–liquid partition chromatography (glpc) Tedder and co-workers (2–4) undertook a systematic study of the vapor phase halogenation of 1- and 2-halo-substituted butanes. A flow reactor system, developed primarily for highly exothermic fluorination reactions, was used to brominate 2-bromobutane at 146°C. One major product (almost 100% of the products detected) was reported, 2,2-dibromobutane. This result was in good agreement with the vapor phase brominations of 2-chloro- and 2-fluorobutanes (4). Here too, high yields of the α-bromo products were reported. These results were interpreted in terms of favorable resonance stabilization of the incipient α radical (3–5). Recently Tedder appears to have confirmed his earlier results in a static system (6).

The solution phase bromination of 2-bromobutane was first reported by Thaler (7). The products formed from a 5:1 molar ratio of 2-bromobutane/bromine at 60°C were reported as: 2,2-dibromobutane (16.3%), *meso*-2,3-dibromobutane (58.3%), and *dl*-2,3-dibromobutane (25.4%). The sharp contrast between Thaler's and Tedder's results has been noted (7, 8). In the same work (7), the solution phase bromination of 2-chlorobutane gave results which are in excellent agreement with Tedder's vapor phase work.

During the course of a study on the mechanism of the solution phase bromination of 2-bromobutane done in this laboratory (9), the vapor phase reaction was reinvestigated. A possible explanation of the current anomaly between vapor and solution phase results is offered.

Discussion and results

The results for a series of liquid phase photobrominations of 2-bromobutane carried out at different temperatures (−20 to 100°C) are shown in Table 1. In contrast to previous vapor phase work (4,6), five products were found: 2,2-dibromobutane, *meso*-2,3-dibromobutane, *dl*-2,3-dibromobutane, 1,2-dibromobutane, and 2,2,3-tribromobutane. The products were isolated by preparative glpc and were identified by a comparison of their ir, nmr, and mass spectra with those of authentic materials.

The product distributions at 0°, 30°, and 100°C in Table 1 are in good agreement with those reported previously for the liquid phase (60°C) bromination by Thaler (7) and by this group (−20 to 20°C) (9). The mechanistic study of the liquid phase photobromination (9) clearly contrasts with the vapor phase results reported by Tedder (6). The production of 2,2,3-tribromobutane can be attributed to the bromination of several of the product dibromides (see Scheme 1). Indeed, it has been shown with optical isomers and isotopically enriched bromine that the products found in the liquid phase are consistent with this scheme (9).

The liquid phase photobromination of 2-bromobutane

[1] Taken in part from the Ph.D. Thesis of T.C.S. Ruo, University of Alberta, 1975.
[2] Postdoctoral Fellow, University of Alberta 1970–1972.
[3] Postdoctoral Fellow, University of Alberta 1982–1983.
[4] Revision received April 25, 1984.

TABLE 1. Liquid phase photobromination of 2-bromobutane over a range of temperatures

Temperature (°C)	[RBr]/[Br_2]	% Yield[a]					
		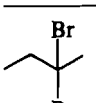	*meso* 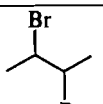	*dl*	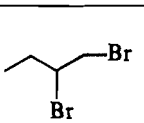	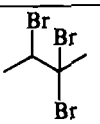	% Yield of bromination products
−20[b]	1:1	3.0	57.7	24.5	2.2	12.7	100.1
0	3:1	4.4(±0.1)	57.5(±0.1)	26.2(±0.1)	2.6(±0.3)	9.2(±0.3)	99.9
5[b]	2:1	5.6	61.2	29.3	1.5	2.4	100.0
17[b]	3:1	7.3(±0.3)	55.9(±2.3)	25.5(±0.1)	1.9(±0.4)	9.5(±0.3)	101.1
20[b]	4:1	9.8	58.0	26.1	Trace	6.1	100.0
30	4:1	10.7	57.6	24.7		3.5	96.5
60[c]	5:1	16.3	58.3	25.4			100
100	3:1	21.7(±0.2)	45.7(±0.2)	25.8(±0.5)	Trace	6.7(±0.9)	99.9

[a] Absolute yield (mol%) based on bromine consumed. The errors indicated are the average deviations from the mean of three independent experiments.
[b] Taken from ref. 9.
[c] Taken from ref. 7.

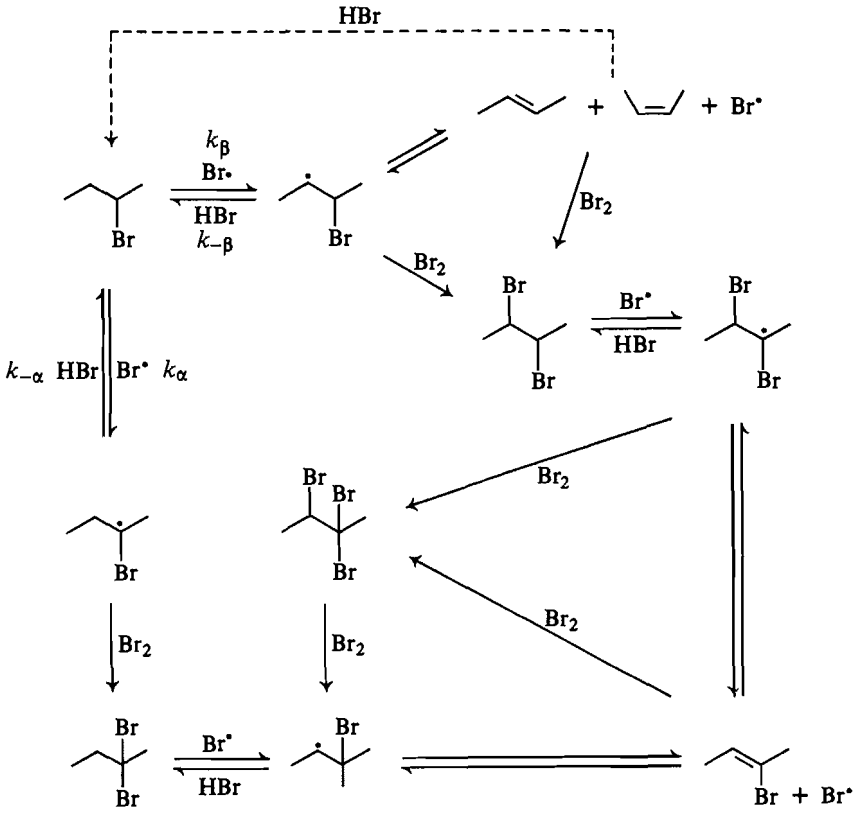

SCHEME 1

carried out at a series of increasing temperatures gives an apparently increasing yield of 2,2-dibromobutane, see Table 1. This can be accommodated by a reaction scheme in which there are two competing reactions that have diffeent activation energies, $E_\alpha > E_\beta$.

At low temperatures $k_\beta > k_\alpha$, but as the temperature rises k_α increases faster than k_β and the yield of 2,2-dibromobutane increases at the expense of the 2,3-dibromide.

Figure 1 shows a plot of the absolute yield of 2,2-dibromobutane vs. temperature. A straight line results; $Y = mT + C$, $m = 0.167$, $c = 5.42$, and the correlation coefficient = 0.981.

If it is assumed that the relative rates of formation of the

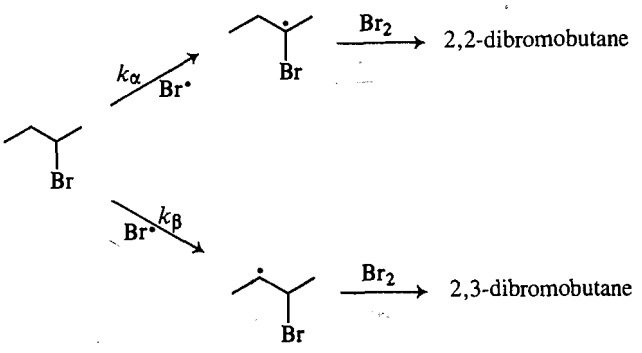

Can. J. Chem. Downloaded from www.nrcresearchpress.com by 210.87.254.5 on 09/06/12
For personal use only.

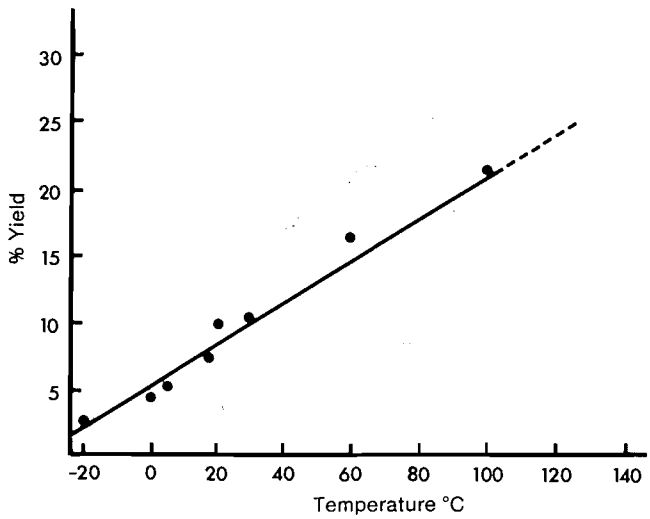

FIG. 1. Plot of % yield of 2,2-dibromobutane produced from the liquid phase photobromination of 2-bromobutane versus temperature.

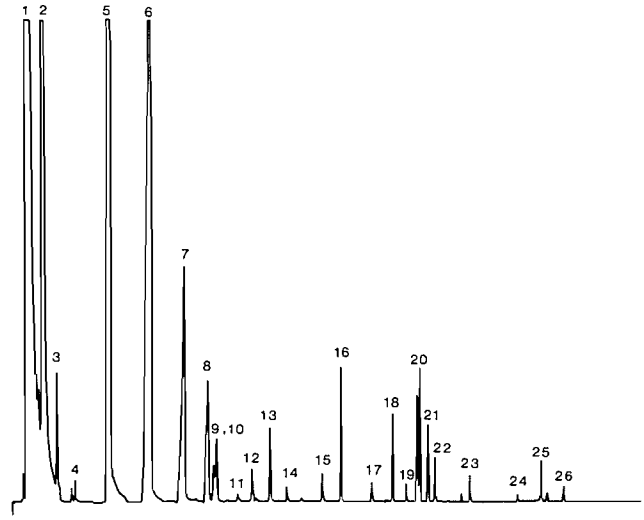

FIG. 2. Gas–liquid partition chromatogram of the reaction mixture obtained from the vapor phase photobromination of 2-bromobutane with molecular bromine, $T = 100°C$.

products in the liquid phase are the same as those in the vapor phase, then extrapolation of the plot predicts that a 30% yield of 2,2-dibromobutane would be expected at 146°C. This is contrary to the almost 100% formation of 2,2-dibromobutane reported by Tedder (4, 6).

In order to clarify these anomalous results the vapor phase bromination of 2-bromobutane was investigated at a series of temperatures in a static system (see Table 2). As well as 2,2-dibromobutane, *meso*- and *dl*-2,3-dibromobutane, many other brominated compounds were identified by gc/mass spectral analysis and, where possible, by comparison of their retention times with those of authentic materials. Capillary column glpc of the reaction mixtures indicated several distinct fractions of brominated materials (see Fig. 2).

The lowest boiling fraction contained three dibromides (2,2-dibromobutane, *meso*- and *dl*-2,3-dibromobutane) and a bromobutene (1-bromo-2-butene).

The intermediate fraction contained traces of two dibromides (1,2- and 1,3-dibromobutane) and six dibromobutenes (one of which was assigned the structure *trans*-1,4-dibromo-2-butene by a comparison of its glpc retention time with that of an authentic sample).

The highest boiling fraction revealed two tribromides, 2,2,3-tribromobutane and 1,2,3-tribromobutane, and five tribromobutenes. Traces of *meso*-1,2,3,4-tetrabromobutane and two other tetrabromobutanes were also indicated. A few other minor peaks were present but were not further characterized.

By using calibration factors determined for the di-, tri-, and tetrabromides on hand as representative values, a satisfactory material balance could be obtained for the brominations carried out at the elevated temperatures (see Table 2). These calculations were made assuming the addition of a bromine atom to the substrate consumed overall one bromine molecule and the formation of an allylic bromide also consumed overall one bromine molecule. Unknown peaks were determined using the calibration factor of the nearest known peak and assuming it was a similar type of compound.

At elevated temperatures the material balance of dibromides formed was very poor. Since the major product(s) at low temperature arises from the abstraction of a β-hydrogen it is conceivable that at elevated temperatures the polyhalogenated materials arise from the reactions of the β-radical (see Scheme 2).

There are numerous precedents for elimination of a bromine atom from β-bromoalkyl radicals (3, 8–15). This elimination is responsible for the rapid vapor phase isomerization of *trans*- and *cis*-alkenes during photoinitiated bromination (16–20). It is also well documented that allylic bromides are formed in high yields in the bromination of alkenes when the bromine concentration is kept low (17). Such an allylic bromination pathway could account for the 1,2,3-tribromobutane, the unsaturated bromides, and the saturated polyhalogenated materials. A similar mechanism was proposed for the vapor phase bromination of 1-bromobutane (20). The fate of the β-bromoalkyl radical can be affected by either the temperature of the system or the concentration of the transfer agents. As the temperature rises the yield of 2,3-dibromobutane decreases, i.e. the β-scission of the 2-bromomethylpropyl radical to alkene is facilitated. At constant temperature the yield of 2,3-dibromobutane decreases with decreasing bromine concentration since the intermediate radical has a longer lifetime in which to fragment. Similarly, the yields of polybromides increase with temperature rise as well as with decreasing bromine concentration (see Table 2).

Of the polybromides formed, the allylic bromides become prevalent at high temperature and low bromine concentration at the expense of 1,2,3-tribromobutane. This is consistent with Scheme 2. As bromine concentration falls, the reversible addition of a bromine atom to a double bond becomes less likely than the irreversible allylic bromination steps. Allylic bromides are unstable and frequently rearrange to the thermodynamic mixtures of all possible isomers (22–24). This would account for the number of polyhalogenated allylic bromides that were observed.

The proposal that allylic bromination preferentially occurs at low bromine concentration (ref. 17, p. 182) was substantiated by a study of the vapor phase bromination of 2-butene (see Table 3). At very low bromine concentration over 90% of the bromination products from either *trans*- or *cis*-2-butene are the allylic bromides. These results are in good accord with the proposed mechanism for the bromination of 2-bromobutane, i.e., 2-butene is formed from the unstable β-bromoalkyl radical and is brominated allylically. The unsaturated bromides produced are in turn brominated allylically to produce unsaturated

Can. J. Chem. Downloaded from www.nrcresearchpress.com by 210.87.254.5 on 09/06/12
For personal use only.

Can. J. Chem. Downloaded from www.nrcresearchpress.com by 210.87.254.5 on 09/06/12
For personal use only.

TABLE 2. The vapor phase photobromination of 2-bromobutane at various temperatures

	Reactants		% Yield[a]												
			Saturated dibromides					Saturated tribromides		Allylic bromides			Saturated tetrabromide		
Temperature °C	$[Br_2]^0$ mmol L^{-1}	$[C_4H_9Br]^0/[Br_2]^0$	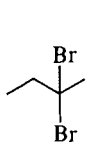	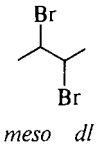 *meso*	*dl*			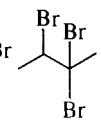	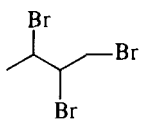	Mono-C_4H_7Br	Di-$C_4H_6Br_2$	Tri-$C_4H_5Br_3$	$C_4H_6Br_4$	$(\alpha/\beta)_{products}$	Balance
35	0.73	4:1	23.4	40.4	13.4	Trace	Trace	4.5	11.6	0.3	0.7	—	1.8	27:73	96.1
65	0.97	3:1	23.1	24.4	8.7	Trace	0.3	4.5	17.6	0.8	4.6	3.6	4.5	31:69	92.1
65	0.56	3:1	17.9	15.9	5.5	0.3	0.4	1.6	13.8	3.3	8.5	10.1	7.8	29:71	85.1
65	0.17	17:1	22.7	12.5	4.9	Trace	1.2	Trace	10.2	8.1	25.4	8.0	1.2	32:68	94.2
100	0.71	4:1	24.0	10.2	4.1	0.1	1.4	0.5	9.0	3.1	24.0	20.0	9.0	35:65	105.4
100	0.63	3:1	22.5	8.8	3.4	Trace	1.3	1.5	6.3	1.7	20.4	21.3	3.8	37:63	91.0
100	0.18	13:1	26.7	6.4	2.8	0.9	2.2	Trace	2.7	8.4	37.9	9.1	Trace	38:62	97.1
100	0.15	20:1	33.1	5.3	2.1	Trace	2.1	Trace	2.1	17.8	37.1	6.0	Trace	40:60	105.6
100	0.08	37:1	34.6	3.9	1.3	Trace	1.6	Trace	1.1	20.3	31.0	4.1	1.2	44:56	99.1
152	0.83	3:1	22.1	5.9	1.8	0.7	1.8	0.4	2.5	1.3	25.1	27.8	2.7	38:62	92.1
152	0.78	4:1	23.3	3.7	1.5	0.3	1.7	Trace	2.2	4.1	28.3	19.2	1.0	41:59	85.3
152	0.17	18:1	29.4	2.3	1.1	1.2	2.0	Trace	Trace	15.6	31.6	3.4	Trace	43:57	88.6
100	0.28	10:1:1[b]	22.5	6.3	2.6	Trace	1.9	Trace	3.8	8.5	39.7	20.2	1.0	32:68	106.5
100	0.15	20:1:3	21.6	5.7	2.1	Trace	2.5	Trace	3.9	14.6	39.1	8.0	Trace	31:69	97.5
100	0.22	14:1:1[c]	20.9	4.5	1.9	0.3	1.6	2.2	3.6	7.0	34.3	9.5	Trace	35:65	85.8
100	0.56	5:1:0.25	23.8	13.7	5.2	0.4	0.9	0.9	12.5	3.7	19.2	13.4	3.3	34:66	97.0

[a] % Yields based on bromine consumed.
[b] HBr added to starting mixture: [2-bromobutane]/[Br_2]/[HBr].
[c] 2,2-Dibromobutane added to starting mixture: [2-bromobutane]/[Br_2]/[2,2-dibromobutane].

TABLE 3. Vapor phase photobromination of 2-butene at room temperature

Substrate	$[Br_2]$ mmol/L	$[RH]/[Br_2]$	Reactor volume	% Yield[a]				
				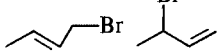		*meso*	*dl*	Balance
	0.081	5:1	5 L	50.5	17.7	29.0	7.3	104.5
	0.040	5:1	5 L	56.3	20.1	18.0	5.5	99.9
	0.019	6:1	5 L	57.7	21.3	17.2	5.9	102.1
	0.031	5:1	12.7 L	60.7	22.5	14.8	5.7	103.4
	0.016	5:1	12.7 L	66.8	24.5	8.7	3.4	103.4
	0.008	5:1	12.7 L	65.8	24.1	6.5	2.3	98.4
	0.005	5:1	22.0 L	66.4	24.2	6.8	2.6	100.0
	0.008	5:1	12.7 L	67.4	24.4	6.8	4.9	102.6
	0.005	5:1	22.0 L	67.7	25.6	5.1	2.2	100.6

[a] % Yields based on bromine consumed.

di- and tribromides (see Scheme 2).

The product yields quoted in Table 2 are based on the amount of bromine consumed. The formation of polybromides causes the overall stoichiometry of the reaction to deviate from a 1:1 bromine-to-substrate ratio. However, assuming all the polybromides and 2,3-dibromobutanes are derived from the β radical, the real ratio of α- and β-radical products can be determined from the experimental data by calculating the overall stoichiometry (see $(\alpha/\beta)_{products}$, Table 2). It is realized that this assumption may not be completely true regarding the production of 2,2,3-tribromobutane since some of this product might arise from further bromination of both 2,2- or 2,3-dibromobutane; however, in the vapor phase reaction 2,2,3-tribromobutane is a very minor product.

Extrapolation of the plot derived from the liquid phase bromination over a temperature range (see Fig. 1) predicts the yields of 2,2-dibromobutane to be 16%, 22%, and 31% at 65°, 100°, and 152°C respectively. The calculated ratios of $(\alpha/\beta)_{products}$ would suggest that the absolute yields of the α-radical product in the vapor phase are slightly higher than the values predicted from the results of the solution phase reactions (see Table 2). Moreover, in the vapor phase the yield appears to be a function of bromine concentration as well as temperature.

As the reaction temperature increases, the amount of α-radical product increases at the expense of β-radical products, i.e. $(\alpha/\beta)_{products}$ increases. This is consistent with the liquid phase results and must be due to a decreasing difference between the activation energies E_α and E_β.

The formation of the α and β radicals in a kinetic distribution is determined by the ratio of the rate constants (k_α/k_β) and is therefore concentration independent. At low bromine concentration the α radical can form product or revert to starting material, whereas the β radical can also undergo elimination. In the vapor phase, the only straightforward way to affect the apparent ratio of products resulting from initial abstraction reactions at the α and β positions, by a change in bromine concentration is for the α or β radicals or a product derived from the β radical to be able to revert to starting material. Two cases are envisaged: (*i*) at low bromine concentration elimination from the β radical effectively competes with its transfer with HBr or Br_2. The resulting product distribution shows less 2,3-dibromobutane and more polyhalogenation (see Table 2). As the concentrations of 2-butene and HBr increase (as the reaction proceeds) the likelihood that 2-bromobutane can reform also increases. (*ii*) At high bromine concentration elimination is less likely and higher yields of dibrominated butanes are produced from the intermediacy of the α and β radicals which either transfer with hydrogen bromide or molecular bromine.

If starting material is reformed it will react again to form the α and β radicals in the ratio set by the absolute rate constants (k_α/k_β). This will lead to a net increase in the amount of 2,2-dibromobutane formed, at the expense of products from the β radical. Therefore, at low bromine concentration, the yield of 2,2-dibromobutane will be partially dependent upon the concentration of the chain transfer agents.

Reaction mixtures containing HBr and (or) bromine at the high concentrations were subjected to the reaction conditions in the absence of light (i.e. 45 min, 100°C). No bromination products were observed. Liquid phase reactions (2 days, 90°C) similarly showed no reaction in the absence of light. These observations would appear to rule out ionic reactions with 2-bromobutane which could conceivably lead to 2,3-dibrominated products. Vapor phase photobrominations with HBr added to the initial reaction mixture showed α/β product ratios slightly lower than those found in reactions run without added HBr under the same conditions (see Table 2). Hydrogen bromide can affect the ratio of 2,2- and 2,3-dibromobutane by two distinct processes. First, the α and β radicals can both competitively transfer with bromine and hydrogen bromide to yield dibromide and starting material, the ratio depending upon the relative ratio of their rate constants and the concentration of the two transfer reagents. By analogy with the bromination of 1-bromobutane (20), where transfer with hydrogen bromide affects the α radical more strongly than it does the β radical, it is predicted that the presence of added HBr in the reaction mixture would lower the ratio of α/β products. However, the

Can. J. Chem. Downloaded from www.nrcresearchpress.com by 210.87.254.5 on 09/06/12
For personal use only.

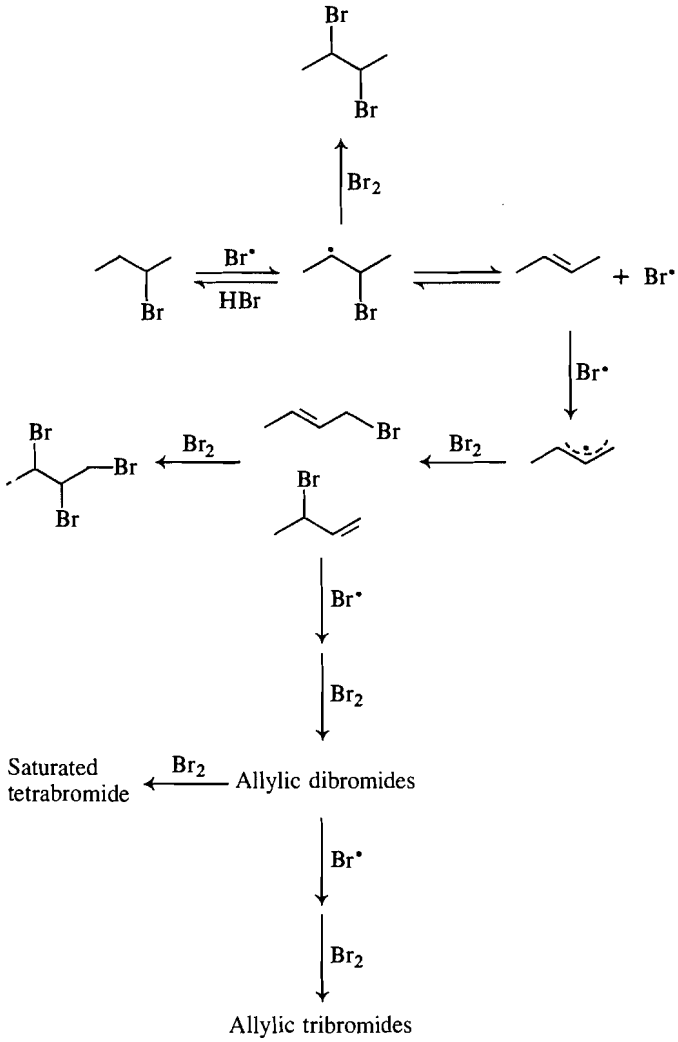

SCHEME 2

second process which regenerates starting material from 2-butene (a product from the β radical) with hydrogen bromide would cause an apparent increase in the ratio of α/β products. Under the conditions of high HBr concentrations apparently the first factor is the most influential (see Table 2). The possibility that 2,2-dibromobutane, itself, reacts further was also discounted. Two reactions which had 2,2-dibromobutane initially added also showed product distributions essentially the same as reactions run without its addition under the same conditions (see Table 2).

Moreover, the results show that the absolute yield of 2,2-dibromobutane formed in the gas phase reactions, as a function of temperature, agree remarkably well with those obtained in the solution phase bromination. The conclusions from these observations are identical with those reached for the bromination of 1-bromobutane under comparable conditions (20). It can be concluded that the α-bromoalkyl radical is stable under these conditions. In sharp contrast the yields of 2,3-dibromobutane are diminished at higher temperatures, due to the instability of the β-bromoalkyl radical.

Clearly, there is a discrepancy between these results and those reported by Fredericks and Tedder (4). This may very well be due to the differing conditions under which the reaction was studied.

In the present work the reaction was done under vacuum in sealed 100-mL glass ampoules. After completion of the reaction the product mixture was condensed, the reaction vessel opened, and the products were extracted with solvent. This ensured that *all* the products were present in the solution when it was analyzed by glpc.

Tedder studied the reaction in a flow system (3, 4); alkyl halide and halogen were fed, with nitrogen as a diluent, via two separate feeds into a heated reaction chamber. The mixture was irradiated with light as it passed through a glass tube. It was then passed through a column to remove hydrogen halide and excess halogen. The mixture was then frozen at −70°C, collected, and subjected to glpc analysis. Under these conditions no material balance could be obtained. It is possible that any polybrominated materials formed in the bromination of 2-bromobutane would not be carried through to the collection trap in this system. At 152°C much more 2,2-dibromobutane is formed relative to 2,3-dibromobutane. If this mixture was collected and analyzed, and the polyhalogenated material was not accounted for, it would give an apparent result similar to the one reported by Tedder.

Experimental

Materials

Bromine, *dl*-2-bromobutane, *meso* and *dl*-2,3-dibromobutane, and 2,2,3-tribromobutane were purified or synthesized as previously reported (9).

2,2-Dibromobutane was obtained by preparative glpc collection (80°C, 10 ft × 1/4 in. 10% Carbowax 20 M glass column) from the product mixture resulting from the liquid phase photobromination of 2-bromobutane.

1-Bromo-2-butene was obtained by preparative glpc collection (50°C, 6 ft × 1/4 in. 10% Carbowax 20 M TPA glass column) from commercially available crotyl bromide (Aldrich Chemical Co. Ltd.). A freshly collected sample had n_D^{25} = 1.4804 (lit. (21) n_D^{22} = 1.4822). The sample isomerized to a mixture of 1-bromo-2-butene and 3-bromo-1-butene on standing (22).

trans-1,4-Dibromo-2-butene was prepared by the method of Shantz (25). Equimolar amounts of 1,3-butadiene and bromine were allowed to react in chloroform at −30°C. The chloroform was removed by distillation and the product isolated by distillation under reduced pressure and recrystallized from methanol (mp 52–53°C (lit. (26) mp 53–54°C); mass spectra show parent peaks 212, 214, 216, 1:2:1 ratio).

1,2,3-Tribromobutane (City Chemical Corp.), and 1,2-dibromobutane (Eastman Kodak Co.) were used as supplied.

Gas–liquid chromatographic analysis

This was carried out as described previously (9).

Liquid phase photobromination of 2-bromobutane with molecular bromine

This was carried out as previously described (9). Brominations run at elevated temperatures proceeded more rapidly. At 100°C the reaction was complete within 10 min. A control reaction, i.e. the reactants were not photoinitiated, revealed no products after 24 h at both 17 and 90°C. Similarly, reaction mixtures containing RBr/Br_2/HBr (10:1:1), thermostated at both 17 and 90°C for 24 h and 0.5 h, also showed no reaction.

Vapor phase photobromination of 2-bromobutane with molecular bromine

Bromine and 2-bromobutane were accurately weighed into capillary tubes and placed in a reaction ampoule previously darkened with aluminium foil. The vessel was attached to a vacuum line and the reactants degassed three times. The ampoule was sealed under vacuum and thermostated, in the absence of light, at the required temperature for at least 10 min. The mixture was photolyzed with a 200-W incan-

Can. J. Chem. Downloaded from www.nrcresearchpress.com by 210.87.254.5 on 09/06/12
For personal use only.

Can. J. Chem. Downloaded from www.nrcresearchpress.com by 210.87.254.5 on 09/06/12
For personal use only.

descent lamp for 5 min. In all cases the bromine color was rapidly discharged. The total of the partial pressures of the products varied from 2 Torr to 20 Torr (1 Torr = 133.3 Pa) depending upon the initial bromine concentration. The total reactant pressure was approximately 80 Torr.[5] After irradiation the products were cooled with liquid nitrogen.

A reaction mixture was prepared and kept at 100°C in the dark for 45 min. Analysis of the mixture showed only 2% of the bromine had been consumed and only traces of products were observed by glpc analysis. Similarly, a reaction mixture containing HBr (0.3 mmol/L) and bromine (0.3 mmol/L) was kept at 100°C for 45 min in the absence of light. Analysis revealed that no reaction had occurred. The HBr had been manometrically measured and condensed into the reaction vessel. Two reaction mixtures with added HBr were photoinitiated and the products analyzed (see Table 2).

After any of the reactions run, aliquots of a chlorobenzene/Freon 113 solution (2 mL, 0.3 mmol/L), Freon 113 solvent (2 mL), and saturated aqueous sodium bicarbonate (2 mL) were each added to the frozen mixture. The resulting solutions were allowed to warm to room temperature and mixed by shaking. The organic layers were separated and dried over anhydrous sodium sulfate.

The reaction mixtures were analyzed by both capillary column glpc (10 meters, Methyl Silicone Fluid) and packed column glpc (10 ft × 1/4 in. 5% Carbowax 20 M on 80/100 Chromosorb PAW). The chromatograms revealed a complex mixture of products (see Fig. 2). The mixtures were subjected to capillary gc/mass spectral analysis and, where possible, this identification was confirmed by comparing their retention times and mass spectra with those of authentic samples.

A bromobutene (P^+ = 134, 136; Br doublet) was identified as 1-bromo-2-butene using an authentic sample. Five dibromobutanes (P^+ = 214, 216, 218; Br_2 triplet) were shown to be 2,2-dibromobutane, *meso*- and *dl*-2,3-dibromobutane, and 1,2- and 1,3-dibromobutane using authentic samples.

Mass spectral analysis revealed the presence of six dibromobutenes (P^+ = 212, 214, 216; Br_2 triplet) at slightly longer retention times. One of these was assigned to *trans*-1,4-dibromo-2-butene by comparison of its mass spectrum and retention time with that of an authentic sample.

A high boiling fraction showed a number of compounds. Two tribromobutanes (P^+ = 292, 294, 296, 298; Br_3 quartet, $[P - Br]^+$ = 213, 215, 217; Br_2 triplet) were seen, one was identified as 2,2,3-tribromobutane and the other as 1,2,3-tribromobutane using the authentic compounds. In the same fraction five tribromobutenes (P^+ = 290, 292, 294, 296; Br_3 quartet, $(P - Br)^+$ = 211, 213, 215, Br_2 triplet) were indicated. A small amount of *meso*-1,2,3,4-tetrabromobutane was detected by comparing its glpc retention time and ms cracking pattern with that of an authentic sample, as was the presence of two other tetrabromobutanes. A few other minor products were not further characterized.

Calibration factors determined for 2,3-dibromobutane, 1,2-dibromobutane, 1,3-dibromobutane, 2,2,3-tribromobutane, 1,2,3-tribromobutane, and *meso*-1,2,3,4-tetrabromobutane were used as representative values for all the products.

Vapor phase photobromination of 2-butene with molecular bromine

Bromine was accurately weighed in a capillary tube and sealed in a breakseal tube which was then attached to a vacuum line. A known amount of 2-butene (*cis or trans*) was manometrically measured. The reactants were allowed to enter a darkened reaction vessel of known volume and to equilibrate for 3 min. The total pressure of the reactants varied from 0.5 to 10 Torr. The reactants were then irradiated with a 200-W incandescent lamp for 5 min. The products were condensed into a collecting tube and treated as described above.

Products were identified by comparison of their glpc retention times with those of authentic materials. The products were: 3-bromo-1-butene, 1-bromo-2-butene, and *meso* and *dl*-2,3-dibromobutane (see Table 3).

[5] The saturation pressure for the reactant 2-bromobutane is 40 Torr at room temperature, while it is 200 Torr for bromine. The saturation pressures are even higher at higher temperature.

Acknowledgments

The authors wish to thank the Natural Sciences and Engineering Research Council of Canada and the University of Alberta for their generous support of this work. We would also like to thank Professor J. M. Tedder of the University of St. Andrews for his comments and for a preview of his unpublished results. Thanks are also expressed to Dr. A. Hogg of the University of Alberta for running the capillary gc/ms analyses.

1. M. S. KHARASCH, W. S. ZIMMT, and W. NUDENBERG. J. Org. Chem. **20**, 1430 (1955).
2. P. C. ANSON, P. S. FREDERICKS, and J. M. TEDDER. J. Chem. Soc. 918 (1959).
3. P. S. FREDERICKS and J. M. TEDDER. J. Chem. Soc. 144 (1960).
4. P. S. FREDERICKS and J. M. TEDDER. J. Chem. Soc. 3520 (1961).
5. P. S. FREDERICKS and J. M. TEDDER. Chem. Ind. 490 (1959).
6. S. Y. ATTO, J. M. TEDDER, and J. C. WALTON. J. Chem. Soc. Perkin Trans. 2, 629 (1983).
7. W. THALER. J. Am. Chem. Soc. **85**, 2607 (1963).
8. W. THALER. *In* Methods in free radical chemistry. Vol. 2. *Edited by* E. S. Huyser. Marcel Dekker, New York, NY. 1969. p. 177.
9. D. D. TANNER, E. V. BLACKBURN, Y. KOSUGI, and T. C. S. RUO. J. Am. Chem. Soc. **99**, 2714 (1977).
10. D. D. TANNER, T. PACE, Y. KOSUGI, E. V. BLACKBURN, and T. RUO. Tetrahedron Lett. 2413 (1976).
11. R. K. FRIEDLINA, U. N. KOST, and M. Y. KHERLINA. Russ. Chem. Rev. **31**, 1 (1962).
12. W. O. HAAG and E. I. HEIBA. Tetrahedron Lett. 3683 (1965).
13. D. S. ASHTON, J. M. TEDDER, and J. C. WALTON. Chem. Commun. 1487 (1971).
14. G. A. RUSSELL and A. ITO. J. Am. Chem. Soc. **85**, 2983 (1963).
15. G. A. RUSSELL, A. ITO, and R. KONAKA. J. Am. Chem. Soc. **85**, 2988 (1963).
16. C. WALLING. Free radicals in solution. Wiley, New York, NY. 1957.
17. A. NECHVATAL. *In* Advances in free radical chemistry. Vol. IV. *Edited by* G. H. Williams. Logos Press, London. 1976. p. 175.
18. B. P. MCGRATH and J. M. TEDDER. Proc. Chem. Soc. **80**, 199 (1961).
19. P. I. ABELL. *In* Free radicals. Vol. 2. *Edited by* J. K. Kochi. Wiley, New York. 1973. Chapt. 13.
20. D. D. TANNER, Y. KOSUGI, R. ARHART, N. WADA, T. PACE, and T. C. RUO. J. Am. Chem. Soc. **98**, 6275 (1976).
21. M. S. KHARASCH, E. T. MARGOLIS, and F. R. MAYO. J. Org. Chem. **1**, 393 (1937).
22. S. WINSTEIN and W. G. YOUNG. J. Am. Chem. Soc. **58**, 104 (1936).
23. L. BATEMAN and J. I. CUNNEEN. J. Chem. Soc. 941 (1950).
24. L. BATEMAN, J. I. CUNNEEN, J. M. FABIAN, and H. P. KOCH. J. Chem. Soc. 936 (1950).
25. E. M. SHANTZ. J. Am. Chem. Soc. **68**, 2553 (1946).
26. R. C. WEAST. Handbook of chemistry and physics. 56th ed. C.R.C. Press, Cleveland, Ohio. 1976.

Décomposition homolytique du peracide phényl-5 pentanoïque: réactivité du radical phényl-4 butyle et compétition entre deux mécanismes en chaïne

JEAN-YVES NEDELEC, JACQUES FOSSEY, DANIEL LEFORT ET JEANINE SORBA
C.N.R.S., G.R. 12, 2, rue H. Dunant, 94320 Thiais, France

Reçu le 28 décembre 1983

JEAN-YVES NEDELEC, JACQUES FOSSEY, DANIEL LEFORT et JEANINE SORBA. Can. J. Chem. **62**, 2317 (1984).

Le peracide phényl-5 pentanoïque, en solution à ébullition dans le cyclohexane, se décompose essentiellement en acide correspondant au lieu de se décarboxyler en phényl-4 butanol comme les termes inférieurs ou supérieurs; cette différence de comportement est expliquée par la cyclisation du radical phényl-4 butyle, lequel ne peut pas propager le mécanisme en chaîne conduisant au phényl-4 butanol et le peracide se transforme alors en acide par un autre mécanisme radicalaire en chaîne compétitif.

JEAN-YVES NEDELEC, JACQUES FOSSEY, DANIEL LEFORT, and JEANINE SORBA. Can. J. Chem. **62**, 2317 (1984).

5-Phenyl pentanoic peracid decomposes in boiling cyclohexane solution to the corresponding acid instead of decarboxylation as is observed for the related cases. This difference in behaviour is explained by the cyclization of the 4-phenyl butyl radical which can then no longer propagate any chain reaction leading to 4-phenyl butanol. The peracid, therefore, reacts by a competitive radical chain mechanism leading to the corresponding acid.

[Journal translation]

Can. J. Chem. Downloaded from www.nrcresearchpress.com by 210.87.254.6 on 09/06/12
For personal use only.

L'intérêt des peracides RCO_3H en chimie radicalaire résulte d'une double spécificité: ils sont à la fois source de radicaux libres $R^{\cdot}$ et substrat pour différents radicaux libres nucléophiles ($R^{\cdot}$) pour former des alcools. Ainsi, la décomposition thermique d'un peroxyacide aliphatique conduit à l'alcool ROH selon le mécanisme en chaîne suivant (I) (1).

[1] $RCO_3H \rightarrow RCO_2^{\cdot} + \dot{O}H$

[2] $RCO_2^{\cdot} \rightarrow R^{\cdot} + CO_2$

[3] $R^{\cdot} + RCO_3H \rightarrow ROH + RCO_2^{\cdot}$

Réactions de terminaison

MÉCANISME 1

Cependant dans certains cas liés au milieu réactionnel (2, 3) (nature du solvant, présence d'oxygène) ou lorsque le radical $R^{\cdot}$ est électrophile (3, 4), le produit principal est l'acide correspondant.

Ainsi nous avons déjà montré (3) que lorsque l'on n'opère pas à ébullition de la solution, l'oxygène dissous bloque le mécanisme I et que l'acide se forme par le mécanisme en chaîne II.

[4] $RCO_3H \rightarrow RCO_2^{\cdot} + \dot{O}H$

[5] $\dot{O}H + RCO_3H \rightarrow H_2O + RCO_3^{\cdot}$

[6] $RCO_3^{\cdot} \rightleftarrows R\dot{C}O + O_2$

[7] $R\dot{C}O + RCO_3H \rightleftarrows RCHO + RCO_3^{\cdot}$

[8] $RCHO + RCO_3H \rightarrow 2\ RCO_2H$

MÉCANISME II

Dans l'étude présentée ici nous allons montrer que ces deux mécanismes, qui diffèrent radicalement par la nature des entités radicalaires mises en jeu ($RCO_2^{\cdot}$ et $R^{\cdot}$ dans I, $RCO_3^{\cdot}$ et $R\dot{C}O$ dans II), évoluent de manière compétitive; nos travaux antérieurs (1−4) ont établi que la chaîne I est généralement plus rapide que la chaîne II quand le radical $R^{\cdot}$ est nucléophile.

Au cours de notre étude sur les transferts intramoléculaires d'hydrogène de cabone à carbone, nous avons produit une série de radicaux ω-phényl alkyle à partir des peracides correspondants.

$\phi\text{-}(CH_2)_n\ CH_2 - CO_3H$

Dans les conditions habituelles (décomposition dans un hydrocarbure à ébullition) la quantité d'acide est inférieure à 20% sauf quand $n = 3$: le peracide phényl-5 pentanoïque conduit en effet à 80% d'acide (5).

Pour expliquer les raisons de la particularité de ce peracide par rapport à ses homoloques et vérifier du même coup notre hyothèse de la compétition des mécanismes I et II, nous avons approfondi l'étude de la décomposition thermique de ce peracide, par comparaison avec la décomposition de l'homologue immédiatement inférieur.

Résultats

Les peracides sont décomposés en solution dans le cyclohexane *à ébullition* pour éliminer l'oxygène dissous.

Le tableau 1 montre la différence très nette de la distribution des produits, pour une même concentration initiale (0,1 *M*), entre les deux peracides phényl-4 butanoïque et phényl-5 pentanoïque. Pour ce dernier, quand on augmente la concentration initiale en peracide on constate, d'une part, que la quantité de phényl-4 butanol croit au détriment de l'acide phényl-5 pentanoïque et, d'autre part, que les quantités de phénylbutane, de tétraline et de cyclohexanol restent faibles et à peu près constantes. On notera qu'à 0,1 *M* le temps de demi-réaction est supérieur pour le peracide phényl-5 pentanoïque; ce ralentissement de la vitesse de décomposition, résultat de plusieurs mesures, est significatif.

Quand on décompose un mélange équimoléculaire des peracides dodécanoïque et phényl-5 pentanoïque (Tableau 2), on observe une augmentation très nette de la quantité de phényl-4 butanol par rapport à celle résultant de la décomposition du peracide phényl-5 pentanoïque seul (tableau 1); de plus, l'augmentation des concentrations initiales a pour conséquence d'accroître les quantités d'alcool RCH_2OH et $\phi\text{-}(CH_2)_3CH_2OH$ issus de chacun des peracides. On note également que la quantité de cyclohexanol est accrue mais que celles de phénylbutane et de tétraline restent du même ordre de grandeur.

Discussion

Il est raisonnable d'admettre que l'énergie de la liaison O—O n'est pas influencée par la position du phényle par rapport à la fonction peroxydique.

Le mécanisme I ne peut donc être ralenti qu'au niveau de la

TABLEAU 1. Décomposition des peracides phényl-4 butanoïque et phényl-5 pentanoïque en solution dans le cyclohexane, à ébullition

Peracide	Conc. (M)	$t_{1/2}$ (min)	Produits formés (en mole par mole de peracide)				Cyclohexanol
$\phi(CH_2)_3CO_3H$	0,1	20	$\phi(CH_2)_2CH_2OH$ 0,7	$\phi(CH_2)_3CO_2H$ 0,16	$\phi(CH_2)_2CH_3$*	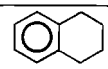	0,15
			$\phi(CH_2)_3CH_2OH$	$\phi(CH_2)_4CO_2H$	$\phi(CH_2)_3CH_3$	Tétraline	
$\phi(CH_2)_4CO_3H$	0,1	30	Traces	0,84	0,10	0,03	0,10
	0,2		0,10	0,60	0,05	0,08	0,07
	0,5	20	0,30	0,35	0,06	0,08	0,07

*Non dosé.

TABLEAU 2. Décomposition de mélanges de peracides dodécanoïque et phényl-5 pentanoïque en solution dans le cyclohexane à ébullition: produits formés en mole par mole de peracide

Mélange des peracides	Conc. (M)	ROH	RCO_2H	$\phi(CH_2)_3CH_2OH$	$\phi(CH_2)_4CO_2H$	$\phi(CH_2)_3CH_3$ 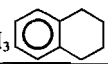	Cyclohexanol
RCO_3H*	0,05	0,36	0,63	0,15	0,70	0,05	0,05	0,12
$\phi(CH_2)_4CO_3H$	0,05							
	$t_{1/2}$ = 37 min							
RCO_3H	0,1	0,50	0,50	0,35	0,50	0,10	0,10	0,20
$\phi(CH_2)_4CO_3H$	0,1							

*$R = CH_3(CH_2)_{10}$.

réaction [2] ou de la réaction [3].

L'hypothèse d'une stabilisation du radical carboxyle par complexation intramoléculaire (6−8) expliquerait le ralentissement de la chaîne I par une diminution de k_2, constante de vitesse de décarboxylation.

[9] 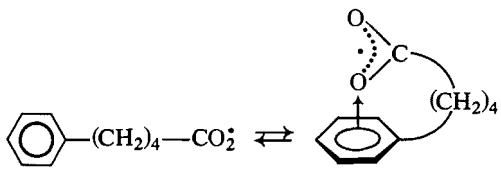

L'acide résulterait alors d'une réaction de ce radical sur le solvant

[10] 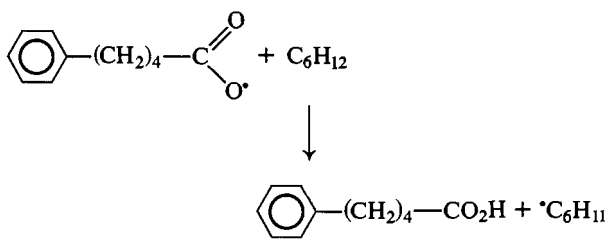

Mais on devrait alors trouver des quantités équivalentes de cyclohexanol

[11] $^{\bullet}C_6H_{11} + RCO_3H \rightarrow C_6H_{11}OH + RCO_2^{\bullet}$

comme c'est le cas pour ϕCO_3H décomposé dans C_6H_{12} à ébullition (2).

De plus, un tel phénomène de complexation devrait jouer dans la décomposition du peroxyde de diacycle correspondant (9, 10), et devrait être accentué, pour des raisons entropiques, avec l'homologue inférieur, ce qui n'est pas le cas (5).

Il y a donc tout lieu de penser que les réactions de rupture homolytique [1] et de décarboxylation [2] sont aussi rapides que pour l'homologue inférieur. D'ailleurs la présence dans le mélange réactionnel de phényl-4 butanol qui se forme à partir du radical phényl-4 butyle montre bien que ces réactions ont lieu mais elles sont moins importantes que celles du mécanisme II pour les raisons que nous allons exposer.

La propagation de la chaîne peut être ralentie au niveau de la réaction [3]. Dans l'expression de la vitesse

$$\left[v_3 = k_3[R^{\bullet}][P]\right]$$

k_3 exprime la réactivité intrinsèque d'un radical carboné primaire $R'—CH_2^{\bullet}$. Or celle-ci ne peut être influencée notablement par un groupement phényle en position 4. C'est donc la concentration $[R^{\bullet}]$ qui doit déterminer la vitesse v_3.

On sait que le radical phényl-4 butyle se cyclise rapidement (9, 11) ($k_{cy} \simeq 5 \times 10^{-4}\ s^{-1}$) (12, 13) et de façon irréversible en Ar_2-6 et réversible en Ar_1-5 (14).

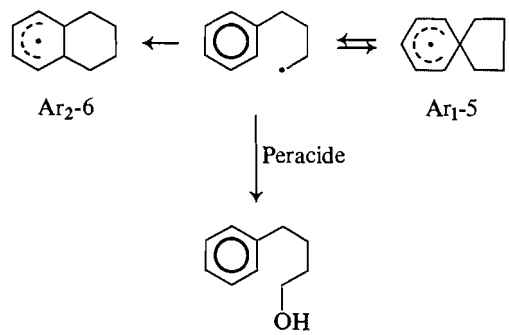

Il y a donc compétition entre la cyclisation et la réaction sur le peracide. La réaction unimoléculaire est la plus rapide quand [P] = 0,1 M puisque dans ce cas l'on trouve des quantités faibles de phényl-butane et de phényl-4 butanol.

On s'attend dès lors à trouver des quantités importantes de produits bicycliques, tétraline et dérivés. Mais le radical Ar_2-6 ne réagit pas sur le peracide ni non plus sur le solvant (il y a peu de cyclohexanol). Ainsi, puisqu'aucun radical ne peut propager

Can. J. Chem. Downloaded from www.nrcresearchpress.com by 210.87.254.6 on 09/06/12
For personal use only.

la chaîne I, celle-ci est tout simplement inhibée et le peracide se décompose essentiellement selon le mécanisme II. Comme les deux chaînes n'ont pas d'entité réactionnelle commune, il ne peut y avoir passage de l'une à l'autre.

Néanmoins ces deux chaînes sont bien compétitives comme le montrent l'étude de l'effet de la concentration et l'étude de la décomposition du mélange de peracides.

Quand on augmente la concentration en peracide, on accélère la réaction [3] qui est l'étape limitante de la chaîne I alors que le mécanisme II n'est pas sensible à la concentration initiale en peracide et l'alcool se forme bien aux dépens de l'acide. Quand la concentration en peracide est supérieure à 0,1 *M* on observe donc le déroulement simultané des deux mécanismes en chaîne.

Quand on décompose le peracide phényl-5 pentanoïque en présence d'une quantité équimolaire de peracide dodécanoïque, on lève l'inhibition du fait que le dernier se décompose normalement: le peracide dodécanoïque produit en effet des radicaux alkyles réactifs qui quand ils réagissent sur ϕ-$(CH_2)_4-CO_3H$ redonnent de l'importance à la décomposition selon le mécanisme I en générant les radicaux ϕ-$(CH_2)_4-CO_2^{\cdot}$

En conclusion: si pour l'essentiel, le détail de chacun des mécanismes en chaîne était établi, la présente étude montre clairement la délicate balance qui régit la compétition des deux mécanismes. Quand le radical alkyle produit par décarboxylation disparait rapidement, soit par réaction avec O_2 soit par réaction unimoléculaire comme la cyclisation, la chaîne I s'interrompt et la chaîne II devient prépondérante.

Partie expérimentale

Le cyclohexane utilisé est de qualité "spectroscopique". Les analyses cpg sont effectuées avec un appareil Girdel-75 et les spectres ir, en solution dans CCl_4, avec un appareil Hitachi-EPI G2. Les indices de peroxyde sont déterminés par iodométrie (15).

Preparation des peracides

On utilise la méthode décrite par Swern et coll. (16), à laquelle nous avons apporté quelques modifications (17) et qui consiste à faire agir H_2O_2 85% sur l'acide en solution dans CH_3SO_3H.

Le peracide est recristallisé dans l'hexane; sa pureté est contrôlée par les spectres ir et par détermination de l'indice de peroxyde. On obtient aisément des peracides à 96−98%.

Décomposition des peracides

Nous utilisons le même protocole que celui décrit précédemment (3). Les mélanges réactionnels sont analysés, après estérification par CH_2N_2, en cpg (Carbowax 20 M, 15%, 2 m, 150 à 160°C) en utilisant pour le dosage quantitatif, comme témoin interne, l'hexadécanoate de méthyle.

1. J. FOSSEY et D. LEFORT. Tetrahedron, **36**, 1023 (1980).
2. J. SORBA, J. FOSSEY, D. LEFORT et J. Y. NEDELEC. Tetrahedron, **37**, 69 (1981).
3. J. SORBA, J. FOSSEY, J. Y. NEDELEC et D. LEFORT. Tetrahedron, **35**, 1509 (1979).
4. J. SORBA, J. FOSSEY, J. Y. NEDELEC et D. LEFORT. Tetrahedron, **38**, 2083 (1982).
5. D. LEFORT et J. Y. NEDELEC. Tetrahedron, **38**, 2681 (1982).
6. M. MARTIN et G. GLEICHER. J. Am. Chem. Soc. **86**, 233 (1964); **86**, 238 (1964).
7. D. NEWKIRK, G. GLEICHER et V. KOCH. Tetrahedron, **28**, 449 (1972).
8. D. Newkirk et G. GLEICHER. J. Am. Chem Soc. **96**, 3543 (1974).
9. D. DETAR et C. WEISS. J. Am. Chem. Soc. **78**, 4296 (1956).
10. D. LEFORT, D. TEMPIER et J. SORBA. Bull. Soc. Chim. Fr. 442 (1960).
11. J. WILT. *Dans* Free radicals. Vol I. *Edité par* J. Kochi. Wiley, New York. 1973. p. 433.
12. J. KOCHI et R. GILLION. J. Am. Chem. Soc. **85**, 5251 (1964).
13. A. BECKWITH. Essays on free radical chemistry. Chem. Soc. Spec. Publ. n° 24, p. 239, Chem. Soc. London (1970).
14. M. JULIA et B. MALASSINE. Tetrahedron, **30**, 695 (1974).
15. R. JOHNSON et I. SIDDIQUI. The determination of organic peroxides. Pergamon Press, Oxford. 1976.
16. L. SILBERT, E. SIEGEL et D. SWERN. J. Org. Chem. **27**, 1336 (1962).
17. J. Y. NEDELEC, J. SORBA et D. LEFORT. Synthesis, 823 (1976).

Can. J. Chem. Downloaded from www.nrcresearchpress.com by 210.87.254.6 on 09/06/12
For personal use only.

Etude vibrationnelle des associations ioniques dans les solvants aprotiques. 7. Solvatation de $(LiNCS)_p$ par les solvants peu polaires

MARTIAL CHABANEL ET ZHENGLIE WANG

Laboratoire de Spectrochimie des Ions, 2, rue de la Houssinière, 44072 Nantes Cedex, France

Reçu le 8 février 1984

MARTIAL CHABANEL et ZHENGLIE WANG. Can. J. Chem. **62**, 2320 (1984).

Les solutions de LiSCN dans des mélanges solvant donneur − benzène ont été étudiées par mesure de solubilité et par spectrométrie infrarouge. L'état d'association de LiSCN a été obtenu à partir des spectres ir dans la région ν(CN) 2100−2000 cm^{-1}. Les solvants étudiés (tétrahydrofuranne, pyridine, acétone, carbonate de diéthyle, acétate de butyle, éthylméthylcétone) sont plus ou moins associants vis à vis de LiSCN. L'addition de benzène renforce leur pouvoir associant. En faisant varier le solvant donneur et la quantité de benzène ajouté, il est possible de modifier les proportions de paire d'ions LiNCS, de dimère $(LiNCS)_2$ et d'agrégats supérieurs. Les vibrations du solvant permettent d'obtenir le nombre de solvatation du lithium. Chacun des processus d'association de LiSCN s'accompagne d'une désolvatation du lithium. Le nombre de coordination de cet ion dans les différentes espèces formées reste égal à 4 ou légèrement inférieur dans certains cas.

MARTIAL CHABANEL and ZHENGLIE WANG. Can. J. Chem. **62**, 2320 (1984).

Solutions of LiSCN in donor solvent − benzene mixtures have been investigated by solubility measurements and by infrared spectrometry. The state of aggregation of LiSCN has been obtained from the ir spectra in the ν(CN) region 2100−2000 cm^{-1}. The selected solvents (tetrahydrofuran, pyridine, acetone, diethylcarbonate, butylacetate, ethylmethylketone) are more or less associating towards LiSCN. The addition of benzene causes an increase of the associating ability of the solvents. By changing the donor solvent and the amount of benzene it has been possible to obtain the ion pair LiNCS, the dimer $(LiNCS)_2$, and higher aggregates in various proportions. The solvation number of lithium has been measured in solvent vibration regions. Each step of aggregation is accompanied by lithium desolvation. The coordination of lithium in all the species which are formed remains equal to 4, or slightly lower in some cases.

Can. J. Chem. Downloaded from www.nrcresearchpress.com by 210.87.254.6 on 09/06/12
For personal use only.

Introduction

En solution dans les solvants donneurs dits aprotiques les cations des sels interagissent fortement avec les molécules de solvant. Dans la première couche de solvatation ces molécules peuvent être suffisamment perturbées pour être spectroscopiquement discernables des autres molécules plus ou moins libres dans la solution. Ainsi la spectrométrie infrarouge est une technique capable en principe de donner les nombres de solvatation des cations, mais les difficultés pratiques apportent des limitations sérieuses. D'abord, les bandes libres et associées sont généralement mal séparées et, sauf en solution très concentrée, la bande associée est peu intense. Enfin son coefficient d'extinction molaire est mal connu. Ces difficultés sont en partie résolues si l'on remplace la plus grande partie du solvant donneur par un solvant suffisamment inerte pour ne pas entrer en compétition avec le solvant donneur dans la première couche de solvatation. Par ordre de pouvoir solvatant croissant on pourra prendre un alcane, le benzène ou le nitrométhane. Bien qu'il soit fortement polaire ce dernier composé a été utilisé (1, 2) car il n'est que faiblement donneur. Cette méthode est d'application facile lorsque le sel est soluble dans le solvant dit inerte, ce qui est souvent le cas pour le nitrométhane. La solvatation de Na^+ a ainsi été étudiée dans le système $NaAlBu_4$ − cyclohexane − solvant donneur (3, 4). Lorsque le solvant inerte ne dissout pas le sel il arrive que le solvant mixte le dissolve. Toutefois l'addition d'un solvant inerte peut aussi favoriser la formation de solvates solides ou la démixtion de la solution.

La connaissance de l'état d'ionisation ou d'association du sel est nécessaire pour déterminer complètement le mode de coordination du cation étudié dans les solvants non-aqueux peu ionisants ou associants. Dans nos travaux antérieurs sur la structure des solutions de LiSCN la plupart des agrégats formés ont été identifiés et leur structure établie. C'est pourquoi, dans le présent travail, ce seront les solutions de LiSCN qui seront étudiées dans des mélanges benzène − solvant donneur. Les espèces formées seront caractérisées par les fréquences ν(CN) du groupement SCN attribuées antérieurement. Les vibrations du solvant permettront d'obtenir par ailleurs le nombre de solvatation du lithium. On remarquera que le benzène joue un rôle non négligeable car nous n'avons pas réussi à préparer les solutions mixtes avec un solvant plus inerte encore, comme le cyclohexane par example.

La formule des thiocyanates à l'état de solide pur est généralement écrite MSCN, ce qui ne préjuge rien sur la liaison entre M^+ et SCN^-. Ainsi la formule de thiocyanate de lithium sera écrite LiSCN. Par contre les agrégats de ce sel ont une structure de type isothiocyanate et leur formule sera écrite $(LiNCS)_p$.

Résultats expérimentaux

Cosolubilité LiSCN − solvant donneur

Le thiocyanate de lithium, comme presque tous les sels inorganiques, est insoluble dans le benzène pur. Les essais préliminaires de solubilité en solvant mixte ont été effectués en utilisant des mélanges de concentration 1 *M* en solvant donneur. Lorsque celui-ci est très polaire (diméthylformamide, diméthylacétamide, carbonate de propylène) ou multidentate (dioxolanne, triglyme), on constate que le système ternaire se sépare en deux phases. La phase inférieure, qui contient la quasi totalité du sel, est donc stabilisée par les interactions à longue et à moyenne distance entre ions solvatés et entre dipôles.

Lorsque le solvant donneur est peu polaire comme le tétrahydrofuranne (THF), le carbonate de diéthyle (DEC), l'acétate de butyle et l'éthylméthylcétone (EMC) la solubilité du thiocyanate de lithium est à peu près proportionnelle à la concentration du solvant donneur dans le mélange. Cependant dans certains cas (pyridine, acétone) les phénomènes sont compliqués par la formation d'un solvate solide.

Si l'on désigne le solvant par *S* la réaction de dissolution s'écrit, pour un agrégat ionique d'ordre *p*,

$$\text{LiSCN (solide)} + nS = \frac{1}{p}\,(\text{LiNCS}, nS)_p$$

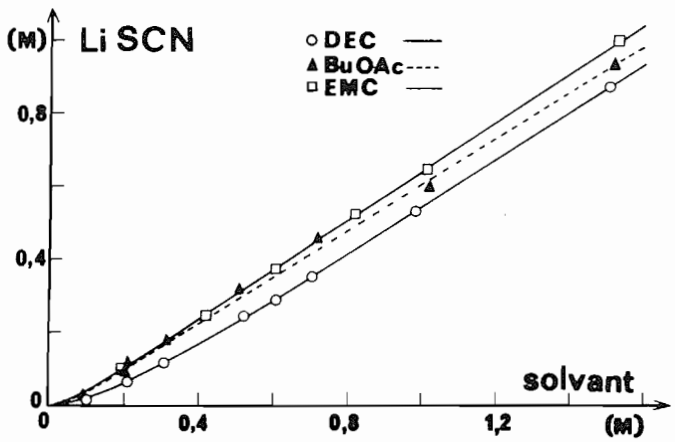

FIG. 1. Courbes de cosolubilité LiSCN – solvant donneur dans le benzène.

Si cette réaction est totale et si le mode d'association en change pas avec la concentration, la courbe de solubilité c de LiSCN en fonction de la concentration c_S en solvant doit être une droite de pente $1/n$ passant par l'origine. Les points expérimentaux (fig. 1) sont effectivement alignés sauf aux basses concentrations ($c < 0{,}1\ M$), ce qui montre que la réaction de dissolution est équilibrée. Les valeurs de n sont sensiblement les mêmes dans le DEC (n = 1,55), l'acétate de butyle (n = 1,6) et l'EMC (n = 1,45). La valeur obtenue dans le THF (n ~ 2,4) est peu précise car la saturation en LiSCN est difficile à obtenir. Puisqu'il reste toujours un peu de solvant libre, ces valeurs donnent une limite supérieure du nombre de solvatation moyen $\bar{n}$ du lithium.

Classification des solvants étudiés

La zone 2120–1980 cm^{-1} sert à caractériser les agrégats lithium–thiocyanate. Chaque agrégat possède une fréquence ν(CN) caractéristique qui varie dans une zone étroite (± 5 cm^{-1} environ) selon la constante diélectrique du solvant. Cette fréquence ν(CN) se situe en infrarouge à 2065 cm^{-1} (5) pour LiNCS, 2040 cm^{-1} pour $(LiNCS)_2$ (6), 2100 cm^{-1} pour LiNCSLi (7, 8), 1995 cm^{-1} pour $(LiNCS)_4$ de symétrie T_d (9).

Les solvants étudiés se classent schématiquement en deux catégories selon leur comportement plus ou moins associant (10) vis à vis de LiSCN. La première catégorie comprend les solvants peu associants (THF, pyridine, acétone) pour lesquels LiSCN en solution ($c \sim 0{,}1\ M$) est presque entièrement sous forme de paires d'ions; en solution concentrée ($c > 1M$) de petites quantités de dimère et d'ion triple apparaissent. La seconde catégorie comprend des solvants "associants" (EMC, acétate de butyle, DEC) pour lesquels on observe un équilibre paire–dimère.

L'addition de benzène rend tous ces solvants plus associants vis à vis de LiNCS. Ainsi, pour une concentration c_S en solvant de l'ordre de $1M$ dans le benzène, on observe, avec les solvants peu associants, que la dimérisation de LiNCS est pratiquement complète. Avec les solvants associants l'association dépasse le dimère, comme le montre l'apparition de trois nouvelles bandes entre 2000 et 2100 cm^{-1}.

Méthode d'analyse des spectres infrarouges

Les spectres infrarouges du solvant mixte et de la solution de LiSCN correspondante sont enregistrés séparément et on en retranche la contribution du spectre du benzène en tenant compte du volume occupé par le solvant donneur. Pour étudier la solvatation, les zones intéressantes du spectre sont celles qui comportent une vibration du solvant donneur à la fois intense et sensible à la fixation du lithium. Dans le spectre S_o du solvant mixte la bande du solvant libre apparaît seule. Pour obtenir la quantité de solvant libre dans la solution on retranche à son spectre S le spectre S_o multiplié par en coefficient ajusté pour que la bande libre disparaisse. On en déduit donc la quantité de solvant lié et le nombre de solvatation $\bar{n}$. La précision de cette méthode est maximale (~ ± 5%) lorsque le solvant libre est en proportion très inférieure à celle du solvant lié. Cette condition est réalisable dans les solvants associants et dans le THF. Par contre, dans la pyridine et l'acétone l'expérience montre qu'une proportion de solvant libre du même ordre que celle du solvant lié est nécessaire pour éviter la précipitation de solvates. Dans ce cas, la méthode ci-dessus est peu précise. C'est pourquoi les spectres ont été décomposés à l'ordinateur, chaque pic étant la somme de contributions de Gauss et de Lorentz.

Résultats

L'ensemble des résultats est rassemblé sur les tableaux 1 et 2. Les fréquences des vibrations utilisées pour le calcul des nombres de solvatation sont données en solution diluée dans le benzène. Les nombres de solvatation sont déterminés avec une incertitude estimée à ±0,1 sauf dans les solvants purs et dans les systèmes contenant de l'acétone ou de la pyridine (±0,2).

Discussion

Tétrahydrofuranne

Pour des concentrations en THF variant entre 0,5 et 2,5 M on a obtenu des nombres de solvatation moyens $\bar{n}$ de Li voisins de 2 (tableau 1). Comme la dimérisation de LiNCS est pratiquement totale à ces concentrations, on en a déduit que le nombre de solvatation de Li dans le dimère est égal à 2. Aux plus fortes concentrations en THF la valeur de $\bar{n}$ est légèrement supérieure à 2 ce qui correspond à l'apparition de paires d'ions plus solvatées que le dimère. La mesure du nombre de solvatation de la paire est possible dans les solutions concentrées LiSCN–THF sans benzène. Elle ne peut être effectuée qu'en film liquide. Dans les solutions en solvant mixte on a remarqué, avec des cellules d'épaisseur connue, que l'intensité intégrée est la même pour le THF à l'état libre ou à l'état associé. Dans le système LiSCN–THF, et pour des concentrations en LiSCN de l'ordre de 1 à $2M$, il apparaît que la paire LiNCS est largement prédominante (fig. 2). Par contre, en solution très concentrée (~ 3 à $4M$), la proportion de dimère et de groupement LiSCNLi, ion triple ou plus probablement agrégat en chaîne (7), augmente rapidement avec la concentration. Les nombres de solvatation ont été mesurés par décomposition des spectres dans la région ν(COC). Ils sont en bon accord avec un nombre de solvatation égal à 3 pour la paire et de l'ordre de 2 pour les autres espèces. L'équilibre de dimérisation s'écrit donc:

$$2\ LiSCN,\ 3THF = (LiNCS)_2,\ 4THF + 2THF$$

Le nombre de solvatation (n = 3) de la paire est égal à celui qui a été obtenu par TOTH *et al.* (11) pour la paire $LiNO_3$ en matrice moléculaire. Mais ces auteurs obtiennent des valeurs plus élevées (n = 4) lorsqu'ils utilisent le DMSO, plus polaire, ou l'acétonitrile, moins encombré.

La bande ν(COC) passe de 1069 cm^{-1} pour les molécules de THF libres à 1048 cm^{-1} pour les molécules de THF associées.

Can. J. Chem. Downloaded from www.nrcresearchpress.com by 210.87.254.6 on 09/06/12
For personal use only.

TABLEAU 1. Fréquences d'absorption, intensités intégrées et nombres de solvatation $\bar{n}$ du lithium dans des systèmes LiSCN (c) − solvant peu associant (c_S) − benzène[a]

THF										
Paramètre	ν(COC)		ν_i = 1069		ν_a = 1048		I_i = 3300		I_a/I_i = 1	
c_S	0,5	0,83	1	1	1,5	2	2,5	11,7[b]	11,25[b]	10,8[b]
c	0,167	0,37	0,28	0,44	0,53	0,6	1	2	3	4
c_S/c	3	2,2	3,6	2,2	2,8	3,3	2,4	5,9	3,7	2,7
$\bar{n}$	1,9	2,0	1,9	2,0	2,1	2,2	2,1	~3,3	2,8	2,5
% paire	<5	<5	~5	~5	~5	~10	20	85	75	50

Pyridine										
Paramètre	ν(CNC)		ν_i = 1437,7		ν_a = 1442,4		I_i = 1600		I_a/I_i = 1	
c_S	1	1	1	2	2	2	3	3	4	4
c	0,35	0,3	0,2	0,6	0,394	0,2	1	0,6	1	0,6
c_S/c	2,9	3,3	5	3,3	5,08	10	3	5	4	6,7
$\bar{n}$	1,9	1,9	2,0	2,1	2,2	~2,1	2,1	2,2	2,2	2,3
% paire	15	25	35	50	65	75	65	80	85	85

Acetone							
Paramètre	ν(CCC)		ν_i = 1219,2		ν_a = 1235,7		I_i = 2500	I_a/I_i = 1
c_S	0,25	0,5	1	2	13,1[b]	12,7[b]	12,2[b]	
c	0,075	0,15	0,3	0,6	2	3	4	
c_S/c	3,3	3,3	3,3	3,3	6,5	4,2	3	
$\bar{n}$	1,6	1,8	2	2,2	2,8	2,6	2,4	
% paire	~5	~10	15	20	~100	90	70	

[a]Les fréquences sont en cm^{-1}, les intensités intégrées en mol^{-1} L cm^{-2} et les concentrations en mol L^{-1}.
[b]Solution sans benzène, spectre en film liquide.

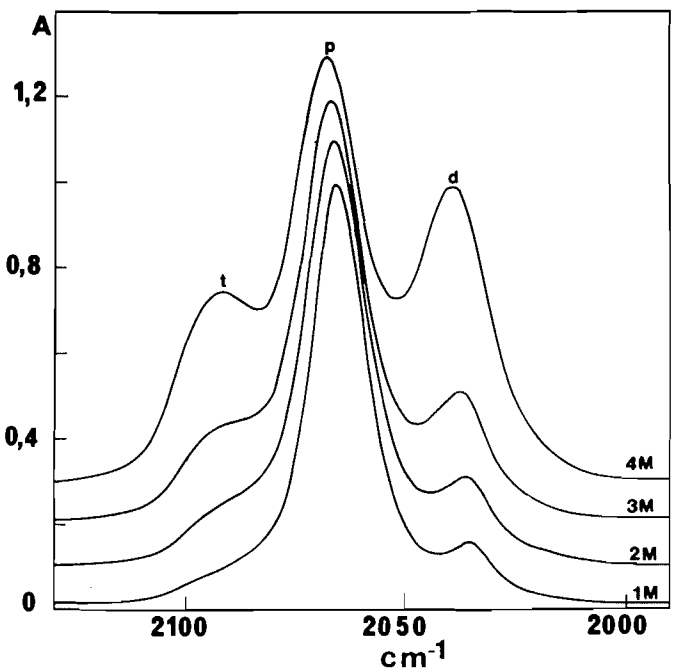

FIG. 2. Spectres infrarouges de LiSCN en solution concentrée dans le THF (film liquide) p = LiNCS, d = $(LiNCS)_2$, t = LiNCSLi.

Cet écart est pratiquement le même pour le dimère, dans le système THF−benzène, et pour la paire dans THF. Le déplacement de fréquence (-21 cm^{-1}) est à peine inférieur à celui observé pour la solvatation par le sodium (12) c'est à dire -19 cm^{-1}. Généralement les perturbations causées par le sodium sont nettement plus faibles que celles causées par le lithium. Ce nivellement pourrait provenir d'un encombrent stérique des molécules de THF autour du lithium.

Pyridine

En solution dans le benzène, la pyridine possède une bande ν(CNC) très fine ($\Delta\nu_{\frac{1}{2}}$ = 4 cm^{-1}) située à 1437,7 cm^{-1}. Cette bande se déplace vers les hautes fréquences d'environ 4 cm^{-1} lorsque la pyridine solvate le lithium, et sa largeur diminue encore ($\Delta\nu_{\frac{1}{2}}$ = 2,7 cm^{-1}). Dans les solutions pyridine−benzène ou a dû utiliser un excès de pyridine libre sinon il y a précipitation d'un solvate solide. Ceci diminue la précision des mesures de $\bar{n}$ qui est estimée à ± 0,2.

La figure 3(a) montre l'effet de la dilution dans le benzène sur une solution pyridine (3 *M*) − LiSCN (0,8 *M*). A chaque dilution d'un facteur 4 les hauteurs d'absorption ont également été mulitpliées par 4. L'examen de la zone ν(CN) (2100−2000 cm^{-1}) montre que la paire prédomine dans la solution concentrée, comme d'ailleurs dans la pyridine pure. La dilution provoque une dimérisation presque totale. Simultanément (fig. 3(b)) on constate le renforcement de la bande ν(CNC) libre, donc une désolvatation du lithium à la suite de la dimérisation. La bande ν(CNC) associée se déplace vers les hautes fréquences; le déplacement de fréquence passe de 4,0 cm^{-1} pour la paire à 4,7 cm^{-1} pour le dimère. L'interaction pyridine−lithium est donc plus forte dans le dimère que dans la paire. Ceci provient sans doute d'une gêne stérique entre les molécules de pyridine dans la paire. Cet effet est sensiblement plus marqué que dans le THF.

Les mesures des nombres de solvatation du lithium par la pyridine ont été faites par décomposition des spectres dans la région ν(CNC). L'intensité intégrée des spectres est indépen-

Can. J. Chem. Downloaded from www.nrcresearchpress.com by 210.87.254.6 on 09/06/12
For personal use only.

TABLEAU 2. Fréquences d'absorption, intensités intégrées et nombres de solvatation $\bar{n}$ du lithium dans des systèmes LiSCN (c) − solvant associant (c_S) − benzène

Acétate de butyle	ν(CO)		ν_l = 1739,$_5$		ν_a = 1708,$_8$		I_l = 12 000		I_a/I_l = 1,25	
Paramètre	ν(CCO)		ν_l = 1244		ν_a = 1287		I_l = 12 400		I_a/I_l = 0,9	
c_S	0,210[a]	0,316[a]	0,51[a]	0,72[a]	1,02[a]	1,52[a]	0,5	1	1	2
c	0,115	0,176	0,315	0,45$_2$	0,59$_3$	0,93	0,19	0,39	0,31	0,89
c_S/c	1,83	1,80	1,62	1,59	1,72	1,63	2,6	2,6	3,2	2,2
$\bar{n}$	1,3$_7$	1,4$_4$	1,4$_2$	1,4$_8$	1,5$_9$	1,5$_9$	1,6$_2$	1,8$_7$	1,9$_2$	2,0$_5$
DEC	ν(CO)		ν_l = 1745,$_2$		ν_a = 1714		I_l = 16 000		I_a/I_l = 1,15	
Paramètre	ν(CCO)		ν_l = 1263,$_3$		ν_a = 1304,$_7$		I_l = 32 000		I_a/I_l = 0,75	
c_S	0,31[a]	0,52[a]	0,60[a]	0,70[a]	1,00[a]	1,50[a]	0,25	0,5	1	1
c	0,117	0,245	0,286	0,35	0,53	0,87	0,096	0,19	0,39	0,23
c_S/c	2,65	2,12	2,10	2,00	1,88	1,72	2,6	2,6	2,6	4,3
$\bar{n}$	1,5$_4$	1,5$_5$	1,5$_3$	1,5$_6$	1,5$_8$	1,5$_5$	1,4$_1$	1,6$_2$	1,8$_2$	1,9$_0$
EMC										
Paramètre	ν(CCC)		ν_l = 1170		ν_a = 1183		I_l = 2000		I_a/I_l = 0,75	
c_S	0,41[a]	0,60[a]	0,81[a]	1,00[a]	1,53[a]	0,50	1			
c	0,242	0,368	0,52	0,64	1,00	0,20	0,40			
c_S/c	1,69	1,63	1,56	1,56	1,53	2,5	2,5			
$\bar{n}$	1,4$_4$	1,3$_9$	1,4$_5$	1,4$_4$	1,4$_5$	1,8$_5$	1,9$_8$			

[a]Solutions saturées. Les unités sont données au tableau 1.

dante du caractère libre ou associé de la pyridine, ce qui montre que les intensités des bandes libre et associée ne sont pas significativement différentes. Les nombres de solvatation ont été obtenus à partir des rapports des intensités intégrées des deux bandes. Ils sont un peu inférieurs aux valeurs attendues (n = 2 pour le dimère et 3 pour la paire) pour un ion Li^+ tétracoordiné. Cet écart, de l'ordre de 20%, est supérieur aux erreurs de mesure (~10%). On le retrouve encore lorsqu'on applique le méthode de soustraction de la bande libre. Même avec ces valeurs le nombre de coordination de Li^+ reste proche de 4 (~3,6). Ces résultats sont en accord avec ceux obtenus dans le pyridine pure par Rouvière *et al.* (13). Par effet Raman ces auteurs ont obtenu un nombre de solvatation de l'ion Li^+ égal à 4, avec une marge d'incertitude assez large qui n'a pas été précisée.

Acétone

Les bandes ν(CO) libre et associée de l'acétone dans les solutions benzéniques de LiSCN se situent à 1715 et 1707 cm^{-1}. Ces valeurs sont les mêmes que celles obtenues en l'absence de benzène (14). Comme la séparation des bandes est insuffisante, il vaut mieux utiliser la vibration ν(CCC) pour étudier la solvatation (ν_l = 1219 cm^{-1} et ν_a = 1236 cm^{-1}). En l'absence de benzène, LiSCN dissous dans l'acétone est presque entièrement sous forme de paire. Les résultats obtenus sont tout à fait comparables à ceux obtenus dans la pyridine. Ainsi les nombres de solvatation de Li^+ semblent légèrement inférieurs à 2 pour le dimère et 3 pour la paire.

Solvants associants

Dans les mélanges solvant associant − benzène (c_S ~ 0,1 à 1 *M*) saturés et LiSCN on observe la formation non seulement du dimère mais aussi d'agrégat(s) supérieur(s). Avec l'acétate de butyle par exemple, de nouvelles bandes ν(CN) situées à 2076, 2018 et 2006 cm^{-1} apparaissent (fig. 4). Elles ne sont attribuables ni à LiNCS (~2065 cm^{-1}), ni à LiNCSLi (~2100 cm^{-1}), ni à $(LiNCS)_4$ de symétrie T_d (~1993 cm^{-1}) mais à un ou plusieurs autres agrégats qui sont les mêmes dans les trois solvants.

Les éléments disponibles ne permettent pas d'établir la structure de ces espèces qui viennent enrichir encore la chimie de coordination de LiSCN. On remarque cependant que les deux pics de basse fréquence ont toujours sensiblement la même intensité. Le pic à 2076 cm^{-1} a une intensité beaucoup plus faible. Dans les solutions saturées en LiSCN la proportion des agrégats est pratiquement indépendante de c_S. Si l'on se fonde sur les intensités intégrées on obtient environ 30 à 50% de LiSCN sous forme d'agrégat dans l'acétate de butyle et l'EMC et 20 à 30% dans le DEC. Dans les solutions saturées le rapport c_S/c est de l'ordre de 1,6. Si l'on augmente ce rapport la proportion d'agrégats supérieurs diminue rapidement. Ainsi pour c_S = 1 *M* et c_S/c = 2,5 ces agrégats ont pratiquement disparu au profit du dimère. Par dilution dans le benzène pur les agrégats supérieurs réapparaissent et la solution finit par précipiter au-delà d'une certaine dilution.

La position des fréquences ν(CN) des agrégats donne, sinon leur structure, du moins des informations sur la coordination des groupements SCN qui y sont engagés. Les fréquences 2018 et 2006 cm^{-1} sont à rapprocher de celles du doublet (2022, Raman et 1993, ir, Raman) caractéristique du tétramère (9). Cette zone de fréquence caractérise les groupements $SCNLi_3$ où l'azote est tridentate. Une bande faible vers 2100 cm^{-1} correspond aux groupements LiSCNLi. Une bande de moyenne intensité à 2076 cm^{-1}, peut-être dédoublée, devrait correspondre à des groupements $LiSCNLi_2$, dans la mesure où les déplacements de fréquence sont additifs. Elle pourrait provenir d'une interaction entre dimères par une liaison Li . . . S.

Dans les esters (BuOAc, DEC) les bandes ν(CO) libre et associée sont bien séparées ($\Delta\nu$ = −31 cm^{-1} dans BuOAc et

Can. J. Chem. Downloaded from www.nrcresearchpress.com by 210.87.254.6 on 09/06/12
For personal use only.

Can. J. Chem. Downloaded from www.nrcresearchpress.com by 210.87.254.6 on 09/06/12
For personal use only.

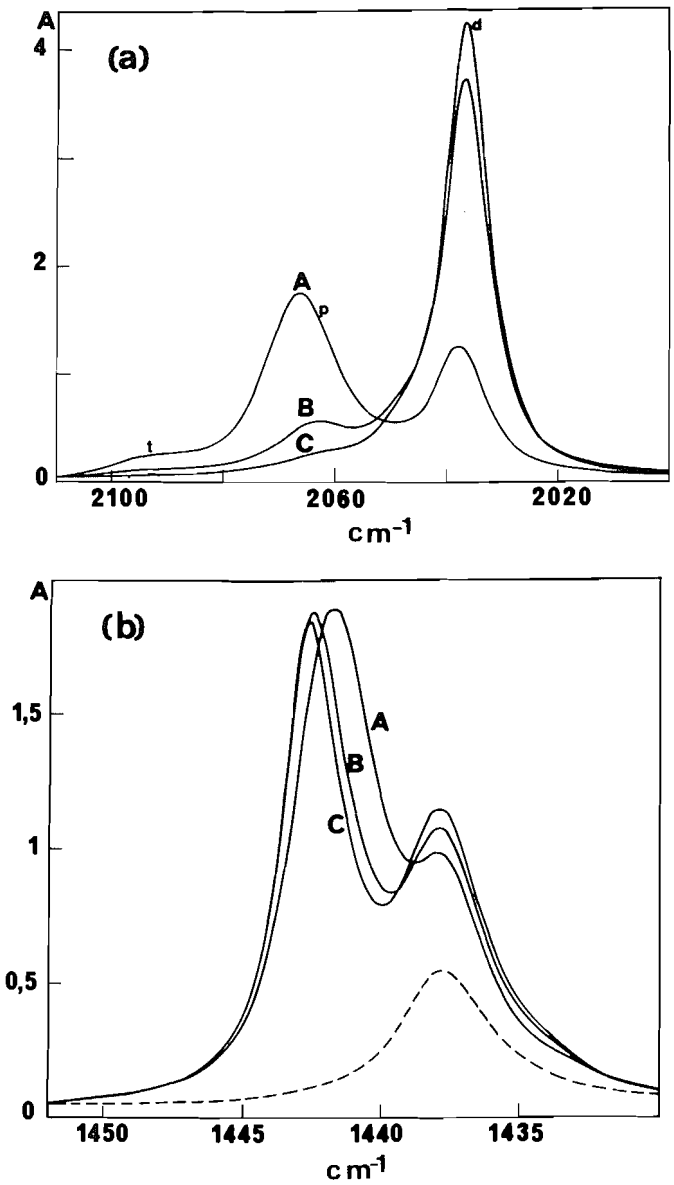

FIG. 3. Spectres infrarouges d'une solution A: LiSCN (0,8 *M*) – pyridine (3 *M*) et des solutions diluées: B 4 fois et C 16 fois dans le benzène. Régions: (a) ν(CN) de SCN et (b) ν(CNC) de la pyridine. Les hauteurs des spectres sont ramenées à 1 *M* en LiSCN (a) ou en pyridine (b). En pointillé le spectre de la pyridine (0.25 *M*) dans le benzène.

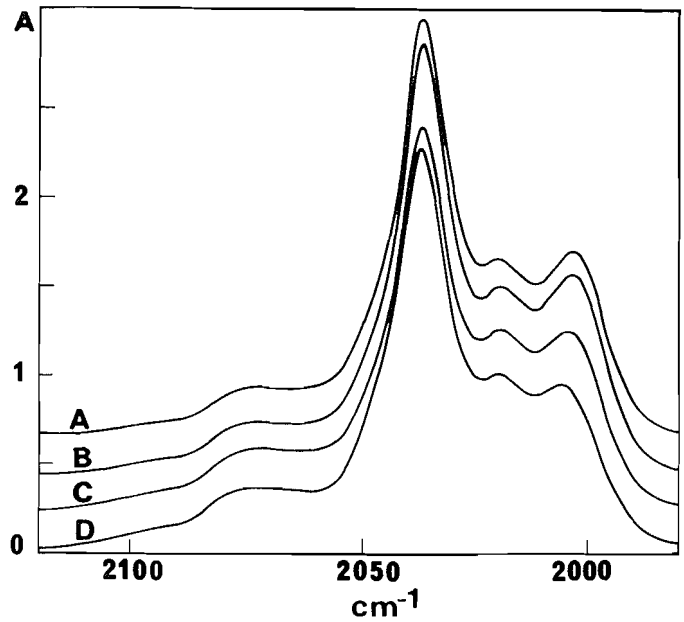

FIG. 4. Spectres infrarouges de solutions mixtes LiSCN – acétate de butyle dans le benzène (région ν(CN)). Concentrations (*M*): A 0,115 et 0,21; B 0,176 et 0,315; C 0,45 et 0,72; D 0,93 et 1,52. Les hauteurs des spectres ont été ramenées à 1 *M* en LiSCN.

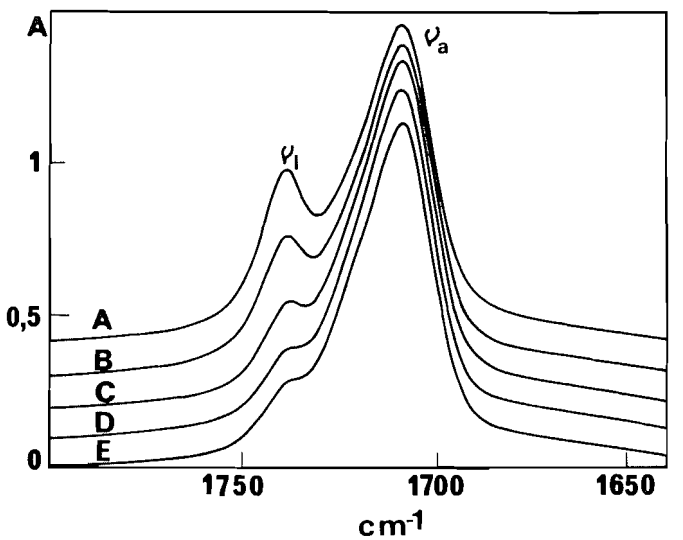

FIG. 5. Spectres infrarouges de solutions mixtes LiSCN – acétate de butyle dans le benzène (région ν(COC)). Concentrations (*M*): A 0,115 et 0,21; B 0,176 et 0,315; C 0,315 et 0,51; D 0,45 et 0,72; E 0,59 et 1,02. Les hauteurs des spectres ont été ramenées à 1 *M* en acétate de butyle.

DEC) de même que les bandes ν(CCO) ($\Delta\nu$ = 41 et 43 cm^{-1} dans BuOAc et DEC). Ces deux zones sont alors utilisables pour la détermination du nombre de solvatation et l'accord entre les résultats est excellent. Dans les solutions saturées l'intensité relative des bandes dues au solvant libre est faible (fig. 5) et elle décroît régulièrement lorsque la concentration augmente. La concentration en solvant libre que l'on en déduit, et qui est nécessaire pour assurer l'équilibre de dissolution, est pratiquement constante (~0,05 *M* dans l'acétate de butyle et ~0,14 *M* dans le DEC) dans tout le domaine de concentration étudié. Les résultats relatifs à l'EMC ont été obtenus, comme pour l'acétone, en utilisant la région ν(CCC) du spectre. Les solutions non saturées en LiSCN (tableau 2) donnent le nombre de solvatation du dimère pur avec $c_S/c \sim 2{,}5$ à 3. Pour les trois solvants ce nombre de solvatation est égal à 2. Dans les solutions saturées la valeur moyenne $\bar{n}$ du nombre de solvatation est comprise entre 1,4 et 1,6. Comme prévu les agrégats sont donc beaucoup moins solvatés que le dimère et leur nombre de solvatation moyen est probablement de l'ordre de 1.

Les résultats obtenus sur les différents systèmes étudiés montrent donc que le réaction de dimérisation de la paire LiNCS s'accompagne d'une désolvatation importante. Ce résultat avait été obtenu de façon indirecte dans un précédent travail (15) où nous avions montré que la dimérisation de LiNCS est un processus contrôlé par le terme entropique, ainsi d'ailleurs que la tétramérisation (16). Le nombre de coordina-

tion global du lithium reste égal à 4 ou voisin de 4 dans toutes les espèces formées. Les réactions d'association entre Li^+ et SCN^- sont donc des réactions où le solvant est remplacé par le ligand SCN dans la première couche de solvatation de Li^+.

Partie expérimentale

Le benzène utilisé est de qualité "pour spectroscopie" ainsi que l'acétone. Les autres solvants ont été distillés sur une colonne à 20 plateaux et séchés sur tamis moléculaire 4 Å. Toutes les manipulations ont été effectuées en boite à gants sèche.

Les spectres en solvant mixte ont été faits dans une cellule en CaF_2 d'épaisseur 26,8 μm. L'appareil utilisé est un spectromètre Bruker IFS 85 à transformée de Fourier. La résolution utilisée est 2 cm^{-1} sauf pour les spectres de la pyridine (0.5 cm^{-1}).

1. M. K. WONG, W. J. MCKINNEY et A. I. POPOV. J. Phys. Chem. **75**, 56 (1971).
2. H. L. YEAGER, J. D. FEDYK et R. J. PARKER. J. Phys. Chem. **77**, 2407 (1973).
3. E. G. HOHN, J. A. OLANDER et M. C. DAY. J. Phys. Chem. **73**, 3880 (1969).
4. N. AHMAD et M. C. DAY. J. Inorg. Nucl. Chem. **40**, 1383 (1978).
5. M. CHABANEL, C. MENARD et G. GUIHENEUF. C. R. Acad. Sci. Paris, **272**, 253 (1971).
6. D. PAOLI, M. LUCON et M. CHABANEL. Spectrochim. Acta, Part A, **35**, 593 (1979).
7. J. VAES, M. CHABANEL et M. L. MARTIN. J. Phys. Chem. **82**, 2420 (1978).
8. P. BACELON, J. CORSET et C. DE LOZE. J. Solution Chem. **9**, 129 (1980).
9. M. CHABANEL, M. LUCON et D. PAOLI. J. Phys. Chem. **85**, 1058 (1981).
10. C. MENARD, B. WOJTKOWIAK et M. CHABANEL. C. R. Acad. Sci. Ser. C, **278**, 553 (1974).
11. J. P. TOTH, G. RITZHAUPT et J. DEVLIN. J. Phys. Chem. **85**, 1387 (1981).
12. J. A. OLANDER et M. C. DAY. J. Am. Chem. Soc. **93**, 3584 (1971).
13. J. ROUVIERE, B. DIMON, B. BRUN et J. SALVINIEN. C. R. Acad. Sci. Ser. C, **274**, 458 (1972).
14. I. S. PERELYGIN et M. A. KLIMCHUK. Russ. J. Phys. Chem. **49**, 76 (1975); A. D. E. PULLIN et J. M. POLLOCK. Trans. Faraday Soc. **54**, 11 (1958).
15. M. CHABANEL et D. PAOLI. J. Chim. Phys. Chim. Biol. **77**, 913 (1980).
16. Y. H. KIM, D. PAOLI et M. CHABANEL. 8th International Conference on Non-Aqueous Solutions, Nantes, 1982.

Can. J. Chem. Downloaded from www.nrcresearchpress.com by 210.87.254.6 on 09/06/12
For personal use only.

Synthèse du (±)-loliolide ou hydroxy-6 tétrahydro-5,6,7,7a triméthyl-4,4,7a(4*H*) benzofurannone-2 (6*S*,7a*R*) par cyclisation de l'acide homogéranique

HENRI ZAMARLIK[1] ET NOUKPO GNONLONFOUN

Laboratoire de Chimie Organique et Biologique, Faculté des Sciences, Université de Tours, 37200 Tours, France

ET

FRANCIS ROUESSAC

Laboratoire de Synthèse Organique, Faculté des Sciences, Université du Maine, 72017 Le Mans, France

Reçu le 14 juin 1983[2]

HENRI ZAMARLIK, NOUKPO GNONLONFOUN et FRANCIS ROUESSAC. Can. J. Chem. **62**, 2326 (1984).

Au départ de l'acide homogéranique (isomère *trans*) **2**, nous décrivons une nouvelle synthèse totale et stéréosélective du (±)-loliolide **1**. La cyclisation de **2** avec le trifluoroacétate de mercure ou le chlorure de phénylsélénium conduit dans un premier temps à l'isodihydroactinidiolide **6** qui est transformé en (±)-loliolide après six étapes simples.

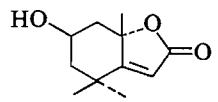

1

HENRI ZAMARLIK, NOUKPO GNONLONFOUN, and FRANCIS ROUESSAC. Can. J. Chem. **62**, 2326 (1984).

Starting from pure homogeranic acid **2**, in a stereoselective fashion, we describe a new synthesis of (±)-loliolide **1**. Cyclization of **2** with mercury trifluoroacetate or phenylselenenyl chloride provides the isodihydroactinidiolide **6** which was converted to the racemate of loliolide after six steps.

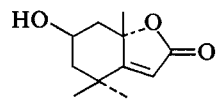

1

Le (±)-loliolide **1**[3] est un composé appartenant à un groupe particulier de lactones terpéniques à onze atomes de carbone qui comprend essentiellement les divers actinidiolides. Le composé **1** a été isolé à l'état de traces à partir de divers végétaux dont le *Lolium perenne* (1, 2), le *Fumaria officinalis* (3), le *Digitalis lanata* (4), le *Digitalis purpurea* (5) et le *Cystophora moniliformis* (algue brune) (6).

Sa structure a été établie par Hodges et Porte (1) ainsi que par Sato *et al.* (5). Sa configuration absolue a été déterminée par Isoe, Hyeon *et al.* (7, 8). Jusqu'à ce jour, quatre synthèses de **1** ont été effectuées à partir de la bromo-2 triméthyl-2,6,6 cyclohexanone (9), de l'isophorone (10), de l'acide homosafranique (11) et de l'hydroxy-4 triméthyl-2,2,6 cyclohexanone optiquement active (12).

Par ailleurs Hoye et Kurth (13) ont obtenu en 1978 et 1979 des composés biologiques, à jonction *trans*, apparentés aux tétrahydroactinidiolides, susceptibles de conduire à **1**.

La méthode retenue pour la synthèse totale du loliolide racémique repose sur la création du système bicyclique lactonique, par cyclisation électrophile de l'acide homogéranique **2** (isomère *trans* pur) (14), soit au moyen du trifluoroacétate de mercure, soit avec le chlorure de phénylsélénium. On obtient dans un premier temps la lactone éthylénique **6**, les intermédiaires réactionnels étant les lactones halogénées **4** ou **5** ou la sélénolactone **7** (15, 16) (schémas 1 et 2).

Traité par le trifluoroacétate mercurique, l'acide homogéranique en solution dans le nitrométhane se cyclise à température ambiante pour donner le tétrahydroactinidiolide substitué en 5 avec le groupement (TFA—Hg) en position équatoriale. Après remplacement de TFA par un atome d'halogène (Br ou I) au moyen d'une solution saturée d'halogénure de

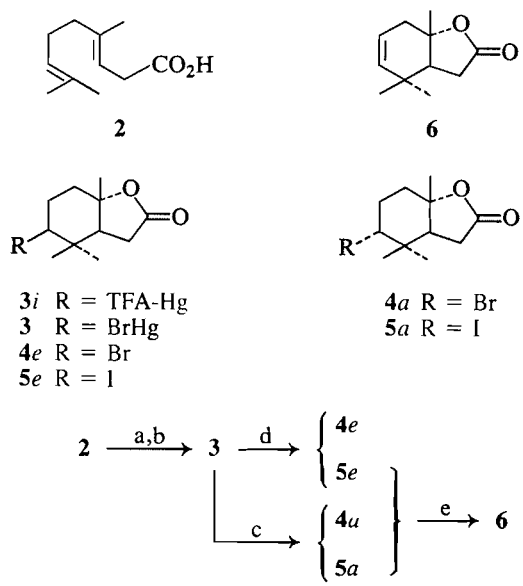

(a) Hg $(CF_3CO_2)_2$; (b) KBr/H_2O/20°C/24 h; (c) X_2 (X = Br ou I)/pyr./*hν*/20°C/10 min; (d) Li I_3/dioxanne/eau/20°C/72 h ou Li Br + Br_2 (2:1)/pyridine/20°C/20 h; (e) LiCl anhydre/DMF/50°C/3 H (réf. 17).

SCHÉMA 1

[1] Auteur à qui adresser toute correspondance.

[2] Revision reçue le 6 avril 1984.

[3] Nom systématique: hydroxy-6 tétrahydro-5,6,7,7a triméthyl-4,4,7a (4*H*) benzofurannone-2 (6*S*,7a*R*).

Can. J. Chem. Downloaded from www.nrcresearchpress.com by 210.87.254.105 on 09/06/12
For personal use only.

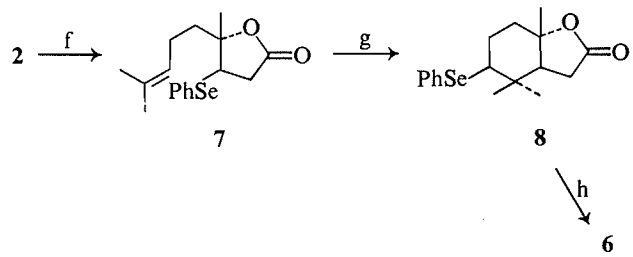

(f) $PhSeCl/CH_2Cl_2/0°C/15$ min; (g) CF_3CO_2H (10% dans CH_2Cl_2)/ 20°C/5 min; (h) $NaIO_4$/acétone/eau (1:1/20°C/20 min

SCHÉMA 2

potassium à l'abri de la lumière, on isole l'organomercuriel **3**, lui-même transformé en lactones bromées **4***e* ou **4***a* selon Hoye et Kurth (13).

Nous avons déjà décrit une méthode de préparation de **4***e* en passant par la bromhydrine terminale de **2** (18), mais les meilleurs intermédiaires halogénés en vue d'accéder par déhydrohalogénation à **6**, sont constitués par les iodolactones **5***e* ou **5***a*. L'iodolactone équatoriale **5***e* est obtenue en agitant le dérivé mercuriel **3**, en solution dans du dioxanne, avec KI_3 à température ambiante (rendement global **2** → **6**:30%). Par contre en traitant **3**, par de l'iode en milieu pyridinique sous irradiation uv pour favoriser un mécanisme radicalaire, on prépare de manière stéréospécifique l'iodolactone axiale **5***a* (19) (rendement global **2** → **6**:25%). L'iodolactone **5***e*, traitée dans du DMF diméthylformamide fraîchement distillé, avec du chlorure de lithium anhydre, permet de préparer la lactone éthylénique **6** avec un rendement de 40%.

L'oxydation–élimination de la lactone séléniée **8** (16) est une autre voie d'accès à la même lactone éthylénique **6**. L'acide homogéranique **2**, en solution dans CH_2Cl_2 et à 0°C, traité par PhSeCl permet de préparer la lactone de monocyclisation **7** (15). En agitant **7** avec CF_3COOH à 10% dans CH_2Cl_2, on obtient la lactone bicyclique séléniée **8**. Le rendement global pour obtenir la lactone **6** par cette méthode est de 30% à partir de **2** ce qui est comparable à la voie précédemment décrite.

Le schéma 3 résume les dernières étapes de la synthèse du (±)-loliolide. La lactone éthylénique **6**, traitée par le *N*-bromoacétamide en milieu eau–acétone (1/3 d'eau), à 0°C ou par le *N*-bromosuccinimide en milieu eau–THF (1:1) à 0°C, conduit à la bromhydrine *trans* diaxiale **9** qui est alors réduite en dihydrololiolide **10** par le nickel de Raney en suspension dans CH_2Cl_2.

La création d'une double liaison en α du carbonyle de **10**, via l'énolate correspondant, conduit au (±)-loliolide. On commence par désactiver la fonction alcool de **10** pour éviter qu'elle soit le siège de réactions secondaires. Pour cela, **10** en solution dans l'éther sec est agité à 0°C avec du dihydropyranne en présence d'acide paratoluènesulfonique. Le dérivé tétrahydropyrannylique **11** obtenu, traité par le diisopropylamidure de lithium à −78°C dans du THF sec, conduit à l'énolate correspondant. On fixe le radical SePh (mélange des deux isomères) en agitant à −78°C l'énolate obtenu avec PhSe—SePh, en solution dans du THF, et en présence d'HMPT sec. L'α-phénylsélénolactone bloquée **12** en solution dans $(C_2H_5)_2O$, est enfin hydrolysée par une solution d'acide chlorhydrique 2 *N*.

Par oxydation–élimination de l'α-phénylsélénolactone **13** en solution dans l'acide acétique à 0°C, et de l'eau oxygénée à 30%, on obtient le (±)-loliolide qui est purifié par chro-

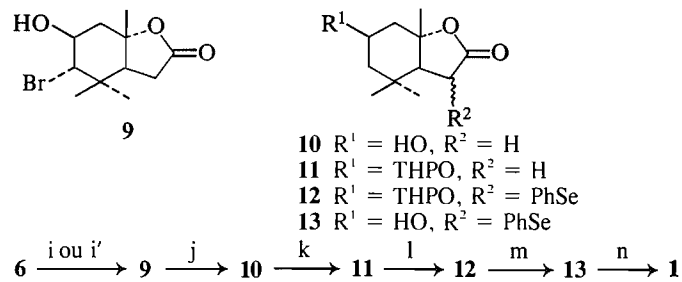

(i) NBS/eau–tétrahydrofuranne (1:1)/0°C puis température ambiante/3 jours; (i') NBA/eau–acétone (1:2)/0°C/ puis température ambiante/1 h; (j) Ni Raney/CH_2Cl_2/20°C/4 h; (k) dihydropyranne/éther/TsOH/20°C/6 h; (l) LiN($^{iPr}_{iPr}$)/tétrahydrofuranne/ −78°C/1 h puis $(PhSe)_2$/−78°C → 40°C/2 h; (m) HCl–H_2O (2 *N*)/Et_2O/20°C/6 h; (n) H_2O_2/AcOH–tétrahydrofuranne (1:10)/ 0°C/2 h

SCHÉMA 3

matographie sur gel de silice (benzène/éther 1:1). Le composé **1**, ainsi formé présente les mêmes caractéristiques que celles indiquées dans la littérature (1).

Cette synthèse s'insère dans les travaux que nous avons effectués pour obtenir des lactones dont le squelette à onze atomes de carbone est commun à celui de la famille des actinidiolides naturels. La préparation des dérivés glycosidés du (±)-loliolide **1** sera la prochaine étape de notre étude.

Partie expérimentale

Conditions générales

Les déterminations physico-chimiques ont été effectuées au moyen des appareils suivants: spectrophotomètre infrarouge Beckman Acculab 2; spectrophotomètre rmn ^1H Varian EM 360 60 MHz et EM 390 90 MHz; le TMS est utilisé comme référence interne; spectromètre de masse Kratos MS 25 couplé à un ordinateur Data Novo System 4 pour l'impact électronique (IE) 70 eV; spectromètre de masse quadrupôle Nermag R 10–10 pour l'ionisation chimique par NH_3 (IC).

Les microanalyses des nouveaux composés ont été effectuées au service central d'analyse du centre national de la recherche scientifique 69390 Vernaison (France). Silice pour chromatographie sur colonne: gel de silice 40 Merck (70–230 mesh ASTM).

1. *Hexahydro-3α,4,5,6,7,7aα (3H) trifluoroacétobromomercuro-5β triméthyl-4,4,7a benzofurannone-2* **3**i

A 1,70 g (9,34 mmol) d'acide homogéranique en solution dans 20 mL de nitrométhane sec, fraîchement distillé, on ajoute rapidement par petites fractions, sous azote, 4,38 g (10,27 mmol) de trifluoroacétate de mercure $(CF_3CO_2)_2Hg$. Le mélange est agité 1 h à température ambiante 20°C. On ajoute 20 mL d'H_2O; on filtre sur laine de verre après extraction au CH_2Cl_2, on sèche sur $MgSO_4$. Après évaporation des solvants on obtient 4,58 g d'une huile brune qui se solidifie lentement; ir (KBr) ν (CO_2): 1770 cm^{-1}; ccm, R_f = 0,14 (éluant: CH_2Cl_2/hexane/éther 1:1:1).

2. *Bromomercuro-5β hexahydro-3aα,4,5,6,7,7aα (3H) triméthyl-4,4,7a benzofurannone-2* **3**

La trifluoroacétomercurolactone brute est solubilisée dans CH_2Cl_2; on ajoute 150 mL d'une solution de KBr. Le mélange est agité à l'abri de la lumière pendant 3 jours. Après extraction, on sèche la phase organique sur $MgSO_4$. On évapore sous vide le solvant et on obtient 4,05 g de produit brut **3**; ccm R_f = 0,29 (éluant: CH_2Cl_2/hexane/éther 1:1:1); sm (IE) *m/e* (%): 462 (<1), 380 (<1), 181 (52,1) (−HgBr), 153 (11,7), 137 (15,5), 135 (12,3), 121 (28,5), 109 (12), 95 (34,9), 93 (12,7), 81 (24,1), 79 (12,5), 69 (100), 67 (23,7); sm (IC au NH_3) *m/e* (%): 463 (53) (M + 1), 479 (70), 480 (100) (M + NH_4^+), 200

Can. J. Chem. Downloaded from www.nrcresearchpress.com by 210.87.254.105 on 09/06/12
For personal use only.

Can. J. Chem. Downloaded from www.nrcresearchpress.com by 210.87.254.105 on 09/06/12
For personal use only.

(52). *Anal.* calc. pour $C_{11}H_{17}HgBrO_2$ (M = 461,77): C 28,61, H 3,72, O 6,93, Br 17,30, Hg 43,44%; tr.: C 28,82, H 3,32, O 7,03%.

3. *Hexahydro-3aα,4,5,6,7,7aα (3*H*) iodo-5β triméthyl-4,4,7a benzofurannone-2* **5**e

A 4 g (8,67 mmol) d'une solution de **3** dans 50 mL d'un mélange eau–dioxanne (10% H_2O) on ajoute goutte à goutte 25 mL d'une solution de KI_3, 1,2 équivalent (2,64 g de I_2 dans 25 mL d'une solution saturée de KI). Une fois l'addition terminée, on agite le mélange 3 jours à température ambiante (20°C). On rajoute 25 mL d'H_2O et on décolore la solution au disulfite de potassium. Après extraction à l'éther, séchage sur $MgSO_4$ et évaporation du solvant, on obtient 2,65 g de **5***e*; ccm R_f = 0,47 (éluant: CH_2Cl_2/hexane/éther 1:1:1); rmn ^1H ($CDCl_3$/TMS) δ en ppm: 1,05, 1,10, 1,40 (3s, CH_3), 4,20 (dd, J = 12 et 6 Hz, *H*—C—I); sm (IE) *m/e* (%): 309 (14) × 10, 293 (2,2) ($-CH_3$), 265 (2,2) ($-CO_2$), 182 (10,6), 181 (76) (−I), 153 (27,5), 137 (11,9), 135 (34,2), 121 (49,4), 111 (15,8), 101 (23,9), 95 (77,1), 69 (65,4), 67 (37,6), 55 (44,2), 43 (100); sm (IC au NH_3) *m/e* (%): 327 (18), 326 (100) (M + NH_4^+), 309 (22) (M + 1). *Anal.* calc. pour $C_{11}H_{17}IO_2$ (M = 308,19): C 42,87, H 5,57, O 10,38, I 41,18%; tr.: C 43,20, H 5,55, O 10,10%.

4. *Hexahydro-3aα,4,5,6,7,7aα (3*H*) iodo-5α triméthyl-4,4,7a benzofurannone-2* **5**a

Dans un mélange de 910 mg (2 mmol) de dérivé **3**, dissous dans 15 mL de pyridine sèche, on ajoute 0,77 g d'iode dissous dans 10 mL de pyridine. Après un barbotage d'azote (10 min), on irradie le mélange durant 10 min avec une lampe Hanovia 100 W, dans un tube Pyrex.

On récupère 580 mg (Rdt 94%) d'iodolactone axiale **5***a*, après traitement habituel. La lactone brute est recristallisée dans un mélange hexane–éther (4:1), F = 127°C (hexane/éther); spectre ir ν(C=O): 1741 cm^{-1}; rmn ^1H ($CDCl_3$/TMS) δ en ppm: 1,12, 1,16, 1,40 (3s, CH_3), 4,63 (dd J = 3 et 2,2 Hz, (*H*—C—I).

5. *Tetrahydro-3aα,4,7,7aα (3*H*) triméthyl-4,4,7a benzofurannone-2* **6**

Les 2,65 g (8,60 mmol) de **5** brut sont mis en solution dans du DMF sec fraîchement distillé et contenant 0,55 g de LiCl anhydre. On agite la solution 3 h à 50°C. Après refroidissement, on rajoute un peu d'eau, extrait à l'éther, et sèche ($MgSO_4$). On évapore le solvant puis on fait la chromatographie du produit brut sur gel de silice, éluant: éther/éther de pétrole (1:2). Rendement (**5***e* → **6**:40%); ccm R_f = 0,50 (même éluant); R_f = 0,67 (toluène/éther 1:1); ir (film) $\nu(CO_2)$: 1765 cm^{-1}; ν(C—H): 940 cm^{-1}; rmn ^1H ($CDCl_3$/TMS) δ en ppm: 1,05 (s, CH_3), 1,08 (s, CH_3), 1,35 (s, CH_3), 2,15 à 3,00 (m, 5H), 5,60 (m, 2H éthyl); sm (IE) *m/e* (%): 180 (6,1), 165 (42,2) ($-CH_3$), 137 (19,4), 136 (6,3) ($-CO_2$), 121 (17,8), 109 (28,1), 95 (21,7), 93 (25,2), 82 (69,7), 79 (19), 67 (35,7), 55 (29,1), 43 (100). $C_{11}H_{16}O_2$, M^+ calculé: 180,11502; trouvé: 180,1150. *Anal.* calc.: C 73,28, H 8,96, O 17,75%; tr.: C 73,31, H 8,96, O 17,81%.

6. *(2S,3R;3S,2R) méthyl-5 (méthyl-4 pentène-3 yl)-5 phénylséléno-4 butyrolactone* **7**

A une solution d'acide homogéranique (1,82 g, 10 mmol) **2** dans 10 mL de CH_2Cl_2, on ajoute 420 mg (7 mmol) d'acide acétique et 610 mg (6 mmol) de triéthylamine anhydre. On agite 5 min à température ambiante, puis on refroidit ce mélange à 5°C. On ajoute alors, goutte à goutte, sous azote, 1,2 g (3,1 mmol) de chlorure de phénylsélénium en solution dans 10 mL de CH_2Cl_2. On poursuit l'agitation durant 8 h à température ambiante avant de laver le mélange réactionnel avec une solution aqueuse de $NaHCO_3$ (40 mL). On extrait à l'éther, sèche ($MgSO_4$) et concentre. Le produit brut est chromatographié sur gel de silice. On recueille 2,4 g (Rdt 70%) de **7**, aux caractéristiques déjà décrites (15).

7. *Hexahydro-3aα,4,5,6,7,7aα (3*H *phénylséléno-5β triméthyl-4,4,7a benzofurannone-2* **8**

On ajoute sous azote à 2 g de **7** en solution dans 10 mL de CH_2Cl_2 anhydre, 0,2 mL d'acide trifluoroacétique. On agite 10 min, dilue avec 50 mL d'eau et 50 mL d'éther puis neutralise avec $NaHCO_3$. Après traitement habituel, le produit réactionnel brut est chromatographié sur silice (éluant C_6H_6), pour éliminer les traces de $(PhSe)_2$. On obtient ainsi 1,6 g de **8** (Rdt 80%), F = 141°C (éther/hexane), aux caractéristiques déjà décrites (16); sm (IE) *m/e* (%): 338 (20), 336 (11), 181 (39), 153 (24), 137 (11), 135 (35), 121 (57), 111 (15), 95 (64), 69 (84), 43 (100). *Anal.* calc. pour $C_{17}H_{22}SeO_2$ (M = 337,35): C 60,52, H 6,59, O 9,49, Se 23,41%; tr.: C 60,89, H 7,09%.

8. *Bromo-5α hexahydro-3aα,4,5,6,7,7aα (3*H*) hydroxy-6 triméthyl-4,4,7α benzofurannone-2* **9**

A 70 mg (0,39 mmol) de **6** solubilisé dans 5 mL d'acétone à 0°C, on ajoute 134,3 mg (0,973 mmol) de *N*-bromoacétamide dissous dans 3,5 mL d'eau. On laisse 2 h à 0°C. Une fois la solution revenue à température ambiante, on laisse 1 h à cette température. On évapore l'acétone, on ajoute de l'eau puis une solution de disulfite de potassium à 10% pour détruire HOBr en excès. On extrait à l'éther, sèche sur $MgSO_4$. Après évaporation du solvant on obtient 103 mg de la bromhydrine **9**; ccm R_f = 0,16 (éluant: CH_2Cl_2/hexane/éther 1:1:1); sm (IE) *m/e* (%): 279 (1), 278 (2,1), 276 (2,3), 263 (12,3) ($-CH_3$), 261 (12,8) ($-CH_3$), 197 (4) (−Br), 183 (2,4) (−Br $-H_2O$), 179 (7,6), 153 (36), 143 (15,1), 136 (31,9), 135 (29,8), 134 (30,1), 109 (14,4), 98 (65,5), 85 (73,5), 71 (76,7), 55 (62), 43 (100); sm (IC au NH_3) *m/e* (%): 296 (87), 294 (100) (M + NH_4^+), 279 (18), 277 (21) (M + 1). *Anal.* calc. pour $C_{11}H_{17}O_3Br$ (M = 277,18): C 47,66, H 6,19, O 17,32, Br 28,83%; tr.: C 47,42, H 6,00, O 17,10%.

9. *Hexahydro-3aα,4,5,6,7,7aα (3*H*) hydroxy-6 triméthyl-4,4,7a benzofurannone-2* ***10***

Les 103 mg de la bromhydrine **9** sont solubilisés dans 15 mL de CH_2Cl_2. On ajoute 1 g de Ni de Raney en suspension dans CH_2Cl_2 sous N_2 (ballon bouché). On agite 4 h à température ambiante. On filtre sur Büchner, puis on sèche le filtrat sur $MgSO_4$. Après évaporation des solvants, le dihydrololiolide obtenu est purifié par chromatographie sur gel de silice (toluène/CH_2Cl_2/éther 13:10:4). On obtient alors 52 mg de **10** pur. Il cristallise lentement; F = 126°C; ir (film) ν (OH): 3480, 920 cm^{-1}; ν (COO): 1785 cm^{-1}; rmn ^1H δ en ppm: 1,0, 1,15, 1,55 (3s, $3CH_3$), 2,10 (s, OH), 4,35 (m, *H*-COH); sm (IE) *m/e* (%): 199 (5) × 10, 198 (1) × 10, 183 (17,5) ($-CH_3$), 165 (14) ($-CH_3$ $-H_2O$), 155 (2,6), 137 (15,2), 136 (12,1), 121 (11,1), 109 (12), 99 (19,1), 98 (45,9), 95 (18,5), 85 (23,7), 83 (33,5), 71 (22,6), 70 (35,5), 69 (85,6), 43 (100); sm (IC au NH_3): 217 (17), 216 (100) (M + NH_4^+), 200 (5), 199 (55) (M + 1). *Anal.* calc. pour $C_{11}H_{18}O_3$ (M = 198,29): C 66,62, H 9,17, O 24,21%; tr.: C 66,54, H 9,38, O 24,10%.

10. *Hexahydro-3aα,4,5,6,7,7aα (3*H*) tétrahydropyrannoxy-6 triméthyl-4,4,7a benzofurannone-2* ***11***

On dissout 52 mg de l'alcool **10** dans l'éther à sec à 0°C; on ajoute quelques mg d'acide paratoluènesulfonique, puis goutte à goutte, le dihydropyranne (1,5 équivalent). On laisse 1 h à 0°C, puis 5 h à température ambiante 20°C. On neutralise par Na_2CO_3 jusqu'à pH basique. Après extraction à l'éther, les phases organiques sont lavées à l'eau saturée de NaCl, et séchées sur $MgSO_4$. On évapore l'éther et on obtient **11** avec un rendement quantitatif; ir ν (COO): 1785, 1200, 1130, 1080, 1030, 810 cm^{-1}.

11. *Hexahydro-3aα,4,5,6,7aα (3*H*) phénylséléno-3-tétrahydro-pyrannoxy-6 triméthyl-4,4,7a benzofurannone-2* ***12***

On ajoute 0,36 mL (2,71 mmol) de diisopropylamine à 1,6 mL de butyllithium (1,6 *M* dans l'hexane) soit 1,28 équivalent, sous azote à −78°C en agitant. Une fois l'addition terminée, le mélange est abandonné 1 h à température ambiante.

On ajoute 3 mL de THF anhydre au LDA formé et on refroidit à −78°C. On additionne goutte à goutte en 1 h 564 mg (2 mmol) de **11** dissous dans 3 mL de THF anhydre puis on agite le mélange 20 min à −78°C et 1 h à température ambiante.

L'énolate formé est ensuite refroidi à −78°C, on rajoute 754 mg (2,4 mmol) de diphényldiséléniде en solution dans 2 mL de THF anhydre et 430 mg (2,4 mmol) de HMPT. Une fois l'addition terminée on agite le mélange 40 min à −78°C, puis 2 h à −40°C. On acidifie le mélange par addition de HCl 1 *M*. On extrait à l'éther, les phases

organiques sont lavées à l'eau saturée de NaCl et séchées sur $MgSO_4$. Après concentration sous vide on fait la chromatographie du produit brut sur une colonne de silice (éluant: hexane/acétate d'éthyle 80:20). En tête de colonne on élue PhSe—SePh et PhSeH puis une huile très légèrement jaune constituée de 440 mg de **12**; Rdt: 50%; ir ν (=C—H) 3030, 1580, 740 cm^{-1}; ν (COO): 1760 cm^{-1}.

12. *Hexahydro-3aα,4,5,6,7,7aα (3H) hydroxy-6 phénylséléno-3 triméthyl-4,4,7a benzofurannone-2* ***13***

A 438 mg (1 mmol) du mélange des 2 épimères de **12** dissous dans 20 mL d'éther, on ajoute 10 mL de HCl 2 *M* et on agite 6 h à température ambiante 20°C. Après décantation, la phase aqueuse est lavée une fois avec 10 mL d'éther. Les phases éthérées sont ensuite lavées à l'eau saturée de NaCl, séchées sur $MgSO_4$, concentrées sous vide. On obtient 352 mg de **13** (rendement quantitatif); ir (film): 3030, 1580, 740 cm^{-1}; ν (OH): 3440 cm^{-1}; ν (COO): 1760 cm^{-1}.

13. *Hydroxy-6 tétrahydro-5,6,7,7a triméthyl-4,4,7a (4H) benzofurannone-2* ***1***

On agite 48 mg (0,135 mmol) de **13** en solution dans 5 mL de THF avec 0,15 mL d'H_2O_2 à 30% et 0,50 mL d'acide acétique à 0°C sous azote pendant 2 h (ballon bouché). Le mélange réactionnel est ensuite versé dans une solution saturée de $NaHCO_3$ et extrait à l'éther. Les phases organiques sont lavées avec H_2O saturées de NaCl, séchées sur $MgSO_4$ et concentrées sous vide. Après chromatographie sur une colonne de gel de silice, éluant benzène/éther (1:1), on obtient 20 mg de **1** pur. Le rendement de la dernière étape est de 75%. Le composé **1** est insoluble dans l'éther et le CCl_4 à froid. Il est recristallisé dans le CCl_4; F = 140°C en accord avec la littérature (1); rmn ^1H ($CDCl_3$/TMS) δ en ppm: 1,25, 1,45, 1,80 (3s, $3CH_3$), 4,35 (pq, 1H, $J \simeq 3,5$ Hz, C*H*OH), 5,70 (s, 1H éthyl).

1. R. HODGES et A. L. PORTE. Tetrahedron, **20**, 1463 (1964).
2. E. P. WHITE. New Zealand J. Agric. Res. **1**, 859 (1958).
3. R. H. F. MANSKE. Can. J. Res. B, **16**, 438 (1938).
4. R. TSCHESCHE et G. BUSCHAUER. Thèse Hamburg, 1957.
5. D. SATO, H. ISHII, Y. OYAMA, T. WADA et T. OKUMURA. Chem. Pharm. Bull. Jpn. **4**, 284 (1956).
6. B. N. RAVI, P. T. MURPHY, R. O. UDGARD, R. G. WARREN et R. J. WELLS. Aust. J. Chem. **35**, 171 (1982).
7. S. ISOE, S. B. HYEON, S. KATSUMURA et T. SAKA. Tetrahedron Lett. 1089 (1972).
8. S. ISOE, S. B. HYEON, S. KATSUMURA et T. SAKA. Tetrahedron Lett. 2517 (1972).
9. Z. HORII, T. YAGAMI et M. HANAOKA. Chem. Commun. 634 (1966).
10. J. N. MARX et F. SONDHEIMER. Tetrahedron, Suppl. 8, part 1, 1, (1966).
11. E. DE MOLE et P. ENGGIST. Helv. Chim. Acta, **51**, 481 (1968).
12. F. KIENZLE, H. MAYER, R. MINDER et H. THOMMEN. Helv. Chim. Acta, **61**, 2616 (1978).
13. T. R. HOYE et M. J. KURTH. J. Org. Chem. **43**, 3693 (1978); **44**, 3461 (1979).
14. P. GOSSELIN et F. ROUESSAC. C. R. Acad. Sci. **295** (série 2), 469 (1982).
15. A. ROUESSAC, F. ROUESSAC et H. ZAMARLIK. Tetrahedron Lett. 2641 (1981).
16. F. ROUESSAC et H. ZAMARLIK. Tetradedron Lett. 2643 (1981).
17. E. J. COREY, M. A. TIUS et J. DAS. J. Am. Chem. Soc. **102**, 7612 (1980).
18. P. GOSSELIN et F. ROUESSAC. Tetrahedron Lett. **23**, 5145 (1982).
19. F. SONDHEIMER et R. L. WIFE. Tetrahedron Lett. 765 (1973).

Can. J. Chem. Downloaded from www.nrcresearchpress.com by 210.87.254.105 on 09/06/12
For personal use only.

Correlation pK_a – activité catalytique des thiols dans la réaction d'hydrolyse de l'acétate de *p*-nitrophényle

ALAIN BREMBILLA, DENIS ROIZARD, JACQUELINE SCHOENLEBER ET PIERRE LOCHON[1]

Laboratoire de Chimie-physique Macromoleculaire, C.N.R.S. – E.R.A. 23, Ecole Nationale Superieure des Industries Chimiques, 1, rue Grandville, 54042 Nancy Cedex, France

Reçu le 6 février 1984

ALAIN BREMBILLA, DENIS ROIZARD, JACQUELINE SCHOENLEBER et PIERRE LOCHON. Can. J. Chem. **62**, 2330 (1984).

L'étude cinétique de l'hydrolyse de l'acétate de *p*-nitrophényle en présence de thiols primaires montre une activité catalytique provenant de l'ion thiolate seul. La comparaison des constantes de second ordre k_{RS^-} met en évidence un comportement différent des thiols primaires purement aliphatiques et des thiols primaires substitués en position α par un groupement aromatique. Dans ce dernier cas apparaît une corrélation de Brönsted log $k_{RS^-} = \beta pK_{SH} + C$ avec $\beta = 0{,}40$ et $C = -0{,}85$.

ALAIN BREMBILLA, DENIS ROIZARD, JACQUELINE SCHOENLEBER, and PIERRE LOCHON. Can. J. Chem. **62**, 2330 (1984).

The kinetic study of the hydrolysis of *p*-nitrophenylacetate in the presence of primary thiols indicates the thiolate anion as the sole catalytic species. Comparison of the true second order rate constants (k_{RS^-}) reveals that purely aliphatic primary thiols behave differently from aromatic α-substituted primary thiols. In the latter group a correlation can be established between the true second order rate constants and the pK_{SH} values by means of the Brönsted equation log $k_{RS^-} = \beta pK_{SH} + C$, with β equal to 0.40 and C equal to −0.85.

Can. J. Chem. Downloaded from www.nrcresearchpress.com by 210.87.254.6 on 09/06/12
For personal use only.

Introduction

Les enzymes protéolytiques comme la papaïne, la ficine ou la bromelaïne possèdent en plus du noyau imidazole de l'histidine un groupe thiol contenu dans le motif cysteïne qui est essentiel pour leur activité d'esterases. Le mécanisme d'action de ce type d'enzymes apparaît comme le résultat probable d'une coopération entre un groupe nucléophile et un site basique dans une catalyse plurifonctionnelle. Cette hypothèse a incité certains chercheurs à réaliser l'association des fonctions précédentes sur des molécules simples (mercaptoalcoyl-4 imidazoles) (1, 2) ou sur des macromolécules formées d'enchaînements peptidiques allant du dipeptide à quelques polypeptides (3, 4). Une première étude a été réalisée au Laboratoire sur de nouvelles molécules formées d'une chaîne alcoylthiol en position 2 d'un cycle benzimidazole, (les mercaptoalcoyl-2 benzimidazoles) (5), dans la réaction d'hydrolyse de l'acétate de *p*-nitrophényle. Cependant, l'interprétation des effets catalytiques particuliers de ces thiols hétérocycliques exige la connaissance des propriétés générales de la fonction sulfhydryle seule dans ce domaine.

Les travaux mentionnés actuellement dans la littérature concernent soit des thiols aliphatiques comportant un substituant susceptible d'engendrer une activité catalytique supplémentaire (6–8), soit des thiols aromatiques (9, 10). Ces composés constituant des cas particuliers, il est apparu nécessaire d'étendre l'étude sur des exemples plus nombreux, en élargissant l'échelle des pK_a et tout en évitant d'introduire des fonctions parasites. Pour permettre une meilleure comparaison avec les molécules bifonctionnelles (en particulier les mercaptoalcoyl-2 benzimidazoles) la structure des mercaptans étudiés présente une certaine similitude (—CH_2—SH) au voisinage du groupe fonctionnel. Les composés répondant le mieux à cette condition sont les benzylmercaptans, facilement synthétisables et dont la nature et la position du substituant (*para* ou *méta*) sur le noyau benzénique permettent d'obtenir une gamme assez étendue de pK_{SH}. L'activité catalytique de ces thiols est comparée à celle de composés présentant une structure voisine comme le furyl-2 méthanethiol et d'autre part à celle d'éthanethiols β substitués tels que la cystéamine, le mercapto-2 éthanol ou le phényl-1 éthanethiol.

Propriétés catalytiques

Les propriétés catalytiques de ces thiols ont été étudiées en prenant comme réaction de base l'hydrolyse de l'acétate de *p*-nitrophényle (PNPA). Celle-ci est suivie à un pH donné en déterminant par spectrométrie uv la quantité d'ion *p*-nitrophénolate (PNP^-) libérée en fonction du temps.

Dans ce type de réaction catalysée par un thiol, il a été démontré (7) que la première étape est l'étape lente avec formation d'un thiolester via un intermédiaire tétraédrique d'addition, qui est ensuite très rapidement hydrolysé si le pH est supérieur à 6,9; il n'est alors plus possible de déceler une quantité appréciable de ce composé dans le milieu réactionnel.

Pour définir un ordre 1 par raport à l'ester, il n'est donc pas

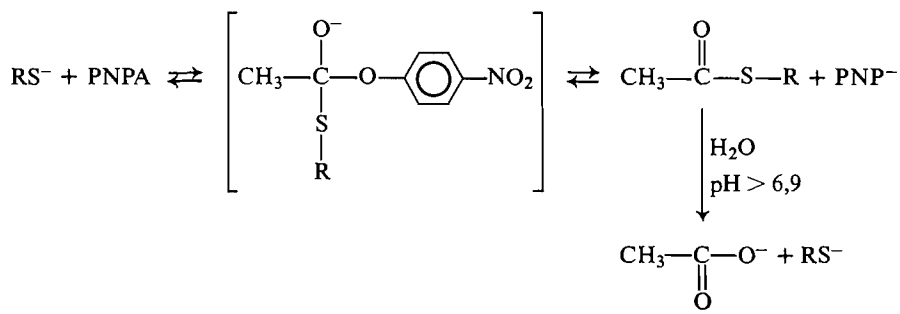

[1] Personne à qui toute correspondance devrait être adressée.

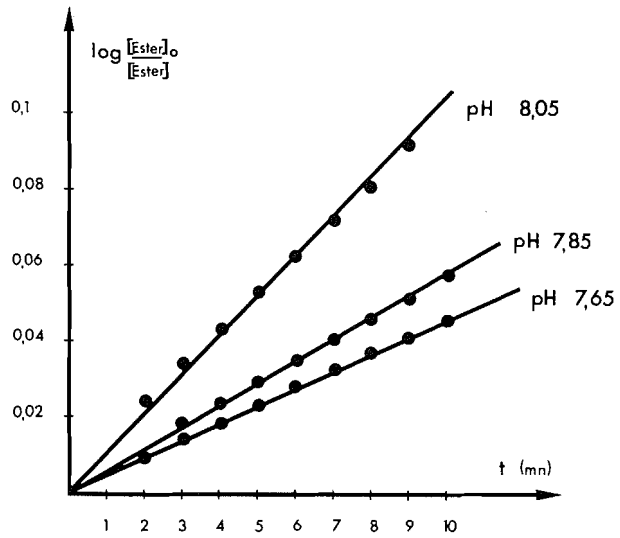

FIG. 1. Représentation de l'avancement de la réaction d'hydrolyse de l'acétate de *p*-nitrophényle (2×10^{-4} *M*) catalysée par le nitro-4 benzylmercaptan à différents pH et à différentes concentrations. Température: 30°C, solvant: eau–éthanol (28,5% d'éthanol vol.), tampon: phosphates (0,134 *M*) $I = 0{,}268$; pH = 7,65, $c = 2{,}23 \times 10^{-4}$ *M*; pH = 7,85, $c = 1{,}69 \times 10^{-4}$ *M*; pH = 8,05, $c = 1{,}96 \times 10^{-4}$ *M*.

nécessaire d'utiliser le thiol en large excès. Dans ces conditions, la cinétique du pseudo premier ordre s'exprime par la relation:

$$V(\text{vitesse globale}) = -\frac{d[PNPA]}{dt} = \frac{d[PNP^-]}{dt} = k_{obs}[PNPA]$$

k_{obs} = constante de vitesse globale de la réaction avec $k_{obs} = k_1 + k_{hydr}$

k_1 = constante de vitesse de pseudo-premier ordre de la réaction catalysée

k_{hydr} = constante de vitesse globale de la réaction non catalysée (hydrolyse propre de l'ester).

Les valeurs de k_{hydr} sont déterminées séparément pour chaque valeur du pH dans des conditions identiques à celles de la catalyse.

$k_{hydr} \times 10^4$ min^{-1}	pH
9,2	7,65
13,9	7,85
19,5	8,05

Comme pour les dérivés imidazoliques simples ne possédant qu'une seule fonction à caractère catalytique nucléophile (l'imidazole et le benzimidazole (11–13)) la réaction d'hydrolyse du PNPA catalysée par ces thiols simples est du pseudo premier ordre pour des concentrations en catalyseur égales et même inférieures à celles du substrat (fig. 1). En effet, pour un pH donné (fixé par la solution tampon), l'expression $x = f(t)$, représentant l'avancement de la réaction, varie linéairement avec le temps. Ce comportement a pu être vérifié pour certains composés jusqu'à un taux de conversion voisin de 50%, mais dans la pratique, les essais ont été limités à 25% d'avancement afin d'analyser principalement le début de la réaction et d'éviter par la suite le phénomène d'oxydation du catalyseur qui intervient de manière non négligeable.

L'examen du tableau 1 montre que la constante apparente du second ordre $k_2' = k_1/[\text{thiol}]_{total}$ qui caractérise l'efficacité du catalyseur à un pH donné, croît avec celui-ci mais reste invariante quelle que soit la valeur de rapport [catalyseur]/[substrat] (supérieur ou inférieur à 1), pour ce même pH.

Dans la série des benzylmercaptans, la constante k_2' dépend, à pH donné de la basicité de l'ion thiolate et par conséquent de la nature du substituant sur le noyau benzénique. Sa variation est identique en première approximation à celle du pouvoir donneur du substituant, ce dernier diminuant selon la séquence de substitution $p\text{-}OCH_3 > \rightarrow > p\text{-}NO_2$.

Séparation des effets catalytiques

L'interprétation de l'activité catalytique des thiols implique la prise en considération des différentes formes sous lesquelles peuvent exister ces composés dans le milieu réactionnel: RS^-, l'ion thiolate, caractérisé par la constante spécifique k_{RS^-}, et éventuellement la forme neutre RSH (constante spécifique k_{RSH}). Ces deux constantes sont reliées à k_1 et k_2' par les relations suivantes:

$$k_1 = k_2'([RS^-] + [RSH]) = k_{RS^-}[RS^-] + k_{RSH}[RSH]$$

En combinant avec la relation donnant la constante d'équilibre acide–base

$$RSH + H_2O \overset{K_{SH}}{\rightleftarrows} RS^- + H_3O^+$$

nous obtenons l'expression:

$$Y \equiv k_2'\left(1 + \frac{K_{SH}}{a_H}\right) = \frac{K_{SH}}{a_H} k_{RS^-} + k_{RSH} \text{ avec } a_H \simeq [H_3O^+]$$

La détermination des constantes spécifiques du deuxième ordre pour la réaction d'hydrolyse du PNPA catalysée par quelques thiols courants associés à une autre fonction conduisait Whitaker (7), puis Ogilvie *et al.* (8) à admettre que seul l'ion thiolate est responsable de l'activité catalytique. Les résultats que nous rapportons portent sur un plus grand nombre de composés ne comportant que la fonction thiol et pour une échelle de pK_a beaucoup plus large. Ils confirment et généralisent la conclusion précédente. En effet, même en tenant compte de l'imprécision expérimentale, le tracé du diagramme $Y = f(1/a_H)$ se compose d'un ensemble de droites passant par l'origine (fig. 2), l'ordonnée à l'origine calculée, qui représente la constante spécifique k_{RSH} de la molécule à l'état neutre, a une valeur négligeable ($-0{,}4 < k_{RSH} < +0{,}4$). L'espèce thiol neutre ne présente donc dans ce cas aucune réactivité sur la fonction carbonyle de l'ester et l'effet catalytique est uniquement attribué à l'ion thiolate. La constante spécifique k_{RS^-} (tableau 1) est déterminée à partir de la pente de la droite $Y = f(1/a_H)$ correspondante (méthode des moindres carrés). Nous observons en outre une bonne concordance entre les valeurs de k_{RS^-} ainsi obtenues et celles calculées (tableau 1) pour chaque valeur du pH et de la concentration en catalyseur, par la relation:

$$k_{RS^-} = k_2'(10^{pK_{SH} - pH} + 1)$$

(l'imprécision étant plus grande dans le cas du cyclohéxylméthanethiol, qui présente une très faible réactivité).

Pour l'ensemble des thiols étudiés, la constante spécifique k_{RS^-} est indépendante de la concentration en catalyseur et du pH. L'invariance de k_{RS^-} montre que même à des pH où la concentration en ions thiolate est faible, la forme non ionique du groupe thiol ou le reste de la molécule (cycle benzénique, furanne) n'ont pas d'action décelable. Ce résultat est également observé dans le cas des thiols comportant une fonction susceptible d'accroître l'activité catalytique à certains pH (supé-

Can. J. Chem. Downloaded from www.nrcresearchpress.com by 210.87.254.6 on 09/06/12
For personal use only.

TABLEAU 1. Constantes de vitesse de premier et second ordre pour la réaction d'hydrolyse de l'acétate de *p*-nitrophényle (2×10^{-4} *M*) catalysée par les différents thiols[a]

Thiols	pK_{SH} ±0,02	pH ±0,02	$[RSH]_t$ 10^4 M^{-1}	$[RS^-]$ 10^4 M^{-1}	$k_{obs} - k_{hydr}$ 10^4 min^{-1}	k'_2(±2%) M^{-1} min^{-1}	k_{RS^-}(±6%)[b] M^{-1} min^{-1}	k_{RS^-}[c] M^{-1} min^{-1}
p-Méthoxybenzyl mercaptan	9,86	7,65	5,14	0,0315	52,1 − 9,2	8,3	1361	1390 log k_{RS^-} = 3,14
			7,24	0,044	68,3 − 9,2	8,2	1332	
		7,85	4,13	0,04	67,7 − 13,9	13	1347	
			6,45	0,063	97,9 − 13,9	13	1345	
		8,05	10	0,152	227 − 19,5	20,8	1365	
			10,47	0,160	239 − 19,5	21	1373	
p-Méthylbenzyl mercaptan	9,76	7,65	5,43	0,042	54,4 − 9,2	8,3	1080	1076 log k_{RS^-} = 3,03
			3,00	0,023	34 − 9,2	8,2	1069	
		7,85	3,85	0,047	64,7 − 13,9	13,2	1086	
			4,8	0,058	76 − 13,9	13	1070	
		8,05	5,86	0,11	139 − 19,5	20,4	1069	
			5,3	0,10	127 − 19,5	20,3	1062	
m-Méthylbenzyl mercaptan	9,58	7,65	7,57	0,088	84,7 − 9,2	10,0	859	827 log k_{RS^-} = 2,92
			3,47	0,04	42,7 − 9,2	9,8	829	
		7,85	4,35	0,08	82 − 13,9	15,7	857	
			3,88	0,07	75,5 − 13,9	15,9	868	
		8,05	7,36	0,21	197 − 19,5	24,1	842	
			6,7	0,19	180,7 − 19,5	24	838	
Benzylmercaptan	9,55	7,65	5,38	0,067	64,3 − 9,2	10,3	824	820 log k_{RS^-} = 2,91
			5,06	0,063	61,7 − 9,2	10,4	834	
		7,85	6,44	0,126	118 − 13,9	16,2	827	
			7,19	0,14	131 − 13,9	16,3	835	
		8,05	6,03	0,185	174 − 19,5	25,6	837	
			4,67	0,143	136,5 − 19,5	25	817	
p-Fluorobenzyl mercaptan	9,50	7,65	5,28	0,074	76,5 − 9,2	12,8	915	898 log k_{RS^-} = 2,95
			5,72	0,08	81,7 − 9,2	12,7	911	
		7,85	1,75	0,038	49 − 13,9	20	913	
			3,9	0,086	92 − 13,9	20	911	
		8,05	4,0	0,137	144 − 19,5	31	906	
			5,8	0,198	199,5 − 19,5	31	905	
p-Chlorobenzyl mercaptan	9,23	7,65	3,5	0,09	69 − 9,2	17	661	687 log k_{RS^-} = 2,84
			4,4	0,112	84 − 9,2	17	665	
		7,85	5,82	0,23	171 − 13,9	27	675	
			5,56	0,22	154 − 13,9	27,7	692	
		8,05	8,0	0,5	353 − 19,5	42	669	
			4,65	0,29	214 − 19,5	42	673	
p-Bromobenzyl mercaptan	9,11	7,65	5,22	0,175	109,6 − 9,2	19,2	574	584 log k_{RS^-} = 2,77
			3,67	0,123	80,9 − 9,2	19,5	582	
		7,85	2,41	0,126	87,4 − 13,9	30,5	585	
			3,5	0,183	119,7 − 13,9	30,2	579	
		8,05	3,76	0,30	195 − 19,5	46,6	582	
			2,00	0,16	113 − 19,5	46,6	582	
m-Fluorobenzyl mercaptan	9,07	7,65	4,19	0,15	77,3 − 9,2	16,3	444	461 log k_{RS^-} = 2,66
			2,50	0,092	50,6 − 9,2	16,5	453	
		7,85	6,78	0,39	188,6 − 13,9	25,8	453	
			4,04	0,23	120 − 13,9	26,2	462	
		8,05	4,06	0,35	185 − 19,5	40,7	467	
			4,89	0,43	209 − 19,5	38,8	445	
(Furyl-2) méthanethiol	9,10	7,65	6,96	0,238	145,8 − 9,2	19,65	573	576 log k_{RS^-} = 2,76
			7,12	0,244	151 − 9,2	19,9	582	
		7,85	5,44	0,289	183 − 13,9	31	585	
			5,52	0,294	183,7 − 13,9	31	579	
		8,05	7,90	0,646	389,8 − 19,5	46,9	573	
			6,74	0,551	339,7 − 19,5	47,5	580	

Can. J. Chem. Downloaded from www.nrcresearchpress.com by 210.87.254.6 on 09/06/12
For personal use only.

TABLEAU 1. (*suite et fin*)

Thiols	pK_{SH} ±0,02	pH ±0,02	$[RSH]_t$ $10^4\ M^{-1}$	$[RS^-]$ $10^4\ M^{-1}$	$k_{obs} - k_{hydr}$ $10^4\ min^{-1}$	$k'_2(\pm 2\%)$ $M^{-1}\ min^{-1}$	$k_{RS^-}(\pm 6\%)^b$ $M^{-1}\ min^{-1}$	$k_{RS^-}{}^c$ $M^{-1}\ min^{-1}$
p-Méthylsulfonyl benzylmercaptan	8,62	7,65	3,94	0,381	157 − 9,2	37,5	388	370
			3,84	0,371	131,4 − 9,2	37,8	369	log k_{RS^-} = 2,57
		7,85	4,87	0,706	271,6 − 13,9	53	365	
			2,17	0,315	131,4 − 13,9	54	374	
		8,05	2,46	0,52	215,7 − 19,5	80	377	
			1,42	0,300	132,3 − 19,5	79,7	376	
m-Nitrobenzyl mercaptan	8,54	7,65	3,31	0,377	160,4 − 9,2	45,7	401	387
			4,83	0,552	235,6 − 9,2	46,8	410	log k_{RS^-} = 2,59
		7,85	2,70	0,457	197,7 − 13,9	68	402	
			5,31	0,900	373 − 13,9	67,6	399	
		8,05	4,53	1,1	456,4 − 19,5	96,5	395	
			5,45	1,3	532,7 − 19,5	96,3	394	
p-Nitrobenzyl mercaptan	8,50	7,65	2,23	0,276	114,4 − 9,2	47,1	381	356
			2,37	0,294	116,4 − 9,2	45,2	365	log k_{RS^-} = 2,55
		7,85	1,69	0,31	125,9 − 13,9	66,2	362	
			2,44	0,446	178,6 − 13,9	67,6	369	
		8,05	1,96	0,513	207,6 − 19,5	96	367	
			2,42	0,632	246,2 − 19,5	94	359	
Cystéamine	8,34	7,65	5,11	0,86	178,5 − 9,2	33,1	195	196
			3,9	0,66	138,7 − 9,2	33,1	195	log k_{RS^-} = 2,29
		7,85	1,91	0,47	107,9 − 13,9	49,2	201	
			2,86	0,70	147,8 − 13,9	46,9	192	
		8,05	1,25	0,42	102,7 − 19,5	66,5	196	
			1,51	0,51	119,1 − 19,5	66	195	
Phényl-2 éthanethiol	9,89	7,65	5,56	0,032	29,5 − 9,2	3,64	634	624
			7,65	0,044	36,7 − 9,2	3,62	625	log k_{RS^-} = 2,80
		7,85	5,83	0,053	47,2 − 13,9	5,7	628	
			7,43	0,067	56,9 − 13,9	5,8	641	
		8,05	3,1	0,044	47,4 − 19,5	8,97	634	
			5,8	0,083	71,2 − 19,5	8,93	623	
Mercapto-2 éthanol	9,45	7,65	10,03	0,157	58,3 − 9,2	4,9	313	282
			10,77	0,168	60,3 − 9,2	4,75	304	log k_{RS^-} = 2,45
		7,85	22,97	0,563	176,9 − 13,9	7,1	290	
			12,47	0,306	102,8 − 13,9	7,13	291	
		8,05	10,37	0,397	136,7 − 19,5	11,30	295	
			5,87	0,225	84,3 − 19,5	11,04	288	
Cyclohéxylméthane thiol	10,60	7,65	9,50	0,011	23,2 − 9,2	1,47	1320	961
			7,05	0,008	19,8 − 9,2	1,50	1325	log k_{RS^-} = 2,98
		7,85	5,62	0,01	26 − 13,9	2,15	1210	
			12	0,021	36,8 − 13,9	1,91	1090	
		8,05	3,94	0,011	32,3 − 19,5	3,25	1163	
			11,4	0,032	53 − 19,5	2,94	1047	

[a] Solvant: eau–éthanol (28,5% d'éthanol vol.), T = 30°C, tampon phosphates (0,134 M) I = 0,268.
[b] k_{RS^-} calculé pour chaque valeur de la concentration en catalyseur et du pH.
[c] k_{RS^-} déterminé par la pente de la droite $Y = f(1/a_H)$; pK_{SH} déterminés dans un mélange eau–éthanol (28,5% d'éthanol vol.), T = 30°C, (solutions 10^{-3} M sans addition de KCl).

rieurs au pK_a) pour le mercapto-2 éthanol et la cystéamine. Dans ce dernier cas, l'espèce $R(NH_3^+)S^-$ est prépondérante aux pH étudiés (7,65 à 8,05) (14) et donc responsable de l'activité catalytique.

Influence de la basicité de l'anion sur sa nucléophilie

La basicité de l'ion thiolate définie par la mesure du pK_{SH} varie avec la nature du substituant dans une série de composés homologues. Dans le cas des benzylmercaptans il est possible d'établir une corrélation de Hammett (fig. 3) entre le pK_{SH} de la fonction thiol et les constantes classiques de substituants (15). Pour les dérivés *para* ou *méta* substitués nous obtenons une droite unique d'équation:

$$pK_{SH} = -1{,}30\sigma + 9{,}5 \text{ avec } R = 0{,}99$$

Le but de cette étude cinétique sur ces thiols simples est essentiellement d'examiner s'il existe une relation entre l'activité catalytique de l'ion thiolate et sa basicité. Pour cela nous utilisons une corrélation de Brönsted entre la constante spécifique de l'anion et le pK_a de la fonction thiol. Le diagramme log k_{RS^-} vs. pK_{SH} (fig. 4) présente un bon alignement des points repré-

Can. J. Chem. Downloaded from www.nrcresearchpress.com by 210.87.254.6 on 09/06/12
For personal use only.

Can. J. Chem. Downloaded from www.nrcresearchpress.com by 210.87.254.6 on 09/06/12
For personal use only.

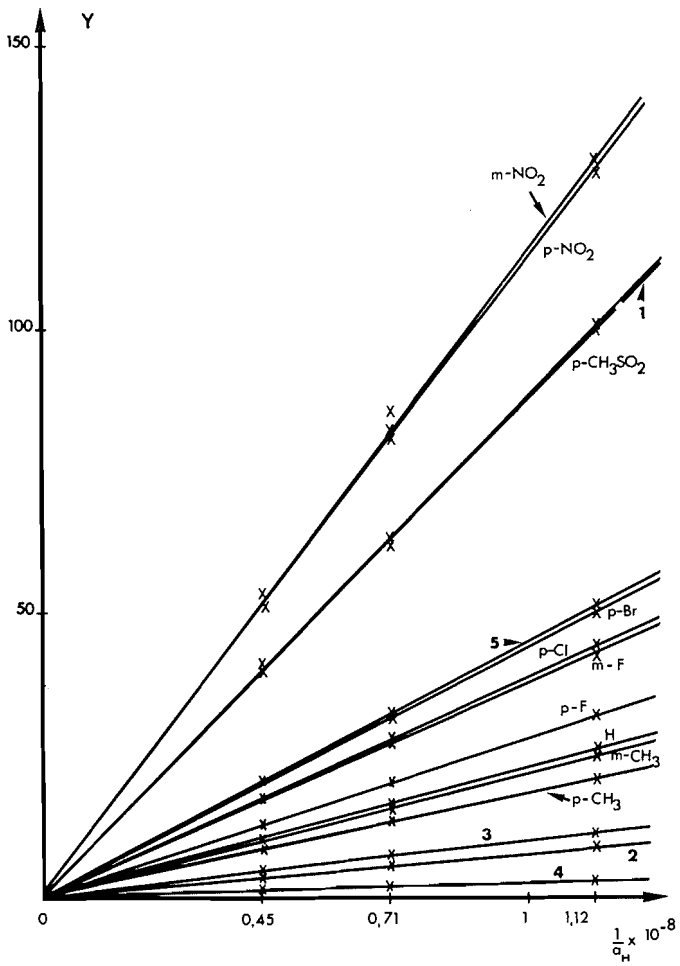

FIG. 2. Représentation de $Y = f(1/a_H)$ pour l'hydrolyse de l'acétate de *p*-nitrophényle catalysée par les différents thiols: benzylméthanethiols *méta* ou *para* substitués, **1** cystéamine, **2** mercapto-2 éthanol, **3** phényl-2 éthanethiol, **4** cyclohexylméthanethiol, **5** (furyl-2) méthanethiol; T = 30°C; mélange eau–éthanol (28,5% d'éthanol vol.); tampon phosphates (0,134 M) I = 0,268.

sentatifs des benzylmercaptans *méta* et *para* substitués ainsi que du composé de même structure, le furyl-2 méthanethiol.

La méthode des moindres carrés conduit à la relation:

$$\log k_{RS^-} = 0{,}4\ pK_{SH} - 0{,}85\ (R = 0{,}99)$$

Pour les ions thiolate avec un environnement stérique et électronique différant peu d'un composé à l'autre, il existe un parallèle entre la vitesse d'attaque du nucléophile sur le centre électrophile et l'affinité de ce même nucléophile pour le proton exprimé par sa basicité.

Dans le cas particulier des dérivés β substitués de l'éthanethiol (cystéamine, mercapto-2 éthanol et phényl-2 éthanethiol), la déviation négative de leurs points représentatifs par rapport à la droite précédente ne peut être attribuée à des erreurs expérimentales, mais plutôt à une diminution de l'activité catalytique de l'anion due à une augmentation de la longueur de la chaîne aliphatique entre le site catalytique et le noyau aromatique ou toute autre fonction. Nous constatons ainsi un accroissement de nucléophilie de l'anion lorsque le centre réactionnel n'est séparé d'un cycle à caractère aromatique que par un seul groupe méthylène. Une observation analogue est faite lors de l'étude de la réactivité d'un thiol comportant un groupe cyclohexyle séparé du site actif par un

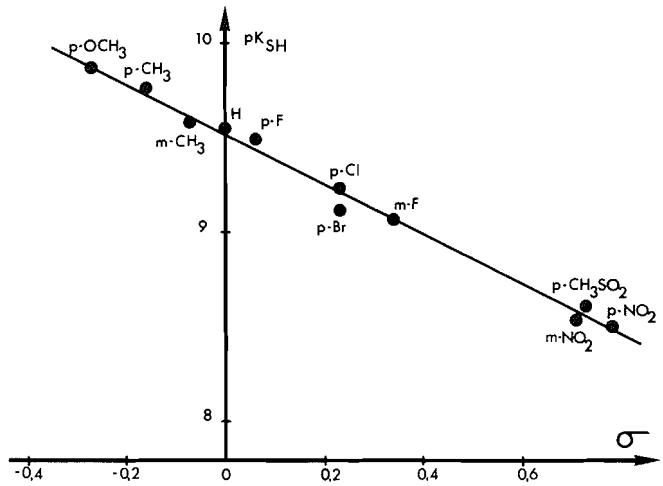

FIG. 3. Corrélation de Hammett pour les pK_{SH} des benzylméthanethiols.

seul méthylène (le cyclohexylmethanethiol). La diminution de nucléophilie de l'anion par rapport à celle d'un benzylmercaptan de même pK_{SH} semble provenir du caractère saturé du groupe fixé en position β.

L'équation de Brönsted trouvée pour la série des benzylmercaptans est très comparable à celle obtenue par Ogilvie *et al.* (8) (0,38 pK_{SH} − 0,75) pour la réaction d'alcanethiols sur le PNPA dans un mélange eau–dioxanne (1% de dioxanne en volume) à 25°C. La valeur β = 0,4 que nous obtenons confirme que la sensibilité à la basicité d'un nucléophile dans les réactions avec l'acétate de *p*-nitrophényle est plus faible dans le cas des bases contenant un atome de soufre que pour les bases oxygénées ou azotées (12). Ce résultat rejoint les conclusions d'Ogilvie *et al.* (8) selon lesquelles, d'un point de vue purement biologique, un thiol possédant un faible pK_{SH} sera un nucléophile très efficace dans le domaine des pH physiologiques. Toutefois, la comparaison des constantes β pour différents types de nucléophiles nécessite certaines réserves dans la mesure où la structure de l'état de transition varie avec la nature des composés (16).

Conclusion

L'étude des propriétés catalytiques sur l'hydrolyse de l'acétate de *p*-nitrophényle d'une série de méthanethiols α substitués par des groupements aromatiques confirme et généralise les premières conclusions avancés par Whitaker (7) en montrant que la fonction thiol est effectivement un catalyseur de type nucléophile uniquement sous la forme thiolate, même à très faible concentration, selon un mécanisme caractérisé par une première étape lente d'attaque sur le groupe carbonyle. La molécule à l'état neutre ne participe aucunement à la réaction.

Partie expérimentale

Méthode générale de préparation des benzylmercaptans

(Méthode à la thiourée – à l'exception des dérivés nitrés, qui nécessitent un procédé particulier).

A partir d'un alcool (17, 18)

On porte à reflux, sous courant d'azote pendant 24 h, un mélange de 0,1 mol d'alcool benzylique approprié, 0,3 mol d'acide bromhydrique à 48% et 0,1 mol de thiourée. Au mélange préalablement refroidi on ajoute 129 mL d'une solution de soude à 10%. On laisse poursuivre la réaction d'hydrolyse pendant 6 h à 100°C. toujours sous courant d'azote, mais sans agitation.

Il se forme une couche huileuse qui est séparée de la phase aqueuse.

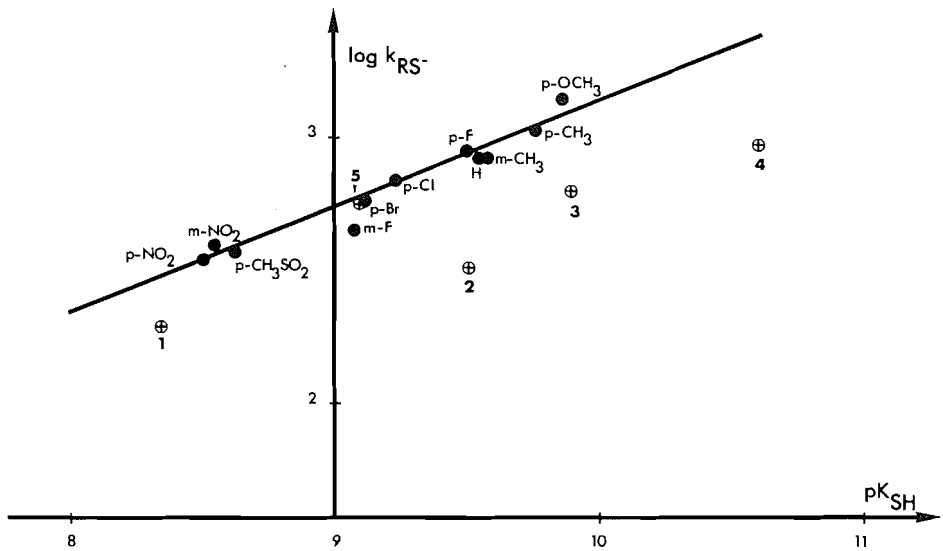

FIG. 4. Corrélation de Brönsted pour la réaction des ions thiolates avec l'acétate de *p*-nitrophényle dans un mélange eau–éthanol (28,5% d'éthanol vol.) à la température de 30°C; ● benzylméthanethiols; ⊕ **1** cystéamine, **2** mercapto-2 éthanol, **3** phényl-2 éthanethiol, **4** cyclohexylméthanethiol, **5** (furyl-2) méthanethiol.

Après refroidissement, la phase aqueuse est acidifiée et le thiol extrait à l'éther. L'extrait éthéré est mélangé à la phase organique, puis séché sur sulfate de calcium. Après évaporation du solvent, l'huile est distillée sous vide pour donner le benzylmercaptan recherché qui est conservé sous argon et à l'abri de la lumière.

Le rendement de la réaction varie entre 60 et 80% selon l'alcool utilisé.

A partir d'un dérivé halogéné

Un mélange de 1,12 mol de thiourée et 0,37 mol de dérivé halogéné dans 60 mL d'eau est porté à reflux sous courant d'azote pendant 6 h. A la solution refroidie on ajoute 2 mol de potasse dans 200 mL d'eau et on laisse poursuivre l'hydrolyse à 100°C pendant 6 h sous courant d'azote et sans agitation. La suite des opérations est identique à celle décrite dans la méthode précedente.

Benzylmercaptans (substituant nucléaire)	Produit de départ	Caractéristiques physiques (solvant de recristallisation, point d'ébullition, point de fusion)
p-CH_3	Alcool	Eb 53°C sous 1 Torr litt. (19) Eb_{14} = 99°C
m-CH_3	Alcool	Eb 49°C sous 1 Torr litt. (19) Eb_{12} = 90°C
p-F	Alcool	Eb 45°C sous 1 Torr
m-F	Alcool	Eb 23°C sous 0,6 Torr litt. (20) Eb_3 = 45°C
p-Br	Bromure	P.F. = 25°C litt. (21) F° = 25°C
p-CH_3SO_2	Bromure	Distillation sous vide F° = 46°C
Cyclohexylmethanethiol	Alcool	Eb_{11} = 54°C sous 11 Torr

La cystéamine, le mercapto-2 éthanol et le phényl-2 éthanethiol sont des produits commerciaux, ainsi que le furyl-2 méthanethiol et les benzylmercaptans (*p*-OCH_3, *p*-Cl, H).

Synthèse du bromure de méthylsulfonyl-4 benzyle

Ce composé n'est pas commercialisé, il a donc fallu envisager sa synthèse à partir de l'acide *p*-méthylsulfonylbenzoïque.

Préparation du chlorure de méthylsulfonyl-4 benzoyle

On porte à reflux pendant 4 h un mélange de 0,101 mol d'acide *p*-méthylsulfonylbenzoïque, 0,303 mol de chlorure de thionyle (23 mL) et 2,3 mL de diméthylformamide. Après élimination du chlorure de thionyle excédentaire par distillation, le chlorure d'acide est ensuite recristallisé dans le benzène; *F* = 129°C, rendement 85%.

Préparation du méthylsulfonyl-4 benzoate d'éthyle

On ajoute à froid, par petites quantités, 0,086 mol du chlorure d'acide dans un mélange alcool–pyridine. Celui-ci est chauffé au bain marie pendant 3 h, tout le chlorure passe alors en solution. Après refroidissement le produit précipite en masse. Il est essoré, puis abondamment lavé à l'eau pour éliminer la pyridine, puis à l'éther de pétrole. L'ester est recristallisé dans le benzène; *F* = 96–97°C. Rendement après recristallisation: 84%.

Réduction de l'ester

Borohydrure de lithium (0,025 mol) à 99% dans 25 mL de diglyme anhydre sont versés dans un ballon tricol équipé d'une agitation. On ajoute par petites portions 0,04 mol de méthylsulfonyl-4 benzoate d'éthyle (9, 12 g) et on chauffe le mélange au bain marie pendant 3 h. La solution obtenue est ensuite versée dans 50 g de glace pilée contenant 5 mL d'acide chlorhydrique concentré. Après extraction à l'éther et évaporation à sec, l'alcool obtenu a un aspect sirupeux et recristallise très difficilement. Il sera utilisé sans autre purification. Rendement en produit brut: 90%. Le diglyme utilisé est purifié selon une méthode décrite par Brown *et al.* (22).

Bromation de l'alcool méthylsulfonyl-4 benzylique

Nous avons adapté une méthode de bromation des alcools décrite par Kamm et Marvel (23). On ajoute goutte à goutte 2 g d'acide sulfurique concentré dans un mélange de 0,04 mol de l'alcool précédent, 0,49 mol d'acide bromhydrique à 48% et 2,5 g d'acide sulfurique concentré. La solution est portée à reflux pendant 6 h, puis versée dans de la glace pilée. Le bromure précipite sous forme de fines plaquettes. Le produit est recueilli sur verre fritté, et lavé à l'eau froide pour éliminer l'acide. Recristallation dans un mélange (méthylcyclohexane–benzène, 50:50 en volume); rendement quantitatif; *F* = 97°C.

Préparation des p- *et* m-*nitrobenzylmercaptans*

Les thiocyanates

A 0,1 mol de chlorure de *p*- ou *m*-nitrobenzyle dissoute dans 150 mL d'alcool absolu, on ajoute par petites quantités et sous bonne agitation 0,1 mol de thiocyanate de potassium sec et on porte le mélange à reflux pendant 6 h. La suspension est ensuite filtrée à chaud afin de séparer le chlorure de potassium qui a précipité au cours de la réaction. Le thiocyanate cristallise après refroidissement du filtrat.

Can. J. Chem. Downloaded from www.nrcresearchpress.com by 210.87.254.6 on 09/06/12
For personal use only.

Can. J. Chem. Downloaded from www.nrcresearchpress.com by 210.87.254.6 on 09/06/12
For personal use only.

Recristallisation dans l'alcool; rendement: 93%; dérivé *para*: F = 86°C; dérivée *méta*: F = 72°C. Caractérisation par spectroscopie infrarouge, ν(SC≡N): bande fine et intense à 2150 cm^{-1}.

Hydrolyse du thiocyanate par l'acide sulfurique

Le dérivé thiocyanaté (1 g) est ajouté dans 10 g d'acide sulfurique 36 *N* refroidi à 0°C. La solution est ensuite maintenue à 0°C sous agitation pendant une nuit, puis versée dans un mélange eau–glace. Le précipité formé (thiolamide) est essoré et lavé plusieurs fois à l'eau; rendement quantitatif.

Le composé *para* est recristallisé dans l'alcool absolu, F = 140–141°C; le dérivé *méta* dans le benzène, F = 122–123°C. Sur le spectre infrarouge on remarque la disparition de la bande ν(SCN) et l'apparition de la bande amide I ν(C=O) à 1660 cm^{-1}.

Hydrolyse de la thiolamide

Un mélange de 0,1 mol de thiolamide dans 150 mL d'acide chlorhydrique 6 *N* est porté à reflux sous azote pendant 12 h. Le mercaptan libéré au cours de la réaction est extrait à l'éther, séché sur sulfate de calcium puis distillé sous vide ou recristallisé; *m*-nitro, Eb 110°C sous 0,6 Torr (1 Torr = 133.3 Pa); *p*-nitro recristallisé dans l'éther de pétrole F = 55°C, litt. (24) F = 55°C.

Caractéristiques spectrales des différents thiols

Spectroscopie infrarouge

Les spectres ir ont été enregistrés sur un spectromètre Unicam SP 1200, cependant, l'absorption liée au mouvement d'élongation ν(SH) se manifeste vers 2550 cm^{-1} mais elle est trop peu intense pour la considérer comme déterminante.

Spectrométrie de résonance magnétique nucléaire (proton)

Les caractéristiques sont obtenues à partir d'un appareil Hitachi R 24-A 60 Mz. Les composés sont étudiés à l'état pur pour les liquides et en solution dans le chloroforme deutérié pour les solides (la référence interne étant le TMS). Le signal qui caractérise la fonction thiol apparaît dans les benzylmercaptans et le cyclohexylmethanethiol sous la forme d'un triplet résultant du couplage du proton SH et des protons méthylèniques. La position du pic central de ce signal se situant aux environs de 1,7 ppm.

Dosage chimique du groupe mercaptan

L'analyse élémentaire ne permet pas de s'assurer que la totalité du soufre contenu dans ces composés est présent uniquement sous la forme de fonctions thiols. Nous avons eu recours à une méthode de caractérisation chimique quantitative du groupe mercaptan décrite par Saville (25). L'évaluation du taux de fonction thiol est en outre rendu nécessaire pour les essais cinétiques.

Etude acidimétrique

Les fonctions thiols incluses dans les composés examinés peuvent être dosées par acidimétrie. Les pK_{SH} correspondants sont obtenus à partir des courbes de neutralisation et les pH mesurés au moyen d'un appareil Tacussel TS 70/N_1. On opère à 30°C ± 0,1, sous atmosphère d'azote dans le mélange eau–éthanol (28,5% d'éthanol en volume). La précision est estimée à ±0,02.

Mesures cinétiques

Les mesures ont lieu dans des milieux constitués, en raison de la solubilité de certains thiols, de 28,5% d'alcool et 71,5% d'eau. Le pH, ainsi que la force ionique du milieu, sont maintenus constants à l'aide de solution tampons, tandis que la température est fixée à 30°C ± 0,1. Les tampons normalement utilisés sont des solutions aqueuses de dihydrogénophosphate de potassium et d'hydrogénophosphate de sodium selon Clark et Lubs (26) à la concentration totale de 0,134 *M* et une face ionique I = 0,268.

La concentration en ester est fixée à 2×10^{-4} *M*. L'ester et le catalyseur sont intimement mélangés puis dissous dans la quantité nécessaire d'alcool. On complète alors au volume désiré (100 mL) par la solution aqueuse tampon à 30°C. Le temps $t = 0$ est pris au moment où l'on atteint le volume final. Une partie de la solution est alors transvasée dans la cellule de mesure. Les vitesses de réaction sont suivies par enregistrement à l'aide d'un spectrophotomètre uv–visible Hitachi 320. Les mesures sont faites à 405 nm maximum d'absorption du *p*-nitrophénolate. La formation d'ions est reliée à la disparition de l'ester par la relation $[\text{ester}] = [\text{ester}]_0 - D/\epsilon_{app} \times l$ avec l = 1 cm, D = densité optique à 405 nm, ϵ_{app} est le coefficient d'extinction molaire apparent à 405 nm et au pH considéré. Il est directement déterminé dans les mêmes conditions que les mesures cinétiques sur le *p*-nitrophénol et varie de 1,38 à 1,85 $\times 10^4$ L M^{-1} cm^{-1} dans le domaine des pH utilisés.

1. F. SCHNEIDER. Hoppe Seyler's Z. Physiol. Chem. **348**, 1034 (1967).
2. F. SCHNEIDER et H. WENCK. Hoppe Seyler's Z. Physiol. Chem. **350**, 1653 (1969).
3. J. C. SHEEHAN, G. B. BENNETT et J. A. SCHNEIDER. J. Am. Chem. Soc. **88**, 3455 (1966).
4. E. KATCHALSKI, G. D. FASMAN, E. SIMONS, R. BLOUT, F. R. N. GURD et N. L. KOLTON. Arch. Biochem. Biophys. **88**, 361 (1960).
5. P. LOCHON et J. SCHOENLEBER. Tetrahedron, **32**, 3023 (1976).
6. W. P. JENCKS et J. CARRIUOLO. J. Am. Chem. Soc. **82**, 1778 (1960).
7. J. R. WHITAKER. J. Am. Chem. Soc. **84**, 1900 (1962).
8. J. W. OGILVIE, J. T. TILDON et B. S. STRAUCH. Biochemistry, **3**, 754 (1964).
9. G. R. SCHONBAUM et M. L. BENDER. J. Am. Chem. Soc. **82**, 1900 (1960).
10. G. GUANTI, C. DELL'ERBA, F. PERO et G. LEANDRI. J. Chem. Soc. Perkin Trans. 2, 212 (1975).
11. T. C. BRUICE et G. L. SCHMIR. J. Am. Chem. Soc. **79**, 1663 (1957).
12. T. C. BRUICE et R. LAPINSKI. J. Am. Chem. Soc. **80**, 2265 (1958).
13. T. C. BRUICE et G. L. SCHMIR. J. Am. Chem. Soc. **80**, 148 (1958).
14. R. E. BENESCH et R. BENESCH. J. Am. Chem. Soc. **77**, 5877 (1955).
15. H. H. JAFFE. Chem. Rev. **53**, 91 (1953).
16. F. G. BORDWELL et W. J. BOYLE. J. Am. Chem. Soc. **94**, 3907 (1972).
17. J. M. SPRAGUE et T. B. JOHNSON. J. Am. Chem. Soc. **58**, 1837 (1937).
18. R. L. FRANK et P. V. SMITH. J. Am. Chem. Soc. **68**, 2103 (1946).
19. J. V. BRAUN, W. MAY et R. MICHAELIS. Ann. **490**, 189 (1931).
20. C. VON SZCEPANSKI, J. HEINDL, E. SCHROEDER, H. J. KESSLER et U. REDMANN. Ger. Offen. 2,114, 653 (C1 C07 C,A 61 k, 5 Oct. 1972, Appl. P 21 14653.2, 23 Mar. 1971).
21. C. L. JACKSON et G. T. HARTSHORN. Am. Chem. J. **5**, 268 (1883).
22. H. C. BROWN, E. J. MEAD et B. C. SUBBA RAO. J. Am. Chem. Soc. **77**, 6209 (1955).
23. O. KAMM et C. S. MARVEL. Org. Synth. Coll. Vol. **1**, 25 (1941).
24. R. POGGI. Atti R. Accad. Naz. Lincei. Vol. II, 423 (1925).
25. B. SAVILLE. Analyst, **86**, 29 (1961).
26. W. M. CLARK et H. A. LUBS. J. Biol. Chem. **25**, 479 (1916).

Electrostatic effects on disproportionation equilibria: dihalogeno and methyl derivatives of benzene

ZDENĚK FRIEDL[1]

Department of Chemistry, University of Alberta, Edmonton, Alta., Canada T6G 2G2

Received December 12, 1984

ZDENĚK FRIEDL. Can. J. Chem. **62**, 2337 (1984).

The disproportionation equilibria of benzene derivatives X—Ph—Y (X, Y = F, Cl, CH_3) in the gas phase, were calculated from their enthalpies and entropies of formation at 298 K. Calculations of the electrostatic energy based on the point charges approximation method predict reasonably well the reaction enthalpies of all *meta*-benzene derivatives and predict nearly as well the other fluoro- and methyl-derivatives. The theory fails if strong resonance and/or steric interactions are present. The generally better ability of the electrostatic theory to treat disproportionation or conformational equilibria than the proton transfer reactions is also discussed.

ZDENĚK FRIEDL. Can. J. Chem. **62**, 2337 (1984).

En utilisant leurs enthalpies et leurs entropies de formation, on a calculé l'équilibre de dismutation, à 298 K et en phase gazeuse, des dérivés benzéniques X—Ph—Y (X, Y = F, Cl, CH_3). Des calculs d'énergie électrostatique, basés sur la méthode d'approximation des charges ponctuelles, permettent de prédire convenablement les enthalpies de réaction de tous les dérivés du benzène substitués en position *méta* et permettent de faire des prédictions presqu'aussi bonnes pour les autres dérivés fluorés et méthylés. La théorie n'est pas adéquate si les molécules étudiées portent des groupes provoquant une forte résonance et/ou de fortes interactions stériques. On discute aussi du fait que la théorie électrostatique est généralement plus apte à traiter des équilibres de dismutation ou conformationnels que les réactions de transfert de proton.

[Traduit par le journal]

Can. J. Chem. Downloaded from www.nrcresearchpress.com by 210.87.254.42 on 09/06/12
For personal use only.

Introduction

In previous papers in this series we have investigated the electrostatic effects on conformational (1–4) and ionization (5–7) equilibria to test the individual assumptions and approximations of the theory. In the cases of proton transfer reactions

[1] R—Z—H + Z^- = R—Z^- + Z—H

and conformational equilibria

[2] R—Z—X—Y (*anti*) = R—Z—X—Y (*syn*)

with a dipolar substituent R, the substituent effect on the equilibrium constant may be expressed within the framework of classical electrostatics. The Gibbs energy is then usually equated to the electrostatic energy

[3] $\Delta G^0 = -RT \ln K = N_A f(z_i, \mu_i, r_i, \theta_i, \epsilon_{ef})$

where r is the distance between charges z and/or dipoles μ, θ the angle between μ's or μ and r, and ϵ_{ef} effective relative permittivity.

The electrostatic theory has been applied to many ionization equilibria, mostly of carboxylic acids in mixed aqueous solvents (8–10). An application of the electrostatic theory in this case is heavily dependent on all of its approximations. One possible failing of the theory is the fact that the Z—H bond energies in the substituted (RZH) and unsubstituted (ZH) acid will probably not be exactly equal (1, 3–4, 6). Another difficulty can be a too strong non-electrostatic interaction, e.g., resonance, between the substituent R and the anion in RZ^-. Nevertheless, the most important complications originate in the experimental conditions. Except for some gas phase results available only recently (11, 12), the equilibrium constants of reaction [1] have been determined mostly in water or in aqueous polar solvents (8–10). Thus all the solute molecules and ions involved in the equilibria appear as solvated species and the solvation energies do not necessarily cancel (13). Finally, the effective relative permittivitiy ϵ_{ef} must be calculated from the solvent bulk permittivity ϵ_{ext} and the internal relative permittivity ϵ_{int} attributed to the solute molecule. In such a calculation the solute molecule is described as a spheroidal (14) or ellipsoidal (15–18) cavity and its geometrical parameters are adjusted in different ways (14–19).

The possibility of measuring proton transfer reactions in the gas phase is apparently the best way to test the electrostatic theory. There are no solvent molecules so that difficulty with the calculations of ϵ_{ef} are eliminated. In spite of these assumptions our recent study (7) of proton transfer reactions in the gas phase has disclosed fundamental shortcomings of the theory even for such condition.

In the case of conformational equilibria (1–4, 20–25), the electrostatic theory has been more successful due primarily to the possibility of working in non-polar solvents. This removes problems with calculating the effective relative permittivity by means of cavity models and ϵ_{ef} is simply set equal to the solvent bulk permittivity ϵ_{ext}, even if the ϵ_{ef} differs slightly from the ϵ_{ext} which occurs when the solute and solvent do not have the same permittivity. In addition, no bond is broken during the conformational change, so that cancellation of bond energies (5–7, 13) loses its importance.

On the other hand, the applicability of the theory is strongly restricted to model compounds in which the remaining non-electrostatic substituent effects are eliminated. This concerns particularly non-bonded interactions, torsional strain and resonance effects. In addition, despite the possibility of measuring the conformational equilibria in non-polar solvents, there still remains the necessity to consider different energies of solvation of both conformers.

For the above reasons we proposed (26) to test the electrostatic theory on the isodesmic equilibria of the disproportionation type (eq. [4]), which had not been discussed in the

[4] R—Z—X—Y + Z—X = R—Z—X + Z—X—Y

literature in this way so far. In general, the disproportionation

[1]Permanent address: Department of Organic Chemistry, Slovak Technical University, CS-81237 Bratislava, Czechoslovakia.

TABLE 1. Thermodynamic parameters, electrostatic energies, and energies derived from CNDO/2 and STO-3G calculations for [5] (in kJ mol^{-1})

No.	X	Y	ΔH^0	$T\Delta S^0$	$T\Delta S_\sigma$	ΔE_{elst}[a]	ΔE_{tot} CNDO	ΔE_{elst}[b] CNDO	ΔE_{tot} STO-3G
1	F	2-F	−21.6	4.2	4.4	−17.5	−15.1	−54.4	−13.0[c]; −38.3[d]
2	F	3-F	−6.1	4.7	4.4	−5.5	−1.0	23.7	0.0[c]; −24.9[d]
3	F	4-F	−8.8	6.1	6.2	−4.2	−4.7	−21.1	−2.9[c]; −12.1[d]
4	Cl	2-Cl	−9.2	4.8	4.4	−18.1	−9.5	−19.9	—
5	Cl	3-Cl	−5.7	4.3	4.4	−6.2	−2.4	3.7	—
6	Cl	4-Cl	−2.3	6.3	6.2	−4.8	−2.9	−7.7	—
7	F	4-CH_3	−1.5	4.3	4.4	0.6	−0.8	−5.6	−0.8[c]
8	F	3-CF_3	−5.9	—	2.7	−3.4	−5.0	−12.3	—
9	CH_3	2-CH_3	−1.9	5.8	4.4	−0.4	3.1	−2.2	—
10	CH_3	3-CH_3	−0.2	4.3	4.4	−0.1	4.3	1.4	—
11	CH_3	4-CH_3	−0.9	5.9	6.2	0.0	3.4	−2.4	—

[a]The point charges taken from the bond moment scheme (ref. 1).
[b]The point charges taken from the CNDO charge distribution.
[c]Reference 32.
[d]Reference 33.

equilibria have the advantage versus the ionization and conformational equilibria that cavity models and differential solvation need not be taken into account, since the equilibria are investigated in the gas phase. In these reactions some bonds are broken but changes in the bond energies may be self-compensating and non-electrostatic interactions should not be stronger than in the preceding cases.

In this paper we investigate the disproportionation equilibria of fluoro-, chloro-, and methyl-disubstituted benzene derivatives.

[5] 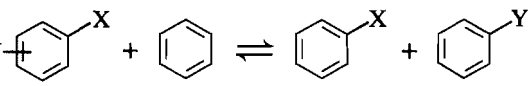

The thermodynamic data are compared with both electrostatic and quantum chemical calculations.

Results

Thermodynamic calculations

The experimental enthalpies ΔH_f^0 and entropies ΔS^0 of formation in the gas phase at 298 K were taken from ref. 27. The relative energies of the disproportionation equilibria ΔH^0 were obtained as a difference of the sums of ΔH_f^0 of reactants and products. To test the premise of a symmetry control of isodesmic reactions (28), the entropy change ΔS^0 was assumed to be due to changes of symmetry during reaction [5]:

$$[6] \quad \Delta S^0 \cong \Delta S_\sigma = R \ln K_\sigma$$

so that eq. [7]

$$[7] \quad \Delta G^0 = \Delta H^0 - T\Delta S^0$$

can be written consequently as

$$[8] \quad \Delta G^0 \cong \Delta E_{elst} - T\Delta S_\sigma$$

The experimental values ΔH^0 and $T\Delta S^0$ are listed in Table 1 together with the calculated terms $T\Delta S_\sigma$.

Electrostatic calculations

For disproportionation equilibrium [4] using the point charges approximation, the ΔE_{elst} term from eq. [8] acquires the form

$$[9] \quad \Delta E_{elst} = (N_A/4\pi\epsilon_o) \sum q_i q_j / r_{ij}$$

where r_{ij} is the distance between the charges q_i and q_j. The summation extends to all molecules involved with the reactants being taken with a negative sign. The charges q on individual atoms were obtained as previously (1) by dividing the bond moments by the bond lengths and summing up at each atom. Standard bond moments were used (29) (in 10^{-30} C m): C_{al}—H −1.0, C_{al}—F 4.67, C_{ar}—F 4.90, C_{ar}—Cl 5.34 plus resonance moment 0.33. The distances r_{ij} were calculated from the standard geometry parameters (30) (in pm): C_{ar}—C_{ar} 139, C_{ar}—H 108, C_{ar}—F 133, C_{ar}—C 170, C_{ar}—C 152, C—H 109, C—F 136. The benzene nucleus was assumed hexagonal and all remaining bond angles were assumed to be 109.5°. The results are listed in Table 1.

Quantum chemical calculations

The total energies and charge distributions of all benzene derivatives were calculated by the CNDO/2 method with the standard parametrizations (31) and standard geometries, which were the same as in the previous paragraph and were not optimized. The *ab initio* STO-3G calculations were taken from refs. 32 and 33 and had also been obtained without optimizing the standard geometry (30). The results are given in Table 1.

Discussion

In the past, several attempts have been made (34–37) to calculate absolute values of enthalpies of formation ΔH_f^0 in the gas phase by a simple electrostatic approach, treating the molecule as a system of discrete point charges in a vacuum. The results agreed generally well with experiments, considering the rough approximation of the theory.

When we had decided to test the electrostatic theory on disproportionation equilibria, we were restricted in the choice of suitable model systems to published ΔH_f^0 or ΔG_f^0 values in the gas phase (27). We chose the set of fluoro-, chloro-, and methyl-substituted benzene derivatives 1–11 (see Table 1), even though we were aware of possible shortcomings, notably possible resonance interactions.

The relative ΔH^0 and ΔE_{elst} energies of reaction [5] are given in Table 1 together with the experimental $T\Delta S^0$ and calculated entropy terms $T\Delta S_\sigma$. When comparing these values, there is an

Can. J. Chem. Downloaded from www.nrcresearchpress.com by 210.87.254.42 on 09/06/12
For personal use only.

Can. J. Chem. Downloaded from www.nrcresearchpress.com by 210.87.254.42 on 09/06/12
For personal use only.

evident agreement with the assumption (eq. [6]), that the entropy change is practically all due to changes of symmetry during reaction [5]. When discussing the ΔE_{elst} data in Table 1, it is advisable to start with *meta*-substituted derivatives **2**, **5**, **8**, and **10**, because in these compounds the bonding, resonance, and steric interactions may be negligible. Provided this condition is fulfilled, only the polar (i.e. electrostatic) interactions will be significant. The agreement is reasonably good considering that the limiting value for the relative permittivity of gaseous molecules, as suggested recently (25), is 1.5. A worse but still reasonable agreement was obtained for the other fluoro and methyl *ortho*/*para*-derivatives **1**, **3**, **9**, and **11**. The reason for the failure of the theory for *ortho*-dichlorobenzene **4**, *para*-dichlorobenzene **6**, and *para*-fluorotoluene **7** is evidently the large polarizability and steric effects in **4**, and strong resonance interactions in **6** and **7** which interfere with the electrostatic interaction.

The results of the CNDO/2 and some STO-3G calculations are only able to qualitatively reproduce the experimental ΔH^0 values. Note the poorer agreement of the *ab initio* calculations (32, 33) in comparison with the simple semi-empirical CNDO/2 method. It is important to note that *ab initio* calculations, done using a minimum basis STO-3G set and without geometry optimization, are generally accepted as a standard method for description of isodesmic reactions (32, 38), but it can be shown that only optimized calculations at STO 4-31G level lead to any essential improvement (39). Electrostatic calculations based on CNDO/2 charge distribution do not agree with ΔH^0 either quantitatively or qualitatively and our preliminary attempts on the same level gave similarly poor results (2, 4). Probably it will be necessary to use a more sophisticated charge distribution (40) than that of the traditional Mulliken population analysis.

In summary, we can state that the electrostatic theory with its point charges approximation as expressed by eq. [10] is reasonably adequate for the description of the disproportionation equilibria investigated in this study. A more accurate proof should be possible in future, if further thermodynamic data of suitable model compounds become available.

Acknowledgements

I am grateful to Professor Otto Exner, Prague, and to Professor Loren G. Hepler for many helpful discussions. I also thank the Natural Sciences and Engineering Research Council of Canada for support of this research and related continuing research.

1. O. EXNER and Z. FRIEDL. Collect. Czech. Chem. Commun. **42**, 3030 (1977).
2. Z. FRIEDL and O. EXNER. Collect. Czech. Chem. Commun. **43**, 2591 (1978).
3. Z. FRIEDL, P. FIEDLER, and O. EXNER. Collect. Czech. Chem. Commun. **45**, 1351 (1980).
4. O. EXNER, Z. FRIEDL, and P. FIEDLER. Collect. Czech. Chem. Commun. **48**, 3086 (1983).
5. O. EXNER and Z. FRIEDL. Collect. Czech. Chem. Commun. **43**, 3227 (1978).
6. Z. FRIEDL, J. HAPALA, and O. EXNER. Collect. Czech. Chem. Commun. **44**, 2928 (1979).
7. K. KALFUS, Z. FRIEDL, and O. EXNER. Collect. Czech. Chem. Commun. **49**, 179 (1984).
8. S. EHRENSON. Prog. Phys. Org. Chem. **2**, 195 (1964).
9. L. M. STOCK. J. Chem. Educ. **49**, 400 (1972).
10. W. F. REYNOLDS. Prog. Phys. Org. Chem. **14**, 165 (1983).
11. P. KEBARLE. Ann. Rev. Phys. Chem. **28**, 445 (1977).
12. R. W. TAFT. Prog. Phys. Org. Chem. **14**, 247 (1983).
13. H. M. SMALLWOOD. J. Am. Chem. Soc. **54**, 3048 (1932).
14. J. G. KIRKWOOD and F. H. WESTHEIMER. J. Chem. Phys. **6**, 506 (1938).
15. F. H. WESTHEIMER and J. G. KIRKWOOD. J. Chem. Phys. **6**, 513 (1938).
16. J. N. SARMOUSAKIS. J. Chem. Phys. **12**, 277 (1944).
17. S. EHRENSON. J. Am. Chem. Soc. **98**, 7510 (1976).
18. S. EHRENSON. J. Org. Chem. **48**, 1884 (1983).
19. C. TANFORD. J. Am. Chem. Soc. **79**, 5348 (1957).
20. R. A. Y. JONES, A. R. KATRITZKY, and A. V. OCHKIN. J. Chem. Soc. B, 1795 (1971).
21. H. WENNERSTRÖM, S. FORSÉN, and B. ROSS. J. Phys. Chem. **76**, 2430 (1972).
22. H. LUMBROSO and C. G. ANDRIEU. Bull. Soc. Chim. Fr. 1575 (1973).
23. I. TVAROŠKA and T. BLEHA. Collect. Czech. Chem. Commun. **43**, 922 (1978).
24. R. D. STOLOW, P. W. SAMAL, and T. W. GIANTS. J. Am. Chem. Soc. **103**, 197 (1981).
25. L. DOŠEN-MICOVIC, D. JEREMIC, and N. L. ALLINGER. J. Am. Chem. Soc. **105**, 1716 (1983); **105**, 1723 (1983).
26. Z. FRIEDL and O. EXNER. First conference on organic and bioorganic chemistry of young scientists. Bechyně, Czechoslovakia. 1980.
27. D. R. STULL, E. F. WESTRUM, and G. C. SINKE. The chemical thermodynamics of organic compounds. John Wiley and Sons, New York. 1969.
28. S. W. BENSON. Thermochemical kinetics. John Wiley and Sons, New York. 1976.
29. O. EXNER. Dipole moments in organic chemistry. Thieme, Stuttgart. 1975. p. 33.
30. J. A. POPLE and M. GORDON. J. Am. Chem. Soc. **89**, 4253 (1967).
31. J. A. POPLE and D. L. BEVERIDGE. Approximate molecular orbital theory. McGraw-Hill, New York. 1970. QCPE Program No. 141.
32. A. PROSS and L. RADOM. Prog. Phys. Org. Chem. **13**, 1 (1981).
33. S. MILLEFIORI, A. MILLEFIORI, and G. GRANOZZI. J. Mol. Struct. **89**, 247 (1982).
34. V. A. PALM and N. V. PALM. Reakts. Sposobnost Org. Soedin. **10**, 391 (1973).
35. V. A. PALM. Reakts. Sposobnost Org. Soedin. **10**, 413 (1973).
36. S. W. BENSON and M. LURIA. J. Am. Chem. Soc. **97**, 704, 3337, 3342 (1975).
37. S. W. BENSON. Angew. Chem. Int. Ed. Engl. **17**, 812 (1978).
38. S. MARRIOTT and R. D. TOPSOM. J. Mol. Struct. **89**, 83 (1982).
39. E. VON NAGY-FELSOBUKI, R. D. TOPSOM, S. POLLACK, and R. W. TAFT. J. Mol. Struct. **88**, 255 (1982).
40. V. SACKWILD and W. G. RICHARDS. J. Mol. Struct. **89**, 269 (1982).

The mass spectra of pyrimidines. II. 2(1*H*)-Pyrimidinethiones and some N(1)-substituted derivatives

ROBIN T. B. RYE,[1] OSWALD S. TEE, AND EVA M. KAZDAN
Department of Chemistry, Concordia University, 1455 de Maisonneuve Blvd., W., Montreal, P.Q., Canada H3G 1M8

Received July 11, 1983[2]

ROBIN T. B. RYE, OSWALD S. TEE, and EVA M. KAZDAN. Can. J. Chem. **62**, 2340 (1984).

The EI induced fragmentation of 2(1*H*)-pyrimidinethione (**1**), some N(1)-substituted derivatives, and 2(1*H*)-pyrimidineselenone (**4**) have been studied. Principal fragmentation pathways have been identified using ^{2}H-labelling, metastable defocussing, and exact mass measurements.

The fragmentations of **1** and **4** generally parallel those reported for 2(1*H*)-pyrimidinone. In contrast to the oxo-compound, however, direct expulsion of the exocyclic hetero atom is significant in the fragmentation of **1**, and dominates the spectrum of **4**.

Based on metastable peak abundances and kinetic energy release measurements, it is postulated that the $[M - H]^+$ entity generated from *N*-ethyl-2-pyrimidinethione has a thiazolinium structure.

ROBIN T. B. RYE, OSWALD S. TEE et EVA M. KAZDAN. Can. J. Chem. **62**, 2340 (1984).

On a étudié la fragmentation, induite par impact électronique, de la (1*H*)-pyrimidinethione-2 (**1**), de quelques-uns de ses dérivés substitués en position N(1) et de la (1*H*)-pyrimidinesélénone-2 (**4**). On a identifié les principales voies de fragmentation en faisant appel au marquage au ^{2}H, à la dispersion des ions métastables et à des mesures de masses exactes.

Les fragmentations des composés **1** et **4** sont généralement semblables à celles rapportées antérieurement pour la (1*H*)-pyrimidone-2. Cependant, contrairement à ce qui est observé avec le composé oxo, l'expulsion directe de l'hétéroatome exocyclique est importante lors de la fragmentation du composé **1** et elle est majoritaire dans le spectre du composé **4**.

En se basant sur les abondances relatives des pics métastables et sur les mesures d'énergie cinétique dégagée, on postule que l'entité $[M - H]^+$ générée par la *N*-éthyl pyrimidinethione-2 a une structure de thiazolinium.

[Traduit par le journal]

Introduction

It has been known for some time that the thio-analogues of the pyrimidine bases show significant biological activity. Lozzio and Wigler (1) interpreted the cytoxicity of 2-thiocytosine and 2-thiouracil in terms of interference with RNA synthesis, and the effect of 2-thiocytosine on mitosis in human lymphocytes has been reported (2). Holy and co-workers reported that 2-pyrimidinethione (**1**) showed marked *in vitro* bacteriostatic activity towards *E. coli* (3). We are interested in **1** and its derivatives as precursors for synthetic nucleosides. As part of this continuing study we have examined the mass spectra of **1**, its seleno-analogue, and the N(1)-substituted pyrimidinethiones listed in Table 1.

Experimental

Synthesis[3]

Preparation of the pyrimidinethiones employed in this study followed the cyclization procedure described previously (4). The 2(1*H*)-pyrimidineselenone, **4**, was prepared in 38% yield from selenourea (Aldrich) via cyclization with 1,1,3,3-tetramethoxy propane; mp 174–176°C. *Anal.* calcd. for $C_4H_4N_2Se$: C 30.20, H 2.53, N 17.61, Se 49.64; found: C 29.99, H 2.58, N 17.57, Se 49.62.

Spectra

The mass spectra were taken on a Hitachi-Perkin-Elmer RMU-7 instrument using 70 V ionizing electrons and the lowest practicable source temperature. First field-free region metastable peaks were recorded by the accelerating voltage scan method, using an instrument modification previously described by McGillivray and co-workers (5). Exact mass measurements and additional metastable peaks data were obtained using a Kratos-AEI MS-902S instrument.

TABLE 1. Compounds studied

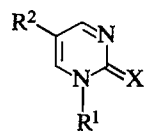

Compound	R^1 (R^2 = H, X = S)	Compound	R^2 (R^1 = H)
1	H	**2**	D, X = S
3	D	**4**	H, X = Se
5	CH_3		
6	C_2H_5		
7	Phenyl		
8	CD_3		
9	CH_2CD_3		
10	CD_2CH_3		
11	CD_2CD_3		
12	Phenyl-2,4,6-d_3		

Results and discussion

The 70 eV mass spectra of the compounds studied are reported in Table 2. Fragmentation pathways leading to the principal daughter ions have been deduced from exact mass measurements and from observed metastable decompositions.

The principal framentation pathways for **1**, shown in Scheme 1, are analogous to those reported for 2-pyrimidinone (4). Like its oxo-analogue, **1** can exist in two main tautomeric forms:

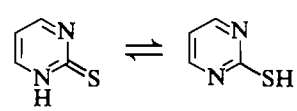

There is, however, little information as to which tautomer predominates in the gas phase. Beak and co-workers (6) studied the gas phase equilibrium of 2-thiopyridine and concluded that

[1] To whom all correspondence should be addressed.
[2] Revision received April 10, 1984.
[3] Full details of all synthetic procedures can be found in refs. 15 and 16.

Can. J. Chem. Downloaded from www.nrcresearchpress.com by 210.87.254.5 on 09/06/12
For personal use only.

TABLE 2. Major fragment ions in the mass spectra of compounds **1–12**

Compound	*m/z* (relative intensity, %)
1	112 ($M^{+\cdot}$, 100), 111(14), 85(17), 84(10), 79(8), 68(33), 59(39), 58(23), 53(31), 52(30), 32(28)
2	113 ($M^{+\cdot}$, 100), 112(35), 111(6), 86(15), 85(13), 80(9), 69(36), 60(13), 59(35), 54(23), 53(32), 32(54)
3	113 ($M^{+\cdot}$, 75), 112(100), 111(22)[a]
4	160 ($M^{+\cdot}$, 100), 159(10), 158(53), 157(22), 156(20), 133(10), 132(7), 131(7), 130(6), 129(6), 107(14), 106(13), 105(10), 104(9), 80(58), 79(58), 68(18), 53(42), 52(37)
5	129 ($M^{+\cdot}$, 100), 125(22), 110(2), 98(6), 93(3), 80(11), 68(22), 66(16), 42(31), 32(31)
6	140 ($M^{+\cdot}$, 100), 139(19), 125(13), 112(78), 111(24), 107(32), 98(18), 85(18), 84(13), 82(40), 81(19), 80(40), 79(16), 68(37), 53(37), 53(32), 42(23)
7	188 ($M^{+\cdot}$, 55), 187(100), 77(36), 51(22), 39(10)
8	129 ($M^{+\cdot}$, 100), 128(13), 127(10), 99(4), 98(4), 95(4), 94(4), 81(10), 71(23), 70(6), 69(9), 45(20)
9	143 ($M^{+\cdot}$, 100), 142(8), 141(8), 125(10), 113(41), 112(13), 109(10), 85(34), 82(14), 81(12), 80(14), 69(21)
10	142 ($M^{+\cdot}$, 100), 141(20), 140(4), 127(9), 113(14), 112(57), 111(15), 109(17), 84(39), 68(22), 53(20)
11	145 ($M^{+\cdot}$, 100), 144(7), 143(11), 127(9), 113(45), 112(13), 111(14), 100(5), 87(18), 83(12), 69(17)
12	191 ($M^{+\cdot}$, 48), 190(40), 189(100), 188(23), 80(43), 79(22), 53(28), 52(27), 40(16), 39(16)

[a]Molecular ion region only; significant back exchanged and/or unlabelled material makes complete spectrum of questionable value.

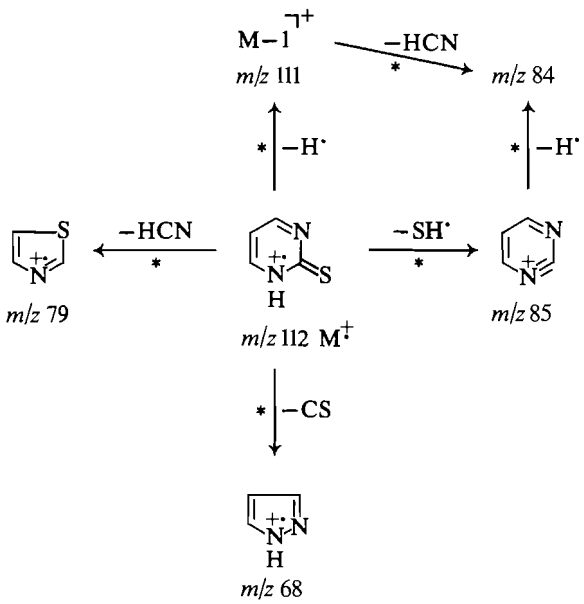

SCHEME 1. Principal fragmentation pathways for the molecular ion of **1**.

the 2-mercapto form predominates, in contrast to the solution results. Similar conclusions were reached by Gronneberg and Undheim (7) on the basis of ionization potential measurements. Few comparable studies have been reported for the thiopyrimidines. Berndt *et al.* (8) applied CNDO/2 methods to calculate that the —NH form of thiopyrimidine was stable with respect to the —SH form by 143 kJ mol^{-1}. Baddar *et al.* (9) investigated tautomerism in a series of 4,6-diarylpyrimidine-2(1*H*)-thiones and concluded that the thione form predominates in solution. Recent X-ray photoelectron spectroscopic measurements (10) on 6-(*m*-chlorophenyl)-4-phenyl pyrimidinethione lead to an estimate of 65% thione in the solid material.

Interpretation of the molecular ion region of the mass spectrum of the 1-d_1-pyrimidinethione, **3**, is complicated by the presence of unlabelled or back-exchanged material and by a kinetic isotope effect for H/D loss of unknown magnitude. An estimate of the relative importance of H· loss versus D· loss from the molecular ion of **3** was made, based on the assumption that H· loss from **3** would be less than or equal to H· loss from **1**. On this basis it was possible to assign limits to the relative intensities of peaks at *m/z* 112 and *m/z* 111 in the spectrum of **3** due to loss of H· and D·, respectively. These calculations put the contribution of D· loss from $M^{+\cdot}$ as 25–30% of the peak intensity at *m/z* 111, with the remainder being due to the H· loss from unlabelled material. Loss of the tautomeric hydrogen would thus appear to be considerably more important in the fragmentation of **1** than was found to be the case for the 2-pyrimidinone, but it should be noted that this does not confirm that there is a significant concentration of the —NH tautomer in the gas phase. If the S—H bond strength in the molecular ion is significantly lower than the N—H bond strength, loss of the tautomeric hydrogen from the thiol form may compete with SH· loss. This latter process is characteristic of the mass spectra of aliphatic, cyclic, and α-cyclic thioketones (11) and thiopyridines, and occurs to a significant extent (R.I. = 8%) in the mass spectrum of **1**.

Calculations similar to those described above were done for the molecular ion region of the spectrum of 5-d_1-pyrimidinethione, **2**, in order to correct for unlabelled material. Within the limits of the method there is no evidence for significant D· loss from the molecular ion of **2**, and we conclude that for **1**, as was found for 2-pyrimidinone, the principal sites of H· loss are C(4) and/or C(6).

2(1H)-Pyrimidineselenone (4)

The general characteristics of the mass spectra of selenoheterocycles have been the subject of several reports, and have been summarized by McCloskey *et al.* (12). Whereas direct loss of the exocyclic heteroatom is absent or occurs only to a minor extent in the fragmentation of the oxo- and thioanalogues, loss of Se or SeH by direct expulsion from $M^{+\cdot}$ is a prominent feature of the mass spectra of selenium containing compounds. Likewise, in the present case *m/z* 79 ($M^{+\cdot}$ − SeH) and *m/z* 80 ($M^{+\cdot}$ − Se) are major peaks in the spectrum of **4**. While the characteristic selenium isotope pattern makes identification of Se containing fragment ions a straightforward matter, comparison with the spectra of **1** and of 2-pyrimidinone is facilitated by presentation of the data as the monoisotopic (^{80}Se) spectra (Fig. 1). The corresponding fragmentation scheme (Scheme 2) shows few other differences from that of **1**.

N(*1*)-R-*Pyrimidinethiones*

The principal fragmentation pathways observed for **5**, **6**, and **7** generally parallel those reported for the oxo-compounds, and

Can. J. Chem. Downloaded from www.nrcresearchpress.com by 210.87.254.5 on 09/06/12
For personal use only.

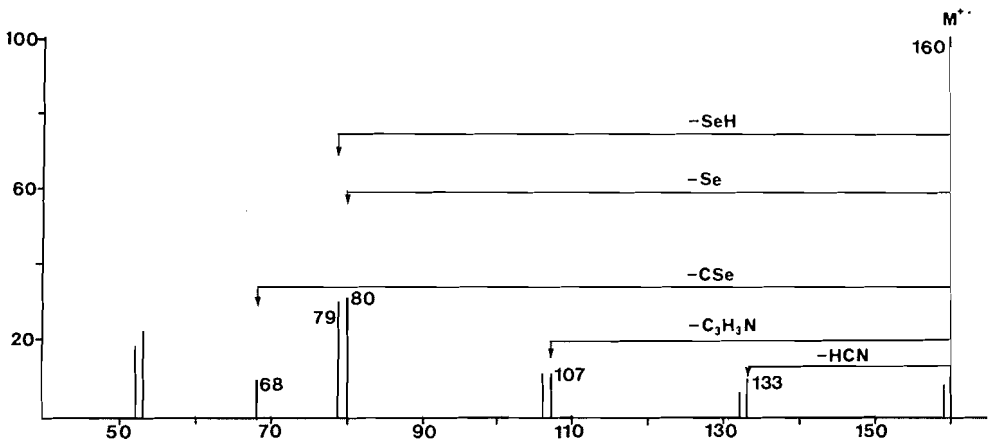

FIG. 1. Monoisotopic (^{80}Se) mass spectrum of **4**.

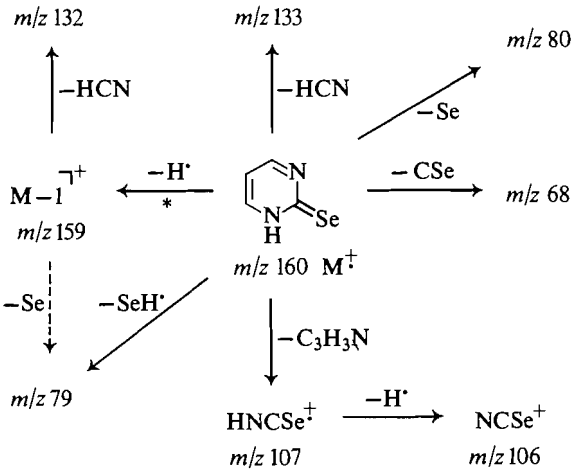

SCHEME 2. Principal fragmentation pathways for the molecular ion of **4**.

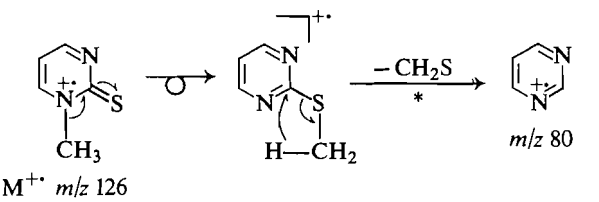

SCHEME 3. Formation of *m/z* 80 from **5**.

only significant differences will be discussed here. The expected loss of SH· from M^{+}· is a significant process (R.I. = 35%) in the fragmentation of **6**; in both **5** and **6** intense metastable peaks were observed for this elimination. The analogous OH· loss from M^{+}· of the pyrimidinones was not observed. Ion peaks at *m/z* 80 in the spectra of **5** and **6** can be explained in terms of migration of the N-alkyl group to sulfur, followed by H atom transfer to the ring and elimination of (R^1—H)S (Scheme 3). When $R^1 = CD_3$ the ion peak shifts to *m/z* 81 as predicted by this mechanism. The driving force for this reaction is presumably the formation of the stable pyrimidinium ion; however, the analogous process was not observed in the oxo-compounds. The spectrum of **7** has *m/z* 187 (M^{+}· − H·) as the base peak, and this ion fragment carries 25% of the total ion current. As was the case for the *N*-phenyl-2-pyrimidinone an intense metastable peak was associated with H· loss. However, in contrast to the fragmentation of the ^{2}H-labelled pyrimidinone, loss of D· from **12** was also associated with an intense metastable peak. Thus while we have previously concluded that the oxazolium structure is, at best, only a minor component of the $(M - H)^{+}$ ion generated from *N*-phenyl-2-pyrimidinone, we propose that rearrangement to give an ion with the thiazolium structure **13** is a significant feature in the fragmentation of **7**, with the stability of **13** accounting for the predominance of the *m/z* 187 peak in the spectrum. It should be noted that stable salts (perchlorates) of **13** are easily prepared (7), although adequate mass spectra were not obtainable in this laboratory. Ions of structures **14** and **15** might reasonably be expected to have stabilities comparable to that of **13**. Loss of H· from the molecular ions of *N*-methyl and *N*-ethyl-2-pyrimidinones has been shown to occur predominantly by simple bond cleavage without prior rearrangement from both ring and alkyl substituent sites. In the case of the thio-compounds **5** and **6**, the observation that moderately intense metastable peaks were associated with H· loss suggested that rearrangement leading to **14** (from **5**) and **15** (from **6**) could be significant reaction pathways.

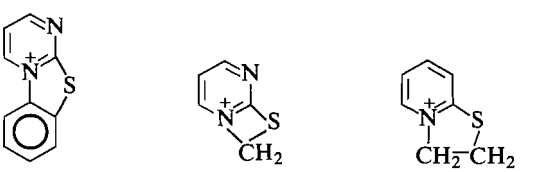

The kinetic energy release, *T*, associated with a metastable decomposition has been widely used (13) to characterize the reacting configurations of gas phase ions. Values of *T* corresponding to the widths of the metastable peaks at half height, $T_{0.5}$, give a convenient basis for the comparison of closely related metastable decompositions.

The metastable peaks for H· loss from **8** ($R^1 = CD_3$) and **11** ($R^1 = CD_2CD_3$) were of low intensity and we assume, therefore, that the relatively intense metastable peaks observed for H· loss from **5** ($R^1 = CH_3$), **9** ($R^1 = CH_2CD_3$) and **10** ($R^1 = CD_2CH_3$) can be assigned to H· loss from the alkyl substituent only, without introducing a significant error in the measured $T_{0.5}$ values (Table 3). There is a significant isotope effect on the abundance of the metastable peak for H· loss from the methylene carbon of the *N*-ethyl substituent. In contrast to the mod-

Can. J. Chem. Downloaded from www.nrcresearchpress.com by 210.87.254.5 on 09/06/12
For personal use only.

TABLE 3. Kinetic energy release ($T_{0.5}$, eV) for H/D loss

		RMU-7[a]		MS-902S[b]	
Cpd.	R^1	$-H\cdot$	$-D\cdot$	$-H\cdot$	$-D\cdot$
5	CH_3	0.09	—	n.d.	n.d.
8	CD_3	[c]	0.20	n.d.	n.d.
6	CH_2CH_3	0.15	—	0.29	—
9	CH_2CD_3	0.08	0.38	0.12	0.48
10	CD_2CH_3	n.d.	n.d.	0.21	[c]
11	CD_2CD_3	[c]	0.43	[c]	0.47

[a] Accelerating voltage = 3 kV.
[b] Accelerating voltage = 8 kV.
[c] Metastable peak too weak for $T_{0.5}$ measurement.

erately intense metastable peak for H· loss from **9**, the metastable peak for D· loss from **10** was too weak to permit an accurate measurement of $T_{0.5}$. Such an isotope effect on metastable peak abundance can be associated with a steep curve for k vs. E_{int}, with deuterium substitution lowering k to a value which puts it outside the range accessible to the metastable window (13). It has been pointed out that a steep k vs. E_{int} curve is associated with a fragmentation having a high entropy of activation (14), i.e. simple cleavage rather than rearrangement. Comparison shows that $T_{0.5}$ for H· loss from **9** is significantly lower than that observed for H· loss from **10**, and is comparable to that for H· loss from **5**. We infer from these observations that loss of H· from the methylene group of **9**, and from **5**, involves predominantly simple cleavage with little prior rearrangement. On these grounds **14** would appear to be ruled out as a major contributor to the ($M^{+\cdot}$ − H) ion generated from **5** and **9**.

A more positive case can be made for the production of **15** in the fragmentation of **9**. Loss of H· from the methyl group of **10** shows only a small isotope effect on the metastable peak abundance, and the significantly larger $T_{0.5}$ is consistent with a rearrangement process. Indirect evidence for the formation of **15** also is found by examination of the source generated ($M^{+\cdot}$ − H) ions from *N*-ethyl-2-pyrimidinone fragmenting further by loss of ethylene. Similar fragmentations were observed for **9**, **10**, and **11**; however, ($M^{+\cdot}$ − D) ions generated from these precursors did not eliminate ethylene in the metastable time frame. This observation is consistent with structure **15**, for which ethylene loss would require the rupture of the stable thiazolinium ring.

Acknowledgements

We thank the Natural Sciences and Engineering Research Council of Canada for operating grants and Dr. J. Krause for invaluable technical assistance. We thank Professor J. L. Holmes for making the mass spectrometry facilities of the University of Ottawa available to us.

1. C. B. LOZZIO and P. W. WIGLER. J. Cell. Physiol. **78**, 25 (1971).
2. J. TIMSON and D. J. PRICE. Chromosomes Today, **3**, 118 (1972).
3. A. HOLY, I. VOTRUBA, and K. JOST. Coll. Czech. Chem. Commun. **39**, 634 (1974).
4. E. M. KAZDAN, R. T. B. RYE, and O. S. TEE. Can. J. Chem. **60**, 1800 (1982).
5. T. K. DAVIES, D. L. MCGILLIVRAY, and T. W. WILEY. Int. J. Mass Spectrom. Ion Phys. **15**, 350 (1974).
6. P. BEAK, F. S. FRY, JR., J. LEE, and F. STEELE. J. Am. Chem. Soc. **98**, 171 (1976).
7. T. GRONNEBERG and K. UNDHEIM. Org. Mass Spectrom. **6**, 823 (1972); **6**, 225 (1972).
8. H. BERNDT, J. S. KWIATKOWSKI, J. BUDZINSKI, and B. SZCZODROWSKA. Chem. Phys. Lett. **19**, 246 (1973).
9. F. G. BADDAR, F. H. AL-HAJJAR, and N. R. EL-RAYYES. J. Heterocyclic Chem. **15**, 105 (1978).
10. A. KATRIB, F. G. BADDAR, N. R. EL-RAYYES, and F. H. AL-HAJJAR. J. Mol. Struct. **60**, 193 (1980).
11. D. PAQUER, L. MORIN, M. VOYEUX, and C. G. ANDRIEU. Rec. Trav. Chim. Pays-Bas. **100**, 36 (1981); **100**, 52 (1981).
12. J. G. LIEHR, C. L. WEISE, P. F. CRAIN, G. H. MILNE, D. S. WISE, L. B. TOWNSEND, and J. A. MCCLOSKEY. J. Heterocyclic Chem. **16**, 1263 (1979).
13. R. G. COOKS, J. H. BEYNON, R. M. CAPRIOLI, and G. R. LESTER. Metastable ions. Elsevier Scientific Publishing Co., New York. (1973); J. L. HOLMES and J. K. TERLOUW. Org. Mass Spectrom. **15**, 383 (1980).
14. M. BERTRAND, J. H. BEYNON, and R. G. COOKS. Org. Mass Spectrom. **7**, 193 (1973).
15. E. M. KAZDAN. Ph.D. Thesis. Concordia University, Montreal. 1980.
16. E. M. KAZDAN. M.Sc. Thesis. Concordia University, Montreal. 1976.

Can. J. Chem. Downloaded from www.nrcresearchpress.com by 210.87.254.5 on 09/06/12
For personal use only.

The simultaneous analysis of chlorine-36, sulphur-35, and phosphorus-32 in urine[1]

GARY H. KRAMER AND SIDNEY JOSEPH[2]

Biomedical Research Branch, Health Sciences Division, Atomic Energy of Canada Limited Research Company, Chalk River Nuclear Laboratories, Chalk River, Ont., Canada K0J 1J0

Received January 16, 1984

GARY H. KRAMER and SIDNEY JOSEPH. Can. J. Chem. **62**, 2344 (1984).

A method has been developed for the simultaneous analysis of phosphorus-32, sulphur-35, and chlorine-36 in urine. The sample must be divided for the analysis; therefore, at least 500 mL of urine is required. Chlorine-36 is estimated by counting AgCl after interferences have been removed by $Fe(OH)_3$, $Ca_3(PO_4)_2$, and $BaSO_4$ precipitations. Sulphur-35 is estimated as $BaSO_4$ and phosphorus-32 is estimated as $BiPO_4$ after interferences have been removed by cation exchange and coprecipitation. Cross-contamination of the radionuclides is negligible and the chemical recoveries and limits of detection are as follows: Cl-36, 90% (269 mBq); S-35, 95% (144 mBq); P-32, 70% (38 mBq).

GARY H. KRAMER et SIDNEY JOSEPH. Can. J. Chem. **62**, 2344 (1984).

On a mis au point une méthode qui permet d'analyser simultanément du phosphore-32, du soufre-35 et du chlore-36 dans l'urine. Pour les fins de cette analyse, l'échantillon doit être divisé; pour ce faire, il faut donc au moins 500 mL d'urine. Pour évaluer le chlore-36, on effectue un comptage sur le chlorure d'argent après avoir éliminé les produits qui interfèrent grâce à des précipitations par le $Fe(OH)_3$, le $Ca_3(PO_4)_2$ et le $BaSO_4$. On évalue le soufre-35 sous forme de $BaSO_4$ et le phosphore-32 sous forme de $BiPO_4$ après avoir éliminé les produits qui interfèrent grâce à des coprécipitations et des échanges de cations. La contamination entre radionuclides est négligeable; les récupérations chimiques et les limites de détection sont les suivantes: Cl-36, 90% (269 mBq); S-35, 95% (144 mBq); P-32 70% (38 mBq).

[Traduit par le journal]

Introduction

The radionuclides in this report, P-32, S-35, and Cl-36, are principally pure β emitters (Cl-36 has two other minor decay pathways, 1.9% electron capture and 0.0012% positron emission) with a variety of half-lives and maximum β energies. These values are P-32, 14.3 d, 1.71 MeV; S-35, 88 d, 0.167 MeV; Cl-36, 3×10^5 a, 0.714 MeV.

It is generally assumed that the chemical form of the radionuclide that is ingested or inhaled in a possible occupational contamination incident is inorganic. It is believed that there is no area in the human body that contains non-exchangeable chloride (1) and that greater than 90% of a radioactive sulphate intake is still excreted in that chemical form after seven days (2). Phosphorus, on the other hand, has a higher metabolic conversion to organically bound phosphorus compounds than either the chloride or the sulphate (3–5); therefore, this method has been developed using an organic form of phosphorus and inorganic forms of chlorine and sulphur to test the procedures.

A search of the literature for a satisfactory method for determining P-32, S-35, or Cl-36 in urine showed that very little work has been carried out on low level measurements of these radionuclides. Phosphorus-32 has previously been determined by extraction of molybdophosphoric acid into an organic solvent (6) but the removal of some of the possible interferences can be lengthy (7). Sulphur-35 has been previously estimated as a barium sulphate precipitate (8), but no account was taken of the whole host of cations and anions that will also be coprecipitated. In particular, K-40 is a problem in urine samples when trying to estimate low levels of S-35 (9). Chlorine-36 appears to have received no attention in the past.

This paper describes the simultaneous analysis of Cl-36, P-32, and S-35 in urine. A 100 mL portion of urine is reserved for the Cl-36 analysis and the remainder used for the S-35 and P-32 determination. The possible cross-contaminations by S-35 and P-32 in the Cl-36 analysis are eliminated by removal of the sulphates and phosphates by precipitation. Chlorine-36 is estimated as a dry silver chloride precipitate using a gas proportional counter. Liquid scintillation cannot be used due to the extreme photosensitivity of wet silver chloride. The portion of urine reserved for S-35 and P-32 analysis is ashed to remove the possible cross-contamination by Cl-36 and to convert some, if not all, of the organic sulphur and phosphorus compounds to the inorganic form. Except for an intake of an organic form of a radionuclide, the amount of activity that would be found in the organic constituents of urine is expected to be very small. The ashed urine residue is redissolved and all the cations, except H^+, are removed by cation exchange. The interfering anion, sulphate or phosphate, is removed by precipitation. Sulphur-35 is estimated as a gel-suspended barium sulphate precipitate in a liquid scintillation counter. Phosphorus-32 can be estimated either as a gel-suspended bismuth phosphate precipitate in a liquid scintillation counter, or as a dry precipitate in a gas proportional counter.

Experimental

Procedure

The urine sample should be at least 500 mL because it will be divided to perform the simultaneous analysis. The sample is initially divided into two portions, 100 mL for the Cl-36 analysis and the remainder for S-35 and P-32.

Chlorine-36

Ferric chloride (50 mg) and calcium nitrate (1.5 g) are added to the raw urine and dissolved. Aqueous ammonia is added, with stirring, until the pH is approximately 10. The precipitates are removed by filtration and washed with 20 mL of a dilute ammonia solution. The precipitates are discarded and the pH of the combined filtrates is adjusted to 1.2. The solution is then heated to approximately 70°C. A barium nitrate solution (1 g/10 mL) is added and the mixture is stirred. The solution is allowed to cool to room temperature before removing the precipitate by filtration. The precipitate is washed with a dilute nitric acid solution (5 mL) and then discarded. The filtrates are combined and 25 mL silver nitrate solution (0.15 g/mL) are added. The solution is stirred and the precipitate allowed to settle overnight.

The bulk of the supernatant is decanted and the precipitate separated from the remaining liquid by centrifugation. The precipitate is washed twice with dilute nitric acid (10 mL); the supernatants being discarded

[1] AECL-8543.

[2] AECL summer student.

Can. J. Chem. Downloaded from www.nrcresearchpress.com by 210.87.254.5 on 09/06/12
For personal use only.

Can. J. Chem. Downloaded from www.nrcresearchpress.com by 210.87.254.5 on 09/06/12
For personal use only.

at each step. The precipitate is dried in an oven at 100°C for approximately 2 h. The dried precipitate is transferred to a weighed 5 cm stainless steel counting dish and the precipitate is ground to an even layer. The precipitate is placed back in the oven until it is completely dried. The cooled dish is counted for β activity.

Sulphur-35 and phosphorus-32

The urine is wet ashed as follows. The sample is made approximately 2 mol/L in nitric acid and boiled to almost dryness. At this point the ashing is continued using fuming nitric acid (CAREFULLY). The orange–brown residue will often catch fire leaving a yellow salt residue with some carbon. Further additions of the fuming nitric acid to the heated salts will remove the carbon and turn the residue white. The residue is dissolved in a minimum of 8 mol/L nitric acid (10–30 mL) and then diluted to 250 mL using distilled water. If necessary, the pH is adjusted to between 2–3 using aqueous ammonia. The solution is passed through a cation exchange column at a flow rate of 1–2 mL/min. After the sample has passed through the column the resin is washed with distilled water (300–400 mL) until the pH of the eluate has reached 4.5. At this point the solution is divided into two equal portions.

Sulphur-35

The pH is adjusted to 1.0 and heated to 90°C. Excess bismuth nitrate is added (15.6 mL of a 10% w/v solution per 0.1 g phosphorus present) and the solution allowed to cool. The precipitate is centrifuged and then discarded after washing with dilute nitric acid (20 mL). The pH of the combined supernatants is adjusted to between 2–3 and heated. Excess barium chloride is added (9 mL of a 10% w/v solution per 0.1 g sulphur present) and the solution allowed to cool. The supernatant is discarded and the precipitate is transferred to a liquid scintillation vial. The volume of the precipitate and liquid is made up to 5 mL with distilled water and 10 mL of scintillation cocktail added. The resulting gel is counted for β activity.

Phosphorus-32

The procedure given for sulphur-35 is reversed. The barium sulphate is removed first and the bismuth phosphate is retained for counting either by liquid scintillation as given above or by transferring the precipitate to a 5 cm diameter stainless steel dish drying and then counting in a gas proportional counter.

Apparatus and tracers

Radioactive counting was performed with either a liquid scintillation (LS) counter or a gas proportional (GP) counter. The approximate counting efficiencies of the radionuclides were S-35, 60% (LS); P-32, 90% (LS), 35% (GP); Cl-36, 10% (GP). The counting efficiency of the GP counter for P-32 and Cl-36 was determined in a similar manner. A known amount of activity was precipitated from aqueous solution by the appropriate reagent (Bi or Ag) and the precipitate plated, dried, and weighed. A second precipitate on the same aqueous solution was used to estimate residual activity (usually less than 0.1%).

The LS counter was calibrated by adding known amounts of precipitate to a known amount of activity. The aqueous layer was well slurried before the LS-cocktail was added to form a gel.

The radionuclides were obtained in the following chemical forms: Cl-36, NaCl from the Radiochemical Company, Ottawa; S-35, Na_2SO_4 from New England Nuclear Ltd.; P-32, Adenosine 5′ [γ-^{32}P] triphosphate from the Radiochemical Centre, Amersham, England. Typically, the amount of activity used to test the analyses was 44 Bq. The amount of activity used for the cross-contamination studies was 0.7 MBq.

The ion exchange column was charged with enough Dowex 50W X12 cation exchange resin to accommodate 650 mEq ($\cong$ 15 g Na^+ or $\cong$ 25 g K^+ or $\cong$ 13 g Ca^{2+}). This amount of resin is capable of absorbing the cationic components of two standard urine samples (10). The resin was used in the H^+ form. The liquid scintillation cocktail was "Scintiverse" supplied by the Fisher Chemical Company, Canada.

Results and discussion

Unlike most radiochemical separations on urine, where a major problem is the presence of large amounts of other interfering elements, the analysis of chlorine-36, sulphur-35, or phosphorus-32 is made difficult by the large amounts of inorganic chloride, sulphate, and phosphate (4.4 g Cl/days urine, 0.8 g S/days urine, and 0.9 g P/days urine — ref. 10). The large quantities of inorganic anions limit the volume of urine that can be analysed. For chlorine-36 the optimum volume was found to be 100 mL (11). The average amount of silver chloride obtained from this volume was found to be 2.3 g which gave a counting efficiency of approximately 10%. The chemical recovery of Cl-36 was found to be 90 ± 5% with 8 ± 3% being lost to the phosphates and 3 ± 1% being lost to the sulphates. Cross-contaminations by S-35 and P-32 were negligible. It was also found necessary to manipulate wet silver chloride under red-light conditions; however, dry silver chloride is able to withstand short exposures to room light with no noticeable effect.

The portion of urine reserved for S-35 and P-32 analysis is ashed thoroughly. All the Cl-36 will be driven off either as Cl_2 or HCl. It was found necessary to remove all the cationic species, except for H^+, due to the coprecipitation problems encountered in estimating S-35 as barium sulphate. Specifically, significant amounts of K-40 were found in the precipitates. It is also well known that barium sulphate will coprecipitate group II elements, actinides, Cu, Cd, Zn, Ni, Mn, Fe(II), Al, Cl^-, I^-, and others, any of which could give rise to estimation problems. The chemical recovery of S-35 was found to be 95 ± 5% with 3 ± 1% lost to the phosphates. The chemical recovery of P-32 was found to be 70 ± 8% with 3 ± 1% lost to the sulphates. The remaining P-32 is unaccounted for because only 4 ± 3% was found in the remaining supernatant. It is postulated that the loss is due to the ashing procedure but the mechanism is unknown. Cross-contaminations of S-35 in the P-32 estimation, or vice versa, were found to be negligible.

The detection limits (12) for S-35, P-32, and Cl-36 at the 95% confidence level are estimated to be: 144 mBq, 38 mBq, and 269 mBq, respectively. These estimates include the effects of ambient background (20 cpm, LS; 1.5 cpm, GP), chemical recoveries counter efficiency, and a 20 min counting time. The detection limits may be halved if the counting time is increased to 60 min.

1. A. GOTTSCHALK and E. POTCHEN (*Editors*). Diagnostic nuclear medicine. Williams and Wilkins, Baltimore. 1976.
2. D. DZIEWIATKOWSKI. J. Biol. Chem. **178**, 389 (1949).
3. H. WEIJER, H. DUGGAN, and D. B. SCOTT. J. Can. Assoc. Radiol. **13**, 81 (1962).
4. L. ERF, L. TUTTLE, and J. LAWRENCE. Ann. Int. Med. **15**, 487 (1941).
5. J. CASTLE, K. SCOTT, and W. A. REILLY. Am. J. Roent. **91**, 1128 (1964).
6. P. PAKALNS. Anal. Chim. Acta, **40**, 1 (1968).
7. R. C. MILHAM. Dupont de Nemours and Company, Savannah River Laboratory. Report DP-MS-73-35, 1973.
8. W. NEWTON, J. MURPHY, and L. MULLINS. J. Lab. Clin. Methods, **69**, 518 (1967).
9. G. H. KRAMER. Atomic Energy of Canada Limited, Report AECL-7162, 1981.
10. International Commission on Radiological Protection. Report of the Task Group on Reference Man. ICRP Publication 23, Pergamon Press, New York, 1975.
11. G. H. KRAMER and S. JOSEPH. Atomic Energy of Canada Limited, AECL-7512, 1982.
12. L. A. CURRIE. Anal. Chem. **40**, 586 (1968).

Photochemistry of 2-phenylbenzophenone. An unusual bichromophoric molecule[1]

J. C. SCAIANO
Division of Chemistry, National Research Council of Canada, Ottawa, Ont., Canada K1A 0R6
AND
DAVID E. NICODEM
Instituto de Quimica, Universidade Federal do Rio de Janeiro, Ilha do Fundão-CEP: 21910, Rio de Janeiro, Brazil

Received January 18, 1984

J. C. SCAIANO and DAVID E. NICODEM. Can. J. Chem. **62**, 2346 (1984).

2-Phenylbenzophenone is proposed to have two nearby triplets, a low lying π,π^* state similar to that of biphenyl and a benzophenone-like triplet lying ~4 kcal/mol higher. The triplet lifetimes of this photostable ketone are extremely short, e.g. 0.56 and 2.5 ns at 300 K in toluene and isooctane, respectively, and are believed to be controlled by population of the benzophenone-like triplet and decay from this state via interaction of the carbonyl chromophore with the phenyl ring in the *ortho* position. The two triplets interconvert via ring rotation. The Arrhenius parameters for triplet decay in five solvents show some dependency with the temperature dependence of the solvent viscosity.

J. C. SCAIANO et DAVID E. NICODEM. Can. J. Chem. **62**, 2346 (1984).

On suggère que la phényl-2 benzophénone possède deux états triplets voisins, soit un état de basse énergie π,π^* semblable à celui du biphényle et un état triplet semblable à celui de la benzophénone dont le niveau énergétique est environ 4 kcal/mol plus élevé. Les temps de vie du triplet de cette cétone photostable sont extrêmement courts, soit 0,56 et 2,5 ns respectivement dans le toluène et l'osooctane à 300 K et on pense qu'ils sont contrôlés par la population du triplet similaire à celui de la benzophénone et sa dégénérescence à partir de cet état se produit par le biais d'une interaction entre le chromophore du carbonyle et le groupe phényle en position *ortho*. Les deux triplets se convertissent l'un dans l'autre par une rotation de cycle. Les paramètres d'Arrhénius pour la dégénérescence du triplet dans cinq solvants montrent qu'il existe une certaine relation avec l'influence de la température sur le viscosité du solvant.

[Traduit par le journal]

Can. J. Chem. Downloaded from www.nrcresearchpress.com by 210.87.254.42 on 09/06/12
For personal use only.

Introduction

The photoreactions of benzophenone and its derivatives are among the best studied photochemical processes (1, 2). It is thus surprising that some rather simple substituted benzophenones behave in a seemingly unpredictable way. For example, 2-phenylbenzophenone does not photoreduce significantly (3, 4) under conditions where 4-phenylbenzophenone does (1). The latter is in turn substantially less reactive than benzophenone itself (5). In the case of 2-phenylbenzophenone, it should be noted that the aromatic ring in the *ortho* position is not expected to be able to lead to an "all planar" configuration; this in turn, would be expected to enhance the carbonyl triplet reactivity, since the reactivity towards photoreduction is expected to decrease with increasing π,π^* character of the triplet state (6).

Several observations in related systems provide, in fact, a basis for the understanding of the unreactivity of 2-phenylbenzophenone: (*a*) 2-methylbenzophenone undergoes photoenolization — involving hydrogen transfer — very efficiently (7), (*b*) 2-hydroxybenzophenone undergoes rapid intramolecular deactivation (8), a process that is widely used in polymer photostabilization (9), (*c*) β-phenylpropiophenone triplets decay via interaction of the excited carbonyl group with the β-phenyl ring, a process that occurs with rate constants in the neighbourhood of $10^9\ s^{-1}$ (10–12), and (*d*) 2-methoxy- and 2-benzyloxybenzophenone decay via intramolecular hydrogen abstraction (13), demonstrating that processes that involve interactions more remote than the conventional 6-center process (e.g. Norrish Type II) can occur quite efficiently (14).

2-Phenylbenzophenone can be regarded as a rather special case of a bichromophoric molecule. This molecule presents a biphenyl, as well as a benzophenone moiety which share one aromatic ring. Examples of energy transfer in bichromophoric systems in the literature frequently involve systems where the rate and efficiency of the process is controlled by the transfer step itself or by the ability of the two chromophores to approach sufficiently for energy transfer to occur (15). In contrast, in the case of 2-phenylbenzophenone we can anticipate intramolecular motion to play an important role.

This paper reports the results of quantum yield and laser flash photolysis studies of the photochemistry of 2-phenylbenzophenone in homogeneous solutions, including the effect of solvents and temperature on the kinetics of triplet deactivation.

Experimental

2-Phenylbenzophenone was prepared by addition of phenyl lithium to 2-phenylbenzoic acid (16). It was purified by column chromatography on silica gel and repeated recrystallization from 2-propanol, followed by sublimation. Melting point and spectral data were in full agreement with literature values (4, 16, 17).

All other reagents and solvents were commercially available and were purified by standard procedures.

Quantum yield and product studies

Quantum yields of photoreduction were measured in deaerated samples using a merry-go-round type of reactor. Typical ketone concentrations were around $1.5 \times 10^{-3}\ M$ which is enough to absorb >99% of the light at 313 nm. This mercury line (from a 450 W Hanovia lamp) was isolated using a K_2CrO_4 filter solution. Benzophenone — 1,3-cyclohexadiene was used as an actinometer system (18). Analysis was performed by opening the ampoules, diluting the sample, and measuring the absorbance at 290 nm for quadruplicate samples that had been irradiated and the same number of nonirradiated samples. It was found that upon extensive irradiation the absorbance at 290 nm was reduced to less than 5% of its original value in 2-propanol and that there was no change in absorbance when *t*-butanol was substituted. The quantum yield for photoreduction in neat 2-propanol was found

[1]NRCC No. 23388.

Can. J. Chem. Downloaded from www.nrcresearchpress.com by 210.87.254.42 on 09/06/12
For personal use only.

to be $(6.2 \pm 1.8) \times 10^{-4}$. When 3.33 *M* 2-propanol in *t*-butanol was used the quantum yield was 45% of the original value.

Laser flash photolysis

All experiments were carried out on deaerated samples using for excitation the pulses (337.1 nm, ~8 ns, up to 10 mJ) from a Molectron UV-24 nitrogen laser. The detection system has a rise time of ~1 ns, but the shortest lifetime that can be accurately determined without deconvolution is about 12 ns. The signals, initially captured by an R-7912 Tektronix transient digitizer, are then transferred to a PDP11/23 computer that also controls the experiment and provides suitable processing, storage, and hardcopy facilities. Further details can be found elsewhere (19).

Some of our experiments involved the addition of 1-methylnaphthalene as a triplet quencher. This approach usually allows the determination of $k_q\tau_T$ from a Stern–Volmer type of analysis on the yield of triplet 1-methylnaphthalene, and has been described in some detail earlier (e.g. ref. 20). In the case of 2-phenylbenzophenone the concentrations of quencher needed were sufficiently high that partial light absorption by 1-methylnaphthalene had to be taken into consideration. The corrections introduced take into account the decreased light absorption by the substrate, as well as the formation of triplet 1-methylnaphthalene via direct excitation (21).

The lifetimes obtained for the 1-methylnaphthalene triplet formed by energy transfer from 2-phenylbenzophenone were the same as those obtained when the triplet was obtained by direct excitation at 308 nm, thus indicating that the energy transfer process is irreversible under our experimental conditions.

Results

By comparison with benzophenone, 2-phenylbenzophenone should be regarded as a photostable ketone. Even in the highly reactive solvent 2-propanol, the quantum yield for photoreduction is only 6.2×10^{-4}. This extremely low yield is the result of the composite effect of a low reactivity towards hydrogen abstraction, and a very short triplet lifetime, controlled by other deactivation pathways (*vide infra*). The quantum yield of photoreduction changes from 6.2×10^{-4} in neat (13.1 *M*) 2-propanol, to $\sim 2.8 \times 10^{-4}$ for 3.3 *M*, with *tert*-butanol as cosolvent. In *tert*-butanol 2-phenylbenzophenone is, for all practical purposes, photostable.

An important implication of the results presented above is that permanent chemical change is, in all cases, sufficiently small ($\Phi < 10^{-3}$) that these processes cannot be expected to play any important role in the transient phenomena studied using laser flash photolysis techniques. These experiments are presented below.

The transient signals observed at room temperature decayed too rapidly for accurate kinetic study; the signals simply followed the shape of the laser pulse.

Figure 1 shows the transient spectrum obtained in isooctane at 190 K, where the triplet lifetime is 115 ns. The decay kinetics were monitored in several solvents at low temperatures and fitted with an Arrhenius expression; the results are given in Table 1, and a summary of the Arrhenius parameters in Table 2; representative plots are shown in Fig. 2. The shape of the decay traces was the same at all wavelengths in the region monitored (345 to 800 nm) and could be fitted by a single exponential. This is consistent with the involvement of a single transient, which decays to yield the parent molecule or permanent products; in this case our quantum yield studies (*vide supra*) indicate that the decay regenerates the parent ketone. Even in the case of 2-propanol, where some photoreduction takes place, the yields are low enough that this process does not need to be taken into account in the interpretation of transient phenomena.

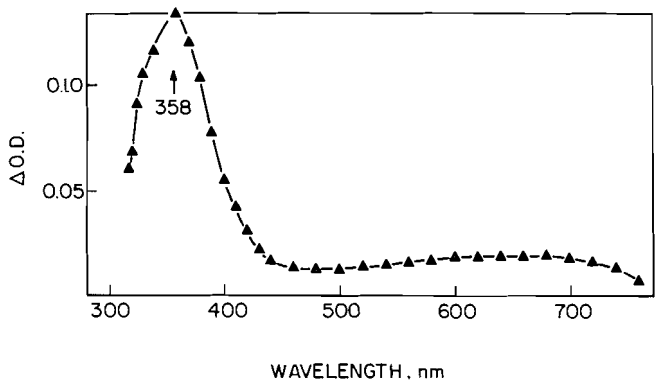

FIG. 1. T–T spectrum of 2-phenylbenzophenone recorded at 190 K in isooctane, between 20 and 70 ns following laser excitation.

TABLE 1. Kinetic data for the decay of triplet 2-phenylbenzophenone at various temperatures and in several solvents

Solvent	*T*/K	k_{decay}[a]
Toluene	181.4	2.40×10^6
	194.4	8.41×10^6
	202.3	1.68×10^7
	208.1	2.18×10^7
	217.1	3.82×10^7
	223.1	5.41×10^7
2-Propanol	188.0	1.23×10^6
	193.1	2.33×10^6
	202.2	4.99×10^6
	212.0	1.03×10^7
	221.6	1.73×10^7
Isooctane	207.0	2.08×10^7
	208.5	2.25×10^7
	219.1	3.12×10^7
	230.1	6.07×10^7
	236.1	6.90×10^7
	243.9	8.20×10^7
Methanol	200.3	4.79×10^6
	210.0	9.95×10^6
	216.4	1.39×10^7
	230.8	3.47×10^7
	234.4	3.64×10^7
	235.1	3.99×10^7
	242.0	5.12×10^7
Diethylether	157.3	4.47×10^6
	167.1	6.73×10^6
	178.9	1.37×10^7
	185.4	2.00×10^7
	199.4	3.97×10^7
	204.0	4.47×10^7

[a]In units of s^{-1}.

The triplet lifetimes at ambient temperatures could also be determined from the integration of the area under the corresponding trace, using the technique described earlier (22). The values obtained were consistent with those calculated from an extrapolation of the Arrhenius plot, but did not represent a substantial improvement.

The assignment of the transient signals observed to the triplet state was also confirmed by addition of 1-methylnaphthalene, which leads to the formation of its triplet state via energy transfer. The yields of triplet 1-methylnaphthalene can be treat-

TABLE 2. Arrhenius parameters for the decay of triplet 2-phenylbenzophenone in several solvents[a]

Solvent	T-range (K)	log A^b	$E_a{}^c$	$\tau_{300K}{}^d$	E_a (viscosity)^{c,e}
Toluene	181–223	13.57±0.51	5.92±0.47	0.56	2.7
2-Propanol	188–222	13.63±0.73	6.42±0.67	1.15	5.8
Isooctane	207–244	11.46±0.52	3.92±0.53	2.51	2.7
Methanol	200–242	12.73±0.33	5.51±0.33	1.98	3.1
Diethylether	157–204	11.46±0.13	3.52±0.11	1.31	2.1

[a]According to $-\log \tau = \log A - E_a/2.3RT$, with $2.3RT$ in kcal/mol. Errors reported as $\pm 2\sigma$.
[b]A in units of s^{-1}.
[c]In kcal/mol.
[d]Nanoseconds, extrapolated.
[e]From a plot of log T/η vs. T^{-1}, where η is the solvent viscosity.

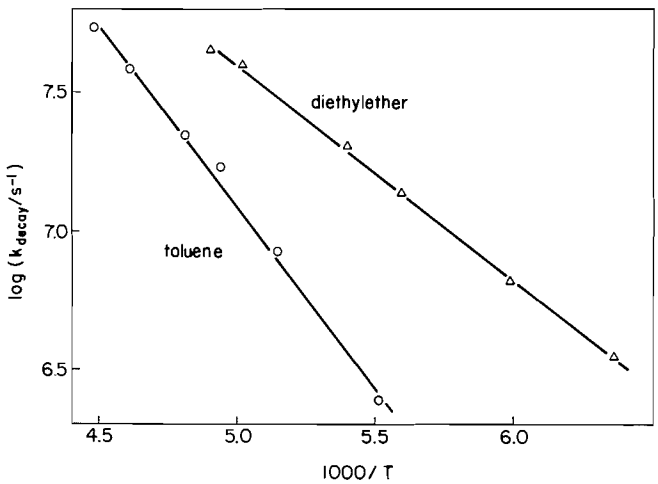

FIG. 2. Representative Arrhenius plots for the decay of triplet 2-phenylbenzophenone in toluene and in diethylether.

ed in a Stern–Volmer type of approach (20), and used to obtain $k_q\tau$, even at temperatures where triplet decay is too fast for direct monitoring: i.e.

$$[1] \quad \frac{1}{\Phi_N} = \frac{1}{\Phi_{ISC}} + \frac{1}{k_q\tau[N]}$$

where Φ_N and Φ_{ISC} are the quantum yields of triplet 1-methylnaphthalene and intersystem crossing, respectively, and [N] is the concentration of 1-methylnaphthalene. In terms of the transient absorbances due to triplet 1-methylnaphthalene (A_N), which were monitored at 420 nm,

$$[2] \quad \frac{1}{A_N} = a + a/k_q\tau[N]$$

where a is a constant that depends on instrumental response, and in a matched series of experiments is also proportional to Φ_{ISC}^{-1}. The values of $k_q\tau$ obtained in this way are given in Table 3. A few representative plots are shown in Fig. 3.

In the cases of benzene and 2-propanol, we also determined Φ_{ISC}. These were based on the intercepts of the Stern–Volmer plots (i.e., a) for 2-phenylbenzophenone and benzophenone, under identical experimental conditions and in samples of the same optical density at the excitation wavelength (337 nm). The values of Φ_{ISC} obtained were 0.67 ± 0.11 and 0.85 ± 0.14 at 300 K in benzene and 2-propanol, respectively. It should be noted that all the data obtained using 1-methylnaphthalene include the corrections due to partial absorption of the light by the quencher, as already mentioned in the Experimental section (21).

TABLE 3. Stern–Volmer slopes obtained using 1-methylnaphthalene in various solvents at 300 K

Solvent	$k_q\tau/M^{-1}$
Diethylether	5.6
Toluene	2.5
Benzene	3.8
Isooctane	9.1
Methanol	12.5
2-Propanol	7.2

Discussion

As a bichromophoric molecule 2-phenylbenzophenone is rather peculiar since the biphenyl and benzophenone chromophores share an aromatic ring. This is naturally the same situation as in 4-phenylbenzophenone; however, in the case of the *ortho*-isomer one can expect steric hindrance to prevent the three rings to approach planarity at any given time. We propose that on a first approximation conformations **I** and **II** are important in understanding the photochemistry of this ketone.

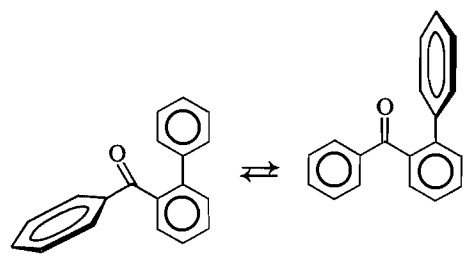

I **II**

We believe that the decay of the triplet state occurs predominantly from conformation **II**, which closely approaches the geometry (**III**) from which β-phenylpropiophenone and related ketones have been shown to undergo triplet deactivation (12).

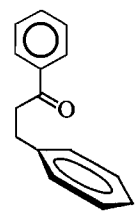

III

Can. J. Chem. Downloaded from www.nrcresearchpress.com by 210.87.254.42 on 09/06/12
For personal use only.

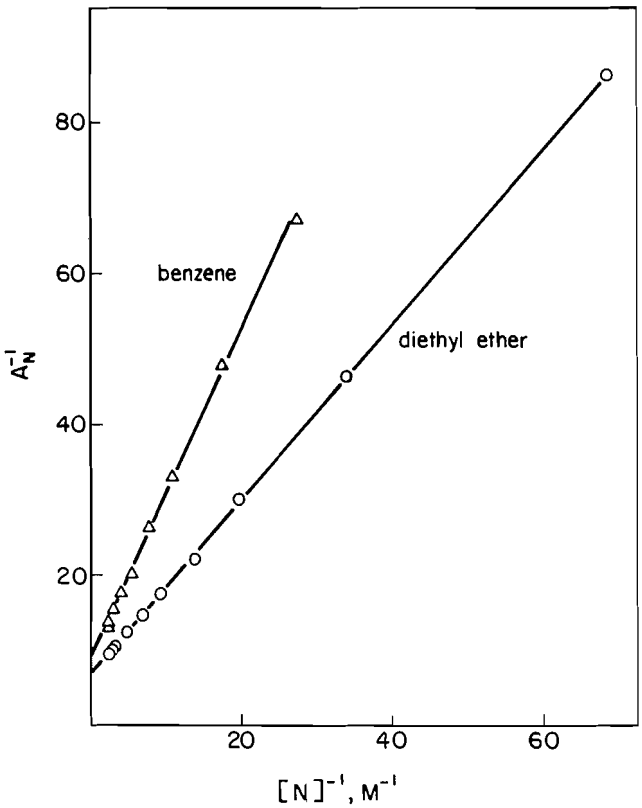

FIG. 3. Stern–Volmer plots according to eq. [2], for benzene and diethylether.

The conclusion that **III** represents the optimum conformation for deactivation was based on the analysis of decay parameters for a series of ketones having β-phenyl rings and cyclopropyl or cyclobutyl rings which introduce conformational restrictions in these molecules (12).

In the case of 2-phenylbenzophenone, the lowest triplet energy conformation is expected to correspond to **I**, since biphenyls have triplet energies somewhat lower than that for benzophenone. Consistently with this, the T–T spectrum (Fig. 1) resembles that of biphenyl (λ_{max} ~365 nm) (23) rather than that of benzophenone (λ_{max} ~525 nm) (e.g. ref. 24). In the case of the ground state, **II** is expected to approach the most favourable conformation, since in this case both chromophores are in their preferred ground state geometry (25, 28); further, the ground state absorption spectrum of 2-phenylbenzophenone at $\lambda >$ 300 nm strongly resembles that of benzophenone, with a well defined n,π* band.

The fact that the values of Φ_{ISC} are below one indicates that triplet **I** is reached inefficiently; our results do not show if this inefficiency occurs at the singlet level, or as a result of partitioning of initially formed triplet **II** between ground state **II** or triplet **I**. This latter possibility, which we favour (*vide infra*), effectively means that triplet **II** is too short-lived to be quencheable by 1-methylnaphthalene.

The essentials of the mechanism proposed are shown in Fig. 4. Several facts make us believe that intersystem crossing occurs from ^{1}**II***, rather than ^{1}**I*** (not included in Fig. 4). First initial excitation takes place predominantly in the n,π* ketone band (337 nm, where biphenyl is transparent), and any ground state equilibrium conformation **I** would not be expected to be excited. Second, ^{1}**I*** is likely to be somewhat higher in energy than ^{1}**II***, and finally, the relaxation ^{1}**II*** → ^{1}**I***, even if the

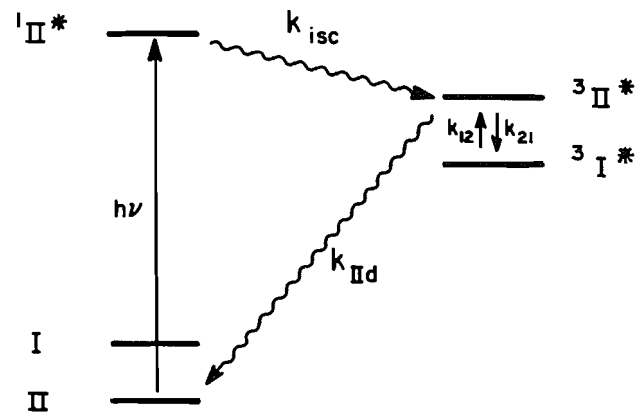

FIG. 4. Proposed mechanism for the photochemistry of 2-phenylbenzophenone in solution.

latter was lower in energy, would be unlikely to compete with ultrafast intersystem crossing processes in the benzophenone moiety (29), while even moderately viscous solvents can affect this process in biphenyl itself (e.g., ref. 30).

Kinetic analysis according to the mechanism of Fig. 4, after the steady state, has been established leads to:

$$[3] \quad \frac{-\partial[^3\mathbf{I}^*]}{\partial t} = k_{12}\frac{k_{IId}}{k_{21} + k_{IId}}[^3\mathbf{I}^*]$$

$$[4] \quad k_{decay} = \frac{k_{12}k_{IId}}{k_{21} + k_{IId}}$$

$$[5] \quad \Phi_{ISC} = \Phi^0_{ISC}\frac{k_{21}}{k_{21} + k_{IId}}$$

where t is the time, k_{decay} is the experimentally determined rate constant for triplet decay (i.e. $\tau_T^{-1} = k_{decay}$) and Φ^0_{ISC} refers to the yield of triplets initially reaching ^{3}**II***, rather than the experimentally determined Φ_{ISC}. Equations [3] and [4] apply only after the initial relaxation of ^{3}**II***, since the steady state assumption has been applied the concentration of ^{3}**II***. Rearranging eq. [5] leads to

$$[6] \quad 1 - \frac{\Phi_{ISC}}{\Phi^0_{ISC}} = \frac{k_{IId}}{k_{21} + k_{IId}}$$

dividing eqs. [4] and [6] gives,

$$[7] \quad k_{12} = \frac{k_{decay}}{1 - \Phi_{ISC}/\Phi^0_{ISC}}$$

If Φ^0_{ISC} is taken as 1.0, as is usually the case for benzophenones, it is possible to estimate the rate constants for the up-conversion, k_{12}. The corresponding values are 5.4×10^9 and 7.6×10^9 s^{-1} at 300 K in benzene and 2-propanol, respectively. The former has been used combining benzene data with the k_{decay} value obtained by extrapolation of the low temperature toluene data.

The decay from the upper triplet, k_{IId} can be expected to have only a small activation energy, since otherwise this process would be unlikely to compete with the internal conversion, k_{21}. The overall activation energy (see Table 1) will be the sum of the energy gap between the two triplets, plus the activation energy corresponding to k_{IId}; thus, the gap between ^{3}**II*** and ^{3}**I*** will be around 4 kcal mol^{-1}. This puts k_{21} in the neighbourhood of 10^{12} s^{-1} or slightly less, assuming, as a first approximation, that entropy changes between the two states can be neglected. Since Φ_{ISC} values indicate $k_{21} > k_{IId}$, then,

Can. J. Chem. Downloaded from www.nrcresearchpress.com by 210.87.254.42 on 09/06/12
For personal use only.

k_{IId} must be around 10^{11} s^{-1}, or about 100 times faster than in the case of β-phenylpropiophenone (12). This probably reflects lower entropic requirements to achieve the transition state (less interval rotations need to be frozen) in the case of 2-phenylbenzophenone.

The quantum yield data for the photoreduction of 2-phenylbenzophenone in 2-propanol can be combined with the laser data to estimate the rate constant for hydrogen abstraction from the solvent, i.e.

$$[8] \quad \Phi_{photored} = \Phi_{ISC} \frac{k_a[Me_2CHOH]}{k_{decay}}$$

where it has been assumed that for these low quantum yields $k_a[Me_2CHOH] \ll k_{decay}$, and k_a is the rate constant for hydrogen abstraction from 2-propanol. From the data presented before, we estimate $k_a \sim 7 \times 10^4\ M^{-1}\ s^{-1}$, which should be compared with values of $\sim 4 \times 10^6\ M^{-1}\ s^{-1}$ for benzophenone (2) and $\sim 1 \times 10^3\ M^{-1}\ s^{-1}$ for 4-phenylbenzophenone (5). The results are entirely consistent with the idea that the three aromatic rings cannot simultaneously approach planarity. Thus, while abstraction 2-phenylbenzophenone may require up-conversion to an upper state, the reactivity for this state is not unlike that of benzophenone itself.

Other carbonyl compounds, in particular those containing *p*-methoxybenzoyl moieties present similar characteristics; i.e. a two-state system in which reaction seems to occur from the upper state, while the spectroscopic properties of the triplet are largely determined by the more heavily populated low lying π,π* state (6, 31, 32). However, these systems do not seem to require the relatively large conformational changes proposed in the case of 2-phenylbenzophenone.

The data in Table 1 suggest a moderate trend of E_a with the temperature dependence of the solvent viscosity, but clearly other factors (such as solvation) must also be playing a role.

Can. J. Chem. Downloaded from www.nrcresearchpress.com by 210.87.254.42 on 09/06/12
For personal use only.

Acknowledgement

Thanks are due to Mr. S. E. Sugamori for technical assistance.

1. N. J. TURRO. Molecular photochemistry. Benjamin, New York. NY. 1967. Chapt. 6.
2. J. C. SCAIANO. J. Photochem. **2**, 81 (1973/74).
3. F. BERGMANN and Y. HIRSHBERG. J. Am. Chem. Soc. **65**, 1429 (1943).
4. H. H. HATT, A. PILGRIM, and E. F. M. STEPHENSON. J. Chem. Soc. 478 (1941).
5. N. J. TURRO and C. G. LEE. Mol. Photochem. **4**, 427 (1972).
6. P. J. WAGNER, A. E. KEMPPAINEN, and H. N. SCHOTT. J. Am. Chem. Soc. **95**, 5604 (1973); P. J. WAGNER and T. NAKAHIRA. J. Am. Chem. Soc. **96**, 3668 (1974); P. J. WAGNER, A. E. KEMPPAINEN, and H. N. SCHOTT. J. Am. Chem. Soc. **92**, 5280 (1970); P. J. WAGNER. Pure Appl. Chem. **49**, 259 (1977).
7. P. K. DAS and J. C. SCAIANO. J. Photochem. **12**, 85 (1980); K. UJI-IE, K. KIKUCHI, and H. KOKOBUN. J. Photochem. **10**, 145 (1979); G. PORTER and M. F. TCHIR. Chem. Commun. 1372 (1979); J. Chem. Soc. A, 3772 (1971); P. K. DAS, M. V. ENCINAS, R. D. SMALL JR., and J. C. SCAIANO. J. Am. Chem. Soc. **101**, 6965 (1979).
8. J. C. SCAIANO. Chem. Phys. Lett. **92**, 97 (1982); S.-Y. HOU, W. M. HETHERINGTON III, G. M. KORENOWSKI, and K. B. EISENTHAL. Chem. Phys. Lett. **68**, 282 (1979).
9. C. BAILEY and O. VOGL. J. Macromol. Sci. Rev. Macromol. C**14**, 267 (1976); D. J. CARLSSON, T. SUPRUNCHUK and D. M. WILES. J. Appl. Polym. Sci. **16**, 615 (1972); K. B. CHAKRABORTY and G. SCOTT. Europ. Polym. J. **15**, 35 (1979); J. C. SCAIANO and J. C. SELWYN. Macromolecules, **14**, 1723 (1981); D. J. CARLSSON and D. M. WILES. J. Macromol. Sci. Rev. Macromol. C**14**, 155 (1976).
10. P. J. WAGNER, P. A. KELSO, A. E. KEMPPAINEN, A. HAUG, and D. R. GRABER. Mol. Photochem. **2**, 81 (1970).
11. R. F. STERMITZ, D. E. NICODEM, V. P. MURALIDHARAN, and C. M. O'DONNELL. Mol. Photochem. **2**, 87 (1970).
12. J. C. SCAIANO, M. J. PERKINS, J. W. SHEPPARD, M. S. PLATZ, and R. L. BARCUS. J. Photochem. **21**, 137 (1983).
13. P. J. WAGNER, M. MEADOR, and J. C. SCAIANO. To be published.
14. P. J. WAGNER, P. A. KELSO, A. E. KEMPPAINEN, and R. G. ZEPP. J. Am. Chem. Soc. **94**, 7500 (1972).
15. A. A. LAMOLA, P. A. LEERMAKERS, G. W. BYERS, and G. S. HAMMOND. J. Am. Chem. Soc. **87**, 2322 (1965); A. A. LAMOLA. J. Am. Chem. Soc. **92**, 5045 (1970); T. TAMAKI. Photochem. Photobiol. **33**, 31 (1981); P. K. DAS and J. C. SCAIANO. Macromolecules, **14**, 693 (1981); R. A. KELLER and L. J. DOLBY. J. Am. Chem. Soc. **91**, 1293 (1969); N. FILIPESCU, J. R. DE MEMBER, and F. L. MINN. J. Am. Chem. Soc. **91**, 4169 (1969); J. P. BAYS, M. V. ENCINAS, R. D. SMALL, JR., and J. C. SCAIANO. J. Am. Chem. Soc. **102**, 727 (1980).
16. D. E. NICODEM and M. L. MARCHIORI. J. Org. Chem. **46**, 3928 (1981); R. C. FUSON, R. J. LOKKEN, and R. L. PEDROTTI. J. Am. Chem. Soc. **78**, 6064 (1956).
17. T. W. J. TAYLOR, J. S. OWEN, and D. WHITTAKER. J. Chem. Soc. 206 (1938).
18. G. V. VESLEY and G. S. HAMMOND. Mol. Photochem. **5**, 367 (1973).
19. J. C. SCAIANO. J. Am. Chem. Soc. **102**, 7747 (1980).
20. J. P. BAYS, M. V. ENCINAS, and J. C. SCAIANO. Macromolecules, **13**, 815 (1980).
21. D. E. NICODEM and J. C. SCAIANO. To be published.
22. J. C. SCAIANO. J. Photochem. **16**, 71 (1981).
23. W. J. LEIGH and J. C. SCAIANO. J. Am. Chem. Soc. **105**, 5652 (1983).
24. M. R. TOPP. Chem. Phys. Lett. **32**, 144 (1975); G. PORTER and M. W. WINDSOR. Proc. R. Soc. London Ser. A, **245**, 238 (1958).
25. P. J. WAGNER. J. Am. Chem. Soc. **89**, 2820 (1967).
26. P. J. WAGNER and B. J. SCHEVE. J. Am. Chem. Soc. **99**, 2888 (1977).
27. G. N. LEWIS and M. KASHA. J. Am. Chem. Soc. **66**, 2100 (1944).
28. M. K. ORLOFF and J. S. BRINEN. J. Chem. Phys. **47**, 3999 (1967); E. C. LIM, and H. Y. LI. J. Chem. Phys. **52**, 6416 (1970); J. MISPELTER. Chem. Phys. Lett. **10**, 539 (1971); A. IMAMURA and R. HOFFMAN. J. Am. Chem. Soc. **90**, 5379 (1968).
29. N. J. TURRO. Modern molecular photochemistry. Benjamin-Cummings, Menlo Park, CA. 1978. Table 6.3.
30. T. FUJII, S. KOMATSU, and S. SUZUKI. Bull. Chem. Soc. Jpn. **55**, 2516 (1982).
31. P. J. WAGNER and T. NAKAHIRA. J. Am. Chem. Soc. **96**, 3668 (1974); **95**, 8474 (1973); J. C. SCAIANO and J. C. SELWYN. Macromolecules, **14**, 1723 (1981).
32. M. V. ENCINAS, E. A. LISSI, E. LEMP, A. ZANOCCO, and J. C. SCAIANO. J. Am. Chem. Soc. **105**, 1856 (1983).

Comparison of the quenching of excited states by 5-DOXYL and 12-DOXYL-stearates in micellar solution[1]

J. C. SCAIANO AND C. I. PARASKEVOPOULOS[2]
Division of Chemistry, National Research Council of Canada, Ottawa, Ont., Canada K1A 0R6

Received February 8, 1984

J. C. SCAIANO and C. I. PARASKEVOPOULOS. Can. J. Chem. **62**, 2351 (1984).

The relative reactivity of the nitroxides tetramethylpiperidin-*N*-oxide, 5-DOXYL-stearic acid and 12-DOXYL-stearic acid in the quenching of excited states in sodium dodecyl sulfate micelles has been examined. 12-DOXYL-stearic acid is a better quencher in the case of very hydrophobic sensitizers, such as pyrene singlets or phenanthrene (singlet or triplet states). The converse is true for the hydrophilic xanthone triplet or excited $Ru(bipy)_3^{2+}$. The results support the idea of preferential solubilization in different regions of the micelle and provide a method for probing this preference.

J. C. SCAIANO et C. I. PARASKEVOPOULOS. Can. J. Chem. **62**, 2351 (1984).

On a étudié les réactivités relatives des nitroxydes suivants, soit le *N*-oxyde de la tétraméthylpipéridine, l'acide DOXYL-5 stéarique et l'acide DOXYL-12 stéarique, comme pièges d'états excités dans des micelles de dodécylsulfate de sodium. L'acide DOXYL-12 stéarique est un meilleur piège dans le cas de sensibilisateurs très hydrophobes comme les états singulets du pyrène ou les états singulet ou triplet de l'anthrène. L'inverse est également vrai pour les sensibilisateurs hydrophiles comme l'état triplet de la xanthone ou l'état excité du $Ru(bipy)_3^{2+}$. Les résultats sont en accord avec l'hypothèse selon laquelle il se produit des solubilisations préférentielles dans différentes portions de la micelle et ils fournissent une méthode de déterminer cette préférence.

[Traduit par le journal]

Can. J. Chem. Downloaded from www.nrcresearchpress.com by 210.87.254.42 on 09/06/12
For personal use only.

Introduction

Singlet and triplet sensitizers are frequently used as probes in organized systems, particularly micellar solution (1–5). Of particular relevance is the question of the effect of probe and/or quencher location on the rates and efficiency of quenching. The most drastic effect is achieved when full separation of the reaction partners between the aqueous and organic pseudo-phases is achieved. Relatively more subtle differences can be expected when quencher and sensitizer are present in the same micellar aggregates, but have preference for different locations within the micelle. Effects of this type have been examined by others; for example, Thulborn and co-workers (5, 6) have used *n*-(9-anthroyloxy)-fatty acids as fluorescent probes. Singer *et al.* (7) have examined the quenching of pyrene-containing cationic fluorescers of different lengths by a surfactant nitroxide. Bales and Kevan (8) have used stearic acid DOXYL probes of the same type employed here to examine spatial effects on electron scavenging in micelles. Smith *et al.* (9) have studied membrane permeability using epr techniques to monitor the behaviour of nitroxide probes.

In this work we examine the quenching of various sensitizers by tetramethylpiperidin-*N*-oxide (TEMPO), 5-DOXYL-stearic acid (5DSA), and 12-DOXYL-stearic acid (12DSA) in micellar and homogeneous solution.

The reactions were examined using fluorescence spectroscopy and laser flash photolysis techniques.

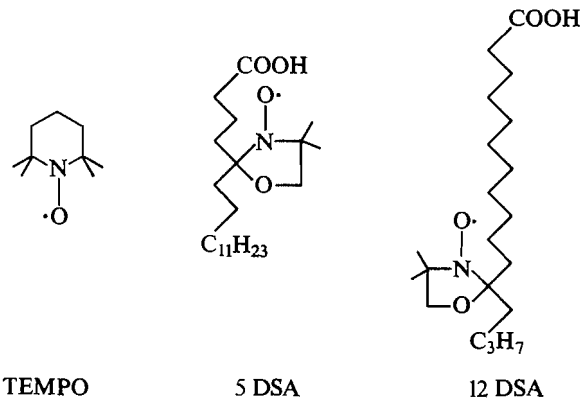

TEMPO 5 DSA 12 DSA

Experimental section

Materials

All spin labels were obtained from Aldrich and were used as received, although concentrations were based on epr measurements, not on the weight of material used (*vide infra*). Sodium dodecyl sulfate (SDS) from BDH (specially purified grade), was used as received. All sensitizers were commercially available and were recrystallized or distilled before use.

Sample preparation

The samples of spin labels were dissolved in absolute ethanol. The concentrations of the stock solutions (typically in the 0.3–0.9 *M* range) were determined by comparing the double integrated epr spectrum of appropriately diluted samples with samples of DPPH standards.

The samples of the sensitizer (usually 0.1 *M* in SDS) were contained in sample tubes made of square 7 × 7 mm^2 (laser photolysis) or 10 × 10 mm^2 (fluorescence) Suprasil tubing. They were deaerated of bubbling oxygen-free nitrogen. The quenchers were added by injecting known volumes of the concentrated stock solutions.

Luminescence

These measurements were carried out in an LS-5 Perkin-Elmer spectrofluorimeter controlled by a Model-3600 data station.

Laser flash photolysis

The samples were excited with the pulses (337.1 nm, ~8 ns, up to 10 mJ/pulse) from a Molectron UV-24 nitrogen laser. The transient absorption signals, initially captured by a Tektronix R-7912 transient digitizer, were transferred to a PDP 11/23 computer that controlled the experiment and provided suitable processing, storage, and hard-copy facilities. Further details have been reported elsewhere (10).

Results

Luminescence quenching

The experiments were carried out in order to establish reactivity differences between the two DOXYL derivatives, and between these and the model compound, TEMPO. The ap-

[1]NRCC No. 23382.
[2]1983 NRCC Summer Student.

Can. J. Chem. Downloaded from www.nrcresearchpress.com by 210.87.254.42 on 09/06/12
For personal use only.

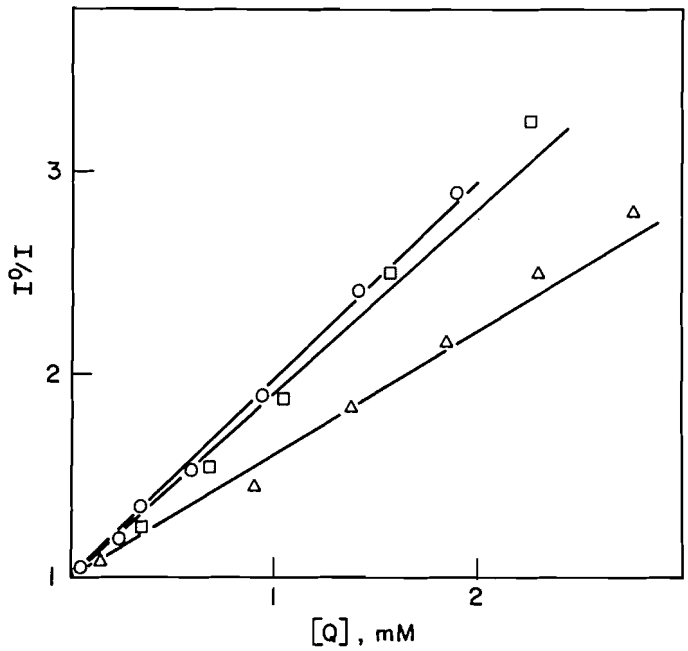

FIG. 1. Stern–Volmer plots for the quenching of pyrene (monomer) fluorescence by TEMPO (○), 5DSA (△), and 12DSA (□) in 0.1 *M* SDS at 300 K.

TABLE 1. Quenching of various luminescent sensitizers by nitroxides in homogeneous and micellar solution at 300 K

Sensitizer	Media[a]	$k_q\tau/M^{-1}$ TEMPO	5DSA	12DSA	$\lambda_{ex}/\lambda_{em}$[b]
Pyrene	Methanol	4230	2540	2380	350/400
Pyrene	SDS	1010	650	1130	350/400
Phenanthrene	Methanol	230			354/380
Phenanthrene	SDS	290	150	310	354/380
Perylene	Methanol	250			355/500
Perylene	SDS	410	385	395	355/500
Anthracene	Methanol	220			350/437
Anthracene	SDS	305	435	420	350/437
$Ru(bipy)_3^{2+}$	Methanol	320			342/615
$Ru(bipy)_3^{2+}$	SDS	575	70.5	37.4	342/615

[a]In the case of SDS its concentration was 0.1 *M*.
[b]Excitation and emission in nm.

proach used involved conventional Stern–Volmer analysis of the quenching data, eq. [1]

$$[1] \quad \frac{I^0}{I} = 1 + k_q\tau[Q]$$

where I^0 and I are the luminescence intensities on the absence and presence of quencher Q, respectively and $k_q\tau$ is the Stern–Volmer constant. These plots were found to be reasonably linear under our experimental conditions. Representative plots are included in Fig. 1, which illustrates the quenching of pyrene singlets; all other systems showed less curvature than this one (*vide infra*). In this particular system the excitation wavelength was 350 nm and the emission was monitored at 400 nm. The results for pyrene and the other luminescent sensitizers have been summarized in Table 1. Experiments with TEMPO were generally used in order to establish the experimental conditions under which studies with the costly DOXYL derivatives were more likely to succeed.

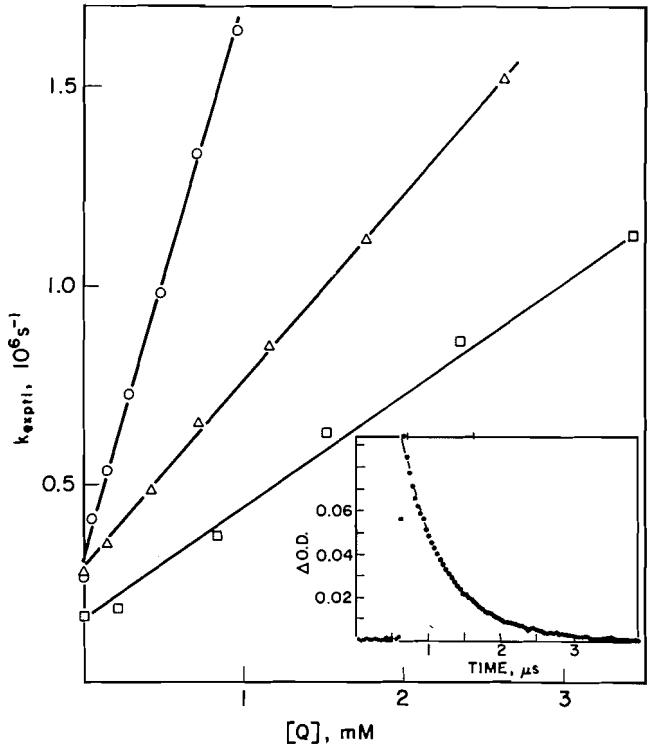

FIG. 2. Quenching of xanthone triplets by TEMPO (○), 5DSA (△), and 12DSA (□) in 0.1 *M* SDS at 300 K. (*Insert*) Decay of xanthone triplets (monitored at 600 nm) in the presence of 0.95 m*M* TEMPO.

Triplet quenching studies using laser-photolysis

In this case the decay of the sensitizers was monitored directly from the time evolution of the triplet–triplet absorption signals at the appropriate wavelengths. For example, in the case of xanthone triplets, the decay can be conveniently monitored at 600 nm (10) (see insert in Fig. 2). We find that the decay profiles can be reasonably fitted with a first order kinetic expression and a quenching rate constant, k_q, can be derived according to eq. [2]

$$[2] \quad k_{exptl} = k_0 + k_q[Q]$$

where k_{exptl} is the pseudo first order rate constant for triplet decay, k_0 is the rate constant in the absence of quencher (i.e., $k_0 = \tau_T^{-1}$), and [Q] the quencher concentration. Figure 2 shows the corresponding plots for xanthone quenching by the three nitroxides in micellar solution, and Table 2 summarizes the data for the various sensitizers used. Experiments with phenanthrene were rather difficult because singlet quenching leads to a substantial decrease in the triplet input at the higher nitroxide concentrations. The relatively large error limits reflect these problems. In the case of anthracene triplets the rate constants for TEMPO were quite slow (11), thus requiring relatively high quencher concentrations; as a result, no experiments were attempted with the costly DOXYL derivatives.

Discussion

It is important to establish under which type of conditions a given type of experiment can be useful in establishing reactivity differences between the two DOXYL derivatives, or between these and the model compound, TEMPO. For example, in the case of static quenching experiments, if we encountered a situation where quenching occurred with 100% efficiency every

TABLE 2. Rate constants obtained by laser photolysis for the quenching of triplet sensitizers by nitroxides at 300 K

Sensitizer (λ)[a]	Media	Quencher	$k_q/M^{-1}\ s^{-1}$ [b]
p-Methoxyacetophenone	Methanol	TEMPO	$(3.0 \pm 0.1) \times 10^9$
(400 nm)	Methanol	5DSA	$(1.37 \pm 0.06) \times 10^9$
	Methanol	12DSA	$(1.32 \pm 0.02) \times 10^9$
	SDS	TEMPO	$(1.7 \pm 0.3) \times 10^9$
	SDS	5DSA	$(8.9 \pm 2.8) \times 10^8$
	SDS	12DSA	$(8.1 \pm 1.4) \times 10^8$
Xanthone	Methanol	TEMPO	$(5.5 \pm 0.4) \times 10^9$
(600 nm)	Methanol	5DSA	$(2.7 \pm 0.1) \times 10^9$
	Methanol	12DSA	$(2.68 \pm 0.05) \times 10^9$
	SDS	TEMPO	$(1.47 \pm 0.07) \times 10^9$
	SDS	5DSA	$(4.72 \pm 0.15) \times 10^8$
	SDS	12DSA	$(2.9 \pm 0.2) \times 10^8$
Phenanthrene	Methanol	TEMPO	$(1.67 \pm 0.27) \times 10^9$
(480 nm)	Methanol	5DSA	$(9.2 \pm 2.1) \times 10^8$
	Methanol	12DSA	$(9.6 \pm 0.3) \times 10^8$
	SDS	TEMPO	$(7.7 \pm 1.7) \times 10^8$
	SDS	5DSA	$(8.8 \pm 3.7) \times 10^6$
	SDS	12DSA	$(3.5 \pm 1.5) \times 10^7$
Anthracene	Methanol	TEMPO	$(2.8 \pm 0.8) \times 10^6$
(420 nm)	SDS	TEMPO	$(5.2 \pm 1.2) \times 10^6$

[a]Monitoring wavelength (in nm) employed in the experiments.
[b]Errors as $\pm 2\sigma$.

time a sensitizer and one quencher molecule were in the same micelle at the time of excitation, no difference would be expected among the various substrates; i.e. quenching experiments would only reflect the statistical distribution of reaction partners. Thus, when sensitizer and quencher are resident in the same micelle at the time of excitation, we need a competition between quenching and some other process, such as luminescent emission and/or exit from the parent micelle.

We find TEMPO to be generally more reactive than the DOXYL derivatives, and the difference is quite large in the case of $Ru(bipy)_3^{2+}$. It seems reasonable to assume that the ruthenium complex will be resident at the micelle–water interphase (whether it is held there by electrostatic interactions or by chemical bonding (12)). Thus, the more efficient quenching by TEMPO must be a reflection of its higher mobility and of the absence of a long hydrophobic chain. Similarly, the higher Stern–Volmer constant for 5DSA compared with 12DSA indicates that the former can access the micellar surface more easily. The converse seems true of at least some of the aromatic hydrocarbons. Thus, in the cases of pyrene and phenanthrene, 12DSA is a better quencher than 5DSA, reflecting that these hydrocarbons spend more time near the non-polar core of the micelle which must be more readily accessible in the case of 12DSA. Such preference is not unexpected, given the hydrophobic nature of these substrates.

The absence of any significant differences in the Stern–Volmer slopes for the DOXYL derivatives in the cases of perylene and anthracene are rather surprising. In these cases we tentatively suggest that there is no preference between the regions around 5 and 12 carbon atoms away from the polar head of the probe. It should also be noted that quenching in these cases must be quite fast, since the singlet lifetimes for anthracene and perylene are only a few nanoseconds.

In the case of time-resolved experiments, one can expect to be able to detect differences in the reactivity of the various quenchers provided that static quenching is not so rapid as to be complete within the response time of our instrumentation. In fact our determinations seem to be quite sensitive in these systems. In all cases we observe that in homogeneous solution 5DSA and 12DSA are equally reactive. In the case of xanthone, the data in micellar solution indicates that 5DSA is almost twice as reactive as 12DSA. The difference is in line with the expected hydrophilicity of the polar xanthone triplet. In fact, in other organized media (13) (e.g. polyelectrolyte–surfactant aggregates) xanthone has been shown to relocate to a more polar environment following excitation into the triplet state.

p-Methoxyacetophenone shows virtually no preference for 5DSA or 12DSA, probably a reflection of a relatively homogeneous distribution within the micelle.

Phenanthrene triplets show a preference for the less polar micellar core, as indicated by the higher rate constant for 12DSA compared with 5DSA. Such preference is consistent with the observations in the case of the singlet state (see Table 1). It should be noted that the ratio of values for 5DSA and 12DSA quenching of phenanthrene are different in Tables 1 and 2. In fact, there is no reason why they should be equal, since they refer to different electronic states; further while the Stern–Volmer approach deals with static and dynamic phenomena, the time-resolved approach relates only to the dynamic component.

Conclusion

Nitroxide probes attached to amphiphilic molecules, such as stearic acid, are useful in the study of the location of excited probes in micellar solutions. Similar applications have been suggested earlier in the case of photoionization processes (8), as well as in studies of lipid membrane permeability (9). An alternative approach, using *n*-(9-anthroyloxy) fatty acids as fluorescent probes has been recently reviewed by Thulborn (5).

The two techniques used show good sensitivity and can easily distinguish between the location of different probes. While all the plots obtained here in the time-resolved and luminescence studies were approximately linear, it should be noted that this need not be the case for all similar probes or in different ranges in concentration. Indeed the reasons leading to curved Stern–Volmer plots in micellar solution are well established (14). Our claim is simply that since the plots show only a very slight curvature, the ratio of slopes can be used as a measure of the preference for the reactive 5 or 12 position in the stearic acid chain.

Acknowledgements

Thanks are due to Drs. A. S. Nazran and J. Lusztyk for their help with the epr measurements and to Mr. S. E. Sugamori for technical assistance.

1. K. KALYANASUNDARAM. Chem. Soc. Rev. **7**, 453 (1978).
2. J. K. THOMAS. Chem. Rev. **80**, 283 (1980); J. K. THOMAS, F. GRIESER, and M. WONG. Ber. Bunsenges. Phys. Chem. **82**, 937 (1978).
3. M. ALMGREN, F. GRIESER, and J. K. THOMAS. J. Am. Chem. Soc. **101**, 279 (1979).
4. G. S. BEDDARD. *In* Fluorescent probes. *Edited by* G. S. Beddard and M. A. West. Academic Press, London. 1981. p. 21.
5. K. R. THULBORN. *In* Fluorescent probes. *Edited by* G. S. Beddard and M. A. West. Academic Press, London. 1981. p. 113.
6. K. R. THULBORN, L. M. TILLEY, W. H. SAWYER, and E. TRELOAR. Biochim. Biophys. Acta, **558**, 166 (1979); A. G.

Can. J. Chem. Downloaded from www.nrcresearchpress.com by 210.87.254.42 on 09/06/12
For personal use only.

ASHCROFT, K. R. THULBORN, J. R. SMITH, H. G. L. COSTER, and W. H. SAWYER. Biochim. Biophys. Acta, **602**, 299 (1980).
7. S. S. ATIK, C. L. KWAN, and L. A. SINGER. J. Am. Chem. Soc. **101**, 5696 (1979).
8. B. L. BALES and L. KEVAN. J. Phys. Chem. **86**, 3836 (1982); M. GIANGRANDE and L. KEVAN. Photochem. Photobiol. **33**, 721 (1981).
9. S. SCHREIER-MUCCILLO, D. MARSH, and I. C. P. SMITH. Arch. Biochem. Biophys. **172**, 1 (1976); K. W. BUTLER, N. H. TATTRIE, and I. C. P. SMITH. Biochim. Biophys. Acta, **363**, 351 (1974).
10. J. C. SCAIANO. J. Am. Chem. Soc. **102**, 7747 (1980).
11. J. C. SCAIANO. Chem. Phys. Lett. **79**, 441 (1981) and references therein.
12. J. H. BAXENDALE and M. A. J. ROGERS. J. Phys. Chem. **86**, 4906 (1982).
13. E. B. ABUIN and J. C. SCAIANO. J. Am. Chem. Soc. In press.
14. S. S. ATIK and L. A. SINGER. Chem. Phys. Lett. **59**, 519 (1978).

Can. J. Chem. Downloaded from www.nrcresearchpress.com by 210.87.254.42 on 09/06/12
For personal use only.

Flash photolysis of phenylacetatopentaminecobalt(III) in aqueous solution. Generation of benzyl radicals and their reversible trapping by cupric ions in homogeneous and micellar solutions[1]

J. C. SCAIANO AND W. J. LEIGH
Division of Chemistry, National Research Council of Canada, Ottawa, Ont., Canada K1A 0R6

AND

G. FERRAUDI
Radiation Laboratory, University of Notre Dame, Notre Dame, IN 46556, U.S.A.

Received February 20, 1984

J. C. SCAIANO, W. J. LEIGH, and G. FERRAUDI. Can. J. Chem. **62**, 2355 (1984).

The photodecomposition of $[Co(NH_3)_5OC(O)CH_2C_6H_5](ClO_4)_2$ is a convenient source of benzyl radicals in aqueous systems. The radicals react with cupric ions with a rate constant of $(2.1 \pm 0.2) \times 10^7\ M^{-1}\ s^{-1}$ to yield a complex that is formed reversibly. This complex can decay to Cu(I), but at high radical concentrations the recombination of benzyl radicals in equilibrium with it can become the predominant decay path. The reaction of benzyl radicals (from 1,3-diphenylacetone) in anionic micelles in the presence of Cu^{2+} leads to strong signals from the same intermediate, $CuCH_2C_6H_5^{2+}$.

J. C. SCAIANO, W. J. LEIGH et G. FERRAUDI. Can. J. Chem. **62**, 2355 (1984).

La décomposition photochimique du $[Co(NH_3)_5OC(O)CH_2C_6H_5](ClO_4)_2$ est une source commode de radicaux benzyles dans des systèmes aqueux. Les radicaux réagissent avec les ions cuivriques avec une constante de vitesse de $(2{,}1 \pm 0{,}2) \times 10^7\ M^{-1}\ s^{-1}$ pour donner un complexe qui est formé d'une façon réversible. Ce complexe peut se dégrader en Cu(I); toutefois, si les concentrations en radical sont élevées, la recombinaison des radicaux benzyles en équilibre avec le complexe peut devenir le processus prédominant de la dégradation. La réaction des radicaux benzyles (provenant de la diphényl-1,3 acétone), dans des micelles anioniques et en présence de Cu^{2+}, permet de déceler de forts signaux attribuables au même intermédiaire, soit le $CuCH_2C_6H_5^{2+}$.

[Traduit par le journal]

Introduction

The widespread use of photochemical free radical sources has largely concentrated on systems in organic solvents, where many convenient precursors are well known (e.g., ref. 1). The situation is quite different in aqueous solutions, where few well documented photochemical sources of organic free radicals are known. In particular, laser photolysis techniques are seldom applied to organic radicals in water. The increase of the interest in free radical processes in organized assemblies and in biological systems (2, 3) has made evident the need of reliable water soluble precursors (2, 3). Thus, it becomes important to understand the mechanism and kinetics of the reactions of relatively hydrophobic radicals in water.

The photodecomposition of cobalt(III) complexes of the type $[Co(NH_3)_5OC(O)R](ClO_4)_2$ has been recognized for over a decade, but their potential use as a free radical source in aqueous systems has received very little attention (5–7).[2] These compounds are stable, easy to prepare and purify, and R can be virtually any group (8). The photochemistry of the phenylacetato complex shows wavelength dependence, but the generation of $C_6H_5CH_2\cdot$ was found to be sufficiently efficient at 308 nm to make it a convenient precursor.

In this paper we report the details of a study of the flash photodecomposition of $[Co(NH_3)_5OC(O)CH_2C_6H_5]^{2+}$ to generate $C_6H_5CH_2\cdot$ and the subsequent reaction of these radicals with cupric ions. This latter reaction is recognized as a very efficient process and has been used as a diagnostic test of radical exit processes in micelles (9). We find the reaction to be considerably slower than we had anticipated, and to involve an intermediate that is formed reversibly.

The question of benzyl radical trapping in micellar systems has also been examined using 1,3-diphenylacetone as the radical precursor.

Experimental

The phenylacetato complex $[Co(NH_3)_5OC(O)CH_2C_6H_5](ClO_4)_2$, was synthesized and purified according to reported procedures (8). Sodium dodecyl sulfate, SDS, was from BDH, specially purified, while cetyltrimethylammonium chloride (CTAC) from K&K was purified by multiple recrystallizations from acetone/methanol. 1,3-Diphenylacetone (Aldrich) was recrystallized from ethanol. All other materials were of the highest purity commercially available and were used as received.

Laser flash photolysis experiments were carried out using for excitation a Lumonics TE-860-2 excimer laser operated with Xe/HCl mixtures (308 nm, ~5 ns, up to 80 mJ/pulse). Similar, but much weaker transient signals were obtained using a Molectron UV-24 nitrogen laser (337.1 nm, ~8 ns, up to 10 mJ/pulse). All experiments were carried out at 300 K using a flow system in which the cell compartment has been built of 7×7 mm^2 Suprasil tubing. The stock solution under study was deaerated with oxygen-free nitrogen in a nearby container; typical flow rates were ca. 0.2 mL/pulse. The transient signals, initially captured by a R-7912 Tektronix transient digitizer, were transferred to a PDP 11/23 computer which controls the experiments and provides suitable processing, storage, and hard-copy facilities. Further details have been reported elsewhere (10).

Conventional flash experiments were carried out using a system which has been described elsewhere (11). Briefly, pulses of white light, with a typical duration of 30 μs were obtained for stored energies of ≤250 J/pulse. In order to ensure light absorption by the cobalt complex in the presence of cupric ions, a solution of $CuSO_4$ (usually ≤0.1 M) was used as a filter; this leads to $\lambda_{excitation} \leq 275$ nm.

The products of reaction were identified by gc–ms, using a Hewlett–Packard Model 5995 instrument.

[1]NRCC No. 23618.

[2]For a review of photochemical properties of Co(III) complexes, see ref. 4.

Can. J. Chem. Downloaded from www.nrcresearchpress.com by 210.87.254.6 on 09/06/12
For personal use only.

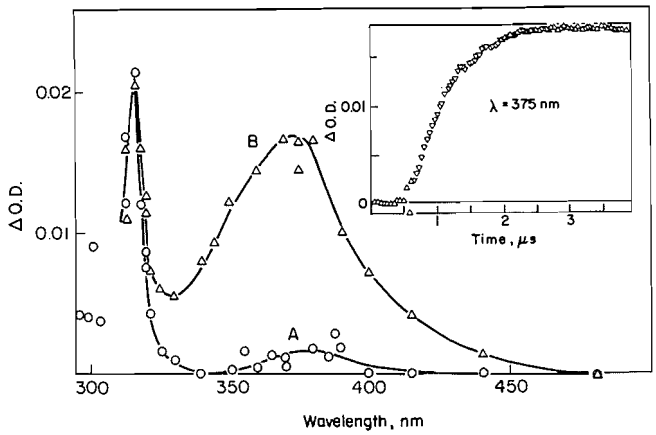

FIG. 1. Spectra recorded immediately (*A*) and 2.5 μs (*B*) after excitation of a solution of 0.0014 *M* $[Co(NH_3)_5OC(O)CH_2C_6H_5]$-$(ClO_4)_2$ and 0.03 *M* $CuSO_4$ at pH 2.8 (flow system, 300 K). (*Insert*) Build-up trace monitored at 375 nm.

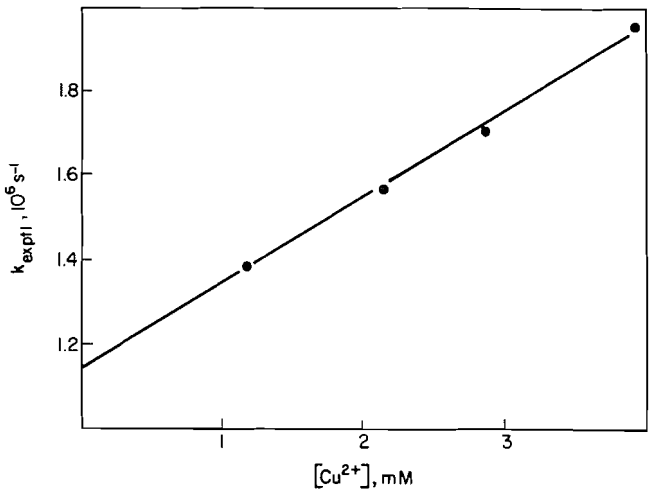

FIG. 2. Dependence of the rate of formation of $CuCH_2C_6H_5^{2+}$ on the concentration of Cu(II), according to eq. [3].

Results

Laser photolysis of deaerated aqueous solutions of $[Co(NH_3)_5OC(O)CH_2C_6H_5]^{2+}$, usually ~0.002 *M*, led to $C_6H_5CH_2\cdot$ (λ_{max} 317 nm) as the only transient species detected (12), reaction [1].

$$[1]\quad [Co(NH_3)_5OC(O)CH_2C_6H_5]^{2+} \xrightarrow{h\nu} Co^{2+} + 5NH_3 + CO_2 + C_6H_5\dot{C}H_2$$

While reaction [1] may involve the intermediacy of $C_6H_5CH_2C(O)O\cdot$ as a discrete transient, our experiments, usually in the 50 ns to 500 ms time domain, show no evidence for this species. Acyloxy radicals, particularly those leading to stabilized radicals, are believed to be very short-lived (13).

In the absence of scavengers benzyl radicals decayed predominantly with second order kinetics in both laser and conventional flash experiments, the radical concentration being substantially lower in the latter.

Cupric ions were added as $CuSO_4$. Optical spectroscopy did not indicate any thermal reaction between the cobalt complex and cupric ions. The pH of the samples was adjusted to 2.8 by addition of $HClO_4$ to prevent the precipitation of cobalt(II) hydroxide on photolysis. Addition of cupric ions led to a small increase of the decay rate of $C_6H_5CH_2\cdot$ and the formation of a new transient with λ_{max} ~ 375 nm; its formation followed pseudo-first order kinetics. Figure 1 shows the spectra obtained at two different times after laser excitation. The formation of a species with absorptions in this region is in line with similar observations for other carbon centered radicals (6, 14) and is attributed to reaction [2].

$$[2]\quad C_6H_5CH_2 + Cu^{2+}_{(aq)} \underset{k_{-2}}{\overset{k_2}{\rightleftharpoons}} CuCH_2C_6H_5^{2+}$$

Such intermediates have been proposed before on the basis of kinetic (15) and product analysis data (16).

A study of the rate of formation of $CuCH_2C_6H_5^{2+}$ for different concentration of $Cu^{2+}_{(aq)}$, under conditions where the decay of $Ph\dot{C}H_2$ is at least one order of magnitude slower, leads to k_2 from a plot of the pseudo-first order rate constant, k_{exptl}, against $[Cu^{II}]$, eq. [3].

$$[3]\quad \ln\frac{A_{eq}}{A_{eq} - A} = k_{exptl}\cdot t = (k_2[Cu^{II}] + k_{-2})t$$

where A_{eq} and A are the transient absorbances at equilibrium and at time t, respectively, and the equation neglects the slow decay in the absence of Cu^{II}. The corresponding plot (Fig. 2) leads to $k_2 = (2.1 \pm 0.2) \times 10^7\ M^{-1}\ s^{-1}$ and $k_{-2} = (1.14 \pm 0.06) \times 10^6\ s^{-1}$ at 27°C (errors as $\pm 2\sigma$). The equilibrium yield of 375 nm transient was proportional to $[Cu^{II}]$, as expected.

The signal intensity at 317 nm (mostly due to the benzyl radical) was reduced, but not eliminated, by addition of cupric ions. Even after the formation of the 375 nm absorption is complete, the 317 nm band remains in exactly the same position, and just as sharp as it is in the absence of Cu^{II} (see Fig. 1).

The decay of the 375 nm species occurs concurrently with that of the benzyl radical (monitored at 317 nm), over a wide range of transient concentrations. In the laser photolysis experiments, which involve higher radical concentrations, the decay incorporated a considerable degree of second order kinetics, particularly at the higher laser doses. In the conventional flash experiments the decay kinetics followed first order, single exponential behavior at both wavelengths 317 and 375 nm; in these the yield of 375 nm transient was linearly proportional to the flash energy at energies below 200 J/pulse, and was also higher for the higher Cu^{2+} concentrations.

The mixed first and second order kinetics observed in the laser experiments at either 317 or 375 nm are expected if the equilibrium conditions (reaction [2]) lead to a competition of radical decay processes via reactions [4] and [5].

$$[4]\quad 2C_6H_5\dot{C}H_2 \xrightarrow{2k_t} C_6H_5CH_2CH_2C_6H_5$$

$$[5]\quad CuCH_2C_6H_5^{2+} \xrightarrow[(H_2O)]{k_5} Cu^{+}_{(aq)} + C_6H_5CH_2OH$$

High $Cu^{2+}_{(aq)}$ and low radical concentrations (as in conventional flash experiments) lead to predominant first order decay via reaction [5], while reaction [4] can predominate in laser experiments. Typical experimental lifetimes for $CuCH_2C_6H_5^{2+}$ are in the 25–70 μs range, but usually involve some second order decay. The correct lifetime for reaction [5], obtained by extrapolation at low transient concentrations, is close to 100 μs (k_5^{-1}). An "apparent" rate constant for the trapping of benzyl by cupric ions can be obtained by monitoring the small changes in the decay at 317 nm and lead to $k_{app} = k_5k_2/k_{-2} = (2.1 \pm 1.0) \times 10^5\ M^{-1}\ s^{-1}$. The large error

Can. J. Chem. Downloaded from www.nrcresearchpress.com by 210.87.254.6 on 09/06/12
For personal use only.

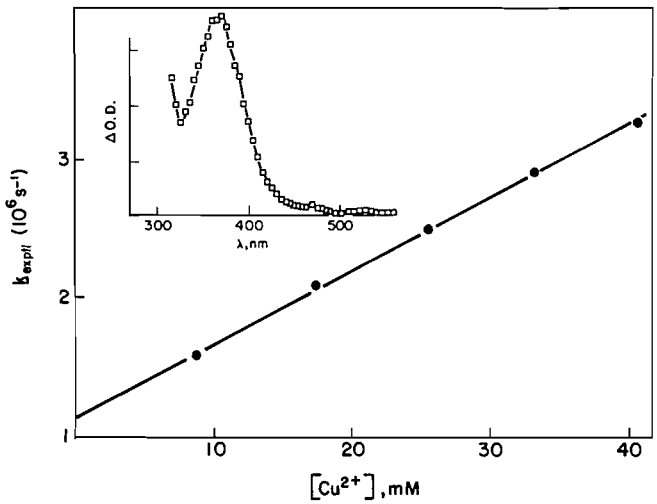

FIG. 3. Dependence of the rate of formation of $CuCH_2C_6H_5^{2+}$ on the concentration of cupric sulfate in 0.2 *M* SDS solution, using 1,3-diphenylacetone as a radical precursor. (*Insert*) Spectrum recorded between 1 and 10 μs following excitation.

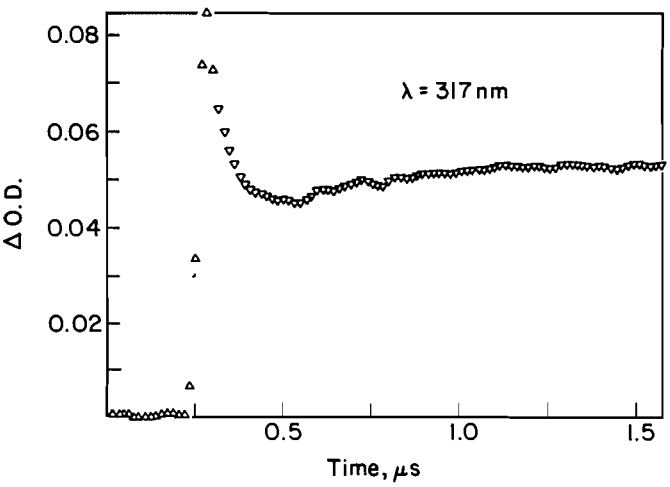

FIG. 4. Trace recorded at 317 nm, for a solution of 0.006 *M* 1,3-diphenylacetone in 0.2 *M* SDS, at 300 K.

results mainly from interference by reaction [4]. An estimate of k_5 that can also be obtained by combining the value of k_{app} with k_2 and k_{-2}; this leads to $k_5 \sim 1.2 \times 10^4$ s^{-1}, in good agreement with the value given above.

Product studies (gc−ms) in steady state irradiations with excitation light centered around 300 nm lead to $C_6H_5CH_2OH$, $C_6H_5CH_2C(O)OCH_2C_6H_5$, and $C_6H_5CH_2CH_2C_6H_5$ as the main products, in approximate ratios 1.0:0.6:0.2. The ester is believed to result from reaction of benzyl radicals with the cobalt complex. A trace of $C_6H_5CH_2Cl$ was also observed, although its origin is unclear. The expected formation of Cu(I) was confirmed by reaction with 2,9-dimethylphenanthroline.

A few laser photolysis experiments were also carried out in micellar solutions using 1,3-diphenylacetone as the radical precursor. In the case of CTAC micelles (typically 0.05 *M* surfactant) the signal at 375 nm is detectable with some difficulty, but definitely much weaker than those in just water. This may reflect a separation of quencher and radical, promoted by the positive micelles.

In SDS micelles, by contrast, the 375 nm transient is easily detectable and virtually identical to the species detected in water. The insert in Fig. 3 illustrates the spectrum obtained under these conditions. The build-up of the complex $CuCH_2C_6H_5^{2+}$ followed pseudo-first order kinetics, and for example had a growth lifetime of ~300 ns for $[Cu^{2+}] = 0.045$ *M* and [SDS] = 0.2 *M*. This rate of formation was linearly dependent on the concentration of cupric ions. The plot shown in Fig. 3 (compare with Fig. 2) leads to an overall rate constant for trapping $k_{trapping} = (5.3 \pm 0.3) \times 10^7$ M^{-1} s^{-1}, to be compared with $k_2 = 2.1 \times 10^7$ M^{-1} s^{-1} in water. Clearly SDS promotes quenching.

In the absence of Cu^{2+}, the signal from $C_6H_5\dot{C}H_2$ can be easily monitored at 317 nm. Under these conditions ([SDS] = 0.2 *M*) we observe a partial decay with a lifetime of ca. 60 ns, followed by a modest growth, with a lifetime in the 200−350 ns range (for this process it is difficult to determine a more accurate value). A representative trace is illlustrated in Fig. 4.

TABLE 1. Representative kinetic parameters for the reaction of carbon centered radicals with cupric ions

Radical	k_2[a,b]	k_{-2}[a,c]	k_5[a,c]	Reference
$\dot{C}H_2CO_2^-$	6.4×10^8	1×10^2	2.8	14
$CH_3\dot{C}HCO_2^-$	5×10^8	8.6×10^3	0.2	14
$\dot{C}H_2OH$	1.6×10^8			14
$\dot{C}H_2CH_2OH$	3.1×10^7		3.3×10^2	14
$CH_3\cdot$	7.4×10^5		7×10^2	6
$C_6H_5\dot{C}H_2$	2.1×10^7	1.1×10^6	1.2×10^4	This work

[a]The reactions refer to $C_6H_5\dot{C}H_2$ or to the equivalent reaction for the radical listed in each case.
[b]In units of M^{-1} s^{-1}.
[c]In units of s^{-1}.

Discussion

The formation of complex intermediates by reaction of carbon centered radicals with cupric ions seem to be a rather general phenomenon; some representative examples studied by pulse radiolysis (14), flash photolysis (16), and laser photolysis have been summarized in Table 1. Judging from the similarity of spectral shape and λ_{max}, the bonding interactions in all these species must be essentially the same. For example, λ_{max} is ~350, 370, and 375 nm for $\dot{C}H_2(CH_3)_2COH$ (14), $\dot{C}H_3$ (6), and $C_6H_5\dot{C}H_2$, respectively.

The apparent rate of benzyl radical scavenging by Cu^{2+} (i.e. k_5k_2/k_{-2}) is only 2.1×10^5 M^{-1} s^{-1}, in fact not a very efficient process. The vast majority of the initial trapping events (~99%) lead to the dissociation of the intermediate, with only ~1% leading to products (compare k_{-2} and k_5 in Table 1).

It is important to examine more quantitatively the implications of these results in terms of the relative contributions of reactions [4] and [5] to the decay of benzyl radicals. Thus, for a 0.1 *M* concentration of Cu^{2+} the ratio of radicals removed by each process is:

$$\frac{\text{termination}}{\text{trapping}} \sim 2k_t \times (1.11 \times 10^{-4})[C_6H_5\dot{C}H_2]_{total}$$

where $[Ph\dot{C}H_2]_{total} = [C_6H_5\dot{C}H_2] + [CuCH_2C_6H_5^{2+}]$ and the value of 1.11×10^{-4} includes all other relevant rates determined herein. Thus, if $2k_t \sim 4 \times 10^9$ M^{-1} s^{-1},[3]

$$\frac{\text{termination}}{\text{trapping}} \cong 4.4 \times 10^5[C_6H_5\dot{C}H_2]_{total}$$

[3]Reported values in water range for ca. 2 to 9×10^9 M^{-1} s^{-1} (17).

Can. J. Chem. Downloaded from www.nrcresearchpress.com by 210.87.254.6 on 09/06/12
For personal use only.

Can. J. Chem. Downloaded from www.nrcresearchpress.com by 210.87.254.6 on 09/06/12
For personal use only.

As a result of this analysis, we conclude that in homogeneous systems, cupric ions will be good traps of benzyl radicals, when the radical concentration is low as in steady irradiation experiments. However, trapping will be inefficient for high radical concentrations, such as those frequently achieved using pulsed techniques. For example, in laser flash photolysis experiments, radical concentrations around or over 10^{-5} M are not uncommon.

The situation may be even more complex in micellar systems (9) where exit–entry processes and electrostatic interactions may play a role in determining the efficiency of trapping. Given the overall trapping rate of $2.1 \times 10^5 M^{-1} s^{-1}$ determined here in water, it would appear that for a benzyl radical in water, its probability of entering a micelle would be, under most experimental conditions, much higher than the probability of irreversible quenching.

Our exploratory experiments in micellar systems using 1,3-diphenylacetone as a benzyl radical precursor illustrate some of the problems mentioned above. The photochemistry of 1,3-diphenylacetone in compartmentalized systems (9, 18) can be expected to follow the mechanism of reactions [6]–[11].

[6] $C_6H_5CH_2COCH_2C_6H_5 \xrightarrow{h\nu} \longrightarrow {}^3[C_6H_5\dot{C}H_2 + C_6H_5CH_2\dot{C}O]$

[7] ${}^3[C_6H_5\dot{C}H_2 + C_6H_5CH_2\dot{C}O] \xrightarrow[\text{ISC}]{k_7} \longrightarrow C_6H_5CH_2COCH_2C_6H_5$

[8] ${}^3[C_6H_5\dot{C}H_2 + C_6H_5CH_2\dot{C}O] \xrightarrow{k_8} {}^3[2C_6H_5\dot{C}H_2] + CO$

[9] ${}^3[C_6H_5\dot{C}H_2 + C_6H_5CH_2\dot{C}O] \xrightarrow{k_9} [C_6H_5CH_2\dot{C}O] + C_6H_5\dot{C}H_2$

[10] $[C_8H_5CH_2\dot{C}O] \xrightarrow{k_{10}} [C_6H_5\dot{C}H_2] + CO$

[11] ${}^3[2C_6H_5\dot{C}H_2] \xrightarrow[\text{ISC}]{k_{11}} \longrightarrow C_6H_5CH_2CH_2C_6H_5$

[12] ${}^3[2C_6H_5\dot{C}H_2] \xrightarrow{k_{12}} [C_6H_5\dot{C}H_2] + C_6H_5\dot{C}H_2$

where square brackets identify species in the same compartment (geminate pairs). Reaction [9] actually corresponds to exit by either radical, since these processes are indistinguishable (i.e. k_9 is the sum of both exit rate constants).

The decay constant of 60 ns observed, corresponds to the composite of reactions [7], [8], and [9]; i.e. $(k_7 + k_8 + k_9) \sim 1.7 \times 10^7$ s^{-1}, the predominant process being reaction [7], since the others would contribute to the kinetics but not to the readily detectable (Fig. 4) depletion of signal. The modest growth observed presumably reflects reaction [10], and is consistent with recent rate measurements for this process in homogeneous solution (19). These processes are not unlike those reported by Turro *et al.* (9, 18), frequently in CTAC, except that our data include a substantial amount of information in the ~50 ns range, which was not examined in detail in earlier reports.

The very weak 375 nm signals detected in CTAC micelles emphasize the efficient separation of free radicals and scavenger caused by the repulsive interaction between Cu^{2+} and the micellar surface, as well as the efficient micellization of $C_6H_5\dot{C}H_2$.

The scavenging of benzyl radicals by cupric ions in SDS micellar solution has already been examined (20). Surprisingly, the intense band at 375 nm escaped comment, apparently undetected. The formation of this band is in fact the dominant feature when the system is examined using laser flash photolysis techniques. Quite clearly micellization leads to a significant enhancement in the formation of $CuCH_2C_6H_5^{2+}$, consistent with the strong binding of Cu^{2+} to the micelle (21).

Acknowledgements

Thanks are due to Mr. S. E. Sugamori for technical assistance. The research discussed herein was partly supported by the Office of Basic Energy Sciences of the U.S. Department of Energy. This is Document No. NDRL-2388 from the Notre Dame Radiation Laboratory.

1. J. K. KOCHI (*Editor*). Free radicals. Vols. 1 and 2. Wiley, New York. 1973.
2. N. J. TURRO and B. KRAEUTLER. Acc. Chem. Res. **13**, 369 (1980); W. A. PRYOR. *In* Free radicals in biology. Vol. I. *Edited by* W. A. Pryor. Academic Press. 1976. Chapt. 1; J. C. SCAIANO. Proc. R. Soc. Can. **21**, 133 (1983).
3. J. H. FENDLER and P. TUNDO. Acc. Chem. Res. **17**, 3 (1984).
4. V. BALZANI and V. CARASSITI. Photochemistry of coordination compounds. Academic Press, New York. 1970; J. F. ENDICOTT. *In* Concepts in inorganic photochemistry. *Edited by* A. Adamson and P. D. Fleischaver. Wiley-Interscience, New York. 1975.
5. E. R. KANTROWITZ, M. Z. HOFFMAN, and J. F. ENDICOTT. J. Phys. Chem. **75**, 1914 (1971).
6. G. FERRAUDI. Inorg. Chem. **17**, 2506 (1978).
7. T. S. ROCHE and J. F. ENDICOTT. Inorg. Chem. **13**, 1575 (1974).
8. R. ROBSON and H. TAUBE. J. Am. Chem. Soc. **89**, 6487 (1967).
9. N. J. TURRO, M.-F. CHOW, C.-J. CHUNG, Y. TANIMOTO, and G. C. WEED. J. Am. Chem. Soc. **103**, 4574 (1981); N. J. TURRO and W. R. CHERRY. J. Am. Chem. Soc. **100**, 7431 (1978); N. J. TURRO, B. KRAEUTLER, and D. R. ANDERSON. J. Am. Chem. Soc. **101**, 7435 (1979); N. J. TURRO and J. MATTAY. J. Am. Chem. Soc. **103**, 4200 (1981).
10. J. C. SCAIANO. J. Am. Chem. Soc. **102**, 7747 (1980).
11. G. FERRAUDI. Inorg. Chem. **17**, 3164 (1978).
12. A. HABERSBERGEROVA, I. JANOVSKY, and J. TEPLY. Rad. Res. Rev. **1**, 109 (1968).
13. W. BRAUN, L. RAJBENBACH, and F. R. EIRICH. J. Phys. Chem. **66**, 1591 (1962); R. KAPTEIN, J. BROKKEN-ZIJP, and F. J. J. DE KANTER. J. Am. Chem. Soc. **94**, 6280 (1972); E. A. TURETSKAYA, E. D. SHAKORSKII, S. V. RIKOV, YU V. GLAZKOV, and YU A. OL'DEKOP. Dokl. Akad. Nauk. USSR, **24**, 57 (1980); R. E. SCHWERZEL, R. G. LAWLER, and G. T. EVANS. Chem. Phys. Lett. **29**, 106 (1974).
14. M. FREIBERG and D. MEYERSTEIN. J. Chem. Soc. Faraday Trans. I, 1825 (1980).
15. J. K. KOCHI, C. L. JENKINS, and BEMIS. J. Am. Chem. Soc. **90**, 4616 (1968).
16. C. L. JENKINS and J. K. KOCHI. J. Am. Chem. Soc. **94**, 856 (1972).
17. D. GRILLER. *In* Radical reaction rates in liquids. *Edited by* H. Fischer. Landolt-Börnstein, New Series, Group II, Springer-Verlag, Berlin. 1984.
18. N. J. TURRO. Proc. Natl. Acad. Sci. USA, **80**, 609 (1983).
19. L. LUNAZZI, K. U. INGOLD, and J. C. SCAIANO. J. Phys. Chem. **87**, 529 (1983); N. J. TURRO, I. R. GOULD, and B. H. BARETZ. J. Phys. Chem. **87**, 531 (1983).
20. Y. SAKAGUCHI, H. HAYASHI, and S. NAGAKURA. J. Phys. Chem. **86**, 3177 (1982).
21. M. GRÄTZEL and J. K. THOMAS. J. Phys. Chem. **78**, 2248 (1974); J. C. DEDEREN, M. VAN DER AUWERAER, and F. C. DE SCHRYVER. Chem. Phys. Lett. **68**, 451 (1979); M. A. J. RODGERS and M. F. DE SILVA E WHEELER. Chem. Phys. Lett. **53**, 165 (1978).

Adsorption of sodium cyclododecylmethanoate and cycloundecylmethanoate at the air/water interface

JAN J. SPITZER[1]

Department of Chemistry, University of Lethbridge, Lethbridge, Alta., Canada T1K 3M4

Received October 25, 1983[2]

JAN J. SPITZER. Can. J. Chem. **62**, 2359 (1984).

Surface tension measurements on aqueous solutions of sodium cyclododecylmethanoate and sodium cycloundecylmethanoate in sodium carbonate/bicarbonate buffers and at constant sodium ion concentration at 25°C were used to obtain the standard free energies of adsorption, the saturation areas per surfactant ion, and the critical "micelle" concentrations of these compounds. Similar measurements were done for solutions of sodium dodecanoate for comparisons.

The standard free energies of adsorption of CH_2 group that is located in a macrocyclic cycloalkyl ring appears to follow the "rule of two" ($-RT$ ln 2) that is also valid for straight chain ionic surfactants. The saturation areas of both cyclododecylmethanoate and cycloundecylmethanoate are about 52 Å^2/ion as compared to about 32 Å^2/ion for normal dodecanoate.

For large ring cycloalkylmethanoates the critical "micelle" concentrations appear to decrease by a factor of about 4/5 for each CH_2 group added to the ring as compared to the factor of about 1/2 for each CH_2 group added to the chain of normal alkanoates. The data suggest that large cycloalkyl rings have "collapsed ring", or "double chain", conformation in aqueous solutions and in the adsorbed state.

JAN J. SPITZER. Can. J. Chem. **62**, 2359 (1984).

Opérant à 25°C, dans des tampons de carbonate et de bicarbonate de sodium et à une concentration constante en ion sodium, on a mesuré les tensions de superficielles de solutions aqueuses de cyclododécylméthanoate de sodium et de cycloundécylméthanoate de sodium et l'on a utilisé les valeurs ainsi déterminées pour obtenir les énergies libres standard d'adsorption, les surfaces de saturation par ion tensioactif et les concentrations critiques de "micelles" de ces composés. Pour fins de comparaison, on a aussi effectué des mesures semblables sur des solutions de dodécanoate de sodium.

Les énergies libres standard d'adsorption du groupe CH_2 situé dans le cycloalkyle macrocyclique semblent suivre la "règle de deux" ($-RT$ ln 2) qui est également valable pour les agents tensioactifs ioniques à chaîne droite. La surface de saturation du cyclododécylméthanoate ainsi que celle du cycloundécylméthanoate sont d'environ 52 Å^2/ion par comparaison avec environ 32 Å^2/ion pour un dodécanoate normal.

Pour les cycloalkylméthanoates à grands cycles, les concentrations critiques de "micelle" semblent diminuer par un facteur d'environ 4/5 pour chaque CH_2 qui est ajouté au cycle; ceci se compare à un facteur 1/2 pour chaque CH_2 ajouté à une chaîne normale d'alkanoates. Les données suggèrent que, en solutions aqueuses et à l'état adsorbé, les cycloalkyles à grands cycles adoptent des conformations de "cycle effondré" ou de "double chaîne".

[Traduit par le journal]

Introduction

As part of our program of measurements leading to interfacial and micellization (or aggregation) data for surfactants that do not have long paraffinic chains in their molecular structure (1, 2), we now report surface tension measurements of aqueous solutions of sodium cyclododecylmethanoate and sodium cycloundecylmethanoate. For comparisons, similar measurements were also done for sodium dodecanoate.

The micellization of straight chain carboxylates has been extensively studied, and there is now a wealth of experimental and theoretical data (3–9). On the other hand the surface activity of normal alkanoates appears to be known only semi-quantitatively. Early workers recognized the large pH effects on the surface tension of solutions of carboxylates (10–12), particularly the effect of atmospheric carbon dioxide (13), but few data seem to have been published since. The most reliable data are probably those of Roe and Brass (14) on potassium dodecanoate and potassium palmitate. Graphical data for sodium decanoate, dodecanoate, and tetradecanoate have large minima in their surface tension vs. logarithms of concentration curves (15). These minima probably indicate the hydrolysis of carboxylate ions, or the presence of impurities (16).

The aggregation behaviour of surfactants with non-paraffinic hydrophobic structures depends on the geometrical structure of the hydrophobic moiety. A useful classification of various types of aggregation has been given by Mukerjee together with a discussion of possible data treatments (17). Most of the relevant aggregation data are for surfactants with structures based on bile acids, and these types of compounds continue to receive attention (18, 19). There are also some thermodynamic data on cycloalkylamine hydrobromides and non-paraffinic potassium carboxylates (20, 21). The surface activity of non-paraffinic hydrophobic solutes has not been much investigated (1) in spite of early elegant experiments by Hartley on double chain ethers of resorcinol (22, 23), even though these kinds of compounds occur naturally in biological systems (24), in crude oil as non-hydrocarbon bases and acids (25), and some are synthesised for technological applications (26). Again there are some data on cholate adsorption at various oil interfaces (27), while the effects of molecular structure on surface activity have been reviewed by Rosen recently (28).

Experimental

Surface tension measurements

Surface tensions were measured by the drop volume method as described earlier (1, 2). This time the Agla (Wellcome) precision microsyringe was used in preference to Gilmont syringe; the all-glass Agla syringe is easy to clean and assemble for measurements. The temperature was 25°C controlled to ±0.1°C. The surface tensions were calculated from volumes of 10–25 drops.

Conductivity measurements

These were done with the LKB 5300B precision conductoanalyzer

---

[1]Present address: Department of Chemistry, Sir Wilfred Grenfell College, Memorial University of Newfoundland, Corner Brook, Nfld., Canada A2H 6P9.

[2]Revision received May 24, 1984.

Can. J. Chem. Downloaded from www.nrcresearchpress.com by 210.87.254.42 on 09/06/12
For personal use only.

Can. J. Chem. Downloaded from www.nrcresearchpress.com by 210.87.254.42 on 09/06/12
For personal use only.

(which was checked against standard resistances) using Yellow Springs Instrument Co. conductivity cell No. 3403 at 25.0°C. The cell was calibrated with a KCl solution in the usual manner.

Preparation of salts

(*a*) Sodium dodecanoate was prepared by neutralization of BDH specially pure lauric acid dissolved in ethanol with 0.5 *M* ACS Certified NaOH in pure water (Gelman Water I System). The reaction mixture was refluxed for 12 h; solvents were then evaporated on a steambath. The sodium dodecanoate was then extracted with ether for two weeks. The solid in the thimble was stirred once a day because the ether drained too fast from the thimble. This resulted in extraction of solids from only along the walls of the thimble. The surface tensions of solutions of this salt in appropriate buffers did not show aging effects over a period of 5–10 min.

(*b*) Sodium cyclododecylmethanoate was prepared from cyclododecylmethanoic acid (Fluka Purum) by the same procedure as sodium dodecanoate. The elemental analysis (Galbraith Laboratories) showed purity of 99.8–100.1% for C, H, and Na. There were no observable aging effects during the surface tension measurements.

(*c*) Sodium cycloundecylmethanoate was prepared from cycloundecylmethanoic acid (Fluka Pract.) as above. The elemental purity was 99.9–100.1% for C, H, and Na. However, the surface tensions of the aqueous solutions of this salt showed surface tension aging. These aging effects could not be reduced by repeated crystallizations from a variety of solvents. The surface tensions in this case are those determined from drops aged 15 min (after which the decrease of surface tension was quite slow). The data for this salt are therefore less accurate than the data from the other salts, which are good to $\pm$ 0.1$_5$ mN m^{-1}.

The surface tension measurements were done in sodium carbonate (Fisher Certified, dried at 270°C for 2 h)/sodium bicarbonate (used as such) buffers to eliminate the hydrolysis of the carboxylate ions. Two buffer solutions were made. The first one, which will be referred to as 0.01 *M* buffer (and the subscript 0.01 used for free energies and cmc's obtained in these buffer solutions), was made up from equimolar mixtures of 0.01 *M* $NaHCO_3$ and 0.01 *M* Na_2CO_3. The second one, which will be referred to as 0.1 buffer, was made up from equimolar mixtures of 0.1 *M* $NaHCO_3$ and 0.1 *M* Na_2CO_3. All the solutions had pH of 10.3 ($\pm$ 0.1), and this gives the concentration of free carboxylic acids at less than 1×10^{-6} *M* even in the most dilute carboxylate solutions. The constant Na^+ concentration experiments were all done in 0.01 buffers. The solutions were made up by mixing appropriate volumes of solutions of the carboxylates in 0.01 buffer with solutions of NaCl (Fisher Certified dried at 550°C for 1 h) in 0.01 buffer. Water from the Gelman System I had surface tension of 71.8 mN m^{-1}.

The conductivity was determined for solutions made up in 0.01 buffer.

Results and discussion

In view of uncertainties in deriving free energies of adsorption from raw data (1, 2), the original data are given in Tables 1, 2, and 3.

The free energies of adsorption were derived by fitting 3rd degree polynomials

$$\gamma = a_0 + a_1C + a_2C^2 + a_3C^3$$

and the Szyszkowski equation

$$\Pi = a \ln (1 + bC)$$

where γ and Π are surface tension and spreading pressure respectively, C is molarity, and a_0, a_1, a_2, a_3, a, b are least-squares coefficients, to the experimental data. Experimental data in the region of saturation adsorption were not used in these least-squares fits. The least-squares coefficients determine the Traube constants (limiting slopes of the function of surface tension or spreading pressure vs. molarity at zero molarity), as $\alpha_3 = -a_1$ and $\alpha_s = ab$, where a_3 and a_s are Traube's constants determined from the 3rd degree polynomial and Szyszkowski least-squares analyses. For calculations of free energies of adsorption from bulk buffer solutions the average values of Traube's constants were used in the expression (29, 30).

$$[1] \quad \Delta G_{ad} = -RT \ln \alpha$$

Other definitions of free energies of adsorption are also possible (31, 32). The free energies of adsorption derived from the 3rd polynomial fit and from the Szyszkowski equation fit agreed to within 2%. The reference states in eq. [1] are surface pressure of 1 mN m^{-1} for the surface phase, and the hypothetical ideal 1 *M* solution of the surfactant in the appropriate buffer solution for the bulk phase. The standard free energies at zero buffer concentration were obtained by extrapolation from the two values of the free energies of adsorption at 0.1 *M* and 0.01 *M* buffer concentration. The values of the free energy of adsorption in 0.01 buffer were only about 0.5 kJ mol^{-1} more negative than the extrapolated infinite dilution values. These values are given in Table 4.

The saturation adsorption areas per ion were obtained from constant Na^+ ion concentration data graphically (1). For cyclo-

TABLE 1. Surface tensions γ as a function of concentration c of cyclododecylmethanoate in buffered solutions and in solutions of constant sodium ion concentration

c (mol dm^{-3})	γ (mN m^{-1})	c (mol dm^{-3})	γ (mN m^{-1})
(*1*) In 0.01 *M* $NaHCO_3$ + 0.01 *M* Na_2CO_3 buffer			
0.00106	70.2	0.0333	51.4
0.00201	69.3	0.0539	46.3
0.00348	68.0	0.0650	44.4
0.00637	65.7	0.0676	44.0
0.00980	63.0	0.0970	41.5
0.0151	59.4	0.101	41.3
0.0222	55.8	0.238	39.5
0.0230	55.6	0.393	38.2
(*2*) In 0.1 *M* $NaHCO_3$ + 0.1 *M* Na_2CO_3 buffer			
0.000113	71.4	0.0154	47.8
0.000387	69.7	0.0317	42.1
0.00151	63.8	0.0490	39.7
0.00288	60.0	0.0565	39.1
0.00540	56.2	0.0805	38.4
0.00888	52.7	0.115	38.0
		0.199	37.2
(*3*) At constant $[Na^+]$ = 0.127 *M*			
0.00115	69.7	0.0388	47.6
0.00485	62.7	0.0582	44.4
0.00970	58.3	0.0776	43.3
0.0194	53.2	0.0970	42.7
(*4*) At constant $[Na^+]$ = 0.095 *M*			
0.00650	61.4	0.0390	48.3
0.0130	56.9	0.0520	46.2
0.0195	53.8	0.0650	44.4
0.0260	51.6		
(*5*) At constant $[Na^+]$ = 0.053 *M*			
0.00460	65.8	0.0138	59.1
0.00690	63.8	0.0184	57.1
0.00920	62.1	0.0230	55.6
0.0120	60.3		

Can. J. Chem. Downloaded from www.nrcresearchpress.com by 210.87.254.42 on 09/06/12
For personal use only.

TABLE 2. Surface tensions γ as a function of concentration c of sodium dodecanoate in buffered solutions and in solutions of constant sodium ion concentration

c (mol dm^{-3})	γ (mN m^{-1})	c (mol dm^{-3})	γ (mN m^{-1})
(*1*) In 0.01 *M* $NaHCO_3$ + 0.01 *M* Na_2CO_3 buffer			
0.0000499	70.9	0.00917	45.1
0.000154	69.7	0.0118	41.6
0.000264	68.9	0.0178	35.4
0.000450	67.9	0.0295	33.6
0.000958	64.6	0.0529	33.2
0.00170	61.4	0.0777	33.3
0.00307	56.7	0.0983	33.1
0.00545	51.5		
(*2*) In 0.1 *M* $NaHCO_3$ + 0.1 *M* Na_2CO_3 buffer			
0.0000277	71.2	0.000555	57.4
0.0000444	70.1	0.000855	53.4
0.0000555	69.1	0.00102	51.4
0.0000832	68.1	0.00160	47.4
0.000166	65.2	0.00201	44.6
0.000222	64.0	0.00286	41.0
0.000351	60.5	0.00392	37.1
(*3*) At constant $[Na^+]$ = 0.057 *M*			
0.00540	48.1	0.0160	34.6
0.00810	43.6	0.0216	33.3
0.0108	40.0	0.0270	33.4
0.0140	36.7		

TABLE 3. Surface tensions γ as a function of concentration c of cycloundecylmethanoate in buffered solutions and in solutions of constant sodium ion concentration

c (mol dm^{-3})	γ (mN m^{-1})	c (mol dm^{-3})	γ (mN m^{-1})
(*1*) In 0.01 *M* $NaHCO_3$ + 0.01 *M* Na_2CO_3 buffer			
0.00603	68.5	0.0849	49.7
0.0100	67.1	0.100	47.1
0.0177	64.4	0.129	45.1
0.0204	63.6	0.137	44.8
0.0395	58.2	0.159	44.2
0.0541	54.5	0.210	42.8
0.0674	52.2	0.281	42.0
(*2*) At constant $[Na^+]$ = 0.167 *M*			
0.0137	61.1	0.0685	49.1
0.0274	56.5	0.110	45.9
0.0411	53.4	0.123	45.1
0.0548	51.0	0.137	44.8

dodecylmethanoate the constant Na^+ concentration was kept both below and above the critical micelle concentration (cmc) in order to check (1) that the saturation area per ion does not depend on the counter ion concentration, Table 1, which the data confirm.

The critical "micelle" concentrations were determined graphically as the intersection of two straight lines in the plot of surface tension against log of molarity and also from the plots of conductivities vs. molarities as shown in Fig. 1. The data are given in Table 4.

The free energies of adsorption appear to follow the rule of "two" ($-RT$ ln 2). This rule gives about 1.7 kJ mol^{-1} for each CH_2 group added to the ring. It is likely that this rule remains valid for larger rings but may not be valid for smaller rings because of their increased rigidity. In conjunction with previous data (28) it appears that this rule is valid for a variety of ionic surfactants, and that the way in which the CH_2 groups in the hydrophobic structures are arranged is not very important. From Table 4, the value of the free energy of adsorption of cyclododecylmethanoate is lower (by an equivalent of about 3 CH_2 groups) than the free energy of adsorption of straight chain dodecanoate. This is a large structural difference because the number of atoms in these two hydrophobic moieties is nearly the same ($CH_{12}H_{23}$ for cyclododecylmethanoate and $C_{11}H_{23}$ for dodecanoate). This suggests that the cyclododecylmethanoate ion exists in aqueous solution in "collapsed ring" conformation, as short as about octanoate, but with thicker "double" chain.

The saturation adsorption areas for both cyclododecylmethanoate and cycloundecylmethanoate are about the same of around 52 ± 1 Å^2/ion, as compared to about 33 Å^2/ion for straight chain dodecanoate. Because straight chain carboxylates have saturation adsorption areas independent of the length of the chain, the value of 33 Å^2/ion is thought to be determined by the size of the solvated charged carboxyl group (32). In our case the saturation adsorption areas are determined by the size of the cycloalkylmethanoate hydrophobic moiety. If we consider that cyclododecylmethanoate ions are standing up at the interface with their rings as two short double chains, then we get a value of 26 Å^2 per chain. These values can be compared with the value of about 21 Å^2 per chain derived from insoluble monolayer studies for paraffinic compounds. The difference of 5 Å^2 is probably a measure of water penetration into the adsorbed monolayer of cyclododecylmethanoate.

A saturation area of 93.2 Å^2 ion has been determined for sodium cyclododecyl sulfate (33). The large difference between our value of 52 Å^2/ion and the cited value is due to different experiments from which the saturation areas were derived. The value of 93.2 Å^2/ion was obtained from experiments with no added salt, whereas our value is derived from experiments at constant counter-ion (sodium) concentration. This is another example of persisting ambiguity about the meaning and determination of saturated areas as has been recently discussed by Ikeda (34). The least unambiguous procedure for the determination of saturated areas of surfactants is to perform constant counter-ion experiments (1, 35). Such experimentally derived saturation areas are independent of the actual but constant counter-ion concentration (e.g., our results for sodium dodecanoate), and yield the surface excess concentration per surfactant ion only (35).

The critical micelle concentrations determined from both the surface tension and conductance measurements are given in Table 4. The cmc determined from the surface tension data are consistently higher. Similar trends were also found in the case of paraffinic carboxylates (15). The reported cmc for cyclododecyl sulfate is 0.070 mol dm^{-3} which can be compared to our mean value of 0.083 mol dm^3 for cyclododecyl carboxylate. The lower value for the sulfate is due to the sulfate ester oxygen which can be counted as part of the hydrophobic moiety (36). This conclusion appears to be collaborated by the cmc value of 0.083 mol dm^{-3} (unfortunately at unknown ionic strength) for the double-chain surfactant undecyl-6-sulfate (37). The conductivity data can be also used to estimate the degree of dissociation of micelles as the ratio of the specific conductance vs. molarity slopes above and below the cmc (38). In the present case the unusually high degrees of over 80% indicate a small aggregation number for the cyclododecyl (80%) and cycloundecyl (86%) carboxylate micelles (38).

TABLE 4. The free energies of adsorption, ΔG, the critical micelle concentrations, cmc, and saturation adsorption areas A_{sa} of the carboxylates

	$-\Delta G_{0.1}$ (kJ mol^{-1})	$-\Delta G_{0.01}$ (kJ mol^{-1})	$-\Delta G^0$ (kJ mol^{-1})	$cmc_{0.01}$ (mol dm^{-3})	$cmc_{0.1}$ (mol dm^{-3})	A_{sa} (Å^2/ion)
$CH_2(CH_2)_{10}CH$—COONa	22.1	17.5	17.0	0.085[a] 0.079[b]	0.057	53
$CH_2(CH_2)_9CH$—COONa	—	15.9	(15.4)	0.105[a] 0.098[b]	—	51
$CH_3(CH_2)_9CH_2$—COONa	26.7	22.7	22.3	0.023	—	33

[a]From surface tension measurements.
[b]From conductivity measurements.

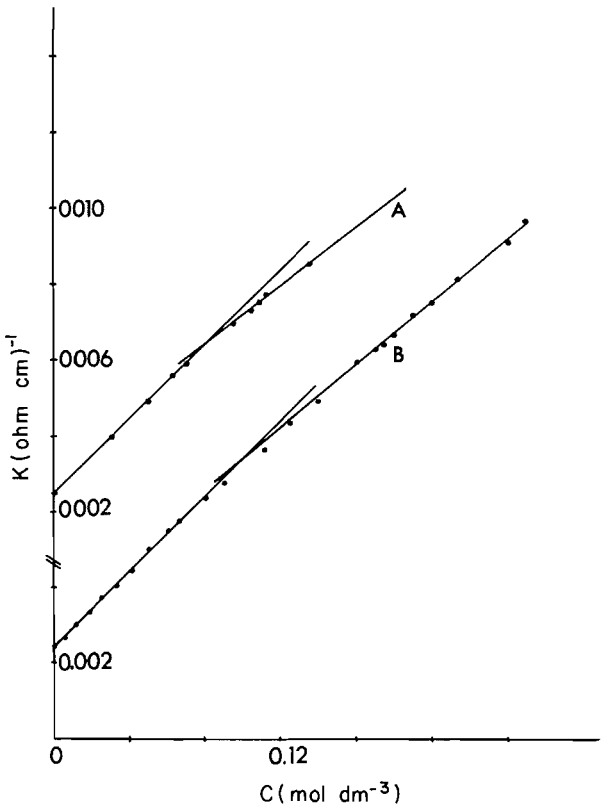

FIG. 1. The plot of specific conductance vs. molarity for determination of cmc: (*A*) cyclododecylmethanoate, (*B*) cycloundecylmethanoate.

Though the data pertain to only two members of the cycloalkylmethanoate homologous series, the critical micelle concentrations seem to follow a "rule" of 4/5 (0.8). That is the cmc decreases by a factor of 0.8 for each CH_2 group added to the ring. For straight chain carboxylates the factor is close to 0.5 for each CH_2 group added to the chain. If it were considered that the cycloalkylmethanoate ring behaves as a double chain that is made longer by one half of the CH_2 group for each CH_2 group that is added to the ring, then the cmc factor would be 0.71 (square root of 0.5). It thus appears that the ring is not quite collapsed into a double chain, and that two CH_2 groups added to the ring make the double chain conformation longer by a little less than one CH_2 group.

Acknowledgements

The authors thanks Doug Dolman and members of this Department for useful advice and the Natural Sciences and Engineering Council of Canada for financial support.

1. A. SKAUGE and J. J. SPITZER. J. Phys. Chem. **87**, 2398 (1983).
2. J. J. SPITZER and L. HEERZE. Can. J. Chem. **61**, 1067 (1983).
3. F. ERIKSSON, J.-C. ERIKSSON, and P. STENIUS. *In* Solution chemistry surfactants. Vol. 1. *Edited by* K. L. Mittal. Plenum Press, New York. 1979. p. 297.
4. P. EKWALL, P. STENIUS, and S. BACKLUND. *In* Thermodynamic and transport properties of organic salts. *Edited by* P. Franzosin and M. Sanesi. Pergamon Press, Oxford. 1980.
5. B. LINDMAN and H. WENNERSTRÖM. *In* Topics in Current Chemistry. Vol. 87. Springer-Verlag, Berlin. 1980. p. 1.
6. C. TANFORD. The hydrophobic effect. 2nd ed. Wiley, New York. 1980.
7. K. SHINODA. Colloidal surfactants. Academic Press, New York. 1963.
8. C. TANFORD. *In* Micellization, solubilization and microemulsions. Vol. 1. *Edited by* K. L. Mittal. Plenum Press, New York. 1977. p. 119.
9. E. W. ANACKER. *In* Cationic surfactants. *Edited by* E. Jungermann. Marcel Dekker, New York. 1970. p. 203.
10. J. POWNEY. Trans. Faraday Soc. **31**, 1510 (1935).
11. J. POWNEY and C. C. ADDISON. Trans. Faraday Soc. **34**, 374 (1938).
13. N. K. ADAM. Trans. Faraday Soc. **32**, 653 (1936).
14. C. P. ROE AND P. D. BRASS. J. Phys. Chem. **58**, 4703 (1954).
15. A. N. CAMPBELL and G. R. LAKSHINARAYANAN. Can. J. Chem. **43**, 1729 (1965).
16. G. NILSSON. J. Phys. Chem. **61**, 1135 (1957).
17. P. MUKERJEE. J. Pharm. Sci. **63**, 972 (1974).
18. P. EKWALL. J. Colloid Sci. Suppl. **1**, 66 (1954).
19. Y. MURATA, G. SUGIHARA, K. FUKUSHIMA, and M. TANAKA. J. Phys. Chem. **86**, 4690 (1982).
20. C. JOLICOEUR, J. BOILEAU, S. BAZINET, and P. PICKER. Can. J. Chem. **53**, 716 (1975).
21. C. JOLICOEUR, J. PAGUETTE, Y. LAVIGNE, and R. ZANA. *In* Solution behaviour of surfactants. Vol. 1. *Edited by* K. L. Mittal and E. J. Fendler. Plenum Press, New York. 1982. p. 389.
22. G. S. HARLTEY. Trans. Faraday Soc. **37**, 130 (1941).
23. G. S. HARTLEY. *In* Micellization, solubilization and microemulsions. Vol. 1. *Edited by* K. L. Mittal. Plenum Press. New York. 1977. p. 23.
24. J. H. FENDLER. Membrane mimetic chemistry. J. Wiley, New York. 1982.
25. W. K. SEIFERT. Prog. Chem. Org. Nat. Prod. **32**, 1 (1975).
26. J. L. MOILLIET, B. COLLIE, and W. BLACK. Surface activity. E. & F. N. Spon, London. 1961.
27. M. K. SHARMA, M. SHARMA, S. P. JAIN, and S. N. SRIVASTAVA. J. Colloid Interface Sci. **64**, 179 (1978).
28. M. J. ROSEN. *In* Solution chemistry of surfactants. *Edited by* K. L. Mittal. Plenum Press, New York. 1978. p. 45.
29. N. H. SAGERT and W. LEE. Can. J. Chem. **58**, 2789 (1980).
30. R. AVEYARD and B. J. BRISCOE. Trans. Faraday Soc. **64**, 2911 (1970).
31. M. J. ROSEN and S. ARONSON. Colloids Surf. **3**, 201 (1981).
32. E. H. LUCASSEN-REYNDERS. *In* Progress in surface and mem-

Can. J. Chem. Downloaded from www.nrcresearchpress.com by 210.87.254.42 on 09/06/12
For personal use only.

brane science. *Edited by* D. A. Cadenhead and J. F. Danielli. Academic Press, New York. 1976. p. 253.
33. T. HIKOTA, M. NAKAMURA, S. MACHIDA, and K. MEGURO. J. Am. Oil Chem. Soc. **48**, 784 (1976).
34. S. IKEDA. Adv. Colloid Interface Sci. **18**, 93 (1982).
35. J. SASAKI, K. TAJIMA, and T. SASAKI. Bull. Chem. Soc. Jpn. **45**, 348 (1972).
36. H. B. KLEVENS. J. Am. Oil Chem. Soc. **30**, 74 (1953).
37. H. C. EVANS. J. Chem. Soc. 579 (1956).
38. R. ZANA. J. Colloid Interface Sci. **78**, 330 (1980).

Can. J. Chem. Downloaded from www.nrcresearchpress.com by 210.87.254.42 on 09/06/12
For personal use only.

Ion/molecule reactions in allene. II. Collisional stabilization of the dimer ion $(C_3H_4)_2^{+\cdot}$ by non-polar molecules

KENZO NAGASE[1] AND JAN A. HERMAN

Centre de Recherches sur les atomes et les molécules et le département de Chimie, Université Laval, Québec (Qué.), Canada G1K 7P4

Received January 31, 1984

KENZO NAGASE and JAN A. HERMAN. Can. J. Chem. **62**, 2364 (1984).

The relative deactivation efficiencies, k_s, for collisional stabilization of $(C_3H_4)_2^{+*}$ ion species, produced by photoionization at 10.03 eV of allene, were obtained in various bath gases, such as rare gases, N_2, CO, CO_2, and CF_4. A linear relationship between ln $(k_s\sqrt{\mu})$ and ϵ_{M-M} was obtained, where ϵ_{M-M} stands for the intermolecular well-depth potential between pairs of neutral M and μ is the reduced mass of colliding partners. Similar relations were examined for other collisionally stabilized ion species.

KENZO NAGASE et JAN A. HERMAN. Can. J. Chem. **62**, 2364 (1984).

Opérant dans divers bains de gaz, tels les gaz rares, le N_2, le CO, le CO_2 et le CF_4, on a déterminé les efficacités de désactivaction relatives, k_s, pour la stabilisation collisionnelle de l'espèce ionique $(C_3H_4)_2^{+*}$ produite par photoionisation, à 10,03 eV, de l'allène. On a obtenu une relation linéaire entre ln $(k_s\sqrt{\mu})$ et ϵ_{M-M}, où ϵ_{M-M} correspond au puit de potentiel intermoléculaire entre les paires neutres M et où μ est la masse réduite des partenaires entrant en collision. On a étudié des relations similaires pour d'autres espèces ioniques stabilisées par collision.

[Traduit par le journal]

Introduction

Ion/molecule reactions of allene have been studied by mass-spectrometry using various types of instruments (1–5). At low pressure ($P < 0.02$ Torr) the major reaction is $C_3H_4^{\cdot+}(C_3H_4,H^{\cdot})C_6H_7^+$ and it is assumed that this reaction proceeds via a long-lived collision complex, $(C_3H_4^{\cdot+}.C_3H_4)$ (5, 6). The cross-section of this reaction is dependent upon the internal energy and diminishes with increasing energy (5). It was also suspected that the collision complex might isomerize into more stable $C_6H_8^{\cdot+}$ species of lower heat of formation, since some of its isomers are considered to have heats of formation lower than the calculated threshold energy for the main reaction leading to $C_6H_7^{\cdot+}$ and $H^{\cdot}$ (5, 7).

However, the $C_6H_8^{\cdot+}$ species (m/z 80) was not observed at low pressure in the mass spectrum of pure allene, probably because of high reactivity of the collision complex or excited dimer ion, $(C_3H_4)_2^{\cdot+*}$. Our recent study of ion/molecule reactions in allene indicates that $C_6H_8^+$ species and even of its solvates are present at high pressure (up to 3.5 Torr), but their fractional abundances are low (<2%) (8). One may expect the mass peak $m/z = 80$ to be more intense if a successful energy transfer from the excited $(C_3H_4^{\cdot+}.C_3H_4)^*$ species to a suitable third body could occur. As shown in Fig. 1 the heats of formation of some $C_6H_8^{\cdot+}$ isomers are below the sum of the heats of formation of $C_6H_7^+ + H^{\cdot}$ species. If the energy barrier towards isomerization is not too high, one can expect to observe a $C_6H_8^{\cdot+}$ peak in the mass spectrum. The mass peak of the $C_6H_8^{\cdot+}$ ion was observed in the present experiments and its fractional intensity increased with increasing pressure of the third body (M) and, moreover, depended on the nature of M. The relative deactivation efficiencies, k_s, for the stabilization of the excited dimer ion, $(C_3H_4)_2^{+*}$, by M could be followed through the variation of the fractional intensity ratio of $C_6H_8^{\cdot+}$ against other ionic species.

Experimental

The apparatus and the experimental procedure have been already described (9, 10). The ion/molecule reactions were studied under field-free conditions inside the collision chamber and with an electric field at low intensity (~5 V/cm) in the ion optics. The distance in the collision chamber between the plane of formation of the parent-ions by photon impact of 10.03 eV krypton resonance line and the exit slit was fixed at 4.2 mm. The temperature of the cell was kept at 25 ± 2°C as measured by a thermocouple connected to the wall of the collision chamber. The mass spectra of allene were measured in the pressure range of 0.1–10 Torr under the above conditions.

The allene from Matheson of 99.5% purity was used without further purification. All other gases, also from Matheson, were of instrumental grade purity. The mixtures of known concentrations were prepared in a conventional high vacuum manifold. The usual concentration of allene in the mixtures was kept around 10%.

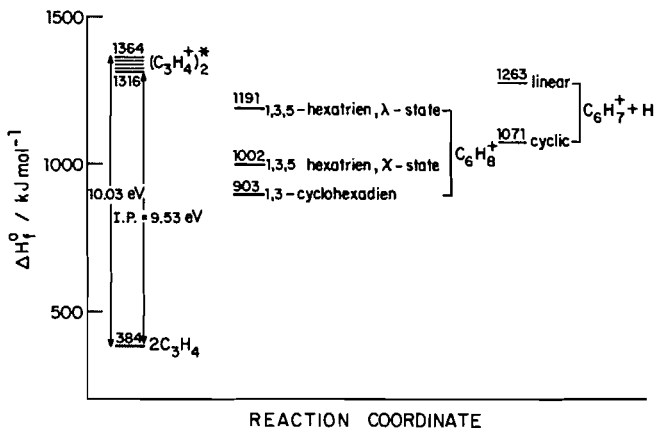

FIG. 1. Energy state of allene, its activated dimer ion, and some isomers of $C_6H_8^{\cdot+}$ and $C_6H_7^+$.

Kinetic considerations

The m/z values and the corresponding fractional intensities of ions produced by photoionization in pure allene in the present experiments agree well with those already published (8). The major products were $C_6H_7^+$, $C_6H_9^+$, $C_7H_7^+$, and their clusters. At this relatively high pressure $C_6H_8^{\cdot+}$ species is also observed, confirming our previous results (8). In the case of mixtures of allene with added gases (rare gases, N_2, CO, CO_2,

[1] Visiting Professor, 1982. Present address: College of General Education, University of Tohoku, Kawauchi, Sendai 980, Japan.

Can. J. Chem. Downloaded from www.nrcresearchpress.com by 210.87.254.40 on 09/06/12
For personal use only.

Can. J. Chem. Downloaded from www.nrcresearchpress.com by 210.87.254.40 on 09/06/12
For personal use only.

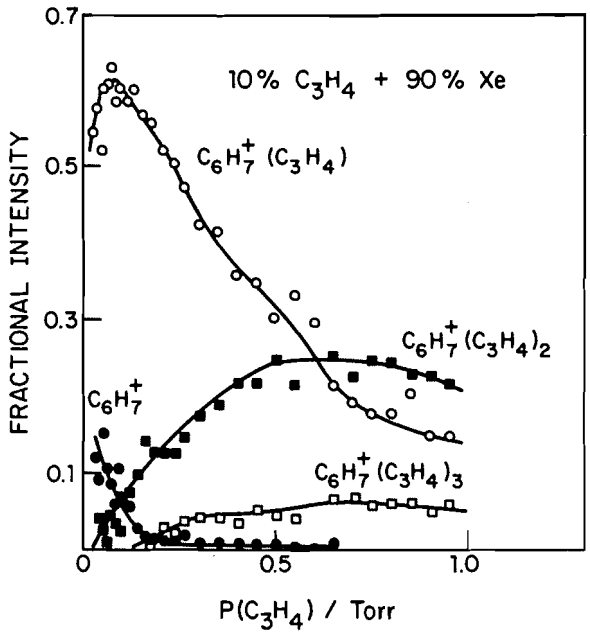

FIG. 2. Fractional intensities for the members of the $C_6H_7^+$ family in the xenon mixture, as a function of the partial pressure of allene.

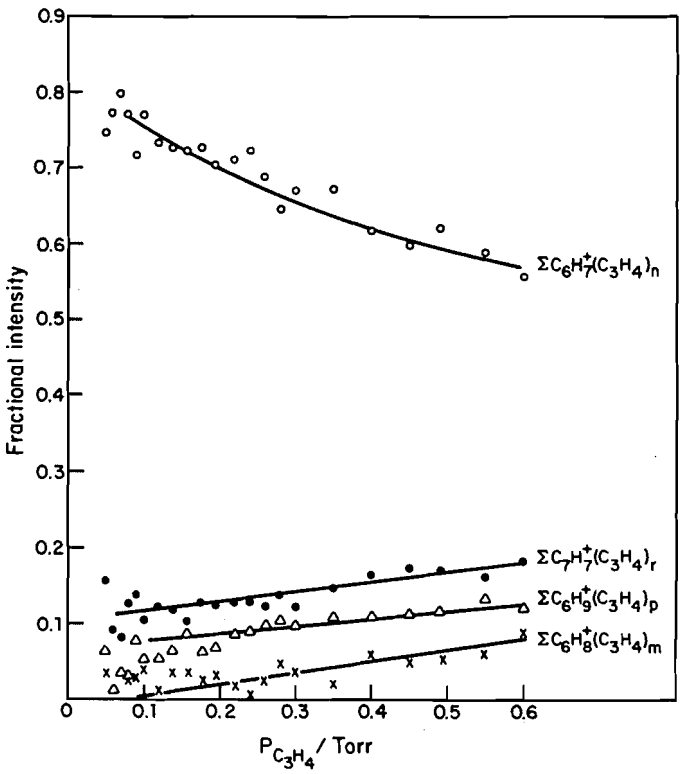

FIG. 3. Pressure dependence of the fractional intensities for the four major ion families of allene (10%) in the Kr (90%) mixture.

and CF_4) a similar mass spectra are obtained, but the fractional intensities of some peaks are different from those in the mass spectrum of pure allene. As an example we show in Fig. 2 the mass spectrum of $C_6H_7^+$ and its clusters $C_6H_7^+(C_3H_4)_n$ in the mixture of 10% allene in Xe. With increasing pressure the highly clustered species tend to increase in abundance, indicating that the condensation processes may occur very rapidly prior to the fragmentation and rearrangement reactions. Therefore, the total abundance of $C_6H_7^+$ may be represented by the sum of $C_6H_7^+(C_3H_4)_n$ species, the same applying to other species. The relative abundances of $C_6H_7^+$, $C_6H_8^{\cdot+}$, $C_6H_9^+$, and $C_7H_7^+$, which are given by the sum of the fractional intensities of the corresponding solvated ion species, change with the partial pressure of allene either pure or in the mixture as shown in Figs. 3–5. Starting from a pressure around 0.2 Torr the abundance of $C_6H_7^+$ ion species decreases, whereas the fractional intensities of other ionic species increase with increasing partial pressure of allene. It was noticed that the rate of abundance decrease of $C_6H_7^+$ and that increasing of $C_6H_8^+$ depended on the nature of bath gas M, whereas the abundances of both $C_6H_9^+$ and $C_7H_7^+$ were only weakly influenced by M. These observations suggest the following reaction scheme (8), (henceforward, we shall abbreviate the ion-dimer $(C_3H_4)_2^+$ by A^+):

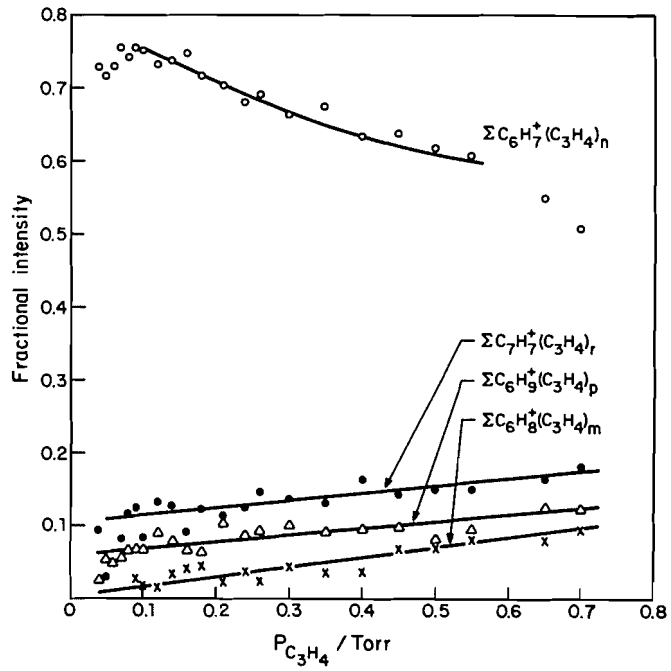

FIG. 4. Pressure dependence of the fractional intensities for the four major ion families of allene (10%) in the Xe (90%) mixture.

[1] $C_3H_4^{\cdot+*} + C_3H_4 \rightarrow (C_3H_4)_2^{\cdot+*} \longrightarrow C_6H_7^+ + H^{\cdot}$

[2] $A^{+*} \xrightarrow{C_3H_4} C_6H_9^+ + C_3H_3^{\cdot}$

[3] $\xrightarrow{C_3H_4} C_7H_7^+ + C_2H_5^{\cdot}$

[4] $\xrightarrow[(k_s \text{ or } k_s)]{C_3H_4 \text{ or M}} C_6H_8^{\cdot+}$

Reaction [1] is a unimolecular decomposition of the activated dimer A^{+*} and reactions [2] and [3] are bimolecular processes of A^{+*} with neutral allene. Reaction [4] is a collisional stabilization (or deactivation) of A^{+*} by M or by allene itself.

On the basis of the above scheme, the following kinetic expressions [5] to [8] can be derived:

[5] $d[(C_6H_7^+)_f] = k_1[A^{+*}]$

[6] $d[(C_6H_9^+)_f] = k_2[A^{+*}][C_3H_4]$

[7] $d[(C_7H_7^+)_f] = k_3[A^{+*}][C_3H_4]$

Can. J. Chem. Downloaded from www.nrcresearchpress.com by 210.87.254.40 on 09/06/12
For personal use only.

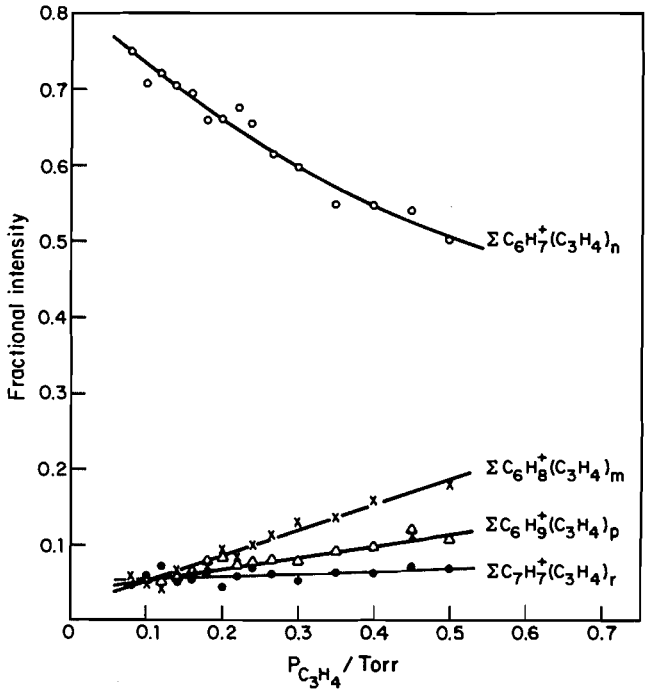

FIG. 5. Pressure dependence of the fractional intensities for the four major ion families of allene (10%) in the CF_4 (90%) mixture.

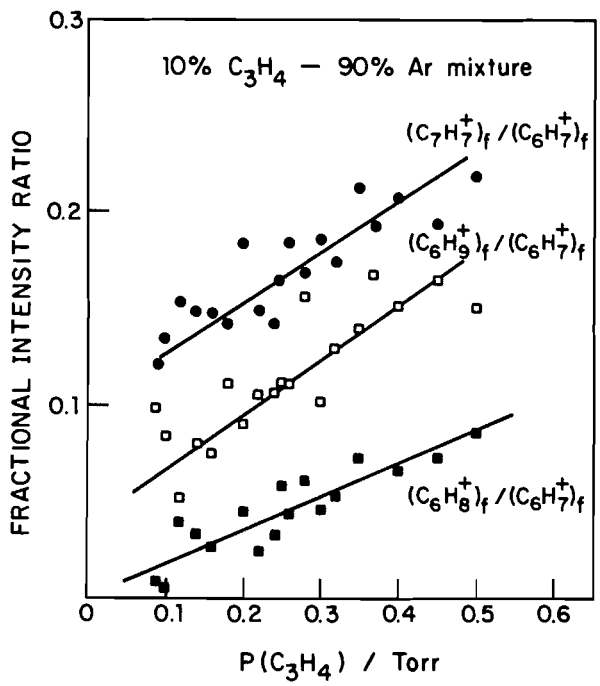

FIG. 6. Fractional intensity ratios of the three ion families against $(C_6H_7^+)_f$ family, as a function of the partial pressure of allene in the argon mixture.

[8] $$d[(C_6H_8^+)_f] = k_s[A^{+*}][M] + k_{s'}[A^{+*}][C_3H_4]$$

The subscript f indicates that the corresponding family of ions is involved. Neglecting the mass discrimination effects the ratios of the rates can be replaced by the ratios of the fractional intensities, and one can derive the following expressions:

[9] $$I(C_6H_9^+)_f/I(C_6H_7^+)_f = (k_2/k_1)P_{C_3H_4}$$

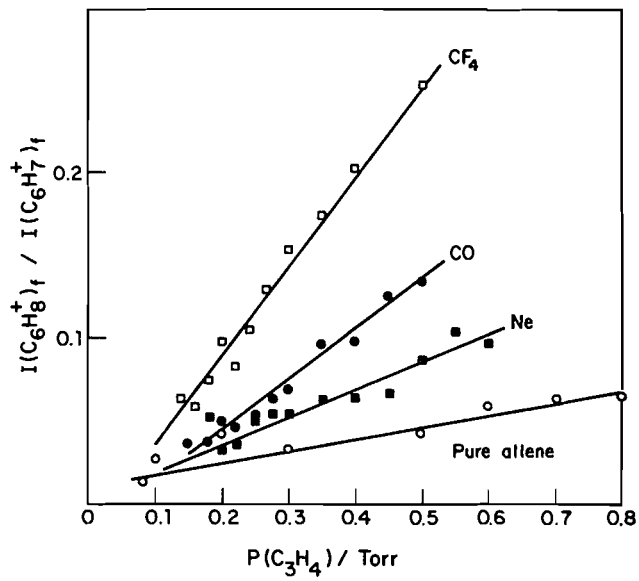

FIG. 7. Fractional intensity ratios for pure allene and the mixtures as a function of the pressure of allene.

[10] $$I(C_7H_7^+)_f/I(C_6H_7^+)_f = (k_3/k_1)P_{C_3H_4}$$

[11] $$I(C_6H_8^+)_f/I(C_6H_7^+)_f = [k_s/(Rk_1) + k_{s'}/k_1]P_{C_3H_4}$$

where $P_{C_3H_4}$ stands for the partial pressure of allene and R stands for the mixing ratio of allene in the mixture, $R = P_{C_3H_4}/P_M$. As an example the plot of the above intensity ratios versus $P_{C_3H_4}$ for the mixture of argon ($R = 0.11$) is shown in Fig. 6. Almost linear lines were obtained for $(C_6H_9^+)_f$, $(C_7H_7^+)_f$, and $(C_6H_8^{\cdot+})_f$ ion species for all mixtures measured in the present experiments. It should be noticed that the line of the $(C_6H_8^{\cdot+})_f$ species passes almost through the origin of the axes, suggesting that the source of this species is the activated ion-dimer only. The lines of the other two species, however, take positive values of the intercept, suggesting that at low pressure they originate not only from the activated ion-dimer but also from other sources. Another source of $C_6H_9^+$ ion might be the condensation reaction of $C_3H_5^+$, since its presence with a fractional intensity, $I = 0.14$ at 0.02 Torr has been reported (4). The reaction $C_4H_4^+(C_3H_4,H)C_7H_7^+$, which has been suggested (2, 4), might be another source of $C_7H_7^+$.

Results and discussion

All "inert" gases showed a linear relation when the ratios $I(C_6H_8^+)_f/I(C_6H_7^+)_f$ were plotted as a function of the partial pressure of allene, Figs. 7–9. From the slopes of these graphs the values of the coefficient $[k_s/(Rk_1) + k_{s'}/k_1]$ can be measured. This value is a measure of the relative efficiency of the total stabilization of the activated ion-dimer, A^{+*}, by "inert" molecules M and allene itself. The value of $k_{s'}/k_1$, which corresponds to the stabilization by allene, was obtained from the slope of the pure allene system and is equal to 0.07 + 0.02 $Torr^{-1}$. A least-square treatment analysis (95% confidence) given the values k_s/k_1 tabulated in Table 1.

The values k_2/k_1 and k_3/k_1, which correspond to the relative rates of reaction of A^{+*} with allene, were obtained for all mixtures from relations [9] and [10] respectively, and are also presented in Table 1. The mean values of k_2/k_1 and k_3/k_1 for the mixtures are 0.24 and 0.20 $Torr^{-1}$, respectively, and are almost equal to the corresponding values in pure allene.

Can. J. Chem. Downloaded from www.nrcresearchpress.com by 210.87.254.40 on 09/06/12
For personal use only.

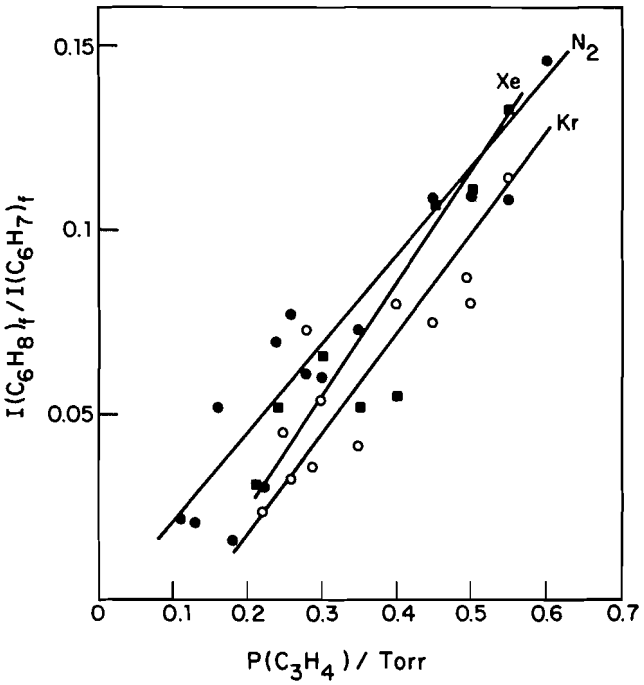

FIG. 8. Fractional intensity ratios for the mixtures as a function of the pressure of allene.

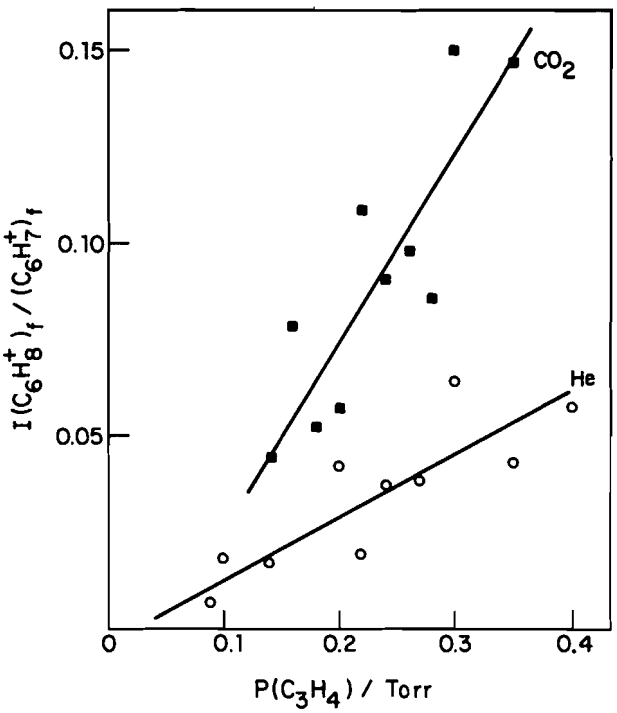

FIG. 9. Fractional intensity ratios for the mixtures as a function of the pressure of allene.

For reasons of comparison, the ratios k_s/k_1, k_2/k_1, and k_3/k_1 were recalculated as relative values and are tabulated in the last three columns of Table 1. For k_s/k_1 the value for the mixture He + allene was chosen as unity, whereas for k_2/k_1 and k_3/k_1, the values corresponding to pure allene were chosen as unity. The values of $k_{s,rel}$ depend on the nature of M, whereas those of $k_{2,rel}$ and $k_{3,rel}$ are almost constant within the experimental error for the mixtures: M + allene. This seems to be a strong addi-

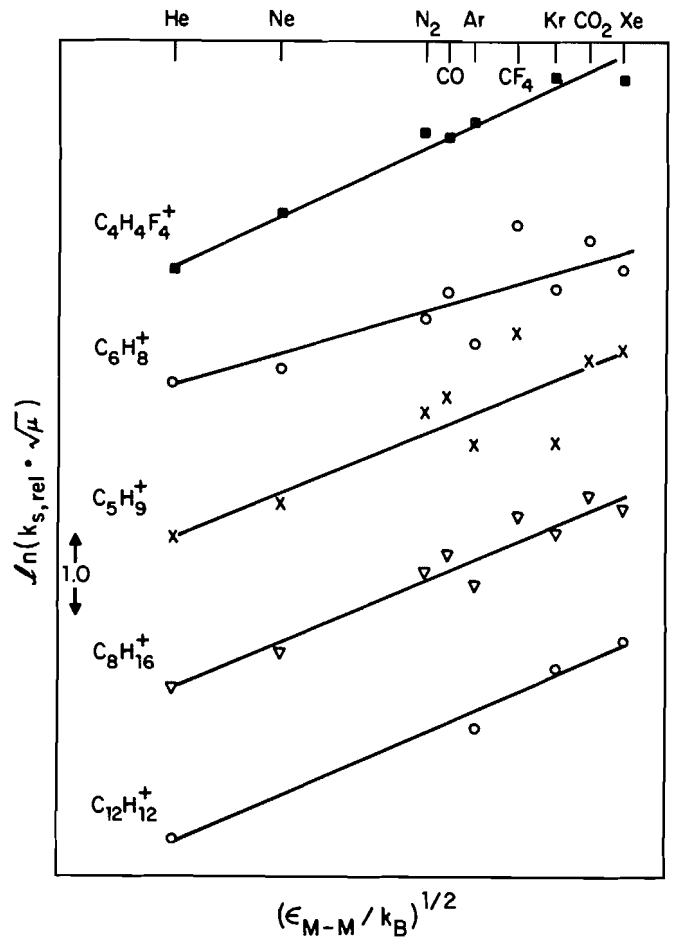

FIG. 10. Correlation between the logarithms of the relative deactivation efficiencies and the square-roots of the potential well-depths, ϵ_{M-M}, between the pairs of the non-polar bath gases, for the five excited ions.

tional support to the reaction scheme [1] to [4].

In the preceding paper on the stabilization by non-polar molecules of the excited dimer $(C_4H_8)_2^{+*}$ formed in photoionized isobutene, we showed that there is a linear relationship between the logarithm of the deactivation (or stabilization) efficiencies (where the differences in collisional rates for various M are taken into account), represented by $(k_s\sqrt{\mu})$, and the square-root of the interaction potential of pairs of M, ϵ_{M-M}, (10). Here, μ is the reduced mass of the system. We tried to apply this correlation for k_s values obtained in the present study and to extend it for k_s values of $C_5H_9^{+*}$, $C_4H_4F_4^{+*}$, and $C_{12}H_{12}^{+*}$ ion species reported elsewhere (11, 12). As shown in Fig. 10, a similar linear relationship is found in all cases. Therefore, we suggest that this relationship (of stabilization processes of excited ions by atomic or by small non-polar polyatomic molecules) may be general.

The slopes of the straight lines in Fig. 10 are different for various A^{+*}. In increasing order the slopes are $C_6H_8^{+*}$ (0.16) < $C_5H_9^{+*}$ (0.20) < $C_8H_{16}^{+*}$ (0.22) ~ $C_{12}H_{12}^{+*}$ (0.22) < $C_4H_4F_4^{+*}$ (0.24). The slopes appear to increase with the increasing size of A^{+*}.

The results shown in Fig. 10 suggest that the collisional stabilization efficiency can be described from a phenomenological point of view by the interaction potential between the excited ion species, A^{+*}, and the neutral M, since the potential can be approximated by the combined rule:

TABLE 1. Kinetic parameters of ion/molecule reactions of pure allene and the 10% C_3H_4 + 90% mixtures

M	k_s/k_1 (Torr^{-1})	k_2/k_1 (Torr^{-1})	k_3/k_1 (Torr^{-1})	$k_{s,rel}$[a]	$k_{2,rel}$[b]	$k_{3,rel}$[c]
C_3H_4	0.076 ± 0.02	0.23 ± 0.1	0.23 ± 0.04	8.8 ± 2.3	1	1
He	0.0086 ± 0.02	0.26 ± 0.2	—	1	1.1 ± 0.8	—
Ne	0.010 ± 0.003	0.25 ± 0.03	0.15 ± 0.07	1.2 ± 0.4	1.1 ± 0.1	0.7 ± 0.3
Ar	0.012 ± 0.005	0.26 ± 0.08	0.20 ± 0.06	1.4 ± 0.6	1.1 ± 0.3	0.9 ± 0.3
Kr	0.021 ± 0.007	0.27 ± 0.04	0.40 ± 0.05	2.4 ± 0.8	1.2 ± 0.2	1.7 ± 0.3
Xe	0.026 ± 0.007	0.21 ± 0.05	0.29 ± 0.08	3.0 ± 0.8	0.9 ± 0.2	1.3 ± 0.4
N_2	0.018 ± 0.007	0.20 ± 0.05	0.14 ± 0.07	2.1 ± 0.8	0.9 ± 0.2	0.6 ± 0.3
CO	0.026 ± 0.006	0.25 ± 0.07	0.22 ± 0.05	3.0 ± 0.7	1.1 ± 0.3	1.0 ± 0.2
CO_2	0.046 ± 0.014	0.17 ± 0.20	0.24 ± 0.12	5.3 ± 1.6	0.7 ± 0.6	1.0 ± 0.5
CF_4	0.051 ± 0.006	0.25 ± 0.05	0.14 ± 0.05	5.9 ± 0.7	1.1 ± 0.2	0.6 ± 0.2

[a] Relative to k_s(He) = 1.
[b] Relative to k_2(pure allene) = 1.
[c] Relative to k_3(pure allene) = 1. The mean values of k_2/k_1 and k_3/k_1 in the mixtures are 0.24 and 0.20 Torr^{-1}, respectively, and they are near the corresponding values in pure allene.

$$\epsilon_{A^{+*}-M} = (\epsilon_{A^{+*}-A^{+*}}\epsilon_{M-M})^{1/2}$$

According to the approach of Parmenter and co-workers (13) the final expression for the stabilization process of A^{+*} by M is

$$[12] \quad \ln k_s = \text{const} + (\epsilon_{A^{+*}-A^{+*}}/k_B T^2)^{1/2}(\epsilon_{M-M}/k_B)^{1/2}$$

where k_B is the Boltzmann constant. At constant temperature and for an A^{+*} species common to all collisional pairs, relation [12] can be replaced by

$$[13] \quad \ln k_s = C + C'\epsilon_{M-M}^{1/2}$$

The linear relation in Fig. 10 agrees with this expression. In this figure ϵ_{M-M} values are taken from ref. 13.

The slopes of the straight lines in Fig. 10 correspond to the respective C' values and as noticed previously, they vary from 0.16 to 0.24 along with the increasing size of A^{+*}. Since polarizability is a measure of the molecular size and the bath gas molecules studied have different polarizabilities, these results indicate that the effect of molecular size on the collisional deactivation efficiency is accounted for by the molecular polarizabilities. This is in agreement with an earlier conclusion of Su and Bowers (14).

Acknowledgement

The authors are indebted to the Natural Sciences and Engineering Research Council of Canada for financial support.

1. J. J. MYHER and A. G. HARRISON. J. Phys. Chem. **72**, 1905 (1968).
2. M. T. BOWERS, D. D. ELLEMAN, R. M. O'MALLEY, and K. R. JENNINGS. J. Phys. Chem. **74**, 2583 (1970).
3. A. NATO, M. NIWA, H. HOMMA, I. TANAKA, and I. KOYANO. Int. J. Mass Spectrom. Ion Phys. **34**, 287 (1980).
4. C. LIFSHITZ, Y. GLEITMAN, S. GEFEN, U. SHAINOK, and I. DOTAN. Int. J. Mass Spectrom. Ion Phys. **40**, 1 (1981).
5. C. LIFSHITZ and Y. GLEITMAN. Int. J. Mass Spectrom. Ion Phys. **40**, 17 (1981).
6. P. R. LEBRETON, A. D. WILLIAMSON, J. L. BEAUCHAMP, and W. T. HUNTRESS. J. Chem. Phys. **62**, 1623 (1975).
7. W. WAGNER, K. LEVSEN, and C. LIFSHITZ. Org. Mass Spectrom. **15**, 271 (1981).
8. D. CARRIER and J. A. HERMAN. Int. J. Mass Spectrom. Ion Phys. **44**, 183 (1984).
9. Z. LUCZYNSKI and J. A. HERMAN. Int. J. Mass Spectrom. Ion Phys. **17**, 237 (1979).
10. K. NAGASE and J. A. HERMAN. J. Phys. Chem. **88**, 1368 (1984).
11. P. G. MIASEK and A. G. HARRISON. J. Am. Chem. Soc. **97**, 714 (1975).
12. V. G. ANICICH and M. T. BOWERS. J. Am. Chem. Soc. **96**, 1279 (1974).
13. H. M. LIN, M. SEAVER, K. Y. TANG, A. E. W. KNIGHT, and C. S. PARMENTER. J. Chem. Phys. **70**, 5442 (1979).
14. T. SU and M. T. BOWERS. J. Am. Chem. Soc. **95**, 7609 (1973).

Can. J. Chem. Downloaded from www.nrcresearchpress.com by 210.87.254.40 on 09/06/12
For personal use only.

Excess volumes of binary mixtures of *n*-octane with each of the hexane isomers at 298.15 K[1]

M. K. KUMARAN[2] AND GEORGE C. BENSON

Division of Chemistry, National Research Council of Canada, Ottawa, Ont., Canada K1A 0R6

Received April 12, 1984

M. K. KUMARAN and GEORGE C. BENSON. Can. J. Chem. **62**, 2369 (1984).

Excess molar volumes, measured at 298.15 K in a tilting dilution dilatometer, are reported for the five binary systems formed by mixing *n*-octane with *n*-hexane, 2-methylpentane, 3-methylpentane, 2,2-dimethylbutane, and 2,3-dimethylbutane. The Flory theory of mixtures provides a reasonable correlation of the results in combination with excess molar enthalpies measured previously.

M. K. KUMARAN et GEORGE C. BENSON. Can. J. Chem. **62**, 2369 (1984).

Faisant appel à un dilatomètre à dilution inclinable et opérant à 298,15 K, on a mesuré les volumes molaires d'excès de cinq systèmes binaires formés par le mélange du *n*-octane avec le *n*-hexane, le méthyl-2 pentane, le méthyl-3 pentane, le diméthyl-2,2 butane et le diméthyl-2,3 butane. La théorie des mélanges de Flory, combinée aux enthalpies molaires d'excès que l'on a mesurées antérieurement, fournit une corrélation raisonable des résultats.

[Traduit par le journal]

Can. J. Chem. Downloaded from www.nrcresearchpress.com by 210.87.254.40 on 09/06/12
For personal use only.

Isomer effects in binary mixtures of hydrocarbons or substituted hydrocarbons have been the subject of a number of previous investigations (1, 2). In particular, considerable effort has been devoted to studying the thermodynamic properties of mixtures of various hydrocarbons with the isomers of hexane (3, 4): *n*-hexane (*n*-C_6), 2-methylpentane (2-MP), 3-methylpentane (3-MP), 2,2-dimethylbutane (2,2-DMB), and 2,3-dimethylbutane (2,3-DMB). Our previous work in this field includes determinations of excess enthalpies (5), excess volumes (6), ultrasonic speeds and isentropic compressibilities (7), and excess isobaric heat capacities (8) for (*n*-heptane + a hexane isomer), and of excess enthalpies and excess volumes (9) for (*n*-dodecane + a hexane isomer). Most recently we reported excess enthalpies (10) for binary mixtures of *n*-octane with each of the hexane isomers. As a continuation of that investigation, we have measured excess volumes at 298.15 K for the same five mixtures.

Experimental

Component liquids

The *n*-octane was Aldrich Chemical Co. Gold Label reagent with a specified purity of 99+ mol%. The isomeric hexanes were Phillips Research Grade reagents with purities 99.88 mol% or greater. At 298.15 K, the densities (in kg m^{-3}) of the samples used for the dilatometric studies were as follows: *n*-octane, 698.63; *n*-C_6, 654.92; 2-MP, 648.50; 3-MP, 659.82; 2,2-DMB, 644.47; 2,3-DMB, 657.06.

Dilatometric measurements

Excess molar volumes V_m^E were determined in a tilting dilution dilatometer. This apparatus and its operation have been described by Kumaran and McGlashan (11). For the present mixtures, the error of the measurements is estimated to be less than 0.0010 cm^3 mol^{-1}.

Results and discussion

The measurements of V_m^E at 298.15 K for $\{xn\text{-}C_8H_{18} + (1 - x)C_6H_{14}\}$ are summarized in Table 1. The results for each mixture were fitted with a polynomial of the form:

$$[1]\quad V_m^E/(cm^3\ mol^{-1}) = x(1 - x)\sum_{j=0}^{n-1} v_j(1 - 2x)^j$$

where x is the mole fraction of *n*-octane. Values of the coefficients v_j determined by the method of least-squares with all points weighted equally are listed in Table 2 along with the standard deviations s of the representations.

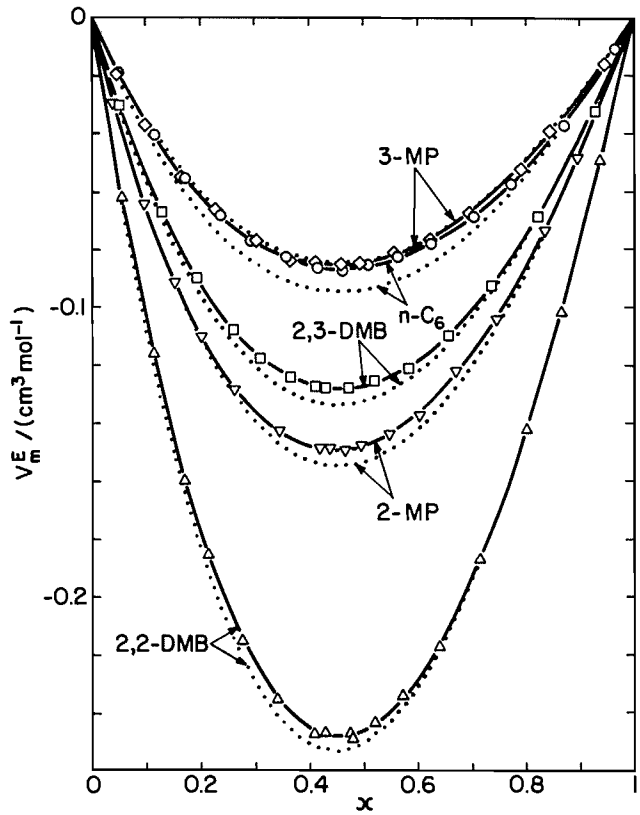

FIG. 1. Excess molar volumes V_m^E for $\{xn\text{-}C_8H_{18} + (1 - x)C_6H_{14}\}$ at 298.15 K. Experimental results: ○, *n*-C_6; ▽, 2-MP; ◇, 3-MP; △, 2,2-DMB; □, 2.3-DMB. Curves: —, calculated from eq. [1] with coefficients from Table 2; ···, calculated from Flory theory.

The experimental results and their representations by eq. [1] are shown in Fig. 1. The curves for *n*-C_6 and 3-MP are very similar, particularly for $x < 0.5$ where their difference is less than their estimated uncertainties. In all cases the curves are only approximately quadratic and exhibit a definite, albeit small, skew toward low mole fractions of the *n*-alkane (*n*-octane). Similar behavior has been observed for mixtures of the

[1]NRCC No. 23631.

[2]National Research Council of Canada Research Associate.

Can. J. Chem. Downloaded from www.nrcresearchpress.com by 210.87.254.40 on 09/06/12
For personal use only.

TABLE 1. Excess molar volumes V_m^E for $\{xn\text{-}C_8H_{18} + (1 - x)C_6H_{14}\}$ at 298.15 K

x	V_m^E / cm^3 mol^{-1}	x	V_m^E / cm^3 mol^{-1}	x	V_m^E / cm^3 mol^{-1}	x	V_m^E / cm^3 mol^{-1}
			n-Octane + *n*-C$_6$				
0.0498	−0.0191	0.3581	−0.0825	0.4675	−0.0865	0.7041	−0.0690
0.1162	−0.0401	0.4167	−0.0862	0.5088	−0.0856	0.7734	−0.0575
0.1716	−0.0552	0.4171	−0.0864	0.5647	−0.0826	0.8699	−0.0371
0.2370	−0.0681	0.4612	−0.0873	0.6254	−0.0783	0.9661	−0.0109
0.2951	−0.0768						
			n-Octane + 2-MP				
0.0416	−0.0298	0.2619	−0.1283	0.4659	−0.1494	0.6724	−0.1221
0.0993	−0.0641	0.3451	−0.1427	0.4951	−0.1478	0.7447	−0.1042
0.1539	−0.0913	0.4174	−0.1484	0.5474	−0.1438	0.8357	−0.0734
0.2029	−0.1101	0.4371	−0.1488	0.6029	−0.1372	0.8952	−0.0486
			n-Octane + 3-MP				
0.0465	−0.0191	0.3629	−0.0833	0.4691	−0.0861	0.6950	−0.0673
0.0985	−0.0367	0.4119	−0.0855	0.4944	−0.0849	0.7899	−0.0521
0.1648	−0.0549	0.4132	−0.0845	0.5569	−0.0813	0.8453	−0.0392
0.2299	−0.0664	0.4576	−0.0854	0.6237	−0.0766	0.9454	−0.0159
0.3023	−0.0767						
			n-Octane + 2,2-DMB				
0.0562	−0.0618	0.3409	−0.2352	0.4769	−0.2487	0.7136	−0.1872
0.1157	−0.1160	0.4091	−0.2474	0.5198	−0.2436	0.8025	−0.1423
0.1725	−0.1597	0.4301	−0.2470	0.5717	−0.2340	0.8660	−0.1018
0.2151	−0.1853	0.4754	−0.2470	0.6392	−0.2174	0.9384	−0.0490
0.2766	−0.2150						
			n-Octane + 2,3-DMB				
0.0506	−0.0299	0.3105	−0.1174	0.4720	−0.1279	0.7361	−0.0925
0.1310	−0.0671	0.3663	−0.1246	0.5211	−0.1255	0.8229	−0.0687
0.1944	−0.0898	0.4116	−0.1275	0.5832	−0.1214	0.9277	−0.0322
0.2607	−0.1078	0.4307	−0.1279	0.6557	−0.1102		

TABLE 2. Coefficients v_j and standard deviation s for representations of $V_m^E/(\text{cm}^3\ \text{mol}^{-1})$ for $\{xn\text{-}C_8H_{18} + (1 - x)C_6H_{14}\}$ at 298.15 K by eq. [1]

	Hexane isomer				
	n-C$_6$	2-MP	3-MP	2,2-DMB	2,3-DMB
v_0	−0.3446	−0.5911	−0.3386	−0.9852	−0.5094
v_1	−0.0511	−0.1198	−0.0640	−0.1761	−0.0835
v_2	−0.0285	−0.0515	−0.0270	−0.0383	−0.0403
v_3	0.0160				
s	0.0004	0.0006	0.0007	0.0008	0.0005

hexane isomers with *n*-heptane (6), *n*-dodecane (9), and *n*-hexadecane (4). A comparison of the results for different *n*-alkanes shows that the skew of the curves increases with the chain length of the *n*-alkane.

The only V_m^E data found in the literature for the present mixtures at 298.15 K are those of Goates *et al.* (12) for (*n*-octane + *n*-C$_6$), and of Handa *et al.* (13) for (*n*-octane + 2,3-DMB). Comparisons of these with our results are given in Fig. 2, where deviations from our smoothing equations are plotted. Both sets of results show more scatter than ours, but in general their smoothed values agree with ours over most of the mole fraction range within the combined uncertainties of the respective investigations.

In our studies of mixtures of *n*-heptane (5, 6) and of *n*-dodecane (9) with the hexane isomers, we found that the excess volumes could be interpreted in terms of the Flory theory (14, 15) when the interchange energy parameter was adjusted to give a fit between the experimental and theoretical excess enthalpy curves. This same treatment was investigated for the present *n*-octane mixtures. The calculation used the molar volumes V_m, isobaric thermal expansivities α_p, and isothermal compressibilities κ_T given in Table 3 for the component liquids at 298.15 K. The properties of the hexane isomers are the same as in our earlier work where their sources are indicated (6). For *n*-octane, α_p was derived from density data (16), and κ_T was estimated from values of the speed of sound and isobaric heat capacity measured in our laboratory. The characteristic pressures p^*, molar volumes V_m^*, and temperatures T^*, obtained from the Flory formalism, are also listed in Table 3 along with the ratio s_{12} of molecular surface areas of contact and the interchange energy parameter X_{12} for each mixture. The values of s_{12} are based on the simple assumption that the molecules are spherical; the values of X_{12} were obtained by fitting the Flory formula for the excess molar enthalpy H_m^E to our smoothed experimental results (10). The dotted curves in Fig. 1 were calculated from the Flory formula for V_m^E using the parameters in Table 3. It can be seen that the theory again predicts the order and asymmetry of the curves correctly. That for 3-MP is nearly identical to the experimental curve. For the other isomers, the theory tends to overestimate the magnitude of V_m^E, as was found for the mixtures with *n*-dodecane (10).

TABLE 3. Component properties and parameters used in calculations for (*n*-octane + hexane isomer) mixtures at 298.15 K by the Flory theory[a]

Component	V_m / cm^3 mol^{-1}	α_p / kK^{-1}	κ_T / TPa^{-1}	p^* / J cm^{-3}	V_m^* / cm^3 mol^{-1}	T^* / K	s_{12}	X_{12} / J cm^{-3}
n-C_8H_{18}	163.51	1.164[b]	1302.4[c]	436.9	127.70	4827.0		
n-C_6	131.57	1.387	1703.9	424.2	99.52	4436.1	0.9203	0.3382
2-MP	132.89	1.426	1838.9	408.3	99.99	4380.8	0.9217	0.9996
3-MP	130.61	1.396	1719.1	424.2	98.68	4423.0	0.9177	0.8284
2,2-DMB	133.73	1.468	2009.6	389.0	100.07	4324.8	0.9219	1.6123
2,3-DMB	131.16	1.391	1790.2	405.3	99.16	4430.2	0.9191	0.8391

[a]Sources of α_p and κ_T for the hexane isomers are given in ref. 6.
[b]Estimated from densities in ref. 16.
[c]Derived from speed of sound and isobaric heat capacity measurements in our laboratory.

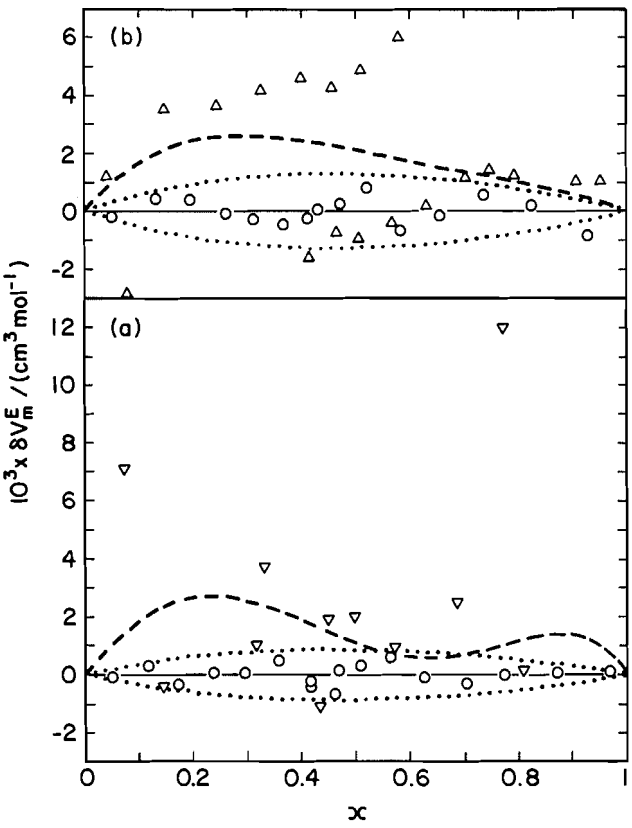

FIG. 2. Plots of the deviations $\delta V_m^E = V_m^E(\text{expt}) - V_m^E(\text{eq. [1]})$ for $\{xn\text{-}C_8H_{18} + (1-x)C_6H_{14}\}$ at 298.15 K. (*a*) *n*-C_6 mixture: ○, our results; ▽, Goates *et al.* (12); (*b*) 2,3-DMB mixture: ○, our results; △, Handa *et al.* (13). Curves: ---, calculated from smoothing equations in refs. 12 and 13; ···, indicates ±1% deviation from eq. [1].

Can. J. Chem. Downloaded from www.nrcresearchpress.com by 210.87.254.40 on 09/06/12
For personal use only.

Acknowledgments

We are indebted to C. J. Halpin and P. J. D'Arcy for technical assistance during this investigation.

1. D. V. FENBY, J. R. KHURMA, Z. S. KOONER, T. E. BLOCK, C. M. KNOBLER, J. REEDER, and R. L. SCOTT. Aust. J. Chem. **33**, 1927 (1980).
2. Y. P. HANDA, C. M. KNOBLER, and R. L. SCOTT. J. Chem. Thermodyn. **9**, 451 (1977).
3. J. A. LARKIN, D. V. FENBY, T. S. GILMAN, and R. L. SCOTT. J. Phys. Chem. **70**, 1959 (1966).
4. J. REEDER, C. M. KNOBLER, and R. L. SCOTT. J. Chem. Thermodyn. **7**, 345 (1975).
5. F. KIMURA, G. C. BENSON, and C. J. HALPIN. Fluid Phase Equilib. **11**, 245 (1983).
6. F. KIMURA and G. C. BENSON. J. Chem. Eng. Data, **28**, 387 (1983).
7. E. AICART, M. K. KUMARAN, C. J. HALPIN, and G. C. BENSON. J. Chem. Thermodyn. **15**, 919 (1983).
8. G. C. BENSON, P. J. D'ARCY, and M. K. KUMARAN. Thermochim. Acta. **75**, 353 (1984).
9. S. E. M. HAMAM, M. K. KUMARAN, and G. C. BENSON. J. Chem. Thermodyn. **16**, 537 (1984).
10. S. E. M. HAMAM, M. K. KUMARAN, and G. C. BENSON. Fluid Phase Equilib. In press.
11. M. K. KUMARAN and M. L. MCGLASHAN. J. Chem. Thermodyn. **9**, 259 (1977).
12. J. R. GOATES, J. B. OTT, and R. B. GRIGG. J. Chem. Thermodyn. **13**, 907 (1981).
13. Y. P. HANDA, J. REEDER, C. M. KNOBLER, and R. L. SCOTT. J. Chem. Eng. Data, **22**, 218 (1977).
14. P. J. FLORY. J. Am. Chem. Soc. **87**, 1833 (1965).
15. A. ABE and P. J. FLORY. J. Am. Chem. Soc. **87**, 1838 (1965).
16. Selected Values of Properties of Hydrocarbons and Related Compounds. Thermodynamics Research Center Hydrocarbon Project. Thermodynamics Research Center, Texas A&M University, College Station, Texas. (See Table 23-2(1.101)-d, page 2 dated June 30, 1973.)

Effet de substitution dans les positions 3, 5 et 7 en série spiropyrannique benzothiazolinique

JACKY KISTER,[1] HENRI PAUL POMMIER ET JACQUES METZGER
L.A. 126. Laboratoire de Chimie Organique A, Centre Universitaire de St-Jérôme, 13397 Marseille Cedex 13, France

ET

ROBERT GUGLIELMETTI
L.A. 322. Laboratoire de Synthèse Organique, Université de Bretagne Occidentale, 6, Avenue Le Gorgeu, 29283 Brest Cedex, France

Reçu le 27 janvier 1984

JACKY KISTER, HENRI PAUL POMMIER, JACQUES METZGER et ROBERT GUGLIELMETTI. Can. J. Chem. **62**, 2372 (1984).

L'étude de la substitution dans les positions 3, 5, 6, 7 et 8 des spiropyrannes benzothiazoliniques a permis de mettre en évidence l'aspect tout-à-fait complémentaire des positions 3 et 5, sur la stabilité du système délocalisé de type mérocyanine. Les interactions de non liaison ont une influence directe sur la fermeture de la molécule de spiropyranne. Les paramètres stéréoélectroniques judicieusement choisis permettent de modifier l'équilibre forme fermée/forme ouverte dès le développement synthétique.

JACKY KISTER, HENRI PAUL POMMIER, JACQUES METZGER, and ROBERT GUGLIELMETTI. Can. J. Chem. **62**, 2372 (1984).

Benzothiazolinic spiropyrans substituted in the 3, 5, 6, 7, and 8 positions have been studied. The results obtained show the equivalent role of the 3 and 5 substituted positions during the synthesis of merocyanin type compounds. Non-bonded interactions play a direct role in ring closing to spiropyran compounds. The relative stabilities of open and closed ring compounds depend on stereoelectronic parameters.

Can. J. Chem. Downloaded from www.nrcresearchpress.com by 210.87.254.5 on 09/06/12
For personal use only.

L'utilisation des spiropyrannes photochromiques comme substrats photosensibles dans des procédés photographiques implique la recherche de composés dont la structure est adaptée au procédé que celui-ci comporte ou non une étape d'amplification du signal photonique primaire (1, 2). Les divers résultats obtenus dans ce domaine (2, 3) nous ont amené à étudier plus particulièrement la série benzothiazolinique substituée principalement dans les positions 3, 6, 8 sur la partie chroménique et 3′, 4′, 6′ sur la partie benzothiazolinique (schéma 1):

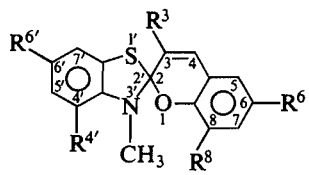

SCHÉMA 1. Nomenclature officielle de la molécule de spiropyranne benzothiazolinique.

La numérotation des atomes est conforme aux règles énoncées dans le "Ring-Index" et la nomenclature officielle est la suivante: spiro [R_3, R_6, R_8 benzo 2*H* [1] pyranne-2,2′ méthyl-3′, R'_4, R'_6 benzothiazoline].

I. Définition des effets de substitution

Si de tels composés sont interessants, en vue de leur utilisation photochimique possible, par contre leur synthèse devient particulièrement complexe et délicate (3, 4) en fonction des substituants choisis correlativement à l'optimisation des paramètres spectro-cinétiques de la réaction de fermeture après irradiation uv (schéma 2).

Il est traditionnellement admis et démontré que le caractère photochromique des spiropyrannes azahétérocycliques est lié à la substituion dans les positions 6 et 8 de la partie benzopyrannique par des couples NO_2/R (3*a*, 5) où R est souvent un groupement OCH_3 intéressant par les propriétés conférées et également par la commodité d'accès synthétique. R peut également être du type CH_2X ou OR′ pour lesquels X = Cl, OR′, $N(R')_2$ avec R′ = H, CH_3, C_2H_5, ...$(CH_2)_nCH_3$, cycle ... (6).

En première approximation, on peut dire que les substituants de chacune des deux parties benzopyrannique et benzothiazolinique affectent les cinétiques de façon indépendante (3, 7−9). En règle générale les substituants électron-attracteurs placés sur la partie benzopyrannique ralentissent la fermeture des photomérocyanines alors que les substituants électron-donneurs l'accélèrent. L'effet est inverse mais très atténué pour la partie benzothiazolinique. Les substituants placés au voisinage du carbone central et dont l'effet est essentiellement stérique accélèrent la décoloration thermique (2, 3, 8, 9). La présence simultanée de plusieurs substituants conduit à des résultats difficilement interprétables (2, 4).

Dans ce présent mémoire, nous nous intéressons aux facteurs sensibilisant la refermeture de la forme ouverte (FO) en forme fermée (FF) sans tenir compte des considérations spectro-cinétiques de l'équilibre photochromique. Par souci d'homogénéité et pour présenter les résultats des études physico-chimiques et l'analyse des effets de substitution en 3, 5 et 7, nous avons réalisé la synthèse des composés dont le couple de substituants en position 6/8 peut être H/H, NO_2/H et H/OCH_3.

En position 3′, nous choisissons un groupement méthyle, lequel est rendu électrophile par ouverture de la liaison C_2—O_1. Il convient de rappeler que la labilité de ce méthyle peut être mesurée en utilisant la réaction de déméthylation par la triphénylphosphine (10).

En position 6′, le substituant placé en position *para* de l'atome d'azote hétérocyclique exerce une influence importante sur la délocalisation électronique du système. C'est ainsi que nous avons placé un groupement méthoxy correspondant à une optimisation des photochromes adaptés aux procédés photographiques avec amplification (3*c*, 4).

En position 3, position adjacente au carbone spiropyrannique, les groupes fonctionnels oxygénés comme le méthoxy et le phénoxy exercent un important ralentissement sur les cinéti-

[1]Auteur à adresser toute correspondance.

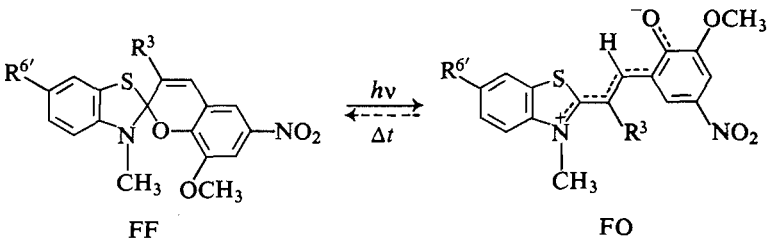

SCHÉMA 2. Equilibre photochromique forme fermée/forme ouverte (FF/FO).

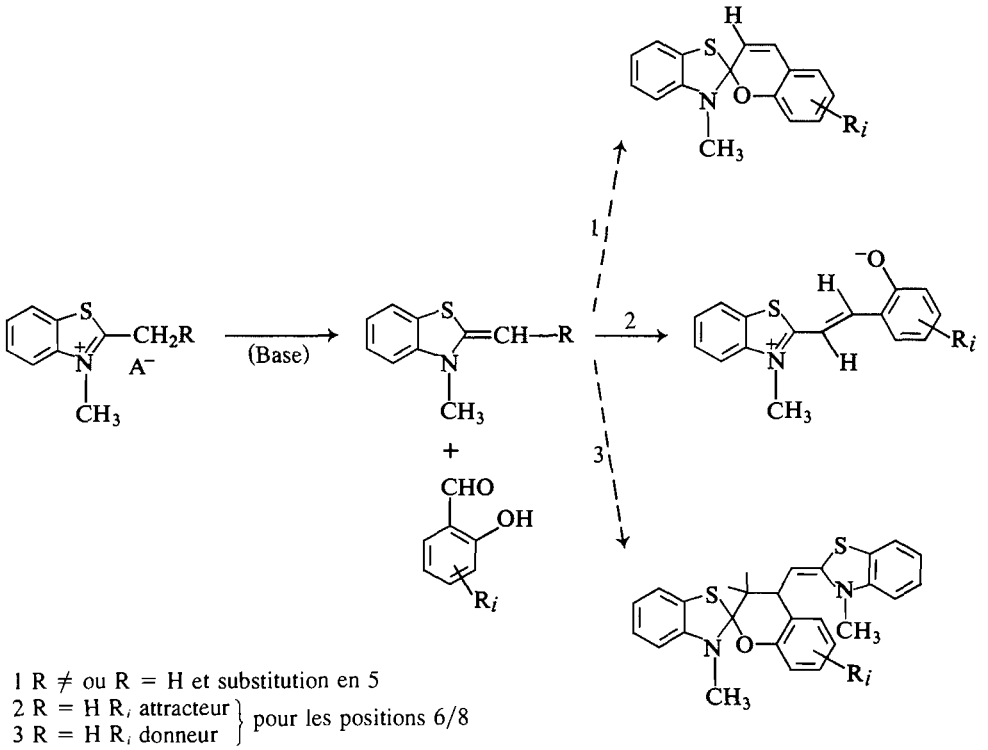

SCHÉMA 3. Reactions de condensation spiropyrannique.

ques de décoloration thermique (3*a*, 7). Cette stabilisation de la FO est d'autant plus forte que le substituant est moins encombrant. La simultanéité de substitution par le groupement méthoxy en position 3 et 6′ a conduit à l'obtention d'une mérocyanine permanente (2, 3*b*, 7), l'équilibre photochromique étant totalement déplacé vers la "photomérocyanine."

En position 5 et 7: ces positions n'ont pas fait l'objet de recherches approfondies en série benzothiazolinique. Nous avons étudié l'influence d'un groupement méthyle en position 5, sur l'obtention de formes fermées alors que la position 3 reste non substituée. Smets et coll. (11) avaient déjà étudié cette position 5 en série benzothiazolinique et ceci simultanément avec la substitution en position 3. La séparation des effets de substitution en 3/5 n'avait pas été réalisée.

La condensation du sel quaternaire de diméthyl-2,3 benzothiazolium (donnant un hydrogène en position 3) sur des aldéhydes salicyliques porteurs de groupements électron-attracteurs, conduit à des mérocyanines (FO permanentes) (12) tandis que la condensation sur des aldéhydes salicyliques porteurs de groupements électron-donneurs conduit à l'obtention de composés tricycliques de type spirodihydropyrannique (12), schéma 3.

Enfin l'étude de composés porteurs de longues chaînes aliphatiques avait été développée dès 1972 (13) et l'influence de ces chaînes grasses sur la solubilisation des FO a été utilisée pour l'étude physicochimique des mérocyanines (14, 15). Les mérocyanines classiques sont en effet particulièrement insolubles dans la plupart des solvants polaires ou apolaires à fortiori. Par ailleurs, il n'était pas venu à l'idée de placer un hydrogène en position 3 puisque l'on cherchait également à accroitre le système π susceptible de former des complexes stables par adsorption sur semi-conducteurs. Les groupements phénoxy et β naphtoxy étaient alors particulièrement intéressants en position 3 (2, 3, 7).

L'ensemble de ces considérations expérimentales nous a conduit à étudier les spiropyrannes et mérocyanines présentés dans les tableaux 1 et 2. Les spiropyrannes **4**−**7** et **11**−**15** sont présentés pour comparaison. Le mode de synthèse est maintenant connu (2 à 7); il nécessite la synthèse intermédiaire de sels quaternaires de benzothiazolium par quaternisation de bases benzothiazoliques. Celles utilisées dans ce mémoire ont fait l'objet d'études et de publications (2−5, 7). L'aldéhyde salicylique utilisé pour la condensation finale avec le sel quaternaire peut-être le classique nitro-5 méthoxy-3 salicylaldéhyde (3, 5). Dans le cas des aldéhydes conduisant aux composés substitués en 5/7, ils résultent de synthèses délicates (13, 16). L'alkylation des aldéhydes se fait par le tosylate d'hexadécyle dans l'éthanol à reflux pendant 12 h; les composés obtenus sont

Can. J. Chem. Downloaded from www.nrcresearchpress.com by 210.87.254.5 on 09/06/12
For personal use only.

TABLEAU 1. Effet de substitution sur la partie benzopyrannique, la partie benzothiazolinique restant fixe et substituée par un groupement méthyle en position 3′

N°	Substitution partie benzopyrannique R_3	R_5	R_6	R_7	R_8	Formes isolées FF MEL	FO MEL	Rendement (%) FF MEL	FO MEL	Photochrome	Solvant de synthèse	θ fusion (°C) FF MEL	FO MEL	Solvant de précipitation de la FF	Ref.
1	H	CH_3	H	$OC_{16}H_{33}$	H	—	+ —	50		Non	EtOH	— rouge		EtOH	—
2	H	H	H	$OC_{16}H_{33}$	H	—	+	—	60	FO stable	EtOH	250 violet		EtOH	—
3	H	$OC_{16}H_{33}$	H	$OC_{16}H_{33}$	H	—	+	50		Non	EtOH	180 marron		EtOH	—
4	H	H	NO_2	H	OCH_3	—	+	—	70	FO stable	EtOH	260		EtOH	3*a*
5	CH_3	H	NO_2	H	OCH_3	+	+	77	85	Oui	EtOH	182	—	EtOH	5
6	OCH_3	H	NO_2	H	OCH_3	+	+	94	94	Oui	EtOH	195	—	EtOH	3*b*

TABLEAU 2. Effet de substitution sur la partie benzopyrannique: partie benzothiazolinique fixe, substituée par un groupement méthyle en 3′ et méthoxy en 6′

N°	Substitution Partie hétérocyclique R_3'	R_6'	Partie benzopyrannique R_3	R_5	R_6	R_7	R_8	Formes isolées FF MEL	FO MEL	Rdt (%) en F isolée FF MEL	FO MEL	Photochrome	Solvant de synthèse	θ fusion (°C) FF	FO	Solvant de précipitation de la FF	Ref.
7	CH_3	OCH_3	CH_3	H	NO_2	H	OCH_3	+	+	85	—	Oui	EtOH	188		Ether de pétrole	5
8	CH_3	OCH_3	H	CH_3	H	$OC_{16}H_{33}$	H	+		70		Non	EtOH	Mélange		EtOH	—
9	CH_3	OCH_3	H	H	H	$OC_{16}H_{33}$	H		+	—	50	—	EtOH	—	165	EtOH	—
10	CH_3	OCH_3	H	H	NO_2	H	OCH_3	—	+	—	70	—	EtOH	—	260	EtOH	(3*a*)
11	CH_3	OCH_3	OCH_3	H	NO_2	H	OCH_3	—	+	—	90	—	EtOH	—	260	EtOH	7
12	CH_3	OCH_3	OC_6H_5	H	NO_2	H	OCH_3	+	+	50	74	Oui	EtOH	214	230	Ether de pétrole	4, 7
13	CH_3	OCH_3	OC_6H_5	H	H	H	H	+	—	92	—	Non	EtOH	146	—	EtOH	1*b*, 2
14	CH_3	OCH_3	OC_6H_5	H	NO_2	H	H	+	+	18	90	Oui	EtOH	156	—	Pentane	1*b*, 2
15	CH_3	OCH_3	OC_6H_5	H	H	H	OCH_3	+	—	81	—	Oui	EtOH	150	—	Pentane	1*b*, 2

recristallisés dans l'acétone. Les rendements sont de l'ordre de 70%. La préparation des spiropyrannes s'effectue par reflux de quantités équimoléculaires de sels de benzothiazolium, d'aldéhyde et de pipéridine dans l'éthanol; les rendements varient de 50 à 70%.

II. Analyses spectroscopiques

Les diverses études spectroscopiques (ir, uv−vis, rmn^{1}H) ont été réalisées. Les composés obtenus peuvent être sous forme de FF pure, de FO pure ou de mélange FF/FO. Les techniques d'identification s'avèrent fiables par le grand nombre de caractérisations FF/FO effectuées sur des séries homogènes de spiropyrannes diversement substitués.

A. spectroscopie infrarouge

La spectroscopie infrarouge apparait comme la méthode la plus adaptée pour différencier rapidement les formes fermées et formes ouvertes et estimer la pureté des produits obtenus (17−19). Les spectres infrarouges ont été enregistrés sur spectrographes Perkin Elmer 125 et 225. Les échantillons ont été examinés sous forme de pastilles KBr (environ 1,50 mg de produit pour 150 mg de KBr).

Les spiropyrannes FF sont caractérisés par (17−19) (fig. 1): (*i*) quatre bandes entre 1700 et 1550 cm^{-1} dont trois sont imputables aux vibrations du noyau benzopyrannique et une au noyau benzothiazolinique. Le sommet ir correspondant au ν(C=C) est faible et ne peut pas être observé; (*ii*) une bande forte vers 1515 cm^{-1} correspondant au $\nu_a(NO_2)$; (*iii*) un sommet intense vers 1490−1470 cm^{-1} dû au noyau benzothiazolinique (17, 19); (*iv*) un maximum vers 1340 cm^{-1} ($\nu_s(NO_2)$; (*v*) des bandes attribuables aux mouvements ν(CO) intracycliques et ν(=C—OR) et aux vibrations du noyau benzothiazolinique entre 1300 et 1200 cm^{-1}.

Les mérocyanines FO sont caractérisées par (17−19): (*i*) la présence d'un massif intense au dessous de 1600 cm^{-1} (quatre absorptions théoriques) résultant du glissement des absorptions du noyau benzopyrannique; (*ii*) un $\nu_a(NO_2)$ inchangée par rapport à la FF; (*iii*) une bande forte vers 1500 cm^{-1} correspondant au glissement de la bande FF (1490−1470); (*iv*) l'apparition d'un sommet intense vers 1400 cm^{-1} qui peut être attribuée à une vibration ν(C=N); (*v*) une bande vers 1200 cm^{-1}, intense non attribuée; (*vi*) un massif complexe entre 1300 et 1200 cm^{-1} comportant les absorptions ν(=C—OR), les vibrations du noyau benzothiazolinique, les ν(C—O) intracycliques intenses et très larges et la bande correspondant aux $\nu_s(NO_2)$ très abaissée par rapport à la FF.

De ces considérations générales on en déduit pour nos composés (tableau 3):

Les composés **1**, **3**, **8** sont obtenus sous forme de mélange FF/FO.

Can. J. Chem. Downloaded from www.nrcresearchpress.com by 210.87.254.5 on 09/06/12
For personal use only.

Can. J. Chem. Downloaded from www.nrcresearchpress.com by 210.87.254.5 on 09/06/12
For personal use only.

TABLEAU 3. Caractéristiques infrarouge des spiropyrannes et mérocyanines (e = épaulement, m = moyen, f = faible, F = fort et FF = intense)

		Fréquences infrarouges et attributions caractéristiques entre 1700−1150 cm^{-1}														
FF	FO	$\nu(CC_{ethylénique})$		$\nu(CC_{benzénique})$			$\nu_a(NO_2)$	ν(noyau)	ν(C—N)	$\nu_s(NO_2)$		$\nu(CO_{cycle})$, ν(C—OR) ν(noyau)				
1	**1**	1667e		1610F				1468					1235m			1183F
			1593FF		1582FF			1504F	1457	1410m			1259F		1224	1204F
	2		1590F			1575FF		1500F	1460	1410m			1255F	1235m	1220m	1190F
3	**3**	1650m		1610	1585				1480F					1235		1180
			1590FF		1585	1577		1502		1410m			1260F		1210	
	4		1595FF		1587F	1575	1558	1515FF		1405F	1301F	1277FF	1260F	1230F	1210F	1190F
5	**5**	1655f		1620	1588			1530F	1476F		1339F		1251FF	1238m	1220F	1188F
			1595FF		1588	1575		1525F	1500F	1405F	1302	1288	1260F		1225f	1203
6	**6**	1652m		1613	1587	1577		1523FF	1470F		1335F			1230F	1246FF	1195F
			1595FF			1577		1527FF	1502F	1405F		1290F	1270FF			1218 1203
7	**7**	1645m		1605f		1573		1518F	1480F		1330F		1250	1238		
			1595FF		1585			1520F	1500F	1402F		1288F	1260F	1235F		1210
8	**8**	1655f				1575			1490F				1245F			1210
			1590	1580		1575			1500F	1410m			1260f	1235F		1205
	9		1590	1580f		1575			1500F	1410m			1260f	1230F		1205F
	10		1590	1585f		1575		1525F	1505F	1395F		1288FF	1260f	1235FF		
	11		1590F	1580f		1568		1525F	1504F	1395F		1280FF		1245FF		1230
12	**12**	1655m		1613F	1587m	1576f		1520F		1487F		1336F		1250F	1242F		1215
			1588F	1580f		1575f		1525F	1505F	1392F		1288FF		1235FF		
13		1645m		1600f	1587m	1573m			1486F				1243F	1230f	1220F	1207F
14	**14**	1645m		1600f	1588m	1575m		1520F		1486F		1337F		1262F	1237F	1222f	1202F
			1595	1575f				1520F	1500F	1394F		1295FF	1265f	1245FF		
15	**15**	1645m		1604m	1586m	1575F				1485F			1250m		1225F	1213f 1203F
			1588F	1600f		1572F				1485F			1260f		1225F	1210F 1203f

Can. J. Chem. Downloaded from www.nrcresearchpress.com by 210.87.254.5 on 09/06/12
For personal use only.

TABLEAU 4. Caractéristiques ultraviolet et visible des spiropyrannes et mérocyanines (longueurs d'ondes d'absorption en nm)

N°		Caractéristiques déterminées par photolyse éclair																			
		Ethanol			Dioxanne						Ethanol			Toluène							
1	FF/FO	545	455	316	296	270	264	560	500	305e	295	238e	218	—					—		
2	FO	560	450	317		277		573	450e	306	285			—					—		
3	FF/FO	550	450	316	290	273		565	485	305	290	240		—					—		
4	FO	FO stable: spectre non enregistré (insoluble)												490	420		600	545	430		
5	FO	490	420																		
	FF			342	280e	252.5	217			345	288	268	253,5	224							
6	FO	532	415												532	415		640		420	340e	302e
	FF			344	270e	250				347	280		255								
7	FF/FO	490	450	323,5		253	224	520	430	355					490	412		520	430	355	
8	FF/FO	545	435	315	290	273		560	485	305	285	270	218	Non photochrome							
9	FO	FO stable: spectre non enregistré (insoluble)																			
10	FO	FO stable: spectre non enregistré (insoluble)																			
11	FO	Mérocyanine permanente (insoluble)																			
12	FF/FO	570		365	284		220			335		270	215	530	400	345	321	630	410	340	323
13	FF			312	283	273	227			312,5	282,5	273,5	218	Non photochrome							
14	FF		350	304		274	227			350	304	277	226		510	355	310	620		350	310
15	FF			305		268	225			317		280	227	Photochrome à basse température non exploitable							

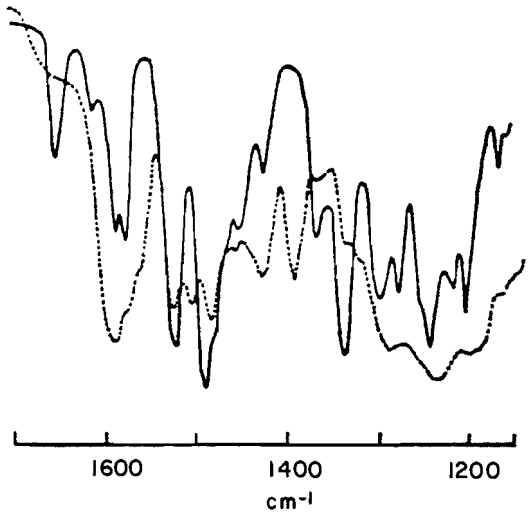

FIG. 1. Différenciation spectroscopique entre la FF (——) et FO (– – –) d'une molécule benzothiazolinique de type **5** dans la région 1100–1700 cm^{-1}.

Les composés **2**, **4**, **9**, **10**, **11** donnent les spectres caractéristiques des FO.

Les composés **5**, **6**, **7**, **12**, **14**, **15** sont obtenus soit en mélange soit en FF ou FO pure selon que le composé issu de la réaction de condensation est analysé sous forme brute en fin de synthèse après refermeture complète dans le toluène chaud (FF pure) ou après ouverture et photoprécipitation (FO pure).

Le composé **13** donne directement la FF, il n'est pas photochrome.

B. Spectroscopies ultraviolette et visible

Les spectres des spiropyrannes benzothiazoliniques ont été réalisés dans le dioxanne et l'éthanol sur un spectrophotomètre Cary 14 à double faisceau et sur un spectrophotomètre Perkin Elmer 137. La faible solubilité des mérocyanines ne permet pas une grande précision pour l'estimation du coefficient d'extinction moléculaire ϵ. L'identification de certaines bandes caractéristiques a été réalisée en décomposant la molécule en deux parties (3*a*, *b*).

P. Appriou *et al.* (20) ont étudié les interactions des deux parties et la redistribution des niveaux d'énergie (20, 21). La durée de vie des FO en solution est généralement courte et leur solubilité faible et la décoloration de la solution montre l'évolution vers la FF. L'on obtient ainsi souvent le spectre d'un mélange FF/FO.

Les résultats sont regroupés dans le tableau 4 et la fig. 2 montre la différenciation entre la FF et la FO. Lors des mesures des constantes cinétiques de refermeture des FO dans l'éthanol et le toluène (2, 3, 7, 9) effectuées par photolyse éclair, les caractéristiques spectroscopiques uv–visible des FF et FO pures ont été mesurées. Ces résultats sont regroupés dans le tableau 4. Ces mesures ne sont fournies que pour les composés photochromes conduisant à des mérocyanines pouvant se refermer en solution (composés **5**, **6**, **7**, **12** et **14**).

Ainsi on peut vérifier que les composés **1**, **3**, **8** sont obtenus sous forme de mélange FF/FO; que les composés **2**, **4**, **9**, **10** et **11** sont des mérocyanines insolubles. Le composé **2** peut être analysé et légèrement solubilisé du fait de la présence d'une chaine grasse en position 7.

C. Analyse de résonance magnétique nucléaire du proton

Les déplacements chimiques sont toujours exprimés en ppm

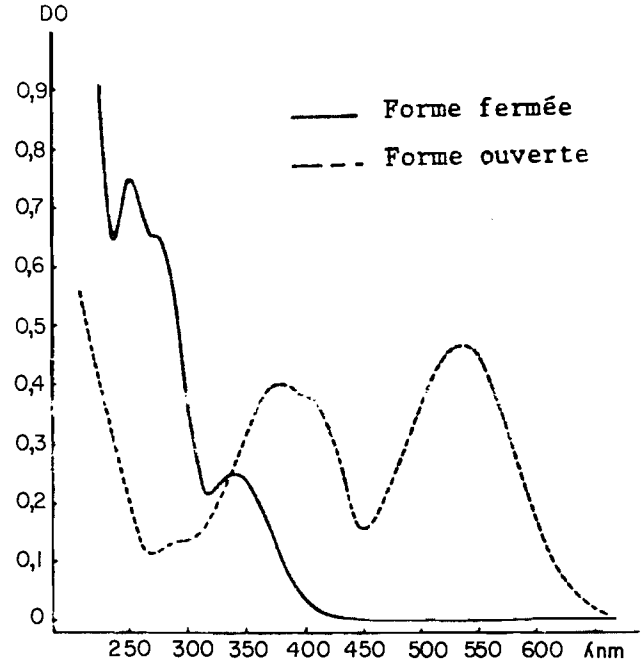

FIG. 2. Spectre d'absorption électronique du spiropyranne **6** et de la photomérocyanine correspondante (EtOH).

par rapport au TMS. Les spectres ont été réalisés sur des appareils de type Varian XL 100 et Cameca 250 MHz. L'enregistrement des spectres de FF pures ne pose aucun problème, leur solubilité étant acceptable (2, 3). Il existe beaucoup moins de résultats relatifs aux FO (22, 23). Cependant la rmn protonique apporte des résultats importants sur la polarité et la structure des FO. Trois problèmes limitent l'étude des FO: la solubilité, la stabilité en solution et l'obtention de FO isolées. La présence de chaînes grasses et l'utilisation d'appareil à transformée de Fourier permet l'étude de solutions peu concentrées évitant la photoprécipitation et la refermeture de la FO dans un solvant polaire tel que DMSO-d_6.

Dans cette étude nous nous intéressons plus spécialement au déplacement chimique du groupe méthyle fixé sur l'azote benzothiazolinique. Ainsi on peut constater une variation de son déplacement chimique de 0,9 à 1,5 ppm lorsque l'on passe d'une Forme Fermée à une Forme Ouverte (2, 23).

Ce résultat confirme la déficience électronique sur la partie azahétérocyclique et les déplacements chimiques observés, comparés à ceux obtenus dans le cas des sels quaternaires de benzothiazolium ($4{,}30 < \delta\overset{+}{N}CH_3 < 4{,}70$ dans le TFA), indiquent une localisation importante de la charge positive sur cette partie de la molécule (ceci est confirmé par le déplacement paramagnétique du proton H_4 (3*b*, 23) et par l'étude radiocristallographique aux rayons X effectuée sur une mérocyanine benzothiazolinique (24).

La rmn des FF et FO montre bien l'existence d'interactions stéréoélectroniques entre le doublet libre de l'oxygène en position 3 et le proton H_5 quand il existe (3*b*, 23). Ainsi le tableau 5 montre les déplacements observés pour les composés **1** à **15**. Les déplacements chimiques δNCH_3 des composés **1**, **2**, **8** sont bien caractéristiques d'un mélange FF/FO avec $1{,}10 < \Delta\delta NCH_3 < 1{,}20$ ppm. Les composés **2**, **4**, **9**, **10** et **11** donnent un déplacement chimique caractéristique d'une FO. Les composés **5**, **6**, **8** et **12** peuvent être analysés à l'état de FO pures ou FF pures. Les composés **7**, **13**, **14** et **15** sont par leur

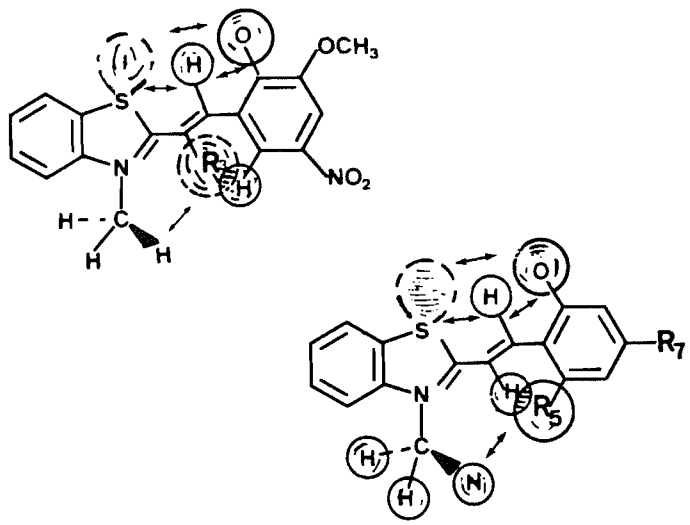

SCHÉMA 4. Visualisation des intéractions de non-liaison d'origine stérique et électronique (H_3/R_5-R_3/H_5).

TABLEAU 5. Analyse résonance magnétique nucléaire de ^1H dans $CDCl_3$ (ref. TMS) des FF/FO (déplacements chimiques en ppm)

N°	δNCH_3 FF	$\delta\overset{+}{N}CH_3$ FO
1	3,0	4,10
2	—	3,80 *DMSO-d_6
3	2,95	4,14
4	—	3,80 *DMSO-d_6 mérocyanine stable
5	3,0	4,14
6	3,02	4,33
7	3,02	—
8	3,04 $CDCl_3$	4,14 *DMSO-d_6
9	—	3,85 *DMSO-d_6
10	—	3,80 *DMSO-d_6
11	—	4,38
12	3,22	4,38
13	3,20	—
14	3,20	—
15	3,24	—

*Solubilité partielle.

déplacement chimique des FF pures. Ainsi pour l'ensemble de ces composés

$$2{,}95 < \delta NCH_{3\ FF} < 3{,}24 \text{ ppm}$$

$$3{,}80 < \delta\overset{(+)}{N}CH_{3\ FO} < 4{,}38 \text{ ppm}$$

Dans un précédent travail, nous avons montré que cette étude comparative permet d'évaluer la capacité d'une mérocyanine à céder son méthyle (2). Cette capacité est mesurée par ailleurs en mettant en oeuvre une réaction de déméthylation (2, 10).

III. Conclusion

Ainsi les trois techniques spectroscopiques confirment bien l'obtention partielle de FF dans le cas de non substitution en position 3 mais avec encombrement stérique en position 5. L'on peut ainsi nettement mettre en évidence les interactions équivalentes H_3/R_5 et R_3/H_5 (schéma 4). Dans le cas des composés **3** et **6**, une stabilisation complémentaire des FO est

Can. J. Chem. Downloaded from www.nrcresearchpress.com by 210.87.254.5 on 09/06/12
For personal use only.

obtenue par les interactions entre les hydrogènes en position 3 ou 5 et l'oxygène du méthoxy en 3 ou de l'hexadecyloxy en 5.

A Samat *et al.* ont effectué des calculs d'interactions de non-liaison dans le cas de mérocyanines et photomérocyanines benzothiazoliniques (25); les résultats obtenus montrent:

1. Une différence très importante de l'ordre de 190 kcal d'énergie pour la forme la plus stable entre la mérocyanine stable (composé n° **4**, H en 3) et la photomérocyanine issue du composé n° **5** (CH_3 en 3). Ceci est en accord avec le fait qu'en série benzothiazolinique la FO est peu contrainte stériquement et la refermeture sous forme spiropyrannique n'a pas lieu.

2. Avec une atome d'hydrogène en position 3, les énergies d'interactions stériques sont faibles, par contre la présence d'un groupement volumineux permet de négliger l'effet électrostatique au profit de l'effet stérique. La série benzoxazolinique (26) conduit en général à des photomérocyanines thermiquement plus stables que leurs homologues benzothiazoliniques. L'atome d'oxygène allie les effets électroniques et stériques favorisant cette stabilisation, par contre on observe en série benzosélénazolique les effets contraires (27).

Il serait intéressant d'examiner dans la même perspective les problèmes liés à la substitution ou non dans les positions 5 et 7 lorsque la position 3 est occupée par un atome d'hydrogène. Il apparaît néanmoins que la position 7 doit jouer un rôle beaucoup plus négligeable que la position 5 dans l'obtention des FF lorsque la position 3 n'est pas substituée. Les interactions stéréoélectroniques entre les groupements situées en position 3 et 5 sur les mérocyanines montrent un effet complémentaire dans l'obtention des FF ou des FO.

Remerciements

Ce travail a été réalisé dans le cadre du contrat DRET 80/084. Nous remercions la DRET pour l'aide financière apportée.

1. (*a*) J. METZGER. Brevet Français, n° 7328538 (1973); (*b*) J. KISTER et J. METZGER. C.R. Acad. Sci. Ser. C, **287**, 281 (1978).
2. J. KISTER. These Sciences, Marseille (1977).
3. (*a*) R. GUGLIELMETTI. Thèse Sciences, Marseille (1967); R. GUGLIELMETTI, E. DAVIN et J. METZGER. Bull. Soc. Chim. Fr. 2812 (1967); (*b*) A. SAMAT. Thèse Sciences, Brest (1976); A. SAMAT, R. GUGLIELMETTI et J. METZGER. Helv. Chim. Acta, **55**, 1782 (1972); (*c*) J. KISTER. Thèse spécialité, Marseille (1974).
4. J. KISTER, A. BLANC, E. DAVIN et J. METZGER. Bull. Soc. Chim. Fr. 2297 (1975).
5. R. GUGLIELMETTI et J. METZGER. Bull. Soc. Chim. Fr. 2824 (1967).
6. (*a*) M. LE BACCON. Thèse Sciences, Brest (1978); (*b*) M. LE BACCON, F. GARNIER et R. GUGLIELMETTI. Bull. Soc. Chim. Fr. 315 (1979).
7. A. SAMAT, J. KISTER, F. GARNIER, J. METZGER et R. GUGLIELMETTI. Bull. Soc. Chim. Fr. 2627 (1975).
8. R. GUGLIELMETTI, M. MOSSE, J. C. METRAS et J. METZGER. J. Chim. Phys. **65**, 454 (1968).
9. A. SAMAT, J. METZGER, F. MENTIENNE, F. GARNIER, J. E. DUBOIS et R. GUGLIELMETTI. J. Phys. Chem. **76**, 3554 (1972).
10. J. KISTER, U. BERG, R. GALLO et J. METZGER. Bull. Soc. Chim. Fr. 484 (1979).
11. P. H. VANDEWYER, J. HOEFNAGELS et G. SMETS. Tetrahedron, **25**, 3251 (1969).
12. A. SAMAT, C. RIOU, J. ROBILLARD et R. GUGLIELMETTI. J. Photogr. Sci. **26**, 34 (1978).
13. H. P. POMMIER. Thèse Docteur-Ingénieur, Marseille (1972).
14. A. LE BEUZE, A. SAMAT, A. BOTREL, P. APPRIOU et R. GUGLIELMETTI. J. Chim. Phys. **75**, 46 (1978).
15. J. P. BESSE, A. SAMAT, A. LE BEUZE, J. Y. LE GALL et R. GUGLIELMETTI Org. Magn. Reson. **11**, 493 (1978).
16. H. P. POMMIER, J. BARIL, I. GRUDA et R. M. LEBLANC. Can. J. Chem. **57**, 1377 (1979).
17. E. DAVIN-PRETELLI, M. GUILIANO, G. MILLE et J. CHOUTEAU. Helv. Chim. Acta, **60**, 215 (1977); **61**, 1092 (1978).
18. M. GUILIANO, G. MILLE, J. CHOUTEAU, J. KISTER et J. METZGER. Anal. Chim Acta, **93**, 33 (1977).
19. (*a*) E. DAVIN-PRETELLI. Thèse Sciences, Marseille (1983); (*b*) E. DAVIN, M. GUILIANO, H. REYMOND, G. MILLE et J. KISTER. Anal. Chim. Acta, **148**, 271 (1983).
20. (*a*) P. APPRIOU. Thèse Sciences, Brest (1977); (*b*) P. APPRIOU, R. GUGLIELMETTI et F. GARNIER. J. Photochem. **8**, 145 (1978).
21. W. D. OLLIS, K. L. ORMAND et J. O. SUTHERLAND. J. Chem. Soc. 1697 (1978).
22. J. B. FLANNERY. J. Am. Chem. Soc. **90**, 5660 (1968).
23. A. SAMAT, G. MARTIN et R. GUGLIELMETTI. C. R. Acad. Sci, Ser. C, **279**, 573 (1974); Org. Magn. Reson. **8**, 62 (1976).
24. E. MILER-SPRENGER et R. GUGLIELMETTI. Acta Crystallogr. Sect. B, **38**, 1980 (1982).
25. A. SAMAT, R. GUGLIELMETTI, Y. FERRE, H. P. POMMIER et J. METZGER. J. Chim. Phys. **69**, 1202 (1972).
26. (*a*) M. MAGUET. Thèse Sciences, Brest (1980); (*b*) D. GAUDE, R. GAUDRON, M. MAGUET et R. GUGLIELMETTI. Helv. Chim. Acta, **66**, 1 (1983); **66**, 342 (1983).
27. R. GUGLIELMETTI, E. DAVIN et J. METZGER. Bull. Soc. Chim. Fr. 556 (1971).

Can. J. Chem. Downloaded from www.nrcresearchpress.com by 210.87.254.5 on 09/06/12
For personal use only.

Etudes des complexes metalliques de Ac-Asp-Val-Asp-Ala-OH par potentiométrie et résonance magnétique nucléaire du ^1H

MARCEL ASSO[1] ET DAVID BENLIAN
Laboratoire de Chimie de Coordination, Centre de St-Jérôme, 13397 Marseille Cedex 13, France
LILIANE ASSO
Laboratoire d'électrochimie, Centre de St-Charles, 13331 Marseille Cedex 3, France
ET
CLAUDE GRANIER
Laboratoire de Biochimie, ERA 617, Secteur Nord, 13326 Marseille Cedex 15, France

Reçu le 23 novembre 1983

MARCEL ASSO, DAVID BENLIAN, LILIANE ASSO et CLAUDE GRANIER. Can. J. Chem. **62**, 2379 (1984).

Les constantes de stabilité des complexes formés entre l'acétylaspartylvalylaspartylalanine (Ac-DVDA-OH) et divers cations métalliques ont été déterminées par mesures potentiométriques. Les spectres rmn des protons ont permis d'apporter des informations sur la conformation des espèces prépondérantes en solution. Les déplacements induits par le cation praseodyme sont fortement dépendant du pH. Au pH physiologique, en présence de Ca(II), les résonances relatives aux deux résidus aspartyl subissent d'importantes modifications. Ces résultats montrent une interaction spécifique entre le tétrapeptide synthétique et les cations Ca^{2+} ou Pr^{3+} au niveau des deux groupements carboxylates des résidus aspartyl en milieu neutre, avec le groupement carboxylate C-terminal en milieu acide.

MARCEL ASSO, DAVID BENLIAN, LILIANE ASSO, and CLAUDE GRANIER. Can. J. Chem. **62**, 2379 (1984).

Formation constants for complexes between acetylaspartylvalylaspartylalanine (Ac-DVDA-OH) and a number of transition metal cations have been determined by potentiometric titrations. The ^1H nmr spectra have been recorded in order to support the potentiometric results and to obtain information concerning the conformation of the detected species. The praseodymium induced shifts of most resonances are observed to be strongly dependent on pH. The Ca^{2+} complexes generate a different ^1H nmr spectrum for the aspartyl resonances at neutral pH. These observations are shown to be consistent with stepwise binding of the Ca^{2+} or Pr^{3+} cations to the carboxylate of Ala C-terminus in acidic medium, and to the carboxylates of aspartyl residues in neutral pH.

Introduction

Les études de la sélection exercée par les systèmes biologiques lors de la fixation d'éléments métalliques mettent en jeu des facteurs liés à la stéréochimie du ligand et à la géométrie de coordination préférentielle du cation métallique (1−5).

Une approche possible est la simulation de la partie active de la protéine par un peptide de synthèse qui constitue un modèle de l'environnement du métal (6−9).

Dans plusieurs protéines telles que la concanavaline (10) et la thermolysine (11), l'élément métallique notamment Ca(II) est lié préférentiellement au groupement carboxylate de résidus aspartyl ou glutamyl. L'examen des séquences actives vis à vis du calcium révèle, pour la thermolysine l'alternance (-Asp^{57}-Ala-Asp^{59}).

Comme les fragments complexants dans ces protéines contiennent séquentiellement soit deux résidus aspartyl soit un résidu aspartyl et un résidu glutamyl séparés par un résidu d'acide aminé non fonctionnel, nous avons réalisé la synthèse d'un peptide représentant un modèle simplifié ayant la séquence suivante: Ac-Asp-Val-Asp-Ala-OH (fig. 1).

Dans ce travail, nous présentons une détermination des groupes fonctionnels coordinants du tétrapeptide synthétique Ac-DVDA-OH (cf abréviations), en présence de divers éléments métalliques afin d'établir un ordre d'affinité sélectif. Les complexes ont été caractérisés en solution acide et neutre par titrages potentiométriques et pour certains d'entre eux, par les mesures des déplacements chimiques des noyaux ^1H.

[1]Auteur à qui adresser toute correspondance.

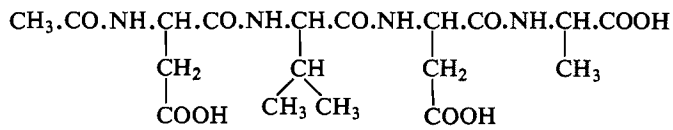

FIG. 1. Acetylaspartylvalylaspartylalanine.

Notations

Tous les acide aminés sont en configuration L. La nomenclature IUPAC des acides aminés a été employée. D: acide aspartique; A: alanine; V: valine; Ac: acetyl; Boc: tertiobutoxycarbonyl.

C_A, C_M: concentration analytique du ligand Ac-DVDA-OH, de l'ion métallique M: M = Ca^{2+}, Cu^{2+} etc...

$H_qA = L_q$: tétrapeptide sous la forme monomère contenant q protons dissociables: q = 0, 1, 2 et 3 (ex: A = L_o: forme trianionique)

$\bar{q}$: nombre moyen de protons échangeables par molécule de ligand

$\bar{r}$: nombre moyen de ligands complexés par atome métallique

k_q: constante de dissociation partielle: $[H_{q-1}A][H]/[H_qA]$

β_{pqr}: constante de stabilité globale issue de l'équilibre $pM + qH + rA \rightleftarrows M_pH_qA_r$

: β_q si $p = 1$ et $r = 1$, cas de complexes mononucléaires à un seul ligand

f_{L_q}, f_{ML_q}: fractions molaires des espèces libres L_q, complexées ML_q

Can. J. Chem. Downloaded from www.nrcresearchpress.com by 210.87.254.105 on 09/06/12
For personal use only.

δ_{L_q}, δ_{ML_q}: déplacements chimiques d'un noyau dans le cas d'espèces libres L_q, complexées ML_q

Δ_{ML_q}: déplacement induit limite: $(\delta_{ML_q} - \delta_{L_q})$

: Δ_q pour les complexes monométalliques à un seul ligand

Principe

Méthode potentiométrique

Le réseau des courbes normalisées pH = $f(\bar{q})$ permet en principe, d'effectuer une estimation des paramètres p, q, r caractérisant l'espèce $M_pH_qA_r$ relative à l'équilibre de complexation:[2]

$$[1] \quad pM + qH + rA \rightleftharpoons M_pH_qA_r$$

La détermination des constantes de formation β_{pqr} est alors effectuée selon un procédé classique (14–16), à partir des relations exprimant la conservation des espèces:

$$[2] \quad C_M = m + \sum p(\beta_{pqr} m^p \cdot h^q \cdot a^r)$$

$$[3] \quad C_H = h - oh + \sum q(\beta_{pqr} m^p \cdot h^q \cdot a^r)$$

$$[4] \quad C_A = a + \sum r(\beta_{pqr} m^p \cdot h^q \cdot a^r)$$

en formulant les différentes combinaisons pour p, q et r. Signalons cependant que les hypothèses peuvent être réduites si l'on procède à une estimation de $\bar{r}$, nombre moyen de coordinats fixés par atome métallique (17):

$$[5] \quad \bar{r} = (C_A - a)/(C_M)$$

Les valeurs des constantes ainsi prétablies sont ensuite optimalisées par un calcul en retour $\bar{q} = f(\text{pH})$.

A l'aide des valeurs de k_p, β_{pqr}, C_A et C_M, on calcule successivement a, m puis $\bar{q}$ ($\bar{q}$ cal) que l'on compare à $\bar{q}$ expérimental (15).

Titrages de la résonance magnétique nucléaire

La constante de complexation β_{pqr} donne le bilan de l'état stationnaire obtenue entre les différents constituants d'une solution. Si les échanges sont rapides par rapport au temps d'observation de la rmn, on n'observe qu'un pic moyen intégrant pour un noyau donné.

Dans ces conditions, en présence d'un cation paramagnétique fort réactif de déplacement chimique (18), et à pH fixe, le déplacement chimique observé est la moyenne pondérée des déplacements des espèces libres et complexées (19, 20).

$$[6] \quad \delta_{obs} = f_{L_q} \cdot \delta_{L_q} + f_{ML_q} \cdot \delta_{ML_q}$$

avec $f_{L_q} + f_{ML_q} = 1$. Cette expression peut être transformée en (20, 21):

$$[7] \quad \delta = f_{ML_q} \cdot \Delta_{ML_q}$$

où $\delta = \delta_{obs} - \delta_{L_q}$ est une fonction linéaire de la quantité de complexe formé en solution.

En donnant à β_{pqr} des valeurs fixées arbitrairement et au moyen des relations [1] à [4], on calcule la quantité $f_{ML_q} = [ML_q]/C_A$ pour chaque rapport C_M/C_A donné, les valeurs de k_q et [H] étant connues.

Les valeurs de β_{pqr} retenues sont celles qui conduisent à des valeurs de f_{ML_q} qui portées dans la relation [7] donnent par régression linéaire le meilleur coefficient de corrélation (20).

Dans le cas d'un complexe unique, mononucléaire, la relation permettant de déterminer f_{ML_q} se réduit à:

$$[8] \quad [ML_q]^2 - [ML_q](1 + \beta_q(C_A + C_M)) + \beta_q \cdot C_A \cdot C_M = 0$$

Dans le cas d'un complexe dit "fort" (β_{pqr} élevé), on peut atteindre sans problème le déplacement induit limite Δ_{ML_q} même si l'échange est rapide par extrapolation à $C_M \gg C_A$ où l'espèce totalement complexée est seule présente (22). La constante de stabilité a alors pour expression:

$$[9] \quad \beta_{pqr} = (Y \cdot C_A)/(C_A - C_M - Y \cdot C_A^2 - Y \cdot C_A \cdot C_M + Y^2 \cdot C_A^2)$$

avec $Y = (\delta_{obs} - \delta_{L_q})/(\delta_{ML_q} - \delta_{L_q})$.

Partie expérimentale

Matériaux

Les sels métalliques $CaCl_2 \cdot 2H_2O$, $MnCl_2 \cdot 6H_2O$, $NiCl_2 \cdot 6H_2O$, $CuCl_2 \cdot 2H_2O$, $CoCl_2 \cdot 6H_2O$, $ZnSO_4 \cdot 7H_2O$, $CdCl_2 \cdot 2{,}5\ H_2O$, KCl et K_2CO_3 sont des produits Fluka.

$PrCl_3$ est obtenu par attaque de l'oxyde Pr_6O_{11} (Fluka) à chaud dans HCl concentré. Les acides aminés N protégés: Nα Boc alanine, Nα Boc valine, Nα Boc, γ Benzyl acide aspartique sont également des produits Fluka.

Le tétrapeptide Ac-DVDA-OH a été synthétisé selon le procédé en phase solide (12), la préparation ayant été effectuée sur 5 g de résine chlorosubstituée UCB. Notons seulement que la fixation du résidu C terminal a été obtenue en préparant au préalable le sel de césium Boc-Ala-Cs suivant la méthode développée par Gisin (13). Le rendement après réaction dans HF est de 61%. La purification a été effectuée par chromatographie liquide à haute pression avec un instrument Waters Associates modèle 204 sur colonnes Merck Lickrosorb RP 18.

L'analyse des acides aminés a été effectuée sur un Analyseur Biotronik CC 7000 et a donnée la composition suivante: Asp: 2,02; Ala: 1,00; Val: 0,99.

Appareillage

Les titrages potentiométriques ont été réalisés à 25 ± 1°C dans une enceinte thermostatée sous azote, à l'aide d'un pHmètre Metrohm E 603 couplé à une micro-électrode Metrohm EA 120. Toutes les mesures ont été effectuées sur des solutions contenant 4×10^{-3} *M* de Ac-DVDA-OH et des concentrations croissantes en sels métalliques (0 à 8×10^{-3} *M*) et en milieu de force ionique KCl = 0,5 *M* et K_2SO_4 = 0,5 *M*.

Les spectres rmn ont été enregistrés sur un spectromètre Bruker 200 MHz équipé d'un microprocesseur Aspect 2000 dans D_2O (pD = pH + 0,39) dans les mêmes conditions de température. La concentration en substrat après deutération de tous les protons échangeables est de $1{,}08 \times 10^{-2}$ *M*, celle en cations varie de 0 à $5{,}40 \times 10^{-2}$ *M*.

Résultats

Titrages potentiométriques

Les réseaux des courbes de neutralisation pH = $f(\bar{q})$ de Ac-DVDA-OH en présence de divers cations métalliques, montre une acidification dans la zone de pH étudié 3 < pH < 7 (fig. 2).

A titre d'exemple nous avons porté sur la figure 3, les courbes obtenues en présence de Ni(II) à différentes concentrations. Un équilibre de complexation existe donc, en milieu acide, lorsque les fonctions carboxyliques des deux résidus aspartyl commencent à être dissociées (pk_2 = 3,70; pk_1 = 4,84).

L'examen des courbes $\bar{r} = f(\log L_q)$ pour les différents rapports C_M/C_A montre que les valeurs de $\bar{r}$ sont faibles (0,1 <

[2]Pour une commodité d'écriture, les charges positives, neutres ou négatives n'ont pas été mentionnées.

Can. J. Chem. Downloaded from www.nrcresearchpress.com by 210.87.254.105 on 09/06/12
For personal use only.

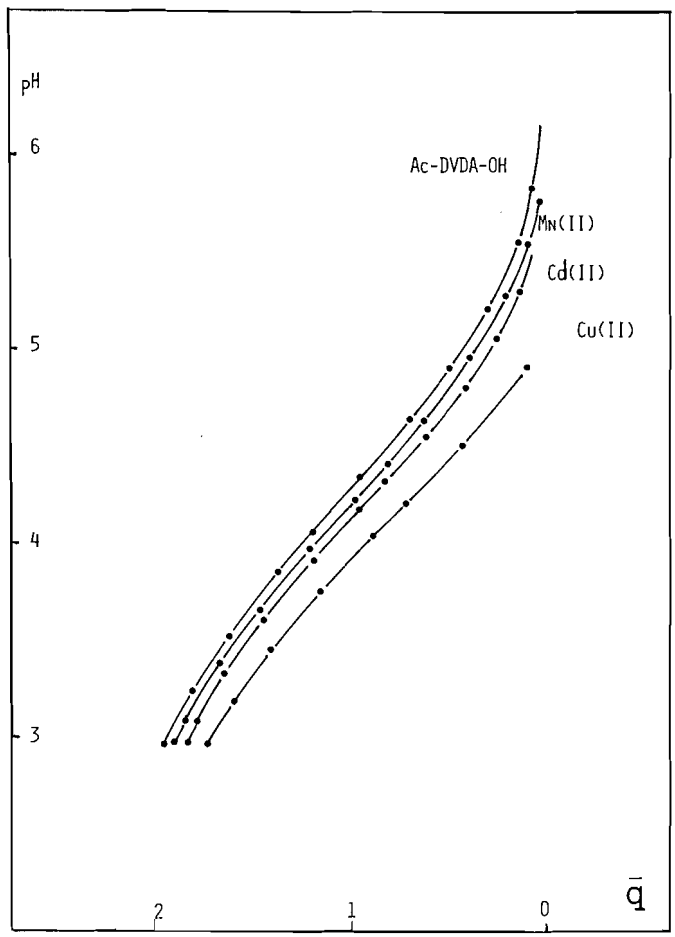

FIG. 2. Courbes de neutralisation pH = $f(\bar{q})$ de Ac-DVDA-OH ($4 \times 10^{-3} M$) en présence de divers cations métalliques ($4 \times 10^{-3} M$).

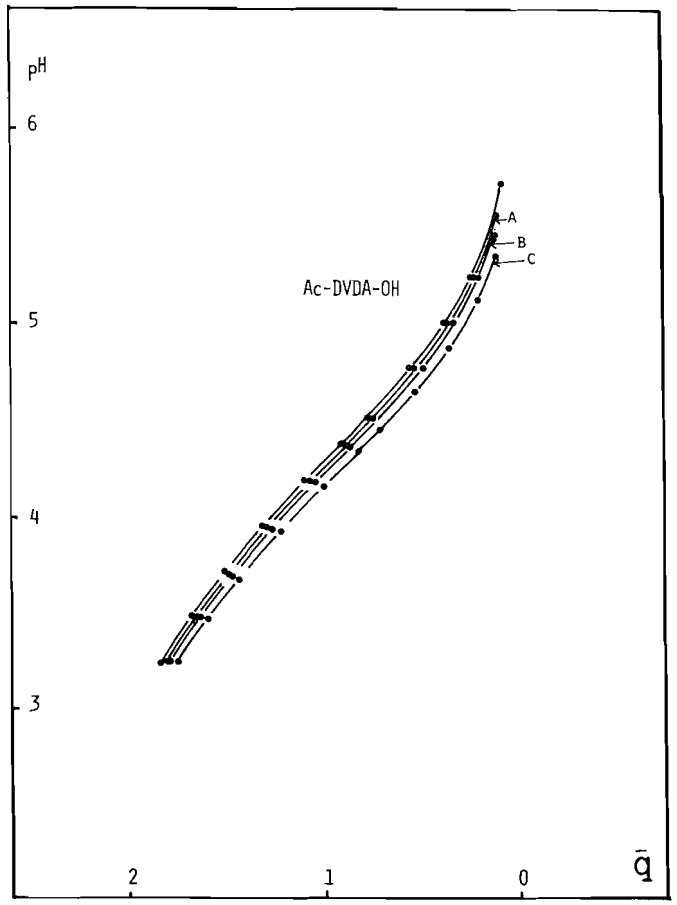

FIG. 3. Courbes de neutralisation pH = $f(\bar{q})$ de Ac-DVDA-OH ($4 \times 10^{-3} M$) en présence de $NiCl_2$: A, $Ni^{2+} = 2 \times 10^{-3} M$; B, $Ni^{2+} = 4 \times 10^{-3} M$; C, $Ni^{2+} = 8 \times 10^{-3} M$.

$\bar{r} < 0{,}4$) pour tout l'intervalle de pH considéré.

Compte tenu de ce résultat, nous nous sommes limités dans un premier temps, à la formation de complexes à un seul ligand. D'autre part, la concentration en sel métallique étant peu élevée (C_M max = $8 \times 10^{-3} M$), nous avons envisagé, en première approximation, la formation des complexes mononucléaires à un seul ligand, issus des équilibres.

$$[10] \quad \begin{aligned} &H_2A \rightleftharpoons Ha + H \ (k_2) \\ &M + HA \rightleftharpoons MHA \ (\beta_{111}) \end{aligned}$$

$$[11] \quad \begin{aligned} &HA \rightleftharpoons A + H \ (k_1) \\ &M + A \rightleftharpoons MA \ (\beta_{101}) \end{aligned}$$

où H_2A, HA et A représentent respectivement le tétrapeptide à 1, 2 et 3 charges négatives. Les constantes de stabilité β_{111} et β_{101} sont déterminées successivement pour $2 < \bar{q} < 1$ puis $1 < \bar{q} < 0$.

La calcul donne alors une valeur approchée de ces constantes. Ces valeurs sont ensuite optimalisées par un calcul complet des courbes de titrage à l'aide d'un microprocesseur Commodore 8032.

Afin de mieux cerner le phénomène de complexation, nous avons tenu compte des équilibres pouvant apparaître dans les zones de pH (ou $\bar{q}$) extrémales du réseau. En milieu acide, pour $q \simeq 2$, la présence du complexe MH_2A formé à partir du tétrapeptide chargé négativement sur le groupement carboxylate du résidu alanine C terminal doit être considérée, même si l'écartement des courbes du réseau pH = $f(\bar{q})$ est peu important. La détermination de la constante β_{121} est de ce fait peu précise. Elle a été estimée à 4 ± 1. Une meilleure approche du milieu acide a pu être effectuée par rmn, grace à l'utilisation du cation paramagnétique Pr^{3+}.

La dernière partie du réseau ($\bar{q} < 0{,}15$) est caractérisée par une évolution très lente des potentiels des solutions, contenant les éléments Zn(II), Cu(II) et Cd(II), peu avant la zone de précipitation. Outre la présence d'hydroxocomplexes du type $M(OH)^+$ établie par certains auteurs (23), il est nécessaire d'envisager la formation possible de complexes polynucléaires. Cependant, les calculs basés sur l'abaissement du pH des solutions dans cette zone instable ne sont pas assez rigoureux pour formuler une estimation convenable du phénomène.

L'ensemble des résultats sont regroupés dans le tableau 1. Des valeurs des constantes β_{pqr}, on tire les concentrations des espèces présentes en solution. Les courbes de répartition en fonction de pH ou de $\bar{q}$ permettent de préciser les proportions relatives des espèces ainsi que leur domaine de formation, comme on peut le constater sur la figure 4.

Cette étude a été nécessaire pour suivre par rmn les variations des déplacements chimiques des protons en présence des cations Ca^{2+} et Pr^{3+}.

Titrages de la résonance magnétique nucléaire

Déplacements chimiques en présence de $PrCl_3$

Les variations de déplacement chimique de tous les protons du tétrapeptide Ac-DVDA-OH ont été suivies sur des solutions

Can. J. Chem. Downloaded from www.nrcresearchpress.com by 210.87.254.105 on 09/06/12
For personal use only.

Can. J. Chem. Downloaded from www.nrcresearchpress.com by 210.87.254.105 on 09/06/12
For personal use only.

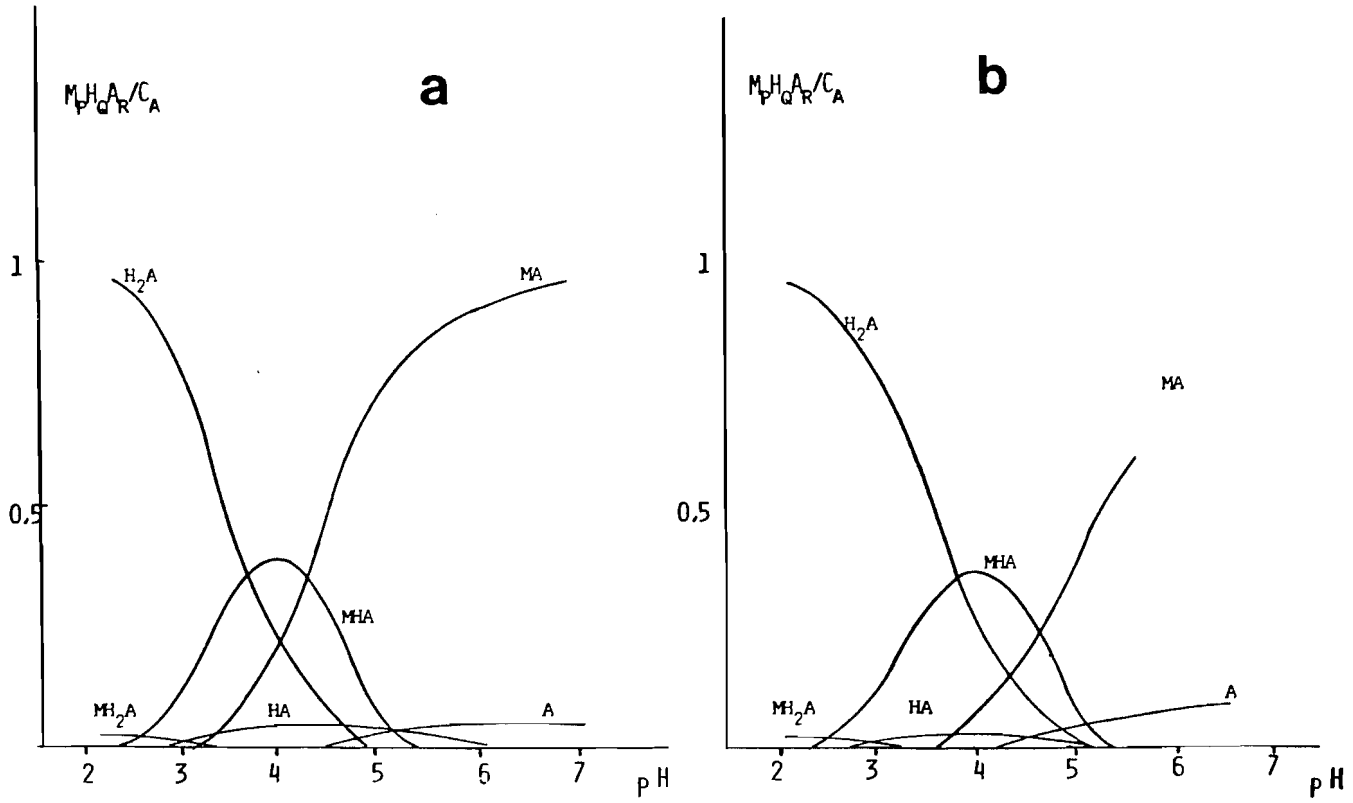

FIG. 4. Répartition en fonction du pH des espèces libres et complexées du tétrapeptide Ac-DVDA-OH: (a) en présence de Ca(II), C_M/C_A = 2; (b) en présence de Zn(II), C_M/C_A = 2.

TABLEAU 1. Constantes de stabilité des complexes métalliques de Ac-DVDA-OH (25°C, KCl = 0,5 *M*, K_2SO_4 = 0,5 *M*)

Constantes de dissociation k_q de Ac-DVDA-OH		
pk_3	pk_2	pk_1
2,2±0,1	3,70±0,02	4,84±0,02

Constantes de stabilité des complexes $M_pH_qA_r$			
	log β_{121}*	log β_{111}	log β_{101}
Ca^{2+}		3,11±0,40	3,60±0,60
Cd^{2+}		2,70±0,30	3,46±0,50
Co^{2+}		2,67±0,30	3,43±0,50
Cu^{2+}		3,30±0,50	4,48±0,60
Mn^{2+}		2,64±0,30	3,40±0,50
Ni^{2+}		2,78±0,30	3,78±0,50
Pr^{3+}	0,78±0,04	2,70±0,30	3,48±0,50
Zn^{2+}		3,18±0,40	3,48±0,50

*Pour les différents cations métalliques étudiés par potentiométrie la valeur moyenne retenue est log β_{121} = 0,60.

de concentration 1,08 × 10^{-2} *M* ajustées à pH = 2,50 et 7,00.

Le fait le plus marquant est le déplacement vers les champs forts des groupements —CH_2 et Hα des deux résidus aspartyl ainsi que celui de H_α du résidu alanyl, lors de la neutralisation. Les expériences ont été ensuite reproduites dans des conditions identiques en présence de quantités croissantes de $PrCl_3$ (0 à 5,4 × 10^{-2} *M*). Les résultats des déplacements des pics sont groupés sur les figures 5 et 6. L'introduction du cation Pr^{3+} provoque: en milieu acide, une variation importante des résonances des protons H_α et —CH_3 de l'alanine, alors que les

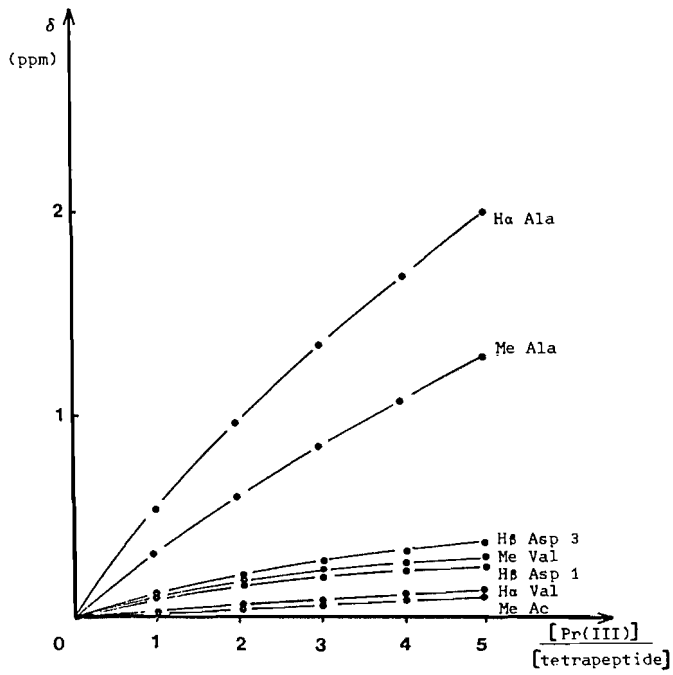

FIG. 5. Variation du déplacement chimique (ppm) des noyaux ^1H de Ac-DVDA-OH en fonction de la concentration en $PrCl_3$ à pH = 2,50.

autres protons sont peu perturbés; en milieu neutre, les groupements —CH_2 des résidus aspartyl subissent le plus fort glissement chimique (fig. 6).

A partir de ces variations nous avons procédé à une estimation des constantes de stabilité au moyen des relations [1] à [4] et [7].

TABLEAU 2. Constantes de stabilité β_2 et déplacements induits limites Δ_2 (Hz) des complexes Ac-DVDA-OH − Pr(III) = ML_2 à pH = 2,50, KCl = 0,5 *M*

Paramètre	H_β (Asp^1)	H_α (Val)	Me (Val)	H_α (Asp^3)	H_β (Asp^3)	H_α (Ala)	Me(Ala)	Me (Ac)
log β_2	0,78	0,83	0,72	0,74	0,80	0,76	0,81	0,80
Δ_2	221	88,3	265	629	309	1766	1148	44

TABLEAU 3. Constantes de couplages $^3J_{HC^\alpha C^\beta H}$ (Hz) et conformères de rotation* autour de la liaison C^α—C^β des résidus aspartyls à pH = 7,00

[Ca^{2+}]	Asp 1					Asp 3				
[Ac-DVDA-OH]	J_{AX}	J_{BX}	P_I	P_{II}	P_{III}	J_{AX}	J_{BX}	P_I	P_{II}	P_{III}
0	5,58	7,77	0,27	0,47	0,26	5,98	7,50	0,30	0,44	0,26
0,5	5,45	8,10	0,26	0,50	0,24	6,82	6,80	0,38	0,38	0,24
1	5,23	8,37	0,24	0,52	0,24	7,61	6,10	0,46	0,32	0,22
2	4,80	8,80	0,20	0,56	0,24	8,65	5,12	0,55	0,23	0,22
3	4,40	9,20	0,16	0,60	0,24	9,53	4,21	0,63	0,15	0,22
4	4,13	9,57	0,14	0,63	0,23	10,2	3,60	0,69	0,09	0,23

*Par convention les protons H_B résonnent à champ fort, les rotamères I, II, III correspondent aux angles de torsion $\chi_1 = -60$ (I), 180 (II), 60 (III).

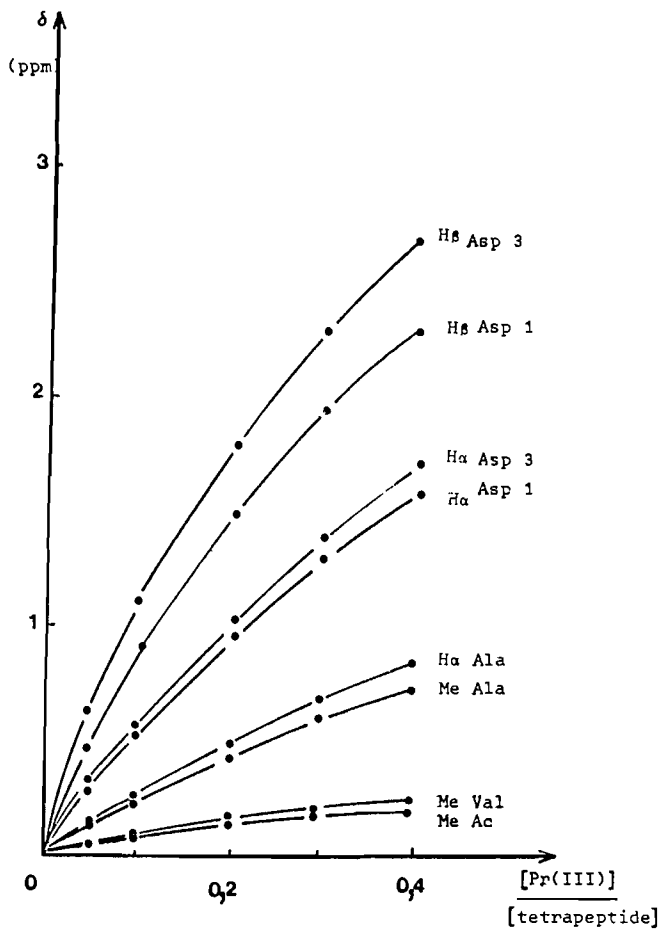

FIG. 6. Variation du déplacement chimique (ppm) des noyaux ^1H de Ac-DVDA-OH en fonction de la concentration en $PrCl_3$ à pH = 7,00.

A pH 2,50 les espèces H_3A, H_2A et MH_2A sont essentiellement présentes. La relation [6] devient:

[12] $\delta_{obs} = f_{L_3} \cdot \delta_{L_3} + f_{L_2} \cdot \delta_{L_2} + f_{ML_2} \cdot \delta_{ML_2}$

qui après transformation s'écrit:

[13] $\delta = f_{ML_2} \cdot \Delta_{ML_2} = f_{ML_2} \cdot \Delta_2$ (cf. notations)

Le meilleur accord est obtenu pour $\beta_{121} = \beta_2 = 6 \pm 1$. Rappelons que la détermination de β_{121} effectuée par potentiométrie a permis d'avoir seulement un ordre de grandeur de la constante de complexation du fait de la faible modification des valeurs de pH.

Les résultats concernant la détermination des constantes β_2 et les déplacements induits limites Δ_2 sont regroupés dans le tableau 2.

Couplages en présence de $CaCl_2$

Alors qu'en milieu acide, l'addition de $CaCl_2$ n'apporte pas de modifications de la partie spectrale correspondant aux résonances des résidus Asp, au pH physiologique les couplages J_{AX} et J_{BX} subissent une variation en fonction du rapport [Ca^{2+}]/[Ac-DVDA-OH]. Nous observons en particulier, une augmentation de J_{AX} (5,98 à 10,2 Hz) pour le résidu aspartyl en position 3 (tableau 3).

L'analyse des constantes de couplage vicinales, effectuée au moyen de la relation de Karplus−Bystrov (24):

[14] $^3J_{HC^\alpha C^\beta H} = 11 \cos^2 \theta - 1{,}4 \cos \theta + 1{,}6 \sin^2 \theta$

donnent un angle dièdre $\theta = 148°$ ($H^\alpha C^\alpha C^\beta H^{\beta 1}$) et $\theta = 70°$ ($H^\alpha C^\alpha C^\beta H^{\beta 2}$) pour le résidu Asp 3.

Le rotamère caractérisé par l'angle χ_1 ($NC^\alpha C^\beta C^\gamma$) = −60° est le principal conformère présent en solution (~69%). Ces résultats sont à rapprocher de ceux obtenus pour un autre peptide transporteur de calcium (25).

Discussion

Les constantes d'équilibre des systèmes Ac-DVDA-OH − cations métalliques établies dans ce travail ont permis de dégager les points suivants.

En milieu acide, l'examen de la constante β_2 obtenue par titrage rmn en présence de $PrCl_3$ montre qu'un complexe labile, certainement monodentate, est formé par interaction entre le cation Pr^{3+} et le groupement —COO^- C terminal du résidu alanine. Les déplacements chimiques ayant pour origine une interaction dipolaire sont exploitables dans un calcul en raison

Can. J. Chem. Downloaded from www.nrcresearchpress.com by 210.87.254.105 on 09/06/12
For personal use only.

Can. J. Chem. Downloaded from www.nrcresearchpress.com by 210.87.254.105 on 09/06/12
For personal use only.

de la relation géométrique simple existant entre la position du cation paramagnétique et celle du noyau perturbé (26). Cette relation, dans le cas où le complexe présente un axe de symétrie principal, s'écrit:

$$[15] \quad \Delta = D(3\cos^2\theta_i - 1)/r_i^3$$

où D est un terme constant pour un complexe donné, r_i est la distance entre le noyau i et le centre paramagnétique, θ_i est l'angle entre l'axe de symétrie principal du complexe et le vecteur $\vec{r_i}$. On remarque, effectivement, que les noyaux les plus proches du site d'interaction subissent la plus forte variation: H_α et le groupement Me de l'alanine. L'interaction s'atténue très rapidement avec la distance $(1/r_i^3)$; de ce fait les autres noyaux subissent peu de variation (fig. 5).

En milieu neutre, l'étude basée sur la variation du pH des solutions et celle des fréquences de résonances des ^1H montre: une forte augmentation de la constante de stabilité (environ 10^3 fois) pour les différents systèmes étudiés; une perturbation importante des noyaux $-CH_2$ des deux groupements aspartyl même en présence de faibles quantités de $PrCl_3$; une augmentation de la constante de couplage J_{AX} relative aux groupements aspartyl notamment pour le résidu Asp^3, lorsque la concentration de $CaCl_2$ est supérieure à celle du ligand. L'affinité relative des cations étudiés vis à vis des groupements carboxylates du tétrapeptide diminue du cuivre au manganèse selon: Cu(II) $\gg$ Ni(II) > Ca(II) > Zn(II) > Pr(III), Cd(II) > Co(II), Mn(II). Par comparaison avec les données établies par Williams (27), il ressort de cette étude que le tétrapeptide Ac-DVDA-OH a une nette affinité vis à vis de Ca^{2+}. Le cuivre montre également une forte interaction avec le modèle synthétisé. Une stabilisation importante due au cuivre est d'ailleurs vérifiée pour la plupart des systèmes peptidiques analogues (28, 29).

Pour rendre compte de ces résultats, il s'impose d'avoir recours à la formation possible d'un chélate où le cation métallique, ici Ca^{2+} ou Pr^{3+}, interagit fortemment, à la fois avec deux groupements carboxylates des deux résidus aspartyl. Cette hypothèse est à comparer aux modèles proposés pour l'interaction Angiotensine$-Yb^{3+}$ (30). Nous ne disposons encore que de données trop peu nombreuses pour formuler des propositions sur une conformation préférentielle. Il est vraisemblable que la portion de la chaîne comprise entre Asp^1 et Asp^3 garde une souplesse importante. Cette étude a permis de souligner l'importance de l'interaction du calcium vis à vis d'un modèle peptidique présentant deux groupements carboxylates rapprochés sur les chaînes latérales. Cette affinité montre donc une coordination sélective de l'élément alcalino terreux dans un environnement favorable. Les mesures de constantes de couplage mettent en évidence une réorientation préférentielle du système en présence de Ca(II), en particulier la formation privilégiée d'un conformère de rotation autour de $C^\alpha—C^\beta$.

Conclusion

Le tétrapeptide Ac-DVDA-OH homologue d'un fragment actif de protéines contenant du calcium, montre une affinité pour Ca^{2+} nettement plus importante que pour d'autres peptides courts étudiés jusqu'ici.

La substitution isomorphe des cations Ca^{2+} par les cations de lanthanides utilisés comme réactifs de déplacement chimique, Pr^{3+} dans l'étude, permet de mettre en évidence en solution aqueuse l'existence de deux modes de complexation dont l'un concerne la fonction carboxylique située en bout de chaine en milieu acide, et l'autre les deux résidus aspartyl des chaines latérales pour le pH physiologique.

Remerciements

Les auteurs remercient bien vivement Mlle. M. Noailly pour l'obtention des spectres rmn.

1. R. J. SUNDBERG et R. B. MARTIN. Chem. Rev. **74**, 492 (1974).
2. P. M. COLMAN, J. N. JANSONIUS et B. W. MATTHEWS. J. Mol. Biol. **70**, 701 (1972).
3. S. LINDSKEG et J. E. COLEMAN. Proc. Nat. Acad. Sci. U.S.A. **70**, 2505 (1973).
4. H. SIGEL, B. E. FISHER et B. PRIJS. J. Am. Chem. Soc. **99**, 4489 (1977).
5. K. D. HARDMAN et C. F. AINSWORK. Biochemistry, **11**, 4910 (1972).
6. T. P. A. KRUCK, S. J. LAU et B. SARKAR. Can. J. Chem. **54**, 1300 (1976).
7. H. LAKUSTA, C. M. DEBER et B. SARKAR. Can. J. Chem. **58**, 757 (1980).
8. K. S. IYER, J. P. LAUSSAC et V. SARKAR. Int. J. Pept. Protein Res. **18**, 468 (1981).
9. M. ASSO, C. GRANIER, J. VAN RIETSCHOTEN et D. BENLIAN. J. Chim. Phys. **79**, 455 (1982).
10. A. D. SHERRY, M. A. LINDORFER, P. ADAMS STEMLER et O. A. MILANES. Biochemistry, **20**, 3492 (1981).
11. A. P. SNYDER, D. R. SUDNICK, V. K. ARKLE et W. DE W. HORROCKS. Biochemistry, **20**, 3334 (1981).
12. R. B. MERRIFIELD. J. Am. Chem. Soc. **85**, 2149 (1963).
13. B. F. GISIN. Helv. Chim. Acta, **56**, 1476 (1973).
14. R. OSTERBERG. Acta Chem. Scand. **19**, 1445 (1965).
15. L. ASSO, M. ASSO, J. MOSSOYAN et D. BENLIAN. J. Chim. Phys. **75**, 561 (1978).
16. L. ABELLO, A. ENSUQUE, M. JOUINI et G. LAPLUYE. J. Chim. Phys. **77**, 537 (1980).
17. J. BJERRUM. Metal amine formation in aqueous solutions. Haase and Son, Copenhague. 1957.
18. C. D. BARRY, A. C. T. NORTH, J. A. GLASEL, R. J. P. WILLIAMS et A. V. XAVIER. Nature (London), **232**, 236 (1971).
19. A. D. SHERRY et E. PASCUAL. J. Am. Chem. Soc. **99**, 5871 (1977).
20. J. MOSSOYAN, M. ASSO et D. BENLIAN. J. Magn. Reson. **46**, 289 (1982).
21. M. ASSO, J. MOSSOYAN, L. ASSO et D. BENLIAN. J. Chim. Phys. **80**, 251 (1983).
22. J. GARIEPY, B. D. SYKES et R. S. HODGES. Biochemistry, **22**, 1765 (1983).
23. S. CHABEREK, R. C. COURTNEY et A. E. MARTELL. J. Am. Chem. Soc. **74**, 5057 (1952).
24. V. F. BYSTROV. Prog. Nucl. Magn. Reson. Spectrosc. **10**, 44 (1976).
25. D. W. HUGHES et C. M. DEBER. Biopolymers, **21**, 169 (1982).
26. H. M. MCCONNEL et R. E. ROBERTSON. J. Chem. Phys. **29**, 1631 (1968).
27. R. J. P. WILLIAMS. Q. Rev. **24**, 231 (1970).
28. T. P. A. KRUCK et B. SARKAR. Can. J. Chem. **51**, 3555 (1973).
29. B. SARKAR, J. P. LAUSSAC et S. J. LAU. Biological aspects of metals and metal related diseases. Raven Press, New York. 1983.
30. R. E. LENKINSKI et R. L. STEPHENS. J. Inorg. Chem. **18**, 175 (1983).

Déplacements homolytiques intramoléculaires. 2. Décomposition du perpentène-4 oate de *tert*-butyle dans les éthers

A. KHARRAT, C. GARDRAT[1] ET B. MAILLARD[2]

Laboratoire de Chimie Appliquée, Université de Bordeaux I, 351, cours de la Libération, 33405 Talence-Cedex, France

Reçu le 10 janvier 1984

A. KHARRAT, C. GARDRAT et B. MAILLARD. Can. J. Chem. **62**, 2385 (1984).

La thermolyse du perpentène-4 oate de *tert*-butyle **1** dans le THF conduit à de nombreux produits; le composé majoritaire, le (tétrahydrofuryl-2)-5 pentanolide-4, obtenu avec un rendement de 42%, provient d'une décomposition induite du perester par suite de l'addition du radical tétrahydrofuryle-2 sur la double liaison. Cette réaction a pu être effectuée à basse température en utilisant un amorceur annexe, le perdicarbonate de butyle, mais il n'a pas été possible de préciser le type de mécanisme (concerté ou en deux étapes). L'intérêt synthétique de la thermolyse de **1** dans d'autres éthers (THP, oxépanne, dioxanne-1,4, éther de dipropyle) a pu être mis en évidence puisqu'un certain nombre de nouvelles γ-lactones ont ainsi été préparées.

A. KHARRAT, C. GARDRAT, and B. MAILLARD. Can. J. Chem. **62**, 2385 (1984).

The thermolysis of *tert*-butyl perpent-4-enoate **1** in THF led to several compounds; the main product, 5-(2-tetrahydrofuryl)-4-pentanolide (yield 42%) comes from an induced decomposition of the perester occurring with the addition of 2-tetrahydrofuryl radical to the double bond. A similar reaction was performed at a lower temperature, using butyl perdicarbonate as initiator, but did not define the mechanism (concerted or two-step). The thermolysis of **1** in ethers (THP, oxepane, 1,4-dioxane, dipropyl ether) appears to be a useful synthetic tool: several new γ-lactones have been obtained in this way.

Introduction

Dans un travail précédent (1) nous avons montré que la thermolyse du perpentène-4 oate de *tert*-butyle **1** dans les cyclanes conduisait à la formation de cycloalkyl-5 pentanolides-4 en quantités relativement importantes. L'obtention de ces lactones est due à une décomposition induite du perester; elle résulte de l'addition d'un radical cycloalkyle sur la double liaison et d'un déplacement homolytique intramoléculaire d'un radical *tert*-butoxyle. La phase de propagation de la réaction, ayant lieu en chaîne, est la suivante:

[1] $S^{\bullet} + H_2C{=}CH{-}(CH_2)_2{-}CO_3tBu \longrightarrow S{-}CH_2{-}\underset{\displaystyle O}{\overset{\displaystyle O}{\langle}}{=}O + tBuO^{\bullet}$

[2] $tBuO^{\bullet} + SH \longrightarrow tBuOH + S^{\bullet}$

Les éthers subissent très facilement un arrachement d'hydrogène par les radicaux *tert*-butoxyle (2−4) conduisant à des radicaux qui s'additionnent aux doubles liaisons de composés éthyléniques fonctionnels ou non (2, 5−9). Nous avons donc décidé d'aborder dans un premier temps l'étude de la thermolyse du perpentène-4 oate de *tert*-butyle dans le tétrahydrofuranne afin d'essayer de préciser le mécanisme réactionnel de la thermolyse de **1**. Dans un deuxième temps, nous avons étendu cette réaction à d'autres éthers afin d'en tester les possibilités synthétiques.

Résultats

Décomposition du perpentène-4 oate de tert*-butyle dans le tétrahydrofuranne*

Ayant décidé de rechercher l'intérêt synthétique de la décomposition induite de **1** par les radicaux dérivant d'éthers, nous avons essayé, avant toute étude, de définir les conditions optimales d'obtention de la lactone à partir d'un composé modèle, le tétrahydrofuranne. Pour cela, nous avons recherché l'influence de la température (donc du temps de chauffage) et des rapports molaires **1**/THF sur les quantités de lactone formée. Le tableau 1 montre les principaux résultats.

TABLEAU 1. Variation du rendement en (tétrahydrofuryl-2)-5 pentanolide-4 en fonction des conditions de la réaction

Rapport molaire **1**/THF	Rendement en **10**%*		
	2 h à 130°C	4 h à 120°C	8 h à 110°C
1:5	20	18	25
1:10	28	24	39
1:20	27	24	42
1:50	26	26	39
1:100	20	20	38

*Calculé par rapport au perester mis en jeu et déterminé par cpg.

Les produits formés par thermolyse de **1** dans le THF sont de deux types comme cela avait été observé lors de la réaction effectuée dans le cyclohexane (1): (*i*) composés provenant uniquement du perester (*tert*-butanol **2**, acétone **3**, butène-1 **4**, gaz carbonique **5**, acide pentène-4 oïque **6**) ou du solvant ((tétrahydrofuryl-2)-2 tétrahydrofuranne **7**); (*ii*) composés comportant dans leur molécule à la fois des motifs provenant du perester et du solvant (butyl-2 tétrahydrofuranne **8**, acide (tétrahydrofuryl-2)-5 pentanoïque **9**, (tétrahydrofuryl-2)-5 pentanolide-4 **10**, *tert*-butoxy-2 tétrahydrofuranne **11**).

Dans le tableau 2 sont rassemblés les nombres de moles de chacun de ces produits formés par la décomposition d'une mole de perester **1**.[3]

[1]Ecole Nationale Supérieure de Chimie et de Physique de Bordeaux, 351, cours de la Libération, 33405 Talence-Cedex, France.

[2]Auteur à qui adresser toute correspondance.

[3]Le butène-1 et le gaz carbonique n'ont pas été dosés pour les deux raisons suivantes: dispositif expérimental ne permettant pas d'être certain de récupérer l'intégralité des produits gazeux; partage probable des produits légers entre les phases liquide et gazeuse.

Can. J. Chem. Downloaded from www.nrcresearchpress.com by 210.87.254.6 on 09/06/12
For personal use only.

TABLEAU 2. Quantité de produits formés en mole par mole de perester **1***

Produits	**2**	**3**	**6**	**7**	**8**	**9**	**10**	**11**
Rdt†	~0,96	Traces	0,06	0,07	0,06	0,17	0,42	0,04

*Conditions: rapport **1**/THF = 1:20; température: 110°C; durée: 8 h.
†Valeurs déterminées par cpg à partir de fractions de distillation et calculées par rapport au perester mis en jeu dans la réaction.

TABLEAU 3. Rendement et composition des lactones isolées*

	Ethers				
	THF	THP	Oxépanne	Dioxanne-1,4	Ether de dipropyle
Rdt†	35	45	37	53	24
Isomères $\alpha/\beta + \gamma$	100/0	84/16	68/32	—	100/0

*Conditions: rapport **1**/éther = 1:20; température: 110°C; durée: 8 h.
†Calculé sur la fraction de distillation par rapport au perester mis en jeu.

Décomposition du perpentène-4 oate de tert-*butyle* **1** *dans divers éthers*

La thermolyse du perpentène-4 oate de *tert*-butyle effectuée dans le tétrahydropyranne, l'oxépanne, le dioxanne-1,4 et l'éther de dipropyle conduit dans les deux premiers cas à plusieurs lactones isomères alors que dans les deux derniers un seul produit de substitution de l'éther semble être obtenu. Les compositions des fractions isolées et leurs rendements sont rapportés dans le tableau 3.

Discussion

Origine des divers produits formés dans la réaction de thermolyse de **1** *dans le THF*

Les composés **2** et **3** sont les produits d'évolution classique des radicaux *tert*-butoxyle alors que **7** est formé par couplage des radicaux tétrahydrofuryle-2.

La présence simultanée de **4**, **5** et **6** pourait être expliquée par l'évolution du radical pentène-4 oyloxyle décrite fig. 1 (R = $(CH_2)_2CH{=}CH_2$, SH:THF). En fait, comme nous le verrons par la suite **6** est obtenu par une autre voie.

Les composés **8** et **9** ont *a priori* deux origines possibles (fig. 2): (*i*) addition radicalaire au butène-1 **4** ou à l'acide pentène-4 oïque **6** formés dans la décomposition de **1**; ou (*ii*) décomposition du (tétrahydrofuryl-2)-5 perpentanoate de *tert*-butyle **1***a* formé à partir du radical A par arrachement d'hydrogène dans l'hypothèse d'une décomposition induite en deux étapes.

Les additions radicalaires du THF au butène-1 **4** et à l'acide pentène-4 oïque **6** amorcées par le peroxyde de di-*tert*-butyle à 140°C conduisent bien à **8** et **9** confirmant la validité de la première hypothèse.

Le (tétrahydrofuryl-2)-5 perpentanoate de *tert*-butyle **1***a* a été préparé à partir de **9** et thermolysé en solution dans le THF (110°C, 8 h, rapport molaire 1:20) afin de montrer la possibilité d'existence du deuxième mécanisme avancé. Après réaction le butyl-2 tétrahydrofuranne **8** et l'acide **9** sont obtenus avec des rendements respectifs de 5% et 80% par rapport au perester mis en jeu. D'autres produits correspondant aux 15% manquants sont observés; ils résultent vraisemblablement des réactions des radicaux dans la cage de solvant, comme cela est généralement observé lors de décomposition de peresters (10, 11).

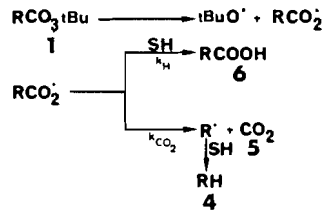

FIG. 1.

La mise en évidence de la formation de **1***a* lors de la décomposition thermique de **1** dans le THF permettrait de montrer que la deuxième hypothèse de formation de **8** et **9** a une réalité. La stabilité thermique de ce perester étant similaire à celle de **1** nous avons décidé d'effectuer la décomposition induite de **1** en initiant la réaction en chaîne par un amorceur annexe se décomposant avec une vitesse très supérieure à **1** et **1***a* à des températures plus basses; le perdicarbonate de n-butyle a été utilisé. Le chauffage à 65°C pendant 13 h d'une solution de ce peroxyde et de **1** dans le THF (rapport 0,2:1:20) a conduit à **10** (rendement 20% par rapport au perester mis en jeu) alors que 50% de **1** sont récupérés inchangés. Le perester **1***a* a été vainement recherché à l'aide de la hplc analytique en comparant le temps de rétention d'un échantillon de référence à celui des produits contenus dans les fractions renfermant le composé peroxydique séparé des produits lourds par chromatographie liquide–solide sur une colonne de silice (éluant: pentane). Dans ces conditions, nous voyons qu'au moins à 65°C si la réaction de décomposition induite se fait en deux étapes, le déplacement homolytique s'effectue avec une vitesse beaucoup plus importante que le transfert d'hydrogène pouvant conduire à **1***a*.

Au niveau de la formation de **9** les deux mécanismes paraissent également plausibles. Par contre, **8** est essentiellement formé par addition radicalaire du THF au butène-1 **4** puisque le rapport **8**/**9** obtenu pour la thermolyse de **1** dans le THF (6:17) est très supérieur à celui (5:80) qui est observé lors de celle du (tétrahydrofurfuryl-2)-5 perpentanoate de *tert*-butyle **1***a* dans les mêmes conditions.

La comparaison des produits de décomposition du perester **1** dans le THF et le cyclohexane, de **1***a* dans le THF et du cyclohexyl-5 perpentanoate de *tert*-butyle **1***b* dans le cyclohexane laisse apparaître la formation d'acide uniquement pour les thermolyses effectuées dans l'éther cyclique.

Dans l'hypothèse d'un mécanisme de décomposition représenté fig. 1, le rapport des quantités d'acide et de carbure formés à partir de **1***a* indique que les valeurs numériques des constantes k_H et k_{CO_2} doivent être voisines. Kaptein (12) ayant estimé que k_{CO_2} est de l'ordre de 10^{10} s^{-1} à 100°C, la valeur calculée pour la constante de vitesse d'arrachement d'hydrogène du THF par les radicaux acyloxyle k_H paraît excessive surtout si on la compare avec celle de la même réaction effectuée par les radicaux *tert*-butoxyle ($k \sim 10^7$ s^{-1} mol^{-1} à 100°C) (4).

De même la comparaison des quantité d'acides et de carbures obtenus lors des décompositions de **1***a* et **1***b*[4] respectivement dans le THF et le cyclohexane permet de trouver, avec la même hypothèse de mécanisme de décomposition (fig. 1), une limite inférieure du rapport des constantes de vitesse d'arrachement

[4]On suppose pour cela que la décomposition de la fonction perester n'est pas affectée par la nature du substituant en 5 (tétrahydrofuryl-2 ou cyclohexyl). Le rapport acide/carbure formés dans la thermolyse de **1***b* dans le cyclohexane est pris égal à 1:99 (valeur maximale de la proportion d'acide compte-tenu de la limite de détection).

Can. J. Chem. Downloaded from www.nrcresearchpress.com by 210.87.254.6 on 09/06/12
For personal use only.

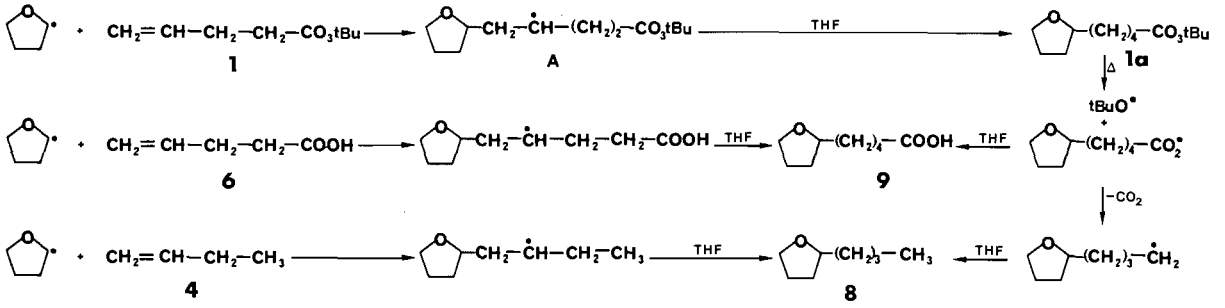

FIG. 2.

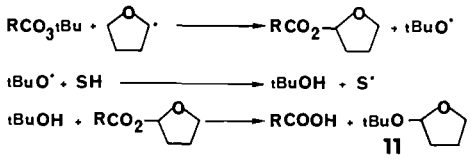

FIG. 3.

d'hydrogène du THF et du cyclohexane par les radicaux acyloxyle: $k_{H_{THF}}/k_{H_{C_6H_{12}}} \sim 10^3$. A partir des résultats de la littérature (3, 4), nous avons pu calculer la valeur du rapport $k_{H_{THF}}/k_{H_{C_5H_{10}}} \sim 10$ pour les radicaux *tert*-butoxyle. Des réactivités voisines des hydrogènes du cyclohexane et du cyclopentane vis-à-vis des mêmes radicaux (13) montrent que l'on peut considérer que $k_{H_{THF}}/k_{H_{C_6H_{12}}}$ est de l'ordre de 10. La comparaison de ces rapports laisse apparaître une grande différence de sélectivité entre les radicaux acyloxyle et *tert*-butoxyle, ce qui peut paraître surprenant.

Dans ces conditions si, dans la thermolyse de peresters dans le THF, les carbures semblent bien se former par décarboxylation des radicaux acyloxyle, il semble qu'il faille rechercher une autre origine pour la formation des acides. Huyser (14) propose une explication sur la formation d'acide et de *tert*-butoxy tétrahydrofuranne **11** dans la thermolyse du peracétate de *tert*-butyle dans le THF par la décomposition induite de ce dernier par les radicaux dérivant du solvant (fig. 3). Bien que dans la décomposition de **1** et **1***a* nous observions une quantité plus faible de **11** que d'acide (0,04:0,06 et 0,57:0,80), il est difficile d'exclure le mécanisme proposé par Huyser.

La γ-lactone **10** est formée dans la décomposition induite du perester **1** par les radicaux tétrahydrofuryle-2; comme dans le cas des cyclanes (1) nous venons de voir qu'il est difficile de savoir si cette réaction a lieu en deux étapes (addition, déplacement homolytique) ou fait appel à un mécanisme concerté du même type que celui qui est avancé par Hart et Chloupeck (15).

Les résultats précédents nous montrent en outre qu'il semble vain de poursuivre dans cette voie pour la mise en évidence d'un mécanisme en deux étapes. La compétition de la réaction de déplacement homolytique avec des réarrangements intramoléculaires sera notre prochain objectif dans la recherche d'une preuve de ce schéma réactionnel. De plus, l'existence d'une telle compétition pourrait permettre une détermination de la constante de vitesse du déplacement (16).

Le composé **11** a déjà été observé au laboratoire dans les réactions de thermolyse du percarbonate de vinyle dans le THF (9). Les auteurs ont attribué la formation au couplage des radicaux *tert*-butoxyle et tétrahydrofuryle-2 comme Sosnovsky lors de sa communication préliminaire (17). Compte-tenu de la valeur de la constante de vitesse ($k_H \sim 10^7$ s^{-1} mol^{-1}) de réaction des radicaux *tert*-butoxyle avec le THF (concentration $\sim$ 10 mol/L), dans l'hypothèse d'une limite du couplage des radicaux par la diffusion moléculaire ($k_t \sim 10^{10}$ s^{-1} mol^{-1}) comme nous avons:

[3] $v_{\text{transfert}} = k_H\,[t\text{BuO}^\cdot]\,[\text{SH}]$

[4] $v_{\text{couplage}} = k_t\,[t\text{BuO}^\cdot]\,[\text{S}^\cdot]$

la concentration stationnaire des radicaux tétrahydrofuryle-2 devra être supérieure à 10^{-2} mol/L pour que la réaction de couplage soit plus rapide que celle de transfert. Si l'on considère la concentration initiale du peroxyde, au moins dans la décomposition du percarbonate de vinyle (~1 mol/L) et la constante de vitesse de décomposition de ce dernier (~10^{-3} s^{-1}) (18), il paraît impossible que les concentrations en radicaux tétrahydrofuryle-2 soient aussi élevées.

La proposition faite par Huyser (14) et reprise par Walling et Azar (19) paraît donc actuellement mieux rendre compte de la formation de **11** que le couplage des radicaux (9, 17).

Thermolyse de 1 dans divers éthers

Les rendements de fonctionnalisation des éthers cycliques sont tout à fait comparables à ceux enregistrés lors de leur acétonylation (8) et de leur formylméthylation (9) ce qui n'était pas le cas avec les cyclanes (13). En outre, alors que dans le cas du THP, les répartitions des attaques en α d'une part, β et γ d'autre part sont les mêmes, pour l'oxépanne, nous pouvons noter une moins grande sélectivité dans cette étude. Nous signalerons que, comme pour l'acétonylation le rapport THP ou oxépanne/perester est sans effet sur la composition du mélange d'isomères. Dans ces conditions, il semble que l'on puisse admettre que les proportions relatives des produits finaux reflètent convenablement les pourcentages initiaux de l'attaque des radicaux *tert*-butoxyle sur les éthers cycliques. Il est probable que la diminution de la sélectivité avec l'augmentation de la taille du cycle est due à des effets stéréoélectroniques (3, 4) comme cela a déjà été envisagé (8).

On outre, il faut noter que le produit d'attaque en β n'est pas observé dans le cas de l'éther de dipropyle. Nous mentionnerons qu'un essai de décomposition de **1** dans l'éther de diisopropyle a été effectué. La γ-lactone recherchée est obtenue en mélange avec de nombreux autres produits.

Conclusion

En conclusion de cette étude sur la thermolyse de **1** dans les éthers nous retiendrons comme point important une certaine généralisation de l'utilisation de cette réaction pour préparer des lactones fonctionnelles. Nous signalerons aussi l'existence d'une décomposition induite de **1** par réaction des radicaux tétrahydrofuryle sur la fonction perester. Comme cela avait été le cas pour les cyclanes, l'analyse des produits secondaires n'a

Can. J. Chem. Downloaded from www.nrcresearchpress.com by 210.87.254.6 on 09/06/12
For personal use only.

pas permis de savoir si la réaction procède par un mécanisme en deux étapes ou concerté malgré la tentative de mise en évidence d'un perester d'addition. Une décomposition induite du perpentène-4 oate de *tert*-butyle par les radicaux tétrahydrofuryle-2 a pu être effectuée à plus basse température ouvrant la voie à la recherche d'une amélioration du procédé; les radicaux ont été engendrés par la thermolyse d'un amorceur annexe dans la solution tétrahydrofurannique de **1**.

Partie expérimentale

L'analyse des produits liquides par chromatographie en phase gazeuse (cpg) a été effectuée sur un appareil Intersmat IGC 112 F (ionisation de flamme; gaz vecteur: azote (débit ~ 30 mL/min)) équipé de colonnes en acier Inox (longueur: 2 m; diamètre intérieur: 2 mm). Deux phases ont été principalement utilisées: OV-275 (10% sur Chromosorb WHP, 80/100 mesh) et FFAP (10% sur Chromosorb WAW, 80/100 mesh). Les identifications ont été réalisées par comparaison des temps de rétention avec ceux d'échantillons préparés en référence ou par couplage avec un spectromètre de masse. Les dosages ont été effectués par la méthode de l'étalon interne.

Les produits gazeux de réaction avec le THF ont été récupérés sur une cuve à eau et analysés par cpg à l'aide d'un appareil Varian 920 (Catharomètre; gaz vecteur: hélium (débit ~ 12 mL/min)) équipé d'une colonne en acier Inox (longueur: 9 m; diamètre intérieur: 2 mm), la phase étant DC-200 (28%) sur Chromosorb PAW (60/80 mesh). Un mélange gazeux a servi de référence. Les échantillons ont été prélevés à l'aide d'une seringue à gaz.

L'étude par hplc a été effectuée sur un appareil Waters (colonne μPorasil (3,9 mm × 30 cm); détecteur: réfractomètre différentiel; solvant: hexane/éther 70:30; débit: 3 mL/min).

Les spectres rmn du proton ont été enregistrés sur un appareil Perkin–Elmer R12 B opérant à 60 MHz à partir de solutions à 10% dans le tétrachlorure de carbone (déplacements chimiques en δ ppm par rapport au TMS).

Les spectres rmn du ^{13}C ont été enregistrés sur un appareil Bruker WP 60 fonctionnant à 15,08 MHz équipé d'un calculateur Nicolet BNC 12 (déplacements chimiques en δ ppm par rapport au TMS) à partir de solutions dans le chloroforme deutéré.

Les spectres de masse ont été obtenus, en général par couplage masse–cpg sur des appareils Micromass 16F et 70-70 sous impact électronique (70 eV). Nous n'indiquons que les pics dont l'abondance dépasse 10%.

Etude des décompositions

Les études analytiques ont été réalisées en introduisant 2 cm^3 de solution dans des ampoules en Pyrex scellées placées pendant le temps adéquat dans un bain thermostaté à la température choisie (110, 120 ou 130°C).

Les études préparatives ont été effectuées sur des volumes de l'ordre de 100 cm^3 dans un autoclave de 125 cm^3 placé dans une étuve thermorégulée préalablement portée à la température souhaitée. Après élimination du solvant en excès, le produit recherché est distillé sous pression réduite puis purifié par chromatographie liquide–solide sur une colonne de gel de silice (Kiesel 60, 35–70 mesh).

Matières premières

Les éthers, le *tert*-butanol, l'acétone et le butène-1 sont des produits commerciaux. Le (tétrahydrofuryl-2)-2 tétrahydrofuranne a été obtenu par décomposition du peroxyde de di-*tert*-butyle dans le THF. Les synthèses de l'acide pentène-4 oïque et du perpentène-4 oate de *tert*-butyle ont été décrites dans réf. (1).

Le butyl-2 THF a été synthétisé par addition radicalaire du THF sur le butène-1 en présence de peroxyde de *tert*-butyle (rapports molaires THF/butène-1/PDTB = 20:1:0,1; température: 140°C; durée: 10 h); pé 68°C/22 Torr; n_D^{20} = 1,4462 (litt. (20) pé 158–159°C/750 Torr; n_D^{20} = 1,4287); rmn δ: 0,7 à 2,1 (1 massif, 13H), 3,3 à 3,9 (1 massif, 3H).

L'acide (tétrahydrofuryl-2)-5 pentanoïque a été préparé par addition radicalaire du THF (2 mol) à l'acide pentènoïque (0,1 mol) en présence de peroxyde de di-*tert*-butyle (0,02 mol) à 140°C pendant 10 h; pé 112°C/0,1 Torr; n_D^{20} = 1,4625; rmn δ: 1,1 à 2,7 (1 massif, 12H), 3,5 à 4,1 (1 massif, 3H), 9,85 (1 signal large, 1H).

Le (tétrahydrofuryl-2)-5 perpentanoate de *tert*-butyle a été obtenu par action du *N*,*N'*-carbonyldiimidazole sur l'acide correspondant dans le THF anhydre suivi d'une addition d'hydroperoxyde de *tert*-butyle. Il a été purifié par passage sur gel de silice; taux de perester déterminé selon (21): 98%; rmn δ: 1,1 à 2,5 (1 massif, 12H), 1,3 (1 s, 9H), 3,4 à 4,0 (1 massif, 3H).

Le *tert*-butoxy-2 tétrahydrofuranne a été préparé par décomposition du perbenzoate de *tert*-butyle dans le THF en présence de bromure de cuivre (17); pé 53°C/22 Torr; n_D^{20} = 1,4221 (litt. (17) pé 40°C/11 Torr; n_D^{25} = 1,4186); rmn δ: 1,2 (1 s, 9H), 1,6 à 2,2 (1 massif, 4H), 3,5 à 4,0 (1 massif, 2H), 5,2 à 5,4 (1 massif, 1H).

Caractéristiques physiques des différentes lactones substituées[5,6]

(Tétrahydrofuryl-2)-5 pentanolide-4 **10**: pé 116–117°C/0,3 Torr; n_D^{20} = 1,4697; rmn ^1H δ: 0,8 à 2,7 (1 massif, 10H), 3,4 à 4,2 (1 massif, 3H), 4,3 à 4,9 (q, 1H); principaux pics du spectre de masse *m*/*z* (abondance): 71 (100), 43 (20), 85 (20).

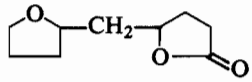

10

(Tétrahydropyrannyl)-5 pentanolide-4 **12**: point d'ébullition du mélange des trois isomères 126–128/0,3 Torr.

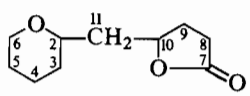

12*a*

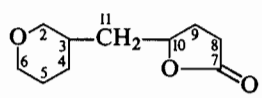

12*b*

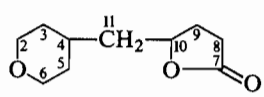

12*c*

[5]Les déterminations par rmn ^{13}C des structures isomères des composés **12** et **13** ont été effectuées par comparaison des valeurs des déplacements chimiques observées et calculés selon réf. 22 à partir de modèles décrits dans la littérature (1, 22, 23). Pour **12***b* et **12***c* nous sommes basés essentiellement sur les déplacements chimiques des carbones C_2 et C_6, pour **13***b* et **13***c* sur ceux des carbones C_2 et C_7.

[6]Toutes les lactones décrites donnent des microanalyses C, H en accord avec les formules proposées. Toutefois pour le produit **15** il faut signaler un écart plus important avec les valeurs théoriques.

Can. J. Chem. Downloaded from www.nrcresearchpress.com by 210.87.254.6 on 09/06/12
For personal use only.

12*a*: séparé sur colonne de gel de silice; n_D^{20} = 1,4752; rmn ^{1}H δ: 0,7 à 2,7 (1 massif, 12H), 3,1 à 4,2 (1 massif, 3H), 4,4 à 5,0 (q, 1H); principaux pics du spectre de masse *m/z* (abondance): 85 (100), 41 (25), 111 (24), 55 (23); rmn ^{13}C:

	C_2	C_3	C_4	C_5	C_6	C_7	C_8	C_9	C_{10}	C_{11}
$\delta_{observé}$	74,07/74,48	31,77/32,38	23,43	26,05	68,29	177,17	27,94/28,48	28,67/28,79	77,84	41,63/42,79
$\delta_{calculé}$	75,41	31,60/32,40	23,90	26,70	68	177,1	28,73	28,73	78,94	43,32

Mélange **12***b* + **12***c*: séparé sur colonne de gel de silice; rmn ^{13}C:

		C_2	C_3	C_4	C_5	C_6	C_7	C_8	C_9	C_{10}	C_{11}
12*b*	$\delta_{observé}$	72,55/73,16	33,17/34,37	30,06	25,50/26,23	68,40	177,11	28,72/29,58		78,40	43,03
	$\delta_{calculé}$	74,70/75,5	34,8	30/31	26,5	68,2	177,1	28,73	28,73	78,94	43,5
12*c*	$\delta_{observé}$	67,8	32,04	32,56	32,04	67,8	177,11	28,72/29,58		79,0	38,59
	$\delta_{calculé}$	67,7	33,0/33,8	32,11	33,0/33,8	67,7	177,1	28,73	28,73	78,94	43,4

(Oxacycloheptyl)-5 pentanolide-4 **13**: point d'ébullition du mélange des trois isomères 146°C/0,8 Torr.

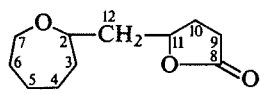

13*a*

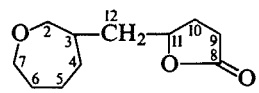

13*b*

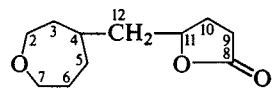

13*c*

13*a*: séparé sur colonne de gel de silice; n_D^{20} = 1,4630; rmn ^{1}H δ: 0,8 à 2,7 (1 massif, 14H), 3,2 à 4,1 (1 massif, 3H), 4,3 à 4,9 (q, 1H); principaux pics du spectre de masse *m/z* (abondance): 99 (100), 55,1 (61), 85 (50), 81 (41), 83 (39), 42 (35), 111 (21); rmn ^{13}C:

	C_2	C_3	C_4	C_5	C_6	C_7	C_8	C_9	C_{10}	C_{11}	C_{12}
$\delta_{observé}$	75,8/76,2	36,0/36,5	25,75/26,11	26,29/26,78	31,04	68,47/68,96	177,23	28,95	27,94/28,42	78,27/78,51	41,87/43,03
$\delta_{calculé}$	76,5	35,4/36,4	26,25	27,0	31,7	68,8	177,17	28,9	28,7	79,4	42,4

Mélange **13***b* + **13***c*: séparé sur colonne de gel de silice; rmn ^{13}C:

		C_2	C_3	C_4	C_5	C_6	C_7	C_8	C_9	C_{10}	C_{11}	C_{12}
13*b*	$\delta_{observé}$	73,4/74,5	37,43	33,17/33,78	24,22	30,74	70,66	177,11	28,73	28,60	79,24	39,14/39,32
	$\delta_{calculé}$	73,3/74,2	37,7	33,0/33,86	24,5	31,7	71	177,17	28,95	28,7	79,5	39,6
13*c*	$\delta_{observé}$	67,74	36,52	35,36	32,26/32,87	30,61	69,57	177,11	28,73	28,60	79,0	43,15/43,33
	$\delta_{calculé}$	67,9	36,7/35,9	34,9	32,4/33,26	29,1	69,8	177,17	28,95	28,5	79,0	41,67/42,83

(Dioxa-1,4 cyclohexyl-2)-5 pentanolide-4 **14**: pé 145-146°C/1,1 Torr; n_D^{20} = 1,4762; rmn ^{1}H δ: 1,2 à 2,7 (1 massif, 6H), 2,9 à 3,9 (1 massif, 7H), 4,3 à 4,9 (q, 1H); principaux pics du spectre de masse *m/z* (abondance): 85 (100), 101 (68), 43 (39), 55 (32), 45 (32).

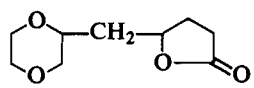

14

Propoxy-6 octanolide-4 **15**: pé 110°C/0,7 Torr; n_D^{20} = 1,4505; rmn ^{1}H δ: 0,7 à 2,7 (1 massif, 16H), 3,1 à 3,6 (1 massif, 3H), 4,3 à 4,8 (q, 1H); principaux pics du spectre de masse *m/z* (abondance): 59 (100), 129 (86), 85 (65), 101 (58), 43 (52).

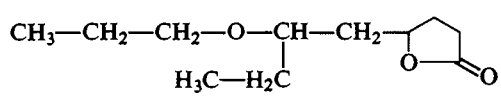

15

Remerciements

Les auteurs remercient Monsieur le Professeur R. Lalande (Université de Bordeaux I) pour l'intérêt qu'il a porté à ce travail ainsi que les Docteurs K. U. Ingold (CNRC, Ottawa) et D. Lefort (CNRS, Thiais) pour leurs nombresuses suggestions.

1. B. MAILLARD, A. KHARRAT et C. GARDRAT. Tetrahedron. Sous presse.
2. T. J. WALLACE et R. J. GRITTER. J. Org. Chem. **26**, 5256 (1961).
3. V. MALATESTA et K. U. INGOLD. J. Am. Chem. Soc. **103**, 609 (1981) et références citées.
4. V. MALATESTA et J. C. SCAIANO. J. Org. Chem. **47**, 1455 (1982).

Can. J. Chem. Downloaded from www.nrcresearchpress.com by 210.87.254.6 on 09/06/12
For personal use only.

5. T. J. WALLACE, R. J. GRITTER et H. G. WALSH. Nature, **198**, 284 (1963).
6. M. I. SHUIKIN et B. L. LEBEDEV. Z. Chem. **6**, 459 (1966).
7. T. N. ABROSKINA, A. O. SOROKIN, R. V. KUDRYAVTSEV et YU. N. CHERDUKOV. Izv. Akad. Nauk SSSR, Ser. Khim. 1823 (1974).
8. R. JAOUHARI, B. MAILLARD, C. FILLIATRE et J-J. VILLENAVE. Tetrahedron, **39**, 1559 (1983).
9. C. FILLIATRE, J-J. VILLENAVE, R. JAOUHARI et M. BARATCHART. Bull. Soc. Chim. Fr. II-352 (1982).
10. R. A. SHELDON et J. K. KOCHI. J. Am. Chem. Soc. **92**, 5175 (1970).
11. C. M. RYNARD, C. THANKACHAN et T. T. TIDWELL. J. Am. Chem. Soc. **101**, 1196 (1979).
12. R. KAPTEIN. *Dans* Advances in free radical chemistry. Vol. 5. *Edité par* G. H. Williams. Elek Science, London. 1975. p. 346.
13. R. JAOUHARI, C. FILLIATRE, B. MAILLARD et J-J. VILLENAVE. Tetrahedron, **38**, 3137 (1982).
14. E. S. HUYSER. *Dans* Free radical chain reactions. Wiley Interscience, New York. 1968. p. 281.
15. H. HART et F. J. CHLOUPECK. J. Am. Chem. Soc. **85**, 1155 (1963).
16. D. GRILLER et K. U. INGOLD. Acc. Chem. Res. **13**, 317 (1980).
17. G. SOSNOVSKY. J. Org. Chem. **25**, 874 (1960).
18. J-J. VILLENAVE, C. FILLIATRE et R. JAOUHARI. Thermochim. Acta, **60**, 353 (1983).
19. C. WALLING et J. C. AZAR. J. Org. Chem. **33**, 3888 (1968).
20. Y. K. YUR'EV et I. P. GRAGEROV. Zh. Obsch. Khim. **19**, 724 (1949).
21. L. S. SILBERT et D. SWERN. Anal. Chem. **30**, 385 (1958).
22. M. BARATCHART, C. FILLIATRE, R. JAOUHARI, J-J. VILLENAVE, B. BARBE et M. PETRAUD. Analusis, **11**, 65 (1983).
23. A. J. DE HOOG. Org. Magn. Reson. **6**, 233 (1974).

Can. J. Chem. Downloaded from www.nrcresearchpress.com by 210.87.254.6 on 09/06/12
For personal use only.

COMMUNICATIONS

Reaction of diphenylcarbene with oxygen: a laser flash photolysis study[1]

N. H. WERSTIUK,[2] H. L. CASAL, AND J. C. SCAIANO
Division of Chemistry, National Research Council of Canada, Ottawa, Ont., Canada K1A 0R6

Received April 18, 1984

N. H. WERSTIUK, H. L. CASAL, and J. C. SCAIANO. Can. J. Chem. **62**, 2391 (1984).

Diphenylcarbene reacts with oxygen with a rate constant of $5 \times 10^9\ M^{-1}\ s^{-1}$ in acetonitrile at 300 K. The reaction leads to an intermediate which absorbs strongly at ~410 nm, believed to be the carbonyl oxide, Ph_2COO.

N. H. WERSTIUK, H. L. CASAL et J. C. SCAIANO. Can. J. Chem. **62**, 2391 (1984).

Le diphénylecarbene réagit avec l'oxygène dans la solution d'acetonitrile avec une constante de vitesse $5 \times 10^9\ M^{-1}\ s^{-1}$ à 300 K. Cette réaction forme un produit intermédiaire possédant une absorption forte à ~410 nm que nous croyons être l'oxyde de carbonyle Ph_2COO.

Can. J. Chem. Downloaded from www.nrcresearchpress.com by 210.87.254.6 on 09/06/12
For personal use only.

Triplet carbenes are known to react readily with oxygen (1–7); but little is known about the kinetics of these reactions (4, 8). In the case of diphenylcarbene (DPC) the reaction ultimately leads to benzophenone and its diperoxide (3). There is some evidence that at least some of the benzophenone is produced in its triplet state in glasses at low temperature (7). Several authors have speculated as to the type of mechanism and reactive intermediates involved in the process; there is some consensus that benzophenone-oxide, Ph_2COO (i.e. the Criegee intermediate (9)) is probably involved; this species has recently been detected in other systems involving cyclopentadienylidene at low temperatures using vibrational spectroscopy (10). While this communication was being considered for publication we learned about the recent detection of 10,10-dimethyl-10-silaanthracen-9[10*H*]-one oxide by laser flash photolysis (11).[3]

Pulsed laser photodecomposition (308 nm, ~4 ns, up to 80 mJ/pulse) of diphenyldiazomethane (typically $10^{-4}\ M$) in acetonitrile at 300 K yields, after carbene intersystem crossing, triplet diphenylcarbene (^{3}DPC), easily detectable by its strong optical absorption around 315 nm (12).[4] The triplet carbene can be readily scavenged by oxygen, as evidenced by the decrease in lifetime in the presence of increasing concentrations of oxygen. The decay of ^{3}DPC follows clean pseudo-first order kinetics in the presence of oxygen. A plot of the corresponding rate constants for carbene decay vs. the oxygen concentrations yields $k_{O_2} = 5 \times 10^9\ M^{-1}\ s^{-1}$, based on the reported solubility of oxygen in acetonitrile (14).

$$[1]\quad Ph_2C^{\uparrow\uparrow} + O_2 \xrightarrow{k_{O_2}} Ph_2COO$$

Oxygen usually does not scavenge singlet carbenes (8) since this process would only be allowed if it yielded a triplet product. This is confirmed by our experiments, where only the lifetime of the triplet, but not its yield, were affected by oxygen.

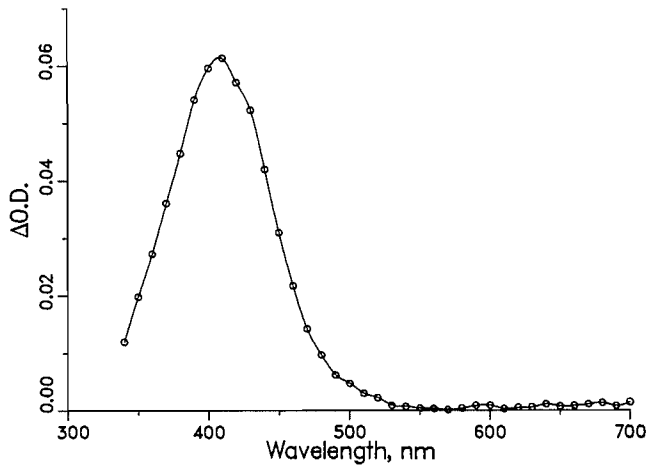

FIG. 1. Transient absorption spectrum obtained 10 μs after laser excitation of a 10^{-4} *M* solution of diphenyldiazomethane in acetonitrile (300 K) containing 7.7×10^{-3} *M* oxygen.

We have observed that quenching by oxygen is accompanied by the formation of a long-lived intermediate ($\tau > 100$ μs) which shows relative intense absorptions with $\lambda_{max} \sim 410$ nm (see Fig. 1). There is only one other recent example where intermediates of this type have been detected by uv–vis spectroscopy (11). We tentatively assign these signals to the carbonyl-oxide Ph_2COO, which is ultimately responsible for the formation of benzophenone. The absorption spectrum is not sufficiently informative to decide on the structure of Ph_2COO; while an ylide structure is quite possible, other possibilities, such as a biradical or 3-member ring cannot be ruled out.

A few experiments have been carried out in order to characterize this transient better. Electron deficient olefins scavenge the 410 nm transient, a common reaction for carbene-derived ylides (15); for example, $k = 1.5 \times 10^6\ M^{-1}\ s^{-1}$ for diethylfumarate. Slow ($k \sim 4 \times 10^5\ M^{-1}\ s^{-1}$), but detectable quenching is also observed in the case of the carbene precursor, diphenyldiazomethane. Oxygen, at pressures of up to 1 atm, does not quench this intermediate. The same intermediate has also been detected in benzene and in methylene chloride solution, thus confirming that the 410 mm band does not result from reactions involving the solvent.

Carbonyl oxides are known to be good oxygen-transfer reagents, reacting readily with a wide range of organic substrates,

[1] NRCC No. 23270.

[2] NRCC Visiting Scientist. Permanent address: Department of Chemistry, McMaster University, Hamilton, Ont., Canada L8S 4M1.

[3] We are grateful to Dr. M. T. H. Liu for bringing this work to our attention.

[4] Details of our laser facility have been reported elsewhere (13). All experiments were carried out using a flow system and employing solutions saturated with O_2/N_2 mixtures of known composition. An excimer laser (Lumonics TE860-2) was used for excitation.

including aromatic hydrocarbons and olefins (e.g. refs. 16, 17). The 410 nm transient was scavenged by 2,5-dimethyl-2,4-hexadiene with a rate constant of $\sim 1 \times 10^6\ M^{-1}\ s^{-1}$ in acetonitrile at 300 K.

Further laser and product studies, including substituent and solvent effects are currently in progress, in an attempt to elucidate further the mechanisms and kinetics of these reactions.[5]

1. G. A. HAMILTON and J. R. GIACIN. J. Am. Chem. Soc. **88**, 1584 (1966).
2. R. W. MURRAY and A. SUZUI. J. Am. Chem. Soc. **93**, 4963 (1971).
3. P. D. BARTLETT and T. G. TRAYLOR. J. Am. Chem. Soc. **84**, 3408 (1962).
4. G. L. CLOSS and B. E. RABINOW. J. Am. Chem. Soc. **98**, 8190 (1976).
5. W. KIRMSE, L. HORNER, and H. HOFFMANN. Ann. **614**, 22 (1958).
6. R. M. ETTER, H. S. SKOVRONEK, and P. S. SKELL. J. Am. Chem. Soc. **81**, 1008 (1959).
7. A. M. TROZZOLO, R. W. MURRAY, and E. WASSERMAN. J. Am. Chem. Soc. **84**, 4990 (1962); A. M. TROZZOLO. Acc. Chem. Res. **1**, 329 (1968).
8. D. GRILLER, A. S. NAZRAN, and J. C. SCAIANO. Acc. Chem. Res. In press.
9. R. CRIEGEE. Record Chem. Prog. **13**, 111 (1957); R. CRIEGEE. Angew. Chem. Int. Ed. Engl. **14**, 745 (1975).
10. G. A. BELL and I. R. DUNKIN. J. Chem. Soc. Chem. Commun. 1213 (1983); O. L. CHAPMAN and T. C. HESS. J. Am. Chem. Soc. **106**, 1842 (1984).
11. T. SUGAWARA, H. IWAMURA, H. HAYASHI, A. SEKIGUCHI, W. ANDO, and M. T. H. LIU. Chem. Lett. 1261 (1983).
12. L. M. HADEL, M. S. PLATZ, and J. C. SCAIANO. J. Am. Chem. Soc. **106**, 283 (1984).
13. J. C. SCAIANO. J. Am. Chem. Soc. **102**, 7747 (1980).
14. J. F. COETZEE and I. M. KOLTHOFF. J. Am. Chem. Soc. **79**, 6110 (1957).
15. P. C. WONG, D. GRILLER, and J. C. SCAIANO. J. Am. Chem. Soc. **104**, 6631 (1982); L. M. HADEL, M. S. PLATZ, and J. C. SCAIANO. Chem. Phys. Lett. **97**, 446 (1983).
16. A. SEKIGUCHI, Y. KABE, and W. ANDO. J. Org. Chem. **47**, 2900 (1982); Y. SAWAKI, H. KATO, and Y. OGATA. J. Am. Chem. Soc. **103**, 3832 (1981).
17. S. K. AGARWAL and R. W. MURRAY. Photochem. Photobiol. **35**, 31 (1982); D. P. HIGLEY and R. W. MURRAY. J. Am. Chem. Soc. **96**, 3330 (1974); R. W. MURRAY and S. KUMAR. *In* Polynuclear aromatic hydrocarbons: physical and biological chemistry. *Edited by* M. Cooke, A. J. Dennis, and G. L. Fisher. Battelle Press, Columbus. 1982. p. 575.

[5] The same intermediate has also been detected in the reaction of singlet oxygen with diphenyldiazomethane (H. L. Casal, S. E. Sugamori, and J. C. Scaiano. Unpublished work).

Can. J. Chem. Downloaded from www.nrcresearchpress.com by 210.87.254.6 on 09/06/12
For personal use only.

Thermolysis of unsymmetrically substituted vinylcyclopropanes. The effect of substituents on the site-selectivity of homo-[1,5]-sigmatropic hydrogen migrations

EDWARD PIERS AND ANDERSON RICHARD MAXWELL

Department of Chemistry, University of British Columbia, 2036 Main Mall, University Campus, Vancouver, B.C., Canada V6T 1Y6

Received June 1, 1984

EDWARD PIERS and ANDERSON RICHARD MAXWELL. Can. J. Chem. **62**, 2392 (1984).

Thermolysis of the unsymmetrical vinylcyclopropanes **18**–**24** reveals a notable substituent effect on the site-selectivity of homo-[1,5]-sigmatropic hydrogen shifts. Rearrangement of **18**–**20** (OMe substituent) produces only products **25**–**27**, respectively (H_A migration). In sharp contrast, thermolysis of **24** (Me_3Si substituent) provides exclusively substance **34** (H_X migration). Thermolysis of substrates bearing methyl (**21**, **22**) or phenyl (**23**) groups provide, in each case, mixtures of the two possible products.

EDWARD PIERS et ANDERSON RICHARD MAXWELL. Can. J. Chem. **62**, 2392 (1984).

La thermolyse des vinylcyclopropanes **18**–**24** révèle l'existence d'un effet important des substituants sur la sélectivité du site des transpositions homo-[1,5]-sigmatropiques d'hydrogènes. Les transpositions des produits **18**–**20** (substituant OMe) ne conduisent respectivement qu'aux produits **25**–**27** (migration de H_A). Par opposition, la thermolyse de **24** (substituant Me_3Si) ne conduit qu'à la substance **34** (migration de H_X). Lors de la thermolyse de substrats portant des groupes méthyles (**21**, **22**) ou phényle (**23**), on obtient dans chaque cas des mélanges des deux produits possibles.

[Traduit par le journal]

Reactions involving thermal homo-[1,5]-sigmatropic hydrogen migrations, exemplified by the "parent" transformation **1** → **2** (eq. [1]) (1, 2), are quite well known (3, 4) and have found some use in organic synthesis (5–7). However, studies which have provided information regarding site-selectivity in the thermolysis of unsymmetrical vinylcyclopropanes (**3** → **4** and (or) **5**, eq. [2])[1] have been rare. High site-selectivity in such processes, apart from being of theoretical interest, could have important consequences for synthetic organic chemistry.

Nearly two decades ago, Ohloff (8) reported that thermolysis of compound **6** produces exclusively products which could have arisen only from initial migration of H_A. More recently (9), work in our laboratory showed, *inter alia*, that thermolysis of substrates **7** and **8** provided, as the sole products, compounds **9** and **10** (eq. [3]). Thus, in all three cases (**6**–**8**), only the hydrogen (H_A) not associated with the oxygen substituent underwent migration.

A number of questions come to mind in connection with the conversions outlined in eq. [3]. For example, (a) does the

[1] For the sake of clarity and brevity, the hydrogens migrating from carbons bearing no substituent are designated H_A, while those migrating from carbons containing a substituent are designated H_X (see eq. [2]). This convention is employed throughout this communication.

including aromatic hydrocarbons and olefins (e.g. refs. 16, 17). The 410 nm transient was scavenged by 2,5-dimethyl-2,4-hexadiene with a rate constant of $\sim 1 \times 10^6\ M^{-1}\ s^{-1}$ in acetonitrile at 300 K.

Further laser and product studies, including substituent and solvent effects are currently in progress, in an attempt to elucidate further the mechanisms and kinetics of these reactions.[5]

1. G. A. HAMILTON and J. R. GIACIN. J. Am. Chem. Soc. **88**, 1584 (1966).
2. R. W. MURRAY and A. SUZUI. J. Am. Chem. Soc. **93**, 4963 (1971).
3. P. D. BARTLETT and T. G. TRAYLOR. J. Am. Chem. Soc. **84**, 3408 (1962).
4. G. L. CLOSS and B. E. RABINOW. J. Am. Chem. Soc. **98**, 8190 (1976).
5. W. KIRMSE, L. HORNER, and H. HOFFMANN. Ann. **614**, 22 (1958).
6. R. M. ETTER, H. S. SKOVRONEK, and P. S. SKELL. J. Am. Chem. Soc. **81**, 1008 (1959).
7. A. M. TROZZOLO, R. W. MURRAY, and E. WASSERMAN. J. Am. Chem. Soc. **84**, 4990 (1962); A. M. TROZZOLO. Acc. Chem. Res. **1**, 329 (1968).
8. D. GRILLER, A. S. NAZRAN, and J. C. SCAIANO. Acc. Chem. Res. In press.
9. R. CRIEGEE. Record Chem. Prog. **13**, 111 (1957); R. CRIEGEE. Angew. Chem. Int. Ed. Engl. **14**, 745 (1975).
10. G. A. BELL and I. R. DUNKIN. J. Chem. Soc. Chem. Commun. 1213 (1983); O. L. CHAPMAN and T. C. HESS. J. Am. Chem. Soc. **106**, 1842 (1984).
11. T. SUGAWARA, H. IWAMURA, H. HAYASHI, A. SEKIGUCHI, W. ANDO, and M. T. H. LIU. Chem. Lett. 1261 (1983).
12. L. M. HADEL, M. S. PLATZ, and J. C. SCAIANO. J. Am. Chem. Soc. **106**, 283 (1984).
13. J. C. SCAIANO. J. Am. Chem. Soc. **102**, 7747 (1980).
14. J. F. COETZEE and I. M. KOLTHOFF. J. Am. Chem. Soc. **79**, 6110 (1957).
15. P. C. WONG, D. GRILLER, and J. C. SCAIANO. J. Am. Chem. Soc. **104**, 6631 (1982); L. M. HADEL, M. S. PLATZ, and J. C. SCAIANO. Chem. Phys. Lett. **97**, 446 (1983).
16. A. SEKIGUCHI, Y. KABE, and W. ANDO. J. Org. Chem. **47**, 2900 (1982); Y. SAWAKI, H. KATO, and Y. OGATA. J. Am. Chem. Soc. **103**, 3832 (1981).
17. S. K. AGARWAL and R. W. MURRAY. Photochem. Photobiol. **35**, 31 (1982); D. P. HIGLEY and R. W. MURRAY. J. Am. Chem. Soc. **96**, 3330 (1974); R. W. MURRAY and S. KUMAR. *In* Polynuclear aromatic hydrocarbons: physical and biological chemistry. *Edited by* M. Cooke, A. J. Dennis, and G. L. Fisher. Battelle Press, Columbus. 1982. p. 575.

[5] The same intermediate has also been detected in the reaction of singlet oxygen with diphenyldiazomethane (H. L. Casal, S. E. Sugamori, and J. C. Scaiano. Unpublished work).

Can. J. Chem. Downloaded from www.nrcresearchpress.com by 210.87.254.105 on 09/06/12
For personal use only.

Thermolysis of unsymmetrically substituted vinylcyclopropanes. The effect of substituents on the site-selectivity of homo-[1,5]-sigmatropic hydrogen migrations

EDWARD PIERS AND ANDERSON RICHARD MAXWELL

Department of Chemistry, University of British Columbia, 2036 Main Mall, University Campus, Vancouver, B.C., Canada V6T 1Y6

Received June 1, 1984

EDWARD PIERS and ANDERSON RICHARD MAXWELL. Can. J. Chem. **62**, 2392 (1984).

Thermolysis of the unsymmetrical vinylcyclopropanes **18**–**24** reveals a notable substituent effect on the site-selectivity of homo-[1,5]-sigmatropic hydrogen shifts. Rearrangement of **18**–**20** (OMe substituent) produces only products **25**–**27**, respectively (H_A migration). In sharp contrast, thermolysis of **24** (Me_3Si substituent) provides exclusively substance **34** (H_X migration). Thermolysis of substrates bearing methyl (**21**, **22**) or phenyl (**23**) groups provide, in each case, mixtures of the two possible products.

EDWARD PIERS et ANDERSON RICHARD MAXWELL. Can. J. Chem. **62**, 2392 (1984).

La thermolyse des vinylcyclopropanes **18**–**24** révèle l'existence d'un effet important des substituants sur la sélectivité du site des transpositions homo-[1,5]-sigmatropiques d'hydrogènes. Les transpositions des produits **18**–**20** (substituant OMe) ne conduisent respectivement qu'aux produits **25**–**27** (migration de H_A). Par opposition, la thermolyse de **24** (substituant Me_3Si) ne conduit qu'à la substance **34** (migration de H_X). Lors de la thermolyse de substrats portant des groupes méthyles (**21**, **22**) ou phényle (**23**), on obtient dans chaque cas des mélanges des deux produits possibles.

[Traduit par le journal]

Reactions involving thermal homo-[1,5]-sigmatropic hydrogen migrations, exemplified by the "parent" transformation **1** → **2** (eq. [1]) (1, 2), are quite well known (3, 4) and have found some use in organic synthesis (5–7). However, studies which have provided information regarding site-selectivity in the thermolysis of unsymmetrical vinylcyclopropanes (**3** → **4** and (or) **5**, eq. [2])[1] have been rare. High site-selectivity in such processes, apart from being of theoretical interest, could have important consequences for synthetic organic chemistry.

Nearly two decades ago, Ohloff (8) reported that thermolysis of compound **6** produces exclusively products which could have arisen only from initial migration of H_A. More recently (9), work in our laboratory showed, *inter alia*, that thermolysis of substrates **7** and **8** provided, as the sole products, compounds **9** and **10** (eq. [3]). Thus, in all three cases (**6**–**8**), only the hydrogen (H_A) not associated with the oxygen substituent underwent migration.

A number of questions come to mind in connection with the conversions outlined in eq. [3]. For example, (a) does the

[1] For the sake of clarity and brevity, the hydrogens migrating from carbons bearing no substituent are designated H_A, while those migrating from carbons containing a substituent are designated H_X (see eq. [2]). This convention is employed throughout this communication.

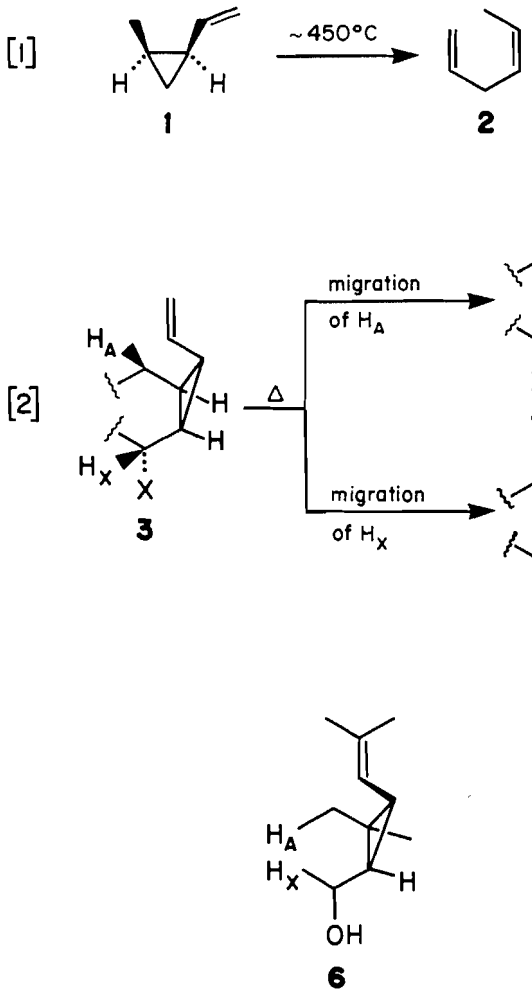

conjugated carbonyl function attached to the vinyl moiety of substrates **7** and **8** influence the site-selectivity of the reaction? (b) What is the effect of substituents other than OR? (c) Is the placement of the oxygen atom (e.g. external vs. internal with respect to the ring) a significant factor in determining the site-selectivity of the rearrangement? We report herein some results which relate to questions (a) and (b), while, hopefully, a future report will provide information regarding question (c).

Conversion (9, 10) of the tetrahydropyranyl ether of 2-cyclohexen-1-ol (**11**) into the dibromocyclopropane **16**,[2] followed by reduction (*n*-Bu_3SnH) of the latter substance, gave a mixture of **17** and the corresponding *exo* bromide (ratio 2.3:1, respectively). Chromatographic separation provided (20% from **11**) the required *endo* bromide **17** which, upon subjection to an appropriate sequence of reactions (2 equiv. *t*-BuLi, Et_2O, −78°C; $HCONMe_2$, Et_2O, −78°C → room temperature; $Ph_3P{=}CH_2$, tetrahydrofuran; pyridinium *p*-toluenesulfonate, EtOH, 50°C; NaH, MeI, tetrahydrofuran, reflux) afforded *trans*-2-methoxy-*endo*-7-vinylbicyclo[4.1.0]heptane (**18**). By use of similar, quite straightforward chemical reactions, the alkenes **12**−**15** were converted into the vinylcyclopropanes **19**−**24**.[3]

TABLE 1. Thermal rearrangement of vinylcyclopropanes **18**−**24**[a]

Experiment	Substrate	Product(s) (ratio)	Yield (%)[b]
1	**18**	**25**	80
2	**19**	**26**	90[c]
3	**20**	**27**	90
4	**21**	**28** + **29** (60:40)	—[d]
5	**22**	**30** + **31** (57:43)	96[e]
6	**23**	**32** + **33** (18:82)	87
7	**24**	**34**	90

[a]Unless otherwise noted, thermolysis of each of the substrates was performed in benzene solution (230−240°C, 6−8 h) in sealed, base-washed, silylated glass tubes. In each case, the cooled reaction mixture was analyzed directly by gas−liquid chromatography (glc). The benzene was removed, the product(s) was (were) distilled and subjected again to analysis (glc, ^1H nmr spectroscopy).

[b]Unless otherwise noted, yield of isolated, distilled product(s).

[c]Rearrangement was carried out both neat and in benzene solution. The yield is given for the neat experiment.

[d]Rearrangement was performed in C_6D_6. The yield was not determined, but the ^1H nmr spectrum of the cooled thermolysis solution indicated clean rearrangement into two products.

[e]Rearrangement of **22** was accomplished by heating this substance (neat) at 215°C for 15 min.

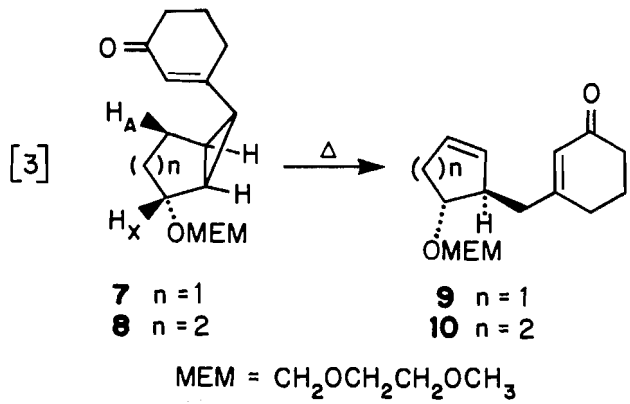

The results obtained from thermal rearrangement of compounds **18**−**24** are summarized in Table 1. The reactions were, in general, very clean and, for experiments 1−3, we were not able to detect any of the products which would have resulted from migration of H_X in substrates **18**−**20**. In contrast, thermolysis of **24** provided exclusively the H_X migration product **34**. The product pairs obtained from each of experiments 5 and 6 were separated and all four compounds (**30**−**33**) were fully characterized.

Although a detailed discussion of the results given in Table 1 is not appropriate here, a few comments should be made. The results obtained from experiments 1−5, along with those summarized by eq. [3], make it clear that the presence or absence

[2]All compounds reported herein exhibited spectra consistent with assigned structures. New compounds were fully characterized and gave satisfactory molecular mass determinations (high-resolution mass spectrometry). The stereochemical assignments for compounds **16**−**24** are based on a number of considerations, including steric approach control arguments, ^1H nmr spectral data, and chemical correlations with known compounds. Details concerning the stereochemical conclusions (see also ref. 9), as well as complete descriptions of the preparation of substrates **18**−**24**, will be given in a full paper.

[3]For methods involved in the conversion of **12** and **13** into substrates **20** and **22**, respectively, see ref. 9. Alkenes **13** and **14** were prepared by $CuBr{\cdot}Me_2S$ catalyzed coupling (Et_2O, 0°C) of CH_3MgI and C_6H_5MgBr with 3-bromocyclohexene (**A**), while **15** was obtained by the coupling (tetrahydrofuran, 5°C → room temperature) of Me_3SiCl and **A** in the presence of magnesium turnings (ref. 11).

Can. J. Chem. Downloaded from www.nrcresearchpress.com by 210.87.254.105 on 09/06/12
For personal use only.

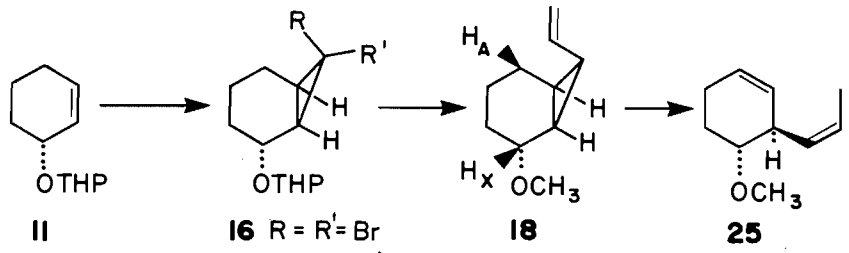

11 **16** R = R' = Br; **17** R = Br, R' = H **18** **25**

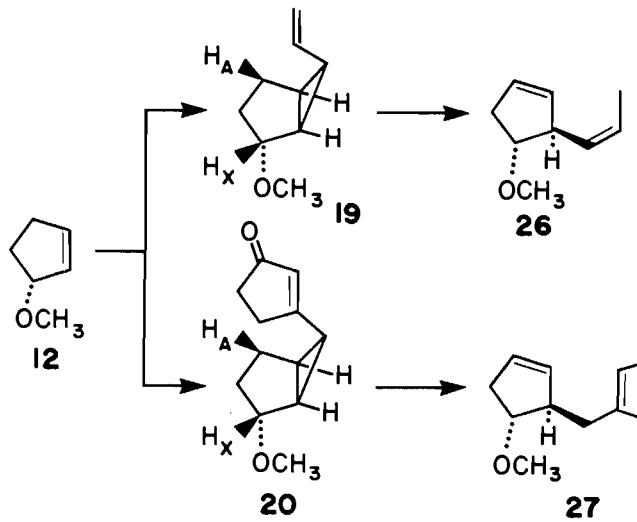

19 **26** **12** **20** **27**

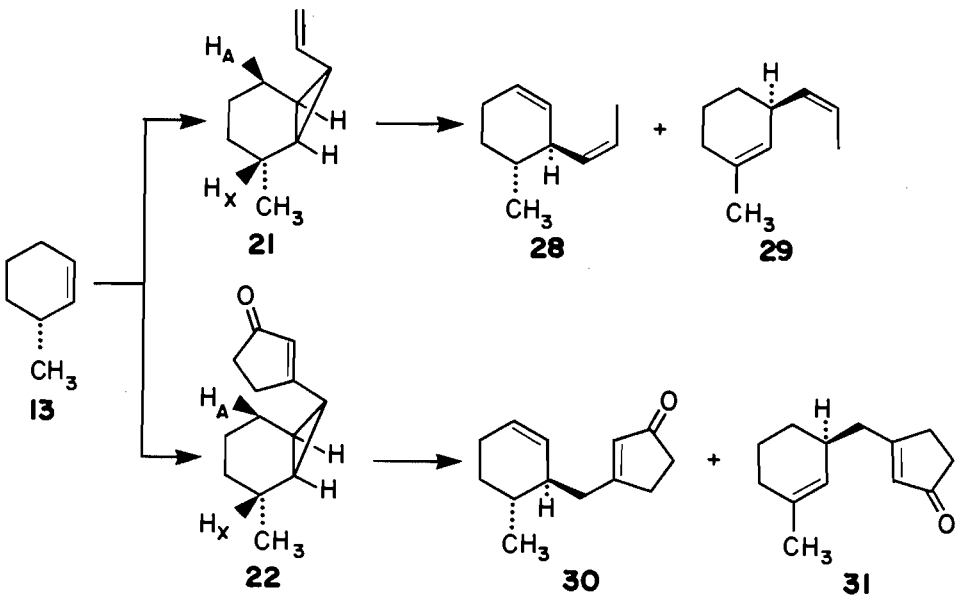

21 **28** **29** **13** **22** **30** **31**

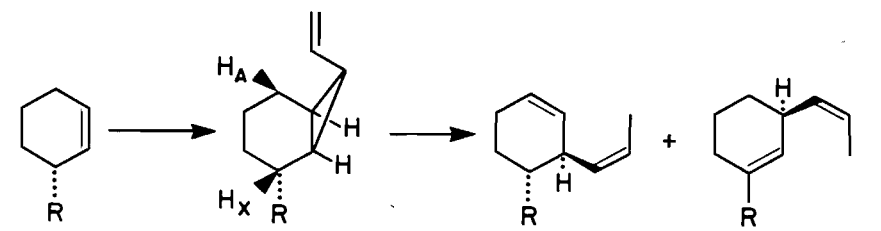

14 R = C_6H_5 **15** R = $SiMe_3$ **23** R = C_6H_5 **24** R = $SiMe_3$ **32** R = C_6H_5 **33** R = C_6H_5 **34** R = $SiMe_3$

Can. J. Chem. Downloaded from www.nrcresearchpress.com by 210.87.254.105 on 09/06/12
For personal use only.

Can. J. Chem. Downloaded from www.nrcresearchpress.com by 210.87.254.105 on 09/06/12
For personal use only.

of a conjugated carbonyl group on the vinyl function is not crucial in determining the site-selectivity of the sigmatropic rearrangements. Thus, question (a), above, may be answered negatively. With respect to the effect of substituents, experiments 1–3 show, in agreement with previous results (9) (eq. [3]), that an oxygen-containing group impressively retards the rate of hydrogen migration. On the other hand, a methyl group has very little effect on the site-selectivity of the process (experiments 4 and 5), while a phenyl substituent moderately facilitates the migration of an adjacent hydrogen (experiment 6). In sharp contrast to the OMe group, the Me_3Si moiety markedly enhances the ease of hydrogen migration (experiment 7). Thus, remarkably, thermolysis of the structurally comparable substrates **18** and **24** provides, exclusively, products resulting from migration of H_A and H_X, respectively. Clearly, quite apart from speculation regarding the underlying cause(s) of this site-selectivity, these observations could well be of considerable value in organic synthesis.

Although a definitive rationalization of the results obtained from this preliminary study is difficult, it is tempting to tentatively postulate that in the transition states of these sigmatropic rearrangements, there is an accumulation of electron density ("partial negative charge") at the carbon from which the hydrogen migrates. On this basis, the slight rate-retarding effect of a methyl group and the moderate rate-enhancing effect of a phenyl group (stabilization of negative charge by resonance and (or) inductive effects) can be understood. Furthermore, the ability of the Me_3Si group to stabilize adjacent negative charge is well documented (12). On the other hand, it is more difficult, on the basis of this postulate, to account for the effect of OR groups.[4] However, it seems possible that the transition states which would be involved in the migration of H_X in substrates **7**, **8**, and **18–20** could be destabilized by interaction of the "partial negative charge" on carbon with the lone pairs of electrons on oxygen.

[4]Does an oxygen atom stabilize or destabilize an adjacent negative charge? It appears that the answer to this question is not clear-cut, although evidence suggests that the effect is destabilizing when the carbanion is planar or nearly planar (negative charge associated with a *p* orbital) (13). For other reports related to this general question, see ref. 14.

Acknowledgements

We are grateful to the Natural Sciences and Engineering Research Council of Canada for financial support and to MacMillan Bloedel Limited and the University of British Columbia for Graduate Fellowships to A.R.M.

1. R. J. Ellis and H. M. Frey. J. Chem. Soc. 5578 (1964).
2. W. R. Roth and J. Konig. Justus Liebigs Ann. Chem. **688**, 28 (1965).
3. C. W. Spangler. Chem. Rev. **76**, 187 (1976).
4. E. M. Mil'vitskaya, A. V. Tarakanova, and A. F. Plate. Russ. Chem. Rev. **45**, 469 (1976).
5. E. J. Corey, H. Yamamoto, D. K. Herron, and K. Achiwa. J. Am. Chem. Soc. **92**, 6635 (1970).
6. E. J. Corey and D. K. Herron. Tetrahedron Lett. 1641 (1971).
7. B. M. Trost and P. L. Ornstein. J. Org. Chem. **47**, 748 (1982).
8. G. Ohloff. Tetrahedron Lett. 3795 (1965).
9. E. Piers, I. Nagakura, and J. E. Shaw. J. Org. Chem. **43**, 3431 (1978).
10. M. Makosza and M. Fedorynski. Synth. Commun. **3**, 305 (1973).
11. C. Eaborn, R. Jackson, and R. Pearce. J. Chem. Perkin Trans 1, 2055 (1974); J. M. Reuter, A. Sinha, and R. G. Salomon. J. Org. Chem. **43**, 2438 (1978).
12. E. W. Colvin. Chem. Soc. Rev. **7**, 15 (1978).
13. J. M. Lehn and G. Wipff. J. Am. Chem. Soc. **98**, 7498 (1976).
14. J. Hine and P. D. Dalsin. J. Am. Chem. Soc. **94**, 6998 (1972); N. D. Epiotis, R. L. Yates, F. Bernardi, and S. Wolfe. J. Am. Chem. Soc. **98**, 5435 (1976); F. G. Bordwell, M. Van Der Puy, and N. R. Vanier. J. Org. Chem. **41**, 1885 (1976); J. F. Biellmann and J. B. Ducep. Org. React. **27**, 1 (1982); J. Hirsch and X. L. Wang. Synth. Commun. **12**, 333 (1982).

A simple and direct method of cyclization for the synthesis of a 10-membered ring[1]

Pierre Deslongchamps, Serge Lamothe,[2] and Ho-Shen Lin

Laboratoire de synthèse Organique, Département de Chimie, Faculté des Sciences, Université de Sherbrooke, Sherbrooke (Qué.), Canada J1K 2R1

Received June 25, 1984

Pierre Deslongchamps, Serge Lamothe, and Ho-Shen Lin. Can. J. Chem. **62**, 2395 (1984).

The malonate anion displacement of allylic chloride in a ten-carbon aliphatic chain containing one additional unsaturation center yields 10-membered cyclic compounds.

Pierre Deslongchamps, Serge Lamothe et Ho-Shen Lin. Can. J. Chem. **62**, 2395 (1984).

Le déplacement intramoléculaire d'un chlorure allylique par l'anion malonate transforme en cycle à dix membres une chaîne aliphatique de dix carbones contenant un autre site d'insaturation.

The study of medium and large rings (1) is an important area of research (2–8) which has not yet been explored in detail and one of the main reasons is the lack of reliable direct methods of synthesis. We wish to report the synthesis of 10-membered rings via a simple direct method of cyclization.[3]

Generally speaking, there are two factors which influence ring closure. The first is the frequency with which atoms placed at the end of a chain will come into reacting distance (entropy

[1]This work was first presented as part of the 1983 Reuben Benjamin Sandin Lecture Series, University of Alberta, June 13–16, 1983.

[2]NSERCC and FCAC predoctoral fellowships, 1983–1985.

[3]For a transition metal-induced cyclization method, see ref. 8.

Can. J. Chem. Downloaded from www.nrcresearchpress.com by 210.87.254.105 on 09/06/12
For personal use only.

of a conjugated carbonyl group on the vinyl function is not crucial in determining the site-selectivity of the sigmatropic rearrangements. Thus, question (a), above, may be answered negatively. With respect to the effect of substituents, experiments 1–3 show, in agreement with previous results (9) (eq. [3]), that an oxygen-containing group impressively retards the rate of hydrogen migration. On the other hand, a methyl group has very little effect on the site-selectivity of the process (experiments 4 and 5), while a phenyl substituent moderately facilitates the migration of an adjacent hydrogen (experiment 6). In sharp contrast to the OMe group, the Me_3Si moiety markedly enhances the ease of hydrogen migration (experiment 7). Thus, remarkably, thermolysis of the structurally comparable substrates **18** and **24** provides, exclusively, products resulting from migration of H_A and H_X, respectively. Clearly, quite apart from speculation regarding the underlying cause(s) of this site-selectivity, these observations could well be of considerable value in organic synthesis.

Although a definitive rationalization of the results obtained from this preliminary study is difficult, it is tempting to tentatively postulate that in the transition states of these sigmatropic rearrangements, there is an accumulation of electron density ("partial negative charge") at the carbon from which the hydrogen migrates. On this basis, the slight rate-retarding effect of a methyl group and the moderate rate-enhancing effect of a phenyl group (stabilization of negative charge by resonance and (or) inductive effects) can be understood. Furthermore, the ability of the Me_3Si group to stabilize adjacent negative charge is well documented (12). On the other hand, it is more difficult, on the basis of this postulate, to account for the effect of OR groups.[4] However, it seems possible that the transition states which would be involved in the migration of H_X in substrates **7**, **8**, and **18–20** could be destabilized by interaction of the "partial negative charge" on carbon with the lone pairs of electrons on oxygen.

[4]Does an oxygen atom stabilize or destabilize an adjacent negative charge? It appears that the answer to this question is not clear-cut, although evidence suggests that the effect is destabilizing when the carbanion is planar or nearly planar (negative charge associated with a *p* orbital) (13). For other reports related to this general question, see ref. 14.

Acknowledgements

We are grateful to the Natural Sciences and Engineering Research Council of Canada for financial support and to MacMillan Bloedel Limited and the University of British Columbia for Graduate Fellowships to A.R.M.

1. R. J. Ellis and H. M. Frey. J. Chem. Soc. 5578 (1964).
2. W. R. Roth and J. Konig. Justus Liebigs Ann. Chem. **688**, 28 (1965).
3. C. W. Spangler. Chem. Rev. **76**, 187 (1976).
4. E. M. Mil'vitskaya, A. V. Tarakanova, and A. F. Plate. Russ. Chem. Rev. **45**, 469 (1976).
5. E. J. Corey, H. Yamamoto, D. K. Herron, and K. Achiwa. J. Am. Chem. Soc. **92**, 6635 (1970).
6. E. J. Corey and D. K. Herron. Tetrahedron Lett. 1641 (1971).
7. B. M. Trost and P. L. Ornstein. J. Org. Chem. **47**, 748 (1982).
8. G. Ohloff. Tetrahedron Lett. 3795 (1965).
9. E. Piers, I. Nagakura, and J. E. Shaw. J. Org. Chem. **43**, 3431 (1978).
10. M. Makosza and M. Fedorynski. Synth. Commun. **3**, 305 (1973).
11. C. Eaborn, R. Jackson, and R. Pearce. J. Chem. Perkin Trans 1, 2055 (1974); J. M. Reuter, A. Sinha, and R. G. Salomon. J. Org. Chem. **43**, 2438 (1978).
12. E. W. Colvin. Chem. Soc. Rev. **7**, 15 (1978).
13. J. M. Lehn and G. Wipff. J. Am. Chem. Soc. **98**, 7498 (1976).
14. J. Hine and P. D. Dalsin. J. Am. Chem. Soc. **94**, 6998 (1972); N. D. Epiotis, R. L. Yates, F. Bernardi, and S. Wolfe. J. Am. Chem. Soc. **98**, 5435 (1976); F. G. Bordwell, M. Van Der Puy, and N. R. Vanier. J. Org. Chem. **41**, 1885 (1976); J. F. Biellmann and J. B. Ducep. Org. React. **27**, 1 (1982); J. Hirsch and X. L. Wang. Synth. Commun. **12**, 333 (1982).

A simple and direct method of cyclization for the synthesis of a 10-membered ring[1]

Pierre Deslongchamps, Serge Lamothe,[2] and Ho-Shen Lin

Laboratoire de synthèse Organique, Département de Chimie, Faculté des Sciences, Université de Sherbrooke, Sherbrooke (Qué.), Canada J1K 2R1

Received June 25, 1984

Pierre Deslongchamps, Serge Lamothe, and Ho-Shen Lin. Can. J. Chem. **62**, 2395 (1984).

The malonate anion displacement of allylic chloride in a ten-carbon aliphatic chain containing one additional unsaturation center yields 10-membered cyclic compounds.

Pierre Deslongchamps, Serge Lamothe et Ho-Shen Lin. Can. J. Chem. **62**, 2395 (1984).

Le déplacement intramoléculaire d'un chlorure allylique par l'anion malonate transforme en cycle à dix membres une chaîne aliphatique de dix carbones contenant un autre site d'insaturation.

The study of medium and large rings (1) is an important area of research (2–8) which has not yet been explored in detail and one of the main reasons is the lack of reliable direct methods of synthesis. We wish to report the synthesis of 10-membered rings via a simple direct method of cyclization.[3]

Generally speaking, there are two factors which influence ring closure. The first is the frequency with which atoms placed at the end of a chain will come into reacting distance (entropy

[1]This work was first presented as part of the 1983 Reuben Benjamin Sandin Lecture Series, University of Alberta, June 13–16, 1983.

[2]NSERCC and FCAC predoctoral fellowships, 1983–1985.

[3]For a transition metal-induced cyclization method, see ref. 8.

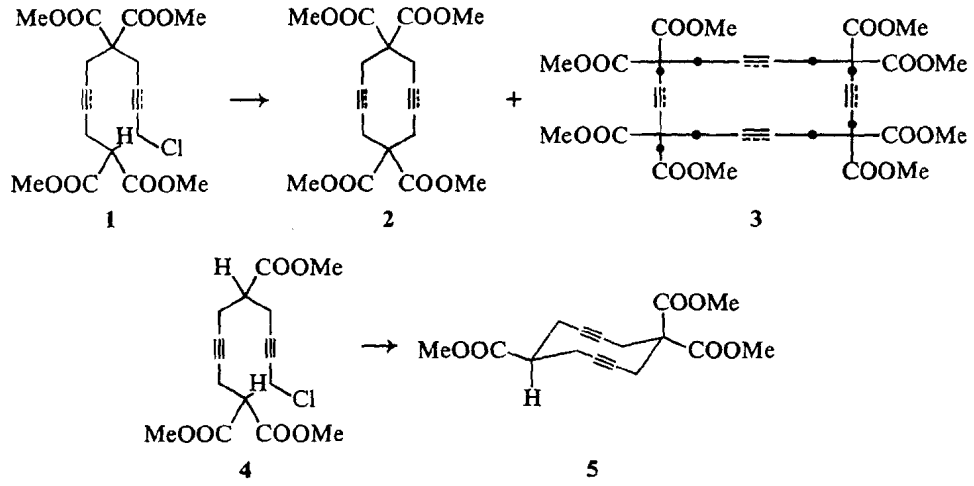

SCHEME 1

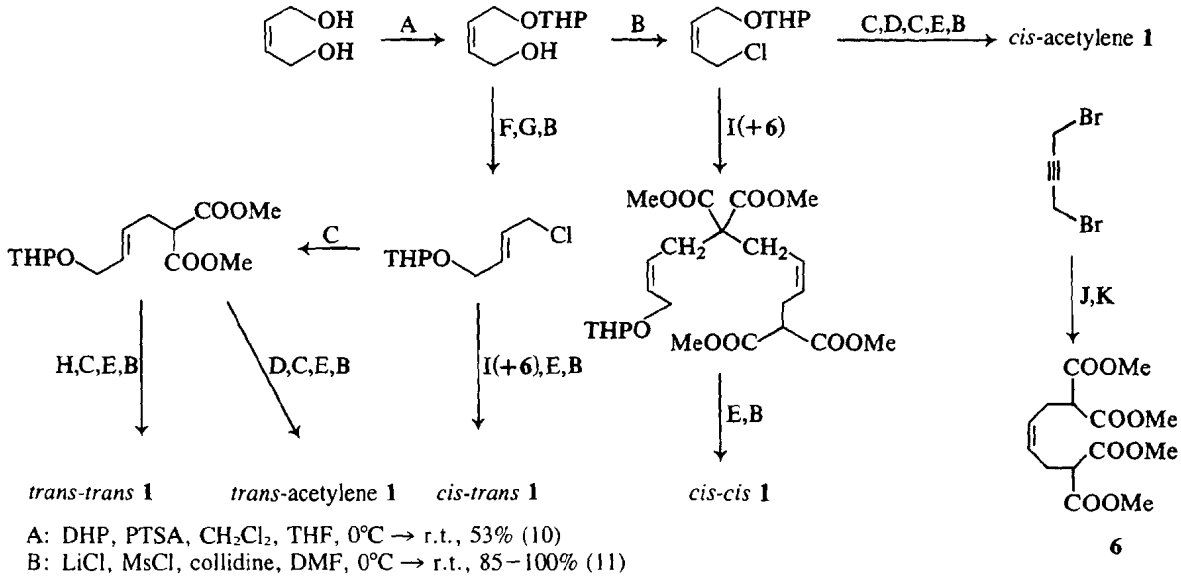

A: DHP, PTSA, CH_2Cl_2, THF, 0°C → r.t., 53% (10)
B: LiCl, MsCl, collidine, DMF, 0°C → r.t., 85–100% (11)
C: $CH_2(CO_2Me)_2$, K_2CO_3, DMF–THF, 90°C, 85–94%
D: $ClCH_2C{\equiv}CCH_2Cl$, K_2CO_3, DMF–THF, 90°C, 55–73%
E: MeOH, PPTS, r.t., 90–96% (12)
F: PCC, AcONa, CH_2Cl_2, M.S. 4 Å, r.t., 80% (13)
G: DIBAH, CH_2Cl_2, 0°C, 89% (14)
H: $ClCH_2CH{=}CHCH_2Cl$ (*trans*), K_2CO_3, DMF–THF, 90°C, 70–85%
I : Benzene, sodium *tert*-amylate, reflux, 31–38%
J : MeONa, $CH_2(CO_2Me)_2$, MeOH, 45°C, 40%
K: Benzene, quinoline, 5% $Pd/BaSO_4$, H_2, r.t., 99%

SCHEME 2

effect) and the second is the sum of steric and stereoelectronic interactions due to ring closure (enthalpy effect). The synthesis of medium rings is disfavored by the entropy effect (the chain is too long and the number of degrees of freedom is too large) and by severe transannular steric interactions.

In principle, a very simple approach for the synthesis of medium rings is to find a device to restrict the rotational possibilities of the chain (9) and to eliminate transannular steric interactions. A very simple device is to replace two methylene groups of a chain by a double (and (or) triple) bond. This has the effect of diminishing the number of degrees of freedom of the chain and, if more than one double (and (or) triple) bond is used and appropriately located in the chain, it could eliminate at the same time most of the transannular steric interaction. Examination of molecular models indicates that this might well be the case for the 10-membered ring system **2** (Scheme 1) having either double bonds (*cis* or *trans*) and (or) triple bonds. Interestingly, in the cyclization **1** → **2**, there are only six degrees of freedom and space filling models do not indicate severe transannular steric interactions, except for **2** having two triple bonds. The appropriate acyclic ten-carbon precursors **1** were synthesized[4] (Schemes 2 and 3) and the cyclization was

[4]For all new substances, the spectra (ir, 250 MHz and 60 MHz ^1H nmr, ^{13}C nmr, and high resolution mass spectra) were in complete agreement with the assigned structures.

Can. J. Chem. Downloaded from www.nrcresearchpress.com by 210.87.254.105 on 09/06/12
For personal use only.

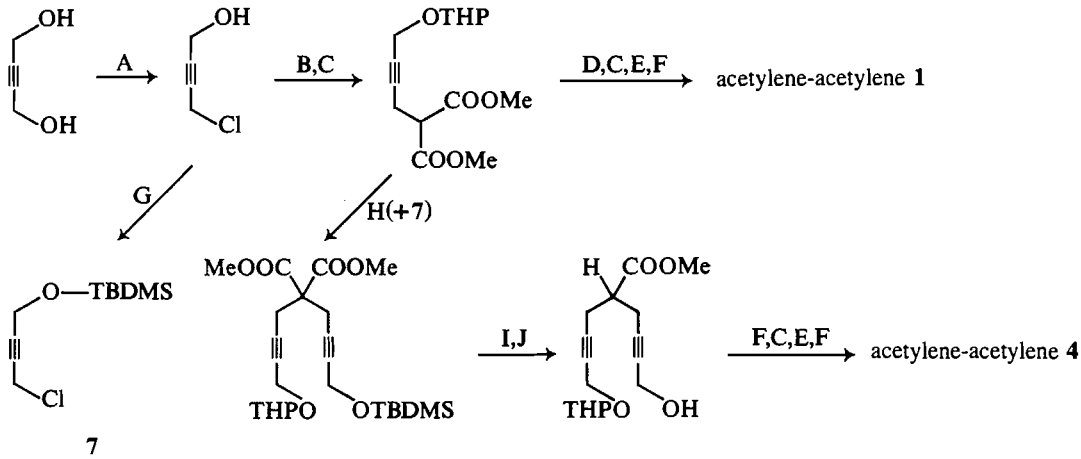

A: $SOCl_2$, Py, Benzene, r.t., 50% (15)
B: DHP, CF_3CO_2H, CH_2Cl_2, r.t., 95%
C: $CH_2(CO_2Me)_2$, K_2CO_3, DMF–THF, 90°C, 91–93%
D: $ClCH_2C{\equiv}CCH_2Cl$, K_2CO_3, DMF–THF, 90°C, 60%
E: MeOH, PPTS, r.t., 94% (12)
F: LiCl, MsCl, collidine, DMF, 0°C → r.t., 92–95% (11)
G: TBDMSCl, Et_3N, CH_2Cl_2, r.t., 84% (16)
H: K_2CO_3, DMF–THF, 90°C
I : *n*-$Bu_4N^+F^-$, THF, r.t., 58% (H + I) (16)
J : NaCN, DMSO, 100°C, 53% (17)

SCHEME 3

TABLE 1. Cyclization products

Starting material 1		*M*	Monomer 2	Dimer 3
cis, *cis**	K_2CO_3/acetone, 4 days	10^{-2}	84	—
cis, *trans*	K_2CO_3/DMF–THF, 32 h	10^{-2}	44	25
trans, *trans*	K_2CO_3/DMF–THF, 26 h	10^{-2}	10	42
		10^{-3}	43	13
Acetylene, *cis*	K_2CO_3/DMF–THF, 24 h	10^{-2}	60	17
		10^{-3}	73	9
Acetylene, *trans*	K_2CO_3/DMF–THF, 26 h	10^{-2}	17	35
		10^{-3}	57	15
Acetylene, acetylene†	K_2CO_3/DMF–THF, 12 h	10^{-2}	26	40
		10^{-3}	39	12

*For a very similar cyclization giving a *cis*,*cis* monomer see ref. 6.
†See ref. 7 for a similar cyclization.

studied at 10^{-2} and 10^{-3} molar solutions, and not high dilution. The results are described in Table 1. Each acyclic precursor **1** gave the corresponding cyclic monomer **2** and dimer **3**, except for the *cis-cis* acyclic case (6) which gave only the cyclic monomer **2**. Even the cyclic monomer **2** (7) having two triple bonds was formed in a reasonable yield. All cyclic compounds are crystalline and it is interesting to notice that the dimerization process yielding the 20-membered ring always competes favorably with polymerization.

In the above cyclization, two of the four carbomethoxy groups of the chain take a pseudo-axial position in the 10-membered ring and this must create additional steric interactions which should disfavor monomer formation. Accordingly, the cyclization of diacetylene **4** (Scheme 1), having only one carbomethoxy group in the middle of the chain, was studied and it was found to give a respectable 70% yield of monomer **5** along with 13% of the corresponding cyclic dimer.

Takahashi *et al.* (4) have recently shown that the intramolecular alkylation of cyanohydrin ethers is an excellent general method for the direct production of 2,6-cyclodecadienones. Previously, Ito and co-workers (3) had demonstrated that the anion-induced cyclization of epoxy-phenyl sulfides was also a convenient and efficient route to macrocyclic germacradienes.

The 10-membered ring is one of the most difficult medium rings to synthesize. The above studies constitute examples (18) that the synthesis of medium and large rings by a simple direct method of cyclization is indeed possible.

The development of new direct methods using various organic reactions for the construction of a large variety of medium and large rings via the above general strategy is now in progress in our laboratory.

Acknowledgements

This research was supported by the Natural Sciences and Engineering Research Council of Canada (NSERCC) and by

Can. J. Chem. Downloaded from www.nrcresearchpress.com by 210.87.254.105 on 09/06/12
For personal use only.

the "Ministère de l'Éducation (F.C.A.C.) du Québec." Financial assistance in the form of an unrestricted grant from Merck Frosst Canada Inc. is also appreciated.

1. (*a*) J. DALE. *In* Topics in stereochemistry. Vol. 9. *Edited by* N. L. Allinger and E. L. Eliel. Interscience, New York, NY. 1976. pp. 199–270; (*b*) Angew. Chem. Int. Ed. Engl. **5**, 1000 (1966); (*c*) V. PRELOG. Pure Appl. Chem. **6**, 545 (1963); (*d*) R. A. RAPHAEL. Proc. Chem. Soc. (London), 97 (1962); (*e*) J. SICHER. Prog. Stereochem. **3**, 202 (1962).
2. (*a*) P. DESLONGCHAMPS. Aldrichimica Acta. In press; (*b*) Bull. Soc. Chim. Fr. In press.
3. (*a*) M. KODAMA, S.-I. YOKOO, H. YAMADA, and S. ITÔ. Tetrahedron, **34**, 3121 (1978); (*b*) M. KODAMA, Y. MATSUKI, and S. ITÔ. Tetrahedron Lett. 3065 (1975); 1121 (1976).
4. (*a*) T. TAKAHASHI, T. NAGASHIMA, and J. TSUJI. Tetrahedron Lett. **22**, 1359 (1981); (*b*) T. TAKAHASHI, H. NEMOTO, and J. TSUJI. Tetrahedron Lett. **24**, 2005 (1983); (*c*) Tetrahedron Lett. **24**, 3485 (1983).
5. (*a*) W. C. STILL. J. Am. Chem. Soc. **99**, 4186 (1977); (*b*) J. Am. Chem. Soc. **101**, 2493 (1979); (*c*) W. C. STILL, S. MURATA, G. REVIAL, and K. YOSHIHARA. J. Am. Chem. Soc. **105**, 625 (1983); (*d*) W. C. STILL and I. GALYNKER. Tetrahedron, **37**, 3981 (1981).
6. M. S. FRAZZA and B. W. ROBERTS. Tetrahedron Lett. **42**, 4193 (1981).
7. A. ETOURNAUD and H. WYLER. Helv. Chim. Acta, **56**, 625 (1973).
8. (*a*) E. J. COREY and E. HAMANAKA. J. Am. Chem. Soc. **89**, 2758 (1976); (*b*) Y. KITAGAWA, A. ITOH, S. HASHIMOTO, H. YAMAMOTO, and H. NOZAKI. J. Am. Chem. Soc. **99**, 3864 (1977); (*c*) M. B. TROST and R. W. WARNER. J. Am. Chem. Soc. **104**, 6112 (1982); (*d*) J. E. MCMURRY and J. R. MATZ. Tetrahedron Lett. **23**, 2723 (1982).
9. W. BAKER, J. F. W. MCOMIE, and W. D. OLLIS. J. Chem. Soc. 200 (1951).
10. K. F. BERNADY, M. B. FLOYD, J. F. POLETTO, and M. J. WEISS. J. Org. Chem. **44**, 1438 (1979).
11. E. W. COLINGTON and A. I. MEYERS. J. Org. Chem. **36**, 3044 (1971).
12. M. MIYASHITA, A. YOSHIKOSHI, and P. A. GRIECO. J. Org. Chem. **42**, 3772 (1977).
13. E. J. COREY and J. W. SUGGS. Tetrahedron Lett. **31**, 2647 (1975).
14. K. E. WILSON, R. T. SEIDER, and S. MASAMUNE. Chem. Commun. 213 (1970).
15. W. J. BAILEY and E. FUJIWARA. J. Am. Chem. Soc. **77**, 165 (1955).
16. E. J. COREY and A. VENKATESWARLU. J. Am. Chem. Soc. **94**, 6190 (1972).
17. A. P. KRAPCHO, G. A. GLYNN, and B. J. GRENON. Tetrahedron Lett. **3**, 215 (1967).
18. R. B. KELLY, D. M. MACDONALD, and K. WIESNER. Nature, **166**, 225 (1950).

Can. J. Chem. Downloaded from www.nrcresearchpress.com by 210.87.254.105 on 09/06/12
For personal use only.

syn–anti Stereoselection in the Diels–Alder reactions of spiro[bicyclo[2.2.2]octane-2,1′-[2,4]cyclopentadiene]

D. JEAN BURNELL, H. BRUCE GOODBRAND, STEPHANIE M. KAISER, AND ZDENEK VALENTA
Department of Chemistry, University of New Brunswick, Bag Service #45222, Fredericton, N.B., Canada E3B 6E2

Received May 28, 1984

D. JEAN BURNELL, H. BRUCE GOODBRAND, STEPHANIE M. KAISER, and ZDENEK VALENTA. Can. J. Chem. **62**, 2398 (1984).

No significant differences were found between the *syn* to *anti* adduct ratios established for the Diels–Alder cycloadditions, both thermal and catalysed, of spiro[bicyclo[2.2.2]octane-2,1′-[2,4]cyclopentadiene] (**1**) to a variety of dienophiles. This suggests that, in the *exo* region, the distance between the addends at the transition state is approximately the same in all the cases studied.

D. JEAN BURNELL, H. BRUCE GOODBRAND, STEPHANIE M. KAISER et ZDENEK VALENTA. Can. J. Chem. **62**, 2398 (1984).

On n'a pas trouvé de différences significatives entre les rapports *syn/anti* d'adduits formés lors des cycloadditions de Diels–Alder, thermiques ou catalysées, du spiro[bicyclo[2.2.2]octane[2.4]cyclopentadiène-2,1] (**1**) avec divers diénophiles. Ceci suggère que dans l'état de transition de la région *exo*, la distance entre les produits qui s'additionnent est approximativement la même dans tous les cas étudiés.

[Traduit par le journal]

Frontier molecular orbital calculations by Houk and Strozier (1) showed that secondary attractive interactions are much stronger in Lewis acid-catalysed Diels–Alder reactions than in thermally-induced reactions. Therefore, they reasoned, the transition state of a catalysed reaction could be expected to be "tighter" than that of a thermal reaction; this accounts well for the enhanced *endo* stereoselectivity and chiral induction observed in catalysed reactions. The tight-transition-state hypothesis has been extended to explain the greater *endo* stereoselectivity in the thermal reactions of more reactive dienophiles, such as maleic anhydride and *N*-phenylmaleimide, compared to less reactive dienophiles, such as acrolein and butenone (2). Consistent with this hypothesis, reactions involving more reactive dienophiles and, especially, catalysed reactions have smaller volumes of activation as determined by high-pressure techniques (3).

If the distance between the addends at the transition state decreases as the reaction rate increases, then, with a given plane-nonsymmetrical diene, the more reactive dienophiles should be closer to the source of plane-nonsymmetry at the transition state; consequently, greater *syn–anti* stereoselectivity should be observed with these dienophiles.

Because of its symmetry and the subtle steric difference between its two faces, compound **1**[1] seemed particularly attrac-

[1]The synthesis of **1** will be described in the full paper.

the "Ministère de l'Éducation (F.C.A.C.) du Québec." Financial assistance in the form of an unrestricted grant from Merck Frosst Canada Inc. is also appreciated.

1. (*a*) J. DALE. *In* Topics in stereochemistry. Vol. 9. *Edited by* N. L. Allinger and E. L. Eliel. Interscience, New York, NY. 1976. pp. 199–270; (*b*) Angew. Chem. Int. Ed. Engl. **5**, 1000 (1966); (*c*) V. PRELOG. Pure Appl. Chem. **6**, 545 (1963); (*d*) R. A. RAPHAEL. Proc. Chem. Soc. (London), 97 (1962); (*e*) J. SICHER. Prog. Stereochem. **3**, 202 (1962).
2. (*a*) P. DESLONGCHAMPS. Aldrichimica Acta. In press; (*b*) Bull. Soc. Chim. Fr. In press.
3. (*a*) M. KODAMA, S.-I. YOKOO, H. YAMADA, and S. ITÔ. Tetrahedron, **34**, 3121 (1978); (*b*) M. KODAMA, Y. MATSUKI, and S. ITÔ. Tetrahedron Lett. 3065 (1975); 1121 (1976).
4. (*a*) T. TAKAHASHI, T. NAGASHIMA, and J. TSUJI. Tetrahedron Lett. **22**, 1359 (1981); (*b*) T. TAKAHASHI, H. NEMOTO, and J. TSUJI. Tetrahedron Lett. **24**, 2005 (1983); (*c*) Tetrahedron Lett. **24**, 3485 (1983).
5. (*a*) W. C. STILL. J. Am. Chem. Soc. **99**, 4186 (1977); (*b*) J. Am. Chem. Soc. **101**, 2493 (1979); (*c*) W. C. STILL, S. MURATA, G. REVIAL, and K. YOSHIHARA. J. Am. Chem. Soc. **105**, 625 (1983); (*d*) W. C. STILL and I. GALYNKER. Tetrahedron, **37**, 3981 (1981).
6. M. S. FRAZZA and B. W. ROBERTS. Tetrahedron Lett. **42**, 4193 (1981).
7. A. ETOURNAUD and H. WYLER. Helv. Chim. Acta, **56**, 625 (1973).
8. (*a*) E. J. COREY and E. HAMANAKA. J. Am. Chem. Soc. **89**, 2758 (1976); (*b*) Y. KITAGAWA, A. ITOH, S. HASHIMOTO, H. YAMAMOTO, and H. NOZAKI. J. Am. Chem. Soc. **99**, 3864 (1977); (*c*) M. B. TROST and R. W. WARNER. J. Am. Chem. Soc. **104**, 6112 (1982); (*d*) J. E. MCMURRY and J. R. MATZ. Tetrahedron Lett. **23**, 2723 (1982).
9. W. BAKER, J. F. W. MCOMIE, and W. D. OLLIS. J. Chem. Soc. 200 (1951).
10. K. F. BERNADY, M. B. FLOYD, J. F. POLETTO, and M. J. WEISS. J. Org. Chem. **44**, 1438 (1979).
11. E. W. COLINGTON and A. I. MEYERS. J. Org. Chem. **36**, 3044 (1971).
12. M. MIYASHITA, A. YOSHIKOSHI, and P. A. GRIECO. J. Org. Chem. **42**, 3772 (1977).
13. E. J. COREY and J. W. SUGGS. Tetrahedron Lett. **31**, 2647 (1975).
14. K. E. WILSON, R. T. SEIDER, and S. MASAMUNE. Chem. Commun. 213 (1970).
15. W. J. BAILEY and E. FUJIWARA. J. Am. Chem. Soc. **77**, 165 (1955).
16. E. J. COREY and A. VENKATESWARLU. J. Am. Chem. Soc. **94**, 6190 (1972).
17. A. P. KRAPCHO, G. A. GLYNN, and B. J. GRENON. Tetrahedron Lett. **3**, 215 (1967).
18. R. B. KELLY, D. M. MACDONALD, and K. WIESNER. Nature, **166**, 225 (1950).

Can. J. Chem. Downloaded from www.nrcresearchpress.com by 210.87.254.6 on 09/06/12
For personal use only.

syn–anti Stereoselection in the Diels–Alder reactions of spiro[bicyclo[2.2.2]octane-2,1′-[2,4]cyclopentadiene]

D. JEAN BURNELL, H. BRUCE GOODBRAND, STEPHANIE M. KAISER, AND ZDENEK VALENTA
Department of Chemistry, University of New Brunswick, Bag Service #45222, Fredericton, N.B., Canada E3B 6E2

Received May 28, 1984

D. JEAN BURNELL, H. BRUCE GOODBRAND, STEPHANIE M. KAISER, and ZDENEK VALENTA. Can. J. Chem. **62**, 2398 (1984).

No significant differences were found between the *syn* to *anti* adduct ratios established for the Diels–Alder cycloadditions, both thermal and catalysed, of spiro[bicyclo[2.2.2]octane-2,1′-[2,4]cyclopentadiene] (**1**) to a variety of dienophiles. This suggests that, in the *exo* region, the distance between the addends at the transition state is approximately the same in all the cases studied.

D. JEAN BURNELL, H. BRUCE GOODBRAND, STEPHANIE M. KAISER et ZDENEK VALENTA. Can. J. Chem. **62**, 2398 (1984).

On n'a pas trouvé de différences significatives entre les rapports *syn/anti* d'adduits formés lors des cycloadditions de Diels–Alder, thermiques ou catalysées, du spiro[bicyclo[2.2.2]octane[2.4]cyclopentadiène-2,1] (**1**) avec divers diénophiles. Ceci suggère que dans l'état de transition de la région *exo*, la distance entre les produits qui s'additionnent est approximativement la même dans tous les cas étudiés.

[Traduit par le journal]

Frontier molecular orbital calculations by Houk and Strozier (1) showed that secondary attractive interactions are much stronger in Lewis acid-catalysed Diels–Alder reactions than in thermally-induced reactions. Therefore, they reasoned, the transition state of a catalysed reaction could be expected to be "tighter" than that of a thermal reaction; this accounts well for the enhanced *endo* stereoselectivity and chiral induction observed in catalysed reactions. The tight-transition-state hypothesis has been extended to explain the greater *endo* stereoselectivity in the thermal reactions of more reactive dienophiles, such as maleic anhydride and *N*-phenylmaleimide, compared to less reactive dienophiles, such as acrolein and butenone (2). Consistent with this hypothesis, reactions involving more reactive dienophiles and, especially, catalysed reactions have smaller volumes of activation as determined by high-pressure techniques (3).

If the distance between the addends at the transition state decreases as the reaction rate increases, then, with a given plane-nonsymmetrical diene, the more reactive dienophiles should be closer to the source of plane-nonsymmetry at the transition state; consequently, greater *syn–anti* stereoselectivity should be observed with these dienophiles.

Because of its symmetry and the subtle steric difference between its two faces, compound **1**[1] seemed particularly attrac-

[1]The synthesis of **1** will be described in the full paper.

TABLE 1. Diels–Alder adducts obtained by reaction with **1**

Dienophile	X	Y	Thermal Yield (%)	Thermal Type I/Type II[a]	Catalysed Yield (%)	Catalysed Type I/Type II[a]
Maleic anhydride	—C(=O)—O—C(=O)—		95	86:14	71	90:10
N-phenylmaleimide	—C(=O)—N(Ph)—C(=O)—		100	86:14	98	93:7
1,4-Benzoquinone	—C(=O)—CH=CH—C(=O)—		100	86:14	95	89:11
Dimethyl maleate	CO_2CH_3	CO_2CH_3	80	89:11	—	—
Acrolein	CHO	H	85	86:14	—	—
Methyl acrylate	CO_2CH_3	H	83	88:12	—	—
Butenone	$COCH_3$	H	61	89:11	—	—

[a]Ratios were determined by signal integration in the 360-MHz ^{1}H nmr spectra of adduct mixtures.

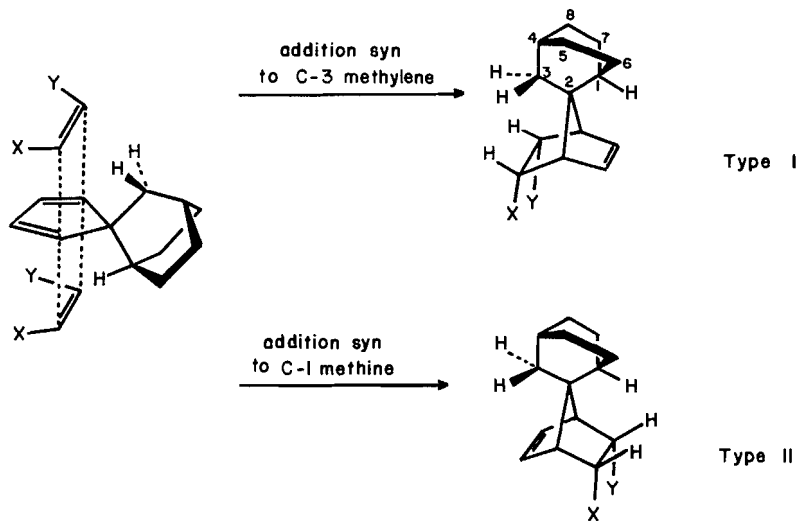

FIG. 1

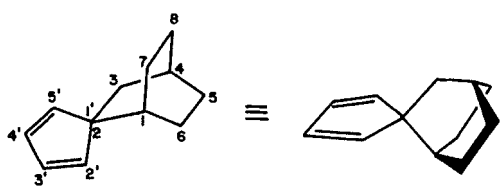

1

tive as a diene substrate with which to test this hypothesis (Fig. 1). Dichloromethane solutions of each of the dienophiles[2] listed in Table 1 were heated under reflux with **1**. Times required for complete reaction varied from a few hours with equimolar amounts of maleic anhydride, *N*-phenylmaleimide, and 1,4-benzoquinone, to a week with more than a forty-fold excess of butenone. Additions of **1** to dichloromethane solutions of three dienophiles, each in the presence of an equivalent of boron trifluoride etherate at −78°C, provided catalysed-reaction products.[3]

Every reaction gave a major and a minor adduct. The major one from the addition of maleic anhydride to **1** was isolated by repeated crystallization. Its Type I structure[4] was proven by irradiating the protons on the carbons α to its carbonyl groups, which resulted in a nuclear Overhauser enhancement of 11% for the signals arising from the protons on C-3 of its bicyclo[2.2.2]octane moiety.[5] Then, a comparison of the relative chemical shifts and the coupling constants of the signals in the 360-MHz ^{1}H nmr spectra of all the reaction products estab-

[2]The dienophiles were chosen to represent a range of reactivity while keeping the potential for steric interaction roughly constant; thus, during cycloaddition, each dienophile projects two hydrogens towards the bicyclo[2.2.2]octane moiety of **1**.

[3]Thermally-induced reaction of **1** with 1,4-benzoquinone proceeds relatively sluggishly at 0°C. However, by quenching the catalysed reaction mixture with an excess of cyclopentadiene, we have shown that, in the presence of the Lewis acid, adduct formation is essentially complete within 30 min at −78°C.

[4]This structure has been confirmed crystallographically by Dr. P. S. White of this Department. Details of this determination will be published in the full paper.

[5]We thank Dr. Thomas T. Nakashima of the University of Alberta for kindly running this experiment.

Can. J. Chem. Downloaded from www.nrcresearchpress.com by 210.87.254.6 on 09/06/12
For personal use only.

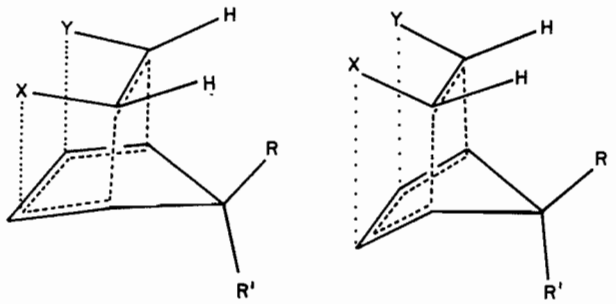

FIG. 2

lished that every major adduct was of Type I and that every minor adduct was of Type II (not an *exo*-addition product).

The Type I/Type II ratios given in Table 1 are very similar,[6] even though the relative rates of reaction must span several orders of magnitude. Steric interactions with the bicyclo-[2.2.2]octane moiety can be assumed to be important at both transition states, because both faces of **1** are much less reactive than cyclopentadiene itself.[7,8] This implies that the difference in steric hindrance between the two faces of **1** is nearly constant, regardless of the reaction rate, which in turn suggests that the relative positions of the sterically interacting groups must be similar in all the reactions summarized in Table 1.

This does not necessarily mean that the tight-transition-state hypothesis is incorrect. This hypothesis was formulated to explain phenomena associated with the *endo* region of a reacting diene. Our results must reflect the geometry of the *exo* region. Refining the hypothesis of Houk and Strozier (1) with the conclusions which we have drawn from our results with **1**, we can postulate a difference in transition-state geometry between a relatively reactive dienophile and a relatively unreactive one as shown in Fig. 2. Thus, in the *exo* region, the two transition states are geometrically very similar. In contrast, in the case of a relatively reactive dienophile, the secondary, ultimately non-bonding, atoms in the *endo* region are significantly closer together at the transition state. As can be appreciated from Fig. 2, the σ-bond-forming carbons of the less reactive system must have more sp^3 character at the transition state because its addends are less planar.[9] Therefore, this system may be regarded as being further along the reaction coordinate (as described by hybridization and not by the distance between the addends). This is in accord with Hammond's postulate (9), and it is still consistent with the volumes of activation data.

Acknowledgements

The support of this work by the Natural Sciences and Engineering Research Council of Canada in the form of an operating grant and a postgraduate scholarship to D.J.B. is gratefully acknowledged.

1. K. N. HOUK and R. W. STROZIER. J. Am. Chem. Soc. **95**, 4094 (1973).
2. K. SEGUCHI, A. SERA, Y. OTSUKI, and K. MARUYAMA. Bull. Chem. Soc. Jpn. **48**, 3641 (1975).
3. J. R. MCCABE and C. A. ECKERT. Acc. Chem. Res. **7**, 251 (1974); K. SEGUCHI, A. SERA, and K. MARUYAMA. Bull. Chem. Soc. Jpn. **47**, 2242 (1974).
4. R. S. ROUSE and W. E. TYLER III. J. Org. Chem. **26**, 3525 (1961).
5. R. GLEITER and L. A. PAQUETTE. Acc. Chem. Res. **16**, 328 (1983).
6. M. HARDY, P.-A. CARRUPT, and P. VOGEL. Helv. Chim. Acta, **59**, 1685 (1976); M. AVENATI, J.-P. HAGENBUCH, C. MAHAIM, and P. VOGEL. Tetrahedron Lett. **21**, 3167 (1980); J.-P. HAGENBUCH, P. VOGEL, A. A. PINKERTON, and D. SCHWARZENBACH. Helv. Chim. Acta, **64**, 1818 (1981); M. AVENATI, O. PILET, P.-A. CARRUPT, and P. VOGEL. Helv. Chim. Acta, **65**, 178 (1982); M. AVENATI, P.-A. CARRUPT, D. QUARROZ, and P. VOGEL. Helv. Chim. Acta, **65**, 188 (1982); M. AVENATI and P. VOGEL. Helv. Chim. Acta, **65**, 204 (1982); C. MAHAIM and P. VOGEL. Helv. Chim. Acta, **65**, 866 (1982); C. MAHAIM, L. SCHWAGER, P.-A. CARRUPT, and P. VOGEL. Tetrahedron Lett. **34**, 3603 (1983).
7. R. E. TOWNSHEND, G. RAMUNNI, G. SEGAL, W. J. HEHRE, and L. SALEM. J. Am. Chem. Soc. **98**, 2190 (1976).
8. L. A. BURKE, G. LEROY, and M. SANA. Theor. Chim. Acta, **40**, 313 (1975); L. A. BURKE and G. LEROY. Theor. Chim. Acta, **44**, 219 (1977).
9. G. S. HAMMOND. J. Am. Chem. Soc. **77**, 334 (1955).

[6]The adducts were not formed under equilibrating conditions, as the following results testify. Heating a dichloromethane solution of the above-mentioned pure Type I adduct under reflux for many hours failed to produce a mixture of Type I and Type II adducts. Furthermore, the *N*-phenylmaleimide adducts of **1** did not equilibrate with cyclopentadiene; neither did the 1,4-benzoquinone adduct of cyclopentadiene equilibrate with **1**.

[7]This was established by competitive experiments. 5,5-Dimethylcyclopentadiene is also much less reactive than cyclopentadiene (4).

[8]Recent studies (5, 6) have demonstrated that hyperconjugation can be important in controlling *syn*−*anti* stereoselection. Certain resonances in the ^{13}C nmr spectrum of **1** are significantly upfield of their expected positions (in $CDCl_3$, C-1 at δ 31.4 and, more significantly, C-3 at δ 28.9), which may be symptomatic of appreciable hyperconjugation of various σ-orbitals of the bicyclo[2.2.2]octane moiety with the diene π-orbital(s). At present, it is uncertain whether hyperconjugative effects in **1** are strong enough to modify the *syn*−*anti* stereoselectivity. We are investigating this possibility.

[9]*Ab initio* calculations of the butadiene plus ethylene system have shown that there is considerable sp^3 character for the reacting carbons at the transition state (7, 8).

Can. J. Chem. Downloaded from www.nrcresearchpress.com by 210.87.254.6 on 09/06/12
For personal use only.

Mechanistic variation in the reactions of substituted acetamides in aqueous sulfuric acid

LINDA M. DRUET AND KEITH YATES[1]

Department of Chemistry, University of Toronto, Toronto, Ont., Canada M5S 1A1

Received February 8, 1984

This paper is dedicated to Professor Peter Yates on the occasion of his 60th birthday

LINDA M. DRUET and KEITH YATES. Can. J. Chem. **62**, 2401 (1984).

The acid-catalyzed reactions of acetamide **1**, *N-tert*-butylacetamide **2**, and several *p*-substituted *N*-benzylacetamides (**3** = H, **4** = CH_3, **5** = OCH_3, **6** = Cl, **7** = NO_2) have been studied as a function of acidity and temperature over a wide range of aqueous sulfuric acid solutions (0–91%). Analysis of the reaction products and rate–acidity profiles revealed that four different mechanisms are operative over different acidity regions depending on the structure of the substrate. These are: two A-2 hydrolysis mechanisms with *N*-acyl fission of the substrate (with participation of one or several water molecules in the rate-determining step); A-1 hydrolysis with *N*-alkyl fission; and sulfonation, followed by hydrolysis. These conclusions are supported by three complementary and detailed kinetic treatments based on the hydration parameter, transition state activity coefficient, and excess acidity approaches. The acidity domains of each mechanism have been established for each substrate. The mechanistic conclusions are fully supported by the different values of $\Delta H^{\ddagger}$ and $\Delta S^{\ddagger}$ obtained in different regions of acidity.

LINDA M. DRUET et KEITH YATES. Can. J. Chem. **62**, 2401 (1984).

Opérant avec des solutions aqueuses d'acide sulfurique à des concentrations variant de 0 à 91%, on a étudié les réactions acido-catalysées de l'acétamide (**1**), du *N-tert*-butylacétamide (**2**) et de plusieurs *N*-benzylacétamides substitués en *para* (**3** = H, **4** = CH_3, **5** = OCH_3, **6** = Cl, **7** = NO_2) en fonction de l'acidité et de la température. Une analyse des produits de réaction ainsi que des courbes reliant les vitesses de réaction et l'acidité révèle que, suivant la nature du substrat, quatre mécanismes différents peuvent intervenir dans diverses régions d'acidité. Il s'agit de: deux mécanismes d'hydrolyse de type A-2 impliquant une rupture *N*-acyle du substrat (avec la participation d'une ou de plusieurs molécules d'eau dans l'étape déterminante); une hydrolyse de type A-1 impliquant une rupture *N*-alkyle; et une sulfonation suivie d'une hydrolyse. Ces conclusions sont en accord avec trois études cinétiques complémentaires et détaillées et qui sont basées sur des approches reliées au paramètre d'hydratation, au coefficient d'activité de l'étape déterminante et aux acidités en excès. Pour chacun des substrats, on a établi les domaines d'acidité associés à chacun des mécanismes. Les différentes valeurs de $\Delta H^{\ddagger}$ et de $\Delta S^{\ddagger}$ obtenues dans diverses régions d'acidité supportent bien les conclusions relatives aux mécanismes.

[Traduit par le journal]

Introduction

Most studies of amides in aqueous acid solution involve the normal acid-catalyzed hydrolysis process (1). In recent years, supporting evidence has appeared for the component processes of this mechanism, including pre-equilibrium oxygen protonation of the amide (2), and subsequent formation of a tetrahedral intermediate via nucleophilic attack by water molecules (3). The ^1H nmr results indicate that the accompanying proton exchange process, postulated to occur via a very small concentration of the *N*-protonated species (4), is consistent with the currently accepted hydrolysis mechanism, shown in eq. [1]. (In eq. [1] the number of water molecules involved in the rate-determining step is designated by *r*. Hydration of the various species by water molecules is not shown.)

The possibility of other types of amide hydrolysis in aqueous acid media has been considered by a few workers. The results of limited temperature, rate, and product studies on *N-tert*-alkylamides have suggested unimolecular *N*-alkyl cleavage of the *N*-protonated amide, shown in eq. [2] (5) although a similar A-1 scission of the predominant *O*-protonated form, to give initially the imido form of the product, cannot be ruled out. Temperature, rate, and substituent studies of nitro-substituted acetanilides led to the proposal (6) of unimolecular *N*-acyl cleavage of the protonated amide at high acid concentrations, as in eq. [3]. Acetanilide derivatives, and benzamides containing electron-donating ring substituents, have been shown to form sulfonated products, which subsequently undergo unimolecular hydrolysis (eq. [4]).

[1] $R'-C(=O)-NHR \underset{(fast)}{\overset{1/K_{AH^+}}{\rightleftharpoons}} R'-C(=OH^+)-NHR$

$R'-C(=OH^+)-NHR \xrightarrow[(slow)]{rH_2O} R'-C(OH)(OH_2^+)-NHR \xrightarrow{fast} R'-C(=O)-OH + RNH_3^+$

More recently, acid-catalysed hydrolyses of acylpyrroles have been shown to involve S_E2 mechanisms rather than typical A2 processes (7). It is thus evident that amide chemistry in aqueous acids does not always consist solely of a relatively straightforward hydrolytic process.

To investigate these possibilities further, the kinetic study reported here was undertaken. This involved acetamide **1**, *N-tert*-butylacetamide **2**, and a series of *N-para*-substituted benzylacetamides **3**–**7**. For these compounds, the occurrence of unimolecular *N*-alkyl fission would result in carbonium ions with varying degrees of inductive and resonance stabilization.

[1] Author to whom correspondence may be addressed.

Can. J. Chem. Downloaded from www.nrcresearchpress.com by 210.87.254.40 on 09/06/12
For personal use only.

Can. J. Chem. Downloaded from www.nrcresearchpress.com by 210.87.254.40 on 09/06/12
For personal use only.

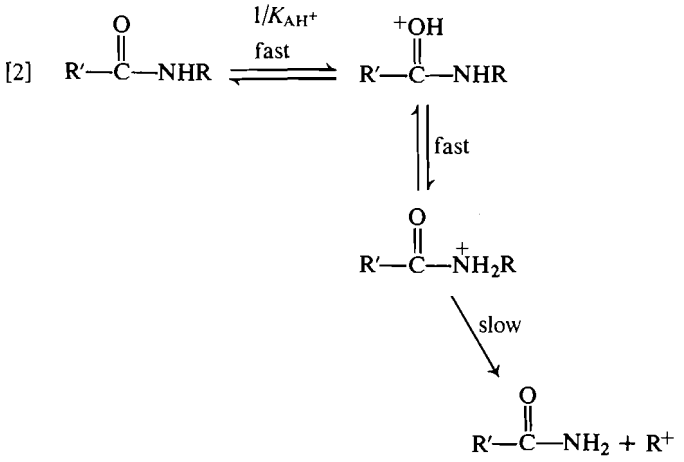

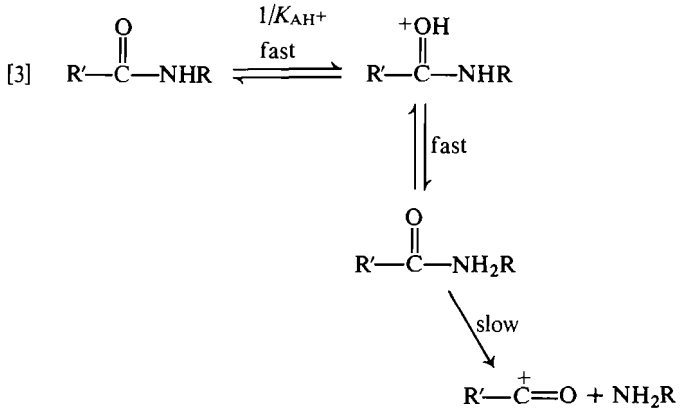

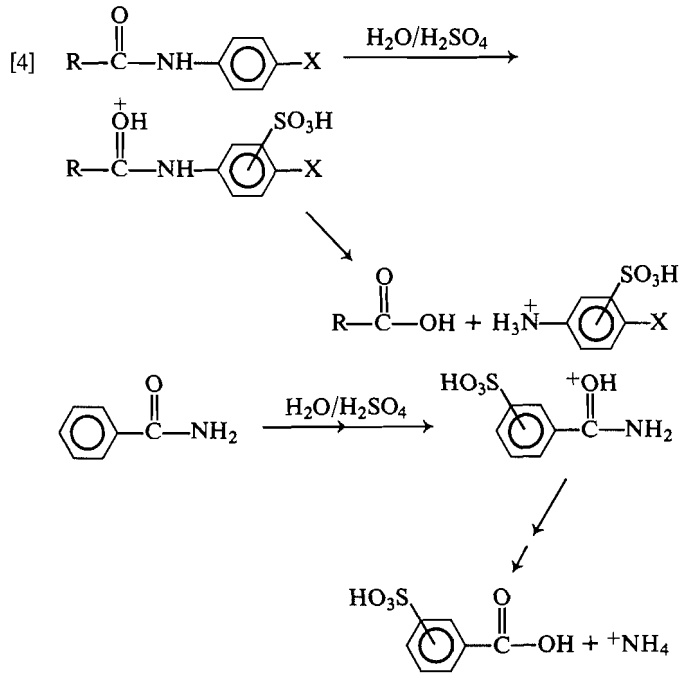

Since the *N*-benzyl substituents used range from strongly electron withdrawing to electron donating, their ability to form sulfonated products should also vary significantly. Acetamides were chosen to obviate possible complications from concurrent acylium ion formation.

Kinetic models currently used for analysis of amide hydrolysis data include the r (8) or ϕ (9) hydration parameter treatments, the transition state activity coefficient approach (10), and the excess acidity treatment (11). The theoretically linear hydration parameter plots are not obtained experimentally for amides. Actual plots for normal bimolecular hydrolysis are gently curved (3*b*, 3*c*, 9, 12). One proposed interpretation is medium variation of the activity coefficient ratio, log $(f_{SH^+}/f_{S^\ddagger_{p+r}})$ where, by conventional notation, f_{i_h} is a hydration activity coefficient and the subscript h is the species' average hydration number. Another explanation considered is a decrease in hydration number of the transition state with increasing acidity and therefore the occurrence of more than one individual rate process (3*c*, 12*c*). An explanation invoking more than one distinct reaction has also been used for substituted acetamides whose hydration plots show sharply changing curvature. This is consistent with a mechanistic change from a bimolecular to a unimolecular process at high acidities (6*e*, 6*f*).

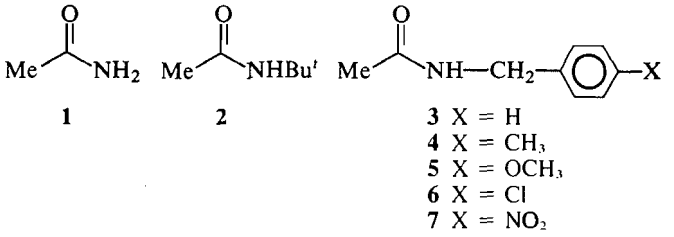

The shape of transition state activity coefficient (TSAC) plots (13) for amides closely parallels the shape for normal bimolecular ester hydrolysis (14), as is expected from the normal amide hydrolysis mechanism. The plot for β-lactam hydrolysis (13*c*) is similar to that for acylium ion formation in ester hydrolysis (15) and different from that for the proposed S_N2-like displacement process for acid-catalyzed oxygen exchange in methanol (16). It is therefore clear that the TSAC plots can provide evidence of diverse amide reaction mechanisms.

Application of the excess acidity treatment of rate data (11*b*, 17) to normal bimolecular amide hydrolysis has shown (18) that a gradual change of mechanism can occur. The observed rate constant can be dissected into two components, involving three water molecules in the rate-determining step in dilute acid, and one water molecule in more strongly acidic solutions. This treatment has yet to be applied to analysis of rate data which indicate abnormal amide behaviour in aqueous acids.

Experimental

Reagents

Sulfuric acid solutions were prepared by diluting CIL reagent grade sulfuric acid (≥95.5% w/w)[2] and were standardized either by titration against standard sodium hydroxide solution or by densitometry (Anton Paar Model DMA-02C). Perchloric acid solutions were prepared by diluting Fisher Reagent A.C.S. perchloric acid (≥70% w/w)[2] and acids were standardized by titration against standard sodium hydroxide solution.

Commercially available **1** was recrystallized from acetone. Compound **2** was prepared by adding acetyl chloride (136 mL) to a cooled solution of *tert*-butylamine (200 mL) in chloroform (400 mL). After filtration of *tert*-butylamine hydrochloride and subsequent solvent evaporation, the crude product was isolated and recrystallized from hexane to yield white crystals, mp 98.0–99.5°C (lit. (19) mp 97–98°C).

[2] All percentage acid values referred to subsequently are in w/w.

Can. J. Chem. Downloaded from www.nrcresearchpress.com by 210.87.254.40 on 09/06/12
For personal use only.

The Schotten–Baumann procedure (20) was used for the preparation of **4**, **6**, and **7**. In each case, recrystallization from toluene and hexane gave white crystals having melting points in good agreement with literature values (21).

Due to their low water solubility, **3** and **5** were prepared by a nonaqueous route. A solution of acetyl chloride (9.8 mL, 0.092 mol) in chloroform (15 mL) was slowly added to an ice-cooled solution of the appropriate benzylamine (20 mL, 0.18 mol) in chloroform (50 mL). After filtration, isolation of the crude product by solvent evaporation, and recrystallization from toluene and hexane, white crystals were obtained whose melting point agreed well with literature values (21*b*, 22). Chromatographic and elemental analyses were used to check the purity of all the amides.

Reaction products

A detailed ^{1}H nmr product study in 5.00–91.50% H_2SO_4 was carried out. For **2**, **3**, **4**, and **5** this involved a comparison of the ^{1}H nmr spectra of aqueous acid solutions containing reacted or unreacted amide both before and after addition of acetamide, acetic acid, ammonium sulfate, and the appropriate amine. For the *p*-methyl-, *p*-methoxy-, and unsubstituted benzylamines and benzyl alcohols, as well as for *tert*-butylamine and *tert*-butyl alcohol, the study involved ^{1}H nmr monitoring of aqueous acid solutions heated under the reaction conditions.

Nuclear magnetic resonance kinetic methods

The ^{1}H nmr chemical shifts of the amide (—*NH*C(O)—), phenyl, and methylene (—CH_2C(O)—) peaks of substituted *N*-benzylacetamides are acidity dependent. At lower acidities the amide, phenyl, and (or) methylene signals are obscured by the water peak, and kinetic measurements involved monitoring of the acetyl methyl signals of the substrate and product acetic acid. Above 82% H_2SO_4 the rate of change from the phenyl singlet of the substrate to that of the corresponding *N*-benzylammonium ion was measurable. The acetyl methyl signal of acetic acid was nearly coincident with that of the substrate at high acidities, necessitating either monitoring the phenyl region or utilization of expanded sweep widths for kinetic measurements. This chemical shift information is summarized in Table 1, which indicates which ^{1}H nmr signals were used for all kinetic measurements.

Three kinetic methods were employed, depending on the stability of the amide and its reactivity in a given aqueous acid. The standard quenching technique involved heating (thermostated oil bath) for recorded times an aqueous acid solution of the amide using sealed, thick-walled ^{1}H nmr tubes as reaction vessels, discontinuing timing when the tubes were removed from the bath and cooled for ^{1}H nmr analysis, and resuming timing upon return to the bath. A Varian T-60 or EM360 spectrometer was used for the analysis. The standard technique was generally employed except for special cases requiring one of the two *in situ* techniques.

In the *in situ* technique for faster reactions, one sealed glass insert containing D_2O and DSS (sodium 2,2-dimethyl-2-silapentane-5-sulfonate) was placed in the bottom of each cooled aqueous acid solution of the amide in regular ^{1}H nmr tubes, which were subsequently sealed. The probe of a Varian XL-100 nmr spectrometer was tuned at reaction temperature using one sample tube which was then quickly replaced by another, with concurrent starting of a timer and recording of peak integrals. In most cases the time required to reach probe temperature (1–3 min) was negligible in terms of the rate of reaction being studied. For the faster reactions, only the integrals obtained from solutions which had reached probe temperature were used to calculate k_ψ values. This procedure was used for following hydrolysis of **1** at 60.0 and 76.9°C in acidities near the maximum of the rate profile, and for hydrolysis of **4** at 60°C in ≥82.5% H_2SO_4 and at 76.9, 87.0, and 92.0°C in 77.7% H_2SO_4.

In the technique used for sparingly soluble amides, ca. 10^{-4} mol of amide and 0.5 mL of aqueous acid were stirred with a glass plunger in a regular ^{1}H nmr tube. A sealed glass insert (D_2O/DSS) was added to each tube, which was then sealed and cooled. One sample tube was inserted into the Varian XL-100 probe for instrument tuning and timing was begun. Peak integrations were obtained at recorded times. Dissolution of the amide was considered to be complete when the ratio of the peak heights of the total acetyl methyl signals (starting material plus product) to the peak height of the methyl signal of DSS from the insert was constant. This method was used to follow the hydrolysis of **6** and **7** in acidites up to 25% H_2SO_4.

With all three methods, 0.125–0.500 *M* amide solutions were employed. Reactions were followed for at least one, and usually two, half-lives. For the amides analyzed by the first two methods, duplicate or triplicate runs were carried out. Kinetics determined by the *in situ* technique for sparingly soluble amides were not generally performed in duplicate, therefore many nmr integrations were obtained to compensate for this. Good pseudo-first-order rate constants (correlation coefficients ≥0.990) were obtained from plots of ln([Pd] + [SM]/[SM]) vs. time, where [SM] and [Pd] are the nmr integral heights of a starting material peak and the corresponding product peak at time *t*. The standard deviations were generally better than ±10%, indicating good results within the limitations of the ^{1}H nmr method. Reduced precision in a few cases was due to either the low substrate concentrations used for sparingly soluble amides, or the short times involved in the case of the fastest reactions of **2**. In some cases, proximity of the monitored peaks of starting material and product also reduced the precision.

Hydration parameter plots[3]

The *r* treatment (8) involves plotting log k_ψ, the logarithm of the protonation-corrected rate constant, versus log a_{H_2O}. As shown in eq.

TABLE 1. ^{1}H nuclear magnetic resonance signals used for rate measurements

R—NHC(O)—CH_3	Acidity range % H_2SO_4	Peaks monitored
H—	4.0–73.5	Acetyl methyls[a]
4-Cl—$C_6H_4CH_2$—	8.2–82.5	Acetyl methyls[a]
	85.9–91.50	Acetyl methyls[b]
4-NO_2—$C_6H_4CH_2$—	8.2–85.9	Acetyl methyls[a]
C_6H_5—CH_2—	4.0–56.5	Acetyl methyls[a]
	63.75–77.7	Acetyl methyls[b]
	82.5	Phenyls[c]
	87.35–91.50	Phenyls[d]
4-CH_3—$C_6H_4CH_2$—	4.0–52.4	Distant methyls[a,e]
	63.75–72.8	Distant methyls[e,f]
	79.0–87.7	Distant methyls[e,g]
4-CH_3O—$C_6H_4CH_2$—	1.9–15.2	Acetyl methyls[a]
	15.2–73.5	Acetyl methyls[b]
	80.2–85.9	Phenyls[d]
$(CH_3)_3C$—	5.1–46.0	Acetyl methyls[b]
	54.7–72.8	Acetyl methyls[h]
	82.5–91.50	Acetyl methyls[i]

[a] Formation of HOAC from starting material.
[b] Formation of HOAC from starting material and acetamide, the latter two acetyl methyl peaks being coincident.
[c] Formation of the corresponding *N*-(*p*-substituted)benzylammonium ion and the corresponding *N*-(*p*-sulfobenzyl)acetamide from starting material.
[d] Formation of the corresponding ring-monosulfonated *N*-benzylacetamide from starting material.
[e] See accompanying text for definition.
[f] Formation of HOAC and acetamide from starting material.
[g] Formation of HOAC and the ring-monosulfonated *N*-(*p*-methylbenzyl)acetamide from starting material.
[h] Formation of HOAC from starting material and acetamide, the latter two acetyl methyl peaks being distinct.
[i] Formation of acetamide from starting material.

[3] All data used in this and subsequent kinetic treatments are available in the Ph.D. Thesis of L. Druet, University of Toronto, 1983.

Can. J. Chem. Downloaded from www.nrcresearchpress.com by 210.87.254.40 on 09/06/12
For personal use only.

[5], log k_p may be defined in terms of the ionization ratio, $I = [SH^+]/[S]$.

$$[5] \quad \log k_p = \log k - \log \frac{[SH^+]}{[SH^+] + [S]} = \log k - \log \frac{I}{I + 1}$$

Temperature-corrected I values were obtained using the excess acidity equation: $I = \text{antilog}\,(m^*X + pK_{AH^+} + \log [H^+])$ (17). Temperature-corrected X values, X_T, were obtained using eq. [6] (17). Temperature-corrected values of log $[H^+]$ were kindly supplied by Dr. R. A. Cox

$$[6] \quad X_T = X\left(\frac{298.15}{(273.15 + T)}\right)$$

(17*a*). Water activities in mole fraction units were available at any temperature by the method of Giauque *et al.* (23). These were later converted via the densities (24) to the molarity units typically used in the excess acidity plots.

Substrate activity coefficients

For the dilute solutions employed, values of D_0 and D_s, the distribution coefficients with water and the aqueous acid solution, respectively, were used to obtain medium effect activity coefficients, f_i, by eq. [7].The distribution coefficients for acetamides at 25°C in

$$[7] \quad f_i = \frac{D_0}{D_s}$$

chloroform/aqueous sulfuric acid mixtures were obtained by the nmr method outlined by McClelland (10*c*). These experimental activity coefficients were not corrected for the extent of protonation of substrate and the symbol f_i was therefore replaced by the more appropriate symbol $f_{([SH^+]+[S])exp}$. These values of $f_{([SH^+]+[S])exp}$ for **2**, **3**, **5**, and **6** were fitted to a polynomial expression of n terms ($y = a_0 + a_1 + a_2x^2 + \ldots + a_nx^n$). Activity values at any acidity were then available by interpolation. However, the validity of the polynomial expression was limited to acidities at most 5% higher than the highest acidity in which experimental values were obtained. For the four amides listed above, the highest acidity used for f_i measurements was 60.3%, 46.0%, 52.4%, and 46.0% H_2SO_4, respectively.

Transition state activity coefficients

As previously reported (10*c*), protonation corrections for the transition state activity coefficient, $f_{S^\ddagger}$, and the experimental activity coefficients f_i were unnecessary in the $f_{S^\ddagger}$ calculation through use of eq. [8]. Hydronium ion activities $a^*_{H^+}$ relative to tetraethylammonium ion are

$$[8] \quad \log f_{S^\ddagger} - \log k_0 = \log a^*_{H^+} + \log f_{([SH^+]+[S])exp} + pK_{AH^+} - \log k$$

available (10*a*). The rate constants for the four substrates (**2**, **3**, **5**, and **6**) were expressed at 25°C using plots of k_ψ vs. log a_{H_2O} (a_{H_2O} in molarity units) at several temperatures. For each water activity used in eq. [8] activation parameters were calculated and used to give k_ψ values at 25°C. The log k_0 values are intercepts of plots of % H_2SO_4 vs. the right-hand side of eq. [8]. Estimates of log $f_{S^\ddagger}$ were obtained by substitution of the other quantities into eq. [8].

Excess acidity treatment

Application of this treatment to rate data (11*b*, 18, 25) for each amide involved curve fitting, to give the optimum combination of two kinetic equations for the component processes. The analysis for **7** used equations for a single reaction temperature (76.9°C) (11*b*). Data for the other substrates were available at three or four temperatures (60, 76.9, 87.0, and 92.0°C) and the component kinetic expressions for these reactions required simple modifications which have been previously reported (11*b*, 18, 25). This modified treatment was used in the analysis of the rate data for **1**, **5**, and **6**.

The kinetic data for **4** and **5** at one temperature (76.9°C) and that for **3** at four temperatures (60.0, 76.9, 87.0, and 92.0°C) were fitted to a combination of equations for three component processes. For each substrate the optimum combination of kinetic expressions was identified by the fact that it gave the smallest root-mean-square error and standard deviation of all tested combinations.

Activation parameters

Two methods were used. The first (26) was a simple least-squares analysis of eq. [9], where h and k are the Planck and Boltzmann constants. It involved plotting ln (k/T) vs. $(1/T)$ at either constant acidity or water activity.

$$[9] \quad \ln k/T = \ln k/h + \Delta S^\ddagger/R - \Delta H^\ddagger/RT$$

Activation parameters at constant water activity (11*c*) were required for calculations of $f_{S^\ddagger}$. In this case temperature corrected values of log a_{H_2O} were used to obtain interpolated rate constants at 25°C for every value of log a_{H_2O} in which activity coefficients had been measured. The second method involved the excess acidity treatment for the five substrates for which kinetic data at several temperatures had been obtained. Solutions for the optimum kinetic expressions resulted in standard state activation parameters for the component processes along with standard state rate constants.

Results and discussion

Analysis of the complex behaviour of these seven acetamides in aqueous sulfuric acid required thorough product studies, which were performed under typical reaction conditions. In 5–80% H_2SO_4 **1**, **6**, and **7** were observed to form only the normal hydrolysis products, acetic acid and either ammonium ion in the case of acetamide hydrolysis or the corresponding *N*-benzylammonium ion in the case of the two latter amides. For the *p*-chloro compound another reaction product was observed and became the exclusive reaction product above 90% H_2SO_4. The peak signalling this new product was the distinctive ^1H nmr signal of ammonium ion (27). Under the reaction conditions, it must arise from normal acid-catalyzed hydrolysis of acetamide. The acetamide, in turn, must have come from *N*-alkyl cleavage of **6**. A unimolecular *N*-alkyl cleavage of the protonated amide is therefore postulated.

For the three other *N*-benzylacetamides (**3**–**5**) the normal hydrolysis products were found to be gradually replaced by *N*-alkyl cleavage products in moderately concentrated sulfuric acid solutions. The acidity at which normal hydrolysis products ceased to form varied from 82.5% to 63.75% to 52.4%, in these three cases, and *N*-alkyl cleavage products were formed in 63.75–87.35%, 60.3–87.7%, and 34.7–73.5% H_2SO_4, for **3**, **4**, and **5** respectively. It is clear that the amide producing the most stable *para*-substituted benzyl carbonium ion shows the onset of *N*-alkyl cleavage in the lowest acidity.

Precipitates were often found to accompany the *N*-alkyl cleavage process. For the reaction of **5** in 73.5% H_2SO_4, the crude material was isolated and the ^1H nmr spectrum in $CDCl_3$/TMS exhibited multiplets at δ 3.63–3.76 and δ 6.61–7.06 with integrals in the ratio 5:3. *p*-Methoxybenzyl alcohol subjected to the same conditions gave identical results, suggesting that dimerization of two molecules to form the ether has occurred in both cases. The precipitate formed by reaction of the amide or alcohol in lower acidities exhibited multiplets with similar chemical shifts and integrals in the ratio 5:4, a value which is in accord with a product resulting from polymerization of more than two molecules. Formation of this polymeric product is analogous to the result from N—C bond fission of *N*-benzylarylsulfonamides with concentrated sulfuric acid (28).

A third reaction pathway was indicated by the formation of other reaction products; the lowest acidity in which these were observed was 83.5%, 79.0%, and 79.0% H_2SO_4 for **3**, **4**, and **5** respectively. Formation of this product was detected by com-

Can. J. Chem. Downloaded from www.nrcresearchpress.com by 210.87.254.40 on 09/06/12
For personal use only.

parison of the ^1H nmr spectra of unreacted and completely reacted **3** in concentrated sulfuric acid. The product exhibits an amide NH signal, phenyl multiplet, methylene doublet, and acetyl methyl singlets. This and the integration support a ring-monosulfonated benzylacetamide as in **8**. Additional support for an amide product was obtained by dilution of the solution with water and subsequent heating. The resultant spectrum indicated acetic acid and a substituted *N*-benzylammonium ion, the expected products from normal amide hydrolysis of **8**. The nmr peaks due to the substituted *N*-benzylammonium ion were similar to those obtained from heating a solution of benzylamine in concentrated sulfuric acid.

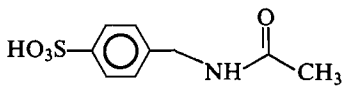

8

Sulfonation reactions of benzene and toluene under similar reaction conditions are well known (29). Several phenyl-substituted amides have been found to sulfonate (6*d*) in more concentrated sulfuric acid solutions, but acetanilide reacts similarly in acidities as low as 70% w/w H_2SO_4 (30). In addition, sulfonation in all acidities greater than 40% H_2SO_4 occurs with 4-chloro-*N*-phenylbenzamide and *N*-benzyl-4-chlorobenzamide (31).

A summary of the more complex results is shown in Fig. 1, which includes results for **1**. Identification of *tert*-butylamine, which results exclusively from normal hydrolysis of this amide, was possible only at 5.1% H_2SO_4, partly due to the coincidence of amine and amide methyl signals, as indicated in Table 1. Products due to *N*-alkyl cleavage were more easily identified: *tert*-butyl alcohol in acidities up to 72.8% H_2SO_4 and acetamide in 54.8–91.5% H_2SO_4. Appearance of the latter in lower acidities is obscured due to coincidence of its acetyl methyl peak with that of the substrate. Structures shown in brackets in Fig. 1(d) are those whose presence can only be inferred from the nmr spectra, due to coincidence of ^1H nmr signals in the case of acetamide and *tert*-butylamine or subsequent reaction in the case of *tert*-butyl alcohol.

Kinetics

For all seven substrates reaction rates were measured via ^1H nmr spectroscopy in dilute to concentrated sulfuric acid solutions. With the exception of **7** (76.9°C) and **1** (60.0, 76.94, 87.0°C), rates were generally measured at four reaction temperatures (60.0, 76.94, 87.0, and 92.0°C). Since the acid concentration is effectively constant in these solutions, good pseudo-first-order rate constants *k* were obtained from the standard analysis (ref. 26, pp. 230–232) of the data. The rate–acidity data obtained at 76.9°C are plotted in Fig. 2.[4]

The rate profiles exhibit four types of acidity dependence. For **1**, as well as for **6** and **7**, there is a rate maximum at intermediate acidities followed by a very slow reaction in more concentrated acids. For **3** and **4**, there is a rate maximum at intermediate acidities, followed by a sharp increase in rate in more concentrated acids. For **5**, there is the normally observed rate maximum at intermediate acidities followed first by a local

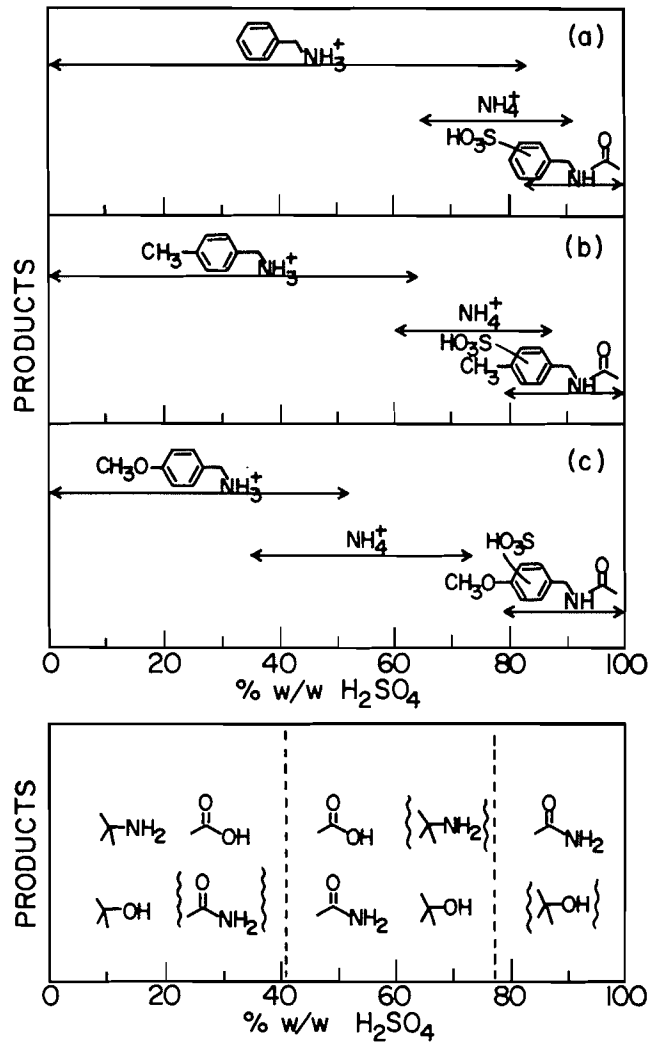

FIG. 1. Product ranges in aqueous acid for the reactions of **3** (a), **4** (b), **5** (c), and **2** (d). In (d) the presence of products shown in brackets is inferred from other products initially formed (see text).

minimum, second by a second local rate maximum at higher acidities, and finally by a sharp increase in rate in the most concentrated acids. Only for **2** is there a monotonic increase in reaction rate with increasing acid concentration.

Several interesting features are shown in Fig. 2. Firstly, the position of the rate maximum for **1** (ca. 22% H_2SO_4) agrees with other reports (12*e*). Secondly, the decreased reactivity of the secondary amides at low acidities relative to that of acetamide is striking but not completely unexpected (12*c*, 12*e*). Thirdly, the double rate maximum in the profile for **5** is a phenomenon unique to this amide. A study of the reactivity of this substrate in aqueous perchloric acid also resulted in a profile which exhibited two local rate maxima. Fourthly, the rate profile for **2** agrees well with earlier work (5*a*, 5*b*). This is the only substrate exhibiting a continuous increase in k_ψ with increasing acidity, with no indication of the typical bell-shaped profile normally found for acid-catalyzed amide hydrolysis.

On the basis of the product studies, it appears that the diversity in these rate profiles is due to at least three types of acid-catalyzed reaction. These include normal bimolecular amide hydrolysis, unimolecular *N*-alkyl cleavage to give a substituted carbonium ion and acetamide (which subsequently hydrolyses), and electrophilic aromatic substitution to give a

[4] Values of the measured pseudo-first-order rate constants for all seven substrates are in tables of supplementary material which are available, at a nominal charge, from the Depository of Unpublished Data, CISTI, National Research Council of Canada, Ottawa, Canada K1A 0S2.

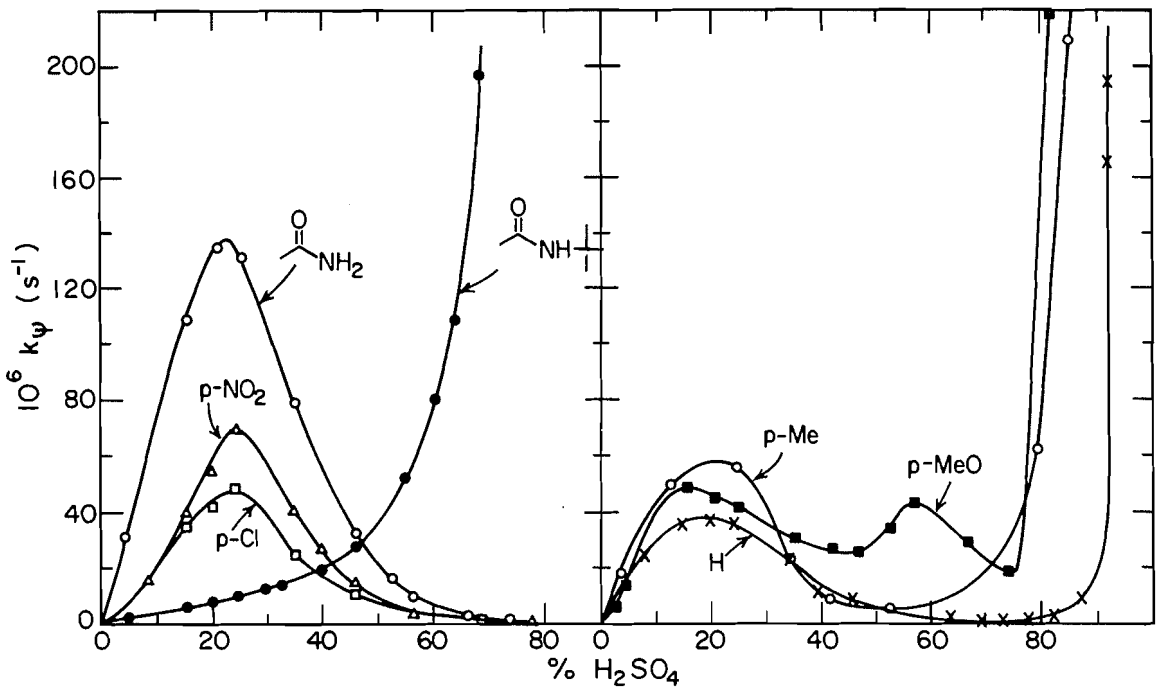

FIG. 2. Rate–acidity profiles for the reactions of acetamide (**1**), *N-tert*-butylacetamide (**2**), and substituted benzylacetamides (**3**–**7**). (all k_ψ measured at 76.9°C, except for **1** at 50.0°C.)

monosulfonated *N*-benzylacetamide. The question arises as to whether these quite different rate–acidity dependences can be treated quantitatively by a uniform approach. The results of three standard kinetic treatments will be presented in an attempt to answer this question, but first the acid dissociation constants of these amides must be considered, since they are needed for all three quantitative analyses.

Acid dissociation constants pK_{AH^+}

Accurate pK_{AH^+} values were obtained by application of the excess acidity method to ^1H chemical shifts of the substrates (16*b*). Differences in δ between pairs of well-spaced protons were employed. There was usually only one suitable set of values for each acetamide due to interference by solvent peaks. A curve-fitting computer analysis gave pK_{AH^+} values at absolute temperatures T_1 and T_2, respectively. Equation [10] assumes that the standard state enthalpy for the acid-dissociation

$$[10] \quad (pK_{AH^+})_2 = (pK_{AH^+})_1 \cdot \frac{T_1}{T_2}$$

reaction is essentially temperature independent. Any error introduced by this assumption should not significantly affect the present kinetic analysis.

The results are shown in Table 2. The trends in four of the pK_{AH^+} values are reasonable, in terms of substituent effects. The anomalously low value for the *p*-methyl compound may be attributable to difficulties encountered in the nmr measurements used for its pK_{AH^+} determination. *N-tert*-butylacetamide with $pK_{AH^+} = -0.41$ is the strongest base of all six amides, as intuitively expected. This was in good agreement with previously reported values for this amide (32).

r *Hydration parameter plots*

Equation [11] for the modified *r* hydration parameter treatment (7, 11*b*) states that if acidity is defined in terms of a function H_s which is strictly appropriate to the type of substrate

TABLE 2. Acid dissociation constants of *N-para*-substituted benzylacetamides[a] *p*-X—C_4H_4—CH_2—NH—C(O)—CH_3 at 25°C

X	pK_{AH^+}
CH_3O	−1.00
CH_3	−0.49
H	−1.13
Cl	−1.31
NO_2	−1.35

[a]The pK_{AH^+} value for acetamide (−0.73) was also obtained by the above method.

$$[11] \quad \log k_p = \log k + H_s = r \log a_{H_2O} + \text{constant}$$

being investigated, the slope of a plot of log k_p vs. log a_{H_2O} should correspond to the average number of water molecules required to convert a protonated substrate molecule to transition state. This is supported by the *r* plots obtained for **1** and **7**, which react solely via normal bimolecular (A-2) hydrolysis. As Fig. 3 shows, an initially steep dependence on water activity gradually changes above 50% H_2SO_4 to a much shallower dependence. This type of behaviour has been observed with other amides (12*c*).

A generally similar result was obtained with **6** up to the high acidity region where a negative curvature is evident. (This is more pronounced in the *r* plots constructed from the data for this substrate at higher temperatures.) Such curvature is in sharp contrast with that for normal A-2 amide hydrolysis (e.g. the published *r* plot of benzamide extends to 80% H_2SO_4 and has a positive curvature throughout (33).) Similar negative curvature in *r* plots for ester hydrolysis (34) has been associated with unimolecular (A-1) cleavage. For the *p*-chloro compound

Can. J. Chem. Downloaded from www.nrcresearchpress.com by 210.87.254.40 on 09/06/12
For personal use only.

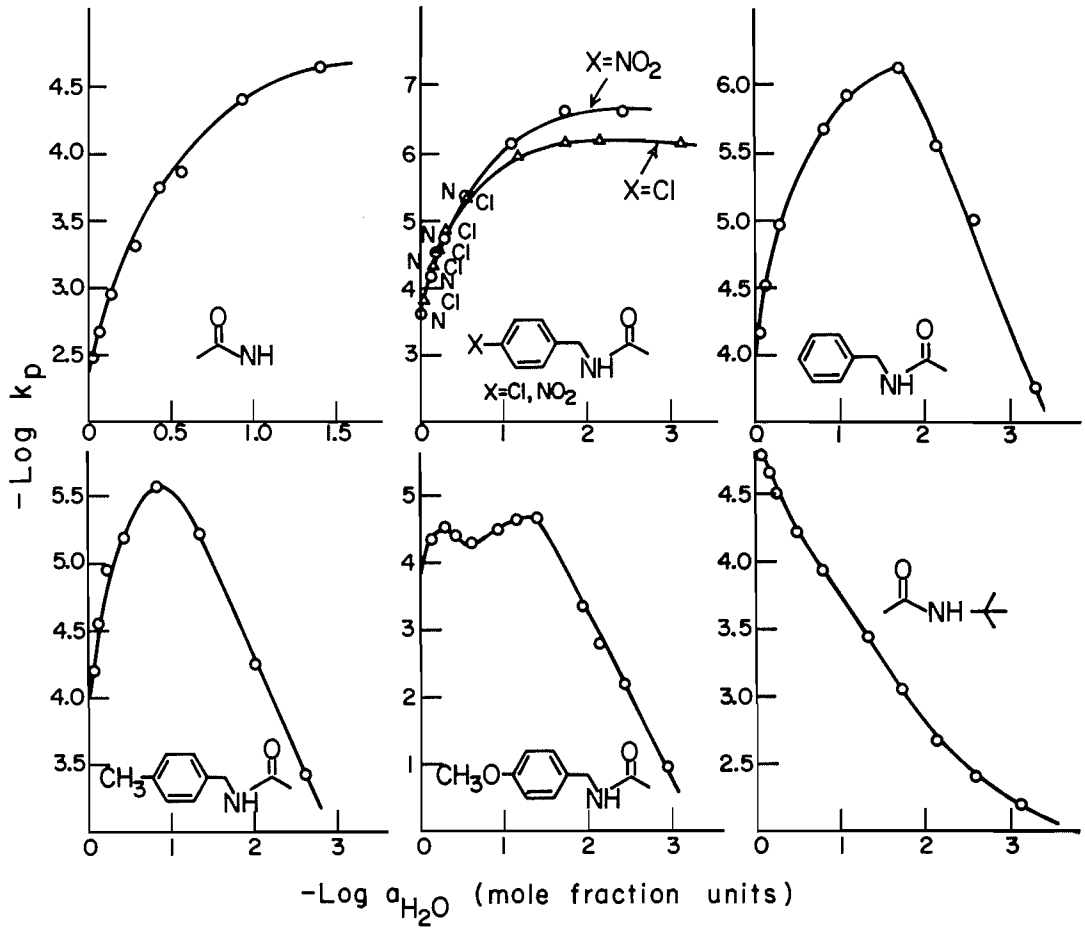

FIG. 3. r Hydration parameter plots of log k_ψ vs. log a_{H_2O} (see text) for substrates **1**–**7** at 76.9°C.

a unimolecular process is consistent with the *N*-alkyl cleavage indicated by the product study in higher acidities.

For **3** a water activity dependence typical of normal amide hydrolysis is observed up to 80% H_2SO_4 although typical hydrolysis products form exclusively only up to 60% H_2SO_4, where *N*-alkyl cleavage products begin to appear. The r plot in 60–80% H_2SO_4 apparently describes a combination of the normal hydrolyses of **3** and **1**, the latter having resulted from fast, prior *N*-alkyl cleavage of **3**. The strongly negative curvature above 80% H_2SO_4 markedly resembles the negative dependence found for *tert*-butyl acetate and *p*-methoxybenzyl acetate hydrolyses (34), for which A-1 reactions are the dominant processes at all acidities. (The sulfonation of **3** is probably a pseudo-first-order process also occurring in this acidity region.)

For **4**, the r-plot curvature expected for normal hydrolysis extends to 63.75% H_2SO_4. Above this acidity the onset of negative curvature indicates unimolecular *N*-alkyl cleavage, which is overtaken above 79% H_2SO_4 by sulfonation.

The sixth r plot in Fig. 3 exhibits a series of unique, sharp changes in slope. The gradually decreasing, positive curvature of the r plot for **5** indicates normal A-2 hydrolysis up to 40% H_2SO_4. The next two changes of slope, the negative curvature of a unimolecular process followed by the positive curvature of normal hydrolysis, may be explained by noting that the k_ψ values obtained by monitoring the acetyl methyl region were influenced by normal hydrolysis and *N*-alkyl cleavage, with each process influencing k_ψ to differing extents, depending on the acidity. In low acidities normal amide hydrolysis dominates k_ψ and the r plot curvature is positive. In 40–60% H_2SO_4 the A-1 cleavage reaction is of comparable importance in the overall k_ψ value and its effect is to make the r plot more negative. Thus the first negative region of the plot results. In 60–70% H_2SO_4 the A-1 cleavage reaction dominates the normal A-2 hydrolysis; therefore, conversion of substrate to acetamide is much faster than the measured formation of acetic acid. The r plot will reflect this slower process and again shows positive curvature for bimolecular hydrolysis of acetamide. The final negative curvature in the highest acidities is representative of the independence of the sulfonation reaction on water, for stabilization of its transition state.

This explanation for the r plot of **5** is consistent with the implications obtained from a comparison of the rate profile for this substrate with those of **1** and **2** in 20–80% H_2SO_4. This is illustrated in Fig. 4. It suggests that the overall reaction rate obtained by monitoring the acetyl methyl signals in 20–40% H_2SO_4 is dominated by amide hydrolysis. The overall rate in 40–60% H_2SO_4 is affected significantly by both hydrolysis and *N*-alkyl cleavage processes. The *N*-alkyl cleavage rate for **5** in 60–80% H_2SO_4 is so fast that only the subsequent acetamide hydrolysis is measured by the ^1H nmr method. The strongly negative water activity dependence exhibited by **2** in Figure 3 is analogous to that for the A-1 cleavage processes of *tert*-butyl acetate and *p*-methoxybenzyl acetate (15). There is no indication of positive r values at low acidities. This fact along with the detection of *tert*-butylamine only in 5.08% H_2SO_4 may

Can. J. Chem. Downloaded from www.nrcresearchpress.com by 210.87.254.40 on 09/06/12
For personal use only.

Can. J. Chem. Downloaded from www.nrcresearchpress.com by 210.87.254.40 on 09/06/12
For personal use only.

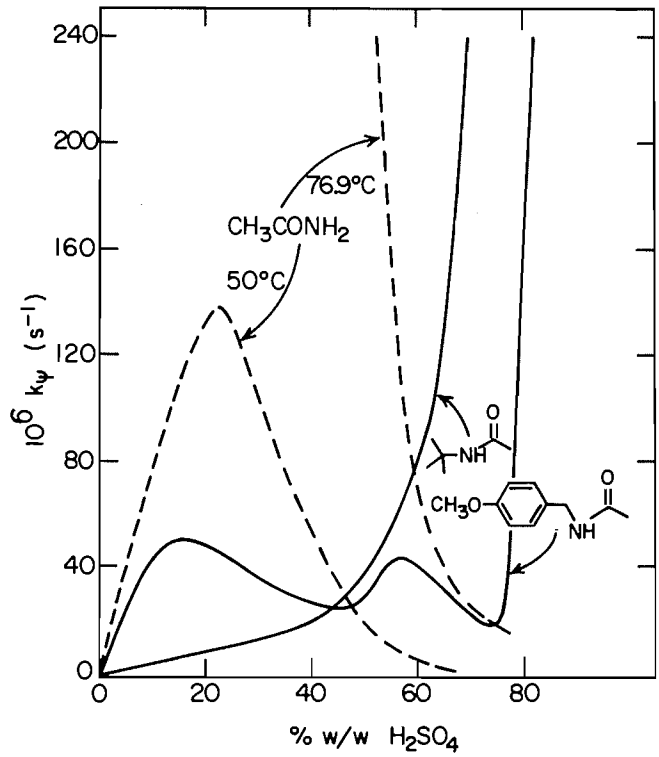

FIG. 4. Schematic comparison of the rate behaviour of **2** and **5** at 76.9°C with that of **1** at 50.0°C and 76.9°C.

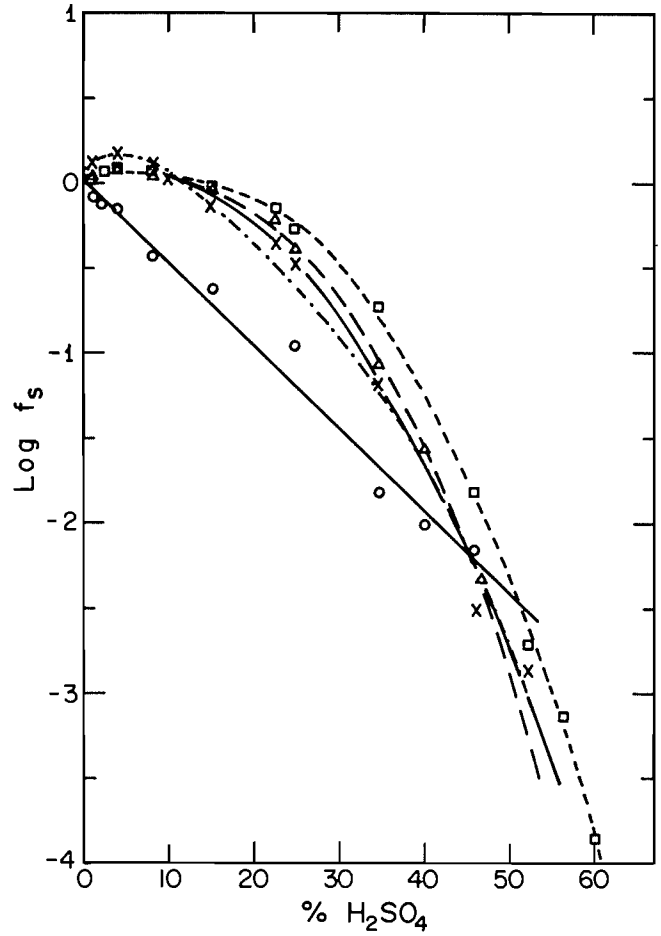

FIG. 5. Activity coefficient (lot f_s) behaviour of substituted acetamides as a function of acidity (% H_2SO_4). Open circles, **2**; triangles, **3**; crosses, **5**; squares, **6**.

mean that normal amide hydrolysis is only important in acidities less concentrated than this. Previous workers have not detected this process at any acidity (*5a*, *5b*, *5c*).

Transition state acidity coefficient treatment

Figure 5 includes values of $\log f_{([SH^+]+[S])exp}$, as well as the curve constructed from the polynomial expression for the logarithm of the activity coefficients $\log f_{([SH^+]+[S])exp}$ for **2**, **3**, **5**, and **6**. The three substituted *N*-benzylacetamides initially demonstrate a weak salting-out (35) at low acidities; that is, the $\log f$ values become increasingly positive with increasing acid concentration. At higher acidities the three display a strong salting-in; that is, with increasing acid concentration the values become increasingly negative. This behaviour is similar to that found for any benzamides and other weak organic bases. On the other hand, **2** is salted-in over the entire acidity range.

Values of $\log f_{S^\ddagger}$ are plotted versus % H_2SO_4 for these four substituted acetamides in Fig. 6. Figure 6 also includes $\log f_{S^\ddagger}$ curves for pertinent literature examples, i.e., benzamide (36), *p*-methoxybenzylacetate (*14a*), and *tert*-butyl acetate (*14a*). TSAC curves for the three substituted benzylacetamides (**3**, **5**, and **6**) exhibit a general conformity with that for normal acid-catalyzed hydrolysis of benzamide (36) and other amides (*13c*). This result is not entirely unexpected since throughout the entire acidity range over which it was possible to make activity coefficient measurements, the normal hydrolysis mechanism is important for all but **2**. Thus in spite of their striking differences in rate profiles, products, and *r*-plot behaviour, the three substituted *N*-benzylacetamides are virtually indistinguishable in terms of their transition state solvation requirements up to 45% H_2SO_4.

The *N-tert*-butyl compound is the only one of the four substituted acetamides with a distinct $\log f_{S^\ddagger}$ curve, but even this difference is not pronounced. In contrast, plots of *p*-methoxybenzyl acetate and particularly *tert*-butyl acetate hydrolyses are very different (8) from those for the three substituted *N*-benzylacetamides. The difference between $\log f_{S^\ddagger}$ of the latter ester and **2** suggests that the transition state solvation requirements for A-1 reactions of amides are quite different from those for A-1 ester reactions. This result does not contradict the previous conclusion that an A-1 process instead of a normal A-2 hydrolysis is operative for **2** over most of the acidity range. It is generally supposed that the hydration requirements of esters and amides differ appreciably (*12c*). Hydration changes upon transition state formation may well reflect this difference. Another possibility is that A-1 reactions of amides can take place via the predominant *O*-protonated form, rather than exclusively from the *N*-protonated form, as has been generally been assumed to be the case (5). This would tend to reduce the difference in $\log f_{S^\ddagger}$ behaviour between A-1 and A-2 reactions, since both would start from a common cationic form of the substrate.

Excess acidity treatment

In the application of the excess acidity treatment (11, 18, 25), the kinetic data were fitted to an optimum combination of the general A-1 and A-2 kinetic expressions, shown in eqs. [12] and [13], respectively, for the reactions of predominantly protonated substrates, at one temperature. Here *r* is the number of

$$[12] \quad \log k_p = (m^\ddagger - 1)\, m^*X + \log k_0$$

Can. J. Chem. Downloaded from www.nrcresearchpress.com by 210.87.254.40 on 09/06/12
For personal use only.

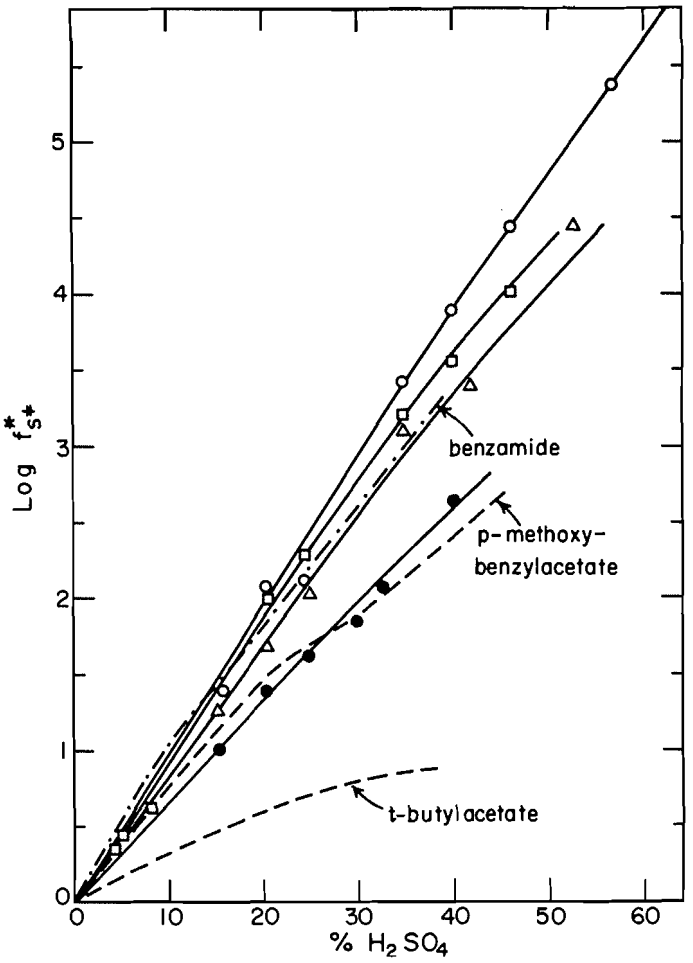

FIG. 6. Variation of the transition state activity coefficient ($\log f_{S^+}$) as a function of acidity for the hydrolyses of **2** (closed circles), **3** (squares), **5** (triangles), and **6** (open circles). Corresponding data for benzamide, *p*-methoxybenzamide, and *tert*-butyl acetate hydrolyses taken from refs. 14*a* and 36.

$$[13]\quad \log k_p = (m^\ddagger - 1)\, m^* X + \log k_0 + r \log a_{H_2O}$$

water molecules involved, $m^\ddagger$ is a slope parameter, and k_0 is the standard state rate constant. For reactions at more than one temperature, substitution into eqs. [12] and [13] of the k_0 definition, given in eq. [14], is necessary:

$$[14]\quad \log k_0 = \left(\frac{k}{h} \ln 10\right) + \log T - \frac{\Delta G^\ddagger_{25°}}{R\theta \ln 10} + \frac{\Delta H^\ddagger_{25°}}{R\theta \ln 10}\left(\frac{(T-\theta)}{T}\right)$$

The resulting expressions allow construction of plots of calculated rate constants for the overall and component processes. The data obtained from the analysis are available for all seven amides in the tables of supplementary material.[4] Excellent agreement between calculated overall rate constants and experimental values was observed in all cases.

For **1** as well as **6** and **7**, the analysis gave similar results, which are illustrated for the former (**6**) at 76.9°C in Fig. 7. The plot of the overall calculated rate constant vs. excess acidity curves downward with increasing acidity. This might be expected (18) from a bimolecular process involving water, whose concentration must decrease as the acid concentration increases. In ≤35% H_2SO_4 the calculated overall rates are indistinguishable from those of one of the component processes, A-2 hydrolysis involving three water molecules designated A-2, $3H_2O$. In ≥65% H_2SO_4 the calculated overall rates are indistinguishable from those calculated for the other component process, A-2 hydrolysis involving one water molecule (designated as A-2, $1H_2O$.) In intermediate acidities the calculated total rates contain significant contributions from both of these processes.

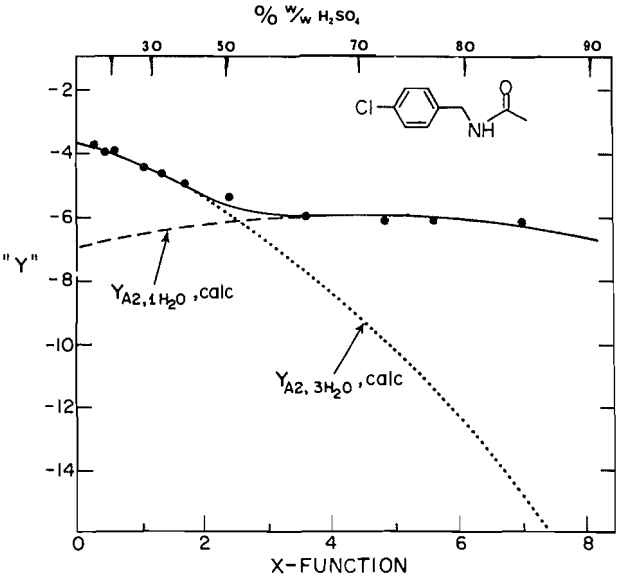

FIG. 7. Plots of calculated rate constant, Y_{nH_2O},calc = ($\log k_\psi$ − log $[SH^+]/([SH^+] + [S])$ − $n \log a_{H_2O}$) versus excess acidity, X = [log $(f_S f_{H^+}/f_{SH^+})]/m^*$, for component reactions of **6** at 76.9°C (see top of figure for corresponding acidity in terms of % H_2SO_4). Circles and upper curve show experimental values for overall reaction.

This result is surprising for **6** above 85% H_2SO_4 where no normal hydrolysis products are formed and *N*-alkyl cleavage must first occur, to give the observed products. However, if the rate of this unimolecular process is large relative to the rate of subsequent acetamide hydrolysis, then the measured rate constants will reflect the slower process, i.e., acetamide hydrolysis. This is apparently not entirely the case, since the r plot shows a significant contribution of the unimolecular process to the k_ψ values. Therefore, it seems that the magnitude of the observed rate constants for *N*-alkyl cleavage and those which might be predicted for normal amide hydrolysis are not vastly different in these acidities.

As Fig. 8 illustrates for **8** at 76.9°C, in ≤73.5% H_2SO_4 the bimolecular three and one water molecule processes dominate in a manner analogous to the foregoing results for the first three amides, and the excess acidity plot exhibits characteristic downward curvature. In 73.5–82.5% H_2SO_4 there is a change to positive curvature as expected (25*b*) of a process described by the A-1 kinetic expression. In >82.5% H_2SO_4 the observed rates are indistinguishable from those calculated for an A-1 reaction. These results confirm the mechanistic proposals for these acidities, with the A-1 rate expression corresponding to the pseudo-first-order sulfonation of **3**. The overall experimental rate profile is therefore best explained as a composite of three processes, i.e., normal bimolecular hydrolyses involving three and one water molecules respectively, and sulfonation in the most concentrated sulfuric acids.

Identical results were obtained from excess acidity analysis

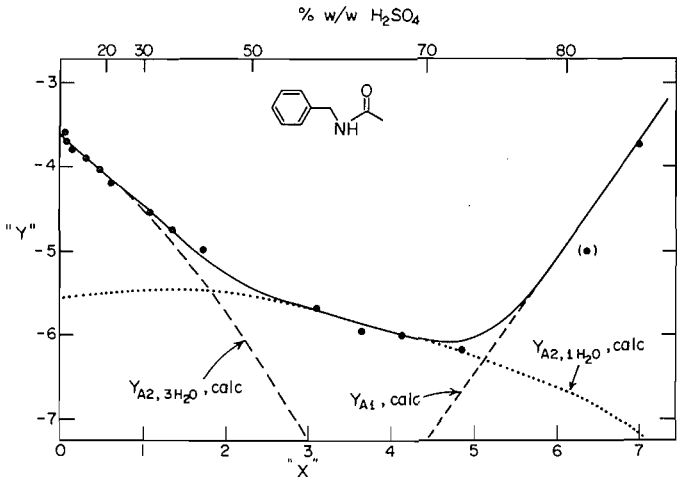

FIG. 8. Plots of Y_{nH_2O},calc versus excess acidity (X) (see caption for Fig. 7) for component reactions of **3** at 76.9°C (see top of figure for corresponding acidity in terms of % H_2SO_4). Circles and upper curve show experimental values for overall reaction.

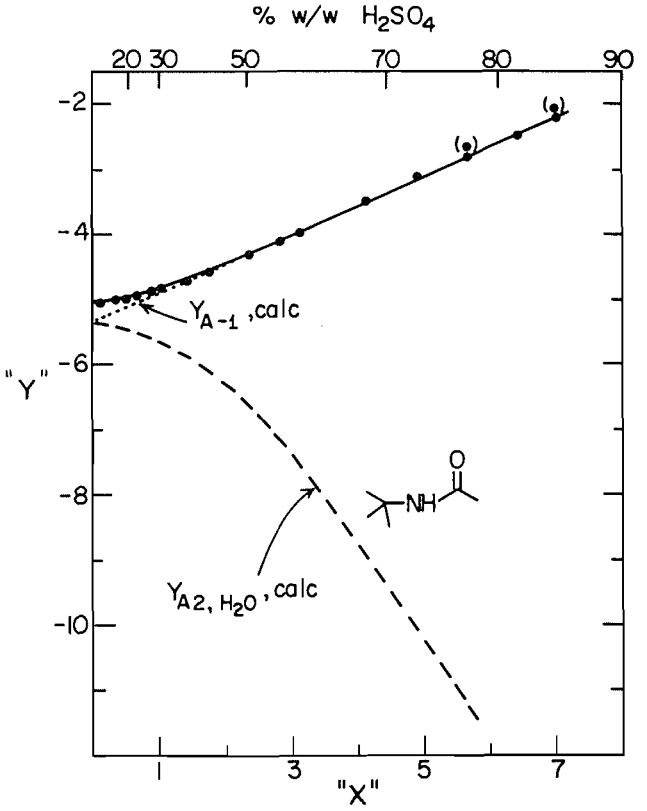

FIG. 9. Plots of Y_{nH_2O},calc (see caption for Fig. 7) versus excess acidity (X) for component reactions of **2** at 76.9°C. Circles and upper curve show experimental values for overall reaction.

of the data for **5** in acidities as high as 85.9% H_2SO_4. Data in acidities up to 85.9% H_2SO_4 were available for this substrate at a single temperature, 76.8°C. It is surprising that an expression for the contribution of the *N*-alkyl cleavage process does not appear in the analysis for this substrate. When the data at four temperatures, available up to 73.5% H_2SO_4, were treated separately, the optimum combination was found to be that of the "bimolecular" three and one water molecule processes; again no contribution from an equation representative of the *N*-alkyl cleavage was required to fit the data. An obvious explanation of the anomalous excess acidity results is that the effect of the *N*-alkyl cleavage process on the k_ψ values does not occur over a range of acidities that is large enough to be recognized by the analysis as a distinct process, due to the early onset of sulfonation. Analysis of the r plot indicates that at most three of the experimental k_ψ values contain a dominant contribution from *N*-alkyl cleavage.

Results from excess acidity analysis of the 76.9°C data for **4** implicated bimolecular three and one water molecule processes followed by an A-1 process, which becomes dominant at a much lower acidity than in the case of **3**. This result is easily explained. As Table 1 and the r plot for this substrate indicate, the *N*-alkyl cleavage process makes a significant and measureable contribution to the k_ψ values. Thus for **3** the positive curvature in the excess acidity plot is due to the occurrence of two A-1 or pseudo-first-order processes. It is initially due to *N*-alkyl cleavage and, at higher acidities, sulfonation. Thus, of the three substituted *N*-benzylacetamides reacting via a unimolecular cleavage pathway, this is the one for which the excess acidity analysis offers the strongest support for the process.

The excess acidity results for **2** consist of a combination of normal bimolecular hydrolysis at low acidities and an A-1 process at higher acidities, with the latter process completely dominating above 40% H_2SO_4. Except for a small region in the lowest acidity region the overall profile exhibits strongly positive slope, as expected for an A-1 process. Figure 9 illustrates the minor extent of the bimolecular process at low acidities, where either of the three or one water molecule kinetic expressions give equally good fits of the data. This obvious limitation of the analysis may reflect the tendency of the excess acidity treatment to compress the data along the x-axis in the very dilute acid region.

The analysis does, however, suggest that for **2**, normal hydrolysis may contribute in acidities as high as 40% H_2SO_4. In contrast, the product study identified normal hydrolysis products only at a single, much lower acidity and the r treatment gave no indication of normal bimolecular hydrolysis. The above treatment has clearly supplied a plausible acidity range for operation of the normal mechanism for this substrate.

Activation parameters

Activation parameters were calculated at constant water activity for **1**, **2**, **3**, **5**, and **6**. Although these are naturally composite values for the various reactions competing in each acidity range, they should reflect the dominant kinetic process at any given acidity. Kinetic data at three or four temperatures were used. The resultant correlation coefficients ($\geq$0.990) and standard deviations in $\Delta H^\ddagger$ and $\Delta S^\ddagger$ ($<\pm$10%) were quite satisfactory for the nmr kinetic method. Table 3 summarizes the results for **1**, **3**, and **6** and includes individual values for **2** and **5**.

For **1** as well as **3** and **6**, in 4–75% H_2SO_4, the activation enthalpies lie within the range 13.4 to 22.4 kcal mol^{-1} and the activation entropies lie in the range -17.2 to -42.5 eu. Although these are fairly typical values for normal amide hydrolysis (1*b*, 1*c*, 1*d*, 12*c*, 18), there is a clear distinction between a dominant bimolecular three water molecule process at low acidities and an analogous one water molecule process at higher acidities, particularly in the $\Delta S^\ddagger$ terms, as will be shown later.

The activation parameters for **3** in 91.5% H_2SO_4 should be representative of the sulfonation process which occurs exclu-

Can. J. Chem. Downloaded from www.nrcresearchpress.com by 210.87.254.40 on 09/06/12
For personal use only.

TABLE 3. Activation parameters, calculated at constant water activities, for the reactions of substituted acetamides in aqueous sulfuric acid solutions

R—NH—$COCH_3$	Acidity range (% H_2SO_4)	Corresponding log a_{H_2O}	Range of $\Delta H^{\ddagger}$ (kcal mol^{-1})	Range of $\Delta S^{\ddagger}$ (eu)
H—	4–73.5	1.722–0.143	15.1–19.9	(−17.2)–(−36.0)
p-Cl—$C_6H_4CH_2$—	15–56.5	1.694–0.985	19.9–20.8	(−19.6)–(−33.6)
$C_6H_5CH_2$	4–75.0	1.733–(−0.169)	13.4–22.4	(−2.15)–(−42.5)
$C_6H_5CH_2$	91.5[a]	[a]	19.5	(−20.2)

N-(*p*-Methoxybenzyl)acetamide

% H_2SO_4	log a_{H_2O} 25°C	$\Delta H^{\ddagger}$ (kcal mol^{-1})	$\Delta S^{\ddagger}$ (eu)	ρ[b]
15.15	1.694	19.5 ± 1.0	−23.3 ± 2.9	0.997
20.35	1.665	20.0 ± 0.6	−21.7 ± 1.8	0.999
24.90	1.632	20.0 ± 0.1	−21.7 ± 0.2	0.999
34.7	1.525	23.3 ± 0.4	−13.1 ± 1.1	0.949
41.76	1.405	26.1 ± 0.6	−5.4 ± 1.6	0.949
46.00	1.311	27.1 ± 1.4	−2.3 ± 3.9	0.998
52.43	1.130	28.2 ± 0.6	1.4 ± 1.7	0.999
56.50	0.985	26.2 ± 1.4	−4.2 ± 4.1	0.997
65.8	0.527	20.7 ± 1.0	−20.8 ± 2.8	0.998
73.5	−0.052	23.1 ± 0.7	−14.5 ± 2.1	0.999

N-tert-Butylacetamide

% H_2SO_4	log a_{H_2O} 25°C	$\Delta H^{\ddagger}$ (kcal mol^{-1})	$\Delta S^{\ddagger}$ (eu)	ρ[b]
15.50	1.692	27.2 ± 1.0	−5.0 ± 2.8	0.999
20.35	1.665	29.0 ± 1.5	0.8 ± 4.4	0.997
24.72	1.633	29.1 ± 1.2	1.4 ± 3.4	0.998
29.74	1.586	29.0 ± 0.9	1.5 ± 2.6	0.999
32.74	1.551	29.6 ± 0.5	3.5 ± 1.4	0.999
39.88	1.441	30.8 ± 0.7	7.9 ± 1.9	0.999
46.00	1.311	30.8 ± 0.4	8.7 ± 1.1	0.998
54.73	1.052	29.5 ± 0.4	6.2 ± 2.4	0.999
60.26	0.826	29.0 ± 0.4	5.6 ± 1.3	0.999
63.75	0.648	28.9 ± 0.4	6.0 ± 1.1	0.998
72.77	0.012	30.8 ± 0.6	14.0 ± 1.7	0.999

[a] These values not calculated at constant water activity.
[b] Correlation coefficient.

sively here. The rate of sulfonation of benzene in 93.4% H_2SO_4 has been reported at three temperatures (29*a*), allowing the following activation parameters to be calculated: $\Delta H^{\ddagger}$ = 17.01 kcal mol^{-1}, $\Delta S^{\ddagger}$ = −11.00 eu (corr. coeff = 0.9998). Comparison with the values for **3** in 91.5% H_2SO_4 shows that the latter are consistent with a dominant sulfonation reaction at this acidity.

While the activation enthalpies for **5** simply support bimolecular amide hydrolysis, the activation entropies provide much more insight into the foregoing complex results for this substrate. In the three lowest acidities $\Delta S^{\ddagger}$ is in the range (−21.7 to −23.3 eu) expected for normal amide hydrolysis. In the next four acidities the $\Delta S^{\ddagger}$ values become increasingly positive, changing progressively from −13.1 eu in 34.7% H_2SO_4 to +1.4 eu in 52.4% H_2SO_4. This result is expected, since the onset of unimolecular *N*-alkyl cleavage should change $\Delta S^{\ddagger}$ from a strongly negative value for bimolecular hydrolysis to a more positive value. In the last three acidities $\Delta S^{\ddagger}$ again becomes more negative. Ranging from −4.2 eu to −20.8 eu, the values reflect the bimolecular hydrolysis of acetamide which occurs after very fast *N*-alkyl cleavage of **4**. Thus, although $\Delta S^{\ddagger}$ values were not available in the highest acidities, where sulfonation occurs, the values in all other acidities provide strong evidence for the mechanistic proposals for this substrate.

Activation parameters for **2** also support the mechanistic interpretations. The $\Delta H^{\ddagger}$ values are generally more positive than for normal bimolecular hydrolysis, as expected for a substrate exhibiting predominant, if not exclusve, unimolecular cleavage (11*b*). In 15.5% H_2SO_4 the small, negative activation entropy (−5.0 eu) may be the result of contributions from both an A-2 process, which alone would produce a large negative value, and an A-1 process, which alone would produce a small positive value. In higher acidities the observed positive $\Delta S^{\ddagger}$ values emphasize the importance of the unimolecular process which dominates above 35% H_2SO_4.

Table 4 shows an attempt to dissect the observed composite $\Delta H^{\ddagger}$ and $\Delta S^{\ddagger}$ behaviour into individual values for the com-

Can. J. Chem. Downloaded from www.nrcresearchpress.com by 210.87.254.40 on 09/06/12
For personal use only.

TABLE 4. Standard state activation parameters and rate constants for the hydrolysis of acetamides in aqueous sulfuric acid: results of the excess acidity treatment[a]

Amide	log k_0', 25°C	Mechanism	$\Delta H^{\ddagger b}$ (kcal mol^{-1})	$\Delta S^{\ddagger b}$ (eu mol^{-1})
Acetamide	−4.509	A-2, $3H_2O$[c]	18.7 ± 0.47	−40.6 ± 1.3
	−6.354	A-2, $1H_2O$[d]	19.9 ± 0.6	−19.3 ± 2.1
N-*p*-Cl-Benzylacetamide	−5.950	A-2, $3H_2O$	21.0 ± 1.2	−39.2 ± 4.0
	−10.001	A-2, $1H_2O$	27.7 ± 1.7	−19.4 ± 5.7
N-Benzylacetamide	−5.812	A-2, $3H_2O$	19.7 ± 0.6	−42.9 ± 2.0
	−8.098	A-2, $1H_2O$	22.9 ± 0.7	−26.8 ± 2.3
	−17.275	A-1[e]	36.4 ± 1.0	−15.5 ± 3.6
N-*p*-CH_3O-Benzylacetamide	−5.407	A-2, $3H_2O$	16.7 ± 0.6	−51.4 ± 2.1
	−7.775	A-2, $1H_2O$	26.2 ± 0.5	−14.2 ± 1.8
N-*tert*-Butylacetamide	−8.084	A-2, $3H_2O$	24.5 ± 1.1	−37.2 ± 3.7
	−8.758	A-1[f]	30.8 ± 0.1	4.8 ± 0.8

[a] Obtained by curve fitting of the kinetic data.
[b] Standard state activation parameters.
[c] Normal bimolecular hydrolysis assisted by three water molecules.
[d] Bimolecular hydrolysis assisted by one water molecule.
[e] Sulfonation.
[f] Unimolecular *N*-alkyl cleavage.

TABLE 5. Summary of the mechanistic behaviour of substituted acetamides in aqueous sulfuric acid solution

R—NHCOCH$_3$	Acidity range (% H_2SO_4)	Predominant mode of reaction
$C_6H_5CH_2$—	4–73	*N*-acyl cleavage[a]
	73–82.5	*N*-acyl plus *N*-alkyl cleavage[b]
	82.5–87	*N*-alkyl cleavage plus sulfonation
	91.5	Sulfonation
4-$CH_3C_6H_4CH_2$—	4–60	*N*-acyl cleavage
	60–64	*N*-acyl plus *N*-alkyl cleavage
	64–79	*N*-alkyl cleavage
	79–88	*N*-alkyl cleavage plus sulfonation
4-$CH_3OC_6H_4CH_2$—	2–35	*N*-acyl cleavage
	35–52.5	*N*-acyl plus *N*-alkyl cleavage
	52.5–73.6	*N*-alkyl cleavage
	73.5–91.5	Sulfonation
4-$ClC_6H_4CH_2$—	15–78	*N*-acyl cleavage
	82.5–86	*N*-acyl plus *N*-alkyl cleavage
	91.5	*N*-alkyl cleavage
4-$NO_2C_6H_4CH_2$—	8–86	*N*-acyl cleavage
t-C_4H_9—	5–33	*N*-acyl plus *N*-alkyl cleavage
	40–91.5	*N*-alkyl cleavage
CH_3—	4–73.5	*N*-acyl cleavage

[a] Bimolecular reaction of protonated amide with water molecules (A-2).
[b] Unimolecular fission of protonated amide to give carbonium ion (A-1).

peting processes. Standard state activation enthalpies and entropies were calculated from the excess acidity analysis of the variable temperature data for five of the substrates. These values complement those of Table 3. For example, although similar $\Delta H^{\ddagger}$ values are calculated for the A-2, $3H_2O$ and A-2, $1H_2O$ processes, the former has consistently lower $\Delta H^{\ddagger}$ values, as might be expected. Also, the $3H_2O$ process has much more negative $\Delta S^{\ddagger}$ values than the $1H_2O$ mechanism, which is in full accord with the higher degree of solvent restriction expected for this type of transition state. The A-1 process for **2** is the only hydrolysis mechanism for which a positive value of $\Delta S^{\ddagger}$ is calculated, as would be expected.

Along with standard state activation parameters, estimates of the standard state rate constants for the individual rate processes were also obtained from the application of the excess acidity treatment. The log k_0 values were calculated by adding the value r log a_{H_2O} (where r is the appropriate number of water molecules) to eq [14]. The resultant values then refer to a standard state of pure water (55.35 M) at 25°C and have been termed log k_0' in Table 4. The data indicate that the intrinsic relative reactivities of the amides toward the bimolecular three and one water molecule hydrolyses are acetamide > *N*-(*p*-methoxybenzyl)acetamide > *N*-benzylacetamide > *N*-(*p*-chlorobenzyl)acetamide > *N*-*tert*-butylacetamide. This order of reactivities is easily rationalized in terms of steric and inductive effects. Thus the least sterically crowded primary amide, acetamide, is most reactive, whereas the most bulky secondary amide, *N*-*tert*-butylacetamide, is least reactive. In addition, the order of reactivity of the three substituted *N*-benzylacetamides, i.e., *p*-methoxy > hydrogen > *p*-chloro, is

Can. J. Chem. Downloaded from www.nrcresearchpress.com by 210.87.254.40 on 09/06/12
For personal use only.

Can. J. Chem. Downloaded from www.nrcresearchpress.com by 210.87.254.40 on 09/06/12
For personal use only.

that of the electron-donating ability of the three substituents, implying a reaction favoured by increased electron supply from the aromatic ring. The ease of amide protonation in the pre-equilibrium step of the hydrolysis pathway would also be expected to be influenced in a similar fashion.

In summary, it may be concluded that rate and product studies, combined with activation parameters and three quantitative analytical treatments have produced an extensive description of the reaction modes available to this series of substituted acetamides. Table 5 is a summary of the overall results, which shows that the chemistry of the protonated amides in aqueous acid solutions encompasses normal bimolecular hydrolytic processes in addition to unimolecular *N*-alkyl cleavage and aromatic sulfonation reactions. There is no evidence for unimolecular acylium ion formation. It is also evident that the three kinetic treatments applied to the rate data provide complementary information, which taken together offers strong support for proposed mechanistic explanations based on rate-profile and product studies alone.

Acknowledgements

The continued financial support of NSERC is gratefully acknowledged. The authors are grateful to Dr. R. A. Cox for fruitful discussions and invaluable assistance with some of the calculations.

1. (*a*) C. O'Connor. Rev. Chem. Soc. **24**, 553 (1970); (*b*) P. D. Bolton. Aust. J. Chem., **19**, 1013 (1966); (*c*) B. S. Rabinovitch and C. H. Winkler. Can. J. Res. **20**(B), 73 (1942); (*d*) P. D. Bolton and I. R. Wilson. Tetrahedron Lett. 847 (1963).
2. (*a*) A. R. Fersht. J. Am. Chem. Soc. **93**, 3504 (1971); (*b*) R. B. Martin. J. Chem. Soc. Chem. Commun. 793 (1972); (*c*) R. B. Martin and W. C. Hutton. J. Am. Chem. Soc. **95**, 4752 (1973); (*d*) E. Benedetti, B. DiBlasio, and P. Baine. J. Chem. Soc. Perkin Trans. 2, 500 (1980); (*e*) J. Catalan and M. Yanez. Tetrahedron, **36**, 665 (1980); (*f*) R. A. McClelland and W. F. Reynolds. J. Chem. Soc. Chem. Commun. 824 (1974); (*g*) C. R. Smith and K. Yates. Can. J. Chem. **50**, 771 (1972); (*h*) A. J. Kresge, P. H. Fitzgerald and Y. Chiang. J. Am. Chem. Soc. **96**, 4698 (1974); (*i*) A. Williams. J. Am. Chem. Soc. **98**, 5645 (1976).
3. (*a*) M. L. Bender. Chem. Rev. **60**, 53 (1960); (*b*) C. A. Bunton, C. J. O'Connor, and T. A. Turney. Chem. Ind. 1835 (1967); (*c*) C. R. Smith and K. Yates. J. Am. Chem. Soc. **94**, 8811 (1972); (*d*) C. A. Bunton, T. A. Lewis, and D. R. Llewellyn. Chem. Ind. 1154 (1954); (*e*) M. L. Bender and R. D. Ginger. J. Am. Chem. Soc. **77**, 348 (1955); (*f*) J. H. Barnett and C. J. O'Connor. J. Chem. Soc. Perkin Trans. 2, 220 (1973); (*g*) R. A. McClelland. J. Am. Chem. Soc. **97**, 5281 (1975).
4. (*a*) C. L. Perrin. J. Am. Chem. Soc. **96**, 5628 (1974); (*b*) R. A. McClelland and W. F. Reynolds. Can. J. Chem. **57**, 2896 (1979); (*c*) S. Forsen and R. A. Hoffman. J. Chem. Phys. **39**, 2892 (1963); (*d*) C. L. Perrin and E. R. Johnston. J. Magn. Reson. **33**, 619 (1979); (*e*) C. L. Perrin and E. R. Johnston. J. Am. Chem. Soc. **101**, 4753 (1979); (*f*) C. L. Perrin, E. R. Johnston, C. P. Lallo, and P. A. Kobrin. J. Am. Chem. Soc. **103**, 4691 (1981); (*g*) C. L. Perrin and E. R. Johnston. J. Am. Chem. Soc. **103**, 4697 (1981); (*h*) E. R. Johnston. Ph.D. Thesis. University of California, San Diego, 1980; (*i*) A. G. Redfield, S. D. Kunz, and E. K. Ralph. J. Magn. Reson. **19**, 114 (1975); (*j*) S. F. Waelder, L. Lee, and A. G. Redfield. J. Am. Chem. Soc. **97**, 2927 (1975); (*k*) S. F. Waelder and A. G. Redfield. Biopolymers, **16**, 623 (1977); (*l*) A. G. Redfield. Methods Enzymol. 253 (1978); (*m*) A. G. Redfield and S. Waelder. J. Am. Chem. Soc. **101**, 6151 (1979).
5. (*a*) H. Itsuki and S. Terasaura. Nippon Kagaku Zusshi, **90**, 1012 (1969); (*b*) T. Yamana, Y. Mizukami, A. Tsuju, and M. Ikuta. Chem. Pharm. Bull. (Tokyo) **20**, 1778 (1972); (*c*) R. N. Lacey. J. Chem. Soc. 1633 (1960).
6. (*a*) J. A. Duffy and J. A. Leisten. J. Chem. Soc. 853 (1960); (*b*) M. I. Vinnik, I. M. Medvetskaya, L. A. Andreeva, and A. E. Tiger. Ress. J. Phys. Chem. **41**, 128 (1967); (*c*) M. I. Vinnik and I. M. Medvetskaya. Russ. J. Phys. Chem. **41**, 947 (1967); (*d*) J. A. Duffy and J. A. Leisten. J. Chem. Soc. 545 (1960); (*e*) J. W. Barnett and C. J. O'Connor. J. Chem. Soc. Commun. 525 (1972); (*f*) J. W. Barnett and C. J. O'Connor. J. Chem. Soc. Perkin Trans. 2, 2378 (1972); (*g*) C. J. Giffney and C. J. O'Connor. J. Chem. Soc. Perkin Trans. 2, 1357 (1975).
7. A. Cipiciani, P. Linda, G. Savelli, and C. A. Bunton. J. Org. Chem. **48**, 1349 (1983).
8. K. Yates, J. B. Stevens and A. R. Katritzky. Can. J. Chem. **42**, 1957 (1964).
9. (*a*) J. F. Bunnett and F. P. Olsen. Can. J. Chem. **44**, 1899 (1966); Can. J. Chem. **44**, 1917 (1966).
10. (*a*) T. A. Modro, K. Yates, and J. Janata. J. Am. Chem. Soc. **97**, 1492 (1975); (*b*) K. Yates and R. A. McClelland. Prog. Phys. Org. Chem. **11**, 331 (1974); (*c*) R. A. McClelland. Can. J. Chem. **58**, 393 (1980).
11. (*a*) R. A. Cox and K. Yates. J. Am. Chem. Soc. **100**, 3861 (1978); (*b*) Can. J. Chem. **57**, 2944 (1979).
12. (*a*) V. C. Armstrong and R. B. Moodie. J. Chem. Soc. (B), 275 (1968); (*b*) K. Yates and J. C. Riordan. Can. J. Chem. **43**, 2328 (1965); (*c*) C. R. Smith and K. Yates. J. Am. Chem. Soc. **93**, 6578 (1971); (*d*) C. A. Bunton, S. J. Farber, A. J. G. Millbank, C. J. O'Connor, and T. A. Turney. J. Chem. Soc. Perkin Trans. 2, 1869 (1972); (*e*) C. J. Hyland and C. J. O'Connor. J. Chem. Soc. Perkin Tran. 2, 1402 (1973).
13. (*a*) R. H. Boyd. J. Am. Chem. Soc. **85**, 1555 (1963); (*b*) T. A. Modro, W. F. Reynolds, and K. Yates. Can. J. Chem. **54**, 1439 (1976); (*c*) P. A. Wan, T. A. Modro, and K. Yates. Can. J. Chem. **58**, 2423 (1980).
14. (*a*) R. A. McClelland, T. A. Modro, M. F. Goldman, and K. Yates. J. Am. Chem. Soc. **97**, 5223 (1975); (*b*) K. Yates and T. A. Modro. Acc. Chem. Res. **11**, 190 (1978).
15. K. Yates and R. A. McClelland. J. Am. Chem. Soc. **89**, 2686 (1967).
16. T. A. Modro and K. Yates. J. Am. Chem. Soc. **98**, 4247 (1976).
17. (*a*) R. A. Cox and K. Yates. J. Am. Chem. Soc. **100**, 3862 (1978); (*b*) Can. J. Chem. **59**, 1560 (1981).
18. R. A. Cox and K. Yates. Can. J. Chem. **59**, 2853 (1981).
19. H. Fernholz and H. J. Schmidt. Angew. Chem. Int. Ed. Engl. **8**, 521 (1969).
20. R. L. Shriner, R. C. Fuson, and D. Y. Curtin. The systematic identification of organic compounds. 5th ed. John Wiley and Sons, New York, NY. 1964. pp. 259–260.
21. (*a*) H. H. Jaffe. Chem. Rev. **53**, 191 (1953); (*b*) C. L. Parris and R. M. Christenson. J. Org. Chem. **25**, 331 (1960); (*c*) J. Krober. Ber. **23**, 1026 (1890); (*d*) F. Lustig. Ber. **28**, 2988 (1895); (*e*) D. Metayer and D. Dat-Xuong. Bull. Soc. Chim. Fr. 615 (1954); (*f*) C. W. Shoppee. J. Chem. Soc. 1225 (1931); (*g*) J. N. Ashley and M. Davis. J. Chem. Soc. 812 (1957).
22. (*a*) R. C. Weast (*Editor*). Handbook of chemistry and physics. 53rd ed. The Chemical Rubber Co., Cleveland, Ohio, C7. 1972. (*b*) H. Goldschmidt and N. Polonowski. Ber. **20**, 24067 (1887); (*c*) W. H. Carothers, C. F. Bickford, and G. J. Hurwitz. J. Am. Chem. Soc. **49**, 2908 (1927).
23. W. F. Giauque, E. W. Hornung, J. E. Kunzler, and T. R. Rubin. J. Am. Chem. Soc. **82**, 62 (1960).
24. International Critical Tables. Vol. 3. McGraw–Hill, New York, NY. 1930. pp. 50–57.
25. R. A. Cox, C. R. Smith, and K. Yates. Can. J. Chem. **57**, 2952

(1979); R. A. COX, M. F. GOLDMAN, and K. YATES. Can. J. Chem. **57**, 2960 (1979).
26. G. M. BARROW. Physical chemistry. 2nd ed. McGraw–Hill, New York, NY. 1961. pp. 495–496.
27. (*a*) N. MULLER and R. H. BIRKHAN. J. Chem. Phys. **43**, 4541 (1965); (*b*) J. D. BALDESCHWIELER. J. Chem. Phys. **36**, 152 (1962).
28. B. B. GAWALI, P. NEELAKANTAN, S. N. RAV, D. S. IYENGAR, and U. T. BHALERAO. Indian J. Chem. **20**B, 616 (1981).
29. (*a*) A. W. KAANDORP, H. CERFONTAIN, F. L. J. SINMA. Recl. Trav. Chim. Pays-Bas, **81**, 969 (1962); (*b*) C. EABORN and R. TAYLOR. J. Chem. Soc. 1480 (1960).
30. J. W. BARNETT and C. J. O'CONNOR. Chem. Ind. 1172 (1970).
31. C. J. O'CONNOR and R. E. RAMAGE. Aust. J. Chem. **30**, 527 (1977).
32. R. A. COX, L. M. DRUET, A. E. KLAUSNER, T. A. MODRO, P. WAN, and K. YATES. Can. J. Chem. **59**, 1568 (1981).
33. C. R. SMITH. Ph.D. Thesis. University of Toronto. 1969. p. 179.
34. R. A. MCCLELLAND. Ph.D. Thesis. University of Toronto. 1969. p. 97.
35. K. YATES and R. A. MCCLELLAND. Prog. Phys. Org. Chem. **11**, 323 (1974).
36. T. A. MODRO, K. YATES, and F. BEAUFAYS. Can. J. Chem. **55**, 3050 (1977).

Can. J. Chem. Downloaded from www.nrcresearchpress.com by 210.87.254.40 on 09/06/12
For personal use only.

Stereocontrolled total synthesis of the triquinane marine sesquiterpene $\Delta^{9(12)}$-capnellene

LEO A. PAQUETTE AND KENNETH E. STEVENS
Evans Chemical Laboratories, The Ohio State University, Columbus, OH 43210, U.S.A.

Received January 10, 1984

This paper is dedicated to Professor Peter Yates on the occasion of his 60th birthday

LEO A. PAQUETTE and KENNETH E. STEVENS. Can. J. Chem. **62**, 2415 (1984).

A total synthesis of $\Delta^{9(12)}$-capnellene, a *cis-anti-cis*-tricyclo[6.3.0.0^{2,6}]undecane sesquiterpene of marine origin, is described. Starting with bicyclic enone **5**, which was prepared by a Nazarov cyclization, the remaining portion of the molecule is elaborated by means of a new and relatively efficient cyclopentenone annulation scheme. The relative stereochemistries of the chiral centers are properly incorporated by taking advantage of prevailing steric factors.

LEO A. PAQUETTE et KENNETH E. STEVENS. Can. J. Chem. **62**, 2415 (1984).

On décrit une synthèse totale de la $\Delta^{3(12)}$-capnellène, un sesquiterpène du type tricyclo[6.3.0.0^{2,6}]undécane-*cis-anti-cis* d'origine marine. Partant de l'énone bicyclique **5** que l'on prépare par une cyclisation de Nazarov, on élabore le reste de la molécule en faisant appel à une méthode, nouvelle et relativement efficace, d'annellation en cyclopentènone. On incorpore correctement les stéréochimies relatives appropriées des centres chiraux en tirant profit de facteurs stériques existants.
[Traduit par le journal]

Can. J. Chem. Downloaded from www.nrcresearchpress.com by 210.87.254.105 on 09/06/12
For personal use only.

The soft coral *Capnella imbricata*[1] has proven to be a rich source of an interesting family of non-isoprenoid sesquiterpenes which share in common the *cis-anti-cis* tricyclo[6.3.0.0^{2,6}]undecane ring system. These marine natural products known as capnellanes occur in various stages of oxidation ranging from purely hydrocarbon[1,2] to polyhydric derivatives[3–7]. $\Delta^{9(12)}$-Capnellene (**1**), the presumed biosynthetic precursor of the capnellenols, reveals the typical arrangement of methyl groups about the linear triquinane nucleus[8]. These features differentiate the capnellanes from their terrestrial counterparts, the hirsutanes (e.g., hirsutene (**2**)), which possess

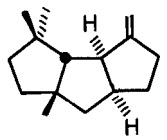

1

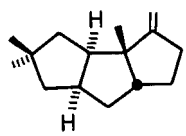

2

a geminal dimethyl unit at C-2 and an angular methyl group at C-10 (ref. 9, hirsutene; ref. 10, hirsutic acid; ref. 11, coriolin).

Although the capnellane group seemingly serves as agents of chemical defense within the coral reef biomass to ward off algal and microbial growth[12] and to prevent larval settlement[13], their detailed biological function is not known. The compelling biosynthetic position held by **1**[4,12] has caused it to become a focal point of substantive synthetic activity[15–20][2]. In this paper, we describe in detail a short, stereocontrolled total synthesis of **1**, which features two different methods for regiospecific cyclopentenone annulation[15].

From the retrosynthetic perspective, bicyclic ketone **6** appeared to be an ideal advanced intermediate for elaboration of the third five-membered ring. Attention was therefore directed to its acquisition. Conjugate addition of lithium dimethylcuprate to **5** was envisioned to be a suitably viable approach to **6** (Scheme 1). With these goals in mind, cyclopentenyl carboxaldehyde **3** was prepared by the method of Magnusson and Thorén[21]. Their protocol provides **3** admixed with approximately 20% of the 3,3-dimethyl isomer. Although the unwanted component could be removed by reaction with an appropriate quantity of Girard's reagent T, it proved more convenient to effect condensation of the mixture with vinylmagnesium bromide and to separate the dienols by high pressure liquid chromatography. Manganese dioxide oxidation of the appropriate vinyl carbinol proceeded smoothly to deliver the sensitive dienone **4** which was subjected directly to Nazarov cyclization[22]. The combination of 8% phosphorus pentoxide in methanesulfonic acid[23] at 20°C for only 2 min sufficed to provide a 68% yield of **5** with the double bond crucially positioned in the central, more highly substituted region of the molecule. In accord with previous experience[24], immediate treatment of **5** with the cuprate reagent led efficiently to **6**. Detailed chromatographic and spectral analysis at this juncture failed to give evidence of isomeric material.

With **6** in hand, [3+2] cyclopentannulation with regiospecific bonding of a new carbonyl group to the site of the old as in **17** was given attention. Several procedures have been developed which effect such a transformation[25]. However, most lack the intrinsic regiochemical control required to deliver exclusively the proper linearly fused tricyclopentanoid framework. The one known exception, that based upon vinylsilane acylation–cyclization[26], proceeds in the desired sense because production of the vinylsilane is usually achieved by proton abstraction from the less substituted α carbon[27].

For this reason, **6** was converted via its triisopropylbenzenesulfonyl hydrazone[28] to **7** (Scheme 2). Attempts to acylate **7** with 3-chloropropionyl chloride according to previously developed procedures[26] proved not to be successful. When application of more forcing conditions than normal led to destruction of the vinylsilane, an alternate route to dienone **9** was sought. Recourse to a smaller electrophilic species, viz. that resulting from the action of aluminum chloride on dichloromethyl methyl ether[29], led successfully to aldehyde **8** from which **9** could be prepared conventionally. However, this dienone failed to undergo Nazarov cyclization as induced by a wide range of Bronsted and Lewis acids. Our inability to arrive at **11**

[1]Collections were made off the coast of Serwaru, Leti Island, Indonesia and Liang Island off the north coast of New Guinea.

[2]For syntheses of $\Delta^{8(9)}$-capnellene, see ref. 20(*a*); for $\Delta^{9(12)}$-capnellene-8α,10α-diol, see ref. 20(*b*).

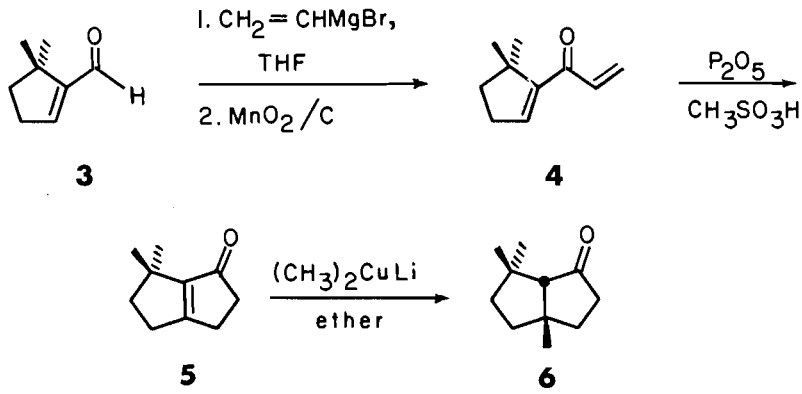

3 4 5 6

SCHEME 1

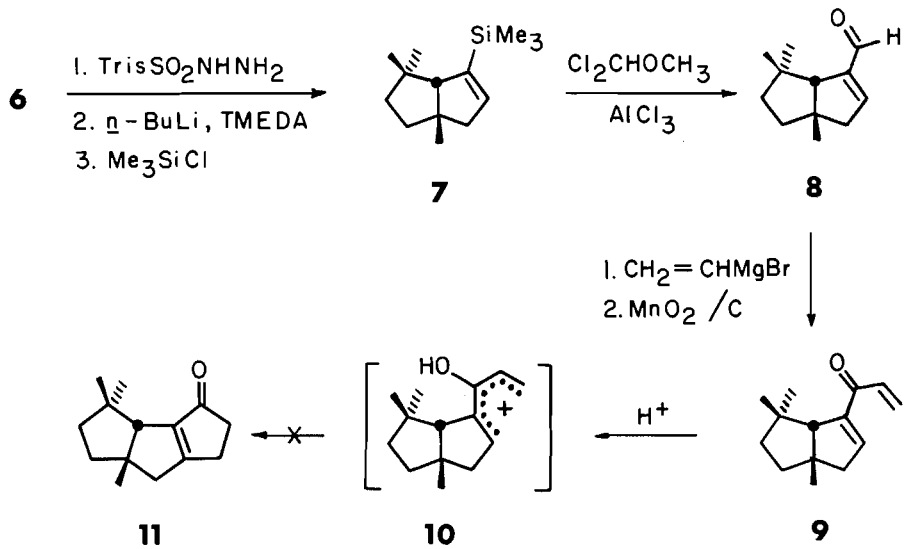

6 7 8 9 10 11

SCHEME 2

in this fashion may be the result of steric impedance by the geminal methyl groups to attainment of planarity within the pentadienyl cation intermediate (**10**) which must experience the requisite conrotatory electrocyclization (cf. Newman's Rule of Six[30]).

Although not previously encountered, this limitation to the Nazarov procedure mandated that an alternative regiospecific cyclopentenone annulation method be developed. From the outset, early introduction of the new carbonyl group was viewed as especially desirable. This issue was addressed by condensing **6** with lithium acetylide[31] and treating propargyl alcohol **12** with formic acid containing sulfuric acid at 90°C to effect Rupe rearrangement[32]. This sequence proved to be highly efficient and to exhibit a high predilection for formation of the lesser substituted enone **13** (Scheme 3). This substance in turn was exposed to vinylmagnesium bromide and cuprous iodide in tetrahydrofuran at −78°C[33]. The isomerically pure substance which was produced proved to be **14**. Although the precise stereochemical relationship of the acetyl and vinyl groups was not known with rigor at the time, *exo* delivery of the vinyl cuprate was anticipated for the usual steric reasons. Since protonation of the resulting enolate from the less hindered β face must compress the acetyl group tightly against the *endo* methyl group of the geminal pair, we deemed it likely that this energy demanding state of affairs might be avoided.

In any event, the ozonolysis of **14** proceeded readily. Resulting keto aldehyde **15** was cyclized with 5% potassium hydroxide in a 2:1 mixture of tetrahydrofuran and ether[34] which also contained a catalytic amount of tetra-*n*-butylammonium hydroxide. Tricyclic enone **16** was isolated in 79% yield. During the $\Delta^{9(12)}$-capnellene synthesis later developed by the Geneva group[18], two isomers of keto aldehyde **15** were obtained. The major isomer (identical to **15**) was again found to cyclize cleanly under the mild two-phase conditions just described. The minor isomer, which was recovered intact from this treatment, was converted to **16** only when more stringent conditions (KOH, C_2H_5OH) were applied. These results agree fully with our original stereochemical assumptions.

To secure the target molecule, **16** was subjected to sequential catalytic hydrogenation and Wittig olefination. The ^1H nmr spectrum of the resulting racemic hydrocarbon was identical with that of the authentic natural product as recorded by Professor Djerassi. Thus, $\Delta^{9(12)}$-capnellene has been stereoselectively assembled in 8 laboratory steps from bicyclic enone **5** in 8.3% overall yield.

Experimental

8,8-Dimethylbicyclo[3.3.0]oct-1(5)-en-2-one (**5**)

2,3-Epoxy-4,4-dimethylcyclohexanol[21] (30.0 g, 0.21 mol) in toluene (240 mL) was added over 2 h to a solution of lithium bromide (41 g, 0.47 mol) and hexamethylphosphoramide (82 g, 0.46 mol) in the same solvent (240 mL) while being heated at reflux under nitro-

Can. J. Chem. Downloaded from www.nrcresearchpress.com by 210.87.254.105 on 09/06/12
For personal use only.

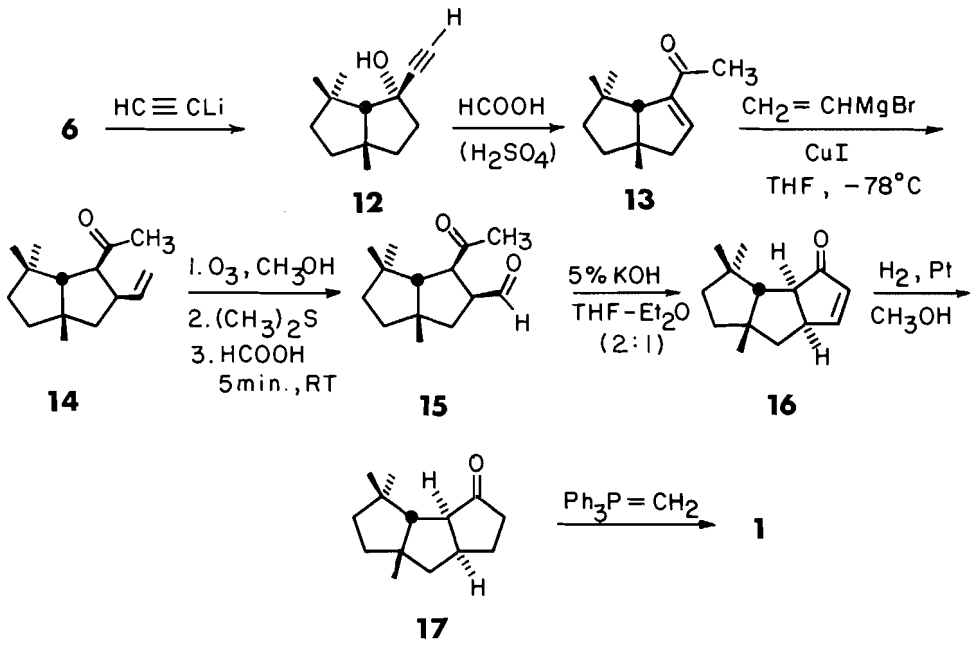

SCHEME 3

gen. Upon completion of the addition, heating was immediately discontinued and the reaction mixture was allowed to cool to room temperature during 1.5 h, diluted with ether (200 mL), washed with water (4 × 100 mL), and dried. The solvents were removed at reduced pressure, leaving the mixture of **3** and its 3,3-dimethyl isomer as a pale yellow oil. This material was dissolved in anhydrous tetrahydrofuran (200 mL) and added during 1.5 h to a cold (10°C) slurry of vinylmagnesium bromide (prepared from magnesium (10 g, 0.42 g-atom) and vinyl bromide (33 mL, 0.44 mol)) in tetrahydrofuran (500 mL). The mixture was allowed to warm to room temperature during 3 h, poured into saturated ammonium chloride solution, and stirred for 1 h. The organic phase was removed and the aqueous layer was extracted with ether (3 × 100 mL). The combined organic solutions were dried and concentrated to leave a colorless oil from which the desired vinyl alcohol was separated by preparative hplc (Waters Prep 500, elution with 9% ethyl acetate in petroleum ether). Distillation afforded 9.55 g (30% overall) of product as a colorless, mobile oil, bp 114°C (43 Torr (1 Torr = 133.3 Pa)). As distillation caused partial polymerization with loss of water, this manipulation was not carried out generally. Under these conditions, the overall yield averaged 14.65 g (46%); *m/z* calcd. (M^+): 152.1201; found: 152.1205.

A mixture of the vinyl alcohol (2.29 g, 15.0 mmol) and manganese dioxide on carbon[35] (22.9 g) in petroleum ether (150 mL) was stirred at room temperature for 24 h. Filtration and solvent evaporation left pure **4** (2.14 g, 95%) which was used without further purification; ir (CCl_4): 1715, 1660, 1605 cm^{-1}; ^1H nmr (CCl_4) δ: 1.24 (s, 6H), 1.58–1.92 (m, 2H), 2.28–2.7 (m, 2H), 5.40–5.68 (m, 1H), 5.94–6.26 (m, 1H), 6.48–6.95 (m, 2H); *m/z*. calcd. (M^+): 150.1045; found: 150.1048.

The analytical sample was obtained by molecular distillation at 100°C and 30 Torr. *Anal.* calcd. for $C_{10}H_{14}O$: C 79.96, H 9.39; found: C 79.96, H 9.50.

The preceding material was placed in a round-bottomed flask equipped with a magnetic stirrer, thoroughly cooled in ice, and treated in one portion with a solution of phosphorus pentoxide in methanesulfonic acid (3.5 mL of 1:10 by weight). A vigorously exothermic reaction resulted. After 2 min, the resulting brown tarry mixture was carefully added to a mixture of ether (50 mL) and saturated sodium bicarbonate solution (75 mL). After neutralization, the aqueous phase was extracted with ether (2 × 20 mL) and the combined organic layers were washed with saturated sodium bicarbonate solution, dried, and concentrated to leave 1.58 g of pale yellow oil. Further purification by mplc on silica gel (elution with 15% ethyl acetate in petroleum ether) gave **5** as a colorless oil (1.45 g, 65% from the alcohol) which darkened considerably on standing and therefore was utilized without undue delay; ir ($CHCl_3$): 1685, 1630 cm^{-1}; ^1H nmr (CCl_4) δ: 1.18 (s, 6H), 2.00–2.28 (m, 2H), 2.28–2.70 (m, 6H); *m/z* calcd. (M^+): 150.1045; found: 150.1039. *Anal.* calcd. for $C_{10}H_{14}O$: C 79.96, H 9.39; found: C 79.84, H 9.39.

5,8,8-Trimethyl-bicyclo[3.3.0]octan-2-one (6)

A solution of lithium dimethylcuprate was prepared by the addition of $CH_3Li \cdot LiBr$ in ether (1.8 mL of 1.4 *M* solution, 2.52 mmol) to a cold (0°C), magnetically stirred slurry of cuprous iodide (241 mg, 1.26 mmol) in ether (5 mL) under nitrogen. A solution of **5** (97 mg, 0.65 mmol) in ether (2 mL) was introduced via cannula. After 30 min, the reaction mixture was siphoned into half-saturated ammonium chloride solution (20 mL) made basic by the addition of concentrated ammonium hydroxide. After the copper salts had been solubilized, the aqueous phase was extracted with ether (2 × 10 mL) and the combined organic layers were washed with saturated ammonium chloride solution (10 mL), dried, and concentrated to leave **6** as a pale yellow oil (87 mg, 80%); ir ($CHCl_3$): 1730 cm^{-1}; ^1H nmr (CCl_4) δ: 0.94 (s, 3H), 1.14 (s, 3H), 1.30 (s, 3H), 1.39–1.91 (series of m, 7H), 2.18 (pseudo t, *J* = 7.5 Hz, 2H); *m/z* calcd. (M^+): 166.1358; found: 166.1361. *Anal.* calcd. for $C_{11}H_{18}O$: C 79.47, H 10.91; found: C 79.47, H 10.89.

The 2,4,6-triisopropylbenzenesulfonylhydrazone derivative was prepared by adding the sulfonylhydrazine (3.20 g, 9.7 mmol) to a magnetically stirred solution of **6** (1.60 g, 9.6 mmol) in acetonitrile (10 mL) at room temperature. Concentrated hydrochloric acid (1 mL) was introduced and the mixture was stirred overnight, allowed to stand in a freezer for 12 h, and suction filtered to recover the precipitated solid. This material was washed with cold methanol and air dried to give 3.40 g (79%) of colorless crystals, mp 148–151°C (from methanol–dichloromethane): *m/z* calcd. (M^+): 446.2967; found: 446.2980. *Anal.* calcd. for $C_{26}H_{42}N_2O_2S$: C 69.91, H 9.48; found: C 69.81, H 9.50.

5,8,8-Trimethyl-2-(trimethylsilyl)-bicyclo[3.3.0]oct-2-ene (7)

A solution of *n*-butyllithium in ether (6.0 mL of 2.26 *M*, 13.5 mmol) was added over 15 min to a cold (−65°C), magnetically stirred slurry of the triisopropylsulfonylhydrazone of **6** (2.00 g, 4.5 mmol) in a solution of tetramethylethylenediamine (2.0 mL) and hexane (20 mL). After 30 min. at −70°C. the reaction mixture was allowed to warm to 0°C over 20 min, giving a clear, pale yellow solution. After 15 min at this temperature, chlorotrimethylsilane (1.8 mL, 14.1 mmol) was added over 10 min. Following this, the

Can. J. Chem. Downloaded from www.nrcresearchpress.com by 210.87.254.105 on 09/06/12
For personal use only.

Can. J. Chem. Downloaded from www.nrcresearchpress.com by 210.87.254.105 on 09/06/12
For personal use only.

solution was poured into a mixture of ice and water (total volume ca. 60 mL). After shaking, the layers were separated and the aqueous phase was extracted with ether (2 × 10 mL). The combined organic layers were washed with water (2 × 20 mL), saturated cupric sulfate solution (20 mL), and water (2 × 10 mL) prior to drying and solvent evaporation. The resulting pale yellow oil (1.81 g) was filtered through a plug of silica gel (elution with petroleum ether) and purified by mplc on silica gel (same eluent). There was isolated 580 mg (58%) of **7** as a colorless oil. The analytical sample was prepared by vpc (3 ft × 0.25 in. 5% SE-30 on Chromosorb P, 120°C); ^{1}H nmr (CCl_4) δ: 0.12 (s, 9H), 0.75 (s, 3H), 1.07 (s, 3H), 1.10 (s, 3H), 1.55 (m, 4H), 2.23 (br s, 3H), 5.83 (m, 1H). *Anal.* calcd. for $C_{14}H_{26}Si$: C 75.59, H 11.78; found: C 75.63, H 11.73.

Formylation of 7

Anhydrous powdered aluminum chloride (0.2 g, 1.5 mmol) was added in one portion under a stream of nitrogen to a cold (−70°C), magnetically stirred solution of dichloromethyl methyl ether (190 mg, 1.65 mmol) and vinylsilane **7** (238 mg, 1.07 mmol) in dichloromethane (10 mL). After 15 min at −70°C, the reaction mixture was allowed to warm to 0°C over 30 min, poured onto ice (25 g), and stirred for 30 min. The layers were separated, the aqueous phase was extracted with dichloromethane (2 × 10 mL), and the combined organic layers were washed with water (10 mL) prior to drying and concentration. Preparative tlc purification of the residue on silica gel (elution with 5% ethyl acetate in petroleum ether) returned 60 mg of unreacted **7** and furnished 72 mg (50% based on consumed silane) of **8** as a colorless oil; ir (CCl_4): 1685 cm^{-1}; ^{1}H nmr (CCl_4) δ: 0.97 (s, 3H), 1.13 (s, 3H), 1.23 (s, 3H), 1.30−2.10 (series of m, 4H), 2.38 (br s, 3H), 6.32−6.58 (m, 1H), 9.77 (s, 1H).

Vinylation−oxidation of 8

A solution of vinylmagnesium bromide under nitrogen was prepared from magnesium turnings (130 mg, 5.34 mg-atoms) and vinyl bromide (0.61 g, 5.66 mmol) in anhydrous tetrahydrofuran (10 mL). The solution was cooled to 0°C and **8** (117 mg, 0.66 mmol) in the same solvent (5 mL) was added. After 1 h at 0°C, the reaction mixture was poured into saturated ammonium chloride solution (20 mL), the layers were separated, and the aqueous phase was extracted with ether (3 × 10 mL). The combined organic layers were dried and evaporated to give the dienol (137 mg), which was dissolved in dry petroleum ether (20 mL), treated with manganese dioxide on carbon (1.4 g), and stirred vigorously for 17 h. The solids were separated by filtration and the filtrate was concentrated to leave pure **9** (134 mg, 100%); ir (CCl_4): 1662, 1605 cm^{-1}; ^{1}H nmr (CCl_4) δ: 0.97 (s, 3H), 1.10 (s, 3H), 1.77 (s, 3H), 1.33−1.75 (m, 4H), 2.28−2.60 (m, 3H), 5.61 (dd, J = 10 and 3 Hz, 1H), 6.17 (dd, J = 17 and 3 Hz, 1H), 6.45 (m, 1H), 6.82 (dd, J = 17 and 10 Hz, 1H).

*2-Ethynyl-5,8,8-trimethyl-bicyclo[3.3.0]octan-2-ol (**12**)*

A solution of lithium acetylide was prepared by bubbling acetylene (dried by passage through a −78°C cold trap) into cold (−78°C), magnetically stirred dry tetrahydrofuran (100 mL) containing *n*-butyllithium (35 mL, 1.37 *M* in hexane, 48.0 mmol). A nitrogen atmosphere was restored and a solution of **6** (832 mg, 5.01 mmol) in anhydrous tetrahydrofuran (15 mL) was added during 15 min. The reaction mixture was allowed to warm to −20°C and was poured into saturated ammonium chloride solution (100 mL). The layers were separated, the aqueous phase was extracted with ether (3 × 10 mL), and the combined organic layers were dried and concentrated. The resulting yellow oil (1.24 g) was purified by mplc on silica gel (elution with 4.5% ethyl acetate in petroleum ether). In addition to recovery of 86 mg of unreacted **6**, there was isolated 677 mg (70.5%) of **12** as a colorless oil; ir (CCl_4): 3605, 3310 cm^{-1}; ^{1}H nmr (CCl_4): δ: 1.02 (s, 3H), 1.11 (s, 3H), 1.32 (s, 3H), 1.4−2.1 (series of m, 10H), 2.31 (s, 1H); m/z calcd. ($M^+ - CH_3$): 177.1279; found: 177.1275. *Anal.* calcd. for $C_{13}H_{20}O$: C 81.20, H 10.48; found: C 81.19, H 10.54.

*2-Acetyl-5,8,8-trimethyl-bicyclo[3.3.0]oct-2-ene (**13**)*

A magnetically stirred solution of **12** (255 mg, 1.33 mmol) in 98% formic acid (6 mL) containing concentrated sulfuric acid (3 drops) was heated at 92°C for 15 min. After cooling, the reaction mixture was diluted with ether (100 mL), washed with water (6 × 10 mL) and saturated sodium bicarbonate solution (3 × 10 mL), dried, and concentrated. There was obtained 227 mg (88.7%) of **13** as a colorless oil; ir (CCl_4): 1670, 1610 cm^{-1}; ^{1}H nmr (CCl_4) δ: 0.68 (s, 3H), 1.16 (s, 6H), 1.36−1.68 (m, 4H), 2.20 (s, 3H), 2.27−2.46 (m, 2H), 2.53 (s, 1H), 6.39 (t, J = 3 Hz, 1H); m/z calcd. (M^+): 192.1514; found 192.1519. *Anal.* calcd. for $C_{13}H_{20}O$: C 81.20, H 10.48; found: C 80.95, H 10.49.

*2-Acetyl-5,8,8-trimethyl-3-vinyl-bicyclo[3.3.0]octane (**14**)*

A solution of vinylmagnesium bromide in anhydrous tetrahydrofuran (3 mL) under nitrogen (prepared from magnesium (61 mg, 2.52 mg-atoms) and vinyl bromide (379 mg, 3.54 (mmol)) was diluted with tetrahydrofuran (5 mL), cooled to −10°C, and treated with cuprous iodide (248 mg, 1.30 mmol). The internal temperature rose to −5°C and after exactly 3 min at −5 to −10°C, the dark mixture was rapidly (< 3 min) cooled to −78°C and a solution of **13** (81 mg, 0.42 mmol) in the same solvent was added dropwise. The reaction mixture was stirred at −78°C for 30 min, allowed to warm to room temperature, poured into weakly basic saturated ammonium chloride solution, and stirred for 30 min. The layers were separated, the aqueous phase was extracted with ether (2 × 10 mL), and the combined organic layers were washed with saturated ammonium chloride solution (10 mL), dried, and concentrated. Purification of the residual yellow oil (108 mg) by mplc on silica gel (elution with 2% ethyl acetate in petroleum ether) gave **14** (51 mg, 54.8%) as a colorless oil; ir (CCl_4): 1713, 1636, 1352, 980, 905 cm^{-1}; ^{1}H nmr (CCl_4) δ: 0.92 (s, 3H), 1.01 (s, 3H), 1.18 (s, 3H), 1.23−1.90 (m, 6H), 1.98 (d, J = 4 Hz, 1H), 2.12 (s, 3H), 2.44−2.84 (m, 1H), 2.84−3.31 (m, 1H), 4.64−5.11 (m, 2H), 5.31−5.99 (m, 1H); m/z calcd. (M^+): 220.1827; found: 220.1832.

Ozonolysis−cyclization of 14

A solution of **14** (70 mg, 0.32 mmol) in methanol (10 mL) was cooled to −78°C and treated with a stream of ozone for 5 min whereupon the solution turned faintly blue, The cold solution was deoxygenated with a stream of nitrogen, dimethyl sulfide (0.5 mL) was added, and the reaction mixture was maintained at −78°C for 30 min prior to warming to 20°C. Removal of the solvent left the dimethyl acetal which was dissolved in formic acid (98%, 2 mL) and swirled at room temperature for 5 min. Ether (50 mL) was added, the solution was washed with water (4 × 10 mL) and saturated sodium bicarbonate solution (10 mL), and the organic phase was dried and evaporated. The resulting aldehyde, which exhibited a single spot on tlc analysis, was dissolved in tetrahydrofuran (10 mL) and ether (5 mL). Aqueous potassium hydroxide (5%, 5 mL) and tetra-*n*-butylammonium hydroxide (40%, 2 drops) were added and the two-phase mixture was vigorously stirred and heated at gentle reflux under nitrogen for 4 h. After cooling, the layers were separated, the aqueous phase was extracted with ether (4 × 10 mL), and the combined organic layers were dried and concentrated. The residue was purified by mplc on silica gel (elution with 9% ethyl acetate in petroleum ether) and gave 55 mg (84,3%) of **16** as a colorless oil; ir (CCl_4): 1712 cm^{-1}; ^{1}H nmr (CCl_4): δ: 0.97 (s, 3H), 0.99 (s, 3H), 1.56 (s, 4H), 1.20−2.19 (series of m, 3H), 2.53 (dd, J = 6 and 3 Hz, 1H), 3.19−3.57 (m, 1H), 5.91 (dd, J = 6 and 2 Hz, 1H), 7.47 (dd, J = 6 and 3 Hz, 1H); m/z calcd. (M^+): 204.1514; found: 204.1518.

*$\Delta^{9(12)}$-Capnellene (**1**)*

Enone **16** (45 mg, 0.22 mmol) was hydrogenated at atmospheric pressure in methanol (10 mL) over platinum oxide (16 mg). The catalyst was separated by filtration and the filtrate was concentrated to give crude **17**.

A solution of potassium *tert*-butoxide was prepared by heating potassium metal (17 mg, 0.43 mg-atom) in *tert*-butyl alcohol (0.5 mL) and benzene (2 mL) under nitrogen. After cooling to room temperature, methyltriphenylphosphonium bromide (120 mg, 0.34 mmol) was added and the deep yellow mixture was stirred at room temperature for 20 min. A solution of **17** in benzene (1 mL) was intro-

duced via cannula and the reaction mixture was heated at reflux for 21 h, cooled, and treated with saturated oxalic acid solution (10 mL). The product was extracted into petroleum ether (2 × 10 mL) and the combined organic layers were washed with saturated brine (10 mL), dried, and evaporated. The residual material (49 mg) was eluted through a plug (10 g) of silica gel with petroleum ether (100 mL) and the eluate was carefully concentrated to furnish 16 mg (36%) of **1** as a colorless oil. The ^{1}H nmr spectrum of this substance was identical in all respects to that of the authentic natural product provided by Professor Djerassi.

Acknowledgements

This investigation was financially supported by the National Institutes of Health through Grant GM-28468. The authors are indebted to Dr. David Dime for preliminary synthetic studies. We are especially pleased to join in this well deserved recognition of Professor Peter Yates' many contributions to the field of organic chemistry on the occasion of his 60th birthday. One of us (K.E.S.) particularly values the direct personal interaction with Professor Yates enjoyed during his graduate years in the Yates' group (Ph.D. Toronto, 1980).

1. E. AYANOGLU, T. GEBREYESUS, C. M. BEECHAN, C. DJERASSI, and M. KAISIN. Tetrahedron Lett. 1671 (1978).
2. M. KAISIN, Y. M. SHEIKH, L. J. DURHAM, C. DJERASSI, B. TURSCH, D. DALOZE, J. C. BRAEKMAN, D. LOSMAN, and R. KARLSSON. Tetrahedron Lett. 2239 (1974).
3. Y. M. SHEIKH, G. SINGY, M. KAISIN, H. EGGERT, C. DJERASSI, B. TURSCH, D. DALOZE, and J. C. BRAEKMAN. Tetrahedron, **32**, 1171 (1976).
4. Y. M. SHEIKH, C. DJERASSI, J. C. BRAEKMAN, D. DALOZE, M. KAISIN, B. TURSCH, and R. KARLSSON. Tetrahedron, **33**, 2115 (1977).
5. R. KARLSSON. Acta Crystallogr. Sect. B, **32**, 2609 (1976).
6. M. KAISIN, B. TURSCH, J. P. DECLERCQ, G. GERMAIN, and M. VAN MEERSSCHE. Bull. Soc. Chim. Belg. **88**, 253 (1979).
7. B. TURSCH, J. C. BRAEKMAN, D. DALOZE, and M. KAISIN. Terpenoids from colenterates. *In* Marine natural products. Vol. II. *Edited by* P. J. Scheuer. Academic Press, New York. 1978. p. 284.
8. L. A. PAQUETTE. Top. Curr. Chem. **79**, 41 (1979); **119**, 1 (1984).
9. (*a*) K. TATSUKA, K. AKIMOTO, and M. KINOSHITA. J. Am. Chem. Soc. **101**, 6116 (1979); (*b*) T. HUDLICKY, T. M. KUTCHAN, S. R. WILSON, and D. T. MAO. J. Am. Chem. Soc. **102**, 6351 (1980); (*c*) A. E. GREENE. Tetrahedron, Lett. 3059 (1980); (*d*) R. D. LITTLE and G. W. MULLER. J. Am. Chem. Soc. **103**, 2744 (1981); (*e*) S. V. LEY and P. J. MURRAY. J. Chem. Soc. Chem. Commun. 1252 (1982); (*f*) P. MAGNUS and D. A. QUAGLIATO. Organometallics, **1**, 1243 (1982); (*g*) P. A. WENDER and J. J. HOWBERT. Tetrahedron Lett. 3983 (1982); (*h*) K. HAYANO, Y. OHFUNE, H. SHIRAHAMA, and T. MATSUMOTO. Tetrahedron Lett. 1991 (1978); (*i*) R. D. LITTLE, R. G. HIGBY, and K. D. MOELLER. J. Org. Chem. **48**, 3139 (1983); (*j*) B. A. DAWSON, A. K. GHOSH, J. L. JURLINA, and J. B. STOTHERS. J. Chem. Soc. Chem. Commun. 204 (1983).
10. (*a*) H. HASHIMOTO, K. TSUZUKI, F. SAKAN, H. SHIRAHAMA, and T. MATSUMOTO. Tetrahedron Lett. 3745 (1974); (*b*) B. M. TROST, C. D. SHUEY, and F. DEVINNO, JR. J. Am. Chem. Soc. **101**, 1284 (1979); (*c*) M. SHIBASAKI, M. YAMAZAKI, K. ISEKI, and S. IKEGAMI. Tetrahedron Lett. 5311 (1982); (*e*) A. E. GREENE, M.-J. LUCHE, and J.-P. DEPRÉS. J. Am. Chem. Soc. **105**, 2435 (1983).
11. (*a*) S. DANISHEFSKY, R. ZAMBONI, M. KAHN, and S. J. ETHEREDGE. J. Am. Chem. Soc. **102**, 2097 (1980); (*b*) M. SHIBASAKI, K. ISEKA, and S. IKEGAMI. Tetrahedron Lett. 3587 (1980); (*c*) K. TATSUTA, K. AKIMOTO, and M. KINOSHITA. J. Antibiot. **33**, 100 (1980); (*d*) K. ISEKI, M. YAMAZAKI, M. SHIBASAKI, and S. IKEGAMI. Tetrahedron, **37**, 4411 (1981); (*e*) B. M. TROST and D. P. CURRAN. J. Am. Chem. Soc. **103**, 7380 (1981); (*f*) T. ITO, N. TOMIYOSHI, K. NAKAMURA, S. AZUMA, M. IZAWA, F. MORUYAMA, M.YANAGIYA, H. SHIRAHAMA, and T. MATSUMOTO. Tetrahedron Lett. 1721 (1982); (*g*) G. METHA, A. V. REDDY, A. N. MURTHY, and D. S. REDDY. J. Chem. Soc. Chem. Commun. 540 (1982); (*h*) P. H. SCHUDA, H. L. AMMON, M. R. HEIMANN, and S. BHATTACHARJEE. J. Org. Chem. **47**, 3434 (1982); (*i*) P. F. SCHUDA and M. R. HEIMANN. Tetrahedron Lett. 4267 (1983); (*j*) C. EXON and P. MAGNUS. J. Am. Chem. Soc. **105**, 2477 (1983).
12. (*a*) L. S. CIERZSKO. Trans. N. Y. Acad. Sci. **24**, 502 (1962); (*b*) P. R. BURKOLDER and L. M. BURKOLDER. Science, **127**, 1174 (1958).
13. L. S. CIERZSKO and T. K. B. KARNS. *In* Biology and geology of coral reefs. Vol. II. *Edited by* O. A. Jones and R. Endean. Academic Press, New York. 1972. Chapt. 6.
14. T. FUJITA, T. OHTSUKA, H. SHIRAHAMA, and T. MATSUMOTO. Tetrahedron Lett. 4091 (1982).
15. K. E. STEVENS and L. A. PAQUETTE. Tetrahedron Lett. 4393 (1981).
16. (*a*) R. D. LITTLE and G. L. CARROLL. Tetrahedron Lett. 4389 (1981). (*b*) R. D. LITTLE, G. W. MULLER, M. G. VENEGAS, G. L. CARROLL, A. BUKHARI, L. PATTON, and K. STONE. Tetrahedron, **37**, 4371 (1981); (*c*) R. D. LITTLE, G. L. CARROLL, and J. L. PETERSEN. J. Am. Chem. Soc. **105**, 928 (1983).
17. J. HUGUET, M. KARPF, and A. S. DREIDING. Helv. Chim. Acta, **66**, 2413 (1983).
18. W. OPPOLZER and K. BÄTTIG. Tetrahedron Lett. 4669 (1982).
19. (*a*) G. MEHTA, D. S. REDDY, and A. N. MURTY. J. Chem. Soc. Chem. Commun. 824 (1983); (*b*) E. PIERS and V. KARUNARATNE. Can. J. Chem. **62**, 629 (1984).
20. (*a*) A. M. BIRCH and G. PATTENDEN. Tetrahedron Lett. 991 (1982); J. Chem. Soc. Perkin Trans. 1, 1913 (1983); (*b*) G. PATTENDEN and S. J. TEAGUE. Tetrahedron Lett. 5471 (1982); E.PIERS and V. KARUNARATNE. Can. J. Chem. **62**, 629 (1984).
21. G. MAGNUSSON and S. THORÉN. J. Org. Chem. **38**, 1380 (1973).
22. (*a*) I. N. NAZAROV and I. I. ZARETSKAYA. J. Gen. Chem. USSR (Engl. Transl.), **29**, 1532 (1959); (*b*) S. DEV. J. Indian Chem. Soc. **34**, 169 (1957); (*c*) W. E. FRISTAD, D. S. DIME, T. R. BAILEY, and L. A. PAQUETTE. Tetrahedron Lett. 1999 (1979); (*d*) F. COOKE, R. MOERCK, J. SCHWINDEMAN, and P. MAGNUS. J. Org. Chem. **45**, 1046 (1980); (*e*) R. M. JACOBSON, G. P. LAHM, and J. W. CLADER. J. Org. Chem. **45**, 395 (1980); (*f*) P. MAGNUS, D. A. QUAGLIATO, and J. C. HUFFMAN. Organometallics, **1**, 1240 (1982); (*g*) S. E. DENMARK and T. K. JONES. J. Am. Chem. Soc. **104**, 2642 (1982).
23. P. E. EATON, G. R. CARLSON, and J. T. LEE. J. Org. Chem. **38**, 4071 (1973).
24. G. H. POSNER. Org. React. **19**, 1 (1972).
25. (*a*) T. HIYAMA, M. TSUKANAKA, and H. NOZAKI. J. Am. Chem. Soc. **96**, 3713 (1974); (*b*) B. M. TROST and M. J. BOGDANOWICZ. J. Am. Chem. Soc. **95**, 289 (1973); **95**, 5298 (1973); **95**, 5311 (1973); B. M. TROST and P. H. SCUDDER. J. Org. Chem. **46**, 506 (1981); (*c*) G. A. MACALPINE, R. A. RAPHAEL, A. SHAW, A. W. TAYLOR, and H.-J. WILD. J. Chem. Soc. Perkin Trans. 1, 410 (1976); (*d*) M. KARPF and A. S. DREIDING. Helv. Chim. Acta, **59**, 1226 (1976); (*e*) M. BAUMANN, W. HOFFMANN, and N. MÜLLER. Tetrahedron Lett. 3585 (1976); (*f*) T. HIYAMA, M. SHINODA, and H. NOZAKI. J. Am. Chem. Soc. **101**, 1599 (1979); Tetrahedron Lett. 771 (1978); (*g*) E. J. COREY and D. L. BOGER. Tetrahedron Lett. 13 (1978).
26. L. A. PAQUETTE, W. E. FRISTAD, D. S. DIME, and T. R. BAILEY. J. Org. Chem. **45**, 3017 (1980).
27. R. H. SHAPIRO. Org. React. **23**, 405 (1976).
28. A. R. CHAMBERLIN, J. E. STEMKE, and F. T. BOND. J. Org. Chem. **43**, 147 (1978).
29. T. H. CHAN, P. W. K. LAU, and W. MYCHAJLOWSKIJ. Tetrahedron Lett. 3317 (1977).

Can. J. Chem. Downloaded from www.nrcresearchpress.com by 210.87.254.105 on 09/06/12
For personal use only.

30. M. S. NEWMAN. J. Am. Chem. Soc. **72**, 4783 (1950).
31. M. M. MIDLAND. J. Org. Chem. **40**, 2250 (1975).
32. S. SWAMINATHAN and K. V. NARAYANAN. Chem. Rev. **71**, 429 (1971).
33. P. M. WEGE, R. D. CLARK, and C. H. HEATHCOCK. J. Org. Chem. **41**, 3144 (1976).
34. P. D. MAGNUS and M. S. NOBBS. Synth. Commun. **10**, 273 (1980).
35. L. A. CARPINO. J. Org. Chem. **35**, 3971 (1970).

Can. J. Chem. Downloaded from www.nrcresearchpress.com by 210.87.254.105 on 09/06/12
For personal use only.

Total assignment of ^1H and ^{13}C spectra of kauradien-9(11),16-oic acid with the aid of heteronuclear correlated 2D spectra optimized for geminal and vicinal $^{13}C-^1H$ coupling constants: or what to do when "INADEQUATE" is impossible

WILLIAM F. REYNOLDS

Department of Chemistry, University of Toronto, Toronto, Ont., Canada M5S 1A1

AND

RAUL G. ENRÍQUEZ, LAURA I. ESCOBAR, AND XAVIER LOZOYA

Unidad de Investigación Biomédica en Medicina Tradicional y Herbolaria, IMSS, Luz Saviñón 214, México, D.F. 03100

Received March 27, 1984

This paper is dedicated to Professor Peter Yates on the occasion of his 60th birthday

WILLIAM F. REYNOLDS, RAUL G. ENRÍQUEZ, LAURA I. ESCOBAR, and XAVIER LOZOYA. Can. J. Chem. **62**, 2421 (1984).

It is shown that heteronuclear correlated spectra in which delay times are optimized for geminal and vicinal $^{13}C-^1H$ couplings rather than direct $^{13}C-^1H$ couplings can be used to assign quaternary carbons in the ^{13}C spectrum of kauradien-9(11),16-oic acid. These spectra in combination with normal heteronuclear correlated spectra plus homonuclear correlated spectra can be used to completely and unambiguously assign the ^{13}C and ^1H spectral peaks for the title compound. The main advantage of this approach over the use of $^{13}C-^{13}C$ connectivity ("INADEQUATE") experiments is sensitivity.

WILLIAM F. REYNOLDS, RAUL G. ENRÍQUEZ, LAURA I. ESCOBAR, et XAVIER LOZOYA. Can. J. Chem. **62**, 2421 (1984).

On démontre que l'on peut utiliser les spectres hétéronucléaires corrélés, dans lesquels on a optimisé les couplages géminal et vicinal $^{13}C-^1H$ plutôt que les couplages $^{13}C-^1H$ directs, pour attribuer les carbones quaternaires du spectre ^{13}C de l'acide kauradiène-9(11),16 oïque. On peut combiner ces spectres avec les spectres hétéronucléaires corrélés normaux et les spectres homonucléaires corrélés normaux pour faire une attribution complète et sans ambiguité des pics présents dans les spectres ^{13}C et ^1H. C'est la sensibilité qui est l'avantage principal de cette approche par rapport aux expériences de connectivité $^{13}C-^{13}C$ ("INADEQUATE").

[Traduit par le journal]

Introduction

As part of a systematic investigation of medicinal properties of natural products isolated from Mexican plants (1), we were interested in using some of the recently developed two dimensional nmr pulse sequences (2, 3) as an aid in characterizing these products and assigning their ^1H and ^{13}C spectra.

The techniques for simultaneously assigning hydrogens and protonated carbons by 2D nmr are now well established (3). For example, one can use heteronuclear ($^1H-^{13}C$) correlated spectroscopy (4) in conjunction with either homonuclear correlated spectroscopy (5, 6) or the more recently developed relayed coherence spectroscopy (7) for this purpose. Either of the latter allow establishment of hydrogen connectivity maps via vicinal $^1H-^1H$ coupling while the former identifies pairs of directly bonded carbons and hydrogens.

However, these experiments provide no assignments for either quaternary carbons or isolated protonated carbons (e.g. methyl groups attached to quaternary carbons) and may also fail in other special cases (see Discussion).

The ultimate approach is either the one-dimensional (8) or two-dimensional (9) $^{13}C-^{13}C$ connectivity experiment which allows assignment of the entire carbon skeleton. Unfortunately, due to the extremely low sensitivity of these experiments, this approach is often impractical. However, recently Richarz *et al.* (10) and Hull (11) have independently suggested the possibility of modifying the heteronuclear correlated experiment by choosing delay times appropriate for transferring magnetization via geminal ($^1\underline{H}—C-^{13}\underline{C}$) or vicinal ($^1\underline{H}—C—C-^{13}C$) couplings rather than the usual direct $^1H-^{13}C$ coupling.[1] In this manuscript, we show that this technique can be used in conjunction with other correlation experiments to provide a total and unambiguous assignment of all ^1H and ^{13}C signals of a typical natural product.

Results and discussion

The compound chosen for initial investigation was kauradien-9(11),16-oic acid, **1**, which was isolated from the plant *Montanoa tomentosa* ("zoapatle" in Mexican folk medicine) (1). This was chosen not only for its interesting and important medicinal properties (1) but also because only limited ^1H spectral data (13) and no ^{13}C spectral data were available for this compound.

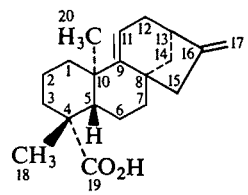

1

A ^1H spectrum (200 MHz in $CDCl_3$, see Fig. 1) indicated the presence of several partially overlapping multiplets in the aliphatic region. However, all peaks were resolved in the ^1H-decoupled ^{13}C spectrum. Consequently, a heteronuclear correlated experiment was carried out (see Fig. 2). This allowed straightforward determination of which ^1H signals were associated (by direct bonding) with which ^{13}C signals. A homonuclear correlated experiment (6) was then carried out in an attempt to determine $^1H-^1H$ connectivity patterns. However, some of the connectivities could not be clearly established, because of multiplet overlap. Consequently, the heteronuclear and homonuclear experiments were repeated in C_6D_6. While the ^{13}C chemical shifts were almost unchanged (see Table 1),

[1]After initial submission of this manuscript, a report appeared demonstrating the utility of this approach for sequencing polypeptides (12).

Can. J. Chem. Downloaded from www.nrcresearchpress.com by 210.87.254.40 on 09/06/12
For personal use only.

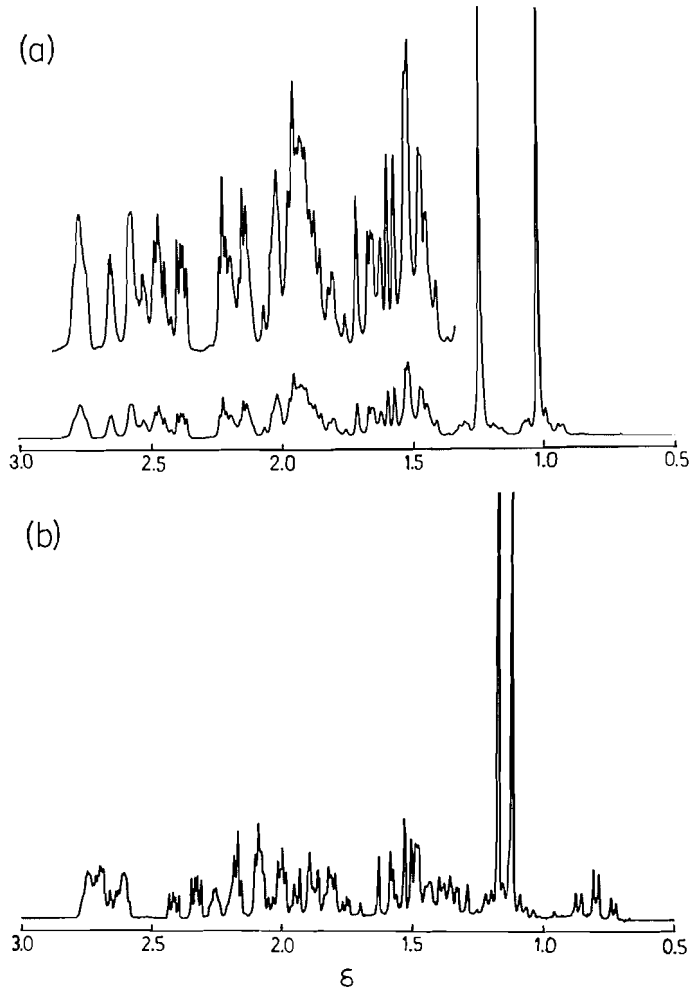

FIG. 1. Aliphatic ^1H spectral region (δ 0.5−3.0) for **1** in (a) $CDCl_3$ (b) C_6D_6.

aromatic solvent-induced shifts altered the ^1H spectrum sufficiently that previously overlapping multiplets could be resolved, allowing completion of the assignment of $^1H-^1H$ connectivities. This was aided by the fact that many of the carbons had two attached hydrogens which provided independent pathways for establishing connectivities.

The two types of 2D experiments in the two solvents allowed unambiguous assignment of most hydrogen and protonated carbon signals. Specifically the fragments —C(5)H—C(6)H_2—C(7)H_2— and —C(11)H—C(12)H_2—C(13)H—C(14)H_2 could be assigned, starting in each case with the underlined hydrogen. The protons of one C(sp^3)H_2 group showed allylic coupling to the C(17) olefinic protons in the homonuclear correlated experiments, allowing identification of this group as C(15)H_2, while C(17)H_2 could be assigned from the heteronuclear correlated experiments as the only C(sp^2)H_2 group. Finally the CO_2H group could be assigned on the basis of its unique ^{13}C chemical shift. However, while we could also identify the fragment —C(1)H_2—C(2)H_2—C(3)H_2 and assign C(2)H_2, it was impossible to determine which of the two remaining groups was C(1)H_2 and which was C(3)H_2, since each end of the sequence was terminated by a quaternary carbon. Similarly, the two CH_3 groups could not be definitively assigned since each is also attached to a quaternary carbon. Finally, the experiments described above provided no basis

TABLE 1. Assigned ^{13}C and ^1H chemical shifts for kauradien-9(11),16-oic acid in ppm to low field of $(CH_3)_4Si$)

Carbon	$\delta_C(CDCl_3)$	$\delta_C(C_6D_6)$	$\delta_{H(\alpha)}$[a]	$\delta_{H(\beta)}$[a]
1	40.75	40.91	1.92(1.84)[b]	1.25(1.15)[c]
2	20.13	20.50	1.49(1.42)[c]	1.89(2.04)[b]
3	38.21	38.36	2.14(2.22)[b]	1.01(0.81)[c]
4	44.74	45.01	—	—
5	46.61	46.85	—	1.65(1.58)[c]
6	18.44	18.82	1.85(1.80)[c]	2.50(2.66)[b]
7	29.67	29.93	1.97(1.96)[b]	1.44(1.34)[c]
8	42.26	42.48	—	—
9	155.93	156.00	—	—
10	38.80	39.07	—	—
11	114.89	115.40	5.21(5.22)	
12	37.91	38.10	2.42(2.36)	1.98(2.02)[d]
13	41.23	41.64	2.77(2.72)	—
14	44.94	45.17	1.48(1.46)	1.61(1.54)[e]
15	50.29	50.42	2.60(2.63)	2.17(2.12)[d]
16	158.49	158.30	—	—
17	105.49	105.96	4.78(4.94)	4.89(5.03)[f]
18	28.23	28.27	—	1.24(1.12)[b]
19	184.72	185.36	~11(~11)[g]	—
20	23.59	23.90	1.02(1.17)[c]	—

[a]The first listed value is the chemical shift of each proton in $CDCl_3$ while the second value (in brackets) is the chemical shift in C_6D_6.
[b]Equatorial proton or methyl group.
[c]Axial proton or methyl group.
[d]Pairs of hydrogens could be interchanged.
[e]Assigned on the basis of an observed cross peak between C(16) and $H(14)_\alpha$ in Fig. 3 (see text).
[f]It cannot be determined which of these olefinic hydrogens is *cis* to C(13) and to C(15). Note that the labels α and β do not apply.
[g]Very broad CO_2H peak.

for assigning the three quaternary sp^3 carbons, C(4), C(8), and C(10), as well as the two quaternary sp^2 carbons, C(9) and (16).

Several of these signals (particularly the two CH_3 groups) could have been tentatively assigned on the basis of previous assignments of closely related compounds (14). However, we were interested in making the assignments with a minimum of *a priori* assumptions since one can never be absolutely confident of the validity of the earlier assignments. Consequently, we decided to try the idea of Richarz *et al.* (10) and Hull (11) of altering the delay times in the heteronuclear correlated experiment to values appropriate for promoting magnetization transfer via geminal ^1H—C—^{13}C and (or) vicinal ^1H—C—C—^{13}C couplings rather than direct $^1H-^{13}C$ couplings, as normally used. The use of magnetization transfer from CH_3 signals seemed particularly promising, both because these sharp singlets should give the most intense peaks in the 2D (heteronuclear correlated) spectrum and because the similar magnitudes of geminal and vicinal $^1H-^{13}C$ couplings involving methyl hydrogens should allow simultaneous establishment of connectivities via both types of couplings in a single experiment.

Inspection of the structure of **1** shows that the C(18)H_3 signal should transfer magnetization to C(3), C(4), C(5), and C(19) while the C(20)H_3 signal should transfer magnetization to C(1), C(5), C(9), and C(10). As shown below, this is sufficient to allow unambiguous assignment of all previously unassigned signals.

The heteronuclear correlated pulse sequence (4*b*) is illustrated in **2**. With the Varian software, one enters a value of J_{CH}

Can. J. Chem. Downloaded from www.nrcresearchpress.com by 210.87.254.40 on 09/06/12
For personal use only.

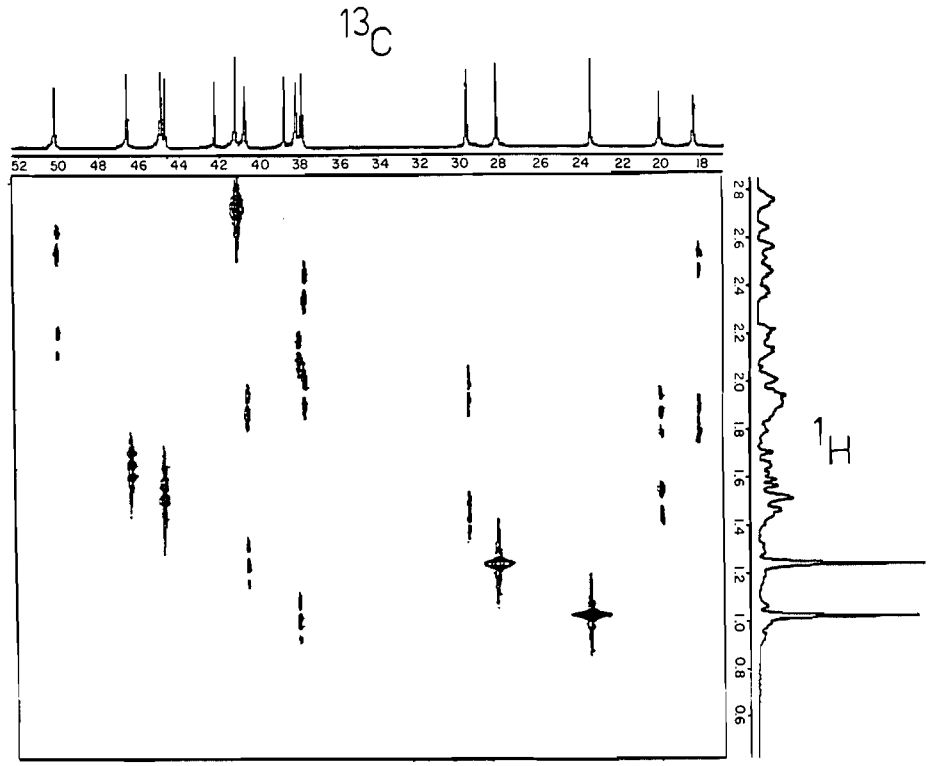

FIG. 2. Normal heteronuclear correlated spectrum for **1** in $CDCl_3$, illustrating the aliphatic ^{13}C (horizontal) and ^{1}H (vertical) spectral regions.

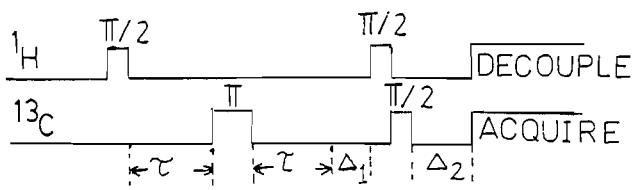

2

(in Hz) with Δ_1 set at $1/2J$ and Δ_2 at $1/3J$. Repeated preliminary experiments with different input J_{CH} values indicated that best results were obtained for $J_{CH} = 10$ Hz (i.e. $\Delta_1 = 0.05$ s, $\Delta_2 = 0.033$ s) even though $^2J_{CH}$ and $^3J_{CH}$ couplings involving methyl hydrogens are typically ca. 5 Hz (15). Two factors are likely responsible for this. First, the value $\Delta_2 = 1/3J$ is actually a compromise value for different CH_n groups with $\Delta_2 \simeq 1/5J$ being optimum for CH_3 groups (2), i.e., optimum $\Delta_2 \simeq 0.2/5 = 0.04$ s. By contrast, the theoretical optimum Δ_1 is independent of the type of CH_n group, i.e. optimum $\Delta_1 = 0.10$ s. However, ^1H magnetization is decaying towards zero during this delay period. Due to short ^1H relaxation times in large molecules, the use of a shorter than theoretically optimum Δ_1 may actually maximize the residual magnetization available for transfer to ^{13}C in the final stage of the pulse sequence.[2]

Results are shown in Figs. 3 and 4. Figure 3 shows the low field ^{13}C region. It is seen that the low field $C\underline{H}_3$ group transfers magnetization to $\underline{C}(19)O_2H$. Thus, this signal corresponds to $C(18)\underline{H}_3$. Similarly the high field $C\underline{H}_3$ group transfers magnetization to the low field quaternary $C(sp^2)$ signal, simultaneously confirming that the former is $C(20)\underline{H}_3$ and that the latter is C(9). The methyl ^{13}C signals can then be assigned from the normal heteronuclear correlated experiment (Fig. 2) while C(16) is assigned on the basis that it is the only remaining quaternary $C(sp^2)$ signal.

Figure 4 illustrates the aliphatic ^{13}C region. The low field $C\underline{H}_3$ peak ($C(18)\underline{H}_3$) transfers magnetization to three peaks on the left hand side of the spectrum, corresponding to C(3), C(4), and C(5). The final assignment of these three peaks is straightforward due to their different numbers of attached protons (respectively 2, 0, and 1). Similarly, one can identify (C1), C(5), and C(9) on the basis of magnetization transfer from $C(20)\underline{H}_3$ and their different numbers of attached protons (respectively 2, 1, and 0). Note that this experiment provides a check of the self-consistency of the approach since it provides two independent assignments of C(5) which can be compared with the earlier assignment of this carbon based on proton–proton connectivities. All three assignments agree. Finally, C(8) can be assigned as the only quaternary sp^3 carbon which receives no magnetization from either $C(18)\underline{H}_3$ or $C(20)\underline{H}_3$, thus completing the assignment. Strong peaks are also observed corresponding to $\underline{C}(18)\underline{H}_3$ and $\underline{C}(20)\underline{H}_3$, even though the chosen delay time is far removed from the optimum value for magnetization transfer via direct $^{13}C-^{1}H$ coupling. However, this is redundant information since these connectivities have already been established (see Fig. 2).

Some additional peaks are observed in Figs. 3 and 4 corresponding to connectivities between methine or methylene hydrogens and adjacent carbons. Most of these correspond to *anti* vicinal $^{13}C-^{1}H$ coupling, as expected, since the chosen delay times are close to optimal (2) for this type of coupling (*anti* $^3J_{CH} \simeq 9$ Hz (15)) but not for the much smaller *gauche* coupling. In all cases, the observed cross peaks support the earlier ^{13}C and ^{1}H assignments. For example, in Fig. 3, there are two cross peaks corresponding to $^{13}\underline{C}O_2H$ plus protons assigned as H(3)β and H(5), both of which are in an *anti* vicinal arrangement with

[2]No attempt was made to independently optimize Δ_1 and Δ_2 since this would be extremely time consuming.

Can. J. Chem. Downloaded from www.nrcresearchpress.com by 210.87.254.40 on 09/06/12
For personal use only.

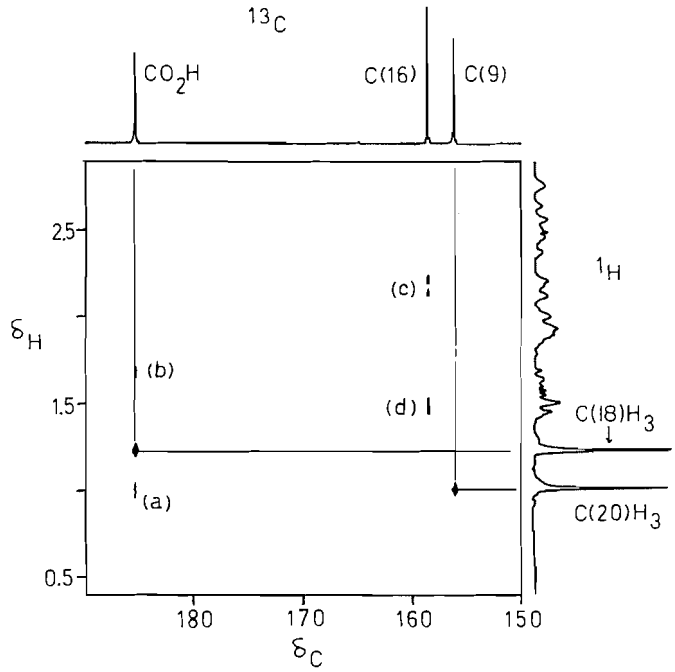

FIG. 3. Long range heteronuclear correlated spectrum (emphasizing $^2J_{CH}$ and $^3J_{CH}$ couplings) for **1** in $CDCl_3$ with the low field ^{13}C spectral region along the horizontal and the aliphatic ^1H spectral region along the vertical. Crossed lines point out the main peaks used for assignment purposes. Redundant peaks discussed in the text include (a) $\underline{C}O_2H—\underline{H}(5)$ (b) $\underline{C}O_2H—\underline{H}(3)\beta$ (c) $\underline{C}(16)—H(15)$ (d) $C(16)—\underline{H}(14)\alpha$.

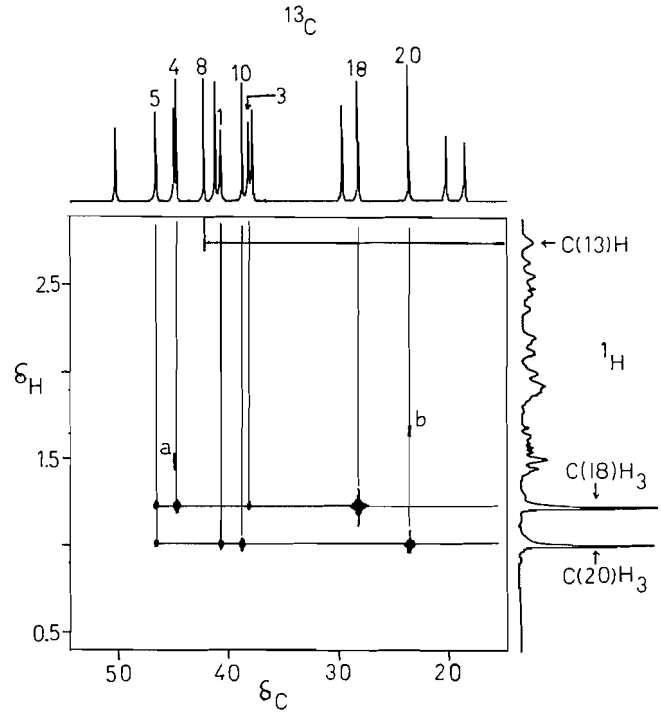

FIG. 4. Long range heteronuclear correlated spectrum for **1** in $CDCl_3$ with the aliphatic ^{13}C spectral region along the horizontal. Crossed lines point out the main peaks used for assignment purposes with the assigned carbons labelled. Redundant peaks discussed in the text include (a) C(14)—H(7)β and (b) C(20)—H(5). Note the absence of a peak for C(18)—H(5).

respect to CO_2H. There are cross peaks between C(16) and one of the C(15) protons plus one of C(14) protons, presumably the one *anti* to C(16), both supporting the assignment of C(16) given above. Similarly in Fig. 4, there is a cross peak between C(8) and the *anti*-vicinal H(13), supporting the assignment of this quaternary carbon. A peak is also observed establishing a connectivity between C(14) and one of the C(7) protons. Interestingly, there is also a cross peak between C(20) and H(5) but not between C(18) and H(5), consistent with the *anti* orientation of the former coupling and the *gauche* orientation of the latter coupling. Thus, the modified heteronuclear correlated experiment can not only be used to establish geminal and vicinal $^{13}C-^1H$ connectivities but can also provide conformational information in the case of vicinal coupling. It should be noted that spectra recorded at higher vertical gain show many additional geminal or vicinal $^{13}C-^1H$ peaks which are consistent with our assignments. The vertical gains for Figs. 3 and 4 were chosen to give relatively clean spectra, emphasizing the key cross peaks involving the methyl hydrogens, since the other peaks provide redundant information.

Final assignments are provided in Table 1. The assignment of methylene hydrogens as α or β is based on the known stereochemistry of **1** plus the presence or absence of a large vicinal coupling constant (indicative of an axial orientation) in individual proton multiplets (cross-sections through each ^{13}C peak in Fig. 1 were used to better determine ^1H multiplet patterns). In three cases, it was impossible to unambiguously assign pairs of methylene hydrogens on a single carbon. Otherwise, the assignment is complete and unambiguous. Furthermore, this assignment has required no prior assumptions, other than the trivial one that can distinguish CO_2H from quaternary sp^2 carbons separated by over 25 ppm.

It is interesting to compare this approach with alternative approaches which could have been used. To begin, we could have used a relayed coherence experiment (7) in place of the homonuclear correlated experiment (6). The former approach also establishes $^1H-^1H$ connectivities between vicinal hydrogens but detects these connectivities via ^{13}C spectral peaks, taking advantage of the much greater resolution in the ^{13}C spectrum (7, 10). This would have avoided the need to carry out measurements in more than one solvent. However, due to the significantly lower sensitivity of this experiment (7), the total measuring time would have been longer than for the homonuclear correlated spectra, negating the advantages of increased resolution in this particular case.

The main advantage of the approach we have used over the use of $^{13}C-^{13}C$ connectivity (INADEQUATE) experiments is sensitivity. For example, the actual spectra in Figs. 2–4 were obtained using 200 mg of **1** and 5-h acquisition times (in view of the high signal-to-noise ratios, 1- to 2-h runs probably would have been sufficient). By contrast, when we carried out a $^{13}C-^{13}C$ connectivity experiment using the same sample, signal-to-noise was still "inadequate" after 36 h. In addition, the long range heteronuclear correlated experiment can be used to establish connectivities even through heteroatoms (e.g. $^1\underline{H}—C—O—^{13}\underline{C}(10)$). Finally, as partially illustrated in Figs. 3 and 4, it provides much redundant information which can be used to confirm the spectral assignments. There are, however, at least two potential limitations to this experiment. First, there must be resolved peaks in the ^1H spectra which can be used to unambiguously assign geminal and vicinal $^1H-^{13}C$ connectivities. This will be a problem particularly for large molecules with complex ^1H spectra but can be partially overcome by increasing digitization for the ^1H spectral domain. There may

Can. J. Chem. Downloaded from www.nrcresearchpress.com by 210.87.254.40 on 09/06/12
For personal use only.

Can. J. Chem. Downloaded from www.nrcresearchpress.com by 210.87.254.40 on 09/06/12
For personal use only.

also be sensitivity problems for larger molecules because their very short ^1H relaxation times result in very significant loss of ^1H magnetization during Δ_1, prior to transfer to ^{13}C. However, subsequent to submission of this manuscript, Kessler *et al.* published a modified heteronuclear correlation pulse sequence (COLOC (16)) which is specifically designed to minimize this problem. Consequently, we conclude that these limitations are not serious and that "long range" heteronuclear correlated experiments, either as used above or as modified by Kessler (16), can often provide a viable alternative to $^{13}C-^{13}C$ connectivity experiments, particularly in cases where sensitivity limitations make INADEQUATE impossible.

Experimental

Full details of the isolation of **1** have been presented elsewhere (17). 2D experiments were performed on a Varian XL-200 spectrometer at a probe temperature of ca. 20°C. Standard Varian software (G and H release) were used.

Homonuclear correlated experiments were carried out using a spectral width of 1000 Hz in each domain (ca. δ 0.5−5.5), a 512 × 512 data matrix, 256 time increments, and 16 transients for each FID. The second mixing pulse in the homonuclear (Jeener) pulse sequence (6) was set at 60° (5.2 μs), as recommended by Bax and Freeman (18). Free induction decays were subjected to "pseudo-echo" processing (18) and diagonal folding (5*b*) was applied to the final spectrum. Normal heteronuclear correlated experiments were carried out using a spectral width of 5500 Hz in the first domain (^{13}C, ca. δ 10−120) and 1000 Hz in the second domain (^1H, ca. δ 0.5−5.5), a 2048 × 512 data matrix, 128 time increments, and 128 transients per FID 2.5-Hz exponential line broadening was applied in each case. Long range heteronuclear correlated experiments were carried out in $CDCl_3$, using $\Delta_1 = 0.05$ s and $\Delta_2 = 0.033$ s. The first experiment used a ^{13}C spectral width of 2500 Hz (ca. δ 10−60) and 500 Hz in the ^1H domain (ca. δ 0.5−3.0) and a 2048 × 512 data matrix, while the second experiment differed only by using a ^{13}C spectral width of 9000 Hz (ca. 10−190) to include CO_2H and quaternary $C(sp^2)$ carbons. It should be noted that the first of the two modified heteronuclear experiments was not strictly necessary and was carried out mainly for esthetic purposes, i.e. to get a spectrum with excellent ^{13}C digital resolution for the aliphatic region (see Fig. 4).

All heteronuclear experiments were carried out in 10-mm tubes, using 200 nmg of **1** in ca. 2 mL of $CDCl_3$ or C_6D_6. Homonuclear experiments were carried out in 5-mm tubes, using aliquots of the samples from the heteronuclear experiments.

Acknowledgments

Financial support from NSERC is gratefully acknowledged (WFR).

1. X. LOZOYA, R. G. ENRIQUEZ, E. BEJAR, A. V. ESTRADA, H. GIRON, H. PONCE-MONTER, and A. J. GALLEGOS. Contraception, **27**, 267 (1983), and references therein.
2. A. BAX. Two-dimensional nuclear magnetic resonance in liquids. D. Reidel, Holland. 1982.
3. R. BENN and H. GUNTHER. Angew. Chem. Int. Ed. Engl. **22**, 350 (1983).
4. (*a*) A. A. MAUDSLEY, L. MULLER, and R. R. ERNST. J. Magn. Reson. **28**, 463 (1977); (*b*) A. BAX and G. A. MORRIS. J. Magn. Reson. **42**, 501 (1981).
5. (*a*) K. NAGAYAMA, K. WURTHRICH, and R. R. ERNST. Biochem. Biophys. Res. Commun. **90**, 305 (1979); (*b*) K. NAGAYAMA, A. KUMA, K. WURTHRICH, and R. R. ERNST. J. Magn. Reson. **40**, 321 (1980).
6. A. BAX, R. FREEMAN, and G. A. MORRIS. J. Magn. Reson. **42**, 169 (1981).
7. P. D. BOLTON. J. Magn. Reson. **48**, 336 (1982).
8. A. BAX, R. FREEMAN, and S. P. KEMPSELL. J. Am. Chem. Soc. **102**, 4849 (1980).
9. T. H. MARECI and R. FREEMAN. J. Magn. Reson. **48**, 158 (1982).
10. R. RICHARZ, W. AMMAN, and T. WIRTHLIN. Varian Applications Note NMR-20 (1982).
11. W. E. HULL. Two-dimensional N.M.R. Bruker, Karlsruhe. 1982.
12. C. WYNANTS, K. HALLENGA, G. VAN BINST, A. MICHEL, and J. ZANEN. J. Magn. Reson. **57**, 93 (1984).
13. F. PIOZZI, S. PANNANNANTI, M. L. MARINO, and V. SPIRO. Can. J. Chem. **50**, 109 (1972).
14. (*a*) K. YAMASAKI, K. KOHDA, T. KOBAYASHI, R. KASAI, and O. TANAKA. Tetrahedron Lett. 1005 (1976); (*b*) I. YAMAUCHI, N. TAKAHASHI, and K. FUJITA. J. Chem. Soc. Perkin Trans. 1, 992 (1975).
15. P. E. HANSEN. Prog. Nucl. Magn. Reson. Spectrosc. **14**, 175 (1981).
16. H. KESSLER, C. GRIESINGER, J. ZARBOCK, and H. R. LOOSI. J. Magn. Reson. **57**, 331 (1984).
17. R. G. ENRIQUEZ, L. I. ESCOBAR, M. L. ROMERO, M. A. CHAVEZ, and X. LOZOYA. J. Chromatogr. **258**, 297 (1983).
18. A. BAX and R. FREEMAN. J. Magn. Reson. **44**, 542 (1981).

On Worrall's dilactams. Structural corrections

DOUGLAS N. BUTLER AND SUSHIL DATTA
Department of Chemistry, York University, Toronto, Ont., Canada M3J 1P3

Received March 21, 1984

This paper is dedicated to Professor Peter Yates on the occasion of his 60th birthday

DOUGLAS N. BUTLER and SUSHIL DATTA. Can. J. Chem. **62**, 2426 (1984).

The structures of a number of polycyclic diamides available via the action of ammonia on *exo,exo*-5,6-dibromonorbornane-*endo,endo*-2,3-dicarboxylic anhydride have been shown to be incorrectly reported. These substances all possess a nortricyclyl skeleton, e.g. **8**, **9**, and **10**.

DOUGLAS N. BUTLER et SUSHIL DATTA. Can. J. Chem. **62**, 2426 (1984).

On a démontré que les structures proposées antérieurement pour un certain nombre de diamides polycycliques disponibles par le biais de l'action de l'ammoniac sur l'anhydride dibromo-5,6 *exo,exo* norbornane dicarboxylique-2,3 *endo,endo* ne sont pas correctes. Le squelette fondamental de chacune de ces substances est le nortricyclyle, comme dans les produits **8**, **9** et **10**.
[Traduit par le journal]

For a number of years we have designed, synthesized, and studied rigid molecules which exhibit specific, intramolecular functional group proximities (2). Recently we observed that the basicity of certain diethers (eg. **1**) was markedly enhanced by the proximity of the two oxygen atoms (3) and we therefore sought to extend this concept to the equivalent diamine **2**. A survey of the literature for potential starting points revealed that the obviously desirable dilactam **3** was apparently known.

The carefully described, though somewhat tedious procedure of Worrall (1) for the "ammonolysis" of *exo,exo*-5,6-dibromonorbornane-*endo,endo*-2,3-dicarboxylic anhydride (4) was repeated and a solid isolated which by melting point, yield (28%), and infrared spectrum corresponded to the compound for which he ascribed the hydroxy-amide-lactam structure **4**. No evidence was presented by Worrall (or by us) as to the fate of the remainder of the starting material. In our hands, repeated recrystallization from methanol of this product raised the melting point considerably – perhaps because water was the solvent originally used. However, the combustion analysis, the mass spectrum, the infrared spectrum, and subsequent chemistry were all consistent with this product being the same as that isolated by Worrall. In particular, thermal deamination to a

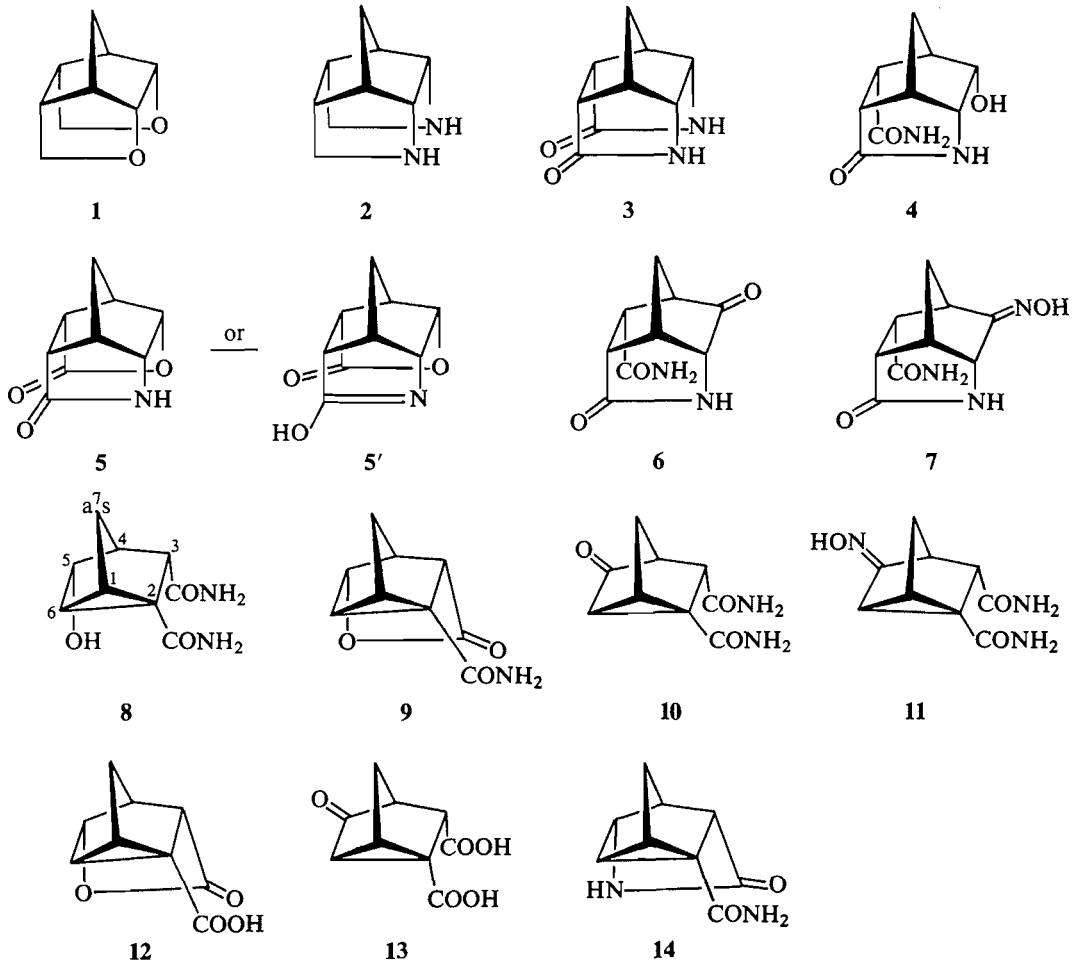

Can. J. Chem. Downloaded from www.nrcresearchpress.com by 210.87.254.5 on 09/06/12
For personal use only.

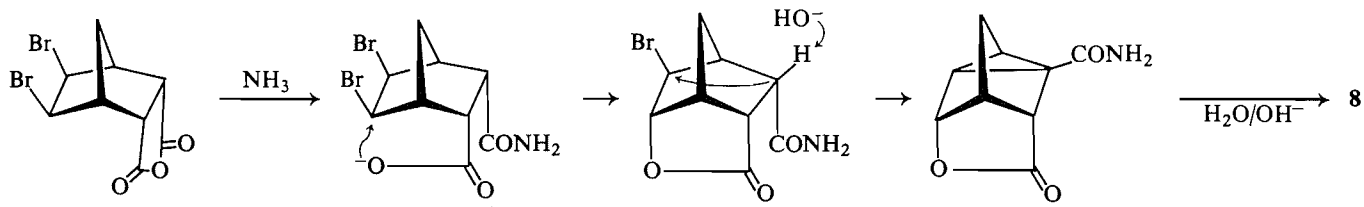

SCHEME 1

lactone-lactam assigned as structure **5** (or **5′**) was readily repeated, giving a product having an identical melting point and infrared spectrum to that described. It also showed the appropriate parent-ion in its mass spectrum. Further, permanganate oxidation to a keto-amide-lactone (given as structure **6**) and its derived oxime (given as structure **7**) was easily followed using the published procedure, once again giving products of like melting points and infrared spectra and again for which appropriate parent-ions were observed. Thus there is little doubt that the compounds that we have made do indeed correspond to those originally prepared.

An examination of the compound given structure **4** by 2D FT nuclear magnetic resonance techniques quickly revealed that the assigned structures were wrong. Structure **4** is reassigned as **8** with **5**, **6**, and **7** becoming **9**, **10**, and **11** respectively. In particular, the 2D $^1H-^1H$ homonuclear shift and $^{13}H-^1H$ heteronuclear shift correlated plots were obtained in DMSO-d_6 solution and these analysed to provide the assignments given herein. Along with the two-proton AB quartet for the 7-methylene protons at δ = 1.32 and 1.48 ppm with ^2J = 10.5 Hz there were two other coupled protons (^3J = 6 Hz) at δ = 1.61 and 1.96 ppm. These correlated with the highest-field carbon lines at δ = 22.5 and 25.64 ppm, both of which showed a $J(^{13}C-^1H)$ = 179 Hz. Such large couplings for high-field carbon resonances are consistent with cyclopropyl structures and similar pairs of such proton coupled high-field carbon resonances were seen in **9**, **10**, and **11** (see Experimental). For compound **8** at 10°C, five D_2O exchangeable protons were all resolved in the ^1H spectrum in DMSO-d_6. After the exchange for deuterium, the ^1H doublet at δ = 3.75 ppm now appeared as a slightly broadened singlet and thus must be assigned as H_5. This was corroborated in the COSY plot (5) which showed the coupled —OH at δ = 5.74 ppm. At room temperature, two of the four NH lines observed upon cooling coalesced into a broad singlet (δ = 6.81 ppm) whilst the remaining two at δ = 7.27 and 7.79 coalesced upon heating to 90°C into a very broad resonance centred near δ = 7.4 ppm. Since, from the thermal cyclization (with ammonia evolution) by which **9** is produced, the *endo–endo* disposition of the functionalities involved is obligatory, we propose that hydrogen bonding between these functions (i.e. 5-hydroxyl and 3-carboxamido) is responsible for the differential behaviour of the pairs of amido protons. The remaining ^1H assignments of δ = 1.98 and 2.69 ppm, as H_4 and H_3 respectively, whilst showing only small coupling in the normal ^1H spectrum, did show weak correlations in the COSY plot with H_3 only coupling to H_4 but H_4 coupling to H_3, H_5, and to both H_7 protons. With these proton assignments in hand, the $^{13}C-^1H$ shift correlation readily allowed the carbon assignments with C_2 δ = 31.08 ppm unattached to any proton and C_7 δ = 31.70 ppm being attached to two protons ($J(^{13}C-^1H)$ = 134 Hz), confirming the corresponding ^1H resonances detailed above and C_3 and C_4 respectively at δ = 50.49 and 40.74 ppm.

These assignments allowed fully consistent analysis of the ^1H and ^{13}C routine spectra of compounds **9**, **10**, and **11** (see Experimental) and thus support our revised structures for these molecules.

Further structural proof was indirectly provided from the literature. Zalkow and Kennedy (6) repeated Worrall's preparations and found that when the lactone-lactam **5** (actually **9**) was heated with 5% hydrochloric acid, an "unusual" *N*-alkyl cleavage took place to give the known tricyclic lactone-acid **12**. Likewise, under the same conditions the ketone **6** (actually **10**) was converted to the known keto-diacid **13**. Since the structures of **12** and **13** were secure (7), the revised tricyclic structures for the starting materials, viz. **9** and **10**, of these reactions were in fact already present and no "unusual" chemistry was involved at all.

The literature preparation (7) of **12**, from alkali treatment of the same dibromo-anhydride as used in Worrall's aqueous ammonia procedure, provided an insight to the formation of **8** as rationalized in Scheme 1.

Although we did not proceed beyond the oxime **11** of Worrall's route, we have little reason to doubt that his reported dilactam **3** is, in fact, compound **14**. We have synthesized diamine **2** via an alternative route and will shortly report this chemistry.

Experimental

General

Melting points were determined an a Fisher–Johns apparatus and are uncorrected. Infrared spectra were recorded on a Unicam SP1000A instrument as Nujol mulls and mass spectra taken at 70 eV on a V. & G. Micro-mass 16F spectrometer. The ^1H and ^{13}C nuclear magnetic resonance spectra were recorded on Varian Associates EM360 (60 MHz), CFT80, or Bruker AM250 (250 MHz) instruments.

*2,3-Bis-carboxamido-5-*endo*-hydroxy tricyclo[2.2.1.0^{2,6}]heptane,* **8**

To saturated ammonium hydroxide (750 mL) was added *exo,exo*-5,6-dibromobicyclo[2.2.1]heptane-*endo,endo*-2,3-dicarboxylic anhydride (4) (76.5 g) and this stoppered mixture was allowed to stand with occasional shaking at room temperature for two weeks (solid goes into solution after 3 days). The solution was partially concentrated under vacuum at 40°C to 500 mL, diluted with an equal volume of water, and then passed through a 125 × 3.8 cm column of Amberlite IRA-400 (approx. 500 g) in the OH^- form in two halves, with the exchange column being regenerated to the OH^- form between each half. The combined effuents and washings (approx. 3 L) were evaporated under vacuum (0.05 Torr; 1 Torr = 133.3 Pa) with the bath at 40–45°C, and the residue recrystallized from hot water to give the product (12.3 g), mp 183–184°C. Four recrystallizations from methanol produced colorless crystals of **8**, mp 219–220°C; ir: 3190, 3300, 1665, 1610 cm^{-1}; ^1H nmr (DMSO-d_6) δ = 1.32 (d, J = 10.5 Hz, 1H = H_{7s}), 1.48 (d, J = 10.5 Hz, 1H = H_{7a}), 1.61 (d, J = 6 Hz, 1H = H_1), 1.96 (d, J = 6 Hz, 1H = H_6), 1.98 (narrow m, 1H = H_4), 2.69 (d, J = 2 Hz, 1H = H_3), 3.75 (d, J = 10 Hz, 1H = H_5), 5.74 (d, J = 10 Hz, 1H = OH), 6.81 (bd s, 2H = NH_2), 7.27 (bd s, 1H = NH), 7.79 (bd s, 1H = NH); ^{13}C nmr (DMSO-d_6) δ: 22.50 (d, J = 179 Hz, C_1), 25.64 (d, J = 179 Hz, C_6), 31.08 (s, C_2), 31.70 (t, J = 134 Hz, C_7), 40.74 (d, J = 149 Hz, C_4), 50.49 (d, J = 138 Hz,

Can. J. Chem. Downloaded from www.nrcresearchpress.com by 210.87.254.5 on 09/06/12
For personal use only.

C_3), 77.59 (d, J = 150 Hz, C_5), 173.42 (s, C=O), 177.08 (s, C=O); *m/e*: 196 $M^{+\cdot}$, 44 (100%). *Anal.* calcd. for $C_9H_{12}N_2O_3$: C 55.10, H 6.17%; found: C 55.04, H 6.24%.

Lactone-amide, 9

Prepared from **8** as described (1) and recrystallized three times from methanol–water (5:1), mp 192.5°C; ir 3434, 3339, 3290, 3239, 3201, 1740, 1651, 1616; ^{1}H nmr ($CDCl_3$) δ: 1.86 (bd s, 2H), 2.48 (AB, 2H), 2.77 (m, 1H), 3.12 (m, 1H), 4.87 (m, 1H), 6.74 (bd m, 4H); ^{13}C nmr (DMSO-d_6) δ: 28.19 (d, J = 179 Hz), 30.02 (t, J = 137 Hz), 31.46 (d, J = 179 Hz), 34.01 (s), 46.14 (d, J = 156 Hz), 47.59 (d, J = 154 Hz), 84.14 (d, J = 166 Hz), 170.69 (s), 176.21 (s); *m/e*: $M^{+\cdot}$, 179, 91 (100%). *Anal.* calcd. for $C_9H_9NO_3$: C 60.33, H 5.06%; found: C 60.54, H 4.88%.

2,3-endo,endo-*Bis-carboxamido-5-oxo tricyclo*[2.2.1.$0^{2,6}$]*heptane,* **10**

Prepared by oxidation of **8** with permanganate as described (1) and recrystallized four times from methanol, mp 235–236°C; ir: 3382, 3319, 3125, 1762, 1661, 1640; ^{1}H nmr ($CDCl_3$) δ: 1.89 (d, J = 11.5 Hz, 1H), 1.91 (d, J = 11.5 Hz, 1H), 2.42 (d, J = 5 Hz, 1H), 2.68 (d, J = 5 Hz, 1H), 2.78 (m, 1H), 2.89 (m, 1H), 4.88 (m, 2H), 5.51 (m, 1H), 6.04 (m, 1H); ^{13}C nmr (DMSO-d_6) δ: 22.72 (d, J = 185 Hz), 23.60 (d, J = 185 Hz), 30.38 (t, J = 139 Hz), 34.96 (s), 43.43 (d, J = 155 Hz), 47.97 (d, J = 140 Hz), 169.84 (s), 172.05 (s), 206.84 (s); *m/e*: $M^{+\cdot}$ 194, 44 (100%). *Anal.* calcd. for $C_9H_{10}N_2O_3$: C 55.67, H 5.19%; found: C 55.48, H 5.28%.

Oxime, 11

Prepared as described (1) and recrystallized from water three times, mp 225–226°C; ir 3406, 3220 (bd), 1614; ^{1}H nmr (DMSO-d_6) δ: 1.62 (d, J = 11 Hz, 1H), 1.68 (d, J = 11 Hz, 1H), 2.06 (d, J = 5 Hz, 1H), 2.44 (s, 1H), 2.80 (d, J = 5 Hz, 1H), 2.84 (s, 1H), 6.85 (s, 1H), 6.94 (m, 1H), 7.00 (m, 1H), 7.21 (s, 1H), 10.06 (s, 1H); ^{13}C nmr (DMSO-d_6) δ: 18.86 (d, J = 181 Hz), 24.74 (d, J = 181 Hz), 33.55 (s), 34.20 (t, J = 135 Hz), 39.60 (d, J = 156 Hz), 50.97 (d, J = 136 Hz), 161.20 (s), 171.87 (s), 172.08 (s); *m/e*: $M^{+\cdot}$ 209, 192 (100%). *Anal.* calcd. for $C_9H_{11}N_3O_3$: C 51.67, H 5.30%; found: C 51.40, H 5.16%.

1. W. Scott Worrall. J. Am. Chem. Soc. **82**, 5707 (1962).
2. (*a*) D. N. Butler, I. Gupta, W. W. Ng, and S. C. Nyburg. J. Chem. Soc. Chem. Commun. 596 (1980); (*b*) D. N. Butler, A. Barrette, and R. A. Snow. Synth. Commun. **5**, 101 (1975).
3. D. N. Butler and T. J. Munshaw. Can. J. Chem. **59**, 3365 (1981).
4. J. A. Berson and R. Swidler. J. Am. Chem. Soc. **76**, 4060 (1954).
5. (*a*) K. Nagayama, A. Kumar, K. Wüthrich, and R. R. Ernst. J. Magn. Reson. **40**, 321 (1980; (*b*) A. Bax, R. Freeman, and G. Morris. J. Magn. Reson. **42**, 164 (1981).
6. L. H. Zalkow and C. D. Kennedy. J. Org. Chem. **28**, 852 (1963).
7. A. Winston and P. Wilder, Jr. J. Am. Chem. Soc. **76**, 3045 (1954).

Can. J. Chem. Downloaded from www.nrcresearchpress.com by 210.87.254.5 on 09/06/12
For personal use only.

Preparation and transformations of allenic ketones and 3(2*H*)-furanones

STEVEN WOLFF AND WILLIAM C. AGOSTA
Laboratories of The Rockefeller University, New York, NY 10021, U.S.A.

Received March 8, 1984

This paper is dedicated to Professor Peter Yates on the occasion of his 60th birthday

STEVEN WOLFF and WILLIAM C. AGOSTA. Can. J. Chem. **62**, 2429 (1984).

Swern oxidation of allenic alcohols **7** and **10** gives the corresponding ketones **3** and **12**. Reaction of **3** with ruthenium tetroxide yields the stable acyl ketene **17** and the acyloxy α-diketone **20** as well as pivalil (**4**). Formation of **20** by way of the 3(2*H*)-furanone **22** is suggested, since oxidation of **3** and **12** with osmium tetroxide followed by dehydration provides the corresponding furanones **22** and **26** in good yield. Epoxidation of **3** furnishes some **20** as well as **27** and **29**, the first stable keto allene oxide and bisepoxide, respectively. On thermolysis **27** rearranges to furanone **22**. The double bond of **22** is cleaved by peracid to form **20**; similar treatment of **31***a, b* leads to cleavage of the double bond accompanied by Baeyer–Villiger oxidation, with formation of the carboxylic acids corresponding to methyl esters **33***a, b* as the major products.

STEVEN WOLFF et WILLIAM C. AGOSTA. Can. J. Chem. **62**, 2429 (1984).

Une oxydation de Swern des alcools alléniques **7** et **10** conduit aux cétones correspondantes **3** et **12**. La réaction de **3** avec le tétroxyde de ruthénium fournit l'acyl cétène stable (**17**), l'acyloxy α-dicétone (**20**) ainsi que le pivalile (**4**). On suggère que la formation de **20** se produit probablement via la (2*H*)-furanone-3 (**22**) puisque l'oxydation des composés **3** et **12** par le tétroxyde d'osmium, suivie d'une déshydratation, conduit aux furanones correspondantes **22** et **26** avec de bons rendements. L'époxydation du composé **3** conduit à un peu de composé **20** aux côtés des composés **27** et **29**, respectivement les premiers céto allène oxyde et bisépoxyde stables. La thermolyse du produit **27** provoque une transposition en furanone **22**. On a coupé la double liaison du composé **22** par traitement avec un peracide et on a ainsi obtenu le composé **20**; un traitement semblable des composés **31***a, b* conduit à une coupure de la double liaison qui est accompagnée d'une réaction d'oxydation de Baeyer–Villiger conduisant à la formation, comme produits majeurs, des acides carboxyliques correspondants aux esters méthyliques **33***a, b*.

[Traduit par le journal]

Irradiation of the α,β-acetylenic ketone **1** and tetramethylethylene in wet benzene leads to efficient formation of the cyclopropenol **2**, a reaction we have explained by the path shown in [1] (1). Part of the evidence for the constitution of **2** is its thermal fragmentation to form conjugated allenic ketone **3** and dimethylcarbene or its equivalent (1). In the course of securing the structure of **3** we treated it with excess ruthenium tetroxide and obtained pivalil (**4**) (1) along with two other oxidation products not yet described in detail. Investigation of these two compounds led us to examine the preparation and reactions both of allenic ketones and of the 3(2*H*)-furanones that were found to be important oxidation products of the allenes. Overall, we have found new routes to both allenic ketones and furanones; we have observed several novel oxidations of both these types of ketones; and we have encountered the first examples of an acyl ketene, an acyl allene oxide, and an acyl allene bisepoxide that are isolable by virtue of steric stabilization. Details are given below.

Investigation of the reactions of **3** with any convenience required a more suitable source of this ketone. This was available through reaction (2) of pivalaldehyde with the lithium derivative **5** of 1,1-dimethyl-3-*tert*-butylallene (**6**) (3), which yielded a 4:1 mixture of alcohol **7** and its acetylenic isomer **8**. Oxidation of these alcohols using oxalyl chloride in dimethyl sulfoxide (4) converted them into **3** and **9**, respectively, in high yield. The properties of **3** prepared in this fashion were identical with those of the compound formed thermally from **2**. Difficulties in oxidation of allenic alcohols to the corresponding ketones are well known (5) and this convenient application of Swern's conditions (4) appeared attractive. We found that they worked equally well on the trisubstituted allenic alcohol **10** to furnish **12**. Alcohol **10**, accompanied by a small amount

[1] $(CH_3)_3C-\overset{O}{\overset{\|}{C}}-C\equiv C-C(CH_3)_3 + (CH_3)_2C=C(CH_3)_2 \xrightarrow[C_6H_6,\ H_2O]{h\nu}$ → $\xrightarrow{H_2O}$ **2**

1

2 $\xrightarrow{-H_2O}$ → **3** **4**

Can. J. Chem. Downloaded from www.nrcresearchpress.com by 210.87.254.105 on 09/06/12
For personal use only.

Can. J. Chem. Downloaded from www.nrcresearchpress.com by 210.87.254.105 on 09/06/12
For personal use only.

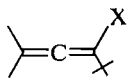

5, X = Li
6, X = H

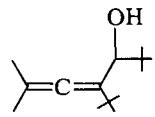

7

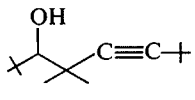

8

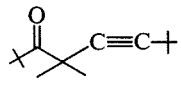

9

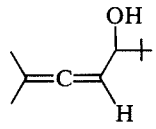

10

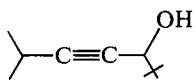

11

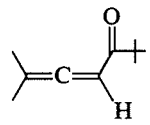

12

of its prototropic isomer **11**, was available from addition of the lithium derivative of 1,1-dimethylallene to pivalaldehyde. In keeping with the previous difficulties mentioned, oxidation of **7** by other methods, including Jones's reagent (6), Collins's reagent (7), and pyridinium chlorochromate (8), gave no allenic ketone. We did, however, isolate pivalil (**4**) and varying amounts of five other products from these attempts. These latter compounds were identified as **13**–**16** from their spectroscopic properties. The assignment of geometry to **13** and **15** follows from comparison of their nuclear magnetic resonance (nmr) spectra with data reported for *E*- and *Z*-3-methyl-3-penten-2-one (9). The stereochemical assignments for **14** and **16** are tentative but supported by nmr data for related systems (10). Related oxidations of hindered secondary allylic alcohols are known, and their possible mechanisms have been discussed (11). Efforts to reach **3** more directly by reaction of **5** with either pivalyl chloride or *N*,*N*-dimethylpivalamide (12) gave mixtures containing little or none of the desired product.

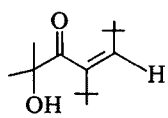

13

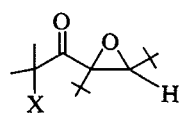

14
a, X = OH; *b*, X = H

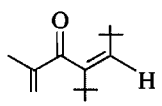

15

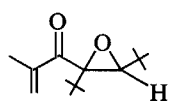

16

We turn now to the two oxidation products from **3**. The simpler of these is formed in very low yield and was recognized from its spectroscopic properties as *tert*-butyl pivalyl ketene (**17**). We confirmed this structure through slow reaction of **17** with warm ethanol to furnish the known (13) β-ketoester **18**. Acyl ketenes have been recognized as transient intermediates for years, but they typically dimerize unless trapped by some dienophile (14). More recently, perfluoro methyl propionyl ketene (**19**) has been isolated; this inductively stabilized ketene does not dimerize but is quite reactive in [4 + 2] cycloadditions (15). Ketene **17** appears to be the first isolable acyl ketene stabilized only by bulky substituents, and its kinetic stability is similar to that of di-*tert*-butyl ketene (16).

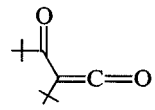

17

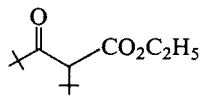

18

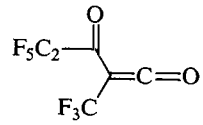

19

The remaining compound formed on oxidation of **3** with ruthenium tetroxide was a yellow oil with surprising spectroscopic properties that were compatible only with ester α-diketone **20**. In justifying this unexpected transformation we reasoned that, if ruthenium tetroxide initially oxidized **3** to **21**, this intermediate might well cyclize to the furanone, **22**. The related cyclization of α′-hydroxy β-diketones to furanones occurs readily under mild conditions (17). Cleavage of **22** at the double bond by ruthenium tetroxide could then furnish **20**.

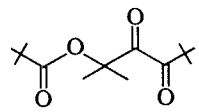

20

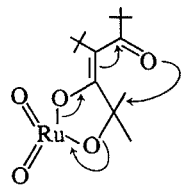

21

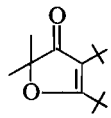

22

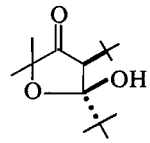

23

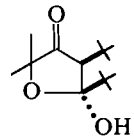

24

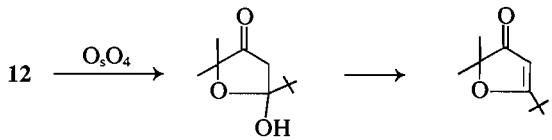

25 26

Support for this explanation came from treatment of **3** with osmium tetroxide (18). Oxidation proceeded smoothly with this milder reagent and furnished the cyclic hemiketals **23** and **24**. Only a few percent of the latter, very congested isomer was obtained, and it lost water to give **22** on attempted purification. Treatment of the crude hemiketal mixture with acid furnished **22** in high yield. The spectroscopic properties of **22** are appropriate for a 3(2*H*)-furanone; especially noteworthy are the characteristic (19) ^{13}C nmr signals for the olefinic carbon atoms at 118 and 190 ppm. Oxidation of **22** with ruthenium tetroxide in carbon tetrachloride yielded the yellow diketone **20**, thus completing experimental support for the suggested path from **3**.

Conversion of **3** into **22** is interesting, since synthesis of 3(2*H*)-furanones has commanded considerable attention in recent years (17). Similar oxidation of **12** with osmium tetroxide gave hemiketal **25**, and subsequent dehydration furnished the known (17) furanone **26** in good yield.

In exploring oxidation of **3** we also examined its reaction with *m*-chloroperbenzoic acid in methylene chloride. This gave two new products along with some **20**. The first of these new compounds was the keto allene oxide **27**, which was sufficiently stable for complete characterization. A particularly distinctive spectroscopic feature of **27** is the infrared (ir) band at 1786 cm^{-1}, an absorption typical of allene oxides (20, 21). Epoxidation of allenes is known to be sensitive to steric hindrance (22) and the effective bulk of peracids is enhanced in

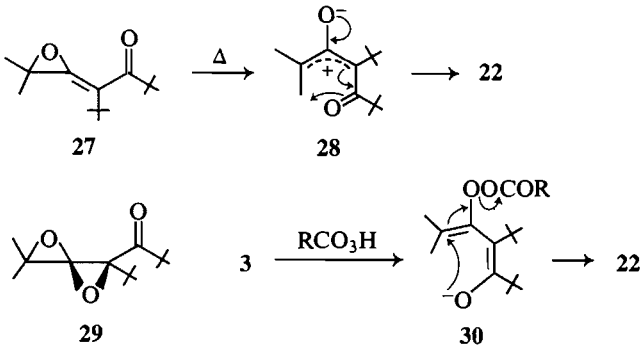

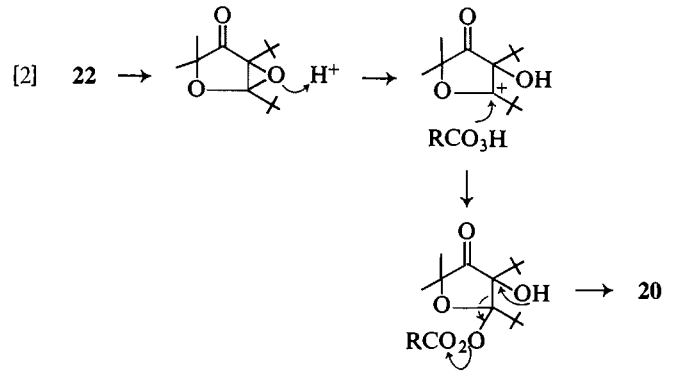

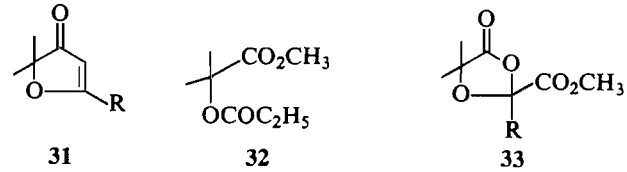

31 32 33

a, R = C_2H_5; *b*, R = $CH(CH_3)_2$

methylene chloride as solvent (23); for these reasons the single allene oxide obtained is considered to be the isomer shown as **27**. Although allene oxides have been known for some time (20, 21), **27** is the first characterized epoxide derived from a conjugated allenic ketone (5). On heating to 125°C it smoothly isomerizes to **22**, presumably by way of zwitterion **28** (21) or the corresponding biradical. This result lends support to the earlier suggestion (24) of an unisolated acyl allene oxide intermediate in conversion of an allenic ketone to a 3(2*H*)-furanone (5–10%) on reaction with hydrogen peroxide in hot formic acid. Related oxidative cyclizations of allenic alcohols and esters are also known (25). The second product from peracid oxidation of **3** was also formed on resubmission of **27** to the conditions of oxidation. This fact, together with previous observations on the oxidation of hindered allenes (22), suggests that the second product is spiro bisepoxide **29**, an assignment supported by the presence of an ir absorption at 1616 cm^{-1} characteristic of such systems (22), carbonyl absorption typical of an ordinary *tert*-butyl ketone (1693 cm^{-1}), and ^{13}C nmr absorption at 90.5 ppm attributable to the spiro carbon atom bearing two oxygen atoms.

The third product from treatment of **3** with peracid was **20**. Since exposure of **27** to mild acid in methylene chloride leads to no reaction and reexposure of **27** to peracid yields only **29**, it appears that neither of these epoxides is an intermediate in oxidation of **3** to **20**. A reasonable possibility is that Michael addition of *m*-chloroperoxybenzoate anion to **3** competes with epoxidation. Cyclization of the resulting enolate **30** with expulsion of *m*-chlorobenzoate anion would then give the furanone **22**, oxidative cleavage of which by peroxy acid could furnish **20**. The last step of this proposed sequence was demonstrated experimentally; **22** undergoes smooth reaction with *m*-chloroperbenzoic acid to give **20**. As depicted in [2], this transformation can be understood as initial epoxidation, followed by ring opening, attack of a second molecule of peracid on the derived alkoxy-stabilized carbonium ion, and subsequent elimination of *m*-chlorobenzoic acid, all in analogy with the long-known scission of simple enol ethers by peroxyacids (26).

We have also investigated this oxidation in two other 3(2*H*)-furanones, **31***a* and *b* (17). Treatment of **31***a* with *m*-chloroperbenzoic acid yielded a mixture of two acidic products that were conveniently isolated and purified after esterification with ethereal diazomethane. The first of these (~10%) was identified as the propionate ester of methyl α-hydroxyisobutyrate (**32**) from its composition and spectroscopic properties. The characteristics of the accompanying major ester (~50%) were most consistent with its formulation as the 1,3-dioxolan-4-one **33***a*. Especially significant in this regard was intense carbonyl absorption in the ir spectrum at 1814 cm^{-1}, since both the high frequency and the intensity of the carbonyl band in such dioxolanones have been noted (27). This structural assignment was verified by independent synthesis of **33***a* through acid-catalyzed ketalization (27) of methyl α-ketobutyrate with α-hydroxyisobutyric acid. Reaction of **31***b* with peroxyacid led to analogous transformations, but in this case too little of the minor product was obtained for characterization. Although various mechanisms may be entertained for these oxidations, in the absence of additional evidence it seems appropriate to write the most economical sequence, and this is shown for **31***a* in the accompanying scheme. Baeyer–Villiger reaction accompanied by epoxidation gives **34** in a process that has analogy in the quantitative conversion of a cyclopentenone into an epoxy δ-lactone (28). Subsequent opening of the epoxide by peroxyacid furnishes the key intermediate **35**. Fragmentation of this along path (a) (see [2] above) (26) leads to the unstable mixed formyl anhydride **36**, which should decompose to product **37**. Alternatively, oxidative elimination of *m*-chlorobenzoate from **35** by path (b) (29) should provide the hydroxyanhydride **38**. Intramolecular acyl transfer through the

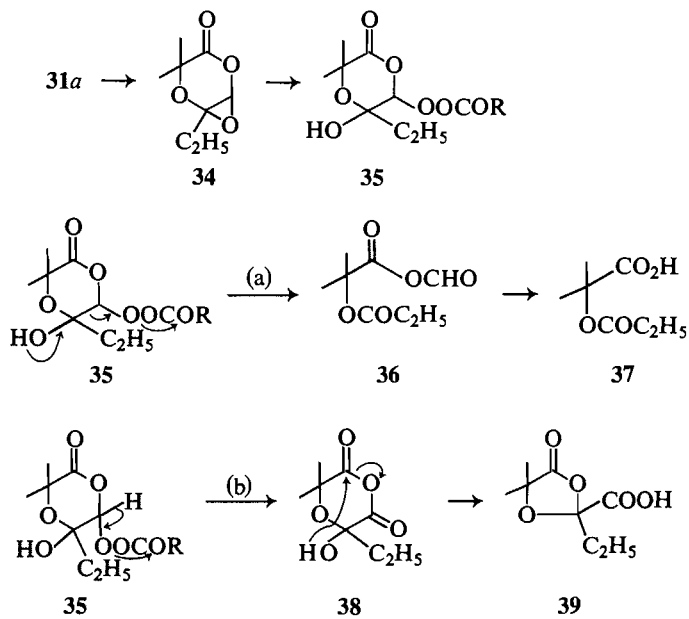

Can. J. Chem. Downloaded from www.nrcresearchpress.com by 210.87.254.105 on 09/06/12
For personal use only.

boat form of **38** could then furnish **39**. Subsequent esterification of **37** and **39** with diazomethane yields the observed products **32** and **33***a*. Thus, peracid oxidation of **31***a* and *b* leads to the Baeyer–Villiger reaction as well as the epoxidation that occurs with **22**. Presumably Baeyer–Villiger attack on the carbonyl group of **22** is prevented by the adjacent *tert*-butyl substituent at C(4). These rather clean oxidations of **22** and **31***a* and *b* with peracid stand in contrast to previous observation of the "massive decomposition" of 3(2*H*)-furanones on exposure to a variety of oxidizing agents (30).

Experimental

Materials and equipment

General procedures have been previously described (1). All vapor phase chromatography (vpc) was carried out by using a Varian Aerograph Model 920 gas chromatograph with one of the following columns: A, 25% QF-1, 10 ft; B, 22.5% Carbowax 20 M, 7 ft; C, 25% QF-1, 3 ft; D, 22.5% Carbowax 20 M, 8 ft; E, 25% Carbowax 20 M, 4 ft. All columns were packed in 0.25-in. aluminum tubing with 45/60 Chromosorb W except column B which used 60/80 Chromosorb P. In addition to a Varian T-60A nmr spectrophotometer, a Nicolet/Oxford NT-300 (300 MHz for ^{1}H) instrument was also employed. Unless otherwise noted, all pure compounds were obtained as colorless oils; melting points are corrected; boiling points are uncorrected; products are usually listed in order of their elution upon column or vapor phase chromatography.

*Reaction of 1,1-dimethyl-3-*tert*-butylallene-3-lithium (**6**) with trimethylacetaldehyde*

To a solution of **6** (3) (1.242 g, 10 mmol) in THF (25 mL), cooled to −40°C under a N_2 atmosphere, was added *tert*-butyllithium (5 mL of a 2 *M* solution, 10 mmol) (12). The mixture was maintained at this temperature for 21 h, then cooled to −78°C before the addition of trimethylacetaldehyde (1.0 g, 11.6 mmol). The reaction was allowed to warm to 25°C, poured into ice/H_2O, and was extracted with Et_2O. The residue obtained after removal of solvent by distillation through a Vigreux column was distilled with a short-path apparatus to give an oil (1.084 g, 52%), bp 95–104°C (12 Torr; 1 Torr = 133.3 Pa) which vpc analysis (column A, 140°C) indicated to be a mixture of 2 components in the ratio of 1:4. These were separated by preparative vpc. The minor, first eluted compound was 2,2,4,4,7,7-hexamethyl-5-octyn-3-ol (**8**); ir: 3645 (w), 3540 (w), 2975 (s), 1469 (m), 1357 (m), 1040 (m), 998 (m) cm^{-1}; nmr (60 MHz) δ: 2.90 (d, J = 8 Hz, 1H), 1.58 (d, J = 8 Hz, 1H), 1.24 (s, 6H), 1.18 (s, 9H), 1.02 (s, 9H). *Anal.* calcd. for $C_{14}H_{26}O$: C 79.93, H 12.46; found: C 80.07, H 12.48. The second compound was 4-*tert*-butyl-2,2,6-trimethyl-4,5-heptadien-3-ol (**7**); ir: 3615 (w), 2960 (s), 1387 (m), 1360 (m), 988 (s), 891 (w) cm^{-1}; nmr (60 MHz) δ: 3.57 (br d, $J \cong$ 8 Hz, 1H) 1.68 (s, 6H), 1.05 (s, 9H), 0.92 (s, 9H), 0.83 (br d, 1H). *Anal.* calcd. for $C_{14}H_{26}O$: C 79.93, H 12.46; found: C 79.99, H 12.41.

Swern oxidation of 7 and 8

A mixture of crude alcohols **7** and **8** (3.766 g, 17.9 mmol) was oxidized with $(COCl)_2$ (2.614 g, 20.6 mmol) and DMSO (3.22 g, 41.2 mmol) in CH_2Cl_2 according to the method of Swern and co-workers (4). Bulb-to-bulb distillation afforded an oil (2.627 g, 70%), bp 90–100°C (20 Torr) which vpc analysis (column A, 140°C) indicated to be a mixture of 2 components in the ratio of 1:4. These were separated by preparative vpc. The first, minor component was 2,2,4,4,7,7-hexamethyl-5-octyn-3-one, mp 35–36°C; ir: 2960 (s), 1697 (s), 1362 (m), 1277 (m), 1050 (m), 986 (m) cm^{-1}; nmr (300 MHz) δ: 1.34 (s, 9H), 1.31 (s, 6H), 1.19 (s, 9H); ^{13}C nmr δ: 215.25, 92.60, 83.25, 45.96, 41.46, 30.90, 29.63, 27.51, 27.27; mass spectrum m/z: 208.1763 (M^+, calcd. for $C_{14}H_{24}O$: 208.1826). The second component was **3**, identical in all respects to the compound obtained previously (1).

Oxidation of 7 with chromium reagents

The allenic alcohol **7** (50.8 mg) in acetone (4 mL), cooled to 5°C, was treated with excess Jones's reagent for 1 h. Standard work-up yielded an oil (46.6 mg, 92%) which vpc analysis indicated to be a mixture of four major components. The first component (10%) was pivalil (**4**). The second component was a mixture of **15** (4%) and **16** (27%). These were separated by flash chromatography with 98:2 hexanes/Et_2O. First eluted was **16**; ir: 2960 (s), 2865 (m), 1664 (s), 1364 (s), 1081 (m), 952 (s), 877 (m), 842 (w) cm^{-1}; nmr (60 MHz) δ: 6.45 (br s, 1H), 5.88 (m, 1H), 2.53 (s, 1H), 1.80 (br s, 3H), 0.93 (s, 9H), 0.83 (s, 9H); mass spectrum m/z: 224.1772 (M^+, calcd. for $C_{14}H_{24}O_2$: 224.1776). The second compound was **15**; ir: 2960 (s), 2860 (m), 1657 (s), 1475 (m), 1360 (m), 1110 (m), 955 (w), 937 (w), 730 (w) cm^{-1}; nmr (60 MHz) δ: 5.88 (br s, 2H), 5.40 (s, 1H), 1.87 (br s, 3H), 1.03 (s, 9H), 0.93 (s, 9H); mass spectrum m/z: 208.1832 (M^+, calcd. for $C_{14}H_{24}O$: 208.1828). The third component (10%) was **14***b*; ir: 2965 (s), 1698 (s), 1475 (s), 1395 (w), 1382 (w), 1365 (s), 910 (m) cm^{-1}; nmr (60 MHz) δ: 3.00 (septet, J = 6.5 Hz, 1H), 2.60 (s, 1H), 1.15 (d, J = 6.5 Hz, 3H), 0.98 (d, J = 6.5 Hz, 3H), 0.97 (s, 9H), 0.90 (s, 9H); mass spectrum m/z: 226.1925 (M^+, calcd. for $C_{14}H_{26}O_2$: 226.1933). The fourth component was a mixture of **13** (14%) and **14***a* (35%); these were separated by flash chromatography using 85:15 hexanes/Et_2O. First eluted was **14***a*, mp 56.5–57°C; ir: 3575 (m), 2955 (s), 1710 (s), 1464 (m), 1366 (m), 1192 (s), 969 (m), 899 (m) cm^{-1}; nmr (60 MHz) δ: 3.07 (br s, 1H), 2.62 (s, 1H), 1.36 (br s, 6H), 1.03 (s, 9H), 0.98 (s, 9H); ^{13}C nmr δ: 212.94, 79.75, 73.04, 68.99, 34.63, 31.59, 31.18, 27.49, 27.24. *Anal.* calcd. for $C_{14}H_{26}O_3$: C 69.38, H 10.81; found: C 69.53, H 10.86. The second eluted compound was **13**, mp 62–63°C; ir: 3560 (w), 2960 (s), 1680 (s), 1475 (m), 1360 (m), 965 (m) cm^{-1}; nmr (60 MHz) δ: 5.37 (s, 1H), 2.28 (br s, 1H), 1.42 (s, 6H), 1.13 (s, 9H), 1.03 (s, 9H). *Anal.* calcd. for $C_{14}H_{26}O_2$: C 74.28, H 11.58; found: C 73.98, H 11.67.

Oxidation of **7** (69.5 mg, 0.33 mmol) in CH_2Cl_2 (3 mL) with pyridinium chlorochromate (172.6 mg, 0.80 mmol) yielded a mixture (60.8 mg, 87%) of **4** (5%), **15** (5%), **14***a* (5%), and **13** (85%).

Oxidation of **7** (60.0 mg, 2 mmol) with the complex prepared from CrO_3 (200 mg, 2 mmol) and pyridine (323 mL) in CH_2Cl_2 (5 mL) yielded an oil (56.4 mg, 94%) consisting of **15** and **16** (18%), **13** (65%), and **14***a* (17%).

Reaction of 1,1dimethylallene-3-lithium with trimethylacetaldehyde

To a solution of dimethylallene (1.362 g, 20 mmol) in THF (30 mL), cooled to −40°C under a N_2 atmosphere, was added *tert*-butyllithium (10 mL of a 2 *M* solution, 20 mmol). The mixture was stirred at −40°C for 2.5 h. It was then cooled to −78°C and trimethylacetaldehyde (1.72 g, 20 mmol) in THF (5 mL) was added. The mixture was allowed to warm to 25°C and was worked up as described above. Short-path distillaiton yielded an oil (2.081 g, 67%) which vpc analysis (column A, 120°C) showed to be a mixture of two components. The first component (12%) was 2,2,6-trimethyl-4-heptyn-3-ol (**11**); ir: 3625 (m), 3475 (w), 2975 (s), 2870 (m), 2235 (w), 1363 (m), 1318 (m), 995 (s) cm^{-1}; nmr (60 MHz) δ: 3.55 (d, J = 1.5 Hz, 1H), 2.58 (m, 1H), 1.43 (br s, 1H), 1.18 (d, J = 7 Hz, 6H), 0.95 (s, 9H). *Anal.* calcd. for $C_{10}H_{18}O$: C 77.86, H 11.76; found: C 77.78, H 11.80. The second component (88%) was 2,2,6-trimethyl-4,5-heptadien-3-ol (**10**); ir: 3625 (w), 3570 (w), 2970 (s), 1958 (w), 1628 (w), 1475 (m), 1358 (s), 1086 (m), 993 (m) cm^{-1}; nmr (60 MHz) δ: 5.08 (septet, J = 3.5 Hz, 1H), 3.63 (d, J = 6 Hz, 1H), 1.72 (d, J = 3.5 Hz, 6H), 1.33 (br s, 1H), 0.88 (s, 9H). *Anal.* calcd. for $C_{10}H_{18}O$: C 77.86, H 11.76; found: C 77.92, H 11.70.

*Swern oxidation of **10** and **11***

A mixture of **10** and **11** (1.137 g, 7.4 mmol) was oxidized with $(COCl)_2$ (0.74 mL) and DMSO (1.25 mL) in CH_2Cl_2 according to the published procedure (4). Short-path distillation gave an oil (884 mg, 78%), bp 79–85°C (16 Torr). Preparative vpc (column B, 135°C) gave 2,2,6-trimethyl-4-heptyn-3-one (18%); ir: 2975 (s), 2930 (s), 2865 (s), 2250 (m), 2200 (s), 1667 (s), 1474 (m), 1362 (w), 1312 (m), 1181 (s), 1127 (s), 918 (s) cm^{-1}; nmr (60 MHz) δ: 2.73 (septet, J = 7 Hz, 1H), 1.28 (d, J = 7 Hz, 6H), 1.15 (s, 9H); mass spectrum m/z: 95.0495 ((M − t-Bu)$^+$, calcd. for C_6H_7O: 95.0497). The second eluted component (82%) was **12**; ir: 2970 (s), 1955 (m), 1668 (s),

Can. J. Chem. Downloaded from www.nrcresearchpress.com by 210.87.254.105 on 09/06/12
For personal use only.

Can. J. Chem. Downloaded from www.nrcresearchpress.com by 210.87.254.105 on 09/06/12
For personal use only.

1388 (m), 1124 (s), 1066 (m), 975 cm^{-1}; nmr (60 MHz) δ: 5.77 (septet, J = 3.5 Hz, 1H), 1.81 (d, J = 3.5 Hz, 6H), 1.17 (s, 9H). *Anal.* calcd. for $C_{10}H_{16}O$: C 79.93, H 12.46; found: C 79.99, H 12.41.

Oxidation of 4-tert-butyl-2,2-6-trimethyl-4,5-heptadien-3-one (3) with ruthenium tetroxide

Oxidation of **3** was carried out as previously described (1). In addition to pivalil (**4**), *tert*-butyl pivalyl ketene (**17**, ~5%) was detected; ir: 2105 (s) and 1658 (m) cm^{-1}; nmr (60 MHz) δ: 1.22 (s) and 1.2 (s). A mixture of **4** and **17** in CCl_4 (4 mL) containing ethanol (1 mL) was allowed to stand at 25°C overnight; no reaction was detected. The mixture was heated at 50°C for 4 h to afford **18**, which was isolated by preparative vpc and whose ir and nmr spectral characteristics were identical to those reported (13). The third compound isolated from this reaction was **20**, a yellow oil: uv λ_{max}: 402 nm (ε = 23.5); ir: 3000 (m), 1711 (s), 1477 (m), 1297 (m), 1132 (m), 900 (w) cm^{-1}; nmr (60 MHz) δ: 1.56 (s, 6H), 1.23 (s, 9H), 1.15 (s, 9H). *Anal.* calcd. for $C_{14}H_{24}O_4$: C 65.59, H 9.44; found: C 66.12, H 9.42.

Osmium tetroxide oxidation of 3

To a solution of OsO_4 (657 mg, 2.58 mmol) in pyridine (10 mL) was added allene **3** (511 mg, 2.45 mmol). The mixture was stirred for 2 days at 25°C. Hydrolysis of the osmate ester was accomplished by the addition of $NaHSO_3$ (1.3 g) in 2:1 H_2O/pyridine (15 mL) and stirring for 5 h. Dilution with H_2O and extraction with Et_2O afforded an oil (635 mg) which vpc analysis (column C, 130°C) indicated to be a mixture of 2 components in a 1:10 ratio. The major component was collected by preparative vpc and was identified as **23**, mp 78–79°C; ir: 3600 (m), 2955 (s), 1750 (s), 1480 (m), 1464 (m), 1390 (m), 1374 (m), 1365 (m), 1095 cm^{-1}; nmr (60 Mz) δ: 2.30 (s, 1H), 2.17 (br s, 1H), 1.30 (s, 6H), 1.20 (s, 9H), 1.02 (s, 9H). *Anal.* calcd. for $C_{14}H_{26}O_3$: C 69.49, H 10.71; found: C 69.38, H 10.81. Attempted purification of the first eluted minor component resulted in partial dehydration to **22**, but the following nmr data were obtained, permitting identification of this material as **24**; nmr (60 MHz) δ: 5.1 (s, 1H), 2.03 (br s, 1H), 1.40 (s, 3H), 1.28 (s, 3H), 1.25 (s, 9H), 1.08 (s, 9H).

Preparation of 2,2-dimethyl-4,5-di-tert-butyl-3(2H)-furanone (22)

A mixture of **23** and **24** (592 mg, 2.44 mmol) in benzene (50 mL) containing a trace of *p*-toluenesulfonic acid was heated to reflux for 4 h with removal of H_2O in a Dean–Stark trap. The reaction mixture was cooled, washed with aqueous $NaHCO_3$, and dried. Removal of solvent yielded a semi-solid (458 mg, 84%); vpc analysis (column C, 120°C) indicated the absence of starting materials and the formation of one product. This was collected preparatively and identified as **22**, mp 51–52°C; uv λ_{max}: 275 (log ε = 3.92); ir: 2995 (s), 1687 (s), 1532 (m), 1339 (m), 1176 (m), 1057 (m), 992 (m) cm^{-1}; nmr (60 MHz) δ: 1.37 (s, 9H), 1.32 (s, 9H), 1.20 (s, 6H); ^{13}C nmr δ: 209.97, 190.25, 118.41, 81.73, 36.86, 31.28, 29.90, 27.08, 23.07; mass spectrum m/z: 224.1775 (M^+, calcd. for $C_{14}H_{24}O_2$: 224.1776).

Oxidation of 2,2,6-trimethyl-4,5-heptadien-3-one (12) with osmium tetroxide

The allenic ketone (**12**) (154 mg, 1.01 mmol) was added to a pyridine solution (4 mL) of OsO_4 (311 mg, 1.22 mmol). The mixture was stirred for 45 h at 25°C and was worked up as above to yield an oil (119 mg); vpc analysis (column A, 140°C) indicated one component which was collected and identified as 2,2-dimethyl-5-*tert*-butyl-3(2*H*)-furanone on the basis of its nmr (60 MHz) and ir spectra, which were identical to those reported (17).

Oxidations of furanone 22

Furanone **22** (~6 mg) in CCl_4 (0.5 mL) was added to RuO_4 (from RuO_2, 10 mg) in CCl_4 (2 mL). Precipitation of black RuO_2 was instantaneous. Excess oxidant was destroyed by the addition of 2-propanol; vpc analysis (column B, 150°C) indicated complete disappearance of starting material and the formation of one product with the retention time of **20**. This was collected and identified spectroscopically as **20**.

The reaction of **22** (47 mg) with *m*-chloroperbenzoic acid (49.2 mg) in CH_2Cl_2 (1 mL) was complete in 1 h as monitored by vpc analysis. The mixture was diluted with Et_2O, washed with aqueous $NaHSO_3$, $NaHCO_3$, and brine, and was dried. After removal of solvent, the residue was purified by preparative vpc to afford **20**, whose nmr and ir spectra were identical to those obtained previously.

Oxidation of allene 3 with m-chloroperbenzoic acid

Allene **3** (111.4 mg, 0.54 mmol) in CH_2Cl_2 (5 mL) was treated with *m*-chloroperbenzoic acid (175.2 mg, 1.0 mmol) for 24 h at 25°C. Work-up as before yielded a residue that vpc analysis (column D, 150°C) indicated to be a mixture of 3 components. These were collected and identified as (in order of elution) **3** (50%), **20** (10%), and **22** (25%).

Similar treatment of **3** (166 mg) with MCPBA (414 mg) in CH_2Cl_2 (4 mL) gave, after flash chromatography with 95:5 hexanes/Et_2O, in addition to small amounts of **3** and **20**, two new products. The first of these was **27** (35 mg, 20%); ir: 2980 (s), 2890 (s), 1786 (w), 1663 (s), 1475 (s), 1387 (m), 1372 (m), 1358 (m), 1261 (m), 1161 (m), 1050 cm^{-1}; nmr (60 MHz) δ: 1.55 (s, 6H), 1.13 (s, 18H); mass spectrum m/z: 224.1782 (M^+, calcd. for $C_{14}H_{24}O_2$: 224.1776). The second eluted new compound was bisepoxide **29** (84 mg, 44%); ir: 2970 (s), 2930 (s), 2875 (m), 1693 (s), 1616 (m), 1477 (s), 1394 (m), 1378 (m), 1366 (m), 1144 (m), 961 (m), 915 (m), 856 (s) cm^{-1}; nmr (60 MHz) δ: 1.50 (s, 6H), 1.21 (s, 9H), 1.05 (s, 9H); ^{13}C nmr nmr δ: 210.49, 90.53, 77.37, 63.17, 45.47, 34.91, 27.33, 27.01, 22.11, 19.92. *Anal.* calcd. for $C_{14}H_{24}O_3$: C 69.96, H 10.07; found: C 70.00, H 9.84.

Treatment of allene oxide 27 with MCPBA

To a solution of **27** (~60 mg, 0.27 mmol) in CH_2Cl_2 (3 mL) was added MCPBA (140 mg, 0.81 mmol). The mixture was stirred at 25°C overnight. The usual work-up afforded an oil (59 mg, 92%) whose nmr and ir spectra indicated it to be **29**.

Thermolysis of allene oxide 27

Preparative vpc (column D, 150°C) of **27**, isolated by flash chromatography, afforded furanone **22**. Alternatively, a benzene solution of **27** was heated at 100°C for 5.5 h. A nmr spectrum of the residue after removal of solvent indicated the formation of **22** (~85% purity).

Oxidation of 2,2-dimethyl-5-ethyl-3(2H)-furanone (31a) with MCPBA

A mixture of **31***a* (167 mg, 1.19 mmol) and MCPBA (653 mg, 3.78 mmol) in CH_2Cl_2 (10 mL) was stirred at 25°C for 3 days; vpc analysis (column E, 135°C) indicated the presence only of starting material. The mixture was filtered and treated with excess diazomethane. After removal of solvent, vpc analysis indicated the presence of 3 additional peaks. The first component was **32** (18 mg, 9%); ir: 2995 (m), 2950 (m), 1748 (s), 1183 (m), 1193 (s), 1168 (s), 1129 (s) cm^{-1}; nmr (60 MHz) δ: 3.65 (s, 3H), 2.26 (q, J = 7 Hz, 2H), 1.48 (s, 6H), 1.10 (t, J = 7 Hz, 3H). *Anal.* calcd. for $C_8H_{14}O_4$: C 55.16, H 8.10; found: C 55.07, H 8.15. Eluted second was unreacted **31***a*. The third component was **33***a* (114 mg, 51%); ir: 3010 (m), 2970 (w), 1814 (s), 1761 (s), 1378 (w), 1175 (m) cm^{-1}; nmr (60 MHz) δ: 3.82 (s, 3H), 1.99 (q, J = 7 Hz, 2H), 1.46 (s, 6H), 0.97 (t, J = 7 Hz, 3H); ^{13}C nmr δ: 174.70, 168.54, 105.20, 77.93, 53.07, 29.07, 25.85, 24.12, 6.22. *Anal.* calcd. for $C_8H_{14}O_5$: C 53.46, H 6.98; found: C 53.66, H 6.94. The last component was methyl *p*-chlorobenzoate.

Oxidation of 2,2-dimethyl-5-isopropyl-3(2H)-furanone (31b) with MCPBA

Similar treatment of **31***b* (72 mg, 0.5 mmol) in CH_2Cl_2 (5 mL) with MCPBA (711 mg, 3.5 mmol) for 45 h at 25°C and then with diazomethane yielded **33***b* (47 mg, 44%); ir: 3005 (m), 1812 (s), 1758 (s), 1262 (m), 1175 (m), 1032 (m) cm^{-1}; nmr (60 MHz) δ: 3.80 (s, 3H), 2.02 (septet, J = 7 Hz, 1H), 1.45 (s, 3H), 1.4 (s, 3H), 0.96 (d, J = 7 Hz, 6H). *Anal.* calcd. for $C_{10}H_{16}O_5$: C 55.54, H 7.46; found: C 55.73, H 7.40.

Preparation of 2-carbomethoxy-2-ethyl-5,5-dimethyl-1,3-dioxolan-4-one (33a)

A mixture of methyl α-keto butyrate (1.78 g, 15.3 mmol), α-hydroxybutyric acid (1.33 g, 12.8 mmol), and *p*-TsOH (371 mg, 1.95 mmol) in benzene (40 mL) was heated to reflux with removal of

H_2O by a Dean–Stark trap for 5 h according to the literature procedure (26). Work-up yielded an oil (2.34 g, 89%) which was further purified by vpc (column C, 120°C) to give **33***a*, having identical nmr and ir spectra with material derived from **31***a*.

Acknowledgments

We thank Professor Amos B. Smith III for generous samples of **31***a*, *b*, Francis Picart for 300-MHz nmr spectra, Phyllis Wilson for technical assistance, and S. T. Bella for microanalyses. This research was supported by the National Science Foundation and the donors of the Petroleum Research Fund, administered by the American Chemical Society. Purchase of the 300-MHz nmr spectrometer was facilitated by funds from the National Science Foundation and from the Camille and Henry Dreyfus Foundation.

1. S. WOLFF and W. C. AGOSTA. J. Am. Chem. Soc. **106**, 2363 (1984).
2. L. BRANDSMA and H. D. VERKRUIJSSE. Synthesis of acetylenes, allenes, and cumulenes. Elsevier, Amsterdam. 1981. Chapt. 3.
3. P. VERMEER, H. WESTMIJZE, H. KLEIJN, and L. A. VAN DIJCK. Recl. Trav. Chim. Pays-Bas, **97**, 56 (1978).
4. A. J. MANCUSO, S.-L. HUANG, and D. SWERN. J. Org. Chem. **43**, 2480 (1978).
5. M. HUCHÉ. Tetrahedron, **36**, 331 (1980).
6. A. BOWERS, T. G. HALSALL, E. R. H. JONES, and A. LEMIN. J. Chem. Soc. 2548 (1953); C. DJERASSI, R. R. ENGLE, and A. BOWERS. J. Org. Chem. **21**, 1547 (1956).
7. R. RATCLIFFE and R. RODEHORST. J. Org. Chem. **35**, 4000 (1970); J. C. COLLINS, W. W. HESS, and F. J. FRANK. Tetrahedron Lett. 3363 (1968).
8. E. J. COREY and J. W. SUGGS. Tetrahedron Lett. 2647 (1975).
9. D. E. MCGREER, N. W. K. CHIN, and M. G. VINJE. Can. J. Chem. **43**, 1398 (1965).
10. P. BARET, J. L. PIERRE, and R. HEILMANN. Bull. Soc. Chim. Fr. 4735 (1967); M. H. GIANNI, E. L. STOGRYN, C. M. ORLANDO, JR. J. Phys. Chem. **67**, 1385 (1963); J. M. COXON, M. P. HARTSHORN, A. J. LEWIS, K. B. RICHARDS, and W. H. SWALLOW. Tetrahedron, **25**, 4445 (1969).
11. P. SUNDARARAMAN and W. HERZ. J. Org. Chem. **42**, 813 (1977), and references cited therein.
12. J. C. CLINET and G. LINSTRUMELLE. Nouv. J. Chim. **1**, 373 (1977).
13. Y. ITO, M. NAKATSUKA, N. KISE, and T. SAEGURA. Tetrahedron Lett. **21**, 2873 (1980).
14. H. STETTER and K. KIEHS. Chem. Ber. **98**, 1181 (1965); **98**, 2099 (1965); G. JÄGER. Chem. Ber. **105**, 137 (1972).
15. D. C. ENGLAND. J. Org. Chem. **46**, 147 (1981); **46**, 154 (1981).
16. M. S. NEWMAN, A. ARKELL, and T. FUKUNAGA. J. Am. Chem. Soc. **82**, 2498 (1960).
17. A. B. SMITH III, P. A. LEVENBERG, P. J. JERRIS, R. M. SCARBOROUGH, JR., and P. M. WOVKULICH. J. Am. Chem. Soc. **103**, 1501 (1981), and references cited therein.
18. M. SCHRÖDER. Chem. Rev. **80**, 187 (1980); M. BIOLLAZ, W. HAEFLIGER, E. VALARDE, P. CRABBÉ, and J. H. FRIED. Chem. Commun. 1322 (1971).
19. M. D. TAYLOR, A. B. SMITH III, G. T. FURST, S. P. GUNASEKARA, C. A. BEVELLE, G. A. CORDELL, N. R. FARNSWORTH, S. M. KUPCHAN, H. UCHIDA, A. R. BRANFMAN, R. G. DAILEY, JR., and A. T. SNEDEN. J. Am. Chem. Soc. **105**, 3177 (1983).
20. R. L. CAMP and F. D. GREENE. J. Am. Chem. Soc. **90**, 7349 (1968).
21. T. H. CHAN and B. S. ONG. Tetrahedron, **36**, 2269 (1980).
22. J. K. CRANDALL, W. W. CONOVER, J. B. KOMIN, and W. H. MACHLEDER. J. Org. Chem. **39**, 1723 (1974).
23. R. G. CARLSON and N. S. BEHN. J. Org. Chem. **32**, 1363 (1967); R. C. EWINS, H. B. HENBEST, and M. A. MCKERVEY. J. Chem. Soc. Chem. Commun. 1085 (1967).
24. W. RIED and A. MARHOLD. Chem. Ber. **107**, 1714 (1974).
25. M. BERTRAND, J. P. DULCÈRE, G. GIL, J. GRIMALDI, and P. SYLVESTRE-PANTHET. Tetrahedron Lett. 1507 (1976); M. BERTRAND, J. P. DULCÈRE, and G. GIL. Tetrahedron Lett. 4403 (1977); P. KOLSAKER and S. BØRRESEN. Acta Chem. Scand. Ser. B, **33**, 133 (1979).
26. B. BELLEAU and T. F. GALLAGHER. J. Am. Chem. Soc. **74**, 2816 (1952); C. L. STEVENS and J. TAZUMA. J. Am. Chem. Soc. **76**, 715 (1954).
27. M. FARINES and J. SOULIER. Bull. Soc. Chim. Fr. 332 (1970); T. B. CAMERON, F. M. EL-KOBBANI, and H. W. PINNICK. J. Am. Chem. Soc. **103**, 5414 (1981).
28. A. PADWA and R. HARTMAN. J. Am. Chem. Soc. **88**, 3759 (1966).
29. L. A. SINGER. *In* Organic peroxides. Vol. 1. *Edited by* D. Swern. Wiley–Interscience, New York. 1970. Chapt. 5. p. 299, and references cited therein.
30. T. F. TAM and B. FRASER-REID. J. Org. Chem. **45**, 1344 (1980).

Can. J. Chem. Downloaded from www.nrcresearchpress.com by 210.87.254.105 on 09/06/12
For personal use only.

Synthesis of some 3-arylisochromene, 3-arylisoquinoline, 6*H*-5-oxachrysene, and benzo[*c*]phenanthridine analogs of some naturally occurring alkaloids

ANTOINE CARTY, I. WESLEY ELLIOTT,[1] AND GREFONDA M. LENIOR
Department of Chemistry, Fisk University, Nashville, TN 37203, U.S.A.

Received March 19, 1984

This paper is dedicated to Professor Peter Yates on the occasion of his 60th birthday

ANTOINE CARTY, I. WESLEY ELLIOT, and GREFONDA M. LENIOR. Can. J. Chem. **62**, 2435 (1984).

A 2-benzopyrylium perchlorate **6** was prepared from the keto ester **5**. Reduction of **6** followed by dilute HCl affords 6*H*-5-oxachrysene **10**. Reaction of **6** with ammonia solution gives the isoquinoline acid **13**. By a short series of steps **13** is cyclized to the dihydrobenzo[*c*]phenanthridine **16**.

ANTOINE CARTY, I. WESLEY ELLIOT et GREFONDA M. LENIOR. Can. J. Chem. **62**, 2435 (1984).

On a préparé le perchlorate du benzopyrylium-2 **6** à partir du céto-ester **5**. La réduction de **6**, suivie d'une hydrolyse par du HCl dilué, conduit au 6*H*-oxo-5 chrysène **10**. La réaction de **6** avec une solution d'ammoniac conduit à l'acide isoquinoléique **13**. Faisant appel à une courte série de réactions, on peut cycliser le composé **13** en dihydrobenzo[*c*] phénanthridine **16**.

[Traduit par le journal]

In early schemes for the biogenesis of isoquinoline alkaloids Robinson boldly proposed that benzo[*c*]phenanthridines **3** (e.g., chelerythrine and sanguinarine) arose from berberine alkaloids **1** (1). The structural change from a dibenzo[*a*,*g*]quinolizine **1** to a benzo[*c*]phenanthridine **3** required a bond cleavage in **1** to form an intermediate 3-arylisoquinoline derivative **2** which subsequently recyclized to **3**. At that time there were no known examples of 3-arylisoquinoline alkaloids. The hypothesis that compounds of type **1** could give rise to related alkaloids of type **3** was shown by Battersby *et al.* to be substantially correct by the biosynthesis of several benzo[*c*]phenanthridine alkaloids from the proposed biogenetic precursors, exemplified by the formation of chelidonine from labeled (−)-stylopine (2). Although the exact sequence for these conversions has not been established, nor all of the specific intermediates identified, there is general agreement that a 3-arylisoquinoline (cf. **2**) is required. Battersby suggested an intermediate with an aldehyde side chain (**2**, Y = O=) and the heterocyclic ring at the 1,2-dihydroisoquinoline stage. Following the discovery of 3-arylisoquinoline alkaloids in nature, labeled (±)-tetrahydrocoptisine, a berberine alkaloid, was shown to be converted in *Corydalis incisa* to the 3-arylisoquinoline alkaloids, corydamine and corydalic acid methyl ester, as well as to corynoline, which is a reduced benzo[*c*]phenanthridine alkaloid (3). Moreover, laboratory syntheses that parallel the biogenetic sequence **1** → **2** → **3** have been reported for chelerythrine and sanguinarine from canadine and protopine respectively (4).

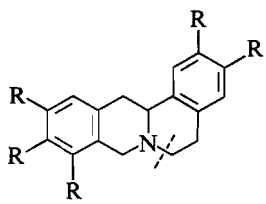

1

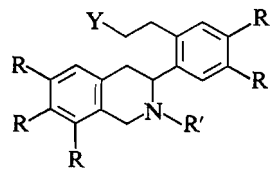

2

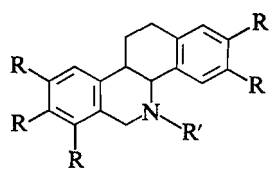

3

In our program of syntheses of structurally diverse, but biogenetically related, isoquinoline alkaloids from 6-homoveratroylhomoveratric acid (the keto acid, **4**), tetrahydropapaverine (5), laudanosine (5), *O*-methylthalisopavine (6), and *O*-methylcryptaustoline iodide (7) have been prepared. Other workers have used **4** to synthesize the aporphine alkaloid, pontevedrine (8), and berberine-type alkaloids (9). We now report the syntheses of some 3-arylisochromene and 3-arylisoquinoline derivatives from **4** and the conversion of these tricyclic compounds to the corresponding 5-oxachrysene and benzo[*c*]phenanthridine compounds (Schemes 1 and 2).

We chose to investigate the preparation and reactions of a 2-benzopyrylium salt derived from **4**, along the lines explored by Dorofeenko and Kuznetsov with aryl benzyl ketones (10), and after our work was in progress Dorofeenko and co-workers reported studies with the keto acid **4** and a derivative of **4** that are similar to ours in some aspects but also differ significantly in others (11).

The oxygen series

Attempted reactions of the keto acid **4** with acetic anhydride and perchloric acid (Scheme 1) did not readily afford a benzopyrylium salt, but when the keto ester **5** was used in place of **4**, a benzopyrylium perchlorate **6** was rapidly formed in good yield. The 2-benzopyrylium perchlorate **6**, and an analogous one **7** derived from desoxyveratroin, were reduced by sodium borohydride in alcohol to the corresponding 3-aryl-1*H*-2-benzopyrans (3-arylisochromenes, **8** and **9**). The 2-benzopyrylium ring was only partially reduced to the dihydro stage

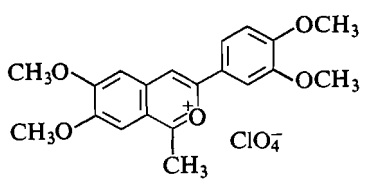

7

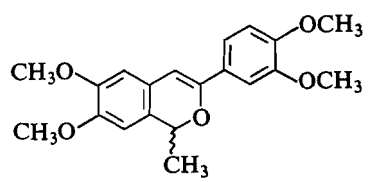

9

[1] Author to whom correspondence may be addressed.

Can. J. Chem. Downloaded from www.nrcresearchpress.com by 210.87.254.105 on 09/06/12
For personal use only.

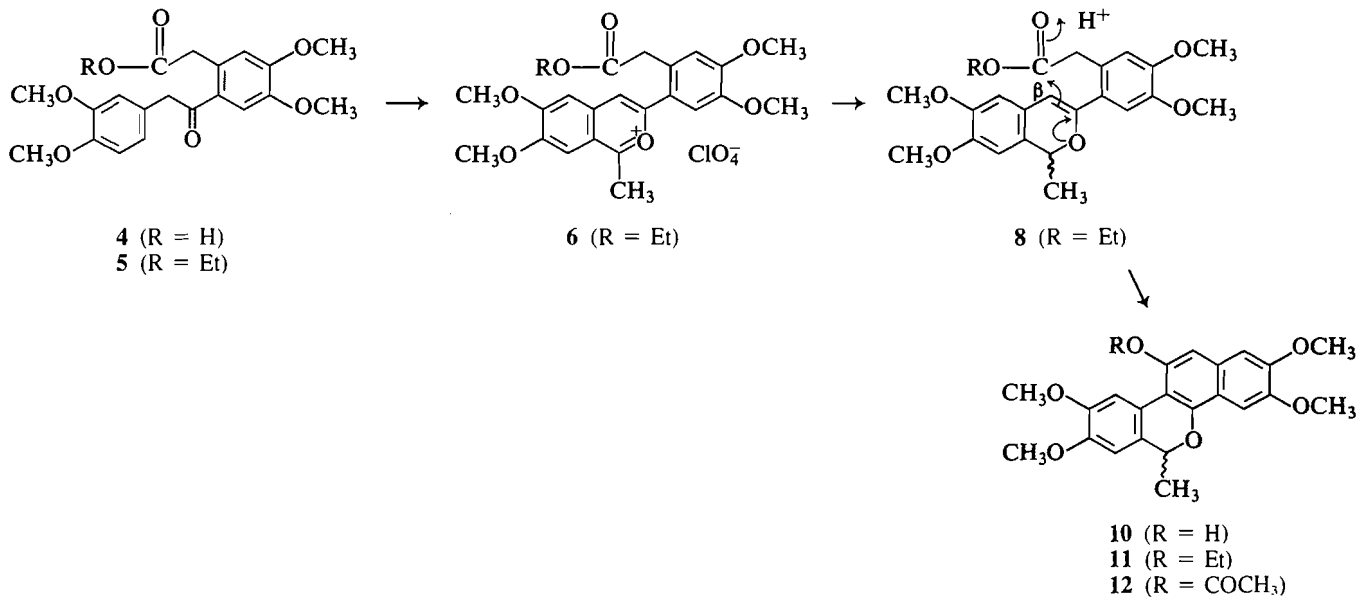

4 (R = H)
5 (R = Et)

6 (R = Et)

8 (R = Et)

10 (R = H)
11 (R = Et)
12 (R = $COCH_3$)

SCHEME 1. Synthesis of 3-arylisochromene **8** and 6*H*-5-oxachrysene **10**.

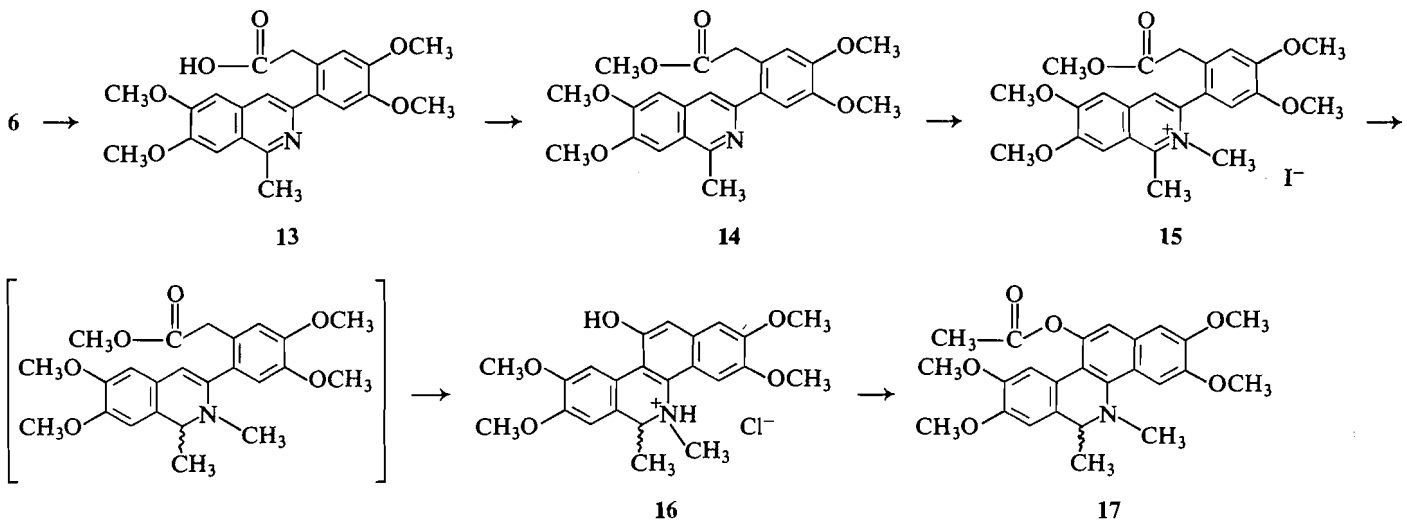

13

14

15

16

17

SCHEME 2. Synthesis of 3-arylisoquinoline **13** and benzo[*c*]phenanthridine **17**.

by sodium borohydride in aqueous alcohol, in contrast to *N*-alkylisoquinolinium salts which are really reduced to the 1,2,3,4-tetrahydroisoquinolines under these conditions (12).

When the isochromene **8** was warmed briefly with EtOH–HCl a new, higher-melting product was obtained that was identified as a difficulty separable mixture of 6*H*-5-oxachrysene derivatives **10** and **11** in which the phenol **10** predominated. The ethyl ether **11** was not detected in the 60-MHz ^{1}H nmr spectrum, probably because of its low concentration and the limited solubility of the tetracyclic compounds, but the presence of both **10** and **11** in the reaction product, even after several recrystallizations, was suggested from the mass spectrum of the product, which showed molecular ion peaks at 382 and 410 for **10** and **11** respectively and parallel fragmentation patterns from each of the parent molecular ions. Liquid chromatographic separation of the product showed two peaks in the approximate ratio of 10 to 1, and when these fractions were examined separately by mass spectral analysis, the two samples showed the peaks matching those for **10** and **11** in the composite spectrum. The reaction mixture of **10** with **11** was treated with Ac_2O–pyridine, and the 11-acetoxy-6*H*-5-oxachrysene **12** was obtained as a useful derivative for further characterization. Attempts to regain the phenol **10** by hydrolysis of **12** were generally accompanied by extensive oxidation to afford dark colored products and were abandoned.

The formation of the 5-oxachrysenes **10** and **11** from **8** under mild acid catalysis can be explained by a push–pull effect in which the β-position of the vinyl ether in **8** serves as a nucleophile that adds to the protonated ethoxycarbonyl group. The mixture of the phenol **10** and the ethyl ether **11** can arise from competing loss of water or ethanol from an intermediate hemiketal. Alternatively, the reaction mixture of **10** and **11** can be rationalized through a series of equilibria involving the keto tautomer of **10** and a hemiketal in a manner similar to the polynuclear phenols studied by Newman *et al.* (13).

The isoquinoline derivatives

Reaction of the 2-benzopyrylium salt **6** with alcoholic am-

Can. J. Chem. Downloaded from www.nrcresearchpress.com by 210.87.254.105 on 09/06/12
For personal use only.

Can. J. Chem. Downloaded from www.nrcresearchpress.com by 210.87.254.105 on 09/06/12
For personal use only.

monium hydroxide solution afforded the isoquinoline derivative **13** (Scheme 2). Surprisingly, hydrolysis of the ester occurred readily and possibly conjunctively under the very mild conditions used for ammonolysis of the 2-benzopyrylium ring of **6** and recyclization of the isoquinoline system. The structure of the isoquinoline acid **13** was supported by both chemical and spectroscopic evidence. Loss of the ethyl group was first suspected by the disappearance of an ir band for the ester carbonyl stretching vibration near 1730 cm^{-1} and the appearance of a medium intensity band at 1620 cm^{-1}, assigned to the carboxyl group. The low frequency for the carboxyl group absorption band suggests that the isoquinoline acid may exist in the zwitterionic form. Initially the mass spectrum showed the highest peak at 379 amu and a base peak at 353, but when spectra were obtained under more careful temperature controls, a weak peak was observed at 397; the presence of this molecular ion peak at 397 was confirmed from a field desorption spectrum. The repeated elemental analyses showed that the compound tenaciously retained solvents, especially water, but eventually recrystallization of **13** from xylene gave analytical samples that provided satisfactory combustion data for $C_{22}H_{23}NO_6$. The ^{13}C nmr spectrum showed the presence of five doublets in the aromatic region and a singlet at 172.4 which is assigned to the carboxyl carbon. Other data from both the ^{13}C and ^{1}H nmr spectra support the structure **13** (see Experimental).

The isoquinoline acid **13** was esterfied to **14** by methyl iodide and potassium carbonate in acetone or alternatively by addition of a sulfuric acid solution of **13** to methanol. The methyl ester **14** was a more tractable compound than **13** for analysis, and both elemental composition and spectral data for **14** fit the assigned constitution. The ester **14** provides access to other isoquinoline derivatives structurally analogous to alkaloids of the 3-arylisoquinoline and benzo[*c*]phenanthridine types.

A methiodide **15** was readily obtained from the ester **14**. Controlled reduction of **15** by sodium borohydride in cold THF, followed by treatment with warm EtOH–HCl solution gave the salt **16**. A 1,2-dihydroisoquinoline derivative, analogous to **8**, is a probable intermediate in the formation of **16** from **15**. The parent ion in the mass spectrum of **16** was at 395 amu, corresponding to the formula $C_{23}H_{25}NO_5$. An ester carbonyl band was not present in the ir, but a broad band appeared at 3400 cm^{-1}, corresponding to an OH. Since the hydrochloride **16** tended to darken on exposure to light and retain hydroxylic solvents, **16** was allowed to react with acetic anhydride in excess pyridine to give a stable crystalline acetyl derivative **17**.

As indicated earlier, Dorofeenko and co-workers (11) used an 1-benzylidene-3-isochromanone **18**, which is obtained from the keto acid **4** by an intramolecular cyclodehydration, to prepare a 2-benzopyrylium perchlorate **19**, and **19** is simply the parent acid of the ester **6**. When **19** was heated with ammonia solution, followed by perchloric acid, these investigators isolated a product to which they assigned the constitution **20**. In more recent papers, this group has offered further support for the oxoberberinum structure (14) and also reported that **4** was successfully converted to a benzopyrylium perchlorate (15).

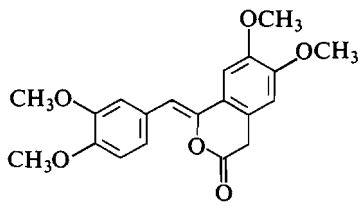

18

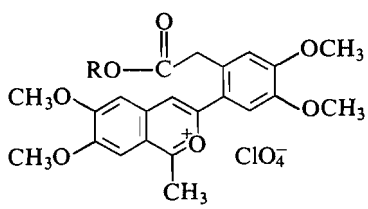

19

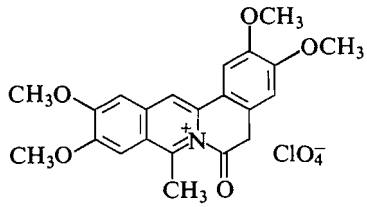

20

Our attempts to prepare a perchlorate **20** from **13** were unsuccessful; although a perchlorate salt was obtained from **13**, it was heavily solvated and apparently not in the tetracyclic, acyliminium form **20**; efforts to dehydrate the perchlorate from **13** resulted in extensive decomposition and no useful products, with the properties described for **20**, could be isolated. However, when our experimental protocol for benzopyrylium salt formation and ammonolysis was applied to **18**, we were able to isolate **13**, but the yields were small and inferior to the results from **5**.

In addition to providing new compounds in the 5-oxachrysene and benzo[*c*]phenanthridine series, this work includes practical examples of intramolecular acylation of a vinyl ether and an enamine with an ester group.

Experimental

General

Melting points were determined on a Mel-Temp apparatus and are uncorrected. Spectra were recorded as indicated: ir on a Perkin Elmer 727 spectrophotometer as paraffin oil mulls; uv on a Carey 14 spectrophotometer; ^{1}H nmr on Varian A60 or EM390 and ^{13}C nmr on a Varian CFT-20 spectrometer as $CDCl_3$ solutions, except where other solvents are specified, with Me_4Si as internal reference; mass spectra on LKB9000 spectrometer. Analyses were performed by Schwarzkopf Microanalytical Laboratory, Woodside, NY. or by MicAnal, Tucson, Arizona.

Ethyl 6-[(3,4-dimethoxyphenyl)acetyl]-3,4-dimethoxyphenylacetate (5)

Compound **5** was prepared from **4** as previously described (5); the preparation of the keto acid **4** in 60% yield was modified as follows: 20 g of 3,4-dimethoxyphenylacetic acid was allowed to react at room temperature in 200 g of polyphosphoric acid for 48 h.

1-Methyl-3-[2-(ethoxycarbonylmethyl)-4,5-dimethoxyphenyl]-6,7-dimethoxy-2-benzopyrylium perchlorate (6)

A suspension of 5 g of the keto ester **5** in 15 mL of acetic anhydride was cooled in an ice bath, and 5 mL of cold 70% $HClO_4$ was added dropwise with stirring over a 20-min period. The reaction mixture immediately developed an orange color, and after 1.5 h the cold paste was filtered and the salt **6** was washed with ether. For routine reductions or aminolyses, the damp perchlorate was used immediately without drying or recrystallizing.[2]

An analytical sample of **6** was recrystallized from acetic acid – nitromethane, with two drops of $HClO_4$, as deep orange prisms; mp 268–270°C (dec.); ir: 1725 cm^{-1} (ester C=O); ^{1}H nmr (trifluoro-

[2] The perchlorates prepared in this work have been stable to shock or heat (**6** decomposes gently at its mp), but organic perchlorates are often unpredictably explosive and should be handled with care.

Can. J. Chem. Downloaded from www.nrcresearchpress.com by 210.87.254.105 on 09/06/12
For personal use only.

acetic acid) δ: 1.21 (t, 3H, J = 6.0 Hz), 3.28 (s, 3H), 3.92 (s, 6H, $2CH_3O$), 4.11 (s, 3H, CH_3O), 4.18 (s, 3H, CH_3O), 4.20 (q, 2H, J = 6.0 Hz), 7.05 (s, 1H), 7.26 (s, 1H), 7.48 (s, 1H), 7.62 (s, 1H), 8.07 (s, 1H). *Anal.* calcd. for $C_{24}H_{27}O_{11}Cl$: C 54.70, H 5.17; found: C 54.30, H 5.20.

1-Methyl-3-[2-(ethoxycarbonylmethyl)-4,5-dimethoxyphenyl]-6,7-dimethoxyisochromene (8)

To the perchlorate salt **6**, freshly prepared from 5 g of **5**, was added 20 mL of methanol, 1 mL of water, and, in portions, 1 g of $NaBH_4$. After 1 h, more water was added to precipitate a gum which was recrystallized from aqueous ethanol as a colorless crystalline solid (2.1 g, 35% from **5**); mp 85–86°C; ir: 1740 cm^{-1}; uv (EtOH), λ_{max} (log ε): 215 (4.82), 270 (4.42), 300 nm (4.18); ^1H nmr δ: 1.24 (t, 3H, J = 7.0 Hz), 1.67 (d, 2H, J = 6.4 Hz), 3.78 (s, 2H), 3.87 (s, 12H, $4CH_3O$), 4.15 (q, 2H, J = 7.0 Hz), 5.31 (q, 1H, J = 6.4 Hz), 5.96 (s, 1H, =CH), 6.82–7.97 (m, 4H, ArH); mass spectrum, m/e: 428 (M^+, base peak), 413 ($M^+ - 15$, 80%); 399 ($M^+ - 29$, 11%). *Anal.* calcd. for $C_{24}H_{28}O_7$: C 67.28, H 6.59; found: C 67.22, H 6.46.

1-Methyl-3-(3,4-dimethoxyphenyl)-6,7-dimethoxyisochromene (9)

To an ice cold suspension of 5 g of desoxyveratroin in 25 mL of acetic anhydride was added 6 mL of 70% $HClO_4$ over a 20-min period. The orange perchlorate was collected by suction filtration, washed with ether, and directly reduced by the addition of 3 g of $NaBH_4$ to an ethanolic mixture of the salt. After standing overnight, the organic product was isolated by the addition of water and recrystallization from ethanol as a colorless solid (4.8 g); mp 141–142°C; ir: 1610 cm^{-1}; uv (EtOH), λ_{max} (log ε): 215 (4.55), 270 (4.23), 300 nm (3.98); mass spectrum, m/e: 342 (17%), 341 ($M^+ - 1$, 62%), 327 ($M^+ - 15$, 100%), 311 ($M^+ - 31$, 5%). *Anal.* calcd. for $C_{20}H_{22}O_5$: C 70.16, H 6.48; found: C 70.45, H 6.48.

2,3,8,9-Tetramethoxy-6-methyl-11-hydroxy-6H-5-oxachrysene (10) and ethyl ester 11

A solution of 1.60 g of **8** in 40 mL of ethanol and 2 mL of concentrated HCl was allowed to reflux 45 min. The red-brown solution was concentrated to yield a tan solid that was recrystallized from ethanol–benzene as a colorless solid (0.95 g, 73%); mp 223–225°C; ir: 3550 and 1638 cm^{-1}; uv (EtOH), λ_{max} (log ε): 215 (4.88), 260 (4.51), 300 nm (4.30); ^1H nmr: ($CDCl_3$ – DMSO-d_6) δ: 1.74 (d, 3H, J = 7.0 Hz), 3.94–3.97 (m, 12H, $4CH_3O$), 5.28 (q, 1H, J = 7.0 Hz), 6.78 (s, 1H), 682 (s, 1H), 6.86 (s, 1H), 7.20 (s, 1H), 8.29 (s, 1H), 9.59 (s, 1H, ArOH); mass spectrum, m/e: 410, 395, 382, 367, 351. *Anal.* found: C 66.48, H 6.63. High-pressure liquid chromatography (hplc) was performed on Radial Pak A (Waters C_{18} reverse phase column) using acetonitrile–water (80:20) as the solvent. The sample separated into two peaks (relative areas 10 to 1), and each fraction was collected, evaporated, and reextracted in $CHCl_3$ for mass spectrometry (LKB9000 probe); fraction 1, m/e: 382 (M^+, 51%); 367 ($M^+ - 15$, 100%), 351 ($M^+ - 13$%); fraction 2, m/e: 410 (M^+), 395 ($M^+ - 15$), 379 ($M^+ - 31$).

2,3,8,9-Tetramethoxy-6-methyl-11-acetoxy-6H-5-oxachrysene (12)

A solution of 0.75 g of the oxychrysene **10** in 7.5 mL of pyridine and 2.5 mL of acetic anhydride was heated on a water bath for 40 min and poured into excess 10% HCl solution. The precipitate was collected and recrystallized from ethanol–benzene as a colorless solid (0.61 g); mp 235–236°C; ir: 1785 cm^{-1}; uv (EtOH), λ_{max} (log ε): 230 (4.46), 280 (4.42), 320 nm (3.96); ^1H nmr δ: 1.65 (d, 3H, J = 6.0 Hz), 2.32 (s, 3H), 3.90–3.99 (m, 12H, $4CH_3O$), 5.28 (q, 1H, J = 6.0 Hz), 6.72 (s, 1H), 6.99 (s, 1H), 7.05 (s, 1H), 7.48 (s, 1H), 7.62 (s, 1H); mass spectrum, m/e: 424 (M^+, 93%), 409 ($M^+ - 15$, 31%), 395 ($M^+ - 29$, 20%), 382 ($M^+ - 42$, 28%), 368 ($M^+ - 56$, 100%). *Anal.* calcd. for $C_{24}H_{24}O_7$: C 67.91, H 5.70; found: C 68.19, H 5.98.

1-Methyl-3-(2-carboxymethyl-4,5-dimethoxyphenyl)-6,7-dimethoxyisoquinoline (13)

2-Benzopyrylium perchlorate **6**, freshly prepared from 10 g of keto ester **5**, was dissolved in 20 mL of ethanol and 20 mL of ammonium hydroxide with loss of orange color. On heating 40 min on a water bath, the solution first became reddish amber and then a tan solid precipitated. The solid was collected from the cooled mixture after 2 h and re-suspended in 150 mL of 10% acetic acid solution for 30 min. The solid was filtered off and recrystallized from pyridine–ethanol as a colorless solid (4.2 g, 43% from **5**); mp 229–230°C; ir: 3450, 1680 sh, 1620, 1520 cm^{-1}; ^1H nmr δ: 2.99 (s, 3H), 3.65 (s, 2H), 3.94 (s, 6H, $2CH_3O$), 4.08 (s, 6H, $2CH_3O$), 7.02 (s, 1H), 7.04 (s, 1H), 7.20 (s, 1H), 7.36 (s, 1H), 7.69 (s, 1H); ^{13}C nmr (DMSO-d_6) δ: 172.42, 154.32, 153.44, 150.28, 148.89, 147.84, 133.74, 131.01, 125.75, 121.35, 118.21, 114.34, 113.86, 105.82, 104.10, 79.13, 55.78, 41.66, 20.26; mass spectrum, m/e: field desorption spectrum 397 (M^+), electron impact spectrum 379 ($M^+ - 18$, 8%), 353 ($M^+ - 44$, 100%), 353 (83%), 338 (64%). *Anal.* calcd. for $C_{22}H_{23}NO_6$: C 66.48, H 5.83, N 3.52; found: C 66.34, H 5.74, N 3.45.

A *perchlorate salt* of **13** was prepared in acetic acid as an ivory solid: mp 164–166°C (dec.); ir: 3480, 1680, 1655, 1610 cm^{-1}. *Anal.* calcd. for $C_{22}H_{24}NO_{10}Cl \cdot 2H_2O$: C 49.51, H 5.29, N 2.62; found: C 49.23, H 5.49, N 2.29.

1-Methyl-3-(2-carbomethoxymethyl-4,5-dimethoxyphenyl-6,7-dimethoxyisoquinoline (14)

(a) *From methyl iodide – K_2CO_3*

A suspension of 4.2 g of the isoquinoline acid **13** in 100 mL of acetone was treated with 6 g of anhydrous potassium carbonate and, with vigorous stirring, 7 mL of methyl iodide was added in portions over a 30-min period. The mixture was warmed and stirred for 1.5 h longer, during which time the solid phase changed in appearance. The solid was filtered by suction and the acetone solution was evaporated. The residual syrup was diluted with methanol and, on scratching and standing, the ester **14** was obtained in three crops and recrystallized from aqueous methanol as a colorless solid (3.5 g, 81%); mp 126–128°C; ir: 1740 cm^{-1} (C=O); ^1H nmr δ: 2.88 (s, 3H, $ArCH_3$), 3.61 (s, 3H, CH_3O), 3.78 (s, 2H), 3.93–4.04 (12H, $4CH_3O$), 6.87 (s, 1H), 7.08 (s, 2H), 7.30 (s, 1H), 7.52 (s, 1H); mass spectrum, m/e: 411 (M^+, 100%), 396 (46%), 354 (92%). *Anal.* calcd. for $C_{23}H_{25}NO_6$: C 67.14, H 6.12, N 3.40; found: C 66.88, H 6.10, N 3.34.

(b) *Alternative preparation of 14*

To 10 mL of cold sulfuric acid was added 4 g of **13**, and after 30 min the acid solution was stirred slowly into 30 mL of cold methanol. A pale yellow solid separated on standing and, after 24 h, 30 mL of ether was added. The salt was collected after 2 h and added to 200 mL of saturated sodium bicarbonate solution. The organic base was extracted with three 30-mL portions of dichloromethane, and evaporation of the organic solvent left an oily residue that was dissolved in hot methanol. The ester **14** was obtained in several crops from aqueous methanol as a colorless solid (3.5 g); mp 126–127°C. This product was identical with the ester **14** from part (a) by ir and nmr comparisons.

1-Methyl-3-(2-carbomethoxymethyl-4,5-dimethoxyphenyl)-6,7-dimethoxyisoquinoline methiodide (15)

The methiodide **15** was obtained from 0.3 g of **14**, 3 mL of methyl iodide, and 2 drops of DMF, after 18 h at room temperature, as a yellow crystalline solid (0.18 g); mp 194–195°C. *Anal.* calcd. for $C_{24}H_{28}NO_6I$: C 52.09, H 5.10, N 2.53, I 22.93; found: C 51.73, H 5.19, N 2.66, I 22.94.

2,3,8,9-Tetramethoxy-5,6-dimethyl-11-hydroxy-5,6-dihydrobenzo[c]phenanthridine hydrochloride (16)

Into an ice cold solution of 2.6 g of **15** in 60 mL of dry THF was stirred 0.2 g of $NaBH_4$ over a 5-min period. After 20 min an additional 0.1 g of $NaBH_4$ was introduced, and the reaction mixture was stirred 20 min longer at 0°C. The mixture was filtered to remove insoluble salts, and the filtrate was treated with 20 mL of a 1:1 solution of methanol – concentrated HCl. A solid precipitated immediately, but this redissolved when the mixture was heated on a water bath for 30 min. Addition and evaporation of two 20-mL portions of benzene, followed by dilution of the residue with ether, gave a solid (1.2 g, 44%) that was recrystallized from benzene–ethanol as a colorless solid; mp 274–276°C; ir: 3400, 1620, 1520, 1475 cm^{-1}; mass spec-

trum, *m/e*: 395 (M^+ − HCl, 21%), 380 (100%). *Anal.* calcd. for $C_{23}H_{26}NO_5Cl$: C 63.96, H 6.07, N 3.32, Cl 8.21; found: C 63.58, H 6.18, N 3.22, Cl 8.15.

2,3,8,9-Tetramethoxy-5,6-dimethyl-11-acetoxy-5,6-dihydrobenzo-[c]phenanthridine (17)

A solution of 0.8 g of the hydrochloride **16** in 3 mL of pyridine and 2 mL of acetic anhydride was warmed on a water bath 30 min and diluted with water to give a precipitate. Recrystallization of the product from ethanol–benzene gave colorless needles (0.65 g, 82%); mp 187–188°C; ir: 1760 cm^{-1}; ^1H nmr δ: 1.20 (d, 3H, J = 2.0 Hz), 2.33 (s, 3H), 2.56 (s, 3H), 3.45 (q, 1H, J = 2.0 Hz), 4.00 (m, 12H, $4CH_3O$), 6.77 (s, 1H), 7.06 (s, 1H), 7.30 (s, 1H), 7.64 (s, 1H), 7.70 (s, 1H); mass spectrum, *m/e*: 437 (M^+, 76%), 422 (100%), 380 (64%). *Anal.* calcd. for $C_{25}H_{27}NO_6$: C 68.63, H 6.22, N 3.20; found: C 68.71, H 6.42, N 3.16.

Acknowledgements

We thank Dr. Helen Lloyd, National Institute of Health, for some of the mass spectral data and assistance with the hplc experiment, Dr. Edward White, National Bureau of Standards, Analytical Chemistry Division, for the field desorption mass spectrum, and Professor Peter Yates for mass and ^{13}C nmr spectra and useful interpretations of them. This research was supported by a grant (RR08062) from the National Institute of Health.

1. R. ROBINSON. The structural relations of natural products. Oxford University Press, London. 1955. p. 89.
2. (*a*) A. R. BATTERSBY, R. J. FRANCIS, M. HIRST, E. A. RUVEDA, and J. STAUNTON. J. Chem. Soc. Perkin Trans. 1, 1140 (1975); (*b*) A. R. BATTERSBY, J. STAUNTON, H. R. WILTSHIRE, R. J. FRANCIS, and R. SOUTHGATE. J. Chem. Soc. Perkin Trans 1, 1147 (1975); (*c*) A. R. BATTERSBY, J. STAUNTON, H. R. WILTSHIRE, B. J. BIRCHER, and C. FUGANTI. J. Chem. Soc. Perkin Trans. 1, 1162 (1975).
3. A. YAGI, G. NONAKA, S. N. KAYAMA, and I. NISHIOKA. Phytochem. **16**, 1197 (1977).
4. (*a*) M. ONDA, K. YONEZAWA, and K. ABE. Chem. Pharm. Bull. **19**, 31 (1971); (*b*) M. ONDA, K. YUASA, J. OKADA, K. KATAOKA, and K. ABE. Chem. Pharm. Bull. **21**, 1333 (1973); (*c*) T. KAMETANI, M. TAKEMURA, M. IHARA, K. FUKUMOTO, and K. TAKAHASHI. Heterocycles, **6**, 99 (1977).
5. I. W. ELLIOTT. J. Heterocycl. Chem. **9**, 853 (1972).
6. I. W. ELLIOTT. J. Org. Chem. **44**, 1162 (1979).
7. I. W. ELLIOTT. J. Org. Chem. **47**, 5398 (1982).
8. L. CASTEDO, R. ESTEVEZ, J. M. SAA', and R. SUAU. Tetrahedron Lett. 2179 (1978).
9. G. D. PANDEY and K. P. TIWARI. J. Sci. Res. (Bhopal, India), **1**, 93 (1979); Chem. Abstr. **93**, 72051 (1980).
10. G. N. DOROFEENKO and E. V. KUZNETSOV. Chem. Heterocycl. Compd. USSR, 207 (1970); Chem. Abstr. **76**, 14014h (1972).
11. E. V. KUZNETSOV, I. V. SHCHERBAKOVA, and G. N. DOROFEENKO. Chem. Heterocycl. Compd. USSR, **13**, 1183 (1977); Chem. Abstr. **88**, 89499g (1978).
12. R. MIRZA. J. Chem. Soc. 4400 (1957).
13. M. S. NEWMAN, V. SANKARAN, and D. R. OLSON. J. Am. Chem. Soc. **98**, 3237 (1976).
14. I. V. SHCHERBAKOVA, O. E. SHELEPIN, N. A. KLYUEV, G. N. DOROFEENKO, and E. V. KUZNETSOV. Chem. Heterocycl. Compd. USSR, 1072 (1982); Chem. Abstr. **98**, 71889F (1983).
15. I. V. SHCHERBAKOVA, G. N. DOROFEENKO, and E. V. KUZNETSOV. Chem. Heterocycl. Compd. USSR, 221 (1981); Chem. Abstr. **95**, 80653q (1981).

Can. J. Chem. Downloaded from www.nrcresearchpress.com by 210.87.254.105 on 09/06/12
For personal use only.

Photoinduced isomerization reactions of azetidinodiazepines

THÉOPHILE TSCHAMBER, JACQUES STREITH,[1] AND HENRI STRUB
Ecole Nationale Supérieure de Chimie, Université de Haute-Alsace, F-68093 Mulhouse Cédex, France
HANS FRITZ
Zentrale Funktion Forschung Physik, Ciba–Geigy AG, CH-4002 Basel, Switzerland
AND
DAVID J. WILLIAMS
Department of Chemistry, Imperial College of Science and Technology, London SW7 2AZ, Great Britain

Received February 15, 1984

This paper is dedicated to Professor Peter Yates on the occasion of his 60th birthday

THÉOPHILE TSCHAMBER, JACQUES STREITH, HENRI STRUB, HANS FRITZ, and DAVID J. WILLIAMS. Can. J. Chem. **62**, 2440 (1984).

Ultraviolet irradiation of the azetidinodiazepines **3** leads in good yield to the expected tricyclic isomers **4** which represent potential precursors for the synthesis of 3-azacarbapenam derivatives. The rigid boat-shaped topology of the photoisomers **4** could be ascertained by detailed ^1H and ^{13}C nmr measurements, and in particular by the determination of nuclear Overhauser effects. That only the *syn* stereoisomers **4** are formed is most likely due to the conformation of the precursors **3** in which the convex side of the seven-membered ring is *syn* with respect to the β-lactam ring. Triplet sensitized irradiation of **3**, which should specifically give a $\pi^* \leftarrow n$ transition of the azetidinocarbonyl function, leads to the highly strained anti-Bredt isomers **5** whose structures were determined by ^1H and, especially, by ^{13}C nmr measurements. The structure of **5***a* was also established by an X-ray analysis which shows, in particular, that the bridgehead imine double bond is twisted out of plane by about 20°. Thermal activation of the anti-Bredt compound **5***a* leads to a mixture of the two isomers **8** and **9** which are more stable than **5***a* by about 40 kcal/mol as determined by differential scanning calorimetry.

THÉOPHILE TSCHAMBER, JACQUES STREITH, HENRI STRUB, HANS FRITZ et DAVID J. WILLIAMS. Can. J. Chem. **62**, 2440 (1984).

L'irridation ultraviolette des azétidinodiazépines **3** conduit, avec de bons rendements, aux isomères tricycliques attendus **4** qui représentent des précurseurs potentiels pour la synthèse de dérivés aza-3 carbapénames. Des mesures de rmn du ^1H et du ^{13}C et, en particulier, des mesures d'effet Overhauser nucléaire permettent d'établir que le photoisomère **4** possède une topologie de forme bateau rigide. Le fait que seuls les stéréoisomères *syn* **4** se forment est probablement dû à la conformation des précurseurs **3** dans lesquels la portion convexe du cycle à sept chaînons est en position *syn* par rapport au cycle du β-lactame. L'irradiation, sensibilisée par un triplet, du composé **3**, qui devrait conduire d'une façon spécifique à une transition $\pi^* \leftarrow n$ de la fonction azétidinocarbonyle, conduit plutôt aux isomères **5** qui sont fortement tendus et qui n'obéissent pas à la règle de Bredt; on a déterminé leurs structures en faisant appel à la rmn du ^1H et plus encore à la rmn du ^{13}C. On a également établi la structure du composé **5***a* par diffraction des rayons-X qui montre, en particulier, que la double liaison de l'imine sur la tête de pont est tordue hors du plan d'environ 20°. L'activation thermique du produit anti-Bredt **5***a* conduit à un mélange des deux isomères **8** et **9**. La calorimétrie différentielle à balayage montre que ces derniers sont plus stables que leur précurseur **5***a* d'environ 40 kcal/mol.

[Traduit par le journal]

Introduction

The pharmacologically active β-lactam antibiotics, such as penicillins, cephalosporins, or monobactams, are produced by microorganisms. Starting from these naturally occurring products, slightly modified molecules have been synthesized in the pharmaceutical industry; these play an ever-increasing role in modern medicine (1). On the other hand, medicinal chemists are focusing their attention and efforts towards the total synthesis of non-natural monocyclic or bicyclic β-lactams, which would hopefully have some antimicrobial activity.

Although to our knowledge none of the "artificial" β-lactams synthesized so far have made their way to the market, major pharmaceutical companies are striving to find new β-lactam antibiotics by total synthesis (2–5).

Azetidinodiazepines **3** can be prepared easily by cycloaddition of methylketene with the imino double bond of the corresponding 1,2-diazepines (6). We surmised that the conjugated diene moiety of **3** would undergo a facile photochemical ring closure, leading to the new tricyclic system **4**. These latter compounds represent annelated azacarbapenam derivatives whose partial structure (azetidinone and five-membered ring) is similar to that of the penicillin and the thienamycin skeleton.

We describe herein some experimental data, which agree with the above mentioned expectation, as well as some unexpected results which were obtained during photosensitized uv irradiation of the four azetidinodiazepines **3***a*–**3***d*.

Direct ultraviolet irradiation of azetidinodiazepines 3*a*–3*d*

Ultraviolet irradiation of the diazepine **1***a* has been shown to lead in moderate yield to the bicyclic isomer **2** (7). Similar results have been obtained by us (7, 8) and by others (9) during uv irradiation of a series of diazepines which gave the corresponding bicyclic isomers having the same skeleton as **2**. We expected, therefore, that the azetidinodiazepines **3** would undergo a similar disrotatory ring closure during direct ultraviolet irradiation of their conjugated diene moiety.

Ultraviolet irradiation of **3***a* through Corex glass – which permits the specific electronic excitation of the diene portion – gives the expected tricyclic isomer **4***a* in 69% yield. A minor photoisomer **5***a* also forms in this experiment (yield: 14%); the

[1]Author to whom correspondence may be addressed.

Can. J. Chem. Downloaded from www.nrcresearchpress.com by 210.87.254.42 on 09/06/12
For personal use only.

TABLE 1. 360 MHz proton magnetic resonance spectrum of compound **4***a* measured in $CDCl_3$*

H-3	H-4	H-6	H-7	H-8	Me-5	Me-8	CH_2CH_3	CH_2CH_3
5.27	5.83	3.69	3.44	3.01	1.79	1.48	4.20†	1.30

$J_{8,Me\text{-}8} = 7.5$	$J_{3,6} = 3.5$	$J_{Me\text{-}5,6} = 1$	$J_{3,8} = 0.5$
$J_{7,8} = 2$	$J_{4,3} = 0.5$	$J_{Me\text{-}5,3} = 1.5$	$J_{CH_2—CH_3} = 7$
$J_{6,7} = 6.5$	$J_{4,Me\text{-}5} = 1.5$	$J_{4,6} = 1.5$	

*Chemical shifts in δ (ppm) and coupling constants J in Hz.
†Center of the AB part of an ABX_3 spectrum (J_{AB} = 10.5 Hz; $\Delta\nu$(AB) = 9.4 Hz).

TABLE 2. 90.5-MHz ^{13}C magnetic resonance spectrum of the photoproduct **4***a* measured in $CDCl_3$*

	δ	$^1J_{C,H}$	$^{n>1}J_{C,H}$
C-9	180.06		6 (Me-8); 6 (H-8); 9 (H-7)
—CO_2—	156.08		1(H-3); 3(CH_2—CH_3)
C-5	147.84		Complex coupling pattern with Me-5, H-3, H-6, and H-7; $\Sigma J = 37$
C-4	132.63	174.5	2.5 (H-3); 8 (H-6); 7 (Me-5)
C-3	67.00	159.9	3 (H-4?); 4.5 (H-6?); 1 (Me-5)
CH_2—CH_3	62.71	148.0	4.4 (CH_2—CH_3)
C-7	59.23	157.7	5 (Me-8)
C-6	53.60	146.3	2 (Me-5); 13 (H-4); 2.5, 2.5, 2.5 (H-8, H-7, H-3)
C-8	45.76	140.2	5 (Me-8)
Me-5	16.35	126.9	1.5 (H-4)
Me-8	14.87	128.9	4 (H-8); 3 (H-7)
CH_2—CH_3	14.47	127.2	2.6 (CH_2—CH_3)

*Chemical shifts in δ (ppm); coupling constants $J_{C—H}$ in Hz.

structure and the mechanism of formation of this isomer will be discussed in the next section (*vide infra*).

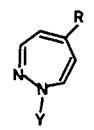

1

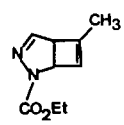

2

	R	Y
a	CH_3	CO_2Et
b	CH_3	$CONH_2$
c	CH_3	COPh
d	H	CO_2CH_2Ph

The structure and relative configuration of **4***a* follow from its spectral data. The ir spectrum shows a band at 1785 cm^{-1} which is indicative of a β-lactam ring; this means that the four-membered ring stayed intact during uv excitation. In Table 1 chemical shifts and coupling constants of the ^1H nmr spectrum of **4***a* are reproduced. We notice, in particular, that the $J_{6,7}$ coupling constant of 6.5 Hz is in favour of a *cis* configuration for H-6 and H-7, and therefore of a rigid boat-shaped topology for this tricyclic molecule. The ^{13}C nmr spectrum of **4***a* (Table 2) fits the proposed structure, although the β-lactam carbonyl function appears at an unexpectedly low field (180.06 ppm). In the starting material **3***a* the carbonyl of the β-lactam moiety appears at 164.64 ppm (6); the β-lactam carbonyls show up between 165 and 168 ppm for penicillins (10, 11), at about 165 ppm for cephalosporin (12), and at 166.1 ppm for thienamycin (13). The low-field chemical shift we observe for the β-lactam carbonyl of **4***a* clearly indicates that there is very little amide character in the four-membered ring and that the N-1 nitrogen atom is likely to have a pronounced pyramidal geometry.

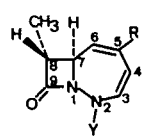

3

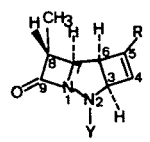

4

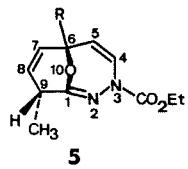

5

	R	Y
a	CH_3	CO_2Et
b	CH_3	$CONH_2$
c	CH_3	COPh
d	H	CO_2CH_2Ph

The ^{13}C spectrum of **4***a* agrees well with a *syn* configuration for this tricyclic molecule: the coupling constants $J_{Me\text{-}8,H\text{-}7}$ (3 Hz) and $J_{C\text{-}6,H\text{-}8}$ (2.5 Hz) indicate that Me-8 and H-7 on the one hand, and C-6 and H-8 on the other hand, are both *cis* to each other (14). Together with the ^1H nmr data cited above, these findings are good evidence in favour of the relative configuration as shown in formula **4***a* (Table 2).

That the structure of the tricyclic compound is indeed as shown in formula **4***a* — not considering stereochemistry — is demonstrated by the $^{13}C—^{13}C$ coupling constant parameters which were obtained from satellites observed in the broad-band-decoupled ^{13}C nmr spectra of a concentrated solution of **4***a* in $CDCl_3$ (14). Table 3 gives the values of the one-bond

Can. J. Chem. Downloaded from www.nrcresearchpress.com by 210.87.254.42 on 09/06/12
For personal use only.

TABLE 3. $^1J(^{13}C-^{13}C)$ coupling constants and values for the $^{13}C-^{13}C$ isotope effects on the chemical shifts (in Hz at 90.5 MHz) for compound **4***a*

(*i*, *j*)	$J(i, j)$ Hz	$j\Delta(i)$ Hz	$i\Delta(j)$ Hz
5–4	58.4	−3.0	−2.9
5–6	35.6	−0.8	−1.1
5-Me-5	42.8	−0.4	*
4–3	39.6	−0.8	−0.9
3–6	25.5	−0.8	−1.2
6–7	38.0	−1.0	−0.9
7–8	33.0	−0.7	−1.0
8–9	40.0	−1.8	*
8-Me-8	35.0	−0.3	*

*Not measured.

TABLE 4. Nuclear Overhauser effect measurements determined at 360 MHz by selective irradiation of several protons of compound **4***a*

Irradiated protons	Intensity enhancements observed with neighbourhood protons
H-3	H-4: +10.3%; H-6: +10.8%
H-6	H-3: +17% ; H-7: +14.9%
H-7	H-6: +13.4%; H-8: no change
Me-8	H-7: +14.6%; H-8: +19.4%
Me-5	H-4: +9.7% ; H-6: +5.8%; H-8: +15.5%

coupling constants and of the $^{13}C-^{13}C$ isotope effects on the chemical shifts.

The results obtained with nuclear Overhauser effect (nOe) measurements fully agree with the proposed relative configuration as shown in formula **4***a* (Table 4). The most pronounced nOe effects are those observed for H-8, during irradiation of the methyl group Me-5, and for H-3 and H-7 during irradiation of H-6. On the other hand, no nOe effect could be detected for H-8 when H-7 was irradiated. These data clearly indicate that H-7 and H-8 are in a *trans* configuration and that H-3, H-6, and H-7 are all three located on the convex side of the rigid boat-shaped molecule **4***a*.

The exclusive formation of stereoisomer **4***a* can be accounted for as follows. The X-ray diagram of the azetidinodiazepine **6** (15), a compound whose topology is similar to that of **3***a*, shows that the boat-shaped conformation of the seven-membered ring and the plane of the β-lactam ring are *syn*. It also shows that the H-3 and H-6 hydrogen atoms point towards the "backside" of the azetidinodiazepine. A photochemical disrotatory ring closure, starting from this *syn* conformation, would then lead to the stereoisomer **4***a*.

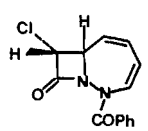

6

Ultraviolet irradiation of the azetidinodiazepines **3***b*–**3***d* leads likewise to the corresponding tricyclic isomers **4***b*–**4***d* (see Experimental).

Triplet-sensitized irradiation of the azetidinodiazepine 3*a*

In the above unsensitized photochemical experiments there was always formed a minor photoisomer **5** together with **4**. When the uv irradiation of **3***a* is carried out in the presence of fluorenone as triplet-sensitizer (E_T = 53.3 kcal/mol), **4***a* is no longer formed. Instead, the compound **5***a*, which was obtained as a minor by-product during the direct irradiation, is now the major photoproduct. These results show that the products **4***a*–**4***d* are most likely produced starting from an excited singlet state of the corresponding educts **3***a*–**3***d*, whereas the by-products are formed from an excited triplet state.

Determination of the structure of the by-products **5** could be achieved with the usual spectrophotometric methods, except for the relative configuration of the two asymmetric centres. The ir spectrum of **5***a* shows a strong carbonyl band at 1708 cm^{-1} which indicates the absence of a β-lactam ring in this photoproduct. The 360-MHz ^1H nmr spectrum, measured in $CDCl_3$, shows a single two-proton band at δ 5.74 ppm which could be resolved by using a solvent mixture ($CDCl_3/C_6D_6$ 1:1): these two vinylic protons have a coupling constant of 9.2 Hz. Two additional vinylic protons appear at δ 6.90 and 4.94 ppm (AB spectrum) with a coupling constant of 9.5 Hz. Clearly neither of these two pairs of olefinic protons can be attached to unsaturated five-membered rings. The ^{13}C nmr spectral data, which are reproduced in the experimental part, led us to postulate the bicyclic "anti-Bredt" structure **5***a* for this unexpected photoproduct.[2] To be noted in particular is a fully substituted sp^3 carbon atom giving rise to a singlet at δ 86.49 ppm; such a low-field chemical shift seemed to indicate that this doubly allylic carbon atom is attached to an oxygen atom. An X-ray investigation of **5***a* confirmed the postulated structure (see below) and led to the determination of the relative configuration of the two asymmetric centres.

For the time being, there is no clear-cut mechanistic interpretation for the triplet-photosensitized formation of the "anti-Bredt" isomer **5***a*. Formally, **5***a* results from a Cope-type rearrangement. Nevertheless it is obvious that this photoproduct cannot be formed in a concerted fashion, starting from **3***a* in its triplet state: Cope-rearrangements are initiated from a singlet ground state!

Whatever the real mechanism for the formation of **5***a*, a diradical intermediate of type **10** – first in its triplet state and thence in its singlet ground state – must be ruled out, since it is precisely this singlet ground state **10** which seems to be the obvious intermediate during the thermal rearrangement of **5***a* (*vide infra*).

Crystallographic analysis of 5*a*

Crystal data

$C_{12}H_{16}N_2O_3$ fw = 236.26

Monoclinic, a = 8.634(1), b = 14.853(2), c = 9.529(1) Å, β = 92.02(1)°, U = 1221 $Å^3$, Z = 4, ρ_c = 1.29 g cm^{-3}, $F(000)$ = 504, μ(Cu-$K\alpha$) = 7 cm^{-1}, space group (uniquely determined from systematic absences) $P2_1/a$. Refined unit cell parameters were obtained by centering 15 reflections on a Nicolet R3m diffractometer. 1529 independent reflections were measured ($\theta \leq 55°$) with Cu-$K\alpha$ radiation (graphite monochromator) using the ω-scan measuring technique. 1447 reflections had $|F_o| > 3\sigma(|F_o|)$ and were considered to be ob-

[2]Some so-called anti-Bredt compounds have been synthesized; some of them could be isolated at room temperature as stable entities, provided that the two-bridged cycles were sufficiently large rings, so that the bridgehead double bonds are only slightly twisted out of plane (16). For the evaluation and prediction of the stability of bridgehead olefinic compounds, see ref. 17; for a review, see ref. 18.

Can. J. Chem. Downloaded from www.nrcresearchpress.com by 210.87.254.42 on 09/06/12
For personal use only.

Can. J. Chem. Downloaded from www.nrcresearchpress.com by 210.87.254.42 on 09/06/12
For personal use only.

TABLE 5. Atom coordinates ($\times 10^4$) and temperature factors (Å^2 $\times$ 10^3) of the anti-Bredt compound **5***a*

Atom	*x*	*y*	*z*	U_{eq}
C(1)	862(2)	146(1)	3113(2)	38(1)*
N(2)	45(2)	−504(1)	2645(2)	41(1)*
N(3)	884(2)	−1081(1)	1756(1)	43(1)*
C(4)	1571(2)	−713(1)	571(2)	48(1)*
C(5)	2285(2)	77(1)	486(2)	49(1)*
C(6)	2744(2)	684(1)	1686(2)	47(1)*
C(7)	1843(2)	1553(1)	1734(2)	55(1)*
C(8)	774(3)	1696(1)	2646(2)	56(1)*
C(9)	201(2)	993(1)	3661(2)	46(1)*
O(10)	2427(1)	190(1)	2962(1)	41(1)*
C(11)	4472(2)	850(2)	1717(3)	61(1)*
C(12)	−1554(2)	1001(1)	3725(2)	56(1)*
C(13)	571(2)	−1985(1)	1789(2)	49(1)*
O(13)	1007(2)	−2504(1)	923(2)	69(1)*
O(14)	−212(2)	−2205(1)	2925(2)	58(1)*
C(15)	−507(3)	−3158(1)	3130(3)	69(1)*
C(16)	778(4)	−3596(2)	3917(3)	89(1)*

*Equivalent isotropic *U* defined as one third of the trace of the orthogonalised U_{ij} tensor.

TABLE 6. Selected torsion angles* of the anti-Bredt compound **5***a*

Atoms	Angle	Atoms	Angle
C(1)N(2)N(3)C(4)	−56.8(2)	N(2)N(3)C(4)C(5)	39.4(3)
N(3)C(4)C(5)C(6)	10.8(3)	C(4)C(5)C(6)C(7)	−111.3(2)
C(5)C(6)C(7)C(8)	105.8(2)	C(6)C(7)C(8)C(9)	−6.2(3)
C(7)C(8)C(9)C(1)	−12.2(3)	C(8)C(9)C(1)N(2)	−117.0(2)
C(9)C(1)N(2)N(3)	159.4(1)	O(10)C(1)N(2)N(3)	−10.3(2)

*With esd's in parentheses.

served. The data were corrected for Lorentz and polarisation factors. No absorption correction was applied.

The structure was solved by direct methods and the non-hydrogen atoms refined anisotropically. All the hydrogen atoms were clearly located in a difference electron density map. The hydrogen positions were idealized (C—H = 0.96 Å), assigned isotropic thermal parameters, $U(H) = 1.2U_{eq}(C)$ and allowed to ride on their parent carbon atoms. The methyl groups were refined as rigid bodies. Refinement was by block-cascade full matrix least-squares to $R = 0.040$, $R_w = 0.051$, ($w^{-1} = \sigma^2(F) + 0.00065F^2$). The maximum residual electron density in the final ΔF map was 0.17 e A^{-3}, and the mean and maximum shifts/error in the final refinement cycle were 0.03 and 0.25 respectively. Computations were carried out on an Eclipse S140 computer using the SHELXTL program system.

Tables 5–7 list the fractional atomic coordinates, some selected torsion angles, bond lengths, and bond angles, respectively. The anisotropic thermal parameters, the structure factors, and the hydrogen coordinates and temperature factors (tables) have been placed in the Depository of Unpublished Data.[3]

The X-ray analysis of **5***a* has confirmed the postulated structure (Fig. 1) and showed that this highly strained arrangement can only be achieved by sacrificing the planarity of the C(1)—N(2), C(4)—C(5), and C(7)—C(8) double bonds. This is most

[3]Data are available, at a nominal charge, from the Depository of Unpublished Data, CISTI, National Research Council of Canada, Ottawa, Ont., Canada K1A 0S2.

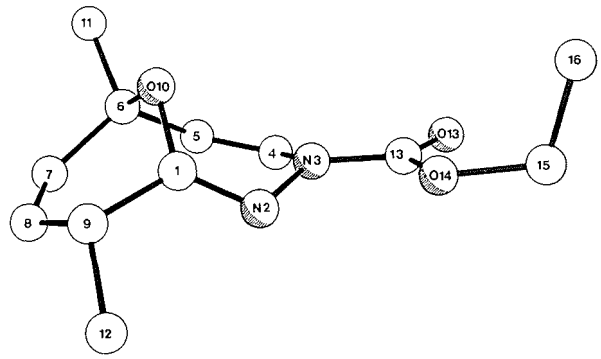

FIG. 1. Perspective view of the anti-Bredt compound **5***a* as determined by X-ray analysis.

pronounced for the bridgehead imine double bond which is twisted out of plane by 20°. This is accompanied by a pyramidal distortion of C(1) which lies 0.066 Å (in the direction of H(9)) from the plane of N(2), C(9), and O(10). N(3) is also slightly pyramidilized, being displaced 0.156 Å above the plane formed by N(2), C(4), and C(13). Table 6 lists selected torsion angles and Table 7 the bond lengths and valence angles. There are no short intermolecular contacts.

Thermal rearrangement of the anti-Bredt photoproduct 5*a*

Thermolysis of the strained photoproduct **5***a* leads to the more stable isomers **7** (85%) and **8** (7%), whose structures follow from their nmr data (see Experimental). To be noted in particular are two close peaks (δ 5.83) corresponding to H-4 and H-5 on **7**. The corresponding protons in **8** appear respectively at δ 5.60 and 5.85 ppm with a coupling constant of 9.6 Hz. The H-7 and H-8 protons show coupling constants of 4.4 Hz for **7** and 4.3 Hz for **8**; the magnitude of these coupling constants is compatible with olefinic protons in a five-membered ring.

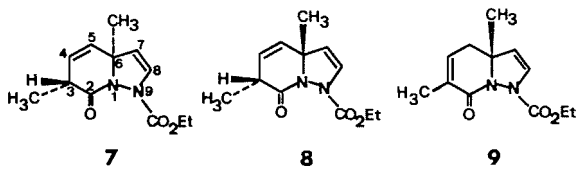

7 **8** **9**

The ^{13}C nmr spectra agree with the stereostructures which are assigned to the diastereomers **7** and **8**. For example Me-3 of **9** shows two coupling constants of 6.5 and 4.0 Hz, respectively with H-3 and with H-4, whereas Me-3 of **7** shows coupling only with H-3 (^2J = 7 Hz) but no coupling constant with H-4. The absence of any coupling with H-4 is due to the fact that the dihedral angle between the C-3—Me-3 and the C-4—H-4 bonds is close to 90°: according to the Karplus equation, ^3J for such a dihedral angle should indeed be close to zero. These data show that the two methyl groups of diastereomer **7** are located on the same side of the molecule: they are *cis* to one another. To be noted, furthermore, are the Me-3 chemical shifts of **7** (δ = 29.2) and of **8** (δ = 14.55): this large difference is not due to a so-called δ-effect between Me-3 and Me-6! It is rather the result of the steric interaction, in **8**, between Me-3 and one of the carbonyl lone electron pairs. A Dreiding model shows that the carbonyl double bond and the C-3—Me-3 bond are indeed quasi coplanar.

Differential scanning calorimetry of the reaction **5***a* → **7** + **8** gave an enthalpy of 40.5 kcal/mol for this rearrangement.

TABLE 7. Bond lengths (Å) and angles (deg) of **5***a*

Bond	Length	Bond	Length
C(1)—N(2)	1.268(2)	C(1)—C(9)	1.483(2)
C(1)—O(10)	1.366(2)	N(2)—N(3)	1.422(2)
N(3)—C(4)	1.405(2)	N(3)—C(13)	1.370(2)
C(4)—C(5)	1.329(3)	C(5)—C(6)	1.499(3)
C(6)—C(7)	1.509(3)	C(6)—O(10)	1.455(2)
C(6)—C(11)	1.511(3)	C(7)—C(8)	1.307(3)
C(8)—C(9)	1.518(3)	C(9)—C(12)	1.518(3)
C(13)—O(13)	1.200(3)	C(13)—O(14)	1.337(2)
O(14)—C(15)	1.452(2)	C(15)—C(16)	1.469(4)
Bond	**Angle**	**Bond**	**Angle**
N(2)—C(1)—C(9)	123.6(2)	N(2)—C(1)—O(10)	122.7(2)
C(9)—C(1)—O(10)	113.0(1)	C(1)—N(2)—N(3)	112.3(1)
N(2)—N(3)—C(4)	118.9(1)	N(2)—N(3)—C(13)	118.1(1)
C(4)—N(3)—C(13)	119.3(2)	N(3)—C(4)—C(5)	127.0(2)
C(4)—C(5)—C(6)	126.6(2)	C(5)—C(6)—C(7)	114.5(2)
C(5)—C(6)—O(10)	106.4(1)	C(7)—C(6)—O(10)	107.1(1)
C(5)—C(6)—C(11)	110.4(2)	C(7)—C(6)—C(11)	111.7(2)
O(10)—C(6)—C(11)	106.3(2)	C(6)—C(7)—C(8)	122.5(2)
C(7)—C(8)—C(9)	124.4(2)	C(1)—C(9)—C(8)	102.8(1)
C(1)—C(9)—C(12)	114.7(2)	C(8)—C(9)—C(12)	111.6(2)
C(1)—O(10)—C(6)	109.1(1)	N(3)—C(13)—O(13)	123.2(2)
N(3)—C(13)—O(14)	111.4(2)	O(13)—C(13)—O(14)	125.4(2)
C(13)—O(14)—C(15)	116.3(2)	O(14)—C(15)—C(16)	111.6(2)

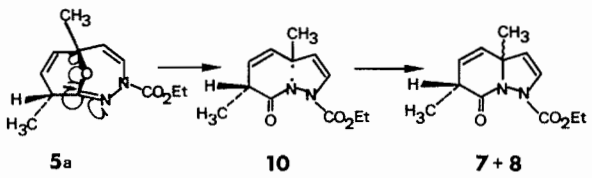

SCHEME 1. Proposed mechanistic scheme for the thermal rearrangement of the anti-Bredt compound **5***a* to the isomers **7** and **8**.

Such a large exothermic value is to be attributed to relief of the ring strain present in the bridged anti-Bredt compound **5***a*. Treatment of the DSC (differential scanning calorimetry) curve using Ellerstein's method (19) leads to the determination of the activation energy (E_a = 31.1 kcal/mol) and the pre-exponential factor ($\ln A$ = 32.0 s^{-1}) of the Arrhenius equation for this thermal isomerization.

The mechanism of this latter ground-state rearrangement seems to be straightforward: homolytic fragmentation of the C_6—O_{10} bond leads to a singlet diradical **10** which is doubly allylic at carbon, and of the "push-pull" type (20) or of the capto-dative type (21) at nitrogen (Scheme 1). Recombination of these two delocalized radicals leads to compounds **7** and **8**, which are thermodynamically more stable than their strained precursor **5***a*.

That **7** and **8** are diastereoisomers can easily be demonstrated: both lead, after equilibration, to the same conjugated enamide **9** when treated with DBU in boiling chloroform (about 65°C) for 15 h. A similar experiment with **7** in the presence of DBU but in boiling methylene chloride (ca. 43°C), under equilibrating conditions when no **9** was formed, gave mainly **8**, suggesting that it is the thermodynamically more stable isomer of the two. Yet, in the thermolysis of **5** leading to **7** and **8**, the latter – though more stable – is the minor isomer formed.

This may indicate that the carbon radical of **10** combines with its neighbouring nitrogen radical in a very fast intramolecular process, thereby retaining to a large degree its original configuration.

Ultraviolet irradiation of the azetidinodiazepines **3***a*–**3***d* led to the expected tricyclic isomers **4***a*–**4***d* as the major photoproducts. Taking advantage of these model reactions, one should now be in a position (*i*) to attach an acid, other than carboxyl, to the nitrogen atom N-2; (*ii*) to induce a fragmentation reaction between C-3 and C-4 and between C-5 and C-6 of products having the overall structure **4**. This synthetic planning would ultimately yield 3-azacarbapenam derivatives.

The photochemical formation of the highly strained anti-Bredt isomers **5***a*–**5***d* was rather unexpected. It shows once more how specific photochemical reactions can be, when compared to thermally induced ones, provided that the proper wavelengths and spin multiplicities are chosen.

Experimental

Microanalyses were carried out by the Service Central de Microanalyses of the C.N.R.S. Melting points were taken with Büchi SMP-2 and Mettler FP5 apparatus and are not corrected. The uv spectra (λ_{max} nm (ϵ)) were recorded on a Varian Techtron 635 spectrophotometer. The ir spectra (cm^{-1}) were determined on a Perkin–Elmer 157 G spectrophotometer. The ^1H and ^{13}C nmr spectra were obtained with Varian T-60 (60 MHz), Bruker WP 80 (80 MHz), Bruker WH 360 (360 MHz), and Bruker WM 400 (400 MHz) instruments, with Me_4Si as an internal reference (δ ppm, J Hz). Normal ms as well as high resolution ms were measured with a MAT 311 mass spectrometer by the Centre de Mesures Physiques of the University of Rennes. Differential Scanning Calorimetry was performed with the fully automated Perkin–Elmer DSC-2C apparatus. Flash chromatographies (22) were carried out with silica gel (Merck 60; 230–400 mesh) and thin-layer chromatographies on aluminium roll (Merck 60 F_{254}). The photochemical experiments were carried out under an argon atmosphere in a Pyrex glass vessel using a water-cooled Hanovia immersion well (Corex glass) equipped with a Philips HPK 125 medium pressure mercury vapour lamp.

Can. J. Chem. Downloaded from www.nrcresearchpress.com by 210.87.254.42 on 09/06/12
For personal use only.

Can. J. Chem. Downloaded from www.nrcresearchpress.com by 210.87.254.42 on 09/06/12
For personal use only.

Synthesis of 1-benzoyloxycarbonyl 1,2-diazepine **1**d

(*i*) To a stirred solution of hydroxylamin-O-sulfonic acid at 0°C (14.13 g; 0.125 mol) in water (31 mL) are successively added potassium hydroxide (8.8 g) in water (13 mL) and pyridine (18.8 mL) over 30 min at about 5°C. After 2 days of continuous stirring at room temperature, potassium carbonate (8.75 g) is slowly added. After 2 h the precipitated solids are filtered off; ethanol is added to the solution, leading to additional precipitates which are filtered. The resulting solution is diluted with ethanol (250 mL) and stirred at 10°C. To this stirred solution potassium carbonate (25 g) and benzyl chloroformate (18 mL) are added, the latter dropwise, and the reaction mixture is kept at room temperature for 24 h and then filtered over sinter glass. The resulting solution is evaporated to dryness *in vacuo*. The resulting crude pyridinium ylide is purified by column chromatography (AcOEt/EtOH 8:2) followed by crystallization in toluene; the resulting brown crystals are further purified by dissolution in a mixture of acetone and petrol ether, whereby a brown product precipitates; after filtration, the mother liquors lead to the pure pyridinium ylide (4.60 g; 16% overall yield) as colourless crystals (toluene), mp 113°C; ir (KBr): 1630, 1605 cm^{-1}; uv (MeOH) λ_{max} (ϵ): 312 nm (6400); ^1H nmr ($CDCl_3$ at 60 MHz) δ: 8.87 (dm, J = 7 Hz, H-2 and H-6), 7.8–7.2 (m, H-3, H-4, H-5, and H-arom.), and 5.20 ppm (s, CH_2). *Anal.* calcd. for $C_{13}H_{12}N_2O_2$ (228.24): C 68.41, H 5.30, N 12.27; found: C 68.30, H 5.25, N 12.46.

(*ii*) A solution of the above described pyridinium ylide (4.60 g; 20.2 mmol) in toluene (2.0 L) is irradiated for 7 h under nitrogen in a "falling-film" type photoreactor (23) equipped with a 700-W medium pressure mercury vapour lamp, the reaction being followed by uv spectroscopy and by tlc until complete disappearance of the pyridinium ylide absorption band. After evaporation of the solvent *in vacuo* and column flash chromatography (AcOEt/cyclohexane 3:7) of the crude reaction mixture, diazepine **1***d* is obtained as an orange oil which solidifies in the cold; mp 67–68°C (hexane); ir (KBr): 1701 cm^{-1}; uv (MeOH) λ_{max} (ϵ): 216 nm (15 200) and 357 nm (280); ^1H nmr ($CDCl_3$ at 60 MHz) δ: 7.40 (m, H-3 and H-arom.), 6.52 (ddd, J = 11, 5, and 1 Hz, H-5), 6.24 (d, J = 7.2 Hz, H-7), 6.20 (partly hidden by H-7; resolved when determined in C_6D_6: dd, J = 11 and 3.5 Hz, H-4), 5.72 (ddd, J = 7.2, 5, 1.5 Hz, H-6), and 5.33 ppm (s, CH_2). *Anal.* calcd for $C_{13}H_{12}N_2O_2$ (228.24): C 68.41, H 5.30, N 12.27; found: C 68.32, H 5.27, N 12.17.

[7α,8α] 8-Methyl 2-benzoyloxycarbonyl 9-oxo 1,2-diazabicyclo-[5.2.0] 3,5-nonadiene **3**d

Through a solution of diazepine **1***d* (3.27 g; 14.3 mmol) in 200 mL toluene is passed the pyrolysis gas of butanone which is produced in a ketene lamp (3) for about 3 h at room temperature, until disappearance of **1***d* as shown by tlc. After evaporation of the solvent *in vacuo*, the crude reaction mixture is separated into its components by flash chromatography (AcOEt/cyclohexane 2:8), which gives mainly the expected β-lactam **3***d* (3.42 g; 84%) as a colourless solid (ether); mp 78°C; ir (KBr): 1773, 1728 cm^{-1}; uv (MeOH) λ_{max} (ϵ): 274 nm (9600); ^1H nmr ($CDCl_3$ at 60 MHz) δ: 7.40 (s, H-arom.), 6.88 (d, J = 9 Hz, H-3), 5.93 (s, H-6), 5.87 (m, H-5), 5.27 (s, CH_2), 5.12 (ddd, J = 9, 7, and 2 Hz, H-4), 4.17 (m, H-7), 2.68 (qd, J = 7.5 and 2.0 Hz, H-8), and 1.38 ppm (d, J = 7.5 Hz, Me-8). *Anal.* calcd. for $C_{16}H_{16}N_2O_3$ (284.30): C 67.59, H 5.67, N 9.85; found: C 67.63, H 5.75, N 9.89.

[3α,6α,7α,8α] 5,8-Dimethyl 2-ethoxycarbonyl 9-oxo 1,2-diazatricyclo[5.2.0.0^{3,6}] 4-nonene **4**a *and [1α,6α,9β] 6,9-dimethyl 3-ethoxy-carbonyl 10-oxa 2,3-diazabicyclo[4.3.1] 1,4,7-decatriene* **5**a

A solution of the azetidinodiazepine **3***a* (3) (3.10 g; 13.1 mmol) in 400 mL methylene chloride is irradiated by uv light until complete consumption of the starting material, the reaction medium being monitored by tlc. Two photoproducts appear which are separated by column flash chromatography (AcOEt/cyclohexane 2:8). Compound **5***a* (435 mg; 14%), being the less polar one, is eluted first; it is followed by its isomer **4***a* (2.127 g; 69%).

Photoisomer **4**a: colourless crystals (ether/petrol ether), mp 92°C; ir (KBr): 1785, 1695 cm^{-1}; uv (MeOH) λ_{max} (ϵ): 238 nm (770); ms: 236 (M^+; 11%); 180 (100%). *Anal.* calcd. for $C_{12}H_{16}N_2O_3$ (236.26): C 61.00, H 6.83, N 11.86; found: C 61.15, H 6.76, N 12.32.

Photoisomer **5**a: colourless crystals (*n*-hexane), mp 54°C; ir (KBr): 1708, 1700, and 1635 cm^{-1}; uv (MeOH) λ_{max} (ϵ): 240 nm (8400); ^1H nmr ($CDCl_3$ at 360 MHz) δ: 6.90 (d, J = 9.5 Hz, H-4), 5.74 (s, H-7 and H-8), 4.94 (d, J = 9.5 Hz, H-5), 4.34 and 4.28 (two ABX systems; twice dq, J_{AB} = 11 Hz, J_{AX} = J_{BX} = 7 Hz, OCH_2CH_3), 3.31 (qd, J = 7 Hz and J < 1 Hz; H-9), 1.50 (s, Me-6), 1.35 (t, J = 7 Hz, OCH_2CH_3), 1.27 (d, J = 7 Hz, Me-9); ^1H nmr ($CDCl_3/C_6D_6$ 1:1 at 360 MHz) δ: 5.52 (d, J = 9.2 Hz, H-7) and 5.50 ppm (d, J = 9.2 Hz, H-8); ^{13}C nmr ($CDCl_3$ at 100.6 MHz) δ: ($^1J_{i,j}$) 167.40 (s, C-1), 153.90 (s, CO), 132.36 (ddq, 167 Hz, C-8), 131.86 (dm, 163 Hz, C-7), 125.91 (dd, 180.5 Hz, C-4), 115.61 (d, 162 Hz, C-5), 86.49 (s, C-6), 63.10 (tq, 149 Hz, CH_2CH_3), 35.94 (dm, 133 Hz, C-9), 28.06 (qs, 129 Hz, Me-6), 14.45 (qt, 127 Hz, CH_2CH_3), 14.45 (q, about 130 Hz, Me-9); ^{13}C nmr ($CDCl_3$ at 100.6 MHz) ^1J ($^{13}C_i - ^{13}C_j$) coupling constants ± 0.3 Hz: J(1, 9) = 55.9 Hz; J(9, Me-9) = 35.9 Hz; J(9, 8) = 36.8 Hz; J(6, Me-6) = 39.7 Hz; J(6, 5) = 47.5 Hz; J(6, 7) = 45.3 Hz; J(5, 4) = 80 Hz; ms: 236 (M^+, 12%), 121 (100%). *Anal.* calcd. for $C_{12}H_{16}N_2O_3$ (236.26): C 61.00, H 6.83, N 11.86; found: C 61.00, H 6.89, N 11.78.

Fluorenone-sensitized formation of the bicyclic product **5**a

A stirred solution of the azetidinodiazepine **3***a* (1.416 g; 6.00 mmol) and of fluorenone (270 mg; 1.5 mmol) in 250 mL acetone is irradiated by uv light (Philips HPK 125) through Pyrex for 9 h, the disappearance of the starting material being determined by tlc. After evaporation of the solvent *in vacuo*, the crude reaction mixture is separated into its components by column flash chromatography (AcOEt/cyclohexane 1:9). The main compound proved to be the photoisomer **5***a* (1.041 g; 73%).

[3α,6α,7α,8α] 5,7-Dimethyl 2-carboxamido 9-oxo 1,2-diazatricyclo-[5.2.0.0^{3,6}] 4-nonene **4**b *and [1α,6α,9β] 6,9-dimethyl 3-carboxamido 10-oxa 2,3-diazabicyclo[4.3.1] 1,4,7-decatriene* **5**b

A solution of azetidinodiazepine **3***b* (3) (995 mg; 4.80 mmol) in 300 mL methylene chloride is irradiated by uv light for 6 h until complete disappearance of the starting material. After evaporation of the solvent *in vacuo* the crude reaction mixture is dissolved in a mixture of ethyl acetate and cyclohexane 6:4 whereby compound **4***b* (368 mg) crystallizes out. Flash chromatography of the remaining mother liquors (AcOEt/cyclohexane 6:4) leads to the successive isolation of the photoisomers **5***b* (130 mg; 13%) and **4***b* (193 mg; combined yield of **4***b*: 56%).

Photoisomer **4**b: colourless crystals (methylene chloride/petrol ether), mp 160–161°C (dec.); ir (KBr): 1779, 1690 cm^{-1}; uv (MeOH) λ_{max} (ϵ): 241 nm (720); ^1H nmr ($CDCl_3$ at 80 MHz) δ: 5.83 (m, H-4), 5.45 (m, H-3), 3.70 (dm, H-6), 3.44 (dd, H-7), 3.07 (qd, H-8), 1.82 (m, Me-5), 1.50 (d, Me-8), 5.4 (s large, NH_2); ^1H-J (i, j) mostly determined by selective irradiation experiments: 3,6 = 3 Hz; 3, Me-5 = 1.5 Hz; 4,6 = 1.5 Hz; 4,Me-5 = 1.5 Hz; 6,7 = 7 Hz; 6,Me-5 = 1.5 Hz; 7,8 = 1.8 Hz; 8,Me-8 = 7 Hz. *Anal.* calcd. for $C_{10}H_{13}N_3O_2$ (207.23): C 57.96, H 6.32, N 20.28; found: C 57.65, H 6.18, N 20.24.

Photoisomer **5**b: colourless crystals (methylene chloride/petrol ether), mp 110–111°C (turns yellow); ir (KBr): 1695 cm^{-1}; uv (MeOH) λ_{max} (ϵ): 243 nm (8800); ^1H nmr ($CDCl_3$ at 80 MHz) δ : 7.07 (d, J = 9.5 Hz, H-3), 5.75 (s, H-6 and H-7), 5.8 (s large, exchangeable with D_2O; NH_2), 4.91 (d, J = 9.5 Hz, H-4), 3.31 (qd, J = 7 and 1 Hz, H-8), 1.54 (s, Me-5), 1.24 (d, J = 7 Hz, Me-8). *Anal.* calcd. for $C_{10}H_{13}N_3O_2$ (207.23): C 57.96, H 6.32, N 20.28; found: C 57.97, H 6.51, N 21.07.

[3α,6α,7α,8α] 5,8-Dimethyl 2-benzoyl 9-oxo 1,2-diazatricyclo-[5.2.0.0^{3,6}] 4-nonene **4**c *and [1α,6α,9β] 6,9-dimethyl 3-benzoyl 10-oxa 2,3-diazabicyclo[4.3.1] 1,4,7-decatriene* **5**c

A solution of azetidinodiazepine **3***c* (3) (2.005 g; 7.47 mmol) in 250 mL methylene chloride is irradiated by uv light for 14 h until

Can. J. Chem. Downloaded from www.nrcresearchpress.com by 210.87.254.42 on 09/06/12
For personal use only.

complete disappearance of the starting material. After evaporation of the solvent *in vacuo*, the crude reaction mixture is separated into its components by flash chromatography (AcOEt/cyclohexane 2:8). The two isomers **5***c* (55 mg; 3%) and **4***c* (402 mg; 20%) are isolated in that order.

Photoisomer **4**c: colourless crystals (ether), mp 138−139°C; ir (KBr): 1775, 1655 cm^{-1}; uv (MeOH) λ_{max} (ϵ): 228 nm (14 100); ^1H nmr ($CDCl_3$ at 60 MHz) δ: 7.93 (m, H-arom.), 7.47 (m, H-arom.), 5.95 (m, H-4), 5.77 (m, H-3), 3.72 (dm, J = 7 Hz, H-6), 3.37 (dd, J = 7 and 1.5 Hz, H-7), 3.07 (qd, J = 7.5 and 1.5 Hz, H-8), 1.85 (m, Me-5), 1.37 (d, J = 7.5 Hz, Me-8); ms: 268 (M^+; 4%), 105 (100%). *Anal.* calcd for $C_{16}H_{16}N_2O_2$ (268.30): C 71.62, H 6.01, N 10.44; found: C 71.50, H 5.84, N 10.41.

Photoisomer **5**c: colourless crystals (methylene chloride, petrol ether), mp 115−117°C (dec.); ir (KBr): 1670, 1640 cm^{-1}; uv (MeOH) λ_{max} (ϵ): 280 (8000), 227 (7400), and 204 nm (14 900); ^1H nmr ($CDCl_3$ at 60 MHz) δ: 7.77 (m, H-arom.), 7.45 (m, H-arom.), 7.30 (d, J = 10 Hz, H-4), 5.78 (s, H-7 and H-8), 5.13 (d, J = 10 Hz, H-5), 3.30 (q, J = 7 Hz, H-9), 1.53 (s, Me-6), and 1.10 ppm (d, J = 7 Hz, Me-9); ms: 268 (M^+; 8%), 105 (100%). *Exact Mass* calcd. for $C_{16}H_{16}N_2O_2$ (ms): 268.121169; found: 268.1217.

[3α,6α,7α,8α] 8-Methyl 2-benzyloxycarbonyl 9-oxo 1,2-diazatricyclo[5.2.0.0^{3,6}] 4-nonene **4**d *and [1α,6α,9β] 9-methyl 3-benzyloxycarbonyl 10-oxa 2,3-diazabicyclo[4.3.1] 1,4,7-decatriene* **5**d

A solution of azetidinodiazepine **3***d* (1.11 g; 3.89 mmol) in 150 mL methylene chloride is irradiated with uv light for 9 h until consumption of the starting material. After evaporation of the solvent *in vacuo*, the crude reaction mixture is separated into its components by flash chromatography (AcOEt/cyclohexane 2:8). The two isomers **5***d* (144 mg; 13%) and **4***d* (785 mg; 71%) are isolated in that order.

Photoisomer **4**d: yellow oil; ir ($CHCl_3$): 1785, 1718 cm^{-1}; uv (MeOH) λ_{max} (ϵ): 242 nm (770); ^1H nmr ($CDCl_3$ at 60 MHz) δ: 7.40 (s, H-arom.), 6.18 (s, H-4 and H-5), 5.45 (dm, J = 3 Hz, H-3), 5.22 (s, CH_2), 3.93 (dd, J = 6.5 and 3 Hz, H-6), 3.43 (dd, J = 6.5 and 1.5 Hz, H-7), 3.04 (qd, J = 7.5 and 1.5 Hz, H-8), 1.45 (d, J = 7.5 Hz, Me-8); ms: 284 (M^+; less than 1%), 91 (100%). *Exact Mass* calcd. for $C_{16}H_{16}N_2O_3$ (ms): 284.116083; found: 284.1153.

Photoisomer **5**d: colourless oil; ir ($CHCl_3$): 1715, 1645, 1395, 1325, 1305 cm^{-1}; uv (MeOH) λ_{max} (ϵ): 229 (10 700) and 207 nm (13 500); ^1H nmr ($CDCl_3$ at 60 MHz) δ: 7.4 (s, H-arom.), 7.02 (dd, J = 10 and 2 Hz, H-4), 5.80 (m, H-7 and H-8), 5.37 (dd, J = 4 and 2 Hz, H-6), 5.30 (s, CH_2), 5.01 (dd, J = 10 and 4 Hz, H-5), 3.34 (qm, J = 7 Hz, H-9), and 1.27 (d, J = 7 Hz, Me-9); ms: 284 (M^+; 6%); 91 (100%). *Exact Mass* calcd. for $C_{16}H_{16}N_2O_3$ (ms): 284.116084; found: 284.1162.

[3α,6α] And [3α,6β] 3,6-dimethyl 9-ethoxycarbonyl 2-oxo 1,9-diazabicyclo[4.3.0] 4,7-nonadiene 7 and 8

The anti-Bredt compound **5***a* (2.10 g; 8.89 mmol) is heated under an argon atmosphere for 30 min at 140°C; tlc shows that the starting material has disappeared and that two new products have formed. Flash chromatography of the reaction mixture (AcOEt/cyclohexane 3:7) leads to the isolation of compound **8** (146 mg; 7%) and thence of its diasteroisomer **7** (1.78 g; 85%).

Diastereoisomer **7**: colourless crystals (ether/petrol ether), mp 68°C; ir (KBr): 1740, 1718, 1680 cm^{-1}; uv (MeOH) λ_{max} (ϵ): 230 nm (9200); ^1H nmr ($CDCl_3$ at 80 MHz) δ: 6.79 (d, J = 4.4 Hz, H-8), 5.83 (d, J = 2.2 Hz, H-4 and H-5), 5.36 (d, J = 4.4 Hz, H-7), 4.30 (q, J = 7 Hz, CH_2CH_3), 3.04 (qt, J = 7.3 and 2.2 Hz, H-3), 1.46 (d, J = 7.3 Hz, Me-3), 1.43 (s, Me-6), 1.35 (t, J = 7 Hz, CH_2CH_3); ^{13}C nmr ($CDCl_3$ at 100.6 MHz) δ ($^1J_{C-H}$): 172.44 (s, C-2), 152.80 (s, CO_2Et), 127.24 (dd, 194 Hz, C-8), 126.98 (d, 163 Hz, C-4 or C-5), 126.96 (d, 163 Hz, C-5 or C-4), 116.22 (ddq, 181 Hz, C-7), 71.71 (sm, C-6), 62.72 (tq, 149 Hz, CH_2CH_3), 38.63 (dm, 134 Hz, C-3), 29.12 (qs, 129 Hz, Me-6), 20.52 (qd, 130 Hz, Me-3), 14.38 (qt, 128 Hz, CH_2CH_3); ^{13}C nmr ($CDCl_3$ at 100.6 Hz) ^1J ($^{13}C-^{13}C$) coupling constants ± 0.3 Hz: J(2,3) = 50.8 Hz; J(3,4) = 38.7 Hz; J(3,Me-3) = 31.6 Hz; J(6,Me-6) = 36.6 Hz; $J(CH_2,CH_3)$ = 38.3 Hz; J(6,7) = 40.2 Hz; J(7,8) = 76.8 Hz; ms: 236 (M^+; 7%); 121 (100%). *Anal.* calcd. for $C_{12}H_{16}N_2O_3$ (236.26): C 61.00, H 6.83, N 11.86; found: C 61.25, H 6.92, N 11.96.

Diastereoisomer **8**: colourless crystals (ether/petrol ether), mp 83°C; ir (KBr): 1740, 1683 cm^{-1}; uv (MeOH) λ_{max} (ϵ): 230 nm (8800); ^1H nmr ($CDCl_3$ at 80 MHz) δ: 6.75 (d, J = 4.3 Hz, H-8), 5.85 (dd, J = 9.6 and 3.2 Hz, H-4), 5.60 (dd, J = 9.6 and 1.4 Hz, H-5), 5.27 (d, J = 4.3 Hz, H-7), 4.28 (q, J = 7 Hz, CH_2—CH_3), 3.25 (qdd, J = 7.3, 3.2, and 1.4 Hz, H-3), 1.38 (s, Me-6), 1.31 (t, J = 7 Hz, CH_2—CH_3), 1.30 (d, J = 7.3 Hz, Me-3); ^{13}C nmr ($CDCl_3$ at 20.1 MHz) δ($^1J_{C-H}$): 171.29 (sm, C-2), 152.09(st, CO_2Et), 128.20 (dm, 167 Hz, C-4 or C-5), 127.38 (ddq, 168 Hz, C-5 or C-4), 126.74 (dd, 196 Hz, C-8), 114.99 (dm, 180 Hz, C-7), 72.26 (sm, C-6), 62.29 (tq, 148.5 Hz, CH_2CH_3), 34.28 (ddq, 128 Hz, C-3), 27.31 (qs, 130 Hz, Me-6), 14.55 (qdd, 129 Hz, Me-3), 14.05 (qt, 128 Hz, CH_2CH_3); ms: 236 (M^+; 6%); 121 (100%). *Anal.* calcd. for $C_{12}H_{16}N_2O_3$ (236.26): C 61.00, H 6.83, N 11.86; found: C 60.97, H 6.79, N 12.02.

Base-catalyzed equilibration of the two diastereoisomers 7 and 8

(*i*) A solution of compound 7 (945 mg; 4.00 mmol) in 5 mL methylene chloride, to which is added DBU (0.30 mL; 2.00 mmol), is heated at reflux temperature for 90 min, the reaction being followed by tlc. After cooling to room temperature and addition of silicic acid (4 g), the solvent is evaporated *in vacuo*. Flash chromatography of the reaction mixture (AcOEt/cyclohexane 3:7) leads to the isolation of isomer **8** as the major product (530 mg; 56%) and of isomer 7 (388 mg; 41%).

(*ii*) A solution of compound **8** (590 mg; 2.50 mmol) is treated with identical reaction conditions whereby **8** is again isolated as the major product (330 mg; 56%) and 7 as the minor isomer (207 mg; 35%). In addition, compound **9** also forms in low yield (22 mg; 4%).

3,6-Dimethyl 9-ethoxycarbonyl 2-oxo 1,9-diazabicyclo[4.3.0] 3,7-nonadiene **9**

A solution of compound 7 (472 mg; 2.00 mmol) in 8 mL chloroform, to which is added DBU (0.30 mL; 2.00 mmol), is heated at reflux temperature for 15 h. The reaction is followed by tlc which shows that the equilibration between 7 and **8** occurs rapidly. After a few hours a new compound appears which is the sole product at the end of the reaction. After addition of some silicic acid (2 g) the solvent is evaporated *in vacuo* and the crude reaction mixture separated by flash chromatography (AcOEt/cyclohexane 3:7). Compound **9** is obtained (408 mg; 86%) as colourless crystals (ether/petrol ether), mp 62°C; ir (KBr): 1745, 1675, 1642, 1615 cm^{-1}; uv (MeOH) λ_{max} (ϵ): 212 (13 400) and 273 nm (1700; shoulder); ^1H nmr ($CDCl_3$ at 80 MHz) δ: 6.71 (d, J = 4.5 Hz, H-8), 6.10 (m, H-4), 5.30 (d, J = 4.5 Hz, H-7), 4.27 (q, J = 7 Hz, CH_2CH_3), 2.70 (ddq, J = 16, 2.5, and 2.5 Hz, H-5), 2.37 (dd, J = 16 and 6 Hz, H-5), 1.98 (m, Me-3), 1.39 (s, Me-6), and 1.34 ppm (t, J = 7 Hz, CH_2CH_3); ^{13}C nmr ($CDCl_3$ at 20.1 MHz) δ ($^1J_{C-H}$): 160.17 (sm, C-2), 153.61 (st, $CO_2CH_2CH_3$), 131.02 (sm, C-3), 128.24 (dm, 163 Hz, C-4), 128.10 (dd, 195 Hz, C-8), 116.35 (dm, 179 Hz, C-7), 66.84 (sm, C-6), 62.47 (tq, 149 Hz, CH_2CH_3), 33.77 (tm, 131 Hz, C-5), 25.57 (qdd, 129 Hz, Me-6), 16.24 (qdd, 128 Hz, Me-3), 13.91 (qt, 128 Hz, CH_2CH_3); ms: 236 (M^+; 13%), 82 (100%). *Anal.* calcd. for $C_{12}H_{16}N_2O_3$ (236.26): C 61.00, H 6.83, N 11.86; found: C 61.13, H 6.87, N 11.85.

Differential scanning calorimetry of the thermal isomerization of **5**a *into the mixture of 7 and 8*

The thermal rearrangement of the neat anti-Bredt compound **5***a* to its isomers **7** and **8** (melt process) was determined by DSC with a Perkin−Elmer DSC-2C apparatus coupled with a Perkin−Elmer TADS-computer. This latter permits one to memorize and to process the DSC curve according to the standard Perkin−Elmer DSC program. Measurements were determined in a dynamic mode, with a constant heating rate of 80°/min. Results: reaction enthalpy: ΔH = 169 ± 2.0 kJ/mol (40.5 kcal/mol); order of the reaction: n = 1.09 ± 0.02; activation energy: E_a = 130 ± 2.8 kJ/mol (31.1 kcal/mol); logarithm of the Arrhenius pre-exponential factor: ln (A) = 32.0 ±

0.7 (A in s^{-1}). According to the ^1H nmr (80-MHz FT) and to the tlc analysis of the reaction mixture, compound **7** is by far the major thermoisomer formed at the end of the DSC experiment with educt **5***a*.

Acknowledgements

We thank the Centre National de la Recherche Scientifique for financial support. We are also grateful to Michelle Martigneaux for her aid in preparing the diazepines **1***a*–**1***d*.

1. R. B. MORIN and M. GORMAN. Chemistry and biology of β-lactam antibiotics. Vols. 1–3. Academic Press, New York. 1982.
2. P. SAMMES. Topics in antibiotic chemistry. Vol. 4. Ellis Horwood Ltd.; Chichester, England. 1980.
3. H. R. PFAENDLER, J. GOSTELI, and R. B. WOODWARD. J. Am. Chem. Soc. **102**, 2039 (1980); V. M. GIRIJAVALLABHAN, A. K. GANGULY, P. PINTO, and R. VERSACE. J. Chem. Soc. Chem. Commun. 908 (1983).
4. A. G. BROWN. J. Antimicrob. Chemother. 15 (1981); N. IKOTA, O. YOSHINO, and K. KOGA. Chem. Pharm. Bull. **30**, 1929 (1982).
5. C. M. CIMARUSTI, H. E. APPLEGATE, H. W. CHANG, D. M. FLOYD, W. H. KOSTER, W. A. SLUSARCHYK, and M. G. YOUNG. J. Org. Chem. **47**, 179 (1982).
6. J. STREITH and T. TSCHAMBER. Justus Liebigs Ann. Chem. 1993 (1983).
7. J. P. LUTTRINGER, N. PEROL, and J. STREITH. Tetrahedron, **31**, 2435 (1975).
8. J. STREITH, J. P. LUTTRINGER, and M. NASTASI. J. Org. Chem. **36**, 2962 (1971).
9. G. KAN, M. T. THOMAS, and V. SNIECKUS. J. Chem. Soc. Chem. Commun. 1022 (1971).
10. C. R. HARRISON and P. HODGE. J. Chem. Soc. Perkin Trans. 1, 1772 (1976).
11. E. H. FLYNN. Cephalosporins and penicillins. Academic Press, New York. 1972.
12. R. MONDELLI and P. VENTURA. J. Chem. Soc. Perkin Trans. 2, 1749 (1977); J. W. PASCHAL, D. E. DORMAN, P. R. SRINIVASAN, and R. L. LICHTER. J. Org. Chem. **43**, 2013 (1978).
13. G. ALBERS-SCHÖNBERG, B. H. ARISON, O. D. HENSENS, J. HIRSHFIELD, K. HOOGSTEEN, E. A. KACZKA, R. E. RHODES, J. S. KAHAN, F. M. KAHAN, R. W. RATCLIFFE, E. WALTON, L. J. RUSWINKLE, R. B. MORIN, and B. G. CHRISTENSEN. J. Am. Chem. Soc. **100**, 6491 (1978).
14. J. L. MARSHALL. *In* Carbon–carbon and carbon–proton NMR couplings in the series stereochemical analysis. Vol. 2. *Edited by* A. P. Marchand. Verlag Chemie International, Deerfield Beach, Florida. 1983, and references cited therein.
15. R. ALLMANN and T. DEBAERDEMAEKER. Cryst. Struct. Commun. **3**, 365 (1974).
16. S. SHIOTANI, T. KOMETANI, A. KUROBE, and K. MITSUHASHI. J. Org. Chem. **41**, 4106 (1976); H. J. BESTMANN and G. SCHADE. Tetrahedron Lett. **23**, 3543 (1982); H. KATO, Y. ARIKAWA, and M. MASUZAWA. Heterocycles, **20**, 118 (1983).
17. W. F. MAIER and P. VON R. SCHLEYER. J. Am. Chem. Soc. **103**, 1891 (1981).
18. G. SZEIMIES. *In* Reactive intermediates. Vol. 3. *Edited by* R. A. Abramovitch. Plenum Publishers, New York. 1983.
19. L. W. CRANE, P. J. DYNES, and D. H. KAELBLE. J. Polym. Sci. Polymer Lett. Ed. **11**, 533 (1973).
20. A. T. BALABAN. Rev. Roum. Chim. **16**, 725 (1971).
21. H. G. VIEHE, R. MERÉNYI, L. STELLA, and Z. JANOUSEK. Angew. Chem. **91**, 982 (1979); Angew. Chem. Int. Ed. Engl. **18**, 917 (1979).
22. W. C. STILL, M. KAHN, and A. MITRA. J. Org. Chem. **43**, 2923 (1978).
23. F. BELLAMY and J. STREITH. J. Chem. Res. (S), 18 (1979).

Can. J. Chem. Downloaded from www.nrcresearchpress.com by 210.87.254.42 on 09/06/12
For personal use only.

Rates of detritiation of the strychninesulfonic acids at the 11-position in alkaline solution

JOHN T. EDWARD AND SIN CHEONG WONG
Department of Chemistry, McGill University, 801 Sherbrooke St. W., Montreal (Que.), Canada H3A 2K6

AND

A. J. KRESGE AND M. F. POWELL
Department of Chemistry, University of Toronto, 80 St. George St., Toronto, Ont., Canada M5S 1A1

Received June 22, 1983[1]

This paper is dedicated to Professor Peter Yates on the occasion of his 60th birthday

JOHN T. EDWARD, SIN CHEONG WONG, A. J. KRESGE, and M. POWELL. Can. J. Chem. **62**, 2448 (1984).

Tritium was incorporated into the 11-position of strychnine, and of strychninesulfonic acids-I, -II, and -III, and the rate of detritiation from the four compounds in 0.5 *M* sodium hydroxide at 25°C was measured. Rates were reduced by the negative sulfonate groups, the extent of reduction varying inversely with the distance of the sulfonate group from the negative oxygen of the enolate intermediate. Experimental rates were in reasonable agreement with values expected at zero ionic strength from the Kirkwood–Westheimer equation. The problem of correcting experimental values for the effect of ionic strength is discussed.

JOHN T. EDWARD, SIN CHEONG WONG, A. J. KRESGE et M. POWELL. Can. J. Chem. **62**, 2448 (1984).

On a incorporé du tritium en position 11 de la strychnine et des acides strychninesulfoniques-I, II et III et on a mesuré la vitesse de détritiation des quatre composés, dans l'hydroxyde de sodium 0,5 *M*, à 25°C. Les groupes sulfonates négatifs réduisent la vitesse; le taux de la réduction varie de façon inverse avec la distance du groupe sulfonate par rapport à l'oxygène négatif de l'énolate intermédiaire. Les vitesses expérimentales sont raisonablement en accord avec les valeurs attendues à partir de l'équation de Kirkwood–Westheimer pour une force ionique de zéro. On discute de la façon de corriger les valeurs expérimentales pour tenir compte de l'effet de la force ionique.

[Traduit par le journal]

Can. J. Chem. Downloaded from www.nrcresearchpress.com by 210.87.254.6 on 09/06/12
For personal use only.

Strychnine (**1***a*), brucine, and their derivatives condense readily with benzaldehyde (1) and amyl nitrite (2) in alkaline solution. It may be assumed that these reactions involve the enolate ion **2** as an intermediate. The same ion must be involved in the incorporation of tritium from TOH into strychnine, which we find to take place readily under alkaline conditions. This reaction is reversible. In the present paper we report on the rate of removal in alkali of tritium from tritiated strychnine and from the tritiated anions derived from strychninesulfonic acids-I (**1***b*), -II (**1***c*), and -III (**1***d*). The structures of these acids have been elucidated only recently (3, 4). The anions **3***b*–**3***d*, with the charged SO_3^- group at various distances from the developing negative centre of **2**, would seem good model compounds for testing the validity of Kirkwood–Westheimer theory (5) for the kinetics of detritiation.

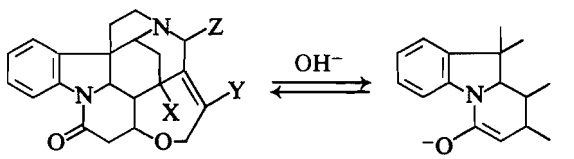

1*a* X = Y = Z = H
b X = SO_3^-, Y = Z = H
c Y = SO_3^-, X = Z = H
d Z = SO_3^-, X = Y = H

2

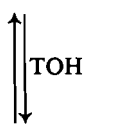

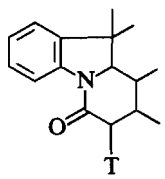

3

Experimental

Materials

Tritiated strychnine was prepared by stirring a suspension of strychnine in tetrahydrofuran and tritiated water with a small amount of sodium hydroxide added as a catalyst. After 24 h, the tritium exchange was quenched by acid. The solid was filtered, washed thoroughly with ordinary water, and dried under high vacuum to remove any unreacted TOH. It was then used for detritiation studies without further purification.

Tritiated strychninesulfonic acids-I, -II, and -III were similarly prepared, except that sulfonic acid-III was not washed with water because of its high water solubility.

Detritiation of strychnine

A small amount of tritiated strychnine was added to a 50 mL volumetric flask containing aqueous sodium hydroxide solution of an appropriate concentration (and KCl to keep the ionic strength at 0.5), thermally pre-equilibrated to 25.0°C in a thermostatted water bath. The flask was shaken vigorously and placed back in the water bath. Five-milliliter aliquots of the solution were removed at regular intervals and quenched with acid in a separatory funnel; 30 mL of carbonate buffer (pH 10) and exactly 7 mL of toluene were added. The funnel was vigorously shaken and the aqueous layer was discarded. The toluene layer was washed 3 more times with 30-mL portions of carbonate buffer and 5 mL of th toluene solution was pipetted into a scintillation counting vial containing 15 mL of Bray's solution (6). The residual radioactivity of the tritiated strychnine was then counted by a Packard Tricarb Model 314 EX scintillation counter.

Detritiation of strychninesulfonic acids

Due to their low solubilities in toluene as well as in Bray's solution, the above procedure used for strychnine had to be modified. Five-milliliter aliquots of the substrate in aqueous sodium hydroxide were again removed at regular intervals and quenched in acid. They were

[1] Revision received April 3, 1984.

Can. J. Chem. Downloaded from www.nrcresearchpress.com by 210.87.254.6 on 09/06/12
For personal use only.

left in round bottom flasks and evaporated to dryness, and then kept several hours under high vacuum to remove any TOH formed in the detritiation process. The residue was redissolved in 5 mL of dilute aqueous sodium hydroxide, and 3 mL of it was the pipetted into a scintillation counting vial containing 15 mL of the water-tolerant scintillation solution due to Kennedy (7) and counted.

Results and discussion

Order of reaction

In the large excess of sodium hydroxide employed, detritiation of strychnine (**3***a*) followed pseudo-first-order kinetics. Over the range 0.1–0.5 *M* sodium hydroxide, the rate constant k_ψ was roughly linear with hydroxide ion concentration, but was somewhat higher than predicted by a linear relationship in the highest concentrations of hydroxide.

Such behaviour is consonant with a mechanism having a transition state **4**, in which δ− of the carbonyl oxygen approaches a unit electronic charge, and breaking of the

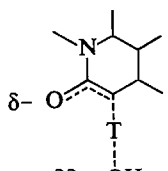

4

C(11)—T bond to form T—OH is largely complete (δδ− very small). For such a mechanism the Bronsted–Bjerrum treatment gives

$$[1] \quad k_\psi = k_0[OH^-] f_{ST} f_{OH^-}/f_{S^\ddagger}$$

where ST stands for **3***a*, $S^\ddagger$ for the transition state **4**, k_0 for the rate constant at zero ionic strength, and the *f*'s are activity coefficients. If the equilibrium ionization of **3***a* in sodium hydroxide solution is governed by the h_- function established with thioacetamide (8) (which is likely to be only approximately true), then we can write

$$[2] \quad f_{ST} f_{OH^-}/f_{S^-} = K_w/h_- [OH^-]$$

where K_w is the autoprotolysis constant for water. Since **4** is close to **2** in structure, $f_{S^\ddagger} \approx f_{S^-}$, and we obtain from [1] and [2]

$$[3] \quad k_\psi = k_0 K_w/h_-$$

Values of k_ψ thus calculated are given in Table 1 and are in fair agreement with experimental results.

Effect of negatively-charged groups

The presence of negatively-charged sulfonate groups in **3***b–d* depresses k_ψ, as shown by the positive values of $\Delta\log k_\psi$ ($\equiv \log k_\psi^P - \log k_\psi$, where k_ψ^P is the rate constant for the "parent" compound, strychnine) in Table 2. This is in agreement qualitatively with Kirkwood–Westheimer theory: the negative charges of the sulfonate groups will make the change from the formally uncharged carbonyl group of **3** to the negatively charged group of the transition state **4** more difficult. Furthermore, this electrostatic effect diminishes as the distance of the sulfonate groups from the carbonyl group increases, in going from strychninesulfonic acid-I to -II to -III.

Calculation of the electrostatic effect by the Kirkwood–Westheimer equation

According to Kirkwood and Westheimer (9), the change in rate of hydrolysis brought about by the variously-placed sulfonate groups is given by

$$[4] \quad \Delta\log k_0 = \log k_0^P - \log k_0 = e^2/2.3\ kTRD_{eff}$$

where k_0 stands for rate constants obtained by extrapolation of $k_\psi/[OH^-]$ to zero ionic strength, *e* is the electronic charge, *k* Boltzmann's constnat, *T* the absolute temperature, *R* the intercharge distance, and D_{eff} the effective dielectric constant.

To obtain *R* we assumed that in the transition state the negative charge resides completely on the carbonyl oxygen, i.e. that the transition state **4** is very close to **2**. *R* was obtained by measurements on scale models of **2** set up using the Tacoma flexible molecular model kit,[2] and is given in Table 2. From *R* the eccentricity λ_0 of a prolate ellipsoid modelling the transition state was calculated according to Tanford (10), and D_{eff} thence obtained from the published $D_{eff} - \lambda_0$ relation (9).

The $\Delta\log k_0$ values given by eq. [4] were as follows ($\Delta\log k_\psi$ from Table 2 in parentheses):

Strychninesulfonic acid-I	0.60	(0.68)
Strychninesulfonic acid-II	0.41	(0.50)
Strychninesulfonic acid-III	0.38	(0.34)

These results are surprising, since the k_ψ values were obtained in 0.5 *M* sodium hydroxide. In a solution of this ionic strength $\Delta\log k_\psi$ might be expected to be considerably lower than $\Delta\log k_0$ because shielding of the negative sulfonate groups by counterions should reduce the electrostatic effects of these groups. However, the estimate of this shielding effect is uncertain in concentrated solutions because of the limitations of Debye–Hückel theory (11). Westheimer *et al.* (5) found that

TABLE 1. Effect of concentration of sodium hydroxide on the rate of detritiation of strychnine-C(11)-t

	$10^4\ k_\psi(s^{-1})$	
$[OH^-]^a$	Exptl.	Calcd.[b]
0.1	4.32 ± 0.14	4.17
0.2	8.46 ± 0.32	8.13
0.3	11.5 ± 0.3	12.6
0.4	16.6 ± 0.8	17.8
0.5	24.5 ± 1.2	22.9

[a] Ionic strength kept constant at 0.5 *M* by addition of requisite amount of KCl.
[b] From [3], with $k = 5.25 \times 10^{-3}$, and using h_- values from ref. 8 with the assumption that they are unaffected by the KCl added to the NaOH solutions.

TABLE 2. Rates of detritiation from C(11)-position of strychninesulfonic acid-I, -II, and -III in 0.5 *M* sodium hydroxide at 25°C

Acid	Formula	*R* (Å)	$10^4\ k_\psi(s^{-1})$	$\Delta\log k_\psi$
I	**1***b*	6.5	5.07 ± 0.09	0.68
II	**1***c*	8.4	7.75 ± 0.11	0.50
III	**1***d*	8.9	11.1 ± 0.12	0.34

[2] These models are more convenient than the Dreiding models when models of strained cage molecules must be constructed.

the second-order rate constant k for the hydrolysis of the negative monoethyl adipate ion by hydroxide ion in water at 20°C in solutions having ionic strength μ up to 0.273 obeyed the equation:

$$[5] \quad \text{Log } k = \log k_0 + 2\alpha\sqrt{\mu} + \beta\mu$$

where α is the Debye–Hückel constant and β is an empirically-determined constant (obtained as the slope of the straight line given by plotting ($\log k - 2\alpha\sqrt{\mu}$) against μ). For the hydrolysis of monoethyl adipate ion β was -1.03. On the other hand, the second-order rate constant for the hydrolysis of the uncharged diethyl adipate molecule by hydroxide ion under the same conditions was almost independent of ionic strength. If we assume similar relationships to hold for the detritiation by hydroxide ion of the neutral strychnine molecule and the negatively charged sulfonate ions in 0.5 *M* sodium hydroxide, the fairly close correspondence between $\Delta\log k_\psi$ and $\Delta\log k_0$ can be accounted by a value for β of about -1.4. This would seem a reasonable value, and could be confirmed experimentally by obtaining rates of detritiation at several lower values of μ. However, the counting methods for the water-soluble sodium salts of the sulfonic acids are tedious, and the accuracy of measurements would drop for the slower reactions in more dilute alkali. Consequently, it was decided that it would be more profitable to look for more simply monitored reactions of salts of strychnine sulfonic acids. However, the present work does suggest that Kirkwood–Westheimer calculations may indicate trends for reaction rates even in solutions of high ionic strength.

Acknowledgments

Grateful acknowledgment is made to the Natural Sciences and Engineering Research Council of Canada and to the Ministry of Education of Quebec (under the Programme de Coopération entre les Collèges et entre les Universités des Québec et de l'Ontario) for financial support.

1. W. H. PERKIN and SIR R. ROBINSON. J. Chem. Soc. **132**, 964 (1929).
2. H. WIELAND and W. GUMLICH. Ann. **494**, 191 (1932); H. WIELAND and K. KAZIRO. Ann. **506**, 60 (1933).
3. J. T. EDWARD, P. G. FARRELL, S. A. SAMAD, R. WOJTOWSKI, and S. C. WONG. Can. J. Chem. **58**, 2380 (1980).
4. L. COLEBROOKE, W. CHAZIN, and J. T. EDWARD. Can. J. Chem. **61**, 1749 (1983).
5. F. H. WESTHEIMER, W. A. JONES, and R. A. LAD. J. Chem. Phys. **10**, 478 (1942).
6. G. A. BRAY. Anal. Biochem. **1**, 279 (1960).
7. J. F. KENNEDY. Experientia, **25**, 1120 (1969).
8. J. T. EDWARD and I. C. WANG. Can. J. Chem. **40**, 399 (1962).
9. J. G. KIRKWOOD and F. H. WESTHEIMER. J. Chem. Phys. **6**, 506 (1938); **6**, 513 (1938).
10. C. TANFORD. J. Am. Chem. Soc. **79**, 5348 (1957).
11. L. P. HAMMETT. Physical organic chemistry. 2nd ed. McGraw–Hill, New York. 1970. pp. 187–219; K. B. WIBERG. Physical organic chemistry. John Wiley, New York. 1964. pp. 394–395.

Can. J. Chem. Downloaded from www.nrcresearchpress.com by 210.87.254.6 on 09/06/12
For personal use only.

Addition initiated ring closure: synthesis of substituted spiro[2.4]hepta-4,6-dienes via cyclopentadiene intermediates from fulvene precursors

KAZIMIERZ ANTCZAK, JOHN F. KINGSTON, AND ALEX G. FALLIS

Department of Chemistry, Memorial University of Newfoundland, St. John's, Nfld., Canada A1B 3X7

Received March 20, 1984

This paper is dedicated to Professor Peter Yates on the occasion of his 60th birthday

KASIMIERZ ANTCZAK, JOHN F. KINGSTON, and ALEX G. FALLIS. Can. J. Chem. **62**, 2451 (1984).

The reactivity of the epoxy-fulvene **1**, prepared by pyrrolidine catalyzed condensation of cyclopentadiene and epoxybutanone, has been examined with various nucleophiles. It is a versatile intermediate for the preparation of spiro[2.4]hepta-4,6-diene synthons via nucleophilic addition to the C_6 position of the fulvene followed by intramolecular cyclization of the substituted cyclopentadiene anion generated *in situ*.

KASIMIERZ ANTCZAK, JOHN F. KINGSTON et ALEX G. FALLIS. Can. J. Chem. **62**, 2451 (1984).

On a étudié la réactivité de l'époxy-fulvène **1**, préparé par une condensation catalysée par la pyrrolidine du cyclopentadiène sur l'époxybutanone, avec divers nucléophiles. C'est un intermédiaire versatil dans la préparation de synthons spiro[2,4]-heptadiènes-4,6 accessibles par le biais d'une addition nucléophile en position C_6 du fulvène qui est suivie d'une cyclisation intramoléculaire de l'anion cyclopentadiène substitué, généré *in situ*.

[Traduit par le journal]

Can. J. Chem. Downloaded from www.nrcresearchpress.com by 210.87.254.5 on 09/06/12
For personal use only.

Introduction

Synthetic routes involving sequential nucleophilic addition with the generation of a new nucleophilic centre that can react intramolecularly with another electrophile have particular appeal. These schemes require intermediates bearing several electrophilic sites and, in principle, offer rapid synthetic access to an array of bridge, fused, conjoint, and spiro ring systems. This strategy holds considerable potential and is frequently initiated by a Michael addition (Michael initiated ring closure) (1–3). Recently Danishefsky *et al.* reported a stereospecific 2 + 2 + 2 annulation which involves two sequential Michael additions followed by an aldol reaction (4, 5).

Cyclopentadiene is an economical and readily available cyclopentane unit; however, the use of substituted cyclopentadienes in natural product synthesis has frequently been complicated by the facile 1,5-sigmatropic rearrangements which these species undergo. One solution we have developed is to block the rearrangement with a cyclopropyl unit which may serve as a source of latent functionality (6, 7). In the course of these investigations we have devised a general route to spiro[2.4]-hepta-4,6-dienes ("blocked cyclopentadienes") from fulvene intermediates via *in situ* generation of substituted cyclopentadiene anions. It is well established that the exocyclic double bond in fulvenes is polarized and of similar reactivity to a carbonyl group (8). Thus fulvenes have served as a source of substituted cyclopentadienes by both hydride reduction (9–11) and nucleophilic addition (11, 12). However, with the exception of work by Büchi *et al.* (13) leading to the spiro-sesquiterpenes hinesol and β-vetivone, they have been underutilized in total synthesis. As illustrated in Scheme 1, after nucleophilic addition intramolecular alkylation may proceed to give spiro and (or) fused ring systems (more than one cyclopentadiene isomer is possible but only one is illustrated). The major products will depend upon the relative ease of cyclization for the competing pathways and in most instances should be predictable, based on the nature of the electrophiles and the chain lengths involved. The system studied by Büchi *et al.* (13), in which the electrophilic site was four carbons removed from the fulvene, gave spiro[4.5]deca-1,3-dienes and no hydroazulenes were formed. This is in contrast to earlier results of Hafner (10), who found that spiro ring formation was

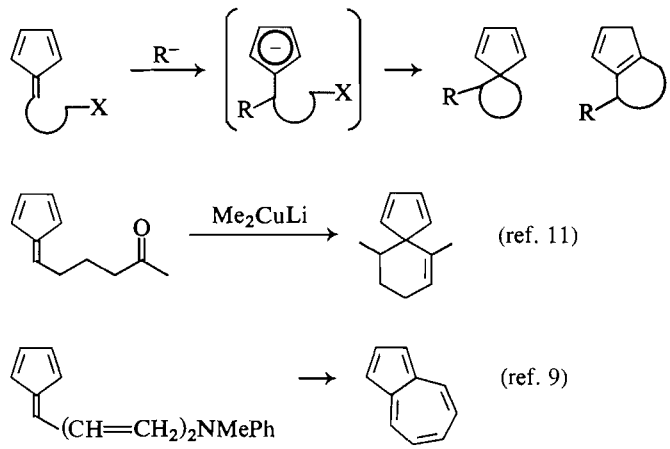

SCHEME 1

inhibited by the presence of unsaturation in the connecting chain and afforded azulene exclusively.

We wish to report the results of our initial studies, which permit the introduction of diverse functionality into the epoxy-fulvene **1**. These investigations have established that the preferred mode of intramolecular cyclization affords the spiro[2.4]hepta-4,6-diene system **3** (Scheme 2), a key intermediate in our approach to longifolene. These addition initiated ring closures provide direct access to useful bicyclic synthons for subsequent Diels–Alder reactions, as synthetic equivalents for 5,5-disubstituted cyclopentadienes (14), and in cases where the cyclopropane contains olefinic substituents for subsequent vinyl cyclopropane type rearrangements to diverse ring systems. The extension of this approach to polyquinanes such as capnellene (15) and pentalenene (16) also appears feasible.

Results and discussion

A variety of bases have been employed for fulvene preparation (8) from carbonyl compounds, although the mildest and most efficient tend to be amines (17). In these studies a significant improvement in yield was achieved by using pyrrolidine as the catalyst. Thus condensation of cyclopentadiene with the epoxide derived from 3-butenone (30% H_2O_2, CH_3OH,

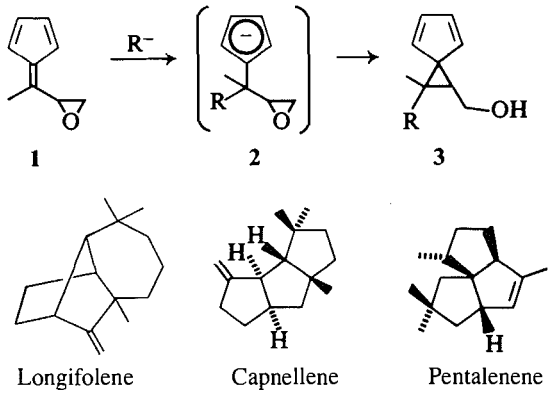

SCHEME 2

60–71%) in the presence of pyrrolidine (0°C, 2 h) afforded the epoxy-fulvene **1** in 86% yield.[1] The ^{1}H nmr spectrum of this material displayed a characteristic four-proton multiplet at δ 6.35 for the vinyl protons, a vinyl methyl singlet at 1.91, a multiplet at 2.82 for the methylene hydrogens, and a doublet of doublets (J = 1.5, 1 Hz) at 3.90 due to the methine hydrogen. These features support the assigned structure.

In principle, nucleophilic attack may occur at any of the three major electrophilic sites present in **1** and the epoxide may be opened at either end to generate several different structures.

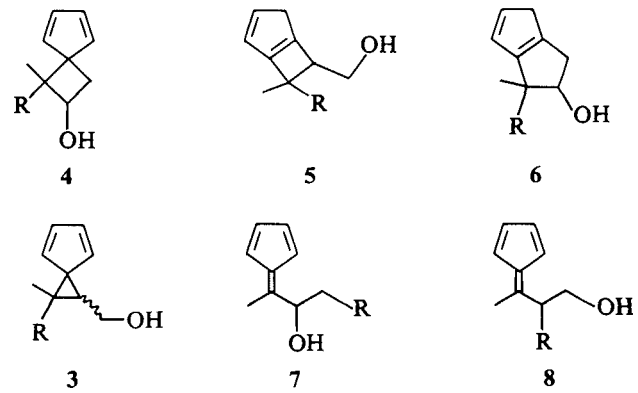

The carbocyclic skeletons **3**–**6** and the fulvene alcohols **7**–**8** are all possible. However, in the majority of cases nucleophilic addition occurred preferentially at the C_6 fulvene centre to generate the cyclopentadiene intermediate **2** which cyclized to form the cyclopropyl unit by *exo* cleavage of the epoxide. These results are summarized for a variety of lithio nucleophiles in Table 1. The alternative cyclization to form the cyclobutane **4** requires an *endo-tet* ring opening which is disfavoured (18–21), as is the spiro[3.4]octa-1,3-diene system itself (22–24). In a typical example, addition of methyllithium to the fulvene-epoxide **1** at −78°C in tetrahydrofuran followed by warming to 0°C afforded the spiro-alcohol **9** as the sole product after work-up and chromatography. The ^{1}H nmr spectrum displayed methyl singlets at δ 1.38 and 1.40, the cyclopropyl hydrogen appeared as a triplet (J = 7 Hz) at 2.22, the methylene protons as a doublet (J = 7 Hz) at 3.71, and the four cyclopentadienyl hydrogens as two overlapping multiplets at

TABLE 1. Addition of lithium nucleophiles to fulvene **1**

Nucleophile	Product	Yield
MeLi	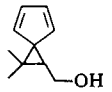 **9**	55%
*n*BuLi	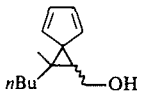 **10**	52% (~1:1)
*s*BuLi	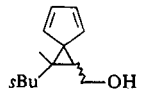 **11**	40% (~3:1)
VinylLi	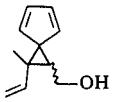 **12**	46%

6.30, all of which were consistent with the assigned structure. There was no evidence for any of the fused ring structures **5** or **6**. In all cases 10–15% of the unreacted fulvene was recovered even in the presence of excess nucleophile. Thus, based on reacted starting material, the yields are 10–15% higher than listed.

Lithium reagents were the most efficient although their use is influenced by their steric bulk. These results were consistent with related studies on Michael initiated ring closure of methyl 4-bromocrotonate (3), where it was also found that the better nucleophiles afforded the best yields of cyclopropanes. In contrast to the results for methyllithium, methyl Grignard and related reagents were unreactive towards both the fulvene and the epoxide. Apparently as a consequence of its size, *tert*-butyllithium also failed to add. In this case most of the fulvene-epoxide decomposed and the major product was the fulvene-alcohol **13** (35%). This unexpected product resulted, formally at least, from the net addition of hydrogen to **1**. The exact mechanism is uncertain, but it appears, as recommended by a referee, that the fulvene-alcohol arose via electron transfer from *tert*-butyllithium to epoxyfulvene **1** followed by protonation on work-up, rather than from deprotonation, rearrangement, and bond cleavage. Analogy for this electron transfer pathway (Scheme 3) is provided by the work of Ashby and Wiesemann (25) with *tert*-butylmagnesium chloride, where it was established that the Grignard addition to benzophenone involved a radical anion – radical cation pair which collapsed to addition products or dissociated to form *tert*-butyl radical and benzopinacol. Similarly, the synthesis of carbocyclic rings upon treatment of diiodoalkanes with *tert*-butyllithium (26) is assumed to proceed via initial metal–halogen interchange, a reaction for which the intermediacy of anion radicals, formed by electron transfer, is implicated (27).

Sodium dimethyl malonate did not add to the fulvene, but after prolonged reflux (3 h) a low yield (<10%) of alcohols was obtained. In contrast, 2-lithio-1,3-dithiane occupied an intermediate position, since it reacted at both the fulvene terminus to give **14** and the primary epoxide centre to generate the secondary alcohol **15** (Table 2). Some control over the relative

[1]Since acceptance of this manuscript Stone and Little (30) have reported similar observations in a detailed account of pyrrolidene induced fulvene preparation.

Can. J. Chem. Downloaded from www.nrcresearchpress.com by 210.87.254.5 on 09/06/12
For personal use only.

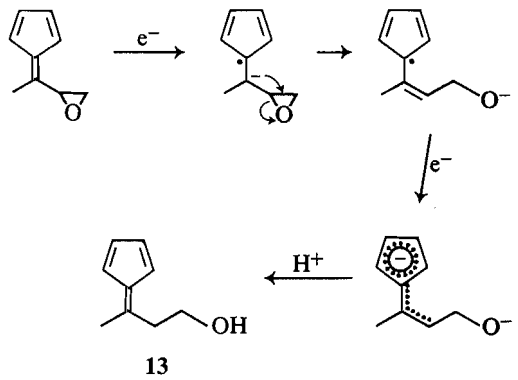

13

SCHEME 3

amounts of these two products was achieved by varying the temperature and the *cis* and *trans* cyclopropane isomers were separated by chromatography. These results are summarized in Table 2. The spiro compound **14** was the major product (31%) and the fulvene **15** the minor one (16%) when the reaction was conducted for 10 min at −60°C followed by 2 h at 22°C.

A number of other reagents, including the lithium salt of nitromethane and alkoxymethyllithiums (28, 29), which should serve to introduce a functionalized carbon atom, did not add in useful yields. In contrast, the potassium anion of nitromethane was generated with potassium hydride but addition to the fulvene occurred only in the presence of 18-crown-6 ether (Table 2). However, unlike the examples above, the reaction stopped at the cyclopentadiene stage to give **16** as a mixture of interconverting double bond isomers (~1:2). The 400-MHz ^{1}H nmr spectrum displayed four separate methyl singlets at δ 0.90, 0.96, 1.00, and 1.05 due to the individual isomers. Subsequent base treatment (KH, MeLi) of the isolated cyclopentadiene failed to produce any of the corresponding spiro compound **17**. This appears to be a consequence of the similarity in acidity of the two potential anionic centres, so that intramolecular proton exchange takes precedence over nucleophilic displacement. Treatment of **16** with two equivalents of methyllithium formed the dianion by proton abstraction from both the cyclopentadiene and the nitromethylene centres but instead of the spiro product the conjoint system **18** resulted. This material was a mixture of positional (~1:1) and stereochemical isomers. The methyl singlets were shifted downfield (δ 2.16−2.18) compared to the starting material, reflecting their rigid anisotropic environment. The cyclopropyl hydrogen adjacent to the nitro function appeared as a multiplet at 3.46, while the other cyclopropyl proton gave rise to a broadened triplet (J ~ 7 Hz) at 1.75. The structure of **18** was further established by conversion into the diacetate **19**. This involved reduction of the nitro group with lithium aluminum hydride (86%) followed by acetylation with acetic anhydride in pyridine.

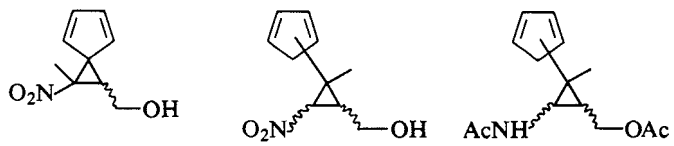

17 18 19

Work is in progress to prepare the fulvene-epoxide **1** in chiral form, both for use in the asymmetric total synthesis of sesquiterpenes and to provide insight into the diastereofacial selection of these reactions. In addition, these investigations are being extended to other fulvenes bearing electrophilic centres for the preparation of various spiro and fused rings.

TABLE 2. Addition of functionalized nucleophiles to fulvene **1**

Nucleophile	Product(s)	
DithianylLi	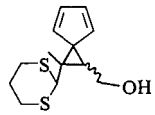 **14**	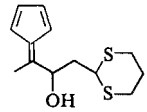 **15**
10 min, −60°C, 2.5 h, 22°C	31% (~1:2)	16%
5 h, −60°C	20% (~2:3)	28%
2.5 h, −60°C, 40 Torr, 22°C	25% (~2:3)	26%
KCH_2NO_2	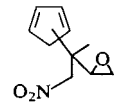 **16**	
	46% (~1:2)	

Experimental

Infrared spectra were recorded on a Perkin−Elmer 237B or 451 grating spectrophotometer, and were calibrated with the 2850 and 1601 cm^{-1} bands of polystyrene film. Ultraviolet spectra were recorded on a Perkin−Elmer 202 uv−visible spectrophotometer and were calibrated with the 279.4-nm band of a Holmium oxide filter. Proton magnetic resonance spectra were measured at 80 MHz with a Bruker WP80 spectrometer employing a chloroform lock or at 60 MHz with a Varian EM 360 spectrometer or at 400 MHz with a Bruker WH 400 spectrometer at the University of Alberta. Signal positions are reported in ppm downfield from tetramethylsilane (δ scale) as an internal standard; the number of protons, multiplicity, coupling constants, and proton assignments are indicated in parentheses. Mass spectra were determined on a V.G. Micromass 7070 HS instrument using an ionization energy of 70 eV.

Gas−liquid chromatographic analyses were conducted on a Hewlett Packard 402B gas chromatograph equipped with a column (3 m × 6 mm id) containing 1.5% OV-17 supported on Gas Chrome Q using helium as the carrier gas. Thin-layer chromatographic analyses were carried out on commercial precoated silica gel plates with a fluorescent indicator (Eastman Kodak silica gel 13181). Preparative thin-layer chromatography was conducted on 20 × 20 cm glass plates coated with silica gel $PF_{254+366}$ type 60 (E. Merck). Flash chromatography using BDH silica gel Kieselgel 60, 230−400 mesh, was employed for all column chromatography.

Petroleum ether refers to a fraction with boiling range 30−60°C. Anhydrous diethyl ether (ether), tetrahydrofuran (THF), dimethoxyethane (DME), and dioxane were obtained by distillation from lithium aluminum hydride or potassium/benzophenone. Absolute ethanol and methanol were dried by distillation from magnesium. Dry hexamethylphosphoramide (HMPA), dimethylformamide (DMF), dimethyl sulfoxide (DMSO), and diisopropylamine were prepared by distillation from calcium hydride. Solutions in organic solvents were dried over anhydrous magnesium sulphate and stripped of solvent with a Büchi rotary evaporator connected to a water aspirator. Unless otherwise indicated all reactions were conducted under an atmosphere of dry nitrogen.

1,2-Epoxy-3-butanone

3-Butenone (56 g, 0.8 mol, Aldrich) was dissolved in methanol (400 mL) containing 30% hydrogen peroxide (230 mL) and the solution cooled to 0°C with an external ice bath. Aqueous sodium hydroxide (2 *M*, 200 mL) was added dropwise to the stirred solution (caution: initially the reaction is very exothermic) maintaining the temperature

Can. J. Chem. Downloaded from www.nrcresearchpress.com by 210.87.254.5 on 09/06/12
For personal use only.

Can. J. Chem. Downloaded from www.nrcresearchpress.com by 210.87.254.5 on 09/06/12
For personal use only.

below 20°C. Stirring was continued for a further 2 h at 22°C after addition was complete, the reaction was extracted with dichloromethane (5×), the extracts dried, filtered, concentrated, and the product purified by distillation to give the epoxy-ketone, 42 g (60%), bp 45–46°C/12 Torr (1 Torr = 133.3 Pa) (the yield was 71% on a smaller scale); ir (film): 1715 (C=O), 1260, 865 (C—O) cm^{-1}; ^1H nmr (CCl_4) δ: 1.99 (s, 3H, CH_3), 2.92 (m, 2H, CH_2-O), 3.28 (dd, 1H, J = 1.5, 1 Hz, O=C-CH-O). *Exact Mass* calcd. for $C_4H_6O_2$: 86.0368; found: 86.0352.

6-Methyl-6-oxiranyl fulvene (1)

A stirred, methanol solution (12 mL) of cyclopentadiene (3.30 g, 0.05 mmol, Aldrich) and 1,2-epoxy-3-butanone (4.30 g, 0.05 mol) was cooled to 0°C and pyrrolidine (0.25 mL) added. The yellow colour due to the fulvene was immediately observed and stirring was continued for 2 h at 0°C, 2 h at 22°C, and the reaction poured into cold, dilute aqueous HCl and extracted with petroleum ether. The combined organic layers were washed with saturated aqueous sodium bicarbonate, followed by brine, dried, filtered and concentrated to give the fulvene (**1**), 5.8 g (86%). The fulvene was sufficiently pure for direct use; upon storage at −20°C it formed yellow crystals, and it was kept anhydrous by addition and evaporation of anhydrous benzene; ir (film): 3060 (H-C=), 1635 (s, C=C) cm^{-1}; ^1H nmr (CCl_4) δ: 1.91 (s, 3H, CH_3), 2.82 (m, 2H, CH_2-O), 3.90 (dd, 1H, J = 1.5, 1 Hz, CH-O), 6.35 (m, 4H, H-C=C). *Exact Mass* calcd. for $C_{10}H_{10}O$: 134.0732; found: 134.0708.

General procedure for the addition of lithium reagents to fulvene (1)

The appropriate lithium reagent (Aldrich or ROC/RIC, 1.2 equiv.) was added dropwise to a stirred tetrahydrofuran (20 mL) solution containing the fulvene (**1**) (2.01 g, 15 mmol) maintained at −78°C by an external solid CO_2/acetone bath. After stirring for 10 min at −78°C, it was allowed to warm to 0°C and saturated aqueous ammonium chloride was added. The mixture was extracted with ether, the combined ether extracts dried, filtered, concentrated, and the product purified by chromatography (25% ethyl ether/*n*-hexane) to give the spiro-alcohols **9**–**14**. In each case 10–15% of the fulvene **1** was also recovered.

2,2-Dimethyl-1-hydroxymethylspiro[2.4]hepta-4,6-diene (9): 1.24 g (55%); ir (film): 3350 (br, OH), 3090, 3060 (H-C=), 1650 (C=C) cm^{-1}; ^1H nmr (CCl_4) δ: 1.38 (s, 3H, CH_3), 1.40 (s, 3H, CH_3), 2.22 (t, 1H, J = 7 Hz, cyclopropyl H), 3.18 (br s, 1H, OH), 3.71 (d, 2H, J = 7 Hz, CH_2-O), 6.20 (m, 2H, H-C=), 6.36 (m, 2H, H-C=C). *Exact Mass* calcd. for $C_{10}H_{14}O$: 150.1044; found: 150.1025.

2-Methyl-2-(1-butyl)-1-hydroxymethylspiro[2.4]hepta-4,6-diene (10): 1.50 g (52%, ~1:1 isomer ratio); ir (film): 3330 (br, OH), 3085, 3060 (H-C=), 1630 (C=C) cm^{-1}; ^1H nmr (CCl_4) δ: 0.91 (br t, 3H, CH_2CH_3), 1.38 (s, 3H, CH_3), 2.21 (t, 1H, J = 7 Hz, cyclopropyl H), 3.22 (br s, 1H, OH), 3.73 (d, 2H, J = 7 Hz, CH_2-O), 6.18 (m, 2H, HC=C), 6.39 (m, 2H, H-C=C). *Exact Mass* calcd. for $C_{13}H_{20}O$: 192.1514; found: 192.1511.

2-Methyl-2-(1-methyl-1-propyl)-1-hydroxymethylspiro[2.4]hepta-4,6-diene (11): 1.15 g (40%), the major isomer (~3:1) was separated by tlc although the minor isomer could not be fully resolved; major, ir (film): 3325 (br, OH), 3070 (sh), 3055 (H-C=), 1645 (C=C) cm^{-1}; ^1H nmr (CCl_4) δ: 0.80 (d, 3H, J ~ 6 Hz, CH_3-CH), 1.05 (m, 3H, CH_2CH_3), 1.21 (s, 3H, CH_3), 2.23 (t, 1H, J = 7 Hz, cyclopropyl H), 2.78 (br s, 1H, OH), 3.71 (d, 2H, J = 7 Hz, CH_2-O), 6.20 (m, 2H, H-C=C), 6.40 (m, 2H, H-C=C). *Exact Mass* calcd. for $C_{13}H_{20}O$: 192.1514; found: 192.1516; minor, ir (film): 3350 (br, OH), 3080 (sh), 3055 (H-C=), 1650 (C=C) cm^{-1}; ^1H nmr (CCl_4) δ: 0.70–1.08 (m, 6H, overlapping CH_3's), 1.22 (s, 3H, CH_3), 2.20 (m, 1H, cyclopropyl H), 3.70 (m, 2H, CH_2-O), 6.17 (m, 2H, H-C=C), 6.39 (m, 2H, H-C=C). *Exact Mass* calcd. for $C_{13}H_{20}O$: 192.1514; found: 192.1516.

2-Methyl-2-vinyl-1-hydroxymethylspiro[2.4]hepta-4,6-diene (12): 1.12 g (46%); ir (film): 3340 (br, OH), 3060 (H-C=), 1665 (C=C) cm^{-1}; ^1H nmr (CCl_4) δ: 1.50 (s, 3H, CH_3), 2.53 (t, 1H, J = 7 Hz, cyclopropyl H), 3.10 (br s, 1H, OH), 3.80 (d, 2H, J = 7 Hz, CH_2-O), 4.93 (m, 1H, H-C=), 5.15 (m, 1H, H-C=), 5.7–6.1 (m, 1H, C=CH-C), 6.28 (m, 4H, cyclopentadiene H). *Exact Mass* calcd. for $C_{11}H_{14}O$: 162.1044; found: 162.1050.

6-Methyl-6-(1-ethyl-2-hydroxy)fulvene (13): 35%; ir (film): 3325 (br, OH), 3085, 3060 (H-C=), 1635 (s, C=C) cm^{-1}; ^1H nmr (CCl_4) δ: 1.12 (s, 3H, CH_3), 2.54 (t, 2H, J = 7 Hz, =C-CH_2-), 3.28 (br s, 1H, OH), 3.63 (t, 2H, J = 7 Hz, CH_2-O), 6.32 (s, 4H, H-C=C). *Exact Mass* calcd. for $C_9H_{12}O$: 136.0888; found: 136.0873.

Addition of 2-lithio-1,3-dithiane to fulvene 1

A solution of tetrahydrofuran (6 mL) containing 1,3-dithiane (0.96 g, 8 mmol, Aldrich) was cooled to −60°C with an external solid CO_2/methanol bath. *n*-Butyllithium (0.74 mL, 9.5 *M*, 7 mmol, Aldrich) was added dropwise, after 5 min the reagent was warmed to 0°C, recooled to −60°C, fulvene **1** (0.804 g, 6 mmol) in tetrahydrofuran (3 mL) added dropwise, and the reaction stirred for 10 min at −60°C followed by 2.5 h at 22°C. Aqueous saturated ammonium chloride (10 mL) was added, the mixture extracted with ether, the combined ether extracts dried, filtered, concentrated, and the product purified by chromatography (20% ethyl ether/*n*-hexane) to give **14**, 0.470 g (31%, ~1:2) and **15**, 0.240 g (16%); when the reaction was conducted for 5 h at −60°C the relative amounts changed, **14**, 0.310 g (20%, ~2:3) and **15**, 0.430 g (28%); when the reaction was conducted for 2.5 h at −60°C followed by 40 min at 22°C the products were **14**, minor isomer 0.140 g (10%), major isomer 0.230 g (15%) and **15**, 0.390 g (26%).

2-Methyl-2-(2-(1,3-dithianyl)-1-hydroxymethylspiro[2.4]hepta-4,6-diene (14): major, ir (film): 3380 (br, OH), 3070 (sh), 3055 (H-C=), 1635 (C=C), cm^{-1}; ^1H nmr (CCl_4) δ: 1.45 (s, 3H, CH_3), 1.91 (m, 2H, ring CH_2), 2.28 (t, 1H, J = 7 Hz, cyclopropyl H), 2.73 (m, 4H, CH_2-S), 3.91 (s, 1H, S-CH-S), 6.14 (m, 2H, H-C=C), 6.39 (m, 2H, H-C=C). *Exact Mass* calcd. for $C_{13}H_{18}OS_2$: 254.0799; found: 254.0808; minor, ir (film): 3420 (br, OH), 3055 (H-C=), 1635 (C=C) cm^{-1}; ^1H nmr (CCl_4) δ: 1.53 (s, 3H, CH_3), 1.97 (m, 2H, ring CH_2), 2.41 (m, 1H, cyclopropyl H), 2.73 (m, 4H, CH_2-S), 3.76 (m, 2H, CH_2-O), 4.36 (s, 1H, S—CH—S), 6.14 (m, 2H, H-C=C), 6.44 (m, 2H, H-C=C). *Exact Mass* calcd. for $C_{13}H_{18}OS_2$: 254.0799; found: 254.0813.

6-Methyl-6-(1-propyl-1-hydroxy-3-(2-(1,3-dithianyl)fulvene (15): ir (film): 3415 (OH), 3090, 3060 (H-C=), 1640 (s, C=C), cm^{-1}; ^1H nmr (CCl_4) δ: 2.08 (m, 4H, CH_2), 2.18 (s, 3H, CH_3), 2.87 (m, 4H, CH_2-S), 4.15 (dd, 1H, J = 6, 8 Hz, S-CH-S), 5.23 (m, 1H, CH-O), 6.52 (s, 4H, H-C=C). *Exact Mass* calcd. for $C_{13}H_{18}OS_2$: 254.0799; found: 254.0800.

Addition of potassium nitromethane to fulvene 1: preparation of (1-nitro-2-oxiranylpropyl)cyclopentadiene (16)

Potassium hydride (7.43 g, 65 mmol, 35% suspension in oil, Aldrich) after washing with dry hexane, was suspended in tetrahydrofuran (100 mL) and nitromethane (6.5 mL, 120 mmol) added to the stirred mixture. Stirring was continued at 22°C until all the potassium hydride has dissolved. The solution was cooled to 0°C, 18-crown-6 ether (0.2 g, Aldrich) added, followed by the fulvene **1** (8.04 g, 60 mmol) in tetrahydrofuran (20 mL) which was added dropwise. After 1 h at 0°C saturated aqueous ammonium chloride (30 mL) was slowly added, the mixture was extracted with ether, the combined ether extracts were dried, filtered, concentrated, and the product purified by chromatography (25%–50% ethyl ether/*n*-hexane) to give recovered fulvene (1 g) plus **16**, 5.4 g (46%), ~1:2 isomer ratio; ir (film): 3040 (H-C=), 1535 (NO_2), 1565 (NO_2) cm^{-1}; ^1H nmr (CCl_4) δ: 1.16, 1.28 (s, 3H, CH_3), 2.59 (m, 2H, CH_2-O), 3.01 (m, 2H, C=C-CH_2-C=C), 3.11 (m, 1H, CH-O), 4.54 (m, 2H, CH_2NO_2), 6.15–6.65 (m, 3H, H-C=C); (400 MHz, $CDCl_3$) δ: 0.90, 0.96, 1.00, 1.05 (s, 3H, CH_3's), 2.00 (overlapping m, 2H, CH_2-O), 2.58, 2.70 (m, 2H, C=C-CH_2-C=C), 2.70, 2.89 (m, 1H, CH-O), 3.80–4.09 (overlapping m, 2H, CH_2NO_2), 5.83, 6.03, 6.19, 6.40 (m, 3H, H-C=C). *Exact Mass* calcd. for $C_{10}H_{13}NO_3$: 195.0895; found: 195.0880.

*Treatment of cyclopentadiene-epoxide **16** with methyllithium: preparation of (1-methyl-2-nitro-3-hydroxymethylcyclopropyl)-cyclopentadiene (**18**)*

The cyclopentadiene-epoxide **16** (1.95 g, 10 mmol) was dissolved in THF (5 mL) and added dropwise to a stirred THF (30 mL) solution containing methyllithium (14 mL, 22 mmol, 1.56 *M*, Aldrich) maintained at −78°C with an external solid CO_2/acetone bath. Stirring was continued for a further 10 min after addition was complete, the reaction was allowed to warm to 22°C, and saturated aqueous ammonium chloride added slowly. The mixture was extracted with ether, the combined ether extracts washed with brine, dried, filtered, concentrated, and the product purified by chromatography (50% ether/*n*-hexane) to give the cyclopropyl alcohol **18**, 1.37 g, (70%); ir (film): 3300−3500 (OH), 3050 (H-C=), 1630 (C=C), 1540 (sh), 1515 (NO_2), 1365 (sh), 1335 (NO_2) cm^{-1}; ^1H nmr (360 MHz, $CDCl_3$) δ: 1.75 (br t, 1H, $J \sim 7$ Hz, cyclopropyl H), 2.16, 2.17, 2.18 (overlapping s, 3H, CH_3), 2.88, 3.04 (m, 2H, C=C-CH_2-C=C), 3.46 (m, 1H, cyclopropyl H-C-NO_2), 3.94 (m, 2H, CH_2-O), 6.22, 6.37, 6.46 (m, 3H, H-C=), 7.08 (m, 1H, OH).

*(1-Methyl-2-amino(*N*-acetoxy)-3-acetoxymethylcyclopropyl)-cyclopentadiene (**19**)*

The nitro compound **18** (2.34 g, 12 mmol) dissolved in ether (20 mL) was added dropwise to a stirred suspension of lithium aluminum hydride (1.14 g, 30 mmol) in ether (100 mL) maintained at 0°C by an external ice bath. Stirring was continued at 0°C for 2 h after addition was complete and water (2 mL) was added carefully to the reaction mixture, followed by aqueous 20% sodium-potassium tartrate (80 mL). The mixture was extracted with ether, the combined ether extracts washed with brine, dried, filtered, and concentrated to give the amino-alcohol, 1.7 g (86%). This material was dissolved in pyridine (15 mL), the solution cooled to 0°C with an external ice bath, and acetic anhydride (6 mL) added. The reaction was stirred at 0°C overnight, poured into 3 *N* HCl at 0°C, extracted with ether, the combined ether extracts dried, filtered, concentrated, and the product purified by chromatography (100% ethyl ether to 5% 2-propanol/ether) to give **19**, 0.55 g (18%); ir (film): 3275 (NH), 3050 (H-C=), 1735 (C=O), 1650 (C=C) cm^{-1}; ^1H nmr (CCl_4) δ: 0.96 (m, 2H, cyclopropyl H), 1.95 (s, 3H, CH_3), 2.00 (s, 6H, CH_3C=O), 2.98 (m, 2H, C=C-CH_2-C=C), 4.30 (m, 2H, CH_2-OAc), 6.18−6.53 (m, 3H, H-C=), 7.79 (br, 1H, NH).

Acknowledgements

We are grateful to Memorial University of Newfoundland and to the Natural Sciences and Engineering Research Council of Canada for financial support of this research; B. Gregory for high resolution mass spectra; H. J. Liu (University of Alberta) for 400 MHz ^1H nmr spectra; C. R. Jablonski for a 360 MHz ^1H nmr spectrum; E. Kozma and R. Bukownik for preliminary experiments; S. J. Alward for fruitful discussions; and a referee for constructive comments.

1. R. D. LITTLE and J. R. DAWSON. Tetrahedron Lett. **21**, 2609 (1980).
2. G. H. POSNER, J. P. MALLAMO, and A. Y. BLACK. Tetrahedron, **37**, 3921 (1981).
3. P. PREMPREE, S. RADVIROONGIT, and Y. THEBTARANONTH. J. Org. Chem. **48**, 3553 (1983).
4. S. DANISHEFSKY, S. CHACKALAMANNIL, M. SILVESTRI, and J. SPRINGER. J. Org. Chem. **48**, 3615 (1983).
5. S. DANISHEFSKY, P. HARRISON, M. SILVESTRI, and B. SEGMULLER. J. Org. Chem. **49**, 1319 (1984).
6. S. K. ATTAH-POKU, G. GALLACHER, A. S. NG, L. E. B. TAYLOR, S. J. ALWARD, and A. G. FALLIS. Tetrahedron Lett. **24**, 677 (1983); G. GALLACHER, A. S. NG, S. K. ATTAH-POKU, K. ANTCZAK, S. J. ALWARD, J. F. KINGSTON, and A. G. FALLIS. Can. J. Chem. **62**, 1709 (1984).
7. S. K. ATTAH-POKU, S. J. ALWARD, and A. G. FALLIS. Tetrahedron Lett. **24**, 681 (1983); S. K. ATTAH-POKU, K. ANTCZAK, S. J. ALWARD, and A. G. FALLIS. Can. J. Chem. **62**, 1717 (1984).
8. P. YATES. Adv. Alicyclic Chem. **2**, 59 (1968).
9. K. ZIEGLER, H.-G. GELLERT, H. MARTIN, K. NAGEL, and J. SCHNEIDER. Ann. Chem. **589**, 91 (1954).
10. K. HAFNER. Ann. Chem. **606**, 79 (1957).
11. D. D. STERNBACH, J. W. HUGHES, and D. F. BURDI. J. Org. Chem. **49**, 201 (1984).
12. W. F. LITTLE and R. C. KOESTLER. J. Org. Chem. **26**, 3247 (1961).
13. G. BÜCHI, D. BERTNET, R. DECORZANT, A. GRIEDER, and A. HAUSER. J. Org. Chem. **41**, 3209 (1976).
14. E. J. COREY, C. S. SHINER, R. P. VOLANTE, and C. R. CYR. Tetrahedron Lett. 1161 (1975).
15. E. AYANOGLU, T. GEBREYESUS, C. M. BEECHAN, C. DJERASSI, and M. KAISIN. Tetrahedron Lett. 1671 (1978).
16. H. SETO and H. YONEHARA. J. Antibiot. **33**, 92 (1980).
17. W. FREIESLEBEN. Angew. Chem. **75**, 576 (1963).
18. J. E. BALDWIN. J. Chem. Soc. Chem. Commun. 734 (1976).
19. G. STORK and J. F. COHEN. J. Am. Chem. Soc. **96**, 5270 (1974).
20. K. ANTCZAK, J. F. KINGSTON, S. J. ALWARD, and A. G. FALLIS. Can. J. Chem. **62**, 829 (1984).
21. P. DESLONGCHAMPS. Stereoelectronic effects in organic chemistry. Pergamon Press, Oxford. 1983. pp. 166−172.
22. C. F. WILCOX, JR. and G. C. WHITNEY. J. Org. Chem. **32**, 2933 (1967).
23. R. D. MILLER, M. SCHNEIDER, and D. L. DOLCE. J. Am. Chem. Soc. **95**, 8468 (1973).
24. A. DE.MEIJERE and L. U. MEYER. Chem. Ber. **110**, 2561 (1977).
25. E. C. ASHBY and T. L. WIESEMANN. J. Am. Chem. Soc. **100**, 189 (1978).
26. W. F. BAILEY and R. P. GAGNIER. Tetrahedron Lett. **23**, 5123 (1982).
27. J. F. GARST, R. D. ROBERTS, and J. A. PACIFICI. J. Am. Chem. Soc. **99**, 3528 (1977).
28. E. J. COREY and T. M. ECKRICH. Tetrahedron Lett. **24**, 3163 (1983).
29. E. J. COREY and T. M. ECKRICH. Tetrahedron Lett. **24**, 3165 (1983).
30. K. J. STONE and R. D. LITTLE. J. Org. Chem. **49**, 1849 (1984).

Can. J. Chem. Downloaded from www.nrcresearchpress.com by 210.87.254.5 on 09/06/12
For personal use only.

Reactive intermediates in the photochemistry of 4-diazo-2-pyrazolin-5-ones

PESI UMRIGAR AND GARY W. GRIFFIN
Department of Chemistry, University of New Orleans, New Orleans, LA 70122, U.S.A.

SEYHAN N. EGE AND ALAN D. ADAMS
Department of Chemistry, University of Michigan, Ann Arbor, MI 48109, U.S.A.

AND

PARITOSH K. DAS
Radiation Laboratories, University of Notre Dame, Notre Dame, IN 46556, U.S.A.

Received March 12, 1984

This paper is dedicated to Professor Peter Yates on the occasion of his 60th birthday

PESI UMRIGAR, GARY W. GRIFFIN, SEYHAN N. EGE, ALAN D. ADAMS, and PARITOSH K. DAS. Can. J. Chem. **62**, 2456 (1984).

Photolysis of 4-diazo-2-pyrazolin-5-ones in methanol gives a mixture of stereoisomeric methyl 3-aryl-(or alkyl-)azo-2-alkenoates. A study of the absorption spectra of the species generated upon steady-state photolyses in glasses at 77 K, in solution at 296 K, and by laser and lamp flash photolysis experiments suggests that a long-lived heterocyclic intermediate that we formulate as a carbene or its valence isomer, as well as a ketene generated by ring opening, are precursors to the esters.

PESI UMRIGAR, GARY W. GRIFFIN, SEYHAN N. EGE, ALAN D. ADAMS et PARITOSH K. DAS. Can. J. Chem. **62**, 2456 (1984).

La photolyse des diazo-4 pyrazoline-2 ones-5 dans le méthanol conduit à un mélange des stéréoisomères des aryl-3 (ou alkyl-3) azo-2 alcènoates de méthyle. Sur la base d'une étude des spectres d'absorption des espèces générées dans les états stationnaires de photolyses réalisées dans des verres à 77 K et en solution à 296 K ainsi que ceux des espèces générées lors d'expériences de photolyse éclair provoquées par des lampes ou des laser, on suggère que les précurseurs des esters sont d'une part un intermédiaire hétérocyclique à longue vie que l'on formule sous forme de carbène ou de son isomère de valence et d'autre part un cétène généré par son ouverture de cycle.

[Traduit par le journal]

Can. J. Chem. Downloaded from www.nrcresearchpress.com by 210.87.254.6 on 09/06/12
For personal use only.

Introduction

Diazo compounds are classical thermal and photochemical precursors of carbenes (1). We became interested in 4-diazo-2-pyrazolin-5-ones (**1**) as possible sources of heterocyclic carbenes **2** (Scheme 1) when we failed to find products derived from such carbenes during experiments on the photochemical fragmentation of 1-oxa-5,6-diazaspiro[2.4]hept-6-ene-4-ones, pyrazolinone spirooxiranes (**5***b*), even when aryl aldehydes **7** were isolated in high yields (2) (Scheme 2). The intervention of another reactive intermediate, carbonyl ylides **6**, in the photochemical reactions of oxiranes **5***b* complicates the search for carbenes **2**, hence we attempted to create **2** in an alternative and more conventional manner by photolysis of diazopyrazolinones **1**, prepared by diazo transfer reactions (3) from the corresponding pyrazolinones (Table 1).

Results and discussion

No carbene addition products, as have been observed upon photolysis of 1-methyl-3-diazooxindole (4) in alkenes, are found when diazopyrazolinone **1***a* is photolyzed in 2,3-dimethyl-2-butene or cyclohexene. The mixture of products is not separable by chromatography, an outcome that was not surprising in light of similar mixtures obtained when oxiranes **5***b* are photolyzed in the presence of alkenes (2). Nor do we have evidence of cycloaddition of the diazopyrazolinones to the alkenes as has been observed in a thermal reaction of **1***a* with an electron-deficient alkene (5).

Photolysis of **1***a* in acetone, attempted to see whether carbene **2***a* may have been intercepted by acetone (6) to give oxirane **5***a* (isolated as the chief photoproduct when 5-methyl-2-phenyl-3-pyrazolidinone is irradiated in acetone (7)), also gave no isolable products and no chromatographic evidence of the formation of **5***a*.

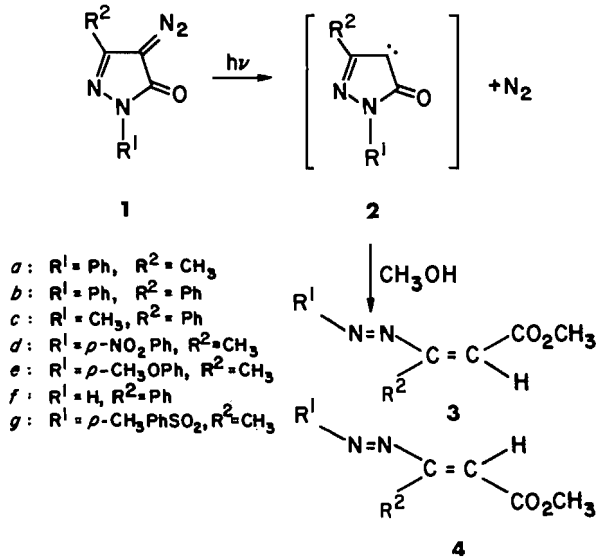

SCHEME 1. Esters isolated from **1***a*, **1***b*, **1***c*, and **1***e*.

Diazopyrazolinone **1***a* upon photolysis in methanol gives chiefly methyl (*Z*)-3-phenylazo-2-butenoate (**3***a*), which, upon standing in deuteriochloroform, is converted over a week to the thermodynamically more stable (*E*)-isomer, **4***a*. A similar acid-catalyzed isomerization of (*Z*)-3-phenylazo-2-butenenitrile to the (*E*)-isomer has been reported (8). Experimentally, we determined that the isomerization did not occur thermally in the photolysis mixture and that the two stereoisomers were not photochemically interconvertible. Thus it is certain that the photochemical reaction leads predominantly to the thermodynamically less stable isomer.

The assignment of the phenylazo ester structures **3***a* and **4***a*

TABLE 1. Physical properties of diazopyrazolinones **1**

Diazo compound[a]	Method, yield (%)	Melting point (°C), solvent	Spectral data[b]	Calculated (%) [found (%)]
1*a*	A, 76	94–96 Ethanol/water (1:1)	*m/e* 200	Ref. 20
1*b*	A, 73	109.5–110[c] 95% ethanol	*m/e* 262 δ 7.27–7.90 (m)	$C_{15}H_{10}N_4O$ C 68.68, H 3.85, N 21.37 [C 68.57, H 3.81, N 21.42]
1*c*	A, 34	76.5–77.5 95% ethanol	*m/e* 200 δ 3.90 (s, 3H), 7.39–7.92 (m, 5H)	$C_{10}H_8N_4O$ C 59.98, H 4.04, N 27.99 [C 59.91, H 4.00, N 27.88]
1*d*	B, 21	180–185 Carbon tetrachloride	*m/e* 245 δ 2.42 (s, 3H), 7.34–8.26 (m, 4H)	$C_{10}H_7N_5O_3$ C 48.98, H 2.88, N 28.57 [C 48.69, H 2.83, N 28.66]
1*e*	C, 64	117–118 Ethanol	λ_{max} ($CHCl_3$): 2100, 1675; δ 2.3 (s, 3H), 3.7 (s, 3H), 6.7, 7.6 (m, 4H)	$C_{11}H_{10}N_4O_2$ C 57.38, H 4.38, N 24.34 [C 57.43, H 4.49, N 24.22]
1*f*	A, 61	180–181 Ethanol	*m/e* 186	Ref. 10
1*g*	C, 71	168–170 95% ethanol	*m/e* 278 δ 2.30 (s, 3H), 2.43 (s, 3H), 7.29–7.98 (m, 4H)	$C_{11}H_{10}N_4O_3S$ C 47.47, H 3.63, N 20.14, S 11.52 [C 47,28, H 2.61, N 20.22, S 11.39]

[a] References for the pyrazolinones used in these syntheses are: for **1***a*, 30; **1***b*, 31; **1***c*, 32; **1***d*, 33; **1***e*, 34; **1***f*, 32; **1***g*, 35.
[b] ^1H nmr ($CDCl_3$) relative to tetramethylsilane.
[c] Literature (36) mp 103–105°C for **1***b* prepared by another route.

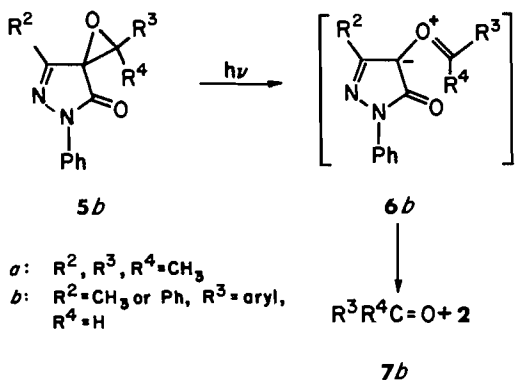

SCHEME 2

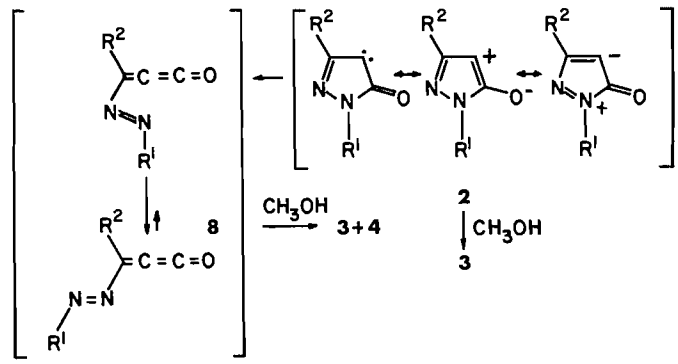

SCHEME 3

to the photoproducts of **1***a* was based on the formation of the known (9) ethyl (*E*)-3-phenylazo-2-butenoate when **1***a* was photolyzed in ethanol. In both sets of stereoisomeric esters, as well as in the case of the stereoisomeric phenylazobutenenitriles (8), the methyl group on the carbon–carbon double bond has the smaller chemical shift: δ 2.04 for **3***a*, δ 2.05 for the (*Z*) ethyl ester, δ 2.13 for the nitrile, as compared to δ 2.41 for **4***a*, δ 2.40 for the (*E*) ethyl ester, and δ 2.28 for the (*E*)-nitrile. Similarly for both sets of esters, the vinylic hydrogen in the (*Z*)-ester is upfield, δ 6.20 for **3***a* and δ 6.24 for the ethyl ester compared to δ 6.77 for **4***a* and the (*E*)-isomer of the ethyl ester. These values were also used to assign stereochemistry to the azoesters obtained as photoproducts from other diazopyrazolinones **1**. Along with the esters **3***a* and **4***a*, polymeric materials were separated from the photolysis mixture.

Similar mixtures of (*Z*)- and (*E*)-arylazoalkenoic acid esters **3** and **4**, as well as polymeric material, have been obtained from **1***b* and **1***e*, and an unstable yellow oil having the ^1H nmr spectrum expected of methyl (*Z*)-3-methylazo-3-phenylpropenoate (**3***c*) was obtained when **1***c* was photolyzed in methanol. The two diazopyrazolinones bearing electron-withdrawing groups on the ring nitrogen atom, **1***d* with a *p*-nitrophenyl group and **1***g* with a tosyl group, do not give such esters as photoproducts, and **1***f*, which is unsubstituted on the nitrogen atom, gives only polymeric material. These findings are summarized in Scheme 1. The photochemical reactivity of **1***f* is in direct contrast to its thermal stability (10). It withstands refluxing xylene, but heating of **1***f* in benzyl alcohol to reflux gives 4-benzyl-3-phenyl-2-pyrazolin-5-one, an unusual reduction reaction (10).

Two mechanisms account for the formation of open-chain azoesters **3** and **4**, as depicted in Scheme 3. The electronic charge distribution in **2** may be such that this transient has zwitterionic character. Concerted or non-concerted nucleophilic attack and protonation of **2** in methanol results in the formation of the (*Z*)-esters **3**, but fails to account for the presence of the (*E*)-isomers **4** unless we assume tht rotation of the carbonyl function about the carbon-3 – carbon-4 axis is possible in the transition state.

In the alternate mechanism shown in Scheme 3, carbene **2**

Can. J. Chem. Downloaded from www.nrcresearchpress.com by 210.87.254.6 on 09/06/12
For personal use only.

undergoes ring opening to ketene **8**, which subsequently is intercepted by methanol to give **3** and **4**. The stereochemical outcome of the photolyses of the diazopyrazolinones described above is difficult to rationalize on the basis of a ring-opened ketene intermediate, which should give approximately equal quantities of **3** and **4**, if not indeed an excess of the thermodynamically more stable **4**. The formation of the (*Z*)-ester **3***c* exclusively from the photolysis of diazopyrazolinone **1***c*, especially, points to a direct attack of the nucleophilic solvent on carbene **2**. In this case, the presence of the electron-donating methyl group on the nitrogen atom of the pyrazolinone ring facilitates the development of positive charge on the nitrogen, precluding ring opening of the carbene to ketene.

It might be argued that if an electron-donating substituent at the 1-position of the pyrazolinone ring system provides additional driving force for the formation of the azoesters, then the reverse should also hold true; that is, an electron-withdrawing substituent at this position should inhibit the conversion of diazopyrazolinones **1** to azoesters by this mechanism. In fact, because this mechanism appears to be the more important one, even in the case of **1***a* and **1***b*, a powerful electron-withdrawing substituent at the 1-position of the ring may destabilize the transition state for the ring opening of the carbene to such an extent that the reaction path is altered. Indeed, the two diazopyrazolinones **1***d* and **1***g* that have substitution on the ring nitrogen atom that would destabilize one zwitterionic form of **2** do not give esters as products upon photolysis.

Ketenes have been proposed as reactive intermediates in the ring contraction reactions of a number of heterocyclic α-diazoketones. Among these are 3-diazo-4-oxo-3,4-dihydroquinolines, which give derivatives of 3-indolecarboxylic acids (11, 12) as well as 3-diazo-4-oxo-3,4-dihydropyridine (12) and diazopyridazine derivatives (13). The ring contraction reaction is also seen for analogs of 3-diazo-4-oxoindanes in which the methylene group of the five-membered ring is replaced by sulfur or oxygen, but not in 3-diazooxoindoles (4, 14). To our knowledge, however, ring opening of heterocyclic carbenes has been reported only for thermolysis reactions of 3-diazoindazoles (15) and of 3-diazopyrazole (16), in which products are postulated to arise from such rearrangement of a carbene to a cyanonitrene. Photolysis of these compounds gives primarily carbene insertion products (16, 17), though the carbenes derived from diazopyrazoles are reported to be electrophilic enough to react with the oxygen atom of ethers giving products interpreted to arise from the ionic cleavage of the resulting oxonium ions (16).

Carbenes usually react with alcohols to give ethers; the reactivity of an alcohol with a carbene in this manner depends upon the acidity of the alcohol and upon the electronic character of the carbene (18). Photolysis of diazoimidazoles in alcohols, however, gives, along with ethers, significant amounts of products derived from insertion into carbon–hydrogen bonds (19), a reaction seen previously only at low temperatures in alcohol matrices (20). The reaction that we see differs from both of these modes of reactivity.

In contrast to the reactions we observed, photolyses of 3-carbethoxy-4-diazo-1-phenyl-2-pyrazolin-5-one in dioxane, ethanol, benzene, or tetrahydrofuran are reported (21) to give a variety of decomposition products, the only isolable one being a compound derived from insertion of the terminal nitrogen atom of the diazo group in a carbon–hydrogen bond in tetrahydrofuran. Thus 4-diazo-2-pyrazolin-5-ones appear to have a range of thermal (5, 10) and photochemical (21) reactions that depends heavily on the substituents on the pyrazolinone ring.

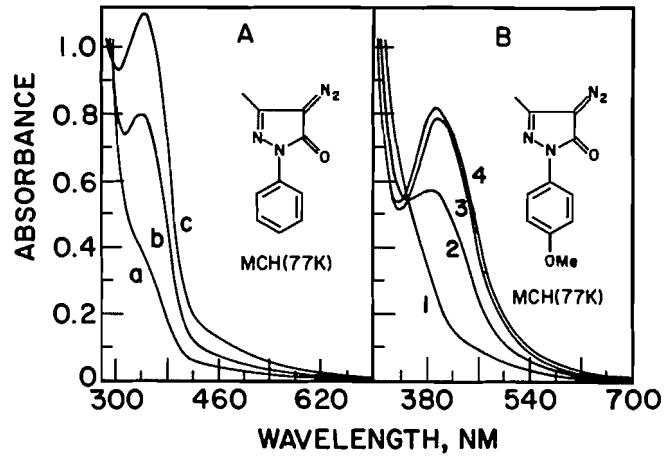

FIG. 1. Absorption spectral changes from steady-state photolysis of **1***a* (A) and **1***e* (B) at 366 nm in methylcyclohexane glass at 77 K. Irradiation times are: 0, 5, and 15 min for the spectra marked a, b, and c, respectively in Fig. A and 0, 2.5, 5, and 7.5 minutes for the spectra marked 1, 2, 3, and 4, respectively, in Fig. B.

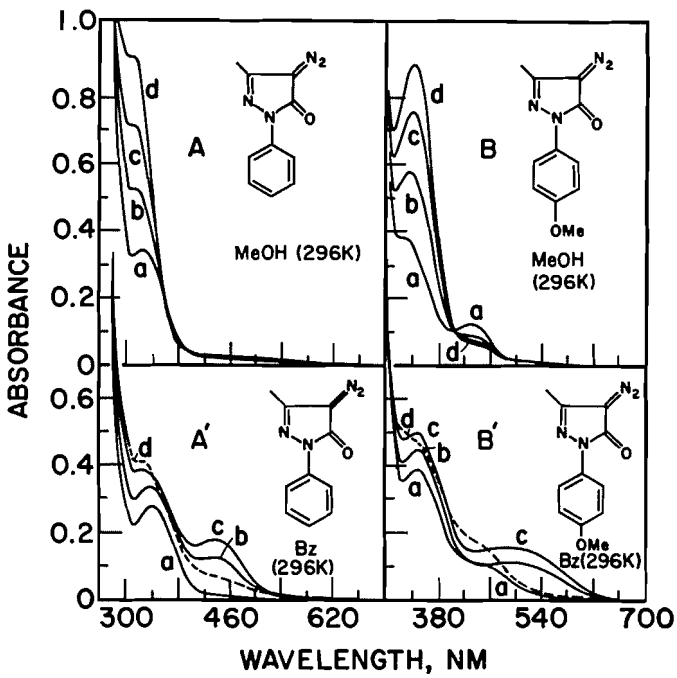

FIG. 2. Absorption spectral changes from steady-state photolysis (366 nm) of **1***a* and **1***e* at 296 K. **1***a* (A) in methanol; irradiation times: 0, 1, 2, and 3 min for a, b, c, and d, respectively. **1***e* (B) in methanol; irradiation times: 0, 1, 2, and 3 min, respectively. **1***a* in benzene (A′); irradiation times: 0, 1, and 3 min for a, b, and c, respectively; the spectrum d (dotted line) was obtained 25 min after adding methanol to the irradiated solution (to make 0.6 *M* in MeOH). **1***e* in benzene (B′); irradiation times: 0, 2, and 3 min for a, b, and c, respectively; the spectrum d (dotted line) was recorded at 10 min, following the addition of methanol to the irradiated solution (to make 0.6 *M* in MeOH).

The nature of the intermediates formed from diazopyrazolinones **1** was further investigated by studying the absorption spectra of the species generated upon steady-state photolyses in glasses at 77 K (Fig. 1), in solution at 296 K (Fig. 2), and by laser (Figs. 3 and 4) and conventional lamp flash

Can. J. Chem. Downloaded from www.nrcresearchpress.com by 210.87.254.6 on 09/06/12
For personal use only.

TABLE 2. Absorption maxima (λ_{max}, nm) observed upon photolyses of diazopyrazolinones under different conditions

Diazopyrazolinone	Steady-state irradiations		Flash photolyses	
	77 K (solvent glasses)[a]	296 K (solvent)[a]	Laser (solvent, lifetime)[a,b]	Lamp (solvent, lifetime)[a]
1*a*	342 (MCH) 350 (MTHF)	314,460 (MeOH) 327,442 (ϕH) 322,435 (MCH)	345 (MeOH, >150 μs) 345 (CH, >150 μs) 350 (ϕH, >150 μs)	
1*c*			315–320 (ϕH, >150 μs) 315–320 (MeOH, 90 μs) 315–320 (*i*-PrOH, >1 ms)	
1*e*	394 (MCH)	340,520 (MeOH) 350,495 (ϕH)	400 (MeOH, >150 μs) 400 (CH, >150 μs) 405 (ϕH, >150 μs)	400 (CH, >100 ms) 400,450 (MeOH, 2 ms)[c]
1*f*			305–310 (ϕH, >150 μs) 305–310 (MeOH, 18 μs) 305–310 (EtOH, 75 μs) 305–310 (*i*-PrOH, 700 μs)	
1*g*			No transient absorption in ϕH, MeOH	

[a] MCH = methylcyclohexane; MTHF = 2-methyltetrahydrofuran; CH = cyclohexane.
[b] The lifetimes of the transients formed here are not affected by cyclohexene and dimethyl acetylenedicarboxylate (for **1***c*, **1***e*, and **1***f*).
[c] Absorption at 340 nm, corresponding to the photoproduct seen upon steady-state irradiation in MeOH, develops.

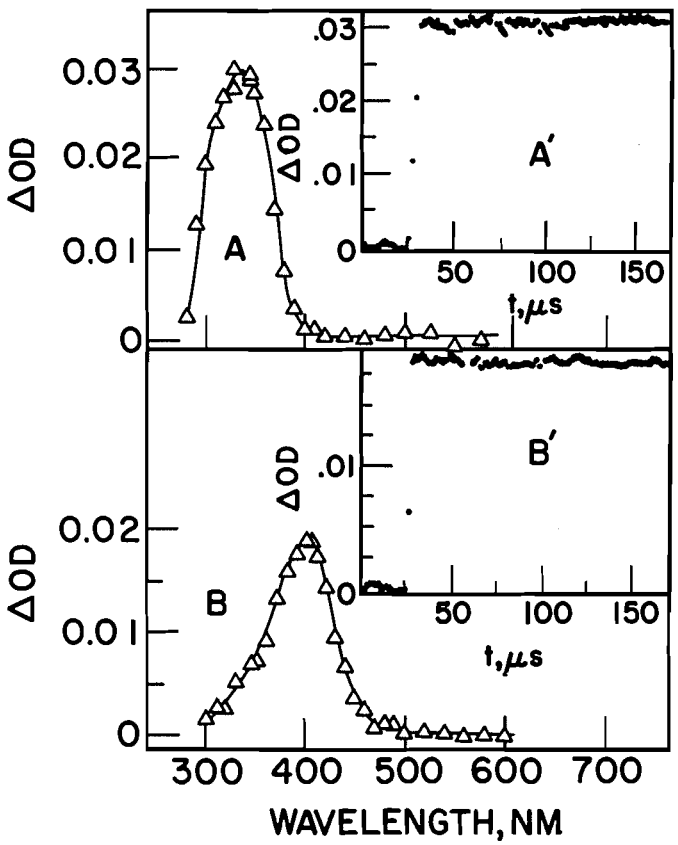

FIG. 3. Transient absorption spectra observed at 10 μs following 337.1-nm laser flash photolysis of **1***a* (A) and **1***e* (B) in degassed methanol. Insets: typical experimental traces in degassed methanol for **1***a* at 350 nm (A′) and **1***e* at 400 nm (B′).

photolysis experiments. The most significant findings of these experiments are summarized in Table 2. Two findings correlate directly with the preparative scale steady-state experiments described above. First, diazopyrazolinone **1***g*, which gives no isolable product, also exhibits no absorption attributable to a transient upon laser flash photolysis. Second, the absorption spectrum developed upon steady-state irradiation of **1***a* in methanol at room temperature (Fig. 2A, λ_{max} 314 nm) corresponds closely with those of the product azoesters (λ_{max} 308 nm for **3***a*; 311 nm for **4***a*). This second finding is significant because two other species with different transient absorption spectra have also been observed for diazopyrazolinones **1***a* and **1***e*. In methylcyclohexane glass at 77 K, steady-state irradiation of **1***a* and **1***e* at 366 nm leads to the formation of photoproducts with absorption maxima at 342 and 394 nm and isobestic points at 298 and 345 nm, respectively (Figs. 1A and B). When the glass from the photolysis of **1***a* is allowed to warm up, bands at 322 and 435 nm develop. This same spectrum is obtained when **1***a* is subjected to steady-state irradiation at 296 K in methylcyclohexane.

The species observed in matrix have spectra similar to those observed upon laser flash photolysis of **1***a* and **1***e* in methanol, benzene, and cyclohexane. Diazopyrazolinone **1***a* in methanol, for example, gives a photoproduct with λ_{max} 345 nm that does not decay over 100–150 μs. A similar intermediate, λ_{max} 400 nm, is observed for **1***e*. These experimental results, including insets A′ and B′ showing the persistence over time of the species formed, are shown in Figs. 3A and 3B. Observation of transient phenomena within ~20 ns following the laser pulse shows that the products are formed within that time period. Experiments with **1***e* in methanol at temperatures as low as −100°C indicate no formation or decay process that can be attributed to a precursor of the long-lived photoproduct observed at 400 nm.

Conventional flash photolysis of diazopyrazolinone **1***e* allows us to observe the intermediate over longer periods of time. The same transient with λ_{max} 400 nm is observed in cyclohexane and does not decay over 100 ms. In methanol, however, we observe that the intermediate has a lifetime of 2 ms and that decay is coincident withe the development of a band at 340 nm, corresponding to the absorption maximum seen when **1***e* is subjected to steady-state irradiation in methanol at 296 K (Fig. 2B).

In contrast to the results obtained at 77 K and upon flash photolysis, diazo compound **1***a* gives rise to another species with significant absorption at 327 and 442 nm when subjected

Can. J. Chem. Downloaded from www.nrcresearchpress.com by 210.87.254.6 on 09/06/12
For personal use only.

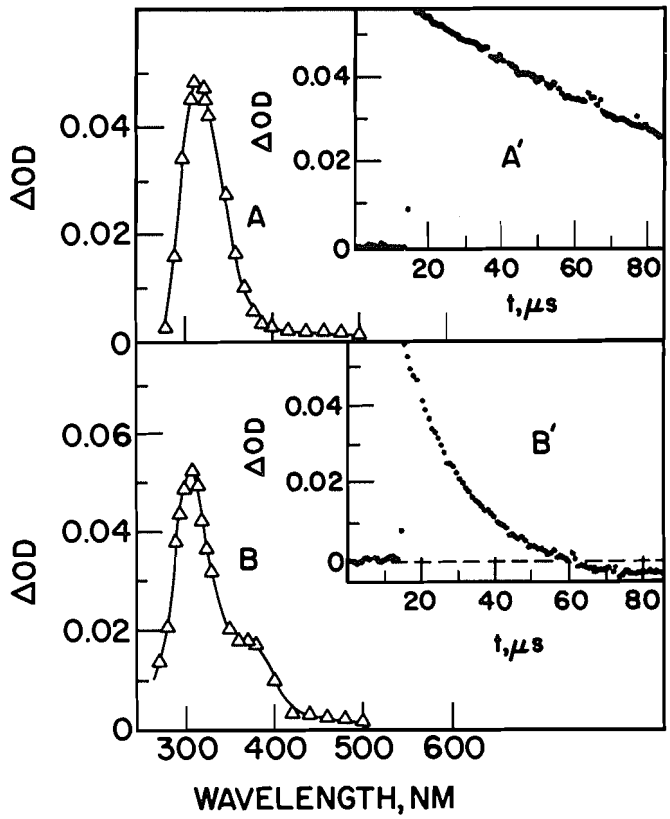

FIG. 4. Transient absorption spectra observed at 10 μs following 337.1-nm laser flash photolysis of **1***c* (A) and **1***f* (B) in degassed benzene. Insets: experimetnal decay curves in degassed methanol for **1***c* at 320 nm (A′) and **1***f* at 310 nm (B′).

to steady-state irradiation at 296 K in benzene (Fig. 2A′). The corresponding experiment in benzene for **1***e* gives a spectrum (Fig. 2B′) with absorption at 350 and 495 nm. When methanol is added to these benzene solutions in the dark, the species observed appear to be converted into the products seen when **1***a* and **1***e* are irradiated in methanol (cf. traces d in Figs. 2A′ and 2B′ with Figs. 2A and 2B).

Laser flash photolyses (Fig. 4) of diazopyrazolinones **1***c* and **1***f*, which do not have phenyl groups on nitrogen, give transients that have shorter lifetimes and an interesting sensitivity to the alcohol used in quenching experiments. The transient from **1***c* has a lifetime of 90 μs in methanol, but over 1 ms in 2-propanol. That from **1***f* has a lifetime of 18 μs in methanol, 75 μs in ethanol, and 70 μs in 2-propanol. If the transients observed are carbenes, they show a much larger range of reactivity with different alcohols than has been previously observed (18*b*).

Upon the photolysis of compounds **1***a* and **1***e*, we appear to observe three distinct species. The spectra generated upon steady-state irradiation at 296 K in methanol are assigned to the azoesters **3** and **4**. The species with the long-wavelength absorption that are generated in benzene and methylcyclohexane at 296 K and that are converted to azoesters upon the addition of methanol are assigned arylazoketene structures **8**.

Assignment of structure to the third species, observed at low temperatures and in laser flash photolysis experiments, is more difficult. These species, absorbing at ~342–345 nm when generated from **1***a* and at ~394–400 nm for **1***e*, are very long-lived with lifetimes extending into milliseconds. While lifetimes for many carbenes have not been determined, the ones

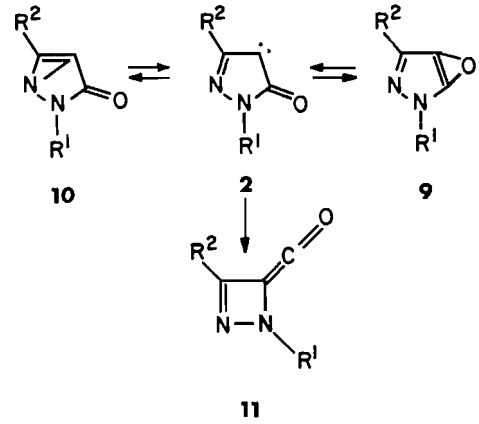

SCHEME 4

reported vary from 27 ns for triplet fluorenylidene (22) to values in the μs range for triplet diphenylmethylene (23), *p*-nitrophenylmethylene (2*b*), and 10,11-dihydrobenzo[*a*,*d*]-cycloheptenylidene (24). Dimesitylcarbene, with a lifetime of ~200 μs, has been recently characterized as a particularly long-lived carbene (25).

In view of the isolation of the (*Z*)-azoesters **3** as the major photoproducts in methanol, we are inclined to assign a cyclic structure to the species observed upon flash photolysis. The species from **1***e*, for example, seems to react directly with methanol to give the azoester.

The observed lifetimes of the transients and their lack of conventional carbenoid reactivity suggest alternative structures for the species. Valence isomers such as oxirenes **9**, well-known intermediates in the photochemistry of α-diazocarbonyl compounds (26), azirenes **10**, or diazetine-ketenes **11** derived from contraction of the ring in carbene **2** are possibilities (Scheme 4). Such formulations require, however, that the precursor of these species, carbene **2**, be very short-lived ($\tau < 5$ ns) for all of the systems that we have examined under different conditions.

The data now available do not allow us to distinguish among the several possibilities. Infrared spectroscopy of matrix-isolated species at low temperatures may permit a more definitive assignment of structure to the unusual heterocyclic intermediate observed. We continue to investigate the properties of these interesting species.

Experimental

The photolyses from which products were isolated were carried out in 17 cm × 2.5 cm id Pyrex test tubes, which were then sealed with rubber serum caps wired into place. The samples were deoxygenated by nitrogen sparging for 30 min prior to irradiation. Irradiations were conducted in a Rayonet Photochemical Reactor (Southern New England Ultraviolet Co., Middletown, Conn.) employing, unless otherwise specified, sixteen 8-W G8T5 (254 nm) or F8T5/BLB (350 nm) low-pressure mercury lamps (General Electric Company). Solutions were usually stirred magnetically during irradiation.

In experiments to measure the spectral changes that occur upon steady-state irradiation at 366 nm, the excitation source was a Bausch and Lomb SP-200 medium pressure mercury lamp coupled with a Bausch and Lomb 33-86-07 monochromator and a Corning filter (CS 0-54). Photolyses at room temperature were performed on degassed solutions (4 mL, ~10–4 *M*) contained in quartz cells (1 cm^2). Solutions (~10–4 *M*) contained in rectangular quartz cells with a path-length of ~3 mm were immersed in liquid nitrogen in a Dewar fitted with flat-faced quartz windows for the experiments at 77 K.

Can. J. Chem. Downloaded from www.nrcresearchpress.com by 210.87.254.6 on 09/06/12
For personal use only.

Can. J. Chem. Downloaded from www.nrcresearchpress.com by 210.87.254.6 on 09/06/12
For personal use only.

Ultraviolet and visible spectra were obtained on a Cary Model 17 spectrophotometer. Mass spectra were determined with a Hitachi Perkin–Elmer RMU-6E spectrometer. Infrared spectra were recorded on Beckman and Perkin–Elmer 237B spectrometers. The ^{1}H nmr were obtained on Varian A-60, T-60, or Hitachi Perkin–Elmer R-20B spectrometers or a JEOL FX-90Q spectrometer. Deuteriochloroform was generally used as the solvent with 1% tetramethylsilane as the internal standard.

Fischer spectroscopic grade solvents were used as received for irradiation experiments, except when otherwise indicated. Solutions were evaporated on a rotary evaporator under vacuum. Melting points were obtained in capillary tubes on a Thomas–Hoover apparatus and are uncorrected. Silica Gel G (PF 254; Brinkman Co.) on glass plates was used for thick-layer, Eastman Kodak No. 6060 sheets for thin-layer chromatography (tlc). Oils recovered by chromatography were further purified by bulb-to-bulb distillation under vacuum before elemental analysis. Elemental analyses were performed by Galbraith Laboratories, Inc., Knoxville, Tennessee, or Spang Microanalytical Laboratory, Eagle Harbor, Michigan.

Flash photolyses

All laser flash photolysis experiments (27*a*) were carried out in rectangular quartz cells (3 mm × 7 mm) using pulses (337.1 nm, 8 ns, 3 mJ) from a Molectron UV-400 nitrogen laser system for excitation. The transients were monitored by a kinetic spectrophotometer consisting of an Eimac 150-W xenon lamp (pulsed), a high-intensity Bausch and Lomb monochromator, and an RCA 4840 photomultiplier tube. The signal from the photomultiplier tube was terminated via 93 ohm into a Tektronix transient digitizer, which, in turn, was interphased with a multiuser PDP 11/55 computer system that controlled experiments, processed data, and stored information. Electromechanical shutters in the paths of exciting and analyzing lights, as well as suitable Corning filters, were used to minimize undue exposure of samples to actinic lights. The response of the detector system was ≤1 ns. The apparatus used for conventional flash photolyses is described elsewhere (27*b*). Solutions used for laser flash photolyses experiments were $0.5–1 \times 10^{-3}$ *M*; those for conventional flash photolyses were $1–3 \times 10^{-6}$ *M*.

Preparation of 4-diazo-2-pyrazolin-5-ones

Method A

The pyrazolinone (0.01 mol) was dissolved in dimethylformamide (25 mL) and triethylamine (0.005 mol) was added to the stirred solution. Tosyl azide (28) (0.01 mol) was added in one portion and the solution stirred rapidly for 0.25 h. Hydrochloric acid (6 *N*, 50 mL) was then added to the solution and the resultant brown mixture was diluted with water (500 mL) and twice extracted with benzene (500 mL). The benzene layer was washed with water (300 mL) containing silica gel (20–25 g), dried over magnesium sulfate, and the benzene removed under reduced pressure for **1***c* and **1***f*. Alternatively, for **1***a* and **1***b*, the original benzene extracts were dried, then filtered through silica gel (dry column, 6 in. × 1 in.). The column was eluted with benzene (100–200 mL), and the benzene evaporated to give the product.

Method B

In the preparation of diazopyrazolinone **1***d*, acetonitrile (100 mL) was the solvent and triethylamine was increased to 0.01 mol. The reaction with tosyl azide took 1 h, after which the solvent was removed and the residue triturated with ether (100 mL). The ether solution was shaken with sodium hydroxide (3%, 25 mL) and the aqueous layer extracted twice more with ether (100 mL). The combined ether extracts were washed successively with hydrochloric acid (6 *M*, 200 mL) and water. Drying of the ether (magnesium sulfate) and removal of the solvent gave the product.

Method C

A solution of the pyrazolinone (0.01 mol) in dimethylformamide/water (50 mL, 4:1) was adjusted to pH 3–4 with a hydrochloric acid – sodium acetate (1 *M* in each component) buffer. To this was added a similarly pH-adjusted solution of 2-azido-3-ethylbenzo-1,3-thiazolium tetrafluoroborate (29) (0.01 mol) in the same solvent (50 mL). The mixture was allowed to stand in the dark for 1 h. It was then diluted with water (400–500 mL) and extracted with benzene (500–1000 mL). The benzene layer was washed successively with hydrochloric acid (1 *M*, 300 mL) and water, dried (mganesium sulfate), and evaporated.

*Photolysis of 4-diazo-3-methyl-1-phenyl-2-pyrazolin-5-one (1*a*) in alkenes or acetone*

Diazopyrazolinone **1***a* (200 mg, 1.00 mmol) was dissolved in acetone (distilled from anhydrous calcium sulfate), 2,3-dimethyl-2-butene, or cycloehexene (45 mL) and irradiated at 350 nm for 24 h. Removal of solvent yielded a dark tarry residue that proved unresolvable upon chromatography (silica gel; benzene; chloroform; benzene/chloroform; ethyl acetate/hexane). In the case of acetone, no chromatographic evidence was found for the presence of oxirane **5***a* (7).

*Photolysis of 4-diazo-3-methyl-1-phenyl-2-pyrazolin-5-one (1*a*) in alcohols*

Diazopyrazolinone **1***a* (200 mg, 1.00 mmol) in absolute methanol (50 mL) was irradiated at 350 nm for 24 h. Removal of the solvent, trituration of the residue with ether (5 mL), and preparative thick-layer chromatography (benzene/petroleum ether, 3:2) of the ether-soluble portion of the product, after removal of the ether, gave two fractions. Fraction I was *methyl* (E)*-3-phenylazo-2-butenoate*, red oil, (**4***a*) (13 mg, 6%); λ_{max} (methanol): 540 (ε 94), 433 (ε 3.9×10^2), 311 nm (ε 2.1×10^4); ^{1}H nmr ($CDCl_3$): 2.41 (d, J = 1.2 Hz, 3H), 3.82 (s, 3H), 6.77 (q, J = 1.2 Hz, 1H), 7.40–7.92 (m, 5H) ppm; *m/z* 204. *Anal.* calcd for $C_{11}H_{12}N_2O_2$: C 64.69, H 5.92, N 13.72; found: C 64.76, H 6.04, N 13.61.

Fraction II was methyl (*Z*)-3-phenylazo-2-butenoate, red oil, (**3***a*) (87 mg, 43%); λ_{max} (methanol): 549 (ε 57), 440 (ε 2.4×10^2), 308 (ε 1.6×10^4); ^{1}H nmr ($CDCl_3$): 2.04 (d, J = 0.8 Hz, 3H), 3.76 (s, 3H), 6.20 (q, J = 0.8 Hz, 1H), 7.35–7.91 (m, 5H) ppm; *m/z* 204.

The ether-insoluble residue was a brownish-white solid that decomposed without melting at 212–215°C; ^{1}H nmr ($CDCl_3$): 1.0–2.8 (br), 7.0–7.7 (br); not volatilized in the mass spectrometer.

Diazopyrazolinone **1***a* was photolyzed again under identical conditions, but allowed to stand in the dark for two days before work-up. The ratio of (*Z*)- to (*E*)-esters **3***a* and **4***a* obtained was the same as that above. When the nmr sample of the (*Z*)-ester was allowed to stand for 1 week and the spectrum taken again, the solution contained only (*E*)-isomer.

An identical photolysis experiment was carried out with **1***a* in absolute ethanol (distilled from magnesium in the presence of iodine). The products were ethyl (*E*)-3-phenyl-azo-2-butenoate (16 mg, 7%), mp 48°C (lit. (9) mp 50°C); ^{1}H nmr ($CDCl_3$): 1.37 (t, J = 6.0 Hz, 3H), 2.40 (d, J = 1.2 Hz, 3H), 4.28 (q, J = 6.0 Hz, 2H), 6.77 (q, J = 1.2 Hz, 1H), 7.39–7.94 (m, 5H) ppm; *m/z* 218; and ethyl (*Z*)-3-phenyl-azo-2-butenoate, red oil (92 mg, 42%), ^{1}H nmr ($CDCl_3$): 1.30 (t, J = 6.3 Hz, 3H), 2.05 (d, J = 0.8 Hz, 3H), 4.25 (q, J = 6.3 Hz, 2H), 6.24 (q, J = 0.8 Hz, 1H), 7.38–7.95 (m, 5H) ppm; *m/z* 218.

Investigation of the photochemical interconvertability of (Z)*- and* (E)*-phenylazobutenoates* 3a *and* 4a

(*E*)-Ester **4***a* (30 mg) in methanol (10 mL) was irradiated at 350 nm for 24 h. The ^{1}H nmr analysis of the oil after removal of solvent showed some deterioration of the sample, but no conversion to (*Z*)-isomer **3***a*. Similarly, a mixture of the two isomers **3***a* and **4***a* (30 mg) in methanol (10 mL) was irradiated at 350 nm for 24 h, with no nmr evidence, as judged by the relative intensities of bands at δ 2.41 and δ 2.04, that one isomer had been photochemically converted to the other.

*Photolysis of 4-diazo-1,3-diphenyl-2-pyrazolin-5-one (1*b*) in methanol*

Diazopyrazolinone **1***b* (262 mg, 1.00 mmol) in absolute methanol (50 mL) was irradiated at 350 nm for 24 h. Removal of the solvent, trituration of the residue with ether (5 mL), and preparative thick-layer chromatography (benzene/petroleum ether, 1:1) of the ether-soluble

Can. J. Chem. Downloaded from www.nrcresearchpress.com by 210.87.254.6 on 09/06/12
For personal use only.

portion after removal of the ether gave two fractions. Fraction I was *methyl* (E)-*3-phenyl-azo-3-phenylpropenoate* (**4***b*), red oil (11 mg, 4%); ^{1}H nmr ($CDCl_3$): 3.79 (s, 3H), 6.87 (s, 1H), 7.35–7.95 (m, 10H) ppm; *m/z* 266. *Anal.* calcd for $C_{16}H_{14}N_2O_2$: C 72.15, H 5.31, N 10.52; found: C 72.32, H 5.28, N 10.66.

Fraction II was methyl (*Z*)-3-phenylazo-3-phenylpropenoate (**3***b*), red oil (104 mg, 39%); ^{1}H nmr ($CDCl_3$): 3.67 (s, 3H), 6.03 (s, 1H), 7.39–8.00 (m, 10H) ppm; *m/z* 266.

Photolysis of 4-diazo-1-methyl-3-phenyl-2-pyrazolin-5-one (1c) in methanol

Diazopyrazolinone **1***c* (285 mg, 1.42 mmol) in absolute methanol (45 mL) was irradiated at 350 nm for 24 h. Removal of the solvent, trituration with ether (5 mL), and preparative thick-layer chromatography (benzene/petroleum ether, 3:2) of the ether-soluble portion after removal of solvent gave a yellow oil (78 mg, 27%), assigned structure as methyl (*Z*)-3-methylazo-3-phenylpropenoate (**3***c*) on the basis of spectroscopic evidence; ^{1}H nmr ($CDCl_3$): 3.66 (s, 3H), 4.06 (s, 3H), 5.95 (s, 1H), 7.35 (s, 5H) ppm; *m/z* 204.

Photolysis of 4-diazo-3-methyl-1-(p-nitrophenyl)-2-pyrazolin-5-one (1d) in methanol

Diazopyrazolinone **1***d* (245 mg, 1.00 mmol) in methanol (50 mL) was irradiated at 350 nm for 24 h. Removal of the solvent gave a dark brown residue that could not be resolved by chromatography (silica gel; benzene; chloroform; benzene/chloroform; ethyl acetate/hexane).

Photolysis of 4-diazo-1-(p-methoxyphenyl)-3-methyl-3-pyrazolin-5-one (1d) in methanol

Diazopyrazolinone **1***e* (70 mg) in absolute methanol (70 mL) was irradiated (eleven 350-nm lamps in use) for 12.5 h. Removal of solvent gave an oil, the ^{1}H nmr spectrum of which indicated that methyl (*Z*)-3-(*p*-methoxyphenyl)azo-2-butenoate (**3***a*), ($CDCl_3$) δ 2.10 and 6.20 ppm, is the major product, and the (*E*)-isomer **4***e*, ($CDCl_3$) δ 2.39 and 6.65 ppm, is the minor one. The nmr sample was inspected at intervals of 1, 3, 5, 7, and 13 days, during which time a decrease in the intensity of the bands at δ 2.10 and 6.20 and a corresponding increase at δ 2.39 and 6.65 ppm could be observed.

A small sample (15 mg) of a red oil with ^{1}H nmr ($CDCl_3$): 2.39 (d, 3H), 3.79 (s, 3H), 3.86 (s, 3H), 6.65 (m, 1H), 6.8–7.8 (m, 4H) ppm, consistent with an assignment of structure as methyl (*E*)-3-(*p*-methoxyphenyl)azo-2-butenoate (**4***e*), was obtained by preparative thick-layer chromatography (ether).

Photolysis of 4-diazo-3-phenyl-2-pyrazolin-5-one (1f) in methanol

Diazopyrazolinone **1***f* (313 mg, 1.68 mmol) in absolute methanol (45 mL) was irradiated at 350 nm for 24 h. Trituration with ether (5 mL) of the residue from the removal of the solvent gave a white precipitate (278 mg) that was polymeric, mp > 200°C with decomposition; ^{1}H nmr ($CDCl_3$): 2.1–3.0 (br), 4.5 (br), 7.3–7.9 (m) ppm; *m/z* >500. Analysis of the ether-soluble portion by tlc (silica gel; benzene; chloroform; chloroform/petroleum ether; ethyl acetate/petroleum ether) showed only intractable material present.

Photolysis of 4-diazo-3-methyl-1-tosyl-2-pyrazolin-5-one (1g) in methanol

Diazopyrazolinone **1***g* (278 mg, 1.00 mmol) in methanol (50 mL) was irradiated at 350 nm for 24 h. Trituration with ether (5 mL) of the residue from the removal of the solvent gave a white precipitate (201 mg), mp 167–168°C, which was not further characterized. The tlc of the ether-soluble portion of the residue failed to yield any azoesters.

Acknowledgments

The work described herein was supported in part by the Office of Basic Energy Sciences of the Department of Energy (P.K.D.) and the National Science Foundation (G.W.G.). This is Document NDRL 2565 from the Notre Dame Radiation Laboratory. We are grateful to Dr. G. Ferraudi for giving us access to his conventional flash photolysis set-up and for his assistance in using it. We thank Professor A. M. Trozzolo for helpful discussions.

1. W. J. Baron, M. R. DeCamp, M. E. Hendrick, M. Jones, Jr., R. H. Levin, and M. B. Sohn. Carbenes. Vol. 1. *Edited by* M. Jones, Jr. and R. A. Moss. John Wiley and Sons, New York. 1973. Chapt. 1.
2. (*a*) S. N. Eğe, E. J. Gess, A. Thomas, P. Umrigar, G. W. Griffin, P. K. Das, A. M. Trozzolo, and T. M. Leslie. J. Chem. Soc. Chem. Commun. 1263 (1980); (*b*) P. Umrigar, G. W. Griffin, B. A. Lindig, M. A. Fox, P. K. Das, T. M. Leslie, A. M. Trozzolo, S. N. Eğe, and A. Thomas. J. Photochem. **22**, 71 (1983).
3. M. Regitz. Synthesis, **1**, 351 (1972).
4. E. J. Moriconi and J. J. Murray. J. Org. Chem. **29**, 3577 (1964).
5. A. D. Woolhouse, T. C. Caruso, and A. Padwa. Tetrahedron Lett. **23**, 2167 (1982).
6. J. N. Bradley and A. Ledwith. J. Chem. Soc. 3480 (1963).
7. S. N. Eğe, C. J. Tien, A. Dlesk, B. E. Potter, and B. K. Eagleson. J. Chem. Soc. Chem. Commun. 682 (1972).
8. P. A. S. Smith, G. J. Breen, M. K. Hajek, and D. V. C. Awang. J. Org. Chem. **35**, 2215 (1970).
9. S. Searles, Jr. and W. R. Hine, Jr. J. Am. Chem. Soc. **79**, 3175 (1957).
10. D. G. Farnum and P. Yates. J. Am. Chem. Soc. **84**, 1399 (1962).
11. J. T. Carlock, J. S. Bradshaw, B. Stanovnik, and M. Tišler. J. Org. Chem. **42**, 1883 (1977); J. T. Carlock, J. S. Bradshaw, B. Stanovnik, and M. Tišler. J. Heterocycl. Chem. **14**, 519 (1977); B. Stanovnik, M. Tišler, and J. T. Carlock. Synthesis, 754 (1976).
12. O. Süs, M. Glos, K. Moller, and H. Eberhardt. Justus Liebigs Ann. Chem. **583**, 150 (1953); O. Süs. Justus Liebigs Ann. Chem. **579**, 133 (1953); O. Süs and K. Moller. Justus Liebigs Ann. Chem. **593**, 91 (1955); **597**, 233 (1956); **617**, 20 (1958).
13. B. Stanovnik, M. Tišler, B. Kirin, and I. Kovač. J. Heterocycl. Chem. **16**, 195 (1979).
14. E. Voigt and H. Meier. Chem. Ber. **110**, 2242 (1977).
15. H. Dürr and H. Schmitz. Chem. Ber., **111**, 2258 (1978).
16. W. L. Magee and H. Schechter. J. Am. Chem. Soc. **99**, 633 (1977).
17. U. Simon, O. Süs, and L. Horner. Justus Liebigs Ann. Chem. **697**, 17 (1966).
18. (*a*) W. Kirmse. Justus Liebigs Ann. Chem. **666**, 9 (1963); (*b*) D. Bethell and R. D. Howard. J. Chem. Soc. B, 745 (1969); (*c*) D. Bethell, A. R. Newall, and D. Whittaker. J. Chem. Soc. B, 23 (1971).
19. U. G. Kang and H. Schechter. J. Am. Chem. Soc. **100**, 651 (1978).
20. H. Tomioka and Y. Izawa. J. Am. Chem. Soc. **99**, 6128 (1977).
21. A. Schmitz, U. Kraatz, and F. Korte. Heterocycles, **10**, 199 (1978).
22. P. C. Wong, D. Griller, and J. C. Scaiano. J. Am. Chem. Soc. **104**, 663 (1982).
23. L. M. Hadel, M. S. Platz, and J. C. Scaiano. J. Am. Chem. Soc. **106**, 283 (1984).
24. I. Moritani, S. I. Murahashi, H. Ashitaka, K. Kimura, and H. Tsubomura. J. Am. Chem. Soc. **90**, 5918 (1968).
25. A. S. Nazran and D. Griller. J. Am. Chem. Soc. **106**, 543 (1984).
26. I. G. Csizmadia, J. Font, and O. P. Strausz. J. Am. Chem. Soc. **90**, 7360 (1968); D. E. Thornton, R. K. Gosavi, and O. P. Strausz. J. Am. Chem. Soc. **92**, 1768 (1970); G. Frater and O. P. Strausz. J. Am. Chem. Soc. **92**, 6654 (1970); S. A. Matlin and P. G. Sammes. J. Chem. Soc. Chem. Commun. 11 (1972).
27. (*a*) P. K. Das, M. V. Encinas, and J. C. Scaiano. J. Am. Chem. Soc. **101**, 6965 (1979); P. K. Das and S. N. Bhattacha-

RYYA. J. Phys. Chem. **85**, 1391 (1981); P. K. DAS and K. BOBROWSKI. J. Chem. Soc. Faraday Trans. 2, **77**, 1009 (1981); (*b*) D. R. PRASAD and G. FERRAUDI. Inorg. Chem. **22**, 1672 (1983).
28. T. CURTIUS and G. KRAEMER. J. Prakt. Chem. **125**, 303 (1930).
29. H. BALLI and R. GIPP. Justus Liebigs Ann. Chem. **699**, 133 (1966).
30. L. KNORR. Justus Liebigs Ann. Chem. **238**, 137 (1888).
31. P. N. DAHL, T. E. ACHARY, and A. NAYAK. J. Indian Chem. Soc. **52**, 1196 (1975).
32. A. MICHAELIS, W. RASSMAN, T. VON DER HAGEN, H. DORN, and H. WREDE. Justus Liebigs Ann. Chem. **352**, 152 (1907).
33. W. HAENSEL. Justus Liebigs Ann. Chem. 1380 (1976).
34. P. A. LEWIN. Zh. Prikl. Khim. **34**, 2803 (1961); Chem. Abstr. **56**, 12871i (1962).
35. Swiss Patent 310,137, December, 1955; Chem. Abstr. **51**, P5127e (1957).
36. M. CROCI, A. FIGERIO, E. GREMMO, and P. VITA-FINZI. Gazz. Chim. Ital. **103**, 179 (1973).

Can. J. Chem. Downloaded from www.nrcresearchpress.com by 210.87.254.6 on 09/06/12
For personal use only.

Electron transfer reactions from alkali metal surfaces to (±) and (*S*)-(−)-1,3-dimethoxy-1,1-diphenylbutane. Studies on 1,3-elimination

HARRY M. WALBORSKY[1] AND MARTHA PASS MURARI
Department of Chemistry, Florida State University, Tallahassee, FL 32306 U.S.A.

Received February 7, 1984

This paper is dedicated to Professor Peter Yates on the occasion of his 60th birthday

HARRY M. WALBORSKY and MARTHA PASS MURARI. Can. J. Chem. **62**, 2464 (1984).

The 1,3-elimination of methoxide by carbanions generated from the reaction of (±)-1,3-dimethoxy-1,1-diphenylbutane with the alkali metals, lithium, sodium, and potassium, in various solvents was studied to determine the significance of cation–methoxyl coordination due to decreasing charge/radius ratio of the cations and also the cation complexing ability of the solvent. The stereochemistry of cyclization in the reaction of (*S*)-(−)-1,3-dimethoxy-1,1-diphenylbutane with lithium metal in tetrahydrofuran and with sodium metal in methylcyclohexane to yield 1-methyl-2,2-diphenylcyclopropane was determined. The reaction proceeded by an intramolecular S_N2-type displacement to yield optically pure product of inverted configuration.

HARRY M. WALBORSKY et MARTHA PASS MURARI. Can. J. Chem. **62**, 2464 (1984).

Dans le but de déterminer l'importance de la coordination du méthoxyle par le cation dû à une diminution du rapport charge à rayon des cations ainsi que l'habilité du solvant à complexer le cation, on a étudié la réaction d'élimination 1,3 du méthylate par des carbanions générés par la réaction, dans divers solvants, du (±)-diméthoxy-1,3 diphényl-1,1 butane avec les métaux alcalins, lithium, sodium et potassium. On a déterminé la stéréochimie de la réaction du (*S*)-(−)-diméthoxy-1,3 diphényl-1,1 butane avec le lithium métallique dans le tétrahydrofuranne et avec le sodium métallique dans le méthylcyclohexane qui conduit, par cyclisation, au méthyl-1 diphényl-2,2 cyclopropane. La réaction se produit par un mécanisme, de type déplacement S_N2- intramoléculaire, qui conduit à une produit optiquement pur dont la configuration est inversée.

[Traduit par le journal]

Introduction

An established method for preparation of cyclopropane compounds is the use of the base-induced 1,3-elimination reaction. Two examples, *inter alia*, of this process are the conversion of **1** to **2** by Yates and Anderson (1) (eq. [1]) and **3** to **4** by Bumgardner (2) (eq. [2]).

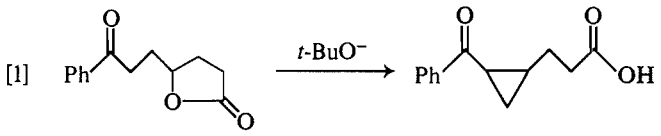

1 **2**

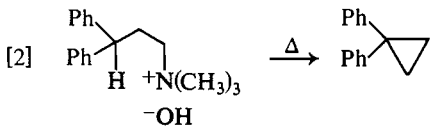

3 **4**

Some general features of base-induced 1,3-elimination reactions have been covered in an early review (3), and various mechanistic aspects, conformational and stereochemical, have also been discussed (4, 5). Considerable experimental evidence has accumulated to support the view that for base-induced 1,3-elimination reactions a two-step reaction process is preferred and a one-step concerted reaction is rare, if it exists at all. A consequence of this two step process is inversion of confuguration at the carbon atom that is the object of nucleophilic attack.

The two-step process is enhanced by relatively unreactive leaving groups. A leaving group which belongs to that classification is alkoxyl. The nucleophilic displacement of alkoxide has been studied in some detail by Köbrich and Baumann (6) and observed on several other occasions (7–9).

A stereochemical study of cyclopropane formation by displacement of an alkoxide has not been made but, in view of some interesting results obtained by Sugita *et al.* (10) in a 1,2-elimination of methoxide, such a study is warranted. The 1,2-elimination of methoxide in the reaction of *erythro-* and *threo*-1-bromo-2-methoxy-1,2-diphenylethane (**5** and **6**) with *n*-butyllithium in diethyl ether gave *cis*- (**7**) and *trans*-stilbene (**8**), respectively (eqs. [3] and [4]). These results show that a

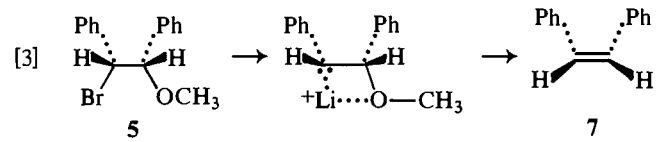

5 **7**

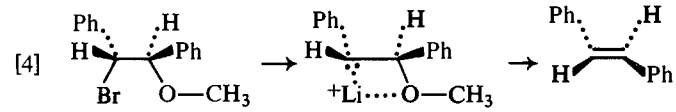

6 **8**

stereospecific *syn*-elimination has occurred. The factor expected to be the driving force for the production of **7** from the *erythro* isomer (**5**), even against the large thermodynamical instability of the product, is the coordination between the lithium cation and the oxygen of the methoxyl group. This was indicated by the observation that the stereospecificity decreased on changing the solvent from the low polarity solvents, diethyl ether and benzene, to the more polar, cation complexing solvents, tetrahydrofuran and diglyme. Table 1 summarizes the relevant data of Sugita *et al.* (10).

The binding energies of lithium cations with the nonbonding electrons of the oxygen in ethers is substantial (~38 kcal/mol) (11). Such bonding plays an important role in Cram's cyclic model (12) for asymmetric syntheses, Meyers (13) asymmetric syntheses model (chiral lithio-oxazoline), Helmchen's (14) chiral lithium enolates of esters, and Masamune's (15) lithium enolates of aldehydes and ketones which lead to directed aldol condensations. This type of binding also

[1] Author to whom correspondence may be addressed.

Can. J. Chem. Downloaded from www.nrcresearchpress.com by 210.87.254.42 on 09/06/12
For personal use only.

TABLE 1.[a] Elimination reactions of *erythro*- and *threo*-1-bromo-2-methoxy-1,2-diphenylethane with *n*-butyllithium

Time (min)	Isomer	Solvent	% Yield	*cis* : *trans*
30	*erythro*	Et_2O	48	100 : Trace
15	*erythro*	THF	59	52 : 48
10	*erythro*	Diglyme	76	22 : 78
10	*threo*	Et_2O	53	Trace : 100
15	*threo*	THF	48	Trace : 100
10	*threo*	Diglyme	93	Trace : 100
30	*erythro*	Benzene[b]	22	100 : Trace

[a] Data from ref. 10.
[b] Room temperature.

accounts for the stability of 2-lithio-7-*syn*-methoxy-norbornane which, although a secondary organolithium, is more stable than the primary *n*-butyllithium (16). A similar effect accounts for the stabilization of α-halocyclopropyllithium reagents (carbenoids) (17).

Moreover, for reactions believed to involve intramolecular coordination of alkali metal cations with ligands containing heteroatoms, it is found that the reaction course is specific for lithium (18). Changing the cation from lithium to sodium or potassium or adding solvents capable of complexing with lithium competitively with internal complexation can critically affect the course of the reaction.

This investigation into 1,3-elimination is designed to study the parameters known to affect internal lithium–alkoxyl coordination. The effects of varying the solvent and the cation will be presented, as will the stereochemistry of the reaction.

Results and discussion

Synthesis of substrate

The choice of substrate to study the effect of lithium–alkoxyl coordination on 1,3-elimination reactions was determined by the scope of the investigation. To make a systematic study, the substrate was required to have structural features that would (1) permit generation of a carbanionic nucleophile with lithium, sodium, or potassium as cation, (2) have an alkoxyl group attached to an asymmetric center capable of being displaced, and (3) allow cyclization to a cyclopropane with known absolute configuration. The molecule 1,3-dimethoxy-1,1-diphenylbutane (9) fulfilled these requirements. As can be seen in eq. [5], **9** possesses the diphenylcarbinylmethyl ether moiety

[5] 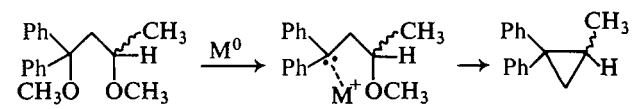

9 **10** **11**

M = Li, Na, K

which can be cleaved (19) with alkali metals to form **10**. The 2° carbon to which the methoxyl group is attached can be chiral and nucleophilic attack is possible since it is not sterically hindered. Cyclization of **10** would give 1-methyl-2,2-diphenylcyclopropane (**11**) whose absolute configuration was determined many years ago (20). (±)-1,3-Dimethoxy-1,1-diphenylbutane (**9**) was simply prepared by the reaction of the dilithium derivative of benzophenone (21) with racemic propylene oxide to form (±)-1,1-diphenyl-1,3-butanediol (**12**), which upon treatment with sodium hydride and methyl iodide (eq. [6]) produced the desired substrate.

Chiral **9** was prepared by the same reaction sequence illustrated in eq. [6] but using chiral (*S*)-(−)-propylene oxide (22) to yield (*S*)-(+)-**12** in 84% yield. The chiral diol produced (*S*)-(−)-**9** in 95% yield upon treatment with sodium hydride and methyl iodide.

[6] 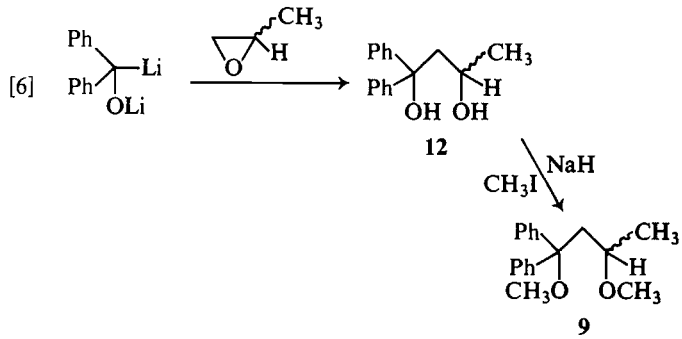

Effect of solvent and cation

To determine the effect of solvent on the lithium–methoxyl coordination, three solvents were chosen that represent a range of polarities. Nonpolar methylcyclohexane, tetrahydrofuran (THF) with intermediate polarity, and the very polar hexamethylphosphoramide (HMPA) were used. Finely dispersed lithium was prepared and was allowed to react with racemic 1,3-dimethoxy-1,1-diphenylbutane (**9**). In each solvent sufficient time was allowed to cleave the diphenylcarbinyl ether and for subsequent cyclization to occur. The main products observed in these reactions were 1-methyl-2,2-diphenylcyclopropane (**11**) and 2-methoxy-4,4-diphenylbutane (**13**) (eq. [7]). The product of interest (**11**) was not stable under

[7] 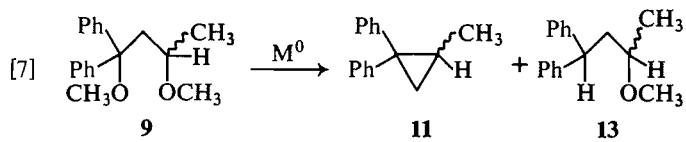

9 **11** **13**

[8] 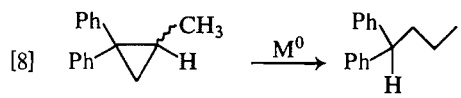

11 **14**

these conditions and reacted with excess metal to form 1,1-diphenylbutane (**14**) (23) (eq. [8]). The yields of 1-methyl-2,2-diphenylcyclopropane (**11**) and 1,1-diphenylbutane (**14**) for this series of reactions are given in Table 2.

As is evident from the data in Table 2, fair yields of cyclization product were observed in methylcyclohexane and THF but not in HMPA. In hydrocarbon solvents, it is known that the ion pair consisting of a lithium cation attached to a delocalized carbanion exists as an unreactive contact ion pair, whereas in THF the ion pair exists as a reactive solvent-separated ion pair (24). By analogy, the observed cyclization in THF would be expected to take place from a solvent-separated ion pair in which the diphenylcarbinyl anion is a reactive nucleophile. However, it would seem that in methylcyclohexane the diphenylcarbinyl anion would not have been a reactive nucleophile and cyclization should not have occurred. The fact that cyclization did occur in methylcyclohexane indicates that the lithium–methoxy coordination produced a reactive solvent-separated lithium diphenylcarbinyl anion ion pair (**15**).

If a reactive nucleophile is the only prerequisite for obtaining cyclization, then HMPA should have promoted cyclization in-

Can. J. Chem. Downloaded from www.nrcresearchpress.com by 210.87.254.42 on 09/06/12
For personal use only.

TABLE 2. Effect of solvent on the reaction of 1,3-dimethoxy-1,1-diphenylbutane with lithium[a, b]

Time (h)	T (°C)	Solvent	% Yield[c] 11	13	14[d]
72	100	Methylcyclohexane	33[e]	15	—
72	25	THF	32	34	4.8
48	25	HMPA	12	26	5.7

[a] Substrate conc. = 0.06 *M*.
[b] Lithium/substrate = 10.
[c] Yields determined by glc analysis.
[d] See ref. 23.
[e] Isolated yield.

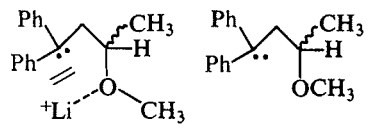

15

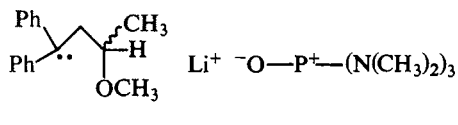

16

stead of diminishing cyclization since HMPA is known to dissociate ion pairs into free ions (25). For the reaction in HMPA, a species such as **16** in which the lithium cation is out of binding distance can be envisioned. Both intermediates, **15** and **16**, have the diphenylcarbinyl anion as a reactive nucleophile but only **15** has the lithium–methoxy coordination. Therefore it appears that the displacement of the methoxyl group is facilitated by coordination with the lithium cation (Lewis acid) and is retarded when the lithium cation is unable to coordinate. The coordination of the lithium cation to the methoxyl group weakens the C—OCH_3 bond. Furthermore, cyclization in THF must be occurring through **15** and this conclusion indicates that the internal solvation of the lithium cation by the methoxyl group competes effectively with the external solvation of the lithium cation by THF.

The tendency for ligand attraction decreases for other alkali metal ions like sodium and potassium due to decreasing charge/radius ratio (26) and, for the same reason, the fraction of reactive solvent-separated ion pairs decreases according to the sequence Li > Na > K (27). Thus it was of interest to determine the existence of a species corresponding to **15** for the reaction of 1,3-dimethoxy-1,1-diphenylbutane (**9**) with sodium and potassium in both methylcyclohexane and THF.

The reaction of **9** with sodium in methylcyclohexane gave 1-methyl-2,2-diphenylcyclopropane (**11**) and 2-methoxy-4,4-diphenylbutane (**13**) as the main products but the reaction of **9** with potassium in methylcyclohexane gave mainly **13**. The yields of the cyclization product **11** for these two reactions and for the previously discussed reaction of lithium with **9** in methylcyclohexane are given in Table 3. In the reactions of **9** with sodium and potassium in tetrahydrofuran mainly **13** was obtained. However, the reaction of **9** with potassium in THF to form intermediate **10**, followed by cation exchange with anhydrous lithium perchlorate ($LiClO_4$), gave both **11** and **13**. The yields of cyclization product **11** for these three reactions and for the previously discussed reaction of lithium with **9** in THF are given in Table 4. It was noted that longer reaction times were necessary for the reaction of **9** with lithium because the lithium metal floats and contact with solution is not very good.

Inspection of Tables 2 and 4 shows that for the reaction of **9** with sodium in methylcyclohexane, an intermediate, **17**,

TABLE 3. Reactions of 1,3-dimethoxy-1,1-diphenylbutane with metals in methylcyclohexane[a, b]

Time (h)	T (°C)	Metal	% Yield[c] 11	14[d]
72	100	Li	33	—
24	100	Na	63	—
24	100	K	<1[e]	1.5[e]

[a] Substrate conc. = 0.06 *M*.
[b] Metal/substrate = 10.
[c] Isolated yields.
[d] See ref. 23.
[e] Yield determined by glc analysis.

corresponding to **15** for lithium, must be present. In **17** the sodium cation is internally solvated by the methoxyl group so that the diphenyl carbinyl anion is not part of a contact ion pair with the sodium cation but instead is reactive and able to initiate nucleophilic attack. Since the unit positive charge on the sodium cation is dispersed over a larger area than that for the lithium cation, the sodium cation cannot effectively coordinate to the methoxyl group in the presence of external solvation by THF. Hence **17** cannot form and cyclization does not occur.

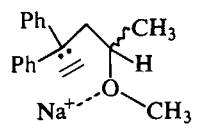

17

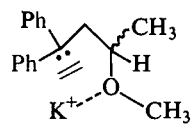

18

For the reaction of potassium with **9** in both methylcyclohexane and THF, intermediate **18**, corresponding to **15** for lithium, must not be present to any large extent. Thus, for the potassium cation in which the unit positive charge is dispersed over an area greater than that for either lithium or sodium cations, ligand coordination is ineffective even in the absence of external solvation (methylcyclohexane). An ion pair consisting of the potassium cation and the diphenylcarbinyl anion must be the predominant species in the reactions with potassium. This is unreactive and does not cyclize.

The significance and existence of the lithium–methoxyl coordination is further substantiated by the cation exchange reaction. As shown in Table 4, in the addition of excess lithium cation (from $LiClO_4$), the diphenylcarbinyl–potassium exchanges potassium cation for lithium cation and cyclization can then occur through the intermediate, **15**.

Stereochemistry

The solvent and cation studies showed that lithium in THF and sodium in methylcyclohexane resulted in reasonable yields of **11** from **9** and these conditions were chosen to evaluate the stereochemistry of the reaction (eq. [9]).

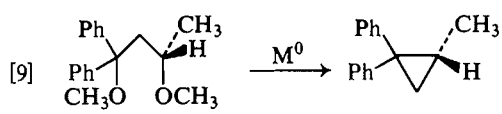

[9]

(*S*)-(−)-**9** (*R*)-(−)-**11**

Reaction of (*S*)-(−)-**9** with lithium metal in THF at 25°C gave a 20% yield of (*R*)-(−)-**11** with 99% optical purity. The same reaction of sodium metal in methylcyclohexane at 100°C

Can. J. Chem. Downloaded from www.nrcresearchpress.com by 210.87.254.42 on 09/06/12
For personal use only.

TABLE 4. Reactions of 1,3-dimethoxy-1,1-diphenylbutane with metals in tetrahydrofuran[a, b]

Time (h)	T (°C)	Metal	Additive	% Yield[c] 11	% Yield[c] 14[d]
72	25	Li	—	32	4.8
64[e]	25[e]	Na	—	7.7	<1
64[e]	25[e]	K	—	<1	2.0
23	25	K	$LiClO_4$[f]	28[g]	—

[a] Substrate conc. = 0.06 *M*.
[b] Metal/substrate = 10.
[c] Yield based on glc and on starting material considered.
[d] See ref. 23.
[e] With 40 h at 25°C and 24 h at reflux.
[f] $LiClO_4$/substrate = 6.
[g] Isolated yield.

gave a 63% yield of (*R*)-(−)-**11** with 96% optical purity. Thus the overall reaction (eq. [9]) proceeds in a stereospecific manner with complete inversion of configuration at C-3 of **9**.

(*S*)-(+)-2-Methoxy-4,4-diphenylbutane (**19**) was prepared by reaction of lithium diphenylmethide with (*S*)-1-(*p*-toluenesulfonoxy)-2-(tetrahydro-2-pyranoxy) propane (22), hydrolysis to remove the tetrahydropyranyl blocking group, and the resulting (*S*)-(+)-4,4-diphenyl-2-butanol etherified with sodium hydride and methyl iodide. The metalation of (*S*)-(+)-**19** with *n*-butyllithium in methylcyclohexane/THF (35:1) at 25°C resulted in a 28% yield of (*R*)-(−)-**11** with 99% optical purity (eq. [10]).

[10] 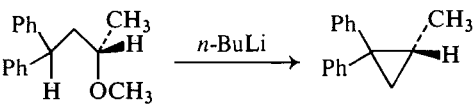

(*S*)-(+)-**19** (*R*)-(−)-**11**

The foregoing results show that in all cases inversion of configuration has occurred and speak strongly for an intermediate like **15** in which the cation is strongly coordinated with the oxygen of the leaving methoxyl group and in which the cation is solvent separated from the diphenylcarbanion moiety. The ring closure then proceeds as depicted in eq. [11].

[11] 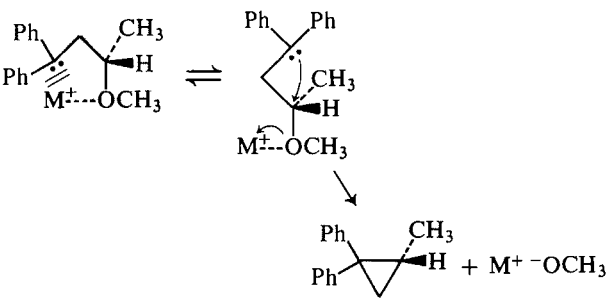

Experimental

Melting points were measured in open capillaries with a Mel-Temp apparatus. Melting points and boiling points are uncorrected. The ir spectra were recorded on a Perkin–Elmer Model 257 spectrophotometer; band positions are reported in wave numbers (cm^{-1}). The nmr spectra were recorded as $CDCl_3$ solutions on Varian Associates Model A-60 and on JEOL Model C-60 HL spectrometers unless specified otherwise; chemical shifts are reported in δ (ppm) downfield from internal tetramethylsilane and coupling constants are in hertz (Hz). Low resolution mass spectra were obtained on a Nuclide Model 12-90 G electron impact mass spectrometer. Microanalyses were performed by the Beller Laboratories, Göttingen, Germany.

Optical rotations were measured at either the 546.1-nm mercury line or at the 589.3-nm sodium line using a Bendix–Ericsson Model 987 ETL/NPL polarimeter with a digital display attachment. The cell length was 0.4 dm and all solvents used were spectrophotometric grade. Error limits for rotations were calculated by multiplying the relative standard deviation by the specific rotation. The relative standard deviation was determined by dividing the standard deviation (0.002) by the observed rotation. Percent optical purity was determined as follows: (observed specific rotation ÷ maximum specific rotation) multiplied by 100. The maximum specific rotation for (*R*)-(−)-1-methyl-2,2-diphenylcyclopropane is $[\alpha]_{Hg}^{25}$ −150.6° (*c* 1.18, $CHCl_3$) or, as reported, $[\alpha]_D^{26}$ −127° (28).

Qualitative gc analyses were performed on a Hewlett Packard Model 5710A gas chromatograph (thermal conductivity detectors with helium as carrier gas) using packed columns (column A, 15% Carbowax-20 M on acid-washed 80/100 Chromosorb P, 10 ft × 1/8 in., 220°C; and column B, 15% Lexan on acid-washed 60/80 Chromosorb P, 4 ft × 1/8 in., 200°C) and on a Varian Model 1200 Series gas chromatograph (flame ionization detector with nitrogen as carrier gas) using a J & W Scientific, Inc., glass capillary column (column C, wall coated SE 30, 30 m × 0.2415 mm, 165°C). Quantitative glpc analyses were performed on column A using diphenylmethane as internal standard. Peak areas were measured as height × width at half-height.

Product separations obtained by high-pressure liquid chromatography (hplc) were conducted on Waters Associates ALC 202 Liquid Chromatograph equipped with an Instrument Specialities Co. "Golden Retriever" automatic sample collector and a Rikadenki recorder (dfifferential refractometer detection) using two Porasil B columns (4 ft × 3/8 in. each) under the conditions described. Thin-layer chromatography (tlc) and preparative thick-layer chromatography (ptlc) were performed using glass plates coated with Merck silica gel 60 PF-254 + 366. Flash chromatography was carried out on a 20 × 5 cm column of silica gel 60 (400–230 mesh, E. Merck No. 9385).

(±)-1,1-Diphenyl-1,3-butanediol (12)

A modification of the procedure of Askinazi and Ioffe (21) was used. To a cooled (0°C) purple solution of the dilithium dianion of benzophenone prepared (*vide supra*) from 9.1 g (0.050 mol) benzophenone, 1.3 g (0.010 mol) of naphthalene, and 0.85 g (0.12 g-atom) of lithium in 63 mL of dry THF under an argon atmosphere was added slowly a solution of 3.8 g (0.065 mol) racemic propylene oxide in 15 mL dry THF. The reaction mixture was stirred at 25°C for 3 h as it decolorized, cooled, and was cautiously quenched with 20 mL saturated ammonium chloride. After removing the THF *in vacuo*, the basic aqueous layer was extracted with 100 mL ether and the ether extract was washed with saturated ammonium chloride, dried over anhydrous sodium sulfate, and evaporated to leave an oil (14.1 g) which crystallized to a white solid upon scratching. The solid was refluxed overnight with low boiling petroleum ether to dissolve the naphthalene and leave the insoluble product. After cooling and filtering, there was obtained 9.3 g (77%) of (±)-1,1-diphenyl-1,3-butanediol: mp 80–82°C; ir ($CHCl_3$): 3571 (s), 3531–3111 (s, br), 3091–2791 (s), 1981–1721 (w), 1596 (w), 1491 (s), 1451 (s), 1376 (s), 1131 (s), 1066 (s) cm^{-1}; nmr ($CDCl_3$) δ: 1.10 (3H, d, *J* 6 Hz), 2.30 (2H, m), 3.23 (1H, br d, *J* 3 Hz), 3.73 (1H, br m), 4.85 (1H, s), 7.30 (10H, m). *Anal.* calcd. for $C_{16}H_{18}O_2$: C 79.31, H 7.49; found: C 79.46, H 7.55.

(S)-(+)-1,1-Diphenyl-1,3-butanediol (12)

The procedure is identical to that for the preparation of (±)-1,1-diphenyl-1,3-butanediol except that (*S*)-(−)-propylene oxide (22), $[\alpha]_D^{29}$ −8.7 was used. The yield of (*S*)-(+)-1,1-diphenyl-1,3-butanediol was 84% and gave mp 105–107°C; $[\alpha]_{Hg}^{24}$ +65.4 ± 0.5 (*c* 1.02, $CHCl_3$). The ir and nmr spectra were identical with those of racemic diol. *Anal.* calcd. for $C_{16}H_{18}O_2$: C 79.31, H 7.49; found: C 79.34, H 7.36.

Can. J. Chem. Downloaded from www.nrcresearchpress.com by 210.87.254.42 on 09/06/12
For personal use only.

Can. J. Chem. Downloaded from www.nrcresearchpress.com by 210.87.254.42 on 09/06/12
For personal use only.

(±)-1,3-Dimethoxy-1,1-diphenylbutane (9)

To a slurry of 19.7 g (0.821 mol) of sodium hydride in 250 mL of dry THF at 25°C was added dropwise (30 min) a solution of 25.6 g (0.106 mol) of (±)-1,1-diphenyl-1,3-butanediol in 250 mL of dry THF. After a 2-h reflux, the reaction mixture was cooled (0°C) and 106 mL (1.70 mol) of freshly distilled methyl iodide was added dropwise (15 min). The reaction mixture was stirred at 25°C for an additional 15 h, poured slowly with stirring onto 2000 g of ice, and extracted twice with ether. The combined ethered extracts were washed with saturated ammonium chloride, water, saturated sodium chloride, dried over anhydrous sodium sulfate, and concentrated *in vacuo* to afford 27.9 g of product. The tlc analysis with hexane–ether (1:1) showed two components. The mixture was separated into two portions by flash chromatography (hexane bed). Eluting first with hexane and then with 10% ether in hexane gave 20.8 g (73%) of 1,3-dimethoxy-1,1-diphenylbutane. Elution continued with ether gave 5.0 g of impure 1,3-dimethoxy-1,1-diphenylbutane. Distillation of the 20.8-g portion gave 19.0 g of (±)-1,3-dimethoxy-1,1-diphenylbutane; bp 116–119°C (0.25 Torr (1 Torr = 133.3 Pa); mp 54–56°C; ir ($CHCl_3$): 3001–2791 (m), 1901–1745 (w), 1446 (m), 1059, 1036 (s) cm^{-1}; 270-MHz nmr ($CDCl_3$) δ: 0.96 (3H, d, $J(CH_3—H_x)$ 6 Hz), 2.34 ($1H_B$, dd, J(AB) 15 Hz, J(BX) 8 Hz), 2.67 ($1H_A$, dd, J(AB) 15 Hz, J(AX) 6 Hz), 3.03 (3H, s), 3.05 (3H, s), 3.17 ($1H_X$, m), 7.29 (10H, m). *Anal.* calcd. for $C_{18}H_{22}O_2$: C 79.96, H 8.20; found: C 80.06, H 8.31.

(S)-(−)-1,3-Dimethoxy-1,1-diphenylbutane (9)

(*S*)-(−)-**9** was prepared in an identical manner to (±)-**9**. The yield was 95% and gave bp 118–120°C (0.2 Torr); mp 52–54°C; $[\alpha]_{Hg}^{24}$ −15.4 g ± 0.7 (*c* 0.770, $CHCl_3$). The ir and nmr spectra were identical with those of (±)-**9**. *Anal.* calcd. for $C_{18}H_{22}O_2$: C 79.96, H 8.20; found: C 80.02, H 8.09.

(S)-4,4-Diphenyl-2-(tetrahydro-2-pyranoxy)butane

To a solution of lithium diphenylmethide (15°C) prepared from 50.5 g (0.301 mol) of diphenylmethane was added 34.9 g (0.301 mol) of TMEDA, 300 mL of dry ether, and 139 mL (0.30 mol) of (*S*)-1-(*p*-toluenesulfonoxy)-2-(tetrahydro-2-pyranoxy)propane in 150 mL of anhydrous ether under nitrogen. The reaction mixture was stirred at 25°C overnight, refluxed 4 h, cooled, and hydrolyzed with 100 mL of cold water. The ether layer was separated, washed with cold 3 *N* hydrochloric acid, saturated sodium bicarbonate, and saturated sodium chloride, dried over anhydrous sodium sulfate, and concentrated *in vacuo* to give an oil (80.6 g). A portion of this oil (13.9 g) was chromatographed on a column of alumina. Elution with pentane removed diphenylmethane and pentane–chloroform (1:1) gave 10.9 g of (*S*)-4,4-diphenyl-2-(tetrahydro-2-pyranoxy)butane; ir (CCl_4): 3051–3021 (w), 2938–2849 (s), 2000–1670 (w), 1596, 1491, 1451, 1376 (s), 1138, 1080, 1036, 1025 (s), 696 (s) cm^{-1}; nmr ($CDCl_3$) δ: 1.10 and 1.20 (3H, doublets, *J* 3 Hz and *J* 3 Hz), 1.37–1.93 (5H, br), 2.0–2.5 (3H, m), 3.17–4.77 (5H, m), 7.32 (10H, s). *Anal.* calcd. for $C_{21}H_{26}O_2$: C 81.25, H 8.44; found: C 81.31, H 8.42.

The remaining 66.7 g of the oil was used without further purification as described below to prepare (*S*)-(+)-4,4-diphenyl-2-butanol.

(S)-(+)-4,4-Diphenyl-2-butanol

To 66.7 g of crude (*S*)-4,4-diphenyl-2-(tetrahydro-2-pyranoxy)butane from the above experiment dissolved in 250 mL of anhydrous methanol was added 3 mL of 12 *N* hydrochloric acid. After standing 48 h, the solution was brought to neutral pH with 30 mL of saturated sodium bicarbonate. The methanol was evaporated and replaced with ether. The ether solution was dried over anhydrous sodium sulfate and concentrated *in vacuo* to give 51.4 g of product which was purified by alumina chromatography. Diphenylmethane was eluted with pentane and chloroform eluted the alcohol which was distilled to give 37.0 g of (*S*)-(+)-4,4-diphenyl-2-butanol; bp 103–105°C (0.025 Torr); $[\alpha]_{Hg}^{24}$ +33.1 ± 0.17° (*c* 2.95, $CHCl_3$). The values reported for (*R*)-(−)-4,4-diphenyl-2-butanol are bp 107–109°C (0.1 Torr); $[\alpha]_D$ −27.1 ± 0.9° (*c* 2.77, $CHCl_3$); the nmr spectrum reported is identical with that of (*S*)-(+)-4,4-diphenyl-2-butanol prepared here.

(S)-(+)-2-Methoxy-4,4-diphenylbutane (19)

To 1.4 g (0.058 mol) of sodium hydride was added a solution of 6.6 g (0.029 mol) of (*S*)-(+)-4,4-diphenyl-2-butanol in 50 mL of dry THF at 25°C and the mixture was refluxed for 2 h. The reaction mixture was cooled (25°C) and 17 g (0.12 mol) of freshly distilled methyl iodide was added. After stirring overnight, the reaction mixture was poured slowly with stirring onto ice and extracted twice with ether.The combined ethereal extracts were washed with saturated ammonium chloride, water, saturated sodium chloride, dried over anhydrous sodium sulfate, and concentrated *in vacuo* to give 7.2 g of product which was distilled to yield 5.5 g (79%) of (*S*)-(+)-2-methoxy-4,4-diphenylbutane; bp 150–151°C (3.0 Torr); mp 39–40°C $[\alpha]_{Hg}^{25}$ +19.2 ± 0.2° (*c* 2.10, $CHCl_3$); ir (CCl_4): 3098–3038 (m), 2978–2838 (s), 1946–1754 (w), 1598, 1496, 1453, 1377 (s), 1143, 1083 (s), 693 (s) cm^{-1}; nmr ($CDCl_3$) δ: 1.12 (3H, d, *J* 6 Hz), 2.17 (2H, m), 2.83–3.47 (1H, m), 3.20 (3H, s), 4.2 (1H, dd, *J* 6.3, 7 Hz), 7.2 (10H, s). *Anal.* calcd. for $C_{17}H_{20}O$: C 84.96, H 8.39; found: C 85.03, H 8.35.

General procedure for preparing metal dispersions (ref. 29)

The desired amount of metal was rinsed with heptane to remove mineral oil, cut into small pieces, and placed in a dry 500-mL Morton-type flask along with 25 mL of a dry hydrocarbon solvent (methylcyclohexane was used in the case of potassium, decane was used for sodium, and dodecane was used for lithium) under an atmosphere of dry argon. The flask was heated until the solvent boiled and the metal was molten. The heating mantle was quickly replaced by a metal pail loosely packed with glass wool and the contents of the flask were stirred at high speed (7500 rpm) for 1 min. The flask was then allowed to cool slowly. A change of solvent was made by removing the hydrocarbon solvent with a syringe attached to a long needle. The high-speed stirrer was replaced by a glass-enclosed magnetic stirring bar.

Reaction of (±)-1,3-dimethoxy-1,1-diphenylbutane (9) with lithium in methylcyclohexane

A lithium dispersion was made from 0.104 g (0.0151 g-atom; 2.45 cm of 1/8-in. diameter wire) of lithium in dodecane under an argon atmosphere. The dodecane was replaced with 25 mL dry methylcyclohexane. To this dispersion was added 0.405 g (0.0015 mol) of (±)-1,3-dimethoxy-1,1-diphenylbutane as a solid and the mixture was stirred at reflux for 72 h. The progress of the reaction was monitored by glpc on column C at 24-h intervals to check for the disappearance of starting material and for an increase in the amount of product, 1-methyl-2,2-diphenylcyclopropane. The starting material disappeared within 48 h and there was no further increase in the amount of 1-methyl-2,2-diphenylcyclopropane during the next 24 h, as shown by a constant area ratio between 1-methyl-2,2-diphenylcyclopropane and 2-methoxy-4,4-diphenylbutane. The color of the reaction solution throughout reflux varied from an initial yellow or green to gray. After the usual work-up procedure, the product mixture (0.880 g) was separated by hplc using 5% ether in heptane into 0.529 g of a hydrocarbon mixture containing dodecane and 1-methyl-2,2-diphenylcyclopropane, 0.159 g (44%) of 2-methoxy-4,4-diphenylbutane, and 0.0585 g (15%) of 3-methoxy-1,1-diphenyl-1-butanol. The 0.529-g hydrocarbon fraction was resubmitted to hplc separation with heptane as eluant to give 0.102 g (33%) of 1-methyl-2,2-diphenylcyclopropane. Products present in trace amounts were not identified. The nmr spectrum for each was identical with that of an authentic sample.

Reaction of (S)-(−)-1,3-dimethoxy-1,1-diphenylbutane with sodium in methylcyclohexane

A sodium dispersion was made from 0.240 g (0.0104 g-atom) of sodium in decane under an argon atmosphere. The decane was replaced with 17 mL of dry methylcyclohexane. To this dispersion was added 0.272 g (0.0010 mol) of (*S*)-(−)-1,3-dimethoxy-1,1-diphenylbutane as a solid and the mixture was refluxed 24 h. During this time, an orange color developed and disappeared. After the usual work-up procedure, the product mixture (0.215 g) was analyzed by gc on column C and found to contain two components which were separated by hplc using 5% ether in heptane to give 0.131 g (63%) of (*R*)-(−)-1-methyl-2,2-diphenylcyclopropane and 0.0451 g (19%) of

Can. J. Chem. Downloaded from www.nrcresearchpress.com by 210.87.254.42 on 09/06/12
For personal use only.

(*S*)-(+)-2-methoxy-4,4-diphenylbutane. The (*R*)-(−)-1-methyl-2,2-diphenylcyclopropane was further purified by Kugelrohr distillation (120°C bath, 0.4 Torr) and gave $[\alpha]_{Hg}^{24}$ −144.5 ± 0.8° (*c* 0.628, $CHCl_3$), 96% optical purity. The (*S*)-(+)-2-methoxy-4,4-diphenylbutane, without further purification, gave $[\alpha]_{Hg}^{24}$ +20.2 ± 0.8° (*c* 0.60, $CHCl_3$), 100% optical purity. The nmr spectrum for each was identical with that of an authentic sample.

Reaction of (±)-1,3-dimethoxy-1,1-diphenylbutane (9) with potassium in methylcyclohexane

A potassium dispersion was made from 0.660 g (0.0169 g-atom) of potassium in 25 mL of dry methylcyclohexane under an argon atmosphere. To this dispersion was added 0.412 g (0.0015 mol) of (±)-1,3-dimethoxy-1,1-diphenylbutane as a solid and the mixture stirred at reflux for 24 h. The reaction mixture became dark red immediately and the color was maintained during reflux. After the usual work-up procedure, the product mixture (0.359 g) was separated by hplc using 5% ether in heptane into 0.0257 g of a hydrocarbon mixture, 0.217 g (60%) of 2-methoxy-4,4-diphenylbutane, 0.0414 g (11%) of 3-methoxy-1,1-diphenyl-1-butanol, and two minor components which were not identified. Analysis of the hydrocarbon mixture by gc on columns A and C showed three components that gave enhancement with authentic samples of 1-methyl-2,2-diphenylcyclopropane, 1,1-diphenylbutane, and 1,1-diphenyl-1-butene. Quantitative glpc analysis on column A with diphenylmethane as internal standard gave the following yields: <1% of 1-methyl-2,2-diphenylcyclopropane, 1.5% of 1,1-diphenylbutane, and 4.0% of 1,1-diphenyl-1-butene. The nmr spectrum for each pure component was identical with that of an authentic sample.

Reaction of (S)-(−)-1,3-dimethoxy-1,1-diphenylbutane (9) with lithium in tetrahydrofuran

A lithium dispersion was made from 0.069 g (0.010 g-atom; 1.6 cm of 1/8-in. diameter wire) of lithium in dodecane under an argon atmosphere. The dodecane was replaced with 17 mL of dry THF. To this dispersion was added 0.271 g (0.0010 mol) of (*S*)-(−)-1,3-dimethoxy-1,1-diphenylbutane as a solid and the mixture was stirred at 25°C for 27 h. A red color developed and persisted after 2 h of rapid stirring. After the usual work-up procedure, the product mixture (0.282 g) was analyzed by gc on column C and found to contain five components which were separated by hplc using 5% ether in heptane into 0.217 g of a hydrocarbon mixture, 0.0796 g (33%) of (*S*)-(+)-2-methoxy-4,4-diphenylbutane with $[\alpha]_{Hg}^{24}$ +19.0 ± 0.3° (*c* 1.59, $CHCl_3$) and 99% optical purity, and 0.0115 g (4.5%) of (*S*)-(+)-3-methoxy-1,1-diphenyl-1-butanol with $[\alpha]_{Hg}^{24}$ +34.7 ± 2° (*c* 0.230, $CHCl_3$) and unknown optical purity. Analysis of the hydrocarbon mixture by gc on columns A and C showed four components that gave enhancement with authentic samples of 1-methyl-2,2-diphenylcyclopropane, 1,1diphenylbutane, 1,1-diphenyl-1-butene, and dodecane. The dodecane was removed by preparative tlc with heptane to give 0.0629 g of an aromatic hydrocarbon mixture which was distilled by the Kugelrohr method to yield 0.0387 g which gave $[\alpha]_{Hg}^{24}$ −100.4 ± 0.8° (*c* 0.610, $CHCl_3$), 66.7% optical purity. Quantitative gc analysis on column A with diphenylmethane as internal standard showed the mixture to be composed of 67.5% (*R*)-(−)-1-methyl-2,2-diphenylcyclopropane, 17.3% of 1,1-diphenylbutane, and 15.1% of 1,1-diphenyl-1-butene, and the corrected specific rotation for (*R*)-(−)-1-methyl-2,2-diphenylcyclopropane is $[\alpha]_{Hg}^{24}$ −148.7 ± 0.8° (99% optical purity). The yields based on internal standardization are 20% of (*R*)-(−)-1-methyl-2,2-diphenylcyclopropane, 5.2% of 1,1-diphenylbutane, and 4.6% of 1,1-diphenyl-1-butene. The nmr spectrum for each pure component was identical with that of an authentic sample.

Reaction of (±)-1,3-dimethoxy-1,1-diphenylbutane (9) with lithium in tetrahydrofuran

A lithium dispersion was made from 0.104 g (0.0151 g-atom; 2.45 cm of 1/8-in. diameter wire) of lithium in dodecane under an argon atmosphere. The dodecane was replaced with 25 mL of dry THF. To this dispersion was added 0.405 g (0.0015 mol) of (±)-1,3-dimethoxy-1,1-diphenylbutane as a solid and the mixture stirred at 25°C, becoming red and decoloring in 72 h. After the usual work-up procedure, the product mixture (0.391 g) was separated by hplc using 5% ether in heptane into 0.149 g of a hydrocarbon mixture, 0.124 g (34%) of 2-methoxy-4,4-diphenylbutane, 0.0160 g (4.2%) of 3-methoxy-1,1-diphenyl-1-butanol, and a minor component which was not identified. Analysis of the hydrocarbon mixture by gc on columns A and C showed four components that gave enhancement with authentic samples of 1-methyl-2,2-diphenylcyclopropane, 1,1-diphenylbutane (under these conditions, in a separate experiment, it was found that **11** formed 1,1-diphenylbutane), 1,1-diphenyl-1-butene, and dodecane. Quantitative gc analysis on column A with diphenylmethane as internal standard gave the following yields: 32% of 1-methyl-2,2-diphenylcyclopropane, 4.8% of 1,1-diphenylbutane, and 5.7% of 1,1-diphenyl-1-butene. The nmr spectrum for each pure component was identical with that of an authentic sample.

Reaction of (±)-1,3-dimethoxy-1,1-diphenylbutane (9) with sodium in tetrahydrofuran

A sodium dispersion was made from 0.350 g (0.0152 g-atom) of sodium in decane under an argon atmosphere. The decane was replaced with 25 mL of dry THF. To this dispersion was added 0.407 g (0.0015 mol) of (±)-1,3-dimethoxy-1,1-diphenylbutane as a solid and the mixture stirred at 25°C for 40 h and at reflux for 24 h, since gc analysis on column A of a sample showed minor conversion to 1-methyl-2,2-diphenylcyclopropane at 25°C. After the usual work-up procedure, the product mixture (0.338 g) was separated by hplc using 5% ether in heptane into 0.0415 g of a hydrocarbon mixture, 0.131 g (50%) of 2-methoxy-4,4-diphenylbutane, 0.114 g (28%) of 1,3-dimethoxy-1,1-diphenylbutane, 0.0232 g (8.2%) of 3-methoxy-1,1-diphenyl-1-butanol, and a minor component which was not identified. Analysis of the hydrocarbon mixture by gc on columns A and C showed three components that gave enhancement with authentic samples of 1-methyl-2,2-diphenylcyclopropane, 1,1-diphenylbutane, and 1,1-diphenyl-1-butene. Quantitative gc analysis on column A with diphenylmethane as internal standard gave the following yields: 7.7% of 1-methyl-2,2-diphenylcyclopropane, <1% of 1,1-diphenylbutane, and 2.6% of 1,1-diphenyl-1-butene. The nmr spectrum for each pure component was identical with that of an authentic sample.

Reaction of (±)-1,3-dimethoxy-1,1-diphenylbutane (9) with potassium in tetrahydrofuran

A potassium dispersion was made from 0.590 g (0.0151 g-atom) of potassium in methylcyclohexane under an argon atmosphere. The methylcyclohexane was replaced with 25 mL of dry THF. To this dispersion was added 0.407 g (0.0015 mol) of (±)-1,3-dimethoxy-1,1-diphenylbutane as a solid and the mixture stirred at 25°C for 40 h and at reflux for 24 h, since gc analysis on column A of a sample showed minor conversion to the 1-methyl-2,2-diphenylcyclopropane at 25°C. After the usual work-up procedure, the product mixture (0.339 g) was separated by hplc using 5% ether in heptane into 0.0313 g of a hydrocarbon mixture, 0.223 g (62%) of 2-methoxy-4,4-diphenylbutane, 0.0132 g (3.4%) of 3-methoxy-1,1-diphenyl-1-butanol, and a minor component which was not identified. Analysis of the hydrocarbon mixture by gc on columns A and C showed three components that gave enhancement with authentic samples of 1-methyl-2,2-diphenylcyclopropane, 1,1-diphenylbutane, and 1,1-diphenyl-1-butene. Quantitative gc analysis on column A with diphenylmethane as internal standard gave the following yields: <1% of 1-methyl-2,2-diphenylcyclopropane, 2.0% of 1,1-diphenylbutane, and 4.5% of 1,1-diphenyl-1-butene. The nmr spectrum for each pure component was identical with that of an authentic sample.

Reaction of (±)-1,3-dimethoxy-1,1-diphenylbutane (9) with potassium in tetrahydrofuran and cation exchange with lithium perchlorate

A potassium dispersion was made from 0.600 g (0.0153 g-atom) of potassium in methylcyclohexane under an argon atmosphere. The methylcyclohexane was replaced with 25 mL of dry THF. To this dispersion was added 0.405 g (0.0015 mol) of (±)-1,3-dimethoxy-1,1-diphenylbutane as a solid and the mixture stirred at 25°C for 3 h, becoming deep red. The red solution was filtered through a Schlenck apparatus (medium frit; 0.25-Torr vacuum) into a receiving

flask containing a glass-covered magnetic stirrer and anhydrous $LiClO_4$ which was prepared by treating under vacuum (250°C bath, 0.25 Torr) of 1.0 g (0.009 mol) of $LiClO_4 \cdot 3H_2O$ for 20 min, resolidifying, and storing under an argon atmosphere. The reaction flask and Schlenck apparatus were rinsed with 5 mL of dry THF and the receiving flask was maintained under argon as the reaction mixture stirred for 23 h and complete decolorization occurred. After the usual work-up procedure, the product mixture (0.341 g) was analyzed by gc on column C and found to contain four main components which were separated by hplc using 5% ether in heptane into 0.0820 g (28%) of 1-methyl-2,2-diphenylcyclopropane, 0.137 g (41%) of 2-methoxy-4,4-diphenylbutane, 0.0193 g (4.8%) of 1,3-dimethoxy-1,1-diphenylbutane, 0.0187 g (5.2%) of 3-methoxy-1,1-diphenyl-1-butanol, and a minor component which was not identified. The nmr spectrum for each pure component was identical with that of an authentic sample.

Acknowledgement

Acknowledgement is made to the donors of The Petroleum Research Fund, administered by the American Chemical Society, for support of this research.

1. P. YATES and C. D. ANDERSON. J. Am. Chem. Soc. **85**, 2937 (1963).
2. C. L. BUMGARDNER. J. Am. Chem. Soc. **83**, 4423 (1961).
3. D. J. CRAM. Fundamentals of carbanion chemistry. Academic Press, New York, NY. 1965. pp. 243–256.
4. W. H. SAUNDERS, JR. and A. F. COCKERILL. Mechanisms of elimination reactions. Wiley Interscience, New York, NY. 1973. pp. 566–586.
5. A. F. COCKERILL. Elimination reactions. *In* Comprehensive chemical kinetics. Vol. 9. *Edited by* C. H. Bamford and C. F. H. Tipper. Eds., Elsevier, Amsterdam. 1973. pp. 328–343.
6. G. KÖBRICH and A. BAUMANN. Angew. Chem. Int. Ed. Engl. **12**, 856 (1973).
7. O. BRUNNER and P. HANKE. Monatsh. Chem. **83**, 1485 (1952).
8. N. RABJOHN and M. S. COHEN. J. Am. Chem. Soc. **74**, 6290 (1952).
9. M. CHASTRETTE, G. P. AXIOTIS, and R. GAUTHIER. C. R. Acad. Sci. Ser. C, 697 (1978).
10. T. SUGITA, J. NAKAGAWA, K. NISHIMOTO, Y. KASAI, and K. ICHIKAWA. Bull. Chem. Soc. Jpn. **52**, 871 (1979).
11. R. H. STALEY and J. L. BEAUCHAMP. J. Am. Chem. Soc. **97**, 5920 (1975).
12. D. J. CRAM and D. R. WILSON. J. Am. Chem. Soc. **85**, 1245 (1963).
13. A. I. MYERS. Acc. Chem. Res. **11**, 375 (1978).
14. G. HELMCHEN, A. SALIM, D. DORSCH, and I. TAUFER. Tetrahedron Lett. 3213 (1983).
15. S. MASAMUNE, J. W. ELLINGHOE, and W. CHOY. J. Am. Chem. Soc. **104**, 5526 (1982).
16. E. BOERHORST, R. F. SCHMITZ, and G. W. KLUMPP. Tetrahedron Lett. 3347 (1975).
17. K. G. TAYLOR, W. E. HOBBS, and M. SAQUET. J. Org. Chem. **136**, 369 (1971).
18. (*a*) D. A. EVANS, G. C. ANDREWS, and B. BUCKWALTER. J. Am. Chem. Soc. **96**, 5560 (1974); (*b*) R. D. LITTLE and J. R. DAWSON. J. Am. Chem. Soc. **100**, 4607 (1978).
19. E. STANDE and F. PATAT. *In* The chemistry of the ether linkage. *Edited by* S. Patai. Interscience, New York, NY. 1967. pp. 70–73.
20. H. M. WALBORSKY and C. G. PITT. J. Am. Chem. Soc. **84**, 4831 (1962).
21. B. Z. ASKINAZI and D. V. IOFFE. Zh. Org. Khim. **3**, 367 (1967).
22. R. G. GHIRARDELLI. J. Am. Chem. Soc. **95**, 4987 (1973).
23. H. M. WALBORSKY and J. B. PIERCE. J. Org. Chem. **33**, 4102 (1968).
24. T. E. HOGEN-ESCH and J. SMID. J. Am. Chem. Soc. **88**, 307 (1966); R. WAACK, M. A. DORAN, and P. E. STEVENSON. J. Am. Chem. Soc. **88**, 2109 (1966); M. SWARC, A. STREITWIESER, and P. C. MOWERY. *In* Ions and ion-pairs in organic reactions. Vol. 2. *Edited by* M. Swarc. Wiley Interscience, New York, NY. 1974. p. 167.
25. A. SZERHEGYI, J. CHANDHURI, E. FRANTA, and M. SWARC. J. Am. Chem. Soc. **89**, 7129 (1967).
26. R. T. SANDERSON. Chemical periodicity. Reinhold Publishing Corp., New York, NY. 1960. p. 312.
27. T. E. HOGEN-ESCH. *In* Advances in physical organic chemistry. Vol. 15. *Edited by* V. Gold and D. Bethell. Academic Press, New York. 1977. p. 205.
28. H. M. WALBORSKY and F. J. IMPASTATO. J. Am. Chem. Soc. **81**, 5835 (1959).
29. R. A. BENKESER, A. E. TRAVILLYAN, and J. HOOZ. J. Am. Chem. Soc. **84**, 4971 (1962).

Can. J. Chem. Downloaded from www.nrcresearchpress.com by 210.87.254.42 on 09/06/12
For personal use only.

Controlled coupling of aminoglycoside antibiotics to proteins for use in homogeneous enzyme immunoassays

PRITHIPAL SINGH,[1] MARCEL PIRIO, DANTON K. LEUNG, AND YUH-GENG TSAY
Syva Company,[2] Palo Alto, CA 94303, U.S.A.

Received March 23, 1984

This paper is dedicated to Professor Peter Yates on the occasion of his 60th birthday

PRITHIPAL SINGH, MARCEL PIRIO, DANTON K. LEUNG, and YUH-GENG TSAY. Can. J. Chem. **62**, 2471 (1984).

Selective *N*-acylation of aminoglycoside antibiotics with the *N*-hydroxysuccinimide ester of methyldithioacetic acid, followed by reaction with methanethiol or dithioerythritol, gives sulfhydryl labeled antibiotics. Alternatively, the nucleophilic sulfhydryl group is incorporated into an antibiotic by treatment with *N*-acetyl-*d,l*-homocysteine thiolactone. These derivatives couple readily with proteins that have previously been modified with bromoacetylglycyl groups to provide conjugates for use in the development of homogeneous enzyme immunoassays.

PRITHIPAL SINGH, MARCEL PIRIO, DANTON K. LEUNG et YUH-GENG TSAY. Can. J. Chem. **62**, 2471 (1984).

La *N*-acylation sélective d'antibiotiques aminoglycosidiques, à l'aide de l'ester *N*-hydroxysuccinimide de l'acide méthyldithioacétique, suivie d'une réaction avec du méthanethiol ou du dithioérythritol conduit à des antibiotiques portant des groupes sulfhydryles marqués. On peut aussi incorporer le groupe sulfhydryle nucléophile dans un antibiotique en le faisant réagir avec de la *N*-acétyl *d,l*-homocystéine thiolactone. Grâce à un couplage facile de ces dérivés avec des protéines qui auraient préalablement été modifiées à l'aide de groupes bromoacétylglycyles, on peut obtenir des dérivés conjugués qui peuvent être utilisés pour développer des méthodes immunologiques homogènes de détermination des enzymes.

[Traduit par le journal]

Can. J. Chem. Downloaded from www.nrcresearchpress.com by 210.87.254.5 on 09/06/12
For personal use only.

Aminoglycoside antibiotics, products of mold metabolites, are commonly given intravenously to patients suffering from severe infection of Gram-negative bacteria. Serious oto- and nephrotoxic side effects are often encountered during the course of therapy (1, 2). This generally happens when the concentration of an antibiotic in patient blood is kept abnormally high for an extended period of time. The optimum therapeutic window for these antibiotics, which differs somewhat from drug to drug, is narrow (3). For example, in serum the therapeutic range of the two most commonly used drugs, gentamicin and tobramycin, is between 2–8 μg/mL while that of amikacin, a semi-synthetic antibiotic, is between 5–25 μg/mL. Titration of the plasma concentration of these antibiotics is often practiced as an aid to therapy and to decrease the risk of undesirable side effects during the course of treatment.

A number of analytical methods based on chromatographic, microbiological, and immunochemical techniques have been used to monitor blood level concentration of aminoglycosides (4, 5). Homogeneous enzyme immunoassay (EMIT®)[3] (6, 7), one of the more versatile immunochemical methods, has found wide acceptance by commercial clinical laboratories for routine monitoring of drugs in biological fluid. It utilizes drug specific antibodies and drug enzyme conjugate as the key reagents. The antidrug antibodies are generally harvested from animals injected at regular intervals with immunogens (drugs coupled to proteins). The conjugates are readily prepared by reacting an activated carboxylic acid derivative of an appropriately functionalized drug with the amino groups of enzymes and carrier proteins. Since the aminoglycoside antibiotics, **1**–**6**, are polyamino compounds (Fig. 1), this coupling method is of limited application for preparation of their protein conjugates. Activation of their carboxylic acid derivatives would result in polymerization. During the course of development of EMIT assays for these antibiotics, we solved this problem by application of a novel three-stage heterobifunctional coupling method (8, 9). It involves (*a*) selective modification of an antibiotic with a nucleophilic sulfhydryl group, (*b*) labeling of the protein with electrophilic bromoacyl groups, (*c*) coupling under gentle experimental conditions.

Although a host of nucleophilic and electrophilic groups can be considered (10), the sulfhydryl and bromoacyl groups were preferred for ease of their reactivity at 0°C in aqueous buffered media.

Appropriately derivatized antibiotics (haptens)[4] are required to achieve their chemical attachment to proteins. Preparation of gentamicin, amikacin, and tobramycin haptens requires only subtle chemical modifications in such a way that most of the structural integrity of these drugs is kept intact. Only a limited chemistry of these aminoglycosides has been reported in the literature. This is presumably due to their complex structures and insolubility in most of the organic solvents. Our approach to preparing their haptens rests on modification of the antibiotic amines with a sulfhydryl group. Because of the general lability of sulfhydryl groups to aerial oxidation, the antibiotic was selectively acylated with methyldithioacetic acid. Cleavage with dithioerythritol or methanethiol gave the desired drug hapten. Alternatively, the nucleophilic suflhydryl group was generated by controlled reaction of an antibiotic with *N*-acetyl-*d,l*-homocysteine thiolactone.

Proteins were modified with a number of bromoacetylglycyl groups. Coupling with the sulfhydryl haptens afforded the desired drug immunogens and the drug enzyme conjugates (Scheme 1).

Gentamicin hapten

Perhaps the most commonly utilized antibiotic of its class, gentamicin is available as a mixture of at least three components, **1**–**3**. It is commonly resolved through liquid–liquid partition chromatography (11). This method is both tedious and time consuming. Because of the quantities of material needed,

[1] Author to whom corespondence may be addressed.

[2] Contribution no. 106 from Syva Research Department.

[3] EMIT® is a trademark for homogenous enzyme immunoassays and is held by Syva Corporation, Palo Alto, California.

[4] A hapten is a compound carrying suitable functionalities, for coupling to proteins.

FIG. 1. Chemical structures for some of the commonly used aminoglycoside antibiotics.

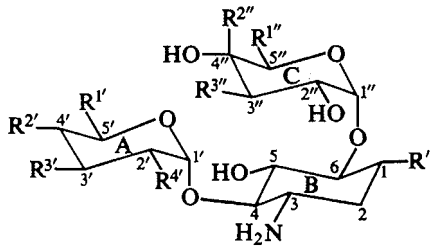

Antibiotic	R^1	$R^{1'}$	$R^{2'}$	$R^{3'}$	$R^{4'}$	$R^{1''}$	$R^{2''}$	$R^{3''}$
1 Gentamicin C_1	NH_2	$CH(CH_3)NHCH_3$	H	H	NH_2	H	CH_3	$NHCH_3$
2 Gentamicin C_1a	NH_2	CH_2NH_2	H	H	NH_2	H	CH_3	$NHCH_3$
3 Gentamicin C_2	NH_2	$CHCH_3NH_2$	H	H	NH_2	H	CH_3	$NHCH_3$
4 Tobramycin	NH_2	CH_2NH_2	OH	H	NH_2	CH_2OH	H	NH_2
5 Kanamycin A	NH_2	CH_2NH_2	OH	OH	OH	CH_2OH	H	NH_2
6 Amikacin	NH $\vert$ $COCH(OH)(CH_2)_2NH_2$	CH_2NH_2	OH	OH	OH	CH_2OH	H	NH_2

Protein — Drug

Protein—[Lys-$NHCOCH_2NHCOCH_2Br$]$_n$ + Drug—$NHCO\sim SH$

Protein—[Lys-$NHCOCH_2NHCOCH_2S\sim COHN$—Drug]$_n$

Protein = bovine serum albumin, glucose-6-phosphate dehydrogenase
Drug = Gentamicin C_1, amikacin, tobramycin

SCHEME 1. Selective coupling of aminoglycosides to proteins.

we considered this procedure to be less attractive and developed a more practical high-pressure liquid chromatographic method for separation. Gram quantities of the pure, individual components are readily available by using this technique.

Each of the antibiotic components **1**–**3** has a number of amino and hydroxyl functionalities. Since gentamicin C_1, **1**, has the least number of primary amino groups and the design of a hapten involved selective *N*-acylation, it was chosen as a starting material. The more reactive $R^{4'}$ amino group was protected by reaction with *S*-ethyl trifluorothioacetate (12). Careful acylation of the product **7** with the *N*-hydroxysuccinimide

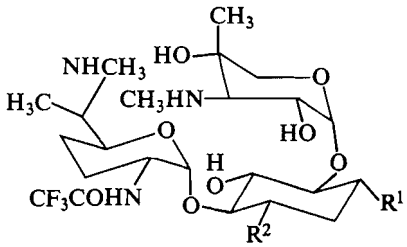

7 $R^1 = R^2 = NH_2$
8 $R^1 = R^2 = NHCOCH_2SSCH_3$
9 $R^1 = R^2 = NHCOCH_2SH$

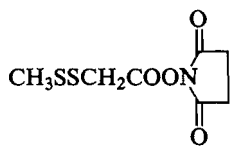

10

ester of methyldithioacetic acid, **10**, gave a mixture from which diacylated compound **8** was isolated in moderate yields. A small amount of a by-product, considered to be a monoacylated derivative (R^1 or R^2 = $NHCOCH_2SSCH_3$ in **8**) by nmr analysis, could also be obtained. All attempts to improve the yield of the

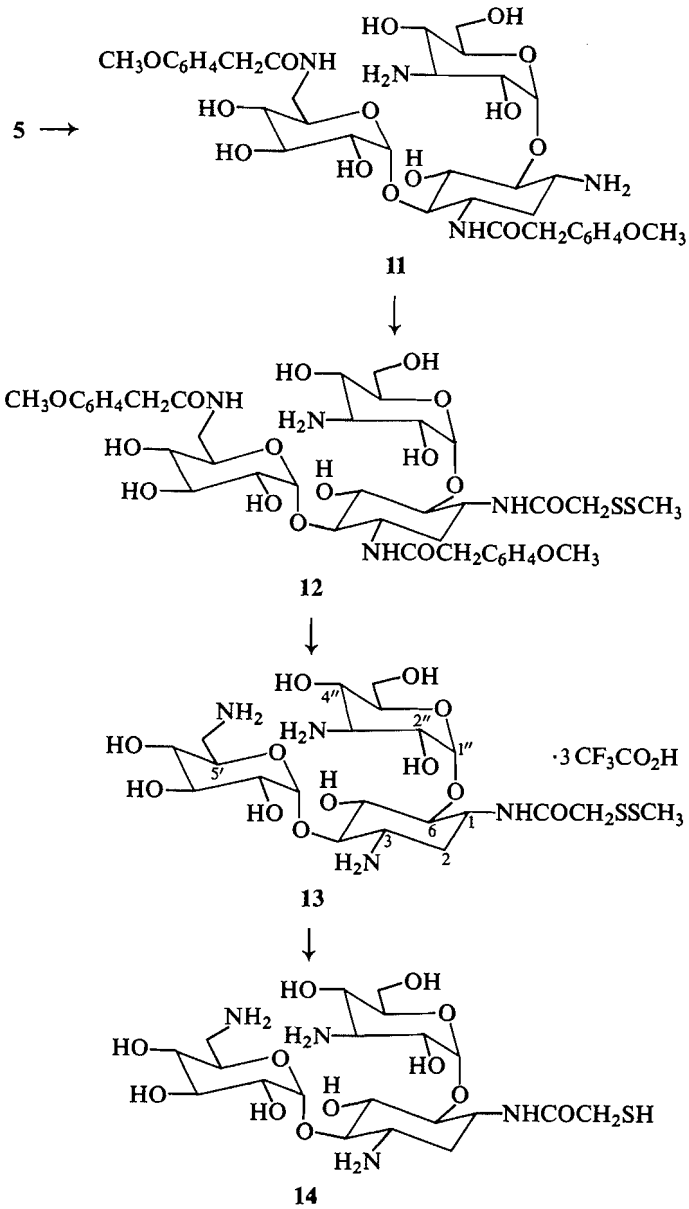

11

12

13

14

Can. J. Chem. Downloaded from www.nrcresearchpress.com by 210.87.254.5 on 09/06/12
For personal use only.

TABLE 1. Carbon-13 chemical shifts, δ values, of kanamycin A, amikacin, and amikacin pro-hapten (structurally significant carbons)

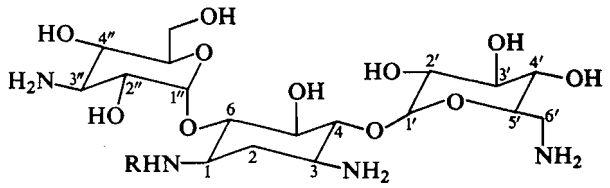

5 R = H, kanamycin A
6 R = $COCH(OH)CH_2CH_2NH_2$, amikacin
13 R = $COCH_2SSCH_3$, amikacin pro-hapten

Carbon nucleus	Kanamycin A			Amikacin			Amikacin pro-hapten		
	pH ≤4	≥11	Δ	≤4	≥11	Δ	≤4	≥11	Δ
1	50.6	51.2		49.5	50.4		49.9	50.4	
2	28.2	35.8	−7.6	30.8	35.0	−4.2	31.0	35.0	−4.0
3	48.4	49.6		48.6	49.4		48.6	49.5	
4	78.8	86.8	−8.0	79.9	87.7	−7.8	80.0	87.6	−7.6
5	73.4	74.9		73.2	75.4		73.2	75.2	
6	84.5	88.5	−4.0	81.2	81.3	0	81.7	82.0	−0.3
5′	69.4	73.0	−3.6	69.5	73.8	−4.3	69.5	73.7	−4.2
2″	68.9	72.5	−3.6	68.8	72.9	−3.9	68.7	72.7	−4.0
4″	66.3	70.0	−3.7	66.4	70.2	−3.8	66.4	70.1	−3.7

monoacylated product failed. The bismethyldithioacetyl derivative was cleaved to hapten **9** with methanethiol for *in situ* coupling to the bromoacetylglycyl modified enzyme, glucose-6-phosphate dehydrogenase (G6PDH) (8).

Amikacin hapten

A relatively new member in its class for treatment of Gram-negative bacteria, amikacin is particularly useful for patients having strains resistant to all other aminoglycosides (13). Hapten **14** was designed so that most of the structural topology of the drug would remain intact and exposed after coupling to proteins. Such a conjugate should produce drug specific antibodies.

Our synthetic approach for amikacin hapten **14** followed that of the parent drug from kanamycin A (14, 15). The order of reactivity for acylation of amino groups in kanamycin A, **5**, has been determined as C-6′ > C-1 > C-3 > C-3″, which makes its direct transformation to **14** by reaction with **10** less attractive. A more involved route, utilizing the protection of amino groups before acylation, was therefore followed. The C-1 and C-3″ amino groups of **5** were first protected by reacting it with nickel acetate in dimethyl sulfoxide. Treatment of the nickel complex with *p*-methoxybenzyl-5-(4,6-dimethylpyrimidine-2-yl)thiocarbonate, followed by removal of the metal with hydrogen sulfide, gave 3,6′-di-*N*-*p*-methoxybenzyloxycarbonyl kanamycin A, **11**, identical in all respects to an authentic sample (16). Based on the findings of Hanessian and Patel (17) that the vicinal C-3″ amino and C-4″ hydroxyl groups selectively complex with the Group II transition metals such as Cu^{2+} in protic media, **11** was stirred with Ni^{2+} acetate in a 1:1 mixture of tetrahydrofuran and water. The resulting nickel complex, which now has a free C-1 amino group, was then condensed with the activated methyldithioacetic acid **10**. Removal of the metal with Chelex-100® resin gave **12**, which after cleavage of the *p*-methoxybenzyloxycarbonyl protecting groups with trifluoroacetic acid afforded the desired pro-hapten **13** in an overall yield of 15% from kanamycin A. The hapten **14** was readily obtained by stirring it with dithioerythritol under an inert atmosphere for *in situ* coupling to modified proteins. The pure hapten could not be isolated, presumably due to its sensitivity to aerial oxidation.

The chemical structure **13** of the amikacin pro-hapten is in accord with its elemental analysis and spectral data. The exact site of acylation was determined from the pH-dependent ^{13}C nmr chemical shift of its carbon nuclei β to amino groups (Table 1). A change in pH from 4 to 11 caused 2,5′, 2″, and 4″ carbon nuclei to experience downfield shifts of ~4 ppm, similar to the ones observed for amikacin (18). As expected, the C-6 nucleus showed insignificant change and the shift of approximately 4 ppm in the C-2 nucleus, one half the value of the same carbon atom in kanamycin A (7.6 ppm shift), is in accord with acylation only at the C-1 amino group.

Tobramycin hapten

Our strategy to prepare its hapten directly from the parent drug by selective acylation of the C-6 amino group of **4** relied heavily on the relative basicities of the five amino groups of tobramycin, which by pH-dependent nmr studies have been reported in the order C-6′ > C-3 > (C-2′, C-3″) > C-1 (19). Such a hapten would furthermore provide the maximum exposure of the antibiotic ring C after attachment to proteins, the part of structures at which tobramycin differs substantially from gentamicins **1**–**3**. More selective anti-tobramycin antibodies are therefore expected.

Reaction of tobramycin (**4**) with the *N*-hydroxysuccinimide ester of 2,4-dinitrophenylthioglycolic acid afforded monoacylated product **15**. Analysis of its ultraviolet spectrum at 331 nm and comparison with the benzamide derivative **20** of 2,4-dinitrophenylthioglycolic acid as a model compound clearly showed that only one 2,4-dinitrophenyl moiety had been incorporated into a molecule of **4**. That the monoacylation had indeed taken place only at the C-6 amino group was in accord with the mass spectral fragmentation of the derivative **15**. As expected, appropriate fragments attributed to the cleavage of

Can. J. Chem. Downloaded from www.nrcresearchpress.com by 210.87.254.5 on 09/06/12
For personal use only.

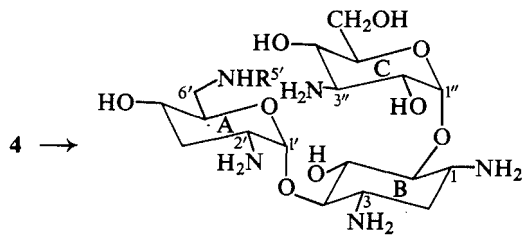

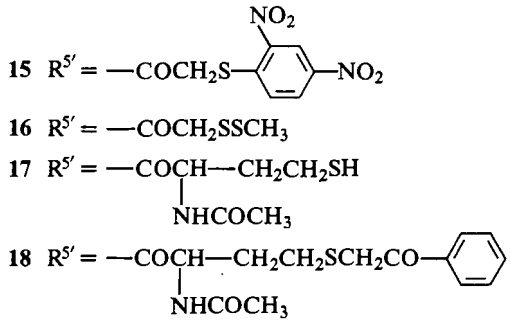

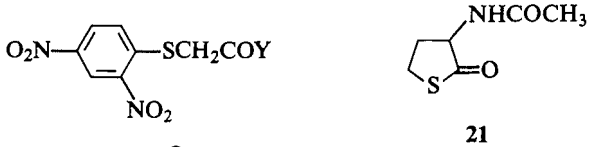

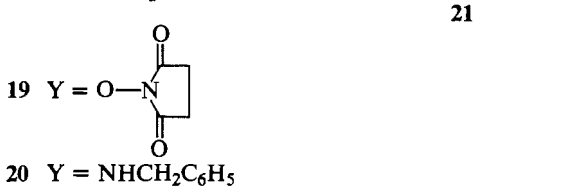

unmodified glycosidic rings B and C were observed (20).

Formation of **15** as the sole monoacylated product established that the selective acylation of tobramycin at the C-6′ amino group was indeed achievable. Our attempt to extend this reaction further by acylation with **10**, with the object of preparing the pro-hapten **16**, failed. The product had an amide carbonyl infrared absorption at 1650 cm^{-1} and showed complete absence of an SCH_3 signal in it proton nmr spectrum. We rationalize these observations as due to the presumed instability of the disulfide group in the product to the experimental conditions.

Amines are reported to open *N*-acetyl-*d,l*-homocysteine thiolactone, **21**, quantitatively (21). Our attention was therefore turned to using this thiolactone as a potential synthon for introduction of a mercapto group into tobramycin. Indeed, when aqueous tobramycin, under high dilution, was stirred under argon, with 0.5 mol-equivalents of the thiolactone **21**, a new compound **17** was obtained as the sole product by tlc analysis. That it is the monoacylated derivative **17** was proven by reaction, without further purification, with ω-bromoacetophenone and by comparing the spectral data of the product **18** with 2-hydroxyethylmercaptophenone as a model compound.

The tobramycin hapten **17**, prepared *in situ*, was used directly for coupling to bromoacetylglycyl modified G6PDH and bovine serum albumin.

Modification of proteins for coupling to aminoglycosides

Development of an EMIT® assay for an aminoglycoside antibiotic requires drug specific antibodies and active drug enzyme conjugates. The immunogens needed for raising the antibodies to antibiotics are often prepared by coupling an aminoglycoside with a carrier protein in the presence of 1-ethyl-3(3-dimethylaminopropyl)carbodiimide (EDAC). Such a method would lead to random coupling of antibiotics, resulting in an heterogeneous mixture of immunogens. This not only leads to a lot-to-lot variation for preparation of immunogens but, in our experience, elicits poor quality (low titer) antisera. As an attempt to solve this problem, the antibiotic immunogens were prepared by using a more controlled heterobifunctional coupling procedure, shown in Scheme 1. For example, the amikacin and tobramycin immunogens were readily prepared by coupling at pH ~ 8 bovine serum albumin, modified with a number of bromoacetylglycyl groups, with the sulfhydryl labeled antibiotic haptens **14** and **17**. Selective reaction of the modified proteins with the sulfhydryl groups of antibiotics is expected because of more than hundred-fold greater reactivity of thiols as compared to amino groups with bromoacyl groups (22). This is in agreement with the observation that only a single product **18** is formed upon reacting **17** with ω-bromoacetophenone under similar conditions. Use of radiolabeled drugs showed that 8–12 haptens could be readily incorporated into proteins using this procedure. Superior titer antibodies were obtained from sheep injected with these immunogens.

Labeling of the enzyme, glucose-6-phosphate dehydrogenase, with aminoglycosides using the direct EDAC coupling procedure turned out to be a more serious problem. The method afforded enzyme conjugates which were generally found inactive, presumably due to extensive polymerization, and therefore could not be used in EMIT® assays. Extension of the protocol similar to the one used for the preparation of antibiotic immunogens afforded useable enzyme conjugates. The procedure has been described previously in detail for preparation of the G6PDH–gentamicin conjugates (8). The method has now been extended for preparation of the G6PDH conjugates of other aminoglycosides, including tobramycin, netilmicin, and amikacin. These conjugates are found useful for development of their EMIT® assays (23, 24).

A brief mention of the method for preparation of the enzyme–amikacin conjugate for use in development of its EMIT® assay is provided as an example. The enzyme, G6PDH, was labeled with a number of bromoacetyl groups by reaction in a buffer at pH ~6, with bromoacetylglycyl-*N*-hydroxysuccinimide ester. The modified enzyme was then treated at 0°C, under an inert atmosphere, with the freshly prepared amikacin hapten **14** in a buffered medium at pH 8. The amikacin–G6PDH conjugate, with a residual activity of ~25% of the native enzyme, was readily inhibited by anti-amikacin antibodies. The conjugate was used to develop its EMIT® assay in the range of 2.5–50 μg/mL. The assay has the usual convenient protocol like other EMIT® assays and provides patient sample quantitation in less than a minute (6, 7).

Experimental

Melting points are uncorrected and were determined with a Thomas–Hoover capillary apparatus. The ir spectra were measured on a Perkin–Elmer 297 spectrometer and the proton nmr spectra were recorded on a 90 MHz Varian EM-390 instrument using tetramethylsilane as an internal standard. The ^{13}C nmr were taken on a Bruker WM-300 with dioxane as an internal standard and uv spectra were recorded on a Cary-15 instrument. Enzyme activity of drug–enzyme conjugates was measured on a Gilford Stasar III spectrometer. Analytical tlc analyses were performed on Analtech silica gel GF and E Merck silanized silica gel 60 plates, using 5% ammonium molybdate – sulfuric acid or 0.1% ninhydrin in isopropanol as sprays for viewing of the developed plates. Preparative tlc work was carried using Analtech 1000-μm thick silica G plates.

Can. J. Chem. Downloaded from www.nrcresearchpress.com by 210.87.254.5 on 09/06/12
For personal use only.

Can. J. Chem. Downloaded from www.nrcresearchpress.com by 210.87.254.5 on 09/06/12
For personal use only.

Separation of gentamicin isomers 1–3

Ammonia gas was bubbled through a stirring suspension of gentamicin sulfate (60 g) in 750 mL of methanol. After 3 h, the slurry was filtered and the filtrate was evaporated to give 35 g of gentamicin-free base as a white foam. The tlc analysis ($CHCl_3/CH_3OH/NH_4OH$, 10:10:3) showed two major and one minor spots.

Two silica cartridges (Waters preparative 500), in series, were equilibrated with the lower phase of a 2:1:1 mixture of chloroform, isopropanol, and 14% aqueous ammonium hydroxide. A solution of gentamicin-free base (10 g) in methylene chloride (total volume, 15 mL) was loaded onto the first column. Elution with the same mixture of solvents at 300 mL/min afforded fractions which after evaporation gave tlc pure gentamicin C_1 (**1**, 3.39 g). The elution solvent was then made more basic by changing it to the lower layer of a 2:2:1 mixture of chloroform, isopropanol, and concentrated ammonium hydroxide. The fractions were continuously monitored by analytical tlc. Pooling of the like fractions followed by evaporation afforded the remaining two components, namely gentamicin C_2 (**3**, 1.5 g) and gentamicin C_{1a} (**2**, 2.1 g).

N-*Hydroxysuccinimide ester of methyldithioacetic acid (10)*

Into a 50-mL round-bottom flask was placed 1.2 g (8.86 mmol) of methyldithioacetic acid (8), 35 mL of dichloromethane, and 1.09 g (9.54 mmol) of *N*-hydroxysuccinimide (crystallized from ethyl acetate). The solution was cooled in an ice bath, to which was then added 1.96 g (9.54 mmol) of freshly distilled *N,N'*-dicyclohexylcarbodiimide. The reaction mixture was stirred, and after 4 h the solution was filtered through a sintered glass funnel. Precipitated urea was washed with dichloromethane. The light brown filtrate was concentrated under vacuum at ambient temperature. The residue was dissolved in 10 mL of methylene chloride and applied to the top of a 2.5 × 43 cm dry glass column packed with 110 g of silanized silica gel (70–230 mesh, E Merck reagent). Elution with a mixture of hexane/methylene chloride (1:1) afforded **10** as a white solid (1.2 g, 60%). Recrystallization from methylene chloride/hexane afforded crystals, mp 79–81°C; ir (KBr): 1760, 1790, 1830 cm^{-1}; nmr ($CDCl_3$) δ: 2.5 (s, 3H, SCH_3), 2.85 (s, 4H), and 3.74 (s, 2H, CH_2); ms, *m/e*: 235 (M^+), 120, 93. *Anal.* calcd. for $C_7H_9NO_4S_2$: C 35.73, H 3.85, N 5.95, S 27.25; found: C 36.22, H 4.02, N 6.18, S 27.25.

*Preparation of 3-*N*-methyldithioacetyl-2'-*N*-trifluoroacetyl gentamicin C_1 (8)*

Into a 250-mL 3-necked round-bottom flask, equipped with an argon inlet, rubber septum, and magnetic stirrer, was placed 2'-*N*-trifluoroacetyl gentamicin C_1 (**7**, 1.5 g, 2.6 mmol), prepared from gentamicin C_1 according to the literature procedure (11), in 80 mL of dry tetrahydrofuran. To this was added dropwise over 2 h the activated ester **10** of methyldithioacetic acid (560 mg, 2.8 mmol) (8) in 15 mL dimethylformamide. The mixture was allowed to stir overnight at room temperature and the solvent was removed under reduced pressure at 40°C. Careful chromatography of the crude product on a column of silica gel using chloroform/methanol (2:1) followed by chloroform/methanol/17% NH_4OH (2:1:1) yielded two products.

The minor product, R_f 0.3 ($CHCl_3/CH_3OH$/17%NH_4OH, 2:1:1), considered to be a monoacylated derivative, exhibited the following spectral data: ir (KBr): 3300 (NH_2,OH), 1720 (CF_3CO), and 1660 (amide CO) cm^{-1}; ^1H nmr ($CDCl_3$) δ: 1.1 (d, $CHCH_3$ J = 6 Hz), 1.2 (s, CH_3), 2.4 (s, $NHCH_3$), 2.5 (s, S—CH_3), 2.7 (s, $NHCH_3$), 3.4 (s, CH_2SS). The major product, identified as **8**, had its R_f 0.6 and showed bands in its ir spectrum identical to the monoacylated derivative mentioned above. It showed signals in its nmr ($CDCl_3$) spectrum at δ: 1.1 (d, J = 6 Hz, $CHCH_3$), 1.26 (s, $C(OH)CH_3$), 3.40 (s, SCH_2CO). *Anal.* calcd. for $C_{29}H_{50}N_5O_{10}F_3S_4$: C 42.80, H 6.15, N 8.61, F 7.01, S 15.72; found: C 42.47, H 6.17, F 6.90, N 8.32, S 15.98.

*3,6'-Di-*N*-p-methoxybenzyloxycarbonyl kanamycin A (11)*

A solution of 1 *N* sodium hydroxide in deionized water was passed through a column (35 cm × 4 cm) packed with 350 mL of Bio-Rad Ag1X8 resin (20–50 mesh, chloride form) until the eluent showed a negative test for chloride ions. An aqueous solution of kanamycin A sulfate (23 g, Sigma Company) in 2 L of deionized water was then passed through the column at 8 mL/min and the solution collected. The column was further washed with 3 L of deionized water. The total eluent was concentrated under vacuum at 45°C to approximately 400 mL. Methanol (400 mL) was added to the concentrate, which was kept stirring and maintained at about 45°C. A white amorphous precipitate of the free kanamycin A (**5**), mp >245°C (dec.), was formed and collected by filtration. Treatment of the filtrate with an additional 400 mL of methanol afforded a second crop of **5**.

A solution of the kanamycin free base **5** (4.6 g, 9.5 mmol) and nickelous acetate (15 g, 60 mmol) in anhydrous DMSO was stirred in a round-bottomed flask for 30 min. A deep green solution was formed, to which was added dropwise, with stirring, *p*-methoxybenzyl-*S*-(4,6-dimethylpyrimidine-2-yl)thiocarbonate (7.22 g, 23.7 mmol) in 60 mL of DMSO. After stirring overnight the green solution was placed in a 2-L Erlenmeyer flask and treated with a liter of diethylether. The mixture was swirled vigorously, allowed to settle, and the ethereal phase decanted. This was repeated three more times, when a green semisolid material was obtained. The semisolid residue was dissolved in methanol (300 mL) and filtered. Hydrogen sulfide was slowly bubbled through the filtrate for 30 min and the reaction set aside with stirring for 24 h.

The mixture was filtered through a bed of Celite and washed with methanol. To the concentrated filtrate (~300 mL) was added an excess of ethyl acetate and the pH adjusted to 9.0 with ammonium hydroxide. The crude aminoglycoside product **11** separated out as an oily solid. The semisolid material was redissolved in a minimum amount of methanol and reprecipitated with a 1:1 mixture of acetonitrile and ethyl acetate. The solid was filtered, washed with ethyl acetate, and dried under vacuum over P_2O_5. The title compound **11** was obtained as a white solid (5.1 g, 65%), mp 220–235°C (dec.); ir (KBr): 3395 (br), 1700, 1620 cm^{-1}. Its R_f value on a silica tlc plate (CH_3OH/NH_4OH, 9.5:05) and infrared spectrum were identical to those of the authentic sample (16). *Anal.* calcd. for $C_{36}H_{52}N_4O_{17}$: C 53.19, H 6.44, N 6.89; found: C 52.99, H 6.29, N 6.90.

*1-*N*-Methyldithioacetyl-3,6'-di-*N*-p-methoxybenzyloxycarbonyl kanamycin A (12)*

A mixture of **11** (2.5 g, 3 mmol) and nickelous acetate (4 g, 16 mmol) in 100 mL of 1:1 tetrahydrofuran–water was stirred for 1 h. A deep green solution was formed. To the stirring green solution was added dropwise a solution of the activated ester **10** of methyldithioacetic acid (1 g, 4.5 mmol) in tetrahydrofuran (30 mL). The reaction mixture was stirred for 16 h and treated with an excess of Bio-Rad Chelex-100 resin. The mixture was stirred overnight and filtered. The resin was washed with a mixture of tetrahydrofuran–water (1:1) until the filtrate was free of aminoglycoside by tlc analysis. The colorless filtrate was concentrated under vacuum at 20°C, when a white suspension was formed. The mixture was centrifuged. The supernatant was removed and made alkaline to pH 9.5 with ammonium hydroxide. A white precipitate was formed and removed by centrifugation. The precipitate was washed twice with deionized water and once with methanol by repeatedly suspending and centrifuging it in these liquids. The white solid was lyophilized, affording **12** as a tlc pure white powder (1.4 g, 50%), mp 200–205°C (dec.). Its proton nmr spectrum (DMF-d_7) showed signals at δ: 2.46 (s, 3H, S—CH_3), 3.2–4.2 (m), 3.8 (s, OCH_3) 5.0 (br s, 4H, —O—CH_2 Ar), and AA'XX' doublet of a doublet centered at 7.1 (aromatics, 8H) and ir absorption bands (KBr) at 3350 (br), 1700, 1645 cm^{-1}. *Anal.* calcd. for $C_{39}H_{56}N_4O_{18}S_2$: C 50.20, H 6.05, N 6.00, S 6.87; found: C 50.50, H 6.12, N 5.90, S 6.89.

*Amikacin pro-hapten, 1-*N*-methyldithioacetyl kanamycin A, (13)*

Into a dry two-necked flask was placed 1.5 g (1.50 mmol) of **12** (previously dried at 60°C/0.1 Torr over P_2O_5 (1 Torr = 133.3 Pa) and a stream of argon was passed over it. The contents of the flask were cooled in an ice bath and 25 mL ice-cooled trifluoroacetic acid (distilled from P_2O_5) was added with swirling. After 5 min the acid, from the deep purple colored mixture, was removed at room temperature under vacuum (0.1 Torr). The residual solid material was pulverized

Can. J. Chem. Downloaded from www.nrcresearchpress.com by 210.87.254.5 on 09/06/12
For personal use only.

and washed with diethyl ether. This was repeated twice with ether and twice with dichloromethane, leaving **13** as an off-white solid. Chromatography on a 250-g silanized silica gel RP-2 column using a gradient of 0–20% of methanol in methylene chloride afforded the pure hapten as a white solid (670 mg, 45%), mp > 185°C (dec.). It showed signals in its ^{1}H nmr spectrum (CD_3OD) at δ: 2.46 (s, 3H, S—CH_3), 5.15 (br s, 1H, —O*CH*O—), 5.5 (br s, 1H, O*CH*O), along with multiplets for other protons between δ 2.8–4.4. *Anal.* calcd. for $C_{21}H_{40}N_4O_{12}S_2 \cdot 3CF_3CO_2H \cdot H_2O$: C 33.60, H 4.69, N 5.80, F 17.70, S 6.64; found: C 33.25, H 4.66, N 5.78, F 17.40, S 6.53.

The ^{13}C nmr spectrum of **13** (D_2O–dioxane) exhibited its carbon signals at the following chemical shifts: for pH ≤4.0, δ: 49.94 (C-1), 30.98 (C-2), 48.60 (C-3), 79.98 (C-4), 73.15 (C-5), 81.70 (C-6), 96.33 (C-1′), 72.86 (C-2′), 71.59 (C-3′ and C-4′), 69.54 (C-5′), 41.09 (C-6′), 98.99 (C-1″), 68.73 (C-2″), 55.98 (C-3″), 66.39 (C-4″), 73.15 (C-5″), 60.57 (C-6″), 22.76 (S—CH_3), 41.65 (S—CH_2), and 173.15 (C=O); for pH ≥11.0, δ: 50.39 (C-1), 35.02 (C-2), 49.51 (C-3), 87.62 (C-4), 75.23 (C-5), 82.02 (C-6), 99.51 (C-1′), 72.69 (C-2′), 71.82 (C-3′ and C-4′), 73.73 (C-5′), 42.27 (C-6′), 100.26 (C-1″), 72.69 (C-2″), 54.42 (C-3″), 70.29 (C-4″), 73.25 (C-5″), 61.0 (C-6″), 42.27 (S—CH_2), and 179.0 (C=O).

2,4-Dinitrophenylthioglycolic acid N-*hydroxy succinimide ester (**19**)*

To a mixture of 2,4-dinitrophenylthioglycolic acid (0.774 g, 3 mmol) and *N*-hydroxysuccinimide (0.345 g, 3 mmol) in 25 mL of freshly distilled THF at 0°C under nitrogen was added *N,N′*-dicyclohexylcarbodiimide (DCC) (0.927 g, 4.5 mmol). The mixture was stirred. After 4 h, a white precipitate was formed and was filtered. The solvent was removed from the filtrate under reduced pressure and the solid residue was triturated with 10% dichloromethane in hexanes. The solid which remained undissolved was collected by filtration. Recrystallization of the solid from ethyl acetate – DMF gave **19** as a light yellow solid (0.854 g, 80% yield), mp 198–199°C; ir (KBr): 1820, 1775, 1740 cm^{-1}; ^{1}H nmr (DMSO-d_6) δ: 8.88 (d, J = 1.5 Hz, 1H), 8.47 (q, J_1 = 5.0, J_2 = 1.5, 1H), 7.90 (d, J = 5.0 Hz, 1H), 4.85 (s, 2H), 2.83 (s, 4H). *Anal.* calcd. for $C_{12}H_9N_3O_8S$: S 40.51, H 2.55, N 11.58, S 9.17; found: C 40.56, H 2.53, N 11.83, S 9.00.

*Reaction of tobramycin with 2,4-dinitrophenylthioglycolic acid NHS ester (**19**)*

To a stirring solution of tobramycin (**4**, 0.92 g, 2 mmol) in 200 mL of water at 0°C, pH 10.76, was added very slowly a solution of 2,4-dinitrophenylthioglycolic acid NHS ester **18** (0.365 g, 1 mmol) in 25 mL of anhydrous DMF. The pH of the solution was maintained at 10.5–10.9 throughout the reaction (10% sodium hydroxide). After addition, the mixture was stirred at 0°C for 2 h and filtered. The filtrate was washed several times with ethyl acetate. The aqueous layer was evaporated to dryness under reduced pressure to give a solid residue. The solid residue was chromatographed on preparative silica gel plates, using chloroform/methanol/ammonium hydroxide (v/v 1:2:1) for elution, to give **15** as an orange solid (0.2 g, 28.3%), mp 210°C (dec.); ir (KBr): 3700–2400, 1645 cm^{-1}; uv (H_2O): 331 nm (ε 6532); EI ms, *m/e* (relative abundance): 163(8), 203(2), 306(1.5), 323(3), 351(2), 407(2.5). *Anal.* calcd. for $C_{26}H_{41}N_7O_{14}S$: S 4.53; found: S 4.74.

*Preparation of benzamide derivative **20***

To a solution of 2,4-dinitrophenylthioglycolic acid NHS ester **18** (0.19 g, 0.54 mmol) in 5 mL of anhydrous DMF at 0°C under nitrogen, was added dropwise a solution of benzylamine (0.06 g, 0.54 mmol). After addition, the mixture was stirred at 0°C for 3 h. The solvent was removed under reduced pressure to give an orange solid residue. Preparative tlc on silica plates using chloroform/methanol (95:5) gave **20** (0.16 g, 85%), which upon recrystallization from methanol gave deep yellow needles, mp 148–151°C; ir (KBr): 3300, 1640 cm^{-1}; uv (50% THF in water): 335 (ε 9000); nmr (DMSO-d_6) δ: 8.78 (d, 1H), 8.35 (q, 1H), 7.80 (d, 1H), 7.20 (s, 5H), 4.28 (d, 2H), 4.05 (s, 2H); *Anal.* calcd. for $C_{15}H_{13}N_3O_5S$: C 51.60, H 3.80, N 12.00, S 9.32; found: C 51.72, H 3.80, N 12.69, S 9.20.

*Reaction of tobramycin with activated methyldithioacetic ester (**10**)*

To a stirring solution of tobramycin (0.723 g, 1.55 mmol) in 20 mL of dimethylformamide, 20 mL of water, and 10 drops of triethylamine at 0°C and under nitrogen was added very slowly a solution of methyldithioacetic acid NHS ester (**10**, 0.364 g, 1.55 mmol) in 4 mL of anhydrous DMF. After addition, the mixture was stirred at 0°C for 2 days. The solvent was removed under reduced pressure to give a white residue. The solid residue was chromatographed on silica plates, elution with methanol/acetic acid/water (3:1:1) or methanol/chloroform/ammonium hydroxide (2:1:1) gave a solid product which showed in its ir spectrum an amide band at 1650 cm^{-1}. Its ^{1}H nmr spectrum, however, showed the absence of an S—CH_3 signal.

Reaction of tobramycin with N-*acetyl*-d,l-*homocysteine thiolactone (**21**)*

A steady stream of dry nitrogen was bubbled through a solution of tobramycin (0.934 g, 2 mmol) in 75 mL of water at pH 10.12 for 30 min. To this stirring solution was added slowly (15 drop/s) a solution of the homocysteine thiolactone **20** (0.159 g, 1 mmol, Sigma Chemicals) in 5 mL of oxygen-free tetrahydrofuran. The pH of the mixture was maintained at 10.12–10.25 throughout the addition with 10% sodium hydroxide. After addition, the mixture was stirred for 1 h. The pH of the solution was adjusted to 7 with 5% hydrochloric acid. The solution was washed carefully with oxygen-free ethyl acetate (4 × 30 mL) and the aqueous layer was collected. The pH of the solution was adjusted to 10.12 with 10% sodium hydroxide. Lyophilization of the solution gave a white solid (ca. 800 mg). The analytical silica gel tlc showed a single new product (R_f 0.39) and the unreacted starting tobramycin (R_f 0.10) using methanol/chloroform/ammonium hydroxide (2:1:1) as the solvent system.

The mixture obtained by the addition of tobramycin to *N*-acetylhomocysteine thiolactone (**4** + **17**, 700 mg) was dissolved in 25 mL of oxygen-free water. The pH of the solution was adjusted to 7.5 with 5% hydrochloric acid. To this solution was added slowly a solution of ω-bromoacetophenone (0.1 g, 0.5 mmol) in 5 mL of THF at 0°C under nitrogen. The pH of the reaction mixture was maintained at 7.1–7.5 with 10% sodium hydroxide solution. After addition, the mixture was stirred for 2 h and filtered. The filtrate was washed with ethyl acetate and lyophilized to give a white solid residue. The solid was chromatographed on silica tlc plates; elution with chloroform/methanol/ammonium hydroxide (1:2:1) gave **18** as a white solid (60 mg); ir (KBr): 3700–2400, 1640 cm^{-1}; uv (H_2O): 250 nm (ε 10 496). The 2-hydroxyethylmercaptoacetophenone, prepared in 91% yield by condensing bromoacetophenone with 2-mercaptoethanol, had its ultraviolet maxima in ethanol at 242 nm (ε 10 014).

Bromoacetylglycine N-*hydroxysuccinimide ester*

To a solution of bromoacetylglycine (463 mg, 2.37 mmol) and *N*-hydroxysuccinimide (273 mg, 2.37 mmol) in 15 mL of anhydrous tetrahydrofuran at 0°C, under nitrogen, was added *N,N′*-dicyclohexylcarbodiimide (DCC) (732 mg, 50% excess). The resulting solution was stirred at 0°C for 4 h, when a white precipitate had formed. The precipitate was removed by filtration and the filtrate evaporated to dryness under vacuum. The solid residue was triturated with a 1:4 mixture of dichloromethane in hexanes. The solid was collected by filtration, and recrystallization from dichloromethane – ethyl acetate – hexanes gave the title compound as ten colored crystals (400 mg, 58%), mp 122–123°C; ir (KBr); 3270, 1830, 1780, 1650 cm^{-1}; ^{1}H nmr ($CDCl_3$ – DMSO-d_6) δ: 2.88 (s, 4H), 3.90 (s, 2H), 4.55 (d, 2H), 8.50 (m, 1H). *Anal.* calcd. for $C_8H_9NO_5Br$: C 32.76, H 3.07, N 9.56, Br 27.30; found: C 32.62, H 2.99, N 9.42, Br 27.53.

Labeling of bromoacetylglycine–NHS ester to bovine serum albumin (BSA)

To a solution of BSA (644 mg, 0.01 mmol) in 32 mL of 0.1 *M* borate buffer, pH 8.44, at 0°C was added dropwise a solution of bromoacetylglycine–NHS ester (293 mg, 1 mmol) in 5 mL of dry DMF. All solutions were saturated with argon before use. The addition took 20 min. The conjugation was closely monitored by pH meter. While the initial pH of the protein solution was 8.44, it dropped

Can. J. Chem. Downloaded from www.nrcresearchpress.com by 210.87.254.5 on 09/06/12
For personal use only.

to around 8.0 and was maintained to ±0.5 pH units with 0.1 *N* sodium hydroxide or 0.1 *N* hydrochloric acid. The pH, after additions of the NHS ester, was adjusted to 8.04; the solution was allowed to stir in an ice bath for 40 min, after which time the pH had changed to 7.15. This pH was again adjusted to 6.8 with the acid. The bromoacetylglycyl labeled BSA conjugate, about 50 mL, was purified by passing through a 100-ml G-50 Sephadex column using deionized water as eluent. Appropriate fractions were pooled and used either immediately or the following day (stored in cold room).

Conjugation of amikacin hapten ***14*** *to BSA. Formation of an immunogen*

The amikacin pro-hapten **13** (44 mg) was dissolved in 2 mL of methanol and taken into a 10-ml round-bottomed (or a pear shaped) flask. A slow stream of argon was bubbled through the solution for 30 min. To this stirring solution under argon was now added dithioerythritol (180 mg) in degassed methanol (6 mL), along with a drop of triethylamine. Progress of the reaction was continuously monitored by using silica tlc plates. After completion of the reaction (ca. 2 h), the solution was dried by evaporation and the residue stored under nitrogen.

The bromoacetylglycyl-labeled BSA solution (ca. 10 mL) prepared from 60 mg of BSA was degassed by bubbling a slow stream of argon. The pH of the solution was maintained around 7.3 using 0.2 *M* phosphate buffer. To this solution at 0°C was now added dropwise the cleaved amikacin hapten **14** in 0.5 mL of DMF (degassed with argon). The reaction mixture was stirred overnight in the cold room. The BSA–amikacin conjugate was dialyzed in a Spectropor membrane tubing (mol. wt. cutoff 6000–8000), dialyzed against 4 L of deionized water, and adjusted to pH 8.0 with ammonium hydroxide. The dialyzing medium was changed three times after every 3 h. The residual conjugate in the membrane tube was centrifuged at ~10,000 rpm (to remove any suspended material) and the liquid was lyophilized to give 56 mg of the conjugate.

*Conjugation of tobramycin-*N*-acetyl-*d,l*-homocysteine thiolactone (17) with bromoacetylglycine-labeled G6PDH*

To a solution of bromoacetylglycine-labeled G6PDH (3.3 mL, 0.0245 μmol of G6PDH) prepared as described elsewhere (8), at 0°C, pH 7.7 (adjusted with 10% NaOH), was added in 5-μL portions a solution of **17** (36.8 mg, only 25% of which is assumed to be the desired mercaptotobramycin) in 0.5 mL of 0.01 *M*, pH 6.8 phosphate buffer. The pH of the reaction solution was maintained at around 7.5–7.7 throughout the reaction with 5% hydrochloric acid. The reaction was constantly followed by checking the enzyme activity on a Gilford spectrophotometer. The reaction was stopped when a total of 240 μL of the tobramycin sulfhydryl derivative **17** had been added. No loss of the enzyme activity was noticed throughout the reaction. The solution of tobramycin–G6PDH conjugate was stored at 0°C for 5 days and chromatographically purified by a Sephadex G-50 column (eluting with 0.01 *M*, pH 6.8 phosphate buffer) for use in an EMIT® assay.

Conjugation of amikacin hapten ***14*** *to glucose-6-phosphate dehydrogenase*

The amikacin hapten **14**, freshly prepared by cleaving the disulfide linkage of **13** as described above, was coupled to bromoacetylglycine-labeled G6PDH by a procedure identical to the one described for the preparation of gentamicin–G6PDH conjugates (8). The amikacin–G6PDH conjugate, with 25–30% of the native enzyme activity, was ~75% inhibitable by addition of anti-amikacin antibodies. Most of the inhibited activity was reversible by addition of the drug.

Acknowledgements

We thank Waren F. Colvin and Dr. Pyare L. Khanna for developing a high-pressure liquid chromatography method used for resolution of the gentamicin mixture. Helpful discussions with Dr. Edwin F. Ullman throughout the course of this work are gratefully acknowledged.

1. G. KAHLMETER. Scand. J. Infect. Dis. Suppl. **18**, 1 (1979).
2. F. D. PIEN and P. W. HO. Am. J. Hosp. Pharm. **38**, 981 (1981).
3. (*a*) D. REEVES. Infection, **8**, S313 (1980); (*b*) J. FOLLATH, M. WENK, and S. VOZEH. J. Antimicrob. Chemother. Suppl. A, **8**, 37 (1981).
4. J. P. ANHALT. Antimicrob. Agents Chemother. **11**, 651 (1977).
5. S. K. MAITRA, T. T. YOSHIKAWA, L. B. GUZE, and M. C. SCHATZ. Clin. Chem. **25**, 1361 (1979).
6. K. E. RUBENSTEIN, R. S. SCHNEIDER, and E. F. ULLMAN. Biochem. Biophys. Res. Commun. **47**, 846 (1972).
7. (*a*) K. E. RUBENSTEIN. Scand. J. Immunol. Suppl. 7. **8**, 57 (1978); (*b*) P. SINGH. Non isotopic immunoassays and their applications. *Edited by* G. P. Talwar. Vikas Publications, India. 1983. pp. 105–124.
8. P. SINGH, D. K. LEUNG, G. L. ROWLEY, C. GAGNE, and E. F. ULLMAN. Anal. Biochem. **104**, 51 (1980).
9. G. L. ROWLEY, D. LEUNG, and P. SINGH. U.S. Patent 4328311 (1982).
10. T. KITAGAWA and T. AIKEWA. J. Biochem. **79**, 233 (1976).
11. D. J. COOPER, M. D. YUDIS, H. M. MARIGLIANO, and T. TRAUBEL. J. Chem. Soc. (C), **17**, 2876 (1971).
12. P. J. L. DANIELS, J. WEINSTEIN, and T. L. NAGABHUSHAN. J. Antibiotics, **27**, 889 (1974).
13. F. P. TALLY, T. J. LOAVE, U. M. WEINSTEIN, J. G. BARTLETT, and S. L. GORBAD. Ann. Intern. Med. **83**, 484 (1975).
14. H. KAWAGUCHI, T. NAIT, S. NAKAGAWA, and K. FUJISAWA. J. Antibiot. **25**, 695 (1972).
15. T. L. NAGABHUSHAN, W. N. TURNER, and A. COOPER. U.S. Patent 4136254 (1979).
16. T. L. NAGABHUSHAN, A. B. COOPER, W. N. TURNER, H. TSAI, S. MCCOMBIE, A. K. MALLAMS, D. RANE, J. J. WRIGHT, P. REICHERT, D. L. BOXSTER, and J. WEINSTEIN. J. Am. Chem. Soc. **100**, 5253 (1978).
17. S. HANESSIAN and G. PATEL. Tetrahedron Lett. 1035 (1978).
18. T. L. NAGABHUSHAN, A. B. COOPER, H. TSAI, P. J. C. DANIES, and G. H. MILLER. J. Antibiot. **31**, 681 (1978).
19. K. F. KOCH, J. A. RHODES, E. W. HAGAMAN, and E. WENKERT. J. Am. Chem. Soc. **96**, 3300 (1974).
20. P. J. L. DANIELS, A. K. MALLAMS, J. WEINSTEIN, and J. J. WRIGHT. J. Chem. Soc. Perkin Trans. 1, 1078 (1976).
21. R. BENESCH and R. E. BENESCH. J. Am. Chem. Soc. **78**, 1597 (1956).
22. G. E. MEANS and R. E. FEENEY. *In* Chemical modifications of proteins. Holden–Day, San Francisco. 1971. p. 109.
23. D. K. LEUNG, P. SHERIDAN, A. JAKLITSCH, P. SINGH, and D. S. KABAKOFF. Curr. Chemother. Infec. Dis. Vol. 1. *Edited by* J. D. Nelson and C. Grassi. Am. Soc. Microbiol. 1980. p. 516.
24. M. WENK, R. HEMMANN, and F. FOLLATH. Antimicrob. Agents Chemother. **22**, 954 (1982).

Photoisomerization of *N,N'*-disubstituted indigos. A search for energy storage

JOSEPH POULIQUEN, VÉRONIQUE WINTGENS, VICENTE TOSCANO,[1] BRAHIM BEN JAAFAR, SADHANA TRIPATHI, AND JEAN KOSSANYI[2]

Laboratoire de Photochimie Solaire, Equipe de Recherche 241 du C.N.R.S., 2–8 rue Henry Dunant, 94320 Thiais, France

AND

PIERRE VALAT

Institut Curie, Bâtiment 112, Centre Universitaire d'Orsay, 91405 Orsay, France

Received April 4, 1984

This paper is dedicated to Professor Peter Yates on the occasion of his 60th birthday

JOSEPH POULIQUEN, VÉRONIQUE WINTGENS, VICENTE TOSCANO, BRAHIM BEN JAAFAR, SADHANA TRIPATHI, JEAN KOSSANYI, and PIERRE VALAT. Can. J. Chem. **62**, 2478 (1984).

The photochemical behaviour of *N,N'*-disubstituted indigo dyes has been investigated. The *trans* to *cis* and *cis* to *trans* photoisomerization quantum yields are found to be of the order of 0.25 or less (down to 0.03). These dyes, which fluoresce only weakly in solution and at room temperature, show a drastic increase in their fluorescence when inserted into a polymer matrix or at 77 K in butyronitrile glass. This has been interpreted in terms of the inhibition of formation of a twisted excited intermediate as well as of the rotation of the substituent on the nitrogen atom. An important electron transfer occurs from the singlet excited state when the indigo dyes are placed in the presence of electron-donating molecules. When irradiating with visible light, the photostationary state is always in favour of the *trans* isomers. This, and kinetic as well as thermodynamic considerations, excludes these compounds as candidates for solar energy storage.

JOSEPH POULIQUEN, VÉRONIQUE WINTGENS, VICENTE TOSCANO, BRAHIM BEN JAAFAR, SADHANA TRIPATHI, JEAN KOSSANYI et PIERRE VALAT. Can. J. Chem. **62**, 2478 (1984).

Le comportement des indigos substitués **1**–**4** a été examiné. On trouve que les rendements quantiques de photoisomerisation sont faibles (de l'ordre de, ou inférieurs à, 0,20). Ces composés qui fluorescent faiblement en solution et à 20°C, présentent une augmentation considérable de leur fluorescence quand ils sont inclus dans un polymère ou bien lorsque la température est abaissée à 77 K dans le butyronitrile. Ceci a été interprêté comme un empêchement à la rotation autour de la double liaison centrale, et comme une gêne à la rotation du substituant sur l'azote ainsi que de l'inversion de cet atome. L'irradiation en lumière blanche est toujours en faveur des isomères *trans*. Ceci, ainsi que des considérations cinétiques et thermodynamiques excluent ces composés pour le stockage de l'énergie solaire.

Introduction

In the search for new sources of energy, photochemical transformations have been examined as a potential means of obtaining energy-rich stable products. Criteria for efficient photochemical conversion of solar energy are: absorption in the visible or near-ultraviolet region, high quantum efficiencies, large positive ground state enthalpies, and stable photoproducts. In addition, the reactant must be inexpensive and not dangerous.

The importance of dyes has been widely recognized in different converting systems related to photobiology (1, 2), photoelectrochemistry (3, 4), and photochemistry (5).

Photochemical systems mostly involve (Fig. 1) absorption of visible light by a reagent R to produce a high energy content product P which can later release the stored energy while reverting to the starting material. Among the systems reported thus far, one finds intramolecular cycloadditions (the best system investigated seems to be the norbornadiene-quadricyclane one (6) which can store about 26 kcal/mol (7)) and valence isomerization (such as the photochemical transformation of 1-methyl 5-phenyl Δ-2 pyrazoline into 2-phenylcyclopropylazomethane (8).

E/Z isomerizations have been recognized for a long time as efficient photochemical reactions which can occur by either direct irradiation or triplet sensitization. These reactions, which have been investigated in great detail, include the cases of azobenzene (9) and stilbene derivatives (10), but they usually suffer from the fact that the materials absorb mainly in the uv region. The use of *E/Z* isomerization for energy storage has been proposed tentatively (11) for cyanines and indigos as well. These two series of compounds have the advantage of absorbing light in the visible region but the difference in energy between the excited states of the geometrical isomers is around 10 kcal/mol in the 500-nm region (*vide infra*) and decreases as the molecules absorb at longer wavelengths.

In several cases, the reactivity of the compounds towards oxygen or their low solubility in both organic solvents and water put a limit to the feasibility of their isomerization as a source of energy storage. In addition, a compromise must be found between two opposing requirements: to absorb visible light and to gain enough energy for the isomerization. Such an energy gain will depend on the energy gap between the singlet (or triplet) excited states of the two isomers and on the height of the energy barrier between them. A gain of 10 kcal/mol or more seems to be a reasonable goal. This can be obtained when the excited states are separated by 150 nm in the 600–750 nm region or by 100 nm in the 500–600 nm region. Trying to store 15 kcal/mol is only reasonable for the 400–500 nm region and this explains why the best results are given by systems which absorb light in the near-uv region. A reasonable compromise can be achieved when the singlet excited states are localized in the 500–600 nm range. This is precisely the case of the *N,N'*-diacyl substituted indigos.

Experimental

Melting points were determined with a Mettler FP1 automatic appa-

[1]Present address: Instituto de Quimica da Universidade Sao Paulo, Caixa Postal 20780, Sao Paulo, Brazil.

[2]Author to whom correspondence may be addressed.

Can. J. Chem. Downloaded from www.nrcresearchpress.com by 210.87.254.40 on 09/06/12
For personal use only.

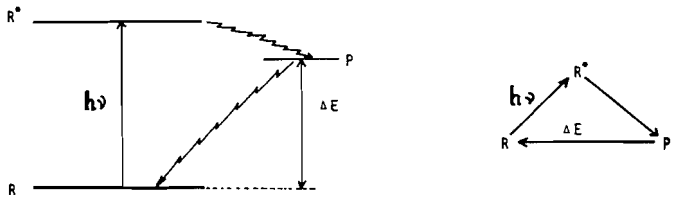

FIG. 1. Photochemical conversion (by direct irradiation or by triplet energy transfer) of a reagent R into the product P. ΔE is the stored energy which can be released in the back reaction P → R.

ratus. Infrared spectra were obtained with a Perkin–Elmer 357 model spectrophotometer and uv–visible absorption spectra were recorded on a Varian Cary 219 model. Emission spectra were performed using a Perkin–Elmer MPF 44B spectrofluorimeter; the spectra are corrected with a DCS 2U unit and a calibrated tungsten lamp.

A. *Materials*

The amines used as electron donors were purified by distillation with the exception of triphenylamine which was used without purification, of *N,N'*-diphenylparaphenylenediamine which was chromatographed on silica gel (elution with benzene), and of phenothiazine which was purified in the same way but using a 50:50 mixture of benzene with petroleum ether (60–80°C) as eluent. Naphthalene (scintillation grade), 1,4-dimethoxybenzene, and 1,3,5-trimethoxybenzene were used without purification. 1,2-Dimethoxybenzene was distilled.

The *trans* isomers of *N,N'*-disubstituted indigos were prepared according to the procedure of Blanc and Ross (12) for the *N,N'*-diacetyl derivative **1***t* and by Posner's method (13) for the *N,N'*-dibenzoyl **2***t*, *N,N'*-diparachlorobenzoyl **3***t*, and *N,N'*-diparamethoxybenzoyl **4***t* derivatives.

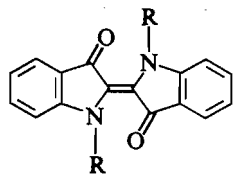

trans-Indigos: **1***t* R = CH_3—C(=O)— **2***t* R = C_6H_5—C(=O)—

3*t* R = *p*-Cl—C_6H_4—C(=O)— **4***t* R = *p*-CH_3O—C_6H_4—C(=O)—

The purity of the compounds was verified by thin-layer chromatography on silica gel (elution with benzene/ethylacetate 80:20).

(a) trans *Derivatives*

The chemical yields and characteristics of the *trans* derivatives were the following.

trans-N,N'-*diacetylindigo* (**1***t*): yield 57%; mp 269°C (lit. (12*a*) mp 263–264°C); ir (KBr): 1700, 1685, 1600, 1472, 1460, 1362, 1320, 1300, 1278, 1250, 1200, 1170, 1064, 925, and 755 cm^{-1}; uv λ_{max} (toluene) (ϵ): 560 nm (6,400 L mol^{-1} cm^{-1}).

trans N,N'-*dibenzoylindigo* (**2***t*): yield 79%; mp 254°C (lit. (14) mp 256–257°C); ir (KBr): 1705, 1670, 1600, 1472, 1460, 1320, 1270, 1240, 1187, 1105, 1070, 1040, 1020, 912, 800, 790, 758, 750, and 740 cm^{-1}; uv λ_{max} (toluene) (ϵ): 577 nm (7,700 L mol^{-1} cm^{-1}).

trans-N,N'-*diparachlorobenzoylindigo* (**3***t*): yield 42%; mp 254°C; ir (KBr): 1710, 1690, 1660, 1605, 1476, 1460, 1320, 1300, 1290, 1255, 1187, 1175, 1043, 1010, 877, 847, 830, 760, and 750 cm^{-1}; uv λ_{max} (toluene) (ϵ): 575 nm (8,350 L mol^{-1} cm^{-1}).

trans-N,N'-*diparamethoxybenzoylindigo* (**4***t*): yield 52%; mp 255°C; ir (KBr): 1690, 1665, 1600, 1575, 1510, 1455, 1420, 1320, 1295, 1250, 1183, 1165, 1065, 1040, 1020, 872, 860, 840, 760, and 750 cm^{-1}; uv λ_{max} (toluene) (ϵ): 580 nm (8,900 L mol^{-1} cm^{-1}).

(b) *Irradiation; general procedure*

The *cis* isomers were prepared by photochemical isomerization of the *trans* isomers, according to the procedure already described (14). Irradiations were carried out with a Philips HPLN 400 medium-pressure mercury arc in a water-cooled Pyrex jacket; the light emitted by the mercury lamp was filtered with a circulating solution of 80 g cobalt sulphate, 4.3 g potassium chromate, and 16 g sodium carbonate dissolved in 1 L of water.

The general procedure consisted of the irradiation of a 1:1 benzene – *n*-hexane solution saturated with the *trans* isomer and cooled at a temperature between 0° and 10°C by an external cooling jacket. As the *cis* isomer was formed, additional aliquots of the *trans* isomer were introduced into the irradiated solution. After several hours of irradiation, the solution was enriched in the *cis* isomer which began to crystallize.

This procedure enabled the *cis* isomer to be separated in a pure form. Only for the *N,N'*-diparamethoxybenzoyl indigo did this procedure fail, as the *cis* isomer reverted rapidly in the solution to the *trans* isomer when the light was switched off, even at −5°C.

(c) cis *Derivatives*

The characteristics of the isolated *cis* isomers were the following.

cis-N,N'-*diacetylindigo* (**1***c*): mp 266°C (lit. (14) mp 244–246°C);[3] ir (KBr): 1725, 1695, 1600, 1560, 1472, 1460, 1370, 1325, 1300, 1268, 1260, 1210, 1168, 1100, 1085, 1000, 885, 750, and 740 cm^{-1}; uv λ_{max} (toluene) (ϵ): 432 nm (4,050 L mol^{-1} cm^{-1}).

cis-N,N'-*dibenzoylindigo* (**2***c*): mp 260°C (lit. (14) mp 246°C);[3] ir (KBr): 1724, 1670, 1595, 1560, 1460, 1445, 1325, 1285, 1227, 1170, 1087, 1050, 1020, 1010, 922, 900, 855, 782, 750, and 740 cm^{-1}; uv λ_{max} (toluene) (ϵ): 460 nm (4,800 L mol^{-1} cm^{-1}).

cis-N,N'-*diparachlorobenzoylindigo* (**3***c*): mp 257°C; ir (KBr): 1720, 1675, 1597, 1585, 1560, 1460, 1395, 1325, 1285, 1230, 1180, 1167, 1085, 1050, 1008, 902, 845, 830, 780, 760, and 746 cm^{-1}; uv λ_{max} (toluene) (ϵ): 460 nm (2,600 L mol^{-1} cm^{-1}).

(d) *Solvents*

Solvents for absorption, emission, and quantum yield measurements were of spectrograde (Merck) quality and used without further purification. Experiments for the photochemical preparation of the *cis* isomers of the indigo derivatives were carried out in distilled benzene – *n*-hexane 1:1 solution.

B. *Emission*

(a) *Spectra*

All four *trans* isomers fluoresced when excited in their long-wavelength charge transfer band; the excitation spectra matched the absorption bands. No phosphorescence emission could be detected from them, even at liquid nitrogen temperature.

The *cis* isomers showed no fluorescence or phosphorescence.

(b) *Lifetimes*

The fluorescence decay of the *trans* isomers **1***t*–**4***t* was measured with a YAG laser from Quantel.

Frequency doubling of the fundamental light (1064 nm) by a prism gave a 532-nm light beam which passed through a diaphragm before traversing a quartz cell of dimensions 1 cm × 1 cm which contained the sample in chloroform solution. The emitted light was received at right angles by the photocathode of a high-speed photodiode (type S 11; rise time less than 150 ps). A gelatin filter (Kodak nb 21) was inserted between the photocathode and the cell, in order to eliminate the Rayleigh scattering. The photodiode signal was transmitted to a Tektronix 7104 oscilloscope with a risetime of about 350 ps and the oscilloscope trace was recorded on a Polaroid film. A 30-ps laser pulse produced an electronic echo in the detection system about 1 ns

[3]The mp of the *cis* isomers might be higher than the one given here since they can revert thermally to more stable *trans* isomers. This would be more pronounced for **1***c* (which has a lower mp than **1***t*) than for **2***c* and **3***c* (which melt at higher temperature than **2***t* and **3***t*).

Can. J. Chem. Downloaded from www.nrcresearchpress.com by 210.87.254.40 on 09/06/12
For personal use only.

after the signal; treatment of the data enabled this perturbation to be removed.

The light beam was split before passing through the cell and one part was focused on a GenTec pyroelectric detector; the signal obtained was proportional to the energy of the excitation light. A linear relationship between the fluorescence intensity and the excitation energy was obtained for all the compounds studied. The power density at the sample was less than 1 MW cm^{-2}.

(c) *Quantum yields*

The fluorescence quantum yields were determined using the Perkin–Elmer MPF-44B spectrofluorometer coupled to the DCS-2U device. The optical density of the solutions of the indigo derivatives in chloroform solution (Uvasol quality) was adjusted to 0.05 at the excitation wavelength. Fluorescein was used as the standard under the following experimental conditions: buffer solution at pH 10, optical density 0.05 at an excitation wavelength of 436 nm. A value of 0.85 has been reported (15) for the fluorescence quantum yield at this wavelength.

C. *Isomerization quantum yields*

The quantum yields of the *trans* to *cis* and *cis* to *trans* isomerizations of the indigo derivatives were measured using a 150-W Xenon lamp, the light being focused on a 1 cm × 1 cm quartz cell through a water filter and a Jobin–Yvon H 20 monochromator adjusted at 580 nm. The second-order spectra of the grating were removed by a 400-nm cut-off glass filter.

All the measurements were carried out at 20°C, the optical density of the toluene solution of the sample being adjusted to 0.13 at 580 nm. Under these conditions, the irradiation time varied from 0.3 to 0.6 h, depending on the starting material.

In the case of the *cis* to *trans* isomerization quantum yield measurements, a blank was run simultaneously in the dark to take into account the amount of isomerization which occurs thermally.

D. *Photostationary equilibrium*

The photostationary state equilibrium was determined for each couple of the *cis–trans* isomeric indigo derivatives. The irradiations were carried out with a 150-W Xenon lamp using an optical bench; the light beam was focused through a Pyrex lens and a diaphragm into a 1 cm × 1 cm Pyrex cuvette held firmly by a holder and containing the solution of the sample to be analyzed. A 400-nm cut-off filter was put between the lamp and the cuvette. Experiments were carried out at both 10°C and 22°C, starting from pure *cis* or *trans* isomers (10^{-4} *M* in chloroform) except for **4***c* where a 60% *cis*-rich mixture was used.

Degassed and undegassed solutions were used for comparison. Direct irradiations in the presence or in the absence of triplet inhibitors (oxygen-saturated solution, or perylene) as well as sensitized irradiations (benzophenone, anthracene, xanthone, thioxanthone) were performed for the sake of comparison, but aromatic ketones react rapidly with the indigo derivatives and form addition products (*vide infra*).

E. *Fluorescence quenching*

The quenching of the fluorescence of the indigo derivatives **1***t*, **2***t*, and **3***t* was carried out in acetonitrile solution at 20°C. The indigo derivative concentration was adjusted to about a 0.1 optical density at the excitation wavelength which was chosen at the maximum of the visible absorption band. The apparent rate constant K_{CT} for the quenching of the fluorescence by the electron donor was deduced from the slope of the Stern–Volmer plot. The process was repeated for all the electron-donor molecules. The quenching rate constant can be evaluated, as the lifetime of the singlet excited state was known (*vide supra*). The decimal logarithm of this constant is plotted vs. the free energy ΔG of the charge-transfer complex formation (Fig. 2).

F. *Electrochemistry*

Redox potentials were obtained by cyclic voltammetry using a P.A.R. model 173 potentiostat monitored by a P.A.R. model 175 programmer coupled to a TGM X-Y Sefram recorder. The electrochemical measurements were performed in acetonitrile solution using 0.1 *M* tetrabutylammonium perchlorate as supporting electrolyte. The reference electrode was a calomel electrode saturated with KCl and separated from the main solution by a bridge consisting of a glass tube closed by a medium-porosity glass frit and containing the supporting electrolyte. The working electrode was a platinum gauze and the counter electrode was a 1 cm × 1 cm platinum surface.

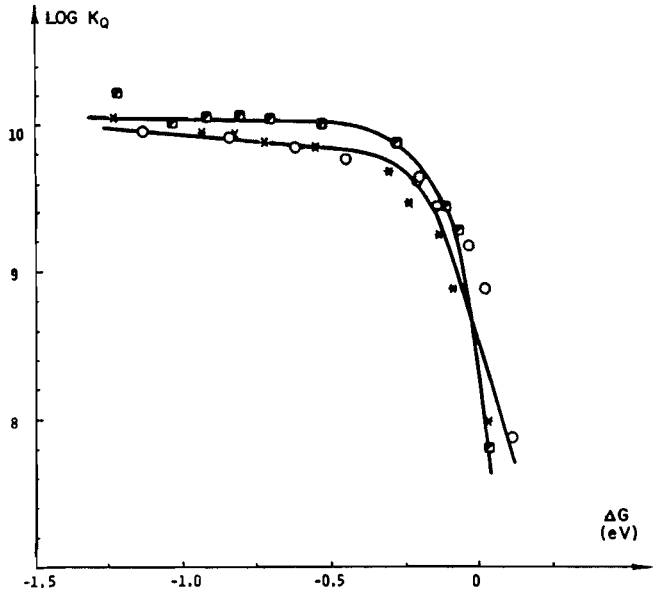

FIG. 2. Plot of the logarithm of the quenching rate constant versus ΔG for **1***t* (◪◪◪), **2***t* (○○○○○), and **3***t* (*****).

Results and discussion

A. *Excited state involved in the isomerization*

Knowledge of the excited state(s) from which the $t \rightarrow c$ and $c \rightarrow t$ isomerizations of the substituted indigos originate is of importance since it governs the thermodynamic data and the energy content of the process.

It is known that the isomerization of stilbenes results from a singlet excited state (10, 16) and that for thioindigo derivatives, molecules which are closely related to the series studied here, it depends on the geometry of the starting material with the *trans* isomer undergoing a photoisomerization via the triplet excited state (17–19), while the reverse photochemical reaction occurs from the singlet state (20, 21). When the $c \rightarrow t$ isomerization of thioindigo derivatives was studied in a toluene-containing solution, the isomerization quantum yield was found to vary with the temperature and to reach a maximum value (ca. 0.9) at 180 K; this effect could be rationalized (22) on the basis of the formation of an exciplex between the excited *cis*-indigos and toluene. The multiplicity of the excited state involved in the $t \rightarrow c$ isomerization has been questioned by Haucke and Paetzold (20) who found that oxygen quenches this process, but not completely (about 90%); such a quenching was already described by Kirsch and Wyman (17).

All the *trans N*-substituted indigo dyes **1***t*–**4***t* studied here fluoresce weakly at room temperature (Table 1) but do not phosphoresce. On the other hand, the *cis* isomers **1***c*–**4***c* show no emission at all, even at liquid nitrogen temperature; when a weak fluorescence was observed for a *cis* derivative, it had to be attributed to a trace of the corresponding *trans* isomer (the method described in the experimental part for preparing the *cis* isomers appears to be particularly well adapted for obtaining them in a pure form). Radiative lifetimes of the *trans* isomers are reasonable for singlet excited states (Table 1); if one com-

Can. J. Chem. Downloaded from www.nrcresearchpress.com by 210.87.254.40 on 09/06/12
For personal use only.

TABLE 1. Fluorescence lifetimes, quantum yields, rate constants, and photostationary equilibrium of indigo dyes **1**–**4** in chloroform solution

	1		**2**		**3**		**4**	
	t	*c*	*t*	*c*	*t*	*c*	*t*	*c*
Fluorescence								
λ_{max}	620	No	626	No	628	No	632	No
τ_s (ns)	2.1		2.7		1.8		2.1	
$\phi_f \times 10^3$	22		5		5		4	
$k_f \times 10^{-6}\ s^{-1}$	10.7		1.8		2.7		1.8	
Isomerization								
$\phi_{t\rightarrow c}$[a]	0.25		0.06		0.03			
$k_{t\rightarrow c}$[b] $\times 10^{-7}\ s^{-1}$	12		2.2		1.7			
$\phi_{c\rightarrow t}$[a]		0.16		0.12		0.09		
$([t]/[c])_{PSS}$[c]	1		3		5.6		9	

[a]At 10°C; λ_{exc} = 580 nm.
[b]Assuming a singlet reaction.
[c]Photostationary state at 10°C; $\lambda_{exc} > 400$ nm (Corning 3-74 cut-off filter).

pares with the thioindigos, one would expect the latter to show a shorter singlet lifetime and a smaller fluorescence quantum yield than the corresponding indigo derivatives; simultaneously, the intersystem crossing efficiency should be larger due to the heavy atom effect from the sulphur atom. In fact, the intersystem crossing efficiency value is (19) reasonably high (0.42) for thioindigo, but its singlet lifetime (13.4 ns) and fluorescence efficiency (0.56) are both unexpectedly high (23) compared to the indigo derivatives and are not consistent with a heavy atom effect from sulphur in the thioindigo derivatives.

When the temperature is decreased from room temperature to 77 K, the fluorescence efficiency increases by a factor of 16, 110, and 140 respectively for compounds **1***t*, **2***t*, and **3***t* in butyronitrile solution. Under the same conditions, the singlet lifetime increases by factors of only 4.4, 5.4, and 7.1 respectively. Such a decrease in lifetime when the temperature increases is not uncommon and can be attributed to several processes which already have precedents in the literature. One is a hindrance to the rotation around the central double bond as a result of the increased viscosity of the medium; this is usually the case for *cis*–*trans* isomerization which involves a twisted intermediate state (24). Another, which has been reported already for a few rigid aromatic molecules (25), is a modification of the singlet to triplet intersystem crossing which is found to increase with the temperature; if this is effectively the case, both the *cis* to *trans* and *trans* to *cis* isomerizations could have a double singlet and triplet origin. A third process could be a net decrease of the rotation of the substituents linked to the nitrogen atom.

A similar increase, although less pronounced than the one found in liquid nitrogen, of the fluorescence quantum yields is observed at room temperature when the compounds are inserted in a poly(methyl methacrylate) matrix. The factor by which ϕ_f increases is now 2, 28, and 23 for **1***t*, **2***t*, and **3***t* respectively, by comparison with the values in glycerol triacetate (GTA) solution. More striking, just as at 77 K, is the absence of isomerization to the *cis* isomers after prolonged irradiation of the *trans* isomers in their absorption band. This can be interpreted in terms of a steric hindrance to the formation of the twisted intermediate by the rigid medium.

Different processes can contribute to the deactivation of the singlet excited state: fluorescence (rate constant k_f), intersystem crossing (k_{isc}), formation of a twisted intermediate (k_{tw}) by a 90° rotation of one moiety of the molecule around the central double bond, and rotation of the substituents on the nitrogen atoms (k_{rot}) as well as radiationless internal conversion (k_{nr}).

In a fluid liquid medium, all five processes are competitive. Inversion at the level of the nitrogen might occur also in the excited state although the N atom is expected to be planar in the ground state.[4] Argument for a change in the excited state is obtained with the Stokes shift of the fluorescence. This process, if it occurs, should be strongly restricted at 77 K (26). Its rate constant has been included in k_{rot}. In the polymeric matrix the twisted intermediate is no longer formed since no photoisomerization is then observed. At 77 K the rotation of the R—CO substituents becomes considerably hindered, as is the formation of the twisted intermediate; fluorescence, intersystem crossing, and radiationless internal conversion become the principal deactivation paths of the singlet excited state.

At room temperature, in fluid solution, the inverse of the singlet excited lifetime τ_s^{293} can be written as:

$$[1]\quad \frac{1}{\tau_s^{293}} = k_f + k_{isc} + k_{tw} + k_{nr} + k_{rot}$$

In the polymeric matrix the twisting around the central double bond of the two bulky moieties is considerably restricted as no *trans* to *cis* isomerization occurs under irradiation. Since this observation is made at room temperature, the rotation of the acyl groups around the N—C single bond must still take place.

The lifetime τ_s^{PMMA} of the singlet excited state of the *trans* indigo dyes **1***t*–**3***t* in PMMA can be expressed, then, by the relation [2]:

$$[2]\quad \frac{1}{\tau_s^{PMMA}} = k_f + k_{isc} + k_{rot} + k_{nr}$$

At liquid nitrogen temperature, one would expect the rotation around the N—C single bond to be strongly hindered; the quantum yield of the other processes would consequently increase, since the rate constants of the intrinsic deactivation processes are not expected to vary appreciably. If one considers

[4]We thank one of the referees for pointing out the planarity of the nitrogen atom in the ground state.

Can. J. Chem. Downloaded from www.nrcresearchpress.com by 210.87.254.40 on 09/06/12
For personal use only.

TABLE 2. Fluorescence emission, quantum yields, and rate constants of *trans*-indigo dyes **1***t*−**3***t* under different conditions ($CHCl_3$ = chloroform; CH_3CN = acetonitrile; GTA = glycerol triacetate; C_3H_7CN = butyronitrile; MTHF = methyltetrahydrofuran; PMMA = poly(methyl methacrylate)

	Temperature (K)	Medium	**1***t*	**2***t*	**3***t*
$\phi_f \times 10^2$	293	$CHCl_3$	2.4	0.5	0.6
	293	CH_3CN	1.5	0.2_5	0.3
	293	GTA	2.8	0.5	0.7
	293	PMMA	5.8	14.	16.
	77	C_3H_7CN	24.	29.	42.
τ_s (ns)	293	$CHCl_3$	2.1	2.7	1.8
	293	CH_3CN	1.5	1.3	0.9
	293	GTA	2.6	2.7	2.4
	293	PMMA	5.3	5.9	3.4
	77	MTHF	10.	14.3	12.8
	77	C_3H_7CN	6.6	7.0	6.4
$k_f \times 10^{-7}$ s^{-1}	293	CH_3CN	1.1	0.2	0.4
$k_{tw} \times 10^{-8}$ s^{-1} [a]	293	CH_3CN	2.2	2.2	1.4
ϕ_{tw} ($= k_{tw} \times \tau_s^{CH_3CN}$)	293	CH_3CN	0.35	0.28	0.13
$k_{isc} \times 10^{-8}$ s^{-1} [b]	293	CH_3CN	<1.3	<1.4	<1.6
ϕ_{isc} ($= k_{isc} \times \tau_s^{CH_3CN}$)	293	CH_3CN	<0.20	<0.18	<0.14
$k_{rot} \times 10^{-8}$ s^{-1} [c]	293	CH_3CN	1.2	1.4	1.4
ϕ_{rot} ($= k_{rot} \times \tau_s^{CH_3CN}$)	293	CH_3CN	0.18	0.18	0.13

[a]Deduced from relations [1] and [2].
[b]Deduced from relation [3].
[c]Deduced from relations [2] and [3].

the lifetime of the singlet excited state to be subordinated mainly to k_f, k_{nr}, and k_{isc}, the knowledge of k_f and that of τ_s^{77} (relation [3]) can give ($k_{nr} + k_{isc}$) and, consequently, the upper limit of

$$[3] \quad \frac{1}{\tau_s^{77}} \simeq k_f + k_{isc} + k_{nr}$$

the singlet to triplet intersystem crossing quantum yield, if no radiationless transition occurs.

Thus, measurement of the fluorescence quantum yield and singlet lifetime under the different conditions can give a reasonable idea of the various deactivation process rate constants. These are listed in Table 2.

In the case of *trans*-thioindigo, different mechanisms have been postulated for the rotation process; in the first one, the isomerization occurs from the singlet excited state through the twisted state which subsequently can undergo the intersystem crossing to the triplet excited state (20); in the second one, the planar singlet excited state crosses over to the triplet excited state which then undergoes the internal rotation to the twisted form (27).

If a triplet excited state has to be involved in the isomerization of the indigo derivatives **1***t*−**3***t*, this process could be both sensitized and inhibited. The isomerization of thioindigos has been claimed to be sensitized by tin(IV) tetraphenylporphyrin (E_T = 36.1 kcal/mol) in benzene or toluene solution, and argument has been taken from this to postulate a double singlet and triplet origin to the isomerization (28); it has been verified also that the ratio of the *cis* to *trans* isomers is different in the sensitized reaction compared to its value for direct irradiation.

Sensitizing the isomerization of **1***t*−**3***t* has been tried, using tetraphenylporphine (TPP) as sensitizer. Unfortunately, no triplet sensitization could be characterized, but rather a very efficient quenching of the fluorescence of TPP by the *N*,*N*′-disubstituted indigos has been observed; the rate constant for the quenching process is found to be of the same order as that of the diffusion. As will be discussed later, an electron-transfer mechanism has been put forward for this process.

Inhibition of the *trans* to *cis* isomerization of **1***t*−**3***t* by oxygen failed, the quantum yield for the isomerization process being the same whether oxygen is present or absent.

Thus, unlike the thioindigo derivatives for which the *trans* to *cis* isomerization could be partly quenched by oxygen (20), compounds **1***t*−**3***t* apparently isomerize solely from the singlet excited state.

Similarly, no quenching of the isomerization occurs when perylene (E_T = 36 kcal/mol) or anthracene (E_T = 42 kcal/mol) are used as triplet quenchers in degassed toluene solution, the irradiation ($\lambda > 450$ nm) being carried out at the temperature of +10°C.

That the singlet excited state is the only one involved in the *trans* to *cis* photoisomerizations has been verified by additional experiments: (*i*) the photostationary state between the two isomers is the same, whether the solution is degassed or enriched with oxygen; this holds as long as the excitation wavelength is higher than 400 nm; (*ii*) attempts to sensitize the *trans* to *cis* isomerization by perylene (E_T = 36 kcal/mol) in degassed toluene solution with monochromatic light at 435 nm were unsuccessful; under such conditions the sensitizer absorbs more than 97% of the light, but after 2 h irradiation, only 4% of the *trans* isomer had disappeared; (*iii*) the same failure was experienced when sensitization by anthracene (E_T = 42 kcal/mol) was carried out under 360-nm irradiation.

However, a weak isomerization, resulting from direct ab-

Can. J. Chem. Downloaded from www.nrcresearchpress.com by 210.87.254.40 on 09/06/12
For personal use only.

Can. J. Chem. Downloaded from www.nrcresearchpress.com by 210.87.254.40 on 09/06/12
For personal use only.

sorption (ca. 3% of the light) by the indigo derivatives could not be excluded in the last two cases. In the presence of *N*,*N*-diethylaniline, the photoisomerization of compounds **1***t* and **2***t* was totally inhibited; no singlet or triplet energy transfer from the indigo derivatives ($E_s \sim 49$ kcal/mol) to *N*,*N*-diethylaniline ($E_s \sim 95$ kcal/mol; $E_T \sim 73$ kcal/mol) could be involved in this deactivation process, as the energies of the excited states do not match each other.

This effect could be attributed to an electron donor–acceptor interaction between the two species, since the oxidation potential of diethylaniline is +0.76 V vs. SCE. That there is effectively such an effect is supported by the fact that the irradiation ($\lambda > 500$ nm) of a (**1***t* + **1***c*) or (**2***t* + **2***c*) mixture reduces rapidly the percentage of the *cis* isomer in the mixture.

No characterization of the triplet of the *trans* isomers could be obtained, even by laser flash photolysis using a ruby laser, although the *T*–*T* absorption spectra of **1***t* has already been found (27). Indeed, as we have discussed above on the basis of the kinetics, intersystem crossing to the triplet state should apparently occur,[5] the most striking result that we found being the absence of quenching or sensitization of this excited state.

That an electron transfer reaction occurs in most cases is evidenced in the subsequent discussion.

B. *Electron-acceptor behaviour*

As has been discussed above, no quenching of the triplet excited state of the *trans* indigo derivatives **1***t*–**3***t* could be characterized, in contrast to thioindigo derivatives which show triplet quenching by oxygen (17, 20) as well as triplet sensitization by tin(IV) tetraphenylporphyrin (28).

Thioindigo derivatives have been found to interact with hydroxyl compounds such as phenols (29) and alcohols (30); they have been reported also to behave like electron acceptors (22) in donor–acceptor interactions. This prompted us to investigate the effect of electron donors on the excited state of the indigo derivatives **1***t*, **2***t*, and **3***t*.

The voltamogram curves of these *trans* isomers show two distinct reversible reduction waves (at −0.58 V and −1.18 V vs. SCE for **2***t*) and an oxidation wave (at +0.64 V vs. SCE for **2***t*) in acetonitrile solution. This oxidation wave, 1.22 V above the first reduction wave, lies below the reduction potential of the corresponding excited states. Consequently, a serious effect on the photochemical behaviour of the indigo derivatives might be expected.

The reduction potentials of the ground (E_{red}) and singlet (E^*_{red}) excited states of an acceptor molecule can be related to each other by relation [4]:

$$[4] \quad E^*_{red}(A^*/A^{\cdot-}) = E_{red}(A/A^{\cdot-}) + E_s$$

where E_s is the energy of the singlet excited state. This relation neglects the work functions of ion-pair and encounter-complex formation.

For compounds **1***t*–**3***t*, E_s is about 2.1 eV, as deduced from the fluorescence emission. Irradiation of an acetonitrile solution of the *trans* indigo derivatives, in the long-wavelength absorption band, yields the lowest excited state which fluoresces weakly. Addition of an electron-donor molecule to the solution yields an encounter complex which can revert to the ground-state starting molecules or form a charge-transfer complex. The electron transfer can be viewed as irreversible at the very early stage, since then the reverse reactions are negligible (31). Usually, quenching of the lowest singlet excited state by an electron donor–acceptor exchange process forms no detectable separate ions, in contrast to the ion pairs arising from the triplet state, thus showing an expected spin selection rule (32).

The absorption spectra of mixtures of the indigo derivatives with the electron-donor molecules proved to be additive with respect to the acceptor and quencher component spectra. Furthermore, the weak fluorescence and fluorescence excitation spectra of **1***t*–**3***t* show no change in the presence of the quencher but only a decrease of the emission intensity. This process, which increases with the concentration of the electron donor, gives a linear Stern–Volmer plot according to relation [5]:

$$[5] \quad \phi^0_f/\phi_f = 1 + K_q\tau_s[\text{quencher}]$$

If the quenching process occurs from an electron acceptor–donor exchange, as is the case for the thioindigo derivatives (22), then the rate constant K_q should vary with the oxidation potential of the donor E^{ox}_D. According to the pioneering work of Leonhard and Weller (33), the rate constant K_q for the fluorescence quenching process should increase with decreasing E^{ox}_D of the donor, until a plateau is reached when K_q is equal to the diffusion rate constant of the solvent (34, 35).

The oxidation potentials of the electron donors used as quenchers lie between 0.35 and 1.60 V versus the saturated calomel electrode. No quenching by toluene ($E^{ox}_D = 1.97$ V) has been observed, in contrast to the thioindigo compounds (22), the reduction potentials (−0.5 V) of which are slightly less negative than that of the indigo derivatives (−0.58 V).

The quenching of the fluorescence of compounds **1***t*–**3***t* in acetonitrile solution gives a linear Stern–Volmer plot for all the series of electron donors used as quencher. Since the lifetime of the singlet excited state of the *trans* derivatives has been measured directly by fluorescence decay after excitation by a frequency-doubled YAG laser, it was possible to calculate the quenching rate constant from the slope of the linear plot. The decimal logarithms of the values thus obtained are reported in Table 3.

No new luminescence has been detected, in different solvents, which could be attributed to an exciplex or a charge-transfer complex emission. Consequently, it must be ensured that the standard free energy change ΔG^0 of the exciplex formation varies with the oxidation potential of the electron donor.

The energy of the charge-transfer complex E_e in solution is related to the energy of the pure charge-transfer complex E^0_e in the gaseous phase by a relationship which includes the solvation enthalpy of the complex. This involves several factors including the radius ρ of the solvent spherical cavity occupied by the complex in the Kirkwood and Onsager model. By taking ρ = 9 Å for the cavity radius, as deduced from molecular volume calculations (36), and by assuming that the distance between the electron donor and electron acceptor in the complex is 5 Å, one obtains the value 0.35 for the solvation term in acetonitrile solution. This leads to expression [6] for the variation of the free energy change ΔG:

$$[6] \quad \Delta G = E^{ox}_D - E^{red}_A - E_s \ (\pm 0.10 \text{ eV})$$

The rate constant K_q for the charge-transfer complex formation is correlated to ΔG by an expression of the type

$$[7] \quad K_q = A \exp(-\Delta G^{\neq}/RT)$$

[5] Further studies for characterizing the triplet excited state of **1**–**3** are in progress.

TABLE 3. Values of the oxidation potential of the electron-donor molecule, of the reduction potential of the electron-accepting indigo derivatives **1***t*, **2***t*, and **3***t*, and of the logarithm of the quenching rate constant log k_q for the different values of the free energy change ΔG of the charge-transfer complex formation

		1*t*		**2***t*		**3***t*	
		$E^{A}_{red} = -0.58$ V[a]		$E^{A}_{red} = -0.60$ V[a]		$E^{A}_{red} = -0.55$ V[a]	
Electron donor	E^{D}_{ox}[a] (V)	ΔG	log k_q	ΔG	log k_q	ΔG	log k_q
N,*N*′-diphenyl *p*-phenylenediamine	0.35	−1.21	10.22	−1.13	9.97	−1.23	10.05
Phenothiazine	0.53	−1.03	10.01	—	—	—	—
N,*N*-dimethyl *p*-toluidine	0.65	−0.91	10.05	−0.83	9.93	−0.93	9.94
N,*N*-diethyl aniline	0.76	−0.80	10.05	−0.72	9.88	−0.82	9.92
Triphenylamine	0.86	−0.70	10.03	−0.62	9.85	−0.72	9.87
N-methylaniline	1.03	−0.53	10.00	−0.45	9.77	−0.55	9.84
Aniline	1.28	−0.28	9.87	−0.20	9.62	−0.30	9.68
1,4-Dimethoxy benzene	1.34	−0.22	9.61	−0.14	9.44	−0.24	9.47
1,2-Dimethoxy benzene	1.45	−0.11	9.44	−0.03	9.19	−0.13	9.24
1,3,5-Trimethoxy benzene	1.49	−0.07	9.27	+0.01	8.88	−0.09	8.86
Naphthalene	1.60	+0.04	7.80	+0.12	7.89	+0.02	7.99

[a]Versus SCE.

Can. J. Chem. Downloaded from www.nrcresearchpress.com by 210.87.254.40 on 09/06/12
For personal use only.

which assumes that the electron-transfer process occurs according to an outer-sphere mechanism, $\Delta G^{\neq}$ being the standard free activation energy. Since ΔG can be measured for a thermodynamically reversible electron-transfer reaction, and as $\Delta G^{\neq}$ can be expressed, in principle, as a function of ΔG, the quenching rate constant will vary only with ΔG. Thus, plotting log K_q versus ΔG yields a curve which increases as ΔG decreases and which should reach a maximum value equal to the diffusion-controlled rate constant $2.7 \times 10^{10}\ M^{-1}\ s^{-1}$ in acetonitrile solution (37) whatever ΔG may be. The variation of log K_q versus ΔG is depicted in Fig. 2.

The results obtained by this method agree with an electron-transfer mechanism in which the excited singlet state of the *trans* indigo derivatives behaves like an electron acceptor.

Porphyrins are known to be good electron donors in EDA complex formation, their oxidation potential (versus SCE) being of the order of 1 V (38*a*, as quoted in ref. 38*b*). Thus, in benzene solution, the fluorescence of tetraphenylporphine has been found to be quenched by the *trans* indigo derivatives **1***t* and **2***t* with a rate constant ($6 \times 10^9\ M^{-1}\ s^{-1}$) close to that for diffusion ($1.5 \times 10^{10}\ M^{-1}\ s^{-1}$ for benzene), while with the parachlorobenzoyl derivative **3***t* this rate constant is $1.8 \times 10^{10}\ M^{-1}\ s^{-1}$. By analogy with this result and in accord with the recently reported electron-acceptor behaviour of thioindigos (22), one should consider the possibility that isomerization of thioindigos in the presence of tin tetraphenylporphyrin (28) is the result of an electron transfer mechanism rather than a triplet−triplet energy transfer.

C. *Photostationary state*

The photostationary equilibrium has been determined in chloroform solution at 10° and 20°C. Due to the tendency of the *cis* isomers to revert thermally to the corresponding *trans* isomer, better results are obtained at 10°C. A Corning 3-74 glass filter was placed between the 150-W Xenon lamp and the cuvette containing the sample in order to eliminate the λ < 400 nm uv light. The photostationary state was reached starting from both the pure *cis* and pure *trans* isomers; the evolution of the *trans*/*cis* ratio is shown in Fig. 3 and the values at the steady state are tabulated in Table 2. In each case, the same equilibrium is obtained whether or not the solution is flushed through with argon for 15 min prior to the experiment.

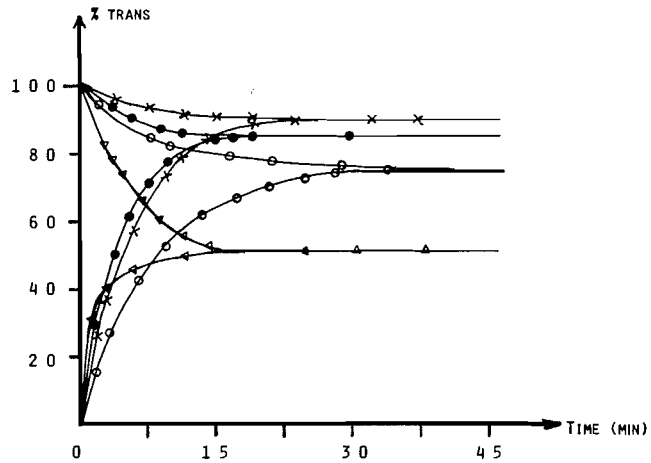

FIG. 3. Photostationary state composition versus time, obtained by irradiation of the indigo derivatives **1** (ΔΔΔΔ), **2** (○○○○), **3** (●●●●), and **4** (××××) with visible light (λ > 400 nm).

No change in the *trans*/*cis* ratio was observed when the well-degassed photostationary equilibrium was irradiated with visible light (λ > 400 nm) in the presence of anthracene or with λ > 440 nm in the presence of perylene. Under these conditions neither anthracene nor perylene absorbs light. Consequently, there seems to be no triplet quenching by *T*−*T* energy transfer from the excited indigo dyes to anthracene or perylene. We have indicated already that no sensitization could be observed using either tetraphenylporphine, anthracene, or

Can. J. Chem. Downloaded from www.nrcresearchpress.com by 210.87.254.40 on 09/06/12
For personal use only.

perylene.

As indicated in Table 1, the photostationary state is always in favor of the *trans* isomer when the irradiation is carried out with polychromatic light of wavelength > 400 nm. The *N,N'*-diacetyl derivative **1** is the only compound for which the *cis* isomer is present in equal quantity with the *trans* one at the steady state under these conditions.

When the irradiation is extended in order to include the uv region, a slow disappearance of the dyes is observed. If, in addition, the irradiation is carried out in toluene solution, then a very rapid bleaching of the dye is observed; thus irradiation, using exclusively the 330−380 nm region (Corning band-pass 7-37), causes a degassed 6×10^{-5} *M* toluene solution of **2***t* to fade in less than 1 h while, under the same conditions but in acetonitrile solution, 25% of **2***t* is transformed into **2***c*. A rapid bleaching is observed also when irradiating a deaerated acetone solution (Merck, spectroscopic quality) of **2***t* at 254 nm.

Formation of a charge-transfer complex between the excited dye and toluene can hardly be put forward as an explanation for this bleaching since the same solution gives the normal *trans*−*cis* isomerization when the excitation wavelength is limited to the long-wavelength absorption band of the dye, or if the irradiation is carried out in benzene solution instead of toluene. We believe that the indigo dye, in its second excited singlet state S_2, abstracts a hydrogen atom from the solvent and adds subsequently to the formed $C_6H_5CH_2$· radical. At this stage, a more efficient intersystem crossing to the triplet state from S_2 cannot be excluded completely, but we have observed no phosphorescence of the compounds when excited at 77 K with 360-nm light.

Bleaching of the indigo dyes was also observed during the attempts at sensitization by xanthone, thioxanthone, or benzophenone in toluene solution using the Corning 7-37 band-pass filter (360 nm).

If a trace of tertiary amine, such as *N,N*-diethylaniline (E_D^{ox} = +0.76 V), is added to the photostationary equilibrium between the two isomers, the *cis* reverts rapidly to the *trans*; in the same way, the *trans* derivatives do not isomerize to their corresponding *cis* derivatives when irradiated at their long-wavelength maximum in the presence of a tertiary amine. If this is relevant to an intermediate charge-transfer complex formation, the oxidation potential of the donor must be critical since neither TPP (E_D^{ox} = +0.97 V) nor perylene (+0.85 V) are effective under the same conditions.

D. *Energy storage feasibility*

As already mentioned, the *trans* → *cis* photoisomerization of *N,N'*-disubstituted indigo derivatives has been proposed as a potential system for solar energy conversion and storage (11). The practical efficiency of the process has been discussed also (39). It appears that one of the disadvantages of the system overcomes its advantages, the main drawback being the low amount of the stored energy: 34 kJ mol^{-1} for *N,N'*-diacetyl indigo **1**, and from 14 to 24 kJ mol^{-1} for various *N,N'*-dibenzoyl derivatives (11, 39). Increasing the bulk of the *N*-substituent does not increase the energy difference (and so the stored energy) between the *cis* and the *trans* isomers: ΔH = 13.4 kJ mol^{-1} for *N,N'*-dibenzoyl derivatives and 8 kJ mol^{-1} for *N,N'*-di-(1-naphthoyl) derivatives. *N,N'*-diacetylindigo is also the more suitable compound for the stored energy content per gram of compound: 100 J g^{-1}, but only 29 J g^{-1} for compound **2**. The amount stored in this way corresponds at the most to an increase by 25° of the temperature of 1 g of water.

In solution, the *cis* isomers exhibit a low kinetic stability since the activation free energy is about 100 kJ mol^{-1} (14); for instance, the lifetime of **1***c* in benzene solution and at 42.5°C is 0.55 h if we assume a first-order kinetics; this kinetic stability increases slightly from **1***c* to **2***c*, the relative isomerization rate being 7.9:1. This observation implies that the *cis*-rich solution should be stored or handled at low temperature, and the ir part of the solar spectrum eliminated during the irradiation process.

In addition to these unfavourable thermodynamic and kinetic data, the photochemical results do not look much better. Our results show that the isomerization quantum yields $\phi_{t\rightarrow c}$ are rather low, although no by-product can be detected when irradiating with $\lambda > 400$ nm. As mentioned already, decomposition occurs slowly if the irradiation is carried out with an irradiation light which includes the uv part. Also, it has been demonstrated that minute amounts of amines or alcohols quench the *trans* to *cis* photoisomerization and catalyze the reverse reaction. Consequently, this point implies high purity and expensive solvents which forbid the proposed energy extraction process (11*b*).

Catalysis by the amines, which speeds up the $c \rightarrow t$ reaction, allows one to gather the stored energy in a reasonable time but prevents any recycling of the system. And, finally, it should be recognized that at best the photostationary state is 1:1 (in the case of **1**) when exciting with visible light, so that, in order to get *cis*-rich mixtures, one has to use filtered light ($\lambda >$ 580 nm), and this results in long and inconvenient irradiation times.

Thus, although the indigo dyes show interesting photochemical behaviour, and are claimed as ranking among the best photochemical energy storage systems, we believe from our study that, even ignoring their cost, they show little promise as a convenient system.

1. M. CALVIN. *In* Photochemical conversion and storage of solar energy. *Edited by* J. S. Connolly. Academic Press, New York. 1981. p. 1.
2. J. J. KATZ and J. C. HINDMAN. *In* Photochemical conversion and storage of solar energy. *Edited by* J. S. Connolly. Academic Press, New York. 1981. p. 27.
3. (*a*) P. CLECHET, C. MARTELET, J. R. MARTIN, and R. OLIER. Actual. Chim. **11**, 17 (1978); (*b*) A. J. NOZIK. Ann. Rev. Phys. Chem. **29**, 189 (1978).
4. M. A. BUTLER and D. S. GINLEY. J. Mater. Sci. **15**, 1 (1980).
5. G. JONES, S. H. CHIANG, and P. T. XUANG. J. Photochem. **10**, 1 (1979).
6. (*a*) R. R. HAUTALA, J. LITTLE, and E. SWEET. Sol. Energy, **19**, 503 (1977); (*b*) D. P. SCHWENDIMAN and C. KUTAL. J. Am. Chem. Soc. **99**, 5677 (1977); (*c*) P. GRUTSCH and C. KUTAL. J. Am. Chem. Soc. **99**, 6460 (1977).
7. K. B. WIBERG and H. A. CONNON. J. Am. Chem. Soc. **98**, 5411 (1976).
8. H. GIEZENDANNER, H. J. ROZENKRANZ, H. J. HANSON, and H. SCHMID. Helv. Chim. Acta, **56**, 2588 (1973).
9. (*a*) A. W. ADAMSON, A. VOGLER, H. KUNKELY, and R. WACHTER. J. Am. Chem. Soc. **100**, 1298 (1978); (*b*) J. RONAYETTE, R. ARNAUD, P. LEBOURGEOIS, and J. LEMAIRE. Can. J. Chem. **52**, 1958 (1974); **52**, 1848 (1974); (*c*) D. P. FISHER, V. PIERMATTIE, and J. C. DABROWIAK. J. Am. Chem. Soc. **99**, 2811 (1977).
10. F. MALLORY and S. MALLORY. Org. React. **30**, 1 (1983).
11. (*a*) R. A. NATHAN, R. E. SCHWERZEL, A. H. ADELMAN, and R. E. WYANT. US Patent No. 4,004,572; Jan. 25 (1977)/June (1975); (*b*) R. E. SCHWERZEL, N. E. KLOSTERMAN, J. R. KELLY,

and L. J. HILLENBRAND. US Patent No. 4,105,014; Aug. 8 (1978)/Jan. 24 (1977).
12. J. BLANC and D. L. ROSS. (*a*) J. Phys. Chem. **72**, 2818 (1968); (*b*) *In* Photochromism. *Edited by* G. H. Brown. John Wiley, New York. 1971. p. 497.
13. T. POSNER. Ber. Dtsch. Chem. Ges. **59**, 1977 (1926).
14. Y. OMOTE, S. IMADA, R. MATSUZAKI, K. FUJIKI, T. NISHIO, and C. KASHIMA. Bull. Chem. Soc. Jpn. **52**, 3397 (1979).
15. J. UMBERGER and V. LAMER. J. Am. Chem. Soc. **67**, 1099 (1945).
16. J. L. CHARLTON and J. SALTIEL. J. Phys. Chem. **81**, 1940 (1977).
17. A. D. KIRSCH and G. M. WYMAN. J. Phys. Chem. **81**, 413 (1977).
18. K. H. GRELLMANN and P. HENTZSCHEL. Chem. Phys. Lett. **53**, 545 (1978).
19. C. P. KLAGES, K. KOBS, and R. MEMMING. Ber. Bunsenges. Phys. Chem. **86**, 716 (1982).
20. G. HAUCKE and R. PAETZOLD. J. Prakt. Chem. **321**, 978 (1979).
21. R. MEMMING and K. KOBS. Ber. Bunsenges. Phys. Chem. **85**, 238 (1981).
22. R. MEMMING and K. KOBS. J. Phys. Chem. **85**, 2771 (1981); Chem Phys. Lett. **80**, 475 (1981).
23. G. WYMAN and B. ZARNEGAR. J. Phys. Chem. **77**, 831 (1973).
24. (*a*) E. D. LIPPERT, W. LÜDER, and M. MÖLL. Spectrochim. Acta, **10**, 258 (1959); (*b*) M. A. EL BAYOUMI and F. M. A. HALIM. J. Chem. Phys. **48**, 2536 (1968); (*c*) J. TURNBULL and A. BOWD. Isr. J. Chem. **17**, 225 (1978); (*d*) G. BARTOCCI and U. MAZZUCATO. J. Lumin. **27**, 163 (1982), and references therein.
25. A. KEARVELL and F. WILKINSON. *In* Transitions non-radiatives dans les molécules. J. Chim. Phys. 125 (1970).
26. H. KESSLER. Angew. Chem. Int. Ed. Engl. **9**, 219 (1970).
27. H. GÖRNER and D. SCHULTE-FROHLINDE. Chem. Phys. Lett. **66**, 363 (1979).
28. G. M. WYMAN, B. M. ZARNEGAR, and D. G. WHITTEN. J. Phys. Chem. **77**, 2584 (1973).
29. G. M. WYMAN and B. M. ZARNEGAR. J. Phys. Chem. **77**, 1204 (1973).
30. T. KARSTENS. Ber. Bunsenges. Phys. Chem. **86**, 311 (1982).
31. F. SCANDOLA, V. BALZANI, and G. B. SCHUSTER. J. Am. Chem. Soc. **103**, 2519 (1981).
32. D. HOLTEN, M. GOUTERMAN, W. W. PARSON, N. W. WINDSOR, and M. G. ROCKLEY. Photochem. Photobiol. **23**, 415 (1976).
33. H. LEONHARD and A. WELLER. Ber. Bunsenges. Phys. Chem. **67**, 791 (1963).
34. H. BEENS and A. WELLER. *In* Organic molecular photophysics. Vol. 2. *Edited by* J. B. Birks. J. Wiley, London. 1975. p. 159.
35. A. WELLER. *In* The exciplex. *Edited by* M. Gordon and W. R. Ware. Academic Press, New York. 1975. p. 23.
36. J. T. EDWARDS. J. Chem. Educ. **47**, 261 (1970).
37. S. MUROV. Handbook of Photochemistry. Marcel Dekker Inc., New York. 1973. p. 55.
38. (*a*) A. STANIENDA and G. BIEBL. Z. Phys. Chem. (Frankfurt am Main) **52**, 254 (1967); (*b*) G. DRYHURST. Electrochemistry of biological molecules, Academic Press, New York. 1977. p. 461.
39. H. D. SCHARF, J. FLEISCHHAUER, H. LEISMANN, I. RESSLER, W. SCHLEKER, and R. WEITZ. Angew. Chem. Int. Ed. Engl. **18**, 652 (1979).

Can. J. Chem. Downloaded from www.nrcresearchpress.com by 210.87.254.40 on 09/06/12
For personal use only.

Synthesis, stereochemistry, and transformations of (*E*)-1,2-bis(benzenesulfonyl)ethylene cycloadducts to 2-oxa substituted 1,3-dienes

OTTORINO DE LUCCHI, VITTORIO LUCCHINI, MORENO ZAMAI, AND GIORGIO MODENA[1]

Centro Studi Meccanismi di Reazioni Organiche del C.N.R., Istituto di Chimica Organica, Via Marzolo 1, 35131 Padova, Italy

AND

GIOVANNI VALLE

Centro di Studi Biopolimeri del C.N.R., Istituto di Chimica Organica, Via Marzolo 1, 35131 Padova, Italy

FOR ERRATA SEE
1133 1985 P. 787

Received April 2, 1984

This paper is dedicated to Professor Peter Yates on the occasion of his 60th birthday

OTTORINO DE LUCCHI, VITTORIO LUCCHINI, MORENO ZAMAI, GIORGIO MODENA, and GIOVANNI VALLE. Can. J. Chem. **62**, 2487 (1984).

The cycloaddition of (*E*)-1,2-bis(benzenesulfonyl)ethylene (**2**) to 2-acetoxy- and 2-silyloxy-1,3-cyclodienes occurs in high yields and with high steroselectivity. Structure assignment has been based largely on ^{1}H nmr nuclear Overhauser effect (nOe) experiments on the isolated products. The cycloadducts **4***a* and **4***b* derived from the 2-oxa substituted cyclopentadienes have been further elaborated to the parent norbornenone, to the respective unsaturated sulfones **5**, and to the β-hydroxy substituted sulfone **6**. The vinyl sulfones **5** have also been independently synthesized via cycloaddition of benzenesulfonyl acetylene. The sulfones obtained are potentially important starting molecules for the preparation of more complex targets.

OTTORINO DE LUCCHI, VITTORIO LUCCHINI, MORENO ZAMAI, GIORGIO MODENA et GIOVANNI VALLE. Can. J. Chem. **62**, 2487 (1984).

La cycloaddition du (*E*)-bis(benzènesulfonyl)-1,2-éthylène (**2**) sur les acétoxy-2 et silyloxy-2 cyclodiènes-1,3 se produit avec des rendements élevés et avec une stéréosélectivité élevée. La détermination des structures repose principalement sur des expériences d'effet Overhauser nucléaire (eOn) et rmn du ^{1}H qui ont été réalisées sur les produits isolés. De plus, une filiation a pu être établi entre les cycloadduits **4***a* et **4***b*, obtenus à partir des oxa-2 cyclopentadiènes, et la norbornénone apparentée ainsi qu'avec la sulfone insaturée **5** et la β-hydroxysulfone **6**. Faisant appel à une cycloaddition du benzènesulfonylacétylène, on a également synthétisé les vinylsulfones **5** d'une façon indépendante. Les sulfones obtenues peuvent éventuellement être d'importantes molécules de départ dans la synthèse de composés plus complexes.

[Traduit par le journal]

Can. J. Chem. Downloaded from www.nrcresearchpress.com by 210.87.254.40 on 09/06/12
For personal use only.

We have recently reported on the high dienophilic reactivity of (*Z*)- and (*E*)-1,2-bis(benzenesulfonyl)ethylenes **1** (1) and **2** (2) towards cyclic 1,3-dienes and on the reductive elimination of the two sulfonyl groups from the adducts with the formation of the corresponding carbon–carbon single (3) or double (1, 2) bond, depending upon the reaction conditions.

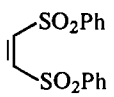

1

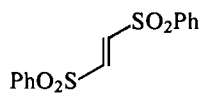

2

Lately we became interested in utilizing these reagents for the synthesis of polycyclic ketones in order to exploit fully their synthetic potential. Preparation of polycyclic saturated and especially unsaturated ketones has in fact remarkable importance because of their verstatility as building blocks for the preparation of complex natural products (4) and especially of prostaglandins (5).

As represented in Scheme 1, two possible approaches to bicyclic unsaturated ketones of type **3** are practicable. Path (a) entails the reaction of a ketene equivalent (as ketenes usually undergo [2+2]-cycloadditions) with a 1,3-diene, while path (b) takes advantage of the easy hydrolysis of the products derived by the acetylene equivalent cycloaddition to 2-oxa substituted 1,3-dienes. While there are a number of reagents capable of performing path (a) (6), and even **1** and **2** have been shown to be potential ketene equivalents (3), maleic anhydride is so far the only acetylene equivalent that can realize path (b), as shown by Yates and co-workers (7) as well as by others (8).

Herewith we report on the use of (*E*)-1,2-bis(benzenesulfonyl)ethylene (**2**) for the synthesis of bicyclic unsaturated ketones of type **3** through path (b), with a procedure that entails reductive processes, as an alternative to the strong oxidative conditions necessary with the use of maleic anhydride. The isomeric dienophile **1** behaves similarly, but in the present study **2** was preferred for its greater reactivity.

The cycloaddition of a *trans* dienophile to an asymmetric diene necessarily leads to a mixture of isomers of type **4**; they have been obtained in variable ratios and their structure determined by nuclear Overhauser effect (nOe) experiments.

Finally, in view of the growing interest in sulfones as building blocks of complex molecules (9), we provide access to vinyl sulfones of type **5** and to the β-hydroxy sulfone **6**, which are polyfunctionalized molecules amenable to a variety of more complex transformations.

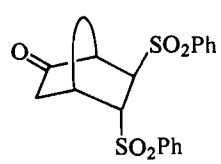

4

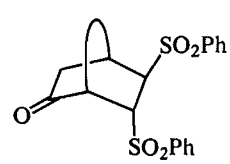

4′

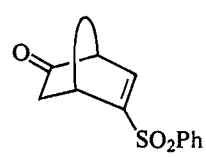

5

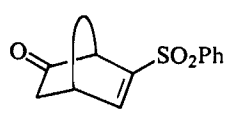

5′

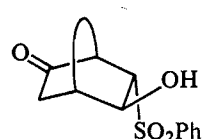

6

[1]Author to whom correspondence may be addressed.

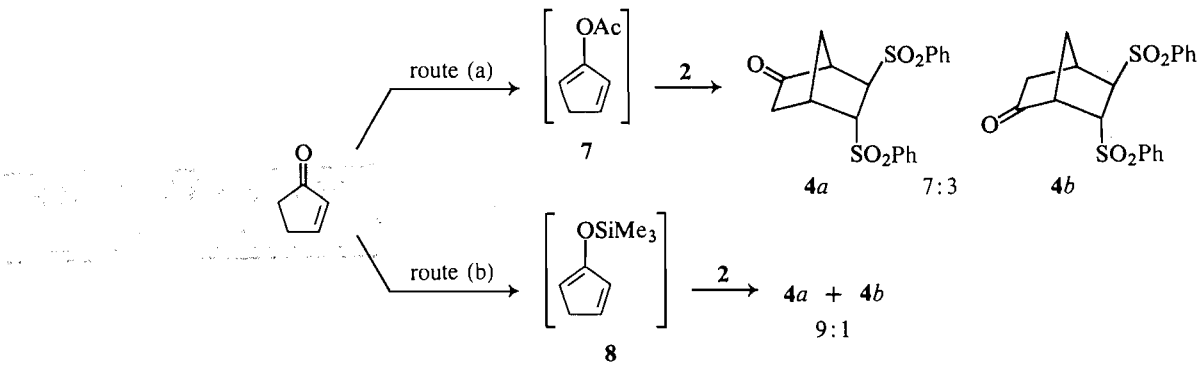

CHART 1

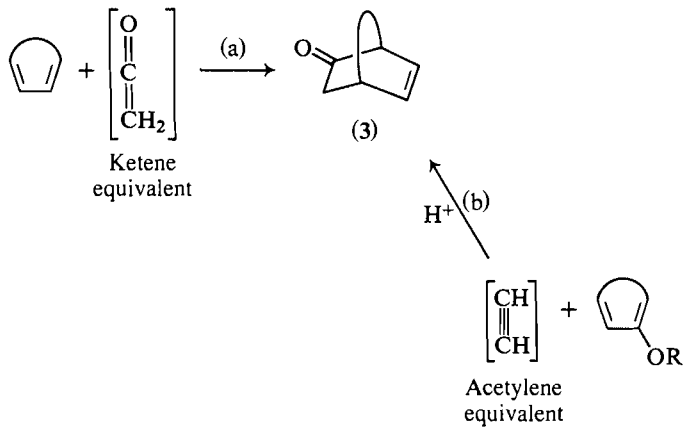

SCHEME 1

Results

Ketones **4***a* and **4***b* are obtained via cycloaddition of (*E*)-1,2-bis(benzenesulfonyl)ethylene (**2**) to *in situ* generated 2-acetoxycyclopentadiene (**7**) or 2-silyloxycyclopentadiene (**8**) (routes (a) and (b) in Chart 1). Route (a) is performed by refluxing an isopropenyl acetate solution of 2-cyclopentenone and **2** with catalytic amounts of *p*-toluenesulfonic acid for 2 h (8). After silica gel low pressure chromatography, adducts **4***a* and **4***b* are obtained in ca. 50 and 20% yields respectively. Alternatively (route (b)), the cycloaddition of **2** to 2-silyloxycyclopentadiene, generated *in situ* from 2-cyclopentenone and trimethylsilyl chloride with zinc chloride in triethylamine (10), furnishes a 9:1 mixture of adducts **4***a* and **4***b* in ca. 90% yield with respect to the dienophile. Similarly as above, the resulting isomeric adducts can be separated by silica gel column chromatography. The generation of **8** by other different procedures as, for example, with 1,8-diazabicyclo[5.4.0]undec-7-ene (DBU) (11), is less efficient, and also the isolation of **8** upon quenching of the 2-cyclopentenone anion with trimethylsilyl chloride (12) prior to cycloaddition gives poorer results.

No attempts were undertaken for the isolation of the intermediate enol-acetate adducts derived from route (a) or the silyl enol-ethers from route (b).

Beside the correct C,H composition by combustion analysis, the ^1H, ^{13}C nmr, ir spectral data, and especially nOe experiments were essential for the structure elucidation and for the determination of their relative stereochemistry (see below).

The same set of reactions of Chart 1 can be accomplished with 2-cyclohexenone with some differences in the product distribution. The isopropenyl acetate route leads with 2-cyclohexenone mainly to products derived from the cycloaddition of **2** to the thermodynamically more stable isomer 1-acetoxy-1,3-cyclohexadiene, while products of type **4***c* and **4***d* derived from cycloaddition to 2-acetoxy-1,3-cyclohexadiene (**9**) are obtained only in low yields. The cycloaddition of **2** to the more reactive 2-trimethylsilyloxy-1,3-cyclohexadiene (**10**) (13) (eq. [1]) affords adduct **4***c* almost exclusively. The isomeric **4***d* is produced in such a small quantity that it could not be isolated from runs carried out with ca. 1.5 mmol of dienophile.

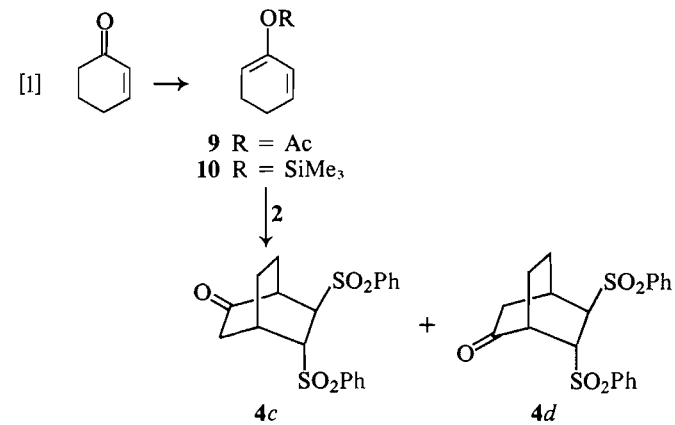

In contrast to the 2-cyclopentenone case, the *in situ* generation of **10** is of little convenience for the preparation of **4***c*, and good results are obtained only when pure **10** is reacted.

The structures of **4***c* and **4***d* have been determined by C,H composition and by spectral data. The relative stereochemistry has been assigned on the basis of nOe experiments.

The isomeric adducts **4***a* and **4***b* from cyclopentenone have been transformed into 5-norbornen-2-one (**11**) with the set of reactions shown in eq. [2]. After protection of the ketone function as the ethylene ketal, the two benzenesulfonyl groups have

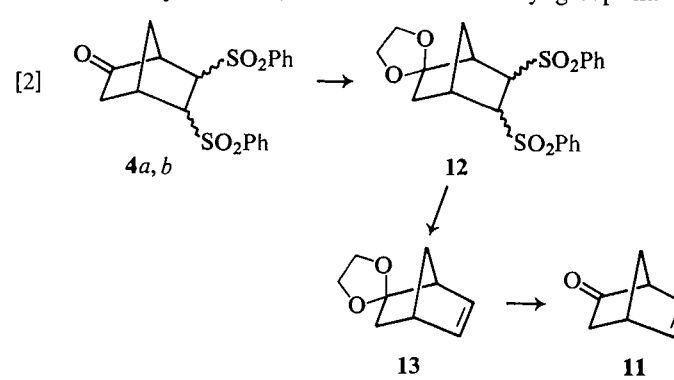

Can. J. Chem. Downloaded from www.nrcresearchpress.com by 210.87.254.40 on 09/06/12
For personal use only.

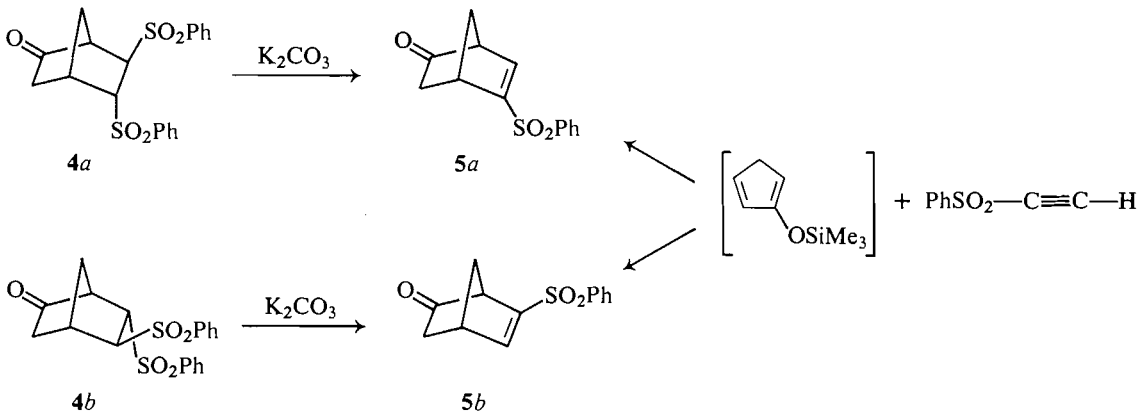

CHART 2

been efficiently removed with the recently reported method of sodium amalgam in buffered methanol (1), to give protected norbornenone (**13**) in 94% overall yield. Acidic deprotection furnishes **11**, whose structure has been confirmed by independent synthesis (14).

A mixture of **4***a* and **4***b* treated with potassium carbonate in aqueous dioxane gives a mixture of isomeric vinyl sulfones **5** in a ratio comparable to that of the starting adducts. This fact suggested that the reaction is stereo- and regiospecific in each isomer. Consequently **4***a* and **4***b* were independently reacted with potassium carbonate and transformed into the isomeric vinyl sulfones **5***a* and **5***b* respectively as single products (Chart 2). A mixture of the same vinyl sulfones **5***a* and **5***b* in a ratio of ca. 8:2 was also obtained via addition of benzensulfonylacetylene to the *in situ* generated 2-trimethylsilyloxycyclopentadiene, thus confirming by chemical means the structure of the products.

The individual structure assignment has been made on the basis of ^{1}H nmr spectral data. In fact, in both isomers the bridgehead proton 4, which couples with four methylenic protons,is readily distinguishable from the other bridgehead proton in 1, which couples only with two methylenic protons. In the isomer **5***a*, proton 1 shows a further coupling (confirmed by decoupling experiments) with the vinylic proton, which is not observed in the case of isomer **5***b*.

The reaction of adducts **4***a* and **4***b* with sodium hydroxide is remarkably different. On treatment of a mixture of **4***a* and **4***b* in dioxane with a ca. 0.5 *N* sodium hydroxide solution, a mixture of β-hydroxyalcohol **6** and ether **14** is obtained in ca. 50% yield.

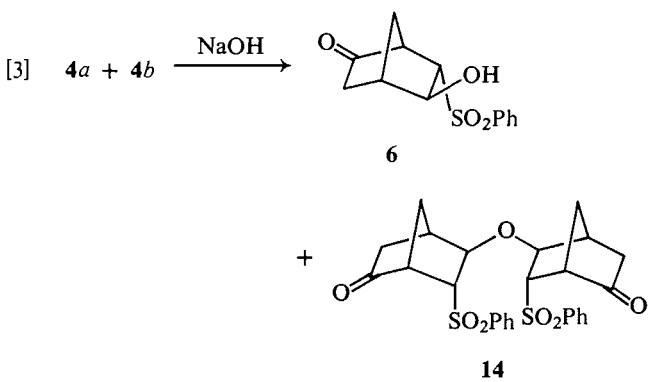

The two products have been separated through low pressure column chromatography and identified by elemental analysis and spectral data. The stereochemistry of the functional groups in **6** has been determined by nOe experiments. The relative position of the alcoholic and sulfonyl functionalities with respect to the carbonyl one was confirmed with an X-ray structure determination.

Treatment of pure adduct **4***a* with sodium hydroxide gives, in low yields (ca. 10%), alcohol **6** plus lower yields of unidentified products. In contrast, adduct **4***b* furnishes upon the same treatment both **6** and **14** in 40 and 10% yield respectively. A mixture of **6** and **14** is also obtained in comparable yields via hydroxide ion reaction with vinyl sulfone **5***b*, but only low yields of unidentified products are obtained from **5***a* under the same conditions. Work is in progress to gain a better understanding of this reaction.

Determination of the absolute configurations by the nOe technique

Isomers **4**a *and* **4**b

In these isomers the two *endo* protons are either in the 1,3 or in the 1,4 reciprocal position, so that the measurement of the nOe enhancements between them should allow the assignment of the absolute stereochemistry. To this aim, the resonances of the 3-*endo* proton and of the *endo* proton α to the sulfonyl group should be predetermined.

The ^{1}H nmr spectra are given in Figs. 1 and 2, while the nOe enhancements induced by individual saturation of all the alkyl resonances are reported in Tables 1 and 2.

In both spectra, the two multiplets at low field are to be attributed to the α-sulfonyl protons. Other safe assignments are those of the methylenic protons at the 7 position (isomer **4**: multiplets at δ 2.48 and 1.87; isomer **4***b*: multiplets at δ 2.47 and 1.76) and of the methylenic protons at the 3 position (separated multiplets for the isomer **4***a*, resonating at δ 3.09 and 2.18; almost coincident resonances at δ 2.27 for the isomer **4***b*).

In the case of **4***a*, the saturation of the low field α-sulfonyl resonance at δ 4.36 brings about positive and negative enhancements of the multiplets at δ 2.48 and 1.87, which are therefore attributed to protons 7′ and 7 in that order, while the α-sulfonyl proton is *exo* oriented.

Analogously, in the isomer **4***b* the resonance at δ 4.19 belongs to the *exo* α-sulfonyl proton since its saturation causes positive and negative nOe enhancements of the multiplets at δ 2.47 and 1.76 (respectively 7′ and 7 protons). These attributions are confirmed, for both isomers, by the reverse nOe experiments.

The other α-sulfonyl proton is necessarily *endo* and resonates in the isomer **4***a* at δ 3.78. Its saturation allows us to

Can. J. Chem. Downloaded from www.nrcresearchpress.com by 210.87.254.40 on 09/06/12
For personal use only.

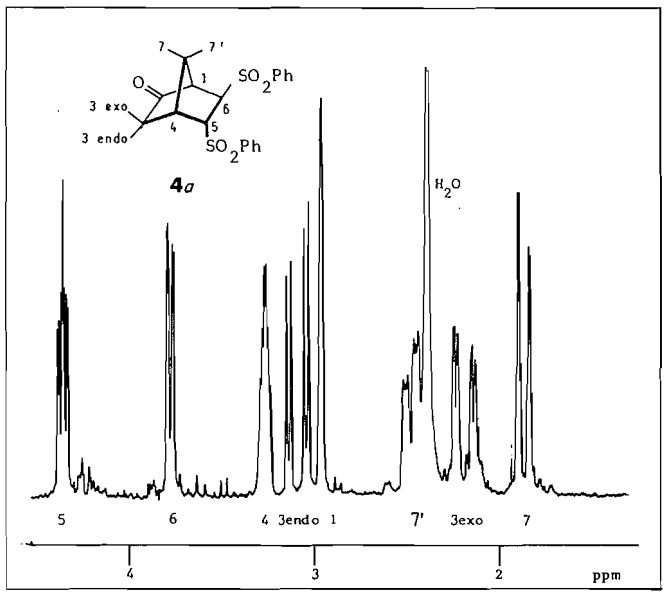

FIG. 1. 200-MHz ^{1}H nmr spectrum of the aliphatic region of cycloadduct **4***a*.

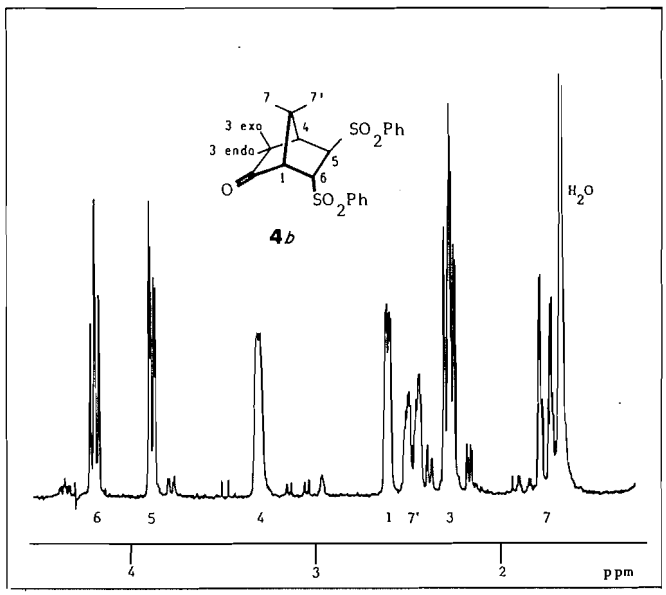

FIG. 2. 200-MHz ^{1}H nmr spectrum of the aliphatic region of cycloadduct **4***b*.

individuate the 3-*endo* resonance at δ 3.09. The nOe enhancement is small (1.4%), because of the relatively efficient relaxation induced by the nearby 3-*exo* proton. The reverse experiment gives a more significant 4.3% enhancement of the *endo* α-sulfonyl proton.

This result is to be compared with the outcome of the similar experiment carried out on the isomer **4***b*. The irradiation of the multiplet at δ 2.27 induces the contemporary saturation of both 3-*exo* and 3-*endo* protons; the result is a 13.4% enhancement of the *endo* α-sulfonyl proton resonating at δ 3.88. It is evident from this comparison that the 3 and α-sulfonyl protons with *endo* orientation are in the 1,4 position in isomer **4***a* and in the 1,3 position in isomer **4***b*.

Isomers **4**c *and* **4**d

The ^{1}H nmr spectra and the results of nOe experiments are reported in Fig. 3 and Table 3 for isomer **4***c* and in Fig. 4 and Table 4 for isomer **4***d*. The criterion for the structure assignment is, also for this pair of isomers, the measurement of the nOe enhancements between the two *endo* protons.

From the onset, only the α-sulfonyl protons can be safely attributed to the two low field multiplets (isomer **4***c*: δ 4.09 and 4.03; isomer **4***d*: δ 4.09 and 3.96). The protons in position 3 are easily identifiable, in the case of **4***c*, with the relatively isolated doublets at δ 3.11 and 2.26. The assignment is less certain for the other isomer **4***d*, where the methylenic 3 protons resonate around δ 2.5, together with one bridgehead and one ethano resonance.

It is therefore relatively easy, in the case of the first isomer **4***c*, to establish that the 3-*exo* proton is that at δ 2.26, since its saturation causes a small but significant 1.2% enhancement of the ethano resonance at δ 1.87 (proton 8); the saturation of this two-proton resonance causes positive and negative enhancements of the 3-*exo* and 3-*endo* resonances respectively, because of the obtuse angle between the 3-*exo*, 3-*endo*, and 8 protons. From the saturation of the 3-*endo* resonance at δ 3.11 follows a rather small (1.6%) enhancement of the α-sulfonyl proton resonating at δ 4.09 (therefore in the *endo* orientation). The modesty of this value suggests that the relative position of the *endo* protons is 1,4 and that the structure of the isomer is that reported in formula **4***c*.

TABLE 1. Nuclear Overhauser effect enhancements of compound **4***a*

	Observed							
Saturated	1	3-*exo*	3-*endo*	4	5	6	7	7′
1						7.2	2.5[a]	2.1[a]
3-*exo*			26.7	5.6			4.5	
3-*endo*		26.6		[b]		4.3		
4		4.2	[b]		9.9		2.9[a]	2.5[a]
5				8.8		6.6	−1.4[c]	4.5
6	6.4		1.4[a]		5.6			
7	5.6	3.7		4.3	−0.4[c]			35.2
7′	4.5			3.6	7.5		31.6	

[a]Reduced enhancement due to efficient relaxation induced by nearby protons.
[b]Not measurable because of the proximity of the saturated and observed resonances.
[c]Negative enhancement due to "quasi" linearity of 5, 7, and 7′ protons.

TABLE 2. Nuclear Overhauser effect enhancements of compound **4***b*

	Observed							
Saturated	1	3-*exo*	3-*endo*	4	5	6	7	7′
1						10.5	3.7	[a]
3-*exo*			[a]					
3-*endo*		[a]		13.9[b]	13.4			
4			3.0[b,c]		5.5		2.8	2.6
5			2.1[c]	4.3		5.6		
6	9.9				6.1		−1.6[d]	3.0[c]
7	4.8	2.1		3.7		−1.9[d]		29.5
7′	[a]			3.4		8.4	30.2	

[a]Not measurable because of the proximity of the saturated and observed resonances.
[b]The coincidence of 3-*exo* and 3-*endo* resonances does not allow the separate determination of nOe enhancements.
[c]Reduced enhancements due to efficient relaxation induced by nearby protons.
[d]Negative enhancement due to "quasi" linearity of 6, 7, and 7′ protons.

Can. J. Chem. Downloaded from www.nrcresearchpress.com by 210.87.254.40 on 09/06/12
For personal use only.

FOR ERRATA SEE
V.63#3 1985 P. 787

Can. J. Chem. Downloaded from www.nrcresearchpress.com by 210.87.254.40 on 09/06/12
For personal use only.

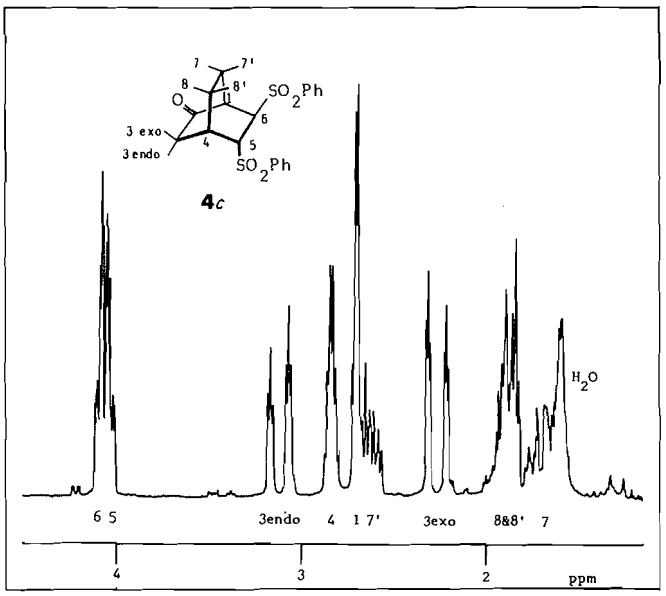

FIG. 3. 200-MHz ^{1}H nmr spectrum of the aliphatic region of cycloadduct **4***c*.

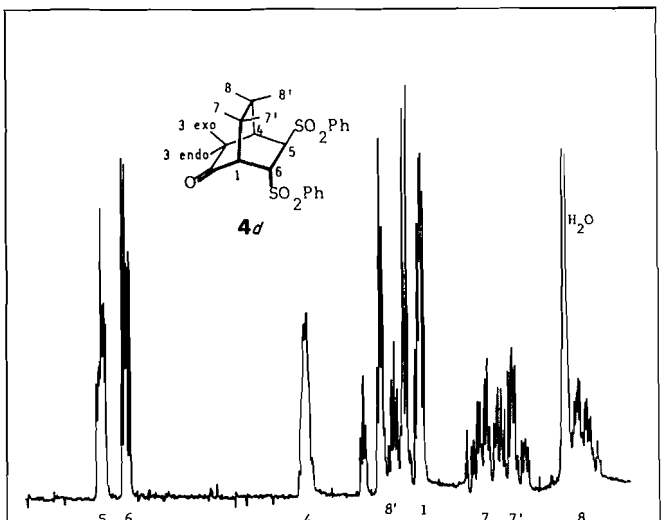

FIG. 4. 200-MHz ^{1}H nmr spectrum of the aliphatic region of cycloadduct **4***d*.

Regarding the isomer **4***d*, it is more convenient to determine firstly the orientation of the α-sulfonyl protons, since protons 3 resonate in a crowded region. The saturation of the high field part of the two-proton ethano resonance at δ 1.9 induces a nOe enhancement of the α-sulfonyl proton resonating at δ 3.96, which is therefore in the *exo* orientation. The perturbation of the other α-sulfonyl proton at δ 4.09 (necessarily *endo*) allows the identification of the 3-*endo* resonance at δ 2.61. The enhancement is a modest 3.3% (because of efficient relaxation induced by the geminal proton), while the reverse experiment brings about a 9.8% enhancement of the *endo* α-sulfonyl resonance. This value is indicative of a 1,3 relative position of the *endo* protons and a proof for the structure of the isomer as reported in formula **4***d*.

*Adducts **6** and **14***

The ^{1}H nmr spectra for alcohol **6** and ether **14** (reported in Figs. 5 and 6 respectively) are very similar, as are the results of nOe experiments (Table 5 and 6), except for one significant point to be dealt with later.

In both spectra the methylenic 3 protons resonate at the same frequency (**6**: δ 2.19; **14**: δ 2.24); furthermore, in the alcohol **6** the resonance of one methylenic 7 proton overlaps with that of proton 3. All that makes the discussion of nOe results rather difficult. It is, however, possible to assign, by saturation of the *ortho* protons in the phenyl ring, the α-sulfonyl proton to the resonance at δ 3.44 (alcohol **6**) or 3.61 (ether **14**).

Regarding the alcohol **6**, the saturation of the high field 7 methylenic doublet at δ 1.77 has the effect of a 0.7% negative enhancement of the α-sulfonyl proton resonance, so that this latter is almost collinear with the 7 methylenic protons, and *exo* oriented. No such effect is noted for the resonance at δ 4.78, to be attributed to the α-hydroxy proton, with *endo* orientation. Actually, the small (2.5%) mutual nOe which is observed between the α-sulfonyl and the α-hydroxy protons is indicative of a *trans* reciprocal orientation. A significant (9.8%) nOe is induced on the α-hydroxy resonance from saturation of the methylenic 3 resonance, suggesting the 1,3 reciprocal position of the *endo* protons and the structure given in formula **6**.

Exactly the same perturbational pattern holds for the ether **14**, except that the nOe reciprocal enhancements between α-sulfonyl 6 and α-hydroxy 5 protons are noticeably greater (5{6}: 9.8%; 6{5}: 11.8%). Because the saturation of the 7 methylenic resonances affects only the α-sulfonyl resonance 6, their orientation is again *trans*. The greater nOe is due to the fact that the 5 (or 6) proton in one monomeric unit can come very close to the 6 (or 5) proton in the second unit.

*X-ray analysis of hydroxysulfone **6***

Positional parameters are given in Table 7. Table 8 lists bond lengths and Table 9 bond angles. The perspective drawing is represented in Fig. 7. As independently shown by nOe experiments, the hydroxy group is *exo* oriented, while the sulfonyl group is *endo* on the same side of the carbonyl group. No intramolecular hydrogen bonding is effective between the hydroxy and the sulfonyl group (O(2)—O(4) = 3.60 Å) but it is observed intermolecularly. Each O(2) atom binds reciprocally with an inversion centre with an O(4) of another molecule (O(2)—O(4) $(1-x, -y, 1-z)$ = 2.763 Å). It is, however, likely that in solution the hydrogen bonding is actually intramolecular.

Discussion

The method of choice for the preparation of **4***a* and **4***b* is based on the acid-catalyzed reaction of 2-cyclopentenone with isopropenyl acetate and simultaneous reaction with **2** (route (a) in Chart 1). This method has already been used by several other authors (8) for the *in situ* generation of 2-acetoxy dienes and their reaction with maleic anhydride. Indeed this procedure is convenient for the reaction with **2** when reactive dienic substrates such as 2-acetoxycyclopentadiene are formed, but it fails to give good yields of the expected cycloadducts when 2-acetoxy-1,3-cyclohexadiene is the intermediate diene. In this case, in fact, the need of a higher temperature to promote the cycloaddition of the dienophile favours the allowed 1,5-sigmatropic proton shift in **9**, with formation of the thermodynamically more stable (and probably more reactive) isomer **15**.

TABLE 3. Nuclear Overhauser effect enhancements of compound **4c**

	Observed									
Saturated	1	3-*exo*	3-*endo*	4	5	6	7	7′	8	8′
1					4.6	10.0	[a]	12.2[b]		
3-*exo*			36.8	4.1					1.2	
3-*endo*		33.7		3.7		1.6			0.0	
4		4.9	5.6		8.4	3.6			2.6[c]	
5	3.7			7.1		[a]				1.8[d]
6	5.2		0.8[d]	3.1	[a]					
7	[a]							12.2	4.5[c]	
7′	14.6[b]						15.4		[a]	[a]
8		2.1	−0.6[e]					[a]		[a]
8′				7.5[c]	6.7		4.5[c]	[a]	[a]	

[a]Not measurable because of the proximity of the saturated and observed resonances.
[b]Enhancement induced by multiple saturation of protons with similar chemical shift and geometrically close to the observed proton.
[c]The chemical shift coincidence of protons 8 and 8′ does not allow separate determination of nOe enhancements.
[d]Reduced enhancement due to efficient relaxation induced by nearby protons.
[e]Negative enhancement due to "quasi" linearity of 3-*endo*, 3-*exo*, and 8 protons.

TABLE 4. Nuclear Overhauser effect enhancements of compound **4d**

	Observed									
Saturated	1	3-*exo*	3-*endo*	4	5	6	7	7′	8	8′
1						9.7	1.7[a]	[b]		
3-*exo*			[b]	6.4[c]					10.0[c]	
3-*endo*		[b]		4.4	9.8				7.2[c]	
4		4.2	3.5		10.3				1.9[a]	1.8[a]
5			3.3[a]	8.2		[b]				
6	8.7				[b]		−1.1[d]	2.3[a]		
7	8.1					−0.6[d]		[b]	2.9[a]	[b]
7′	[b]					7.6	[b]			7.3[c]
8		10.1	[c]	4.0			7.5			18.1
8′				8.0[c]			[b]	3.3[a]	14.5	

[a]Reduced enhancement due to efficient relaxation induced by nearby protons.
[b]Not measurable because of the proximity of the saturated and observed resonances.
[c]Enhancement induced by multiple saturation of protons with similar chemical shift and geometrically close to the observed proton.
[d]Negative enhancement due to "quasi" linearity of 6, 7′, and 7 protons.
[e]Not discernible from the enhancement of nearby resonances.

[4] 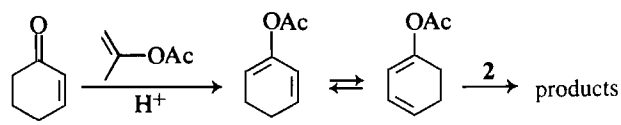

9

The desired cycloadduct of type **4** from 2-cyclohexenone is, however, readily obtainable from the reaction of **2** with the 2-silyloxy-1,3-cyclohexadiene **10**, because of the higher activation given by the ether functionality with respect to the acetoxy one. This trend of reactivity has also been observed in the reaction with maleic anhydride (12), although in this case the observation of the preferential stereoselectivity exerted by a *trans* dienophile was precluded. To the best of our knowledge, no studies on the stereoselectivity in the cycloaddition to 2-oxy substituted 1,3-cyclodienes have been reported (15).

Our results indicate that the reaction of a *trans* dienophile such as (*E*)-1,2-bis(benzenesulfonyl)ethylene (**2**) with 2-oxy substituted 1,3-cyclodienes leads with high stereoselectivity to the isomer in which the activating group of the dienophile is *endo* with respect to the unsubstituted part of the molecule. The observed steric course of addition can be easily explained by the rules of secondary orbital interaction associated with the consideration of the magnitude of the orbital coefficients that usually controls regioselectivity (16). The effect exerted by the silyloxy group to the atomic orbital coefficients in the HOMO of the diene, as compared to that of the acetoxy one, is the probable cause of the higher stereoselectivity. Furthermore, an added steric contribution caused by the trimethylsilyl group may play some role in determining the observed stereopreference. A more in-depth investigation of the real factors that govern the stereoselectivity of these reactions is in progress and it will be published in due time.

For the preparation of norbonenone (**11**) it has been shown that there is no need to use separated isomers and that the overall yield of the reaction is reasonably comparable with that of other routes to the same molecule (14). However, it is to be pointed out that the present method, engaging a very powerful dienophile, may be broader in scope and can be used when functional groups sensitive to oxidants are present in the

Can. J. Chem. Downloaded from www.nrcresearchpress.com by 210.87.254.40 on 09/06/12
For personal use only.

TABLE 5. Nuclear Overhauser effect enhancements of compound **6**

	Observed								
Saturated	1	3-*exo*	3-*endo*	4	5	6	7	7′	*ortho*
1						7.8	2.8[a]	[b]	1.7
3-*exo*				15.5[c]			38.8[c]		
3-*endo*					9.8				
4			3.0[d]		11.7[e]		2.2	3.0[d]	
5			2.1[a]	4.1		2.5			1.0
6	8.6				2.5		−0.8[f]	1.2[a]	2.5
7	6.5	23.5[d]		3.8		−0.7[f]		23.5	
7′	[b]			15.5[c]		7.2	38.8[c]		
ortho	2.5				0.9	3.3			

[a]Reduced enhancement due to efficient relaxation induced by nearby protons.
[b]Not measurable because of the proximity of the saturated and observed resonances.
[c]Enhancement induced by multiple saturation of protons with similar chemical shift and geometrically close to the observed proton.
[d]Not discernible from the enhancement of nearby resonances.
[e]Affected also by the saturation of the OH resonance.
[f]Negative enhancement due to "quasi" linearity of 6, 7′, and 7 protons.

TABLE 6. Nuclear Overhauser effect enhancements of compound **14**

	Observed								
Saturated	1	3-*exo*	3-*endo*	4	5	6	7	7′	*ortho*
1						11.5	2.3[a]	2.1[a]	3.0
3-*exo*				12.3[b]			4.9[c]		
3-*endo*					10.1				
4			2.4		9.8		2.9[a]	2.5[a]	
5			2.4[a]	10.6		11.8[d]			1.2
6	14.2				9.8[d]		−1.4[e]	4.0[a]	4.0
7	5.2	1.1		4.4		−2.2[e]		37.0	
7′	4.9			4.5		7.7	39.6		
ortho	3.3				1.0	3.7			

[a]Reduced enhancement due to efficient relaxation induced by nearby protons.
[b]Enhancement obtained by simultaneous saturation of 3-*exo* and 3-*endo* protons.
[c]Enhancement induced by multiple saturation of protons with similar chemical shift and geometrically close to the observed proton.
[d]Enhancement induced by multiple saturation of the 5 (or 6) proton in both monomeric units.
[e]Negative enhancement due to "quasi" linearity of 6, 7, and 7′ protons.

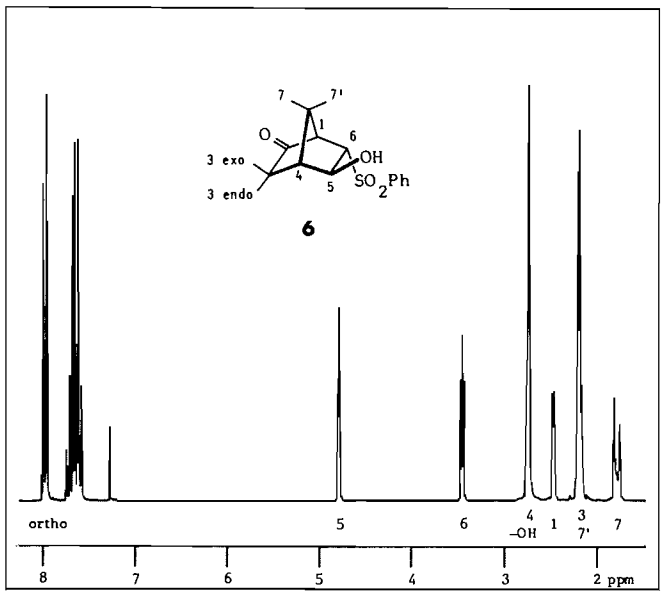

FIG. 5. 200-MHz ^{1}H nmr spectrum of the β-hydroxysulfone **6**.

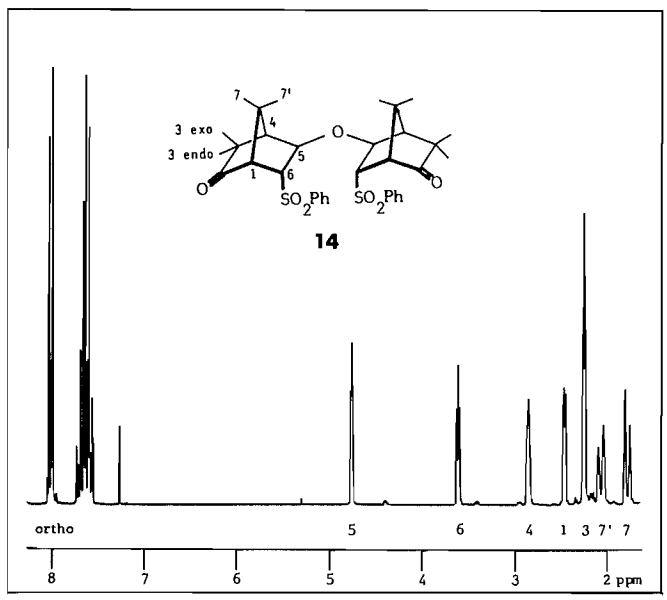

FIG. 6. 200-MHz ^{1}H nmr spectrum of the ether **14**.

Can. J. Chem. Downloaded from www.nrcresearchpress.com by 210.87.254.40 on 09/06/12
For personal use only.

Can. J. Chem. Downloaded from www.nrcresearchpress.com by 210.87.254.40 on 09/06/12
For personal use only.

TABLE 7. Fractional coordinates of compound **6**

Atom	*x/a*	*y/b*	*z/c*
S(1)	0.6276(0)	0.1750(1)	0.6832(1)
O(1)	0.6245(2)	0.0132(5)	0.7755(3)
O(2)	0.6341(2)	0.0969(5)	0.5656(3)
O(3)	0.5793(2)	0.3378(6)	0.9771(2)
O(4)	0.4516(2)	0.2517(5)	0.5238(2)
C(1)	0.5517(2)	0.3429(5)	0.6689(3)
C(2)	0.5410(2)	0.4871(5)	0.7784(3)
C(3)	0.5395(2)	0.3379(6)	0.8856(3)
C(4)	0.4727(2)	0.2005(7)	0.8567(3)
C(5)	0.4405(2)	0.2891(6)	0.7360(3)
C(6)	0.4831(2)	0.2033(5)	0.6421(3)
C(7)	0.4265(2)	0.5365(6)	0.7445(3)
C(8)	0.7327(2)	0.3451(11)	0.8426(4)
C(9)	0.7851(3)	0.4900(16)	0.8811(6)
C(10)	0.8017(3)	0.6509(14)	0.8066(8)
C(11)	0.7667(3)	0.6723(11)	0.6910(8)
C(12)	0.7133(2)	0.5186(8)	0.6495(5)
C(13)	0.6970(2)	0.3584(6)	0.7280(3)

TABLE 8. Bond lengths (Å) of compound **6**

Bond	Length	Bond	Length
S(1)—O(1)	1.436(3)	S(1)—O(2)	1.438(3)
S(1)—C(1)	1.765(3)	S(1)—C(13)	1.749(3)
O(3)—C(3)	1.194(4)	O(4)—C(6)	1.417(4)
C(1)—C(2)	1.554(4)	C(1)—C(6)	1.558(4)
C(2)—C(3)	1.515(5)	C(2)—C(7)	1.536(5)
C(3)—C(4)	1.525(6)	C(4)—C(5)	1.512(5)
C(5)—C(6)	1.531(5)	C(5)—C(7)	1.542(5)
C(8)—C(9)	1.356(8)	C(9)—C(10)	1.353(10)
C(10)—C(11)	1.387(11)	C(11)—C(12)	1.409(7)
C(12)—C(13)	1.380(6)	C(8)—C(13)	1.378(6)

molecule, since it requires reductive conditions.

The preparation of vinyl sulfones **5***a* and **5***b* represents an example of synthetic transformation of the adducts. Vinyl sulfones are continuously receiving remarkable interest in organic synthesis, and recent work in a number of laboratories witnesses their importance (9). The regioselective formation of **5***a* from **4***a* and **5***b* from **4***b* can be explained on the basis of the stereochemistry of the molecules and of the higher exposure of the *exo* hydrogen to the base attack.

Finally, the preparation of β-hydroxysulfone **6** is a further example of synthetic modification of the adducts derived from cycloaddition of (*E*)-1,2-bis(benzenesulfonyl)ethylene (**2**), where three versatile functional groups have been stereo- and regiospecifically constituted in a single molecule.

Experimental

Melting points are uncorrected. The nmr spectra were recorded on a Bruker WP 200SY, operating at 200 MHz or 50.3 MHz respectively for ^{1}H and ^{13}C. Alternatively a Varian EM 360A or a Bruker WP 60, both operating at 60 MHz, were used. All nmr spectra were recorded in $CDCl_3$ solution. The ir spectra were recorded on a Perkin Elmer 580B spectrophotometer and were taken in $CHCl_3$ solution. Microanalyses were performed by Mr. G. Biasioli of Prof. E. Celon "Laboratorio di Microanalisi" staff. Commercial reagents and solvents were purified to match reported physical and spectral data. Known compounds used in this research were either purchased from standard chemical suppliers or prepared according to literature procedures and purified to match the reported physical and spectral data.

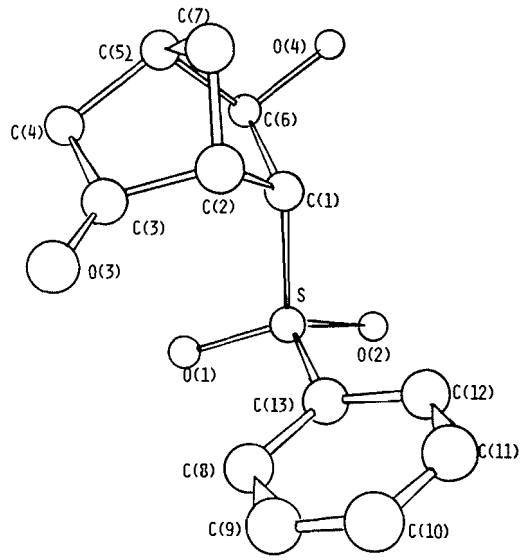

FIG. 7. Perspective drawing of the crystal structure of β-hydroxysulfone **6**.

*Nuclear Overhauser effect measurements (17*a)

The measurement tubes were freed from oxygen by repeated freeze–thaw cycles and then sealed under vacuum.

The usual pulse sequence for differential nOe experiments was adopted (17*b*); as the only modification, a multiplet was saturated with the least decoupling power by a 5-s cyclic perturbation of all multiplet lines. The percent enhancements were obtained from the coefficients of the reference spectrum when it was brought to exact matching with the perturbed spectrum. Errors are estimated as about 1%.

Preparation of 5,6-bis(benzenesulfonyl)bicyclo[2.2.1]heptan-2-one **4***a and* **4***a*

(a) *Through cycloaddition of* **2** *to* in situ *generated 2-acetoxycyclopentadiene*

(*E*)-1,2-bis(benzenesulfonyl)ethylene (**2**) (18) (2.7 g, 8.8 mmol) is added to a solution of 2-cyclopentenone (2.6 g, 31.9 mmol) and *p*-toluenesulfonic acid (30 mg) in 6.0 mL of isopropenyl acetate, and the reaction mixture is refluxed for 2 h with stirring. The cooled, clear yellow solution is concentrated on the rotatory evaporator and the residue is flash chromatographed through a silica gel column (>230 mesh, weight ratio adsorbant/substrate ca. 15:1) eluting with a 9:1 mixture chloroform – ethyl acetate. The first eluted product is ketone **4***a* (1.81 g, 53%); mp 204–206°C; ir ν_{max}: 1759, 1449, 1310, 1293, 1154, 1085 cm^{-1}; ^{1}H nmr δ: 1.87 (H_7, dq, $J_{7,7'}$ = 11.5, $J_{6,7}$ = $J_{1,7}$ = $J_{4,7}$ = 1.5, 1H), 2.18 ($H_{3\text{-}exo}$, dd, $J_{3\text{-}endo,3\text{-}exo}$ = 18.9, $J_{3\text{-}exo,4}$ = 4.3, 1H), 2.48 ($H_{7'}$, dm, 1H), 2.96 (H_1, bs, 1H), 3.09 ($H_{3\text{-}endo}$, dd, $J_{3\text{-}endo,4}$ = 4.6, 1H), 3.26 (H_4, m, 1H), 3.78 (H_6, dd, $J_{5,6}$ = 5.5, 1H), 4.36 (H_5, m, 1H), 7.53–7.82, 7.91–7.97 (C_6H_5, series of m, 10H); ^{13}C nmr δ: 36.59 (t), 39.54 (d), 40.49 (t), 54.34 (d), 62.40 (d), 65.23 (d), 128.51 (d), 128.62 (d), 129.43 (d), 129.71 (d), 134.40 (d), 134.61 (d), 137.83 (s), 139.30 (s), 209.25 (s); *m/e*: 249, 125, 107, 79, 77, 66, 51, 39. *Anal.* calcd. for $C_{19}H_{18}O_5S_2$: C 58.44, H 4.65; found: C 58.10, H 4.59.

The second product eluted is ketone **4***b* (0.77 g, 23%); mp 205–206°C; ir ν_{max}: 1761, 1449, 1310, 1154, 1084 cm^{-1}; ^{1}H nmr δ: 1.76 (H_7, dq, $J_{7,7'}$ = 11.6, $J_{5,7}$ = $J_{1,7}$ = $J_{4,7}$ = 1.8, 1H), 2.23 and 2.31 ($H_{3\text{-}endo}$ and $H_{3\text{-}exo}$, split AB quartet, $J_{3\text{-}endo,3\text{-}exo}$ = 18.0, $J_{3\text{-}endo,4}$ = 3.7, $J_{3\text{-}exo,4}$ = 4.3, 2H), 2.47 ($H_{7'}$, dm, 1H), 2.61 (H_1, m, 1H), 3.30 (H_4, m, 1H), 3.88 (H_5, dd, $J_{5,6}$ = 4.9, 1H), 4.19 (H_6, t, $J_{1,6}$ = 4.9, 1H), 7.57–7.80, 7.89–8.02 (C_6H_5, series of m, 10H); ^{13}C nmr δ: 36.40 (t), 38.29 (d), 42.43 (t), 51.77 (d), 65.37 (d), 65.43 (d), 128.88 (d), 129.03 (d), 129.53 (d), 129.57 (d), 134.52 (d), 134.61 (d), 137.47 (s), 138.32 (s), 208.51 (s); *m/e*: 249, 125, 107, 79, 77, 51.

TABLE 9. Bond angles (deg) of compound **6**

Bonds	Angle	Bonds	Angle
O(1)—S(1)—O(2)	118.4(2)	O(1)—S(1)—C(1)	109.2(2)
O(1)—S(1)—C(13)	109.1(2)	O(2)—S(1)—C(1)	106.8(2)
O(2)—S(1)—C(13)	107.7(2)	C(1)—S(1)—C(13)	104.9(2)
S(1)—C(1)—C(2)	116.9(2)	S(1)—C(1)—C(6)	112.4(2)
C(2)—C(1)—C(6)	104.1(2)	C(1)—C(2)—C(3)	109.5(3)
C(1)—C(2)—C(7)	98.8(2)	C(3)—C(2)—C(7)	100.2(3)
C(2)—C(3)—O(3)	127.6(4)	C(2)—C(3)—C(4)	105.4(3)
O(3)—C(3)—C(4)	126.8(4)	C(3)—C(4)—C(5)	102.8(3)
C(4)—C(5)—C(6)	108.8(3)	C(4)—C(5)—C(7)	102.2(3)
C(6)—C(5)—C(7)	101.3(3)	O(4)—C(6)—C(1)	107.7(2)
O(4)—C(6)—C(5)	113.1(3)	C(1)—C(6)—C(5)	102.3(2)
C(2)—C(7)—C(5)	94.7(3)	C(9)—C(8)—C(13)	120.6(6)
C(8)—C(9)—C(10)	119.4(6)	C(9)—C(10)—C(11)	122.0(5)
C(10)—C(11)—C(12)	118.8(6)	C(11)—C(12)—C(13)	117.9(5)
C(8)—C(13)—C(12)	121.2(4)	S(1)—C(13)—C(8)	119.3(3)
S(1)—C(13)—C(12)	119.4(3)	C(8)—C(13)—C(12)	121.2(4)

Anal. calcd. for $C_{19}H_{18}O_5S_2$: C 58.44, H 4.65; found: C 58.31, H 4.57.

(b) *Through cycloaddition to* in situ *generated 2-silyloxacyclopentadiene*

A 100-mL, three-necked, round-bottomed flask is charged with 2.3 mL (16.8 mmol) of freshly distilled triethylamine and ca. 3 mg (0.22 mmol) of anhydrous zinc chloride (10). The mixture is stirred 1 h under nitrogen at room temperature and then added through a rubber septum, via syringe, to 0.59 g (7.7 mmol) of 2-cyclopentenone in 4 mL of dry benzene, followed by 1.9 mL (14.4 mmol) of trimethylchlorosilane with a drop of triethylamine. After 12 h at 40°C under vigorous stirring, the mixture is cooled to room temperature and 0.5 g (1.62 mmol) of **2** are added. The mixture is further stirred at room temperature for 1 day, then rotoevaporated. The residue is chromatographed through silica gel (70–230 mesh, weight ratio adsorbant/substrate ca. 10:1), eluting with dichloromethane. The first eluted product is ketone **4***a* (0.52, 82.2%), the second is ketone **4***b* (52 mg, 8.2%).

Preparation of 5,6-bis(benzenesulfonyl)bicyclo[2.2.2]octan-2-one **4**c *and* **4**d

(a) *Through cycloaddition of* **2** *to* in situ *generated 2-acetoxy-1,3-cyclohexadiene*

(*E*)-1,2-bis(benzenesulfonyl)ethylene (**2**) (0.45 g, 1.46 mmol), 2-cyclohexenone (0.19 g, 1.97 mmol), and *p*-toluenesulfonic acid (6 mg) in 1 mL of isopropenyl acetate are refluxed 90 min into a Pyrex vial sealed with a screw cap. The resulting reaction mixture is concentrated on the rotatory evaporator and the residue chromatographed through silica gel (>230 mesh, weight radio adsorbant/substrate ca. 20:1), eluting with dichloromethane. Except for products probably derived from cycloaddition of **2** to the isomeric acetate **15**, **4***c* is the first eluted adduct (0.10 g, 14%); mp 179–180.5°C (EtOH); ir ν_{max}: 2955, 1735, 1449, 1322, 1150, 1086 cm^{-1}; ^1H nmr δ: 1.70 (H_7, m, 1H), 1.87 (H_8 and $H_{8'}$, m, 2H), 2.26 ($H_{3\text{-}exo}$, dm, $J_{3\text{-}exo,3\text{-}endo}$ = 19.8, 1H), 2.63 ($H_{7'}$, m, 1H), 2.70 (H_1, m, 1H), 2.84 (H_4, m, 1H), 3.11 ($H_{3\text{-}endo}$, dm, 1H), 4.03 and 4.09 (H_5 and H_6, split AB quartet, $J_{5,6}$ = 5.5, 2H), 7.52–7.95 (C_6H_5, series of m, 10H). *Anal.* calcd. for $C_{20}H_{20}O_5S_2$: C 59.39, H 4.98; found: C 59.50, H 5.11.

As second adduct, **4***d* is eluted (30 mg, 5%); mp 215°C (EtOH); ir ν_{max}: 2929, 1738, 1451, 1328, 1153, 1088, cm^{-1}; ^1H nmr δ: 1.51 (H_8, m, 1H), 1.87 (H_7, m, 1H), 2.04 ($H_{7'}$, m, 1H), 2.36 (H_1, m, 1H) 2.50 ($H_{8'}$, m, 1H), 2.41 and 2.61 ($H_{3\text{-}exo}$ and $H_{3\text{-}endo}$, split AB quartet, $J_{3\text{-}endo,3\text{-}exo}$ = 18.6, 2H), 2.99 (H_4, m, 1H), 3.96 (H_6, dd, $J_{5,6}$ = 4.6, $J_{1,6}$ = 2.7, 1H), 4.09 (H_5, m, 1H), 7.55–7.82, 7.98–8.04 (C_6H_5, series of m, 10H). *Anal.* calcd. for $C_{20}H_{20}O_5S_2$: C 59.39, H 4.98; found: 59.09, H 4.82.

(b) *Through cycloaddition of* **2** *to 2-silyloxy-1,3-cyclohexadiene*

(*E*)-1,2-bis(benzenesulfonyl)ethylene (**2**) (0.5 g, 1.62 mmol), 2-trimethylsilyloxy-1,3-cyclohexadiene (0.5 g, 2.97 mmol), and 1.5 mL of toluene are deposited into a screw-capped vial and sealed under nitrogen. After heating at 120°C for 90 min, the reaction mixture is cooled and the precipitated, unreacted **2** is filtered off. The filtrate is concentrated on the rotatory evaporator and chromatographed through silica gel (70–230 mesh, weight ratio adsorbant/substrate ca. 15:1), eluting with dichloromethane to obtain **4***c* as the only recognizable product (0.44 g, 67%).

*Preparation of 5,6-bis(benzenesulfonyl)bicyclo[2.2.1]heptan-2-one ethylene ketal (***12***)*

A mixture of the isomeric ketone **4***a* and **4***b* (0.8 g, 2.05 mmol), ethylene glycol (0.3 g, 4.83 mmol), and *p*-toluenesulfonic acid (70 mg) in 30 mL of anhydrous toluene is refluxed with azeotropic water removal (Dean Stark apparatus) for 7 h. The resulting reaction mixture is rotoevaporated to dryness, dissolved in a few drops of dichloromethane, and ether added to form colorless crystals of ketal (**13**: 0.86 g, 97%); mp 203–205°C; ^1H nmr δ: 1.62–2.00 (series of m, 3H), 2.52–2.80 (series of m, 3H), 3.38–4.29 (series of m, 6H), 7.49–8.05 (C_6H_5, series of m, 10H). *Anal.* calcd. for $C_{21}H_{21}O_6S_2$: C 58.05, H 5.10; found: C 57.62, H 5.12.

Desulfonylation and hydrolysis of ketal **12**. *Preparation of 5-norbornen-2-one (***11***)*

A mixture of ketals **12** (0.5 g, 1.15 mmol), obtained as above, was suspended in methanol (20 mL) containing ca. 2.5 g of sodium dihydrogenphosphate and ca. 4.8 g of finely grounded sodium amalgam (ca. 4%, 8.5 mg-atoms of sodium). The reaction mixture is kept under continuous stirring at room temperature overnight, filtered, water added, and extracted with dichloromethane (3 × ca. 20 mL). The organic phase is washed with brine (3 × ca. 30 mL), dried over anhydrous sodium sulfate, and carefully concentrated on the rotatory evaporator. The residue (**13**, 0.16 g, 91%; ^1H nmr δ: 1.43 (H_7, dd, $J_{7,7'}$ = ca. 13 and 3, 1H), 1.62 (H_6, dm, $J_{6\text{-}endo,6\text{-}exo}$ = ca. 10, 1H), 1.69 (H_6, d, 1H), 1.80 (H_7, dd, J_d = ca. 3, 1H), 2.61 ($H_{1(4)}$, m, 1H), 2.80 ($H_{1(4)}$, m, 1H), 6.05 ($H_{2(3)}$, dd, $J_{2,3}$ = ca. 6 and 3, 1H), 6.28 ($H_{2(3)}$, dd, J_d = ca. 3, 1H)) has been directly submitted to hydrolysis.

The crude ketal is dissolved in dichloromethane (ca. 10 mL) and a few drops of concentrated hydrochloric acid are added with stirring. After 30 min water is added, and the organic phase is separated and washed to neutrality. Rotoevaporation of the dried (Na_2SO_4) resulting solution and Kugel-rohr distillation of the residue affords an oil (0.08 g, 80%) whose ir and ^1H nmr spectral data are identical to those of an authentic sample of **11** independently synthesized as described (14).

Can. J. Chem. Downloaded from www.nrcresearchpress.com by 210.87.254.40 on 09/06/12
For personal use only.

Can. J. Chem. Downloaded from www.nrcresearchpress.com by 210.87.254.40 on 09/06/12
For personal use only.

Potassium carbonate treatment of ketones **4**a and **4**b

(a) *Preparation of 5- and 6-benzenesulfonylnorbornen-2-one* **5**a *and* **5**b *as a mixture*

Potassium carbonate (0.96 g, 6.91 mmol) in ca. 6 mL of water is added, while stirring, to a solution of a mixture of **4***a* and **4***b* (0.45 g, 1.15 mmol) in ca. 13 mL of dioxane. After 45 min at 45°C, dichloromethane (ca. 15 mL) is poured into the reaction mixture and the organic phase is separated. The aqueous layer is neutralized by addition of 1 *N* hydrochloric acid and thoroughly extracted with dichloromethane (3 × 20 mL). The combined organic extracts are dried over anhydrous sodium sulfate and rotoevaporated to dryness to afford a pale yellow oily residue of the two isomeric vinylsulfones (**5***a* and **5***b*; 0.25 g, 88%). Though it is possible to separate them by silica gel chromatography (see later), this specific mixture has not been further purified since **5***a* and **5***b* can be prepared as single products from the separated isomers **4***a* and **4***b*.

(b) *Preparation of vinylsulfone* **5**a *from adduct* **4**a

To a solution of ketone **4***a* (0.7 g, 1.79 mmol) in ca. 16 mL of dioxane 1.49 g (10.8 mmol) of potassium carbonate in ca. 9 mL of water are added with stirring at 45°C. After 1 h, dichloromethane (ca. 15 mL) is added and the aqueous layer neutralized with dilute hydrochloric acid. After separation of the two layers, the aqueous phase is extracted with more dichloromethane (2 × 10 mL) and the organic extracts washed with brine (3 × 30 mL), dried over anhydrous sodium sulfate, and rotoevaporated to dryness to afford an oil (**5***a*; 0.4 g, 90%) that was crystallized from ethanol; mp 74.5–76°C; ir ν_{max}: 2953, 1750, 1579, 1308, 1172, 1150, 1091 cm^{-1}; ^1H nmr δ: 1.61 (H_8, dd, $J_{7,8}$ = 17.1, $J_{8,3\text{-}endo}$ = 4.6, 1H), 2.01 (H_7, dd, $J_{4,7}$ = 3.4, 1H), 2.08 ($H_{3\text{-}exo}$, dm, $J_{3\text{-}exo,3\text{-}endo}$ = 9.8, 1H), 2.39 ($H_{3\text{-}endo}$, dm, 1H), 3.33 (H_1, m, 1H), 3.40 (H_4, m, 1H), 6.83 (H_6, m, 1H), 7.53–7.74, 7.87–7.95 (C_6H_5, series of m, 5H); *m/e*: 248, 206, 141, 125, 97, 81, 77, 53, 51, 39. *Anal.* calcd. for $C_{13}H_{12}O_3S$: C 62.89, H 4.87; found: C 63.40, H 4.93.

(c) *Preparation of vinylsulfone* **5**b *from adduct* **4**b

On treatment of adduct **4***b* (0.9 g, 2.30 mmol) in 12 mL of dioxane with potassium carbonate (1.79 g, 13.0 mmol) in 11 mL of water, at 45°C for 30 min and work-up as before, there was obtained 0.52 g (90%) of vinylsulfone **5***b* that was recrystallized from ethanol; mp 81°–82.5°C; ir ν_{max}: 2947, 1765, 1579, 1320, 1170, 1150, 1071 cm^{-1}; ^1H nmr δ: 1.83 (H_8, dd, $J_{7,8}$ = 17.09, $J_{3\text{-}endo,8}$ = 4.6, 1H), 2.04 (H_7, dd, $J_{4,7}$ = 3.4, 1H), 2.08 ($H_{3\text{-}exo}$, dm, $J_{3\text{-}endo,3\text{-}exo}$ = 10.1, 1H), 2.45 ($H_{3\text{-}endo}$, dm, 1H), 3.29 (H_1, m, 1H), 3.39 (H_4, m, 1H), 7.39 (H_5, d, $J_{4,5}$ = 3.0, 1H), 7.50–7.71, 7.84–7.92 (C_6H_5, series of m, 5H); *m/e*: 248, 206, 141, 125, 97, 81, 77, 53, 51, 39. *Anal.* calcd. for $C_{13}H_{12}O_3S$: C 62.89, H 4.87; found: C 62.24, H 4.80. Depending on the runs, this sample may be contaminated with ether **14** (see below).

(d) *Cycloaddition of benzenesulfonyl acetylene to* in situ *generated 2-acetoxycyclopentadiene. Preparation of a mixture of vinylsulfones* **5**a *and* **5**b

A 10-mL Pyrex vial equipped with a screw cap and a rubber septum, containing benzenesulfonyl acetylene (19) (0.5 g, 3.01 mmol), 2-cyclopentenone (0.32 g, 3.9 mmol), and *p*-toluenesulfonic acid (30 mg) in 2 mL of isopropenyl acetate is sealed under nitrogen and heated at reflux for 2 h. The reaction mixture is rotoevaporated and the resulting dark residue is chromatographed through a silica gel column (70–230 mesh, weight ratio adsorbant/substrate ca. 10:1) eluted with dichloromethane. The products are eluted in the sequence **5***a* (0.48 g, 64%) and **5***b* (0.12 g, 12%), as determined by comparison of the tlc and ^1H nmr spectral data with those of the previously obtained samples.

Sodium hydroxide treatment of adducts **4**a *and* **4**b. *Preparation of ketohydroxysulfone* **6**

To a solution of 1.10 g (2.82 mmol) of ketones **4***a* and **4***b*, as obtained from cycloaddition of **2** to 2-acetoxycyclopentadiene in 23 mL of dioxane, is added, while stirring, a 0.5 *N* solution (30 mL) of sodium hydroxide. The mixture is stirred at room temperature for 30 min and extracted with dichloromethane (20 mL). The aqueous phase is neutralized with 1 *N* hydrochloric acid and further extracted with dichloromethane (2 × 20 mL). The organic extracts are washed with brine (3 × 30 mL), dried over anhydrous sodium sulfate, and rotoevaporated. The residue is flash chromatographed through a silica gel column (>230 mesh, weight ratio adsorbant/substrate ca. 15:1), eluting with a 8:2 mixture chloroform – ethyl ether. The first eluted product is the ketohydroxysulfone **6** (0.3 g, 40%); mp 263–267°C; ir ν_{max}: 3601, 3493, 2983, 1754, 1448, 1311, 1290, 1153, 1084 cm^{-1}; ^1H nmr δ: 1.77 ($H_{7'}$, dm, $J_{7,7'}$ = 11.0, 1H), 2.19 ($H_{3\text{-}endo}$, $H_{3\text{-}exo}$, and $H_{7'}$, m, 3H), 2.47 (H_1, m, 1H), 2.74 (H_4, m, 1H), 4.78 (H_5, m, 1H), 7.56–7.72, 7.94–7.80 (C_6H_5, series of m, 5H); *m/e*: 267, 249, 125, 107, 79, 77. *Anal.* calcd. for $C_{13}H_{14}O_4S$: C 58.63, H 5.30; found: C 58.48, H 5.31.

Crystal data of **6** are as follows:

$C_{13}H_{14}O_4S$ fw = 266

Monoclinic, a = 19.314(7), b = 6.001(3), c = 11.348(5) Å, β = 98.7(3)°, V = 1300 $Å^3$, ρ_o = 1.35(1), ρ_c = 1.359 g cm^{-3} (20°C, MoKα, λ = 0.71069 Å), space group $P2_{1/\alpha}$ (N. 14).

3116 independent reflections were collected on a Philips PW1100 four-circle diffractometer, θ–2θ scan mode up to 2θ = 50°. 2005 reflections were considered observed with $I > 3\sigma(I)$. The structure solution was obtained by the direct method using the "Multan" program. All non-hydrogen atoms were refined anisotropically by full-matrix least-squares ($w = 1/(\sigma^2 F + 0.0102 F^2)$). Hydrogen atoms were located on a ΔF map, but not refined. The final agreement index R = 0.064. The scattering factors and all the calculations were obtained by Shelx-76 programs (G. M. Sheldrick, Cambridge).

The second eluted product is ether **14** (0.15 g, 20%); mp 150–152°C (EtOH); ir ν_{max}: 2938, 1756, 1448, 1321, 1155, 1076 cm^{-1}; ^1H nmr δ: 1.77 (H_7, dm, $J_{7,7'}$ = 11.0, 2H), 2.06 ($H_{7'}$, dm, 2H), 2.24 ($H_{3\text{-}endo}$ and $H_{3\text{-}exo}$, m, 4H), 2.46 (H_1, m, 2H), 2.85 (H_4, m, 2H), 3.61 (H_6, m, 2H), 4.76 (H_5, m, 2H), 7.54–7.73, 7.97–8.04 (C_6H_5, series of m, 10H); *m/e*: 372, 267, 249, 125, 107, 79, 77, 55, 41. *Anal.* calcd. for $C_{26}H_{22}O_7S_2$: C 60.68, H 5.09; found: C 60.70, H 5.10.

Under the same reaction conditions adduct **4***a* and vinyl sulfone **5***a* give, with sodium hydroxide, ca. 10% yield of **6**, while a mixture of **6** (ca. 40%) and **14** (ca. 10%) is produced from pure **4***b* or **5***b*. Work is in progress to gain a better understanding of these reactions.

1. O. DE LUCCHI and G. MODENA. J. Chem. Soc. Chem. Commun. 914 (1982); Phosphorus Sulfur, **14**, 229 (1983).
2. O. DE LUCCHI and G. MODENA. Tetrahedron Lett. **24**, 1653 (1983).
3. O. DE LUCCHI and L. PASQUATO. Gazz. Chim. Ital. In press.
4. M. DEMUTH and K. SCHAFFNER. Angew. Chem. Int. Ed. Engl. **21**, 820 (1982); C. LE DRIAN and A. E. GREENE. J. Am. Chem. Soc. **104**, 5473 (1982).
5. J. S. BINDRA and R. BINDRA. Prostaglandin synthesis. Academic Press, New York, NY. 1977; A. MITRA. The synthesis of prostaglandins. Wiley–Interscience, New York, NY. 1977.
6. S. RANGANATHAN, D. RANGANATHAN, and A. K. MEHROTRA. Synthesis, 289 (1977).
7. P. YATES and H. AUKSI. Can. J. Chem. **57**, 2853 (1979); P. YATES and G. E. LANGFORD. Can. J. Chem. **59**, 344 (1981).
8. (*a*) C. M. CIMARUSTI and J. WOLINSKY. J. Am. Chem. Soc. **90**, 113 (1968); J. Org. Chem. **36**, 1871 (1971); (*b*) S. GERIBALDI, G. TORRI, and M. AZZARO. Bull. Soc. Chim. Fr. 2521 (1973); 2836 (1973).
9. (*a*) P. D. MAGNUS. Tetrahedron, **33**, 2019 (1977); (*b*) L. A. PAQUETTE and G. D. CROUSE. J. Org. Chem. **48**, 141 (1983); (*c*) B. M. TROST and D. M. T. CHAN. J. Am. Chem. Soc. **101**, 6429 (1979); (*d*) S. DANISHEFSKY, T. HARAYAMA, and R. K. SINGH. J. Am. Chem. Soc. **101**, 7008 (1979); (*e*) W. BOELL. Justus Liebigs Ann. Chem. 1665 (1979); (*f*) R. E. DONALDSON, J. C. SADDLER, S. BYRN, A. T. MCKENZIE, and P. L. FUCHS. J. Org. Chem. **48**, 2167 (1983) and preceding work in the series; (*g*) G. DE CHIRICO, V. FIANDANESE, G. MARCHESE, F. NASO, and O. SCIACOVELLI. J. Chem. Soc. Chem. Commun. 523 (1981).
10. S. DANISHEFSKY, C.-F. YAN, R. K. SINGH, R. B. GAMMILL,

P. M. MCCURRY, JR., N. FRITSCH, and J. CLARDY. J. Am. Chem. Soc. **101**, 7001 (1979).
11. Y. TANIGUCHI, J. INANAGA, and M. YAMAGUCHI. Bull. Chem. Soc. Jpn. **54**, 3229 (1981).
12. G. M. RUBOTTOM and D. S. KRUEGER. Tetrahedron Lett. 611 (1977).
13. C. GIRARD and J. M. CONIA. Tetrahedron Lett. 3327 (1974).
14. C. LE DRIAN and A. E. GREENE. J. Am. Chem. Soc. **104**, 5473 (1982), and cited references.
15. M. PETRZILKA and J. I. GRAYSON. Synthesis, 753 (1981).
16. I. FLEMING. Frontier orbitals and organic chemical reactions. John Wiley and Sons, London. 1976; T. L. GILCHRIST and R. C. STORR. Organic reactions and orbital symmetry. Cambridge Press, London. 1979.
17. (*a*) J. H. NOGGLE and R. E. SCHIRMER. The nuclear Overhauser effect. Academic Press, New York. 1971; (*b*) Bruker Analytische Messtechnick GMBH, Aspect 2000 Pulse Programmer. Rheinstetten, West Germany. 1981.
18. O. DE LUCCHI, V. LUCCHINI, L. PASQUATO, and G. MODENA. J. Org. Chem. **49**, 596 (1984).
19. S. N. BHATTACHARYA, B. M. JOSIAH, and D. R. M. WALTON. Organomet. Chem. Synth. **1**, 145 (1970).

Can. J. Chem. Downloaded from www.nrcresearchpress.com by 210.87.254.40 on 09/06/12
For personal use only.

Stereospecific cyclization of β-hydroxy aryl amides to β-lactams[1]

AJAY K. BOSE, M. S. MANHAS, D. P. SAHU, AND V. R. HEGDE
Department of Chemistry and Chemical Engineering, Stevens Institute of Technology, Hoboken, NJ. 07030, U.S.A.

Received January 17, 1984

This paper is dedicated to Professor Peter Yates on the occasion of his 60th birthday

AJAY K. BOSE, M. S. MANHAS, D. P. SAHU, and V. R. HEGDE. Can. J. Chem. **62**, 2498 (1984).

N-Aryl-β-lactams can be prepared conveniently by an intramolecular reaction of β-hydroxyarylamides under the influence of diethyl azodicarboxylate (DEAD) and triphenylphosphine (TPP). Optically active 3-amino-2-azetidinone derivatives can be prepared by this method starting with a suitably protected α-amino-β-hydroxy carboxylic acid amide. This cyclization involves the retention of configuration at C2 and complete inversion at C3 of the starting acid. In some cases diamides of azodicarboxylic acid have been used by replacing TPP with the more reactive tributyl phosphine. Other phosphorus reagents such as phosphite esters and hexamethyl phosphorus triamide could also be used.

AJAY K. BOSE, M. S. MANHAS, D. P. SAHU et V. R. HEGDE. Can. J. Chem. **62**, 2498 (1984).

Grâce à une réaction intramoléculaire des β-hydroxyarylamides, qui se produit sous l'influence de l'azodicarboxylate de diéthyle (DEAD) et de la triphénylphosphine (TPP), on peut facilement préparer des *N*-aryl β-lactames. Utilisant cette méthode, on peut préparer des dérivés optiquement actifs de l'amino-3 azètidone-2 en partant de l'amide d'un acide α-amino β-hydroxy carboxylique convenablement protégé. Cette cyclisation implique une rétention de configuration en C2 et une inversion complète en C3 de l'acide de départ. Dans quelques cas, on a utilisé les diamides de l'acide azodicarboxylique en remplacant la TPP par la tributyl phosphine qui est plus réactive. On pourrait aussi utiliser d'autres réactifs phosphorés comme les esters de phosphites et le HMPT (hexaméthyl phosphore triamide).

[Traduit par le journal]

Can. J. Chem. Downloaded from www.nrcresearchpress.com by 210.87.254.105 on 09/06/12
For personal use only.

In recent years monocyclic β-lactams have become a center of attention in many laboratories. This type of heterocycle has been found in nature (2); also, suitably substituted moncyclic β-lactams can be converted to bicyclic (or polycyclic) β-lactams including naturally occurring penicillins, cephalosporins, cephamycins, and their analogs (3). In a preliminary communication (4) we have reported some aspects of our studies on the conversion of α-amino-β-hydroxy acid derivatives to optically active β-lactams by an intramolecular Mitsunobu type reaction (5). We present here details of these studies as well as new observations made by us.

Characteristics of the Mitsunobu reaction

In essence the Mitsunobu reaction (5) is the replacement of a hydroxyl group by an anion under the influence of triphenylphosphine (TPP) and diethyl azodicarboxylate (DEAD) (6); the elements of water are removed by combining hydrogen with DEAD to form the hydrazine derivative and by converting TPP to its oxide (Scheme 1). The replacement of the hydroxyl group is stereospecific and occurs with complete inversion.

Even such weak acids as active methylene compounds can undergo reactions with alcohols under the influence of DEAD/TPP. For example, ethyl cyanoacetate and propyl alcohol have been reported to produce mono- and dipropylcyanoacetate (6*c*).

Carlock and Mack (7) have shown that intramolecular dehydration of diols to cyclic ethers (8) and amino alcohols to cyclic amines takes place under the conditions of the Mitsunobu reaction (Scheme 2).

Synthesis of 1-aryl-3-carbamato-2-azetidinones

In the light of the successful synthesis by Carlock and Mack of azacyclic compounds by an internal Mitsunobu reaction, and of our earlier work (9), we attempted the cyclization of the *p*-toluidide **1** of N-Cbz serine (Scheme 3). Under the influence of DEAD/TPP at room temperature, **1** was converted in 53% yield to the desired β-lactam **2** (4). The clearest indication of

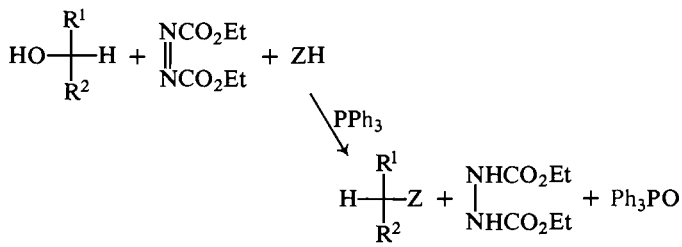

SCHEME 1

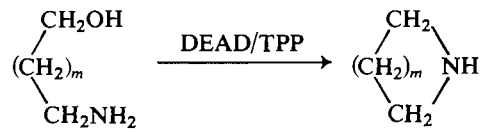

SCHEME 2

β-lactam formation was the infrared absorption of **2** at 1770 cm^{-1} and the ^1H nmr spectrum.

While this research was in progress, Miller and co-workers (10,11) reported the synthesis of β-lactams **4** from β-hydroxyhydroxamic acids **3** under the Mitsunobu reaction conditions (Scheme 3). According to these authors, the key to their success in cyclization was the acidity ($pK_a \sim 6-10$) of the —CO—NH— bond of the hydroxamic acid.

In a later publication Townsend and Nguyen (12) have reported the formation of the *N*-alkyl-β-lactam **6** from the dipeptide **5**, the —CO—NH bond of which is not expected to be particularly acidic (Scheme 4).

Our detailed studies on the internal Mitsunobu reaction of arylamides of β-hydroxy-α-amino acids disclosed that the acidity of the —CO—NH— bond is but one of several factors that affect the course of the reaction. Our findings are discussed below.

Steric course of β-lactam formation

The reaction of the *p*-toluidide **7***c* of phenylserine with DEAD and TPP led to two products, in about equal amounts,

[1] Studies on lactams, Part 70. For part 69, see ref. 1.

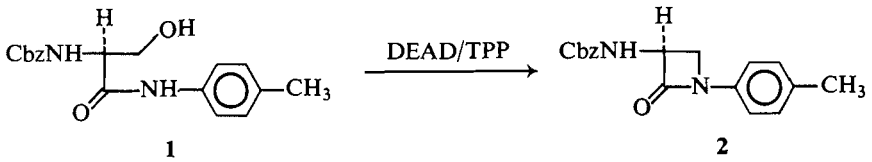

1 2

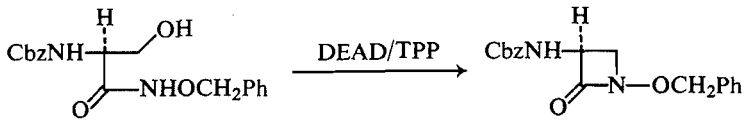

3 4

SCHEME 3

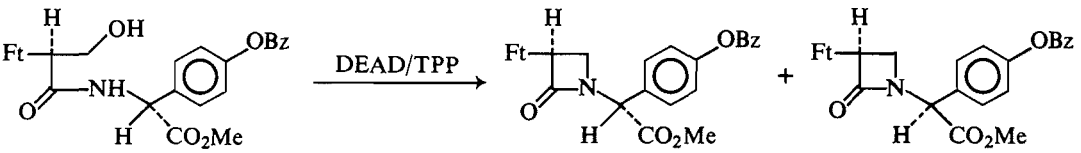

5 6

SCHEME 4

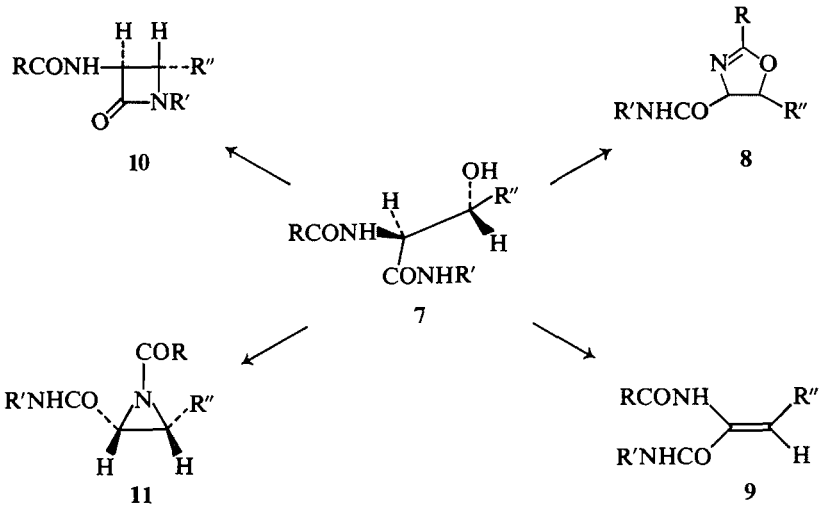

	R	R′	R″
a	OCH_2Ph	$C_6H_4CH_3(p)$	H
b	OCH_2Ph	$C_6H_4CH_3(p)$	CH_3
c	OCH_2Ph	$C_6H_4CH_3(p)$	C_6H_5
d	OCH_2Ph	$C_6H_3(OCH_3)_2$,2:4	H
e	OC_4H_9'	$C_6H_4OCH_3(p)$	H
f	OC_4H_9'	$C_6H_4CH_3(p)$	H
g	OC_4H_9'	$C_6H_4CH_3(p)$	CH_3
h	OC_4H_9'	$C_6H_4CH_3(p)$	C_6H_5

SCHEME 5

which could be separated by chromatography. Loss of the elements of water from **7***c* could possibly lead to four different types of compounds (Scheme 5). The ^1H nmr spectra of the two products obtained were incompatible with the oxazoline (**8***c*) and the eneamide (**9**) structures, but these spectra were in agreement with the four-membered and three-membered ring structures **10** and **11**, respectively.

Of the two products, one showed infrared absorption peaks at 1740, 1730, 1620 cm^{-1} and the other at 1730, 1665, 1600 cm^{-1}. Clearly, the former is the β-lactam **10***c* and the latter the aziridine **11***c*. The ^1H nmr spectrum of **10***c* showed signals δ ($CDCl_3$): 7.4–6.9 (m, 14H), 6.1 (bd, J = 9 Hz, 1H), 5.03 (s, 2H), 4.9 (bs, 1H), 4.45 (bd, J = 8 Hz, 1H), 2.2 (s, 3H). The broad singlet at δ 4.9 could be resolved into a doublet (J = 2 Hz) by adding the shift reagent $Eu(fod)_3$ to the nmr sample.

The J value of 2 Hz for the coupling of C3 and C4 protons in **10***c* is evidence for the *trans* stereochemistry of the β-lactam. Since the starting compound **7***c* had the *erythro* or (2*SR*,3*RS*) configuration, the internal Mitsunobu-type reaction must proceed with inversion at C3 of **7***c*. The *cis* or *trans* configuration of the β-lactam, therefore, can be controlled by selecting a *threo*- or *erythro*-β-hydroxy-α-amino acid as the

Can. J. Chem. Downloaded from www.nrcresearchpress.com by 210.87.254.105 on 09/06/12
For personal use only.

starting material.

The second product, **11***c*, which is isomeric with **10***c*, is best described by the aziridine structure **11**. The two ring protons of **11***c* which resonate at 3.6 and 4.0 ppm show a coupling constant of 7 Hz and are therefore *cis* to each other. During cyclization to the 3-membered ring, inversion must have occurred at C3 of the starting material **7***c*.

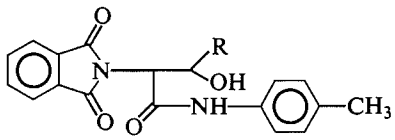

12

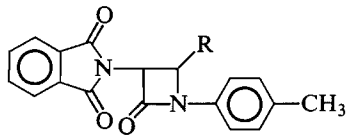

13

a = H
b = CH_3
c = Ph

A simple way of preventing the formation of aziridine is to use the *N*-phthaloyl derivative of a β-hydroxy-α-amino acid. Thus, the phthalimido derivative **12** was smoothly converted to the β-lactam **13** under the DEAD/TPP reaction conditions.

Previously we (4) have reported that the acyl hydrazide **14** can be cyclized to the β-lactam **15** – although in low yield – under the influence of DEAD/TPP at room temperature. It should be possible to prepare an *N*-unsubstituted β-lactam by taking advantage of N—N bond scission under dissolving metal reduction conditions.

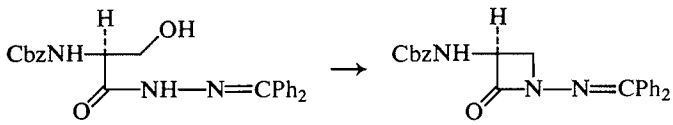

14 **15**

Chiral synthesis

The chiral nature of the synthesis described here was established by converting the *p*-toluidide **7***a* of *N*-carbobenzyloxy-L-serine to the β-lactam **10***a*. Attempts to determine the optical purity of **10***a* by using the chiral shift reagent Eu(tfac)$_3$ for nmr spectral studies were unsuccessful. To induce stronger binding with the shift reagent, the β-lactam **14** containing a free amino group was then generated by catalytic hydrogenation of **10***a*. The shift in the signal for the 4H proton *trans* to the 3H proton (shown by J = 1.5 Hz) in the ^{1}H nmr spectrum of **10***a* was studied. The quartet pattern for this proton in DL-**10***a* derived from DL-serine was shifted to form two sets of quartets of equal area. Under the same conditions **10***a* from L-serine showed only the quartet at lower field. Hence, in the course of β-lactam formation there was retention of the chirality of the α-amino acid.

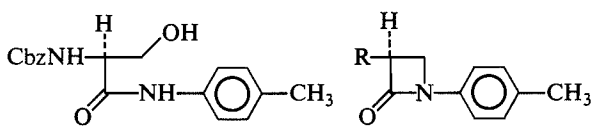

7*a* **10***a* R = CbzNH
16 R = NH_2

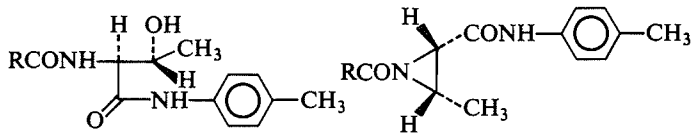

7 **11**

R = OCH_2Ph
R = $OC_4H_9^t$

Influence of various parameters

The L-threonine amides **7***b* and **7***g* on DEAD/TPP reaction gave no β-lactam; the aziridine derivatives **11***b* and **11***g* were formed instead. This indicates the importance of the group attached to the carbinol carbon in directing the course of the reaction. The *cis*-stereochemistry of the C2 and C3 protons in **11***b* and **11***g* was as expected.

2′,4′-Dimethoxybenzamide of carbobenzyloxyserine failed to undergo any reaction with DEAD/TPP under similar conditions. The nature of the group attached to the amide nitrogen also appears to play a significant role in this reaction. Thus, the 2′,4′-dimethoxylbenzamide **7***d* and the *p*-methoxybenzamide **7***b* produced only dehydration products of the type **9** under the influence of DEAD and tributylphosphine or triethyl phosphite.

We have studied the effect of changing the nature of the phosphorus and the hydrazine compounds used in our β-lactam synthesis. Table 1 shows the conversion of **7***a* to **10***a* using various phosphorus compounds and diethyl azodicarboxylate. Triphenylphosphite failed to produce any β-lactam in 2 h at room temperature. In the light of later work (11, 12), that 2 h appears to have been inadequate reaction time. Morrison and Miller (11) have shown that β-lactam formation using triphenylphosphite and DEAD requires several days at room temperature.

The effect of changing the azo reagent was also studied. Several azo reagents were prepared by heating diethyl azodicarboxylate with secondary amines in ether (13). These reagents were tested for the cyclization of **7***a* to **10***a* (Table 2). It was found that **17**, **18**, and **19** failed to produce **10***a* when triphenylphosphine was used as the phosphorus compound. However, these compounds reacted with **7***a* in the presence of tri-n-butyl phosphine. Table 2 shows the yields of β-lactam **10***a* obtained with these reagents.

3-Unsubstituted-2-azetidinones

We have found that an α-carbamato or α-phthlimido group is not necessary for cyclization to β-lactams. Thus, benzoylacetanilide (**20**) was reduced with sodium borohydride in methanol to the corresponding β-hydroxy derivative (**21**) which on treatment with DEAD/TPP gave the β-lactam **22** (15) in 61% yield. The structure of this compound was established

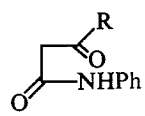

20 R = Ph
23 R = CH_3

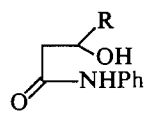

21 R = Ph
24 R = CH_3

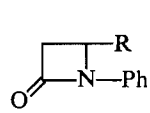

22 R = Ph
25 R = CH_3

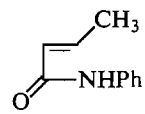

26

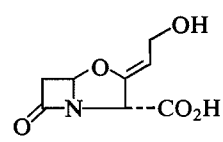

27

Can. J. Chem. Downloaded from www.nrcresearchpress.com by 210.87.254.105 on 09/06/12
For personal use only.

TABLE 1. Cyclization of **7***a* to **10***a*

Phosphorus reagent	Yield* of **10***a* (%)
$P(C_6H_5)_3$	74
$P(n\text{-}Bu)_3$	68
$P(OEt)_3$	79
$P[N(CH_3)_2]_3$	67
$P(OPh)_3$	0

*The yields were not optimized.

TABLE 2. Cyclization of **7***a* to **10***a* using n-Bu_3P

Azo reagent		Yield of **10***a* (%)
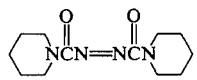	(**17**)	57
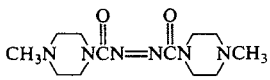	(**18**)	57
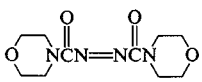	(**19**)	47

through its spectral analysis. Acetoacetanilide **23**, under similar conditions, gave a mixture of the expected β-lactam **25** and crotonanilide **26**. The β-lactams obtained are unsubstituted on C3 and are thus similar in structure to a series of naturally occurring β-lactams, a representative example of which is clavulanic acid **27**.

Conclusions

The reaction of a phosphine and an azo compound with an arylamide of a β-hydroxycarboxylic acid constitutes a convenient synthesis of substituted β-lactams under mild conditions. This method involves the retention of the configuration at C2 and total inversion of the configuration at C3 of the β-hydroxy-α-amino acid starting material. Therefore, knowledge about the steric disposition of the starting compound permits one to predict the absolute and relative configuration of the β-lactam formed. Extension of the scope of this reaction is possible (16); further studies are in progress in our laboratory.

Experimental

The melting points are uncorrected. The ^1H nmr spectra were recorded on a Varian EM-390 nmr spectrometer. Chemical shifts are reported in parts per million from tetramethylsilane as internal standard, with the downfield direction taken as positive. Mass spectra were taken with a Hitachi RMU-7 mass spectrometer and a CIMS-Biospec instrument. The infrared spectra were recorded on a Perkin–Elmer 1310 infrared spectrophotomer. Microanalyses were performed by Schwarzkopf Microanalytical Laboratory, Inc., Woodside, N.Y.

Formation of amides from protected amino acids

To a mixture of carbobenzyloxyamino acid (0.05 *M*) and dicyclohexylcarbodiimide (0.055 *M*) in 100 mL of chloroform, was added *p*-toluidine (0.05 *M*) and the solution was stirred at room temperature for about 5 h. The cooled solution was filtered to remove precipitated dicyclohexylurea. The filtrate was washed successively with 0.5 *N* hydrochloric acid, 5% sodium bicarbonate, and water. The solution was then dried ($MgSO_4$). Removal of the solvent under reduced pressure gave the crude amide as a gummy solid which on crystallization from chloroform and petroleum ether afforded the pure product. The compounds listed in Table 3 were synthesized by using this procedure.

Preparation of diazenecarboxamides

To a solution of 2 g of diethyl azodicarboxylate in 20 mL of dry ether at 0°C was added dropwise with stirring 2 g of the secondary amine in 20 mL dry ether. After 2 h at 0°C the crystallized product was filtered, dried, and recrystallized from ether and petroleum ether to obtain pure diazenecarboxamide. Compounds **17** and **19** were prepared by this method (13).

Cyclization of β-hydroxy-α-amino acid amides

To a mixture of carbobenzyloxyamino acid amide (0.003 *M*) and triaryl (or trialkyl) phosphine (0.004 *M*) in 30 mL of dry tetrahydrofuran, was added diethyl azodicarboxylate (or diazenecarboxamide) in 15 mL of tetrahydrofuran, dropwise with stirring, over a period of 30 min. The course of the reaction was monitored with thin-layer chromatography. The reaction mixture was stirred at room temperature for 2 h. Removal of the solvent afforded a gummy mass which on passing through silica gel column gave the pure product. The compounds shown in Table 4 were obtained by this method.

Sodium borohydride reduction of β-keto acid anilides

To a cold (5°C) solution of β-keto acid anilide (0.01 *M*) in methanol was added sodium borohydride (0.015 *M*) in small portions with stirring. After 2 h of stirring, methanol was removed under reduced pressure. To the resulting solid were added ethyl acetate and water and the mixture was well shaken. The contents (ethyl acetate and water layers) were slowly neutralized with dilute hydrochloric acid. The ethyl acetate layer was separated, dried, and solvent evaporated to get a white solid which was further crystallized from ethyl acetate and hexane to obtain the β-hydroxyanilides. Compounds **21** and **24** were prepared by this method.

Cyclization of β-hydroxy acid anilides

Cyclizations of β-hydroxy acid anilides were effected using the DEAD/TPP reaction. The method is similar to the one explained in the case of cyclization of β-hydroxy-α-amino acid amides. Compounds **22**, **25**, and the amide **26** were obtained by using this procedure.

cis-*1-Carbobenzyloxy-2-methyl-3-(*N-p-*tolyl)amidoaziridine* (**11***b*) was obtained as an oily liquid in 66% yield; ir (neat): 3300, 1715, 1660 cm^{-1}; nmr ($CDCl_3$) δ: 1.26 (d, 3H, J = 6 Hz), 2.3 (s, 3H), 2.83 (quintet, 1H, J = 6 Hz), 3.30 (d, 1H, J = 6 Hz), 5.26 (s, 2H), 7.08 (d, 2H, J = 9 Hz), 7.28 (s, 5H), 7.52 (d, 2H, J = 9 Hz), 9.11 (b, 1H).

cis-*1-*tert-*butoxycarbonyl-2-methyl-3-(*N-p-*tolyl)amidoaziridine* (**11***g*) was obtained as a viscous liquid in 54% yield; ir (neat): 3300, 1715, 1635 cm^{-1}; nmr ($CDCl_3$) δ: 1.30 (d, 3H, J = 6 Hz), 1.52 (s, 9H), 2.26 (s, 3H), 2.28 (quintet, 1H, J = 6 Hz), 3.16 (d, 1H, J = 6 Hz), 7.15 (d, 2H, J = 9 Hz), 7.45 (d, 2H, J = 9 Hz), 8.20 (s, H).

cis-*1-Carbobenzyloxy-2-phenyl-3-(*N-p-*tolyl)amidoaziridine* (**11***h*) was isolated in 39% yield, mp 107°C; ir (Nujol): 1730, 1665, 1600 cm^{-1}; nmr ($CDCl_3$) δ: 2.2 (s, 3H), 3.6 (d, 1H, J = 7 Hz), 4.0 (d, 1H, J = 7 Hz), 5.2 (s, 2H), 6.9–7.5 (m, 14H), 7.64 (b, 1H); mass spectrum (CIMS, NH_3 reagent gas) m/z: 387 ($M^+ + 1$). *Anal.* calcd. for $C_{24}H_{22}N_2O_3$: C 74.59, H 5.74, N 7.25%; found: C 74.57, H 5.74, N 7.31%.

α-*Carbobenzyloxyamino-*N-*(2,4-dimethoxyphenyl)acrylamide* (**9***d*) was isolated as a white crystalline solid in 48% yield, mp 101°C; ir (Nujol); 3300, 1710, 1660 cm^{-1}; nmr (DMSO-d_6) δ: 3.66 (s, 6H), 4.98 (s, 2H), 5.40 (s, 1H), 5.55 (s, 1H), 6.42 (m, 2H), 7.20 (s, 5H), 7.42 (m, 1H) 8.60 (b, 1H), 8.96 (b, 1H); mass spectrum (CIMS, NH_3 reagent gas) m/z: 357 ($M^+ + 1$). *Anal.* calcd. for $C_{19}H_{20}N_2O_5$: C 64.04, H 5.61, N 7.86%; found: C 65.03, H 5.71, N 7.87%.

α-tert-*Butoxycarbonylamino-*N-*(*p-*anisyl)acrylamide* (**9***e*) was obtained in 55% yield, mp 153–155°C; nmr ($CDCl_3$) δ: 1.50 (s, 9H), 3.47 (s, 3H), 5.2 (b, 1H), 6.06 (b, 1H), 6.90 (d, 2H, J = 9 Hz), 7.30 (b, 1H), 7.40 (d, 2H, J = 9 Hz), 7.90 (b, 1H). *Anal.* calcd. for $C_{15}H_{20}N_2O_4$: C 61.64, H 7.53, N 9.58%; found: C 61.62, H 7.46, N 9.53%.

Crotonanilide (**28**) was formed in 21% yield from **24**, mp 112°C;

Can. J. Chem. Downloaded from www.nrcresearchpress.com by 210.87.254.105 on 09/06/12
For personal use only.

Can. J. Chem. Downloaded from www.nrcresearchpress.com by 210.87.254.105 on 09/06/12
For personal use only.

TABLE 3. β-Hydroxyamides

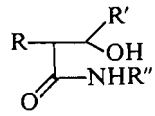

Entry	R	R′	R″	Melting point (°C)	Yield (%)	Molecular formula
7*a*	CbzNH	H	$C_6H_4CH_3(p)$	163–165	86	$C_{18}H_{20}N_2O_4$
7*b*	CbzNH	CH_3	$C_6H_4CH_3(p)$	155–156	92	$C_{19}H_{22}N_2O_4$
7*c*	CbzNH	C_6H_5	$C_6H_4CH_3(p)$	172	57	$C_{24}H_{24}N_2O_4$
7*d*	CbzNH	H	$C_6H_3(OCH_3)$ (2,4)	123–125	85	$C_{19}H_{22}N_2O_6$
7*e*	*t*-BocNH	H	$C_6H_4OCH_3$	98–99	98	$C_{15}H_{22}N_2O_5$
7*f*	*t*-BocNH	H	$C_6H_4CH_3$	165–167	64	$C_{15}H_{22}N_2O_4$
7*g*	*t*-BocNH	CH_3	$C_6H_4CH_3(p)$	153–155	89	$C_{16}H_{24}N_2O_4$
7*h*	*t*-BocNH	PH	$C_6H_4CH_3(p)$	153–154	58	$C_{21}H_{26}N_2O_4$
12*a*	Ft	H	$C_6H_4CH_3(p)$	Semi-solid	50	$C_{18}H_{16}N_2O_4$
12*b*	Ft	CH_3	$C_6H_4CH_3(p)$	138–140	86	$C_{19}H_{18}N_2O_4$
12*c*	Ft	Ph	$C_6H_4OCH_3(p)$	219–220	95	$C_{24}H_{20}N_2O_5$
14	CbzNH	H	$-N{=}CPh_2$	146–148	25	$C_{24}H_{23}N_3O_4$
24	H	CH_3	Ph	109	81	$C_{10}H_{13}NO_2$

* Values in parentheses refer to calculated values.

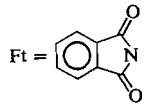

Can. J. Chem. Downloaded from www.nrcresearchpress.com by 210.87.254.105 on 09/06/12
For personal use only.

Spectral data	Analysis C	H	N
Infrared (Nujol): 3280, 1700, 1660 cm^{-1}; nmr ($CDCl_3$) δ: 2.33 (s, 3H), 3.68 (b, 1H, exchangeable with D_2O), 4.18 (m, 1H), 4.30 (m, 2H), 5.33 (s, 2H), 5.88 (b, 1H), 7.18 (d, 2H, J = 9 Hz), 7.34 (m, 2H), 7.40 (s, 5H), 8.66 (b, 1H); mass spectrum (PC1, NH_3 reagent gas) m/z: 329 ($M^+ + 1$), 346 ($M^+ + 18$)	65.22 (65.85)*	6.18 (6.14)	8.44 8.53
Infrared (Nujol): 3330, 1689, 1644 cm^{-1}; nmr ($CDCl_3$) δ: 1.14 (d, 3H J = 6 Hz), 2.33 (s, 3H), 3.54 (b, 1H, exchangeable with D_2O), 4.18 (m, 1H), 4.60 (m, 1H), 5.14 (s, 2H), 5.93 (b, 1H), 7.18 (d, 2H, J = 9 Hz), 7.36 (m, 2H), 7.46 (s, 5H), 8.83 (b, 1H); mass spectrum (PC1, NH_3 reagent gas) m/z: 343 ($M^+ + 1$), 360 ($M^+ + 18$)	66.66 (66.65)	6.43 (6.48)	8.18 (8.18)
Infrared (Nujol): 3450, 3360, 1730, 1640, 1600 cm^{-1}; nmr ($CDCl_3$) δ: 2.3 (s, 3H), 2.55 (dd, 1H, J = 5 Hz), 5.0 (s, 2H), 5.3 (m, 1H), 5.4 (d, 1H, J = 5 Hz), 6.3 (d, 1H, J = 9 Hz), 7.0–7.5 (m, 14H), 9.12 (b, 1H)	71.38 (71.27)	6.49 (5.98)	7.12 6.93
Infrared (Nujol): 3300, 1710, 1640 cm^{-1}; nmr ($CDCl_3$) δ: 3.42 (b, 1H, exchangeable with D_2O), 3.50 (m, 1H), 3.78 (s, 6H), 4.10 (m, 1H), 4.36 (m, 1H), 5.13 (s, 2H), 5.92 (b, 1H), 6.16 (d, 1H, J = 7.5 Hz), 6.46 (m, 2H), 7.36 (s, 5H), 8.13 (m, 1H), 8.66 (b, 1H); mass spectrum (PC1, NH_3 reagent gas) m/z: 375 ($M^+ + 1$), 357 ($M^+ - H_2O + 1$)			
Infrared (Nujol): 3300, 1700, 1635 cm^{-1}; nmr ($CDCl_3$) δ: 3.40 (s, 9H), 3.70 (s, 3H), 3.73 (b, 1H, exchangeable with D_2O), 4.33 (m, 1H)			
Infrared (Nujol): 3500, 3300, 1708, 1680 cm^{-1}; nmr ($CDCl_3$ + DMSO-d_6) δ: 1.48 (s, 9H), 2.25 (s, 3H), 3.78 (m, 2H, 1H exchangeable with D_2O), 4.23 (m, 1H), 4.74 (m, 1H), 6.10 (bd, 1H), 7.06 (d, 2H, J = 9 Hz), 7.40 (d, 2H, J = 9 Hz), 9.28 (b, 1H)	60.80 (61.21)	7.74 (7.53)	9.58 (9.52)
Infrared (Nujol): 3300, 1695, 1645 cm^{-1}; nmr ($CDCl_3$) δ: 1.13 (d, 3H, J = 6 Hz), 1.44 (s, 9H), 2.33 (s, 3H), 3.40 (b, 1H, exchangeable with D_2O), 4.18 (dd, 1H, J = 1.5 Hz and J = 6.0 Hz), 4.40 (m, 1H), 5.56 (d, 1H, J = 6 Hz), 7.03 (d, 2H, J = 9 Hz) 7.20 (d, 2H, J = 9 Hz), 8.53 (b, 1H)	62.10 (62.32)	7.99 (7.84)	9.13 (9.09)
Infrared (Nujol): 3350, 1705, 1680 cm^{-1}; nmr ($CDCl_3$) δ: 1.38 (s, 9H), 2.28 (s, 3H), 3.80 (b, 1H, exchangeable with D_2O), 4.52 (m, 1H), 5.08 (m, 1H), 5.20 (m, 1H), 7.08 (d, 2H, J = 9 Hz), 7.28 (s, 5H), 7.36 (d, 2H, J = 9 Hz), 8.40 (b, 1H); mass spectrum (CIMS, NH_3 reagent gas) m/z: 371 ($M^+ + 1$), 388 ($M^+ + 18$)			
Infrared (Nujol): 3300, 1740, 1710, 1650 cm^{-1}; nmr ($CDCl_3$) δ: 1.4 (s, 3H), 3.70 (b, 1H, exchangeable with D_2O), 4.13 (m, 2H), 5.03 (m, 1H), 7.03 (d, 2H, J = 9 Hz), 7.36 (d, 2H, J = 9 Hz); mass spectrum (CIMS, NH_3 reagent gas) m/z: 325 ($M^+ + 1$), 342 ($M^+ + 18$)			
Infrared (Nujol): 3250, 1745, 1715, 1648 cm^{-1}; nmr ($CDCl_3$) δ: 1.6 (d, 3H, J = 6 Hz), 2.66 (s, 3H), 3.70 (b, 1H, exchangeable with D_2O), 4.68 (m, 1H), 4.90 (d, 1H, J = 6 Hz), 7.06 (d, 2H, J = 9 Hz), 7.36 (d, 2H, J = 9 Hz), 7.80 (m, 4H), 8.93 (bs, 1H); mass spectrum (CIMS, NH_3 reagent gas) m/z: 339 ($M^+ + 1$), 356 ($M^+ + 18$)			
Infrared (Nujol): 1730, 1694, 1666 cm^{-1}; nmr (DMSO-d_6) δ: 3.70 (s, 3H), 4.60 (b, 1H, exchangeable with D_2O), 5.10 (d, 1H, J = 7 Hz), 5.72 (d, 1H, J = 7 Hz), 6.80 (d, 2H, J = 9 Hz), 7.38 (m, 6H), 7.92 (s, 5H), 9.40 (b, 1H).	69.09 (69.23)	4.94 (4.84)	6.65 (6.73)
Infrared (Nujol): 3300, 1695, 1640 cm^{-1}; nmr ($CDCl_3$ + DMSO-d_6) δ: 3.60 (b, 1H, exchangeable with D_2O), 4.1 (m, 2H), 5.10 (s, 2H), 5.20 (m, 1H), 6.43 (b, 1H), 7.43 (s, 10H), 7.63 (m, 5H), 8,53 (b, 1H); mass spectrum (NCl, NH_3 + NH_4Cl) m/z: 416 $(M - 1)^-$, 452 $(M + 35)^-$			
Infrared (Nujol): 3150, 1660, 1600 cm^{-1}; nmr ($CDCl_3$) δ: 1.23 (d, 3H, J = 9 Hz), 2.48 (d, 2H, J = 9 Hz), 3.65 (b, 1H), 4.23 (m, 1H), 6.9–7.6 (m, 5H), 8.27 (b, 1H)	67.29 (67.02)	7.57 (7.31)	7.84 (7.82)

Can. J. Chem. Downloaded from www.nrcresearchpress.com by 210.87.254.105 on 09/06/12
For personal use only.

TABLE 4. β-Lactams

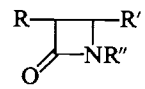

Entry	R	R′	R″	Melting point (°C)	Yield (%)	Molecular formula	Analysis C	Analysis H	Analysis N	Spectral data
10*a*	CbzNH	H	$C_6H_4CH_3(p)$	181–183	53	$C_{18}H_{18}N_2O_3$	69.80 (69.66)	5.94 (5.85)	8.97 (9.03)	Infrared (Nujol): 3300, 1770, 1700 cm^{-1}; nmr ($CDCl_3$) δ: 2.34 (s, 3H), 3.60 (dd, 1H, J = 3 Hz), 3.92 (t, 1H), 4.90 (m, 1H), 5.12 (s, 2H), 5.36 (b, 1H), 7.33 (m, 9H); mass spectrum (CIMS, NH_3 reagent gas) m/z: 311 ($M^+ + 1$)
10*c*	CbzNH	Ph	$C_6H_4CH_3(p)$	136	42	$C_{24}H_{22}N_2O_3$	74.17 (74.59)	5.76 (5.74)	7.16 (7.25)	Infrared (Nujol): 1740, 1730, 1620 cm^{-1}; nmr ($CDCl_3$) δ: 2.2 (s, 3H), 4.45 (d, 1H, J = 8 Hz), 4.9 (bs, 1H, d with $Eu(fod)_3$, J = 2 Hz), 5.03 (s, 2H), 6.1 (bd, 1H, J = 8 Hz), 6.9–7.4 (m, 14H); mass spectrum (CIMS, NH_3 reagent gas) m/z: 387 ($M^+ + 1$)
10*f*	*t*-BocNH	H	$C_6H_4CH_3(p)$	228–229	64	$C_{15}H_{22}N_2O_3$				Infrared (Nujol): 3450, 1778, 1708 cm^{-1}; nmr ($CDCl_3$) δ: 1.40 (s, 9H), 2.30 (s, 3H), 3.58 (dd, 1H, J = 3 Hz and J = 6 Hz), 3.98 (t, 1H, J = 6 Hz), 4.83 (m, 1H), 5.13 (m, 1H), 7.10 (d, 2H, J = 9 Hz), 7.20 (m, 2H, J = 9 Hz)
10*h*	*t*-BocNH	Ph	$C_6H_4CH_3(p)$	190–191	83	$C_{21}H_{24}N_2O_3$				Infrared (Nujol): 3380, 1760, 1718 cm^{-1}; nmr ($CDCl_3$) δ: 1.43 (s, 9H), 2.36 (s, 3H), 4.32 (m, 1H), 4.96 (d, 1H, J = 2.5 Hz), 5.0 (m, 1H), 7.0 (d, 2H, J = 9 Hz), 7.22 (d, 2H, J = 9 Hz), 7.33 (s, 5H); mass spectrum (CIMS, NH_3 reagent gas) m/z: 353 ($M^+ + 1$) 370 ($M^+ + 18$)
12*a*	Ft	H	$C_6H_4CH_3(p)$	208–210	78	$C_{18}H_{14}N_2O_3$	70.45 (70.58)	4.66 (4.61)	9.21 (9.15)	Infrared (Nujol): 1775, 1738, 1712 cm^{-1}; nmr ($CDCl_3$) δ: 2.33 (s, 3H), 4.0 (d, 2H, J = 4 Hz), 5.55 (t, 1H, J = 4.5 Hz), 7.16 (d, 2H, J = 9 Hz), 7.30 (d, 2H, J = 9 Hz), 7.83 (m, 4H); mass spectrum (CIMS, NH_3 reagent gas) m/z: 307 ($M^+ + 1$), 324 ($M^+ + 18$)
12*b*	Ft	CH_3	$C_6H_4CH_3(p)$	198–200	41	$C_{19}H_{16}N_2O_3$	70.95 (71.25)	5.66 (5.03)	8.91 (8.75)	Infrared (Nujol): 1772, 1740, 1715 cm^{-1}; nmr ($CDCl_3$) δ: 1.6 (d, 3H, J = 6 Hz), 2.32 (s, 3H), 4.50 (dd, 1H, J = 3 Hz and J = 6 Hz), 5.05 (d, 1H, J = 3 Hz), 7.15 (d, 2H, J = 9 Hz), 7.23 (d, 2H, J = 9 Hz), 7.8 (m, 4H); mass spectrum (CIMS, NH_3 reagent gas) m/z: 321 ($M^+ + 1$), 338 ($M^+ + 18$)
12*c*	Ft	Ph	$C_6H_4OCH_3(p)$	188–190	58	$C_{24}H_{18}N_2O_4$	72.61 (72.35)	4.61 (4.55)	6.93 (7.03)	Infrared (Nujol): 1769, 1709, 1666 cm^{-1}; nmr ($CDCl_3$) δ: 3.73 (s, 3H), 5.34 (d, 1H, J = 1.5 Hz), 5.36 (d, 1H, J = 1.5 Hz), 6.88 (d, 2H), 7.37 (d, 2H), 7.45 (s, 5H), 7.88 (s, 4H); mass spectrum (CIMS, NH_3 reagent gas) m/z: 399 ($M^+ + 1$)
15	CbzNH	H	N=CPh_2	104–106	30	$C_{24}H_{21}N_3O_3$	71.89 (72.18)	5.54 (5.26)	10.37 (10.52)	Infrared (Nujol): 3290, 1770, 1680 cm^{-1}; nmr ($CDCl_3$) δ: 2.86 (dd, 1H, J = 3 Hz), 3.17 (t, 1H, J = 6 Hz), 4.62 (b, 1H), 5.04 (s, 2H), 5.4 (m, 1H), 7.45 (m, 15H); mass spectrum (CIMS, NH_3 reagent gas) m/z: 410 ($M^+ + 1$)
22	H	CH_3	Ph	Oily liquid	41	$C_{10}H_{11}NO$				Infrared (neat): 1770 cm^{-1}; nmr ($CDCl_3$) δ: 1.5 (d, 3H, J = 6 Hz), 2.6 (dd, 1H, J = 6 Hz and J = 9 Hz), 4.13 (m, 1H), 6.9–7.3 (m, 5H)
25	H	Ph	Ph	153	61	$C_{15}H_{13}NO$				Infrared (Nujol): 1760 cm^{-1}; nmr ($CDCl_3$) δ: 1.9 (dd, 1H, J = 3 Hz and J = 9 Hz), 3.53 (dd, 1H, J = 6 Hz and J = 9 Hz), 5.0 (dd, 1H, J = 3 Hz and J = 3 Hz), 6.9–7.4 (m, 10H)

ir (Nujol): 1660 cm^{-1}; nmr ($CDCl_3$) δ: 1.8 (dd, 3H, J = 2 Hz and J = 6 Hz), 6.0 (dd, 1H, J = 2 Hz and J = 15 Hz), 6.67–7 (m, 6H), 8.6 (b, 1H).

Acknowledgements

We are grateful to Stevens Institute of Technology for partial support of this work through Stanley Funds and to Drs. R. F. Cotellessa, Jack Fajans, and F. T. Jones for their interest.

1. A. K. BOSE, K. GUPTA, and M. S. MANHAS. J. Chem. Soc. Chem. Commun. 86 (1984).
2. M. S. MANHAS and A. K. BOSE. *In* Beta lactams: natural and synthetic. Wiley–Interscience, New York, NY. 1971.
3. P. G. SAMMES (*Editor*). Topics in antibiotic chemistry. Vol. 4. Ellis Harwood Limited, New York. 1980.
4. A. K. BOSE, D. P. SAHU, and M. S. MANHAS. J. Org. Chem. **46**, 1229 (1981).
5. O. MITSUNOBU. Synthesis, 1 (1981).
6. (*a*) A. K. BOSE, W. A. HOFFMAN III, and M. S. MANHAS. J. Chem. Soc. Perkin Trans 1, 2344 (1976); (*b*) F. DININNO. J. Am. Chem. Soc. **100**, 3251 (1978); (*c*) M. WADA and O. MITSUNOBU. Tetrahedron Lett. 1279 (1972).
7. J. T. CARLOCK and M. P. MACK. Tetrahedron Lett. 5153 (1978).
8. R. MENGEL and M. BARTKE. Angew. Chem. **90**, 725 (1978).
9. (*a*) B. LAL, B. N. PRAMANIK, M. S. MANHAS, and A. K. BOSE. Tetrahedron Lett. 1977 (1977); (*b*) A. K. BOSE and B. LAL. Tetrahedron Lett. 3937 (1973).
10. P. G. MATTINGLY, J. F. KERWIN, JR., and M. J. MILLER. J. Am. Chem. Soc. **101**, 3983 (1979).
11. M. A. MORRISON and M. J. MILLER. J. Org. Chem. **48**, 4421 (1983).
12. (*a*) C. A. TOWNSEND and L. T. NGUYEN. J. Am. Chem. Soc. **103**, 4582 (1981); (*b*) C. A. TOWNSEND, A. M. BROWN, and L. T. NGUYEN. J. Am. Chem. Soc. **105**, 919 (1983).
13. E. M. KOSOWER and H. KANAETY-LONDNER. J. Am. Chem. Soc. **98**, 3001 (1975).
14. D. P. SAHU, P. MASHAVA, M. S. MANHAS, and A. K. BOSE. J. Org. Chem. **48**, 1142 (1983).
15. I. L. KNUNYANTS and N. P. GAMBARYAN. Izv. Akad. Nauk SSSR Otd. Khim. Nauk, 834 (1957).
16. P. MASHAVA. Ph.D. Thesis, Stevens Institute of Technology, 1984.

Can. J. Chem. Downloaded from www.nrcresearchpress.com by 210.87.254.105 on 09/06/12
For personal use only.

Dipolar cycloaddition reactions of diazoindene and the thermal behavior of the cycloadducts

ALBERT PADWA[1] AND STEVEN I. GOLDSTEIN
Department of Chemistry, Emory University, Atlanta, GA 30322, U.S.A.

Received February 7, 1984

This paper is dedicated to Professor Peter Yates on the occasion of his 60th birthday

ALBERT PADWA and STEVEN I. GOLDSTEIN. Can. J. Chem. **62**, 2506 (1984).

A study of the dipolar cycloaddition behavior of diazoindene toward electron-deficient acetylenic and olefinic dipolarophiles has been carried out. Reactions with alkynes afford transient 1,3-dipolar cycloadducts. Product formation can be attributed to a substituent-dependent partitioning between spiro 3*H*-pyrazole adducts and ring opened diazoalkenes. The initially formed cycloadducts lose nitrogen to give a spirocyclopropene derivative or undergo the van Alphen – Huttel rearrangement. When olefinic dipolarophiles are used, nitrogen deficient 1 : 1 adducts are isolated. The formation of the product involves the further loss of nitrogen from the initially formed spiropyrazoline adduct.

ALBERT PADWA and STEVEN I. GOLDSTEIN. Can. J. Chem. **62**, 2506 (1984).

On a réalisé une étude du comportement, lors de réactions de cycloadditions dipolaires, du diazoindène vis-à-vis de dipolarophiles oléfiniques et acétyléniques déficients en électrons. Les réactions avec les alcynes fournissent des cycloadduits 1,3-dipolaires intermédiaires. On peut attribuer la formation de ces produits à une partition, qui dépend des substituants, entre les adduits spiro 3*H*-pyrazoles et les diazoalcènes à cycle ouvert. Les cycloadduits qui se forment initialement peuvent soit perdre de l'azote pour conduire à un dérivé spirocyclopropène ou subir une transposition de van Alphen – Huttel. Lorsqu'on utilise des dipolarophiles oléfiniques, on isole des adduits 1 : 1 déficients en azote. La formation du produit implique une perte subséquente d'azote par l'adduit spiropyrazoline qui se forme initialement.

[Traduit par le journal]

Higher order dipolar cycloadditions of diazo compounds can occur when the diazo system contains more than four π-electrons (1–12). The use of extended diazoalkanes with six or more electrons has received little attention despite the obvious synthetic and theoretical interest in such processes. Selection rules for higher order dipolar cycloadditions are similar to those of the corresponding isoelectronic polyenes and are allowed in the suprafacial-suprafacial mode when the total number of participating electrons is $4n + 2$ (13, 14). Derivatives of the diazocyclopentadiene and certain diazoazole ring systems are ideally suited to a study of the various possible modes of extended dipolar cycloaddition. As part of a general program to study profiles of reactivity of diazoalkanes (15–17), we became interested in determining whether diazoindene (**1**) could undergo a higher order dipolar cycloaddition reaction. This paper summarizes our observations in this area.

Results and discussion

Diazoindene **1** could in principle react with acetylenic dipolarophiles via several plausible pathways: by either or both of two competing modes (1,3 or 1,7) of cycloaddition giving respectively **2** or **3**, or via loss of nitrogen to give the carbene derived product **4**. Previous work in this area has shown that while the analogous diazacyclopentadiene system reacts almost exclusively by 1,3-addition to acetylenes (7–10), the aza-heterocyclic analogues give products resulting from 1,7-cycloaddition (1, 2). In an effort to establish the preferred mode of cycloaddition, we allowed diazoindene **1** to react with dimethyl acetylenedicarboxylate. The cycloaddition was carried out in benzene solution and the reaction was monitored qualitatively by the disappearance of the diazo compound according to both infrared and tlc analyses. The reaction of **1** with dimethyl acetylenedicarboxylate furnished (94%) dimethyl *Z*-diazo-1*H*-

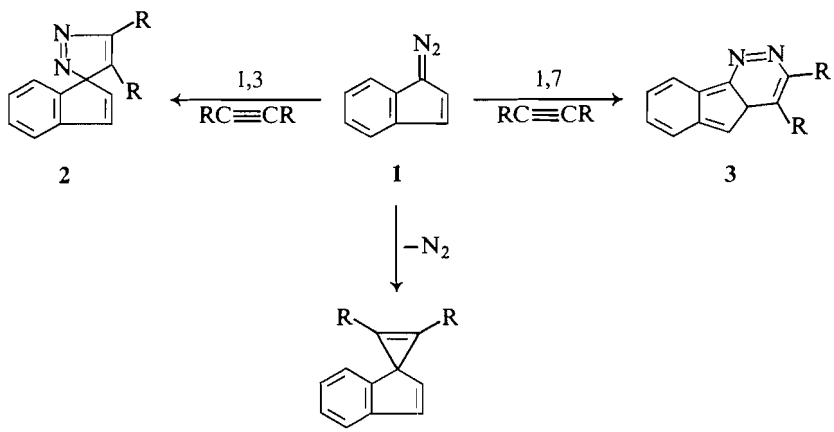

[1]Alexander von Humboldt Senior Visiting Scientist, University of Wurzburg, 1983–1984.

Can. J. Chem. Downloaded from www.nrcresearchpress.com by 210.87.254.105 on 09/06/12
For personal use only.

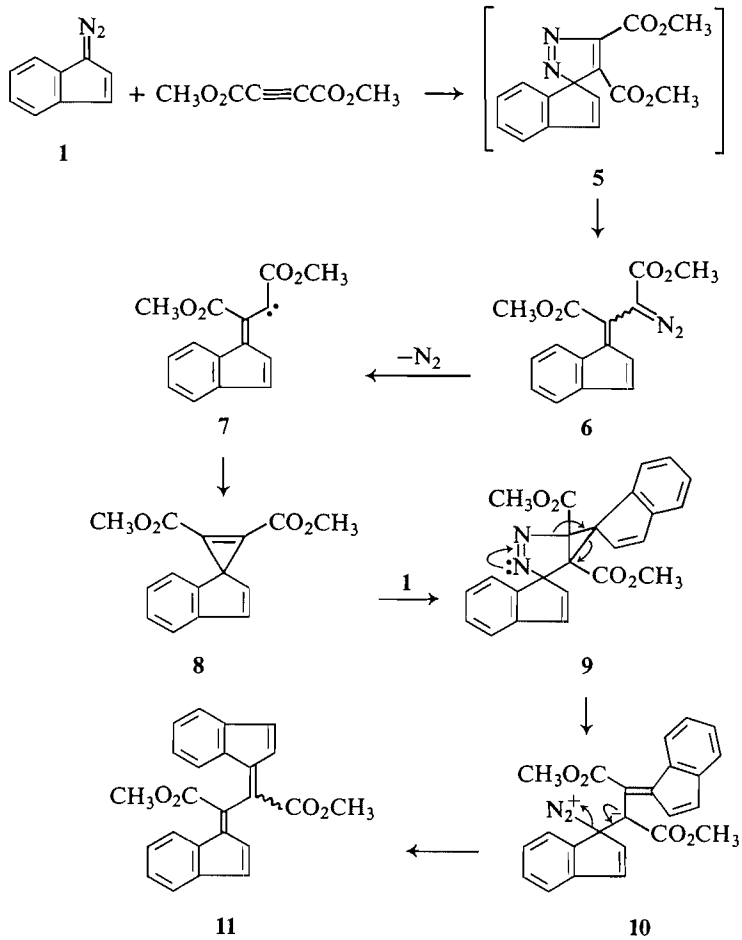

SCHEME 1

inden-1-ylidenebutanedioate (**6**). The formation of **6** can be regarded as proceeding by an initial 1,3-dipolar cycloaddition followed by a thermally allowed (3+2)-cycloreversion (for a review of 1,3-dipolar cycloreversions, see ref. 18). The conversion of **1** to **6** represents an interesting example of a 1,3-dipole metathesis process since the diazoalkane obtained is different from the one used initially (19).[2]

Structure **6** liberated nitrogen on heating in benzene to give spirocyclopropene **8**. This reaction undoubtedly involves cyclization of the initially formed vinylcarbene intermediate **7**. The thermolysis of vinyldiazomethanes is well known to give cyclopropenes as products, thereby providing a good analogy for this process (20). Heating a sample of diazoindene **1** and dimethyl acetylenedicarboxylate at 80°C for longer periods of time produced a 2:1 adduct (i.e. **9**, 92%) in addition to spiroindene **8**. The formation of **9** is believed to proceed by cycloaddition of **1** onto spirocyclopropene **8**. This could be confirmed by allowing **1** to react with a sample of **8** at 25°C. When diazabicyclohexene **9** was heated at 160°C, nitrogen was lost and the major product obtained corresponded to diene **11**. The formation of **11** can be viewed in terms of a process involving initial carbon–nitrogen bond cleavage to yield zwitterion **10** followed by loss of nitrogen to give diene **11**. This reaction is similar to that encountered on thermal or photochemical decomposition of related derivatives of 2,3-diazabicyclo[3.1.0]hex-2-enes (21, 22).

There are a number of reports in the literature which describe 1,3-dipolar cycloadditions to cyclopropene derivatives (21–43). The rates of these 1,3-dipolar cycloadditions are quite high, indicating that considerable strain in the olefin is relieved in the transition state for addition (43). The initial cycloadducts often rearrange by valence bond tautomerization, and secondary products are frequently isolated. In view of our interest in the cycloaddition behavior of cyclopropene derivatives (44), we initiated a study dealing with the reaction of **8** with several dipoles. When spirocyclopropene **8** was treated with diazomethane in ether solution at 25°C, a clean cycloaddition reaction occurred to give diazabicyclohexene **12**. Thermolysis of a sample of **12** at 110°C in benzene or photolysis in benzene resulted in the formation of the isomeric diazabicyclohexene **13**. Interestingly, structure **13** could not be isomerized back to **12** on heating or on irradiation. The stereochemistry of the individual isomers could be readily discerned by examination of their nmr spectra. The appearance of the 6-*endo* proton in **12** (δ 3.98) at high field relative to proton H6 in **13** (δ 5.13) is compatible with the anisotropic shielding of this proton by the adjacent aromatic ring. As is the case with most 1,3-dipolar cycloadditions (45), the 1,3-dipole added from the least hindered side of the π-bond to give structure **12**. An attractive rationale for the interconversion of **12** to **13** (Path A) involves an initial cycloreversion to give **14** followed by a subsequent intramolecular cycloaddition. An alternate mechanism (Path B) consists of cleavage of the cyclopropane ring to give diradical **15**, which undergoes ring flipping followed by ring closure. This path seems less likely since diazabicyclohexenes are

[2]No signs of the initially formed cycloadduct **5** could be detected in the crude reaction mixture.

Can. J. Chem. Downloaded from www.nrcresearchpress.com by 210.87.254.105 on 09/06/12
For personal use only.

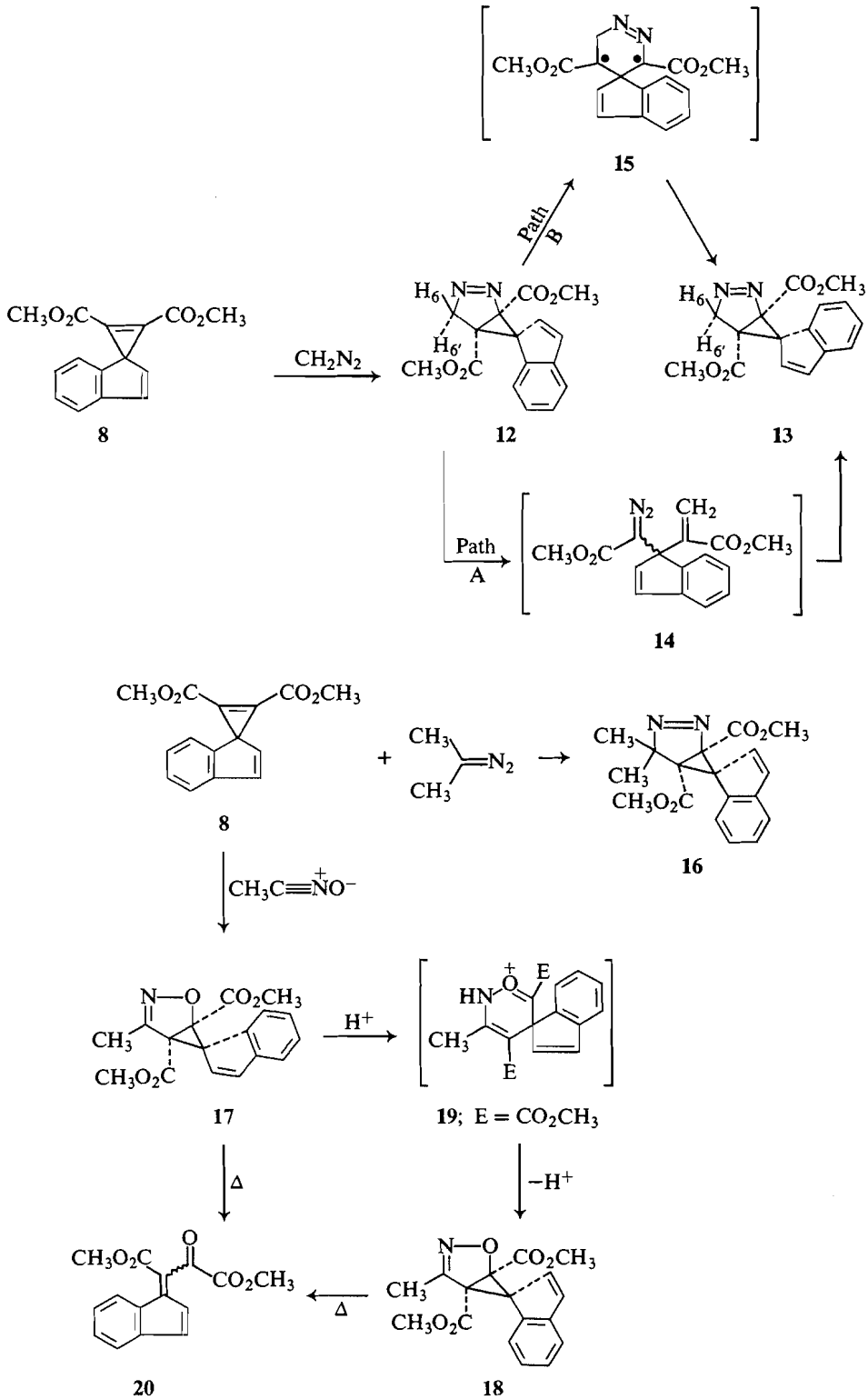

known to produce β,γ-unsaturated diazoalkenes on heating (21, 22). In fact, the thermolysis of a sample of **12** at 145°C produced diazoalkene **14**. The nmr absorptions due to **14** disappeared on standing at room temperature, cleanly reproducing the spectrum of **13**. These results clearly indicate that the intramolecular dipolar cycloaddition reaction of **14** is highly stereoselective and produces the thermodynamically more stable diazabicyclohexene isomer.

A related set of results was encountered when spirocyclopropene **8** was allowed to react with 2-diazopropane. We also found that **8** gave the dipolar cycloadduct **17** when treated with α-chloroacetaldoxime in the presence of triethylamine. Silica gel chromatography of **17** produced the isomeric oxadiazabicyclohexene **18**. A similar rearrangement occurred when **17** was stirred in benzene with a trace of *p*-toluene sulfonic acid. The stereochemistry of cycloadduct **17** was easily assigned on the basis of its nmr spectrum. The appearance of the indenyl proton in **17** at a higher field (δ 5.80) than the corresponding proton in **18** (δ 6.57) is consistent with the expected shielding effect of the C=N double bond. Thermolysis of **17** (or **18**)

Can. J. Chem. Downloaded from www.nrcresearchpress.com by 210.87.254.105 on 09/06/12
For personal use only.

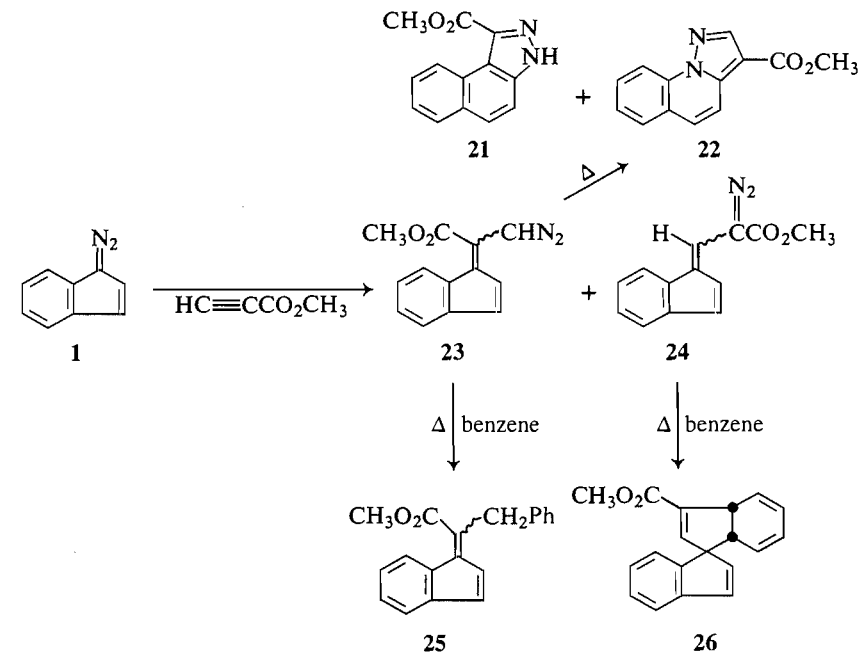

SCHEME 2

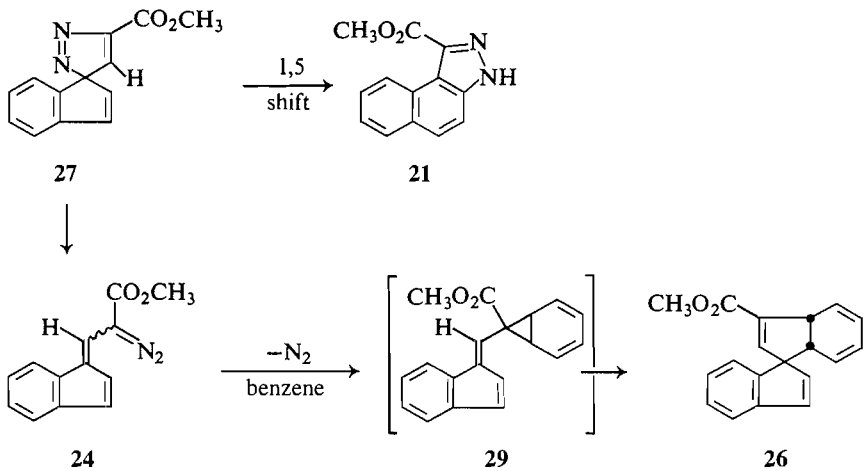

results in the loss of acetonitrile and formation of enone **20**. The isomerization of **17** to **18** is an interesting transformation and merits some discussion. The reaction most likely involves cleavage of the central bond of the cyclopropane ring to give **19**, which undergoes ring flipping followed by a subsequent ring closure.

In an effort to establish the regiochemical cycloaddition behavior of diazoindene, the reaction of **1** with methyl propiolate was investigated. In this case the cycloaddition produced a complex mixture of products which could be separated by silica gel chromatography. The products were assigned as indazole **21**, pyrazoloquinoline **22**, and diazoalkenes **23** and **24** (*E*,*Z*-mixture). The structures of **21**–**24** were in accord with the nmr, uv, ir, and mass spectral data (see experimental section). Heating diazoalkenes **23** and **24** in a sealed tube in benzene at 160°C produced pyrazole **22**, benzylidene indene **25**, and spiroindene **26**, respectively (see Scheme 2).

The mechanism by which these reactions proceed is worthy of comment in view of the diversity of structures obtained. We believe that the initial reaction involves a 1,3-dipolar cycloaddition of **1** with methyl propiolate to give a mixture of regioisomeric cycloadducts (i.e. **27** and **28**). The reactions of simple diazoalkanes are generally HO (1,3-dipole) – LU (dipolarophile) controlled (46) (Type I process (47)). 3-Substituted pyrazolines are the major products produced, a result of union of the larger diazoalkane HO coefficient on carbon with that of the larger dipolarophile LU coefficient on the unsubstituted carbon (46). We suspect that the formation of a mixture of regioisomers (*vide infra*) is a result of the Type II dipolar cycloaddition behavior of diazoindene **1** (Sustmann's classification (47)). Introduction of an aryl group onto diazomethane is known to result in a mixture of regioisomeric cycloadducts (45). The initially formed cycloadduct **27** aromatizes under the reaction conditions via a thermally allowed 1,5-sigmatropic shift of the phenyl group to give compound **21**. Interestingly, this type of isomerization (van Alphen – Huttel rearrangement), for which ample precedence exists (48, 49), proceeds by exclusive migration of the phenyl bond to the carbon atom. The major path followed by **27** involves a 3+2-cycloreversion to give diazoalkene **24**. Further heating of this material in benzene results in the formation of spiroindene **26**. The formation of **26** involves loss of nitrogen followed by carbene addition across

Can. J. Chem. Downloaded from www.nrcresearchpress.com by 210.87.254.105 on 09/06/12
For personal use only.

Can. J. Chem. Downloaded from www.nrcresearchpress.com by 210.87.254.105 on 09/06/12
For personal use only.

the π-bond of benzene to give a transient norcaradiene intermediate (i.e. **29**) which rearranges to **26** via a vinylcyclopropane–cyclopentene rearrangement.

The isomeric cycloadduct (i.e. **28**) obtained from the initial 1,3-dipolar cycloaddition could not be isolated. It is assumed that this species is converted into diazoalkene **23** by means of a 3+2-cycloreversion. A control experiment showed that **23** is stable at room temperature but is converted into pyrazoloquinoline **22** upon heating in a sealed tube at 178°C. This transformation can be rationalized in terms of an intramolecular electrocyclization reaction to produce **28** followed by a van Alphen – Huttel rearrangement. The exclusive migration of the phenyl group to the nitrogen atom in this case is probably associated with stabilization of the developing negative charge by the carbomethoxy group in the transition state. Steric factors may also play a role in the migration. Structure **23** also undergoes the loss of nitrogen and the resulting carbene inserts into the carbon–hydrogen bond of benzene to give **25**.

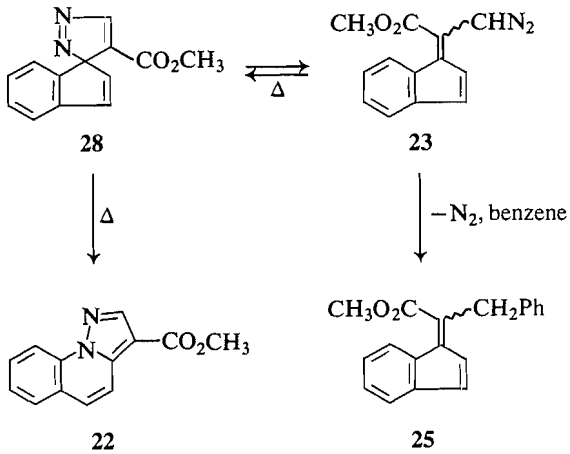

We also examined the thermal cycloaddition of diazoindene **1** with methyl phenylpropiolate in cyclohexane. From the reaction two products were isolated by preparative thick layer chromatography. The major species (34%) corresponded to 1-cyclohexylindene (**30**). This material is formed by insertion of the carbene derived from diazoindene into the C—H bond of solvent. In addition to **30**, the minor component obtained was a white solid whose structure was assigned as methyl pyrazolo[1,5-*a*]quinoline-2-phenyl-3-carboxylate (**31**) on the basis of its spectral properties. Here again the formation of **31** can be most conveniently rationalized as arising from a simple 1,3-dipolar cycloaddition followed by a van Alphen – Huttel rearrangement of the initial spiro adduct.

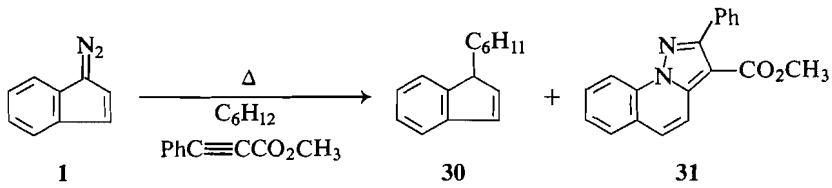

As an extension of our studies with diazoindene **1**, we also investigated its cycloaddition behavior with electron deficient alkenes. In each case, nitrogen deficient 1:1 adducts, the structures of which have been assigned as the spiro-cyclopropylindenes **32–36**, were isolated in yields of 80–95%. Whereas the reaction of **1** with methyl acrylate (or nitroethylene) afforded a mixture of stereoisomers, diazoindene gave rise to a single product when diethyl fumarate was used as the trapping agent. This same adduct was also obtained when diethyl maleate was used as the alkene. The isomer in which the cyclopropyl methoxycarbonyl group is *syn* to the aromatic ring (i.e. **33**) has been assigned on the basis of a comparison of resonances due to the ester methoxyls. Specifically, the appearance of a high-field signal at δ 2.52 can only be rationalized by assuming a configuration in which shielding due to the anisotropic properties of the aromatic benzene ring is invoked. The isomer to which the *anti* configuration has been assigned (i.e. **32**) exhibits the same signal at δ 3.63. Because only minimal steric and anisotropic interactions are likely to be incurred with spiro adducts **35** and **36**, it is not possible to establish the stereochemistry of substitution on the cyclopropane ring.

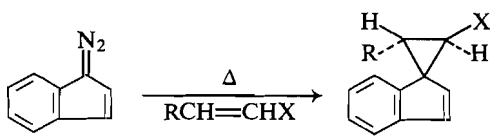

32 and **33** R = H; X = CO_2CH_3
34 R = X = CO_2CH_3
35 and **36** R = H; X = NO_2

It is of some interest to note that diazoindene **1** is stable under the reaction conditions used for the cycloadditions. This would suggest that the reaction of **1** with electron deficient alkenes does not proceed by initial loss of nitrogen from diazoindene followed by carbene addition to the olefinic π-bond. Instead, the formation of cycloadducts **32–36** can be thought of as resulting from a thermally induced extrusion of nitrogen from intermediate spiro pyrazoline adducts (**37**) which are formed in a manner analogous to those derived from propiolate cycloadditions.

Since the theory of spiroconjugation was formulated over fifteen years ago (50, 51), a number of spiroconjugated compounds have been prepared and their spectral data and chemical reactivity have been evaluated. Several dialkyl derivatives of spiro[2.4]heptatriene (**39**) have been experimentally isolated and spectroscopically studied with particular emphasis on the stability of the system (52–54). Spiroconjugation theory suggests that the HOMO level of **39** should be stabilized (50). Using MINDO/3 calculations, Gordon *et al.* (54) concluded

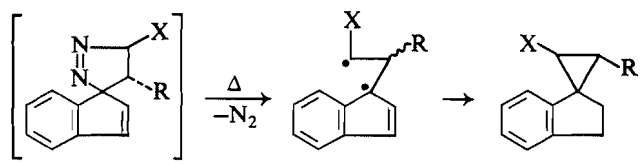

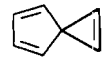

39

Can. J. Chem. Downloaded from www.nrcresearchpress.com by 210.87.254.105 on 09/06/12
For personal use only.

that spiroconjugation adds little, if any, contribution to the stabilization of molecules like **39**. On the other hand, Kao and Radom argued that the spiroconjugated stabilization of spiro-[2.4]heptatriene is reflected in the calculated strain (55). This comes out to 58.5 kcal/mol, which is less than the sum of the strains of the cyclopropene and cyclopentadiene rings despite the deformed bond angles about the spiro carbon. This result was interpreted as being consistent with a favorable orbital interaction (56).

As a continuation of our interest in this area, we decided to study the thermal chemistry of spiroindene **8**. Heating a sample of **8** at 160°C gave dimethyl 2a*H*-cyclopent[*c*,*d*]inden-1,2-dicarboxylate (**40**) in good yield. The rate of reaction of **8** is very similar to related cyclopropenes (57) and it does not appear that this molecule is stabilized by spiroconjugation. The rearrangement can be interpreted in terms of an initial ring opening to produce a vinylcarbene intermediate (**41**) which

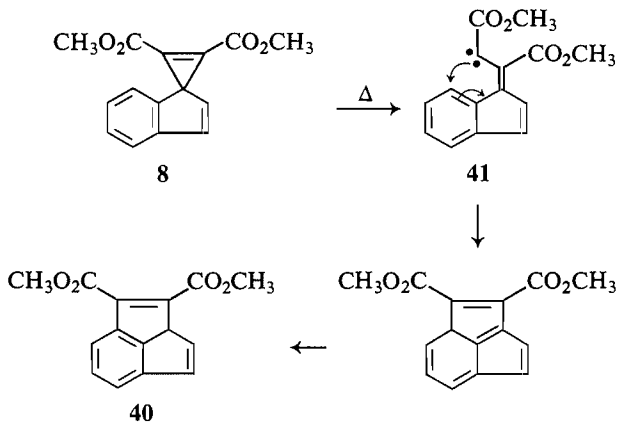

undergoes 1,5-electrocyclization followed by a 1,5-sigmatropic hydrogen shift. Other mechanisms are also conceivable and can not be ruled out without further evidence.

Experimental[3]

Reaction of diazoindene (1) with dimethyl acetylenedicarboxylate

To a solution containing 220 mg of diazoindene **1** in 10 mL of anhydrous benzene was added 250 mg of dimethyl acetylenedicarboxylate. After stirring for 17 h at 25°C, the solvent was removed under reduced pressure and the residue was chromatographed on a silica gel column using a 10% acetone–hexane mixture as the eluent to give 413 mg (94%) of a red oil which was identified as dimethyl *Z*-diazo-1*H*-inden-1-ylidenebutanedioate (**6**); ir (neat): 2990, 2100, 1700, 1435, 1340 cm^{-1}; nmr (CCl_4, 90 MHz) δ: 3.88 (s, 3H), 3.92 (s, 3H), 6.92 (d, 1H, J = 6.0 Hz), 6.96 (d, 1H, J = 6.0 Hz), and 7.00–7.34 (m, 4H). *Anal.* calcd. for $C_{15}H_{12}N_2O_4$: C 63.38, H 4.26, N 9.86; found: C 63.19, H 4.17, N 9.84.

A solution containing 400 mg of **6** in 10 mL of benzene was heated at reflux for 20 min. The solvent was removed under reduced pressure and the residue was chromatographed on a silica gel column using a 10% acetone–hexane mixture to give 256 mg (71%) of a pale yellow solid, mp 86–87°C, whose structure was assigned as dimethyl spiro[2-cyclopropene-1,1-[1*H*]indene]-2,3-dicarboxylate (**8**); ir (KBr): 3000, 1870, 1730, 1430, 1260, 1050 and 750 cm^{-1}; uv (95% ethanol): 292 (ε 1,470), 266 (7,330), and 227 nm (16 660); nmr (CCl_4, 90 MHz) δ: 3.81 (s, 6H), 6.16 (d, 1H, J = 7.0 Hz), 6.96 (d, 1H, J = 7.0 Hz), and 7.00–7.46 (m, 4H); *m/e*: 256 (M^+), 226, 225, 224 (base), 197, 166, 139, and 138. *Anal.* calcd. for $C_{15}H_{12}O_4$: C 70.30, H 4.72; found: C 70.44, H 4.75.

Reaction of dimethyl spiro[2-cyclopropene-1-1′-[1H]indene]-2,3-dicarboxylate (8) with diazoindene (1)

To a solution containing 26 mg of **8** in 20 mL of benzene was added 30 mg of diazoindene. The solution was heated at reflux for 15 min. At the end of this time the solvent was removed under reduced pressure and the residue was chromatographed on a silica gel column using a 10% acetone–hexane mixture as the eluent. The first component isolated contained 55 mg (92%) of a white crystalline solid, mp 137–138°C, whose structure was assigned as dimethyl dispiro-[indene-1,4′-[2,3]diazabicyclo[3.1.0]hexane-6′,1′-indene]-1′,5′-dicarboxylate (**9**); ir (KBr): 3020, 1740, 1450, 1430, 1280, 1260, 1190, and 1090 cm^{-1}; uv (95% ethanol): 229 nm (ε 26 840); nmr (CCl_4, 90 MHz) δ: 3.06 (s, 3H), 3.96 (s, 3H), 5.69 (d, 1H, J = 6.0 Hz), 6.18 (d, 1H, J = 6.0 Hz), 7.00 (d, 1H, J = 6.0 Hz), 7.03 (d, 1H, J = 6.0 Hz), 7.10–7.37 (m, 8H); *m/e*: 370, 339, 311, 296, 280, and 252 (base). *Anal.* calcd. for $C_{24}H_{18}N_2O_4$: C 72.35, H 4.55, N 7.03; found: C 72.06, H 4.73, N 6.98.

A solution containing 31 mg of **9** in 20 mL of anhydrous benzene was heated in a sealed tube for 2.5 h at 128°C. The solvent was removed under reduced pressure leaving behind a red oil which was chromatographed on a silica gel column using a 10% acetone–hexane mixture as the eluent to give 26 mg (88%) of an orange oil which was identified as dimethyl bimethyleneindene-1,1′-dicarboxylate (**11**);[4] ir (neat): 3100, 3000, 1730, 1600, 1450, 1220, and 750 cm^{-1}; uv (95% ethanol): 355 (ε 4,320) and 250 nm (14 530); nmr (CCl_4, 90 MHz) δ: 3.73 (s, 3H), 3.76 (s, 3H), 6.20 (d, 1H, J = 6.0 Hz), 6.63 (d, 1H, J = 6.0 Hz), 6.80 (d, 1H, J = 6.0 Hz), 6.73–7.26 (m, 6H), 7.33 (d, 1H, J = 6.0 Hz), 7.70–8.00 (m, 1H), and 8.25–8.40 (m, 1H); *m/e*: 370 (M^+), 229, 227, 311, 310, 308, 280, 279, 252, and 125. *Anal.* calcd. for $C_{24}H_{18}O_4$: C 77.82, H 4.90; found: C 77.72, H 4.94.

Reaction of dimethyl spiro[2-cyclopropene-1,1′-[1H]indene]-2,3-dicarboxylate (8) with diazomethane

To a solution containing 286 mg of dimethyl spiro[2-cyclopropene-1,1′-[1*H*]indene]-2,3-dicarboxylate (**8**) in 20 mL of ether was added an excess of diazomethane. This mixture was allowed to stir for 8 h and the solid that formed was filtered to give 90 mg of a colorless crystalline material, mp 152–153°C, whose structure was assigned as *endo* dimethyl spiro[2,3-diazabicyclo[3.1.0]hex-2-ene-6,1′-indene]-1,5-dicarboxylate (**12**); ir (KBr): 3000, 1740, 1430, 1300, 1250, 1200, and 1110 cm^{-1}; uv (95% ethanol): 236 nm (ε 14 300) and 220 nm (16 250); nmr ($CDCl_3$, 90 MHz) δ: 3.76 (s, 3H), 3.85 (s, 3H), 3.98 (d, 1H, J = 18.0 Hz), 5.25 (d, 1H, J = 7.0 Hz), 5.48 (d, 1H, J = 18.0 Hz), 6.93 (d, 1H, J = 7.0 Hz), and 7.10–7.56 (m, 4H). *Anal.* calcd. for $C_{16}H_{14}O_4N_2$: C 64.42, H 4.73, N 9.39; found: C 64.52, H 4.71, N 9.20.

Thermolysis of dimethyl spiro[2,3-diazabicyclo[3.1.0]hex-2-ene-6,1′-indene]-1,5-dicarboxylate (12) in benzene

A solution containing 80 mg of **12** in 25 mL of anhydrous benzene was heated in a sealed tube at 110°C for 10 min. The solvent was removed under reduced pressure and the residue was chromatographed on a silica gel column using a 10% acetone–hexane mixture as the eluent. The first material to be eluted from the column contained 443 mg of a pale yellow oil whose structure was assigned as *exo*-dimethyl spiro[2,3-diazabicyclo[3.1.0]hex-2-ene-6,1′-indene]-1,5-dicarboxylate (**13**); ir (neat: 2990, 1730, 1530, 1450, 1430, 1260, 1120, and 780 cm^{-1}; uv (95% ethanol): 242 (ε 14 420) and 215 nm (22 050); nmr (CCl_4, 90 MHz) δ: 3.73 (s, 3H), 3.87 (s, 3H), 5.13 (d, 1H, J = 18.0 Hz), 5.47 (d, 1H, J = 18.0 Hz), 6.20 (d, 1H, J = 7.0

[3]All melting points and boiling points are uncorrected. Elemental analyses were performed by Atlantic Microlabs, Atlanta, GA. The infrared absorption spectra were determined on a Perkin–Elmer 467 infrared spectrophotometer. The ultraviolet absorption spectra were measured with a Cary Model 14 recording spectrophotometer by using 1-cm matched cells. The proton magnetic resonance spectra were determined at 90 MHz by using a Varian EM-390 spectrometer. Mass spectra were determined with a Finnegan 4000 mass spectrometer at an ionizing voltage of 70 eV.

[4]The sterochemistry of **11** is plausible but not proven.

Can. J. Chem. Downloaded from www.nrcresearchpress.com by 210.87.254.105 on 09/06/12
For personal use only.

Hz), 6.60–7.30 (m, 5H); *m/e*: 298 (M^+), 270, 211, 210, and 152. *Anal.* calcd. for $C_{16}H_{14}N_2O_4$: C 64.42, H 4.73, N 9.39; found: C 64.40, H 4.75, N 9.30.

A solution containing 100 mg of **12** in 10 mL of benzene was also heated in a sealed tube at 145°C for 35 min. The solvent was removed under reduced pressure and the residue was chromatographed on a medium pressure chromatography column using a 10% acetone–hexane mixture as the eluent. The first fraction contained 80 mg of a yellow oil whose structure was assigned as 1-(methyl diazoacetate)-1-(methyl ethylene-1-acetate)indene (**14**); ir (neat): 3400, 2130, 1720, 1440, 1315, 1210, 1180, 1130, and 860 cm^{-1}; uv (95% ethanol): 250 (ε 11 030) and 210 nm (26 530); nmr (CCl_4, 90 MHz) δ: 3.70 (s, 3H), 3.76 (s, 3H), 5.70 (s, 1H), 6.03 (s, 1H), 6.73 (d, 1H, J = 5.0 Hz), 6.83 (d, 1H, J = 5.0 Hz), 7.06–7.33 (m, 3H), and 7.60–7.77 (m, 1H); *m/e*: 270, 212, 180, 179, 168, 167, 146 (base), and 145. *Anal.* calcd. for $C_{16}H_{14}O_4N_2$: C 64.42, H 4.73, N 9.39; found: C 64.62, H 4.78, N 9.16.

Reaction of dimethyl spiro[2-cyclopropene-1-1′-[1H]indene]-2,3-dicarboxylate (8) with diazopropane

To a solution containing 40 mg of **8** in 20 mL of anhydrous ether at 0°C was slowly added an ether solution of diazopropane until the orange color persisted. The mixture was allowed to stir for 12 h and the solvent was removed under reduced pressure. The residue was chromatographed on a silica gel column using a 10% acetone–hexane mixture as the eluent. The major fraction contained 51 mg (98%) of a white crystalline solid, mp 114–115°C, whose structure was assigned as dimethyl spiro[2,3-diazo-4,4-dimethylbicyclo[3.1.0]hex-2-ene-6,1′-[1*H*]indene]-1,5-dicarboxylate (**16**); ir (KBr): 3000, 1740, 1450, 1430, 1270, 1240, 1200, and 1080 cm^{-1}; uv (95% ethanol): 232 nm (ε 19 010); nmr (CCl_4, 90 MHz) δ: 1.33 (s, 3H), 1.60 (s, 3H), 3.62 (s, 3H), 3.83 (s, 3H), 5.49 (d, 1H, J = 6.0 Hz), 6.90 (d, 1H, J = 6.0 Hz), and 7.10–7.40 (m, 4H). *Anal.* calcd. for $C_{18}H_{18}N_2O_4$: C 66.24, H 5.56, N 8.58; found: C 66.18, H 5.63, N 8.31.

Thermal rearrangement of dimethyl spiro[2-cyclopropene-1,1′-[1H]-indene]-2,3-dicarboxylate (8) in benzene

A solution containing 60 mg of **8** in 100 mL of anhydrous benzene was heated in a sealed tube at 176°C for 30 min. The solvent was removed under reduced pressure and the residue was chromatographed by hplc on a Zorbax-Cn preparative column using a 3% acetone–hexane mixture. The major component contained 28 mg of a yellow oil whose structure was assigned as dimethyl 2a*H*-cyclopent[*c,d*]-inden-1,2-dicarboxylate (**40**); ir (neat): 2990, 1720, 1700, 1430, 1280, 1100, 900, 770, and 720 cm^{-1}; uv (95% ethanol): 320 (ε 4,100), 275 (6,160), 245 (8,210), 238 (8,360), and 215 nm (10 560); nmr (CCl_4, 90 MHz) δ: 3.69 (s, 3H), 3.83 (s, 3H), 5.18 (s, 1H), 6.75 (d, 1H, J = 5.5 Hz), and 7.15–7.46 (m, 4H); *m/e*: 256 (M^+), 241, 225, and 166. *Anal.* calcd. for $C_{15}H_{12}O_4$: C 70.30, H 4.72; found: C 70.15, H 4.69.

Reaction of dimethyl spiro[2-cyclopropene-1,1-[1H]indene]2,3-dicarboxylate (8) with chloroacetaldoxime

To a solution containing 200 mg of **8** and 80 mg of α-chloroacetaldoxime and 20 mL of anhydrous ether at 0°C was slowly added 100 mg of triethylamine. The mixture was stirred at 0°C for 1 h and the solution was filtered in order to remove the triethylamine hydrochloride salt. The solvent was removed under reduced pressure, leaving behind 240 mg of a pale yellow oil which was identified as dimethyl spiro[4-methyl-2-oxa-3-azabicyclo[3.1.0]hex-3-ene-6,1′-indene]-1,5-dicarboxylate (**17**); ir (neat): 3000, 1760, 1450, 1390, 1280, 1240, 1210, 1110, 1090, 940, 870, and 750 cm^{-1}; uv (95% ethanol): 247 (ε 13 770) and 210 nm (14 910); nmr (CCl_4, 90 MHz) δ: 2.03 (s, 3H), 3.70 (s, 6H), 5.80 (d, 1H, J = 6.0 Hz), 6.90 (d, 1H, J = 6.0 Hz), and 6.98–7.23 (m, 4H); ^{13}C nmr ($CDCl_3$, 30 MHz) δ: 12.28 (q), 42.80 (s), 53.16 (q), 58.54 (s), 79.10 (s), 122.31 (d), 124.87 (d), 125.19 (d), 127.68 (d), 129.29 (d), 134.75 (d), 137.00 (s), 145.27 (s), 157.32 (s), and 162.70 (s); *m/e*: 272, 213 (base), 154 and 114. *Anal.* calcd. for $C_{17}H_{15}NO_5$: C 65.17, H 4.82, N 4.47; found: C 65.09, H 4.76, N 4.53.

Chromatography of this material on a silica gel column using a 10% acetone–hexane mixture as the eluent resulted in an epimerization reaction to give *endo*-dimethyl spiro[4-methyl-2-oxa-3-azabicyclo-[3.1.0]-hex-3-ene-6,1′-indene]-1,5-dicarboxylate (**18**); ir (neat): 3000, 1750, 1440, 1380, 1280, 1240, 1110, 870, and 730 cm^{-1}; uv (95% ethanol): 242 (ε 11 050) and 221 nm (10 730); nmr (CCl_4, 90 MHz) δ: 2.1 (s, 3H), 3.80 (s, 3H), 3.83 (s, 3H), 6.57 (d, 1H, J = 6.0 Hz), 6.83 (d, 1H, J = 6.0 Hz), and 7.00–7.45 (m, 4H); ^{13}C nmr ($CDCl_3$, 20 MHz) δ: 12.46 (q), 40.26 (s), 53.40 (q), 58.87 (s), 84.49 (s), 122.31 (d), 122.72 (d), 125.50 (d), 128.18 (d), 131.18 (d), 132.27 (d), 136.12 (s), 145.51 (s), 154.67 (s), 163.51 (s), and 164.72 (s); *m/e*: 272, 213 (base), 154, and 114. *Anal.* calcd. for $C_{17}H_{15}NO_5$: C 65.17, H 4.82, N 4.47; found: C 65.10, H 4.68, N 4.31.

A solution containing 100 mg of **17** (or **18**) in 10 mL of anhydrous benzene was heated at 160°C for 10 min. The solvent was removed under reduced pressure leaving behind a pale oil whose structure was assigned as pyruvate **20**;[5] ir (neat): 3000, 1730, 1700, 1600, 1450, 1380, 1310, 1240, 1150, 1050, and 750 cm^{-1}; uv (95% ethanol): 245 (ε 5,900) and 247 nm (16 550); nmr (CCl_4, 90 MHz) δ: 3.83 (s, 3H), 3.87 (s, 3H), 6.87 (d, 1H, J = 6.0 Hz), 7.00–7.20 (m, 4H), and 7.35 (d, 1H, J = 6.0 Hz); ^{13}C nmr ($CDCl_3$, 20 MHz) δ: 52.77 (q), 53.61 (q), 126.31 (s), 126.88 (d), 127.04 (d), 127.44 (s), 131.36 (d), 131.78 (d), 133.30 (s), 140.37 (d), 141.32 (d), 144.54 (s), 152.89 (d), 154.25 (d), 182.92 (s), and 185.15 (s); *m/e*: 272 (M^+), 213 (base), 154, and 114. *Anal.* calcd. for $C_{15}H_{12}O_5$: C 66.17, H 4.44; found: C 66.03, H 4.27.

Reaction of diazoindene (1) with methyl propiolate

To a solution containing 200 mg of diazoindene **1** in 20 mL of anhydrous benzene was added 200 mg of methyl propiolate. The mixture was allowed to stir at 25°C for 18 h and the red solution was filtered to give 75 mg of a white crystalline material, mp 254–255°C, whose structure was assigned as methyl-1*H*-benz[*e*]indazole-3-carboxylate (**21**); ir (KBr): 3250, 1730, 1470, 1440, 1270, 1220, 1060, 1020, 980, 820, and 760 cm^{-1}; uv (95% ethanol): 333 (ε 6,340), 317 (6,890), 292 (12 410), 281 (12 690), 270 (15 720), 255 (17 930), 237 (48 000), and 230 nm (41 380); nmr (C_5D_6, 90 MHz) δ: 4.0 (s, 3H), 7.63–7.80 (m, 3H), 8.10–8.30 (m, 2H), 8.45–8.65 (m, 1H), and 14.5 (s, 1H); *m/e*: 266 (M^+), 195, 140, and 138 (base). *Anal.* calcd. for $C_{13}H_{10}N_2O_2$: C 69.01, H 4.46, N 12.38; found: C 69.21, H 4.47, N 12.40.

The solvent was removed from the mother liquor and the residue was chromatographed on a medium pressure silica gel column using a 5% acetone–hexane mixture as the eluent. The major diazo compound isolated from the column (120 mg) was assigned the structure of methyl (*Z*)-diazo-1*H*-inden-1-ylidenepropanoate (**24**) on the basis of its spectral data; ir (neat): 3300, 2110, 1720, 1620, 1440, 1400, 1310, 1250, 1220, and 1100 cm^{-1}; uv (95% ethanol): 363 (ε 15 790), 298 (12 680), 287 (12 620), 252 (14 660), 245 (14 150) and 210 nm (28 990); nmr (CCl_4, 90 MHz) δ: 3.83 (s, 3H), 6.56 (d, 1H, J = 6.0 Hz), 6.66 (s, 1H), 6.86 (s, 1H, J = 6.0 Hz), 7.00–7.33 (m, 3H), and 7.46–7.66 (m, 1H).

A solution containing 150 mg of the above oil in 10 mL of benzene was heated in a sealed tube at 178°C for 12 h. The solvent was removed under reduced pressure and the residue was chromatographed to give 135 mg of methyl spiro[3a,7a-dihydroindene-1,1′-indene]-3-carboxylate (**26**); ir (neat: 2990, 2900, 1720, 1620, 1440, 1330, 1230, 1110, 1090, and 960 cm^{-1}; uv (95% ethanol): 258 (ε 11 240) and 218 nm (27 720); nmr (CCl_4, 90 MHz) δ: 3.45 (dd, 1H, J = 12.0, J = 5.0 Hz), 3.72 (s, 3H), 4.11 (brd, 1H, J = 12.0 Hz), 5.10–5.26 (m, 1H), 5.66–5.86 (m, 3H), 6.16 (d, 1H, J = 6.0 Hz), 6.22 (brs, 1H), 6.58 (d, 1H, J = 6.0 Hz), and 7.00–7.30 (m, 4H); ^{13}C nmr ($CDCl_3$, 20 MHz) δ: 43.83 (d), 44.86 (d), 51.54 (q), 70.96 (s), 121.16 (d), 121.72 (d), 122.47 (d), 123.01 (d), 124.22 (d), 125.51 (d), 127.45 (d), 131.10 (d), 139.64 (d), 139.87 (s), 144.29 (s), 147.50 (d), 148.87 (s), 164.69 (s). *Anal.* calcd. for $C_{19}H_{16}O_2$: C 82.58, H 5.84; found: C 82.20, H 5.80.

The next component isolated from the chromatography of the resi-

[5]The stereochemistry of **20** is unknown.

Can. J. Chem. Downloaded from www.nrcresearchpress.com by 210.87.254.105 on 09/06/12
For personal use only.

due derived from diazoindene with methyl propiolate contained 26 mg of methyl pyrazolo[1,5-*a*]quinoline-3-carboxylate (**22**): ir (neat): 1710, 1540, 1450, 1380, 1320, 1280, 1220, 1200, 1170, 1100, 800, and 770 cm^{-1}; uv (95% ethanol): 335 (ε 8,500), 320 (6,860), 265 (29 410), 258 (28 100), and 208 (25 000); nmr (CCl_4, 90 MHz) δ: 3.90 (s, 3H), 7.1 (d, 1H, J = 7.0 Hz), 7.60–7.80 (m, 3H), 8.25 (d, 1H, J = 7.0 Hz), 8.33 (s, 1H), and 9.80–9.93 (m, 1H); *m/e*: 226 (M^+), 195 (base), 167, 141, and 180. *Anal.* calcd. for $C_{13}H_{10}N_2O_2$: C 69.01, H 4.46, N 12.38; found: C 68.87, H 4.31, N 12.46.

The third component isolated from the column contained a mixture of isomeric diazo compounds (**23**, *Z* and *E*) which could not be separated. A solution containing 80 mg of this oil in 10 mL of benzene was heated at 178°C for 10 min. Removal of the solvent left a yellow oil which was chromatographed on a silica gel column to give 55 mg of methyl β-benzylindenylindene-β-carboxylate (**25**)[6]; ir (neat): 3090, 2980, 1720, 1460, 1440, 1240, 1040, and 760 cm^{-1}; uv (95% ethanol): 310 (ε 4,090) and 250 nm (20 460); nrm (CCl_4, 90 MHz) δ: 3.16 (brs, 2H), 3.70 (s, 3H), 5.8–6.4 (2H), 7.00–7.50 (m, 9H), ^{13}C nmr ($CDCl_3$, 20 MHz) δ: 39.16 (t), 52.36 (q), 119.17 (d), 123.89 (d), 125.25 (d), 126.31 (d), 127.80 (d), 128.51 (d), 128.39 (d), 132.01 (d), 134.85 (s), 144.20 (s), and 168.05 (s); *m/e*: 276 (M^+), 245, 217 (base), and 215. *Anal.* calcd. for $C_{19}H_6O_2$: C 82.58, H 5.84; found: C 82.70, H 5.83.

In addition, 25 mg of pyrazoloquinoline **22** was also isolated.

Reaction of diazoindene with methyl phenylpropiolate

To a solution containing 100 mg of diazoindene (**1**) in 10 mL of anhydrous cyclohexane was added 124 mg of methyl phenylpropiolate. The mixture was heated in a sealed tube at 160°C for 1 h. At the end of this time the solvent was removed under reduced pressure and the residual oil was chromatographed on a medium pressure chromatography column using a 10% acetone–hexane mixture as the eluent. The first compound isolated from the column contained 65 mg of a pale yellow oil which was identified as 1-cyclohexylindene (**30**); ir (neat): 3070, 2930, 2860, 1460, 1450, 800, 760, 750, and 720 cm^{-1}; nmr (CCl_4, 90 MHz) δ: 0.53–2.20 (m, 11H), 3.25–3.40 (m, 1H), 6.40 (dd, 1H, J = 6.0, J = 1.5 Hz), 6.20 (dd, 1H, J = 6.0, J = 2.0 Hz), and 6.90–7.43 (m, 4H); *m/e*: 198 (M^+), 116 (base), 115, and 83. *Anal.* calcd. for $C_{15}H_{18}$: C 90.85, H 9.15; found: C 90.81, H 9.10.

The next compound isolated from the column contained 30 mg of a white solid, mp 109–110°C, whose structure was assigned as methyl pyrazolo[1,5-*a*]quinoline-2-phenyl-3-carboxylate (**31**); ir: 1370, 1330, 1160, and 1110 cm^{-1}; uv (95% ethanol): 337 (ε 6,400), 321 (5,700), and 265 nm (40 515); nmr (CCl_4, 90 MHz) δ: 3.70 (s, 3H), 6.93 (d, 1H, J = 8.0 Hz), 7.20–7.63 (m, 8H), 8.16 (d, 1H, J = 8.0 Hz), and 9.10–9.30 (m, 1H); *m/e*: 302 (M^+), 271 (base), 244, 243, and 140. *Anal.* calcd. for $C_{19}H_{14}N_2O_2$: C 75.48, H 4.67, N 9.27; found: C 75.36, H 4.72, N 9.20.

Reaction of diazoindene with methyl acrylate

To a 100-mg sample of diazoindene (**1**) was added 129 mg of methyl acrylate. After stirring for 6 h at 25°C, the reaction mixture was chromatographed on a medium pressure column using a 5% acetone–hexane mixture as the eluent. The first compound isolated contained 88 mg (63%) of a colorless oil whose structure was assigned as methyl *cis*-spiro[cyclopropane-1,1′-[1*H*]indene]-2-carboxylate (**32**); ir (neat): 3050, 2975, 1740, 1460, 1440, 1390, 1320, 1280, 1180, 1090, 1070, 1000, 960, 940, 850, and 820 cm^{-1}; uv (95% ethanol): 290 (ε 960), 272 (1,330), 245 (5,790), and 227 nm (26 060); nmr (CCl_4, 90 MHz) δ: 1.80 (dd, 1H, J = 8.5 Hz, J = 5.5 Hz), 2.23 (dd, 1H, J = 6.5 Hz, J = 5.5 Hz), 2.60 (dd, 1H, J = 8.5 Hz, J = 6.5 Hz), 3.63 (s, 3H), 6.53 (d, 1H, J = 6.0 Hz), 6.83 (d, 1H, J = 6.0 Hz), and 6.90–7.40 (m, 4H); ^{13}C nmr ($CDCl_3$, 20 MHz) δ: 19.37 (t), 28.46 (d), 40.20 (s), 51.68 (qd), 117.45 (d), 121.45 (d), 124.61 (d), 135.36 (d), 143.47 (s), 145.56 (s), and 171.82 (s); *m/e*: 200 (M^+), 185, 169, 168, 141 (base), 128, and 115. *Anal.* calcd. for $C_{13}H_{12}O_2$: C 77.98, H 6.04; found: C 77.82, H 6.09.

The next component isolated from the column contained 48 mg (32%) of a colorless oil whose structure was assigned as methyl *trans*-spiro[cyclopropane-1,1′-[1*H*]indene]-2-carboxylate (**33**); ir (neat): 3100, 3000, 1730, 1400, 1390, 1360, 1280, 1210, 1170, 1090, 1020, 940, 840, 810, 760, and 720 cm^{-1}; uv (95% ethanol): 300 (ε 1,500), 290 (1,880), 263 (5,640), and 230 nm (21 430); nmr (CCl_4, 90 MHz) δ: 1.80 (dd, 1H, J = 8.5 Hz, J = 4.5 Hz), 2.19 (dd, 1H, J = 7.5 Hz, J = 4.5 Hz), 2.60 (dd, 1H, J = 8.5 Hz, J = 7.5 Hz), 2.52 (s, 3H), 5.89 (d, 1H, J = 5.7 Hz), 6.78 (d, 1H, J = 5.7 Hz), and 6.97–7.48 (m, 4H); ^{13}C nmr ($CDCl_3$, 20 MHz) δ: 17.66 (t), 27.76 (d), 40.21 (s), 51.26 (q), 121.35 (d), 121.45 (d), 124.57 (d), 126.28 (d), 130.00 (d), 139.07 (d), 142.20 (s), 144.44 (s), and 169.90 (s); *m/e*: 200 (M^+), 169, 168, and 115 (base). *Anal.* calcd. for $C_{13}H_{12}O_2$: C 77.98, H 6.04; found: C 77.73, H 6.09.

Reaction of diazoindene with diethylfumarate

To a solution containing 200 mg of diazoindene in 10 mL of anhydrous benzene was added 240 mg of diethylfumarate. After stirring for 53 h at 25°C, the solvent was removed under reduced pressure and the resulting residue was chromatographed on a silica gel column using a 1% acetone–hexane solution as the eluent. The first compound isolated from the column contained 320 mg (82%) of a white solid, mp 91–92°C, whose structure was assigned as diethyl *trans*-spiro[cyclopropane-1,1′-indene]-2,3-dicarboxylate (**34**); ir (KBr): 3010, 1730, 1450, 1370, 1330, 1310, 1280, 1210, 1160, 1080, 1020, and 850 cm^{-1}; uv (95% ethanol): 295 (ε 1,420), 260 (2,960), and 232 nm (25 800); nmr (CCl_4, 90 MHz) δ: 1.15 (t, 3H, J = 6.0 Hz), 1.23 (t, 3H, J = 6.0 Hz), 3.25 (s, 2H), 4.07 (q, 2H, J = 6.0 Hz), 4.16 (q, 2H, J = 6.0 Hz), 6.46 (d, 1H, J = 6 Hz), 6.83 (d, 1H, J = 6.0 Hz), and 7.00–7.52 (m, 4H); *m/e*: 286 (M^+), 241, 240, 213, 168, and 139 (base). *Anal.* calcd. for $C_{17}H_{18}O_4$: C 71.31, H 6.34; found: C 71.21, H 6.28.

Reaction of diazoindene with nitroethylene

To a solution containing 215 mg of diazoindene in 10 mL of benzene was added 200 mg of nitroethylene. After stirring for 4 h the solvent was removed under reduced pressure and the residue was chromatographed on a medium pressure chromatography column using a 1% acetone–hexane solution as the eluent. The first component contained 169 mg (67%) of a colorless oil whose structure was assigned as 2-nitrospiro[cyclopropane-1,1′-[1*H*]indene] (**35**); ir (neat): 3230, 1560, 1460, 1420, 1370, 1220, 1090, 1080, 1000, 960, 880, 820, and 740 cm^{-1}; uv (95% ethanol): 298 (ε 1,990) and 242 nm (17 340); nmr (CCl_4, 90 MHz) δ: 2.00 (t, 1H, J = 6 Hz), 2.86 (t, 1H, J = 6 Hz), 4.93 (brd, 1H, J = 6 Hz), 6.45 (d, 1H, J = 5.7 Hz), 6.80–7.45 (m, 5H); *m/e*: 187 (M^+), 158, 144, 141, 139 (base), 128, and 115. *Anal.* calcd. for $C_{11}H_9NO_2$: C 70.58, H 4.85, N 7.48; found: C 70.35, H 4.87, N 7.33.

The second component to be eluted from the column contained 70 mg (28%) of a colorless oil whose structure was assigned as the isomeric 2-nitro-spiro[cyclopropane-1,1[1*H*]indene] (**36**); ir (neat): 3040, 1560, 1470, 1430, 1370, 1210, 1100, 960, 860, 820, and 770 cm^{-1}; uv (95% ethanol): 301 (ε 2,190) and 246 nm (11 700); nmr (CCl_4, 90 MHz) δ: 2.01 (dt, 1H, J = 6.5 Hz, J = 2.0 Hz), 2.63 (dt, 1H, J = 6.5 Hz, J = 2.0 Hz), 4.83 (brt, 1H, J = 6.5 Hz), 5.80 (brd, 1H, J = 6.5 Hz), 6.82 (d, 1H, J = 6.5 Hz), and 7.00–7.40 (m, 4H); *m/e*: 187 (M^+), 158, 141 (base), and 115. *Anal.* calcd. for $C_{11}H_9NO_2$: C 70.58, H 4.85, N 7.48; found: C 70.30, H 4.86, N 7.33.

Acknowledgments

We wish to thank the National Institute of Health for generous support of this work. A.P. also wishes to thank the organic faculty at the University of Wurzburg for their gracious hospitality during his stay at the Institute as an Alexander von Humboldt Senior Awardee. Use of the high field nmr spectrometer used in these studies was made possible through a NSF equipment grant.

[6]The stereochemistry of compounds **23–25** is unknown.

Can. J. Chem. Downloaded from www.nrcresearchpress.com by 210.87.254.105 on 09/06/12
For personal use only.

1. G. EGE, K. GILBERT, and H. FRANZ. Synthesis, 556 (1977).
2. G. EGE, K. GILBERT, and H. FRANZ. Tetrahedron Lett. 1567 (1979).
3. H. SHECHTER, and W. L. MAGEE. J. Am. Chem. Soc. **99**, 633 (1977).
4. K. N. HOUK and L. J. LUSKUS. Tetrahedron Lett. 4029 (1970).
5. P. CARAMELLA, P. FRATTINI, and P. GRUNANGER. Tetrahedron Lett. 3817 (1971).
6. A. R. KATRITZKY, N. DENNIS, G. J. SABONGI, and L. TURKER. J. Chem. Soc. Perkin Trans. 1, 1525 (1979), and references cited therein.
7. H. DURR, A. C. RANADE, and A. F. HALBERSTADT. Synthesis, **12**, 878 (1974).
8. H. DURR and H. SCHMITZ. Chem. Ber. **111**, 2258 (1978).
9. H. DURR and W. SCHMIDT. Justus Liebigs Ann. Chem. 1140 (1974).
10. H. DURR and R. SERGIO. Chem. Ber. **107**, 2027 (1974).
11. G. EGE and R. GILBERT. Tetrahedron Lett. 4253 (1979).
12. R. GOMPPER. Angew. Chem. Int. Ed. Engl. **8**, 312 (1969).
13. I. FLEMING. Frontier orbitals and organic chemical reactions. Wiley, New York. 1976.
14. R. B. WOODWARD and R. HOFFMANN. Angew. Chem. Int. Ed. Engl. **8**, 781 (1969).
15. A. PADWA and H. KU. J. Org. Chem. **45**, 3756 (1980); A. PADWA and T. KUMAGI. Tetrahedron Lett. 1199 (1981).
16. A. D. WOOLHOUSE, T. C. CARUSO, and A. PADWA. Tetrahedron Lett. 2167 (1982); J. Org. Chem. **48**, 2330 (1983).
17. A. PADWA, A. RODRIGUEZ, M. TOHIDI, and T. FUKUNAGA. J. Am. Chem. Soc. **105**, 933 (1983).
18. G. BIANCHI, C. DEMICHELI, and R. GANDOLFI. Angew. Chem. Int. Ed. Engl. **18**, 721 (1979).
19. E. J. YORK, W. DILTMAR, J. R. STEVENSON, and R. G. BERGMAN. J. Am. Chem. Soc. **95**, 5680 (1973); J. A. PINCOCK and K. P. MURRAY. Can. J. Chem. **57**, 1403 (1979).
20. D. F. EATON, R. G. BERGMAN, and G. S. HAMMOND. J. Am. Chem. Soc. **94**, 1351 (1972); P. G. GASSMAN and W. GREENLEE. J. Am. Chem. Soc. **95**, 980 (1973).
21. P. LUGER, C. TUCHSCHERER, M. GROSSE, and D. REWICKI. Chem. Ber. **109**, 2596 (1976); W. BURGERT, M. GROSSE, and D. REWICKI. Chem. Ber. **115**, 309 (1982).
22. H. PRINZBACH and U. FISCHER. Helv. Chim. Acta, **50**, 1692 (1967).
23. S. MASAMUNE and K. FUKUMOTO. Tetrahedron Lett. 4647 (1965).
24. K. T. POTTS and J. BAUM. J. Chem. Soc. Chem. Commun. 833 (1973).
25. M. I. KOMENDANTOV and V. BERMUKHAMETOV. Zh. Org. Khim. **7**, 427 (1971).
26. G. EGE, K. GILBERT, and B. HAHN. Tetrahedron Lett. 1571 (1979).
27. T. UCHIDA. J. Chem. Soc. Perkin Trans. 1, 1315 (1978).
28. K. MATSUMOTO and Y. KONO. J. Chem. Soc. Chem. Commun. 1045 (1976); K. MATSUMOTO and T. UCHIDA. Synthesis, 207 (1978).
29. A. KASCHERES and D. MARCHI. J. Chem. Soc. Chem. Commun. 275 (1976).
30. H. D. MARTIN and M. HEKMAN. Angew. Chem. **84**, 995 (1972).
31. H. MATSUKUBO, M. KOJIMA, and H. KATO. Chem. Lett. 1153 (1975).
32. J. P. FREEMAN and R. C. GRABIAK. J. Org. Chem. **41**, 3970 (1976).
33. K. T. POTTS, J. BAUM, and E. HOUGHTON. J. Org. Chem. **41**, 818 (1976).
34. A. OHSAWA, I. WADA, H. IGETA, T. AKIMOTO, and A. TSUJI. Tetrahedron Lett. 4121 (1978).
35. H. M. COHEN. J. Heterocycl. Chem. **4**, 130 (1967).
36. M. SCHNEIDER and B. CSACSKO. Angew. Chem. Int. Ed. Engl. **16**, 867 (1977).
37. M. F. NEUMANN and C. BUCHECKER. Angew. Chem. **85**, 259 (1973); M. F. NEUMANN and J. J. LOHMANN. Angew. Chem. **89**, 331 (1977).
38. M. F. NEUMANN and C. BUCHECKER. Tetrahedron Lett. 1139 (1973); **21**, 671 (1980); 2659 (1969).
39. M. F. NEUMANN, D. MARTINA, and C. D. BUCHECKER. Tetrahedron Lett. 1763 (1975).
40. M. REGITZ and W. WELTER. Tetrahedron Lett. 1473 (1976).
41. M. REGITZ and B. MATHIEU. Chem. Ber. **113**, 1632 (1980); M. REGITZ, W. WELTER, and A. HARTMANN. Chem. Ber. **112**, 2509 (1979); H. HEYDT, K. H. BUSCH, and M. REGITZ. Justus Liebigs Ann. Chem. 590 (1980); A. HARTMANN, W. WELTER, and M. REGITZ. Tetrahedron Lett. 1825 (1974).
42. D. H. AUE, R. B. LORENS, and G. S. HELWIG. Tetrahedron Lett. 4795 (1973); D. AUE and G. S. HELWIG. Tetrahedron Lett. 721 (1974); D. H. AUE, M. J. MESHISHNEK, and D. F. SHELLHAMER. Tetrahedron Lett. 4799 (1973); D. H. AUE and G. S. HELWIG. J. Chem. Soc. Chem. Commun. 925 (1974); 603 (1975); 604 (1975); D. H. AUE, R. B. LORENS, and G. S. HELWIG. J. Org. Chem. **44**, 1202 (1979).
43. A. PADWA. Acc. Chem. Res. **12**, 310 (1979).
44. R. HUISGEN, R. GRASHEY, and J. SAUER. The chemistry of alkenes. *Edited by* S. Patai. Interscience, New York. 1964. p. 806.
45. K. N. HOUK, J. SIMS, C. R. WATTS, and L. J. LUSKUS. J. Am. Chem. Soc. **95**, 7301 (1973).
46. R. SUSTMANN. Tetrahedron Lett. 2717 (1971).
47. J. VAN ALPHEN. Recl. Trav. Chim. Pays-Bas, **62**, 485 (1943).
48. R. HUTTEL, J. REIDL, H. MARTIN, and K. FRANKE. Chem. Ber. **93**, 1425 (1960).
49. H. E. SIMMONS and T. FUKUNAGA. J. Am. Chem. Soc. **89**, 5208 (1967).
50. R. HOFFMANN, A. IMAMURA, and G. D. ZEISS. J. Am. Chem. Soc. **89**, 5215 (1967).
51. R. BOSCHI, A. S. DREIDING, and E. HEILBRONNER. J. Am. Chem. Soc. **92**, 123 (1970).
52. H. DURR, B. RUGE, and H. SCHMITZ. Angew. Chem. Int. Ed. Engl. **12**, 577 (1973).
53. P. BISCHOF, R. GLEITER, H. DURR, B. RUGE, and P. HERBST. Chem. Ber. **109**, 1412 (1976).
54. M. D. GORDON, T. FUKUNAGA, and H. E. SIMMONS. J. Am. Chem. Soc. **98**, 8401 (1976).
55. J. KAO and L. RADOM. J. Am. Chem. Soc. **100**, 760 (178).
56. A. PADWA. Acc. Chem. Res. **12**, 310 (1979).
57. H. DURR and V. FUCHS. Tetrahedron Lett. 4049 (1976).

Structural effects on reactivity in intramolecular catalysis. The hydrolysis of *N*-alkylated monoamides derived from norbornene-2,3-dicarboxylic acid

RONALD KLUGER AND MICHAEL BRANDL

Lash Miller Laboratories, Department of Chemistry, University of Toronto, Toronto, Ont., Canada M5S 1A1

Received April 27, 1984

This paper is dedicated to Professor Peter Yates on the occasion of his 60th birthday

RONALD KLUGER and MICHAEL BRANDL. Can. J. Chem. **62**, 2515 (1984).

Monoamides of 2,3-*endo-cis*-5-norborene dicarboxylic acid (compounds **1**–**5**) were prepared by addition of primary alkyl amines (*n*-propyl-, 2-methoxyethyl-, 2-fluoroethyl-, 2,2-difluoroethyl-, 2,2,2-trifluoroethyl-) to 2,3-*endo-cis*-5-norborene dicarboxylic anhydride. The rates of hydrolysis of each compound in solutions whose acid concentration ranged from 0.01 *M* to 9 *M* were determined. Rates increase with acidity above 0.1 *M* until a maximum rate is achieved in strong acid. The results are consistent with a mechanism involving intramolecular catalysis of the hydrolysis of the amide by the adjacent carboxylic acid. The dependence of rate on acidity can be interpreted in terms of a multistep mechanism involving formation of an intramolecular tetrahedral adduct, tautomerization of the adduct, and expulsion of the amine to give the anhydride. The identity of the rate-determining step is a function of the basicity of the substrate and the acidity of the medium. Analysis of the data in terms of the proposed mechanism suggests that the effective molarity of the groups involved in tautomerization of the tetrahedral internal addition intermediate is higher than in other rigid systems which lack the norbornene structure. It is proposed that ring strain and rotational entropy control cyclization and elimination steps. Interactions of the solvent with the entire substrate control reorganization of the intermediate. Conjugation of the interacting functional groups does not appear to have a significant effect upon their reactivity.

RONALD KLUGER et MICHAEL BRANDL. Can. J. Chem. **62**, 2515 (1984).

Faisant réagir des amines aliphatiques primaires (*n*-propyl-, méthoxy-2 éthyl-, fluoro-2 éthyl-, difluoro-2,2 éthyl- et trifluoro-2,2,2 éthyl-) sur l'anhydride de l'acide norbornène-5 dicarboxylique-2,3 (*endo, cis*), on a préparé les monoamides de l'acide norbornène-5 dicarboxylique-2,3 (*endo, cis*) (composés **1** à **5**). On a déterminé les vitesses d'hydrolyse de chacun de ces composés dans des solutions dont la concentration en acide variait de 0,01 à 9 *M*. Les vitesses augmentent avec une augmentation de l'acidité (au-dessus de 0,1 *M*) jusqu'à ce qu'elles atteignent un maximum en milieu fortement acide. Ces résultats sont en accord avec un mécanisme impliquant une catalyse intramoléculaire, due à l'acide carboxylique voisin, lors de l'hydrolyse de l'amide. On peut interpréter la relation qui existe entre les vitesses et l'acidité en faisant appel à un mécanisme en plusieurs étapes impliquant la formation d'un adduit tétraédrique intramoléculaire, une tautomérisation de l'adduit et l'expulsion de l'amine pour donner l'anhydride. La nature de l'étape déterminante est une fonction de la basicité du substrat et de l'acidité du milieu. L'analyse des données en relation avec le mécanisme proposé suggère que la molarité efficace des groupes impliqués dans la tautomérisation de l'intermédiaire tétraédrique provenant d'une addition interne est plus élevée que dans d'autres systèmes rigides qui ne comportent pas la structure norbornène. On suggère que les tensions de cycle et l'entropie de rotation sont les facteurs qui contrôlent les étapes de cyclisation et d'élimination. Les interactions du solvant avec l'ensemble du substrat contrôleraient la réorganisation de l'intermédiaire. Il ne semble pas que la conjugaison entre les groupes fonctionnels qui interagissent ait un effet important sur leur réactivité.

[Traduit par le journal]

Carboxylic acids may promote the hydrolysis of an adjacent amide through a mechanism involving intermediate formation of an anhydride (1, 2). The mechanism of this type of reaction has been investigated in detail and a number of factors which contribute to the effectiveness of the intramolecular participation phenomenon have been identified. The geometric relationship of the functional groups has been shown to be a key factor in determining the efficiency of the reaction (3). In addition, steric effects due to substituents on the departing amine cause variations in reactivity (4). The basicity of the departing amine may also have an observable effect which can be related to the detailed mechanism of the formation of the anhydride (5).

A key part of the mechanism involves conversion of an uncharged tetrahedral intermediate (**T**) to the zwitterion (**T′**) by net internal transfer of a proton. This transfer may occur with or without acid catalysis (3, 5, 6).

Kinetic analysis of the hydrolysis of amides derived from rigid systems containing neighboring amide and carboxylic acid groups has provided valuable information on the reactivity of tetrahedral intermediates. In particular, substrates which have provided information about proton transfer have been derived from acyclic conjugated monoamide monocarboxylic

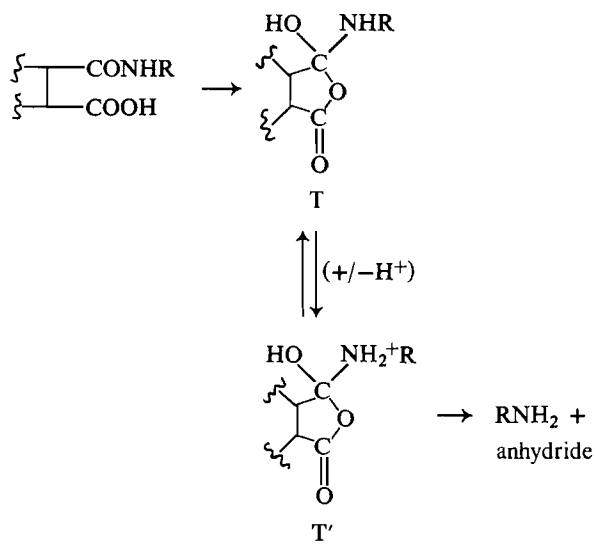

acids (maleamic acids (3, 6) and 2,3-dimethylmaleamic acids (3, 5)). Since interactions between functional groups are affected by conjugation, it is important to examine in detail the kinetics of similar reactions in rigid but nonconjugated sub-

Can. J. Chem. Downloaded from www.nrcresearchpress.com by 210.87.254.40 on 09/06/12
For personal use only.

strates. This allows the effects on reactivity of the structure connecting the interacting functional groups in each step to be determined. We have now determined the reactivity in acidic solutions of a series of sterically similar monoamides derived from norbornene-2,3-dicarboxylic acid (structures **1**–**5**).

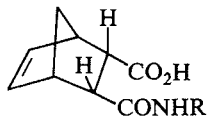

1 R = $—CH_2CH_2CH_3$
2 R = $—CH_2CH_2OCH_3$
3 R = $—CH_2CH_2F$
4 R = $—CH_2CHF_2$
5 R = $—CH_2CF_3$

In this series, the groups are held in proximity while the connection does not cause the interacting groups to be conjugated. The reactivities can be analyzed in terms of the mechanisms established for related conjugated compounds. Our results indicate that the reactivity patterns of these compounds are affected by the structure of the hydrocarbon connecting the amide and acid at each stage of the reaction process. No specific effects due to conjugation of the interacting functional groups are apparent.

Materials and methods

All chemicals used for which preparations are not given were obtained from the Aldrich Chemical Company or Fisher Scientific. All inorganic materials were reagent grade.

endo-cis-5-Norbornene-2,3-dicarboxylic acid monoamides were prepared by addition of the appropriate amine to *endo-cis*-5-norbornene-2,3-dicarboxylic anhydride in ether. Amines which are available as free bases (propylamine, 2-methoxyethylamine, and 3-hydroxypropylamine) were purified by distillation and added directly to a solution of 1 equivalent of the anhydride. The amides precipitated as they formed and were collected by filtration. For the other amines, the free base was generated by stirring the hydrochloride salt (which had been recrystallized prior to use) with triethylamine in tetrahydrofuran for several hours. The mixture was then filtered and the filtrate reacted with the anhydride in ether as above. 2,2-Difluoroethylamine was prepared from 2,2-difluoroacetic acid by a procedure which has previously been reported (5). All amides thus prepared gave satisfactory nmr and ir spectra as well as elemental analyses (Galbraith Laboratories). The uv spectra of the amides, products, and intermediate anhydride were determined under the reaction conditions, and extinction coefficients were determined at 220 nm (the wavelength at which kinetic data were collected).

Kinetics

The amides were subjected to hydrolysis in aqueous solutions at 38.0°C. Dilute acid solutions (less than 1.0 *M*) were prepared by adding aqueous potassium chloride to concentrated hydrochloric acid, maintaining ionic strength at 1.0. The diluted solutions were used as standards for measurement of empirical pH values. The pH values of the solutions were determined with a glass electrode and Fisher 119 pH meter based on the calibration from diluted hydrochloric acid solutions. For solutions of acid strength 1 *M* and more, concentrated sulphuric acid was diluted with distilled water, with acidity measured by the Hammett acidity function. Solutions of phosphoric acid – sodium phosphate buffers were prepared by neutralizing 1 *M* phosphoric acid with 1 *M* sodium hydroxide solutions and diluting with 1 *M* KCl. Buffer concentrations refer to the total phosphate concentration. Phosphoric acid solutions of 1 *M* and higher concentrations were prepared by adding distilled water to 85% phosphoric acid.

Hydrolysis reactions were initiated by adding the amide, dissolved in a minimal volume of methanol or water, to the acid solution at the reaction temperature in a cuvette contained in a jacketed holder in the spectrophotometer. Temperature in the sample compartment was kept constant at 38.0 (+/− 0.1)°C with a Neslab Exacal EX-100 Circulator.

Hydrolysis reactions were followed by monitoring the decrease in absorbance at 220 nm for all compounds studied. The measurements were performed with a Varian Cary 210 spectrometer and the data were collected through a digital interface and microprocessor with a Commodore 2001 computer. The data were transferred to diskettes for storage and retrieval using a Commodore 2031 disk drive. The microprocessor-based controller for the interface was built by Comspec Communications. In all cases the reactions were followed for at least three half-lives. Observed first-order rate constants were determined from the data using a computer program based on the method of "over-relaxation" as described by Swain *et al.* (7).

Results

Kinetic data were obtained from observations of changes in absorbance due to the conversion of the amides (**1**–**5**) to norbornene dicarboxylic acid and the corresponding amine at 220 nm. Since the amides are not conjugated, there is no significant change in absorbance at longer wavelengths. The initial product of the reaction is the anhydride, which is converted to an equilibrium mixture with the dicarboxylic acid (see Scheme 1). The rate of hydrolysis of the anhydride (rate constant k') is comparable to the rate of conversion of the amide to the anhydride and amine (rate constant k_0). The observed process is also first order ($v = k_{obs}$[amide]).

$$\text{Amide} \xrightarrow{k_0} \text{amine} + \text{anhydride} \overset{k'}{\rightleftharpoons} \text{dicarboxylic acid}$$

SCHEME 1

The value of k' was determined independently, as were the extinction coefficients for each species in Scheme 1 at 220 nm. These data were substituted into the integrated rate law for consecutive first-order reactions, following the procedure reported by Wiberg and Lepse (8) for their analysis of the oxidation of benzaldehyde by chromyl acetate. We find that the observed rate constant for the hydrolysis of the anhydride, k' ($= 4.5 \times 10^{-3}\ M^{-1}\ s^{-1}$), is independent of acidity. Our first trial value for k_0 for each amide at each acidity is the observed rate constant, k_{obs}. We then computed a best fit (least squares) of the observed absorbance changes to that predicted from the Wiberg–Lepse treatment by varying k_0. The absorbance change for the anhydride to acid conversion is small compared to that for the amide cleavage. Since the difference between k_{obs} and k_0 depends on the relative degree of spectral change in the two steps, the final values of k_0 were close to each k_{obs}.

The kinetic results for the hydrolysis of amides **1**–**5** are summarized in Fig. 1 and Table 1. The plot relates the first-order rate constant for cleavage of the amides (k_0) to the acidity of the solution. Since the study involves strongly acidic media as well as dilute acids, acidity is reported as measured by the Hammett acidity function, H_0 (9), in strongly acidic solutions. The rates increase with acidity to varying extents and reach maxima. For **5**, which is the least basic substrate, the maximum appears just to be reached at $H_0 = -3$. Data collected for the reaction of **5** in 9 *M* sulfuric acid (beyond the scale of Fig. 1, presented in Table 1) were used to determine the maximum. The maxima are clearly attained for the other amides.

Since the reactions of the least basic compounds are subject to hydronium catalysis, we wished to determine if other Bronsted acids will accelerate the reaction. We note that catalysis is observable only at hydronium ion concentrations near

Can. J. Chem. Downloaded from www.nrcresearchpress.com by 210.87.254.40 on 09/06/12
For personal use only.

Can. J. Chem. Downloaded from www.nrcresearchpress.com by 210.87.254.40 on 09/06/12
For personal use only.

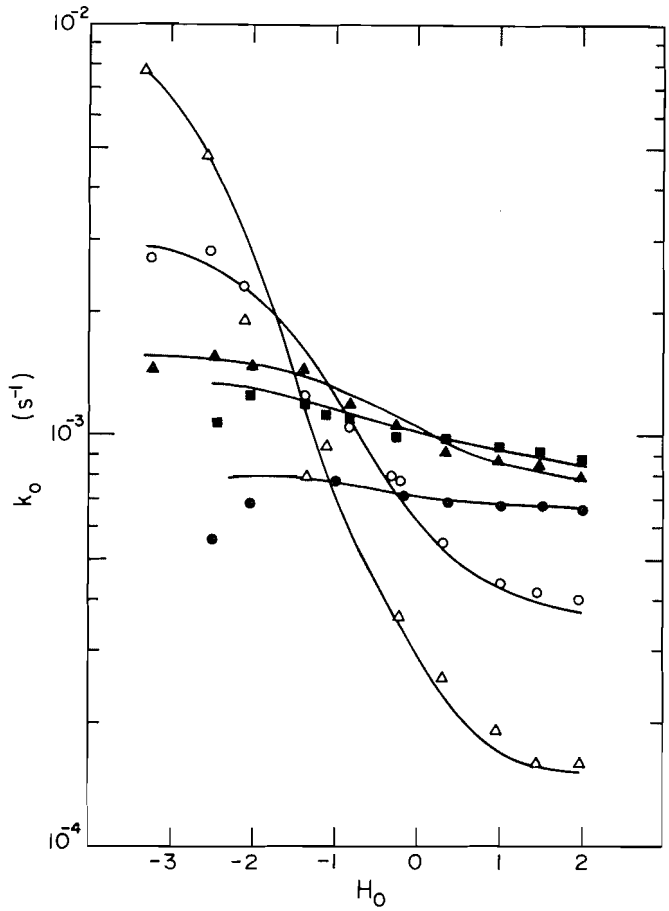

FIG. 1. Dependence on acidity of first-order rate constant for conversion of **1** (●), **2** (■), **3** (▲), **4** (○), and **5** (△) to norbornene-2,3-dicarboxylic acid anhydride and the corresponding amine at 38°C. The acidity scale is the Hammett acidity function at acid concentrations above 1 *M*. The lines are plots of eq. [1] using parameters in Tables 2 and 3.

1 *M* and above, indicating that the "uncatalyzed" mechanism competes very effectively. Since the hydrolysis of **5** shows the largest susceptibility to hydronium ion catalysis, we studied the effects of phosphoric acid and phosphate buffers on its hydrolysis. The results of these experiments are presented in Table 1. The rates do not increase at low phosphoric acid concentrations. At higher concentrations, the rates follow the H_0 correlation as in Fig. 1.

The data in Fig. 1 are consistent with the mechanism in Scheme 2. This mechanism is similar to mechanisms for other reactions in which an adjacent carboxylic acid promotes the hydrolysis of an amide (3, 5).

This mechanism involves a branch via specific acid − general base catalysis (k_5k_4) as well as a direct equivalent of intramolecular proton transfer (k_2). These branches were proposed by Kirby and co-workers to explain the observation of buffer catalysis in reactions of alkylated maleamic acids (3).

An expression for observed first-order rate constants based on Scheme 2 is presented in eq. [1], which depends explicitly on hydrogen ion activity.

$$[1] \quad k_0 = (k_2k_3K_1 + k_3k_4K_5[H^+]K_1)/(k_3 + k_{-2} + k_{-4}[H^+])$$

Equation [1] contains seven dependent variables (rate constants and equilibrium constants). Many of these parameters can be estimated independently. The equilibrium constants K_5 and K_2 (that is, k_2/k_{-2}) are dissociation constants which can be estimated using linear free energy relationships following the procedure used in an earlier study (5). The value of K_4 is the product of the other two equilibria. The rate constant k_{-4} is for a diffusion-controlled proton transfer and therefore should have a value of about $10^{10}\ M^{-1}\ s^{-1}$ (10). The resulting values are presented in Table 2.

TABLE 1. First-order rate constants (k_0) for conversion of **5** to norbornene dicarboxylic acid anhydride and trifluoroethylamine at 38°C[a]

Buffer or acid	Concentration	H_0 or pH[b]	$k_0 \times 10^4$, s^{-1}
HCl	0.01 *M*	2.15	1.65
H_3PO_4/NaH_2PO_4	0.2 *M*	2.15	1.64
	0.4 *M*	2.15	1.66
	0.8 *M*	2.15	1.68
	1.0 *M*	2.15	1.67
	0.3 *M*	0.8	1.97
	0.5 *M*	0.8	1.96
	0.7 *M*	0.8	1.90
H_3PO_4	10%	0.75	2.24
	20%	0.3	2.85
	30%	−0.12	4.03
	44%	−0.6	4.86
	52%	−1	8.08
H_2SO_4	9 *M*	−4.5	200

[a]Rate constants listed are for data that does not duplicate results presented in Fig. 1. Ionic strength was maintained at 1.0 for all concentrations of buffers and acids less than 1.0 *M*.

[b]"pH" as measured by glass electrode for first eight points. H_0 values are from ref. 17.

Other rate and equilibrium constants can be obtained by fitting the data to appropriate versions of eq. [1]. At low acidity, we observe that the rate for all substrates is independent of acidity. Thus, the pathway involving the protonated intermediate, $\mathbf{TH}^+$ does not make a significant contribution under these conditions.

$$[2] \quad k_0 = K_1k_2k_3/(k_3 + k_{-2})$$

In more acidic solutions, terms containing proton concentrations become dominant so that eq. [1] simplifies to eq. [3].

$$[3] \quad k_0 = K_1K_2k_3$$

As acidity is increased, the observed rate constants for each substrate increase to varying extents. At the point where the rate is twice that at low acidity, flux through the protonated and neutral intermediates is equal. Using eq. [1] with the data for compound **5**, we derive the acidity at which the fluxes through the two pathways are equal. This acidity gives the ratio of rate constants.

$$[4] \quad [H^+] = k_2/k_4K_5 = k_{-2}/k_{-4}$$

The terms k_{-2} and k_{-4} are thermodynamically favorable proton transfers. Since k_{-4} represents an intermolecular process, we set its value at $10^{10}\ M^{-1}\ s^{-1}$ (10). The values of k_{-2} and k_{-4} should be independent of the amine substituent since the rest of the molecule remains unchanged. We find k_{-2} by noting the acidity at which rates are twice the low acid minimum for **5**. The rate at this acidity must be made up of equal contributions from the acid catalysis pathway and the uncatalysed route ($k_{-2} = k_{-4}[H^+]$). Our data suggest the acidity at which rates are equal is that produced by 1 *M* sulfuric acid. Therefore, k_{-2}/k_{-4} is 1 *M*. The data in Fig. 1 were fitted to eq. [1] using K_1 and

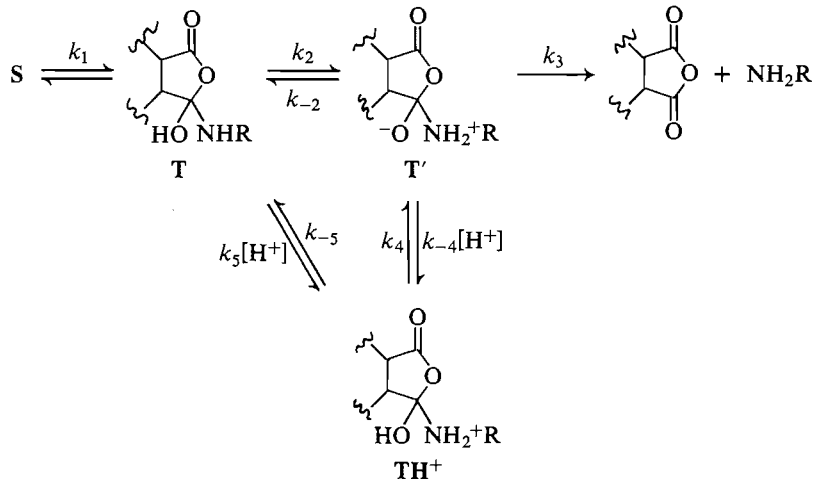

SCHEME 2

TABLE 2. Derived and calculated rate and equilibrium constants for reactions of monoamide derivates of norbornene 2,3-dicarboxylic acid (compounds **1**–**5**), according to Scheme 2 in text[a]

Leaving amine	pK_a[b]	K_2	K_5, M^{-1}	K_4, M	k_4, M^{-1} s^{-1}
Propyl-	10.58	1.6×10^{-3}	2.1×10^{4}	7.6×10^{-8}	7.6×10^{2}
2-Methoxyethyl-	9.68	2.5×10^{-4}	2.6×10^{3}	9.6×10^{-8}	9.6×10^{2}
2-Fluoroethyl-	9.19	8.9×10^{-5}	8.3×10^{2}	1.1×10^{-7}	1.1×10^{3}
2,2-Difluoroethyl-	7.45	2.0×10^{-6}	1.3×10	1.5×10^{-7}	1.5×10^{3}
2,2,2-Trifluoroethyl-	5.40	3.4×10^{-8}	1.3×10^{-1}	2.6×10^{-7}	2.6×10^{3}

[a]The methods used to calculate these values are described in the Results section of the text.
[b]pK_a values are for the conjugate acids of the listed bases from ref. 16.

TABLE 3. Rate and equilibrium constants for reactions of monoamide derivatives of norbornene 2,3-dicarboxylic acid at 38°C, ionic strength 1.0, as described in Scheme 2

Substrate	k_2, s^{-1}	K_1	k_3, s^{-1}
1	1.6×10^{7}	2.5×10^{-10}	2×10^{9}
2	2.5×10^{6}	1.0×10^{-10}	6×10^{9}
3	8.9×10^{5}	1.8×10^{-9}	1×10^{10}
4	2.0×10^{4}	2.0×10^{-8}	8×10^{10}
5	3.4×10^{2}	4.4×10^{-7}	9×10^{11}

k_3 as adjustable parameters within the restrictions we have presented. The values giving the best fit to the data are presented in Table 3. The curves in Fig. 1 are plots of these parameters substituted into eq. [1].

Discussion

Reactivity patterns

The amides derived from the least basic amines are less reactive than those derived from the more basic amines in dilute acid; the order of reactivity is reversed in strong acid. This is consistent with the mechanisms presented in Scheme 2. The intermediate formed by the addition of the carboxyl group (**T**) must become protonated on its nitrogen atom and its hydroxyl group must be deprotonated in order for the amine to be expelled (**T′**). In solutions of low acidity, the tautomeric shift of a proton from the hydroxyl group to the amino group is the most effective route for generating the alkyl ammonium ion. If expulsion of the amine from the zwitterionic intermediate is completely rate determining for a particular substrate, then addition of acid to the solution will not further increase the rate of reaction. Therefore, we observe very little acid catalysis for the derivatives with the most basic leaving groups. However, if proton transfer, k_2, is rate determining or partly rate determining, then addition of acid can produce a more effective reaction through the conjugate acid of T. This will lead to an increase in rate with acidity until the rate-determining step becomes elimination, k_3. At this point, the rate should not increase with additional acidity, which is consistent with the patterns in Fig. 1.

The rate-determining step in the acid-catalyzed process in Scheme 2 is removal of the hydroxyl proton of the protonated intermediate by water to give the zwitterion. This step is a thermodynamically unfavourable proton transfer and should be subject to general base catalysis with β near unity for weak bases (3, 10). Since a prior protonation is involved, the observed phenomenon should be general acid catalysis with α near zero. As we have noted in the Results section, we do not observe buffer catalysis although the mechanism involves a step which should be subject to such catalysis. However, the uncatalysed process (k_2) is very efficient so that high acid concentrations are needed to see catalysis by acid. Furthermore, since hydronium ion is much more effective than predicted by Bronsted plots in related cases (3), it overwhelms any catalysis that we might have observed from other Bronsted acids.

Alternatively, one could interpret our results as indicating that the hydronium ion catalysis we observe is the result of a mechanism involving specific acid catalysis. However, we find that a less likely possibility. Since decomposition of the tetrahedral intermediate, rather than cyclization, is rate deter-

Can. J. Chem. Downloaded from www.nrcresearchpress.com by 210.87.254.40 on 09/06/12
For personal use only.

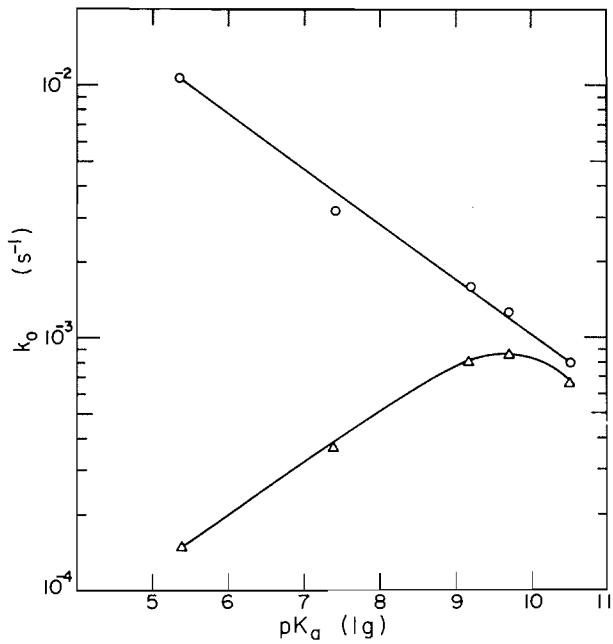

FIG. 2. The dependence of the maximal (○) and minimal (△) rate constants (k_0) upon the pK_a of the conjugate acid of the leaving amine ("lg" = leaving group) for compounds **1**–**5**. The pK_a values are listed in Table 2.

mining (3, 5), a mechanism involving specific acid catalysis must provide a means for direct decomposition of the protonated tetrahedral intermediate, $\mathbf{TH}^+$. In Fig. 2, a pK_a vs. rate plot for the rates at low acid concentration is concave downward, indicating that there is a change in rate-determining step within a common mechanism amongst the substrates. The plot for the rate maxima in high acid concentration is a straight line with the high pK_a portion in common with the plot for the minima. This suggests that acid catalysis is enhancing the rate within a mechanism involving the same intermediates as in the uncatalysed process. A specific acid catalysis route involving direct decomposition of $\mathbf{TH}^+$ would provide an alternative mechanism, resulting in all rates at high acid concentration being significantly above those at low acidity, with the greatest effect on the substrate with the poorest leaving group (**1**). This is contrary to the observed results.

Effective molarities

Effective molarity measures the relative concentrations of interacting functional groups within a molecule as the ratio of the intramolecular rate or equilibrium constant to the analogous quantity for a bimolecular reaction (11). It is a useful calibration of the efficiency of intramolecular catalysis.

The addition of a carboxylic acid to an amide in water, the bimolecular analogue of the equilibrium between **S** and **I**, has not been observed. However, an appropriate bimolecular analogue has been estimated in an earlier study from our laboratory, based on methods that have been developed by Guthrie (5, 12). Thus, it was estimated that the equilibrium constant for addition of acetic acid to dimethyl acetamide is $10^{-18}\,M^{-1}$. The equilibrium constant for the conversion of **S** to **I** can be estimated from the kinetic data we have obtained. The closest analogy to the dimethyl acetamide case is that in which n-propylamine is the leaving group in the intramolecular reaction. Since K_1 is 10^{-10}, the effective molarity of the carboxyl group in these reactions is about $10^8\,M$.

The effective molarity for the proton transfer step, k_{-2}, in the tautomerization of the intermediate, **T**, can also be estimated. The analogous bimolecular process is a thermodynamically favorable proton transfer. The rate should be diffusion controlled with a rate constant of $10^{10}\,M^{-1}\,s^{-1}$. This is k_4 in Scheme 2. Since k_{-2} is $10^{10}\,s^{-1}$, the effective molarity of the internal ammonium ion is 1 M.

These effective molarities differ from values that have been obtained for the similar hydrolysis reactions of *N*-alkyl maleamic acids and *N*-alkyl 2,3-dimethylmaleamic acids (5, 6). The effective molarity of the cyclization equilibrium, K_1, is two orders of magnitude smaller than that for the maleamic acids and four orders of magnitude smaller than for the 2,3-dimethylmaleamic acids. Intramolecular processes are most effective when there is a minimal amount of rotational entropy lost upon cyclization (11). The norbornene system should equal the maleamic acids in this respect since the interacting functional groups are held *cis* and coplanar in both systems. Beyond this, the norbornene system is subject to additional steric strain upon cyclization, due to the fusing of the additional ring onto the bicyclic system, while the maleamic acid systems will be monocyclic, relieving interactions between other substituents on the carbon–carbon double bond. It is also apparent that there is no special effect due to the conjugation of the functional groups in the maleamic acids since the norbornene derivatives, in which the connection between functional groups is saturated, show similar reaction patterns.

The effective molarity for the proton transfer step is much larger than in the monocyclic cases by about three orders of magnitude. Bernasconi *et al.* have considered the general question of effective molarities in formal 1,3-proton transfers between nitrogen and oxygen (13). The transfer in these cases involves intermediate participation by the solvent. The value of 1 M is in the upper range of possibilities that was considered. Our results suggest that the structure of the nonreacting portion of the substrate has a significant influence on the effective molarities in the reacting portion with respect to the proton transfer step.

Since the solvent is an essential participant in the 1,3 prototopic shift, it is likely that any effect that disrupts the structure of the solvent will have an effect on the rate of this process. The norbornenyl derivatives contain large hydrocarbon regions which do not fit into the hydrogen-bonded water lattice. By comparison, derivatives of maleic acid contain no large hydrocarbon region and will better accommodate themselves to aqueous solvation. The norbornenyl derivatives then may effectively direct the proton transfer away from the backbone and reduce the entropic barrier to the proton shift associated with smaller substrates.

Amine expulsion

A plot of the maximum rate constants versus pK_a of the leaving group is linear (Fig. 2). As stated earlier, this is evidence that these rates involve a common mechanism with a common rate-limiting step. The slope of the plot of log k vs. pK_a for the maximum rate constants is −0.27. This value suggests that the amine has about 0.27 units less positive charge associated with it in the transition state of the rate-determining step than it does in the initial amide (14). This is consistent with a transition state for the expulsion step in which considerable bond breaking has occurred. In the product, the amine is uncharged while in the intermediate it has a charge of +1. In the starting amide, we expect a charge of about 0.5 to 0.6 on nitrogen (14, 15).

Can. J. Chem. Downloaded from www.nrcresearchpress.com by 210.87.254.40 on 09/06/12
For personal use only.

Conclusions

Our results illustrate how the interactions of functional groups involved in intramolecular reactions are influenced by the chain which connects them. However, for amides and carboxylic acids, conjugation of the interacting functional groups appears to have no significant effect on reactivity. The principal enthalpic effects in these systems are widely recognized and can be considered in terms of buttressing and ring strain (16). However, we now see that additional complications, probably arising from perturbations of the solvent, also affect observed rates by affecting the reactivity of intermediates. As a result, we feel that further generalizations concerning rate constants for reactive intermediates must describe ranges rather than specific values of rate constants.

Acknowledgements

This work has been supported by an operating grant from the Natural Sciences and Engineering Research Council. Michael Brandl is the recipient of a postgraduate fellowship from that Council.

1. M. L. BENDER. J. Am. Chem. Soc. **79**, 1258 (1957).,
2. A. BRUYLANTS and F. J. KÉZDY. Rec. Chem. Prog. **21**, 213 (1960).
3. M. F. ALDERSLEY, A. J. KIRBY, P. W. LANCASTER, R. S. MCDONALD, and C. R. SMITH. J. Chem. Soc. Perkin Trans. 2, 1487 (1974).
4. I. H. PITMAN, K. UEKAMA, T. HIGUCHI, and W. E. HALL. J. Am. Chem. Soc. **94**, 8147 (1972).
5. R. KLUGER, J. CHIN, and W. W. CHOY. J. Am. Chem. Soc. **101**, 6976 (1979).
6. R. KLUGER and J. CHIN. J. Am. Chem. Soc. **104**, 2891 (1982).
7. C. G. SWAIN, M. S. SWAIN, and L. F. BERG. J. Chem. Inf. Comput. Sci. **20**, 47 (1980).
8. K. B. WIBERG and A. LEPSE. J. Am. Chem. Soc. **86**, 2612 (1964).
9. M. PAUL and F. A. LONG. Chem. Rev. **57**, 1 (1957).
10. M. EIGEN. Angew. Chem. Int. Ed. Engl. **3**, 1 (1964).
11. A. J. KIRBY. Adv. Phys. Org. Chem. **17**, 183 (1980).
12. J. P. GUTHRIE. J. Am. Chem. Soc. **96**, 3608 (1974).
13. C. F. BERNASCONI, S. A. HIBDON, and S. E. MCMURRY. J. Am. Chem. Soc. **104**, 3459 (1982).
14. W. P. JENCKS, B. SCHAFFHAUSEN, K. TORNHEIM, and H. WHITE. J. Am. Chem. Soc. **9**, 3917 (1971).
15. R. KLUGER and J. C. HUNT. J. Am. Chem. Soc. In press.
16. A. J. KIRBY and P. W. LANCASTER. J. Chem. Soc. Perkin Trans. 2, 1206 (1972).
17. C. H. ROCHESTER. Acidity functions. Academic Press, New York, NY. 1970. p. 50.

Can. J. Chem. Downloaded from www.nrcresearchpress.com by 210.87.254.40 on 09/06/12
For personal use only.

A synthesis of hirsutene: a simple route via β-enolization[1]

BRIAN A. DAWSON, ASHIM K. GHOSH,[2] JEFFREY L. JURLINA,[3] ARTHUR J. RAGAUSKAS, AND J. B. STOTHERS
Department of Chemistry, University of Western Ontario, London, Ont., Canada N6A 5B7

Received May 31, 1984

This paper is dedicated to Professor Peter Yates on the occasion of his 60th birthday

BRIAN A. DAWSON, ASHIM K. GHOSH, JEFFREY L. JURLINA, ARTHUR J. RAGAUSKAS, and J. B. STOTHERS. Can. J. Chem. **62**, 2521 (1984).

A simple sequence from dicyclopentadiene to the *cis,anti,cis*-tricyclopentanoid carbon skeleton of the hirsutanes is described. A key step employs a β-enolate rearrangement to generate the ring system having the desired stereochemistry. The route to the requisite ketone for this rearrangement utilizes efficient ring expansion via homoketonization.

BRIAN A. DAWSON, ASHIM K. GHOSH, JEFFREY L. JURLINA, ARTHUR J. RAGAUSKAS et J. B. STOTHERS. Can. J. Chem. **62**, 2521 (1984).

On décrit une série simple de réactions qui permettent de transformer le dicyclopentadiène en squelette carboné tricyclopentanoïde-*cis,anti,cis* des hirsutanes. L'étape clé fait intervenir une transposition β-énolique qui permet de générer le système cyclique comportant la stéréochimie appropriée. Afin d'obtenir la cétone requise pour cette transposition, on utilise une méthode efficace d'extension de cycle par le biais d'une homocétonisation.

[Traduit par le journal]

Can. J. Chem. Downloaded from www.nrcresearchpress.com by 210.87.254.42 on 09/06/12
For personal use only.

The linearly fused tricyclopentanoid ring system of *cis,anti,cis*-tricyclo[6.3.0.0^{2,6}]undecane constitutes the skeleton of several naturally occurring sesquiterpenes having antibiotic and (or) antitumor activity (1) and consequently has attracted considerable attention in recent years. Representative examples of this group of compounds are hirsutene (**1**) and coriolin (**2**). Several different syntheses have been devised for (±)-**1** (2–5), which has been considered the biosynthetic precursor of **2** and hirsutic acid (2) as originally suggested from results of study of the synthesis of the latter (6) even though **1** had not been isolated and characterized at the time. We describe here a simple stereocontrolled sequence leading from

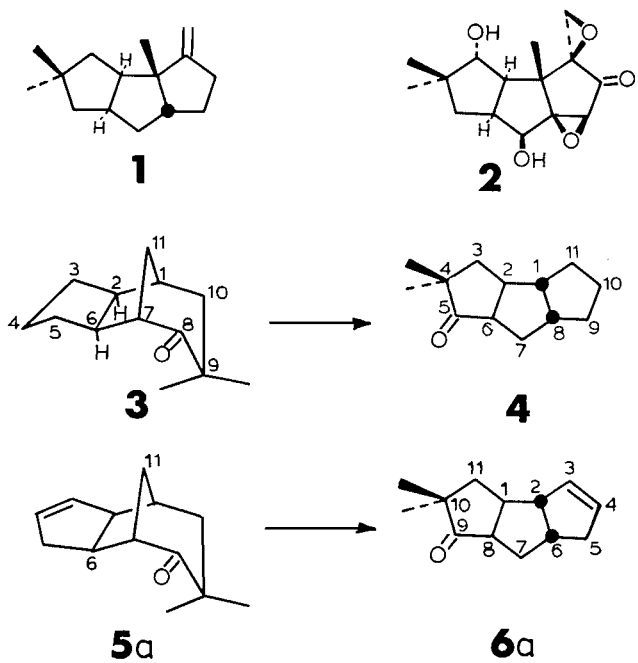

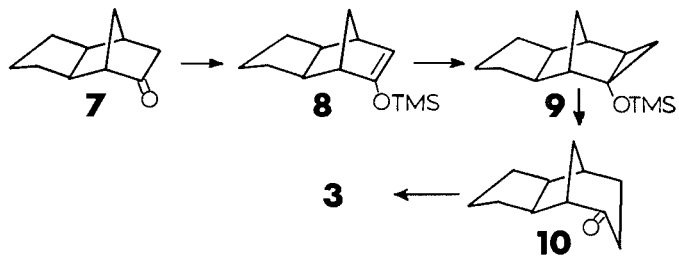

SCHEME 1

dicyclopentadiene to **1** which employs ring expansion by ketonization of a cyclopropoxide and skeletal rearrangement through a β-enolate. A major feature of this synthesis is that the stereochemistry at three of the four chiral centres is established essentially at the outset of the sequence and the constraints are such that the β-enolate rearrangement specifically generates the correct configuration at the fourth centre exclusively. A preliminary report of this sequence has appeared (5).

The notion that the key β-enolate rearrangement could provide the desired ring system arose from our earlier results for 3,3-dimethylbicyclo[3.2.1]octan-2-one which had been found to rearrange unidirectionally to the isomeric 3,3-dimethylbicyclo[3.3.0]octan-2-one (7). As an exploratory case, the potential isomerization of 9,9-dimethyltricyclo[5.3.1.0^{2,6}]undecan-8-one (**3**) to *cis,anti,cis*-4,4-dimethyltricyclo[6.3.0.0^{2,6}]-undecan-5-one (**4**) through β-enolate formation at C-11 of **3** was examined initially. Upon finding that the conversion of **3** → **4** indeed occurs, we turned our attention to an examination of the behavior of **5***a* under the same reaction conditions, namely, *t*-BuO$^-$/*t*-BuOH at 185°C, since the transformation of **5***a* → **6***a* provides the needed functionality in the third cyclopentane ring for generation of the appropriate substitution for the hirsutene molecule.

For the initial case, ketone **3** was prepared from commercially available tricyclo[5.2.1.0^{2,6}]decan-8-one (**7**) as outlined in Scheme 1, utilizing ring expansion via ketonization of the cyclopropoxide analog (8). Treatment of **7** with lithium diisopropylamide (LDA) at −78°C followed by reaction with trimethylsilyl chloride and triethylamine gave silyl enol ether **8** in 98% yield. Cyclopropanation of **8** using a zinc–silver couple and CH_2I_2 provided the tetracyclic ether **9** in 94% yield. On the

[1] Part 113 of the series ^{13}Cmr studies; for Part 111 see ref. 15; for Part 112 see ref. 16.

[2] Present Address: Department of Biochemistry, St. Louis Medical Centre, St. Louis, MI 63104, U.S.A.

[3] Present Address: Department of Pharmacology, School of Medicine, University of Auckland, Auckland, New Zealand.

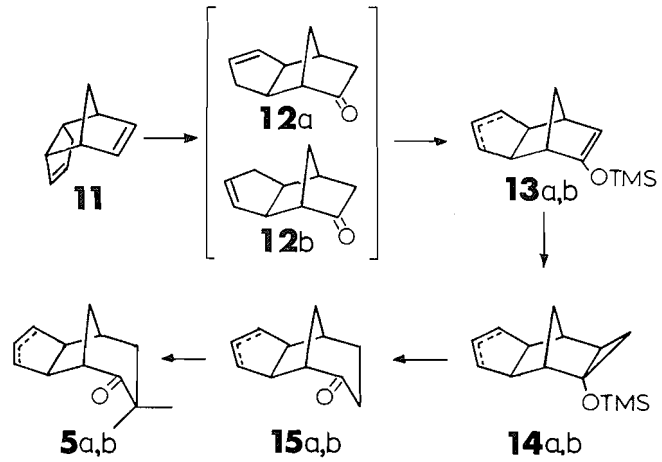

SCHEME 2

basis of our earlier results for the homoketonization of polycyclic cyclopropoxides (8), we anticipated that base-catalyzed cleavage of **9** would strongly favor ring expansion to the desired ketone **10** rather than generation of the 9-methyl derivative of **7**. This was indeed the case; upon treatment of **9** with NaOH–MeOH at 0°C a single ketone lacking methyl absorption in both its ^{1}H and ^{13}Cmr spectra was obtained in 96% yield. Dimethylation of **10** with $NaNH_2$–Et_2O–MeI (9) furnished the required ketone **3**. The ^{13}Cmr spectra of **3** and **7**–**10** have been reported previously (10).

Treatment of **3** with *t*-BuO^-/*t*-BuOH at 185°C for extended reaction times gave a neutral fraction in >90% yield which, by glc analysis, consisted of two components, readily separable by preparative glc. The ratio of the two compounds was a function of reaction time, with equal quantities apparent after ca. 120 h. One was easily identified as recovered starting material **3** while the second was a new ketone, containing a cyclopentanone moiety on the basis of its carbonyl absorption (1737 cm^{-1}, δ_C 224.6) which was distinctly different from that of **3** (1710 cm^{-1}, δ_C 218.0). Furthermore, its ^{13}Cmr spectrum contained signals for two methyl, five methylene, four methine, and one quaternary carbon which are entirely consistent with structure **4**. Although the formation of β-enolates can be envisaged by proton abstraction from C-6, -10, -11, and the methyl carbons of **3**, rearrangement via cleavage of each of these intermediates leads to a different isomeric ketone, each of which has different numbers of methyl, methylene, methine, and quaternary carbons. Only the β-enolate formed by 11-proton abstraction yields a ketone fitting the observed data. The parent system, 3,3-dimethylbicyclo[3.2.1]octan-2-one, undergoes β-enolization at the centres corresponding to C-6 and -11 in **3** (7). If rearrangement of **3** proceeded by proton abstraction at C-6, the product, 8,8-dimethyltricyclo[4.3.2.$0^{1,5}$]undecan-9-one, would have six methylene and each of two methyl, methine, and quaternary signals, contrary to the spectral data. Structure **4** was confirmed by Wolff–Kishner reduction to the corresponding hydrocarbon, as discussed later.

Experiments at 200°C revealed that the conversion of **3** → **4** is >95% complete after 140 h and the half-life for the transformation is ca. 30 h.

With clear evidence that **3** is smoothly transformed to **4** under homoenolization conditions, we turned our attention to the preparation of ketone **5** (see Scheme 2) as the key intermediate for our planned sequence leading to **1**. Dicyclopentadiene (**11**) was readily converted to **12** by reaction with HCOOH and alkaline hydrolysis (11) followed by oxidation (12); this product is a 30:70 mixture of the Δ^3- and Δ^4-isomers, **12***a* and *b*, respectively. It should be noted that, at this stage, three of the chiral centres (C-1, -2, and -6) have the stereochemistry required in the target skeleton. Treatment of **12** with LDA at −78°C followed by Me_3SiCl afforded a 30:70 mixture of **13***a*,*b*, in 95% yield, cyclopropanation of which gave **14***a*,*b* in 82% yield. For the latter step, the mole ratio of CH_2I_2/**13***a*,*b* was reduced to 1.1 from 1.7 used for the cyclopropanation of **8** → **9**; this was done to avoid reaction at the second double bond in the unsaturated series that occurs if a larger excess of CH_2I_2 is used. As in the case of **9**, ether cleavage and ketonization of **14***a*,*b* in methanolic NaOH at 0°C furnished a "single" product in the sense that a 30:70 mixture of **15***a*,*b* was obtained exclusively. It may be mentioned that with relatively short reaction times (1–2 h) and (or) at higher temperatures glc analysis reveals the presence of small amounts of the 9-methyl derivative of **12** in the ketonization product. Since these derivatives were prepared in another project (10), their identification was straightforward. While higher reaction temperatures are known to increase the proportion of the α-methyl isomers in closely related homoketonizations (8), the α-methyl derivatives can also arise from thermal decomposition of the cyclopropanols formed from TMS ethers analogous to **14**. We have found that although the TMS ethers are generally stable to glc analysis the corresponding cyclopropanols decompose on the column to give the α-methyl products exclusively. To avoid this complication, the ketonizations were performed at 0°C for relatively long reaction times (24 h). Dimethylation of **15***a*,*b* ($NaNH_2$–Et_2O–MeI) furnished the required ketone **5** as the expected 30:70 mixture of Δ^3- and Δ^4-isomers. For all products in this sequence, **5** and **12**–**15**, the mixtures of *a* and *b* isomers gave a single band in the glc traces; the composition of the mixtures was judged from the ^{13}Cmr spectra of each product, which have been reported previously (10).

The behavior of **5***a*, *b* upon reaction with *t*-BuO^-/*t*-BuOH at 185°C was very similar to that found for **3**, in that glc analysis of the neutral product indicated the presence of only two "components", each of which, of course, is a mixture of two double bond isomers. One of the components was easily shown to be the initial ketone **5**, differing from the starting material only in the proportion of *a* and *b* isomers. With increasing reaction times, the proportion approached 50:50 but a detailed study of the rate of change was not done. Since proton abstraction from C-5 (**5***a*) and C-3 (**5***b*) generates the same allylic carbanion, one can expect equilibration of the Δ^3- and Δ^4-isomers to occur under these strongly basic conditions. Because of this, separation of the isomeric mixtures **5** and **12**–**15** is unwarranted. The new component generated under these reaction conditions was also found to be an approximately 50:50 mixture of isomers (by ^{13}Cmr) which contain a five-membered ring ketone (1736 cm^{-1}, δ_C 224.7). By analogy with the results discussed earlier, β-enolate **16** could be envisaged to arise by proton abstraction from C-11 in **5** and cleavage, as indicated, to form **6**. The ^{13}C spectrum of this product contain-

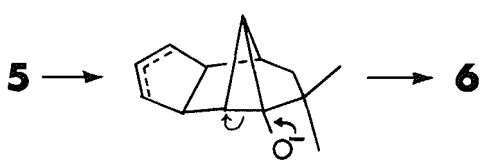

16

Can. J. Chem. Downloaded from www.nrcresearchpress.com by 210.87.254.42 on 09/06/12
For personal use only.

Can. J. Chem. Downloaded from www.nrcresearchpress.com by 210.87.254.42 on 09/06/12
For personal use only.

ed the expected signals for an approximately 1:1 mixture of **6***a*,*b* although there were four accidental equivalencies with two methyl, the two quaternary, both carbonyls, and a methylene and methine carbons exhibiting the same shieldings. To confirm the presence of two isomeric ketones a small sample of **6***a*,*b* was treated with LAH and the resulting mixture of alcohols, giving a single major spot on tlc, was isolated and examined by ^{13}Cmr. The ^{13}C spectrum contained two sets of thirteen signals in a ratio of ca. 55:45 with each set consisting of two methyl, three methylene, five methine, one quaternary, and two olefinic CH signals. These results are entirely consistent with the reduction of **6***a*,*b* to the corresponding alcohols, presumably having *endo*-hydroxyl groups, but their orientation was not established. At 185°C, the half-life for the conversion of **5** → **6** is ca. 225 h. A few runs were also performed at 205–210°C and exhibited a half-life of ca. 70 h; in the longest runs (150 h) at this temperature the neutral product contained 80% of **6** whereas even after >300 h at 185°C the maximum amount of **6** was ca. 65%.

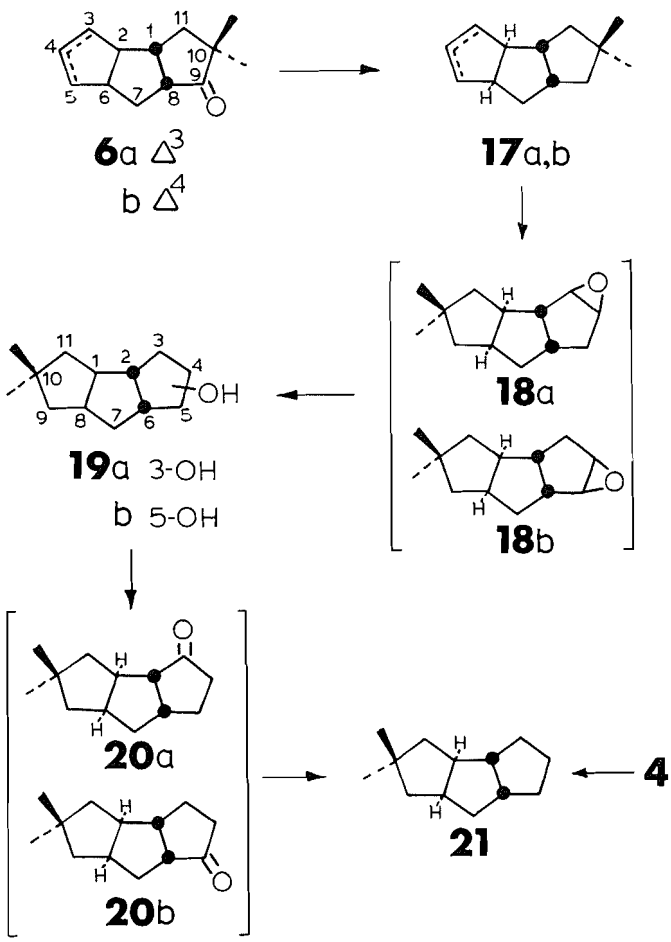

Wolff–Kishner reduction of **6***a*,*b* gave **17***a*,*b* in 90% yield after isolation by column chromatography and, upon treatment with *m*-chloroperbenzoic acid, furnished a 50:50 mixture of **18***a*,*b* in 85% yield after bulb-to-bulb distillation. This mixture was treated with LAH to furnish an oily product which on the basis of its ^{13}C spectrum consisted mainly of a 1:1 mixture of the 3- and 5-alcohols together with a small amount (<5%) of a third alcohol. The total product was subsequently oxidized in 92% yield to the corresponding mixture of ketones from which samples of the ketones **20***a* and *b* were isolated by preparative hplc. For the series **6** and **17**–**20**, all attempts with glc failed to effect a separation of the isomers. Spectral data (ir, ^{1}Hmr, ^{13}Cmr) for **20***a* were found to be identical to those for the same ketone described by Little and Muller (3). Wolff–Kishner reduction of the mixture of ketones furnished a single hydrocarbon **21**, confirming that **20***b* had the same carbon skeleton. As mentioned earlier, ketone **4** also gave **21** exclusively upon Wolff–Kishner reduction, thus confirming the transformation of **3** → **4**.

Since **20***a* has previously been converted into (±)-hirsutene (3), our synthesis is complete, demonstrating the utility of a stereocontrolled β-enolate rearrangement for the generation of the *cis,anti,cis*-tricyclopentane ring system of the hirsutanes. As noted earlier, the configuration at three of the four chiral sites is established at an early stage in the sequence and the constraints of the β-enolate rearrangement are such that only the correct configuration is realized at the fourth centre upon the conversion of **5** → **6**. It can be mentioned that, in principle, resolution of the enantiomeric intermediates could be performed at an early stage in the sequence, thereby providing an asymmetric synthesis of this ring system.

Experimental

Thin-layer chromatography (tlc) was done on Kiesel gel 60 F_{254} plates. Gas–liquid chromatography (glc) was performed using a 6% FFAP on Chromosorb W (3 m × 0.6 cm) with a Varian 920 or 3700 instrument. Tetrahydrofuran (THF) and ether were distilled from Na/benzophenone before use. Pyridine and *tert*-butyl alcohol were distilled from CaH_2 and stored over 4A molecular sieves. Dicylopentadiene and *exo*-tricyclo[5.2.1.$0^{2,6}$]decan-8-one were obtained commercially (Aldrich).

Infrared spectra were recorded with a Beckman 4250 spectrophotometer and mass spectra with a Varian MAT-311A system at 70 eV (direct inlet). Routine ^{1}Hmr spectra were recorded on Varian T-60 or EM-360 instruments, while the data for pure samples were obtained using a Varian XL-200 spectrometer. The latter instrument was employed for the ^{13}C spectra (50.3 MHz) and comparison of the fully decoupled spectra with those obtained with either the APT (13) or INEPT (14) sequences served to identify the methyl, methylene, methine, and quaternary signals.

Trimethylsilyl enol ether of tricyclo[5.2.1.$0^{2,6}$]decan-8-one (8)

A solution of diisopropylamine (5.22 mL) in THF (22 mL) was cooled to −78°C and, after stirring for 10 min, n-butyllithium (12.78 mL, 2.5 *M* in hexane) was added dropwise. After the slow addition of **7** (4.0 g, 7 mmol) in THF (10 mL), the solution was stirred for 0.5 h. A quenching solution (triethylamine (1.86 mL), THF (8 mL), and chlorotrimethylsilane (5.4 mL)) was prepared in a flame-dried centrifuge tube, sealed with a syringe cap, and purged with nitrogen. After centrifugation for 10 min, the clear solution was transferred to the reaction mixture using a syringe and the mixture stirred for 1 h at −78°C before it was allowed to warm to room temperature and stirred for 3 h. The mixture was cooled to 0°C, cold saturated Na_2CO_3 solution (60 mL) was added with vigorous stirring, and the product isolated by pentane extraction (4 × 40 mL). The combined extracts were washed with saturated Na_2CO_3, then with saturated NaCl solution, dried over $MgSO_4$, and the solvent removed by evaporation. Short path distillation of the residue gave **8** (5.81 g, 98%), bp ~ 92–94°C/0.4 Torr (1 Torr = 133.3 Pa); ir ($CHCl_3$): 1610, 1315, 1250, 850 cm^{-1}. *Exact Mass* calcd. for $C_{13}H_{22}OSi$: 222.1440; found: 222.1445.

Cyclopropanation of 8 and (9)

Anhydrous ether (5 mL) and methylene iodide (2.05 g, 7.7 mmol) were added to a flame-dried flask containing Zn/Ag couple (0.88 g) and the mixture refluxed for 15 min before the addition of **8** (1.00 g, 4.5 mmol) in anhydrous ether (5 mL). After heating under reflux for 18 h, the mixture was cooled to 0° and pyridine (2 mL) was added

Can. J. Chem. Downloaded from www.nrcresearchpress.com by 210.87.254.42 on 09/06/12
For personal use only.

slowly. The solids were removed by filtration and washed with ether (20 mL). The ether solution was dried over Na_2SO_4 before removal of the solvent by evaporation. Bulb-to-bulb distillation of the residue gave a single product, **9** (bp ~ 70°C/0.2 Torr, 1.00 g, 94%); ir ($CHCl_3$): 1250, 840 cm^{-1}. *Exact Mass* calcd. for $C_{14}H_{24}OSi$: 236.1596; found: 236.1596.

*Tricyclo[5.3.1.0^{2,6}]undecan-8-one (**10**)*

A solution of **9** (3.47 g, 14.7 mmol) in methanolic NaOH (66 mL, 3.13 *M* in NaOH) was stirred at ice temperature for 26 h, after which time 10% NaCl solution (50 mL) was added and the product extracted with pentane (4 × 40 mL). The pentane extracts were washed with 10% NaCl (2 × 30 mL), and water (2 × 30 mL). The aqueous extracts were extracted again with pentane (2 × 50 mL) and the combined extracts dried over $MgSO_4$. Removal of the pentane gave a clear oil (2.31 g, 96%) which was >99% pure **10** by glc analysis; ir ($CHCl_3$): 1705 cm^{-1}. *Exact Mass* calcd. for $C_{11}H_{16}O$: 164.1201; found: 164.1199.

*9,9-Dimethyltricyclo[5.3.1.0^{2,6}]undecan-8-one (**3**)*

To a stirred suspension of $NaNH_2$ (1.78 g, 46 mmol) in dry Et_2O (50 mL) under nitrogen was added **10** (1.50 g, 9.2 mmol) and the mixture gently refluxed for 3 h. Methyl iodide (1.14 mL, 18 mmol) was added slowly and three further additions of CH_3I (1.14 mL) were made after 2, 9, and 5-h reflux periods; finally the mixture was gently refluxed for 3 h. After cooling to 0°C and the addition of 10% NaCl solution (40 mL) slowly, the product was isolated by pentane extraction (4 × 35 mL) as a viscous colorless liquid (1.56 g, 89%), >99% pure by glc analysis; ir ($CHCl_3$): 1710 cm^{-1}. *Exact Mass* calcd. for $C_{13}H_{20}O$: 192.1514; found: 192.15135.

*Rearrangement of **3** to* cis,anti,cis-*4,4-dimethyltricyclo[6.3.0.0^{2,6}]-undecan-5-one (**4**)*

Our general procedure for homoenolization studies (7) was employed whereby a solution of **3** in *t*-BuO^-/*t*-BuOH (H_2O content ~ 30 μg/mL, made by dissolving potassium metal in dry *t*-BuOH) was prepared under nitrogen having a molar ratio of ketone/*t*-BuO^-/*t*-BuOH of 1:4:40. Aliquots were quickly transferred to predried, thick-walled glass tubes which were degassed and sealed under vacuum before heating. After cooling, the reaction mixture was diluted with 10% NaCl and the neutral product isolated by ether extraction. The extracts were washed with 10% NaCl, dried over $MgSO_4$, and the solvent evaporated to afford a pale yellow oil which was examined by glc (6% FFAP). The product was a two-component mixture, separable by preparative glc, containing **3** and a new ketone **4**; ir ($CHCl_3$): 1738 cm^{-1}; ^{13}Cmr ($CDCl_3$) δ_C: 24.8, 25.2 (2 × CH_3), 26.7, 33.7, 34.2, 35.5, 43.8 (5 × CH_2), 44.2, 46.1, 51.4, 52.0 (4 × CH), 47.1 (quat C), 224.6 (C=O). *Exact Mass* calcd. for $C_{13}H_{20}O$: 192.1514; found: 192.1519.

Experiments at 185°C indicated the half-life for the conversion of **3** → **4** to be ca. 120 h, which was reduced to ca. 30 h at 200°C. After 140 h at 200°C only traces of **3** were detectable by glc.

*Trimethylsilyl enol ethers of Δ^3- and Δ^4-**12** (**13**a,b)*

A 30:70 mixture of **12***a* and *b* (3 g, 20 mmol), prepared in 72% yield from dicyclopentadiene following literature procedures (11, 12), was dissolved in THF (5 mL) and added by syringe to a stirred solution of diisopropylamine (3.6 mL) in THF (10 mL) containing *n*-butyllithium (9 mL, 2.3 *M* in hexane), maintained at −78°C. Stirring was continued for 0.5 h during which time a quenching solution (Et_3N (2.4 mL), THF (18 mL), and trimethylsilyl chloride (4.8 mL)) was prepared in a flame-dried centrifuge tube as described for **8**, and then the clear solution was added to the reaction mixture. After isolation of the crude product as above for **8**, bulb-to-bulb distillation furnished a 30:70 mixture of **13***a,b* (4.2 g, 95%); ir ($CHCl_3$): 1610, 1320, 1250, 850 cm^{-1}. *Exact Mass* calcd. for $C_{13}H_{20}OSi$: 220.1284; found: 220.1280.

*Cyclopropanation of **13**a,b (**14**a,b)*

Following the procedure described above for **9**, the reagent was prepared in dry ether (15 mL) using 4.15 g of Zn/Ag couple and 9.4 g of CH_2I_2 and cooled to room temperature before the addition of the mixture of **13***a,b* (7.0 g). The reaction mixture was stirred at room temperature for 18 h and cooled to 0°C before pyridine (5.5 g) was added. Bulb-to-bulb distillation (75°C/0.2 Torr) of the crude product afforded **14***a,b* (6.13 g, 85%); ir ($CHCl_3$): 1240, 865, 830 cm^{-1}. *Exact Mass* calcd. for $C_{14}H_{22}OSi$: 234.1440; found: 234.1432.

*Δ^3- and Δ^4-tricyclo[5.3.1.0^{2,6}]undecan-8-one (**15**a,b)*

Ketonization of **14***a,b* (6.1 g) was accomplished with aqueous NaOH (10 mL, 2 *M*) and methanol (50 mL) at 0°C for 24 h and the product isolated as described for **10**. The glc analysis indicated a single product and bulb-to-bulb distillation (80°C/0.3 Torr) furnished 3.68 g (87%) of **15***a,b*; ir ($CHCl_3$): 1700 cm^{-1}. *Exact Mass* calcd. for $C_{11}H_{14}O$: 162.1045; found: 162.1042.

*Δ^3- and Δ^4-9,9-dimethyltricyclo[5.3.1.0^{2,6}]undecan-8-one (**5**a,b)*

To a stirred suspension of $NaNH_2$ (6.0 g, 0.154 mol) in dry Et_2O (50 mL) under nitrogen was added **15***a,b* (5.0 g, 0.031 mol) and the mixture refluxed for 3 h. After cooling to room temperature, methyl iodide (27 g, 0.19 mol) was added slowly along with more Et_2O (20 mL) and this mixture refluxed for 15 h before cooling to room temperature. Methyl iodide (8 g, 0.056 mol) was added and then refluxing continued for 3 h. The product was isolated by ether extraction as described for **3**. Bulb-to-bulb distillation (80°C/0.3 Torr) furnished **5***a,b* (4.89 g, 83%); glc analysis indicated the presence of a single component; ir ($CHCl_3$): 1705 cm^{-1}. *Exact Mass* calcd. for $C_{13}H_{18}O$: 190.1358; found: 190.1349.

*Rearrangement of **5**a,b (**6**a,b)*

Our general procedure for homoenolizations, described above, was employed using 30:70 mixtures of **5***a,b* and the neutral product, isolated by pentane extraction in 70–80% yield, was examined by glc. Two prominent bands, the ratios of which varied with reaction time, were evident. One was found, by ^{13}Cmr, to contain a mixture of the initial ketones differing only from the starting material in terms of the ratio of **5***a/b*; with increasing reaction times the ratio approached 50:50 but the rate of approach was not determined. The second band also contained a mixture of two ketones on the basis of its ^{13}Cmr spectrum; ir ($CHCl_3$): 1736 cm^{-1}; ^{13}Cmr ($CDCl_3$) δ: 24.8, 25.1(2), 25.2 (4 × CH_3), 33.3, 36.6, 40.5, 41.4, 43.6, 44.1 (6 × CH_2), 41.4, 44.1, 47.6, 48.4, 51.4, 51.6, 52.4, 58.5 (8 × CH), 129.5, 130.1, 133.5, 133.9 (4 × —CH=), 47.1 (2 quat C), 224.7, (2C=O). *Exact Mass* calcd. for $C_{13}H_{18}O$: 190.1358; found: 190.1351. The ratio of these two ketones (**6***a,b*) was close to 50:50 but was not precisely determined. The half-life for conversion of **5** → **6** was ca. 225 h at 185°C and ca. 75 h at 205°C. All attempts to separate **6***a* and *b* by glc were uniformly unsuccessful.

Additional evidence that the carbon skeleton is as assigned was provided by the ^{13}C spectrum of the alcohol mixture produced by LAH reduction. A sample of **6***a,b* (39 mg) was added to a mixture of LAH (39 mg) in THF (3 mL) and the mixture refluxed for 8 h. After isolation by ether extraction the product (39 mg) was examined by tlc (n-pentane/EtOAc, 95:5) which showed one major and one very minor spot. Bulb-to-bulb distillation (85°C/0.3 Torr) gave a colorless oil (34 mg, 87%) and the ^{13}C spectrum indicated the presence of two alcohols in a 55:45 ratio giving rise to the following signals ($CDCl_3$). δ: (major component) 19.8, 26.6 (2 × CH_3), 36.9, 38.4, 46.5 (3 × CH_2), 40.9, 42.7, 51.2, 60.0, 85.6 (5 × CH), 42.6 (quat C), 128.3, 135.3 (2 olefinic CH); (minor component): 20.7, 27.3 (2 × CH_3), 36.5, 39.8, 45.9 (3 × CH_2), 47.4, 51.1, 52.3, 52.6, 87.4 (5 × CH), 44.0 (quat C), 129.0, 135.4 (2 olefinic CH).

*Δ^3- and Δ^4-*cis,anti,cis-*10,10-dimethyltricyclo[6.3.0.0^{2,6}]undecane (**17**)*

A mixture of **6***a,b* (250 mg, 1.3 mmol), hydrazine hydrate (705 mg, 13 mmol), KOH (1.11 g), and diethylene glycol (10 mL) was placed in a thick-walled glass tube; the tube was sealed and heated at 182°C for 64 h. After cooling and dilution with H_2O (10 mL), the reaction mixture was extracted with Et_2O (3 × 10 mL) and the extracts washed with water before drying over $MgSO_4$. Evaporation of the ether gave an oil (228 mg) which was purified by chromatography on silica gel,

Can. J. Chem. Downloaded from www.nrcresearchpress.com by 210.87.254.42 on 09/06/12
For personal use only.

elution with n-pentane, to furnish a colorless oil (206 mg, 90%) characterized as **17***a,b*; ^{13}Cmr ($CDCl_3$) δ: 27.8, 29.2, 29.6, 30.6 (4 × CH_3), 39.0, 39.1, 39.8, 40.9, 47.5, 47.9, 48.3, 49.6 (8 × CH_2), 40.9, 44.0(2), 48.0, 48.7, 52.9, 53.9, 59.3 (8 × CH), 128.1, 129.1, 135.3, 135.6 (4 × —CH=), 41.6, 41.0 (2 × quat C). *Exact Mass* calcd. for $C_{13}H_{20}$: 176.1565; found: 176.1562.

Preparation of ***18***a,b

The mixture of **17** isomers (200 mg, 1.14 mmol) was dissolved in CH_2Cl_2 (10 mL) and cooled in an ice-bath before the addition of *m*-chloroperbenzoic acid (237 mg, 1.37 mmol). This mixture was stirred at room temperature for 16 h, at which point tlc indicated the absence of starting material. Excess peracid was destroyed by the addition of 10% sodium sulfite solution (negative starch–iodide test) before washing with 10% $NaHCO_3$ solution (3 × 20 mL), water, and finally with saturated NaCl solution. The organic layer was dried over $MgSO_4$ and the solvent evaporated to leave an oil which was purified by bulb-to-bulb distillation (70°C/1 Torr) to furnish a 50:50 mixture of **18***a,b* (185 mg, 85%) which was used directly for the next step; ^{13}Cmr ($CDCl_3$) δ: 26.7, 28.4, 29.0, 29.8 (4 × CH_3), 33.3, 33.4, 33.5, 39.2, 47.8, 48.2, 48.7, 49.6 (8 × CH_2), 42.9, 43.5, 44.4, 44.5, 45.7, 45.9, 48.2, 52.2, 56.6, 58.4, 60.0, 61.1 (12 × CH), 41.1(2) (2 quat C).

Cleavage of ***18***a,b *(****19****a,b)*

The mixture of epoxides **18***a,b* (175 mg, 0.9 mmol) was added to a solution of LAH (171 mg, 4.5 mmol) in dry Et_2O (25 mL) and the reaction mixture was refluxed overnight. After the cautious destruction of the excess LAH with 5% NaOH solution, the ether layer was separated, washed with H_2O (3 × 10 mL), and dried over $MgSO_4$. Removal of the ether gave a clear oil (175 mg, 99%) which was judged to consist mainly of two major alcoholic components (**19***a,b*) in equal amounts together with a small amount (<5%) of a third alcohol on the basis of its ^{13}C spectrum; ^{13}Cmr ($CDCl_3$) δ: 28.1, 28.5, 29.9, 30.1 (4 × CH_3), 29.3, 30.0, 30.7, 34.8, 35.1, 36.7, 40.9, 47.7, 48.0, 48.7 (10 × CH_2), 42.8, 43.8, 44.1, 48.8, 49.7, 51.4, 53.6, 60.8 (8 × CH), 79.1, 80.0 (2 × —CHOH), 41.1, 41.6 (quat C). The total product was used directly for the next step.

Oxidation of ***19***a,b *(****20****a,b)*

The above mixture of alcohols **19***a,b* (175 mg, 0.9 mmol) was dissolved in acetone (5 mL) and titrated with Jones' reagent until the brown color persisted. Isolation by ether extraction afforded a crude product (160 mg, 92%) consisting of a mixture of isomeric ketones; ir ($CHCl_3$): 1735 cm^{-1}. *Exact Mass* calcd. for $C_{13}H_{20}O$: 192.1514; found: 192.1512. All attempts to separate this mixture by glc were unsuccessful but hplc examination indicated the presence of two major components and a minor one in an approximate ratio of 10:10:1. Although poorly resolved, hplc on a semipreparative scale (Prep LC 500 system, semiprep column, silica gel, hexane/CH_2Cl_2 60:1, flow rate 0.1 L/min) furnished small samples of the two major components which, on the basis of their ^{13}Cmr spectra, were reasonably pure (>98%). Fraction 1, **20***a* (49 mg), ir ($CHCl_3$): 1735 cm^{-1}; ^{1}Hmr ($CDCl_3$) δ: 0.9 (s, 3H), 1.04 (s, 3H), 1.0–3.0 complex absorption, 14H with discernible multiplets centred at 1.4 (1H), 2.2 (1H), 2.28 (3H), 2.69 (1H), 2.85 (1H), 2.95 (1H); ^{13}Cmr ($CDCl_3$) δ: 26.6, 28.9 (2 × CH_3), 23.8, 35.8, 37.0, 48.0, 49.1 (5 × CH_2), 40.6, 43.9, 45.9, 61.3 (4 × CH), 41.1 (quat C), 222.7 (C=O). Fraction 2, **20***b* (32 mg), ir ($CHCl_3$): 1735 cm^{-1}; ^{1}Hmr ($CDCl_3$) δ: 0.92 (s, 3H), 1.04 (s, 3H), 1.0–1.15 (m, 2H), 1.5–3.0 (multiplets, 12H); ^{13}Cmr ($CDCl_3$) δ: 27.1, 29.1 (2 × CH_3), 26.9, 34.9, 38.1, 48.4, 48.5 (5 × CH_2), 44.1, 49.6, 50.4, 53.0 (4 × CH), 41.6 (quat C), 222.1 (C=O).

cis, anti, cis-*4,4-Dimethyltricyclo[6.3.0.0^{2,6}]undecane (****21****)*

A sample (21 mg, 0.109 mmol) of the product from the preceding reaction, hydrazine hydrate (54 mg, 1.1 mmol), KOH (108 mg, 1.91 mmol), and diethylene glycol (0.5 mL) were placed in a thick-walled glass tube; the tube was sealed and heated at 182°C for 60 h. After cooling and dilution with H_2O (5 mL), the reaction mixture was extracted with Et_2O (3 × 10 mL) and the extracts washed with H_2O before drying over $MgSO_4$. After removal of the ether, the residual oil was passed through a short column (1 × 5 cm) of SiO_2 with n-pentane (30 mL) as eluent to furnish **21** (13 mg, 65%) as a colorless oil; ^{1}Hmr ($CDCl_3$) δ: 0.84 (s, 3H, Me), 1.00 (s, 3H, Me), 1.0–2.8 (complex absorption, 16H); ^{13}Cmr ($CDCl_3$) δ_C: 28.1, 29.9 (2 × CH_3), 25.8, 32.0, 33.3, 39.8, 49.1, 49.0 (6 × CH_2), 44.0, 44.2, 50.9, 52.1 (4 × CH), 41.2 (quat C); *m/e* relative intensity): 178 (M^+, 10), 163 (42), 122 (100), 95 (26), 93 (31), 81 (49), 67 (33). *Exact Mass* calcd. for $C_{13}H_{22}$: 178.17215; found: 178.17227.

In an analogous experiment, a sample of **4** (63 mg, 0.33 mmol) was heated at 185°C for 57 h with hydrazine hydrate (170 mg, 3.4 mmol), KOH (280 mg, 5 mmol), and diethylene glycol (3.5 mL) in a sealed, thick-walled Pyrex tube. After cooling to 0°C, the tube was opened and the contents washed from the tube with 10% aqueous NaCl (6 mL). This solution was acidified with 50% aqueous HCl and extracted with pentane (3 × 10 mL). The combined extracts were washed with 10% aqueous NaCl solution (2 × 8 mL) and dried over $MgSO_4$. Removal of the pentane by distillation gave a colorless oil (58 mg, 99%) which was identical to **21** described above.

Acknowledgements

We are grateful for the financial support of this project provided by the Natural Sciences and Engineering Research Council of Canada through operating grants and a scholarship (A.J.R.). We wish to thank Professor R.D. Little for kindly providing a 300-MHz proton spectrum and the ^{13}Cmr data for ketone **20***a*.

1. W. A. AYER and L. M. BROWNE. Tetrahedron, **37**, 2199 (1981); R. D. LITTLE and G. W. MULLER. J. Am. Chem. Soc. **101**, 7129 (1979).
2. S. NOZOE, J. FURUKAWA, U. SANKAWA, and S. SHIBATA. Tetrahedron Lett. 195 (1976).
3. R. D. LITTLE and G. W. MULLER. J. Am. Chem. Soc. **103**, 2744 (1981) and references therein.
4. G. MEHTA and A. V. REDDY. J. Chem. Soc. Chem. Commun. 756 (1981); S. MISUMI, H. MATSUSHIMA, H. SHIRAHAMA, and T. MATSUMOTO. Chem. Lett. 855 (1982); S. V. LEVY and P. J. MURRAY. J. Chem. Soc. Chem. Commun. 1252 (1982); P. A. WENDER and J. J. HOWBERT. Tetrahedron Lett. **23**, 3983 (1982).
5. B. A. DAWSON, A. K. GHOSH, J. L. JURLINA, and J. B. STOTHERS. J. Chem. Soc. Chem. Commun. 204 (1983).
6. T. C. FELINE, G. MELLOWS, R. B. JONES, and L. PHILLIPS. J. Chem. Soc. Chem. Commun. 63 (1974).
7. A. L. JOHNSON, N. O. PETERSEN, M. B. RAMPERSAD, and J. B. STOTHERS. Can. J. Chem. **52**, 4143 (1974).
8. Y. HOYANO, V. PATEL, and J. B. STOTHERS. Can. J. Chem. **58**, 2730 (1980).
9. E. J. COREY, R. HARTMANN, and R. A. VATAKENCHERRY. J. Am. Chem. Soc. **94**, 2611 (1962).
10. B. A. DAWSON and J. B. STOTHERS. Org. Magn. Reson. **21**, 217 (1983).
11. S. J. CRISTOL, W. K. SEIFERT, and S. B. SOLWAY. J. Am. Chem. Soc. **82**, 2351 (1960).
12. H. C. BROWN, C. P. GARG, and K. T. LIU. J. Org. Chem. **36**, 387 (1971).
13. S. L. PATT and J. M. SHOOLERY. J. Mag. Reson. **46**, 535 (1982).
14. G. A. MORRIS and R. FREEMAN. J. Am. Chem. Soc. **107**, 760 (1979).
15. J. E. HOLENSTEIN, A. STOESSL, H. KERN, and J. B. STOTHERS. Can. J. Chem. **62**, 1971 (1984).
16. V. DAVE, J. B. STOTHERS, and E. W. WARNHOFF. Can. J. Chem. **62**, 1965 (1984).

Evidence for molecular complexes in the mechanism of additions of iodine monochloride to alkenes

GEORGE H. SCHMID[1] AND JAMES W. GORDON

Department of Chemistry, University of Toronto, Toronto, Ont., Canada M5S 1A1

Received February 8, 1984

This paper is dedicated to Professor Peter Yates on the occasion of his 60th birthday

GEORGE H. SCHMID and JAMES W. GORDON. Can. J. Chem. **62**, 2526 (1984).

Immediately upon mixing ICl and 2,3-dimethyl-2-butene in CCl_4 at 25°C a new absorption band due to an alkene−ICl molecular complex appears at 295 ± 5 nm and decreases rapidly with time. The rate law under conditions of $(alkene)_0 \gg (ICl)_0$ for the electrophilic addition of ICl to 2,3-dimethyl-2-butene, *E*- and *Z*-2-butene, and *E*- and *Z*-1-phenylpropene is $-d(ICl)/dt = k_{expt}(alkene)(ICl)^3/\{1 + K_{AD}(alkene)\}^3$ where K_{AD} is the equilibrium constant for the formation of a 1:1 alkene−ICl molecular complex. The addition of ICl to the *Z* and *E* isomers of 2-butene and 1-phenylpropene occurs by *anti*-stereospecific addition. The negative enthalpy of activation for the addition of ICl to 2,3-dimethyl-2-butene is evidence that one or more complexes are involved on the reaction coordinate prior to the rate-determining step. On the basis of analysis of the enthalpy changes during the reaction, it is proposed that both a 1:1 and a 1:2 alkene−ICl molecular complex is involved in the mechanism prior to the rate-determining step.

GEORGE H. SCHMID et JAMES W. GORDON. Can. J. Chem. **62**, 2526 (1984).

Dès que l'on mélange du ICl et du diméthyl-2,3 butène-2 dans du CCl_4 à 25°C, il y a apparition, à 295 ± 5 nm, d'une nouvelle bande d'absorption qui est due à un complexe moléculaire alcène−ICl; l'intensité de cette bande diminue rapidement avec le temps. La loi de vitesse qui s'applique, si $(alcène)_0 \gg (ICl)_0$, pour l'addition électrophile de ICl sur le diméthyl-2,3 butène-2, sur les butènes-2 (*E* ou *Z*) ou sur les phényl-1 propènes (*E* ou *Z*) est $-d(ICl)/dt = k_{expt}(alcène)(ICl)^3/\{1 + K_{AD}(alcène)\}^3$, où K_{AD} est la constante d'équilibre pour la formation d'un complexe moléculaire 1:1 alcène−ICl. La stéréochimie de l'addition du ICl sur les isomères *E* et *Z* du butène-2 et du phényl-1 propène est stéréospécifiquement *anti*. Le fait que l'enthalpie d'activation de l'addition du ICl sur le diméthyl-2,3 butène-2 soit négative est une preuve qu'un ou plusieurs complexes sont impliqués dans les coordonnées de la réaction avant d'atteindre l'étape déterminante. Sur la base d'une analyse des changements d'enthalpie au cours de la réaction, on propose que des complexes moléculaires alcène−ICl 1:1 ainsi que 1:2 sont impliqués dans le mécanisme avant d'atteindre l'étape déterminante.

[Traduit par le journal]

Can. J. Chem. Downloaded from www.nrcresearchpress.com by 210.87.254.42 on 09/06/12
For personal use only.

The stoichiometry of the addition of iodine monochloride (ICl) to alkenes is 1:1 in a number of solvents (1−5). Because of this fact, solutions of ICl in acetic acid (Wijs' solution) are used to determine iodine values of fats and oils (6). Despite such widespread use, little work has been done on the kinetics and mechanism of this addition of ICl to alkenes and some of the work is contradictory. White and Robertson (1) reported that the addition of ICl to allyl acetate in acetic acid follows an overall third-order rate law, first order in alkene and second order in ICl. A similar rate law was reported by Viswanathan and co-workers (2) for ICl addition to some allyl and vinyl compounds in acetic acid, and by Sergeev and Smirnov (3) for the addition of ICl to both cyclohexene and 1-hexene in CCl_4. In contrast, Heublein (4) reported a second-order rate law, first order in both ICl and alkene, for the addition of ICl to *trans*-stilbene in acetic acid, dibutyl ether, and acetonitrile.

The products of addition of ICl to alkenes are sometimes formed by *anti*-stereospecific addition (4−7), while in other cases by *anti*-stereoselective addition (8). Regiospecific addition to styrene (9) is reported, while nonregiospecific addition occurs to 1-hexene (10). Furthermore, solvent incorporated (10) and rearranged products have also been reported (11).

The work reported in the literature is fragmented, with each worker or group of workers employing different compounds and different solvent systems. Frequently only the rates of addition with no product study are carried out or vice versa. It is clear that a systematic study of both the rates and products of this reaction is long overdue. We have undertaken such a study. In this first paper we report the rate law, the effect of temperature on the rate, and the stereo- and regiochemistry of the addition of ICl to 2,3-dimethyl-2-butene, *E*- and *Z*-1-phenylpropene, and *E*- and *Z*-2-butene.

[1]Author to whom correspondence may be addressed.

Results and discussion

Kinetic and thermochemical study

The rate of addition of ICl to 2,3-dimethyl-2-butene in CCl_4 at 25°C was measured by monitoring the disappearance with time of ICl at 460 nm by means of a Durrum−Gibson stopped-flow spectrophotometer. The rate measurements were made with $(alkene)_0 \gg (ICl)_0$.

Immediately on mixing ICl and 2,3-dimethyl-2-butene a new absorption band, absent in either reactant or product, appears at 295 ± 5 nm and decreases rapidly with time. This new band is attributed to the presence of an intermediate ICl−alkene molecular complex. Reversible formation of labile molecular complexes between alkenes and halogens are well documented (2). While fewer data are available for alkene−interhalogen complexes, cyclohexene and 1-hexene are known to form molecular complexes with ICl in CCl_4 at room temperature, characterized by absorbances at 267 and 257 nm respectively (3). The molecular complexes of ICl and several allyl and vinyl compounds have characteristic absorbances in dry acetic acid in the region 290−310 nm (2). The position of the band for the complex of ICl and 2,3-dimethyl-2-butene at longer wavelength (295 nm), compared to the complexes of ICl and cyclohexene (267 nm) and 1-hexene (257 nm), is expected for the more highly substituted alkene (12*a*). Thus we conclude that the band at 295 nm in CCl_4 at 25°C is consistent with the formation of a molecular complex between ICl and 2,3-dimethyl-2-butene.

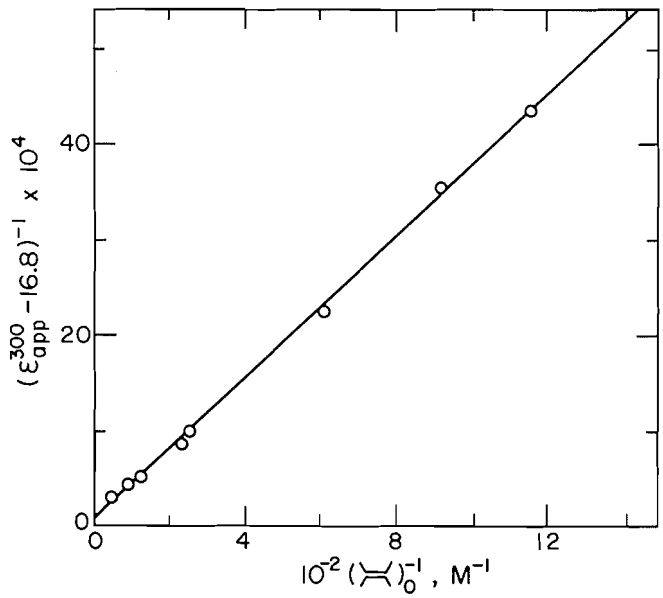

FIG. 1. Ketelaar plot for the 2,3-dimethyl-2-butene-ICl system measured at 300 nm in CCl_4 at 25°C.

The Ketelaar equation (13) was used to obtain the equilibrium constant for the formation of the molecular complex, K_{AD}. Briefly, the method is to measure the variation of initial absorbance values with varying initial concentrations of alkene under conditions where $(\text{alkene})_0 \gg (\text{ICl})_0$. The analysis was carried out in CCl_4 at 25°C and at 300 nm. The equation is as follows:

$$[1] \quad \frac{1}{\epsilon_{app} - \epsilon_{ICl}} = \frac{1}{\epsilon_{AD} - \epsilon_{ICl}} + \frac{1}{K_{AD}(\epsilon_{AD} - \epsilon_{ICl})(\text{alkene})_0}$$

where ϵ_{app} is the apparent extinction coefficient and ϵ_{AD} is the extinction coefficient of the molecular complex. The apparent extinction coefficient is defined by eq. [2].

$$[2] \quad \epsilon_{app} = \text{Abs}_0\, l^{-1}\, (\text{ICl})_0^{-1}$$

The straight line obtained by plotting $1/(\epsilon_{app} - \epsilon_{ICl})$ versus $1/(\text{alkene})_0$ is shown in Fig. 1. Values of $K_{AD} = 19 \pm 6\ M^{-1}$ and $\epsilon_{AD} = 1.4 \pm 0.5 \times 10^4\ M^{-1}\ \text{cm}^{-1}$ are obtained from the values of the slope, intercept with the ordinate axis, and their ratio. The value of K_{AD} obtained in this study is larger than the value of $2\ M^{-1}$ for the equilibrium constant of the formation of the molecular complex in the reaction of 1-hexene and ICl in CCl_4 at 25°C obtained by Sergeev *et al.* (14*a*).

If it is assumed that the ICl–alkene molecular complex is rapidly established relative to the rate of addition of ICl (14*b*), then Beer's law (eq. [3]) will be valid for the total or stoichiometric ICl concentration at all times t under the conditions $(\text{alkene})_0 \gg (\text{ICl})_0$.[2]

$$[3] \quad \text{Abs}_t - \text{Abs}_\infty = \epsilon_{app} l (\text{ICl})_t$$

The pseudo-order rate law, eq. [4], is third order with respect to ICl.

$$[4] \quad -\text{d(ICl)}/\text{d}t = k_{app}(\text{ICl})_t^3$$

Substituting eq. [3] into the integrated form of eq. [4] and rearranging gives the pseudo-order experimental rate equation [5].

$$[5] \quad (\text{Abs}_t - \text{Abs}_\infty)^{-2} = \{\epsilon_{app} l (\text{ICl})_0\}^{-2} + \{2k_{app}/(\epsilon_{app} l)^2\}t$$

The plot of a typical run is given in Fig. 2. The apparent pseudo-order rate constant is readily calculated from the intercept, slope, and $(\text{ICl})_0$. As shown by the data in Table 1, there is no apparent trend in the values of the slope as required by eq. [4] for a series of solutions of constant $(\text{alkene})_0$ and varying $(\text{ICl})_0$. Furthermore, the values of K_{app} are not dependent on the wavelength used to follow the kinetics.

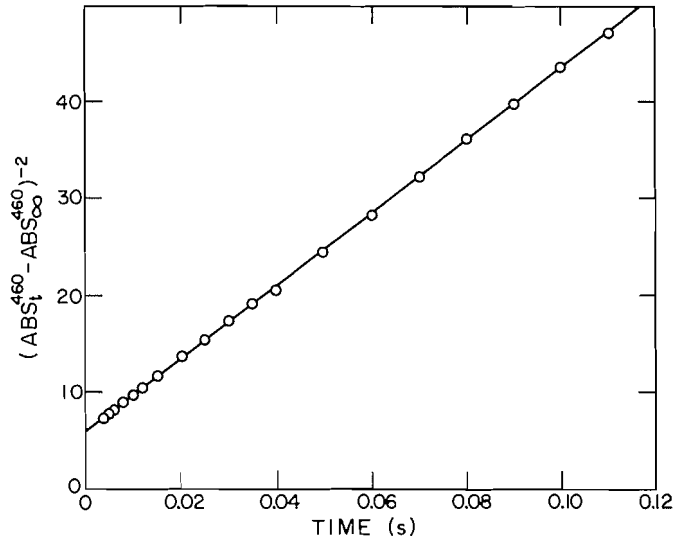

FIG. 2. Third-order kinetic plot for the addition of ICl to 2,3-dimethyl-2-butene in CCl_4 at 25°C.

TABLE 1. Slope and intercept obtained by fitting eq. [4] to the data from the reactions of a series of solutions of constant $(2,3\text{-dimethyl-2-butene})_0 = 0.1188\ M$ and varying $(\text{ICl})_0$ in CCl_4 at 25°C

$(\text{ICl})_0$ $(M) \times 10^3$	Intercept	Slope
5.59	2.74	620
3.31	7.55	415
2.24	15.8	500
1.68	19.3	396
1.33	32.9	425
1.12	51.1	410

The initial concentration of alkene was varied over the range from $3.33 \times 10^{-3}\ M$ to $4.25 \times 10^{-1}\ M$ to determine the dependence of alkene in the rate law. Equation [6] describes the experimentally observed variation of the pseudo-third-order rate constant k_{app} with initial alkene concentration where C_1 and C_2 are constants.

$$[6] \quad \frac{C_1(\text{alkene})_0}{\{1 + C_2(\text{alkene})_0\}^3} = k_{app}$$

The linear plot of $\{(\text{alkene})_0/k_{app}\}^{1/3}$ versus $(\text{alkene})_0$ is shown in Fig. 3. From the intercept and the ratio of slope to intercept, values of $C_1 = 9 \pm 1 \times 10^8\ M^{-3}\ \text{s}^{-1}$ and $C_2 = 17.8 \pm 0.8\ M^{-1}$ are obtained.

The complete rate law describing the rate of addition of ICl to 2,3-dimethyl-2-butene in CCl_4 at 25°C in terms of their total

[2]The symbol (X) represents the total, stoichiometric, or analytical concentration of X in solution in mol/L; [X] represents the free, uncomplexed concentration of X in solution in mol/L.

Can. J. Chem. Downloaded from www.nrcresearchpress.com by 210.87.254.42 on 09/06/12
For personal use only.

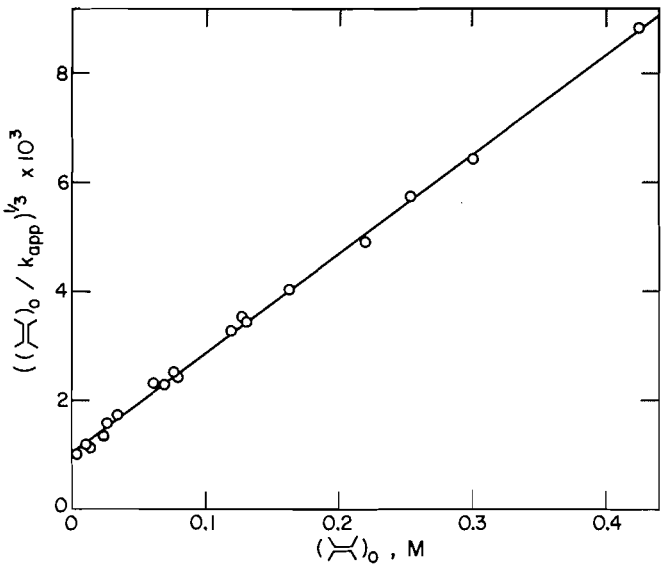

FIG. 3. Experimental test of eq. [6] for the addition of ICl to 2,3-dimethyl-2-butene in CCl_4 at 25°C.

or stoichiometric concentrations is given in eq. [7] for $(\text{alkene})_0 \gg (\text{ICl})_0$. The constants C_1 and C_2 can be identified as a rate

$$[7] \quad -\text{d(ICl)}/\text{d}t = \frac{C_1(\text{alkene})_0(\text{ICl})^3}{\{1 + C_2(\text{alkene})_0\}^3}$$

constants k and K_{AD} respectively in the following way. Equations [8] and [9] relate the stoichiometric and free concentrations of both 2,3-dimethyl-2-butene and ICl at time t under the condition $(\text{alkene})_0 \gg (\text{ICl})_0$. Comparison of eqs. [7] and [9]

$$[8] \quad [\text{alkene}] = (\text{alkene})_0$$

$$[9] \quad [\text{ICl}] = \frac{(\text{ICl})}{1 + K_{AD}(\text{alkene})_0}$$

strongly suggests that the experimental parameter C_2 be identified as the equilibrium constant K_{AD}. This assignment is further substantiated by the fact that the value of C_2 is identical within experimental error with the value of K_{AD} obtained independently from analysis of the initial absorbance data.

The experimental rate law can now be written in terms of the actual, free or uncomplexed, concentrations of ICl and 2,3-dimethyl-2-butene as given in eq. [10].

$$[10] \quad -\text{d(ICl)}/\text{d}t = k[\text{alkene}][\text{ICl}]^3$$

In eq. [10], the experimental parameter C_1 has been redefined as rate constant k. Since C_1 and C_2 are identified, the complete rate law when $(\text{alkene})_0 \gg (\text{ICl})_0$ can be written as given in eq. [11].

$$[11] \quad -\text{d(ICl)}/\text{d}t = \frac{k(\text{alkene})_0(\text{ICl})^3}{\{1 + K_{AD}(\text{alkene})_0\}^3}$$

The rate law given in eq. [11] is not unique to 2,3-dimethyl-2-butene since the additions of ICl to *E*- and *Z*-2-butene and *E*- and *Z*-1-phenylpropene in CCl_4 at 25°C follow exactly the same rate law. Treating the rate data in the same way as described for 2,3-dimethyl-2-butene allows us to determine the values of k and K_{AD} for both pairs of *Z* and *E* isomers. The data are summarized in Table 2.

The structure–reactivity pattern of these five compounds

TABLE 2. Values of k and K_{AD} for the addition of ICl to selected alkenes in CCl_4 at 25°C

Alkene	k (M^{-3} s^{-1})	K_{AD} (M^{-1})
E-$CH_3CH{=}CHCH_3$	$(2.27\pm0.06)\times10^7$	3.7±0.1
Z-$CH_3CH{=}CHCH_3$	$(7.1\pm0.4)\times10^7$	5.8±0.1
E-$C_6H_5CH{=}CHCH_3$	$(5.2\pm0.2)\times10^6$	1.4±0.1
Z-$C_6H_5CH{=}CHCH_3$	$(3.1\pm0.1)\times10^6$	1.4±0.1
$(CH_3)_2C{=}C(CH_3)_2$	$(9\pm1)\times10^8$	17.8±0.8

given in Table 2 is consistent with a reaction that occurs by an electrophilic addition mechanism (15). Further evidence for an ionic mechanism is the fact that the rate of addition is unaffected by the presence of small amounts of I_2. Furthermore, chlorocyclohexane is not formed when the addition of ICl to 2,3-dimethyl-2-butene is carried out in cyclohexane.

The product of the addition of ICl to alkenes reacts further with ICl to form a vicinal dichloro compound. This subsequent reaction has been shown to be much slower and does not compete with the fast addition of ICl to any of the alkenes reported here under conditions where $(\text{alkene})_0 \gg (\text{ICl})_0$ (16).

The observation of a molecular complex in the reaction of ICl and alkenes does not necessarily mean that it is on the reaction coordinate. In order to establish that the molecular complex is involved in the reaction, variation in k and K_{AD} with temperature was determined for the addition of ICl to 2,3-dimethyl-2-butene. The data are given in Table 3. The rate of the addition actually *decreases* with increasing temperature. Furthermore, the value of the enthalpy of activation is an extremely large negative value. Such temperature dependence of the rate of reaction is good evidence for a complex reaction mechanism (17). Thus the negative enthalpy of activation observed for this reaction may be taken as kinetic proof that a complex or several complexes are involved *on the reaction coordinate prior* to the rate determining transition site.

Product stereo- and regiochemistry

The products of the addition of ICl to *E*- and *Z*-2-butene and *E*- and *Z*-1-phenylpropene were examined to establish the stereo- and regiochemistry of this reaction in CCl_4 at 25°C. The addition to *Z*-2-butene forms a single adduct while addition to the *E* isomer also forms only one product whose ^1H nmr, given in Table 4, is different from that of the product of addition to the *Z* isomer. Such a result is consistent with a stereospecific addition of ICl. The *vicinal* methine H—H coupling constants (J_{ab}) of the products can be used to determine the stereochemistry of the adducts. Usually the *vicinal* methine H—H coupling constant in 1,2-disubstituted-1,2-dihaloethanes is larger for the *erythro* (or *meso*) than the corresponding *threo* (or *dl*) isomer (18). On this basis we can assign the *threo* configuration to the product of addition of ICl to *Z*-2-butene and the *erythro* configuration to the product formed by addition of ICl to *E*-2-butene.

To verify this stereochemical assignment the two adducts were independently synthesized by the series of reactions shown in Fig. 4. The addition of iodine to a mixture of *Z*-2-butene and yellow mercuric oxide in 80% aqueous acetonitrile forms *threo*-3-iodo-2-butanol. The *threo* configuration of the product was established by means of a base-induced ring closure reaction to form the epoxide. This reaction is known to occur with a single inversion of configuration at the carbon atom bearing the halogen atom (19). Thus treatment of *threo*-3-iodo-2-butanol with moist sodium aluminate in methylene

Can. J. Chem. Downloaded from www.nrcresearchpress.com by 210.87.254.42 on 09/06/12
For personal use only.

TABLE 3. Thermodynamic parameters obtained from the temperature dependence of k and K_{AD} for the addition of iodine monochloride to 2,3-dimethyl-2-butene in CCl_4

T(°C)	$10^{-8} \cdot k$ (M^{-3} s^{-1})	$\Delta H^{\ddagger}$(expt) (kcal mol^{-1})	$\Delta S^{\ddagger}$(expt) (cal deg^{-1} mol^{-1})	$K_{AD}(M^{-1})$	ΔH_{AD} (kcal mol^{-1})	ΔS_{AD} (cal deg^{-1} mol^{-1})
25.0	9±1			17.8±7		
34.7	3.8±0.6	−17	−75	11.3±7	−9	−24
43.0	1.8±0.2			7.6±4		

TABLE 4. ^{1}H nuclear magnetic resonance spectra of adducts of addition of ICl to E and Z isomers of 2-butene and 1-phenylpropene

Adduct	Configuration	Chemical shift (δ)[a] H^{α}	H^{β}	H^{γ}	H^{δ}	$J_{\beta,\gamma}$
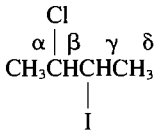	*erythro*	1.67d	3.96dq	4.23dq	2.00d	7.6
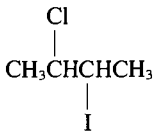	*threo*	1.62d	4.11dq	4.48dq	1.96d	3.0
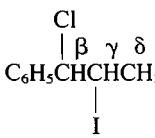	*erythro*	—	4.99d	4.50dq	2.12d	9.0
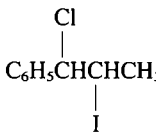	*threo*	—	4.96d	4.56dq	1.87d	6.0
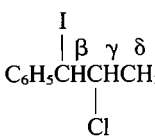	*erythro*	—	5.21d	4.30q	1.85d	10.0
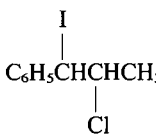	*threo*	—	5.10d	4.47dq	1.48d	6.5

[a]In ppm downfield from $(CH_3)_4Si$. Abbreviations are d = doublet, q = quartet, dq = double quartet.

chloride forms the known *cis*-2,3-dimethyloxirane (19*c*).

Reaction of *threo*-3-iodo-2-butanol with neat thionyl chloride forms 2-chloro-3-iodobutane whose ^{1}H nmr spectrum is identical to the product formed by addition of ICl to *Z*-2-butene. The configuration of the product of the thionyl chloride reaction is assigned on the basis of the mechanism of this reaction (20). In neat thionyl chloride, replacement of the hydroxy group by chloride occurs with retention of configuration. Retention of configuration is also expected because of the involvement of the iodine atom as a neighboring group (21). Consequently the product of the reaction of *threo*-3-iodo-2-butanol with neat thionyl chloride has the *threo* configuration.

The *erythro*-3-iodo-2-butanol was synthesized by an identical series of reactions starting with *E*-2-butene as shown in Fig. 4. The ^{1}H nmr spectrum of 2-chloro-3-iodobutane prepared in this way is identical to the product formed by the addition of ICl to *E*-1-butene. Thus these results are conclusive evidence that the addition of ICl to *Z*- and *E*-2-butene occurs in an *anti* stereospecific manner.

To determine the regiochemistry as well as the stereochemistry, the addition of ICl to *E*- and *Z*-1-phenylpropene was carried out. As in the case of the 2-butenes, the ^{1}H nmr spectrum of the product of addition to *Z*-1-phenylpropene is different than that of the product obtained by addition of *E*-1-phenylpropene as shown in Table 4. To unambigously determine the stereo- and regiochemistry of addition in this system,

Can. J. Chem. Downloaded from www.nrcresearchpress.com by 210.87.254.42 on 09/06/12
For personal use only.

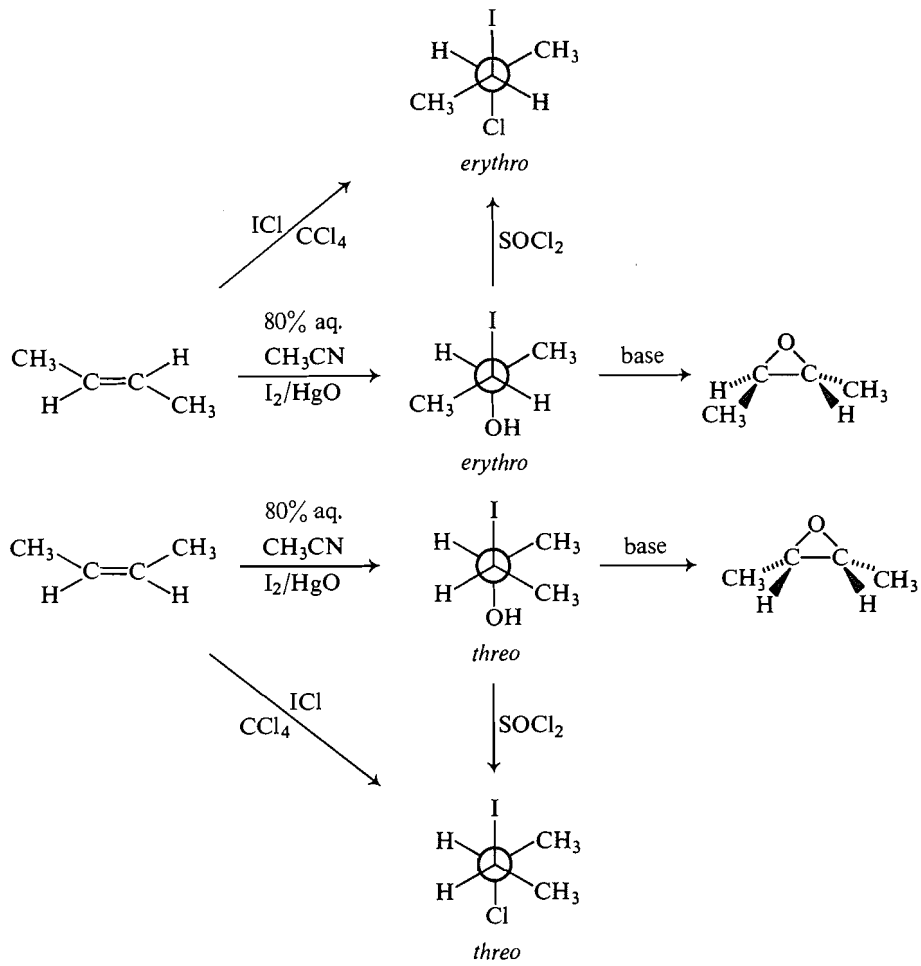

FIG. 4. Synthetic scheme for preparation of *erythro*- and *threo*-2- chloro-3-iodobutane.

it is necessary to prepare authentic samples of the four possible adducts: *erythro*- and *threo*-1-chloro-2-iodo-1-phenylpropane and *erythro*- and *threo*-2-chloro-1-iodo-1-phenylpropane. The synthesis of the two stereoisomers of 1-chloro-2-iodo-1-phenylpropane has been reported (16). The *threo* and *erythro* isomers of 2-chloro-1-iodo-1-phenylpropane were synthesized as shown in Fig. 5.

erythro-1-Chloro-1-phenyl-2-propanol was prepared from *E*-1-phenylpropene by using the oxymercuration reaction (22) followed by a chlorodemercuration reaction (23). Reaction of the chlorohydrin product with base forms *trans*-2-methyl-3-phenyloxirane. This reaction again establishes the configuration of the chlorohydrin as being *erythro*. The position of the chlorine atom in the chlorohydrin was established by means of the ring opening of *trans*-2-methyl-3-phenyloxirane by HCl. Such acid-catalyzed ring opening reactions of oxiranes are known to form the product resulting from the more stable carbonium ion (24). Thus the reaction of *trans*-2-methyl-3-phenyloxirane with aqueous concentration HCl forms a mixture of 45% *erythro*- and 55% *threo*-1-chloro-1-phenyl-2-propanol.

The treatment of *erythro*-1-chloro-1-phenyl-2-propanol with *o*-phenylene phosphorochloridite in pyridine followed by iodine in CCl_4 forms a mixture of 41% *threo*- and 59% *erythro*-2-chloro-1-iodo-1-phenylpropane (25). The same mixture of products could be prepared by the same series of reactions starting with *Z*-1-phenylpropene as shown in Fig. 5. The ^1H nmr spectra of these two compounds are different than those of *erythro*- and *threo*-1-chloro-2-iodo-1-phenylpropane. The data are summarized in Table 4.

The value of preparing all four stereo- and regioisomers is that we can now use well-established ^1H nmr relationships to verify their structure and stereochemistry. For a pair of *threo*–*erythro* stereoisomers, it is known that the methyl protons of the *threo* isomer of 1,2-disubstituted-2-arylpropanes are found at higher field than those of the *erythro* isomer (26). Thus the methyl protons of *threo*-1-chloro-2-iodo-1-phenylpropane are found at δ 1.87 while those of its *erythro* isomer are found further downfield at δ 2.12 ppm. A similar relationship exists between the *threo* (δ 1.48 ppm) and the *erythro* (δ 1.85 ppm) isomers of 2-chloro-1-iodo-1-phenylpropane. As well, the $J_{H,H}$ coupling constant of the *erythro* isomer is larger than that of the *threo* isomer. Thus the proton magnetic resonance spectra are in accord with our assignment of stereochemistry.

The chemical shift of a proton next to iodine is further downfield than the same proton next to chlorine (27). We can make use of this relationship to verify the regiochemistry of the four compounds. Compare the methyl protons first. In *erythro*-1-chloro-2-iodo-1-phenylpropane, the methyl protons are found at δ 2.12 ppm downfield from the methyl protons of the isomeric *erythro*-2-chloro-1-iodo-1-phenylpropane at δ 1.85 ppm. The same relationship exists for the *threo* isomers ($ICHCH_3$ δ 1.87 ppm; $ClCHCH_3$ δ 1.48 ppm). A similar relationship exists for protons at benzylic carbons bonded to

Can. J. Chem. Downloaded from www.nrcresearchpress.com by 210.87.254.42 on 09/06/12
For personal use only.

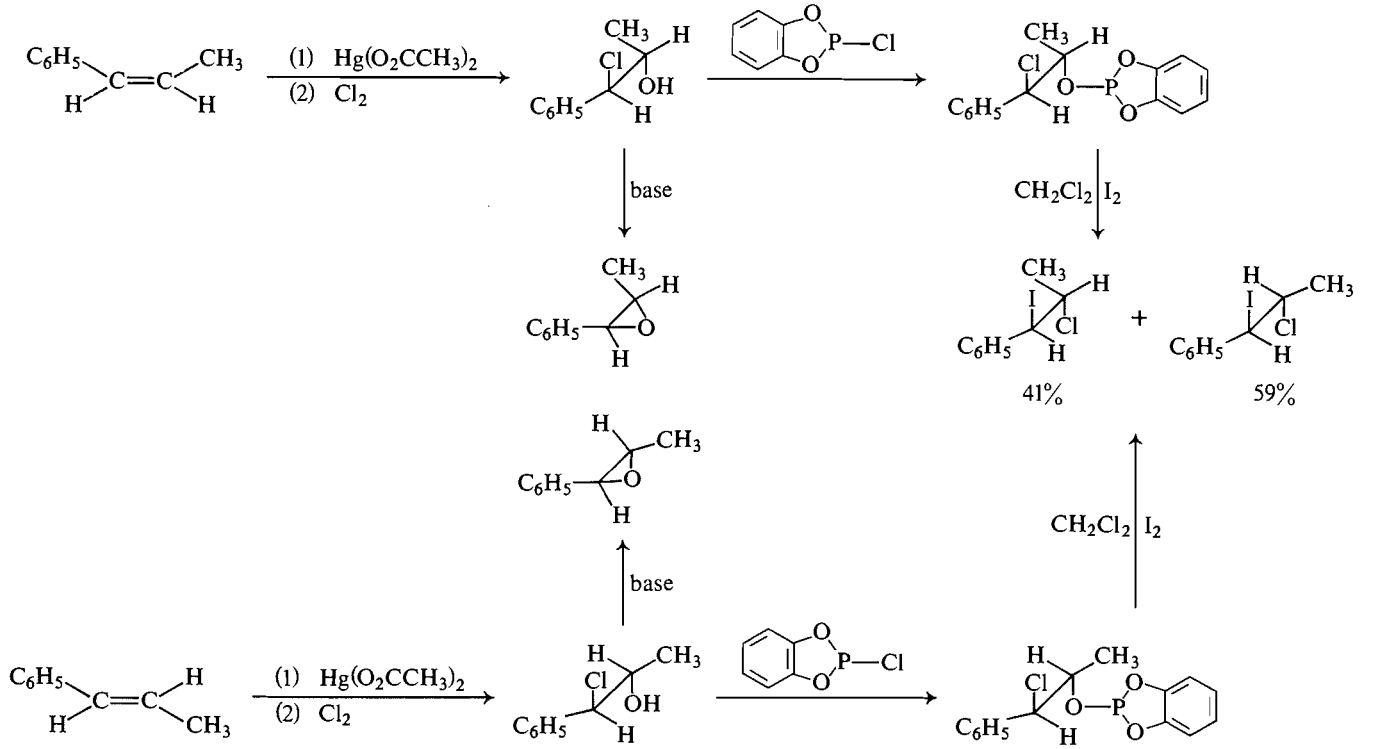

FIG. 5. Synthetic scheme for the preparation of *erythro*- and *threo*-2-chloro-1-iodo-1-phenylpropane.

chlorine and iodine. Thus the proton magnetic resonance spectra of these four isomers are in accord with our assignment of both the stereochemistry and regiochemistry of the compounds.

In summary, addition to all four alkenes is *anti*-stereospecific. Furthermore, addition to the 1-phenylpropenes is regiospecific: only the product of Markownikoff orientation is formed. No Markownikoff to *anti*-Markownikoff isomerization of the products of addition to *Z*- or *E*--1phenylpropene has been observed (28).

Proposed mechanism

Two possible mechanisms for this reaction are shown in Fig. 6. Both mechanisms involve only bimolecular processes, a rate-determining step that contains 3 molecules of ICl and one of alkene, and two equilibria prior to the rate-determining step. The first equilibrium in both mechanisms is the formation of a 1:1 alkene−ICl molecular complex. Formation of an ICl dimer is the second equilibrium in mechanism A while formation of a 1:2 alkene−ICl molecular complex is the second equilibrium in mechanism B. Both mechanisms are consistent with our data. Johnson and Bowen (29) have shown that linear Benesi−Hildebrand (B−H) or Ketelaar plots can be obtained for reactions that involve both 1:1 and 1:2 molecular complexes. Thus both mechanisms are in accord with our linear Ketelaar plot.

When $(\text{alkene})_0 \gg (\text{ICl})_0$, the concentration of the product of the second equilibrium in either mechanism (ICl dimer in mechanism A or 1:2 alkene−ICl molecular complex in mechanism B) will always be small compared to the concentration of the 1:1 alkene−ICl complex.[3] As a result, the stoichiometric concentration of ICl can be approximated within experimental error by eq. [9]. The predicted rate law for both mechanisms is then given by eq. [10] where $k = k_3 K_{AD} K_{A_2}$ (for mechanism A) or $k = k_3 K_{AD} K_2$ (for mechanism B). Again substituting for $[\text{ICl}]_t$ in eq. [10], we obtain the rate law given in eq. [11]. Thus both mechanisms are in accord with the experimentally determined rate law.

Mechanism A.

$$A + D \rightleftharpoons AD \quad (K_{AD})$$
$$A + A \rightleftharpoons A_2 \quad (K_{A_2})$$
$$AD + A_2 \xrightarrow{k_3} \text{Product}$$

A = ICl D = Alkene
AD = 1:1 Alkene−ICl molecular complex
A_2D = 1:2 Alkene−ICl molecular complex
A_2 = ICl dimer

Mechanism B.

$$A + D \rightleftharpoons AD \quad (K_{AD})$$
$$A + AD \rightleftharpoons A_2D \quad (K_2)$$
$$A + A_2D \xrightarrow{k_3} \text{Product}$$

FIG. 6. Two proposed mechanisms for the addition of ICl to alkenes in CCl_4 at 25°C.

The assumption of two equilibria can be substantiated by quantitative consideration of the enthalpy changes in the reaction as shown in Fig. 7. It is clear that the enthalpy change, ΔH_{AD}, for the formation of a 1:1 alkene−ICl complex (−9 kcal/mol) cannot account for the large negative enthalpy of activation (−17 kcal/mol). Another intermediate is needed whose value of $\Delta H_x \leq -8$ kcal/mol.[4]

Dimers of halogens are known and the equilibrium constants

[3]For example, when the ratio K_{A_2D}/K_{AD} is 100, the ratio $[A_2D]/(AD)$ will be less than 0.01.

[4]If the enthalpy of activation for step 3 is taken into account, ΔH_x becomes even more negative than −8 kcal/mol.

Can. J. Chem. Downloaded from www.nrcresearchpress.com by 210.87.254.42 on 09/06/12
For personal use only.

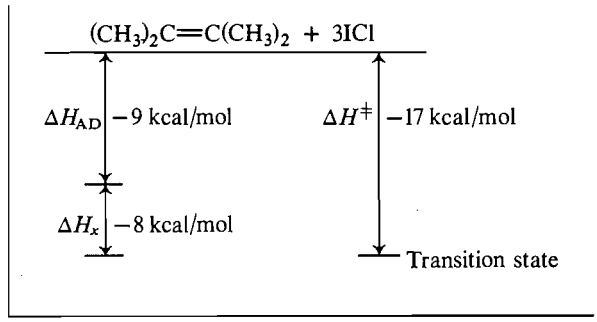

FIG. 7. Enthalpy change in the addition of ICl to 2,3-dimethyl-2-butene in CCl_4 at 25°C.

TABLE 5. Values of $K_{A_2}\epsilon^{\lambda}_{A_2}$ at selected wavelengths in CCl_4 at 25°C

λ (nm)	$K_{A_2}\epsilon^{\lambda}_{A_2}$ ($L^2\ mol^{-2}\ cm^{-1}$)
270.0	685±90
280.0	291±20
290.0	150±6
300.0	89.2±3.5
310.0	49.9±1.7
320.0	35.6±1.7
330.0	28.6±1.3
340.0	22.7±0.9
350.0	20.4±0.7
360.0	20.3±1.0
370.0	20.9±0.8
380.0	19.4±1.5

and enthalpies of formation for the dimers of several halogens in solution and in the gas phase have been determined (30). The most common method for determining these quantities is to examine deviations from the Beer–Lambert Law (31). If ICl and its dimer both contribute to the uv absorbance, eq. [12] can be written.

$$[12]\quad \mathrm{Abs}^{\lambda} l^{-1} = \epsilon^{\lambda}_{ICl}[ICl] + \epsilon^{\lambda}_{A_2}[\mathrm{dimer}]$$

where $\epsilon^{\lambda}_{A_2}$ is the extinction coefficient of the dimer. If the extent of dimer formation is very small than eq. [12] becomes

$$[13]\quad \epsilon^{\lambda}_{app} = \frac{\mathrm{Abs}^{\lambda}}{l(ICl)} = \epsilon^{\lambda}_{ICl} + K_{A_2}\epsilon^{\lambda}_{A_2}(ICl)$$

From linear plots of ϵ^{λ}_{app} versus (ICl), values of $K_{A_2}\epsilon^{\lambda}_{A_2}$ were obtained and are given in Table 5.

From our data, it is impossible to determine K_{A_2} from the product $K_{A_2}\epsilon_{A_2}$. It is possible, however, to obtain an upper limit to K_{A_2} in the following way. If K_{A_2} were appreciable, the exact equation for ϵ^{λ}_{app} is as follows:

$$[14]\quad \epsilon^{\lambda}_{app} = \epsilon^{\lambda}_{ICl} + (\epsilon^{\lambda}_{A_2} - 2\epsilon^{\lambda}_{ICl})\{1 + 4K_{A_2}(ICl) - [1 + 8K_{A_2}(ICl)]^{1/2}(8K_{A_2})^{-1}$$

Synthetic data were generated from eq. [14] using values of $\epsilon^{\lambda}_{ICl} = 10$ and $\epsilon_{A_2}K_{A_2} = 100$, which correspond closely to the experimental values obtained in CCl_4 at 290 to 310 nm. Sets of values of ϵ^{λ}_{app} were calculated for various values of K_{A_2} (0.1 to 5.0 M^{-1}). The values of ϵ^{λ}_{app} obtained for a particular value of K_{A_2} were then plotted according to eq. [13]. Any value of K_{A_2} greater than 0.5 M^{-1} causes a definitive curvature of plots of eq. [13]. Thus the value of $K_{A_2} \leq 0.5\ M^{-1}$ in order to account for the experimentally observed linear plots of eq. [13].

The enthalpy of formation of the ICl dimer was estimated by the method of Keefer and Allen (32). Literature values of ΔH_{AD} and ΔG_{AD} for a wide range of donor–ICl complexes in CCl_4 at 25°C are given in Table 6. When ΔG_{AD} is plotted against ΔH_{AD} the following linear relationship is obtained:

$$[15]\quad \Delta G_{AD} = 2.8 + 0.77\ \Delta H_{AD}$$

Equation [15] should be valid for the ICl dimer. A K_{AD} value of 0.5 M^{-1} predicts a value of ΔH_{A_2} of −3 kcal/mol, very similar to the literature values of ΔH_{A_2} for the iodine dimer in CCl_4 at 25°C (−1.0 ± 0.2 kcal/mol (41); −1.96 kcal/mol (42); −1.52 ± 0.29 (43). We may state with some confidence that ΔH_{A_2} for the ICl dimer is more positive than −4 kcal/mol. Returning to Fig. 7, it is clear that ΔH_{A_2} is not sufficient to account for the value of ΔH_x. On this basis, it is concluded that the ICl dimer, while present in CCl_4, is not involved on the reaction coordinate of the addition of ICl to 2,3-dimethyl-2-butene.[5]

Mechanism B, Fig. 6, involves successive equilibria for the formation of 1:1 and 1:2 alkene–ICl molecular complexes. There is no experimental evidence for such 1:2 alkene–ICl molecular complexes. However, experimental data are available for 1:2 alkene–Br_2 complexes. Kimer'fel'd *et al.* (44) have observed both 1:1 and 1:2 cyclohexene-Br_2 complexes in solid solutions at −185°C in ir and Raman spectroscopy. Sergeev *et al.* and Lishnevskii *et al.* have demonstrated the existence of a 1:1 and 1:2 propene–Br_2 complexes at low temperatures by thermographic (45), uv (46), and ir (46) studies. Sergeev *et al.* (47) have also postulated a 1:2 cyclohexene–Br_2 complex in Freon 113 at ambient temperature on the basis of a uv study in the range 250–270 nm. A structure of these 1:2 alkene–Br_2 complexes has been proposed in which the two bromine molecules are on opposite sides and perpendicular to the plane of the double bond (44). A similar structure would be expected for a 1:2 alkene–ICl complex. While it seems reasonable to propose the existence of a 1:2 alkene–ICl complex on the reaction coordinate of ICl additions to alkenes, its verification awaits further data.

Summary

Observation of a negative activation enthalpy for the reaction of ICl and 2,3-dimethyl-2-butene in CCl_4 at 25°C provides strong evidence for the existence of one or more molecular complexes on the reaction coordinate. The rate law requires a rate-determining step that contains one molecule of alkene and three of ICl. Quantitative analysis of the enthalpy change in the reaction rules out the involvement of the ICl dimer on the reaction coordinate. The involvement of a 1:2 alkene–ICl complex in the mechanism is proposed.

Experimental

All boiling and melting points are uncorrected. The glc analysis was carried out using a Varian Aerograph Series 2740 analytical instrument equipped with a FID. Proton magnetic resonance spectra were recorded on a Varian T-60 or HA-100 spectrometer in $CDCl_3$ containing $(CH_3)_4Si$ as internal standard. ACS grade CCl_4, CH_2Cl_2, and CH_3CN were used without further purification. *E*- and *Z*-1-phenylpropene, *E*- and *Z*-2-butene, and 2,3-dimethyl-2-butene were

[5]We estimate the errors in $\Delta H^{\ddagger}$(expt) and ΔH_{AD} to be ±10% using the method of Benson (17*a*).

Can. J. Chem. Downloaded from www.nrcresearchpress.com by 210.87.254.42 on 09/06/12
For personal use only.

TABLE 6. Literature thermodynamic parameters for selected donor − iodine monochloride complexes in CCl_4 at 25°C

Donor	K_{AD} (M^{-1}), 25°C	ΔH_{AD} (kcal mol^{-1})	ΔS_{AD} (cal deg^{-1} mol^{-1})[a]	References
Ph_2SeO	36 000.0	−10.87±0.27	−15.6±1.2	33
Ph_3PO	3 000.0	−9.79±0.14	−16.9±1.0	33
Ph_2SO	410.0	−7.62±0.08	−13.6±0.3	33
Ph_2CO	9.59	−6.05±0.25	−15.8±0.9	33
1,2-Epoxycyclohexane	90.5	−8.3	−20.0	34
4-Chlorotoluene	0.35	−2.1	−9.1	35, 36
Benzene	0.54	−3.2	−12.0	35, 36
p-Xylene	1.51	−4.1	−13.0	35, 36
1,2,4-Triethylbenzene	2.5	−4.7	−14.0	35, 36
Mesitylene	4.59	−5.1	−14.0	35, 36
Pentamethylbenzene	6.43	−5.5	−15.0	35, 36
Hexamethylbenzene	22.7	−5.7	−13.0	35, 36
Hexaethylbenzene	1.24	−3.8	−12.0	35, 36
Dichloroacetonitrile	0.69±0.05	−3.7	−13.0	37
Monochloroacetonitrile	2.41±0.24	−5.3	−16.0	37
Acetonitrile	8.4 ±0.8	−4.9 ±0.7	−12.0	37
Propionitrile	8.3 ±0.2	−5.2 ±0.2	−13.0	38
Dimethylcyanamide	130.0	−7.3	−15.0	39
N,*N*-dimethylacetamide	1 100.0 ±100	9.5 ±0.2	−18.0	40

[a] ΔS_{AD} (average) was calculated to be −(14.3 ± 2.5) eu.

obtained commercially and used without further purification. Iodine monochloride was purified by fractional crystallization from the melt, discarding the remaining liquid portion (48).

threo-*3-Iodo-2-butanol* was prepared by adding 8.0 g (0.035 mol) of finely ground iodine in several portions over 5−10 min to a vigorously stirred solution of 40 g (0.0185 mol) of yellow mercuric oxide and excess *Z*-2-butene in 15 mL of 80% aqueous acetonitrile at room temperature. After an additional 10−15 min, the reaction mixture was filtered by suction to remove the red mercuric iodide using a small amount of acetonitrile as a rinse solution. The filtrate was poured into a separatory funnel containing a two-fold excess of ether. The resulting solution was washed successively with a 5% aqueous KI solution, a 5% aqueous $NaHSO_3$ solution, and a saturated NaCl solution. The organic layer was separated, dried over anhydrous $MgSO_4$, filtered, and solvent removed at reduced pressure to yield 3.28 g (0.0164 mol, 52%), bp 45−47°C/5 Torr (1 Torr = 133.3 Pa) (lit. (49) bp 43.0°C/2.5 Torr); ^{1}H nmr δ: 1.23 (d, J = 6.0 Hz, 3H), 1.92 (d, J = 7.0 Hz, 3H), 3.20 (dq, J = 4.5, 6.0 Hz, 1H), 4.15 (dq, J = 3.5, 7.0 Hz, 1H).

erythro-*3-Iodo-2-butanol* was prepared in 80% yield by the same method as the *threo* isomer but using *E*-2-butene as the starting alkene, bp 50−52°C/5 Torr (lit. (49) bp 34.3−34.9°C/0.9 Torr); ^{1}H nmr δ: 1.21 (d, J = 6.0 Hz, 3H), 1.82 (d, J = 7.0 Hz, 3H), 4.31 (dq, J = 3.5, 7.0 Hz, 1H), 3.32 (dq, J = 3.5, 6.0 Hz, 1H).

cis-*2,3-Dimethyloxirane* was prepared by adding excess moist sodium aluminate to 2.00 g (0.010 mol) of *threo*-3-iodo-2-butanol in 10 mL CS_2. The sodium aluminate was prepared by adding with stirring 1 mL of 10 *N* NaOH solution per 5 g of chromatographic grade alumina. A three-fold excess of base was used. The reaction mixture was allowed to stand for 10 h with occasional stirring. The mixture was filtered and the solid was thoroughly washed with CH_2Cl_2. The solvent was removed at reduced pressure to yield 0.56 g (80% yield) of product, bp 55−57°C (lit. (53) bp 53.5−53.7°C); ^{1}H nmr δ: 1.22 (d, J = 6 Hz, 3H), 2.91 (m, 1H).

trans-*2,3-Dimethyloxirane* was prepared in 67% yield by the same method as the *cis* isomer except that *erythro*-3-iodo-2-butanol was used as the starting iodohydrin, bp 55−56°C (lit. (49) bp 53.5−54.0°C); ^{1}H nmr δ 1.27 (d, J = 5Hz, 3H), 2.62 (m, 1H).

threo-*2-Chloro-3-iodobutane* was prepared by adding 16.6 g (0.014 mol) $SOCl_2$ to 20 g (0.010 mol) *threo*-3-iodo-3-butanol. After copious evolution of HCl, the solution was stirred for 30 min at room temperature. The reaction mixture was transferred to a separatory funnel containing a 10-fold excess of CH_2Cl_2. The organic layer was washed with a 5% aqueous $NaHCO_3$ solution, a 5% aqueous $NaHSO_3$ solution, and a saturated NaCl solution. The organic layer was dried over K_2SO_3, filtered, and the solvent removed at reduced pressure to give 1.5 g (68%) of product, bp 35−37°C/5 Torr (lit. (49) bp 32.2−33.5/4 Torr).

erythro-*2-Chloro-3-iodobutane* was prepared in 88% yield by the same method as the *threo* isomer except that *erythro*-3-iodo-2-butanol was used as the starting iodohydrin; bp 35−37°C 5 Torr (lit. (49) bp 34.8−35.3°C/5 Torr).

threo-*1-Chloro-1-phenyl-2-propanol* was prepared by adding 4.72 g (0.040 mol) of *Z*-1-phenylpropene to a stirred ice-cold solution of 15.9 g (0.050 mol) of mercuric acetate in 200 mL of 50% aqueous acetonitrile. Stirring was continued for 4 days at room temperature. To the reaction mixture was added 50 mL of a saturated NaCl solution. Stirring was continued for an additional 15 min. The resulting mixture was poured into 200 mL of water and extracted with 3 × 125 mL portions of ether. The combined ether extracts were washed with 2 × 100 mL portions of water and 100 mL of saturated NaCl solution. The ether layer was dried over $MgSO_4$, filtered, and the ether removed to give 9.6 g of *threo*-2-hydroxy-1-methyl-2-phenylethyl mercuric chloride. A solution of 1.60 g (4.31 mmol) of the organomercurial in 25 mL of dry pyridine in a 50-mL flask fitted with a magnetic stirrer, $CaCl_2$ drying tube, and a gas bubbler was cooled to between −50 and −60°C and Cl_2 was bubbled through for 5 min. The reaction mixture was poured into 150 mL of ether. The ether solution was washed with 2 × 50 mL 5% aqueous HCl solution, 2 × 50 mL 5% aqueous $NaHCO_3$ solution, 25 mL of a 1% aqueous $NaHSO_3$ solution, and 50 mL saturated NaCl solution. The ether layer was dried over anhydrous $MgSO_4$, filtered, and the solvent removed at reduced pressure to give 0.60 g (81%) of product; ^{1}H nmr δ: 1.05 (d, J = 6.0 Hz, 3H), 4.00 (dq, J = 6.0, 7.0 Hz, 1H), 4.68 (d, J = 7.0 Hz, 1H), 7.27 (s, 5H).

erythro-*1-Chloro-1-phenyl-2-propanol* was prepared in 75% yield by the same method as the *threo* isomer except that *E*-1-phenylpropene was used as the starting alkene; ^{1}H nmr δ: 1.22 (d, J = 6.0 Hz, 3H), 4.04 (dq, J = 6.0 Hz, 1H), 4.74 (d, J = 6.0 Hz, 1H), 7.27 (s, 5H).

Reaction of the 2-methyl-3-phenyloxirane and HCl

A solution of epoxide in CH_2Cl_2 cooled in an ice bath was treated with enough concentrated HCl solution so that a 1.5 to 2.0-fold excess of HCl was present. After stirring for 1 h, the reaction mixture was diluted with an equal volume of CH_2Cl_2. The CH_2Cl_2 layer was separated and washed with 3 portions of H_2O and one portion of saturated NaCl solution. The organic layer was dried over anhydrous $MgSO_4$,

Can. J. Chem. Downloaded from www.nrcresearchpress.com by 210.87.254.42 on 09/06/12
For personal use only.

filtered, and the solvent removed at reduced pressure to give the crude chlorohydrin. The product of the reaction of the *trans* isomer was determined to be 45% *erythro*- and 55% *threo*-1-chloro-1-phenyl-2-propanol. The *cis* isomer formed 57% *threo*- and 17% *erythro*-1-chloro-1-phenyl-2-propanol and 26% *threo*-2-chloro-1-phenyl-1-propanol (16). The ratios of products were determined from the areas of non-overlapping methyl peaks in the ^{1}H nmr spectrum (26).

erythro- *And* threo-*2-chloro-1-iodo-1-phenylpropane* were prepared from the corresponding *erythro* or *threo*-1-chloro-1-phenyl-2-propanol using the method of Corey and Anderson (25*b*). Starting with either isomer, a mixture containing 59% *erythro*- and 41% *threo*-2-chloro-1-iodo-1-phenylpropane was obtained as determined from the relative areas of the non-overlapping methyl peaks in the ^{1}H nmr spectrum. Anal. ($C_9H_{10}ICl$)C,H.

Acknowledgment

Financial assistance by the Natural Sciences and Engineering Research Council of Canada is gratefully acknowledged.

1. E. P. WHITE and P. W. ROBERTSON. J. Chem. Soc. 1509 (1939).
2. N. AMIRTHA, S. VISWANATHAN, and R. GAMESAN. Bull. Chem. Soc. Jpn. **56**, 314 (1983).
3. G. B. SERGEEV and V. V. SMIRNOV. Kinet. Catal. USSR, **16**, 1142 (1975).
4. G. HEUBLEIN. Z. Chem. **6**, 186 (1966).
5. A. GERO, J. J. KERSHNER, and R. E. PERRY. J. Am. Chem. Soc. **75**, 5119 (1953).
6. L. F. FIESER and M. FIESER. Reagents for organic synthesis. John Wiley and Sons Inc., New York. 1967. p. 502.
7. R. C. CAMBIE, W. I. NOALL, G. J. POTTER, P. S. RUTLEDGE, and P. D. WOODGATE. J. Chem. Soc. Perkin Trans. 1, 226 (1977).
8. G. DANA, O. CONVERT, and C. PERRIN. J. Org. Chem. **40**, 2133 (1975).
9. R. E. BUCKLES and D. F. KNACK. J. Chem. Educ. **37**, 298 (1960).
10. D. F. SHELLHAMER, V. L. HEASLEY, L. E. HEASLEY, G. E. HEASLEY, and J. SABINE. Paper presented at 177th National Meeting ACS, Honolulu, HI. Abstract No. 299.
11. (*a*) A. HASSNER and J. S. TEETER. J. Org. Chem. **35**, 3397 (1970); (*b*) N. H. WERSTIUK, I. VANCAS, J. WARKENTIN, and F. R. S. CLARK. Can. J. Chem. **50**, 291 (1972); (*c*) G. MEHTA, S. K. KAPOOR, and B. G. B. GUPTA. Ind. J. Chem. **14B**, 364 (1976); (*d*) G. MEHTA, P. K. DUTTA, and P. N. PANDEY. Ind. J. Chem. **14B**, 307 (1976).
12. (*a*) J. E. DUBOIS and F. GARNIER. Spectrochim. Acta Part A, **23**, 2279 (1967); (*b*) J. E. DUBOIS and F. GARNIER. J. Chim. Phys. **63**, 351 (1966); (*c*) D. R. LONG and R. W. NEUZIL. Anal. Chem. **27**, 1110 (1955); (*d*) S. FUKUZUMI and J. K. KOCHI. J. Am. Chem. Soc. **104**, 7599 (1982).
13. H. A. BENESI and J. H. HILDEBRAND. J. Am. Chem. Soc. **71**, 2703 (1949).
14. (*a*) G. B. SERGEEV, Y. A. SERGUCHEV, and V. V. SMIRNOV. Russ. Chem. Rev. **42**, 697 (1973); (*b*) R. FOSTER. *In* Molecular complexes. Vol II. P. Elek Science, London. 1973. Chapt. 1. p. 2.
15. G. H. SCHMID and D. G. GARRATT. *In* The chemistry of double bonded functional groups. *Edited by* S. Patai. John Wiley and Sons, Inc., New York. 1977. Chapt. 8.
16. G. H. SCHMID and J. W. GORDON. J. Org. Chem. **48**, 4010 (1983).
17. (*a*) S. W. BENSON. The foundations of chemical kinetics. McGraw–Hill, New York. 1960. p. 305; (*b*) G. M. HARRIS. Chemical kinetics. Health, Boston. 1966. p. 51; (*c*) G. B. SERGEEV. Mendeleev Chem. J. **19**, 57 (1974); (*d*) G. B. SERGEEV and I. A. LEENSON. Russ. Chem. Rev. **41**, 726 (1972).
18. (*a*) A. A. BOTHNER-BY and C. J. NAAR-COLIN. J. Am. Chem. Soc. **84**, 743 (1962); (*b*) C. A. KINGSBURY and D. C. BEST. J. Org. Chem. **32**, 6 (1967); (*c*) R. C. FAHEY. J. Am. Chem. Soc. **88**, 4681 (1966).
19. (*a*) J. W. CORNFORTH, R. H. CORNFORTH, and K. K. MATHEW. J. Chem. Soc. 112 (1959); (*b*) G. GOLUMBIC and D. L. COTTLE. J. Am. Chem. Soc. **61**, 996 (1939); (*c*) J. W. CORNFORTH and D. T. GREEN. J. Chem. Soc. (C), 846 (1970).
20. (*a*) D. J. CRAM. J. Am. Chem. Soc. **75**, 332 (1953); (*b*) T. G. SQUARES, W. W. SCHMIDT, and C. S. MCCANDLISH, JR. J. Org. Chem. **40**, 134 (1975).
21. H. J. LUCAS and H. K. GARNER. J. Am. Chem. Soc. **72**, 2145 (1950).
22. J. G. NOLTES and D. SEYFERTH. Organometallics in chemical synthesis. Vol. 1. Elsevier, New York. 1970. p. 70.
23. F. R. JENSEN and B. RICKBORN. Electrophilic substitution of organomercurials. McGraw–Hill, New York. 1968. p. 75.
24. J. G. BUCHANAN and H. Z. SABLE. *In* Selective organic transformations. Vol 2. *Edited by* B. S. Thyagarajan. Wiley–Interscience, New York. 1972. Chapt. 1.
25. (*a*) P. A. GRIECO and B. S. FINKELHOR. J. Org. Chem. **38**, 2245 (1973); (*b*) E. J. COREY and J. E. ANDERSON. J. Org. Chem. **32**, 4160 (1967); (*c*) J. P. FORSMAN and D. LIPKIN. J. Am. Chem. Soc. **75**, 3145 (1953).
26. G. H. SCHMID. Can. J. Chem. **46**, 3115 (1970).
27. J. ZUBICKY and S. EHRLICH-TAGOZINSKI. *In* The chemistry of the carbon–halogen bond. Part 1. *Edited by* S. Patai. Wiley, London. 1973. Chapt. 3.
28. G. H. SCHMID, V. M. CSIZMADIA, V. J. NOWLAN, and D. G. GARRATT. Can. J. Chem. **50**, 2457 (1972).
29. C. D. JOHNSON and R. E. BOWEN. J. Am. Chem. Soc. **87**, 1655 (1965).
30. (*a*) P. A. D. DE MAINE. Can. J. Chem. **35**, 573 (1957); (*b*) A. A. PASSCHIER and N. W. GREGORY. J. Phys. Chem. **72**, 2697 (1968); (*c*) E. A. OGRYZLO and B. C. SANCTUARY. J. Phys. Chem. **69**, 4422 (1965).
31. (*a*) G. KORTUM and G. FRIEDHEIM. Z. Naturforsch. Teil A, **2**, 20 (1947); (*b*) M. TAMRES, W. K. DUERKSEN, and J. M. GOODENOW. J. Phys. Chem. **72**, 2697 (1968); (*c*) R. M. NOYES and W. Y. WEN. J. Phys. Chem. **76**, 1017 (1972).
32. R. M. KEEFER and T. L. ALLEN. J. Phys. Chem. **24**, 1901 (1956).
33. V. H. P. SIEPER and R. PACTZOLD. Z. Phys. Chem. Leipzig, **255**, 1125 (1974).
34. G. B. SERGEEV, Z. NAIZAREK, and V. V. SMIRNOV. Russ. J. Phys. Chem. **49**, 1417 (1975).
35. N. OGIMACHI, L. J. ANDRES, and R. M. KEEFER. J. Am. Chem. Soc. **77**, 4202 (1955).
36. L. J. ANDREWS and R. M. KEEFER. J. Am. Chem. Soc. **74**, 4500 (1952).
37. W. B. PERSON, W. C. GOLTON, and A. I. PLPOV. J. Am. Chem. Soc. **85**, 891 (1963).
38. P. J. KOAEBOE. J. Am. Chem. Soc. **85**, 871 (1963).
39. E. AUGDAHL and P. KLAEBOE. Acta Chem. Scand. **19**, 807 (1965).
40. R. S. DRAGO and W. A. WENZ. J. Am. Chem. Soc. **84**, 526 (1962).
41. R. M. KEEFER and T. L. ALLEN. J. Chem. Phys. **24**, 1059 (1956).
42. P. A. D. DE MAINE. J. Chem. Phys. **24**, 1091 (1956).
43. M. M. DE MAINE, P. A. D. DE MAINE, and G. E. MCALONIE. J. Mol. Spectrosc. **4**, 271 (1960).
44. (*a*) Y. M. KIMEL'FEL'D, A. B. MOSTOVOI, and L. I. FAINSHTEIN. Dokl. Adak. Nauk SSSR, **209**, 299 (1973); (*b*) Y. M. KIMEL'-FEL'D, A. B. MOSTOVOI, A. V. BOBROV, and Y. Z. VOLKOV. Theor. Exp. Chem. USSR, **10**, 322 (1974).
45. V. A. LISHNEVSKII, and G. V. SERGEEV. Kinet. Catal. USSR, **5**, 355 (1964).
46. V. A. LISHNEVSKII, I. A. ORESHKIN, G. B. SERGEEV, and E. I. YAKOVENKO. Dokl. Adak. Nauk SSSR, **172**, 121 (1967).
47. G. B. SERGEEV, V. V. SMIRNOV, G. A. BAKARINOVA, and M. A. VETROVA. Dokl. Akad. Nauk. SSSR, **203**, 225 (1972).
48. G. V. CALDER and W. F. GIAUQUE. J. Phys. Chem. **69**, 2443 (1965).
49. H. J. LUCAS and H. K. GARNER. J. Am. Chem. Soc. **72**, 2145 (1950).

Can. J. Chem. Downloaded from www.nrcresearchpress.com by 210.87.254.42 on 09/06/12
For personal use only.

A general route to the synthesis of 3-alkylidene derivatives of 4-thiochromanone 1,1-dioxide

IAN W. J. STILL[1] AND FRED J. ABLENAS

J. Tuzo Wilson Research Laboratories, Erindale Campus, University of Toronto in Mississauga, Mississauga, Ont., Canada L5L 1C6

Received May 1, 1984

This paper is dedicated to Professor Peter Yates on the occasion of his 60th birthday

IAN W. J. STILL and FRED J. ABLENAS. Can. J. Chem. **62**, 2535 (1984).

The reactions of the trimethylsilyl enol ethers of both 4-thiochromanone and 4-thiochromanone 1,1-dioxide with various carbonyl compounds complexed with titanium tetrachloride give moderate yields of the previously unknown 3-alkylidene condensation products under mild conditions. Other Lewis acids, with the exception of boron trifluoride, were found to be ineffective in this transformation.

IAN W. J. STILL et FRED J. ABLENAS. Can. J. Chem. **62**, 2535 (1984).

Opérant sous des conditions expérimentales douces, les réactions des éthers énoliques triméthylsilylés de la thio-4 chromanone et de la thio-4 chromanone dioxyde-1,1 avec divers composés carbonylés complexés avec du tétrachlorure de titane conduisent, avec des rendements modérés, à des produits de condensation alkylidène-3 qui étaient inconnus antérieurement. On a trouvé que les autres acides de Lewis, à l'exception du trifluorure de bore, sont inefficaces pour cette transformation.
[Traduit par le journal]

Can. J. Chem. Downloaded from www.nrcresearchpress.com by 210.87.254.5 on 09/06/12
For personal use only.

Introduction

The synthesis of 3-methylene-4-thiochromanone 1,1-dioxide **1** has been reported for the first time in a recent paper by Holshouser and Loeffler (1). This compound was synthesized as part of a systematic investigation (2) of the effectiveness of various α-methylene carbonyl compounds as anti-tumor agents and was shown to be marginally active in this respect. Of more immediate chemical interest, **1** was also found to undergo very facile dimerization at 25°C, via a Diels–Alder reaction to the pentacyclic compound **2**, this process being reversible at 250°C.

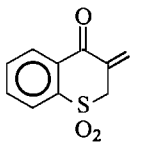

1

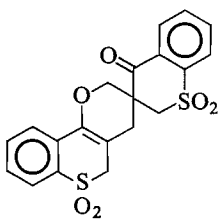

2

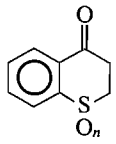

3*a*, $n = 0$
b, $n = 2$

Given our previous interest in 4-thiochromanone chemistry (3–6), we wished to undertaken a more general investigation of synthetic routes to higher homologs of **1**. Somewhat surprisingly, very few analogs of **1** have been reported in the literature to date, although 3-arylidene deivatives derived from 4-thiochromanone **3***a* itself have been known for many years (7, 8). The dichloromethylene derivative of **3***a* was also obtained earlier by us (3) in an unusual reaction of 4-thiochromanone with carbon tetrachloride. The Mannich procedure (1) used to prepare **1** and the acid-catalyzed route to the arylidene derivatives of **3***a* employed by Orlov *et al.* (8) proved to be incapable of extension to the condensation of **3***a*, or its dioxide **3***b*, with ketones. In addition, the well-documented (8, 9) tendency for the α-carbanions of **3***a* and **3***b* to undergo ring-opening reactions in preference to alkylation at the C-3 carbon meant almost certain failure for any approach to the condensation along these lines. The use of milder reaction conditions seemed to offer the only hope of success and constitutes the subject of this paper.

Results and discussion

In the light of the difficulties mentioned above, it seemed to us that an approach to the condensation of **3***a* (or **3***b*) with ketones would be most effective if an additional electron-withdrawing group were present at C-3 to facilitate carbanion formation at this site under mild conditions. The 3-hydroxymethylene compound **4**, reported by Tilak and co-workers (10), seemed ideal for this purpose and was readily prepared in 95% yield by reaction of **3***a* with ethyl formate, using sodium hydride as the base. (In contrast to the earlier report (10), sodium methoxide was found to be ineffective as a catalyst for the formylation and compound **4**, when pure, is a reasonably stable compound which can be stored for several weeks without appreciable decomposition.) Unfortunately, **4** did not react under acid- or base-catalyzed Knoevenagel reaction conditions at room temperature with cyclopentanone or cyclohexanone, and attempts to ensure reaction by resorting to higher temperatures led only to the destruction of the keto-aldehyde.

Compound **4** did undergo successful alkylation with chloromethyl phenyl sulfide in the presence of sodium hydride to produce **5**, albeit in only 24% yield. We had thought that it might be possible to selectively oxidize the acyclic sulfur atom in **5** to the corresponding sulfoxide or sulfone and then carry out a combined deformylation and elimination of benzenethiolate ion with alkali to provide an alternative route to the 3-methylene derivative of **3***a*, but the low yield of the alkylation step discouraged further exploration of this route. Attempted alkylation of **4** with chloromethyl phenyl sulfone directly to avoid the awkward selective oxidation step was completely without success, again presumably for steric reasons.

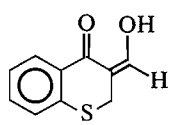

4

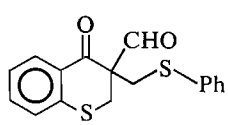

5

[1]Author to whom all correspondence may be addressed.

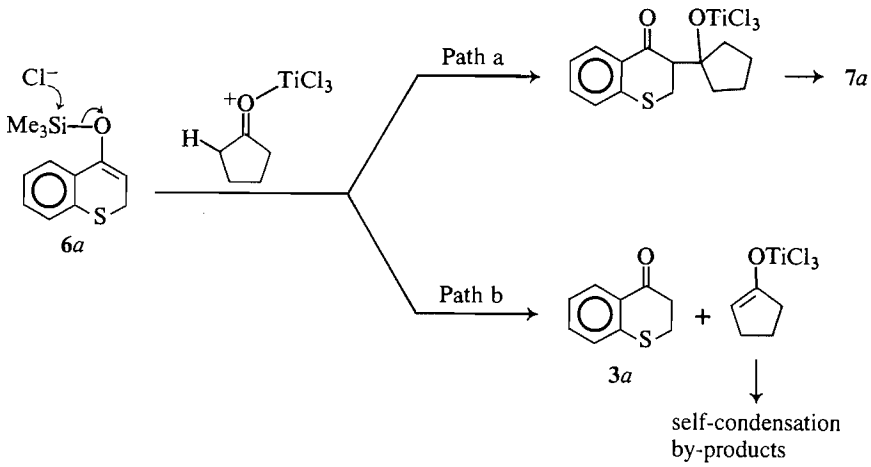

SCHEME 1

An alternative approach which presented itself was to use the enol silyl ether of **3***a* or **3***b* for the condensation with the appropriate ketone, in the presence of a Lewis acid catalyst, by the procedure developed recently by Paterson and Fleming (11). Here an immediate difficulty presented itself in that one of the most commonly employed routes to enol silyl ethers is via the (lithium) enolate and we have already noted the propensity of the enolates derived from **3***a* and **3***b* to undergo preferential ring cleavage reactions. The enol silyl ether **6***a* of 4-thiochromanone had been reported earlier by Hellberg and Juarez (12) as resulting from the reaction of 4-thiochromanone with dimethylaminotrimethylsilane. We have found, however, that a recent modification to the lithium enolate procedure by Fleming *et al.* (13), whereby the ketone and the chlorotrimethylsilane are added *simultaneously* to the strong base used (here LDA) instead of treating the preformed enolate with the silylating agent, works very well and affords **6***a* in 94% yield and the corresponding enol silyl ether **6***b* derived from **3***b* in 96% yield. Compound **6***a* may be purified by short-path distillation but the higher-boiling **6***b* was used directly for the condensation reactions without purification. Both compounds were found to be stable towards water and brief exposure to 1 *M* hydrochloric acid.

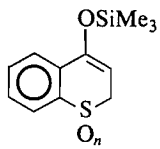

6*a*, *n* = 0
b, *n* = 2

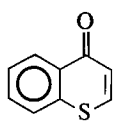

9

The enol silyl ethers **6***a*,*b* were initially reacted with cyclopentanone and cyclohexanone in dichloromethane at −78°C, with titanium tetrachloride as the catalyst, to establish the potential of this method. The reaction of **6***a* with cyclopentanone is illustrative. Three compounds could be isolated: the desired 3-cyclopentylidene-4-thiochromanone **7***a* (22%), accompanied by 4-thiochromaone **3***a* (24%) and thiochromone **9** (20%). Since **3***a* can be recycled via the enol silyl ether, the corrected figure for the isolated yield of the alkylidene derivative **7***a* is 29%. Initially it was felt that the 4-thiochromanone was being formed from the enol silyl ether during work-up, or possibly because of contamination of the titanium tetrachloride used by traces of hydrogen chloride, but the latter cause can now be

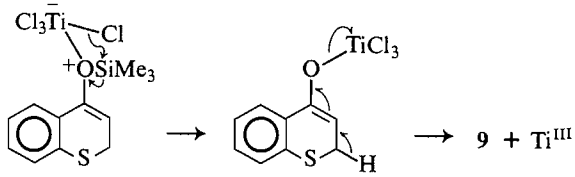

SCHEME 2

eliminated. It is quite possible, however, that proton transfer from cyclopentanone to the enol silyl ether, with concomitant formation of the cyclopentanone enolate, is responsible, since in almost all of the reactions which we have carried out significant amounts of ketone self-condensation products were found. A plausible mechanistic rationale for these reactions is shown in Scheme 1, where path a accounts for the formation of the desired aldol product and path b for the unproductive trans-enolization process.

The formation of thiochromone **9** is more surprising, since this formally involves an oxidation step, but Kuwajima and co-workers (14) have very recently noted the rapid (5−15 min) conversion of enol silyl ethers from cyclohexanones into the corresponding trichlorotitanium enolates, with $TiCl_4$ in halocarbon solvents at 20−35°C. While this process is unlikely to be complete under our reaction conditions (−78°C), a significant amount of the trichlorotitanium enolate must be formed which could then react, given the particularly stable, quasi-aromatic nature of the thiochromone produced, by the redox mechanism shown in Scheme 2 to give **9**. The formation of a violet color, perhaps indicative of Ti^{III}, is observed during the reaction. Once again, modification of the conventional reaction conditions was instrumental in eliminating this problem. It was found that by pre-coordinating the ketone with titanium tetrachloride at −78°C, *followed by* addition of the enol silyl ether, the amount of thiochromone formed became negligible and no violet coloration was observed during the reaction. Conversion yields of the alkylidene derivatives did not change dramatically but the corrected yields were higher (see Table 1).

In one experiment the *tert*-butyldimethylsilyl ether analog of **6***a* was used but the conversion to **7***a* achieved (26 vs. 22%) was only marginally better. The remaining aspect which we examined in our preliminary investigation was the importance of the Lewis acid catalyst used. The results of a number of reactions of enol silyl ethers **6***a*,*b* with cyclopentanone or cyclohexanone using a variety of Lewis acids and, in one

Can. J. Chem. Downloaded from www.nrcresearchpress.com by 210.87.254.5 on 09/06/12
For personal use only.

TABLE 1. Lewis acid catalysis used for condensation reactions of **6***a*,*b* with cyclopentanone **10** or cyclohexanone **11**

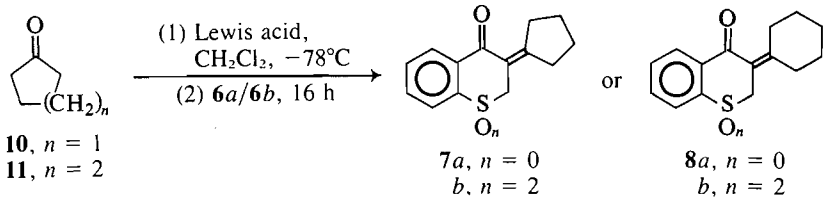

10, *n* = 1
11, *n* = 2

7*a*, *n* = 0
b, *n* = 2

8*a*, *n* = 0
b, *n* = 2

Entry	Ketone	Lewis acid	Enol ether	Method	Condensation product (%)[a] 7a	8a	7b	8b
1	**10**	$TiCl_4$	**6***a*	A	30	—	—	—
2	**10**	$ZnBr_2$	**6***a*	A	0	—	—	—
3	**11**	$TiCl_4$	**6***a*	A	—	86	—	—
4	**11**	0.5 $TiCl_4$ + 0.5 Ti $(O^iPr)_4$	**6***a*	A	—	24	—	—
5	**10**	$^nBu_4NF.nH_2O$[b]	**6***a*	A	0	—	—	—
6	**10**	$TiCl_4$	**6***b*	B	—	—	93	—
7	**10**	$MgCl_2$	**6***b*	B	—	—	0	—
8	**11**	$TiCl_4/Et_3N$	**6***b*	B	—	—	—	24[c]
9	**11**	$TiCl_4/Et_3N$	**6***b*	B	—	—	—	33
10	**11**	$ZnCl_2$	**6***b*	B	—	—	—	0[d]
11	**10**	BF_3	**6***b*	C	—	—	25	0[e]

[a]Isolated yield of pure product, corrected for recovered **3***a* or **3***b*. Reactions normally run for 16 h.
[b]In this case the catalyst was added to the mixture of the enol ether and the carbonyl compound.
[c]Yield after 4 h. The ^1H nmr indicated 51% enol ether unreacted at this point.
[d]After 18 h. The ^1H nmr showed unreacted enol silyl ether and ketone **3***b* to be the only species present.
[e]Ketone **3***b* was detected but not isolated.

TABLE 2. Formation of 3-alkylidene-4-thiochromanone 1,1-dioxides

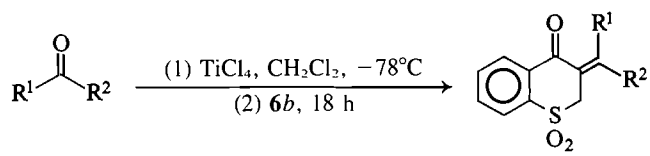

7*b*, **8***b*, **12**–**15**

R^1	R^2	Condensation product (%)[a]	^1H nuclear magnetic resonance data (δ)
—$(CH_2)_4$—		**7***b* (39)	1.6–1.9 (m, 4H), 2.55 (t, 2H), 2.9 (t, 2H), 4.3 (s, 2H), 7.6–8.0 (m, 3H), 8.0–8.3 (m, 1H)
—$(CH_2)_5$—		**8***b* (33)	1.4–2.1 (m, 6H), 2.3 (t, 2H), 2.6 (t, 2H), 4.3 (s, 2H), 7.6–8.0 (m, 3H), 8.0–8.2 (m, 1H)
CH_3	CH_3	**12** (42)	2.15 (s, 3H), 2.35 (s, 3H), 4.45 (s, 2H), 7.5–8.3 (m, 4H)
H	$^iC_3H_7$	**13** (30)	1.1 (d, 6H, *J* = 7 Hz), 2.65 (m, 1H), 4.3 (d, 2H, *J* = 2 Hz), 7.0 (dd, 1H, *J* = 2 Hz, 10 Hz), 7.5–8.2 (m, 4H)
H	C_6H_5	**14** (18)	4.55 (s, 2H), 7.4 (s, 5H), 7.7–8.0 (m, 3H), 8.05–8.3 (m, 2H)
CH_3	$^nC_5H_{11}$	**15** (11)	0.7–1.7 (m, 11H), 2.2 (s, 3H), 4.3 (s, 2H), 7.5–8.0 (m, 3H), 8.1–8.3 (m, 1H)

[a]Isolated yields, uncorrected for recovered **3***b*.

instance, tetrabutylammonium fluoride as catalyst have been summarized in Table 1. The yields of the condensation products have been corrected to allow for substantial recovery (0–95%) of **3***a* or **3***b* in almost all cases. It is quite clear from these results that, while the list of Lewis acids is not exhaustive, only $TiCl_4$ and BF_3 are effective in catalyzing this difficult condensation reaction. The use of triethylamine in conjunction with the titanium tetrachloride appeared to have little effect on the success of the reaction.

Returning to our original goal of establishing a viable synthetic route to 3-alkylidene-4-thiochromanone 1,1-dioxide analogs, we have now successfully extended our investigation of the utility of the method to a fairly large variety of ketones and aldehydes, as shown by Table 2. Since the purpose of these reactions is primarily synthetic, the yields shown in this table are *uncorrected* and represent conversion to isolated products in each case. The yields are modest but represent the only viable general route so far reported to these novel derivatives of 4-thiochromanone, a ring system of continuing biological interest (1, 2, 15). Benzophenone did not react with **6***b* under these conditions, while acetophenone gave only a trace of the expected product.

The application of a modern variant of the classical aldol reaction described in this study has revealed once again the impressive ability of enolate equivalents to overcome serious problems arising from the use of strongly basic, or acidic, reaction conditions. A convenient route to the otherwise difficulty accessible 3-alkylidene-4-thiochromanones is thereby revealed.

Can. J. Chem. Downloaded from www.nrcresearchpress.com by 210.87.254.5 on 09/06/12
For personal use only.

Can. J. Chem. Downloaded from www.nrcresearchpress.com by 210.87.254.5 on 09/06/12
For personal use only.

Experimental

Infrared spectra were recorded in chloroform on a Perkin–Elmer 298 grating spectrophotometer. The ^{1}H nmr spectra were obtained on a EM-360 spectrometer in $CHCl_3$-*d* solution unless otherwise indicated. Routine (low-resolution) mass spectra were obtained with a Du Pont 21-490 spectrometer and the high-resolution data on the AEI-MS 3074 instrument. Column chromatography and tlc (analytical and preparative) were carried out on silica gel supplied by E. Merck (Darmstadt). Elemental analyses were performed by the Scandinavian Microanalytical Laboratory, Box 25 DK2730, Herlev, Denmark. Melting points are uncorrected.

DME (1,2-dimethoxyethane) was dried from sodium benzophenone ketyl. Triethylamine, diisopropylamine, and toluene were dried by distillation over sodium. Chloroform and dichloromethane were dried with calcium chloride. Carbonyl compounds were routinely distilled on a Büchi–Brinkmann Kugelrohr apparatus. Titanium tetrachloride, if yellow, was distilled from zinc, although this additional precaution did not appear to affect the product yields obtained.

Preparations of enol silyl ethers **6**a,b

(a) *4-Trimethylsilyloxy-3-thiochromene,* **6**a

Potassium iodide (7.52 g, 45 mmol) was stirred in dry chloroform (25 mL), cooled to 0°C under N_2, and chlorotrimethylsilane (2.0 mL, 16 mmol) added, followed by the slow addition of a solution of 4-thiochromanone (**3***a*) (1.13 g, 6.9 mmol) and triethylamine (2.0 mL, 27 mmol) in dry chloroform (25 mL). The solution was allowed to warm to 25°C, then refluxed 16 h in the dark. Filtration and removal of solvent yielded crude **6***a* (1.47 g, 94%). This was distilled (Kugelrohr) at 130–140°C/0.9 torr (1 Torr = 133.3 Pa) (lit. (12) bp 115–118°C/0.75 Torr); ir ν: 1255 (C—O), 1640 (C=C) cm^{-1}; ^{1}H nmr δ: 0.2 (s, 9H), 3.4 (d, J = 6 Hz, 2H), 5.13 (t, J = 6 Hz, 1H), 6.8–7.3 (m, 3H), 7.3–7.6 (m, 1H) ppm (lit. (12) δ 5.12 (t, J = 5.1 Hz) ppm).

(b) *4-Trimethylsilyloxy-3-thiochromene 1,1-dioxide,* **6**b[2]

Dissopropylamine (3.02 mL, 22 mmol) was dissolved in dry DME (40 mL) and cooled to −78°C under N_2. 2.5 *M* n-Butyllithium (8.40 mL, 22 mmol) was added, followed 30 min later by the addition of a solution of 4-thiochromanone 1,1-dioxide **3***b* (4.01 g, 21 mmol) and chlorotrimethylsilane (6.50 mL, 51 mmol) in DME (40 mL). The red solution was allowed to warm to room temperature, then filtered and the solvent removed. The solid was redissolved in dichloromethane (60 mL) and the solution washed with saturated sodium bicarbonate solution (50 mL). The organic layer was dried ($MgSO_4$), filtered, and evaporated to yield **6***b* as a red oil (5.16 g, 96%). This crude product was satisfactory for further use and was not amenable to further purification by recrystallization, distillation, or chromatography (silica gel or alumina); ir ν: 1155 (SO_2), 1260 (C—O), 1320 (SO_2), 1642 (C=C) cm^{-1}; ^{1}H nmr δ: 0.2 (s, 9H), 3.85 (d, J = 6 Hz, 2H), 5.3 (t, J = 6 Hz, 1H), 7.4–7.7 (m, 3H), 7.8–8.0 (m, 1H) ppm.

3-Hydroxymethylene-4-thiochromanone, **4**

The procedure of Tilak (10) was modified by substituting an equimolar quantity of sodium hydride for sodium methoxide and an equal volume of toluene for benzene. Compound **4** was obtained in 95% yield and was distilled (Kugelrohr) at 140°C/1.5 Torr; ^{1}H nmr δ: 3.5 (s, 2H), 7.0–7.3 (m, 3H), 7.8–8.0 (m, 1H), 8.3 (s, 1H), 14.7 (s, 1H, disappears in D_2O) ppm. The red oil was stable and storable at 0°C.

3-Formyl-3-phenylthiomethyl-4-thiochromanone, **5**

Sodium hydride (0.27 g, 9.0 mmol) was slurried in dry DME (5.0 mL) and a solution of 3-hydroxymethylenethiochromanone **4** (1.71 g, 8.9 mmol) in DME (5.0 mL) added slowly at 0°C. Chloromethyl phenyl sulfide (1.20 mL, 8.9 mmol) was slowly added and the red slurry warmed to 25°C for 13 h, then refluxed a further 5 h, by which time the red color had disappeared. The solution was cooled and water added (1.0 mL) before evaporation of the solvent. The resultant red oil was dissolved in dichloromethane (50 mL) and washed with 1 *M* hydrochloric acid (20 mL). The acid layer was washed twice with dichloromethane (30 mL), the organic layers combined, dried ($MgSO_4$), filtered, and solvent removed to yield a red oil (2.80 g). This was chromatographed on a silica-gel thick-layer plate (dichloromethane) wtih a "pre-concentration" zone to yield **5** as a yellow oil (24%); ^{1}H nmr δ: 3.75 (s, 2H), 3.8 (s, 2H), 7.0–7.5 (m, 8H), 7.9–8.1 (m, 1H), 9.85 (s, 1H) ppm; ms *m/z*: 314(M^+, 1), 284(32), 175(100).

General procedures for Lewis acid catalyzed reactions of **6**a,b *with ketones/aldehydes*

Method A

3-Cyclohexylidene-4-thiochromanone, **8**a

4-Trimethylsilyloxy-3-thiochromene **6***a* (1.02 g, 4.3 mmol) and cyclohexanone **11** (0.50 mL, 4.9 mmol) were dissolved in dry dichloromethane (10 mL) and cooled to −78°C under N_2. Titanium tetrachloride (0.50 mL, 4.6 mmol) was added, turning the yellow solution black. The solution was allowed to warm to 25°C and stirred 18 h, before diluting with dichloromethane (50 mL) and washing with 1 *M* hydrochloric acid (50 mL), followed by saturated sodium bicarbonate (50 mL). Drying ($MgSO_4$), filtration, and evaporation yielded a dark oil which was chromatographed on silica gel. Dichloromethane/carbon tetrachloride (50:50) eluted **8***a* as a yellow oil (0.34 g, 32%); ir ν: 1682 (C=O) cm^{-1}; ^{1}H nmr δ: 1.4–2.1 (m, 6H), 2.3 (t, 2H), 2.6 (t, 2H), 4.3 (s, 2H), 7.6–8.0 (m, 3H), 8.0–8.2 (m, 1H) ppm; ms *m/z*: 244(100), 163(33), 136(53). *Exact mass* calcd. for $C_{15}H_{16}OS$: 244.0918; found (high resolution ms): 244.0925.

Dichloromethane/carbon tetrachloride (75:25) eluted 4-thiochromanone **3***a* (0.45 g, 63%).

3-Cyclopentylidene-4-thiochromanone, **7**a

Compound **6***a* (1.03 g, 4.4 mmol) and cyclopentanone **10** (0.40 mL, 4.5 mmol) were dissolved in dry dichloromethane (10 mL), cooled to −78°C under N_2, and titanium tetrachloride (0.38 mL, 3.5 mmol) added.

Work-up as above yielded a black oil (0.91 g) which was chromatographed on a silica gel thick-layer plate (dichloromethane) to yield **7***a* as a pale yellow oil (0.22 g, 22%); ^{1}H nmr δ: 1.5–1.8 (m, 4H), 2.4 (t, 2H), 2.75 (t, 2H), 3.7 (s, 2H), 7.0–7.3 (m, 3H), 7.9–8.2 (m, 1H) ppm; ms *m/z*: 230(100), 201(22), 197(26), 136(57).

4-Thiochromanone **3***a* was also recovered (0.24 g, 24%), as well as thiochromone **9** (0.14 g, 20%).

Method B

3-Cyclohexylidene-4-thiochromanone 1,1-dioxide, **8**b

Titanium tetrachloride (0.35 mL, 3.2 mmol) was added to a solution of cyclohexanone (0.33 mL, 3.2 mmol) at 0°C in chloroform (15 mL) under N_2. The addition of triethylamine (0.80 mL) turned the yellow solution red. A solution of 4-trimethylsilyloxy-3-thiochromene 1,1-dioxide **6***b* (0.80 g, 3.0 mmol) in dichloromethane (3 mL) was slowly added and the solution allowed to warm up to 25°C. After 18 h, the solution was diluted with dichloromethane (50 mL) and washed with 1 *M* hydrochloric acid (50 mL), saturated sodium bicarbonate (50 mL), dried ($MgSO_4$), filtered, and evaporated to yield a brown oil (0.75 g) which was chromatographed on silica gel. Dichloromethane/carbon tetrachloride (50:50) eluted **8***b* (0.28 g, 33%). This was recrystallized from 95% ethyl alcohol to yield pale yellow crystals, mp 138–139°C. (No 4-thiochromanone 1,1-dioxide was recovered in this case.) *Anal.* calcd. for $C_{15}H_{16}O_3S.\frac{1}{2}C_2H_5OH$: C 64.21, H 6.35, S 10.70; found: C 64.55, H 6.08, S 10.71.

3-Isopropylidene-4-thiochromanone 1,1-dioxide, **12**

Method B was used, with acetone (0.39 mL, 5.3 mmol) and titanium tetrachloride (0.57 mL, 5.3 mmol) in dichloromethane (5 mL) at −78°C, followed by the addition of **6***b* (1.39 g, 5.2 mmol) in dichloromethane (5.0 mL). Work-up afforded a brown oil (0.85 g) from which **12** (42%) was isolated by chromatography on a silica-gel thick-layer plate, mp 107–108°C. *Anal.* calcd. for $C_{12}H_{12}O_3S$: C 61.00, H 5.12, S 13.57; found: C 61.01, H 5.32, S 13.41.

[2]Silyl ether **6***a* could also be made conveniently using this procedure.

3-Isobutylidene-4-thiochromanone 1,1-dioxide, 13

Method B was used, with isobutyraldehyde (0.41 mL, 4.5 mmol), titanium tetrachloride (0.48 mL, 4.5 mmol) in dichloromethane (10 mL) at −78°C, followed by the addition of **6***b* (1.18 g, 4.4 mmol) in dichloromethane (10 mL). Work-up afforded a brown oil (0.95 g) from which pure **13** was isolated (0.32 g, 30%) as a yellow solid, mp 98°C (95% EtOH); ms *m/z*: 250(20), 186(72), 171(52), 132(100). *Exact Mass* calcd. for $C_{13}H_{14}O_3S$: 250.0646; found (high resolution ms): 250.0663.

3-Benzylidene-4-thiochromanone 1,1-dioxide, 14

Method B was used, with a solution of **6***b* (1.39 g, 5.2 mmol) in dichloromethane (5 mL) being added to a solution of titanium tetrachloride (0.58 mL, 5.3 mmol) and benzaldehyde (0.54 mL, 5.3 mmol) at −78°C. Chromatography of the oil (0.34 g) resulting from work-up afforded pure **14** (0.27 g 18%) on elution with dichloromethane/carbon tetrachloride (50:50), as a solid, mp 172°C (95% EtOH); ir *ν*: 1155, 1320 (SO_2), 1675 (C=O) cm^{-1}; ms *m/z*: 284(82), 220(85), 192(100). *Exact Mass* calcd. for $C_{16}H_{12}O_3S$: 284.0503; found (high resolution ms): 284.0510.

3-(2-Heptylidene)-4-thiochromanone 1,1-dioxide, 15

Method B was used, with a solution of **6***b* (1.39 g, 5.2 mmol) in dichloromethane (7 mL) being added to a solution of 2-heptanone (0.75 mL, 5.3 mmol) and titanium tetrachloride (0.58 mL, 5.3 mmol) in dichloromethane. Work-up afforded a dark oil (1.40 g) from which pure **15** (0.17 g, 11%) was obtained by column chromatography with dichloromethane/carbon tetrachloride (75:25) as eluant. Attempted recrystallization from 95% ethanol yielded only a tan oil; ir *ν*: 1150, 1318 (SO_2), 1677 (C=O) cm^{-1}; ms *m/z*: 292(5), 166(11), 149(100). *Exact Mass* calcd. for $C_{16}H_{20}O_3S$: 292.1127; found (high resolution ms): 292.1140.

Method C

*3-Cyclopentylidene-4-thiochromanone 1,1-dioxide, 7*b

Silyl ether **6***b* (1.14 g, 4.3 mmol) and **10** (0.38 mL, 4.3 mmol) were dissolved in dry dichloromethane (25 mL) and cooled to −78°C. A slow stream (1 bubble/s) of boron trifluoride was passed through the solution in a N_2 stream (3 bubbles/s) until fuming was observed in the sodium hydroxide solution exit trap. The flow of gases was continued for an additional 15 min before the reaction flask was allowed to warm to room temperature and stirred a further 16 h. The mixture was then poured into saturated sodium bicarbonate solution (50 mL) and extracted three times with dichloromethane (30 mL). The organic layers were combined, dried ($MgSO_4$), filtered, and evaporated to yield a brown oil (1.07 g), from which **7***b* was obtained (0.28 g, 25%), mp 126.7°C (95% EtOH); ir *ν*: 1155, 1322 (SO_2), 1670 (C=O) cm^{-1}; ms *m/z*: 262(100), 197(48), 169(40). *Exact Mass* calcd. for $C_{14}H_{14}O_3S$: 262.0660; found (high resolution ms): 262.0664.

Acknowledgements

We are grateful to the Natural Sciences and Engineering Research Council of Canada for generous financial support.

1. M. H. HOLSHOUSER and L. J. LOEFFLER. J. Pharm. Sci. **71**, 715 (1982).
2. M. H. HOLSHOUSER, J. L. LOEFFLER, and I. H. HALL. J. Med. Chem. **24**, 853 (1981).
3. I. W. J. STILL and S. B. ABHYANKAR. J. Org. Chem. **47**, 373 (1982).
4. I. W. J. STILL, P. C. ARORA, S. K. HASAN, G. W. KUTNEY, L. Y. T. LO, and K. TURNBULL. Can. J. Chem. **59**, 199 (1981).
5. I. W. J. STILL and T. S. LEONG. Can. J. Chem. **58**, 369 (1980).
6. R. O. LOUTFY, I. W. J. STILL, M. THOMPSON, and T. S. LEONG. Can. J. Chem. **57**, 638 (1979).
7. F. ARNDT, W. FLEMMING, E. SCHOLTZ, V. LOWENSOHN, G. KALLNER, and B. EISTERT. Chem. Ber. **58**B, 1612 (1925).
8. V. D. ORLOV, O. A. NODEL'MAN, and E. I. MIKHED'KINA. Zh. Obshch. Khim. **51**, 1153 (1981).
9. I. W. J. STILL, M. S. CHAUHAN, and M. T. THOMAS. Can. J. Chem. **51**, 839 (1973).
10. V. N. GOGTE, K. A. R. SASTRY, and B. D. TILAK. Ind. J. Chem. **12**, 1147 (1974).
11. I. PATERSON and I. FLEMING. Tetrahedron Lett. 2179 (1979).
12. L. H. HELLBERG and A. JUAREZ. Tetrahedron lett. 3553 (1974).
13. I. FLEMING, J. IQBAL, and E.-P. KREBS. Tetrahedron, **39**, 841 (1983).
14. E. NAKAMURA, J. SHIMADA, Y. HORIGUCHI, and I. KUWAJIMA. Tetrahedron Lett. **24**, 3341 (1983).
15. K. RAMALINGAM, G. X. THYVELIKAKATH, K. D. BERLIN, R. W. CHESNUT, R. A. BROWN, N. N. DURHAM, S. E. EALICK, and D. VAN DER HELM. J. Med. Chem. **20**, 847 (1977).

Can. J. Chem. Downloaded from www.nrcresearchpress.com by 210.87.254.5 on 09/06/12
For personal use only.

High temperature catalytic hydrogenolysis and alkylation of anisole and phenol

R. K. M. R. KALLURY AND T. T. TIDWELL
Department of Chemistry, University of Toronto, Toronto, Ont., Canada M5S 1A1
AND
D. G. B. BOOCOCK AND D. H. L. CHOW
Department of Chemical Engineering, University of Toronto, Toronto, Ont., Canada M5S 1A4

Received March 2, 1984

This paper is dedicated to Professor Peter Yates on the occasion of his 60th birthday

R. K. M. R. KALLURY, T. T. TIDWELL, D. G. B. BOOCOCK, and D. H. L. CHOW. Can. J. Chem. **62**, 2540 (1984).

Hydrogenation of phenol at 2.8 MPa pressure with $MoO_3-NiO-Al_2O_3$ catalyst at 450°C gave 60% benzene, 16% cyclohexane, and 7% methylcyclopentane, while anisole under the same conditions gave 60–70% less of each of these products and 52% methylated benzenes. In the presence of added methanol either phenol or anisole give 47–63% of methylbenzenes and 22% of methylated phenols. At 350–400°C significant yields of cyclohexylbenzene and cyclohexylphenol were formed. The reactions are interpreted as involving electrophilic methylation or cyclohexylation of phenol concurrent with ring hydrogenation and hydrogenolysis of C—O bonds. Cyclohexyl cations are proposed as reactive intermediates that act as cyclohexylating agents or rearrange to methylcyclopentyl cations, and the methylating species is derived from methanol or the methyl group of anisole. When phenol was reacted with H_2 and CD_3OH the methylated aromatic products were only partially deuterated, indicating exchange with the H_2 atmosphere was occurring. Control experiments involving possible intermediates in the reaction are consistent with these conclusions. Nickel catalysts favour ring saturation over C—O bond cleavage.

R. K. M. R. KALLURY, T. T. TIDWELL, D. G. B. BOOCOCK et D. H. L. CHOW. Can. J. Chem. **62**, 2540 (1984).

L'hydrogénation du phénol à une pression de 2,8 MPa, à 450°C et utilisant un catalyseur de $MoO_3-NiO-Al_2O_3$ fournit un mélange formé de 60% de benzène, 16% de cyclohexane et 7% de méthylcyclopentane; dans les mêmes conditions, l'anisole fournit de 60 à 70% de moins de chacun de ces produits et 52% de benzènes méthylés. Si on ajoute du méthanol au milieu réactionnel, le phénol ainsi que l'anisole conduisent à 47–63% de méthylbenzènes et 22% de phénols méthylés. A des températures de 350 à 400°C, il se forme des quantités importantes de cyclohexylbenzène et de cyclohexylphénol. On suppose que ces réactions impliquent que, concurrement avec l'hydrogénation du cycle et l'hydrogénolyse des liaisons C—O, il se produit des réactions de méthylation ou de cyclohexylation électrophiles du phénol. On propose les cations cyclohexyles comme intermédiaires réactionnels qui agissent comme agents cyclohexylants ou qui se transposent en cations méthylcyclopentyles; les espèces méthylantes proviendraient soit du méthanol soit du groupe méthyle de l'anisole. Lorsqu'on fait réagir du phénol avec du H_2 et du CD_3OH, les produits aromatiques méthylés qui se forment ne sont que partiellement deutérés; ceci indique qu'il se produit un échange avec le H_2 du milieu. Des réactions de contrôle impliquant des intermédiaires réactionnels possibles sont en accord avec ces conclusions. Les catalyseurs de nickel favorisent la saturation du cycle plutôt que la rupture de la liaison C—O.

[Traduit par le journal]

Can. J. Chem. Downloaded from www.nrcresearchpress.com by 210.87.254.105 on 09/06/12
For personal use only.

Introduction

The thermal liquefaction of wood is a process for biomass conversion that has recently been the object of study in many different laboratories (1–7). Analysis of the chemical composition of the liquefaction products has revealed the presence of alkylphenols as well as cyclic ketones that may be derived at least in part from phenols (8–11). The present investigation was undertaken for the purpose of understanding some of the chemical pathways that may occur during liquefaction and also for studying the reactivity of the phenols themselves in processes that might form upgraded products with increased value as fuels. Increased yields of aromatics and decreased oxygen content would be particularly desirable for the latter goal.

Previous studies on the hydrogenolysis of phenol indicate that under most conditions for removal of the OH function saturation of the ring also occurs (12–14). However, it has been demonstrated that the use of molybdenum-based catalysts gives significant yields of aromatic hydrocarbons (15). Accordingly this study has concentrated on hydrogenation in the presence of a molybdenum catalyst.

Experimental

A. Procedure for hydrogenolysis

Approximately 10 g of the substrate was placed in a 1 L stirred autoclave reactor (AE Autoclave of Canada Ltd.) with approximately 1.5 g of BASF catalyst M 8-21 (15% MoO_3, 3% NiO on activated alumina) enclosed in two stainless steel mesh baskets suspended in the vapour region of the reactor. The autoclave was sealed, hydrogen-flushed twice, and charged with hydrogen to the desired cold pressure (2.8–9.8 MPa). The autoclave was heated to the desired temperature (350–450°C) at the rate of approximately 5°/min, with the reported reaction time commencing from the point of reaching the desired temperature. After the contemplated reaction period the heaters were removed and the reactor cooled. After venting of the gases the reactor was opened and the liquid product collected and weighed.

B. Analysis of the liquid products

The dried ($MgSO_4$) liquid was analyzed by a three-step procedure: (*i*) initially, the product mixture from each reaction was subjected to analytical gas chromatography and peak retention times compared with those of standards (which include commercial or synthesized methylcyclopentane, cyclohexane, cyclohexene, benzen, toluene, *o*-, *m*-, and *p*-xylenes, 1,2,4- and 1,3,5-trimethylbenzenes, 1,2,4,5-tetramethylbenzene, phenol, *o*-, *m*-, and *p*-cresols, 2,4- and 2,6-dimethylphenols, and *o*- and *p*-cyclohexylphenols, diphenyl, and cyclohexylbenzene); (*ii*) each product mixture was then subjected to gc–ms and comparison of each peak from the resulting mass chromatogram (a plot of the total ion current against time/scan number) with the analytical gc of the same product mixture confirmed the structure of the substance corresponding to each peak; and finally (*iii*) the reaction product from each substrate was subjected to preparative gas chromatography and the structures of individual products isolated there

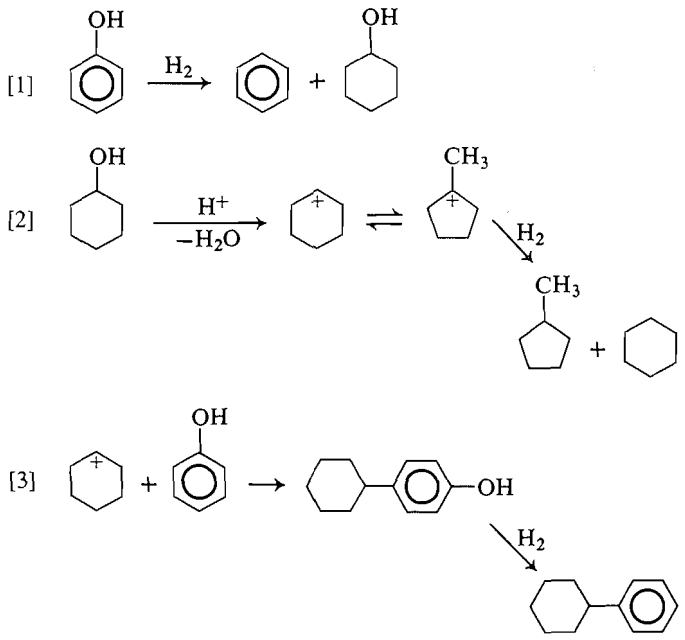

SCHEME 1

from unequivocally established by ^{1}H-nmr and mass spectra. The instrumentation used has been described previously (11).

Results and discussion

The reaction of phenol using the MoO_3-NiO catalyst at 450°C and 2.8 MPa gave essentially complete conversion of the reactant after 45 min reaction time, with formation of benzene (60%), cyclohexane (16%), and methylcyclopentane (7%) as the major products. In addition, a group of products were formed that were presumably derived from coupling of two phenol-derived units, namely, cyclohexylcyclohexane (2%), diphenyl (3%), and cyclohexylbenzene (2%). These results indicate that benzene is essentially inert to these reaction conditions and this was confirmed experimentally (Table 1).

A mechanism to explain these observations is shown in Scheme 1 (reactions [1]–[3]).[1] A key feature of this proposed pathway is the intermediacy of cyclohexanol as the precursor to cyclohexane, methylcyclopentane, and the C_{12}-products, so this was tested by examining the reactivity of various cyclic C_6 compounds under the same conditions (Table 1). The failure of benzene, cyclohexane, cyclohexene, or cyclohexanone to form major amounts of methylcyclopentane or the C_{12}-products indicates that these reactants are not major participants as reactive intermediates in phenol reduction, whereas the observed formation of methylcyclopentane and cyclohexane from cyclohexanol is in accord with Scheme 1. The isomerization of cyclohexane to methylcyclopentane has been observed on heating with catalysts (16), but, as shown in Table 1, is not significant under our reaction conditions. The intervention of a cyclohexyl cation as shown in Scheme 1 can accommodate this product, as the rearrangement of the cyclohexyl cation to the methylcyclopentyl system is a known process (17). The intervention of the cyclohexyl cation provides a reasonable pathway for formation of the C_{12}-products as well by the known electrophilic aromatic substitution on phenol (18). Free radical intermediates are excluded on the basis that rearrangement of the cyclohexyl radical to the methylcyclopentyl system is not normally observed (19). The failure to form C_{12}-products from cyclohexanol itself is expected in the absence of phenol.

In an interesting analogue of this reaction cyclohexanol was reacted with hydrogen and iodine at 7 MPa at 300°C to give a 40% yield of hydrocarbons in the ratio shown (reaction [4]) (20).

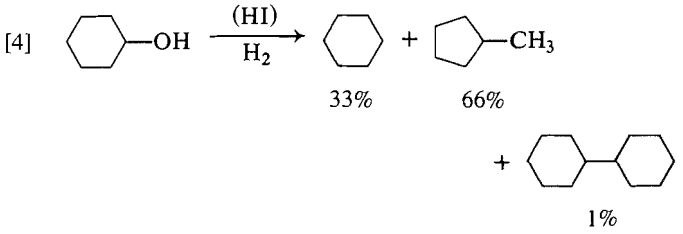

This process was shown to involve alkyl iodides and while the mechanism of their reaction was left open, the formation of cyclohexylcyclohexane was attributed to a free radical dimerization. As already noted, free radical intermediates would not provide a route to the large amounts of methylcyclopentane, whereas the alkyl iodides should be good sources of carbonium ions so such intermediates are strongly implied in this reaction. The similarity of the products observed in our work and in this latter study also suggests that our MoO_3-NiO catalyst does not play a crucial role in the cyclohexyl/methylcyclopentyl interconversion.

At lower temperatures (350 or 400°C, Table 2) the conversion of phenol is not complete even after 2 h, and the proportion of saturated products has increased at the expense of the benzene. Evidently the reaction mechanism for the hydrogenolysis of phenol to benzene and the ring saturation to cyclohexanol are quite different, and the former process becomes much more favourable at higher temperatures. This effect has been observed before by Cawley (21) who found that ammonium molybdate on charcoal converted phenol to cyclohexane and benzene in 37 and 25% yields at 400°C, and 35 and 44%, respectively, at 450°C.

The reaction of *o*-cyclohexylphenol under comparable conditions (Table 1) provides a further insight into this reaction sequence. The product mixture resembled that from phenol itself, and the formation of methylbenzenes provides a clue to the origin of these products from phenol. Degradation of the cyclohexylarene to a methylarene (reaction [5]) evidently occurs as one of the reaction pathways, although it cannot be specified whether this reaction precedes hydrogenolysis of the phenolic OH. This reaction also explains why significant yields of cyclohexylphenols are observed at 350–400°C but not at 450°C (Table 2). Evidently these products do not survive the higher temperature.

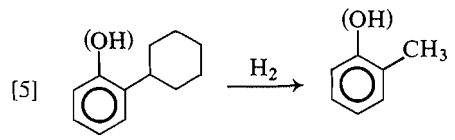

Anisole was 98% consumed on reaction with the MoO_3-NiO catalyst at 450°C and 2.8 MPa (Table 1), but in comparison to phenol gave only about a third of the amounts of methylcyclopentane, cyclohexane, and benzene. Instead tolu-

[1]This description of a mechanism for a reaction at high temperature in the presence of inhomogeneous catalysts in terms of specific reaction intermediates familiar from reactions in solution near room temperature is surely naive. Nevertheless, a consistent and useful rationalization does emerge from this analysis.

Can. J. Chem. Downloaded from www.nrcresearchpress.com by 210.87.254.105 on 09/06/12
For personal use only.

Can. J. Chem. Downloaded from www.nrcresearchpress.com by 210.87.254.105 on 09/06/12
For personal use only.

TABLE 1. Hydrogenation with BASF catalyst, 450°C, 2.8 MPa initial H_2 pressure

Substrate	% conversion	Methylcyclopentane	Cyclohexane	Cyclohexene	Benzene	Toluene	Me_2benzene[c]	Me_3benzene[d]	Me_4benzene	Me_5benzene	Other
Cyclohexane	2		98		2						
Cyclohexene	100		85		15						
Cyclohexanol	100	20	65		0.3	0.1	0.1				
Cyclohexanone	100	3	40	36	0.5	0.1	0.1				[e]
Phenol	100	7	16		60	2	2	2	2		[f]
Anisole	98	2	5		20	18	12	15	5		[g]
Phenol/MeOH[a]	98	1	2	1	7	7	8	16	20	10	[h]
Phenol/CD_3OH[b]	75	1	1		10	8	6	3	5	2	[i]
Anisole/MeOH[a]	96	0.5	1		2	5	5	13	16	8	[j]
Benzene	0										
Benzene/MeOH[a]	2				98	2					
m-Xylene	15					6	85				[k]
m-Xylene/MeOH[a]	15					4	85	4[m]	2		
o-Cyclohexylphenol	91	14	16		20	3	2				[l]

[a]1/1 (by wt.).
[b]2/1 (by wt.), 2.1 MPa.
[c]*o*/*m*,*p* = 1/2.5.
[d]1,2,3/1,2,4/1,3,5 = 1/3/6.
[e]Cyclohexylbenzene (7), biphenyl (4), phenol (4).
[f]Cyclohexylbenzene (2), biphenyl (3), cyclohexylcyclohexane (2).
[g]Phenol (10), mono- and dimethylphenol (10).
[h]Methylphenols (3), dimethylphenols (15), trimethylphenols (5), hexamethylbenzene (2).
[i]Methylphenols (15), dimethylphenols (13), trimethylphenol (3), hexamethylbenzene (2).
[j]Phenol (5), methylphenols (4), dimethylphenols (14), trimethylphenols (14), tetramethylphenols (4),methylcyclohexane (3), dimethylcyclohexane (1).
[k]1,3-Dimethylcyclohexane (3).
[l]Phenol (10), cyclopentane (2), cyclohexylbenzene (11), bicyclohexyl (3), biphenyl (4).
[m]1,2,4-Isomer.

TABLE 2. Reaction variables in the BASF catalyst hydrogenation of phenol[a]

T(°C)	Pressure (MPa)	Time (h)	Phenol	Benzene	Cyclohexane	Methylcyclopentane	Cyclohexylbenzene	Biphenyl	Other[c]
400	9.8	2	13	23	24	16	5	4	
400	9.8	0.5	38	22	13	2	8	5	[d]
350	9.8	1	35	15	14		2		[e]
400	3.5	2	27	30	7	7	4	4	[f]
350	2.8	2	53	17	15		4	1	[g]
450[b]	2.8	0.3	47	26	12	7			[h]
450[b]	2.8	0.7		60	16	7			
450[b]	2.8	1.3		58	20	13			
450[b]	2.8	1.8		55	19	12			

[a]Catalyst concentration 20% with 100 g substrate except as noted.
[b]Catalyst concentration 15% with 10 g substrate.
[c]Methylated benzenes were formed in yields up to 9% total (cf. Table 1).
[d]Cyclohexylphenols (7).
[e]Cyclohexylphenol (19), dicyclohexylphenol (12).
[f]Cyclohexylphenols (3), dicyclohexylphenols (2).
[g]Bicyclohexyl (2), cyclohexylphenol (7).
[h]Cyclohexene (5).

ene, xylenes, and tri- and tetramethylbenzenes constituted 52% of the volatile product, along with 20% of phenol and mono- and dimethylphenols. If methanol was added to the reaction of either phenol or anisole then the formation of C_6 products decreased still further and methylated benzenes and phenols made up at least 80% of the product.

Evidently phenol is methylated by a reactive species derived from methanol, and the methyl group of anisole is also active in ring methylation. The alkylation of the phenol nucleus must precede cleavage of the OH group, as benzene is unreactive under these conditions and xylene gives only 15% conversion to other products (Table 1). The much greater reactivity of phenol compared to benzene and xylene is consistent with an electrophilic attack on the phenol to give methylated phenols, which then undergo hydrogenolysis to the methylbenzenes (reaction [6]).

[6] 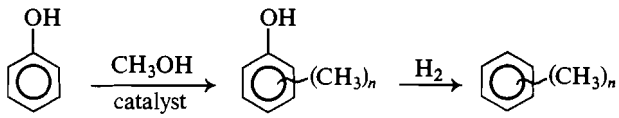

There have been previous reports of methylation of phenol by methanol and MoO_3 catalysts, for example, that of Inoue and Enomoto shown in reaction [7] (22). A similar preference for *o*-methylation was observed for reaction of phenol and methanol with ThO_2 (23).

[7] 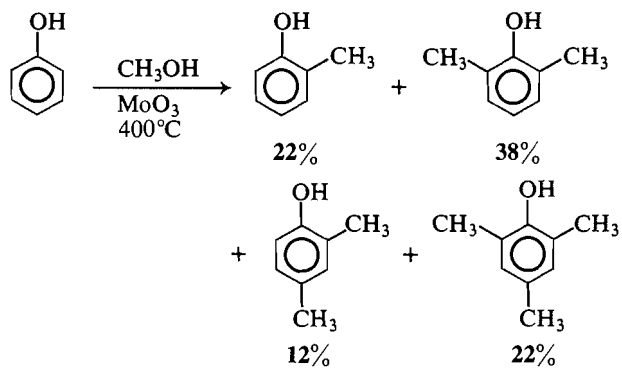

The preference for substitution *ortho* to the OH group was ascribed by these latter authors (23) to coordination of phenol and methanol to neighboring sites on the catalyst surface and delivery of the methyl group in an electrophilic attack to the nearby *ortho* position (reaction [8]). Inoue and Enomoto (22) also suggested that electrophilic attack on the ring by an alkyl cation on the catalyst surface could occur. The *p*-position of the phenol ring would also be accessible for such a process and this mechanism provides a satisfactory explanation of our results.

[8] 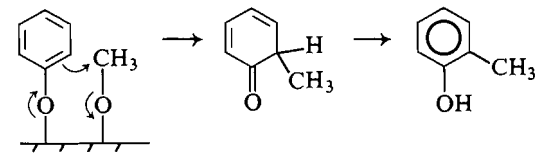

The details of the alkylation process were elucidated further in an experiment in which phenol was reacted with CD_3OH (Table 1). The product distribution resembled that for the comparable reaction with CH_3OH, but in the former case the conversion of phenol dropped to 75% instead of 90%, and the yield of polymethylated benzenes was greatly reduced (18% vs. 56%) while the amount of methylphenols was significantly greater (15% vs. 3%). The lower extents of methylation and hydrogenolysis are presumably due to the proportionally lower amount of methanol and the somewhat lower pressure used in the CD_3OH experiment.

The deuterium contents[2] of the products in the CD_3OH experiment were monitored using CIMS and gc–ms, with the following results: benzene (d_0/d_1 = 1/0.3), toluene ($d_0/d_1/d_2/d_3$ = 1/0.6/0.5/0.4), phenol (d_0/d_1 = 1/0.3), cyclohexane (d_0/d_1 = 1/0.5), xylenes ($d_0/d_1/d_2/d_3/d_4/d_5/d_6$ = 1/0.6/0.3/0.2/0.1/0.05/0.03). The alkylphenols showed comparable deuterium incorporation.

These results show that there has been considerable isotopic exchange by hydrogen for deuterium in the methylated aromatic products. One plausible pathway for this exchange would be isotopic exchange of the methanol through dedeuteration to a formaldehyde intermediate on the catalyst surface which is then hydrogenated to methanol which attacks the aryl ring as depicted in reaction [8]. An alternative pathway would involve attack by the formaldehyde unit (reaction [9]), and is similar to

[2]Corrected for natural isotopic abundance.

Can. J. Chem. Downloaded from www.nrcresearchpress.com by 210.87.254.105 on 09/06/12
For personal use only.

TABLE 3. Effect of catalyst variation on hydrogenation anisole (7 MPa)

Catalyst	T(°C)	Anisole	Cyclohexyl methyl ether	Cyclohexane	Cyclohexanol	Phenol	Cyclohexanone	Benzene	Phenylcyclohexene	Other
Ni/Al (H_2O)	350	45	25	5	14	1				
Ni/Al	350	26		26	3	18	10	2		
Ni/Al (H_2O)	250	82	4		4	3	2			
Ni/Al	250	68	10	2	2	2	5			
$NiCO_3$ (H_2O)	350	72			7	3	4		2	
$NiCO_3$	350	16		46	10					
$NiCO_3$ (H_2O)	250	98				2				
$NiCO_3$	250	15	45	26	15					
Raney Ni	250	5		49		8		16	5	[a]
Raney Ni (MeOH)	250	28	10	8	24	2	2	5		[b]

[a]Methylcyclopentane (7).
[b]Methylphenols (16).

a process proposed by Inoue and Enomoto for MgO catalyst (22). A third alternative would be the exchange of the aryl-methyls by hydrogen after ring-substitution has occurred; there is evidence for such a reaction using Ni catalysts (24). However, under these latter conditions exchange of the aryl hydrogens in both benzene and alkylbenzenes occurred, whereas under our conditions this is evidently not the case.

[9] 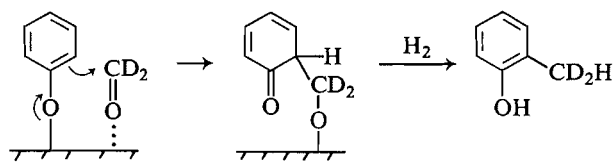

The benzene and cyclohexane formed had each undergone monodeuteration to the extent of about 30%, with very little, if any, higher deuteration. This result indicates that the deuterium is incorporated in the hydrogenolysis of the OH group and not in the hydrogenation of the ring. This reaction could occur by nucleophilic substitution with concomitant formation of formaldehyde as shown in reaction [10].

[10] 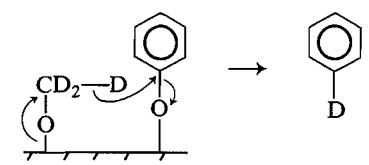

The recovered phenol was shown by its mass spectrum to have the deuterium incorporated as PhOD. This result shows that deuterium originally present as CD_3OH has been converted to part of the hydroxylic hydrogen pool.

The reaction of cyclohexanone with MoO_3–NiO catalyst (Table 1) gives a product composition significantly different from that of cyclohexanol, so it is apparent that reduction of cyclohexanone to cyclohexanol is not a major reaction pathway under these conditions. In particular 36% of cyclohexene is observed, as well as 4% of phenol and 11% of cyclohexylbenzene and biphenyl which are evidently derived from phenol. The formation of phenol from cyclohexanone on catalytic treatment has been observed before (25) and presumably occurs via enolization of the cyclohexanone (reaction [11]). A metal enolate (**1**) could undergo hydrogenolysis to provide the observed cyclohexene (reaction [12]). This suggestion is related to the proposal of a "π-allylic intermediate" (**2**) in the reaction of cyclohexanol on platinum (25), and similar oxo-π-allylpalladium complexes have been reported (26) and provide an alternative to the enolate **1**.

[11] 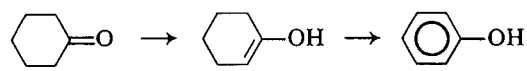

[12] 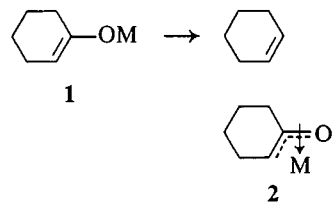

The strong effect of MoO_3-based catalysts in removing oxygen from organic molecules appears in the conversions of both phenol to benzene, and cyclohexanone to cyclohexene. The active molybdenum species under the reaction conditions of high temperatures and hydrogen atmosphere has been shown to be Mo(IV) (27), and evidently this species has a high affinity for oxygen which facilitates cleavage of the C—O bond by hydrogen.

The reduction of anisole with nickel catalysts (Table 3) gave quite different results from the reaction with the molybdenum-based catalyst. Raney nickel without solvent was the most active catalyst, and the predominant reaction was saturation of the aromatic ring. No ring methylated products were observed.

The NiO in the BASF catalyst clearly does not have the catalytic activity of the nickel catalysts surveyed in Table 3, for even at the higher temperatures used in the former reactions the extent of benzene hydrogenation is low. The specificity of this MoO_3–NiO on alumina catalyst is emphasized by the observation that MoO_2 supported on nickel is an effective catalyst for the hydrogenation of benzene to cyclohexane (28).

In summary, the use of MoO_3-NiO catalyst is quite effective for the hydrogenation of phenol to benzene and this process shows promise for the upgrading of wood oils. The conversion of anisole or of phenol and methanol to methylated aromatics by the catalyst indicates that this process will also occur in wood oils because of the presence of aryl methyl ethers in the original lignin. The observations of the degradation of o-cyclohexylphenol and the isotopic exchange of the CD_3OH-

Can. J. Chem. Downloaded from www.nrcresearchpress.com by 210.87.254.105 on 09/06/12
For personal use only.

derived products demonstrate the severity of the reaction conditions and the complexity of the processes which occur.

Acknowledgement

Financial support by a Strategic Grant from the Natural Sciences and Engineering Research Council of Canada and by Imperial Oil, Limited, is gratefully acknowledged.

1. R. L. EAGER, J. F. MATHEWS, J. M. PEPPER, and H. ZOHDI. Can. J. Chem. **59**, 2191 (1981).
2. F. SHAFIZADEH. Prog. Biomass. Convers. **3**, 51 (1982).
3. D. G. B. BOOCOCK, D. MACKAY, H. FRANCO, and P. LEE. Can. J. Chem. Eng. **58**, 466 (1980); **60**, 802 (1982).
4. T. J. ELDER and E. J. SOLTES. Wood Fibre, **12**, 217 (1980).
5. K. W. HANSELMANN. Experientia, **38**, 176 (1982).
6. M. B. POLK and M. PHINGBODHIPAKKIYA. Nucl. Chem. Waste Manage. **1**, 111 (1980); Chem. Abstr. **95**, 17666f (1981).
7. K. GRAVES. Holz Roh-Wehrkst. **40**, 41 (1982); Chem. Abstr. **96**, 124731 (1982).
8. I. J. MILLER and S. K. FELLOWS. Nature, **289**, 398 (1981).
9. YU. K. SHAPOSHNIKOV and L. V. KOSYUKOVA. Gidroliz. Lesokhim. Prom. **19**, 19 (1966); Chem Abstr. **66**, 56740w (1966).
10. R. L. EAGER, J. M. PEPPER, J. C. ROY, and J. F. MATHEWS. Can. J. Chem. **61**, 2010 (1983).
11. D. G. B. BOOCOCK, R. K. M. R. KALLURY, and T. T. TIDWELL. Anal. Chem. **55**, 1689 (1983).
12. P. N. RYLANDER. Catalytic hydrogenation in organic syntheses. Academic Press, New York. 1979. pp. 192–212.
13. M. LJ. MIHAILOVIC and Z. CEKOVIC. *In* The chemistry of the hydroxyl group. Part 1. *Edited by* S. Patai. Interscience, London. 1971. pp. 577–581.
14. L. J. BAGNELL and E. A. JEFFERY. Aust. J. Chem. **34**, 697 (1981).
15. N. J. SHUIKIN and L. A. ERIVANSKAYA. Usp. Khim. **29**, 648 (1960); Russ. Chem. Rev. **29**, 309 (1960).
16. A. K. KHASANOV, I. KADYROV, and A. M. MADZHIDOV. Uzb. Khim. Zh. **16**, 72 (1972); Chem Abstr. 77, 61297p (1972).
17. (*a*) E. M. ARNETT and C. PETRO. J. Am. Chem. Soc. **100**, 5408 (1978); (*b*) V. ILLÉS and H. SCHINDLBAUER. Acta Chim. Acad. Sci. Hung. **82**, 449 (1974).
18. J. F. BARTLETT and C. E. GARLAND. J. Am. Chem. Soc. **55**, 2064 (1933).
19. A. L. J. BECKWITH and K. U. INGOLD. Free radical rearrangement. *In* Rearrangements in ground and excited states. Vol. 1. *Edited by* P. deMayo. Academic Press, New York. 1980.
20. W. W. PAUDLER and T. E. WALTON. J. Org. Chem. **46**, 4306 (1981).
21. C. M. CAWLEY. Fuel, **11**, 217 (1932).
22. M. INOUE and S. ENOMOTO. Chem. Pharm. Bull. **24**, 2199 (1976).
23. S. KARUPPANNASAMY, K. NARAYANAN, and C. N. PILLAI. J. Catal. **66**, 281 (1980).
24. (*a*) L. M. MAMALADZE, N. V. NEKRASOV, B. S. GUDKOV, and S. L. KIPERMAN. Acta Chim. Acad. Sci. Hung. **92**, 73 (1977); (*b*) P. M. POJER. Tetrahedron Lett. **25**, 2507 (1984).
25. I. MANNINGER, Z. PAAL, and P. TETENYI. J. Catal. **48**, 422 (1977).
26. (*a*) T. MUKAIYAMA, M. OHSHIMA, and T. NAKATSUKA. Chem. Lett. 1207 (1983); (*b*) Y. ITO, H. AOYAMA, T. HURAO, A. MOCHIZUKI, and T. SAEGUSA. J. Am. Chem. Soc. **101**, 494 (1979); (*c*) N. YOSHIMURA, S.-I. MURAHASHI, and I. MORITANI. J. Organomet. Chem. **52**, C58 (1973).
27. L. A. WOODWARD and A. T. GLOVER. Trans. Faraday Soc. **44**, 608 (1948).
28. M. ASTIER, A. BERTRAND, and S. J. TEICHNER. C. R. Seances Acad. Sci. Ser. C, **290**, 333 (1980); Bull. Soc. Chim. Fr. 191 (1980).

Can. J. Chem. Downloaded from www.nrcresearchpress.com by 210.87.254.105 on 09/06/12
For personal use only.

Spectroscopic studies of the compatibility of small molecules in polymers

RAFIK O. LOUTFY AND BENG S. ONG
Xerox Research Centre of Canada, 2660 Speakman Drive, Mississauga, Ont., Canada L5K 2L1

Received March 16, 1984

This paper is dedicated to Professor Peter Yates on the occasion of his 60th birthday

RAFIK O. LOUTFY and BENG S. ONG. Can. J. Chem. **62**, 2546 (1984).

A spectroscopic technique has been developed to study the compatibility and stability of small molecules in polymers. The technique was applied to investigate the compatibility of an electron-acceptor molecule, *n*-butyl 9-dicyanomethylene fluorene-4-carboxylate (BDFC), **1**, in six different polymers. The electronic absorption of the small molecule **1** in polymer films as a function of concentration and temperature was examined. The deviation in the absorption of **1** from the molecular absorption properties was taken to indicate the degree of incompatibility (phase separation). The small molecule **1** was found to be most compatible with halogenated and electron-donating polymers.

In general, our results indicated the existence of very strong intermolecular interaction between the small molecules and weaker small molecule – polymer interaction, which lead to the small molecule aggregation, i.e., incompatibility. The extent of aggregation of **1** in various polymers varied with the concentration of **1**, the speed of drying the film, and the post-casting heat treatment. Aggregation of **1** in polycarbonate was drastically suppressed by incorporating a donor molecule into the matrix.

RAFIK O. LOUTFY et BENG S. ONG. Can. J. Chem. **62**, 2546 (1984).

On a développé une technique spectroscopique permettant d'étudier la compatibilité et la stabilité des petites molécules dans des polymères. On a appliqué la technique pour étudier la compatibilité d'une molécule acceptrice d'électrons, le dicyanométhylène-9 fluorènecarboxylate-4 de *n*-butyle (BDFC) (**1**), dans six polymères différents. On a aussi évalué, en fonction de la concentration et de la température, l'absorption électronique de la petite molécule **1** dans des films de polymère. On a utilisé la déviation dans l'absorption de **1**, par rapport aux propriétés moléculaires d'absorption, comme mesure de l'incompatibilité (séparation de phase). On a trouvé que la compatibilité de la petite molécule **1** est maximale avec les polymères halogénés et les polymères donneurs d'électrons.

D'une façon générale, nos résultats indiquent qu'il existe de très fortes interactions intermoléculaires entre les petites molécules et des interactions plus faibles entre la petite molécule et les polymères; ceci conduit à une aggrégation des petites molécules, donc à une incompatibilité. Le taux d'aggrégation de **1** dans divers polymères varie avec la concentration de **1**, la vitesse de séchage du film et avec les traitements par la chaleur opérés après le moulage. L'incorporation d'une molécule donneur dans la matrice supprime d'une façon dramatique l'aggrégation de **1** dans le polycarbonate.

[Traduit par le journal]

Introduction

The idea of dispersing or dissolving small electron-acceptor or -donor molecules into solid polymer matrices has attracted a great deal of interest in industry, mainly because such devices are simple to fabricate, economical, and have wide technological applications. Xerographic applications in charge carrier generation layer (1, 2), and charge transport layer (3, 4) have been documented. The unique feature of stable molecularly-doped polymer systems is that the reactants are held apart at fixed distance which is controlled by the concentration and the molecular size of the charge rely molecule. In practice, it has been shown that the microscopic structure of these small molecules in the matrix has a profound effect on the performance of these devices. Inhomogeneity due to microcrystallization or aggregation of the small molecule in the polymer matrix can dramatically change the electrical properties of such layers. The crystallization and aggregation phenomena are dominated by intermolecular interaction forces between the small molecules (molecule–molecule interaction) and with the host polymer (molecule–polymer interaction). In order to have better control over the properties of a given device, knowledge of the microscopic characteristics of the material package is essential.

In this work the photophysical properties of an electron-acceptor molecule butyl 9-dicyanomethylene fluorene-4-carboxylate (BDFC) **1** (5) in different polymer matrices were studied. This material when incorporated into a polymer matrix was shown to exhibit good electron mobility (5).

We used spectroscopic techniques to probe the microscopic properties of BDFC **1** in six different polymers and to monitor the stability of the small molecules in these matrices. We observed broadening and decrease in the absorption coefficient as the concentration of **1** increased or the polymer films were heated for extended periods above 60°C.

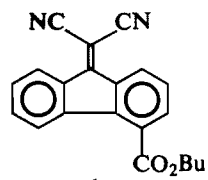

1

Experimental section

Materials

n-Butyl 9-dicyanomethylene fluorene-4-carboxylate was synthesized (5) via the condensation of *n*-butyl fluorenone-4-carboxylate with malononitrile in methanol in the presence of piperidine. The product was purified by recrystallization from acetone/methanol. Polyvinylcarbazole, polyvinylchloride, and copolyvinylidene chloride – vinylacetate (10%) were obtained from Poly Science; polyvinyl butyral was obtained from Aldrich; polyvinylidene chloride – acrylonitrile (SF-310) from Dow Chemical Company; and bisphenol – a polycarbonate, (Makrolon) obtained from Bayer. All polymers except polyvinylcarbazole were used as received. Polyvinylcarbazole was purified by dissolving in methylene chloride and precipitating with methanol. Glass substrates were obtained from Corning (7059) and were washed with soapy water and distilled water (twice) in an ultrasonic bath; they were then dried before use. Methylene chloride (glass distilled) was from BDH.

Preparation of the small molecule-in-polymer films

Various concentrations of the polymers and **1** in methylene chloride

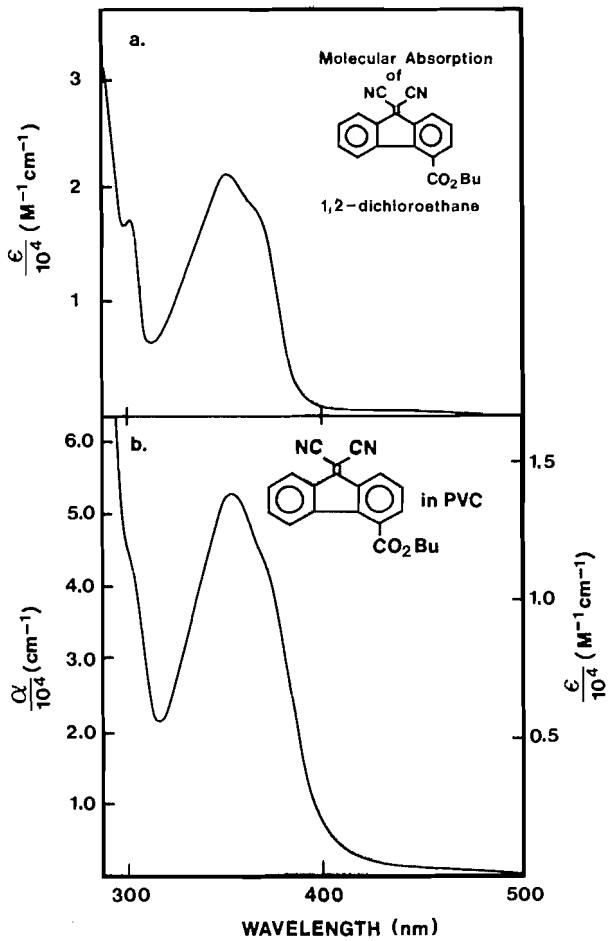

FIG. 1. Molecular electronic absorption of **1**, (*a*) in 1,2-dichloroethane and (*b*) at low concentration (21% by weight) in polyvinylchloride.

were prepared by vibrating in an ultrasonic bath until a clear solution was achieved. The solutions were filtered through 1 μm Millipore filters and then spin coated onto precleaned 2 in. × 2 in. glass substrate, using a Model 1-EC-101 Headway Research photoresist spinner. Uniform and optically clear films were obtained. The film thickness was controlled by the spin rate, typically between 500–4000 rpm. The optical density and the thickness of the resulting films were measured with a Cary 17 spectrophotometer and a Talystep instrument, respectively. The heat treatment studies were carried out by placing the samples in a forced air oven Delta Design 2300 at 60°C for 30 min.

Results and discussion

Absorption spectroscopy

Figure 1*a* shows the molecular electronic absorption spectrum of **1** in 1,2-dichloroethane. The electron acceptor molecule **1** exhibits an intense uv absorption (ϵ_{max} 2.15 × 10^4 M^{-1} cm^{-1}) at λ_{max} 352 nm. The width of the absorption band at half-height is approximately 55 nm. The cause of the yellow–orange color of this material is a weak visible absorption band centred around 440 nm. In Fig. 1*b* the absorption spectrum of a solid-solution of **1** at low concentration (21% by weight) in polyvinyl chloride is shown. The spectrum resembles closely the molecular absorption of **1** in solution, indicating that the small molecules are randomly dispersed into the polymer. The density of the film is about 1.36 g/mL. The molarity, C_m, of **1** in the polymer was calculated accordingly:

TABLE 1. The decadic absorption of **1** at 352 nm (3 mmol/g polymer) in various polymers

Number	Polymer	$\alpha_{352}/10^4$ cm^{-1}
1	Polyvinyl butyral	3.93
2	Polyvinyl carbazole	4.2
3	Polycarbonate	4.7
4	Polyvinyl chloride	4.9
5	Copolyvinylidene chloride – vinyl acetate	5.13
6	Co-polyvinylidene chloride – acrylonitrile	5.6
7	Polycarbonate/TPB	7.8

$$[1]\quad C_m = \frac{\rho W_f \times 1000}{\text{M.wt.}}$$

where M.wt. is the molecular weight of **1** (328 g/mol), W_f is the weight fraction of **1** ($\omega_1/(\omega_1 + \omega_2)$), and ρ is the density of the film. The density of **1** (1.25 g/mL) is very close to the density of most polymers used (1.1–1.39 g/mL). The decadic absorption coefficients, α, were calculated from the optical density, O.D., according to:

$$[2]\quad \alpha = \frac{\text{O.D.}}{LV_f}$$

where L is the film thickness and V_f is the volume fraction of **1** in the polymer. The decadic absorption coefficient α is related to the molar extinction coefficient ε (ε = O.D. × M.wt./$L\rho W_f$ 1000) according to:

$$[3]\quad \alpha(\lambda) = \epsilon(\lambda)C_M$$

where C_M is the molar concentration of **1** (for pure **1**, C_M = 3.808).

The solid absorption coefficient, α of **1** in PVC at 352 nm is 5.3 × 10^4 cm^{-1} which corresponds to an ϵ_{max} of 1.39 × 10^4 M^{-1} cm^{-1}. This value is only slightly lower than the molecular absorption coefficient in solution, 2.15 × 10^4 M^{-1} cm^{-1}. Similar results were obtained for the absorption coefficient of **1** at low concentration in other polymers.

For most practical applications the concentration of the electroactive species molecularly dispersed into polymers is usually high, > 35%. Therefore, we determined the absorption characteristic of films consisting of 50% by weight of **1** in the various polymers. Figure 2*a–f* show the electronic absorption of **1** at the 50% by weight (3.1 mmol/g polymer) in polyvinyl butyral, polyvinylcarbazole, polyvinyl choride, polycarbonate, copolyvinylidene chloride – acrylonitrile, and copolyvinylidene chloride – vinylacetate, respectively. In contrast to the absorption at low concentrations, the absorption bands become broader and less intense. In Table 1 the decadic absorption coefficient of **1** at λ_{max} (352 nm) in the various polymers studied is listed. The values of α_{max} vary from 3.9 to 5.6 × 10^4 cm^{-1}; depending on the host polymer. In general, higher absorption coefficients were observed in halogenated polymers. The lowest α value of **1** was obtained in polyvinyl butyral.

The loss of absorption intensity and broadening of the electronic absorption band of **1** can be attributed to aggregation and phase separation of the small molecule from the polymer. It is evident that at high concentration **1** is incompatible with polyvinyl butyral, polyvinyl carbazole and polycarbonate, however, it is more compatible with polyvinyl chloride copolyvinylidene chloride – vinylacetate and most compatible with

TABLE 2. Spectroscopic data for **1** in PVC

Sample	Concentration[a] (mmol **1**/g)	V_f[b]	C_m[c]	$\alpha_{max}/10^4$ (cm^{-1})[d]	$\epsilon/10^4$ M^{-1} cm^{-1}[e]
1	10	0.785	2.99	3.65	0.96
2	5.3	0.66	2.51	4.7	1.24
3	2.58	0.485	1.85	5.02	1.32
4	0.82	0.23	0.878	5.3	1.39

[a] In mmol **1**/g polymer.
[b] d_1 = 1.25 g/mL. d_{PVC} = 1.39 g/mL.
[c] Equation [1].
[d] Equation [2], λ_{max} = 350 nm.
[e] Equation [3].

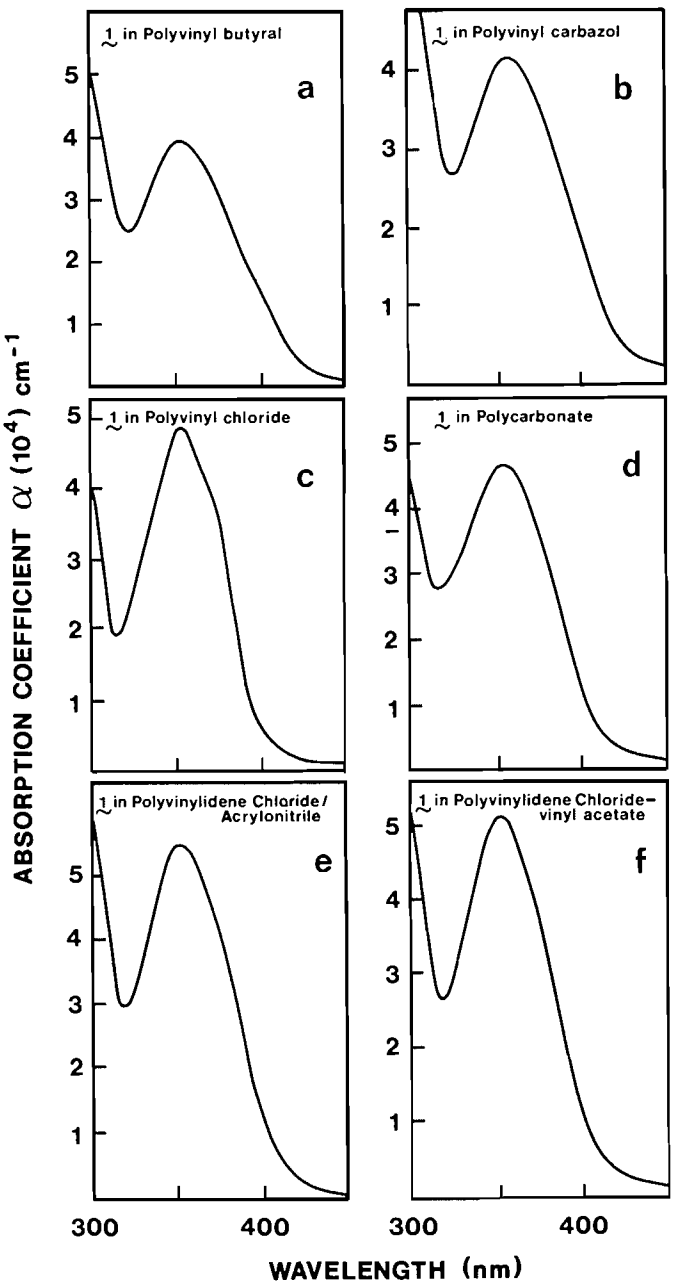

FIG. 2. The electronic absorption spectra of **1** at 50% by weight in (*a*) polyvinyl butyral, (*b*) polyvinylcarbazole, (*c*) polyvinyl chloride, (*d*) polycarbonate, (*e*) copolyvinylidene chloride – acrylonitrile, and (*f*) copolyvinylidene chloride – vinylacetate.

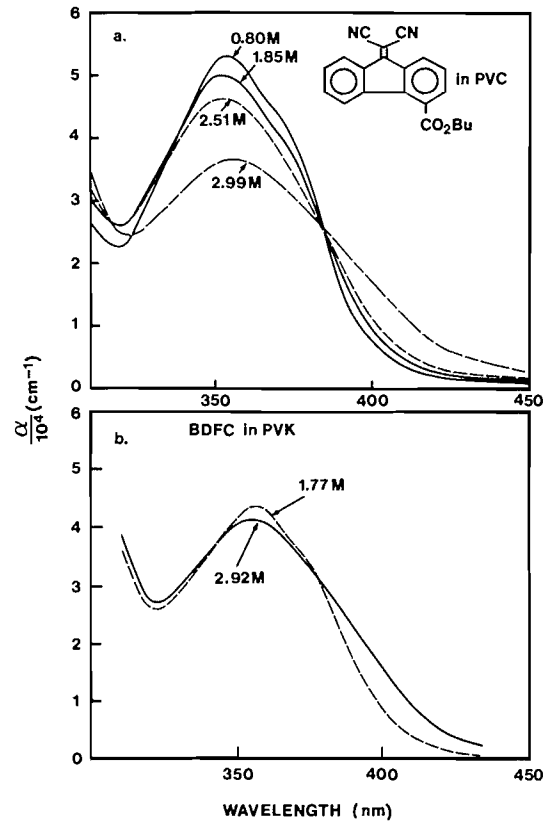

FIG. 3. The concentration-dependent uv absorption of **1** in (*a*) PVC and (*b*) PVK.

copolyvinylidenechloride – acrylonitrile. It, thus, appears that the electron-acceptor small molecule is more compatible with polymers possessing electronegative atoms such as chlorine.

The aggregation of the small molecule **1** in polymer matrices was further studied by investigating the dependence of the absorption spectra on the concentration of **1** in polyvinylchloride and polyvinyl carbazole. Figure 3 (*a* and *b*) shows the concentration-dependent uv absorption coefficients of **1** in PVC and PVK, respectively. The absorption band became broader, less intense, and shifted slightly to the red as the concentration of **1** in the polymer increases. The spectroscopic results for PVC are summarized in Table 2. An isosbestic point at ~380 nm was observed, indicating a specific stoichiometry of aggregates. The aggregates must have absorption bands to the red and blue of the monomer absorption and exhibit lower absorption coefficients. The large difference between the molecular absorption of many small molecules and that of their

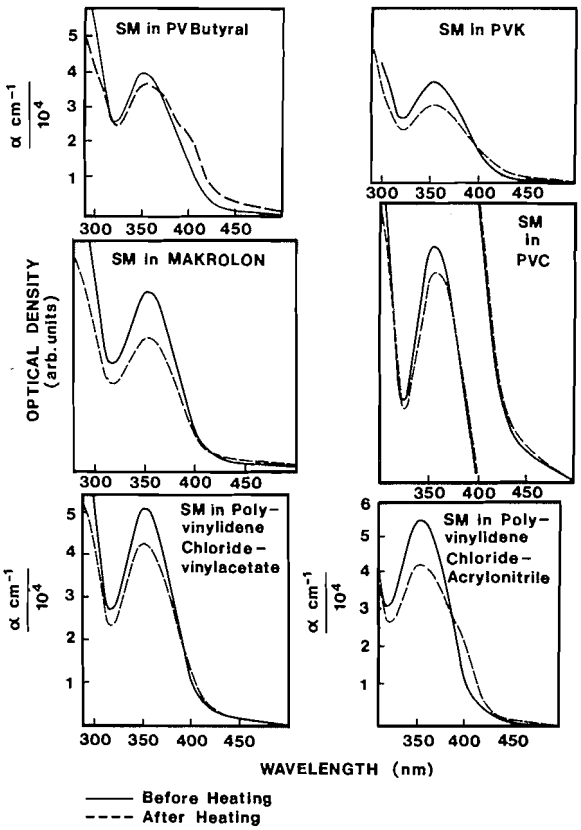

FIG. 4. Test of the stability of **1** in various polymers. Effect of heating the films for 30 min at 60°C (—) before heating, (- - -) after heating.

aggregates permit the use of electronic absorption spectroscopy as a tool to probe the compatibility of the small molecule in polymers.

For xerographic applications the concentration of the small molecule in polymer is typically 3 mmol/g or about 50% by weight, which corresponds to molar concentration of ~1.95 *M* depending on the density of the polymer. At such concentration **1** appears to exhibit significant aggregation in all polymers studied.

Stability of 1 in polymer matrices

The thermal stability of **1** in the six polymers chosen was investigated by heating films of **1** at 50% by weight in polymers for 30 min at 60°C. This temperature is below the glass transition, T_g, of all polymeric solid-solutions studied. During the thermal treatment the diffusion of the small molecule in the matrix is greatly accelerated. Figure 4*a–f* shows the electronic absorption spectra of **1** in polymers before and after heat treatment. Again, it is evident that the absorption coefficient of **1** decreases and the absorption bands broaden, indicating increase in aggregate level upon heat treatment. The magnitude of absorption band broadening and loss of absorption intensity depend on the host polymer. The absorption spectra of **1** in polyvinyl butyral and copolyvinylidene chloride – acrylonitrile after heating show a distinct shoulder around 400 nm, indicating the increase in aggregate concentration.

In the other polymer matrices, namely, polyvinylcarbazole, polycarbonate, polyvinylchloride, and copolyvinylidene chloride-vinylacetate, the effect of heating is much less severe. This test is an extremely mild test of stability of the small molecule in the polymer and the results indicate that none of the chosen polymers is a good host for the small molecule. This is in a large part due to the strong affinity of the small molecule to aggregate, i.e., strong molecule–molecule interaction force.

TABLE 3. The effect of the electron donor **2** on the absorption of **1** in polycarbonate[a]

Sample No.	**2** (mg)	V_f (**2**)	V_f (**1**)	Molar ratio 1:2	α **1**/10^{4b} cm^{-1}
1	118	0.314	0.36	1.8	5.43
2	60.4	0.19	0.43	3.55	7.81
3	39.16	0.13	0.46	5.5	7.45
4	9.93	0.037	0.51	21	5.67
5	0.00	0.00	0.53	∞	4.7

[a] 0.1363 g **1** and 0.1035 g polycarbonate.
[b] λ_{max} = 350 nm.

Stabilization of 1 in polymer matrices

It has been noted that the addition of donor molecules to **1** in polymer matrices generally increases the absorption coefficient. This can be attributed to the formation of charge-transfer complexes between the electron acceptor, **1**, and the electron donor which minimize acceptor–acceptor interactions. We investigated the effect of the electron-donor molecule tetraphenyl benzidene derivative (TPB) (6), **2**, on the dispersability and stability of **1** in polycarbonate. To solutions of 0.136 g of **1**, 0.104 g of polycarbonate in 5 mL methylene chloride various amounts of **2**, ranging from zero to 0.118 g was added. The solutions were then spin coated onto 2 in. × 2 in. precleaned glass slides. Analysis of the absorption spectra of the resulting films are complicated by the absorption of **2** in the same wavelength region as **1**. We have previously determined the absorption coefficient of **2** in polycarbonate and found that $\alpha_{350} = 4.5 \times 10^4$ cm^{-1}. Knowing α_{350} for **2**, its volume fraction V_f (2), and film thickness *L*, the contribution of **2** to the optical absorption can be determined from eq. [2] and subtracted to get the absorption due to **1**.

Table 3 lists the results of the effect of **2** on the absorptivity of **1** in polycarbonate. It is evident that the addition of **2** to

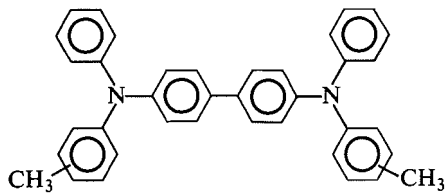

2

1/PC matrix increases the absorption coefficient of **1**, which approaches the molecular absorption values at the **2**-to-**1** molar ratio of 1:4. Figure 5 shows the correlation between **1** absorption coefficient onto **2**:**1** ratio. The highest α values obtained at molar ratio of 1:3 to 1:4. These results indicate that one molecule of the electron donor **2** forms a charge transfer complex with four molecules of the electron acceptor **1**. This charge transfer complexation diminishes the interaction force between the acceptor molecules and results in an absorption curve very closely similar to molecular absorption. An additional absorption band at 600 nm was also observed, this can be assigned to the charge-transfer complex (CT state), see Fig. 6. Figure 7 shows the effect of heat treatment on the absorption characteristics of a polycarbonate film containing ~50% by weight of **1**

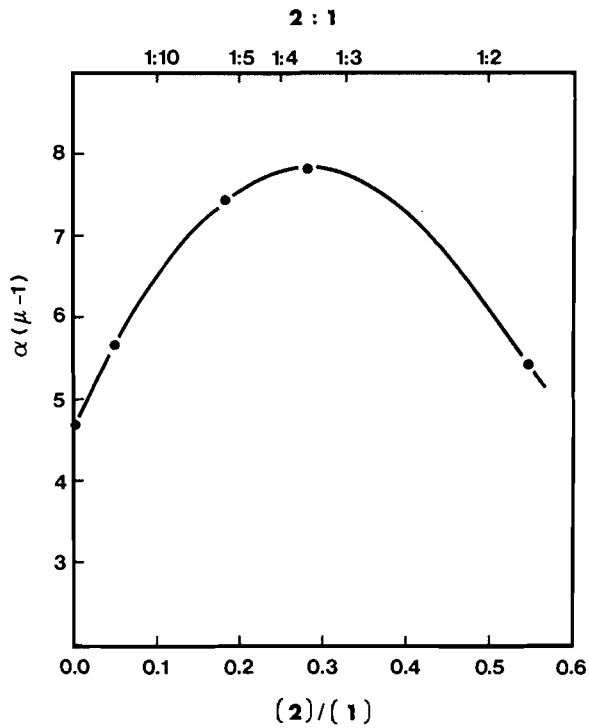

FIG. 5. Effect of **2** on the absorption coefficient of **1** in polycarbonate.

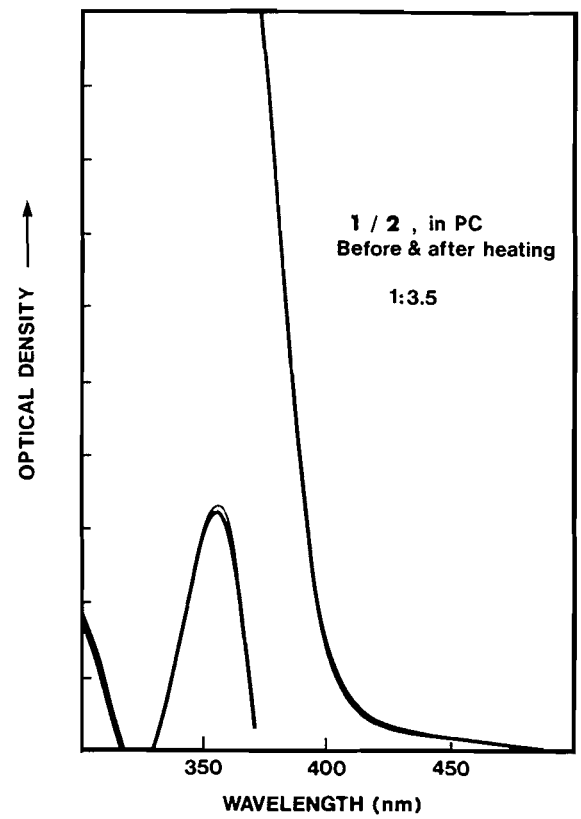

FIG. 7. Effect of heating on the absorption characteristics of **1** in PC in presence of **2**.

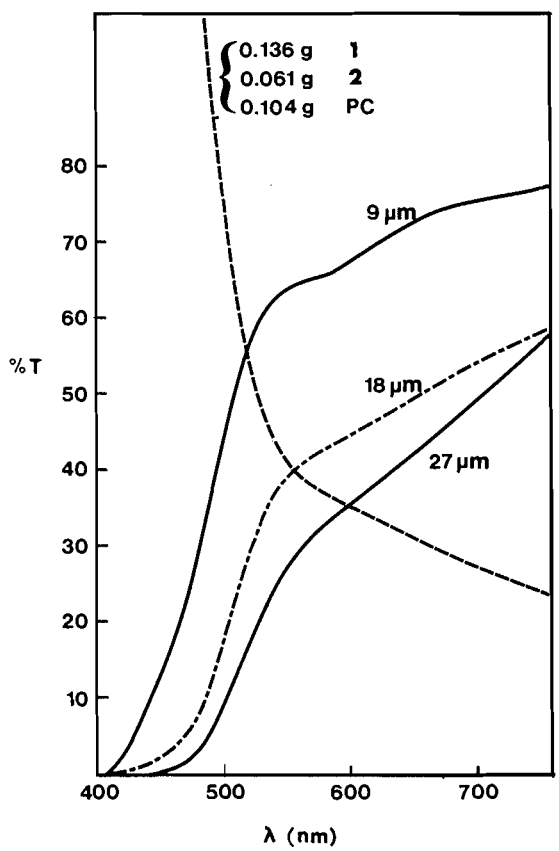

FIG. 6. The absorption spectra of thick polycarbonate film containing **1** and **2** at a molar ratio of 3.5:1.

and also incorporates **2** (**2**:**1** molar ratio 1:3.5). The absorption spectra before and after heat treatment are virtually identical (cf. Fig. 4*c*). The presence of the electron donor **2** had a dramatic stabilizing effect on the diffusion and aggregation of the electron acceptor **1**.

Conclusion

We have utilized electronic absorption spectroscopy to study the compatibility and stability of a small molecule, *n*-butyl 9-dicyanomethylene fluorene-4-carboxylate, **1**, in polymer matrices. At low concentration the electronic absorption of **1** in various polymers closely resembled the molecular absorption, indicating random distribution. As the concentration of **1** increases the absorption bands become broader, less intense, and red-shifted. These results implied aggregation and phase separation of **1** from the polymer (incompatibility). The small molecule **1** was found to be more compatible with halogenated polymers than with polyesters of polyvinyl carbazole. Heating the film causes diffusion of the small molecules and enhances aggregation and phase separation.

The addition of electron donor molecules to the matrix of **1** in polycarbonate caused dramatic increase in the absorptivity and the stability of **1**. This was attributed to the formation of large charge transfer complexes.

1. W. J. DUMAGE, W. A. LIGHT, S. J. MARINO, C. D. SALZBERG, D. L. SMITH, and W. J. STAUDENMAYER. J. Appl. Phys. **49**, 5543 (1978); P. M. BORSENBERGER, A. CHOWDRY, D. C. HOESTEREY, W. MEY. J. Appl. Phys. **49**, 5555 (1978).
2. W. D. GILL. Amorphous and liquid semiconductors. *Edited by* J.

Stuke, and W. Brenig. J. Wiley and Son Inc., NY. 1973. p. 901; R. M. SCHAFFERT. IBM J. Res. Develop. **15**, 75 (1971); J. Appl. Phys. **43**, 5033 (1972).
3. U.S. Patents 4140529 and 4141729; D. M. PAI and J. YANUS. Photograph. Sci. Eng. **27**, 14 (1983); J. E. KUDER, J. M. POCHAN, S. R. TURNER, and D. F. HINMAN. J. Electrochem. Soc. **125**, 1750 (1978).
4. W. WOLFGANG. Eup. Patent No. 0040402. 1981.
5. R. O. LOUTFY, B. S. ONG, and B. KEOSHKERIAN. J. Electroanal. Chem. To be published.
6. M. STOLKA, D. M. PAI, and J. YANUS. US Patent 4 265 990. 1981.

Electron transfer from anthracenes. Comparison of photoionization, charge-transfer excitation and electrochemical oxidation

J. M. MASNOVI, E. A. SEDDON, AND J. K. KOCHI[1]

Departments of Chemistry, Indiana University, Bloomington, IN 47405, U.S.A.; University of Houston, University Park, Houston, TX 77004, U.S.A; and School of Molecular Sciences, University of Sussex, Brighton BN1 9QJ, England

Received March 26, 1984

This paper is dedicated to Professor Peter Yates on the occasion of his 60th birthday

J. M. MASNOVI, E. A. SEDDON, and J. K. KOCHI. Can. J. Chem. **62**, 2552 (1984).

Quantitative measures of electron detachment from anthracene and various *meso*-substituted derivatives (D) are examined in the gas phase and in solution. The photoelectron spectra show well-resolved bands for E_I corresponding to the first ionization (i.e., $D \rightarrow D^{+\cdot} + e$) from a π-molecular orbital (HOMO) with maximum electron density at the 9,10-positions. The same series of anthracenes form 1:1 electron donor–acceptor complexes with tetracyanoethylene [D,TCNE], which exhibit distinctive colors associated with charge transfer transitions $h\nu_{CT}$ to the ion pair $[D^{+\cdot},TCNE^{-\cdot}]$. These measures of the gas phase energetics of electron transfer from the anthracenes are compared with their standard oxidation potentials E^0_{Ar} determined from the reversible cyclic voltammograms in methylene chloride and trifluoroacetic acid solutions. Although there are direct, linear free energy relationships between E_I and $h\nu_{CT}$ as well as E_I and E^0_{Ar}, the best correlation is observed between E^0_{Ar} and $h\nu_{CT}$. The validity of the latter is discussed in terms of offsetting effects arising from differences in solvation energy and steric effects attendant upon 9,10-substitution in anthracenes.

J. M. MASNOVI, E. A. SEDDON et J. K. KOCHI. Can. J. Chem. **62**, 2552 (1984).

Opérant en phase gazeuse ainsi qu'en solution, nous avons effectué des mesures quantitatives d'enlèvement d'électrons de l'anthracène et de divers dérivés substitués en position méso (D). Les spectres photoélectroniques présentent des bandes bien résolues pour E_I qui correspondent à la première ionisation (soit $D \rightarrow D^{+\cdot} + e$) d'une orbitale moléculaire π(OM-HO) avec une densité électronique maximale aux positions 9 et 10. La même série d'anthracènes forme des complexes électroniques donneur–accepteur 1:1 avec le tétracyanoéthylène [D,TCNE] qui présentent des couleurs caractéristiques associées avec des transitions de transfert de charge $h\nu_{CT}$ conduisant à la paire d'ions $[D^{+\cdot},TCNE^{-\cdot}]$. Nous comparons les énergies impliquées en phase gazeuse lors du transfert d'électrons provenant d'anthracènes avec leurs potentiels standard d'oxydation E^0_{Ar} déterminés, en solutions dans le chlorure de méthylène et dans l'acide trifluoroacétique, à partir de voltammogrammes cycliques réversibles. Quoique les relations linéaires d'énergie libre entre E_I et $h\nu_{CT}$ ainsi qu'entre E_I et E^0_{Ar} soient directes, la meilleure corrélation est celle qui relie E^0_{Ar} et $h\nu_{CT}$. Nous discutons de la validité de cette dernière en fonction d'effets qui se compensent et qui découlent de différences dans les énergies de solvatation et dans les effets stériques qui sont reliées à la présence de substituants dans les positions 9 et 10 des anthracènes.

[Traduit par le journal]

Can. J. Chem. Downloaded from www.nrcresearchpress.com by 210.87.254.42 on 09/06/12
For personal use only.

Introduction

Electron transfer from aromatic hydrocarbons to form such reactive intermediates as arene cation radicals is playing an increasingly important role in various oxidative processes in organic chemistry (1–3). In these situations, the quantitative evaluation of the feasibility of electron transfer as a reaction pathway depends critically on the knowledge of the energetics of electron detachment from the aromatic compound ArH (4). Such information *in the gas phase* can be obtained as vertical or adiabatic ionization energies

$$[1] \quad ArH \xrightarrow{E_i} ArH^{+\cdot} + e$$

which are readily evaluated by photoelectron spectroscopy (5). A more convenient, although less direct, method is based on the charge transfer absorption energy $h\nu_{CT}$ for electron donor–acceptor or EDA complexes (6). For a series of aromatic hydrocarbons with an electron acceptor (A) in common, the charge transfer excitation of the EDA complex leads to the ion pair (7), i.e.,

$$[2] \quad [ArH,A] \xrightarrow{h\nu_{CT}} [ArH^{+\cdot},A^{-\cdot}]$$

According to the Mulliken theory (8), the value of $h\nu_{CT}$ for weak complexes is directly proportional to the first vertical ionization energy E_I (or equivalently the ionization potential I_P) of ArH according to the relationship

$$[3] \quad h\nu_{CT} = I_P - E_A - \omega$$

where E_A is the electron affinity of the common acceptor. The term ω is to first order the electrostatic energy of the ion pair formed in eq. [2], and is commonly considered to be invariant in such a series of related donors.

The assessment of electron transfer from aromatic compounds *in solution* requires knowledge of the standard or reversible oxidation potential for the process

$$[4] \quad ArH_s \overset{-E^0_{Ar}}{\rightleftharpoons} ArH^{+\cdot}_s + e$$

where subscript s refers to the solvated species (9). Electrochemical methods, particularly cyclic voltammetry, offer the most direct and convenient access to oxidation potentials. When electron transfer in reaction [4] is reversible, the cyclic voltammogram consists of anodic and cathodic waves with current maxima of equal magnitudes at potentials E^a_P and E^c_P, respectively. Under these circumstances the standard potential E^0_{Ar} is within 0.030 V of the average, namely $(E^a_P + E^c_P)/2$. Unfortunately, most aromatic hydrocarbons do not afford reversible cyclic voltammograms at sweep rates attainable with standard instrumentation. Therefore we focused our attention in this study on anthracene and its derivatives substituted in the 9- and 10- or *meso* positions to represent structurally related

[1] To whom all correspondence should be addressed.

Can. J. Chem. Downloaded from www.nrcresearchpress.com by 210.87.254.42 on 09/06/12
For personal use only.

TABLE 1. Ionization energies of 9,10- mono- and di-substituted anthracenes[a]

Substituent	E_1 HOMO (eV)	E_2 SHOMO (eV)	Δ^b (eV)
None	7.43 (7.43)	8.53 (8.53)	1.10 (1.10)
9-Bromo	7.47 (7.48)	8.68 (8.67)	1.21 (1.19)
9,10-Dibromo	7.54	8.81	1.27
9-Phenyl	(7.18)	(8.37)	(1.19)
9,10-Diphenyl	7.04	8.32	1.28
9-Methoxy	(7.21)	(8.47)	(1.26)
9,10-Dimethoxy	7.09	8.48	1.39
9-Methyl	7.25 (7.24)	8.45 (8.41)	1.20 (1.17)
9,10-Dimethyl	7.11	8.41	1.30
9-Cyano	7.84 (7.80)	8.94 (8.90)	1.10 (1.10)
9,10-Dicyano	8.25	9.34	1.09
9-Acetoxy	7.35	8.56	1.21
9-Carboxy	7.56	8.72	1.16
9-Hydroxymethyl	7.47	8.62	1.15
9-Chloro	7.48 (7.45)	8.71 (8.65)	1.23 (1.20)
9-Formyl	7.69 (7.67)	8.83 (8.74)	1.14 (1.07)
9-Carbomethoxy	7.48	8.62	1.14
9-Acetyl	7.52	8.73	1.21
9-Nitro	(7.88)	(8.99)	(1.11)
9-Formyl-10-chloro	7.74	9.09	1.35

[a] Determined by He(I) photoelectron spectroscopy for the vertical process. Numbers in parentheses are from ref. 10.
[b] Splitting between E_1 and E_2.

compounds in which the energetics of electron detachment can be systematically varied by appropriate substituents. This series of aromatic compounds is particularly well suited to study the relationships among the various measures of electron detachment both in the gas phase and in solution. Thus the anthracenes are sufficiently volatile for the photoelectron spectra to be measured directly in the gas phase (10). Moreover, they form an extensive series of EDA complexes with tetracyanoethylene or TCNE, in which the charge transfer absorption bands are exceptionally well resolved from those of the components (11). Most importantly, the cyclic voltammograms of these anthracenes are reversible (12), which allows a direct relationship to be established between values of E^0_{Ar} in solution and E_1 or I_P in the gas phase. The latter will permit an evaluation of solvation effects on electron transfer from this aromatic system (12, 13).

Results

Photoelectron spectra of anthracene and its derivatives

The comparison of the He(I) and He(II) photoelectron spectra of anthracene with those of benzene and naphthalene has established the first ionization E_1 at 7.43 eV to occur from a π-orbital (HOMO according to Koopmans' theorem) of b_{2g} symmetry with maximum electron density at the 9- and 10-positions (10). The second ionization E_2 at 8.53 eV occurs from the subjacent π-orbital (SHOMO) of b_{1g} symmetry with a node at the 9- and 10-positions. In order to examine the polar effects of substituents at both of these positions, we measured the photoelectron spectra of the series of anthracene derivatives included in Table 1. Uniformity in the PES measurements was ensured by recording all the spectra under a single set of standard conditions using a small amount of methyl iodide as an internal calibrant (with E_1 9.53_8 eV and E_2 10.16_5 eV (5*b*)).

The lowest energy bands of the photoelectron spectra for most anthracenes are well resolved — the adiabatic and vertical ionization energies being within ~0.02 eV of one another, and showing a progression of vibrational fine structure, as typically illustrated in Fig. 1 for 9-acetoxy, 9-bromo, and 9,10-dibromoanthracene. The reliability in the values of E_1 and that of the second ionization energy E_2 listed in Table 1 was established by a comparison with those obtained independently by Klasinc and co-workers (10). The trend, as reported earlier, is for both E_1 and E_2 to generally increase with values of the Hammett σ constant — that is, the presence of electron-attracting substituents leads to the stabilization of the HOMO as well as the SHOMO.

Charge transfer transitions in electron donor–acceptor complexes of substituted anthracenes with tetracyanoethylene

When a methylene chloride solution of anthracene is mixed with tetracyanoethylene or TCNE, a transient blue coloration is observed immediately (11), and it persists for slightly longer times if the reactants are cooled prior to mixing (14). Analogously, 9-cyanoanthracene and tetracyanoethylene afford a green solution which lasts for a prolonged period. The other substituted anthracenes yield similarly colored solutions of varying shades of blue and green as illustrated by the absorption spectra in Fig. 2. These broad, featureless absorption bands are characteristic of weak intermolecular electron donor–acceptor or EDA complexes, and the visible absorptions have been assigned to charge transfer transitions in the 1:1 EDA complex (11), e.g.

[5] 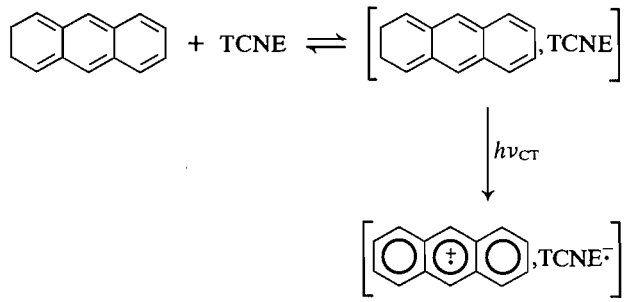

The color as such is a measure of the electron donor property of the particular anthracene (see eq. [3]), and it is quantitatively indicated in Table 2 by the value of $h\nu_{CT}$, i.e., the absorption maximum. Since neither the parent anthracenes (see Fig. 3) nor tetracyanoethylene absorb beyond 500 nm, the charge transfer transitions in this series of EDA complexes are unambiguously indicated by these clearly resolved visible absorptions. With some of the anthracene–tetracyanoethylene complexes, a second absorption band was apparent in the far uv region. More often, the second band was obscured by the long wavelength tail of the parent anthracene absorption. The CT transition energy of the visible band (I) and that of the uv band (II), when resolved, are included in Table 2. Since the splittings between bands I and II are the same as the first and second bands E_1 and E_2 in the PE spectra (see Table 1), band II is most likely to be associated with charge transfer transitions from the SHOMO (14*b*).

Electrochemical oxidation of substituted anthracenes. Evaluation of the standard oxidation potential E^0_{Ar}

The cyclic voltammogram of a 5×10^{-3} *M* solution of 9,10-diphenylanthracene in methylene chloride (containing 0.1 *M* tetrabutylammonium perchlorate as supporting electrolyte) is reversible at a platinum electrode at sweep rates less

Can. J. Chem. Downloaded from www.nrcresearchpress.com by 210.87.254.42 on 09/06/12
For personal use only.

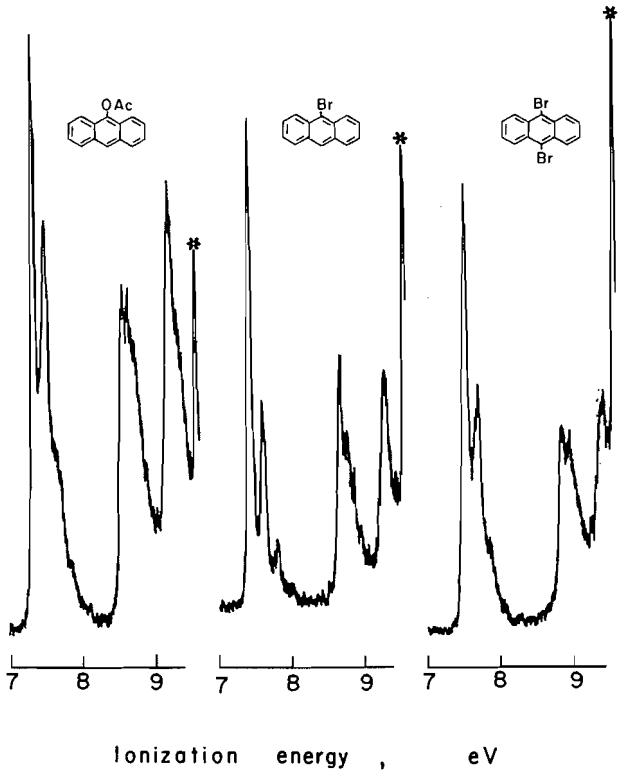

FIG. 1. Low energy portion of the He(I) photoelectron spectra of 9-acetoxy-, 9-bromo-, and 9,10-dibromoanthracene with methyl iodide* as calibrant (E_1 9.53$_8$ eV).

than 0.05 V s^{-1}. Under the same conditions, the cyclic voltammogram of 9,10-dimethylanthracene is irreversible (the cathodic wave on the return sweep simply being unobserved), but it becomes reversible at a higher sweep rate of 0.20 V s^{-1} (see Fig. 4). Although the cyclic voltammogram of the parent anthracene remains irreversible in methylene chloride up to sweep rates exceeding 100 V s^{-1}, the addition of trifluoroacetic acid is sufficient to promote reversibility in the cyclic voltammogram (CV), even at a sweep rate of 1 V s^{-1}. The CV waves correspond to a one-electron process (as in reaction [6]), based on the calibration of the peak current with ferrocene.

[6] 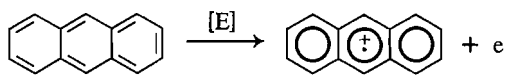 + e

Thus for each anthracene derivative, the CV reversibility can be achieved by the appropriate adjustment of the sweep rate and/or by the addition of trifluoroacetic acid. Both of these factors relate directly to the varying lifetimes of the respective anthracene cation radicals which are known to be more persistent in acidic media such as trifluoroacetic acid (15, 16).[2] (Note also that the intrinsic heterogeneous rate constant k_s appears to be fast for aromatic hydrocarbons (13).) Indeed, each of the substituted anthracenes in Table 3 shows distinctive CV behavior as indicated by the sweep rate v at which reversibility is observed in a standard medium consisting of methylene chloride and 20 %v trifluoroacetic acid. Most importantly for each anthracene, the average of the anodic and cathodic peak potentials, i.e. $(E_P^a + E_P^c)/2$, remains constant with variations in the

[2] For the chemical reactivity of the radical cations of anthracene and related compounds, see ref. 16.

TABLE 2. Charge transfer transitions in electron donor–acceptor complexes of substituted anthracenes and tetracyanoethylene[a]

Substituent	$h\nu_{CT}$ (eV) I	II	Substituent	$h\nu_{CT}$ (eV) I
None	1.73	2.79	9-Formyl	1.90
9-Phenyl	1.59	2.8	9-Cyano	2.01
9,10-Diphenyl	1.56		9-Nitro	2.03
9,10-Dibromo	1.76	2.76	9-Methoxy	1.65
9-Chloro	1.74	2.8	9-Methyl	1.55[b]
9-Bromo	1.74	2.86	2-Methyl	1.67
9-Acetoxy	1.75	2.86	9-Hydroxymethyl	1.73
9-Acetyl	1.84	2.82	9,10-Dimethoxy	1.56
9-Carbomethoxy	1.84	2.89	9,10-Dimethyl	1.44[b]
9-Formyl-10-chloro	1.96			

[a] In methylene chloride containing ~0.05 *M* anthracene and 0.05 *M* tetracyanoethylene.
[b] From ref. 21.

scan rate (17). The values of E^0_{Ar} obtained in this manner are listed in Table 3, and they show a marked dependence on the presence of *meso* substituents.

The effect of solvent on the values of the standard oxidation potentials of substituted anthracenes was also examined in methylene chloride (without added trifluoroacetic acid), trifluoroacetic acid alone, and in acetonitrile. Each solvent system contained 0.1 *M* tetra-*n*-butylammonium perchlorate as the supporting electrolyte. The values of E^0_{Ar} in these pure solvents are presented in Table 4. The standard oxidation potentials of the anthracenes are not always reported for each solvent owing to difficulties in attaining reversibility of the cyclic voltammogram.

Direct evidence for the formation of anthracene cation radicals according to reaction [6] was obtained by a spectroelectrochemical examination of anthracene oxidation. For example, the absorption spectrum of the radical cation of anthracene shown in Fig. 5 represents the average of the multiple accumulation of spectra (>50) measured through a 0.1 mm gold minigrid electrode maintained at constant potential in 30 %v trifluoroacetic acid – methylene chloride containing 0.1 *M* tetra-*n*-butylammonium perchlorate. Figure 5 emphasizes the pronounced red spectral shift which accompanies the oxidation of the anthracene to its radical cation. (The absorption spectrum of anthracene cation radical in Fig. 5 is the same as that generated independently by γ-irradiation of the parent hydrocarbon immobilized in a polymer matrix (18).) The absorption spectra of 9-nitro and 9-carbomethoxyanthracene as well as their radical cations are also included in Fig. 5 for comparison. The radical cations of 9-methoxy-, 9,10-dimethoxy-, 9-cyano-, 9,10-dicyano-, 9-formyl-, 9-formyl-10-chloro-, and 9,10-diphenylanthracene were also generated in sufficient concentrations to observe by the same spectroelectrochemical method.

Discussion

The availability of the independent measures for effecting electron detachment from the anthracenes listed in Tables 1–4 allows us to examine the relationships between various gas phase and solution processes. Let us first examine how the vertical ionization energy E_1 of anthracenes obtained from the photoelectron spectrum relates to the charge transfer transition energy $h\nu_{CT}$ of their EDA complexes with tetracyanoethylene. The linear correlation of $h\nu_{CT}$ and E_1 shown in Fig. 6 includes

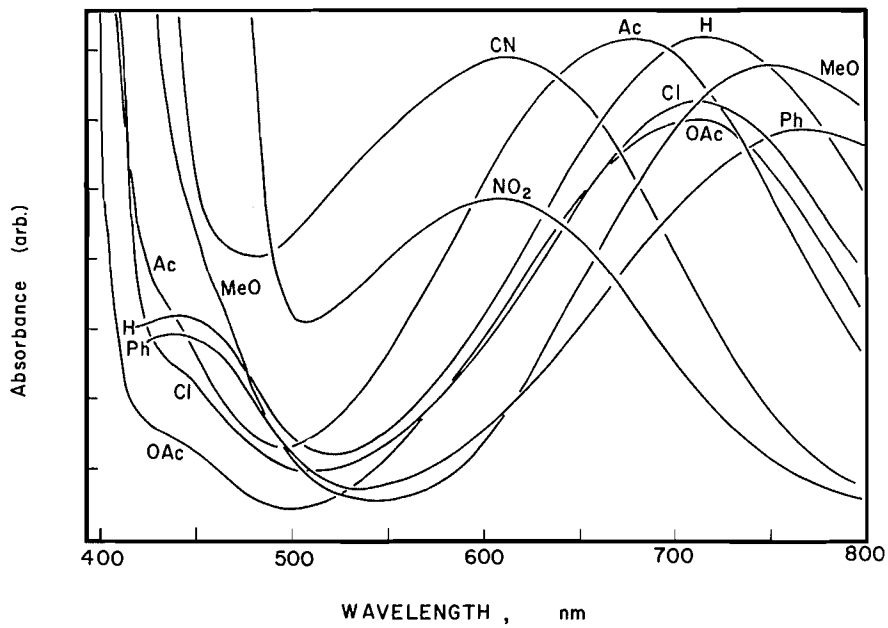

FIG. 2. Charge transfer spectra of a series of EDA complexes of 9-substituted anthracenes (~0.05 *M*) with tetracyanoethylene (0.05 *M*) in methylene chloride.

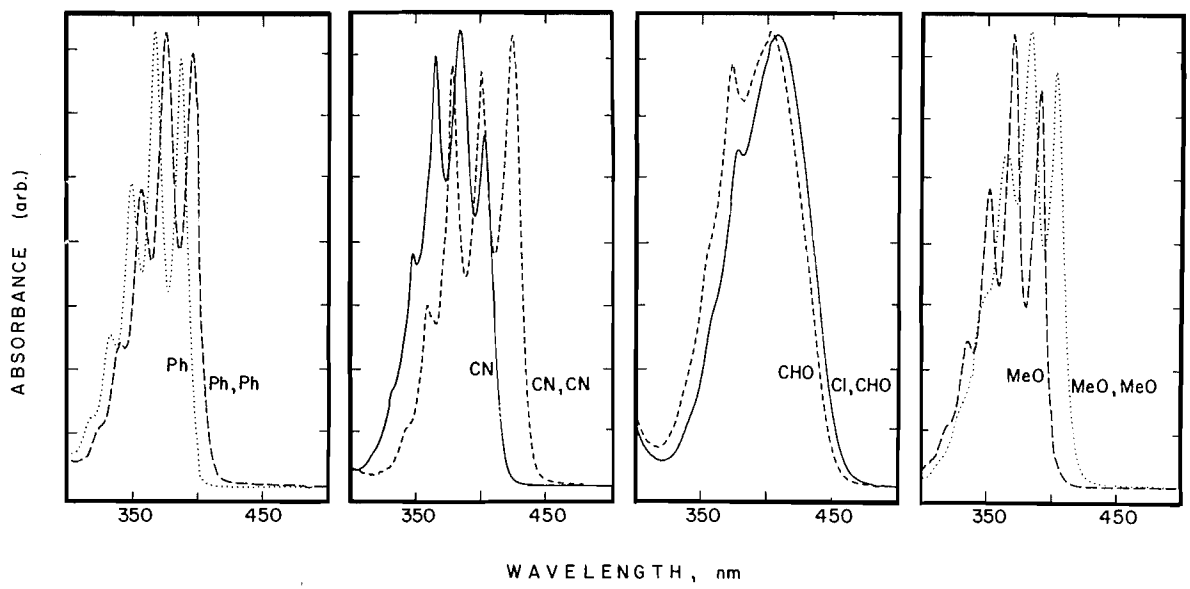

FIG. 3. Absorption spectra of representative pairs of 9,10-mono- and disubstituted anthracenes (~10^{-4} *M*) in methylene chloride.

all eighteen of the 9-monosubstituted as well as the 9,10-disubstituted anthracenes. The least-squares line in the graph describes the relationship

$$[7] \quad h\nu_{CT} = 0.63E_I - 2.93$$

with a correlation coefficient of 0.97. Since the photoionization of an anthracene and the charge transfer excitation of its EDA complex both represent vertical transitions, the slope of the correlation should be close to unity if the interaction energy ω in eq. [3] were invariant in the series. Thus a slope of only 0.6 in eq. [7] suggests that ω actually decreases in proportion to the donor property of the anthracene. Such a trend could arise from increasing steric hindrance at the *meso* positions attendant upon disubstitution required for better donor properties. The adverse steric effect would be expected to decrease the magnitude of ω owing to its large electrostatic component which is inversely proportional to the mean separation *r* of the anthracene and TCNE in the EDA complex.[3]

The comparison of the vertical ionization energy E_I and the standard oxidation potential E^0_{Ar} is illustrated in Fig. 7. The line in the graph describes the relationship

$$[8] \quad E^0_{Ar} = 0.86E_I - 4.91$$

with a correlation coefficient of 0.98 for fourteen mono- and disubstituted anthracenes. A slope of considerably less than unity indicates that the energetics of the gas phase ionization are not completely mirrored in the solution oxidation. In partic-

[3] For a discussion of steric effects on the charge transfer transition energy of EDA complexes, see ref. 19.

Can. J. Chem. Downloaded from www.nrcresearchpress.com by 210.87.254.42 on 09/06/12
For personal use only.

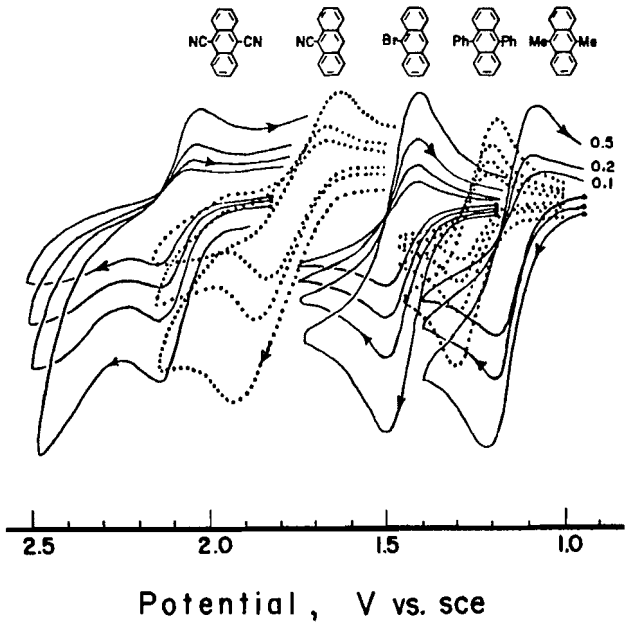

FIG. 4. Cyclic voltammograms of substituted anthracenes (0.005 *M*) using a platinum electrode at various sweep rates in the presence or absence of trifluoroacetic acid: 9,10-diphenyl- and 9,10-dimethylanthracene in CH_2Cl_2, 9-bromoanthracene in 20 %v CF_3CO_2H–CH_2Cl_2, 9-cyano- and 9,10-dicyanoanthracene in CF_3CO_2H — all containing 0.1 *M* tetra-*n*-butylammonium perchlorate as supporting electrolyte. CV sweep rates from top to bottom are 0.5, 0.2, 0.1, and 0.05 (where applicable) V s^{-1}.

TABLE 3. Cyclic voltammetry of substituted anthracenes[a]

Substituent	E^0_{Ar} (V vs. sce)	ΔE_P[b] (V)	ν[c] (V s^{-1})
9-Nitro	1.83	0.25	2
9-Formyl	1.70	0.12	2
None	1.49	0.12	1
9-Cyano	1.78	0.29	20
9-Carbomethoxy	1.57	0.12	0.05
9-Formyl-10-chloro	1.69	0.12	0.5
9,10-Dimethyl	1.13	0.11	0.1
9-Bromo	1.45	0.10	0.2
9,10-Dibromo	1.54	0.18	2
9,10-Diphenyl	1.26	0.13	0.05
9,10-Dimethoxy	1.14	0.16	2
9-Methoxy	1.30	irrev	> 50
9-Methyl	1.26		
9,10-Dicyano	2.23	0.11	0.2

[a] At a platinum electrode in 20 %v trifluoroacetic acid – methylene chloride containing 0.1 *M* tetra-*n*-butylammonium perchlorate.

[b] Separation of the anodic and cathodic peak potentials at a scan rate of 0.5 V s^{-1}.

[c] Approximate scan rate at which anodic and cathodic peak currents become equal.

ular, the contribution from solvation is implicit in the values of E^0_{Ar}, whereas it is not in the values of E_1. Furthermore, values of the vertical E_1 do not include any reorganization energy arising from a Jahn–Teller distortion. Inclusion of these terms (13) leads to

$$[9] \quad E^0_{Ar} = E_1 + (\Delta G^0_s + \Delta G^0_r)/F + C$$

TABLE 4. Solvent effects on the standard oxidation potentials of substituted anthracenes[a]

Substituent	E^0_{Ar} (V vs. sce)		
	CH_2Cl_2	CH_3CN	CF_3CO_2H
9-Bromo	1.47	1.38	
9,10-Dibromo	1.54	1.46	
9-Methyl		1.23	
9,10-Dimethyl	1.17	1.09	
9-Nitro		1.74	1.79
9-Cyano			1.78
9,10-Dicyano		1.93	2.29
9,10-Dimethoxy	1.07	0.98	
9-Formyl-10-chloro	1.69	1.56	
9-Carbomethoxy	1.58		
9-Formyl	1.72		
9,10-Diphenyl	1.27	1.22	

[a] In the pure solvent, each containing 0.1 *M* tetraalkylammonium perchlorate.

where ΔG^0_s and ΔG^0_r represent the free energies of solvation and reorganization of the radical ion $ArH^{\ddagger}$, respectively.[4] (*F* is the Faraday constant and *C* is a constant determined by the particular working and reference electrode.) Comparison of eq. [9] with the experimental relationship in eq. [8] indicates that $(\Delta G^0_s + \Delta G^0_r)$ cannot be considered as a constant term for the series of anthracenes under consideration. Instead, it varies with E_1 or E^0_{Ar}, as given by the combination of eqs. [8] and [9], i.e.

$$[10] \quad \Delta G^0_s + \Delta G^0_r = -0.14FE_1 + \text{constant}$$

From the limited difference observed between the magnitudes of the vertical and adiabatic ionization energies for the first photoelectron band E_1 (see Results section), we infer that the reorganization energies of the anthracene cation radicals are rather small and constant (5*b*). If so, the relationship in eq. [10] suggests that the solvation energy decreases by about 0.2 eV or ~5 kcal mol^{-1} in covering the gamut of anthracenes from 9-nitroanthracene to 9,10-dimethoxyanthracene at the extremes. Interestingly, this trend also parallels the structural changes of increasing size of the anthracene moiety resulting from disubstitution of both *meso* positions. Furthermore, the point for 9,10-diphenylanthracene falls furthest off the line in Fig. 7, in accord with an expected large decrease in the solvation energy associated with extensive delocalization of the charge in the corresponding radical cation.

Steric size thus appears to be a common factor which diminishes the slope of the correlation in Fig. 6 as well as that in Fig. 7. The limited slopes in both instances suggest that a reasonable correlation would be found between the standard oxidation potential E^0_{Ar} and the charge transfer transition energy $h\nu_{CT}$. Indeed, the result shown in Fig. 8 includes the least-squares line which describes the relationship

$$[11] \quad E^0_{Ar} = 1.22\, h\nu_{CT} - 0.67$$

with a correlation coefficient of 0.98 for thirteen substituted anthracenes. It is interesting to note that all the points (includ-

[4] For a discussion of these energy terms as they relate to aromatic cation radicals, see refs. 12 and 13. Note the contribution arising from the neutral arenes is negligible owing to their much smaller solvation energies; see ref. 20.

Can. J. Chem. Downloaded from www.nrcresearchpress.com by 210.87.254.42 on 09/06/12
For personal use only.

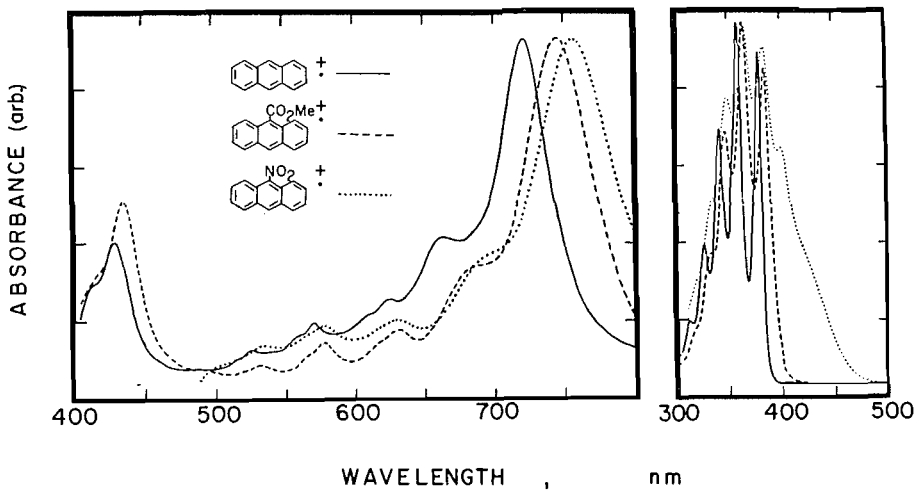

FIG. 5. Left: absorption spectra of the radical cations of 9-nitro- (···), 9-carbomethoxy- (- - -), and anthracene (—) generated at a gold minianode at constant potentials of 2.0, 1.8, and 1.7 V vs. sce, respectively, in 30 %v trifluoroacetic acid – methylene chloride containing 0.1 *M* tetra-*n*-butylammonium perchlorate. Right: absorption spectra of the parent anthracenes ($\sim 10^{-4}$ *M*). Absorbance units are arbitrary.

ing those for the disubstituted anthracenes) are better accommodated by this correlation than those presented in either Fig 6 or 7. (Note especially the points for 9,10-diphenylanthracene in these comparisons.) The reason could lie in the partial offset of steric factors in the measurements of E^0_{Ar} (owing to differences in the solvation energy) and $h\nu_{CT}$ (owing to changes in the mean separation). In any case, the validity of this type of correlation is supported in Fig. 9 which utilizes the recent electrochemical data obtained for the homologous methylbenzenes (13). The least-squares line in Fig. 9 has a slope close to unity, viz., $E^0_{Ar} = 0.99h\nu_{CT} - 0.58$. Indeed, the foregoing correlations of E^0_{Ar} and $h\nu_{CT}$ may be a general one applicable to other electron donors. If so, it would provide a very convenient method for the evaluation of standard oxidation potentials of organic compounds which are otherwise not directly measurable.[5]

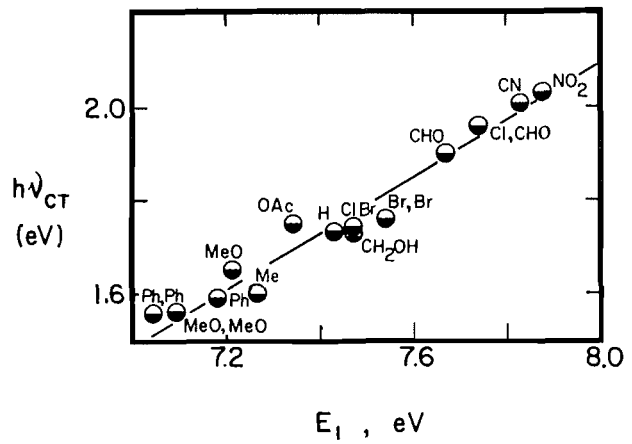

FIG. 6. Correlation of the vertical ionization energy E_i of various anthracenes with the charge transfer transition energy $h\nu_{CT}$ of their EDA complexes with tetracyanoethylene.

Experimental section

Materials

Tetracyanoethylene (Aldrich) was purified by repeated sublimation, first *in vacuo* and then several times at atmospheric pressure. 9-Cyanoanthracene, 9-anthraldehyde, 10-chloro-9-anthraldehyde, 9-methylanthracene, 9,10-dimethylanthracene, 9-acetylanthracene, 9-bromoanthracene, and 9-anthracenemethanol (Aldrich) were each purified by three recrystallizations from ethanol. 9-Chloroanthracene (Pfaltz and Bauer) was recrystallized from alcohol. Anthracene, 9-phenylanthracene, and 9,10-diphenylanthracene (Aldrich, Gold Label) were used without further purification. 9-Nitroanthracene (23), 9-methoxyanthracene (24), 9,10-dimethoxyanthracene (25), 9-anthryl acetate (24), methyl 9-anthroate (26), and 9,10-dibromoanthracene (27) were synthesized according to the procedures in the literature indicated. 9,10-Dicyanoanthracene was a gift from Professor N. C. Yang and was used as received.

Methylene chloride (Aldrich, Gold Label) was distilled from P_2O_5 under argon prior to use and was stored under argon in a Schlenk flask. Trifluoroacetic acid was a gift from Halocarbon Corporation and was distilled from a small amount of trifluoroacetic anhydride. The middle half was collected under argon in a Schlenk flask. Manipulation of trifluoroacetic acid was carried out with a platinum needle attached to an all-glass syringe under an argon atmosphere. Acetonitrile (HPLC grade from Fisher Scientific) was further purified by distillation from CaH_2 through a 15-plate Oldershaw column, followed by stirring overnight with $KMnO_4$ and Na_2CO_3 (5 g of each per liter). The mixture was filtered, distilled under reduced pressure, and finally fractionated from P_2O_5 under an argon atmosphere and stored in a Schlenk flask.

Tetra-*n*-butylammonium perchlorate (G.F. Smith Co.) was recrystallized from an isooctane – ethyl acetate mixture, and was dried *in vacuo* for 2 days prior to use. Tetraethylammonium perchlorate (G.F. Smith Co.) was further dried under vacuo.

Instrumentation

Photoelectron spectra were measured for gaseous compounds using a Perkin-Elmer PS 16/18 photoelectron spectrometer fitted with an Helectros lamp capable of generating both He(I) and He(II) radiation. Spectra were calibrated with respect to methyl iodide and the He (1s) band. The photoelectron spectra of the anthracenes demonstrate sharp peaks with well-resolved vibrational fine structure for ionizations involving the lower energy π-orbitals (Fig. 1). The vibrational progressions for the first (E_1) ionization energies of the anthracenes were measured as reported below (in cm^{-1}): *H*, 1300; *9-Me*, 1400; *9-OCOMe*, 1300; *9-Br*, 1500; *9-Cl*, 1500; *9-CH_2OH*, 1200; *9-CHO*, 1300; *9-COOH*, 1300; *9-CN*, 1400; *9-COOMe*, 1400; *9-COMe*, 1400; *9,10-DCN*, 1400; *9,10-DMe*, 1400; *9,10-DPh*, 1400; *9,10-DBr*, 1400; *9-CHO-10Cl*, 950. The sharpness of the bands and the similarity

[5] For similar correlations of the ionization energy and various electrochemical measures of oxidation, see ref. 22.

Can. J. Chem. Downloaded from www.nrcresearchpress.com by 210.87.254.42 on 09/06/12
For personal use only.

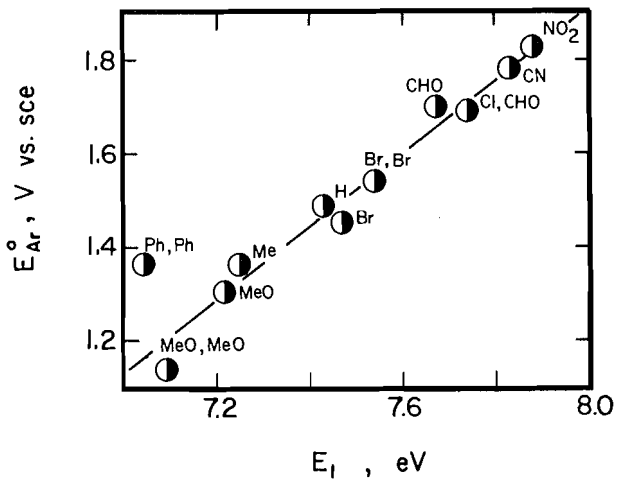

FIG. 7. Correlation of the standard oxidation potentials E^0_{Ar} of various anthracenes with the first vertical ionization energies E_I.

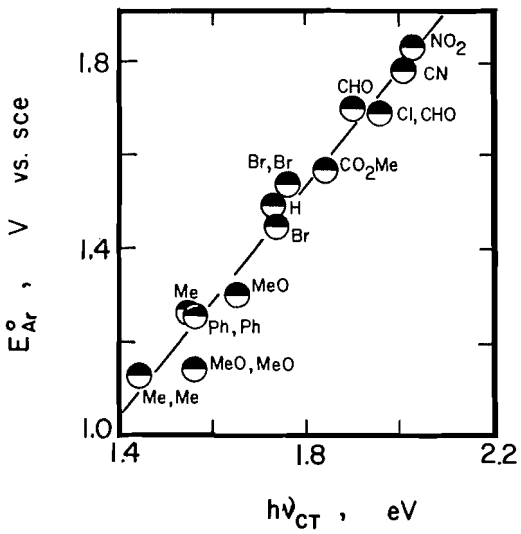

FIG. 8. Correlation of the standard oxidation potential E^0_{Ar} of 9,10-substituted anthracenes with the charge transfer transition energy $h\nu_{CT}$ of the corresponding EDA complex with tetracyanoethylene.

of the energies of the vibrational progression to those observed in the absorption spectra of the neutral, uncomplexed arenes (~1400 cm^{-1}, see Figs 3 and 5) indicates that a similarity exists in the geometries of the ground and excited states of the anthracene chromophore and the respective cation radical. That is, excitation or ionization generates a species in which the equilibrium geometry has not changed greatly, so that the internal reorganization energy is very small.

Electronic spectra were obtained on a Hewlett-Packard 8450A diode-array spectrometer. Absorption spectra of the anthracenes were measured on ~10^{-4} *M* solutions in methylene chloride and were normalized at their maxima to facilitate comparison (see Figs. 3 and 5). The absorption of the electron donor–acceptor complexes of anthracenes with TCNE were measured on solutions ~0.05 *M* in arene and in TCNE. The relative intensities in Fig. 2 are on an arbitrary scale.

Cyclic voltammetry was conducted with 5 × 10^{-3} *M* solutions of arene containing 0.1 *M* electrolyte (tetra-*n*-butylammonium perchlorate in methylene chloride or trifluoroacetic acid solvent systems and tetraethylammonium perchlorate in acetonitrile). All electrochemical experiments were performed using a flame-dried, air-tight cell under an atmosphere of argon. The instrumentation consisted of a Princeton Applied Research (PAR Model 173) potentiostat equipped with a current-to-voltage converter (PAR Model 176) for suitable

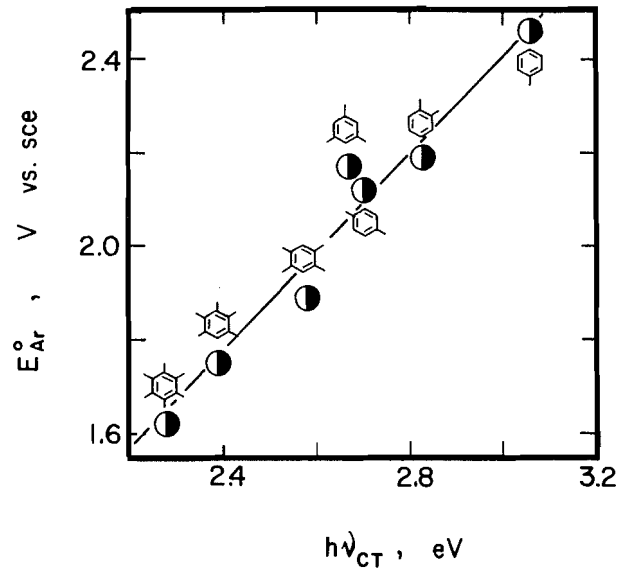

FIG. 9. Correlation of the standard oxidation potentials E^0_{Ar} for the homologous methylbenzenes with the charge transfer transition energy $h\nu_{CT}$ of the corresponding EDA complex with tetracyanoethylene.

ohmic drop compensation and a high impedance voltage amplifier (PAR model 178). The working electrode consisted of a 1 mm diameter platinum disc embedded in a cobalt glass seal. The counter electrode was a grid of platinum mesh with a 1 cm^2 surface area. The reference electrode was a saturated calomel electrode (sce) which was contained in a separate compartment separated by a cracked-glass tip capillary. Prior to use it was immersed in solvent of the same composition as that contained within the cell. However, methylene chloride was used in the reference cell compartment for cyclic voltammograms taken in trifluoroacetic acid solvent in order to limit exposure to this solvent. The system was calibrated relative to an anthracene standard (28). To obtain E^0_{Ar} relative to ferrocene, subtract 0.14_5 from each value. The addition of trifluoroacetic acid to methylene chloride solutions was found to be particularly effective in the stabilization of the cation radicals of monosubstituted anthracenes (15). The values of the standard oxidation potentials for the homologous methylarenes (see Fig. 9) are from ref. 13 after correction by 0.06 V for the change in solvent to 20 %v trifluoroacetic and in methylene chloride.

The absorption spectra of the anthracene radical cations were the result of electronically averaging multiple accumulations of spectra measured through a 0.1 mm gold minigrid (Buckbee-Mears Co., St. Paul, MN) electrode maintained at a constant potential ~0.2 V more positive than the E_0 determined by cyclic voltammetry. Spectroelectrochemistry was carried out by positioning the working electrode in a bulk electrolysis cell fused to a 1.0 cm Pyrex uv cuvette. The interrogating beam of the Hewlett-Packard 8450A spectrometer was directed through the gold minigrid electrode and was balanced prior to oxidation. Spectra were accumulated every 1 s starting simultaneously with the application of an oxidizing potential to the minigrid. The spectra of the immediately formed transients were the result of 40–100 balance-accumulation measurements.

Acknowledgment

We wish to thank Dr. Christian Amatore for assistance with the electrochemical studies and helpful discussion, and the National Science Foundation and Science and Engineering Council (EAS) for financial support.

1. I. P. BELETSKAYA and D. I. MAKHON'KOV. Russ. Chem. Rev. **50**, 1007 (1981).
2. R. A. SHELDON and J. K. KOCHI. Metal-catalyzed oxidation of

Can. J. Chem. Downloaded from www.nrcresearchpress.com by 210.87.254.42 on 09/06/12
For personal use only.

organic compounds. Academic Press, New York. 1981.
3. K. YOSHIDA. Electrooxidation in organic chemistry. Wiley, New York. 1984.
4. C. J. SCHLESENER, C. AMATORE, and J. K. KOCHI. J. Am. Chem. Soc. **106**, 3567 (1984).
5. (*a*) E. HEILBRONNER. Organic chemical photoelectron spectroscopy. *In* Molecular spectroscopy. *Edited by* A. R. West. Heyden and Son, London. 1977. p. 422; (*b*) J. W. RABALAIS. Principles of ultraviolet photoelectron spectroscopy. Wiley, New York. 1977.
6. R. FOSTER. Organic charge transfer complexes. Academic Press, New York. 1969.
7. E. F. HILINSKI, J. M. MASNOVI, C. AMATORE, J. K. KOCHI, and P. M. RENTZEPIS. J. Am. Chem. Soc. **105**, 6167 (1983).
8. R. S. MULLIKEN. J. Am. Chem. Soc. **74**, 811 (1952); R. S. MULLIKEN and W. B. PERSON. Molecular complexes: a lecture and reprint volume. Wiley, New York. 1969.
9. A. J. BARD and L. R. FAULKNER. Electrochemical methods. Wiley, New York. 1980.
10. L. KLASINC, B. KOVAČ, and H. GÜSTEN. Pure Appl. Chem. **55**, 289 (1983); L. KLASINC, B. KOVAČ, S. SCHOOF, and H. GÜSTEN. Croat. Chem. Acta, **51**, 307 (1978); R. BOSCHI, E. CLAR, and W. SCHMIDT. J. Chem. Phys. **60**, 4406 (1974); P. A. CLARK, F. BROGLI, and E. HEILBRONNER. Helv. Chim. Acta, **55**, 1415 (1972).
11. L. J. ANDREWS and R. M. KEEFER. J. Am. Chem. Soc. **73**, 3776 (1953). S. FUKUZUMI and J. K. KOCHI. Tetrahedron, **38**, 1035 (1982).
12. V. D. PARKER. J. Am. Chem. Soc. **98**, 98 (1976); V. D. PARKER and O. HAMMERICH. Acta Chem. Scand. B**31**, 883 (1977).
13. J. O. HOWELL, J. GONCALVES, C. AMATORE, L. KLASINC, R. M. WIGHTMAN, and J. K. KOCHI. J. Am. Chem. Soc. **106**, 3968 (1984).
14. (*a*) V. D. KISELEV and J. G. MILLER. J. Am. Chem. Soc. **97**, 4036 (1975); M. LOFTI and R. M. G. ROBERTS. Tetrahedron, **35**, 2123 (1979); **35**, 2131 (1979); (*b*) S. PIGNATARO and G. ALOISI. Z. Naturforsch. A**27**, 1165 (1972).
15. O. HAMMERICH and V. D. PARKER. J. Chem. Soc. Chem. Commun. 156 (1972); J. Am. Chem. Soc. **96**, 4289 (1974).
16. A. J. BARD, A. LEDWITH, and H. J. SHINE. Adv. Phys. Org. Chem. **13**, 156 (1976); K. E. FRIEND and W. E. OHNESORGE. J. Org. Chem. **28**, 2435 (1963); H. LUND. Acta Chem. Scand. **11**, 1323 (1957).
17. R. J. KLINGLER and J. K. KOCHI. J. Phys. Chem. **85**, 1731 (1981).
18. T. SHIDA and S. IWATA. J. Am. Chem. Soc. **95**, 3473 (1973); H. HIRATSUKA and Y. TANIZAKI. J. Phys. Chem. **83**, 2501 (1979).
19. S. FUKUZUMI and J. K. KOCHI. J. Phys. Chem. **84**, 608 (1980) and related papers.
20. M. H. ABRAHAM. J. Am. Chem. Soc. **104**, 2085 (1982); M. LOFTI and R. M. G. ROBERTS. Tetrahedron, **35**, 2137 (1979).
21. J. SAUER, J. BENDIG, and M. SIEGMUND. Z. Chem. **17**, 308 (1977).
22. (*a*) L. L. MILLER, G. D. NORDBLOM, and E. A. MAYEDA. J. Org. Chem. **37**, 916 (1972); W. C. NEIKAM. G. R. DIMELER, and M. M. DESMOND. J. Electrochem. Soc. **111**, 1190 (1964); E. S. PYSH and N. C. YANG. J. Am. Chem. Soc. **85**, 2124 (1963).
23. N. RABJOHN (*Editor*). Organic syntheses. Vol. 4. Wiley and Sons, New York. 1963. p. 711.
24. J. S. MEEK, P. A. MONROE, and C. J. BOUBOULIS. J. Org. Chem. **28**, 2572 (1963).
25. E. B. BARNETT, J. W. COOK, and M. A. MATHEWS. J. Chem. Soc. **123**, 1994 (1923).
26. R. C. PARISH and L. M. STOCK. J. Org. Chem. **30**, 927 (1965).
27. H. GILMAN (*Editor*). Organic syntheses. Vol. 1. Wiley and Sons, New York. 1961. p. 207.
28. R. R. GAGNE, C. A. KOVAL, and G. C. LISENSKY. Inorg. Chem. **19**, 2854 (1980).

Can. J. Chem. Downloaded from www.nrcresearchpress.com by 210.87.254.42 on 09/06/12
For personal use only.

The Py scale of solvent polarities

DAO CONG DONG[1] AND MITCHELL A. WINNIK[2]

Lash Miller Laboratories, Department of Chemistry and Erindale College, University of Toronto, Toronto, Ont., Canada M5S 1A1

Received March 26, 1984

This paper is dedicated to Professor Peter Yates on the occasion of his 60th birthday and to Professor J. T. Edward on the occasion of his 65th birthday

DAO CONG DONG and MITCHELL A. WINNIK. Can. J. Chem. **62**, 2560 (1984).

The relative intensities I_1/I_3 of the vibronic bands of pyrene fluorescence in 94 solvents and the vapor phase are reported. These values, ranging from 0.47 (vapor) to 1.95 (dimethyl sulfoxide) form the Py scale of solvent polarities. This scale is compared to other scales of solvent polarity, particularly the π^* scale of Kamlet and Taft in order to assess the contributions of various factors (dipolarity/polarizability, hydrogen bonding, etc.) to the solute–solvent interaction.

DAO CONG DONG et MITCHELL A. WINNIK. Can. J. Chem. **62**, 2560 (1984).

On rapporte les intensités relatives I_1/I_3 des bandes vibroniques de la fluorescence du pyrène dans 94 solvants et en phase vapeur. Ces valeurs, qui s'étalent de 0,47 (vapeur) à 1,95 (diméthyl sulfoxyde) forment l'échelle Py des polarités de solvant. Dans le but d'évaluer les contributions de divers facteurs (dipolarité/polarisabilité, liaison hydrogène, etc) sur l'interaction soluté–solvant, on compare cette échelle à d'autres échelles de polarité de solvants, en particulier avec l'échelle π^* de Kamlet et Taft.

[Traduit par le journal]

Can. J. Chem. Downloaded from www.nrcresearchpress.com by 210.87.254.6 on 09/06/12
For personal use only.

Introduction

Empirical solvent polarity parameters represent simple and straightforward means for characterizing and ranking the polarity of solvent media (1–5). When these media are structured or anisotropic, as in micelles, biological membranes, polymer blends, or swollen polymer resins, they provide unique insights into the effective polarity within individual microdomains (6, 7). The problem is that there are now many such parameters. Among the more well known are Kosower's Z parameter (5), the Dimroth E_T30 scale (3), Hildebrand's δ_H parameter (8), the Py scale (9), and the (π^*, α, β) treatment of Kamlet and Taft (1, 10). These parameters tend to be differently sensitive to various aspects of solvent–solute interactions.

Important progress has been made over the last ten to fifteen years in understanding the relationships between these various scales. While the early dream has vanished that a single parameter would somehow serve to describe a solvent, one still believes that there are a small number of identifiable classes of interactions between solvents and solutes (1). These can in principle be identified and measured, and through them the magnitude of any solvent-sensitive process can be understood. It is particularly noteworthy that all attempts to understand solvent sensitivity in terms of the bulk properties of the solvent — its dielectric constant and its index of refraction — have in the end failed. One now recognizes that interactions between molecules must be treated at the molecular level (1). The molecular theory of solvent–solute interactions is not very advanced but progress can be anticipated.

Among the most significant discoveries was the recognition that all solvent polarity scales can be expressed as linear combinations of other polarity parameters (1). This is in accord with the simple concept of linear free energy relationships and also supports the belief that the different scales are simply sensitive to different combinations of fundamental interactions between solutes and solvents. The current problem is one of identifying those interactions and separating experimental observations into the contributions of each of the individual components.

Kamlet and Taft (1, 10) and co-workers have played a leading role in this development. They write an equation which describes any observable XYZ as a linear combination of individual components

$$[1] \quad XYZ = XYZ_0 + S(\pi^* + d\delta) + a\alpha + b\beta + h\delta_H + e\xi$$

where π^* is an index solvent dipolarity/polarizability. The α scale is an index of hydrogen bond donor capability; β, of hydrogen bond acceptor basicities; and ξ, a coordinate covalency measure for electron pair donors. The δ_H term is the Hildebrand solubility parameter (8), a measure of solvent/solvent interactions which are interrupted in creating a cavity for the solute. The S, a, b, h, and e coefficients describe the sensitivity of a process to each of the individual contributions. Their hope is that each of the parameters in eq. [1] describe a truly fundamental aspect of solute–solvent interactions. For any given process, the coefficients of these parameters would measure the relative importance of each type of interaction.

Our concern is with the Py scale of solvent polarity. Py values are obtained in a very simple manner, either as the ratio of two absorbances within the fine structure of the uv spectrum of pyrene (6, 9, 11), or as the ratio of two intensities within the vibrational bands of pyrene fluorescence. Pyrene is readily available. One introduces it into a sample in only trace amounts. Detection by fluorescence means that one can examine optically awkward systems such as powders, suspensions, and other turbid mixtures. Values obtained by different laboratories agree to within a few percent (6, 9, 11).

In this paper we report Py values for 95 solvents. We review the origin of the phenomena underlying this effect and compare the Py scale to other measures of solvent polarity. Because of the extensive studies of Kamlet, Taft, and co-workers, we examine in more detail the relationship between the Py values and their π^* scale. Both are suggested to be independent of the hydrogen bonding nature of solvent media.

Results

The fluorescence spectra of pyrene at 1 μm in hexane and in

[1] Present address: Uniroyal Research Laboratories, Guelph, Ont., Canada N1H 6N3.

[2] To whom all correspondence should be addressed.

Can. J. Chem. Downloaded from www.nrcresearchpress.com by 210.87.254.6 on 09/06/12
For personal use only.

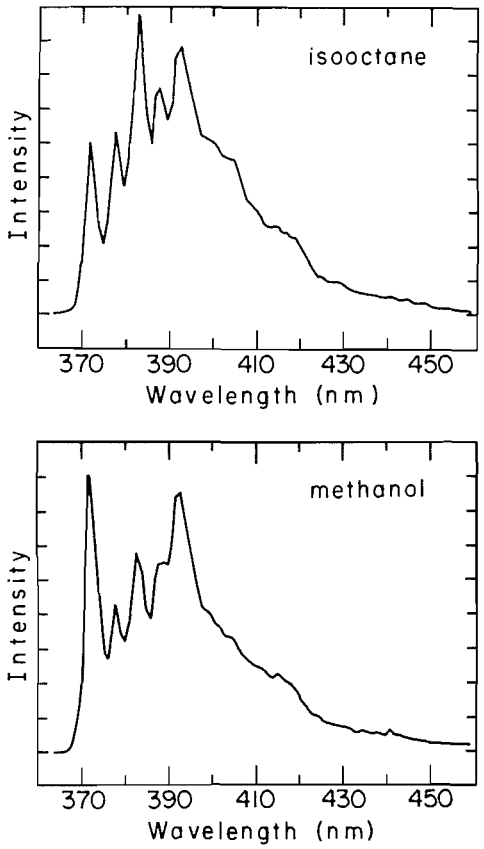

FIG. 1. Fluorescence spectra of pyrene in hexadecane and methanol showing differences in the fine structure of the spectra due to solvent change.

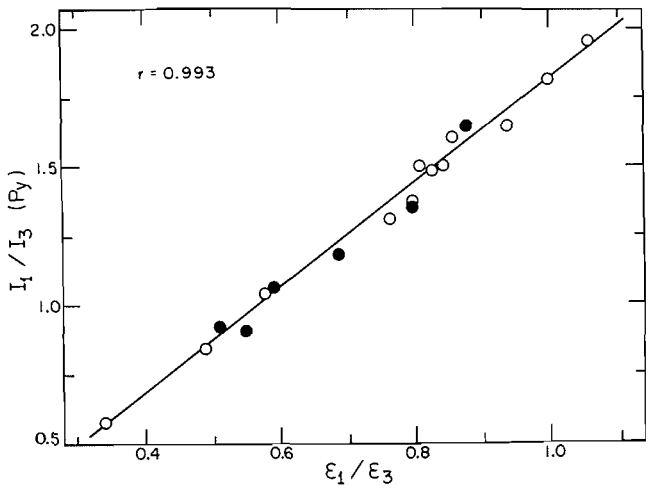

FIG. 2. Plot of Py values vs. extinction coefficients ratio ϵ_1/ϵ_3. Protic solvent (●); aprotic solvents (○).

methanol are shown in Fig. 1. Following Nakajima (11) these are normalized at the (0,2) band. One notices a pronounced enhancement of the intensity (I_1) of the (0,0) peak at 375 nm relative to that (I_3) of the (0,2) peak at 384 nm. Values of "Py" = I_1/I_3 range from 0.41 in the gas phase (11*a*) and 0.58 in hexane to 1.95 in dimethyl sulfoxide. Measurements are reproducible typically to ±0.02, and the results from different laboratories tend to fall within this range. Table 1 contains I_1/I_3 values measured for 95 solvents.

Pyrene fluorescence is suceptible to quenching by certain solvents such as amines and carbon tetrachloride. Py values in these solvents can be obtained by measuring the Beer's law extinction coefficient of the lowest energy peak (the (0,0) band) at 374 nm in the uv absorption spectrum of pyrene. These ϵ values increase linearly with I_1/I_3 (12). We have found it operationally less tedious to measure the ratio of the peak absorbance at ca. 374 nm to that at ca. 362 nm; which we denote as ϵ_1/ϵ_3. These are related to I_1/I_3 values (for 18 solvents, Fig. 2) by the equation

$$[2] \quad \frac{I_1}{I_3} = 1.84\frac{\epsilon_1}{\epsilon_3} - 0.054 \qquad \text{corr. } 0.991$$

Empirical correlations of Py with other solvent polarity scales are described below.

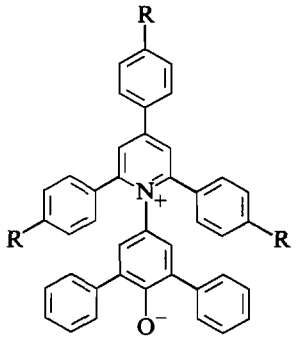

I, R = H
II, R = CH_3

Dimroth et al.*'s betaine*

E_T scale of Dimroth, Reichardt, Siepmann, and Bohlmann (3*a*) is based on the solvatochromic band of the pyridinium-*N*-phenolbetaines, **I** and **II**. The E_T value is the transition energy (in kcal mol^{-1}) of the intramolecular charge transfer band of **I**.

Compound **I** is insoluble in aliphatic and aromatic hydrocarbons, but the scale may be extended using the more soluble compound **II**. An excellent correlation exists between the transition energies of **I** and **II**, and the E_T scale has been extended to include value for *n*-hexane (13). As has been described in previous papers (9), plotting Py values against E_T values gives separate correlations for aprotic and protic solvents (Fig. 3). Py values for 37 aprotic solvents (except dioxane (solvent 73) and *o*-dichlorobenzene (solvent 24)) are nicely linear with corresponding E_T values. The correlation, represented by the regression line in Fig. 3, is as shown in eq. [3] with r (the correlation coefficient) = 0.946 and sd (the standard deviation) = 0.34. If the data for dioxane and *o*-dichlorobenzene are included, n = 39 solvents, r becomes 0.924, sd = 0.36. The

$$[3] \quad \text{Py} = 0.080E_T - 1.74$$

correlation equation for 19 protic solvents (except 2-methoxyethanol (solvent 80)), represented by the regression line in Fig. 3, is as shown in eq. [4] with r = 0.921, sd = 0.28. If the data for 2-methoxyethanol is included r becomes 0.892, sd = 0.28

$$[4] \quad \text{Py} = 0.0584E_T - 1.750$$

Different correlations for protic and aprotic solvents can be explained by the fact that solvent polarity and polarizability are dominant effects influencing E_T values in aprotic solvents whereas in protic solvents, in addition to polarity and polarizability, there are contribution from hydrogen bonding inter-

TABLE 1. Solvent dependence of the relative band intensities I_1/I_3 for pyrene fluorescence

Number	Solvent	I_1/I_3	Number	Solvent	I_1/I_3
0	Vapor	0.41	48	2-Methyl-1,4-pentanediol	1.28
1	Perfluorodecalin	0.52	49	3-Octanone	1.31
2	Perfluoromethylcyclohexane	0.52	50	Tetrahydrofuran	1.35
3	Perfluoro-2-butylTHF	0.55	51	Methylene chloride	1.35
4	Hexane	0.58	52	Methanol	1.35
5	Cyclohexane	0.58	53	*n*-Butyl acetate	1.35
6	Methylcyclohexane	0.58	54	1,5-Pentanediol	1.36
7	Dodecane	0.59	55	Acetic acid (glacial)	1.37
8	Isooctane	0.59	56	Ethyl acetate	1.37
9	Hexadecane	0.60	57	3-Heptanone	1.39
10	1-Octene	0.66	58	2-Methylcyclohexanone	1.41
11	Pentadecylbenzene	0.78	59	2-Heptanone	1.41
12	2,6-Di-*t*-butylpyridine	0.80	60	Pyridine	1.42
13	*n*-Butyl ether	0.84	61	2-Ethoxyethanol	1.43
14	*n*-Octanoic acid	0.91	62	Pinacolone	1.43
15	3,3-Dimethyl-2-butanol	0.92	63	1,4-Butanediol	1.45
16	*n*-Octanol	0.92	64	2-Chloroethanol	1.45
17	*iso*-Propyl ether	0.93	65	1,2-Propanediol	1.45
18	1,1-Dimethylpropanol	0.94	66	1,2-Dichloroethane	1.46
19	*p*-Xylene	0.95	67	Cycloheptanone	1.46
20	Mesitylene	0.97	68	Cyclohexanone	1.47
21	1,2,4-Trichlorobenzene	0.97	69	*N*-Methylacetamide	1.48
22	*o*-Xylene	0.99	70	Methyl acetate	1.48
23	m-Xylene	1.01	71	4-Methyl-2-pentanone	1.48
24	*o*-Dichlorobenzene	1.02	72	Dimethoxyethane	1.48
25	2-Methylcyclohexanol	1.02	73	Dioxane	1.50
26	*n*-Pentanol	1.02	74	Diethyl malonate	1.50
27	2-Methylpropanol	1.02	75	2-Pentanone	1.50
28	Ethyl ether	1.02	76	Cyclopentanone	1.56
29	1-Methylpropanol	1.03	77	Formamide	1.57
30	Toluene	1.04	78	Triethylene glycol	1.57
31	Benzene	1.05	79	2-Butanone	1.58
32	*n*-Butanol	1.06	80	2-Methoxyethanol	1.58
33	Bromobenzene	1.07	81	Diglyme	1.60
34	Chlorobenzene	1.08	82	Glycerol	1.60
35	Dihydropyran	1.08	83	Triglyme	1.62
36	1-Methylethanol	1.09	84	Acetic anhydride	1.63
37	*n*-Propanol	1.09	85	Acetone	1.64
38	Cyclohexanol	1.09	86	Ethylene glycol	1.64
39	*o*-Methylanisol	1.11	87	Propionitrile	1.68
40	2,6-Lutidine	1.17	88	2,2,2-Trifluoroethanol	1.69
41	Butyric acid	1.18	89	Formic acid	1.69
42	Ethanol	1.18	90	*N*,*N*-Dimethylacetamide	1.79
43	2-Undecanone	1.23	91	Acetonitrile	1.79
44	Anisol	1.24	92	*N*,*N*-Dimethylformamide	1.81
45	Benzyl alcohol	1.24	93	Water	1.87
46	Chloroform	1.25	94	Dimethyl sulphoxide	1.95
47	Propionic acid	1.28			

Can. J. Chem. Downloaded from www.nrcresearchpress.com by 210.87.254.6 on 09/06/12
For personal use only.

actions (4) on E_T values. Hydrogen bonding to phenoxide oxygen should stabilize the ground state relative to electronic state, and the effect in protic solvents should be hypsochromic (14) as is observed.

Kosower's 1-ethyl-4-carbomethoxypyridinium iodide

Kosower's Z scale (5) is based on the pronounced solvatochromism of 1-ethyl-4-carbomethoxypyridinium oxide. The Z value is calculated from the position of the absorption maximum. The stronger the stabilization effect of the solvent on the ion-pair relative to that in the less polar excited state, the higher the transition energy and the Z value.

Correlation equation of Py value of 18 aprotic solvents (except benzene (solvent 31) and dimethoxyethane (solvent 72)) with Z values represented by the regression line in Fig. 4, is shown in eq. [5] with $r = 0.920$, sd = 0.25. If the data for benzene and dimethoxyethane are included $n = 25$, r becomes 0.896, sd = 0.25

$$[5] \quad \text{Py} = 0.0671Z - 2.870$$

The Z value for water was reported by Kosower (5*a*) to be 94.6, but it was later proposed by Griffiths and Pugh (5*c*) to be 91.8.[3] The correlation of Py values with Z values for 17 protic solvents (except 2-ethoxyethanol (solvent 61) and *N*-methylacetamide (solvent 69)) is represented by the regression

[3] The Z value could not be obtained directly as the charge transfer band is masked by the intense absorption band of the pyridinium cation. It was obtained by extrapolating from the correlation with Winstein's Y value (15) of binary solvent mixtures (5*a*).

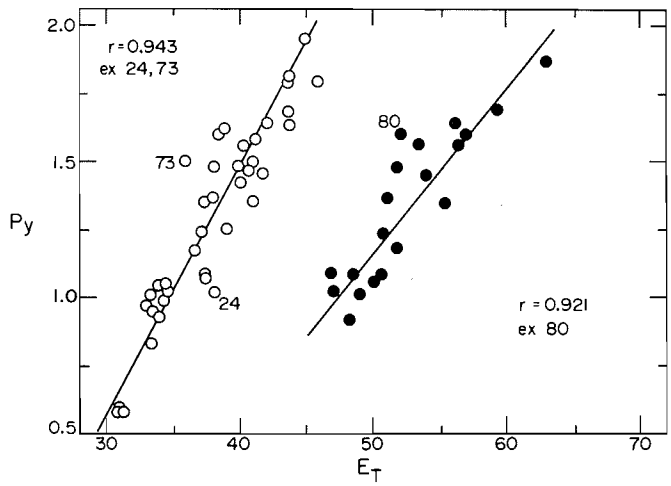

FIG. 3. Plot of Py values vs. Dimroth's E_T values. Protic solvents (●); aprotic solvents (○).

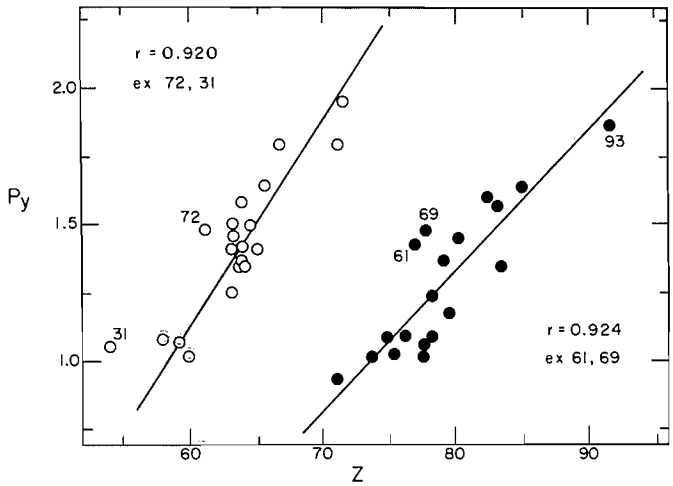

FIG. 4. Plot of Py values vs. Kosower's Z values. Protic solvents (●); aprotic solvents (○).

line in Fig. 4, and is given by eq. [6] with $r = 0.924$, sd = 0.27 when the value 91.8 is used for water.

[6] $\quad Py = 0.052Z - 2.82$

If the results for solvents 61, 69 are included r becomes 0.866, sd = 0.26.

The contribution of hydrogen bonding on Z values of protic solvents was recognized by Kosower (5*a*) in agreement with our separate correlation with aprotic and with protic solvents (Fig. 4).

Smith, Fainberg, and Winstein's log k_{ion} *values*

Fainberg and Winstein (15) introduced the ionization of *p*-methoxyneophenyl-*p*-toluenesulphonate as a standard reaction for characterizing the polarity of solvents. The rate of this reaction at 75°C was termed the log k_{ion} value.

Py values for eight aprotic solvents (Et_2O, THF, EtOAc, Ac_2O, acetone, CH_3CN, DMF, Me_2SO; excluding pyridine (solvent 60)) are nicely linear with their correlation equation represented by

[7] $\quad Py = 0.250 \log k_{ion} + 2.85$

with $r = 0.987$, sd = 0.30. If value for pyridine is included one obtains $r = 0.939$, sd = 0.29, slope = 0.239, intercept = 2.77.

For six protic solvents (*n*-octanoic acide, EtOH, MeOH, AcOH, HCOOH, H_2O) against log k_{ion} values, the correlation equation obtained is $r = 0.969$, sd = 0.34:

[8] $\quad Py = 0.27 \log k_{ion} + 2.08$

Taft's P *value*

Taft's *P* parameter (16) is defined as the chemical shift (in ppm) of the fluorine resonance in the nmr spectrum of *p*-nitrosofluorobenzene in a given solvent relative to the same quantity in the standard solvent cyclohexane. The *P* values appear to be related to the ability of the solvents to form specific 1:1 complexes with the polar nitroso group. Py gives only a very poor correlation with *P* values, i.e. for 23 aprotic and 3 protic solvents

[9] $\quad Py = 0.46P + 0.6$

with $r = 0.79$ and sd = 0.31.

Allerhand and Schleyer's G *values*

The *G* value (17) is based on the relative wave number difference in the gas phase and in solution of ir stretching vibration absorption of X=O and X—H . . . B groups (X = C, S, N, O, P; B = solvent). A plot of Py vs. *G* gives the regression equation

[10]. $\quad Py = 0.0165G - 0.16$

with $r = 0.858$, $S = 0.36$, $n = 13$. If the results for chloroform (high Py value) and acetonitrile (low Py value, but similar *G* values) are excluded, r becomes 0.938.

Kamlet, Abboud, and Taft's π^* *scale*

Recently Kamlet, Abboud, and Taft introduced the π^* solvent polarity scale (10) on the basis of the average solvatochromic behavior of a large number of indicator solutes rather than on a single one. A plot of Py vs. π^* values for 44 solvents is shown in Fig. 5. The correlation equation is as shown in eq. [11], with $r = 0.832$ and sd = 0.32.

[11] $\quad Py = 0.64 + 1.109\pi^*$

Interestingly, if solvents are divided by classes: aprotic aliphatics, protic aliphatics, aprotic aromatic, each class gives excellent correlation of Py vs. π^* values as shown in eqs. [12]–[14]:

[12] $\quad Py = 0.64 + 1.329\pi^*$

for aprotic aliphatic solvents ($n = 23$, $r = 0.976$, sd = 0.37)

[13] $\quad Py = 0.46 + 1.304\pi^*$

for protic aliphatic solvents ($n = 9$, $r = 0.982$, sd = 0.28)

[14] $\quad Py = 0.54 + 0.972\pi^*$

for aprotic aromatic solvents ($n = 8$, $r = 0.979$, sd = 0.16)

For chlorinated aliphatics (three solvents) and protic aromatic solvents (one solvent), data are insufficient for correlation.

Discussion

Spectroscopy

The variation of I_1/I_3 with solvent polarity is one of many examples of intensification of symmetry-forbidden bands in polar solvents. The effect was first observed in benzene by Ham (18) and later studied by Durocher and Sandorfy (19). It is frequently referred to as the Ham effect. This effect is partic-

Can. J. Chem. Downloaded from www.nrcresearchpress.com by 210.87.254.6 on 09/06/12
For personal use only.

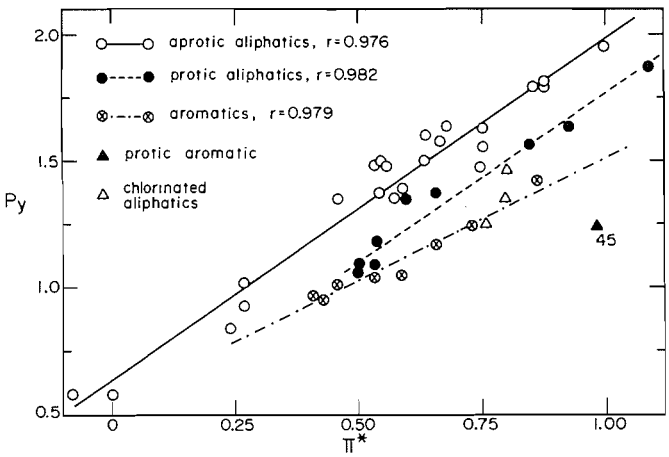

FIG. 5. Plot of Py values vs. Taft's π^* values.

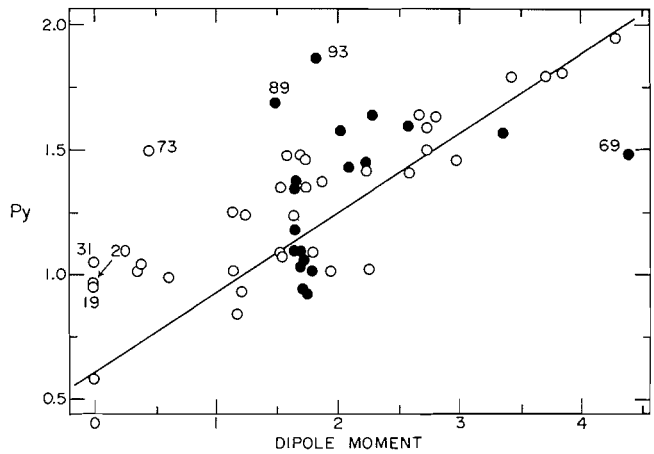

FIG. 6. Plot of Py values vs. dipole moment. Protic solvents (●); aprotic solvents (○).

ularly pronounced in pyrene where it has been studied by several research groups including those of Nakajima (11), Kalyanasundaram and Thomas (6), Hara and Ware (12), Lianos and Georghiou (20), and ourselves (9). Hara and Ware (12) demonstrated that polar solvents effected an increase of the radiative transition rate of the (0,0) band in fluorescence. This is the most compelling of many indications that polar solvents enhance the oscillator strength of symmetry-forbidden transitions. Other factors indicate that they do so through a reduction of local symmetry.

Lianos and Georghiou (20) compared pyrene with 1-methylpyrene and noted that the I_1/I_3 value of the latter in heptane was comparable to that of the former in water. Furthermore, the vibrational fine structure in 1-methylpyrene is broadened and much less sensitive to solvent polarity than that of pyrene itself. These symmetry-breaking features of the local field about the pyrene group ought also to affect the selection rules for vibronic transitions in pyrene. Solvent-enhancement of weakly allowed infrared bands in pyrene were also reported. Polar solvents cause peak broadening and intensity enhancements comparable in magnitude to those caused by methyl substitution.

The origin and nature of the local field is still not clear. Four factors can be cited. (*i*) Dipole interactions between the transition moment of the pyrene and the permanent dipole moment of the solvent molecules; (*ii*) inductive interactions with the quadrupole moment of the solvent molecules; (*iii*) dispersive interactions, and (*iv*) hydrogen bonding interactions. The first three effects have been discussed by Nakajima (11) and by Hara and Ware (12). If (*i*) were dominant, one would anticipate a correlation by Py with molecular dipole moment μ. As Fig. 6 emphasizes, this correlation is rather poor. Kamlet and Taft (1, 10) report a correlation of their π^* scale with μ for *select solvents*. Their presumption is that for these solvents, other factors affecting π^* are relatively unimportant.

Lianos and Georghiou (20) believe that molecular complex formation is the major factor. For protic solvents they see pyrene as a hydrogen bond acceptor with alcohols and even solvents as weakly acidic as CH_2Cl_2 acting as hydrogen bond donors. To substantiate this point of view he finds from infrared studies that pyrene forms weakly-bound 1:1 complexes with simple alcohols in dilute solution in CCl_4, and that these complexes have red-shifted O—H stretching frequencies. On the other hand we find only very small H/D isotope effects on I_1/I_3. Thus we obtain Py values of 1.20 in EtOD (1.18 in EtOH), 1.36 in CD_3OD (1.35 in CH_3OH), 1.44 in CH_3CO_2D (1.44 in CH_3CO_2H),[4] and 1.91 in D_2O (1.87 in H_2O).

Comparison with eq. [1]

According to eq. [1], π^* is an index of solvent dipolarity and polarizability. Under some circumstances, it overcompensates for the additional polarizability of aromatic and halogenated solvents, so that a correction term $d\delta$ is introduced. We noted in discussing Fig. 5 that Py correlated poorly with π^* but that there were indications of local correlations within families of solvents. This observation suggests that a correlation of Py ≡ XYZ ought to be possible in terms of eq. [1].

$$[15]\quad XYZ = XYZ_0 + S(\pi^* + d\delta) + a\alpha$$

Equation [1] can be simplified since pyrene is not a hydrogen bond donor: $b = 0$. We also assume that h and e are likewise zero, although the neglect of the $h\delta_H$ term is based only on the observation of similar Py values in alkanes that differ by about 1 unit in δ_H. With these assumptions we find an excellent correlation, Fig. 7, to the expression

$$[16]\quad Py^{calcd} = 0.64 + 1.33(\pi^* - 0.24\delta) - 0.25\alpha$$

with certain exceptions. The perfluorodecalin, perfluoromethylcyclohexane (Py = 0.52), and gas phase (Py = 0.41) points fall far off the line and are not included in the correlation. For the gas phase, eq. [16] predicts a Py^{calcd} value of −0.8. Trifluoroethanol has a Py^{calcd} value substantially smaller than its actual Py value, with the difference exacerbated by the -0.25α term ($\alpha[CF_3CH_2OH] = 1.51$). Acetonitrile and formamide also seem conspicuously far from the correlation line. These differences are particularly striking since dimethylformamide, dimethyl acetamide, and dimethylsulfoxide fall directly on the correlation line.

We suggest the possibility that the π^* values for fluorocarbons, acetonitrile, and formamide may need revision. For acetonitrile, where the $a\alpha$ term is very small, a π^* value of 0.90 (rather than 0.75) is in better accord with our data. In treating the fluorocarbons, we have set $\delta = 0$ in our correlation using eq. [15]. To improve the fit, we would suggest $\pi^* = -0.09$ instead of −0.33. For formamide, we question whether a somewhat smaller π^* value coupled with a larger value of a α might not also accommodate the other data from which the

[4] In freshly dried (glacial) acetic acid, Py = 1.37, as reported in Table 1.

Can. J. Chem. Downloaded from www.nrcresearchpress.com by 210.87.254.6 on 09/06/12
For personal use only.

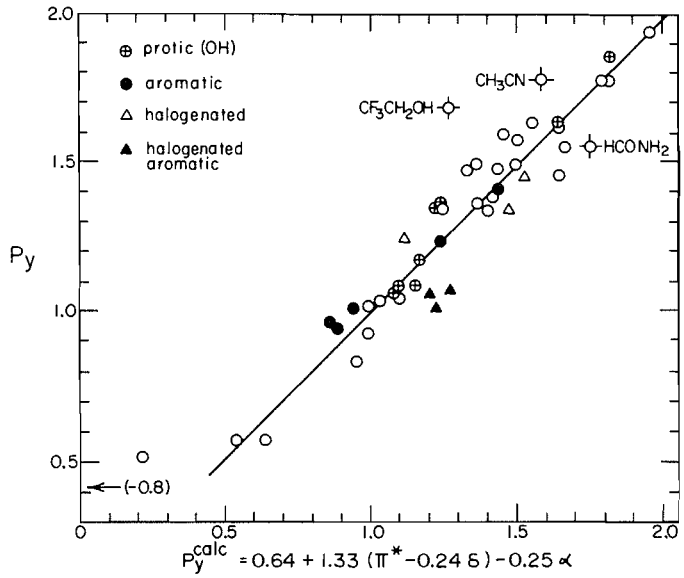

FIG. 7. Plot of Py values vs. Py^{calcd} values obtained from the Kamlet and Taft parameters and the correlation equation (15): $Py^{calcd} = 0.64 + 1.33\ (\pi^* - 0.24\delta) - 0.25\alpha$; slope = 0.988, intercept = 0.02, corr. = 0.959.

original values were derived.

It is curious that the coefficient of the α-term in eq. [14] is negative. This implies that solvent hydrogen bond donor ability acts to *lower* Py values over those inferred from ($\pi^* + 0.24\delta$) values (see Fig. 5). Yet in Table 1 it appears that solvents which are strong hydrogen bond donors have larger Py values (e.g. water, formic acid, trifluoroethanol) than those which are weaker hydrogen bond donors (e.g. ethanol, methanol). The small absolute value of the coefficient of the α-term indicates that the Py scale is much less sensitive to hydrogen bonding effects than to dipolarity–polarizability effects of the solvent. Its negative sign raises the question of whether there might be some residual hydrogen-bond-acceptor sensitivity contained within Kamlet and Taft's π^* scale for protic solvents.

Summary and future directions

The Py scale of solvent polarities is an empirical scale. Its values are easily determined with good precision. They span a significant range, varying from 0.41 in the gas phase to 1.95 in dimethylsulfoxide. Comparison with eq. [1] based upon the work of Kamlet, Taft, and co-workers (1, 10) emphasizes that the Py scale is relatively insensitive to the hydrogen bonding capability of protic solvents. Under other circumstances, these values might have served to parameterize the π^* scale for protic solvents.

In the spirit of Kamlet and Taft's research (1, 10), one would like a series of independent measurements which could be used to parameterize a solvent polarity scale in which dipolarity–polarizability terms were indeed separated from those describing hydrogen bond donor or acceptor capabilities. This is of course the aim of eq. [1]. This ought to be possible by examining solvent-induced emission intensity and absorption enhancements for other aromatic molecules. Mukhopadhyay and Georghiou (21) report enhancement factors (DMSO vs. *n*-heptane) of 2.93 (fluorescence) and 3.84 (absorption) for 1,12-benzoperylene, 2.10 (fluorescence) and 3.47 (absorption) for naphthalene, with somewhat smaller enhancements for 1-methylnaphthalene. Nakajima reported a value of 3.95 (fluorescence) for coronene (11*b*). Each of these molecules could serve as a probe for its own independent solvent polarity scale.

Experimental

Pyrene was purified as described previously (9). Solvents used were either reagent grade or spectral grade and were purified further by distillation. Fluorescence spectra were run at 22° on an SLM model 4800 spectrometer using 0.5 nm slits. Details were as previously reported (9).

Acknowledgments

The authors thank NSERC Canada for its support of this research. Discussions with Dr. S.T. Cheung are greatly appreciated.

1. M. KAMLET. Prog. Phys. Org. Chem. **13**, 485 (1981) and references therein.
2. T. R. GRIFFITHS and D. C. PUGH. Coord. Chem. Rev. **29**, 129 (1979).
3. (*a*) K. DIMROTH, C. REICHARDT, T. SIEPMANN, and F. BOHLMANN. Liebigs Ann. Chem. **661**, 1 (1963); (*b*) K. DIMROTH and C. REICHARDT. Leibigs Ann. Chem. **727**, 93 (1969); (*c*) C. REICHARDT. Leibigs Ann. Chem. **752**, 64 (1971); (*d*) C. REICHARDT. Angew. Chem. Int. Ed. Engl. **18**, 98 (1979).
4. (*a*) J. FIGUERAS. J. Am. Chem. Soc. **93**, 3255 (1971); (*b*) F. W. FOWLER, A. R. KATRITZKY, and J. D. RUTHERFORD. J. Chem. Soc. B 460 (1971).
5. (*a*) E. M. KOSOWER. J. Am. Chem. Soc. **80**, 3253 (1958); **80**, 3261 (1958); **80**, 3267 (1958); (*b*) E. M. KOSOWER and J. A. SKOREZ. J. Am. Chem. Soc. **82**, 2188 (1960); (*c*) T. R. GRIFFITHS and D. C. PUGH. J. Sol. Chem. **8**, 247 (1979).
6. K. KALYANASUNDARAM and J. K. THOMAS. J. Am. Chem. Soc. **99**, 2039 (1977).
7. P. LIANOS, A. K. MUKHOPADHYAY, and S. GEORGHIOU. Photochem. Photobiol. **32**, 415 (1980).
8. J. H. HILDEBRAND and R. L. SCOTT. The solubility of nonelectrolytes. 3rd ed. Reinhold, New York. 1950.
9. D. C. DONG and M. A. WINNIK. Photochem. Photobiol. **35**, 17 (1982).
10. (*a*) M. J. KAMLET, J. L. ABBOUD, and R. W. TAFT. J. Am. Chem. Soc. **99**, 6027 (1977); (*b*) M. J. KAMLET, J. L. ABBOUD, and R. W. TAFT. J. Am. Chem. Soc. **99**, 8325 (1977); (*c*) M. J. KAMLET, T. N. HALL, J. BOYKIN, and R. W. TAFT. J. Chem. Soc. Perkin Trans. 2, 2559 (1979).
11. A. NAKAJIMA. (*a*) Bull. Chem. Soc. Jpn. **44**, 3272 (1977); (*b*) J. Lumin. **11**, 429 (1976); (*c*) J. Mol. Spectrosc. **61**, 467 (1976); (*d*) Kagaku No. Ryoiki, **33**, 40 (1979); (*e*) Spectrochim. Acta. Part A, **39A**, 913 (1983).
12. K. HARA and W. WARE. Chem. Phys. **51**, 61 (1980).
13. C. REICHARDT and E. HARBUSCH-GÖRNERT. Liebigs. Ann. Chem. 721 (1983).
14. R. W. TAFT and M. J. KAMLET. J. Am. Chem. Soc. **98**, 2886 (1976).
15. A. R. FAINBERG and S. WINSTEIN. J. Am. Chem. Soc. **78**, 2770 (1956).
16. (*a*) R. W. TAFT, G. B. KLINGENSMITH, E. PRICE, and I. R. FOX. Prepr. Pa. Symp. LFE Relat. 265 (1964); (*b*) C. D. RITCHIE. *In* Solute–solvent interactions. *Edited by* J. F. Coetzee and C. D. Ritchie. Marcel Dekker Inc., New York. 1969. p. 281.
17. A. ALLERHAND and P. R. SCHLEYER. J. Am. Chem. Soc. **85**, 371 (1963).
18. J. S. HAM. J. Chem. Phys. **21**, 756 (1953).
19. G. DUROCHER and C. SANDORFY. J. Mol. Spectrosc. **20**, 410 (1966).
20. P. LIANOS and S. GEORGHIOU. Photochem. Photobiol. (*a*) **30**, 355 (1979); (*b*) **30**, 843 (1979).
21. A. K. MUKHOPADHYAY and S. GEORGHIOU. Photochem. Photobiol. **31**, 407 (1980).

Can. J. Chem. Downloaded from www.nrcresearchpress.com by 210.87.254.6 on 09/06/12
For personal use only.

Restricted rotation about arene–oxygen bonds in some 1,3-di-*tert*-butyl-2-methoxyarenedicarbonylphosphorus(III)chromium compounds

EVA M. CAMPI, BRYAN M. K. GATEHOUSE, W. ROY JACKSON, IAN D. RAE,[1] AND MARGARET G. WONG
Department of Chemistry, Monash University, Clayton, Victoria, Australia 3168

Received March 6, 1984

This paper is dedicated to Professor Peter Yates on the occasion of his 60th birthday

EVA M. CAMPI, BRYAN M. K. GATEHOUSE, W. ROY JACKSON, IAN D. RAE, and MARGARET G. WONG. Can. J. Chem. **62**, 2566 (1984).

The ^{1}H nmr spectra of 1,3-di-*tert*-butyl-2-methoxybenzenedicarbonyltriphenylphosphinechromium (**5**) and some related compounds at low temperatures show the presence of two species which interconvert with free energy of activation near 50 kJ mol^{-1}. The species differ in the orientation of the methoxy with respect to the chromium, since the same type of process is observed in a chelate complex in which a phosphinite ligand on chromium is also attached to the arene. Hindered rotation about the arene–chromium axis is not involved. The crystal structure of **5** shows the Ph_3P *anti* to the methoxy and the O-methyl group proximal to chromium.

EVA M. CAMPI, BRYAN M. K. GATEHOUSE, W. ROY JACKSON, IAN D. RAE et MARGARET G. WONG. Can. J. Chem. **62**, 2566 (1984).

Les spectres rmn du ^{1}H, obtenus à basse température, du di-*tert*-butyl-1,3 méthoxy-2 benzènedicarbonyltriphénylphosphinechrome (**5**) et de quelques composés apparentés démontrent l'existence de deux espèces qui se convertissent l'une dans l'autre avec une énergie libre d'activation de près de 50 kJ mol^{-1}. Considérant que l'on observe le même type de processus dans le chélate complexe dans lequel un ligand phosphinite du chrome est aussi attaché à l'arène, on en conclut que la différence entre les espèces se manifeste dans l'orientation du groupe méthoxyle par rapport au chrome. L'empêchement à la rotation autour de l'axe arène–chrome n'est pas impliquée. La structure cristalline du composé **5** démontre que le Ph_3P est en position *anti* par rapport au groupe méthoxyle alors que le groupe O-méthyle est proximal par rapport au chrome.

[Traduit par le journal]

Can. J. Chem. Downloaded from www.nrcresearchpress.com by 210.87.254.42 on 09/06/12
For personal use only.

Introduction

Arenetricarbonyl chromium compounds (**1**) are believed to exist in solution as equilibrium mixtures of eclipsed conformers (**1***a*, **1***b*) (1, 2), although staggered conformers (**2**) are often observed in the solid state, e.g. for benzenetricarbonylchromium itself (3). The position of equilibrium is determined by the steric and electronic properties of substituents on the arene ring, with **1***b* being favoured when R is electron releasing, but **1***a* if R is large and (or) electron withdrawing (1).

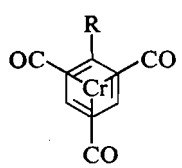

1*a*

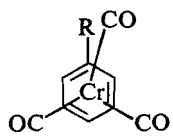

1*b*

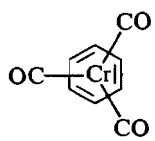

2

The interchange between these two eclipsed conformations is extremely rapid, with an electron diffraction study indicating that there was practically unhindered motion about the arene–Cr axis in gaseous benzenetricarbonylchromium (4). In the solid state a phase change at 108 K was attributed to the freezing-out of this motion (5). Nonetheless there have been numerous attempts to prepare arenechromium compounds in which this rotation would be sufficiently hindered to permit the observation of individual conformers by low-temperature nmr spectroscopy. We had great hopes (6) for 1,3,5-tri-*tert*-butylbenzenedicarbonyltriphenylphosphinechromium, but no evidence for restricted rotation could be found above 183 K, the lowest temperature at which we could keep the compound in solution. Others have succeeded in demonstrating restricted rotation about an arene–metal bond in the complexes (*p*-*t*-$BuC_6H_4Me)Ru(CO)(SiCl_3)_2$ (7) and (*p*-*t*-$BuC_6H_4Me)_2Cr$ (8).

When hexaethylbenzenetricarbonylchromium was studied at low temperature (9), the arene ligand was found to be eclipsed with respect to the carbonyls and alternate methyl groups were distal and proximal to the chromium. The ethyl groups changed orientation by a complex series of rotations having, overall, $\Delta G‡$ about 48 kJ mol^{-1}. When one of the carbonyls was replaced by Ph_3P, however, the crystal structure showed a staggered conformation with all of the methyls distal to the chromium, and solutions of the complex showed no dynamic nmr behaviour down to 148 K (9).

More recently McGlinchey *et al.* have reported low-temperature nmr studies of hexaethylbenzenedicarbonylthiocarbonylchromium (10) in which it is proposed that arene–Cr rotation is slow at 163 K and that $\Delta G‡$ for the rotation is 48 kJ mol^{-1}. This attribution has been challenged by Hunter and Mislow (11), who feel that changes in the nmr spectrum at low temperatures can be explained by permutation among the side-chains as described above.

In pursuing this same goal of restricted arene–Cr rotation we have used as ligands some 1,3-di-*tert*-butyl-2-methoxyarenes in which the three contiguous arene substituents were expected to buttress each other and increase the hindrance they offer to rotation of the $Cr(CO)_3$, $Cr(CO)_2P(OPh)_3$, and $Cr(CO)_2PPh_3$ moieties. Theoretical work had indicated (12) that electron donation by the arene substituents would increase the barrier to rotation, and the methoxy substituent was expected to help in this regard.

Experimental

Synthesis

The arenetricarbonylchromium complexes were prepared from hexacarbonylchromium and the appropriate arenes in a mixture of butyl ether and tetrahydrofuran (13) and purified by flash chro-

[1]Author to whom correspondence should be addressed.

matography on silica gel. Replacement of one CO by a phosphorus(III) ligand was achieved by irradiation of the ligand and chromium complex with ultraviolet light. Details of the preparation and characterization of **3**, **4**, **5**, and **7** are to be found in our recent publication (14).

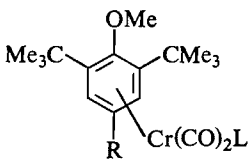

Compound	R	L
3	H	CO
4	H	$P(OPh)_3$
5	H	PPh_3
6	D	PPh_3
7	Me	PPh_3

Cyclic phosphinite (8)

A solution of 3,5-di-*tert*-butyl-4-methoxytoluene (17.6 g, 0.075 mol), recrystallized *N*-bromosuccinimide (13.35 g, 0.075 mol), and benzoyl peroxide (100 mg) in carbon tetrachloride (100 mL) was stirred and refluxed for 18 h while under irradiation from a photoflood lamp. The mixture was cooled and filtered, the precipitated succinimide being washed with a little CCl_4 which was added to the filtrate. The solvent was then removed on the rotary evaporator and the residue distilled at reduced pressure to give the *bromomethyl compound* as an oil (14.7 g, 62%), bp 126–128°C/0.5 Torr (1 Torr = 133.3 Pa), which solidified to a yellowish solid with mp 41–43°C and was sufficiently pure for use in the next step.

The bromomethyl compound (13.5 g, 0.043 mol) and sodium acetate (10.2 g, 0.125 mol) were dissolved in glacial acetic acid (50 mL) and the solution refluxed for 9 h. The cooled mixture was partitioned between water (150 mL) and diethyl ether (150 mL) and the ether layer was separated, washed with aqueous $NaHCO_3$ and then water (2 × 50 mL), dried over Na_2SO_4, and finally evaporated to give crude *acetoxymethyl compound* (11.2 g) which was shown by nmr to contain some aldehyde impurity.

The acetoxymethyl compound (10 g, 0.034 mol) was dissolved in dry methanol (30 mL) and treated at room temperature with a solution of sodium methoxide prepared from sodium (0.80 g, 0.035 mol) in methanol (15 mL). The solution was stirred under a N_2 atmosphere for 18 h and then diluted with concentrated NaCl solution (80 mL). Extraction with diethyl ether (4 × 50 mL) and a conventional work-up gave the crude product as a liquid, which slowly solidified. Recrystallization from ethyl acetate – hexane gave 3,5-di-*tert*-butyl-4-methoxybenzenemethanol (5.09 g, 59%) as white crystals, mp 101.5–102.5°C; infrared (KBr) ν_{max}: 3300, 1120 cm^{-1}; ^{1}Hmr ($CDCl_3$/TMS) δ: 1.43 (s, 18), approx. 1.4 (br, 1), 3.69 (s, 3), 4.62 (br d, 2, J = 4 Hz), 7.26 (s, 2). *Anal.* calcd. for $C_{16}H_{26}O_2$: C 76.75, H 10.47; found: C 76.82, H 10.80.

This alcohol (2.33 g, 9 mmol) and hexacarbonylchromium (2.0 g, 9 mmol) reacted in dibutyl ether – tetrahydrofuran as described (13, 14) for 18 h, and the solvent was removed at reduced pressure. Recrystallization of the residue from ether–hexane gave several crops of the *tricarbonylchromium complex* (0.95 g, 26%) as bright yellow crystals, mp 144–146°C; infrared (KBr) ν_{max}: 3440, 1950, 1870, 1815 cm^{-1}; ^{1}Hmr ($CDCl_3$/TMS) δ: 1.47 (s, 18), approx. 1.4 (br, 1), 3.86 (s, 3), 4.25 (d, 2, J = 7 Hz), 5.9 (s, 2). *Anal.* calcd. for $C_{19}H_{26}CrO_5$: C 59.06, H 6.78; found: C 58.76, H 6.82.

The above complex (0.68 g, 1.8 mmol) in diethyl ether (25 mL) with triethylamine (0.27 g, 2.7 mmol) was treated with $ClPPh_2$ (0.409 g, 1.8 mmol) under a N_2 atmosphere at 0°C. After stirring for 1 h, the solution was filtered through a glass sinter into a quartz test tube. The precipitate was washed with C_6H_6 (30 mL) and then cyclohexane (30 mL), which were added to the filtrate. This solution was then irradiated for 7 h with annular discharge lamps (254, 310 nm) and then evaporated to dryness. The residue was taken up in toluene – light petroleum (1:4) and flash chromatographed on silica gel, the product eluting as an orange band. Evaporation of the solvents and recrystallization from light petroleum gave the *chelate complex* **8** (140 mg, 15%) as orange needles, mp 180–182°C; infrared (KBr) ν_{max}: 1875, 1820 cm^{-1}; ^{1}Hmr (CD_2Cl_2/TMS) δ: 1.36 (s, 18), 3.90 (s, 3), 4.39 (d, 2, J = 13.8 Hz), 4.97 (d, 2, J = 2.6 Hz), 7.2–7.7 (m, 10). *Anal.* calcd. for $C_{30}H_{35}CrO_4P$: C 66.41, H 6.50; found: C 66.45, H 6.83.

Deuterated complex 6

2,6-Di-*tert*-butyl-1-methoxybenzene (11.23 g, 0.051 mol) was stirred for 24 h at room temperature with bromine (8.16 g, 0.051 mol) and anhydrous $FeCl_3$ (0.2 g) in methylene chloride (50 mL). The reaction mixture was then washed with water (2 × 50 mL), dried over sodium sulfate, and evaporated. Distillation under reduced pressure gave 4-bromo-2,6-di-*tert*-butyl-1-methoxybenzene (12.2 g, 80%) as a colourless liquid, bp 130°C/2 Torr, which soon solidified, mp 48–49°C (lit. (15) bp 149–150°C/9 Torr). The bromo compound (7.0 g, 0.023 mol) in anhydrous ether (50 mL) was added dropwise to a Grignard reagent prepared from iodoethane (0.85 g, 0.005 mol) and magnesium (0.85 g, 0.036 mol). The solution was refluxed for 2 h, the D_2O (2 mL) was added, and the mixture was worked up to give the neutral product.

Flash chromatography on silica gel with pentane gave the 4-deutero compound as a liquid whose spectroscopic properties were similar to those of the protio-analogue. Mass spectrum m/z: 221 (mol. ion), 206 (base peak). Conversion to the complex **6** was accomplished in the usual way (14) and the product had mp 179–180°C.

Nuclear magnetic resonance spectra

^{1}H and ^{13}C nmr spectra were recorded at 90 MHz and 22.62 MHz respectively with Bruker WH90 and HX90 spectrometers operating in the pulse-FT mode. Digital resolution was 0.15 or 0.3 Hz for ^{1}H and 0.75 or 1.5 Hz for ^{13}C spectra and probe temperatures were measured with the Bruker temperature controller. Theoretical spectra were calculated using the computer program DMNR5 (16) assuming a two-site exchange from unequally populated sites, and the exchange rates derived from visual matching were used in the Eyring equation to calculate $\Delta G\ddagger$ values. Error limits are ±2 kJ mol^{-1}.

Crystal structure determination

Diffraction data for compound **5** were collected for Mo-Kα radiation on a Phillips PW1100 automated diffractometer and the structure solved by conventional methods. Details are given in our preliminary communication (17) and atomic coordinates are available on request from the Cambridge Crystallographic Data Centre. The structure is shown in Fig. 1.

Results

The ^{1}H nmr spectra of the tricarbonyl (**3**) and dicarbonyltriphenylphosphite (**4**) complexes did not change over the temperature range 303–183 K, and we deduce that all possible intramolecular rotations in these molecules remain very fast at the lowest temperature. The triphenylphosphine complexes **5**–**7** did show temperature-variable spectra, those of the latter two being easier to analyze because of the simpler aromatic region. In the spectra of **6** taken below 223 K in CD_2Cl_2, the signals of the methoxy group, the *tert*-butyl groups, and the aromatic hydrogens were all doubled. The two solute species were in the ratio 6:5 with the major one giving the more shielded methoxy signal ($\Delta\nu$ 56 Hz) and the less shielded aromatic ($\Delta\nu$ 52 Hz). The $\Delta G\ddagger$ for interconversion was 48.2 kJ mol^{-1}. Some ^{13}C spectra were also recorded but, because of the concentrated solutions required for these measurements, we were unable to maintain solutions below 233 K, at which temperature only the methoxy carbon and the ring carbon Cl signals had broadened extensively. Complex **5** had $\Delta G\ddagger$ 47.2 ($CDCl_3$) and 48.1 (CD_2Cl_2) and complex **7** 48.0 ($CDCl_3$) and 48.3 (CD_2Cl_2) kJ mol^{-1}.

The chelate complex **8** was synthesized from 3,5-di-*tert*-butyl-4-methoxytoluene and it also showed temperature dependent ^{1}H nmr spectra in CD_2Cl_2, with $\Delta G\ddagger$ 49.7 kJ mol^{-1}.

Can. J. Chem. Downloaded from www.nrcresearchpress.com by 210.87.254.42 on 09/06/12
For personal use only.

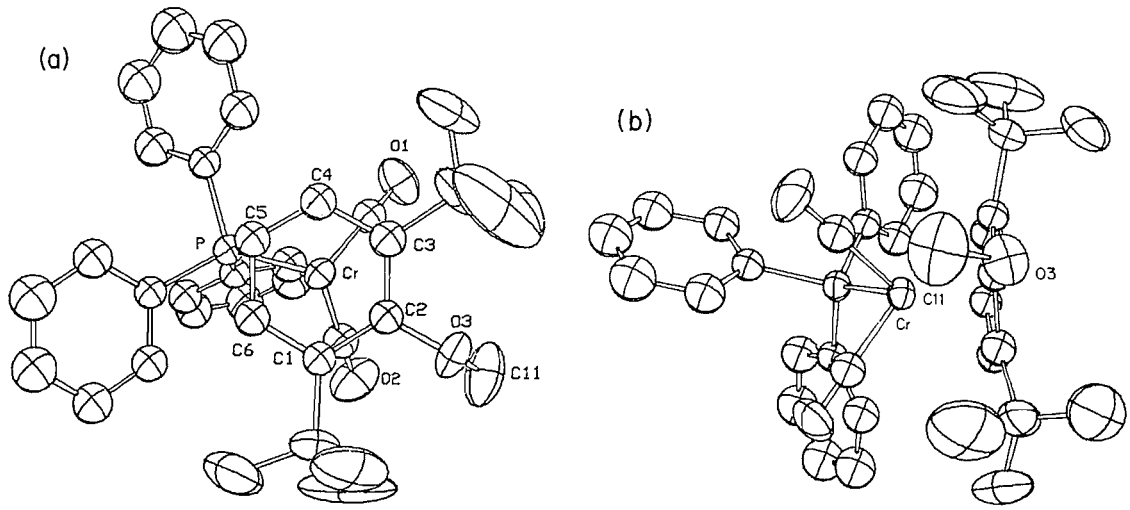

FIG. 1. ORTEP drawing of **5** showing thermal ellipsoids at 50% probability level; (a) viewed down the arene–chromium axis, with the chromium below the arene; (b) side view showing the disposition of the methoxy group.

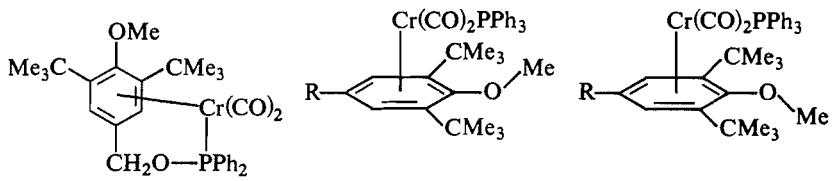

8 **10*a*** **10*b***

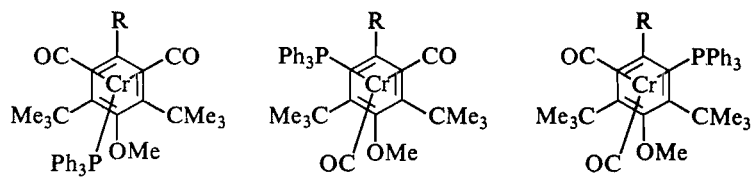

9a ***9b*** ***9c***

Discussion

Two intramolecular rotations need to be considered as causes of the temperature dependence of the nmr spectra: rotation about the arene–chromium axis and hindered rotation of the methoxy group about the arene–oxygen bond. These alternatives are depicted in formulae **9***a–c* and **10***a,b*, and the second was initially unattractive because of the difference in behaviour between the $Cr(CO)_2PPh_3$ compound **5** and its less bulky analogues **3** and **4**. It was only in the bulkiest of these compounds, complex **5**, that we observed restricted rotation, whereas in other cases, where the side chain rotates about a complexed arene, the free energies of activation normally lie in the reverse order: free ligand > ligand$(CO)_3Cr$ > ligand$(CO)_2P(OPh)_3Cr$ > ligand$(CO)_2PPh_3Cr$ (18).

In the first proposal, the two species giving rise to nmr spectra at low temperatures would be **9***a*, which has a mirror plane, and a 1:1 mixture of **9***b* and **9***c*, which interconvert rapidly when PPh_3 passes the substituent R. The energy maximum is the movement of PPh_3 past a *tert*-butyl group. This scheme became less likely, however, when the X-ray crystal structure (Fig. 1) showed the PPh_3 ligand eclipsing R, i.e. *trans* to the methoxy and as far as possible from the *tert*-butyls. Similar conformations probably exist in solution because we had previously noted (14) some shielding of groups at R which we now ascribe to the anisotropic effects of the aromatic rings on the PPh_3 ligand.

Other possible explanations are that rotation about the arene–Cr bond is very slow, with the preferred conformation being **9***a* or the one shown in Fig. 1 (with the phosphorus in the C1—C4—Cr plane), and that rotation about the aryl–oxygen bond is being observed. Rapid rotation about the arene–chromium axis and slow aryl–oxygen rotation would also produce this result.

A final decision in favour of methoxy group rotation was made on the basis that the chelate compound **8** also showed restricted rotation at low temperatures, and the arene–Cr rotation in this compound is prevented by attachment of the phosphinite ligand to the arene. There remains the anomaly of the steric considerations discussed above: we are unable to explain why our series should show the opposite behaviour to those in the literature. Significantly though, the $\Delta G\ddagger$ values for all of our complexes and for Mislow's hexaethylbenzene complex (9) were close to 50 kJ mol^{-1}. The McGlinchey work (10) produced a $\Delta G\ddagger$ of about this size, too, and it seems possible that all of these cases involve restricted rotation of the side chain in the complexed arene.

Crystal structure

The crystal structure (Fig. 1) shows the chromium atom to be almost centered with respect to the aromatic ring, and at a distance of 173.6(2) pm from the mean ring plane. The average Cr—C(arene) distance is 223.6 pm, similar to the 219.8 pm

Can. J. Chem. Downloaded from www.nrcresearchpress.com by 210.87.254.42 on 09/06/12
For personal use only.

found in (methylbenzoate)dicarbonyltriphenylphosphinechromium (19) and slightly longer than the 220.2 pm for the only other chelate complex (a phosphite) studied by X-ray crystallography (20). The Cr—P bond distance is even shorter than that found in the methyl benzoate complex above, 231.5 vs. 233.7 pm, but not as short as that in the chelate complex, 220.1 pm.

The carbonyls and the phosphorus are approximately eclipsed with aromatic ring carbons, the angle defined by C1, the ring centre and the C17 carbonyl being 16.4(5)°. The importance of this structure is that the PPh_3 ligand is *anti* to the methoxy, as far as possible from the *tert*-butyls, and in a position where its aromatic rings can shield C5 (Fig. 1).

An interesting feature of the structure is that the methoxy methyl group is proximal to the chromium, the torsion angle C3, C2, 3, C11 being −98.0(9)°. This places it in the apparently more crowded region of the molecule, and a similar preference has been observed for the central methoxy group in the crystal structure of (1,2,3-trimethoxybenzene)tricarbonylchromium (21). There might be some stereoelectronic reason for this seemingly contra-steric preference, but the nature of it is not apparent to us and invites further investigation.

Acknowledgments

M.G.W. acknowledges the award of a Monash Graduate Scholarship. The authors thank Professor K. Mislow (Princeton) and Dr. G. Hunter (Dundee) for their interest in this work and for a good deal of helpful discussion. We also thank Professor M. J. McGlinchey for his comments and for making available to us a preprint of his recent communication on this matter (22).

1. W. R. JACKSON, W. B. JENNINGS, S. C. RENNISON, and R. SPRATT. J. Chem. Soc. C, 1214 (1969).
2. A. SOLLADIÉ-CAVALLO and J. SUFFERT. Org. Magn. Reson. **5**, 426 (1980).
3. P. CORRADINI and G. ALLEGRA. J. Am. Chem. Soc. **81**, 2271 (1959).
4. N-S. CHIU and L. SCHÄFER. J. Organomet. Chem. **101**, 331 (1975).
5. P. DELISE, G. ALLEGRA, E. R. MOGNASCHI, and A. CHIERICO. J. Chem. Soc. Faraday Trans. 2, **71**, 207 (1975).
6. W. R. JACKSON, C. F. PINCOMBE, I. D. RAE, D. RASH, and B. WILKINSON. Aust. J. Chem. **29**, 2431 (1976).
7. R. K. POMEROY and D. J. HARRISON. J. Chem. Soc. Chem. Commun. 661 (1980).
8. U. ZENNECK, C. H. ELSCHENBROICH, and R. MOCKEL. J. Organomet. Chem. **219**, 177 (1981).
9. D. J. IVERSON, G. HUNTER, J. F. BLOUNT, J. R. DAMEWOOD, JR., and K. MISLOW. J. Am. Chem. Soc. **103**, 6073 (1981).
10. M. J. MCGLINCHEY, J. L. FLETCHER, B. G. SAYER, J. BOUEGARD, R. FAGGIANI, C. J. L. LOCK, A. D. BAIN, C. RODGER, E. P. KÜNDIG, D. ASTRUC, J-R. HAMON, P. LE MAUX, S. TOP, and G. JAOUEN. J. Chem. Soc. Chem. Commun. 634 (1983).
11. G. HUNTER and K. MISLOW. J. Chem. Soc. Chem. Commun. 172 (1984).
12. T. A. ALBRIGHT. Acc. Chem. Res. **15**, 149 (1982).
13. C. A. MAHAFFY and P. L. PAUSON. Inorg. Synth. **19**, 154 (1979).
14. W. R. JACKSON, I. D. RAE, and M. G. WONG. Aust. J. Chem. **36**, 1563 (1984).
15. K. S. DHAMI and J. B. STOTHERS. Can. J. Chem. **44**, 2855 (1966).
16. G. BINSCH and H. KESSLER. Angew. Chem. Int. Ed. Engl. **19**, 411 (1980).
17. E. M. CAMPI, B. M. K. GATEHOUSE, W. R. JACKSON, I. D. RAE, and M. G. WONG. J. Chem. Soc. Chem. Commun. 175 (1984).
18. D. J. IVERSON and K. MISLOW. Organometallics, **1**, 3 (1982).
19. V. G. ANDRIANOV, Y. T. STRUCHKOV, N. K. BARANETZKAYA, V. N. SETKINA, and D. N. KURSANOV. J. Organomet. Chem. **101**, 209 (1975).
20. A. N. NESMEYANOV, Y. T. STRUCHKOV, V. G. ANDRIANOV, V. V. KRIVYKH, and M. I. RYBINSKAYA. J. Organomet. Chem. **164**, 51 (1979).
21. J. Y. SAILLARD, D. GRANDJEAN, P. LE MAUX, and G. JAOUEN. Nouv. J. Chim. **5**, 153 (1981).
22. M. J. MCGLINCHEY, P. BOUGEARD, B. G. SAYER, R. HOFER, and C. J. L. LOCK. J. Chem. Soc. Chem. Commun. 789 (1984).

Can. J. Chem. Downloaded from www.nrcresearchpress.com by 210.87.254.42 on 09/06/12
For personal use only.

A definitive synthesis of 2-[(5-methyl-*s*-triazolo[4,3-*c*]quinazolin-3-yl)thio]-*N*-benzylacetanilide and other reactions of its precursors[1]

ELLI SMAKULA HAND AND DAVID C. BAKER
Department of Chemistry, University of Alabama, Tuscaloosa, AL 35486, U.S.A.

Received May 2, 1984

This paper is dedicated to Professor Peter Yates on the occasion of his 60th birthday

ELLI SMAKULA HAND and DAVID C. BAKER. Can. J. Chem. **62**, 2570 (1984).

Treatment of 2-methyl-4-chloroquinazoline **2** with hydrazine gave 2-methyl-4-hydrazinoquinazoline **3** which was converted to 5-methyl-3-mercapto-*s*-triazolo[4,3-*c*]quinazoline **4**, followed by *S*-alkylation with chloro-*N*-benzylacetanilide to give **6**. The hydrazine **3** was converted to the hydrazone **9** with acetone, to 3,5-dimethyltriazolo[4,3-*c*]-quinazoline **10** with acetic anhydride, and to 5-methyl-*s*-tetrazolo[1,5-*c*]-quinazoline **12** via a nitroso intermediate **11** with nitrous acid. Compound **3** and its derivatives **4**, **6**, **10**, and **12** differed from those alleged to have these structures. The previously reported compounds cannot have these structures since X-ray diffraction studies established that the structure of the common precursor is **3**. The mercaptotriazole **4** was air oxidized to the disulfide **20** and hydrolyzed to 2-methyl-3-hydrazinothiocarbonyl-4(3*H*)-quinazolinone **19**. The reaction of **4** with carbon disulfide gave a side-product for which the 5-methylquinazolino[3,4-*c*]-1,2,4-thiadiazol-2-thione **21** is suggested. The ^{1}H nmr chemical shifts of the quinazoline methyl substituent are near δ 3 ppm in the fully aromatic compounds and at higher field when the heterocycle is non-aromatic.

ELLI SMAKULA HAND et DAVID C. BAKER. Can. J. Chem. **62**, 2570 (1984).

La réaction de la méthyl-2 chloro-4 quinazoline **2** avec de l'hydrazine conduit à la méthyl-2 hydrazino-4 quinazoline **3** que l'on a transformée en méthyl-5 mercapto-3-*s*-triazolo[4,3-*c*] quinazoline **4**; une *S*-alkylation de ce dernier composé, à l'aide de la chloro--benzylacétanilide, conduit au produit **6**. L'hydrazine **3** est transformée en hydrazone **9** par réaction avec de l'acétone, en diméthyl-3,5 triazolo[4,3-*c*] quinazoline **10** par réaction avec de l'anhydride acétique et en méthyl-5-*s*-tétrazolo[1,5-*c*]quinazoline **12**, via l'intermédiaire nitroso **11**, par réaction avec de l'acide nitreux. Le composé **3** et ses dérivés **4**, **6**, **10** et **12** diffèrent de ceux qui seraient censés posséder ces structures. Les composés rapportés antérieurement ne peuvent pas posséder les structures qui leur ont été attribuées puisque des études de diffraction des rayons-X ont permis d'établir la structure du composé **3** qui est un précurseur commun. Le mercaptotriazole **4** a été oxydé par l'air en disulfure **20** et son hydrolyse conduit à la méthyl-2 hydrazinothiocarbonyl-3 (3*H*)-quinazolinone-4 **19**. La réaction du composé **4** avec le bisulfure de carbone fournit un produit secondaire pour lequel on suggère la structure méthyl-5 quinazolino[3,4-*c*] thiadiazole-1,2,4 thione-2 **21**. Dans les spectres rmn du ^{1}H, les déplacements chimiques des substituants méthyles sont de l'ordre de 3 ppm dans les composés complètement aromatiques et à des champs plus élevés lorsque l'hétérocycle n'est pas aromatique.

[Traduit par le journal]

The reactions shown in Scheme 1 are reported (1) to give the alkylthiotriazoloquinazoline **6**, a compound of interest to our program in the synthesis and evaluation of heterocyclic compounds as potential anti-tumor agents. Our attempted synthesis of **6** by the published procedure (1), however, led to products distinctly different from **6** and its precursors **3** and **4**. We describe here a definitive synthetic route to **6** and show that the hydrazine previously obtained (1) cannot have structure **3**.

4-Chloro-2-methylquinazoline, 2

2-Methyl-4(3*H*)-quinazolinone (**1**) was converted to **2** by the reported procedure (2). Since other workers reported (3) that **2**, prepared according to ref. 2, gave **1**·HCl upon standing for 1 week at refrigerator temperatures, and since other 4-chloroquinazolines are heat-sensitive as well (4), we modified the procedure (2) by keeping both work-up time and temperatures to a minimum and immediately purifying crude **2** by chromatography on neutral alumina. Such preparations of **2** were stable at room temperature for at least 1 month.

The reactions of 4-chloro-2-methylquinazoline (2) with hydrazine

Hydrazinolysis of **2** has been reported by two research groups (1, 5) to give in ≥80% yield compounds (**A** and **B**, Table 1) of decidedly different characteristics to which, however, the same structure, **3***a*, was assigned. Our attempts to repeat these procedures led to conflicting results, intractable mixtures, or both. (See parts (a) and (b) in the experimental section.) The conditions advocated by one group (5), for instance, gave the hydrochloride **7**, formed by ethanolysis of **2**,[2] as the major product (45%), along with **3** (10%) and small amounts of **8** (Scheme 2.)

Gradual addition of an ethanolic solution of **2** to a 10-fold excess of aqueous 85% hydrazine hydrate at 0°C gave the desired hydrazine **3** in 80% yield. Its structure was established by (a) elemental analysis; (b) a ^{1}H nmr spectrum (Table 2) which shows the presence of a methyl group, four aromatic protons, and protons that exchanged with deuterium oxide; (c) a mass spectrum which gave the expected molecular ion ($M^{\ddagger}$ = 174) as the base peak; and (d) formation of the hydrazone **9** on treatment with acetone.

Inasmuch as the physical properties of our preparation differed from those reported (1, 5), and **3** was essential to our scheme, its structure was unequivocally established by single-crystal X-ray analysis (Fig. 1). The diffraction study also shows that the N1—C2 and N3—C4 bond lengths are equal (1.36 Å); the crystalline solid, obtained from chloroform, therefore has the aromatic structure **3***a* (Scheme 1). Solution ^{1}H nmr data (Table 2) are in better accord with the 4-(3*H*)quinazolinone structure **3***b* (Scheme 2) or an equilibrium mixture of both forms (*vide infra*).

The hydrazine **3**, which is stable at −15°C in the dark,

[1] Aspects of this work have been presented in preliminary form. See ref. 16.

[2] Similarly, when the parent 4-chloroquinazoline is dissolved in absolute methanol, the HCl salt of 4-methoxyquinazoline is formed (6).

Can. J. Chem. Downloaded from www.nrcresearchpress.com by 210.87.254.5 on 09/06/12
For personal use only.

TABLE 1. Melting points (°C) of isomeric hydrazines and their derivatives

Hydrazines (ref.)	Triazolo derivative (ref.)	Nitrosation product (ref.)	Tetrazolo (derivative (ref.)
3 175–176.5	**10** 200–201	**11** 190–191	**12** 157–158
A 199 (1)	155 (1)		180 (1)
B 180–182 (5)		197–198 (5)	162–163 (5)
13 172 (7)	196 (7)		151 (7)

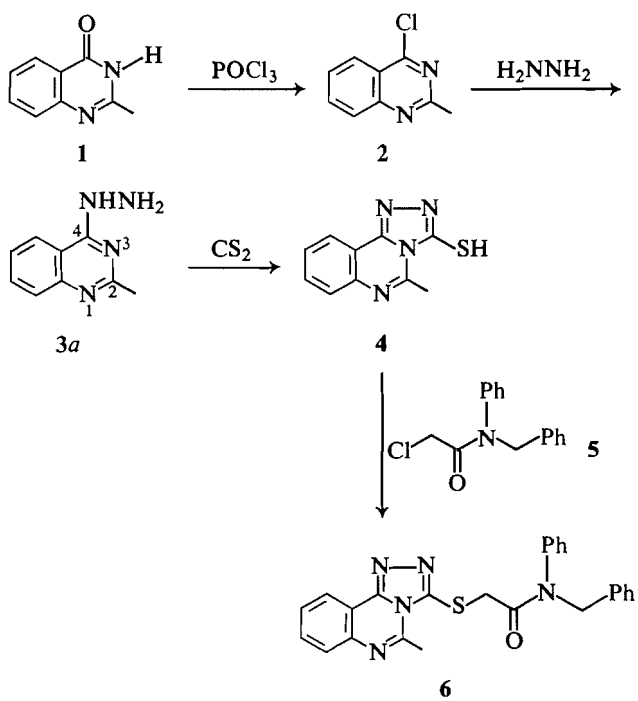

SCHEME 1

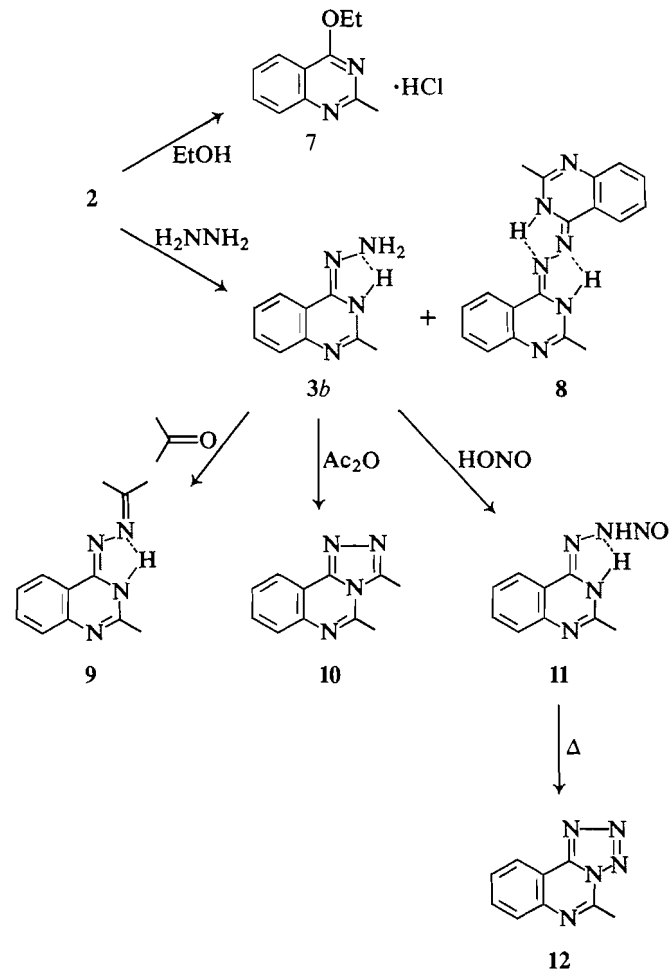

SCHEME 2

gradually forms the *N,N'*-disubstituted compound **8** on exposure to air and light. Compound **8** is also formed when **2** is treated with hydrazine under various conditions (see Experimental). The symmetrical structure **8** shown (Scheme 2) conforms to elemental analysis data, a mass spectrum (*m/z* 316 $M^{\ddagger}$, 100%), and ^1H nmr data which indicate the presence of a non-aromatic 4-(3*H*)-pyrimidone system.[3] The N3—H (**8**) rather than the tautomeric N1—H structure is shown, since in this arrangement internal hydrogen bonding is possible.

The identity of our compound **3** with **B** (5) and its dissimilarity to **A** (1) is established by comparison of the properties of some derivatives (Table 1). Compound **3** was converted by nitrous acid to a nitroso compound **11** that was in turn converted to the tetrazoloquinazoline **12** by heating at its melting point (~190°C). Compounds **3**, **11**, and **12** have melting points similar to those reported (5). The melting point and ir spectrum of the tetrazoloquinazoline prepared in ref. 1 differ from those of both **11** and **12**. Treatment of **3** with acetic anhydride gave the triazoloquinazoline **10**, which also differed from that reported (1). The structures of **10**–**12** are supported by ^1H nmr (Table 2) and ms data (Experimental).

The question of the structure of the hydrazine compound **A** (1) remains unresolved. As possible candidates for **A** one might consider the three isomers, **13**, **14**, and **15**, which could undergo reactions analogous to those of **3**. Compound **13** is excluded on the basis of its melting point and those of the derivatives (Table 1). Neither **14** nor **15** has been reported. It seemed plausible that **3** might have rearranged to give **14** under the conditions employed for the preparation of **A** (1). Alternatively, the precursor of **3**, i.e. **2**, could have decomposed to give the quinazolinone hydrochloride **1**·HCl (3), which upon treatment with hydrazine might have given **14**. Neither hypothesis was substantiated by experiment. Thus, attempts to induce the rearrangement of **3** to **14** by refluxing ethanolic solutions of **3** with hydrazine or hydrazine and acid failed, and the reaction

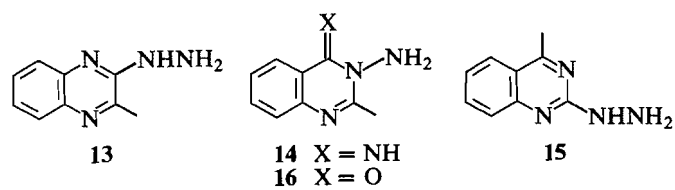

13 **14** X = NH **15**
16 X = O

[3] The ^1H nmr data thus exclude the alternate unsymmetrical structure, in which the system must be aromatic.

Can. J. Chem. Downloaded from www.nrcresearchpress.com by 210.87.254.5 on 09/06/12
For personal use only.

Can. J. Chem. Downloaded from www.nrcresearchpress.com by 210.87.254.5 on 09/06/12
For personal use only.

TABLE 2. ^{1}H nuclear magnetic resonance data for 2-methylquinazoline derivatives[a]

Compound no.	Solvent[b]	δ (ppm)		
		CH_3	NH/SH[c]	Aromatic protons
1	A	2.35	12.2 (b)	8.07 (d, 1), 7.77 (t, 1), 7.57 (d, 1), 7.45 (t, 1)
2	B	2.87		8.24 (d, 1), 7.88–8.0 (m, 2), 7.67 (t, 1)
3	A	2.33	5.4 (vb)	7.91 (d, 1), 7.50 (t, 1), 7.21–7.32 (m, 2)
	B	2.61	3.9 (vb)	7.67–7.73 (m, 3), 7.38–7.42 (m, 1)
4	A	2.86	3.4 (b)[d]	8.35 (d, 1), 8.0 (b, 2), 7.83 (b, 1)
6[e]	A	2.82		8.29 (d, 1), 7.91–7.97 (m, 2), 7.77 (t, 1), 7.37–7.49 (m, 5), 7.22 (s, 5)
	B	2.89		8.34 (d, 1), 7.95 (d, 1), 7.81 (t, 1) 7.65 (t, 1), 7.14–7.37 (m, ~10)
7[f]	A	2.83		8.26 (d, 1), 8.13 (m, 2), 7.83 (t, 1)
8	A	2.40	10.69 (s, 1[g])	8.54 (d, 1), 7.54 (t, 1), 7.29–7.34 (m, 2)
	B	2.45	9.84 (b)	8.22 (d, 1), 7.53 (m, 2), 7.34 (t, 1)
9	B	2.38, 2.21, 2.10	9.75 (vb)	8.20 (d, 1), 7.3–7.6 (m, 3)
10	B	3.04, 3.02		8.55 (d, 1), 7.83 (d, 1), 7.72 (t, 1), 7.59 (t, 1)
11	A	2.12	10.51 (s, 1) 3.5 (vb)	8.22 (d, 1), 7.88 (d, 1), 7.56 (t, 1), 7.31 (t, 1)
12	B	3.20		8.65 (d, 1), 8.09 (d, 1), 7.95 (t, 1), 7.80 (t, 1)
16	A	2.61	5.83 (b, 2)	8.13 (d, 1), 7.66 (m, 3)
19	A	2.07	13.85 (s, 1), 13.80 (s, 1), 10.09 (s, 1)	8.18 (d, 1), 7.76 (d, 1), 7.49 (t, 1), 7.24 (t, 1)
20	A	2.89		8.37 (d, 1), 7.88–7.97 (m, 2), 7.76 (t, 1)
	B	3.00		8.47 (d, 1), 7.96 (d, 1), 7.82 (t, 1), 7.66 (t, 1)
21	A	2.96		8.21 d, 1), 8.1 (m[h], 2), 7.84–7.92 (m, 1)
24[i]	B	1.83		8.35 (d, 1), 7.09–7.42 (m, ~12), 6.77 (d, 1)

[a] Relative to internal TMS; symbols in parentheses are multiplicity, area; all CH_3 groups are singlets, 3 protons; b = broad; vb = very broad; s = singlet; d = doublet; t = triplet; q = quartet; m = multiplet; the doublets generally show further fine splitting.
[b] A = DMSO-d_6; B = $CDCl_3$.
[c] Protons exchangeable with D_2O.
[d] This signal (area 3) is attributed to H_2O + SH.
[e] Other signals: A: 4.92 (s, 2), 4.12 (s, 2); B: 4.94 (s, 2), 3.98 (s, 2).
[f] Other signals: 4.76 (q, 2), 1.49 (t, 3).
[g] Number of protons relative to one CH_3 group.
[h] This multiplet appears as an intense "singlet" flanked by small peaks.
[i] Other signals: 4.92 (s, 2), 4.45 (q, 2), 4.08 (s, 2), 1.40 (t, 3).

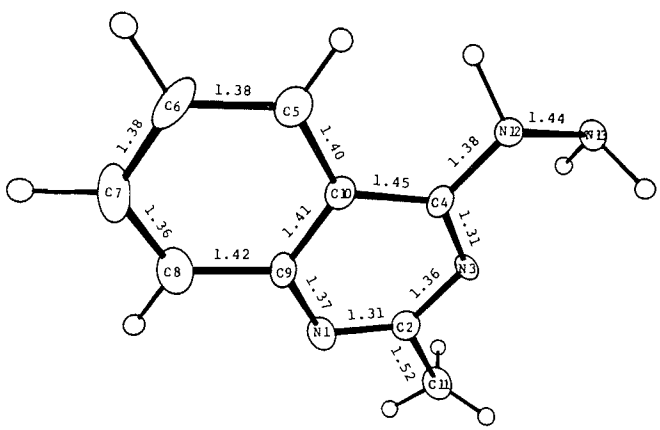

FIG. 1. Molecular structure and interatomic distances (Å) of 2-methyl-4-hydrazinoquinazoline (**3**).

of **1**·HCl with hydrazine gave instead another rearrangement product, **16**, identified by its melting point (8)[4] and spectral data. An attempt to produce **14** from 2-acetamidobenzonitrile gave 2-aminobenzonitrile (**18**) and **3** in 42 and 35% yield, respectively.[5]

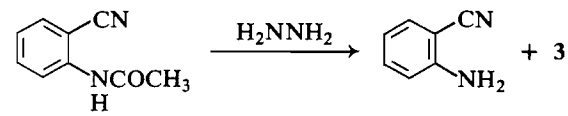

17 **18**

*The reaction of 4-hydrazino-2-methylquinazoline **3** with carbon disulfide*

Treatment of **3** with carbon disulfide in *N*,*N*-dimethylformamide gave **4** as the major product (in ~50% yield),[6] along

[4] The previous synthesis of **16** from **1** was achieved in the absence of acid (8).

[5] Although the yield of **3** from commercially available **18** (via the *N*-acetyl derivative **17**) is low, the process, based on a single experiment, is recommended since the work-up is simpler and the compounds do not have the tenacious unpleasant odor associated with **2**.

[6] Other methods, including the use of potassium trithiocarbonate/acetic acid, carbon disulfide/pyridine, or carbon disulfide/potassium hydroxide (1), gave much lower yields of **4**, in part expected, since **3** is known to decompose in the presence of air and base (5) and since the 2-methyl group in other quinazolines undergoes condensation reactions in the presence of even weak bases, such as sodium acetate or piperidine (9).

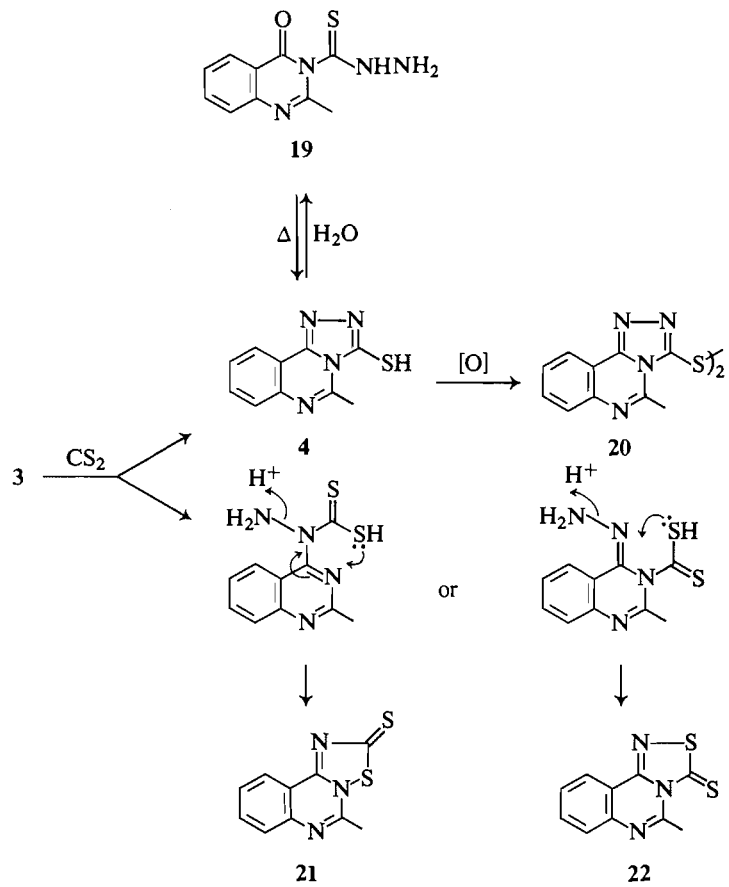

SCHEME 3

with at least nine other products, including **19**, **20**, and **21** (Scheme 3).

The structure of the unstable **4** is assigned on the basis of (a) spectral data, and conversion to stable derivatives by (b) oxidation to **20**, and by (c) hydrolysis to **19**, as well as by alkylation to give **6**.

(a) The elemental composition of $C_{10}H_8N_4S$ is indicated by the mass and isotopic distribution of the molecular ion, *m/z* 216, 217, 218 (100, 13, 4.3%; calcd. 100, 13.2, 5.1%). The presence of an aromatic methyl group and four aromatic protons is established by a ^{1}H nmr spectrum (Table 2), and a broad band in an ir spectrum at 2600 cm^{-1} is attributable to the stretch of the SH function.

(b) On exposure to air and light, **4** was converted to a compound that displays neither —NH nor —SH absorption in its ir spectrum, contains only aromatic and methyl protons in a ratio of 4:3 as shown by a ^{1}H nmr spectrum, and has a molecular weight of 430 as indicated by the molecular ion (base) peak in its mass spectrum. These data, together with an elemental analysis, establish the disulfide structure **20**.[7]

(c) Compound **4** was converted to **19** by refluxing a solution of **4** in 95% ethanol for 1 h. The spectral evidence for **19** includes broad —NH ir absorption from 2600 to 3300 cm^{-1}; a molecular ion *m/z* 234 (1.6%) and a low-mass fragmentation pattern which is the same as that of **4**; and ^{1}H nmr signals corresponding to one methyl group, four aromatic protons, and three protons exchangeable with deuterium oxide (Table 2). Elemental analysis data are in accord with structure **19**.

A fourth product isolated from the reaction of carbon disulfide and **4** must have structure **21** or **22** on the basis of the following data. Its ^{1}H nmr spectrum shows only four aromatic protons and a methyl group, its ir spectrum lacks —NH, —OH, and —SH absorption, and a mass spectrum has molecular ion isotopic distribution peaks, *m/z* 233, 234, 235 (53, 8, 5.5%), in accord with a formula $C_9H_7N_3S_2$ (calcd. 53, 6.6, 4.7%). This formula is supported by elemental analysis of a derivative (**24**, *vide infra*). Of the two possible strutures, **21** is preferred on mechanistic grounds. Reaction of **3** at H_2N—*N*== or the *N*3 ring nitrogen with CS_2 would give initial adducts (Scheme 3) in equilibrium with **3** and CS_2. Such reactions may well have similar energy requirements. Subsequent cyclization to **21** or **22**, however, should be energetically more favorable from the former adduct since an sp^3 rather than an sp^2 bond must be broken. It is estimated that ~15% of **3** was converted to the thiadiazole.

*Alkylation of **4** to give 2-[(5-methyl-*s*-triazolo[4,3-c]quinazolin-3-yl)thio]-N-benzylacetanilide **6***

Reaction of the mercaptotriazole **4** with chloro-*N*-benzylacetanilide in ethanolic sodium hydroxide gave a product ($C_{25}H_{21}N_5SO$) in 63% yield to which the structure **6** is assigned, in accord with predominant *S*-alkylation observed with other mercaptotriazoles (11). The similarity of the ^{1}H nmr chemical shifts of the protons of **6** and the corresponding protons of the disulfide **20** provides strong evidence that the ring systems and the substitution patterns are the same in both of these compounds. Since in **20** the ring system must be aromatic, possible *N*-alkylation of **4**, which gives a non-aromatic system, is ex-

[7] For other examples of oxidation of mercaptotriazoles to the disulfides, see ref. 10.

Can. J. Chem. Downloaded from www.nrcresearchpress.com by 210.87.254.5 on 09/06/12
For personal use only.

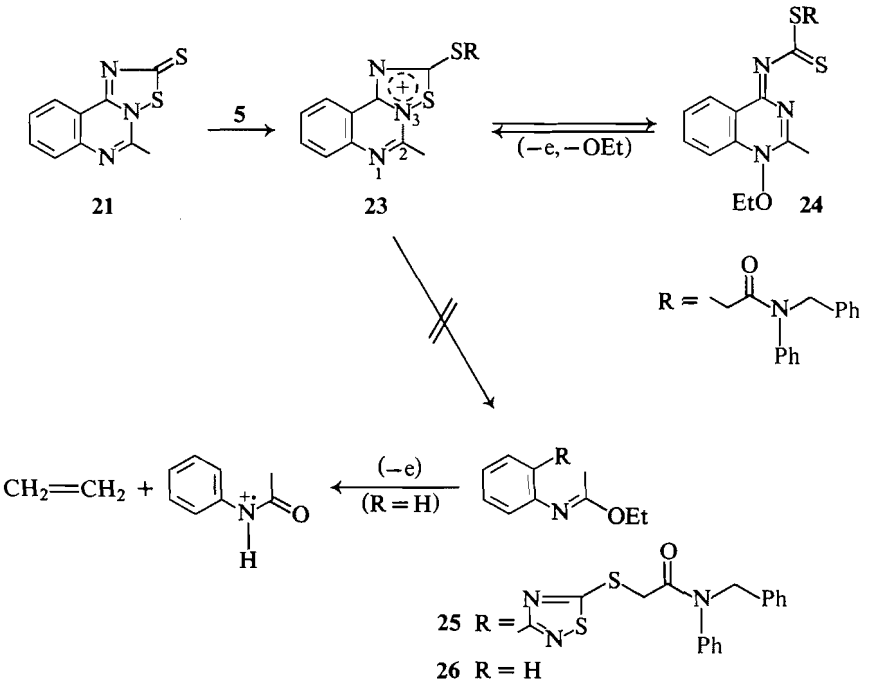

SCHEME 4

cluded. Further, the mass spectrum of **6** has a fragment,[8] m/z 201, which indicates the alkyl group is bonded to sulfur. This fragment, which has the same intensity (16%) as the parent ion, can arise by loss of $OCN(Ph)CH_2Ph$ and N_2. A possible path via the fragment m/z 229 (56%) is shown below.

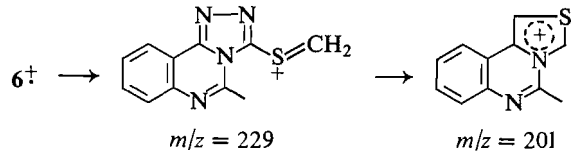

Since **4** was contaminated with small amounts of **19**, **20**, and **21**, and attempted purification led to increased amounts of **19** and **20**, the alkylation with **5** was carried out on crude **4**. From that mixture another alkylation product **24** was obtained. The ^1H nmr spectrum (Table 2) showed the presence of the $—CH_2CON(Ph)CH_2Ph$ group, four additional aromatic protons, plus a methyl and an ethyl group. Elemental analysis gave a composition of $C_{27}H_{26}N_4O_2S_2$. These data indicate that **24** was formed from **21** (or **22**) by addition of the elements $CH_3CH_2O—$ and $—CH_2CON(Ph)CH_2Ph$. This was confirmed by tlc analysis of the alkylation reaction of pure **21**.

Structure **24**, which is derived by *S*-alkylation of **21**, followed by nucleophilic attack of solvent ethanol at N1 and cleavage of the N3—S bond (Scheme 4), is suggested for this product. The alternative imido ester structure **25**, obtained by reaction of ethanol at C2, is contraindicated by ir and mass spectral data. Compound **24** shows a single ir absorption band in the 1600–1700 cm^{-1} region at 1640 cm^{-1}, attributable to the amide function of the alkyl side chain. The model imido ester **26** absorbs at 1670 cm^{-1}. In its mass spectrum compound **24** gave no detectable fragment attributable to loss of $CH_2=CH_2$, the expected product of McLafferty rearrangement of an ethyl imido ester.[9] The high-mass region is characterized by the molecular ion (11%), a fragment due to the loss of $\cdot CH_3$ (3%), and an intense fragment due to loss of $\cdot OEt$ (76%). The latter fragmentation is expected for **24** since it results in the formation of a resonance-stabilized species, **23**. The ^1H nmr data are also in accord with structure **24**. The low-field chemical shift (δ 4.45) of the methylene protons of the $—OCH_2CH_3$ group suggests that this group is attached to an electron-withdrawing moiety,[10] and the high-field chemical shift of one of the aromatic doublets (δ 6.77) is indicative of the presence of an NR_2 function.[11] Attempts to formulate a corresponding derivative from **22** led to no reasonable postulates.

Proton magnetic resonance spectra

The chemical shifts of the 2-methyl substituents in the above compounds tend to fall in two general ranges (Table 2). When the ring system is aromatic, as in the simple 4-substituted compounds (**2** and **7**) or in those fused with a five-membered aromatic heterocycle (**6**, **10**, **12**, and **20**), the 2-methyl protons exhibit signals near δ 3 ppm. Similar low-field resonances of the 2-methyl groups in **4** and **21** suggest that the mercaptotriazole **4** exists as the SH tautomer as shown (Scheme 1) and that the thiadiazole **21** (Scheme 3) is also a fully aromatic system.

The methyl signals of the quinazolinones **1**, **16**, and **19**, in which the heterocycle is not aromatic, are observed at higher field (δ 2.35, 2.61, and 2.07, respectively). Since compounds

[8] Other fragments of potential diagnostic value, i.e., those containing sulfur and the alkyl side chain or portions thereof, coincidentally have the same masses as fragments containing the heterocycle. The position of alkylation cannot be inferred from such fragments. For example m/z 256 can be due to both RS^+ and $ArSCHCO^+$ and m/z 257 can be due to both RSH^+ and $ArSCH_2CO^+$

[9] The $(M - CH_2=CH_2)^+$ fragment of the model imido ester, $PhN=C(CH_3)OEt$ (**26**), has half the intensity (19%) of the parent ion (39%); other high-mass peaks are attributable to the loss of $\cdot OEt$ (20%) and $CH_2=CH_2 + \cdot CH_3$ (20%).

[10] Compare with δ 3.48 for $—CH_2CH_3$ in diethyl ether and δ 4.21 for $PhN=C(CH_3)OCH_2CH_3$.

[11] Compare with δ 6.7 for the *ortho* protons in $PhNR_2$.

Can. J. Chem. Downloaded from www.nrcresearchpress.com by 210.87.254.5 on 09/06/12
For personal use only.

3, **8**, **9**, and **11** exhibit methyl signals in the higher-field region, it is suggested that the heterocyclic ring of these compounds exists predominantly as the non-aromatic tautomer in solution.

Experimental

General

Melting points were taken on a Thomas–Hoover capillary melting point apparatus or, if >250°C, on a Mel-Temp capillary block; both are uncorrected. Thin-layer chromatography (tlc) was carried out on E. Merck's silica gel plates (60F-254 aluminum-backed plates, catalog no. 5539). Column chromatography was carried out as indicated using either Woelm neutral alumina (activity grade III) or E. Merck Silica Gel 60 (70–230 mesh, catalog no. 7734). Spectra were determined as follows: infrared (ir) on a Beckman IR-33 double-beam spectrophotometer as Nujol mulls; proton nuclear magnetic resonance (^{1}H nmr) at 200 MHz on ~1% solutions (tetramethylsilane, internal standard) using a Nicolet NT-200 FT-NMR instrument; mass spectra (ms) at 70 eV using the direct-inlet probe on a Hewlett–Packard 5985A GLC–MS instrument. Elemental analyses were performed by Atlantic Microlab, Inc., Atlanta, Georgia.

Preparation of 4-chloro-2-methylquinazoline (2)

A mixture of 2-methyl-4(3*H*)-quinazolinone (**1**, Aldrich, mp 232.5–233°C, 4.8 g, 30 mmol), *N*,*N*-dimethylaniline (5.5 g, 45 mmol), and dry benzene (100 mL) was briefly boiled to remove water; aged phosphorus oxychloride (3.7 g, 24 mmol) was added, and the mixture was stirred and refluxed for 2 h under protection of a Drierite-filled tube. The mixture was then filtered, and the insoluble material was extracted with benzene (100 mL). The combined solutions were rapidly extracted sequentially with ice water, 20% sodium hydroxide (2 × 50 mL) diluted with ice, ice water, saturated sodium chloride, and then dried over sodium sulfate. Evaporation of solvent at ~30°C under reduced pressure gave a liquid which was directly applied to a column of alumina (300 g) packed in hexane. Hexane eluted dimethylaniline. 50% Hexane–benzene gave **2** (3.2 g, 60%), pure by tlc (chloroform), mp 78–79°C (lit. (2) mp 81.5–83°C); ms *m/z* (%): 178, 180 ($M^{\ddagger}$, 25, 9).

Reactions of 4-chloro-2-methylquinazoline (2) with hydrazine

(a) When 85% hydrazine hydrate (0.90 g, 15 mmol) was added to a solution of **2** (1.25 g, 7.0 mmol) in absolute ethanol (10 mL) (1), **2** was consumed at once (tlc, chloroform). After the solution had been refluxed for the requisite 5 h, 4 major and 7 minor products were present (tlc, ~10% absolute ethanol – chloroform). Attempted work-up according to ref. 1 gave a mixture (0.45 g) that was not further investigated.

(b) An attempt to duplicate the formation of **3** in 80% yield by stirring an emulsion of **2** (500 mg, 2.8 mmol) with 5 equivalents of hydrazine hydrate (0.75 g, 13.8 mmol) in benzene (15 mL) for two h (5), gave a benzene-insoluble gum which was treated with water (8 mL) to give **3** (50 mg, 10%, mp 171–174°C (dec)). Evaporation of solvent from the benzene-soluble fraction gave a residue which was rinsed with water and air dried (0.4 g). An ir spectrum displayed all of the bands present in the starting material **2**. Crystallization of the residue (90 mg) from absolute ethanol (10 mL) afforded a mixture (20 mg) which contained **8** according to a mass spectrum (*m/z* (%) 316 ($M^{\ddagger}$, 100)). Evaporation of the ethanolic mother liquor, extraction of the resulting residue with chloroform, evaporation of the solvent, and treatment of the residue with ether gave 4-ethoxy-2-methylquinazoline hydrochloride (**7**, 65 mg, 45%); ir: ~2350 and 1880 (both broad) cm^{-1}; ms *m/z* (%): 188, 189 ((M-HCl)‡, 28, 4.4), 173 ((M-HCl-CH_3)$^+$, 51), 160 ((M-HCl-CH_2=CH_2)‡, 100). The presence of halogen was verified by a green flame with a copper wire.

(c) To a stirred solution of 85% aqueous hydrazine hydrate (11.5 g, 200 mmol) in absolute ethanol (15 mL), cooled in ice, was added dropwise during 15 min a freshly prepared solution of pure **2** (3.2 g, 18 mmol) in absolute ethanol (60 mL). The ice bath was then removed, and stirring was continued for 1.75 h. After the mixture was clarified by filtration, the filtrate was concentrated *in vacuo*. The residual oil dissolved in water (35 mL) and then suddenly set to a crystalline mass. Filtration, rinsing with water, and air drying gave a hydrate of nearly pure **3** as pale yellow needles (3.05 g), mp (partial melting) 80°C, gas evolution, resolidification, partial melting 165°C, resolidification with gas evolution 168°C.

A chloroform solution (100 mL) of the hydrate (2.54 g) was boiled down (to 40 mL) to give off-white needles of **3** (1.92 g). Treatment of the mother liquor with charcoal, followed by concentration to ~10 mL yielded a second crop of **3** (0.23 g, 81% total). An analytical sample had mp 175–176.5°C (dec.); another sample had mp 179–180°C; on occasion the melt resolidified on further heating; other times resolidification occurred prior to complete melting (lit. (1) mp 199°C; lit. (5) mp 180–182°C); ms *m/z* (%): 174, 175 ($M^{\ddagger}$, 100, 12). *Anal.* calcd. for $C_9H_{10}N_4$: C 62.05, H 5.79, N 32.16; found: C 61.97, H 5.82, N 32.12. The compound became contaminated with **8** (tlc, chloroform), gradually in the presence of air, rapidly in the presence of air and light, but was stable at −15°C in the dark.

(d) In other experiments, when hydrazine was added to **2**, or when **2** was added rapidly to hydrazine, or when the latter was not cooled, varying amounts of the disubstituted hydrazine **8** were formed. Treatment with water of the residue obtained after evaporation of ethanol led to selective dissolution of **3**. Rapid filtration gave the solid **8**; the filtrate then either spontaneously or upon seeding deposited the hydrate of **3**.

N,*N*′-di(2-methylquinazolin-4-yl)-hydrazine (**8**) crystallized from 2-propanol as fine, bright yellow needles; mp 287°C (dec.) (depends on rate of heating) (lit. (5) mp 280°C); ms *m/z* (%): 316, 317 ($M^{\ddagger}$, 100, 22). *Anal.* calcd. for $C_{18}H_{16}N_6 \cdot 0.42\ C_3H_7OH$: C 67.78, H 5.63, N 24.62; found: C 67.95, H 5.82, N 24.67. The presence of 2-propanol was confirmed by a ^{1}H nmr spectrum.

(e) Refluxing an ethanolic solution (3 mL) of **3** (200 mg, 1.15 mmol) and aqueous 85% hydrazine hydrate (100 mg, 1.7 mmol) for 5 h, evaporation of solvent, and treatment of the residue with water gave starting material **3** (130 mg), contaminated with **8** (tlc, 15% absolute ethanol – chloroform). A similar experiment, in which ~90% of the hydrazine was present as its hydrochloride salt, gave a ten-component mixture (tlc).

*Acetone 2-methyl-4(3*H*)-quinazolinone azine (9)*

A solution of crude **3** (0.65 g) in acetone was left to stand for several days when the solvent had evaporated to give a solid form which the hydrazone **9** (0.50 g) was isolated by chromatography on silica gel (30 g, 2.5% absolute ethanol – chloroform). Crystallization from hexane, followed by sublimation (80°C/0.1 Torr) (1 Torr = 133.3 Pa), gave **9** as a colorless solid, mp 118.5–120.5°C; ms *m/z* (%): 214, 215 ($M^{\ddagger}$, 22, 3.4), 199 ((M − CH_3)$^+$, 100). The compound turned deep yellow on exposure to light and air. *Anal.* calcd. for $C_{12}H_{14}N_4$: C 67.27, H 6.59, N 26.15; found: C 67.07, H 6.61, N 26.09.

*3,5-Dimethyl-*s*-triazolo[4,3-*c*]quinazoline (10)*

A solution of **3** (100 mg, 0.58 mmol) in acetic anhydride (0.7 mL, 7.5 mmol) was heated for 1 h in a 150°C oil bath. The solvents were evaporated in a stream of nitrogen, and the residual solid was crystallized from ethyl acetate to give colorless needles of **10** (80 mg, 73%). Two recrystallizations gave an analytical sample, mp 200–201°C (lit. (1) mp 155°C); ms *m/z* (%): 198, 199 ($M^{\ddagger}$, 100, 22), 197 ((M − H)$^+$, 22). *Anal.* calcd. for $C_{11}H_{10}N_4$: C 66.66, H 5.08, N 28.27; found: C 66.73, H 5.09, N 28.23.

*5-Methyltetrazolo[1,5-*c*]quinazoline (12) via 11*

Compound **3** (120 mg, 0.69 mmol) was treated with aqueous hydrochloric acid (2.9 *N*, 3 mL). A small amount of orange material was removed by filtration, and the colorless filtrate, stirred in ice, was treated dropwise with aqueous (~0.3 mL) sodium nitrite (~50 mg, 0.73 mmol). A solid which separated almost at once was filtered after 50 min and rinsed with water to give colorless **11** (135 mg, 96%, pure by tlc (~30% absolute ethanol – chloroform)) which crystallized from ethanol as a light yellow powder, mp 190–191°C (dec.) (lit. (5) mp 197–198°C); ms *m/z* (%): 203, 204 ($M^{\ddagger}$, 100, 11).

Compound **11** (55 mg, 0.27 mmol) was heated for 2 min at its

Can. J. Chem. Downloaded from www.nrcresearchpress.com by 210.87.254.5 on 09/06/12
For personal use only.

Can. J. Chem. Downloaded from www.nrcresearchpress.com by 210.87.254.5 on 09/06/12
For personal use only.

melting point in a beaker covered with a watch glass when no further gas evolved. The mixture was cooled, treated with ethanol and charcoal, and filtered through Celite. Evaporation of the filtrate to ~1 mL afforded **12** (20 mg, 40%) as off-white needles; mp 157–158°C (lit. (5) mp 162–163°C); ms *m/z* (%): 185, 186 (M^+, 40, 4.7), 157 ($(M - N_2)^+$, 90), 156 (100).

*Reaction of 2-methylquinazolinone (**1**) with hydrazine*

A solution of **1** (1.6 g, 10 mmol), concentrated HCl (0.83 mL, 10.4 mmol), and 95% hydrazine hydrate (1 mL, ~20 mmol) in absolute ethanol (60 mL) was refluxed for 2 h. Since tlc indicated the presence of only **1**, another portion of hydrazine (2 mL, ~60 mmol, total) was added, and refluxing was continued overnight when some of the product had formed (tlc, 5% methanol–chloroform). Most of the solvent was then boiled off, and heating was continued for 2 h. On cooling, the residue set to a solid mass which was treated with ice and water. Insolubles were filtered and rinsed with water to give **16** (0.63 g, 36%). When the remaining ethanol in the filtrate was evaporated under reduced pressure, a second crop of **16** (0.67 g) contaminated with **1** separated. A third crop (0.34 g) was obtained by extraction of the aqueous filtrate with chloroform (2 × 20 mL). Crystallization of the combined latter crops from benzene gave a solid (0.48 g) enriched in **1**. The material remaining in the benzene was recrystallized from aqueous 60% ethanol to give pure **16** (0.38 g, 58% total), mp 144–145.5°C (lit. (8) mp 146–148°C); ms *m/z* (%): 175, 176 (M^+, 100, 11.3), 146 ($(M - COH)^+$, 72).

*Reaction of 2-acetamidobenzonitrile (**17**) and hydrazine*

A solution of 2-acetamidobenzonitrile (11) (640 mg, 4 mmol) and aqueous 85% hydrazine hydrate (3.4 g, 55 mmol) in absolute ethanol (10 mL) was refluxed overnight. Since tlc (20% absolute ethanol – chloroform) indicated the presence of starting material, ethanol was boiled off, and the residual liquid was heated for an additional 1.5 h at 100°C. The cooled solution was diluted with water (5 mL) and extracted with chloroform (3 × 15 mL). The extracts were dried over sodium sulfate and stripped of solvent under reduced pressure to give a light brown liquid (660 mg) which partially solidified. Treatment with hot hexane (2 × 60 mL) gave an insoluble solid, **3** (240 mg, 35%), which after crystallization from chloroform (charcoal) was nearly colorless (180 mg, 25%), mp 179–180°C (dec.).[5] The hexane-soluble fraction was subjected to chromatography on alumina (35 g). Elution with chloroform afforded 2-aminobenzonitrile (0.20 g, 42%) which, after sublimation (50°C/0.1 Torr), had mp 47–48°C and the same ir spectrum (melt) as a commercial (Aldrich) sample (mp 45–47.5°C).

*Reaction of 4-hydrazino-2-methylquinazoline with carbon disulfide: formation of **4**, **19**, **20**, and **21***

After a solution of **3** (1.4 g, 8 mmol), carbon disulfide (20 mL, 330 mmol), and dry *N,N*-dimethylformamide (2 mL) was refluxed overnight, a solid had separated. Carbon disulfide was boiled off, the mixture was cooled, and the yellow solid was filtered and rinsed with small amounts of *N,N*-dimethylformamide (filtrate A) and absolute ethanol. The insoluble product **4** (0.90 g, 52%) was contaminated (tlc, 15% absolute ethanol – chloroform) with sulfur (ms: S–S8, e.g., S8 *m/z* (%) 256, 258 (M^+, 100, 34)), the disulfide **20**, and the yellow compound **21**.

Crystallization of **4** from ethanol gave less pure product (tlc), larger amounts of **20**, as well as the hydrolysis product **19** being formed. Subsequent treatment of **4** (80 mg) with hot chloroform gave a colorless insoluble solid **19**, 2-methyl-3-hydrazinothiocarbonyl-4(3*H*)-quinazolinone (25 mg). Compound **19** was also isolated from the filtrate A, above, as follows. The filtrate was diluted with water (20 mL), and the insoluble materials (0.16 g, ten components (tlc, 10% absolute ethanol – chloroform)) were filtered and discarded. After standing for 2 weeks, the filtrate had deposited a five-component mixture (0.33 g) from which colored materials (0.01 g) were removed by extraction with hot benzene (10 mL). Subsequent crystallization from ethanol failed to give separation; the recombined mixture was then triturated with boiling chloroform (15 mL), cooled, and filtered to give **19** (0.16 g, 8.5% total). Two crystallizations from absolute ethanol afforded colorless crystals, mp 249.5–250°C (dec.) (depends on rate of heating); ir: 3290 (br), 3100 (br), 1680 (s), 1620 (s), 1590 (s), 1535 (s), 1310 (s) cm^{-1}; ms: same as mass spectrum of **4**, except for the additional molecular ion peak, *m/z* (%) 234 (1.6). *Anal.* calcd. for $C_{10}H_{10}N_4OS \cdot 0.25\ H_2O$: C 50.30, H 4.43, N 23.47, S 13.43; found: C 50.30, H 4.41, N 23.45, S 13.49.

A pure sample of the disulfide **20** was obtained as follows. After refluxing a solution of **3** (250 mg, 1.4 mmol) in carbon disulfide (2.5 mL, 41 mmol) and dry *N,N*-dimethylformamide (0.3 mL) for 19 h, the carbon disulfide was boiled off and the cooled residual mixture was triturated with ether. Filtration of the mixture gave a yellow solid (300 mg) which was heated with chloroform (5 mL) and then cooled. The chloroform-soluble fraction (170 mg) was treated with water (5 mL) and 2.5 *N* sodium hydroxide (pH ~ 10) to give an insoluble yellow solid (20 mg), which was primarily **21** according to its ^1H nmr spectrum. Treating the filtrate with 1 *N* hydrochloric acid (to pH ~3) gave a precipitate of primarily **4**, **19**, and **20** (tlc, ~5% absolute ethanol – chloroform). A similar mixture precipitated upon standing overnight. On further standing, the aqueous solution deposited colorless needles of **20** (25 mg, 15% total). An analytical sample, prepared by dissolving **20** (45 mg) in chloroform (3 mL), filtering, adding absolute ethanol (5 mL) to the filtrate, and boiling the solution down to incipient crystal formation, cooling, and filtering, had mp 244–245°C; ir: 1625 (s), 1525 (m), 1285 (s) cm^{-1}; ms *m/z* (%): 430, 431, 432, (M^+, 100, 28, 13), 216 (8), 215 (17). *Anal.* calcd. for $C_{20}H_{14}N_8S_2$: C 55.80, H 3.28, N 26.05, S 14.89; found: C 55.52, H 3.29, N 25.94, S 14.75.

*Interconversion of **4** and **19***

(a) Compound **19** (35 mg, 0.15 mmol) was heated in a beaker at its melting point for ~3 min. The nearly colorless crystals of **4** (15 mg, 46%), which deposited on the walls, had mp 210–211.5°C and displayed in an ir spectrum all of the major bands present in the spectrum of crude **4** (obtained from **3** and carbon disulfide, *vide supra*): 2650 (br); 1640 (s), 1530 (s), 1310 (s) cm^{-1}; ms *m/z* (%): 216, 217, 218 (M^+, 100, 13, 4.3), 215 (12).

(b) When a solution of crude **4** (12.2 mg, 0.056 mmol) in aqueous 70% ethanol (0.7 mL) was refluxed for 1 h, none of 4 remained and **19** had formed (tlc, 15% absolute ethanol – chloroform). Ethanol was boiled off and the mixture was cooled and filtered to give a solid (8.3 mg, 63%). After crystallization from absolute ethanol, the colorless solid had an ir spectrum identical to that of the analytical sample of **19** (*vide supra*).

*Reaction of crude **4** with 2-chloro-*N*-benzylacetanilide, **5**; formation of **6** and **24**; isolation of 5-methyl-1,2,4-thiadiazolo[2,3-c]-quinazolin-2-thione, **21***

The chloroamide **5**, prepared by a general method (12), was treated with several portions of hexane to remove unreacted benzylaniline. The product was then pure according to its ^1H nmr spectrum and had mp 64–66°C (lit. (13) mp 75–76°C); ^1H nmr δ ($CDCl_3$): 3.85 (s, 2), 4.90 (s, 2), 6.99–7.36 (m, 10); ms *m/z* (%): 259, 261 (M^+, 5.2, 1.6), 91 (100).

A stirred mixture of crude **4** (0.9 g, ~4.2 mmol) and absolute ethanol (40 mL) was treated with aqueous 2.5 *N* sodium hydroxide (1.67 mL, 4.2 mmol) to give a green solution to which the chloroamide **5** (1.08 g, 4.2 mmol) was added. Shortly after the latter had dissolved, a colorless solid began to precipitate. The solid was filtered after 2 h (filtrate A), rinsed with absolute ethanol, and then triturated with water to give **6** (1.15 g, 63%). After recrystallization from absolute ethanol, **6** had mp 149.5–150.5°C (lit. (1) mp 89°C); ir: 1665 (s), 1620 (s), 1520 (s), 1385 (s), 1190 (s) cm^{-1}. *Anal.* calcd. for $C_{25}H_{21}N_5SO$: C 68.31, H 4.82, N 15.93, S 7.29; found: C 68.20, H 4.85, N 15.90, S 7.19.

The combined green-blue filtrate A and rinse liquid were concentrated *in vacuo* to give a solid (0.37 g), primarily **6** and **24** (tlc, chloroform), which was fractionated by elution with chloroform from silica gel (40 g). Early fractions gave **24** (0.17 g, 8% based on crude **4**), which after crystallization from ethanol had mp 156.5–157.5°C; ir: 1640 (s), 1590 (m), 1490 (m), 1390 (m), 1290 (m), 1280 (m) cm^{-1};

ms m/z (%): 502, 503 (M^{+}, 11, 3), 487 ($(M - CH_3)^{+}$, 3.3); 457, 458, 459 ($(M - OC_2H_5)^{+}$, 76, 19, 11), 91 (100). *Anal.* calcd. for $C_{27}H_{26}N_4S_2O_2$: C 64.52, H 5.21, N 11.15, S 12.76; found: C 64.33, H 5.22, N 11.13, S 12.80.

In a similar experiment less than one equivalent of sodium hydroxide (1.9 mmol for 0.57 g, (2.6 mmol) of crude **4**) was used. As above, the initially green solution (pH ~ 10) deposited a solid, but the supernatant solution turned bright yellow (pH ~ 6). Filtration of the mixture and rinsing of the solids with ethanol and water gave a mixture of **21** and **6** (0.75 g) which was treated with hot ethanol (75 mL). An insoluble, bright yellow solid, **21** (~20 mg, 3%), was filtered. Concentration of the filtrate to ~15 mL gave impure **6** (0.50 g) which was subjected to chromatography on alumina (40 g). 40% Chloroform–ether eluted colorless **6** (0.42 g, 35%).

Compound **21** had mp 275°C (sudden dec.); ir: 1600 (s), 1550 (w), 1400 (s), 1040 (s) cm^{-1}; ms m/z (%): 233, 234, 235 (M^{+}, 53, 8, 5.5), 201 ($(M - S)^{+}$, 2), 175 ($(M - NCS)^{+}$, 5). Its R_f (chloroform) was the same as that of the yellow contaminant in crude **4**. According to tlc analysis (chloroform), reaction of a chloroform–ethanol (1:2) solution of **21** (~1 mg) with **5** in the presence of sodium hydroxide gave **24**.

Ethyl N-*phenylacetimidate (26)*

The imido ester **26** (14) had bp 119°C/40 Torr (lit. (14) bp 94.5°C/12.5 Torr); ^{1}H nmr δ ($CDCl_3$): 1.32 (t, 3), 1.80 (s, 3), 4.25 (q, 2), 6.65–7.45 (m, 5) ppm; ms, see footnote 9.

Crystallographic structure determination of **3**[12]

$C_9H_{10}N_4$ fw = 174.2

Monoclinic, space group $P2_1/n$, a = 4.941(2), b = 15.008(6), c = 11.928(5) Å, β = 100.20(4)°, V = 870.5 Å^3, Z = 4, ρ_c = 1.33 g cm^{-1}, MoK_α radiation, λ = 0.71069 Å, $\mu(MoK_\alpha)$ = 0.51 cm^{-1}.

Data were collected on an Enraf–Nonius CAD-4 diffractometer out to a 2θ value of 40°. A total of 408 observed reflections were obtained, and the structure was refined to a conventional R value of 0.044. Details of data collection are given in ref. 15.

Acknowledgments

The authors are grateful to W. E. Hunter and J. L. Atwood for the X-ray crystallographic study of **3**. This work was supported in part by contract no. NO1-CM-07355 from the National Cancer Institute of the National Institutes of Health.

[12] This work was carried out by W. E. Hunter and J. L. Atwood of this department; details will be published elsewhere.

1. M. R. CAURASIA and S. K. SHARMA. Heterocycles, **14**, 1759 (1980).
2. H. C. SCARBOROUGH, B. C. LAWES, J. L. MINIELLI, and J. L. COMPTON. J. Org. Chem. **27**, 957 (1962).
3. T. YAMAZAKI, K. MATOBA, A. SHIROKAWA, and R. N. CASTLE. J. Heterocycl. Chem. **15**, 467 (1978).
4. W. L. F. ARMAREGO. *In* The chemistry of heterocyclic compounds, fused pyrimidines. Part I. *Edited by* D. J. Brown. Interscience, New York. 1967 p. 223.
5. I. YA. POSTOVSKII, N. N. VERESHCHAGINA, and S. L. MERTSALOV. Khim. Geterotsikl. Soedin. Akad. Nauk Latv. SSR, **1**, 130 (1966); Chem. Abstr. **65**, 710h (1966).
6. A. J. TOMISEK and B. E. CHRISTENSEN. J. Am. Chem. Soc. **67**, 2112 (1945).
7. D.-I. SHIHO and S. TAGAMI. J. Am. Chem. Soc. **82**, 4044 (1960).
8. N. J. LEONARD and W. V. RUYLE. J. Org. Chem. **13**, 903 (1948).
9. L. N. YAKHONTOV, G. P. ZHIKHAREVA, E. V. PRONINA, G. N. PERSHIN, S. S. LIBERMAN, E. N. PADEISKAYA, T. N. ZYKOVA, T. A. GUSKOVA, and E. A. BERLYAND. Khim. Farm. Zh. **9**, 12 (1975); Chem. Abstr. **84**, 43974x (1976).
10. C. TEMPLE, JR. *In* The chemistry of heterocyclic compounds, 1,2,4-triazoles. Vol. 37. *Edited by* A. Weissberger and E. C. Taylor. John Wiley & Sons, Inc., New York. 1981. Chapt. 10.
11. J. PINNOW and C. SAMANN. Ber. **29**, 623 (1896); K. W. BREUKINK, L. H. KROL, P. E. VERKADE, and B. M. WEPSTER. Recl. Trav. Chim. Pays-Bas, **76**, 401 (1957).
12. A. J. SPEZIALE and P. C. HAMM. J. Am. Chem. Soc. **78**, 2556 (1956).
13. P. B. PATEL and J. J. TRIVEDI. J. Indian Chem. Soc. **50**, 287 (1973).
14. R. H. DEWOLFE. J. Org. Chem. **27**, 490 (1962).
15. J. HOLTON, M. F. LAPPERT, D. G. H. BALLARD, R. PEARCE, J. L. ATWOOD, and W. E. HUNTER. J. Chem. Soc. Dalton Trans. 45 (1979).
16. E. S. HAND and D. C. BAKER. Abstracts of papers, 34th Southeast Regional Meeting of the American Chemical Society, Birmingham, AL. November 3–5, 1982. ORGN/MEDI 314.

Can. J. Chem. Downloaded from www.nrcresearchpress.com by 210.87.254.5 on 09/06/12
For personal use only.

Enzymes in organic synthesis. 32.[1] Stereospecific horse liver alcohol dehydrogenase-catalyzed oxidations of *exo*- and *endo*-oxabicyclic *meso* diols

J. Bryan Jones and Christopher J. Francis
Department of Chemistry, University of Toronto, Toronto, Ont., Canada M5S 1A1

Received March 7, 1984

This paper is dedicated to Professor Peter Yates on the occasion of his 60th birthday

J. Bryan Jones and Christopher J. Francis. Can. J. Chem. **62**, 2578 (1984).

Preparative-scale horse liver alcohol dehydrogenase-catalyzed oxidation of *meso exo*- and *endo*-7-oxabicyclo[2.2.1]heptane diols provides a direct one-step route to enantiomerically pure chiral γ-lactones of the oxabicyclic series.

J. Bryan Jones et Christopher J. Francis. Can. J. Chem. **62**, 2578 (1984).

L'oxydation préparative, catalysée par l'alcool déshydrogénase du foie de cheval, des oxa-7 bicyclo[2.2.1] heptanediols-*exo* et -*endo méso* s'avère être une route directe en une étape conduisant aux γ-lactones chirales énantiomériquement pures de la série oxabicyclique.

[Traduit par le journal]

Can. J. Chem. Downloaded from www.nrcresearchpress.com by 210.87.254.6 on 09/06/12
For personal use only.

The abilities of enzymes to discriminate between enantiotopic groups of compounds that possess prochiral centres or that are *meso* compounds are being exploited to an ever-increasing extent in asymmetric synthesis (2). Horse liver alcohol dehydrogenase (HLADH),[2] a commercially available NAD-dependent alcohol dehydrogenase that catalyzes CH(OH) ⇌ C=O oxidoreductions of a wide range of substrates, is one of the most versatile enzymes in this regard. In its oxidative mode, it has been shown to operate stereospecifically on only one of the enantiotopic hydroxyl groups of acyclic and monocyclic *meso*-diols (1, 3). In this paper we report that preparative-scale HLADH-catalyzed oxidations are also enantiotopically specific for *meso* oxabicyclic diols such as **1** and **2**.

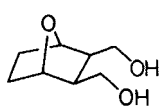

1

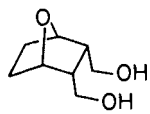

2

Results

The *exo*- and *endo*-diol substrates **1** and **2**, the racemic lactones **5** and **6**, and racemic diols **7** and **8** required as reference compounds were obtained as shown in Scheme 1.

Both **1** and **2** were found to be excellent substrates of the enzyme. Their rates of HLADH-catalyzed oxidations, relative to the usual benchmark of cyclohexanol = 1.0 under equivalent assay conditions, were found to be 0.63 for **1** and 0.21 for **2**. Such oxidation rates indicate that multi-gram HLADH-catalyzed oxidations will be viable.[3] The results of the preparative-scale enzyme-mediated oxidations are summarized in Scheme 2.

The enantiomeric excesses of the *exo*-(+)-**5** and *endo*-(+)-**6** lactones of Scheme 2 were determined by ^{1}H nmr spectroscopic

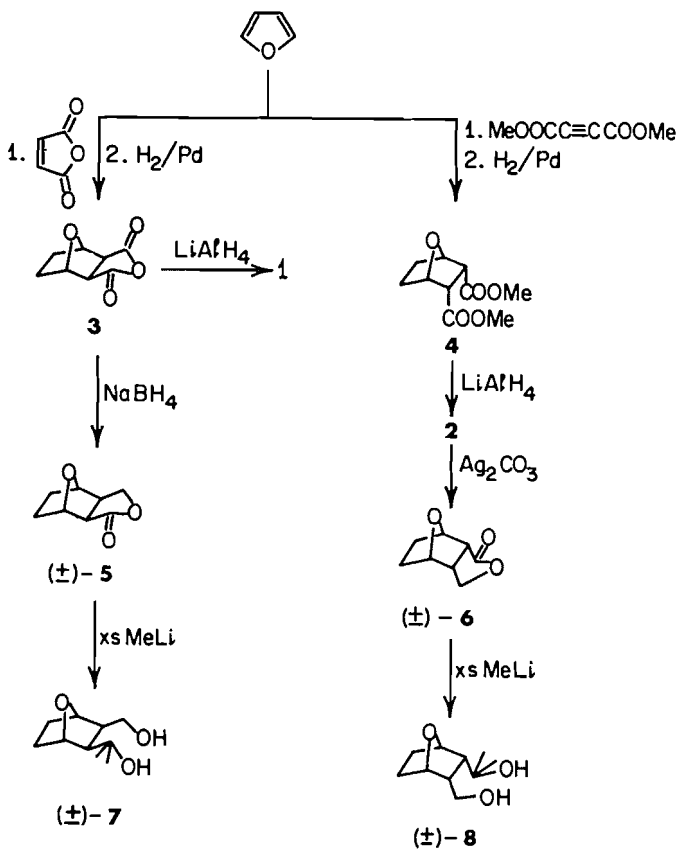

SCHEME 1

examination (4) of the dimethyl diols, (+)-**7** and (+)-**8** respectively, obtained using excess methyllithium as shown for the racemic series in Scheme 1. In the presence of 0.4 equivalents of Eu(hfc)$_3$, the protons of the *gem*-dimethyl groups of the racemic reference diols *exo*-(±)-**7** and *endo*-(±)-**8** were cleanly resolved into two doublets with ΔΔδ values of 0.03 and 0.11 ppm respectively. The spectra of (+)-**7** and (+)-**8** showed no trace of splitting under the same conditions, thereby demonstrating that their precursor lactones (+)-**5** and (+)-**6** respectively were enantiomerically pure.[4]

[1]For Part 31, see ref. 1.

[2]Abbreviations used: HLADH, horse liver alcohol dehydrogenase; NAD, nicotinamide adenine dinucleotide; FMN, flavin mononucleotide (riboflavin phosphate); Eu(hfc)$_3$, tris[3-(heptafluoropropylhydroxymethylene)-*d*-camphorato]europium^{III}; PLE, pig liver esterase.

[3]Good preparative-scale oxidations can be expected when the rate of oxidation of a new substrate is >0.05 of that of cyclohexanol under the same assay conditions.

[4]The nmr ee (enantiomeric excess) determination method is considered accurate to <±2%.

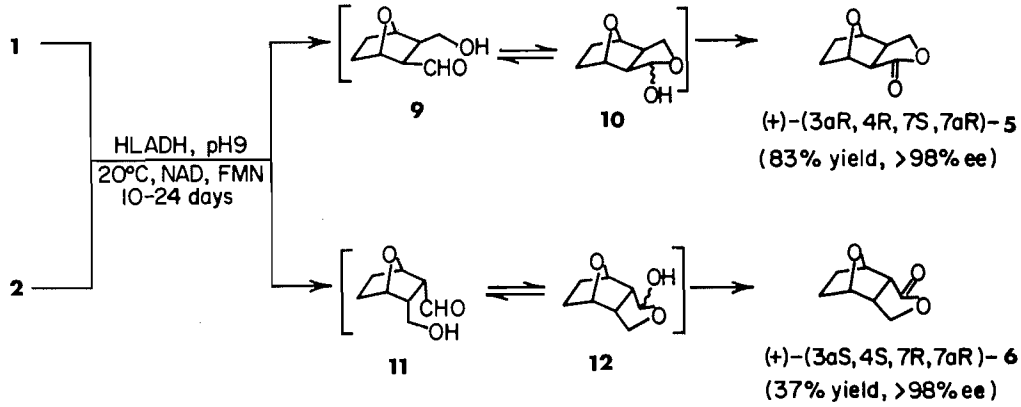

SCHEME 2

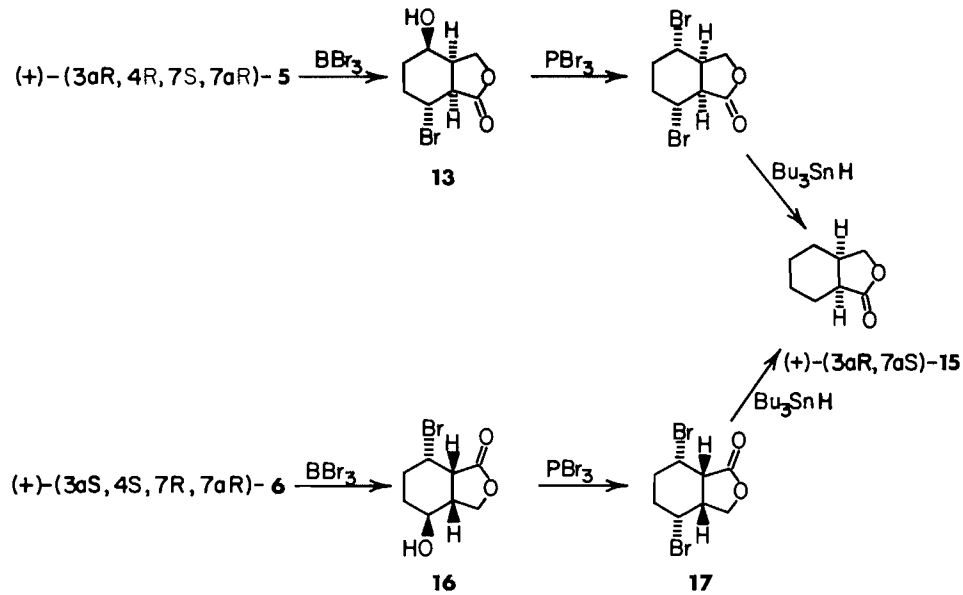

SCHEME 3

The absolute configurations of (+)-**5** and (+)-**6** were established by their conversion to the known (3*a*) (+)-(3a*R*,7a*S*)-perhydroisobenzofuranone (**15**) by the methods summarized in Scheme 3.

In view of the stereospecificities reported for pig liver esterase-catalyzed hydrolyses of *meso*-diesters (5), the ability of PLE to exert enantiotopic discrimination in its hydrolyses of diesters within the oxabicyclic series was evaluated on the *meso* diesters *exo*-**18** and *endo*-**4**. The diester **4** had been prepared earlier (Scheme 1) and **18** was readily produced from **3** by Fischer esterification in methanol. Disappointingly, neither diester was a substrate of PLE.[5]

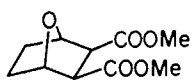

18

Discussion

The substrates and required reference compounds were readily prepared by the Scheme 1 routes. The *exo*- and *endo*-diols **1** and **2** were both very good substrates for HLADH under the preliminary assay conditions, exhibiting very high relative oxidation rate values of 0.63 and 0.21 respectively.[3] In view of this, the 2−3 week reaction times required for the preparative-scale reactions were unexpectedly lengthy. For such excellent substrates, HLADH-catalyzed oxidations on the 2-g scale of the Scheme 2 reactions should have been complete in a few hours and the enzyme may be experiencing product inhibition by one or all of the hydroxy aldehydes **9** and **11** formed initially, their hemiacetal isomers **10** and **12**, or the hydroxyacid precursors of **3** and **4** that are the final products before work-up of the pH 9 reaction medium. In contrast to previous *meso*-diol oxidations, in which some hemicaetal intermediates were isolated (3), only the lactone products (+)-**3** and (+)-**4** were obtained from the Scheme 2 reactions.

Both HLADH-derived lactones were shown to be enantiomerically pure within the accuracy limits of the nmr method used. The absolute configuration determinations (Scheme 3) were straightforward. While only one bromoalcohol structure is shown for each of **13** and **16**, the positions of the hydroxyl and bromo substituents could be reversed. In fact, the ^{1}H nmr spectrum of **16** indicated that it was a mixture of isomers. In contrast, **13** appeared to be a single stereoisomer. The spectral data did not permit unequivocal isomeric

[5]The experimental conditions applied were those described by Chen *et al.* in ref. 5.

Can. J. Chem. Downloaded from www.nrcresearchpress.com by 210.87.254.6 on 09/06/12
For personal use only.

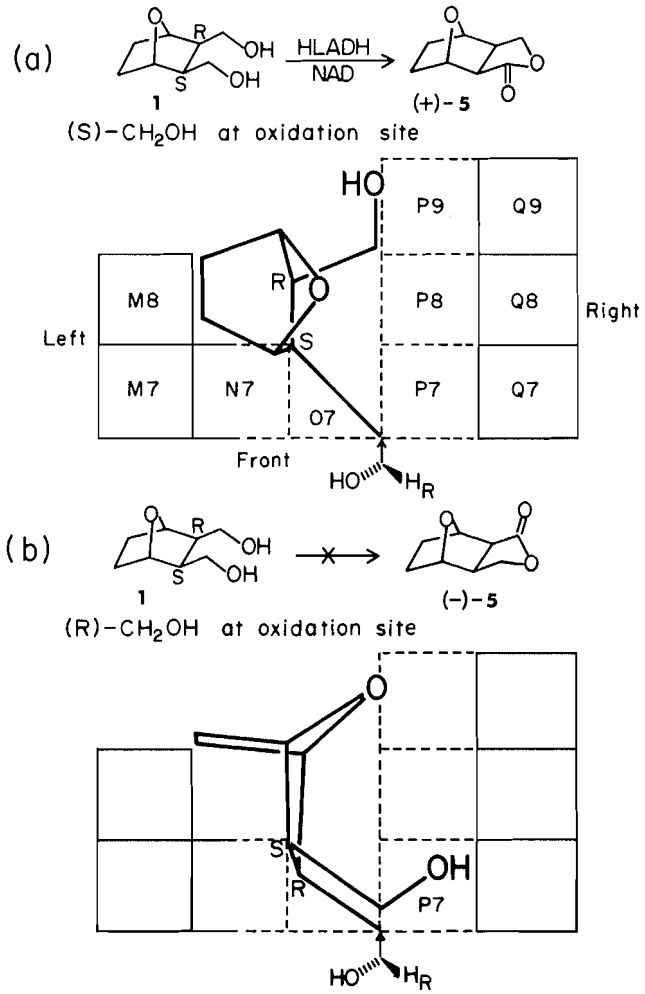

FIG. 1. Cubic active-site section analysis of the stereospecificity of HLADH-catalyzed oxidation of the *exo*-diol **1**. The model, the analytical procedure applied, and the alphanumeric assignments of the cube locations are as described previously (6). In this analysis, the top elevation perspective is used to depict the substrate orientations. The orientations shown are the most favourable for the reactive ES-complex and the least unfavourable for the unreactive orientations. Cubes bounded by solid lines are "forbidden" regions where substrate groups cannot be accommodated because the space is filled with amino-acid residues or by coenzyme. The regions in front, underneath, and above the defined cubic section are forbidden for the same reason. Cubes bordered by broken lines represent "limited access" spaces where substrate binding is possible, but not favoured owing to their proximity to forbidden locations. The negative effects of limited region binding are synergistic. Violation of two limited regions is equivalent to a forbidden location. The open areas are "allowed" space where substrate can be freely accommodated. For oxidation to occur the alcohol moiety must locate at the enzymic oxidation site, indicated by ↑. HLADH-catalyzed oxidations of primary alcohols require abstraction of the *pro-R* hydrogen (3, 7). This ensures a unique —CH_2OH group orientation. In (a) oxidation of the —CH_2OH group attached to the (*S*)-centre is considered. All of the substrate can be accommodated in allowed space. Productive ES-complex formation is therefore possible and oxidation to (+)-**5** occurs via the Scheme 2 pathway. In (b), the consequences of placing the (*R*)-CH_2OH group at the oxidation site are considered. No orientations are possible that do not involve unfavourable interactions. In the best fit shown, the (*S*)-CH_2OH would penetrate limited region **P7**, an interaction that would be particularly adverse because **P7** is a hydrophobic region that would accept a polar OH function with great reluctance. Productive ES-complex formation is therefore precluded and (−)-**5** is not produced.

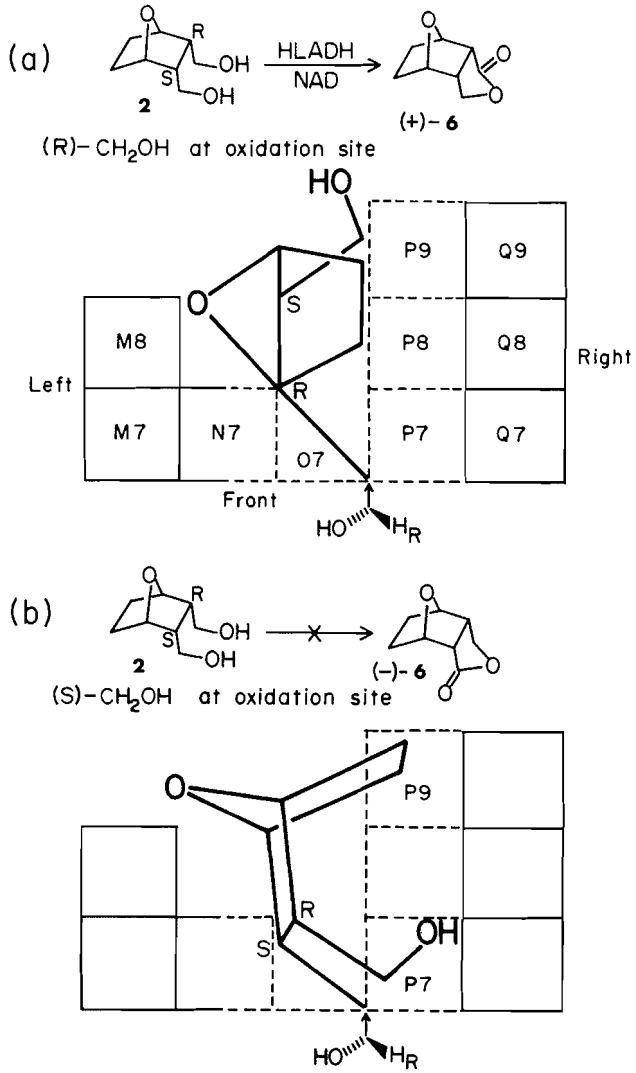

FIG. 2. Cubic active-site section analysis of the stereospecificity of HLADH-catalyzed oxidation of the *endo*-diol **2**. Again, the top elevation perspective (6) is used. (a) With (*R*)-CH_2OH correctly positioned at the oxidation site, all substrate groups can locate in allowed space and oxidation to (+)-**6** therefore occurs readily. (b) A productive ES-complex cannot form for (*S*)-CH_2OH oxidation and (−)-**6** is therefore not produced. The least unfavourable orientation shown would require penetration of two limited regions, **P7** and **P9**, an energetically prohibitive combination.

structure distinctions to be made.

The active site model employing cubic space descriptors developed recently (6) enables the stereospecificities of the enzyme-catalyzed oxidations of **1** and **2** to be readily interpreted. The analyses are depicted in Figs. 1 and 2.

The results of this study provide a further demonstration of the value of the approach for the preparation of useful chiral synthons. Lactones **5** and **6**, which are of potential value as oxaprostaglandin precursors, are not easily available in enantiomerically pure form by any other route.

Experimental

Analytical and instrumental procedures and sources of materials were as described previously (3*a*). All distillations were performed in a Kugelrohr apparatus.

cis-exo-*2,3-(Bishydroxymethyl)-7-oxabicyclo[2.2.1]heptane (1)*

exo-4,7-Epoxyisobenzofuran-1,3-dione (**3**, 5 g, 30 mmol, obtained

Can. J. Chem. Downloaded from www.nrcresearchpress.com by 210.87.254.6 on 09/06/12
For personal use only.

Can. J. Chem. Downloaded from www.nrcresearchpress.com by 210.87.254.6 on 09/06/12
For personal use only.

by the literature (8, 9) method) in dry THF (300 mL) was reduced with lithium aluminum hydride (2.5 g, 66 mmol) in the usual way to yield the *exo*-diol **1** (2.7 g, 57% yield after recrystallization from ethyl acetate/ether (1:2)), mp 63°C (lit. (9) mp 62°C); ^{1}H nmr ($CDCl_3$) δ: 2.18 (2H, d of t, J = 5 Hz, 1.5 Hz), 3.4−3.8 (4H, m), 4.1 (2H, broad s, OH), and 4.35 (2H, t, J = 3 Hz) ppm.

cis-endo-*2,3-(Bishydroxymethyl)-7-oxabicyclo[2.2.1]heptane (2)*

cis-endo-2,3-(Biscarbomethoxy)-7-oxabicyclo[2.2.1]heptane (**4**, 5.35 g, 25 mmol, prepared by the method of Eberbach *et al.* (10)) in dry THF (300 mL) was reduced with lithium aluminum hydride (2.1 g, 55 mmol) to give the *endo*-diol **2** (2.6 g, 66% yield), bp 120°C (0.4 Torr (1 Torr = 133.3 Pa)), mp 49−51°C (lit. (11) mp 49−50°C); ^{1}H nmr ($CDCl_3$) δ: 1.55 (4H, s), 2.2−2.6 (2H, m), 3.4−3.82 (4H, m), 4.1 (2H, broad s, OH), and 4.5 (2H, broad s) ppm.

exo-*Perhydro-4,7-epoxyisobenzofuranone ((±)-5)*

The anhydride **3** was reduced with sodium borohydride by the procedure of Eggelte *et al.* (11) to give the *exo*-lactone (±)-**5** (63% yield after recrystallization from acetone), mp 113°C (lit. (11) mp 112−113°C); ir ($CHCl_3$): 1770 cm^{-1}, ^{1}H nmr ($CDCl_3$) δ 1.4−1.9 (4H, m), 2.6−2.9 (2H, m), and 3.9−4.9 (4H, m) ppm.

endo-*Perhydro-4,7-epoxyisobenzofuranone ((±)-6)*

Using the method of Fetizon and Golfier (12), *cis-endo*-2,3-(bishydroxymethyl)-7-oxabicyclo[2.2.1]heptane (**2**, 1.0 g, 6.3 mmol) was refluxed in the dark for 16 h in benzene (60 mL) containing freshly prepared silver carbonate on Celite (16 g). Filtration followed by rotary evaporation gave the *endo*-lactone (±)-**6** (0.92 g, 91% yield), mp 108−109°C (lit. (11) mp 108−109°C); ir ($CHCl_3$): 1765 cm^{-1}; ^{1}H nmr ($CDCl_3$) δ: 1.8 (4H, broad s), 3.1−3.3 (2H, m), 4.0−4.3 (2H, m), and 4.5−4.9 (2H, m) ppm.

Relative rates of HLADH-catalyzed oxidations of diols 1 and 2

The oxidation rates were determined by monitoring the change in the 340-nm absorption of NAD as in the general HLADH kinetic assay method (13). The assays were performed at 25°C at pH 9.0 with the following stock solutions: HLADH, 1 mg mL^{-1} in 0.05 *M* Tris−HCl buffer, pH 7.4; NAD, 10 mg mL^{-1} in 0.1 *M* glycine−NaOH buffer, pH 9.0; diols, 2×10^{-2} *M* solutions in 0.05 *M* glycine−NaOH buffer, pH 9.0. A reference assay was performed under the same conditions with cyclohexanol. The rates observed, relative to cyclohexanol = 1.0, were 0.63 for **1** and 0.21 for **2**.

Preparative-scale HLADH-catalyzed oxidations

(a) *Of the* exo-*diol 1*

The *exo*-diol **1** (2.0 g, 12.7 mmol), NAD (720 mg, 1.1 mmol), and FMN[6] (9.72 g, 20 mmol) were dissolved in 0.1 *M* glycine−NaOH buffer (600 mL, pH 9.0) at room temperature (20°C) and the pH adjusted to 9.0 by the addition of 15% aqueous NaOH. HLADH (50 mg) was then added and the mixture kept at room temperature (20−25°C). The clear, orange solution soon turned black as the reaction proceeded, and the pH was readjusted periodically to 9.0 with 15% aqueous NaOH. The course of the reaction was monitored by glc analysis and, when no more **1** remained (10 days), the mixture was acidified to pH 3 with 5 *N* hydrochloric acid and continuously extracted with $CHCl_3$ for 2 days. The $CHCl_3$ extract was dried ($MgSO_4$), decolourized with Norite, and rotoevaporated to a pale yellow oil (2 g) which was purified by column chromatography on silica gel (60−200 mesh, 50 g) with ethyl acetate elution. (+)-(3a*R*,4*R*,7*S*,7a*R*)-perhydro-4,7-epoxyisobenzofuranone (**5**) was obtained as a white crystalline solid (1.62 g, 83% yield, >98% ee), mp 112°C; $[\alpha]_D^{25}$ +91.9° (*c* 0.1, $CHCl_3$); ir ($CHCl_3$) and ^{1}H nmr ($CDCl_3$) as for (±)-**5** above. *Anal.* calcd. for $C_7H_{10}O_3$: C 62.34, H 6.49; found: C 62.51, H 6.53%.

(b) *Of the* endo-*diol 2*

The *endo*-diol **2** (2.0 g, 12.7 mmol) was oxidized as described above for 12 days. At this time, glc analysis indicated only 16% conversion of **2**. More NAD (720 mg, 1.1 mmol) and HLADH (50 mg) were added and the reaction was continued for a further 14 days, by which time ~50% of **2** had disappeared. The reaction mixture was terminated at this stage and worked up as described above to give (+)-(3a*S*,4*S*,7*R*,7a*R*)-4,7-epoxyisobenzofuranone (**6**, 712 mg, 37% yield, >98% ee); $[\alpha]_D^{25}$ +31.3° (*c* 0.1, MeOH); ir ($CHCl_3$) and ^{1}H nmr ($CDCl_3$) as for (±)-**6** above. *Anal.* calcd. for $C_7H_{10}O_3$: C 62.34, H 6.49; found: C 62.15, H 6.24%.

Enantiomeric excess determinations

The ee's of the (+)-lactones **5** and **6** were determined by reacting 100 mg of each with excess MeLi as described previously (4) and examining the ^{1}H nmr spectra of the *gem*-dimethyl groups of the product diols **7** and **8** respectively in CCl_4 solution in the presence of 0.4 equivalents of Eu(hfc)$_3$. For the racemic references diols (±)-**7** and (±)-**8**, ΔΔδ values of 0.03 and 0.11 ppm respectively were observed. Only one enantiomer was detectable for the (+)-**7** and (+)-**8** diols obtained from the enzyme-derived lactones.[4] The properties of the dimethyl diols **7** and **8** were as follows. *cis-exo*-2-Hydroxymethyl-3-(1′-hydroxy-1′-methyl)ethyl-7-oxabicyclo[2.2.1]heptane ((±)-**7**, 84% yield from (±)-**3**), mp 89−91°C; ir ($CHCl_3$): 3700−3780 cm^{-1}; ^{1}H nmr (CCl_4) δ: 1.3 (6H, *gem*-diMe) ppm; (+)-**7** (82% yield from (+)-**3**), mp 88−89°C; $[\alpha]_D^{25}$ +21.3°C (*c* 0.1, MeOH). *cis-endo*-2-Hydroxymethyl-3-(1′-hydroxy-1′-methyl)ethyl-7-oxabicyclo[2.2.1]-heptane ((±)-**8**, 85% yield from (±)-**4**), mp 76−77°C; ir ($CHCl_3$): 3710−3100 cm^{-1}; ^{1}H nmr (CCl_4) δ: 1.15 (6H, *gem*-diMe) ppm; (+)-**8** (90% yield from (+)-**4**), mp 77−78°C; $[\alpha]_D^{25}$ +12.8°C (*c* 0.1, MeOH).

Absolute configuration determinations

(a) *Of (+)-(3a*R*,4*R*,7*S*,7a*R*)-Perhydro-4,7-epoxyisobenzofuranone ((±)-5)*

Based on the procedure of McOmie *et al.* (15), boron tribromide (0.42 g, 1.7 mmol) was added dropwise with stirring to the *exo*-lactone (+)-**5** (1.54 g, 0.01 mol) in dry CH_2Cl_2 (25 mL) at −78°C and the resulting light brown solution stirred for 1 h. The mixture was then allowed to warm slowly to room temperature during 2 h and was then washed with brine (2 × 25 mL). The brine solution was reextracted with CH_2Cl_2 (2 × 25 mL) and the combined CH_2Cl_2 solutions (75 mL) washed successively with saturated aqueous $NaHCO_3$ (2 × 30 mL), water (25 mL), and brine (2 × 20 mL) and then dried ($MgSO_4$). Rotoevaporation gave 7-bromo-4-hydroxyperhydroisobenzofuranone (**13**, or its 4-bromo-7-hydroxy isomer) as a white solid (842 mg, 75% yield), mp 90−91°C; $[\alpha]_D^{25}$ +31.3° (*c* 0.1, MeOH); ir ($CHCl_3$): 3500, 1760 cm^{-1}; ^{1}H nmr ($CDCl_3$) δ: 1.4−2.6 (4H, m), 2.6−3.12 (2H, m), 3.9 (1H, broad s, OH), and 3.4−4.38 (4H, m) ppm.

Using the methodology of Noller and Dinsmore (16), phosphorous tribromide (100 mg, 0.34 mmol) was added dropwise with stirring to the bromohydroxy lactone (+)-**13** (235 mg, 1 mmol) in dry CH_2Cl_2 (10 mL) at −78°C. The mixture was kept at −78°C for 90 min, then allowed to warm slowly to room temperature and stirred for a further 3 h. The mixture was then washed with water (2 × 10 mL), saturated aqueous $NaHCO_3$ (2 × 10 mL), and finally with brine (2 × 10 mL). The dried ($MgSO_4$) CH_2Cl_2 solution was rotoevaporated to give the dibromo lactone **14** as a viscous oil (300 mg, ir (film): 1770 cm^{-1}). This was dissolved immediately in dry benzene (20 mL) and, based on the method of van der Kerk *et al.* (17), freshly prepared (18) tri-n-butyltin hydride (1.4 g, 5 mmol) was added. The mixture was kept at 20°C in the dark for 40 h and then refluxed for 30 min. The mixture was rotovaporated and the residual oil chromatographed on silica gel (75 g, 60−200 mesh, ethyl acetate/hexane (1:1) elution) to give, after Kugelrohr distillation at 120-C (0.3 Torr), (+)-(3a*R*,7a*S*)-perhydroisobenzofuranone (**15**, 63 mg, 50% yield); $[\alpha]_D^{25}$ +43.8° (*c* 0.1, MeOH) (lit. (3*a*) $[\alpha]_D^{25}$ +48.8° (*c* 0.5, $CHCl_3$)).

(b) *Of (+)-(3a*S*,4*S*,7*R*,7a*R*)-perhydro-4,7-epoxyisobenzofuranone ((+)-6)*

Using the same procedures as described above, the *endo*-lactone (+)-**6** (500 mg, 3.3 mmol) was treated with boron tribromide (270 mg, 1.1 mmol) to give a C-4,C-7-mixture of isomers of the

[6]FMN is used to recycle the catalytic amount of NAD used (14).

bromohydroxy lactone **16** (600 mg), mp 69–71°C; ir ($CHCl_3$): 3650, 1765 cm^{-1}, ^1H nmr ($CDCl_3$) δ: 1.0–2.6 (4H, m), 2.6–3.0 (2H, m), and 3.3–4.95 (5H, m, includes OH) ppm. This mixture was converted to the dibromolactone **17** (ir (film): 1760 cm^{-1}) with phosphorus tribromide (230 mg, 0.86 mmol) and the product (500 mg) immediately reduced with tri-n-butyltin hydride (1.95 g, 10 mmol) to give (+)-(3a*R*,7a*S*)-perhydroisobenzofuranone (**15**, 60 mg, 13% overall yield from (+)-**6**), bp 120°C (0.2 Torr); $[\alpha]_D^{25}$ +21.2° (*c* 0.1, MeOH) (lit. (3*a*) $[\alpha]_D^{25}$ +48.8° (*c* 0.5, $CHCl_3$)).

Acknowledgements

We thank the Natural Sciences and Engineering Research Council for generous financial support.

1. A. J. BRIDGES, P. S. RAMAN, G. S. NG, and J. B. JONES. J. Am. Chem. Soc. **106**, 1461 (1984).
2. (*a*) A. FISCHLI. *In* Modern synthetic methods. *Edited by* R. Scheffold. Salle/Sauerländer, Frankfurt. 1980 pp. 269–350; (*b*) J. B. JONES. *In* Enzymic and non-enzymic catalysis. *Edited by* P. Dunnill, A. Wiseman, and N. Blakeborough. Ellis Horwood/Wiley, Chichester/New York. 1980. pp. 54–83; (*c*) C.-H. WONG and G. M. WHITESIDES. Aldrichimica Acta, **16**, 27 (1983).
3. (*a*) I. J. JAKOVAC, H. B. GOODBRAND, K. P. LOK, and J. B. JONES. J. Am. Chem. Soc. **104**, 4659 (1982); (*b*) G. S. Y. NG, L.-C. YUAN, I. J. JAKOVAC, and J. B. JONES. Tetrahedron **40**, 1235 (1984).
4. I. J. JAKOVAC and J. B. JONES. J. Org. Chem. **44**, 2165 (1979).
5. Y. ITO, T. SHIBATA, M. ARITA, H. SAWAI, and M. OHNO. J. Am. Chem. Soc. **103**, 6739 (1981); C.-S. CHEN, Y. FUJIMOTO, and C. J. SIH. J. Am. Chem. Soc. **103**, 3580 (1981); S. IRIUCHIJIMA, K. HASEGAWA, and G. TSUCHIHASHI. Agric. Biol. Chem. **46**, 1907 (1982); P. MOHR, N. WAESPE-SARCEVIC, C. TAMM, K. GAWRONSKA, and J. C. GAWRONSKI. Helv. Chim. Acta, **66**, 2501 (1983); M. SCHNEIDER, N. ENGEL, and H. BOENSMANN. Angew. Chem. **96**, 52, 55 (1984); G. SABBIONI, M. L. SHEA, and J. B. JONES. Chem. Commun. 236 (1984).
6. J. B. JONES and I. J. JAKOVAC. Can. J. Chem. **60**, 19 (1982).
7. C. DONNINGER and G. RYBACK. Biochem. J. **91**, 11P (1964); H. GERLACH and B. ZAGALAK. J. Chem. Soc. Chem. Commun. 274 (1973).
8. O. DIELS and K. ALDER. Ann. **470**, 62 (1972); S. TAKANO and K. OGASAWARA. Synthesis, 42 (1976).
9. J. JOHVET. Ann. Chim. (Paris) **5**, 1198 (1960).
10. W. EBERBACH, M. PERROUD-HRGUELLES, H. HCKENBACH, E. DRUCKY, and E. PRINZBACH. Helv. Chim. Acta, **54**, 2579 (1971).
11. T. A. EGGELTE, H. DE KONING, and H. O. HUISMAN. Tetrahedron, **29**, 2445 (1973).
12. M. FETIZON and M. GOLFIER. Ct. R. Acad. Sci. **267**, 900 (1968).
13. J. M. H. GRAVES, A. CLARK, and H. J. RINGOLD. Biochemistry, **4**, 2655 (1965).
14. J. B. JONES and K. E. TAYLOR. Can. J. Chem. **55**, 2969 (1976).
15. J. F. MCOMIE, M. L. WATTS, and D. E. WEST. Tetrahedron, **24**, 2289 (1968).
16. C. R. NOLLER and R. DINSMORE. Org. Synth. Coll. Vol. **2**, 358 (1943).
17. G. J. M. VAN DER KERK, J. G. NOLTES, and J. G. H. SUIJTEN. J. Appl. Chem. **7**, 366 (1937).
18. H. G. KUIVILA and O. F. BEUMEL. J. Am. Chem. Soc. **83**, 1264 (1961).

Can. J. Chem. Downloaded from www.nrcresearchpress.com by 210.87.254.6 on 09/06/12
For personal use only.

Amino derivatives of anhydrotetracycline

MARY D. MENACHERY AND MICHAEL P. CAVA[1]
Department of Chemistry, University of Pennsylvania, Philadelphia, PA 19104, U.S.A.

Received March 7, 1984

This paper is dedicated to Professor Peter Yates on the occasion of his 60th birthday

MARY D. MENACHERY and MICHAEL P. CAVA. Can. J. Chem. **62**, 2583 (1984).

Nitrosation of anhydrotetracycline (**5**) affords 9-nitrosoanhydrotetracycline (**6**), which is converted by sodium dithionite into 9-aminoanhydrotetracycline (**7**). Alkaline coupling of anhydrotetracycline with diazotized sulfanilic acid gives an azo dye which is reduced by sodium dithionite to give 7-aminoanhydrotetracycline (**9**). Reductive methylation of amines **7** and **9** with formaldehyde and sodium cyanoborohydride yields 9-dimethylaminoanhydrotetracycline (**8**) and 7-dimethylaminoanhydrotetracycline (**10**), respectively.

MARY D. MENACHERY et MICHAEL P. CAVA. Can. J. Chem. **62**, 2583 (1984).

La nitrosation de l'anhydrotétracycline (**5**) conduit à la nitroso-9 anhydrotétracycline (**6**) qui, par réaction avec le dithionite de sodium, peut être transformée en amino-9 anhydrotétracycline (**7**). Un couplage en milieu alcalin de l'anhydrotétracycline avec l'acide sulfanilique diazoté conduit à un colorant azo qui, par réduction avec du dithionite de sodium, fournit l'amino-7 anhydrotétracycline (**9**). Des méthylations réductrices des amines **7** et **9**, par réaction avec le formaldéhyde et le cyanoborohydrure de sodium, fournissent respectivement les diméthylamino-9 anhydrotétracycline (**8**) et diméthylamino-7 anhydrotétracycline (**10**).

[Traduit par le journal]

Tetracycline (**1**) is one of the most widely used of all antibiotics. Its bacteriostatic properties are usually decreased by structural modification, but this is not always the case. Thus, the mutant-derived analog sancycline (**2**) has activity similar to that of tetracycline; chemical introduction of a 7-dimethylamino group into sancycline yields minocycline (**3**), an expensive but valuable antibiotic which is clinically active against

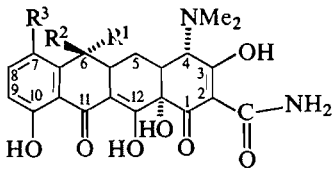

1 R^1 = OH; R^2 = CH_3; R^3 = H
2 R^1, R^2, R^3 = H
3 R^1, R^2 = H; R^3 = NMe_2

a number of tetracycline-resistant organisms. By contrast, anhydrotetracycline (**5**), the acid-catalyzed dehydration product of tetracycline, is clinically useless. Anhydrotetracycline-type structures are not, however, necessarily inactive per se, as shown by the broad-spectrum antibiotic properties of the naturally-produced compound chelocardin (cetotetrin, **4**). In

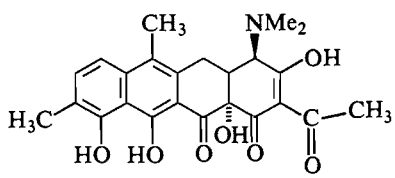

4

view of the facts outlined above, we felt that it would be of interest to attempt the synthesis of several amino and dimethylamino derivatives of anhydrotetracycline, in the hope that these compounds might show enhanced biological activity over the parent substance. No compounds of this type have been

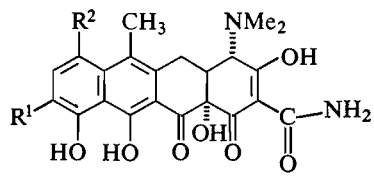

5 R^1 = R^2 = H
7 R^1 = NH_2; R^2 = H
8 R^1 = NMe_2; R^2 = H
9 R^1 = H; R^2 = NH_2
10 R^1 = H; R^2 = NMe_2

reported previously.[2]

Anhydrotetracycline reacted rapidly with nitrous acid in a cold aqueous solution to give a single nitroso derivative, which was easily isolated in almost quantitative yield as its red-orange hydrochloride. Its nmr spectrum indicated the absence of any appreciable chemical shift difference for the C-6 methyl, indicating that substitution had taken place at C-9 rather than C-7. The absence of a green nitroso chromophore and the observed red end-absorption were consistent with its formulation as the *o*-quinone oxime tautomer **6**, as in the case of 2-nitroso-1-naphthol (2). It may be noted that several tetracyclines have been found previously to undergo degradative nitrosation with the formation of dimethylnitrosamine, but no aromatic nitrosation products were detected (3).

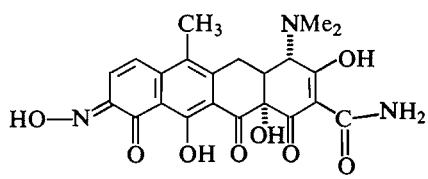

6

The "nitroso" compound **6** was easily reduced by excess sodium dithionite in a dilute alkaline solution. The resulting 9-aminoanhydrotetracycline (**7**) was isolated in good yield by

[1]Author to whom correspondence may be addressed.

[2]For a comprehensive review of tetracycline chemistry, see ref. 1.

Can. J. Chem. Downloaded from www.nrcresearchpress.com by 210.87.254.40 on 09/06/12
For personal use only.

Can. J. Chem. Downloaded from www.nrcresearchpress.com by 210.87.254.40 on 09/06/12
For personal use only.

chloroform extraction at pH 4.5, followed by conversion to the dihydrochloride. The nmr spectrum of this salt showed the aromatic protons as an AB system (J = 9 Hz) centered at δ 7.89 and 7.63, attributable to the C-7 *peri* proton and the C-8 proton deshielded by a protonated amino group. Reductive alkylation of **7** by aqueous formaldehyde and sodium cyanoborohydride afforded 9-dimethylaminoanhydrotetracycline (**8**), isolated as the dihydrochloride.

In contrast to nitrosation, diazonium coupling of anhydrotetracycline led to substitution at C-7. Thus, coupling of anhydrotetracycline with diazotized anthranilic acid in an alkaline solution, followed by sodium dithionite reduction of the resulting dye, afforded 7-aminoanhydrotetracycline (**9**), isolated in good (57%) overall yield as its dihydrochloride. The nmr spectrum of this salt was in accord with the assigned structure. Thus, the C-9 proton of the aromatic AB system appeared at δ 6.88, due to the absence of a strongly deshielding *ortho* substituent. In addition, the C-6 methyl protons were deshielded by the adjacent protonated amino group of the extent of 0.17 ppm as compared to the 9-substituted isomer. Reductive methylation of **9** was carried out as described for the 9-isomer to give, in low yield, 7-dimethylaminoanhydrotetracycline (**10**).

The nmr spectra of all compounds studied showed only one peak for the 4-dimethylamino group at around δ 3, indicating no appreciable contamination by 4-*epi* isomers.

The new anhydrotetracycline derivatives were much less active than tetracycline, and showed no useful activity against a number of gram-negative bacteria which were either tetracycline-susceptible or tetracycline-resistant. Minimum inhibitory concentrations (MIC, 18 h, 35°C, mcg/mL) of ≧128 were observed for all five compounds against strains *Escherichia coli*, *Klebsiella pneumoniae*, *Enterobacter aerogenes*, *E. cloacae*, *Serratia marcescens*, *Proteus morganii*, *P. rettgeri*, *Salmonella sp.*, *Acinetobacter calcoaceticus*, and *Pseudomonas aeruginosa*. The 9-amino derivative (**7**) was the only member of the series to show significant activity among a few gram-positive strains tested. It gave m.i.c. values of ≦0.06 and 8 for *Staphyloccuus aureus* (Smith) and *Micrococcus lutea*, respectively; the tetracycline values against the same organisms were 0.06 and 0.25, respectively.

Experimental

The nmr spectra were obtained on a Bruker 250 nmr spectrometer with tetramethylsilane as internal standard. Ultraviolet spectra were determined using a Perkin Elmer 202 spectrometer. Analyses were carried out at Galbraith Labs, Knoxville, Tennessee.

9-Nitrosoanhydrotetracycline (6)

To a solution of anhydrotetracycline hydrochloride (2.15 g, 4.65 mmol), in distilled water (70 mL) at 0°C, was added a solution of $NaNO_2$ (0.38 g, 5.62 mmol) in a few mL of water. Concentrated HCl was added to lower the pH to 1. The precipitated red-orange nitroso salt was filtered and further purified by dissolving in methanol and precipitating with ether to give the hydrochloride of **6** (2.25 g, 98%); uv (MeOH): 225 (log ε 4.46), 242 sh (4.53), 258 (4.64), 275 (4.63), 292 sh (4.28), 298 sh (4.17), 322 (4.00), 341 (3.91), and 445 nm (4.14); nmr (CD_3OD) δ: 7.00, 6.94 (d, 1H each, J = 10 Hz), 4.22 (s, 1H, C_4-H), 3.22 (s, 6H, NMe_2), 2.34 (s, 3H, C6Me). *Anal.* calcd. for $C_{22}H_{27}N_3O_8Cl.2H_2O$: C 50.03, H 5.15, N 7.96, Cl 6.71; found: C 49.59, H 5.10, N 7.89, Cl 6.57.

9-Aminoanhydrotetracycline (1)

Excess $Na_2S_2O_4$ was added to a solution of 9-nitrosoanhydrotetracycline hydrochloride (1.82 g, 3.70 mmol) in 0.1 *N* aqueous NaOH (150 mL). The 9-amino compound was extracted into chloroform at pH 4.5. The red-orange solution was washed with a little distilled water and the chloroform layer was then acidified with concentrated HCl to give the dihydrochloride on evaporation to dryness (1.61 g, 84%); uv (MeOH): 226 (log ε 4.37), 244 sh (4.42), 274 4.62), 305 sh (4.22), 315 sh (4.13), 327 sh (4.00), 4.18 (3.70), 474 sh (3.40), and 494 nm sh (3.31); nmr (CD_3OD) δ: 7.89, 7.63 (d, 1H each, J = 9 Hz), 4.36 (s, 1H, C4-H), 3.13 (s, 6H, NMe_2), 2.46 (s, 3H, C6Me). *Anal.* calcd. for $C_{22}H_{25}N_3O_7Cl_2.3H_2O$: C 46.47, H 5.49, N 7.39, Cl 12.4; found: C 46.32, H 5.46, N 7.17, Cl 11.78.

9-Dimethylaminoanhydrotetracycline (8)

9-Aminoanhydrotetracycline dihydrochloride (0.038 g, 0.07 mmol) was dissolved in 3 mL of water, and to this solution was added one drop of aqueous HCHO followed by excess $NaBH_3CN$. The 9-dimethylamino derivative was extracted into $CHCl_3$ at pH 6.0, the solution washed with a little distilled water, and the chloroform layer acidified with concentrated HCl and evaporated to dryness, giving the dihydrochloride of **8** (0.017 g, 42%); uv (MeOH): 244 (log ε 4.38), 278 (4.68), 320 sh (3.74), and 408 nm (3.77); nmr (CD_3OD) δ: 8.01, 7.44 (d, 1H each, J = 9 Hz), 4.32 (s, 1H, C4-H), 3.37 (s, 6H, C9-NMe_2), 3.09 (s, 6H, C4-NMe_2), 2.51 (s, 3H, C6-Me). High resolution mass spectrum (Cl) calcd. for $C_{24}H_{27}N_3O_7$: 469.1839; found: 469.1853.

7-Aminoanhydrotetracycline (9)

To a solution of sulfanilic acid (0.347 g, 2.00 mmol) and sodium carbonate (0.08 g, 0.75 mmol), in a few mL of cold distilled water, $NaNO_2$ (0.107 g, 1.55 mmol) was added. To about 10 g of ice, 0.3 mL of concentrated HCl was added, followed by the sodium sulfanilate solution. The anhydrotetracycline hydrochloride (0.462 g, 1 mmol) was dissolved in 40 mL of 0.1 *N* NaOH and the cooled solution was added to the cold diazonium compound solution. After stirring for 15 min, excess $Na_2S_2O_4$ was added to reduce the azo dye and the 7-amino derivative was extracted into chloroform, as in the case of 9-amino derivative, at pH 4.7 and converted into the dihydrochloride (0.29 g, 57%); mp 220−223°C (dec); uv (MeOH): 230 sh (og ε 4.44), 268 (4.88), 340 sh (3.53), and 408 nm (3.89); nmr (CD_3OD) δ: 7.75, 6.88 (d, 1H each, J = 8 Hz), 4.32 (s, 1H, C4-H), 3.18 (s, 6H, NMe_2), 2.63 (s, 3H, C6-H_3). *Anal.* calcd. for $C_{22}H_{25}N_3O_7Cl_2.H_2O$: C 49.61, H 5.11, N 7.89, Cl 13.3; found: C 49.49, H 5.89, N 7.44, Cl 13.68. High resolution mass spectrum (Cl). calcd. for $C_{22}H_{23}N_3O_7$: 441.1527; found: 441.1535.

7-Dimethylaminoanhydrotetracycline (10)

To 7-aminoanhydrotetracycline dihydrochloride (0.065 g, 0.126 mmol) in 3 mL distilled water, excess formaldehyde was added and the solution was stirred for 2 min. Excess sodium cyanoborohydride was then added and the solution was stirred for 30 min. The 9-dimethylamino derivative was extracted into chloroform at pH 4.7−5.0 (0.008 g, 12%); uv (MeOH): 230 sh (log ε 4.38), 270 (4.81), 329 (3.55), and 410 nm (3.43). High resolution mass spectrum (Cl) calcd. for $C_{24}H_{27}N_3O_7$: 469.1839; found: 469.1880.

Chromatographic characterization

The new aminoanhydrotetracycline hydrochlorides were characterized by chromatography on Analtech Micropolyamide plates (ML = 1515) using acetonitrile−water (45:55) as developer. The R_f values were as follows: 0.65 (**1**), 0.53 (**8**), 0.50 (**9**), and 0.79 (**10**).

Acknowledegments

Partial support of this work by NIH grant AI 14717 is gratefully acknowledged. We also thank Dr. R. Wilkinson, Lederle Laboratories, for the antibacterial assay results.

1. L. MITSCHER. The chemistry of the tetracycline antibiotics. Marcel Dekker, New York, NY. 1978.
2. H. S. FRENCH and D. J. PERKINS. J. Am. Chem. Soc. **59**, 1182 (1937).
3. H. ROEPER and K. HEYNS. Z. Naturforsch. Teil C, **32**, 696 (1977); Chem. Abstr. **88**, 74230p (1978).

Adriamycin analogues. Synthesis of the α and β anomers of 7-*O*-(3-amino-3,5-dideoxy-D-ribofuranosyl)adriamycinone and some related compounds[1]

NARENDRA KUMAR AND MERVYN ISRAEL[2]

Department of Pharmacology, University of Tennessee Center for the Health Sciences, Memphis, TN 38163, U.S.A.

Received March 26, 1984

This paper is dedicated to Professor Peter Yates on the occasion of his 60th birthday

NARENDRA KUMAR and MERVYN ISRAEL. Can. J. Chem. **62**, 2585 (1984).

2-*O*-Acetyl-3,5-dideoxy-3-trifluoracetamido-D-ribofuranosyl bromide, prepared by an improved 10-step synthesis from 1,2-isopropylidene-D-xylofuranose, was coupled under Koenigs–Knorr glycosidation conditions with a side-chain protected aglycone derivative of the antitumor antibiotic adriamycin. Complete removal of the blocking groups from the anomeric coupling products afforded glycoside ring-contracted analogs of adriamycin. Selective removal of blocking groups resulted in analogs of *N*-trifluoroacetyladriamycin-14-valerate (AD 32), an non-DNA binding analog of adriamycin with clinical activity and reduced toxicity. Anomeric assignment of coupling products was derived from nmr spectral data consistent with Karplus equation considerations. In vitro growth-inhibition and DNA binding assays were performed with a number of the target compounds. Of interest is the observation that, although binding to calf thymus DNA to a lesser extent than adriamycin, the isosteric 7-*O*-(3-amino-3,5-dideoxy-β-D-ribofuranosyl)adriamycinone produced a greater inhibition of growth of CCRF–CEM human-derived lymphoblastic leukemic cells in culture.

NARENDRA KUMAR et MERVYN ISRAEL. Can. J. Chem. **62**, 2585 (1984).

Le 2-*O*-acetyl-3,5-trifluoroacetamido-D-ribofuranosyl de bromure, preparé de 1,2-isopropylidene-D-xylofuranose en 10 étapes, était attaché, sous les conditions de la glycosidation de Koenings–Knorr, à la chaîne de côté protégée d'une aglycone dérivée de l'antitumeur antibiotique adriamycine. L'enlèvement complet des groupes de stoppage des produits anomériques fournit des analogues d'adriamycine dont l'anneau de la glycoside est réduit. Le déplacement sélective d'un groupe de stoppage produit l'analogues *N*-trifluoroacetyladriamycine-14-valerate (AD 32), même qui se ne réagit pas avec les ADN, manifeste une activité supérieure en clinique, et en même temps moins toxique. L'anomérique assignée de ces produits qui était dérivée de data de spectre de rmn est compatible aux considérations de l'équation de Karplus. L'inhibition de croissance de la culture, in vitro, et l'essai de l'attachement à ADN, étaient exécutés avec plusieurs produits d'objectif; et c'était intéressant d'observer que malgré l'attachement aux ADN de thymus de veau est moins que cel d'adriamycine, il inhibe considérablement la croissance des cellules lymphoblastiques leucémiques (CCRF–CEM) d'origine humaine en culture.

For some time, these laboratories have been engaged in a broad program of anthracycline pharmacology, including new drug development. The anthracyclines are a diverse family of antibiotic substances containing hydroxylated anthraquinone chromophores connected to one or more glycosidic units. Adriamycin (doxorubicin, **1**), the prototypical anthracycline antitumor agent, continues to be of major importance in cancer medicine because of its broad spectrum of activity against leukemias, lymphomas, and a range of solid tumors, including soft-tissue sarcomas, otherwise refractory towards chemotherapeutic intervention (1). Dose-limiting toxicities (acute myelosuppression and chronic accumulated dose-related cardiomyopathy), however, complicate its use, and the desire for reduced toxicity and enhanced activity, particularly against advanced carcinomatous disease, has led to a variety of efforts to develop analogs with improved therapeutic properties.

Mechanistically, based upon early evidence, adriamycin has generally been considered to exert its antitumor effects through DNA binding, with resultant steric interference of DNA polymerase action (2). Thus, with respect to the synthesis of analogs, many investigators have adhered closely to this mechanistic hypothesis and the published restriction that the glycosidic amino group must be unsubstituted in order for DNA binding and antitumor effects to be expressed. At the outset of our program, we were not entirely convinced of these arguments, and so, in addition, sought to explore structure–activity relationships among semisynthetic analogs with reduced or absent DNA binding capability. This approach has led to the development of *N*-trifluoroacetyladriamycin-14-valerate (AD 32, **2**), a non-DNA binding analog with experimentally superior in vivo antitumor activity and significantly reduced toxicity compared to **1** (3–8). Compound **2** continues in Phase II clinical trial, with documented activity against a number of different human tumor types (9, 10). Recently, we described the synthesis and biological evaluation of *N*-trifluoroacetyladriamycin-14-*O*-hemiadipate (**3**), a second-generation analog of **2** with improved water solubility (11, 12); this agent is currently in late preclinical development.

The profound biological effects exhibited by **2** and **3**, to-

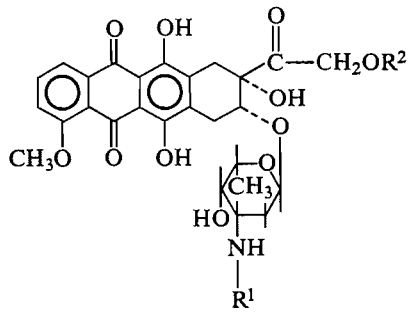

1 $R^1 = R^2 = H$ (adriamycin)
2 $R^1 = COCF_3$, $R^2 = CO(CH_2)_3CH_3$
3 $R^1 = COCF_3$, $R^2 = CO(CH_2)_4COOH$
4 $R^1 = COCF_3$, $R^2 = H$

[1]Work started at the Dana–Farber Cancer Institute, Boston, Massachusetts.

[2]Author to whom correspondence should be addressed.

Can. J. Chem. Downloaded from www.nrcresearchpress.com by 210.87.254.5 on 09/06/12
For personal use only.

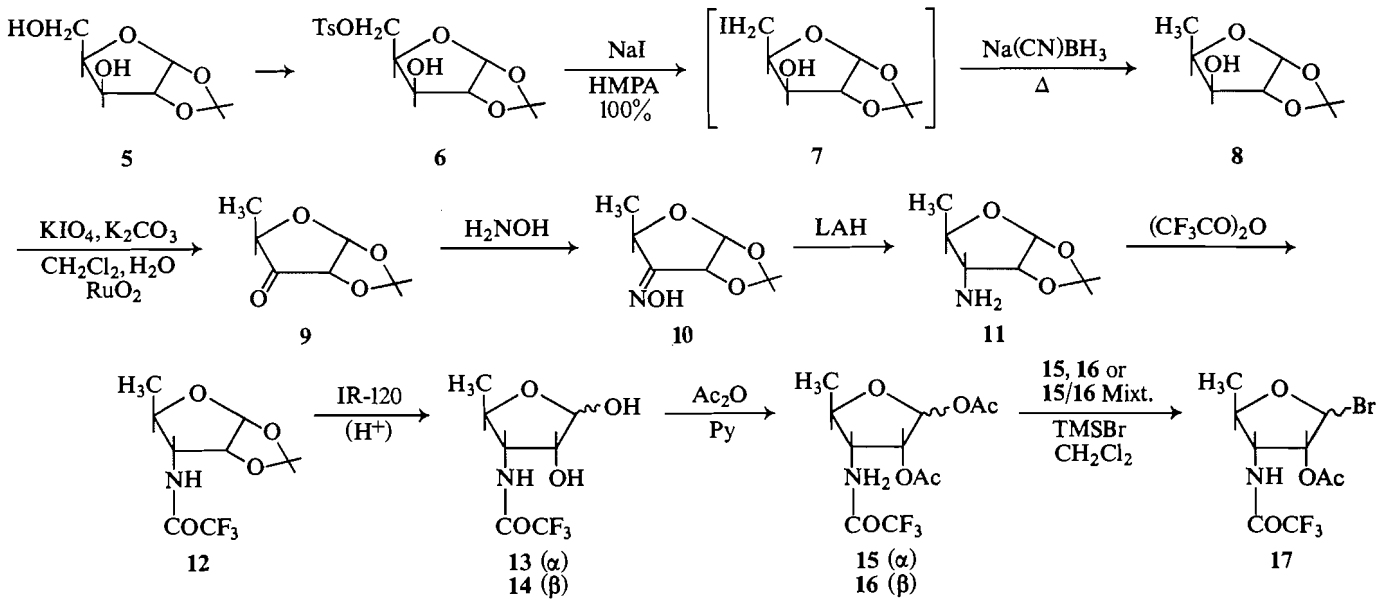

SCHEME 1

gether with other evidence, have done much to alter the overly simplistic DNA-binding hypothesis for **1** and related compounds, and has encouraged us to explore other more diverse structural variants in the search for novel analogs. Since the activity of the system appears to be inherent in the chromophore, with the natural daunosamine sugar possibly serving as a carrier, we have also been examining various analogs of **1** containing fraudulent glycosidic units, which agents have been shown to exhibit significant in vivo antitumor activity in murine tumor systems despite greatly altered DNA binding capability (13, 14).

We now wish to report on the synthesis and in vitro biological evaluation of the anomeric 7-*O*-(3-amino-3,5-dideoxy-D-ribofuranosyl)adriamycinones, **29** and **30**, and their trifluoroacetamides, **25** and **26**, compounds which may be viewed as glycoside ring-contracted isosteres of **1** and **4**, respectively. Compound **4** (*N*-trifluoroacetyladriamycin) is the initially-formed metabolite of **2** and **3**, and has been shown to be biologically active in its own right.

Chemistry

The synthesis of the target compounds was accomplished utilizing the following stepwise approach: (*a*) preparation of an appropriately protected bromosugar; (*b*) preparation of a side-chain protected adriamycin aglycone; (*c*) coupling of the aglycone and bromosugar under Koenings–Knorr conditions; (*d*) separation of the anomeric coupling products; and (*e*) selective removal of protecting groups, in each instance, to give the trifluoroacetamide and the fully-deblocked anomeric product.

The requisite bromosugar, 2-*O*-acetyl-3,5-dideoxy-3-trifluoroacetamido-D-ribofuranosyl bromide (**17**), was prepared in 10 steps from commercially available 1,2-*O*-isopropylidene-D-xylofuranose (**5**), as shown in Scheme 1. This sequence is similar to the route previously developed by us (14), but with a number of significant improvements. Deoxygenation at C-5 via tosylation, followed by iodide displacement and reductive deiodination, was adapted from a procedure used by Almquist and Vince (15). Previously, the iodination step was accomplished under pressure in a sealed Pyrex pressure bottle. However, in attempts to prepare larger amounts of the 5-deoxyxylofuranoside **8** for our current and future needs, we found this pressure reaction to be both arduous and hazardous.[3] The use of elevated temperature instead of pressure for the conversion of **6** into **7** proved highly successful, with a quantitative yield of product being formed when the reaction was carried out at 100°C in HMPA (the reaction did not go when attempted in hot DMF). The iodide was then reduced to **8** in the same flask by means of sodium cyanoborohydride.

Similarly, the use of the earlier described (15) DMSO-based oxidizing system for the conversion of **8** into **9**, in connection with placing an amino function in the *ribo* configuration at C-3, proved inadequate for larger scale reactions because of a complex work-up and the formation of accompanying thioethers, which made isolation of **9** difficult and resulted in poor yields. As an alternative for situating the riboamino function at C-3, we considered the preparation of an azide precursor, which had the attraction of allowing, after coupling, for a novel anthracycline azide derivative for evaluation as a new analog type, as well as providing for an intact glycoside precursor for reduction to the corresponding amine.

Although reports exist of failure in displacing the 3-xylotosyloxy function by azide (16), the possibility of displacing a triflyl group appeared worth attempting in view of the greater leaving character of this function. Unfortunately, only very poor yields of the 3-azidoribofuranose were produced when the 3-triflyl ester of **8** was treated with excess lithium azide in DMF at 100°C. Instability of **8** triflyl ester precluded the possibility of success at higher temperature; attempts led to extensive decomposition and a complex mixture of products, of which the elimination product was most prominent. Attention was then redirected to improving the oxidation of the C-3 hydroxyl. This was successfully accomplished by an adaptation of a procedure described by Lawton *et al.* (17), involving as oxidant ruthenium tetraoxide derived from catalytic amounts of ruthenium dioxide. Ketone **9**, obtained in excellent yields by this

[3]In an attempted scale-up of the reaction an explosion of the bottle was encountered.

Can. J. Chem. Downloaded from www.nrcresearchpress.com by 210.87.254.5 on 09/06/12
For personal use only.

Can. J. Chem. Downloaded from www.nrcresearchpress.com by 210.87.254.5 on 09/06/12
For personal use only.

method, was then converted into the 3-riboamine **11** in quantitative yield by LAH reduction of the corresponding oxime **10**. The amino group of **11** was trifluoroacetylated, and the acetonide group removed by treatment with ion-exchange resin, to give a mixture of the anomeric diols **13** and **14**, which were not separable by tlc. Following acetylation, the anomeric diacetates **15**(α) and **16**(β) could be separated by preparative hplc. Anomeric bromination of **15** and **16** separately, or of the mixture **15/16**, was accomplished by means of the TMS bromide procedure developed earlier in these laboratories (18); this conversion was done just prior to use, because of the instability of **17** on storage.

Adriamycinone, the aglycone of **1**, is easily obtained from the parent antibiotic by mild acid hydrolysis. Protection of the C-14 primary alcohol function prior to coupling was essential, both to eliminate this function as an alternate site for glycosidation and to preserve the base-labile but biologically important dihydroxyacetone side-chain during subsequent operations to remove glycosidic protecting groups after coupling. For this purpose, the *p*-anisyldiphenylmethyl ether (19, 20) was preferred over the dioxolane (13) or other acid-sensitive side-chain protecting groups (21), based upon (*a*) the ease of its formation in high purity without recourse to chromatography, (*b*) its lipophilic character, imparting to the molecule the desired solubility in organic solvents for extraction from aqueous media, (*c*) its inability to produce overlapping proton signals in the diagnostically crucial region in the nmr spectrum of the coupled products, and (*d*) the ease of removal under mild acidic conditions. In contrast to the *p*-anisyldiphenylmethyl function, the otherwise unsubstituted trityl function was found to be less desirable as a protecting function because it required, for removal, acidic conditions drastic enough to produce a significant degree of hydrolytic cleavage of the glycoside.

The coupling of the bromosugar **17** onto the C-7 hydroxyl of the protected adriamycinone **18** was accomplished under Koenigs–Knorr conditions in dry methylene dichloride (Scheme 2). The progress of the reaction was monitored by a combination of tlc and analytical hplc. Maximum conversion of **18** into the product mixture **19/20** was conveniently determined by injecting aliquots withdrawn from the reaction mixture from time to time onto the hplc column and measuring the quantitative ratios of the integrated peak areas of starting material and products on the recorder trace of the detector response. Best results were obtained when a ratio of 2:1 of **17** to **18** was employed. The anomeric products, **19**(β) and **20**(α), were formed in a ratio of 2:3, a relationship which varied only slightly from the results obtained in different small-scale practice runs. Separation of the anomeric coupling products and removal, in each instance, of the *p*-anisyldiphenylmethyl protecting group produced the doubly-blocked ribofuranosyl adriamycinones **21**(β) and **22**(α). When the acidic removal of the *p*-anisyldiphenylmethyl group was effected after removal of the sugar *O*-acetyl function, the desired ribofuranoside analogs of **4** (**25** and **26**) were obtained. Removal of *p*-anisyldiphenylmethyl groups after sequential hydrolysis of both the *O*- and *N*-acyl blocking groups afforded the glycoside ring-contracted adriamycin analogs **29** and **30**. Samples of **25** and **26** made by trifluoroacetylation of **29** and **30** were identical to those derived, as shown, from **23** and **24**, respectively.

The appearance of the C-1′ proton in the nmr spectra (Table 1) of the coupled products **19** and **20** as a singlet in one instance, and a doublet (J = 4 Hz) in the other, provided

TABLE 1. Proton magnetic resonance spectral data for ribofuranosyladriamycinones[a]

Assignment	**19** (β)	**20** (α)	**21** (β)	**23** (β)	**24** (α)	**25** (β)[b]	**26** (α)	**27** (β)	**28** (α)
Aromatic protons	6.80–8.10, 17H	6.80–8.06, 17H	7.33–8.06, 3H	6.83–7.76, 17H	6.76–8.03, 17H	7.26–8.00, 3H	7.23–8.00, 3H	6.83–7.86, 17H	6.63–8.00, 17H
H-7	5.14,[c] 1H, m	5.45,[c] 1H, m	5.26, 1H, m	4.66, 1H, m	5.45, 1H, m	5.13, 1H, m	5.56, 1H, m	5.06, 1H, m	5.45, 1H, m
H-8a	2.10, 2H	1.98, 2H	2.20, 2H	2.10, 2H	2.28, 1H, br d (16)	2.36, 2H	2.56, 1H, br d (16)	2.53, 1H, d (16)	2.13, 2H
H-8b	AB center	AB center	AB center	AB center	1.88, 1H, br d (16)	AB center	2.00, 1H, br d (16)	1.93, 1H, d (16)	AB center
H-10a	2.83, 2H	3.10, 1H, d (18.5)	3.10, 2H	2.66, 2H	2.91, 2H	2.60, 2H	3.10, 2H	2.86, 2H	2.91, 2H
H-10b	AB center	2.70, 1H, d (18.5)	AB center	AB center	AB center	AB center	AB center	AB center	AB center
H-14	4.46, 2H	4.43, 2H, br s	4.76, 2H AB center	4.43, 2H	4.38, 2H	4.68, 2H AB center	4.73, 2H	4.53, 2H	4.51, 2H
C-4 OMe	4.00, 3H	4.06, 3H	4.06, 3H	3.76,[c] 3H	4.03, 3H	4.00, 3H	4.10, 3H	4.00, 3H	4.04, 3H
Trityl-OMe	3.75, 3H	3.81, 3H	—	3.76,[c] 3H	3.76, 3H	—	—	3.85, 3H	3.78, 3H
H-1′	5.40, 1H	5.45,[e] 1H, d (4)	5.50, 1H	5.23, 1H	5.25, 1H, d (3.5)	5.43, 1H	5.40, 1H, d (4)	5.36, 1H	5.08, 1H, d (4)
H-2′	5.14,[c] 1H, d (4)	5.06, 1H, dd (4, 7)	5.26,[c] 1H	4.03,[d] 1H	4.20[d]	4.10,[d] 1H, m	4.41, 1H, dd (4, 7)	4.00,[d] 1H	4.24,[d] 1H
H-5′	1.20, 3H, d (7)	1.41, 3H, d (7)	1.43, 3H, d (7)	1.20, 3H, d (7)	1.36, 3H, d (7)	1.45, 3H, d (7)	1.43, 3H, d (7)	1.20, 3H. d (7)	1.40, 3H, d (7)
Phenolic OH	12.60 & 11.93 (1H, each)	13.26 & 12.26 (1H, each)	14.66 & 13.86 (1H, each)	14.20 & 13.66 (1H, each)	15.13 & 14.00 (1H, each)	14.66 & 13.80 (1H, each)	15.06 & 13.86 (1H, each)	— —	— —
NH	6.50, 1H, br d (8)	—	6.36, 1H, m	—	—	—	—	—	—
C-2′ OAc	2.06, 3H	1.83, 3H	2.16, 3H	—	—	—	—	—	—

[a]Run in $CDCl_3$ at 60 MHz, unmarked signals are singlets. Frequencies in ppm downfield from TMS as internal standard. Coupling constants (in parentheses) in Hz.
[b]Recorded in $CDCl_3$ + DMSO (19:1), TMS as internal standard.
[c]Overlapping signals.
[d]Obscured signals.

Can. J. Chem. Downloaded from www.nrcresearchpress.com by 210.87.254.5 on 09/06/12
For personal use only.

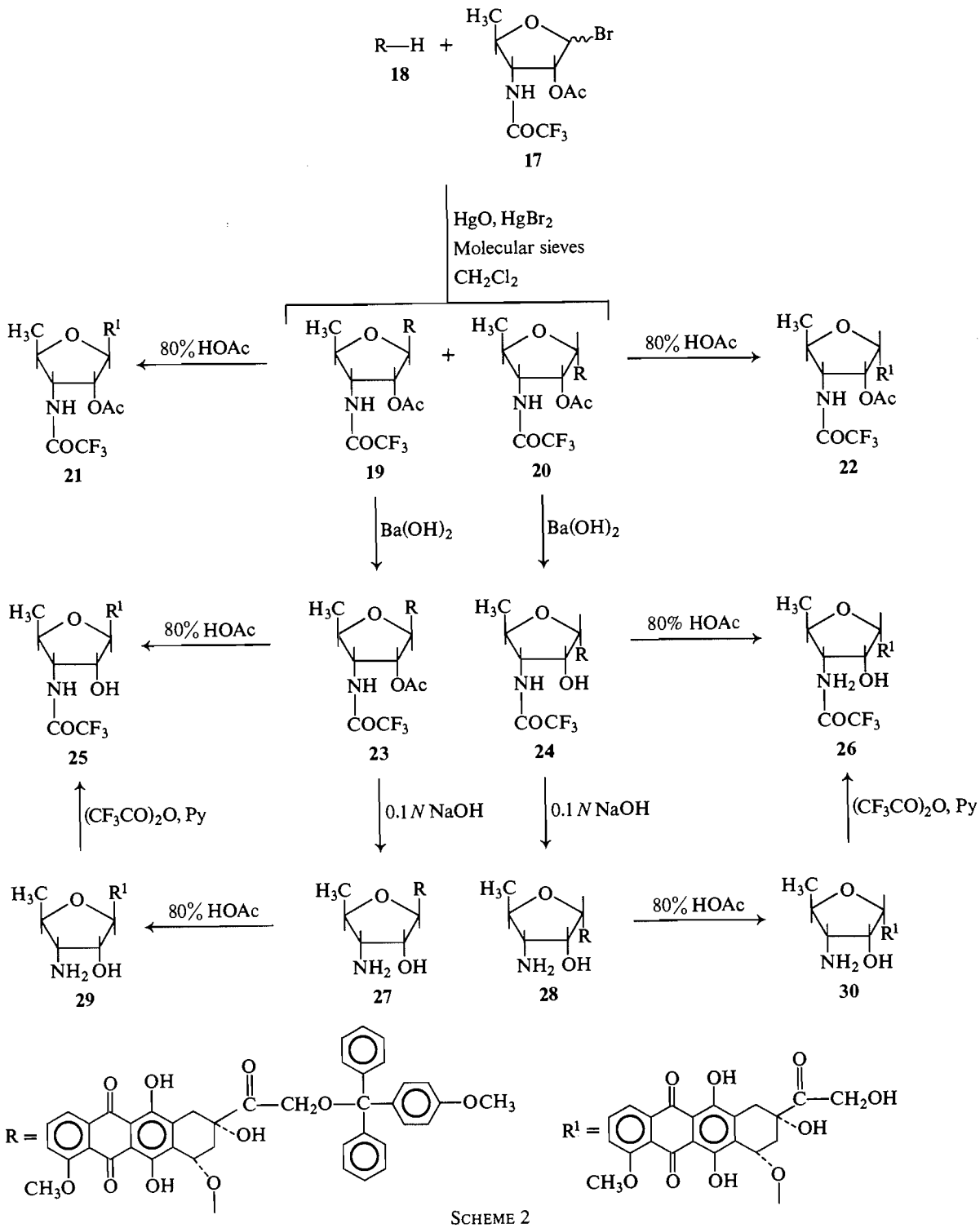

SCHEME 2

evidence for the β- and α-anomeric stereochemical assignments, as depicted in Scheme 2. The assignments are in agreement with the Karplus calculations (22), which require that the observed coupling constants involving H-1′ and H-2′ ($J_{1',2'}$) be in the range of 3.5−8.0 Hz for the α-glycoside and 0.0−8.0 Hz for the β anomer. Dreiding models for **20** showed a dihedral angle for H-1′—H-2′ of about 30°, whereas for **19** the value was closer to 90°. The stereochemical assignments were also consistent with the doublet and double−doublet nature of the H-2′ proton of the anomeric glycosides, and with the relative chemical shifts of the proton under the glycosidic bond (H-7), as described in Table 1 (21). Removal of the protecting groups in the side-chain and in the sugar produced expected proton shifts in the nmr spectra of the deprotected products.

Biological evaluation

Compounds **21**, **22**, **25**, **26**, **29**, and **30** were evaluated in vitro for growth-inhibitory activity against human leukemic cells. Compounds **29** and **30**, which possess an unaltered adriamycin aglycone and an unsubstituted aminoglycoside, were additionally assayed for their DNA binding capability. The results of these assays are summarized in Table 2, which also

TABLE 2. In vitro properties of some ribofuranosyladriamycinones

Compound	ID_{50},[a] μM	Extent of DNA binding: A/A_0[b] (λ 480 nm)
Adriamycin (**1**)	0.05	0.62
AD 32 (**2**)	0.23	0.98
21 (β)	1.0	
22 (α)	>1.0	
25 (β)	0.28	
26 (α)	>1.0	
29 (β)	0.04	0.70
30 (α)	>1.0	0.76

[a]Versus CCRF–CEM cells in culture; 48-h continuous drug exposure.
[b]Calf thymus DNA; pH 7.0 Tris buffer; drug/DNA molar ratio = 0.1.

includes corresponding values for key reference compounds.

The growth-inhibition assay (23, 24) utilized CCRF–CEM cells, a lymphoblastic leukemic cell line of human origin, maintained as suspension cultures. The ID_{50} value represents the concentration of drug which results in a 50% inhibition of growth of treated (48 h) cultures, compared to untreated controls. Adriamycin (**1**) is highly growth inhibitory in this system, the ID_{50} generally being in the range of 0.05–0.06 μM. In an internally consistent test system, **29**, which is isosteric with **1**, actually proved to be more growth inhibitory. Just as **1** shows anomeric specificity in its biological action, the α anomer **30** shows greatly reduced activity compared to the β anomer. A similar structure–activity relationship as exists between **1** and **2**, or **4** (ID_{50} 0.23 μM), is seen for **29** and its trifluoroacetamide **25**; again, activity is greater in the β-anomeric configuration than in the α configuration. The sugar-diprotected analogs (*O*-acetoxy-*N*-trifluoroacetamido) **21** and **22** were inactive, regardless of anomeric configuration.

The extent of DNA binding of **29** and **30** was determined by a spectral method (25). This procedure measures the ratio of the absorbances of drug–DNA mixtures, under defined conditions, to drug alone at 480 nm. By this technique, A/A_0 values close to unity represent little or no drug–DNA interaction, while values significantly less than 1.0 represent extensive interaction. A/A_0 values in our laboratories for adriamycin in the range 0.60–0.65 are in close agreement with other published data (26); values for AD 32 (**2**) indicate essentially no drug–DNA interaction. Both **29** and **30** by this procedure show significant DNA binding, but not nearly to the extent of adriamycin. More DNA interaction is shown by **29** and **30** than by the corresponding (14) ribofuranosyldaunomycinones (9-methylketone side-chain in place of the adriamycin 9-hydroxymethylketone), thus providing further support for the importance of the C-14 hydroxyl function of **1** as an additional site for hydrogen bonding. Somewhat greater DNA interaction is exhibited by the β anomer **29** (anomerically equivalent to **1**) than by the α anomer, in which the amino function is somewhat buried beneath the chromophore.

Interestingly, **29**, which is isosteric with **1** and is more growth inhibitory than **1** in the CEM assay, does not interact with DNA to as great an extent as **1**. Compound **30**, on the other hand, interacts to a reasonable extent with DNA, but is not active in the growth-inhibition assay. These findings continue to support our general considerations that cytotoxicity and antitumor effects among anthracyclines may have much less to do with direct DNA binding than has generally been regarded. We hope that other adriamycin analogs under development in our laboratories, including those with more drastically altered glycosidic functions, will help to further probe these structure–activity relationships.

Experimental

Melting points were recorded on a Kofler hot stage with microscope and are uncorrected. The ir spectra were determined as KBr disks on Perkin–Elmer Model 137B and Model 1320 spectrophotometers. The uv spectra were recorded on a Perkin–Elmer Model Lambda 3 system linked with their Model 3600 Data Station. Proton nmr spectra were recorded on a Varian Associates Model T60-A system spectrometer, with tetramethylsilane as internal standard, and are expressed as δ values. Elemental analyses were performed by Galbraith Laboratories, Inc., Knoxville, TN. Thin-layer chromatography (tlc) was done using analytical silica gel G glass-backed plates (Analtech), with chloroform–methanol (9:1 by volume, System A), chloroform–methanol (19:1, System B), or chloroform–methanol–water (120:20:1, System C) as irrigant. Analytical hplc determinations utilized a Waters Associates Model 202 chromatograph, with a U6K universal loop injector and dual Model M6000-A solvent delivery pumps controlled by a Model 660 Programmer. The column material was μ-Bondapak/phenyl, operating in reverse phase, with linear gradient elution (32% to 65% acetonitrile in ammonium formate buffer, pH 4.0, at 3.5 mL/min over 6 min). Signals were monitored by means of flow fluorescence detection (Schoeffel Model FS970 fluorescence detector, excitation wavelength 484 nm, emission cut-off at 580 nm). Preparative separations were done by gravity-flow column chromatography on silicic acid (Bio-Sil A, Bio-Rad), by preparative tlc using silica gel G Uniplates (Analtech) and by hplc, using a preparative (1-in. od × 1 ft) column packed with silica gel mounted in the above Waters Associates instrument and operating in normal phase, with signal detection by uv and refractive index. Moisture or oxygen-sensitive reactions were carried out in flame-dried glassware in a nitrogen atmosphere.

1,2-O-Isopropylidene-5-deoxy-D-xylofuranose (8)

1,2-*O*-Isopropylidene-5-xylofuranose (**5**), purchased from Pfanstiehl, was converted into 1,2-*O*-isopropylidene-5-tosyloxy-α-D-xylofuranose (**6**), as previously described (15). Reaction of **6** (5 g), dissolved in HMPA (150 mL), with NaI (10 g) at 100°C for 12 h, with stirring, afforded **7** *in situ*. To the flask was added $Na(CN)BH_3$ (7.5 g) and heating was continued for an additional 15 h. The mixture was cooled, diluted with H_2O, and extracted with ether. The ether extract was washed with H_2O, dried, and evaporated *in vacuo* to give a syrup, which was crystallized from $CHCl_3$ – petroleum ether to give **8** (3 g, 60% yield), identical to previously obtained samples (14, 15).

1,2-O-Isopropylidene-5-deoxy-α-D-erythropentofuran-3-ulose (9)

Compound **8** (3 g) was dissolved in alcohol-free CH_2Cl_2 (40 mL), and to this solution was added 30 mL of H_2O. Powdered KIO_4 (5 g), K_2CO_3 (0.5 g), and RuO_2 (Engelhardt Industries; 0.1 g)[4] were added simultaneously and the mixture was stirred vigorously for 2 h. At that time, additional quantities of KIO_4 (0.15 g), K_2CO_3 (0.22 g), and RuO_2 (0.05 g) were added and vigorous stirring was continued for another hour or until tlc no longer showed the presence of starting material. Residual RuO_4 was destroyed by isopropyl alcohol (5 mL) and the mixture filtered. The filtrate was evaporated under reduced pressure and the residue taken into $CHCl_3$. The $CHCl_3$ solution was washed with H_2O, dried, and the solvent removed to give **9** as a syrup (2.7 g, 90%). The spectral properties of this material were identical with those previously reported (15) for **9**.

[4]Best yields were obtained with ruthenium dioxide supplied by Engelhardt Industries; use of material from other supplies gave unsatisfactory results.

Can. J. Chem. Downloaded from www.nrcresearchpress.com by 210.87.254.5 on 09/06/12
For personal use only.

Can. J. Chem. Downloaded from www.nrcresearchpress.com by 210.87.254.5 on 09/06/12
For personal use only.

2-O-Acetyl-3,5-dideoxy-3-trifluoroacetamido-α- and β-D-ribofuranosyl bromide 17

Ketone **9** (5 g) was converted into 3-amino-3,5-dideoxy-1,2-*O*-isopropylidene-α-D-ribofuranose (**11**) in 2 steps (3.75 g, 75%), according to the procedure of Almquist and Vince (15). Bromosugar **17** was obtained from **11** in 4 steps, as previously described (14).

7-O-(2-Acetoxy-3,5-dideoxy-3-trifluoroacetamido-α- and β-D-ribofuranosyl)-14-O-p-anisyldiphenylmethyladriamycinones (19 and 20)

14-*O*-*p*-Anisyldiphenylmethyladriamycinone (**18**) was prepared according to the published procedure (19); mp 192°C; tlc (system B) R_f 0.78. To a solution of **18** (500 mg) dissolved in dry and alcohol-free CH_2Cl_2 (70 mL) was added finely-ground preignited type 3A molecular sieves (3.0 g), moisture-free yellow HgO (0.75 g), and $HgBr_2$ (0.25 g). Freshly prepared bromosugar (900 mg) was dissolved in dry CH_2Cl_2 (10 mL). Half of this solution was added, dropwise in a N_2 atmosphere, to the solution of **18**. After stirring for 30 min, another batch of molecular sieves (1.0 g), yellow HgO (0.25 g), and $HgBr_2$ (0.015 g) was added, followed by the dropwise addition of the remainder of the bromosugar solution. The mixture was stirred at room temperature for an additional 0.5 h, at which time no further conversion of **18** into **19**/**20** could be detected (hplc). The mixture was filtered and the solvent removed under reduced pressure to give a red residue, which was dissolved in CH_2Cl_2 (10 mL). Addition of petroleum ether (70 mL) precipitated an orange solid, which was collected and dried under vacuum. This crude product showed 3 major red spots on tlc (System B), R_f 0.8, 0.78, and 0.64; hplc analysis showed 2 peaks, corresponding to **19** and **20** in a ratio of 3:2, and a third small signal corresponding to unchanged **18**. Chromatography on silica gel afforded 350 mg of **19**, 210 mg of **20**, and 30 mg of starting material.

Compound **19**: mp 133–34°C; tlc (System B) R_f 0.80; hplc, retention time (RT) 12.89 min; ir (KBr): 3450 (br), 1740, 1730, 1720, 1620, 1580, 1510, and 1225 cm^{-1}; nmr given in Table 1. *Anal.* calcd. for $C_{50}H_{44}F_3NO_{14}$: C 63.90, H 4.68, F 6.07, N 1.49; found: C 63.56, H 5.13, F 5.60, N 1.29.

Compound **20**: mp 145°C; tlc (System B) R_f 0.64; hplc, RT 12.17 min; ir (KBr): 3460, 1750, 1730, 1615, 1515, and 1230 cm^{-1}; nmr Table 1. *Anal.* calcd. for $C_{50}H_{44}F_3NO_{14}\cdot 2H_2O$: C 61.50, H 4.71, F 5.84, N 1.43; found: C 61.83, H 4.92, F 6.16, N 1.42.

Final elution of the column with $CHCl_3$–CH_3OH (9:1) gave a mixture of products (**21**/**22**) which were separated by preparative tlc (System B); R_f 0.46 and 0.36. These materials, which arose as a result of loss of the *p*-anisyldiphenylmethyl group during chromatography, were identical with samples of **21** and **22** obtained by hydrolysis of **19** and **20** respectively, as described below.

7-O-(2-Acetoxy-3,5-dideoxy-3-trifluoroacetamido-β-D-ribofuranosyl)-adriamycinone (21)

Compound **19** (50 mg) was dissolved with stirring in 80% HOAc (5 mL) at 0°C, and the solution was let stand overnight in the refrigerator. Lyophilization, followed by crystallization of the residue from $CHCl_3$ – petroleum ether, afforded **21** as a red powder (30 mg), mp 138–139°C; tlc (System B) R_f 0.46; hplc, RT 6.10 min; ir (KBr): 3500, 1725 (br), 1620, 1580, and 1230 cm^{-1}; nmr Table 1. *Anal.* calcd. for $C_{30}H_{28}F_3NO_{13}\cdot H_2O$: C 52.55, H 4.37, F 8.31, N 2.04; found: C 52.96, H 4.39, F 7.77, N 2.03.

7-O-(2-Acetoxy-3,5-dideoxy-3-trifluoroacetamido-α-D-ribofuranosyl)-adriamycinone (21)

The hydrolysis procedure was identical to that described for the preparation of **21** from **19**. Hydrolysis of **20** (10 mg) gave 28 mg of **22**, mp 146°C after crystallization from $CHCl_3$ – petroleum ether; tlc (System B) R_f 0.36; hplc, RT 6.23 min; ir (KBr): 3500, 1730 (br), 1625, and 1590 cm^{-1}; nmr Table 1. *Anal.* calcd. for $C_{30}H_{28}F_3NO_{13}\cdot 2H_2O$: C 51.10, H 4.55, F 8.10, N 1.99; found: C 50.61, H 4.20, F 8.65, N 2.11.

7-O-(3,5-Dideoxy-3-trifluoroacetamido-β-D-ribofuranosyl)-14-O-p-anisyldiphenylmethyladriamycinone (23)

A solution of **19** (0.63 g) in 30 mL of acetone was cooled in an ice bath and to it was added dropwise an ice-cold solution of $Ba(OH)_2$ $8H_2O$ in CH_3OH (6 mL of a 10 g/100 mL solution). The resulting violet solution was stirred at 0°C for 1–5 h, then treated with dry CO_2 until the red color returned, and extracted with $CHCl_3$. The $CHCl_3$ layer was washed with H_2O, dried, and the solvent removed. The product was purified by preparative tlc to give **23**, which gave, from $CHCl_3$ – petroleum ether, an orange-red amorphous powder (0.36 g); mp 156–157°C; tlc (System B) R_f 0.70; hplc, RT 0.61 min; ir (KBr): 3450, 1728, 1720, 1615, and 1580 cm^{-1}; nmr Table 1. *Anal.* calcd. for $C_{48}H_{42}F_3NO_{13}\cdot H_2O$: C 62.95, H 4.80, F 6.35, N 1.53; found: C 62.94, H 5.01, F 6.42, N 1.53.

7-O-(3,5-Dideoxy-3-trifluoroacetamido-α-D-ribofuranosyl)-14-O-p-anisyldiphenylmethyladriamycinone (24)

Compound **20** (500 mg) was converted into **24** using the above described procedure for **23**. The product was purified by preparative tlc to give 200 mg of red powder after crystallization from $CHCl_3$ – petroleum ether, mp 161–162°C; tlc (System B) R_f 0.52; ir (KBr): 3440, 1740, 1616, and 1580 cm^{-1}; nmr Table 1. *Anal.* calcd. for $C_{48}H_{42}F_3NO_{13}$: C 64.20, H 4.68, F 6.35, N 1.56; found: C 64.01, H 4.64, F 6.12, N 1.35.

7-O-(3,5-Dideoxy-3-trifluoroacetamido-β- and α-D-ribofuranosyl)-adriamycinone (25 and 26)

Compounds **23** and **24** (50 mg each) were treated separately with 80% HOAc, as described before for the preparation of **21**. Crystallization of the products from $CHCl_3$ – petroleum ether gave **25** (32 mg, mp 148–149°C; tlc (System B) R_f 0.35; ir (KBr): 3400, 1720 (br), 1618, and 1578 cm^{-1}; nmr Table 1. *Anal.* calcd. for $C_{28}H_{26}F_3NO_{12}\cdot H_2O$: C 52.24, H 4.35, F 8.86, N 2.17; found: C 52.08, H 4.06, F 8.92, N 1.95); and **26** (35 mg, mp 165–166°C; tlc (System B) R_f 0.40; ir (KBr): 3450, 1720 (br), 1618, and 1580 cm^{-1}; nmr Table 1. *Anal.* calcd. for $C_{28}H_{26}F_3NO_{12}\cdot H_2O$: C 52.45, H 4.35, F 8.86, N 2.17; found: C 52.47, H 4.54, F 8.59, N 1.99.

7-O-(3-Amino-3,5-dideoxy-β-D-ribofuranosyl)-14-O-p-anisyldiphenylmethyladriamycinone (27)

Compound **23** (250 mg) was dissolved in 50 mL of acetone and the solution cooled to 0°C. NaOH solution (0.1 *N*, 2.5 mL) was added dropwise under N_2 with stirring. The blue solution was allowed to stir at 0°C for 1 h, at which time the hplc trace (reverse phase) of an aliquot of the solution showed the total replacement of the signal from **23** by a new one. The pH of the solution was adjusted to 8.5 by dropwise addition of 0.1 *N* HCl at 0°C, acetone (20 mL) was added, and the mixture was evaporated at 0°C. The concentrate was repeatedly extracted with $CHCl_3$–CH_3OH (9:1) until no orange color was further extracted. The combined $CHCl_3$–CH_3OH extracts were washed with 5 mL of H_2O and the water washings were extracted back. The colored organic layers were combined, dried, and evaporated. The residue was chromatographed on preparative tlc and the pure **27** was crystallized from $CHCl_3$ – petroleum ether (100 mg), mp 161–162°C; tlc (System A) 0.50; ir (KBr): 3450, 1730, 1720, 1615, and 1579 cm^{-1}; nmr Table 1. *Anal.* calcd. for $C_{46}H_{43}NO_{12}$: C 68.91, H 5.36, N 1.74; found: C 68.61, H 5.44, N 1.67.

7-O-(3-Amino-3,5-dideoxy-α-D-ribofuranosyl)-14-O-anisyldiphenylmethyladriamycinone (28)

Compound **28** was obtained from **24** in a manner similar to that used to prepare **27** from **23**. Thus, 200 mg of **24** afforded, after preparative tlc, 75 mg of **28**, mp 169–170°C; tlc (System A) 0.62; ir (KBr): 3450, 1730, 1617, and 1580 cm^{-1}; nmr Table 1. *Anal.* calcd. for $C_{46}H_{43}NO_{12}\cdot H_2O$: C 67.39, H 5.49, N 1.70; found: C 67.05, H 5.40, N 1.53.

7-O-(3-Amino-3,5-dideoxy-β- and α-D-ribofuranosyl)adriamycinones (29 and 30)

Compounds **27** and **28** (50 mg of each), from above, were dissolved separately in ice-cold 80% HOAc (5 mL) and the solutions stored at 0°C for 10 h. Lyophilization, followed by chromatography of the residues on silica gel, afforded pure **29** and **30** as deep-red amorphous powders from $CHCl_3$–ether. Compound **29** (25 mg): mp 232–233°C;

tlc (System C) R_f 0.22; ir (KBr): 3400, 3220, 1720, 1612, and 1580 cm^{-1}. *Anal.* calcd. for $C_{26}H_{21}NO_{11} \cdot 4H_2O$: C 55.91, H 5.82, N 2.32; found: C 55.78, H 5.57, N 2.17. Compound **30** (20 mg): mp 209–210°C; tlc (System C) R_f 0.40; ir (KBr): 3440, 3240 (br), 1724, 1718, 1618, and 1578 cm^{-1}. *Anal.* calcd. for $C_{26}H_{27}NO_{11} \cdot 2H_2O$: C 55.24, H 5.48, N 2.47; found: C 55.78, H 5.57, N 2.17.

Hydrochloride salts of **29** and **30** were prepared by adding equivalent amounts of methanolic HCl to their $CHCl_3-CH_3OH$ solutions, evaporating the solutions below 0°C, and precipitating the hydrochloride salts. The two hydrochlorides had the same tlc behavior and hplc retention times as the free amines **29** and **30**.

N-*Trifluoracetylation of* ***29*** *and* ***30****: alternate preparation of* ***25*** *and* ***26***

Free amines **29** and **30** (3 mg each) were separately dissolved in 1 mL of pyridine and cooled to −78°C. An ice-cold solution of 0.1 mL of trifluoroacetic anhydride in 2 mL of ether was added to each of the above solutions, and the mixtures stirred at −78°C for 0.5 h. Ice-cold water (5 mL) was then added, and the solutions extracted with $CHCl_3$. The $CHCl_3$ extracts were washed with H_2O (2 mL), dried, and evaporated. Methanol (5 mL) was added to each residue and the solutions heated at reflux for 0.5 h. Removal of the methanol in each instance gave products identical with **25** and **26** (tlc, hplc).

Acknowledgement

This investigation was supported by Research Grants CA 17263, CA 19118, CA 37082, and CA 37209 from the National Cancer Institute, National Instituted of Health, U.S. Public Health Service. The authors are grateful to Dr. John M. Idriss and Mrs. Yael Schwartz of these laboratories for the cell culture determinations and DNA binding assays, respectively. We thank Farmitalia-Carlo Erba, Milan, Italy, and Adria Laboratories, Inc., Columbus, Ohio, for the generous supplies of bulk adriamycin used in this work.

1. R. H. BLUM and S. K. CARTER. Ann. Intern. Med. **80**, 249 (1974).
2. A. DIMARCO and F. ARCAMONE. Arzneim. Forsch. **25**, 368 (1975).
3. M. ISRAEL, E. J. MODEST, and E. FREI III. Cancer Res. **35**, 1365 (1975).
4. L. M. PARKER, M. HIRST, and M. ISRAEL. Cancer Treatment Rep. **62**, 119 (1978).
5. A. VECCHI, M. CAIRO, A. MANTOVANI, M. SIRONI, and F. SPREAFICO. Cancer Treatment Rep. **62**, 111 (1978).
6. I. C. HENDERSON, M. BILLINGHAM, M. ISRAEL, A. KRISHAN, and E. FREI III. Proc. Am. Assoc. Cancer Res. Am. Soc. Clin. Oncol. **19**, 158 (1978).
7. D. DANTCHEV, V. SLIOUSSARTCHOUK, V. PAINTRAND, M. HAYAT, C. BOURUT, and G. MATHÉ. Cancer Treatment Rep. **63**, 875 (1979).
8. T. J. LAMPIDIS, L. V. JOHNSON, and M. ISRAEL. J. Mol. Cell. Cardiol. **13**, 913 (1981).
9. R. H. BLUM, M. B. GARNICK, M. ISRAEL, G. P. CANELLOS, I. C. HENDERSON, and E. FREI III. *In* New drugs in cancer chemotherapy. *Edited by* S. K. Carter, Y. Sakurai, and H. Umezawa. Springer Verlag, Berlin–Heidelberg–New York. 1981. p. 7.
10. M. B. GARNICK, J. D. GRIFFIN, M. J. SACK, R. H. BLUM, M. ISRAEL, and E. FREI III. *In* Anthracycline antiobiotics in cancer therapy. *Edited by* F. M. Muggia, C. W. Young, and S. K. Carter. Martinus Nijhoff Publ., The Hague. 1982. p. 541.
11. M. ISRAEL and P. G. POTTI. U.S. Patent No. 4,299,822 (November 10, 1981).
12. M. ISRAEL, R. SESHADRI, and N. KUMAR. Proc. 13th Intl. Cancer Congress. Seattle, WA. 1982. p. 407.
13. M. ISRAEL and R. J. MURRAY. J. Med. Chem. **25**, 24 (1982).
14. M. ISRAEL, J. E. AIREY, R. J. MURRAY, and J. W. GILLARD. J. Med. Chem. **25**, 28 (1982).
15. R. G. ALMQUIST and R. VINCE. J. Med. Chem. **16**, 1396 (1973).
16. M. L. WOLFROM, J. BERNSMANN, and D. HORTON. J. Org. Chem. **27**, 4505 (1962).
17. B. T. LAWTON, W. A. SZAREK, and J. K. N. JONES. Carbohydr. Res. **10**, 456 (1969).
18. J. W. GILLARD and M. ISRAEL. Tetrahedron Lett. **22**, 513 (1981).
19. B. R. VISHNUVAJJALA, T. KATAOKA, F. D. CAZER, D. T. WITIAK, and L. MALSPEIS. J. Labelled Compd. Radiopharm. **14**, 77 (1978).
20. G. POTTI and M. ISRAEL. J. Med. Chem. **25**, 478 (1981).
21. F. ARCAMONE, S. PENCO, A. VIGEVANI, S. REDAELLI, G. FRANCHI, A. DIMARCO, A. M. CASAZZA, T. DASDIA, F. FORMELLI, A. NECCO, and C. SORANZO. J. Med. Chem. **18**, 703 (1975).
22. M. KARPLUS. J. Chem. Phys. **30**, 11 (1959).
23. G. E. FOLEY, H. LAZARUS, S. FARBER, B. G. UZMAN, B. A. BOONE, and R. E. MCCARTHY. Cancer, **18**, 522 (1965).
24. G. E. FOLEY and H. LAZARUS. Biochem. Pharmacol. **16**, 659 (1967).
25. I. H. GOLDBERG, M. RABINOWITZ, and E. REICH. Proc. Natl. Acad. Sci. U.S.A. **48**, 2094 (1962).
26. A. RUSCONI. Biochim. Biophys. Acta, **123**, 627 (1966).

Can. J. Chem. Downloaded from www.nrcresearchpress.com by 210.87.254.5 on 09/06/12
For personal use only.

Some photochemical rearrangements of vinylcyclopentadienes. Mechanistic and exploratory organic photochemistry[1,2]

HOWARD E. ZIMMERMAN AND WILLIAM D. RAMSDEN
Department of Chemistry, University of Wisconsin, Madison, WI 53706, U.S.A.

Received March 8, 1984

This paper is dedicated to Professor Peter Yates on the occasion of his 60th birthday

HOWARD E. ZIMMERMAN and WILLIAM D. RAMSDEN. Can. J. Chem. **62**, 2592 (1984).

The photochemistry of 2,3-diphenyl-1,4,5-trimethyl-5-vinylcyclopentadiene and 1,2-diphenyl-3,4,5-trimethyl-5-vinylcyclopentadiene was studied. The triplet of the 2,3-diphenyl isomer was found to undergo a 1,5-vinyl migration; in contrast, the 1,2-diphenyl diene was unreactive. On direct irradiation, in addition to vinyl migration, four photoproducts were formed from the cyclopentadienes. These were shown to be 5,6-diphenyl-1,2,7-trimethylbicyclo[3.2.0]hepta-2,6-diene, 1,5-diphenyl-2,6,7-trimethylbicyclo[3.2.0]hepta-2,6-diene, 6,7-diphenyl-1,2,5-trimethylbicyclo[3.2.0]hepta-2,6-diene, and 1,7-diphenyl-2,5,6-trimethylbicyclo[3.2.0]hepta-2,6-diene. A number of experimental observations led to a mechanism involving: (*a*) electrocyclic closure of the vinylcyclopentadienes to give vinyl housenes, (*b*) bicycling which interconverts isomeric housenes, and (*c*) thermal Cope rearrangement of the vinyl housenes to afford bicyclo[3.2.0]hepta-2,6-dienes. In addition, evidence was adduced for 1,5-vinyl shifts occurring in the vinylcyclopentadiene reactants.

HOWARD E. ZIMMERMAN et WILLIAM D. RAMSDEN. Can. J. Chem. **62**, 2592 (1984).

On a étudié la photochimie du diphényl-2,3 triméthyl-1,4,5 vinyl-5 cyclopentadiène et du diphényl-1,2 triméthyl-3,4,5 vinyl-5 cyclopentadiène. On a trouvé que l'état triplet de l'isomère diphényl-2,3 subit une migration 1,5 du vinyle; par opposition, le diphényl-1,2 diène n'est pas réactif. Par irradiation directe, les cyclopentadiènes conduisent, en plus du produit de migration du groupe vinyle, à quatre photoproduits; on a démontré qu'ils ont les structures suivantes: diphényl-5,6 triméthyl-1,2,7 bicyclo[3.2.0] heptadiène-2,6; diphényl-1,5 triméthyl-2,6,7 bicyclo[3.2.0] heptadiène-2,6; diphényl-6,7 triméthyl-1,2,5 bicyclo[3.2.0] heptadiène-2,6 et diphényl-1,7 triméthyl-2,5,6 bicyclo[3.2.0] heptadiène. Sur la base d'un certain nombre de données expérimentales, on propose un mécanisme impliquant: (*a*) une cyclisation électrocyclique des vinylcyclopentadiènes conduisant aux vinyl housènes; (*b*) des réactions de bicyclisation permettant de provoquer des interconversions entre les divers housènes isomères; (*c*) une transposition thermique de Cope qui transforme les vinyl housènes en bicyclo[3.2.0] heptadiènes-2,6. De plus, on a obtenu des données permettant de supposer qu'il se produit des déplacements 1,5 de groupes vinyles dans les réactifs vinylcyclopentadiènes.

[Traduit par le journal]

Can. J. Chem. Downloaded from www.nrcresearchpress.com by 210.87.254.42 on 09/06/12
For personal use only.

Introduction

One of our main research objectives has been the elucidation of new photochemical organic reactions. It is clear that the number of ground state organic reactions is immense, a result of a century and a half of intensive efforts. In comparison, the number of photochemical reactions is minuscule. Nevertheless, the known photochemical reactions are often fascinating, primarily because of their departure from intuitive ground state expectation, and promising, primarily because patterns of behavior demonstrate the presence of understandable mechanistic factors.

In recent years we have uncovered some unique rearrangements of vinylcyclopropenes affording cyclopentadienes (1*c*, 2; note also work by Padwa *et al.* (3)). We thus proceeded to investigate the photochemical behavior of the homologous vinylcyclopentadienes.

Results

Synthesis of reactants of interest

For our study we selected 2,3-diphenyl-1,4,5-trimethyl-5-vinylcyclopentadiene **1**. The synthesis of this compound is outlined in Scheme 1. Also included in Scheme 1 is the synthesis of 1,2-diphenyl-3,4,5-trimethyl-5-vinylcyclopentadiene **2** whose photochemistry proved to be intimately intertwined with that of vinylcyclopentadiene **1**.

*Reactivity of vinylcyclopentadiene **1** on direct irradiation and structure elucidation of photoproducts*

Irradiation of vinylcyclopentadiene **1** afforded four photoproducts **A**, **B**, **C**, and **D** in a ratio of 8:4:1:2 as outlined in eq. [1].

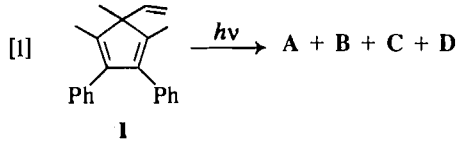

1

The nmr spectra of these photoproducts revealed a three-hydrogen pattern attributable to a $CH_2CH=$ moiety. Additionally, one methyl peak was weakly coupled with these hydrogens, and the chemical shift was suggestive of a vinyl methyl group, thus further defining the group as $CH_2CH=CCH_3$ in all four photoproducts. Further, the proton nmr spectra showed two additional methyl peaks in each photoproduct. Beyond this, the Cmr spectra of each photoproduct had two absorbances in the range of δ 50–75 ppm, characteristic of quaternary ring junction carbon atoms. At this point we considered the basic structure **14** for the four photoproducts. The ultraviolet spectrum of **A** suggested the presence of a styryl moiety, that of **B** only unconjugated phenyl groups, the uv of

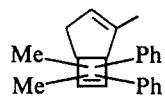

14

[1] This is paper 141 of our photochemical series.

[2] For paper 140, note ref. 1*a*. For paper 139, see ref. 1*b*, and for paper 138, see ref. 1*c*.

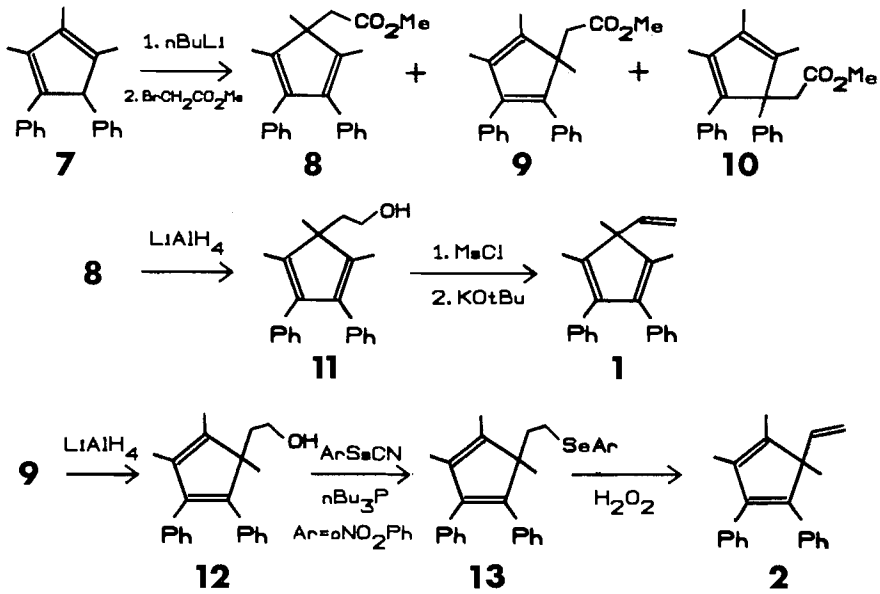

SCHEME 1. Synthesis of photochemical reactants.

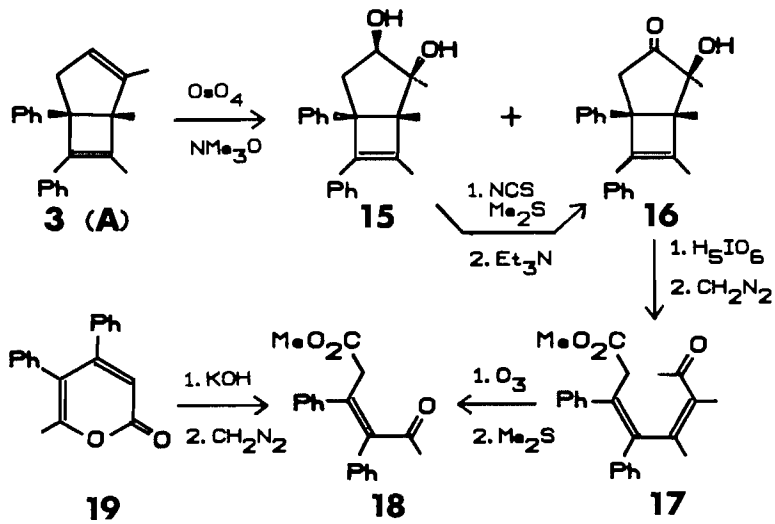

SCHEME 2. Structure elucidation of photoproduct A by degradation.

C a stilbenyl chromophore, and that of **D** a styryl group as in **A**. Since rigorous structural assignments seem a necessary requisite to mechanistic understanding (4), we proceeded to establish the structures of the photoproducts by degradation and X-ray determination.[3]

The structure of photoproduct **A** was established by a degradation beginning with osmium tetroxide oxidation, which afforded a vicinal diol **15** as well as a ketol **16**. For simplicity in presentation, the degradation is outlined in Scheme 2 with final structural assignments.

Surprisingly, periodic acid oxidation of ketol **16** afforded a ketoester which, after esterification, possessed *two* double bonds while the ketol reactant had only *one*. This resulted from the remarkably facile electrocyclic ring opening of the cyclobutene oxidation product (*vide infra*). The degradation scheme led ultimately to enone ester **18** which was independently prepared from pyrone **19**.

The validity of the degradation scheme was established by an X-ray determination of the structure of ketol **16** derived from photoproduct **A**. Figure 1 provides the ORTEP drawing. Hence photoproduct **A** is assigned structure **3**.

A degradation of photoproduct **B**, beginning in similar fashion, led as depicted in Scheme 3 to the terphenyl aldehyde **22**. Routine X-ray structure determination of terphenyl **22** confirmed its structure. Note Fig. 2. This led to formulation of photoproduct **B** as **4**.

We next turned our attention to photoproduct **D**. Hydroboration–oxidation of **D** led to hydroxylated product **23**. With the strong implication of a bicyclo[3.2.0] skeleton for **D**, coupled wih nmr evidence suggesting the placement of all substituents except for possible interchange of phenyl and methyl

[3] Currently X-ray has become a routine tool for structure elucidation in our group. Such powerful programs as MULTAN 80 (*5a*) and SHELX 76 (*5b*) coupled with a VAX/750 provide unrefined structures in 15–20 min; refinement does take some additional time. The X-ray structure determinations are to be published by K. J. Haller and W. D. Ramsden.

Can. J. Chem. Downloaded from www.nrcresearchpress.com by 210.87.254.42 on 09/06/12
For personal use only.

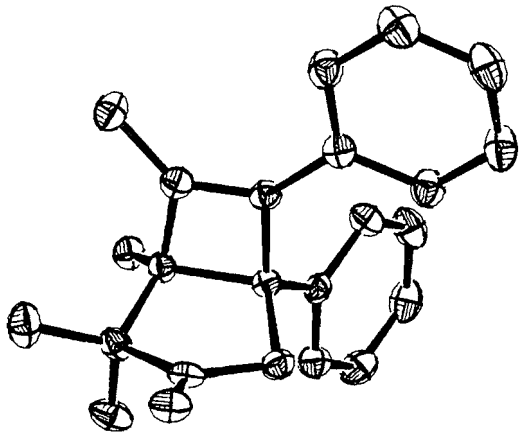

FIG. 1. ORTEP drawing for ketol **16**.

groups, we independently synthesized the hydroxylated product **23** as outlined in Scheme 4. The most critical step involved the useful cyclopropene cycloaddition of van Tilborg *et al.* (6). Finally, we note that photoproduct **D** was assigned structure **6**.

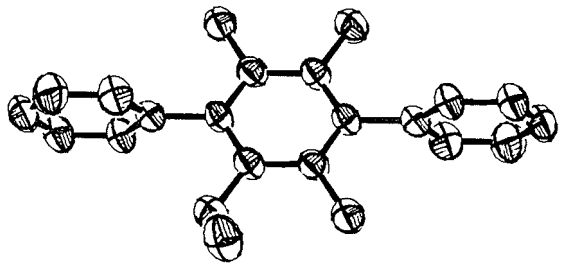

FIG. 2. ORTEP drawing for terphenyl **22**.

Photoproduct **C** was the most minor photoproduct and thus the least available for study. Its structure derived from the presence of two junction methyl groups (δ 1.36 and 1.38 singlets), the usual $CH_2CH{=}CCH_3$ moiety as determined by nmr, and the presence of a *cis*-stilbenyl chromophore as evidenced in the ultraviolet spectrum. This led to formulation of **C** as **5**.

As a consequence of the structure elucidations, one may describe the photochemical transformation of vinylcyclopentadiene **1** as in eq. [2]. Additionally, the product distribution at 8°C is included and is discussed below.

[2] 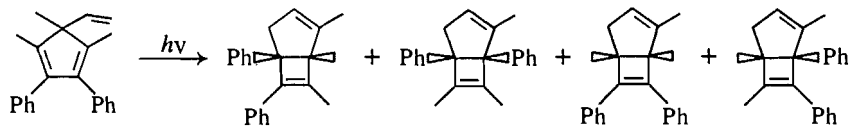

	1	**3 (A)**		**4 (B)**		**5 (C)**		**6 (D)**
Temperature: 30°C		8	:	4	:	1	:	2
8°C		4	:	13	:	1	:	2

Reactivity of vinylcyclopentadiene 2 on direct irradiation

Irradiation of vinylcyclopentadiene **2** rapidly led to vinylcyclopentadiene **1** with very minor formation of **3**, **4**, **5**, and **6**. The irradiation was carried out with a solution filter preventing absorption of light by product vinylcyclopentadiene **1**. This transformation is depicted in eq. [3]. The significance of this is considered below in connection with the reaction mechanism.

[3] 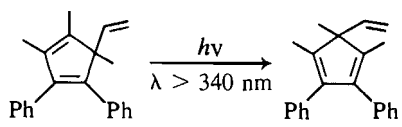

Reactivity of the vinylcyclopentadienes on sensitized irradiation

When the corresponding photolysis of vinylcyclopentadiene **2** was carried out with sensitization, using *p*-dimethylaminobenzophenone (E_T 62 kcal/mol (7)[4]), no reaction occurred. In contrast, when the same sensitization was carried out with vinylcyclopentadiene **1** as the reactant, a facile conversion to diene **2** was observed. Note eq. [4]. Here, the energy of vinylcyclopentadiene **1** triplet should be no higher than the 58 kcal/mol reported (8) for cyclopentadiene itself and E_T for vinylcyclopentadiene **2** should be no higher than the 57 kcal/mol reported (9) for *cis*-stilbene.

[4] 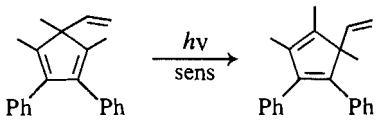

[4]The estimated triplet energy is taken as that of *p*-aminobenzophenone as in ref. 7*a* and 7*b*.

Labeling studies necessary for mechanistic understanding

Since two different mechanisms – a 1,5-vinyl shift and a bicycle migration (10) – seemed plausible possibilities for the interconversion of vinylcyclopentadienes **1** and **2**, it was necessary to have available these molecules properly labeled to differentiate between these pathways. Reaction of vinylcyclopentadiene **1** with Streitwieser's base (11, 12), however containing deuterium (12), led to selective deuteration of the C-1 and C-4 methyl groups as shown in eq. [5].

[5] 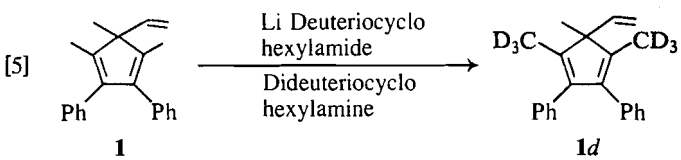

Direct irradiation of **1***d* to appreciable conversion (77%) led to the expected formation of the usual bicyclic photoproducts. In addition, a very minor (3%) amount of vinylcyclopentadiene **2** was isolable. Interestingly, the nmr spectrum showed the methyl groups to be statistically scrambled, each being 1/3 CH_3 and 2/3 CD_3. The recovered starting material (i.e. vinylcyclopentadiene **1**) also had its methyl groups close to statistically scrambled. Note eq. [6]. As might be surmised, the bicyclic photoproducts **3**, **4**, **5**, and **6** each possessed nmr spectra showing that two-thirds of the methyl groups in each location were replaced by CD_3. Note eq. [7]. Clearly, scrambling of the

Can. J. Chem. Downloaded from www.nrcresearchpress.com by 210.87.254.42 on 09/06/12
For personal use only.

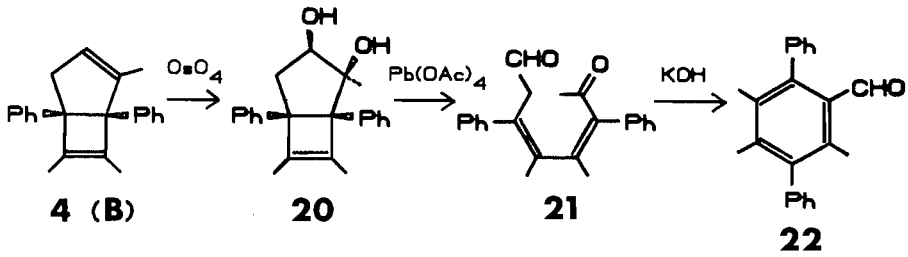

SCHEME 3. Structure elucidation of photoproduct B by degradation.

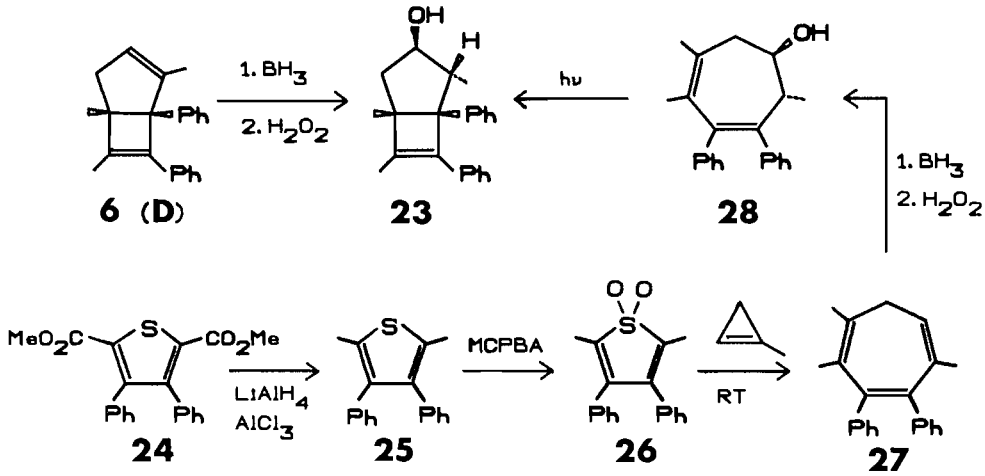

SCHEME 4. Independent synthesis of alcohol **23**.

deuterium labeled methyl groups in vinylcyclopentadiene **1** and the product vinylcyclopentadiene **2** accounts of the scrambling of the bicyclic photoproducts. In lower conversion runs, vinylcyclopentadiene **2** was formed in too minor amounts to be isolated. However, scrambling methyl groups could be monitored by observing distribution of the deuterated methyl groups in recovered vinylcyclopentadiene **1** and in the bicyclic photoproducts **3**, **4**, **5**, and **6**. Note eqs. [6] and [7].

[6]

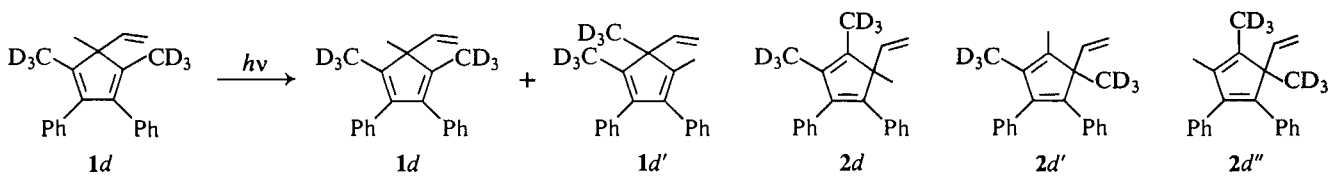

19% Conv: 95 5 ⟵ not detected ⟶

[7]

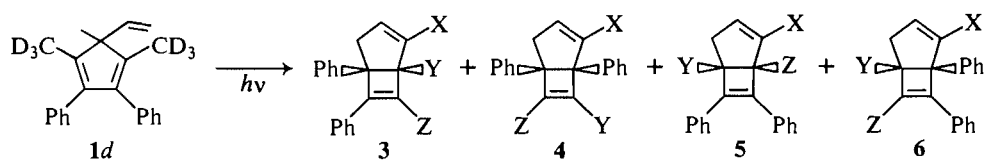

Relative amounts of CH_3 at given positions

	3			4			5 and 6		
	X	Y	Z	X	Y	Z	X	Y	Z
19% Conversion:	89	6	5	77	16	7	—		

In another study of labeled reactant, methyl deuterated vinylcyclopentadiene **1***d* was irradiated under sensitized conditions to afford vinylcyclopentadiene **2***d′* but no bicyclic products. Strikingly, and in contrast to the direct irradiation, not only was reactant not scrambled, but also the photoproduct consisted of one isomer resulting from a simple vinyl migration with no methyl scrambling. Note eq. [8].

[8]

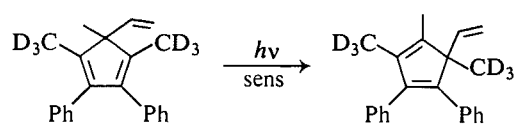

Can. J. Chem. Downloaded from www.nrcresearchpress.com by 210.87.254.42 on 09/06/12
For personal use only.

With specifically labeled **2** (i.e. **2***d*′) available it was of interest to investigate its photochemistry. Direct irradiation of **2***d*′ led to partially scrambled **1** (i.e. **1***d* and **1***d*′). Recovered reactant was unscrambled. In addition the usual photoproducts were observed. Of most interest were **3** and **4**. In **3**, the C-2 methyl group was completely deuterated while the remaining label was equally distributed between C-1 and C-7. In product **4** C-2, again, was completely deuterated while the remaining label was unequally distributed between C-6 and C-7. The photolysis of labeled **2** is described in eq. [9]. The significance of these labeling studies is considered in the section on Discussion of results.

TABLE 1. Quantum yields in the photochemistry of vinylcyclopentadiene **1**

Sensitizer	Product	Quantum yield
None	Bicyclic photoproduct **3**	0.030
None	Bicyclic photoproduct **4**	0.0098
None	Bicyclic photoproduct **5**	0.001_5
None	Bicyclic photoproduct **6**	0.0040
p-Dimethylamino benzophenone	Vinylcyclopentadiene **2**	0.075

[9]

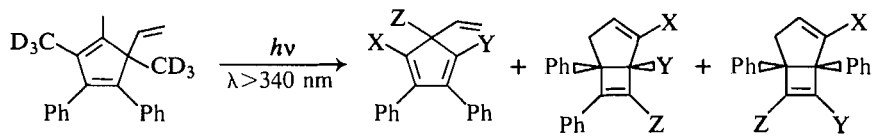

2*d*′ **1***d* (86%) **3***d* (8.5%) **4***d* (5.5%)

Relative amounts of CH_3 at given positions:

1*d*	**3***d*	**4***d*
X Y Z	X Y Z	X Y Z
46:46:8	0:50:50	0:68:32

Equation [2] includes the effect on the distribution of photoproducts resulting from lowering the irradiation temperature from 30 to 8°C. Although the overall conversion was not appreciably affected, the ratio of photoproducts **A** to **B** was decreased by a factor of ca. 6. This suggested a still lower temperature run, and at −70°C, in place of the bicyclic photoproducts, there was observed the vinyl shifted cyclopentadiene **2**. Note eq. [10].

[10]

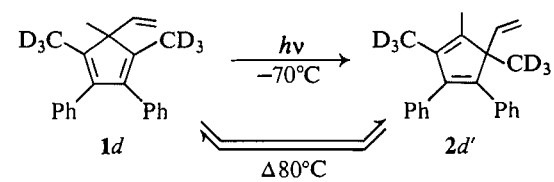

1*d* **2***d*′

Beyond this simple low temperature run, we used deuterium labeled **1***d* to check on the nature of the rearrangement process. This, too, is included in eq. [10]. It is seen that the low temperature photolysis affords **2***d*′ which is derived from vinylcyclopentadiene **1***d* by a simple 1,5-vinyl shift rather than by a bicycle process.

Quantum yields, quenching experiments, and product photostability

Quantum yields for the reactions of interest were obtained (note Experimental section) and are detailed in Table 1. These include the direct irradiation efficiencies for photolysis of vinylcyclopentadiene **1** and for the sensitized irradiation of this compound.

A related item of consequence is the very low photoreactivity of the four photoproducts **3**, **4**, **5**, and **6**, coupled with the observation that these compounds neither interconvert nor afford any of the compounds of the present study.

Finally, it was of some importance to test for the presence of triplet species in the direct irradiation of vinylcyclopentadiene **1**, since intersystem crossing was a possibility and any such triplets would be candidates for the rearranging excited state. At 0.002 *M*, 3,3,4,4-tetramethyl-1,2-diazetine-1,2-dioxide (E_T 40 kcal/mol) did not quench the rearrangement to photoproducts **3**, **4**, **5**, and **6** (note Experimental section for details).

Observation of ground state chemistry

It seemed necessary to establish the limits of thermal stability of the photochemical reactants **1** and **2**. At 30°C these proved quite stable. However, at 80°C in benzene facile equilibration was encountered, the steady-state distribution being 1:1. Furthermore, deuterium labeling showed that the rearrangement derived from a vicinal vinyl shift rather than a bicyclic step. Note eq. [10], which includes the deuterium substitution.

Interpretative discussion

The overall mechanism of bicyclic photoproduct formation

The two phenyl groups and three methyl groups provided markers which clarified the nature of the skeletal transformation on direct irradiation of vinylcyclopentadiene **1**. Even more definitive was the photolysis of the di-deuteriomethyl reactant **1***d*. Note eq. [7]. For the transformation of vinylcyclopentadiene **1** or **1***d* into photoproduct **A** (i.e. **3**) or its deuterated counterpart, an electrocyclic closure of **1** to afford housene **29**, followed by a Cope rearrangement, leads nicely to the skeletal pattern of phenyl, methyl, and trideuteriomethyl substitution in photoproduct **A** (**3**). This mechanism is outlined as eq. [11] in Scheme 5.

Also, the same mechanistic process accounts for the conversion of vinylcyclopentadiene **2** into the observed bicyclic photoproduct **B** (i.e. **4**) with the correct disposition of phenyl and methyl groups. This route proceeds via housene **30** as depicted in eq. [12] of Scheme 5. Additionally, the alternative Cope regiochemistry can be seen to lead to photoproduct **C** (i.e. **5**).

Thus far we have considered just two mechanistic processes, namely electrocyclic closure of the vinylcyclopentadiene reactants to afford housenes and the Cope rearrangement of the housenes thus formed. It is clear that more than these two processes are occurring. We see, for example, that irradiation

Can. J. Chem. Downloaded from www.nrcresearchpress.com by 210.87.254.42 on 09/06/12
For personal use only.

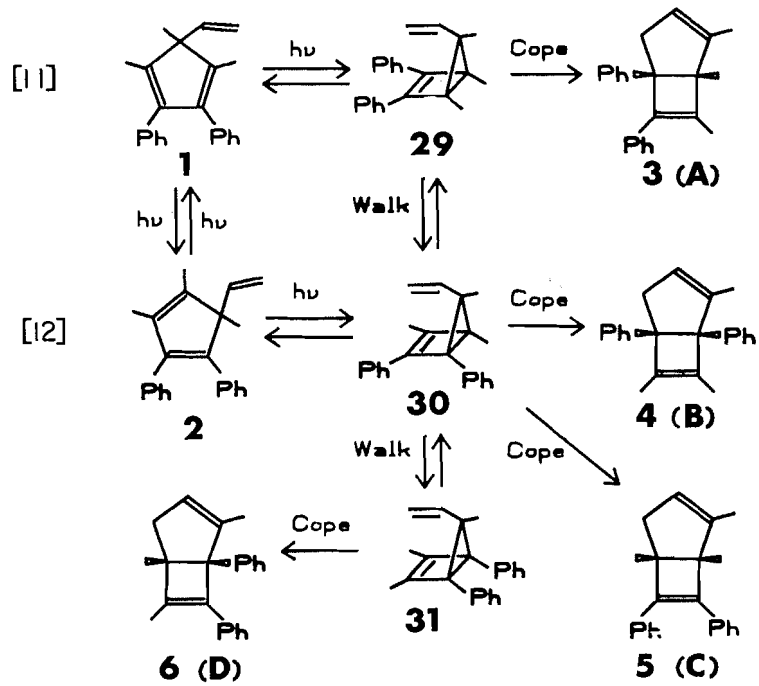

SCHEME 5. Mechanism of conversion of vinylcyclopentadienes **1** and **2** into photoproducts.

of vinylcyclopentadiene **1** affords all four of the photoproducts – **A**, **B**, **C**, and **D** – rather than just **A** as predicted by the above. Similarly, photolysis of **2** leads to more photoproducts than just **B** and **C**.

It appears that two additional mechanistic processes are operating and account for the additional products observed in each case. The first is a vinyl shift in which a vinyl moiety moves to the adjacent carbon of the five-membered ring. An illustration of the process is found in Scheme 5 in the interconversion of **1** and **2**.

A second mechanistic process which seems to be operating is a bicycle rearrangement (10, 13) in which the out-of-plane carbon atom of the housene molecule moves to the adjacent bond. This is illustrated in Scheme 5 in the conversion of housene **29** to **30** and the conversion of **30** to **31**.

Clear evidence for these processes came from irradiation of the deuterated vinylcyclopentadiene **2***d*′ (note eq. [13]) where the major (86% of the converted reactant) photoproduct is vinylcyclopentadiene **1** with labeling demonstrating 92% bicycling to give **1***d*′ and 8% vicinal (i.e. 1,5) vinyl shifting to give **1***d*.

[13]

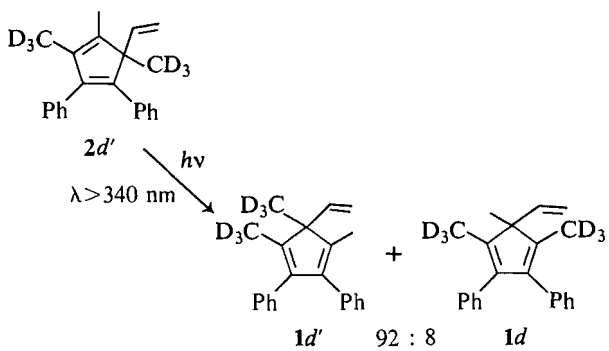

Thus four basic processes – (*a*) electrocyclic closure to afford the vinylcyclopentadienes, (*b*) bicycling of C-5 of the housenes, (*c*) vicinal vinyl shifting, and (*d*) Cope rearrangement of the housenes – permit formulation of the overall mechanistic pathways in Scheme 5 leading from reactant vinylcyclopentadienes to bicyclic photoproducts.

A check on the mechanisms leading to bicyclic photoproducts provided by deuterium labeling

As noted above, the bistrideuteriomethyl vinylcyclopentadienes **1***d* and **2***d*′ promised to shed light on the mechanisms of both the vinylcyclopentadiene interconversions and on the conversions to bicyclic photoproducts **3**–**6**. The latter require discussion first. Referring to Scheme 6, we note that bis-deuteriomethyl vinylcyclopentadiene **1***d* affords primarily bicyclic photoproduct with the deuteriomethyl groups in locations in accordance with the proposed mechanism; as a consequence of the plane of symmetry in the housene precursor **29***d*, the subsequent Cope rearrangement affords only one bicyclic product (i.e. **3***d*). The competitive 1,5-vinyl shift to afford **2***d*′ does not obscure the results, since the formation of bicyclic products **3***d*′ and **3***d*″ is of lower efficiency. Similarly, scrambling of reactant **1***d* is a lower efficiency process.

More informative is the photolysis of the bis-deuteriomethyl vinylcyclopentadiene **2***d*′, also shown in Scheme 6, which portrays the relevant transformations. Here the irradiation wavelength was such that any vinylcyclopentadiene **1***d* formed would not absorb light and thus would not mar the simplicity of the experiment. The formation of the two bicyclic regioisomers **3***d*′ and **3***d*″ in a 1:1 ratio confirms the mechanism. Thus, housene intermediate **29***d*′ has a pseudo plane of symmetry, and the two Cope rearrangements depicted have equal probability, barring any minor secondary deuterium isotope effects.

Nature of the bicycle and Cope rearrangement steps

A priori, it appeared possible that the bicycle rearrangements were either thermal or photochemical, since both have precedent (12–14). Scheme 7 depicts the photochemistry relevant to this question. Housene **31***d* has no extended chromophore and should not absorb under the conditions of the irradiation of **2***d*′.

Can. J. Chem. Downloaded from www.nrcresearchpress.com by 210.87.254.42 on 09/06/12
For personal use only.

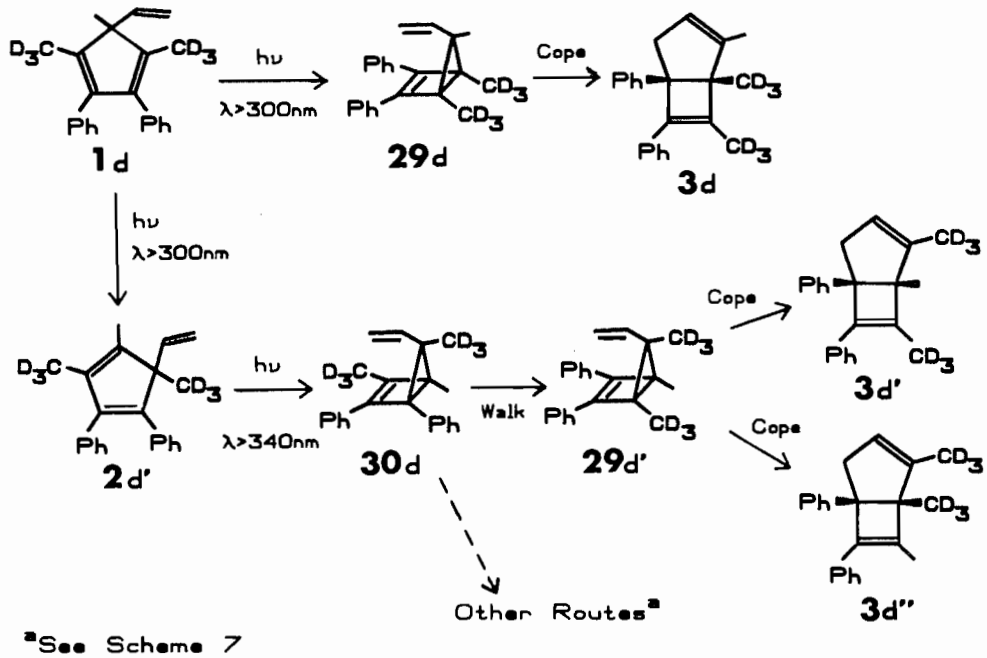

SCHEME 6. Selected transformations in the photochemistry of bis-deuteriomethyl vinylcyclopentadienes 1*d* and 2*d'* giving product A.

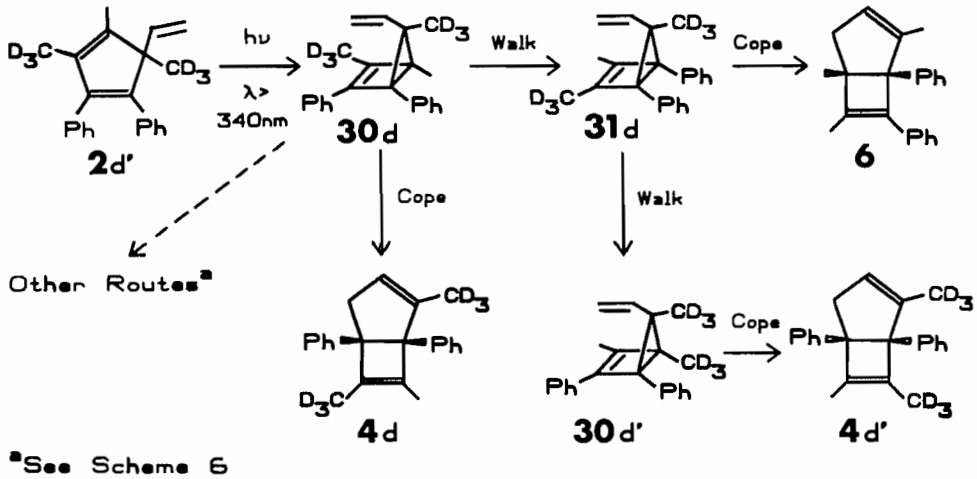

SCHEME 7. Selected transformations in the photochemistry of bis-deuteriomethyl vinylcyclopentadiene 2*d'* giving photoproducts B and D.

Nevertheless, experimentally, housene **31***d* leads onwards by bicycle and Cope rearrangements to afford bicyclic photoproduct **4***d'*. In absence of light absorption by **31***d*, the bicycle rearrangement must thus be thermal.

A similar point derives from the observation of photoproduct **D** (i.e. **6**) under these conditions. This means that the Cope rearrangement step converting **31** (or **31***d*) must be occurring under conditions where no light is absorbed by the housene precursor **31***d*, and the Cope rearrangement also must be occurring thermally.

Since the various bicycle steps are similar structurally, the thermal nature of one step strongly suggests that all of the bicycle rearrangements observed are thermal. Similarly, the observation of one thermal Cope step provides evidence that the remaining Cope rearrangements are thermal rather than photochemical.

Regarding the reaction stereochemistry, we note that an *endo*-vinyl configuration in the housenes is required for each Cope rearrangement. The simplest rationale is that the electrocyclic closure of the vinylcyclopentadienes **1** and **2** gives rise to some *endo* stereoisomer. The *endo* stereoisomer (e.g. **30**), then, would be capable of undergoing either the Cope rearrangement to afford product (e.g. **4**) or a stereospecific bicycle rearrangement, giving rise to product housene (e.g. **31**) still having an *endo*-vinyl group. The low quantum yields, in the range of 0.03 and lower, imply that some *exo*-vinyl stereoisomer might be formed and revert to initial reactant, being unable to undergo the Cope rearrangement. Reversion of the housenes to afford vinylcyclopentadienes is quite likely in view of the reported[5] (15) thermal instability of housenes, coupled with our not finding nmr indication of the presence of housenes surviving at 0°C (note Experimental section).

In much simpler systems the thermal walk reaction of housenes is known from the work of Klärner and Adamsky (13), who have shown these to proceed in a thermally allowed fashion with retention of the *endo* vs. *exo* configuration, that is,

[5] Housenes tend to revert to cyclopentadienes at 0–50°C (13, 15).

Can. J. Chem. Downloaded from www.nrcresearchpress.com by 210.87.254.42 on 09/06/12
For personal use only.

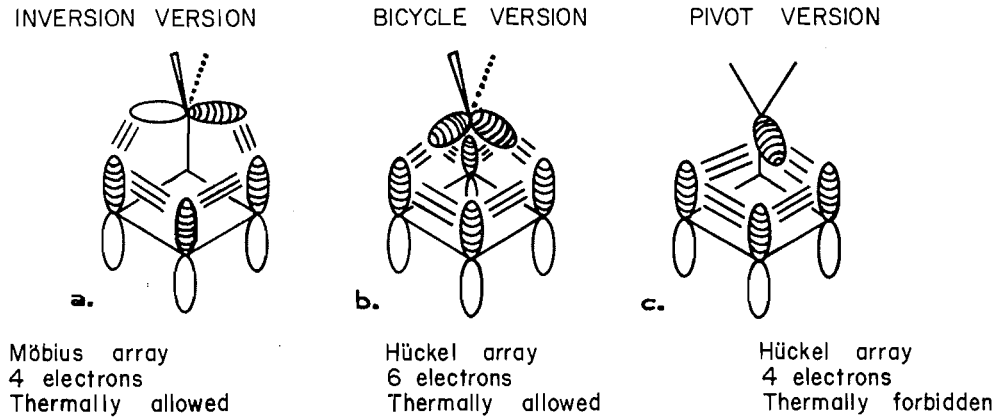

FIG. 3. Electronics of the bicycle (walk) rearrangement for bicyclo[2.1.0]pentenes.

with stereochemistry corresponding to our photochemical bicycle rearrangements (13) and ground state bicycle walk rearrangements of Type A zwitterions[6–8] (16–18). The reaction is seen to be allowed in the Woodward–Hoffmann sense (19), being a 1,3-suprafacial rearrangement with inversion of configuration of the bicycling carbon.

An alternative and useful analysis of this type of "walk rearrangement" (20) has been presented in connection with the rearrangement of Type A zwitterions. This uses the Möbius–Hückel treatment (21). Applied to the case in hand, we consider Figs. 3a and 3b and see that, with bicycling (i.e. inversion of migrating carbon configuration), there are 4 delocalized electrons in a Möbius system (21). With 4N electrons and a ground state Möbius array, a closed shell is predicted by the Zimmerman circle mnemonic (21). This contrasts with pivoting as in Fig. 3c where there are 4N electrons in a Hückel array (21), which predicts a higher energy and open shell transition state using the Frost counterpart mnemonic (22).

The bicycle description of the mechanism, as in Fig. 3b, depends on our recognition (21*e*) that two sp^5 orbitals are precisely equivalent to an sp^2 and a *p*-orbital (Fig. 3a). When we use the bicycle equivalent, we again apply the Möbius–Hückel treatment by including the six delocalized orbitals.

Unusual Cope selectivity[9]

The rather interesting regioselectivity observed in the preferential conversion of vinyl housene **30** to afford photoproduct **4** (i.e. **B**) over photoproduct **5** (i.e. **C**) needs consideration. A simple rationale might be applicable if the phenyl group at C-1 is selectively twisted into a conformation not permitting full overlap with σ bond 1–5, and thus not able to stabilize the transition state leading to photoproduct **5** (i.e. **C**). The ORTEP drawing in Fig. 1 for the analogous bicyclic ketol **16** does show the ring junction phenyl group as conformationally twisted, while the remaining phenyl is not. This explanation is less than ideal, since crystal lattice forces may control the phenyl conformation in solid ketol **16**.

A more intriguing possibility is found in an analysis which considers the effect of a phenyl group substituted in each of two locations in a Cope transition state. Figure 4 poses the problem of two alternative transition states and thus the question of which location for phenyl substitution is most helpful energetically. The Cope rearrangement under discussion is a special case of the 1,2-divinylcyclopropane rearrangement which is known to be particularly facile (23) as a result of release of three-ring strain energy. Hence the rearrangement under consideration is one which should have an early transition state compared to that for the usual acyclic systems[10] which have received attention.

The two cyclic arrays included in Fig. 4 correspond to the two modes of rearrangement of vinylhousene **30**. For a divinylcyclopropane, a model is selected which assumes an early transition state, and thus has appreciable residual 3,4-σ bonding compared with new π–π (i.e. 1,6) overlap. We consider two types of effects. The first is inclusion of *s*-character in the orbitals of the original 3,4-σ bond; the second is inclusion of *s*-character in the bond itself. Dissection of the two effects – on the diagonal matrix element and on the off-diagonal matrix elements – is artificial but does reveal the consequence of inclusion of the two independently. From even simple Hückel calculations we find that it is the phenyl group remote from the site of σ-bond fission which has the greater stabilizing effect. This is quite different from the situation[10] observed where 1,6-σ-bond formation is more complete than 3,4-σ-bond fission as in the ordinary Cope cases and where phenyl substitution on the central carbon of each allylic moiety has a dominating effect.

Temperature control of vinylcyclopentadiene reactivity

Two effects were noted on lowering temperature. One was seen at −70°C (note eq. [10]) where vinylcyclopentadiene **1** isomerization still occurred and the Cope rearrangement was inhibited. The second effect is the changed product distribution on photolysis of **1** (note eq. [2]) where the trend is toward inhibition of the Cope rearrangement of the initially formed housene **9** relative to processes which lead to the isomeric housene **30**. The overall reaction efficiency did not appear to be

[6] The stereochemistry of the zwitterion rearrangement by motion of two bonds rather than pivoting of one was first outlined in refs. 16*a* and 16*b*.

[7] The first non-photochemically generated bicyclo[3.1.0] system rearranging was described in ref. 16*c*.

[8] The equivalence of the "inversion" and "bicycling" mechanisms was shown in refs. 17*a–c*.

[9] Subsequent examples of bicycling of ground state bicyclo[3.1.0]-hexyl species are described in refs. 18*a–c*.

[10] Literature experiment (24*a–d*) reveals that phenyl at the central carbon of the allylic moiety in the Cope rearrangement accelerates the reaction by ca. 17-fold, while phenyl substitution at the σ-bonded end causes an acceleration of ca. 69-fold. However, it has already been noted by Gajewski and Conrad (24*d*) that a divinylcyclopropane is likely to have an early transition state.

Can. J. Chem. Downloaded from www.nrcresearchpress.com by 210.87.254.42 on 09/06/12
For personal use only.

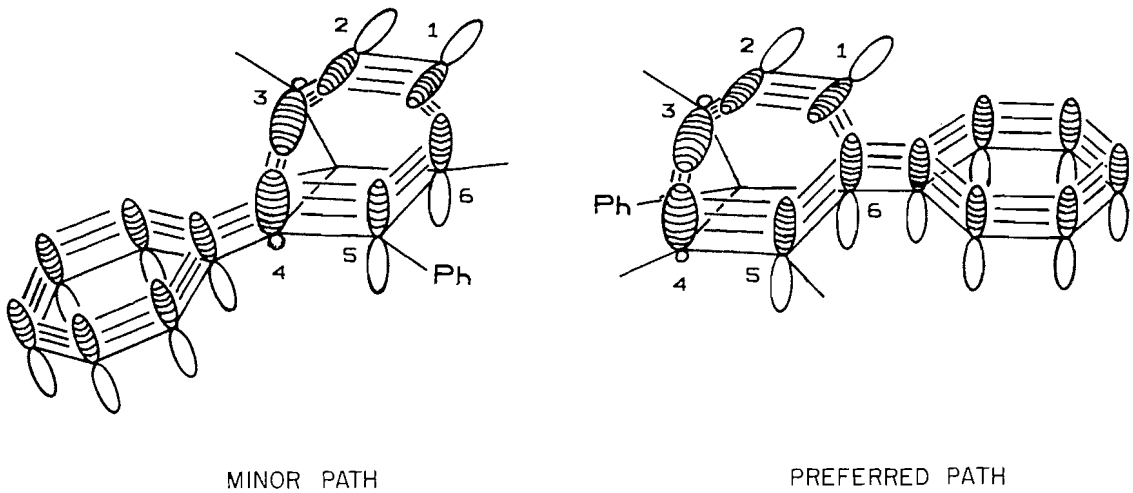

FIG. 4. The effect of phenyl substitution on Cope rearrangements of divinylcyclopropanes.

inhibited, at least qualitatively, and thus the initial electrocyclic closure seems to be relatively temperature independent. In contrast to such a photochemical process, one might expect a ground state Cope rearrangement to be inhibited at lower temperature in accord with these observations.

Finally, relative to the low temperature photochemistry we see from the deuterium labeling (note eq. [10]) that the rearrangement of vinylcyclopentadiene **1***d* to afford **2***d'* involved a 1,5-vinyl sigmatropic rearrangement rather than bicycling which also was an a priori possibility. Hence low temperature inhibits both the Cope rearrangement, as noted above, and also the bicycling, leaving the vinyl shift process.

Multiplicity control of reactivity. Differing triplet behavior

In recent years we have been particularly interested in examples where a given reactant exhibits different photochemistry depending on multiplicity. The major challenge here is development of a mechanistic framework which eventually may predict such dependences.

In the present study, sensitization of vinylcyclopentadiene **1** led exclusively to vinylcyclopentadiene **2** as initially described in eq. [4]. The use of the tagged methyl groups as described in eq. [8] permitted description of the rearrangement as a vicinal 1,5-vinyl shift rather than a bicycle process.

The exact counterpart direct irradiation experiment is not available, since direct irradiation of vinylcyclopentadiene **1** affords both primary and secondary photoproducts. However, direct irradiation of **2** should be quite similar mechanistically, and here the long wavelength chromophore permits selective light absorption by reactant only. This direct irradiation of vinylcyclopentadiene **2** affords primarily (86%) isomeric vinylcyclopentadiene **1** (note eq. [9]), and the deuterium label showed that this arose 92% by electrocyclic closure followed by a bicycle process and only 8% by vicinal vinyl shifting. In addition, the 14% of bicyclic photoproducts **3** and **4** have been shown to arise by bicycling of the vinylhousene **30**.

Hence there is a dramatic difference, wherein T_1 vinylcyclopentadienes prefer vicinal vinyl shifting while S_1 vinylcyclopentadienes prefer electrocyclic closure. This appears to be still another example of the exchange integral (i.e. K) control of photochemical reactions. In this work (12*g*, 25, 26) and related early discussions (27–29), the type of reactions undergoing triplet processes was postulated to be quite different than those undergoing singlet transformations. Figure 5 outlines the

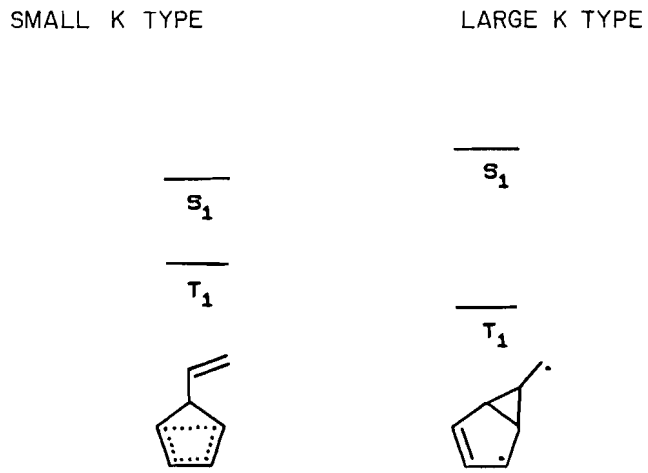

FIG. 5. Exchange integral control of vinylcyclopentadiene reactivity.

present situation. As in our general postulate, singlets prefer the small K mechanism while triplets prefer the large K route. As has been noted earlier, pericyclic processes are small K type reactions while large K reactions include diradical rearrangements in which the odd electrons are distributed over a delocalized system.[11]

Electronic nature of the 1,5-vinyl shift

The 1,5-vinyl shift process, observed both thermally and photochemically, is reminiscent of the MO Following description (21*c*, 32) of the 1,2-vinyl shift for cations, radicals, and carbanions. In that case (e.g. the radical) an odd-electron containing *p*-orbital was on a carbon adjacent to the vinyl group and was left in the new *p*-orbital generated by the 1,2-shift. In the current system, there is a string of three *p*-orbitals con-

[11] (a) Large K photochemical reactions include 1,3-vinyl shifts in di-π-methane systems (26), triplet di-π-methane rearrangements of bicyclics (30) and reactive acyclics (12*g*, 25), stereoisomerization of vinylcyclopropanes via ring opening to diradicals (28), *cis–trans* isomerization of styrenes (27). (b) Small K reactions include such pericyclic processes as electrocyclic ring closure as in the present study, cycloaddition (26), electrocyclic ring opening (e.g.) of cyclohexadienes (28), and concerted di-π-methane rearrangements (12*a*, *b*, *d*, *e*, 27, 31).

Can. J. Chem. Downloaded from www.nrcresearchpress.com by 210.87.254.42 on 09/06/12
For personal use only.

Can. J. Chem. Downloaded from www.nrcresearchpress.com by 210.87.254.42 on 09/06/12
For personal use only.

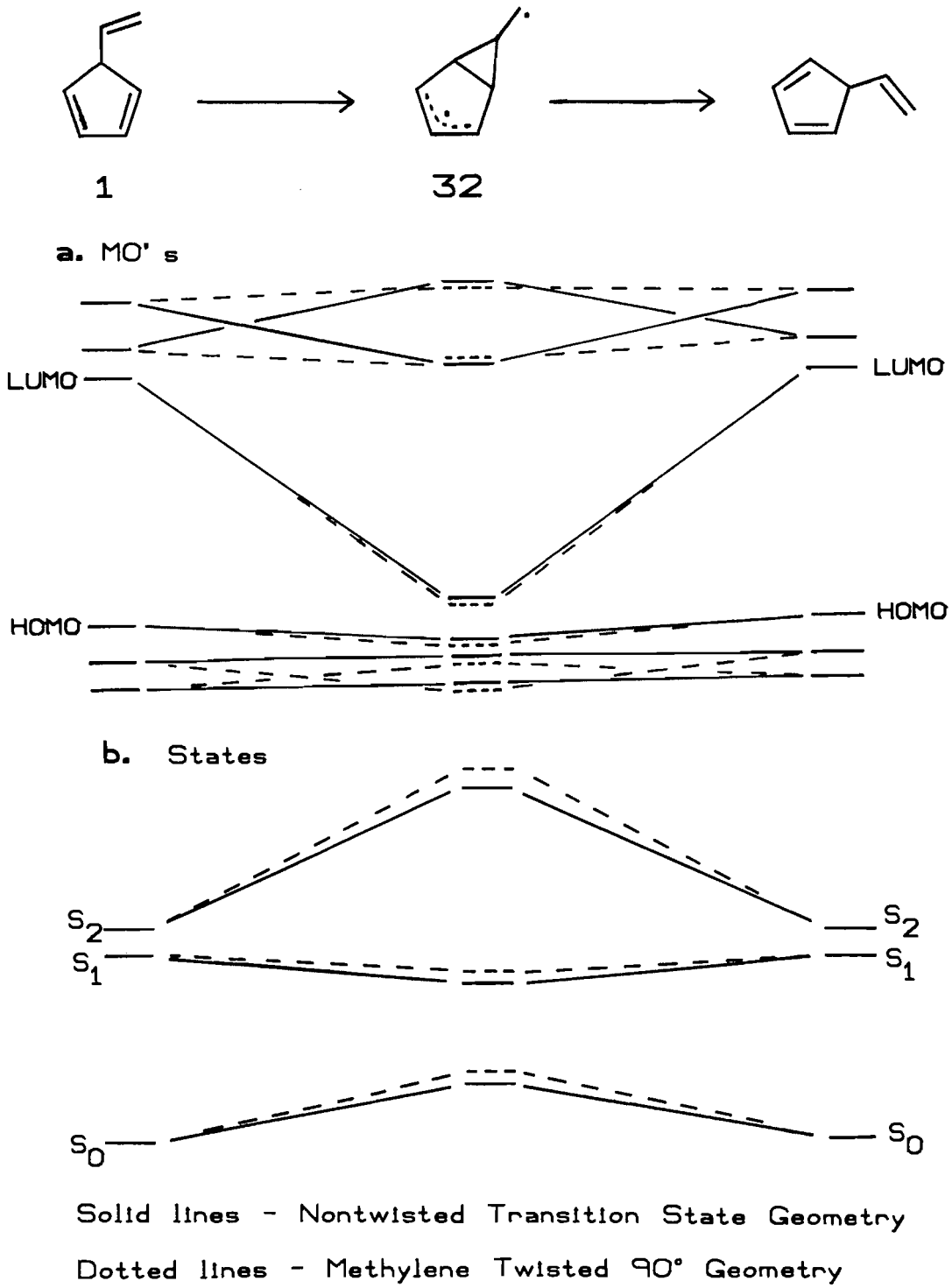

FIG. 6. Correlation diagram for 1,5-vinyl migration.

necting the two *p*-orbitals constituting the origin and terminus of the vinyl shift.

The present case is considerably more complex, and was analyzed by quantum mechanical calculation[12] of the starting vinylcyclopentadiene **1**, the diradical **32**, and the product vinylcyclopentadiene. For simplicity, the calculations were performed on a truncated model with phenyl and methyl groups removed; note Fig. 6a which depicts only the highest few bonding MO's and lowest few antibonding MO's. Figure 6b provides the results of configuration interaction and the state surfaces.

It is seen that there is no crossing of bonding and antibonding MO's although there is a near degeneracy with approach of bonding and antibonding MO's. The situation is quite reminiscent of the correlation obtained in our earlier treatment (32)

[12] (a) All calculations were run on a Digital Equipment VAX/750; (b) To obtain geometry of the species, "Tribble", D. Pensak and J. J. Wendoloski, was employed; (c) SCF and CI calculations were run on "Gamess", as written by M. DuPuis, D. Spangler, and J. J. Wendoloski, NRCC, Berkeley, and modified by M. W. Schmidt and S. T. Elbert, Iowa State University.

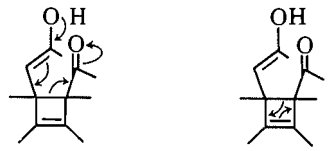

FIG. 7. Equivalency of reverse Michael and electrocyclic processes.

of phenyl migration where the bonding MO rose in energy transiently. The net result in the present system is a correlation diagram which provides an approach of excited and ground state surfaces to provide the bifunnel (12*f*, 12*i*, 12*j*, 29) required for a successful photochemical reaction with decay of the reacting excited state to the S_0 surface. Furthermore, the conclusions appear independent of any terminal twisting of the carbinyl carbon (i.e. the terminal methylene).

One interesting point is that the bridged species is precedented in the cyclopropyldicarbinyl diradicals of the di-π-methane and bicycle rearrangements. In any case, it appears that the reaction is also photochemically allowed.

Finally, the correlation provides a sufficiently low barrier to permit successful thermal rearrangement in a situation quite similar to that observed in the phenyl migration study (32). Hence the reaction is predicted to be thermally allowed, consonant with the experimentally observed facile vinyl migration compared with alkyl shifts (33) and in agreement with literature conclusions.

Interpretation of interesting ground state chemistry encountered

Several observations made in the synthetic portions of this endeavor deserve comment. Both deal with the oxidative degradation of the bicyclic photoproducts **3** (i.e. **A**) and **4** (i.e. **B**); note Schemes 2 and 3. The cyclobutene openings proceeded under very mild conditions.[13] While the ring openings of ketol **16** and diol **20** seem formally to be electrocyclic processes, they also may be considered to be reverse Michael reactions which by precedent are also facile (note Fig. 7). With these two views of the same process, it is clear that an electrocyclic cyclobutene opening should be facile when there is a capable electron donor attached to one sp^3 hybridized ring carbon and an electron withdrawing group attached to the other as in these examples. This point has literature precedent (35).

Finally, selective formation of the tautomers of **17** and **21** in this reaction seems likely to derive from a preferential protonation of the resulting, ring-opened enolate at a site α to the carbonyl, a kinetic preference noted by us (36) quite some years ago.

Experimental

Melting points were determined using a calibrated hot-stage apparatus. Elemental analyses were performed by Galbraith Laboratory, Inc., Knoxville. TE.

All reactions were run under dry nitrogen. High-pressure liquid chromatography (hplc) was performed on a liquid chromatograph employing a LDC 254 nm detector, a LDC 6000 psi minipump, and a 0.95 × 50 cm polished stainless steel column packed with 5–15 μm porous silica micro beads.[14] Column chromatography was performed on silica gel (Matheson, Coleman, and Bell, grade 62, 60–200 mesh) mixed with Sylvania 2282 phosphor and slurry packed into quartz columns permitting monitoring by a hand uv lamp. Preparative thick-layer chromatography was carried out with MN-Kieselgel G/UV 254 silica gel. Acetonitrile and *tert*-butanol utilized for irradiation experiments were distilled from calcium hydride before use. Pentane utilized for irradiation experiments was washed with concentrated sulfuric acid, water, saturated $NaHCO_3$, brine, dried over anhydrous magnesium sulfate, and distilled from calcium hydride. THF was purified by storage over KOH, followed by successive distillation under a nitrogen atmosphere from calcium hydride, lithium aluminium hydride, and sodium/benzophenone ketyl.

Neutral work-up refers to dilution with ether, washing with water and brine, drying over anhydrous magnesium sulfate or sodium sulfate, filtering, and concentration *in vacuo*. Acidic work-up added an initial 5% HCl wash after dilution. Basic work-up added an initial saturated Na_2CO_3 wash after dilution. Basic–acidic work-up used both the acid and base washes after dilution.

5-(Carbomethoxymethyl)-2,3-diphenyl-1,4,5-trimethyl-1,3-cyclopentadiene, 5-(carbomethoxymethyl)-1,2-diphenyl-3,4,5-trimethyl-1,3-cyclopentadiene, and 5-(carbomethoxymethyl)-1,5-diphenyl-2,3,4-trimethyl-1,3-cyclopentadiene

To 33.6 g (0.130 mol) of 4,5-diphenyl-1,2,3-trimethyl-1,3-cyclopentadiene (37) in 200 mL of THF at 0°C was added 90 mL (0.135 mol) of a 1.5 *M* solution of *n*-BuLi in hexane. After 0.5 h, 22.7 g (0.127 mol) of HMPA was added, followed by 19.5 g (0.130 mol) of methyl bromoacetate dropwise. After 18 h at room temperature, acidic work-up gave 49 g of an oil. Trituration with 150 mL of pentane and cooling gave 13.9 g of ester, mp 79–82°C. Recrystallization from ether–hexane gave 10.3 g (24%) of 5-(carbomethoxymethyl)-2,3-diphenyl-1,4,5-trimethyl-1,3-cyclopentadiene, mp 89–89.5°C. The mother liquors were treated as below.

The spectral data were: ir ($CHCl_3$): 3012, 2967, 2932, 2924, 2873, 2857, 1760, 1613, 1577, 1497, 1443, 1324, 1280, 1163, 1090, 1080, 1024 cm^{-1}; H nmr ($CDCl_3$) δ: 6.80–7.35 (m, 10H, arom), 3.52 (s, 3H, —O—CH_3), 2.64 (s, 2H, CH_2), 1.91 (s, 6H, 2 vinyl CH_3), 1.20 (s, 3H, CH_3); Cmr ($CDCl_3$) δ: 170.56, 143.61, 139.90, 136.42, 129.62, 127.52, 126.06, 55.48, 51.04, 40.91, 21.46, 10.80; ms, *m/e*: 332.1777 (calcd. for $C_{23}H_{24}O_2$, *m/e*: 332.1775). *Anal.* calcd. for $C_{23}H_{24}O_2$: C 83.10, H 7.28; found: C 83.26, H 7.29.

Chromatography of 1.68 g of the mother liquors (34.0 g) on a 3 × 230 cm silica gel column eluted with 2 L hexane and 17 L 1% ether–hexane, collecting 40-mL fractions, was monitored at 252 nm to give: fractions 339–368, 248 mg of 5-(carbomethoxymethyl)-1,2-diphenyl-3,4,5-trimethyl-1,3-cyclopentadiene as an oil; 369–373, 16.8 mg of overlap as an oil; 374–388, 129 mg of 5-(carbomethoxymethyl)-2,3-diphenyl-1,4,5-trimethyl-1,3-cyclopentadiene as an oil; 389–398, 89.7 mg of overlap as an oil; 399–413, 90.2 mg of 5-(carbomethoxymethyl)-1,5-diphenyl-2,3,4-trimethyl-1,3-cyclopentadiene as an oil.

Trituration and cooling of fractions 339–368 gave crystals, mp 25–55°C, which were recrystallized from ether–hexane to give 161 mg of 5-(carbomethoxymethyl)-1,2-diphenyl-3,4,5-trimethyl-1,3-cyclopentadiene, mp 54–55°C.

The spectral data were: ir ($CHCl_3$): 3160, 3010, 2970, 2930, 2870, 1725, 1605, 1578, 1498, 1440, 1389, 1327, 1280, 1200, 1150, 1100, 1076, 1020, 910, 693 cm^{-1}; 200-MHz H nmr ($CDCl_3$) δ: 7.00–7.20 (m, 10H, arom), 3.43 (s, 3H, OCH_3), 2.61 (d, J = 13.5 Hz, 1H, —C*H*H—), 2.44 (d, J = 13.5 Hz, 1H, —CH*H*—), 1.81 (bs, 3H, vinyl CH_3), 1.68 (bs, 3H, vinyl CH_3), 1.13 (s, 3H, CH_3); Cmr ($CDCl_3$) δ: 170.63, 147.00, 143.64, 142.20, 137.02, 136.58, 133.45, 130.25, 129.42, 127.50, 126.12, 56.14, 51.02, 40.16, 21.71, 12.07, 10.36; ms, *m/e*: 332.1777 (calcd. for $C_{23}H_{24}O_2$, *m/e*: 332.1775). *Anal.* calcd. for $C_{23}H_{24}O_2$: C 83.10, H 7.28; found: C 83.25, H 7.45.

[13] Phenyl substitution on the cyclobutene double bond seems not to affect the facility of electrocyclic opening, while such substitution on the sp^3 carbons markedly lowers the activation energy (34*a–e*) by ca. 5–6 kcal/mol per phenyl group (34*e*). Thus the 1,2,3,4-tetraphenylcyclobutene stereoisomers open at room temperature (34*b–d*).

[14] H. E. Zimmerman, T. R. Welter, D. Tartler, R. A. Bunce, W. D. Ramsden, and R. K. King. Unpublished results.

Can. J. Chem. Downloaded from www.nrcresearchpress.com by 210.87.254.42 on 09/06/12
For personal use only.

Can. J. Chem. Downloaded from www.nrcresearchpress.com by 210.87.254.42 on 09/06/12
For personal use only.

Fractions 388–413 were further purified by hplc, eluting with 20% ether–pentane at 1.8 mL/min collecting the major band, k' 0.84, cutting fronts and tails to give 71.5 mg of 5-(carbomethoxymethyl)-1,5-diphenyl-2,3,4-trimethyl-1,3-cyclopentadiene as an oil.

The spectral data were: ir (thin film): 3085, 3060, 3025, 2975, 2950, 2917, 2858, 1740, 1727, 1592, 1485, 1435, 1368, 1317, 1270, 1220, 1178, 1155, 1080, 1060, 1039, 1020, 998, 940, 918, 898, 840, 810, 772, 746, 728, 685, 625 cm^{-1}; 270-MHz H nmr ($CDCl_3$) δ: 6.75–7.25 (m, 10H, arom), 3.46 (s, 3H, —OCH_3), 2.99 (d, J = 12.2 Hz, 1H, —C*H*H—), 2.87 (d, J = 12.2 Hz, 1H, —CH*H*—), 1.95 (s, 3H, C-2 CH_3), 1.89 (bs, 3H, vinyl CH_3), 1.64 (bs, 3H, vinyl CH_3); Cmr ($CDCl_3$) δ: 170.25, 145.41, 143.38, 140.07, 139.63, 136.33, 136.16, 129.12, 128.23, 127.35, 126.14, 125.98, 63.43, 50.88, 37.06, 12.66, 11.12, 10.46; ms, *m/e*: 332.1770 (calcd. for $C_{23}H_{24}O_2$, *m/e*: 332.1775). *Anal.* calcd. for $C_{23}H_{24}O_2$: C 83.10, H 7.28; found: C 82.93, H 7.24.

2,3-Diphenyl-5-(2-hydroxyethyl)-1,4,5-trimethyl-1,3-cyclopentadiene

To 12.3 g (37.0 mmol) of 5-(carbomethoxymethyl)-2,3-diphenyl-1,4,5-trimethyl-1,3-cyclopentadiene in 250 mL of ether at 0°C was added 0.920 g (24.2 mmol) of LAH. After stirring 3.5 h, 150 mL of 10% HCl was slowly added, and neutral work-up gave 11.0 g of alcohol, mp 88–100°C. Decolorization with charcoal and recrystallization from ether–hexane gave 8.67 g (77%) of 2,3-diphenyl-5-(2-hydroxyethyl)-1,4,5-trimethyl-1,3-cyclopentadiene, mp 117–118°C.

The spectral data were: ir ($CHCl_3$): 3154–3700, 3058, 3003, 2958, 2932, 1949, 1859, 1742, 1709, 1642, 1558, 1495, 1445, 1385, 1360, 1340, 1241, 1060, 1012, 943 cm^{-1}; H nmr ($CDCl_3$) δ: 6.80–7.35 (m, 10H, arom), 3.36 (t, J = 6.9 Hz, 2H, CH_2—C*H*$_2$—O), 2.04 (t, J = 6.9 Hz, 2H, C*H*$_2$—CH_2—O), 1.90 (s, 6H, 2 vinyl CH_3), 1.60 (bs, 1H, —OH), 1.18 (s, 3H, C-5 CH_3); Cmr ($CDCl_3$) δ: 144.81, 139.72, 136.18, 129.60, 127.61, 126.15, 60.268, 56.030, 38.698, 22.502, 10.992; ms, *m/e*: 304.1828 (calcd. for $C_{22}H_{24}O$, *m/e*: 304.1826). *Anal.* calcd. for $C_{22}H_{24}O$: C 86.80, H 7.95; found: C 87.00, H 8.02.

2,3-Diphenyl-5-(2-methanesulfonylethyl)-1,4,5-trimethyl-1,3-cyclopentadiene

To 9.78 g (32.1 mmol) of 2,3-diphenyl-5-(2-hydroxyethyl)-1,4,5-trimethyl-1,3-cyclopentadiene and 6.5 g (64 mmol) of triethylamine in 150 mL methylene chloride at 0°C was added 5.51 g (48.1 mmol) of methanesulfonyl chloride dropwise. After 2 h, acidic work-up gave a semi-solid. Chromatography on a 5 × 35 cm silica gel column eluted with 500 mL of 20% methylene chloride – hexane, 500 mL of 30% methylene chloride – hexane, and 7 L of 50% methylene chloride – hexane gave 11.25 g (92%) 2,3-diphenyl-5-(2-methanesulfonylethyl)-1,4,5-trimethyl-1,3-cyclopentadiene, mp 103–117°C, as the first band. Recrystallization from ether–hexane brought the mp to 116–117°C.

The spectral data were: ir ($CHCl_3$): 3021, 2958, 2924, 2865, 1751, 1721, 1698, 1639, 1610, 1492, 1462, 1445, 1360, 1339, 1230, 1181, 1080, 1055, 1024, 980, 961 cm^{-1}; H nmr ($CDCl_3$) δ: 6.80–7.40 (m, 10H, arom), 3.84 (t, J = 6.6 Hz, 2H, CH_2—C*H*$_2$—O), 2.89 (s, 3H, SCH_3), 2.20 (t, J = 6.6 Hz, 2H, C*H*$_2$—CH_2—O), 1.89 (s, 6H, 2 vinyl CH_3), 1.20 (s, 3H, C-5 CH_3); ms, *m/e*: 382.1601 (calcd. for $C_{23}H_{26}O_3S$, *m/e*: 382.1601). *Anal.* calcd. for $C_{23}H_{26}O_3S$: C 72.22, H 6.85; found: C 72.30, H 6.85.

2,3-Diphenyl-1,4,5-trimethyl-5-vinyl-1,3-cyclopentadiene

To 11.1 g (29.1 mmol) of 2,3-diphenyl-5-(2-methanesulfonylethyl)-1,4,5-trimethyl-1,3-cyclopentadiene in 125 mL of DMSO at 0°C was added 5.60 g (50.0 mmol) of potassium *tert*-butoxide. After 8 h at room temperature, an additional 5.60 g of potassium *tert*-butoxide was added. After 2.5 h more, 100 mL of saturated NH_4Cl was added, and neutral work-up gave 8.13 g of an oil which crystallized on standing, mp 66–79°C. Chromatography on a 3 × 30 cm silica gel column eluted with hexane gave 6.75 g of product, mp 78–80°C, as the first band. Recrystallization from pentane gave 5.16 g (62%) of 2,3-diphenyl-1,4,5-trimethyl-5-vinyl-1,3-cyclopentadiene, mp 79.5–80.0°C.

The spectral data were: ir ($CHCl_3$): 3077, 3003, 2967, 2932, 2907, 2849, 1631, 1608, 1492, 1445, 1195, 1080, 1015, 917 cm^{-1}; uv (EtOH): 226 (sh, ε 15 700), 234 (ε 17 200), 256 (sh, ε 5160) nm; 200-MHz H nmr ($CDCl_3$) δ: 6.95–7.40 (m, 10H, arom), 5.40 (dd, J = 18.5, 10.0 Hz, 1H, C*H*=CH_2), 5.10–5.30 (m, 2H, —CH=C*H*$_2$), 1.82 (s, 6H, 2 vinyl CH_3), 1.25 (s, 3H, C-5 CH_3); Cmr ($CDCl_3$) δ: 144.35, 140.93, 139.77, 136.29, 129.56, 127.46, 126.02, 113.66, 60.72, 17.20, 12.20; ms *m/e*: 286.1722 (calcd. for $C_{22}H_{22}$, *m/e*: 286.1720). *Anal.* calcd. for $C_{22}H_{22}$: C 92.26, H 7.74; found: C 92.06, H 7.82.

1,2-Diphenyl-5-(2-hydroxyethyl)-3,4,5-trimethyl-1,3-cyclopentadiene

To 773 mg (2.32 mmol) of 5-(carbomethoxymethyl)-1,2-diphenyl-3,4,5-trimethyl-1,3-cyclopentadiene in 25 mL of ether at 0°C was added 66.3 mg (1.74 mmol) of LAH. After 3 h, 5.0 g (14 mmol) of sodium sulfate decahydrate was added. After 2 h more, acidic work-up gave 710 mg of an oil; hplc eluting with 20% ether – 40% pentane – 40% methylene chloride gave a major band, k' 3.1, 381 mg of an oil. Trituration and cooling with pentane gave 342 mg (48%) of 1,2-diphenyl-5-(2-hydroxyethyl)-3,4,5-trimethyl-1,3-cyclopentadiene, mp 106–107°C.

The spectral data were: ir ($CHCl_3$): 3610, 3300–3580, 3055, 3000, 2960, 2920, 2860, 1605, 1578, 1500, 1450, 1390, 1373, 1347, 1110, 1082, 1060, 1042, 1023, 1009, 999, 975, 920, 704 cm^{-1}; 270-MHz H nmr (C_6D_6) δ: 6.90–7.20 (m, 10H, arom), 3.41 (ddd, J = 14.1, 8.55, 5.70 Hz, 1H, CH_2—C*H*H—OH), 3.29 (ddd, J = 14.3, 8.30, 6.17 Hz, 1H, CH_2—CH*H*—OH), 2.03 (ddd, J = 13.7, 8.18, 5.64 Hz, 1H, C*H*H—CH_2OH), 1.78 (m, 1H, —CH*H*—CH_2OH), 1.76 (bs, 3H, vinyl CH_3), 1.73 (bs, 3H, vinyl CH_3), 1.15 (s, 3H, C5-CH_3); ms *m/e*: 304.1828 (calcd. for $C_{22}H_{24}O$, *m/e*: 304.1826). *Anal.* calcd. for $C_{22}H_{24}O$: C 86.80, H 7.95; found: C 86.62, H 7.91.

1,2-Diphenyl-5-(2-(2-nitroselenophenyl)ethyl)-3,4,5-trimethyl-1,3-cyclopentadiene

Following the general method of Grieco *et al.* (38), to 396 mg (1.30 mmol) of 1,2-diphenyl-5-(2-hydroxyethyl)-3,4,5-trimethyl-1,3-cyclopentadiene and 352 mg (1.55 mmol) of 2-nitrophenylselenocyanate (39) in 5.0 mL of THF at room temperature was added, dropwise, 313 mg (1.55 mmol) of tri-*n*-butylphosphine. After 3 h, concentration *in vacuo* gave 1.13 g of a red oil which was chromatographed on a 1 × 60 cm silica gel column eluted with 100 mL of hexane, 100 mL of 5% ether–hexane, and 400 mL of 10% ether–hexane collecting the initial band to yield 467 mg of an oil. Crystallization from hexane gave 427 mg (67%) of 1,2-diphenyl-5-(2-(2-nitroselenophenyl)ethyl)-3,4,5-trimethyl-1,3-cyclopentadiene, mp 136–138°C.

The spectral data were: ir (thin film): 3060, 3030, 2970, 2930, 2870, 1599, 1572, 1520, 1510, 1468, 1460, 1450, 1440, 1340, 1314, 1260, 1180, 1109, 1083, 1048, 920, 861, 792, 761, 740, 710 cm^{-1}; 200-MHz H nmr ($CDCl_3$) δ: 8.16–8.30 (m, 1H, *o*-NO_2 H), 7.00–7.30 (m, 13H, arom), 2.63 (td, J = 13.0, 5.0 Hz, 1H, CH_2—C*H*H—Se), 2.35 (td, J = 13.0, 5.0 Hz, 1H, —CH_2—CH*H*—Se), 1.90–2.20 (m, 2H, C*H*$_2$—CH_2—Se), 1.89 (bs, 3H, vinyl CH_3), 1.88 (bs, 3H, vinyl CH_3), 1.30 (s, 3H, C-5 CH_3); ms, *m/e*: 489.1208 (calcd. for $C_{28}H_{27}NO_2Se$, *m/e*: 489.1205). *Anal.* calcd. for $C_{28}H_{27}NO_2Se$: C 68.84, H 5.57; found: C 68.70, H 5.76.

1,2-Diphenyl-3,4,5-trimethyl-5-vinyl-1,3-cyclopentadiene

Following the general method of Reich *et al.* (40), to a rapidly stirred solution of 410 mg (0.839 mmol) of 1,2-dimethyl-5-(2-(2-nitroselenophenyl)ethyl)-3,4,5-trimethyl-1,3-cyclopentadiene and 130 mg (1.70 mmol) of pyridine in 5.0 mL of methylene chloride at room temperature was added 250 mg (2.24 mmol) of 30% H_2O_2. After 36 h, basic–acidic work-up gave 362 mg of an oil which was chromatographed on a 1 × 70 cm silica gel column eluted with hexane in 100-mL fractions. Fraction 1, nil; 2, 66.1 mg of colorless product, mp 55–73°C; 3, 69.1 mg of more product as an orange oil (total crude yield 56%). Recrystallization of fraction 2 from pentane gave 48.1 mg of 1,2-diphenyl-3,4,5-trimethyl-5-vinyl-1,3-cyclopentadiene, mp 78–79°C.

The spectral data were: ir ($CHCl_3$): 3775, 3445, 2990, 2960, 2915,

Can. J. Chem. Downloaded from www.nrcresearchpress.com by 210.87.254.42 on 09/06/12
For personal use only.

2855, 1639, 1600, 1575, 1497, 1445, 1409, 1387, 1367, 1341, 1110, 1090, 1078, 1002, 958, 915, 698 cm^{-1}; uv (EtOH): 232 (ε 19 000), 310 (ε 8100), tails to 370 nm; 200-MHz H nmr ($CDCl_3$) δ: 7.00–7.30 (m, 10H, arom), 5.55 (dd, J = 17.19, 10.77 Hz, 1H, CH=CH_2), 5.15–5.30 (m, 2H, —CH=CH_2), 1.78 (bs, 3H, vinyl CH_3), 1.76 (bs, 3H, vinyl CH_3), 1.16 (s, 3H, C-5 CH_3); Cmr ($CDCl_3$) δ: 146.84, 143.10, 141.45, 136.96, 136.44, 134.02, 129.45, 128.89, 127.85, 127.24, 126.36, 125.65, 113.04, 60.95, 16.52, 12.39, 10.24; ms m/e: 286.1722 (calcd. for $C_{22}H_{22}$, m/e: 286.1720). *Anal.* calcd. for $C_{22}H_{22}$; C 92.26, H 7.74; found: C 91.92, H 7.82.

General procedure for exploratory photolysis

All direct and sensitized exploratory irradiations were performed using a 450-W medium-pressure mercury lamp immersion apparatus fitted with a Pyrex filter sleeve and cooled with a recirculating filter solution. The filter solutions employed were: Filter A, 0.0020 *M* sodium metavanadate in 0.1 *M* NaOH; transmission, 0% below 300 nm, 40% at 328 nm, 90% above 370 nm; Filter B, 0.020 *M* sodium metavanadate in 0.10 *M* NaOH; transmission, 0% below 340 nm, 90% above 380 nm; Filter C, 0.010 *M* $FeCl_3$ in 0.5 *M* HCl; transmission, 0% below 380 nm, 3.0% at 420 nm, 55% above 460 nm. The filter solutions remained unchanged after photolysis. All runs were purged with purified nitrogen (41) for at least 1 h before and during photolysis and the temperature was monitored during the run using a calibrated thermistor.

Exploratory direct photolysis of 2,3-diphenyl-1,4,5-trimethyl-5-vinyl-1,3-cyclopentadiene

Run A, at 30°C

Using the general photolysis procedure, 300 mg (1.05 mmol) of 2,3-diphenyl-1,4,5-trimethyl-5-vinyl-1,3-cyclopentadiene in 230 mL of *tert*-butanol was irradiated through Filter A for 17 h at 30 ± 2°C. Concentration *in vacuo* gave 311 mg of a yellow oil which was chromatographed on a 3 × 100 cm 7% (by weight) silver nitrate – silica gel column, gradient eluted with ether–hexane, collecting 40 mL fractions and monitoring at 240 nm. Column fraction compositions were determined by integration of their 200-MHz nmr spectra. Fractions 1–280, 0% (per cent ether–hexane), nil; 281–331, 0.5%, 4.8 mg of an unidentified oil; 332–338, 0.5%, 7.0 mg of an oil, nearly pure photoisomer **D**; 339–346, 0.5%, 24.9 mg of an oil, 65% photoisomer **D** and 35% photoisomer **A**; 347–394, 0.5%, 96.0 mg, mp 77–94°C, nearly pure photoisomer **A**; 395–414, 1%, 24.6 mg of an oil, 72% photoisomer **A** and 27% photoisomer **C**; 415–442, 1%, 27.6 mg, mp 35–62°C, 87% recovered starting material, 9% photoisomer **C**, and 5% photoisomer **A**; 443–460, 1%, 9.5 mg, mp 65–77°C, nearly pure recovered starting material; 461–506, 3%, 29.9 mg, mp 47–66°C, 52% recovered starting material and 37% photoisomer **B**; 507–540, 5%, 31.7 mg, mp 30–62°C, nearly pure photoisomer **B**; 541–601, 5%, 30.7 mg of an oil, 50% photoisomer **B** and 50% unidentified material. Results: 52.0 mg of recovered starting material, 123.8 mg of photoisomer **A**, 58.1 mg of photoisomer **B**, 23.2 mg of photoisomer **D**, and 9.1 mg of photoisomer **C**. Mass balance: 89%.

Recrystallization of fractions 347–394 from pentane gave 51.2 mg of 5,6-diphenyl-1,2,7-trimethylbicyclo[3.2.0]hepta-2,6-diene (photoisomer **A**), mp 98–99°C.

Recrystallization of fractions 507–540 from ether–pentane gave 19.5 mg of 1,5-diphenyl-2,6,7-trimethylbicyclo[3.2.0]hepta-2,6-diene (photoisomer **B**), mp 90–91°C.

High-pressure liquid chromatography, using 1% isopropanol–pentane, of fractions 332–338 combined with the corresponding fractions from 2 identical photolysates (total of 27.1 mg), collecting the center of the major band, gave 19.8 mg of 1,7-diphenyl-2,5,6-trimethylbicyclo[3.2.0]hepta-2,6-diene (photoisomer **D**) as an oil.

High-pressure liquid chromatography of fractions 395–414 eluting with 6% methylene chloride – pentane at a flow rate of 2.4 mL/min yielded fraction 1, k' 1.75, 4.2 mg of 6,7-diphenyl-1,2,5-trimethylbicyclo[3.2.0]hepta-2,6-diene (photoisomer **C**) as an oil; 2, k' 2.47, photoisomer **A**.

The spectral data for 5,6-diphenyl-1,2,7-trimethylbicyclo[3.2.0]-hepta-2,6-diene were: ir ($CHCl_3$): 3085, 3062, 3008, 2965, 2920, 2850, 1600, 1493, 1447, 1583, 1572, 1520, 1495, 1208, 1133, 1095, 1082, 1070, 1038, 1021, 1008, 998, 945, 910, 812, 690 cm^{-1}; uv (EtOH) 217 (sh, ε 15 900), 268 (ε 10 900) nm; 200-MHz H nmr ($CDCl_3$) δ: 6.60–7.20 (m, 10H, arom), 5.40 (bs, 1H, vinyl), 2.90 (qd, J = 2.21, 1.10 Hz, 2H, CH_2), 2.08 (s, 3H, C-7 CH_3), 1.75 (td, J = 2.40, 1.47 Hz, 3H, C-2 CH_3), 0.647 (s, 3H, C-1 CH_3); Cmr ($CDCl_3$) δ: 149.84, 144.23, 143.06, 137.96, 134.22, 128.90, 127.80, 127.07, 126.24, 125.59, 124.88, 65.78, 59.98, 39.59, 14.94, 13.17; ms, m/e: 286.1713 (calcd. for $C_{22}H_{22}$, m/e: 286.1720). *Anal.* calcd. for $C_{22}H_{22}$: C 92.26, H 7.74; found: C 92.31, H 7.90.

The spectral data for 1,5-diphenyl-2,6,7-trimethylbicyclo[3.2.0]-hepta-2,6-diene were: ir ($CHCl_3$): 3040, 3004, 2918, 2853, 1606, 1497, 1450, 1382, 1314, 1158, 1122, 1085, 1040, 1030, 973, 954, 840, 830, 903; uv (EtOH) 254 (ε 182), 261 (ε 208), 267 (ε 156), 272 (ε 113) nm; 200-MHz H nmr ($CDCl_3$) δ: 6.77–7.06 (m, 10H, arom), 5.61 (m, 1H, vinyl), 2.85 (ddq, J = 18.0, 2.2, 2.2 Hz, 1H, CHH), 2.63 (ddq, J = 18.0, 2.2, 2.2 Hz, 1H, CHH), 1.86 (bs, 3H, C-7 CH_3), 1.84 (bs, 3H, C-6 CH_3), 1.73 (bq, J = 2.16 Hz, 3H, C-2 CH_3); Cmr ($CDCl_3$) δ: 145.90, 143.08, 139.77, 139.16, 128.44, 127.50, 127.34, 127.22, 126.51, 125.40, 125.12, 75.52, 65.80, 37.84, 15.80, 11.60, 9.45; ms, m/e: 286.1722 (calcd. for $C_{22}H_{22}$, m/e: 286.1720. *Anal.* calcd. for $C_{22}H_{22}$: C 92.26, H 7.74; found: C 92.33, H 7.79.

The spectral data for 1,7-diphenyl-2,5,6-trimethylbicyclo[3.2.0]-hepta-2,6-diene were: ir ($CHCl_3$): 3070, 3045, 2990, 2950, 2900, 2850, 2830, 1645, 1595, 1492, 1445, 1375, 1305, 1170, 1105, 1080, 1025, 995, 960, 945, 910, 830, 695 cm^{-1}; uv (EtOH): 216 (ε 25 000), 266 (ε 17 000), 295 (sh, ε 1300) nm; 200-MHz H nmr ($CDCl_3$) δ: 7.05–7.40 (m, 10H, arom), 5.46 (bs, 1H, vinyl), 2.42 (bd, J = 16 Hz, 1H, CHH), 2.05 (bd, J = 16 Hz, 1H, CHH), 2.05 (s, 3H, C-6 CH_3), 1.78 (bs, 3H, C-2 CH_3), 0.67 (s, 3H, C-5 CH_3); Cmr ($CDCl_3$) δ: 145.30, 143.54, 143.38, 140.13, 134.84, 128.40, 127.79, 127.57, 126.86, 126.69, 126.09, 125.54, 70.588, 56.822, 38.377, 20.041, 16.462, 11.287; ms, m/e: 286.1722 (calcd. for $C_{22}H_{22}$, m/e: 286.1720). *Anal.* calcd. for $C_{22}H_{22}$: C 92.26, H 7.74; found: C 91.96, H 8.02.

The spectral data for 6,7-diphenyl-1,2,5-trimethylbicyclo[3.2.0]-hepta-2,6-diene were: ir ($CHCl_3$): 2958, 2920, 2860, 2838, 1599, 1496, 1460, 1440, 1375, 1018, 1000, 993, 910, 690, 640 cm^{-1}; uv (pentane): 222 (ε 27 000), 256 (sh, ε 12 000), 278–282 (ε 15 000) nm; 270-MHz H nmr ($CDCl_3$) δ: 7.10–7.40 (m, 10H, arom), 5.26 (bd, J = 1.8 Hz, 1H, vinyl), 2.77 (dp, J = 17.0, 2.0 Hz, 1H, CHH), 2.21 (dp, J = 17.0, 2.2 Hz, 1H, CHH), 1.64 (bd, J = 1.8 Hz, 3H, C-2 CH_3), 1.38 (s, 3H, CH_3), 1.36 (s, 3H, CH_3); Cmr ($CDCl_3$) δ: 144.31, 143.71, 135.83, 134.35, 128.07, 127.08, 126.97, 126.80, 123.61, 62.26, 52.69, 39.64, 20.65, 15.42, 14.98; ms, m/e: 286.1722 (calcd. for $C_{22}H_{22}$, m/e: 286.1720). *Anal.* calcd. for $C_{22}H_{22}$: C 92.26, H 7.74; found: C 92.15, H 7.86.

Run B, at 8°C

Using the general photolysis procedure, 305 mg (1.06 mmol) of 2,3-diphenyl-1,4,5-trimethyl-5-vinyl-1,3-cyclopentadiene in 270 mL of acetonitrile was irradiated through Filter A for 18.25 h. The photolysis well was externally cooled with recirculating ice-water. The temperature inside the well during the run was found to be 8–9°C. Concentration *in vacuo* gave 318 mg of a yellow oil which was chromatographed on a 2.5 × 100 cm 10% (by weight) silver nitrate – silica gel column, collecting 40 mL fractions monitoring at 244 nm. Column fraction compositions were determined by integration of their 200-MHz H nmr spectrum. Fractions 1–383, 0% (per cent ether–hexane), nil; 384–408, 0%, 10.6 mg of an oil, nearly pure photoisomer **D**; 409–429, 1%, 15.1 mg of an oil, 25% photoisomer **D** and 75% photoisomer **A**; 430–441, 1%, 8.2 mg, mp 38–70°C, 16% photoisomer **C** and 84% photoisomer **A**; 442–470, 1%, 43.5 mg, mp 25–42°C, 12% photoisomer **C**, 25% photoisomer **A**, and 62% recovered starting material; 471–494, 1%, 17.9 mg, mp 46–65°C, recovered starting material; 495–518, 1%, 6.3 mg, mp 52–68°C, recovered starting material; 519–541, 1%, 15.4 mg, mp 37–54°C, 18% recovered starting material and 82% photoisomer **B**; 542–589,

Can. J. Chem. Downloaded from www.nrcresearchpress.com by 210.87.254.42 on 09/06/12
For personal use only.

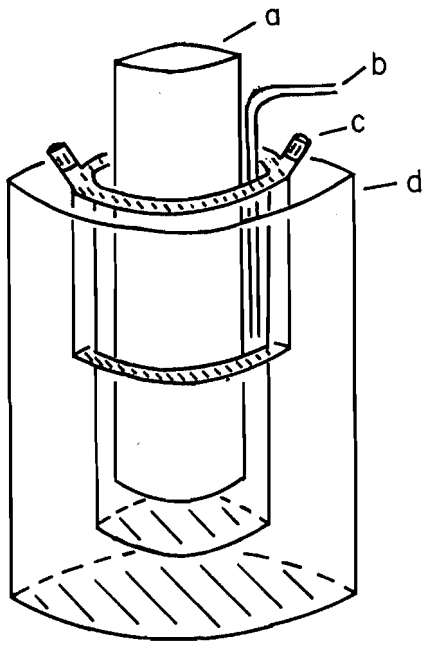

FIG. 8. Low temperature photolysis apparatus. a: Hanovia well and lamp; b: dry nitrogen purge to remove excess heat and moisture; c: sample cell, 100-mL volume; d: low temperature bath.

1.5%, 42.1 mg, mp 34–59°C, photoisomer **B**; 590–663, 1.5%, 45.1 mg, mp 28–51°C, photoisomer **B** and 20% unidentified material; 664–686, 2%, 1.5 mg, mp 25–34°C, 60% photoisomer **B** and 40% unidentified material; 687–738, 2%, 12.0 mg of an oil containing some photoisomer **B**. Results: 54.0 mg recovered starting material, 29.1 mg of photoisomer **A**, 91.7 mg of photoisomer **B**, 14.4 mg of photoisomer **D**, and 6.5 mg of photoisomer **C**. Mass balance: 64%.

Run C, at −70°C

Using a low temperature photolysis apparatus (consisting of a toroidal 100-mL Pyrex vessel with two ground-glass joint openings fused to a Pyrex cyclinder of the same id, closed on the bottom with dimensions such that a Hanovia lamp well fit down the center of the apparatus with the lamp center coincident with the toroid's center, note Figure 8), 91.1 mg (0.318 mmol) of 2,3-diphenyl-1,4,5-trimethyl-5-vinyl-1,3-cyclopentadiene in 100 mL of pentane was irradiated for 2.6 h in a −78°C bath using the general photolysis procedure through Filter A. After photolysis, the solution was kept at −78°C for 1.5 h with continued nitrogen purging, then at room temperature for 5 h. Concentration *in vacuo* gave 93.4 mg of an oil; hplc eluting with 6% methylene chloride – pentane at 2.4 mL/min gave: fraction 1, k' 1.8, 47.1 mg (52%) of recovered starting material, mp 64–73°C; 2, k' 2.1, 20.0 mg (22%) of a 4:1 mixture of 1,2-diphenyl-3,4,5-trimethyl-5-vinyl-1,3-cyclopentadiene (16 mg, 17.6%) and starting material as an oil; 3, k' 2.6, 8.3 mg (9.1%) of an oil containing small amounts of 1,2-diphenyl-3,4,5-trimethyl-5-vinyl-1,3-cyclopentadiene and photoisomer **A**, along with at least two unknown products.

Exploratory p-*dimethylaminobenzophenone sensitized photolysis of 2,3-diphenyl-1,4,5-trimethyl-5-vinyl-1,3-cyclopentadiene*

Using the general photolysis procedure, 100 mg (0.349 mmol) of 2,3-diphenyl-1,4,5-trimethyl-5-vinyl-1,3-cyclopentadiene and 0.391 g (1.74 mmol) of *p*-dimethylaminobenzophenone in 260 mL of *tert*-butanol was irradiated through Filter B at 31°C for 25 min. After concentration *in vacuo*, the residue was chromatographed on a 3 × 50 cm silica gel column eluted with 1 L of hexane, 500 mL of 1% ether–hexane, 500 mL of 2% ether–hexane, 1 L of 5% ether–hexane, and 500 mL of 10% ether–hexane collecting 500-mL fractions. Fraction 2 gave 94.8 mg (95%) of product, mp 69–72°C, fractions 8 and 9 gave 397 mg recovered *p*-dimethylaminobenzophenone, mp 70–86°C. Other fractions contained no material. Recrystallization of fraction 2 from hexane gave 48.2 mg of 1,2-diphenyl-3,4,5-trimethyl-5-vinyl-1,3-cyclopentadiene, mp 77–78.5°C, whose spectral data were identical with those of independently synthesized material (*vide supra*).

Exploratory direct photolysis of 1,2-diphenyl-3,4,5-trimethyl-5-vinyl-1,3-cyclopentadiene

Using the general photolysis procedure, 300 mg (1.046 mmol) of 1,2-diphenyl-3,4,5-trimethyl-5-vinyl-1,3-cyclopentadiene in 270 mL of acetonitrile was irradiated through Filter B at 31°C for 20 min. After concentration *in vacuo*, 305 mg, mp 53–68°C, were obtained. 200-MHz H nmr analysis showed 95% 2,3-diphenyl-1,4,5-trimethyl-5-vinyl-1,3-cyclopentadiene and ca. 5% bicyclics. Recrystallization from ether–pentane gave 173 mg (58%) of 2,3-diphenyl-1,4,5-trimethyl-5-vinyl-1,3-cyclopentadiene, mp 77–79°C, identical in all respects to independently synthesized material (*vide supra*).

Exploratory sensitized photolysis of 1,2-diphenyl-3,4,5-trimethyl-5-vinyl-1,3-cyclopentadiene

Using the general photolysis procedure, 63.0 mg (0.220 mmol) of 1,2-diphenyl-3,4,5-trimethyl-5-vinyl-1,3-cyclopentadiene and 295 mg (1.10 mmol) of *p*-dimethylaminobenzophenone in 260 mL of acetonitrile were irradiated through Filter C at 31°C for 6 h. After concentration *in vacuo*, 375.5 mg, mp 152–162°C, were obtained. Chromatography on a 1 × 65 cm silica gel column eluted with 250 mL 5% ether–hexane, and 1 L ether, collecting 75-mL fractions: 1, nil; 2, 58.0 mg of starting material; 3, nil; 4–13, 295 mg of recovered sensitizer, mp 148–162°C.

Photolysis apparatus for quantum yield determinations

All quantum yield determinations were run on the microoptical bench (42). Light output was measured for each run by digital electronic actinometer (43) calibrated by ferrioxalate actinometry (44). Photolyses employed an Osram HBO 200-W high-pressure mercury lamp and a Bausch and Lomb Model 33-86-79 high intensity monochromator. All quantum yield photolyses were in 40 mL of *tert*-butanol, were purged with purified nitrogen (41) for 1 h before and during each run, and were maintained at 30°C using a jacketed cell and a recirculating constant temperature apparatus. Runs were analyzed by 200-MHz H nmr, expanded peaks being integrated using a Summagraphics Bit Pad interfaced with a PDP-11/T55 computer. The internal standard employed was methyl diphenylglycolate.

Summary of direct quantum yield results for 2,3-diphenyl-1,4,5-trimethyl-5-vinyl-1,3-cyclopentadiene

All runs were conducted at 315 nm with a 3.6-mm entrance slit and 2.0-mm exit slit (half-height band pass, 15 nm). All runs are reported in Table 2.

Summary of p-*dimethylaminobenzophenone sensitized quantum yield results for 2,3-diphenyl-1,4,5-trimethyl-5-vinyl-1,3-cyclopentadiene*

Photolyses were conducted at 370 nm with a 3.6-mm entrance slit and 4.0-mm exit slit (band pass, 0% transmittance beyond ±30 nm). *p*-Dimethylaminobenzophenone, absorbing ≥ 99% of the light, was used as the sensitizer. After concentrating the photolysates *in vacuo*, the sensitizer was removed by column chromatography on a 2 × 40 cm silica gel column using pentane and collecting all of the intial band. Runs are reported in Table 3.

Thermolysis of 2,3-diphenyl-1,4,5-trimethyl-5-vinyl-1,3-cyclopentadiene

A solution of 103 mg (0.360 mmol) of 2,3-diphenyl-1,4,5-trimethyl-5-vinyl-1,3-cyclopentadiene in 15 mL of benzene was refluxed for 23 h. Concentration *in vacuo* gave 127 mg of an oil. 200-MHz H nmr analysis revealed a 1:1 mixture of starting material and 1,2-diphenyl-3,4,5-trimethyl-5-vinyl-1,3-cyclopentadiene. High-pressure liquid chromatography eluting with 6% methylene chloride – pentane at a flow rate of 2.3 mL/min gave: 1, k' 2.18, 39.6 mg of recovered starting material, mp 64–74°C; 2, k' 2.48, 52.1 mg of 1,2-diphenyl-3,4,5-trimethyl-5-vinyl-1,3-cyclopentadiene, mp 54–63°C. Re-

TABLE 2. Direct quantum yield photolyses of 2,3-diphenyl-1,4,5-trimethyl-5-vinyl-1,3-cyclopentadiene

Reactant (mmol)	Light absorbed (mEinsteins)	% Conversion	Photoproduct (mmol × 100)				Quantum yield (× 100)			
			A	B	C	D	A	B	C	D
0.143	0.0997	2.0	0.29	[a]	[a]	[a]	2.88	[a]	[a]	[a]
0.140	0.0764	5.0	0.26	[a]	0.031	[a]	3.35	[a]	0.40	[a]
0.134	0.352	22.0	1.10	[a]	0.061	[a]	3.12	[a]	0.17	[a]
0.134	0.365	24.6	1.21	0.34	0.17	[a]	3.31	0.93	0.48	[a]
0.133	0.424	15.0	1.28	0.39	0.19	[a]	3.02	0.91	0.46	[a]
0.146	0.663	34.0	2.26	0.85	0.32	0.10	3.41	0.85	0.48	0.15

[a] Amount of photoproduct too low to assay.

TABLE 3. *p*-Dimethylaminobenzophenone sensitized quantum yield photolyses of 2,3-diphenyl-1,4,5-trimethyl-5-vinyl-1,3-cyclopentadiene

Reactant (mmol × 100)	Sensitization (mmol)	Light absorbed (mEinsteins)	% Conversion	Photoproduct (mmol × 100)	Quantum yield (× 100)
5.27	0.295	0.0135	1.5	0.809	5.99
5.83	0.283	0.0375	4.0	2.33	6.22
5.24	0.259	0.198	8.6	4.49	2.27

Can. J. Chem. Downloaded from www.nrcresearchpress.com by 210.87.254.42 on 09/06/12
For personal use only.

crystallization of fraction 1 from pentane gave 30.3 mg of recovered starting material (29%), mp 78–80°C. Recrystallization of fraction 2 from ether–pentane gave 42.2 mg of product (41%), mp 77–78°C.

Thermolysis of 1,2-diphenyl-3,4,5-trimethyl-5-vinyl-1,3-cyclopentadiene

A solution of 41.7 mg (0.146 mmol) of 1,2-diphenyl-3,4,5-trimethyl-5-vinyl-1,3-cyclopentadiene in 1.0 mL of benzene was refluxed for 24 h. Concentration *in vacuo* gave 44.0 mg of an oil. 200-MHz H nmr analysis revealed a 1.1:1 mixture of starting material and 2,3-diphenyl-1,4,5-trimethyl-5-vinyl-1,3-cyclopentadiene.

2,3-(exo,exo)-Dihydroxy-5,6-diphenyl-1,2,7-trimethylbicyclo[3.2.0]hept-6-ene

Using a modification of the general method of Ray and Matteson (45), a mixture of 142 mg (0.495 mmol) of photoproduct **A**, 95 mg (0.86 mmol) of trimethylamine *N*-oxide dihydrate, 2 mg (0.008 mmol) of osmium tetroxide, 0.15 mL of pyridine, 0.3 mL of water, and 2 mL of *tert*-butanol were heated with stirring at 80°C for 6 h. After cooling, 5 mL of saturated sodium bisulfite solution were added, and neutral work-up gave 179 mg of an oil, which was chromatographed on a 7 × 20 cm silica gel thick-layer plate eluted with 50% ether–hexane to give: 1, R_f 0.8, 15.2 mg of an unidentified oil; 2, R_f 0.5, 21 mg (13%) of crude 5,6-diphenyl-2-*exo*-hydroxy-1,2,7-trimethylbicyclo[3.2.0]hept-6-en-3-one (note below for identification), as an oil; 3, R_f 0.2, 102.3 mg (64%) of diol as an oil. Recrystallization of fraction 3 from ether–hexane gave 84.1 mg (53%) of 2,3-*exo,exo*-dihydroxy-5,6-diphenyl-1,2,7-trimethylbicyclo[3.2.0]hept-6-ene, mp 116–117°C.

The spectral data were: ir (thin film): 3610, 3542, 3440 (br), 3080, 3058, 3000, 2960, 2925, 2885, 1602, 1497, 1450, 1382, 1371, 1235, 1117, 1082, 1060, 1038, 1010, 960, 915, 885, 828, 704 cm^{-1}; H nmr ($CDCl_3$) δ: 6.80–7.40 (m, 10H, arom), 4.02 (dd, J = 6.3, 10.0 Hz, 1H, —C*H*OH—), 2.20–2.60 (bs, 2H, 2—OH's), 2.48 (dd, J = 6.3, 12.0 Hz, 1H, C*H*H), 2.26 (dd, J = 10.0, 12.0 Hz, 1H, CH*H*), 1.87 (s, 3H, C-7 CH_3), 1.20 (s, 3H, C-2 CH_3), 0.67 (s, 3H, C-1 CH_3); Cmr ($CDCl_3$) δ: 141.56, 141.42, 139.02, 133.74, 128.25, 127.87, 127.69, 126.99, 126.61, 125.73, 77.85, 76.44, 61.23, 57.96, 36.35, 21.58, 12.91, 11.51; ms, *m/e*: 320.1776 (calcd. for $C_{22}H_{24}O_2$, *m/e*: 320.1775). *Anal.* calcd. for $C_{22}H_{24}O_2$: C 82.46, H 7.55; found: C 82.68, H 7.64.

5,6-Diphenyl-2-exo-hydroxy-1,2,7-trimethylbicyclo[3.2.0]hept-6-en-3-one

Using the general method of Corey and Kim (46), to a slurry of 147 mg (1.10 mmol) of *N*-chlorosuccinimide in 3.0 mL of toluene at 0°C, 143 mg (2.30 mmol) of dimethyl sulfide was added. After cooling to −20°C, 133 mg (0.146 mmol) of 2,3-*exo,exo*-dihydroxy-5,6-diphenyl-1,2,7-trimethylbicyclo[3.2.0]hept-6-ene in 1 mL of toluene was added dropwise. After 2 h, 110 mg (1.10 mmol) of triethylamine was added dropwise, the mixture stirred 1 h at −20°C, then warmed to room temperature over 2 h. Neutral work-up gave 154 mg of an oil which was chromatographed on a 20 × 20 cm silica gel thick-layer plate eluted twice with 30% ether–hexane to give: 1, R_f 0.9, 11.2 mg of an unidentified oil; 2, R_f 0.6, 94 mg of product, mp 51–53°C; 3, R_f 0.1, 19.0 mg of recovered starting material as an oil. Recrystallization of fraction 2 from 20% ether–hexane gave 76.7 mg (58%) of 5,6-diphenyl-2-*exo*-hydroxy-1,2,7-trimethylbicyclo[3.2.0]-hept-6-en-3-one, mp 160.5–161.5°C.

The spectral data were: ir ($CHCl_3$): 3575, 3450 (br), 3078, 3050, 3012, 3000, 2980, 2960, 2920, 2858, 1742, 1651, 1600, 1495, 1445, 1408, 1380, 1370, 1322, 1292, 1183, 1130, 1112, 1080, 1070, 1009, 998, 939, 922, 883, 810, 697 cm^{-1}; uv (EtOH): 216 (sh, ε 12 000), 224 (sh, ε 9100), 256 (sh, ε 8900), 265 (ε 10 400), 277 (sh, ε 6900), 292 (sh, ε 550) nm; H nmr ($CDCl_3$) δ: 7.00–7.60 (m, 10H, arom), 3.54 (d, J = 18.0 Hz, 1H, C*H*H), 2.83 (d, J = 18.0 Hz, 1H, CH*H*), 2.50 (bs, 1H, —OH), 2.04 (s, 3H, C-7 CH_3), 1.35 (s, 3H, C-2 CH_3), 0.83 (s, 3H, C-1 CH_3); ms, *m/e*: 318.1619 (calcd. for $C_{22}H_{22}O_2$, *m/e*: 318.1619). *Anal.* calcd. for $C_{22}H_{22}O_2$: C 82.99, H 6.94; found: C 82.70, H 7.04.

Single-crystal X-ray structures of 5,6-diphenyl-2-(exo)-hydroxy-1,2,7-trimethylbicyclo[3.2.0]hept-6-en-3-one and 3,5,6-trimethyl-1,4-terphenyl-2-carboxaldehyde[15]

Preliminary examinations and collection of the diffraction data were carried out on a Syntex–Nicolet P_1 diffractometer equipped with a graphite monochromated MoK_α radiation source (and a modified LT-1 low temperature device.) Structure amplitudes and their standard deviations were calculated from the intensity data by procedures similar to those described previously (47). Crystal data and details of the intensity data collections are given in Table 4.

The structures were solved by direct methods using the MULTAN (48) package and refined by full-matrix least-squares refinement. The final cycles of the least-squares refinement[15] assumed the non-hydrogen atoms to vibrate anisotropically and the hydrogen atoms to vibrate isotropically. Final electron density difference maps showed no significant features. Final discrepancy indices are included in Table 4.

[15] (a) Atomic form factors were from ref. 49. (b) The atomic factor for hydrogen was from ref. 50.

Can. J. Chem. Downloaded from www.nrcresearchpress.com by 210.87.254.42 on 09/06/12
For personal use only.

TABLE 4. Summary of crystal data and intensity collection

Parameters	Ketol *16*	Terphenyl **22**
Empirical formula	$C_{22}H_{22}O_2$	$C_{22}H_{20}O$
Molecular weight	318.4	300.4
Crystal dimensions (mm)	0.4×0.4×0.15	0.3×0.35×0.2
Temperature (K)	198 ± 5	248 ± 3
Cell parameters *a* (Å)	16.017(3)	8.126(2)
b (Å)	9.365(2)	7.217(1)
c (Å)	12.490(2)	14.381(2)
β (°)	112.95(1)	91.77(2)
Space group	$P2_1/c$	$P2_1/c$
Z	4	2
Density, calcd. (g/cm^3)	1.23	1.18
Absorption coefficient (cm^{-1})	0.42	0.37
Scan range (deg below 2θ $k_{\alpha 1}$)	0.85	0.9
(deg above 2θ $k_{\alpha 2}$)	0.85	0.9
Scan speed (deg/min)	2.0–24.0	3.4–24.0
Scan type	θ–2θ	θ–2θ
2θ limits (°)	3.5–54.9	3.5–54.9
Sin θ/λ max (Å^{-1})	0.649	0.649
Unique data, theoretical	3943	1947
$F_o > 3\sigma$ (F_o)	2473	1128
Discrepancy index, R_1	0.054	0.056
R_2	0.055	0.065
Goodness of fit	1.37	1.71

Degradation of 5,6-diphenyl-2-(exo)-hydroxy-1,2,7-trimethylbicyclo[3.2.0]hept-6-en-3-one to methyl 3,4-diphenyl-5-oxo-3-hexenoate

To 61.0 mg (0.191 mmol) of 5,6-diphenyl-2-*exo*-hydroxy-1,2,7-trimethylbicyclo[3.2.0]hept-6-en-3-one in 1.0 mL of *tert*-butanol and 0.25 mL of ethyl acetate at room temperature was added 43.5 mg (0.191 mmol) of periodic acid in 1.5 mL of water. After 18 h, ether was added, the solution extracted with saturated sodium bicarbonate, the water layers acidified to Congo red with 10% HCl, then ether extracted, dried over anhydrous sodium sulfate, and concentrated *in vacuo* to yield 31.4 mg (0.094 mmol, 49%) of one isomer of 5,6-dimethyl-3,4-diphenyl-6-oxo-3,5-octadienoic acid as a slightly yellow oil.

The spectral data were: ir ($CHCl_3$): 3600–2500 (br), 1710 (br), 1670 cm^{-1}; H nmr ($CDCl_3$) δ: 7.00–7.70 (m, 10H, arom), 3.48 (s, 2H, CH_2), 1.78 (s, 3H, CH_3), 1.70 (s, 6H, 2 CH_3).

The acid in 3 mL of ether was added to 2 mmol of diazomethane[16] in 20 mL of ether at 0°C. After 10 min, the excess diazomethane was removed with a stream of nitrogen. Concentration *in vacuo* gave 31.1 mg (0.0892 mmol, 95%) methyl 5,6-dimethyl-3,4-diphenyl-6-oxo-3,5-octadienoate as a slightly yellow oil.

The spectral data were: ir ($CHCl_3$): 1735, 1690 cm^{-1}; H nmr ($CDCl_3$) δ: 7.00–7.70 (m, 10H, arom), 3.57 (s, 3H, OCH_3), 3.46 (s, 2H, CH_2), 1.76 (s, 3H, CH_3), 1.70 (s, 3H, CH_3), 1.64 (s, 3H, CH_3).

The methyl ester in 10 mL of ethyl acetate in a −23°C bath was treated with a stream of ozone in dry oxygen (0.05 mmol/min, Welsbach Ozonator) for 4.3 min, followed by addition of 0.25 g (4.1 mmol) of dimethyl sulfide. After 2 h, concentration *in vacuo* gave 33.4 mg of a yellow oil, which was chromatographed on a 5 × 20 cm thick-layer silica gel plate eluted with 50% ether–hexane to give 9.4 mg, R_f 0.5, methyl 3,4-diphenyl-5-oxo-3-hexenoate as a yellow oil. Crystallization from hexane gave 9.0 mg (32% from the acid, 16% overall) crystals, mp 94–105°C. The spectral data proved identical with those of independently synthesized material (*vide supra*).

4,5-Diphenyl-6-methyl-2-pyrone

To 0.25 g (1.6 mmol) of methyl phenylpropiolate and 0.21 g (1.6 mmol) of phenylacetone in 2 mL of ether at room temperature was added 0.084 g (1.6 mmol) of sodium methoxide. After 3 h, 5.0 mL of saturated NH_4Cl was added, and neutral work-up gave an oil which was chromatographed on a 3 × 40 cm silica gel column eluted with 1 L 2% ether–hexane and 1 L 10% ether–hexane collecting 500 mL fractions. Fraction 1, nil; 2, recovered phenylacetone; 3, nil; 4, 0.170 g of product as a yellow oil. Recrystallization from methanol gave 31.0 mg of 4,5-diphenyl-6-methyl-2-pyrone (7.6%), mp 137–138°C (lit.[17] mp 135°C).

The spectral data were: ir ($CHCl_3$): 2996, 1720, 1633, 1621, 1602, 1580, 1533, 1490, 1448, 1394, 1380, 1295, 1266, 1156, 1080, 1028, 1011, 998, 927, 908, 868, 845 cm^{-1}; H nmr ($CDCl_3$) δ: 7.00–7.40 (m, 10H, arom), 6.34 (s, 1H, vinyl), 2.23 (s, 3H, CH_3).

Methyl 3,4-diphenyl-5-oxo-3-hexenoate

A 140-mg (0.534 mmol) sample of 4,5-diphenyl-6-methyl-2-pyrone was dissolved in 4.0 mL of 5% KOH in CH_3OH by warming for 10 min and then kept at room temperature for 18 h. The solution was poured into water, acidifed with 10% HCl, ether extracted, dried over anhydrous magnesium sulfate, and concentrated *in vacuo* to give 116.4 mg of the two product acids as an oil.

The acids in 6.0 mL of ether were added to 2.0 mmol of diazomethane[16] at 0°C in 20 mL of ether. After 10 min, excess diazomethane was removed with a stream of nitrogen, and the solution concentrated *in vacuo* to give 93.0 mg of a yellow oil. Column chromatography on a 1 × 30 cm silica gel column eluted with 10% ether–hexane, collecting the initial band, gave 65.2 mg of an oil which was further purified by hplc, eluting with 45% methylene chloride – 45% pentane – 10% ether to give: 1, *k'* 0.71, 6.2 mg of unidentified oil; 2, *k'* 0.88, 24.4 mg of the major product isomer, mp 78–95°C; 3, *k'* 1.83, 9.0 mg of the minor product isomer as an oil. Recrystallization of fraction 2 gave 19.7 mg, mp 99–100°C, (13%) of the major isomer of methyl 3,4-diphenyl-5-oxo-3-hexenoate, identical in all respects to the ester obtained from degradation of photoproduct **A**.

The spectral data were: ir ($CHCl_3$): 3000, 2956, 1739, 1692, 1495, 1447, 1440, 1418, 1359, 1340, 1267, 1165, 1081, 1028, 706 cm^{-1}; uv (EtOH): 248 (ε 8300) nm; 200-MHz H nmr ($CDCl_3$) δ: 7.00–7.30 (m, 10H, arom), 3.56 (s, 3H, OCH_3), 3.40 (s, 2H, CH_2), 1.92 (s, 3H, CH_3); Cmr ($CDCl_3$) δ: 204.08, 170.81, 145.28, 139.89, 136.64, 136.25, 128.65, 128.45, 128.19, 51.719, 40.478, 30.667; ms, *m/e*: 294.1256 (calcd. for $C_{19}H_{18}O_3$, *m/e*: 294.125). *Anal.* calcd. for $C_{19}H_{18}O_3$: C 77.53, H 6.16; found: C 77.59, H 6.37.

Crystallization of fraction 3 from pentane gave 6.2 mg of the minor isomer of methyl 3,4-diphenyl-5-oxo-3-hexenoate, mp 67–68°C. The spectral data were: ir ($CHCl_3$): 3080, 3060, 3030, 3005, 2955, 1740, 1688, 1617, 1600, 1580, 1497, 1449, 1441, 1420, 1360, 1345, 1242, 1200, 1176, 1090, 1077, 1038, 1023, 1010, 955, 704 cm^{-1}; 200-MHz H nmr ($CDCl_3$) δ: 6.90–7.20 (m, 10H, arom), 3.76 (s, 2H, CH_2), 3.69 (s, 3H, OCH_3), 2.10 (s, 3H, —C=O—CH_3); ms, *m/e*: 294.126 (calcd. for $C_{19}H_{18}O_3$, *m/e*: 294.125).

2,3-(exo,exo)-Dihydroxy-1,5-diphenyl-2,6,7-trimethylbicyclo-[3.2.0]hept-6-ene

To 175 mg (0.61 mmol) of photoisomer **B** in 3.0 mL of pyridine at 0°C was added 140 mg (0.550 mmol) of osmium tetroxide. After 5 h, the pyridine was removed *in vacuo* and 50 mL of sodium bisulfite-saturated 95% ethanol added. After stirring 15 h, the solvent was removed *in vacuo*, and neutral work-up gave 282 mg of an oil. Chromatography on a 8 × 20 cm thick-layer silica gel plate eluted twice with 20% ether–hexane, twice with 30% ether–hexane, and twice with ether gave: 1, R_f 1.0, 56.3 mg of recovered starting material as an oil; 2, R_f 0.2, 77.4 mg of diol as an oil. Recrystallization from ether gave 48.3 mg (25%) of 2,3-*exo*,*exo*-dihydroxy-1,5-diphenyl-2,6,7-trimethylbicyclo[3.2.0]hept-6-ene, mp 167–167.5°C.

The spectral data were: ir ($CHCl_3$): 3550–3600, 3090, 3060, 3005,

[16] Generated by distillation from 0.70 g of *N,N'*-dinitroso-*N,N'*-dimethyl terephthalamide (Du Pont EXR-101), 1.24 g KOH, 2.5 mL ethoxyethoxyethanol, 25 mL ether, and 4.0 mL water.

[17] 4,5-Diphenyl-6-methyl-2-pyrone has been previously reported (51) but the details of its preparation are not readily available, nor is the preparation a straightforward one.

Can. J. Chem. Downloaded from www.nrcresearchpress.com by 210.87.254.42 on 09/06/12
For personal use only.

2962, 2930, 2860, 1655, 1612, 1497, 1445, 1405, 1379, 1330, 1266, 1188, 1169, 1107, 1083, 1046, 1034, 1008, 960, 909, 883, 834, 691 cm^{-1}; 200-MHz H nmr ($CDCl_3$) δ: 6.85–7.40 (m, 10H, arom), 4.15 (bdd, J = 6.0, 10.0 Hz, 1H, —C*H*OH—), 2.41 (dd, J = 10.0, 12.5 Hz, 1H, C*H*H), 2.40 (bs, 1H, —OH) 2.22 (dd, J = 6.0, 12.5 Hz, 1H, CH*H*), 2.03 (bs, 3H, vinyl CH_3), 1.58 (bs, 1H, OH), 1.43 (bs, 3H, vinyl CH_3), 1.25 (s, 3H, C-2 CH_3); Cmr ($CDCl_3$) δ: 143.49, 140.07, 137.04, 136.66, 129.78, 127.41, 126.86, 125.76, 77.75, 70.97, 60.95, 33.59, 22.30, 13.60, 8.92; ms, *m/e*: 320.1776 (calcd. for $C_{22}H_{24}O_2$, *m/e*: 320.1775). *Anal.* calcd. for $C_{22}H_{24}O_2$: C 82.46, H 7.55; found: C 82.62, H 7.74.

3,5,6-Trimethyl-1,4-terphenyl-2-carboxaldehyde

To 50.5 mg (0.158 mmol) of 2,3-*exo,exo*-dihydroxy-1,5-diphenyl-2,6,7-trimethylbicyclo[3.2.0]hepta-6-ene in 1.0 mL of benzene at room temperature was added 69.8 mg (0.158 mmol) of lead tetraacetate. After 10 min, neutral work-up gave 54.7 mg of 4,5-dimethyl-3,6-diphenyl-3,5-ocatadien-7-one-1-carboxaldehyde as an oil. This material was used below without further purification.

The spectral data were: ir (thin film): 1713, 1677 cm^{-1}; 200-MHz H nmr ($CDCl_3$) δ: 9.70 (t, J = 2.2 Hz, 1H, CHO), 6.70–7.50 (m, 10H, arom), 3.49 (d, J = 2.2 Hz, 2H, CH_2), 2.05 (s, 3H, —CO—CH_3), 1.62 (s, 3H, CH_3), 1.60 (s, 3H, CH_3); ms, *m/e*: 318.1619 (calcd. for $C_{22}H_{22}O_2$, *m/e*: 318.1618).

To the crude aldehyde in 1 mL of methanol was added 3.4 mg (0.061 mmol) of KOH at room temperature. After 15 min, neutral work-up gave 69.4 mg of solid, mp 106–211°C. Recrystallization from ether–hexane gave 30.3 mg of 3,5,6-trimethyl-1,4-terphenyl-2-carboxaldehyde, (64%), mp 217–220°C (sealed tube).

The spectral data were: ir ($CHCl_3$): 3067, 3017, 2880, 2778, 1683, 1603, 1568, 1557, 1498, 1464, 1445, 1411, 1387, 1320, 1290, 1075, 1032, 1004, 993, 920, 848, 820, 697 cm^{-1}; uv (EtOH): 222 (ε 36 000), 267 (ε 13 000), 307 (ε 3700) nm; 200-MHz H nmr ($CDCl_3$) δ: 9.77 (s, 1H, CHO), 7.07–7.53 (m, 10H, arom), 2.24 (s, 3H, CH_3), 2.02 (s, 3H, CH_3), 2.01 (s, 3H, CH_3); Cmr ($CDCl_3$) δ: 195.55, 145.19, 143.04, 141.27, 140.54, 138.87, 134.75, 132.90, 131.75, 130.01, 129.22, 128.62, 128.33, 127.42, 126.88, 19.06, 18.33, 17.06; ms, *m/e*: 300.1514 (calcd. for $C_{22}H_{20}O$, *m/e*: 300.1513). *Anal.* calcd. for $C_{22}H_{20}O$: C 87.96, H 6.71; found: C 88.04, H 6.80.

2,5-Dimethyl-3,4-diphenylthiophene

Using a modification of the general method of Dabard and Le Bihan (52), to a suspension of 3.22 g (84.7 mmol) of LAH in 120 mL of ether, with mechanical stirring in an ice-bath, was slowly added, 11.3 g (84.7 mmol) of aluminum trichloride. After 1 h, 4.28 g (12.1 mmol) of 2,5-bis(carbomethoxy)-3,4-diphenylthiophene (53) suspended in 200 mL of ether was added, and the solution refluxed 9 h. After recooling in an ice-bath, 30 mL of ethyl acetate was slowly added, followed by 100 mL of 10% HCl. Basic work-up gave 3.9 g of an oil, which was chromatographed on a 3 × 33 cm silica gel column eluted with hexane to give 1.8 g of product as the initial band as an oil. Recrystallization from hexane gave 1.38 g (43%) of 2,5-dimethyl-3,4-diphenylthiophene, mp 101–102°C.

The spectral data were: ir ($CHCl_3$): 3060, 3000, 2922, 2860, 1610, 1492, 1450, 1285, 1175, 1140, 1084, 1025, 928, 708 cm^{-1}; 270-MHz H nmr ($CDCl_3$) δ: 6.90–7.30 (m, 10H, arom), 2.36 (s, 6H, $2CH_3$); Cmr ($CDCl_3$) δ: 138.99, 136.74, 131.28, 130.20, 127.66, 126.20, 13.90; ms, *m/e*: 264.0973 (calcd. for $C_{18}H_{16}S$, *m/e*: 264.0972). *Anal.* calcd. for $C_{18}H_{16}S$: C 81.77, H 6.10; found: C 81.84, H 6.19.

2,5-Dimethyl-3,4-diphenylthiophene-1,1-dioxide

To 1.38 g (5.23 mmol) of 2,5-dimethyl-3,4-diphenylthiophene, in 20 mL of chloroform at room temperature was added dropwise 198 g (11.5 mmol) of *meta*-chloroperbenzoic acid in 15 mL of chloroform. After 2 h, basic work-up gave 1.70 g of crude product, mp 150–190°C (dec.). Recrystallization from chloroform–ether gave 0.642 g (41%) of 2,5-dimethyl-3,4-diphenylthiophene-1,1-dioxide, mp 209–210°C.

The spectral data were: ir ($CHCl_3$): 3080, 3060, 3024, 2910, 2844, 1595, 1580, 1497, 1448, 1383, 1293, 1235, 1199, 1180, 1114, 1082, 1024, 1010, 1001, 983, 929, 913, 870, 846, 702 cm^{-1}; 270-MHz H nmr ($CDCl_3$) δ: 7.20–7.50 (m, 6H, arom), 6.85–7.00 (m, 4H, arom), 2.15 (s, 6H, 2 CH_3); Cmr ($CDCl_3$) δ: 133.67, 131.24, 130.19, 128.93, 128.49 (C4 Ph), 127.99, 8.264 (CH_3); ms, *m/e*: 296.0872 (calcd. for $C_{18}H_{16}O_2S$, *m/e*: 296.0960). *Anal.* calcd. for $C_{18}H_{16}O_2S$: C 72.94, H 5.44; found: C 72.95, H 5.50.

3,4-Diphenyl-1,2,5-trimethyl-1,3,5-cycloheptatriene

Using the general method of van Tilborg *et al.* (6), to 800 mg (2.72 mmol) of 2,5-dimethyl-3,4-diphenylthiophene-1,1-dioxide in 5 mL of methylene chloride at room temperature was added a solution of 370 mg (6.8 mmol) of 1-methylcyclopropene (54) in 2.0 mL of methylene chloride at −78°C in a stoppered flask. The mixture was stirred at room temperature for 4 h. Concentration *in vacuo* gave 1.2 g of an oil, which was chromatographed ona 3 × 33 cm alumina column eluted with hexane to yield: 1, 500 mL, nil; 2, 1 L, 0.575 g of product, mp 71–76°C. Recrystallization from ether–pentane gave 0.4127 g (53%) of 3,4-diphenyl-1,2,5-trimethyl-1,3,5-cycloheptatriene, mp 86–87°C.

The spectral data were: ir ($CHCl_3$): 3085, 3063, 3016, 2963, 2935, 2892, 2863, 1600, 1490, 1450, 1440, 1378, 1310, 1072, 840, 696, 645 cm^{-1}; 270-MHz H nmr ($CDCl_3$) δ: 6.80–7.20 (m, 10H, arom), 5.60 (t, J = 8.1 Hz, 1H, vinyl), 2.52 (bs, 2H, CH_2), 1.98 (s, 3H, CH_3), 1.68 (s, 3H, CH_3), 1.54 (s, 3H, CH_3); Cmr ($CDCl_3$) δ: 145.62, 141.98, 141.71, 141.43, 134.00, 131.40, 130.47, 130.30, 126.83, 125.40, 122.98, 35.10, 21.49, 20.66, 17.08; ms, *m/e*: 286.1722 (calcd. for $C_{22}H_{22}$, *m/e*: 286.1720). *Anal.* calcd. for $C_{22}H_{22}$: C 92.26, H 7.74; found: C 92.08, H 7.94.

*3,4-Diphenyl-*trans*-2,5,6-trimethylcyclohepta-3,5-dienol*

Using the general method of Zweifel and Brown (55), to 288 mg (1.00 mmol) of 3,4-diphenyl-1,2,5-trimethylcyclohepta-1,3,5-triene in 2.0 mL of THF at 0°C was added 6.9 mg (0.50 mmol, 0.51 mL) of 0.98 *M* borane in THF) of borane. After 30 min, 1.5 mL of 5 *N* NaOH solution was added, followed by 1.0 mL of 30% H_2O_2 solution. After 3 h, neutral work-up gave an oil which nmr analysis showed as approximently 50% converted starting material. This material was again treated with borane as above to yield 317 mg of an oil, which was chromatographed on two 5 × 20 cm silica gel thick-layer paltes eluted once with 10% ether–hexane and once with 20% ether–hexane to give: 1, R_f 0.71, 43.2 mg of recovered material as an oil; 2, R_f 0.50, 5.8 mg of an unidentified oil; 3, R_f 0.21, 133.9 mg of alcohol, mp 114–118°C; 4, R_f 0.00, 82.0 mg of an unidentified solid, mp 70–100°C. Recrystallization of fraction 3 from ethyl acetate – pentane gave 129.2 mg (42%) of 3,4-diphenyl-*trans*-2,5,6-trimethylcyclohepta-3,5-dienol, mp 122–123°C.

The spectral data were: ir ($CHCl_3$): 3590, 3300–3500, 3075, 3055, 2998, 2956, 2922, 2865, 1603, 1494, 1454, 1445, 1385, 1330, 1245, 1190, 1160, 1136, 1110, 1077, 1045, 1032, 996, 867, 705 cm^{-1}; uv (EtOH): 234 (ε 14 000/, 269 (sh, ε 6800) nm; 270-MHz H nmr ($CDCl_3$) δ: 6.80–7.20 (m, 10H, arom), 4.07 (m, 1H, —C*H*OH—), 2.77 (dd, J = 13.3, 4.3 Hz, 1H, C*H*H), 2.67 (p, J = 7.22 Hz, 1H, —C*H*CH_3—), 2.31 (dd, J = 13.3, 4.0 Hz, 1H, CH*H*), 2.02 (s, 3H, vinyl CH_3), 1.56 (s, 3H, vinyl CH_3), 1.05 (d, J = 7.06 Hz, 3H, —CHCH_3—); Cmr ($CDCl_3$) δ: 142.84, 142.29, 141.91, 140.62, 131.28, 132.51, 130.11, 129.85, 127.25, 125.79, 87.453, 45.962, 43.072, 21.408, 16.852, 16.561; ms, *m/e*: 304.1828 (calcd. for $C_{22}H_{24}O$, *m/e*: 304.1826). *Anal.* calcd. for $C_{22}H_{24}O$: C 86.80, H 7.95; found: C 87.14, H 7.96.

*1,7-Diphenyl-*endo*-2,5,6-trimethylbicyclo[3.2.0]hept-6-ene-2-*exo*-ol*

*Method A, photolysis of 3,4-diphenyl-*trans*-2,5,6-trimethylcyclohepta-3,5-diene-1-ol*

Using the general photolysis procedure, 75.1 mg (0.247 mmol) of 3,4-diphenyl-*trans*-2,5,6-trimethylcyclopheta-3,5-diene-1-ol in 185 mL of acetonitrile was irradiated for 5 h through Filter A at 30°C. Concentration *in vacuo* yielded 79.5 mg of an oil, which was chromatographed on a 1 × 60 cm silica gel column eluted with 20% ether–hexane, collecting 50-mL of fractions to give: 1, nil; 2, 5.6 mg of an unidentifid oil; 3–4, 29.3 mg of product as an oil. Recrystallization from ether–pentane gave 19.1 mg (25%) of 1,7-

Can. J. Chem. Downloaded from www.nrcresearchpress.com by 210.87.254.42 on 09/06/12
For personal use only.

diphenyl-*endo*-2,5,6-trimethylbicyclo[3.2.0]hept-6-ene-2-*exo*-ol, mp 112–113°C.

The spectral data were: ir ($CHCl_3$): 3620, 3300–3550, 3093, 3064, 3015, 2972, 2940, 2882, 1603, 1500, 1450, 1378, 1210, 1120, 1086, 1052, 1028, 1008, 968, 725, 699 cm^{-1}; 270-MHz H nmr ($CDCl_3$) δ: 7.10–7.40 (m, 10H, arom), 3.82 (td, J = 9.5, 6.0 Hz, 1H, —C*H*OH—), 2.40 (dq, J = 9.0, 6.8 Hz, 1H, —C*H*CH_3—), 2.20 (dd, J = 12.5, 6.0 Hz, 1H, C*H*H), 1.98 (s, 3H, vinyl CH_3), 1.56 (bs, 1H, —OH), 1.25 (dd, J = 12.4, 9.9 Hz, 1H, CH*H*), 1.00 (d, J = 6.8 Hz, 3H, —CHC*H*$_3$—), 0.65 (s, 3H, C-5 CH_3); Cmr ($CDCl_3$) δ: 145.03, 141.12, 136.22, 135.69, 128.01, 127.86, 127.75, 126.38, 126.14, 63.74, 53.88, 44.30, 41.11, 17.96, 13.96, 10.75; ms, m/e: 304.1828 (calcd. for $C_{22}H_{24}O$, m/e: 304.1826). *Anal.* calcd. for $C_{22}H_{24}O$: C 86.80, H 7.95; found: C 86.92, H 8.02.

Method B: Hydroboration–oxidation of photoproduct D

Using the general method of Zweifel and Brown (55), to 28.8 mg (0.100 mmol) of photoproduct D in 0.6 mL of THF at room temperature was added 1.4 mg (0.10 mmol, 0.010 mL of 0.98 *M* borane in THF) of borane. After 12 h, 0.20 mL of 5.0 *N* NaOH was added, followed by 0.2 mL of 30% H_2O_2, stirred for 10 h, and neutral work-up gave 39.4 mg of an oil. High-pressure liquid chromatography eluting with 1:1 ether–pentane at a flow rate of 4.5 mL/min gave: 1, k' 0.0, 2.9 mg of an unidentified oil; 2, k' 1.0, 0.4 mg of an unidentified oil; 3, k' 2.47, 3.6 mg of an unidentified oil; 4, k' 8.05, 12.8 mg of product as an oil. Recrystallization of fraction 4 from ether–pentane gave 6.7 mg of 1,7-diphenyl-*endo*-2,5,6-trimethylbicyclo[3.2.0]hept-6-ene-2-*exo*-ol, mp 112–113°C, whose spectral data were identical to those of independently synthesized material.

1,4-Bis(trideuteriomethyl)-2,3-diphenyl-5-methyl-5-vinyl-1,3-cyclopentadiene

Using the general method of Zimmerman *et al.* (12*b*), to 1.0 g (3.5 mmol) of 2,3-diphenyl-1,4,5-trimethyl-5-vinyl-1,3-cyclopentadiene in 8.80 g (8.80 mmol) of *N,N*-dideuteriocyclohexyl amine (12*b*) (>98% D) at room temperature was added 2.4 mL of 1.5 *M* (3.5 mmol) *n*-BuLi in hexane. After 12 h, 0.40 mL of D_2O was added, the solution poured into 220 mL of 5% HCl, and neutral work-up gave 1.01 g, mp 74.5–78°C, 90% deuterated (nmr). The above procedure was repeated to yield 0.988 g, mp 74.5–78°C, 94% deuterated, and once more repeated to yield 0.982 g, mp 38–65°C. Recrystallization from pentane gave 0.702 g (70%) of 1,4-bis(trideuteriomethyl)-2,3-diphenyl-5-methyl-5-vinyl-1,3-cyclopentadiene, mp 77.5–78°C, 96.5% deuterated (nmr).

Direct photolysis of 1,4-bis(trideuteriomethyl)-2,3-diphenyl-5-methyl-5-vinyl-1,3-cyclopentadiene

High conversion run

Using the general photolysis procedure, 82.0 mg (0.281 mmol) of 1,4-bis(trideuteriomethyl)-2,3-diphenyl-5-methyl-5-vinyl-1,3-cyclopentadiene in 170 mL of acetonitrile was irradiated for 3 h through Filter A at 31–33°C. Concentration *in vacuo* gave 80.8 mg of an oil, which was chromatographed using hplc eluting with 6% methylene chloride – pentane at a flow rate of 2.4 mL/min. Fraction compositions were determined by integration of their 200-MHz H nmr spectra. Fraction 1, k' 1.48, 1.8 mg of an unidentified oil; 2, k' 1.67, 2.5 mg of an oil, 60% photoisomer **D** and 40% photoisomer **C**; 3, k' 1.87, 19.0 mg of recovered starting material, mp 51–67°C; 4, k' 2.03, 8.5 mg of an oil, 67% photoisomer **B** and 33% 1,2-diphenyl-3,4,5-trimethyl-5-vinyl-1,3-cyclopentadiene; 5, k' 2.33, 27.1 mg of an oil, 43% photoisomer **B** and 57% photoisomer **A**. Results: 19.0 mg (23%) of recovered starting material, 15.4 mg (18.8%) of photoisomer **A**, 17.3 mg (21.1%) of photoisomer **B**, 1.5 mg (1.8%) of photoisomer **D**, 1.0 mg (1.2%) of photoisomer **C**, and 2.8 mg (3.4%) of 1,2-diphenyl-3,4,5-trimethyl-5-vinyl-1,3-cyclopentadiene. The recovered starting material had 36% CH_3 on C-5 (1.25 ppm) and 64% CH_3 on the vinyl positions (1.82 ppm). All the products had 33 ± 1% CH_3 in all positions.

Low conversion run

Using the general photolysis procedure, 30.3 mg (0.104 mmol) of 1,4-bis(trideuteriomethyl)-2,3-diphenyl-5-methyl-5-vinyl-1,3-cyclopentadiene in 170 mL acetonitrile was irradiated through Filter A for 22 min at 27°C. Concentration *in vacuo* gave 28.9 mg of a semi-solid. High-pressure liquid chromatography eluting with 6% methylene chloride – pentane at 1.1 mL/min gave: 1, k' 1.47, 0.1 mg of an unidentified oil; 2, k' 2.38, 24.5 mg (81%) of recovered starting material, 95% CH_3 on C-5 (1.25 ppm) and 5% CH_3 on the vinyl positions (1.82 ppm); 3, k' 3.75, 2.0 mg (6.6%) of a mixture of 78% photoisomer **A** (5.1%) and 22% photoisomer **B** (1.5%). Photoisomer **A** had 89% CH_3 on C-2 (1.75 ppm), 6% CH_3 on C-1 (0.65 ppm), and 5% CH_3 on C-7 (2.08 ppm). Photoisomer **B** had 77% CH_3 on C-2 (1.73 ppm), 16% CH_3 on C-7 (1.86 ppm), and 7% CH_3 on C-6 (1.84 ppm).

At −70°C

Using the low temperature photolysis apparatus described above (note Fig. 8), 47.7 mg (0.163 mmol) of 1,4-bis(trideuteriomethyl)-2,3-diphenyl-5-methyl-5-vinyl-1,3-cyclopentadiene in 100 mL pentane was irradiated for 164 min in a −78°C bath using the general photolysis procedure through Filter A. The solution was kept at −78°C with continued nitrogen purging for an additional 1.5 h, followed by 4 h at room temperature. Concentration *in vacuo* gave 47.3 mg of a yellow solid, mp 23–43°C, which 270-MHz nmr analysis showed consisted of a 3.75:1 mixture of recovered starting material and 3,5-bis(trideuteriomethyl)-1,2-diphenyl-4-methyl-5-vinyl-1,3-cyclopentadiene, with small amounts (<5%) of unidentified material. Neither component showed detectable scrambling of the methyl groups.

Sensitized photolysis of 1,4-bis(trideuteriomethyl)-2,3-diphenyl-5-methyl-5-vinyl-1,3-cyclopentadiene

Using the general photolysis procedure, 42.1 mg (0.114 mmol) of 1,4-bis(trideuteriomethyl)-2,3-diphenyl-5-methyl-5-vinyl-1,3-cyclopentadiene and 162.4 mg (0.721 mmol) of *p*-dimethylaminobenzophenone in 250 mL acetonitrile were irradiated through Filter C for 40 min at 30°C. Concentration *in vacuo* gave 217 mg of an oil which was chromatographed on a 1 × 28 cm silica gel column eluted with 100 mL 1% ether–pentane and 500 mL ether collecting 50-mL fractions to give: 1, nil; 2, 41.2 mg of a mixture of starting material and product; 3–4, nil; 5–6, 171.8 mg of recovered sensitizer, mp 80–87°C. High-pressure liquid chromatography of fraction 2 eluting with 6% methylene chloride – pentane at a flow rate of 2.2 mL/min gave: 1, k' 1.9, 4.2 mg of recovered starting material as an oil, retaining its label on the vinyl methyl groups; 2, k' 1.95, 3.3 mg of overlap; 3, k' 2.0, 27.0 mg of 3,5-bis(trideuteriomethyl)-1,2-diphenyl-4-methyl-5-vinyl-1,3-cyclopentadiene, mp 66–73°C.

Direct photolysis of 3,5-bis(trideuteriomethyl)-1,2-diphenyl-4-methyl-5-vinyl-1,3-cyclopentadiene

Using the general photolysis procedure, 23.0 mg (0.0788 mmol) of 3,5-bis(trideuteriomethyl)-1,2-diphenyl-4-methyl-5-vinyl-1,3-cyclopentadiene in 160 mL acetonitrile was irradiated through Filter A for 10 min at 27°C. Concentration *in vacuo* gave 21.0 mg of an oil; hplc eluting with 6% methylene chloride – pentane at a flow rate of 2.2 mL/min gave: 1, k' 2.29, 14.2 mg of 2,3-diphenyl-1,4,5-trimethyl-5-vinyl-1,3-cyclopentadiene, mp 61–72°C, 92% CH_3 on the vinyl positions (1.82 ppm), and 8% CH_3 on C-5 (1.25 ppm); 2, k' 2.78, 4.1 mg of recovered starting material as an oil, labeled as before the photolysis; 3, k' 3.21, 2.3 mg of a mixture of 59% photoisomer **A** and 41% photoisomer **B** as an oil. Photoisomer **A** had 0% CH_3 on C-2 (1.75 ppm), 50% CH_3 on C-1 (0.65 ppm), and 50% CH_3 on C-7 (2.08 ppm). Photoisomer **B** had 0% CH_3 on C-2 (1.73 ppm), 68% CH_3 on C-7 (1.86 ppm), and 32% CH_3 on C-6 (1.83 ppm).

Thermolysis of 1,4-bis(trideuteriomethyl)-2,3-diphenyl-5-methyl-5-vinyl-1,3-cyclopentadiene

A solution of 16.1 mg of 1,4-bis(trideuteriomethyl)-2,3-diphenyl-5-methyl-5-vinyl-1,3-cyclopentadiene in 1 mL of benzene was re-

Can. J. Chem. Downloaded from www.nrcresearchpress.com by 210.87.254.42 on 09/06/12
For personal use only.

fluxed 23 h. Concentration *in vacuo* gave 15.5 mg of an oil, which 200-MHz H nmr analysis showed consisted of a 1:1 mixture starting material, labeled unchanged, and 3,5-bis(trideuteriomethyl)-1,2-diphenyl-4-methyl-5-vinyl-1,3-cyclopentadiene.

Photolysis of 2,3-diphenyl-1,4,5-trimethyl-5-vinyl-1,3-cyclopentadiene in the presence of 3,3,4,4,-tetramethyl-1,2-diazetine-1,2-dioxide

Using the general photolysis procedure, 120 mg (0.419 mmol) of 2,3-diphenyl-1,4,5-trimethyl-5-vinyl-1,3-cyclopentadiene and 46.9 mg (0.326 mmol, 2.03×10^{-3} *M*) of 3,3,4,4-tetramethyl-1,2-diazetine-1,2-dioxide (56) in 160 mL of acetonitrile was irradiated through Filter A for 3 h at 31–33°C. Concentration *in vacuo* gave 152.2 mg of an oil. 200-MHz H nmr analysis revealed 84.5% recovered starting cyclopentadiene, 9.3% photoisomer **A**, 5.0% photoisomer **B**, and 1.1% photoisomer **D**. An identical run was conducted using 122.9 mg (0.4291 mmol) of 2,3-diphenyl-1,4,5-trimethyl-5-vinyl-1,3-cyclopentadiene, but omitting the quencher. Concentration *in vacuo* gave 119.7 mg of an oil. Analysis by 200-MHz H nmr revealed 81.4% recovered starting material, 10.4% photoisomer **A**, 6.2% photoisomer **B**, and 1.9% photoisomer **D**. Within experimental error, the two runs provided photoproducts in the same ratios.

Photolysis of 2,3-diphenyl-1,4,5-trimethyl-5-vinyl-1,3-cyclopentadiene at −20°C in an nmr tube

In a 5-mm od nmr tube was put 1.5 mg of 2,3-diphenyl-1,4,5-trimethyl-5-vinyl-1,3-cyclopentadiene in 0.5 mL trideuterioacetonitrile. After purging with purified nitrogen (41) for 0.5 h, the nitrogen inlet was raised above the surface of the solution ca. 3 cm, and the tube placed inside a Pyrex tube through which nitrogen cooled to −20°C (via a coil immersed in liquid nitrogen) was continually blown. The tube was then placed ca. 1 cm from a 450-W medium-pressure mercury lamp and irradiated through Filter A for 4 h. Analysis by 200-MHz H nmr at −40°C revealed only recovered starting material.

Investigation of the secondary photochemistry

Photoisomer A

Using the general photolysis procedure, 15.3 mg (0.0534 mmol) of photoisomer **A** in 170 mL *tert*-butanol was irradiated at 30°C for 11.7 h. Concentration *in vacuo* gave 17.1 mg of an oil; nmr analysis showed ca. 20% remaining starting material, along with several unknown products. None of the other bicyclic photoproducts were present.

Photoisomer C

After purging with purified nitrogen (41) for 1 h prior to and during photolysis, 4.4 mg (0.015 mmol) of photoisomer **C** in 40 mL acetonitrile was irradiated at 28°C on the microoptical bench (42) at 330 nm with an entrance slit of 3.6 mm and an exit slit of 4.0 mm (band pass: 100% transmittance at ±15 nm, decreasing to 0% transmittance at ±30 nm) until digital actinometry (43) indicated 0.322 mEinsteins (20.9 equivalents) of light had been absorbed. Concentration *in vacuo* gave 4.6 mg of an oil, to which 3.3 mg (0.014 mmol) of methyl diphenylglycolate was added as internal standard; nmr analysis showed 79% recovered starting material for a quantum yield of disappearance of 0.0098. None of the unidentified products were the other bicyclic photoproducts.

Photoisomer D

Using the general photolysis procedure, 27.4 mg (0.0957 mmol) of photoisomer **D** in 170 mL acetonitrile was irradiated for 5.7 h at 30°C. Concentration *in vacuo* gave 25.0 mg of an oil; nmr analysis showed 21% remaining starting material, along with several unknown products. None of the other bicyclic photoproducts were present.

Quantum mechanical calculations

All quantum mechanical calculations were performed using the "GAMESS" program package (12*c*). The geometry of 5-vinyl-1,3-cyclopentadiene was obtained using the molecular mechanics portion of the "Tribble" program package (12*b*) and was optimized using the MNDO program contained therein. The geometry for the transition states was constructed using standard bond lengths and angles and was not optimized. In all cases, an STO-3G basis set was used. For 5-vinyl-1,3-cyclopentadiene, the Restricted Hartree–Fock method yielded MO's which, after configuration interaction involving the two highest energy HOMO's and the two lowest energy LUMO's, yielded the energies of the three lowest energy singlet states. For the non-twisted transition state geometry and the 90-deg methylene twisted transition state geometry, the Restricted Open Shell Hartree–Fock method yielded MO's which, after configuration interaction involving the three highest energy HOMO's and the three lowest energy LUMO's yielded the energies of the three lowest energy singlet states.

Acknowledgments

Support of this research by NIH Grant GM07487 and the National Science Foundation is gratefully acknowledged. Mechanistic aspects were supported by NSF while exploration of the synthetic aspects was supported by NIH.

1. (*a*) H. E. ZIMMERMAN and R. L. SWAFFORD. J. Org. Chem. **49**, 3069 (1984); (*b*) H. E. ZIMMERMAN and G.-S. WU. Can. J. Chem. **61**, 866 (1983); (*c*) H. E. ZIMMERMAN and S. A. FLEMING. J. Am. Chem. Soc. **103**, 622 (1983).
2. (*a*) H. E. ZIMMERMAN and S. AASEN. J. Am. Chem. Soc. **99**, 2342 (1977); (*b*) H. E. ZIMMERMAN and S. M. AASEN. J. Org. Chem. **43**, 1493 (1978); (*c*) H. E. ZIMMERMAN and M. C. HOVEY. J. Org. Chem. **44**, 2331 (1979); (*d*) H. E. ZIMMERMAN and D. J. KREIL. J. Org. Chem. **47**, 2060 (1982).
3. (*a*) A. PADWA, T. J. BLACKLOCK, D. GETMAN, N. HATANAKE, and R. LOZA. J. Org. Chem. **43**, 1481 (1978); (*b*) A. PADWA, T. J. BLACKLOCK, and R. LOZA. J. Org. Chem. **47**, 3712 (1982).
4. (*a*) H. E. ZIMMERMAN and L. M. TOLBERT. J. Am. Chem. Soc. **97**, 5497 (1975), footnote 12; (*b*) H. E. ZIMMERMAN and T. R. WELTER. J. Am. Chem. Soc. **100**, 4131 (1978), footnote 4.
5. (*a*) P. MAIN, S. J. FISKE, S. E. HULL, L. LESSINGER, G. GERMAIN, J.-P. DECLERCQ, and M. M. WOOLFSON. MULTAN 80 – a system of computer programs for the automatic solution of crystal structures from X-ray diffraction data. University of York, England and University of Louvain, Belgium. 1980; (*b*) G. M. SHELDRICK. SHELX 76. A program for crystal structure determination. University of Cambridge, England. 1976.
6. W. J. M. VAN TILBORG, P. SMAEL, J. P. VISSER, C. G. KOUWENHOVEN, and D. N. REINHOUDT. Recl. Trav. Chim. Pay-Bas, **94**, 85 (1975).
7. (*a*) G. PORTER and P. SUPPAN. Trans. Faraday Soc. **61**, 1664 (1965); (*b*) E. J. O'CONNELL, JR. J. Chem. Soc. Chem. Commun. 571 (1969).
8. D. F. EVANS. J. Chem. Soc. 1735 (1960).
9. W. G. HERKSTROETER and G. S. HAMMOND. J. Am. Chem. Soc. **88**, 4769 (1966).
10. (*a*) H. E. ZIMMERMAN, D. F. JUERS, J. M. MCCALL, and B. SCHRÖDER. J. Am. Chem. Soc. **92**, 3474 (1970); (*b*) H. E. ZIMMERMAN, P. HACKETT, D. F. JUERS, J. M. MCCALL, and B. SCHRÖDER. J. Am. Chem. Soc. **93**, 3653 (1971); (*c*) H. E. ZIMMERMAN, J. M. MCCALL, and B. SCHRÖDER. J. Am. Chem. Soc. **93**, 3662 (1971); (*d*) H. E. ZIMMERMAN and T. P. CUTLER. J. Chem. Soc. Chem. Commun. 232 (1978); (*e*) H. E. ZIMMERMAN AND T. P. Cutler. J. Org. Chem. **43**, 3283 (1978); (*f*) H. E. ZIMMERMAN and R. E. FACTOR. J. Am. Chem. Soc. **102**, 3538 (1980); (*g*) H. E. ZIMMERMAN and R. E. FACTOR. Tetrahedron, **37**, Suppl. 1, 125 (1981); (*h*) H. E. ZIMMERMAN. Chimia, **36**, 423 (1982); (*i*) H. E. ZIMMERMAN. Top. Curr. Chem. **100**, 45 (1982); (*j*) H. E. ZIMMERMAN. Acc. Chem. Res. **10**, 312 (1982).
11. A. STREITWIESER, JR., D. E. VAN SICKLE, and W. C. LANGWORTHY. J. Am. Chem. Soc. **84**, 244 (1962).
12. (*a*) H. E. ZIMMERMAN, R. W. BINKLEY, R. S. GIVENS, and M. A. SHERWIN. J. Am. Chem. Soc. **89**, 3932 (1967); (*b*) H. E. ZIMMERMAN, R. W. BINKLEY, R. S. GIVENS, G. L. GRUNEWALD,

Can. J. Chem. Downloaded from www.nrcresearchpress.com by 210.87.254.42 on 09/06/12
For personal use only.

and M. A. SHERWIN. J. Am. Chem. Soc. **91**, 3316 (1969); (*c*) H. E. ZIMMERMAN, R. S. GIVENS, and R. M. PAGNI. J. Am. Chem. Soc. **90**, 6096 (1968); (*d*) H. E. ZIMMERMAN and C. O. BENDER. J. Am. Chem. Soc. **91**, 7516 (1969); (*e*) H. E. ZIMMERMAN and C. O. BENDER. J. Am. Chem. Soc. **92**, 4366 (1970).

13. (*a*) F.-G. KLÄRNER and F. ADAMSKY. Angew. Chem. Int. Ed. Engl. **18**, 674 (1979); (*b*) Chem. Ber. **116**, 299 (1983).
14. (*a*) G. D. ANDREWS and J. E. BALDWIN. J. Am. Chem. Soc. **99**, 4851 (1977); (*b*) J. Am. Chem. Soc. **99**, 4853 (1977).
15. (*a*) W. R. ROTH, F.-G. KLÄRNER, and H. W. LENNARTZ. Chem. Ber. **113**, 1818 (1980); (*b*) J. I. BRAUMAN, L. E. ELLIS, and E. E. VAN TAMELEN. J. Am. Chem. Soc. **88**, 846 (1966); (*c*) S. MCLEAN and D. M. FINDLAY. Can. J. Chem. **48**, 3107 (1970); (*d*) J. E. BALDWIN and G. D. ANDREWS. J. Am. Chem. Soc. **94**, 1775 (1972).
16. (*a*) H. E. ZIMMERMAN and D. I. SCHUSTER. J. Am. Chem. Soc. **84**, 4527 (1962); (*b*) H. E. ZIMMERMAN. Adv. Photochem. **1**, 183 (1963); (*c*) H. E. ZIMMERMAN, D. DÖPP, and P. S. HUYFFER. J. Am. Chem. Soc. **88**, 5352 (1966).
17. (*a*) H. E. ZIMMERMAN, D. S. CRUMRINE, D. DÖPP, and P. S. HUYFFER. J. Am. Chem. Soc. **91**, 434 (1969); (*c*) H. E. ZIMMERMAN and D. S. CRUMRINE. J. Am. Chem. Soc. **90**, 5612 (1968); (*d*) H. E. ZIMMERMAN. Angew. Chem. **81**, 45 (1969); Angew. Chem. Int. Ed. Engl. **8**, 1 (1969).
18. (*a*) D. W. SWATTON and H. HART. J. Am. Chem. Soc. **89**, 5075 (1967); (*b*) R. F. CHILDS and S. W. WINSTEIN. J. Am. Chem. Soc. **90**, 7146 (1968); (*c*) R. F. CHILDS and S. W. WINSTEIN. J. Am. Chem. Soc. **96**, 6409 (1974).
19. R. B. WOODWARD and R. HOFFMANN. Angew. Chem. **81**, 797 (1969); Angew. Chem. Int. Ed. Engl. **8**, 781 (1969).
20. H. E. ZIMMERMAN and W. EBERBACH. J. Am. Chem. Soc. **95**, 3970 (1973).
21. H. E. ZIMMERMAN. (*a*) J. Am. Chem. Soc. **88**, 1564 (1966); (*b*) Acc. Chem. Res. **4**, 272 (1971); (*c*) Acc. Chem. Res. **5**, 393 (1972); (*d*) Tetrahedron, **38**, 753 (1982); (*e*) Quantum mechanics for organic chemists. Academic Press, New York. 1975; (*f*) *In* Pericyclic reactions. *Edited by* A. P. Marchand and R. E. Lehr. Academic Press, New York. 1977. Chapt. 2.
22. A. FROST and B. MUSULIN. J. Chem. Phys. **21**, 572 (1953).
23. (*a*) E. VOGEL, K.-H. OTT, and K. GAJEK. Justus Liebigs Ann. Chem. **644**, 172 (1961); (*b*) W. VON E. DOERING and W. R. ROTH. Tetrahedron, **19**, 715 (1963); (*c*) J. M. BROWN, B. T. GOLDING, and J. J. STOFKO, JR. J. Chem. Soc. Perkin Trans. 2, 436 (1978); (*d*) M. SCHNEIDER and J. REBELL. J. Chem. Soc. Chem. Commun. 283 (1975).
24. (*a*) R. P. LUTZ, W. BERNAL, R. J. BOGGIO, R. O. HARRIS, and M. W. MCNICHOLAS. J. Am. Chem. Soc. **93**, 3985 (1971); (*c*) M. J. S. DEWAR and L. E. WADE, JR. J. Am. Chem. Soc. **99**, 4417 (1977); (*d*) J. J. GAJEWSKI and N. D. CONRAD. J. Am. Chem. Soc. **101**, 6693 (1979); (*e*) R. P. LUTZ and H. A. J. BERG. J. Org. Chem. **45**, 3915 (1980).
25. H. E. ZIMMERMAN, D. ARMESTO, M. G. AMEZUA, T. P. GANNETT, and R. P. JOHNSON. J. Am. Chem. Soc. **101**, 6367 (1979).
26. H. E. ZIMMERMAN, J. H. PENN, and M. R. JOHNSON. Proc. Natl. Acad. Sci. USA, **78**, 2021 (1981).
27. H. E. ZIMMERMAN and A. C. PRATT. J. Am. Chem. Soc. **92**, 1409 (1970).
28. H. E. ZIMMERMAN and G. A. EPLING. J. Am. Chem. Soc. **94**, 8749 (1972).
29. J. MICHL. Mol. Photochem. **4**, 243 (1972).
30. H. E. ZIMMERMAN. *In* Rearrangements in ground and excited states. Vol. 3. *Edited by* P. DeMayo. Academic Press, New York. 1980.
31. (*a*) H. E. ZIMMERMAN and R. PAGNI. J. Am. Chem. Soc. **90**, 6096 (1968); (*b*) H. E. ZIMMERMAN and D. R. AMICK. J. Am. Chem. Soc. **95**, 3977 (1973); (*c*) H. E. ZIMMERMAN and D. R. AMICK. J. Am. Chem. Soc. **95**, 4606 (1973).
32. H. E. ZIMMERMAN and A. ZWEIG. J. Am. Chem. Soc. **83**, 1196 (1961).
33. (*a*) D. J. FIELD, D. W. JONES, and G. KNEEN. J. Chem. Soc. Chem. Commun. 873 (1976); (*b*) D. J. FIELD and D. W. JONES. J. Chem. Soc. Chem. Commun. 688 (1977); (*c*) D. J. FIELD and D. W. JONES. J. Chem. Soc. Perkin Trans. 1, 714 (1980); (*d*) M. F. SEMMELHACK, H. N. WELLER, and J. S. FOOS. J. Am. Chem. Soc. **99**, 292 (1977); (*e*) M. F. SEMMELHACK, H. N. WELLER, and J. CLAUDY. J. Org. Chem. **43**, 3791 (1978).
34. (*a*) M. A. BATTISTE and M. E. BURNS. Tetrahedron Lett. 523 (1966); (*b*) H. H. FREEDMAN, G. A. DOORAKIAN, and V. R. SANDEL. J. Am. Chem. Soc. **87**, 3019 (1965); (*c*) G. A. DOORAKIAN and H. H. FREEDMAN. J. Am. Chem. Soc. **90**, 3582 (1968); (*d*) G. A. DOORAKIAN and H. H. FREEDMAN. J. Am. Chem. Soc. **90**, 5310 (1968); (*e*) M. POMERANTZ and P. H. HARTMAN. Tetrahedron Lett. 991 (1968).
35. (*a*) K. C. BRANNOCK, R. D. BURPITT, V. W. GOODLETT, and J. G. J. G. THWEATT. J. Org. Chem. **28**, 1464 (1963); (*b*) D. N. REINHOUDT, H. C. VOLGER, and C. G. KOUWENHOVEN. Tetrahedron Lett. 5269 (1972); (*c*) R. CRIEGEE, D. SEEBACH, R. E. WINTER, B. BÖRRETZEN, and H.-A. BRUNE. Chem. Ber. **98**, 2339 (1965); (*d*) N. D. Epiotis. Angew. Chem. Int. Ed. Engl. **13**, 751 (1974).
36. H. E. ZIMMERMAN. *In* Molecular rearrangements. *Edited by* P. DeMayo. Interscience, New York. 1963. Chapt. 6.
37. P. BLANDON, MCS. VEY, P. L. PAUSON, G. D. BROADHEAD, and W. M. HORSPOOL. J. Chem. Soc. (C), 306 (1966).
38. P. A. GRIECO, S. GILMAN, and M. NISHIZAWA. J. Org. Chem. **41**, 1485 (1976).
39. K. B. SHARPLESS and M. W. YOUNG. J. Org. Chem. **40**, 947 (1975).
40. H. J. REICH, J. M. RENGA, and I. L. REICH. J. Am. Chem. Soc. **97**, 5434 (1975).
41. L. MEITES and T. MEITES. Anal. Chem. **20**, 984 (1948).
42. H. E. ZIMMERMAN. Mol. Photochem. **3**, 281 (1971).
43. H. E. ZIMMERMAN, T. P. CUTLER, V. R. FITZGERALD, and T. WEIGHT. Mol. Photochem. **8**, 379 (1977).
44. C. G. HATCHARD and C. A. PARKER. Proc. R. Soc. London, Ser. A, **235**, 518 (1956).
45. R. RAY and D. S. MATTESON. Tetrahedron Lett. 449 (1980).
46. E. J. COREY and C. U. KIM. Tetrahedron Lett. 287 (1974).
47. K. J. HALLER and J. H. ENEMARK. Inorg. Chem. **17**, 3552 (1978).
48. G. GERMAIN, P. MAIN, and M. M. WOOLFSON. Acta Crystallogr. Sect. A, **27**, 368 (1971).
49. D. T. CROMER and J. B. MANN. International tables for X-ray crystallography. Vol. 4. Kynoch Press, Birmingham, England. 1974. pp. 99–101. Table 2.2B.
50. R. F. STEWART, E. R. DAVIDSON, and W. T. SIMPSON. J. Chem. Phys. **42**, 3175 (1965).
51. G. TRAVERSO. Boll. Sci. Fac. Chim. Ind. Bologna, **13**, 53 (1955); Chem. Zent. **30**, 5474 (1959).
52. R. DABARD and J-Y. LE BIHAN. Bull. Soc. Chim. Fr. 4280 (1972).
53. H. J. BACKER and STEVENS. Recl. Tray. Chim. Pay-Bas, **59**, 423 (1940).
54. R. KÖSTER, S. ARORA, and P. BINGER. Justus Liebigs Ann. Chem. **1973**, 1219 (1973).
55. G. ZWEIFEL and H. C. BROWN. Org. React. **13**, 1 (1963).
56. E. F. ULLMAN and P. SINGH. J. Am. Chem. Soc. **94**, 5077 (1972).

Synthesis of dodecahedrane precursors. 3. Synthesis of alkylidene-1,3-cyclopentanediones and attempts to roof peristylanes

PHILIP E. EATON[1] AND WILLIAM H. BUNNELLE
Department of Chemistry, The University of Chicago, Chicago, IL 60637 U.S.A.

AND

PETER ENGEL
Laboratorium für chemische und mineralogische Kristallographie, Universität Bern, Bern, Switzerland

Received April 4, 1984

This paper is dedicated to Professor Peter Yates on the occasion of his 60th birthday

PHILIP E. EATON, WILLIAM H. BUNNELLE, and PETER ENGLE. Can. J. Chem. **62**, 2612 (1984).

Phenylsulfenylation of 2-alkyl-1,3-cyclopentanediones followed by oxidation and elimination is shown to give easy access to 2-alkylidene-1,3-cyclopentanediones, a heretofore rare class of highly reactive compounds with good synthetic potential as dienophiles, Michael acceptors, etc. The synthesis of 2-phenylthio-1,3-cyclopentanedione is given and its use as synthon for introduction of the 2-alkylidene-1,3-cyclopentadione group into other systems is described. The methodology is applied to the preparation of a substituted peristylane containing a complete complement of carbons, proper functionality, and correct stereochemistry for closure to a dodecahedrane. The X-ray structure analysis of an example of this ring system is given. Efforts to effect the closure are described.

PHILIP E. EATON, WILLIAM H. BUNNELLE et PETER ENGLE. Can. J. Chem. **62**, 2612 (1984).

On démontre que la phénylsulfénylation des alkyl-2 cyclopentanediones-1,3, suivie d'une oxydation et d'une élimination, s'avère une voie d'accès facile aux alkylidène-2 cyclopentanediones-1,3, une classe de composés qui était jusqu'à maintenant rare, qui sont très réactifs et qui présentent beaucoup de potentiel en synthèse soit comme diénophiles, comme accepteurs dans les réactions de Michael, etc. On rapporte la synthèse de la phénylthio-2 cyclopentanedione-1,3 et on l'utilise comme synthon pour introduire le groupe alkylidène-2 cyclopentanedione-1,3 dans d'autres systèmes. On a appliqué la méthodologie pour préparer un péristylane substitué contenant un complément complet de carbones, la fonctionalité appropriée et la bonne stéréochimie pour effectuer une fermeture conduisant à un dodécaédrane. Faisant appel à la diffraction des rayons-X, on a déterminé la structure d'un composé faisant partie de ce système cyclique. On décrit les essais effectués en vue de réaliser la fermeture désirée.

[Traduit par le journal]

Can. J. Chem. Downloaded from www.nrcresearchpress.com by 210.87.254.105 on 09/06/12
For personal use only.

Introduction

Dodecahedrane (**1**) is an exceptional molecule. Its symmetry, rigidity, and near lack of angular strain provide a special opportunity for the study of fundamental chemistry (for a general overview, see Eaton (1)). The synthesis of dodecahedrane continues to be pursued with great vigor both here and elsewhere (1), even in view of the recent fine achievement of its first preparation by Paquette *et al.* (2). The challenge and importance of the system are sufficient to merit development of other synthetic methodologies. We report here some of our continuing efforts along these lines (3).

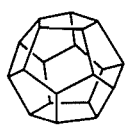

1

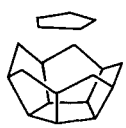

2

We view dodecahedrane as a peristylane (**2**) roofed by a five-membered ring. In 1972 we reported the first synthesis of the peristylane ring system (3*a*,*b*), and have since modified and improved this synthesis to the point that the peristylane **3** can now be considered a fairly readily accessible material (3*d*). We have examined the chemistry of this peristylane at some length and have presented detailed methodology for its further functionalization at carbons 8 and 15, and for substitution at carbon 4 (3*c*). These methods depend on the preparation of unsaturated peristylenones and the high reactivity of these strained olefins. We have shown also how certain *exo*-substituents on the peristylane frame, particularly at C-4, can be transformed into the corresponding *endo*-substituents positioned properly for ultimate integration into the dodecahedrane frame (3*c*). A proposal is sketched out in Scheme 1 to bring these successes together into a tactical synthesis of a peristylane substituted and suited functionally, at least in theory, for closure into a dodecahedrane. This paper describes the real-world travails by which the ideas in Scheme 1 were brought to fruition and then some of our attempts to carry on further toward dodecahedrane.

Results and discussion

The roof: initial attachment

The 1,7-bisselenide **4** can be made readily from **3** by reaction with phenylselenenyl chloride in ethyl acetate (3*c*). Heating **4** with 1,3-cyclopentanedione in basic 2,2,2-trifluoroethanol gave the expected *exo*-adduct **5**. The material, like most 1,3-cyclopentanedione derivatives, was an equilibrating mixture of the enolized forms, as evidenced by the single absorption for the four methylene protons in its ^{1}Hmr spectrum, as well as ir bands characteristic of β-hydroxycyclopentenones (2700, 1580 cm^{-1}). As a result of this enolization, **5** was quite insoluble in most organic solvents; as an organic acid, however, it was readily soluble in basic solutions.

Selenenylation of **5** was easily achieved by reaction of its

[1]Author to whom correspondence may be addressed.

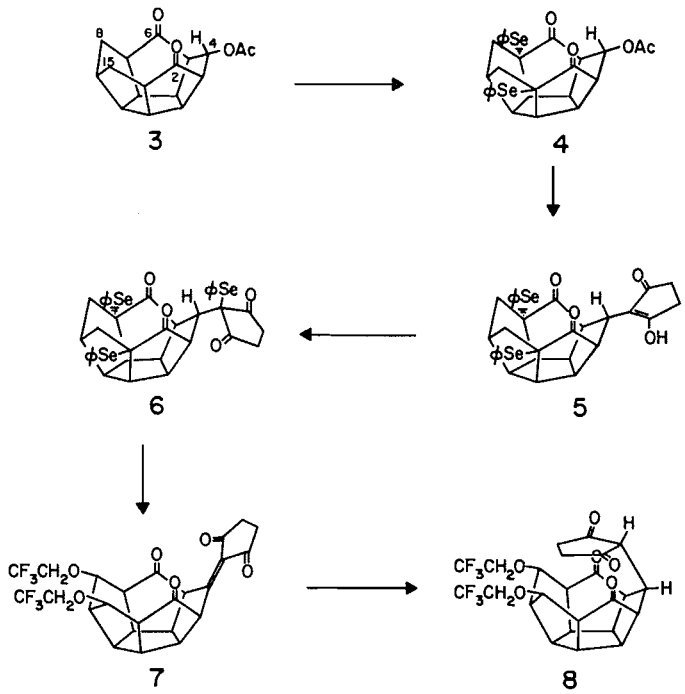

SCHEME 1

solution in pyridine with phenylselenenyl chloride.[2] Substitution took place at the nucleophilic carbon of the 1,3-dione system, and not at the oxygen of the enolate, providing the trisselenide **6**. As enolization of the β-dione was now blocked, **6** was easily handled as a typical hydrophobic compound. Its ^{1}Hmr spectrum was consistent with the plane of symmetry in the molecule.

With the successful preparation of trisselenide **6**, it seemed that functionalization of the remote peristylane methylenes (C-8 and C-15) as well as part of an *exo* → *endo* inversion sequence at C-4 could be attempted, all in one fell swoop, following the methods developed here previously. However, treatment of **6** at −70°C with ozone, conditions appropriate to selenoxide formation, followed by warming to room temperature in basic trifluoroethanol, gave a hopeless mixture of products. The addition of ethyl vinyl ether as a selenenic acid trap, a useful technique developed here (*3c*), failed to improve the situation. Even gross simplification of the system failed to help: although condensation of acetoxyperistylanedione **3** and 1,3-cyclopentanedione gave adduct **9** easily enough, and selenenylation produced the C-selenide **10**, oxidation/elimination gave only low yields of unidentified products.

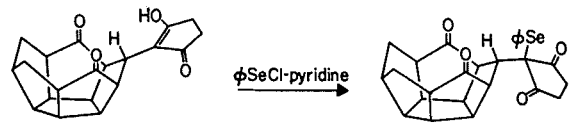

2-Alkylidene-1,3-cyclopentanediones

Faced with this, it was prudent to backtrack and investigate the chemistry of simple 2-alkylidene-1,3-cyclopentanediones (6). A search of the literature revealed that very little was known about such compounds (7). Although the "parent" 2-alkyl-1,3-cyclopentanediones are accessible by a variety of routes, the conceptually simple transformation to the unsaturated 2-alkylidene compounds had never been reported. With this rather puzzling lack of precedent, work on the formal dehydrogenation of 2-isopropyl-1,3-cyclopentanedione (**11**) was begun. The compound was prepared as described by Hiraga (8). The ^{1}Hmr spectrum of **11** in pyridine-d_5 solution showed the anticipated four-proton singlet for the ring methylene hydrogens and the heptet−doublet pair characteristic of an isopropyl group. The relative simplicity of this spectrum and the spectra of the reaction products from **11** proved a great asset in subsequent structural assignments.

Selenenylation of **11** in pyridine with phenylselenenyl chloride gave, after chromatographic work-up, a good yield of a product whose ir and ^{1}Hmr spectra were consistent with the *C*-selenenylated structure **12**. Confirmation of this structure was obtained by ^{13}Cmr spectroscopy. There were nine lines in the proton-decoupled spectrum, consistent in number and position with the *C*-selenide, but not the alternative enol *O*-selenenylated isomer. As samples of **12** degraded upon

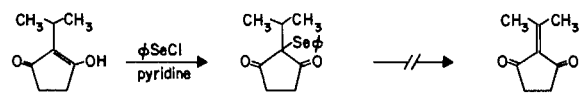

[2]The conditions of this selenenylation are worthy of comment. When these experiments were first carried out in 1978, literature precedent for selenenylation of β-dicarbonyl compounds dictated very much more drastic conditions (4). Typically, the β-dicarbonyl system would first be deprotonated with a strong base (potassium hydride or lithium diisopropylamide) and the enolate then quenched with phenylselenenyl chloride. When other enolizable carbonyl groups were present, as in **5**, the amount of base had to be controlled carefully to avoid over-selenenylation. We found here that pyridine was a strong enough base to allow selenenylation of the β-diketone via the enolate, while isolated carbonyl groups were quite inert. The use of pyridine/phenylselenenyl chloride as a general reagent for effecting selenenylation of β-dicarbonyl compounds has since been developed independently by Liotta *et al.* (5).

Can. J. Chem. Downloaded from www.nrcresearchpress.com by 210.87.254.105 on 09/06/12
For personal use only.

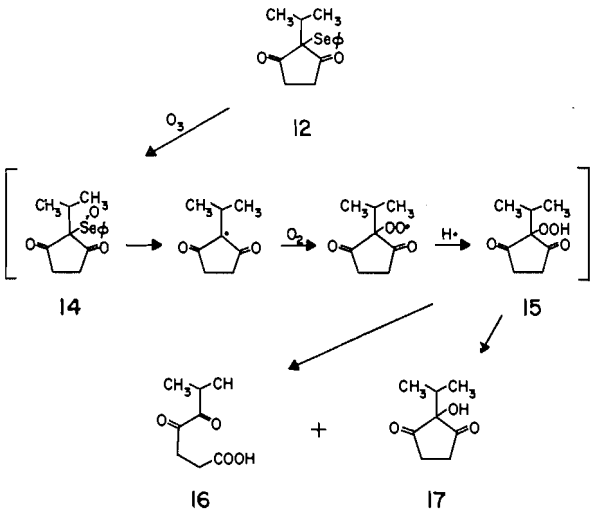

SCHEME 2

standing, attempts to convert it to **13** had to be done with freshly prepared material. Even so, although a variety of oxidation–elimination conditions were tried, in no case could any of the desired ene-dione **13** be isolated. Instead, more or less complex mixtures of products were obtained. The cleanest reaction occurred on low-temperature ozonization of a methylene chloride solution of **12**, followed by warming to room temperature. In addition to deselenenylated material **11**, two major products were obtained in a 3:1 ratio (see Scheme 2). The major component, shown by mass spectroscopy to have molecular formula $C_8H_{12}O_{14}$, was assigned structure **16** on the basis of the spectral evidence (isopropyl group methine at 3.36 ppm, AA′BB′ pattern centered at 2.80 ppm in ^{1}Hmr; CO_2H band in ir). The minor product was likewise identified as the tertiary alcohol **17** ($C_8H_{12}O_3$; isopropyl methine at 2.15 ppm, AA′BB′ pattern centered at 2.84 ppm in the ^{1}Hmr). Low-temperature ^{1}Hmr studies indicated that these products were formed rapidly even at −60°C. We believe (Scheme 2) that selenoxide **14** was formed initially but then fragmented, not in the desired pericyclic sense, but rather homolytically at the carbon–selenium bond to give the stabilized cyclopentanedione radical.[3] This in turn could have captured oxygen to give a peroxide radical and then, through hydrogen abstraction, the hydroperoxide **15**. This compound finally could have decomposed along two pathways: the major product **16** arising from fragmentation of the peroxide (11); the minor product **17** resulting from reduction of the peroxide (by available selenium species?) to the observed tertiary alcohol.

By now it seemed certain that a selenenylation–oxidation–elimination route to compounds like **13** would not work. We looked for alternative routes. Partial hydrogenation of the known 2-isopropylidene-4-cyclopenten-1,3-dione **19** appeared promising. This compound was prepared by the procedure of Skorianetz *et al.* (10); sensitized photooxygenation of dimethylfulvene (Rose Bengal, O_2, pyridine) gave (in part) the ketodienol **18**, which was converted to the bright yellow crystalline diene-dione **19** on oxidation with Jones reagent.

Catalytic hydrogenation of **19** over palladium-on-carbon at 0°C using methylene chloride as solvent, gave fairly selective reduction of the disubstituted double bond. The ^{1}Hmr spectrum of the crude yellow product showed only two lines, a four-proton singlet at 2.64 ppm and a six-proton singlet at 2.54 ppm, completely consistent with the formation of enedione **13**. The uv spectrum could not be determined precisely as the material was unstable, converting to a dimeric compound, isolated as colorless crystals from ether–hexanes.

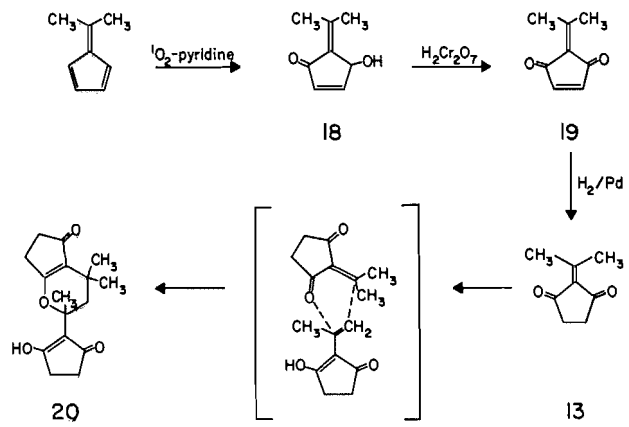

The mass spectrum of the dimer gave a parent ion corresponding to $C_{16}H_{20}O_4$ and a major fragment ion for the monomer $C_8H_{10}O_2$. The presence of an enolized 1,3-cyclopentanedione was indicated in the ir by bands at 2700, 1693, and 1636 cm^{-1}, and in the uv by an absorption at 250 nm (ϵ = 24 300) that shifted to 260 nm (ϵ = 26 000) in base. The ^{1}Hmr spectrum of the dimer showed the presence of three methyl group (singlets), as well as one isolated geminal methylene proton pair. Taken with knowledge of the compound's origin, this spectroscopic information was sufficient to assign structure **20** to the dimer, a formal Diels–Alder adduct between the heterodiene system of one molecule of **13** and the terminal olefin of the dienol form of a second.[4] A few attempts were made to intercept these components (maleic anhydride as dienophile for the former; furan as diene for the other), but these were not successful. Only dimer **20** was isolated.

With the knowledge that 2-alkylidene-1,3-cyclopentanediones could be handled and characterized (albeit requiring some speed), new attempts were made to obtain them directly from the much more readily available 2-alkyl-1,3-cyclopentanedione precursors. As proposed in Scheme 2, the problem with the initial approach is thought to be the homolytic frangibility of the carbon–selenium bond. Carbon–sulfur bonds are stronger than those to selenium (11), it seemed therefore that substitution of sulfur for selenium might be exploited with success. With this change, the desired pericyclic elimination might be able to compete successfully with the homolytic bond cleavage pathway.

The sulfenylation of ketones has generally been achieved by reaction of the ketone enolate with diphenyl disulfide (12). To this end, the potassium enolate of 2-isopropyl-1,3-cyclopentanedione was prepared by reaction with potassium hydride in tetrahydrofuran. However, this stabilized β-dione enolate did not react with diphenyl disulfide or even the more electrophilic phenyl benzenethiosulfonate. 1,3-Cyclopentanediones have been sulfenylated with phenylsulfenyl chloride (13), but the

[3]Cyclic 1,3-diketones are easily peroxygenated without basic catalysts (9).

[4]Its regioisomer was excluded based on the high field position of the methylene protons of the dihydropyran sub-unit.

Can. J. Chem. Downloaded from www.nrcresearchpress.com by 210.87.254.105 on 09/06/12
For personal use only.

instability of this reagent makes it impractical for general use. On the other hand, sulfenimides are stable, crystalline solids and have been shown to be effective sulfenylating reagents for active methylene compounds (14). Indeed, treatment of 2-isopropyl-1,3-cyclopentanedione with *N*-phenylthiosuccinimide in triethylamine and benzene resulted in its efficient conversion to the desired phenyl sulfide **21**. The ^{1}Hmr and ir spectral data for **21** were certainly consistent with this structure but, as before with the corresponding selenide **12**, it was ^{13}Cmr spectroscopy that permitted unambiguous determination that sulfenylation had occurred on carbon and not on oxgyen.

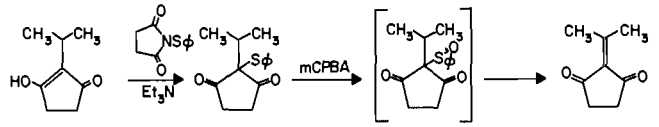

11 21 13

Oxidation of **21** was carried out with *m*-chloroperoxybenzoic acid (mCPBA). Experimentally, it was most convenient to add the peracid to a cold (−70°C) solution of **21**. Oxidation was sluggish at this temperature, but proceeded smoothly as the mixture was warmed toward room temperature. The presumed intermediate sulfoxide was not isolated, but was taken to 40°C, effecting elimination of phenylsulfenic acid and clean generation of the desired ene-dione **13**. This route gave for the first time a simple and direct conversion of a 2-alkyl-1,3-cyclopentanedione to the corresponding 2-alkylidene-1,3-cyclopentanedione.

Although it was outside our purpose to explore fully the application of this sulfenylation−oxidation−elimination to compounds not on the path to dodecahedrane, we did consider briefly the synthesis of the simplest 2-alkylidene-1,3-cyclopentanedione, the 2-methylene compound **23** (see Scheme 3). Phenylsulfenylation of the readily available 2-methyl-1,3-cyclopentanedione with *N*-phenylthiosuccinimide in benzene with triethylamine as base proceeded smoothly to give **22** in 90% yield. Reaction of **22** with *m*-chloroperoxybenzoic acid, as in the conversion **21** → **13**, gave (presumably) 2-methylene-1,3-cyclopentanedione. It was not possible to isolate this compound. Apparently, this unhindered, cross-conjugated enedione is exceptionally reactive. In the case at hand, it was trapped by Michael addition of cognate phenylsulfenic acid (15) to give a crystalline adduct assigned the sulfoxide structure **24**, consistent with the AB quartet in the ^{1}Hmr spectrum arising from the diastereotopic protons on the sulfoxide methylene group.

The exceptional reactivity of 2-alkylidene-1,3-cyclopentanediones can be put to very good use, for not only are the compounds active Michael acceptors, they are reactive dienophiles. Thus, when **23** was generated at 40°C in the presence of isoprene the major product (70% isolated yield overall from **22**) was a Diels−Alder adduct, the [4.5]spirocycle **25**.[5] Such spiro systems are common elements in the acorane and spirovetivane sesquiterpenes, etc. Clearly, this chemistry could be developed

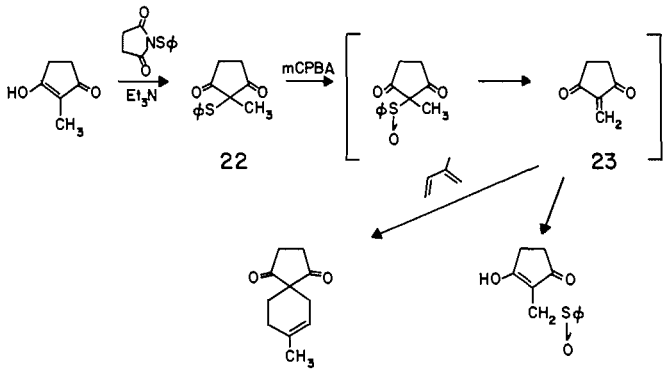

22 23 25 24

SCHEME 3

fruitfully with such goals in miond. Here, however, we turn to apply it to elaboration of peristylane.

2-(Peristylylidene)-1,3-cyclopentanediones

With the simple model work completed satisfactorily, we were able to apply sulfoxide elimination methodology successfully to the preparation of the peristylane ene-tetraone **27**. Phenyl sulfenylation of the peristylanedione-cyclopentanedione **9** with *N*-phenylthiosuccinimide gave **26**. Oxidation to the sulfoxide with *m*-chloroperoxybenzoic acid followed by warming to 40°C produced the desired ene-tetraone **27** as the major product (Scheme 4).

The important features of the ^{1}Hmr spectrum of **27** were the obvious simplifications due to symmetry, the broadened doublet at 5.15 ppm for the allylic methines (H-3 and H-5), and the absence of a signal for a proton at C-4. The molecular formula was confirmed by high resolution mass spectroscopy. This yellow, microcrystalline 2-alkylidene-1,3-cyclopentadione was completely stable to dimerization, no doubt due to the steric effects of the bulky peristylane substituent. The enedione chromophore could now be characterized precisely (see Experimental). The compound was, however, exceptionally sensitive to nucleophilic attack. If aqueous base were used in its work-up, substantial amounts of a by-product were formed. This is thought to have structure **28***a* (R = H) on mechanistic grounds supported by ^{1}Hmr and mass spectral evidence. Even carefully controlled attempts to perform Michael additions (CF_3CH_2OH, Et_3N) to the conjugated olefin of **27** resulted instead in facile, vinylogous retrograde-Claisen reaction, probably initiated by attack of the nucleophile at a carbonyl center on the peristylane ring as shown for the formation of **28***b* (R = CH_2CF_3).

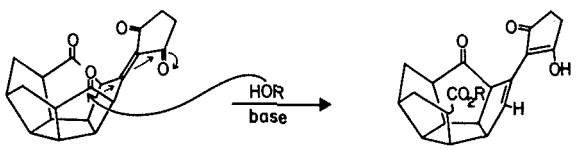

27 28

The overall yield of ene-tetraone **27** from peristylanedione-cyclopentanedione **9** by the sulfenylation−oxidative elimination was 50%. It was good finally to have the material in hand, but this first synthesis was not altogether satisfying. There was, *ex post facto*, no reason to sulfenylate compound **9**, which was difficult to make and handle efficiently (enolized β-dicarbonyl). Why not instead have the sulfur substituent already attached to the cyclopentanedione ring at the time this

[5]The expected "*para*" regiochemistry was confirmed by converting **25** (ketalization, photochemical olefin migration, ketal hydrolysis) to its exocyclic double bond isomer, the nmr spectrum of which was in complete accord with the C_{2v} symmetry: δ 4.72 (2H, s), 2.81 (4H, 2), 2.41 (4H, t, $J \sim 5$ Hz), and 1.73 ppm (4H, t, $J \sim 5$ Hz), *quod erat demonstrandum*.

Can. J. Chem. Downloaded from www.nrcresearchpress.com by 210.87.254.105 on 09/06/12
For personal use only.

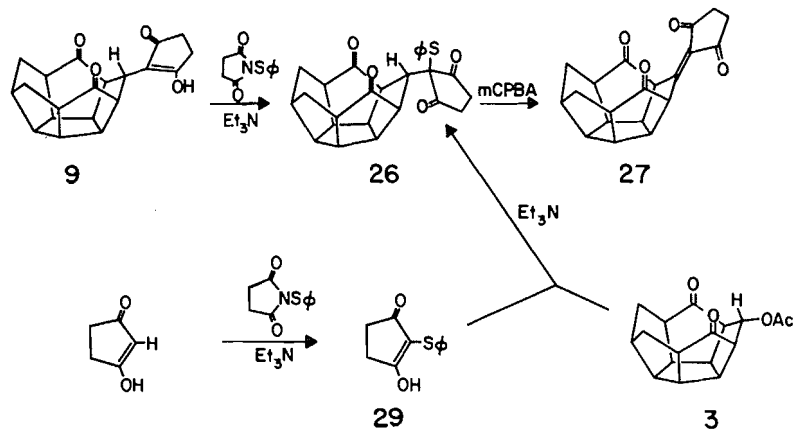

SCHEME 4

is put on the readily available peristylane **3**? The synthetic scheme would be more convergent, and **9** could be bypassed altogether.

The previously unknown 2-phenylthio-1,3-cyclopentanedione **29** was easily prepared in 90% yield by phenylsulfenylation of 1,3-cyclopentanedione with one equivalent of *N*-phenylthiosuccinimide. It was isolated as stable, colorless needles from ethyl acetate. Initial alkylation experiments using 4-acetoxyperistylane-2,6-dione (**3**) in methylene chloride with triethylamine afforded mainly the *O*-alkylated product. A simple change of solvent, from methylene chloride to benzene, resulted in exclusive *C*-alkylation; 80–85% yields of the crystalline (phenylthiocyclopentanedionyl)-peristylanedione **26** were then obtained from **3** in this single laboratory operation. This compound was taken as before to be **27**. A 70% yield of pure material was obtained directly. The major by-product was the desulfenylated material **9**, which could be recovered and recycled, bringing the total yield for this step to 80–85%. Overall then, ene-tetraone **27** could be prepared from **3** in 60–70% yield using just two simple laboratory operations on this most available peristylane. This sequence was altogether satisfactory for the preparation of multigram quantities of the ene-tetraone.

Before moving on to the next section the point should be made that 2-phenylthiocyclopentane-1,3-dione is easily made and should, in turn, make readily available a large variety of 2-alkylidene cyclopentane-1,3-diones to whose utility we have already alluded.

Stereochemistry at C-4

Hydrogenation of the olefin bond in ene-tetraone **27** from the outer, less-hindered face can be imagined to give the *endo* roofed compound **30***a*. The close geometrical relationship between this product and dodecahedrane is obvious. However, this conceptual drawing is illusory. It does not give proper weight to the steric congestion of groups about the peristylane rim nor to the ways that simple changes can minimize these interactions. Enolization and slight rotation about the peristylane–cyclopentane connecting bond (C-4, C-16) would move the "roof" out from close proximity to the peristylane rim (→ **30***b*). It was obvious therefore from the start that some conformational difficulties would pertain to further closures of **30** towards dodecahedrane.

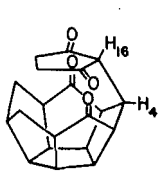

30*a*

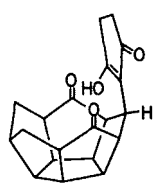

30*b*

Ene-tetraone **27** smoothly absorbed hydrogen over a palladium catalyst to give an equilibrating mixture of dihydro isomers, from which one eventually crystallized from chloroform solution. This compound was assigned structure **31**, formed via enolization of the hydrogenation product **30** and then internal hemiketalization. Molecular models of **31** suggest a low-energy conformation in which the dihydropyran so formed exists in a flattened half-chair conformation **31***a*. Minimization of steric interactions about the peristylane cavity would put one of the *endo*-peristylane protons (H_a) within the shielding region of the enone sub-system; the dihedral angles to the vicinal protons would be about 160°. Consistent with this, the ^{1}Hmr spectrum of **31** showed a signal for one proton unusually upfield at 0.38 ppm, appearing appropriately as a doublet of triplets (J_{gem} = 15 Hz, J_{vic} = 12 Hz). Complementarily, the other *endo* proton (H_b) appeared as a slightly broadened doublet at 2.08 ppm. In conformation **31***a* the dihedral angles for this proton to its vicinal neighbors are close to 90°, so only geminal coupling is observable.

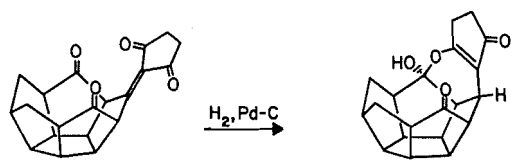

27 **31**

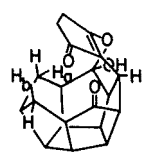

31*a*

A sample of **31** was heated in acetic acid-d_4 with sodium acetate. At 50°C, exchange of deuterium for protium occurred over a period of hours at the four sites adjacent to carbonyls and potential carbonyls on the peristylane ring (C-1,3,5,7 by

Can. J. Chem. Downloaded from www.nrcresearchpress.com by 210.87.254.105 on 09/06/12
For personal use only.

Can. J. Chem. Downloaded from www.nrcresearchpress.com by 210.87.254.105 on 09/06/12
For personal use only.

peristylane numbering).[6] The exchange was monitored conveniently by ^{1}Hmr, following the loss of vicinal spin coupling to the protons at C-4, C-8, and C-15. We interpret this exchange to mean that **31** under these conditions was in equilibrium with its open forms.

These results showed that the ready enolization of the β-diketone of the roof fragment would be little more than a nuisance. Conformational flexibility about the C-4, C-16 bond was surely to be more troublesome as there was no reason for the roof to assume a conformation consistent with the required bonding ahead. Our plan from the beginning therefore was to set in the appropriate conformation by Diels–Alder addition to (rather than reduction of) the electron deficient olefin of **27**. This incidentally would also solve the enolization problem. We were encouraged in this with the results from simple model systems, e.g. **23** → **25**. Indeed, reaction of **27** with excess 2,3-dimethylbutadiene in a sealed tube at 130°C gave the crystalline, 1:1 Diels–Alder adduct **32** in 85% yield. Examination of its ^{1}Hmr and ^{13}Cmr spectra confirmed this assignment of structure fully.

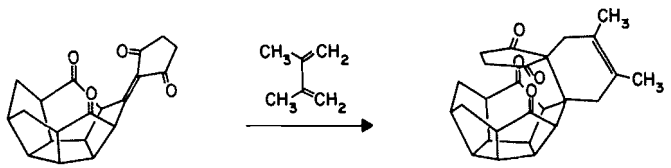

27 32

Further functionalization

Compound **32**, available in just three synthetic steps from acetoxyperistylanedione **3**, is a very attractive dodecahedrane intermediate. All twenty carbon atoms are there and are suitably arranged for incorporation into the dodecahedrane skeleton. The nuisance enolization of the β-dione system has been blocked, and rotation around the peristylane–cyclopentane connective bond (C-4, C-16) has at least been partially restricted. Construction of only four carbon–carbon bonds would complete the dodecahedrane cage. On paper, all that seems necessary for two of these bonds is the introduction of leaving groups at C-8 and C-15, followed by intramolecular alkylation α to each carbonyl group of the roof.

Methodology for the functionalization of the C-8 and C-15 positions had been described in our earlier paper (3*c*, cf. Scheme 1); now it was a matter of integrating it into the evolving scheme. Reaction of the known (3*c*) 1,7-bis(phenylselenenyl)-4-*exo*-acetoxyperistylane-1,5-dione (**4**) with 2-thiophenyl-1,3-cyclopentanedione and triethylamine in benzene formed the desired C-4 alkylated product **33** in 84% yield (Scheme 5). Low temperature ozonization of **33**, as expected, oxidized the selenide groups cleanly and selectively without affecting the sulfide portion of the molecule. No attempts was made to isolate this bisselenoxide-sulfide (**34**); it was allowed instead to decompose in the presence of triethylamine and trifluoroethanol. The expected eliminations of phenylselenenic acid and the Michael additions of trifluoroethanol to the transient enones so formed occurred smoothly, but (distressingly)

[6]The methylene protons of the enolized cyclopentanedione underwent exchange at a substantially slower rate; extended enolization of an already enolized system is not easy. Exchange of two of these cyclopentane protons (presumably those in the *exo*-position) was eventually effected by raising the temperature to 100°C.

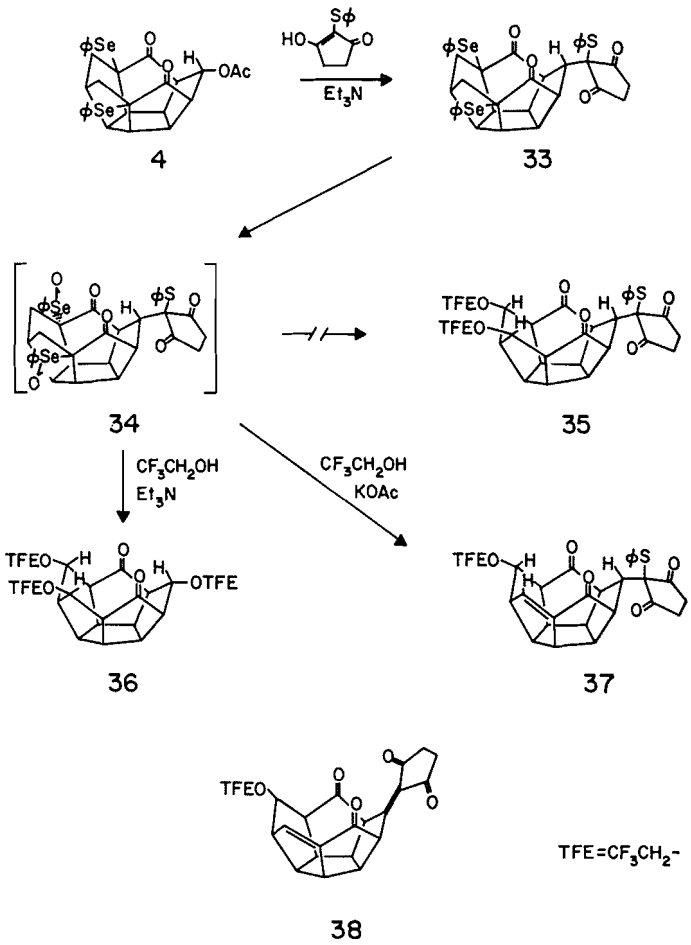

4 33 34 35 36 37 38

SCHEME 5

the product finally isolated was the tris(trifluoroethyl ether) **36** (3*c*). None of the desired compound **35** could be isolated.

Apparently, under the conditions of the reaction, reverse Michael loss of the highly-stabilized anion of 2-thiophenyl-1,3-cyclopentanedione occurred to give the familiar peristyl-3(4)-enone system, which then added the third trifluoroethanol unit. We thought it should be possible to suppress this retro-Michael elimination by using a weaker base than triethylamine. To test this, the simpler phenylthiocyclopentanedione-peristylanedione **26** was put through a series of model experiments to determine the range of conditions compatible with the thiophenylcyclopentanedione moiety. Alkyl amines, alkali metal carbonates, and bicarbonate bases in trifluoroethanol all promoted retro-Michael reactions at ambient temperature. Pyridine and alkali metal carboxylate salts were unreactive under these conditions, meriting further consideration for use in the conversion **33** → **35**. Pyridine proved unsuitable in the real case – intractable mixtures were produced. Potassium acetate was used somewhat more successfully. When **33** was ozonized in methylene chloride at −70°C, and the solution then allowed to warm to room temperature in the presence of added trifluoroethanol and potassium acetate, the thiophenylcyclopentanedione moiety remained intact, and the elimination–addition chemistry on the rest of the molecule went well, if somewhat astray. The major product isolated was now the ene-trifluoroethyl ether **37**. A bit, but not enough, of the more desirable bis(trifluoroethyl ether) **35** could be detected spectroscopically.

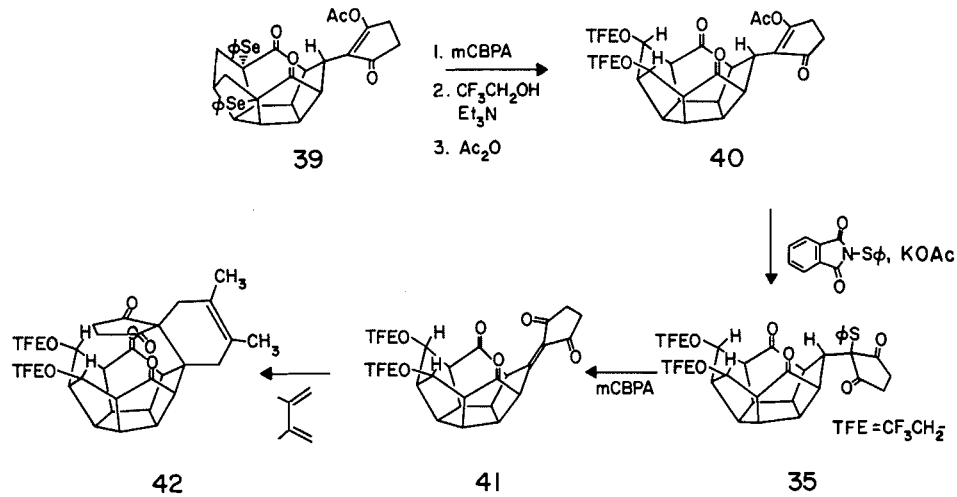

SCHEME 6

Although the ene-ether **37** might at first be considered functionally equivalent to **35** with regard to the projected enolate closure reactions, there are some unfortunate problems with this idea. The alkylidene cyclopentanedione **38**, of which **37** could be parent, would certainly react first in a Diels–Alder addition at the peristylenone double bond rather than at the ene-dione; we have shown already that such strained, twisted olefins are exceptionally reactive in these diene additions (3*c*). On the other hand, there is no possibility of being able to achieve selective Michael addition to the peristylenone double bond in the presence of the much more Michael-receptive enedione moiety; recall the reverse Claisen cleavage of **27** → **28**. The only remaining remedy is to effect addition to the peristylenone **37** before oxidative elimination of the phenylthio group. Disappointingly, all attempts to do this, extending over a wide variety of nucleophiles, were without significant reward.

More devious ways around this stalemate were sought. If the sulfide group in **33** could be oxidized to the exclusion of the selenide groups, then elimination and Diels–Alder addition at C-4 could be carried out first, without interference from sensitive groups on the peristylane ring. Unfortunately, no method to achieve such selectivity is known; on the contrary, selenides are oxidized much more easily than sulfides. But if the sulfur group were to be oxidized prior to its introduction into the molecule, the presence of the selenides would offer no problem. To this end, 2-phenylthio-1,3-cyclopentanedione was oxidized to the corresponding sulfoxide with 2-hydroperoxyhexafluoroisopropanol (16). The sulfoxide was heated in benzene with triethylamine and 4-acetoxyperistylanedione. Under the conditions of the experiment, had any of the *C*-alkylated adduct formed, it would have immediately suffered thermolysis to the known ene-tetraone **27**. Unfortunately, none of this material was obtained.

Since the development of proper substitution at the C-8 and C-15 positions of peristylane required nucleophilic conditions incompatible with a fragile group or good nucleofuge at C-4, we turned to placing the enolate ion of a 1,3-cyclopentanedione at C-4. The negative charge on this ion would effectively prevent it from being attacked by nucleophiles or behaving as a leaving group. The plan (Scheme 6), unhappily less convergent than before, was to carry out the selenoxide elimination – Michael addition sequence to functionalize C-8 and C-15 on compound **5** (from **39**)[7] in which cyclopentane-1,3-dione was already in place as the C-4 appendage. Under the basic conditions of the reaction the β-diketone would of course be in its ionized, enolic form. After functionalization of the peristylane methylenes had been completed, sulfenylation, oxidative elimination, and Diels–Alder addition should then provide the desired, fully-developed dodecahedrane precursor **42**.

Condensation of cyclopentane-1,3-dione with bis(phenylselenenyl)acetoxyperistylanedione **4** in triethylamine and benzene, followed by treatment of the crude adduct with acetic anhydride, gave the beautifully crystalline enol acetate **39** in 95% overall yield. Oxidation of the selenide groups of **39** with ozone, even at low temperature, also gave substantial oxidation at the enol double bond. Fortunately, the use of *m*-chloroperoxybenzoic acid at −70°C avoided this complication and provided the bisselenoxide with a minimum of side reactions. When trifluoroethanol and triethylamine were added to the cold solution of the (unisolated) bisselenoxide, and the mixture was allowed to warm to room temperature, sequential elimination and Michael addition occurred without interference. Of course, these conditions were sufficient to take the enol acetate of the dione to the desired enolate anion, shielding the group from displacement or attack. Work-up and reacetylation (Ac_2O) gave the enol acetate **40**. This was then subjected to a very mild deprotection–sulfenylation sequence with *N*-phenylthiosuccinimide, trifluoroethanol, and potassium acetate. Isolation by preparative thin-layer chromatography provided finally the elusive sulfenylated bis(trifluoroethyl ether) **35** in 45–50% overall yield from **39**.

Oxidative elimination of phenyl sulfenic acid from **36** was effected smoothly as before with *m*-chloroperoxybenzoic acid. Buffered work-up followed by trituration with diethyl ether gave a 73% yield of the bright yellow ene-tetraone **41**, whose identity followed from its ^{1}Hmr spectrum. After so much frus-

[7]In practice, it was much more satisfactory to work with this enol acetate than with the free β-diketone **5**. The derivative had the advantage of high solubility in common organic solvents and under the reaction conditions to be used for C-8/C-15 functionalization, trifluoroethanol and triethylamine (or even potassium acetate), the enol acetate was rapidly converted to the enolate anion. Thus, **39** served as a synthetic equivalent of **5**, while conferring the convenience of solubility.

Can. J. Chem. Downloaded from www.nrcresearchpress.com by 210.87.254.105 on 09/06/12
For personal use only.

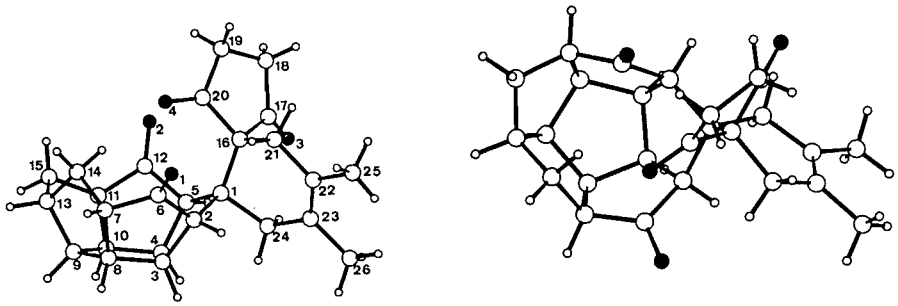

FIG. 1. Two views of compound **32** derived from X-ray crystallographic data; cf. the idealized drawing **32** in which the trans-skeletal interactions are ignored. (The numbering system pertains to the crystallographic analysis; C-8, 18, 15, 19 in the discussion correspond to C-15, 18, 14, 19, respectively, in this figure.)

Can. J. Chem. Downloaded from www.nrcresearchpress.com by 210.87.254.105 on 09/06/12
For personal use only.

tration, this was indeed a pleasing result.

Reaction of **41** with 2,3-dimethylbutadiene in a sealed tube at 100°C gave the desired Diels–Alder adduct **42**. The reaction proved capricious; yields ranged, without apparent reason, from 0 to 100%. It proved wise therefore to do only small-scale runs.[8] Nevertheless, it was possible to prepare and characterize **42** and to bring up sufficient material to investigate the chemistry of this crucial intermediate. The mass spectrum was in agreement with the assigned structure, and the ^{1}Hmr spectrum was readily recognizable as that of an 8,15-substituted peristylane.

The conformation problem

At this point our synthetic plan called for generation of an enolate anion in the roof five-membered ring and its bonding into the peristylane portion via one of two possible mechanisms: the first, simply S_N2 displacement of the appropriately sited trifluoroethoxy group in an intramolecular alkylation; alternatively, base-induced elimination of trifluoroethanol would give a peristylenone to which the roof enolate could add in Michael fashion. Done twice over, either of these internal alkylations would produce the desired bissecododecahedrane, from which a dodecahedrane could then be obtained by, for example, pinacol closure. This plan requires a proper orientation of the reactive sites within the molecule (C-8 must bond with C-18; C-15 with C-19). The necessary stereochemical alignment is possible, but by no means comfortable. The required conformation in **42** involves significant non-bonded interactions between opposing *endo*-oriented protons. At this point in our work the solid-state structure of the closely related Diels–Alder adduct **32** was obtained by single crystal X-ray analysis. The drawings in Fig. 1 generated from this analysis clearly show the fused 6-membered ring of **32** in its half-chair conformation and the cyclopentanedione unit in an orientation skewed to the peristylane mirror plane. Thus, even with the extra rigidity provided by the annulated cyclohexene ring, the molecule can still flex away from the necessary conformational arrangement.

A molecule with a yet more rigid skeleton was needed. Diels–Alder adducts of ene-tetraone **41** to cyclic rather than

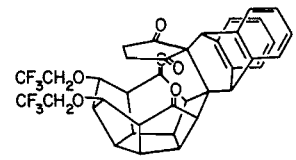

43

acyclic dienes would, with the extra bridge, have much less conformational flexibility. For example, in the anthracene adduct **43** the cyclopentanedione "roof" would be locked into position symmetrically over the peristylane bowl with very little torsional movement possible.

Exploratory reactions were carried out with the readily available ene-tetraone **27**. Even with prolonged reaction times at 100–200°C, none of the desired adduct could be obtained with anthracene or the more highly reactive 9,10-dimethylanthracene. Under forcing conditions, charring of the ene-tetraone occurred. Attempted catalysis with Lewis acids gave only unreacted starting materials, even after long reaction times. Tries at additions of cyclic, non-aromatic dienes (e.g. cyclohexa-1,3-diene) were equally without reward. Even furan at very high pressures failed to add. Diels–Alder reactions are often easily reversible, and here it now seems probable that the steric congestion enforced in the desired adduct sets the equilibrium position well to the side of the starting materials.

A variety of other attempts was made to provide locks on the conformation of the roof: light-induced 2+2 cycloadditions (e.g. cyclopentene) and thermal 2+2 and 1,3-dipolar cycloadditions (e.g. 1,1-dimethoxyethylene, diazomethane). These reactions often gave interesting chemistry, but none proved useful for solution of the problem at hand.

Attempts at closure

Although it was clear that the conformational preferences of **42** were not ideal for the necessary bond-forming reactions, neither were they forbidding. With little other choice available we proceeded to examine the reactions of **42** under enolate-generating conditions. Heating it under equilibrating conditions in trifluoroethanol with potassium carbonate caused loss of trifluoroethanol from the peristylane rim. Escalation of the reaction conditions to higher temperatures or longer reaction times caused only unproductive destruction of starting material. Use of amine bases (triethylamine or 1,4-diazabicyclo-[2.2.2]octane led to similar results. Potassium *tert*-butoxide in *tert*-butyl alcohol caused resinification. Many other systems were tried. In one, on the supposition that a complexing cation might favor bond-closing conformations by association

[8]Much effort was expended to bring the reaction under control, but this was not achieved. In one case, the two major wayward products had molecular formula $C_{38}H_{44}O_4$, implying double elimination of trifluoroethanol and net uptake of three equivalents of dimethylbutadiene. One product gave a ^{1}Hmr spectrum indicative of a time average plane of symmetry, consistent with a tris Diels–Alder adduct. The isomeric product quite likely resulted from at least one ene-type addition.

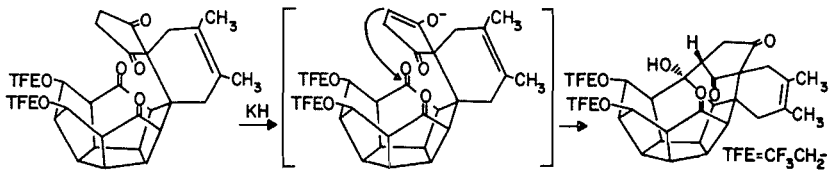

42 44

with the carbonyl oxygens, the reaction was attempted with magnesium methoxide as the base; only starting material was recovered.

Kinetic deprotonation conditions were tried next. When a tetrahydrofuran solution of **44** was added to a slurry of potassium hydride in tetrahydrofuran at −70°C, there was no reaction at all. Quenching with acetic acid-*O-d* gave only starting material without any deuterium incorporation. When the reaction mixture was allowed to warm to −45°C, a yellow color developed, signaling some kind of reaction. Quenching with acetic acid-*O-d*, followed by work-up with H_2O at room temperature, gave a new compound. Prominent peaks in the mass spectrum were observed at *m/e*'s corresponding to loss of water and to loss of trifluoroethanol from the starting material. No deuterium incorporation was evident. By ^{1}Hmr, the compound was clearly non-symmetric; both trifluoroethoxy groups were intact; one D_2O-exchangeable proton could be detected. The ir spectrum showed a weak band consistent with the presence of a tertiary alcohol and obvious carbonyl group absorptions. The structure was assigned as **44**, the product of an internal aldol reaction between a cyclopentanedione enolate at C-19 and a peristylane carbonyl group at C-6. Reference to Fig. 1 provides rationalization for this product without lengthy comment; the juxtaposition of the peristylane carbonyl center with the cyclopentanedione methylene group permits facile intramolecular reaction.

The conformation of **42** works against the desired bond closure reactions. The *endo*-oriented hydrogens at C-8 and C-15 are responsible, at least in part, for the conformational difficulty. This would be eliminated by conversion of **42** to the bis olefin **45**. We thought this very highly strained molecule might be made available transiently by oxidative elimination from bisselenide **46** done *in the absence of nucleophiles*. If this worked, then if the cyclopentanedione enolate could be formed (non-nucleophilic base), the desired intramolecular Michael addition might subsequently occur spontaneously.

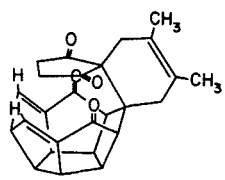

45

The necessary bisselenide **46** was prepared in good yield by selenenylation of tetraketone **32**. Low temperature oxidation with *m*-chloroperoxybenzoic acid gave (presumably) the corresponding bisselenoxide **47**. The reaction mixture was allowed to warm to room temperature in the presence of a large excess of triethylamine. The product (80% yield!) was the extraordinary ene-alcohol **50**, the first peristylane with a basal plane substituent. Its molecular formula was established by mass spectroscopy, and the structure was deduced from extensive ^{1}Hmr decoupling experiments which established the connectivity in the system. As proposed in the progression **47** → **50**, the first selenoxide elimination probably occurred along the peristylane rim as normal, giving enone **48**. All previous eliminations of peristylane bisselenoxides had been performed under conditions of high nucleophile concentration wherein this kind of enone would have undergone Michael addition prior to the second elimination. In the case at hand, with only adventitious water available as nucleophile, this sub-unit can survive. Apparently its presence alters markedly the elimination pathway of the second selenoxide. Probably the conformation of the peristylenone is such that the *syn* arrangement necessary for concerted loss of phenylselenenic acid along the rim is less available, whereas that for loss toward the basal position is not. By default, then, elimination would occur towards the base giving the very strained olefin **49** which in turn would hydrate readily. Further discussion of such compounds will be reserved for a later paper, with less complex examples.

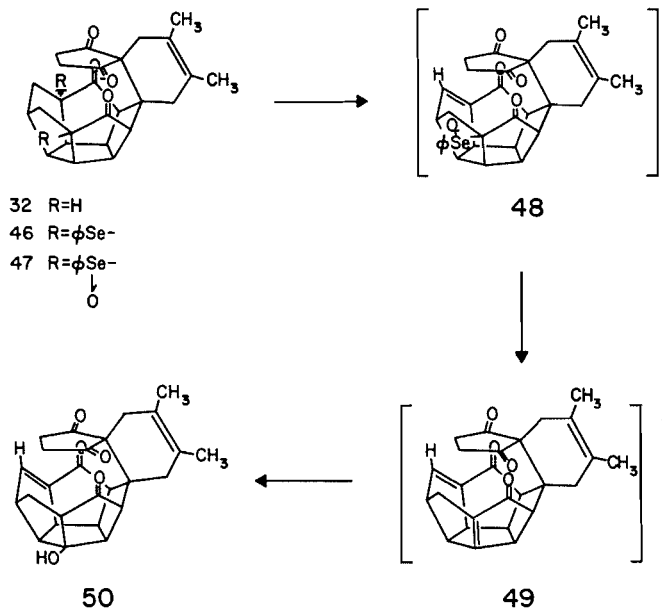

A brief excursion with another approach

Bonding reactions of the kind anticipated clearly require more rigid geometric control than we have yet achieved. A small torsional displacement at the single connective bond between roof and peristylane in **42** causes a drastic misalignment of the bonding positions C-8 and C-18, C-15 and C-19. This distortion is much less severe between the pairs of carbonyl positions. Geometrically, it might be easier to construct bonds between these carbonyl centers. Two-fold pinacol coupling within **32** would provide a bissecododecahedrane. (Of course, the loss of the carbonyl groups would necessitate a new strategy for closure of the final bonds.) Unfortunately, tetraketone **32** proved completely inert to treatment with magnesium amalgam

Can. J. Chem. Downloaded from www.nrcresearchpress.com by 210.87.254.105 on 09/06/12
For personal use only.

Can. J. Chem. Downloaded from www.nrcresearchpress.com by 210.87.254.105 on 09/06/12
For personal use only.

in refluxing dioxane and variations on such classical pinacol coupling conditions. Suffice it to say, although many reagents and conditions were tried, none of them – from simple zinc and magnesium metal systems to the more exotic low-valent titanium species – led to any of the desired pinacol product.

Only one reduction system ever gave an identifiable, symmetrical material. Lithium – liquid ammonia reduction of tetraketone **32** provided a 30–40% yield of a crystalline material, tentatively assigned tetraol structure **53** on the basis of nmr and mass spectroscopy. Under these reducing conditions, the 1,4-diketone bonding within the cyclopentanedione was apparently cleaved reductively to the bisenolate **51**. Two-fold intramolecular aldol reaction (→**52**) and subsequent reduction of the ketones would account for the observed product. Although a very interesting ring system of highly convex topology, tetraol **53** is not especially well suited for development to dodecahedrane. The twenty-carbon framework has been effectively scrambled.

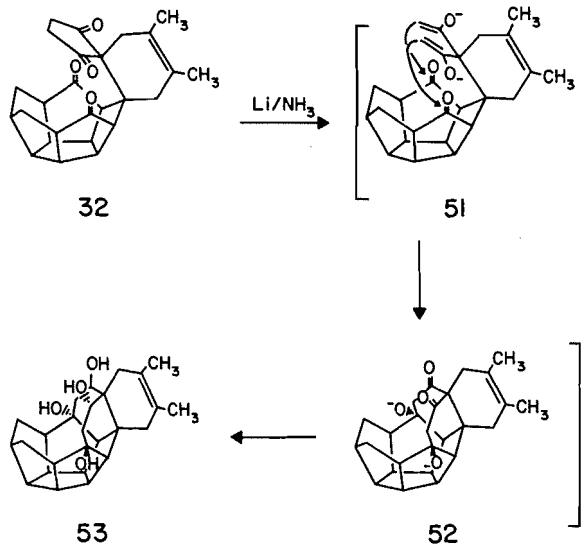

Conclusion

The cyclopentanedione-peristylanedione route to dodecahedrane has been examined from many different angles in this work; much has been learned, but our goal has not yet been reached. One point in particular has been driven home repeatedly – the effect of steric congestion around the peristylane cavity is to discourage much more dramatically than expected those reactions originally projected to complete the scheme.

Experimental

Proton nmr spectra of solutions in deuteriochloroform were taken in pulsed-Fourier mode at 500 MHz unless indicated otherwise and were referenced to internal chloroform (δ = 7.26 ppm). Chemical shifts are reported to a precision of ±0.02 ppm and coupling constants to ±1 Hz. Carbon-13 nmr spectra of solutions in deuteriochloroform were obtained in pulsed-Fourier mode at 22.63 MHz. Chemical shifts, referenced to the center line of deuteriochloroform (δ = 77.0 ppm), are reported to the nearest 0.1 ppm.

High-resolution mass spectra were obtained at an ionizing potential of 50–70 eV with perfluorokerosene as an internal reference. In most cases samples were homogeneous by tlc.

Infrared spectra were referenced to the 1602 cm^{-1} band of polystyrene for calibration. Spectra were recorded as solutions in chloroform unless otherwise noted. Absorptions are reported to a precision of ±3 cm^{-1} for bands of importance.

Analytical thin-layer chromatography (tlc) was performed on fluorescent-indicating silica gel on plastic sheets precoated to a thickness of 0.25 mm (Machery–Nagel Co.). Visualization was accomplished under ultraviolet light or with iodine vapor. Preparative thin-layer chromatography was performed on silica gel precoated on glass plates to a thickness of 1 mm (Brinkman Instruments, Inc.). Column chromatography was done using slurry-packed columns of 60–200 mesh silica gel (J. T. Baker Chemical Co.). Eluting solvents are reported as volume-to-volume mixtures, with the minor component given first.

Reactions were generally run under an inert atmosphere of either dry nitrogen or argon. Concentration of solutions during work-up procedures refers to the evaporation of solvent on a rotary evaporator under house vacuum (about 40 Torr; 1 Torr = 133.3 Pa) at 20–30°C. Pumping down of a sample refers to initial removal of solvent on the rotary evaporator, followed by removal of residual volatiles on a vacuum line at 20 mTorr.

Solvents were bulk reagent grade and were dried and distilled before use: methylene chloride and ethyl acetate were distilled from phosphorous pentoxide; hexane and pentane were distilled over concentrated sulfuric acid; benzene was dried azeotropically, then distilled; methanol was distilled over magnesium metal and a catalytic amount of iodine.

Ozone was generated to a concentration of ca. 5% in a stream of oxygen using an Orec Model E3V5-O Ozonator. The effluent stream was dried with sulfuric acid before use.

Melting points are uncorrected. Microanalyses were performed by MicAnal Laboratories.

exo-*4-(1-Phenylselenenocyclopentyl-2,5-dione)-1,7-bis(phenylselenenyl)hexacyclo[7.5.1.$0^{3,13}$.$0^{5,12}$.$0^{7,11}$.$0^{10,14}$]pentadecane-2,6-dione* (**6**)

Compound **4** (100 mg, 0.17 mmol), prepared as described previously (3*c*), and 1,3-cyclopentanedione (60 mg, 0.61 mmol) were put into a resealable Carius tube with potassium carbonate (100 mg, 0.72 mmol) and 2,2,2-trifluoroethanol (3 mL). The tube was sealed and the mixture stirred at 70°C for 40 h. After cooling, the contents of the tube were rinsed into a separatory funnel with 1 *M* HCl (10 mL) and the whole extracted with methylene chloride (6 × 10 mL). The extract was dried ($MgSO_4$), filtered, and concentrated to leave a yellow solid contaminated with 1,3-cyclopentanedione. Trituration with cold isopropanol (2 mL), followed by drying under vacuum, left **5** as a white solid (75 mg, 70%). (This material was characterized as its enol acetate, compound **39**, *vide infra*.)

A solution of crude **5** (32 mg, 0.05 mmol) in methylene chloride (11 mL), ethyl acetate (3 mL), and pyridine (5.5 mL) was stirred at room temperature as solid phenylselenenyl chloride (29 mg, 0.151 mmol) was added. The resulting pale yellow solution was stirred 4 h, then pumped down to leave an orange-yellow residue. The product was purified by column chromatography, eluting first with methylene chloride to remove diphenyl diselenide, then 5% ethyl acetate – methylene chloride to elute the tris(phenylselenide) **6** (32 mg, 80%). Purification of this material could not be effected satisfactorily but, as its ^{1}Hmr spectrum was sufficiently in accord with expectation, it was used as it was; ^{1}Hmr δ: 7.8–7.3 (15H), 3.77 (1H, q, *J* = 10 Hz), 3.53 (1H, br s), 3.38 (2H, m), 3.27 (2H, m), 2.94 (2H, d of d, *J* = 7, 17 Hz), 2.90 (1H, m), 2.79 (2H, br d, *J* = 9 Hz), 2.45 (2H, d of d, *J* = 7, 17 Hz), 2.24 (2H, d of d, *J* = 10, 15 Hz), 2.04 (2H, d of d, *J* = 4, 15 Hz) ppm.

exo-*4-(Cyclopentyl-2,5-dione)-hexacyclo[7.5.1.$0^{3,13}$.$0^{5,12}$.$0^{7,11}$.$0^{10,14}$]-pentadecane-2,6-dione* (**9**)

Acetoxyperistylanedione (**3**, 57 mg, 0.20 mmol), 1,3-cyclopentanedione (20 mg, 0.20 mmol), and triethylamine (0.20 mL, 1.4 mmol) were refluxed together in benzene (8 mL) for 4 h. The mixture was then cooled; the volatiles were removed *in vacuo*. Water (4 mL) and a trace of phenolphthalein were added. Aqueous 1 *M* NaOH was added to the suspension very slowly with good agitation until a just pink endpoint was sustained. Filtration gave a white powder (3 mg)

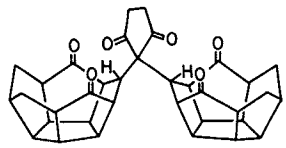

54

identified spectroscopically as the double adduct **54**; ^{1}Hmr δ: 3.64 (4H, m), 3.58 (2H, q, J = 10 Hz), 3.37 (2H, br s), 3.30 (4H, m), 2.84 (4H, br d, J = 9 Hz), 2.74 (4H, s), 2.75–2.65 (6H, m), 2.30 (4H, d of t, J = 15, 10 Hz), 1.75 (4H, d of t, J = 15, 4 Hz) ppm.

Acidification of the filtrate with excess 10% hydrochloric acid gave a white precipitate which was extracted into methylene chloride (3 × 10 mL). The extract was dried (Na_2SO_4), filtered, and evaporated to dryness. Trituration with ether left 55 mg (85%) of **9** of reasonable quality; this was usually taken on without further purification. Crystallization (with difficulty) of a small sample from methanol gave a bit better material, mp >290°C; ir (KBr) ν: 2700, 1730, 1575 cm^{-1}; ^{1}Hmr ($CDCl_3$ with a drop of C_5D_5N) δ: 3.89 (3H, m), 3.43 (1H, q, J = 9 Hz), 3.20 (2H, q, J = 10 Hz), 2.76 (2H, m), 2.61 (2H, m), 2.54 (1H, m), 2.33 (4H, s), 1.88 (2H, d of t, J = 13, 9 Hz), 1.54 (2H, d of t, J = 13, 5 Hz) ppm; m/e: 324.1411 ($C_{20}H_{20}O_4$ requires 324.1362).

*exo-4-(1-Phenylselenenocyclopentyl-2,5-dione)-hexacyclo[7.5.1.0^{3,13}.0^{5,12}.0^{7,11}.0^{10,14}]pentadecane-2,6-dione (**10**)*

Crude compound **9** (32 mg, 0.1 mmol) was dissolved in pyridine (500 μL) and ethyl acetate (1 mL). Solid phenylselenenyl chloride (21 mg, 0.11 mmol) was added. The yellow solution was stirred for 2 h at room temperature under nitrogen. The reaction mixture was diluted with methylene chloride (10 mL) and washed with 1 *M* sulfuric acid (10 mL). The organic phase was dried ($MgSO_4$), filtered, and concentrated. The residue was purified by trituration with pentane, followed by quick chromatography on silica gel with ethyl acetate. Evaporation left a yellow-orange crystalline solid which could not be purified further efficiently, but was of sufficient quality to use in trial oxidations; ^{1}Hmr δ: 7.7–7.3 (5H, aromatics), 3.77 (1H, q, J = 10 Hz), 3.53 (1H, br s), 3.38 (2H, m), 3.27 (2H, m), 2.94 (2H, d of d, J = 7, 17 Hz), 2.90 (1H, m), 2.79 (2H, br d, J = 9 Hz), 2.45 (2H, d of d, J = 7, 17 Hz), 2.24 (2H, d of d, J = 10, 13 Hz), 2.04 (2H, d of d, J = 4, 15 Hz) ppm.

Preparation and oxidation of 2-isopropyl-2-(phenylselenenyl)-1,3-cyclopentanedione

A stirred solution of 2-isopropyl-1,3-cyclopentanedione (**11**, 100 mg, 0.70 mmol) in ethyl acetate (10 mL) and pyridine (60 μL) was treated with phenylselenenyl chloride (160 mg, 0.83 mmol, added as a solid). The yellow solution was stirred for 2 h, then poured into 25 mL of 0.04 *M* H_2SO_4. The layers were separated, and the aqueous phase was extracted twice with methylene chloride (10 mL total). The combined organic phase was dried (Na_2SO_4) and concentrated to a yellow oil which was purified by column chromatography (methylene chloride). Selenide **12** (200 mg, 95%) was obtained as a pale yellow oil and used directly without further purification; ^{1}Hmr (350 MHz) δ: 7.55 (2H, d, J = 8 Hz), 7.44 (1H, t, J = 8 Hz), 7.34 (2H, t, J = 8 Hz), 2.65 (2H, m), 2.46 (2H, m), 2.26 (1H, heptet, J = 7 Hz), 1.17 (6H, d, J = 7 Hz) ppm; ^{13}Cmr δ: 208.2 (s), 137.6 (d), 130.2 (d), 129.2 (d), 125.7 (s), 64.8 (s), 34.8 (t), 29.9 (d), 18.4 (q) ppm.

A stream of ozone in oxygen was bubbled through a cold (−70°C) solution of selenide **12** (50 mg) in methylene chloride (5 mL) until the bright blue color of ozone developed. Excess ozone was removed in a nitrogen stream until the effluent gave a negative starch–iodide test. The cold bath was removed, and the solution was stirred at room temperature for 2 h. The yellow solution was concentrated. By ^{1}Hmr analysis the residue was shown to contain three aliphatic products in a 6:3:2 ratio. These were identified as diketo acid **16**, deselenenylated dione **11**, and tertiary alcohol **17**, respectively. Although rather sensitive to chromatography, pure samples of **16** and **17** could be isolated by preparative tlc (10% ethyl acetate − methylene chloride); **16** (R_f = 0.4); ir ν: 3100, 1720 cm^{-1}; ^{1}Hmr (270 MHz) δ: 3.30 (1H, heptet, J = 7 Hz), 2.97 (2H, m), 2.53 (2H, m), 1.04 (6H, d, J = 7 Hz) ppm; m/e: 172.0743 ($C_8H_{12}O_4$ requires 172.0735); **17** (R_f = 0.3); ^{1}Hmr δ: 3.05 (2H, m), 2.70 (2H, m), 2.15 (1H, heptet, J = 7 Hz), 0.95 (6H, d, J = 7 Hz) ppm; m/e: 156.0826 ($C_8H_{12}O_3$ requires 156.0786).

*2-Isopropylidene-1,3-cyclopentanedione (**13**) and 3-(cyclopentyl-2,5-dione)-3,5,5-trimethyl-2-oxabicyclo[4.3.0]non-1,6-en-7-one (**20**)*

Method A

Palladium catalyst (38 mg, 10% on carbon support) which had been washed free of carbonate was suspended in methylene chloride (15 mL). The flask was attached to an atmospheric pressure hydrogenator and agitated vigorously (Vibromixer shaking) for 30 min under hydrogen. The suspension was then cooled to 0°C; diene-dione **18** (136 mg, 1.00 mmol) was added as a solid. The mixture was shaken at 0°C for 1 h, at which time hydrogen uptake had reached 24 mL (1.1 equiv.). The reaction mixture was filtered through a pad of Celite, then concentrated to leave a yellowish semi-solid consisting mostly of ene-dione **13**; uv (CH_2Cl_2) λ_{max}: 239 (ε ~7,900), 264 (~3,200) and 390 nm (~12), cf. text; ^{1}Hmr (270 MHz) δ: 2.64 (4H, s), 2.54 (6H, s) ppm.

The ene-dione **13**, on standing in the concentrated state for several hours at room temperature, converted to dimer **20**. This was purified by crystallization from ether–hexanes to give colorless prisms (96 mg, 70% from **18**), mp 200–202°C (dec.); ir ν: 2800, 1692, 1635 cm^{-1}; uv (ethanol) λ_{max}: 250 nm (ε = 24 300), shifts to λ_{max} = 260 nm (ε = 26 000) upon addition of a small amount of 10% aqueous K_2CO_3; ^{1}Hmr δ: 9.04 (1H, br s), 2.62–2.30 (5H, m), 1.99 (1H, d, J = 16 Hz), 1.63 (3H, s), 1.29 (3H, s), 1.11 (3H, s) ppm; ^{13}Cmr ($CDCl_3$ + py-d_5) δ: 204.0, 193.2 (2 carbons), 183.1, 121.2, 118.2, 82.3, 43.1, 33.6, 30.8 (2 carbons), 28.8, 28.4, 27.6, 26.3, 25.6 ppm; m/e: 276.1383 ($C_{16}H_{20}O_4$) requires 276.1361).

Method B

A solution of 2-isopropyl-2-phenylthio-1,3-cyclopentanedione **21** (*vide infra*, 248 mg, 1.0 mmol) in methylene chloride (10 mL) was prepared in a 25-mL round-bottomed flask equipped with a stirring bar and addition funnel. The mixture was cooled in a Dry Ice/methanol bath; a solution of *m*-chloroperoxybenzoic acid (216 mg, 80% titre, 1.0 mmol) in methylene chloride (5 mL) was added dropwise over 5 min. The cold bath was removed, and the mixture allowed to warm toward room temperature. After 5 min, a reflux condenser was fitted to the system, and the white suspension was warmed to reflux on a steam bath. The solids quickly dissolved, and a bright yellow color developed. After 30 min, the yellow solution was cooled, diluted with methylene chloride (10 mL), and washed with 20 mL of 0.15 *M* phosphate buffer (pH 7.5) to remove *m*-chlorobenzoic acid (17). After drying ($MgSO_4$), the solvent was removed *in vacuo*. Analysis of the residue by ^{1}Hmr showed only signals for **13** and its dimer **20** in the aliphatic region.

*2-Isopropyl-2-phenylthio-1,3-cyclopentanedione (**21**)*

2-Isopropyl-1,3-cyclopentanedione (280 mg, 2.00 mmol) and *N*-phenylthiosuccinimide (414 mg, 2.00 mmol) were stirred together in benzene (10 mL). Triethylamine (0.6 mL) was added, and the solution was heated at reflux for 2 h. The mixture was then cooled to room temperature and concentrated. The brown semi-solid residue was extracted with hot hexane (4 × 10 mL). Concentration of the extract left **21** (480 mg, 97%) as a light yellow oil of reasonable purity by ^{1}Hmr; ^{1}Hmr (270 MHz) δ: 7.45 (2H, d, J = 8 Hz), 7.41 (1H, t, J = 8 Hz), 7.33 (2H, t, J = 8 Hz), 2.48 (4H, s), 2.27 (1H, heptet, J = 7 Hz), 1.14 (6H, d, J = 7 Hz) ppm; ^{13}Cmr δ: 209.7 (s), 136.7 (d), 130.0 (d), 128.6 (d), 128.0 (s), 35.6 (t), 31.0 (d), 17.9 (q) ppm; m/e: 248.0870 ($C_{14}H_{16}O_2S$ requires 248.0870). This material was used without further purification.

*2-Methyl-2-phenylthio-1,3-cyclopentanedione (**22**)*

A mixture of 2-methyl-1,3-cyclopentanedione (1.12 g, 10 mmol),

Can. J. Chem. Downloaded from www.nrcresearchpress.com by 210.87.254.105 on 09/06/12
For personal use only.

Can. J. Chem. Downloaded from www.nrcresearchpress.com by 210.87.254.105 on 09/06/12
For personal use only.

N-phenylthiosuccinimide (2.07 g, 10 mmol), and triethylamine (1.1 g, 11 mmol) in benzene (50 mL) was heated at reflux for 2 h. The solution was cooled to room temperature, washed with 1 *M* H_2SO_4, dried over Na_2SO_4, and concentrated. The residue was taken up in CCl_4 (10 mL) and filtered to remove succinimide. After removal of the solvent, the crude product was crystallized from ether–hexanes to give 2.0 g (90%) of **22** as white needles, mp 67–68°C (lit. (14) mp 69–70°C); ir ν: 1765, 1730 cm^{-1}; ^{1}Hmr δ: 7.47 (3H, m), 7.37 (2H, t, J = 8 Hz), 2.95 (2H, m), 2.61 (2H, m), 1.38 (3H, s) ppm. *Anal.* calcd. for $C_{12}H_{12}O_2S$: C 65.41, H 5.49; found: C 65.45, H 5.54.

2-(Phenylsulfoxymethyl)-1,3-cyclopentanedione (24)

A solution of 2-methyl-1,3-cyclopentanedione (**22**, 220 mg, 1.0 mmol) in ether (7 mL) was prepared in a 25-mL round-bottomed flask equipped with a stirring bar and addition funnel. The stirred solution was cooled in an ice-water bath as *m*-chloroperoxybenzoic acid (216 mg, 80% titre, 1.0 contained mmol) in ether (8 mL) was added dropwise over a period of 5 min. The cold solution was stirred for 5 min more at 0°C. The flask was fitted with a reflux condenser, and the clear, colorless solution was warmed to reflux on a steam bath for 30 min. A white crystalline precipitate began forming almost immediately. The mixture was cooled overnight at 0°C. The precipitate was isolated by filtration to give 215 mg (91%) of **24**, mp >200°C (dec.); ir (KBr) ν: 2900, 1620, 1020, 985 cm^{-1}; ^{1}Hmr (acetone-d_6) δ: 7.58 (5H, m), 4.08 and 3.76 (2H, AB quartet, J = 14 Hz), 2.38 (4H, br, s) ppm; *m/e*: no parent ($C_{12}H_{12}O_3S$), major fragments at 110.0368 (P − C_6H_5 − SOH requires 110.0368) and 126.0182 (P − $C_6H_6O_2$ requires 126.0139). *Anal.* calcd. for $C_{12}H_{12}O_3S$: C 61.00, H 5.12, S 13.57; found: C 60.77, H 5.42, S 11.61. Attempts to purify the material further were thwarted by its ready disproportionation.

8-Methylspiro[4.5]dec-7-ene-1,4-dione (25)

A solution of 1.10 g (5 mmol) of sulfide **22** in methylene chloride (10 mL) was prepared in a 100-mL, round-bottomed flask fitted with a stirring bar and addition funnel. The mixture was cooled in an ice bath and stirred as a solution of *m*-chloroperoxybenzoic acid (1.10 g, 80% titre, 5 mmol) in methylene chloride (10 mL) was added dropwise over 15 min. Isoprene (25 mL) was then added in one portion. A reflux condenser was fitted to the top of the addition funnel; the cold bath was removed, and the mixture was warmed to reflux on a steam bath for 1 h. After cooling, the light yellow solution was diluted with methylene chloride (10 mL) and washed with saturated aqueous $NaHCO_3$ (25 mL). The organic phase was dried ($MgSO_4$) and concentrated. The residue was crystallized from hexanes (3 crops) to give 620 mg (70%) of spirodiketone **25**, mp 81.5–83°C; ir ν: 1730 cm^{-1}; ^{1}Hmr δ: 5.41 (1H, m), 2.89 (2H, m), 2.69 (2H, m), 2.14 (2H, m), 2.03 (2H, m), 1.75 (2H, t, J = 6 Hz), 1.70 (3H, br, s) ppm; *m/e*: 178.0999 ($C_{11}H_{14}O_2$ requires 178.0994).

exo-*4-(1-Phenylthiocyclopentyl-2,5-dione)hexacyclo[7.5.1.$0^{3,13}$.$0^{5,12}$.$0^{7,11}$.$0^{10,14}$]pentadecane-2,6-dione (26)*

A solution of acetoxyperistylanedione **3** (3.04 g, 10.6 mmol) and 2-phenylthio-1,3-cyclopentanedione (**29**, 2.62 g, 12.7 mmol) in benzene (750 mL) and triethylamine (9 mL) was stirred and heated at reflux for 40 h. (This reaction must be run under dilute conditions to suppress formation of compound **54**; cf. the procedure for **5**.) After cooling, the yellow solution was washed with 1 *M* H_2SO_4 (100 mL), dried (Na_2SO_4), and concentrated. The brownish residue was absorbed on a small column of silica gel which was then eluted with 30% ethyl acetate − methylene chloride (200 mL) to give, after concentration, 4.20 g of an off-white solid. Crystallization from ethyl acetate (400 mL, 4 crops) gave colorless plates of **26** (3.72 g, 81%), mp 215–217°C (dec.); ir ν: 1720 cm^{-1}; ^{1}Hmr δ: 7.61 (2H, d, J = 8 Hz), 7.40 (1H, t, J = 8 Hz), 7.35 (2H, t, J = 8 Hz), 3.88 (2H, m), 3.69 (1H, q, J = 10 Hz), 3.46 (1H, s), 3.44 (2H, q, J = 10 Hz), 3.14 (2H, br d, J = 10 Hz), 2.75 (3H, m), 2.69 (4H, m), 2.09 (2H, d of t, J = 15, 9 Hz), 1.71 (2H, d of t, J = 15, 4 Hz) ppm; ^{13}Cmr δ: 223.3, 206.8, 136.9, 130.4, 129.4, 64.0, 58.5, 55.6, 55.5, 53.9, 51.8, 47.3, 38.1, 34.9 ppm (one phenyl carbon not observed, two aliphatic carbons overlapping); *m/e*: 432.1472 ($C_{26}H_{24}O_4S$ requires 432.1393).

4-(Cyclopentyliden-2,5-dione)hexacyclo[7.5.1.$0^{3,13}$.$0^{5,12}$.$0^{7,11}$.$0^{10,14}$]-pentadecane-2,6-dione (27)

A solution of 1.76 g sulfide **26** (4.08 mmol) in methylene chloride (80 mL) was placed in a 250-mL, round-bottomed flask with stirring bar and fitted with an addition funnel. The stirred solution was cooled to −70°C. A solution of *m*-chloroperoxybenzoic acid (880 mg, 80% titre, 4.08 contained mmol) in methylene chloride (50 mL) was added dropwise over 5 min. The cold bath was then removed, and succinic anhydride (1.0 g, 2.5 equiv.) in 35 mL of methylene chloride was added rapidly to the reaction mixture according to the method of Schlessinger and co-workers (18). The flask was warmed on a steam bath, and the contents gently refluxed for 30 min. The solution developed a bright yellow color during this time. After cooling to room temperature, the solution was washed with aqueous sodium phosphate buffer (100 mL, 0.15 *M*, pH 7.5) and dried (Na_2SO_4). It was concentrated to leave a yellow solid. This, on trituration with ethyl acetate (30 mL), gave 970 mg (74%) of yellow, microcrystalline ene-tetraone **27**. A small sample was crystallized from ethyl acetate, mp >290°C (dec.); ir ($CHCl_3$) ν: 1750, 1692, 1608 cm^{-1}; uv (methylene chloride) λ_{max}: 286 (ϵ = 12 200), 310 (8,700), and 415 nm (225); ^{1}Hmr δ: 5.09 (2H, br d, J = 10 Hz), 3.69 (3H, m), 3.46 (2H, q, J = 10 Hz), 2.98 (2H, t of d, J = 10, 3 Hz), 2.90–2.60 (5H, m), 2.17 (2H, d of t, J = 16, 10 Hz), 1.73 (2H, d of t, J = 16, 4 Hz) ppm; *m/e*: 322.1214 ($C_{20}H_{18}O_4$ requires 322.1204).

2-Phenylthio-1,3-cyclopentanedione (29)

Triethylamine (0.4 mL) was added to a stirred suspension of 1,3-cyclopentanedione (326 mg, 3.69 mmol) and *N*-phenylthiosuccinimide (764 mg, 3.69 mmol) in benzene (10 mL). The mixture was heated at reflux for 3 h, during which time all of the solids dissolved and the *N*-phenylthiosuccinimide reacted (tlc analysis; 5% ethyl acetate − methylene chloride). The solution was cooled to room temperature and concentrated. The brown residue was taken up in methylene chloride (10 mL), and this solution poured into 0.5 *M* H_2SO_4 (4 mL). The mixture was cooled in an ice bath for 15 min to complete precipitation of the product, which was isolated by filtration. Crystallization from ethyl acetate (60 mL) gave 690 mg (90%) of **29** as white needles, mp 191–192°C; ir (KBr) ν: 2900, 2600, 1665, 1560, 1400 cm^{-1}; ^{1}Hmr ($CDCl_3$ with a drop of C_5D_5N, 350 MHz) δ: 7.05 (2H, t, J = 8 Hz), 6.93 (3H, m), 6.55 (1H, br s), 2.65 (4H, s) ppm. *Anal.* calcd. for $C_{11}H_{10}O_2S$: C 64.03, H 4.89; found: C 63.68, H 5.01.

Reduction of enetetraone 27. Formation of 31

A 10-mL flask containing a suspension of neutralized 10% palladium-on-carbon (10 mg) in acetone (3 mL) under a hydrogen atmosphere was shaken vigorously for 2 h. A solution of ene-tetraone **27** (7 mg, 0.022 mmol) in acetone (1 mL) and methylene chloride (2 mL) was added, and agitation under hydrogen was continued for 2 h longer. At the end of this time, tlc analysis (30% ethyl acetate − methylene chloride eluent) indicated complete consumption of starting material. The hydrogen atmosphere was replaced by nitrogen in the usual way, and the mixture was filtered through a pad of Celite. The solvents were removed under vacuum, and the residue taken up in $CDCl_3$ (400 μL). Hemiketal **32** separated as fine white needles (4 mg, 57%), mp 213–217°C (dec.); ir (KBr) ν: 3440, 1725, and 1625 cm^{-1}; *m/e*: 324.1339, $C_{20}H_{20}O_4$ requires 324.1362. The key features of the otherwise uselessly complex ^{1}Hmr spectrum are discussed in the text.

Hexacyclo[7.5.1.$0^{3,13}$.$0^{5,12}$.$0^{7,11}$.$0^{10,14}$]pentadecane-2,6-dione-4-spiro-1′-4′,5′-dimethylcyclohex-4′-ene-2′-spiro-2″-cyclopentane-1″,3″-dione (32)

Ene-tetraone **27** (285 mg, 0.88 mmol), dimethylbutadiene (17 mL), and a small stirring bar were placed in a resealable Carius tube (Fischer and Porter Co.). The sealed tube was immersed in a 130°C oil bath, and the yellow suspension heated with stirring for 19 h. By the end of this time, the yellow color had faded leaving a colorless mixture with a lot of white solid present. The mixture was cooled to room temperature, the tube opened, and the solid collected. Purification by column chromatography on silica gel (30% ethyl acetate −

Can. J. Chem. Downloaded from www.nrcresearchpress.com by 210.87.254.105 on 09/06/12
For personal use only.

methylene chloride) gave 285 mg of adduct **33**. An additional 25 mg was obtained from the dimethylbutadiene solution after concentration and column chromatography to remove substantial quantities of polymeric material (methylene chloride, then 30% ethyl acetate – methylene chloride). The total yield was 310 mg (87%). Crystallization from 1,2-dimethoxyethane gave small prisms of **32**, mp 247–252°C (dec.); ir ν: 1720 cm^{-1}; ^{1}Hmr δ: 3.61 (2H, m), 3.52 (1H, q, J = 9 Hz), 3.26 (2H, m), 2.93 (2H, m), 2.82–2.68 (4H, m), 2.67–2.60 (3H, m), 2.50–2.35 (4H, br m), 2.01 (2H, d of t, J = 15, 8 Hz), 1.82 (2H, br m), 1.66 (3H, s), 1.63 (3H, s) ppm; ^{13}Cmr δ: 221.0, 211.1, 124.3, 121.4, 64.2, 61.9, 57.8, 56.2, 55.3, 52.9, 51.3, 48.4, 48.0, 37.3, 36.4, 33.9, 18.9, 18.4 ppm; m/e: 404.2030 ($C_{26}H_{28}O_4$ requires 404.1986).

X-ray crystal structure analysis of ***32***

Small colourless crystals of **32**, 0.1–0.5 mm in size, were used. The shape is prismatic, elongated along the a-axis with prominent monoclinic prism {0.23} and pinacoid {101}. Preliminary Weissenberg photographs with CuK_α radiation indicated that the crystals belong to the monoclinic system. Systematic extinctions are $h0l$, $h+l = 2n+1$, and $0k0$, $k = 2n+1$, thus defining the space group $P2_1/n$. The determination of the lattice parameters and the intensity measurements were made with the Nonius CAD4-diffractometer, with graphite monochromatized $MoK_{\bar{\alpha}}$ radiation. A small crystal fragment with approximate dimensions 0.22 × 0.22 × 0.25 mm was used. 25 reflections determined with the Nonius peak-hunting procedure in the range $10° < 2\theta < 25°$ were carefully centered. Cell parameters were calculated by a least-squares procedure. All independent reflections in the range $2° \leq 2\theta \leq 54°$ were measured at T = 20(1)°C by the $\omega-2\theta$ scan technique. Every 200 reflections the orientation of the crystal was controlled and every 2.5 h the intensities of the $6\bar{3}2$ and $7\bar{1}4$ reflections were checked. During the measurement no significant deviation (less than 3σ) could be observed. A total of 4587 reflections were measured. After averaging multiple measurements 4142 independent reflections remained, of which 1235 were unobserved with $I < 2.58\,\sigma(I)$. The intensities were corrected for Lorentz and polarization effects but no absorption correction was applied ($\mu(MoK_{\bar{\alpha}})$ = 1.010 cm^{-1}).

Crystal data:

$C_{26}H_{28}O_4$ fw = 404.5

Monoclinic, $P2_1/n$, a = 10.260(5), b = 11.583(5), c = 16.004(7) Å, β = 90.7(1)°, V = 1901.7 $Å^3$, Z = 4, ρ_c = 1.41 gcm^{-3} (20°C; $MoK_{\bar{\alpha}}$, λ = 0.71069 Å). Statistical tests are in good agreement with a centrosymmetric structure viz. $\langle E\rangle$ = 0.791, $\langle E^2\rangle$ = 1.0, $\langle E^2-1\rangle$ = 0.968. The structure was solved with direct phasing according to the symbolic addition procedure. The E-map clearly showed 28 out of the 30 non-hydrogen atoms. The complete molecule was then determined with structure factor and successive Fourier calculations. The hydrogen atoms could all be seen in a difference Fourier synthesis. The structure was refined with block-diagonal least-squares calculations. In the last few cycles of refinement the hydrogen atoms were included with isotropic temperature factors, and anisotropic temperature factors for the C and O atoms were applied. The function minimized being $\Sigma w(|F_o| - |F_c|)^2$ and $w = 1/\sigma^2$ (F). The atomic scattering factors were taken from ref. 19. The final agreement index was R = 0.048 for observed reflections and R = 0.084 for all reflections.[8] A final difference Fourier synthesis did not show any peak higher than $\mp$ 0.3 e/A^3. All calculations and drawings were done using the program system KRIPROG (20).

exo-*4-(1-Phenylthiocyclopentyl-2,5-dione)-1,7-bis(phenylselenenyl)-hexacyclo[7.5.1.0^{3,13}.0^{5,12}.0^{7,11}.0^{10,14}]pentadecane-2,6-dione* (***33***)

Compound **4** (176 mg, 0.29 mmol), described previously (3*c*), and 2-(phenylthio)-1,3-cyclopentanedione (70 mg, 0.34 mmol) were combined in benzene (10 mL) in a 25-mL, round-bottomed flask. Triethylamine (0.5 mL) was added, and the resulting solution was heated at reflux for 40 h. The amber solution was cooled to room temperature and concentrated. The crude residue was taken up in methylene chloride and filtered through a short column of silica gel with 10% ethyl acetate – methylene chloride (30 mL). Evaporation of the eluate gave the solid bisselenide-sulfide **33** (187 mg, 84%); ir ν: 1730 cm^{-1}; ^{1}Hmr δ: 7.66 (2H, d, J = 8 Hz), 7.52 (4H, d, J = 8 Hz), 7.42 (1H, t, J = 8 Hz), 7.35 (6H, t, J = 8 Hz), 7.28 (2H, t, J = 8 Hz), 3.87 (1H, q, J = 10 Hz), 3.46 (1H, s), 3.39 (2H, m), 3.26 (2H, t, J = 11 Hz), 2.91 (3H, m), 2.78 (2H, m), 2.54 (2H, m), 2.24 (2H, d of d, J = 16, 10 Hz), 1.99 (2H, d of d, J = 16, 3 Hz) ppm. *Anal.* calcd. for $C_{38}H_{32}O_4Se_2S$: C 61.46, H 4.34; found: C 61.87, H 4.34. Further purification was ineffective; the phenylthio group suffered easy nucleophilic displacement.

exo-*4-(1-Phenylthiocyclopentanyl-2,5-dione)*-exo-*15-(2,2,2-trifluoroethoxy)hexacyclo[7.5.1.0^{3,13}.0^{5,12}.0^{7,11}.0^{10,14}]pentadec-7-ene-2,6-dione* (***37***)

A solution of bisselenide-sulfide **34** (60 mg, 0.081 mmol) in methylene chloride was cooled to −70°C. A stream of ozone in oxygen was bubbled through the solution until a bright blue color developed. The excess ozone was removed in a nitrogen purging stream until the effluent gas did not color moistened starch–iodide test paper. A solution of potassium acetate (100 mg, 1.02 mmol) in trifluoroethanol (5 mL) was added to the cold mixture along with 1 mL of ethyl vinyl ether. The cold bath was removed, and the reaction mixture was allowed to stir at ambient temperature for 8 h. The yellow solution was concentrated, and the residue purified by preparative tlc (10% ethyl acetate – methylene chloride) to give as the major peristylane-based product, ene-ether **37** (R_f = 0.55, 20 mg, 39%); ir ν: 1730, 1625, 1285, 1180 cm^{-1}; ^{1}Hmr δ: 7.57 (2H, d, J = 8 Hz), 7.42 (1H, t, J = 8 Hz), 7.36 (2H, t, J = 8 Hz), 5.63 (1H, s), 4.49 (1H, s), 3.90–3.50 (8H, m), 3.22 (1H, s), 3.16 (1H, d, J = 12 Hz), 3.06 (1H, d, J = 7 Hz), 3.01 (1H, d, J = 10 Hz), 2.86 (2H, m), 2.62 (2H, m) ppm; m/e: 528.1193 ($C_{28}H_{23}O_5F_3S$ requires 528.1218).

exo-*4-(2-Acetoxycyclopentyl-1-en-5-one)-1,7-bis(phenylselenenyl)-hexacyclo[7.5.1.0^{3,13}.0^{5,12}.0^{7,11}.0^{10,14}]pentadecane-2,6-dione* (***39***)

The bisselenide acetate **4** (700 mg, 1.17 mmol), 1,3-cyclopentanedione (142 mg, 1.45 mmol), benzene (21 mL), and triethylamine (1 mL) were combined in a 50-mL, round-bottomed flask equipped with a stirring bar and reflux condenser. The mixture was stirred at reflux for 4 h, then cooled to room temperature and treated with acetic anhydride (2 mL). After being stirred for 20 min at room temperature, all of the solids had dissolved. The stirring was continued for 40 min more. Concentration of this mixture left a dark residue which was filtered through silica gel with 5% ethyl acetate – methylene chloride (120 mL). This eluate was pumped down to leave a light yellow, crystalline solid. Crystallization from ethyl acetate provided fine white needles of **39** (730 mg, 92%), mp (206–208°C (dec.); ir ν: 1775, 1730, 1705, 1650, 1180 cm^{-1}; ^{1}Hmr δ: 7.49 (4H, d, J = 8 Hz), 7.35 (2H, t, J = 8 Hz), 7.27 (4H, t, J = 8 Hz), 3.88 (1H, s), 3.76 (1H, q, J = 10 Hz), 3.67 (2H, m), 3.23 (2H, t of m, J = 10 Hz), 2.91 (1H, m), 2.89 (2H, d, J = 9 Hz), 2.80 (2H, m), 2.46 (2H, m), 2.35 (3H, s), 2.24 (2H, d of d, J = 15, 10 Hz), 1.96 (2H, d of d, J = 15, 4 Hz) ppm; ^{13}Cmr δ: 216.7, 204.4, 176.2, 136.6, 133.6, 129.2, 128.9, 127.9, 63.3, 63.0, 59.2, 59.0, 54.2, 45.3, 34.8, 26.9, 21.0 ppm (one aromatic and one aliphatic signal are not accounted for, presumably due to fortuitous overlap with neighboring lines); m/e: 678.0336 ($C_{34}H_{30}O_5Se_2$ requires 678.0424). *Anal.* calcd. for $C_{30}H_{30}O_5Se_2$: C 60.36, H 4.47; found: C 60.25, H 4.53.

exo-*4-(2-Acetoxycyclopentyl-1-en-5-one)*-exo,exo-*8,15-bis(2,2,2-trifluoroethoxy)hexacyclo[7.5.1.0^{3,13}.0^{5,12}.0^{7,11}.0^{10,14}]pentadecane-2,6-dione* (***42***)

A solution of bisselenide **39** (156 mg, 0.23 mmol) in methylene chloride (6 mL) was placed with a stirring bar in a 25-mL round-

[8]Tables of observed and calculated structure factor amplitudes, of bond length and bond angles, and of torsion angles are available, at a nominal charge, from the Depository of Unpublished Data, CISTI, National Research Council of Canada, Ottawa, Ont., Canada K1A 0S2.

Can. J. Chem. Downloaded from www.nrcresearchpress.com by 210.87.254.105 on 09/06/12
For personal use only.

bottomed flask fitted with two 10-mL addition funnels, arranged one atop the other. The lower funnel contained a solution of *m*-chloroperoxybenzoic acid (153 mg, 60% titre, 0.53 contained mmol) in methylene chloride (5 mL); the upper, a mixture of trifluoroethanol (9 mL) and triethylamine (1 mL). The reaction solution was cooled to −70°C; oxidizing solution was added dropwise with stirring over 3 min. The cold reaction mixture was stirred for 2 min more, whereupon the contents of the upper addition funnel were added all at once. The cooling bath was removed, and the reaction mixture was allowed to warm to room temperature. After 16 h, the yellow-orange solution was concentrated; the residue was taken up in methylene chloride (5 mL) and acetic anhydride (2 mL). The reddish-brown mixture was stirred for 2 h at room temperature. This solution was then pumped down, and the dark brown residue was dissolved in methylene chloride (15 mL). The solution was washed with 0.1 *M* H_2SO_4 (15 mL), then 10% aqueous Na_2CO_3 (10 mL), dried (Na_2SO_4), and concentrated to give crude enol acetate **40**, contaminated chiefly with diphenyl diselenide. This was conveniently removed by partitioning the crude between trifluoroethanol (4 mL) and pentane (3 mL). The alcohol solution contained the enol acetate in reasonable purity as shown by ^{1}Hmr analysis; ^{1}Hmr δ: 3.97 (2H, br s), 3.95 (4H, m), 3.84 (4H, q, J = 8 Hz), 3.58 (2H, q, J = 11 Hz), 2.93 (2H, d, J = 11 Hz), 2.82 (3H, m), 2.76 (2H, d, J = 11 Hz), 2.50 (2H, m), 2.41 (3H, s) ppm. This was used directly in the next step.

exo-*4-(1-Phenylthiocyclopentanyl-2,5-dione)*-exo,exo-*bis(2,2,2-trifluoroethoxy)hexacyclo[7.5.1.0^{3,13}.0^{5,12}.0^{7,11}.0^{10,14}]pentadecane-2,6-dione (**35**)*

The trifluoroethanol solution of **40** as just obtained was heated at 70°C with potassium acetate (48 mg, 0.49 mmol) and *N*-phenylthiophthalimide (69 mg, 0.27 mmol). The progress of the reaction was most conveniently followed by ^{1}Hmr analysis of aliquots. Deprotection of the enol acetate was rapid; the free, enolized cyclopentadione gave rise to a signal at 2.4 ppm for the methylene protons. Subsequently this disappeared to be replaced by the AA′BB′ pattern for the methylene protons of **35**. The conversion was complete after 8 h. The mixture was cooled, diluted with methylene chloride (30 mL), and the solution was washed with 0.1 *M* H_2SO_4. The organic layer was dried (Na_2SO_4) and concentrated. The dark brown residue was purified by preparative tlc (10% ethyl acetate − methylene chloride, R_f = 0.7) to yield 74 mg of **35** (51% overall from bisselenide **39**). A small sample was crystallized from benzene − petroleum ether, mp 185.5−187°C; ir ν: 1730, 1280, 1170 cm^{-1}; ^{1}Hmr δ: 7.67 (2H, d, J = 8 Hz), 7.45 (1H, t, J = 8 Hz), 7.39 (2H, t, J = 8 Hz), 3.95 (2H, s), 3.94 (1H, q, J = 10 Hz), 3.84 (6H, m), 3.58 (2H, q, J = 11 Hz), 3.44 (1H, s), 3.15 (2H, br d, J = 10 Hz), 2.93 (2H, d, J = 11 Hz), 2.80 (3H, m), 2.65 (2H, m) ppm; *m/e*: 628.1336 ($C_{30}H_{26}O_6F_6S$ requires 628.1354).

4-(Cyclopentyliden-2,5-dione)-exo,exo-*8,15-bis(2,2,2-trifluoroethoxy)hexacyclo[7.5.1.0^{3,13}.0^{5,12}.0^{7,12}.0^{10,14}]pentadecane-2,6-dione (**41**)*

A solution of sulfide **35** (100 mg, 0.16 mmol) in methylene chloride (15 mL) was placed with a stirring bar in a 50-mL, round-bottomed flask equipped with an addition funnel. The stirred solution was cooled to −70°C. A solution of *m*-chloroperoxybenzoic acid (58 mg, 60% titre, 0.20 contained mmol) in methylene chloride was added dropwise over 30 min. The cold mixture was stirred for 1 h more, then the cold bath was removed and the reaction warmed to reflux on the steam bath for 20 min. A bright yellow color developed over this time. The solution was cooled, diluted with methylene chloride (50 mL), and washed with sodium phosphate buffer solution (40 mL, 0.15 *M*, pH 7.5). The organic layer was dried (Na_2SO_4) and concentrated to leave a yellow semisolid (110 mg). Trituration with ether (3 mL) left 60 mg (73%) of yellow, microcrystalline ene-tetraone (**41**), mp 199−201°C (dec.); ir ν: 1750, 1690, 1610, 1280, 1170 cm^{-1}; uv (CH_2Cl_2) λ_{max}: 281 (ε = 8,800), 315 (4,500) 420 nm (~150); ^{1}Hmr δ: 5.07 (2H, d, J = 8 Hz), 4.06 (1H, q, J = 11 Hz), 3.95 (2H, s), 3.81 (4H, q, J = 8 Hz), 3.75 (4H, m), 3.12 (2H, d, J = 11 Hz), 2.87 (3H, m), 2.68 (2H, m) ppm; *m/e*: 518.1216 ($C_{24}H_{20}O_6F_6$ requires 518.1164). *Anal.* calcd. for $C_{24}H_{20}O_6F_6$: C 55.19, H 3.89; found: C 55.61, H 3.80.

exo,exo-*8,15-Bis(2,2,2-trifluoroethoxy)hexacyclo[7.5.1.0^{3,13}.0^{5,12}.0^{7,11}.0^{10,14}]pentadecane-2,6-dione-4-spiro-1′-4′,5′-dimethylcyclohex-4′-ene-2′-spiro-2″-cyclopentane-1″,3″-dione (**42**)*

Ene-tetraone **41** (17 mg, 0.033 mmol) and dimethylbutadiene (1 mL) were placed in a resealable Carius tube (7-mL capacity, Fischer and Porter Co.) containing a small stirring bar. The sealed tube was immersed in a 100°C oil bath and stirred for 3 h. The initial yellow color faded to give a colorless solution. The tube was cooled; the solution was concentrated to give a semi-solid residue. This was freed of polymeric material by preparative tlc (10% ethyl acetate − methylene chloride, R_f = 0.55) and gave 15 mg of adduct **42**. A sample was crystallized from hexane, mp 221−222°C (dec., bubbling); ir ν: 1723, 1280, 1170 cm^{-1}; ^{1}Hmr δ: 4.19 (2H, br s), 4.03 (2H, m), 3.95 (2H, m), 3.83 (1H, q, J = 11 Hz), 3.66 (2H, m), 3.51 (2H, br q, J = 10 Hz), 2.90−2.78 (7H, m), 2.67 (2H, br d, J = 10 Hz), 2.42 (4H, br m), 1.66 (3H, s), 1.63 (3H, s) ppm; *m/e*: 600.2008 ($C_{30}H_{30}O_6F_6$ requires 600.1944).

*3,4-Dimethyl-20-hydroxy-16,18-bis(2,2,2-trifluoroethoxy)nonacyclo[19.2.1.0^{1,6}.0^{6,13}.0^{7,20}.0^{8,12}.0^{9,19}.0^{10,17}.0^{11,15}]tetracos-3-ene-14,23,24-trione (**44**)*

Oil-free potassium hydride (20 mg, 0.50 mmol) and tetrahydrofuran (2 mL, freshly distilled from sodium-benzophenone ketyl) were placed in a dry, 10-mL, pear-shaped flask with a septum inlet and a magnetic stirring bar. The stirred suspension was cooled to −70°C under a nitrogen atmosphere. A solution of **42** (13 mg, 0.022 mmol) in dry tetrahydrofuran (1.5 mL) was added via syringe over 10 min. After 5 min more, the mixture was allowed to warm to −45°C (Dry Ice/acetonitrile bath). The suspension slowly turned yellow, then orange. After 2 h at −45°C the cold reaction mixture was quenched by rapid addition of acetic acid (0.3 mL, 5 mmol). The color was discharged to light yellow during the quench. The mixture was warmed to room temperature and concentrated. The residue was taken up in methylene chloride (7 mL) and washed with saturated aqueous $NaHCO_3$ (7 mL). The organic phase was dried (Na_2SO_4) and concentrated to a pale yellow oil. Preparative tlc (5% ethyl acetate − methylene chloride) gave, at R_f = 0.23, the aldol product **44** (8 mg, 62%); ir ν: 3510, 1740 cm^{-1}; ^{1}Hmr δ: 4.17 (1H, s, disappeared on treatment with D_2O), 3.99 (1H, s), 3.94 (2H, m), 3.83 (1H, s), 3.78 (2H, q, J = 9 Hz), 3.38 (1H, br t, J = 6 Hz), 3.04 (1H, q, J = 7 Hz), 2.98 (1H, br d, J = 5 Hz), 2.90 (2H, m), 2.71 (1H, q, J = 8 Hz), 2.55 (3H, m), 2.40 (1H, t, J = 10 Hz), 2.35 (1H, m), 2.25−2.02 (4H, m), 1.75 (1H, d, J = 18 Hz), 1.63 (3H, s), 1.59 (3H, s), 1.49 (1H, d, J = 18 Hz) ppm; *m/e*: 582.1862, 500.1837 ($C_{30}H_{30}O_6F_6$ minus H_2O requires 582.1840, $C_{30}H_{30}O_6F_6$ minus CF_3CH_2OH requires 500.1809).

*1,7-Bis(phenylselenenyl)hexacyclo[7.5.1.0^{3,13}.0^{5,12}.0^{7,11}.0^{10,14}]pentadecane-2,6-dione-4-spiro-1′-4′,5′-dimethylcyclohex-4′-ene-2′-spiro-2″-cyclopentane-1″,3″-dione (**46**)*

Diels−Alder adduct **32** (285 mg, 0.705 mmol) was dissolved in ethyl acetate (15 mL), and the solution was stirred at 50°C as solid phenylselenenyl chloride (325 mg, 1.70 mmol) was rinsed in with 4 mL of ethyl acetate. The orange mixture was stirred at 50°C for 2 h; the color gradually faded to yellow. The solution was cooled to room temperature and concentrated. The residue was purified by column chromatography (5% ethyl acetate − methylene chloride). Crystallization from 20 mL of isopropyl ether − ethyl acetate (3:1, v/v) gave 2 crops of bisselenide **46** (300 mg, 60%), mp 136.5−139°C; ir ν: 1720 cm^{-1}; ^{1}Hmr δ: 7.55 (4H, d, J = 8 Hz), 7.36 (2H, t, J = 8 Hz), 7.28 (4H, 1, J = 8 Hz), 3.67 (1H, q, J = 9 Hz), 3.27 (2H, m), 3.22 (2H, m), 2.90 (2H, m), 2.70 (2H, m), 2.63 (2H, br d, J = 9 Hz), 2.58 (1H, m), 2.30 (2H, br s, $w_{\frac{1}{2}}$ = 12 Hz), 2.2 (2H, br s, $w_{\frac{1}{2}}$ = 20 Hz), 2.05 (4H, m), 1.63 (3H, s), 1.57 (3H, s) ppm; *m/e*: 716.1019 ($C_{38}H_{36}O_4Se_2$ requires 716.0944).

11-Hydroxyhecacyclo[7.5.1.0^{3,13}.0^{5,12}.0^{7,11}.0^{10,14}]pentadec-7-ene-2,6-dione-4-spiro-1'-4',5'-dimethylcyclohex-4'-ene-2'-spiro-2"-cyclopentane-1",3"-dione (50)

Bisselenide **46** (49 mg, 0.069 mmol) and methylene chloride were placed with a stirring bar in a 10-mL, round-bottomed flask equipped with an addition funnel. The solution was cooled to −70°C, and a solution of *m*-chloroperoxybenzoic acid (37 mg, 80% titre, 0.17 contained mmol) in methylene chloride (2.5 mL) was added dropwise over 5 min. The cold reaction mixture was stirred for 3 min more, then triethylamine (2 mL) was added and the cold bath was removed. The reaction was allowed to warm to room temperature with stirring overnight (10 h). In the morning, the solution was pumped down and the residue redissolved in fresh methylene chloride (25 mL). This was washed with 1 *M* H_2SO_4 (10 mL), then 10% aqueous Na_2CO_3 (10 mL). The organic phase was dried (Na_2SO_4) and concentrated to a yellow oil which was purified by preparative tlc (30% ethyl acetate − methylene chloride, R_f = 0.19) to give ene-alcohol **52** (23 mg, 79%): ir *ν*: 3590, 1720 cm^{-1}; ^{1}Hmr δ: 5.58 (1H, br s), 3.70 (1H, m), 3.64 (1H, t, *J* = 8 Hz), 3.55 (1H, m), 3.43 (1H, t, *J* = 11 Hz), 3.21 (1H, t, *J* = 7 Hz), 3.03 (1H, br d, *J* = 17 Hz), 2.95 (1H, d of d, *J* = 11, 2 Hz), 2.90−2.60 (7H, m), 2.59 (1H, d, *J* = 8 Hz), 2.48 (2H, m), 1.95 (1H, d, *J* = 17 Hz), 1.68 (1H, d, *J* = 17 Hz), 1.64 (3H, s), 1.61 (3H, s) ppm; *m/e*: 418.1757 ($C_{26}H_{26}O_5$ requires 418.1779).

1,13,15,24-Tetrahydroxy-18,19-dimethynonacyclo[14.6.2.0^{2,9}.0^{4,8}.0^{6,13}.0^{7,11}.0^{10,22}.0^{12,21}.0^{16,21}]tetracos-18-ene (52)

Diels−Alder adduct **32** (28 mg, 0.069 mmol) was placed with a stirring bar in a 50-mL, three-necked flask fitted with a Dry Ice condenser. Tetrahydrofuran (7 mL, freshly distilled from sodium-benzophenone ketyl) was added. The flask was cooled in a Dry Ice/methanol bath, and the condenser was filled with Dry Ice and methanol. Ammonia was distilled directly into the flask from a blue solution of lithium in ammonia (about 25 mL transferred). The cold bath was removed, and the contents of the flask were stirred at reflux. Lithium wire (12 mg, 1.7 mmol, low sodium, Foote Mineral Company) was added. A deep blue color developed immediately. The reaction was allowed to proceed for 90 min, after which the deep blue solution was quenched by cautious addition of solid ammonium chloride (220 mg, 4.0 mmol). The white mixture was allowed to warm to room temperature overnight with evaporation of most of the ammonia. The residual slurry was pumped down, suspended in boiling methylene chloride (25 mL), and filtered hot. The residue was washed with hot methylene chloride (15 mL), and the combined filtrate was evaporated. The crude product (20 mg) was purified by preparative tlc (30% ethyl acetate − methylene chloride). The component at *Rf* = 0.18 was crystallized from benzene as feathery crystals of tetraol **52** (12 mg, 42%), mp 243−244°C; ir *ν*: 3400, 2960, 1075 cm^{-1}; ^{1}Hmr δ: 4.81 (2H, m), 3.11 (1H, q, *J* = 8 Hz), 2.90 (2H, m), 2.60 (1H, q, *J* = 8 Hz), 2.54 (2H, t, *J* = 8 Hz), 2.48 (2H, m), 2.28 (2H, t, *J* = 2 Hz), 2.23 (4H, br s), 1.84 (2H, m), 1.76 (4H, m), 1.69 (3H, s), 1.63 (2H, d, *J* = 13 Hz), 1.57 (3H, s) ppm; ^{13}Cmr δ: 127.4, 125.8, 88.2, 77.6, 60.2, 59.7, 57.4, 54.1, 52.5, 48.4, 44.1, 41.2, 38.8, 32.3, 30.7, 17.9 ppm (2 lines not resolved); *m/e*: 392.2343 ($C_{26}H_{34}O_4$ minus H_2O requires 392.2350).

Acknowledgments

The research of the Principal Investigator is supported by the National Institutes of Health (GM 29258-11) and the National Science Foundation (CHE 8118391). We are grateful to these agencies also for their contributions to the high field nmr facility at The University of Chicago (CA 14599). We thank Professor John Gladysz for attempting high pressure Diels−Alder additions to some of our compounds, and Dr. A. Srikrishna and Mr. Ronald Martin for filling in some experimental details. W.H.B. is grateful to the NSF for a graduate fellowship.

1. P. E. Eaton. Tetrahedron, **35**, 2189 (1979); P. Deslongchamps and P. Soucy. Tetrahedron, **37**, 4385 (1981); W. P. Roberts and G. Shoham. Tetrahedron Lett. **22**, 4895 (1981); M. A. McKervey, P. Vibuljan, G. Ferguson, and P. Y. Siew. J. Chem. Soc. Chem. Commun. 912 (1981); J. E. Baldwin and P. L. M. Beckwith. J. Chem. Soc. Chem. Commun. 279 (1983); G. Mehta and M. S. Nair. J. Chem. Soc. Chem. Commun. 439 (1983); D. G. Farnum and T. Mogeno. Tetrahedron Lett. **24**, 1361 (1983); W. D. Fessner, H. Prinzbach, and G. Rihs. Tetrahedron Lett. **24**, 5857 (1983).
2. L. A. Paquette, R. J. Ternansky, D. W. Balough, and G. Kentgen. J. Am. Chem. Soc. **105**, 5446 (1983).
3. (*a*) P. E. Eaton and R. H. Mueller. J. Am. Chem. Soc. **94**, 1014 (1972); (*b*) P. E. Eaton, R. H. Mueller, G. R. Carlson, D. A. Cullison, G. F. Cooper, T.-C. Chou, and E.-P. Krebs. J. Am. Chem. Soc. **99**, 2751 (1977); (*c*) P. E. Eaton, G. D. Andrews, E.-P. Krebs, and A. Kunai. J. Org. Chem. **44**, 2824 (1979); (*d*) P. E. Eaton, A. Srikrishna, and F. Uggeri. J. Org. Chem. **49**, 1728 (1984).
4. H. J. Reich, J. M. Renga, and I. L. Reich. J. Am. Chem. Soc. **97**, 5434 (1975).
5. D. Liotta, C. Barnum, R. Puleo, G. Zima, C. Bayer, and H. S. Kezar III. J. Org. Chem. **46**, 2920 (1981).
6. P. E. Eaton and W. H. Bunnelle. Tetrahedron Lett. **25**, 23 (1984).
7. (*a*) N. Acton, A. Brossi, D. L. Newton, and M. J. Sporn. J. Med. Chem. **23**, 805 (1980); (*b*) T. Tsujikawa, Y. Nakagawa, K. Tsukamura, and K. Masuda. Chem. Pharm. Bull. **25**, 2775 (1977); (*c*) M. L. Bolte, W. D. Crow, and S. Yoshida. Aust. J. Chem. **35**, 1411 (1982).
8. K. Hiroga. Chem. Pharm. Bull. **13**, 1359 (1967).
9. (*a*) H. Bredereck, R. Franz, and G. Bauer. Angew. Chem. Int. Ed. Engl. **7**, 299 (1968); (*b*) C. Bischoff and A. Rieche. Z. Chem. **8**, 384 (1968).
10. W. Skorianetz, K. H. Schulte-Elte, and G. Ohloff. Helv. Chim. Acta, **54**, 1913 (1971).
11. L.-B. Agenäs. *In* Organic selenium compounds: their chemistry and biology. *Edited by* D. L. Klayman and W. H. Günther. John Wiley and Sons, Inc., New York. 1973.
12. B. M. Trost, T. N. Salzmann, and K. Hiroi. J. Am. Chem. Soc. **98**, 4887 (1976).
13. Ae. de Groot and B. J. M. Jansen. Recl. Trav. Chim. Pays-Bas, **98**, 487 (1979).
14. T. Kumamota, S. Kobayashi, and T. Mukaiyama. Bull. Chem. Soc. Jpn. **45**, 866 (1972).
15. J. R. Shelton and K. E. Davis. J. Am. Chem. Soc. **89**, 718 (1967).
16. B. Ganem, A. J. Biloski, and R. P. Heggs. Tetrahedron Lett. 689 (1980).
17. N. W. Schwartz and J. H. Blumbergs. J. Org. Chem. **29**, 1976 (1964).
18. J. L. Hermann, M. H. Berger, and R. H. Schlessinger. J. Am. Chem. Soc. **95**, 7923 (1973).
19. I. A. Ibers and W. C. Hamilton. International tables for X-ray crystallography. Vol. IV. The Kynoch Press, Birmingham. 1974. p. 71.
20. P. Engel. Acta Crystallogr. Sect. A, **34**, S 348 (1978).

Can. J. Chem. Downloaded from www.nrcresearchpress.com by 210.87.254.105 on 09/06/12
For personal use only.

COMMUNICATION

A construction of the angularly hydroxylated *cis* 1,8-naphthalenedione system typical of the tetracyclines

GILBERT STORK[1] AND YING K. YEE
Department of Chemistry, Columbia University, New York, NY 10027, U.S.A.

Received March 30, 1984

This article is dedicated to Professor Peter Yates on the occasion of his 60th birthday

GILBERT STORK and YING K. YEE. Can. J. Chem. **62**, 2627 (1984).

This paper demonstrates the feasibility of constructing the angularly hydroxylated 1,8-decalindione system typical of the tetracycline group of antibiotics. The α-hydroxy-β-diketone structure is constructed by the action of fluoride ion on an enediol disilyl ether. The siloxyketone enolate thus generated is then intramolecularly trapped by an appositely placed ester.

GILBERT STORK et YING K. YEE. Can. J. Chem. **62**, 2627 (1984).

Cet article montre qu'il est possible de construire le système d'une 1,8-décalinedione portant un hydroxyle dans l'angle qui est typique du groupe d'antibiotiques apparentés à la tétracycline. La fonctionalité α-hydroxy β-dicétone est formée par l'action de l'anion fluorure sur le bis-silyl ether d'un ènediol. L'énolate de siloxy cétone ainsi formé est alors piégé intramoléculairement par un ester approprié.

This communication reports the construction of a molecule **1** (as its trimethylsilyl ether **1***a*) embodying the α-hydroxy-β-diketone array which is a common feature of the a/b ring system of antibiotics such as tetracycline, **2** (1). Our goal was to develop a process which would specifically produce the *cis*-fused 8a-hydroxy-1, 8-napthalenedione arrangement rather than the mixture of *cis* and *trans* isomers which results when the hydroxydiketone construction depends, as it classically has (2), on the hydroxylation of a precursor enolic β-diketone system.

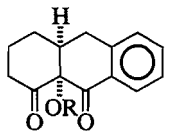

1 R = H

1*a* R = Si

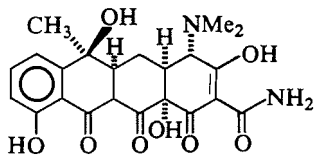

2

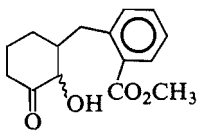

3

We envisaged that a cyclization formally represented by **3** → **1** would, if feasible, lead to the required structure and stereochemistry, as a result of well-understood geometric constraints on the transition state for the cyclization process.

Our initial attempts were centered on the possibility of achieving base-catalyzed cyclization of some enolate species derivable from ketols like **3**. The ketol **3** was simply constructed by alkylation of the isobutyl enol ether of cyclohexane-1,2-dione with methyl 2-bromomethylbenzoate (LDA–THF; HMPA, 1 h, −20°C) to **4** (61% yield), which was then transformed to the desired **3** by reduction with sodium borohydride followed by hydrolysis of the enol ether with 50% acetic acid.

[1] Author to whom correspondence may be addressed.

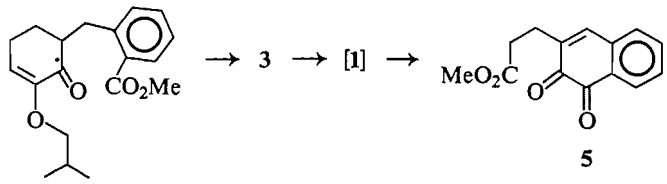

4 → **3** → [1] → **5**

Treatment of the ketol **3** with 1 equiv. of sodium hydride in THF for 2 h at room temperature resulted in the isolation, after flash chromatography, of the α-naphthoquinone **5** as orange crystals, mp 89.5–91.5°C; ir ($CHCl_3$): 1735 (s), 1695 (w), 1662 (s), 1627 (w) cm^{-1}; nmr (δ): 1.67–2.02 (m, 2H), 2.10–2.55 (m, 4H), 3.60 (s, 3H), 6.85–7.65 (m, 4H), 7.87–8.06 (m, 1H); ms (EI): 258. This result strongly suggests that the desired cyclization (**3** → **1**) had taken place but had been followed by cleavage of the β-diketone system and air oxidation (the latter, presumably, during chromatography).

The desired cyclization was finally achieved by a modification of the general scheme above.

Alkylation of cyclohexanone (LDA/THF/−78°C) with phenyl-2-bromomethylbenzoate (HMPA, −10°C) gave **6**, mp 70–71.5°C in 76% yield. The silyl enol ether **7** (75%) obtained via kinetic deprotonation with LDA[2] was converted to the ketol TMS ether **8** (*m*-CPBA; TMSCl, NEt_3; ~2:1 mixture of stereoisomers, 82% yield) (3).

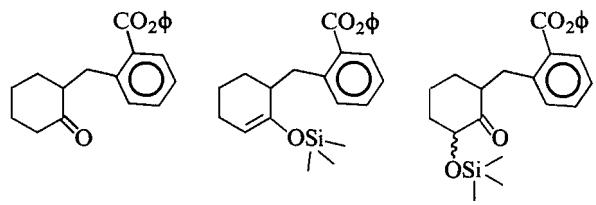

6 **7** **8**

After various attempts at cyclization of the kinetic lithium enolate of **8** had met with failure, success was finally achieved

[2] About 20% of the tricyclic enol lactone, mp 104.5°C, derived from the enolate precursor of **7** was also obtained.

by the use of the crucial silylated enediol **9**[3] obtained from the kinetic enolate of **8**: Treatment of **9** with a dry (molecular sieves) THF solution of tetrabutylammonium fluoride at −78 to −20°C, followed by quenching with *N*-trimethylsilylimidazole, gave **1***a* in 74% yield (mp 69.5–70°C from hexane; ir (neat): 1735 (s), 1725 (s), 1690 (s), 1677 (s), 1603 (m) cm^{-1}; nmr (δ): 0.13 (s, 9H), 1.53–2.15 (m, 4H), 2.35–2.70 (m, 3H), 2.77 (db of db, incompletely resolved, J = 6.3, 16.2 Hz, 1H), 3.47 (db, J = 4.5, 16.2 Hz, 1H), 7.15–7.67 (m, 3H), 7.90–8.07 (m, 1H); ms (EI): 302 (M^+). The identity of **1***a* was further established by conversion (Zn/AcOH) to the β-diketone **10**, mp 74–76°C, identical with an unambiguously synthesized sample. The ring fusion in **1***a* is shown as *cis*, as it is in the tetracyclines, for mechanistic reasons.[4] It is of some interest that the conditions which were successful with the phenyl ester **9** were unsuccessful with the corresponding methyl ester.

[3] For related reactions, see ref. 4.

[4] This is a consequence of geometric requirements for the cyclization reaction (cf. "Baldwin rules").

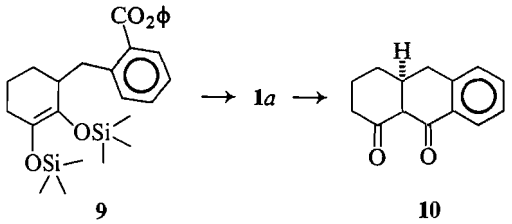

9 **10**

Acknowledgments

We thank the National Institutes of Health and the National Science Foundation for support of this work.

1. L. A. MITSCHER. The chemistry of the tetracycline antibiotics. Marcel Dekker, Inc., New York. 1978.
2. H. MUXFELDT, G. HAAS, G. HARDTMANN, F. KATHAWALA, J. B. MOOBERY, and E. VEDEJS. J. Am. Chem. Soc. **101**, 689 (1979); B. GLATZ, G. HELMCHEN, H. MUXFELDT, H. PORCHER, R. PREWO, J. SENN, J. J. STEZOWSAKI, R. J. STOJDA, and D. R. WHITE. J. Am. Chem. Soc. **101**, 2171 (1979).
3. G. M. RUBBOTTOM, M. A. VASQUEZ, and D. R. PELEGRINA. Tetrahedron Lett. 4319 (1974); A. G. BROOK and D. M. MACRAE. J. Organomet. Chem. **77**, C19 (1974); A. HASSNER, R. H. REUSS, and H. W. PINNICK. J. Org. Chem. **40**, 3427 (1975).
4. E. NAKAMURA, M. SHIMIZU, I. KUWAJIMA, J. SAKATA, K. YOKOHAMA, and R. NOYORI. J. Org. Chem. **48**, 932 (1983).

Comparison of solvent extraction efficiencies for toxic organic compounds on flyash

R. E. CLEMENT
Ontario Ministry of the Environment, P.O. Box 213, Rexdale, Ont., Canada M9W 5L1

AND

A. C. VIAU AND F. W. KARASEK[1]
Guelph–Waterloo Centre for Graduate Work in Chemistry, Department of Chemistry, University of Waterloo, Waterloo, Ont., Canada N2L 3G1

Received February 16, 1984

R. E. CLEMENT, A. C. VIAU, and F. W. KARASEK. Can. J. Chem. **62**, 2629 (1984).

The extraction efficiencies of various solvents for toxic organic compounds on municipal incinerator flyash were examined. Soxhlet extraction by the solvent was followed by benzene Soxhlet extraction for determination of the non-extracted material. Benzene was found to be the best solvent when considering purity and extraction of hazardous compounds.

R. E. CLEMENT, A. C. VIAU et F. W. KARASEK. Can. J. Chem. **62**, 2629 (1984).

On a étudié l'efficacité de divers solvants pour extraire des composés organiques toxiques qui sont présents dans les jets de cendre d'incinérateurs municipaux. L'extraction par le solvant se fait à l'aide d'un appareil Soxhlet et, dans le but de déterminer les quantités de produits qui n'ont pas été extraits, on procède à une autre extraction par du benzène, à l'aide d'un appareil Soxhlet. On a trouvé que le benzène est le meilleur solvant lorsqu'on veut déterminer la pureté ou extraire des composés dangereux.

[Traduit par le journal]

Introduction

Toxic compounds found on flyash from combustion of waste are a recognized problem (1). Among the toxic compounds found worldwide on flyash are polychlorinated dibenzo-*p*-dioxins (PCDD). The toxicological implications of PCDD on flyash are being elucidated (2). It has been found that rats fed flyash particles containing PCDD absorb all the congeners and isomers into their livers (2). A similar mechanism of absorption could occur in humans.

The precision of PCDD quantitation has increased with the methods of analysis. It is common to see solvent extraction with some form of clean-up procedure involving hplc and analysis with gc–ms. More recently, attention has focussed on the extraction of PCDD from flyash. Various solvents have been reported for extraction of PCDD but the use of acid treatment prior to solvent extraction has gained popularity (3). The original work used 1 *N* HCl; however, researchers are now using 12 *N* HCl in an attempt to puncture the flyash particulate releasing the PCDD found in the interior of the particle for extraction (4). This approach has been found satisfactory if PCDD are the only compounds of interest, but acid treatment ultimately will decompose many other organic compounds. As a result the original composition of organic compounds found on the flyash has been altered and no conclusions can be reached with respect to formation mechanisms and the presence of other toxic compounds such as PAH on flyash particles.

An extraction procedure is needed where the maximum amount of organic compounds including PCDD are extracted unaltered in composition. Such a procedure is proposed in this study. It consists of sequential soxhlet extraction with two solvents. It is found that methanol followed by benzene results in extraction efficiencies which are equal to toluene or benzene for total screening of PAH and PCDD. However, this sequential extraction resulted in better extraction of selected PAH and tetrachlorodibenzo-*p*-dioxins than toluene or benzene.

[1]To whom all correspondence should be addressed.

Experimental

Sample preparation

Three flyash grab samples, from municipal incinerators located in southern Ontario, were combined in equal weights, approximately 50 g each, in a large flint glass jar. The jar was shaken and rotated prior to the removal of each sub-sample, to minimize heterogeneity of the bulk composite.

Sample extraction and concentration

Approximately 10 g samples of the composite flyash were extracted in medium porosity glass fritted extraction thimbles, for 20 filling and draining cycles with 200 mL of each of five solvents; benzene, toluene, and methanol ("Distilled in Glass" grade, Caledon Laboratories Ltd., Georgetown, Ont.) and cyclohexane and dichloromethane ("Distilled in Glass" grade, Burdick and Jackson, Inc., Muskegon, MI) in a soxhlet apparatus. Duplicate extracts for each solvent were prepared in this matter.

Each extract was concentrated to approximately 5 mL by rotary evaporation at 56–69°C under water aspirator vacuum. The extract was transferred, with three washings of 1–2 mL, to a 25 mL pear-shaped flask for further concentration. The concentrated extract was transferred, with three washings of 50–100 μL, to a 1 mL "Mini-Vial" (Alltech Associates, Inc., Arlington Heights, IL) equipped with screw-caps fitted with Teflon-faced liners. A final volume reduction to approximately 100 μL was achieved by direction of a slow stream of high purity argon or nitrogen onto the surface of the extract in the vial. All concentrated extracts were stored in a freezer at approximately −5°C.

After the first extraction with a particular solvent, each flyash sample was subjected to a second extraction with 200 mL of benzene under the same conditions outlined above. The benzene re-extract of each sample was concentrated in the same manner as the original solvent extract.

In addition to the flyash samples, a procedure blank for each solvent was prepared by carring 200 mL of the solvent through each extraction and concentration step, using an empty extraction thimble in a soxhlet apparatus. No contamination could be detected upon gc/fid and gc/ms/sim analysis.

All glassware, vials, and Pasteur pipets were cleaned via the following procedure: ultrasonic agitation in an aqueous solution of Alconox detergent (Alconox, Inc., New York, NY.) for a minimum of 30 min, rinsed with copious quantities of tap water, followed by

rinsing with deionized water, and heated in a laboratory oven for 1 h at 350°C.

Measurement of final extract volume

The following final extract volume calculation was used to reduce measurement errors: 100 μL of pure solvent was dispensed into a vial with a 1000 μL syringe, the weight of the pure solvent in the vial was obtained. The volume of the extract was obtained by multiplying a weight ratio; the weight of extract divided by the weight of the 100 μL of pure solvent, times 100 μL. The assumption that the extract density may be approximated by the density of the pure solvent was justified by the fact that approximately 98% of the peak area, determined via gc/fid, of each extract was attributable to the solvent.

Due to the excessive amount of polar inorganic material co-extracted by methanol, the methanol extracts were successively concentrated by gaseous evaporation until a milky white precipitate formed and centrifuged at 3000 rpm for 10 min. The supernatant was transferred to another vial and the process repeated two more times. The final volume of the methanol extracts was estimated by the graduated vials markings, as any inorganic material still dissolved in the extract would have altered the density of the extract and invalidated the mass ratio technique.

Gas chromatographic analysis

A Hewlett-Packard 5830A digital gas chromatograph (gc) was equipped with a 2.6 m long, 2 mm id column packed with Aue packing, 0.2% w/w Carbowax 20M deposited on 100/120 mesh acid wash Chromosorb W (5). A flame ionization detector (fid) was employed for the determination of the total organic carbon (toc) content of each extract. Chromatographic conditions were as follows: initial temperature, 50°C; program rate, 4°C/min; final temperature, 250°C; time at final temperature, 15 min; helium carrier gas flow, 45 mL/min; attenuation 32; slope sensitivity, 0.01 mV/min, and area reject, 500.

Gas chromatography/mass spectrometry analysis

A Hewlett-Packard 5992A gas chromatograph/mass spectrometer (gc/ms), equipped with a single floppy disk and an X−Y plotter was employed for the selected ion monitoring (sim) analysis of each extract. The glass-packed column employed in the gc/fid analysis was transferred to the gc/ms and identical chromatographic conditions were used. Selected ion monitoring areas generated by the gc/ms were used for quantification. Three standards were employed for the sim analyses. An *n*-alkane standard was employed for the evaluation of response factors for all of the *n*-alkanes from C14 to C30 which were observed in the extracts. A standard containing 1,2,3,4-TCDD was employed for the quantitation of all the PCDD's, assuming all isomers had a relative response factor of one. Although this assumption is not exact, this method is valid for comparative evaluations (6). The third standard contained six *n*-alkanes, three PAH compounds which were employed for the quantitation of the appropriate compounds in each extract. Table 1 lists the components, concentration, and selected ions for all standards. Anthracene was assumed to have a response factor intermediate to fluorene and fluoranthene. A response factor similar to fluoranthene was used for pyrene.

Before operating in sim, the mass spectrometer was tuned daily by the manufacturer-supplied program AUTOTUNE using a perfluorotributylamine calibration standard.

Results and discussion

The gc/ms/sim analysis for *n*-alkanes are shown in Fig. 1. The various solvents used for primary extraction are denoted with each reconstructed ion chromatogram. All chromatograms are plotted to the same full scale for a more direct comparison. This can be done since all the variables such as sample weight are approximately equal. It is seen that benzene, toluene, and cyclohexane extract all of the *n*-alkanes. Dichloromethane extracts other unidentified components which prohibits confident identification and quantitation of some of the *n*-alkanes. It is found that methanol extracts a substantially lower amount of alkanes than any of the other solvents.

The benzene re-extraction of the flyash following the respective solvent extraction indicates that benzene and toluene primary extraction is efficient since relatively little alkanes are extracted. This is not true for the cyclohexane extraction. The re-extract from dichloromethane extraction shows that some alkanes are recovered. The benzene re-extraction of methanol extraction expectedly has the *n*-alkanes since previously little was removed from the flyash by the methanol.

An arbitrary division of the alkanes into low (14−19), medium (20−25), and high (26−30) concentration (ng/g) was done to compare the concentrations extracted with each procedure. These values are listed in Table 2. These data show that primary extraction with benzene extracts more alkanes than any other solvent. Cyclohexane and toluene extract approximately

TABLE 1. Concentration of standard components and ions monitored during selected ion monitoring mass spectrometry

Compound classification	Compound	Concentration in standard (ng/μL)	Ion monitored
n-Alkanes	*n*-$C_{14}H_{30}$	12	85.1
	n-$C_{18}H_{38}$	99	85.1
	n-$C_{20}H_{42}$	103	85.1
	n-$C_{24}H_{50}$	103	85.1
	n-$C_{26}H_{54}$	102	85.1
	n-$C_{30}H_{62}$	100	85.1
Polyaromatic hydrocarbons	Biphenyl	126	154.1
	Fluorene	102	166.1
	Anthracene	—	178.1
	Fluoranthene	111	202.1
	Pyrene	—	202.1
Polychlorinated dibenzo-*p*-dioxins	Tetra-CDD	30(1,2,3,4-TCDD)	321.9
	Penta-CDD	—	355.9
	Hexa-CDD	—	389.8
	Hepta-CDD	—	425.8
	Octa-CDD	—	459.7

TABLE 2. Concentration (ng/g) of *n*-alkanes on flyash extracted with solvent and re-extracted with benzene

	Low (14−19)		Medium (20−25)		High (26−30)		Total of means
Benzene							
Ex	845	917	1007	864	2037	1462	3566
Rex	43	48	21	11	24	16	81
Toluene							
Ex	316	335	631	823	1061	1308	2237
Rex	26	50	22	43	16	47	102
Cyclohexane							
Ex	375	287	928	696	1709	1278	2636
Rex	193	241	172	316	307	577	903
Dichloromethane							
Ex	190	353	376	707	527	1141	1647
Rex	90	88	110	97	94	107	293
Methanol							
Ex	46	89	140	211	25	0	755
Rex	199	199	613	527	1295	944	1888

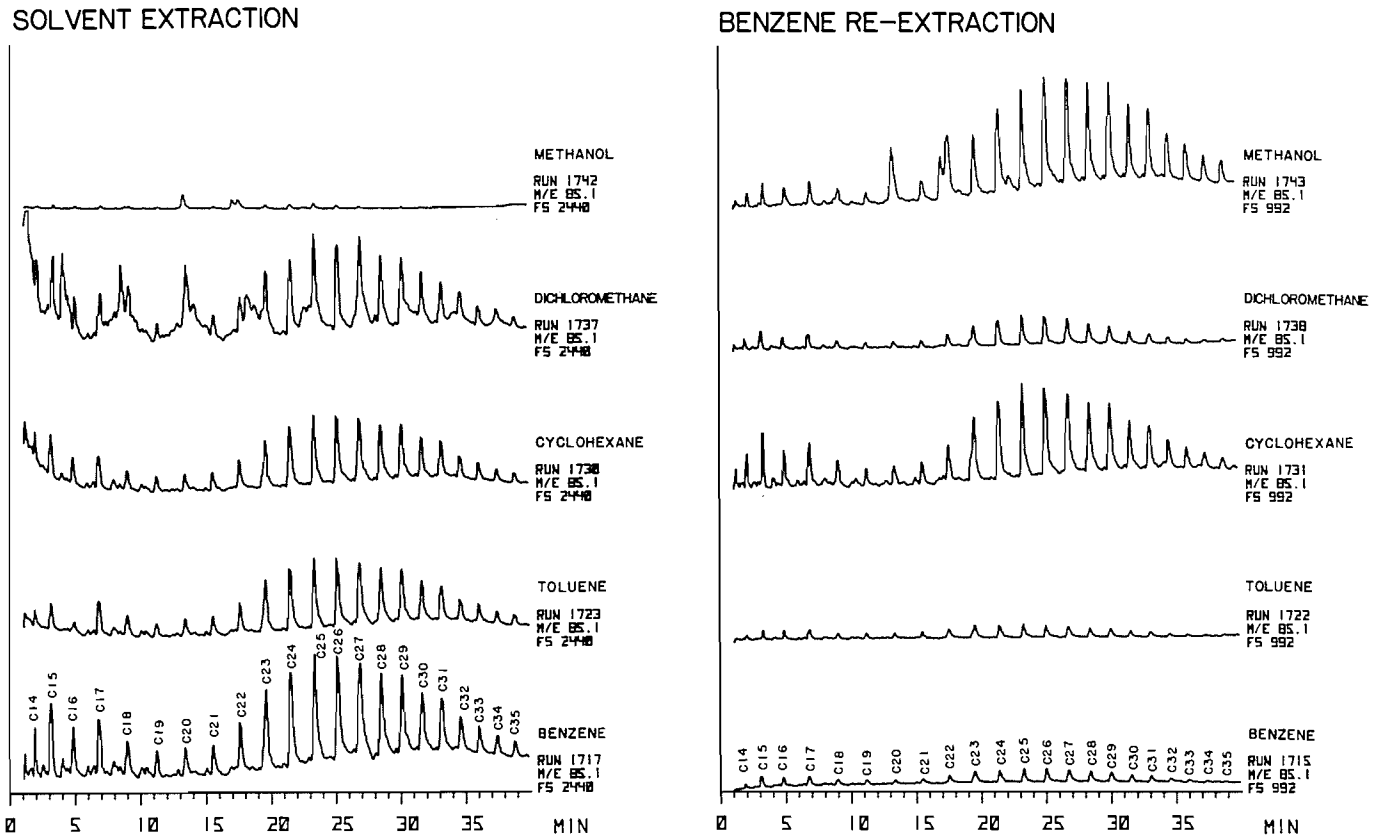

FIG. 1. Selected ion chromatograms demonstrating the differences in extraction of *n*-alkanes by various solvents.

TABLE 3. Concentrations (ng/g) of selected PAH from flyash extracted with solvent and re-extracted with benzene

	Biphenyl		Fluorene		Fluoranthene		Pyrene		Anthracene		Total of means
Benzene											
Ex	168	176	9	11	76	80	28	30	217	223	509
Rex	8	9	0	0	5	9	1	2	11	27	36
Toluene											
Ex	106	98	0	0	79	73	29	33	189	187	397
Rex	13	13	0	0	5	7	1	2	0	0	20
Cyclohexane											
Ex	19	34	0	0	4	4	2	2	16	18	42
Rex	102	129	18	23	55	81	22	29	151	189	399
Dichloromethane											
Ex	92	120	4	6	14	21	4	8	62	96	179
Rex	59	48	5	3	64	49	19	18	125	113	250
Methanol											
Ex	24	26	0	0	3	0	0	0	6	6	32
Rex	106	117	20	21	59	59	20	16	209	210	418

equal amounts while the more polar dichloromethane and methanol extract substantially less than the other solvents. The re-extraction with benzene shows that the alkanes are not totally recovered if the primary solvent was very polar.

The sim chromatogram for two selected PAH, fluoranthene and pyrene, are shown in Fig. 2. Different extraction efficiencies for each primary solvent are seen as compared to alkanes. Benzene and toluene extract those components fairly readily but the other solvents do not. The benzene re-extraction confirms this observation since these compounds are recovered from the cyclohexane, dichloromethane, and methanol but are not evident in the benzene, toluene re-extracts.

The quantitative data for other PAH are shown in Table 3. The trends observed in Fig. 2 are also seen for other PAH. Furthermore, unlike the alkanes, the PAHs are almost totally recovered from flyash following benzene re-extraction. The

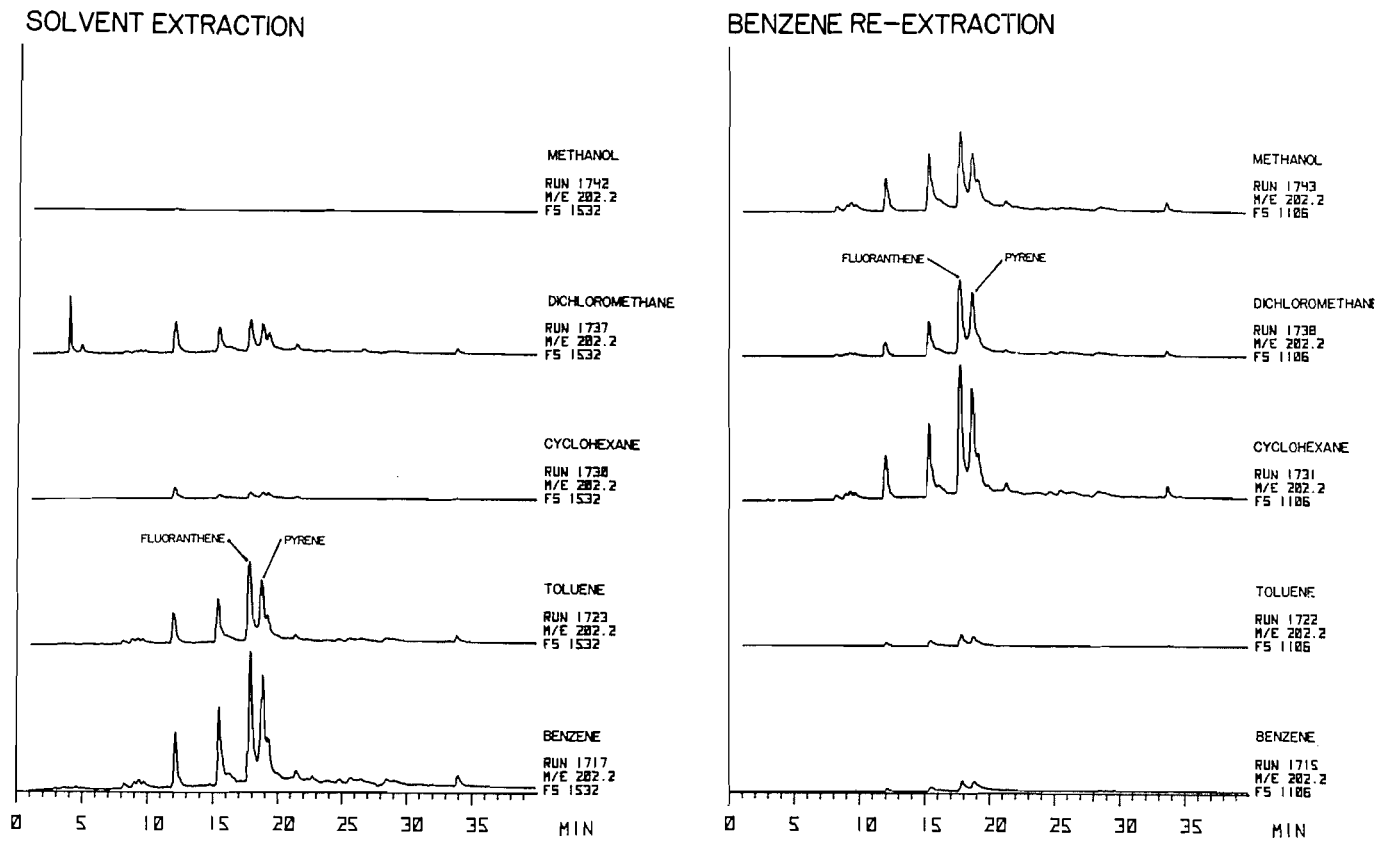

FIG. 2. Selected ion chromatograms of fluoranthene and pyrene showing the extraction efficiencies of the various solvents and the recovery of these compounds by benzene re-extraction.

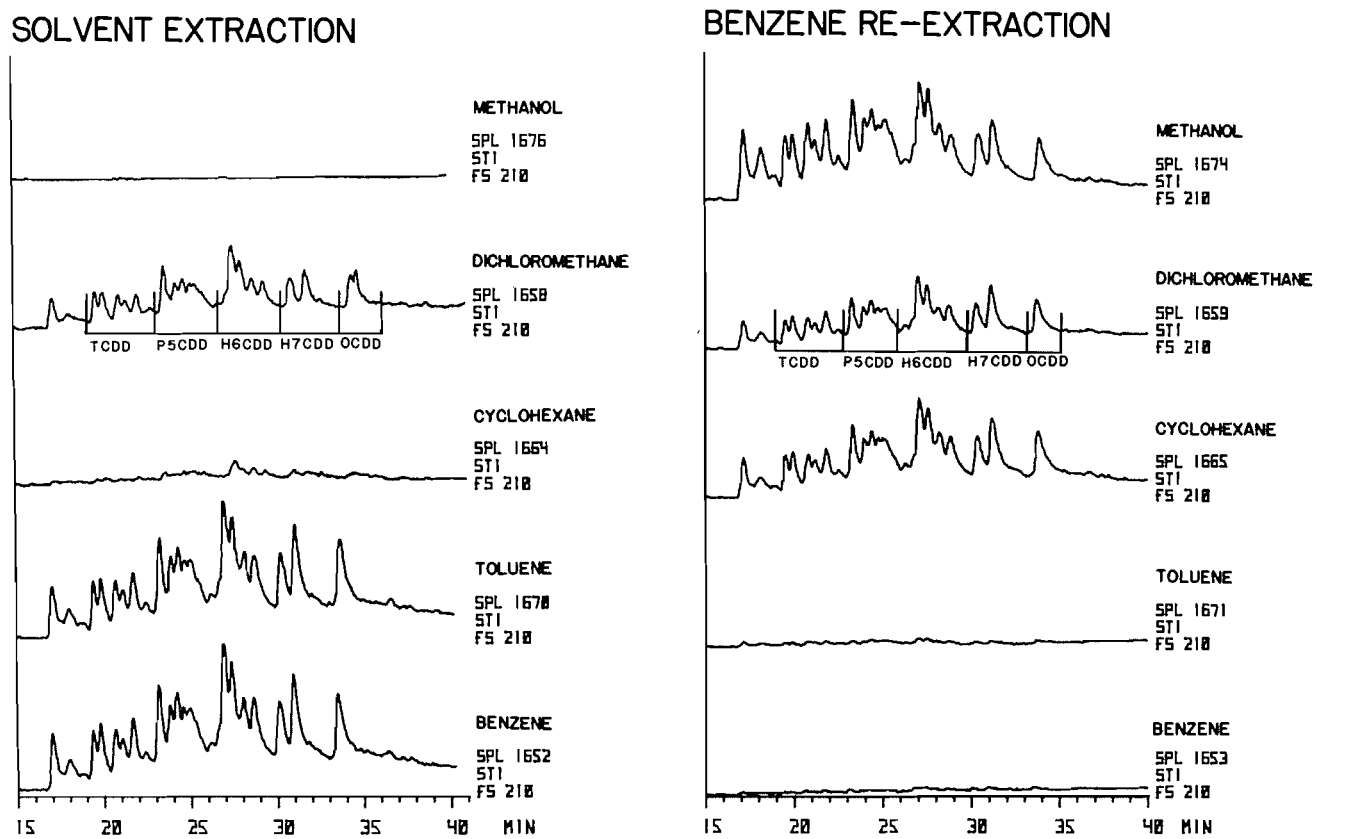

FIG. 3. Selection ion monitoring total ion chromatograms for PCDD showing the extraction of these compounds from flyash by the various solvents and benzene re-extraction.

TABLE 4. Concentrations (ng/g) of PCDD isomeric groups with extracted solvent and re-extracted with benzene

	TCDD		P_5CDD		H_6CDD		H_7CDD		OCDD		Total of means
Benzene											
Ex	22	21	35	31	45	41	30	32	37	37	165
Rex	1	1	1	1	2	2	3	3	0	0	7
Toluene											
Ex	26	25	41	37	53	52	38	38	50	50	205
Rex	1	2	1	2	2	3	0	3	0	0	14
Cyclohexane											
Ex	2	2	2	2	3	3	3	3	0	6	10
Rex	15	19	23	28	29	36	22	24	25	31	127
Dichloromethane											
Ex	11	14	16	16	22	21	16	16	19	19	85
Rex	12	13	20	20	24	24	19	22	25	19	99
Methanol											
Ex	2	1	1	0	2	0	0	0	0	0	3
Rex	33	32	42	42	52	50	32	35	31	37	193

best second extraction recovery is seen with the methanol primary extract. Primary benzene extraction is found to remove the most total PAH than any other solvent. Toluene does not extract any fluorene and a lower amount of biphenyl and anthracene than benzene. The total PAH extracted by toluene is less than that of the sequential methanol–benzene extract which has all the PAHs. Sequential methanol–benzene extraction is also seen to extract more fluorene than any other method. The reason for the differential solvent extraction observed for PAH may lie in π-electron interactions. Thus, cyclohexane would not be as efficient as benzene, toluene, or dichloromethane. This may also help to explain why benzene extracts fluorene better than toluene.

It is to be noted that the concentrations obtained from duplicate extracts are often very close. This is especially observed with solvents which are efficient extractors.

The sim total ion (sti) current chromatogram for PCDD is plotted for all the extracts in Fig. 3. The sim total ion is a program developed for this gc/ms system which allows the user to plot the summed abundances of all the ions monitored (7). The elution times for each PCDD isomeric group are identified in Fig. 3 from the single ions previously plotted. The PCDD are easily identified because of previous work done with flyash from this site (6). It is evident that the extraction of PCDD follows the extraction behaviour of PAH on flyash. Benzene and toluene can extract most of the PCDD while dichloromethane is less efficient in this process. Cyclohexane and methanol extract very little PCDD. The benzene re-extraction only recovers PCDD from the cyclohexane, dichloromethane, methanol primary extracts. The π-electron interactions may again be responsible for the efficient removal of the PCDD from the flyash particle.

The concentrations of PCDD are given in Table 4. It is ascertained that toluene extracts the most PCDD. However, the greatest difference between benzene and toluene is with OCDD; otherwise toluene extracts slightly more than benzene. Cyclohexane virtually does not extract PCDD and benzene re-extraction does not recover all the PCDD. Dichloromethane extracts approximately one-half the benzene amount. It is interesting that although methanol essentially does not extract PCDD, benzene re-extraction results in more PCDD being extracted than by benzene extraction alone. The total amount of PCDD extract by this sequential method is close to that extracted by toluene. An important difference is noted. Whereas toluene extracted a greater amont of OCDD, sequential methanol–benzene extracts more TCDD. The other PCDD concentrations approach the values obtained for toluene.

One of the objectives in the study of toxic compounds on flyash is to extract the components of interest while minimizing interferant and nontoxic compounds. Benzene is found to extract all of the PAH and PCDD sought but many alkanes are also extracted. Toluene extracts less alkanes but does not extract all the PAH compounds and the improvement in PCDD extraction is not very substantial. Cyclohexane and dichloromethane are found to be unsuitable for extraction of the PAH and PCDD from flyash. Sequential extraction of flyash with methanol followed by benzene allows the extraction of all PAH and PCDD. Enhancement of certain compounds such as TCDD and fluorene is found. It can be ascertained that benzene and sequential methanol–benzene extraction of flyash yields the best results for specific trace analysis of the PAH and PCDD compounds. The other solvent methods are found to be less satisfactory.

1. G. A. EICEMAN, R. E. CLEMENT, and F. W. KARASEK. Anal. Chem. **51**, 2343 (1979).
2. M. VAN DER BERG, K. OLIE, and O. HUTZINGER. Chromosphere **12**, 537 (1983).
3. R. M. M. KOOKE, J. W. A. LUSTENBOWER, K. OLIE, and O. HUTZINGER. Anal. Chem. **53**, 461 (1981).
4. D. K. W. WONG, D. H. CHIU, P. K. LEUNG, R. S. THOMAS, and R. C. LAO. *In* Human and environmental risks of chlorinated dioxins and related compounds. *Edited by* R. E. Tucker, A. L. Young, and A. P. Gray. Plenum Press, New York. 1983. p. 113.
5. W. A. AUE, C. R. HASTINGS, and S. KAPILA. J. Chromatogr. **27**, 299 (1973).
6. A. C. VIAU and F. W. KARASEK. J. Chromatogr. **280**, 235 (1983).
7. L. C. DICKSON, F. W. KARASEK, and R. E. CLEMENT. J. Chromatogr. **280**, 23 (1983).

Etude structurale et thermodynamique des interactions entre des dérivés chlorés et bromés du méthane et des amides tertiaires

J. M. DUMAS, C. GERON, A. R. KRIBII ET M. LAKRAIMI

Laboratoire de Physicochimie des diélectriques, Université de Poitiers, 40, avenue du Recteur Pineau, 86002 Poitiers Cedex, France

Reçu le 23 janvier 1984

J. M. DUMAS, C. GERON, A. R. KRIBII et M. LAKRAIMI. Can. J. Chem. **62**, 2634 (1984).

Une étude par polarisation diélectrique, microcalorimétrie et spectrométrie infrarouge a permis de mettre en évidence le rôle joué par l'halogène dans les interactions entre une série de dérivés chlorés et bromés du méthane, pris comme représentants d'anesthésiques halogénés et deux amides tertiaires prises comme modèle de constituant de la membrane des cellules nerveuses. Cette étude a eu lieu en solution diluée dans un solvant organique inerte, le cyclohexane. Les interactions sont de type liaison hydrogène et/ou liaison halogène.

J. M. DUMAS, C. GERON, A. R. KRIBII, and M. LAKRAIMI. Can. J. Chem. **62**, 2634 (1984).

A study by dielectric polarization, microcalorimetry, and infrared spectrometry has allowed us to demonstrate the role played by the halogen in interactions between a series of chlorinated and brominated derivatives of methane (considered as types of halogenated anesthetics) and two tertiary amides taken as models for an element of the membranes of the nervous cells. The inert organic solvent used was cyclohexane. The interactions are of the hydrogen bonding and (or) halogen bonding types.

Can. J. Chem. Downloaded from www.nrcresearchpress.com by 210.87.254.40 on 09/06/12
For personal use only.

Introduction

L'activité biologique et, en particulier, les propriétés anesthésiques des dérivés halogénés ont retenu notre attention. Le mécanisme de l'anesthésie générale semble pouvoir être lié à des phénomènes d'interactions entre les anesthésiques volatils et différents sites d'action au sein de la membrane des cellules nerveuses (1–3). Aussi, les résultats des études sur la recherche des interactions entre les dérivés halogénés et des molécules simples prises pour modèle d'un site d'action possible, paraissent donc importants.

Des études effectuées par Sandorfy et coll. (4–8) ont montré que les dérivés halogénés peuvent entraver la formation de liaison hydrogène. D'autre part, les résultats des recherches menées dans notre laboratoire (9) ont permis de signaler l'existence très générale d'interactions moléculaires de type liaison hydrogène et/ou liaison halogène entre des bases organiques et des dérivés halogénés et d'étudier l'évolution de ces interactions en fonction de l'halogène. Notre contribution à une meilleure connaissance de ces interactions repose sur une étude structurale et thermodynamique de systèmes formés par des dérivés halogénés du méthane (essentiellement chlorés et bromés) et par des amides tertiaires (*N*,*N*-diméthylacétamide et *N*-méthylpyrrolidone) utilisées comme modèle de constituant de la membrane et choisies pour leur caractère polaire (une part importante de notre étude s'appuyant sur la polarisation diélectrique).

Pour cette étude nous avons suivi une démarche méthodologique rigoureuse qui s'appuie sur une sélection de techniques physicochimiques: (*i*) la polarisation diélectrique qui permet de conduire simultanément à la stabilité (constante d'équilibre) et à des informations sur la structure des complexes formés. Tous les systèmes ont été étudiés par cette technique; (*ii*) la microcalorimétrie qui procure des valeurs d'enthalpie accompagnant les interactions étudiées et permet de comparer ces valeurs à celles habituellement mises en jeu dans le cas d'interactions non spécifiques (de l'ordre de 2 à 5 kJ mol^{-1}). Seuls quelques systèmes sont concernés; (*iii*) la spectrométrie d'absorption infrarouge qui, par l'intermédiaire d'une étude à basse température, apporte des compléments d'information sur la structure des complexes. Cette étude est très partielle.

Techniques et méthodes utilisées

En polarisation diélectrique

Nous avons adopté la méthode de Cleverdon *et al.* (10) qui, dans le cadre de la théorie de Debye, permet d'accéder simultanément à la constante d'association K_{AB}, à l'incrément de polarisation ΔP et au moment dipolaire global μ_{AB}, liés à la formation du complexe AB. Cette méthode consiste à déterminer la polarisation molaire du soluté A extrapolée à dilution infinie au sein d'un solvant inerte S (le cyclohexane) et dans une série de solvants mixtes BS.

La relation fondamentale sur laquelle repose la détermination de la polarisation molaire du complexe AB de stoechiométrie 1:1 est

$$\frac{1}{P'_{A_\infty/BS} - (P_{A_\infty/BS})_{cal.}} = \frac{1}{K_{AB}\,\Delta P} \cdot \frac{M_B\,V_{BS}}{W'_B} + \frac{1}{\Delta P}$$

où K_{AB}: constante de formation du complexe AB; V_{BS}: volume massique de la solution BS; M_B: masse molaire du soluté B; W'_B: fraction massique du soluté B dans le solvant S; ΔP: incrément de polarisation lié à la formation du complexe AB tel que $\Delta P + P_{A/S} + P_{B/S} = P_{AB/S}$; $P'_{A_\infty/BS}$: polarisation molaire apparente, à dilution infinie, de A dans BS. L'expression précédente tient compte de l'effet normal de solvant lorsque le soluté A en solution dans un solvant inerte S, se trouve en solution dans un solvant mixte BS.

$(P_{A_\infty/BS})_{cal.}$ représente la polarisation molaire, à dilution infinie, de A dans un solvant inerte fictif de même permittivité que BS. Elle est calculée à partir de l'expression suivante:

$$(P_{A_\infty/BS})_{cal.} = \frac{\left[1 + \frac{\epsilon_{BS} - 1}{\epsilon_{BS} + 2}\,e^{\epsilon^2} - \frac{n_{BS}^2}{n_A^2}\right]\left[P_{A_\infty/S} - \frac{n_A^2 - 1}{n_A^2 + 2} \cdot \frac{M_A}{\rho_A}\right]}{1 + \frac{\epsilon_S - 1}{\epsilon_S + 2}\left(e^{\epsilon^2} - \frac{n_S^2}{n_A^2}\right)} + \frac{n_A^2 - 1}{n_A^2 + 2} \cdot \frac{M_A}{\rho_A}$$

Can. J. Chem. Downloaded from www.nrcresearchpress.com by 210.87.254.40 on 09/06/12
For personal use only.

$P_{A_\infty/S}$: polarisation molaire à dilution infinie du soluté A dans un solvant S; n_A, n_{BS}: indices de réfraction respectifs du soluté A et du solvant mixte BS; M_A: masse molaire du soluté A; ρ_A: masse volumique du soluté A; ϵ_S, ϵ_{BS}: constantes diélectriques respectives du solvant S et du solvant mixte BS; e^{x^2}: caractéristique du soluté A; $x^2 = \frac{c^2 - a^2}{a^2}$ si $a > b > c$; $x^2 = \frac{c^2 - a^2}{b^2}$ si $b > a > c$; $x^2 = \frac{c^2 - a^2}{c^2}$ si $b > c > a$; a, b, c: dimensions de la molécule de soluté A; a: dimension suivant la direction du moment dipolaire; b, c: dimensions suivant les directions perpendiculaires à celle du moment.

Il a été vérifié par l'étude de systèmes témoins: dérivés halogénés (tétrahalogénés (18), trihalogénés (15)), chlorocyclohexane, cyclohexane, que la méthode utilisée corrige de toutes les interactions type van der Waals. Le graphe

$$\frac{1}{P'_{(A_\infty/BS)} - P_{(A_\infty/BS)cal.}} = f\left(\frac{M, v}{w}\right)$$

conduit alors aux valeurs de K_{AB} et du ΔP (11).

Les mesures diélectriques ont été effectuées à l'aide d'un dipolemètre de type DMO1 "Wissenshaftlich-Technische Werkstatten" équipé soit d'une cellule DFL1 (capacité 20 cm^3) soit d'une cellule DFL2 (capacité 8 cm^3) thermorégularisées. Les masses volumiques des corps purs et des solutions ont été mesurées à l'aide d'un densimètre digital AP.PAAR.DMA45 thermorégularisé.

En microcalorimétrie

Nous avons utilisé la relation de Lamberts et Zeegers-Huyskens (12) qui fournit simultanément les valeurs des constantes d'équilibre et les variations d'enthalpie au cours de la formation des complexes. Nous nous sommes placés dans les conditions expérimentales proches de celles préconisées par Deranleau (13) qui permettent de mesurer des valeurs de constantes d'association très faibles (<1 L mol^{-1}).

$$\Delta H = \frac{2Q_C}{V\left[C_A^0 + C_B^0 + \frac{1}{K_{AB}} - \sqrt{\left(C_A^0 + C_B^0 + \frac{1}{K_{AB}}\right)^2 - 4C_A^0 C_B^0}\right]}$$

où V: volume total de la solution; C_A^0, C_B^0: concentrations initiales en A et B en mol L^{-1}; Q_C: chaleur de complexation obtenue à partir des chaleurs de dilution de A (dont la concentration C_A^0 est fixe dans le solvant mixte BS à plusieurs concentrations C_B^0) corrigées de la chaleur de dilution de A dans le solvant S et de celle de S dans le solvant mixte BS pour les concentrations C_B^0 précédemment utilisées.

Les graphes $\Delta H = f(C_B^0)$ établis pour diverses valeurs de K_{AB} permettent de trouver la valeur de K_{AB} liée à une valeur de ΔH constante.

Le calorimètre utilisé est un calorimètre CRMT (SETARAM), avec une cellule de 80 cm^3, couplé à un intégrateur.

En spectrométrie infrarouge

Nous avons étudié la bande d'absorption caractéristique du vibrateur C=O des amides tertiaires (nombre d'onde de vibration de l'ordre de 1680 cm^{-1}) à basse température, sur un spectrophotomètre Perkin Elmer 621. Le principe a été décrit par Asselin et Sandorfy (14). L'intervalle de température était compris entre 30°C et −80°C. Le solvant utilisé était le méthylcyclohexane afin de pouvoir atteindre les basses températures souhaitées.

Purification des produits

Le cyclohexane, produit de très grande pureté pour spectroscopie, a été utilisé sans traitement préalable. Tous les autres produits ont été distillés sous pression réduite d'azote et à l'abri de la lumière, puis conservés sur tamis moléculaire. Le trichlorométhane a été lavé avec un mélange de H_2SO_4 + H_2O et séché sur $MgSO_4$ préalablement à la distillation. Le tétrabromométhane a été sublimé sous vide.

Résultats et interprétation

D'une façon générale, les valeurs de ΔP, ΔH et K_{AB} déterminées dans l'hypothèse d'un complexe 1:1 (cf. tableau 1) pour les systèmes étudiés, mettent en évidence l'existence d'interactions spécifiques entre les deux amides et les dérivés halogénés. Les composés tétrahalogénés en particulier donneraient lieu à des interactions de type liaison halogène. L'étude des systèmes témoins dérivés halogénés (tétrahalogénés (18), trihalogénés (15)), chlorocyclohexane, cyclohexane a montré que toutes les interactions type liaison de van der Waals étaient corrigées.

I. *Informations structurales sur le type de complexe formé*

I. 1. *Par polarisation diélectrique*

En nous appuyant sur des travaux déjà publiés (15, 16) nous avons suivi dans les complexes formés de A et B l'évolution de l'incrément de moment dipolaire $|\vec{\Delta\mu}|$ (noté par la suite $\Delta\mu$) défini vectoriellement comme $\vec{\mu}_{AB} = \vec{\Delta\mu} + (\vec{\mu}_A + \vec{\mu}_B)$.

La figure 1 relative à un complexe formé entre la *N,N*-diméthylacétamide, et un trihalogénométhane, illustre le fait que: (*i*) la direction de $\vec{\Delta\mu}$ est celle de la liaison intermoléculaire; (*ii*) son sens correspond aux exigences du modèle (c'est-à-dire que le déplacement des charges positives doit avoir lieu du site accepteurs d'électrons vers le site donneur: il est vraisemblablement positif dans tous les cas considérés). L'ordre de grandeur de $\Delta\mu$ doit être comparable à celui trouvé pour des complexes présentant des liaisons intermoléculaires semblables et pour lesquels la structure est bien établie. Dans le cas d'un complexe de type liaison hydrogène, nous avons retenu comme valeur probable de référence ($\Delta\mu_{réf}$), celle qui concerne les complexes formés par le pyrrole et les cétones (17): 0,1 D pour une interaction avec les électrons π, 0,6 D pour une interaction avec les électrons n. Dans le cas d'un complexe de type liaison halogène, la valeur de $\Delta\mu_{réf}$ pour les dérivés chlorés a été calculée à partir des systèmes étudiés ici et mettant en jeu le tétrachlorométhane ($\Delta\mu_{réf}$ voisin de 0,5 D). Les mélanges de tétrabromométhane et d'amides tertiaires menant à la formation de combinaisons solides insolubles dans le cyclohexane, il est impossible d'accéder à une valeur sûre de $\Delta\mu_{réf}$ pour les dérivés bromés. Des études faites sur les interactions entre les dérivés tétrahalogénés du méthane (18) et diverses bases organiques ont montré que $\Delta\mu(CBr_4) > \Delta\mu(CCl_4)$, on peut donc estimer, dans le cas d'une interaction par liaison halogène dont l'atome de brome est responsable, une valeur de $\Delta\mu_{réf}$ supérieure à celle calculée précédemment pour CCl_4.

Compte tenu de nos résultats expérimentaux, nous avons éliminé tous les modèles fournissant des valeurs de $\Delta\mu$ trop éloignées des valeurs de référence. Nous ne présentons que les résultats afférant au modèle que nous avons considéré comme le plus probable car permettant de calculer des valeurs de $\Delta\mu$ les plus rapprochées des valeurs de référence.

TABLEAU 1. Systèmes A (dérivés organohalogénés) – B (base) – S (cyclohexane). Constantes d'équilibre K_{AB} (L mol^{-1}), incréments de polarisation ΔP_{AB} (cm^3 mol^{-1}), enthalpies de réaction ΔH_{AB} (kJ mol^{-1}) à 25 ± 0,1°C

		Polarisation dielectrique		Microcalorimetrie	
B	A	K_{AB}	ΔP_{AB}	K_{AB}	$-\Delta H_{AB}$
NNDMA[a]	CCl_4	0,36 ± 0,07	74 ± 4	0,16 ± 0,05	16 ± 2
	$CBrCl_3$	0,7 ± 0,14	75 ± 4		
	CBr_4[b]	2,0 ± 0,7	64 ± 3		
	$CHCl_3$	2,5 ± 0,5	200 ± 10		
	$CHCl_2Br$	2,7 ± 0,5	190 ± 9	2,5 ± 0,2	19 ± 2
	$CHClBr_2$	2,7 ± 0,5	176 ± 8		
	$CHBr_3$	2,7 ± 0,5	155 ± 8		
	CH_2Cl_2	1,2 ± 0,3	93 ± 5	1,6 ± 0,2	17 ± 2
	CH_2BrCl	1,6 ± 0,3	71 ± 4		
	CH_2Br_2	2,0 ± 0,4	61 ± 3	1,7 ± 0,2	15 ± 2
NMP	CCl_4	0,41 ± 0,08	37 ± 2		
	CBr_4[b]	2,2 ± 0,7	55 ± 3		
	$CHCl_3$	2,7 ± 0,5	207 ± 10	2,7 ± 0,3	21 ± 2
	$CHBr_3$	4,7 ± 0,9	135 ± 7	3,6 ± 0,3	16 ± 2
	CH_2Cl_2	1,1 ± 0,2	115 ± 5	0,7 ± 0,2	26 ± 6
	CH_2Br_2	3,6 ± 0,7	50 ± 3		

[a] NNDMA est l'abréviation de *N,N*-diméthylacétamide; NMP est l'abréviation de *N*-méthylpyrrolidone.
[b] Le solvant utilisé est le benzène.

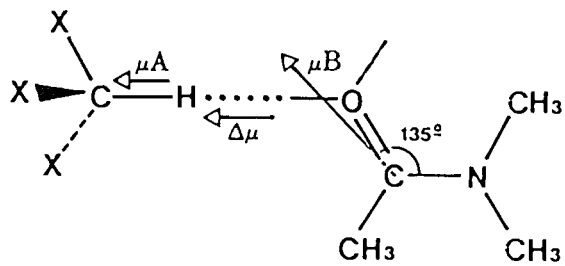

Liaison hydrogène

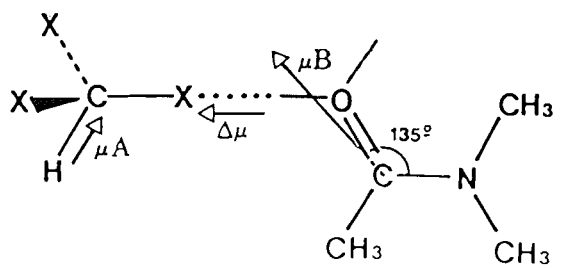

Liaison halogène

FIG. 1. Modèle structural le plus probable dans le cas d'une liaison hydrogène et dans celui d'une liaison halogène.

Pour le système *N,N*-diméthylacétamide (B), trihalogénométhane (A), le modèle le plus probable est schématisé fig. 1. La liaison intermoléculaire se fait suivant l'axe de l'orbitale occupée par une paire d'électrons *n* qui est du côté du groupement CH_3. Le modèle retenu correspond, dans le cas d'une libre rotation autour de l'axe, au cas particulier où les dipôles s'orientent de manière à ce que l'énergie électrostatique du système soit minimisée. Sur la figure 1, il est indiqué le sens des moments de A et de B. La direction du moment de la *N,N*-diméthylacétamide est celle donnée par Nasyrov *et al.* (19).

Les valeurs de $\Delta\mu$ calculées pour ce modèle (cf. tableau 2) sont comparées aux valeurs de $\Delta\mu_{réf}$ retenues et précisées ci-dessus. La comparaison de ces valeurs mène aux remarques suivantes: dans le cas de $CHCl_3$ il est vraisemblable que la liaison soit de type hydrogène, dans celui de $CHBr_3$ une liaison halogène rendrait compte de nos résultats expérimentaux, dans ceux de CH_2Cl_2 et CH_2Br_2 il faudrait envisager une compétition entre les deux modes de liaison intermoléculaire.

En conclusion, pour le modèle structural retenu (le seul pouvant mener à des valeurs d'incrément de moment dipolaire susceptibles de rendre compte de nos résultats expérimentaux) seul le dérivé chloré $CHCl_3$ présente des résultats compatibles avec l'hypothèse d'une liaison hydrogène, et seul le dérivé bromé $CHBr_3$ présente des résultats compatibles avec l'hypothèse d'une liaison halogène. Compte tenu des grandes incertitudes rattachées aux valeurs de $\Delta\mu$ et de l'interprétation donnée aux résultats obtenus sur des systèmes voisins (9, 15, 16), il nous paraît préférable d'émettre, pour tous les cas envisagés ici, l'hypothèse d'une compétition entre les deux modes d'interaction: l'interaction par liaison hydrogène étant prépondérante lorsque l'halogéne est le chlore, l'interaction par liaison halogène devenant prépondérante lorsque l'halogène est le brome.

Les électrons *n* de l'amide seraient les seuls concernés dans cette interaction.

I. 2. *Par spectrométrie infrarouge*

La région spectrale comprise entre 1630 et 1680 cm^{-1}, dans laquelle se trouve la bande caractéristique du vibrateur C=O de la *N,N*-diméthylacétamide, a été explorée. Les spectres des mélanges *N,N*-diméthylacétamide (NNDMA) – dérivés halogénés ($CHCl_3$, $CHCl_2Br$, CCl_4), obtenus dans le solvant méthylcyclohexane pour différentes températures ou différentes concentrations en dérivé halogéné sont comparés au spectre de la NNDMA en solution dans ce même solvant (cf.

Can. J. Chem. Downloaded from www.nrcresearchpress.com by 210.87.254.40 on 09/06/12
For personal use only.

TABLEAU 2. Systèmes A (dérivés organohalogénés) – B (base) – S (cyclohexane). Incréments de moment $\Delta\mu$ (debye), moments dipolaires μ_A, μ_B (± 0,02) D, μ_{AB} (± 0,1) D[a]

B (μ_B)		A (μ_A) $CHCl_3$ (1,15)	$CHBr_3$ (0,97)	CH_2Cl_2 (1,60)	CH_2Br_2 (1,93)
NNDMA[b] (3,74)	μ_{AB}	5,0	4,7	4,6	4,4
	Liaison hydrogène $\Delta\mu$	0,6	0,4	1,1	0,8
	Liaison halogène $\Delta\mu$	1,0	0,8	0,2	−0,2
NMP (3,84)	μ_{AB}	5,1	4,7	4,8	4,4
	Liaison hydrogène $\Delta\mu$	0,6	0,3	1,2	0,8
	Liaison halogène $\Delta\mu$	1,1	0,6	0,5	−0,3

[a] Liaison hydrogène: $\Delta\mu_{réf} = 0,6$ D; liaison halogène par atome Cl: $\Delta\mu_{réf} = 0,5$ D; liaison halogène par atome Br: $\Delta\mu_{réf} > 0,5$ D.
[b] NNDMA = *N*,*N*-diméthylacétamide; NMP = *N*-méthylpyrrolidone.

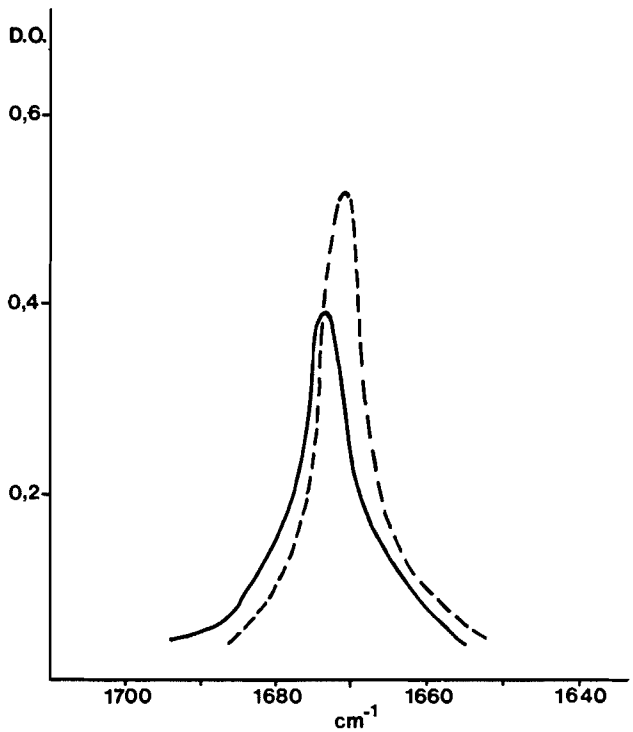

FIG. 2. Région de la vibration CO du spectre infrarouge de la *N*,*N*-diméthylacétamide en solution dans le méthylcyclohexane. c = 0,0084 mol L^{-1}; e = 0,425 mm; — t = 30°C; - - - - t = −56,6°C.

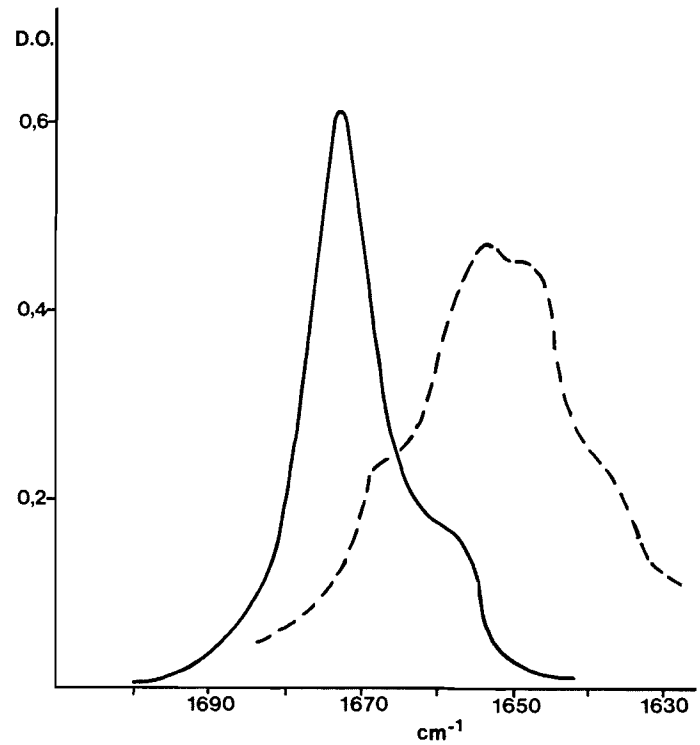

FIG. 3. Région de la vibration CO du spectre infrarouge de la *N*,*N*-diméthylacétamide (c = 0,00239 mol L^{-1}) dans une solution de trichlorométhane (c = 0,0455 mol L^{-1}) et de méthylcyclohexane. e = 0,225 mm; — t = 28,9°C; - - - t = −73,3°C.

fig. 2). Cette comparaison mène aux remarques suivantes.

À 30°C et pour des concentrations pour les deux solutés (NNDMA et dérivé halogéné) peu différentes, c'est-à-dire dans des conditions expérimentales proches de celles des études en polarisation diélectrique et en microcalorimétrie, une bande aux environs de 1655 cm^{-1} apparaît (cf. figs. 3–5). Suivant les résultats obtenus en polarisation diélectrique cette bande pourrait être attribuée à l'existence d'un seul type de complexe de stoechiométrie 1 : 1 dont la liaison intermoléculaire se ferait par l'intermédiaire des électrons *n* de la NNDMA.

À basse température ou à forte concentration en dérivé halogéné, c'est-à-dire loin des conditions expérimentales utilisées en polarisation diélectrique ou en microcalorimétrie, on note un déplacement de la bande du CO "libre" vers les faibles nombres d'onde. D'autre part la bande vers 1655 cm^{-1} se dédouble et une nouvelle bande vers 1640 cm^{-1} apparaît pour les plus fortes concentrations en dérivés halogénés ou pour les plus basses températures (cf. fig. 6). Ces conditions expérimentales particulières favoriseraient la formation de complexes de stoe-

Can. J. Chem. Downloaded from www.nrcresearchpress.com by 210.87.254.40 on 09/06/12
For personal use only.

Can. J. Chem. Downloaded from www.nrcresearchpress.com by 210.87.254.40 on 09/06/12
For personal use only.

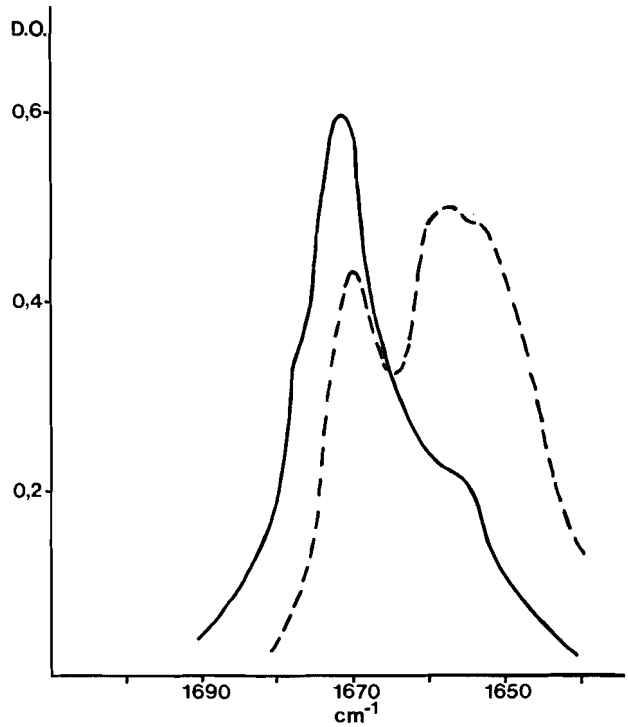

FIG. 4. Région de la vibration CO du spectre infrarouge de la *N,N*-diméthylacétamide (c = 0,0145 mol L^{-1}) dans une solution de bromodichlorométhane (c = 0,0634 mol L^{-1}) et de méthylcyclohexane. e = 0,403 mm; — t = 28,9°C; ---- t = −51,6°C.

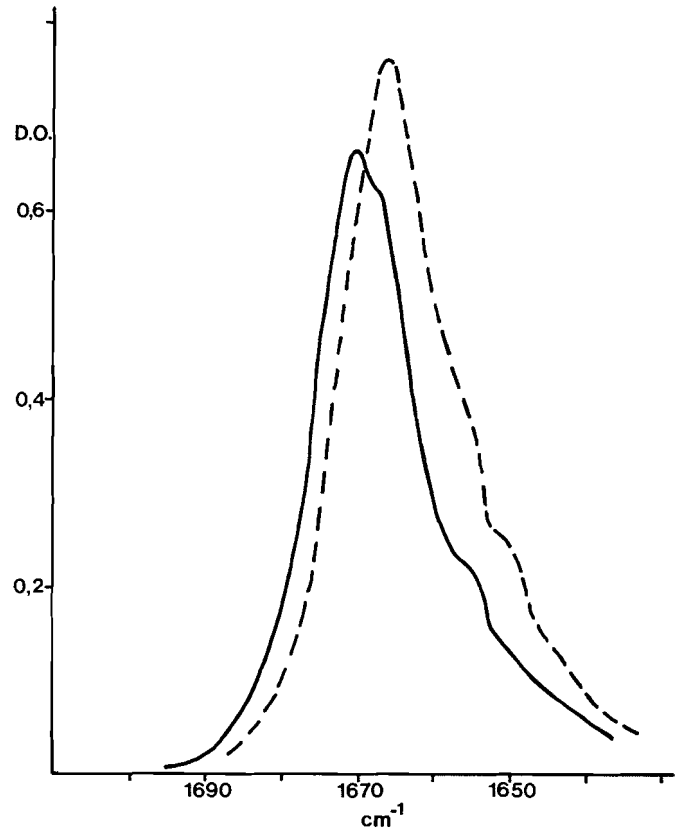

FIG. 5. Région de la vibration CO du spectre infrarouge de la *N,N*-diméthylacétamide (c = 0,0241 mol L^{-1}) dans une solution de tétrachlorométhane (c = 2,076 mol L^{-1}) et de méthylcyclohexane. e = 0,393 mm; — t = 31,0°C; ---- t = −36,6°C.

chiométrie différente de 1:1 ou de complexes présentant différents types de configuration (par l'intermédiaire des électrons n et/ou π de la NNDMA). Ce fait est révélé à l'extrême dans le cas du composé CF_2Br-CF_2Br, qui a pu être étudié jusqu'à la température de −80°C (cf. fig. 7).

II. *Comparaison des valeurs de* K *et* ΔH

Les résultats de l'analyse structurale précédente nous ont conduit à postuler, pour l'interaction décelée entre les amides tertiaires et les dérivés CH_qX_r étudiés, dans le domaine expérimental utilisé, l'existence de complexes de type 1:1 formés par liaison hydrogène (LH) et/ou liaison halogène (LX). Il est donc nécessaire, pour interpréter des résultats issus de techniques différentes, d'élucider la signification des grandeurs à interpréter.

Un développement des équations utilisées en polarisation diélectrique (pd) et en calorimétrie (cal) pour i complexes de type 1:1 en équilibre compétitif mène aux résultas suivants (15):

$$K_{pd} = K_{cal} = \Sigma K_i \ (= \text{par exemple } K_{LH} + K_{LX})$$

$$\Delta H = \frac{\Sigma n_i \Delta H_i}{\Sigma n_i} \left(= \text{par exemple } \frac{K_{LH}}{K_{LH} + K_{LX}} \Delta H_{LH} + \frac{K_{LX}}{K_{LH} + K_{LX}} \Delta H_{LX} \right)$$

LH: interaction par liaison hydrogène; LX: interaction par liaison halogène.

Les résultats portés dans le tableau 1 montrent qu'il apparaît bien une similitude entre les valeurs des constantes d'équilibre issues de ces deux techniques confirmant ainsi que les corrections d'effets secondaires ont été correctement faites. Mais une comparaison des valeurs de K ou de ΔH s'avère difficile car elle nécessite la connaissance de ces grandeurs thermodynamiques pour chaque équilibre mis en jeu. On peut toutefois envisager cette comparaison dans les deux cas extrêmes c'est-à-dire dans l'hypothèse d'une interaction unique par liaison hydrogène ou par liaison halogène. Dans ce cas, lors du passage du dérivé chloré au dérivé bromé on peut prévoir une décroissance de K et de $|\Delta H|$ pour une interaction unique par liaison hydrogène et une croissance de K et de $|\Delta H|$ pour une interaction unique par liaison halogène (15).

Suivant nos résultats expérimentaux (cf. tableau 1), on constate que les valeurs des constantes d'équilibre, qui augmentent lorsque le numéro atomique de l'halogène augmente, ne permettent pas d'admettre l'existence d'un unique mode d'interaction par liaison hydrogène mais elles ne seraient pas incompatibles avec celle d'un unique mode d'interaction par liaison halogène. Ces constatations, dans les quelques cas expérimentaux étudiés, sont inversées pour les valeurs de $|\Delta H|$. Les valeurs de ΔS n'ont pas été notées, car les domaines d'incertitude sont tels que ces valeurs n'ont pas de signification. Toutefois, les résultats de l'analyse structurale nous ont amené à faire intervenir l'existence compétitive de ces deux modes d'interaction. Dans ce cas, pour expliquer une quelconque variation des valeurs de ΔH il est nécessaire de connaitre les valeurs respectives de K_{LH}, ΔH_{LH} et K_{LX}, ΔH_{LX} (voir ci-dessus). Par contre, un sens de variation des valeurs de K, représentant une somme de constantes ($K_{LH} + K_{LX}$), peut être interprété suivant le sens de variation probable de chacune des constantes d'équilibre (18): une augmentation de K lorsque le

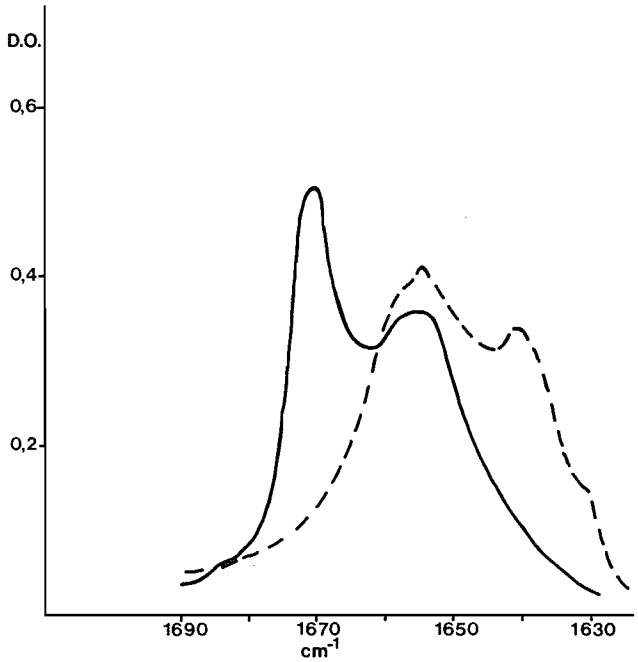

FIG. 6. Région de la vibration CO du spectre infrarouge de la *N,N*-diméthylacétamide (c = 0,023 mol L^{-1}) dans deux solutions de trichlorométhane (— c = 0,0455 mol L^{-1}, ---- c = 0,4511 mol L^{-1}) et de méthylcyclohexane. e = 0,225 mm; t = −36,6°C.

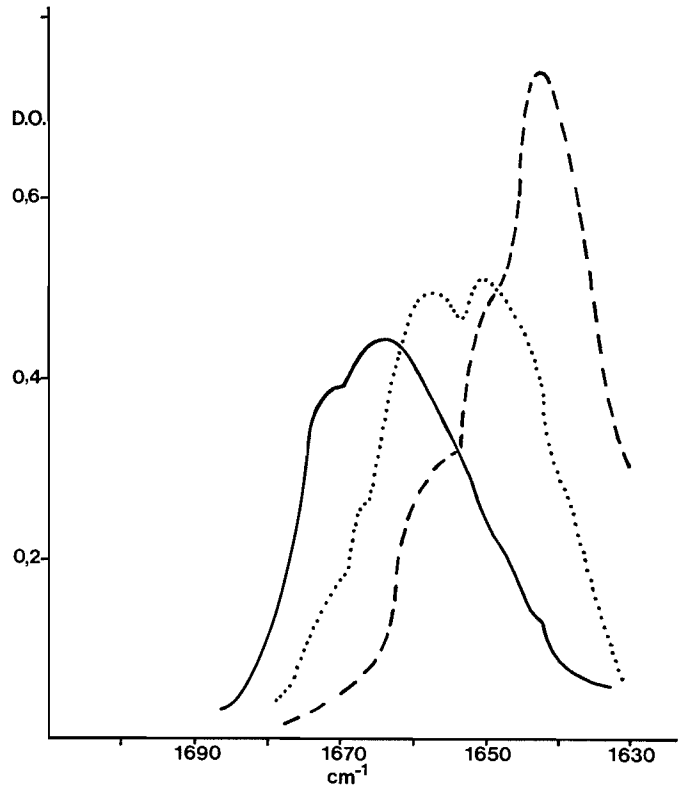

FIG. 7. Région de la vibration CO du spectre infrarouge de la *N,N*-diméthylacétamide (c = 0,0145 mol L^{-1}) dans une solution de tétrafluoro-1,1,2,2 éthane (c = 1,498 mol L^{-1}) et de méthylcyclohexane. e = 0,393 mm; — t = 28,9°C, ... t = −37°C; ---- t = −80,5°C.

numéro atomique de l'halogène croît indique que K_{LX} croît plus vite que K_{LH} ne décroît.

Conclusion

Une étude menée par trois techniques différentes (polarisation diélectrique, spectrométrie infrarouge, microcalorimétrie) nous a permis de mettre en évidence l'existence d'interactions moléculaires faibles entre les dérivés halogénés du méthane et des amides tertiaires.

L'étude structurale par polarisation diélectrique, à partir de modèles structuraux caractéristiques faisant intervenir les électrons n et les électrons π des amides tertiaires, a permis d'une part, de minimiser le rôle des électrons π et maximaliser le rôle des électrons n, d'autre part, de préciser la nature de l'interaction. Les résultats plaident en faveur d'une compétition entre deux modes d'interaction (par liaison hydrogéne et par l'intermédiaire d'un atome d'halogène ou liaison halogène), à l'exception de $CHCl_3$ et $CHBr_3$, pour lesquels respectivement une liaison hydrogène seule et une liaison halogène seule pourrait suffire à expliquer les résultats expérimentaux.

L'étude vibrationnelle par spectrométrie infrarouge a montré que dans les conditions expérimentales sélectionnées pour les deux autres techniques (25°C; concentrations molaires de l'ordre de 0,05 M), les liaisons intermoléculaires (hydrogène ou halogène) donneraient lieu à un complexe de stoechiométrie 1:1, d'autres types de complexes n'apparaissant qu'à basse température.

Les valeurs identiques des grandeurs thermodynamiques déterminées par polarisation diélectrique et microcalorimétrie, dans le domaine d'incertitude considéré, confirment la validité des corrections d'effets secondaires apportées dans chacune des méthodes adoptées. La stoechiométrie des complexes étant postulée 1:1, la variation de ces grandeurs thermodynamiques en fonction du numéro atomique de l'halogène au sein d'une même molécule est incompatible avec une interaction unique par liaison hydrogène et pourrait être interprétée par une interaction par liaison halogène seule. Ce résultat associé aux résultats de notre analyse structurale et à ceux obtenus par ailleurs (9, 15, 16) nous permettent en fait, d'émettre l'hypothèse de l'intervention compétitive de ces deux types d'interaction, l'une ou l'autre devenant plus ou moins prépondérante suivant le type d'halogène porté par le dérivé halogéné.

En conclusion, cette étude des interactions entre une série de composés organohalogénés pris pour représentants d'anesthésiques halogénés et deux amides tertiaires prises comme modèles d'un constituant de la membrane des cellules nerveuses, nous a permis de mettre en évidence, en particulier, le rôle joué par l'halogène dans ces interactions (liaison halogène). Les systèmes simples utilisés dans cette étude sont, bien sûr, loin des systèmes biologiques mais nous proposons l'intervention de ce type d'interaction dans ces milieux plus complexes et sa prise en compte dans un classement des anesthésiques généraux (1–3) suivant le type d'interactions principales auquel ils peuvent participer.

Remerciements

Les spectres infrarouge ont été réalisés par l'un d'entre nous dans le laboratoire du Professeur Sandorfy (Université de Montréal) que nous tenons ici, à remercier. Ce séjour à Montréal a été rendu possible grâce à un programme d'échange scientifique France–Québec.

1. G. TRUDEAU, J. M. DUMAS, P. DUPUIS, M. GUÉRIN et C. SANDORFY. *Dans* Topics in current chemistry. Vol. 93. Springer, Berlin. 1980. pp. 91–125.

Can. J. Chem. Downloaded from www.nrcresearchpress.com by 210.87.254.40 on 09/06/12
For personal use only.

2. C. SANDORFY. *Dans* Progress in anesthesiology. Vol. 2. *Édité par* B. R. Fink. Raven Press, New York. 1980. pp. 353–359.
3. J. M. Dumas. Nouv. J. Chem. **8**, 349 (1984).
4. T. DI PAOLO et C. SANDORFY. J. Med. Chem. **17**, 809 (1974).
5. T. DI PAOLO et C. SANDORFY. Can. J. Chem. **52**, 3612 (1974).
6. A. NAGYRÉVI et C. SANDORFY. Can. J. Chem. **55**, 1593 (1977).
7. R. MASSUDA et C. SANDORFY. Can. J. Chem. **55**, 3211 (1977).
8. G. TRUDEAU, K. C. COLE, R. MASSUDA et C. SANDORFY. Can. J. Chem. **56**, 1681 (1978).
9. J. M.DUMAS, M. GOMEL et M. GUÉRIN. *Dans* The chemistry of functional groups. supp. D, part 2. *Édité par* S. Pataï et Z. Rappoport. John Wiley, New York. 1983. pp. 985–1020.
10. D. CLEVERDON, G. B. COLLINS et J. W. SMITH. J. Chem. Soc. 4499 (1956).
11. J. MONTEAU, H. HUSER, M. GUÉRIN et M. GOMEL. J. Chem. Res. (S) 256, (M) 3217 (1978).
12. L. LAMBERTS et T. ZEEGERS-HUYSKENS. j. Chim. Phys. **60**, 435 (1963).
13. D. A. DERANLEAU. J. Am. Chem. Soc. **91**, 4044 (1969).
14. M. ASSELIN et C. SANDORFY. J. Chem. Phys. **52**, 6130 (1970).
15. C. GÉRON et M. GOMEL. J. Chim. Phys. **75**, 241 (1978).
16. C. GÉRON et M. GOMEL. J. Chim. Phys. **76**, 411 (1979).
17. B. CASTAGNA. Thèse de Doctorat d'Etat, Poitiers, France. 1975.
18. J. M. DUMAS, C. GÉRON, H. PEURICHARD et M. GOMEL. Bull. Soc. Chim. Fr. 720 (1976).
19. D. M. NASYROV et A. N. VERESHCHAGIN. Izv. Akad. Nauk SSSR, Ser. Khim. **3**, 571 (1981).

Can. J. Chem. Downloaded from www.nrcresearchpress.com by 210.87.254.40 on 09/06/12
For personal use only.

Permanganate peroxidation of cyclohexene. II. Temperature, solvent, and concentration effects

JAY. E. TAYLOR
Department of Chemistry, Kent State University, Kent, OH 44242, U.S.A.

Received December 23, 1983

JAY E. TAYLOR. Can. J. Chem. **62**, 2641 (1984).

An investigation of the peroxidation of cyclohexene to form *cis*-1,2-cyclohexanediol has been continued using an improved turbulent stirring apparatus. Varying conditions of temperature, methanol concentration, dilution, and permanganate/cyclohexene ratios have been evaluated by the method of comparative product yields. The temperature effect was quite modest since only at the extremes of −20 and 40°C were decreases in yields noted. Added methanol in low concentrations, >10%, gave slightly increased yields, but decreased yields were observed when methanol was added in 75% concentration. Under the new stirring conditions, 83−86% yields were obtained with ~0.05 *M* added potassium permanganate, but only 70−74% yields were obtained at higher concentrations. This effect appeared to relate to the increased viscosity of the mixture which results from the formation of gelatinous manganese oxides. Ratios of cyclohexene to permanganate ion greater than 2:1 gave no significant yield increases, based on permanganate utilization. All of the above data have been interpreted with the assumption of an intermediate alkene − permanganate ion addition complex. Preparative scale syntheses of *cis*-1,2-cyclohexanediol have produced 83−87% yields with either 0.2 or 0.5 molar quantities of cyclohexene.

JAY E. TAYLOR. Can. J. Chem. **62**, 2641 (1984).

Utilisant un appareil à agitation turbulente amélioré, on a poursuivi l'étude de la peroxydation du cyclohexène conduisant au cyclohexanediol-1,2-*cis*. Faisant appel à la méthode des comparaisons des rendements en produits, on a pu évaluer l'effet d'une variation des conditions de la température, de la concentration en méthanol, de la dilution et des rapports permanganate/cyclohexène. L'influence de la température est faible puisque les rendements ne diminuent qu'aux températures extrêmes, soit à −20 et à 40°C. L'addition de faibles concentrations, <10%, de méthanol provoque une légère augmentation des rendements; toutefois, on observe une diminution des rendements lorsque la concentration de méthanol ajouté est égale ou supérieure à 75%. Les nouvelles conditions d'agitation permettent d'obtenir des rendements de l'ordre de 83 à 86% pour une concentration de permanganate de potassium de 0,05 *M*; toutefois, le rendement n'est que de 70 à 74% pour des concentrations plus élevées. Cet effet semble être relié à une augmentation de la viscosité du mélange qui résulte de la formation d'oxydes de manganèse gélatineux. En tenant compte de l'utilisation du permanganate, des rapports de cyclohexène/permanganate supérieurs à 2:1 ne provoquent pas d'augmentation appréciable des rendements. On interprète tous ces résultats en faisant l'hypothèse qu'il y a formation d'un intermédiaire complexe provenant de l'addition de l'alcène sur l'ion permanganate. A une échelle préparative, impliquant de 0,2 − 0,5 moles de cyclohexène, on peut obtenir le cyclohexanediol-1,2-*cis* avec des rendements de 83 à 87%.

[Traduit par le journal]

Can. J. Chem. Downloaded from www.nrcresearchpress.com by 210.87.254.6 on 09/06/12
For personal use only.

Yields of *cis*-1,2-cyclohexanediol formed by the permanganate peroxidation of cyclohexene (1) may vary from >0 to <88% as a result of stirring efficiency. This unusual stirring effect appears to be the result of competing reactions, one of which is minimized under turbulent stirring conditions.

It is the purpose of this paper to elucidate further the conditions and the mechanism by which this stirring effect occurs. The paper, as was its predecessor (1), is concerned primarily with the peroxidation reaction. Comparative product yields have provided a convenient method of evaluation of a reaction for which many of the classical procedures are inapplicable.

Experimental

A revised stirring arrangement is shown in Fig. 1. The addition of cross bars to the stirring shaft and a baffle in the 1-L bottle reactor enhanced the stirring efficiency of the previously described "Lightnin" stirrer (1). Also an ice water condenser, through which methanol was added, minimized cyclohexene vapor loss. Varying flow rates were attained by using selected lengths of 0.5-mm id tubing at appropriate heights. It was found that the flow rates of $KMnO_4$ solutions and water were essentially the same, but methanol was quite different. Calibrations were done, (s/5 mL) with methanol and with water. Mixtures of methanol and water have significantly slower flow rates (higher viscosities) than either water or methanol (2).

The same general set-up using an enlarged baffle and the same stirrer, but without the cross pieces, has been used in 5-L and 12-L reactors. See Fig. 2.

The cyclohexene (Aldrich Chemical Co.) was redistilled and the product boiling over a range of 0.3°C was used. However, in a duplicate run the unpurified cyclohexene gave the same yield of *cis*-1,2-cyclohexanediol as the redistilled reagent. The cyclohexene was preserved at −20°C.

Descriptions of typical experiments follow.

cis-*1,2-Cyclohexanediol. Procedure A*

The reactor was set up as in Fig. 1. Methanol, 125 mL, was placed in flask A; 7.78 g (0.0492 *m*) $KMnO_4$ in 375 mL water were added to flask B; and 140 mL water, 10 mL of 1 *M* sodium hydroxide, 4.036 g (0.0492 *m*) cyclohexene from a 5-mL pipet (20.0°C) calibrated by weighing the cyclohexene delivered at 20.0°C, followed by 50 mL methanol were placed in reactor J. With the ice water condenser and stirrer in operation, flask A was inverted into C and flask B into D to start the reaction. The length of capillaries and (or) heights of C and D had been previously adjusted to allow the delivery of both the $KMnO_4$ solution and methanol in 1 h. The temperature in J was maintained at 20 ± 2°C. Five minutes after completion of the additions, sulfur dioxide was bubbled in to just dissolve the precipitated manganese dioxide. The stirring was then stopped, and sodium bicarbonate was added to attain pH 8 (slow). The resulting slowly-formed precipitate of manganese sulfites and carbonates was allowed to settle, the solution was decanted and filtered and then extracted continuously over a period of 1−4 days with dichloromethane as previously described (1). The dichloromethane−glycol solution was then concentrated to 25−30 mL, cooled to room temperature, and then to ~4°C. The resulting crystals were filtered and washed twice with CH_2Cl_2 precooled to −15°C. Yield 4.513 g, mp 98−98.5°C (uncorrected). The filtrate was further concentrated and treated as above. Yield 0.230 g, mp 97−98°C. Total yield 83.1%.

Can. J. Chem. Downloaded from www.nrcresearchpress.com by 210.87.254.6 on 09/06/12
For personal use only.

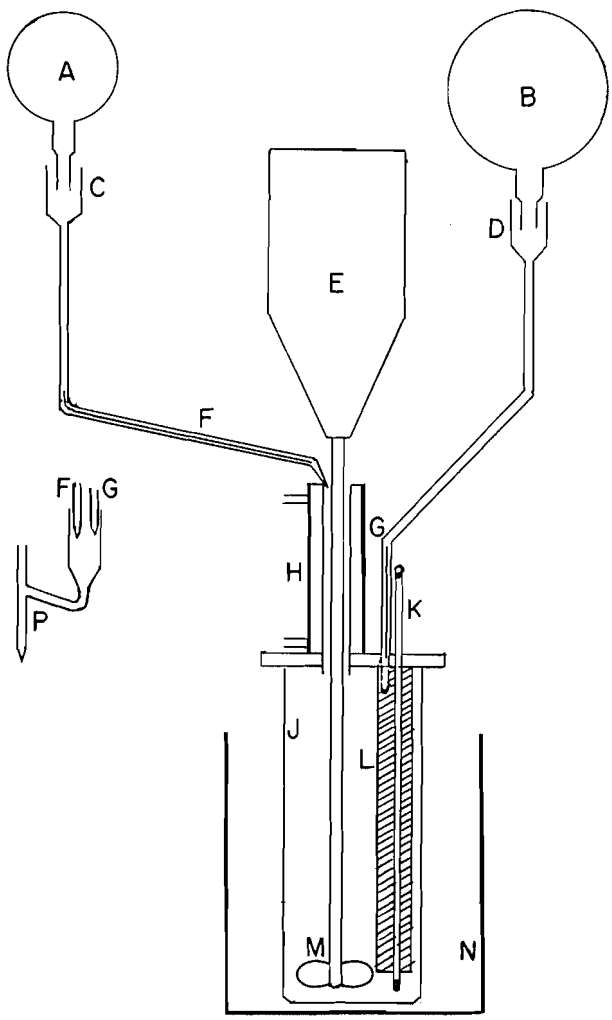

FIG. 1. Small scale reactor. A, methanol reservoir; B, $KMnO_4$ solution reservoir; C and D, liquid leveling devices; E, 1/30-hp, 1600-rpm Lightnin stirrer; F and G, 0.5-mm capillary tubing for liquid flow control; H, ice water condenser; J, 1-L square bottle reactor with a 3/8-in. thick Plexiglas top and rubber tubing seals around inlets G and K; K, thermometer; L, stainless steel baffle; M, 5-cm diameter, 3-blade, 45° angle stirrer; N, water or ice bath; P, auxiliary addition tube for addition of methanol and permanganate solutions as a unit mixture whereby P is substituted for G.

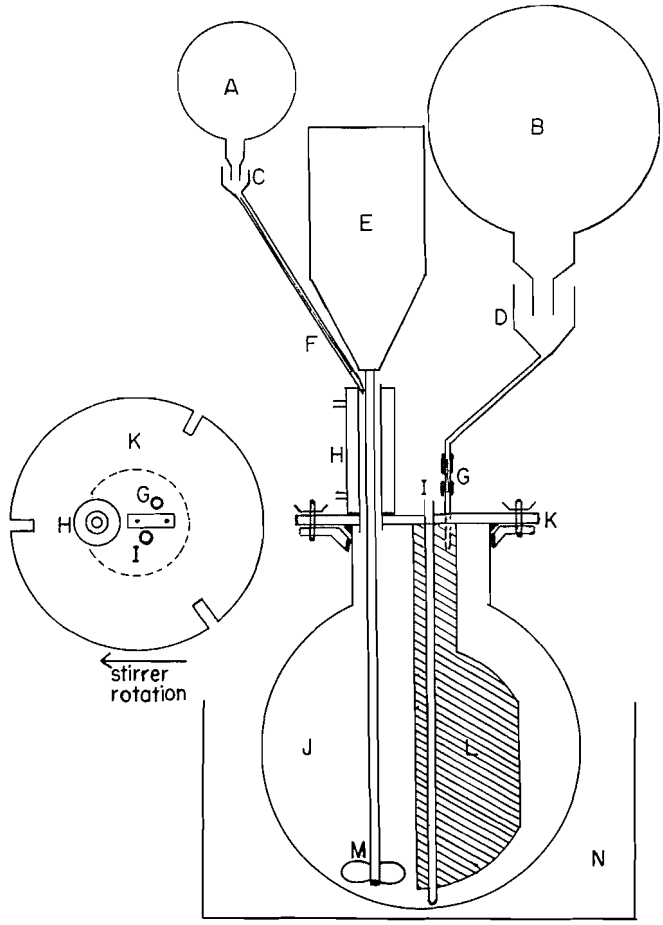

FIG. 2. Preparatory scale reactor. A, methanol reservoir; B, $KMnO_4$ solution reservoir; C and D, liquid leveling devices; E, 1/30-hp, 1600-rpm Lightnin stirrer; F and G, 0.5-mm capillary tubes for flow control; H, ice water condenser; I, thermometer; J, 12-L wide mouth reactor and extension support (Ace Glass Co.); K. 1/2-in. thick Plexiglas top for the reactor with rubber tubing seals around inlets I and G; L, baffle; M, 5-cm diameter, 3-blade, 45° angle stirrer; N, ice bath.

Variations on the above procedure included changes in temperature, methanol concentration, and reactant concentrations. In all experiments described, unless otherwise indicated, the methanol concentrations were continuously maintained by adding methanol at the appropriate rate concurrent with the potassium permanganate solution. Extractions with dichloromethane were made directly on solutions containing up to 50% methanol. With the 75% methanol experiments, it was necessary to remove part of the methanol by vacuum distillation.

Not all experiments used the apparatus precisely as shown in Fig. 1. For certain experiments, indicated in the tables, the methanol was added without passing through the condenser. Through-the-condenser addition was found to increase yields significantly only for the most dilute solutions.

In another set of experiments in which the effect of premixing the potassium permanganate and methanol was investigated, the alternate addition tube, P, shown in Fig. 1 was employed. With this set-up, the potassium permanganate solution and methanol or methanol–water mixtures, each flowing at prescribed rates, dripped into a receiver which then emptied into the reactor. In this manner the concentration of potassium permanganate, as added, was always constant, but the solvent varied in relative concentrations of methanol and water. The reason for the use of the flow mixing arrangement was to minimize the oxidation of methanol by the permanganate ion.

cis-1,2-Cyclohexanediol. Procedure B, for preparative utility

The reactor was set up as in Fig. 2. Methanol, 1 L, was placed in reservoir A; 79 g (0.5 *m*) $KMnO_4$ dissolved in 6 L water were added to reservoir B; then 3 g sodium hydroxide, 1.0 L water, 50.75 mL at 20.0°C (0.500 *m*) cyclohexene followed by 100 mL methanol were placed in reactor J. With the temperature in J at about 12°C and with the ice water condenser and stirrer activated, A and B were inverted into C and D to initiate the reaction. Since C and D served as automatic leveling devices, no further attention, except to replenish ice, was needed until the $KMnO_4$ addition was complete. The temperature remained at 12 ± 2°C, during the time of addition, 3.3 h. A and B, as shown, may be substituted by 2-L and 6-L stoppered separatory funnels with 6-mm and 12-mm bore stopcocks, respectively.

Upon completion of the $KMnO_4$ addition plus 5 min additional stirring, sulfur dioxide was bubbled in to reduce the manganese oxides. The solution was then neutralized (pH 8) with $NaHCO_3$ and extracted with dichloromethane. Using a 120-cm long vertical extraction tube, the extraction was continued until no more product was obtained. Yield 44.36 g, mp 97.5–98.5°C, plus 4.69 g, mp 96–98°C, total yield 85%.

TABLE 1. Effects of temperature and added methanol[a]

Expt. No.	Temperature (°C)	CH_3OH[b] (%)	$KMnO_4$[b] m/L as added	Product (g)	Melting point (°C)	Yield (%)
1	−20	50	0.197	3.985	97.5−98.5	78
				0.476	83−88	
2		75	0.394	2.358	95−97	60
				1.066	93−96	
3	0	0	0.098	4.394	95−96.5	80
				0.148	93.5−95.5	
4		25	0.131	4.449	97.5−98.5	83
				0.305	95−96.5	
5		50	0.197	3.451	96−97.5	81
				1.179	87−93	
6		75	0.394	3.478	97.5−98.5	69
				0.431	87−90	
7	20	0	0.098	3.976	97−98	74
				0.227	95−96.5	
8		25	0.131	4.513	98−98.5	83
				0.230	97−98	
9		50	0.197	4.249	97−98	83
				0.482	88−92	
10		75	0.394	3.505	97−98	69
				0.433	83−87	
11	40	0	0.098	3.826	95.5−97	71
				0.197	86−89.5	
12		25	0.131	3.933	97.5−98.5	79
				0.579	93.5−96	
13		50	0.197	3.218	96.5−98	78
				1.257	85−88	

[a]In all experiments 0.0492 m $KMnO_4$ was reacted with 0.0492 m cyclohexene by procedure A except that the methanol was not added through the condenser. All yields are based on cyclohexene.

[b]The specific volumes added were 75% methanol = 375 mL methanol, 125 mL $KMnO_4$, 50% methanol = 250 mL methanol, 250 mL $KMnO_4$; 25% methanol = 125 mL methanol, 375 mL $KMnO_4$; 0% methanol = 500 mL $KMnO_4$.

Can. J. Chem. Downloaded from www.nrcresearchpress.com by 210.87.254.6 on 09/06/12
For personal use only.

Using 0.2-m reactants in a 5-L reactor similar to Fig. 2, 83−87% yields were obtained.

All yields are based on the initial charge of cyclohexene except for experiments 7−9, Table 3, where excesses of cyclohexene were used. The two yields given are based on unrecovered cyclohexene and on potassium permanganate assuming a 1:1 reaction ratio.

Based on duplicate runs which were made, the average deviation of yields was ±1%.

Discussion

Variations in yields of *cis*-1,2-cyclohexanediol have been evaluated under a variety of conditions including alterations in temperature, methanol concentrations, dilution of reactants, and permanganate/cyclohexene ratios.

Since the existence of the permanganate−alkene complex for alkenes other than cyclohexene has been established by Lee and Brownridge (3) and Wiberg *et al.* (4), with further support by Ogino and Mochizuki (5), the concept was also applied to cyclohexene in the form of the following proposed mechanism.

[1] $MnO_4^- +$ $\xrightarrow{\text{rapid}}$ 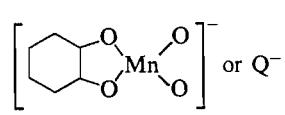 or Q^-

[2] $Q^- + H_2O \longrightarrow$ 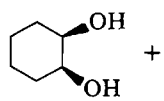 $+ MnO_3^-$

[2a] $3MnO_3^- + H_2O \longrightarrow MnO_4^- + 2MnO_2 + 2OH^-$

[3] $Q^- + MnO_4^- \longrightarrow {}^-O_2C(CH_2)_4CO_2^- + MnO_2$

other oxidations

Temperature

The effects of alterations in temperature were surprisingly minimal. See Table 1, comparing experiments at the same methanol concentrations. Only at the extremes of temperature (−20°C and 40°C) were detectable variations in yields observed. This small temperature coefficient may be attributed to the rapidity of formation of Q^- by reaction [1] followed by conversion to glycol by reaction [2] in the absence of excess MnO_4^-. However, at the low temperature of −20°C, the rate of Q^- formation appeared to decrease sufficiently so that presumably excess MnO_4^- accumulated and reacted with the previously formed Q^- by reaction [3]. This is further supported by the observation of a significant induction period in initial MnO_4^- uptake at −20°C. It is possible therefore that very

TABLE 2. Effects of continuous premixing of methanol and potassium permanganate solutions[a]

0.0492 *m* $KMnO_4$[b] in		CH_3OH	Product	Melting point	Yield
mL H_2O	mL CH_3OH	(%)	(g)	(°C)	(%)
375	125	25	4.670	97–98	86
			0.210	95–96	
250	250	50	4.407	93–95.5	84
			0.373	95–96.5	
125	375	75	2.678	92–96	68
			1.208	80–85	

[a]Temperature 20 ± 2°C. Addition 1 h.

[b]The methanol and $KMnO_4$ solution were mixed continuously before addition using the auxiliary device of Fig. 1. The 0.0492 *m* $KMnO_4$ reacted with 0.0492 *m* (5.00 mL) cyclohexene).

slow addition at −20°C may increase the yield. This has not been tried. Also yields were not as reproducible as at higher temperatures.

In contrast, the modest decrease in yield noted at the high temperature of 40°C may have been the result of other oxidative side reactions or possibly cyclohexene vapor loss.

Methanol

The effect of methanol on yields is not large, as may be seen in Table 1. In the total absence of methanol, the percent yields were 3 to 9% less than with added methanol. With methanol absent, a distinctly greenish color of the reaction mixture (indicating the presence of MnO_4^{2-}) persisted as long as 15 min, particularly at the lower temperatures. In the presence of methanol, this greenish color was seen for only 1–2 min or less. There did appear, therefore, to be some minor effect of the added methanol on the mechanism of the reaction. The methanol also appeared to enhance dispersion of the cyclohexene in the aqueous suspension, and this was probably its major effect.

For the data of Table 1 the permanganate solutions and methanol were added separately. To attain the different concentrations, the amount of water dissolving a given amount of potassium permanganate was varied as shown in note *b*, Table 1. There was then the possibility that the decreased yields at high methanol concentrations were due to the high concentration of added permanganate ion. In view of this possibility, another set of experiments, described in Table 2, was done so that each permanganate solution had the same concentration, 0.098 *M*, as it contacted the surface of the reaction mixture. The only differences were in the methanol content. The concentrated permanganate solutions were diluted continuously with methanol or methanol–water mixtures as described in the Experimental section using the mixing tube, P, shown in Fig. 1.

Essentially the same yields under corresponding conditions were obtained for experiments 8–10, Table 1, and those of Table 2. It is therefore concluded that the stirring was sufficiently adequate and that the direct addition of either dilute or concentrated permanganate solutions had no effect on yields. Therefore, the 75% methanol data of Table 1 are a direct reflection of the influence of that substance.

The explanation of the decrease in yields at 75% methanol concentration appears to relate to the decrease in activity of water with increased concentration of methanol. Since by reaction [2], water is a reactant, any decrease in its activity must correspondingly influence the rate of reaction [2]. In summary, there are then two opposing factors by which methanol may affect yields: rate enhancement of reaction [1] by improved dispersion of the cyclohexene, and retardation of reaction [2] by decreased water activity.

Dilution

In Table 3, experiments 1–6, lower yields were obtained at 0.0985 *m* added permanganate, but roughly equal yields resulted with either 0.0492 or 0.0197 *m*. This apparent optimization of yields with ~0.05 *m* permanganate suggests that factors other than stirring efficiency were operative. If there were inadequacies in mixing of simple aqueous solutions, these should have been evident at all concentration ranges.

As previously noted, adding either a dilute or a concentrated permanganate solution to the reaction mixture made no difference in yields under otherwise equal conditions. Compare again Tables 1 and 2. Thus, it was demonstrated that the specific concentration of the added potassium permanganate did not affect yields, providing the final product concentrations were the same. This observation also is supportive of the above conclusion that mixing efficiency for a low viscosity solution was optimal.

The lowered yields at higher concentrations as seen in Table 3 (experiments 1, 2, 4, 5) may then be attributed to the increased viscosity of the reaction mixture due to the greater concentrations of accumulated manganese dioxide. Since from the outset of any given reaction the cyclohexene distribution was obviously consistent, each drop of added permanganate provided a localized excess of that reagent. Under initial conditions, or dilute concentrations, the viscosity effect was minimal, the permanganate reacted with the available cyclohexene by reaction [1], and the excess was rapidly dispersed. But in the presence of greater accumulations of gelatinous manganese dioxide, the apparent viscosity was significantly increased, the rate of dispersion of excess permanganate ion was retarded, and the undispersed MnO_4^- reacted with the available complex Q by reaction [3], thereby decreasing the glycol yield. Entrainment of a combination of permanganate ions and the complex in a manganaese dioxide matrix may also have been a contributing factor. The stirring efficiency was adequate to overcome the effect of roughly 0.05 *m* of gelatinous manganese dioxide per 700 mL of solution. Yields obtained in either the apparatus of Fig. 1 or of Fig. 2 were equal.

Varying cyclohexene ratios

In another series of experiments, the permanganate concentration was held constant and the cyclohexene concentrations were increased. See Table 3, experiments 7–9. The excess cyclohexene was recovered, and yields were calculated on the basis of unrecovered cyclohexene and on initial potassium permanganate. Due to cyclohexene vapor losses and solubility in the water–alcohol mixture, the yields based on cyclohexene were of little significance. However, the permanganate yields were relevant since these experiments indicated that a 1:1 ratio of MnO_4^-/cyclohexene was the most effective ratio. The yields based on 1:1 $KMnO_4$ utilization (assuming one mole C_6H_{10} consumed 1 mole MnO_4^-) were 93%, 94%, 94% with 2:1, 4:1, and 8:1 ratios respectively. If, however, a 3:2 ratio by the equation

$$[4]\quad 3C_6H_{10} + 2MnO_4^- + 4H_2O \rightarrow 3C_6H_{12}O_2 + 2MnO_2 + 2OH^-$$

is assumed, the yields correspondingly become 62%, 63%, 62%. It is clear, therefore, that if the stoichiometry of equation

Can. J. Chem. Downloaded from www.nrcresearchpress.com by 210.87.254.6 on 09/06/12
For personal use only.

TABLE 3. Effect of dilution and varied reactant ratios

Expt. No.	Temperature (°C)	$KMnO_4$ (*m*)	C_6H_{10} (*m*)	MnO_4^-/C_6H_{10}	CH_3OH (%)	Product (g)	Melting point (°C)	Yield (%)
1	20	0.0985	0.0985	1:1	25[a]	7.503 0.551	97–98 95.5–97	70
2	20	0.0492	0.0492	1:1	25[a,b]	4.513 0.230	98–98.5 97–98	83
3	20	0.0197	0.0197	1:1	25[a]	1.839 0.125	94–96 93–95.5	86
4	20	0.0985	0.0985	1:1	50[a,b]	7.817 0.636	98–98.5 92–95	74
5	20	0.0492	0.0492	1:1	50[a,b]	4.249 0.482	97–98 88–92	83
6	20	0.0197	0.0197	1:1	50[a]	1.424 0.485	96.5–98 86–90	83
7	0	0.0492	0.0985	1:2	15[c]	5.022 0.314	96–97.5 86–89	54[d] 93[e]
8	0	0.0492	0.197	1:4	15[c]	5.148 0.251	96–97.5 86–90	48[d] 94[e]
9	0	0.0492	0.394	1:8	15[c]	4.991 0.357	96–97.5 81–86	41[d] 94[e]

[a]Procedure A was followed except as indicated. Final volume for each experiment was 700 mL plus cyclohexene on which yields were based.
[b]The methanol was not added through the condenser.
[c]Initial concentration. No methanol was added during the course of the reaction.
[d]The yield was based on unrecovered cyclohexene.
[e]The yield was based on $KMnO_4$ assuming a 1:1 reaction ratio with cyclohexene.

[4] is applicable, other side reactions must decrease its efficiency. Previously, it was shown (1) that *at lesser stirring efficiencies*, where the 1:1 ratio gave a yield of 15%, increased cyclohexene/MnO_4^- ratios did give greatly increased yields, ~42%. It appears, therefore, that these increases were the result of better reactant contact efficiencies as the cyclohexene concentration was increased, and were not due to a mass action effect on some phase of the mechanism.

1. J. E. TAYLOR, D. WILLIAMS, K. EDWARDS, D. OTONNAA, and D. SAMANICH. Can. J. Chem. **62**, 11 (1984).
2. M. DIZECHI and E. MARSCHALL. J. Chem. Eng. Data, **27**, 358 (1982).
3. D. G. LEE and J. R. BROWNRIDGE. J. Am. Chem. Soc. **95**, 3033 (1973).
4. K. B. WIBERG, C. J. DEUTSCH, and J. ROCEK. J. Am. Chem. Soc. **95**, 3034 (1973).
5. T. OGINO and K. MOCHIZUKI. Chem. Lett. 443 (1979).

Can. J. Chem. Downloaded from www.nrcresearchpress.com by 210.87.254.6 on 09/06/12
For personal use only.

Conformational features of acyclonucleosides: structure of acyclovir, an antiherpes agent[1]

GEORGE I. BIRNBAUM AND MIROSLAW CYGLER
Division of Biological Sciences, National Research Council of Canada, Ottawa, Ont., Canada K1A 0R6
AND
DAVID SHUGAR
Institute of Biochemistry and Biophysics, Academy of Sciences, 02-532 Warszawa, Poland

Received March 29, 1984

GEORGE I. BIRNBAUM, MIROSLAW CYGLER, and DAVID SHUGAR. Can. J. Chem. **62**, 2646 (1984).

Crystals of acyclovir belong to the space group $P2_1/n$, and the cell dimensions are a = 25.459(1), b = 11.282 (1), c = 10.768(1) Å, β = 95.16(1)°. Intensity data were measured on a diffractometer and the structure was determined by direct methods. The asymmetric unit was found to contain three independent molecules of acyclovir and two molecules of water. Least-squares refinement, which included all hydrogen atoms, converged at R = 0.053 for 3970 observed reflections. In two of the molecules the side chain is partially folded, while in the third one it is fully extended. The glycosidic torsion angles are in the range 91.4−104.3°. The conformational features are compared with those in other known acyclonucleosides. They are also examined in relation to the behavior of acyclonucleosides and acyclonucleotides in various enzymatic systems, including those related to antiviral activities.

GEORGE I. BIRNBAUM, MIROSLAW CYGLER et DAVID SHUGAR. Can. J. Chem. **62**, 2646 (1984).

Les cristaux d'acyclovir appartiennent au groupe d'espace $P2_1/n$ et les dimensions de maille sont a = 25,459(1), b = 11,282(1), c = 10,768(1) Å, β = 95,16(1)°. On a mesuré les intensités à l'aide d'un diffractomètre et on a déterminé la structure par des méthodes directes. On a trouvé que l'unité asymétrique comporte trois molécules indépendantes d'acyclovir et deux molécules d'eau. Un affinement par la méthode des moindes carrés, qui inclut tous les atomes d'hydrogène, converge vers une valeur de R = 0,053 pour 3970 réflexions observées. Dans deux des molécules, la chaîne latérale est partiellement repliée alors qu'elle est totalement allongée dans la troisième. Les angles de torsion autour des liaisons glycosidiques s'étalent de 91,4 à 104,3°. On compare les caractéristiques conformationnelles à celles d'autres acyclonucléosides connus. On les examine aussi en relation avec les comportements des acyclonucléosides et des acyclonucléotides dans divers systèmes enzymatiques, y compris ceux reliés aux activités antivirales.

[Traduit par le journal]

Introduction

It was initially demonstrated by Elion *et al.* (1) that replacement of the ribose moiety of guanosine by an acyclic chain corresponding to the "upper" portion of the ribose ring led to an analogue, 9-[(2-hydroxyethoxy)methyl]guanine (acycloG, acyclovir, ACV), with potent antiherpes activity. Interest in this compound, now licensed for clinical use, was further enhanced by the finding that, in HSV-infected cells, its mechanism of action was due to its specific phosphorylation by the viral-encoded (but not cellular) thymidine kinase to acyclo-GMP (1), followed by further phosphorylation by cellular GMP and GDP kinases to the triphosphate, acycloGTP, which is a selective and potent inhibitor of the HSV DNA polymerase (2).

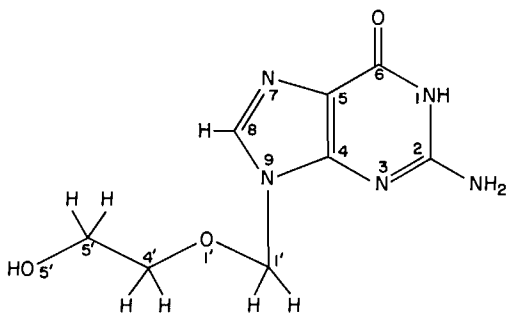

Concurrently it was found that an acyclic analogue of adenosine, in which the sugar ring is replaced by its "lower" fragment, 9-(2,3-dihydroxypropyl)adenine (DHPA), also exhibits significant antiviral activity (3), although the mechanism of action in this instance remains to be clarified. More recently a new analogue of acyclovir has been reported from several laboratories, 9[(1,3-dihydroxy-2-propoxy)methyl]guanine (DHPG), which is an even more active antiherpes agent than acyclovir and is more rapidly phosphorylated by the viral thymidine kinase than acyclovir (4−6).

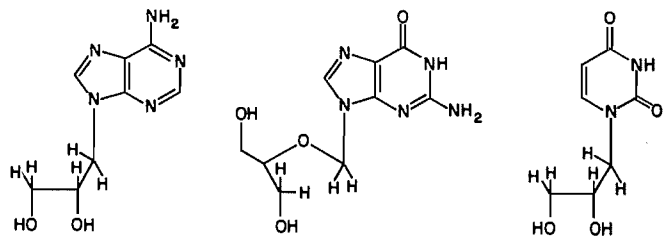

DHPA DHPG DHPU

The foregoing findings have stimulated widespread interest in, and led to the synthesis of a large number of, purine and pyrimidine acyclonucleosides (7). Their antiviral activities and, in some instances, their substrate/inhibitor properties towards both viral and cellular enzymes involved in the anabolism (or "activation") and catabolism of nucleoside analogues with chemotherapeutic activities have been evaluated (7).

Crystal structures have now been reported for the *S* form of DHPA and of its *RS* racemate (8), as well as that of the 2′,3′-*O*-isopropylidene derivative of the *S* form of 1-(2,3-di-

[1]NRCC No. 23630.

TABLE 1. Final parameters and their estimated standard deviations[a]

	Molecule A				Molecule B				Molecule C			
Atom	x	y	z	B_{eq}	x	y	z	B_{eq}	x	y	z	B_{eq}
N(1)	22573(8)	6927(2)	2037(2)	2.4	23157(8)	9636(2)	8783(2)	2.4	21517(8)	9613(2)	5370(2)	2.3
C(2)	17738(9)	6627(2)	1466(2)	2.3	18235(10)	9923(2)	8236(2)	2.4	16691(10)	9911(2)	4783(2)	2.4
N(2)	16611(9)	5473(2)	1365(2)	3.2	17077(9)	11074(2)	8118(3)	3.4	15584(10)	11068(2)	4725(2)	3.3
N(3)	14170(8)	7422(2)	1041(2)	2.3	14659(8)	9125(2)	7833(2)	2.3	13245(8)	9117(2)	4286(2)	2.4
C(4)	15835(9)	8543(2)	1258(2)	2.2	16438(9)	8002(2)	8011(2)	2.1	14963(9)	8003(2)	4461(2)	2.3
C(5)	20593(9)	8930(2)	1818(2)	2.2	21281(9)	7630(2)	8535(2)	2.3	19658(9)	7612(2)	5091(2)	2.2
C(6)	24382(9)	8074(2)	2267(2)	2.4	25082(9)	8489(2)	8966(2)	2.3	23334(9)	8468(2)	5576(2)	2.2
O(6)	28829(7)	8244(2)	2819(2)	3.1	29609(7)	8327(2)	9461(2)	3.0	27750(6)	8294(2)	6133(2)	2.7
N(7)	20730(8)	10156(2)	1884(2)	2.5	21571(8)	6402(2)	8527(2)	2.6	19906(8)	6386(2)	5092(2)	2.4
C(8)	16145(10)	10489(2)	1362(3)	2.6	16988(10)	6069(2)	8014(3)	2.8	15512(10)	6049(2)	4485(2)	2.6
N(9)	12982(8)	9554(2)	954(2)	2.4	13680(8)	6995(2)	7676(2)	2.3	12348(8)	6980(2)	4070(2)	2.4
C(1′)	7511(10)	9591(2)	412(3)	2.8	8238(10)	6937(2)	7095(2)	2.7	7330(11)	6898(3)	3336(3)	3.0
O(1′)	3965(7)	9356(2)	1312(2)	2.9	4556(7)	7182(2)	7939(2)	2.8	3301(8)	6852(2)	4131(2)	3.9
C(4′)	3227(11)	10342(3)	2120(3)	3.4	4421(11)	6307(2)	8894(3)	3.1	−1519(14)	6633(4)	3389(4)	5.3
C(5′)	−65(13)	9962(3)	3135(3)	4.2	144(12)	6590(3)	9704(3)	3.5	−5996(14)	6743(5)	4139(4)	5.8
O(5′)	−5160(9)	9554(2)	2680(3)	4.8	−4820(9)	6336(4)	9051(3)	6.3	−10617(11)	6417(4)	3435(4)	7.6
O(W1)	38199(9)	8513(3)	5740(3)	6.3								
O(W2)	−10866(10)	6900(3)	6778(3)	5.8								

[a]The x coordinates were multiplied by 10^5, the y and z coordinates by 10^4.

hydroxypropyl)uracil (DHPU) (9); a preliminary account of the solid state structure of acyclovir has also appeared (10). We present here full details of the solid state structure and conformation of acyclovir and several examples of its relevance to the role of such compounds in various enzyme systems and in chemotherapy.

Experimental

Acyclovir was crystallized from aqueous dimethylformamide to give thin plates of a hydrate. Precession photographs indicated space group $P2_1/n$. A crystal fragment measuring 0.550 × 0.125 × 0.025 mm was mounted on an Enraf–Nonius CAD4 diffractometer; it provided the following data:

$C_8H_{11}N_5O_3.2/3H_2O$ fw = 237.23

Monoclinic, a = 25.459(1), b = 11.282(1), c = 10.768(1) Å, β = 95.16(1)°, V = 3080.3 Å^3, ρ_c = 1.53 g cm^{-3}, Z = 12 (20°C; CuKα$_1$, λ = 1.54056 Å); $F(000)$ = 1496, μ(CuKα) = 10.1 cm^{-1}.

Cell dimensions were determined from angular settings of 22 reflections. Intensities were measured with Ni-filtered CuKα radiation, using ω/2θ scans with variable scan ranges and speeds. Of the 6343 unique reflections with 2θ ≤ 150°C, there were 3978 with $I \geq 1.5\sigma(I)$ which were considered observed. The intensities were corrected for Lorentz and polarization factors; absorption corrections were considered unnecessary in view of the low value of μ.

The statistics of normalized structure factors indicated a hypercentric distribution, particularly for the $h0l$ zone, and the E values ranged up to 5.60. Repeated attempts to determine the structure with MULTAN (11) and SAP (12) programs were unsuccessful. Removal of $h0l$ reflections also produced uninterpretable E maps. Success was finally achieved when 60 reflections with $E > 3.03$ were removed from the dataset. The MULTAN solution with the highest combined figure of merit gave rise to an E map on which three molecules of acyclovir (48 nonhydrogen atoms) could be located. In addition, the asymmetric unit was found to contain two molecules of water. The difficulties in the structure determination can be attributed to the parallel stacking of all guanine residues (see below). Atomic parameters were refined by block-diagonal least squares with anisotropic thermal parameters for the 50 nonhydrogen atoms and isotropic ones for 34 hydrogen atoms. Three hydrogen atoms were placed in calculated positions and their parameters were not refined. All scattering factors were taken from the "International tables for X-ray crystallography" (13). A weighting scheme was chosen which made the average values of $w(\Delta F)^2$ almost independent of $|F_o|$ and $\sin^2\theta$. Eight strong reflections suffered from extinction effects and were given zero weights. After the final least-squares cycle the average parameter shift equalled 0.03σ and the final value of R was 0.053 (R' = 0.064) for 3970 observed reflections. The coordinates and equivalent isotropic temperature parameters of nonhydrogen atoms are listed in Table 1. Their anisotropic temperature parameters as well as lists of hydrogen atom parameters and of observed and calculated structure factors are available.[2]

Results and discussion

Solid state conformation

The conformations of molecules A and B are fairly similar while that of molecule C is different. The two types of conformations can be seen in the stereoscopic views (Fig. 1) and the details are given in Table 2. In molecule C, the bonds in the side chain attached to N(9) are all in the *trans* conformation, giving rise to an almost planar, zig-zag, arrangement. The *trans* orientation of the C(4′)—O(1′) and C(5′)—O(5′) bonds, corresponding to the gauche$^-$ rotamer in nucleosides, is energetically the least stable one (14). In the other two molecules, these two bonds are in the preferred *gauche* conformation, but the increased stability is estimated to be only 0.65 kcal/mol (15). If the 2:1 equilibrium found in the crystal structure existed in solution as well, the energy difference between the two conformers would amount to about 0.4 kcal/mol. In *S*-DHPA the two C—OH bonds were found to be *trans* to one another, while in the crystal of the racemate (*RS*-DHPA) they were *gauche* oriented (8). In DHPG there are two C—O/C—OH interactions which may be viewed as corresponding to C(4′)—O(1′)/C(5′)—O(5′) and C(4′)—O(1′)/C(3′)—O(3′). Again, one of these interactions is *gauche* and the other *trans* (16). The conformation resembles a xylofuranosyl nucleoside with a *gauche*$^-$ side chain. These examples demonstrate the flexibility of such side chains which is a consequence of the previously mentioned small energy difference between the

[2]These tables may be obtained, at a nominal charge, from the depository of Unpublished Data, CISTI, National Research Council of Canada, Ottawa, Ont., Canada K1S 0S2.

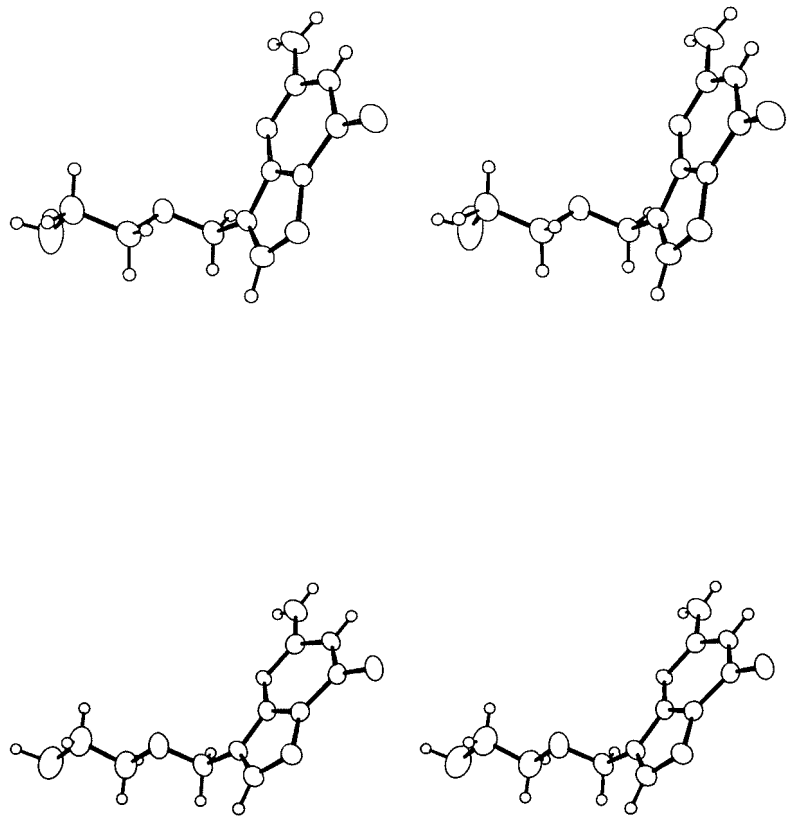

FIG. 1. (Top) Stereoscopic view of molecule B, showing the partially folded conformation of the side chain. Molecule A has essentially the same conformation. (Bottom) Stereoscopic view of molecule C, showing the extended conformation of the side chain.

TABLE 2. Torsion angles (in degrees)

Angle	Molecule A	Molecule B	Molecule C
C(8)—N(9)—C(1′)—O(1′) (χ_{CN})	97.3	104.3	91.4
C(4)—N(9)—C(1′)—O(1′)	−76.5	−74.4	−90.5
N(9)—C(1′)—O(1′)—C(4′)	−76.9	−66.3	−173.3
C(1′)—O(1′)—C(4′)—C(5′)	173.2	−176.2	−171.9
O(1′)—C(4′)—C(5′)—O(5′)	60.6	73.5	−174.4

various possible conformers (see also below). In the crystal structure, the conformation is likely to be dominated by intermolecular hydrogen bonds (see below), while in solution these molecules will easily adopt a conformation in which they can serve as substrates for the appropriate kinase.

In all three molecules of acyclovir the glycosidic torsion angle χ_{CN}[C(8)—N(9)—C(1′)—O(1′)] is in the range 91.4−104.3°. It should be noted that these are absolute values, because in centrosymmetric space groups the signs of torsion angles may be reversed. In DHPG χ_{CN} was found to have a value of 109.3°. In DHPA χ_{CN} cannot be determined owing to the absence of O(1′). We note, however, that the torsion angles C(8)—N(9)—C(1′)—C(2′) are −69.1 and 87.4° in *S*-DHPA and in *RS*-DHPA, respectively. In the DHPU derivative the C(6)—N(1)—C(1′)—C(2′) torsion angle is 85° (9). Thus, all acyclonucleosides in which C(1′) is a secondary carbon atom adopt a conformation about N—C(1′) in which the C(1′)—X bond (X = O or C) is approximately perpendicular (90 ± 20°) to the aglycon. In this conformation the bonds adjoining N—C(1′) are maximally staggered, giving rise to a minimum of steric interactions.

Bond lengths and bond angles

With two exceptions, all bond lengths (Table 3) in the guanine residues are in very good agreement with recently published "standard" values derived from crystal structure analyses (17). The exceptions are in molecule C, where N(3)—C(4) is 0.016 Å shorter, and C(4)—C(5) is 0.015 Å longer, than normal. We do not observe any unique features in the environment of this molecule which would explain what seems to be abnormal electron distribution in part of its ring system. We also note a significant difference between the lengths of the glycosidic bond N(9)—C(1′) in molecules A and B and that in molecule C. This bond can be expected to be somewhat shorter in acyclonucleosides because of decreased substitution at C(1′). Furthermore, its length is influenced by backbonding from the nitrogen p_z-orbital to the antibonding (σ*) orbital of C(1′)—O(1′), an interaction which is at an optimum for χ_{CN} = 90°. The bond length can also be correlated with the torsion angle N(9)—C(1′)—O(1′)—C(4′) as a result of backbonding from the oxygen lone pair to the antibonding orbital of N(9)—C(1′). This torsion angle, approximately *trans* in normal nucleosides, is *gauche* in molecules A and B and *trans*

TABLE 3. Bond lengths (in Ångströms)[a]

Bond	Molecule A	Molecule B	Molecule C
N(1)—C(2)	1.368	1.374	1.372
N(1)—C(6)	1.388	1.391	1.383
C(2)—N(2)	1.336	1.335	1.336
C(2)—N(3)	1.328	1.325	1.332
N(3)—C(4)	1.348	1.353	1.339
C(4)—C(5)	1.375	1.374	1.392
C(4)—N(9)	1.376	1.367	1.379
C(5)—C(6)	1.419	1.418	1.412
C(5)—N(7)	1.385	1.388	1.385
C(6)—O(6)	1.245	1.239	1.241
N(7)—C(8)	1.304	1.300	1.301
C(8)—N(9)	1.375	1.370	1.374
N(9)—C(1′)	1.462	1.470	1.443
C(1′)—O(1′)	1.408	1.391	1.394
O(1′)—C(4′)	1.436	1.428	1.424
C(4′)—C(5′)	1.499(5)	1.490	1.460(5)
C(5′)—O(5′)	1.421	1.419	1.391(5)

[a]Esd's are 0.003–0.004 Å unless otherwise indicated.

TABLE 4. Bond angles (in degrees)[a]

Angle	Molecule A	Molecule B	Molecule C
C(2)—N(1)—C(6)	125.6	125.1	125.1
N(1)—C(2)—N(2)	117.1	117.0	115.9
N(1)—C(2)—N(3)	123.2	123.6	123.4
N(2)—C(2)—N(3)	119.7	119.3	120.7
C(2)—N(3)—C(4)	112.3	112.2	112.3
N(3)—C(4)—C(5)	128.7	128.4	128.4
N(3)—C(4)—N(9)	125.8	125.7	126.9
C(5)—C(4)—N(9)	105.5	106.0	104.7
C(4)—C(5)—C(6)	118.6	119.1	118.4
C(4)—C(5)—N(7)	110.9	110.4	110.7
C(6)—C(5)—N(7)	130.5	130.5	130.9
N(1)—C(6)—C(5)	111.7	111.6	112.2
N(1)—C(6)—O(6)	120.1	120.0	120.1
C(5)—C(6)—O(6)	128.3	128.4	127.7
C(5)—N(7)—C(8)	104.3	104.2	104.7
N(7)—C(8)—N(9)	113.1	113.5	113.1
C(4)—N(9)—C(8)	106.2	106.0	106.7
C(4)—N(9)—C(1′)	125.7	126.3	126.9
C(8)—N(9)—C(1′)	128.0	127.8	126.4
N(9)—C(1′)—O(1′)	111.5	112.2	109.3
C(1′)—O(1′)—C(4′)	113.5	113.3	107.9(3)
O(1′)—C(4′)—C(5′)	109.4(3)	109.9	110.6(3)
C(4′)—C(5′)—O(5′)	113.2(3)	109.4(3)	109.9(4)

[a]Esd's are 0.2° unless otherwise indicated.

in molecule C. We can infer that this accounts for the observed differences in the lengths of N(9)—C(1′). In DHPG, where the corresponding torsion angle is *trans* (16), the glycosidic bond has the same length, 1.441(5) Å, as the one found in molecule C.

Most bond angles (Table 4) in the guanine moiety agree very well with normal values (17). Again, the exception is at C(4) in molecule C where the C(5)—C(4)—N(9) angle is more acute than in the other molecules. Attempts have been made in the past to correlate the relative values of C(4)—N(9)—C(1′) and C(8)—N(9)—C(1′) in purine nucleosides with the conformation about the glycosyl bond (18, 19). The limited data available to date (six independent molecules) suggest that in acyclonucleosides there is a preference for C(8)—N(9)—C(1′) being slightly larger (0–3°) than C(4)—N(9)—C(1′). In molecules A and B the bond angles at C(1′) and O(1′) are considerably larger than in molecule C. This can be attributed to a 1,3-interaction between a C(4′)—H bond and the C(1′)—N(9) bond. The opening of these angles is necessary in order to reduce the nonbonded N(9)···H distance.

Planarity of the guanine residue

As shown in Table 5, the planarity of the guanine residue varies from molecule to molecule. The deviations from planarity are statistically significant, even in molecule B. The χ^2 values are 171.3, 41.1, and 418.6 for A, B, and C, respectively. In most of the cases in which the displaced atom or its substituent participates in a hydrogen bond, the donor, or acceptor, atom in the other molecule is on the same side of the mean plane. This supports our recent conclusion (20) that deviations from planarity in nucleic acid bases, often observed in crystal structure determinations, can be attributed to intermolecular hydrogen bonds.

TABLE 5. Deviations (in Ångströms) from guanine least-squares planes[a]

Atom	Molecule A	Molecule B	Molecule C
N(1)	−0.006	−0.002	0.015
C(2)	−0.013	0.009	−0.025
N(3)	0.006	0.000	−0.010
C(4)	0.009	−0.008	0.007
C(5)	0.021	−0.007	−0.011
C(6)	0.001	0.000	0.015
N(7)	−0.003	0.004	−0.017
C(8)	−0.016	0.004	−0.002
N(9)	−0.002	0.000	0.021
N(2)[b]	−0.069	0.027	−0.077
O(6)[b]	−0.020	0.000	0.037
C(1′)[b]	−0.105	−0.019	0.085

[a]Plane of molecule A: $0.4624X - 0.0186Y - 0.8865Z - 1.3759 = 0$. Plane of molecule B: $0.4356X + 0.0208Y - 0.8999Z + 6.0501 = 0$. Plane of Molecule C: $0.5063X + 0.0265Y - 0.8620Z + 2.1826 = 0$.
[b]Atoms not included in the calculations of the planes.

Hydrogen bonding and packing

Each molecule of acyclovir has four protons capable of participating in hydrogen bonds. With the two molecules of water, there are thus 16 possible hydrogen bonds in the crystal structure. Table 6 lists 15 such bonds, all of them intermolecular, and only H(22A) is missing from this list. Although the latter has O(W1) as its nearest intermolecular neighbour, we do not regard this contact as a proper hydrogen bond because the distance between them is rather long (2.61 Å) and because the H—O—H angles at O(W1) indicate a planar coordination, with only one proton, H(5′B), being accepted. As commonly observed in X-ray analyses, the O—H and N—H bonds appear shorter than their true values of 0.97 and 1.04 Å, respectively. By extending the covalent bond lengths to their nominal values, one obtains corrected H···*A* distances which reflect more accurately the strengths of these hydrogen bonds. It can be seen that most hydrogen bonds are fairly linear and of medium strength. Two of them, however, deviate considerably from linearity and are therefore much weaker. On the basis of the hydrogen bonds involving the two water molecules, one can postulate that the O(6) and O(5′) atoms play an important role

TABLE 6. Distances and angles for hydrogen bonds

			Distances (Å)			Angles (deg)
D	*A*	*A* at	*D*···*A*	H···*A*	H···A_{corr}	*D*—H···*A*
N(1A)—H···N(7A)	$3/2-x, \frac{1}{2}+y, 3/2-z$	2.809	1.96	1.78	173
N(2A)—H(21A)···O(6A)	$3/2-x, \frac{1}{2}+y, 3/2-z$	2.874	2.01	1.88	160
N(1B)—H···N(7C)	$\frac{1}{2}-x, \frac{1}{2}+y, 3/2-z$	2.846	2.05	1.83	166
N(2B)—H(21B)···O(6C)	$\frac{1}{2}-x, \frac{1}{2}+y, 3/2-z$	2.910	2.13	1.91	162
N(2B)—H(22B)···O(5′A)	$\bar{x}, 2-y, 1-z$	3.159	2.43	2.32	139
O(5′A)—H···N(3B)	$\bar{x}, 2-y, 1-z$	2.852	2.07	1.96	154
N(1C)—H···N(7B)	$\frac{1}{2}-x, \frac{1}{2}+y, 3/2-z$	2.864	2.02	1.83	177
N(2C)—H(21C)···O(6B)	$\frac{1}{2}-x, \frac{1}{2}+y, 3/2-z$	2.927	2.10	1.93	161
N(2C)—H(22C)···O(W2)	$\bar{x}, \bar{y}, 1-z$	2.995	2.41	2.28	129
O(W2)—H(W21)···O(6A)	$-\frac{1}{2}+x, 3/2-y, \frac{1}{2}+z$	2.949	1.98	1.99	168
O(W2)—H(W22)···O(5′B)	x, y, z	2.844	2.03	1.88	171
O(5′B)—H···O(W1)	$-\frac{1}{2}+x, 3/2-y, \frac{1}{2}+z$	2.660	1.72	1.69	174
O(W1)—H(W11)···O(6C)	x, y, z	2.742	1.91	1.84	155
O(W1)—H(W12)···O(5′C)	$\frac{1}{2}+x, 3/2-y, \frac{1}{2}+z$	2.892	2.10	1.96	162
O(5′C)—H···O(6B)	$-\frac{1}{2}+x, 3/2-y, -\frac{1}{2}+z$	2.827	1.79	1.87	170

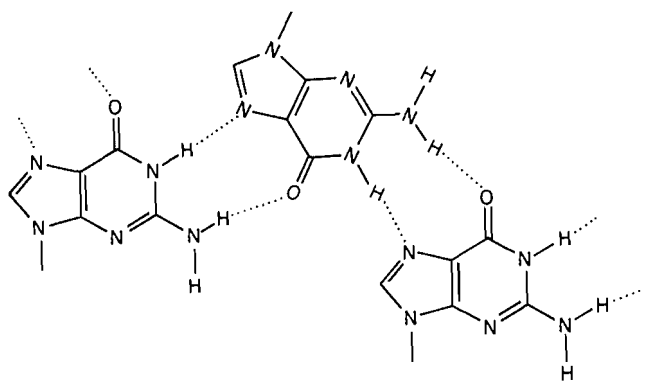

FIG. 2. Hydrogen bonding network in acyclovir.

in acyclovir's interaction with its receptor.

The hydrogen bonding scheme is remarkable, as it joins all guanine bases into infinite sheets. Each base is connected to the next one by two hydrogen bonds: N(1)—H···N(7) and N(2)—H···O(6) (Fig. 2). There are two such sheets in the crystal structure, one formed by symmetry-related A molecules and the other by alternating B and C molecules. The geometry of these hydrogen bonds is very similar: all H···N distances are 1.80 ± 0.03 Å and all H···O distances are 1.90 ± 0.03 Å. The packing diagram (Fig. 3) shows that the ···A···A··· and the ···B···C··· sheets are almost parallel to each other. The dihedral angles between the three guanines in the asymmetric unit are 2.8° for A/B, 3.9° for A/C, and 4.6° for B/C.

Stacking interactions between bases contribute substantially to the stability of nucleic acid structures. The crystal structure of acyclovir is also stabilized by stacking which is illustrated in Fig. 4. A remarkable feature of this arrangement are the continuous dipole–dipole interactions of the carbonyl groups, the electron-rich oxygen atoms overlapping the electron-deficient carbon atoms. This arrangement is maintained despite the fact that the orientation of the A molecules is different from that of the B and C molecules. There is considerable overlapping of bases, particularly between the A/C and B/A pairs. The distances between the successive bases are 3.37 Å for A/C, 3.34 Å for C/B, and 3.37 Å for B/A. These distances are essentially the same as those found between adjacent base pairs in DNA.

Solution conformation and biological activity

In view of the anticipated extensive flexibility of the acyclic chains in acyclonucleosides, it is not unexpected that the standard ^1H and ^{13}C nmr data hitherto reported for such compounds (4, 21) are inadequate for determination of preferred solution conformations. This is further underlined by the results of quantum mechanical calculations of preferred conformation(s) in *S*-DHPA (22), which revealed only the existence of several close energy minima, with no single conformation explicitly favoured. Preliminary attempts to determine some features of the solution conformation of acyclovir by ^1H nmr spectroscopy revealed only free rotation about the terminal C(5′)—O(5′) bond with comparable populations of the three classical rotamers, as compared to the observed *gauche*$^-$ rotamer for molecule C, and *gauche*$^+$ for molecules A and B, in the solid state. Clearly, the use of long-range couplings and, possibly, of nOe methods will be required to obtain more explicit data. The conformation about C—O bonds, which determines the conformation of the entire chain, might be resolved by measurements of carbon–proton coupling constants.

In contrast to the conformational flexibility of the isolated acyclic nucleosides and nucleotides in solution, the biological activities of some of them point to the adoption of defined conformations on interaction with specific enzymes, e.g. the preferential phosphorylation of acyclovir by herpes virus thymidine kinase (see above), and the weak substrate/inhibitor properties of acycloGMP in the 5′-nucleotidase system (10). In tubulin polymerization, which is accompanied by hydrolysis of exchangeably bound GTP to GDP, the former is replaced by acycloGTP with only minimal loss of activity (23). A number of pyrimidine acyclonucleosides are specific reversible inhibitors of mammalian uridine phosphorylase, the most potent being 1-[(2-hydroxyethoxy)methyl]thymine, with a K_i of 3 μM (24, 25). Several bacterial ribonucleases cleave the 2′,3′-cyclic phosphates of DHPU, and of its corresponding thymine analogue, when these are in the *S*, but not *R*, configuration (26), consistent with the fact that only the *S* derivatives imitate the conformation of the natural β-D-ribofuranosyl nucleosides. Investigations of the foregoing enzyme/substrate/inhibitor reactions, and associated conformational changes, should be facilitated with the aid of solid state and solution data for these acyclic nucleoside analogues.

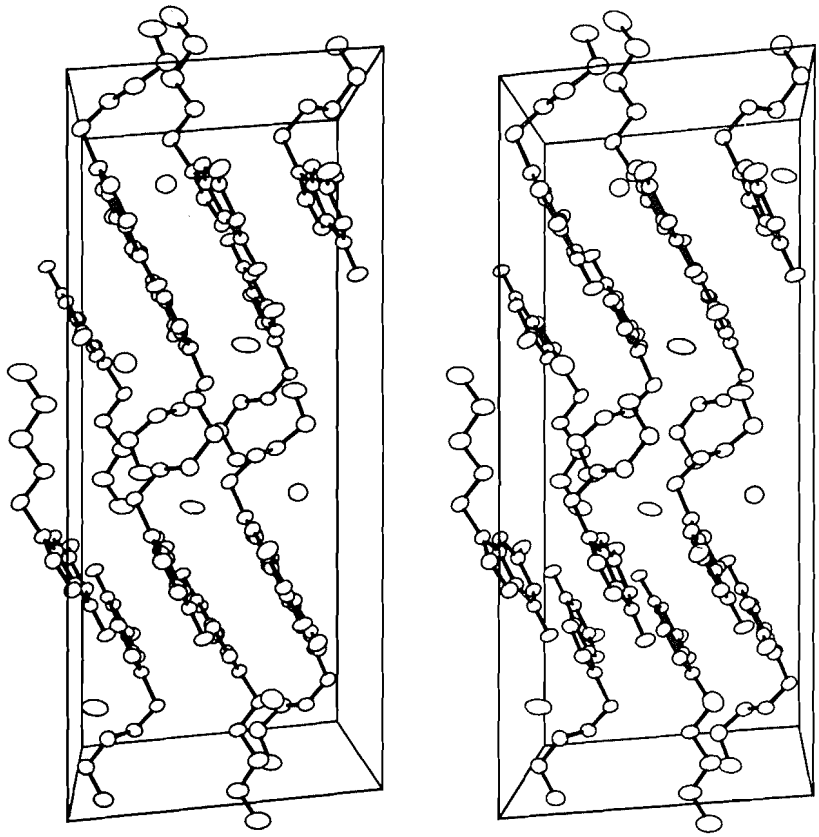

FIG. 3. Stereoscopic view, along the *y* axis, of molecular packing in the crystal.

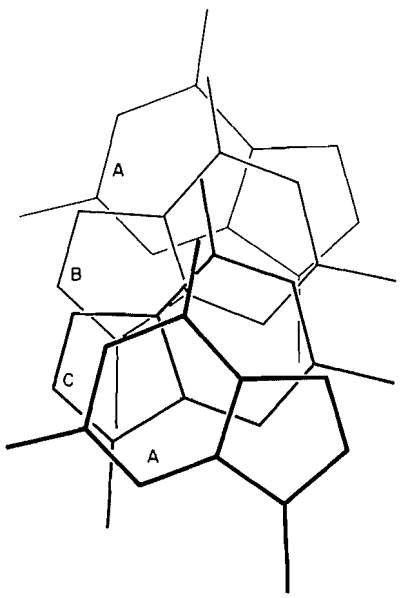

FIG. 4. Guanine stacking in acyclovir; note the dipole–dipole interactions of the carbonyl groups.

Acknowledgments

Apart from MULTAN 78 (11), all crystallographic computations were carried out with programs written by Ahmed *et al.* (12). We are grateful to Dr. G. B. Elion for the gift of a sample of acyclovir and to Dr. R. L. Tolman for providing us with the results of the X-ray analysis of DHPG. Part of this investigation was supported by the Polish National Cancer Research Program (PR-6/1701).

1. G. B. ELION, P. A. FURMAN, J. A. FYFE, P. DE MIRANDA, L. BEAUCHAMP, and H. J. SCHAEFFER. Proc. Natl. Acad. Sci. U.S.A. **74**, 5716 (1977).
2. J. A. FYFE, P. M. KELLER, P. A. FURMAN, R. L. MILLER, and G. B. ELION. J. Biol. Chem. **253**, 8721 (1978).
3. E. DE CLERCQ and A. HOLY. J. Med. Chem. **22**, 510 (1979).
4. J. C. MARTIN, C. A. DVORAK, D. F. SMEE, T. R. MATTHEWS, and P. H. VERHEYDEN. J. Med. Chem. **26**, 759 (1983).
5. A. K. FIELD, M. E. DAVIES, C. DEWITT, H. C. PERRY, R. LIOU, J. GERMERSHAUSEN, J. D. KARKAS, W. T. ASHTON, D. B. R. JOHNSTON, and R. L. TOLMAN. Proc. Natl. Acad. Sci. U.S.A. **80**, 4139 (1983).
6. K. O. SMITH, K. S. GALLOWAY, W. L. KENNELL, K. K. OGILVIE, and B. K. RADATUS. Antimicrob. Agents Chemother. **22**, 55 (1982).
7. G. I. BIRNBAUM and D. SHUGAR. *In* Topics in nucleic acid structure. Part 3. *Edited by* S. Neidle. Macmillan Press, London. 1985. In press.
8. G. S. D. KING and L. SENGIER. J. Chem. Res. (M), 1501 (1981).
9. P. M. KAISER and H. J. LINDNER. *In* Nucleosides, nucleotides and their biological applications. *Edited by* F. C. Alderweireldt and E. L. Esmans. University of Antwerp, Antwerpen. 1982. pp. 293–302.
10. G. I. BIRNBAUM, M. CYGLER, J. T. KUSMIEREK, and D. SHUGAR. Biochem. Biophys. Res. Commun. **103**, 968 (1981).
11. P. MAIN, S. E. HULL, L. LESSINGER, G. GERMAIN, J.-P. DECLERCQ, and M. M. WOOLFSON. MULTAN 78, University of York, England, and University of Louvain, Belgium. 1978.
12. F. R. AHMED, S. R. HALL, M. E. PIPPY, and C. P. HUBER. J. Appl. Crystallogr. **6**, 309 (1973).
13. J. A. IBERS and W. C. HAMILTON (*Editors*). International tables for X-ray crystallography. Vol. IV. Kynoch Press, Birmingham, England. 1974.
14. H. P. M. DE LEEUW, C. A. G. HAASNOOT, and C. ALTONA. Isr. J. Chem. **20**, 108 (1980).

15. N. S. ZEFIROV, V. V. SAMOSHIN, O. A. SUBBOTIN, V. I. BARANENKOV, and S. WOLFE. Tetrahedron, **34**, 2953 (1978).
16. J. HIRSCHFIELD and K. HOOGSTEEN. To be published.
17. R. TAYLOR and O. KENNARD. J. Am. Chem. Soc. **104**, 3209 (1982).
18. S. T. RAO and M. SUNDARALINGAM. J. Am. Chem. Soc. **92**, 4963 (1970).
19. G. I. BIRNBAUM, M. CYGLER, I. EKIEL, and D. SHUGAR. J. Am. Chem. Soc. **104**, 3957 (1982).
20. G. I. BIRNBAUM and G. A. GENTRY. J. Am. Chem. Soc. **105**, 5398 (1983).
21. K. K. OGILVIE, U. O. CHERIYAN, B. K. RADATUS, K. O. SMITH, K. S. GALLOWAY, and W. L. KENNELL. Can. J. Chem. **60**, 3005 (1982).
22. L. HAVLAS, H. HREBABECKY, and J. BERANEK. Nucleic Acids Res. **8**, 6233 (1980).
23. J. LUSTBADER and E. HAMEL. Biochim. Biophys. Acta, **719**, 215 (1982).
24. J. G. NIEDZWICKI, M. H. EL KOUNI, S. H. CHU, and S. CHA. Biochem. Pharmacol. **30**, 2097 (1981).
25. J. G. NIEDZWICKI, S. H. CHU, M. H. EL KOUNI, E. C. ROWE, and S. CHA. Biochem. Pharmacol. **31**, 1857 (1982).
26. A. HOLY and G. S. IVANOVA. Nucleic Acids Res. **1**, 19 (1974).

Proton transfer reactions from 4-X-phenyl-4-nitrophenylcyanomethanes to tetramethylguanidine in acetonitrile solvent

MAHMOOD HOJATTI AND KENNETH T. LEFFEK
Department of Chemistry, Dalhousie University, Halifax, N.S., Canada B3H 4H6

Received December 14, 1983

MAHMOOD HOJATTI and KENNETH T. LEFFEK. Can. J. Chem. **62**, 2653 (1984).

The reactions of 4-X-phenyl-4-nitrophenylcyanomethanes with tetramethylguanidine in acetonitrile solvent give carbanionic products absorbing in the range λ_{max} 580–650 nm. The equilibrium constants are all large, in excess of 6000 $dm^3\ mol^{-1}$. For a series of deprotonation reactions with X = NO_2, Cl, Br, H, and OCH_3, the Hammett ρ value is 2.03 ± 0.03. For the same compounds, the primary deuterium isotope effect, k_H/k_D, varies from 8.9 for X = NO_2 to 14.0 for X = OCH_3 at 25°C.

MAHMOOD HOJATTI et KENNETH T. LEFFEK. Can. J. Chem. **62**, 2653 (1984).

Les réactions des X-4 phényl nitro-4 phénylcyanométhanes avec la tétraméthylguanidine dans l'acétonitrile comme solvant fournissent des produits carbanioniques qui absorbent à des longueurs d'onde allant de 580 à 650 nm. Les valeurs des constantes d'équilibre, qui sont toutes très grandes, dépassent toutes 6000 $dm^3\ mol^{-1}$. Pour une série de réactions de déprotonation, alors que X = NO_2, Cl, Br, H et OCH_3, la valeur ρ de Hammett est égale à 2,03 ± 0,03. Pour les mêmes composés, l'effet isotopique primaire du deutérium, k_H/k_D, varie de 8,9 pour X = NO_2 à 14,0 pour X = OCH_3 à 25°C.

[Traduit par le journal]

Can. J. Chem. Downloaded from www.nrcresearchpress.com by 210.87.254.5 on 09/06/12
For personal use only.

Introduction

The reaction of 4-nitrophenylphenylcyanomethane with tetramethylguanidine in acetonitrile solvent was shown to be a proton transfer with a large equilibrium constant (1). The reaction, shown in eq. [1],

[1] $NO_2C_6H_4\underset{\displaystyle C_6H_4X}{\underset{|}{C}}HCN + HN{=}C(N(CH_3)_2)_2 \underset{k_f}{\overset{k_b}{\rightleftharpoons}} NO_2C_6H_4\overset{-}{\underset{\displaystyle C_6H_4X}{\underset{|}{C}}}CN\ldots H_2\overset{+}{N}{=}C(N(CH_3)_2)_2$

where X = H, was found to have characteristics quite similar to the proton transfer reaction to the same base from 4-nitrophenylnitromethane studied by Caldin and Mateo (2). The cyanomethane reaction gave a primary deuterium isotope, k_H/k_D = 10.7 at 25°C, slightly less than the 11.8 found for the nitromethane. The observed solvent effect on the second-order rate constant between benzonitrile and acetonitrile led to the postulate (1) that the transition state must come early along the reaction coordinate, before much charge development has taken place.

In this paper, further insight into the nature of the transition state is sought by the study of the correlation of the second-order rate constants with the σ value of the substituent, for a series of substrates with different *para*-substituted phenyl groups.

Results and discussion

The reaction of each 4-substituted phenyl-4-nitrophenylcyanomethane with tetramethylguanidine (TMG) in acetonitrile solvent gave a blue–violet product λ_{max} = 582 ± 2 nm, except for bis(4-nitrophenyl)cyanomethane which gave an absorption peak at λ_{max} = 646 nm. An attempt to determine the equilibrium constants by the Hildebrand–Benesi method (3) showed that these constants were all large, greater than 6000 $dm^3\ mol^{-1}$, since the absorption remained virtually unchanged when the base concentration was varied. However, the reaction of 4-nitrophenylphenylcyanomethane with TMG in benzonitrile solvent was previously shown (1) to react as in reaction [1] to give an ion-pair product.

Pseudo first-order rate constants were obtained for each reaction by monitoring the growth of the product peak with time using a stopped-flow spectrophotometer. Each reaction was followed at the wavelength corresponding to the absorption maximum. Initial carbon acid concentrations of $1 \times 10^{-5}\ M$ were used, except for the bis(4-nitrophenyl)cyanomethane reaction for which this had to be reduced to $0.25 \times 10^{-5}\ M$ because of the very rapid rate of the reaction. A range of base concentrations was used with the base always in large excess over the acid to maintain pseudo first-order conditions.

The pseudo first-order rate constants, k_{obs}, were fitted to eq. [2] by a least-squares calculation to yield k_f and k_b, the rate constants for the forward and backward reactions of eq. [1],

[2] $k_{obs} = k_f[\text{base}] + k_b$

which are collected in Table 1. The rate constants at 25°C for the unsubstituted carbon acid (1) are included for comparison purposes.

The second-order rate constants give a very good Hammett plot when the $\log_{10} k_f$ values are plotted against σ^0, the scale appropriate for reactions in which through conjugation is either absent or does not change on going from the initial state to the transition state. The σ^0 values determined for aqueous solutions (4) give a correlation coefficient of 0.9997, whereas σ^0(non-aq) values give a slightly poorer correlation with a coefficient of 0.994. The correlation is poor when σ^- is used for the *p*-nitro substituted compound. A good correlation with σ^0 rather than σ^- was also observed by Boyle (5) for *p*-substituted phenylnitromethane substrates in aqueous solutions. Thus, resonance structures such as **I** may not be important in the transition state of the deprotonation.

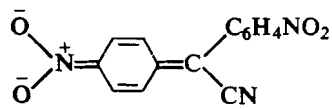

I

TABLE 1. Rate constants for the reaction of 4-X-phenyl-4-nitrophenylcyanomethanes with tetramethylguanidine in acetonitrile solvent

X	T (°C)	10^4 [Base] (M)	k_{obs} (s^{-1})	10^{-3} k_f (dm^3 mol^{-1} s^{-1})	k_b (s^{-1})
NO_2	20.0	0.5–2.5	77.4–129	258 ± 25	61 ± 4
	25.0	0.5–2.5	89.8–166	389 ± 26	66 ± 4
	30.0	0.5–2.5	95.2–203	539 ± 45	69 ± 7
	35.0	0.5–2.5	114–275	824 ± 54	64 ± 9
	40.0	0.5–2.5	137–339	1020 ± 60	76 ± 10
Cl	20.0	1.0–9.0	3.67–15.6	21.2 ± 0.6	2.1 ± 0.3
	25.0	1.0–9.0	3.92–25.4	25.3 ± 0.1	1.4 ± 0.1
	30.0	1.0–9.0	4.15–32.1	32.4 ± 0.8	0.3 ± 0.5
	35.0	1.0–9.0	4.24–35.8	37.1 ± 1.2	−0.2 ± 0.7
	40.0	1.0–9.0	4.78–38.4	42.9 ± 1.5	−0.8 ± 0.9
Br	20.0	1.0–9.0	2.5–19.3	21.3 ± 0.5	0.6 ± 0.3
	25.0	1.0–9.0	3.7–23.2	25.0 ± 1.1	1.4 ± 0.6
	30.0	1.0–9.0	4.6–31.0	32.4 ± 0.7	1.8 ± 0.4
	35.0	1.0–9.0	5.2–38.2	40.5 ± 0.9	1.2 ± 0.5
	40.0	1.0–9.0	6.7–44.0	46.9 ± 1.1	2.3 ± 0.6
H*	25.0	4.9–19.7	5.4–16.9	7.86 ± 0.2	1.5 ± 0.2
OMe	20.0	10.0–50.0	3.8–19.7	3.93 ± 0.1	0.1 ± 0.2
	25.0	10.0–50.0	4.1–21.9	4.46 ± 0.2	−0.2 ± 0.5
	30.0	10.0–50.0	4.5–24.0	4.89 ± 0.2	−0.6 ± 0.5
	35.0	10.0–50.0	4.8–27.8	5.97 ± 0.3	−1.5 ± 0.8
	40.0	10.0–50.0	5.1–30.1	6.39 ± 0.2	−1.7 ± 0.6

* Reference 1.

This could be either because the transition state comes very early along the reaction path or that the developing negative charge remains localized on the carbon atom. Since the ρ value for σ^0(aq) is 2.03 ± 0.03 at 25°C, quite large compared to those observed by Boyle in the range 1.0 to 1.4 in aqueous solution, it appears that there is some amount of negative charge developed in the transition state. Thus, the transition state must have the structure **II** in which the developing charge is mostly localized on the carbon atom.

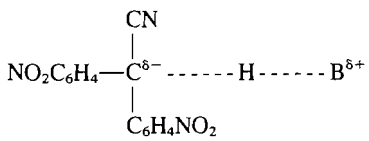

II

The better correlation coefficient with σ^0(aq) than that obtained for σ^0(non-aq) is unexpected. The two scales differ for the substituents used in this study in that σ^0(aq) for NO_2 is 0.82 compared to 0.73 for σ^0(non-aq) and also σ^0(aq) for OCH_3 is −0.12 compared to −0.16 for σ^0(non-aq). The better correlation with σ^0(aq) may be merely an artifact arising from the fact that σ_{NO_2} for this reaction is slightly higher than the standard value of 0.78 but well below the σ^- value for NO_2 of 1.25. If σ_{NO_2} = 0.82 is the best value for this reaction, then the substrate molecule is stabilized by some through conjugation, but this amount of through conjugation increases only very slightly during the activation process.

A correlation $\log_{10} k_f$ may also be made using the dual substituent parameter treatment of Taft (6). This treatment uses eq. [3] in which both σ and ρ values are separated into polar (I)

$$[3] \quad \log_{10} k_f = \log k_{f0} + \sigma_I\rho_I + \sigma_R\rho_R$$

and π delocalization (R) effects. The best fit was obtained when the σ_I and σ_R^0 scales were used with log k_{f0} equal to 3.90, the value corresponding to the observed k_f for the unsubstituted compound from Table 1. This gave ρ_I = 2.1 ± 0.1 and ρ_R = 1.9 ± 0.1, indicating that the substituent effect on the rate constant arises roughly equally from inductive and resonance interactions.

TABLE 2. Activation parameters for the reaction of 4-X-phenyl-4-nitrophenylcyanomethanes with tetramethylguanidine in acetonitrile solvent

X	$\Delta H^{\ddagger}$ (kcal mol^{-1})	$\Delta S^{\ddagger}$ (cal mol^{-1} deg^{-1})
NO_2	12.2 ± 0.6	7.8 ± 2.0
Cl	6.0 ± 0.4	−18.4 ± 1.2
Br	6.9 ± 0.4	−15.1 ± 1.3
H	3.7 ± 0.2	−28.3 ± 0.7
OCH_3	4.0 ± 0.4	−28.4 ± 1.2

The activation parameters, derived from the second-order rate constants of Table 1, are shown in Table 2. All substrates, except the bis-4-nitrophenyl compound, show low enthalpies of activation and negative entropies of activation, typical of proton transfer reactions. The *p*-nitro substituent substantially increases $\Delta H^{\ddagger}$ and brings about a positive $\Delta S^{\ddagger}$. The less powerful electron-withdrawing substitutents Cl and Br exert the same type of influence to a lesser extent, but the electron-releasing substituent OCH_3 has an effect which is not significantly different from that of the unsubstituted substrate.

The most likely explanation of these changes is that the major contribution to $\Delta H^{\ddagger}$ is the energy required to break the initial state solvation shell. Electron withdrawal towards the nitro groups in the bis-4-nitrophenyl compound gives a strongly bound solvation shell in the initial state relative to that of the other substrates. More energy is required to break it and allow

Can. J. Chem. Downloaded from www.nrcresearchpress.com by 210.87.254.5 on 09/06/12
For personal use only.

TABLE 3. Primary deuterium isotope effects for the reaction of 4-X-phenyl-4-nitrophenylcyanomethanes with tetramethylguanidine in acetonitrile solvent at 25°C

X	$10^{-3}\ k_{fD}$ ($dm^3\ mol^{-1}\ s^{-1}$)	k_{fH}/k_{fD}
NO_2	43.7 ± 1.6	8.9 ± 0.7
Cl	2.06 ± 0.2	12.3 ± 0.1
Br	2.10 ± 0.04	11.9 ± 0.6
H	0.73 ± 0.03	10.7 ± 0.5
OCH_3	0.318 ± 0.026	14.0 ± 1.2

proton transfer. The positive ΔS^* arises from a decrease in the strength of solvation between the initial and transition states. This phenomenon is much reduced for the halogen-substituted compounds, resulting in a smaller ΔH^* and a transition state more strongly solvated than the initial state, yielding a negative ΔS^*.

The primary deuterium isotope effects on the second-order rate constants for the reactions are given in Table 3. In order to verify that the k_{fD} values were not in error due to exchange between the deuterated acid and the proton of TMG, a series of experiments was carried out with the *p*-chloro-substituted acid and TMG-*d*. The deuterated TMG was prepared by repeated exchange with D_2O and redried in the usual manner. The second-order rate constants obtained for TMG and TMG-*d* were the same within experimental error.

The value of k_H/k_D appears to increase with the electron-releasing power of the substituent, although the change is not smooth in that the unsubstituted compound has a low value (1) compared to those observed in the present work. However, the standard errors in the k_f values are in some cases quite large, so only the general trend in the isotope effect may be interpreted. It was concluded previously (1) that the unsubstituted compound probably reacted with a significant contribution from proton tunnelling. However, it is not possible to deduce from the present results whether the variation in k_H/k_D arises from changes in the tunnelling contribution or changes arising from vibrational frequency sources. Nevertheless, the variation in k_H/k_D can be qualitatively correlated with the ΔpK for the reactions. The isotope effect is at a maximum when $\Delta pK \sim 0$ and decreases with both positive and negative ΔpK (7). The pK_a of the OCH_3-substituted substrate will be larger than that of the NO_2-substituted substrate. Thus, for a strong base, ΔpK will be smaller for the OCH_3-substituted compound than for the NO_2-substituted compound. Thus, it is expected that k_H/k_D will be larger for the OCH_3 than for the NO_2 compound. Therefore, the change of isotope effect with substrate could arise from vibrational frequency sources with a constant contribution from tunnelling combined with it, although there is no theoretical reason why the tunnelling contribution should not also change with substrate structure.

The suggestion was considered (8) but rejected, that the residual water remaining after very careful drying of TMG, about 1% (9), might give rise to ^-OH base in the form of an ion-pair, which could be the proton-abstracting base rather than TMG. This conclusion was supported when it was shown in a previous publication (1) that replacing this ^-OH by ^-OD gave rise to no isotope effect. Since an isotope effect of 50 to 80% would be expected for these two bases it was concluded that $TMG^+{}^-OH$ contributed to the proton abstraction in a negligible amount.

Tetra-*n*-butylammonium hydroxide was prepared and reacted with 4-chlorophenyl-4-nitrophenylcyanomethane at 25°C under pseudo first-order conditions. This gave $k_f = 3.6 \pm 0.2 \times 10^5\ dm^3\ mol^{-1}\ s^{-1}$, about 15 times greater than that with TMG. Caldin and Mateo (9) determined that equilibrium constant for the reaction of water with TMG to yield the ^-OH ion-pair to be 1.4 in toluene solvent.

If the reactivity of $(C_4H_9)_4N^+{}^-OH$ is assumed to be the same as $TMG^+{}^-OH$, the residual water does not interfere significantly with the TMG reaction, even if the equilibrium constant for $TMG^+{}^-OH$ is as high as 1000 in acetonitrile.

Experimental

Materials

4-Chlorophenyl-4-nitrophenylcyanomethane, 4-bromophenyl-4-nitrophenylcyanomethane, and 4-methoxylphenyl-4-nitrophenylcyanomethane were prepared according to the procedure of Davis and Pizzini (10). The melting points of the compounds were 110–111°C (lit. (10) 110–112°C), 96–97°C, and 69–70.5°C (lit. (10) 69–71°C), respectively.

Bis(4-nitrophenyl)cyanomethane was prepared by nitrating 4-nitrophenylphenylcyanomethane (11) with fuming nitric acid as described by Minch *et al.* (12). The resulting gum was triturated under dry ether at dry ice temperature to yield a yellow powder. After crystallization from ethanol, the slightly yellow crystals melted at 93–94.5°C (lit. (12) 40–45°C). Nmr $CDCl_3$ δ: 5.4 (1H, s), 7.5 (4H, d, J = 9.0 Hz), 8.2 (4H, d, J = 9.0 Hz).

The deuterated analogues of the substrates were prepared as previously described (1). The deuterated materials showed no nmr peak for the aliphatic proton and were, therefore, at least 98% deuterated.

Acetonitrile was purified by the method of O'Donnell *et al.* (13), fractionally distilled over P_2O_5, and collected at 81.5–82.0°C.

Tetramethylguanidine (TMG) was dried over KOH, fractionally distilled over BaO under nitrogen, and collected at 161°C.

Deuterated TMG was made according to the method described by Caldin *et al.* (2). The nmr spectrum showed an isotopic purity of about 98%.

Tetra-*n*-butylammonium hydroxide was prepared from the iodide with Dowex-1-X8 Resin using the method of Harlow (14).

Kinetic measurements

The reaction rates were measured with a Durrum–Gibson stopped-flow spectrophotometer. One hundred optical density measurements were taken for each run using a Hewlett Packard multiprogrammer. Six consecutive trials were made for each set of reactant concentrations and the average value for each of the hundred points was calculated. The first-order rate constant was then calculated using a least-squares fit by a Pet microcomputer from the six-trial-averaged points using the Guggenheim method (15).

1. A. JARCZEWSKI, P. PRUSZYNSKI, and K. T. LEFFEK. Can. J. Chem. **61**, 2029 (1983).
2. E. F. CALDIN and S. MATEO. J. Chem. Soc. Faraday Trans. I, **71**, 1876 (1975).
3. H. A. BENESI and H. H. HILDEBRAND. J. Am. Chem. Soc. **71**, 2703 (1943).
4. P. R. WELLS. Linear free energy relationships. Academic Press, London. 1968. Chapt. 2.
5. W. J. BOYLE, JR. Ph.D. Thesis. Northwestern University. 1971.
6. S. EHRENSON, R. T. C. BROWNLEE, and R. W. TAFT. Prog. Phys. Org. Chem. **10**, 1 (1973).
7. K. T. LEFFEK. *In* Isotopes in organic chemistry. Vol. 2. *Edited by* E. Buncel and C. C. Lee. Elsevier, Amsterdam. 1976. Chapt. 3.
8. I. HEGGEN, J. LINDSTROM, and O. ROGNE. J. Chem. Soc. Faraday Trans. I, **74**, 1263 (1978).

Can. J. Chem. Downloaded from www.nrcresearchpress.com by 210.87.254.5 on 09/06/12
For personal use only.

9. E. F. CALDIN and S. MATEO. J. Am. Chem. Soc. **103**, 202 (1981).
10. R. B. DAVIS and L. C. PIZZINI. J. Org. Chem. **25**, 1884 (1960).
11. H. NERESHEIMER and W. RUPPLE. U.S. Pat. 2,080,057 (1937).
12. M. J. MINCH, M. GIACCIO, and R. WOLF. J. Am. Chem. Soc. **97**, 3766 (1975).
13. J. F. O'DONNELL, J. T. AYERS, and C. K. MANN. Anal. Chem. **37**, 1161 (1965).
14. G. A. HARLOW, C. N. NOBLE, and G. E. A. WYLD. Anal. Chem. **28**, 787 (1956).
15. E. A. GUGGENHEIM. Philos. Mag. **2**, 538 (1926).

Can. J. Chem. Downloaded from www.nrcresearchpress.com by 210.87.254.5 on 09/06/12
For personal use only.

Synthesis of aminoalcohol compounds of platinum and crystal structure of *trans*-[Pt(2-amino-2-methyl-1-propanol)$_2$Cl$_2$]

F. D. ROCHON, P. C. KONG, AND R. MELANSON

Département de chimie, Université du Québec à Montréal, C.P. 8888, Succ. A, Montréal, (Qué.), Canada H3C 3P8

Received October 6, 1983[1]

F. D. ROCHON, P. C. KONG, and R. MELANSON. Can. J. Chem. **62**, 2657 (1984).

Three types of complexes, *trans*-[Pt(LH)$_2$Cl$_2$], [Pt(L)$_2$], and [Pt(LH)$_2$(SR)$_2$] where LH = NH_2—$C(CH_3)_2(CH_2OH)$ and NH_2—$C(CH_2OH)_3$ and L are the deprotonated ligands, have been synthesized.

The crystal structure of *trans*-[Pt(NH_2—$C(CH_3)_2CH_2OH)_2Cl_2$] has been determined by X-ray diffraction methods. The crystals are monoclinic, space group $P2_1/c$, with a = 6,282(3), b = 20,901(13), c = 10,769(10) Å, β = 92,64(6)°, and Z = 4. The structure was refined by full-matrix least-squares analysis to a conventional R factor of 0.049 and R_w = 0.042. The coordination around the platinum atom is square planar. The Pt—Cl distances are 2.306(2) and 2.309(3) Å and the Pt—N bonds are 2.060(8) and 2.071(7) Å. The hydroxyl oxygen atoms are disordered; the disorder is different for each organic ligand. The structure is stabilized by an extensive hydrogen bonding system.

F. D. ROCHON, P. C. KONG et R. MELANSON. Can. J. Chem. **62**, 2657 (1984).

Trois types de composés *trans*-[Pt(LH)$_2$Cl$_2$], [Pt(L$_2$)] et [Pt(LH)$_2$(SR)$_2$] où LH = NH_2—$C(CH_3)_2CH_2OH$ et NH_2—$C(CH_2OH)_3$ et L sont les mêmes ligands déprotonés, ont été synthétisés.

La structure cristalline de *trans*-[Pt(NH_2—$C(CH_3)_2CH_2OH)_2Cl_2$] a été déterminée par diffraction des rayons-X. Les cristaux sont monocliniques, groupe d'espace $P2_1/c$, a = 6,282(3), b = 20,901(13), c = 10,769(10) Å, β = 92,64(6)° et Z = 4. Les coordonnées et les facteurs thermiques anisotropes ont été affinés par moindres-carrés (matrice entière) jusqu'à R = 0,049 et R_w = 0,042. La coordination autour de l'atome de platine est plane. Les distances Pt—Cl sont 2,306(2) et 2,309(3) Å et les liens Pt—N sont 2,060(8) et 2,071(7) Å. Les atomes d'oxygène des ligands sont désordonnés, le désordre étant différent sur chacun des deux ligands organiques. La structure est stabilisée par de nombreux ponts hydrogènes.

Can. J. Chem. Downloaded from www.nrcresearchpress.com by 210.87.254.5 on 09/06/12
For personal use only.

Introduction

Stetsenko *et al.* (1, 2) prepared *trans*-[Pt(LH)$_2$Cl$_2$] (LH = NH_2—$C(CH_2OH)_3$) in a 30% yield from the hot aqueous reaction of Na_2PtCl_4 + 2LH. By heating this product with LH in a Pt:LH ratio of 1:2 in water, the authors obtained [Pt(L)$_2$].2.5-H_2O where L = NH_2—$C(CH_2OH)_2CH_2O^-$. On repeating these experiments, we have found that the yield in the first reaction depends critically on the amount of LH and the heating time, while in the second, the amount of LH is not important and an excess of LH can be used. Furthermore, we found a different content of hydration water in [Pt(L)$_2$].

We have modified these methods to prepare *trans*-[Pt(LH)$_2$-Cl_2] and [Pt(L)$_2$]. Compounds of NH_2—$C(CH_3)_2CH_2OH$ (identified below as L'H) were also synthesized. Organic sulphur compounds R—SH (thiophenol and thiouracil) can react with [Pt(L)$_2$] or [Pt(L')$_2$] to form [Pt(LH)$_2$(SR)$_2$] (or L'H).

The three types of complexes [Pt(LH)$_2$Cl$_2$], [Pt(L)$_2$], and [Pt(LH)$_2$(SR)$_2$] (or L'H) are believed to be *trans*-isomers. In order to confirm these hypotheses, we wanted to determine the crystal structures of one compound of each type. Unfortunately, up to now, only [Pt(L'H)$_2$Cl$_2$] gave suitable crystals for X-ray diffraction. Its crystal structure is reported below.

Experimental

[Pt(L$_2$)] and [Pt(L')$_2$]

K_2PtCl_4 and LH or L'H were dissolved in water in a ratio of LH:Pt > 5. The mixture was heated to 50−70°C for about 1 h and then cooled to room temperature. The light yellow precipitate was filtered, washed with water, and dried with a vacuum pump overnight. The compounds crystallized with one (L) and two (L') molecules of water (Table 1). Yield: 80%.

trans-*[Pt(LH)$_2$Cl$_2$] and* trans-*[Pt(L'H)$_2$Cl$_2$]*

The compounds [Pt(L$_2$)] or [Pt(L')$_2$] were slightly heated in 1 *M* hydrochloric acid until completely dissolved. Upon cooling, yellow crystals slowly formed and they were washed with water and dried under vacuum overnight. Yield: 90%.

[Pt(LH)$_2$(SR)$_2$] and [Pt(L'H)$_2$(SR)$_2$]

[Pt(L)$_2$] or [Pt(L')$_2$] and thiophenol (or thiouracil) were suspended in water in a ratio of RSH:Pt = 2. The mixture was stirred overnight. The precipitate was then filtered, washed with water, and dried under vacuum. The yield was quantitative.

The crystals of *trans*-[Pt(L'H)$_2$Cl$_2$] used for X-ray diffraction were obtained by slow crystallization from a solution of [Pt(L')$_2$] in 1 *M* HCl.

A set of precession photographs showed that the crystals belong to the $P2_1/c$ space group. The cell parameters were calculated by least-squares refinement from the setting angles of 15 centered reflections on a Syntex P$\bar{1}$ diffractometer using graphite-monochromatized MoKα radiation.

Crystal data

$C_8H_{22}N_2O_2Cl_2Pt$ mw = 444.27

Monoclinic, $P2_1/c$, a = 6.282(3), b = 20.901(13), c = 10.769(10) Å, β = 92.64(6)°, V = 1412.5(2) Å^3, Z = 4, D_x × 2.089, D_m = 2.10(2) Mg m^{-3}, λ(MoKα) = 0.71069 Å, μ(MoKα) = 10.40 mm^{-1}, and T = 295 K.

A total of 4140 independent reflections were measured with 2θ < 60° by the θ−2θ scan technique using MoKα radiation. The scan rate was 1° (2θ) min^{-1} for most reflections, but rates as high as 24° min^{-1} were selected for strong reflections by the autocollection program. A 2θ scan range of 1° below $K\alpha_1$ and 1° above $K\alpha_2$ was chosen. The background time to scan time ratio was 0.50. Reflections with I_{net} < 2.5σ(I) were considered as unobserved, where σ(I) was calculated as already described (3). An absorption correction based on the equations of the crystal faces was applied to all reflections. The transmission factors varied from 0.197 to 0.263. The data were then corrected for Lorentz-polarization effects. This set of 2372 observed reflections was used for the structure determination.

The atomic scattering factors of Cromer and Waber (4) were used for Pt, Cl, O, N, and C atoms and those of Stewart, Davidson, and Simpson (5) were used for H. The anomalous-dispersion terms (6) of Pt and Cl were included in the calculations.

The position of the Pt atom was found from the three-dimensional Patterson map. The positions of all other non-hydrogen atoms were

[1]Revision received May 28, 1984.

Can. J. Chem. Downloaded from www.nrcresearchpress.com by 210.87.254.5 on 09/06/12
For personal use only.

TABLE 1. Elemental analysis of the $[Pt(L—H)_2]$ and $[PtL_2(SR)_2]$ complexes (the top row shows the calculated values)

Compound	% C	% H	% O	% S	% Pt
$[Pt(NH_2—C(CH_3)_2CH_2O)_2].H_2O$	24.55	6.14	12.18		49.87
	24.54	5.87	12.04		
	24.57	5.67			49.67
$[Pt(NH_2—C(CH_2OH)_2CH_2O)_2].2H_2O$	20.38	5.10			41.40
	20.34	5.38			40.66
$[Pt(NH_2—C(CH_2OH)_3)_2(PhS)_2]$	36.64	4.92		9.78	
	36.11	4.61		10.30	
$[Pt(NH_2—C(CH_2OH)_3)_2(C_4H_3N_2OS)_2]$	27.79	4.08		9.27	
	27.23	4.23		9.49	
$[Pt(NH_2—C(CH_3)_2(CH_2OH)(C_4H_3N_2OS)_2]$	30.62	4.50		10.22	
	29.32	4.18		9.85	

TABLE 2. Positional parameters, with their esd's and temperature factors ($\times 10^4$)

Atom	x	y	z	U_{eq} (Å^2)*
Pt	1735.4(5)	2418.8(2)	1389(3)	349
Cl(1)	−851(4)	2036(1)	2647(2)	524
Cl(2)	4296(4)	2805(1)	114(2)	564
N(1)	−318(11)	3143(3)	796(7)	395
N(2)	3775(12)	1702(4)	2001(7)	425
C(1)	−356(17)	3768(5)	1515(10)	541
C(2)	1954(19)	4059(5)	1566(14)	774
C(3)	−1328(24)	3661(6)	2802(13)	901
C(4)	−1900(19)	4211(6)	762(16)	782
C(5)	3890(17)	1063(5)	1329(11)	539
C(6)	1604(21)	777(6)	1194(15)	810
C(7)	4896(25)	1166(6)	43(13)	851
C(8)	5381(21)	619(6)	2134(13)	714
O(1)	−1880(30)	4855(9)	1012(18)	688
O(1′)	−1312(24)	4335(7)	−289(15)	742
O(2)	5024(25)	619(6)	3295(15)	824
O(2′)	803(34)	609(11)	2268(29)	936

*$U_{eq} = \frac{1}{3}(U_{11} + U_{22} + U_{33} + 2U_{13}\cos\beta)$.

obtained by a series of full-matrix least-squares refinements followed by electron density difference syntheses. The two oxygen atoms were found to be disordered. Each oxygen atom was located at two different positions. The occupancy factors of the four different positions were refined, keeping the isotropic thermal parameters at 3.0 Å^2. The occupancy factors were then fixed at 0.415, 0.585, 0.386, and 0.614 for O(1), O(1′), O(2), and O(2′), respectively, and the thermal parameters refined. An isotropic secondary-extinction correction (7) was included in the calculations. Individual weights $w = 1/\sigma^2(F)$ were finally applied. The H atoms on the —NH_2 groups were fixed at their calculated positions (N—H = 0.85 Å) and assigned isotropic temperature factors β = 6.0 Å^2. The refinement of the scale factor, the coordinates and anisotropic temperature factors of all non-hydrogen atoms converged to $R = \Sigma||F_o| - |F_c||/\Sigma|F_o| = 0.049$ and a weighted $R_w = \{\Sigma w(|F_o| - |F_c|)^2/\Sigma w|F_o|^2\}^{1/2} = 0.042$.

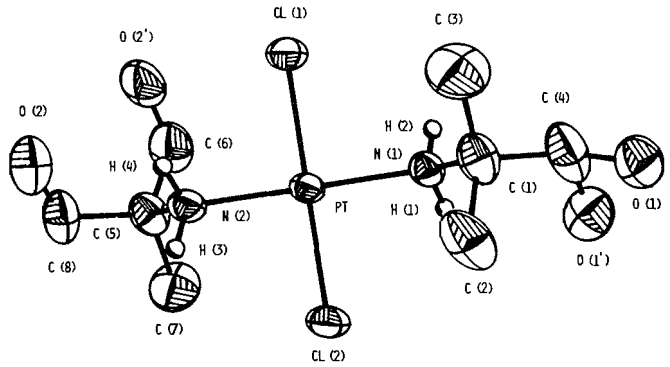

FIG. 1. Labelled diagram of the molecule *trans*-$[Pt(NH_2—C(CH_3)_2CH_2OH)_2Cl_2]$.

The calculations were carried out with a Cyber 171 computer using previously described programs (3). Tables of observed and calculated structure factors and anisotropic thermal parameters are available from the Depository of Unpublished Data.[2]

Results and discussion

The $[Pt(L \text{ or } L')_2]$ compounds have been prepared by heating K_2PtCl_4 with an excess of LH or L′H in water. The light yellow compounds were identified as $[Pt(L)_2].H_2O$ and $[Pt(L')_2].2H_2O$ after drying with a vacuum pump overnight. The syntheses were repeated several times and the elemental analyses were always identical. Stetsenko *et al.* (1, 2) reported $[Pt(L)_2].2.5H_2O$ which was prepared by a different method. They obtained a higher hydration content because they did not dry their compound. They washed it with ethanol and ether and determined its hydration content by thermal analysis.

When $[Pt(L \text{ or } L')_2]$ was dissolved in warm hydrochloric acid solution, yellow crystals of *trans*-$[Pt(LH \text{ or } L'H)_2Cl_2]$ were gradually formed. The reactions are as follows:

$$K_2PtCl_4 + 2LH \text{ or } 2L'H \xrightarrow[H_2O]{50-70°C} [Pt(L \text{ or } L')_2].xH_2O + 2KCl + 2HCl$$

$$[Pt(L \text{ or } L')_2].xH_2O \xrightarrow{1\ M\ HCl} trans\text{-}[Pt(LH \text{ or } L'H)_2Cl_2]$$

[2]Lists of structure factors and anisotropic thermal parameters are available, at a nominal charge, from the Depository of Unpublished Data, CISTI, National Research Council of Canada, Ottawa, Ont., Canada K1A 0S2.

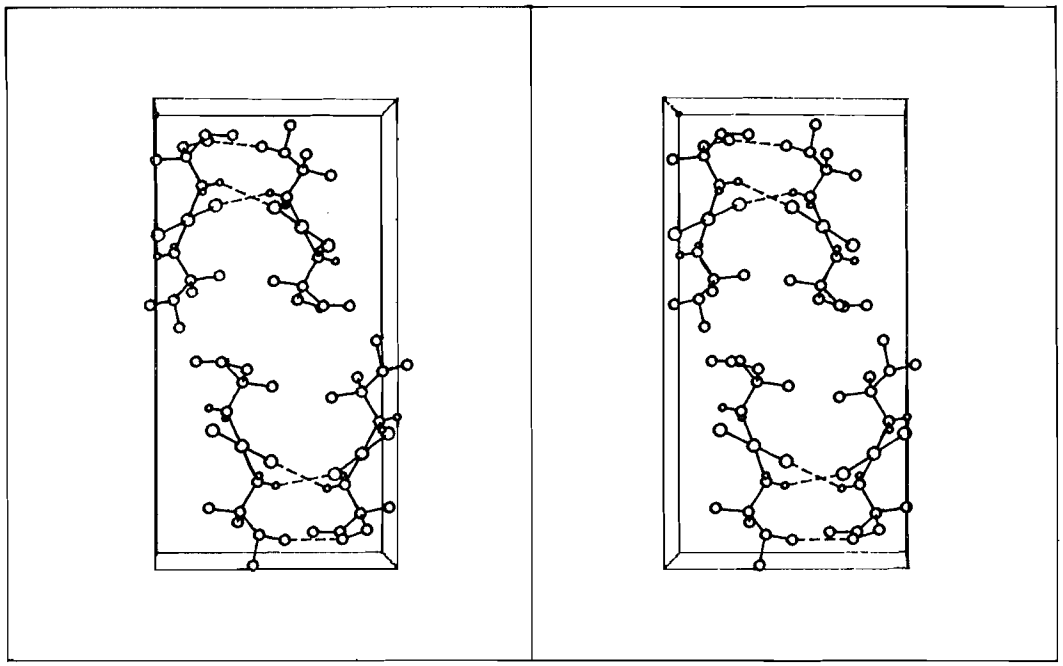

FIG. 2. Stereoscopic diagram of the packing in the *trans*-[Pt(NH_2—$C(CH_3)_2CH_2OH)_2Cl_2$] crystal (*c* axis horizontal and *b* axis vertical).

TABLE 3. Bond distances and angles

Bond	Distance (Å)	Atoms	Angle (deg)
Pt—Cl(1)	2.306(2)	Cl(1)—Pt—Cl(2)	179.4(1)
Pt—Cl(2)	2.309(3)	Cl(1)—Pt—N(1)	89.4(2)
Pt—N(1)	2.071(7)	Cl(1)—Pt—N(2)	90.3(2)
Pt—N(2)	2.060(8)	Cl(2)—Pt—N(1)	90.1(2)
N(1)—C(1)	1.52(1)	Cl(2)—Pt—N(2)	90.2(2)
N(2)—C(5)	1.52(1)	N(1)—Pt—N(2)	179.4(3)
C(1)—C(2)	1.57(2)	Pt—N(1)—C(1)	119.7(6)
C(1)—C(3)	1.56(2)	Pt—N(2)—C(5)	121.9(6)
C(1)—C(4)	1.54(2)	N(1)—C(1)—C(2)	108.3(8)
C(5)—C(6)	1.56(2)	N(1)—C(1)—C(3)	110.4(9)
C(5)—C(7)	1.56(2)	N(1)—C(1)—C(4)	105.8(9)
C(5)—C(8)	1.55(2)	N(2)—C(5)—C(6)	108.5(9)
C(4)—O(1)	1.37(2)	N(2)—C(5)—C(7)	109.3(9)
C(4)—O(1′)	1.23(2)	N(2)—C(5)—C(8)	107.4(9)
C(8)—O(2)	1.28(2)	C(2)—C(1)—C(3)	115.1(9)
C(6)—O(2′)	1.33(3)	C(2)—C(1)—C(4)	110.0(9)
		C(3)—C(1)—C(4)	106.9(10)
		C(6)—C(5)—C(7)	112.3(10)
		C(6)—C(5)—C(8)	110.7(10)
		C(7)—C(5)—C(8)	108.6(10)
		C(1)—C(4)—O(1)	119.0(13)
		C(1)—C(4)—O(1′)	113.6(13)
		C(5)—C(8)—O(2)	114.7(12)
		C(5)—C(6)—O(2′)	113.9(15)

where $x = 1$ (L) or 2 (L′).

The compounds [Pt(L or L′)$_2$] can react with organic sulphur compounds R—SH (thiophenol and thiouracil) to form [Pt(LH or L′H)$_2$(SR)$_2$]. The reactions are as follows:

$$[\text{Pt(L or L')}_2] + 2\text{RSH} \xrightarrow{H_2O} [\text{Pt(LH or L'H)}_2(\text{RS})_2]$$

The results of the elemental analysis of the [Pt(L or L′)$_2$] and [Pt(LH or L′H)$_2$(SR)$_2$] compounds are shown in Table 1.

The three types of compounds, [Pt(L or L′)$_2$], [Pt(LH or L′H)$_2$Cl$_2$], and [Pt(LH or L′H)$_2$(SR)$_2$] are probably *trans*-isomers. The infrared spectrum of [Pt(L′H)$_2$Cl$_2$] showed only one ν_{Pt-Cl} band at 329 cm^{-1} (vs), which is typical of *trans*-compounds. The ν(N—H) vibrations appeared at 3360 (vs br) and 3210 cm^{-1} (vs br) and the $\delta(NH_2)$ deformation absorbed at 1572 cm^{-1} (vs). Since the Pt—N bonds are fairly strong and stable in the conditions used for the preparation of the three types of compounds, we can reasonably assume that [Pt(L or L′)$_2$] and [Pt(LH or L′H)$_2$(SR)$_2$] have the same configuration as *trans*-[Pt(L′H)$_2$Cl$_2$].

The crystal structure analysis of [Pt(L′H)$_2$Cl$_2$] confirmed its *trans* configuration. The refined atomic parameters are listed in Table 2. A labelled diagram of the molecule is shown in Fig. 1. The coordination around the Pt is square planar. The deviations from the least-squares weighted plane are as follows: Pt, −0.0002(3); Cl(1), 0.007(3); Cl(2), 0.008(3); N(1), −0.010(8); and N(2), −0.010(8) Å. The bond lengths and angles are given in Table 3. The angles around the Pt atom are close to the expected values of 90° and 180°.

The Pt—Cl bond lengths (2.306(2) and 2.309(3) Å) are normal and agree well with published values on *trans*-dichloroplatinum(II) compounds (8–11).

The Pt—N bond lengths (2.071(7) and 2.060(8) Å) are also normal and agree with published values on similar compounds (10–12). For example, the Pt—N distances in *trans*-[Pt(NH_2—CH_2—CH_2—$OH)_2I_2$] are 2.05 and 2.08 Å (12). In *trans*-[Pt(NH_2—$C(CH_3)_2CH_2OH)_2Cl_2$], the two organic ligands are arranged so that one ligand is above the platinum plane and the second below it (Fig. 1). The bond lengths and angles in L′H seem normal except that the oxygen atoms are disordered. The disorder is different on each of the two ligands. The disorder of C(4)—O(1) and C(4)—O(1′) is due to redirection of the ROH group while C(6)—O(2) and C(8)—O(2′) are due to disordered —CH_2OH groups. The occupancy ratio for each oxygen atom is about 2:3.

The structures of several copper(II) compounds with this ligand (L′H) has been determined (13–15) where L′H is either neutral or deprotonated. In all these structures, the ligand is

Can. J. Chem. Downloaded from www.nrcresearchpress.com by 210.87.254.5 on 09/06/12
For personal use only.

TABLE 4. Distances and angles involved in possible hydrogen bonds

Atoms	Transformation (on second atom)	Distance (Å)	Atoms	Angle (deg)
N(1)···Cl(1)	$x, \frac{1}{2}-y, z-\frac{1}{2}$	3.41(1)	C(1)—N(1)···Cl(1)	126.7(5)
			Pt—N(1)···Cl(1)	104.9(3)
N(1)···Cl(2)	$x-1, y, z$	3.50(1)	C(1)—N(1)···Cl(2)	104.1(5)
			Pt—N(1)···Cl(2)	119.9(3)
N(2)···Cl(1)	$x+1, y, z$	3.49(1)	C(5)—N(2)···Cl(1)	101.8(5)
			Pt—N(2)···Cl(1)	120.0(3)
N(2)···Cl(2)	$x, \frac{1}{2}-y, \frac{1}{2}+z$	3.51(1)	C(5)—N(2)···Cl(2)	135.1(6)
			Pt—N(2)···Cl(2)	96.9(3)
O(1)···O(2)	$-x, \frac{1}{2}+y, \frac{1}{2}-z$	2.67(2)	C(4)—O(1)···O(2)	129(1)
O(1)···O(1′)	$-x, 1-y, -z$	2.76(2)	C(4)—O(1)···O(1′)	123(1)
O(1)···O(2′)	$-x, \frac{1}{2}+y, \frac{1}{2}-z$	2.50(3)	C(4)—O(1)···O(2′)	139(1)
O(1′)···O(1)	$-x, 1-y, -z$	2.76(2)	C(4)—O(1′)···O(1)	129(1)
O(1′)···O(2)	$x-1, \frac{1}{2}-y, z-\frac{1}{2}$	2.70(2)	C(4)—O(1′)···O(2)	104(1)
O(2)···O(1)	$-x, y-\frac{1}{2}, \frac{1}{2}-z$	2.67(2)	C(8)—O(2)···O(1)	116(1)
O(2)···O(1′)	$1+x, \frac{1}{2}-y, \frac{1}{2}+z$	2.70(2)	C(8)—O(2)···O(1′)	112(1)
O(2′)···O(1)	$-x, y-\frac{1}{2}, \frac{1}{2}-z$	2.50(3)	C(6)—O(2′)···O(1)	135(2)
O(2′)···Cl(1)	x, y, z	3.19(2)	C(6)—O(2′)···Cl(1)	90(1)

bidentate forming a chelate with the metal. Platinum is a soft metal, and is not expected to form strong Pt—O bonds with alcohols or other neutral oxygen ligands as do most first row transition metals. For example, DMSO coordinates to platinum through the sulphur atom (3, 16, 17) and not through the oxygen atom like most transition metals of the first row. Therefore L′H does not form a chelate with platinum unless it is deprotonated.

The packing of the molecules is shown in Fig. 2. The crystal is stabilized by an extensive hydrogen bonding system. The most favorable hydrogen bonds are shown in Table 4. All the amine groups are hydrogen bonded to the chlorine atoms. The hydroxy groups are also hydrogen bonded between themselves or possibly to one chlorine atom.

Acknowledgments

The authors are grateful to the Natural Sciences and Engineering Research Council of Canada, to the National Cancer Institute of Canada, and to the Ministère de l'Education (FCAC) for financial support.

1. A. I. STETSENKO, L. I. SHIGINA, and L. S. TIKHONOVA. Russ. J. Inorg. Chem. **26**, (3), 371 (1981).
2. A. I. STETSENKO, L. I. SHIGINA, L. S. TIKHONOVA, and M. V. SHIRAI. Russ. J. Inorg. Chem. **26**, (11), 1682 (1981).
3. R. MELANSON and F. D. ROCHON. Can. J. Chem. **53**, 2371 (1975).
4. D. T. CROMER and J. T. WABER. Acta Crystallogr. **18**, 104 (1965).
5. R. F. STEWART, E. R. DAVIDSON, and W. T. SIMPSON. J. Chem. Phys. **42**, 3175 (1965).
6. D. T. CROMER. Acta Crystallogr. **18**, 17 (1965).
7. P. COPPENS and W. C. HAMILTON. Acta Crystallogr. A**26**, 71 (1970).
8. F. D. ROCHON, P. C. KONG, and R. MELANSON. Can. J. Chem. **59**, 195 (1981); **58**, 97 (1980).
9. G. ZANOTTI, A. DELPRA, G. BOMBIERI, and A. M. TAMBURRO. Acta Crystallogr. B**34**, 2138 (1978).
10. C. J. L. LOCK and M. ZVAGULIS. Inorg. Chem. **20**, 1817 (1981).
11. B. LIPPERT, C. J. L. LOCK, and R. A. SPERANZINI. Inorg. Chem. **20**, 808 (1981).
12. F. D. ROCHON and R. MELANSON. Acta Crystallogr. B**38**, 1133 (1982).
13. H. MUHONEN and R. HÄMÄLÄINEN. Acta Chem. Scand. A**32**, 121 (1978).
14. H. MUHONEN. Acta Crystallogr. B**37**, 951 (1981); B**38**, 2041 (1982).
15. J. A. BERTRAND, E. FUJITA, and D. G. VANDERVEER. Inorg. Chem. **19**, 2022 (1980).
16. R. MELANSON and F. D. ROCHON. Can. J. Chem. **54**, 1002 (1976).
17. R. MELANSON and F. D. ROCHON. Acta Crystallogr. B**33**, 3571 (1977); B**34**, 941 (1978); B**34**, 1125 (1978).

Can. J. Chem. Downloaded from www.nrcresearchpress.com by 210.87.254.5 on 09/06/12
For personal use only.

Linear oligopeptides. 118.[1] Preferred conformations and modes of self-association of the fluoren-9-ylmethoxycarbonyl amino acid derivatives

GIOVANNI VALLE, GIAN MARIA BONORA, AND CLAUDIO TONIOLO[2]

Biopolymer Research Centre, C.N.R., Institute of Organic Chemistry, University of Padova, 35131 Padova, Italy

Received December 20, 1983

GIOVANNI VALLE, GIAN MARIA BONORA, and CLAUDIO TONIOLO. Can. J. Chem. **62**, 2661 (1984).

An analysis of the preferred conformations and modes of self-association of the *N*-fluoren-9-methoxycarbonyl derivatives of L-alanine and α-aminoisobutyric acid was performed in solution and in the solid state using infrared absorption, ^{1}H nuclear magnetic resonance, and X-ray diffraction. In a solvent of low polarity (deuterochloroform) non-associated and self-associated species (involving predominantly the hydroxyl and carbonyl groups of the carboxylic acid moiety) simultaneously occur. At high dilution, where self-association is absent, the amount of intramolecularly H-bonded forms, if any, should be extremely small. *Z*(*trans*) $\rightleftharpoons$ *E*(*cis*) isomerism about the amide bond of the secondary urethane moiety was observed only for the less bulky L-alanine derivative. In the solid state all H-bonding donors and acceptors of the L-alanine and α-aminoisobutyric acid derivatives take part to complex schemes of intermolecular H-bonds. In the L-alanine derivative, crystallized as monohydrate, most of the intermolecular H-bonds involve the water molecule. Intramolecular H-bonds are not observed in either compound. The conformation about the secondary urethane CO—NH bond is *Z*(*trans*) in both compounds. Both L-alanine and α-aminoisobutyric acid residues are partially folded. The observation of the long C(sp^3)—O bond of the fluoren-9-ylmethoxycarbonyl moiety might contribute to explain the unexpected experimental result that this protecting group can be removed by catalytic hydrogenation.

GIOVANNI VALLE, GIAN MARIA BONORA et CLAUDIO TONIOLO. Can. J. Chem. **62**, 2661 (1984).

Opérant en solution ainsi qu'à l'état solide et faisant appel à la spectroscopie d'absorption infrarouge, à la résonance magnétique nucléaire du ^{1}H et à la diffraction des rayons-X, on a effectué une analyse des conformations priviligiées et des modes d'auto-association des dérivés *N*-fluorèneméthoxycarbonyle-9 de la L-alanine et de l'acide α-aminoisobutyrique. Dans un solvant de faible polarité (deutérochloroforme), les espèces non associées et auto-associées (impliquant d'une façon prépondérante les groupes hydroxyle et carbonyle de la portion acide carboxylique) se forment simultanément. A grande dilution, alors qu'il n'y a pas d'auto-association, le nombre de molécules liées par des liaisons hydrogènes intramoléculaires, s'il y en a, doit être extrêmement faible. Ce n'est que dans le cas du dérivé le moins encombré de la L-alanine que l'on a pu observer une isomérisation *Z*(*trans*) $\rightleftharpoons$ *E*(*cis*) autour de la liaison amide de l'unité uréthane secondaire. A l'état solide, tous les groupes des dérivées de la L-alanine et de l'acide α-aminoisobutyrique qui peuvent agir comme donneurs ou comme accepteurs de liaisons hydrogènes participent à des formes complexes de liaisons hydrogènes intermoléculaires. Dans le dérivé de la L-alanine, qui cristallise sous forme de monohydrate, la plupart des liaisons hydrogènes intermoléculaires impliquent la molécule d'eau. On n'a pas observé de liaisons hydrogènes intramoléculaires ni dans l'un ni dans l'autre de ces composés. La conformation autour de la liaison uréthane secondaire CO—NH est *Z*(*trans*) dans les deux composées. Les résidus L-alanine et acide α-aminoisobutyrique sont partiellement repliés. La présence, dans la portion fluorèneméthoxycarbonyle-9, d'une liaison C(sp^3)—O qui est plus longue que prévue peut contribuer à expliquer le fait inattendu que l'on peut éliminer ce groupe protecteur par hydrogénation catalytique.

[Traduit par le journal]

Introduction

This work is part of our continuing study on the preferred conformations and modes of self-association of amino acids protected at the amino function with urethane-type groups (2, 3). The fluoren-9-ylmethoxycarbonyl (Fmoc) (**1**) group, currently adopted for routine use in peptide synthesis as a N^{α}-protecting group (4, 5), is most attractive because of the following favorable properties: (*i*) the ready preparation of

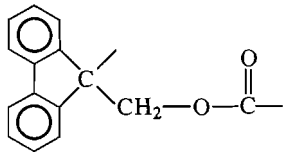

1

crystalline Fmoc-amino acids (5, 6), active esters (7*a*, 7*b*, 8), symmetrical anhydrides (5*b*), 5(4*H*)-oxazolones (9), and oxazolidinones (10); (*ii*) the rapid, quantitative cleavage under racemization-free, nonhydrolytic, mild base treatment via a β-elimination process (abstraction of the acidic benzylic hydrogen atom on the β-carbon of the bulky fluorenyl annular system by the base is the rate-limiting step) (4–7); and (*iii*) the strong uv absorption maxima (11), particularly advantageous for a facile reaction monitoring (5).

In addition: (*i*) the blocking of N^{ω}-amino groups with Fmoc (7*a*, 7*b*) and the blocking of the C-terminal —COOH and side-chain —SH functions in the form of fluoren-9-ylmethyl esters (7*c*, 7*d*) and thioethers (7*e*), respectively, have also been found useful in peptide synthesis; (*ii*) a Fmoc-amino acid derivative containing an isothiocyanate function has been synthesized and assessed for potential application as a chiral Edman reagent to test for racemization after peptide coupling (12); and (*iii*) the 2-sulpho derivative of Fmoc has been proposed as a N^{α}-protecting group for the elimination of side products from the peptides synthesized by the solid-phase method (13).

In this paper we describe the results of an ir absorption, ^{1}H nmr, and X-ray diffraction investigation of Fmoc-Aib-OH (Aib, α-aminoisobutyric acid) and Fmoc-L-Ala-OH in a solvent of low polarity and in the solid state. This study represents *inter alia* the *first* X-ray diffraction analysis of the electronic structure, preferred conformation, and mode of self-association of Fmoc-amino acid and peptide derivatives. The combined in-

[1]For part 117: see ref. 1.

[2]To whom all correspondence should be addressed.

Can. J. Chem. Downloaded from www.nrcresearchpress.com by 210.87.254.40 on 09/06/12
For personal use only.

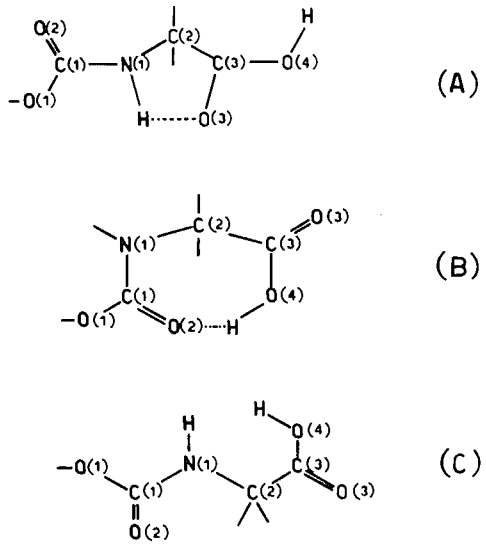

FIG. 1. (*A*) The C_5 conformer of an urethane-protected α-amino acid residue stabilized by the N—H...O=C (carboxylic acid) intramolecular H-bond. (*B*) An oxy-C_7 conformer of an urethane-protected α-amino acid residue stabilized by the O—H...O=C (urethane) intramolecular H-bond. (*C*) The open (no intramolecular H-bond), extended conformer.

vestigation of the Aib and L-Ala derivatives was expected to be particularly relevant, since the former amino acid exhibits severe restrictions to its conformational freedom due to the presence of *gem*-dimethylation at the α-carbon (14), whereas the latter amino acid is free to assume a wide range of conformations owing to the presence of a single, small, side chain (15).

In particular this study could allow us to obtain more information on the following points: (*i*) What are the conformational preferences about the O—C (=O) and (O=) C—N bonds of the secondary urethane moieties (2, 3)? (*ii*) Are the molecules extended (Fig. 1*A* and *C*), e.g. with the formation of the N—H...O=C (carboxylic acid) intramolecular H-bond of the C_5-type (Fig. 1*A*) (16), or rather, folded up to adopt the oxy-analogs of the C_7 conformation (Fig. 1*B*) with the formation of the O—H...O=C (urethane) intramolecular H-bond (16)? Is folding facilitated by the presence of *gem*-dimethylation (Aib derivative) (14)? (*iii*) In the absence of intramolecular H-bonding do these achiral compounds containing a —COOH group form cyclic dimers, as most of the carboxylic acids do (17, 18)? Are the urethane N—H and C=O groups involved in the intermolecular H-bonding schemes? (*iv*) Can the results of this study provide a contribution to explain the unexpected experimental observation that the Fmoc group is completely removed by hydrogenolysis giving 9-methylfluorene in quantitative yield (7*f*)?

Concerning the N-blocked derivatives of these two amino acid residues, it is pertinent to recall that the molecular and crystal structures of *t*-Boc-Aib-OH (*t*-Boc, *tert*-butyloxycarbonyl) (19, 20), *t*-Boc-D-Ala-OH·½H_2O (21), and *t*-Boc-DL-Ala-OH (21) have already been determined by X-ray diffraction.

Experimental

Materials

Fmoc-L-Ala-OH (6*b*, 6*d*, 22) was obtained from Fluka (Büchs, Switzerland).

Fmoc-Aib-OH was prepared as described by Meienhofer *et al.* (22). Mp 179–180°C (from ethyl acetate – petroleum ether). *Anal.* calcd. for $C_{19}H_{19}NO_4$ (325.3): C 70.1, H 5.9, N 4.3; found: C 69.8, H 5.9, N 4.4.

Infrared absorption

Infrared absorption spectra were recorded using a Perkin-Elmer Model 580 spectrophotometer. For the solid-state measurements the KBr disk technique was employed. For the solution measurements 0.1-mm and 1.0-mm cells with CaF_2 windows were used. Deuterochloroform (99.8% *d*) was purchased from Merck, (Darmstadt, West Germany). The band positions are accurate to ±1 cm^{-1}.

^1H Nuclear magnetic resonance

The ^1H nuclear magnetic resonance spectra were recorded using a Bruker WP200SY spectrometer. Measurements were carried out in deuteriochloroform (99.96% *d*; Merck), with tetramethylsilane as the internal standard.

X-ray diffraction

Colorless crystals of Fmoc-L-Ala-OH monohydrate were obtained from an acetone–water solution. Crystal data are:

$C_{18}H_{17}NO_4$ fw = 311.3

Orthorhombic, a = 25.054(4), b = 9.226(6), c = 7.360(6) Å, V = 1701.25 Å^3, ρ_o = 1.20(1), ρ_c = 1.21, Z = 4 (20°C; MoK_α, λ = 0.7107 Å). Space group $P2_12_12_1$.

Colorless crystals of Fmoc-Aib-OH were obtained from an acetone solution. Crystal data are:

$C_{19}H_{19}NO_4$ fw = 325.3

Orthorhombic, a = 29.785(9), b = 12.119(4), c = 9.556(4) Å, V = 3449.37 Å^3, ρ_o = 1.24(1), ρ_c = 1.25, Z = 8 (20°C; MoK_α, λ = 0.7107 Å). Space group *Pbcn*.

A total of 1401 (Fmoc-L-Ala-OH·H_2O) and 2921 (Fmoc-Aib-OH) independent reflections, respectively, were collected on a Philips PW 1100 four-circle diffractometer, using graphite monochromatized MoK_α radiation at $4° < 2\theta < 50°$ with the $\theta-2\theta$ scan mode. The structures were solved by direct methods using MULTAN (23), and refined by full-matrix least-squares with anisotropic thermal parameters for all non-hydrogen atoms. All hydrogen atoms of Fmoc-L-Ala-OH.H_2O were found on the difference Fourier map and refined. Part of the hydrogen atoms of Fmoc-Aib-OH were found on the difference Fourier map; the others were calculated, but not refined. The final R values for 1326 (Fmoc-L-Ala-OH.H_2O) and 1124 (Fmoc-Aib-OH) observed reflections with $I \geq 3.0\sigma(I)$ were 0.047 and 0.086, respectively. For Fmoc-Aib-OH the low (38.5) percentage of observed reflections might tentatively be attributed to the tiny crystals obtained and to the peculiar hypercentricity of the structure. The final atomic coordinates and thermal parameters for the two structures are presented in Tables 1 and 2, respectively. Lists of observed and calculated structure factors are available from the Depository of Unpublished Data.[3]

Results and discussion

Solution conformational analysis

In a diluted (6×10^{-4} M) $CDCl_3$ solution only two bands, at about 3510 cm^{-1} and 3440 cm^{-1}, are visible in the 3550–3300 cm^{-1} region of the ir absorption spectrum of both Fmoc-L-Ala-OH and Fmoc-Aib-OH. They are assigned to absorptions of free (solvated) carboxylic acid —OH and urethane —NH groups, respectively (21, 24, 25). At higher concentration (3×10^{-2} M), conversely, the intensity of the 3510 cm^{-1} band is markedly reduced relative to the 3440 cm^{-1} band. These is no evidence for bands below 3400 cm^{-1}, where H-bonded N—H groups are expected to absorb (21, 25, 26). For

[3]These tables may be obtained, at a nominal charge, from the Depository of Unpublished Data, CISTI, National Research Council of Canada, Ont., Canada K1A 0S2.

Can. J. Chem. Downloaded from www.nrcresearchpress.com by 210.87.254.40 on 09/06/12
For personal use only.

Can. J. Chem. Downloaded from www.nrcresearchpress.com by 210.87.254.40 on 09/06/12
For personal use only.

TABLE 1. Final atomic coordinates with estimated standard deviations for Fmoc-L-Ala-OH.H_2O

Atom	x/a	y/b	z/c	$U_{eq}\times10^4$*
O(1)	0.9051(1)	0.4215(3)	0.5006(4)	566
O(2)	0.9339(1)	0.6107(3)	0.6686(4)	571
O(3)	0.9962(1)	0.7715(3)	0.3177(4)	670
O(4)	1.0475(2)	0.8379(4)	0.5478(6)	853
N(1)	0.9892(1)	0.4954(3)	0.4739(5)	528
C(1)	0.8316(2)	0.1656(4)	0.5742(6)	490
C(2)	0.8778(2)	0.0882(5)	0.5577(7)	609
C(3)	0.8800(2)	−0.0532(5)	0.6263(7)	697
C(4)	0.8357(2)	−0.1124(5)	0.7094(7)	754
C(5)	0.7897(2)	−0.0362(5)	0.7289(7)	752
C(6)	0.7869(2)	0.1074(2)	0.6600(6)	553
C(7)	0.7440(2)	0.2117(5)	0.6591(6)	577
C(8)	0.6928(2)	0.2043(6)	0.7264(7)	738
C(9)	0.6588(2)	0.3177(8)	0.7004(8)	844
C(10)	0.6751(2)	0.4404(7)	0.6060(9)	869
C(11)	0.7265(2)	0.4494(5)	0.5389(7)	709
C(12)	0.7608(2)	0.3346(5)	0.5669(6)	561
C(13)	0.8186(2)	0.3187(4)	0.5074(6)	523
C(14)	0.8536(2)	0.4352(4)	0.5851(7)	601
C(15)	0.9422(2)	0.5188(4)	0.5559(6)	480
C(16)	1.0337(2)	0.5883(4)	0.5141(6)	516
C(17)	1.0228(2)	0.7416(4)	0.4483(6)	509
C(18)	1.0839(2)	0.5296(6)	0.4272(8)	726
OH	0.5245(2)	0.3966(4)	0.5155(6)	920

*$U_{eq} = (1/3)\Sigma_i\Sigma_j U_{ij}a_i^0a_j^0a_ia_j$.

TABLE 2. Final atomic coordinates with estimated standard deviations for Fmoc-Aib-OH

Atom	x/a	y/b	z/c	$U_{eq}\times10^4$
O(1)	0.3541(3)	0.9143(6)	0.5302(7)	540
O(2)	0.3738(3)	1.0346(6)	0.6996(7)	532
O(3)	0.4718(3)	1.0619(6)	0.6437(8)	634
O(4)	0.4644(4)	1.2421(7)	0.6712(9)	705
N(1)	0.3977(3)	1.0549(7)	0.4761(8)	400
C(1)	0.2962(4)	0.6639(9)	0.6679(11)	478
C(2)	0.2522(5)	0.6744(10)	0.7011(12)	600
C(3)	0.2334(5)	0.5963(14)	0.7913(15)	810
C(4)	0.2587(7)	0.5186(14)	0.8532(15)	930
C(5)	0.3036(6)	0.5085(12)	0.8237(15)	824
C(6)	0.3224(4)	0.5831(9)	0.7282(12)	537
C(7)	0.3679(4)	0.5886(9)	0.6734(11)	493
C(8)	0.4053(5)	0.5224(12)	0.6991(15)	722
C(9)	0.4444(6)	0.5457(15)	0.6333(18)	906
C(10)	0.4465(5)	0.6319(16)	0.5365(20)	955
C(11)	0.4094(5)	0.6973(11)	0.5092(14)	656
C(12)	0.3700(4)	0.6767(8)	0.5782(11)	423
C(13)	0.3256(4)	0.7349(9)	0.5743(11)	482
C(14)	0.3272(4)	0.8513(10)	0.6249(12)	549
C(15)	0.3572(4)	1.0025(10)	0.5779(10)	414
C(16)	0.4190(3)	1.1610(9)	0.4957(11)	385
C(17)	0.4460(5)	1.1863(13)	0.3609(12)	612
C(18)	0.3848(4)	1.2504(10)	0.5226(13)	577
C(19)	0.4537(4)	1.505(10)	0.6128(10)	441

both compounds this trend is paralleled by an analogous trend in the carbonyl stretching region (1800−1600 cm^{-1}). Upon increasing concentration, a considerable decrease in intensity of the 1755 cm^{-1} band (free C=O of the un-ionized carboxylic acid group) (21, 24−26) is seen, relative to the band near 1720 cm^{-1} (free C=O of the urethane group) (21, 25, 26). These results, taken together, indicate that the modes of self-association of the Fmoc-L-Ala-OH and Fmoc-Aib-OH molecules in $CDCl_3$ solution involve primarily the —OH and C=O groups of the carboxylic acid moiety. In addition, at high dilution the amount of the intramolecularly H-bonded C_5-form (16) (Fig. 1*A*) and oxy-C_7 form (16) (Fig. 1*B*), if any, should be extremely small.

In $CDCl_3$ (1.8×10^{-2} *M* concentration) the ^1H nmr spectrum of Fmoc-L-Ala-OH shows two peaks for the NH proton (at 5.29 ppm and 6.32 ppm, respectively) (6*c*, 27*a*). The approximate ratio is 5:1. The low-field peak tends to disappear upon heating. The effects of decreasing concentration (to 1.7×10^{-3}) and heating on the chemical shift of the high-field peak are negligible, again suggesting that the mode of self-association of Fmoc-L-Ala-OH in $CDCl_3$ solution does not involve the NH group as the H-bonding donor. According to Branik and Kessler (25, 27*b*), the two NH peaks exhibited by amino acids protected at the N^α-atom as a secondary urethane group have to be related to the *E*(*cis*) ⇌ *Z*(*trans*) conformational equilibrium about the CO—NH bond. Conversely, in the ^1H nmr spectrum of Fmoc-Aib-OH only the high-field peak (5.34 ppm) is observed. This finding is not unexpected in view of the results obtained on N^α-benzyloxycarbonyl Aib derivatives and peptides, and should be related to the enhanced bulkiness and conformational restrictions characteristic of α,α-dialkylated amino acid residues (14).

Solid-state conformational analysis

We started our conformational analysis of Fmoc-L-Ala-OH and Fmoc-Aib-OH in the solid state using ir absorption. Interestingly, the H-bonding schemes in the solid state for both compounds are more complex than those observed in $CDCl_3$ solution. For Fmoc-L-Ala-OH three bands are seen in the region corresponding to the O—H and N—H stretching vibrations (3550−3300 cm^{-1}): two weak bands at 3516 cm^{-1} (free OH) and 3419 cm^{-1} (weakly H-bonded N—H), and an intense band at 3344 cm^{-1} (N—H involved in a H-bond of moderate strength) (21, 24). In the C=O stretching region (1800−1600 cm^{-1}) three bands of comparable intensities are visible, at 1720, 1703, and 1688 cm^{-1}. They are attributed to complex contributions arising from H-bonded C=O of the carboxylic acid group, and free and H-bonded C=O of the urethane group (21, 24, 26, 28). As for Fmoc-Aib-OH, the ir absorption spectrum resembles qualitatively that of Fmoc-L-Ala-OH. Minor differences are as follows. (*i*) The band of the —OH group is absent, suggesting an H-bonded state for this proton. (*ii*) The intensity of the band associated with weakly H-bonded N—H is even furtherly reduced. (*iii*) The intense band of H-bonded N—H falls at 3303 cm^{-1}, suggesting an enhancement in the strength of the corresponding H-bond. (*iv*) The three bands in the C=O stretching region are seen at 1720, 1701, and 1692 cm^{-1}, with an enhancement in the relative intensity of the low-frequency band (H-bonded C=O of the urethane group). It is safe to conclude that the molecules of both Fmoc-protected amino acids tend to self-associate in the solid state. Most of the H-bonding donor and acceptor group seem to be involved in the aggregation process. The molecules of Fmoc-Aib-OH appear to be held together by stronger H-bonds than those of Fmoc-L-Ala-OH.

The solid-state conformational analysis of Fmoc-L-Ala-OH and Fmoc-Aib-OH was extended to X-ray diffraction. This investigation, *inter alia*, allowed us to solve the ambiguity of the assignment of the modes of self-association made on the

TABLE 3. Bond lengths (in Å)

(*A*) Fmoc-L-Ala-OH.H_2O (σ = 0.008 Å)

Bond	Length	Bond	Length	Bond	Length
C(1)—C(2)	1.365	C(2)—C(3)	1.390	C(3)—C(4)	1.378
C(4)—C(5)	1.374	C(5)—C(6)	1.427	C(6)—C(7)	1.440
C(7)—C(8)	1.388	C(8)—C(9)	1.373	C(9)—C(10)	1.376
C(10)—C(11)	1.390	C(11)—C(12)	1.378	C(7)—C(12)	1.390
C(1)—C(6)	1.392	C(1)—C(13)	1.531	C(12)—C(13)	1.512
C(13)—C(14)	1.506	O(1)—C(14)	1.447	O(1)—C(15)	1.358
O(2)—C(15)	1.211	N(1)—C(15)	1.333	N(1)—C(16)	1.436
C(16)—C(17)	1.518	C(16)—C(18)	1.497	O(3)—C(17)	1.204
O(4)—C(17)	1.305				

(*B*)Fmoc-Aib-OH (σ = 0.015 Å)

Bond	Length	Bond	Length	Bond	Length
O(1)—C(14)	1.441	O(1)—C(15)	1.320	O(2)—C(15)	1.227
O(3)—C(19)	1.237	O(4)—C(19)	1.282	N(1)—C(15)	1.340
N(1)—C(16)	1.446	C(1)—C(2)	1.353	C(1)—C(6)	1.378
C(1)—C(13)	1.519	C(2)—C(3)	1.398	C(3)—C(4)	1.344
C(4)—C(5)	1.374	C(5)—C(6)	1.402	C(6)—C(7)	1.453
C(8)—C(9)	1.347	C(7)—C(8)	1.381	C(9)—C(10)	1.396
C(10)—C(11)	1.384	C(11)—C(12)	1.369	C(12)—C(13)	1.500
C(13)—C(14)	1.492	C(16)—C(17)	1.549	C(16)—C(18)	1.509
C(16)—C(19)	1.530				

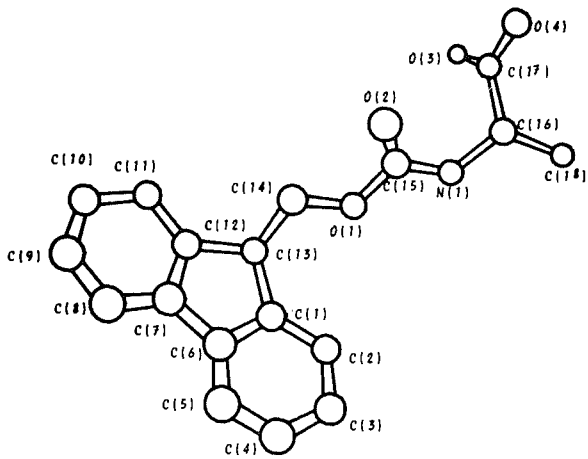

FIG. 2. Molecular structure of Fmoc-L-Ala-OH.H_2O.

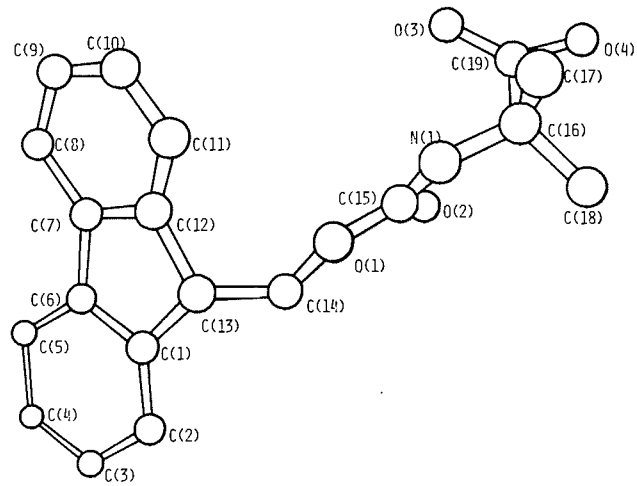

FIG. 3. Molecular structure of Fmoc-Aib-OH.

basis of the ir absorption properties. The molecular structures of Fmoc-L-Ala-Aib-OH.H_2O and Fmoc-Aib-OH are illustrated in Figs. 2 and 3, respectively. Bond lengths and bond angles of the two compounds are listed in Tables 3 and 4, respectively.

Bond lengths and bond angles of the two Fmoc-amino acids compare well with those found in other fluorene (29), urethane (2, 3), alanine (30), and Aib derivatives (19, 31). In particular, we note the following points. (*i*) The C(6)—C(7), C(12)—C(13), and C(1)—C(13) bond lengths of the fluorene system are 1.440 and 1.453 Å, 1.512 and 1.500 Å, and 1.531 and 1.519 Å for Fmoc-L-Ala-OH.H_2O and Fmoc-Aib-OH, respectively. (*ii*) The tetrahedral bond angles about the C(13) atom are considerably spread (101.9° to 113.7° and 103.1° to 114.1° for Fmoc-L-Ala-OH.H_2O and Fmoc-Aib-OH, respectively) to help to relieve the unfavorable interactions between the tricyclic moiety and the methoxycarbonylaminoacyl chain. (*iii*) The C(13)—C(14) bond lengths (1.506 Å for Fmoc-L-Ala-OH.H_2O and 1.492 Å for Fmoc-Aib-OH) are significantly shorter than that quoted as standard for a paraffinic C—C single bond, 1.541(3) Å (32); in contrast, the C(14)—O(1) bond lengths (1.447 Å for Fmoc-L-Ala-OH.H_2O and 1.441 Å for Fmoc-Aib-OH) are longer than that quoted as standard for an ether C—O single bond, 1.430(5) Å (32). The corresponding C—O bond length in N^{α}-benzyloxycarbonyl amino acid and peptide derivatives is on the average 1.454 Å (3).

The fluorene ring system, and the urethane and carboxylic acid groups are close to planarity. The dihedral angle between the average planes of the two aromatic rings of the fluorene system is 3.35° for Fmoc-L-Ala-OH.H_2O and 3.47° for Fmoc-Aib-OH. The dihedral angles between the average plane of the urethane group and the average planes of the fluorene system and the carboxylic acid group are 61.5° and 106.1°, re-

Can. J. Chem. Downloaded from www.nrcresearchpress.com by 210.87.254.40 on 09/06/12
For personal use only.

Can. J. Chem. Downloaded from www.nrcresearchpress.com by 210.87.254.40 on 09/06/12
For personal use only.

TABLE 4. Bond angles (in deg)

(*A*) Fmoc-L-Ala-OH.H_2O (σ = 0.4°)

Bonds	Angle	Bonds	Angle
C(2)—C(1)—C(6)	120.9	C(2)—C(1)—C(13)	130.2
C(6)—C(1)—C(13)	108.9	C(1)—C(2)—C(3)	119.8
C(2)—C(3)—C(4)	120.1	C(3)—C(4)—C(5)	121.5
C(4)—C(5)—C(6)	118.3	C(1)—C(6)—C(5)	119.3
C(5)—C(6)—C(7)	130.6	C(1)—C(6)—C(7)	110.1
C(6)—C(7)—C(8)	131.0	C(6)—C(7)—C(12)	108.6
C(8)—C(7)—C(12)	120.4	C(7)—C(8)—C(9)	118.4
C(8)—C(9)—C(10)	121.1	C(9)—C(10)—C(11)	121.1
C(10)—C(11)—C(12)	117.8	C(7)—C(12)—C(11)	121.1
C(11)—C(12)—C(13)	128.4	C(1)—C(13)—C(12)	101.9
C(1)—C(13)—C(14)	113.7	C(12)—C(13)—C(14)	111.9
O(1)—C(14)—C(13)	107.0	C(14)—O(1)—C(15)	115.1
O(1)—C(15)—O(2)	123.1	O(1)—C(15)—N(1)	111.2
O(2)—C(15)—N(1)	125.6	C(15)—N(1)—C(16)	119.8
N(1)—C(16)—C(18)	110.6	N(1)—C(16)—C(17)	110.7
C(17)—C(16)—C(18)	110.3	C(16)—C(17)—O(3)	124.3
C(16)—C(17)—O(4)	112.0	O(3)—C(17)—O(4)	123.7

(*B*) Fmoc-Aib-OH (σ = 1.0°)

Bonds	Angle	Bonds	Angle
C(14)—O(1)—C(15)	118.7	C(15)—N(1)—C(16)	123.1
C(2)—C(1)—C(6)	121.2	C(2)—C(1)—C(13)	129.9
C(6)—C(1)—C(13)	108.8	C(1)—C(2)—C(3)	118.0
C(2)—C(3)—C(4)	121.3	C(3)—C(4)—C(5)	121.3
C(4)—C(5)—C(6)	117.7	C(1)—C(6)—C(5)	120.3
C(1)—C(6)—C(7)	110.2	C(5)—C(6)—C(7)	129.5
C(6)—C(7)—C(8)	131.5	C(8)—C(7)—C(12)	120.5
C(6)—C(7)—C(12)	108.0	C(7)—C(8)—C(9)	120.4
C(8)—C(9)—C(10)	119.5	C(9)—C(10)—C(11)	121.1
C(10)—C(11)—C(12)	119.3	C(7)—C(12)—C(11)	119.3
C(7)—C(12)—C(13)	109.5	C(11)—C(12)—C(13)	131.2
C(1)—C(13)—C(12)	103.1	C(1)—C(13)—C(14)	111.3
C(12)—C(13)—C(14)	114.1	O(1)—C(14)—C(13)	108.5
O(1)—C(15)—O(2)	124.6	O(1)—C(15)—N(1)	111.7
O(2)—C(15)—N(1)	123.7	N(1)—C(16)—C(17)	107.2
N(1)—C(16)—C(18)	111.3	C(17)—C(16)—C(18)	110.5
N(1)—C(16)—C(19)	108.6	C(17)—C(16)—C(19)	105.9
C(18)—C(16)—C(19)	113.0	O(3)—C(19)—O(4)	122.7
O(3)—C(19)—C(16)	122.7	O(4)—C(19)—C(16)	114.5

spectively, for Fmoc-L-Ala-OH.H_2O, while 89.2° and 73.1°, respectively, for Fmoc-Aib-OH. The secondary urethane linkage in both compounds adopt one of its most common conformations (*trans*, *trans*, or *b* (2, 3)), the corresponding torsional angles being 178.1° and 179.1° for Fmoc-L-Ala-OH.H_2O, and ±168.2° and ∓173.6° for Fmoc-Aib-OH (33). The L-Ala and Aib moieties are partially folded, the sets of ϕ, ψ_T torsional angles (−65.5° and 150.2°, respectively, for Fmoc-L-Ala-OH.H_2O and ±78.6° and ∓158.6°, respectively, for Fmoc-Aib-OH) falling in the *F* region (or in the enantiomeric *F** region for Fmoc-Aib-OH) (34) of the conformational energy map. The carboxylic acid group in both compounds adopts a conformation with respect to the C(16)—N(1) bond intermediate between the *synplanar* and *synclinal* conformations (35), the N(1)—C(16)—C(17)—O(3) torsional angle being −32.2° for Fmoc-L-Ala-OH.H_2O and the corresponding N(1)—C(16)—C(19)—O(3) torsional angle being ±25.2° for Fmoc-Aib-OH.

There are no *intramolecular* H-bonds in either Fmoc-L-Ala-OH.H_2O or Fmoc-Aib-OH. Rather, all potential donors and acceptors of Fmoc-L-Ala-OH.H_2O are involved in a complex scheme of *intermolecular* hydrogen bonds, most of them involving the water molecule: (*i*) O(2)...H_1—O(W) (x, y, $1 + z$), O...O distance 2.754 Å; (*ii*) O(3)...H_2—O (W) (x, y, z), O...O distance 2.773 Å; (*iii*) O(W)...H—O(4) ($2 - x$, $y - 1/2$, $1/2 - z$), O...O distance 2.554 Å; and (*iv*) O(3)...H—N(1) ($2 - x$, $1/2 + y$, $1/2 - z$), O...N distance 3.000 Å. These results are in line with the observation that, in molecules containing the —CONH— moiety, hydration of the C=O group occurs more frequently than hydration of the N—H group (21). Conversely, in the Fmoc-Aib-OH molecules an intermolecular H-bond is seen between the urethane N—H and C=O groups, the O(2)...N(1) (x, $2 - y$, $z - 1/2$) distance being 2.942 Å. Two additional intermolecular distances shorter than 3.0 Å involve the un-ionized carboxylic acid group: (*i*) O(3)...O(3) ($1 - x$, y, $3/2 - z$) = 2.636 Å, and O(4)...O(4) ($1 - x$, y, $3/2 - z$) 2.599 Å.

Conclusion

In this work we have shown that in a solvent of low polarity (deuteriochloroform) non-associated and self-associated species simultaneously occur for both Fmoc-L-Ala-OH and Fmoc-Aib-OH. Self-association involves primarily the hydroxyl and carbonyl groups of the carboxylic acid moiety. The extent of self-association decreases with dilution. At high dilution, where self-association is absent, the amount of intramolecularly H-bonded C_5-form and oxy-C_7 form, if any, should be extremely small. *Z(trans)* ⇌ *E(cis)* isomerism about the amide bond of the secondary urethane moiety was observed only for the less bulky L-Ala derivative.

In the solid state all H-bonding donors and acceptors of the L-Ala and Aib derivatives take part to complex schemes of intermolecular H-bonds. In the L-Ala derivative, crystallized as monohydrate, most of the intermolecular H-bonds involve the water molecule. Intramolecular H-bonds are not observed in either compound, thereby excluding the formation of the C_5-and oxy-C_7 forms. The conformation of the secondary urethane —CONH— group is *Z(trans)* in both compounds. Both L-Ala and Aib residues are partially folded. The observation of the long C(14)—O(1) bond might contribute to explain the unexpected experimental result that the Fmoc group can be removed by catalytic hydrogenation.

1. A. F. SPATOLA, T. J. OWEN, G. ZANOTTI, and C. TONIOLO. Biopolymers. To be published.
2. E. BENEDETTI, C. PEDONE, C. TONIOLO, G. NÉMETHY, M. S. POTTLE, and H. A. SCHERAGA. Int. J. Peptide Protein Res. **16**, 156 (1980).
3. E. BENEDETTI, C. PEDONE, C. TONIOLO, M. DUDEK, G. NÉMETHY, and H. A. SCHERAGA. Int. J. Peptide Protein Res. **21**, 163 (1983).
4. (*a*) E. ATHERTON, H. FOX, D. HARKISS, C. J. LOGAN, R. C. SHEPPARD, and B. J. WILLIAMS. J. Chem. Soc. Chem. Commun. 537 (1978); (*b*) E. ATHERTON, M. CAVIEZEL, H. FOX, D. HARKISS, H. OVER, and R. C. SHEPPARD. J. Chem. Soc. Perkin Trans. 1, 65 (1983).
5. (*a*) C. CHANG and J. MEIENHOFER. Int. J. Peptide Protein Res. **11**, 246 (1978); (*b*) E. P. HEIMER, C. CHANG, T. LAMBROS, and J. MEIENHOFER. Int. J. Peptide Protein Res. **18**, 237 (1981).
6. (*a*) L. A. CARPINO and G. Y. HAN. J. Am. Chem. Soc. **92**, 5748 (1970); (*b*) L. A. CARPINO and G. Y. HAN. J. Org. Chem. **37**, 3404 (1972); (*c*) G. F. SIGLER, W. D. FULLER, N. C. CHATURVEDI, M. GOODMAN, and M. VERLANDER. Biopolymers, **22**, 2157 (1983); (*d*) M. TESSIER, F. ALBERICIO, E. PEDROSO,

A. GRANDAS, R. ERITJA, E. GIRALT, C. GRANIER, and J. VAN RIETSCHOTEN. Int. J. Peptide Protein Res. **22**, 125 (1983).
7. (*a*) A. BODANSZKY, M. BODANSZKY, N. N. CHANDRAMOULI, J. Z. KWEI, J. MARTINEZ, and J. C. TOLLE. J. Org. Chem. **45**, 72 (1980); (*b*) M. BODANSZKY, J. C. TOLLE, M. A. BEDNAREK, and P. W. SCHILLER. Int. J. Peptide Protein Res. **17**, 444 (1981); (*c*) M. A. BEDNAREK and M. BODANSZKY. Int. J. Peptide Protein Res. **21**, 196 (1983); (*d*) H. KESSLER and R. SIEGMEIER. Tetrahedron Letters. 281 (1983); (*e*) M. A. BODANSZKY and M. BEDNAREK. Int. J. Peptide Protein Res. **20**, 434 (1982); (*f*) M. BODANSZKY and J. MARTINEZ. *In* The peptides: analysis, synthesis, biology. Vol. 5. *Edited by* E. Gross and J. Meienhofer. Academic Press, New York. N.Y. 1983. pp. 111–216.
8. L. KISFALUDY and I. SCHÖN. Synthesis, 325 (1983).
9. N. L. BENOITON. *In* The peptides: analysis, synthesis, biology. Vol. 5. *Edited by* E. Gross and J. Meienhofer. Academic Press, New York, N.Y. 1983. pp. 217–284.
10. R. M. FREIDINGER, J. S. HINKLE, D. S. PERLOW, and B. H. ARISON. J. Org. Chem. **48**, 77 (1983).
11. J. SAGIV, A. YOGEV, and Y. MAZUR. J. Am. Chem. Soc. **99**, 6861 (1977).
12. J. S. DAVIES, A. K. MOHAMMED, and E. HAKEEM. *In* Peptides 1982. *Edited by* K. Blaha and P. Malon. de Gruyter, Berlin. 1983. pp. 431–435.
13. R. B. MERRIFIELD and A. E. BACH. J. Org. Chem. **43**, 4808 (1978).
14. C. TONIOLO, G. M. BONORA, A. BAVOSO, E. BENDETTI, B. DI BLASIO, V. PAVONE, and C. PEDONE. Biopolymers, **22**, 205 (1983).
15. M. VASQUEZ, G. NÉMETHY, and H. A. SCHERAGA. Macromolecules, **16**, 1043 (1983).
16. C. TONIOLO. C.R.C. Crit. Rev. Biochem. **9**, 1 (1980).
17. L. LEISEROWITZ. Acta Crystallogr. Sect. B, **32**, 775 (1976).
18. A. T. HAGLER, P. DAUBER, and S. LIFSON. J. Am. Chem. Soc. **101**, 5131 (1979).
19. E. BENEDETTI, C. TONIOLO, and G. M. BONORA. *In* Peptides 1980. *Edited by* K. Brunfeldt. Scriptor, Copenhagen. 1981. pp. 619–624.
20. W. MAYR, G. JUNG, and J. STRÄHLE. Liebigs Ann. Chem. 715 (1980).
21. E. BENEDETTI, B. DI BLASIO, V. PAVONE, C. PEDONE, C. TONIOLO, and G. M. BONORA. Biopolymers. **20**, 1635 (1981).
22. J. MEIENHOFER, M. WAKI, E. P. HEIMER, T. J. LAMBROS, R. C. MAKOFSKE, and C. CHANG. Int. J. Peptide Protein Res. **13**, 35 (1979).
23. G. GERMAIN, P. MAIN, and M. M. WOOLFSON. Acta Crystallogr. Sect. A, **27**, 368 (1971).
24. A. BAVOSO, E. BENEDETTI, B. DI BLASIO, V. PAVONE, C. PEDONE, C. TONIOLO, and G. M. BONORA. Macromolecules, **15**, 54 (1982).
25. M. BRANIK and H. KESSLER. Chem. Ber. **108**, 2176 (1975).
26. C. M. DEBER. Macromolecules, **7**, 47 (1974).
27. (*a*) A. MARSTON and E. HECKER. Zeit. Naturforsch. **38**b, 1015 (1983). (*b*) M. BRANIK and H. KESSLER. Tetrahedron, **30**, 781 (1974).
28. C. TONIOLO, M. PALUMBO, and E. BENEDETTI. Macromolecules, **9**, 420 (1976).
29. (*a*) D. M. BURNS and J. IBALL. Proc. R. Soc. London Ser. A. **227**, 200 (1955); (*b*) X. SOLANS, C. MIRAVITTLES, J. P. DECLERCQ, and G. GERMAIN. Acta Crystallogr. Sect. B, **36**, 2677 (1980); (*c*) R. DESTRO, T. PILATI, and M. SIMONETTA. Acta Crystallogr. Sect. B. **36**, 2500 (1980); (*d*) M. VAN MEERSSCHE, G. GERMAIN, J. P. DECLERCQ, and R. TOUILLAUX. Cryst. Struct. Commun. **8**, 119 (1979); (*e*) M. VAN MEERSSCHE, G. GERMAIN, J. P. DECLERCQ, R. TOUILLAUX, M. ROBERFROID, and C. RAZZOUK. Cryst. Struct. Commun. **9**, 515 (1980); (*f*) M. HAISA, S. KASHINO, T. UENO, N. SHINOZAKI, and Y. MATSUZAKI. Acta Crystallogr. Sect. B, **36**, 2306 (1980).
30. G. VALLE, G. M. BONORA, and C. TONIOLO. Gazz. Chim. Ital. In press.
31. Y. PATERSON, S. M. RUMSEY, E. BENEDETTI, G. NÉMETHY, and H. A. SCHERAGA. J. Am. Chem. Soc. **103**, 2947 (1981).
32. L. E. SUTTON (*Editor*). *In* Tables of interatomic distances and configuration in molecules and ions, Supplement. The Chemical Society, London. U.K. 1965.
33. IUPAC-IUB Commission on Biochemical Nomenclature. Biochemistry, **9**, 3471 (1970).
34. S. S. ZIMMERMAN, M. S. POTTLE, G. NÉMETHY, and H. A. SCHERAGA. Macromolecules, **10**, 1 (1977).
35. J. D. DUNITZ and P. STRICKLER. *In* Structural chemistry and molecular biology. *Edited by* A. Rich and N. Davidson. Freeman, San Francisco, CA. 1968. pp. 595–602.

Can. J. Chem. Downloaded from www.nrcresearchpress.com by 210.87.254.40 on 09/06/12
For personal use only.

The chloroindolenine – imino ether – oxindole sequence. A reexamination[1]

DENNIS V. C. AWANG,[2] ANDRÉ VINCENT, AND DARYL KINDACK
Bureau of Drug Research, Health and Welfare Canada, Sir Frederick G. Banting Research Centre, Ottawa, Ont., Canada K1A 0L2

Received July 15, 1983[3]

DENNIS V. C. AWANG, ANDRÉ VINCENT, and DARYL KINDACK. Can. J. Chem. **62**, 2667 (1984).

The chloroindolenines of deserpidine and reserpine, and the isomeric chloroindolenines derived from yohimbine – characterized for the first time – have been treated with methanol and methoxide ion under a variety of conditions. In the traditional medium of methanolic hydroxide, chlorodeserpidine partially undergoes rearrangement to imino ether, whereas chlororeserpine suffers only substitution of chloride by methoxide; only the α-isomer of the two yohimbine chlorides undergoes rearrangement to a methyl imino ether, the β-isomer being degraded to an intractable mixture. In refluxing neat methanol, the α-chloride of yohimbine rearranges readily and cleanly to imino ether at a rate comparable to that of chlorodeserpidine rearrangement, but vastly greater than that of the β-chloride. However, under silver oxide catalysis all the chloroindolenines rearrange at closely similar rates. The rearrangement of chloroindolenine to methyl imino ether is stereospecific, α-chloride leading to α-spiro imino ether and β-chloride to β-spiro imino ether. The results are rationalized on the basis of stereoelectronic considerations applied to a process of addition of methanol to the imine bond, followed by elimination of hydrogen chloride from the methanol adduct.

DENNIS V. C. AWANG, ANDRÉ VINCENT et DARYL KINDACK. Can. J. Chem. **62**, 2667 (1984).

Opérant sous diverses conditions, on a traité les chloroindolénines de la déserpidine et de la réserpine ainsi que les chloroindolénines isomères dérivées de la yohimbine – que l'on a caratérisées pour la première fois – avec du méthanol et avec l'ion méthanolate. Traitée dans des conditions traditionnelles par l'ion hydroxyde dans le méthanol, la chlorodéserpidine subit une transposition partielle en iminoéther tandis que la chlororéserpine subit uniquement une substitution du chlore par le méthanolate; seul l'isomère α des deux chlorures de yohimbine se transpose en iminoéther méthylique alors que l'isomère β est décomposé en un mélange que l'on ne peut séparer. Par reflux dans du méthanol pur, le chlorure α de la yohimbine se transpose facilement et proprement en un iminoéther; la vitesse de cette réaction est comparable à celle de la transposition de la chlorodéserpidine, mais cette vitesse est de beaucoup supérieure à celle de la transposition du chlorure β. Cependant, lors de la réaction catalysée par l'oxyde d'argent, toutes les chloroindolénines se transposent avec des vitesses très voisines. La transposition de la chloroindolénine en iminoéther méthylique est stéréospécifique, le chlorure α conduit à un spiroiminoéther α alors que le chlorure β conduit à un spiroiminoéther β. On rationalise les résultats en faisant appel à des considérations stéréoélectroniques intervenant dans la réaction d'addition du méthanol sur la liaison de l'imine qui est suivie par une élimination de chlorure d'hydrogène à partir de l'adduit.

[Traduit par le journal]

The most common route to oxindoles from indole alkaloids of the tetrahydro-β-carboline variety involves an initial reaction with *tert*-butyl hypochlorite which produces highly reactive chloroindolenines (1).

Finch and Taylor (2) developed a two-step procedure whereby the crude product of indole chlorination is treated first with aqueous methanolic hydroxide and then hydrolyzed under acidic conditions.[4] The initial phase of this procedure was viewed as producing a unique imino ether (**10**) from *one* of the two epimeric chloroindolenines (see Scheme 1); acid hydrolysis of the rearranged ether yielded the corresponding oxindole which then underwent isomerization to the observed mixture of oxindoles **A** and **B**. Finch and Taylor depicted the isomeric chloroindolenines as having chlorine in axial and equatorial dispositions, and further suggested that it is only in the product of a postulated methanol addition[5] to the *equatorially chlorinated* β-*isomer* that the stereochemistry is appropriate for their suggested four-centred rearrangement to imino ether. It was also claimed that chlorodeserpidine was resistant to methanolysis (except for loss of the trimethoxybenzoyl group), and that therefore this unique product of deserpidine chlorination bore axially oriented chlorine.

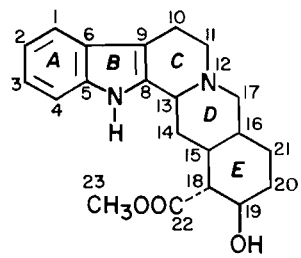

1

In the study here reported, the epimeric chloroindolenines derived from yohimbine (**1**) have been separated and characterized, then treated with aqueous methanolic hydroxide, as have the unique chlorides obtained from reserpine and deserpidine.

Under such conditions, 9-chloro-9*H*-reserpine[6] (**4***a*) is efficiently converted into 9-methoxy-9*H*-reserpine, identical with the product of reaction of reserpine with iodosobenzene diacetate (IBD) in methanol (6). These reserpine derivatives are

[1] Presented in part at the 62nd Annual Conference of the Chemical Institute of Canada. Vancouver, B.C., June 3–6, 1979.

[2] Author to whom all correspondence should be addressed.

[3] Revision received May 23, 1984.

[4] Zinnes and Shavel (3) effected the conversion of chloroindolenines into oxindoles by refluxing in aqueous methanol which had been adjusted to pH 6 by addition of acetic acid, a process which clearly obviates imino ether formation.

[5] Kuehne and Hafter (4) also favour methanol addition to the imine function as a prerequisite to rearrangement.

[6] The numbering system is that used by Wehrli (5), which seems more suitable to general application than the older systems which would designate such compounds as 7-substituted indolenines.

Can. J. Chem. Downloaded from www.nrcresearchpress.com by 210.87.254.40 on 09/06/12
For personal use only.

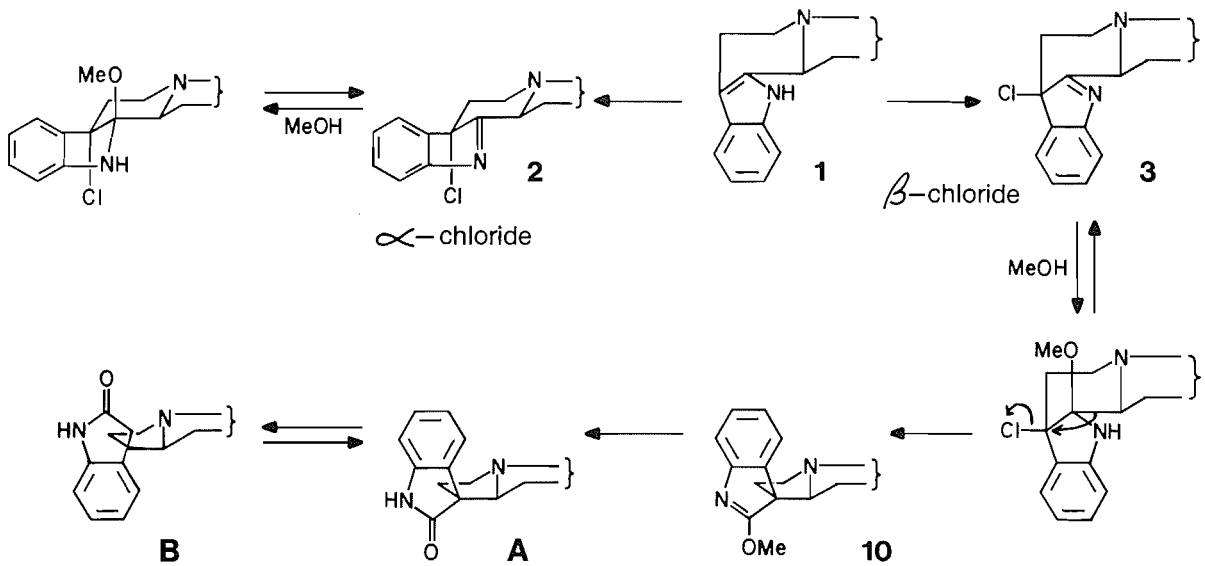

SCHEME 1. Formation of oxindoles from indoles via chloroindolenines (ref. 2).

unquestionably of β configuration,[7] and this methanolysis almost certainly proceeds by way of a benzylic carbonium ion, and not by an S_N2 mechanism as suggested by Owellen (7) for the analogous reaction of the chloroindolenine of tetrahydrocarbazole. The chlororeserpine reaction produced no spiro imino ether, the expected product of rearrangement for which Owellen indicated a carbonium ion intermediate. 9-Chloro-9*H*-deserpidine (**4***b*), under the same conditions, was readily converted to a mixture of methyl 9-methoxy-9*H*-deserpidate and the pair of methyl imino ethers of methyl 13-isodeserpidate, isomeric at C-9.[8]

Treatment of yohimbine (**1**) with *tert*-butyl hypochlorite in the presence of triethylamine (1) produced a mixture of the epimeric 9-chloro-9*H*-yohimbines, the α isomer (**2**) predominating. These chlorides, illustrated as three-dimensional line diagrams in Scheme 2, were separated by column chromatography in roughly a 4:1 ratio of α/β isomers, and subjected to detailed spectroscopic analysis, which is offered later in the text.

The corresponding 9-methoxy derivatives of yohimbine were synthesized, for comparison, by the IBD–methanol reaction (6) and separated by preparative tlc on silica gel in the ratio

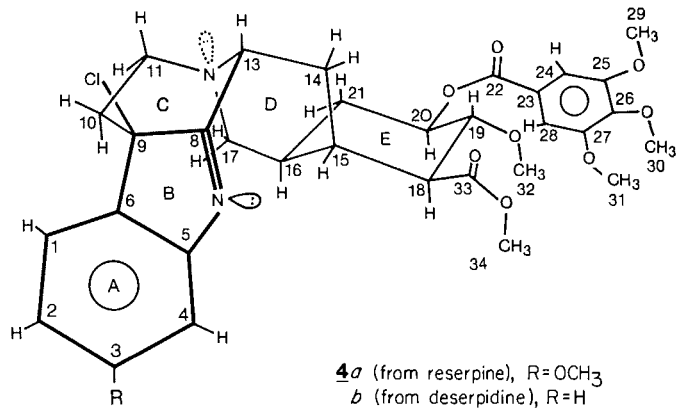

35α:65β.[9] The isomeric chlorides and methyl ethers showed closely corresponding R_f's in the tlc system used, the α-chloro and α-methoxy derivatives having values of 0.27 and 0.30 and the β-isomers, 0.16 and 0.17, respectively. It is interesting to note that lower R_f in silica gel chromatography of epimeric chlorindolenines has been associated with greater basicity, and led Dolby and Gribble (9) to an assignment of epimer configuration contrary to ours. These authors isolated "about equal amounts" of epimeric chlorides from the tetracyclic base, 1,2,3,4,6,7,12,12b-octahydroindolo[2,3-*a*]quinolizine (**5**) and assigned the β configuration (see **3**) to the faster-moving *trans*-chloroindolenine,[10] on the basis that the isomer bearing chlorine *trans* to the N-5 nitrogen would have a less-hindered N-5

[7] The absolute configuration of 9α-acetoxy-9*H*-yohimbine has been established by X-ray crystallographic analysis of its methiodide salt (10). Comparison of the C^{13} nmr spectrum of this acetoxy yohimbine with those of the two epimeric methoxy derivatives leaves no doubt as to their relative configurations. The choice between chlorides seems easy when one makes a similar comparison between methoxy and chloro derivatives, supported by close correspondence of R_f values upon thin-layer chromatography of the chloro and methoxy pairs.

[8] The protons of the methoxyl group attached to the saturated C-9 carbon of 9-methoxyindolenines are easily distinguishable in the ^1H nmr spectrum, giving rise to a methyl spike in the vicinity of δ_{TMS} ($CDCl_3$) 3 ppm (reserpine, 2.78; deserpidine 2.96). The protons of the methoxyl group attached to the C=N carbon resonate much farther downfield, at δ 4.07 and 4.14 ppm, in the imino ethers of methyl 13-isodeserpidate. In the case of 9-chloro-9*H*-reserpine, attack by methanol at C-9 is so rapid that 9-methoxy-9*H*-reserpine precipitates out of solution, thus preventing the hydrolysis of the benzoate group which occurs in the deserpidine case.

[9] Contrary to the claim of Finch and Taylor (2) no quantitation of the isomeric ratio has hitherto been published for the products of chlorination of either yohimbine or yohimbane; these authors reported a "50:50 mixture" for the former and made an unsubstantiated claim that "equal amounts" (of epimers) have been "proved conclusively" in the case of the chloroyohimbanes by Shavel and Zinnes (8). In this study, the ratios of epimers in the crude reaction products from yohimbine were estimated from peak areas of chromatograms following hplc analysis; the ratios of α/β were observed to be 3:1 for the chlorides and 1:3 for the methyl ethers.

[10] *Cis* and *trans* refer to the spatial arrangement of the chlorine atom and the C-12b methine hydrogen.

Can. J. Chem. Downloaded from www.nrcresearchpress.com by 210.87.254.40 on 09/06/12
For personal use only.

Can. J. Chem. Downloaded from www.nrcresearchpress.com by 210.87.254.40 on 09/06/12
For personal use only.

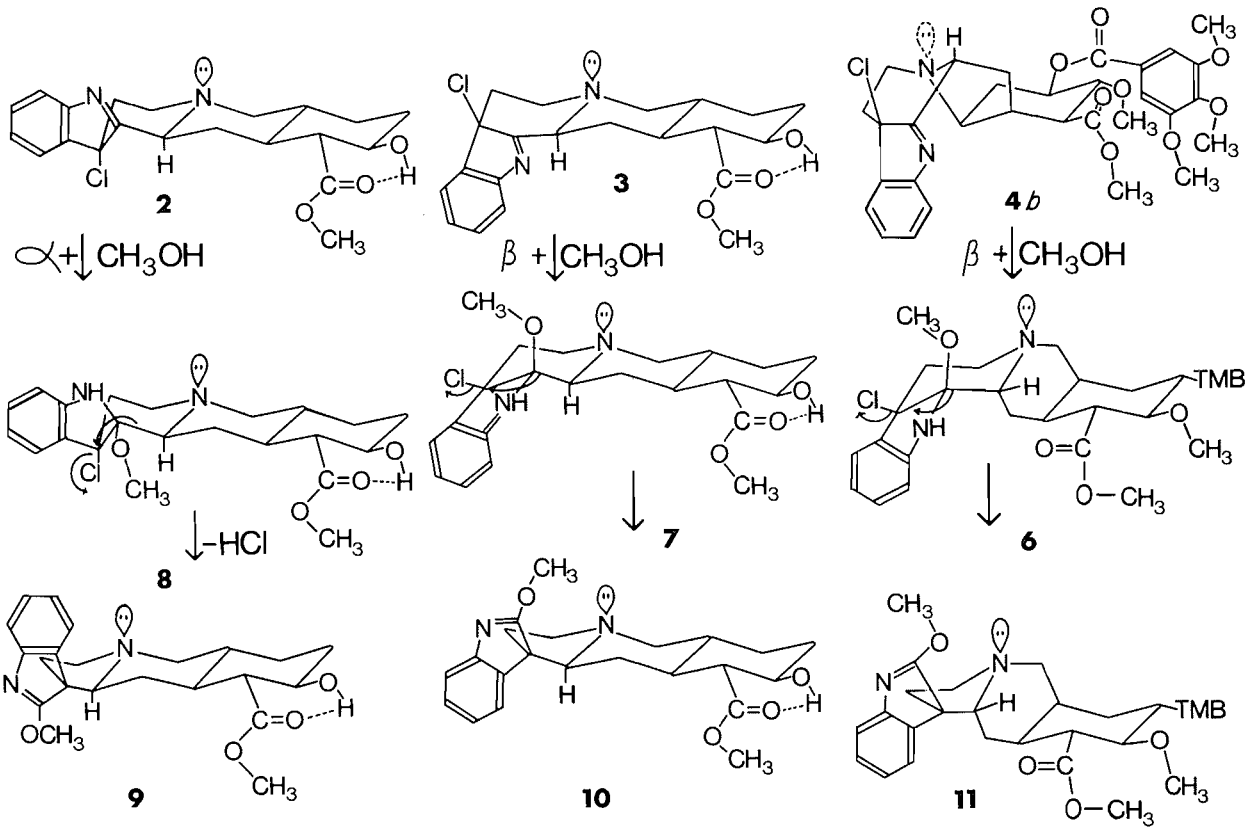

SCHEME 2. Mechanism of formation of imino ethers from chloroindolenines.

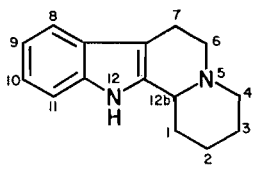

5

lone pair, resulting in stronger adherence to silica gel and enhanced reactivity towards methyl iodide;[11] these authors also cite ^{1}H nmr evidence to support their stereochemical assignments. On the other hand, Finch *et al.* (10) conclude that the epimer of chloroyohimbane that moves faster on silica gel tlc plates – and is positively rotating of polarized light – has the α configuration, parallel to positively rotating 9-acetoxyyohimbine, whose structure and stereochemistry have been established by X-ray crystallography.[12]

The ^{13}C nmr spectra of 9-acetoxyyohimbine, and the epimeric chloro- and methoxyyohimbines, illustrated as bar graphs in Figure 1,[13] confirm the α configuration for the epimers of greater R_f on silica gel and provide a ready means of differentiating indolenine epimers. Comparison of the generally closely similar spectral patterns for the indolenines with that of yohimbine reveals the marked changes that take place in the resonances of ring A and B carbon atoms upon alteration of the indole ring B. The most pronounced effect (of the order of 50 ppm) is observed in the chemical shift of C-8, the imine carbon, undoubtedly due to the highly polar character of the C=N bond; the appreciably reduced chemical shift (by about 10 ppm) of the acetoxyyohimbine C-8 resonance is attributed to shielding by the acetoxy carbonyl group.

It appears clear from models of the indolenine epimers that the C-9 substituents of the β-isomers would have the greater effect, interspatially, on the tertiary nitrogen lone pair and on the carbon electrons of ring D. Compared with the α-isomers, it is observed that C-16 and C-17 of the β-isomers are significantly shielded, whereas the β-carbons-13 are comparably deshielded; as well, β-carbons-10 and especially carbons-11 in ring C are notably shielded, probably a result of transannular influence of the imine double bond.

The mechanism of rearrangement of chloroindolenines to spiro imino ethers

All published accounts (2, 3, 14) of rearrangement of chloroyohimbine to yohimbine oxindoles in basic medium, so far discovered, indicate that the unresolved amorphous *mixture* of epimeric chlorides, the product of yohimbine – *tert*-butyl hypochlorite reaction, was not purified before treatment with methanolic hydroxide. In this study, the pure crystalline epimeric chlorides were separately refluxed in the basic medium and the products of reaction analyzed. It was observed that *only the α-chloro isomer underwent rearrangement to the imino ether*

[11] The anchimeric participation of chlorine in nitrogen lone-pair binding to acidic sites appears not to have been considered.

[12] This stereochemistry could now have been more readily deduced by measuring the nuclear Overhauser effect (nOe) between acetoxy methyl protons and the C-13 methine proton. Our experiments indicate an increase of more than 20% in the integrated intensity of the signal due to H-13 (4.19 ppm) upon irradiation of the acetoxy methyl protons. Also, selective on-resonance decoupling dictates a reversal of the published (11) assignments of ^{13}C resonances for C-13 and C-19 in yohimbine: irradiating the cleanly separated H-13 methine proton at 4.22 ppm resulted in collapse of the *downfield* doublet.

[13] Chemical shifts are listed in Table 1.

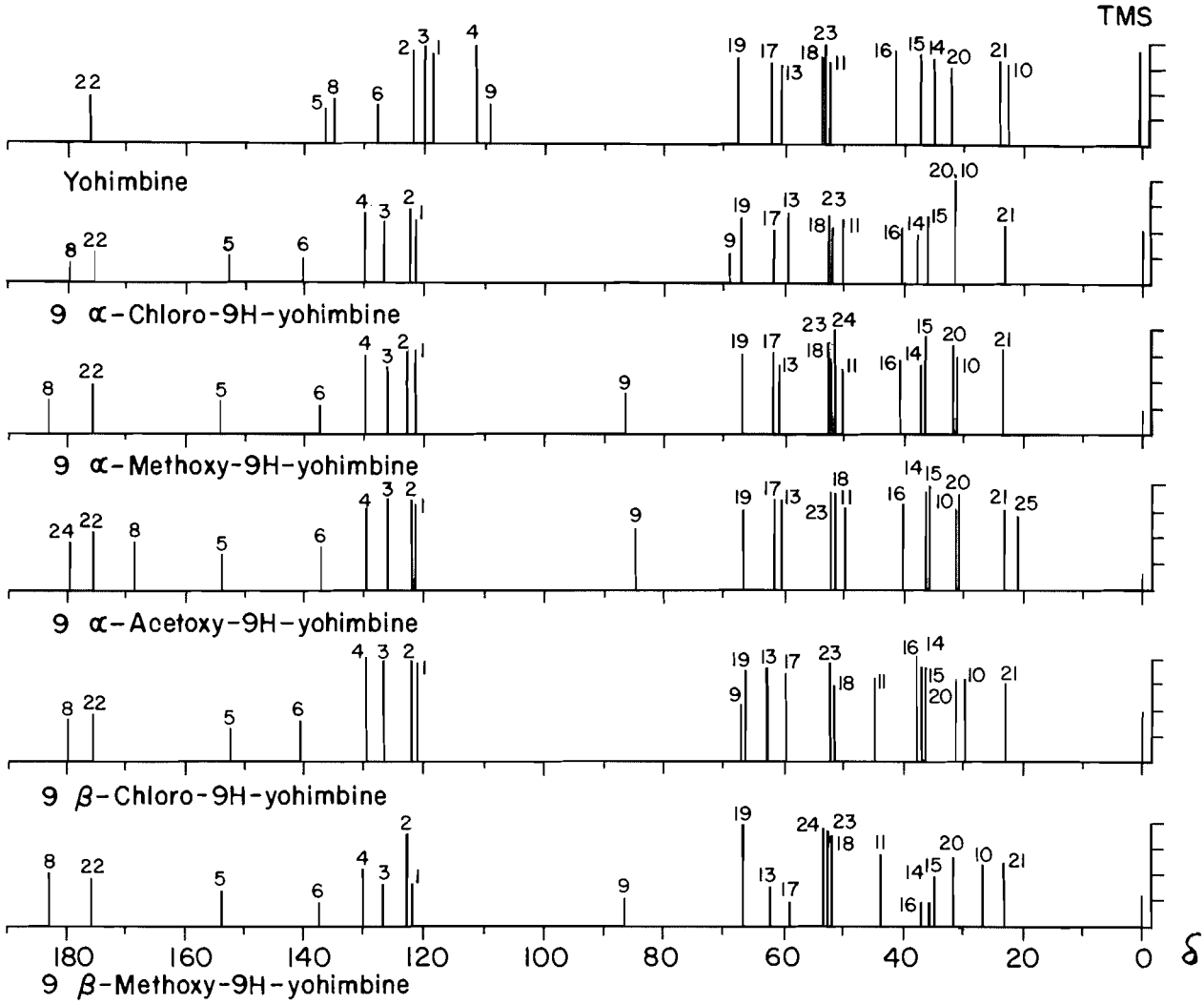

FIG. 1. Bar graphs of ^{13}C spectra of yohimbine and derivatives.

precursor of yohimbine oxindoles. The β-chloride yielded neither imino ether nor the epimeric methoxy yohimbine substitution products formed by IBD reaction in methanol; tlc of the intractable reaction product indicated a predominance of polar (probably polymeric) material close to the origin, accompanied by traces of at least three other compounds.

The fact that under these conditions *only* the α-chloro isomer from yohimbine (**2**) undergoes rearrangement to imino ether further discredits the proposal by Owellen (7) of a carbonium ion mechanism for the rearrangement: one would expect that *both* isomers of 9-chloro-9*H*-yohimbine would yield the same carbonium ion at C-9 even if at different rates, and lead to the same product.

The presence of hydroxide in the traditional reaction medium suggested the possibility of an intermediate cyclopropimine bridging C-9 and C-13, produced by elimination of hydrogen chloride (Fig. 2); such an intermediate would be analogous to the cyclopropanone intermediate widely supported for the Favorskii rearrangement of α-chloroketones under basic influence. Owellen and Hartke (12) discounted such a mechanism for analogous rearrangements of tetrahydrocarbazole derivatives on the plausible grounds that such structures would demand too much distortion – and attendant strain – in the five-membered indole B ring. *No other authors have considered any*

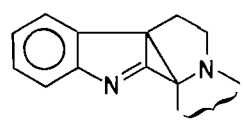

FIG. 2

mechanistic role for hydroxide ion. In view of this apparent oddity, the popularity of the methanol-addition mechanism, and the relatively recent support of Dmitrienko *et al.* (13) for methanol addition to imine being an *acid-catalysed* process, the reaction of neat methanol with the chloroindolenines of yohimbine, deserpidine, and reserpine was examined.

In neat refluxing methanol, α-chloroyohimbine underwent ready rearrangement to methyl imino ether; hplc analysis of the reaction mixture indicated that all substrate disappeared within 90 min. By comparison, after the same period of refluxing, 89% of β-chloroyohimbine was left unreacted; overnight refluxing was needed to complete the rearrangement. Chlorodeserpidine (**4***b*) rearranged to methyl imino ether (without loss of benzoate) almost as readily as α-chloroyohimbine, taking just over 2 h reflux for completion of reaction; at the 1-h mark there were, respectively, 25% and 11% of unreacted chloride. However, as was the case in methanolic hydroxide medium, chlororeserpine underwent quantitative conversion to methoxy-

Can. J. Chem. Downloaded from www.nrcresearchpress.com by 210.87.254.40 on 09/06/12
For personal use only.

TABLE 1. ^{13}C chemical shifts of yohimbine and its 9-indolenine derivatives*

C	Yohimbine	α-Chloro	β-Chloro	α-Methoxy	β-Methoxy	α-Acetoxy
1	118.5	121.77	121.46	121.71	121.52	121.77
2	121.7	122.80	122.56	123.04	122.92	122.43
3	119.8	126.99	127.05	126.44	126.56	126.50
4	111.0	130.27	130.09	130.03	130.03	130.15
5	136.5	153.04	152.83	155.44	154.08	154.38
6	127.8	140.59	141.02	137.68	137.50	137.62
7	—	—	—	—	—	—
8	134.9	179.83	180.19	183.35	182.92	169.02
9	108.7	68.93	67.29	86.54	86.48	85.02
10	21.9	31.40	29.88	31.28	26.90	31.34
11	53.1	50.16	44.76	50.16	43.67	49.98
12	—	—	—	—	—	—
13	67.2	59.40	63.04	60.79	62.74	60.67
14	31.6	37.65	36.38	36.80	36.14	36.32
15	36.9	36.14	36.92	36.32	35.35	36.14
16	41.0	40.39	37.96	40.57	37.77	40.39
17	61.6	61.58	59.94	61.76	59.64	61.58
18	52.7	52.35	51.93	52.47?	51.80	52.05
19	60.1	67.05	66.68	67.17	66.80	66.93
20	31.6	31.40	31.28	31.52	31.46	31.03
21	23.4	23.14	23.08	23.26	23.14	23.20
22	176.0	175.76	176.06	176.00	175.94	176.12
23	52.1	51.99	52.35	52.23?	52.53	52.29
24†				51.99?	52.96	179.89
25†						21.01

*$CDCl_3$ solution, internal TMS.

†C-24 refers to C-9 methoxy and imino ether methyl carbons and, in the case of acetoxyyohimbine, C-24 and C-25 correspond to the acetoxy carbonyl and acetoxy methyl carbons, respectively.

reserpine. The failure of chlororeserpine to yield a rearranged product is attributed to activation of S_N1 substitution at the C-9 position by the C-3 methoxyl group.

The above results are consistent with addition of methanol to the imine bond of the chloroindolenines. Hydroxide ions are clearly unnecessary to the rearrangement, as are protons (since the rearrangement also proceeds under strongly basic conditions), although in the case of neat methanol its addition may be catalysed by hydrogen chloride produced in the course of the reaction. Addition of methanol to the imine bond of 9α- and 9β-chloro-9*H*-yohimbine may occur from α and β faces of the plane of the ring network, with strikingly different results. In the case of each of the three substrates which undergo rearrangement, only one of the two possible addition products (as illustrated in Scheme 2) provides the appropriate *anti* alignment of the C8—C13 and C—Cl bonds,[14] namely the products of β addition of methanol to 9β-chloro-9*H*-deserpidine and 9β-chloro-9*H*-yohimbine (**6** and **7**, respectively) in which the alignment is almost ideal for a planar four-centred transition state, and the product of α addition of methanol to 9α-chloro-9*H*-yohimbine (**8**) in which only relatively unencumbered rotation about the C8—C9 bond is needed to optimize alignment of the skewed C—Cl bond. However, in the first two cases, the benzene ring attached to C9 must adopt an *axial* configuration, a factor which would be expected to disfavour their rearrangement relative to the third substrate (**2**) for which the benzene ring in the addition compound (**8**) is *equatorially* oriented. The dramatic difference in the rates of rearrangement of **4***b* and **3** is likely due to the additional steric hindrance to approach of methanol presented by the C14 methylene group in **3**: the C—Cl and C13—C14 bonds almost coplanarly flank the route to the imine nitrogen orbital; this judgement implies that both methanol addition and bond migration contribute to the rate-determining process.

While the mechanism of Dmitrienko *et al.* (13) involving acid-catalysed addition of methanol to the imine bond of chloroindolenines followed by S_N1 ionization of chloride to form a benzylic carbonium ion seems plausible under those conditions, S_N2 displacement of chloride would appear more likely in strongly basic medium such as employed by Owellen (7). The fact that under Owellen's optimum "substitution" conditions (sodium methoxide in methanol at −10°C)[15] the chloroindolenines of yohimbine undergo rearrangement, exclusively, suggests that their rigid fused ring system militates against the S_N2 mechanism that is dominant in the simpler 2,3-dimethylindole and tetrahydrocarbazole derivatives.

The fact that, in our experiments, no products derived from substitution of chloride by methoxide were observed in refluxing methanol, whereas Dmitrienko *et al.* (13) reported exclusive substitution when methylene chloride solutions of chloroindolenines from 2,3-dimethylindole and tetrahydrocarbazole were treated with methanol at −5°C, prompted ex-

[14] α-Addition of methanol to 9β-chloro-9*H*-yohimbine (**3**) and chlorodeserpidine (**4***b*) produces boat conformations of ring C and unfavourable *syn* alignment of C8—C13 and C—Cl bonds; β-addition of methanol to 9α-chloro-9*H*-yohimbine (**2**) produces a chair conformation of ring C, but also a *syn* alignment of the critical bonds.

[15] Under these conditions the chloroindolenine of tetrahydrocarbazole yielded 80% substitution product vs. 20% rearranged, whereas refluxing methanolic sodium hydroxide (65°C) produced 87% rearrangement and 13% substitution, in both cases after only 30 min.

Can. J. Chem. Downloaded from www.nrcresearchpress.com by 210.87.254.40 on 09/06/12
For personal use only.

Can. J. Chem. Downloaded from www.nrcresearchpress.com by 210.87.254.40 on 09/06/12
For personal use only.

amination of the behaviour of the yohimbine chloroindolenines at low temperature. Under the conditions employed by Dmitrienko *et al.*, the β-chloroindolenine of yohimbine (**3**) is inert, no change being observed after 72 h at −5°C. After 2 weeks all of the β-chloride (**3**) was eventually transformed to the pair of methyl imino ethers, without a trace of substitution products being observed. By contrast, all α-chloroindolenine (**2**) disappears in just over a day, yielding 80% of rearranged product (**9**) in the ratio 6:1::**9**/**10** and 20% 9α-methoxy-9*H*-yohimbine, *uncontaminated by any 9β-methoxy-9*H*-yohimbine*. The predominance of the α imino ether (**9**) indicates a stereospecific rearrangement which also finds support in the methanolic methoxide reaction data later reported. The only rationale suggested for the retention of configuration in the substitution product involves α attack of methanol on the benzylic carbonium ion derived from the product of β addition of methanol to the α chloride. Chlorodeserpidine also degrades completely after 24 h at −5°C in methanol, but no trace of substitution product is observed either by hplc or nmr analysis.

The relative rates of α- and β-chloride rearrangement under the influence of methoxide ion paralleled those observed in refluxing methanol, but the reactions are considerably slower than reported by Owellen for the chloroindolenine of tetrahydrocarbazole. After 2 h at −10°C, 82% and 94% of α- and β-chlorides, respectively, were left unreacted. The reaction mixtures were stored in the refrigerator (15°C) and analyzed by hplc daily. After 1 day at 15°C, 38% and 72% respectively of the α- and β-chlorides remained, at which time both reaction vessels were stored at room temperature; it took fully 2 further days to complete the rearrangement of α-chloride (30% β-chloride remaining), and roughly another 3 days for disappearance of all the β-chloride.

A most interesting result was obtained from treatment of methanolic solutions of the yohimbine chloroindolenines with silver oxide at room temperature.[16] Whereas the exclusive product of reaction is that of rearrangement to spiro methyl imino ether, as in refluxing methanol and low-temperature methanolic sodium methoxide, in this case the rates of reaction of α- and β-chlorides are virtually identical, in contrast with the vast superiority of the α-isomer in the other media; after 2 h 50 and 51% of the α- and β-chlorides, respectively, had been consumed. This result may be rationalized on the basis that complexation of chloride with silver on the surface of silver oxide leads to polarization of the C—Cl bond and facilitation of C8—C13 bond migration; distortion of the half-boat conformation of ring C as a result of unfavourable 1,4-interaction between chlorine and nitrogen lone-pair electrons of the β-chloride would also be relieved as a result. Attack of methanol from the opposite face of the ring planes could take place *in concert* with C8—C13 bond migration, a mechanism which would afford no particular advantage to either of the isomeric chlorides, since both bear chlorine in pseudo-axial conformation relative to the equatorial C8—C13 bond. This silver oxide procedure should be particularly useful where temperature-sensitive indolenine chlorides are involved and where product requirements do not render use of silver economically prohibitive.

The stereochemistry of spiro imino ether formation and the isomerization of spiro imino ethers

Finch and Taylor (2) reported the formation of a single "imido" (imino) ether from rearrangement of the mixture of chloroyohimbines and deduced its structure from a consideration of their proposed mechanism of its formation (Scheme 1), coupled with their judgement that the ether was stereochemically related (via its methiodide) to the less basic oxindole **A**; the more basic oxindole **B** predominated after acid treatment, presumably on account of stabilization of its conjugate acid by hydrogen bonding to the oxindole carbonyl group (see Scheme 1). During the course of this investigation, our observation of *two* epimeric imino ethers was confirmed by Herlem and Khuong-Huu (14) who reported ^{13}C nmr spectra of both imino ether and oxindole pairs; one imino ether, which crystallized from a methanolic solution of the isomeric pair, had a melting point similar to that reported for Finch and Taylor's ether and was likewise dextrorotatory; the other ether was separated by preparative tlc but did not crystallize.[17] Herlem and Khuong-Huu express support for the stereochemistry of Finch and Taylor's imino ether and oxindoles, the structures of the latter pair having been earlier reinforced by Zinnes and Shavel (3).

In this study both imino ethers were obtained pure by preparative tlc and examined by nmr. While excellent ^1H nmr spectra[18] could be obtained from freshly prepared solutions of the imino ethers, it was found difficult to get clean ^{13}C nmr spectra using normal concentration and number of scans: invariably one observed the spectrum of the mixture of epimeric ethers, obviously readily isomerized in solution. However, the use of high concentrations and a relatively low number of scans allowed identification of the respective resonances, their relative growth and decay easily observed with the passage of time and leading to the ascendancy of the isomer of higher R_f in $CDCl_3$ and CD_3OD solution.

The isomeric methyl imino ethers **9** and **10** exist at equilibrium in $CDCl_3$ in a ratio of 1.8:1::**9**/**10**, ether **A** (**9**) predominating presumably because of the destabilizing influence of the methoxy–nitrogen lone-pair interaction in ether **B** (**10**).[19] Under acid conditions at room temperature the rapidity of isomerization makes it difficult to observe the kinetic product of chloride-to-ether rearrangement, but data obtained from the reaction in methanolic methoxide medium support the stereospecificity and concerted character of the rearrangement of both isomeric chlorides, α-chloride leading to ether **A** and

[16] We are grateful to Dr. A. J. Bell for suggesting this procedure and for performing preliminary experiments with it.

[17] It seems curious to note that Herlem and Khuong-Huu generate oxindole **A** by refluxing the crystalline imino ether in trifluoroacetic acid, and oxindole **B** by refluxing the same compound in acetic acid. Finch and Taylor found **B** to predominate after acid treatment while **A** was ascendant after reflux in pyridine.

[18] Our observations are at variance with Herlem and Khuong-Huu, who cite values of 3.53 and 3.90 ppm for the chemical shifts of the respective carbomethoxy protons, 4.06 ppm for the imino ether protons, in $CDCl_3$ solution. We find values of 3.56 and 3.52 for carbomethoxy and 4.07 and 4.03, respectively, for imino ether protons. Their reported value of 3.90 (3.49?) is close to that for the carbomethoxy protons of yohimbine (3.96) and would not be consistent with the appreciably greater shielding by the aromatic ring A which is attendant with such significant departure from the plane of rings B, C, and D as obtains in the indolenines and spiro derivatives; the observed difference in chemical shift for β- and α-substituted indolenines (β, 0.7 ppm > α) is not helpful in assigning configuration in the spiro derivatives on account of the smaller shift differences and not strictly analogous stereochemistry.

[19] This rationale is supported by the relative shielding of the imine methoxy protons of ether **B** (**10**); in the ^1H nmr spectrum, **B** protons appear 0.04 ppm upfield.

TABLE 2. High pressure liquid chromatography retention times of yohimbine and its derivatives

Compound	Time (min)
Spiro imino methyl ether A	3.9
9-α-Chloro-9*H*-yohimbine	5.3
9-α-Methoxy-9*H*-yohimbine	7.6
9-β-Chloro-9*H*-yohimbine	9.8
Spiro imino methyl ether B	12.0
Yohimbine	17.6
9-β-Methoxy-9*H*-yohimbine	18.7

β-chloride to ether **B**; for the α-chloride a ratio of as high as 6:1::**A**/**B**[20] was observed at the outset of the reaction while for the β-isomer the initial ratio observed was as low as 0.6, both ratios gradually approaching the equilibrium value as the reaction progressed.

Consistent with the stereochemistry indicated in the mechanistic outline of Scheme 2, rearrangement of chlorodeserpidine in refluxing methanol yielded predominantly imino ether **B** (**11**); ^{1}H nmr examination of the total crude product, soon after completion of the reaction, indicated a ratio of 4:1 for the integrated intensities of proton resonances (4.11 and 4.19 ppm) due to methoxyl groups attached to the C=N bond, the more highly shielded dominant. Preparative tlc allowed separation of the major reaction product (the pair of imino ethers, in their equilibrium ratio of 4:3) from a minor product of lesser R_f, which is probably the pair of corresponding oxindoles[21] resulting from degradation by hydrogen chloride liberated in the course of the rearrangement.

Experimental

Melting points were determined on a Thomas–Hoover capillary melting point apparatus and are uncorrected. Nuclear magnetic resonance spectra were recorded on a Bruker Spectrospin WP-80 spectrometer (chloroform-*d* solvent and tetramethylsilane internal standard) and chemical shifts reported in parts per million on the δ scale, followed by multiplicity, associated number, and assignment of protons, in parenthesis. Mass spectrometry (ms) was performed on a Hewlett–Packard 5985 gc/ms system using the EI mode at 70 eV. Precise mass determinations were performed on a Kratos MS50 system.

High pressure liquid chromatography (hplc) was done on a Laboratory Data Control (LDC) solvent delivery system fitted with a Valco valve and a 20-μL injection loop. An LDC variable-wavelength detector, set at 254 nm, a Honeywell Electronik 196 recorder, and a Spectraphysics Minigrator completed the system. Yohimbine products were chromatographed on a Brownlee Laboratories SI-5A silica column (4.6-mm id × 25 cm) with a mobile phase of hexane, methylene chloride, and 97% aqueous isopropyl alcohol in the ratio 30:7:3. Reserpine and deserpidine products were chromatographed on a Brownlee Laboratories RP-18 column (4.6-mm id × 25 cm) with an 80% aqueous methanol mobile phase. In every case the flow rate was 2 mL/min. Representative hplc retention times for yohimbine and its derivatives are recorded in Table 2.

Satisfactory elemental analyses were obtained for all individual products isolated as well as ms highest mass peaks consistent with their molecular formulation.

Indoles

Yohimbine hydrochloride, reserpine, and deserpidine were obtained commercially and their purity checked by thin-layer chromatography (tlc); yohimbine free base was generated from the hydrochloride by neutralization with bicarbonate and standard work-up, to yield chromatographically pure material whose physical constants were in agreement with literature values.

Chloroindolenines

Chloroindolenines were prepared from indoles using the procedure of Godtfredsen and Vangedal (1) by reaction with commercial *tert*-butyl hypochlorite in the presence of triethylamine. Unique monochlorinated products were obtained from reserpine and deserpidine: 9-chloro-9*H*-reserpine (**4***a*) had mp 178–183°C, ^{1}H nmr: 7.4–6.8 (m, 5H, aromatic H), 3.92 (s, 9H, benzoate-OCH_3), 3.87, 3.85 (s, s, 6H, ring E-OCH_3 and ring E-$COOCH_3$), 3.54 (s, 3H, ring E-OCH_3); ^{13}C nmr: C-1 122.98, C-2 112.31, C-3 161.57, C-4 107.43, C-5 132.21, C-6 154.20, C-8 178.84, C-9 70.32, C-10 37.77, C-11 50.13, C-13 (C-34?) 51.85 (52.08?), C-14 22.23, C-15 34.57, C-16 31.44, C-17 47.06, C-18 53.66, C-19 (C-20?) 77.94 (78.14?), C-21 29.65, C-22 165.48, C-23 125.47, C-24 106.98, C-25 153.03, C-26 142.44, C-27 153.03, C-28 106.98, C-29 56.33, C-30 60.89, C-31 56.33, C-32 60.89, C-33 172.48, C-35 55.70. 9-Chloro-9*H*-deserpidine (**4***b*) had mp 190–196°C (lit. (1) mp 191–196°C); ^{1}H nmr: 7.6–7.2 (m, 6H, aromatic H), 3.92 (s, 9H, benzoate-OCH_3), 3.84 (s, 3H, ring E-$COOCH_3$), 3.54 (s, 3H, ring E-OCH_3); ^{13}C nmr: C-1 126.54, C-2 129.92, C-3 122.57, C-4 121.62, C-5 140.27, C-6 152.60, C-8 177.40, C-9 70.21, C-10 37.49, C-11 50.13, C-13 (C-34?) 51.84 (52.05?), C-14 22.24, C-15 34.55, C-16 31.40, C-17 49.02, C-18 53.60, C-19 (C-20?) 77.91 (78.06?), C-21 29.62, C-22 165.48, C-23 125.48, C-24,28 106.97, C-25,27 153.03, C-29,31 56.33, C-30,32 60.89, C-33 172.44.

*Separation of isomeric 9-chloro-9*H*-yohimbines*

Generally 5.0 g of the crude chlorinated product were applied to a 3 × 50 cm glass column containing 150 g of neutral alumina (Bio-rad AG7), activity III (6% water, by weight). One of two eluent systems was used, namely, methylene chloride followed by methylene chloride – methanol (19:1), or benzene followed by benzene–ether (9:1).

A Büchler Fractomette 200 automatic fraction collector was used to collect the eluent in 10–15-mL portions. The composition of the fractions was monitored by tlc on silica gel GF 254 precoated plates (0.25 mm) using benzene–ether–methanol (7:2:1) as the developing solvent system. Representative yields of chromatographically pure α- and β-chloroyohimbines from such a run were 2.4 g and 0.8 g, respectively.

*9α-Chloro-9*H*-yohimbine* (**2**) had mp 78–82°C; ^{1}H nmr: 7.7–7.0 (m, 4H, aromatic H), 3.77 (s, 3H, OCH_3). (See Table 1 for ^{13}C nmr chemical shifts of yohimbine derivatives.) *Anal.* calcd. for $C_{21}H_{25}N_2O_3Cl$: C 64.86, H 6.48, N 7.20, Cl 9.12; found: C 65.14, H 6.65, N 6.63, Cl 8.69.

*9β-Chloro-9*H*-yohimbine* (**3**) had mp 85–90°C; ^{1}H nmr: 7.7–7.2 (m, 4H, aromatic H), 3.71 (s, 3H, OCH_3). *Anal.* calcd. for $C_{21}H_{25}N_2O_3Cl$: C 64.86, H 6.48, N 7.20, Cl 9.12; found: C 64.22, H 6.49, N 6.76, Cl 9.41.

Methoxyindolenines

The procedure developed by Awang and Vincent (6) was applied to the synthesis of methoxyindolenines from reserpine and yohimbine. Reserpine yielded pure 9β-methoxy-9*H*-reserpine.

*Separation of 9-methoxy-9*H*-yohimbines*

The methoxyyohimbines were separated by preparative tlc on silica gel GF 254 precoated glass plates (1 mm, 20 × 20 cm) using benzene–ether–methanol (7:2:1) as developing solvent system. The resulting discrete bands were eluted with methanol and the extracts

[20] In one freak instance the initial chromatogram for α-chloride reaction showed only ether **A** and none of ether **B**. This is consistent with the results of α-chloride reaction with methanol at −5°C, discussed earlier in the text.

[21] Cleavage of the C9—C13 bond of spiro imino ethers and oxindoles according to Finch and Taylor's mechanism (2), affords the opportunity for isomerization at C-13. However, in the case of deserpidine such isomerization would lead to unstable boat forms of ring C.

Can. J. Chem. Downloaded from www.nrcresearchpress.com by 210.87.254.40 on 09/06/12
For personal use only.

Can. J. Chem. Downloaded from www.nrcresearchpress.com by 210.87.254.40 on 09/06/12
For personal use only.

evaporated to dryness. Representative yields of chromatographically pure α- and β-methoxyyohimbines were 125 mg and 225 mg, respectively, from 500 mg of the crude mixture.

9α-Methoxy-9H-yohimbine had mp 70–74°C; ^{1}H nmr: 7.8–7.0 (m, 4H, aromatic H), 3.76 (s, 3H, $COOCH_3$), 2.83 (s, 3H, OCH_3); ms M^+: 384.2051 (calcd. for $C_{22}H_{28}N_2O_4$: 384.2049).

9β-Methoxy-9H-yohimbine had mp 88–92°C; ^{1}H nmr: 7.8–7.0 (m, 4H, aromatic H), 3.69 (s, 3H, $COOCH_3$), 2.83 (s, 3H, OCH_3); ms M^+: 384.2051 (calcd. for $C_{22}H_{28}N_2O_4$: 384.2049).

9α-Acetoxy-9H-yohimbine

To 0.25 g (1.4 mmol) of yohimbine dissolved in 25 mL of methylene chloride was added 0.626 g (1.4 mmol) of lead tetraacetate, with stirring. After a couple of minutes the contents of the reaction vessel were filtered and the filtrate passed through 13.0 g of neutral alumina, activity III, in a 6 × 15 cm glass column. The column was eluted with 4 × 50-mL portions of methanol, and the collected fractions (5 mL) analyzed by tlc. All fractions containing only reaction product were combined and the solvent removed under reduced pressure. The resultant colourless crystalline residue had mp 118–120°C (lit. (15) mp 123–124°C); ^{1}H nmr: 7.8–7.0 (m, 4H, aromatic H), 3.76 (s, 3H, $COOCH_3$), 2.05 (s, 3H, CH_3—COO).

Reaction of chloroindolenines with methanolic hydroxide

*Chloroyohimbines (**2**, **3**)*

A solution of 400 mg of chloroyohimbine in 10 mL of methanol was treated with 2.25 mL of 0.43 *N* potassium hydroxide. The resulting solution was refluxed under nitrogen for 90 min, at the end of which it was allowed to cool to room temperature, diluted with a roughly equivalent volume of water, and extracted with methylene chloride. The organic layer was dried over anhydrous sodium sulphate and the dried filtrate evaporated to dryness under reduced pressure.

*Chlorodeserpidine (**4**b)*

A solution of 1.30 g of chlorodeserpidine in 80 mL of methanol was treated with 18.0 mL of 0.43 *N* potassium hydroxide. The resulting solution was refluxed for 90 min under nitrogen and worked up as described above for the chloroyohimbines.

*Chlororeserpine (**4**a)*

A solution of 1.0 g of chlororeserpine in 30 mL of methanol was treated with 4.0 mL of 0.43 *N* potassium hydroxide. The resulting solution was refluxed under nitrogen for 1 h (after approximately 45 min some precipitation was noticeable). At the end of the refluxing period the reaction vessel was cooled in an ice bath, the precipitate filtered, washed with a minimum of cold methanol, and left to dry in the open air.

Separation of isomeric methyl spiro imino ethers of yohimbine

The product of methanolysis of 9α-chloro-9*H*-yohimbine was chromatographed as previously described for the separation of methoxyyohimbines. The separated isomers assessed by analytical tlc were chromatographically pure just after separation but isomerized rapidly in solution. As observed by previous workers, the faster-moving α isomer (N=OCH_3 group *below* the plane of the yohimbine skeleton) had mp in the vicinity of 200°C (194–198°C), whereas the β isomer did not crystallize (14).

*α-Iminoether (**9**)*: ^{1}H nmr: 7.6–7.0 (m, 4H, aromatic H), 4.06 (s, 3H, N=C—OCH_3), 3.55 (s, 3H, $COOCH_3$) (ref. 14).

*β-Iminoether (**10**)*: ^{1}H nmr: 7.4–6.9 (m, 4H, aromatic H), 4.09 (s, 3H, N—C—OCH_3), 3.58 (s, 3H, $COOCH_3$) (ref. 14).

Reaction of chloroindolenines with neat methanol

A solution of 50–200 mg of chlorindolenine was dissolved in 5 mL methanol and the solution refluxed under nitrogen. Aliquots were withdrawn periodically, evaporated to dryness under reduced pressure, dissolved in methylene chloride, and analyzed by hplc. When reaction was complete the reaction vessel was cooled and the product isolated from solvent. In the case of chlororeserpine the product precipitated upon cooling and was filtered off, washed with cold methanol, and dried in the open air prior to hplc analysis; in all other cases the solution was treated in the same manner as the periodic aliquots.

Reaction of chloroyohimbines with silver oxide

To 25 mg (0.064 mmol) of chloroyohimbine dissolved in 1 mL of methanol was added 25 mg (0.11 mmol) of silver oxide. The reaction mixture was sampled periodically, the sample filtered through glass wool, and the filtrate evaporated to dryness under a stream of dry nitrogen. The residues were dissolved in methylene chloride and analyzed by hplc.

Reaction of chloroyohimbines with sodium methoxide at low temperature

A 50-mg (0.13 mmol) sample of chloroyohimbine dissolved in a minimum of cold methanol was added to 10 mg (0.19 mmol) of sodium methoxide, dissolved in 5 mL of methanol and cooled to −10°C in an ice–salt bath. After 3 h at −10°C the reactions were transferred to a refrigerator (15°C). Aliquots taken from the reaction medium were quenched with water, extracted with methylene chloride, dried, and analyzed by hplc.

Reaction of chloroindolenines with methanol at −5°C

Chloroyohimbines

To 200 mg of chloroyohimbine, dissolved in 5 mL of methylene chloride and cooled to −5°C in an ice bath, was added dropwise, over a period of roughly 10 min, 10 mL of cold methanol. After 5 h at −5°C the reaction solution was transferred to the freezing compartment of a refrigerator (−5°C). Periodic aliquots of the solution were withdrawn, evaporated to dryness, dissolved in methylene chloride, and analyzed by hplc. Upon completion of the reaction, solvent was removed under reduced pressure, the residue dissolved in chloroform, washed with saturated aqueous sodium bicarbonate, dried over anhydrous sodium sulphate, and evaporated to dryness.

Chlorodeserpidine

By a procedure essentially similar to that outlined above for the chloroyohimbines, 20 mL of cold methanol were added dropwise to 150 mg of chlorodeserpidine dissolved in 5 mL of methylene chloride at −5°C, under nitrogen, an additional 5 mL of methylene chloride being required to maintain solution of chlorodeserpidine.

Acknowledgements

The authors acknowledge the technical assistance of Mssrs. H. Avdovich, H. D. Beckstead, J.-C. Ethier, and D. Legault, and helpful discussions with Drs. A. By, G. A. Neville, and N. Beaulieu, all of the Bureau of Drug Research, Health and Welfare Canada, Ottawa. Special thanks are due to Dr. A. Bell for her contribution to the silver oxide aspect of our studies, Mr. H. Séguin of the National Research Council of Canada for conducting elemental analyses, and Mr. W. Miles of Agriculture Canada for conducting precise mass determinations.

1. W. O. Godtfredsen and S. Vangedal. Acta Chem. Scand. **10**, 1414 (1956).
2. N. Finch and W. I. Taylor. J. Am. Chem. Soc. (*a*) **84**, 1318 (1962); (*b*) **84**, 3871 (1962).
3. H. Zinnes and J. Shavel, Jr. J. Org. Chem. **31**, 1765 (1966).
4. M. E. Kuehne and R. Hafter. J. Org. Chem. **43**, 3702 (1978).
5. F. W. Wehrli. Adv. Mol. Relaxation Processes, **6**, 139 (1974).
6. D. V. C. Awang and A. Vincent. Can. J. Chem. **58**, 1589 (1980).
7. R. J. Owellen. J. Org. Chem. **39**, 69 (1974).
8. J. Shavel, Jr. and H. Zinnes. J. Am. Chem. Soc. **84**, 1320 (1962).
9. L. J. Dolby and G. W. Gribble. J. Org. Chem. **32**, 1391 (1967).
10. N. Finch, C. W. Gemenden, I. H.-C. Hsu, A. Kerr, G. A. Sim, and W. I. Taylor. J. Am. Chem. Soc. **87**, 2229 (1965).

11. (*a*) E. WENKERT, C.-J. CHANG, H. P. S. CHAWLA, D. W. COCHRAN, E. W. HAGAMAN, J. C. KING, and K. ORITO. J. Am. Chem. Soc. **98**, 3645 (1976); (*b*) R. H. LEVIN, J.-Y. LALLEMAND, and J. D. ROBERTS. J. Org. Chem. **38**, 1983 (1973).
12. R. J. OWELLEN and C. A. HARTKE. J. Org. Chem. **41**, 102 (1976).
13. G. I. DMITRIENKO, E. A. GROSS, and S. F. VICE. Can. J. Chem. **58**, 808 (1980).
14. D. HERLEM and F. KHUONG-HUU. Tetrahedron, **35**, 633 (1979).
15. N. FINCH, C. W. GEMENDEN, I. H.-C. HSU, and W. I. TAYLOR. J. Am. Chem. Soc. **85**, 1520 (1963).

Can. J. Chem. Downloaded from www.nrcresearchpress.com by 210.87.254.40 on 09/06/12
For personal use only.

The total synthesis of (±)-petasitolone

HSING-JANG LIU AND TENG KO NGOOI
Department of Chemistry, University of Alberta, Edmonton, Alta., Canada T6G 2G2

Received March 5, 1984

HSING-JANG LIU and TENG KO NGOOI. Can. J. Chem. **62**, 2676 (1984).

The total synthesis of petasitolone (**1**), a sesquiterpenoid of the eremophilane family, has been accomplished. The key step of this efficient synthesis is the Lewis acid catalyzed Diels–Alder addition of 2-carbomethoxy-2-cyclohexenone (**3**) to diene **9**. The cycloaddition, which gives adduct **16** in good yield, facilitates the rapid construction of the parent ring system of the target molecule and allows an excellent control of the required stereochemistry.

HSING-JANG LIU et TENG KO NGOOI. Can. J. Chem. **62**, 2676 (1984).

On a réalisé la synthèse totale de la pétasitolone (**1**), un sesquiterpène de la famille de l'érémophilane. L'étape fondamentale de cette synthèse efficace est une addition de Diels–Alder, catalysée par un acide de Lewis, de la carbométhoxy-2 cyclohexène-2 one (**3**) sur le diène **9**. La cycloaddition, qui conduit à l'adduit **16** avec un bon rendement, facilite l'édification rapide du système cyclique parent de la molécule recherchée et permet un excellent contrôle de la stéréochimie requise.

[Traduit par le journal]

We wish to report the first total synthesis, in racemic form, of petasitolone (**1**), a sesquiterpene of the eremophilane family which has been isolated from *Petasites japonicus* Maxim (1). The synthesis also demonstrates a new approach to eremophilane sesquiterpenes which are widely distributed in nature (2). These naturally occurring compounds have attracted a great deal of synthetic effort during the past two decades (3). Although a rapid construction of the required decalin framework can conceivably be achieved by an intermolecular Diels–Alder reaction, the difficulty[1] in controlling the desired *cis* stereochemistry of the vicinal methyl groups has hampered the efficient use of such an approach to the synthesis of eremophilanes. During a recent study of the dienophilicity of 2-carbomethoxy-2-cyclohexenone (**3**) (5), it was observed that the Diels–Alder reactions of this enone ester with 1-substituted and 1,3-disubstituted dienes led, in each case, to the preferential formation of the adduct that arose from secondary orbital overlap between the diene and the ester moeity of **3**. For example, its reaction with *trans*-piperylene at −78°C and under stannic chloride catalysis gave a 5:3 mixture of adducts **4** and **5**. The major adduct **4**, which has the all-*cis* stereochemistry for the three contiguous chiral centers, was formed by *endo* addition of the diene to the ester group of **3**. It was also observed that addition of *trans*-2-methyl-1,3-pentadiene to enone ester **3** under the same conditions led to a mixture of adducts **6** and **7**. In this case, an improved stereoselectivity of 13:1 in favor of adduct **6** was obtained. The remarkable ability of the ester group to reverse the course of stereoselectivity normally observed for 2-cyclohexenones makes possible the direct control of the eremophilane stereochemistry using a Diels–Alder reaction. This is illustrated with the efficient total synthesis of petasitolone described below.

Although the Diels–Alder reaction of enone ester **3** and *trans*-piperylene resulted in the preferential formation of adduct **4** possessing the desired stereochemistry, the degree of selectivity was rather unsatisfactory. Since 1,3-disubstituted dienes were shown to be more stereoselective (*vide supra*), two such dienes **8** (6) and **9**[2] were chosen as the diene component

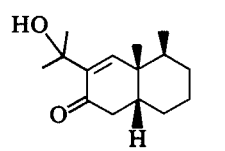

1

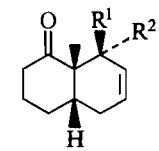

2 R' = H, R² = CH₃

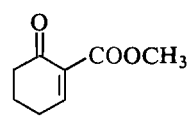

3

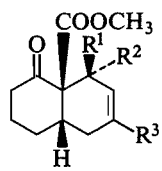

4 R' = CH₃, R² = R³ = H
5 R' = R³ = H, R² = CH₃
6 R' = R³ = CH₃, R² = H
7 R' = H, R² = R³ = CH₃
16 R' = CH₃, R² = H, R³ = OPO(OCH₂CH₃)₂
17 R' = H, R² = CH₃, R³ = OPO(OCH₂CH₃)₂

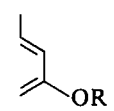

8 R = Si(CH₃)₃
9 R = PO(OCH₂CH₃)₂

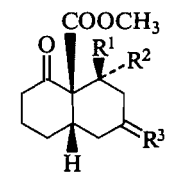

10 R' = CH₃, R² = H, R³ = O
11 R' = H, R² = CH₃, R³ = O
12 R' = CH₃, R² = H, R³ = SCH₂CH₂S
13 R' = H, R² = CH₃, R³ = SCH₂CH₂S
14 R' = CH₃, R² = H, R³ = H₂
15 R' = H, R² = CH₃, R³ = H₂

[1] The reaction of 2-methyl-2-cyclohexenone with *trans*-piperylene, for instance, gave predominantly adduct **2** (4). With the far less reactive *cis*-piperylene, no significant reaction was observed (unpublished results of this laboratory).

[2] Diene **9** was prepared in 44% yield by trapping the kinetic enolate of *trans*-3-penten-2-one, generated *in situ* in tetrahydrofuran at −78°C using lithium diisopropylamide as a base, with diethylchlorophosphate. This diene is rather stable and can be purified by silica gel chromatography.

Can. J. Chem. Downloaded from www.nrcresearchpress.com by 210.87.254.105 on 09/06/12
For personal use only.

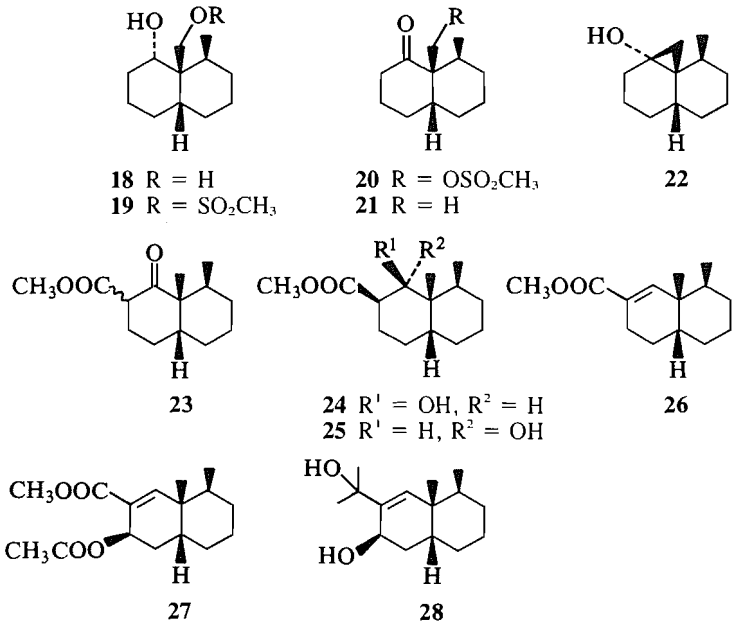

in the reaction. In each case, the additional substituent at C-2, after serving as an element for stereochemical control, could be easily removed.

Treatment of enone ester **3** with diene **8** (5 equiv.) in ether–dichloromethane (1:1) in the presence of stannic chloride (0.5 equiv.) at −50°C for 6 h gave, after aqueous work-up, an inseparable mixture of diketones **10** and **11** in 46% yield and in 7:1 ratio (^{1}Hmr analysis). The mixture was treated with 5 equiv. of 1,2-ethanedithiol and 1 equiv. of boron trifluoride etherate in methylene chloride at 0°C for 30 min to effect the selective thioketalization of the less hindered ketone carbonyl. Desulfurization of the resulting thioketals **12** and **13** (7:1; 90% yield) with W-2 Raney nickel (7) in refluxing ethanol gave, after chromatographic separation, a 60% yield of the desired keto ester **14** along with a small amount (~9%) of its epimer **15**[3].

A shorter and more efficient route leading to the desired keto ester **14** involves the stannic chloride catalyzed addition of enone ester **3** to diene phosphate **9**[4]. When the reaction was carried out in ether at −30°C for 6 h using 1.5 equiv. of the diene and 0.5 equiv. of the catalyst, it afforded a 6:1 mixture of adducts **16** and **17** in 66% yield. Treatment of the mixture with Adams catalyst in ethyl acetate at 1 atmosphere (101.3 kPa) of hydrogen pressure resulted in the reduction of the double bond as well as the cleavage of the phosphoryloxy group (9) to give keto esters **14** and **15** in 76% and 11% yield respectively.

Reduction of keto ester **14** with sodium bis(2-methoxyethoxy)aluminum hydride in ether at 0°C gave almost quantitatively a single crystalline diol (mp 97–99°C) showing 12 lines in the ^{13}Cmr spectrum. Assuming that the reduction of the ketone carbonyl occurred from the sterically less-hindered convex face of the molecule, the resulting diol would have the relative stereochemistry as shown in structure **18** in which the proton adjacent to the secondary hydroxyl group would be axial. This was confirmed by the presence, in the ^{1}Hmr spectrum, of a doublet of doublets at δ 3.83 with a large diaxial coupling constant of 14 Hz and a small axial–equatorial coupling constant of 6 Hz.

Selective mesylation of the primary hydroxyl group of diol **18** was effected by treatment with 1 equiv. of methanesulfonyl chloride in pyridine–dichloromethane (1:10) at −20°C. Jones oxidation of hydroxy mesylate **19** thus obtained in 86% yield afforded the corresponding keto mesylate **20** (85% yield). This compound was subjected to reduction with zince dust and sodium iodide (10) in refluxing *N*,*N*-dimethylformamide (DMF). Two isomeric products were obtained. The major isomer isolated in 60% yield was characterized as the expected ketone **21** and the minor isomer (21% yield) was found to possess the interesting structure of cyclopropanol **22**. This compound was readily converted into ketone **21** upon treatment with aqueous sodium hydroxide in refluxing DMF.

Carbomethoxylation of ketone **21** with dimethyl carbonate and sodium hydride in refluxing benzene gave an 88% yield of two epimeric keto esters **23** existing partially in the corresponding enol form. Sodium borohydride reduction of this mixture furnished two isomeric alcohols, **24** in 20% yield and **25** in 69% yield. The stereochemical assignments were made based on the following spectral data. In the ^{1}Hmr spectrum of the minor alcohol, a signal appearing at δ 3.62 as a doublet of doublets with coupling constants of 6 and 5 Hz was assigned to the proton adjacent to the hydroxyl group. Another signal, due to the methine proton on the α-carbon of the methyl ester, appeared at δ 2.83 as a multiplet. It showed discernible coupling constants of 10 and 5 Hz. A third signal due to the hydroxyl proton appeared at δ 3.35 as a doublet (J = 6 Hz). On deuterium exchange with D_2O, this latter signal disappeared and the signal at δ 3.62 collapsed to a doublet with a coupling constant of 5 Hz. This observation indicated that the proton on the carbon bearing the hydroxyl group was equatorially disposed. Together with the presence of a diaxial coupling constant of 10 Hz for the signal at δ 2.83, it led to the assignment of the structure **24** for the minor alcohol, where the methine proton (at δ 2.83) on the α-carbon of the methyl ester would be axial. The major isomer showed, in the ^{1}Hmr spectrum, a

[3] Compounds **14** and **15** were found to be identical respectively with the products obtained from the hydrogenation of unsaturated keto esters **4** and **5** carried out with W-2 Raney nickel in ethanol.

[4] It is worth noting that very few phosphoryloxy-substituted dienes have been used in Diels–Alder reactions. The only known example is that derived from methyl vinyl ketone (8).

Can. J. Chem. Downloaded from www.nrcresearchpress.com by 210.87.254.105 on 09/06/12
For personal use only.

Can. J. Chem. Downloaded from www.nrcresearchpress.com by 210.87.254.105 on 09/06/12
For personal use only.

signal at δ 2.73 which was assigned to the methine proton on the α-carbon of the methyl ester. It appeared as a doublet of doublets of doublets with coupling constants of 13, 11, and 4.5 hz. The presence of two large coupling constants of 13 and 11 Hz indicated that this proton was axial and further coupled to two adjacent axial protons. One of these axial protons had to be on the carbon bearing the hydroxyl group. That this was so, was confirmed by the presence of a signal at δ 3.53 with coupling constants of 11 and 4.5 assigned to the proton adjacent to the hydroxyl group. On deuterium exchange with D_2O, this signal collapsed to a doublet with a coupling constant of 11 Hz and the doublet at δ 2.46 (J = 4.5 Hz) disappeared.

Treatment of a mixture of alcohols **24** and **25** (~2:7) with dicyclohexylcarbodiimide in refluxing DMF in the presence of a small amount of copper(I) chloride (11) afforded unsaturated ester **26** in 75% yield. Introduction of an oxygen functionality to the allylic carbon of this compound was achieved with selenium dioxide oxidation. When **26** was reacted with an excess of selenium dioxide in refluxing acetic acid for two days, the crystalline acetate **27** (mp 119–120°C) was isolated in 61% yield. The stereochemistry of the newly created asymmetric center was assigned on the basis of the ^{1}Hmr spectrum in which the allylic proton appeared at δ 5.74 as a doublet of doublets with small coupling constants of 4 and 1.5 Hz indicating the equatorial disposition of this proton.

Acetate **27** was converted into petasitolone (**1**) as follows. Treatment of **27** with excess methyllithium in tetrahydrofuran at −78°C resulted in the formation of diol **28** in 93% yield. Oxidation of this diol with 8 *N* Jones reagent (12) gave rise to a 79% yield of (±)-petasitolone (**1**) whose ir, ^{1}Hmr, and ^{13}Cmr spectral data were found to be in agreement with those of the natural material.

Experimental

General

Melting points were determined on a Kofler hot stage apparatus and are uncorrected. Elemental analyses were performed by the microanalytical laboratory of this department. Infrared (ir) spectra were recorded on a Perkin–Elmer model 457 or Nicolet 7-199 FT-IR spectrophotometer and, except where otherwise stated, were obtained on solutions in carbon tetrachloride. Proton nuclear magnetic resonance (^{1}Hmr) spectra were recorded on Varian HA-100, HA-100/Digilab, Bruker WH-200 and WH-400 spectrometers. Unless otherwise stated, deuterochloroform was used as solvent and tetramethylsilane as internal standard. Carbon-13 nuclear magnetic resonance (^{13}Cmr) spectra were recorded on a Bruker WH-200, WH-400, or Bruker HFX-90/Nicolet 1085 system and were obtained on solutions in deuterochloroform using tetramethylsilane as internal reference. Mass spectra (ms) were recorded using A.E.I. model MS9, MS12, or MS50 mass spectrometers. Chemical ionization mass spectra (cims) were recorded on an AEI-MS12 spectrometer using ammonia gas as the ionizing medium. Unless otherwise stated, anhydrous magnesium sulfate was used for drying organic solutions.

Materials

Benzene, ether, and tetrahydrofuran were freshly distilled over lithium aluminum hydride. Pyridine was distilled over barium oxide and stored over potassium hydroxide pellets. Methylene chloride used for reactions was washed with an equal volume of 10% aqueous sodium carbonate and distilled over powdered calcium chloride. Acetone was treated with potassium permanganate, dried over anhydrous potassium carbonate, and distilled. Diisopropylamine was distilled over calcium hydride. *N,N*-Dimethylformamide was distilled over phosphorus pentoxide. Methanol and ethanol were dried over magnesium turnings at elevated temperature and distilled. Enone ester **3** was prepared from 2-carbomethoxycyclohexanone according to the reported procedure (13).

*8aβ-Carbomethoxy-8β-methyl-2,3,4,4aβ,5,7,8,8a-octahydro-1,6-naphthalenedione (**10**) and 8aβ-carbomethoxy-8α-methyl-2,3,4,4aβ,5,7,8,8a-octahydro-1,6-naphthalenedione (**11**)*

At −50°C, anhydrous stannic chloride (261 mg, 1 mmol) was added to a solution of enone ester **3** (369 mg, 2 mmol) and *trans*-2-trimethylsilyloxy-1,3-pentadiene (**8**) (936 mg, 6 mmol) in ether and methylene chloride (2.5 mL each). An additional amount of **8** (624) mg, 4 mmol) in a 1:1 mixture of ether and methylene chloride (5 mL) was added. After stirring under an atmosphere of argon for 6 h, the reaction mixture was warmed to room temperature and water was added. The resulting mixture was extracted with methylene chloride. The organic extracts were dried, filtered, and concentrated. Column chromatography of the residue on silica gel, eluting with 10–15% ethyl acetate in *n*-hexane, gave an impure mixture of **10** and **11**. Another purification by flash chromatography on silica gel, eluting with 10% ethyl acetate in *n*-hexane, gave a 7:1 mixture (by ^{1}Hmr integration) of diketones **10** and **11** (218 mg; 46% yield). The mixture of diketones **10** and **11** showed the following spectral data: ir: 1740 (ester C=O) and 1714 (ketone C=O) cm^{-1}; ms: M$^+$ 238.1205 (calcd. for $C_{13}H_{22}O_4$: 238.1205). The ^{1}Hmr spectrum showed two sets of signals in an integral ratio of 7:1. The major set, assignable to **10**, showed signals at δ 3.73 (s, 3H, —$COOCH_3$) and 0.90 (d, 3H, J = 7 Hz, —CH_3) and the minor set, attributed to **11**, showed signals at δ 3.82 (s, 3H, —$COOCH_3$) and 1.15 (d, 3H, J = 7 Hz, —CH_3).

*8aβ-Carbomethoxy-6,6-ethylenedithio-8β-methyl-3,4,4aβ,5,6,7,8,8a-octahydro-1(2H)-naphthalenone (**12**) and 8aβ-carbomethoxy-6,6-ethylenedithio-8α-methyl-3,4,4aβ,5,6,7,8,8a-octahydro-1(2H)-naphthalenone (**13**)*

At 0°C, 1,2-ethanedithiol (333 mg, 3.54 mmol) and boron trifluoride etherate (104 mg, 0.73 mmol) were sequentially added to a solution of a 7:1 mixture of diketones **10** and **11** (167 mg, 0.7 mmol) in methylene chloride (10 mL). After stirring under an atmosphere of argon for 30 min, the reaction mixture was poured into ice-cold 2 *N* aqueous sodium hydroxide and extracted with methylene chloride. The organic extracts were washed with water, dried, filtered, and concentrated. Column chromatography of the residue on silica gel, eluting with 5% ether in *n*-hexane, gave a 7:1 mixture of thioketals **12** and **13** (198 mg; 90% yield) which showed the following spectral data: ir: 1740 (ester C=O) and 1713 (ketone C=O) cm^{-1}; ms: M$^+$ 314.1008 (calcd. for $C_{15}H_{22}O_3S_2$: 314.1010). The ^{1}Hmr spectrum of the mixture showed two sets of signals in an integral ratio of 7:1. The major set, attributed to **12**, consisted of signals at δ 3.74 (s, 3H, —$COOCH_3$) and 1.02 (d, 3H, J = 7.5 Hz, —CH_3). The minor set, attributed to **13**, showed signals at δ 3.80 (s, 3H, —$COOCH_3$) and 1.10 (d, 3H, J = 7.5 Hz, —CH_3).

Diethyl trans*-1,3-pentadien-2-yl phosphate (**9**)*

To a solution of diisopropylamine (4.1 g, 40.3 mmol) in tetrahydrofuran (50 mL) at −78°C and under an atmosphere of argon, was added a 1.1 *M* solution of methyllithium in *n*-hexane (36.3 mL, 40.3 mmol) with stirring. After 10 min, a solution of *trans*-3-penten-2-one (3.1 g, 36.7 mmol) in tetrahydrofuran (20 mL) was added dropwise over 10 min. After another 15 min, diethylchlorophosphate (13.8 g, 80 mmol) was added. The reaction mixture was allowed to warm up to room temperature. Ice-cold water was added and the resulting mixture extracted with *n*-pentane. The organic extracts were washed with water, dried, filtered, and concentrated. Flash chromatography of the resulting dark yellow oil, eluting with a solution of 50% ether in petroleum ether, gave diene **9** (3.5 g, 44% yield); ir: 1275 and 1270 (P=O) cm^{-1}; ^{1}Hmr δ: 5.70–6.32 (m, 2H, —CH=CH—), 4.82, 4.60 (both m, 1H each, =CH_2), 4.17 (dq, 4H, $J = J'$ = 7 Hz, 2 × —CH_2—), 1.80 (d, 3H, J = 5.5 Hz, =CH—CH_3), and 1.35 (t, 6H, J = 7 Hz, 2 × —OCH_2CH_3); ms: M$^+$ 220.0865 (calcd. for $C_9H_{17}O_4P$: 220.0865).

*8aβ-Carbomethoxy-6-diethylphosphoryloxy-8β-methyl-3,4,4aβ,5,8,8a-hexahydro-1(2H)-naphthalenone (**16**) and 8aβ-carbomethoxy-6-diethylphosphoryloxy-8α-methyl-3,4,4aβ,5,8,8a-hexahydro-1(2H)-naphthalenone (**17**)*

At −30°C, anhydrous stannic chloride (294 mg, 1.13 mmol) was

Can. J. Chem. Downloaded from www.nrcresearchpress.com by 210.87.254.105 on 09/06/12
For personal use only.

added to a solution of enone ester **3** (348 mg, 2.26 mmol) and diene phosphate **9** (698 mg, 3.17 mmol) in ether (10 mL). After stirring under an atmosphere of nitrogen for 6 h, the reaction mixture was warmed to room temperature. Water was added and the resulting mixture extracted with methylene chloride. The organic extracts were combined, dried, filtered, and concentrated. Flash chromatography of the residue on silica gel, eluting with 50% ethyl acetate in *n*-hexane, gave diene **9** (180 mg; 26% recovery). Continued elution gave a mixture of enol phosphates **16** and **17** (555 mg; 66% yield) in a ratio of 6:1. The mixture showed the following spectral data: ir: 1750 (ester C=O) and 1720 (ketone C=O) cm^{-1}; ms: M^+ 374.1495 (calcd. for $C_{17}H_{27}O_7$: 374.1495). The ^{1}Hmr spectrum of the mixture of adducts showed two sets of signals in an integral ratio of 6:1. The major set, assignable to **16**, showed signals at δ 5.47 (m, 1H, =CH—), 4.15 (m, 4H, 2 × —OCH_2—), 3.75 (s, 3H, —$COOCH_3$), 1.37 (t, 6H, J = 7 Hz, 2 × —OCH_2CH_3), and 0.92 (d, 3H, J = 7 Hz, —CH_3); the other set, assignable to **17**, showed signals at δ 5.34 (m, 1H, =CH—), 4.15 (m, 4H, 2 × —OCH_2—), 3.80 (s, 3H, —$COOCH_3$), 1.37 (t, J = 7 Hz, 6H, 2 × —OCH_2CH_3), and 1.24 (d, 3H, J = 7 Hz, —CH_3).

*aβ-Carbomethoxy-8β-methyl-3,4,4aβ,5,6,7,8,8a-octahydro-1(2H)-naphthalenone (**14**) and 8aβ-carbomethoxy-8α-methyl-3,4,4aβ,5,6,7,8,8a-octahydro-1(2H)-naphthalenone (**15**)*

*From thioketals **12** and **13***

Raney nickel (ca. 2 g; grade W-2) was added to a solution of a 7:1 mixture of thioketals **12** and **13** (181 mg, 0.58 mmol) in ethanol (10 mL). The resulting mixture was heated to reflux under a nitrogen atmosphere for 2.5 h. Filtration and concentration gave a light yellow oil which was purified by column chromatography on silica gel. Elution with 1–2% ether in *n*-hexane gave keto ester **15** (11 mg; 9% yield) as a colorless oil; ir (neat): 1739 (ester) and 1712 (ketone) cm^{-1}; ^{1}Hmr δ 3.79 (s, 3H, —$COOCH_3$) and 1.18 (d, 3H, J = 7 Hz, —CH_3); ms: M^+ 224.1410 (calcd. for $C_{13}H_{20}O_3$: 224.1407). Continued elution gave the keto ester (78 mg; 60% yield) which crystallized on standing, mp 37–39°C; ir: 1740 (ester) and 1714 (ketone) cm^{-1}; ^{1}Hmr δ 3.72 (s, 3H, —$COOCH_3$) and 0.86 (d, 3H, J = 7 Hz, —CH_3); ms: M^+ 224.1411 (calcd. for $C_{13}H_{20}O_3$: 224.1407). *Anal.* calcd. for $C_{13}H_{20}O_3$: C 69.91, H 8.99; found: C 69.77, H 9.01.

*From enol phosphates **16** and **17***

A 6:1 mixture of enol phosphates **16** and **17** (528 mg, 1.41 mmol) was dissolved in ethyl acetate (20 mL) and platinum oxide (52 mg) was added. The reaction mixture was hydrogenated at 1 atmosphere of hydrogen pressure for 1 h. Filtration and concentration gave an oil which was purified by flash chromatography on silica gel. Elution with 10% ether in petroleum ether gave keto ester **15** (35 mg; 11% yield). Continued elution gave the isomeric keto ester **14** (241 mg; 76% yield).

*1α-Hydroxy-8aβ-hydroxymethyl-8β-methyl-1,2,3,4,4aβ,5,6,7,8,8a-perhydronaphthalene (**18**)*

At 0°C, a 3.5 *M* solution of sodium bis(2-methoxyethoxy)-aluminium hydride in toluene (2.5 mL, 8.75 mmol) was added to a solution of keto ester **14** (340 mg, 1.53 mmol) in tetrahydrofuran (20 mL). After stirring under an atmosphere of nitrogen for 8 h, the reaction mixture was cooled to 0°C and ice-cold water was added to destroy excess reducing agent. Ice-cold aqueous 2 *N* hydrochloric acid was added and the resulting mixture extracted with ether. The ethereal extracts were washed with water, dried, filtered, and concentrated. Column chromatography of the residue on silica gel, eluting with 50% ether in *n*-hexane, gave diol **18** (289 mg; 96% yield). Recrystallization from a solution of ether and petroleum ether gave white needles of pure **18**, mp 97–99°C; ir: 3317 (—OH) cm^{-1}; ^{1}Hmr δ: 4.35 (d, 1H, J = 12 Hz, —CH*H*—OH), 3.83 (dd, 1H, J = 14, J' = 6 Hz, —C*H*—OH), 3.71 (d, 1H, J = 12 Hz, —C*H*H—OH), 2.74, 2.26 (both br s, 1H each, 2 × —OH), and 1.17 (d, 3H, J = 7 Hz, —CH_3); ^{13}Cmr δ: 79, 66, 44, 38, 32, 30, 29, 27, 26, 25, 21, and 19; ms *m/e*: 180.1517 (M^+ − 18; calcd. for $C_{12}H_{20}O$: 180.1515). *Anal.* calcd. for $C_{12}H_{22}O_2$: C 72.68, H 11.18; found: C 72.58, H 11.06.

*1α-Hydroxy-8aβ-methanesulfonyloxymethyl-8β-methyl-1,2,3,4,4aβ,5,6,7,8,8a-perhydronaphthalene (**19**)*

Diol **18** (215 mg, 1.08 mmol) was dissolved in methylene chloride (10 mL) and cooled to −10°C. Pyridine (1 mL) and methanesulfonyl chloride (120 mg, 1.08 mmol) were sequentially added. After stirring under an atmosphere of argon for 28 h, the reaction mixture was warmed to 0°C. A solution of 2 *N* aqueous hydrochloric acid was added and the resulting mixture extracted with methylene chloride. The organic extracts were washed with water, dried, filtered, and concentrated. Column chromatography of the residue on silica gel, eluting with 50% ether in *n*-hexane, gave mesylate **19** (274 mg; ~86% yield based on consumed starting material) which was contaminated with a small amount (~10%) of the regioisomer. Continued elution gave diol **18** (11 mg, 5% recovery). The following spectral data were recorded for **19**: ir: 3550 (—OH), 2357 and 1173 (S=O) cm^{-1}; ^{1}Hmr δ: 4.73, 4.48 (both d, 1H each, J = 10 Hz each, CH_2O—), 3.68 (m, 1H, —C*H*OH), 3.08 (s, 3H, —OSO_2CH_3), and 1.01 (d, 3H, J = 7 Hz, —CH_3); ms *m/e*: 180.1514 (M^+ − 96; calcd. for $C_{12}H_{20}O$: 180.1515) and 162.1408 (M^+ − 114; calcd. for $C_{12}H_{18}$: 162.1409).

*8aβ-Methanesulfonyloxymethyl-8β-methyl-3,4,4aβ,5,6,7,8,8a-1(2H)-naphthalenone (**20**)*

Mesylate **19** (260 mg, ~90% pure, ~0.85 mmol) was dissolved in acetone (8 mL) and cooled to 0°C. Jones reagent (2 mL of 8 *N*, 16 mmol) was added. After stirring for 30 min, the reaction mixture was diluted with ice-cold water and extracted with methylene chloride. The organic extracts were washed with water, dried, filtered, and concentrated. Column chromatography of the residue on silica gel, eluting with 30% ether in *n*-hexane, gave pure keto mesylate **20** (199 mg, ~85% yield); ir (neat): 1703 (C=O), 1356 and 1175 (S=O) cm^{-1}; ^{1}Hmr δ: 4.70, 4.33 (both d, 1H each, J = 9 Hz each, —CH_2O—), 3.10 (s, 3H, —OSO_2CH_3), and 0.68 (d, 3H, J = 7 Hz, —CH_3); ms: M^+ 274.1233 (calcd. for $C_{13}H_{22}O_4S$: 274.1233).

*8β,8aβ-Dimethyl-3,4,4aβ,5,6,7,8,8a-octahydro-1(2H)-naphthalenone (**21**) and 1α-hydroxy-1β,8aβ-methano-8β-methyl-1,2,3,4,4aβ,5,6,7,8,8a-perhydronaphthalene (**22**)*

Keto mesylate **20** (170 mg, 0.62 mmol), anhydrous sodium iodide (930 mg, 6.20 mmol), and zinc dust (811 mg, 12.4 mmol) were placed in *N,N*-dimethylformamide (10 mL). The resulting mixture was heated to reflux under a nitrogen atmosphere for 52 h. After cooling to room temperature, the reaction mixture was filtered. The organic filtrate was washed with ice-cold 2 *N* aqueous hydrochloric acid and water, dried, filtered, and concentrated. Column chromatography of the residue on silica gel, eluting with 2% ether in *n*-hexane, gave ketone **21** (67 mg; 60% yield); ir: 1706 (C=O) cm^{-1}; ^{1}Hmr δ: 1.08 (s, 3H, —CH_3) and 0.67 (d, 3H, J = 7 Hz, —C*H*CH_3); ^{13}Cmr δ: 216.0, 51.0, 45.0, 38.0, 31.7, 30.0, 26.8, 26.4, 21.0, 16.0, and 14.6; ms: M^+ 180.1515 (calcd. for $C_{12}H_{20}O$: 180.1509). Further elution with 5% ether in *n*-hexane gave cyclopropanol **22** (23 mg; 21% yield); ir: 3443 (—OH) cm^{-1}; ^{1}Hmr δ: 1.07 (d, 3H, J = 7 Hz, —C*H*CH_3), 0.69 (d, 1H, J = 5.5 Hz, cyclopropyl H), and 0.25 (dd, 1H, J = 5.5, J' = 1.5 Hz, cyclopropyl H); ms: M^+ 180.1521 (calcd. for $C_{12}H_{20}O$: 180.1509).

*Conversion of cyclopropanol **22** to ketone **21***

A solution of cyclopropanol **22** (21 mg, 0.12 mmol) and sodium hydroxide (25 mg, 0.63 mmol) in water and *N,N*-dimethylformamide (1:2; 2 mL) was heated to reflux under a nitrogen atmosphere. After 8 h, the reaction mixture was cooled to room temperature and diluted with *n*-hexane. A saturated aqueous ammonium chloride solution was added and the resulting mixture separated. The aqueous phase was extracted with *n*-hexane. The organic extracts were washed with water, dried, filtered, and concentrated. Column chromatography of the residue on silica gel, eluting with 2% ether in *n*-hexane, gave the ketone **21** (10 mg; 48% yield).

*2-Carbomethoxy-8β,8aβ-dimethyl-3,4,4aβ,5,6,7,8,8a-octahydro-1(2H)-naphthalenones (**23**)*

Sodium hydride (60% dispersion in oil, 0.57 g, 14.3 mmol) was

Can. J. Chem. Downloaded from www.nrcresearchpress.com by 210.87.254.105 on 09/06/12
For personal use only.

added to a solution of dimethyl carbonate (4.3 g, 47.8 mmol) in benzene (50 mL) under a nitrogen atmosphere. The resulting mixture was heated to reflux. A solution of ketone **21** (733 mg, 4.07 mmol) in benzene (20 mL) was added dropwise over 20 min. After refluxing for 50 h, the reaction mixture was cooled to 0°C and methanol was added with vigorous stirring to destroy excess sodium hydride. An ice-cold aqueous 10% solution of acetic acid was added. The resulting mixture was extracted with methylene chloride. The organic extracts were washed with water, dried, filtered, and concentrated. Flash chromatography of the residue on silica gel, eluting with 2% ether in petroleum ether, gave a mixture of two epimeric keto esters **23** and the corresponding enol (890 mg; 88% yield). The ^{1}Hmr spectrum showed three sets of signals corresponding to the three compounds. Signals appeared at δ 12.72 (s, ~0.5H, enolic H), 3.74, 3.73, 3.70 (each s, total 3H, —$COOCH_3$), 1.15, 1.11, 1.05 (each s, total 3H, —CH_3), 0.95, 0.73, and 0.66 (each d, total 3H, —$CHCH_3$); ir: 1748, 1702, 1640 and 1604 (β-keto ester) cm^{-1}; ms: M^+ 238.1572 (calcd. for $C_{14}H_{22}O_3$: 238.1563). *Anal.* calcd. for $C_{14}H_{22}O_3$: C 70.56, H 9.30; found: C 70.27, H 9.31.

*2β-Carbomethoxy-1β-hydroxy-8β,8aβ-dimethyl-1,2,3,4,4aβ,5,6,7,8,8a-perhydronaphthalene (**24**) and 2β-carbomethoxy-1α-hydroxy-8β,8aβ-dimethyl-1,2,3,4,4aβ,5,6,7,8,8a-perhydronaphthalene (**25**)*

A mixture of keto esters **23** and the corresponding enol (65 mg, 0.27 mmol) obtained from the preceding experiment was dissolved in methanol (2 mL). The solution was cooled to 0°C and sodium borohydride (33 mg, 0.87 mmol) was added with stirring. After 30 min, water and then saturated aqueous ammonium chloride were introduced. The resulting mixture was extracted with methylene chloride. The organic extracts were washed with water, dried, filtered, and concentrated. Flash chromatography of the residue on silica gel, eluting with 10% ether in petroleum ether, gave alcohol **24** (13 mg, 20% yield) as a colorless oil; ir: 3480 (—OH) and 1728 (C=O) cm^{-1}; ms: M^+ 240.1720 (calcd. for $C_{14}H_{24}O_3$: 240.1726); ^{1}Hmr δ: 3.76 (s, 3H, —$COOCH_3$), 3.62 (dd, 1H, J = 6, J' = 5 Hz, —$CHOH$), 3.35 (d, 1H, J = 6 Hz, —OH), 2.83 (ddm, 1H, J = 10, J' = 5 Hz, —$CHCOOCH_3$), 1.00 (s, 3H, —CH_3), and 0.91 (d, 3H, J = 7 Hz, —$CHCH_3$). After D_2O exchange, the signal at δ 3.35 disappeared and the dd at δ 3.62 collapsed to a doublet (J = 5 Hz). Continued elution gave alcohol **25** (45 mg, 69% yield), mp 82–84°C (ether – petroleum ether); ir: 3510 (—OH) and 1719 (C=O) cm^{-1}; ms: M^+ 240.1723 (calcd. for $C_{14}H_{24}O_3$: 240.1726); ^{1}Hmr δ 3.74 (s, 3H, —$COOCH_3$), 3.53 (dd, 1H, J = 11, J' = 4.5 Hz, —$CHOH$), 2.73 (ddd, 1H, J = 13, J' = 11, J'' = 4.5 Hz, —$CHCOOCH_3$), 2.46 (d, 1H, J = 4.5 Hz, —OH), 1.12 (s, 3H, —CH_3), and 0.98 (d, 3H, J = 7 Hz, —$CHCH_3$). After D_2O exchange, the doublet at δ 2.46 disappeared and the signal at δ 3.53 changed to a doublet (J = 11 Hz). *Anal.* calcd. for $C_{14}H_{24}O_3$: C 69.96, H 10.66; found: C 70.10, H 10.15.

*2-Carbomethoxy-8β,8aβ-dimethyl-3,4,4aβ,5,6,7,8,8a-octahydronaphthalene (**26**)*

A mixture of alcohols **24** and **25** (~2:7, 217 mg, 0.9 mmol) was dissolved in *N*,*N*-dimethylformamide (5 mL) under an atmosphere of nitrogen. Dicyclohexylcarbodiimide (279 mg, 1.36 mmol) and copper(I) chloride (43 mg, 0.43 mmol) were added. The reaction mixture was heated under reflux for 10 h, then cooled to room temperature and diluted with methylene chloride (10 mL). An aqueous 10% solution of acetic acid was added. After stirring for 1.5 h, the mixture was diluted with water and extracted with methylene chloride. The organic extracts were washed with water, dried, filtered, and concentrated. Flash chromatography of the residue on silica gel, eluting with 5% ether in petroleum ether, gave unsaturated ester **26** (150 mg; 75% yield) as a colorless oil; ir: 1717 (C=O) and 1642 (C=C) cm^{-1}; ^{1}Hmr δ: 6.90 (dd, 1H, J = 2, J' = 1.5 Hz, =CH—), 3.76 (s, 3H, —$COOCH_3$), 2.43 (dddd, 1H, J = 17, J' = 6, J'' = 3, J''' = 1.5 Hz, =C—CHH—), 2.19 (dddd, 1H, J = 17, J' = 10, J'' = 6, J''' = 2 Hz, =C—CHH—), 1.04 (s, 3H, —CH_3), and 0.91 (d, 3H, J = 7 Hz, —$CHCH_3$); ms: M^+ 222.1618 (calcd. for $C_{14}H_{22}O_2$: 222.1625). *Anal.* calcd. for $C_{14}H_{22}O_2$: C 75.63, H 9.97; found: C 75.75, H 10.06.

*3β-Acetoxy-2-carbomethoxy-8β,8aβ-dimethyl-3,4,4aβ,5,6,7,8,8a-octahydronaphthalene (**27**)*

Selenium dioxide (63 mg, 0.57 mmol) was added to a solution of unsaturated ester **26** (105 mg, 0.47 mmol) in glacial acetic acid (4 mL) under a nitrogen atmosphere. The resulting mixture was heated at reflux with stirring. After 24 h, an additional batch of selenium dioxide (63 mg, 0.57 mmol) and glacial acetic acid (2 mL) were added. After heating for an additional period of 25 h, the reaction mixture was cooled to room temperature and potassium acetate (200 mg) was added. The resulting mixture was filtered and the residue washed thoroughly with methylene chloride. The filtrate was washed with water, dried, filtered, and concentrated. Flash chromatography of the residue on silica gel, eluting with 10% ether in petroleum ether, gave acetate **27** (81 mg; 61% yield), mp 119–120°C (ether – petroleum ether); ir: 1737 (acetate) and 1723 (α,β-unsaturated ester) cm^{-1}; ^{1}Hmr δ: 7.22 (s, 1H, =CH—), 5.74 (dd, 1H, J = 4, J' = 1.5 Hz, —CHO—), 3.75 (s, 3H, —$COOCH_3$), 2.03 (s, 3H, —$OCOCH_3$), 1.10 (s, 3H, —CH_3), and 0.89 (d, 3H, J = 7 Hz, —$CHCH_3$); ms: M^+ 280.1650 (calcd. for $C_{16}H_{24}O_4$: 280.1675). *Anal.* calcd. for $C_{16}H_{24}O_4$: C 68.55, H 8.63; found: C 68.54, H 8.59.

*8β-Hydroxy-2-(2-hydroxy-2-propyl)-8β,8aβ-dimethyl-3,4,4aβ,5,6,7,8,8a-octahydronaphthalene (**28**)*

At −78°C, a 1.6 *M* solution of methyllithium in ether (0.77 mL, 1.22 mmol) was added to a solution of acetate **27** (57 mg, 0.2 mmol) in tetrahydrofuran (5 mL) under an atmosphere of argon. The reaction mixture was allowed to warm up to room temperature. Ice-cold water was slowly added to destroy excess methyllithium. The resulting mixture was extracted with methylene chloride. The organic extracts were washed with water, dried, filtered, and concentrated. Flash chromatography of the residue on silica gel, eluting with 25% ethyl acetate in petroleum ether, gave diol **28** (45 mg; 93% yield); ir: 3480 and 3377 (—OH) cm^{-1}; ^{1}Hmr δ: 5.74 (s, 1H, =CH—), 4.51 (dd, 1H, J = 4.5, J' = 2 Hz, —$CHOH$), 1.47, 1.39 (both s, 3H each, —$C(CH_3)_2$), 1.00 (s, 3H, —CH_3), and 0.84 (d, 3H, J = 7 Hz, —$CHCH_3$); cims M^+: 238 ($C_{15}H_{26}O_2$).

*Petasitolone (**1**)*

Diol **28** (12.9 mg, 0.05 mmol) was dissolved in acetone (2 mL) and cooled to 0°C. Jones reagent (0.5 mL of 8 *N*, 4 mmol) was added. After stirring for 10 min, the reaction mixture was poured into water and extracted with methylene chloride. The organic extracts were washed with water, dried, filtered, and concentrated. Flash chromatography of the residue on silica gel, eluting with 20% ethyl acetate in petroleum ether, gave petasitolone (**1**) (10.1 mg, 79% yield); ir: 3450 (—OH) and 1719 (C=O) cm^{-1}; ^{1}Hmr δ: 6.73 (s, 1H, =CH—), 4.55 (s, 1H, —OH), 2.73 (dd, 1H, J = 16, J' = 12 Hz, —$COCHH$—), 1.46 (s, 6H, —$C(CH_3)_2$), 1.07 (s, 3H, —CH_3), and 0.97 (d, 3H, J = 7 Hz, —$CHCH_3$); ^{13}Cmr δ: 202.6, 154.7, 141.3, 71.7, 40.7, 39.4, 38.6, 35.8, 30.2, 29.3, 29.1, 26.9, 20.7, 20.4 and 15.8; ms: M^+ 236.2141 (calcd. for $C_{15}H_{24}O_2$: 236.2142).

Acknowledgements

We are grateful to the Natural Sciences and Engineering Research Council of Canada and the University of Alberta for financial support, to the Alberta Heritage Foundation for Med-

ical Research for a Studentship to T.K.N., and to Professor K. Naya and Mr. M. Shimizu of Kwansei Gakuin University for the ir, ^{1}Hmr, and ^{13}Cmr spectra of the natural petasitolone.

1. K. NAYA, F. YOSHIMURA, and I. TAKAGI. Bull. Chem. Soc. Jpn. **44**, 3165 (1971).
2. A. R. PINDER. Fortschr. Chem. Org. Naturst. **34**, 81 (1977).
3. J. A. MARSHALL and A. R. HOCHSTETLER. Chem. Commun. 732 (1967); E. PIERS and R. J. KEZIERE. Can. J. Chem. **47**, 137 (1969); R. M. COATES and J. M. SHAW. J. Org. Chem. **35**, 2597 (1970); E. PIERS and D. R. SMILIE. J. Org. Chem. **35**, 3997 (1970); E. PIERS, M. B. GERAGHTY, and R. D. SMILIE. Chem. Commun. 614 (1971); J. A. MARSHALL and T. M. WARME. J. Org. Chem. **36**, 178 (1971); J. A. MARSHALL and R. A. RUDEN. J. Org. Chem. **36**, 596 (1971); J. A. MARSHALL and G. M. COHEN. J. Org. Chem. **36**, 877 (1971); E. PIERS and M. B. GERAGHTY. Can. J. Chem. **51**, 2166 (1973); K. P. DASTUR. J. Am. Chem. Soc. **95**, 6509 (1973); H. M. MCGUIRE, H. C. ODOM, and A. R. PINDER. J. Chem. Soc. Perkin Trans. 1, 1879 (1974); F. E. ZIEGLER and P. A. WENDER. Tetrahedron Lett. 449 (1974); J. E. MCMURRY, J. H. HUSSER, M. S. AHMAD, and L. C. BLASZCJAK. J. Org. Chem. **40**, 1829 (1975); I. NAGAKURA, S. MAEDA, M. UENO, M. FUNANIZU, and Y. KITAHARA. Chem. Lett. 1143 (1975); F. BOHLMANN, H. J. FORSTER, and C. H. FISHER. Ann. 1487 (1976); F. E. ZIEGLER, G. R. REID, W. L. STUDT, and P. A. WENDER. J. Org. Chem. **42**, 1991 (1977); J. FICINI and A. M. TOUZIN. Tetrahedron Lett. 1081 (1977); K. YAMAKAWA and T. SATOH. Chem. Pharm. Bull. **26**, 3704 (1978); F. NAF, R. DECORZANT, and W. THOMMEN. Helv. Chim. Acta, **62**, 114 (1979); T. YANAMI, M. MIYASHITA, and A. YOSHIKOSHI. Chem. Commun. 525 (1979); T. HIYAMA, M. SHINODA, and H. NOZAKI. Tetrahedron Lett. 3529 (1979).
4. R. BESLIN, R. BLOCH, G. MOINET, and J. M. CONIA. Bull. Soc. Chim. Fr. 509 (1969); I. NAGAKURA, H. OGATA, M. UENO, and Y. KITAHARA. Bull. Chem. Soc. Jpn. **48**, 2995 (1975); F. FRINGUELLI, F. PIZZO, A. TATICHI. T. D. HALLS, and E. WENKERT. J. Org. Chem. **47**, 5056 (1982); J. DAS. Ph.D. Dissertation. University of New Brunswick. 1977.
5. H. J. LIU and T. K. NGOOI. Synth. Commun. 715 (1982).
6. Y. OHFUNE and M. TOMITA. J. Am. Chem. Soc. **104**, 3511 (1982).
7. R. MOZINGO. Org. Synth. Coll. Vol. **3**, 181 (1955).
8. F. KIENZLE and P. ROSEN. Helv. Chim. Acta, **62**, 442 (1979).
9. A. JUNG and R. ENGEL. J. Org. Chem. **40**, 3652 (1978).
10. Y. FUJIMOTO and T. TATSUNO. Tetrahedron Lett. 3325 (1976).
11. C. ALEXANDRE and F. ROUSSEAU. Bull. Soc. Chim. Fr. 1837 (1971).
12. C. DJERASSI, R. R. ENGLE, and A. BOWERS. J. Org. Chem. **21**, 1547 (1956).
13. H. J. REICH, J. M. RENGA, and I. L. REICH. J. Am. Chem. Soc. **97**, 5434 (1975).

Can. J. Chem. Downloaded from www.nrcresearchpress.com by 210.87.254.105 on 09/06/12
For personal use only.

Synthesis of thiaprotoberberines[1]

RICHARD MARSDEN AND DAVID B. MACLEAN[2]
Department of Chemistry, McMaster University, Hamilton, Ont., Canada L8S 4M1

AND

LAJOS FODOR
Central Laboratory, County Hospital, H-5701 Gyula, POB 46 Hungary

Received April 13, 1984

RICHARD MARSDEN, DAVID B. MACLEAN, and LAJOS FODOR. Can. J. Chem. **62**, 2682 (1984).

6,7-Dimethoxy-(2*H*)-1,3-benzothiazine undergoes reaction with phthalide anions yielding 13-hydroxy-8-oxo-5-thiaprotoberberines. The latter dehydrate readily to thia analogues of 8-oxoprotoberberines and in one case have been reduced to 5-thiaprotoberberines by treatment with phosphorus oxychloride followed by sodium borohydride. These compounds are members of a new heterocyclic ring system.

RICHARD MARSDEN, DAVID B. MACLEAN et LAJOS FODOR. Can. J. Chem. **62**, 2682 (1984).

La diméthoxy-6,7 (2*H*)-benzothiazine-1,3 réagit avec les anions phtalides en fournissant les hydroxy-13 oxo-8 thia-5 protoberbérines qui se déshydratent facilement pour conduire aux analogues thia des oxo-8 protoberbérines et qui, dans un cas, ont pu être réduites en thia-5 protoberbérines par un traitement avec de l'oxychlorure de phosphore suivi par une réaction avec du borohydrure de sodium. Ces composés font partie d'un nouveau système hétérocyclique.

[Traduit par le journal]

The reaction of phthalide anions with cylic imines in the form of 3,4-dihydroisoquinolines (1, 2) and with acyclic imines (2–4) has been described in several recent publications. Here we report the reaction of 6,7-dimethoxy-(2*H*)-1,3-benzothiazine **1** (5, 6) with anions derived from phthalide **2***a* and 5,6-dimethoxyphthalide **2***b*. The condensation products and their various transformation products are 5-thia analogues of the protoberberine ring system and represent a new heterocyclic ring system. A different approach to this ring system has recently been discovered and communicated (7). The ring system is systematically named and numbered as shown below.[3]

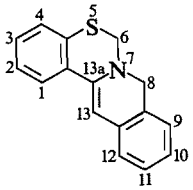

6*H*,8*H*-Isoquino[2,3-*c*][1,3]benzothiazine

A single product of condensation **3***a* was obtained when **1** and **2***a* were condensed together as shown in Scheme 1. Spectroscopic examination of the product and its *O*-acetate led to the structure shown in the formula. The ir spectrum supported the presence of an OH group and a lactam carbonyl in **3***a*. In the aliphatic region of the ^{1}H nmr spectrum the signals at δ 4.27 and δ 5.72 are assigned, respectively, to the protons at H-6_{ax} and H-6_{eq}. The shielding of the equatorial proton is in keeping with similar observations made for protons in the same environment in the 8-oxoprotoberberines (2). A two-proton signal at δ 4.8–4.9 has been assigned to H-13 and H-14, in **3***a*. Upon acetylation of **3***a* to **3***c* these protons now appeared at 4.99 and 6.39 as doublets (J = 8.0 Hz) and are assigned to H-14 and H-13, respectively. The observed coupling constant is compatible with a *trans* relationship between the two hydrogens. Other signals in the nmr spectra of **3***a* and **3***c* corroborate the assigned structures.

The condensation of **1** with **2***b* provided **3***b* as a single product of the reaction. The ir and ^{1}H nmr spectra of **3***a* and **3***b* are very similar. In the nmr, it is noteworthy that the signals associated with the protons at C-6, C-13, and C-14 show analogous behaviour to those in **3***a*, while the differences in the aromatic region are associated with the introduction of the two methoxy groups. It is evident therefore that the two compounds have the same structure and the same stereochemistry about C-13 and C-14.

The ^{13}C nmr spectra of **3***a* and **3***b* confirm the conclusions drawn from the other spectroscopic data, supporting as they do the substitution pattern in each case, and the presence of the lactam carbonyl. No attempt was made to assign the signals attributed to the aromatic carbon atoms other than to separate them on the basis of their coupling into two groups, one bearing hydrogen, and the other quaternary.

Both **3***a* and **3***b* suffer dehydration readily to the compounds **4***a* and **4***b*. The ir, ^{1}H nmr, and ^{13}C nmr spectra of these compounds support the structures assigned to them. The signals associated with H-13 and H-14 in the precursor molecules have disappeared and a new signal of area one attributed to H-13 has appeared in the aromatic region of the ^{1}H nmr but has not been specifically assigned.

Several unsuccessful attempts were made to reduce the lactam function of **3***a*. Complex mixtures, as judged by tlc, were obtained with lithium aluminum hydride in tetrahydrofuran, or with diborane in THF. When triethyloxonium fluoroborate followed by $NaBH_4$ was employed (8) the product was **4***a* and a similar result was observed when tetra-n-butyl ammonium borohydride was used (9).

The reduction of **4***b* with $POCl_3$–$NaBH_4$ (10) proceeded normally, however, yielding **5***b* in a 65% yield. The product lacked lactam absorption in its ir spectrum and displayed nmr properties that are compatible with the assigned structure. Unfortunately, in both the ^{13}C and ^{1}H nmr spectra the presence of several overlapping signals did not allow the unambiguous assignment of the structure, although the weight of evidence is in accord with the proposed structure.

[1] This paper may be regarded as Part 2 of the series "Thiaalkaloids". Part 1: see ref. 7.

[2] Author to whom correspondence may be addressed.

[3] We are indebted to K. L. Loening, Director of Nomenclature, Chemical Abstracts Service, for this information.

Can. J. Chem. Downloaded from www.nrcresearchpress.com by 210.87.254.42 on 09/06/12
For personal use only.

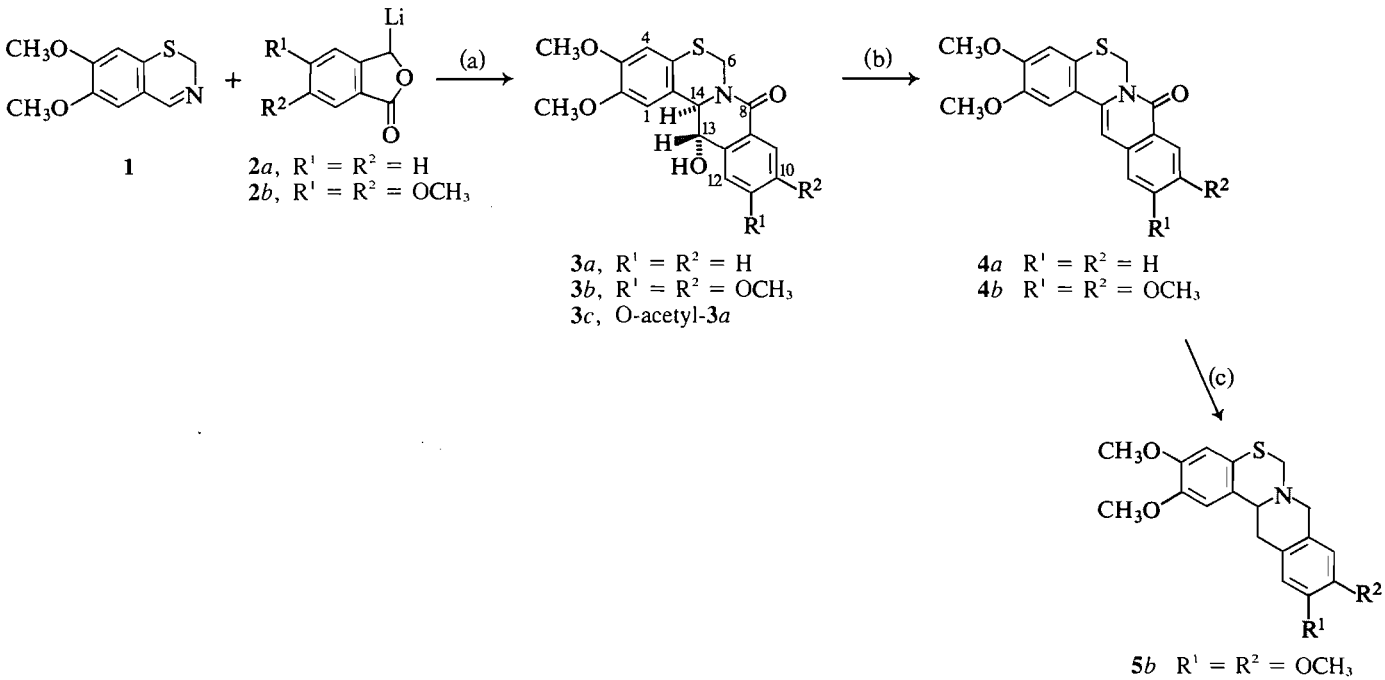

(a) THF, −35°C; (b) TsOH, C_6H_6; (c) $POCl_3$, $NaBH_4$ in MeOH

SCHEME 1

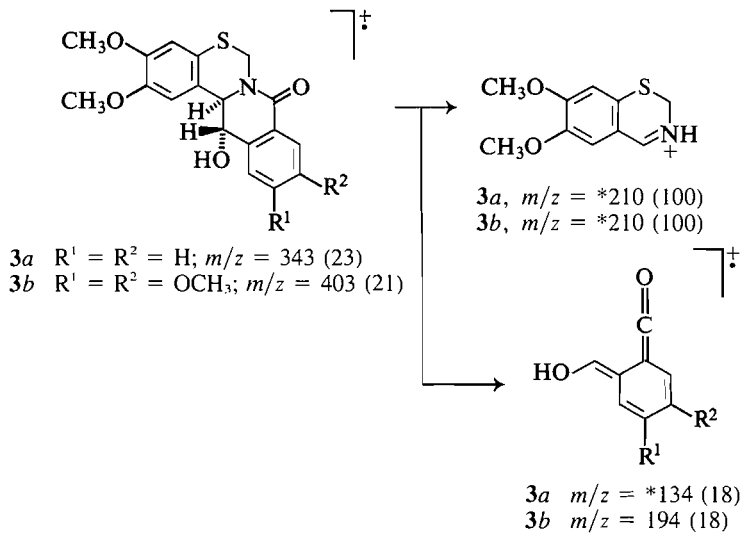

*Compositions verified by accurate mass analysis

SCHEME 2

Compound **4***a* failed to undergo reduction under conditions similar to those used successfully for **4***b*; the reaction product was mainly starting material, based on tlc examination, although a small amount of material of slightly higher R_f value was present. Under forcing conditions (refluxing $POCl_3$, 2 h, followed by $NaBH_4$) the starting material had disappeared, but we were unable to identify the product. Presumably the $POCl_3$–$NaBH_4$ procedure involves formation of a quaternary intermediate, bearing either Cl or $OPOCl_2$ at C-8, which then undergoes reduction by sodium borohydride. The formation of this intermediate would be aided by the methoxyl group at C-11 and this may account for the successful reduction of **4***b* but not of **4***a*.

The mass spectra of these compounds have been recorded and compared with similar structures in the protoberberine series. In the case of **3***a* and **3***b* the spectra are strictly analogous to the spectra of 13-hydroxy-8-oxoprotoberberines of similar substitution pattern (2). The fragmentation pattern is illustrated in Scheme 2. The composition of the fragment ions was established by accurate mass measurement. Compounds **4***a* and **4***b* both display strong molecular ions in their spectra and only a single intense fragment ion at $M - 33$. In both compounds this ion arises by loss of SH from the molecular ion as established by accurate mass measurement. Compound **5***b* behaves much as a tetrahydroprotoberberine alkaloid with a methoxyl substituent at C-10 and C-11 (11). It has, as shown

Can. J. Chem. Downloaded from www.nrcresearchpress.com by 210.87.254.42 on 09/06/12
For personal use only.

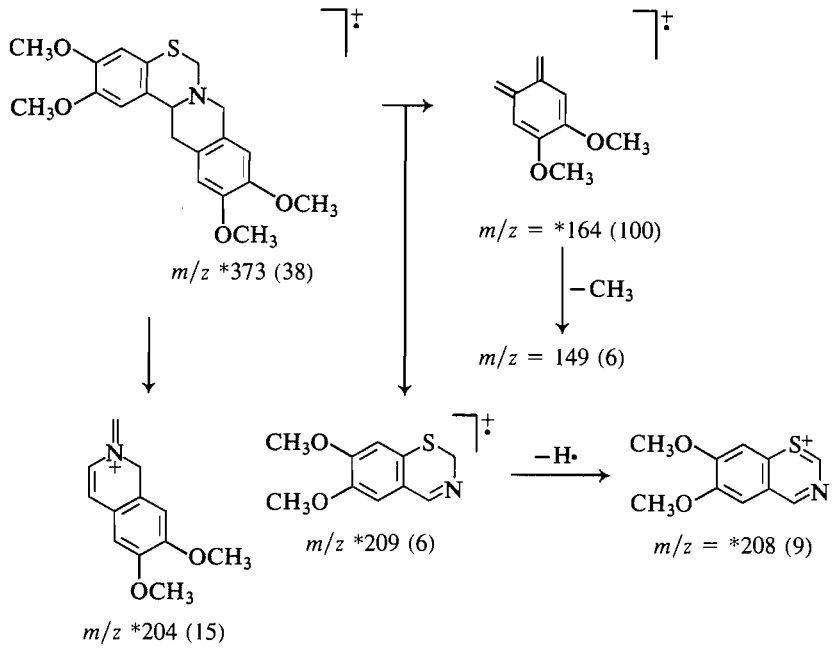

*Compositions verified by accurate mass analysis

SCHEME 3

in Scheme 3, a molecular ion of moderate intensity and a single intense fragment ion at m/z 164 which on further fragmentation yields an ion of low intensity at m/z 149. Ions of low intensity at m/z 208 and 209 represent the benzothiazine portion of the molecule and again the low intensity of these ions strictly parallels the situation with the protoberberines of comparable substitution pattern (11). It is proposed that the peak at m/z 204 may arise by fission of the S—C-6 bond followed by extrusion of the phenyl group by breaking of the bond between C-14 and C-14a. A comparable ion is not found in the spectra of the protoberberines. The mass spectral fragmentation patterns of the compounds studied show many similarities to those of the protoberberines and lend further support to the proposed structures.

It is apparent that **3***a* and **3***b* are formed stereoselectively in the same way that the 13-hydroxy-8-oxoprotoberberines are derived from lithium phthalides and 3,4-dihydroisoquinolines (2).

Experimental

Apparatus, materials, and methods

Unless otherwise stated, the ^{1}H nmr spectra were continuous wave, run at 90 MHz on a Varian EM 390 spectrometer. The samples were dissoved in $CDCl_3$ using tetramethylsilane (TMS) as the internal standard. Chemical shifts, quoted as δ values, were measured in relation to TMS. The symbols s, singlet, d, doublet, t, triplet, q, quartet, and m, multiplet are used in reporting spectra. The Fourier transform spectra were run on either a Bruker WP80 (80 MHz) or WM250 (250 MHz) spectrometer. The ^{13}C nmr spectra were run at 62.9 MHz on a Bruker WM250 FT spectrometer or at 20.115 MHz on a Bruker WP80 FT spectrometer, both at ambient temperature.

Mass spectra were recorded on a V.G. Micromass 7070 F mass spectrometer at 70 eV. Infrared spectra were recorded on a Perkin–Elmer 283 spectrometer in $CHCl_3$ solution. Melting points were determined using a Gallenkamp apparatus and are uncorrected. The microanalyses were performed by the Guelph Chemical Laboratories Ltd., Guelph, Ontario.

Thin-layer chromatography (tlc) was performed using Polygram Sil G/UV$_{254}$ plates. Flash column chromatography (12) was employed using Kieselgel 60 (230–400 mesh).

All reactions involving lithiation steps were carried out in flame-dried apparatus under a blanket of argon, using septa and syringes for transfer of reagents. Diisopropylamine was refluxed over calcium hydride and distilled onto molecular sieves (4A). THF was dried by distillation from Na/benzophenone under a nitrogen atmosphere just prior to use.

The following compounds were prepared by standard methods and gave satisfactory physical data: *m*-meconin (13) and 6,7-dimethoxy-(2*H*)-1,3-benzothiazine (5, 6).

trans-*13-Hydroxy-2,3-dimethoxy-8-oxo-5-thia-tetrahydroproto-berberine* **3***a*

To a stirred solution of diisopropylamine (0.14 mL, 1 mmol) in dry THF (5 mL) at −10°C was added n-BuLi (0.67 mL of a 1.65 *M* solution in hexane, 1.1 mmol). After 5 min the LDA solution was cooled to −70°C and treated dropwise with a solution of phthalide **2***a* (0.134 g, 1 mmol) in dry THF (5 mL), producing initially an orange solution. Towards the end of the addition a suspension was observed; homogeneity was restored by adjusting the temperature to −35°C. After stirring the solution at this temperature for 20 min, imine **1** (0.21 g, 1 mmol) in dry THF (5 mL) was added and the mixture stirred at −35°C for 1 h, allowed to warm to room temperature, and stirred overnight. Evaporation of solvent gave a yellow solid which was crystallized from EtOH following treatment with activated charcoal, yielding **3***a* as a cream colored crystalline powder (190 mg, 55.4%), mp 250–252°C (EtOH); ir: ν_{max}: 3600, 1655 cm^{-1}; ^{1}H nmr (DMSO-d_6) δ: 3.71 (3H, s, —OCH_3), 3.74 (3H, s, —OCH_3), 4.27 (1H, d, J = 12.0 Hz, H-6$_{ax}$), 4.8–4.9 (2H, d (collapsed AB quartet), H-13 and H-14), 5.72 (1H, d, J = 12.0 Hz, H-6$_{eq}$), 6.87 (1H, s, H-1 or H-4), 7.03 (1H, s, H-1 or H-4), 7.25–7.75 and 7.85–8.0 (4H, m, H-9, H-10, H-11, and H-12); ^{13}C nmr: 43.4 (C-6), 55.5, 55.7 (2 × OCH_3), 61.7 (C-14), 67.4 (C-13), 112.0, 114.4, 125.6, 127.1, 127.6, 132.1 (ArCH), 124.1, 124.7, 126.6, 141.0, 146.0, 148.0 (ArC), 161.7 (C-8); ms, m/z (%): 343 (23) M$^+$, 210 (100), 134 (18). *Anal.* calcd. for $C_{18}H_{17}NO_4S$: C 62.97, H 4.96, N 4.08; found: C 63.04, H 4.93, N 4.12%.

The 13-acetoxy derivative **3***c* was prepared by heating **3***a* under reflux in acetic anhydride and pyridine overnight. The solvent was

Can. J. Chem. Downloaded from www.nrcresearchpress.com by 210.87.254.42 on 09/06/12
For personal use only.

Can. J. Chem. Downloaded from www.nrcresearchpress.com by 210.87.254.42 on 09/06/12
For personal use only.

evaporated under high vacuum and the residue analysed by ^{1}H nmr ($CDCl_3$) δ: 2.10 (3H, s, $OCOCH_3$), 3.80 (3H, s, —OCH_3), 3.85 (3H, s, —OCH_3), 4.23 (1H, d, J = 12.0 Hz, H-6_{ax}), 4.99 (1H, d, J = 8.0 Hz, H-14), 5.87 (1H, d, J = 12.0 Hz, H-6_{eq}) 6.39 (1H, d, J = 8.0 Hz, H-13), 6.74 (1H, s, H-1 or H-4), 6.80 (1H, s, H-4 or H-1), 7.2–7.7 (3H, m, H-10, H-11, and H-12), 8.05–8.25 (1H, m, H-9).

trans-*13-Hydroxy-2,3,10,11-tetramethoxy-8-oxo-5-thiatetrahydroprotoberberine* **3**b

An LDA solution (1.5 mmol), prepared by the procedure described above, was treated dropwise at −70°C with a solution of *m*-meconin **2***b* (0.291 g, 1.5 mmol) in dry THF (15 mL). The resulting clear orange solution was stirred at −70°C for 20 min and treated with a solution of imine **1** (0.314 g, 1.5 mmol) in dry THF (10 mL). After stirring the solution at −70°C for 1 h the mixture was allowed to warm to room temperature and stirred overnight. The solvent was evaporated, water added, and the whole extracted with $CHCl_3$. Drying the extract (Na_2SO_4) and evaporation gave a yellow oil. Flash chromatography (silica, eluting with $CHCl_3$ + 0.5% MeOH) furnished **3***b* as a white powder (305 mg, 50.5%), mp 219–221°C (EtOH); ir: ν_{max}: 3610, 1650 cm^{-1}; ^{1}H nmr ($CDCl_3$) δ: 3.79 (3H, s, —OCH_3), 3.85 (3H, s, —OCH_3), 3.93 (3H, s, —OCH_3), 3.97 (3H, s, —OCH_3), 3.96 (1H, d (partially obscured by methoxy signal), H-6_{ax}), 4.77 (2H, s, H-13 and H-14), 5.78 (1H, d, J = 13.0 Hz, H-6_{eq}), 6.77 (1H, s, aromatic), 6.91 (1H, s, aromatic), 7.22 (1H, s, aromatic), 7.52 (1H, s, H-9); ^{13}C nmr: 44.5 (C-6), 56.4 (4 × OCH_3), 63.6 (C-14), 70.2 (C-13), 107.2, 111.2, 113.2, 114.0 (ArCH), 119.9, 123.8, 127.2, 134.5, 147.3, 149.0, 149.3, 153.2 (ArC), 163.2 (C-8); ms, *m*/*z* (%): 403 (21) M$^+$, 210 (100), 194 (18). *Anal.* calcd. for $C_{20}H_{21}NO_6S$: C 59.55, H 5.21, N 3.47; found: C 59.45, H 5.35, N 3.32%.

13,14-Didehydro-2,3-dimethoxy-5-thiaberbin-8-one, **4**a

Lactam **3***a* (145 mg) in benzene was treated with *p*-toluenesulfonic acid (50 mg) as in the case of **3***b*. Evaporation of solvent and crystallization of the residue from EtOH gave **4***a* as a white crystalline powder (125 mg, 91%), mp 222–224°C; ir: ν_{max}: 1640 cm^{-1}; ^{1}H nmr δ: 3.93 (3H, s, —OCH_3), 4.00 (3H, s, —OCH_3), 5.39 (2H, s, H-6_{ax} and H-6_{eq}), 6.80 (1H, s, aromatic H), 6.90 (1H, s, aromatic H), 7.30 (1H, s, aromatic H), 7.35–7.80 (3H, m, H-10, H-11, and H-12), 8.48 (1H, d, J = 8 Hz, H-9); ms, *m*/*z* (%): 325 (89) M$^+$, 292 (100). *Mol. wt.* calcd. for $C_{18}H_{15}NO_3S$: 325.077; found (hrms): 325.074.

13,14-Didehydro-2,3,10,11-tetramethoxy-5-thiaberbin-8-one, **4**b

Lactam **3***b* (120 mg) in benzene (40 mL) was heated under reflux in a Dean–Stark apparatus overnight over *p*-toluenesulfonic acid (50 mg). The cooled solution was washed with water (3 × 50 mL), evaporated to dryness, and crystallized from EtOH as a pale green powder (100 mg, 87.2%), mp 212–214°C; ir ν_{max}: 1650 cm^{-1}; ^{1}H nmr δ: 3.94 (3H, s, —OCH_3), 4.00 (3H, s, —OCH_3), 4.03 (6H, s, 2 × —OCH_3), 5.39 (2H, s, —SCH_2N—), 6.75 (1H, s, aromatic), 6.90 (1H, s, aromatic), 6.96 (1H, s, aromatic), 7.27 (1H, s, aromatic), 7.83 (1H, s, aromatic); ^{13}C nmr: 43.0 (C-6), 56.3, 56.4, 56.7 (4 × OCH_3), 104.1, 106.6, 108.3, 110.3, 111.4 (ArCH), 118.7, 124.0, 126.6, 132.2, 135.9, 148.6, 149.6, 150.4, 154.4 (ArC), 160.3 (C-8); ms, *m*/*z* (%): 385 (100), 352 (62). *Mol. wt.* calcd. for $C_{20}H_{19}NO_5S$: 385.098; found: 385.092.

2,3,10,11-Tetramethoxy-5-thiatetrahydroprotoberberine, **5**b[4]

The didehydro compound **4***b* (100 mg, 0.26 mmol) was dissolved in dry, ethanol-free chloroform (6 mL), treated with $POCl_3$ (4.5 mL, 48 mmol), and refluxed under argon for 1 h. The orange solution was evaporated to dryness, dry methanol (30 mL) was added, and the cooled stirred methanolic suspension was treated with $NaBH_4$ (120 mg, 3.2 mmol) in portions. The mixture was stirred for 0.5 h at room temperature, the solvent evaporated, water (15 mL) was added, and the crude product extracted with $CHCl_3$. The dried (Na_2SO_4), evaporated extract yielded a yellow oil which was subjected to flash chromatography (silica, eluting with $CHCl_3$). Crystallization of the major fraction from EtOH furnished white needles of **5***b* (63 mg, 65%), mp 171–173°C; ir ν_{max}: 2840 cm^{-1}; ^{1}H nmr (250 MHz) δ: 3.1–3.35 (2H, m, H-13_{ax} and H-13_{eq}), 3.75 (3H, s, —OCH_3), 3.80 (3H, s, —OCH_3), 3.82 (3H, s, —OCH_3), 3.85 (3H, s, —OCH_3), 4.05 (1H, t, J = 5.4 Hz, H-14), 4.22 (1H, d, J = 11.4 Hz, H-6_{ax}), 4.64 (1H, d, J = 11.4 Hz, H-6_{eq}), 6.47 (1H, s, aromatic), 6.65 (1H, s, aromatic), 6.67 (2H, s, 2 × aromatic). The integral of the 4 × —OCH_3 protons suggests an additional two protons, H-8_{ax} and H-8_{eq}, are present in the region δ 3.7–3.9; ^{13}C nmr: 33.0 (C-13), 51.7 (C-6 and C-8), 56.1 (C-14), 56.1, 56.3, 56.5, 56.9 (4 × OCH_3), 109.8, 111.2, 111.4, 111.9 (ArCH), 124.8, 125.0, 126.1, 126.2, 146.9, 147.9, 148.1, 148.5 (ArC); ms, *m*/*z* (%): 373 (38) M$^+$, 209 (6), 208 (9), 204 (15), 164 (100), 149 (6). *Anal.* calcd. for $C_{20}H_{23}NO_4S$: C 64.34, H 6.17, N 3.75; found: C 64.26, H 6.21, N 3.69%.

[4] The systematic names of the thiaberberines prepared in this study are listed: **3***a* (13*R**,13a*S**)-13,13a-dihydro-13-hydroxy-2,3-dimethoxy-6*H*,8*H*-isoquino[2,3-*c*][1,3]benzothiazin-8-one; **3***b* (13*R**,13a*S**)-13,13a-dihydro-13-hydroxy-2,3,10,11-tetramethoxy-6*H*,8*H*-isoquino[2,3-*c*][1,3]benzothiazine-8-one; **4***a* 2,3-dimethoxy-6*H*,8*H*--isoquino[2,3-*c*][1,3]benzothiazin-8-one; **4***b* 2,3,10,11-tetramethoxy-6*H*,8*H*-isoquino[2,3-*c*][1,3]benzothiazin-8-one; **5***b* (±)-13, 13a-dihydro-2,3,10,11-tetramethoxy-6*H*,8*H*-isoquino[2,3-*c*][1,3]benzothiazine.

Acknowledgements

The work at McMaster University was supported through an operating grant from the Natural Sciences and Engineering Research Council of Canada to whom we express our thanks. We thank F. Ramelan for the mass spectra and B. Sayer and I. Thompson for the nmr spectra.

1. R. MARSDEN and D. B. MACLEAN. Tetrahedron Lett. **24**, 2063 (1983).
2. R. MARSDEN and D. B. MACLEAN. Can. J. Chem. **62**, 1392 (1984).
3. D. J. DODSWORTH, M. P. CALIAGNO, U. E. EHRMANN, and P. G. SAMMES. Tetrahedron Lett. **21**, 5075 (1980).
4. D. J. DODSWORTH, M. P. CALCAGNO, E. U. EHRMANN, A. M. QUESADA, O. NUÑEZ S., and P. G. SAMMES. J. Chem. Soc. Perkin Trans. 1, 1453 (1983).
5. J. SZABO, L. FODOR, I. VARGA, E. VINKLER, and P. SOHAR. Acta Chim. Acad. Sci. Hung. **92**, 317 (1977).
6. J. SZABÓ, L. FODOR, I. VARGA, and P. SOHÁR. Acta Chim. Acad. Sci. Hung. **88**, 149 (1976).
7. L. FODOR, J. SZABÓ, G. BERNÁTH, and P. SOHÁR. Tetrahedron Lett. **25**, 2013 (1984).
8. R. F. BORCH. Tetrahedron Lett. 61 (1968).
9. D. J. RABER and W. C. GUIDA. J. Org. Chem. **41**, 690 (1976).
10. V. I. OGNYANOV, M. A. HAIMOVA, and N. M. MOLLOV. Heterocycles, **19**, 1069 (1982).
11. C. Y. CHEN and D. B. MACLEAN. Can. J. Chem. **46**, 2501 (1968).
12. W. C. STILL, M. KAHN, and A. MITRA. J. Org. Chem. **43**, 2923 (1978).
13. G. A. EDWARDS, W. H. PERKIN, JR., and F. W. STOYLE. J. Chem. Soc. **127**, 195 (1925).

The free energy barrier to rotation about the Csp^2—N bond in 4-bromo-2,6-difluoro-N-methylaniline. Molecular orbital calculations and experiments. Inversion

TED SCHAEFER, GLENN H. PENNER, KIRK MARAT, AND RUDY SEBASTIAN
Department of Chemistry, University of Manitoba, Winnipeg, Man., Canada R3T 2N2

Received March 21, 1984

TED SCHAEFER, GLENN H. PENNER, KIRK MARAT, and RUDY SEBASTIAN. Can. J. Chem. **62**, 2686 (1984).

The free energy barrier to internal rotation about the Csp^2—N bond in 4-bromo-2,6-difluoro-N-methylaniline in dimethylether solution is 23.1 ± 0.4 kJ/mol at 120 ± 2 K, as determined by demagnetization (lineshape) measurements of ^{19}F nmr spectra. In the same solvent, $\Delta G^{\ddagger}$ is some 7 kJ/mol higher for N-methylaniline. STO 3G MO calculations of the barrier in 2,6-difluoro-N-methylaniline are compared with calculations for the parent compound and its 2,6-dichloro derivative. The calculated barriers can be fit to a twofold potential and are V (kJ/mol) = (19.1 ± 0.9) $\sin^2$ (ϕ − 141.5 ± 0.7°) for N-methylaniline and V (kJ/mol) = (22.2 ± 0.8) $\sin^2$ (ϕ − 120.9 ± 0.8°) for the 2,6-difluoro derivative. The errors are given for the 95% confidence intervals. The angle ϕ is the C_2C_1NC dihedral angle. The barrier in the title compound is presumably a subtle compromise between opposing components consisting of conjugation, intra and intermolecular hydrogen bonding, and steric interactions. For 2,6-dimethyl-N-methylaniline in dimethyl ether no relative broadening of the ^{13}C nmr peaks was observed at 130 K, consistent with a very low barrier or with a ground state conformation in which, via inversion at nitrogen, the C-2 and C-6 relative chemical shift is averaged to zero. The computed geometry of an analogous compound implies that the N—H and N—(CH_3) bonds lie on opposite sides of the benzene plane in the conformation of lowest energy, so that inversion can coalesce the C-2 and C-6 shifts; the methyl group does not have to pass through the benzene plane for inversion to occur.

TED SCHAEFER, GLENN H. PENNER, KIRK MARAT et RUDY SEBASTIAN. Can. J. Chem. **62**, 2686 (1984).

Opérant à 120 ± 2 K et faisant appel à des mesures de démagnétisation (forme des raies) des spectres rmn du ^{19}F, on a trouvé que la barrière (énergie libre) à la rotation interne autour de la liaison Csp^2—N dans la bromo-4 difluoro-2,6 N-méthylaniline, en solution dans l'éther diméthylique, est de 23,1 ± 0,4 kJ/mol. Dans le même solvant, le $\Delta G^{\ddagger}$ de la N-diméthylaniline est environ 7 kJ/mol plus élevé. On compare des calculs d'orbitales moléculaires, sur la base STO 3G, de la barrière dans la difluoro-2,6 N-méthylaniline avec ceux effectués sur le composé de base et sur son dérivé dichloro-2,6. On peut adapter les barrières calculées à un potentiel binaire; pour la N-méthylaniline, V (kJ/mol) = (19,1 ± 0,9) $\sin^2$ (ϕ − 141,5 ± 0,7°), alors que pour le dérivé difluoro-2,6, V (kJ/mol) = (22,2 ± 0,8) $\sin^2$ (ϕ − 120,9 ± 0,8°). On rapporte les erreurs pour les intervalles de confiance de 95%. L'angle ϕ est l'angle dièdre C_2C_1NC. La barrière observée dans le composé mentionné dans le titre est probablement un compromis subtil entre des composantes qui s'opposent comme la conjuguaison, les liaisons hydrogènes intra- et intermoléculaires et les interactions stériques. Dans le cas de la diméthyl-2,6 N-méthylaniline en solution dans l'éther diméthylique que l'on a examinée par rmn du ^{13}C à 130 K, on n'a pas observé d'élargissement relatif des raies; ce résultat est en accord avec la présence d'une barrière à la rotation qui serait très faible ou avec l'existence d'une conformation dans l'état fondamental de laquelle la moyenne des déplacements chimiques relatifs des carbones C-2 et C-6 est égale à zéro. La géométrie que l'on a calculée pour un composé analogue implique que, dans la conformation de plus basse énergie, les liaisons N—H et N—(CH_3) se trouvent de part et d'autre du plan du benzène de façon à ce que l'inversion puisse provoquer une coalescence des déplacements des carbones en C-2 et en C-6; il n'est pas nécessaire que le groupe méthyle passe à travers le plan du benzène pour que l'inversion se produise.

[Traduit par le journal]

Introduction

The free energy of activation, $\Delta G^{\ddagger}$, for rotation about the Csp^2—N bond in N-methylaniline in dimethylether solution is 30.29 ± 0.08 kJ/mol, somewhere between 147 and 160 K (1). Substitution at the *para* position by a π electron donor (acceptor) leads to decreases (increases) in $\Delta G^{\ddagger}$, as expected if the barrier to rotation depends on the mobile bond order of the C—N bond (2). It also appears that there is a substantial solvent effect on the internal rotational barrier (2–4). Vapour phase infrared experiments (4), together with an assumption of a twofold cosine potential, yield 14.5 ± 2.0 kJ/mol as the magnitude of the barrier, to be compared with 25.5 kJ/mol for $\Delta G^{\ddagger}$ in $CHFCl_2$–CHF_2Cl solution and with the 30.3 kJ/mol in ether solution. An STO 3G MO computation gave 37.9 kJ/mol (1).

The heavy atoms in N-methylaniline are unlikely to be coplanar in the minimum-energy conformation (4–6), aniline having a pyramidal arrangement at nitrogen (7, 8). Large *ortho* substituents could possibly produce a conformation of lowest energy in which the N—C(H_3) bond tends towards a plane perpendicular to the benzene plane, thereby relieving steric repulsions between the methyl group and the *ortho* substituents. Thus, for 2-methyl-N-methylaniline and for its 4-nitro derivative (2), only the one conformer, that with the two methyl groups in a *trans* orientation, could be detected. Substitution by two *ortho* substituents might therefore lead to a perpendicular conformation.

Such is *not* found for derivatives of N-methylaniline with two *ortho* nitro groups (9, 10), the Arrhenius activation energy, E_a, rising to 52.3 ± 0.8 kJ/mol in 2,6-dinitro-Nmethylaniline and to 60.7 ± 1.3 kJ/mol in the presence of an additional nitro substituent at the *para* position (CD_2Cl_2 solution). These relatively large barriers probably arise from intramolecular hydrogen bonding in the ground state, suggested as 21 to 29 kJ/mol (9, 10), together with the decrease in the C—N double bond character as the transition state is approached. A *para* nitro substituent increases $\Delta G^{\ddagger}$ for N-methylaniline by about 17 kJ/mol (2, 3). *Ortho* nitro substituents should induce similar changes in the C—N mobile bond order, so that the barrier in these picrates may also include destabilization of the ground

Can. J. Chem. Downloaded from www.nrcresearchpress.com by 210.87.254.40 on 09/06/12
For personal use only.

Can. J. Chem. Downloaded from www.nrcresearchpress.com by 210.87.254.40 on 09/06/12
For personal use only.

state by steric repulsions between the nitro groups and the *N*-alkyl substituent. In that way the much smaller barrier in the *N-tert*-butyl picrate, too small to be measurable by the lineshape methods employed for the smaller alkyl groups (11, becomes plausible.

Now, a *para* fluorine substituent decreases the internal barrier by 1.4 ± 0.3 kJ/mol (2) in dimethylether solution, no doubt because fluorine is a π electron donor. As an *ortho* substituent, fluorine may again reduce the C—N mobile bond order, but it may also act as a hydrogen bond acceptor in the form C—F . . . H—N (an electrostatic interaction). Furthermore, a C—F bond presents a larger van der Waals volume to a methyl group than does a C—H bond. For example, the twofold barrier to rotation about the Csp^2—Csp^3 bond for the ethyl group in ethylbenzene is raised by as much as 20 kJ/mol when hydrogen is replaced by fluorine to yield the 2,6-difluoro derivatives (11). This increase may well be predominantly steric in origin.

Of course, in 2,6-difluoro-*N*-methylaniline the geometry about nitrogen deviates rather more from tetrahedral (including the lone pair as a direction) than it does about the α carbon in ethyl benzene. Consequently, the ground state conformation will not be analogous to **1**, the preferred conformation of the

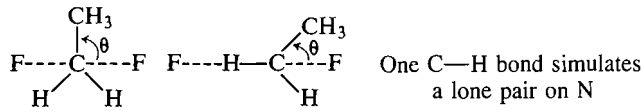

1 **2**

latter, with θ = 90°, but will have θ rather less than 60°, similar to **2**. In fact, the N—H and C—CH_3 bonds are later calculated to lie above the benzene plane for the 2,6-difluoro-*N*-methylaniline (see **3** below), yet do fall on opposite sides of this plane for the 2,6-dichloro derivative (see **5** below).

The actual barrier to internal rotation could be smaller or larger than in *N*-methylaniline, depending on the interplay of the opposing factors mentioned above. Of course, if the steric repulsions were large enough to overcome the conjugation energy, then the conformation might resemble **1** and perhaps lead to only very small Larmor frequency differences for nuclei acting as marker sites in a dynamic nuclear magnetic resonance experiment (dnmr).

In this paper, dnmr experiments are reported for 4-bromo-2,6-difluoro-*N*-methylaniline in dimethylether solution. The bromine substituent, like a chlorine substituent in 4-chloro-*N*-methylaniline (2), serves to raise the barrier sufficiently so as to be measurable with the technology available in this laboratory. The barrier in 2,6-difluoro-*N*-methylaniline is computed at the STO 3G level of *ab initio* molecular orbital theory (12) and is compared with calculations on *N*-methylaniline and its 2,6-dichloro derivative. These calculations give *some* insight into the ground and transition state geometries.

Experimental

The 2,6-difluoroaniline (Aldrich) was brominated in acetic acid solution in the usual way to yield its 4-bromo derivative. *N*-methylation was carried out exactly as described by Johnstone *et al.* (13), giving a compound with the expected ^1H nmr spectrum and mass peaks.

A solution in dimethylether, containing 0.11 g of the aniline, 0.11 g of acetone-d_6, 1.5 mL of dimethylether, and 1 drop of C_6F_6 was transferred on a vacuum line to a 5-mm od nmr sample tube. The latter was flame sealed and stored in a refrigerator while not in use. The

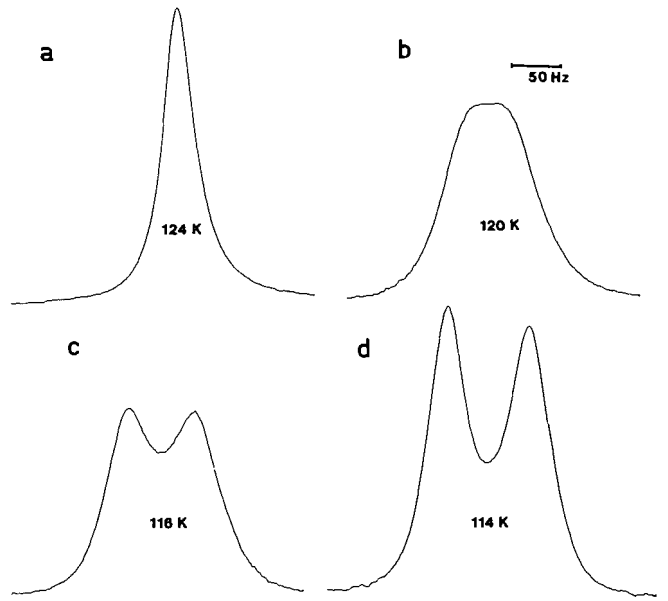

FIG. 1. The ^{19}F nmr spectrum of 2,6-difluoro-*N*-methylaniline in dimethyl ether solution at 84.700 MHz. The spectra were accumulated as described in the text. The coalescence temperature is very near 120 K and complete separation of the doublet has not occurred at 114 K, the lowest temperature attained.

acetone-d_6 was used for internal locking purposes and C_6F_6 served as a linewidth standard.

The ^{19}F nmr spectra were recorded in the FT mode on a WH90 nmr spectrometer at 84.700 MHz (centerband), under conditions of ^1H noise decoupling. The amplitude of the decoupling field was kept low enough to prevent significant sample heating. The pulse width was 5 μs, roughly a 90° pulse, the digitized response was accumulated for 1.02 s into 4 K and the sweep width was 2000 Hz. These conditions applied at temperatures where the peak widths were rather large. As many as 64 scans were performed. At the lowest temperatures, shimming was performed on the FID of the C_6F_6 and the sample was not spun. A very high flow rate of cooling gas was necessary in order to reach 114 K and the temperature was checked by means of a copper–constantan thermocouple. Spectra were accumulated at a given temperature reached from lower as well as from higher temperatures, so that a check on lineshapes obtained near and at coalescence temperatures was possible.

STO 3G MO computations employed an Amdahl 470/V8 system.

Results and discussion

The free energy barrier, $\Delta G^{\ddagger}$

Some typical ^{19}F spectra are displayed in Fig. 1. At 114 K a distinct asymmetry in the unresolved doublet is observable. It is conceivable that stereospecific coupling over three bonds between ^{14}N and ^{19}F nuclei causes a slight broadening of one of the peaks in the doublet. As the temperature increases, the ^{14}N quadrupolar relaxation rate would increase and the asymmetry would decrease. More likely is the presence of a small impurity also yielding a broad peak and lying under the taller peak. A weak impurity peak, lying near the main band, was noticeable at higher temperatures. It was not observable at the low temperatures used during the experiment and may have broadened and moved in the spectral region of interest. In any event, although the source of the peak was not identified, our estimate is that the observed asymmetry caused a negligible contribution to the error quoted for $\Delta G^{\ddagger}$ below.

It is quite clear that the available range of temperatures, 114 K to 135 K, in which a noticeable linewidth difference exists

Can. J. Chem. Downloaded from www.nrcresearchpress.com by 210.87.254.40 on 09/06/12
For personal use only.

between reference and substrate peaks, is too small for a reliable decomposition of $\Delta G^{\ddagger}$ into $\Delta H^{\ddagger}$ and $\Delta S^{\ddagger}$ parameters, particularly as a complete separation into two peaks could not be achieved at the lowest attainable temperature, 114 K. From the repeated experiments at 118 to 120 K, together with thermocouple measurements of the temperatures indicated by the dial settings on the Bruker B-VT-1000 variable temperature controller, it is safe to state that the coalescence temperature, T_c, is 120 ± 2 K. Furthermore, a conservative estimate of $\delta\nu$, the peak separation at zero exchange rate, is 96 ± 5 Hz. The total width at half height at coalescence is the sum of the static splitting and the natural width (14). The width at coalescence was 100 ± 2 Hz and the reference peak had a width of 4 ± 1 Hz. Accordingly, the value of $\Delta G^{\ddagger}_{120}$ can be written (15) as $\Delta G^{\ddagger}_{120}$ (kJ/mol) = $1.914 \times 10^{-2} T_c[9.972 + \log (T_c/\delta\nu)]$ or 23.1 ± 0.4 kJ/mol, using eq. 7.13 of ref. 15. As in the previous studies (2, 3), a transmission coefficient of unity was assumed. This $\Delta G^{\ddagger}_{120}$ is 7 kJ/mol lower than for *N*-methylaniline in the same solvent (1, 3) at 138 K, presumably too large a difference to account for by differences in $\Delta S^{\ddagger}$ for the two compounds.

Molecular orbital calculations

It would be preferable to use a basis set larger than minimal, the one employed in the present STO 3G computations. It would also be very expensive. It may be noted, however, that a recent set of geometry optimizations (16) with STO 3G for benzoyl X compounds (X = H, F, CH_3) gave internal rotational barriers 3.1 kJ/mol too high but in the correct order, and that for phenol the STO 3G barrier was 4.0 kJ/mol too large.

For 2,6-difluoro-*N*-methylaniline, geometry optimization of the sidechain, as well as of the exocyclic bond angles and lengths (keeping the benzene carbon skeleton as a regular hexagon) gave the geometry in Fig. 2, as well as the dihedral angles in **3**. The C_1—N bond direction is tilted 3.9° from the benzene plane, **4**. Furthermore, the methyl group is calculated to be

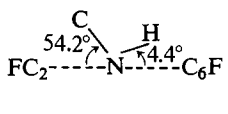

3

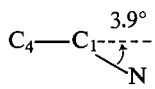

4

almost exactly staggered with respect to the C_1—N bond (61.4, 181.4, and 301.4°). With reference to **3**, the corresponding calculated angles for *N*-methylaniline are 32.5 and 23.8°, whereas they are 76.0 and −16.0° for the 2,6-dichloro derivative, as in **5** and **6**. With reference to **4**, the tilt angles are 3.7° and 2.7° for the compounds depicted in **5** and **6**, respectively. The H—C—N—C_1 dihedral angles are 72.6, 192.6, 312.6° and 58.5, 178.5, and 298.5° (methyl protons constrained to define an equilateral triangle) for **5** and **6**.

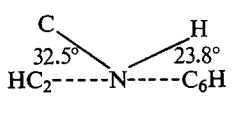

5

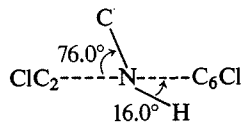

6

Comparison of **3**, **5**, and **6** implies increasing steric repulsion between the methyl group and the *ortho* C—X bond. As X changes from H to F to Cl, the CNC_1C_2 dihedral angle increases from 32.5 to 54.2 to 76.0°. The Csp^2—N bond is also calculated to increase from 1.449 to 1.451 to 1.454 Å (1 Å ≡ 100 pm). In going from **5** to **3**, the HNC_1C_6 dihedral angle decreases by nearly 20°, probably because of twisting about the Csp^2—N bond and increased electrostatic interaction between the N—H^+ and C—F^- dipoles (hydrogen bonding). In the 2,6-dichloro derivative, the N—H and N—$C(H_3)$ bonds lie on opposite sides of the benzene plane. Considerable loss of conjugation between the lone pair on nitrogen and the π orbitals is implied on stepping from H to F to Cl as *ortho* substituents.

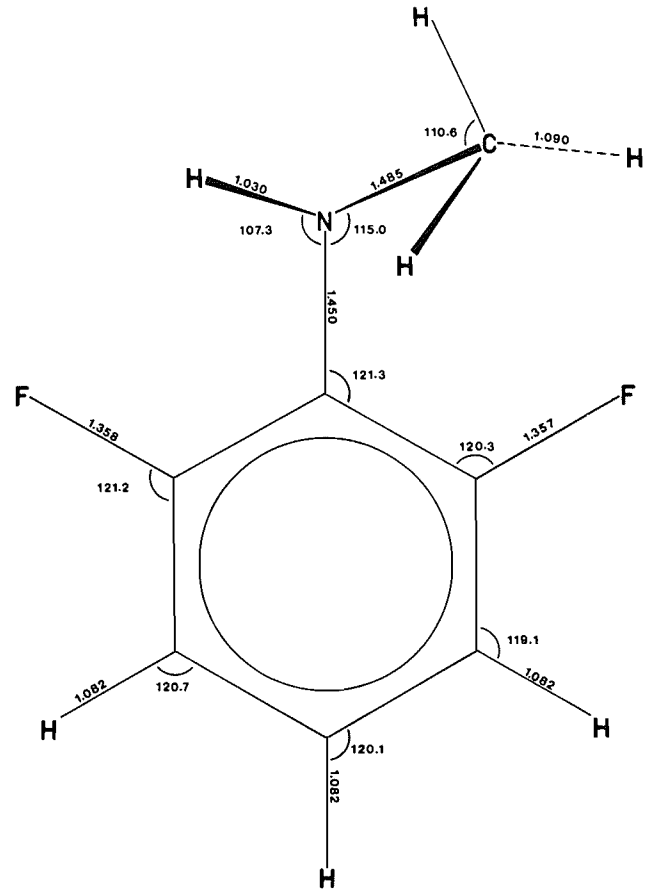

FIG. 2. The computed ground-state structure of 2,6-difluoro-*N*-methylaniline at the STO-3G level of molecular orbital theory. A regular hexagon was assumed for the carbon atom arrangement in the benzene ring. Dihedral angles can be found in the text. One C—H bond of the methyl group lies in a plane at 11° to the ring plane.

The computed barriers

In Figs. 3 and 4 the STO 3G MO energies, relative to their respective ground states, are plotted for *N*-methylaniline and its 2,6-difluoro derivative. The curves represent least-squares fits to the computed points for twofold barriers of the form *V* (kJ mol) = (19.1 ± 0.9) $\sin^2$ (ϕ − 141.5 ± 0.7°) for the parent molecule and *V* (kJ mol) = (22.2 ± 0.8) $\sin^2$ (ϕ − 120.9 ± 0.8°) for the fluorinated compound. The errors are given for 95% confidence intervals. Part of the error arises from difficulties experienced in the geometry optimizations insofar as the computed energies at ϕ = 0° and 180° are unequal. The optimization procedure, sequential variation of bond angles and lengths, proceeded by 15° increments from ϕ = 0° to 180°. The final energy depended somewhat on the starting geometry for ϕ = 180°, which was that for ϕ = 165°. It must therefore be true that at least some of the computed points in the figures

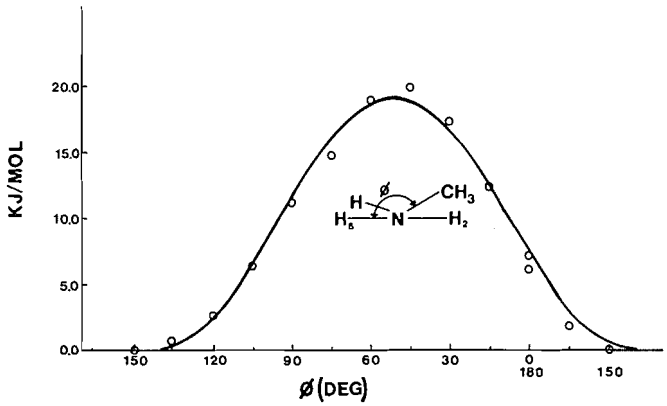

FIG. 3. The computed energies for *N*-methylaniline are plotted as a function of the dihedral angle, ϕ. The solid curve represents a twofold potential fit to the points and is given by V (kJ mol) = (19.1 ± 0.9) $\sin^2$ (ϕ − 141.5 ± 0.7°). The quoted errors are for a 95% confidence interval. The ground-state energy is −320.78804 au for the STO 3G MO computation.

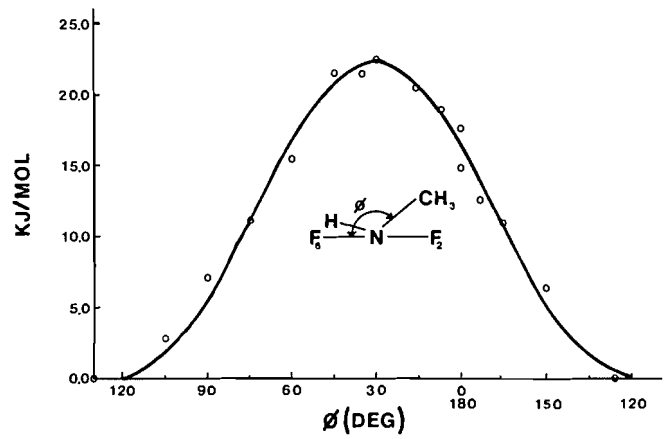

FIG. 4. As for Fig. 3, for 2,6-difluoro-*N*-methylaniline and V (kJ mol) = (22.2 ± 0.8) $\sin^2$ (ϕ − 120.9 ± 0.8°). The STO 3G MO energy for the ground state is −515.70377 au.

have an uncertainty[1] of perhaps as large as 1 kJ/mol. The ground state energies of *N*-methylaniline and 2,6-difluoro-*N*-methylaniline were computed as −320.788044 and −515.703773 au, respectively, at ϕ values of 147.5° and 125.8°.

Comparison of these angles with the fitted twofold potentials above shows that the latter are not exact representations of the computed barriers, as expected. However, they are a good approximation and support the assumption of twofold barriers in the treatment of torsion data (4). Such data imply that the barrier to C_1—N rotation in *N*-methylaniline is 9.8 ± 2.5 kJ/mol lower than in aniline (4, 17). A lower barrier is likely due to steric repulsion between the methyl group and the *ortho* C—H bond, leading to destablization of the ground state in *N*-methylaniline. The shielding of the C-4 nucleus in *N*-methylaniline is very nearly that of C-4 in aniline (18), implying very similar $2p \ldots \pi$ conjugation in the two compounds. That CH_3 repulsive interactions are present is made plausible by the twofold steric barrier of 5.0 kJ/mol in ethylbenzene (19), where the top of the barrier is reached when the methyl group lies in the benzene plane.

Turning to the 2,6-difluoro derivative, an augmented repulsive interaction between the methyl group and the *ortho* C—F bond is expected. This expectation is supported by the smaller calculated ϕ value in the ground state relative to the parent compound and by the observation that the repulsive barrier in 2,6-difluoroethylbenzene (11) is 20 ± 8 kJ/mol higher than in ethylbenzene. That the computed barrier in 2,6-difluoro-*N*-methylaniline is about 3 kJ/mol *higher* than in *N*-methylaniline can be attributed partly to the breaking of the attractive N—$H^+ \ldots {}^-F$—C interaction (the internal hydrogen bond in planar 2-fluorophenol has an energy of about 6 kJ/mol (20)), but also to the fact that the phases and amplitudes of the repulsive and attractive components of the barriers in the two compounds are different. The nitrogen lone pair also has steric requirements (21). At present a further decomposition of the calculated torsion barriers seems infeasible.

However, the inversion barriers are also of interest. In *N*-methylaniline, the inversion barrier is 2.3 ± 0.5 kJ/mol (4); our calculation gives 16 kJ/mol, an overestimate similar to that found for aniline itself (8). Clearly, a larger basis set is needed, as demonstrated for aniline (8). Presumably the inversion barrier in 2,6-difluoro-*N*-methylaniline will be larger than in *N*-methylaniline.

Our calculations for the barrier to rotation of the methyl group in the latter gave 11.7 kJ/mol, the methyl torsion data yielding 12.9 ± 0.2 kJ/mol on the assumption of a threefold potential (4).

Correlations of $\Delta G^{\ddagger}$ *with* V_2 *in* para *substituted thiophenols*

For thiophenol and its *para* substituted derivatives, the *J* method (22, 23) has been used to derive twofold potentials, V_2, for rotation about the C—S bonds. The preferred conformation is planar for thiophenol. V_2 decreases for π electron donors. Indeed, in the *para* amino and methoxy derivatives the preferred conformations have the S—H bond in a plane perpendicular to the benzene plane.

For the five *para* substituents (H, OCH_3, F, Cl, NO_2) common to the thiophenol (23) and *N*-methylaniline (2) derivatives, the correlation between V_2 and $\Delta G^{\ddagger}$ is reasonably good, having a correlation coefficient of 0.965, significant at the 95% confidence level. The V_2 values are derived from data for CCl_4 solutions and assume a twofold cosine potential. In view of the solvent effects on $\Delta G^{\ddagger}$ for the *N*-methylaniline derivatives and the fact that $\Delta G^{\ddagger}$ *may* contain an entropy contribution, the correlation is perhaps as good as could be expected. The correlation is here offered as evidence that both sets of barriers are a reflection of the changes induced in the mobile bond orders of the C—S and C—N bonds by the *para* substituents and that a *para* methoxy substituent does indeed change the ground state conformational preference of the sulfhydryl group.

Furthermore, the correlation can be used to estimate the increase in the $\Delta G^{\ddagger}$ value caused by a *para* bromine substituent in *N*-methylaniline as 2.1 ± 0.3 kJ/mol; the V_2 for the corresponding bromothiophenol being known (23). This estimate may be compared with the increase of 1.9 ± 0.3 kJ/mol in $\Delta G^{\ddagger}$ measured for the 4-chloro substituent (2) in *N*-methylaniline. Consequently, the $\Delta G^{\ddagger}$ for 2,6-difluoro-*N*-methylaniline in dimethyl ether solution could well be as low as 21 kJ/mol and would not be measurable at 114 K and 84.7 MHz because the rate constant would be about 600 s^{-1} instead of near 60 s^{-1} for the title compound.

[1] An automatic geometry optimization procedure is now available to us and gives a ground state geometry for the 2,6-difluoro compound insignificantly different from that in Fig. 2.

Can. J. Chem. Downloaded from www.nrcresearchpress.com by 210.87.254.40 on 09/06/12
For personal use only.

TABLE 1. Experimental and theoretical rotational barriers about the Csp^2—N bond in *N*-methylaniline and 2,6-difluoro-*N*-methylaniline

	$\Delta G^{\ddagger}$ (kJ/mol)		V_2 (kJ/mol)	
Compound	DME[a]	Freon[b]	Gas[c]	STO 3G MO
N-methyl	30.3 ± 0.08	25.5 ± 0.4	14.5 ± 2.0	19.1 ± 0.9[f]
2,6-diF	21.0 ± 0.7[d]	—	17.6 ± 3.7[e]	22.2 ± 0.8[f]

[a] Dimethyl ether solution (1).
[b] $CHFCl_2$–CHF_2Cl (1 to 4 by vol.), from ref. 3.
[c] From torsion data (4).
[d] The 4-bromo-2,6-difluoro-*N*-methylaniline in ether solution has 23.1 ± 0.4 kJ/mol; see text for an estimate of 21.0 kJ/mol for the 2,6-difluoro-*N*-methylaniline.
[e] Estimated as explained in the text.
[f] For geometry optimized conformations.

The barriers in solution and the gas phase

In dimethyl ether solution, the free energy barrier in 2,6-difluoro-*N*-methylaniline is definitely smaller than in the parent compound, contrary to the computed values above. One may reason as follows. In the gas phase, V_2 is 14.5 ± 2.0 kJ/mol for *N*-methylaniline (4). As mentioned, for a series of benzoyl X compounds (X = H, F, CH_3) and for phenol (16) the computational methods employed here yielded barriers between 3 and 4 kJ/mol higher than experimental, estimated in the gas phase. Comparison of V_2 with the STO 3G MO number for *N*-methylaniline suggests a similar situation, in that the computed barrier is 4.6 ± 2.9 kJ/mol too high. Application of this number to the computed barrier of 22.2 kJ/mol for 2,6-difluoro-*N*-methylaniline implies a gas phase barrier of 17.6 ± 3.7 kJ/mol, that is, higher than for the parent compound. A gas phase torsion study would be of interest.

Turning to the ether solutions, the solvent increases the barrier of *N*-methylaniline by 15.8 ± 2.1 kJ/mol, that is by more than its gas phase magnitude.[2] In the previous section, an estimate for 2,6-difluoro-*N*-methylaniline was made as 21.0 ± 0.7 kJ/mol. Therefore, the ether solvent appears to have increased the internal barrier by only 3.4 ± 3.3 kJ/mol, as expected if the *ortho* fluorine substituents with their polar $^{+}C—F^{-}$ bonds severely restrict hydrogen bonding between N—H and the lone pairs on the solvent oxygen atoms, $^{-}O—C_2^{+}$, or, at least, interfere with the approach of the solvent molecules to the $NHCH_3$ moiety.

Table 1 contains data summarizing the reasoning employed in the last few paragraphs.

Because the computed dipole moments of the ground and transition states of *N*-methylaniline differ by only 0.14 D, being 1.35 and 1.49 D, respectively,[3] it appears unlikely that dielectric continuum models (24) could account for the large increase in the barrier in ether solution, at least at the dipole level. In fact, the transition state would be stabilized by such an interaction (unless, of course, quadrupole interaction energies were to reverse this expectation).

All these comparisons are based on the assumption that $\Delta S^{\ddagger}$ is unimportant. The sparse data on *N*-methylaniline in ether solution (1) indicate as much.

*Concerning 2,6-dimethyl-*N*-methylaniline*

The methyl group is larger than a fluorine substituent. The following experiments and calculations were performed on 2,6-dimethyl-*N*-methylaniline (Bader, Aldrich). The ^{13}C nmr spectra at 23.63 MHz were recorded from a solution containing 1 g of the compound, 3 mL of dimethyl ether, and 0.5 g of acetone-d_6. At 130 K, the temperature at which precipitation of the compound became marked, no relative broadening of the C-2, C-6 peak was observable. In *N*-methylaniline itself the shift difference between C-2 and C-6 is 6.0 ppm at 140 K. If this were also true for the dimethylaniline, then it would follow that an upper limit to $\Delta G^{\ddagger}$ would be 24.6 kJ/mol. However, in *N-tert*-butylaniline, the corresponding shift difference is only 3.6 ppm, presumably because the conformation of the ground state is one in which the *tert*-butyl group lies nearer a plane perpendicular to the benzene ring than does the methyl group in the ground state of *N*-methylaniline. If the C-2,C-6 internal shift in the 2,6-dimethyl-*N*-methylaniline is only 3.6 ppm, then an upper limit to $\Delta G^{\ddagger}$ for rotation about the C_1—N bond becomes 25.2 kJ/mol.

These conclusions may well be vitiated by the following arguments. STO-3G MO computations gave 75° for the $C_2C_1N(CH_3)$ dihedral angle in the minimum energy conformation (see **6**), that is, a geometry near that of the 2,6-dichloro derivative. Repeated attempts at full geometry optimizations, as done for *N*-methylaniline and the 2,6-difluoro derivative, resulted in nonconvergence even after 9-h runs. In any event, it seems likely that the ground state is strongly destabilized by the two *ortho* methyl substituents.

This supposition is supported by the chemical shift of C-4. After a correction for the presence of the two methyl substituents, δ_4 is 122.0 at 200 K. In *N*-methylaniline in the same solvent at 200 K, δ_4 is 115.8(3). δ_C in benzene is 128.5. The high-field shift due to π electron donation by the lone pair on nitrogen is therefore reduced by a factor of one half in the presence of the *ortho* methyl groups.

The photoelectron spectrum (26) of 2,6-dimethyl-*N*-methylaniline may in interpreted to mean that the angle between the lone-pair direction and the plane perpendicular to the benzene ring is as large as 44°. Referring to **3** to **6**, it seems reasonable that the angle between the N—(CH_3) bond and ring plane is therefore near 75°.

Now, if the N—(CH_3) bond were in a plane perpendicular to the benzene ring, inversion at nitrogen, as in **7** ⇌ **8**, would lead to a coalescence of the chemical shifts of C-2 and C-6. Even if the N—(CH_3) bond direction deviates somewhat from the perpendicular but leaves the N—H bond on the opposite side of

[2] In view of the experimental errors, any discrimination between V_2 and other barrier forms (questions of ground state energies and the difference between $\Delta H^{\ddagger}$ and V_2, etc) is immaterial at present.

[3] The dipole moment of *N*-methylaniline is 1.67 D in benzene solution (25).

Can. J. Chem. Downloaded from www.nrcresearchpress.com by 210.87.254.40 on 09/06/12
For personal use only.

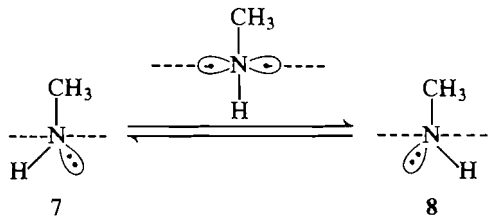

7 8

the benzene plane, as appears probable for 2,6-dimethyl-*N*-methylaniline from the STO-3G MO computations, then inversion will average the C-2 and C-6 relative shift to zero because the N—(CH_3) bond need only move a little near its energy minimum. However, when the N—H and N—(CH_3) bonds lie on the same side of the benzene plane, inversion will not cause such an averaging process.

Although the C_1—N rotational barrier could not be computed for 2,6-dimethyl-*N*-methylaniline, some calculations were done for the 2,6-dichloro derivative, in which the N—H and N—(CH_3) bonds apparently also sit on opposite sides of the benzene plane in the low-energy conformation (see **6**). For example, as the dihedral angle in **6**, C_2C_1NC, decreases to zero, the energy of the molecule increases by 24.2 kJ/mol and this value is still below the maximum barrier. However, torsion by 20° from the equilibrium conformation requires only about 7 kJ/mol, so that a concerted motion to yield the mirror image of **6** is very likely much faster than rotation by 180° about the C_1—N bond.

It appears, therefore, that inversion at nitrogen causes coalescence of the C-2 and C-6 chemical shifts in 2,6-dimethyl-*N*-methylaniline and that, in general, barriers to rotation about the C_1—N bond in *ortho* disubstituted *N*-methylaniline derivatives will not be available from dnmr experiments if the N—H and N—(CH_3) bonds are situated on opposite sides of the benzene plane; the inversion rate will then always be much larger than the rotation rate and too large for the measurement of the dephasing of magnetization due to Larmor site exchange.

Further molecular orbital calculations

For aniline itself, the STO-3G geometry is reasonably good, having an angle of 51° between the NH_2 and benzene plane (8); the experimental value is 38° (27). At the 4-21G level of theory, our calculations yield a planar aniline geometry and a very similar result for *N*-methylaniline, the H—N—C(H_3) plane lying within a degree or two of the benzene plane. Clearly, the introduction of other orbital-type functions (28) is necessary if an improvement over the STO 3G geometries in this paper is to be achieved.

Acknowledgments

We are grateful to the Natural Sciences and Engineering Research Council of Canada for financial support and to the University of Manitoba Computer Center for generous allocations of computing time.

1. L. Lunazzi, C. Magagnoli, M. Guerra, and D. Macciantelli. Tetrahedron Lett. 3031 (1979).
2. L. Lunazzi, C. Magagnoli, and D. Macciantelli. J. Chem. Soc. Perkin Trans. 2, 1705 (1980).
3. F. A. L. Anet and M. Ghiaci. J. Am. Chem. Soc. **101**, 6857 (1979).
4. R. A. Kydd and A. R. C. Dunham. J. Mol. Struct. **98**, 39 (1983).
5. R. Cervellati, G. Corbelli, A. DalBorgo, and D. G. Lister. J. Mol. Struct. **73**, 31 (1981).
6. R. Cervellati, A. DalBorgo, and D. G. Lister. J. Mol. Struct. **65**, 293 (1980).
7. D. G. Lister, J. K. Tyler, J. N. Høg, and N. W. Larsen. J. Mol. Struct. **23**, 253 (1974).
8. A. Wolf, U. Voets, and H.-H. Schmidtke. Theor. Chim. Acta (Berl.) **54**, 175 (1979).
9. J. Heidberg, J. A. Weil, G. A. Janusonis, and J. K. Anderson. J. Chem. Phys. **41**, 1033 (1964).
10. J. v. Jouanne and J. Heidberg. J. Am. Chem. Soc. **95**, 487 (1973).
11. T. Schaefer, R. P. Veregin, R. Laatikainen, R. Sebastian, K. Marat, and J. L. Charlton. Can. J. Chem. **60**, 2611 (1982).
12. W. J. Hehre, W. A. Lathan, R. Ditchfield, M. D. Newton, and J. A. Pople. Quantum Chemistry Program Exchange, **11**, 236 (1979).
13. R. A. W. Johnstone, D. W. Payling, and C. Thomas. J. Chem. Soc. (C), 2223 (1969).
14. G. Binsch and H. Kessler. Angew. Chem. Int. Ed. Engl. **19**, 411 (1980).
15. J. Sandström. Dynamic NMR spectroscopy. Academic Press, New York. 1982. p. 96.
16. T. Schaefer, T. A. Wildman, and R. Sebastian. J. Mol. Struct. (Theochem.) **89**, 93 (1982).
17. N. W. Larsen, E. L. Hansen, and F. M. Nicolaisen. Chem. Phys. Lett. **43**, 584 (1976).
18. V. Formacek, L. Desnoyer, H. P. Kellerhals, and J. T. Clerc. ^{13}C Data Bank. Vol. 1. Copyright Bruker-Physik, Karlsruhe. 1976.
19. T. Schaefer, L. Kruczynski, and W. Niemczura. Chem. Phys. Lett. **38**, 498 (1976).
20. G. L. Carlson, W. G. Fateley, A. S. Manocha, and F. F. Bentley. J. Phys. Chem. **76**, 1553 (1972).
21. D. Gust and M. W. Fagan. J. Org. Chem. **45**, 2511 (1980).
22. W. J. E. Parr and T. Schaefer. Acc. Chem. Res. **13**, 400 (1980).
23. T. Schaefer and T. A. Wildman. Chem. Phys. Lett. **80**, 280 (1981).
24. R. J. Abraham and E. Bretschneider. *In* Internal rotation in molecules. *Edited by* W. J. Orville-Thomas. Wiley & Sons, New York. 1974. Chapt. 13.
25. G. A. Barclay, R. J. W. LeFevre, and B. M. Smythe. Trans. Faraday Soc. **46**, 812 (1950).
26. S. A. Cowling and R. A. W. Johnstone. J. Electron Spectrosc. Rel. Phenom. **2**, 161 (1973).
27. D. G. Lister, J. K. Tyler, J. H. Høg, and N. W. Larsen. J. Mol. Struct. **23**, 253 (1974).
28. A. Szabo and N. S. Ostund. Modern quantum chemistry. Macmillan, New York. 1982. p. 202.

Can. J. Chem. Downloaded from www.nrcresearchpress.com by 210.87.254.40 on 09/06/12
For personal use only.

The phenyl group as a hydrogen bond acceptor in 2-phenylphenol derivatives. Substituent comparisons

TED SCHAEFER, TIMOTHY A. WILDMAN, RUDY SEBASTIAN, AND DAVID M. MCKINNON
Department of Chemistry, University of Manitoba, Winnipeg, Man., Canada R3T 2N2

Received April 13, 1984

TED SCHAEFER, TIMOTHY A. WILDMAN, RUDY SEBASTIAN, and DAVID M. MCKINNON. Can. J. Chem. **62**, 2692 (1984).

The disagreement about the free energy of formation, ΔG, of the intramolecular O—H . . . π bond in 2-phenylphenol is resolved by the measurement of stereospecific spin–spin coupling constants between ring protons and the hydroxyl proton. In CCl_4 solution at 305 K, ΔG is $5.1_5 \pm 1.06$ kJ/mol, in reasonable agreement with a value from hydroxyl stretching band studies. The free energy preferences of the phenyl group relative to chlorine, iodine, and the allyl group are also estimated from long-range couplings in the appropriate derivatives of 2-phenylphenol. A ranking of free energy preferences is given for twelve *ortho* substituents in phenol derivatives in CCl_4 solution. Relative to a methyl group, the free energy difference favoring the O—H . . . π interaction is 1500 ± 350 J/mol for an allyl and is 6500 ± 1030 J/mol for a phenyl group.

TED SCHAEFER, TIMOTHY A. WILDMAN, RUDY SEBASTIAN et DAVID M. MCKINNON. Can. J. Chem. **62**, 2692 (1984).

On a résolu le désaccord qui existait relativement à l'énergie libre de formation, ΔG, de la liaison intramoléculaire O—H . . . π dans le phényl-2 phénol, en mesurant les constantes de couplage spin–spin stéréospécifiques entre les protons du cycle et le proton hydroxyle. A 305 K et en solution dans le CCl_4, le ΔG est égal à $5,1_5 \pm 1,06$ kJ/mol; cette valeur est en bon accord avec une valeur obtenue en étudiant les bandes de vibration de la liaison hydroxyle. Utilisant les couplages à longue distance dans les dérivés appropriés du phényl-2 phénol, on a aussi évalué les préférences, du point de vue de l'énergie libre, du groupe phényle par rapport au chlore, à l'iode ou au groupe allyle. On a établi un ordre, du point de vue de l'énergie libre, des préférences de douze groupes *ortho* dans des dérivés phénoliques en solution dans le CCl_4. Par rapport à un groupe méthyle, la différence d'énergie libre favorisant l'interaction O—H . . . π est égale à 1500 ± 350 J/mol pour un groupe allyle et elle est égale à 6500 ± 1030 J/mol pour un groupe phényle.

[Traduit par le journal]

Introduction

The intramolecular OH . . . π hydrogen bond in 2-phenylphenol, **1** (R^2 = phenyl, $R^4 = R^6$ = H), has been examined by means of hydroxyl stretching (1–4) and torsional (5) frequencies, and by dipole moment measurements (6). Over a range of 50°C in CCl_4 solution, the temperature dependence of the intensities of the hydroxyl stretching bands assigned to **1***b* and **1***a* yielded an enthalpy difference, ΔH, of -6070 ± 1130 J/mol favoring **1***b*. The entropy difference, ΔS, was reported as -1.4 ± 3.5 J/mol K (2), implying a free energy difference, ΔG, of -5640 ± 2200 J/mol at 305 K. For reasons given in an examination of errors inherent to such studies (7), it may well be that this ΔS value is uncertain. Repetition of such experiments indicated ΔH as either greater than 10.4 kJ/mol or smaller than 2.1 kJ/mol (5). Another investigation (3) also reports infrared measurements for **1** in CCl_4 solution, presumably near room temperature. The ratio of the intensities of the hydroxyl stretching bands is 6.4, interpretable as a free energy difference of 4700 J/mol at 305 K or 4600 J/mol at 298 K if the absorptivities of the two bands are equal. There is some evidence for their equality to within about 5% (8). The most recent infrared measurements (4) on **1** in various solvents report an intensity ratio of 6.7, at 35°C, but it is unclear in which solvent this value was found.

Although there were difficulties with the assignment of the torsional frequencies of the hydroxyl group in cyclohexane solution, a potential energy of 11.4 kJ/mol (roughly equivalent to ΔH) favoring **1***b* was tentatively suggested. The dipole moment of **1** was consistent with a preferred OH . . . π interaction (6).

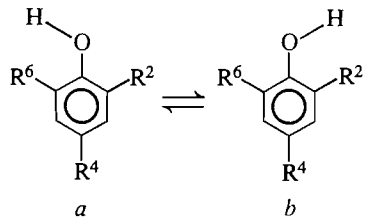

1: R^2 = phenyl, $R^4 = R^6$ = H
2: $R^2 = R^6$ = phenyl, R^4 = H
3: R^2 = phenyl, R^6 = allyl, R^4 = H
4: R^2 = phenyl, $R^4 = R^6$ = I
5: R^2 = phenyl, R^4 = H, R^6 = Cl
6: R^2 = phenyl, R^4 = I, R^6 = H

The existence of an attractive OH . . . π interaction is supported by the crystal structure of 2,6-diphenylphenol, **2** ($R^2 = R^6$ = phenyl, R^4 = H), in which to within experimental error the hydrogen atom of the hydroxyl group lies above the C_1—C_2 bond of R^2 at a distance of 2.42 Å from the two carbon atoms. The hydroxyl group appears to be twisted by 5° away from coplanarity with its own phenyl group. The 6-phenyl group is twisted by 44° and the other phenyl group, involved in the OH . . . π bond, by 52° out of the plane of the phenol ring (9). The latter angle is substantiated by ultraviolet spectra, interpreted to yield 50° in **1** (3).

Ultraviolet and infrared spectra (3) indicate an increased OH . . . π interaction as the dihedral angle between the two benzene rings increases. One conclusion (3) has it that the interaction depends mainly on the π orbital of C-1 on the phenyl ring, giving rise to a charge transfer between the antibonding orbital of the hydroxyl group and the donating occupied π orbital. This conclusion is at variance with the geometry of **2**, with the very similar infrared absorbances of phenol and **1** (8), and very likely also with some recent photoelectron spectroscopy data (10) on OH . . . π systems. These imply a predominantly electrostatic OH . . . π hydrogen bonding energy, requiring little charge transfer.

Now, it has been shown (11–13) that the stereospecific spin–spin coupling constant over five formal bonds between the hydroxyl proton and the ring protons in the *meta* position, $^5J_m^{OH,H}$, yields reliable free energy differences between *a* and *b* conformers of phenol derivatives in solution.[1] This approach

[1] An exception is 2-*tert*-butylphenol (14), but not its 6-substituted derivatives.

Can. J. Chem. Downloaded from www.nrcresearchpress.com by 210.87.254.6 on 09/06/12
For personal use only.

TABLE 1. The ^{1}H nmr spectral parameters for 2-phenylphenol at 100.001 MHz in CCl_4 solution at 305 K

Parameter	1.9 mol%	4.6 mol%	Parameter	1.9 mol%	4.6 mol%
ν_{OH}	497.938(13)[a]	499.750(5)[b]	$^3J_{45}$	7.357(11)	7.366(8)
ν_3	711.805(9)	710.495(5)	$^3J_{56}$	8.132(13)	8.136(8)
ν_4	686.677(9)	685.567(5)	$^4J_{35}$	1.718(10)	1.732(6)
ν_5	714.813(10)	713.065(5)	$^4J_{46}$	1.182(2)	1.183(5)
ν_6	687.280(7)	685.384(4)	$^5J_{36}$	0.437(13)	0.419(8)
$^5J_m^{OH,3}$	0.05(2)[c]	0.06(2)[c]	rms deviation	0.0151	0.0153
$^5J_p^{OH,4}$	[d]	[d]			
$^5J_m^{OH,5}$	0.434(11)	0.403(6)	Observed peaks	33	42
$^4J_o^{OH,6}$	[d]	[d]	Assigned transitions	35	75
$^3J_{34}$	7.610(11)	7.614(7)	Calculated transitions	79[e]	81[e]

[a] In Hz at 100.001 MHz to low field of internal tetramethylsilane.
[b] Numbers in parentheses are standard deviations in the last one or two significant figures.
[c] Estimated from linewidth changes in H-3 and H-5 peaks and spectral simulations while decoupling the hydroxyl protons.
[d] No evidence found for finite magnitudes.
[e] Above a relative intensity of 0.05; note that the signal-to-noise ratio for the 1.9 mol% solution was poor, leading to fewer assigned transitions and larger errors in the spectral parameters.

assumes $^5J_m^{OH,5} \equiv {}^5J_m^{OH,H\text{-}5} = 0$ in *a* and $^5J_m^{OH,3} \equiv {}^5J_m^{OH,H\text{-}3} = 0$ in *b*, so that ΔG can be found from $-RT \ln ({}^5J_m^{OH,5}/{}^5J_m^{OH,3})$. Because of the disagreements among the techniques mentioned above, it was decided to use $^5J_m^{OH,H}$ as an indicator of ΔG for **1** in CCl_4 solution. Furthermore, because the allyl group and the halogens had previously been examined by this method as hydrogen bond acceptors in phenol derivatives (12, 15), **3** (R^2 = phenyl, R^6 = allyl, R^4 = H), **4** (R^2 = phenyl, $R^4 = R^6$ = I), **5** (R^2 = phenyl, R^6 = Cl, R^4 = H), and **6** (R^2 = phenyl, R^6 = H, R^4 = I) were also studied in an attempt to rank the phenyl group as a hydrogen bond acceptor. Compound **2** was also examined. Full analyses of the ^{1}H nmr spectra were performed.

This paper reports the results of these experiments and concludes that the phenyl group ranks below the halogens but above allyl, trifluoromethyl, and saturated hydrocarbon groupings as a hydrogen bond acceptor. No evidence is found for a significant decrease in entropy on formation of the intramolecular OH . . . π bond in 2-phenylphenol.

Experimental

Compounds **1**, **2**, and **5** came from Aldrich Chemical Co. Compounds **4** and **6** were minor and major products, respectively, of a standard iodination procedure. Thin-layer chromatography on silica gel with 10 v/v% $CHCl_3$ in CCl_4 gave 2-phenyl-4-iodophenol, **6**, and 2-phenyl-4,6-diiodophenol, **4**, which yielded satisfactory ^{1}H nmr and mass spectra. Compound **3**, 6-allyl-2-phenylphenol, was prepared via 2-allyloxybiphenyl. The latter was made by reaction of equimolar quantities of **1**, allyl chloride, and NaOH in ethanol. This mixture was heated at reflux for 3 h and worked up by dilution with water. The material was purified by chromatography on silica gel in petroleum ether. The compound (1 g) was heated at 230°C under nitrogen for 1 h. The crude product, **3**, was dissolved in 1:1 v/v benzene/petroleum ether and chromatographed on silica gel. A fast-running colorless band was removed and purified by rechromatography (thick-layer) in benzene/petroleum ether. Compound **3** was obtained as a viscous colorless oil.

Samples for ^{1}H nmr spectroscopy were prepared in 5-mm od Pyrex tubes and were degassed by eight freeze–pump–thaw cycles before being flame sealed. Intermolecular hydroxyl proton exchange was retarded by procedures previously described (15). Concentrations of **1** to **6** in various solvents are given in the tables below. The ^{1}H nmr spectra were calibrated on an HA100 nmr spectrometer at a probe temperature of 305 K. The calibration procedures for this instrument have been described in detail and yield typical standard deviations of the peak frequencies of $\leq$0.02 Hz (16).

Results and discussion

1. *Spectral analyses*

These were performed with the computer program LAME (17, 18). The protons of the phenyl groups in all but **5** were too tightly coupled for an analysis. For **5** an analysis of the complete spectrum was made. Table 1 presents the spectral parameters obtained for two different samples of **1** in CCl_4 solution. Table 2 gives only those spectral parameters of immediate interest to the discussion for **1** to **6**. Figure 1 demonstrates the spectral quality obtained for those compounds. Some inter-ring proton coupling may have contributed to the observed linewidths. Certainly for **6**, some coupling exists between the hydroxyl proton and the phenyl ring protons. The allyl spectrum for **3** was analyzed, yielding coupling parameters very similar to those found for 2-allylphenol and some derivatives (12).

2. *The phenyl group as an acceptor of and competitor for the hydrogen bond*

In the following discussion, $^5J^{OH,H}$ numbers are used: first, to establish the free energy preference of **1***b* in 2-phenylphenol; second, to show the phenyl group in competition with other hydrocarbon substituents for the hydrogen bond; third, to make similar comparisons with halogen substituents. Finally, based on $^5J^{OH,H}$ values, there is given a ranking of the phenyl group as a hydrogen bond acceptor for a variety of substituents.

(i) 2-Phenylphenol, 1

It has been successfully argued previously (11–15) that the free energy difference, ΔG, between conformers *a* and *b* is given simply by $-RT \ln ({}^5J_m^{OH,5}/{}^5J_m^{OH,3})$. For **1**, dilution from 4.6 to 1.9 mol% in CCl_4 causes a highfield shift of 0.02 ppm in δ_{OH}, implying negligible intermolecular self-association at

Can. J. Chem. Downloaded from www.nrcresearchpress.com by 210.87.254.6 on 09/06/12
For personal use only.

TABLE 2. Some spectral parameters for compounds **1** to **6** at 305 K in CCl_4

Compound	R^2	R^4	R^6	Mol%	$^5J_m^{OH,5}$	$^5J_m^{OH,3}$	ν_{OH}
1	C_6H_5	H	H	1.9	0.434(11)[a]	0.05(2)	497.9[b]
1	C_6H_5	H	H	4.6	0.403(6)	0.06(2)	499.8
2	C_6H_5	H	C_6H_5	3.0	0.321(4)	0.321(4)	510.8
3	C_6H_5	H	Allyl[c]	4	0.577(6)	0.08(2)[d]	506.6
4	C_6H_5	I	I	4.3	0.204(8)	0.394(8)	535.2
5	C_6H_5	H	Cl	4.5	0.085(20)[d]	0.534(5)	550.1
5	C_6H_5	H	Cl	7.0[e]	[e]	0.523(7)	547.5
6	C_6H_5	I	H	4.2	0.396(10)	0.05(2)[d]	501.0
6	C_6H_5	I	H	2.8[f]	0.401(3)	0.169(3)	460.7

[a] Numbers in parentheses are the standard deviations in the last one or two significant figures.
[b] In Hz at 100.001 MHz to low field of internal tetramethylsilane.
[c] Long-range couplings from the methylene protons to the ring protons are $^4J_o = -0.609(5)$, $^5J_m = 0.282(5)$, and $^6J_p = -0.413(5)$ Hz.
[d] Simulation of peak widths obtained under single resonance and double resonance (decoupling of hydroxyl proton) conditions.
[e] In CS_2 solution, $^5J_m^{OH,5}$ not measured.
[f] In C_6D_6 solution.

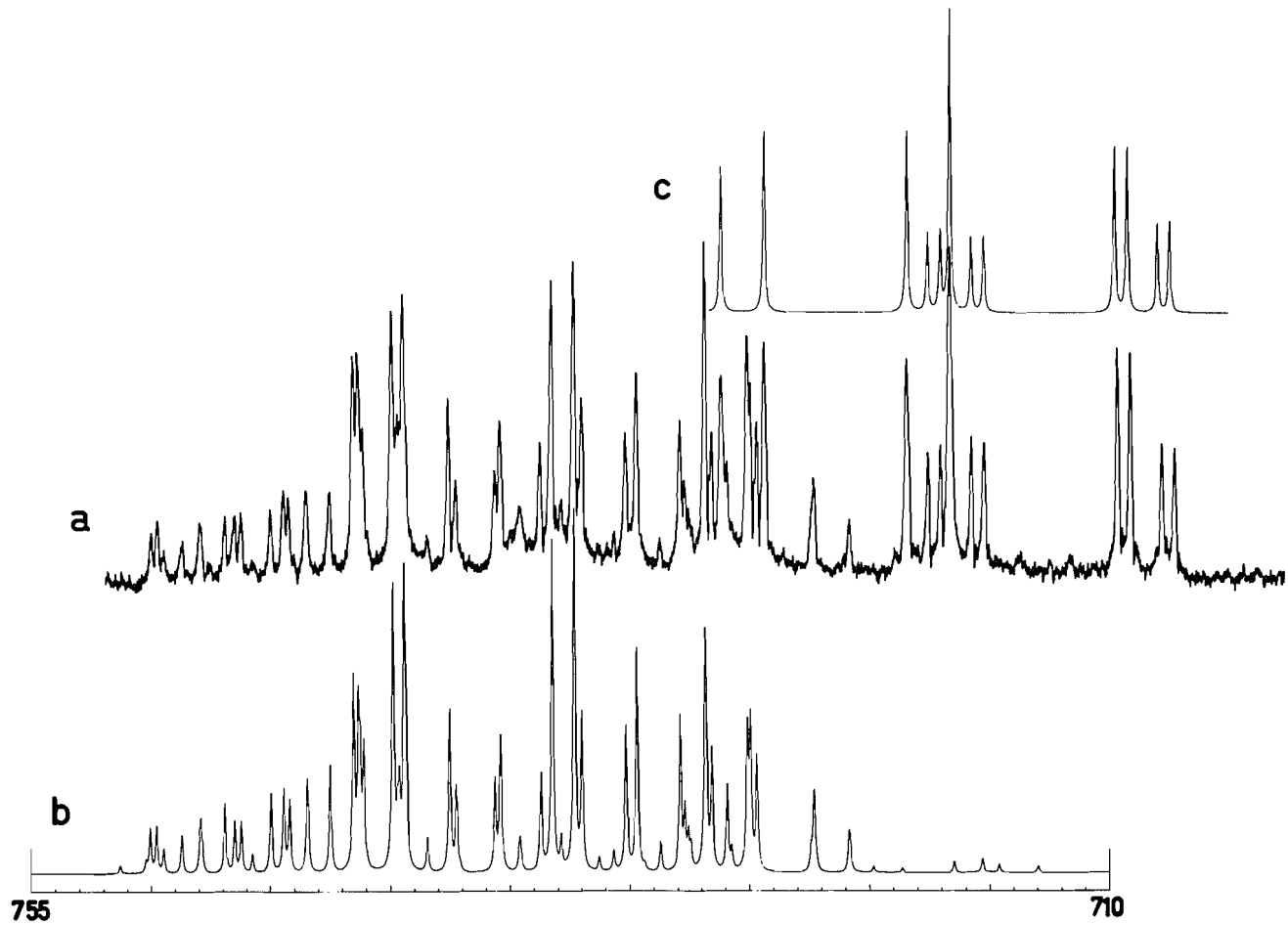

FIG. 1. In (a) a region of the aromatic ^1H nmr spectrum at 100 MHz and 305 K is shown for 2-phenyl-6-chlorophenol, **5**, as a 4.5 mol% solution in CCl_4. The spectrum of H-4 does not occur in this region. In (b) the computed spectrum of the phenyl protons is displayed, and in (c) the computed spectrum of H-3 and H-5 is given. Some impurity peaks are evident in the experimental spectrum. The linewidths at halfheight, $\Delta\nu_{1/2}$, are substantial for some peaks, indicating unresolved coupling to the hydroxyl proton. Thus, the four peaks due to H-3, centered at 717 and 725 Hz relative to internal TMS, decrease in width from 0.22 to 0.15 Hz upon strong irradiation of the hydroxyl proton peaks, while the doublets due to H-5 collapse to single peaks having $\Delta\nu_{1/2}$ as 0.15 Hz. Many of the peaks from the phenyl protons also sharpen under these conditions.

these concentrations. It may also be noted that a detailed dilution study of 2-methyl-4-chlorophenol (11) showed that at these concentrations intermolecular association does not alter the free energy differences calculated for the intramolecular equilibrium from $^5J_m^{OH,H}$. For **1** at 1.9 mol% in CCl_4, signal-to-noise problems lead to higher errors in $^5J_m^{OH,H}$ than for the 4.6 mol% solution (Tables 1 and 2). Nevertheless, the data for the more dilute solution are included in the calculation of ΔG,

Can. J. Chem. Downloaded from www.nrcresearchpress.com by 210.87.254.6 on 09/06/12
For personal use only.

Can. J. Chem. Downloaded from www.nrcresearchpress.com by 210.87.254.6 on 09/06/12
For personal use only.

leading to 5150 ± 1060 J/mol at 305 K favoring conformation *b*, the intramolecularly hydrogen bonded form. The relatively large error in ΔG has its origin in the small magnitude of ${}^5J_m^{OH,3}$ and the concomitant large relative error in this parameter.

Comparison with the infrared data, discussed above, clearly favors the initial results from the hydroxyl stretching band intensities (2) over the estimates obtained from torsional frequencies. The former gave ΔG as 5640 ± 2200 J/mol, in agreement with the coupling constant data, although, to within experimental error, the latter also agree with the ΔH of 6070 ± 1130 J/mol found from the temperature dependence of the intensities of the stretching bands. Our numbers do not affirm the existence of a negative entropy of formation for the OH . . . π bond in **1**.

(ii) 2-Phenyl-6-allylphenol, 3

In 2-allylphenol, the free energy favoring conformer *a* in CCl_4 solution is 90 ± 190 J/mol (12), based on ${}^5J_m^{OH,H}$. On an additive basis, it follows that ΔG in 2-phenyl-6-allylbenzene, **3**, is 5240 ± 1250 J/mol, whereas the coupling data in Table 2 yield 5010 ± 680 J/mol favoring *b*, that is, a hydrogen bond to the phenyl group.

Now, comparison of ${}^5J_m^{H,OH}$ values in 2-allylphenol, 2-methylphenol, and 2-allyl-6-methylphenol shows, first, that ΔG for the last of these three compounds is obtained by addition of the ΔG values for the first two compounds and, second, that the OH . . . π bond in 2-allylphenol has a free energy preference of 1500 ± 350 J/mol at 305 K (12). This number is based on the assumption that the increased population of the conformer with the OH bond *cis* to the substituent in 2-allyphenyl *relative to* 2-*methylphenol* is a consequence of the OH . . . π bond to the allyl substituent.

Because the internal equilibrium constants in the 2- and the 2,6-disubstituted phenols vary substantially for allyl, methyl, and phenyl substituents, the self-consistent additivity schemes above provide no support for substantial negative entropies of formation (2, 5) of the O—H . . . π bond in 2-allylphenol or 2-phenylphenol, unless the entropy differences coincidentally cancel for all these substituents. This coincidence seems unlikely.

It has been suggested (5) that in 2-phenylphenol an entropy decrease of about 18 J/mol K could occur on formation of the OH . . . π hydrogen bond. In our opinion a decrease of less than I J/mol K is more likely. Thus, the internal barrier to rotation in biphenyl is not less than 8 kJ/mol (19–23). Insertion of a 2-hydroxy substituent raises the internal barrier even in the absence of the OH . . . π interaction. An estimate of this increase is available from a comparison of the increased internal rotational barriers in some biphenyl derivatives (Table 3 of ref. 22) caused by 2-fluoro and 2-hydroxy substituents, suggesting a *minimum* value of 11 kJ/mol. Formation of the OH . . . π bond will contribute a further increase of at most 6 kJ/mol. Accordingly, the decrease in entropy on formation of *b* from *a* can be estimated[2] as 1.3 J/mol K on the basis of a hindered rotor model (24). An estimate based on the harmonic oscillator model (25) yields 1.2 J/mol K. The infrared data gave 1.4 ± 3.5 J/mol K for **1***a* ⇌ **1***b* (2). The experimental estimate of the internal entropy of biphenyl itself is 0.9 J/mol K (23), so that these numbers are probably too large. See also ref. 26.

The infrared studies also found ΔS as 3.8 ± 1.8 J/mol K for the equilibrium in 2-allylphenol. In view of the remarks in the introduction concerning the reliability of such numbers, and because of our present results for ΔG, it seems that very small values for ΔS are more likely. Unfortunately, simple calculations show that a temperature change of 50°C, the useful range for CCl_4 solutions, will not yield a reliable ΔS via measurements of ${}^5J_m^{OH,H}$.

In any event, relative to a methyl group, the present results yield free energy differences favoring an OH . . . π interaction of 1500 ± 350 J/mol for allyl and 6500 ± 1030 J/mol for phenyl. The comparison with a methyl group as a 2-substituent seems more appropriate than with hydrogen as a 2-substituent.

(iii) 2-Phenyl-4,6-diiodophenol, 4, and 2-phenyl-6-chlorophenol, 5

In **4** the free energy difference is 1670 ± 150 J/mol to the advantage of the OH . . . I hydrogen bond. Note that for **6**, 2-phenyl-4-iodophenol, in CCl_4 solution (Table 2), ΔG is 5250 ± 1140 J/mol, implying that a 4-iodo substituent does not perturb the equilibrium for **1** or **4**.

Turning to **5**, one has a free energy of 4660 ± 770 J/mol favoring the OH . . . Cl interaction. Now, in a study of halophenol derivatives it was established that the ΔG value to the advantage of Cl over I was 1920 ± 250 J/mol (15). Proceeding as before, one has (4660 ± 630) − (1920 ± 250) or 2740 ± 890 J/mol as a prediction for the OH . . . I over the OH . . . π bond in **4**. The observed value is 1670 ± 150 J/mol.

Clearly, for the chlorine, iodine and phenyl substituents, combined as pairs of 2,6-substituents, an additivity scheme is much less satisfactory than for the allyl, methyl, phenyl triplet. For the latter, the ΔG values for the 2-substituents alone also fit into the additivity scheme. Unfortunately, the equilibrium for 2-iodophenol in CCl_4 solution is shifted so far to the intramolecularly hydrogen bonded conformer that a ΔG value is not available from ${}^5J_m^{OH,H}$ (27).

(iv) Ranking of the phenyl group as a hydrogen bond acceptor

${}^5J_m^{OH,H}$ values are now available for a substantial number of phenol derivatives. Table 3 gives a tabulation of the derived free energy preferences of the hydroxyl group for twelve relatively weak hydrogen-bond acceptors or repellors. The fourth column represents experimental data and the other columns follow directly from it. The first column arranges these preferences relative to the *tert*-butyl group as zero, purely for convenience. Other columns in Table 3 compare free energy preferences for pairs of *ortho* substituents, also derived from ${}^5J_m^{OH,H}$, with the appropriate differences taken from the first column. In general, the agreement is satisfactory, indicating the validity of an additive scheme which includes hydrogen as a substituent.

However, one discrepancy is unsatisfactory and occurs for iodine as a substituent competing with the phenyl group (footnote *e* in Table 3). The iodine substituent provides an entry into the hydrocarbon substituent series, the latter forming a self-consistent set ranging from phenyl, preferring the hydroxyl group by about 5.0 kJ/mol, to *tert*-butyl, repelling the hydroxyl group by about 6.6 kJ/mol. According to Table 3, iodine should have a free energy preference of 2.7 kJ/mol over phenyl, yet the observed value is only 1.7 kJ/mol. Chlorine, on the other hand, does not misbehave in such a comparison. One possibility, unprovable here, is that the *relatively* large iodine substituent causes an increased OH . . . π overlap in **4**.

Table 3 does not contain comparisons of certain other substituents, also studied by nmr. For example, mercapto and chlorine as competing *ortho* substituents (29) yield ${}^5J_m^{OH,H}$ val-

[2] The reduced moment of inertia of 2-phenylphenol is 1.00×10^{-38} g cm^2.

TABLE 3. Free energy preferences of the hydroxyl group in some phenol derivatives in CCl_4 solution at 305 K in J/mol

2-Substituent	ΔG^a	2-X,6-Y[b]	$\Delta G(J)^c$	$\Delta G(2)^d$	2-X,6-Y[b]	$\Delta G(J)^c$	$\Delta G(2)^d$
Cl (Br)	16,000	Cl,I	1,920(250)	2,000	H,allyl	380(630)	400
F	14,300	Cl,F	1,610(200)	1,700	allyl,CH_3	1,640(150)	1,450
I	14,000	F,I	310(80)	300	H,CH_3	1,590(170)	1,850
C_6H_5	11,300	I,C_6H_5	1,670(150)[e]	2,700[e]	H,$CH(CH_3)_2$	2,510(290)	3,000
CF_3	8,700	Cl,C_6H_5	4,660(630)	4,700	CH_3,$CH(CH_3)_2$	1,170(300)	1,150
H	6,400	I,CF_3	5,150(840)	5,300	H,$C(CH_3)_3$	6,570[f]	6,400
$CH_2CH{=}CH_2$ (allyl)	6,000	I,H	>7,800	7,600	CH_3,$C(CH_3)_3$	4,350(570)	4,550
$CH_2C_6H_5$	5,700						
CH_3	4,550	CF_3,H	2,130(210)	2,300			
$CH(CH_3)_2$	3,400	C_6H_5,allyl	5,010(680)	5,300			
$C(CH_3)_3$	0	C_6H_5,H	5,150(1060)	4,900			

[a] These numbers are deduced from $^5J_m^{OH,H}$ measurements for a variety of phenol derivatives (11–15, 27, 28), but see footnote *f*, and are relative to zero for 2-*tert*-butyl phenol.
[b] The conformer with the hydroxyl group oriented towards the first substituent of the pair has the lower free energy.
[c] Derived from the measured $^5J_m^{OH,H}$ for the pairs in the previous column.
[d] Appropriate differences taken from column 2.
[e] This discrepancy is discussed in the text.
[f] From infrared band intensities (33).

ues which suggest that SH falls between I and CF_3 in Table 3. However, formation of the OH . . . S bond twists the mercapto group into a perpendicular conformation, causing a loss of 3.3 kJ/mol in $3p,\pi$ conjugation (29, 30), perhaps implying that the OH . . . S bond strength is as large as the OH . . . Cl interaction. Again, in salicylaldehyde, the OH . . . O=C bond strength is estimated as 29.7 kJ/mol on the basis of δ_{OH} (31), in rough agreement with molecular orbital calculations. The 2-methoxy substituent has also been studied by nmr (32) and by far infrared techniques (5). $^5J_m^{OH,H}$ did not yield ΔG values (32) but is consistent with an energy (enthalpy) preference of 8.4 kJ/mol for the OH . . . O bond derived from the torsional frequencies.

Conclusions

In CCl_4 solution the OH . . . π bond in 2-phenylphenol has a free energy preference of $5.1_5 \pm 1.0_6$ kJ/mol at 305 K. In a ranking of substituents as intramolecular hydrogen bond acceptors in phenol derivatives, the phenyl group falls below the halogens but above the CF_3 group. Comparison with other hydrocarbon groupings does not support the notion of a significant decrease in entropy on formation of the OH . . . π bond, but does show that the OH . . . π bond in 2-phenylphenol is appreciably stronger than in 2-allyl and 2-benzylphenols, in which the nonbonded conformers are actually most abundant at 305 K.

Acknowledgements

We are grateful to the Natural Sciences and Engineering Research Council of Canada for financial assistance and to the referees for useful suggestions.

1. A. W. BAKER and A. T. SHULGIN. J. Am. Chem. Soc. **80**, 5358 (1958).
2. M. OKI and H. IWAMURA. Bull. Chem. Soc. Jpn. **33**, 717 (1960).
3. M. OKI and H. IWAMURA. J. Am. Chem. Soc. **89**, 576 (1967), and references therein.
4. S. UEJI. Bull. Chem. Soc. Jpn. **51**, 1799 (1978).
5. G. L. CARLSON and W. G. FATELEY. J. Phys. Chem. **77**, 1157 (1973).
6. T. DEVANATHAN. Proc. Indian Acad. Sci. **57**, Part A, 25 (1963).
7. H. BRAUN and W. LÜTTKE. J. Mol. Struct. **28**, 415 (1975).
8. A. W. BAKER and A. T. SHULGIN. Spectrochim. Acta, **19**, 1611 (1963).
9. K. NAKATSU, H. YOSHIOKA, K. KUNIMOTO, T. KINUGASA, and S. UEJI. Acta Crystallogr. Sect. B, **34**, 2357 (1978).
10. R. S. BROWN and R. W. MARCINKO. J. Am. Chem. Soc. **99**, 6500 (1977).
11. T. SCHAEFER and K. CHUM. Can. J. Chem. **56**, 1788 (1978).
12. T. SCHAEFER, R. SEBASTIAN, and T. A. WILDMAN. Can. J. Chem. **57**, 3005 (1979).
13. T. SCHAEFER and J. B. ROWBOTHAM. Can. J. Chem. **54**, 2243 (1976).
14. T. SCHAEFER, R. SEBASTIAN, and S. R. SALMAN. Can. J. Chem. **62**, 113 (1984).
15. J. B. ROWBOTHAM and T. SCHAEFER. Can. J. Chem. **52**, 3037 (1974).
16. T. SCHAEFER and R. SEBASTIAN. J. Magn. Reson. **41**, 395 (1980).
17. S. CASTELLANO and A. A. BOTHNER-BY. J. Chem. Phys. **41**, 3863 (1964).
18. C. W. HAIGH. Ann. Rep. NMR Spectrosc. **4**, 311 (1971).
19. J. D. MCKINNEY, K. E. GOTTSCHALK, and L. PEDERSEN. J. Mol. Struct. **104**, 445 (1983).
20. A. CARREIRA and T. G. TOWNS. J. Mol. Struct. **41**, 1 (1977).
21. W. B. RUSING. J. Am. Chem. Soc. **104**, 4829 (1982).
22. G. BOTT, L. D. FIELD, and S. STERNHELL. J. Am. Chem. Soc. **102**, 5618 (1980).
23. J. E. KATON and E. R. LIPPINCOTT. Spectrochim. Acta, **19**, 627 (1959).
24. K. S. PITZER and L. BREWER. Thermodynamics. McGraw–Hill, New York. 1961.
25. J. O. HALFORD. J. Chem. Phys. **15**, 364 (1947).
26. Z. SLANINA. Ber. Bunsenges. Phys. Chem. **87**, 28 (1983).
27. T. SCHAEFER, R. SEBASTIAN, and T. A. WILDMAN. Can. J. Chem. **59**, 3021 (1981).
28. T. SCHAEFER, B. M. ADDISON, R. SEBASTIAN, and T. A. WILDMAN. Can. J. Chem. **59**, 1656 (1981).
29. T. SCHAEFER, R. P. VEREGIN, and D. M. MCKINNON. Can. J. Chem. **59**, 3026 (1981).
30. T. SCHAEFER, T. A. WILDMAN, and S. R. SALMAN. J. Am. Chem. Soc. **102**, 107 (1980).
31. T. SCHAEFER, R. SEBASTIAN, R. LAATIKAINEN, and S. R. SALMAN. Can. J. Chem. **62**, 326 (1984).
32. T. SCHAEFER and T. A. WILDMAN. Can. J. Chem. **57**, 450 (1979).
33. K. U. INGOLD and D. R. TAYLOR. Can. J. Chem. **39**, 471 (1961).

Can. J. Chem. Downloaded from www.nrcresearchpress.com by 210.87.254.6 on 09/06/12
For personal use only.

A new efficient synthesis of the 16-epimers of (±)-3-hydroxy-16,17-butanomorphinan

JOHN DIMAIO
Clinical Research Institute of Montreal, Department of Chemical Biology and Peptide Research, 110 Pine Avenue West, Montreal, P.Q., Canada H2W 1R7

AND

BERNARD BELLEAU
Department of Chemistry, McGill University, 801 Sherbrooke Street West, Montreal, P.Q., Canada H3A 2K6

Received February 7, 1984

JOHN DIMAIO and BERNARD BELLEAU. Can. J. Chem. **62**, 2697 (1984).

A novel synthetic route to the 16α- and 16β-epimers of (±)-3-hydroxy-16,17-butanomorphinan is described. The method involves the key intermediate 4a-(2-piperidinylmethylene)-1,2,3,4,4a,9-hexahydro-6-methoxyphenanthrene **9**. Deprotection of the intermediate epoxy trifluoroacetamide **10** with sodium borohydride provides exclusively the 9α-hydroxyhasubanan which is rearranged to the 14-dehydromorphinan with PBr_3. Hydrogenation of the intermediate olefin followed by *O*-demethylation afforded th desired (±)-3-hydroxy-16,17-butanomorphinan epimers which were separated by crystallization. Single crystal X-ray crystallography confirmed the 16β configuration and chair conformation of ring D in **1***b* which contrasts with the 16α configuration and boat conformation for ring D in **1***a*, a compound identical to that previously synthesized using an extension of the Grewe-type methodology.

JOHN DIMAIO et BERNARD BELLEAU. Can. J. Chem. **62**, 2697 (1984).

On décrit une nouvelle voie de synthèse des épimères 16α et 16β des (±)-hydroxy-3 butano-16,17 morphinanes. La méthode implique le (pypéridinyl-2 méthylène)-4a hexahydro-1,2,3,4,4a,9 méthoxy-6 phénanthrène **9** comme intermédiaire clé. La déprotection de l'intermédiaire époxy trifluoroacétamide **10** par le borohydrure de sodium conduit exclusivement à l'hydroxy-9α hasubanane qui se transpose en déhydro-14 morphinane sous l'action du PBr_3. L'hydrogénation de l'oléfine intermédiaire, suivie d'une *O*-déméthylation, conduit aux épimères (±)-hydroxy-3 butano-16,17 morphinanes désirés que l'on peut séparer par cristallisation. Une étude par diffraction des rayons-X sur des cristaux uniques a permis de confirmer la configuration de l'isomère 16β pour le composé **1***b* et d'établir que son cycle D existe dans une conformation chaise; ceci est en opposition avec une configuration 16α et une conformation bateau du cycle D pour l'isomère **1***a*, un composé identique à celui synthétisé antérieurement en faisant appel à une extension d'une méthodologie du type Grewe.

[Traduit par le journal]

Among the many parameters that contribute to the agonistic activity of rigid opiates of the morphinan and benzomorphan type (1), the spatial orientation of the *N* lone pair plays a role which has formed the basis of much controversy (2, 3). Douglas and Meunier (4) described the synthesis of one of two possible epimers of (±)-3-hydroxy-16,17-butanomorphinan (Fig. 1) and reported that it was inactive either as an agonist or as an antagonist. Recently we reported (5) that this inactive epimer has the structure **1***a* (Fig. 1). The 16α-configuration rigidly locks ring D in the boat conformation. It is difficult to force ring D into the chair form because of the severe steric interactions that are created between the butano bridge and the aromatic ring.[1] As a result, the *N* lone pair of this latter epimer can only be oriented toward the phenyl ring in a manner analogous to the lone pair of an inactive ring D normorphinan described previously (6).

In order to provide additional evidence for the relevance of the *N* lone pair orientation to productive in vivo opiate receptor interactions, we sought a method to invert the *N* lone pair into the favoured orientation (away from the phenyl ring). In order to achieve this, we oxidized the *O*-acetyl-16α,17-butanomorphinan derivative of **1***a* with mercuric acetate (Scheme 1) and obtained the enamine **2** which was reduced with sodium cyanoborohydride followed by hydrolytic removal of the *O*-acetyl group to give the morphinan **1***b*. Single crystal X-ray analysis of the latter established (7) the 16β-configuration and the chair conformation for ring D. This arrangement fixes the

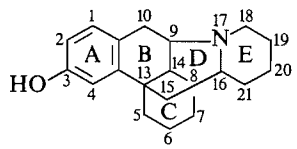

1

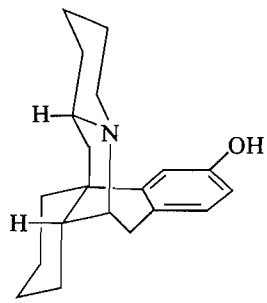

1*a*

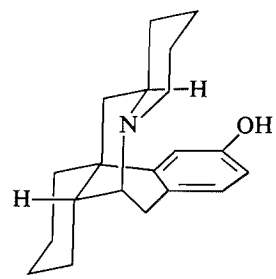

1*b*

FIG. 1

N lone pair orientation in the direction opposite to that of **1***a* (away from the phenyl ring). It was gratifying to discover that this epimer displayed analgesic activity in mice (writhing assay, ED_{50} (mean effective dose) 3 ± 0.5 mg/kg sc) at a level comparable to that of pentazocine as the standard, but was inactive as an antagonist (oxymorphone Straub tail test).[2] The

[1] Using the SCRIPT computer programme, Dr. N. C. Cohen of Roussel–UCLAF estimated this chair form to be disfavored by 2.9 kcal/mol over the boat form.

[2] We are indebted to Dr. Anthony W. Pircio of Bristol Laboratories, Syracuse, New York, for providing us with this data.

Can. J. Chem. Downloaded from www.nrcresearchpress.com by 210.87.254.40 on 09/06/12
For personal use only.

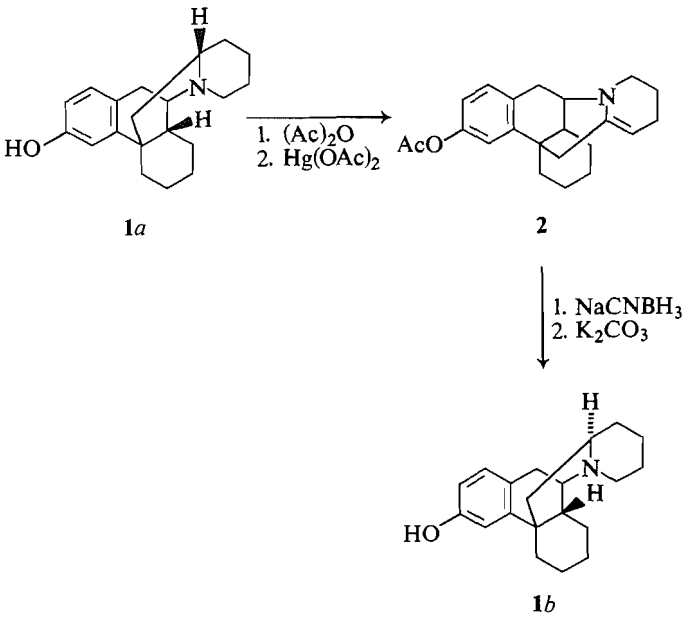

1*a* 2 1*b*

SCHEME 1

original synthesis of Douglas and Meunier generated a single but inactive epimer **1***a* and did not permit access to analogs functionalized at or near the 14-position, although it allowed us to generate (albeit inefficiently) the desired 16β-epimer **1***b* as outlined above. In order to overcome these limitations and acquire a complete pharmacological profile for this and related analogs, access to a more versatile and efficient synthesis became necessary. In this communication we described an alternative strategy which satisfies our requirements.

Results and discussion

Our synthetic approach to (±)-3-hydroxy-16,17-butanomorphinan is shown in Scheme 2 and begins with the known spiro ketone **3** (8). The latter was reacted with the carbanion of α-picoline (generated with phenyllithium) and the adduct **4** quaternized to give the methiodide **5**. Catalytic hydrogenation of the latter over PtO_2 proceeded smoothly to afford **6** without affecting the sensitive benzylic hydroxyl group. It is noteworthy that **6** consisted of a mixture of diastereomers that were readily separable by fractional crystallization of the hydrochloride salts. However, this exercise is obviously superfluous because Wagner–Meerwein rearrangement of each isomer generates the same mixture of racemic diastereomers **7** nonstereospecifically. The resulting tertiary amine **7** was *N*-demethylated using trichloroethyl chloroformate and the resulting carbamate **8** decomposed by the method of Just and Grozinger (9) to yield secondary amine **9** (Scheme 3). As the hydrochloride salt, the latter is soluble in chloroform and in that solvent unequivocal evidence for the expected presence of diastereomers was adduced by nmr spectroscopy which revealed chemical shift differences arising from the olefinic and methoxy protons.

The next step involved oxidation followed by cyclization through the secondary amine nitrogen. However, we attempted initially to isomerize the double bond to the benzylic position with the hope of generating the desired morphinan directly through a subsequent base-catalyzed cyclization (10). Unfortunately, migration of the double bond to the conjugated position did not occur in this instance, no matter the nature of

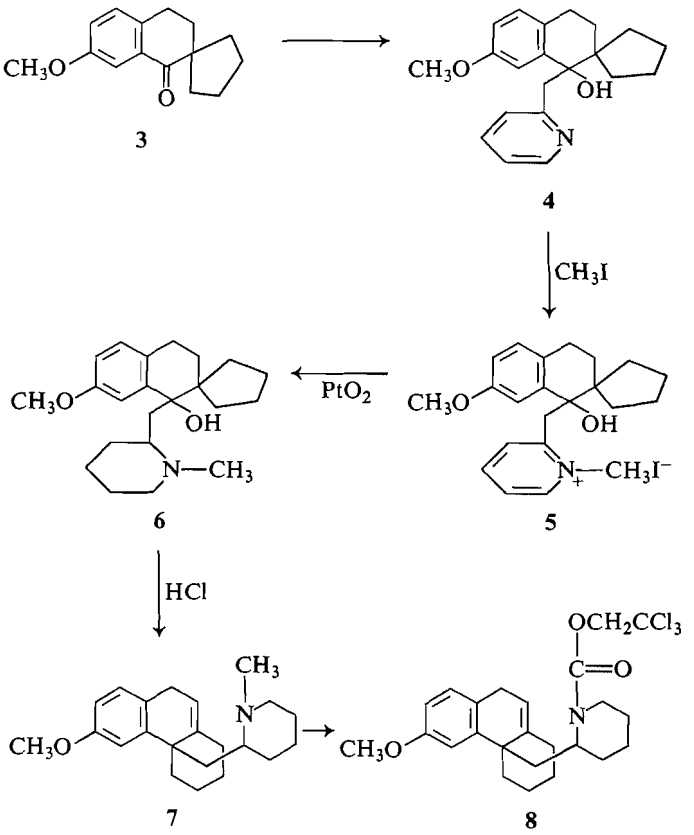

3 4 5 6 7 8

SCHEME 2

the base used (*tert*-butoxide/DMSO, dimsyl sodium/DMSO, n-butyllithium/THF, LDA). Presumably the electron-donating properties of the aromatic methoxy group are counter productive. An alternative strategy involved the direct oxidative cyclization of **9** with mercuric acetate (11). However, the only product isolated using this method was the hasubanan analog, a not unprecedented result (12).

A different route was therefore adopted where the *N*-trifluoroacetyl epoxide **10** served as the key intermediate. It was generated by reaction of the diastereomeric **9** with trifluoroacetic anhydride, followed by epoxidation using *m*-chloroperbenzoic acid, which proceeded in a regiospecific fashion (*trans* relative to the piperidinemethyl face) to afford **10**. Deprotection of the amine with K_2CO_3 or $NaBH_4$ induced cyclization to give exclusively the 9α-hydroxy-16,17-butanohasubanan **11** as a mixture of two diastereomers.[3] The latter readily underwent rearrangement to the desired ring system simply by treatment with excess phosphorus tribromide in boiling ether. After neutralization, the $\Delta^{8,14}$-morphinan **12** was isolated as a mixture of diastereomers, as evidenced by nmr spectroscopy (two triplet signals for the olefinic protons at 5.25 and 5.75 ppm). This mixture of olefins was hydrogenated over PtO_2 and the *O*-methyl group removed with BBr_3. After workup the 16β-epimer **1***b* separated spontaneously from ethanol while the more soluble 16α-isomer remained in the mother liquors. The two isomers thus obtained were characterized by

[3] The two isomers of this 9α-hydroxyhasubanan co-crystallize as their hydrochloride salts. However, subsequent experiments on reversed phase liquid chromatography, in the solvent system 1:1 0.1% trifluoroacetic acid/methanol, revealed two peaks in a one-to-one ratio.

Can. J. Chem. Downloaded from www.nrcresearchpress.com by 210.87.254.40 on 09/06/12
For personal use only.

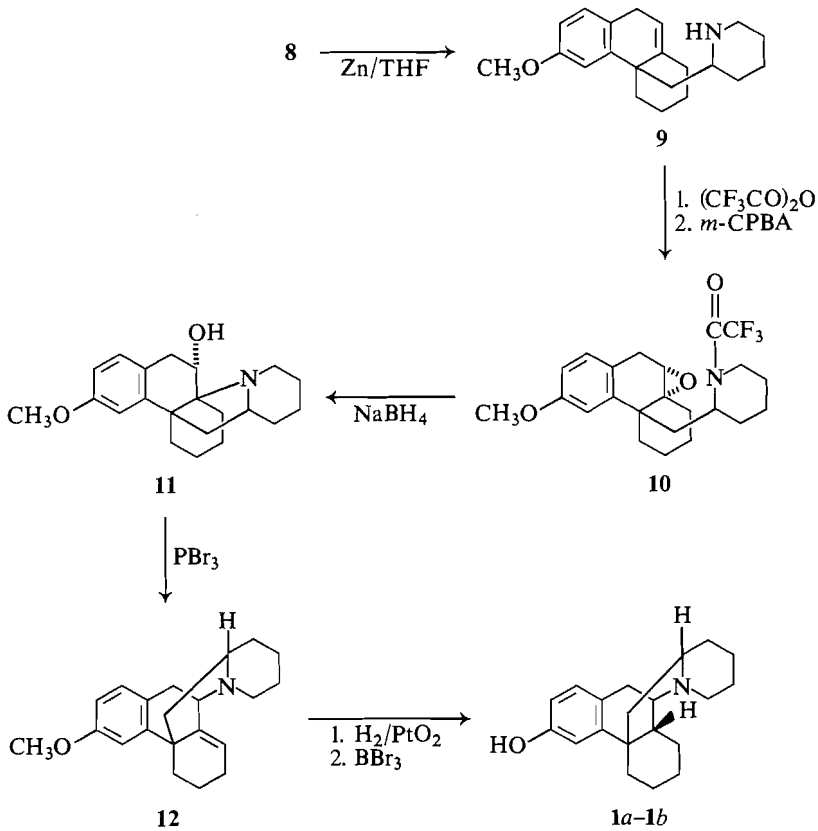

SCHEME 3

ir, hplc, and X-ray crystallography. Their properties were identical to those already observed for the previously synthesized (±)-3-hydroxy-16,17-butanomorphinans, the 16-epimers of which were characterized by X-ray analysis (7).

This new synthetic method also provides entry into analogs as yet unknown, such as 3,14-dihydroxy-16,17-butanomorphinans. Our results along this line will be described later, together with the detailed pharmacological properties of these interesting morphinans.

Experimental

The nmr spectra were recorded on a Varian EM-390 spectrometer using $CDCl_3$ as solvent. The chemical shifts are expressed as values relative to tetramethylsilane. Melting points were determined on a Gallenkamp apparatus and are uncorrected. The tlc analyses were done on Merck Kieselgel $60F_{254}$ silica gel and column chromatography was done on an equivalent Merck Kieselgel 60 gel 230–400 mesh. The ir spectra were recorded on a Beckman ir 4240 spectrophotometer. The hplc experiments were performed on a Waters model 600 A solvent delivery system equipped with a model 450 variable wavelength detector and U6K injector. Microanalyses were performed by Canadian Micro Analytical Services Ltd., Vancouver, B.C.

1-(2-Pyridylmethylene)-7-methoxy-1,2,3,4-tetrahydro-2,2-tetramethylene-1-naphthol (4)

In a 1-L three-neck flask (under nitrogen) containing 100 mL of anhydrous ether was added phenyllithium 2.4 *M* (150 mL) followed by the dropwise addition of 19.4 mL (200 mmol) of α-picoline. After stirring for 15 min, the solution was cooled (MeOH – Dry Ice) and treated dropwise with 57.5 g (240 mmol) of **3**. The solution was stirred at room temperature for 24 h and the reaction quenched with H_2O. The organic layer was separated and the aqueous phase extracted several times with ether. The combined extracts were extracted with cold 6 *N* HCl and the acidic solution made basic with ammonium hydroxide and extracted several times with ether. The combined extracts were dried (Na_2SO_4) and evaporated *in vacuo*. A pure product was obtained (50 g, 80% yield) by crystallization from petroleum ether 80–60°C, mp 63–65°C; ir (KBr): 3400 cm^{-1}; nmr ($CDCl_3$) δ: 5.8–9.7 (7H, m), 3.5 (3H, s), 2.8–3.3 (4H, m), 1.0–2.2 (1H, m). *Anal.* calcd. for $C_{21}H_{25}NO_2$: C 77.96, H 7.81, N 4.33; found: C 77.97, H 7.97, N 4.35.

1-(2-N-methylpyridylmethylene-7-methoxy-1,2,3,4-tetrahydro-2,2-tetramethylene-1-naphthol iodide (5)

To a solution of 4.64 g of **4** (10 mmol) in 30 mL of absolute ethanol was added a three-fold excess of methyl iodide. The solution was allowed to stand for 24 h. Crystalline material deposited, was collected by filtration, and the crystals washed with cold ethanol followed by ether, yield 3.2 g (73%), mp 211–213°C. An analytical sample was prepared by recrystallization from methanol; nmr ($CDCl_3$/DMSO) δ: 1.2–2.4 (10H, m), 2.7–3 (2H, m), 3.3 (3H, s), 3.8 (3H, s). *Anal.* calcd. for $C_{22}H_{28}NO_2I$: C 56.75, H 6.08, N 3.01; found: C 56.51, H 5.95, N 3.05.

1-(2-N-methylpiperidinylmethylene)-7-methoxy-1,2,3,4-tetrahydro-2,2-tetramethylene-1-naphthol (6)

A mixture of 13.6 g of **5** (32 mmol) and 1 g of PtO_2 in 300 mL of methanol was shaken in a Parr instrument (40 psi; 1 psi = 6.89 kPa) until uptake of hydrogen ceased (about 2 h). The catalyst was removed (Celite) and the filtrate evaporated *in vacuo*. The residue was suspended in water, and the mixture made basic with ammonium hydroxide and extracted several times with ether. The combined extracts were washed with 6 *N* HCl and the ether layer discarded. The aqueous phase was made basic with NH_4OH while cooling, the mixture extracted with ether, and the organic phase dried and evaporated *in vacuo*. The residue was dissolved in 200 mL of anhydrous ether and dry HCl introduced into the solution, whereupon a white solid deposited. The hydrochloride salt was collected and dried, yield 9.8 g (90%); nmr free base ($CDCl_3$) δ: 1.85 (N—CH_3, s, 3H), 2.3

Can. J. Chem. Downloaded from www.nrcresearchpress.com by 210.87.254.40 on 09/06/12
For personal use only.

Can. J. Chem. Downloaded from www.nrcresearchpress.com by 210.87.254.40 on 09/06/12
For personal use only.

(N—CH_3, s, 3H), diastereomers. Fractional crystallization from ethanol ether of this product yielded two compounds, one with mp 270–273°C and the other 219–220°C. *Anal.* calcd. for $C_{22}H_{34}N_1O_2Cl$: C 69.69, H 9.06, N 3.70; found: C 69.35, H 9.20, N 3.56.

*4a-(2-*N*-methylpiperidinylmethylene)-1,2,3,4,4a-9-hexahydro-6-methoxyphenanthrene (7)*

The preceding mixture of isomers (4.6 g, 12 mmol) was added to 50 mL of concentrated aqueous HCl and 100 mL of ether and the mixture refluxed for 24 h after which time the layers were separated. The acidic phase was diluted with 50 mL of H_2O, made basic with ammonium hydroxide, and extracted with ether. The combined organic extracts were dried (Na_2SO_4) and evaporated *in vacuo* affording 3.8 g (98% yield) of a clear viscous oil; nmr ($CDCl_3$) δ: 7.1–6.6 (3H, m), 5.7 (1H, m), 3.8 (3H, s), 3.3 (2H, m), 2.2 (1.4H, s), 1.8 (1.5H, s). For purposes of analysis, the HBr salt was prepared and had mp 219–220°C. *Anal.* calcd. for $C_{22}H_{32}NOBr$: C 64.99, H 7.96, N 3.45; found: C 64.42, H 8.08, N 3.39.

*4a-(2-*N*-trichloroethoxycarbonylpiperidinylmethylene)-1,2,3,4,4a,9-hexahydro-6-methoxyphenanthrene (8)*

To a solution of 1.3 g (4 mmol) of **7** in 50 mL of benzene was added 500 mg (6 mmol) of $NaHCO_3$ and 1 mL (6 mmol) of trichloroethyl chloroformate. The solution was heated to reflux while monitoring the reaction by tlc. After 18 h the reaction was complete. The mixture was extracted sequentially with H_2O, 6 *N* HCl (3×), 10% NaOH (3×), and then water again. The organic phase was dried ($MgSO_4$) and evaporated to give a thick oil. The product was purified by flash chromatography eluting with chloroform. The clear viscous oil (1.5 g, 75% yield) resisted crystallization and was used as such in the next step.

4a-(2-Piperidinylmethylene)-1,2,3,4,4a,9-hexahydro-6-methoxyphenanthrene (9)

To a solution of 9.3 g (19 mmol) of **8** in 200 mL of THF was added 20 g of granular Zn, followed immediately by a 50-mL portion of 1 *M* KH_2PO_4. The solution was stirred at room temperature for 4 h, filtered over Celite, the filtrate evaporated *in vacuo*, the residue suspended in water, and the mixture extracted with ether. The combined extracts were washed with 6 *N* HCl and the organic layer discarded. The acidic phase was extracted with chloroform several times, and the extract dried (Na_2SO_4) and evaporated *in vacuo*. A crystalline pure material was obtained from ethanol/ether, yield 4 g (60%), mp 244–245°C; nmr ($CDCl_3$) δ: 5.75 (1H, t, CH=C), 5.55 (1, t, CH=C), 3.8 (3H, s, OCH_3), 3.60 (3H, s, OCH_3). An analytical sample was prepared by recrystallization from ethanol/ether. *Anal.* calcd. for $C_{21}H_{28}NOCl$: C 72.47, H 8.71, N 4.03; found: C 72.08, H 8.96, N 3.97.

*10,10a-α-Epoxy-4a-[2-(*N*-trifluoroacetylpiperidine)methyl]-1,2,3,4,4a,9,10,10a-octahydro-6-methoxyphenanthrene (10)*

To a solution of 1.6 g (5.2 mmol) of **9** in 50 mL of anhydrous ether was added 1.5 g (7 mmol) of trifluoroacetic anhydride and the solution stirred at room temperature overnight. The clear solution was cooled and neutralized with aqueous bicarbonate. The organic phase was extracted with 1 *N* HCl, washed with H_2O, dried, and evaporated *in vacuo* to give 2.1 g (91% yield) of a clear viscous oil; tlc, ($CHCl_3$): two spots R_f 0.4 and 0.45 corresponding to the diastereomeric mixture.

The compound was dissolved in CH_2Cl_2 (50 mL) and treated at 0°C with 1.2 g (7 mmol) of *m*-CPBA. The ice bath was removed and the solution stirred for 2 h and extracted with 5% sodium sulfite, 2 *N* NaOH (3×), 1 *N* HCl (3×), H_2O, and dried. Removal of the solvent *in vacuo* gave 2.2 g of a yellow viscous oil which was submitted to flash chromatography (Merck silica gel). The $CHCl_3$ eluent yielded 1.8 g (90%) of a clear viscous oil that resisted crystallization.

9α-Hydroxy-3-methoxy-16,17-butanohasubanan (11)

The preceding epoxy trifluoroacetamide (2.1 g, 5 mmol) in 50 mL of ethanol was treated with 378 mg (10 mmol) of $NaBH_4$. The solution was heated under reflux for 24 h after which time the reaction had reached completion (tlc). The mixture was concentrated *in vacuo*, diluted with 50 mL of H_2O, and extracted with ether. The combined extracts were re-extracted with 2 *N* HCl and the aqueous phase made basic with NH_4OH followed by extraction with chloroform. After drying (Na_2SO_4) and evaporation of the solvent, a brownish viscous oil consisting of a single component (tlc) was obtained.[3] Yield: 1.5 g (94%); ir (neat): 3400 cm^{-1}; nmr ($CDCl_3$) δ: 6.6–7.1 (3H, m), 3.9 (1H, t), 3.7 (3H, s, OCH_3). A portion was converted to the hydrochloride salt and the solid dried over P_2O_5. Crystallization from ethanol–ether afforded colorless crystals, mp 153–155°C. *Anal.* calcd. for $C_{21}H_{30}NO_2Cl$: C 69.46, H 8.35, N 3.86; found: C 69.20, H 8.61, N 3.80.

3-Methoxy-16,17-butano-$\Delta^{8,14}$-morphinan (12)

To a solution of 654 mg (2 mmol) of the hydroxyhasubanan **11** in 30 mL of anhydrous ether was added 1.6 g (6 mmol) of phosphorus tribromide. The mixture was heated under reflux for 24 h, cooled in an ice bath, and subjected to a dropwise addition of 2 *N* NaOH while maintaining the temperature between 60–70°C. The mixture was then extracted with ethyl acetate and the combined extracts re-extracted with 3 *N* HCl. The aqueous phase was made basic with NH_4OH and extracted with chloroform. The combined extracts were dried (Na_2SO_4) and evaporated *in vacuo*, affording 400 mg of a reddish oil; nmr ($CDCl_3$) δ: 7.1–6.6 (3H, m), 5.7 (0.5H, t), 5.2 (0.5H, t), 3.8 (3H, s, OCH_3). The product appeared sufficiently pure (tlc) for use in the next step.

(±)-3-Hydroxy-16,17- and 16,17-butanomorphinan (1a, 1b)

The preceding $\Delta^{8,14}$-morphinan **12** (324 mg, 1 mmol) was dissolved in 20 mL of ethanol and hydrogenated over PtO_2 in a Parr instrument. After 8 h the catalyst was removed and the filtrate evaporated *in vacuo*, yielding 320 mg of a clear viscous oil. After drying over P_2O_5, the oil was dissolved in 10 mL of CH_2Cl_2 and treated with 750 mg (3 mmol) of BBr_3 to give a clear solution which was stirred at room temperature for 2 h. After quenching with water, it was made strongly basic with 2 *N* NaOH and extracted several times with methylene chloride. The combined extracts were dried (Na_2SO_4), evaporated *in vacuo*, and the residue treated with 15 mL of warm ethanol. The suspended material was collected and washed with some cold ethanol. The hydrobromide salt of this fraction was prepared by suspending the solid in methanol containing aqueous HBr (48%) and the resulting solution evaporated *in vacuo* and the residue dried over P_2O_5. Crystallization from ethanol–ether gave pure crystals (50 mg, 34%), mp 209–210°C; ir (KBr): 3400 cm^{-1}.

The ethanol filtrate was evaporated *in vacuo* to yield a viscous oil which was purified by flash chromatography using the solvent system 20:1 chloroform/0.1% NH_4OH in MeOH. The eluted product was crystallized by slow evaporation of an ethyl acetate solution, yielding 20 mg (15% yield), mp 250°C; ir (KBr): 3400 cm^{-1}.

The two isomers proved identical in every respect (ir, hplc, nmr, X-ray diffraction) to the 16,17-butanomorphinans previously synthesized.

Acknowledgments

This work was supported by an operating grant from the National Research Council of Canada (NSERC-A1529). The authors would like to thank Ms. H. Zalatan for typing the manuscript.

1. G. DE STEVENS (*Editor*). Analgesics. Academic Press, New York. NY. 1965.
2. K. OPHEIM and B. M. COX. J. Med. Chem. **19**, 857 (1976).
3. S. SHIOTANI, T. KOMETANI, Y. ITAKA, and A. ITAI. J. Med. Chem. **21**, 153 (1978), and references therein.
4. J. L. DOUGLAS and M. MEUNIER. Can. J. Chem. **53**, 3681 (1975).
5. J. DIMAIO, F. R. AHMED, P. W. SCHILLER, and B. BELLEAU. *In* Recent advances in receptor chemistry. *Edited by* F. Gualtieri, M. Giannella, and C. Melchiori. Elsevier/North Holland. 1979. p. 221.

6. B. BELLEAU, T. CONWAY, F. R. AHMED, and T. HARDY. J. Med. Chem. **17**, 907 (1974).
7. F. R. AHMED. Acta Crystallogr., Sect. B, **37**, 188 (1981).
8. I. MONCOVIC, H. WONG, B. BELLEAU, I. J. PACHTER, and Y. G. PERRON. Can. J. Chem. **53**, 2515 (1975).
9. G. JUST and K. GROZINGER. Synthesis, 457 (1976).
10. T. T. CONWAY, T. W. DOYLE, Y. G. PERRON, J. CHAPUIS, and B. BELLEAU. Can. J. Chem. **53**, 245 (1975).
11. H. INOUE and E. MAY. J. Med. Chem. **19**, 259 (1976).
12. H. HODJAT, A. LATTES, J. P. LAVAL, J. MOULINÈS, and J. J. PÉRIÉ. J. Heterocycl. Chem. **9**, 1081 (1972).

Can. J. Chem. Downloaded from www.nrcresearchpress.com by 210.87.254.40 on 09/06/12
For personal use only.

Synthesis of antiviral compounds. Preparation and rearrangement of 6-methoxyglyceropurines

KELVIN K. OGILVIE[1] AND H. RIZK HANNA
Department of Chemistry, McGill University, Montreal, P.Q., Canada H3A 2K6

Received January 9, 1984

KEVIN K. OGILVIE and H. RIZK HANNA. Can. J. Chem. **62**, 2702 (1984).

The synthesis of 6-methoxypurine (**4**) and 6-methoxyguanine (**11** and **12**) derivatives of the glyceropurine series is described. The N-7 guanine derivatives rearrange to the N-9 isomers under certain conditions. The 6-methoxyguanine derivative **12** was found to have a remarkably specific activity against equine herpesvirus.

KEVIN K. OGILVIE and H. RIZK HANNA. Can. J. Chem. **62**, 2702 (1984).

On décrit les synthèses des méthoxy-6 purine (**4**) et méthoxy-6 guanines (**11** et **12**) dérivées de la série de la glycéropurine. Sous certaines conditions, les dérivés de la N-7 guanine se transposent en isomères N-9. On a trouvé que le dérivé **12** de la méthoxy-6 guanine possède une activité spécifique remarquable contre le virus herpès de cheval.

[Traduit par le journal]

Can. J. Chem. Downloaded from www.nrcresearchpress.com by 210.87.254.6 on 09/06/12
For personal use only.

Introduction

In our development of the "glycerosides" as a novel class of nucleoside analogues (1–5) having antiviral activity, we have found that some of the glyceropurines have powerful antiherpes activity. In particular, the guanine derivative 9-[[2-hydroxy-1-(hydroxymethyl)ethoxy]methyl]guanine (BIOLF-62) has perhaps the strongest and widest activity against herpesviruses of any reported compound (6–8). The 6-chloroguanine derivative also has significant activity against herpesviruses (4). Because substitution at C-6 of other purine nucleosides has led to a range of biological activity (4,9,10), we sought selective changes at C-6 in the glyceropurine series. In this report we wish to describe the preparation of the 6-methoxypurine and 6-methoxyguanine compounds **4**, **11**, and **12**. In the latter case we have found that the N-7 isomer rapidly rearranges to the more stable N-9 isomer under specific conditions. The 6-methoxy compounds **4**, **11**, and **12** have been tested for activity against a range of herpesviruses with only the N-9 guanine derivative **12** having activity and, in this case, only against equine HSV-2.

The 6-chloropurine (**1**) and 6-chloroguanine (**6**, **7**) derivatives were chosen as starting materials. Alkaline displacement of chlorine at C-6 of purines has led to mixed results, according to the literature. In some reports, ring opening has been the major result (11–14) while in others smooth displacement of chlorine has been observed (15–17). The general trend indicates that 9-alkyl-6-chloropurines are smoothly converted under alkaline conditions, while the nucleosides of 6-chloropurines often lead to ring opening (18). Conversion of 6-methoxy to 6-hydroxypurines with aqueous base has been established (11).

The 6-chloropurine **1** (4) was converted to the 6-methoxypurine **2** in 93% yield using sodium methoxide in methanol for 30 min at room temperature. Interestingly, the same result is obtained when **1** is treated with sodium hydroxide in methanol–water at room temperature for 15 min. However, if the latter reaction is carried out at reflux temperature the hypoxanthine derivative **3** is produced. Compound **2** can be converted to **3** on refluxing with sodium hydroxide in methanol–water. Both compounds, **2** and **3**, are easily deprotected to **4** and **5** respectively using boron trichloride solution.

In the preparation of the 6-chloroguanine derivative a mixture of the N-7 (**6**) and N-9 (**7**) isomers is obtained (ref. 4, ratio 2:3 by nmr). The mixture can be separated at this stage or (and generally more easily) after conversion of the chlorine. The 6-chlorine of the guanine derivative (2-amino-6-chloropurine derivative) is more difficult to displace than in the 6-chloropurine **1**. However, after reflux with sodium methoxide in methanol for 1.5 h, the 6-methoxy products **8** and **9** were obtained in virtually the same ratio as the starting mixture.

When the mixture of **6** and **7** was heated at reflux with sodium hydroxide in methanol–water (1.5 h) only the N-9 guanine derivative **10** was obtained. Furthermore, pure **6** (the N-7 isomer) yielded only the N-9 isomer **10** when subjected to the same conditions. Pure compound **8** and pure compound **9** are each completely converted to the guanine derivative **10** under reflux with sodium hydroxide in methanol–water.

The pure 6-methoxy derivative **9** was smoothly deprotected using boron trichloride (19) giving only the guanine derivative **12**. The N-7 isomer **8** was more sensitive to the conditions used. While tlc indicated that only the N-7 isomer **11** was produced during the actual reaction with boron trichloride, the product was affected by work-up conditions. With heating or during concentration of the reaction mixture, **11** was converted to **12** to varying degrees. Once isolated, **11** was quite stable and was unaffected by most solvents including hot ethanol. However, if after the removal of solvents during the work-up of the reaction the residue was heated in ethanol, significant conversion of **11** to the N-9 isomer occurred. Complete conversion of **11** to **12** could be achieved in this manner. It has previously been reported that the N-7 isomers of purine derivatives can be converted to the more stable N-9 isomers on heating in the presence of salts (20, 21). Pure compound **11** is stable in ethanolic sodium hydroxide (0.05 *N*) for at least 1.5 h at room temperature. However, pure **11** is rapidly converted to the N-9 isomer **12** in 0.05 *N* HCl in ethanol (aqueous) at room temperature.

The new compounds described in this manuscript were tested against a number of herpesviruses including human HSV-1, HSV-2, and CMV, canine herpesvirus, feline herpesvirus, bovine herpesvirus type 4, and equine herpesvirus type 1. In general, **4**, **11**, and **12** were inactive against all of these viruses at a level less than 100 μg/mL. However, the exception was compound **12** which was uniquely active against equine herpesvirus with an ED-50 of 2.8 μg/mL.

[1]Author to whom correspondence may be addressed.

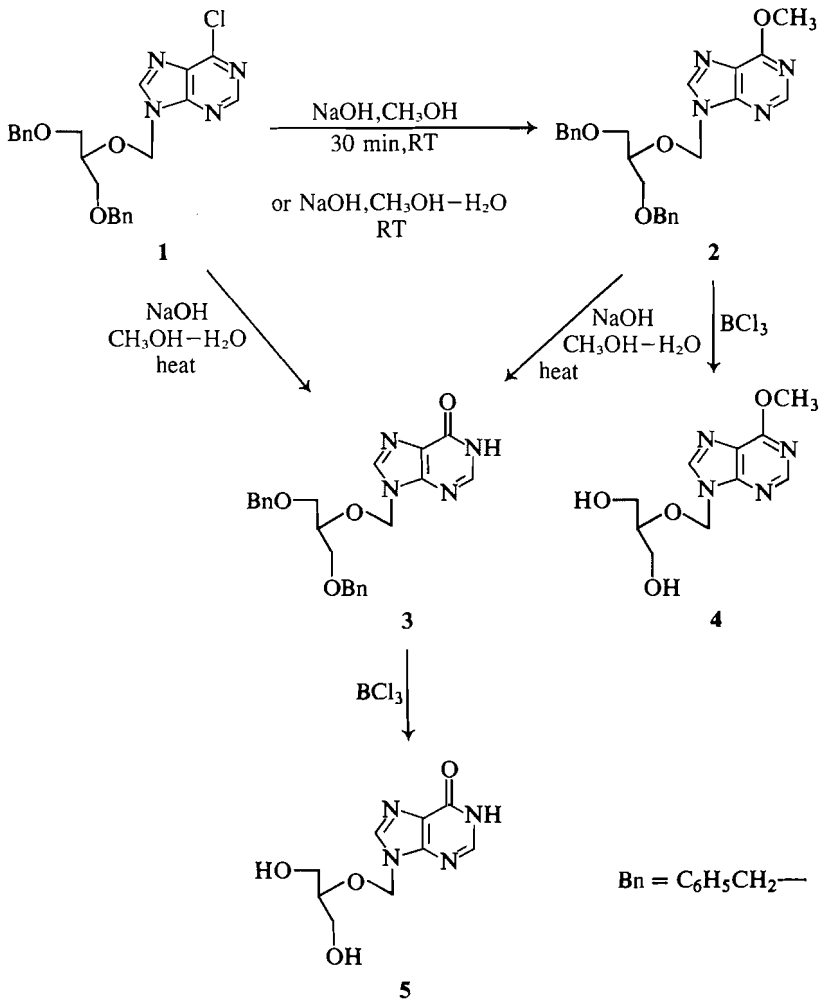

SCHEME 1

Experimental

General methods

Products from preparative scale reactions were isolated by column chromatography using Merck silica gel 60 (230–400 mesh) packed in glass columns (15 g of silica per gram of crude material). Thin-layer chromatographic data (R_f values) are recorded from Merck Kieselgel 60F254 analytical sheets. Purine bases were purchased from Sigma Chemical Co. The uv spectra were recorded on a Cary 17 spectrometer. Nuclear magnetic resonance spectra were recorded using a Bruker WH-90, a Varian XL-200, and a Varian T60A spectrometer.

The 6-chloropurine derivatives 9-[[2-benzyloxy-1-(benzyloxymethyl)ethoxy]methyl]-6-chloropurine **1** and the N-7 and 9-[[2-benzyloxy-1-(benzyloxymethyl)ethoxy]methyl]-2-amino-6-chloropurines **6** and **7** were prepared as previously described (4). Compounds **6** and **7** were obtained as a mixture in a ratio of ~2:3 as judged by nmr (4).

9-[[2-Benzyloxy-1-(benzyloxymethyl)ethoxy]methyl]-6-methoxypurine 2

A. Compound **1** (1 g) was dissolved in methanol (25 mL) containing sodium (0.3 g). The solution was stirred at room temperature for 30 min at which point tlc (EtOAc–hexane, 5:2) indicated complete conversion of **1** (R_f 0.5) to a new compound of R_f 0.2. The solvent was removed at reduced pressure and the residue was dissolved in dichloromethane. The organic layer was washed twice with water followed by drying over magnesium sulfate. The solution was collected by filtration and concentrated. The residue was chromatographed over silica gel eluted with ethyl acetate – hexane (5:7). The product **2** was obtained in 93% yield (0.92 g). The ^{1}Hpmr spectrum of **2** in DMSO-d_6 showed signals (δ, ppm) at 3.49 (m, 4H), 4.0 (m, 1H), 4.17 (s, 3H, OCH_3), 4.43 (s, 4H), 5.8 (s, 1H), 7.28 (10H, aromatic), 8.05 (s, 1H), and 8.56 (s, 1H). The uv characteristics for **2** were λ_{max} in nm(ε) at pH 1: 247 (8200); pH 7: 247 (8800); pH 13: 247 (8500).

B. Compound **1** (0.5 g) was dissolved in methanol (38 mL) to which water (4 mL) and sodium hydroxide (10.5 g) were added. After 5 min at room temperature tlc showed complete conversion of **1** to **2**. After a total of 15 min the solution was diluted with cold water (20 mL) and the solution was carefully neutralized (with cooling) with HCl (3*N* solution). The product was extracted into ether which was dried over magnesium sulphate. Evaporation of the ether gave 0.48 g (97%) of remarkably pure **2**.

9-[[2-Benzyloxy-1-(benzyloxymethyl)ethoxy]methyl]-6-hydroxypurine 3

A. Compound **1** (1 g, 2.3 mmol) was treated with sodium hydroxide (21 g) in methanol (75 mL) to which water (9 mL) had been added. A tlc taken immediately showed only a compound having the same R_f as **2**. The solution was heated at reflux for 1 h at which point tlc indicated the presence of a single spot of R_f 0.06 (ethyl acetate – methanol, 10:0.1). The solution was concentrated at reduced pressure, the residue was dissolved in water, and the solution was neutralized with acetic acid whereupon a precipitate formed. The precipitate was collected by filtration and was allowed to crystallize from ethyl acetate to yield **3** (0.57 g, 60%), mp 131–132°C. Compound **3** had uv properties (λ_{max} in nm (ε)) as follows: pH 1, 247 (9100); pH 7, 247 (10 100); pH 13, 253 (10 700). The ^{1}Hpmr spectrum in DMSO-d_6 showed signals at δ(ppm) of 3.42 (m, 4H), 4.03 (m, 1H), 4.38 (s, 4H), 5.64 (s, 1H), 7.24 (10H, aromatic), 8.06 (s, 1H), and 8.21

Can. J. Chem. Downloaded from www.nrcresearchpress.com by 210.87.254.6 on 09/06/12
For personal use only.

Can. J. Chem. Downloaded from www.nrcresearchpress.com by 210.87.254.6 on 09/06/12
For personal use only.

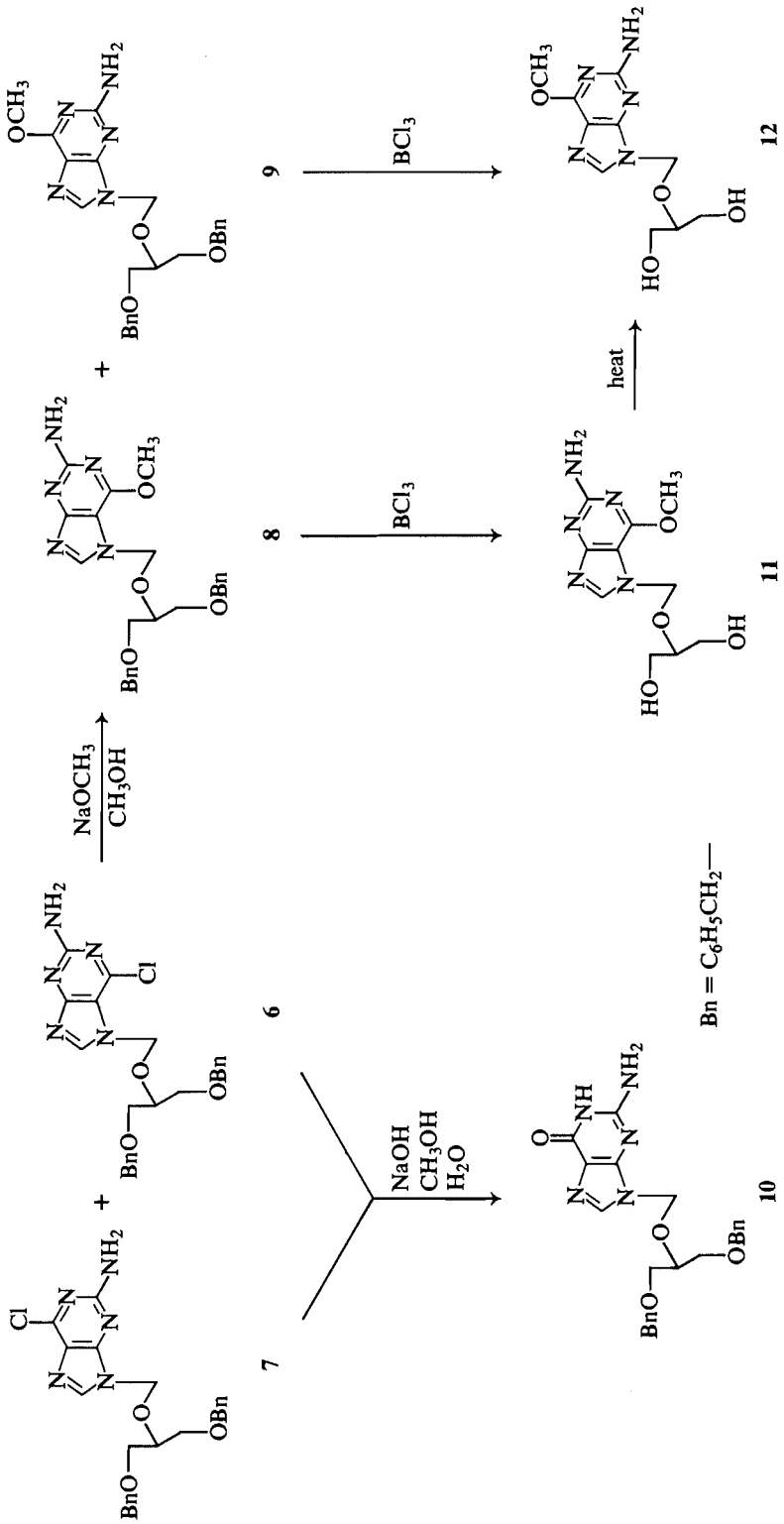

SCHEME 2

Can. J. Chem. Downloaded from www.nrcresearchpress.com by 210.87.254.6 on 09/06/12
For personal use only.

(s, 1H). The ^{13}C spectrum of **3** (DMSO-d_6) showed signals at δ(ppm) of 148.47 (C-2), 145.99 (C-4), 124.14 (C-5), 156.73 (C-6), 140.6 (C-8), 72.25 (C-1′), 76.94 (C-3′), 69.71 (C-4′), and 72.25 (—$CH_2\phi$). *Anal.* calcd. for $C_{23}H_{24}N_4O_4$: C 65.70, H 5.75, N 13.32; found: C 65.52, H 5.64, N 13.34.

Compound **3** was further characterized by treatment with boron trichloride in the standard way (ref. 4, see below) to give the known 6-hydroxypurine derivative **5** in 60% isolated yield. The properties of **5** were identical to those of an authentic sample (4).

B. Compound **2** (1.3 g) was heated in methanol (75 mL) containing water (9 mL) and sodium hydroxide (21 g) at reflux for 30 min. The reaction mixture was worked up as above to yield **3** in 60% yield. No other uv-absorbing material was detected.

*9-[[2-Hydroxy-1-(hydroxymethyl)ethoxy]methyl]-6-methoxypurine **4***

Compound **2** (0.9 g) was dissolved in dichloromethane (50 mL, spectrograde) and boron trichloride (8 mL, 1 *N* in dichloromethane) was added to the solution maintained at −78°C under a nitrogen atmosphere. A tlc showed that after 1 h all of **2** (R_f 0.7, methanol − ethyl acetate (1:3)) had been converted to a new compound of R_f 0.3. The solution was then neutralized with triethyl amine in methanol and the pH was raised to between 8 and 9. The solvents were removed at reduced pressure and the residue was chromatographed on silica gel (eluting first with hexane (500 mL), ethyl acetate (1 L), and ethyl acetate − methanol (18:1, 2 L). The product **4** was collected and after crystallization from methanol−dichloromethane pure crystals of **4** were obtained (70%, mp 135−136°C). The uv properties showed λ_{max} (nm, (ε)) at pH 1: 247 (11 100); pH 7: 247 (12 000); pH 13: 247 (12 100). The ^{1}Hpmr spectrum of **4** in DMSO-d_6 showed signals at δ(ppm) of 3.31 (m, 4H), 3.58 (m, 1H), 4.08 (s, 3H, —OCH_3), 4.58 (t, 2H, —OH), 5.72 (s, 1H), 8.48 (s, 1H), and 8.55 (s, 1H). The ^{13}C spectrum (DMSO-d_6) showed signals at δ(ppm) of 152.19 (C-2), 151.87 (C-4), 120.53 (C-5), 160.34 (C-6), 144.05 (C-8), 72.25 (C-1′), 80.88 (C-3′), 60.97 (C-4′), and 53.96 (—OCH_3). *Anal.* calcd. for $C_{10}H_{14}N_4O_4$: C 47.24, H 5.55, N 22.04; found: C 47.17, H 5.64, N 22.01.

*Conversion of **6** and **7** to the guanine derivative **10***

A. A mixture of **6** and **7** (5.5 g, 2:3 by ^{1}Hpmr) was dissolved in methanol (300 mL) to which water (21 mL) and sodium hydroxide (84 g) were added. The solution was heated at reflux and after 1.5 h, tlc (methanol − ethyl acetate − dichloromethane, 1:3:3) showed that the starting material (R_f 0.75) had been completely converted to material having R_f 0.3. The solution was concentrated at reduced pressure and the residue was dissolved in water. The solution was neutralized with acetic acid whereupon a precipitate formed that was collected by filtration. The material gave, after crystallization from ethanol−water, 3.8 g (70%) of **10**, which was identical in all respects (mp, ^{13}C, ^{1}Hpmr, R_f, uv) to authentic material previously described (2,4)).

B. Pure N-7 isomer **6** (280 mg) was subjected to the above conditions. The sole product was compound **10** isolated in 95% yield (256 mg).

*Conversion of the mixture of **6** and **7** into the 6-methoxyguanine derivatives **8** and **9***

A mixture of **6** and **7** (2.5 g, 2:3 by ^{1}Hpmr) was added to a solution of sodium (0.7 g) in methanol (50 mL). The solution was heated at reflux for 1.5 h at which point tlc (ethyl acetate − hexane, 3:1) showed the starting material (R_f 0.5) had been completely converted to two materials having R_f 0.3 and 0.1. The solvent was removed at reduced pressure and water (50 mL) was added. The pH was adjusted to ~5.5 with acetic acid. The product was extracted into dichloromethane. After drying over magnesium sulfate the solvent was evaporated to leave a dark syrup (2.56 g) which was chromatographed on silica gel. The column was eluted with ethyl acetate − hexane (1:1, 1 L; 2:1, until the first product was completely eluted; 3:1, to collect the second product). The first product, **9**, had R_f 0.3 in ethyl acetate − hexane (3:1) and was obtained as a viscous oil. The material crystallized from ethyl acetate − hexane (mp 83−84°C, 0.87 g, 44%). Compound **9** had λ_{max} (nm (ε)) at pH 1: 289 (8600), 244 (8600); pH 7: 282 (10 100), 247 (11 300); pH 13: 282 (9700), 247 (11 300). The ^{1}Hpmr spectrum in $CDCl_3$ showed signals at 3.49 (m, 4H), 3.97 (m, 1H), 4.05 (s, 3H), 4.44 (s, 4H), 5.60 (s, 2H), 4.92 (NH_2), 7.26 (10H, aromatic), 7.7 (s, 1H). The ^{13}C spectrum (DMSO-d_6) showed signals at δ(ppm) of 160.72 (C-2), 154.24 (C-4), 113.78 (C-5), 160.08 (C-6), 139.79 (C-8), 71.60 (C-1′), 76.56 (C-3′), 69.66 (C-4′), 53.09 (—OCH_3), and 72.19 (—$CH_2\phi$). *Anal.* calcd. for $C_{24}H_{27}N_5O_4$: C 64.13, H 6.05, N 15.58; found: C 64.42, H 6.18, N 15.32.

The second fraction (R_f 0.1) was obtained as a viscous oil (**8**, 0.53 g, 27%). Compound **8** had λ_{max} (nm (ε)) at pH 1: 288 (6600), 247 (7200); pH 7: 283 (7200), 253 (9900); pH 13: 283 (6800), 253 (9700). The ^{1}Hpmr spectrum in $CDCl_3$ showed signals at 3.5 (m, 4H), 3.96 (s, 3H), 4.05 (m, 1H), 4.44 (s, 4H), 5.65 (s, 2H), 6.27 (NH_2), 7.23 (10H, aromatic), 7.7 (s, 1H). *Anal.* calcd. for $C_{24}H_{27}N_5O_4$: C 64.13, H 6.05, N 15.58; found: C 63.96, H 5.95, N 15.41.

*Conversion of **9** to **10***

Compound **9** (0.5 g) was dissolved in methanol (30 mL) and water (3 mL) and sodium hydroxide (10.5 g) were added. The solution was heated at reflux for 1.5 h whereupon tlc showed complete conversion to **10**. The solvents were removed at reduced pressure and the residue was dissolved in water (80 mL). The solution was acidified with acetic acid whereupon a precipitate formed. The solid was collected by filtration, washed with water, and dried to yield 0.41 g (85%) of pure **10**.

*Conversion of **8** to **10***

The above procedure was repeated using 400 mg of **8**. Compound **8** was converted to **10** in 88% isolated yield.

*Conversion of **8** to 7-[[2-hydroxy-1-(hydroxymethyl)ethoxy]methyl]-2-amino-6-methoxypurine (**11**)*

Compound **8** (500 mg) was treated with boron trichloride in the usual manner. After 1 h, tlc (methanol − ethyl acetate, 1:2) showed complete conversion of **8**, R_f 0.7, to a new material of R_f 0.2. The solution was neutralized with triethyl amine in methanol and the pH was adjusted to 8. The solvent was removed at reduced pressure to give a solid that was dissolved in methanol. Dichloromethane was added and a fine precipitate was obtained. This material was identified as compound **11** (0.17 g, 57%, mp 211−212°C). The mother liquor contained both **11** and **12**.

In a repeat of the above reaction the solid obtained directly from the reaction was dissolved in ethanol and allowed to stand; tlc showed that **11** was completely converted to **12** with time and the process was hastened by heating the solution. However, once isolated pure, **11** is stable on heating in ethanol.

Compound **11** showed λ max (nm (ε)) at pH 1: 287 (5900), 246 (6800); pH 7: 283 (7200), 253 (9700); pH 13: 283 (7100), 253 (9700). The ^{1}Hpmr spectrum of **11** in DMSO-d_6 showed signals at 3.33 (m, 4H), 3.6 (m, 1H), 3.98 (s, 3H), 4.62 (OH), 5.58 (s, 2H), 7.40 (NH_2), and 8.01 (s, 1H). *Anal.* calcd. for $C_{10}H_{15}N_5O_4 \cdot \frac{1}{2}H_2O$: C 43.16, H 5.79, N 25.17; found C 43.37, H 5.66, N 24.91.

*Stability of **11** in acid and base*

Compound **11** was dissolved in (a) 0.05 *N* HCl in ethanol (aqueous) and (b) 0.05 *N* NaOH in ethanol (aqueous). Both solutions were stirred at room temperature. After 1.5 h compound **11** had been completely converted to **12** under the acid conditions (a) but was unaffected by the basic conditions (b).

*Conversion of **9** to **12***

Compound **9** (3 g) was treated with boron trichloride solution in the normal manner. The product was isolated pure following chromatography on silica gel using methanol − ethyl acetate (1:6). Compound **12** (mp 167−168°C) was obtained in 63% yield (1.1 g). Compound **9** showed λ max (nm (ε)) at pH 1: 288 (5800), 245 (6100); pH 7: 282 (6600), 247 (7500); pH 13: 282 (6500), 247 (7700). The ^{1}Hpmr spectrum in DMSO-d_6 showed signals δ(ppm) at 3.35 (m, 4H), 3.54 (m, 1H), 3.97 (s, 3H), 4.62 (OH), 5.52 (s, 2H), 6.48 (NH_2), and 7.98 (s, 1H). The ^{13}C spectrum (DMSO-d_6) showed signals at δ (ppm)

of 160.88 (C-2), 154.35 (C-4), 113.78 (C-5), 160.18 (C-6), 140.11 (C-8), 71.65 (C-1′), 80.28 (C-3′), 61.02 (C-4′), and 53.31 (—OCH_3). *Anal.* calcd. for $C_{10}H_{15}N_5O_4 \cdot \frac{1}{2}H_2O$: C 43.16, H 5.79, N 25.17; found C 43.65, H 5.71, N 25.34.

Acknowledgements

We gratefully acknowledge financial support from the Natural Sciences and Engineering Research Council of Canada and from Bio Logicals. We are also grateful to Dr. K. O. Smith and to Bio Logicals for obtaining the level of activity against the indicated viruses.

1. K. K. OGILVIE AND M. F. GILLEN. Tetrahedron Lett. **21**, 327 (1980).
2. K. K. OGILVIE, U. O. CHERIYAN, B. K. RADATUS, K. O. SMITH, K. S. GALLOWAY, and W. L. KENNELL. Can. J. Chem. **60**, 3005 (1982).
3. K. K. OGILVIE, R. G. HAMILTON, M. F. GILLEN, B. K. RADATUS, K. O. SMITH, and K. S. GALLOWAY. Can. J. Chem. **62**, 16 (1984).
4. K. K. OGILVIE, N. NGUYEN-BA, M. F. GILLEN, B. K. RADATUS, U. O. CHERIYAN, H. R. HANNA, K. O. SMITH, and K. S. GALLOWAY. Can. J. Chem. **62**, 241 (1984).
5. K. K. OGILVIE, D. M. DIXIT, B. K. RADATUS, and K. O. SMITH. Nucleosides Nucleotides, **2**, 147 (1983).
6. K. O. SMITH, K. S. GALLOWAY, W. L. KENNEL, K. K. OGILVIE, and B. K. RADATUS. Antimicrob. Agents Chemother. **22**, 55 (1982).
7. (a) K. O. SMITH, K. S. GALLOWAY, K. K. OGILVIE, and U. O. CHERIYAN. Antimicrob. Agents Chemother. **22**, 1026 (1983); (b) K. O. SMITH, K. S. GALLOWAY, S. L. HODGES, K. K. OGILVIE, B. K. RADATUS, S. S. KALTER, and R. L. HEBERLING. Am. J. Vet. Res. **44**, 1032 (1983).
8. (a) W. T. ASHTON, J. D. KARKAS, A. K. FIELD, and R. L. TOLMAN. Biochem. Biophys. Res. Commun. **108**, 1716 (1982); (b) J. C. MARTIN, C. A. DVORAK, D. F. SNEE, T. R. MATTHEWS, and J. P. H. VERHEYDEN. J. Med. Chem. **26**, 759 (1983); (c) V-C. CHENG, E-S. HUANG, J-C. LIN, E-C. MAR, J. S. PAYANO, G. E. DUTSCHMAN, and S. P. GRILL. Proc. Natl. Acad. Sci. U.S.A. **80**, 2767 (1983).
9. G. H. MILNE and L. B. TOWNSEND. J. Med. Chem. **17**, 263 (1974).
10. B. KIERDASZUK, R. STOLARSKI, and D. SHUGAR. FEBS Lett. **158**, 128 (1983).
11. J. A. MONTGOMERY AND H. J. TOMASZ. J. Org. Chem. **36**, 1962 (1971).
12. M. P. GORDON, V. S. WELIKY, and G. D. BROWN. J. Am. Chem. Soc. **79**, 3245 (1957).
13. B. R. BAKER and K. HEWSON. J. Org. Chem. **22**, 959 (1957).
14. A. BENDICH, P. J. RUSSELL, and J. J. FOX. J. Am. Chem. Soc. **76**, 6073 (1954).
15. K. KIKUGAWA, H. SUEHIRO, and M. ICHINO. J. Med. Chem. **16**, 1389 (1973).
16. G. L. SZEKERES, R. K. ROBINS, K. H. BOSWELL, and R. A. LONG. J. Heterocycl. Chem. **12**, 15 (1975).
17. J. F. GERSTER, J. W. JONES, and R. K. ROBINS. J. Org. Chem. **28**, 945 (1963).
18. J. A. MONTGOMERY and C. TEMPLE. J. Am. Chem. Soc. **79**, 5238 (1957).
19. J. SEELA and S. MENKHOFF. Justus Liebigs Ann. Chem. 813 (1982).
20. T. ITOH, T. SUGAWARA, and Y. MIZUNO. Nucleosides Nucleotides, **1**, 179 (1982).
21. K. A. WATANABE, D. H. HOLLENBERG, and J. J. FOX. J. Carbohydr. Nucleosides Nucleotides, **1**, 1 (1974).

Can. J. Chem. Downloaded from www.nrcresearchpress.com by 210.87.254.6 on 09/06/12
For personal use only.

Correlation of nuclear magnetic resonance spectra and structure of *trans*-camphane-2,3-diols

M. S. ALLEN, J. H. HUTCHINSON, AND T. MONEY
Department of Chemistry, University of British Columbia, Vancouver, B.C., Canada V6T 1Y6

Received March 8, 1984

M. S. ALLEN, J. H. HUTCHINSON, and T. MONEY. Can. J. Chem. **62**, 2707 (1984).

Evidence is provided to demonstrate that a recent correction in the published nmr spectra of *trans*-camphane-2,3-diols is unjustified.

M. S. ALLEN, J. H. HUTCHINSON et T. MONEY. Can. J. Chem. **62**, 2707 (1984).

On démontre, évidences à l'appui, qu'une correction parue récemment pour les spectres de rmn de *trans*-camphanediols-2,3 est injustifiée.

[Traduit par le journal]

Can. J. Chem. Downloaded from www.nrcresearchpress.com by 210.87.254.40 on 09/06/12
For personal use only.

In a recent paper (1) it was suggested that the nmr spectra previously assigned by Anet (2) to the *trans*-camphane-2,3-diols, **4** and **5** (3–5), should be reversed. During our investigations (6) on the chemical and microbiological oxidation or bornyl acetate, **1**, we found that a minor product in the microbiological transformation of this compound was 3-*exo*-hydroxyborneol, **4**. In addition, chemical oxidation of bornyl acetate produced a small amount of 3-oxobornyl acetate which was subsequently reduced to 3-*exo*-hydroxyborneol, **4**. The ir and nmr spectra of our *trans*-diol (**4**) (δ ($CDCl_3$): 3.55 (d, $J \sim 2$ Hz), 3.97 (m); δ (C_5H_5N, D_2O): 1.95 (d, $J = 4.5$ Hz), 4.05 (d, $J = 2.5$ Hz), 4.45 (m)) was very similar to that reported by Takeshita and Kitajima (4) and Anet (2) respectively. Furthermore the published nmr spectra (7) for borneol **2**, isoborneol **3**, epiborneol **6**, and epiisoborneol **7** lead to the expectation that Δδ for the C(2) and C(3)-hydrogens in 2-*exo*-3-*endo*-camphanediol (**5**) would be significantly greater than that for the 2-*endo*-3-*exo*-diol (**4**). Anet's recorded spectra (2) for the *trans*-2,3-camphanediols are consistent with this prediction. In addition, the C(4) bridgehead hydrogen in our *trans*-diol (**4**) (2-*endo*-3-*exo*) appears as a doublet at δ 1.95 ($J = 4.5$ Hz) in the 100-MHz spectrum (pyridine-d_5/D_2O). By comparison, the corresponding hydrogen in camphor (**8**) is a triplet ($J = 4.5$ Hz) while in 5-*exo*-hydroxycamphor,[1]

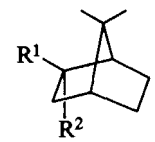

1 R^1 = H, R^2 = OAc
2 R^1 = H, R^2 = OH (δ3.95)
3 R^1 = OH, R^2 = H (δ3.55)

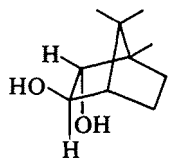

4

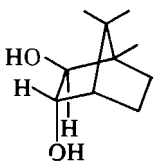

5

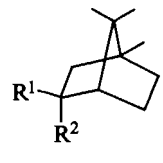

6 R^1 = H, R^2 = OH (δ4.55)
7 R^1 = OH, R^2 = H (δ3.75)

*δ in $CDCl_3$ or CCl_4

[1] D. Dolphin and C. Welborn, University of British Columbia, unpublished results.

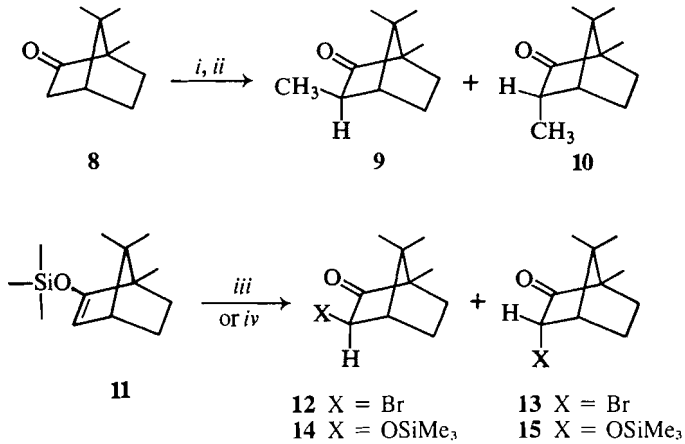

8 **9** **10**

11 **12** X = Br **13** X = Br
14 X = $OSiMe_3$ **15** X = $OSiMe_3$

i LDA–THF/HMPA (20:1)/0°C *ii* CH_3I/0°C
iii Br_2–dioxane/C_5H_5N/CH_2Cl_2 *iv* O_3/CH_2Cl_2/−78°C

SCHEME 1

5-*exo*-hydroxyborneol (3, 8), 5-*exo*-acetoxybornyl acetate (6), and 5-*exo*-deuterioborneol (9) it appears as a doublet ($J \sim 4.5$ Hz).

The proposed correction (1) in the nmr spectra (2) of *trans*-camphane-2,3-diols was based on the assumption that hydroboration of camphor enol trimethylsilyl ether **11** would occur preferentially on the "less hindered" *endo* face of this compound. In recent studies we have established that kinetic methylation of camphor enolate occurs preferentially on the *exo* face to provide a mixture (~4:1) of 3-*exo*-methylcamphor **9** and 3-*endo*-methylcamphor **10** (12). In addition we have shown that treatment of camphor enol trimethylsilyl enol ether **11** (10) with Br_2–dioxane/C_5H_5N (11) produces a mixture (~1:1) of 3-*exo* and 3-*endo* bromo derivatives, **12** and **13**. It has also been reported (13, 14) that ozone reacts with camphor enol trimethylsilyl ether **11** to give a mixture (1.3:1) of 3-*exo*-trimethylsilyloxycamphor **14** and its 3-*endo* epimer **15**. Thus the assumption that the reactions of camphor enolate in camphor enolate derivatives occur preferentially on the *endo* face of the enolate system is not supported by experimental evidence.

On the basis of the chemical and spectroscopic evidence cited above we suggest that the proposed correction (1) of Anet's original assignment (2) of nmr spectra to the *trans*-camphane-2,3-diols is unwarranted.

Acknowledgement

We acknowledge financial support for this research from the Natural Sciences and Engineering Research Council of Canada.

1. M. A. JOHNSON and M. P. FLEMING. Can. J. Chem. **57**, 318 (1979).
2. F. A. L. ANET. Can. J. Chem. **39**, 789 (1961).
3. S. J. ANGYAL and R. J. YOUNG. J. Am. Chem. Soc. **81**, 5467 (1959).
4. T. TAKESHITA and M. KITAJIMA. Bull. Chem. Soc. Jpn. **32**, 985 (1959).
5. I. FLEMING and R. B. WOODWARD. J. Chem. Soc. (C), 1289 (1968).
6. M. S. ALLEN, N. DARBY, P. SALISBURY, E. R. SIGURDSON, and T. MONEY. Can. J. Chem. **57**, 733 (1979).
7. E. HEINÄNEN. Suom. Kemistil. B, **43**, 462 (1970), and references cited therein.
8. A. MARQUET and J. GABARD. Bull. Soc. Chim. Fr. 128 (1967).
9. J. GLOUX and M. GUGLIELMI. Tetrahedron Lett. 2935 (1969).
10. (*a*) G. C. JOSHI and L. M. PANDE. Synthesis, 450 (1975); (*b*) G. SIMCHEN and W. KOBER. Synthesis, 259 (1976).
11. (*a*) R. H. REUSS and A. HASSNER. J. Org. Chem. **39**, 1785 (1974); (*b*) B. M. TROST and P. G. MCDOUGAL. J. Am. Chem. Soc. **104**, 6110 (1982).
12. J. H. HUTCHINSON and T. MONEY. Can. J. Chem. **62**, 1899 (1984).
13. C. W. JEFFORD and C. G. RIMBAULT. J. Am. Chem. Soc. **100**, 6437 (1978).
14. R. D. CLARK and C. H. HEATHCOCK. J. Org. Chem. **41**, 1396 (1976).

Can. J. Chem. Downloaded from www.nrcresearchpress.com by 210.87.254.40 on 09/06/12
For personal use only.

A synthesis of 2-deoxy-2-{^{18}F}fluoro-D-glucose using accelerator-produced ^{18}F-fluoride ion generated in a water target

PHILIP A. BEELEY, WALTER A. SZAREK, GEORGE W. HAY, AND MILTON M. PERLMUTTER

Carbohydrate Research Institute and Department of Chemistry, Queen's University, Kingston, Ont., Canada K7L 3N6

Received March 13, 1984

PHILIP A. BEELEY, WALTER A. SZAREK, GEORGE W. HAY, and MILTON M. PERLMUTTER. Can. J. Chem. **62**, 2709 (1984).

A synthesis of 2-deoxy-2-{^{18}F}fluoro-D-glucose (2-{^{18}F}DFG) from 1,2-anhydro-3,4:5,6-di-*O*-isopropylidene-1-*C*-nitro-D-mannitol has been developed. The procedure employed ^{18}F produced by the $^{16}O(^3He,p)^{18}F$ reaction using a water target. The label was introduced using KH{^{18}F}F_2 dried by microwave heating; the ^{18}F-labeled derivative, upon treatment with 80% trifluoroacetic acid, afforded 2-{^{18}F}DFG in a radiochemical yield of 10%. The total time of the synthesis was less than 110 min.

PHILIP A BEELEY, WALTER A. SZAREK, GEORGE W. HAY et MILTON M. PERLMUTTER. Can. J. Chem. **62**, 2709 (1984).

On développé une méthode de synthèse du déoxy-2 {^{18}F}fluoro-2 D-glucose ({^{18}F}-2 DFG) à partir de l'anhydro-1,2 di-*O*-isopropylidène-3,4:5,6 *C*-nitro-1 D-mannitol. La méthode implique l'utilisation de ^{18}F produit par une réaction $^{16}O(^3He,p)^{18}F$ faisant appel à une cible aqueuse. On a introduit le marqueur en utilisant du KH{^{18}F}F_2 qui avait été séché par micro-ondes; la réaction du dérivé marqué au ^{18}F avec de l'acide trifluoroacétique à 80% fournit le {^{18}F}-2 DFG avec un rendement radiochimique de 10%. Le temps total de la synthèse est inférieur à 110 min.

[Traduit par le journal]

Can. J. Chem. Downloaded from www.nrcresearchpress.com by 210.87.254.40 on 09/06/12
For personal use only.

Introduction

The use of 2-deoxy-2-{^{18}F}fluoro-D-glucose (2-{^{18}F}DFG) for the measurement of regional cerebral glucose metabolism by positron emission tomography (PET) is now well established (1–3) and has generated a widespread interest in the application of this technique. Concomitantly, there has been expended a substantial effort to find alternative routes for the synthesis of this radiopharmaceutical. The first synthesis (4) of 2-{^{18}F}DFG, involving the addition of ^{18}F-labeled F_2 to tri-*O*-acetyl-D-glucal, gave a radiochemical yield of 10%. Recently, this yield has been increased by the use of {^{18}F}-acetyl hypofluorite (5) or {^{18}F}-xenon difluoride (6, 7). However, these syntheses employ molecular fluorine, thereby restricting the theoretical incorporation of ^{18}F to 50%; these methods involve the production of isotope by the $^{20}N(d,\alpha)$ ^{18}F reaction. In contrast, synthetic procedures based on ^{18}F-fluoride ion would, in principle, allow all of the radioisotope to be incorporated into the required product, and would allow a choice from a wider range of nuclear reactions. For example, Levy *et al.* (8) have synthesized 2-{^{18}F}DFG in a radiochemical yield of 10%, by the displacement of the trifluoromethanesulfonyloxy group in methyl 4,6-*O*-benzylidene-3-*O*-methyl-2-*O*-trifluoromethanesulfonyl-β-D-mannopyranoside. The low yield obtained by Levy *et al.* (8) is attributable in part to the low yield of CsH{^{18}F}F_2 obtained by trapping H^{18}F on CsF, and in part to the difficulties in effecting the quantitative hydrolysis of the 1-*O*- and 3-*O*-methyl groups of the substrate. More recently Tewson (9) has synthesized the same compound in a radiochemical yield of 40% by a nucleophilic reaction at C-2 in methyl 4,6-*O*-benzylidene-β-D-mannopyranoside 2,3-cyclic sulfate. Tewson (9) reported an excellent (>90%) incorporation of ^{18}F into the required fluorosulfate, a value approaching the theoretical maximum. However, hydrolysis of the glycoside resulted in a considerably reduced yield of 2-{^{18}F}DFG. Nevertheless, the radiochemical yield obtained is the highest reported at present.

In this laboratory, a synthesis of 2-deoxy-2-fluoro-D-glucose has been achieved (10) in high yield by the reaction of KHF_2 with the acyclic α-nitroepoxide, 1,2-anhydro-1-deoxy-3,4:5,6-di-*O*-isopropylidene-1-*C*-nitro-D-mannitol (**1**). We now report the reaction of KH{^{18}F}F_2 with **1** (see Fig. 1), followed by the removal of the blocking groups to afford 2-{^{18}F}DFG in a radiochemical yield of 10%; the overall synthesis time was less than one half-life of ^{18}F.

Experimental

Production of ^{18}F and labeling of KHF_2

The production of ^{18}F was achieved by the $^{16}O(^3He,p)^{18}F$ reaction using the Queen's University 4-MeV Van de Graaff accelerator. Beam degradation in this low energy accelerator was circumvented by the use of a windowless ice target. The target consisted of a gold-plated, liquid nitrogen-cooled, cold finger located in the vacuum beam line of the accelerator. An external reservoir containing high purity water[1] supplied a constant jet of water vapor to the cold finger, and the ice layer thus formed was bombarded with the 4-MeV ^{3}He beam. This arrangement afforded approximately 0.5 mCi of ^{18}F per μA, accompanied by the production of a similar quantity of ^{15}O from the $^{16}O(^3He,\alpha)^{15}O$ reaction. Normally a 2-μA beam was used and approximately 1 mCi of ^{18}F could be recovered from the target at the end of bombardment. A stoichiometric quantity of ^{19}F-fluoride ion-carrier in the form of KHF_2 (0.5 mole per mole of **1**) was added as a 0.1 *M* aqueous solution to the $^{18}F-H_2O$ (~3 mL) in a Teflon vial and the solution evaporated to dryness in a microwave oven.[2]

*Reaction of the α-nitroepoxide **1** with KH{^{18}F}F_2*

The α-nitroepoxide **1** was synthesized by the method of Szarek *et al.* (10). A weighed amount of **1** (40–60 μmol) was dried over P_2O_5 in a vacuum desiccator for 1 h prior to reaction. The solvent employed in this reaction, namely ethylene glycol, was initially treated with CaO and distilled under reduced pressure; it was then heated at reflux temperature in the presence of 4A molecular sieves and distilled. The distillate was stored over 4A molecular sieves; immediately prior to its use it was treated with Na under N_2 and distilled under reduced pressure. The sample of **1** was added to the KH{^{18}F}F_2 (20–30 μmol) and the vial was sealed with a septum. The freshly distilled ethylene glycol (1 mL) was added to the vial and the solution heated, under N_2, at 135°C for 20–25 min. Thin-layer chromatography[3] (tlc)

[1]HPLC-grade water; Fisher W5.

[2]CEM Corporation; model MDS-81.

[3]Thin-layer chromatography was performed using Merck plates precoated with silica gel 60 F-254. The developed plates were dried and compounds located by heating the plates at ~150°C after they had been sprayed with 10% aqueous sulfuric acid containing 1% cerium sulfate and 1.5% molybdic acid.

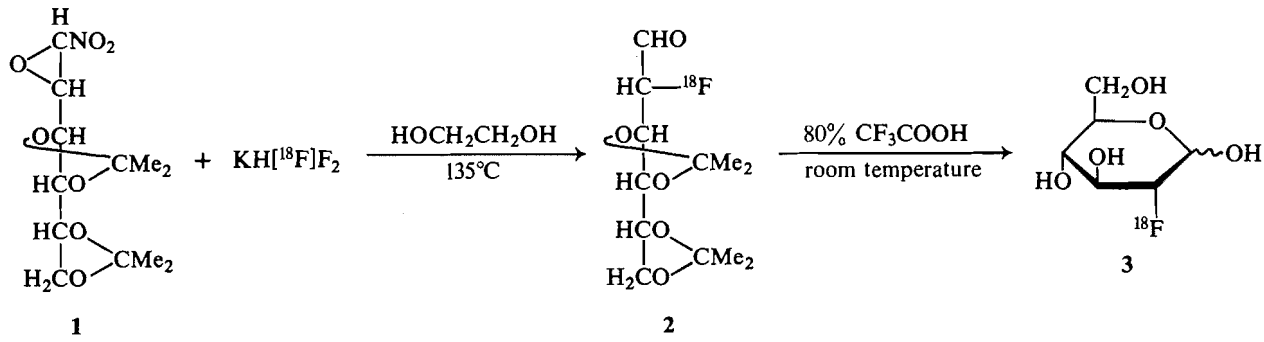

FIG. 1. Synthesis of 2-deoxy-2-{^{18}F}fluoro-D-glucose.

(toluene – ethyl acetate, 1:1 (v/v)) indicated the presence of a trace of starting material **1** (R_f 0.8), and of a component (R_f 0.42) containing 15% (mean value obtained from 8 runs) of the total activity on the plate, the remainder of the activity being at the origin. The reaction mixture was cooled rapidly, diluted with distilled water (10 mL), and the solution was extracted with dichloromethane (3 × 5 mL). The activity distribution between the organic and aqueous layers was comparable to that observed above by tlc; this thin-layer chromatographic examination indicated that more than 90% of the activity present in the organic extracts was attributable to the product having R_f 0.42, the remainder arising from a minute amount of non-migrating material carried over in the extraction procedure. The combined organic extracts were dried over anhydrous Na_2SO_4 and concentrated under reduced pressure.

*Deprotection of 2-deoxy-2-{^{18}F}fluoro-3,4:5,6-di-O-isopropylidene-*aldehydo-*D-glucose (2)*

Method (a)

Trifluoroacetic acid (80% (v/v), 2 mL) was added to the residue obtained from the organic extracts, and the solution was heated to 50°C for 5 min. The acid was removed under reduced pressure (bath temperature < 50°C) and the residue was dissolved in aqueous acetonitrile (0.3% water (v/v), 2 mL). Thin-layer chromatography (acetonitrile–water, 95:5 (v/v)) indicated that the major radioactive product migrated at the same rate as an authentic sample of 2-deoxy-2-fluoro-D-glucose[4] (R_f 0.43). The component giving rise to the most intense spot in tlc (R_f 0.11) did not contain any radioactivity. The presence of a minor component having R_f 0.32 was observed occasionally; this component migrated at the same rate as the product resulting from the treatment of the α-nitroepoxide **1** with trifluoroacetic acid. Thin-layer chromatography indicated the following activity distribution: 2-deoxy-2-fluoro-D-glucose, 80%; solvent front, 15%; origin, 5%.

Method (b)

Trifluoroacetic acid (80% (v/v), 2 mL) was added to the residue obtained from the organic extracts, and the solution was stirred at room temperature for 10 min; the reaction mixture was processed as described in Method (a). Thin-layer chromatography indicated the following activity distribution: 2-deoxy-2-fluoro-D-glucose, ~86%; solvent front, 8%; origin ~6%.

Column chromatography and high performance liquid chromatography (hplc) analysis

The aqueous acetonitrile solution (0.3% water (v/v)) of 2-{^{18}F}DFG was chromatographed on a column (0.7 × 10 cm) of dry silica gel 60 using the same solvent as eluent. The initial 6-mL portion of the eluate was discarded and the product was obtained from the subsequent 10-mL portion. The solvent was removed under reduced pressure; hplc-grade water (~2.5 mL) and washed alumina (~50 mg) were added and the solution filtered through a 0.2-μm Millipore membrane. The product was analyzed by hplc (Bio-Rad Carbohydrate Column HPX-87; Varian 5000 Liquid Chromatograph; 85°C, water, flow rate 0.6 mL/min; differential refractometer and NaI (Tl) well counter detectors). The retention time of the product, detected by the refractometer, was 9.7 min, corresponding to that of an authentic sample[4] of 2-deoxy-2-fluoro-D-glucose. Only one major radioactive component was detected; this had a retention time of 10.0 min and a radiochemical purity greater than 97%. The retention times indicated by the two detectors corresponded to those obtained using a sample of 2-{^{18}F}DFG provided by the Montreal Neurological Institute. Chemical and radiochemical yields of 2-deoxy-2-fluoro-D-glucose were of a comparable value, namely ~10% (mean value obtained from 8 runs).

Activity measurements

Activity distribution on the plates was measured by fractional counting after charring using 10% H_2SO_4 in methanol. The activities in aqueous and organic solutions were measured by counting 100-μL samples at a fixed geometry to the detector system. For relative activity distributions, a 7.62 × 7.62 cm NaI (Tl) detector coupled to a single-channel analyzer, or an intrinsic Ge detector coupled to a multichannel analyzer, was used. The absolute activity of ^{18}F-fluoride ion and of 2-{^{18}F}DFG was measured by counting 100-μL samples at a fixed geometry to the calibrated Ge detector.

Results and discussion

This article described a new synthesis of 2-{^{18}F}DFG in a radiochemical (decay-corrected) yield of 10%. Although this yield is lower than some of those recently reported, nevertheless the synthetic method is a viable alternative for the "in-house" production of 2-{^{18}F}DFG. Because the chemical yield of 2-deoxy-2-fluoro-D-glucose was comparable to the radiochemical yield, it was considered to be unnecessary to treat the accelerator-derived ^{18}F-H_2O with a cation-exchange resin, as was necessary in the method of Tewson (9). Such treatment may result in a loss of ^{18}F, thereby reducing the radiochemical yield of the radiopharmaceutical when based on the starting activity of ^{18}F. The starting material, 1,2-anhydro-3,4:5,6-di-*O*-isopropylidene-1-*C*-nitro-D-mannitol (**1**), has been isolated (10) in crystalline form in 72% yield from a mixture of 1,2-anhydro-3,4:5,6-di-*O*-isopropylidene-1-*C*-nitro-D-mannitol and -D-glucitol which was obtained in 80% yield by treatment of 1,2-dideoxy-3,4:5,6-di-*O*-isopropylidene-1-*C*-nitro-D-*arabino*-hex-1-enitol with 30% hydrogen peroxide; this nitroolefin can be obtained from D-arabinose in a good overall yield. The substrate **1** is a crystalline solid that is stable when stored at 0°C. Full details of the carbohydrate synthesis will be published separately.

In the reaction of the α-nitroepoxide **1** with KHF_2 it has been found that a 12-fold molar-equivalent excess of KHF_2 affords 2-deoxy-2-fluoro-D-glucose in a yield greater than 30% based on **1** and that further increasing the concentration of the fluoride salt enhances the yield. However, reactions using up to 2.5

[4]Calbiochem-Behring Corporation.

Can. J. Chem. Downloaded from www.nrcresearchpress.com by 210.87.254.40 on 09/06/12
For personal use only.

molar equivalents of KHF_2 did not afford yields of 2-deoxy-2-fluoro-D-glucose beyond 10%, in experiments leading to either labeled or unlabeled product. A decrease in the amount of KHF_2 carrier to 5 μmol per 50 μmol of **1** resulted in a 15% incorporation of ^{18}F into the fluoro aldehyde **2**; thus the use of less than 1 molar equivalent of KHF_2 allows the specific activity of the product to be increased, if so desired.

The use of ethylene glycol as the solvent in the reaction of the α-nitroepoxide with fluoride ion resulted in the formation of a component the R_f of which was similar to that of the product, fluoro aldehyde **2**; however, treatment of the mixture of products with 80% trifluoroacetic acid converted this component into one (R_f 0.11, acetonitrile–water, 95:5 (v/v)) which was well separated from 2-deoxy-2-fluoro-D-glucose (R_f 0.43). Competing reactions with ethylene glycol have been observed (11–13) previously with carbohydrate substrates. The use of a variety of other solvents, together with a number of different fluoride salts as well as crown-ether systems (14), has been investigated and the results will be reported in the separate publication.

In the present study the fluoro aldehyde **2** has also been obtained by treatment of the α-nitroepoxide **1** with ^{18}F-labeled tetra-*n*-butylammonium fluoride in ethylene glycol; the reagent salt was dried by the repeated addition of acetonitrile and distillation using a rotary evaporator. In these experiments the yields (~10%) of **2** that were obtained were lower than was the case with KHF_2 and were less reproducible. The use of the technique of microwave drying (15) combined with the performance of the reactions in Teflon vials greatly reduce the loss of ^{18}F prior to its reaction and give better reproducibility.

The deprotection of the fluoro aldehyde **2** was originally accomplished using boron trichloride in dichloromethane. However, the time required for the efficient removal of boron salts during processing prompted the use of 80% trifluoroacetic acid. On the small scales employed in the experiments no epimerization of the fluoro aldehyde to the *manno* epimer was observed with the use of this reagent. If the reaction were performed at room temperature for 10 min, rather than at 50°C for 5 min, less radioactivity was observed at the solvent front in tlc; however, there was slightly more radioactivity at the origin, possibly resulting from the liberation of ^{18}F-fluoride ion. Nevertheless, the room-temperature reaction provided a higher radiochemical purity of the final product **3**.

The use of the α-nitroepoxide substrate **1** is currently being adapted for the synthesis of 2-{^{18}F}DFG employing ^{18}F produced with the McMaster University nuclear reactor.

Conclusion

The methodology described in this article provides an alternative route to 2-{^{18}F}DFG using a water target. Although the beam-energy constraints of the accelerator employed necessitated the use of an unconventional target, it seems reasonable to assume that the method is applicable to any PET facility employing a conventional target. The amounts of radioactivity incorporated, of course, depend upon the concentrations of ^{18}F achieved by the accelerator.

Acknowledgements

The authors are grateful for financial support in the form of grants from the Medical Research Council of Canada and the Natural Sciences and Engineering Research Council of Canada. The high performance liquid chromatograph employed in this study was purchased by funds provided by the Medical Research Council of Canada. The authors also wish to thank the members of the Nuclear Physics Laboratory of Queen's University, especially Drs. W. McLatchie and H.-B. Mak, for their cooperation in the production of ^{18}F.

1. M. REIVICH. Neurosci. Res. Program Bull. **14**, 502 (1976).
2. M. REIVICH, D. KUHL, A. WOLF, J. GREENBERG, M. PHELPS, T. IDO, V. CASELLA, J. FOWLER, E. HOFFMAN, A. ALAVI, P. SOM, and L. SOKOLOFF. Circ. Res. **44**, 127 (1979).
3. M. E. PHELPS, S. C. HUANG, E. J. HOFFMAN, C. SELIN, L. SOKOLOFF, and D. E. KUHL. Ann. Neurol. **6**, 371 (1979).
4. T. IDO, C.-N. WAN, V. CASELLA, J. S. FOWLER, A. P. WOLF, M. REIVICH, and D. E. KUHL. J. Labelled Compd. Radiopharm. **14**, 175 (1978).
5. C.-Y. SHIUE, P. A. SALVADORI, A. P. WOLF, J. S. FOWLER, and R. P. MACGREGOR. J. Nucl. Med. **23**, 899 (1982); M. DIKSIC and D. JOLLY. Int. J. Appl. Radiat. Isot. **34**, 893 (1983); M. J. ADAM. J. Chem. Soc. Chem. Commun. 730 (1982).
6. C.-Y. SHIUE, K.-C. TO, and A. P. WOLF. J. Labelled Compd. Radiopharm. **20**, 157 (1983).
7. S. SOOD, G. FIRNAU, and E. S. GARNETT. Int. J. Appl. Radiat. Isot. **34**, 743 (1983).
8. S. LEVY, D. R. ELMALEH, and E. LIVNI. J. Nucl. Med. **23**, 918 (1982).
9. T. J. TEWSON. J. Nucl. Med. **24**, 718 (1983).
10. W. A. SZAREK, G. W. HAY, and M. M. PERLMUTTER. J. Chem. Soc. Chem. Commun. 1253 (1982).
11. J. E. G. BARNETT. Adv. Carbohydr. Chem. **22**, 177 (1967); see p. 179.
12. L. EVELYN and L. D. HALL. Carbohydr. Res. **47**, 285 (1976).
13. H. C. SRIVASTAVA and V. K. SRIVASTAVA. Carbohydr. Res. **60**, 210 (1978).
14. T. IRIE, K. FUKUSHI, T. IDO, and T. NOZAKI. J. Labelled Compd. Radiopharm. **18**, 9 (1981).
15. T. IRIE, K. FUKUSHI, and T. IDO. Int. J. Appl. Radiat. Isot. **33**, 445 (1982).

Can. J. Chem. Downloaded from www.nrcresearchpress.com by 210.87.254.40 on 09/06/12
For personal use only.

Penicillin formation by cell-free extracts of *Streptomyces clavuligerus*. Behaviour of aminoadipyl-modified analogs of the natural peptide precursor δ-(L-α-aminoadipyl)-L-cysteinyl-D-valine (ACV)

SUSAN E. JENSEN AND DONALD W. S. WESTLAKE
Department of Microbiology, University of Alberta, Edmonton, Alta., Canada T6G 2E9

AND

RAYMOND J. BOWERS, CHRISTOPHER F. INGOLD, MARC JOUANY, LEAH LYUBECHANSKY, AND SAUL WOLFE
Department of Chemistry, Queen's University, Kingston, Ont., Canada K7L 3N6

Received March 26, 1984

Can. J. Chem. Downloaded from www.nrcresearchpress.com by 210.87.254.42 on 09/06/12
For personal use only.

SUSAN E. JENSEN, DONALD W. S. WESTLAKE, RAYMOND J. BOWERS, CHRISTOPHER F. INGOLD, MARC JOUANY, LEAH LYUBECHANSKY, and SAUL WOLFE. Can. J. Chem. **62**, 2712 (1984).

Six analogs of ACV, the biosynthetic precursor of the penicillin nucleus, have been synthesized, in which the δ-(L-α-aminoadipyl) moiety has been replaced by : β-(L-aspartyl), γ-(L-glutamyl), δ-(D-α-aminoadipyl), adipyl, glycyl-δ-(L-α-aminoadipyl), and *N*-acetyl-δ-(L-α-aminoadipyl) side chains have also been synthesized. Several improvements have been made in earlier routes to ACV and related peptides, including a simplified preparation of a dipeptide precursor, and a new synthesis of α-aminoadipic acid from lysine. A new reagent, 2-acetoximino-2-phenylacetonitrile, has been synthesized, which allows ready *N*-acetylation of amino hydroxyacids in aqueous acetone at room temperature. The peptide analogs have been examined as substrates of the enzyme isopenicillin N synthetase, which converts ACV to isopenicillin N in the presence of oxygen, ferrous ions, and ascorbate. The enzyme has been isolated from the prokaryotic organism *Streptomyces clavuligerus*, and has been employed either as a crude salt precipitate or in semi-purified form, freed from other enzymes of the penicillin–cephalosporin pathway. With the crude enzyme preparation, three of the analogs are active substrates, viz., adipyl, glycyl-δ-(L-α-aminoadipyl), and *N*-acetyl-δ-(L-α-aminoadipyl), but the latter two are converted, only via ACV, to isopenicillin N, the normal cyclization product. That the crude enzyme preparation contains a protease that deacylates *N*-substituted ACV analogs to ACV is confirmed, *inter alia*, by the behaviour of the purified enzyme; of the various analogs, only the adipyl compound is an active substrate, but the conversion of this analog to carboxybutylpenicillin proceeds with only 1–2% efficiency, compared to the natural substrate.

SUSAN E. JENSEN, DONALD W. S. WESTLAKE, RAYMOND J. BOWERS, CHRISTOPHER F. INGOLD, MARC JOUANY, LEAH LYUBECHANSKY et SAUL WOLFE. Can. J. Chem. **62**, 2712 (1984).

On a synthétisé six analogues de l'ACV, le précurseur biosynthétique du noyau de la pénicilline, dans lesquel on a remplacé l'unité δ-(L-α-aminoadipyl) par les unités suivantes: β-(L-aspartyl), γ-(L-glutamyl), δ-(D-α-aminoadipyl), adipyl, glycyl-δ-(L-α-aminoadipyl) et *N*-acétyl-δ-(L-α-aminoadipyl). On a également synthétisé des pénicillines ayant des groupes adipyl, glycyl-δ-(L-α-aminoadipyl) et *N*-acétyl-δ-(L-α-aminoadipyl) comme chaînes latérales. On a apporté plusieurs améliorations aux voies d'accès à l'ACV et aux peptides apparentés que nous avions décrites antérieurement; ces améliorations comprennent entre autre une préparation simplifiée d'un dipeptide précurseur ainsi qu'une nouvelle synthèse de l'acide α-aminoadipique à partir de la lysine. On a synthétisé un nouveau réactif, l'acétoxymino-2 phényl-2 acétonitrile, qui permet d'effectuer facilement une *N*-acétylation des hydroxy-acides aminés en opérant dans l'acétone aqueuse et à la température ambiante. On a étudié le comportement des analogues peptidiques comme substrats de l'enzyme isopénicilline *N*-synthétase qui transforme l'ACV en isopénicilline N en présence d'oxygène, d'ions ferreux et d'ions ascorbate. On a isolé l'enzyme à partir de l'organisme prokaryotique *Streptomyces clavuligerus* et on l'a utilisé soit sous la forme d'un sel précipité brut ou sous une forme semi-purifiée, alors que l'enzyme a été débarassé des autres enzymes de la voie pénicilline–céphalosporine. Avec la préparation brute de l'enzyme, les trois analogues portant les groupes adipyl, glycyl-δ-(L-α-aminoadipyl) et *N*-acétyl-δ-(L-α-aminoadipyl) sont des substrats actifs; toutefois, les deux derniers composés ne sont transformés en isopénicilline N, le produit normal de la cyclisation, que via l'ACV. Le fait que la préparation brute de l'enzyme contient un protéase qui peut enlever les groupes acétyles de l'ACV pour les transformer en ACV est confirmé, entre autre, par le comportement de l'enzyme purifié; des divers analogues, seul le composé portant un groupe adipyl s'avère un substrat actif, mais l'efficacité de la transformation de cet analogue en carboxybutylpénicilline n'est que de 1 à 2% par rapport au substrat naturel.

[Traduit par le journal]

Introduction

Streptomyces clavuligerus is a Gram positive, filamentous bacterium which produces a variety of β-lactam compounds including penicillin N, cephamycin C, and clavulanic acid (1, 2). The biosynthetic versatility of this organism, in terms of the synthesis of β-lactam compounds, has prompted an investigation of the enzymatic steps involved in the natural production of these antibiotics (3–5). Concurrent studies on the penicillin and cephalosporin-producing enzymes of *Cephalosporium acremonium* have been undertaken by several groups, and continue at the present time (6–8). One of these enzymes, variously referred to as cyclizing enzyme (3), cyclase (9), or isopenicillin N synthetase (10), leads to oxidative cyclization of the linear tripeptide δ-(L-α-aminoadipyl)-L-cysteinyl-D-valine (**1**) (ACV) into isopenicillin N (**2**). This enzymatic step constitutes the single β-lactam ring forming reaction which leads from the amino acid oxidation level to penicillins and cephalosporins (cephamycins).

In both the prokaryotic (*S. clavuligerus*) and eukaryotic (*C. acremonium*) systems, this oxidative cyclization is carried out by an enzyme with remarkably similar characteristics. In both cases, the enzymes are soluble, require iron and ascorbate as cofactors, and consume molecular oxygen (3, 6, 9, 11).

As noted above, *S. clavuligerus* also produces clavulanic

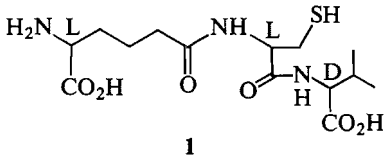

1

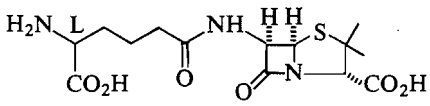

2

acid (**3**), a non-classical β-lactam compound which contains oxygen in the nucleus. The nature of the β-lactam ring forming enzyme associated with clavulanic acid biosynthesis is not known. It is conceivable that a single cyclizing enzyme of broad specificity could lead to the synthesis of penicillin–cephalosporin type compounds and also clavulanic acid (12). It seems more likely, however, that clavulanic acid biosynthesis involves a different pathway (13). Investigations into the substrate specificity of the cyclizing enzyme of *C. acremonium* have already indicated this enzyme to have a narrow substrate specificity (6, 9, 14).

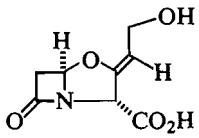

3

The present work is concerned with the behaviour of the cyclizing enzyme of *S. clavuligerus* towards analogs of ACV modified in the aminoadipyl residue. Certain specific modifications were of particular interest, because some β-lactam producing organisms also synthesize peptides, penicillins, and cephalosporins with side chains other than aminoadipyl. For example, ACV was first isolated from the mycelium of *Penicillium chrysogenum* (15), but was later found (16) to be contaminated with an additional peptide containing glycine. The structure and stereochemistry of ACV were established by Loder and Abraham (17) who isolated the peptide from the mycelium of *Cephalosporium* sp. C91, together with a tetrapeptide containing glycine, in addition to aminoadipic acid, cysteine, and valine. The constitution Aad-Cys-Val-Gly was suggested for this tetrapeptide, but a shortage of material prevented proof of this sequence. A peptide, apparently identical to Loder and Abraham's tetrapeptide, has been isolated from the β-lactam producing organism *Paecilomyces persicinus* P10 (18), and found to have the constitution Gly-Aad-Cys-Val (GACV). It was suggested that ACV is a precursor of penicillins, and that GACV may be a precursor of cephalosporins.

However, it has since become clear (3–5) that ACV is a precursor of both penicillins and cephalosporins. The biosynthetic significance of GACV therefore remains unknown.

N-Acetyldesacetoxycephalosporin C (**4**) has been isolated from a mutant of *C. acremonium* which is blocked in the synthesis of cephalosporin C (19). More recently, *N*-acetylisopenicillin N has been isolated from the culture broth of *Streptomyces tokunonensis* sp. nov., an organism that also produces isopenicillin N, penicillin N (**5**), and several carbapenems (20). The compound is considered in this case to be a shunt metabolite of isopenicillin N.

Cephalosporins containing fewer than six carbons in the side

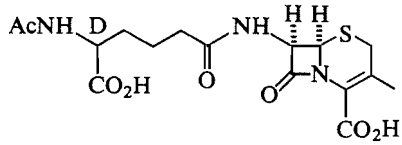

4

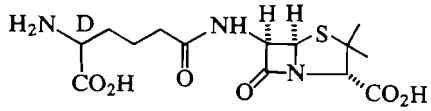

5

chain, or lacking an amino group in the side chain, have been isolated from *Cephalosporium* spp. (21) and *Streptomyces* spp. (22). The side chains of these compounds are thought to be derived from the aminoadipyl side chains of cephalosporin precursors.

In view of these various observations, analogs of ACV were synthesized in which the δ-(L-α-aminoadipyl) moiety was replaced by: β-(L-aspartyl) (**6**), γ-(L-glutamyl) (**7**), δ-(D-α-aminoadipyl) (**8**), adipyl (**9**), *N*-acetyl-δ-(L-α-aminoadipyl) (**10**), and glycyl-δ-(L-α-aminoadipyl) (**11**). Each of these peptides was then subjected to the action of the cyclizing enzyme of *S. clavuligerus*. To facilitate the identication of possible cyclization products, glycyl-isopenicillin N (**12**), *N*-acetylisopenicillin N (**13**), and carboxybutylpenicillin (**14**) were also synthesized. All of the peptides were supplied for enzymatic experiments in the disulfide form. Reduction to the monomeric peptides was performed immediately prior to assays, using dithiothreitol (3).

During the course of the work, two improvements were made in the published synthesis of ACV (23): a technically simpler preparation of *S*-trityl-L-cysteinyl-D-valine benzhydryl ester (**15**) was developed, based on preferential removal of a *tert*-butoxycarbonyl protecting group in the presence of a benzhydryl ester; and a new synthesis of L-α-aminoadipic acid from L-lysine was found. Difficulties encountered in the conversion of α-aminoadipic acid to *N*-acetyl-α-aminoadipic acid led to the development of a new reagent for *N*-acetylation under mild conditions in aqueous media. Details of all of these syntheses are provided.

Experimental

Materials

S-Trityl-L-cysteinyl-D-valine benzhydryl ester (15)

N-tert-Butoxycarbonyl-*S*-trityl-L-cysteinyl-D-valine benzhydryl ester (23) (2.00 g, 2.74 mmol) was dissolved in ethyl acetate (2.0 mL) to give a mobile yellow oil. To this was added 98% formic acid (200 mL) and the resultant solution was stirred vigorously at room temperature. After 15 min the reaction mixture was frozen using liquid nitrogen and then freeze-dried. The residual oil was azeotroped twice with methylene chloride, under reduced pressure, to leave a white foam. The crude formate salt was dissolved in ethyl acetate (100 mL) and washed with saturated sodium bicarbonate (2 × 80 mL, with brine added to minimize the formation of an emulsion), followed by saturated brine (80 mL). The solvent was dried over sodium sulfate and evaporated to leave a syrup which, after azeotroping with methylene chloride and drying under high vacuum, afforded a white foam, 1.49 g (87.5%).

A portion (724 mg) of the product was dissolved in chloroform (1.5 mL), diluted with hexane to the cloud point, and seeded to give white microprisms (517 mg), mp 155–156°C, $[\alpha]_D$ +34.7° (*c* 1.0, CH_2Cl_2); ir (KBr): 3355 (m), 3290 (w), 3160 (m, NH, NH_2), 1726, 1662 (s, ester, amide carbonyl) cm^{-1}; ^{1}Hmr (200 MHz, $CDCl_3$) δ:

Can. J. Chem. Downloaded from www.nrcresearchpress.com by 210.87.254.42 on 09/06/12
For personal use only.

Can. J. Chem. Downloaded from www.nrcresearchpress.com by 210.87.254.42 on 09/06/12
For personal use only.

0.74 (3H, d, J = 7 Hz, $CHCH_3$), 0.84 (3H, d, J = 7 Hz, $CHCH_3$), 1.46 (2H, br, NH_2), 2.17 (1H, m, collapses to quintet, J = 7 Hz, on irradiation at 4.55 ppm; valine C3 methine), 2.47 (1H, q, J = 9, 12 Hz) and 2.75 (1H, q, J = 4, 12 Hz, A and B quartets for cysteine methylene which collapse to two doublets, J = 12 Hz, on irradiation at 2.90 ppm), 2.90 (1H, q, J = 4, 9 Hz, cysteine methine), 4.55 (1H, q, J = 5, 9 Hz, collapses to doublet, J = 9 Hz, on irradiation at 2.17 ppm, valine C2 methine), 6.87 (1H, s, benzhydryl methine), 7.16–7.53 (~26H, aromatic and amide NH). *Anal.* calcd. for $C_{40}H_{40}N_2O_3S$: C 76.40, H 6.41, N 4.45; found: C 75.98, H 6.48, N 4.30.

Bis-β-(L-aspartyl)-L-cysteinyl-D-valine (6)

This compound was synthesized from **15** and N-BOC-L-aspartic acid-α-benzhydryl ester as described for ACV (23), except that the final deprotection was accomplished with formic acid (16 h). Thin-layer chromatography (tlc): R_f 0.12 (butanone – acetic acid – water, 4:1:1); ^{1}Hmr (D_2O) δ: 0.95 (12H, t, 6 Hz), 2.17 (2H, m), 2.99 (4H, m), 3.05 (2H, q, 8, 14 Hz), 3.18 (2H, q, 6.5, 14 Hz), 4.05 (2H, q, 6.5, 8 Hz), 4.20 (2H, d, 6.4 Hz), 4.8 (2H, m).

Bis-γ-(L-glutamyl)-L-cysteinyl-D-valine (7)

This compound was synthesized from **15** and N-BOC-L-glutamic acid-α-benzhydryl ester as described for **6**; tlc: R_f 0.12 (butanone – acetic acid – water, 4:1:1); ^{1}Hmr (D_2O) δ: 2.17 (4H, m), 2.51 (4H, m), 3.00 (2H, q, 8, 14 Hz), 3.18 (2H, q, 6, 14 Hz), 3.77 (2H, t), 4.17 (2H, d), 4.78 (2H, m).

Bis-δ-(D-α-aminoadipyl)-L-cysteinyl-D-valine (8)

This compound has $[\alpha]_D^{20}$ −35.8 (*c* 0.8, 2 *N* HCl); tlc: 0.18 (butanone – acetic acid – water, 4:1:1); ^{1}Hmr (D_2O) δ: 0.92 (12H, t, 7 Hz), 1.73 (4H, m), 1.88 (4H, m), 2.18 (2H, m), 3.00 (2H, q, 8.2, 15 Hz), 3.20 (2H, q, 6.5, 15 Hz), 3.78 (2H, br t), 4.21 (2H, d, 6 Hz), 4.81 (2H, m).

Bis-adipyl-L-cysteinyl-D-valine (9)

Adipic acid (730 mg, 5 mmol) was dissolved in a mixture of methanol (5 mL) and methylene chloride (30 mL), and a solution of diphenyldiazomethane (970 mg, 5 mmol) was added in portions during 8.5 h. When the addition was complete, the solvent was removed and the residue was triturated with ethyl acetate (15 mL) and filtered to give 220 mg of unreacted adipic acid. The filtrate was evaporated, ether (2 mL) was added, and this solution was treated with dicyclohexylamine (519 mg, 3.49 mmol). Hexane was then added to the cloud point and the mixture was chilled overnight. The crystals were then collected (1.1 g, mp 101–104°C) and recrystallized from ethyl acetate – ether (0.92 g, mp 103.5–105°C). The salt (420 mg) was partitioned between ethyl acetate (15 mL) and 10% potassium bisulfate (5 mL), and the organic layer was washed successively with 10% potassium bisulfate (2 × 5 mL) and brine (5 mL), dried, and evaporated. The residue crystallized from hexane (279 mg). Recrystallization from methylene chloride – hexane afforded 197 mg (mp 84.5–85.5°C) of the monobenzhydryl ester of adipic acid. Coupling of this ester with **15**, and further treatment as described for **6** led to **9**, R_f 0.66 (95% ethanol – acetic acid, 20:1).

Conversion of pipecolic acid to α-aminoadipic acid

Thionyl chloride (50.3 mL) was added dropwise, with cooling at 0°C, to a solution of pipecolic acid (50 g, 0.387 mol) in absolute methanol (400 mL). The reaction mixture was allowed to warm to room temperature, stirred for 12 h, and the solvent was then removed under reduced pressure. The crystalline residue was dissolved in dry methylene chloride (900 mL), the solution was cooled to 0°C, stirred, and dry triethylamine (110 mL, 0.785 mol) was added during 15 min followed, dropwise, by a solution of acetyl chloride (28 mL, 0.39 mol) in methylene chloride (100 mL). This mixture was stirred for 12 h, allowed to warm to room temperature, and water (750 mL) was added. The aqueous phase was extracted with methylene chloride (2 × 250 mL), and the combined organic phases were dried and evaporated. The residual oil was distilled (bp 100–110°C/2 Torr; 1 Torr = 133.3 Pa).

A mixture of methyl *N*-acetylpipecolate (46.4 g, 0.25 mol), ruthenium trichloride trihydrate (5 g), sodium periodate (1.073 L of 10% solution), and chloroform (1 L) was stirred vigorously. After 4 h the mixture turned black and was filtered through glass wool. The organic phase was separated, dried, and evaporated. The residue (47.1 g, 0.24 mol) was refluxed for 10 h in 8 *N* hydrochloric acid (1.41 L) and the resulting solution was then cooled to room temperature and concentrated under reduced pressure to a volume of 150 mL. The pH was adjusted to 2.9 with 10 *N* sodium hydroxide and the mixture was stored at 0°C overnight. Subsequent filtration afforded α-aminoadipic acid (24 g), identified by ir, nmr, and tlc.

Conversion of L-α-amino-ω-hydroxycaproic acid (24) to N-BOC-L-α-aminoadipic acid benzhydryl ester

To the amino acid alcohol **18** (92.5 mg, 0.63 mmol) in 50% acetone–water (1 mL) containing triethylamine (95.4 mg, 0.94 mmol) was added BOC-ON (155 mg, 0.63 mmol). The resulting yellow solution was stirred for 2 days and the solvent was then removed. The semi-solid residue was dissolved in water (40 mL) and this solution was extracted with ether (3 × 10 mL). These ether extracts were discarded. The aqueous phase was acidified with 10% potassium bisulfate and extracted with ethyl acetate (3 × 30 mL). The organic phase was dried and evaporated to afford the N-BOC derivative (135 mg, 87%) as a colourless oil. This oil (94.5 mg, 0.38 mmol) was dissolved in methylene chloride (2.5 mL) and treated with diphenyldiazomethane (74 mg, 0.38 mmol). After 5 min, the solvent was evaporated, and the residue was chromatographed (methylene chloride – ethyl acetate 5:1) to give the N-BOC benzhydryl ester (157 mg, 100%). A suspension of platinum oxide (100 mg) in water (1 mL) was stirred under a hydrogen atmosphere for 30 min, purged with nitrogen for 30 min, and then placed under an oxygen atmosphere. Sodium bicarbonate (32 mg, 0.38 mmol) was added, followed by the N-BOC benzhydryl ester (157 mg) in 66% acetone (5 mL). Stirring was continued under oxygen for 16 h and the mixture was then centrifuged and the supernatant acidified with 2% potassium bisulfate. Extraction with methylene chloride, followed by drying and evaporation of the organic extract, yielded N-BOC-L-α-aminoadipic acid benzhydryl ester (156 mg, 96%) as a semi-solid. Dicyclohexylamine salt: mp 156–158°C (lit. (23) mp 156.5–157.5°C); $[\alpha]_D^{25}$ −21.6° (*c* 2, methanol) (lit. (23) $[\alpha]_D$ −20.5 (*c* 2, methanol)).

2-Acetoximino-2-phenylacetonitrile

To 2-oximino-2-phenylacetonitrile (25) (3.1 g, 0.021 mol) in pyridine–benzene (10 mL of a 1:2 mixture) was added acetyl chloride (1.5 mL, 2.08 g, 0.026 mol). The reaction mixture was stirred at 0°C for 3 h, and the solvent was then removed under reduced pressure. The residue was dissolved in a mixture of water and ether and the organic layer was separated, dried, and evaporated. The crystalline residue was recrystallized from ether–hexane to give 3.1 g, mp 70–71°C; ^{1}Hmr ($CDCl_3$) δ: 2.28 (3H, s), 7.35–7.72 (5H, m). *Anal.* calcd. for $C_{10}H_8N_2O_2$: C 63.82, H 4.38, N 14.89; found: C 63.95, H 4.44, N 14.63.

Conversion of L-α-amino-ω-hydroxycaproic acid to N-acetyl-L-α-aminoadipic acid benzhydryl ester (21)

The amino acid alcohol **18** (73.5 mg, 0.5 mmol) was dissolved in 50% acetone (1.5 mL), and triethylamine (1.5 equiv., 100 μL) and 2-acetoximino-2-phenylacetonitrile (113 mg, 0.77 mmol) were added. The resulting solution was stirred at room temperature for 4 h, and the solvent was then removed under reduced pressure. The residue was dissolved in dry methanol (3 mL) and a solution of diphenyldiazomethane (100 mg, 0.52 mmol) in methylene chloride (0.5 mL) was added. The mixture was stirred for 30 min, concentrated, and the residue was chromatographed on silica gel. Elution with methylene chloride – methanol (10:1) gave 110 mg (62%) of **25**; $[\alpha]_D^{24}$ − 9.5° (*c* 2, chloroform); ir (KBr): 3270, 1730, 1650 cm^{-1}; ^{1}Hmr ($CDCl_3$) δ: 1.02–1.95 (6H, m, $CH_2CH_2CH_2$), 1.96 (3H, s, $COCH_3$), 3.51 (2H, t, 6 Hz, CH_2), 4.75 (1H, sextet, 5.5, 7.5 Hz, CH), 6.1 (1H, d, 7.5 Hz, NH), 6.9 (1H, s, CH), 7.33 (10H, s).

Platinum oxide (1 g) was suspended in 50% aqueous acetone (10 mL), containing sodium bicarbonate (168 mg, 2 mmol), and the suspension was stirred under hydrogen for 30 min, purged with nitro-

Can. J. Chem. Downloaded from www.nrcresearchpress.com by 210.87.254.42 on 09/06/12
For personal use only.

gen, and then placed under an oxygen atmosphere. The protected alcohol **25** (510 mg, 1.44 mmol) was added, and vigorous stirring was continued, under oxygen, for 12 h. The mixture was then centrifuged, the residue washed with water (2 × 2 mL), and the combined supernatant was evaporated under reduced pressure. The residue was dissolved in water, the pH was adjusted to 3.0, and the resulting precipitate was extracted with ethyl acetate. This extract was washed successively with 10% potassium bisulfate (10 mL), water (10 mL), and brine (10 mL), then dried and evaporated to yield **21** (340 mg, 64%) as a foam; $[\alpha]_D^{25}$ −7.8° (*c* 2, chloroform); ir (KBr): 1720, 1705, 1660 cm^{-1}; ^{1}Hmr ($CDCl_3$) δ: 1.35−1.95 (4H, m), 1.97 (3H, s), 2.27 (2H, m), 4.75 (1H, sextet, 5.5, 7.5 Hz), 6.29 (1H, d, 7.5 Hz), 6.88 (1H, s), 7.33 (10H, s).

N-Acetylation of L-α-aminoadipic acid-α-benzhydryl ester

The ester **22** (60 mg, 0.18 mmol) was suspended in 50% acetone (1.5 mL), and 2-acetoximino-2-phenylacetonitrile (36 mg, 0.19 mmol) and triethylamine (1.5 equiv.) were added. The suspension dissolved and the resulting solution was stirred for 4 h and then evaporated. Chromatography on silica gel (methylene chloride − methanol, 4:1) afforded 60 mg (90%) of **21**.

*Bis-N-acetyl-δ-(L-α-aminoadipyl)-L-cysteinyl-D-valine (**10**)*

This compound was synthesized from **15** and *N*-acetyl-L-α-aminoadipic acid-α-benzyhydryl ester; tlc: R_f 0.56 (butanone − acetic acid − water, 4:1:1); ^{1}Hmr (DMSO-d_6) δ: 0.96 (6H, d, 7.5 Hz), 0.98 (6H, d, 7.5 Hz), 1.76 (8H, m), 2.00 (6H, s), 2.22 (2H, m), 2.34 (4H, br t), 2.97 (2H, q, 9, 14 Hz), 3.20 (2H, q, 6, 14 Hz), 4.33 (2H, m), 4.38 (2H, m).

*Bis-glycyl-δ-(L-α-aminoadipyl)-L-cysteinyl-D-valine (**11**)*

This compound was synthesized from N-BOC-glycyl-L-α-aminoadipic acid-α-benzhydryl ester (26) and **15**: tlc: R_f 0.1 (butanone − acetic acid − water, 4:1:1), ^{1}Hmr (D_2O) δ: 0.89 (6H, d, 7 Hz), 0.94 (6H, d, 7 Hz), 1.70−2.30 (10H, m), 2.39 (4H, m), 2.98 (2H, q, 8.6, 14 Hz), 3.21 (2H, q, 5.5, 14 Hz), 3.87 (4H, s), 4.16 (2H, d, 6 Hz), 4.28 (2H, m), 4.76 (2H, q, 5.5, 8.6 Hz). *Anal.* calcd. for $C_{34}H_{58}N_8S_2O_{18}\cdot H_2O$: C 43.03, H 6.37, N 11.81; found: C 43.00, H 6.84, N 12.30.

*Glycylisopenicillin N (**12**)*

A solution of L-α-aminoadipic acid-α-benzhydryl ester (321 mg, 0.98 mmol) and dicyclohexylamine (0.4 mL) in methanol (16 mL) and dimethoxyethane (5 mL) was treated with *N*-carbobenzoxyglycine succinimidyl ester (306 mg, 1.0 mmol) (27), and then stirred at room temperature for 72 h. The solvent was removed, and the residue was redissolved in methylene chloride (25 mL), washed with 10% potassium bisulfate (3 × 30 mL) and brine (20 mL), dried, and evaporated. The resulting syrup (565 mg) was redissolved in methylene chloride (10 mL), and the solution was filtered and reevaporated to give a yellow foam (504 mg). A portion of this carbobenzoxyglycyl-L-α-aminoadipic acid-α-benzhydryl ester was purified by rapid chromatography; ^{1}Hmr ($CDCl_3$) δ: 1.58 (4H, m), 2.19 (2H, m), 3.87 (2H, m), 4.71 (1H, m), 5.08 (2H, s), 5.89 (1H, m), 6.86 (1H, s), 7.30 (16H, m), 9.45 (1H, br s). This compound was then converted to glycyl-isopenicillin N, as described for the syntheses of isopenicillin N and penicillin N (4); ir (KBr): 1768 cm^{-1}; ^{1}Hmr (D_2O) δ: 1.52 (3H, s), 1.65 (3H, s), 1.76 (4H, m), 2.40 (2H, m), 3.91 (2H, s), 4.26 (1H, s), 5.49 (1H, d, 4 Hz), 5.57 (1H, d, 4 Hz).

*N-Acetylisopenicillin N (**13**)*

This compound was synthesized from *N*-acetyl-L-α-aminoadipic acid-α-benzhydryl ester and the benzhydryl ester of 6-aminopenicillanic acid (4), as described for **12**, ir (KBr): 1767 cm^{-1}; ^{1}Hmr (D_2O) δ: 1.49 (3H, s), 1.62 (3H, s), 2.03 (3H, s), 1.65−2.45 (6H, m), 4.24 (1H, s), 5.47 (1H, d, 4.0 Hz), 5.57 (1H, d, 4.0 Hz).

*Carboxybutylpenicillin (**14**)*

This compound was synthesized from the monobenzhydryl ester of adipic acid and the benzhydryl ester of 6-aminopenicillanic acid, as described for **12**; ir (KBr): 1765 cm^{-1}; ^{1}Hmr (D_2O) δ: 1.49 (3H, s), overlapping with 1.56 (4H, br m), overlapping with 1.63 (3H, s), 2.17 (2H, m), 2.37 (2H, m), 4.25 (1H, s), 5.66 (1H, d, 3.6 Hz), 5.75 (1H, d, 3.6 Hz).

Organism and cultural conditions

Streptomyces clavuligerus NRRL 3585 was maintained and cultivated as previously described (3). Cells from 40-h cultures were harvested by filtration, washed, and resuspended to 1/10 of the original culture volume (approximately 1.8 mg dry weight/mL) in 0.05 *M* Tris-HCl buffer, pH 7.0, containing 0.1 m*M* dithiothreitol (TD buffer) for preparation of cell-free extracts.

Enzyme preparations

Washed cell suspensions were broken, in 25-mL aliquots, by sonic oscillation for 2 × 15 s at setting 5 with a Sonifier Cell Disruptor 350, Branson Sonic Power, using a standard flat-tipped probe (1.9 cm diameter). Broken cell suspensions were centrifuged 30 min at 25 000 × *g* to remove unbroken cells and cell envelope material. The resulting supernatant, termed cell-free extract, was partially purified by ammonium sulfate precipitation. Solid ammonium sulfate was gradually added to cell-free extract (typically 100 mL) with gentle stirring at 4°C. Material which precipitated between 40% and 70% saturation was collected by centrifugation (15 min at 25,000 × *g*) and resuspended to 1/10 of the original culture volume in TD buffer. This salt-precipitated cell-free extract was concentrated tenfold by ultrafiltration (PM-10 filter, Amicon Corporation), returned to its original volume with TD buffer, and again concentrated tenfold to remove residual ammonium sulfate. The resulting crude enzyme concentrate contained 40−60 mg protein/mL.

Partially purified cyclizing enzyme was prepared by anion exchange chromatography of the crude enzyme concentrate using DEAE-trisacryl resin, as described in ref. 5. This partially purified cyclizing enzyme is functionally pure, since it contains none of the other enzyme activities associated with penicillin/cephalosporin biosynthesis.

Assays

Cyclization activity was measured in a 0.4-mL standard cyclization assay system containing: ascorbic acid 2.8 m*M*, $FeSO_4$ 45 μ*M*, Tris HCl buffer (pH 7.0) 50.0 m*M*, and enzyme 0.1 mL. One hundred micrograms of each peptide substrate was reacted with 25 μL of 66.7 m*M* dithiothreitol for 15 min at 21°C before addition to the standard assay system. The mixtures were incubated for 2 h at 20°C and the reactions were then terminated by the addition of 0.4 mL of methanol. Under these conditions this corresponds to >90% consumption of ACV. Antibiotic formation was monitored by biological assay of reaction mixtures and by hplc analysis.

Biological assays of reaction mixtures were conducted using the agar diffusion procedure with *Micrococcus luteus* ATCC 9341 as the indicator organism.

The protein contents of cell-free extract and salt precipitated cell-free extract were determined by the method of Bradford (28).

High pressure liquid chromatographic analysis of reaction mixtures

Methanol-inactivated reaction mixtures were centrifuged for 5 min at 12 000 × *g* before analysis. Equipment used for hplc analyses consisted of: an M6000 A pump, a WISP Model 710B automatic injector, and M-480 variable wavelength detector, an M420 data module, a Model 720 systems controller, and a C_{18} column (RadPak A in a Z module). All equipment was from Waters Scientific Ltd. The mobile phase consisted of methanol−KH_2PO_4 (0.05 *M* adjusted to pH 4.0 with H_3PO_4) in proportions which varied with the particular separation. The flow rate was 2 mL/min for 5 min and then 3 mL/min for the remaining analysis time. Detection of uv-absorbing materials was at 220 nm at a sensitivity of 0.02 absorbance units full scale.

Results

Syntheses of substrates

A. *Improved synthesis of* S-*trityl-L-cysteinyl-D-valine benzhydryl ester (**15**)*

In an earlier synthesis of ACV (23), **15** was prepared by *N*-detritylation of a *N*,*S*-ditritylated precursor. It has now been

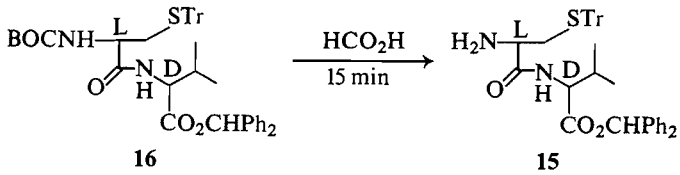

found that a 15-min treatment with a 98–100% formic acid leads to selective removal of the *tert*-butoxycarbonyl protecting group of **16** (23), and provides the intermediate **15** as a crystalline compound in over 80% yield. This is an improvement over the earlier sequence, because of the higher yield in the introduction of the nitrogen protecting group, and the greater ease of coupling of the cysteinyl and valinyl moieties when *N*-*tert*-butoxycarbonyl is employed in place of *N*-trityl.

B. *A new synthesis of* L-α-*aminoadipic acid*

Hungarian workers have recently observed deamination of amino acids, using sodium nitroprusside as the formal source of NO^+ (24). Applied to L-lysine, this reaction leads to L-pipecolic acid (**17**) (40%), and the amino acid alcohol **18** (40%). In the present work, oxidation of *N*-acetylpipecolic acid methyl ester with ruthenium tetroxide (29) led smoothly to **19**. Hydrolysis of this lactam provided α-aminoadipic acid.

However, since α-aminoadipic acid is normally employed in our peptide syntheses in the form of the diprotected derivative **20**, the preparation of **20** from **17** requires six steps. The alcohol **18** is, therefore, a more useful intermediate since only three steps are then needed. In practice, these consisted of reaction with BOC-ON, reaction with diphenyldiazomethane, and oxidation with Pt/O_2. The yield of **20** from **18** was 83%.

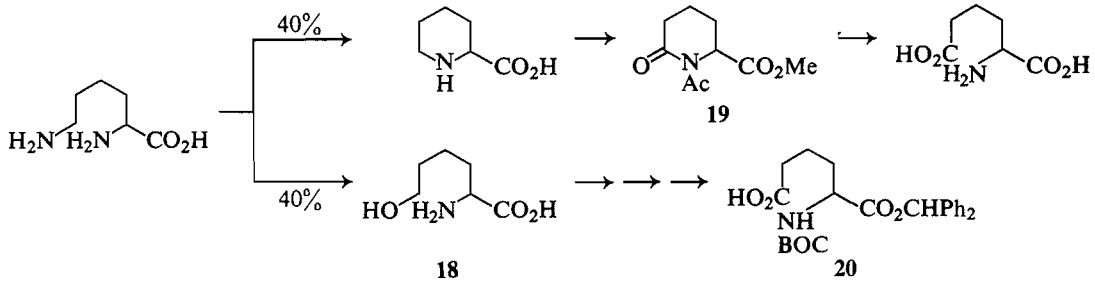

C. *A new reagent for* N-*acetylation in aqueous media*

For the syntheses of the peptide **10** and the penicillin **13**, the *N*-acetylated α-aminoadipic acid derivative **21** was required. However, several attempts to acetylate **22** led to piperidone formation, and **21** could not be detected. Since BOC-ON (**23**) reacts smoothly with **22**, the analog **24** was synthesized from 2-oximino-2-phenylacetonitrile. This compound solved the problem. In aqueous acetone it acetylated **22** in 90% yield, and also *N*-acetylated the amino alcohol **18**.

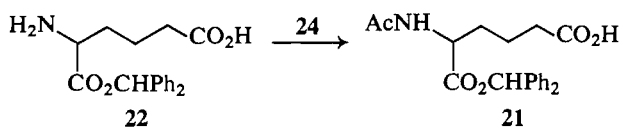

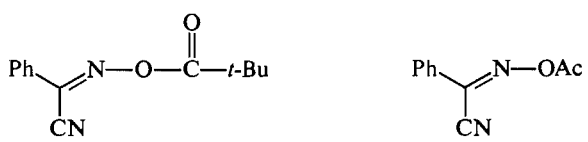

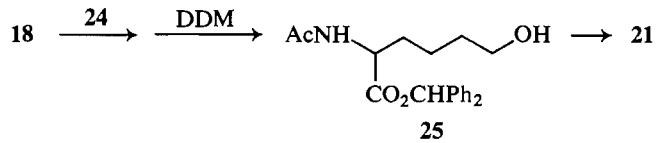

D. *Syntheses of peptides*

These followed the general strategy of ref. 23, with the modifications noted above. Condensation of **15** with the appropriately protected diacid or amino acid led to compounds of the general structure **26**. These were deprotected in two steps: detritylation with iodine in methanol; and removal of *tert*-butoxycarbonyl and benzhydryl protecting groups by overnight treatment with formic acid.

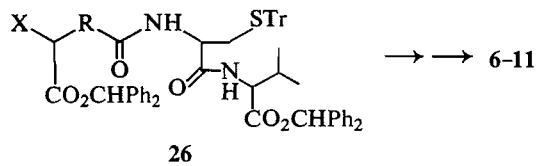

X = BOC-GLY, BOC-NH, AcNH, H

E. *Syntheses of penicillins*

These followed the strategy devised in ref. 4 for the syntheses of isopenicillin N and penicillin N. Condensation of the appropriately protected diacid or amino acid **27** with **28**, the benzhydryl ester of 6-APA (4) afforded the fully protected penicillins. These were deprotected by hydrogenolysis.

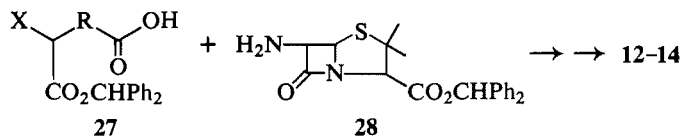

X = Z-GLY, AcNH, H

Cyclization of unnatural peptide substrates

A. *Biological assays*

In control reaction mixtures, none of the peptide substrates **1**, **6**–**11** exhibited antibacterial activity. Reaction mixtures containing enzyme, but no peptide substrate, also showed no activity.

Table 1 summarizes the results of experiments conducted under identical conditions for test reaction mixtures containing both substrate and enzyme. The L-aspartyl (**6**), L-glutamyl (**7**),

Can. J. Chem. Downloaded from www.nrcresearchpress.com by 210.87.254.42 on 09/06/12
For personal use only.

TABLE 1. Cyclization of aminoadipyl-modified analogs of ACV by cell-free extract from *S. clavuligerus*

Substrate	Zone of inhibition (mm)[a]
1 (ACV)	31.5 (30.5)[b]
6 (Asp-CV)	0
7 (Glu-CV)	0
8 (D-ACV)	0
9 (Ad-CV)	12.0 (12.0)[b]
10 (Ac-ACV)	28.0 (0)[b]
11 (GACV)	15.0 (0)[b]

[a]Twenty microlitre aliquots of methanol-inactivated reaction mixtures were bioassayed against *M. luteus* ATCC 9341 as the indicator organism.

[b]Data in parentheses refer to functionally purified cyclase. All other data refer to salt-precipitated cell-free extract.

TABLE 2. High pressure liquid chromatography retention times

Compound	Retention time (min) Method A[a]	Method B[b]
1	19.9	5.0
6	14.1	
7	17.5	
8	19.9	
9		14.1
10		6.3
11	21.7	
2	5.4	
5	5.4	
12	8.0	
13		2.9
14		8.3

[a,b]See text for description of these conditions.

and D-α-aminoadipyl (**8**) containing peptides are inactive substrates. However, antibacterial activity is observed when the adipyl (**9**), *N*-acetyl-L-α-aminoadipyl (**10**), and glycyl-L-α-aminoadipyl (**11**) containing peptides are employed as substrates.

B. *High pressure liquid chromatographic analyses*

The retention times of all monomeric peptide substrates and the putative cyclization products of the active substrates **1**, **9**−**11** were established prior to the analysis of test reaction mixtures. These are summarized in Table 2. Two sets of conditions were necessary because **9**, **10**, **13**, and **14** are retained by the stationary phase under the optimum conditions for elution of the other substrates and penicillins. For **1**, **6**, **7**, **8**, **11**, and **12**, the mobile phase consisted of 5% methanol − 95% KH_2PO_4 (0.05 *M* adjusted to pH 4.0 with H_3PO_4) (method A). For **9**, **10**, **13**, and **14**, the methanol content of the mobile phase was increased to 20% (method B).

Figure 1 shows hplc data obtained using method A, for a no-substrate control and for reaction mixtures containing ACV and **9**−**11**. In the case of the natural substrate ACV, the unreacted peptide is observed at 19.9 min, and there is a large peak at 5.4 min, corresponding to an unresolved mixture of isopenicillin N and penicillin N ((iso)penicillin N) (3−5). In the cases of the inactive substrates **6**−**8**, (data not shown in Fig. 1), hplc profiles of reaction mixtures are identical to the no-substrate control, with the addition of the peaks corresponding to unreacted peptide substrate. These peptides are, therefore, not undergoing transformation to biologically inactive products.

With GACV (**11**) as the substrate, unreacted peptide is observed at 21.7 min, and *(iso)penicillin N is observed at 5.4 min*. In addition, there is a minor peak, corresponding to ACV, at 19.9 min. The latter peak is not seen in control GACV reaction mixtures incubated without enzyme. Since no peak corresponding to glycyl-isopenicillin N is seen at 8.0 min, these observations represent a first indication (confirmed below) that GACV is converted in part to ACV under these conditions, and that the antibacterial activity reported in Table 1 refers to the cyclization of the latter compound.

A similar result is obtained with acetyl-ACV (**10**). The chromatogram shows a small ACV peak at 19.9 min, and a large (iso)penicillin N peak at 5.4 min. No peak is observed at 19.9 min in control reaction mixtures incubated without enzyme. However, the presence or absence of *N*-acetyl-ACV and *N*-acetylisopenicillin N in the reaction mixture cannot be established using method A, because of their retention by the stationary phase. For the same reason, the chromatogram, obtained using method A, of the reaction mixture containing adipyl-CV (**9**) is identical to that of the no-substrate control.

Figure 2 shows the hplc data obtained by method B for reaction mixtures containing **9** and **10**. With **10** as the substrate, all of the substrate is consumed, an ACV peak is seen at 5.0 min, but no penicillin peak corresponding to **13** can be found at 2.9 min. As will be seen below, the acetyl-ACV substrate has been converted completely to ACV *prior to* cyclization in the normal manner.

On the other hand, with **9** as the substrate, a considerable amount of the substrate remains unreacted, and is observed at 14.1 min. A new peak, corresponding to the penicillin **14**, is observed at 8.3 min. The low conversion of **9** that is observed in Fig. 2 is consistent with the low antibacterial activity noted in Table 1. Since zones of inhibition are related exponentially to the concentration of antibiotic, zones of 31.5 mm and 12 mm from ACV and from **9** would have suggested an antibiotic concentration about eighty times lower in the latter case, assuming the two antibiotics to have equal activity.

To check the conclusion that GACV (**11**) and acetyl-ACV (**10**) do not cyclize directly to (iso)penicillin N but, rather, undergo prior deacylation to ACV, cyclization assays were performed on these substrates in mixtures lacking iron and ascorbate. These are the essential cofactors for cyclization activity to be observed (3). Figure 3 shows the hplc data, using method A, obtained from such reactions. The no-substrate control differs in this case from that seen in Fig. 1, because the relative amounts of the oxidized and reduced forms of dithiothreitol (14.3 min and 9.3 min, respectively) are not the same in the absence of the cofactors. In particular, absence of ferrous ions permits the reduced form of dithiothreitol to persist for much longer times.

With **10** as the substrate for this experiment, the chromatogram shows a large ACV peak at 19.9 min, but no (iso)penicillin peak is observed at 5.4 min (and the reaction mixture shows no antibacterial activity). The chromatogram obtained using method B shows no residual **10**. On the other hand, GACV is somewhat more stable. The chromatogram obtained using method A shows unreacted GACV at 21.7 min,

Can. J. Chem. Downloaded from www.nrcresearchpress.com by 210.87.254.42 on 09/06/12
For personal use only.

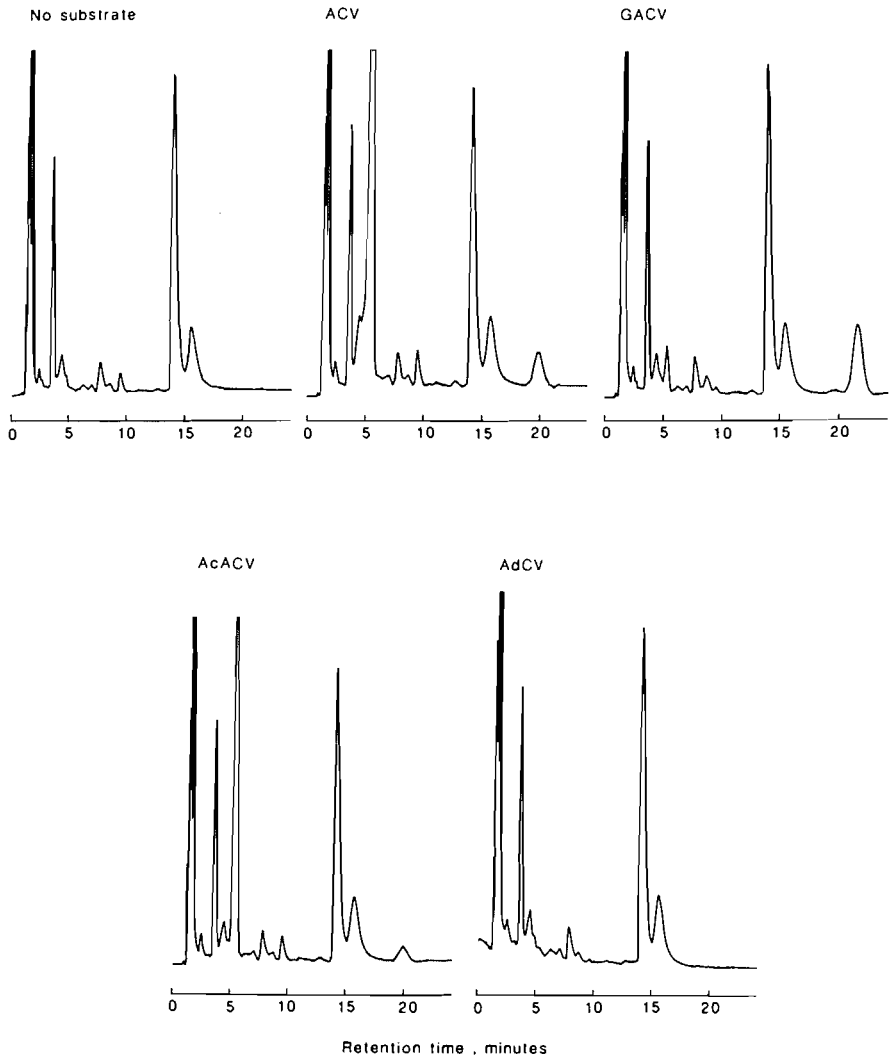

FIG. 1. Analysis of 2-h cyclization reaction mixtures by hplc with a mobile phase of 5% methanol − 95% KH_2PO_4 (0.05 *M* adjusted to pH 4.0 with H_3PO_4) (method A). Twenty microlitre aliquots of methanol-inactivated reaction mixtures were analyzed.

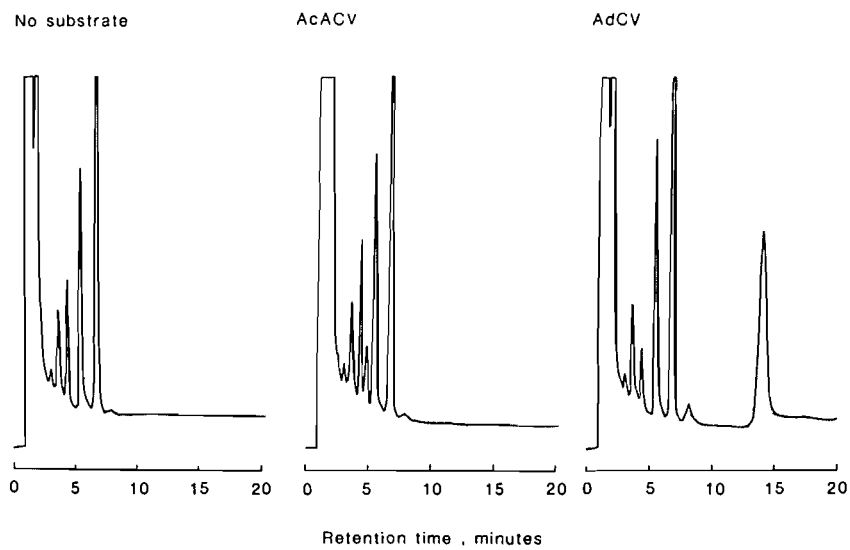

FIG. 2. Analysis of 2-h cyclization reaction mixtures by hplc with a mobile phase of 20% methanol − 80% KH_2PO_4 (0.05 *M* adjusted to pH 4.0 with H_3PO_4) (method B). Twenty microlitre aliquots of no-substrate control, AcACV and AdCV-containing cyclization reaction mixtures were analyzed after methanol inactivation.

Can. J. Chem. Downloaded from www.nrcresearchpress.com by 210.87.254.42 on 09/06/12
For personal use only.

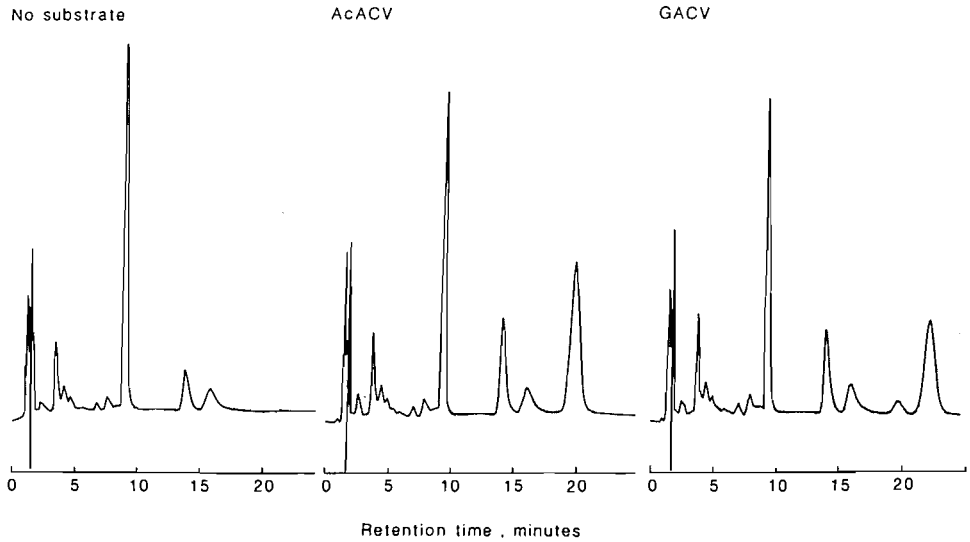

FIG. 3. The hplc analysis of cyclization reaction mixtures lacking iron and ascorbate using method A.

and ACV at 19.9 min. Again, no (iso)penicillin N is observed (and the reaction mixture shows no antibacterial activity).

It is clear that the activities observed from **10** and **11** in Table 1 reflect the extent to which these peptides were converted to ACV under the conditions of those experiments. Once formed, ACV resists further degradation, and there is no evidence that ACV is converted to CV or to free amino acids, either by *S. clavuligerus* cell-free extract or by non-specific proteases. Proteolytic activity, as measured by degradation of azocasein, was not detectable in cell-free extracts or semi-purified enzyme preparations. Similarly, addition of benzylsulfonyl fluoride to reaction mixtures at a final concentration of 1 m*M* had no effect on activity.

C. *Behaviour of functionally purified cyclizing enzyme*

The zones of inhibition shown in parentheses in Table 1 refer to cyclization experiments conducted with functionally purified enzyme. These data demonstrate that only ACV and adipyl-CV (**9**) are true substrates for the cyclizing enzyme, and confirm the conclusions reached in the preceding section.

Discussion

The present study has revealed that the cyclizing enzyme of *S. clavuligerus* has a high degree of specificity for the α-aminoadipyl moiety of ACV. Although this portion of the peptide is well removed from the sites of bond formation, and has no known role in the formation of the penicillin nucleus, modifications to this residue have a profound effect upon the activity of the peptide. A change in the configuration of the α-aminoadipyl residue from L to D or a decrease in the chain length by one or two carbons abolishes cyclizing activity. Although *N*-acylated derivatives of ACV exhibit some cyclization activity, the antibiotic produced in such cases is (iso)penicillin N, the natural product of ACV cyclization. That *N*-deacylation precedes cyclization with these substrates was demonstrated by the formation of ACV following preincubation of reaction mixtures under iron- and ascorbate-free conditions.

Of the analogs tested, only AdCV, which lacks the α-amino group of ACV, is an active substrate, but it is only 1−2% as active as ACV. All of these observations concerning the substrate specificity of the cyclizing enzyme of *S. clavuligerus* are very similar to those reported previously for the cyclizing enzyme of *C. acremonium* (6, 9).

Acknowledgements

This research was supported by grants from the Natural Sciences and Engineering Research Council of Canada and the Alberta Medical Heritage Research Fund. The authors thank L. Wulf for technical assistance and Dr. H. Auksi for preliminary synthetic work related to GACV.

1. R. NAGARAJAN, L. D. BOECK, M. GORMAN, R. L. HAMILL, C. E. HIGGINS, M. M. HOEHN, W. M. STARK, and J. G. WHITNEY. J. Am. Chem. Soc. **93**, 2308 (1971).
2. C. READING and M. COLE. Antimicrob. Agents Chemother. **11**, 852 (1977).
3. S. E. JENSEN, D. W. S. WESTLAKE, and S. WOLFE. J. Antibiot. **35**, 483 (1982).
4. S. E. JENSEN, D. W. S. WESTLAKE, R. J. BOWERS, and S. WOLFE. J. Antibiot. **35**, 1351 (1982).
5. S. E. JENSEN, D. W. S. WESTLAKE, and S. WOLFE. Can. J. Microbiol. **29**, 1526 (1983).
6. E. P. ABRAHAM, J. A. HUDDLESTON, G. S. JAYATILAKE, J. O'SULLIVAN, and R. L. WHITE. *In* Recent advances in the chemistry of β-lactam antibiotics. 2nd International Symposium. *Edited by* G. L. Gregory. Chemical Society Special Publication No. 38. The Chemical Society, London, England. 1981. p. 125.
7. P. A. FAWCETT, J. J. USHER, J. A. HUDDLESTON, R. C. BLEANEY, J. J. NISBET, and E. P. ABRAHAM. Biochem. J. **151**, 651 (1976).
8. J. KUPKA, Y.-Q. SHEN, S. WOLFE, and A. L. DEMAIN. FEMS Lett. **16**, 1 (1983).
9. J. KUPKA, Y.-Q. SHEN, S. WOLFE, and A. L. DEMAIN. Can. J. Microbiol. **29**, 488 (1983).
10. J. E. BALDWIN, E. P. ABRAHAM, R. M. ADLINGTON, B. CHAKRAVARTI, A. E. DEROME, J. A. MURPHY, L. D. FIELD, N. B. GREEN, H.-H. TING, and J. J. USHER. J. Chem. Soc. Chem. Commun. 1317 (1983).
11. Y. SAWADA, J. E. BALDWIN, P. D. SINGH, N. A. SOLOMON, and A. L. DEMAIN. Antimicrob. Agents Chemother. **18**, 465 (1980).
12. S. W. ELSON and R. S. OLIVER. J. Antibiot. **31**, 586 (1978).
13. S. W. ELSON, R. S. OLIVER, B. W. BYCROFT, and E. A. FARUK. J. Antibiot. **35**, 81 (1982).
14. G. A. BAHADUR, J. E. BALDWIN, J. J. USHER, E. P. ABRAHAM, G. S. JAYATILAKE, and R. L. WHITE. J. Am. Chem. Soc. **103**, 7651 (1981).

Can. J. Chem. Downloaded from www.nrcresearchpress.com by 210.87.254.42 on 09/06/12
For personal use only.

15. H. R. V. ARNSTEIN and D. MORRIS. Biochem. J. **76**, 357 (1960).
16. H. R. V. ARNSTEIN, M. ARTMAN, D. MORRIS, and E. J. TOMS. Biochem. J. **76**, 353 (1960).
17. P. B. LODER and E. P. ABRAHAM. Biochem. J. **123**, 471 (1971).
18. L. A. ERIQUEZ and M. A. PISANO. Antimicrob. Agents Chemother. **16**, 392 (1979).
19. P. TRAXLER, H. J. TREICHLER, and J. NÜESCH. J. Antibiot. **37**, 605 (1975).
20. J. SHOJI, H. HINOO, R. SAKAZAKI, T. KATO, K. MATSUMOTO, Y. TAKAHASHI, and E. KONDO. J. Antibiot. **35**, 1646 (1982).
21. K. KITANO, Y. FUJISAWA, K. KATAMOTO, K. NARA, and Y. NAKAO. J. Ferment. Technol. **54**. 712 (1976).
22. J. SHOJI, R. SAKAZAKI, K. MATSUMOTO, T. TANIMOTO, Y. TERUI, S. KOZUKI, and E. KONDO. J. Antibiot. **36**, 167 (1983).
23. S. WOLFE and M. G. JOKINEN. Can. J. Chem. **57**, 1388 (1979).
24. L. KISFALUDY, F. KORENCZKI, and A. KATHO. Synthesis, 163 (1982).
25. M. ITOH, D. HAGIWARA, and T. KAMIYA. Tetrahedron Lett. 4393 (1975).
26. S. WOLFE, R. J. BOWERS, S. K. HASAN, and P. M. KAZMAIER. Can. J. Chem. **59**, 406 (1981).
27. G. W. ANDERSON, J. E. ZIMMERMAN, and F. M. CALLAHAN. J. Am. Chem. Soc. **86**, 1839 (1964).
28. M. BRADFORD. Anal. Biochem. **72**, 248 (1976).
29. S. YOSHIFUJI, H. MATSUMOTO, K. TANAKA, and Y. NITTA. Tetrahedron Lett. **21**, 2963 (1980).

Can. J. Chem. Downloaded from www.nrcresearchpress.com by 210.87.254.42 on 09/06/12
For personal use only.

Study of electrolytic solution process using the scaled particle theory. 4. Standard free energy of transfer from aqueous to mixed aqueous binary solvent systems

UTPAL SEN

Central Electrochemical Research Institute, Karaikudi – 623 006, Tamil Nadu, India

Received February 7, 1984

UTPAL SEN. Can. J. Chem. **62**, 2721 (1984).

A unified approach which considers the electrolyte solution process as a combination of two steps, viz. (*1*) creation of a cavity of suitable size to accommodate the ionic solute species in the solvent system and (*2*) introduction of the ionic solute species into the cavity which interacts with the solvent system, proposed earlier along with the assumption that the overall ion–solvent interaction is the resultant of the electrostatic field and structural contributions, has been extended to study the free energy of transfer of electrolytes from water to a number of mixed aqueous binary solvent systems. The results of such theoretical analysis suggest that electrolytes can possibly be solvated preferentially by water molecules, particularly in the water-rich regions of the binary solvent system, with comparatively more ease in the solvent systems with dipolar aprotic co-solvents rather than in the binary solvent systems with protic co-solvents. This may be attributed to the possibility of strong interactions of water molecules with the protic co-solvent molecules through the hydrogen bonding. Dipolar aprotic co-solvents do not provide the facility for such hydrogen bonding. This observation seems to be consistent with most of the present day understandings about ion-solvent interactions in different binary solvent systems.

UTPAL SEN. Can. J. Chem. **62**, 2721 (1984).

Dans le but d'étudier l'énergie libre de transfert d'électrolytes de l'eau vers un certain nombre de systèmes de solvants binaires aqueux mixtes, on a essayé de rendre plus générale l'hypothèse selon laquelle l'interaction globale ion–solvant est la résultante de contributions structurales et de contributions du champ électrostatique ainsi que l'approche unifiée proposée antérieurement qui considère le processus de dissolution des électrolytes comme une combinaison de deux étapes, soit (*1*) la création d'une cavité ayant une dimension suffisante pour accomoder les espèces ioniques dissoutes dans le système de solvant et (*2*) l'introduction de l'espèce ionique dissoute dans la cavité qui interagit avec le système de solvant. Les résultats de telles analyses théoriques suggèrent qu'il est possible que les électrolytes puissent être solvatés préférentiellement par les molécules d'eau (en particulier dans les régions riches en eau du système de solvant binaire) et avec une facilité relativement plus grande dans les systèmes de solvant ayant des co-solvants aprotiques dipolaires plutôt que dans les systèmes ayant des co-solvants protiques. On peut attribuer ce comportement à la possibilité qu'ont les molécules d'eau de créer des interactions fortes avec les molécules de co-solvants protiques au moyen de liaisons hydrogènes. Par ailleurs, avec les co-solvants aprotiques dipolaires il n'est pas possible de former de telles liaisons hydrogènes. Cette observation semble être en accord avec la plupart des connaissances actuelles portant sur les interactions ion–solvant dans différents systèmes de solvants binaires.

[Traduit par le journal]

Can. J. Chem. Downloaded from www.nrcresearchpress.com by 210.87.254.40 on 09/06/12
For personal use only.

Introduction

Studies of the interaction of electrolytes (ions) in various binary solvent systems are of considerable current interest (1–3). Covington and Newman (4) visualized solvation around an ion in a mixed solvent as a competition between the solvent components for available solvation sites. They also identified this competition to be a useful measure of the solvating ability of the different solvents. Thus for many aqueous binary solvent mixtures it has frequently been suggested that water is the dominant hydrogen bond donor in aqueous solutions, leaving little or no chance for other hydrogen bond donors to compete with water for available acceptor sites as the solute species (5). Consequently, the idea of preferential solvation comes into picture (3). On the other hand, many binary mixtures, particularly of strongly interacting solvent components, may form an entirely new solvent system as the result of the overall interactions among different solvent molecules present (in the absence of the solute species). The behavior of the new solvent system thus formed with respect to the electrolyte solute may be quite different from that of any of the pure components. Consequently, the idea of preferential solvation of ions in such particular mixed solvent systems may get somewhat confused except probably in regions where one particular component in the solvent mixture is so much in excess that almost all the molecules just do not feel at all that there might be any other type of solvent molecules in the system. Obviously, at such given conditions only one component is available for solvation free from the influence of any other type of solvent molecules. As such there would be no competition between the components as they are in the same conditions as in the pure single component solvent state. With this kind of dual understanding in the background a theoretical look into the interaction phenomenon of ions in various mixed solvent systems may be worthwhile.

Calculation of various thermodynamic properties of electrolytes in solution from purely theoretical consideration has long been one of the important objectives of various theories of electrolytes. Many such theoretical approaches are based on various models. Frank and Evans (6), Gurney (7) and others developed their chemical model according to which changes in the water properties are assumed when the water passes from the bulk region far from an ion into a small region (cosphere) next to an ion. The attractive proposal of multilayer hydration zones around a solute ion in solution due to Frank and Wen (8) came almost simultaneously. Many subsequent attempts to theoretically account for the thermodynamic and other behaviours of ions in solution are based on those concepts in one way or another. Excellent recent reviews are available on this subject (9–11).

In our recent work, we have found that the overall interaction phenomenon in electrolyte–solvent systems can be conveniently split into two additive parts, viz. (*i*) the interaction due to the presence of an ionic species of finite size into a uniform dielectric solvent system, and (*ii*) the so-called specific interactions occurring at various distances apart from the incorporated ion which may result in the formation of the

Can. J. Chem. Downloaded from www.nrcresearchpress.com by 210.87.254.40 on 09/06/12
For personal use only.

so-called multilayer solvation zones around the solute ion (12). The free energy involved in the first part of the interaction process as mentioned above may be conveniently estimated with the help of the Born charging equation (13). A prior fixation of the value of the interaction free energy for the second part (denoted as ΔG^*), on the other hand, seems to be difficult and may require various kinds of speculation. It has, however, been realized that ΔG^*, which apparently has its major contribution in the strong interactions in the vicinity of a dissolved ion, would be relatively insensitive to temperature variations (14). Consequently, some interesting possibilities arise for accurate theoretical predictions of the related thermodynamic properties of the system at different temperatures (14, 15).

According to the above theory (16) proposed on the basis of the scaled particle approach (12) the solvation process of electrolytes (or ions) can be seen as the simple combination of two steps, viz. (*a*) the formation of a cavity of appropriate size in the solvent system for the accommodation of the solute species, and (*b*) the introduction of the solute ion into the cavity which interacts with the surrounding solvent. Consequently, when this interaction process is again subdivided as stated above into the (*i*) Born-type electrostatic interaction and (*ii*) the sum of the other various kind specific interactions occurring in the various regions around the incorporated solute ion, which the Born continuum model cannot recognise, the standard free energy of solvation, ΔG_s^0, for electrolytes can be represented as

$$[1] \quad \Delta G_s^0 = \Delta G_c^0 + \Delta G_i^0 + \Delta G_x^0$$

$$[2] \quad \Delta G_s^0 = \Delta G_c^0 + (\Delta G_{Born}^0 + \Delta G^*) + \Delta G_x^0$$

where ΔG_c^0, ΔG_{Born}^0, ΔG^*, and ΔG_x^0 are the Gibbs free energy of cavity formation, of Born type electrostatic interaction, of specific interactions which the Born equation cannot recognise, and the free energy change due to the standard state conversion, respectively.

In a slightly different approach Roseman and Jencks (17) divided the solution process into three parts: (*1*) the formation of cavities in the solvent, (*2*) the development of relatively "nonpolar" solvent–solute interactions in which they included dispersion, dipole – induced-dipole and quadrupole forces, and (*3*) the development of "polar" interactions that involve the polarity of both the solvent and the solute species, i.e., primarily the strong solvent–solute interactions. The overall Gibbs free energy of transfer of a solute from the gas phase to the solvent (in the solvation process) is thus given by eq. [3]

$$[3] \quad \Delta G_{tr} = \Delta G^{cav} + \Delta G_{nonpolar}^{int} + \Delta G_{polar}^{int}$$

The free energy of transfer for a solute from water to a water cosolvent binary mixture, ΔG_{tr} (h $\rightarrow$ c) is given by the difference between the values of ΔG_{tr} (g $\rightarrow$ l) from eq. [3] for two solvents and may be expressed in forms of eq. [4]

$$[4] \quad \Delta G_{tr}\,(h \rightarrow c) = \delta\Delta G^{cav} + \delta\Delta G_{nonpolar}^{int} + \delta\Delta G_{polar}^{int}$$

in which each $\delta\Delta G$ term represents the difference in the free energy of that component in the two solvents. The cavity free energy term in eq. [3] may be estimated by assuming the solute and solvent molecules to be hard spheres. None of the two interaction free energy terms, however, can be estimated without difficulty. Moreover, eq. [3] has apparently been formulated to deal with nonelectrolytic solutes. Another matter to be considered is the free energy change due to the changes of standard states of solutes in different solvent systems, the magnitude of which may not be always considered as negligible when other than molar scale are used (10).

Scaled particle theory (SPT) (18) alone has been used by several workers (19–25) for predicting some thermodynamic functions of transfer from water to mixed and other aqueous solvent systems. Most of the cases solutes involved are nonpolar and it was assumed that the similarity of the solvents for each transfer could cause a cancellation of the interaction terms which was by any means comparatively less significant in magnitude because of nonpolar nature of the solute involved. It was thus implied that a good prediction of the transfer properties may be possible from the cavity formation contribution alone which may be calculated from the SPT. Desrosiers and Desnoyers (23) used the SPT to predict the signs, magnitudes, and the trends on the co-solvent concentration dependence of the enthalpies, volumes, and heat capacities of transfer of Bu_4N^+ from water to aqueous *tert*-butanol binary solvent mixtures considering the cavity formation contributions only.

In the present paper eq. [2] has been used for the theoretical prediction of the Gibbs free energy transfer of electrolytes from water to the mixed aqueous solvent systems. Here, unlike earlier occasions involving nonpolar or hydrophobic solutes where all other interaction contributions were ignored, only a part of the overall interaction for energy contributions (viz., the specific interaction term, ΔG^*) has been probingly assumed to be more or less the same in both the aqueous and mixed aqueous solvent systems. Aqueous mixtures of some typical protic solvent such as methanol (MeOH) and of some typical dipolar aprotic solvents such as dimethyl sulfoxide (Me_2SO) and acetonitrile (MeCN) have been chosen and found convenient for the comparison of the experimentally available and theoretically predicted values of free energy of transfer for electrolytes because the required experimental data related to the free energy transfer values as well as the essential physical parameters of this binary aqueous mixtures required for the theoretical computations may be obtained from literature (26–28).

Method of calculations

Following eq. [1] the standard free energy for transfer of electrolytes from one solvent (S_1) to another (S_2) can be expressed as

$$[5] \quad \Delta G_{tr(S_1-S_2)}^0 = \Delta G_{c(tr)}^0 + \Delta G_{Born(tr)}^0 + \Delta G_{tr}^* + \Delta G_{x(tr)}^0$$

$$[6] \quad \Delta G_{S_2}^0 - \Delta G_{S_1}^0 = [\Delta G_{c(2)}^0 - \Delta G_{c(1)}^0] + [\Delta G_{Born(2)}^0 - \Delta G_{Born(1)}^0] + [\Delta G_2^* - \Delta G_1^*] + [\Delta G_{x(2)}^0 - \Delta G_{x(1)}^0]$$

The first term inside the square brackets on the right side can be calculated by computing the standard free energy for cavity formation for ions in individual solvents and taking the difference. The cavity free energy expressions according to the scaled particle theory (11) are as follows:

$$[7] \quad \Delta G_c^0 = K_0 + K_1 d_{12} + K_2 d_{12}^2 + K_3 d_{12}^3$$

$$[8] \quad K_0 = RT[-\ln(1-y) + 4.5\{y/(1-y)^2\}] - PN\pi d_1^3/6$$

$$[9] \quad K_1 = -(RT/d_1)[\{6y/(1-y)\} + 18\{y/(1-y)\}^2] + PN\pi d_1^2$$

$$[10] \quad K_2 = (RT/d_1^2)[\{12y/(1-y)\} + 18\{y/(1-y)\}^2] - 2PN\pi d_1$$

$$[11] \quad K_3 = 4PN\pi/3$$

where $d_{12} = (d_1 + d_2)/2$ and d_1 and d_2 are the hard sphere

Can. J. Chem. Downloaded from www.nrcresearchpress.com by 210.87.254.40 on 09/06/12
For personal use only.

diameters of solvent and solute molecules, respectively, and $y(=\pi N d_1^3/6V_1)$ is the corresponding compactness factor of the solvent. The details of cavity free energy calculations with the help of SPT have been reported elsewhere (12). The solute species and the solvent molecules have been assumed to be hard spheres. The problem of selecting the so-called hard sphere diameter of a mixed solvent system has been discussed by Desrosiers and Desnoyers (23). In one of the methods they suggested the use of the experimental isothermal compressibility value of the mixed solvent has been recommended for the calculation of the solvent diameter using the Mayer's equation (29). Obviously, the mixed solvent system is assumed to be a uniform solvent system having average molecular diameter d_1. We have followed the same technique and used the average values of molecular weight (M) and molar volume (V) along with the experimental values of dielectric constant (D) for the SPT calculation for cavity free energy contributions. The Born free energy transfer contribution and that of the standard states conversion may be calculated using the following equations:

$$[12]\quad \Delta G^0_{\text{Born(tr)}} = \frac{N(Ze)^2}{2T}\left[\frac{1}{D_2} - \frac{1}{D_1}\right]$$

$$[13]\quad \Delta G^0_{\text{x(tr)}} = RT \ln \frac{RTM_2}{V_2} - RT \ln \frac{RTM_1}{V_1}$$

$$= RT \ln (M_2V_1/M_1V_2) = RT \ln (\rho_2/\rho_1)$$

where r $(= d_2/2)$ is the radius of the solute ion which is assumed to be equal to the Pauling's crystal radius of the ion (30). D_1, D_2; M_1, M_2; V_1, V_2, and ρ_1, ρ_2 are the static dielectric constants, molecular weights, molar volumes, and densities of the solvent systems S_1 and S_2, respectively. Other symbols have the usual significance. To estimate the value of the transfer free energy for specific interactions, which could include many complicated interaction terms theoretically according to the presently known ion–solvent interactions, may be a difficult task. In some earlier attempts of theoretical predictions of thermodynamic functions of transfer of mostly uncharged or feebly charged solutes, the overall interaction contribution as a whole was ignored by assuming the same interaction (which is presumably weak) in both the pure solvent and in mixed solvent systems. With electrolyte solute, as in the present case, one perhaps cannot do the same. However, one may assume that the part of the interaction free energy which the classical Born equation cannot recognise will be approximately the same in pure water as in mixed solvent system containing water. Therefore, the magnitude of $(\Delta G_2^* - \Delta G_1^*)$ in eq. [2] may be considered to be negligible. Consequently, the value of ΔG^0_{tr} $(S \leftarrow W)$ where S_1 is water (W) and S_2 is the corresponding mixed aqueous solvent systems (S), can be calculed theoretically as

$$[14]\quad \Delta G^0_{tr}(S \leftarrow W) = [\Delta G^0_c + \Delta G^0_{\text{Born}} + \Delta G^0_x]_{tr}(S \leftarrow W)$$

Results

As we have seen in the above section, the theoretical estimation of the various contributions of the free energy of transfer for ions from one solvent to the other needs a number of physical parameters, relating particularly to the solvent systems under study and the actual value of such parameters used in these calculations will largely determine the magnitude of each free energy contribution. It is therefore important to define

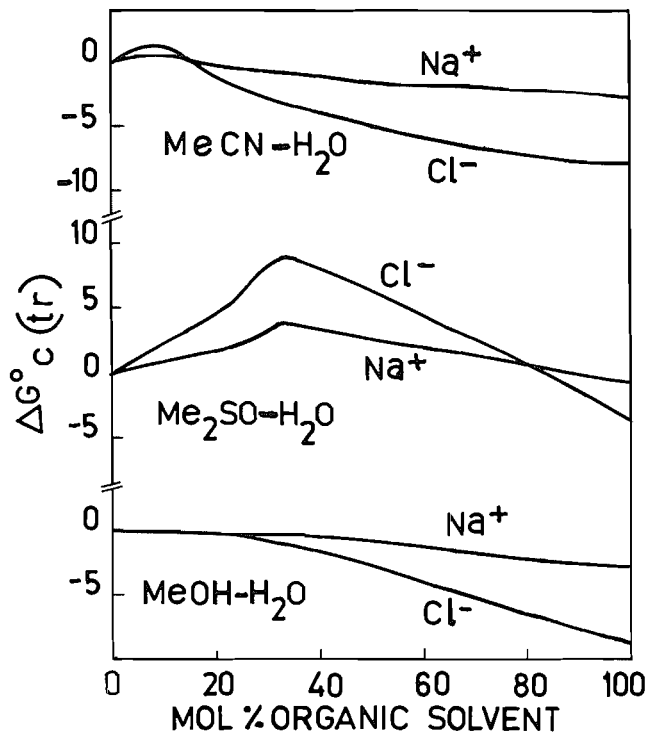

FIG. 1. Variation of transfer free energy due to cavity formation ($\Delta G^0_{c(tr)}$, kJ mol^{-1}) for typical ions with solvent composition.

those parameters which have been actually used. Table 1 shows such parameters. Overall effective average parameters such as molar volume (V), molecular diameter (d_1), compactness factor (y), etc., are calculated from the respective experimental values of the corresponding physical properties such as density (ρ_T), isothermal compressibility (β_T), etc., of the aqueous binary solvent mixtures and hence would be assumed to represent the effective behaviour of the mixed solvent systems with respect to the solute ions. The average molecular diameter (d_1) for the different solvent systems have been estimated from the corresponding isothermal compressibility data (β_T). For the MeOH–H_2O and Me_2SO–H_2O solvent systems, direct experimental values of β_T are not available (22) for the entire range of the solvent compositions where the components of the binaries would be present in the mixture from zero to 100%. Hence the available experimental values of β_T are plotted against the corresponding solvent composition and the values of β_T at all the desired solvent compositions have been generated by interpolation from the smooth master curves. The same β_T values (see Table 1) for solvent mixtures were used for the calculation of the corresponding d_1 values of the solvent mixture. For the Me_2SO–H_2O systems β_T values at 35°C and not at 25°C are available (27). In this case the d_1 values have been calculated for 35°C and subsequently been corrected for 25°C using the available value of the corresponding temperature coefficient $(\delta d_1/\delta T)_P$ of water and of Me_2SO (31). One of the coefficients (K_3) of the equations representing free energy for cavity formation has the same value ($K_3 = 0.2556$ J mol^{-1} Å^{-3}), irrespective of the solvent systems used and is given at the bottom of Table 1.

The free energy of cavity formation is by definition a function of the actual size of the solute ion and not of the charge on it. Figure 1 which plots the calculated cavity free energy of transfer for Na^+ ($r = 0.95$ Å) and Cl^- ($r = 1.81$ Å) from water to the corresponding mixed solvents would give an idea how

TABLE 1. Physical parameters used in the thermodynamic calculations (at 25°C)[a]

Solvent Mol%	Solvent Wt%	M_{ave} (g/mol)	V_{ave} (cm^3/mol)	ρ_T (g/cm^3)	$-\beta_T$[b] (10^{-5} atm^{-1})	Y	d_1 (Å)	D	K_0 (J mol)	K_1/J_{-1} (mol Å^{-1})	K_2/J_{-1} (mol Å^{-2})
					(*a*) MeOH–H_2O system						
0	0	18.015	18.07	0.9971	4.524	0.3510	2.719	78.36	4335	7753	3937
5	8.56	18.717	19.04	0.9850	4.429	0.3596	2.790	75.5	4594	7975	3908
10	16.50	19.418	20.01	0.9722	4.312	0.3685	2.860	71.9	4908	8284	3933
20	30.78	20.820	22.08	0.9443	4.286	0.3805	2.987	65.1	5360	8623	3887
30	43.25	22.223	24.04	0.9256	4.629	0.3814	3.075	59.4	5393	8422	3686
40	54.25	23.625	26.19	0.9030	5.010	0.3822	3.166	54.2	5422	8222	3489
50	64.01	25.028	28.52	0.8783	5.657	0.3780	3.246	49.9	5251	7778	3230
60	72.74	26.430	30.79	0.8590	6.510	0.3707	3.308	46.0	4971	7243	2962
70	80.58	27.833	33.13	0.8407	7.70	0.3597	3.355	42.4	4577	6598	2682
80	87.68	29.235	35.41	0.8258	9.00	0.3492	3.397	38.9	4226	6042	2443
90	94.12	30.638	37.47	0.8178	10.57	0.3369	3.421	35.9	3845	5485	2222
100	100.	32.04	40.73	0.7866	12.58	0.3261	3.479	32.6	35357	4975	1996
					(*b*) MeCN–H_2O system[d]						
5	10.70	19.16	19.74	0.9710	4.10	0.3727	2.858	74.3	5063	8540	4088
10	20.18	20.31	21.39	0.9495	3.82	0.3902	2.982	70.1	5761	9251	4146
20	36.26	22.57	24.62	0.9187	4.88	0.3783	3.092	62.3	5272	8196	3573
30	49.38	24.91	27.94	0.8916	5.56	0.3778	3.224	56.1	5247	7824	3272
40	60.27	27.14	31.37	0.8674	6.56	0.3720	3.333	51.1	5021	7255	2941
50	69.47	29.51	34.91	0.8453	7.57	0.3678	3.441	47.0	4858	6812	2682
60	77.34	31.82	38.52	0.8257	8.48	0.3661	3.550	44.0	4791	6514	2489
70	84.15	34.10	42.08	0.8104	9.35	0.3650	3.652	41.5	4749	6272	2330
80	90.10	36.41	45.62	0.7979	10.15	0.3648	3.751	39.3	4736	6092	2201
90	95.35	38.71	49.20	0.7867	10.87	0.3656	3.849	37.5	4757	5962	2096
100	100.	41.00	52.71	0.778	11.54	0.3636	3.943	36.0	4786	5853	2008
					(*c*) Me_2SO–H_2O system						
5	18.58	21.020	20.61	1.0216	3.70[c]	0.3865	2.934	77.5	5607	9163	4188
10	32.56	24.024	23.09	1.0420	3.23	0.4148	3.120	76.9	6891	10487	4418
20	52.01	30.032	28.05	1.0717	2.59	0.4605	3.447	74.9	9602	13021	4820
30	65.01	36.047	33.15	1.0881	1.80	0.5146	3.782	71.7	14259	17318	5653
40	74.29	42.049	38.40	1.0955	1.77	0.5307	4.013	67.7	16054	18284	5569
50	81.26	48.058	43.78	1.0982	2.00	0.5318	4.195	64.0	16175	17610	5125
60	86.67	54.066	49.23	1.0985	2.34	0.5284	4.353	60.7	15757	16548	4644
70	91.00	60.075	54.72	1.0980	2.62	0.5280	4.508	56.5	15698	16916	4314
80	94.55	66.083	60.21	1.0977	3.24	0.5165	4.620	53.0	14401	14293	3803
90	97.50	72.092	65.74	1.0966	4.10	0.5019	4.712	49.9	12916	12619	3318
100	100	78.10	71.29	1.0956	5.30	0.4843	4.784	46.4	11334	10966	2866

[a] K_3 = 0.2556 J mol^{-1} Å^{-3}, ref. 26.
[b] Reference 27.
[c] Values at 35°C, d_1 calculated at 35°C and then corrected for values at 25°C.
[d] Reference 28.

the magnitude of the cavity free energy transfer for ions changes with the change of the solvent compositions. The electrostatic contributions of free energy of transfer for ions which has been calculated with the help of Born charging equation essentially depends on the respective static bulk dielectric constants (D) of the solvent systems involved. Figure 2 may give an idea how, for monovalent ions (Na^+ and Cl^-), the value of $\Delta G^0_{Born}(tr)$ changes with the solvent compositions of the three particular solvent systems in this study. Table 2 lists the magnitude of the free energy change due to the change of the standard states in these three different aquo-organic solvent systems.

In their excellent review Cox and Waghorne (1) listed the experimental values of free energies of transfer for several electrolytes from water to a number of mixed solvent binaries, obtained by various workers using different experimental techniques. All these experimental values from different sources, which are reported in molar scale, have been converted to the corresponding values in the molal scale (15) and graphically plotted against the respective solvent compositions in mol%. From the smooth average master curves subsequently drawn from the plot the experimental values of free energy of transfer for different electrolytes have been obtained by interpolation at regular intervals of solvent compositions. These ΔG^0_{tr} values in MeOH–H_2O, Me_2SO–H_2O, and MeCN–H_2O binary solvent systems have been listed in Table 3. The values of free energies of transfer for NaCl (a typical electrolyte) from water to the corresponding mixed solvent systems calculated using eq. [14], i.e., by assuming ΔG^*_{tr} to be negligible are plotted along with the corresponding experimental values from Table 3 have been plotted against the corresponding solvent composition in Fig. 3 for comparison.

Can. J. Chem. Downloaded from www.nrcresearchpress.com by 210.87.254.40 on 09/06/12
For personal use only.

Can. J. Chem. Downloaded from www.nrcresearchpress.com by 210.87.254.40 on 09/06/12
For personal use only.

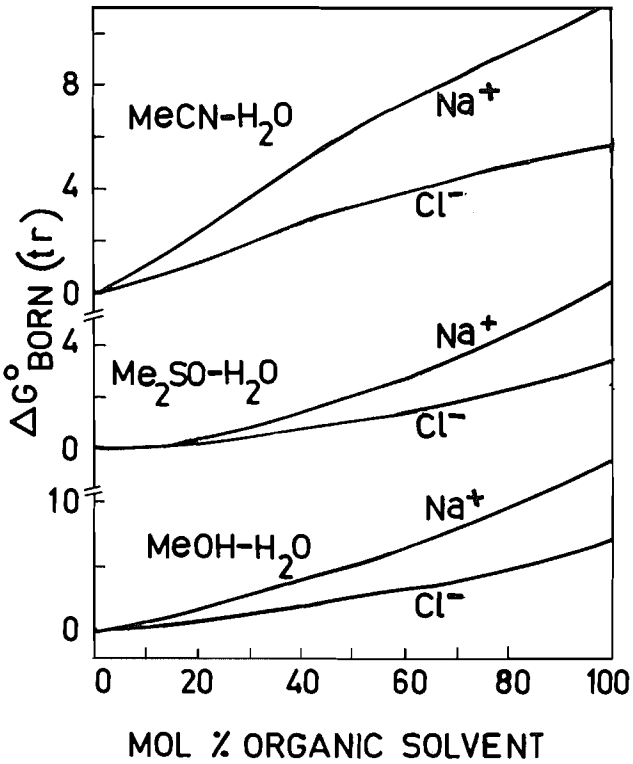

FIG. 2. Variation of transfer free energy due to electrostatic field effect ($\Delta G^0_{Born(tr)}$, kJ mol^{-1}) for typical ions with solvent composition.

Discussion

In mixed aqueous binary solvent systems, the water molecules understandably interact with different kinds of available solvent molecules including those of the cosolvent. The presence of a solute ion in the system obviously disturbs the equilibrium and eventually the ion becomes solvated in one way or other. Normally interactions of water molecules with those of some protic co-solvent (such as alcohols) is believed to be strong due to hydrogen bonding (2). From Fig. 3 it is evident that the value of ΔG^*, free energy of specific interaction, of electrolytes with the methanol–water binary solvent systems is different from that in water. This is true for almost all the different compositions of the binary mixtures. This probably suggests that due to strong interactions between water and methanol molecules in the binary systems there may not be much chance that the solute ions would get preferentially solvated by water molecules as they are present in pure water as solvent. From detailed nmr studies Symons recently reported similar conclusion for ions in alcohol–water binary systems (32).

Interactions of water molecules with dipolar aprotic co-solvents (such as dimethyl sulfoxide, acetonitrile, etc.) are comparatively weaker obviously due to the lack of facilities for hydrogen bonding. Figure 3 shows that in dimethyl sulfoxide – water binary systems, the value of ΔG^* of NaCl is not much different from that in pure water, at least, upto around 50 mol% of dimethyl sulfoxide in the mixture. This probably suggests that solute ions may be getting preferentially solvated by water molecules making the value of the specific interaction free energy, ΔG^*, more or less unchanged. However, when the proportion of dimethyl sulfoxide becomes more than 50 mol% or so the solvation picture becomes complicated and the so-called preferential solvation of electrolytes with water molecules becomes confused with progressively more and more dimethyl sulfoxide molecules interfering with the solvation process. Solvation experience of ions in acetonitrile and its aqueous binary mixtures has been found to be somewhat puzzling (33). Solvation free energy of individual cations and anions obtained from some experimental results through the help of some kind or other extrathermodynamic assumption also did not solve the puzzle (33, 34). Conflicting reports are available stating some cations being preferentially solvated by water and some other by the co-solvent acetonitrile molecules (34), whereas halide anions are thought not to be preferentially solvated by water in acetonitrile–water binary mixtures (33). Considering this somewhat confusing background the present analysis probably (Fig. 3) can only say that the value of the specific interaction free energy in acetonitrile water binary mixtures is different from that in pure water when the propor-

TABLE 2. $\Delta G^0_{x((tr)}$ (kJ mol^{-1}) from water to mixed solvents for ions at 25°C (molal scale)

Mol% of organic solvents	MeOH–H_2O system	MeCN–H_2O system	Me_2SO–H_2O system
0.0	0.00	0.00	0.00
5.0	−0.03	−0.07	0.06
10.0	−0.06	−0.12	0.11
20.0	−0.13	−0.20	0.18
30.0	−0.19	−0.28	0.22
40.0	−0.25	−0.35	0.23
50.0	−0.31	−0.41	0.24
60.0	−0.37	−0.47	0.24
70.0	−0.42	−0.51	0.24
80.0	−0.47	−0.55	0.24
90.0	−0.49	−0.59	0.24
100.0	−0.59	−0.62	0.24

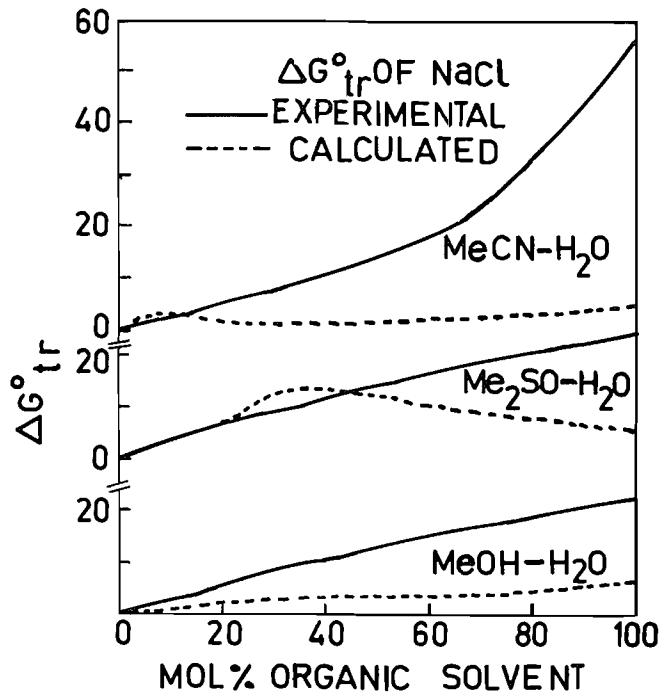

FIG. 3. Comparison of the experimental and calculated (assuming preferential specific interaction by water) values of transfer free energy (ΔG^0_{tr}, kJ mol^{-1}) for a typical electrolyte (NaCl) for different solvent compositions.

TABLE 3. ΔG^0_{tr}(exptl) (kJ mol^{-1}) from water to mixed solvents, at 25°C[a] (molal scale)

Salt	$-\Delta G^0_h$ in H_2O	Mol% of organic solvents										
		5	10	20	30	40	50	60	70	80	90	100
						(*a*) MeOH–H_2O system						
HCl		0.69	1.30	2.36	3.17	4.13	5.53	7.06	9.09	11.03	15.63	24.77
HBr		0.48	0.96	1.61	2.17	2.75	3.77	4.97	7.00	8.94	13.53	22.60
LiCl	452.21	1.15	2.22	4.20	6.14	7.81	9.50	11.20	12.85	14.53	16.17	17.74
NaCl	719.98	1.53	2.93	5.67	8.36	10.868	13.47	15.89	17.62	19.60	21.40	22.93
KCl	647.60	1.57	3.14	5.92	8.57	10.99	13.56	15.97	18.29	20.47	22.32	24.19
RbCl	623.50	1.53	3.05	5.79	8.40	10.87	13.52	15.97	18.25	20.68	22.74	24.61
CsCl	592.79	1.48	2.72	5.54	7.90	10.37	12.81	15.22	17.79	20.31	22.91	25.02
AgCl	781.40	1.23	2.43	4.75	6.94	11.51	11.51	13.58	15.74	17.84	19.90	22.46
NaF		1.61	3.26	6.67	10.247	13.30	16.32	18.69	20.97	22.90	24.41	25.44
NaBr	677.22	1.44	2.68	5.21	7.31	9.53	11.63	13.63	15.61	17.46	19.10	20.46
NaI	669.15	1.19	2.26	4.12	5.64	7.40	9.08	10.78	12.23	14.20	15.42	16.87
						(*b*) MeCN–H_2O system						
LiCl	452.21	2.06	3.67	6.31	9.17	11.90	15.55	19.93	26.80	35.41	16.91	67.34
NaCl	719.98	2.02	3.05	5.76	8.46	11.15	14.79	18.51	24.54	33.91	44.48	57.30
KCl	647.60	1.30	2.67	5.43	8.25	11.03	13.37	16.84	22.79	30.81	40.51	51.44
RbCl	623.50	1.22	2.42	5.26	7.69	10.90	14.00	18.01	24.88	32.99	41.89	51.44
CsCl	592.79	1.18	2.21	4.30	6.37	8.81	11.95	16.29	22.37	30.14	38.83	49.77
AgCl	781.40	−4.64	−6.37	−8.13	−8.65	−7.13	−4.41	−0.53	3.71	8.05	12.47	17.55
KBr	604.84	0.89	1.83	4.09	6.41	11.49	11.49	14.74	20.19	26.92	33.39	39.73
KI	596.76	0.30	0.54	1.75	3.15	5.08	7.01	9.47	12.41	15.87	20.42	28.01
						(*c*) Me_2SO–H_2O system						
LiCl	452.21	0.84	1.71	3.41	4.76	6.27	7.89	10.02	12.91	14.84	18.36	22.96
NaCl	719.98	1.89	3.55	6.59	9.73	12.30	14.17	16.67	18.77	20.86	22.88	25.06
KCl	647.60	1.64	3.59	7.59	11.53	14.51	16.50	18.89	20.53	22.54	24.21	25.89
RbCl	623.50	1.64	3.55	7.51	11.28	14.89	16.80	19.19	21.28	23.25	25.26	27.15
CsCl	592.79	1.60	3.42	6.88	9.90	12.42	14.58	16.30	18.52	20.74	22.88	25.47
AgCl	781.40	0.17	0.26	0.26	−0.02	−0.05	0.36	0.98	2.16	3.29	4.26	5.56
KBr	604.84	0.97	2.21	4.16	5.84	7.11	7.85	8.60	9.27	9.98	10.62	11.25
KI	596.76	0.11	0.17	0.26	0.36	0.45	0.52	0.60	0.64	0.70	0.74	0.79

[a] Interpolated values from the smooth plots of the experimental values of ΔG^0_{tr} obtained from ref. 1 (after converting to the corresponding molal scale), against solvent compositions.

Can. J. Chem. Downloaded from www.nrcresearchpress.com by 210.87.254.40 on 09/06/12
For personal use only.

tion of acetonitrile in the mixture is more than ~20 mol%. This suggests that the so-called preferential solvation of electrolytes by water molecules in the present binary systems may be possible only when the mixture contains a high percentage (~80 mol%) of water. Further experimental and theoretical studies involving different approaches with electrolytes in aqueous mixtures of various dipolar aprotic co-solvents seem to be necessary to have a clearer picture of ion–solvent interactions in those systems and to know whether a generalized picture can be drawn.

The above approach no doubt is essentially associated with some approximations such as the assumptions of hard sphere molecules of particular dimension for the binary solvent mixtures. The corresponding average diameters have been estimated from the experimental values of the respective isothermal compressibility in order to calculate the free energy contribution for cavity formations in the solvent systems to accommodate the solute ions. Nevertheless, it appears that the splitting of the ion–solvent interaction phenomenon into the electrostatic field and the structural contributions which is the basis of eq. [2] may be useful to study the so-called preferential solvation and related aspects of behaviours of electrolytes in mixed binary solvent systems. The theory seems to go along well with most of the recent concepts and understandings.

Acknowledgement

The author thanks Dr. K. S. Rajagopalan, Director, Central Electrochemical Research Institute, Karaikudi, for his interest in the present work.

1. B. G. COX and W. E. WAGHORNE. Chem. Soc. Rev. **9**, 381 (1980) and references therein; B. G. COX. Soc. Chem. Ann. Rep. **78**C, 4 (1981).
2. J. B. F. N. ENGBERTS. Water, a comprehensive treatise. Vol. 6. *Edited by* F. Franks. Plenum, New York. 1979. p. 139. Chapt. 4.
3. A. K. COVINGTON and K. E. NEWMAN. Thermodynamic behaviour of electrolytes in mixed solvents. *Edited by* W. F. Furter. Adv. Chem. Ser. No. 155. Am. Chem. Soc. Washington, DC. 1976. p. 153.
4. A. K. COVINGTON and K. E. NEWMAN. Modern aspects of electrochemistry. Vol. 12. *Edited by* J. O'M.Bockris and B. E. Conway. Plenum, New York. 1977. p. 108.
5. I. M. KLOTZ and J. S. FRANZEN. J. Am. Chem. Soc. **84**, 3461 (1962).
6. H. S. FRANK and M. W. EVANS. J. Chem. Phys. **13**, 507 (1945).
7. R. W. GURNEY. Ionic Processes in solution. McGraw Hill, New York. 1958.
8. H. S. FRANK and W. Y. WEN. Discuss. Faraday Soc. **24**, 133 (1957).

9. J. E. DESNOYERS and C. JOLICOEUR. *In* Modern aspects of electrochemistry. Vol. 5. *Edited by* J. O'M. Bockris and B. E. Conway. Plenum, New York. 1969. Chapt. 1.
10. C. V. KRISHNAN and H. L. FRIEDMAN. *In* Water, a comprehensive treatise. *Edited by* F. Franks. 1973. Chapt. 1.
11. P. P. S. SALUJA. International Rev. Sci. Ser. 2. Vol. 6. *Edited by* J. O'M Bockris. Butterworths, London. 1976. Chapt. 1.
12. U. SEN. J. Am. Chem. Soc. **101**, 2531 (1979).
13. M. BORN. Z. Phyk. **1**, 45 (1920).
14. U. SEN. J. Am. Chem. Soc. **102**, 2181 (1980).
15. U. SEN. J. Chem. Soc. Faraday 1, **77**, 2883 (1981).
16. U. SEN. Proceedings of Sir J. C. Ghosh Memorial Conference on Strong Electrolytes. Calcutta. March, 1982.
17. M. ROSEMAN and W. P. JENCKS. J. Am. Chem. Soc. **97**, 631 (1975).
18. R. PIEROTTI. Chem. Rev. **76**, 717 (1976); J. Phys. Chem. **67**, 1840 (1963); **69**, 281 (1965).
19. N. DESROSIERS and J. P. MOREL. Can. J. Chem. **59**, 1 (1981).
20. P. R. PHILIP and C. JOLICOEUR. J. Sol. Chem. **4**, 105 (1975).
21. M. LUCAS. J. Phys. Chem. **80**, 359 (1976).
22. M. LUCAS and R. BURY. J. Phys. Chem. **80**, 999 (1976).
23. N. DESROSIERS and J. E. DESNOYERS. Can. J. Chem. **54**, 3800 (1976).
24. J. P. MOREL and N. DESROSIERS. J. Sol. Chem. **8**, 579 (1979).
25. J. P. MOREL and N. DESROSIERS. J. Sol. Chem. **10**, 451 (1981).
26. G. J. JANZ and R. P. T. TOMKINS. Nonaqueous handbook. Vol. 1. Academic Press, New York. 1972.
27. K. H. JUNG and J. B. HYNE. Can. J. Chem. **48**, 2423 (1970).
28. D. F. G. TAYLOR and D. D. MCDONALD. Can. J. Chem. **54**, 2815 (1976).
29. S. W. MAYER. J. Phys. Chem. **67**, 2160 (1963).
30. L. PAULING. The nature of chemical bonds. 3rd ed. Cornell Univ. Press, Ithaica, NY. 1960. p. 514.
31. E. WILHELM. J. Chem. Phys. **58**, 3558 (1973).
32. M. C. R. SYMONS. Chem. Soc. Rev. **12**, 1 (1983).
33. T. R. STENGLE, Y. E. PAN, and C. H. LANGFORD. J. Am. Chem. Soc. **94**, 9039 (1972).
34. B. G. COX, R. NATARAJAN, and W. E. WAGHORNE. J. Chem. Soc. Faraday 1, **75**, 86 (1979).

Can. J. Chem. Downloaded from www.nrcresearchpress.com by 210.87.254.40 on 09/06/12
For personal use only.

The hex-5-enose degradation: zinc dust cleavage of 6-deoxy-6-iodo-α-D-galactopyranosidic linkages in methylated di- and trisaccharides[1]

GERALD OLIVER ASPINALL,[2] DELPHI CHATTERJEE, AND LEV KHONDO
Department of Chemistry, York University, Downsview, Toronto, Ont., Canada M3J 1P3

Received April 23, 1984

GERALD OLIVER ASPINALL, DELPHI CHATTERJEE, and LEV KHONDO. Can. J. Chem. **62**, 2728 (1984).

The Bernet–Vasella reaction of 6-deoxy-6-halohexopyranosides with zinc dust to give hex-5-enoses has been explored as the basis for a new procedure for the selective cleavage of glycosidic linkages in complex oligo- and polysaccharides. The overall reaction sequence involves: (a) the generation of primary hydroxyl groups in otherwise fully methylated oligo- or polysaccharides; (b) the formation of 6-deoxy-6-iodohexopyranosides by iodide displacement of reactive sulfonate esters; and (c) treatment with zinc dust followed by the formation of suitable derivatives from the liberated hex-5-enoses. Oligosaccharides carrying β-D-xylopyranosyl substituents at the 2-*O*- (**4**), 3-*O*- (**17**), 4-*O*- (**12**), and both 3-*O*- and 4-*O*- (**8**) positions have been converted into otherwise fully methylated derivatives, each containing methyl 6-deoxy-6-iodo-α-D-galactopyranoside residues, to serve as model substrates for different structural environments. In each case the derived 5,6-dideoxy-hex-5-enoses formed on treatment with zinc dust have been characterized by conversion into the corresponding 1,2-dideoxy-hex-1-enitol acetates. During preparations of 6-deoxy-6-iodo-α-D-galactopyranosides from the corresponding 6-sulfonate esters, solvolytic side reactions have been observed which may include the formation of 3,6-anhydro-α-D-galactopyranosides with intramolecular participation of 3-*O*-methyl or 3-*O*-glycosyl substituents and subsequent loss of such substituents.

GERALD OLIVER ASPINALL, DELPHI CHATTERJEE et LEV KHONDO. Can. J. Chem. **62**, 2728 (1984).

On a examiné la possibilité d'utiliser la réaction de Bernet–Vasella, qui permet de transformer des désoxy-6 halogéno-6 hexopyrannosides en hexène-5 oses par action de la poudre de zinc, comme base d'une nouvelle méthode pour cliver d'une façon sélective les liaisons glycosidiques d'oligo- et de polysaccharides complexes. Dans l'ensemble, la série de réactions implique: (a) qu'il faut générer des groupes hydroxyles primaires dans des oligo- et des polysaccharides qui sont par ailleurs complètement méthylés; (b) la formation de désoxy-6 iodo-6 hexopyrannosides grâce à un déplacement de sulfonates réactifs par de l'iode et (c) un traitement par de la poudre de zinc qui est suivi par la formation de dérivés appropriés des hexène-5 oses libérés. On a pu transformer les oligosaccharides portant des substituants β-D-xylopyrannosyles en positions 2-*O*- (**4**), 3-*O*- (**17**), 4-*O*- (**12**) et 3-*O*- ainsi que 4-*O*- (**8**) en dérivés qui sont par ailleurs complètement méthylés, qui contiennent chacun des résidus désoxy-6 iodo-6 α-D-galactopyrannosides de méthyle et qui peuvent servir de substrats modèles pour différents environnements structuraux. Dans chaque cas, on a caractérisé les didésoxy-5,6 hexène-5 oses qui se forment par traitement avec de la poudre de zinc en les transformant en acétates des didésoxy-1,2 hexène-1 itols correspondants. Lors de la préparation des désoxy-6 iodo-6 α-D-galactopyrannosides à partir des sulfonates-6 correspondants, on a observé des réactions de solvolyses secondaires qui peuvent conduire à la formation des anhydro-3,6 α-D-galactopyrannosides par le biais d'une participation intramoléculaire des substituants 3-*O*-méthyles ou 3-*O*-glycosyles et d'une perte subséquente de ces substituants.

[Traduit par le journal]

Can. J. Chem. Downloaded from www.nrcresearchpress.com by 210.87.254.5 on 09/06/12
For personal use only.

Bernet and Vasella (1) have shown that 6-deoxy-6-halo-glycosides react with zinc dust under mild conditions with glycoside cleavage and formation of hex-5-enoses. In order to assess this reaction for the selective cleavage of glycosidic linkages in polysaccharide derivatives we have examined reactions of selected oligosaccharides. Methylated oligosaccharide glycosides, each of which contained a single primary hydroxyl group, were synthesized in standard reaction sequences. The reactions shown in Scheme 1 were studied, (*i*) the formation of 6-deoxy-6-iodohexopyranosides, and (*ii*) the zinc dust cleavage reaction followed by derivative formation suitable for the characterization of hex-5-enose residues thus generated. The oligosaccharides were all α-D-galactopyranosides, which were chosen as models for different structural regions in carboxyl-reduced methylated pectins and related α-D-galacturonans. Since nucleophilic displacements at C-6 occur least readily in galactopyranosides (2), it is likely that transformations which proceed satisfactorily for these glycosides will take place without difficulty for the corresponding gluco- and mannopyranosides. Two recent methods for halogenation at C-6 involve the formation of highly reactive sulfonates followed by halide displacement under mild conditions (3, 4). These reactions

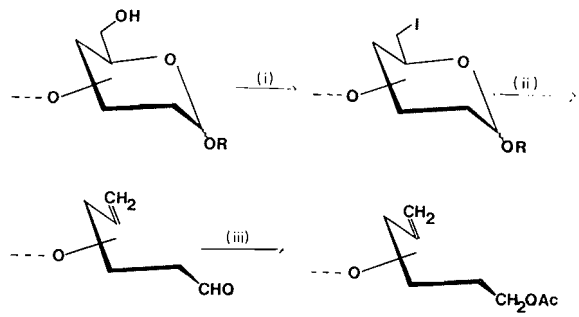

SCHEME 1. Generation of hex-5-enoses and formation of derivatives: (i) sulfonylation, followed by displacement of sulfonate ester with $Bu_4N^+ I^-$; (ii) Zn dust; and (iii) $NaBH_4$, followed by Ac_2O/Pyr (unchanged substituents are omitted).

appeared to offer the greatest chance for the successful introduction of 6-halo substituents into sterically hindered galactopyranose residues in even less reactive environments in polysaccharides where polymer chain conformations may impose additional restrictions. Displacement by iodide ion was chosen as the reaction least likely to be accompanied by competing elimination (3, 4).

Oligosaccharide syntheses

The most readily accessible (1 → 2)-linked disaccharide glycoside (**4**) was synthesized without ambiguity as to linkage type. Condensation of 2,3,4-tri-*O*-acetyl-α-D-xylopyranosyl

[1] Presented in part at the Canadian Institute of Chemistry Conference, Montreal, Quebec, June 3–6, 1984, and at the 12th International Symposium on Carbohydrate Chemistry, Utrecht, The Netherlands, July 2–6, 1984.

[2] Author to whom correspondence should be addressed.

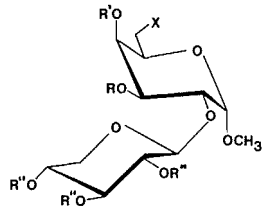

1 R,R′ = $C(CH_3)_2$, R″ = Ac, X = OBn
2 R = R′ = R″ = H, X = OBn
3 R = R′ = R″ = Me, X = OBn
4 R = R′ = R″ = Me, X = OH
18 R = R′ = R″ = Me, X = O—SO_2—Imidazolyl
19 R = R′ = R″ = Me, X = I
29 R = R′ = R″ = Me, X = O—CHO

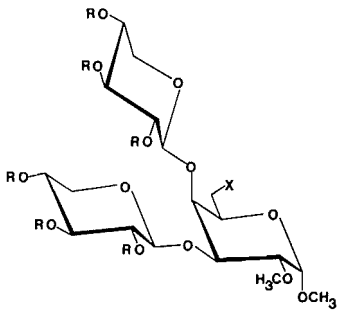

5 R = Ac, X = OBn
6 R = H, X = OBn
7 R = Me, X = OBn
8 R = Me, X = OH
20 R = Me, X = I
30 R = Me, X = O—CHO

bromide with methyl 6-*O*-benzyl-3,4-*O*-isopropylidene-α-D-galactopyranoside (5) afforded methyl 2-*O*-(2,3,4-tri-*O*-acetyl-β-D-xylopyranosyl)-6-*O*-benzyl-3,4-*O*-isopropylidene-α-D-galactopyranoside (**1**), which was successively treated with trifluoroacetic acid for de-isopropylidenation and sodium methoxide for de-*O*-acetylation to give crystalline methyl 6-*O*-benzyl-2-*O*-(β-D-xylopyranosyl)-α-D-galactopyranoside (**2**). The disaccharide benzyl ether (**2**) furnished a fully methylated derivative (**3**) which was hydrogenolyzed to give methyl 3,4-di-*O*-methyl-2-*O*-(2,3,4-tri-*O*-methyl-β-D-xylopyranosyl)-α-D-galactopyranoside (**4**).

In order to have available derivatives of linkage types likely to be encountered in tragacanthic acid (6) and related galacturonan derivatives, syntheses were extended to the isomeric (1 → 3)- and (1→4)-linked disaccharide and the (1 → 3)- and (1 → 4)- linked branched trisaccharide series using generally similar reaction sequences. In each series of reactions all crystalline compounds including end products (**8**, **12**, and **17**) were obtained in analytically pure form. The syrupy intermediates were isolated in chromatographically homogeneous form, gave nmr spectra in accord with the structures shown, and were used directly for the next stages of the syntheses. Methyl 6-*O*-benzyl-2-*O*-methyl-α-D-galactopyranoside (7) was a convenient starting material for each synthetic sequence. When 2,3,4-tri-*O*-acetyl-α-D-xylopyranosyl bromide was condensed with this compound, regardless of the molar ratios of glycosyl halide to aglycone, two products only, although in varying proportions, were observed on tlc and these were separated by preparative chromatography. The first product was methyl

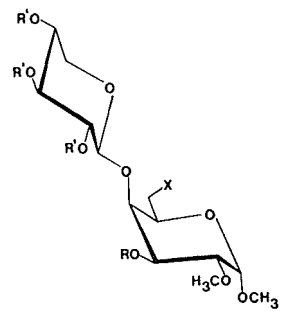

9 R = H, R′ = Ac, X = OBn
10 R = R′ = H, X = OBn
11 R = R′ = Me, X = OBn
12 R = R′ = Me, X = OH
21 R = R′ = Me, X = I

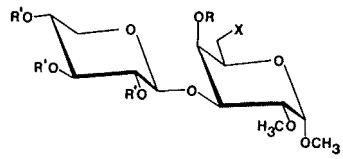

14 R′ = Ac, R = Bz, X = OBn
15 R = R′ = H, X = OBn
16 R = R′ = Me, X = OBn
17 R = R′ = Me, X = OH
22 R = R′ = Me, X = I
31 R = R′ = Me, X = O—CHO
32 R = R′ = Me, X = OAc

3,4-di-*O*-(2,3,4-tri-*O*-acetyl-β-D-xylopyranosyl)-6-*O*-benzyl-2-*O*-methyl-α-D-galactopyranoside (**5**), which on deacetylation, methylation, and debenzylation afforded the trisaccharide derivative, methyl 2-*O*-methyl-3,4-di-*O*-(2,3,4-tri-*O*-methyl-β-D-xylopyranosyl)-α-D-galactopyranoside (**8**). Surprisingly, the second compound from mono-*O*-glycosylation was shown to be methyl 4-*O*-(2,3,4-tri-*O*-acetyl-β-D-xylopyranosyl)-6-*O*-benzyl-2-*O*-methyl-α-D-galactopyranoside (**9**), whose structure was established by methylation–deacetylation, debenzylation, remethylation, and methylated sugar analysis to give *inter alia* 2,3,6-tri-*O*-methylgalactose, identified by glc–ms of the derived partially methylated alditol acetate. In contrast to the preferential glycosylation of equatorial 3-hydroxyl over 4-axial hydroxyl groups in α-D- (8) and β-D-galactopyranosides (9), the present observation provides an example of the opposite selectivity. The methylated disaccharide derivative (**12**) was then prepared in the same way as for the trisaccharide derivative (**8**). Entry was gained to the (1 → 3)-linked disaccharide series by reaction of methyl 6-*O*-benzyl-2-*O*-methyl-α-D-galactopyranoside (7) with trimethyl orthobenzoate followed by acid-catalyzed rearrangement to give the axial 4-benzoate (**13**) (10). Condensation of this compound with 2,3,4-tri-*O*-acetyl-α-D-xylopyranosyl bromide gave methyl 3-*O*-(2,3,4-tri-*O*-acetyl-β-D-xylopyranosyl)-4-*O*-benzoyl-6-*O*-

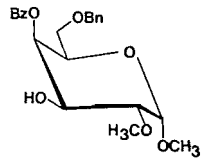

13

Can. J. Chem. Downloaded from www.nrcresearchpress.com by 210.87.254.5 on 09/06/12
For personal use only.

benzyl-2-*O*-methyl-α-D-galactopyranoside (**14**). The linkage position in this disaccharide was confirmed, as for the (1 → 4)-linked disaccharide, by methylation analysis which gave 2,4,6-tri-*O*-methylgalactose from the galactose moiety. The disaccharide benzoate (**14**) was then converted into the methylated derivative (**17**).

Preparation of 6-deoxy-6-iodo oligosaccharides via sulfonate esters and competing 3,6-anhydrogalactopyranoside formation

The 2-linked methylated disaccharide glycoside (**4**) was reacted with sodium hydride and *N,N'*-sulfuryldiimidazole in oxolane, as described by Hanessian and Vatèle (4), and gave the crystalline imidazolylsulfonate (imidazylate) (**18**) which was quite stable provided that care was taken to minimize contact with polar solvents. The imidazylate was converted smoothly into methyl 6-deoxy-6-iodo-3,4-di-*O*-methyl-2-*O*-(2,3,4-tri-*O*-methyl-β-D-xylopyranosyl)-α-D-galactopyranoside (**19**) on heating with tetrabutylammonium iodide in benzene. Alternatively, the iodo disaccharide derivative (**19**) was prepared in comparable yield by reaction of the methylated disaccharide glycoside (**4**) with triflic anhydride in pyridine (3) followed by direct iodide displacement. This procedure was adopted as the method of choice and was used for the conversion of trisaccharide **8** and disaccharides **12** and **17** into the respective 6-deoxy-6-iodo derivatives **20**, **21**, and **22** in good yield.

When an attempt was made to prepare the iododisaccharide (**19**) from the imidazylate (**18**) by activation on nitrogen by reaction with methyl iodide in *N,N'*-dimethylformamide (4), a second product was formed in almost equal amount. The formation of this compound, methyl 3,6-anhydro-4-*O*-methyl-2-*O*-(2,3,4-tri-*O*-methyl-β-D-xylopyranosyl)-α-D-galactopyranoside (**23**), was difficult to suppress entirely in any reaction

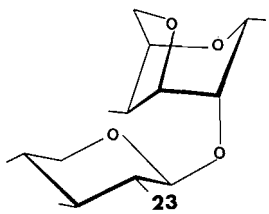

23

involving formation or further reaction of either reactive sulfonate ester unless extreme precautions were taken to exclude moisture and avoid contact with polar solvents. The compound (**23**) was isolated as the major product when the imidazylate (**18**) was allowed to solvolyze in DMF at room temperature. Fragment ions observed in the mass spectrum and ^{1}Hmr data showed loss of sulfonate ester and of a methoxyl group consistent with anhydride formation. The Cmr data showed a downfield shift for C-6 (δ_C 69.69) indicative of etherification, and the alteration in the signal for the anomeric carbon (δ_C 97.52, $J_{^{13}C_1\text{-}^1H_1}$ = 161.6 Hz) was consistent with change from the $^4C_1$ to a $_4C^1$ conformation for the α-D-galactopyranoside residue. In support of these assignments methyl 3,6-anhydro-2,4-di-*O*-methyl-α-D-galactopyranoside (**24**) showed signals for C-6 at δ_C 69.08 and for C-1 at δ_C 98.63 with $J_{^{13}C_1\text{-}^1H_1}$ = 161.1 Hz. Compound **23** may therefore be assigned the structure, methyl 3,6-anhydro-4-*O*-methyl-2-*O*-(2,3,4-tri-*O*-methyl-β-D-xylopyranosyl)-α-D-galactopyranoside. Supporting chemical evidence for the formation of the 3,6-anhydro derivative was obtained by glc–ms analysis of the products of methanolysis

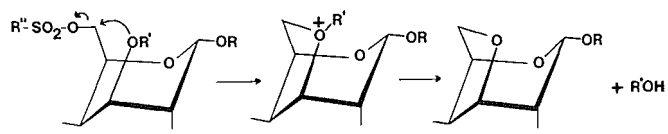

SCHEME 2. Formation of 3,6-anhydro-α-D-galactopyranosides during solvolysis of 6-sulfonates with intramolecular participation and subsequent loss of 3-*O*-methyl or 3-*O*-glycosyl (R') substituent (other substituents are not specified).

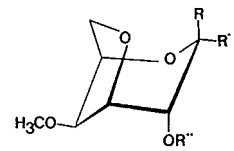

24 R = H, R' = OMe, R'' = Me
25 R = R'' = H, R' = OMe
26 R = H, R' = OMe, R'' = Ac
27 R = OMe, R' = H, R'' = Ac

Unspecified substituents in formulae **23** and **33–36** are OMe

followed by acetylation which showed the formation *inter alia* of the same mixture of anomeric methyl glycoside acetates (**26** and **27**) and acetylated dimethyl acetal (**28**) that was obtained from synthetic methyl 3,6-anhydro-4-*O*-methyl-α-D-galactopyranoside (**25**) (11). The formation of 3,6-anhydro-D-galactopyranose derivatives by intramolecular displacement of 6-sulfonate esters with alkoxyl group participation was first shown by Brimacombe and Ching (12). Volkova *et al.* (13) have previously reported 3,6-anhydride formation during the reaction of benzyl 2,3,4-tri-*O*-benzyl-6-deoxy-6-tosyl-β-D-galactopyranoside with sodium iodide in both acetone and *N,N*-dimethylformamide.

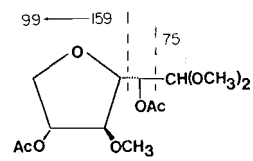

28

Further examination of the solvolysis products from the imidazylate (**18**) showed the formation of a second compound (**29**). Although the anhydride (**23**) was still the major product, the second compound was formed in relatively greater yield when the triflate ester of disaccharide **4** was treated in the same way. Spectroscopic data, including the typical mass spectral fragment ions at *m/z* 293 and 233 for the galactosyl moiety, a characteristic one proton singlet in the ^{1}Hmr spectrum at δ 8.15, and a carbonyl band in the ir spectrum at 1730 cm^{-1}, coupled with characterization of otherwise unaltered sugar constituents on hydrolysis, showed that this second product was the disaccharide 6-formate (**29**). *N,N*-Dimethylformamide used as solvent has been observed to be the source of formylation as a side reaction in other transformations (14, 15).

In order to assess the extent to which variously substituted galactopyranoside 6-sulfonate esters were susceptible to solvolytic side reactions, and in particular to see if 3,6-anhydride formation could occur with participation of a 3-*O*-glycosyl substituent and liberation of that substituent on collapse of an intermediate oxonium ion (Scheme 2), the solvolysis products

Can. J. Chem. Downloaded from www.nrcresearchpress.com by 210.87.254.5 on 09/06/12
For personal use only.

Can. J. Chem. Downloaded from www.nrcresearchpress.com by 210.87.254.5 on 09/06/12
For personal use only.

from the triflate esters of disaccharides **12** and **17** and trisaccharide **8** were examined. In the case of derivatives of disaccharide **12** and the branched trisaccharide **8**, where participation by the 3-*O*-substituents might be expected to lead to the formation of the same 3,6-anhydro derivative, with liberation of 2,3,4-tri-*O*-methylxylose in the latter instance, no evidence was obtained for the formation of such a compound. The major product from the trisaccharide (**8**) was the corresponding 6-formate (**30**). Solvolysis of the triflate ester of disaccharide **17** also led to formation of the disaccharide 6-formate (**31**) as the major product. However, the occurrence of 3-*O*-glycosyl participation in 3,6-anhydride formation was clearly established. Direct examination of the solvolysis products by glc – mass spectrometry showed the formation of methyl 3,6-anhydro-2,4-di-*O*-methyl-D-galactopyranoside (**24**) (in 30% yield based on 1,6-anhydro-2,3,4-tri-*O*-methyl-β-D-galactopyranose as internal standard), together with the disaccharide 6-formate (**31**). When a portion of the solvolysis products was treated with sodium borohydride and then acetylated, glc – mass spectrometry showed the presence of the anhydride (**24**), together with 2,3,4-tri-*O*-methylxylitol diacetate from the liberated glycosyl substituent and a disaccharide derivative now converted into the 6-acetate (**32**).

Cleavage of 6-deoxy-6-iodo-oligosaccharide glycosides with zinc dust and characterization of 5,6-dideoxy-hex-5-enoses

Each of the methylated 6-deoxy-6-iodo oligosaccharides was treated for short periods with freshly prepared activated zinc dust in boiling ethanol or 1-propanol and furnished the corresponding 5,6-dideoxy-hex-5-enose. In the case of the 4-linked 6-deoxy-6-iodo disaccharide glycoside (**21**), extended reaction time or the use of the higher-boiling solvent resulted in the liberation of 2,3,4-tri-*O*-methylxylose to a much greater extent than with the corresponding 2- and 3-linked disaccharide derivatives (**19** and **22**). It is possible that sufficient acidity, not otherwise detected, was generated from the basic zinc iodide formed in the reaction to cause hydrolysis of the resulting 5,6-dideoxy-hex-5-enose, proceeding by a mechanism involving O-allyl rather the normal glycosyl-oxygen cleavage during glycoside hydrolysis. Each 5,6-dideoxy-hex-5-enose-terminated oligosaccharide was conveniently characterized by reduction and acetylation to give the corresponding 1,2-dideoxy-hex-1-enitol acetate (**33**–**36**). These derivatives in the di- and trisaccharide series were amenable to analysis by glc–ms as for the corresponding saturated oligosaccharide alditol derivatives (16). The accompanying structures for these derivatives show the most important fragment ions in the mass spectra, including those which clearly establish the substitution patterns of the methylated 1,2-dideoxy-hex-1-enitol acetate residues. In the case of the trisaccharide derivative (**34**) the V ion at m/z 215 pointed to the presence of vicinal glycosyl substituents (17). Additionally, the ^{1}Hmr spectra of the oligosaccharide derivatives showed characteristic signals for the allyl group of 1,2-dideoxy-hex-1-enitol residues. Furthermore, the oligosaccharide derivatives were hydrolyzed without detectable rearrangement of the 1,2-dideoxy-hex-1-enitol residues so that normal methylated sugar analysis by glc–ms of the partially methylated alditol acetates (18) could be performed. The various partially methylated 1,2-dideoxy-hex-1-enitol acetates gave fragment ions indicative of substitution patterns.

These results clearly show that 5,6-dideoxy-hex-5-enose formation by zinc dust cleavage of 6-deoxy-6-iodo-α-D-galactopyranosides, and presumably of other hexopyranose derivatives, may be used for the selective cleavage of glycosidic linkages. It is necessary that care should be exercised in the introduction of the halo substituent. In the examples studied to date, glycosyl substituents at all positions in the ring are retained in hexenose formation. An application of this non-hydrolytic degradative procedure to a polysaccharide substrate is described in the accompanying paper (6).

Experimental

Evaporations were carried out under diminished pressure at temperatures of 40°C or less. Optical rotations were measured with a Perkin–Elmer model 141 polarimeter at 20 ± 2°C. The ir spectra were measured on a Unicam SP 200 spectrophotometer. The nmr spectra were recorded in deuteriochloroform with tetramethylsilane as internal standard with Varian EM 360 (for ^{1}H), Varian CFT 80A (for ^{13}C), and Bruker WH 400 (for both ^{1}H and ^{13}C) spectrophotometers. Gas–liquid chromatography (glc) was performed on a Perkin–Elmer Sigma 3B chromatograph using (A) a packed column of 3% of silicone gum Silar 10 CP on Chromosorb W-HP (100/200 mesh) or (B) a S.C.O.T. column coated with silicone gum OV-225. For glc – mass spectrometry, capillary columns of (C) silicone gum DB225-15N and (D) DB5-15N (permanently bonded OV-54) were attached by a jet separator to a VG Micromass 16F mass spectrometer operated with an inlet temperature of 250°C, an ionization potential of 70 eV, and an ion-source temperature of ~250°C. Preparative tlc (thin-layer chromatography) was performed on precoated silica gel plates (Baker tlc plate silica gel 60-F (250 μm)). For column chromatography silica gel 60, 0.05–0.2 mm/70–270 mesh ASTM (Macherey Nagel), was used without activation. Zinc dust was activated by the procedure of Frank and Smith (19).

Methyl 6-O-benzyl-2-O-(β-D-xylopyranosyl)-α-D-galactopyranoside (2)

Drierite (pre-dried, 25 g) was added to methyl 6-*O*-benzyl-3,4-*O*-isopropylidene-α-D-galactopyranoside (5) (6.8 g, 20.9 mmol) in dry benzene and nitromethane (500 mL, 1:1) and solvent (200 mL) was removed by distillation with exclusion of moisture. Mercuric cyanide (6 g, 23.7 mmol) was added to the reaction flask at room temperature, followed by 2,3,4-tri-*O*-acetyl-α-D-xylopyranosyl bromide (8 g, 23.5 mmol). The reaction mixture was stirred for 12 h, further quantities of mercuric cyanide (1.5 g, 2.5 mmol) and glycosyl bromide (2.1 g, 2.5 mmol) were added, and the mixture was stirred for another 8 h. The filtrate from the reaction mixture was diluted with dichloromethane, extracted with *M* potassium bromide solution (2 × 50 mL) and water (3 × 50 mL), dried, and concentrated to a syrup (14 g). The syrup was chromatographed on silica gel in chloroform–ether (1:1) to give methyl 2-*O*-(2,3,4-tri-*O*-acetyl-β-D-xylopyranosyl)-6-*O*-benzyl-3,4-*O*-isopropylidene-α-D-galactopyranoside (**1**) (9 g, 77%) as a syrup, R_f 0.51; $[\alpha]_D$ +21.3° (*c*, 1.37 in chloroform); nmr δ: 7.25–7.37 (m, 5H, Ph), 3.39 (s, 3H, CO_2CH_3), 2.07 (s, 3H, OAc), 2.05 (s, 6H, 2 × OAc), 1.33 and 1.50 (2s, 2 × 3H, Me_2C); δ_C: 101.6 ($J_{1',2'}$ 165.4 Hz (C-1')), 99.1 ($J_{1,2}$ 169.5 Hz (C-1)).

This isopropylidene compound **1** (3.1 g) was kept in trifluoroacetic acid (30 mL, 90%) for 1 h, the solution was diluted with water, concentrated, and repeatedly concentrated after further addition of water to ensure removal of trifluoracetic acid. The crude product was treated with 0.1 *M* methanolic sodium methoxide. When deacetylation was complete the solution was treated with Amberlite IR-120 (H) resin to remove sodium ions, and the filtrate was concentrated to a crystalline residue which was recrystallized from ethanol and then chloroform–methanol (10:1) to give the disaccharide glycoside **2** (1.8 g, 80%), mp 180–182°C; $[\alpha]_D$ +53° (*c*, 4.3 in methanol). *Anal.* calcd. for $C_{19}H_{28}O_{10}$: C 54.80, H 6.73; found: C 54.60, H 6.55.

Methyl 3,4-di-O-methyl-2-O-(2,3,4-tri-O-methyl-β-D-xylopyranosyl)-α-D-galactopyranoside (4)

Sodium hydride (0.93 g, 38.7 mmol) was added to disaccharide

Can. J. Chem. Downloaded from www.nrcresearchpress.com by 210.87.254.5 on 09/06/12
For personal use only.

glycoside **2** (1.2 g, 2.9 mmol) in dry oxolane (50 mL), the mixture was stirred for 4 h at room temperature, cooled to 0°C, methyl iodide (4 mL) was added, and the mixture was stirred overnight. Excess of sodium hydride was destroyed by the addition of methanol (0.3 mL), solvent was removed, and the residue was partitioned between water and chloroform. The dried organic layer was concentrated to a syrup which was chromatographed on silica gel in chloroform–ether (1:1) to give methyl 6-*O*-benzyl-3,4-di-*O*-methyl-2-*O*-(2,3,4-tri-*O*-methyl-β-D-xylopyranosyl)-α-D-galactopyranoside (**3**) (0.9 g, 65%), mp 68–71°C; nmr δ: 4.85 (d, 1H, $J_{1,2}$ 3.7 Hz, H-1), 4.41 (d, 1H, $J_{1',2'}$ 6.9 Hz, H-1′); δ_C: 105.92 (C-1′), 100.08 (C-1). *Anal.* calcd. for $C_{24}H_{38}O_{10}$: C 59.24, H 7.87; found: C 58.74, H 8.00. The fully etherified disaccharide glycoside **3** (0.587 g) in ethanol (50 mL) was hydrogenolyzed over 10% palladium-on-charcoal (0.17 g) for 16 h, the solution was filtered, and the filtrate was concentrated to a residue which was crystallized from ether–hexane to give the disaccharide glycoside **4** (0.458 g, 96%), mp 125–126°C. *Anal.* calcd. for $C_{17}H_{32}O_{10}$: C 51.51, H 8.14; found: C 51.41, H 8.21.

*Methyl 3,4-di-*O*-(2,3,4-tri-*O*-acetyl-β-D-xylopyranosyl)-6-*O*-benzyl-2-*O*-methyl-α-D-galactopyranoside (**5**) and methyl 4-*O*-(2,3,4-tri-*O*-acetyl-β-D-xylopyranosyl-6-*O*-benzyl-2-*O*-methyl-α-D-galactopyranoside (**9**)*

Powdered Drierite (15 g) and mercuric cyanide (4.72 g, 18.7 mmol) were added to methyl 6-*O*-benzyl-2-*O*-methyl-α-D-galactopyranoside (7) (4.3 g, 14.4 mmol) in benzene–nitromethane (350 mL, 1:1) and solvent (100 mL) was removed by distillation at atmospheric pressure to remove moisture. 2,3,4-Tri-*O*-acetyl-α-D-xylopyranosyl bromide (5.58 g, 18.7 mmol) was added and the mixture was stirred at room temperature for 3 h; tlc (chloroform–acetone, 5:1) showed the formation of two products, R_f 0.75 and 0.48, together with some starting material, R_f 0.25. Further portions of acetobromoxylose (3.0 g, 10.1 mmol) and mercuric cyanide (2.55 g, 10.1 mmol) were added, and the mixture was stirred for 2 h, at which time tlc showed complete disappearance of starting material. The reaction mixture was filtered through Celite and the filtrate was concentrated to a residue which was extracted with chloroform. The extract was washed with *M* potassium bromide solution and water alone, dried, and concentrated to a syrup which was chromatographed on silica gel in benzene – ethyl acetate (2:1) to give (*i*) trisaccharide glycoside **5** (5.3 g, 45%) as a syrup, R_f 0.75, $[\alpha]_D$ −0.3° (*c*, 1.0 in chloroform); nmr δ: 7.34 (s, 5H, Ph), 4.85 (d, 1H, $J_{1,2}$ 3.57 Hz, H-1), 4.70 (d, 1H, $J_{1',2'}$ 7.62 Hz, H-1′ or H-1″), 4.55, 4.51 (ABq, 2H, J_{AB} 11.7 Hz, CH_2-Ph), 3.41, 3.40 (s, each 3H, 2 × OMe), 2.07, 2.05, 2.02 (s, each 3H, 3 × OAc); δ_C: 102.4 (C-1″, 4-linked), 100.0 (C-1′, 3-linked), 97.4 (C-1); and (*ii*) disaccharide glycoside **9** (2.65 g, 33%), mp 128–129°C (from ether), R_f 0.48; $[\alpha]_D$ +9.1° (*c*, 1.0 in chloroform); nmr δ: 7.38 (s, 5H, Ph), 4.60 (s, 2H, CH_2-Ph), 3.53, 3.45 (s, each 3H, 2 × OMe), 2.10 (m, 9H, 3 × OAc); δ_C: 103.2 (C-1′), 98.2 (C-1). *Anal.* calcd. for $C_{26}H_{36}O_{13}$: C 56.11, H 6.52; found: C 55.84, H 6.07. A sample of the disaccharide glycoside **9** was subjected to the following series of reactions: debenzylation, deacetylation, methylation, hydrolysis, reduction ($NaBD_4$), and acetylation. The derived partially methylated alditol acetates were characterized by glc–ms on column C (180°C) as formed from 2,3,4-tri-*O*-methylxylitol and 2,3,6-tri-*O*-methylgalactitol (fragment ions at *m/z* 233, 173, 162, 131, 118, and 102).

*Methyl 2-*O*-methyl-3,4-di-(2,3,4-tri-*O*-methyl-β-D-xylopyranosyl)-α-D-galactopyranoside (**8**)*

Acetylated trisaccharide glycoside **5** (4.9 g, 6.0 mmol) in methanol (50 mL) was treated with a catalytic quantity of sodium methoxide for 1 h. Sodium ions were removed by treatment with Dowex 50W-X8 (H^+) resin and the filtrate was concentrated to syrupy methyl 6-*O*-benzyl-2-*O*-methyl-3,4-di-*O*-β-D-xylopyranosyl-α-D-galactopyranoside (**6**) (2.91 g, 86%), $[\alpha]_D$ +44.5° (*c*, 1.0 in methanol). Sodium hydride (0.51 g, 21 mmol) was added to the trisaccharide glycoside **6** (1.97 g, 3.5 mmol) in oxolane (60 mL). The mixture was stirred at room temperature for 2 h, cooled to 0°C, and, after addition of methyl iodide, stirred at room temperature overnight. Excess sodium hydride was destroyed by careful addition of methanol to a stirred pre-cooled solution, the solution was concentrated, and the residue was extracted with chloroform. The extract was washed with water, dried, and concentrated to a syrup which was chromatographed on silica gel in chloroform–ether (3:1) to give methyl 6-*O*-benzyl-2-*O*-methyl-3,4-di-*O*-(2,3,4-tri-*O*-methyl-β-D-xylopyranosyl)-α-D-galactopyranoside (**7**) as a syrup (1.67 g, 74%), $[\alpha]_D$ +10.6° (*c*, 1.6 in chloroform); nmr δ: 7.33 (s, 5H, Ph), 4.91 (d, 1H, $J_{1,2}$ 3.61 Hz, H-1), 4.71 (d, 1H, $J_{1',2'}$ 7.36 Hz, H-1′), 4.59, 4.52 (ABq, 2H, J_{AB} 11.8 Hz), 4.52 (d, 1H, $J_{1'',2''}$ 7.52 Hz, H-1″), 3.44–3.62 (8s, each 3H, 8 × OMe); δ_C: 104.4 (C-1′, 3-linked), 103.4 (C-1″, 4-linked), 97.9 (C-1). Trisaccharide glycoside **7** (1.62 g, 2.5 mmol) in ethanol (25 mL) was hydrogenolyzed over 10% palladium-on-charcoal (1.1 g) for 2 h at 505 kPa. The filtered solution was concentrated to a syrup which was crystallized from isopropyl ether to give trisaccharide glycoside **8** (1.15, 83%), mp 129–130°C, $[\alpha]_D$ +20.5° (*c*, 1.0 in chloroform); nmr δ: 4.86 (d, 1H, $J_{1,2}$ 3.10 Hz, H-1), 4.67 (d, 1H, $J_{1',2'}$ 7.53 Hz, H-1′), 4.51 (d, 1H, $J_{1'',2''}$ 7.51 Hz, H-1″), 3.42–3.62 (8s, each 3H, 8 × OMe); δ_C: 104.7 (C-1′, 3-linked), 104.4 (C-1″, 4-linked), 98.1 (C-1). *Anal.* calcd. for $C_{24}H_{44}O_{14}$: C 51.79, H 7.97; found: C 52.01, H 8.14.

*Methyl 2,3-di-*O*-methyl-4-*O*-(2,3,4-tri-*O*-methyl-β-D-xylopyranosyl)-α-D-galactopyranoside (**12**)*

Acetylated disaccharide glycoside **9** (2.5 g, 4.5 mmol) was de-*O*-acetylated as described for compound **5** and crystallization of the product from chloroform–methanol gave methyl 6-*O*-benzyl-2-*O*-methyl-4-*O*-β-D-xylopyranosyl-α-D-galactopyranoside (**10**) (1.76 g, 91%), mp 172–173°; $[\alpha]_D$ +75.5° (*c*, 0.6 in methanol). *Anal.* calcd. for $C_{20}H_{30}O_{10}$: C 55.80, H 7.03; found: C 55.84, H 7.05. Compound **10** was methylated as described for compound **6** and column chromatography afforded methyl 6-*O*-benzyl-2,3-di-*O*-methyl-4-*O*-(2,3,4-tri-*O*-methyl-β-D-xylopyranosyl)-α-D-galactopyranoside (**11**) (1.53 g, 90%) as a syrup, $[\alpha]_D$ +29.0° (*c*, 1.1 in chloroform); nmr δ: 7.34 (s, 5H, Ph), 4.89 (d, 1H, $J_{1,2}$ 3.62 Hz, H-1), 4.65 (d, 1H, $J_{1',2'}$ 7.23 Hz, H-1′), 4.59, 4.53 (ABq, 2H, J_{AB} 11.7 Hz, CH_2Ph), 3.62–3.46 (6s, each 3H, 6 × OMe); δ_C: 103.2 (C-1′), 98.1 (C-1). The foregoing disaccharide glycoside **11** (1.46 g, 3 mmol) was hydrogenolyzed as described for compound **7** and recrystallization of the solid product from isopropyl ether furnished disaccharide glycoside **12** (1.07 g, 90%), mp 69–70°C; $[\alpha]_D$ +47.5° (*c*, 1.0 in chloroform); nmr δ: 4.83 (d, 1H, $J_{1,2}$ 2.81 Hz, H-1), 4.55 (d, 1H, $J_{1',2'}$ 7.41 Hz, H-1′), 3.63–3.39 (6s, each 3H, 6 × OMe); δ_C: 104.2 (C-1′), 98.3 (C-1). *Anal.* calcd. for $C_{17}H_{32}O_{10}$: C 51.51, H 8.14; found: C 51.30, H 7.95.

*Methyl 4-*O*-benzoyl-6-*O*-benzyl-2-*O*-methyl-α-D-galactopyranoside (**13**)*

Methyl 6-*O*-benzyl-2-*O*-methyl-α-D-galactopyranoside (2.0 g, 6.7 mmol), trimethyl orthobenzoate (2.3 mL, 13.4 mmol) and toluene-*p*-sulfonic acid (15 mg) were dissolved in dry benzene and solvent was removed under diminished pressure. Thin-layer chromatography (chloroform–ether, 1:1) showed disappearance of starting material and formation of a new compound of R_f 0.72. The residue was kept in 80% acetic acid (10 mL) for 0.5 h at room teperature and tlc showed disappearence of the compound of R_f 0.72 and formation of a new compound, R_f 0.50. The solution was concentrated several times with toluene to a residue which was chromatographed on silica gel in hexane – ethyl acetate (1:1) and recrystallized from isopropyl ether to give the *O*-benzoyl glycoside **13** (1.99 g, 74%), mp 75°; $[\alpha]_D$ +66.3° (*c*, 1.0 in chloroform); nmr δ: 8.08–7.25 (m, 10H, 2 × Ph), 5.68 (m, 1H, H-4), 5.05 (d, 1H, $J_{1,2}$ 3.52 Hz, H-1), 4.52, 4.42 (ABq, 2H, J_{AB} 11.8 Hz, CH_2Ph), 3.52, 3.48 (s, 3H each, 2 × OMe); δ_C: 97.4 (C-1). *Anal.* calcd. for $C_{22}H_{26}O_7$: C 65.66, H 6.51; found: C 65.45, H 6.59.

*Methyl 2,4-di-*O*-methyl-3-*O*-(2,3,4-tri-*O*-methyl-β-D-xylopyranosyl)-α-D-galactopyranoside (**17**)*

Powdered Drierite (5 g) and mercuric cyanide (1.35 g, 5.3 mmol) were added to the foregoing galactoside **13** (1.65 g, 4.1 mmol) in benzene–nitromethane (150 mL, 1:1) and solvent (50 mL) was removed by distillation. 2,3,4-Tri-*O*-acetyl-α-D-xylopyranosyl bromide (1.81 g, 5.3 mmol) was added and the mixture was stirred at room temperature for 4 h. The filtrate from the reaction mixture was concen-

Can. J. Chem. Downloaded from www.nrcresearchpress.com by 210.87.254.5 on 09/06/12
For personal use only.

trated to a residue which was dissolved in chloroform, and the extract was washed with *M* potassium bromide solution and water alone, dried, and concentrated to a syrup. The syrup was chromatographed on silica gel in chloroform–ether (3:1) to give syrupy methyl 3-*O*-(2,3,4-tri-*O*-acetyl-β-D-xylopyranosyl)-4-*O*-benzoyl-6-*O*-benzyl-2-*O*-methyl-α-D-galactopyranoside (**14**) (1.97 g, 73%); $[\alpha]_D$ +35.8° (*c*, 1.0 in chloroform); nmr δ: 8.08–7.29 (m, 10H, 2 × Ph), 5.72 (m, 1H, H-4), 4.53, 4.48 (ABq, 2H, J_{AB} 11.8 Hz, CH_2Ph), 3.53, 3.50 (s, each 3H, 2 × OMe), 2.07, 1.97, 1.77 (s, each 3H, 3 × OAc); δ_C: 100.9 (C-1′), 97.7 (C-1). The linkage type in compound **14** was confirmed as described for disaccharide glycoside **9**, by methylation analysis which furnished *inter alia* 2,4,6-tri-*O*-methylgalactitol triacetate which was characterized by glc–ms on column C (180°C) with fragment ions at *m/z* 277, 245, 234, 203, 202, 174, 161, 129, 118, and 101. Acetylated disaccharide glycoside **14** (1.92 g, 2.9 mmol) was de-*O*-acylated with sodium methoxide for 48 h and chromatography on silica gel by elution with a chloroform–methanol gradient afforded syrupy methyl 6-*O*-benzyl-2-*O*-methyl-3-*O*-β-D-xylopyranosyl-α-D-galactopyranoside (**15**) (1.15 g, 92%), $[\alpha]_D$ +76° (*c*, 1.4 in methanol). Disaccharide glycoside **15** (1.08 g, 2.5 mmol) was methylated as described for compound **6** and chromatography on silica gel in chloroform–ether (4:1) afforded methyl 6-*O*-benzyl-2,4-di-*O*-methyl-3-*O*-(2,3,4-tri-*O*-methyl-β-D-xylopyranosyl)-α-D-galactopyranoside (**16**) (0.95 g, 78%), $[\alpha]_D$ +34.0° (*c*, 1.0 in chloroform); nmr δ: 7.34 (s, 5H, Ph), 4.88 (d, 1H, $J_{1,2}$ 3.60 Hz, H-1), 4.60, 4.52 (ABq, 2H, J_{AB} 11.8 Hz, CH_2Ph), 4.56 (d, 1H, $J_{1',2'}$ 7.42 Hz, H-1′), 3.61–3.42 (6s, each 3H, 7 × OMe); δ_C: 104.4 (C-1′), 97.8 (C-1). Disaccharide glycoside **16** (0.90 g, 1.85 mmol) in ethanol (15 mL) was hydrogenolyzed as described for compound **7** and recrystallization of the solid product from isopropyl ether furnished disaccharide glycoside **17** (0.58 g, 79%), mp 83–84°C; $[\alpha]_D$ +40.8° (*c*, 0.9 in chloroform); nmr δ: 4.93 (d, 1H, $J_{1,2}$ 3.63 Hz, H-1), 4.54 (d, 1H, $J_{1',2'}$ 7.43 Hz, H-1′), 3.61–3.43 (6s, each 3H, 6 × OMe); δ_C: 104.5 (C-1′), 97.9 (C-1). *Anal.* calcd. for $C_{17}H_{32}O_{10}$: C 51.51, H 8.14; found: C 51.81, H 8.32.

*Methyl 6-deoxy-6-iodo-3,4-di-*O*-methyl-2-*O*-(2,3,4-tri-*O*-methyl-β-D-xylopyranosyl)-α-D-galactopyranoside (**19**)*

A. *Synthesis via imidazolylsulfonate (**18**)*

Sodium hydride (0.048 g, 2 mmol) was added to methylated disaccharide glycoside **4** (0.397 g, 1 mmol) in freshly distilled dry oxolane (10 mL) at 0°C, the suspension was stirred for 2 h, cooled to −40°C, and *N,N′*-sulfuryldiimidazole (0.619 g, 3 mmol) in oxolane (5 mL) was added. The reaction mixture was kept at −40°C for 20 min and then stirred at room temperature for 2 h. Thin-layer chromatography showed complete disappearance of starting material and formation of a single product, and excess of sodium hydride was destroyed by the addition of dry methanol (0.2 mL) to the reaction mixture at 0°C. The reaction mixture was diluted with dichloromethane (15 mL), and the solution was extracted with water until the aqueous extracts were neutral (pH 6.5). The dried organic extract was concentrated to a syrup which crystallized on storage at 0°C and was recrystallized from ether to give methyl 6-*O*-imidazolysulfonyl-3,4-di-*O*-methyl-2-*O*-(2,3,4-tri-*O*-methyl-β-D-xylopyranosyl)-α-D-galactopyranoside (**18**) (0.500 g, 95%), mp 95–99°C. *Anal.* calcd. for $C_{20}H_{34}N_2O_{12}S$: C 45.60, H 6.46, N 5.32, S 6.08; found: C 45.63, H 6.43, N 5.18, S 6.16.

The imidazylate **18** (0.229 g, 0.435 mmol) was heated in boiling benzene (10 mL) with tetrabutylammonium iodide (0.5 g, 1.35 mmol) for 25 min. Solvent was removed, the residue was diluted with dichloromethane, and the organic solution was extracted with aqueous sodium thiosulfate, washed with water, dried, and concentrated to a crystalline residue. Purification by chromatography on silica gel in chloroform–ether (1:1) afforded the iododisaccharide **19** (0.179 g, 81%), mp 120–121°C. The mass spectrum showed prominent fragment ions at *m/z* 415, 375, 315, 175, and 143. *Anal.* calcd. for $C_{17}H_{31}O_9I$: C 40.31, H 6.12, I 25.0; found: C 40.26, H 6.39, I 25.0.

B. *Synthesis via trifluoromethanesulfonate*
(with V. Puvanesarajah)

Trifluoromethanesulfonic anhydride (50 μL) in dichloromethane (0.5 mL) was added dropwise with stirring to dry pyridine (25 μL) in dichloromethane (0.5 mL) at −10°C. Methylated disaccharide glycoside **4** (50 mg) in dichloromethane (1 mL) was added dropwise and the mixture was stirred at −10°C for 2 h. Thin-layer chromatography (dichloromethane–acetone, 10:1) showed complete disappearance of starting material. The reaction mixture was poured into ice-water, and the combined separated organic layer and dichloromethane extracts were washed with aqueous sodium hydrogen carbonate and then with water until free from pyridine, dried, and concentrated to a syrup which showed strong absorption at 1420 cm^{-1} (sulfonate) but none at 3400 cm^{-1} (OH). The triflate ester was heated in boiling benzene (4 mL) with tetrabutylammonium iodide (100 mg) for 2 h. After removal of solvent the residue was chromatographed on silica gel in dichloromethane–acetone (10:1) to yield iododisaccharide **19** (45 mg, 70%) which was identical (mp and glc – mass spectrometry) to the previous sample. A polar component (~2 mg) was also isolated from the column and shown to be indistinguishable (glc – mass spectrometry) from the anhydro disaccharide **23**.

C. *Synthesis from imidazolylsulfonate (**18**) in* N,N-*dimethylformamide*

Imidazylate **18** in *N,N*-dimethylformamide containing imidazole (0.5 equiv.) was treated with methyl iodide and kept for 24 h at room temperature. Thin-layer chromatography showed complete disappearance of starting material with formation of iododisaccharide **19** as the major product with a second component, later identified as the anhydrodisaccharide **23**. The mixture was chromatographed on silica gel in chloroform–acetone (4:1) to give crystalline iododisaccharide **19** (65%), which was identical to the previously isolated sample, and syrupy anhydrodisaccharide **23** (20%). The latter compound gave a single peak on glc on column B (210°C) and the mass spectrum showed fragment ions at *m/z* 233, 175, 173, and 143.

*Solvolysis of imidazolylsulfonate (**18**) in* N,N-*dimethylformamide*

Imidazylate **18** (36 mg) was kept in dry *N,N*-dimethylformamide (2 mL) for 36 h. The acidic solution was neutralized with sodium hydrogen carbonate, diluted with water, and extracted with chloroform. Examination of the chloroform extract by glc – mass spectrometry (column C, 170°C, 1 min, 170 → 200°C, 6°/min) showed anhydrodisaccharide **23** as the major component with a second minor component, later identified as methylated disaccharide 6-formate **29**, which showed fragment ions at *m/z* 293, 233, 201, 175, and 143. The extract was chromatographed on silica gel in chloroform–acetone (4:1) to give syrupy methyl 3,6-anhydro-4-*O*-methyl-2-*O*-(2,3,4-tri-*O*-methyl-β-D-xylopyranosyl)-α-D-galactopyranoside (**23**) (16 mg); nmr δ: 4.84 (d, 1H, $J_{1,2}$ 2.85 Hz, H-1), 3.46–3.70 (5s, each 3H, 5 × OMe); δ_C: 102.84 ($J^{13}C_{1'}\text{-}^{1}H_{1'}$ 160.5 Hz, (C-1′)), 97.52 ($J^{13}C_{1}\text{-}^{1}H_{1}$ 161.1 Hz (C-1)), 69.69 (C-6). A sample was boiled under reflux with methanolic 2% hydrogen chloride for 2 h, and the cooled solution was neutralized and concentrated to a syrup which was treated with acetic anhydride in pyridine. Examination of the products by glc on column B (150 → 180°C, 5°/min, hold) showed the presence of methyl glycosides of 2,3,4-tri-*O*-methylxylose together with three components which were identical (glc – mass spectrometry on column C) to those (**26**–**28**) similarly formed from methyl 3,6-anhydro-4-*O*-methyl-α-D-galactopyranoside (**25**).

*Solvolysis of trifluoromethanesulfonate esters of methylated oligosaccharides (**4**, **8**, and **17**) in* N,N-*dimethylformamide*

Samples (~20 mg) of methylated oligosaccharides were converted into triflate esters using procedure B, and the esters were kept in dry *N,N*-dimethylformamide (1 mL) for 1 h at which time tlc (benzene–methanol, 5:1) showed complete disappearance of starting material. Solutions were diluted with dichloromethane (10 mL), washed several times with water, dried, and concentrated.

Examination of the solvolysis products from the triflate ester of methylated disaccharide **4** by glc – mass spectrometry (as above) showed the formation of anhydro disaccharide **23** and methylated disaccharide 6-formate (**29**) in the molar ratio of 1.3:1. A sample of compound **29** was isolated by preparative tlc; ν_{max} 1730 cm^{-1}; nmr δ: 8.15 (s, 1H, —O—CHO). Hydrolysis of the disaccharide derivative,

Can. J. Chem. Downloaded from www.nrcresearchpress.com by 210.87.254.5 on 09/06/12
For personal use only.

followed by reduction and acetylation, afforded acetates of 2,3,4-tri-*O*-methylxylitol and 3,4-di-*O*-methylgalactitol which were characterized by glc–ms on column C and shown to be identical to derivatives formed similarly from methylated disaccharide **4**.

The solvolysis products from the triflate ester of methylated disaccharide **17** were formed in the presence of 1,6-anhydro-2,3,4-tri-*O*-methyl-β-D-galactopyranose as an internal standard. The glc analysis of the products on column B (130 → 180°C, 4°/min, hold) showed the formation of methyl 3,6-anhydro-2,4-di-*O*-methyl-α-D-galactopyranoside (**24**) in 30% yield. The identity of the latter compound was confirmed by glc – mass spectrometry on column C (180 → 200°C, 6°/min, hold) with fragment ions at *m/z* 173, 113, 101, 71 as for a synthetic sample. The major reaction product had a high retention time and fragment ions at *m/z* 293, 175, 143, 101, and 88 were consistent with those of the 6-formate (**31**) of the methylated disaccharide **17**. A sample of the 6-formate **31** was isolated by preparative tlc and methylated sugar analysis gave the same products as from the parent disaccharide **17**. A sample of the solvolysis mixture was treated with sodium borohydride and then with acetic anhydride in pyridine. Analysis of the products by glc – mass spectrometry as for the solvolysis mixture showed the presence of 2,3,4-tri-*O*-methylxylitol diacetate, anhydro derivative **24**, and a disaccharide derivative identical to a synthetic sample of the 6-acetate of methylated disaccharide **17** (fragment ions at *m/z* 307, 187, 175, 143, 127).

The reaction mixture from solvolysis of the triflate ester of methylated trisaccharide **8** afforded a single major product, a sample of which was isolated by preparative tlc. The ^{1}Hmr spectrum of this compound (**30**) showed signals at δ 8.08 (s, 1H, —O—CHO), 4.90 (d, 1H, $J_{1,2}$ 3.56 Hz, H-1), 4.65 (d, 1H, $J_{1',2'}$ 7.39 Hz, H-1′), 4.51 (d, 1H, $J_{1'',2''}$ 7.37 Hz, H-1″) and the mass spectrum (direct insertion) showed fragment ions at *m/z* 453, 393, 247, 175, 143 which were consistent with its formulation as the 6-formate of methylated trisaccharide (**12**).

*Methyl 6-deoxy-6-iodo-2-*O*-methyl-3,4-di-*O*-(2,3,4-tri-*O*-methyl-β-D-xylopyranosyl)-α-D-galactopyranoside (20)*

The iodo trisaccharide (**20**) was synthesized in 73% yield from methylated trisaccharide glycoside **8** by method B as described for compound **19**, and had $[\alpha]_D$ +19.6° (*c*, 0.7 in chloroform); nmr δ_C: 104.6 (C-1′, 3-linked), 103.6 (C-1″, 4-linked), 98.0 (C-1), 4.8 (C-6); *m/z*: 535, 475, 329, 269, 253, 175, 143.

*Methyl 6-deoxy-6-iodo-2,3-di-*O*-methyl-4-*O*-(2,3,4-tri-*O*-methyl-β-D-xylopyranosyl)-α-D-galactopyranoside (21)*

The iodo disaccharide (**21**) was synthesized in 74% yield from methylated disaccharide glycoside **12** by method B as described for compound **19**, and after recrystallization from hexane had mp 115–116°C; $[\alpha]_D$ +55.3° (*c*, 0.8 in chloroform); nmr δ_C: 103.4 (C-1′), 98.2 (C-1), 4.6 (C-6). *Anal.* calcd. for $C_{17}H_{31}O_9I$: C 40.32, H 6.17, I 25.06; found: C 40.33, H 6.37, I 24.91.

*Methyl 6-deoxy-6-iodo-2,4-di-*O*-methyl-3-*O*-(2,3,4-tri-*O*-methyl-β-D-xylopyranosyl)-α-D-galactopyranoside (22)*

The iododisaccharide (**22**) was synthesized in 75% yield from methylated disaccharide glycoside **17** by method B as described for compound **19**, and after recrystallization from hexane had mp 111–112°C; $[\alpha]_D$ +41.1° (*c*, 1.6 in chloroform); nmr δ: 4.86 (d, 1H, $J_{1,2}$ 3.65 Hz, H-1), 4.56 (d, 1H, $J_{1',2'}$ 7.54 Hz, H-1′), 3.47–3.65 (6s, each 3H, 6 × OMe); δ_C: 104.4 (C-1′), 97.9 (C-1), 2.6 (C-6); *m/z*: 375, 315, 255, 223, 195, 175, 143. *Anal.* calcd. for $C_{17}H_{31}O_9I$: C 40.32, H 6.17, I 25.06; found: C 40.15, H 6.05, I 24.51.

*1,2-Dideoxy-3,4-di-*O*-methyl-5-*O*-(2,3,4-tri-*O*-methyl-β-D-xylopyranosyl)-L-*lyxo*-hex-1-enitol acetate (33)*

Methylated iododisaccharide **19** (169 mg, 0.33 mmol) in 1-propanol – water (5 mL, 14:1) was boiled under reflux with freshly activated zinc dust (0.4 g, 6.1 mmol). After 1 h tlc showed formation of a single product and complete disappearance of starting material. The cooled mixture was filtered through Celite, the filtrate was concentrated, and the residue in oxolane–water (2:1) was treated with sodium borohydride for 4 h at room temperature. The reaction mixture was worked up in the usual way, and the product was acetylated with

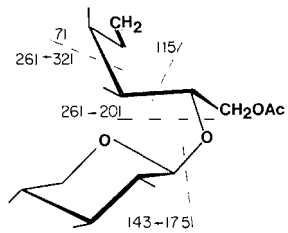

33

acetic anhydride in pyridine. The resulting acetylated derivative (**33**) was chromatographed on silica gel in chloroform–ether (1:1) to give the title compound as a syrup (90 mg, 69%); nmr δ: 5.85 (ddd, 1H, $J_{5,6(trans)}$ 17 Hz, $J_{5,6(cis)}$ 10.3, $J_{4,5}$ 7.9 Hz, —C*H*=CH$_2$), 5.50 (m, 2H, —CH=C*H*$_2$), 4.28 (d, 1H, $J_{1',2'}$ 7.3 Hz, H-1′), 3.60–3.20 (5s, each 3H, 5 × OMe), 2.10 (s, 3H, OAc). Examination by glc–ms on column D (140°C, 1 min, 140 → 200°C, 8°/min, hold) showed a single peak with fragment ions at the *m/z* values shown in structure **33**. *Anal.* calcd. for $C_{18}H_{32}O_9$: C 55.10, H 8.16; found: C 55.24, H 8.15. A portion of the unsaturated disaccharide alditol was hydrolyzed as in methylation analysis, reduced, and acetylated to give two compounds which were characterized by glc–ms on column C as 2,3,4-tri-*O*-methylxylitol diacetate and 1,2-dideoxy-3,4-di-*O*-di-*O*-methyl-L-*lyxo*-hex-1-enitol diacetate (fragment ions at *m/z* 189, 129, 115, 87, and 71).

*1,2-Dideoxy-5-*O*-methyl-3,4-di-*O*-(2,3,4-tri-*O*-methyl-β-D-xylopyranosyl)-L-*lyxo*-hex-1-enitol acetate (34)*

Methylated iodotrisaccharide **20** (67 mg, 0.1 mmol) was reacted with zinc dust in 1-propanol – water as above for 30 min. Thin-layer chromatography indicated a single product which was reduced with sodium borohydride and then acetylated to give the trisaccharide hex-1-enitol acetate **34**; nmr δ: 5.98 (ddd, 1H, $J_{5,6(trans)}$ 17.3 Hz, $J_{5,6'(cis)}$ 10.7 Hz, $J_{4,5}$ 6.1 Hz, H-5), 5.32 (d, 1H, $J_{5,6(trans)}$ 17.26 Hz, H-6), 5.17 (d, 1H, $J_{5,6'(cis)}$ 10.66 Hz, H-6′), 3.60 (s, 6H, 2 × OMe), 3.58–3.45 (5s, each 3H, 5 × OMe), 2.07 (s, 3H, OAc). Analysis by glc–ms on column D (180°C, 2 min, 180 → 230°C, 4°/min, hold) showed a single peak with fragment ions at the *m/z* values shown with structure

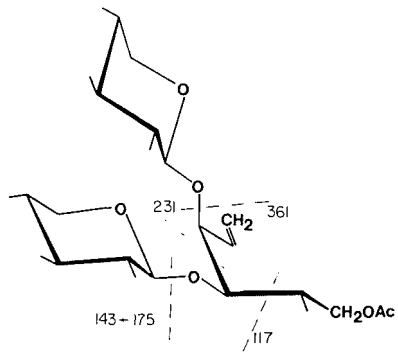

34

34. Hydrolysis etc. as described for compound **33** gave 2,3,4-tri-*O*-methylxylitol diacetate and 1,2-dideoxy-5-*O*-methyl-L-*lyxo*-hex-1-enitol 3,4,6-triacetate (fragment ions at *m/z* 215, 189, 155, 129, and 99).

*1,2-Dideoxy-4,5-di-*O*-methyl-3-*O*-(2,3,4-tri-*O*-methyl-β-D-xylopyranoxyl)-L-*lyxo*-hex-1-enitol acetate (35)*

Methylated iododisaccharide **21** was treated with zinc dust in ethanol–water (14:1) at a bath temperature of 85°C for 30 min. Under these conditions essentially a single product was observed and reduction followed by acetylation afforded the disaccharide hex-1-enitol acetate **35** which was analyzed by glc–ms on column C (180°C, 1 min, 180 → 200°C, 4°/min, hold). Hydrolysis etc. as described for compound **33** gave 2,3,4-tri-*O*-methylxylitol diacetate and 1,2-

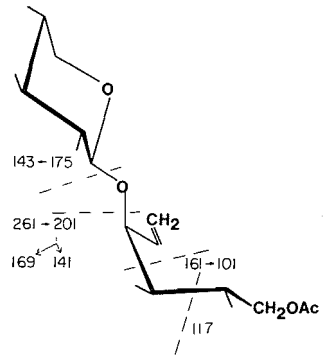

35

dideoxy-4,5-di-*O*-methyl-L-*lyxo*-hex-1-enitol diacetate (fragment ions at *m/z* 161, 143, 127, 117, 101, and 99). When the zinc dust treatment was performed in 1-propanol for longer periods a second product was detected by tlc and was shown to be 2,3,4-tri-*O*-methylxylose by conversion into the corresponding partially methylated alditol acetate.

*1,2-Dideoxy-3,5-di-*O*-methyl-4-*O*-(2,3,4-tri-*O*-methyl-β-D-xylopyranosyl)-L-*lyxo*-hex-1-enitol acetate (36)*

Methylated iododisaccharide **22** was treated with zinc dust in 1-propanol – water as described for compound **19** to give a single product which was reduced and acetylated to furnish the disaccharide 1,2-dideoxy-hex-1-enitol acetate **36** whose structure was confirmed by glc–ms on column C (100°C, 2 min, 100 → 200°C, 8°/min, hold). Hydrolysis etc. for compositional analysis afforded 2,3,4-tri-*O*-methylxylitol diacetate and 1,2-dideoxy-3,5-di-*O*-methyl-L-*lyxo*-hex-1-enitol diacetate (fragment ions at *m/z* 189, 187, 129, 127, 117, and 71.

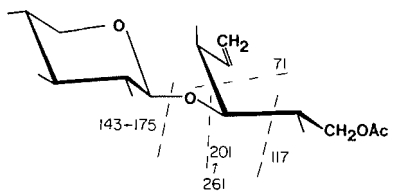

36

Derivatives of methyl 3,6-anhydro-α-D-galactopyranoside

Samples of the 2,4-di-*O*-methyl (**24**) and 4-*O*-methyl (**25**) derivatives of methyl 3,6-anhydro-α-D-galactopyranoside were prepared by incomplete methylation as described by Anderson *et al.* (11). The ^{13}C nmr spectrum of **24** included signals at δ_C 98.63 ($J_{^{13}C_1\text{-}^1H_1}$ 161 Hz) and 69.08 (C-6). The acetylated derivative (**26**) of compound **25** when examined by glc – mass spectrometry on column C showed fragment ions at *m/z* 201 (M − OCH_3), 129, 116, 103, and 71. A sample of glycoside **25** was treated with boiling methanolic 2% hydrogen chloride for 2 h and the products were acetylated; glc – mass spectrometry showed the presence of 3 components, the first indistinguishable from **26**, the second well separated but giving a similar mass spectrum (presumably the β-D-glycoside **27**), and a third and major component for which the acetylated dimethylacetal structure (**28**) may be proposed in the light of prominent fragment ions at *m/z* values shown (compare Chizhov *et al.* (20)).

Acknowledgements

The authors are grateful to the Natural Sciences and Engineering Research Council of Canada for financial support. They also thank Dr. V. Puvanesarajah for performing the experiment cited, Drs. B. H. Khouw and K. R. Sharma for recording the mass spectra and some of the ^{13}C nmr spectra, and the Southwestern Ontario NMR Centre at the University of Guelph for recording high field ^{13}C and ^1H nmr spectra.

1. B. BERNET and A. VASELLA. Helv. Chim. Acta, **62**, 1990 (1979); **62**, 2400 (1979); **62**, 2411 (1979).
2. A. C. RICHARDSON. Carbohydr. Res. **10**, 395 (1969).
3. R. W. BINKLEY, M. G. AMBROSE, and D. G. HEHEMANN. J. Org. Chem. **45**, 4387 (1980).
4. S. HANESSIAN and J.-M. VATÈLE. Tetrahedron Lett. **22**, 3679 (1981).
5. C. E. BALLOU and H. O. L. FISCHER. J. Am. Chem. Soc. **76**, 3188 (1954).
6. G. O. ASPINALL and V. PUVANESARAJAH. Can. J. Chem. **62**, 2736 (1984).
7. P. P. SINGH and G. A. ADAMS. Carbohydr. Res. **13**, 229 (1970).
8. H. M. FLOWERS. Carbohydr. Res. **4**, 312 (1967).
9. C. AUGÉ and A. VEYRIÈRES. Carbohydr. Res. **54**, 45 (1977).
10. P. J. GAREGG and H. HULTBERG. Carbohydr. Res. **72**, 276 (1979); S. JOSEPHSON and D. R. BUNDLE. J. Chem. Soc. Perkin Trans. 1, 297 (1980).
11. N. S. ANDERSON, T. C. S. DOLAN, and D. A. REES. J. Chem. Soc. C, 596 (1968).
12. J. S. BRIMACOMBE and O. A. CHING. Carbohydr. Res. **9**, 287 (1969).
13. L. V. VOLKOVA, M. G. LUCHINSKAYA, N. G. MOROZOVA, N. B. ROZANOVA, and R. P. EVSTIGNEEVA. J. Gen. Chem. (U.S.S.R.) **42**, 2101 (1972).
14. V. POZSGAY and P. NÁNÁSI. Carbohydr. Res. **68**, 157 (1979).
15. L. HOUGH and A. W. LEWIS. Carbohydr. Res. **42**, 173 (1975).
16. J. LÖNNGREN and S. SVENSSON. Adv. Carbohydr. Chem. Biochem. **29**, 41 (1973).
17. B. FOURNET, J.-M. DHALLUIN, G. STRECKER, J. MONTREUIL, C. BOSSO, and J. DEFAYE. Anal. Biochem. **108**, 35 (1980).
18. P.-E. JANSSON, L. KENNE, H. LIEDGREN, B. LINDBERG, and J. LÖNNGREN. Chem. Commun. Univ. Stockholm, **8**, 1 (1976).
19. R. L. FRANK and P. V. SMITH. Org. Synth. Coll. Vol. **3**, 410 (1955).
20. O. S. CHIZHOV, B. M. ZOLOTAREV, A. I. USOV, M. A. RECHTER, and N. K. KOCHETKOV. Carbohydr. Res. **16**, 29 (1971).

Can. J. Chem. Downloaded from www.nrcresearchpress.com by 210.87.254.5 on 09/06/12
For personal use only.

The hex-5-enose degradation: cleavage of 6-deoxy-6-iodo-α-D-galactopyranosidic linkages in modified carboxyl-reduced methylated tragacanthic acid[1]

GERALD OLIVER ASPINALL[2] AND VELUPILLAI PUVANESARAJAH

Department of Chemistry, York University, Downsview, Toronto, Ont., Canada M3J 1P3

Received April 23, 1984

GERALD OLIVER ASPINALL and VELUPILLAI PUVANESARAJAH. Can. J. Chem. **62**, 2736 (1984).

Reduction of galacturonic acid residues in permethylated tragacanthic acid, followed by transformation of the resulting galactose residues to those of 6-deoxy-6-iodogalactose, affords a modified polysaccharide which undergoes depolymerization by the Bernet–Vasella reaction on treatment with zinc dust. The two main products of depolymerization have been characterized, after reduction and acetylation, as 3,6-di-*O*-acetyl-1,2-dideoxy-5-*O*-methyl-4-*O*-(2,3,4-tri-*O*-methyl-β-D-xylopyranosyl)-L-*lyxo*-hex-1-enitol (**1**) and *O*-(2,3,4-tri-*O*-methyl-α-L-fucopyranosyl)-(1 → 2)-*O*-(3,4-di-*O*-methyl-β-D-xylopyranosyl)-(1 → 4)-3,6-di-*O*-acetyl-1,2-dideoxy-5-*O*-methyl-L-*lyxo*-hex-1-enitol (**2**). The fragmentation provides the first example of a chemical degradation of an α-D-galacturonan to furnish oligosaccharides in which side-chain units remain attached to modified galacturonic acid residues. Under the conditions used for the introduction of iodo substituents no evidence could be obtained for loss of 3-*O*-glycosyl substituents through side reactions involving solvolysis of 6-sulfonates.

GERALD OLIVER ASPINALL et VELUPILLAI PUVANESARAJAH. Can. J. Chem. **62**, 2736 (1984).

La réduction de résidus d'acide galacturonique dans de l'acide tragacanthique, suivie par une transformation des résidus de galactose qui en résultent en désoxy-6 iodo-6 galactose, fournit un polysaccharide modifié qui subit une dépolymérisation, sous l'influence de la poudre de zinc, par une réaction de Bernet–Vasella. Après la réduction et une acétylation, on a caractérisé les deux produits principaux de la réaction de dépolymérisation comme étant le di-*O*-acétyl-3,6 didésoxy-1,2 *O*-méthyl-5 *O*-(tri-*O*-méthyl-2,3,4 β-D-xylopyrannosyl)-4 L-*lyxo*-hexène-1 itol (**1**) et le *O*-(tri-*O*-méthyl-2,3,4 α-L-fucopyrannosyl)-(1 → 2)-*O*-(di-*O*-méthyl-3,4 β-D-xylopyrannosyl)-(1 → 4)-di-*O*-acétyl-3,6 didésoxy-1,2 *O*-méthyl-5 L-*lyxo*-hexène-1 itol (**2**). Cette fragmentation est le premier exemple d'une dégradation chimique d'un α-D-galacturonane qui conduit à des oligosaccharides dans lesquels les unités des chaînes latérales restent attachées à des résidus d'acide galacturonique modifiés. Sous les conditions utilisées pour l'introduction des substituants iodo, on n'a pas pu observer de pertes de substituants *O*-glycosyles-3 provenant de réactions de solvolyses secondaires des sulfonates-6.

[Traduit par le journal]

Methods developed recently for the selective cleavage of non-terminal glycosiduronic acid or glycosiduronamide linkages in permethylated polysacharides have been based on structural modifications to yield altered sugar residues at which controlled depolymerization may be carried out with no detectable hydrolysis of normal glycosidic linkages. Thus treatment of glycosiduronic acids with lead tetraacetate effects decarboxylation–acetoxylation to give 5-acetoxypentopyranosides which may be cleaved reductively with sodium borohydride (1). Alternatively, Curtius rearrangements of glycosiduronamides furnish carbamates, 5-*tert*-butyloxycarbonylamino- or 5-benzyloxycarbonylamino-pentopyranosides, which may be cleaved respectively by mild acid treatment or hydrogenolysis (2). The procedures have been applied successfully to the fragmentation of both exterior (1, 2) and interior (3) chains containing β-D-glucosiduronic acid units with the formation of xylitol-terminated oligosaccharides carrying unaltered neutral sugar residues. In this way it is now possible to obtain information on difficultly accessible or previously inaccessible regions of polysaccharide structure. However, the corresponding reactions involving scission of α-D-galactopyranosiduronic acid linkages proceed with difficulty. Even for mono- (4) and disaccharides (2), extended reaction times are often required and (or) products from competing reactions are detected. To an even greater extent (5, 6), derivatives of α-D-galacturonans either fail to react significantly or give rise to incompletely characterized products other than the desired pentitol-terminated fragments.

Bernet and Vasella (7) showed that the reaction of 6-deoxy-6-halohexopyranosides with zinc dust under mild conditions results in glycoside cleavage with the formation of hex-5-enoses. In the accompanying paper (8) it has been shown that permethylated oligosaccharides containing various *O*-substituted methyl 6-deoxy-6-iodo-α-D-galactopyranosides undergo selective glycoside cleavage on treatment with zinc dust and that the resulting hex-5-enoses are conveniently characterized as the derived hex-1-enitol acetates. In principle, the reaction could be initiated through conversion of primary hydroxyl groups at C-6 of hexopyranose residues, however generated, to 6-deoxy-6-halohexopyranose residues in otherwise protected polysaccharides. We describe here an application of this reaction to the selective fragmentation of a permethylated polysaccharide in which the primary hydroxyl groups are formed from the reduction of hexuronic acid residues in a methylated α-D-galacturonan. Although this use of the hex-5-enose-forming reaction involves an indirect approach to structure determination of glycuronans, the overall sequence achieves an objective not otherwise obtained for α-D-galacturonans by chemical degradation, namely, the formation of modified sugar units originating from hexuronic acid residues with neutral glycosyl substituents still attached.

Tragacanthic acid has one of the more completely established structures amongst pectins and structurally related α-D-galacturonans. The 4-linked main chain, which is interrupted only infrequently by the insertion of 2-linked L-rhamnopyranose residues, carries side chains through O-3 of D-galacturonic acid residues (9, 10). These side chains are of D-xylopyranose residues, some of which are further substituted at O-2 by α-L-fucopyranose or, less frequently, β-D-galactopyranose residues. In an earlier study (9), assignments of anomeric configurations for glycosidic linkages of side-chain units were made for terminal α-L-fucopyranose and β-D-xylo-

[1] Presented in part at the Canadian Institute of Chemistry Conference, Montreal, Quebec, June 3–6, 1984, and at the 12th International Symposium on Carbohydrate Chemistry, Utrecht, The Netherlands, July 2–6, 1984.

[2] Author to whom correspondence should be addressed.

Can. J. Chem. Downloaded from www.nrcresearchpress.com by 210.87.254.6 on 09/06/12
For personal use only.

Can. J. Chem. Downloaded from www.nrcresearchpress.com by 210.87.254.6 on 09/06/12
For personal use only.

pyranose residues on the basis of optical rotations of oligosaccharides formed on partial fragmentation, but no specific information was available in respect of the non-terminal D-xylopyranose units.

Fractional precipitation of the water-soluble portion of gum tragacanth afforded a sample of tragacanthic acid whose sugar composition (galacturonic acid, 50%; xylose, 27%; fucose, 20%; galactose and arabinose, traces) was qualitatively similar to, but differed slightly in the proportions of sugar constituents from, those of a previously studied sample of the polysaccharide (9).

Lithium aluminum hydride treatment of permethylated tragacanthic acid afforded the carboxyl-reduced derivative. A sample of the reduced polysaccharide was further alkylated with trideuteriomethyl iodide, and methylated sugar analysis by glc–ms of the derived partially methylated alditol acetates showed the following relative proportions of the main constituents: 2,3,4-tri-*O*-methylxylose and 2,3,4-tri-*O*-methylfucose (28%), 3,4-di-*O*-methylxylose (21%), 2,3,6-tri-*O*-methylgalactose (15%), and 2,6-di-*O*-methylgalactose (36%). The last two sugars contained trideuteriomethyl groups at O-6 in confirmation of their origin in galacturonic acid residues. The small proportions of galactose-terminated side chains found in the earlier sample of tragacanthic acid were apparently absent from the present material.

Carboxyl-reduced permethylated tragacanthic acid was treated carefully with triflic anhydride in pyridine (11) and, as soon as ir examination showed virtual disappearance of hydroxyl absorption at 3600 cm^{-1} together with appearance of sulfonate ester absorption at 1420 cm^{-1}, the reaction mixture was worked up and the product reacted with tetrabutylammonium iodide. Completeness of reaction was ascertained by disappearance of the sulfonate ester band at 1420 cm^{-1}. Reaction of the 6-deoxy-6-iodogalactose residues in the modified polysaccharide with zinc dust in boiling 1-propanol was followed by treatment of the products with sodium borohydride and acetylation to give a mixture of partially methylated oligosaccharide alditol acetates. The two main products were separated chromatographically. Fraction T1 gave on hydrolysis 2,3,4-tri-*O*-methylxylose and a 1,2-dideoxy-5-*O*-methylhex-1-enitol, both of which were characterized by glc–ms of the derived alditol acetates. The ^{1}Hmr spectrum of T1 showed a single anomeric signal at δ 4.42 (doublet, $J_{1,2}$ = 7.26 Hz) characteristic of a β-D-xylopyranose residue. The structure, 3,6-di-*O*-acetyl-1,2-dideoxy-5-*O*-methyl-4-*O*-(2,3,4-tri-*O*-methyl-β-D-xylopyranosyl)-L-*lyxo*-hex-1-enitol (**1**), may therefore be advanced for this compound. Fraction T2 gave on hydrolysis 2,3,4-tri-*O*-methylfucose, 3,4-di-*O*-methylxylose, and the same hexenitol derivative, and the ^{1}Hmr spectrum showed two anomeric signals at δ 5.46 (doublet, $J_{1,2}$ = 3.7 Hz) and 4.51 (doublet, $J_{1,2}$ = 7.3 Hz), assignable to α-L-fucopyranose and β-D-xylopyranose residues respectively. Structure **2**, *O*-(2,3,4-tri-*O*-methyl-α-L-fucopyranosyl)-(1 → 2)-*O*-(3,4-di-*O*-methyl-β-D-xylopyranosyl)-(1 → 4)-3,6-di-*O*-acetyl-1,2-dideoxy-5-*O*-methyl-L-*lyxo*-hex-1-enitol, may be proposed for oligosaccharide alditol T2.

The glc–ms examination of the mixture of partially methylated oligosaccharide alditol acetates provided supporting evidence for structures **1** and **2** for the two main components and *m/z* values are shown for the more significant fragment ions in the mass spectra. A third minor component T3 was observed, whose retention time and mass spectrum were consistent with those of an *O*-(2,3,4-tri-*O*-methylfucopyranosyl)-(1 → 2)-3,4-di-*O*-methylxylitol (**3**), which presumably resulted from a side reaction that involved breakdown of a segment otherwise generating oligosaccharide **2**.

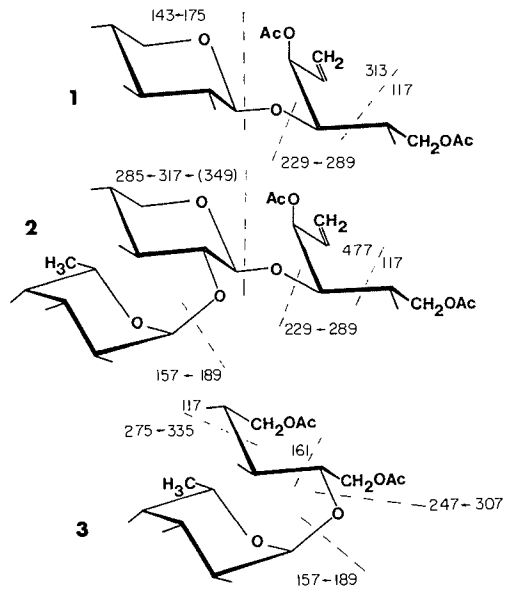

Unless otherwise specified, substituents are OCH_3

The successful application of the hex-5-enose degradation to carboxyl-reduced permethylated tragacanthic acid provides the first example of a chemical (as opposed to enzymic) fragmentation of an α-D-galacturonan derivative which furnishes oligosaccharides containing the full complement of unaltered neutral glycosyl substituents. Since the oligosaccharides are terminated by hex-5-enose units originating from former galacturonic acid residues, the characterization of these substances defines the nature and sites of attachment of side chains, as in structure **4**. The degradative procedure should be applicable to

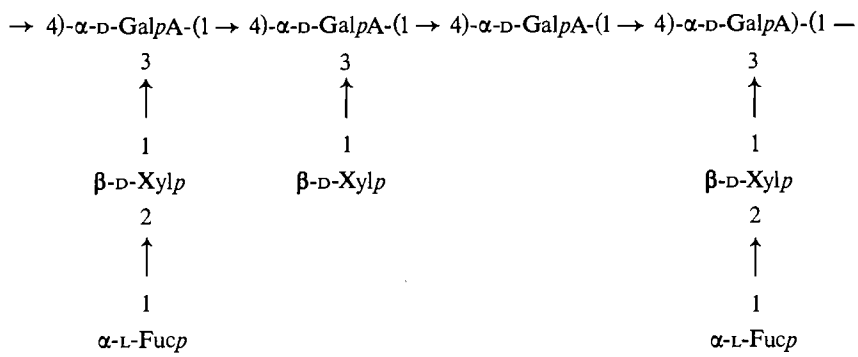

4

Can. J. Chem. Downloaded from www.nrcresearchpress.com by 210.87.254.6 on 09/06/12
For personal use only.

structure determination of otherwise inaccessible regions of pectins and structurally-related galacturonanas and rhamnogalacturonans.

In the accompanying paper (8) evidence was presented for 3,6-anhydro-α-D-galactopyranoside formation through intramolecular participation of 3-*O*-methyl or 3-*O*-glycosyl substituents and subsequent loss of such substituents when the corresponding α-D-galactopyranoside 6-sulfonates undergo solvolysis. Such a solvolytic reaction competes with iodide displacement when reaction is performed in *N,N'*-dimethylformamide, but is of no detectable significance when α-D-galactopyranoside 6-sulfonates are treated with tetrabutylammonium iodide in benzene. Under these latter conditions 6-deoxy-6-iodogalactosides are isolated in high preparative yields. In order to assess whether 3,6-anhydride formation with accompanying loss of 3-*O*-glycosyl substituents would be of any significance in polysaccharide studies, either as an unfavourable side reaction or as an alternative degradation which might be turned to advantage in structural analysis, the solvolysis of methylated carboxyl-reduced tragacanthic acid 6-imidazylate was examined. Chromatographic separation of the products gave modified methylated polysaccharide as the major fraction with a minor fraction containing some material which migrated on tlc. In order to detect the formation of derivatives of 3,6-anhydrogalactose, samples of carboxyl-reduced methylated tragacanthic acid and the methylated polysaccharide recovered from the solvolysis were methanolyzed and the resulting methyl glycosides were acetylated. The glc–ms analysis of the methyl glycoside acetates from the latter polysaccharide sample showed the presence *inter alia* of methyl 3,6-anhydro-2-*O*-methyl-β-D-galactopyranoside 4-acetate. Quantitative estimation placed an upper limit of 2% for the proportion of anhydrogalactose residues in the modifed polysaccharide and for the proportion of 3-*O*-glycosyl side chains which could have been lost in the solvolysis reaction. Furthermore, at least some of the anhydrogalactose residues could have been formed from methoxy rather than glycosyloxy participation in the sulfonate solvolysis. Attempts to detect glycosyl substituents liberated during the solvolysis were unsuccessful. We conclude that, for this 4-linked polysaccharide derivative, sulfonate solvolysis, even under the most favourable conditions, does not result in degradation with liberation of 3-*O*-glycosyl substituents in amounts which could be used to gain structural information. It is even less likely that such a side reaction will compete significantly during the introduction of iodo substituents when sulfonate displacement by iodide ion is performed in a nonpolar solvent in the key step preceding the hex-5-enose degradation.

Experimental

General experimental methods were as described in the preceding paper (8).

Carboxyl-reduced methylated tragacanthic acid

Tragacanthic acid was isolated by fractional precipitation of the water-soluble part of gum tragacanthic acid by graded addition of ethanol. The precipitated polysaccharide was dispersed in water and freeze-dried to give a sample which contained 50% of galacturonic acid residues (12) and gave on hydrolysis (13) xylose (27%), fucose (20%), and traces of galactose and arabinose, which were converted into alditol acetates (14) for analysis by glc on column A. Methylated tragacanthic acid was prepared by the Hakomori procedure (15) in dimethylsulfoxide using sodium methylsulfinylmethanide in ~30% excess of the quantity required to ensure ionization of carboxyl and hydroxyl groups present, as checked with triphenylmethane (16), with subsequent addition of methyl iodide (2 molar proportions). Methylated tragacanthic acid (150 mg) was heated with lithium aluminum hydride (400 mg) in boiling oxolane (10 mL). Excess hydride was destroyed by addition of ethyl acetate and the solution was neutralized to pH 4 by dropwise addition of dilute sulfuric acid. The mixture was diluted with water, concentrated to remove organic solvent, and then extracted with dichloromethane. Concentration of the dried extract afforded carboxyl-reduced methylated tragacanthic acid (125 mg). A portion of the methylated polysaccharide was realkylated using trideuteriomethyl iodide, the product was hydrolyzed, and the resulting sugars were converted into partially methylated alditol acetates which were analyzed by glc – mass spectrometry (15) using column B. The results indicated the presence of derivatives of 2,3,4-tri-*O*-methylxylose and 2,3,4-tri-*O*-methylfucose (28% combined from incompletely separated components), 3,4-di-*O*-methylxylose (21%), 2,3-di-*O*-methyl-6-*O*-($^2H_3$)methylgalactose (15%), and 2-*O*-methyl-6-*O*-($^2H_3$)methylgalactose (36%).

Formation and selective cleavage of 6-deoxy-6-iodogalactopyranosyl residues in carboxyl-reduced methylated tragacanthic acid

Trifluoromethanesulfonic anhydride (300 μL) in dichloromethane (2 mL) was added dropwise, with stirring, to dry pyridine (150 μL) in dichloromethane (1 mL) at −10°C. After 15 min, carboxyl-reduced methylated tragacanthic acid (100 mg) in dichloromethane (2 mL) was added dropwise and the mixture was stirred at −10°C for 2.5 h. The reaction mixture was poured into ice-water (5 mL), the organic layer was separated, and the aqueous layer was extracted with dichloromethane. The combined organic layers were washed with cold dilute sodium hydrogen carbonate and then water until free of base. Concentration of the dried solution yielded polysaccharide sulfonate which showed ir absorption (NaCl) at 1420 cm^{-1} (—SO_2—) but none at 3600 cm^{-1} (OH). The polysaccharide sulfonate was heated in boiling benzene (4 mL) containing tetrabutylammonium iodide (200 mg) for 24 h. After removal of solvent the residue was chromatographed on Sephadex LH-20 in dichloromethane to furnish iodinated methylated polysaccharide (60 mg) whose ir spectrum showed absence of sulfonyl absorption at 1420 cm^{-1}. Iodinated methylated polysaccharide was heated in boiling 1-propanol – water (3 mL, 14:1) with freshly activated zinc (100 mg) for 15 h. The filtered solution combined with methanol washings was concentrated, and the residue in oxolane–water (1:1, 3 mL) was treated with sodium borohydride (75 mg) for 15 h. After normal work-up the product was acetylated with acetic anhydride in pyridine. Examination of a portion of the resulting mixture of partially methylated oligosaccharide alditol acetates by glc – mass spectrometry on column D (180°C, 4°/min → 230°C, hold) showed two major components T1 and T2, eluted at 6.0 and 20.2 min, which were isolated preparatively, together with a minor component T3, eluted at 7.9 min, whose mass spectrum and retention time were consistent with those of an *O*-(2,3,4-tri-*O*-methylfucopyranosyl)-(1 → 2)-3,4-di-*O*-xylitol diacetate. The major part of the above mixture was chromatographed on silica gel with dichloromethane–acetone (10:1) to give samples of hex-1-enitol-terminated oligosaccharides T1 and T2 whose structures were established from the ^{1}Hmr and mass spectra and by methylated sugar analysis. The 1,2-dideoxy-5-*O*-methylhex-1-enitol triacetate formed from both oligosaccharides was identical (glc – mass spectrometry) to the derivative reported in the preceding paper (8).

Solvolysis of carboxyl-reduced methylated tragacanthic acid 6-imidazylate (with L. Khondo)

Carboxyl-reduced methylated tragacanthic acid (30 mg) in dry oxolane (1 mL) was added to sodium hydride (6 mg) in dry oxolane (0.5 mL) and the suspension was stirred for 4 h at room temperature. *N,N'*-Sulfuryldiimidazole (45 mg) was added to the reaction mixture at −40°C, and the mixture was stirred at −40°C for 20 min and at room temperature for 2 days. Progress of reaction was monitored from the ir spectra of isolated polysaccharide samples which showed appearance of a band at 3120 cm^{-1} (imidazole C—H) and the corresponding disappearance of absorption at ~3500 cm^{-1} (OH). Methanol

(0.1 mL) was added to destroy residual sodium hydride, the reaction mixture was concentrated, the residue was extracted with dichloromethane, and the extract was washed several times with water, dried, and concentrated to give modified polysaccharide (36 mg).

The methylated polysaccharide imidazylate (36 mg) was kept in dry *N,N'*-dimethylformamide at room temperature for 5 days. Progress of the solvolysis was monitored by disappearance of ir absorption at 3120 cm^{-1} (imidazole C—H). On completion of reaction the solution was diluted with dichloromethane, washed with water, dried, and concentrated. The residue in *N,N'*-dimethylformamide – water (2 mL, 1:1) was absorbed on a Waters C_{18} reverse-phase Sep-Pak cartridge (17, 18). Elution of the cartridge with methanol–water (1:1) afforded a minor fraction (1.6 mg) which showed traces of chromatographically mobile carbohydrate on tlc in benzene–methanol (5:1). Elution of the cartridge with methanol furnished as a major fraction modified methylated polysaccharide (20 mg). A portion of this material was boiled with methanolic 2.5% hydrogen chloride for 2.5 h and the methanolysate was acetylated. The resulting mixture of methyl glycosides and methyl glycoside acetates was examined by glc–ms on column C, and shown to contain derivatives of 2,3,4-tri- and 3,4-di-*O*-methylxylose, and 2,3,4-tri-*O*-methylfucose, together with small amounts of methyl 4-*O*-acetyl-3,6-anhydro-2-*O*-methyl β-D-galactopyranoside. A parallel experiment showed that this latter compound comprised 67% of the mixture of products formed when methyl 3,6-anhydro-2-*O*-methyl-α-D-galactopyranoside (19) was methanolysed and acetylated under identical conditions. Under these conditions of analysis derivatives of 2,3-di- and 2-*O*-methylgalactose (from caboxyl-reduced galacturonic acid residues) were not conveniently estimated. Based on the above-determined composition of carboxyl-reduced methylated tragacanthic acid and on the ratio of methyl 4-*O*-acetyl-3,6-anhydro-2-*O*-methyl-β-D-galactopyranoside to the above-mentioned methyl glycosides, it is calculated that residues of 3,6-anhydro-D-galactose are present in the modified polysaccharide in an amount not exceeding 2%. The minor fraction from the polysaccharide solvolysis was treated with sodium borodeuteride and then acetylated. The glc–ms analysis of the products showed some non-carbohydrate impurities but neither 2,3,4-tri-*O*-methylxylitol nor the disaccharide alditol **3** could be detected.

Acknowledgements

The authors thank the Natural Sciences and Engineering Research Council of Canada for financial support, Dr. B. H. Khouw for recording mass spectra, and the Southwestern Ontario NMR Centre at the University of Guelph for recording nmr spectra. They also thank Mr. L. Khondo for the experiments cited.

1. G. O. ASPINALL, H. K. FANOUS, N. S. KUMAR, and V. PUVANESARAJAH. Can. J. Chem. **59**, 935 (1981).
2. G. O. ASPINALL, H. K. FANOUS, N. S. KUMAR, and V. PUVANESARAJAH. Can. J. Chem. **61**, 1858 (1983).
3. G. O. ASPINALL and V. PUVANESARAJAH. Can. J. Chem. **61**, 1864 (1983).
4. I. KITAGAWA, M. YOSHIKAWA, and A. KADOTA. Can. Pharm. Bull. **26**, 484 (1978).
5. H. K. FANOUS. Ph.D. Thesis, York University (1983).
6. V. PUVANESARAJAH. Ph.D. Thesis, York University (1983).
7. B. BERNET and A. VASELLA. Helv. Chim Acta, **62**, 1990 (1979); **62**, 2400 (1979); **62**, 2411 (1979).
8. G. O. ASPINALL, D. CHATTERJEE, and L. KHONDO. Can. J. Chem. **62**, 2728 (1984).
9. G. O. ASPINALL and J. BAILLIE. J. Chem. Soc. 1702 (1963).
10. G. O. ASPINALL, D. B. DAVIES, and R. N. FRASER. J. Chem. Soc. 1086 (1967).
11. R. W. BINKLEY, M. G. AMBROSE, and D. G. HEHEMANN. J. Org. Chem. **45**, 4387 (1980).
12. N. BLUMENKRANTZ and G. ASBOE-HANSEN. Anal. Biochem. **54**, 184 (1973).
13. P. ALBERSHEIM, D. J. NEVINS, P. D. ENGLISH, and A. KARR. Carbohydr. Res. **5**, 340 (1967).
14. J. H. SLONEKER. Methods Carbohydr. Chem. **6**, 20 (1972).
15. P.-E. JANSSON, L. KENNE, H. LIEDGREN, B. LINDBERG, and J. LÖNNGREN. Chem. Commun. Univ. Stockholm, **8**, 1 (1976).
16. H. RAUVALA. Carbohydr. Res. **72**, 257 (1979).
17. A. J. MORT, S. PARKER, and M.-S. KUO. Anal. Biochem. **133**, 380 (1983).
18. T. J. WAEGHE, A. G. DARVILL, M. MCNEIL, and P. ALBERSHEIM. Carbohydr. Res. **123**, 281 (1983).
19. N. S. ANDERSON, T. C. S. DOLAN, and D. A. REES. J. Chem. Soc. C, 596 (1968).

Can. J. Chem. Downloaded from www.nrcresearchpress.com by 210.87.254.6 on 09/06/12
For personal use only.

Microbial hydroxylation of steroids. 9. Epoxidation of Δ^6-3-ketosteroids by *Rhizopus arrhizus* ATCC 11145, and the mechanism of the 6β hydroxylase enzyme

HERBERT L. HOLLAND, P. CHINNA CHENCHAIAH, EVERTON M. THOMAS, BEATRIX MADER, AND (IN PART) MICHAEL J. DENNIS

Department of Chemistry, Brock University, St. Catharines, Ont., Canada L2S 3A1

Received March 2, 1984

HERBERT L. HOLLAND, P. CHINNA CHENCHAIAH, EVERTON M. THOMAS, BEATRIX MADER, and MICHAEL J. DENNIS. Can. J. Chem. **62**, 2740 (1984).

A series of Δ^6-3-ketosteroids has been incubated with the C-6β hydroxylating fungus *Rhizopus arrhizus* ATCC 11145. Ring A aromatic steroids are not metabolized by this fungus, nor are 3-chloro- and 3-(*N*-pyrrolideno)-androsta-3,5-dienes. $\Delta^{4,6}$-3-Ketosteroids are epoxidized at the 6,7 position by *R. arrhizus* with β stereochemistry; in contrast, both 5α- and 5β-Δ^6-3-ketosteroids are epoxidized with α stereochemistry by fungal and peracid reagents. The results of this and previous studies now make it possible to define the nature of the hydroxylating/epoxidizing species of the 6β hydroxylase enzyme of *R. arrhizus*. Evidence is presented for a stepwise reaction mechanism in both cases. Improved methods of synthesis are described for 6-methylene-testosterone and estra-4,6-dien-17β-ol-3-one.

HERBERT L. HOLLAND, P. CHINNA CHENCHAIAH, EVERTON M. THOMAS, BEATRIX MADER et MICHAEL J. DENNIS. Can. J. Chem. **62**, 2740 (1984).

On a procédé à l'incubation d'une série de Δ^6 céto-3 stéroïdes en présence du champignon *Rhizopus arrhizus* ATCC 11145 qui provoque des réactions d'hydroxylation en C-6β. Les stéroïdes comportant un cycle A aromatique ainsi que les chloro-3 ou (*N*-pyrrolidéno)-3 androstadiènes-3,5 ne sont pas métabolisés par ce champignon. Sous l'influence du *R. arrhizus*, les $\Delta^{4,6}$ céto-3 stéroïdes subissent une réaction d'époxydation en position 6,7 et la stéréochimie de la réaction est β; par opposition, les Δ^6 céto-3 stéroïdes tant de la série 5α que de la série 5β subissent des réactions d'époxydation dont la stéréochimie est α tant sous l'action des champignons que des peracides. Grâce aux résultats de la présente étude ainsi que ces obtenus antérieurement, il est maintenant possible de définir la nature des espèces, présentes dans l'enzyme hydroxylase 6β du *R. arrhizus*, qui provoquent les réactions d'hydroxylation et d'époxydation. Dans chacun de ces cas, on présente des données qui suggèrent un mécanisme réactionnel par étapes. On décrit des méthodes améliorées de synthèse pour la méthylène-6 testostérone ainsi que pour l'estradiène-4,6 ol-17β one-3.

[Traduit par le journal]

Can. J. Chem. Downloaded from www.nrcresearchpress.com by 210.87.254.40 on 09/06/12
For personal use only.

Introduction

The enzymic introduction of a hydroxy group at the C-6β position of Δ^4-3-ketosteroids (the conversion of **1** to **2**) is a common example of a biotransformation which can be carried out efficiently by mammalian (1) or microbial (2) systems. We have studied the latter reaction, performed by the fungus *Rhizopus arrhizus*, and have demonstrated that the substrate is hydroxylated in its $\Delta^{3,5}$-dienol form (eq. [1]) (3–8).

[1] 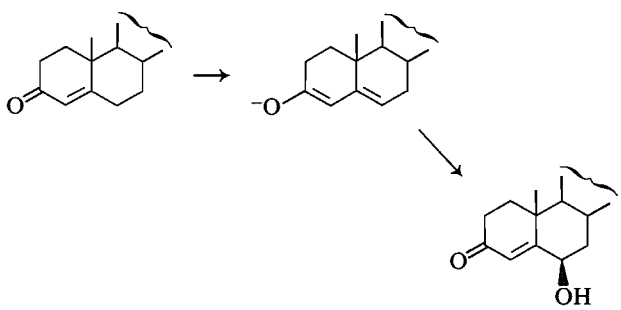

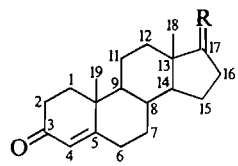

1 *a* R = O
b R = βOH, αH
c R = βOAc, αH

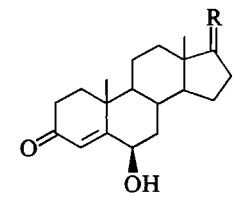

2 *a* R = O
b R = βOH, αH
c R = βOAc, αH

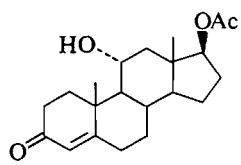

3

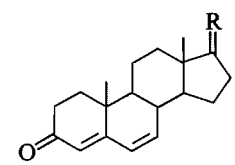

4 *a* R = O
b R = βOH, αH
c R = βOAc, αH

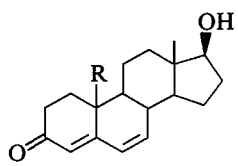

5 *a* R = H
b R = OH

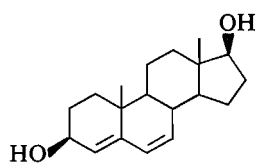

6

The mammalian enzyme which carries out this reaction is a cytochrome P-450 dependent mono-oxygenase (1, 9). Steroid hydroxylating enzymes from microbial sources appear to have similar cofactor requirements (10), and to function by a similar mechanism (2). Analogous enzymes from mammalian or microbial sources are also responsible for the detoxification by hydroxylation of endogenous organic material (11), and are implicated in the metabolism of arenes to arene oxides (12).

The nature of the active site oxidizing species has been formulated as the iron–oxygen complex shown in Scheme 1 (13); the weight of available evidence favours a non-concerted, radical mechanism (pathway B, Scheme 1) for its reaction with a saturated C—H bond (2). A closely related reaction, also carried out by cytochrome P-450 dependent mono-oxygenases (14), is the epoxidation of olefinic substrates (2). This reaction may proceed via one of the mechanisms of Scheme 2, anal-

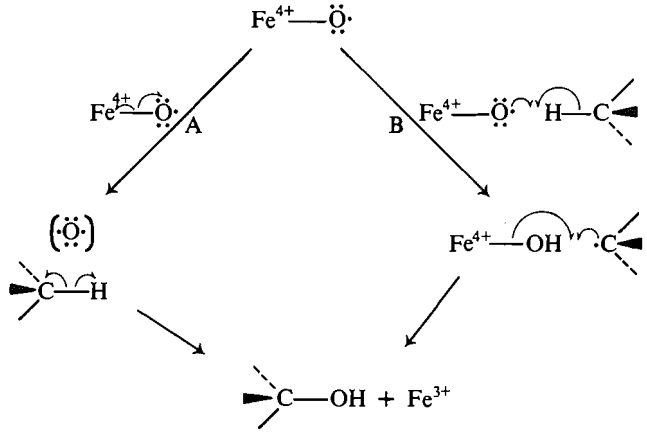

SCHEME 1. Possible routes for hydroxylation at saturated carbon by cytochrome P-450 dependent mono-oxygenases.

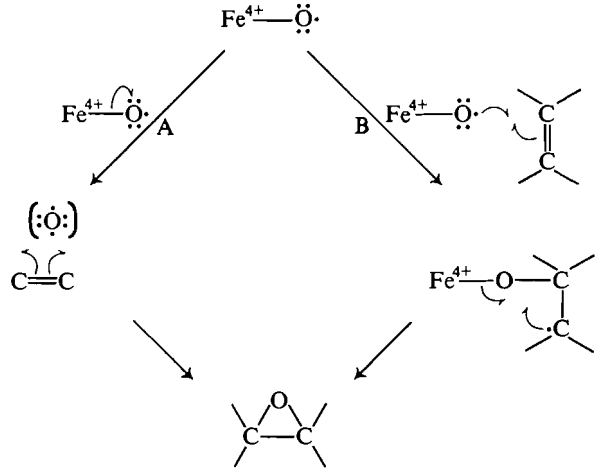

SCHEME 2. Possible routes for epoxidation of olefins by cytochrome P-450 dependent mono-oxygenases.

ogous to the corresponding concerted (path A) or stepwise (path B) routes of Scheme 1; little discriminating evidence is available in support of either pathway (14, 15, and references therein).

We have now extended our study of the microbial hydroxylation of Δ^4-3-ketosteroids at C-6β to include the epoxidation of $\Delta^{4,6}$-diene-3-ones and Δ^6-3-ketosteroids, and propose herein that both processes occur via stepwise rather than a concerted reaction pathway.

Results

Of the substrates used in this study, only 6-methylene-testosterone (10) was synthesized by a new route (Scheme 3), that developed by Danishefsky *et al.* for the synthesis of 6-methylene-progesterone (16).

The determination of the structure of biotransformation products in this study relied heavily on the interpretation of ^{13}C nmr spectral data. For this reason, the ^{13}C nmr spectra of the Δ^6 androstenes used as substrates are reported in Table 1. The resonances assigned to carbons 4 and 6, and to carbons 9 and 14, respectively, of **4***a* and **4***c* represent a reversal of the literature values (17). Our assignments of the carbons 9 and 14 resonance positions of **4***a*–*c*, **5***a*, **5***b*, and **13** reflect the anticipated effects of substitution at C-10 and C-16 (18), while the chemical shifts of C-4 and C-6 of the same compounds were

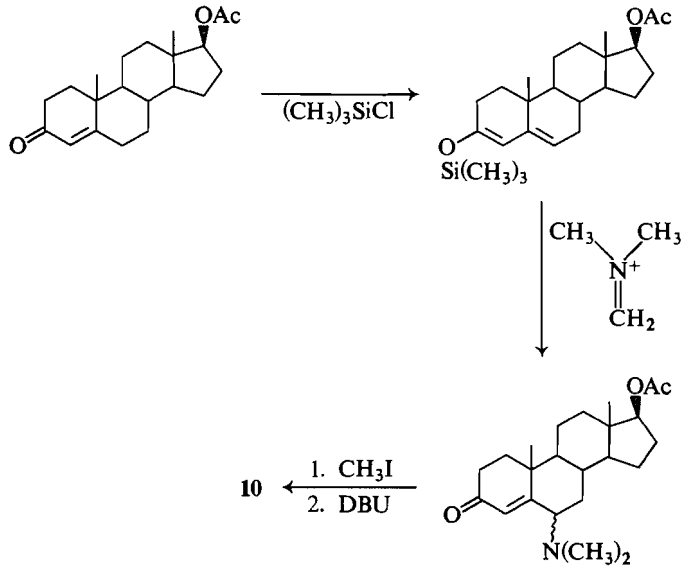

SCHEME 3. Synthesis of 6-methylene testosterone (**10**) (ref. 16).

reassigned following a consideration of the spectra of the 6,7β-epoxides **12** (see below) in which C-4 and C-5 chemical shifts are essentially unchanged from those of the corresponding olefins **4** and **5**. The assignments of the carbon resonances of the Δ^6 estrogens **8***a* and **8***b* were straightforward, while those of the 5α- and 5β-Δ^6-androstenes **11***a*, **11***b*, and **17** follow readily from the spectra of the corresponding saturated compounds (18) and a consideration of the effect of the introduction of unsaturation in the 6,7 position (19).

Following the successful use of $\Delta^{3,5}$ enol acetates as substrates for C-6β hydroxylation by *Rhizopus arrhizus* (4, 7) the $\Delta^{3,5}$-3-chloro steroid **9***a* and the $\Delta^{3,5}$ dienamine **9***b* were

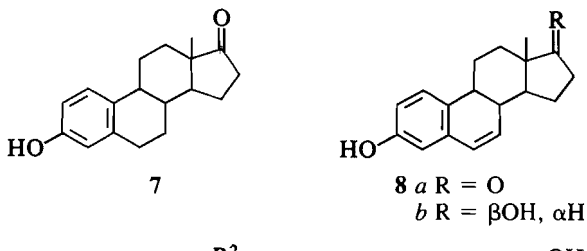

7

8 *a* R = O
b R = βOH, αH

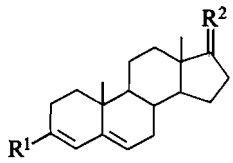

9 *a* R¹ = Cl, R² = βOAc, αH
b R¹ = 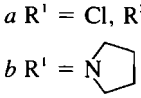 , R² = O

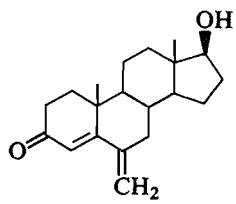

10

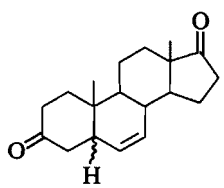

11 *a* 5αH
b 5βH

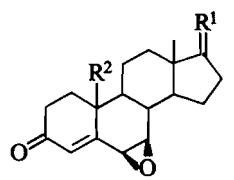

12 *a* R¹ = O, R² = CH_3
b R¹ = βOH, αH, R² = CH_3
c R¹ = βOH, αH, R² = H

Can. J. Chem. Downloaded from www.nrcresearchpress.com by 210.87.254.40 on 09/06/12
For personal use only.

TABLE 1. ^{13}C nuclear magnetic resonance spectra of androst-6-enes and related compounds

	δ C ppm											
Carbon	**4***a*†	**4***b*	**4***c*†	**5***a*	**5***b*	**8***a*	**8***b*	**10**	**11***a*	**11***b*	**13**	**17**
1	33.9	33.7*	33.9	26.7	35.9	128.7	127.4	35.5	35.8	34.5	33.6*	34.7
2	33.9	33.9*	33.9	37.8	33.1	113.4*	112.8*	34.1	38.0	36.3	33.8*	30.7
3	199.2	199.8	199.1	200.2	200.1	155.8	155.1	200.3	211.0	212.1	199.5	71.6
4	128.7	128.1	128.1	128.8	126.4	113.8*	113.1*	122.1	42.6	43.6	128.9	36.1
5	162.9	163.9	163.2	159.0	159.7	135.2	134.9	169.5	45.8	43.9*	162.9	45.2
6	124.1	123.7	123.7	124.4	123.9	124.2	123.7	146.4	128.0	127.1	124.3	128.4
7	138.3	140.6	139.9	141.8	142.2	130.6	132.1	39.5	130.1	130.2	138.8	131.0
8	37.0	37.7	37.3	41.5	32.8	38.3	38.5	36.1	37.4	36.2	36.3	38.2
9	50.7	50.9	50.6	46.2	47.6	42.1	41.6	53.0	52.2	43.6*	50.7	52.9
10	36.1	36.2	36.5	41.0	67.4	129.5	129.7	39.5	34.5	33.7	35.1	34.4
11	20.0	20.3	20.1	25.1	19.5	23.7	23.8	21.0	20.4	20.2	20.1	20.8
12	31.3	36.4	36.0	36.3	36.5	31.1	35.8	36.7	31.6	31.8	36.1	36.9
13	48.3	43.9	43.4	43.9	43.4	48.4	43.3	43.2	48.4	48.2	43.3	44.0
14	48.7	48.3	48.0	48.0	50.4	48.7	47.9	51.2	49.6	49.7	42.6	49.4
15	21.4	23.0	23.1	22.9	22.8	21.4	22.5	23.6	21.7	21.5	36.1	23.3
16	35.6	30.4	27.4	30.3	29.9	35.7	29.7	30.8	35.7	35.7	216.2	31.5
17	219.3	81.2	82.0	81.4	80.6	220.4	80.5	81.8	220.0	219.9	85.9	81.7
18	13.7	11.0	12.0	10.9	10.7	13.6	10.5	11.4	13.5	13.8	11.3	11.5
19	16.3	16.3	16.3					17.4	11.0	21.1	16.3	11.2
Other								114.4				

*Chemical shifts marked with asterisks may be interchanged.

†These assignments are based on those of ref. 17, with the transposition of the resonances assigned therein to carbons 4 and 6, and 9 and 14.

Can. J. Chem. Downloaded from www.nrcresearchpress.com by 210.87.254.40 on 09/06/12
For personal use only.

incubated with this fungus. The former was not metabolized by *R. arrhizus*, and the latter gave only those products produced by rearrangement and auto-oxidation following its hydrolysis to androst-5-ene-3,17-dione (6, 20). The successful use of testosterone acetate (**1***c*) as a substrate, giving the 6β and 11α hydroxy derivatives **2***c* and **3**, respectively, confirms that the 6β hydroxylase enzyme can accept a 17-acetoxy steroid substrate, so that the presence of this functional group in the substrate cannot account for the failure of *R. arrhizus* to metabolize **9***a*.

The 6-methylene steroid **10** and the Δ^6 estrogens **8***a* and **8***b* were recovered unchanged from incubation with *R. arrhizus*. This fungus also fails to hydroxylate estrone (**7**), so its failure to metabolize **8***a* and **8***b* is not unexpected.

The $\Delta^{4,6}$-diene-3,17-dione **4***a* gave two products on incubation with *R. arrhizus*, the 6,7β epoxide **12***a* and the 17β-hydroxy-16-ketone **13**. The structure of **12***a* follows from a comparison of its carbon nmr spectral properties (Table 2) with those of the corresponding 6,7α epoxide (**20**) prepared by chemical synthesis or by incubation of **4***a* with the C-7α hydroxylator *Mucor griseocyanus*. The upfield position of the resonances assigned to carbons 9 and 14 in the latter compound with respect to those reported for **12***a* confirm the respective stereochemistry of substitutions in ring B (γ-*gauche* effects). The assignment of the C-8 resonance of **12***a* at δ 36.1 ppm with respect to that of **20** at 35.6 ppm is in accord with the presence of a γ-*gauche* effect (ca −5 ppm) in the former moderated by a change from axial to equatorial oxygen substitution at C-7 (ca +4 ppm at C-8) (18). A similar effect occurs at C-12 in 9(11) epoxides.[1] Other spectral data (^1H nmr, ir, uv, mass spectra) for **12***a* are in agreement with the proposed structure. The structure proposed for the metabolite **13** is in accord with its proton and carbon nmr data. The assignment of the C-17α hydrogen resonance to the singlet at δ 3.81 and the appearance of the C-18

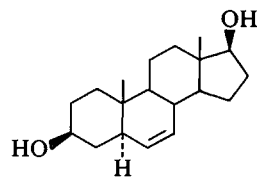

17

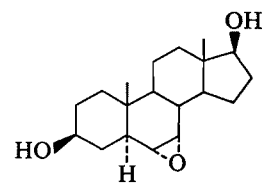

18

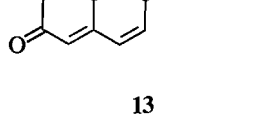

13

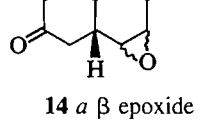

14 *a* β epoxide
b α epoxide

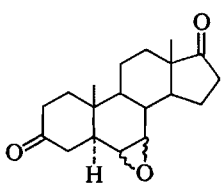

15 *a* β epoxide
b α epoxide

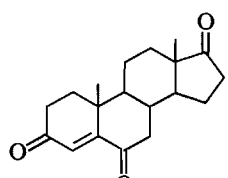

16

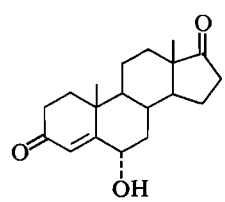

19

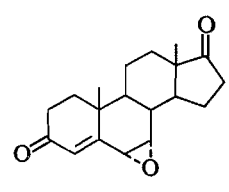

20

[1]H. L. Holland and E. Riemland. Unpublished data.

TABLE 2. ^{13}C nuclear magnetic resonance spectra of 6,7-epoxy-androstanes

	δ C ppm						
Carbon	**12***a*	**12***b*	**12***c*	**14***b*	**15***b*	**18**	**20**
1	35.0	35.5	26.4	34.8	35.2	34.5	34.0
2	34.0	34.1	37.2	35.6	37.5	30.6	33.9
3	198.0	198.4	198.7	211.6	209.7	71.0	199.2
4	120.8	129.4	129.9	38.9	42.0	35.7	131.5
5	162.1	163.3	159.8	40.3	45.3	45.2	161.8
6	55.6	55.6	54.8	53.3	53.5	54.3	52.6
7	57.7	58.6	58.7	54.3	54.8	55.8	53.5
8	36.1	36.1	40.4	33.9	35.2	35.7	35.6
9	51.7	51.8	47.2*	37.7	47.0	47.0	46.8
10	36.6	36.8	36.9	32.6	33.8	33.6	34.3
11	20.6	20.9	25.0	19.7	20.2	20.5	19.2
12	31.0	36.2	36.2	31.2	31.4	36.6	31.1
13	48.3	43.8	44.0	47.8	48.1	43.8	47.8
14	48.0	47.6	47.1*	47.1	46.1	46.6	40.9
15	21.5	23.2	22.9	21.3	21.4	22.9	21.4
16	35.5	30.4	30.3	35.7	35.7	31.0	35.6
17	219.8	81.2	81.2	219.1	219.5	81.3	219.5
18	13.7	10.9	10.9	13.6	13.9	11.2	13.7
19	16.9	16.9		22.2	12.3	12.5	17.3

*Chemical shifts marked with asterisks may be interchanged.

methyl signal at δ 0.83 are characteristic of the substitution pattern proposed for ring D, as are the resonances of carbons 12–18 (Table 1).

Androsta-4,6-dien-17β-ol-3-one (**4***b*) gave only the product of 6,7β epoxidation on incubation with *R. arrhizus*, as did the corresponding diol **6** (following oxidation at C-3). Comparison of carbon spectral data for this product (**12***b*), that for **12***a*, and the epoxide **12***c* (derived from **5***a*) with that for **20** (Table 2) confirms the common β stereochemistry of epoxide in **12***a–c*. The only differences within this series are those anticipated for substitution at C-10 and C-17 (18).

The 19-nor-steroid **5***a* gave, in addition to the epoxide **12***c* as described above, a product **5***b* resulting from hydroxylation at C-10. The structure of **5***b* is entirely in accord with that predicted from application of the ^{13}C nmr shift parameters for a C-10β hydroxy group (22) to **5***a*, and with other spectral data.

The 5α and 5β-androst-6-enes **11***a* and **11***b* each gave a single product on incubation with *R. arrhizus*. These products were identical with those obtained by peracid oxidation of the corresponding olefins, and were assigned the 6,7α epoxy structures **15***b* and **14***b* respectively. The stereochemistry of the epoxide grouping in these compounds can be readily deduced from their ^{13}C nmr spectra (Table 2), the γ upfield shifts of carbons 9 and 14 with respect to those of the corresponding saturated diones being particularly diagnostic (18).

Discussion

The formation of the minor products **13** (from **4***a*) and **5***b* (from **5***a*) may be rationalized as follows. The 16-ketone **13** can arise via the 16β-hydroxy-17-ketosteroid **21** (eq. [2]); steroids with the latter functionality rearrange readily under acidic or basic conditions to the more stable 17β-hydroxy-16-one (23). The pH of the incubation medium is 5.2. Hydroxylation of **5***a* at C-10β parallels the observed hydroxylation of 19-nortestosterone (22) and the corresponding dione (5) at C-10β by *R. arrhizus*. Both **13** and **5***b* may therefore be the result of the enzyme's predilection for axial hydroxylation at

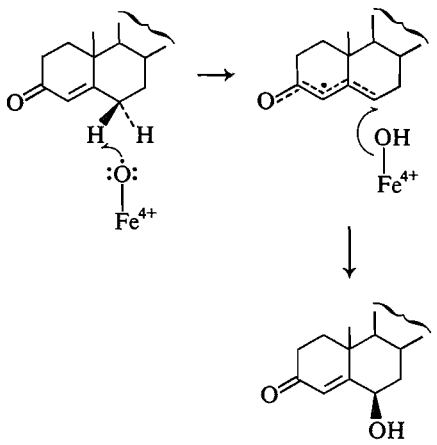

SCHEME 4. Mechanism of C-6β hydroxylation of Δ^4-3-ketosteroids by *R. arrhizus*.

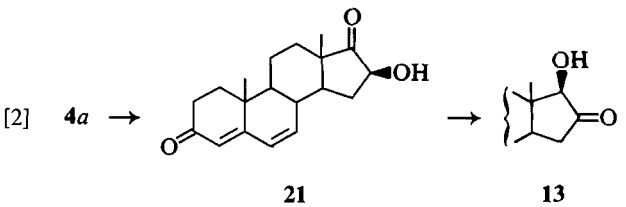

enolizable carbon.

The enzymic formation of the β epoxides **12***a–c* from $\Delta^{4,6}$-diene-3-ones **4**, and the β hydroxylation at C-6 of Δ^4-3-ketosteroids (1) is in contrast to the α epoxidation of **11** reported herein, the stereospecific α epoxidation of the Δ^5 bond in *B*-norsteroids (8), and the C-6α hydroxylation of 5α-androstan-17β-ol-3-one by *R. arrhizus* (24).

Inspection of models of **1**, **4**, and **11**, with the assumption of a fixed relationship between the sites of substrate binding (C-3 and C-17(2)) and oxidation, fails to provide any plausible explanation for the observed changes in the stereochemistry of oxidation at C-6 noted above. In the absence of any clearly definable effect due to substrate binding, we suggest that the reason for these stereochemical changes may be attributable to steric and (or) stereoelectronic effects associated with the individual substrates themselves.

We have previously argued that the β stereochemistry of oxidation at C-6 in the conversion of **1** to **2** is not necessarily a restraint of enzyme specificity, but can be a result of stereoelectronic factors inherent in the conversion of the $\Delta^{3,5}$-dienol intermediate to product (6) (eq. [1]). This reaction has been shown to involve a product-like transition state with the C-6β bond approaching an axial position (25, 26).

If our previous argument is correct, then the enzymic 6β hydroxylation of **1** is most satisfactorily represented as the stepwise process (analogous to route B of Scheme 1) presented in Scheme 4. The alternative concerted proposal (analogous to route A of Schemes 1 and 2) requires a stereospecific β epoxidation at the 5,6 position, followed by rearrangement to give the product (eq. [3]). The data presented herein demonstrate, however, that in the absence of stereoelectronic contraints, enzymic oxidation at C-6 occurs with only α stereochemistry. We therefore conclude that, since the concerted epoxidation of eq. [3] would occur independently of stereoelectronic factors, this reaction pathway is not consistent with the available data.

Can. J. Chem. Downloaded from www.nrcresearchpress.com by 210.87.254.40 on 09/06/12
For personal use only.

Can. J. Chem. Downloaded from www.nrcresearchpress.com by 210.87.254.40 on 09/06/12
For personal use only.

[3]

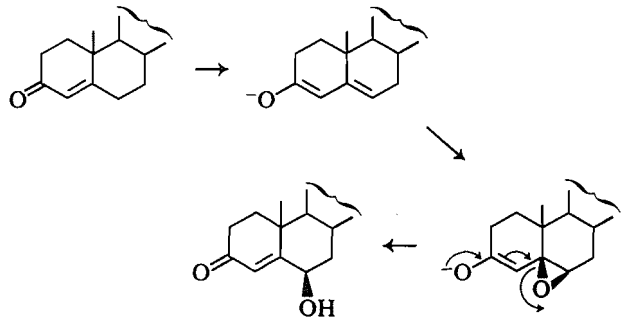

The β stereochemistry of enzymic epoxidation observed for the $\Delta^{4,6}$-dien-3-ones (**4**) can also be rationalized in terms of a stepwise process whose stereochemistry is dictated, not by enzyme specificity, but by the steric and stereoelectronic properties of the substrate. By analogy with the enzymic and chemical conversions of **11** to **14***b* and **15***b*, simple concerted epoxidation of the Δ^6 bond of **4** by *R. arrhizus* should proceed with α stereochemistry. Such is indeed the case for the peracid oxidation of **4** (21). The observed β epoxidation of **4** by *R. arrhizus*, however, in the absence of any discernable effects due to substrate binding (*vide supra*) cannot be attributed simply to enzyme specificity (cf. the α epoxidation of **11**).

Scheme 5 proposes a route for this reaction which is consistent with both the known features of the enzyme (Schemes 1 and 2), and the known steric and stereoelectronic properties exhibited during the epoxidation of the substrate and related molecules (27). The route proposed involves addition of the enzymes active site specie at C-7 of **4**, a process parallel to that of route B, Scheme 2. This process may give either resonance stabilized intermediate **22** or **23** but, by analogy with the preferred addition at C-5 of Δ^4-3-ketosteroids (20, 27), should proceed mainly from the β face to produce **22** whose subsequent closure to **12** would proceed without appreciable steric hindrance (27). In any event, the alternative C-7α intermediate **23** would, if formed, experience severe 1,3-diaxial interactions with the C-14 and C-15 hydrogens when correctly oriented for subsequent epoxide ring closure. An entirely analogous state of affairs prevents the formation of 4,5α epoxides from Δ^4-3-ketosteroids when bulky oxidants are used (27).

The enzymic 6,7α epoxidation of **4***a* to give **20** does in fact proceed with the C-7α hydroxylating fungus *Mucor griseocyanus*. This finding accords with the general observation (28) that fungi capable of introducing an axial hydroxyl group into a saturated steroid epoxidize analogous olefinic steroids with corresponding stereochemistry. In the case of *M. griseocyanus* and other fungi which epoxidize remote from existing functionality in the substrate, however, this effect follows from a spatial similarity of axial C—H and π electron density (2); such cannot be the case for the 6β hydroxylase of *R. arrhizus*, in view of the preferred α stereochemistry of epoxidation in the absence of the Δ^4 bond. The epoxidation of **11***a* and **11***b*, either chemical or enzymic, provides only the α epoxides **14***b* and **15***b*.

For the reasons discussed above, the results of the incubations of the Δ^6-3-ketosteroids **4** and **11** with *R. arrhizus* described herein are therefore most consistent with a stepwise oxidation mechanism for the enzymes as outlined in Schemes 4 and 5. This conclusion adds additional weight to the evidence now accumulating that the cytochrome P-450 mono-oxygenase enzymes act by the non-concerted one-electron pathways outlined in route B, Schemes 1 and 2.

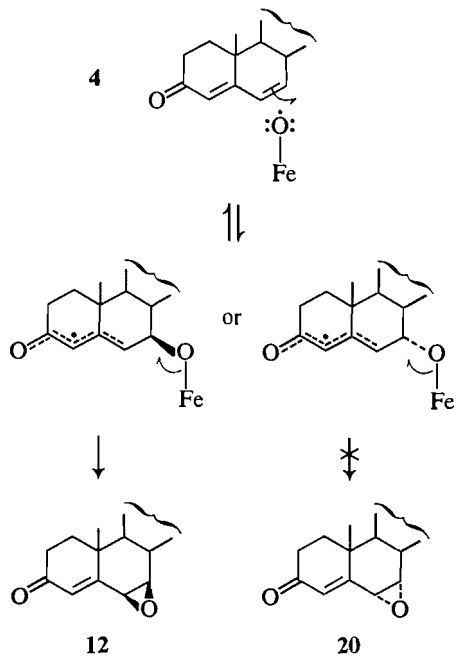

SCHEME 5. Mechanism of 6,7β epoxidation of Δ^4-3-ketosteroids by *R. arrhizus*.

Experimental

Apparatus, materials, and methods

Melting points were determined on a Kofler heating stage and are uncorrected. Infrared spectra were recorded with a Perkin–Elmer 237B spectrometer. The nmr spectra were obtained with a Bruker WP 60, WP80 CW, or WH 400 (at the Southwestern Ontario NMR Centre, Guelph) using $CDCl_3$ as solvent and TMS as internal standard. Mass spectra were obtained with an AEI MS 30 spectrometer fitted with a Kratos DS-55 data system. Thin-layer chromatography was performed on Merck silica gel 60 F-254, and column chromatography on silica gel (60–200 mesh) or alumina. Elemental analyses were performed by Guelph Chemical Laboratories, Guelph, Ontario.

Incubations with fungi

Incubations with *Rhizopus arrhizus* ATCC 11145 (3) or *Mucor griseocyanus* ATCC 1207 (29) were performed as reported, unless otherwise stated.

Preparation of substrates

The following were prepared by published methods and gave satisfactory analytical data: androsta-4,6-diene-3,17-dione (**4***a*) (30), androsta-4,6-dien-17β-ol-3-one (**4***b*) (30), 17β-acetoxy-3-chloroandrosta-3,5-diene (**9***a*) (31), 3-(*N*-pyrrolideno)-androsta-3,5-dien-17-one (**9***b*) (32), 5β-androst-6-ene-3,17-dione (**11***b*) (33), and 5α-androst-6-ene-3β,17β-diol (**17**) (34). The following compounds were commercial samples: **1***a*, **1***b*, **1***c*, **7**, **8***a*, and **8***b*. Hitherto unpublished ^{13}C nmr spectra are presented in Table 1.

*Estra-4,6-dien-17β-ol-3-one (5*a*)*

This was prepared by a modification of the published method (35). A solution of estr-4-ene-17β-ol-3-one (5 g) and chloranil (3.35 g) in ethanol (500 mL) was stirred at 50°C for 2 h, and then evaporated to dryness under reduced pressure. The residue (8.3 g) was dissolved in chloroform (100 mL) and the solution allowed to stand until precipitation of the phenolic by-product was complete. The solution was then filtered, and the filtrate evaporated *in vacuo*. The residue so obtained comprised the desired product and starting material in approximately equal amounts. It was therefore redissolved in ethanol (500 mL) and the above reaction procedure repeated. The final residue from the evaporation of the chloroform solution was filtered through a column of basic alumina (150 g) in chloroform (200 mL). Evapo-

Can. J. Chem. Downloaded from www.nrcresearchpress.com by 210.87.254.40 on 09/06/12
For personal use only.

ration of the resulting solution gave crude **5***a* (3.06 g) which was crystallized from ethyl acetate – hexane to give a sample (2.1 g) of mp 168–170°C; ^{1}H nmr included signals at δ 0.82 (3H, s, C-18 H), 3.70 (1H, t, J = 8 Hz, C-17α H), 5.78 (1H, br s, C-4 H), 6.20 (2H, s, C-6 and -7 H's) ppm; ^{13}C nmr: see Table 1.

*Androsta-4,6-diene-3β,17β-diol (**6**)*

A slurry of lithium tri-*tert*-butoxy aluminum hydride (2.5 g) in THF (100 mL) was added to a stirred solution of **4***b* (1 g) in THF (75 mL), and the mixture heated under reflux for 1 h. Following the usual work-up, the product **6** (0.8 g) was isolated, mp 192–195°C (lit. (36) mp 194–196°C); ^{1}H nmr include signals at δ 0.79 (3H, s, C-18 H), 0.98 (3H, s, C-19 H), 3.5–3.8 (1H, t, C-17α H), 4.0–4.4 (1H, m, C-3α H), 5.46 (1H, m, C-4 H), 5.62 and 5.96 (2H, AB q, J = 9 Hz, C-6 and C-7 H's) ppm.

*6-Methylene androst-4-en-17β-ol-3-one (**10**)*

This was prepared using synthetic methodology developed by Danishefsky *et al.* (16), and outlined in Scheme 3.

3-Trimethylsilyloxyandrosta-3,5-diene-17β-ol, acetate

Freshly distilled chlorotrimethylsilane (25 mL) followed by triethylamine (5 mL) were added to a stirred solution of testosterone acetate (**1***c*) in dry DMF (30 mL) and the resulting mixture refluxed with stirring for 48 h. The mixture was then cooled, diluted with pentane (100 mL), and washed with sodium bicarbonate solution. The aqueous washings were back extracted with pentane and the combined organic extracts washed rapidly with HCl (1.5 *M*) and aqueous sodium bicarbonate. The organic extract was then dried and evaporated to give a residue (1.6 g) which was dissolved in ether–hexane (1:3) and filtered through a short column of silica gel (60 g). In this way was obtained 1.35 g of the title compound, mp 86–88°C, which was used directly in the next step.

6ξ-Dimethylaminoandrost-4-en-17β-ol-3-one, 17 acetate

Working under a nitrogen atmosphere, Eshenmosher's salt (1 g, Aldrich) was dissolved in dry chloroform (20 mL, acid free) by heating for 10 min, after which time the enol silyl ether (above) (1.3 g) was added in three portions at 2-min intervals. The resulting mixture was stirred and refluxed for 45 min, cooled, and then acidified (concentrated HCl, 20 mL). The reaction mixture was stirred for a further 10 min, and the aqueous layer then separated. The organic layer was washed (dilute HCl, water), and the combined aqueous washings were basified and then extracted with ether (2 × 50 mL). The ethereal extract was evaporated to give a thick oil (1.1 g), ^{1}H nmr of which indicated the presence of the dimethylamino group (δ 2.24 ppm). This material was used directly in the next step.

*6-Methylene androst-4-ene-17β-ol-3-one (**10**)*

To a solution of the above Mannich base (1 g) in dry ether (20 mL) was added methyl iodide (7 mL). The resulting mixture was refluxed for 1h, cooled, filtered, and concentrated to half-volume, and refiltered. The quaternary iodide thus obtained (1.19 g) was dried *in vacuo* and used directly in the next step.

A mixture of the above salt (0.99 g) and DBU (0.1 g) in dry THF (5 mL) was refluxed for 1 h. The solvent was then removed by filtration, and the residue washed twice with ether. The combined organic extracts were evaporated to give a residue which was redissolved in ether. The resulting solution was washed (water), dried, and evaporated to give the product **10** (0.465 g). Recrystallization from chloroform–hexane gave a sample (0.4 g) of mp 167–168°C (lit. (37) mp 175°C; lit. (38) mp 110–112°C); ^{1}H nmr included signals at δ 0.81 (3H, s, C-18 H), 1.12 (3H, s, C-19 H), 3.65 (1H, t, C-17α H), 5.0 (2H, br d, =CH_2), and 5.9 (1H, s, C-4 H) ppm; ^{13}C nmr: see Table 1. *Anal.* calcd. for $C_{20}H_{28}O_2$: C 79.96, H 9.39%; found: C 80.06, H 9.03%.

*5α-Androst-6-ene-3,17-dione (**11**a)*

This was prepared by Jones' oxidation of 5α-androst-6-ene-3β,17β-diol (**17**) (34) (1.3 g). Conventional work-up afforded **11***a* (0.95 g from ethyl acetate), mp 156–158°C; ^{1}H nmr included signals at δ 1.06 (3H, s, C-18 H), 1.2 (3H, s, C-19 H), and 5.5 (2H, ABq, C-6 and -7 H's) ppm; ^{13}C nmr: see Table 1. *Anal.* calcd. for $C_{19}H_{26}O_2$: C 79.68, H 9.15%; found: C 79.79, H 9.32%.

Incubations with R. arrhizus

*Androst-4-en-17β-ol-3-one, acetate (**1**c)*

Incubation of **1***c* (4 g) gave extracts from the growth medium (3.4 g) and mycelia (2.8 g).

Starting material (1.34 g) was recovered from the latter extract as the only isolable steroid. Chromatography of the medium extract (silica gel, benzene/ether gradient) afforded further **1***c* (0.22 g) followed by androst-4-ene-11α,17β-diol-3-one, 17 acetate (**3**) (0.48 g), mp 153–155°C (ethyl acetate/hexane); ^{1}H nmr included signals at δ 0.88 (3H, s, C-18 H), 1.34 (3H, s, C-19 H), 2.06 (3H, s, OAc), 3.8–4.25 (1H, m, C-11β H), 4.66 (1H, t, C-17α H), and 5.77 (1H, s, C-4 H) ppm. *Anal.* calcd. for $C_{21}H_{30}O_4$: C 72.80, H 8.73%; found: C 72.89, H 8.91%. Further elution gave androst-4-ene-6β,17β-diol-3-one, 17 acetate (**2***c*) (0.53 g), mp 206–209°C (ethyl acetate/hexane) (lit. (39) mp 206–208°C); ^{1}H nmr included signals at δ 0.88 (3H, s, C-18 H), 1.50 (3H, s, C-19 H), 2.07 (3H, s, OAc), 4.34 (1H, br s, C-6α H), 4.68 (1H, t, C-17α H), and 5.80 (1H, s, C-4 H) ppm.

*Androsta-4,6-diene-3,17-dione (**4**a)*

Incubation of **4***a* (1.7 g) gave an extract from the growth medium (1.8 g) which was chromatographed as described above. Purification of intermediate fractions by preparative tlc afforded the following quantities of product. 6,7β-Epoxyandrost-4-ene-3,17-dione (**12***a*) (0.23 g), mp 210–213°C. ^{1}H nmr included signals at δ 0.97 (3H, s, C-18 H), 1.25 (3H, s, C-19 H), 3.46 (2H, br s, C-6,7 H's), and 6.18 (1H, s, C-4 H) ppm; ^{13}C nmr: see Table 2. *Anal.* calcd. for $C_{19}H_{24}O_3$: C 75.97, H 8.05%; found: C 75.82, H 7.87%. Androsta-4,6-diene-3,16-dione-17β-ol (**13**) (0.16 g), mp 178–180°C; ^{1}H nmr included signals at δ 0.83 (3H, s, C-18 H), 1.15 (3H, s, C-19 H), 3.81 (1H, s, C-17α H), 5.71 (1H, s, C-4 H), and 6.08 (2H, br s, C-6,7 H's) ppm; ^{13}C nmr: see Table 1. *Anal.* calcd. for $C_{19}H_{24}O_3$: C 75.97, H 8.05%; found: C 75.90, H 8.04%, and androsta-4,6-dien-17β-ol-3-one (**4***b*) (0.16 g), identical with an authentic sample.

*Androsta-4,6-dien-17β-ol-3-one (**4**b)*

Incubation of **4***b* (2 g) afforded extracts from medium (0.85 g) and fungal mycelia (3.01 g). The latter extract gave starting material (1.35 g) on column chromatography. Chromatography of the growth medium extract afforded **4***b* (0.28 g) followed by 6,7β-epoxyandrost-4-ene-17β-ol-3-one (**12***b*) (0.41 g), mp 197–199°C (ethyl acetate–hexane); ^{1}H nmr included signals at δ 0.82 (3H, s, C-18 H), 1.22 (3H, s, C-19 H), 3.34 (2H, s, C-6,7 H's), 3.65 (1H, t, C-17α H), and 6.14 (1H, s, C-4 H) ppm; ^{13}C nmr: see Table 2. *Anal.* calcd. for $C_{19}H_{26}O_3$: C 75.46, H 8.66%; found: C 75.26, H 8.70%.

*Estra-4,6-diene-17β-ol-3-one (**5**a)*

Incubation of **5***a* (1 g) gave extracts from the growth medium (0.85 g) and fungus (0.52 g). The latter afforded recovered **5***a* (0.18 g), while the former extract gave, following chromatography as described above, the following steroids.

Recovered **5***a* (0.48 g), followed by 5,6β-epoxyestr-4-en-17β-ol-3-one (**12***c*) (0.295 g), mp 194–197°C (ethyl acetate/hexane); ^{1}H nmr included signals at δ 0.82 (3H, s, C-18 H), 3.32 and 3.45 (2H, ABq, J = 4 Hz, C-6 and 7 H's), 3.72 (1H, t, C-17α H), and 6.25 (1H, d, J = 1.8 Hz, C-4 H) ppm; ^{13}C nmr: see Table 2. *Anal.* calcd. for $C_{18}H_{24}O_3.H_2O$: C 70.58, H 8.5%; found: C 70.67, H 8.0%. Mass spectrum indicated a molecular ion at m/z 288 of composition $C_{18}H_{24}O_3$. Also eluted was estra-4,6-diene-10β,17β-diol-3-one (**5***b*), mp 237–240°C (dec.) (ethyl acetate); ^{1}H nmr included signals at δ 0.77 (3H, s, C-18 H), 3.55 (1H, t, C-17α H), 5.57 (1H, s, C-4 H), and 6.10 (2H, s, C-6 and 7 H's) ppm; ^{13}C nmr: see Table 1. *Anal.* calcd. for $C_{18}H_{24}O_3$: C 74.97, H 8.39%; found: C 74.97, H 8.57%.

*Androsta-4,6-diene-3β,17β-diol (**6**)*

Incubation of **6** (0.5 g) for 36 h gave extracts from the medium (0.35 g) and fungus (0.2 g). Compound **6** (0.19 g) was recovered from the latter, and the former extract chromatographed to give 6,7β-epoxyandrost-4-en-17β-ol-3-one (**12***b*) (0.11 g), identical with the sample described above.

Can. J. Chem. Downloaded from www.nrcresearchpress.com by 210.87.254.40 on 09/06/12
For personal use only.

*3-(*N*-pyrrolideno)-androsta-3,5-dien-17-one (**9***b*)

Incubation of **9***b* (2.0 g) for 36 h gave **1***a* (0.88 g) from the mycelial extract, and an extract of growth medium (1.54 g) which was chromatographed in the usual way to yield further **1***a* (0.21 g), androst-4-ene-3,6,17-trione (**16**) (0.09 g), androst-4-en-6β-ol-3,17-dione (**2***a*) (0.04 g), and androst-4-en-6α-ol-3,17-dione (**19**) (0.04 g). These compounds were all identical with authentic samples (5). A similar distribution of products was obtained from an incubation in which the *R. arrhizus* enzymes were denatured by autoclaving prior to the addition of substrate.

*5α-Androst-6-ene-3,17-dione (**11**a)*

Incubation of **11***a* (0.9 g) for 64 h gave an extract from the medium (1.3 g) from which **11***a* (0.7 g) was recovered. The medium extract was chromatographed to give 6,7α-epoxy-5α-androstane-3,17-dione (**15***b*) (0.04 g). Crystallization from chloroform–hexane gave a sample of mp 174–176°C; ^{1}H nmr included signals at δ 1.1 (3H, s, C-18 H), 1.16 (3H, s, C-19 H), and 2.8 and 3.2 (2H, m, 6β, 7β H's) ppm; ^{13}C nmr see Table 2. *Anal.* calcd. for $C_{19}H_{26}O_3$: C 75.50, H 8.61%; found: C 75.47, H 8.79%.

*5β-Androst-6-ene-3,17-dione (**11**b)*

Incubation of **11***b* (1 g) for 72 h gave an extract of fungus (0.35 g) from which **11***b* (0.27 g) was recovered, and an extract of growth medium (0.8 g) which was chromatographed to afford further **11***b* (0.23 g) followed by 6,7α-epoxy-5β-androstane-3,17-dione (**14***b*) (0.4 g), mp 165–166°C; ^{1}H nmr included signals at δ 0.86 (3H, s, C-19 H), 0.90 (3H, s, C-18 H), and 3.1 and 3.2 (2H, m, C-6β,7β H's) ppm; ^{13}C nmr: see Table 2. *Anal.* calcd. for $C_{19}H_{26}O_3$: C 75.50, H 8.61%; found: C 75.37, H 8.80%.

The following compounds, on incubation with *R. arrhizus*, gave no detectable trace of biotransformation. Only starting material was recovered in all cases. Estrone (**7**), estra-1,3,5(10),6-tetraene-3-ol-17-one (**8***a*), estra-1,3,5(10),6-tetraene-3,17β-diol (**8***b*), 3-chloro-androsta-3,5-diene-17β-ol, acetate (**9***a*), and 6-methyleneandrost-4-en-17β-ol-3-one (**10**).

Incubations with M. griseocyanus

*Androsta-4,6-dien-17β-ol-3-one (**4**b)*

Incubation of **4***b* (1.2 g) gave an extract of fungus from which **4***b* (0.8 g) was recovered, and a growth medium extract (0.2 g) which by spectral analysis (ir, ^{1}H nmr) was shown to consist of a mixture of starting material (**4***b*) and androsta-4,6-diene-3,17-dione (**4***a*) in approximately equal amounts. This mixture proved difficult to separate and was therefore not investigated further.

*Androsta-4,6-diene-3,17-dione (**4**a)*

Incubation of **4***a* (1 g) gave an extract of growth medium (0.82 g) which was chromatographed to give **4***a* (0.34 g) and 6,7α epoxy-androst-4-ene-3,17-dione (**20**), identical in all respects with an authentic sample (21); ^{13}C nmr: see Table 2.

Epoxidations of Δ^6 steroids

*5α-Androst-6-ene-3β,17β-diol (**17**)*

To an ice-cold, stirred solution of **17** (0.112 g) in dichloromethane (5 mL) was added a solution of *m*-chloroperoxybenzoic acid (0.1 g) in dichloromethane (5 mL). The reaction mixture was stirred overnight and then worked up in the usual manner to give **18** (0.94 g), mp 211–212°C; ^{1}H nmr included signals at δ 0.78 (6H, s, C-18 and -19 H's), 2.65 and 2.88 (2H, m, C-6β,7β H's), and 3.4–3.8 (2H, m, C-3α and 17α H's); ^{13}C nmr: see Table 2. *Anal.* calcd. for $C_{19}H_{30}O_3.H_2O$: C 70.33, H 9.94%; found: C 70.32, H 9.64%.

*5α-Androst-6-ene-3,17-dione (**11**a)*

Reaction of **11***a* (0.112 g) with *m*-chloroperoxybenzoic acid (0.1 g) as described above gave 6,7α-epoxy-5α-androstane-3,17-dione (**15***b*) (0.094 g), identical in all respects with the sample obtained by fungal oxidation of **11***a*.

*5β-Androst-6-ene-3,17-dione (**11**b)*

Reaction of **11***b* (0.286 g) with *m*-chloroperoxybenzoic acid (0.22 g) as described above gave 6,7α-epoxy-5β-androstane-3,17-dione (**14***b*) (0.27 g), identical in all respects with the sample obtained by fungal oxidation of **11***b*.

Acknowledgements

Financial support was provided by the Natural Sciences and Engineering Research Council of Canada. We are grateful to T. Jones of Brock University, to B. Sayer of McMaster University, and to the Southwestern Ontario NMR Centre at the University of Guelph for their assistance in obtaining spectra.

1. K.-C. CHENG and J. B. SCHENKMAN. J. Biol. Chem. **258**, 11738 (1983).
2. H. L. HOLLAND. Chem. Soc. Rev. **11**, 371 (1982).
3. H. L. HOLLAND and B. J. AURET. Can. J. Chem. **53**, 2041 (1975).
4. H. L. HOLLAND and B. J. AURET. Tetrahedron Lett. 3787 (1975).
5. H. L. HOLLAND and P. R. P. DIAKOW. Can. J. Chem. **56**, 694 (1978).
6. H. L. HOLLAND and P. R. P. DIAKOW. Can. J. Chem. **57**, 436 (1979).
7. H. L. HOLLAND and P. R. P. DIAKOW. Can. J. Chem. **57**, 1585 (1979).
8. H. L. HOLLAND. Can. J. Chem. **59**, 1651 (1981).
9. A. W. WOOD, D. E. RYAN, P. E. THOMAS, and W. LEVIN. J. Biol. Chem. **258**, 8839 (1983).
10. D. GHOSH and T. B. SAMANTA. J. Steroid Biochem. **14**, 1063 (1981).
11. R. SATO and T. OMURA (*Editors*). Cytochrome P-450. Academic Press, New York. 1978.
12. D. DUTTA, D. K. GHOSH, A. J. MISHRA, and T. B. SAMANTA. Biochem. Biophys. Res. Commun. **115**, 692 (1983).
13. J. T. GROVES, S. KRISHNAN, G. E. AVARIA, and T. E. NEMO. *In* biomimetic chemistry. *Edited by* D. Dolphin, C. McKenna, V. Murakami, and I. Tabushi. American Chemical Society, Washington, DC. 1980. p. 277.
14. P. R. ORIZ DE MONTELLANO, B. L. K. MANGOLD, C. WHEELER, K. L. KUNZE, and N. O. REICH. J. Biol. Chem. **258**, 4208 (1983).
15. J. R. LINDSAY SMITH and P. R. SLEATH. J. Chem. Soc. Perkin Trans. 2, 1009 (1982).
16. S. DANISHEFSKY, M. PRISBYLLA, and B. LIPISKO. Tetrahedron Lett. **21**, 805 (1980).
17. J. R. HANSON and M. SIVERNS. J. Chem. Soc. Perkin Trans. 1, 1956 (1975).
18. J. W. BLUNT and J. B. STOTHERS. Org. Magn. Reson. **9**, 439 (1977).
19. H. L. HOLLAND and JAHANGIR. Can. J. Chem. **61**, 2165 (1983).
20. D. N. KIRK and M. P. HARTSHORN. Steroid reaction mechanisms. Elsevier, London. 1968. p. 187.
21. H. L. HOLLAND and E. M. THOMAS. Can. J. Chem. **60**, 160 (1982).
22. J. FAVERO, J. MARCHAND, and F. WINTERNITZ. Bull. Soc. Chim. Fr. 312 (1977).
23. M. NUMAZAWA and M. NAGAOKA. Chem. Commun. 530 (1982).
24. A. M. BELL, I. M. CLARK, W. A. DENNY, SIR EWART R. H. JONES, G. D. MEAKINS, W. E. MÜLLER, and E. E. RICHARDS. J. Chem. Soc. Perkin Trans. 1, 2131 (1973).
25. S. K. MALHOTRA and H. J. RINGOLD. J. Am. Chem. Soc. **86**, 1997 (1964).
26. G. SUBRAMANYAN, S. K. MALHOTRA, and H. J. RINGOLD. J. Am. Chem. Soc. **88**, 1332 (1966).
27. H. L. HOLLAND, E. RIEMLAND, and U. DAUM. Can. J. Chem. **60**, 1919 (1982).
28. B. M. BLOOM and G. M. SHULL. J. Am. Chem. Soc. **77**, 5767 (1955).
29. K. SINGH, S. N. SEHGAL, and C. VEZINA. Can. J. Microbiol. **13**, 1271 (1967).
30. S. K. PRADHAN and H. J. RINGOLD. J. Org. Chem. **29**, 601 (1964).
31. J. SCHMITT, J. J. PANOUSE, H. PLUCKET, A. HALLOT, P. J. CORNU, and P. COMOY. Bull. Soc. Chim. Fr. 2768 (1964).

32. F. W. HEYL and M. E. HERR. J. Am. Chem. Soc. **75**, 1918 (1953).
33. D. N. KIRK and D. R. A. LEONARD. J. Chem. Soc. Perkin Trans. 1, 1836 (1973).
34. I. KHATTAK and D. N. KIRK. J. Chem. Soc. Perkin Trans. 1, 2010 (1974).
35. H. J. BRODIE, C. E. HAY, and T. A. WITTSTRUCK. J. Org. Chem. **37**, 3361 (1972).
36. F. NEUMANN, G. ROSENKRANZ, J. ROMO, and C. DJERASSI. J. Am. Chem. Soc. **73**, 5478 (1951).
37. D. N. KIRK and V. PETROW. U.S. Patent No 3,112,305 (Nov. 26th, 1963). Chem. Abstr. **60**, 9337d (1964).
38. R. SCIAKY, U. PALLINI, and B. PATELLI. Gazz. Chim. Ital. **96**, 1268 (1966).
39. C. DJERASSI, G. STORK, G. ROSENKRANZ, and F. SONDHEIMER. U.S. Patent No. 2,885,397 (May 5th, 1959). Chem. Abstr. **54**, 1621h (1960).

Can. J. Chem. Downloaded from www.nrcresearchpress.com by 210.87.254.40 on 09/06/12
For personal use only.

Charge distributions and chemical effects. XXXV. Polyunsaturated hydrocarbons, energy calculations from C-13 nmr spectra

S. FLISZÁR AND G. CARDINAL

Department of Chemistry, Université de Montréal, C.P. 6210, Succ. A, Montreal, Quebec, H3C 3V1

Received March 30, 1984

S. FLISZÁR and G. CARDINAL. Can. J. Chem. **62**, 2748 (1984).

Conjugated and nonconjugated dienes are well described in terms of bond energies featuring explicitly the electronic charges of the bond forming atoms. Using charges deduced from ^{13}C nuclear magnetic resonance shifts, this approach evaluates, ultimately, enthalpies of formation of conjugated molecules from ^{13}C nmr spectra, with an accuracy comparable to that achieved for nonconjugated molecules. The examples include typical dienes (like 1,3-butadiene, isoprene, dimethyl-1,3-butadiene, and 1,3-cyclohexadiene) which permit comparisons with experimental results, as well as predictions for larger systems (e.g., *trans*-1,4,9-decatriene and squalene).

S. FLISZÁR et G. CARDINAL. Can. J. Chem. **62**, 2748 (1984).

Les dienes conjugués et non conjugués sont bien décrits par l'utilisation d'énergies de liaison dépendant explicitement des charges électroniques des atomes liés. Les charges déduites de spectres de résonance magnétique nucléaire du carbone-13 conduisent, finalement, à des enthalpies de formation d'hydrocarbures conjugués avec une précision comparable à celle obtenue pour des molécules non conjuguées. Les systèmes étudiés comprennent des dienes typiques (tels que le butadiène-1,3, l'isoprène, le diméthyl butadiène-1,3 et le cyclohexadiène-1,3) permettant des vérifications expérimentales, ainsi que des prédictions pour des molécules plus complexes (le *trans* décatriène-1,4,9 et le squalène, par exemple).

Can. J. Chem. Downloaded from www.nrcresearchpress.com by 210.87.254.6 on 09/06/12
For personal use only.

Introduction

The theoretical evaluation of molecular energies in terms of electron distributions offers a vivid insight into fundamental, basically simple aspects relating to the nature of chemical bonding. This approach has the merit of permitting calculations at the level of experimental accuracy. Here we describe conjugated and non-conjugated double bond systems, and their energies, using charges deduced from ^{13}C nmr shifts — an approach leading, ultimately, to a calculation of enthalpies of formation from ^{13}C nmr spectra. Of course, the derivation of enthalpies also requires an adequate knowledge about vibrational energy. This, however, is another probem. Let us first look at chemical bonding.

The energy of atomization, ΔE_a^*, of a molecule in its hypothetical vibrationless state at 0 K is well described by a sum of individual bond energy terms,

$$[1] \quad \Delta E_a^* \simeq \sum_{j>i} \epsilon_{ij}$$

This approximation yields valid results because the omitted nonbonded Coulomb-type contributions are small in the first place (typically ~0.02−0.05% of ΔE_a^*), nearly additive and, finally, differ little between structural isomers so that they can easily (although not exactly) be incorporated in the ϵ_{ij}'s (1). For a representative group of 19 alkanes, for example, the average deviation between calculated and experimental ΔE_a^*'s is 0.16 kcal mol^{-1} when nonbonded terms are explicitly taken into account and 0.22 kcal mol^{-1} otherwise (1).

Structural effects are included in the *ij*-bond energy terms through the charges carried by atoms *i* and *j* (1, 2),[1]

$$[2] \quad \epsilon_{ij} = \epsilon_{ij}^0 + a_{ij}\Delta q_i + a_{ji}\Delta q_{ji}$$

So, for example, in ethane and cyclohexane the ϵ_{CC}'s are 69.633 and 72.783 kcal mol^{-1}, respectively, because the C atoms are somewhat electron richer in the latter molecule. It follows from eqs. [1] and [2] that

$$[3] \quad \Delta E_a^* \simeq \Sigma\epsilon_{ij}^0 + \Sigma_i\Sigma_j a_{ij}\Delta q_j$$

where $\Sigma_i\Sigma_j a_{ij}\Delta q_i$ clearly describes the role of atomic charges, showing that structural isomers differing in their electron distributions (as a consequence of changes in their molecular wave functions) differ in the overall stability of their chemical bonds. This approach has proven highly successful in over 120 comparisons with experimental energies (1).

The present study concerns unsaturated hydrocarbons, particular attention being focussed on conjugated dienes, in an analysis involving only the basic physical content summarized in eqs. [2] and [3]. Equation [2] results primarily from an effort in developing simplified realistic models that capture the essence of the phenomena: that bond energies should depend on the charges of the bond-forming atoms comes as no surprise. The question asked here is one regarding the applicability of this approach to conjugated systems, and the way conjugation is perceived in a scheme essentially constructed in terms of localized bonds.

Outline of calculations

To begin with, let us describe the steps involved in numerical applications of eq. [3]. The proper evaluation of atomic charges may often enough turn into a problem (1). Luckily, on many occasions, carefully established correlations between theoretical charges and nuclear magnetic resonance shifts (3) provide the required information. Numerical details are given in Appendix 1, showing that the evaluation of the Δq_i's is straightforward, indeed, for the molecules considered in this work.

The next step consists in a calculation of the appropriate a_{ij}'s. This is done following the methods explained elsewhere (1, 2) and which are summarized in Appendix 2. Table 1 indicates the numerical a_{ij}'s which are required in this study.

The $\Sigma_i\Sigma_j a_{ij}\Delta q_i$ term of eq. [3] is most efficiently evaluated as follows. Using the a_{ij}'s of Table 1, we begin with a calcu-

[1] In eq. [2], ϵ_{ij}^0 is the energy contribution of the bond formed by atoms *i* (with net atomic charge q_i^0) and *j* (with net atomic q_j^0); ϵ_{ij} is the energy of the same type of bond in which, however, the net charges of atoms *i* and *j* differ by Δq_i and Δq_j, respectively, from those of the "reference" bond with energy ϵ_{ij}^0. The a_{ij}'s indicate by how much a bond energy is affected by a unitary change in net charge at atom *i* bonded to *j*.

Can. J. Chem. Downloaded from www.nrcresearchpress.com by 210.87.254.6 on 09/06/12
For personal use only.

TABLE 1. Theoretical a_{ij} parameters, kcal mol^{-1} me^{-1}*

Bond i–j	a_{ij}
C(sp^3)—C(sp^3)	−0.488
C(sp^3)—C(sp^2)	−0.488
C(sp^2)—C(sp^3)	0.275
C(sp^2)—C(sp^2)	0.258
C(sp^2)=C(sp^2)	−0.183
C(sp^3)—H	−0.247
C(sp^2)—H	0.454
H—C(sp^3, sp^2)	−0.632

*Conversion factor: 1 au = 627.51 kcal mol^{-1}.

TABLE 2. Numerical evaluation of $\Sigma_i\Sigma_j a_{ij}\Delta q_i$ for (*E*)-1,3-pentadiene*

Atom i	δ^{TMS}	Δq_i	$\Sigma_j a_{ij}$	$\Sigma_j a_{ij}\Delta q_i$
C-1	113.90	−1.335	0.725	−0.968
C-2	137.45	2.198	0.529	1.162
C-3	132.93	1.520	0.529	0.804
C-4	129.03	0.935	0.546	0.510
C-5	17.55	−1.769	−1.229	2.174
$\Sigma\Delta q_H$		26.152	−0.632	−16.528

*Charges and energies are in me and kcal mol^{-1}, respectively. The sum of all the $\Sigma_i\Sigma_j a_{ij}\Delta q_i$ terms gives $\Sigma_i\Sigma_j a_{ij}\Delta q_i$ = = −12.846 kcal mol^{-1}.

TABLE 3. Reference energies, kcal mol^{-1}, of bonds formed by atoms i and j with net charges as indicated in me*

Bond i—j	Reference charge i	Reference charge j	ϵ_{ij}^0
C(sp^3)—C(sp^3)	35.1	35.1	69.633
C(sp^3)—C(sp^2)	35.1	7.7	77.69
C(sp^2)—C(sp^2)	7.7	7.7	89.70
C(sp^2)=C(sp^2)	7.7	7.7	139.27
C(sp^3)—H	35.1	−11.7	106.806
C(sp^2)—H	7.7	−11.7	110.68

*Results extracted from refs. 1, 2, and 4, except for the C(sp^2)—C(sp^2) bond.

lation of $\Sigma_j a_{ij}$ for each individual carbon atom. (A methyl-C atom attached to another carbon, for example, gives $\Sigma_j a_{ij}$ = 3(−0.247) + (−0.488) = −1.229 kcal mol^{-1} me^{-1}.) By means of the Δq_C's deduced from nmr shifts (Appendix 1), we now obtain $\Delta q_i\Sigma_j a_{ij} = \Sigma_j a_{ij}\Delta q_i$. The sum of these atomic terms over all carbon centers i gives the corresponding part of $\Sigma_i\Sigma_j a_{ij}\Delta q_i$. The contribution of the hydrogens is included in the final result by adding the appropriate $\Sigma_i a_{HC}\Delta q_{Hi} = a_{HC}\Sigma\Delta q_H$ term, where $\Sigma\Delta q_H$ is deduced from charge normalization (Appendix 1). A detailed numerical example is worked out in Table 2, illustrating the simplicity of this approach.

The final step consists in the evaluation of the sum of reference bond energies, $\Sigma\epsilon_{ij}^0$. All the ϵ_{ij}^0's (Table 3) are known from previous work on alkanes (1, 2) and alkenes (1, 4) with one exception, namely, the ϵ_{CC}^0 describing the CC "single" bond formed by two sp^2 carbons at a distance of ~1.46 Å (like the central CC bond in 1,3-butadiene). For the latter, a theoretical estimate (Appendix 3) suggests a value in the neighborhood of ~93 kcal mol^{-1} in a planar conjugated system. This sort of result from SCF data, however, is limited in precision. It turns out, from a comparison with experimental energies, that 89.70 kcal mol^{-1} represents a more realistic estimate, at the very demanding level of experimental accuracy. The agreement with its theoretical counterpart is surely acceptable, considering the uncertainties associated with the latter (Appendix 3).

There is one final point to be considered. Energy calculations (1, 4) indicate that the results for *cis*-, *gem*-disubstituted and trialkylsubstituted ethylenes deviate slightly but consistently from experimental ΔE_a^*'s, quite unlike what is observed for mono-alkyl- and *trans*-dialkylsubstituted ethylenes, and tetramethylethylene. This effect is possibly due to differences in local geometries about the ethylenic carbons (3*b*) and the ensuing changes in hydridization (5) affecting charge-shift relationships (1, 4). Presently, small effects of this sort unfortunately resist their theoretical evaluation, at least at the degree of accuracy required in the present work. For mono-olefins, the simplest way of handling this problem is to treat all olefins as indicated above and to include a correction of +0.56 kcal mol^{-1} into $\Sigma_i\Sigma_j a_{ij}\Delta q_i$ for each double bond presenting a *cis*-, *gem*-disubstitution, or trisubstitution situation (4) — an approach which is followed also in the present study of poly-olefins. This correction is primarily made to accommodate possible users of our methods in thermochemical problems: it does not alter the basic tenet of this theory, i.e., the charge dependence of the individual bond energy contributions which is predicted by eq. [2].

We can now proceed with applications and assess the validity of the methods outlined in this section.

Results

In order to offer valid comparisons with theoretical results, we must first deduce "experimental" atomization energies from experimental enthalpies of formation, ΔH^0_f (gas, 298.15 K), zero-point and heat-content energies, ZPE + H_T − H_0, and from the enthalpies of formation, ΔH^0_f(A), of the atoms. The latter are taken from literature (6), i.e., ΔH^0_f(C) = 170.89 and ΔH^0_f(H) = 52.09 kcal atg^{-1}. The appropriate equation is, for nonlinear molecules, at 298.15 K,

$$[4]\quad \Delta E_a^* = \Sigma n_i[\Delta H^0_f(A_i) - \tfrac{5}{2}RT] + \mathrm{ZPE} + H_T - H_0 - \Delta H^0_f$$

Vibrational energy data are relatively scarce, however. Fortunately they can be constructed to a good approximation by means of additivity rules (1), e.g., ZPE + H_T − H_0 ≃ 33.35 + 18.213(n − 2) − 0.343n_{br} for mono-olefins with n carbon atoms and n_{br} = number of branchings. Similar equations are also found to apply in other homologous series of compounds. Along these lines, we use the following appoximation for dienes, based on the experimental ZPE + H_T − H_0 value (55.19 kcal mol^{-1}) deduced for 1,3-butadiene in the harmonic oscillator approximation (1):

$$[5]\quad \mathrm{ZPE} + H_T - H_0 \simeq 55.19 + 18.213(n-4) - 0.343n_{br}\ \text{kcal mol}^{-1}$$

While this type of estimate usually carries an uncertainty not exceeding ~0.2 kcal mol^{-1}, it remains that for the dienes (as for mono-olefins) no spectroscopic information is presently available which would discriminate ZPE + H_T − H_0 energies of *cis* and *trans* isomers in a reliable manner. It is thus possible that part of the correction of 0.56 kcal mol^{-1} discussed pre-

TABLE 4. Energy analysis of selected diolefins (kcal mol^{-1})*

Molecule	ΔH^0_f	ZPE+$H_T - H_0$	$\Sigma\epsilon^0_{ij}$	$\Sigma_i\Sigma_j a_{ij}\Delta q_i$	ΔE^*_a Calcd.	ΔE^*_a Exptl.
1 1,3-Butadiene	26.33	55.19	1032.32	−22.41	1009.9	1010.1
2 (*Z*)-1,3-Pentadiene	19.77	73.40	1319.75	−14.09	1305.7	1305.6
3 (*E*)-1,3-Pentadiene	18.77	73.40	1319.75	−12.85	1306.9	1306.6
4 Isoprene	18.06	73.06	1319.75	−13.09	1306.7	1306.9
5 1,4-Pentadiene	25.25	73.40	1311.61	−11.61	1300.0	1300.1
6 1,5-Hexadiene	20.11	91.60	1594.86	−0.99	1593.9	1594.0
7 DiMe-1,3-butadiene	10.78	90.93	1607.18	−4.20	1603.0	1602.7
8 1,3-Cyclohexadiene	25.38	77.80	1463.20	10.98	1474.2	1473.7

*The ΔH^0_f values are taken from ref. 7 (**1**–**3**) and ref. 8 (**4**–**8**). The ZPE + $H_T - H_0$ values are deduced following the rules given in ref. 1, as indicated in the text. The appropriate ^{13}C nmr shifts are literature values (see Appendix 1).

NOTE ADDED IN PROOF. From experimental Raman and infrared vibrational frequencies given by Compton *et al.* (27), we find in the harmonic oscillator approximation that ZPE + $H_T - H_0$ = 73.32 kcal mol^{-1} for **3**. Similarly, we find for **2** that ZPE + $H_T - H_0$ = 73.28 kcal mol^{-1}, using experimental frequencies given by the same authors and results calculated by Panchenko *et al.* (28). Finally, using frequencies calculated by the latter authors and, whenever available, experimental results from Durig and Compton (29), we find for **7** that ZPE + $H_T - H_0$ = 91.08 kcal mol^{-1}.

TABLE 5. Predicted energies (kcal mol^{-1}) of selected di- and polyolefins*

Molecule	$\Sigma\epsilon^0_{ij}$	$\Sigma_i\Sigma_j a_{ij}\Delta q_i$	ΔE^*_a	ZPE+$H_T - H_0$	ΔH^0_f
1 (*E*,*E*)-2,4-Hexadiene	1607.18	−3.61	1603.57	91.60	10.57
2 (*Z*,*E*)-2,4-Hexadiene	1607.18	−4.68	1602.50	91.60	11.64
3 (*Z*,*Z*)-2,4-Hexadiene	1607.18	−6.07	1601.11	91.60	13.03
4 2-Me-1,5-Hexadiene	1882.29	8.49	1890.78	109.47	11.86
5 3-Me-1,5-Hexadiene	1878.10	10.79	1888.89	109.47	13.75
6 3-Me-1,5-Heptadiene	2165.53	20.00	2185.53	127.68	5.95
7 2,5-diMe-1,5-Hexadiene	2169.71	18.01	2187.72	127.34	3.42
8 2,5-diMe-2,4-Hexadiene	2182.03	13.95	2195.98	127.34	−4.84
9 1,7-Octadiene	2161.35	19.64	2180.99		
10 1,9-Decadiene	2727.84	40.40	2768.24		
11 *trans*-1,4,9-Decatriene	2607.72	17.66	2625.38		
12 Squalene	7945.75	146.48	8092.23		

*The ^{13}C nmr spectra used in these calculations are from ref. 10 (**1**–**3**), ref. 11 (**4**–**11**), and ref. 12 for **12**.

viously covers, in fact, an incomplete description of vibrational energy contributions. Additional spectroscopic analyses would be highly desirable in this area.

With these (minor) reservations in mind, we can now compare atomization energies derived from experimental data with their counterparts deduced from eq. [3]. The results are indicated in Table 4. The average deviation (0.23 kcal mol^{-1}) between calculated and experimental results is well within experimental uncertainty limits and resembles the outcome of earlier energy analyses presented for paraffins, six-membered cycloalkanes, olefins, ethers, and carbonyl compounds (1).

The quality of these results certainly encourages us to offer predictions for related systems (Table 5). The validity of calculated enthalpies rests, of course, largely with the approximations involved in the estimate of ZPE + $H_T - H_0$ energies. The use of vibrational energies constructed on the basis of regular group increments may be regarded acceptable in simple cases like those investigated here (1). However, one should refrain from extrapolations in very large or highly crowded systems until these are adequately supported by spectroscopic evidence. Reversing the approach, one could profit from additional experimental enthalpies of formation obtained by traditional thermochemical methods and/or from appropriate enthalpies of hydrogenation and thus gain access to a new generation of ZPE + $H_T - H_0$ energies using eq. [4] and calculated atomization energies. This type of information would be valuable because it would extend our knowledge concerning ZPE + $H_T - H_0$ energies, and their construction from empirical rules, to classes of compounds which are presently beyond what can be safely inferred from the body of "small" molecules considered in this study. This being said, the predicted ΔH^0_f values given in Table 5 should represent reasonably good estimates.

In selecting the conjugated hydrocarbons indicated in Tables 4 and 5, attention was given to their geometry, essentially planar in their preferred conformations, in order to avoid situations disrupting conjugation. The exception is offered by 1,3-cyclohexadiene, in which a slight departure from planarity (~12–18°) appears to be real for the double bond system (9), thus allowing a staggered conformation for the CH bonds of the two CH_2 groups. Indeed, our calculation appears to overestimate the stability of this compound by a small margin: this could perhaps be taken as an indication for a partial loss in conjugation although, evidently, only limited weight should be given to the numerical value (~0.5 kcal mol^{-1}) describing this discrepancy. Comments on the disruption of conjugation due to changes in geometry are offered further below.

First, it appears interesting to draw attention on a simple method which, besides being instructive in its own way, per-

Can. J. Chem. Downloaded from www.nrcresearchpress.com by 210.87.254.6 on 09/06/12
For personal use only.

TABLE 6. Charge effects in saturated and unsaturated hydrocarbons, the $\Sigma_i\Sigma_j a_{ij}\Delta q_i$ results (kcal mol^{-1}) are "reduced" values*

Parent alkane	$\Sigma_i\Sigma_j a_{ij}\Delta q_i$	Unsaturated hydrocarbon	$\Sigma_i\Sigma_j a_{ij}\Delta q_i$
C_4 Butane	20.82	1-Butene	19.57
		(*Z*)-2-Butene	20.84
		(*E*)-2-Butene	22.01
		1,3-Butadiene	20.90
C_5 Pentane	31.25	1-Pentene	30.18
		(*Z*)-2-Pentene	31.65
		(*E*)-2-Pentene	32.49
		(*Z*)-1,3-Pentadiene	33.41
		(*E*)-1,3-Pentadiene	34.65
		1,4-Pentadiene	27.75
C_{10} Decane	81.31	1-Decene	82.34
		(*E*)-5-Decene	85.06
		1,9-Decadiene	79.76
		(*E*)-1,4,9-Decatriene	80.88
C_6 Cyclohexane	60.60	Cyclohexene	60.59
		1,3-Cyclohexadiene	62.66
		1,4-Cyclohexadiene	59.90

*The value quoted for 1,4-cyclohexadiene is for $\Delta E_a^* = 1471.42$ kcal mol^{-1}, calculated from the ^{13}C nmr spectrum given in ref. 11; assuming ZPE + $H_T - H_0 = 77.8$ kcal mol^{-1} (1), this result corresponds to $\Delta H^0_f = 27.7$ kcal mol^{-1} (1) (gas, 298.15 K). The value for 1-decene was obtained from the experimental ΔE_a^*, eq. [4], using $\Delta H^0_f = -29.48$ kcal mol^{-1} (8) and that for (*E*)-5-decene was deduced from its ^{13}C nmr spectrum (11). The result indicated for decane corresponds to $\Delta H^0_f = -59.64$ kcal mol^{-1} (8). The results for butane, pentane, cyclohexane, and the butene and pentene isomers are extracted from ref. 1. Numerous additional examples follow from $\Sigma_i\Sigma_j a_{ij}\Delta q_i$ results for alkanes and alkenes (1, 2, 4, 13) and those indicated in Tables 4 and 5.

mits a back-of-the-envelope check of ΔE_a^* energies calculated from eq. [3].

Dehydrogenation of hydrocarbons

Up to this point, the appropriate $\Sigma\epsilon_{ij}^0$ sums were deduced from the set of reference bond energies indicated in Table 3. The $\Sigma_i\Sigma_j a_{ij}\Delta q_i$ terms given in Tables 4 and 5 were calculated accordingly. However, one could have selected a simpler set of reference bond energies, namely, the 69.633 value for all CC single bonds, 139.27 for the CC double bond, and 106.806 kcal mol^{-1} for all CH bonds. The latter reference set was, indeed, used in earlier work on olefins (1, 4). Its use renders energy calculations somewhat more involved than those presented in this study because the changes from 69.633 to 77.69 and from 106.806 to 110.68 kcal mol^{-1} for CC and CH bonds, respectively, accompanying the replacement of an sp^3 by an sp^2 carbon, become part of the $\Sigma_i\Sigma_j a_{ij}\Delta q_i$ term. It is instructive to examine the latter $\Sigma_i\Sigma_j a_{ij}\Delta q_i$ term, identified here as "reduced" term. In order to derive it, we calculate ΔE_a^* as shown in this work (which is the "easy" way) and subtract the appropriate $\Sigma\epsilon_{ij}^0$ part involving only $\epsilon_{CC}^0 = 69.633$ (for any single CC bond), $\epsilon_{CH}^0 = 106.806$ (for any CH bond), and $\epsilon_{C=C}^0 = 139.27$ kcal mol^{-1} for each double bond. The results are indicated in Table 6.

The results are self-explanatory. It appears, indeed, that dehydrogenation does not affect the "reduced" $\Sigma_i\Sigma_j a_{ij}\Delta q_i$ energy contribution if we are ready to accept, at this rough level of approximation, discrepancies of a few kcal mol^{-1}. The "quasi constancy" of the "reduced" $\Sigma_i\Sigma_j a_{ij}\Delta q_i$ term during dehydrogenation draws attention on the $\Sigma\epsilon_{ij}^0$ part of eq. [3]: the removal to two CH bonds (-2×106.806) and the replacement of a single CC bond (-69.633) by a double bond ($+139.27$ kcal mol^{-1}) translates into a decrease of $\sim$144 kcal mol^{-1} in ΔE_a^* energy. Briefly, it suffices to subtract $\sim$144 kcal mol^{-1} from the atomization energy of a hydrocarbon in order to obtain a rough estimate for the ΔE_a^* of the corresponding dehydrogenated parent compound. For example, *n*-decane ($\Delta E_a^* = 3057.74$ kcal mol^{-1}) yields estimates of 2769.7 kcal mol^{-1} for decadiene and 2625.7 kcal mol^{-1} for decatriene, in satisfactory agreement with the results given in Table 5. This regularity enables a rapid cross-checking of ΔE_a^* results. More generally, however, it shows the link relating to one another the various classes of saturated and unsaturated hydrocarbons, including allenic, acetylenic, and aromatic hydrocarbons (13).

Conjugation

The electron diffraction investigation of the molecular structure of 1,3-butadiene vapor indicates that the planar *trans* form is predominating: no signs of other conformations were observed (14), a result which is convincingly suported by *ab initio* MO theory (15), at the level of minimal (STO-3G) and extended (4−31G, 6-31G, 6-31G*, (7*s*3*p*|3*s*), and larger) basis set calculations. Structural parameters were determined (14, 16), namely, r(C—C) = 1.463 ± 0.003, r(C=C) = 1.341 ± 0.002, and r(C—H) = 1.090 ± 0.004 Å. While the double bond is, in essence, that of ethylene itself (a fact which led us to treat all double bonds on the same footing), the single CC bond of 1,3-butadiene is significantly shorter than the "usual" single bonds, i.e., those formed by two sp^3 carbon atoms. The short CC single bond and the planar equilibrium conformation have been attributed to π-electron delocalization which gives the single bond some amount of double bond character and is most effective in the planar molecule (17). It became apparent, however, that delocalization was less than predicted by the simple Hückel method (18) and the CC bond shortening was then attributed to the change in hybridization of the bond-forming atoms (19). These points merit attention in the interpretation of anticipated energy effects resulting from steric constraints which would force non-coplanarity of the two double bond systems.

Extended basis set SCF MO calculations indicate that, indeed, resonance is the main factor responsible for the shortening of the CC single bond in the planar *s-trans* conformation of 1,3-butadiene (20, 21). In this conformation the distinction between σ and π electrons is evident. For the perpendicular case, on the other hand, it is always possible to define one localized π MO on each C=C fragment. The SCF localized π MO located on one of the C=C moieties has σ tails on the other C=C fragment and the σ MO's of each C=C moiety have components on the $2p_y$ atomic orbitals associated with the other fragment. This effect which is known as hyperconjugation has been found to stabilize the perpendicular form, largely compensating the lack of π conjugation, and leads to a similar shortening of the central CC bond (21).

Ab initio analyses thus substantiate the concept of π conjugation in the planar conformation and extend it to hyperconjugation in perpendicular forms. Direct calculations of resonance energies lead to estimates in the neighborhood of $\sim$10 kcal mol^{-1} (20, 21). Here, resonance energy is defined in its original sense as the energy difference between the conjugated system and its reference state without resonance, the latter being represented by a model wave function consisting of strictly localized nonresonating π molecular orbitals. Hyperconjugation energy is defined in similar manner (21). The hyperconjugative stabilization in the perpendicular form at

Can. J. Chem. Downloaded from www.nrcresearchpress.com by 210.87.254.6 on 09/06/12
For personal use only.

Can. J. Chem. Downloaded from www.nrcresearchpress.com by 210.87.254.6 on 09/06/12
For personal use only.

its SCF optimum distance (~1.5 Å) turns out to be almost as large (~8.0 kcal mol^{-1}) as the π conjugation energy in the equilibrium planar conformation (~10.4 kcal mol^{-1} at ~1.48 Å) (21). This change from resonance to hyperconjugative stabilization of the central CC bond, however, is not reflected in the $\Sigma_i\Sigma_j a_{ij}\Delta q_i$ term because the latter considers only the effects of varying electron populations at the bond-forming atoms under otherwise identical conditions. Rather, the change in geometry from a planar to a nonplanar form which is at the origin of the loss in conjugation in favor of a hyperconjugative stabilization should be contained in an appropriate change in the reference bond energy ϵ^0_{CC}.

The extent of the change in ϵ^0_{CC}, however, is difficult to evaluate theoretically. A valuable rough estimate is offered by the SCF results discussed above (21) indicating that hyperconjugative stabilization is less effective (by ~2.4 kcal mol^{-1}) than π conjugation. This estimate is similar to the familiar thermochemical resonance energy of some 3 kcal mol^{-1} (22) and suggests that the reference bond energy ϵ^0_{CC} in a markedly nonplanar situation should be lower by approximately that amount relative to that applicable in a planar resonating arrangement.

While π conjugation and/or hyperconjugation are certainly important contributions to the thermochemical stability of CC single bonds embedded in double bond systems, molecules featuring this arrangment (e.g., 1,3-butadiene) still appear to be strongly localized (i.e., poorly conjugated). Of course, this fact is well known from simple π-Hückel theory with equal CC resonance integrals leading to alternating π bond orders. In this sense, keeping in mind the features linked to π conjugation vs. hyperconjugation revealed by SCF theory, it remains valid to apply our bond energy scheme, eqs. [1]–[3], to conjugated systems. The understanding, however, is that π conjugation and/or hyperconjugation effects must be adequately included in the appropriate ϵ^0_{CC} terms.

Conclusion

It is concluded that our bond energy scheme featuring explicitly the charges of the bond-forming atoms can be applied successfully to conjugated hydrocarbons, with an accuracy comparable to that achieved for nonconjugated molecules. In essence, the calculations are carried out in precisely the same manner as for monoolefins. The only new term involved is that of the bond energy contribution, ϵ^0_{CC} = 89.7 kcal mol^{-1}, describing a conjugated CC bond in planar arrangement of the unsaturated moieties. Extention of these views to aromatic hydrocarbons is to be presented shortly.

Acknowledgements

The financial assistance given by the National Research Council of Canada and the cooperation of the "Centre de Calcul de l'Université de Montréal" are gratefully acknowledged.

1. S. FLISZÁR. Charge distributions and chemical effects. Springer-Verlag, New York, NY. 1983.
2. S. FLISZÁR. J. Am. Chem. Soc. **102**, 6946 (1980); S. FLISZÁR. Int. J. Quantum. Chem. In press.
3. S. FLISZÁR, G. CARDINAL, and M.-T. BÉRALDIN. J. Am. Chem. Soc. **104**, 5287 (1982); H. HENRY and S. FLISZÁR. J. Am. Chem. Soc. **100**, 3312 (1978); S. FLISZÁR. Can. J. Chem. **54**, 2839 (1976); S. FLISZÁR, A. GOURSOT, and H. DUGAS. J. Am. Chem. Soc. **96**, 4358 (1974).
4. M.-T. BÉRALDIN and S. FLISZÁR. Can. J. Chem. **61**, 197 (1983).
5. A. VEILLARD and G. DEL RE. Theor. Chim. Acta, **2**, 55 (1964); G. DEL RE, U. ESPOSITO, and M. CARPENTIERI. Theoret. Chim. Acta, **6**, 36 (1966); K. B. WIBERG. Tetrahedron, **24**, 1083 (1968); C. TRINDLE and O. SINANOĞLU. J. Chem. Phys. **49**, 65 (1968); C. TRINDLE and O. SINANOĞLU. J. Am. Chem. Soc. **91**, 853 (1969).
6. D. R. STULL and G. C. SINKE. Adv. Chem. Ser. **18** (1956).
7. S. W. BENSON, F. R. CRUIKSHANK, D. M. GOLDEN, G. R. HAUGEN, H. E. O'NEAL, A. S. RODGERS, R. SHAW, and R. WALSH. Chem. Rev. **69**, 279 (1969).
8. J. D. COX and G. PILCHER. Thermochemistry of organic and organometallic compounds. Academic Press, London, New York. 1970.
9. S. SAEBO and J. E. BOGGS. J. Mol. Struct. **73**, 137 (1981); U. BURKERT and N. L. ALLINGER. Molecular mechanics. ACS Monograph **177**, Am. Chem. Soc., Washington, DC. 1982.
10. J. W. DE HANN and L. J. M. VAN DE VEN. Org. Magn. Res. **5**, 147 (1973).
11. Sadtler standard carbon-13 NMR spectra, Sadtler Research Laboratories Inc., Philadelphia, PA.
12. F. J. WEIGERT, M. JAUTELAT, and J. D. ROBERTS. Proc. Nat. Acad. Sci. U.S. **60**, 1152 (1968).
13. S. FLISZÁR. Can. J. Chem. **61**, 2679 (1983).
14. A. ALMENNINGEN, O. BASTIANSEN, and M. TRAETTEBERG. Acta Chem. Scand. **12**, 1221 (1958); V. SCHOMAKER and L. PAULING. J. Am. Chem. Soc. **61**, 1769 (1939); D. J. MARAIS, N. SHEPPARD, and B. P. STOICHEFF. Tetrahedron, **17**, 163 (1962); A. R. H. COLE, G. M. MOHAY, and G. A. OSBORNE. Spectrochim. Acta, A**23**, 909 (1967).
15. W. J. HEHRE and J. A. POPLE. J. Am. Chem. Soc. **97**, 6941 (1975); L. RADOM and J. A. POPLE. J. Am. Chem. Soc. **92**, 4786 (1970); U. PINCELLI, B. CALDOLI, and B. LEVY. Chem. Phys. Lett. **13**, 249 (1972); B. DUNBACHER. Theoret. Chim. Acta, **23**, 346 (1972); P. N. SKANCKE and J. E. BOGGS. J. Mol. Struct. **16**, 179 (1973).
16. K. KUCHITSU, T. FUKUYAMA, and Y. MORINO. J. Mol. Struct. **1**, 463 (1967); W. HAUGEN and M. TRAETTEBERG. Acta Chem. Scand. **20**, 1726 (1966).
17. C. A. COULSON. Proc. R. Soc. A**169**, 413 (1939).
18. R. S. MULLIKEN. Tetrahedron, **6**, 68 (1959).
19. S. SKAARUP, J. E. BOGGS, and P. N. SKANCKE. Tetrahedron, **32**, 1179 (1976); B. M. MIKHAILOV. Tetrahedron, **21**, 1277 (1965); M. J. S. DEWAR and H. N. SCHMEISING. Tetrahedron, **5**, 166 (1959); H. J. BERNSTEIN. Trans. Faraday Soc. **67**, 1649 (1961); C. W. SHEER. J. Chem. Phys. **21**, 1582 (1953); H. C. LONGUET-HIGGINS and L. SALEM. Proc. R. Soc. A **251**, 172 (1959); A. JULG, P. FRANÇOIS, and R. MOURRE. J. Chim. Phys. **59**, 1363 (1962); P. C. DEN BOER-VEENENDAAL and D. H. DEN BOER. Theoret. Chim. Acta, **6**, 354 (1966).
20. H. KOLLMAR. J. Am. Chem. Soc. **101**, 4832 (1979).
21. J. P. DAUDEY, G. TRINQUIER, J. C. BARTHELAT, and J. P. MALRIEU. Tetrahedron, **36**, 3399 (1980).
22. G. W. WHELAND. Resonance in organic chemistry. Wiley, New York, NY. 1955.
23. J. B. STOTHERS. Carbon-13 NMR spectroscopy. Academic Press, New York, NY. 1972.
24. K. HASEGAWA, R. ASAMI, and K. TAKAHASHI. Bull. Chem. Soc. Jpn. **51**, 916 (1978).
25. D. A. LIGHTNER and B. V. CRIST. Spectrochem. Acta, **38**A, 867 (1982).
26. A. JULG and M. BÉNARD. Tetrahedron, **24**, 5575 (1968).
27. D. A. C. COMPTON, W. O. GEORGE, and W. F. MADDAMS. J. Chem. Soc. Perkin II, 1311 (1977).
28. YU. N. PANCHENKO, V. I. MOCHALOV, P. CSÁSZÁR, F. TÖRÖK, E. BENEDETTI, and M. AGLIETTO. Acta Chim. Hung. **114**, 149 (1983).
29. J. R. DURIG and D. A. C. COMPTON. J. Phys. Chem. **83**, 2879 (1979).

TABLE A1. Carbon-13 nmr shifts used in the calculation of the results indicated in Table 4*

Molecule	Chemical shift (ppm from TMS)					
	C-1	C-2	C-3	C-4	C-5	C(CH_3)
1 1,3-Butadiene	116.6	137.2				
2 (*Z*)-1,3-Pentadiene	116.08	132.21	130.62	126.07	12.87	
3 (*E*)-1,3-Pentadiene	113.90	137.45	132.93	129.03	17.55	
4 Isoprene	113.4	142.9	140.3	116.4		17.6
5 1,4-Pentadiene	115.0	136.4	40.0			
6 1,5-Hexadiene	114.1	137.3	36.0			
7 DiMe-1,3-butadiene	113.0	143.8				20.3
8 1,3-Cyclohexadiene	126.02	124.30			22.07	

*The C-13 results are taken from ref. 23 (**1**, **5**, **6**), ref. 10 (**2**, **3**), ref. 24 (**4**, **7**), and ref. 25 (**8**).

Appendix 1

Evaluation of atomic charges

For typical sp^3 carbons (such as in linear and branched paraffins and six-membered cycloalkanes), the change in net charge (Δq_C) with reference to the ethane-C atom is deduced from eq. [A1] (1)

$$[A1] \quad \Delta q_C(sp^3) = -0.148\delta^{C_2H_6} \text{ me}$$

where $\delta^{C_2H_6}$ is the ^{13}C nmr shift relative to ethane (~5.6 ppm from TMS). Similarly, for ethylenic sp^2 carbons, we use (1, 4)

$$[A2] \quad \Delta q_C(sp^2) \simeq 0.15\delta^{C_2H_4} \text{ me}$$

where $\delta^{C_2H_4}$ is the shift relative to ethylene (taken at 122.8 ppm from TMS) and Δq_C is the change in net charge relative to the ethylene-C atom. The validity of eq. [A1] is well supported by theoretical charges (1, 3) and by numerous energy calculations relying on charges derived from this expression. Its accuracy is important because the saturated hydrocarbon part of organic molecules usually controls a major portion of $\Sigma_i\Sigma_j a_{ij}\Delta q_i$. Unfortunately, the validity of eq. [A2] is presently not assessed as firmly as desired. However, charge contributions of sp^2 carbons generally turn out to be relatively modest so that calculated $\Delta E_a^{\ddagger}$s are not invalidated by uncertainties associated with eq. [A2] — as illustrated by the results obtained for mono-olefins (4).

As regards the hydrogen atoms, we proceed as follows. First, the carbon net charges are calculated from $q_C(sp^3) = 35.1 - 0.148\delta^{C_2H_6}$ and $q_C(sp^2) = 7.7 + 0.15\delta^{C_2H_4}$ me, where 35.1 = C net charge in ethane (1, 2) and 7.7 = ethylene-C net charge (4), in me units. Using these results, the sum (over all C atoms) Σq_C is formed, giving

$$\Sigma q_H = -\Sigma q_C$$

Next, we calculate what the *total* net charge of all the hydrogen atoms of the molecule would have been, had each H net charge been taken at its reference value, −11.7 me (i.e., the H net charge in ethane). Briefly, we calculate $-11.7n_H$, with n_H = number of H atoms in the molecule under scrutiny. (This selection of a reference H charge imposes a constraint in the definition of reference CH bond energies, ϵ_{CH}^0, which is properly taken into account). Finally, we obtain

$$[A3] \quad \Sigma\Delta q_H = \Sigma q_H + 11.7n_H \text{ me}$$

for use in the calculation of $\Sigma_i a_{HC}\Delta q_{Hi} = a_{HC}\Sigma\Delta q_H$.

For the readers' convenience, we indicate in Table [A1] selected ^{13}C nmr results which are used in this work.

Appendix 2

The a_{ij} parameters are deduced from the expression (1, 2)

$$a_{ij} = \frac{1}{\nu_i}\frac{3/7}{K_i^{mol}}\left[\left(\frac{\partial E_i^{vs}}{\partial N_i}\right)^0 - \frac{1}{2}\left(\frac{\partial^2 E_i^{vs}}{\partial N_i^2}\right)^0 \Delta q_i\right] - \frac{3}{7}Z_i^{eff}\langle r_{ij}^{-1}\rangle^0$$

For small Δq_i's (as for C and H), the second order derivative of E_i^{vs} (the valence state energy of atom i) with respect to N_i (the electron population of i) can be safely neglected. The first derivatives $(\partial E_i^{vs}/\partial N_i)^0$ are (from SCF-Xα calculations) −0.735 for C(sp^3), −0.244 for C(sp^2)-π electrons, −0.375 for C(sp^2)-σ electrons and −0.195 au (hartrees) for hydrogen (1, 2, 4). The other quantities are: ν_i = number of atoms bonded to i; K_i^{mol} = constant for each atomic species (= 1/2 for H, ~3/7 for any other atom); Z_i^{eff} = effective nuclear charge of atom i (1 for H, 4 for C); $\langle r_{ij}^{-1}\rangle^0$ = average inverse distance between the electrons of i and nucleus Z_j, corresponding to r_{CH} = 1.08 (σ electrons of sp^3 or sp^2C), r_{CH} = 1.10 (π electrons of sp^2 carbon), r_{CC} = 1.53 (sp^3—sp^3), r_{CC} = 1.34 (sp^2—σ electrons) and r_{CC} = 1.30 (sp^2—π electrons) for double bonds, r_{CC} = 1.46 (sp^2—sp^2 single bond) for σ electrons, viz. 1.48 for π electrons, r_{CC} (sp^2—sp^3) = 1.53 for σ electrons, and 1.55 Å for π electrons of the sp^2 carbon atom. The conversion factors 1 bohr = 0.529 Å and 1 hartree = 627.51 kcal mol^{-1} were used. For ethylenic sp^2 carbons, the appropriate average a_{ij}'s (Table 1), accounting for the fact that electron populations vary at both the σ and π levels, are deduced from the equation (4)

$$a_{ij} = (ma_{ij}^{\sigma} + a_{ij}^{\pi})/(m + 1)$$

with $m = -0.955$. These parameters are precisely those which were described and used in earlier calculations of saturated and unsaturated hydrocarbons.

Appendix 3

The reference bond energies are deduced from the equation (1, 2)

$$[A4] \quad \epsilon_{ij} = K_i^{mol}Z_i\left(\frac{\partial\epsilon_{ij}}{\partial Z_i}\right) + K_j^{mol}Z_j\left(\frac{\partial\epsilon_{ij}}{\partial Z_j}\right) + (K_i^{at} - K_i^{mol}) \times V_{ne}(\text{at } i)/\nu_i + (K_j^{at} - K_j^{mol})V_{ne}(\text{at } j)/\nu_j$$

where V_{ne} (at i) and V_{ne} (at j) are the nuclear−electronic potential energies of the isolated atoms i and j, respectively, and ν_i, ν_j the number of bonds these atoms form in the molecule. The constants K_i^{mol} (=0.4287 for C and 1/2 for H atoms in the molecule) and K_i^{at} (= 0.4276 for C and 1/2 for H, referring to isolated ground-state atoms) were deduced (1, 2) from near Hartree−Fock results. The derivatives $(\partial\epsilon_{ij}/\partial Z_i)$ are obtained from the equation (1, 2)

Can. J. Chem. Downloaded from www.nrcresearchpress.com by 210.87.254.6 on 09/06/12
For personal use only.

TABLE A2. Optimized structure of *trans*-1,3-butadiene in the $[5s3p|3s]$ basis set

Parameter	Calculated value	
	$[5s3p\|3s]$	Skaarup (19)
r(C—C)	1.4704 Å	1.453 Å
r(C=C)	1.3249	1.320
r(C$_2$—H)	1.0758	1.074
r(C$_1$—H)(Z)	1.0741	1.073
r(C$_1$—H)(E)	1.0717	1.071
∠C—C=C	124.34°	124.7°
∠C=C—H(E)	121.85	121.8
∠C=C—H(Z)	121.91	121.8
∠C=C$_2$—H	119.65	119.6

[A5] $$Z_i\Sigma_j\left(\frac{\partial\epsilon_{ij}}{\partial Z_i}\right) \simeq V_{ne}(\text{at } i) - V(i, \text{mol})$$

where, in conventional notations,

$$V(i, \text{mol}) = -Z_i\int\frac{\rho(\boldsymbol{r})}{|\boldsymbol{r} - \boldsymbol{r}_i|}d\boldsymbol{r} + Z_i\sum_{j\neq i}Z_j/r_{ij}$$

is the total (nuclear−electronic and nuclear−nuclear) potential energy involving Z_i, where r_{ij} is the ij internuclear distance.

From $[5s3p|3s]$ SCF results we obtain V_{ne}(at C) = −87.9315 au as well as $\partial\epsilon_{CH}/\partial Z_C \simeq 0.026$ au (1, 2, 13). For 1,3-butadiene in its optimized geometry (using the same basis set), it is found that $V(i, \text{mol}) = -88.42836$ and −88.34076 au for carbons 1 and 2, respectively. Applying eq. [A5] it follows that $\partial\epsilon_{C=C}/\partial Z_C \simeq 0.0308$ au (C-1) and $\partial\epsilon_{C=C}/\partial Z_C + \partial\epsilon_{C-C}/\partial Z_C \simeq 0.0422$ au (C-2). Using these results and eq. [A4] it is found that the sum of the two double bonds plus the CC single bond in butadiene amounts to ~357 kcal mol^{-1}. On the other hand, the ethylenic double bond is ~133.7 kcal mol^{-1} in this basis set (1, 2, 13), giving an estimate of ~89.6 kcal mol^{-1} for the central CC bond. This bond energy is thus 1.343 times that of the ethane CC bond calculated in the same way (66.7 kcal mol^{-1}). Finally, referring now to the appropriate CC bond in ethane (69.633 kcal mol^{-1}), present results lead to an estimate of ~93.5 kcal mol^{-1} for the central CC bond in butadiene. This estimate, however, is not yet the final one. Using eq. [2] and the appropriate a_{ij}'s of Table 1, the charges deduced from $\delta^{C_2H_4} = -6.2$ and 14.4 ppm for C-1 and C-2, respectively, indicate that each butadiene double bond energy is 0.225 kcal mol^{-1} less than that of ethylene (which was used in this evaluation), whereas the central CC bond in butadiene is 1.11 kcal mol^{-1} larger than what would be the case for two sp^2 carbons having the same charge as in ethylene. Taking these corrections into consideration, the final estimate of ϵ^0_{CC} must be lowered by 1.11−0.45 = 0.66 kcal mol^{-1}, giving ~92.9 kcal mol^{-1}. This sort of theoretical prediction is perforce limited in precision. It appears nonetheless to be a realistic one, as indicated by its empirical counterpart, 89.70 kcal mol^{-1}. Possible slight changes of the corresponding C(sp^2)—C(sp^2) bond distance in higher polyenes should not affect the validity of this estimate because any anticipated effect would only be minor (1, 26).

In the $[5s3p|3s]$ contracted basis set, the optimized geometry is as indicated in Table A2. The virial theorem is reasonably well satisfied ($V/T = -1.9989$), which is important because this theorem, as well as the Hellmann−Feynman theorem applied to molecules at equilibrium, are part of the derivation of eqs. [A4] and [A5].

Can. J. Chem. Downloaded from www.nrcresearchpress.com by 210.87.254.6 on 09/06/12
For personal use only.

Binuclear copper(II) complexes of the ligand 1,4-di(1′-methyl-2′-imidazolyl)phthalazine. Structure and magnetism of a hydroxy bridged derivative[1]

LAURENCE KENNETH THOMPSON,[2] FREDERICK W. HARTSTOCK, AND PHILLIP ROBICHAUD
Department of Chemistry, Memorial University of Newfoundland, St. John's, Nfld., Canada A1B 3X7

AND

A. W. HANSON
Atlantic Research Laboratory, National Research Council of Canada, 1411 Oxford St., Halifax, N.S., Canada B3H 3Z1

Received January 26, 1984

LAURENCE KENNETH THOMPSON, FREDERICK W. HARTSTOCK, PHILLIP ROBICHAUD, and A. W. HANSON. Can. J. Chem. **62**, 2755 (1984).

The synthesis and study of a series of copper(II) complexes of a biologically relevant binucleating ligand, 1,4-di(1′-methyl-2′-imidazolyl)phthalazine (MIP) is reported. The binuclear complex $[Cu_2(MIP)(OH)Cl_3(H_2O)]H_2O$ has been characterized by single crystal X-ray diffraction and belongs to the space group $P2_1/n$ with $a = 10.063(1)$, $b = 20.967(1)$, $c = 9.919(1)$ Å, $\beta = 96.48(1)°$, $V = 2079.4$ Å^3, $Z = 4$. The copper coordination geometry is square pyramidal and the two copper(II) centres are bridged by two groups: N_2 (phthalazine) and hydroxide. A large metal–metal separation (3.425 Å) and Cu—O—Cu bridge angle (126.2°) are considered to be a dominant factor responsible for the very large antiferromagnetic exchange present in this system ($-2J = 800$ cm^{-1}). A comparison of $-2J$ and the Cu—O—Cu bridge angle shows that for a related series of complexes with the same basic binuclear centre and a $d_{x^2-y^2}$ copper ion ground state an approximately linear relationship exists.

LAURENCE KENNETH THOMPSON, FREDERICK W. HARTSTOCK, PHILLIP ROBICHAUD et A. W. HANSON. Can. J. Chem. **62**, 2755 (1984).

On rapporte la synthèse et l'étude d'une série de complexes de cuivre(II) d'un ligand bidentate présentant un intérêt du point de vue biologique, soit la di(méthyl-1′ imidazolyl-2′)-1,4 phthalazine (MIP). Faisant appel à la diffraction des rayons-X sur un cristal unique, on a caractérisé le complexe binucléaire $[Cu_2(MIP)(OH)Cl_3(H_2O)]H_2O$ qui appartient au groupe d'espace $P2_1/n$ avec $a = 10{,}063(1)$, $b = 20{,}967(1)$, $c = 9{,}919(1)$ Å, $\beta = 96{,}48(1)°$, $V = 2079{,}4$ Å^3, $Z = 4$. Le cuivre a une géométrie de coordination pyramidale à base carée et les deux ions cuivriques sont reliés par un pont formé de deux groupes: N_2 (phtalazine) et hydroxyde. On considère que la grande distance métal–métal (3,25 Å) et l'angle du pont Cu—O—Cu (126,2°) sont les facteurs les plus responsables de l'échange ferromagnétique important qui est présent dans ce système ($-2J = 800$ cm^{-1}). Si on compare les valeurs de $-2J$ et les angles du pont Cu—O—Cu d'une série de complexes apparentés possédant le même centre binucléaire de base et un état fondamental $d_{x^2-y^2}$ pour l'ion cuivrique, on peut démontrer qu'il existe une relation approximativement linéaire pour ces valeurs.

[Traduit par le journal]

Introduction

Single hydroxy bridges have been shown to mediate strong antiferromagnetic exchange between copper(II) centres, depending on the oxygen bridge angle and the ground state of the metal ion (1–4) and in some cases very large exchange integrals are observed ($-2J > 800$ cm^{-1}) (2, 3) approaching the range observed for binuclear copper protein centres (5, 6). For dihydroxy bridged systems exchange integrals are somewhat smaller, with a linear variation of exchange with oxygen bridge angle (7), and for systems with small oxygen bridge angles ferromagnetic exchange is observed.

Although there appears to be no correlation between oxygen bridge angle and exchange integral for the few systems reported for which X-ray structural evidence indicates a "single hydroxy bridge" (refs. 1–4, 8, and Table 10), it should be emphasized that structurally these compounds are unrelated. In other papers these compounds have been referred to as if they contain just one bridge group, which is a hydroxide bridge, whereas, in reality, most of them contain additional "ligand" bridges. The complex $[Cu_2(bipy)_4(OH)](ClO_4)_3$ has been shown by X-ray crystallography to have just a single hydroxide bridge and other related systems $[Cu_2(phen)_4(OH)](ClO_4)_3$ and $[Cu_2(tren)_2(OH)]X_3$ (X = ClO_4^-, PF_6^-) are expected to be bridged similarly based on other data (8).

In an attempt to correlate the magnetic properties of a binuclear multibridged copper(II) system with a single hydroxy bridge and such variables as oxygen bridge angle and metal–metal separation we have examined the structure and magnetism of a series of closely related binuclear copper(II) compounds based on the phthalazine subunit as a binucleating building block (9, 10). An approximately linear relationship is observed between the exchange integral and the oxygen bridge angle for the compounds $[Cu_2(PAP)(OH)X_3].1.5H_2O$ (X = Cl, Br), $[Cu_2(PAP)(OH)Cl(SO_4)].2H_2O$ and $[Cu_2(PAP4Me)(OH)(H_2O)_2(NO_3)_2]NO_3$ (PAP = 1,4-di-(2′-pyridyl)aminophthalazine, PAP4Me = 1,4-di-(2′-pyridyl-4′-methyl)aminophthalazine). In each case the two copper centres are bridged by a diazine group (=N—N=), a hydroxide, and a variable bridging anion (Cl^-, Br^-, SO_4^{2-}, NO_3^-). Approximately square pyramidal stereochemistries were found for the copper centres in these complexes with $d_{x^2-y^2}$ ground states. The complex $[Cu_2(PAP)(OH)(IO_3)_3].4H_2O$ did not fit the trend and has an exchange much lower than expected based on its oxygen bridge angle. This was attributed to a distorted five-coordinate stereochemistry at the copper centres which approached a trigonal bipyramid, thus indicating a possible d_{z^2} ground state and a possibly different relationship between exchange and bridge angle.

In this report we describe a series of copper(II) complexes of the ligand MIP (1,4-di(1′-methyl-2′-imidazolyl)phthalazine (Fig. 1), which is previously unreported, and which bears a

[1]NRCC No. 23660.

[2]To whom all correspondence should be addressed.

Can. J. Chem. Downloaded from www.nrcresearchpress.com by 210.87.254.42 on 09/06/12
For personal use only.

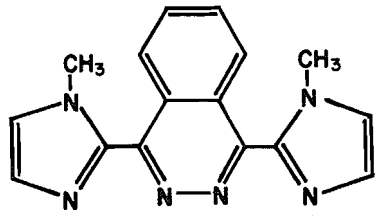

FIG. 1. MIP (1,4-di(1′-methyl-2′-imidazolyl)phthalazine.

resemblance to the ligand 3,6-di(2′-pyridyl)pyridazine (DPPN) (11–13). Also full structural details and a variable temperature magnetic study for the complex $[Cu_2(MIP)(OH)Cl_3(H_2O)].H_2O$ are reported which show that even with structurally different, but related, systems that involve $d_{x^2-y^2}$ ground states, the relationship between exchange integral and bridge angle still appears to hold. The variable temperature magnetism of the complex $[Cu_2(PAP)(OH)(IO_3)_3].4H_2O$ has also been re-examined since the original Gouy data were rather limited.

Experimental

Electronic spectra were recorded with a Cary 17 spectrometer and infrared spectra with a Perkin-Elmer Model 283 spectrometer. Magnetic susceptibilities were obtained at room temperature by the Faraday method using a Cahn Model #7600 Faraday Magnetic Susceptibility system, coupled to a Cahn gram electrobalance. Nuclear magnetic resonance spectra were run as solutions in deuterochloroform using a Bruker WP80 spectrometer and mass spectra were run using a V.G. Micromass 7070 HS spectrometer with a direct insertion probe. Microanalyses were carried out by Canadian Microanalytical Service, Vancouver (C, H, N). Metal analyses were determined by atomic absorption with a Varian Techtron AA-5, after digestion of the samples in concentrated HNO_3 or aqua regia.

Variable temperature magnetic susceptibility data (77–340 K) were obtained courtesy of Mr. B. Van der Griendt, Department of Chemistry, Gorlaeus Laboratories, State University Leiden, Netherlands, using a PAR 150A vibrating sample magnetometer. The data were corrected for underlying diamagnetism and temperature-independent paramagnetism ($N_\alpha = 60 \times 10^{-6}$ cgsu/mol Cu).

Synthesis of 1,4-di(1′-methyl-2′-imidazolyl)phthalazine (MIP)

n-BuLi (37.5 mL of 2.0 *M* solution in hexane) was added to dry (distilled over sodium benzophenone ketyl) THF (300 mL) in an atmosphere of dry nitrogen and the mixture cooled to −70°C. *N*-Methylimidazole (5.8 mL; 0.070 mol) dissolved in dry THF (75 mL) was added dropwise to the solution of *n*-butyllithium in THF over a period of 1/2 h and the mixture stirred for a further 3 h at −70°C. 1,4-Dichlorophthalazine (14) (7.0 g; 0.035 mol) dissolved in dry THF (100 mL) was added dropwise over a period of 1/2 h and the mixture allowed to warm to room temperature overnight. The solvent was removed using a rotary evaporator and the resulting solid extracted into dichloromethane, treated with decolourising charcoal, filtered, and the volume reduced to induce crystallization. The buff solid formed was filtered and recrystallized from 50/50 toluene/ethanol to produce yellow-buff crystals (yield 6 g, 60%) (mp 165–167°C). *Anal.* calcd. for $C_{16}H_{14}N_6.0.75EtOH$: C 64.7, H 5.70, N 25.9; found: C 65.0, H 5.50; N 26.1. Mass spectrum, major mass peaks (*m/e* (relative intensity)) 291(62), 290(100)P, 289(100), 262(87), 248(79), 235(19), 209(51), 183(87), 156(29), 145(26), 129(32), 102(11); ^{1}H nmr ($CDCl_3$) (σ (relative intensity)) 4.08(9) (singlet, CH_3), 7.16(3) (doublet, imidazole, H), 7.34(3) (doublet, imidazole, H), 7.94(3), 9.04(3) (AA′BB′ phthalazine, 2H).

$[Cu_2(MIP)(OH)Cl_3(H_2O)].H_2O$ (I)

$CuCl_2.2H_2O$ (1.0 g; 5.9 mmol) was dissolved in hot water (50 mL) and MIP (0.85 g; 2.9 mmol) dissolved in a minimum volume of hot ethanol. The two solutions were mixed with the formation of a dark green solution. The volume of the solution was reduced by half on a steam bath and allowed to stand. Bright green crystals formed and the product was recrystallised from water.

Compound **III** was prepared in a similar manner while compounds **II** and **V** were prepared using absolute ethanol as solvent for both the ligand and the metal salt. Compound **IV** was obtained as an insoluble green precipitate by addition of excess thiocyanate to an aqueous solution of the green precipitate obtained by reacting MIP and copper nitrate (1:2) in ethanol. The hygroscopic nature of the copper nitrate product prevented adequate characterization of this compound and so it is not described.

Satisfactory analytical data have been obtained for all compounds and are reported in Table 1, which is available from the Depository of Unpublished data.[2]

X-ray crystallographic analysis for $[Cu_2(MIP)(OH)Cl_3(H_2O)].H_2O$

Crystal data (at 24°C) are:

$C_{16}H_{19}N_6O_3Cl_3Cu_2$ fw = 576.82

Monoclinic, $P2_1/n$ (C_{2h}^5; absences $h0l$ for $h + l$ odd, $0k0$ for k odd), $a = 10.063(1)$, $b = 20.967(1)$, $c = 9.919(1)$ Å, $\beta = 96.48(1)°$, $V = 2079.4$ Å^3, $Z = 4$ (CuKα, $\lambda\alpha_1 = 1.54056$ Å); $\mu = 6.4$ mm^{-1}, $D_x = 1.842$ g cm^{-3}.

The crystals were green parallelepipeds with edges corresponding to the unit-cell axes. The specimen used for all measurements was of extreme dimensions 0.04 and 0.20 mm. The cell dimensions were derived from least-squares fitting of the diffractometer settings of 35 well centred reflections for which $111 < 2\theta < 129°$. The relative intensities of the independent reflections with $2\theta < 130°$ were measured with a Picker four-circle diffractometer, using Ni-filtered CuKα radiation. The $\theta-2\theta$ scan method was used, and individual reflection profiles were analysed as described by Grant and Gabe (15). The standard deviations of the measured intensities were evaluated from counting statistics, and those for which $I_{net} < 3\sigma(I_{net})$ were considered to be unobserved, and were omitted from the analysis. The observed reflections numbered 2442, of a possible 3544. Absorption corrections (ranging from 1.30 to 2.58) were applied to the measured intensities.

The structure was solved by the heavy-atom method, and refined by block-diagonal least squares, minimizing $\Sigma w\Delta F^2$, where $w^{-1} = \sigma^2(F_o) + 0.001F_o^2$. Most hydrogen atoms were included in the refinement, with initial positions reasonably assumed, or determined from a difference-Fourier synthesis, and isotropic temperature factors fixed at reasonable values. However, the hydrogen atoms of one water molecule (O(3)) could not be reliably located, and were omitted. The parameters refined were scale factor, secondary extinction coefficient, coordinates of all atoms, and anisotropic temperature parameters of the non-hydrogen atoms. The refinement converged at $R = 0.034$ (observed reflections only; $R_w = 0.046$). Except in the neighbourhood of O(3), where there is a peak of 0.6 e/Å^3, the residual election density lies between the limits −0.4 and 0.3 e/Å^3. The computer program system is specified in ref. 16, and the source of atomic scattering factors in ref. 17. The final atomic coordinates are given in Tables 2 and 3, thermal parameters in Table 4, and observed and calculated structure factors in Table 5.[3]

Results and discussion

Structure description of μ-[1,4-di(1′-methyl-2′-imidazolyl)-phthalazine-N^1,N^3,N^4,N^6]-μ-hydroxotrichloroaquodicopper(II) hydrate

The molecular structure of $[Cu_2(MIP)(OH)Cl_3(H_2O)].H_2O$ (**I**) is shown in Fig. 2 and consists of a pair of copper(II) centres bound simultaneously to the tetradentate phthalazine ligand and bridged by two groups: the phthalazine N_2 and a hydroxide.

[3] Photocopies of Tables 1, 3, 4, 5, 7, and 8 may be obtained at a nominal charge, upon request, from the depository of Unpublished Data, CISTI, National Research Council of Canada, Ottawa, Ont., Canada K1A 0S2.

Can. J. Chem. Downloaded from www.nrcresearchpress.com by 210.87.254.42 on 09/06/12
For personal use only.

TABLE 2. Atomic coordinates and equivalent isotropic temperature factors (esd's) for $[Cu_2(MIP)(OH)Cl_3(H_2O)].H_2O$[a]

Atom	X	Y	Z	B_{iso}
Cu(1)	0.12776(6)	−0.02534(3)	0.18251(6)	2.38(3)
Cu(2)	0.12078(6)	0.13583(3)	0.23777(7)	2.45(3)
Cl(1)	0.29991(12)	−0.07675(6)	0.10814(14)	3.96(6)
Cl(2)	0.29954(11)	0.20067(5)	0.26479(12)	3.11(5)
Cl(3)	0.10176(14)	0.10459(6)	0.49681(12)	3.88(7)
O(1)	0.2063(3)	0.0583(1)	0.1916(3)	2.7(2)
O(2)	0.1629(4)	−0.0361(2)	0.4132(4)	4.2(2)
O(3)	0.3193(6)	0.3039(2)	1.0204(5)	8.6(4)
N(1)	−0.0043(4)	−0.0970(2)	0.1598(4)	2.4(2)
N(2)	−0.2137(4)	−0.1268(2)	0.1068(4)	2.6(2)
N(3)	−0.0492(3)	0.0222(2)	0.1810(3)	2.2(2)
N(4)	−0.0527(3)	0.0853(2)	0.1919(4)	2.2(2)
N(5)	−0.2224(4)	0.2314(2)	0.1445(4)	2.5(2)
N(6)	−0.0161(4)	0.2056(2)	0.2229(4)	2.5(2)
C(1)	−0.0053(5)	−0.1588(2)	0.1201(5)	3.0(2)
C(2)	−0.1345(5)	−0.1780(2)	0.0872(5)	3.1(2)
C(3)	−0.1315(4)	−0.0789(2)	0.1533(4)	2.3(2)
C(4)	−0.3567(5)	−0.1239(2)	0.0547(5)	3.2(2)
C(5)	−0.1595(4)	−0.0124(2)	0.1873(4)	2.2(2)
C(6)	−0.2742(4)	0.0149(2)	0.2357(4)	2.2(2)
C(7)	−0.3774(5)	−0.0210(2)	0.2838(4)	2.7(2)
C(8)	−0.4797(5)	0.0091(2)	0.3386(4)	2.9(2)
C(9)	−0.4823(5)	0.0754(2)	0.3478(5)	3.0(2)
C(10)	−0.3826(5)	0.1123(2)	0.3034(5)	2.9(2)
C(11)	−0.2772(4)	0.0825(2)	0.2453(4)	2.2(2)
C(12)	−0.1646(4)	0.1159(2)	0.2084(4)	2.2(2)
C(13)	−0.1404(4)	0.1849(2)	0.1972(4)	2.3(2)
C(14)	−0.1457(5)	0.2847(2)	0.1378(5)	3.2(2)
C(15)	−0.0186(5)	0.2687(2)	0.1873(5)	3.1(2)
C(16)	−0.3619(5)	0.2265(2)	0.0814(5)	3.4(3)
HO(1)	0.280(5)	0.058(2)	0.201(4)	3.2(0)
HO(2A)	0.141(4)	−0.001(2)	0.439(4)	3.2(0)
HO(2B)	0.122(4)	−0.056(2)	0.406(4)	3.2(0)

[a]An esd of zero denotes a parameter not refined; H atoms bound to carbon are given in Table 3;[2] equivalent positions: $\pm(x, y, z; 1/2 + x, 1/2 - y, 1/2 + z)$.

Selected intramolecular bond distances and angles are given in Table 6. (Other interatomic distances and angles are given in Table 7[2].) The stereochemistry at each copper centre is approximately square pyramidal with the same arrangement of donor atoms in the basal plane. A basal corner is shared at oxygen O(1) by both copper centres. A chlorine atom, Cl(3), is the apical donor to Cu(2) while a water molecule occupies the apical site at Cu(1). A hydrogen bonding contact between Cl(3) and a hydrogen atom of this water molecule is apparent (H....Cl 2.32 Å), while the other hydrogen atom interacts with a corresponding chlorine atom in an adjacent molecule.

The Cu---Cu separation (3.425 Å) is much larger than those found in other monohydroxy bridged systems involving pyridyl aminophthalazine ligands, in which the substituent donor groups are separated from the diazine entity by an additional (nitrogen) atom (9, 10, 18). This has been attributed to the presence of five-membered chelate rings involving MIP as opposed to six-membered chelate rings in the other systems. The geometrical consequence of the five-membered ring is that larger Cu—N—N angles to the diazine group occur in this system (120−121°) than in the others (114−117°). The result of this effect is that the metal−metal separation and the metal−oxygen separations are larger in the MIP complex.

A comparison of the structure of $[Cu_2(MIP)(OH)Cl_3(H_2O)].H_2O$ with that of a related complex $[Cu_2(DPPN)(OH)Cl_3(H_2O)]$ (DPPN = 3,6-bis(pyridyl)pyridazine) reveals a basically similar structure but with some significant differences (13). Bond angles and bond lengths in the coordination sphere of each metal centre and at the diazine function are comparable implying that the basic binuclear centres in each system are very similar but the Cu...Cu separation and the copper−oxygen bridge separations are slightly longer in the MIP complex. Whereas in the DPPN complex the ligand itself is roughly planar (the two pyridyl rings are twisted with respect to the pyridazine moiety by 3.3 and 3.0°, respectively) in the MIP complex significant twisting of the imidazole groups occurs with respect to the mean plane of the phthalazine group. The imidazole rings (A, B) are inclined at 33° to each other and at 31 and 40°, respectively, to the mean plane of the phthalazine entity (*E*). Also this group is bent by 12° about the fused bond C(6)—C(11) (Table 8).[2] This twisting of the ligand is, no doubt, due to steric interactions between the methyl groups on the imidazole rings and protons HC(7) and HC(10) on the "fused" benzene ring of the phthalazine group. This effect would be absent in DPPN and comparable steric interactions would be minimal. The steric effect and the resultant twisting of the ligand in **I** do not significantly alter the overall dimensions of the binuclear centre in this system, when compared with the DPPN complex, other than to create a slightly longer metal−metal separation and copper−oxygen bridge separations. The two copper centres Cu(1) and Cu(2) are displaced by 0.261 and 0.176 Å, respectively, above the mean planes *F* and *G* which describe the basal planes of their square pyramids (Table 8).[2]

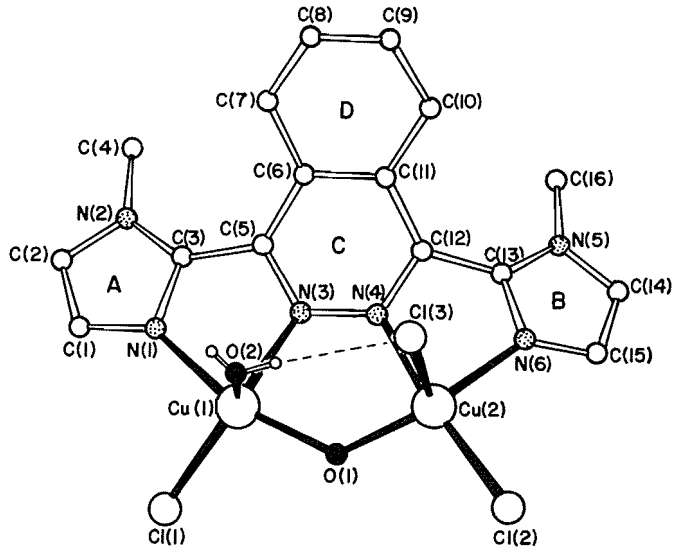

FIG. 2. Molecular structure and labelling scheme for $[Cu_2(MIP)(OH)Cl_3(H_2O)].H_2O$.

Synthesis and characterization of the complexes

Infrared, electronic spectral, and magnetic data are given in Table 9.

Compounds **I** and **III** were prepared from aqueous ethanol while **II** and **V** were prepared from absolute ethanol. On recrystallization of compound **II** from aqueous solvent **I** is obtained. **IV** is obtained by reacting a crude product, obtained from the reaction of copper nitrate and MIP in ethanol, dissolved in water with excess thiocyanate. The copper nitrate complex was, itself, not characterized. While compounds

Can. J. Chem. Downloaded from www.nrcresearchpress.com by 210.87.254.42 on 09/06/12
For personal use only.

Can. J. Chem. Downloaded from www.nrcresearchpress.com by 210.87.254.42 on 09/06/12
For personal use only.

TABLE 6. Selected interatomic distances (Å) and angles (deg) in $[Cu_2(MIP)(OH)Cl_3(H_2O)].H_2O$ (with esd in parentheses)

Atoms	Distance	Atoms	Distance
Cu(1)—Cl(1)	2.235(1)	Cu(2)—Cl(2)	2.247(1)
Cu(1)—O(1)	1.921(3)	Cu(2)—O(1)	1.919(3)
Cu(1)—O(2)	2.286(4)	Cu(2)—Cl(3)	2.679(2)
Cu(1)—N(1)	2.002(4)	Cu(2)—N(6)	2.003(4)
Cu(1)—N(3)	2.039(4)	Cu(2)—N(4)	2.049(3)
Cu(1)—Cu(2)	3.425(1)	O(2)—HO(2A)	0.83(5)
N(3)—N(4)	1.328(5)	OH(2A)···Cl(3)	2.32(4)
Bonds	**Angle**	**Bonds**	**Angle**
Cl(1)—Cu(1)—O(1)	97.2(1)	Cl(2)—Cu(2)—O(1)	99.6(1)
Cl(1)—Cu(1)—O(2)	104.2(1)	Cl(2)—Cu(2)—Cl(3)	100.2(1)
Cl(1)—Cu(1)—N(1)	97.5(1)	Cl(2)—Cu(2)—N(6)	95.8(1)
Cl(1)—Cu(1)—N(3)	160.4(1)	Cl(2)—Cu(2)—N(4)	172.0(1)
O(1)—Cu(1)—O(2)	91.5(1)	O(1)—Cu(2)—Cl(3)	96.0(1)
O(1)—Cu(1)—N(1)	162.7(1)	O(1)—Cu(2)—N(6)	157.6(1)
O(1)—Cu(1)—N(3)	84.8(1)	O(1)—Cu(2)—N(4)	84.4(1)
O(2)—Cu(1)—N(1)	93.7(1)	Cl(3)—Cu(2)—N(6)	97.2(1)
O(2)—Cu(1)—N(3)	95.3(1)	Cl(3)—Cu(2)—N(4)	86.3(1)
N(1)—Cu(1)—N(3)	78.3(1)	N(6)—Cu(2)—N(4)	78.4(1)
Cu(1)—N(3)—N(4)	121.1(3)	Cu(2)—N(4)—N(3)	120.3(3)
Cu(1)—O(1)—Cu(2)	126.3(2)	O(2)—HO(2A)···Cl(3)	172(4)

TABLE 9. Electronic spectra, magnetic moments, and infrared data

Compound	$d-d$, CT (cm^{-1})	μ (BM) (room temperature)	Infrared (cm^{-1})
I $[Cu_2(MIP)(OH)Cl_3(H_2O)].H_2O$	[11800], 14900, 24700	0.62[a]	290, 310(Cu—Cl), 3550(H_2O) 3640(OH)
II $[Cu_2(MIP)Cl_4].2H_2O$	13300, 23000	1.25	305(Cu—Cl), 3460(H_2O)
III $[Cu_2(MIP)(OH)Br_3(H_2O)].H_2O$	[11100], 14000, 26300	0.35	3540(H_2O), 3620(OH)
IV $[Cu_2(MIP)(NCS)_4].4H_2O$	27800	1.10	2095(νCN, NCS), 3400 sh (H_2O)
V $[(MIP)_2Cu(H_2O)_2](ClO_4)_2.5H_2O$	[11500], 14800, 26300	1.95	1080(ClO_4), 3470 sh, 3540(H_2O)

[a]Exchange integral $-2J = 800 \pm 40$ cm^{-1}; $g = 2.00 \pm 0.02$.

I–**IV** are clearly binuclear, **V** is a mononuclear, bis-ligand derivative and no binuclear complex could be isolated.

Compound **I** exhibits $d-d$ bands in the visible region which can be associated with square pyramidal copper(II) and infrared bands indicative of the presence of terminal copper–chlorine bonds, a hydroxy bridge, and water. This compound exhibits a very low room temperature magnetic moment indicative of strong antiferromagnetic exchange. Reaction of copper chloride and MIP in an essentially non-aqueous medium produces a different complex, **II**, which does not have a hydroxy bridge. A lower energy $d-d$ absorption is consistent with a weaker ligand field associated with more coordinated chlorine atoms and a much higher magnetic moment may indicate the presence of a halogen bridge or perhaps no bridge other than the diazine. In the absence of such a bridge two coordinated chlorines per metal seem likely with the possible presence of a coordinated water also at each metal centre. It is of interest to note that an analogous compound involving DPPN has also been reported (13) and a recent X-ray study (19) shows that in $[Cu_2(DPPN)Cl_4(H_2O)]$ the two copper(II) centres are bridged by a chlorine, in addition to the pyridazine bridge, two chlorine atoms are bound to one copper and one chlorine and a water molecule to the other. The structure is similar to that of the μ-hydroxo-bridged analogue and suggests that a similar structure may well exist for **II**.

Compound **III** appears to be the bromo-analogue of **I** with slightly lower energy $d-d$ absorption and similar infrared bands indicative of a hydroxy bridge and the presence of water. However, the room temperature magnetic moment is much lower, which may indicate a more strongly coupled system. Compound **IV** has no discernible $d-d$ absorption in the visible and it is presumably hidden within the intense charge transfer absorption at 27800 cm^{-1}. The stereochemistry at copper is likely, therefore, to be close to square planar. Only one thiocyanate band is observed in the infrared due to CN stretch and this is associated with a terminal nitrogen bound group. The apparent lack of splitting of this absorption does not rule out the presence of two terminal thiocyanates per copper and this seems to be the most likely structure. Since no bridging group other than the diazine, N_2, appears to be present in **IV** the reduction in magnetic moment can be attributed to exchange via the diazine bridge alone.

Compound **V** is clearly anomalous in that it is mononuclear, presumably involving bidentate ligands. A similar situation has been observed with other phthalazine ligands (20–22) although in these cases, in aqueous solution, the pH of the system

TABLE 10. Magnetic exchange and structural data for some binuclear copper(II) complexes with single hydroxy bridges

	Compound	μ (BM) (RT)	$-2J$ (cm^{-1})	Cu—Cu (Å)	Cu—O—Cu (deg)	Stereochemistry[f]	No. bridges	Reference
I	$[Cu_2(MIP)(OH)Cl_3(H_2O)].H_2O$	0.62	800(±40)	3.425	126.2	SP	2	
	$[Cu_2(DPPN)(OH)Cl_3(H_2O)]$		—	3.376	126.5	SP	2	13
VI	$[Cu_2(PAP)(OH)Cl_3].1.5H_2O$[a]	1.60	201	3.001	100.0	SP	3	9
				2.972	101.8			
VII	$[Cu_2(PAP)(OH)Br_3].1.5H_2O$	1.66	191	3.010	101.3	SP	3	9
				2.986	102.9			
VIII	$[Cu_2(PAP)(OH)(IO_3)_3].4H_2O$	1.49	290(±10) 335(ref. 9)	3.165	113.8	SP—TBP	3	
IX	$[Cu_2(PAP)(OH)Cl(SO_4)].2H_2O$	1.01	532(±10)	3.211	115.5	SP	3	10
X	$[Cu_2(PAP4Me)(OH)(H_2O)_2(NO_3)_2]NO_3$[b]	1.02	497(±10)	3.138	115.3	DOH	3	10
XI	$[Cu_2(bipy)_4(OH)](ClO_4)_3$	1.33	322		141.6	TBP	1	8
	$[Cu_2(tren)_2(OH)](PF_6)_3$		700		—		1	1
	$[Cu_2(tren)_2(OH)](ClO_4)_3$		760		—		1	1
	$[Cu_2(phen)_4(OH)](ClO_4)_3$		354		—		1	8
XII	$[Cu_2L(OH)](ClO_4)_3$[c]	1.62	240	3.57	141.7	SP	3	4
XIII	$[Cu_2L(OH)(ClO_4)]^{2+}$[d]	0.29	~1000	3.642	143.7	DSP	4	3
XIV	$[Cu_2L(OH)]^{3+}$[e]	0.48	~820	3.384	132.2	DSP	2	2

[a]PAP = 1,4-di(2′-pyridyl)aminophthalazine.
[b]PAP4Me = 1,4-di(4′-methyl-2′-pyridyl)aminophthalazine.
[c]L = macrocycle derived from condensation of 2,6-diacetylpyridine and 3,6-dioxaoctane-1,8-diamine.
[d]L = sexadentate macrocycle.
[e]L = 1,4-bis[(1-oxa-4,10-dithia-7-azacyclododecan-7-yl)methyl]benzene.
[f]TBP trigonalbipyramid, SP square pyramid, DSP distorted square pyramid, DOH distorted octahedron.

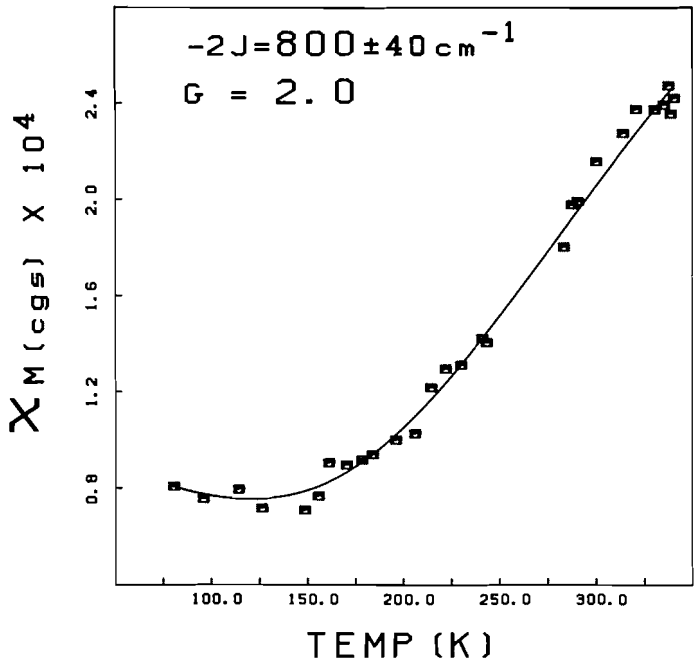

FIG. 3. Magnetic susceptibility data for $[Cu_2(MIP)(OH)Cl_3(H_2O)].H_2O$. The solid line was calculated from eq. [1] with g = 2.00 ± 0.02, $-2J$ = 800 ± 40 cm^{-1}, and $N\alpha$ = 120 × 10^{-6} cgsu/binuclear centre.

turned out to be the controlling factor. A tetragonally distorted six-coordinate structure is proposed for this system involving axially bound water molecules.

Magnetic measurements

Magnetic susceptibility measurements were carried out on powdered samples of **I** and $[Cu_2(PAP)(OH)(IO_3)_3].4H_2O$ (**VIII**; Table 10) in the range 77−340 K. A best fit of the experimental data was obtained using the Van Vleck equation (23) for exchange coupled pairs of copper(II) ions (eq. [1]).

$$[1]\quad \chi_M = \frac{N\beta^2 g^2}{3kT}\left[1 + \frac{1}{3}\exp(-2J/kT)\right]^{-1} + N\alpha$$

In this expression $2J$ (in the spin Hamiltonian $H = -2J\hat{S}_1.\hat{S}_2$) is the singlet−triplet splitting or exchange integral and other symbols have their usual meaning. The parameters giving the best fit were obtained by minimizing the function

$$E = \Sigma_i W_i(\chi_i^{obsd}\chi_i^{calcd})^2$$

(where $W_i = (\chi_i^{obsd})^{-1}$) using a Simplex non-linear fitting routine (24, 25). The results of this fit gave the parameters g = 2.00 ± 0.02 and $-2J$ = 800 ± 40 cm^{-1} (0.5% monomeric paramagnetic impurity) for **I** and g = 2.21 ± 0.02 and $-2J$ = 290 ± 10 cm^{-1} for **VIII**. Figures 3 and 4 illustrate the experimental and theoretical susceptibility curves for **I** and **VIII**, respectively. At temperatures less than 200 K several susceptibility measurements were taken at each temperature for **I**. In some cases significant scatter in these data points were observed. Some of these points have been removed from Fig. 3 for clarity but the best fit of data and error limits were determined using the complete data point set.

Table 10 summarises magnetic and structural data for a number of binuclear copper(II) compounds (including **I** and **VIII**) containing single hydroxy bridges which have been published recently. Figures 5 and 6 illustrate plots of exchange integral ($-2J$) and magnetic moment (RT), respectively, versus oxygen bridge angle for these systems and compound **I**. Reasonable straight lines can be drawn, in both cases, to include compounds **I**, **VI**, **VII**, **IX**, and **X**. For complexes **VI**, **VII**, **IX**, and **X** three bridging entities exist between the copper centres, including the diazine bridge and the hydroxide bridge, and since this feature occurs in **I**, which also falls on the straight line plots, it is this pair of bridges and the $d_{x^2-y^2}$ ground

Can. J. Chem. Downloaded from www.nrcresearchpress.com by 210.87.254.42 on 09/06/12
For personal use only.

Can. J. Chem. Downloaded from www.nrcresearchpress.com by 210.87.254.42 on 09/06/12
For personal use only.

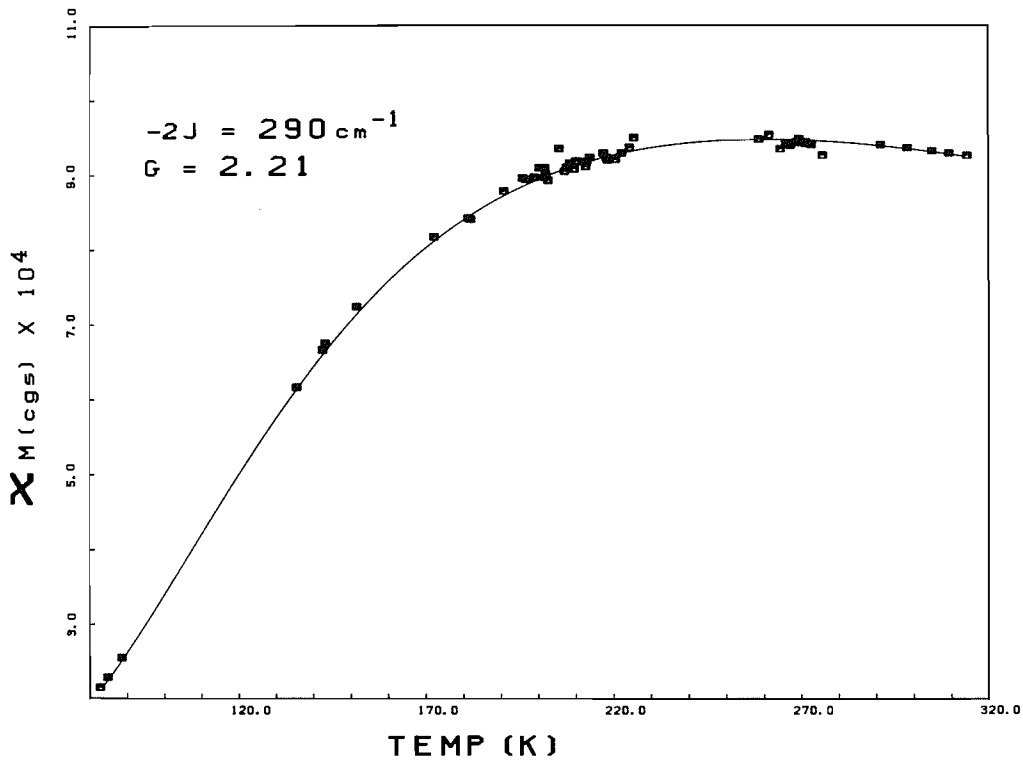

FIG. 4. Magnetic susceptibility data for $[Cu_2(PAP)(OH)(IO_3)_3].4H_2O$. The solid line was calculated from eq. [1] with $g = 2.21 \pm 0.02$, $-2J = 290 \pm 10$ cm^{-1}, and $N\alpha = 120 \times 10^{-6}$ cgsu/binuclear centre.

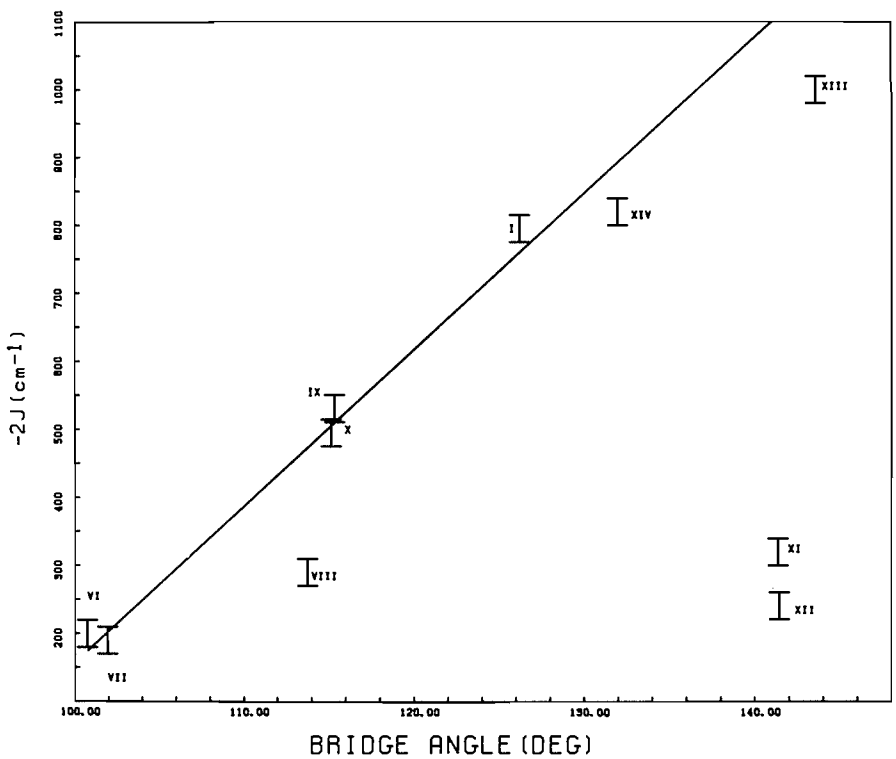

FIG. 5. Plot of $-2J$ against oxygen bridge angle for compounds **I**, **VI**–**XIV** (error bars set arbitrarily).

state which appears to group these five compounds together. The exchange data quoted for **VIII**, $[Cu_2(PAP)(OH)(IO_3)_3].4H_2O$ (26), were obtained originally from a limited set of Gouy measurements. The variable temperature magnetism for this compound has been remeasured because the original data for this compound did not fit the plot of exchange and bridge angle. However, rather than the exchange increasing, as might have been expected, the new data indicate somewhat weaker exchange, confirming the unique position of this compound in the series. The stereochemistry at each copper centre in **VIII**

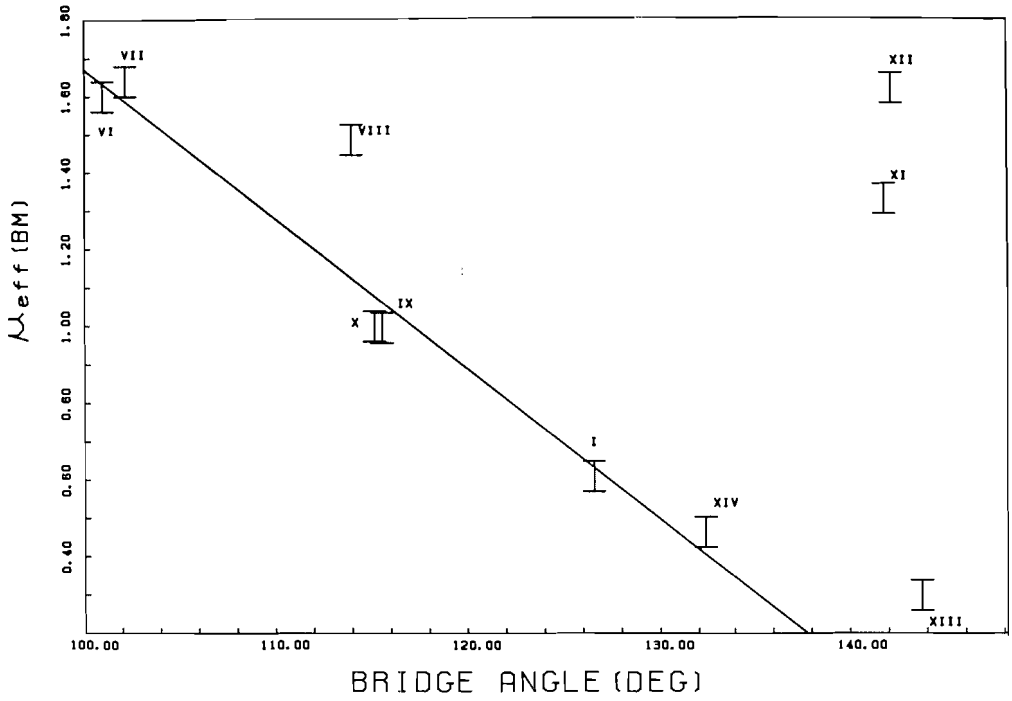

FIG. 6. Plot of μ (RT) against oxygen bridge angle for compounds **I**, **VI**–**XIV** (error bars set arbitrarily).

(9) is in between a square pyramid and a trigonal bipyramid and so the ground state representation may not be $d_{x^2-y^2}$. Such a situation may lead to a different relationship between exchange and bridge angle.

Including data for compounds **XI**–**XIV** in Figs. 5 and 6 shows that compounds **XIII** and **XIV** lie close to the straight line plots but the other two compounds do not. However, the uncertainty of the measurements for compounds **XIII**, **XIV** could place these systems closer to the line generated by compounds **I**, **VI**, **VII**, **IX**, **X**. Compound **XI**, $[Cu_2(bipy)_4(OH)](ClO_4)_3$, has a distorted trigonal bipyramidal structure at the copper centres and orbital overlap with the bridging oxygen atoms occurs via an equatorial metal orbital. d_{z^2} orbital overlap with the oxygen bridge would be much more favourable with an axially bound system, as is expected for $[Cu_2(tren)_2(OH)](ClO_4)_3$ (8), and this leads to much stronger exchange. Surprisingly compound **XII** has a copper ion stereochemistry close to square pyramidal and it is not obvious why this system should display such weak exchange. However, unlike all the other single hydroxide bridged species in which the copper centres are related to each other approximately by a plane of symmetry through the oxygen bridge, the square pyramidal centres in **XII** are twisted with respect to each other by about 90° along the copper–oxygen bonds.

Within the limited scope of this survey most systems with $d_{x^2-y^2}$ ground states and approximately square pyramidal structures relate antiferromagnetic exchange and hydroxide bridge angle in a roughly linear manner. However, within a series of related complexes, with the same copper ion ground state, a much better linear relationship is observed. It is clear that more examples are required to better substantiate these relationships, and that distortions at the copper centres be documented in a systematic way in order to evaluate the molecular orbital situation in the Cu—O—Cu framework.

We have observed that by varying certain bridging groups, X, in the binuclear unit $Cu_2N_2(OH)X$, the dimensions of the binuclear centre, and especially the oxygen bridge angle, can be "tuned" according to the size of X (9, 10). A limit of about 116° for the Cu—O—Cu bridge angle is reached with large bridges, e.g. sulphate, but, on changing from a system with three bridge groups to one with two and decreasing the chelate ring size, enhanced exchange is observed as a result of increased metal–metal separation and bridge angle. Further studies of this sort are ongoing, in which we are attempting to "tune" these systems further by the use of bigger groups, X, and by examining other molecular constraints which might impose, through, e.g., steric factors, other perturbing influences on the dimensions of the binuclear centres. Preliminary structural data indicate that by placing 6-methyl groups on the pyridine rings in ligands like PAP the oxygen bridge angle can be opened up dramatically.

Acknowledgements

We thank the Natural Sciences and Engineering Research Council of Canada for financial support for this study and Dr. B. S. Ramaswamy for computing assistance.

1. M. S. HADDAD and D. N. HENDRICKSON. Inorg. Chim. Acta, **28**, L121 (1978).
2. P. L. BURK, J. A. OSBORN, M.-T. YOUINOU, Y. AGNUS, R. LOUIS, and R. WEISS. J. Am. Chem. Soc. **103**, 1273 (1981).
3. P. K. COUGHLIN and S. J. LIPPARD. J. Am. Chem. Soc. **103**, 3228 (1981).
4. M. G. B. DREW, M. MCCANN, and S. M. NELSON. J. Chem. Soc. Dalton Trans. 1868 (1981).
5. D. M. DOOLEY, R. A. SCOTT, J. ELLINGHAUS, E. I. SOLOMON, and H. B. GRAY. Proc. Natl. Acad. Sci. U.S.A. **75**, 3019 (1978).
6. E. I. SOLOMON, D. M. DOOLEY, R. H. WANG, H. B. GRAY, M. CERDONIO, F. MOGNO, and G. L. ROMANI. J. Am. Chem. Soc. **98**, 1029 (1976).
7. VAN H. CRAWFORD, H. W. RICHARDSON, J. R. WASSON, D. J. HODGSON, and W. E. HATFIELD. Inorg. Chem. **15**, 2107 (1976).
8. M. S. HADDAD, S. R. WILSON, D. J. HODGSON, and

Can. J. Chem. Downloaded from www.nrcresearchpress.com by 210.87.254.42 on 09/06/12
For personal use only.

D. N. HENDRICKSON. J. Am. Chem. Soc. **103**, 384 (1981) and references therein.
9. L. K. THOMPSON. Can. J. Chem. **61**, 579 (1983).
10. L. K. THOMPSON, A. W. HANSON, and B. S. RAMASWAMY. Inorg. Chem. **23**, 2450 (1984).
11. P. W. BALL and A. B. BLAKE. J. Chem. Soc. A, 1415 (1969).
12. P. W. BALL and A. B. BLAKE. J. Chem. Soc. Dalton Trans. 852 (1974).
13. M. GHEDINI, G. DEMUNNO, G. DENTI, A. M. MANOTTI LANFREDI, and A. TIRIPICCHIO. Inorg. Chim. Acta, **57**, 87 (1982).
14. A. HIRSCH and D. ORPHANOS. Can. J. Chem. **43**, 2708 (1965).
15. D. F. GRANT and E. J. GABE. J. Appl. Crystallogr. **11**, 114 (1978).
16. A. C. LARSON and E. J. GABE. Computing in crystallography. Delft University Press, Delft, Holland. 1978.
17. International tables for X-ray crystallography. Vol IV. Kynoch Press, Birmingham, England. 1974. p. 99.
18. G. MARONGIU and E. C. LINGAFELTER. Acta Crystallogr. B**38**, 620 (1982).
19. G. DE MUNNO, G. DENTI, and P. DAPPORTO. Inorg. Chim. Acta, **74**, 199 (1983).
20. J. C. DEWAN and L. K. THOMPSON. Can. J. Chem. **60**, 121 (1982).
21. D. V. BAUTISTA, J. C. DEWAN, and L. K. THOMPSON. Can. J. Chem. **60**, 2583 (1982).
22. G. BULLOCK, F. W. HARTSTOCK, and L. K. THOMPSON. Can. J. Chem. **61**, 57 (1983).
23. J. H. VAN VLECK. The theory of electric and magnetic susceptibilities. Oxford University Press, London. 1932. Chapt. IX.
24. W. SPINDLEY, G. R. HIEXT, and F. R. HIMSWORTH. Technometrics, **4**, 441 (1962).
25. J. N. NELDER and R. MEAD. Comput. J. **7**, 308 (1965).
26. L. K. THOMPSON, V. T. CHACKO, J. A. ELVIDGE, A. B. P. LEVER, and R. V. PARISH. Can. J. Chem. **47**, 4141 (1969).

Can. J. Chem. Downloaded from www.nrcresearchpress.com by 210.87.254.42 on 09/06/12
For personal use only.

Formation and reactivity of transannular sulphur–sulphur bonds in cyclothiazenes and related compounds. A molecular orbital analysis

RICHARD T. OAKLEY

Guelph–Waterloo Centre for Graduate Work in Chemistry, Guelph Campus, Department of Chemistry and Biochemistry, University of Guelph, Guelph, Ont., Canada N1G 2W1

Received March 27, 1984

RICHARD T. OAKLEY. Can. J. Chem. **62**, 2763 (1984).

The structural dichotomy exhibited by heterocyclic thiazenes of the type $E(NSN)_2E$ (E = CR, SR) is analyzed in the light of MNDO molecular orbital calculations on a variety of model structures. For $RS(NSN)_2SR$ molecules the activation energies for inversion at sulphur have been estimated, and the formation of *exo–endo* and *exo–exo* isomers is discussed in terms of the frontier orbitals involved in the free radical and electrophilic oxidation of transannular S—S bonds.

RICHARD T. OAKLEY. Can. J. Chem. **62**, 2763 (1984).

En se basant sur des calculs d'orbitales moléculaires du type MNDO, effectués sur une variété de structures modèles, on a analysé la dichotomie de structure que présentent les thiazènes hétérocycliques du type $E(NSN)_2E$ (E = CR, SR). Dans le cas des molécules $RS(NSN)_2SR$, on a évalué les énergies d'activation pour l'inversion au niveau du soufre et on discute de la formation des isomères *exo–endo* et *exo–exo* en fonction des orbitales frontières impliquées dans les oxydations radicalaire et électrophile des liaisons S—S transannulaires.

[Traduit par le journal]

Introduction

The structural diversity of binary sulphur nitride derivatives has evoked continued debate over the electronic factors which control their shape. The cage-like molecule of S_4N_4 has attracted the most attention (see, for example, ref. 1), and the results of recent structural and theoretical (molecular orbital) studies on the protonated form $S_4N_4H^+$ have illustrated how the energetic balance between different structural modifications can be shifted by a seemingly minor chemical change (2).

In addition to the simple binary molecule, S_4N_4, a variety of heterocyclic derivatives of the type $E(NSN)_2E$ have recently been synthesized and structurally characterized (E = CPh, $CNMe_2$, PMe_2, PPh_2, SCl, $SNMe_2$, $SNPPh_3$) (3–8). The molecular structures of these derivatives fall into two distinct categories exhibiting either an essentially planar shape, e.g. **1**, or a puckered conformation with a close (2.50–2.60 Å) transannular sulphur–sulphur contact, e.g. **2**. Although the reasons

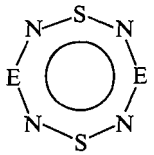

1

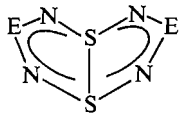

2

for the occurrence of the two structural modifications for different E groups have been investigated by molecular orbital methods (4, 9), no quantitative correlation of electronic structure with observed geometry has been attempted. In addition, for those molecules in which E represents an SR moiety three distinct ligand orientations, here designated as *exo–exo* **3***a*, *endo–endo* **3***b*, and *exo–endo* **3***c*, are possible, but to date no theoretical investigation has been made of the relative stabilities of these isomers, the ease of their interconversion, or the mechanistic factors which might influence the formation of one rather than another.

In the present paper the electronic and energetic criteria underlying the structural reorganization **1** to **2** are evaluated in the light of MNDO molecular orbital calculations on a number of key model compounds. For molecules of the type $RS(NSN)_2SR$ and $S_4N_4R_4$ the observed range of ligand orientations

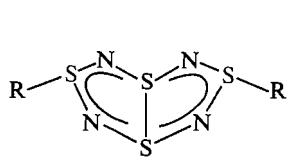

3*a*

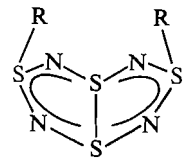

3*b*

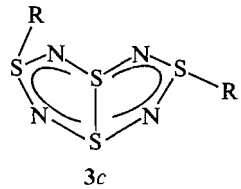

3*c*

is discussed in terms of the stereochemical characteristics of the free radical and electrophilic oxidation of S_4N_4.

Theoretical method and models

The use of the M(odified) N(eglect) of D(iatomic) O(verlap) method (10) and the DFP geometry optimizing algorithm has been used extensively for the study of the conformational characteristics of sulphur nitride compounds. Although the method is somewhat deficient in assessing sulphur(III)–sulphur(III) σ-interactions (11) it has, in many cases, provided reliable predictions of ground state geometries (e.g. S_4N_2, S_3N-, S_4N-, S_4N_4H+) (2, 12–14). In the present study calculations on planar models **1** were carried out with full optimization of the endocyclic bond lengths and angles (within the constraints of D_{2h} symmetry). Bond lengths to the exocyclic ligands (C—H, C—N, S—Cl, S—F, S—N) were also optimized, but for NH_2 ligands, an idealized geometry (planar configuration with d(N—H) = 1.0 Å and ∠NHN = 120°) was used. For the calculations on the puckered models **2**, the transannular S—S distance was fixed at 2.6 Å and each of the ES_2N_2 rings was held planar. Outside of these restrictions, full geometry optimization (within C_{2v} symmetry) was invoked. Bond orders (ρ_{NS}) were calculated as described in ref. 15.

Calculations on the ligand orientations of $RS(NSN)_2SR$ were performed using a restriction of planarity on the two five-membered $(R)SN_2S_2$ rings, the parameters of each being optimized independently (with the exception of the transannular

Can. J. Chem. Downloaded from www.nrcresearchpress.com by 210.87.254.6 on 09/06/12
For personal use only.

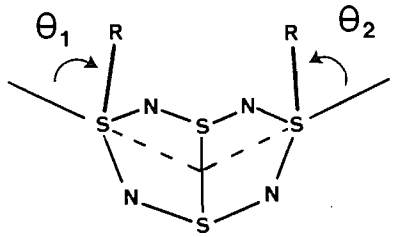

FIG. 1. Definition of ligand orientations in $S_4N_4R_2$ molecules by the two angles θ_1 and θ_2.

S—S distance, which was fixed at 2.6 Å). The two ligand positions were varied by means of the two angles θ_1 and θ_2 defined in Fig. 1.

Results and discussion

$E(NSN)_2E$ isomers

In a recent analysis of the effect of protonation on the shape of the S_4N_4 molecule we emphasized how the redistribution of the π-molecular orbitals following protonation resulted in a net stabilization of the planar conformation relative to the cage structure (2). The structural dichotomy observed for molecules of the type $E(NSN)_2E$ can be interpreted using similar reasoning, and to this end it is useful to compare their electronic structures with that of the unperturbed 10 electron π-system of $S_4N_4^{2+}$. For this latter species the results of extended Hückel, CNDO and *ab initio* Hartree-Fock-Slater molecular orbital studies have confirmed that the π-network of the planar conformation is sufficiently robust to offset the potential gains in σ-bonding occasioned by a puckering of the ring into C_{2v} or D_{2d} symmetry (16, 17). Table 1 summarizes the bond orders obtained from MNDO calculations on a series of $E(NSN)_2E$ molecules, all with a planar skeletal geometry imposed. It is readily apparent that the incorporation of heteroatoms (E = CH, CNH_2) or the covalent attachment of ligands to $S_4N_4^{2+}$ (E = SCl, SF, SNH_2) induces a substantial electronic reorganization, as a result of which the NS bonds of all the $E_2S_2N_4$ molecules are, to varying extents, weakened relative to those of $S_4N_4^{2+}$. Analysis of the π-molecular orbital distributions of the planar models with E = CH, CNH_2 provides an insight into the reasons for this trend.

Figure 2 illustrates the energies and distributions of the π-molecular orbitals of $HC(NSN)_2CH$ and $H_2NC(NSN)_2CNH_2$ (in D_{2h} symmetry). It is evident that while most of the occupied orbitals transform from one molecule to the other with little change in energy or composition, the π-HOMO is altered significantly. In $S_4N_4^{2+}$ the π-HOMO ($2b_{1u}$) is a non-bonding distribution centred on the four sulphur atoms (16, 17) and in $RC(NSN)_2CR$ it evolves progressively under the influences of electronegativity changes and exocyclic conjugation (4) into one ($2b_{1u}$ in R = H and $3b_{1u}$ in R = NH_2) exhibiting strong antibonding characteristics with respect to the SN linkages. Thus of the various orbital modifications which occur in the sequence $S_4N_4^{2+} \rightarrow HC(NSN)_2CH \rightarrow H_2NC(NSN)_2CNH_2$ the changes in this particular orbital are dominant in causing the decrease in ρ_{NS} (Table 1). As a result of the weakening of the planar framework, some deformation should be expected in those molecules with particularly low NS bond orders. The distortion coordinate that transforms the π-HOMO of **1** into the cross ring S—S bond of **2**, and thereby reduces its antibonding character over the NS linkages, has been discussed elsewhere (1*d*, 4, 16, 17). In order to assess the overall energy changes

TABLE 1. NS bond orders (aps)[a] for planar $E_2S_4N_4$ compounds

E	ρ_π	$\rho_{(\sigma+\pi)}$
S^+	0.36	1.23
HC	0.23	1.17
H_2NC	0.21	1.15
ClS[b]	[c]	1.17
FS[b]	[c]	1.13
H_2NS[b]	[c]	1.12

[a]See ref. 15.
[b]$\theta_1 = \theta_2 = 60°$.
[c]No σ/π separation.

TABLE 2. Heats of formation (kcal/mol) of planar (**1**) and puckered[a] (**2**) conformations of $E_2S_2N_4$ compounds

E	ΔH_f(**1**)	ΔH_f(**2**)	ΔH_f(**2**) − ΔH_f(**1**)
S^+	673.6	761.7	88.1
CH	137.3	154.7	17.4
CNH_2	146.6	151.2	4.6
SCl[b]	218.4	221.1	2.7
SF[b]	236.6	221.8	−14.8
SNH_2[b]	303.2	282.4	−20.8

[a]d(S—S) = 2.6 Å.
[b]$\theta_1 = \theta_2 = -60°$.

associated with such a deformation, a series of calculations of the heats of formation of $E(NSN)_2E$ molecules as a function of d(S—S) has been performed. The results are shown in Table 2, which lists the absolute and relative energies of the planar versus the puckered conformations (with d(S—S) set at 2.6 Å) of different models. In a relative sense the trend in ΔH_f(**2**) − ΔH_f(**1**) corresponds remarkably well with the observed structures of $E(NSN)_2E$ derivatives — all are puckered, i.e. **2**, save for $PhC(NSN)_2CPh$ and $S_4N_4^{2+}$, which are both planar. The apparent stability of **1** versus **2** for E = CNH_2 reflects the deficiency of the MNDO method in underestimating the transannular S—S bond of **2** with respect to the π-bonds of **1** (11). Indeed all of the differences ΔH_f(**2**) − ΔH_f(**1**) should probably be adjusted by at least 10 kcal/mol in favour of **2**. Nonetheless the difference in ΔH_f(**2**) − ΔH_f(**1**) for E = CH and CNH_2 illustrates the magnitude of the weakening effect of exocyclic conjugation on the π-system of **1**. The absence of a molecular plane of symmetry in the $R_2S_4N_4$ molecules precludes a rigorous π-orbital analysis. However, the effects of conjugation are still apparent in the relative stabilities of **2** versus **1** for R = Cl, F, and NH_2, the ordering following the expected trend in π-donor capabilities or R (NH_2 > F > Cl).[1]

$RS(NSN)_2SR$ isomers

The preceding analysis focussed attention on the electronic factors which control the skeletal shape of $E(NSN)_2E$ derivatives. In the case of $RS(NSN)_2SR$ compounds, all the known examples of which exhibit puckered geometries (type **2**) in the solid state, the possibility of different orientations (i.e. **3***a*, **3***b*, **3***c*) also exists. X-ray crystallographic studies on $S_4N_4Cl_2$ (6),

[1]Calculations on $E(NSN)_2E$ with E = PH_2 reveal a large preference (33 kcal/mol) for the puckered configuration **2**. However, the planar model converges to a "non-10π" ground state (i.e., the $3b_{1u}$ orbital becomes virtual), indicative of the inability of the restricted MNDO basis set to handle the P(V) valence state.

Can. J. Chem. Downloaded from www.nrcresearchpress.com by 210.87.254.6 on 09/06/12
For personal use only.

Can. J. Chem. Downloaded from www.nrcresearchpress.com by 210.87.254.6 on 09/06/12
For personal use only.

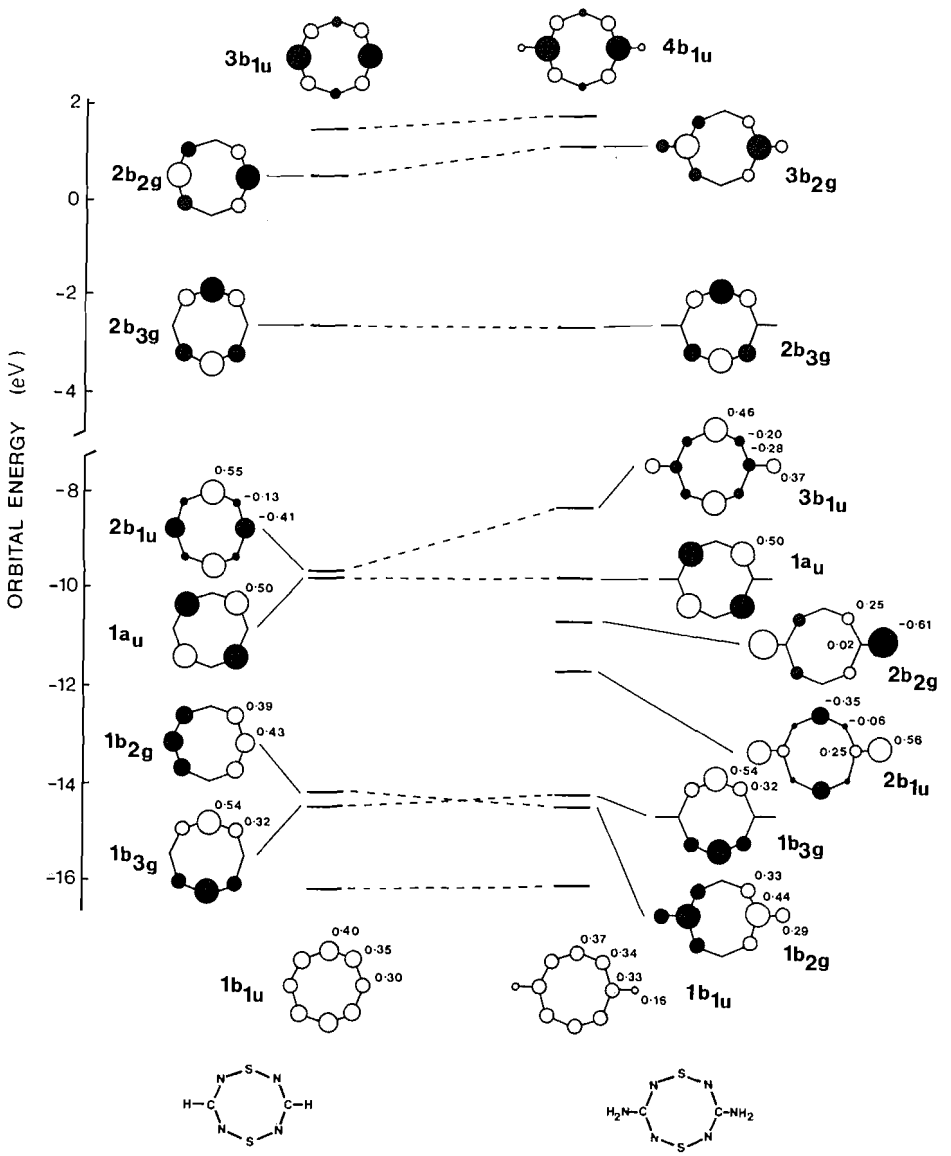

FIG. 2. π-Molecular orbital (MNDO) distributions and energies for $HC(NSN)_2CH$ and $H_2NC(NSN)_2CNH_2$, both in D_{2h} symmetry. Eigenvalue coefficients are indicated for occupied levels.

$S_4N_4(NMe_2)_2$ (7), and $S_4N_4(NPPh_3)_2$ (8) have established the unsymmetrical *exo–endo* ligand orientation **3***c* in the solid state, and nmr studies on all three of these systems (7, 8, 18) have confirmed the non-equivalence of the ligand environments in solution at ambient temperatures.[2] By contrast, the ^{19}F nmr spectra of **3** (R = F and $ON(CF_3)_2$) reveal a single fluorine environment, indicative of one of the two symmetrical isomers **3***a* or **3***b* (19, 20). The interpretation of these observations requires (*i*) an understanding of the energetics of the isomer equilibration process and (*ii*) a consideration of the stereochemistries associated with the preparation of $RS(NSN)_2SR$ compounds.

MNDO calculations on the heats of formation of model $RS(NSN)_2SR$ compounds as a function of the two angles θ_1 and θ_2 (see Fig. 1) provide an estimate of the relative stabilities of the three isomers and the activation barriers which restrict their interconversion. The results of a typical calculation are illustrated in Fig. 3, which shows a plot of the potential energy hypersurface (ΔH_f) for $S_4N_4F_2$. As expected there are three independent minima corresponding to the *exo–exo* ($\theta_1 \simeq \theta_2 \simeq -60°$), *endo–endo* ($\theta_1 \simeq \theta_2 \simeq +60°$) and *exo–endo* ($\theta_1 \simeq \pm 60°$, $\theta_2 \simeq \mp 60°$) geometries. The absolute energies of the three minima and of the transition states between them are listed in Table 3 for a number of different models. The energies of the three "invertomers" **3***a*,*b*,*c* are all very similar, the symmetrical modifications both being slightly more stable than the *exo–endo* form. However, the relative stabilities should not be given too great a significance, since the energy differences are smaller than the limit of reliability of the theoretical model. Of more importance are the barriers to the interconversions (e.g. **3***c* → **3***a*: 27, 47, and 45 kcal/mol for R = Cl, F, and NH_2, respectively), that for R = F being effectively identical to the barrier recently calculated for inversion at sulphur in S_4N_5F, **4** (46.7 kcal/mol) (21).

In view of the thermal instability of all $RS(NSN)_2SR$ derivatives, it seems unlikely that experimental data will be obtained to compare with these calculated values. Nonetheless, the bar-

[2]The ^{15}N nmr spectra of $S_4N_4Cl_2$ shows two distinct resonances at −60°C, consistent with the *exo–endo* geometry **3***c* (see ref. 18). On warming to room temperature the signals broaden but do not coalesce (18*b*).

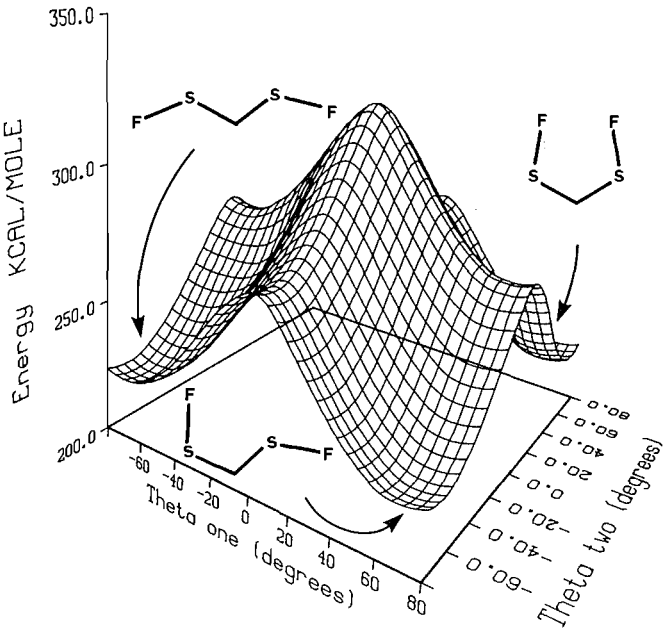

FIG. 3. Heat of formation (kcal/mol) of $S_4N_4F_2$ (d(S—S) = 2.6 Å) as a function of θ_1 and θ_2.

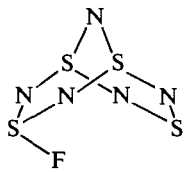

4

riers observed for simpler but related systems provide a useful basis for discussion. Thus, for example, the measured barrier for 1,2,5-thiadiazole-1-oxide **5** (33 kcal/mol) (22) is higher than that found for thiophene-1-oxide **6** (14.8 kcal/mol) (23), but considerably less than that calculated for $(NH_2)_2SO$ (66.5 kcal/mol) (22). For these systems, it has been suggested that conjugation in the cyclic molecules stabilizes the planar transition state, but that this is partially offset in the thiadiazole oxide **5** by the electronegativity effect of nitrogen (which stabilizes

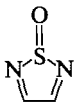

5

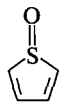

6

the pyramidal structure relative to the transition state). In $RS(NSN)_2SR$ derivatives the latter influences are likely to be even more pronounced, while the effects of conjugation are probably diminished.[3] Consistently the increase in the barrier height along the series R = Cl < NH_2 < F parallels the trend in ligand electronegativity.

[3]The π-electron-rich character of cyclothiazenes inhibits their acceptor capability. This concept is well illustrated by the orbital changes shown in Fig. 2, and is substantiated in the structures of $(Me_2N)_2S_4N_4$ (7) and $(Ph_8P_4N_6S_2)(NMe_2)_2$ (24), both of which exhibit rather long S—N_{exo} distances and pyramidalized nitrogen atoms. Cyclophosphazenes, on the other hand, are better π-acceptors, and aminophosphazene structures are characterized by short P—N_{exo} distances and planar geometries at nitrogen (25).

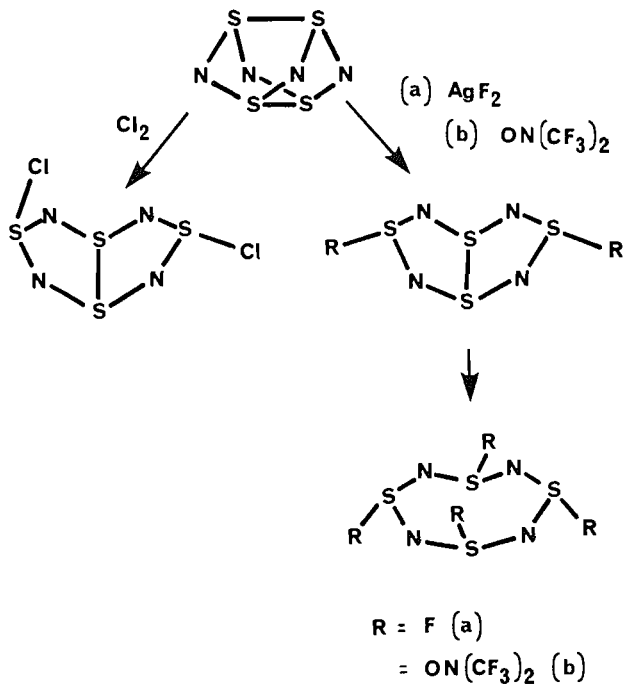

SCHEME 1

TABLE 3. Heats of formation (kcal/mol) of $RS(NSN)_2SR^a$ molecules as a function of θ_1 and θ_2 (deg)

θ_1	60.0	60.0	60.0	0.0	−60.0
θ_2	60.0	0.0	−60.0	−60.0	−60.0
R = Cl	222.4	254.6	226.1	253.1	221.1
R = F	222.4	271.2	224.2	271.0	221.8
R = NH_2	282.8	328.6	283.7	328.7	282.4

[a]d(S—S) fixed at 2.6 Å.

On the basis of the above estimates the stereochemical rigidity of $S_4N_4R_2$ derivatives with respect to inversion at sulphur is to be expected. Moreover, in view of the lack of thermal equilibration of invertomers at ambient temperatures, the range of stereochemistries exhibited by such compounds must reflect fundamental mechanistic differences in the reactions used to prepare them. Scheme 1 summarizes the pertinent synthetic routes to $S_4N_4R_2$ and $S_4N_4R_4$ compounds, i.e. those which involve a direct oxidative addition to the transannular S—S bonds of S_4N_4. It is worth noting that the stereochemistries for $S_4N_4F_4$ (26) and $S_4N_4(ON(CF_3)_2)_4$ (27) support the above assignments, based on nmr evidence, of *exo*−*exo* geometries for the corresponding $S_4N_4R_2$ derivatives, i.e., the ligand orientation patterns of the tetra-substituted products correspond to the sequential oxidation of both S—S bonds of S_4N_4, each step occurring with *exo*−*exo* stereochemistry. While double *endo*−*endo* addition would provide the same $S_4N_4R_4$ geometries, the steric constraints of this pathway make it less attractive. A mechanistic analysis of these reactions further substantiates the *exo*−*exo* geometry.

The stereochemistry of oxidative additions to the transannular S—S bonds of S_4N_4 (and those of $E_2S_2N_4$ derivatives) can be interpreted using the frontier orbital concepts that are commonly used in rationalizing the stereochemistry of organic reactions (28). Indeed recent studies on the electrocyclic additions of olefins to cyclothiazenes have already demonstrated the applicability of these ideas in inorganic thiazyl chemistry

Can. J. Chem. Downloaded from www.nrcresearchpress.com by 210.87.254.6 on 09/06/12
For personal use only.

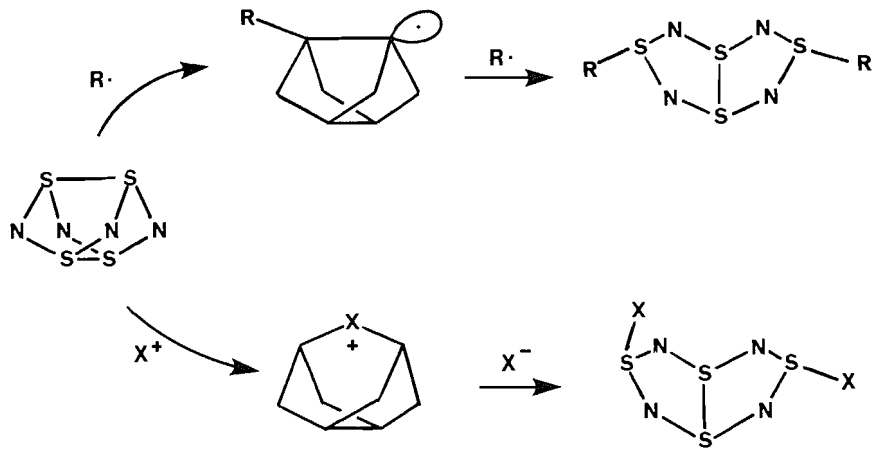

SCHEME 2

(29, 30). In the present instance the interpretation relies on a consideration of the symmetries and spatial distributions of the frontier orbitals of S_4N_4 that are associated with the S—S interactions. The results of many theoretical studies all concur that the high-lying occupied orbital $4b_2$ and the LUMO $6e$ possess overlap and symmetry properties that are characteristic of S—S σ and σ* orbitals (1). The interactions of these orbitals with the corresponding frontier orbitals of an approaching oxidant will determine the stereochemistry of the ensuing product. Thus oxidations involving a polar mechanism, e.g. chlorination, will proceed through the preliminary attack of an electrophilic species, e.g. Cl^+, on the occupied S—S σ-orbital, producing an intermediate with the symmetrical structure shown in Fig. 4. Subsequent attack of Cl^- can then only occur in an *exo* S—S σ-orbital,[4] producing an intermediate with the symmetrical structure shown in Fig. 4. Subsequent attack of Cl^- can then only occur in an *exo* fashion, thereby yielding the *exo–endo* product **3***c* (Scheme 2). By contrast, the reaction of nucleophilic radical oxidants (e.g. AgF_2 and $ON(CF_3)_2$) will be stereochemically coupled to the interaction of the high-lying SOMO of the radical and the low-lying LUMO of S_4N_4.[5] As is illustrated in Fig. 4, such an interaction will lead to attack of the oxidant on the *exo* side of the molecule. Subsequent reaction of a second radical will also be directed *trans* to the S—S bond, resulting in the *exo–exo* isomer **3***a* (Scheme 2).

Finally, some comments on the substitution behaviour of $S_4N_4Cl_2$ are warranted. The stereochemistry of the product $Me_2NS(NSN)_2SNMe_2$ obtained from the reaction of $S_4N_4Cl_2$ with Me_3SiNMe_2 (7) is readily accounted for in terms of a four-centre transition state which retains the configuration of each sulphur atom (31). By contrast, its reaction with ionic nucleophiles should yield the thermodynamically most stable isomer which, according to the above calculations, should be one of **3***a* or **3***b*. Consistently the conversion of $S_4N_4Cl_2$ to

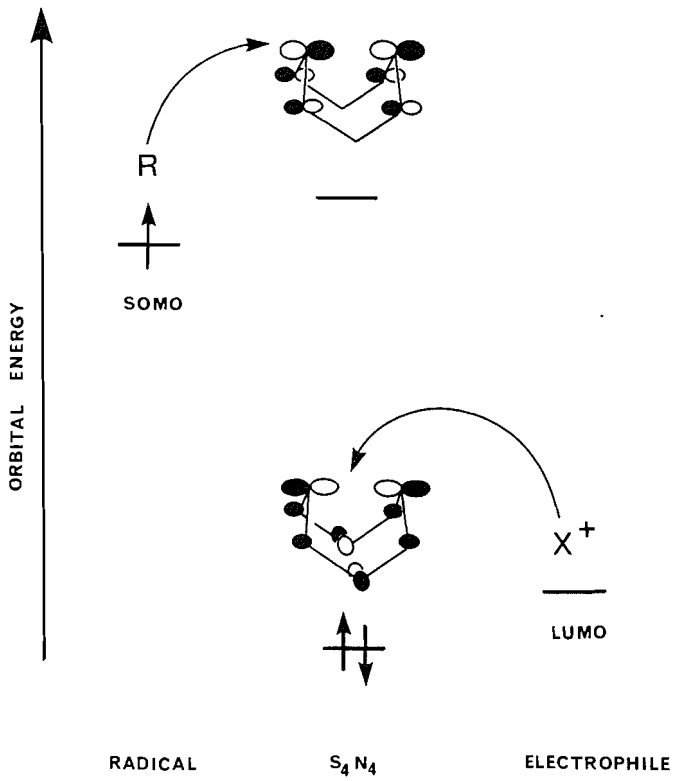

FIG. 4. Dominant interactions between the S—S σ($4b_2$) and σ*($6e$) orbitals of S_4N_4 and the frontier orbitals of radical and polar oxidants.

$S_4N_4F_2$ using excess NaF yields a product whose ^{19}F nmr spectrum is identical to that obtained from S_4N_4 and AgF_2 (19).

Summary

Heteroatom incorporation into the 10 π-electron perimeter of $S_4N_4^{2+}$ transforms its nonbonding π-HOMO into an antibonding orbital localized over the NSN linkages. Puckering of the molecules alleviates the weakness in these bonds by redistributing the orbital into a transannular S—S σ-interaction. The stereochemistry associated with the oxidation of the S—S bonds of S_4N_4 depends on the nature of the oxidants, and the consequent frontier orbital (S—S σ or σ*) with which they interact. Dipolar oxidation proceeds through initial electrophilic attack on the S—S σ-orbital, while the low-lying

[4]There are many occupied orbitals in the molecular orbital stack of S_4N_4 that have non-zero overlap populations between transannular sulphur atoms (1*a*). The cumulative effects (bonding and antibonding) give rise to a very weak but positive interaction, i.e. a partial bond, between cross-ring sulphurs. The $4b_2$ orbital, which is referred to herein as the S—S σ-orbital, is a major contributor to this bond. Energetically, it is the most readily disposed to interact with an approaching electrophile.

[5]The degeneracy of the $6e$ orbitals will be broken upon the approach of an oxidant. In Fig. 4 only one of these orbitals (the one that will interact most strongly with the radical SOMO) is illustrated.

Can. J. Chem. Downloaded from www.nrcresearchpress.com by 210.87.254.6 on 09/06/12
For personal use only.

σ^*(S—S)−SOMO (radical) interaction directs the free radical reactions.

Acknowledgement

I thank the Natural Sciences and Engineering Research Council of Canada for financial support of this work.

1. (*a*) T. CHIVERS, L. FIELDING, W. G. LAIDLAW, and M. TRSIC. Inorg. Chem. Soc. **18**, 3379 (1979); (*b*) R. H. FINDLAY, M. H. PALMER, A. J. DOWNS, R. G. EGDELL, and R. EVANS. Inorg. Chem. **19**, 1307 (1980); (*c*) R. C. HADDON, R. WUDL, and G. R. J. WILLIAMS. J. Am. Chem. Soc. **102**, 6687 (1980); (*d*) R. GLEITER. J. Chem. Soc. A, 3174 (1970).
2. A. W. CORDES, C. G. MARCELLUS, M. C. NOBLE, R. T. OAKLEY, and W. T. PENNINGTON. J. Am. Chem. Soc. **105**, 6008 (1983).
3. I. ERNST, W. HOLICK, G. RIHS, D. SCHOMBURG, G. SHOHAIN, D. WENKERT, and R. B. WOODWARD. J. Chem. Soc. **103**, 1540 (1981).
4. N. BURFORD, T. CHIVERS, P. W. CODDING, and R. T. OAKLEY. Inorg. Chem. **21**, 982 (1982).
5. N. BURFORD, T. CHIVERS, and J. F. RICHARDSON. Inorg. Chem. **22**, 1482 (1983).
6. Z. ZAK. Acta Crystalogr. B**37**, 23 (1981).
7. H. W. ROESKY, C. PELZ, A. GIEREN, and E. HADICKE. Z. Naturforsch. **36**b, 1437 (1981).
8. J. BOJES, T. CHIVERS, A. W. CORDES, G. MACLEAN, and R. T. OAKLEY. Inorg. Chem. **20**, 16 (1981).
9. J. P. BOUTIQUE, J. RIGA, J. J. VERBIST, J. DELHALLE, J. G. FRIPIAT, R. C. HADDON, and M. L. KAPLAN. J. Am. Chem. Soc. **106**, 312 (1984).
10. (*a*) M. J. S. DEWAR and W. THIEL. J. Am. Chem. Soc. **99**, 4899 (1977); (*b*) Quantum Chemistry Program Exchange (1977), No. 353 (MNDO).
11. (*a*) M. J. S. DEWAR and M. L. MCKEE. J. Comp. Chem. **4**, 84 (1983); (*b*) N. C. BAIRD. J. Comp. Chem. **5**, 35 (1984).
12. T. CHIVERS, P. W. CODDING, W. G. LAIDLAW, S. W. LIBLONG, R. T. OAKLEY, and M. TRSIC. J. Am. Chem. Soc. **105**, 1186 (1983).
13. R. J. GLEITER and R. BARTETZKO. Z. Naturforsch. **36**b, 452 (1981).
14. A. W. CORDES, H. KOENIG, R. T. OAKLEY, and W. T. PENNINGTON. Inorg. Chem. **22**, 3375 (1983).
15. D. R. ARMSTRONG, P. G. PERKINS, and J. P. STEWART. J. Chem. Soc. Dalton Trans. 838 (1973).
16. R. J. SHARMA, F. AUBKE, and N. L. PADDOCK. Can. J. Chem. **59**, 3157 (1981).
17. M. TRSIC, W. G. LAIDLAW, and R. T. OAKLEY. Can. J. Chem. **60**, 2281 (1982).
18. (*a*) T. CHIVERS and R. T. OAKLEY. Top. Curr. Chem. **102**, 117 (1982); (*b*) R. T. OAKLEY. Unpublished results.
19. L. ZBORILOVA and P. GEBAUER. Z. Anorg. Allgem. Chem. **448**, 5 (1979).
20. R. MEWS. J. Fluorine Chem. **18**, 155 (1981).
21. W. ISENBERG, R. MEWS, G. SHELDRICK, R. BARTETZKO, and R. GLEITER. Z. Naturforsch. **38**b, 1563 (1983).
22. J. S. AMATO, S. KARADY, R. A. REAMER, H. B. SCHLEGEL, J. P. SPRINGER, and L. M. WEINSTOCK. J. Am. Chem. Soc. **104**, 1375 (1982).
23. W. L. MOCK. J. Am. Chem. Soc. **92**, 7610 (1970).
24. T. CHIVERS, M. N. SUDHEENDRA RAO, and J. R. RICHARDSON. J. Chem. Soc. Chem. Commun. 700 (1983).
25. (*a*) D. P. CRAIG and N. L. PADDOCK. Non-Benzenoid Aromatics, **2**, 273 (1971); (*b*) R. D. SHARMA, S. J. RETTIG, N. L. PADDOCK and J. TROTTER. Can. J. Chem. **60**, 535 (1982).
26. G. A. WIEGERS and A. VOS. Acta Crystallogr. **16**, 152 (1963).
27. H. J. EMELEUS, R. A. FORBER, R. J. POULET, and G. M. SHELDRICK. J. Chem. Soc. Chem. Commun. 1483 (1970).
28. I. FLEMING. Frontier orbitals and organic chemical reactions. John Wiley and Sons. 1976.
29. T. YAMABE, K. TAKANA, A. TACHIBANA, K. FUKUI, and H. KATO. J. Phys. Chem. **83**, 767 (1979).
30. S. W. LIBLONG, R. T. OAKLEY, A. W. CORDES, and M. C. NOBLE. Can. J. Chem. **61**, 2062 (1983).
31. S. OAE, M. YOKOYAMA, M. KISE, and N. KURUKAWA. Tetrahedron Lett. 4131 (1968).

Can. J. Chem. Downloaded from www.nrcresearchpress.com by 210.87.254.6 on 09/06/12
For personal use only.

Evidence for a di-π-methane rearrangement in the photoisomerization of 2,3-benzo-7,8-dimethylbicyclo[4.2.0]octa-2,4,7-triene to 6,7-dimethylbenzotricyclo[3.3.0.0^{2,8}]octa-3,6-diene

CHRISTOPHER OWEN BENDER, IRENE MARIE CASSIS, DOUGLAS DOLMAN, LOUIS DENNIS HEERZE, and FRANCES LINDA SCHULTZ

Department of Chemistry, University of Lethbridge, Lethbridge, Alta., Canada T1K 3M4

Received February 27, 1984

CHRISTOPHER OWEN BENDER, IRENE MARIE CASSIS, DOUGLAS DOLMAN, LOUIS DENNIS HEERZE, and FRANCES LINDA SCHULTZ. Can. J. Chem. **62**, 2769 (1984).

The direct and sensitized (Michler's ketone) irradiations of 2,3-benzo-7,8-dimethylbicyclo[4.2.0]octa-2,4,7-triene (**7**) yield 6,7-dimethylbenzotricyclo[3.3.0.0^{2,8}]octa-3,6-diene (**3**, $\Phi = 0.030$ and 0.093, respectively) and naphthalene ($\Phi = 0.10$ and 0.16, respectively). Deuterium labelling studies suggest that **3** derives from a Zimmerman di-π-methane rearrangement of **7**, and that 1,8-dimethyl-1a,2,7,7a-tetrahydro-1,2,7-metheno-1*H*-cyclopropa[*b*]naphthalene is not an intermediate en route to **3**.

CHRISTOPHER OWEN BENDER, IRENE MARIE CASSIS, DOUGLAS DOLMAN, LOUIS DENNIS HEERZE et FRANCES LINDA SCHULTZ. Can. J. Chem. **62**, 2769 (1984).

La photolyse directe et sensibilisée par le cétone de Michler du benzo-2,3-diméthyl-7,8-bicyclo[4.2.0]octa-2,4,7-trième (**7**) conduit au diméthyl-6,7-benzotricyclo[3.3.0.0^{2,8}]octa-3,6-diène (**3**, $\Phi = 0.030$ et 0.093, respectivement) et au naphtalène ($\Phi = 0.10$ et 0.16, respectivement). Des études de marquages au deuterium suggèrent que **3** dérive d'un réarrangement di-π-méthane de Zimmerman, et que diméthyl-1,8-tetrahydro-1a,2,7,7a-métheno-1,2,7-cyclopropa-1*H*-naphtalène[*b*] n'est pas un composé intermédiaire en route à **3**.

Can. J. Chem. Downloaded from www.nrcresearchpress.com by 210.87.254.42 on 09/06/12
For personal use only.

Introduction

Recently we reported the formation of the mixture of semibullvalenes (SB's) **2** and **3** from the sensitized irradiation of the barrelene **1** (1). The isomers proved difficult to separate (prep. glc). Based on the observations of Sasse and co-workers (2) that the diene **4** could be converted to the SB **6** via the [2 + 2] cycloadduct **5**, we had envisioned that an alternative and perhaps cleaner route to **2** might be available from photoisomerization of the dimethyldiene **7** (i.e., **7** → **8** → **2**, Scheme 1). Here we report that **3** and not the anticipated semibullvalene **2** is the only photoproduct isomeric with reactant **7**, and provide evidence that **3** is formed by a Zimmerman di-π-methane (DPM) rearrangement without the involvement of a symmetric intermediate such as **8**.

Results

2,3-Benzo-7,8-dimethylbicyclo[4.2.0]octa-2,4,7-triene (**7**) was conveniently prepared from the photolysis of 6,7-dimethylbenzocyclooctatetraene (COT **9**) by a modification of the previous method (1). The use of 1-acetonaphthone as sensitizer, instead of chlorobenzene, gave **7** in almost quantitative yield (Scheme 2). Compound **7** was less successfully prepared from the direct irradiation (Pyrex filter) of COT **9** due to secondary photochemistry of initially formed **7** (*vide infra*); at low conversions **7** was the dominant product but naphthalene and 6,7-dimethylbenzotricyclo[3.3.0.0^{2,8}]octa-3,6-diene (**3**) became the major components as the photolysis progressed.

On direct (Pyrex filter) and on sensitized (Michler's ketone) irradiations, **7** gave naphthalene and **3** in the ratio of 3:1 (direct) and 1.7:1 (sensit.). Both COT **9** and SB **2** were absent in photolysates (glc evidence), and **3** was inert under the irradiation conditions used here.

Since the structure of SB **3** was previously assigned on the basis of spectroscopic data alone, the diimide reduction of **3** was carried out in order to provide some chemical support. The reduction of **3** proceeded in a highly stereoselective manner to give **10** quantitatively (Scheme 3). The interpretation of the ^{1}H 400-MHz nmr spectrum of **10** is straighforward. The aliphatic ring protons occur as six distinctly separated one-proton resonances; couplings between protons were confirmed by double irradiation techniques (see Experimental). The stereochemistry of **10** was assigned on the basis that $J_{5,6} = 5$ Hz (cf. $J_{5,6} = 5.4$ Hz in **12** (2), whereas $J_{5,6'} = 0$ Hz in **13** (3)).

Singlet and triplet energies of 7 and quantum yields

The singlet energy of **7** in cyclohexane at room temperature was determined to be 94 kcal/mol from intersection of the absorption and fluorescence spectra. The triplet energy of **7** could not be obtained spectrometrically since no phosphorescence in isopentane–methylcyclohexane glass at 77 K could be detected. However, an "effective" triplet energy at room temperature in cyclohexane solution of $61 \geq E_T \geq 59$ kcal/mol (cf. 61 kcal/mol for styrene) is suggested by triplet sensitization experiments: the conversion of **7** to naphthalene and SB **3** can be sensitized by Michler's ketone ($E_T = 61$ kcal/mol), but not by 2-acetonaphthone ($E_T = 59$ kcal/mol) nor by 1-acetonaphthone ($E_T = 56$ kcal/mol).

The fluorescence quantum yield of **7** at room temperature was determined to be 0.50 by the relative quantum yield method using naphthalene as standard ($\phi_f = 0.23$ (4)) (see Experimental). Product quantum yields for all the transformations observed in this study are summarized in Table 1.

Mechanistic considerations

Unlike the case of **4** → **5** → **6**, the formation of a [2 + 2] cycloadduct in the photoconversion of diene **7** to SB **3** was not detected (glc and nmr monitoring of photolysates). The non-observation of possible intermediate **8** does not, however, preclude its involvement in the production of SB **3**, since **8** may be photo-labile. In order to study this point further, irradiations of the doubly deuterated diene **7***a* (ca. 15%-d_1 at C-4; ca. 90%-d_1 at C-5) were undertaken. The synthesis of **7***a* is outlined in Scheme 4. The structures of compounds **14** and **18** follow from the synthetic route and spectral properties (see Experimental).

The direct and sensitized photolysis of **7***a* led to semibullvalene product **3***a* with deuterium at C-2 (15%-d_1) and at

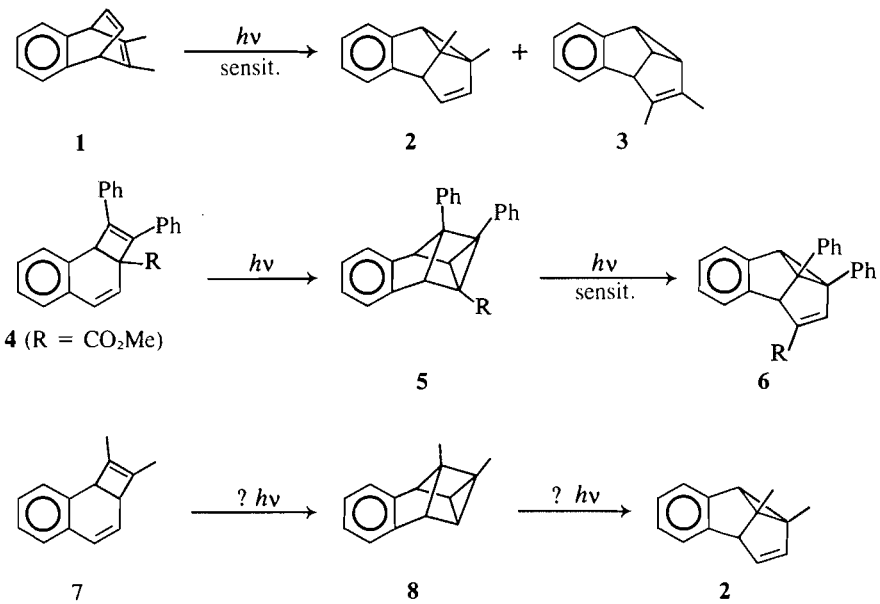

SCHEME 1

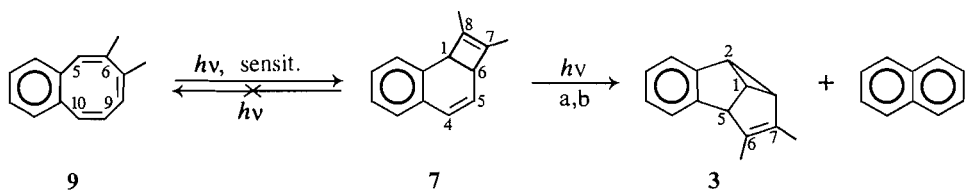

	Yields	
direct (a)	19%	57%
sensit. (b)	24%	41%

SCHEME 2

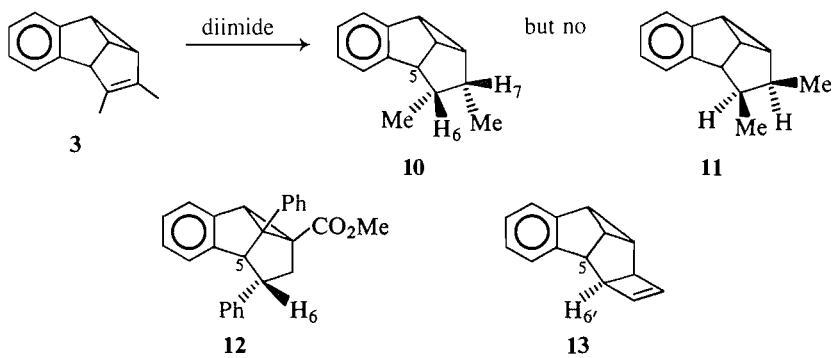

SCHEME 3

C-8 (90%-d_1), as determined by ^{1}H nmr analysis. Recovered reactant showed no label scrambling after >85% consumption.

Three plausible mechanistic routes which rationalize the conversion of diene **7** to SB **3** are given in Scheme 5. A consequence of semibullvalene formation via route ii (Scheme 5), the [2 + 2] cycloaddition pathway, is that both **3***a* and **3***b* should be formed in approximately equal amounts because of the symmetry of the carbon skeleton of **8** (assuming small secondary deuterium isotope effects). Thus the finding that **7***a* gave **3***a* but no **3***b* is persuasive evidence that cycloadduct **8** is not an intermediate en route to **3**.

Inspection of the other pathways shown in Scheme 5 (i.e., routes i and iii) reveals that only route iii can provide the observed labelling pattern of product **3***a*. Route iii is formally equivalent to the ubiquitous Zimmerman di-π-methane rearrangement.

Another aspect of mechanistic interest concerns the formation of SB **3** during the direct irradiations of COT **9** (*vide supra*). By analogy with the isomerization of cyclooctatetraenes to semibullvalenes (5, 6) there exists the possibility that some **3** may derive from 5,9 + 8,10 bonding of an excited state stereoisomer of COT **9** (i.e., **22**; Scheme 6, route i), rather than all of it being produced as a result of secondary photolysis of diene **7** (Scheme 6, route ii).

A means of determining competition between route i and route ii was provided by examining the photolysis of the la-

Can. J. Chem. Downloaded from www.nrcresearchpress.com by 210.87.254.42 on 09/06/12
For personal use only.

TABLE 1. Quantum yield data[a]

Compound	Light wavelength (nm)	Sensitizer	Φ (Product appearance) 7	3	Naphthalene
9	366	1-Acetonaphthone	0.36	—	—
9	300	None	0.04	—	—
7	300	None	—	0.030	0.10
7	335	Michler's ketone	—	0.093	0.16
7	335	1- or 2-acetonaphthone	—	<0.01	<0.01

[a]Ferrioxalate actinometry; cyclohexane solvent. Φ's given are extrapolated to zero conversion; product analyses by glc (internal hydrocarbon standard) at several conversions ≤ 8%. Experimental error of Φ's is ±10%. For sensitized runs, sensitizers absorb >95% of incident light.

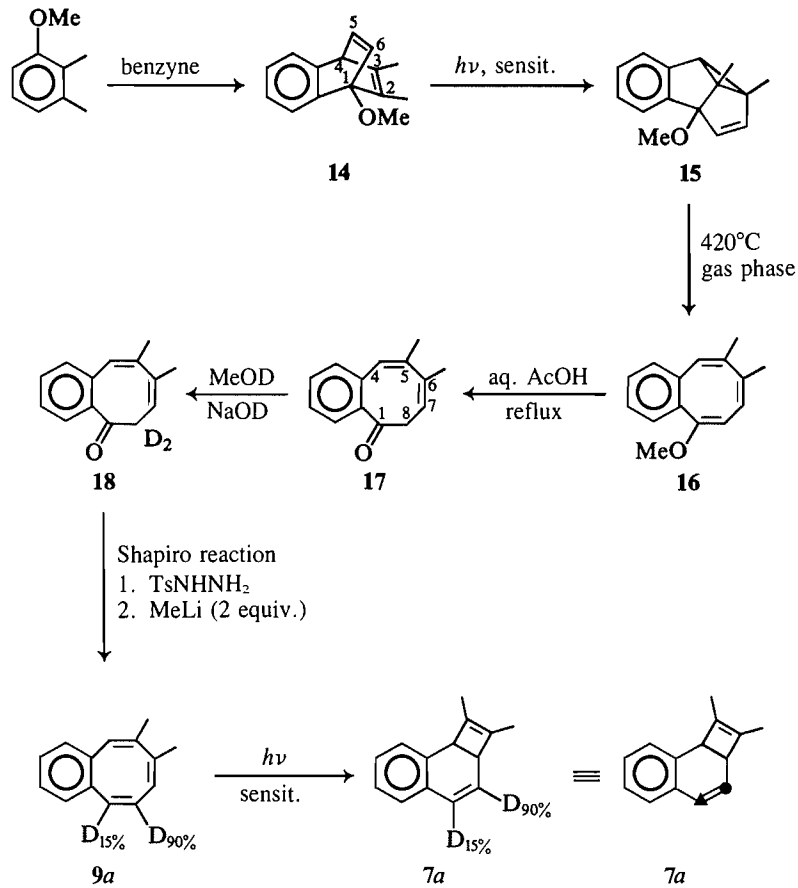

SCHEME 4

belled COT **9***a*. The semibullvalene product isolated from the direct irradiation of **9***a* showed hydrogen distributions consistent with those anticipated for route ii, and which were the same as those found for the conversion of diene **7***a* to SB **3***a* (*vide supra*). Thus **3** is not produced by the traditional 5,9 + 8,10 bonding pathway (route i) usually invoked to rationalize semibullvalene formation in the cases of non aro-fused COT's.

Discussion

The excited state of diene **7** yielding SB **3** and naphthalene upon sensitization with Michler's ketone is assumed to be the triplet, since the products are formed with greater efficiency than when generated from direct irradiation. The multiplicity assignment(s) in the case of the direct irradiation is much less certain. Interpretation of the quantum yield data (Table 1) in terms of the Zimmerman "ratio bracketing rule" (7) indicates that at least ca. 50% of the naphthalene must be singlet derived (i.e., $0.05 \lesssim {}^1\Phi_{Nap} \lesssim 0.1$). But the percentage of singlet involvement in the production of SB **3** cannot be gleaned from this approach. We note, however, that a general preference for triplet initiation of DPM rearrangements has been observed for rigid systems (8), and this situation will hold in the present case if $\Phi_{isc} = 0.33$. This value is not inconsistent with what we know of the fate of excited singlet **7** (i.e., since $\phi_f = 0.5$ and ${}^1\Phi_{Nap} \gtrsim 0.05$, then $\Phi_{isc} \lesssim 0.45$).

With regard to the photoreactions observed for **7**, i.e., cleavage to naphthalene and rearrangement to SB **3**, only the former is well precedented in benzobicyclo[4.2.0]octa-2,4,7-triene derivatives (2). For the latter reaction there may be at least two analogous literature examples.

The first concerns the formation of SB **24** from the photoreaction between naphthalene and dimethyl acetylene-

Can. J. Chem. Downloaded from www.nrcresearchpress.com by 210.87.254.42 on 09/06/12
For personal use only.

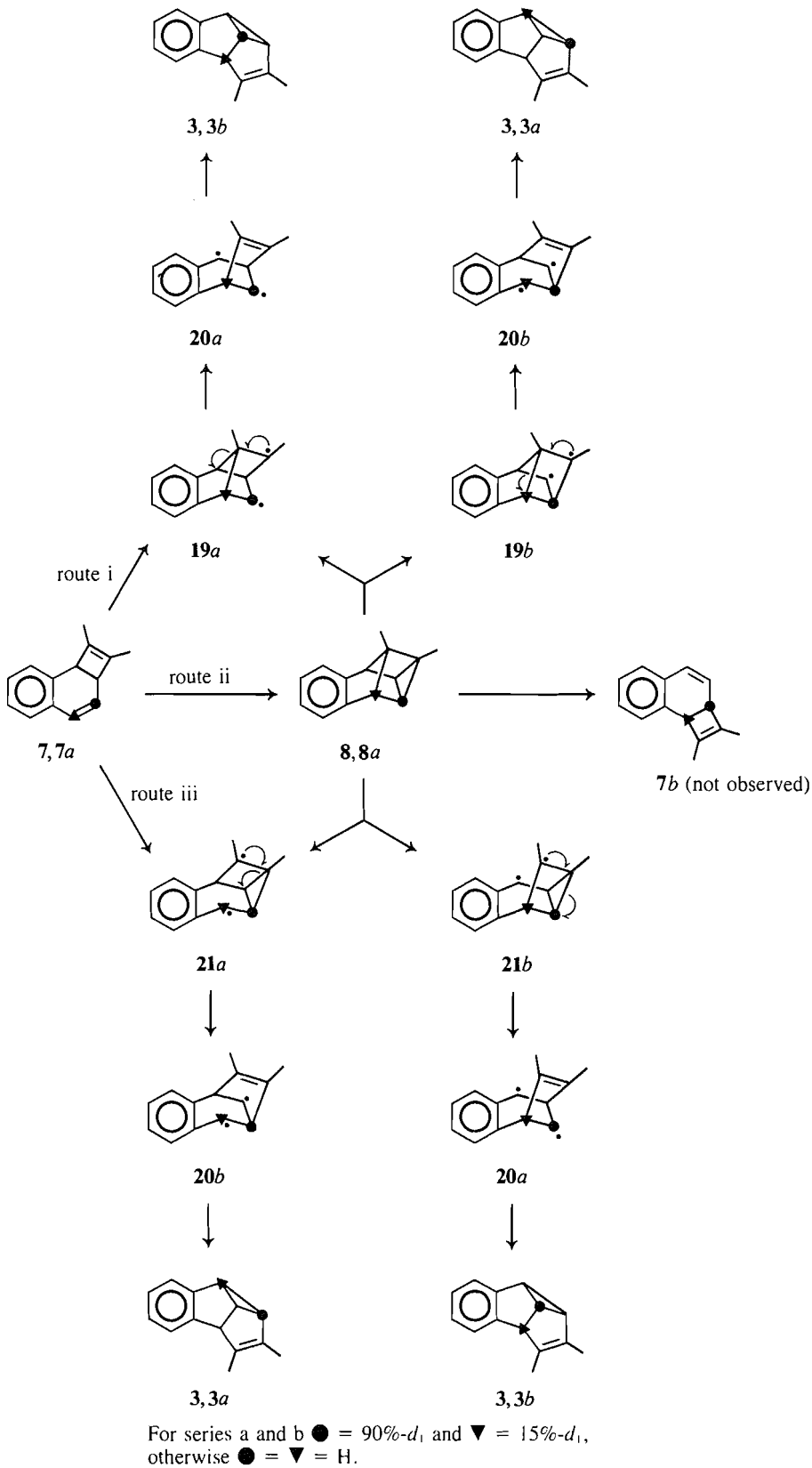

SCHEME 5

dicarboxylate (9). Addition of the acetylene to the diradical species **23** was the suggested product rationalization (Scheme 7). However, naphthalenes are well known to undergo [2 + 2] photocycloadditions with acetylenes (2) (and with alkenes (10)). In light of the present work a plausible alternative pathway to SB **24** is via a DPM rearrangement of initially formed [2 + 2] adduct **25** (Scheme 7).

The second example is the photoconversion of COT **26** to SB

Can. J. Chem. Downloaded from www.nrcresearchpress.com by 210.87.254.42 on 09/06/12
For personal use only.

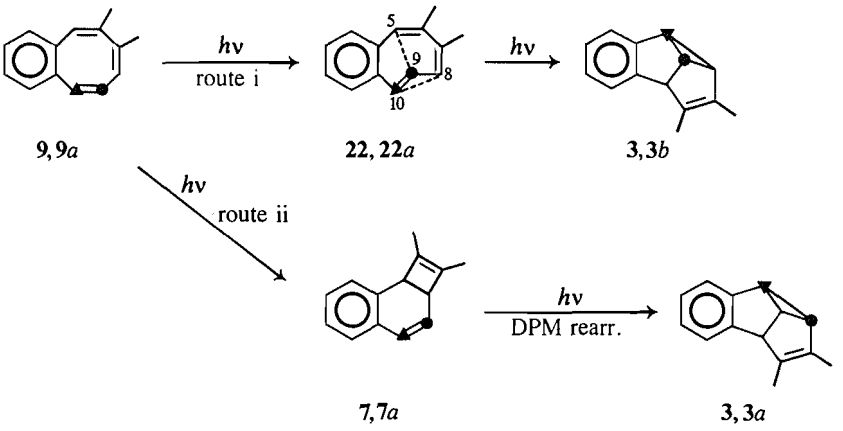

9,9*a* 22,22*a* 3,3*b*

7,7*a* 3,3*a*

For series a and b ● = 90%-d_1 and ▼ = 15%-d_1, otherwise ● = ▼ = H.

SCHEME 6

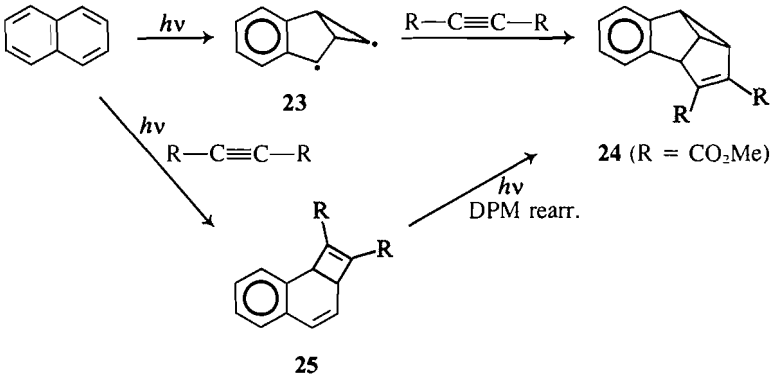

23 24 (R = CO_2Me) 25

SCHEME 7

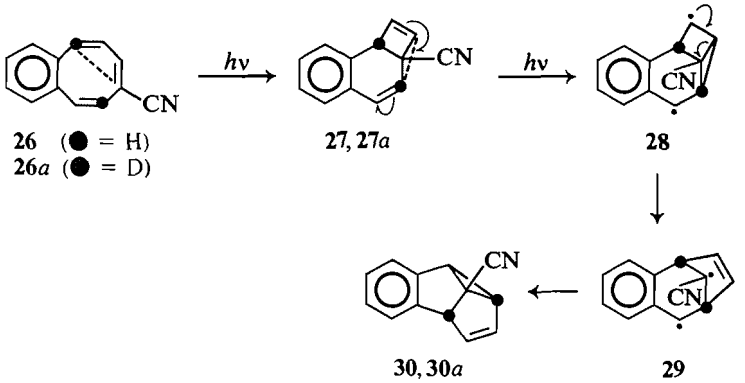

26 (● = H)
26*a* (● = D)
27,27*a* 28
30,30*a* 29

SCHEME 8

30. No previous rationalization of the reaction was given (11). It is readily seen that formation of SB **30** is conveniently accounted for in terms of a DPM rearrangement of initially formed diene **27** (Scheme 8). Note that the mechanism depicted in Scheme 8 predicts the observed location of the cyano group in **30** and both deuterium labels in **30***a*. The photochemistry of COT **26** is presently being reinvestigated,[1] and we report here that diene **27** is indeed an intermediate, and that it further photoisomerizes to SB **30**.

[1] C. O. Bender and D. Dolman, results to be published.

Experimental

The nmr spectra were recorded on a Bruker 400-MHz instrument or on a Varian (EM-360) 60-MHz instrument, with TMS as internal standard. The chemical shifts are in δ units and the coupling constants (J) in Hz. The abbreviations s, d, t, q, and m refer to singlet, doublet, triplet, quartet, and multiplet, respectively. The ir spectra were recorded on a Perkin–Elmer 337 spectrometer and are given in cm^{-1}. The uv spectra (run in cyclohexane solvent) were measured on a Cary 15 spectrometer; maxima are given in nm, with ϵ_{max} values in parentheses; sh = shoulder. Mass spectra were recorded on an MS 9 (A.E.I.) instrument at 70 eV. All melting points are uncorrected. Elemental analyses were performed by Galbraith Labs. Inc., Knoxvil-

Can. J. Chem. Downloaded from www.nrcresearchpress.com by 210.87.254.42 on 09/06/12
For personal use only.

Can. J. Chem. Downloaded from www.nrcresearchpress.com by 210.87.254.42 on 09/06/12
For personal use only.

le, TN. The glc analyses were made on a Varian 3700 instrument (FID) coupled to a Varian CDS 111 computing integrator, and fitted with an OV-101 glass capillary column, 50 m, with helium as carrier gas. Column chromatography was performed with Silica Gel 60 (230–400 mesh; Merck) or Silica Gel H (100–200 mesh; Grace). Cyclohexane for photolyses was prepared by scrubbing with 10% of its volume of 30% fuming sulfuric acid, followed by washing with 10% aqueous sodium hydroxide, drying ($MgSO_4$), and finally distilling from calcium hydride. Sensitizers were distilled or recrystallized prior to use.

General procedures for preparative photolyses

The apparatus consisted of a 450-W Hanovia medium pressure mercury arc surrounded by a water cooled quartz immersion well. For direct irradiations the light was filtered through a cylindrical Pyrex sleeve. For irradiations at wavelengths >340 nm the light was passed through an aqeuous filter jacket (10-mm path length) containing a solution prepared from 750 g NaBr and 8 g $Pb(NO_3)_2$ per 1 L of water. Before irradiations, solutions (35 mL) of reactants contained in 2 cm × 15 cm quartz test-tube-like photolysis cells were deoxygenated by flushing with argon. The tubes were sealed under a positive pressure of argon which was maintained over the stirred solutions throughout the course of the irradiations. The progress of photolyses was followed by glc analyses.

Sensitized irradiation of COT ***9***

A solution of 80.0 mg (0.44 mmol) of **9** (1) and 209.2 mg (1.23 mmol) of 1-acetonaphthone in 35 mL of cyclohexane was photolysed at >340 nm for 1 h (100% conversion by glc). The photolysate was concentrated and the residue chromatographed on Silica Gel 60 (2 cm × 25 cm) with cyclohexane solvent. The first band gave 77.6 mg (97%) of known **7** (1) after short-path distillation at 55°C/0.1 Torr (1 Torr = 133.3 Pa).

Direct irradiation of diene 7

A solution of 45.6 mg (0.25 mmol) of **7** in 35 mL of cyclohexane was photolysed with Pyrex-filtered light for 6 h (100% conversion by glc). The yields of naphthalene and SB **3** were 18.3 mg (57%) and 8.7 mg (19%), respectively, as determined by glc after addition of a known amount of standardized tridecane. The photolysate was concentrated and the residue chromatographed on Silica Gel 60 (2 cm × 45 cm) with cyclohexane solvent. The first band gave 9.6 mg (30%) of naphthalene, mp 78–80°C, after recrystallization from ethanol. The second band gave 7.2 mg (16%) of known SB **3** (1) after short-path distillation at 55°C/0.1 Torr.

Sensitized irradiation of diene 7

A solution of 96.3 mg (0.53 mmol) of **7** and 4.7 mg (0.02 mmol) of Michler's ketone in 35 mL of cyclohexane was photolysed at >340 nm for 2 h (100% conversion by glc). The yields of naphthalene and SB **3** were 27.8 mg (41%) and 23.1 mg (24%), respectively, as determined by glc after addition of a known amount of standardized tridecane. The photolysate, after work-up as in the case of the direct irradiation of **7**, gave 21.3 mg (31%) of naphthalene, mp 78–80°C, and 20.3 mg (21%) of SB **3**.

Diimide reduction of SB ***3***

To a stirred mixture of 47.9 mg (0.26 mmol) of **3** and 3.45 g (17.8 mmol) of potassium azodicarboxylate in 20 mL of methanol at −30°C, 2 mL of acetic acid was added in one portion. The reaction mixture was allowed to warm to room temperature during 1.5 h after which time the solution was added to 200 mL of cyclohexane and was washed with 5% aqueous potassium hydroxide (200 mL) followed by water (2 × 200 mL). The cyclohexane solution was dried ($MgSO_4$), concentrated, and the residue chromatographed on Silica Gel 60 (2 cm × 35 cm) with cyclohexane solvent. The first band gave 47.9 mg (99%) of *endo*-3,4-benzo-6,7-dimethyltricyclo[3.3.0.$0^{2,8}$]oct-3-ene (**10**) as a colourless oil (glc purity >99%) after short-path distillation at 55°C/0.1 Torr; uv: 230 (5 060), 261.5 sh (600), 267 (970), 273 sh (1 300), 275 (1 420), and 282.5 (1 660); nmr (400 MHz, $CDCl_3$): 6.90–7.21 (m, 4**H**, aromatics), 3.34 (t, 1H, **H**-5, $J_{5,1} = J_{5,6} = 5.5$), 2.98 (q, 1H, H-1, $J_{1,2} = J_{1,8} = 6.5$, $J_{1,5} = 5.5$), 2.78–2.88 (m, 1H, H-6, $J_{6,5} = 5.5$, $J_{6,7} = 10.0$, $J_{6,C6\text{-}Me} = 7.0$), 2.47–2.57 (m, 1H, H-7, $J_{7,6} = 10.0$, $J_{7,8} = 6.5$, $J_{7,C7\text{-}Me} = 7.5$), 2.25 (d × d, 1H, H-2, $J_{2,1} = 6.5$, $J_{2,8} = 7.5$), 2.01 (q, 1H, H-8, $J_{8,1} = J_{8,7} = 6.5$, $J_{8,2} = 7.5$), 0.78 (d, 3H, C6-methyl, $J_{C6\text{-}Me,6} = 7.0$), and 0.36 (d, 3H, C7-methyl, $J_{C7\text{-}Me,7} = 7.5$); spin decoupling experiments: irradiation of H-5 collapsed H-1 to a t ($J_{1,2} = J_{1,8} = 6.5$) and modified the H-6 m; irradiation of H-1 collapsed H-5 to a d ($J_{5,6} = 5$), H-2 to a d ($J_{2,8} = 7.5$), and H-8 to a br t ($J_{8,2} = 7.5$, $J_{8,7} = 6.5$); irradiation of H-6 collapsed H-5 to a d ($J_{1,5} = 5.5$), the C6-methyl to an s, and modified H-7; irradiation of H-7 collapsed H-8 to a br t ($J_{8,2} = 7.5$, $J_{8,1} = 6.5$), the C7-methyl to an s, and modified H-6; irradiation of H-2 collapsed H-1 to a br t ($J_{1,5} = 5.5$, $J_{1,8} = 6.5$), and H-8 to a t ($J_{8,1} = J_{8,7} = 6.5$); irradiation of H-8 collapsed H-2 to a d ($J_{2,1} = 6.5$), H-1 to a d × d ($J_{1,2} = 6.5$, $J_{1,5} = 5.5$), and modified H-7; irradiation of the C7-methyl collapsed H-7 to a d × d ($J_{7,8} = 6.5$, $J_{7,6} = 10.0$); irradiation of the C6-methyl collapsed H-6 to a d × d ($J_{6,5} = 5.5$, $J_{6,7} = 10.0$). Mass spectrum showed molecular ion at m/e = 184.1250 (100%), $C_{14}H_{16}$ requires 184.1253.

Quantum yield determinations

Quantum yields were performed on an apparatus previously described (1), which includes an optical bench arranged for beam splitting into ferrioxalate actinometer (12). Sample solutions (4 mL) of reactants (ca. 1×10^{-2} *M*) and sensitizer, if any (1- and 2-acetonaphthone, 3×10^{-2} *M*; Michler's ketone, 0.57×10^{-3} *M*), were deoxygenated prior to irradiation by flushing with argon. A positive pressure of argon was maintained over the stirred solutions throughout the course of the irradiations. For Φ's, and further experimental details, see Table 1.

Fluorescence studies of diene 7

The fluorescence spectrum of **7** was measured in cyclohexane solution at room temperature on an Aminco–Bowman Spectrometer, and showed a maxima at 335 nm. Intersection of emission and absorption spectra occurred at 305 nm corresponding to a singlet energy of 94 kcal/mol. The approximate fluorescence quantum yield of **7** was measured relative to naphthalene as standard. The absorption and emission spectra of these two compounds are similar in the 280–320 nm and 300–400 nm range, respectively. The optical densities of both compounds in cyclohexane solution were matched at 283 nm, the fluorescence excitation λ employed. The fluorescence intensities of the naphthalene and **7** solutions were integrated by cutting and weighing the recorded spectra. Since the ratio was 1.00:2.16, respectively, and $\phi_f = 0.23$ for naphthalene (4), then $\phi_f = 0.50$ for diene **7**.

*2,3-Dimethyl-1-methoxy-4-hydro-1,4-ethenonaphthalene (****14****)*

A mixture of benzene diazonium carboxylate, prepared from 3.5 g (25.6 mmol) of anthranilic acid (1) and 500 mL of 2,3-dimethylanisole was stirred at 50°C overnight under a dry nitrogen atmosphere, and then concentrated. The residue was dissolved in acetone (50 mL), diluted with cyclohexane (500 mL), filtered, and the filtrate concentrated. The residue was chromatographed on Silica Gel H (2.5 cm × 60 cm) with 2% ether–cyclohexane. The first band was residual dimethylanisole. Concentration of the second band gave a yellow residue which yielded 2.90 g (62%) of colourless **14**, mp 83–85°C, after two recrystallizations from ethanol; uv: 248 sh (845), 256.5 (710), 263 (805), 271 (1 040), and 278 (1 000); nmr (60 MHz, CCl_4): 6.56–7.24 (m, 6H, aromatics and vinyls), 4.27 (d × d, 1H, bridgehead, $J_{4,5} = 6$, $J_{4,6} = 1.5$), 3.78 (s, 3H, methoxyl), 1.73 (s, 3**H**, methyl), and 1.66 (s, 3H, methyl). *Anal.* calcd. for $C_{15}H_{16}O$: C 84.87, H 7.60; found: C 84.81, H 7.76.

Sensitized photolysis of barrelene ***14***

A solution of 506.2 mg (2.39 mmol) of **14** and 10 mL of acetone in 250 mL of cyclohexane was irradiated with Pyrex-filtered light for 50 min. The photolysate was concentrated and the residue taken up in 3 mL of 80% aqueous acetic acid. The solution was refluxed for 1 h with stirring, cooled, basified with aqueous KOH, and extracted with cyclohexane. The extract was washed with water, dried ($MgSO_4$),

Can. J. Chem. Downloaded from www.nrcresearchpress.com by 210.87.254.42 on 09/06/12
For personal use only.

concentrated, and the residue chromatographed on Silica Gel H (3 cm × 50 cm) with 2% ether–cyclohexane. The first band gave 82.5 mg (16%) of recovered **14**, and the second band gave 101.2 mg (20%) of 3,4-benzo-1,8-dimethyl-5-methoxytricyclo[3.3.0.$0^{2,8}$]octa-3,6-diene (**15**) (glc purity > 99.5%) as a colourless oil after short-path distillation at 55°C/0.1 Torr; uv: 231 sh (9 000), 269 sh (750), 275 (930), and 282 (810); nmr (60 MHz, CCl_4): 6.63–6.92 (m, 4H, aromatics), 5.30 (d, 1H, H-6, $J_{6,7}$ = 5.0), 4.74 (d, 1H, H-7, $J_{7,6}$ = 5.0), 3.30 (s, 3H, methoxyl), 2.46 (s, 1H, H-2), 1.48 (s, 3H, methyl), and 1.28 (s, 3H, methyl); spin decoupling experiment: irradiation of H-7 collapsed H-6 to an s. Mass spectrum showed molecular ion at m/e = 212.1198 (77%); $C_{15}H_{16}O$ requires 212.1201.

Gas phase thermolysis of SB 15

Over a 45-min period 132.9 mg (0.63 mmol) of **15** was distilled into a Pyrex tube (2 cm × 30 cm) packed with glass beads (0.5 cm diameter) maintained at 420°C. The pressure in the system was kept at 3.5 Torr by the passage of nitrogen. The thermolysis product, collected in a cooled U-trap (Dry Ice – acetone), was chromatographed on Silica Gel 60 (3 cm × 70 cm) with 5% ether–cyclohexane. Crystallization from ethanol of the first band gave 110.0 mg (83%) of colourless 6,7-dimethyl-10-methoxybenzocyclooctatetraene (**16**), mp 68.5–70.5°C; ir (melt): 810, 825, and 840, trisubstituted vinyls; uv: 230 sh (13 300), 253 sh (5 550), and 270 sh (1 650); nmr (400 MHz, $CDCl_3$): 7.18–7.28 (m, 3H, aromatics), 6.97–7.03 (m, 1H, aromatic), 6.35 (br s, 1H, H-5, $J_{5,C6\text{-}Me}$ = 1.5), 5.56 (sym. m, 1H, H-8, $J_{8,9}$ = 3.7, $J_{8,C7\text{-}Me}$ = 1.5), 5.14 (sym. m, 1H, H-9, $J_{9,8}$ = 3.7, $J_{9,C7\text{-}Me}$ = 1.5), 3.68 (s, 3H, methoxy), 1.94 (d, 3H, C6-methyl, $J_{C6\text{-}Me,5}$ = 1.5), and 1.75 (t, 3H, C7-methyl, $J_{C7\text{-}Me,8}$ = $J_{C7\text{-}Me,9}$ = 1.5); spin decoupling experiments: irradiation of H-5 collapsed the C7-methyl to an s; irradiation of H-8 collapsed the C7-methyl to a d ($J_{C7\text{-}Me,9}$ = 1.5) and H-9 to a q ($J_{9,C7\text{-}Me}$ = 1.5); irradiation of H-9 collapsed the C7-methyl to a d ($J_{7,C7\text{-}Me}$ = 1.5) and H-8 to a q ($J_{8,C7\text{-}Me}$ = 1.5); irradiation of the C6-methyl modified H-5 to a sharp s; irradiation of the C7-methyl collapsed H-8 to a d ($J_{8,9}$ = 3.7) and H-9 to a d ($J_{9,8}$ = 3.7). Mass spectrum showed molecular ion at m/e = 212.1200 (90%). *Anal.* found: C 85.02, H 7.69.

Ketone 17

A solution of 287.8 mg (1.45 mmol) of **16** in 3 mL of 80% aqueous acetic acid was refluxed for 1 h, cooled, basified with aqueous KOH, and extracted with cyclohexane. The extract was washed with water, dried ($MgSO_4$), concentrated, and the residue crystallized from ethanol to give 218.5 mg (81%) of 5,6-dimethyl-2,3-benzo-2,4,7-cyclooctatrienone (**17**), mp 72–74°C; ir (KBr): 1670, C=O; uv: 232 (29 800), 304 (3 000), 335 sh (960), 349 sh (600), and 367 sh (195); nmr (60 MHz, CCl_4): 8.01–8.26 (m, 1H, aromatic closest to C=O), 6.97–7.52 (m, 3H, remaining aromatics), 6.53 (br s, 1H, H-4), 5.40 (br t, 1H, H-7, $J_{7,8}$ = $J_{7,8'}$ = 8.0), 3.05–3.52 (m (temperature sensitive), 2H, C8-methylene), 2.07 (d, 3H, C6-methyl, $J_{C6\text{-}Me,7}$ = 1.5), and 1.77 (d, 3H, C5-methyl, $J_{C5\text{-}Me,4}$ = 1.5); spin decoupling experiments: irradiation of C8-methylene collapsed H-7 to a br s; irradiation of C5-methyl modified H-4 to a sharp s. Mass spectrum showed molecular ion at m/e = 198.1046 (100%); $C_{14}H_{14}O$ requires 198.1045. *Anal.* calcd. for $C_{14}H_{14}O$: C 84.81, H 7.12; found: C 84.95, H 7.20.

COT 9 from ketone 17 via the Shapiro reaction (ref. 13)

A solution of 1.0153 g (5.1 mmol) of **17**, 50 mg (0.26 mmol) of *p*-toluenesulfonylchloride, and 1.30 g (7.0 mmol) of *p*-toluenesulfonylhydrazide in 25 mL methanol was stirred at room temperature for 24 h and then cooled to −12°C for 12 h. The precipitate was filtered, washed with cold methanol, and dried *in vacuo* to give 1.7335 g (93%) of the tosylhydrazone as a white solid, mp 166–168°C dec. A solution of 3 mL (0.48 mmol) of 1.6 *M* methyllithium in ether was slowly (1 min) titrated into an ice-cooled, stirred slurry of 345.0 mg (0.95 mmol) of the tosylhydrazone in 20 mL of dry ether under argon until the mixture just maintained an orange colour. A second 3-mL aliquot of the methyllithium was added during 1 min. The orange solution was stirred at room temperature for 2 h, refluxed for 2 h, cooled, and then made slightly acidic by the careful addition of aqueous ammonium chloride solution. The ether layer was extracted with brine, dried ($MgSO_4$), concentrated, and chromatographed on Silica Gel 60 (1.5 cm × 40 cm) with cyclohexane solvent. Short-path distillation (55°C/0.1 Torr) of the first band gave 83.9 mg (49%) of a colourless oil, identical (glc, nmr) to COT **9**.

Labelled COT 9a from ketone 17

To a solution of 200.0 mg (0.94 mmol) of ketone **17** in 20 mL of methanol-d_1 was added 0.15 mL of a 1.43 *M* solution of sodium methoxide in methanol-d_1. The solution was stirred at room temperature for 21.5 h, after which time 2 mL of a 0.72 *M* solution of *p*-toluenesulfonylchloride in methanol-d_1 was added, followed by 260.7 mg (1.40 mmol) of dry *p*-toluenesulfonylhydrazide. The solution was stirred at room temperature for a further 24 h and then cooled to −12°C for 12 h. The precipitate was filtered and washed with cold methanol. The solid was dissolved in 10 mL of acetone and was precipitated by the addition of 30 mL of water. The solid was rapidly filtered, and the precipitation procedure repeated. The tosylhydrazone, after drying *in vacuo*, gave 264.3 mg (74%) of white powder, mp 166–168°C dec. The procedure described above for the preparation of COT **9** was used to convert 234.2 mg (0.67 mmol) of the labelled tosylhydrazone to 61.7 mg (55%) of COT **9***a* (glc purity > 99%); nmr (400 MHz, $CDCl_3$; CW mode): 6.95–7.22 (m, 4.05H, aromatics), 6.52 (br s, 0.85H, H-10), 6.28 (br s, 0.97H, H-5), 6.03 (m, 0.10H, H-9), 5.56 (br s, 0.96H, H-8), 1.94 (d, 3.00H, C6-methyl, $J_{C6\text{-}Me,5}$ = 1.5), and 1.78 (d, 3.00H, C7-methyl, $J_{C7\text{-}Me,8}$ = 1.5), i.e., COT **9***a* is 90%-d_1 labelled at C-9 and 15%-d_1 labelled at C-10. See Table 2, entry 1, for further hydrogen integration details.

Sensitized irradiation of labelled COT 9a

A solution of 97.8 mg (0.53 mmol) of **9***a* and 197.6 mg (1.16 mmol) of 1-acetonaphthone in 35 mL of cyclohexane was photolysed at >340 nm for 1 h (complete conversion by glc). The photolysate was worked up as in the case of the sensitized irradiation of COT **9** to give 96.2 mg (98%) of diene **7***a* (glc purity > 99%); nmr (60 MHz, CCl_4): 6.67–7.06 (m, 4.09H, aromatics), 6.06 (s, 0.83H, H-4), 5.76 (m, 0.09H, H-5), 3.65 (br s, 0.96H, H-1), 3.33 (br s, 0.97H, H-6), 1.40 and 1.63 (two br overlapping singlets, 6.00H, methyls). See Table 2, entry 2, for further hydrogen integration details.

Direct irradiation of labelled diene 7a

A solution of 86.7 mg (0.47 mmol) of **7***a* in 35 mL of cyclohexane was photolysed with Pyrex-filtered light for 4.5 h (85% conversion by glc). The photolysate was worked up as in the case of the direct irradiation of unlabelled diene **7**. Column chromatography gave: 15.1 mg (27%) of labelled naphthalene (from the first band); 12.9 mg (15%) of recovered diene **7***a* (from the second band; see Table 2, entry 3, for hydrogen integration details); and 10.7 mg (14%) of SB **3***a* (from the third band); nmr (60 MHz, CCl_4): 6.72–7.24 (m, 4.10H, aromatics), 3.50 (d, 1.02H, H-5, $J_{5,1}$ = 6.5), 3.15 (t, 0.99H, H-1, $J_{1,5}$ = $J_{1,2}$ = 6.5), 2.77 (d, 0.89H, H-2, $J_{2,1}$ = 6.5), 2.36 (m, 0.13H, H-8), and 1.49 (s, 6.00H, methyls). See Table 2, entry 5, for further hydrogen integration details.

Sensitized irradiation of labelled diene 7a

A solution of 94.9 mg (0.52 mmol) of **7***a* and 4.7 mg (0.02 mmol) of Michler's ketone in 35 mL of cyclohexane was photolysed at >340 nm for 1.75 h (87% conversion by glc). The photolysate was worked up as in the case of the sensitized irradiation of diene **7**. Column chromatography gave: 17.2 mg (30%) of labelled naphthalene (from first band); 10.3 mg (11%) of recovered diene **7***a* (from second band; see Table 2, entry 4, for hydrogen integration details); and 16.0 mg (19%) of SB **3***a* (from third band; see Table 2, entry 6, for hydrogen integration details).

Direct irradiation of labelled COT 9a

A solution of 132.1 mg (0.73 mmol) of **9***a* in 35 mL of cyclohexane was photolysed with Pyrex-filtered light for 25 h (100% conversion by glc). The photolysate was concentrated and the residue chromatographed on Silica Gel 60 (1.7 cm × 45 cm) with cyclohexane

TABLE 2. Nuclear magnetic resonance hydrogen integrations of deuterium labelled compounds[a]

Entry	Aromatics	H-5	H-8	H-10	H-9	Methyls
For COT **9***a*[b]						
1.	4.05 ± 0.13	0.97 ± 0.03	0.96 ± 0.03	0.85 ± 0.02	0.10 ± 0.03	6.00
For diene **7***a*[c]						
	Aromatics	H-1	H-6	H-4	H-5	Methyls
2.	4.09 ± 0.16	0.96 ± 0.04	0.97 ± 0.06	0.83 ± 0.06	0.09 ± 0.03	6.00
3.	4.04 ± 0.09	1.00 ± 0.05	0.97 ± 0.06	0.87 ± 0.06	0.10 ± 0.06	6.00
4.	4.03 ± 0.06	1.00 ± 0.03	1.00 ± 0.03	0.87 ± 0.04	0.05 ± 0.04	6.00
For SB **3***a*[c]						
	Aromatics	H-5	H-1	H-2	H-8	Methyls
5.	4.10 ± 0.08	1.02 ± 0.09	0.99 ± 0.04	0.89 ± 0.04	0.13 ± 0.06	6.00
6.	4.04 ± 0.09	0.94 ± 0.07	1.00 ± 0.05	0.89 ± 0.08	0.05 ± 0.04	6.00
7.	4.08 ± 0.12	1.00 ± 0.03	0.95 ± 0.06	0.85 ± 0.05	0.11 ± 0.04	6.00

[a]Errors estimated from scatter of nmr signal integrations.
[b]400 MHz, $CDCl_3$ solvent.
[c]60 MHz, CCl_4 solvent.

solvent. The first band gave 23.1 mg (25%) of labelled naphthalene, and the second band gave 18.2 mg (14%) of SB **3***a*. See Table 2, entry 7, for hydrogen integration details.

Acknowledgements

The authors thank the Spectroscopic Services Laboratory of the University of Alberta for the 400-MHz nmr and mass spectra, and the Natural Sciences and Engineering Council of Canada for financial support and for two Undergraduate Summer Research Awards (to I.M.C. and F.L.S.).

1. C. O. BENDER, D. L. BENGTSON, D. DOLMAN, C. E. L. HERLE, and S. F. O'SHEA. Can. J. Chem. **60**, 1942 (1982).
2. G. SUGOWDZ, P. J. COLLIN, and W. H. F. SASSE. Aust. J. Chem. **26**, 147 (1973).
3. L. A. PAQUETTE, M. J. KUKLA, and J. C. STOWELL. J. Am. Chem. Soc. **94**, 4290 (1972).
4. I. B. BERLMAN. Handbook of fluorescence spectra of aromatic molecules. Academic Press, New York, NY. 1965. p. 104.
5. R. CRIEGEE and R. ASKANI. Angew. Chem. **80**, 531 (1968).
6. H. E. ZIMMERMAN and H. IWAMURA. J. Am. Chem. Soc. **92**, 2015 (1970).
7. H. E. ZIMMERMAN and R. A. BUNCE. J. Org. Chem. **47**, 3377 (1982).
8. S. S. HIXSON, P. S. MARIANO, and H. E. ZIMMERMAN. Chem. Rev. **73**, 531 (1973).
9. E. GROVENSTEIN, JR, T. C. CAMPBELL, and T. SHIBATA. J. Org. Chem. **34**, 2418 (1969).
10. I. A. AKHTAR, and J. J. MCCULLOUGH. J. Org. Chem. **46**, 1447 (1981); R. M. BOWMAN, T. R. CHAMBERLAIN, C.-W. HUANG, and J. J. MCCULLOUGH. J. Am. Chem. Soc. **96**, 692 (1974); T. S. CANTRELL. J. Am. Chem. Soc. **94**, 5929 (1972).
11. C. O. BENDER, D. W. BROOKS, W. CHENG, D. DOLMAN, S. F. O'SHEA, and S. S. SHUGARMAN. Can. J. Chem. **56**, 3027 (1978).
12. C. G. HATCHARD and C. A. PARKER. Proc. R. Soc. London, Ser. A, **235**, 518 (1956); W. D. BOWMAN and J. N. DEMAS. J. Phys. Chem. **80**, 2434 (1976).
13. R. H. SHAPIRO and M. J. HEATH. J. Am. Chem. Soc. **89**, 5734 (1967); R. M. ADLINGTON and A. G. M. BARRETT. Acc. Chem. Res. **16**, 55 (1983).

Can. J. Chem. Downloaded from www.nrcresearchpress.com by 210.87.254.42 on 09/06/12
For personal use only.

The vibrational spectra of thioketene and deuterothioketenes

MANUEL TORRES, IMRE SAFARIK, ALLAN CLEMENT, RATNAKAR K. GOSAVI, AND OTTO P. STRAUSZ
Department of Chemistry, University of Alberta, Edmonton, Alta., Canada, T6G 2G2

Received January 3, 1984

MANUEL TORRES, IMRE SAFARIK, ALLEN CLEMENT, RATNAKAR K. GOSAVI, and OTTO P. STRAUSZ. Can. J. Chem. **62**, 2777 (1984).

The FTIR spectra of low temperature argon matrix isolated thioketene-d_0, thioketene-d_1, and thioketene-d_2 molecules from the flow thermolysis of the corresponding 1,2,3-thiadiazoles have been recorded and analyzed. Assignment of the normal frequencies has been made by a normal coordinate analysis. Alternatively, vibrational frequencies were computed by *ab initio* MO calculations and the predicted values compared to the experimentally observed ones.

MANUEL TORRES, IMRE SAFARIK, ALLEN CLEMENT, RATNAKAR K. GOSAVI et OTTO P. STRAUSZ. Can. J. Chem. **62**, 2777 (1984).

Opérant à basse température, on a enregistré et analysé les spectres FTIR de molécules, isolées dans des matrices d'argon, de thiocétène-d_0, de thiocétène-d_1 et de thiocétène-d_2 provenant de la thermolyse à flux des thiadiazoles-1,2,3 correspondantes. On a attribué les fréquences normales en se basant sur une analyse normale des coordonnées. On a aussi calculé les fréquences vibrationnelles en faisant appel à des calculs *ab initio* d'orbitales moléculaires et on a alors comparé les valeurs calculées avec les valeurs expérimentales.

[Traduit par le journal]

Can. J. Chem. Downloaded from www.nrcresearchpress.com by 210.87.254.105 on 09/06/12
For personal use only.

Thioketene **1** was first prepared by Howard in 1962 (1) in the thermolysis of *tert*-butylthioacetylene, which produces **1** together with isobutene. Thioketene was described as unstable in solution above −80°C and characterized by a strong ir absorption at 1750 cm^{-1}. Stable substituted thioketenes were subsequently reported by Raasch (2), Elam *et al.* (3), and Seybold (4), and they all feature a characteristic strong ir band at ~1750 cm^{-1}. In 1974 Krantz and Laureni (5) observed the formation of thioketene **1** together with ethynylthiol in the λ>290-nm photolysis of argon-matrix 1,2,3-thiadiazole and reported the observed ir bands of **1** and its deuterated isotopomers assigned on the basis of the similarity of the absorption intensity versus irradiation time plots, Table 1. Each of the observed thioketene absorptions was assigned, presumably intuitively, to a normal mode (Table 1). A subsequent paper by the same authors published in 1981 (6) reports somewhat revised spectral assignments belonging to **1** and its deutero and ^{13}C isotopomers, but none of the normal mode assignments with the exception of the trivial C=C and C—H/D stretching modes, Table 2.

Substituted thioketenes have also been prepared by the flash thermolysis of 1,2,3-thiadiazoles and 1,3-dithietanes (7–9), by the reaction of alkylidene-phosphoranes and α-monosubstituted phosphonate carbanions with CS_2 (10), and by argon-matrix photolysis of 1,2,3-thiadiazoles (11). Unsubstituted thioketene **1** has also been detected in the thermolysis of 1,2,3-thiadiazole and dithioacetic acid (12) and in the argon-matrix photolysis of vinylene trithiocarbonate (13).

The microwave (14, 15) and photoelectron (12) spectra of **1** have been investigated and, although some of the thioketene ir absorptions have been reported (5, 6), to date no serious attempt has been made to assign the thioketene vibrational spectra. Encouraged by the results obtained in the study of the vibrational spectra of argon matrix isolated thiirene (16) and thioformaldehyde (17), we have carried out a study of the vibrational spectra of thioketene and its deuterated isotopomers obtained by flow thermolysis of 1,2,3-thiadiazole **2**, 4-*d*- and 5-*d*-1,2,3-thiadiazole, and 4,5-d_2-1,2,3-thiadiazole, Figs. 1, 2, and 3.

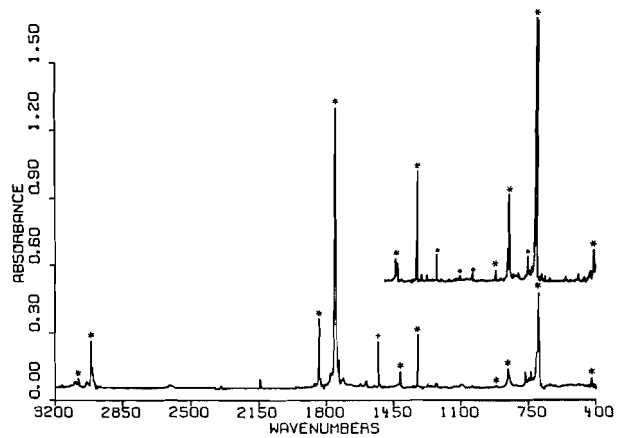

FIG. 1. FTIR spectrum of thioketene-d_0 argon matrix isolated obtained by flow thermolysis of 1,2,3-thiadiazole. Inset: the thioketene-d_0 spectrum isolated in a nitrogen matrix. (*) bands assigned to thioketene-d_0, (+) band assigned to CS_2, (●) bands assigned to unthermolyzed 1,2,3-thiadiazole.

Experimental

An Air-Products and Chemical Inc. Model CS-202 Displex closed-cycle helium refrigeration system coupled to a high vacuum line was employed. The matrix deposit was made on a cesium iodide plate kept at 10 K and the typical host-to-guest ratios were 1:300 with an average deposition time of 30 min at a typical flow rate of 0.2–0.3 μmol/min. Flow thermolyses were carried out in a 6 mm id × 100 mm quartz tube wrapped with a heating filament, maintained at the thermolysis temperature, and placed before the cryostat. The temperature was monitored by an iron versus constantan thermocouple. The residence time at the deposition rate was measured to be ~0.7 s. Alternatively, photolyses were carried out with a Hanovia 30620 medium pressure mercury arc equipped with a 7910 Vycor filter.

1,2,3-Thiadiazole (18), 4-*d*- and 5-*d*-1,2,3-thiadiazole (17, 19), and 4,5-d_2-1,2,3-thiadiazole (17) were prepared as reported before and 4000–400 cm^{-1} ir spectra of matrix isolated species were obtained on a Nicolet 7199 FT infrared spectrophotometer at 1 cm^{-1} resolution and with baseline correction. The ir spectra below 400 were obtained on a Perkin Elmer model 457 spectrophotometer. The MO calculations were carried out on the AMDAHL 5860 computer at the University of Alberta.

Results and discussion

Flow thermolysis of 1,2,3-thiadiazole **2** at 450–520°C resulted in the formation of **1** and nitrogen. Small amounts of

TABLE 1. Infrared bands assigned to thioketenes from ref. 5

Thioketene-d_0	Assignment	Thioketene-d_1	Assignment	Thioketene-d_2	Assignment
3010(w)	$=C\langle^{H}_{H}$ str.	3060(w)	$=C\langle^{H}_{D}$ str.	2240(s)	$=C\langle^{D}_{D}$ str.
1760(vs)	C=C str.	2270(s)	$=C\langle^{H}_{D}$ str.	1735(vs)	C=C str.
1320(m)	C=S str.	1760(vs)	C=C str.	860(w)	CD_2 def.
850(w)	CH_2 wag.	1210(w)	C=S str.	560(s)	CD_2 rock
700(m)	CH_2 rock	870(w)	$C\langle^{H}_{D}$ def.		
400(vw)	C=C=S bend	640(m)	$C\langle^{H}_{D}$ rock		

TABLE 2. Infrared bands of argon-matrix isolated thioketenes from ref. 6

$H_2C=C=S$	3010(m)	$=C\langle^{H}_{H}$ str.	$H_2C=^{13}C=S$	3042(m)	$H\diagdown$ / $D\diagup C^{13}=C=S$	3050
	1840(m)			1822(m)		2259
	1755(vs)	C=C str.		1713(vs)		1741
	1410(w)			1418(w)		686
	1322(m)			1322(m)		619
	692(s)			695(s)		
$H\diagdown$ / $D\diagup C=C=S$	3065	$=C\langle^{H}_{D}$ str.	$H_2{}^{13}C=C=S$	3005(m)	$H\diagdown$ / $D\diagup C=^{13}C=S$	3059
	2273	$=C\langle^{H}_{D}$ str.		1822(m)		
	1760	C=C str.		1737(vs)		2269
	626			1315(m)		1730
				689(s)		1696
						860
						680
						624

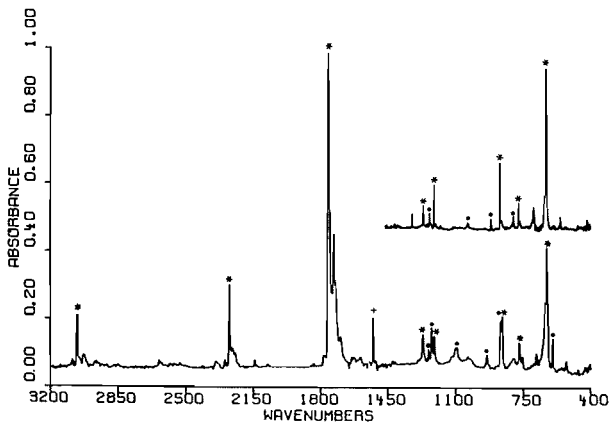

FIG. 2. FTIR spectrum of thioketene-d_1 argon matrix isolated by flow thermolysis of 5-d_1-1,2,3-thiadiazole. Inset: the thioketene-d_1 argon matrix isolated spectrum obtained by flow thermolysis of 4-d_1-1,2,3-thiadiazole. (*) bands assigned to thioketene-d_0, (+) band assigned to CS_2, (●) bands assigned to unthermolyzed 5-d_1 and 4-d_1-1,2,3-thiadiazole, respectively. The band at 1738 cm^{-1} is due to the presence of some thioketene-d_2 impurity.

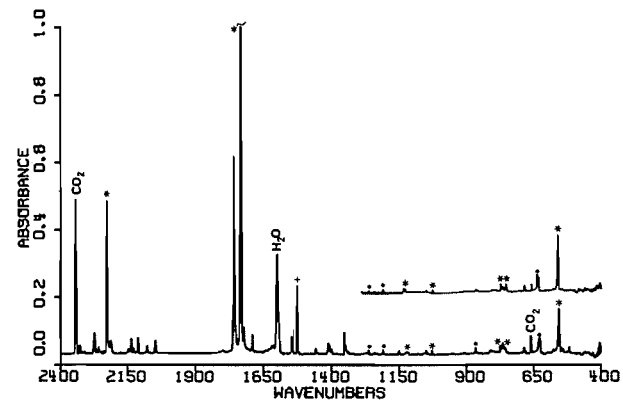

FIG. 3. FTIR spectrum of thioketene-d_2 argon matrix isolated obtained by flow thermolysis of 4,5-d_1-1,2,3-thiadiazole. Inset: the thioketene-d_2 spectrum isolated in a nitrogen matrix. (*) bands assigned to thioketene-d_2, (+) band assigned to CS_2, (●) bands assigned to unthermolyzed 4,5-d_2-1,2,3-thiadiazole. The band at 1760 cm^{-1} is due to the presence of some thioketene-d_1 impurity. Note that band at 1738 cm^{-1} is off scale and had a true absorbance of 2.9.

Can. J. Chem. Downloaded from www.nrcresearchpress.com by 210.87.254.105 on 09/06/12
For personal use only.

TABLE 3. Observed and calculated vibrational frequencies (cm^{-1})[a]

Species	Thioketene-d_0 Observed	Calcd.	% Rel. error[b]	Thioketene-d_2 Observed	Calcd.	% Rel. error[b]	Species	Thioketene-d_1 Observed	Calcd.	% Rel. error[b]
a_1 ν_1	3012(b,m)	3022	0.3	2229(s)	2227	0.1	a'	2274(s)	2266	0.3
ν_2	1755(vs)	1773	1.0	1738(vs)	1727	0.6		1760(vs)	1751	0.5
ν_3	1323(s)	1320	0.2	1030(vw)	1033	0.3		1210(m)	1211	0.1
ν_4	858(m)	858	—	775(w)	777	0.3		770(w)	768	0.3
b_1 ν_5	692(b,s)	689	0.4	555(s)	559	0.7	a''	625(s)	625	—
ν_6	404(w)	397	1.7	375(w)	373	0.5		382(w)	389	1.8
b_2 ν_7	3097,3068(b,w)	3085	0.5	2330[c](w)	2309	—	a'	3060(m)	3056	0.1
ν_8	918(vw)	916	0.2	755(w)	758	0.4		868(m)	871	0.3
ν_9	356(vw)	352	1.1	308(vw)	309	0.3		325(vw)	328	0.9

[a] When the band was split, due to matrix effects, only the strongest band was used in the calculation.

[b] $\left[\frac{\nu_{calcd} - \nu_{obs}}{\nu_{obs}} \times 100\right]$

[c] Tentative, not used for calculation.

unthermolyzed **2** and CS_2, probably resulting from secondary decomposition of the thioketene, were also observed but ethynylthiol was notably absent and this made it possible to obtain the ir spectrum of essentially pure thioketene **1**, Fig. 1. Similarly, flow thermolysis of 4-*d*- or 5-*d*-1,2,3-thiadiazole and 4,5-d_2-1,2,3-thiadiazole resulted in the formation of thioketene-d_1, Fig. 2, and thioketene-d_2, Fig. 3. Owing to the weakness of some of the thioketene bands, assignment of the thioketene d_0, d_1, and d_2 bands was based on the criterion that they be observable in both the flow thermolysis and the λ>210-nm photolysis of **2** under argon-matrix conditions. In addition, bands assigned to thioketene-d_1 were also observed when either 4-*d*- or 5-*d*-1,2,3-thiadiazole was used as source compound. Some of the bands assigned to thioketene appear as doublets but the split is not affected by dilution (200:1 to 500:1), whereas it changes or disappears by changing the matrix environment and therefore has been attributed to different matrix trapping sites (17, 20). In general, ir bands of **1** are found to be sharper and better resolved in nitrogen than in argon matrices and nitrogen causes a hypsochromic shift of 0–10 cm^{-1} as compared to argon, Fig. 1.

As has been established by microwave spectroscopy (14, 15), the thioketene molecule has a planar geometry, and C_{2v} symmetry. The nine normal vibrations form the representation: $4a_1 + 2b_1 + 3b_2$ and the same considerations should apply to thioketene-d_2, whereas thioketene-d_1 has a C_s symmetry and forms the representation: $7a' + 2a''$. In all cases the nine normal vibrations are ir active. The ir spectra of thioketene-d_0, d_1, and d_2, Figs. 1, 2, and 3, respectively, were obtained as described above and the observed frequencies and assignments are listed in Table 3.

C—H stretchings

Two broad bands have been observed for thioketene-d_0 in the C—H stretching region, one at 3012 and a doublet at 3068 and 3097 cm^{-1}, whereas thioketene-d_2 features a single clear absorption at 2229 cm^{-1} and a weak absorption, tentatively assigned to **1**-d_2, at 2330 cm^{-1}. These are assigned to the symmetric and asymmetric C—H stretchings of thioketene-d_0 and thioketene-d_2, respectively. On the other hand, thioketene-d_1 exhibits absorptions at 2274 and 3060 cm^{-1} which are assigned to the two a' C—H stretchings.

C=C and C=S stretchings

The very intense band at 1755 cm^{-1}, which has long been assigned to the C=C stretch of thioketene, shifts upon deuteration to 1738 cm^{-1} for thioketene-d_2. The unusually high wave number for the C=C stretch must be attributed to its coupling with the C=S stretch in a similar manner as observed in ketene for the coupling between the C=O and C=C stretchings, which causes a shift to higher wave numbers for the C=O st, to 2140 cm^{-1} from its normal value of ~1700 cm^{-1}, and at the same time shifts the C=C stretch, usually at ~1650 cm^{-1}, to 1380 cm^{-1} (21). Consequently, the C=S stretch expected in the broad region of 1000–1300 cm^{-1} (22) should be found at substantially lower wave numbers. The next bands identified in the thioketene spectrum appear at 918 and 858 cm^{-1}. These have their counterparts in thioketene-d_2 at 755 and 775 cm^{-1}, respectively. The very weak intensity and larger isotopic shift of the 918-cm^{-1} band made the 858 and 775-cm^{-1} bands a better choice for the C=S stretchings of thioketene-d_0

TABLE 4. Theoretical versus observed product rule ratios[a]

Species	Theoretical	Observed
a_1	0.509	0.515
b_1	0.762	0.744
b_2	0.543	0.540

[a] When the band was split, due to matrix effects, only the strongest band was used in the calculation.

TABLE 5. Calculated force field for thioketene[a] and ketene[b]

	Thioketene	Ketene		Thioketene	Ketene
F_{11}	5.154	5.547	F_{55}	0.126	0.118
F_{12}	−0.099	1.487	F_{56}	0.046	0.113
F_{13}	0.038	0.160	F_{66}	0.471	0.664
F_{14}	0	0	F_{77}	5.002	5.332
F_{22}	8.812	8.387	F_{78}	0	0.120
F_{23}	−0.141	−0.292	F_{79}	0	0
F_{24}	0.562	0.954	F_{88}	0.380	0.348
F_{33}	0.567	0.597	F_{89}	−0.058	0.133
F_{34}	−0.090	0	F_{99}	0.477	0.667
F_{44}	8.341	16.578			

[a] This work.

[b] See ref. 22, p. 70.

Can. J. Chem. Downloaded from www.nrcresearchpress.com by 210.87.254.105 on 09/06/12
For personal use only.

TABLE 6. Calculated potential energy distribution

Frequency (cm^{-1})	Internal coordinates							
	f(C=S)	f(C=C)	f(C—H)	$f(C\langle^{H}_{H})$	$f(CC\langle^{H}$)	$f(\theta)$	$f(\gamma_x)$	$f(\gamma_y)$
3022[a]		1	99					
2227[b]		9	91					
2266[c]		5	95					
1773[a]	27	68		5				
1727[b]	32	60	6	2				
1751[c]	30	63	4	3				
1320[a]	8			92				
1033[b]	29	2		69				
1211[c]	10			82	8			
858[a]	59	38		3				
777[b]	46	25		29				
871[c]	42	21			28			9
689[a]						95	5	
559[b]						96	4	
625[c]						91	9	
397[a]						2	98	
373[b]						17	83	
389[c]						6	94	
3085[a]			100					
2309[b]			100					
3056[c]			100					
916[a]					86			14
758[b]					85			15
768[c]	14	10		12	55			9
352[a]					8			92
309[b]					14			86
328[c]					11			89

[a] Calculated for thioketene-d_0.
[b] Calculated for thioketene-d_1.
[c] Calculated for thioketene-d_2.

and d_2. For thioketene-d_1, the C=C and C=S stretchings are found at 1760 and 770 cm^{-1}, respectively. The small but unusual shift to higher wave numbers of the ν(C=C) upon monodeuteration must lie in the fact that monodeuteration lowers the symmetry of the molecule to a C_s and consequently changes the nature of the coupling, as will be seen later in the potential energy distribution.

A band at 1840 cm^{-1} (m) is always observed in the spectrum of **1**-d_0. This band tends to diminish in intensity on warming the sample and no assignment is possible at this time.

C—H deformations

Two bands are observed at 1413 and 1323 cm^{-1} which fall in the CH_2 symmetric deformation region. For thioformaldehyde the symmetric deformation has been assigned to a band at 1447 cm^{-1} (17, 23, 24). In thioketene, however, this band should be at a much lower wavelength if one follows the parallelism between formaldehyde (1500 cm^{-1}) (25) and ketene (1115 cm^{-1}) (21), and therefore the stronger 1323 cm^{-1} band in thioketene-d_0, with counterparts at 1030 and 1210 cm^{-1} for **1**-d_2 and **1**-d_1 respectively, is assigned to the CH_2 symmetric deformation of thioketene. The other band of thioketene at 1413 cm^{-1} with counterparts at 1130 and 1268 cm^{-1} for thioketene-d_2 and d_1, respectively, is assigned to a $2\nu_5$ overtone (*vide infra*). Of the in-plane and out-of-plane asymmetric deformations, the out-of-plane is expected to be the more intense, and therefore the strong absorptions at 692, 555, and 625 cm^{-1} are assigned to the CH_2 out-of-plane deformations of thioketene-d_0, d_2, and d_1, respectively. As is common in the case of allenes (ref. 2, p. 70), this absorption frequently presents a detectable overtone to which the bands at 1413, 1130, and 1268 cm^{-1} (for **1**-d_0, **1**-d_2, and **1**-d_1) are assigned. Support for this comes from the fact that changing the host from argon to nitrogen causes the broad bands at 1413 and 692 cm^{-1} to split in well-defined doublets at 1430 and 1440 and 705 and 710 cm^{-1}, respectively. Similar effects are observed in the case of **1**-d_2 and **1**-d_1.

Skeletal vibrations

The two remaining vibrations are assigned to the in-plane and out-of-plane skeletal linear bending vibrations. In comparison to ketene, the presence of sulfur, a heavier atom than oxygen, should lower these two fundamentals and therefore they should be the two lowest vibrations. Therefore, the bands at 404 and 365 cm^{-1} for **1**-d_0 and at 375 and 308 cm^{-1} for **1**-d_2 are assigned to the b_1 and b_2 skeletal vibrations and bands at 325 and 382 cm^{-1} for **1**-d_1 to the a' and a'' skeletal vibrations.

Product rule

The theoretical Teller–Redlich rule (26) was applied for thioketene, based on the moments of inertia obtained with the geometrical parameters R(C=S) = 1.554 Å, R(C=C) = 1.314 Å, R(C—H) = 1.090 Å and the α(HCH) = 120.3° determined by Georgiou *et al.* from the microwave spectra (14). The values obtained are in good agreement with the observed values for each symmetry species, Table 4, thus supporting the assignment.

Can. J. Chem. Downloaded from www.nrcresearchpress.com by 210.87.254.105 on 09/06/12
For personal use only.

TABLE 7. Vibrational frequencies (cm^{-1}) of thioketene, observed and calculated by *ab initio* MO calculation with 6-31G* basis set

Symmetry	Assignment	Observed	Calculated	Δ^a
a_1	C—H stretch (sym)	3012	3329	10.5
	C—C stretch	1755	1961	11.7
	C—H bend, in plane	1323	1546	16.9
	C—S stretch	858	902	5.1
b_1	C—H bend, out of plane	692	988	42.8
	C—C—S bend, out of plane	404	449	11.1
b_2	C—H stretch (asym)	3068	3421	11.5
	C—H bend (asym)	918	1088	18.5
	C—C—S bend, in plane	356	393	10.4

$^a\Delta = \frac{\nu_{calcd} - \nu_{obs}}{\nu_{obs}} \times 100$

Normal coordinate analysis

The internal coordinates used in the normal coordinate analysis were the changes in the C=C, C=S, and C—H bond length (ΔR_C, ΔR_S, and Δr), changes in the HCH and HCC angles ($\Delta\alpha$,$\Delta\beta$), change in the angle between the C=C bond and the HCH plane ($\Delta\theta$), and the two perpendicular bendings of the linear C=C=S skeleton ($\Delta\gamma_x$, $\Delta\gamma_y$). The following symmetry coordinates were constructed with these internal coordinates:

$$a_1 : S_1 = (\Delta r_1 + \Delta r_2)/\sqrt{2}$$
$$S_2 = \Delta R_C$$
$$S_3 = \Delta\alpha$$
$$S_4 = \Delta R_S$$
$$b_1 : S_5 = \Delta\gamma_x$$
$$S_6 = \Delta\theta$$
$$b_2 : S_7 = (\Delta r_1 - \Delta r_2)/\sqrt{2}$$
$$S_8 = (\Delta\beta_1 - \Delta\beta_2)/\sqrt{2}$$
$$S_9 = \Delta\gamma_y$$

An initial force field was made up from force constants available in the literature on the basis of structural similarities in analogous molecules (i.e., ketene (27), thioformaldehyde (17)). This force field was then adjusted to fit the observed frequencies for thioketene-d_0, thioketene-d_2, and thioketene-d_1. The vibrational frequencies were calculated using a computer program (VSEC) written by Schachschneider (28).

The calculated normal frequencies together with the observed values are listed in Table 3. As seen, the agreement is quite satisfactory.

The derived force field in terms of the symmetry coordinates given above is listed in Table 5, together with the analogous force field reported for ketene (27) for comparison.

Table 6 shows the potential energy distribution for the calculated vibrational frequencies. The forms of the normal modes agree well with the assignments of the associated frequencies. Beside the strong interaction between the C=C and C=S stretchings, there is a considerable mixing in the normal modes of the thioketene-d_1 molecule.

MO calculation of vibrational frequencies

In a different approach, vibrational frequencies for the ground state ($^1A_1$) thioketene were calculated by the *ab initio* MO method using a 6-31G + polarization functions on the sulfur, 6-31G*, basis set. The calculations were based on an optimized geometry of thioketene obtained as reported (29) by a similar type of calculation. The harmonic vibrational frequencies were then computed at this optimized geometry using the HONDO 76 (IBM version) (30) program and the calculated and experimental values are presented in Table 7. As is common in this type of calculation (31), all the frequencies are predicted at higher wave numbers than the observed experimental values; however, the pattern per each symmetry group is in good agreement with the experimental. In our case, all the frequencies are predicted at 10 to 18% higher values except for the b_1 C—H out-of-plane deformation which is predicted at 43% higher. The deviations between computed and experimental frequencies found here are of similar magnitude to those found before in the case of thiirene (29, 32).

Acknowledgments

The authors are grateful to the Natural Sciences and Engineering Research Council of Canada for continuing financial support and to R. Swindlehurst and J. Hoyle for technical assistance.

1. E. G. HOWARD. U.S. Patent No. 3035030, May 15, 1962; Chem. Abstr. **57**, 13617f (1962).
2. M. S. RAASCH. Chem. Commun. 577 (1966); J. Org. Chem. **35**, 3470 (1970); J. Org. Chem. **37**, 1347 (1972).
3. E. U. ELAM, F. H. RASH, J. T. DOUGHERTY, V. W. GOODLETT, and K. C. BRANNOCK. J. Org. Chem. **33**, 2738 (1968).
4. G. SEYBOLD. Tetrahedron Lett. 555 (1974).
5. A. KRANTZ and J. LAURENI. J. Am. Chem. Soc. **96**, 6768 (1974).
6. A. KRANTZ and J. LAURENI. J. Am. Chem. Soc. **103**, 486 (1981).
7. G. SEYBOLD and C. HEILB. Angew. Chem. Int. Ed. Engl. **14**, 248 (1975); Chem. Ber. **110**, 1225 (1977).
8. E. SCHAUMANN, J. EHLERS, and H. MROTZEK. Justus Liebigs Ann. Chem. 1734 (1979).
9. M. TORRES, A. CLEMENT, and O. P. STRAUSZ. Z. Naturforsch. Teil B, **38**, 1208 (1983).
10. E. SCHAUMANN and F. GRABLEY. Justus Liebigs Ann. Chem. 1702 (1979); 1715 (1979).
11. M. TORRES, A. CLEMENT, J. E. BERTIE, H. E. GUNNING, and O. P. STRAUSZ. J. Org. Chem. **43**, 2490 (1978).
12. H. BOCK, B. SOLOUKI, G. BERT, and P. ROSMUS. J. Am. Chem. Soc. **99**, 1663 (1977).
13. M. TORRES, A. CLEMENT, H. E. GUNNING, and O. P. STRAUSZ. Nouv. J. Chim. **3**, 149 (1979).
14. K. GEORGIOU, H. W. KROTO, and B. M. LANDSBERG. J. Mol. Spectrosc. **77**, 365 (1979).
15. B. BAK, O. J. NIELSEN, H. SVANHOLT, A. HOLMN, N. H. TOUBRO, A. KRANTZ, and J. LAURENI. Acta Chem. Scand. Ser. A, **33**, 161 (1979).

Can. J. Chem. Downloaded from www.nrcresearchpress.com by 210.87.254.105 on 09/06/12
For personal use only.

16. M. TORRES, I. SAFARIK, A. CLEMENT, J. E. BERTIE, and O. P. STRAUSZ. Nouv. J. Chim. **3**, 365 (1979).
17. M. TORRES, I. SAFARIK, A. CLEMENT, and O. P. STRAUSZ. Can. J. Chem. **60**, 1187 (1982).
18. CH. D. HURD and R. J. MORI. J. Am. Chem. Soc. **77**, 5359 (1955).
19. R. A. OLOFSON, J. M. LANDESBERG, K. N. HOUK, and J. S. MICHELMAN. J. Am. Chem. Soc. **88**, 4265 (1966).
20. A. J. BARNES. *In* Matrix isolation spectroscopy. *Edited by* A. J. Barnes, W. J. Orville-Thomas, A. Müller, and R. Gaufrès. NATO Advanced Study Institute Series, Vol. 76. D. Reidel Publishing Company, Holland. 1981.
21. C. B. MOORE and G. C. PIMENTAL. J. Chem. Phys. **38**, 2816 (1963).
22. L. J. BELLAMY. *In* The infrared spectra of complex molecules. Chapman and Hall, London. 1975. p. 399.
23. D. J. CLOUTHIER, C. M. L. KERR, and D. A. RAMSAY. Chem. Phys. **56**, 73 (1981).
24. P. H. TURNER, L. HALONEN, and J. M. MILLS. J. Mol. Spectrosc. **88**, 402 (1981).
25. H. KHOSHKHOO and E. R. NIXON. Spectrochim. Acta Part A, **29**, 603 (1973).
26. E. B. WILSON, JR., J. C. DECIUS, and P. C. CROSS. *In* Molecular vibrations. McGraw–Hill, New York. 1955. p. 183.
27. P. D. MALLINSON and L. NEMES. J. Mol. Spectrosc. **59**, 470 (1976).
28. J. H. SCHACHTSCHNEIDER. Technical Report No. 57-65, Project #31450, Shell Development, Emeryville, CA. 1965.
29. R. K. GOSAVI and O. P. STRAUSZ. Can. J. Chem. **61**, 2596 (1983).
30. M. DUPUIS, J. RYS, and M. F. KING. HONDO 76 (IBM Version) QCPE Program No. 338, Quantum Chemistry Program Exchange, Indiana University, Bloomington, IN 47401, U.S.A.
31. J. A. POPLE, R. KRISHNAN, H. B. SCHLEGEL, and J. S. BINKLEY. Int. J. Quantum Chem. Quantum Chemistry Symp. **13**, 225 (1979).
32. P. ČÀRSKY, B. A. HESS, JR., and L. J. SCHAAD. J. Am. Chem. Soc. **105**, 396 (1983).

Can. J. Chem. Downloaded from www.nrcresearchpress.com by 210.87.254.105 on 09/06/12
For personal use only.

Synthesis and complexation of a tridentate organogallate ligand containing pyrazolyl and pyridylmethoxy donor groups

STEVEN J. RETTIG, ALAN STORR, JAMES TROTTER, AND KALEN UHRICH

Department of Chemistry, University of British Columbia, 2036 Main Mall, Vancouver, B.C., Canada V6T 1Y6

Received March 26, 1984

STEVEN J. RETTIG, ALAN STORR, JAMES TROTTER, and KALEN UHRICH. Can. J. Chem. **62**, 2783 (1984).

The synthesis and complexation of the novel tridentate anionic organogallate ligands $[Me_2Ga(N_2C_3HR_2)\{OCH_2(C_5H_4N)\}]^-$ (where R = H or Me) have been investigated. The ligands, containing both pyrazolyl and pyridyl donor groups, have been incorporated into a variety of octahedral transition metal carbonyl compounds in a *fac* coordination mode. A tetrahedral nickel nitrosyl complex is also described and X-ray crystal structures of bis(pyridine-2-methanolatodimethylgallium) and [dimethyl(3,5-dimethyl-1-pyrazolyl) (2-pyridylmethoxy)gallato-N^2,O,N^3]tricarbonylrhenium(I) are reported. Crystals of bis(pyridine-2-methanolatodimethylgallium) are monoclinic, a = 16.716(2), b = 7.6513(6), c = 7.7591(8) Å, β = 108.349(5)°, Z = 2, space group $C2/m$. The structure was solved by conventional heavy-atom methods and was refined by full-matrix least-squares procedures to R = 0.029 and R_w = 0.032 for 809 reflections with $I \geq 3\sigma(I)$. The dimeric molecule has crystallographically imposed C_{2h} symmetry, the Ga atom having an irregular trigonal bipyramidal coordination geometry. Bond distances (corrected for libration) are Ga—O(eq) = 1.939(3), Ga—O(ax) = 2.086(3), Ga—N(ax) = 2.276(3), and Ga—C(eq) = 1.981(4) Å. Crystals of [dimethyl(3,5-dimethyl-1-pyrazolyl) (2-pyridylmethoxy)gallato-N^2,O,N^3]tricarbonylrhenium(I) are monoclinic, space group $P2_1/n$, a = 9.7457(7), b = 36.991(3), c = 10.8821(8) Å, β = 92.944(3)°, Z = 8. The structure was solved by heavy-atom methods and was refined to 0.042 and R_w = 0.047 for 5321 reflections. Each of the two crystallographically independent molecules displays the expected *fac* octahedral coordination geometry with Re—O = 2.142(6) and 2.143(8), Re—N = 2.166(10)–2.194(8), and Re—CO = 1.89(2)–1.919(11) Å.

STEVEN J. RETTIG, ALAN STORR, JAMES TROTTER et KALEN UHRICH. Can. J. Chem. **62**, 2783 (1984).

On a étudié la synthèse et la complexation des nouveaux ligands organogallates tridentates anioniques $[Me_2Ga(N_2C_3HR_2)\{OCH_2(C_5H_4N)\}]^-$ dans lesquels R = H ou Me. On a incorporé les ligands contenant à la fois les groupes donneurs pyrazolyle et pyridyle dans une variété de composés carbonylés octaédriques du métal de transition qui sont caractérisés par un mode de coordination *fac*. On décrit aussi un complexe tétraédrique du nitrozyle de nickel et, utilisant la diffraction des rayons-X, on a déterminé les structures cristallines du bis(pyridineméthanolato-2 diméthylgallium) et du [diméthyl(diméthyl-3,5 pyrazolyl-1)(méthoxy-2 pyridinyl) gallato-N^2,O,N^3]tricarbonylrhénium(I). Les cristaux du bis(pyridineméthanolato-2 diméthylgallium) sont monocliniques, a = 16,716(2), b = 7,6513(6), c = 7,7591(8) Å, β = 108,349(5)°, Z = 2, groupe d'espace $C2/m$. La structure a été résolue par les méthodes conventionnelles aux atomes lourds et elle a été affinée par la méthode des moindres carrés (matrice entière) jusqu'à des valeurs de R = 0,029 et R_w = 0.032 pour 809 réflexions avec $I \geq 3\sigma(I)$. La molécule dimère possède une symétrie cristallographique C_{2h} imposée et la géométrie de coordination de l'atome de Ga est bipyramidale trigonale irrégulière. Les longueurs des liaisons (corrigées pour la libration) sont: Ga—O(éq) = 1,939(3), Ga—O(ax) = 2,086(3), Ga—N(ax) = 2,276(3) et Ga—C(éq) = 1,981(4) Å. Les cristaux du [diméthyl(diméthyl-3,5 pyrazolyl-1)(méthoxy-2 pyridyl) gallato-N^2,O,N^3]tricarbonylrhénium(I) sont monocliniques, groupe d'espace $P2_1/n$, a = 9,7457(7), b = 36,991(3), c = 10,8821(8) Å, β = 92,944(3)°, Z = 8. La structure a été résolue par la méthode des atomes lourds et elle a été affinée jusqu'à des valeurs de R = 0,042 et R_w pour 5321 réflexions. Chacune des deux molécules, qui sont cristallographiquement indépendantes, possède la géométrie de coordination attendue, *fac* octaédrique, avec Re—O = 2,142(6) et 2,143(8), Re—N = 2,166(10)–2,194(8) et Re—CO = 1,89(2)–1,919(11) Å.

[Traduit par le journal]

Introduction

Unsymmetrical uninegative tridentate chelating organogallate ligands, **1**, have been the subject of a number of recent publications (ref. 1 and references therein).

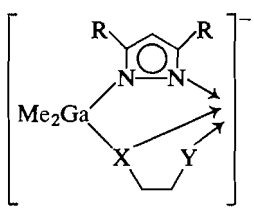

1

X = O; Y = NH_2, NMe_2, SEt, or SPh
X = S; Y = NH_2 or NMe_2

R = H or Me

These ligands all contain a monofunctional donor pyrazolyl moiety in conjunction with a bifunctional donor system, both being attached to a dimethyl gallium grouping. The many novel aspects displayed by compounds containing these ligands prompted us to extend our investigations in this area to include a pyridyl "aromatic" ring in the ligand system to give **2**.

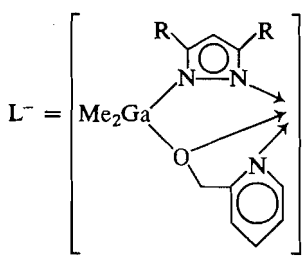

2

R = H or Me

The new ligands have yielded a variety of transition metal complexes and one of these, $LRe(CO)_3$, has been characterized by X-ray crystallographic analysis.

Experimental

Air-sensitive materials were handled in a glove box under an atmosphere of oxygen-free dry nitrogen, in a nitrogen-blanketed apparatus or on a high-vacuum line. Tetrahydrofuran (THF) was dried by refluxing over Na/benzophenone and was used immediately following distillation. Benzene was dried by refluxing over molten potassium followed by distillation. Sodium pyrazolide and sodium 3,5-dimethyl-

Can. J. Chem. Downloaded from www.nrcresearchpress.com by 210.87.254.5 on 09/06/12
For personal use only.

TABLE 1. Analytical and ir data for 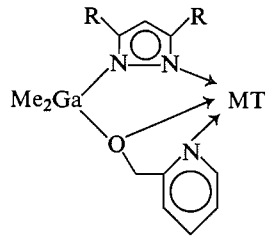

M	R	T	Calcd. (%) C	Calcd. (%) H	Calcd. (%) N	Found (%) C	Found (%) H	Found (%) N	$\nu_{CO}(\nu_{NO})$ cm^{-1} *
Mn	Me	$(CO)_3$	43.48	4.33	9.51	43.56	4.37	9.77	2035, 1943, 1908
Re	Me	$(CO)_3$	33.52	3.34	7.33	33.92	3.52	7.34	2028, 1924, 1898
Ni	Me	NO	39.86	4.89	14.30	39.88	4.92	14.00	(1783)
Mo	H	$(CO)_2(\eta^3\text{-}C_3H_5)$	41.06	4.27	8.98	41.07	4.17	8.86	1942, 1855
Mo	H	$(CO)_2(\eta^3\text{-}C_4H_7)$	42.36	4.60	8.71	42.52	4.62	8.55	1938, 1853

* Measured in cyclohexane.

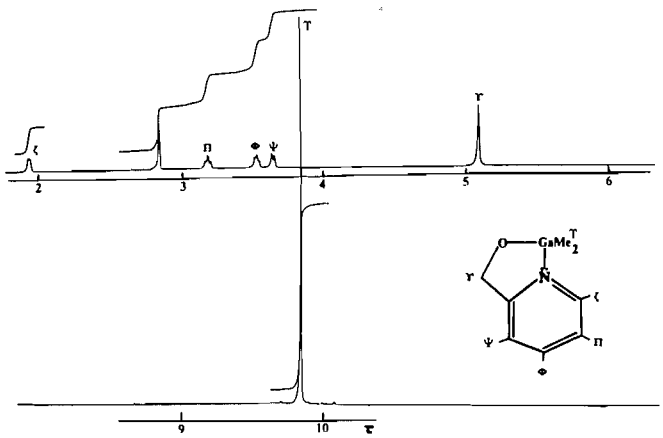

FIG. 1. 400 MHz ^{1}H nmr spectrum of $[Me_2GaOCH_2(C_5H_4N)]$ in C_6D_6.

pyrazolide were prepared by reacting sodium hydride (Alfa) with the appropriate pyrazole (K and K Laboratories) in THF. Trimethyl gallium (2), Ni(NO)I (3), $Mn(CO)_5Br$ (4), and $[Re(CO)_4Cl]_2$ (5) were prepared as previously described. Allyl bromide and 2-methylallyl chloride were distilled before use. $(MeCN)_3Mo(CO)_3$ was prepared from $Mo(CO)_6$ (Strem) by a standard route (6). Pyridyl-2-methanol (Aldrich) was used as supplied.

Preparation of $[Me_2GaOCH_2(C_5H_4N)]_2$

$$Me_3Ga + HOCH_2(C_5H_4N) \rightarrow (1/2)[Me_2GaOCH_2(C_5H_4N)]_2 + MeH$$

To a solution of trimethylgallium (2.42 g, 21.1 mmol) in THF was added pyridine-2-methanol (2.30 g, 21.1 mmol) in the same solvent. The reaction mixture was refluxed for 24 h and the solvent removed under vacuum. The solid obtained was extracted with benzene. The resulting solution afforded white needles of the desired product upon slow evaporation of the solvent. Yield ~85%. *Anal.* calcd. for $[Me_2GaOCH_2(C_5H_4N)]_2$: C 46.22, H 5.82, N 6.74; found: C 45.87, H 6.00, N 6.56. The ^{1}H nmr spectrum of the product is shown in Fig. 1.

Preparation of the ligand L^-

$$Na^+(N_2C_3HR_2)^- + Me_3Ga \rightarrow Na^+[Me_3Ga(N_2C_3HR_2)]^-$$

$$Na^+[Me_3Ga(N_2C_3HR_2)]^- + HOCH_2(C_5H_4N) \rightarrow Na^+L^- + CH_4$$

Typically, trimethylgallium (2.26 g, 19.7 mmol) in 50 mL THF was added to sodium 3,5-dimethylpyrazolide (R = Me) (2.33 g, 19.7 mmol) in 50 mL of the same solvent. After stirring the solution at room temperature for approximately 1 h a 50 mL THF solution of pyridine-2-methanol (2.15 g, 19.7 mmol) was added and the reaction mixture refluxed overnight. The solution was cooled and diluted to 250 mL in a standard flask. Aliquots of this standard solution were used in subsequent reactions.

Preparation of $LMn(CO)_3$

To a stirred solution of $Mn(CO)_5Br$ in THF (0.53 g, 1.97 mmol) was added 25 mL THF solution of the ligand Na^+L^- (R = Me) (1.97 mmol). The reaction mixture was stirred overnight at room temperature and the solvent was then removed under vacuum. The orange residue was extracted with benzene and the solution filtered. The filtrate, on slow evaporation of the solvent, gave dark orange–brown crystals of the product in approximately 70% yield. Analytical, ir, and nmr data for this complex and those described below, are collected in Tables 1 and 2. The $LRe(CO)_3$ complex was prepared similarly using the $[Re(CO)_4Cl]_2$ dimer as starting material. The product was collected in ~70% yield.

Preparation of $LNi(NO)$

To a stirred solution of Ni(NO)I (0.83 g, 3.84 mmol) in 50 mL THF was added 50 mL THF solution of Na^+L^- (R = Me) (3.94 mmol). The reaction mixture was stirred overnight at room temperature and the solvent was then removed under vacuum. The blue residue was extracted with benzene and recrystallization from this solvent afforded a deep blue microcrystalline product in ~65% yield.

Preparation of $Na^+LMo(CO)_3^-$ solution

To a stirred 50 mL THF solution of $(MeCN)_3Mo(CO)_3$ (2.703 g, 8.92 mmol) was added 100 mL THF solution of Na^+L^- (R = H) (8.92 mmol). The resulting mixture was stirred overnight and the resultant orange–brown solution of $Na^+LMo(CO)_3^-$ made up to 250 mL in a standard flask.

Preparation of $LMo(CO)_2(\eta^3\text{-}C_3H_5)$

To a 50 mL solution of $Na^+LMo(CO)_3^-$ (R = H) (1.78 mmol) was added an excess of allyl bromide. The mixture was stirred for 24 h and the solvent removed under vacuum. Recrystallization of the brown residue from benzene yielded waxy orange crystals of the product in ~65% yield.

The $LMo(CO)_2(\eta^3\text{-}C_4H_7)$ complex was prepared similarly, substituting 2-methylallyl chloride as one of the reactants. The product was obtained as orange crystals in ~70% yield.

X-ray crystallographic analyses

$[Me_2GaOCH_2(C_5H_4N)]_2$

A crystal bounded by the six faces (followed by their distances in mm from a common origin): ±(0 0 1), 0.188, ± (1 1 0), 0.094, ±(−1 1 0), 0.094 was mounted in a general orientation. Unit-cell parameters were refined by least-squares on 2 sin θ/λ values for 25 reflections (2θ = 35–44°) measured on a diffractometer with Mo-$K\alpha$

Can. J. Chem. Downloaded from www.nrcresearchpress.com by 210.87.254.5 on 09/06/12
For personal use only.

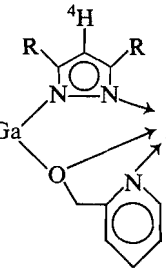

TABLE 2. ^{1}H nmr data for Me_2Ga MT complexes in C_6D_6 solution

M	R	T	τ* —OCH_2—	H^4	R	"allyl"	Ga—Me
Ni	Me	NO	5.33 s	3.98 s	7.06 s, 7.92 s		9.83 s
Re	Me	$(CO)_3$	A = 5.03, B = 5.35 (J = 16 Hz)	4.43 s	7.57 s, 8.15 s		9.79 s, 10.26 s
Mn†	Me	$(CO)_3$	A = 4.71, B = 4.85 (J = 16 Hz)	4.17 s	7.42 s, 7.88 s		10.26 s, 10.38 s
Mo	H	$(CO)_2(\eta^3\text{-}C_3H_5)$	A = 5.38, B = 5.44 (J = 15 Hz)	4.05 t	2.24 d, 3.01 d	8.32 d, 8.50 d (H_{anti} J = 10 Hz) 6.64 d, 6.65 d (H_{syn} J = 6 Hz) 6.08 tt (H_{unique} J = 6, 10 Hz)	10.10 s, 10.56 s
Mo	H	$(CO)_2(\eta^3\text{-}C_4H_7)$	A = 5.15, B = 5.43 (J = 16 Hz)	3.94 t	2.13 d, 2.98 d	8.29 s (allyl Me) 8.37 s, 8.52 s (H_{anti}) 6.81 d, 6.91 d (H_{syn} J = 4 Hz)	9.88 s, 10.77 s

* τ values refer to ($\tau_{C_6H_6}$ = 2.84 ppm), s = singlet, d = doublet, t = triplet, tt = triplet of triplets.
† Measured in acetone-d^6; τ values refer to ($\tau_{acetone}$ = 7.89 ppm).

Radiation ($\lambda(K\alpha_1)$ = 0.70930, $\lambda(K\alpha_2)$ = 0.71359 Å). Crystal data at 22°C are:

$C_{16}H_{24}Ga_2N_2O_2$ fw = 207.91

Monoclinic, a = 16.716(2), b = 7.6513(6), c = 7.7591(8) Å, β = 108.349(5)°, V = 941.9(2) Å^3, Z = 2, ρ_C = 1.466 g cm^{-3}, $F(0\,0\,0)$ = 424, μ(Mo-$K\alpha$) = 28.57 cm^{-1}. Absent reflections: hkl, $h + k$ odd, space group $C2/m$ (C_{2h}^3, No. 12) from structure analysis.

Intensities were measured with graphite-monochromated Mo-$K\alpha$ radiation on an Enraf-Nonius CAD4-F diffractometer. An ω-2θ scan at 1.26–10.06° min^{-1} over a range of (0.60 + 0.35 tan θ) degrees in ω (extended by 25% on both sides for background measurement) was employed. Data were measured to 2θ = 60°. The intensities of three check reflections, measured every 3600 s throughout the data collection, remained constant to within 2%. After data reduction,[1] an absorption correction was applied using the Gaussian integration method (7, 8). Transmission factors ranged from 0.439 to 0.652 for 96 integration points. Of the 1460 independent reflections measured, 809 (55.4%) had intensities greater than $3\sigma(I)$ above background where $\sigma^2(I) = S + 2B + (0.04(S - B))^2$ with S = scan count and B = normalized background count.

The centrosymmetric space group $C2/m$ was indicated by the E-statistics. The coordinates of the Ga atom were determined from the Patterson function and those of the remaining atoms from subsequent difference syntheses. The non-hydrogen atoms were refined with anisotropic thermal parameters and the hydrogen atoms with isotropic thermal parameters. The scattering factors of ref. 9 were used for non-hydrogen atoms and those of ref. 10 for hydrogen atoms. Anomalous scattering factors from ref. 11 were used for the Ga atoms. The weighting scheme, $w = 1/\sigma^2(F)$ where $\sigma^2(F)$ is derived from the previously defined $\sigma^2(I)$, gave uniform average values of $w(|F_o| - |F_c|)^2$ over ranges of both $|F_o|$ and sin θ/λ and was employed in the final stages of refinement. Reflections with $I < 3\sigma(I)$ were not included in the refinement. Convergence was reached at R = 0.029 and R_w = 0.032 for 809 reflections with $I \geq 3\sigma(I)$. For all 1460 reflections R = 0.078. The function minimized was $\Sigma w(|F_o| - |F_c|)^2$, $R = \Sigma||F_o| - |F_c||/\Sigma|F_o|$ and $R_w = (\Sigma w(|F_o| - |F_c|)^2/\Sigma w|F_o|^2)^{1/2}$.

On the final cycle of refinement the mean and maximum parameter shifts corresponded to 0.04 and 0.27σ, respectively. The mean error in an observation of unit weight was 1.402. A final difference map showed maximum fluctuations of −0.81 to +0.67 e Å^{-3} near Ga and ±0.17 e Å^{-3} elsewhere. The final positional and thermal parameters appear in Tables 3 and 7,[2] respectively. Measured and calculated structure factors have been placed in the Depository of Unpublished Data.[2]

The ellipsoids of thermal motion for the non-hydrogen atoms are shown in Fig. 5. The thermal motion has been analysed in terms of the rigid-body modes of translation, libration, and screw motion (12). The rms standard error in the temperature factors σU_{ij} (derived from the least-squares analysis) is 0.0027 Å^2. Analysis of the entire molecule (rms ΔU_{ij} = 0.0071 Å^2) showed significant independent motion of the Me_2Ga units. Fragment consisting of the pyridine ring plus C(6) and the Ga coordination group were separately analysed (rms ΔU_{ij} = 0.0026 and 0.0020 Å^2). The appropriate bond distances have been corrected for libration (12, 13), using shape parameters q^2 of 0.08 for all atoms involved. Corrected bond lengths appear in Table 4 along with the uncorrected values; corrected bond angles do not differ by more than 1σ from the uncorrected values given in Table 5. Intra-annular torsion angles defining the conformations of chelate rings are listed in Table 6 for $[Me_2Ga(N_2C_5H_7)OCH_2(C_5H_4N)]Re(CO)_3$. Bond lengths and angles involving hydrogen and a complete listing of torsion angles (Tables 8–10) are included as supplementary material.

$[Me_2Ga(N_2C_5H_7)OCH_2(C_5H_4N)]Re(CO)_3$

Experimental details are as above except where noted. The bounding planes of the crystal used for data collection were: ±(0 1 0),

[1] The computer programs used include locally written programs for data processing and locally modified versions of the following: ORFLS, full-matrix least-squares, and ORFFE, function and errors, by W. R. Busing, K. O. Martin, and H. A. Levy; FORDAP, Patterson and Fourier syntheses, by A. Zalkin; ORTEP II, illustrations, by C. K. Johnson.

[2] The structure factor table, Table 7 (anisotropic thermal parameters) and other material mentioned in the text are available, at a nominal charge, from the Depository of Unpublished Data, CISTI, National Research Council of Canada, Ottawa, Ont., Canada K1A 0S2.

Can. J. Chem. Downloaded from www.nrcresearchpress.com by 210.87.254.5 on 09/06/12
For personal use only.

TABLE 3. Final positional (fractional × 10^4, Re and Ga × 10^5, H × 10^3) and isotropic thermal parameters ($U \times 10^3$ Å^2) with estimated standard deviations in parentheses*

Atom	x	y	z	U_{eq}/U_{iso}	Atom	x	y	z	U_{eq}/U_{iso}
				$[Me_2GaOCH_2(C_5H_4N)]_2$					
Ga	42417(3)	50000	31230(5)	60	C(7)	4118(3)	2750(6)	1839(7)	95
O	4459(2)	5000	5711(4)	81	H(2)	234(3)	500	679(7)	68(13)
N	2945(2)	5000	3484(4)	64	H(3)	99(4)	500	470(9)	108(18)
C(1)	2977(3)	5000	5215(5)	63	H(4)	100(4)	500	189(7)	81(16)
C(2)	2250(4)	5000	5723(8)	89	H(5)	216(3)	500	94(7)	77(12)
C(3)	1492(4)	5000	4391(9)	103	H(6)	389(2)	393(4)	735(4)	79(9)
C(4)	1456(4)	5000	2614(8)	91	H(7a)	361(2)	240(5)	138(5)	96(13)
C(5)	2189(3)	5000	2203(7)	78	H(7b)	445(3)	252(6)	123(8)	123(17)
C(6)	3851(3)	5000	6557(5)	69	H(7c)	438(4)	208(11)	294(12)	223(37)
				$[Me_2Ga(N_2C_5H_7)\{OCH_2(C_5H_4N)\}]Re(CO)_3$					
Re(1)	34676(4)	28863(1)	45596(3)	39	C(8)	4149(13)	4058(3)	4201(10)	58
Re(2)	63365(5)	9719(1)	37458(4)	52	C(9)	3271(10)	3770(3)	4249(9)	46
Ga(1)	68156(11)	31717(3)	44757(10)	47	C(10)	4134(10)	2813(3)	1901(9)	41
Ga(2)	81173(16)	3474(4)	20287(13)	67	C(11)	4038(11)	2811(3)	617(10)	51
O(1)	5464(7)	2823(2)	3852(7)	49	C(12)	2814(13)	2887(3)	25(10)	60
O(2)	470(8)	2966(3)	5220(9)	84	C(13)	1702(12)	2981(3)	707(11)	59
O(3)	2908(11)	2077(3)	4715(10)	88	C(14)	1879(10)	2978(3)	1973(10)	50
O(4)	4195(10)	2846(3)	7330(8)	89	C(15)	6846(14)	4092(4)	4325(14)	79
O(5)	7750(8)	856(2)	2353(6)	56	C(16)	1727(13)	3780(4)	4204(12)	68
O(6)	4586(12)	1215(4)	5847(12)	128	C(17)	5237(14)	1107(4)	5048(13)	77
O(7)	5726(12)	1737(3)	2774(10)	99	C(18)	5938(14)	1444(4)	3117(11)	70
O(8)	3644(12)	740(4)	2398(12)	123	C(19)	4693(16)	811(4)	2879(15)	86
N(1)	5376(8)	3555(2)	4395(8)	46	C(20)	6641(20)	169(5)	895(16)	110
N(2)	3988(8)	3459(2)	4366(7)	41	C(21)	10076(18)	266(5)	1762(15)	103
N(3)	3087(8)	2897(2)	2571(7)	44	C(22)	8829(15)	1108(3)	2378(10)	64
N(4)	7731(12)	218(3)	3734(9)	67	C(23)	8019(19)	−82(4)	4375(16)	92
N(5)	6911(11)	440(3)	4428(9)	62	C(24)	7329(18)	−70(4)	5480(14)	86
N(6)	8360(9)	1134(2)	4535(7)	45	C(25)	6675(14)	259(4)	5487(12)	72
C(1)	1620(12)	2949(3)	4974(11)	60	C(26)	9319(11)	1180(3)	3701(9)	48
C(2)	3140(11)	2380(3)	4633(10)	50	C(27)	10641(12)	1289(3)	4055(11)	61
C(3)	3951(11)	2869(4)	6290(10)	60	C(28)	10974(12)	1360(3)	5270(11)	61
C(4)	7316(11)	3089(3)	6210(10)	55	C(29)	10002(12)	1302(3)	6112(10)	57
C(5)	8127(12)	3245(4)	3196(11)	71	C(30)	8704(12)	1197(3)	5734(9)	49
C(6)	5423(11)	2692(3)	2627(10)	52	C(31)	8901(26)	−384(5)	3902(21)	135
C(7)	5459(13)	3911(3)	4300(10)	56	C(32)	5869(22)	403(5)	6489(15)	113

* U_{eq} = (1/3) trace (U_{diag}), coordinates having no esd's are fixed.

Can. J. Chem. Downloaded from www.nrcresearchpress.com by 210.87.254.5 on 09/06/12
For personal use only.

0.113, ±(0 0 1), 0.250, ±(1 0 0), 0.263 mm. Reflections employed in the refinement of the unit-cell parameters had 2θ = 35–46°. Crystal data are as follows:

$C_{14}H_{15}GaN_3O_4Re$ fw = 545.21

Monoclinic, a = 9.7457(7), b = 36.991(3), c = 10.8821(8) Å, β = 92.944(3)°, V = 3917.8(5) Å^3, Z = 8, ρ_C = 1.849 g cm^{-3}, F(0 0 0) = 2064, μ(Mo-$K\alpha$) = 76.47 cm^{-1}. Absent reflections: 0k0, k odd, and h0l, $h + l$ odd, uniquely indicate the space group $P2_1/n$ (non-standard setting of $P2_1/c$, C_{2h}^5, No. 14, equivalent positions: ±(x, y, z; 1/2 − x, 1/2 + y, 1/2 − z)).

An ω scan at 1.44–10.06° min^{-1} over a range of (0.65 + 0.35 tan θ)° in ω was employed. Of 8952 independent reflections measured (to 2θ = 55°), 5321 (59.4%) had intensities greater than 3σ(I) above background. The intensities of the three check reflections remained constant to within 2.5%. Data were corrected for absorption using the analytical method (7, 14), transmission factors ranging from 0.057 to 0.199.

The structure was solved by conventional heavy-atom methods, the coordinates of the Re and Ga atoms being determined from the Patterson function and those of the remaining non-hydrogen atoms from subsequent difference maps. All non-hydrogen atoms were refined with anisotropic thermal parameters and hydrogen atoms were included as fixed atoms in idealized positions (C(sp^2)—H = 0.97 and C(sp^3)—H = 0.98 Å). An isotropic Type I extinction correction (Thornley–Nelmes definition of mosaic anisotropy with a Lorentzian distribution) was applied (15–17). The final value of g was 4.5(3) × 10^4. The structure was refined to 0.042 and R_w = 0.047 for 5321 reflections. The mean and maximum parameter shifts on the final cycle of refinement corresponded to 0.06 and 0.40 σ, respectively. The mean error in an observation of unit weight was 1.918. A final difference map showed maximum fluctuations of ±2.6 e Å^{-3} near Re. Calculated coordinates and thermal parameters for hydrogen atoms (Table 11) are included as deposited material. The two independent molecules are shown in Fig. 6.

Results and discussion

Several recent publications have discussed a variety of metal complexes with multidentate ligand systems containing both pyridyl and pyrazolyl donor functions (18, 19). It has been concluded that pyrazolyl has weaker π-acceptor capabilities (20) but stronger σ-donor properties than pyridine (18). The present study extends our work in the area of unsymmetrical uninegative tridentate organogallate ligands to include ligand systems incorporating both a pyrazolyl and a pyridyl donor function. A variety of transition metal complexes bearing these ligands has been characterized by the usual sporting physical

TABLE 4. Bond lengths (Å) with estimated standard deviations in parentheses

Bond	Length Uncorr.	Length Corr.	Bond	Length Uncorr.	Length Corr.
			$[Me_2GaOCH_2(C_5H_4N)]_2$		
Ga—O	1.925(3)	1.939	N—C(5)	1.340(6)	1.347
Ga—N	2.271(3)	2.276	C(1)—C(2)	1.390(7)	1.403
Ga—C(7)	1.967(4)	1.981	C(1)—C(6)	1.504(6)	1.510
Ga—O′	2.073(3)	2.086	C(2)—C(3)	1.360(9)	1.367
O—C(6)	1.373(5)	1.374	C(3)—C(4)	1.361(8)	1.368
N—C(1)	1.328(5)	1.339	C(4)—C(5)	1.360(8)	1.372
			$[Me_2Ga(N_2C_5H_7)\{OCH_2(C_5H_4N)\}]Re(CO)_3$		
Re(1)—O(1)	2.142(6)		N(1)—N(2)	1.397(11)	
Re(1)—N(2)	2.192(9)		N(1)—C(7)	1.326(14)	
Re(1)—N(3)	2.177(8)		N(2)—C(9)	1.347(13)	
Re(1)—C(1)	1.893(12)		N(3)—C(10)	1.321(11)	
Re(1)—C(2)	1.904(12)		N(3)—C(14)	1.348(13)	
Re(1)—C(3)	1.919(11)		N(4)—N(5)	1.396(14)	
Re(2)—O(5)	2.143(8)		N(4)—C(23)	1.33(2)	
Re(2)—N(5)	2.166(10)		N(5)—C(25)	1.364(15)	
Re(2)—N(6)	2.194(8)		N(6)—C(26)	1.346(12)	
Re(2)—C(17)	1.89(2)		N(6)—C(30)	1.351(13)	
Re(2)—C(18)	1.909(15)		C(6)—C(10)	1.518(15)	
Re(2)—C(19)	1.912(15)		C(7)—C(8)	1.39(2)	
Ga(1)—O(1)	1.943(7)		C(7)—C(15)	1.51(2)	
Ga(1)—N(1)	1.993(9)		C(8)—C(9)	1.37(2)	
Ga(1)—C(4)	1.949(11)		C(9)—C(16)	1.504(15)	
Ga(1)—C(5)	1.957(11)		C(10)—C(11)	1.396(14)	
Ga(2)—O(5)	1.950(8)		C(11)—C(12)	1.36(2)	
Ga(2)—N(4)	1.972(10)		C(12)—C(13)	1.39(2)	
Ga(2)—C(20)	1.96(2)		C(13)—C(14)	1.380(15)	
Ga(2)—C(21)	1.97(2)		C(22)—C(26)	1.52(2)	
O(1)—C(6)	1.416(13)		C(23)—C(24)	1.41(2)	
O(2)—C(1)	1.166(13)		C(23)—C(31)	1.52(2)	
O(3)—C(2)	1.147(13)		C(24)—C(25)	1.37(2)	
O(4)—C(3)	1.147(13)		C(25)—C(32)	1.48(2)	
O(5)—C(22)	1.405(15)		C(26)—C(27)	1.39(2)	
O(6)—C(17)	1.17(2)		C(27)—C(28)	1.37(2)	
O(7)—C(18)	1.160(15)		C(28)—C(29)	1.37(2)	
O(8)—C(19)	1.15(2)		C(29)—C(30)	1.37(2)	

methods, and one of them has been further probed by X-ray crystallographic techniques.

The reactivity of pyridyl-2-methanol towards trimethylgallium was first investigated to confirm the expected methane elimination reaction. The product from this reaction, "$[Me_2GaOCH_2(C_5H_4N)]$", was shown to be monomeric in the gas phase, its mass spectrum displaying a weak monomer parent ion (P^+) signal and a very strong $P - Me^+$ signal. Similar dimethylgallium systems have been shown to be associated in the solid state (21, 22) and an X-ray crystal structure of the present pyridyl complex again demonstrated the dimerization of the monomer units via a four-membered [—Ga—O—]$_2$ ring, each gallium having a distorted trigonal bipyramidal arrangement. It is interesting to compare the Ga—N bond lengths in the three complexes $[Me_2GaOCH_2(C_5H_4N)]_2$, $[Me_2NCH_2CH_2OGaMe_2]_2$ (22), and $[Me_2NCH_2CH_2OGaH_2]_2$ (22). The pyridyl complex is comparable with the dihydride (Ga—N = 2.276(3) and 2.279(3) Å respectively), both bonds being considerably shorter than in the $[Me_2NCH_2CH_2OGaMe_2]_2$ dimer (Ga—N = 2.471(4) Å) where severe steric interactions between the "NMe_2" and "$GaMe_2$" moieties lead to bond lengthening.

The ^{1}H nmr of the pyridyl complex in C_6D_6 solution (Fig. 1) shows sharp singlets for both the "$GaMe_2$" protons and the —OCH_2— methylene protons. The spectrum is consistent with an overall planar structure for the monomer in dilute solution with the two GaMe groups and the two methylene protons lying above and below this plane.

The synthesis of the ligands Na^+L^-, **2**, proceeded smoothly as did the subsequent reactions to yield the transition metal complexes listed in Tables 1 and 2. Analysis of mass spectral, ir, and ^{1}H nmr data points to monomeric structures for the whole range of complexes studied. An octahedral structure is proposed for the manganese, rhenium, and molybdenum compounds with the tridentate gallate ligand occupying three facial positions. This arrangement has been proven conclusively for the $LRe(CO)_3$ complex by a crystal structure determination (see below). The LNi(NO) complex is believed to possess a tetrahedral transition metal centre although fluxional behaviour in solution at room temperature must be operative to explain the ^{1}H nmr results for this compound.

Infrared spectra

The ir spectral data reported in Table 1 for the octahedral

Can. J. Chem. Downloaded from www.nrcresearchpress.com by 210.87.254.5 on 09/06/12
For personal use only.

Can. J. Chem. Downloaded from www.nrcresearchpress.com by 210.87.254.5 on 09/06/12
For personal use only.

TABLE 5. Bond angles (deg) with estimated standard deviations in parentheses*

Bonds	Angle (deg)	Bonds	Angle (deg)
	$[Me_2GaOCH_2(C_5H_4N)]_2$		
O —Ga —N	75.26(12)	C(6)—O —Ga′	128.5(3)
O —Ga —C(7)	118.91(15)	Ga —N —C(1)	112.9(3)
O —Ga —O′	73.55(13)	Ga —N —C(5)	128.5(3)
O —Ga —C(7)″	118.91(15)	C(1)—N —C(5)	118.5(4)
N —Ga —C(7)	96.30(14)	N —C(1)—C(2)	121.8(4)
N —Ga —O′	148.81(12)	N —C(1)—C(6)	114.9(4)
N —Ga —C(7)″	96.30(14)	C(2)—C(1)—C(6)	123.3(4)
C(7)—Ga —O′	98.63(15)	C(1)—C(2)—C(3)	118.2(5)
C(7)—Ga —C(7)″	122.2(3)	C(2)—C(3)—C(4)	120.2(5)
O′ —Ga —C(7)″	98.63(15)	C(3)—C(4)—C(5)	118.8(6)
Ga —O —C(6)	125.0(3)	N —C(5)—C(4)	122.4(5)
Ga —O —Ga′	106.45(13)	O —C(6)—C(1)	111.9(3)
	$[Me_2Ga(N_2C_5H_7)\{OCH_2(C_5H_4N)\}]Re(CO)_3$		
O(1)—Re(1)—N(2)	81.6(3)	Re(1)—N(2)—N(1)	118.1(6)
O(1)—Re(1)—N(3)	75.9(3)	Re(1)—N(2)—C(9)	135.4(7)
O(1)—Re(1)—C(1)	172.7(4)	N(1)—N(2)—C(9)	106.5(8)
O(1)—Re(1)—C(2)	93.7(4)	Re(1)—N(3)—C(10)	116.5(7)
O(1)—Re(1)—C(3)	99.7(4)	Re(1)—N(3)—C(14)	125.7(6)
N(2)—Re(1)—N(3)	85.1(3)	C(10)—N(3)—C(14)	117.7(8)
N(2)—Re(1)—C(1)	97.6(4)	Ga(2)—N(4)—N(5)	120.5(7)
N(2)—Re(1)—C(2)	175.0(3)	Ga(2)—N(4)—C(23)	130.6(10)
N(2)—Re(1)—C(3)	94.6(5)	N(5)—N(4)—C(23)	108.6(11)
N(3)—Re(1)—C(1)	96.8(4)	Re(2)—N(5)—N(4)	119.7(7)
N(3)—Re(1)—C(2)	92.3(4)	Re(2)—N(5)—C(25)	133.2(10)
N(3)—Re(1)—C(3)	175.5(4)	N(4)—N(5)—C(25)	107.1(10)
C(1)—Re(1)—C(2)	86.9(5)	Re(2)—N(6)—C(26)	114.3(7)
C(1)—Re(1)—C(3)	87.6(5)	Re(2)—N(6)—C(30)	126.8(7)
C(2)—Re(1)—C(3)	87.6(5)	C(26)—N(6)—C(30)	118.9(9)
O(5)—Re(2)—N(5)	84.0(3)	Re(1)—C(1)—O(2)	176.1(11)
O(5)—Re(2)—N(6)	74.6(3)	Re(1)—C(2)—O(3)	177.2(10)
O(5)—Re(2)—C(17)	173.9(5)	Re(1)—C(3)—O(4)	176.9(11)
O(5)—Re(2)—C(18)	93.2(5)	O(1)—C(6)—C(10)	111.8(8)
O(5)—Re(2)—C(19)	98.1(6)	N(1)—C(7)—C(8)	109.5(10)
N(5)—Re(2)—N(6)	84.4(3)	N(1)—C(7)—C(15)	119.9(12)
N(5)—Re(2)—C(17)	97.4(5)	C(8)—C(7)—C(15)	130.5(12)
N(5)—Re(2)—C(18)	176.7(5)	C(7)—C(8)—C(9)	105.6(10)
N(5)—Re(2)—C(19)	94.6(5)	N(2)—C(9)—C(8)	110.2(9)
N(6)—Re(2)—C(17)	99.6(5)	N(2)—C(9)—C(16)	122.5(10)
N(6)—Re(2)—C(18)	93.0(5)	C(8)—C(9)—C(16)	127.3(11)
N(6)—Re(2)—C(19)	172.7(6)	N(3)—C(10)—C(6)	115.1(8)
C(17)—Re(2)—C(18)	85.1(6)	N(3)—C(10)—C(11)	122.7(10)
C(17)—Re(2)—C(19)	87.7(7)	C(6)—C(10)—C(11)	122.0(9)
C(18)—Re(2)—C(19)	87.6(6)	C(10)—C(11)—C(12)	119.1(10)
O(1)—Ga(1)—N(1)	89.7(3)	C(11)—C(12)—C(13)	119.3(10)
O(1)—Ga(1)—C(4)	111.4(4)	C(12)—C(13)—C(14)	118.0(10)
O(1)—Ga(1)—C(5)	107.4(4)	N(3)—C(14)—C(13)	123.1(9)
N(1)—Ga(1)—C(4)	107.2(4)	Re(2)—C(17)—O(6)	175.3(15)
N(1)—Ga(1)—C(5)	110.8(5)	Re(2)—C(18)—O(7)	177.3(12)
C(4)—Ga(1)—C(5)	124.8(5)	Re(2)—C(19)—O(8)	174(2)
O(5)—Ga(2)—N(4)	91.1(4)	O(5)—C(22)—C(26)	109.4(9)
O(5)—Ga(2)—C(20)	107.7(6)	N(4)—C(23)—C(24)	108.8(14)
O(5)—Ga(2)—C(21)	111.2(6)	N(4)—C(23)—C(31)	123(2)
N(4)—Ga(2)—C(20)	109.9(7)	C(24)—C(23)—C(31)	128.2(15)
N(4)—Ga(2)—C(21)	109.6(6)	C(23)—C(24)—C(25)	106.0(13)
C(20)—Ga(2)—C(21)	122.8(8)	N(5)—C(25)—C(24)	109.4(13)
Re(1)—O(1)—Ga(1)	114.4(3)	N(5)—C(25)—C(32)	124.4(13)
Re(1)—O(1)—C(6)	113.2(6)	C(24)—C(25)—C(32)	126.1(13)
Ga(1)—O(1)—C(6)	122.8(6)	N(6)—C(26)—C(22)	115.0(10)
Re(2)—O(5)—Ga(2)	116.9(4)	N(6)—C(26)—C(27)	121.1(10)
Re(2)—O(5)—C(22)	111.1(6)	C(22)—C(26)—C(27)	123.9(10)
Ga(2)—O(5)—C(22)	120.0(8)	C(26)—C(27)—C(28)	119.7(10)
Ga(1)—N(1)—N(2)	120.0(7)	C(27)—C(28)—C(29)	118.6(10)
Ga(1)—N(1)—C(7)	131.7(8)	C(28)—C(29)—C(30)	120.3(10)
N(2)—N(1)—C(7)	108.3(9)	N(6)—C(30)—C(29)	121.3(10)

*Here and elsewhere primed and double-primed atoms have coordinates related to those in Table 3 by the symmetry operations $1 - x$, $1 - y$, $1 - z$ and x, $1 - y$, z, respectively.

Can. J. Chem. Downloaded from www.nrcresearchpress.com by 210.87.254.5 on 09/06/12
For personal use only.

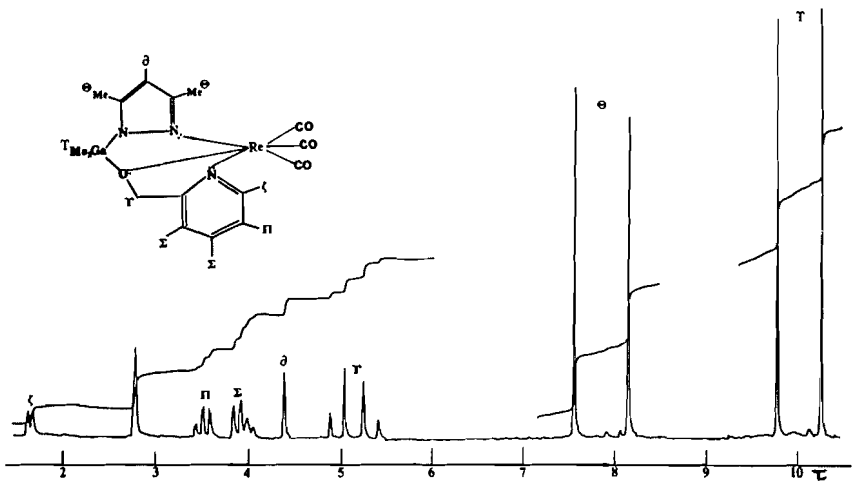

FIG. 2. 100 MHz ^{1}H nmr spectrum of $[Me_2Ga(N_2C_5H_7)\{OCH_2(C_5H_4N)\}]Re(CO)_3$ in C_6D_6.

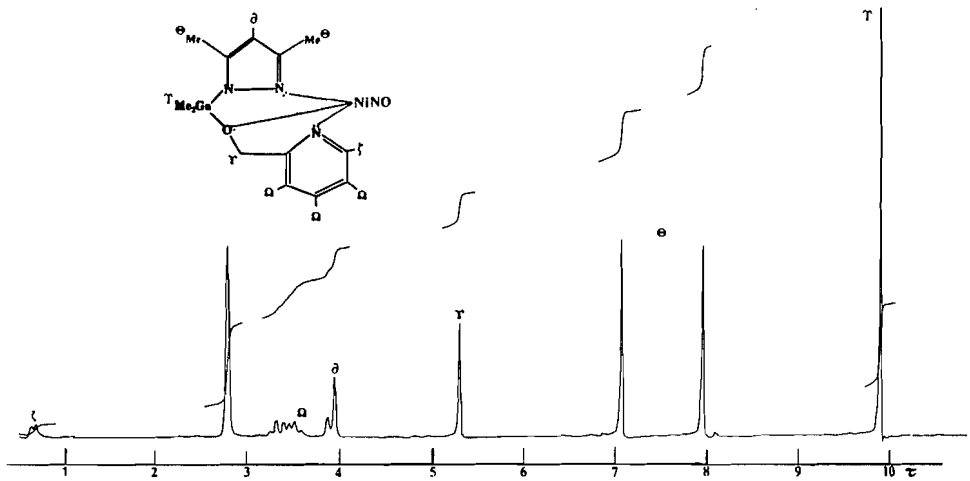

FIG. 3. 100 MHz ^{1}H nmr spectrum of $[Me_2Ga(N_2C_5H_7)\{OCH_2(C_5H_4N)\}]NiNO$ in C_6D_6.

TABLE 6. Intra-annular torsion angles (deg) for $[Me_2Ga(N_2C_5H_7)\{OCH_2(C_5H_4N)\}]Re(CO)_3$ with standard deviations in parentheses

Atoms	Value (deg)
N(2)—Re(1)—O(1)—Ga(1)	38.5(4)
N(1)—Ga(1)—O(1)—Re(1)	−38.7(4)
O(1)—Ga(1)—N(1)—N(2)	20.4(7)
Ga(1)—N(1)—N(2)—Re(1)	4.8(9)
O(1)—Re(1)—N(2)—N(1)	−24.9(6)
N(5)—Re(2)—O(5)—Ga(2)	23.5(4)
N(4)—Ga(2)—O(5)—Re(2)	−28.2(5)
O(5)—Ga(2)—N(4)—N(5)	23.2(9)
Ga(2)—N(4)—N(5)—Re(2)	−10.1(12)
O(5)—Re(2)—N(5)—N(4)	−7.9(8)
N(3)—Re(1)—O(1)—C(6)	−21.8(7)
Re(1)—O(1)—C(6)—C(10)	30.6(10)
O(1)—C(6)—C(10)—N(3)	−23.2(13)
Re(1)—N(3)—C(10)—C(6)	4.6(11)
O(1)—Re(1)—N(3)—C(10)	9.1(7)
N(6)—Re(2)—O(5)—C(22)	−33.5(7)
Re(2)—O(5)—C(22)—C(26)	43.0(11)
O(5)—C(22)—C(26)—N(6)	−27.9(14)
Re(2)—N(6)—C(26)—C(22)	−0.4(12)
O(5)—Re(2)—N(6)—C(26)	18.0(7)

complexes are consistent with a *fac* tridentate gallate ligand in these molecules. Thus, the tricarbonyl complexes give three strong bands in the ν_{CO} region of the spectrum indicative of a facial arrangement of these ligands (23). The molybdenum dicarbonyl "allyl" complexes both show two strong ν_{CO} bands, indicative of a *cis* arrangement of the CO ligands. These data, together with our studies on related complexes (24–26) and the ^{1}H nmr data reported below, confirm a facial tridentate gallate ligand in these compounds. Comparison of the ir data of the pyridyl complexes (Table 1) with that of the corresponding complexes incorporating aminoalcohol moieties (**1**, R = H and Me, X = O, Y = NH_2 or NMe_2) (24) reflects the π-acidity of the pyridyl ring. Thus the frequencies for the pyridyl complexes are consistently ~10 cm^{-1} higher than those for the complexes in ref. 24, suggestive of weaker back-bonding to the ancillary ligands in the present complexes due to competitive back-bonding to the π-system of the pyridyl ring.

^{1}H nmr spectra

Selected ^{1}H nmr data for the transition metal complexes are compiled in Table 2 and representative spectra are shown in Figs. 2–4. The ^{1}H nmr spectra for the tricarbonyl species are consistent with the proposed facial arrangement of the gallate ligand. Thus the Ga—Me groups appear as two singlets and the —OCH_2— methylene protons as an AB quartet (Fig. 2). A

Can. J. Chem. Downloaded from www.nrcresearchpress.com by 210.87.254.5 on 09/06/12
For personal use only.

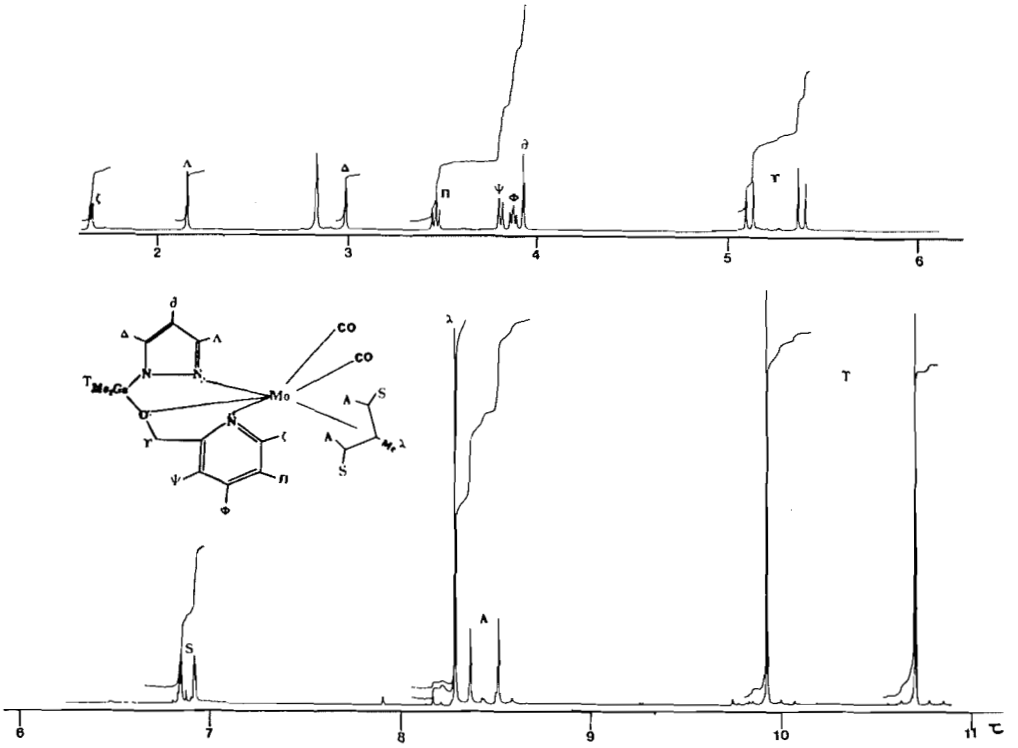

FIG. 4. 400 MHz ^{1}H nmr spectrum of $[Me_2Ga(N_2C_5H_7)\{OCH_2(C_5H_4N)\}]Mo(CO)_2(\eta^3\text{-}C_4H_7)$ in C_6D_6.

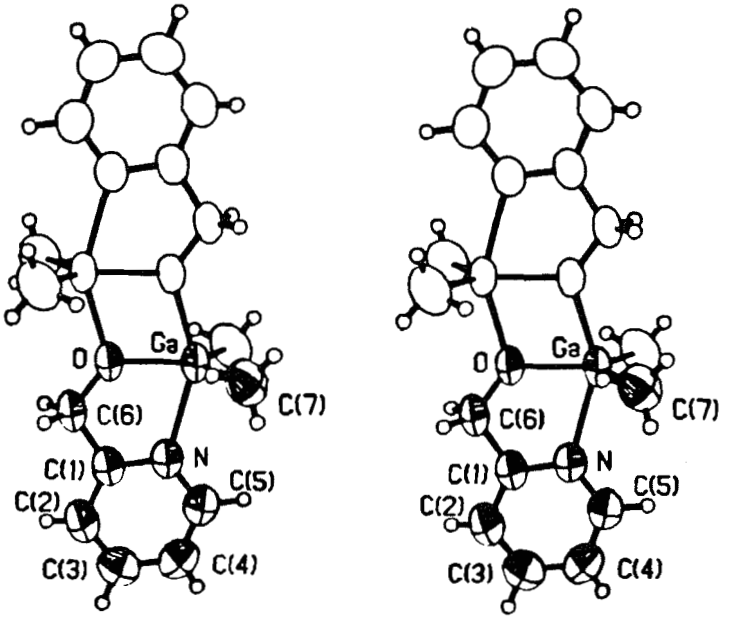

FIG. 5. Stereoscopic view of $[Me_2GaOCH_2(C_5H_4N)]_2$; 50% probability thermal ellipsoids are shown for the non-hydrogen atoms. Hydrogen atoms have been assigned artificially small thermal parameters for the sake of clarity.

meridional arrangement of the gallate ligand, on the other hand, would most probably lead to equivalent Ga—Me groups and equivalent methylene protons and hence singlets in these regions of the spectra. Interestingly the room temperature ^{1}H nmr spectrum of the LNi(NO) complex displays singlets for both of these groupings (see Fig. 3). This result would suggest a square planar arrangement around the Ni centre with a pseudo-meridional gallate ligand. However, the unlikelihood of a square planar arrangement for this complex in light of previous studies which have shown that square planar {MNO}[10] complexes should have an M—N—O bond angle of 120° (27, 28) (contrary to the linear M—N—O grouping suggested by the observed ir results) led us to suspect that a fluxional process was responsible for the observed room temperature spectrum. The closely related $[Me_2Ga(N_2C_3H_3)(OCH_2CH_2NMe_2)]Ni(NO)$ complex has been shown to be fluxional in solution and to have a tetrahedral Ni centre in the solid state (29). On cooling a solution of the above LNi(NO) pyridyl complex to −85°C a marked broadening of both the —$GaMe_2$ and —OCH_2— singlets was observed, indicative of a slowing down of the flux-

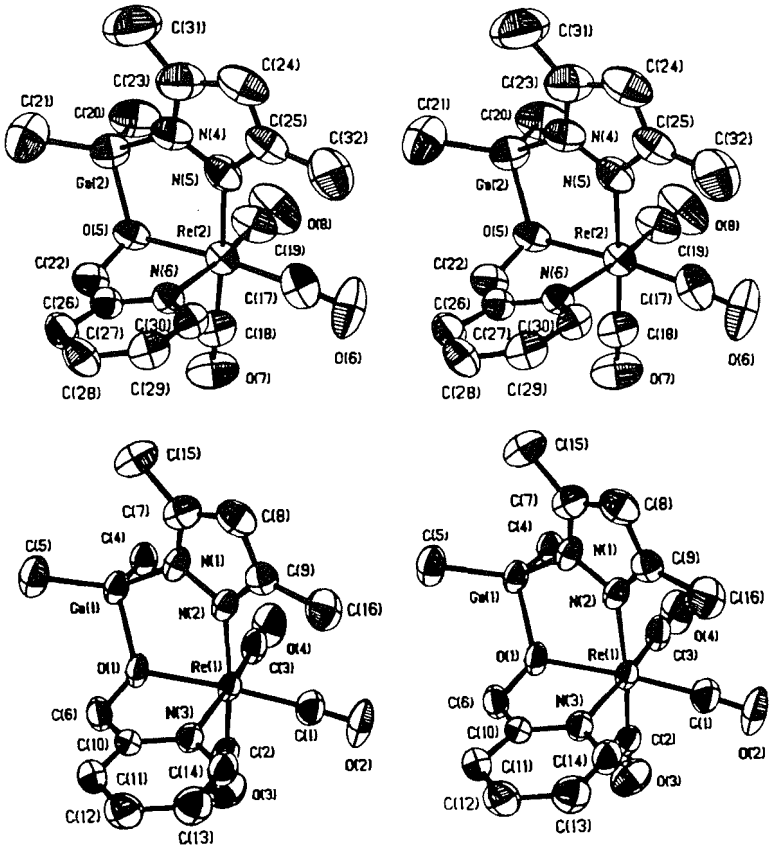

FIG. 6. Stereoscopic views of the two independent $[Me_2Ga(N_2C_5H_7)\{OCH_2(C_5H_4N)\}]Re(CO)_3$ molecules; 50% probability thermal ellipsoids are shown for the non-hydrogen atoms. Hydrogen atoms have been omitted.

ional process. Unfortunately, instrumental limitations precluded the attainment of temperatures low enough to see a clear splitting of these signals.

Both molybdenum dicarbonyl "allyl" complexes in their solution ^1H nmr spectra again showed clearly the presence of inequivalent Ga—Me groups and —OCH_2— methylene protons, supportive of a facial tridentate gallate ligand. With these two complexes, positional isomerism is possible in that substitution of the allyl group for CO in the $LMo(CO)_3^-$ precursor could occur at any one of three positions. It is evident that the allyl group substitutes exclusively at one position only since there is only one set of Ga—Me signals in the spectra (Fig. 4). Molecular models indicate that, sterically, the most favored position is opposite the "pyrazolyl" moiety of the ligand, a position of substitution confirmed crystallographically for the related molecule $[Me_2Ga(N_2C_5H_7)(OCH_2CH_2NH_2)]Mo(CO)_2(\eta^3\text{-}C_4H_7)$ (25). It is interesting, however, that in the similar $\eta^3\text{-}C_7H_7$ dicarbonyl complexes $[Me_2Ga(N_2C_5H_7)(OCH_2CH_2NH_2)]Mo(CO)_2(\eta^3\text{-}C_7H_7)$ (30) and $[Me_2Ga(N_2C_5H_7)(OCH_2CH_2SEt)]Mo(CO)_2(\eta^3\text{-}C_7H_7)$ (1), the $\eta^3\text{-}C_7H_7$ ligand is found opposite the amino nitrogen and the alkyl sulphur donor atoms, respectively.

Crystal structures

$[Me_2GaOCH_2(C_5H_4N)]_2$

The structure of $[Me_2GaOCH_2(C_5H_4N)]_2$ consists of well-separated binuclear molecules having crystallographically imposed C_{2h} symmetry, the system of five fused rings being necessarily planar. The coordination about gallium is distorted trigonal bipyramidal, the angle between axial substituents (N—Ga—O′) being 148.81(12)°. The Ga—N distances have been discussed (see above). The Ga—O distances in the central four-membered ring (1.939(3) and 2.086(3) Å) are similar to the corresponding values of 1.911(3)–1.960(8) and 2.018(2)—2.078(3) Å observed for the bridging alkoxide oxygen atoms in $(Me_2NCH_2CH_2OGaR_2)_2$ (22) and $[MeN(CH_2CH_2O)_2GaH]_2$ (21). These values may also be compared with the distances of 1.933(3) and 2.469(3) Å for the bridging phenoxide oxygen in bis(salicylaldehydatodimethylgallium) (31) and 1.972(2) and 2.551(2) Å for the bridging tropolonato oxygen in bis(tropolonatodimethylgallium) (32). All other geometrical features of the molecule are as expected.

$[Me_2Ga(N_2C_5H_7)OCH_2(C_5H_4N)]Re(CO)_3$

The structure of $[Me_2Ga(N_2C_5H_7)\{OCH_2(C_5H_4N)\}]Re(CO)_3$ consists of discrete molecules separated by normal van der Waals distances. The two crystallographically independent molecules are essentially equivalent, each having the predicted *fac*-octahedral coordination geometry about the central metal atom. The Re—O distances are 2.142(6) and 2.143(8) Å. The equivalence of the Re—N(*pz*) (2.166(10) and 2.192(9) Å) and Re—N(*py*) (2.194(8), 2.177(8) Å) distances as well as the geometry of the Re—CO moieties *trans* to these bonds suggests a balancing of the σ and π effects for the pyrazolyl and pyridyl nitrogen donors (18, 20). Although there are no statistically significant differences between the Re—C or C—O distances, those CO ligands *trans* to oxygen are associated with the shortest Re—C and longest C—O distances.

All aromatic rings in the structure are planar to within experimental error. The conformations of the five-membered chelate rings differ significantly between the two molecules (see Table 6), presumably a result of packing forces. The Ga-containing

Can. J. Chem. Downloaded from www.nrcresearchpress.com by 210.87.254.40 on 09/06/12
For personal use only.

ring in the molecule containing Re(1) deviates more from planarity than does the second chelate ring, this situation being reversed in the second molecule. Other structural parameters are normal.

Acknowledgments

We thank the Natural Sciences and Engineering Research Council of Canada for financial support and the University of British Columbia Computing Centre for assistance.

1. S. J. RETTIG, A. STORR, and J. TROTTER. Can. J. Chem. **59**, 2391 (1981).
2. A. STORR and B. S. THOMAS. Can. J. Chem. **48**, 3667 (1970).
3. B. HAYMORE and R. D. FELTHAM. Inorg. Synth. **14**, 81 (1973).
4. R. B. KING. Organometallic synthesis. Vol. 1. Academic Press, New York. 1965. p. 174.
5. G. DOLCETTI and G. R. NORTON. Inorg. Synth. **16**, 35 (1976).
6. D. P. TATE, W. R. KNIPPLE, and J. M. AUGL. Inorg. Chem. **1**, 433 (1962).
7. P. COPPENS, L. LEISEROWITZ, and D. RABINOVICH. Acta Crystallogr. **18**, 1035 (1965).
8. W. R. BUSING and H. A. LEVY. Acta Crystallogr. **22**, 457 (1967).
9. D. T. CROMER and J. B. MANN. Acta Crystallogr. Sect. A, **24**, 321 (1968).
10. R. F. STEWART, E. R. DAVIDSON, and W. T. SIMPSON. J. Chem. Phys. **42**, 3175 (1965).
11. D. T. CROMER and D. LIBERMAN. J. Chem. Phys. **53**, 1891 (1970).
12. V. SCHOMAKER and K. N. TRUEBLOOD. Acta Crystallogr. Sect. B, **24**, 63 (1968).
13. D. W. J. CRUICKSHANK. Acta Crystallogr. **9**, 747 (1956); **9**, 754 (1956); **14**, 896 (1961).
14. J. DE MEULENAER and H. TOMPA. Acta Crystallogr. **19**, 1014 (1965).
15. P. J. BECKER and P. COPPENS. Acta Crystallogr. Sect. A, **30**, 129 (1974); **30**, 148 (1974); **31**, 417 (1975).
16. P. COPPENS and W. C. HAMILTON. Acta Crystallogr. Sect. A, **26**, 71 (1970).
17. F. R. THORNLEY and R. J. NELMES. Acta Crystallogr. Sect. A, **30**, 748 (1974).
18. A. J. CANTY and C. V. LEE. Organometallics **1**, 1063 (1982).
19. P. J. STEEL, F. LAHOUSSE, D. LERNER, and C. MARTIN. Inorg. Chem. **22**, 1488 (1983).
20. P. SULLIVAN, D. J. SALMON, T. J. MEYER, and J. PEEDIN. Inorg. Chem. **18**, 3369 (1979).
21. S. J. RETTIG, A. STORR, and J. TROTTER. Can. J. Chem. **52**, 2206 (1974).
22. S. J. RETTIG, A. STORR, and J. TROTTER. Can. J. Chem. **53**, 58 (1975).
23. D. M. ADAMS. Metal–ligand and related vibrations. Edward Arnold Ltd., London. 1967. Chapt. 3.
24. K. S. CHONG and A. STORR. Can. J. Chem. **57**, 167 (1979).
25. K. S. CHONG, S. J. RETTIG, A. STORR, and J. TROTTER. Can. J. Chem. **57**, 1335 (1979).
26. K. S. CHONG and A. STORR. Can. J. Chem. **59**, 1331 (1981).
27. K. J. HALLER and J. H. ENEMARK. Inorg. Chem. **17**, 3552 (1978).
28. J. H. ENEMARK and R. D. FELTHAM. Coord. Chem. Rev. **13**, 339 (1974).
29. K. S. CHONG, S. J. RETTIG, A. STORR, and J. TROTTER. Can. J. Chem. **57**, 3107 (1979).
30. K. S. CHONG, S. J. RETTIG, A. STORR, and J. TROTTER. Can. J. Chem. **59**, 1665 (1981).
31. S. J. RETTIG, A. STORR, and J. TROTTER. Can. J. Chem. **54**, 1278 (1976).
32. S. J. RETTIG, A. STORR, and J. TROTTER. Can. J. Chem. **62**, 1705 (1984).

Can. J. Chem. Downloaded from www.nrcresearchpress.com by 210.87.254.40 on 09/06/12
For personal use only.

Coordination compounds of indium. Part 41. The reaction between InX and InX_3 (X = Cl, Br, I) and the stability of the In—In bond

CLOVIS PEPPE AND DENNIS G. TUCK
Department of Chemistry, University of Windsor, Windsor, Ont., Canada N9B 3P4

Received March 27, 1984

CLOVIS PEPPE and DENNIS G. TUCK. Can. J. Chem. **62**, 2793 (1984).

The reaction between InX (X = Cl, Br, I) and InY_3 (Y = Br, I) in toluene/CH_2Cl_2/tmen solution (tmen = *N,N,N',N'*-tetramethylethanediamine) at low temperature (<−20°C) yields the In—In bonded species X(Y)InInY$_2$ as the bis-tmen adduct. Infrared and nmr (^{1}H, ^{13}C) spectra of these indium(II) compounds are reported. No analogous products were obtained from InX + $InCl_3$. The pathway of the InX/InY_3 reaction, and the related problem of the stability of In_2X_4 species, are discussed in terms of a common process involving intramolecular halide transfer.

CLOVIS PEPPE et DENNIS G. TUCK. Can. J. Chem. **62**, 2793 (1984).

La réaction du InX (X = Cl, Br, I) et de l'InY_3 (Y = Br, I), dans une solution de toluène/CH_2Cl_2/tmen (tmen = *N,N,N',N'*-tétraméthyléthanediamine) et à basse température (<−20°C), conduit aux espèces X(Y)InInY$_2$, contenant une liaison In—In, comme adduits bis-tmen. On rapporte les spectres infrarouge et rmn (^{1}H et ^{13}C) de ces composés de l'indium(II). Il ne se forme pas de produits semblables lors de la réaction de InX + $InCl_3$. On discute des mécanismes possibles pour la réaction InX/InY_3 ainsi que le problème relié de la stabilité des espèces In_2X_4 en fonction d'un processus commun impliquant un transfert intramoléculaire d'halogénure.

[Traduit par le journal]

Can. J. Chem. Downloaded from www.nrcresearchpress.com by 210.87.254.40 on 09/06/12
For personal use only.

Introduction

Compounds in which Group IIIA elements are formally in the +2 oxidation state have been the subject of speculation for many years. For gallium dichloride, dibromide, and diiodide, the solid state structure (1) is that of the ionic dimer $Ga^+GaX_4^-$, whereas in contrast the neutral adduct Ga_2Cl_4.2dioxan involves a metal−metal bond (2), as do the anionic derivatives $Ga_2X_6^{2-}$ (X = Cl, Br, I) (3, 4). The general features of the chemistry of the indium dihalides are similar. Spectroscopic studies have shown that both In_2Br_4 and In_2I_4 are ionic dimers in the solid and liquid states (5) and recent X-ray crystallographic work has confirmed this conclusion in the case of In_2I_4 (6). There is some doubt about the structure of solid indium dichloride, but ionic mixed valence species are involved, and the liquid state has been shown to contain $InCl_4^-$ anions (5). The $In_2X_6^{2-}$ anions are metal−metal bonded in the solid (7), and recent work has shown that for this element, as with gallium, neutral adducts of X_2In—InX_2 can be prepared, with the structural assignment being based on both spectroscopic and X-ray crystallographic evidence (8−10). It is important to note immediately that the number of adducts which are stable at room temperature is somewhat limited and apparently dependent on the nature of both halide and neutral donor ligands.

In a recent paper from this laboratory (11), the preparation and synthetic applications of non-aqueous solutions of indium(I) halides (InX; X = Cl, Br, I) were described. The solutions are stable at low temperatures, but decompose at ca. 0°C, generally depositing indium metal and forming neutral adducts of either InX_3 or In_2X_4, depending on halide and neutral ligand. The first step in the reaction was shown to involve the disproportionation

$$[1] \quad 3InX \rightarrow 2In^0 + InX_3$$

and the formation of InX_2 can then be seen as a reaction between InX_3 and excess InX

$$[2] \quad InX + InX_3 \rightarrow In_2X_4$$

We have now investigated reaction [2] as a preparative route to In_2X_4 adducts. The results lead to a discussion of reaction [2] as a reversible process, markedly affected by phase and by ligand, and related to the decomposition reactions of In_2X_4.

Experimental

General

Indium(I) halides were prepared by heating stoichiometric quantities of indium metal and indium trihalide in a sealed tube. Indium trichloride and tribromide were obtained by passing the halogen vapour over molten indium (12). Indium triiodide was prepared by the reaction of indium foil and iodine in refluxing xylene (13).

Methylene dichloride was distilled from phosphorus pentoxide; toluene, diethyl ether, and petroleum ether were dried over sodium; *N,N,N'N'*-tetramethylethanediamine (tmen) was used as supplied.

Infrared spectra were run as Nujol mulls on a Beckman IR-180 instrument; Raman spectra were recorded at McMaster University on a Spectrophysics instrument (264 exciter); ^{1}H nmr spectra were obtained on a Varian EM-360 instrument, and ^{13}C spectra on a Bruker CXP-100 spectrometer.

Analysis was by methods described previously (11). All experimental work was carried out in an atmosphere of dry nitrogen.

Preparative

Equimolar quantities (~3−6 mmol) of InX (X = Cl, Br, I) and InY_3 (Y = Cl, Br, I) were suspended in 50 mL of a toluene/methylene dichloride mixture (1 : 1, v/v), except that 50 mL of toluene alone was used for InI/InI_3. The suspension was cooled (to −20°C for X = Br, I, and to −78°C for X = Cl), and tmen (2−4 mL) syringed into the reaction mixture, at which point the characteristic red colour of solutions of InX in such mixtures was observed (cf. ref. 11). The solution was then allowed to warm up to room temperature over 3−4 h, and the resultant clear solution stirred for a further 30 min period. The subsequent isolation procedures are summarised in Table 1, which also gives the analytical results for the compounds isolated. Yields were close to quantitative.

Results and discussion

Preparative

The method described yields the bis-tmen adducts of a series of In_2X_4 and In_2XY_3 compounds. No such compounds could be obtained from $InCl_3$ with any indium monohalide, but we did isolate the methylene-bridged compounds Cl_2InCH_2-$InCl_2$.2tmen from $InCl_3$ + InCl, and the isostructural

Can. J. Chem. Downloaded from www.nrcresearchpress.com by 210.87.254.40 on 09/06/12
For personal use only.

TABLE 1. Analytical results and isolation procedures for products of InX/InY_3 reactions

Reagents			Analysis: found (calcd) %		
InX	InY_3	Product	In	Halogen[a]	Isolation procedure
InCl	$InBr_3$	$In_2ClBr_3.2tmen$	30.9(31.2)	37.2(37.4)	Some deposition from reaction mixture on standing; removal of solvent in vacuo, addition of petroleum ether
InCl	InI_3	$In_2ClI_3.2tmen.C_7H_8$	23.7(23.7)	43.0(42.9)	As above
InBr	$InBr_3$	$In_2Br_4.2tmen.C_7H_8$	26.6(26.3)	36.7(36.6)	Concentration
InBr	InI_3	$In_2BrI_3.2tmen$	25.0(24.9)	49.7(49.9)	Concentration, addition of diethyl ether
InI	$InBr_3$	$In_2IBr_3.2tmen$	27.9(27.7)	44.3(44.3)	Crystallised on standing
		$In_2IBr_3.2tmen.0.75C_7H_8$	25.3(25.6)	41.5(40.9)	After removal of $In_2IBr_3.2tmen$, addition of diethyl ether
InI	InI_3	$In_2I_4.2tmen$	23.7(23.7)	—	Crystallised on standing

[a]Total halogen for mixed halide complexes.

TABLE 2. The far ir spectra of the tmen adducts of In_2XY_3 (in cm^{-1})

In_2ClBr_3	In_2ClI_3 (C_7H_8)	In_2Br_3I	In_2I_3Br	Assignment
	500 (m)			Unassigned
489 (m)	478 (w)	487 (m)	488 (m)	
464 (w)	466 (m)	462 (w, br)	468 (w)	ν(In—N)
442 (m)	447 (m)	442 (m)	444 (m)	
—	375 (m)	395 (w, br)	—	
—	—	364 (vw)	—	Unassigned
288 (m, br)	290 (s, br)			
212 (vw)		208 (w)		
192 (w)		187 (m)	190 (w)	ν(In—X)
	166 (s)	154 (m, br)	150 (m)	
	140 (s)			
149 (w)				
132 (m)	128 (w)	128 (w)		Bending modes
104 (m)			100 (m, br)	or ν(In—In)

$Cl_2InCH_2InClBr.2tmen$ from $InCl_3$ + InBr. The synthesis and structure of these compounds will be discussed elsewhere (14).

Spectroscopic results

The vibrational spectra of $In_2Br_4.2tmen$ and $In_2I_4.2tmen$ have been discussed previously (8). In addition to vibrations due to the tmen ligand, the ν(In—X) and ν(In—N) modes were identified, as was a strong Raman emission, at 141 cm^{-1} in the bromide and 110 cm^{-1} in the iodide, corresponding to ν(In—In). Table 2 shows that the far infrared spectra of the compounds prepared in this work are readily assigned on the same basis. Complete Raman spectra were not available, but for each compound we were able to identify a strong emission in the 100–150 cm^{-1} region, assigned as ν(In—In) (Table 3).

The ^1H and ^{13}C nmr spectra are presented in Table 4, for both the mixed halide compounds prepared in this work and the symmetrical $In_2X_4.2tmen$ compounds, prepared either from In_2X_4 (8), or by the solution phase reaction described in the Experimental Section. The ^1H spectra of the In_2Br_4 and In_2I_4 adducts show only one set of resonances from tmen, indicating the presence of two equivalent bidentate ligands. For the In_2ClI_3 adduct, we find two sets of sharp singlets, separated by ~2 Hz for the C_2H_4 resonances, and by ~5 Hz for those of $N(CH_3)_2$, corresponding to two non-equivalent non-exchanging tmen ligands whose differing chemical shifts reflect coordination at either ClInI or InI_2 centres. In the other In_2XY_3 systems, the ^1H spectra could not be resolved in this way,

TABLE 3. Raman emissions assigned as ν(In—In) in tmen adducts of In_2XY_3 (in cm^{-1})

Compound	ν(In—In)
In_2ClBr_3	143
In_2ClI_3	105
In_2Br_4	141
In_2Br_3I	131
In_2I_4	110
In_2I_3Br	118

but decoupled ^{13}C spectra show the appropriate set of four singlets from two non-equivalent ligands. The exception was $In_2ClBr_3.2tmen$; this may be due to an accidental coincidence in the chemical shifts, but could equally be due to fast ligand exchange and/or fast halide exchange between the ClInBr and $InBr_2$ sites.

The ^{13}C assignments are based on those for tmen itself (C_2H_4 57.24, NCH_3 46.08 ppm from Me_4Si), and for protonated tmen (shifts of −0.22 and −2.35 ppm) (15). The results in Table 4 suggest that the changes caused by complexation are similar to those due to protonation.

The InX/InY₃ reaction

The stoichiometry of the reaction between InX and InY_3

TABLE 4. ^1H and ^{13}C nmr spectra of tmen adducts of In_2X_4 and In_2XY_3

Compound[a]	^1H[b]		^{13}C[c]		Solvent for ^{13}C
	$N(CH_3)_2$	NC_2H_4N	$N(CH_3)_2$	$N_2C_2H_4N$	
$In_2ClBr_3.L_2$	2.72(3H)	2.82(1H)	47.97	59.00	CD_3CN
$In_2ClI_3.L_2.C_7H_8$[d]	2.70, 2.62(3H)	2.80, 2.77(1H)	49.25, 46.78	56.72, 55.03	CD_3CN
$In_2Br_4.L_2.C_7H_8$[d]	2.72(3H)	2.83(1H)	47.78	56.74	CD_3CN
$In_2Br_3I.L_2$	2.77, 2.70	2.87[e]	49.50, 47.88	56.78, 55.61	$CDCl_3$
$In_2Br_3I.L_2.0.75C_7H_8$[d]	2.64(3H)	2.75(1H)	—	—	—
$In_2I_4.L_2$	2.82(3H)	2.90(1H)	47.78	56.48	CD_3CN
$In_2I_3Br.L_2$	2.64(3)	2.75(1)	49.77, 47.63	56.92, 55.94	$CDCl_3$

[a]L = tmen.
[b]In ppm from Me_4Si; spectra of CD_2Cl_2 solutions; integration not precise; all singlets.
[c]In ppm from Me_4Si; toluene resonances not reported.
[d]Toluene resonance at 7.25 br, 2.55 s.
[e]Integration not possible.

Can. J. Chem. Downloaded from www.nrcresearchpress.com by 210.87.254.40 on 09/06/12
For personal use only.

corresponds formally to the insertion of In^I into an In^{III}—Y bond

[3] $InX + InY_3 \xrightarrow{xs.tmen} X\text{—}In\text{—}In(Y)_2.2tmen$

Analogous insertion reactions with InX have been reported for a wide variety of substrates, including alkyl halides (11, 16, 17), S—S (18), Se—Se and O—O bonded species, and M—M bonded transition metal carbonyls (19, 20). The reaction of InCl and $PtCl(SiPh_3)(PMe_2Ph)_2$ to give $Cl_2InPt(SiPh_3)(PMe_2Ph)_2$ also corresponds to the insertion of indium into an M—X bond (21). There are at least two possible pathways for the overall reaction [3]. The first of these involves the base-catalysed dissociation of InY_3, followed by halide ion transfer to InX, followed by recombination:

[4] $InY_3 + nL \rightarrow InY_3L_n \rightleftharpoons InY_2L_n^+ + Y^-$

[5] $InX + Y^- \rightarrow InXY^-$

[6] $InY_2L_n^+ + InXY^- \xrightarrow{L} LY_2InInX(Y)L$

The chemical evidence for reaction [4] is that non-aqueous solutions of adducts of indium trihalides do show a significant conductivity, which has been explained in terms of ionisation of the type shown (12), while reaction [5], which implies that InX molecules are Lewis acids, is supported by the known existence of InX_2^- anions (X = Cl, Br, I, NCS) (22).

The second pathway depends on the ability of In^I species to function as both electron pair donors and acceptors. The importance of a lone pair in the structure of cyclopentadienylindium(I) has been demonstrated (23), and there is good reason to assume a similar feature in indium(I) halides. The alternative description of reaction [3] is then via a concerted process in which donation from InX into the In—Y bond of InY_3 is accompanied by donation from a halide ligand of InY_3 to InX.

[7] $XIn: + In(Y)_3 \rightleftharpoons X\text{—}In\rightarrow In(Y)_2 \xrightarrow{L} L.X(Y)InInX_2.L$

A similar reaction pathway has been proposed to account for the insertion of InX into various symmetric M—M bonded molecules (19). The essential difference between reaction [7] and the scheme represented by reactions [4]–[6] lies in the existence or otherwise of separate ionic species as part of the halide transfer process. We favour reaction [7] because of its compatibility with the apparent mechanism of other InX insertion reactions (19). For the InX/InY_3 system, the failure to form an In—In bonded product when Y = Cl is a reflection of the poor leaving group properties of this ligand, since in the absence of intramolecular halide transfer, the intermediate will revert to InX and InY_3. For InX itself, the polarisability of the indium, and hence the availability of the lone pair, will go in the order I > Br > Cl, again in keeping with the observed order of reactivity. Finally, the presence of neutral solvating ligands such as tmen may also enhance the availability of the lone pair of InX (see below).

The stability of the In—In bond

The above discussion refers to the solution phase formation of tmen adducts of In_2X_4 (X ≠ Cl) or In_2XY_3 (Y ≠ Cl). In fact, these adducts and those of triethylphosphine (8) are the only such compounds which we have been able to prepare by our methods. Sinclair and Worrall (9) have reported a number of other compounds of $InCl_2$, $InBr_2$, and InI_2 with monodentate donors. The essential difference between their preparations and ours lies in their use of solvent-free conditions, as opposed to the aromatic solvent (or solvent mixtures) used in this and earlier work. Even so, Sinclair and Worrall report that for a number of In_2X_4/ligand combinations, "decomposition to metal always occurred". We have now confirmed our earlier findings (8) that the pyridine adduct of In_2Br_4 cannot be prepared by the reaction of InBr + $InBr_3$ + pyridine in toluene or toluene/CH_2Cl_2. This mixture is stable at or below −20°C, but deposits indium metal when the temperature reaches ~0°C. Equally, no tmen adduct of In_2Cl_4 can be obtained from the reaction of InCl + $InCl_3$ + tmen in toluene; the clear yellow solution which is formed initially precipitates metal when the temperature rises.

These results reflect the differing factors which influence the stability of the In—In bond in such In_2X_4 systems. The discussion is best approached by regarding reaction [2] as a reversible process

[8] $InX + InX_3 \overset{L}{\rightleftharpoons} In_2X_4L_n$

whose equilibrium position depends on temperature, solvent, the properties of X, and the nature of any neutral ligand present.

Can. J. Chem. Downloaded from www.nrcresearchpress.com by 210.87.254.40 on 09/06/12
For personal use only.

In structural terms, it is clear that the solid state of In_2X_4 is best represented as $In^+InX_4^-$ (see Introduction), which can be regarded in the present context as the limiting case of halide transfer from InX to InX_3; in other words, the potential isomerisation

[9] $X_2InInX_2 \rightleftharpoons In^+InX_4$

which requires intramolecular halide transfer, lies completely to the right in the solid state. The treatment of $In^+InX_4^-$ with base does not usually lead to the formation of stable derivatives of In^I cationic complexes, but with crown ether, and with the tetradentate nitrogen base cyclam, $[InL]^+InX_4^-$ species were identified (X = Cl, Br, I) (24). The products of the reaction of InX_2 with aniline and morpholine have also been formulated in this way, although no structural information is available on these materials (25). The general reaction of $In^+InX_4^-$ with base is to yield either neutral In—In bonded adducts, or decomposition products. We propose that in all these cases, the first reaction between solid $In^+InX_4^-$ and neutral ligand is the formation of a salt of a cationic indium(I) complex $[InL_n][InX_4]$ by donation of ligand(s) to In^+. When L = crown ether or cyclam, this salt is the stable final product, either because In^+ is coordinatively saturated, or because steric hindrance prevents close association of the ion pair, thus preventing donor/acceptor interactions (see below). For the more general case, we suggest that the reduction of positive charge density of In^+ due to complexation makes the lone pair more available than it is in the bare ion, or in uncomplexed (or unsolvated) InX, thus giving a species in which insertion of the lone pair into an In—X bond is favoured. The intermediate for this insertion is then

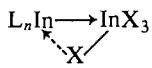

1

If this intermediate is sufficiently stable in the reaction mixture for intramolecular halide transfer to occur, the product will be $L_n(X)In—InX_3$, which with a further halide transfer and rearrangement of the neutral ligand L gives LX_2InInX_2L. The proposed intermediate is therefore similar to that in reaction [7].

An alternative fate of **1** is that it may react with excess L to give a solvated complex **2** which can dissociate to L_nInX and L_mInX_3

[10] 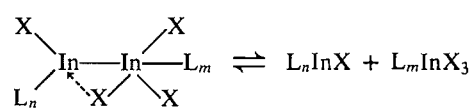 $\rightleftharpoons L_nInX + L_mInX_3$

2

If L_mInX_3 is insoluble, or nearly so, in the reaction mixture, the dissociation of **2** will be driven to the right, leaving essentially a solution of L_nInX, which as we have shown is only stable for special cases of L and X. The most probable reaction observed with L_nInX is the disproportionation (11)

[11] $3L_nInX \rightarrow 2In^0 + L_mInX_3$

so that the solution phase decomposition of In_2X_4 in the presence of base, and the reaction of InX and InX_3 under similar conditions, may give either adducts of In_2X_4, or a mixture of indium metal and an adduct of InX_3. These processes, summarised in the reversible nature of reactions [8] and [10], are fundamentally related by the intermediates **1** and **2**. The stable products $LX(Y)InInY_2L$ (L = tmen) obtained in the present work thus apparently owe their stability in solution to the absence of ligand (halide or tmen) transfer, as shown by the ^1H and ^{13}C nmr spectra which establish the presence of two different tmen ligands in these complexes. The exception is In_2ClBr_3 where the ligand exchange may be rapid on the nmr time scale, although we note that the nmr method can give no information on this aspect of the behaviour of the symmetrical complexes LX_2InInX_2L. Halide transfer yields LInX and $LInX_3$, and this process sets up the conditions for the precipitation of InX_3L and the disproportionation of LInX. We conclude that kinetic rather than thermodynamic stability, specifically in terms of intramolecular halide transfer, is an important factor for In_2X_4 and related adducts. The favourable influence of low temperature in this and earlier preparative work is thus readily explained.

The role of neutral ligand in stabilising In_2X_4 or In_2XY_3 molecules is then understood qualitatively in terms of promoting maximum coordinative saturation at the indium atom. Since intramolecular halide transfer is a destabilising process, a saturated site will favour kinetic stability. Unfortunately, we have no way of quantifying this argument at present, given the lack of information on the coordination chemistry of indium(II).

We noted earlier that Sinclair and Worrall (9) prepared a number of In_2X_4 adducts not accessible via our solution phase reactions by condensing ligand onto solid In_2X_4 at low temperatures, obtaining either a suspension of a solution. Since the colour changes in the solution systems correspond to the formation of InX, these observations are compatible with the mechanism proposed above. Removal of the excess neutral ligand at these low temperatures yields the solid adduct, and halide transfer to InX + InX_3 adducts is prevented, since the solid is not in contact with a solution phase at temperatures at which decomposition is significant. In general, the results reported by these authors appear to be in keeping with the mechanism proposed in the present paper.

Finally, we review earlier work (26) on the equilibrium

[12] $In_2X_6^{2-} \rightleftharpoons InX_2^- + InX_4^-$

which is the analogue of reactions [8] and [10], with the presumed intermediate similar to that proposed in reaction

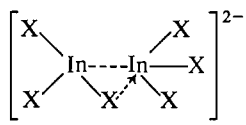

[10]. Our ^{115}In nmr measurements gave approximate values for K_{eq} for reaction [12], with I ⩾ Cl. We now suspect that although equilibrium [12] is correctly stated for X = I, there may be other anionic indium(III) species in the acetonitrile solutions studied. For X = Cl (and possibly X = Br), $[InX_4(CH_3CN)_2]^-$ anions would be stabilised in this medium (cf. $[InCl_4(bpy)]^-$, $[InCl_4(urea)_2]^-$ reported earlier (27, 28) bpy = 2,2′-bipyridine), and such species would not have been identified by the ^{115}In nmr method, which detects only highly symmetrical species. The order of the equilibrium constants may therefore be wrong, although there can be no doubt that a rapid equilibrium between the anionic complexes of indium(II), (I) and (III) is indeed established in solution, and that the qualitative results are in agreement with those for neutral indium(II) complexes.

Acknowledgements

This work was supported in part by Operating Grants (to D.G.T.) from the Natural Sciences and Engineering Research Council of Canada. One of us (C.P.) thanks the Conselho Nacional de Desenvolvimento Cientifico e Tecnólogico (Brasil) for the award of a scholarship. Dr. M. A. Khan is thanked for helpful discussions.

1. N. N. GREENWOOD. Adv. Inorg. Radiochem. **5**, 91 (1963).
2. J. C. BEAMISH, R. W. H. SMALL, and I. J. WORRALL. Inorg. Chem. **18**, 220 (1979).
3. K. L. BROWN and D. HALL. J. Chem. Soc. Dalton Trans. 1843 (1973).
4. M. A. KHAN, C. OLDHAM, M. J. TAYLOR, and D. G. TUCK. Inorg. Nucl. Chem. Lett. **16**, 469 (1980).
5. A. J. CARTY and D. G. TUCK. Prog. Inorg. Chem. **19**, 245 (1975).
6. M. A. KHAN and D. G. TUCK. Inorg. Chim. Acta. In press.
7. B. H. FREELAND, J. L. HENCHER, D. G. TUCK, and J. G. CONTRERAS. Inorg. Chem. **15**, 2144 (1976).
8. M. J. TAYLOR, D. G. TUCK, and L. VICTORIANO. Can. J. Chem. **60**, 691 (1982).
9. I. SINCLAIR and I. J. WORRALL. Can. J. Chem. **60**, 695 (1982).
10. M. A. KHAN, C. PEPPE, and D. G. TUCK. Can. J. Chem. **62**, 601 (1984).
11. C. PEPPE, D. G. TUCK, and L. VICTORIANO. J. Chem. Soc. Dalton Trans. 2165 (1982).
12. A. J. CARTY and D. G. TUCK. J. Chem. Soc. A, 1081 (1966).
13. B. H. FREELAND and D. G. TUCK. Inorg. Chem. **15**, 475 (1976).
14. M. A. KHAN, C. PEPPE, and D. G. TUCK. Unpublished results.
15. J. E. SARNESKI, H. L. SURPRENANT, F. K. MOLEN, and C. N. REILLEY. Anal. Chem. **47**, 2116 (1975).
16. (*a*) L. G. WATERWORTH and I. J. WORRALL. Chem. Commun. 569 (1971); (*b*) M. J. S. GYNANE and I. J. WORRALL. Inorg. Nucl. Chem. Lett. **8**, 547 (1972); (*c*) M. J. S. GYNANE, L. G. WATERWORTH, and I. J. WORRALL. J. Organomet. Chem. **43**, 257 (1972); (*d*) L. G. WATERWORTH and I. J. WORRALL. J. Organomet. Chem. **81**, 23 (1974).
17. J. S. POLAND and D. G. TUCK. J. Organomet. Chem. **42**, 315 (1972).
18. A. F. BERNIAZ, G. HUNTER, and D. G. TUCK. J. Chem. Soc. A 3254 (1971).
19. C. PEPPE and D. G. TUCK. Can. J. Chem. **62**, 2798 (1984).
20. (*a*) D. J. PATMORE and W. A. G. GRAHAM. Chem. Commun. 591 (1965); (*b*) D. J. PATMORE and W. A. G. GRAHAM. Inorg. Chem. **5**, 1586 (1966); (*c*) J. HOYANO, D. J. PATMORE, and W. A. G. GRAHAM. Inorg. Nucl. Chem. Lett. **4**, 201 (1968); (*d*) A. T. T. HSIEH and M. J. MAYS. Inorg. Nucl. Chem. Lett. **7**, 223 (1971).
21. J. CHATT, C. EABORN, and P. N. KAPOOR. J. Organomet. Chem. **23**, 109 (1970).
22. J. J. HABEEB and D. G. TUCK. J. Chem. Soc. Dalton Trans. 866 (1976).
23. C. S. LIN and D. G. TUCK. Can. J. Chem. **60**, 699 (1982).
24. M. J. TAYLOR, D. G. TUCK, and L. VICTORIANO. J. Chem. Soc. Dalton Trans. 928 (1981).
25. P. L. GOGGIN and I. J. MCCOLM. J. Inorg. Nucl. Chem. **28**, 2501 (1966).
26. B. R. MCGARVEY, C. O. TRUDELL, D. G. TUCK, and L. VICTORIANO. Inorg. Chem. **19**, 3432 (1980).
27. R. A. WALTON. J. Chem. Soc. A, 61 (1969).
28. D. G. TUCK and E. J. WOODHOUSE. Chem. Ind. 1363 (1964).

Can. J. Chem. Downloaded from www.nrcresearchpress.com by 210.87.254.40 on 09/06/12
For personal use only.

Coordination compounds of indium. Part 42. The insertion of indium(I) halides into homonuclear bonds in non-aqueous media

CLOVIS PEPPE AND DENNIS G. TUCK
Department of Chemistry, University of Windsor, Windsor, Ont., Canada N9B 3P4

Received March 27, 1984

CLOVIS PEPPE and DENNIS G. TUCK. Can. J. Chem. **62**, 2798 (1984).

Solutions of indium(I) halides (InX; X = Cl, Br, I) in toluene/pyridine or dichloromethane/pyridine are useful reaction media for studying the insertion of InX into various homonuclear R_nM-MR_n systems (M = O, S, Se, Co); the products are generally of the type $(R_nM)_2InX$, obtained as the bis-pyridine adducts. Reaction does not occur under these conditions for M = Sn, Pb, N, P, Te, Mn, Fe. The mechanism of such insertion processes is discussed; the donor and acceptor properties of both In^I and M are important. The InX/benzoyl peroxide system gives rise to a series of products which suggest re-arrangement reactions in solution following insertion of indium into the O—O bond.

CLOVIS PEPPE et DENNIS G. TUCK. Can. J. Chem. **62**, 2798 (1984).

Les solutions d'halogénures d'indium(I) (InX; X = Cl, Br, I) dans des mélanges de toluène/pyridine ou de dichlorométhane/pyridine s'avèrent des milieux réactionnels très utiles pour étudier l'insertion de InX dans divers systèmes homonucléaires R_nM-MR_n (M = O, S, Se, Co); les produits sont généralement du type $(R_nM)_2InX$ et ils sont obtenus sous forme d'adduits bis-pyridine. Dans ces conditions, il ne se produit pas de réaction si M = Sn, Pb, N, P, Te, Mn, Fe. On discute du mécanisme de tels processus d'insertion; les propriétés de donneur et d'accepteur tant du In(I) que du M sont importantes. Le système InX/peroxyde de benzoyle conduit à une série de produits qui suggère qu'en solution il se produit des réactions de transposition après l'insertion de l'indium dans la liaison O—O.

[Traduit par le journal]

Can. J. Chem. Downloaded from www.nrcresearchpress.com by 210.87.254.40 on 09/06/12
For personal use only.

Introduction

The reaction between indium(I) halides (InX, X, = Cl, Br, I) and alkyl halides (RX) has been the subject of a number of reports (1, 2). The products correspond formally to the insertion of InX into a C—X bond

[1] $InX + RX \rightarrow RInX_2$

although the available evidence on these and related processes (1*d*, 2) points to a mechanism more complicated than is implied by reaction [1]. In related studies, we have shown that InX reacts at the S—S bond of 1,2-bis(trifluoromethyl)dithiete (3), as does cyclopentadienylindium(I) (4), and here again the formal stoichiometry implies oxidative insertion. The analogous oxidation of CpIn with iodine (5) and the reactions of InX_2^- and $In_2X_6^{2-}$ with X_2 (X = Cl, Br, I) (6) have also been reported, and possible mechanisms discussed.

A recent paper (7) from this laboratory reported the significant solubility of the indium(I) halides in mixtures of toluene and neutral nitrogen, phosphorus, or oxygen bases. The synthetic applications of such solutions were briefly explored in terms of the InX/RX reaction, and we have now extended these studies to include the reaction of InX (X = Cl, Br, I) with a variety of compounds with homonuclear M—M bonds, where M is a Group IV, V, or VI element, or a transition metal. An analysis of the preparative results leads to a tentative mechanism which is compatible with that proposed for the insertion of InX into In^{III}—X bonds (8).

Experimental

General

The preparative, spectroscopic, and analytical methods were those used in previous work (7, 8). Microanalysis was by Guelph Chemical Laboratories. All experimental procedures were carried out under dry nitrogen.

Preparative: general

In a standard experiment, 5 mmol of InX (X = Cl, Br, I) and an equimolar quantity of substrate were stirred together in a solvent phase of 2–5 mL of pyridine and 50 mL of toluene (or dichloromethane). The temperature was initially −80°C for InCl and −20°C for InBr or InI in toluene solution, and −80°C for InCl or InBr, and −20°C for InI when dichloromethane was used. The cooling bath was gradually removed and the temperature of the reaction mixture allowed to reach ambient over ca. 3 h after which the mixture was filtered to remove any solid material. The details of the isolation procedures are, in summary:

InX/R_2S_2 (X = Cl, Br; R = Ph). At the end of the reaction in CH_2Cl_2/pyridine, the volume of the solution was reduced by approximately 50%, and petroleum ether added to yield a solid which was collected and dried.

InI/Ph_2S_2. The oil obtained by pumping off the solvent toluene was redissolved in CH_2Cl_2 containing a molar equivalent of $^nPr_4NI$. Solvent was removed, and the product recrystallised from methanol, washed with diethyl ether, and dried.

InI/Me_2S_2. Reaction in toluene/pyridine was followed by an isolation procedure similar to that described above for InX/R_2S_2.

InX/Ph_2Se_2. For $InCl/Ph_2Se_2$, the reaction mixture (toluene/pyridine) was pumped to dryness and the resultant solid recrystallised from a CH_2Cl_2/petroleum ether mixture. For InBr and InI, the procedure was similar to that described for InX/R_2S_2.

$InX/Co_2(CO)_8$. Removal of the solvent (CH_2Cl_2/pyridine) by pumping *in vacuo* gave an oil which solidified on stirring with petroleum ether.

The characterisation of the products depended on indium and halogen analysis (Table 1), and on spectroscopic confirmation of the presence of organic ligands and/or cation. Table 2 summarises the ^1H nmr results. The identification of the pyridine and other aromatic resonances was based on the clear downfield separation of the resonance of the *ortho*-hydrogen atoms of pyridine from the rest of the aromatic region.

In a number of cases noted below, no evidence was obtained for any reaction between InX and the M—M species.

Reaction of InCl or InBr with benzoyl peroxide

(*a*) Equimolar quantities (2.6–4.8 mmol) of InX (X = Cl, Br) and dibenzoyl peroxide were mixed together in 50 mL of dichloromethane at −80°C (InCl) or −20°C (InBr). Pyridine (2 mL) was then syringed into the mixture, which was mechanically stirred as the cooling bath was removed. At 0°C, the indium(I) halide had obviously dissolved. The solvents were removed *in vacuo*, leaving a white solid which was collected, washed with diethyl ether, and dried *in vacuo*. The com-

Can. J. Chem. Downloaded from www.nrcresearchpress.com by 210.87.254.40 on 09/06/12
For personal use only.

TABLE 1. Analytical results for indium(III) derivatives produced by oxidation of InX (X = Cl, Br, I)

Product	Analysis found (calcd.) % In	Halogen
$ClIn(SPh)_2py_2$	22.6 (21.8)	7.0 (6.7)
$BrIn(SPh)_2py_2$	20.2 (20.1)	14.1 (14.0)
$Pr^n_4N[In(SPh)_2I_2]$	15.0 (14.9)	32.3 (32.9)
$IIn(SMe)_2py$	27.8 (27.7)	29.8 (30.6)
$ClIn(SePh)_2py_2$	19.2 (18.5)	5.6 (5.7)
$BrIn(SePh)_2py_2$	17.2 (17.3)	12.0 (12.0)
$IIn(SePh)_2py_2$	16.6 (16.2)	17.4 (17.8)
$ClIn[Co(CO)_4]_2py_2$	17.7 (17.7)	5.6 (5.5)
$BrIn[Co(CO)_4]py_2$	16.9 (16.6)	11.7 (11.5)
$IIn[Co(CO)_4]_2py_2$	15.0 (15.5)	18.2 (17.1)

TABLE 2. ^1H nmr spectra of indium(III) products

Compound	Solvent	Resonances[a]
$ClIn(SPh)_2py_2$	$(CD_3)_2SO$	8.6–8.8 (m, 1H), 6.9–8.1 (m, 4H)
$BrIn(SPh)_2py_2$	$(CD_3)_2SO$	8.6–8.8 (m, 1H), 6.9–8.1 (m, 4H)
$Pr^n_4N[In(SPh)_2I_2]$	$CDCl_3$	6.9–7.6 (m, 5H), 2.9 (q, 4H) 1.5 (m, 4H) 0.9 (t, 6H)
$IIn(SMe)_2py$	$(CD_3)_2SO$	8.6–8.9 (m, 2H) 7.1–8.1 (m, 3H) 2.0 (s, 6H)
$ClIn(SePh)_2py_2$	$(CD_3)_2CO$	8.6–8.9 (m, 1H) 6.8–8.1 (m, 4H)
$BrIn(SePh)_2py_2$	$(CD_3)_2CO$	8.6–8.9 (m, 1H) 6.9–8.1 (m, 4H)
$IIn(SePh)_2py_2$	$(CD_3)_2CO$	8.6–8.9 (m, 1H) 6.9–8.1 (m, 4H)
$In_2Cl_3(O_2CPh)_3py_3$	CD_2Cl_2	8.7–9.0 (m, 1H) 7.2–8.1 (m, 4H)
$In_2Br_3(O_2CPh)_3py_3$	CD_2Cl_2	8.7–9.1 (m, 1H) 7.2–8.1 (m, 4H)
$Cl_2In(O_2CPh)py_2$	CD_2Cl_2	8.8–9.1 (m, 4H) 8.2–7.2 (m, 11H)
$IIn(O_2CPh)_2py_2$	CD_2Cl_2	8.8–9.1 (m, 1H) 7.3–8.2 (m, 4H)
$In_2I_3(O_2CPh)_3py_3$	CD_2Cl_2	8.8–9.1 (m, 4H) 7.0–8.0 (m, 11H)

[a]In ppm from Me_4Si; relative intensities in parentheses; s = singlet, t = triplet, q = quartet, m = multiplet.

position of the solids corresponded to the formula $In_2X_3(O_2CC_6H_5)_3py_3$: X = Cl: *Anal.* calcd. for $In_2Cl_3C_{36}H_{30}N_3O_6$: In 24.5, Cl 11.4, C 46.16, H 3.23, N 4.49; found: In 24.2, Cl 11.2, C 46.09, H 3.34, N 4.40. Yield 0.80 g (0.85 mmol), from 2.65 mmol InCl (32%).

X = Br: *Anal.* calcd. for $In_2Br_3C_{36}H_{30}N_3O_6$: In 21.5, Br 22.4; found: In 21.8, Br 23.0. Yield 1.33 g (1.24 mmol) from 4.77 mmol InBr (26%).

(*b*) In a subsequent experiment, the clear colourless solution obtained from 7.7 mmol InCl and 11 mmol Bz_2O_2 in 50 mL dichloromethane and 4 mL pyridine was stirred at room temperature for 5 days. Towards the end of this period, the reaction mixture consisted of a deep red solution and a suspension of a brown solid **A** (0.4 g. *Anal.* calcd. for $InCl_3(C_5H_5N)_3[(C_6H_5CO_2)_2]$: In 16.4, Cl 15.2; found: In 16.1, Cl 14.6. ^1H nmr spectrum 8.66–8.50 (m) (1H), 8.13–7.23, (m) (3H); 3py:2($C_6H_5CO_2$) requires 6H:19H). Addition of diethyl ether yielded 0.55 g of a second brown solid **B** (In 18.7%). Further solid (0.55 g) continued to deposit, and was removed from time to time. The final crop of colourless acicular crystals C (0.60 g) was shown to be $Cl_2In(O_2CC_6H_5)(C_5H_5N)_2$ by X-ray crystallography (9) (*Anal.* calcd. for $Cl_2In(O_2CC_6H_5)(C_5H_5N)_2$: In 24.7, Cl 15.3; found: In 24.5, Cl 15.0). When the final solution was pumped to dryness, the resultant solid **D** had the composition In 14.9, Cl 9.0. Total indium recovered approximately 5.2 mmol (67%).

Reaction of InI with benzoyl peroxide

Equimolar quantities of InI and benzoyl peroxide (5.6 mmol) were mixed in 50 mL dichloromethane and 2 mL pyridine at −20°C. The cooling bath was gradually removed from the stirred mixture, and the temperature allowed to reach ambient. Addition of petroleum ether to the solution precipitated 0.9 g of a yellow solid of unidentified structure (*Anal.* found: In 23.0, I 9.0). The filtrate was allowed to stand overnight, after which 1.2 g of yellow crystalline $IIn(O_2CC_6H_5)_2(C_5H_5N)_2$ deposited (*Anal.* calcd.: In 17. 9, I 19.8; found: In 17.5, I 19.6). Prolonged cooling yielded further solid which analyzed as $In_2I_3(O_2CC_6H_5)_3(C_5H_5N)_3$ (*Anal.* calcd: In 19.0, I 31.5; found: In 19.3, I 32.3). The solid obtained on removing the solvent (0.21 g) had In 20.1, I 28.6. Total indium recovered 83%.

Results and discussion

Group IV and V elements

The addition of 2,4-dinitrophenylhydrazine, tetraphenyl diphosphane, hexaphenyldistannane, or hexaphenyldiplumbane to a solution of InX in toluene/pyridine under the conditions described in the Experimental Section resulted in the deposition of indium metal in quantities corresponding to the process

[2] $3InX \rightarrow 2In^0 + InX_3$

and in the case of InI/Sn_2Ph_6, the tin compound was subsequently recovered unchanged from the reaction mixture. In view of these and other results described below, no further reactions of this type were performed with compounds of Group IV or V elements.

Group VI elements

We have successfully cleaved O—O, S—S, and Se—Se bonds, but Te—Te compounds did not react in this way under the conditions used. In summary, the results obtained were:

(*i*) The reaction of InX (X = Cl, Br, I) with benzoyl peroxide in dichloromethane/pyridine solution gave rise to products containing indium, halogen, and benzoate, with the metal in the +III oxidation state. The nature of the products suggests that the primary process is indeed the insertion

[3] $InX + (C_6H_5COO)_2 \rightarrow XIn(O_2CC_6H_5)_2$

which is followed by the rearrangement reactions

[4] $3XIn(O_2CC_6H_5)_2 \rightarrow In_2X_3(O_2CC_6H_5)_3 + In(O_2CC_6H_5)_3$

[5] $2XIn(O_2CC_6H_5)_2 \rightarrow X_2In(O_2CC_6H_5) + In(O_2CC_6H_5)_3$

The experimental evidence for these processes is summarised in the Experimental Section. No evidence has been found for the presence of $In(O_2CC_6H_5)_3$ in any of the solution phases, however, and the detailed validity of the above equations must therefore remain in question. This not unimportant point aside, there seems to be no doubt that the oxidative insertion process (reaction [3]) does indeed occur.

(*ii*) With a substrate of either Ph_2S_2 or Ph_2Se_2, the products of the reaction, isolated in high yield, correspond to the process

[6] $InX + Ph_2M_2 \xrightarrow[CH_2Cl_2]{py} XIn(MPh)_2py_2$ (M = S, Se)

Can. J. Chem. Downloaded from www.nrcresearchpress.com by 210.87.254.40 on 09/06/12
For personal use only.

In the iodide case the anionic derivative $[I_2In(SPh)_2]^-$ was obtained as the tetra-*n*-propylammonium salt. A similar insertion was observed with InI and Me_2S_2, but the reaction of InI with either $Bu_2''S_2$ or $Bu_2'S_2$ under the conditions described lead to the deposition of indium metal.

(*iii*) When the substrate was Ph_2Te_2, the reaction again followed that in reaction [2], namely, the disproportionation of InX to indium metal and InX_3.

Binuclear metal carbonyls

The synthesis of compounds in which indium is bonded to transition metal carbonyl groups has been achieved by the thermal reaction of InX with a variety of binuclear metal carbonyls. The conditions needed for these reactions depend quite critically on the carbonyl in question (see below).

In the present experiments, we find a smooth and rapid reaction between InX and $Co_2(CO)_8$, leading to the isolation of $XIn[Co(CO)_4]_2py_2$ (X = Cl, Br, I). With indium(I) halides and either $Mn_2(CO)_{10}$ or $[CpFe(CO)_2]_2$, the reaction mixture deposited indium metal, and no evidence could be obtained for the insertion of indium into the metal–metal bond. This behaviour corresponds to that previously reported for the analogous thermal reactions; indium(I) bromide reacts quickly at room temperature with $Co_2(CO)_8$ in tetrahydrofuran (10, 11) but the reaction with either $Mn_2(CO)_{10}$ or $[CpFe(CO)_2]_2$ requires temperatures above 100°C (12, 13), and insertion does not occur under milder conditions.

Reaction mechanism

Solutions of indium(I) halide in the non-aqueous media used in these experiments decompose slowly at room temperature, giving rise to indium metal and adducts of either InX_3 or In_2X_4, depending on the nature of X and the neutral ligand (7, 8). The significance of such processes in the present work is that formation of indium metal is evidence that decomposition is occurring via reaction [2], so that in such cases the substrate resists attack by indium(I) halide. In keeping with this, the products of insertion reactions are isolated in good yield only in those systems in which the precipitation of indium is not observed.

In the previous discussion (8), the properties of indium(I) species were shown to involve both electron pair donor and acceptor properties. Thus the formation of the intermediate in the insertion reaction may involve InX acting as either nucleophile, or electrophile, or both. As in the case of the insertion of InX into an In^{III}—X bond, the proposed mechanism is based on this duality in the chemistry of InX. The reaction of InX at a homonuclear (M—M) bond is unlikely to be a concerted process, since the insertion of a lone pair on InX, presumed to be in the HOMO orbital, into the LUMO of an M—M bond with u-symmetry would be energetically unfavourable. Following the previous discussion (8), we propose that the reaction involves electron pair donation from InX to one M atom, accompanied or followed by donation from the other M to InX. The proposed intermediate

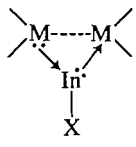

1

then undergoes M—M fission to give the $XInM_2$ kernel. The insertion of InX therefore requires that the M atoms be both acceptor and donor sites, and it remains to show that the pattern of observed reactions, or absence of reaction, supports this mechanism.

TABLE 3. Vibrational spectra (cm^{-1}) of $XIn(SPh)_2py_2$ compounds (X = Cl, Br) (ir), and $[I_2In(SPh_2)]^-$ (ir and Raman)

Vibrational frequency				
		$[I_2In(SPh)_2]^-$		
$ClIn(SPh)_2py_2$	$BrIn(SPh)_2py_2$	Infrared	Raman	Assignment
483 (s)	483 (s)	480 (m)	—	SPh modes
420 (s)	420 (s)	418 (m)	418 (m)	SPh modes
336 (s)	338 (s)	342 (w)	346 (vw)	ν(In—S)
321 (w)	329 (w)	330 (m)	334 (m)	ν(In—S)
286 (vs, br)	—	—	—	ν(In—Cl)
—	275 (vw)	—	—	Unassigned
—	259 (w)	—	—	Unassigned
—	206 (s, br)	—	—	ν(In—Br)
199 (m)	—	—	—	δ(In—Cl)?
—	—	189 (w)	191 (w)	Unassigned
—	—	176 (m)	177 (w)	ν_{as}(In—I)
169 (w-sh)	168 (w-sh)	—	—	Unassigned
156 (m)	156 (m)	156 (w)	155 (vs)	ν_s(In—I)?
135 (m)	—	—	—	Unassigned
—	112 (s, br)	—	—	δ(In—Br)?

For dinuclear transition metal carbonyls, neither $Mn_2(CO)_{10}$ nor $[CpFe(CO)_2]_2$ react under the low temperature/solution phase conditions investigated in the present work, or under the mild condition used by Patmore and Graham (10, 11). The metal atoms in these carbonyls have an 18-electron configuration, and show neither acceptor nor donor functionality, so that an intermediate such as **1** cannot be easily formed. It seems likely that the more extreme conditions under which reaction does occur (12, 13) bring about thermal cleavage of the M—M bond, and that a subsequent free radical reaction with InX leads to the final products. Dicobalt octacarbonyl can exist in two tautomeric forms in solution (14), one with two μ-CO groups and the other the metal–metal-bonded $(CO)_4CoCo(CO)_4$. The latter, like $Mn_2(CO)_{10}$ and $[CpFe(CO)_2]_2$, cannot readily react with InX, but the carbonyl-bridged form, with a bent metal–metal bond, has the correct orientation for attack by InX. This is most easily seen by the interaction of InX with the dipolar canonical form of $Co_2(CO)_8$ to give the intermediate

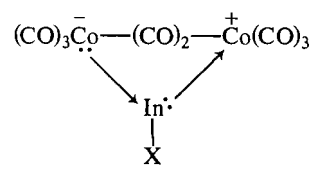

which goes to $XIn[Co(CO_4]_2$ by rupture of the carbonyl bridges.

For the molecules Sn_2Ph_6 and Pb_2Ph_6, the absence of any insertion reaction is easily understood in terms of the lack of donor electrons on the metal. For 2,4-dinitrophenylhydrazine, the nitrogen atoms are potential donors, but cannot act as acceptors, and for tetraphenylphosphane there is little evidence of acceptor properties, even though the phosphorus atoms are known to be potential donors.

The Group VI compounds require more detailed comment. Compounds with S—S, Se—Se, and Te—Te bonds fulfill the required conditions, in that these atoms have potential donor

TABLE 4. Far infrared and Raman spectra (cm^{-1}) of $XIn(SePh)_2py_2$ compounds (X = Cl, Br, I)

$ClIn(SePh)_2py_2$		$BrIn(SePh)_2py_2$		$IIn(SePh)_2py_2$		
Infrared	Raman	Infrared	Raman	Infrared	Raman	Assignment
468 (s)	—	468 (s)	—	467 (vs)	—	SePh modes
409 (s)	—	419 (s)	—	419 (vs)	—	SePh modes
—	305 (m)	—	305 (m)	—	304 (m)	SePh modes
288 vs)	287 (m)	—	—	—	—	ν(In—Cl)
252 (m)	250 (w)	253 (m)	255 (vw)	254 (s)	256 (m)	ν(In—Se)?
242 (vw)	—	243 (w)	246 (w)	243 (m)	247 (w)	ν(In—Se)?
229 (m)	228 (w)	228 (m)	225 (w)	228 (s)	228 (m)	ν(In—Se)?
—	211 (m)	214 (m)	—	208 (m)	211 (m)	ν(In—Se)?
—	—	204 (m)	204 (m, br)	—	—	ν(In—Br)
191 (m)	191 (vw)	192 (m)	—	188 (vs)	186 (m)	—
—	177 (vs)	—	—	—	—	ν(In—Cl)?
—	158 (vw)	162 (w)	161 (vs)	163 (m)	163 (s)	—
154 (m, br)	153 (vw)	150 (m, br)	—	152 (vw)	—	—
—	—	—	—	144 (m)	147 (vs)	ν(In—I)
132 (m)	123 (w)	112 (w)	130 (w)	105 (vw)	—	—

and acceptor properties. No reaction was observed with Ph_2Te_2, and this can be understood in terms of the poor donor ability, given that there is little evidence of such compounds acting as strong ligands. For Ph_2Se_2, the reaction is straightforward, yielding the pyridine adducts of $XIn(SePh)_2$ (X = Cl, Br, I). With disulphides, the easy reaction of Ph_2S_2 and Me_2S_2 contrasts with the absence of any detectable reaction with $Bu_2^nS_2$ or $Bu_2^tS_2$. These results show that the strongest bases undergo reaction, and the order of reactivity is very similar to that reported by Ichimura, Nosco, and Deutsch (15) who studied the electrophile–assisted cleavage of S—S bonds by nucleophiles, reactions which are similar in mechanism to the attack of InX on such bonds via the intermediate **1**.

In general then the reactivities observed in the various InX/M—M systems are readily explained by the proposed mechanism. The previously reported examples of InX insertion processes agree with, but do not confirm, the reaction scheme. Reaction with I_2 (CpIn, InX_2^-) (5, 6) to give In^{III} products are readily accommodated into the scheme, as are reactions with the S—S bond of 1,2-bis(trifluoromethyl)dithiete (3, 4). Similarly, the reaction of InX with RX′ can be viewed as the nucleophilic attack of InX on RX′, with donation from X′ to indium as required by the reaction pathway proposed here.

One final caveat concerns the undetermined effect of the solvation of InX in aromatic/donor solvent solutions used. We have written all the above reactions as though unsolvated InX molecules are involved, but our earlier work (7) demonstrated that solvation by the donor solvent is critically important. We have argued elsewhere (8) that such solvation could increase the availability of the lone pair on InX, but there may well be other effects on these and other features of the reaction.

The InX/benzoyl peroxide system

The complex series of products which are obtained from the InX/benzoyl peroxide reaction systems require some comment. The rapid formation of a clear solution phase implies that reaction [3] occurs readily under the reaction conditions. The reaction is no doubt aided by the presence of carbonyl groups adjacent to the O—O bond, which otherwise lacks the required donor and acceptor properties to form the intermediate **1**. This explains the sharp difference between the N—N and O—O bonded molecules studied.

The simplest system is for X = I, where the major compound isolated is the insertion product $IIn(O_2CC_6H_5)_2py_2$. For X = Cl or Br, the products which are eventually obtained on removing solvent, namely $In_2X_3(O_2CC_6H_5)_3py_2$, correspond to an equimolar mixture of InX_3 and $In(O_2CC_6H_5)_3$. In an earlier paper (16), the nature of a series of some unusual indium(III) acetate compounds was discussed in terms of a polymeric $In(OAc)_3$ lattice which can accommodate various neutral or charged species, and it seems reasonable that a similar structure should apply in the case of $In_2X_3(O_2CC_6H_5)_3py_2$, and this may explain why $In(O_2CC_6H_5)_3$ is not isolated from the reaction mixture (cf. reactions [4] and [5]).

With $InCl/Bz_2O_2$, the complex series of products **A**–**D** isolated from a lengthy reaction include **C**, which is the product of insertion (reaction [3]) followed by rearrangement (reactions [4] and [5]). The structures of substances **A** and **B** are not clear; product **D** corresponds analytically to an $InCl_2$ derivative, and again can be rationalized in terms of reaction [5]. In general, the materials confirm that solution rearrangement reactions which follow the initial insertion reaction play an important role here, as in other indium(III) systems.

Vibrational spectra of $XIn(MC_6H_5)py_2$ complexes (X = Cl, Br, I; M = S, Se)

Table 3 shows the previously unreported far infrared spectra of the neutral phenylthiolate complexes, and the infrared and Raman spectra of the $[I_2In(SPh)_2]^-$ anion. The latter is expected to have C_{2v} symmetry in the InI_2S_2 kernel, with two ν(In—S) and two ν(In—I), all active in both infrared and Raman modes. The ν(In—I) vibrations are readily assigned at 176 and 155 cm^{-1}. The identification of ν(M—S) modes has been the subject of debate (17), with frequencies between 400 cm^{-1} and 160 cm^{-1} being proposed. The ν(In—S) absorptions in indium–dithiolate anionic complexes were assigned in the 300–370 cm^{-1} range (18), and the only reasonable candidates in the spectrum of $[I_2In(SPh)_2]^-$ are the two vibrations at 332 and 344 cm^{-1}, frequencies which are also observed in the spectra of the neutral chloride and bromide compounds. None of the bending modes can be assigned at this stage.

The adducts $XIn(SPh)_2py_2$ (X = Cl, Br) each show one ν(In—X) infrared band, and absorption in the presumed ν(In—S) region, in agreement with the above discussion. The corresponding results for $XIn(SePh)_2py_2$ compounds (X = Cl, Br, I) are given in Table 4, and lend themselves to a similar

Can. J. Chem. Downloaded from www.nrcresearchpress.com by 210.87.254.40 on 09/06/12
For personal use only.

analysis with ν(In—Se) tentatively assigned in the 200–260 cm^{-1} region. The ν(In—N) modes are not identified in this analysis, and may well lie in the spectral region obscured by S—C_6H_5 or Se—C_6H_5 vibrations, since frequencies above 400 cm^{-1} have been reported for ν(In—N) in earlier work (19). The analysis of the spectra does not allow a choice to be made between the various stereochemistries possible for an In-$X(S)_2(N)_2$ kernel, but does confirm that the compounds concerned are mononuclear species.

Acknowledgements

This work was supported in part by Operating Grants (to D.G.T.) from the Natural Sciences and Engineering Research Council of Canada; C.P. thanks the Conselho Nacional de Desenvolvimento Cientifico e Tecnologico (Brasil) for the award of a scholarship.

1. (*a*) L. G. WATERWORTH and I. J. WORRALL. Chem. Commun. 569 (1971); (*b*) M. J. S. GYNANE and I. J. WORRALL. Inorg. Nucl. Chem. Lett. **8**, 547 (1972); (*c*) M. J. S. GYNANE, L. G. WATERWORTH, and I. J. WORRALL. J. Organomet. Chem. **43**, 257 (1972); (*d*) L. G. WATERWORTH and I. J. WORRALL. J. Organomet. Chem. **81**, 23 (1974); (*e*) M. J. S. GYNANE, L. G. WATERWORTH, and I. J. WORRALL. Inorg. Nucl. Chem. Lett. **9**, 543 (1973).
2. J. S. POLAND and D. G. TUCK. J. Organomet. Chem. **42**, 315 (1972).
3. A. F. BERNIAZ, G. HUNTER, and D. G. TUCK. J. Chem. Soc. (A), 3254 (1971).
4. A. F. BERNIAZ and D. G. TUCK. J. Organomet. Chem. **51**, 113 (1973).
5. J. G. CONTRERAS and D. G. TUCK. J. Organomet. Chem. **66**, 405 (1974).
6. J. E. DRAKE, J. L. HENCHER, L. KHASROU, D. G. TUCK, and L. VICTORIANO. Inorg. Chem. **19**, 34 (1980).
7. C. PEPPE, D. G. TUCK, and L. VICTORIANO. J. Chem. Soc. Dalton Trans. 2165 (1982).
8. C. PEPPE and D. G. TUCK. Can. J. Chem. **62**, 2793 (1984).
9. M. A. KHAN, C. PEPPE, and D. G. TUCK. Acta Crystallogr. C**39**, 1339 (1983).
10. D. J. PATMORE and W. A. G. GRAHAM. Chem. Commun. 591 (1965).
11. D. J. PATMORE and W. A. G. GRAHAM. Inorg. Chem. **5**, 1586 (1966).
12. J. HOYANO, D. J. PATMORE, and W. A. G. GRAHAM. Inorg. Nucl. Chem. Lett. **4**, 201 (1968).
13. A. T. T. HSIEH and M. J. MAYS. Inorg. Nucl. Chem. Lett. **7**, 223 (1971).
14. E. W. ABEL and F. G. A. STONE. Q. Rev. **23**, 325 (1969).
15. A. ICHIMURA, D. L. NOSCO, and E. DEUTSCH. J. Am. Chem. Soc. **105**, 844 (1983).
16. J. J. HABEEB and D. G. TUCK. J. Chem. Soc. Dalton Trans. 243 (1973).
17. R. A. HABERKORN, L. QUE, W. O. GILLUM, R. H. HOLM, C. S. LIU, and R. C. LORD. Inorg. Chem. **15**, 2408 (1976).
18. D. G. TUCK and M. K. YANG. J. Chem. Soc. A, 214 (1971).
19. M. J. TAYLOR, D. G. TUCK, and L. VICTORIANO. Can. J. Chem. **60**, 690 (1982).

Can. J. Chem. Downloaded from www.nrcresearchpress.com by 210.87.254.40 on 09/06/12
For personal use only.

ipso Nitration. XXV.[1] Nitration of di-*tert*-butylphenols, α-(3,5-di-*tert*-butylphenoxy)isobutyric acid, and 3,5-di-*tert*-butylphenoxyacetic acid: formation of nitrodienones and nitrodienes containing a secondary nitro group

GORDON G. CROSS, ALFRED FISCHER, AND GEORGE N. HENDERSON
Department of Chemistry, University of Victoria, Victoria, B.C., Canada V8W 2Y2

Received May 8, 1984

GORDON G. CROSS, ALFRED FISCHER, and GEORGE N. HENDERSON. Can. J. Chem. **62**, 2803 (1984).

Nitration of 2,6-di-*tert*-butylphenol in acetic anhydride or chloroform gives 2,6-di-*tert*-butyl-4-nitrophenol and 2-*tert*-butyl-4,6-dinitrophenol. The intermediates 2,6-di-*tert*-butyl-4-nitrocyclohexa-2,5-dienone and 2,6-di-*tert*-butyl-4,6-dinitrocyclohexa-2,4-dienone, have been observed by ^1H and ^{13}C nmr. Nitration of 2,4-di-*tert*-butylphenol gives successively 2,4-di-*tert*-butyl-6-nitrocyclohexa-2,4-dienone, 2,4-di-*tert*-butyl-6-nitrophenol, 2,4-di-*tert*-butyl-4,6-dinitrocyclohexa-2,5-dienone, and 2-*tert*-butyl-4,6-dinitrophenol. Nitration of 3,5-di-*tert*-butylphenol gives successively 3,5-di-*tert*-butyl-6-nitrocyclohexa-2,4-dienone, 3,5-di-*tert*-butyl-2-nitrophenol, 3,5-di-*tert*-butyl-2,4-dinitrocyclohexa-2,5-dienone, and 3,5-di-*tert*-butyl-2,6-dinitrophenol. 3,5-Di-*tert*-butyl-4-nitrocyclohexa-2,5-dienone and 3,5-di-*tert*-butyl-2,6-dinitrocyclohexa-2,4-dienone are also formed as intermediates. Nitration of 3,5-di-*tert*-butylphenoxyacetic and isobutyric acids gives in each case the 2-nitro derivative. Further nitration of 3,5-di-*tert*-butyl-2-nitrophenoxyacetic and isobutyric acids gives a mixture of the adducts 7,9-di-*tert*-butyl-6,10-dinitro-1,4-dioxaspiro[4,5]deca-6,8-dien-2-one and its 6,8-dinitro-6,9-diene isomer from the former and their 3,3-dimethyl derivatives from the latter. No dinitro acids are formed.

GORDON G. CROSS, ALFRED FISCHER et GEORGE N. HENDERSON. Can. J. Chem. **62**, 2803 (1984).

La nitration du di-*tert*-butyl-2,6 phénol, dans l'anhydride acétique ou le chloroforme, conduit au di-*tert*-butyl-2,6 nitro-4 phénol ainsi qu'au *tert*-butyl-2 dinitro-4,6 phénol. Faisant appel à la rmn du ^1H et du ^{13}C, on a pu observé la di-*tert*-butyl-2,6 nitro-4 cyclohexadiène-2,5 one ainsi que la di-*tert*-butyl-2,6 dinitro-4,6 cyclohexadiène-2,4 one qui se forment comme intermédiaires. La nitration du di--*tert*-butyl-2,4 phénol conduit successivement à la di-*tert*-butyl-2,4 nitro-6 cyclohexadiène-2,4 one, au di-*tert*-butyl-2,4 nitro-6 phénol, à la di-*tert*-butyl-2,4 dinitro-4,6 cyclohexadiène-2,5 one et finalement au *tert*-butyl-2 dinitro-4,6 phénol. La nitration du di-*tert*-butyl-3,5 phénol fournit successivement la di-*tert*-butyl-3,5 nitro-6 cyclohexadiène-2,4 one, le di-*tert*-butyl-3,5 nitro-2 phénol, la di-*tert*-butyl-3,5- dinitro-2,4 cyclohexadiène-2,5 one et finalement le di-*tert*-butyl-3,5 dinitro-2,6 phénol. La di-*tert*-butyl-3,5 nitro-4 cyclohexadiène-2,5 one et la di-*tert*-3,5 dinitro-2,6 cyclohexadiène-2,4 one se forment aussi comme intermédiaires. La nitration des acides di-*tert*-butyl-3,5 phénoxyacétique ainsi que phénoxyisobutyrique conduit, dans chaque cas, à la formation du dérivé nitro-2. Des nitrations plus poussées des acides di-*tert*-butyl-3,5 nitro-2 phénoxyacétique ou phénoxyisobutyrique conduisent, dans le cas du dérivé phénoxyacétique, à des mélanges d'adduits de la di-*tert*-7,9 dinitro-6,10 dioxa-1,4 spiro[4,5] décadiène-6,8 one-2 et de son isomère dinitro-6,8 diène-6,9 et aux dérivés diméthyl-3,3, dans le cas de la nitration des dérivés phénoxyisobutiryque. Aucun dérivé dinitré des acides ne se forme.

[Traduit par le journal]

Can. J. Chem. Downloaded from www.nrcresearchpress.com by 210.87.254.6 on 09/06/12
For personal use only.

It is well established that nitration of an aromatic compound generally involves the formation of a cyclohexadienyl cation intermediate by the addition of nitronium ion to the aromatic substrate. The cation is deprotonated to the nitroaromatic in a subsequent step and the overall mechanism is classified as S_E2 (1). There have been a number of reports of the direct observation of the nitrocyclohexadienyl cation intermediate (2–4). However, it appears that most such reports are in error (5*a*) and that the only cyclohexadienyl cation that has a secondary nitro group which is likely to have been observed is that obtained in the nitration of anthracene (2). More extensive observations that point to the existence of the nitrocyclohexadienyl cation have been made for *ipso*-cations, i.e. cations formed by the addition of the nitronium ion at a substituted carbon. Olah *et al.* have observed by nmr the cations obtained by the addition of nitronium ion to hexamethylbenzene and to trifluoromesitylene (6). These nitrobenzenium cations are derived from fully substituted benzenes. In an *ipso* cation derived from a less substituted benzene it is likely that the nitro group would rapidly migrate by a sequence of 1,2-shifts to a proton-bearing carbon, deprotonation would ensue, and the nitrobenzene derivative would be formed (7), precluding direct observation of the cation. However, the methylnitrocyclohexadienyl cation with nitro *ipso* to methyl can be trapped by an appropriate nucleophile to form a pair of diastereoisomeric adducts (8). Such adducts can undergo reactions which are most readily explained in terms of the re-formation of the intermediate methylnitrocyclohexadienyl cation.

The failure either to observe, or to trap as adducts, nitrocyclohexadienyl cations with nitro attached to a proton-bearing carbon reflects the extremely facile deprotonation of such cations. Kinetic isotope effects are not normally observed in nitration, consistent with the deprotonation step being much faster than the reversion of the nitrocyclohexadienyl cation to the nitronium ion and the aromatic substrate. The cyclohexadienyl cation itself is strongly acidic. Introduction of the nitro group at the site of the acidic proton should greatly enhance the acidity. In the exceptional cases in which an isotope effect is observed in nitration and thus the deprotonation step is rate-determining, either the nitrocyclohexadienyl cation is unusually stable and (or) the transition state for the deprotonation reaction is subject to steric strain. Thus for nitration of anthracene an isotope effect is observed (2). The nitrocyclohexadienyl cation from anthracene is unusually stabilized with respect to reactant and product, as there is a relatively small loss of delocalization energy on forming the intermediate. Furthermore, the transition state for deprotonation is subject to steric strain as a result of interactions between the nitro group and the adjacent 1 and 8 hydrogens. An isotope effect is also observed in the nitration of 2-nitro-1,3,5-tri-*tert*-butylbenzene, a case in

[1] For Part XXIV, see ref. 14.

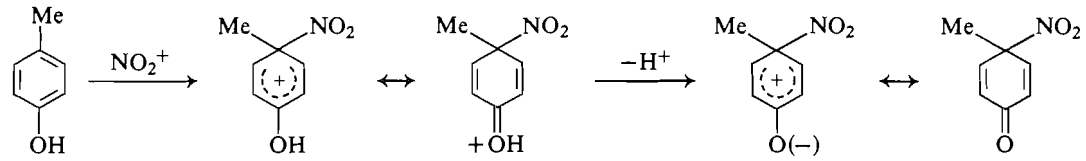

SCHEME 1

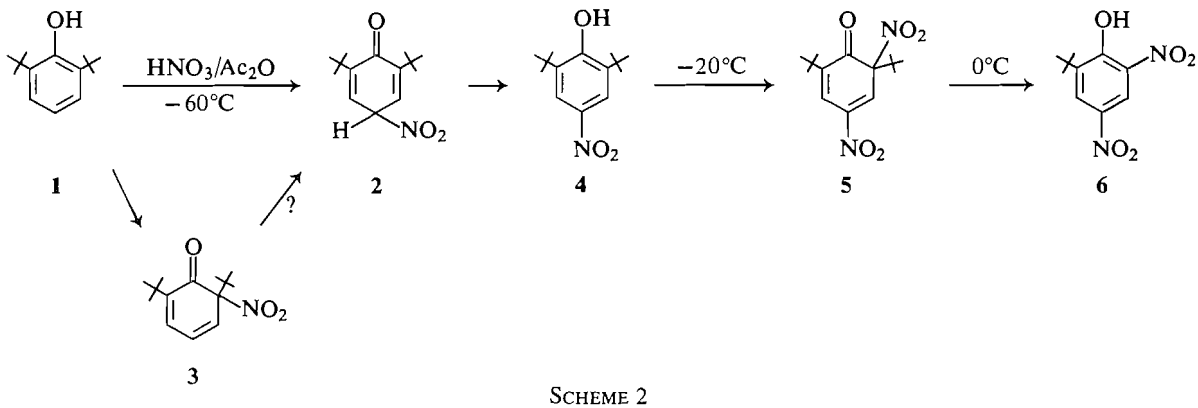

SCHEME 2

Can. J. Chem. Downloaded from www.nrcresearchpress.com by 210.87.254.6 on 09/06/12
For personal use only.

which there is steric strain in the deprotonation step (9). In this case the lifetime of the nitrocyclohexadienyl cation is such that another reaction of the cation also occurs: rearrangement to give (ultimately) 2,4-dinitro-3,5-di-*tert*-butyltoluene (10).

Nitration of phenols which are fully substituted in the reactive 2, 4, and 6 positions to 2,4,6-trisubstituted 4-nitrocyclohexa-2,5-dienones has long been known (11). More recently 4-alkyl-4-nitrocyclohexa-2,5-dienones (12) and 6-alkyl-6-nitrocyclohexa-2,4-dienones (13, 14) have been obtained from the nitration of less substituted phenols or phenyl acetates. The formation of nitrodienones can be viewed as a special case of *ipso* nitration and capture of the *ipso*-methylnitrocyclohexadienyl cation by a nucleophile. In this case the nucleophile is the substituent already present, i.e. hydroxyl. The discrete step of nucleophilic addition has been eliminated. Correspondingly the nitrodienone can be viewed, in one canonical form, as an oxide-substituted nitrocyclohexadienyl cation (Scheme 1). In this communication we report the first detailed observations of nitrodienones containing a secondary nitro group, i.e. oxide-substituted nitrocyclohexadienyl cations with nitro "*ipso*" to hydrogen. We also report the first isolation from a nitration reaction of a nitrocyclohexadiene containing a secondary nitro group. In a recent paper we reported the observation of similar dienones in the nitration of 2,3,6-trimethyl- and 2,3,5,6-tetramethylphenol (14). In those cases, the 2,5-dienone with nitro "*ipso*" to hydrogen was a minor component in a mixture in which the 6-methyl-6-nitrocyclohexa-2,6-dienone predominated and the structural information which could be obtained was limited to ^{1}H nmr observations.

Results and discussion

Nitration of 2,6-di-*tert*-butylphenol (**1**) in both acetic anhydride and chloroform gave, successively, the species **2**, **4**, **5**, and **6** (Scheme 2). The nitrophenols **4** and **6** were isolated and characterized. The nitrodienone **2** was identified in reaction mixtures by ^{1}H and ^{13}C nmr spectra. The symmetry of the spectra, the doublet–triplet splitting in the ^{1}H nmr, and the characteristic dienone peaks at δ_C 80 (saturated carbon) and 184 ppm (carbonyl carbon) in the ^{13}C nmr are all consistent with this assignment. The isomeric 2,4-dienone **3** would exhibit more complex spectra. In some preliminary experiments another intermediate, presumably **3**, was formed but we were unable to find conditions under which this intermediate could be formed reproducibly in substantial amount. In the experiments in which the 2,4-dienone **3** was formed, **4** was the only aromatic product observed when the 2,4-dienone disappeared. It seems likely that the isomerization of **3** to **4** involves the initial rearrangement of **3** to **2** by a dissociation–recombination pathway (*vide infra*) followed by tautomerization of **2** to **4**. The dinitrodienone **5** was identified in reaction mixtures by ^{1}H and ^{13}C nmr. The absence of a plane of symmetry is evident from the spectra and this rules out a 2,5-dienone structure containing a *gem*-dinitro group. Nitration of **4** to **6** has been observed previously (15) and is an example of nitro-de-*tert*-butylation. Formation of the intermediate dienone **5** was not observed by Zlobina and Ershov (15). Loss of the *tert*-butyl group from the dinitrodienone is acid catalysed and presumably involves initial protonation at the carbonyl oxygen followed by loss of the *tert*-butyl cation (16). Note that in the case of the dienone **3** this pathway, which would lead to 2-*tert*-butyl-6-nitrophenol, under the reaction conditions is of higher energy than the **3** → **2** → **4** path and no 2-*tert*-butyl-6-nitrophenol is formed.

On nitration of 2,4-di-*tert*-butylphenol (**7**) in acetic anhydride, successive formation of the species **9**, **10**, and **6** could be observed (Scheme 3). We were not able to observe the nitrodienone **8** even when the reaction was carried out at −70°C. However, we were able to observe the transient formation of **8** in the reaction in chloroform, at −60°C. The 2,4-dienone **8** had three broad singlets in the vinyl-allylic region of the ^{1}H nmr. Its 2,5-dienone isomer would exhibit a 10-Hz vinyl proton coupling and no such coupling was observed. It is not possible to make a similar clear-cut distinction between **10** and its isomer 4,6-di-*tert*-butyl-2,6-dinitrocyclohexa-2,4-dienone. It is possible that the 2,6-dinitro isomer is formed and it, rather than **10**, could even be the observed dinitrodienone. What is clear is that **10** must be the immediate precursor to **6** and that it must be either the observed species, or formed as a transient intermediate from the observed species. Conversion of **10** to **6** is another example of nitro-de-*tert*-butylation and it is observed only when the process of nitro migration and tautomerization to

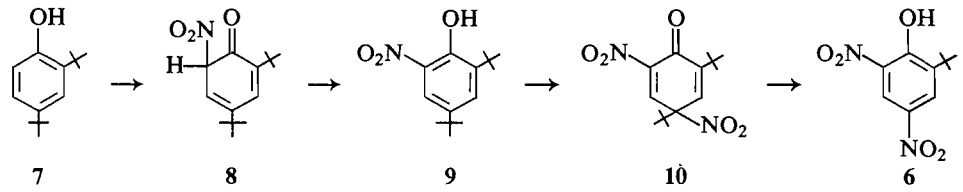

SCHEME 3

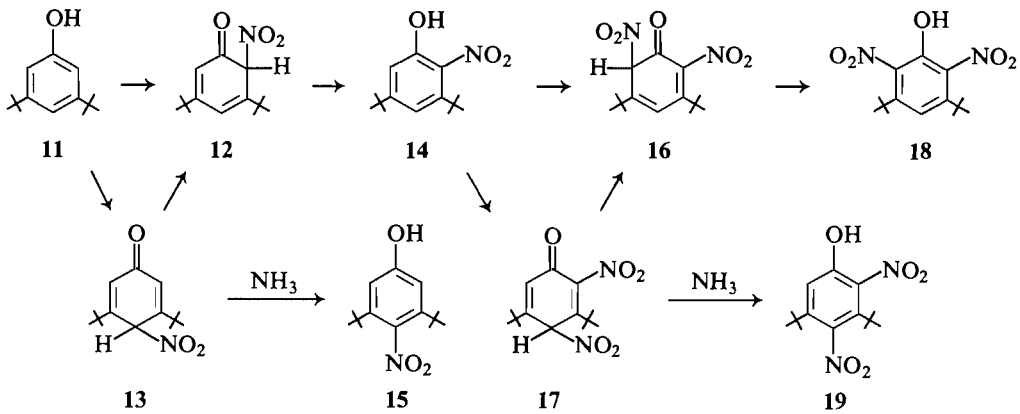

SCHEME 4

a nitrophenol is blocked. The dinitrodienone **10** which, like **5**, readily lost the *tert*-butyl group in the nitration mixture decomposed only slowly at 0°C in chloroform solution when the acid was removed, and even survived for a short period at +35°C, also like **5**. It is likely that these dienones could be isolated free from the dinitrophenol cleavage products although they do appear rather less stable than analogous dienones obtained by nitration of 2,4,6-tri-*tert*-butylphenol (17) and 2,6-di-*tert*-butyl-4-chlorophenol (18). It seems likely that, in accord with its electron-withdrawing effects, the additional nuclear nitro substituent facilitates the cleavage of the dinitrophenol moiety from the incipient *tert*-butyl cation.

Nitration of 3,5-di-*tert*-butylphenol (**11**) in acetic anhydride gave successively the dienone **12** and the nitrophenol **14** (Scheme 4). Precipitation occurred at this stage and the further reactions of **14** were obscured. It is likely that a dinitrodienone and finally the dinitrophenol **18** were formed (*vide infra*). The dienone **12** was identified by ^{1}H and ^{13}C nmr spectra. In the ^{1}H spectrum the three singlets of the ring protons were clearly resolved. In the ^{13}C spectrum peaks for all of the six-ring carbons were observed and in the gated spectrum the C-6 signal at 86 ppm was split into a doublet. The absence of symmetry in the dienone is evident from the spectra and thus the 2,5-dienone **13** is ruled out. Nitration in chloroform gave both nitrodienones **12** and **13**. These rearranged to give the nitrophenol **14**, which was further nitrated to dinitrodienone **17**, which rearranged to the 2,6-dinitrophenol **18**, the final product. The ^{1}H and ^{13}C nmr spectra of **13** are in accord with its symmetry. Further confirmation of the presence of **13** was provided by work-up after quenching with ammonia at low temperature: 3,5-di-*tert*-butyl-4-nitrophenol (**15**) was obtained by the ammonia-catalysed tautomerization of **13**, in addition to the 2-nitro isomer **14**. The assignment of the structure **17** to the dinitrodienone rather than the isomeric structure **16** is based on the experiment in which the reaction mixture from nitration of **14** was quenched with ammonia in methanol at low temperature: the 2,4-dinitrophenol **19** was obtained, as well as the

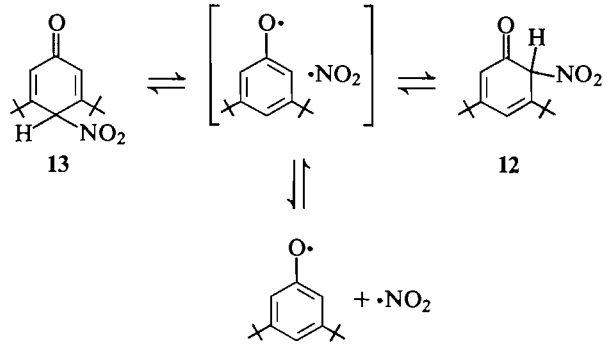

SCHEME 5

2,6-dinitrophenol **18** present in the reaction mixture before quenching.

Nitration of **11** should occur, in principle, at both of the unsubstituted 2 (6) and 4 positions to give, after deprotonation at oxygen, **12** and **13**, respectively. Steric hindrance to nitration would be expected to be greater at the 4 position than at the 2 position, but both products were observed in chloroform. The nitrophenol **15** was not observed under nitration conditions. Conversion of the 4-nitrodienone **13** to the 2-nitrophenol **14** undoubtedly involves the 2-nitrodienone **12** as an intermediate. Barnes and Myhre have shown that 4-methyl-4-nitrocyclohexa-2,5-dienone rearranges to 4-methyl-2-nitrophenol in organic and weakly acidic solvents by a radical dissociation–recombination process involving phenoxy and nitrogen dioxide radicals (19). Barnes and Myhre's mechanism as it applies to **13** is depicted in Scheme 5. Evidently tautomerization of **13** to **15** does not compete with this process unless a base (ammonia) is added, which would greatly enhance the rate of deprotonation. Tautomerization of **12** is much faster than tautomerization of **13**. Use was made of this for the selective aromatization of **12** so that the ^{13}C nmr of **13** could be observed.

Nitration of **14** would be expected to occur at each of the unsubstituted 4 and 6 positions to give **17** and **16**, respectively.

Can. J. Chem. Downloaded from www.nrcresearchpress.com by 210.87.254.6 on 09/06/12
For personal use only.

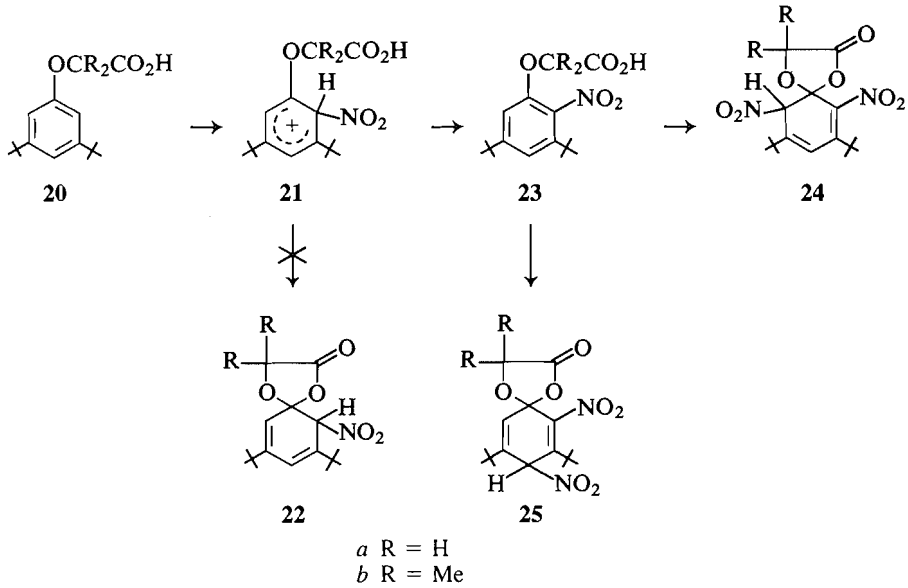

SCHEME 6

Evidently tautomerization of **16** to **18** is rapid since, while **17** was observed, **16** was not, although it must be an intermediate in the formation of **18**. As in the case of the mononitrodienones **12** and **13**, tautomerization of the 2,6-dinitro-2,4-dienone **16** is much faster than tautomerization of the 2,4-dinitro-2,5-dienone **17**, and the isomerization of **17** to **16** followed by tautomerization of the latter to **18** (cf. Scheme 5) is faster than the direct tautomerization of **17** to **19** – unless a base is added to accelerate the deprotonation step.

The nitrodienones **2**, **8**, **12**, **13**, and **17** have nitro attached to the same carbon as hydrogen. We have recently reported the formation of 4-nitro-2,5-dienones containing a secondary nitro group in the nitration of 2,3,6-trimethyl- and 2,3,5,6-tetramethylphenol (14). Together these constitute the first direct observations of monocyclic nitrodienones formed by addition of a nitronium ion to an unsubstituted position of a phenol. We attribute the (relative) stability of the dienones, i.e. the relative slowness of tautomerization, to a combination of steric strain in the transition state for deprotonation at the tetragonal nuclear position and steric hindrance to solvation, and hence protonation, at the carbonyl oxygen. The first factor should be the more important in, e.g., **13**, and the second the more important in, e.g., **2**. Both factors might be important in, e.g., 4-nitro-2,3,5,6-tetramethylcyclohexa-2,5-dienone. An interesting feature of the reactivity of the dienones from **11** is that **13** appears to be more stable than **12**, surviving to a considerably higher temperature than the latter, and **17** more stable than **16**. Yet **13** is proposed to rearrange to **12**, and **17** to **16**. The apparent relative stabilities of **13** and **12** and of **17** and **16** are not necessarily indicative of the relative thermodynamic stabilities. Rather, these reflect the relative stabilities toward deprotonation, i.e. the relative height of the transition state barriers to deprotonation. In the transition state the nitro group has to have moved in the direction of becoming coplanar with the two substituents *ortho* to it. These are the two *tert*-butyl groups in the cases of **13** and **17** (and hence a high barrier), but only one *tert*-butyl group and a smaller hydroxyl group in the cases of **12** and **16** (a lower barrier). We might expect **12** and **16** to be thermodynamically more stable than **13** and **17** since the former, being 2,4-dienones, should have greater resonance stabilization than the latter cross-conjugated 2,5-dienones.

Ershov and Volod'kin (20) isolated 4-bromo-2,6-dialkylcyclohexa-2,5-dienones from bromination of 2,6-dialkylphenols. Ershov *et al.* were not able to isolate or detect the analogous nitrodienones in the nitration of the same phenols (21). The nitrodienones would be expected to be less stable to tautomerization than the bromodienones. From a study of the kinetics of nitration of the 2,6-dialkylphenols, Ershov and coworkers inferred that a transient intermediate was formed during the reaction and they attributed the nitrodienone structure to this intermediate (22). The correctness of this attribution is in some doubt since (*i*) there is no evidence that the 4-nitro-2,6-dialkylphenol is the final reaction product under the reaction conditions employed for the kinetics studies, and (*ii*) in the region in which the formation of the dienone is allegedly rate determining, different 2,6-dialkylphenols exhibit different rates of reaction although, at the sulfuric acid concentration used (82.5% by wt.), these phenols should be nitrated at the encounter rate (5*b*).

Nitration of 3,5-di-*tert*-butylphenoxyacetic acid (**20***a*) in a mixture of acetic anhydride and chloroform at −60°C gave 3,5-di-*tert*-butyl-2-nitrophenoxyacetic acid (**23***a*, Scheme 6). None of the isomeric 4-nitro acid was observed and this presumably reflects the greater steric hindrance at the 4 position of **20***a*, flanked by two *tert*-butyl groups, as compared with the 2 position, flanked by one *tert*-butyl and a smaller ether function. There was no evidence for the formation of the diene **22***a*, which suggests that deprotonation of **21***a* is faster than ring closure. At +20°C the acid **23***a* was converted into a mixed anhydride (probably the phenoxyacetic anhydride), as evidenced by the appearance of an additional methylene peak in the ^{1}H nmr spectrum and the fact that, on reaction with ammonia, 3,5-di-*tert*-butylphenoxyacetamide was obtained. Further nitration of **23***a*, in a mixture of acetic anhydride, trifluoroacetic anhydride, and chloroform, occurred by addition of nitronium ion at both the 6 and 4 positions and was followed in each case by ring closure to give the dinitrodienes, **24***a* and **25***a* respectively, in a 2:1 ratio. These dienes exhibited the characteristic peaks high field to the aromatic region in both the ^{1}H nmr (**24***a*: δ 5.14, 6.47 ppm; **25***a*: δ 6.02, 6.08 ppm) and

Can. J. Chem. Downloaded from www.nrcresearchpress.com by 210.87.254.6 on 09/06/12
For personal use only.

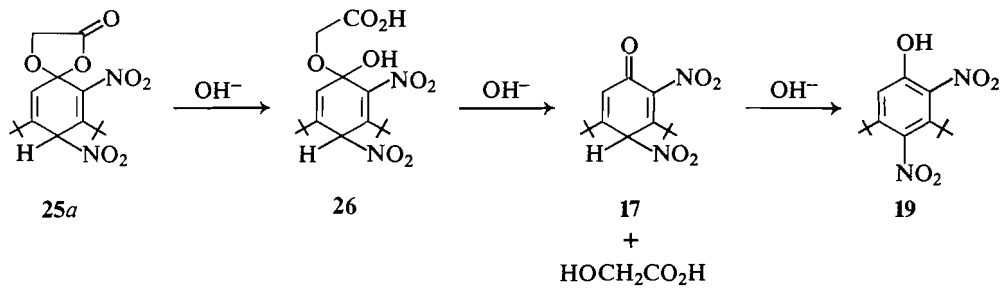

SCHEME 7

^{13}C nmr spectra (**24***a*: δ_C 85.2, 104.8 ppm; **25***a*: δ_C 82.3, 102.6 ppm). Their structures were assigned from the longer wavelength absorption (275 nm) of the extended conjugated system of **24***a*, as compared with the absorption of **25***a* at 223 nm, and from the fact that on treatment with sodium hydroxide **24***a* gave 3,5-di-*tert*-butyl-2,6-dinitrophenoxyacetic acid whereas **25***a* gave 3,5-di-*tert*-butyl-2,4-dinitrophenol. The presence of the nitro group in the 2 position of **23***a* effectively increases the size of the substituted ether group, since it restricts the conformations that the acetic acid moiety could otherwise adopt to reduce hindrance at the 6 position. As a result, addition of the nitronium ion at the 4 position of **23***a* becomes competitive with addition at the 6 position. Ring closure totally dominates deprotonation in the dinitrocyclohexadienyl cation intermediates between **23***a* and **24***a* and **23***a* and **25***a*. Most likely this can be attributed to the increase in steric strain attendant upon aromatization, with all five substituent groups forced into coplanarity with the aromatic ring. It is striking that, whereas **21***a* only deprotonates and does not undergo ring closure at all, its 6-nitro derivative and its regio isomer do not deprotonate at all and only undergo ring closure.

Nitration of 3,5-di-*tert*-butylphenoxyisobutyric acid (**20***b*) with nitric acid in acetic anhydride at −60°C gave the 2-nitro acid **23***b*, which was subsequently converted into the mixed anhydride as evidenced by reaction with ammonia to yield the amide of **23***b*. Nitration of **20***b* was also carried out under conditions designed to avoid the possible prior formation of the mixed anhydride of **20***b* with acetic anhydride (addition of solid **20***b* to the nitrating solution and, also, addition of a solution of **20***b* in [^{2}H]chloroform to the nitrating solution), but only the nitro acid **23***b* was obtained. In particular, no nitrodiene **22***b*, which would arise by ring closure of **21***b*, was observed. Under more vigorous conditions (nitration in trifluoroacetic anhydride/[^{2}H]chloroform) further nitration to the dinitrodiene, **24***b* (85%) and **25***b* (15%) occurred. As in the case of **20***a*, no ring closure occurs in the first nitration step and complete ring closure occurs in the second nitration step.

Each of the dienes **24***a*, **24***b*, **25***a*, and **25***b* can take stereoisomeric forms. The diastereoisomers of *ipso*-nitrocyclohexa-2,4-diene derivatives, in general,[2] and of 10-methyl-10-nitro-1,4-dioxaspiro[4,5]deca-6,8-dien-2-one and 3,3,10-trimethyl-10-nitro-1,4-dioxaspiro[4,5]deca-6,8-dien-2-one, in particular (23*a*), have readily distinguishable nmr spectra and thus it is clear that the compounds **24***a* and **24***b* were isolated as single diastereoisomers. As to the stereochemistry of the diastereoisomers obtained, we rely on the analogy to the *ipso*-nitration of 2-methylphenoxyacetic and 2-methylphenoxyisobutyric acids in which the *E*-diastereoisomer is formed preferentially (23*a*). The addition of nitronium ion to one face of the substrate is expected to shield that face and direct the ring closure, at the adjacent *ortho* position, to the opposite face. It is possible that a small amount of the *Z*-diastereoisomer of each compound could be formed in the nitration reactions, but remain undetected in solution. We estimate that this could not be as much as 5% of the amount of the predominant diastereoisomer and is probably substantially less. The diastereoisomers of 3,3,8-trimethyl-8-nitro-1,4-dioxaspiro[4,5]deca-6,9-dien-2-one, in which the spiro ring is attached *para* to the site of *ipso* addition, have identical nmr spectra. Compound **25***a*, with an identical pattern of nitro group, double bonds, and spiro ring, had a sharp melting point and must therefore have been isolated as a single diastereoisomer. We are unable to assign the stereochemistry of the diastereoisomer. Moreover, it is certainly possible that both diastereoisomers of **25***a* and **25***b* were formed in the nitration reactions since nitration of 4-methylphenoxyisobutyric acid gives both diastereoisomers of the *ipso*-nitrospirodienone (23*a*). However, we did not find any evidence of the presence of the second diastereoisomer when the mother liquor after crystallization of **24***a* was subjected to hplc.

The dienes **24***a*, **24***b*, and **25***a* are quite stable. They are unaffected on washing with aqueous sodium bicarbonate and do not aromatize on warming in organic solvents. The action of strong base (ammonia, sodium hydroxide) on **24***a* and **24***b* results in aromatization through deprotonation and ring opening to form the corresponding 3,5-di-*tert*-butyl-2,6-dinitrophenoxyacetic or isobutyric acid, respectively. Diene **25***a* reacts with aqueous sodium hydroxide to form 3,5-di-*tert*-butyl-2,4-dinitrophenol (**19**). A likely pathway (Scheme 7) involves $B_{AC}2$ cleavage of the lactone function to form hemiketal **26**, which undergoes base-catalysed regression to the dienone **17**, which in turn, under catalysis by the strong base, tautomerizes to **19**. A possible explanation for the proposition that lactone cleavage of **25***a* is preferred to deprotonation and ring opening (to give 3,5-di-*tert*-butyl-2,4-dinitrophenoxyacetic acid) is that deprotonation of **25***a* is sterically hindered and the product and the transition state leading to it would exhibit considerable steric strain as the nitro group moves into the plane of the flanking *tert*-butyl groups, one of which is buttressed. In the case of **24***a* the steric strain in the transition state and product of deprotonation and ring opening would be less and thus the lactone cleavage does not compete. An alternative (or contributing) explanation[3] of the difference in the behavior of **24***a* and **24***b* towards base is that lactone hydrolysis of **24***a* would be sterically hindered by the adjacent nitro group. This factor would be expected to be less significant for the *E*-diastereoisomer, the one obtained, than for the *Z*-diastereoisomer.

The dienes **24***a*, **25***a*, **24***b*, and **25***b* contain a secondary nitro

[2] Sumit Raymahasay. Personal communication.

[3] Suggested by a referee.

Can. J. Chem. Downloaded from www.nrcresearchpress.com by 210.87.254.6 on 09/06/12
For personal use only.

group. Dienes of similar structure have previously been obtained by rearrangement of *ipso*-nitro dienes (23). However, dienes containing a secondary nitro group have not been obtained before from nitration reactions. Normally the precursor secondary nitrocyclohexadienyl cation is too rapidly deprotonated for addition to compete. We may note that the nitrations of **23***a* and **23***b* represent cases in which, because of steric inhibition of deprotonation in the nitrocyclohexadienyl cation, addition of a nucleophile (ring closure) becomes a competitive pathway. The trapping reaction is further assisted by having the nucleophile already attached to the carbonium ion through the ether side chain. An unfavourable entropy factor that would reduce the rate of the trapping reaction is thereby removed.

Experimental

The ^{1}H nmr spectra at 90 MHz were determined on a Perkin–Elmer R32 spectrometer and ^{13}C nmr at 62.9 MHz on a Bruker WM250 instrument. Mass spectra were obtained on a Hitachi Perkin–Elmer RMU 7 spectrometer or a Finnigan 3300 system. Nitric acid was purified by distilling the fuming acid (600 cm^3) at 100 Pa from urea (20 g) and sulfuric acid (1 dm^3). 2,6- 2,4-, and 3,5-di-*tert*-butylphenol were obtained from Aldrich.

*3,5-Di-*tert*-butylphenoxyacetic acid (**20**a)*

A solution of 3,5-di-*tert*-butylphenol (4.0 g, 19 mmol) and sodium methoxide (1.05 g, 19 mmol) in methanol (120 cm^3) was heated under reflux for 2 h. The solution was evaporated to dryness, dry tetrahydrofuran was added, and the solution was again evaporated to dryness. Addition of tetrahydrofuran and evaporation to dryness were repeated. The sodium salt and 18-crown-6 (1.1 g) were dissolved in dry tetrahydrofuran (100 cm^3) and methyl bromoacetate (1.62 cm^3, 19 mmol) was added dropwise. A white solid formed almost immediately. Ether (100 cm^3) and water (100 cm^3) were added. The aqueous layer was separated, mixed with saturated brine (100 cm^3), and this solution was extracted with ether. The combined ether solution was dried and evaporated to yield white crystals (4.95 g) which contained 85% (by ^{1}H nmr) of the desired ester (80% yield). Methyl 3,5-di-*tert*-butylphenoxyacetate had ^{1}H nmr ($CDCl_3$) δ: 1.27 (s, 18, 3- and 5-C(CH_3)$_3$), 3.75 (s, 3, OCH_3), 4.60 (s, 2, CH_2), 6.75 (d, 2, J = 2 Hz, 2- and 6-*H*), and 7.06 (t, 1, J = 2 Hz, 4-*H*) ppm.

A mixture of the methyl ester (4 g) and aqueous KOH (0.5 mol in 250 cm^3) was stirred and heated under reflux for 1 h. The ester dissolved and, when the solution was cooled to ambient temperature, the sodium salt precipitated. This salt was soluble in ether. Acidification with concentrated hydrochloric acid, and extraction with ether (3 × 100 cm^3), followed by washing of the ether extract with brine (100 cm^3), drying ($MgSO_4$), and evaporation of the ether gave colourless crystals of **20***a* (3.45 g, 91%). On recrystallization from ether–pentane **20***a* had mp 141–142°C; ^{1}H nmr ($CDCl_3$) δ: 1.30 (s, 18, 3- and 5-C(CH_3)$_3$), 4.66 (s, 2, CH_2), 6.77 (d, 2, J = 2 Hz, 2- and 6-*H*), 7.08 (t, 1, J = 2 Hz, 4-*H*) ppm; ^{13}C nmr ($CDCl_3$) δ_C: 31.41 (C(CH_3)$_3$), 35.03 (C(CH_3)$_3$), 65.13 (CH_2), 109.21 (*C*-2 and *C*-6), 116.42 (*C*-4), 152.63 (*C*-3 and *C*-5), 157.18 (*C*-1), 174.85 (CO_2H) ppm; ms (70 eV) *m/e* (relative intensity): 265 (5), 264.176 (22, M_r $^{12}C_{16}{}^1H_{24}{}^{16}O_3$ = 264.173), 250 (17), 249 (100), 191 (12), 105 (13) 97 (10), 91 (11), 85 (13), 83 (10), 77 (11), 71 (16), 69 (14). *Anal.* calcd. for $C_{16}H_{24}O_3$: C 72.69, H 9.15; found: C 72.72, H 9.22.

*2-Methyl-2-(3,5-di-*tert*-butylphenoxy)propanoic acid (**20**b)*

3,5-Di-*tert*-butylphenol (8.24 g, 40 mmol) and sodium methoxide (2.16 g, 40 mmol) were dissolved in methanol (250 cm^3). The solution was stirred for 1.5 h and then evaporated to dryness. The sodium salt was dissolved in acetone, chloretone (1,1,1-trichloro-2-methyl-propan-2-ol) dihydrate (17.04 g, 80 mmol) was added, and the solution was stirred at 0°C while powdered sodium hydroxide (4.26 g, 106 mmol) was added. The stirred mixture was warmed to ambient temperature over several hours. The mixture was cooled to 0°C and the addition of sodium hydroxide was repeated twice. The mixture was stirred overnight at ambient temperature and then evaporated to dryness. The residue was dissolved in water (400 cm^3) and acidified (pH < 2) with hydrochloric acid. The suspension was extracted with ether, dried, and evaporated. The residue was heated to 75°C under reduced pressure (<100 Pa) to remove methacrylic acid. Crystallization from ether–pentane gave colourless crystals of **20***b* (7.3 g, 63%), mp 115–116°C; ^{1}H nmr ($CDCl_3$) δ: 1.28 (s, 18, C(CH_3)$_3$), 1.59 (s, 6, CH_3), 6.77 (d, 2, J = 2 Hz, 2- and 6-*H*), 7.09 (t, 1, J = 2 Hz, 4-*H*), 10.38 (br s, 1, CO_2H) ppm; ms (70 eV) *m/e* (relative intensity): 292.209 (22, M_r $^{12}C_{18}{}^1H_{28}{}^{16}O_3$ = 292.204), 206 (60), 191 (100); ms (chemical ionization, methane): 293 (M + 1).

*Nitration of 2,6-di-*tert*-butylphenol (**1**) in acetic anhydride*

A solution of nitric acid (0.95 g, 15 mmol) in acetic anhydride (4.25 cm^3) was prepared at −40°C, warmed to 0°C, and then cooled to −60°C and added, with stirring, to a solution of the phenol **1** (1.03 g, 5 mmol) in acetic anhydride (9.9 cm^3). A sample of the resulting solution was transferred immediately to an nmr tube at −60°C. The transfer pipette had been cooled previously in a cold finger filled with argon and immersed in solid carbon dioxide. The ^{1}H nmr spectrum was monitored at −60°C. The first spectrum showed 2,6-di-*tert*-butyl-4-nitrocyclohexa-2,5-dienone (**2**) (δ 5.93 (t, 1, J = 3 Hz, 4-*H*) and 6.95 (d, 2, J = 3 Hz, 3- and 5-*H*) ppm) and 2,6-di-*tert*-butyl-4-nitrophenol (**4**) (δ 6.97 (s, 1, O*H*) and 8.10 (s, 2, 3- and 5-*H*) ppm). After 60 min at −60°C, **4** was the only species present and the temperature of the nmr sample was then raised slowly. A yellow precipitate formed after 10 min at −40°C, but it dissolved on warming to −20°C. Doublets (J = 2.5 Hz) seen at δ 7.50 and 7.80 ppm were assigned to the 5- and 3- protons, respectively, of 2,6-di-*tert*-butyl-4,6-dinitrocyclohexa-2,4-dienone (**5**). At 0°C doublets (J = 2.5 Hz) appeared at δ 8.43 and 8.88 ppm, which were assigned to the 3- and 5-protons, respectively, of 2-*tert*-butyl-4,6-dinitrophenol (**6**). After 60 min at ambient temperature **6** was the only species present.

After stirring for 2 h at −60°C the bulk reaction mixture was poured into a stirred mixture of 30% aqueous ammonia (30 cm^3) and ether (50 cm^3), at −60°C. The resulting mixture was warmed to ambient temperature and the aqueous layer extracted with ether (3 × 50 cm^3). The ether solutions were combined, dried ($MgSO_4$), and the ether evaporated. Crystallization of the yellow-brown residue from methylene chloride gave **4** as yellow crystals (520 mg, 42%), mp 157–158°C (lit. (21) mp 153–154°C); ^{1}H nmr ($CDCl_3$) δ: 1.46 (s, 18, 2- and 6-C(CH_3)$_3$), 5.92 (s, 1, O*H*), 8.12 (s, 2, 3- and 5-*H*) ppm; ^{13}C nmr ($CDCl_3$) δ_C: 29.9 (C(CH_3)$_3$), 34.5 (C(CH_3)$_3$), 121.3 (*C*-3 and *C*-5), 136.7 (*C*-2 and *C*-6), 140.8 (*C*-4), 159.5 (*C*-1) ppm; ms (70 eV) *m/e* (relative intensity): 251.143 (24, M_r $^{12}C_{14}{}^1H_{21}{}^{14}N^{16}O_3$ = 251.152), 236 (100, M-CH_3), 208 (18).

In the preliminary experiments in which there was less efficient mixing of the nitrating and phenol solutions, and in which there was some warming of the reaction mixture during transfer to the nmr tube, an intermediate was formed which had a broad signal in the ^{1}H nmr spectrum from δ 6.6 to 6.8 ppm as well as a broad singlet at δ 1.29 ppm (recorded in [$^2H_6$]acetic anhydride as described below). This species was more stable than the dienone **2** but after 20 min at −40°C it gave **4**, then **5** and **6**. This intermediate was assigned as 2,6-di-*tert*-butyl-6-nitrocyclohexa-2,4-dienone (**3**). Experiments designed to generate this species in a reproducible significant amount were unsuccessful.

*Nitration of **1** in [$^2H_6$]acetic anhydride*

All solutions were prepared under an argon atmosphere. A stock nitrating mixture was prepared by adding [$^2H_6$]acetic anhydride (340 mm^3, 3.6 mmol) at 0°C to nitric acid (80 mg, 1.2 mmol), also at 0°C. A solution of **1** (21 mg, 0.10 mmol) in [$^2H_6$]acetic anhydride (200 mm^3) at −60°C was added, with stirring, to a portion (105 mm^3) of the nitric acid solution to which tetramethylsilane had been added and which was also at −60°C. The resulting solution was stirred at −60°C for 10 min, then transferred to an nmr tube. The reaction was monitored, initially at −60°C. A singlet at δ 1.24 ppm, which decreased in size with time, was assigned to the *tert*-butyl protons of **2** and a

Can. J. Chem. Downloaded from www.nrcresearchpress.com by 210.87.254.6 on 09/06/12
For personal use only.

Can. J. Chem. Downloaded from www.nrcresearchpress.com by 210.87.254.6 on 09/06/12
For personal use only.

singlet at δ 1.45 ppm, which increased in size with time, was assigned to the *tert*-butyl protons of **4**. On warming, peaks of the ring protons of **5** appeared in conjunction with singlets at δ 1.20 and 1.28 ppm. On further warming the ring proton peaks of **6** appeared in conjunction with a singlet at δ 1.47 ppm.

^{13}C nuclear magnetic resonance spectra of 2 and 5

The reaction mixture was prepared in acetic anhydride, as described above, except that CD_2Cl_2 (1.5 cm^3) was added to the nitrating mixture for a deuterium lock. The mixture was stirred at −60°C for 10 min and then a sample (3 cm^3) was transferred to the nmr sample tube at −60°C, as described. The ^{13}C nmr spectrum of **2** was recorded at −70°C, δ_C: 28.0 (CH_3), 34.8 ($C(CH_3)_3$), 80.0 (*C*-4), 130.1 (*C*-3 and *C*-5), 149.2 (*C*-2 and *C*-6), 184.4 (*C*-1) ppm.

In a separate experiment the reaction mixture was prepared at −60°C and then allowed to warm to −20°C. The yellow nitrophenol **4** crystallized but redissolved after 30 min. The ^1H nmr of the solution at this stage showed that **5** was the only species present in significant amount. The mixture was cooled to −40°C and the ^{13}C nmr spectrum recorded ($CDCl_3$ lock), δ_C: 24.13 ($C(CH_3)_3$), 27.53 ($C(CH_3)_3$), 34.57 (2-$C(CH_3)_3$), 41.72 (6-$C(CH_3)_3$), 99.95 (*C*-6), 127.29 (*C*-5), 131.97 (*C*-3), 145.73 and 146.09 (*C*-2 and *C*-4), 189.44 (*C*-1) ppm.

Nitration of 1 in [^2H]chloroform

A solution of **1** (1.03 g, 5 mmol) in [^2H]chloroform (3 cm^3) at −60°C was added, with stirring, to a mixture of nitric acid (473 mg, 7.5 mmol) and [^2H]chloroform (1 cm^3) at −60°C. After a few minutes a sample was transferred to a cold nmr tube and the reaction was monitored at −60°C. The first spectrum showed two species. The 2,5-dienone **2** (δ 5.62 (t, 1, J = 4 Hz, 4-*H*) and 6.79 (d, 2, J = 4 Hz, 3-*H* and 5-*H*) ppm) disappeared at −40°C. The 2,4-dienone **3** (δ 6.47 (br) ppm) disappeared slowly at ambient temperature. Both intermediates gave 4 (δ 8.05 (s) ppm). In the first experiment **3** was the major species formed initially (75%) but in subsequent experiments **2** was the major species.

Additional nitric acid (473 mg, 7.5 mmol) at −60°C was added, with stirring, to the bulk reaction mixture at −60°C. The solution was allowed to warm to ambient temperature and the solvent evaporated. On crystallization from ether–pentane yellow crystals of **6** were obtained, mp 128–131°C (lit. (24) mp 124–125°C); ^1H nmr ($CDCl_3$) δ: 1.48 (s, 9, $C(CH_3)_3$), 8.41 (d, 1, J = 3.5 Hz, 3-*H*), 8.87 (d, 1, J = 3.5 Hz, 5-*H*) ppm; ms (methane CI) *m/e* (relative intensity): 281 (5, M + 41), 269 (14, M + 29), 242 (12), 241 (100, M + 1).

Nitration of 4 in [^2H]chloroform

Nitric acid (630 mg, 10 mmol) at −40°C was added to trifluoroacetic anhydride (0.88 cm^3, 10 mmol), also at −40°C. The mixture was cautiously warmed to 0°C, [^2H]chloroform was added, and the solution cooled to −40°C to form a white slush. A solution of **4** (1.03 g, 4 mmol) in [^2H]chloroform (4 cm^3) at −40°C was added, with stirring, and a dark red solution was formed. The ^1H nmr spectrum showed **5** (δ 7.55 (d) and 7.82 (d) ppm, J = 3 Hz) and **6** (δ 8.49 (d) and 9.04 (d) ppm, J = 3 Hz), in an 82:18 ratio. At −30°C **5** cleaved to **6**. The bulk reaction mixture was washed twice in a cold (−20°C) separatory funnel with saturated brine, previously cooled at −20°C until it began to freeze. The resulting chloroform solution contained **5** (61%) and **6** (39%). In this washed solution the dienone **5** was more stable, decomposing to **6** slowly at +10°C and surviving for a few minutes at +35°C.

*Nitration of 2,4-di-*tert*-butylphenol (7)*

On nitration of **7** in acetic anhydride the initial ^1H nmr spectrum at −60°C showed **7** and 2,4-di-*tert*-butyl-6-nitrophenol (**9**) (δ 7.75 (d, 1, J = 3 Hz, 3-H) and 7.96 (d, 1, J = 3 Hz, 5-H) ppm). After 15 min at −60°C formation of **9** was complete. No intermediate species was seen and repetition of the reaction at −70°C gave the same result. On warming to −40°C **9** disappeared and equal sized doublets (J = 3 Hz) appeared at δ 7.31 and 8.06 ppm, assigned to 2,4-di-*tert*-butyl-4,6-dinitrocyclohexa-2,5-dienone (**10**). At 0°C **10** disappeared and the doublets (J = 3 Hz) at δ 8.44 and 8.89 ppm of 2-*tert*-butyl-4,6-dinitrophenol **6** appeared. The nitrophenol **9** was isolated after quenching the bulk reaction mixture at −60°C. On crystallization from ethanol–water it had mp 59–61°C (lit. (25) mp 62.5–63°C); ^1H nmr ($CDCl_3$) δ: 1.31 (s, 9, $C(CH_3)_3$), 1.44 (s, 9, $C(CH_3)_3$), 7.65 (d, 1, J = 2.5 Hz, 3-*H*), 7.96 (d, 1, J = 2.5 Hz, 5-*H*); ms (methane CI) *m/e* (relative intensity): 292 (5, M + 41), 281 (3), 280 (14, M + 29), 254 (2), 253 (17), 252 (100, M + 1); ms (70 eV) *m/e* (relative intensity): 251 (11, M), 236 (69), 162 (24), 145 (11), 132 (19), 131 (19), 129 (13), 128 (15), 117 (12), 116 (13), 115 (30), 105 (21), 103 (14), 91 (44), 79 (22), 78 (13), 77 (46).

On nitration of **7** with nitric acid in [^2H]chloroform at −60°C the initial ^1H nmr spectrum showed that all of **7** had reacted and **9** was the major species present. The minor species survived only 10 min at −60°C before conversion into **9** and was assigned as 2,4-di-*tert*-butyl-6-nitrocyclohexa-2,4-dienone (**8**), δ 5.88 (br s, 1,6-*H*), 6.15 (br s, 1,5-*H*), 7.01 (br s, 1,3-*H*) ppm.

Nitration of **9** with nitric acid and trifluoroacetic anhydride in [^2H]chloroform at −40°C gave a mixture of the dienone **10** (65%) (δ 1.20 (s, 9, $C(CH_3)_3$), 1.32 (s, 9, $C(CH_3)_3$), 7.36 (d, 1, J = 3 Hz, 3-*H*), and 8.06 (d, 1, J = 3 Hz, 5-*H*) ppm) and the dinitrophenol **6** (δ 1.57 (s, 9, $C(CH_3)_3$), 8.49 (d, 1, J = 3 Hz, 3-*H*) and 9.03 (d, 1, J = 3 Hz, 5-*H*) ppm). The dienone **10** slowly cleaved to **6** at −40°C and rapidly at −30°C. After washing the bulk nitration solution with cold brine the resulting solution contained **10** and **6** in a 45:55 ratio and in the solution **10** was converted into **6** very slowly at 0°C and even survived for a few minutes at +35°C.

*Nitration of 3,5-di-*tert*-butylphenol (11) in acetic anhydride*

The initial ^1H nmr spectrum at −60°C of the nitration of **11** in acetic anhydride showed a species (40%) assigned as 3,5-di-*tert*-butyl-6-nitrocyclohexa-2,4-dienone (**12**) (δ 5.85 (s, 1, 6-*H*), 5.93 (s, 1, 2-*H*), and 6.70 (s, 1, 4-*H*) ppm), which disappeared with time, and 3,5-di-*tert*-butyl-2-nitrophenol (**14**) (60%) (δ 7.00 (s, 1, 6-*H*), 7.09 (s, 1, 4-*H*), 8.20 (br s, 1, O*H*) ppm), which increased with time and which was the only species present after 45 min at −60°C. On warming to −20°C no additional species was seen and the nmr tube filled with precipitate so that no more spectra could be recorded. The nitrophenol **14** was isolated on quenching the bulk reaction mixture at −60°C and was crystallized from chloroform, mp 122–124°C (lit. (26) mp 127–128°C); ^1H nmr ($CDCl_3$) δ: 1.26 (s, 9, 5-$C(CH_3)_3$), 1.37 (s, 9, 3-$C(CH_3)_3$, 6.86 (br s, 1, O*H*), 6.92 (d, 1, J = 2 Hz, 6-*H*), 7.08 (d, 1, J = 2 Hz, 4-*H*) ppm; ^{13}C nmr ($CDCl_3$) δ_C: 30.95 ($C(CH_3)_3$), 31.04 ($C(CH_3)_3$), 35.24 ($C(CH_3)_3$), 36.39 ($C(CH_3)_3$), 113.02 (*C*-6), 117.87 (*C*-4), 137.66 (*C*-2), 143.72 (*C*-3), 149.13 (*C*-1), 155.57 (*C*-5) ppm; ms (70 eV) *m/e* (relative intensity): 251.141 (47, M_r $^{12}C_{14}{}^1H_{21}{}^{14}N^{16}O_3$ = 251.152), 236 (M − CH_3, 100). No 3,5-di-*tert*-butyl-4-nitrophenol (**15**) was detected. Nitration of **11** in [$^2H_6$]acetic anhydride at −60°C allowed the observation of the *tert*-butyl signals of **12** at δ 1.17 ppm (br s, 18) and of **14** at δ 1.26 (s, 9) and 1.32 (s, 9) ppm, as well as the signals of the nuclear hydrogens. The ^{13}C spectrum of **12** was obtained at −70°C; δ_C: 26.0 ($C(CH_3)_3$), 27.3 ($C(CH_3)_3$), 35.1 ($C(CH_3)_3$), 36.2 ($C(CH_3)_3$), 85.6 (*C*-6), 114.5 (*C*-2), 121.8 (*C*-4), 148.0 (*C*-5), 154.4 (*C*-3), 188.5 (*C*-1) ppm. The gated ^{13}C nmr spectrum was obtained in a separate experiment and the *C*-6 signal was split into a doublet (J_{HC} = 148 Hz).

Nitration of 11 in [^2H]chloroform

Nitration of **11** with nitric acid in [^2H]chloroform at −60°C showed only unreacted starting material in the initial spectrum, but after 10 min at −50°C there were three major species present: **12** (δ 5.68 (br s, 1, 6-*H*), 5.98 (br s, 1, 2-*H*), and 6.60 (br s, 1, 4-*H*) ppm), **14** (δ 6.96 (d, 1, J = 1.5 Hz, 6-*H*) and 7.04 (d, 1, J = 1.5 Hz, 4-*H*) ppm), and 3,5-di-*tert*-butyl-4-nitrocyclohexa-2,5-dienone (**13**) (δ 6.30 (s, 1, 4-*H*), 6.43 (s, 2, 2-*H* and 6-*H*) ppm). Dienone **12** tautomerized to **14** at −30°C. Dienone **13** survived for a few minutes at ambient temperature and also isomerized to **14**. The ^{13}C nmr of **13** was obtained by repeating the nitration using a smaller excess of nitric acid. The reaction mixture was then warmed to −20°C, at which temperature all of the dienone **12** had tautomerized to the nitrophenol **14**. The solution then contained (by ^1H nmr) dienone **13** (28%), nitrophenol **14** (56%), 3,5-di-*tert*-butyl-2,4-dinitrocyclohexa-2,5-dienone (**17**) (6%) (δ 6.49

Can. J. Chem. Downloaded from www.nrcresearchpress.com by 210.87.254.6 on 09/06/12
For personal use only.

(s, 1) and 6.53 (s, 1) ppm), and 3,5-di-*tert*-butyl-2,6-dinitrophenol (**18**) (11%). The solution (~6 cm^3) was concentrated to 1 cm^3 by evaporation at −20°C and the ^{13}C nmr of this solution was recorded at −20°C. Subtraction of the peaks due to phenols **14** and **18** gave the spectrum of **13**: δ_C 28.54 ($C(CH_3)_3$), 37.18 ($C(CH_3)_3$), 82.62 (*C*-4), 127.67 (*C*-2 and *C*-6), 160.31 (*C*-3 and *C*-5), and 189.59 (*C*-1) ppm. Peaks assigned to the dinitrodienone **17** appeared at δ_C 28.30 ($C(CH_3)_3$), 37.45 ($C(CH_3)_3$), 37.74 ($C(CH_3)_3$), 84.06 (*C*-4), and 126.93 (*C*-6).

When the nitration was repeated using equal amounts (5 mmol) of nitric acid and **11** at −60°C, and the reaction quenched with ammonia after warming to −50°C, only unreacted **11** was isolated after work-up. However, when the reaction mixture was warmed to −40°C the dienones **12** (31%) and **13** (31%) and the nitrophenol **14** (38%) were formed. The reaction mixture was then warmed to −20°C, to tautomerize **12** to **14**, and then cooled to −50°C and poured into an excess of ammonia in methanol at −50°C. The solution was warmed to ambient temperature and evaporated to a gum which contained the nitrophenols **14** (77% by ^1H nmr) and **15** (23%). Recrystallization of the residue from pentane gave **14**. Chromatography on silica with pentane and ether–pentane mixtures gave **14** in the initial fractions and **15** in the later fractions. After recrystallization from pentane **15** had mp 129–131°C; ^1H nmr ($CDCl_3$) δ: 1.30 (s, 18, 3- and 5-C(CH_3)$_3$), 6.90 (s, 2, 2-*H* and 6-*H*) ppm; ^{13}C nmr ($CDCl_3$) δ_C: 31.00 ($C(CH_3)_3$), 36.12 ($C(CH_3)_3$), 113.10 (*C*-2 and *C*-6), 143.34 (*C*-3 and *C*-5), 143.69 (*C*-4), 155.04 (*C*-1) ppm; ms (70 eV) *m/e* (relative intensity): 251.160 (24, M_r $^{12}C_{14}{}^1H_{21}{}^{14}N^{16}O_3$ = 251.152), 236 (100); ms (methane CI) *m/e* (relative intensity): 292 (3, *M* + 41), 281 (3), 280 (13, *M* + 29), 253 (17), 252 (100, *M* + 1), 251 (14).

Nitration of ***14*** *in [^2H]chloroform: 3,5-di-*tert*-butyl-2,6-dinitrophenol (**18**) and 3,5-di-*tert*-butyl-2,4-dinitrophenol (**19**)*

A solution of **14** (1.0 g, 4 mmol) in [^2H]chloroform (4 cm^3) at −40°C was added to nitric acid (252 mg, 4 mmol) at −40°C. After stirring for a few min at −40°C and 20 min at −30°C the solution was shown (^1H nmr) to contain both the dinitrodienone **17** (δ 1.26 (s, 9), 1.31 (s, 9), 6.46 (s, 1), and 6.50 (s, 1) ppm) and the dinitrophenol **18** (δ 1.37 (s, 18) and 7.30 (s, 1) ppm). On warming this nmr sample to ambient temperature and dissolving all of the material which precipitated by addition of acetone, the only compound present was **18**. The bulk reaction mixture, which had been maintained at −30°C, was poured into a solution of excess ammonia in methanol (30 cm^3) at −50°C. Hydrogen chloride was passed into the resulting solution, stirred at 0°C, until the solution was strongly acidic. Ammonium chloride was removed by filtration. The filtrate contained (^1H nmr, after evaporation) **18** and its 2,4-dinitro isomer **19** (δ 1.34 (s, 9), 1.42 (s, 9), 7.35 (s, 1) ppm) in a 60:40 ratio. This mixture was absorbed onto silica (3 g), then chromatographed on silica (20 g), eluting with ether–pentane (1:19). The first fraction (200 cm^3) contained only **18**, the second contained both **18** and **19**, and the third contained pure **19**. The dinitrophenol **18** was recrystallized from ether–pentane and had mp 196–197°C; ^1H nmr ($CDCl_3$) δ: 1.37 (s, 18, 3- and 5-C(CH_3)$_3$), 7.28 (s, 1, 4-*H*) ppm; ^{13}C nmr ($CDCl_3$) δ_C: 30.56 ($C(CH_3)_3$), 36.73 ($C(CH_3)_3$), 120.02 (*C*-4), 138.86 (*C*-2 and *C*-6), 142.72 (*C*-1), 145.11 (*C*-3 and *C*-5) ppm; ms (methane CI) *m/e* (relative intensity): 337 (5, *M* + 41), 326 (3), 325 (14, *M* + 29), 299 (2), 297 (100, *M* + 1), 296 (8). Dinitrophenol **19** had mp 175°C (dec.); ^1H nmr ($CDCl_3$/[$^2H_6$]acetone) δ: 1.33 (s, 9), 1.40 (s, 9), 7.36 (s, 1) ppm; ms (70 eV) *m/e* (relative intensity): 297 (16), 296.128 (100, M_r $^{12}C_{14}{}^1H_{20}{}^{14}N_2{}^{16}O_5$ = 296.137), 282 (15), 281 (98), 279 (18).

*Nitration of 3,5-di-*tert*-butylphenoxyacetic acid (**20**a) in acetic anhydride/[^2H]chloroform*

A solution of the acid **20***a* (1 mmol) in [^2H]chloroform (1 cm^3) was added dropwise over 5 min, with stirring, to a mixture of nitric acid (3 mmol) and acetic anhydride (1 cm^3) at −60°C. After a further 10 min at −60°C, a sample was transferred to an nmr tube at −78°C using a precooled pipette. The bulk of the reaction mixture was cooled to −78°C. The ^1H nmr spectra taken at −70°C and at −20°C showed only 3,5-di-*tert*-butyl-2-nitrophenoxyacetic acid (**23***a*); δ: 4.78 (s, CH_2), 6.92 (d, *J* = 2 Hz, 6-*H*), 7.18 (d, *J* = 2 Hz, 4-*H*) ppm. At +20°C an additional CH_2 group, attributed to the mixed anhydride of acetic acid and nitrophenoxyacetic acid, appeared at δ 4.98 ppm. There was no significant change in the aromatic region. After 5 min at +20°C there was 90% acid and 10% mixed anhydride. After 40 min at +40°C, 40% of the mixture was the mixed anhydride and the sample was poured into ether at −78°C. Ammonia gas was blown into the stirred solution until it was strongly alkaline. Water was added and the mixture was warmed to ambient temperature. The organic layer was separated and the aqueous layer was extracted with methylene chloride (2 × 25 cm^3). Drying and removal of the solvent from the combined organic extract gave reddish brown crystals of 3,5-di-*tert*-butyl-2-nitrophenoxyacetamide, ^1H nmr ($CDCl_3$) δ: 1.31 (s, 9, C(CH_3)$_3$), 1.37 (s, 9, C(CH_3)$_3$), 4.55 (s, 2, CH_2), 6.43 (br s, 2, NH_2), 6.88 (d, 1, *J* = 1.5 Hz, 6-*H*), 7.18 (d, 1, *J* = 1.5 Hz, 4-*H*) ppm. The aqueous layer was acidified (pH 1) with concentrated hydrochloric acid and extracted with ether (3 × 25 cm^3). Evaporation of the solvent from the dried ether solution gave the acid **23***a* as pale yellow crystals. Aqueous $NaHCO_3$ was added to the bulk of the reaction mixture at −78°C. It was allowed to warm to ambient temperature and enough solid $NaHCO_3$ to neutralize all the acid was added. After stirring for 3 h at ambient temperature, it was acidified (pH 1), extracted with ether (3 × 35 cm^3), and the ether solution was dried ($MgSO_4$). Removal of solvent gave the acid **23***a*.

Repetition of the nitration on a 2.2-mmol scale, at −60°C for 10 min followed by work-up, gave **23***a* (96%). After recrystallization from ether–pentane, **23***a* was obtained as pale yellow crystals, mp 187–188°C; ^1H nmr in $CDCl_3$ δ: 1.27 (s, 9, C(CH_3)$_3$), 1.35 (s, 9, C(CH_3)$_3$), 4.66 (s, 2, CH_2), 6.80 (d, 1, *J* = 2 Hz, 6-*H*), 7.17 (d, 1, *J* = 2 Hz), and 8.12 (br s, 1, CO_2H) ppm; ^{13}C nmr ($CDCl_3$) δ_C: 30.79 and 31.14 (3- and 5-C(CH_3)$_3$), 35.39 and 36.06 (3- and 5-$C(CH_3)_3$), 66.37 (CH_2), 109.16 (*C*-6), 118.49 (*C*-4), 139.97 (*C*-2), 141.59 (*C*-3), 149.03 (*C*-5), 153.62 (*C*-1), and 172.97 (CO_2H).

Nitration of ***23***a *in [^2H]chloroform*

A mixture of nitric acid (3 mmol) and acetic anhydride (1 cm^3) was cooled to −40°C and trifluoroacetic anhydride (423 mm^3, 3 mmol) was added with stirring. A solution of **23***a* (1 mmol) in [^2H]chloroform (1 cm^3) was added dropwise to the resulting mixture. Some precipitate was formed. After 10 min at −40°C, an nmr sample was removed using a precooled pipette and the bulk of the reaction mixture was cooled to −78°C. The reaction of the nmr sample at −40°C was followed by ^1H nmr. The results are qualitative because the sample was withdrawn from a heterogeneous mixture. After 20 min at −40°C, 48% of the starting material had reacted to give two new compounds, namely, 7,9-di-*tert*-butyl-6,10-dinitro-1,4-dioxaspiro[4,5]deca-6,8-dien-2-one (**24***a*, 31%) and 7,9-di-*tert*-butyl-6,8-dinitro-1,4-dioxaspiro[4,5]deca-6,9-dien-2-one (**25***a*, 17%). The sample was warmed to −30°C and, after 10 min, the reaction mixture had the composition 14% **23***a*, 56% **24***a*, and 30% **25***a*. After 20 min at −30°C, the reaction mixture was homogeneous and all the starting material had disappeared to give **24***a* (65%) and **25***a* (35%). No noticeable change took place on standing at −20°C for 15 min.

The above nmr sample was added to the bulk of the reaction mixture at −78°C and the mixture was sitrred at −30°C for 15 min and then at −20°C for 10 min. The mixture became homogenous after 3 min at −20°C. The ^1H nmr taken at −30°C, of a sample withdrawn from the reaction mixture after stirring for 10 min at −20°C, showed that all of the starting material had reacted to give **24***a* (67%) and **25***a* (33%). The mixture was poured with stirring into a mixture of excess $NaHCO_3$ solution and ice, in an ice bath, and stirred for 1 h. Extraction with ice-cold ether (3 × 20 cm^3), drying, and removal of the solvent at −20°C gave a pale yellow solid (320 mg). The ^1H nmr spectrum of the solid in $CDCl_3$ at 0°C showed only **24***a* (67%) and **25***a* (33%).

Nitration of ***20***a *in [^2H]chloroform – acetic anhydride – trifluoroacetic anhydride. Preparation of dienes* ***24***a *and* ***25***a

A preliminary small scale (1 mmol) nitration of **20***a* showed that the acid **23***a*, formed at −60°C, can be made to react further to give dienes **24***a* and **25***a*, thus eliminating the need for the preparation of the

Can. J. Chem. Downloaded from www.nrcresearchpress.com by 210.87.254.6 on 09/06/12
For personal use only.

mononitrophenoxyacetic acid.

Acid **20***a* (5 mmol) in $CDCl_3$ (5 cm^3) was added, dropwise with stirring (5 min), to a nitrating mixture, prepared from HNO_3 (20 mmol) and Ac_2O (5 cm^3), at −60°C. The mixture was stirred for a further 10 min at −60°C. The ^1H nmr (at −70°C) showed only the mononitrophenoxyacetic acid (**23***a*). The temperature of the reaction mixture was raised to −40°C and trifluoracetic anhydride (20 mmol, 2.8 cm^3) was added over 2 min and the mixture was stirred for 5 min at −40°C, 15 min at −30°C, and 10 min at −20°C. At −40°C a precipitate was formed that completely dissolved after 5 min at −20°C to give a clear yellow solution. The ^1H nmr of a sample at this stage showed only **24***a* (67%) and **25***a* (33%).

The reaction mixture was poured with stirring into excess saturated $NaHCO_3$–ice mixture at 0°C, cooled in an ice bath, and stirred for 1 h. The mixture was extracted with cold (0°C) ether (3 × 150 cm^3) and the extract was dried over $MgSO_4$. Removal of the solvent at −20°C gave a pale yellow solid (1.69 g) composed of **24***a* (68%) and **25***a* (32%). When the nmr sample was heated to 35°C for 10 min no change in the spectrum was noted.

Two recrystallizations of the crude product from ether–pentane gave pure **24***a* (474 mg), mp 149–150°C (dec.); uv (hexane): 274.8 (185) and 208.9 nm (274 m^2 mol^{-1}); ir (KBr): 1213 (C—O), 1360, 1522 (vinylic NO_2), 1558 (alkyl NO_2), and 1809 (C=O) cm^{-1}; ^1H nmr ($CDCl_3$) δ: 1.16 (s, 9, $C(CH_3)_3$), 1.21 (s, 9, $C(CH_3)_3$), 4.43 (d, 1, J = 14 Hz, 3-*H*), 4.51 (d, 1, J = 14 Hz, 3-*H*), 5.14 (s, 1, 10-*H*), 6.47 (s, 1, 8-*H*); ^{13}C nmr ($CDCl_3$, 0°C) δ_C: 27.88 and 28.09 (7- and 9-$C(CH_3)_3$), 36.41 and 36.67 (7- and 9-$C(CH_3)_3$), 64.51 (*C*-3), 85.22 (*C*-10), 104.81 (*C*-5), 124.04 (*C*-8), 136.94 (*C*-6), 142.17 (*C*-9), 143.08 (*C*-7), and 167.97 (*C*-2); ms *m/e*: 354.149 (M_r $^{12}C_{16}{}^1H_{22}{}^{14}N_2{}^{16}O_7$ = 354.143). *Anal.* calcd. for $C_{16}H_{22}N_2O_7$: C 54.23, H 6.25, N 7.90; found: C 54.26, H 6.20, N 7.80.

Part of the mother liquor containing **24***a* and **25***a* was subjected to preparative hplc on a semipreparative silica column using CH_2Cl_2 and hexane as eluents, and **25***a* (46 mg) was separated. Crystallization from ether–pentane gave colourless crystals of **25***a* (24 mg), mp 102–104°C (dec.); uv (hexane): 223 nm (312 m^2 mol^{-1}); ir (KBr): 1215 (C—O), 1370, 1532 (vinylic NO_2), 1568 (alkyl NO_2), 1820 (C=O) cm^{-1}; ^1H nmr ($CDCl_3$, 250 MHz) δ: 1.24 (s, 9, $C(CH_3)_3$), 1.27 (s, 9, $C(CH_3)_3$), 4.35 (d, 1, J = 15.1 Hz, 3-*H*), 4.45 (d, 1, J = 15.1 Hz, 3-*H*), 6.02 (s, 1, 8-*H* or 10-*H*), and 6.08 (s, 1, 10-*H* or 8-*H*) ppm; ^{13}C nmr ($CDCl_3$, 0°C) δ_C: 28.20 (9-$C(CH_3)_3$), 29.11 (7-$C(CH_3)_3$), 36.69 (9-$C(CH_3)_3$), 37.87 (7-$C(CH_3)_3$), 64.02 (*C*-3), 82.34 (*C*-8), 102.63 (*C*-5), 124.03 (*C*-6), 126.70 (*C*-10), 139.97 (*C*-9), 148.21 (*C*-7), 168.94 (*C*-2). *Anal.* calcd. for $C_{16}H_{22}N_2O_7$: C 54.23, H 6.25, N 7.90; found: C 53.68, H 6.21, N 7.78.

*Reaction of **24**a with aqueous sodium hydroxide in tetrahydrofuran*

Aqueous NaOH solution (2 cm^3, 0.2 mmol) was added dropwise (2 min) to a well-stirred solution of spirodiene **24***a* (35.4 mg, 0.1 mmol) in THF (1 cm^3), and stirring was continued for a further 30 min. As soon as the NaOH was added, the solution turned yellow. After the reaction, excess solid NH_4Cl was added to neutralize the excess NaOH. THF was removed on a rotavapor, saturated NaCl (5 cm^3) was added, and the mixture was extracted with ether (3 × 15 cm^3). The extract was dried ($MgSO_4$). Removal of the solvent gave 3,5-di-*tert*-butyl-2,6-dinitrophenoxyacetic acid as a light yellow solid (32 mg); ^1H nmr ($(CD_3)_2CO$) δ: 1.41 (s, 18, 3- and 5-$C(CH_3)_2$), 4.57 (s, 2, CH_2), 7.72 (s, 1, 4-*H*) ppm.

*Reaction of **25**a with aqueous sodium hydroxide in tetrahydrofuran*

Aqueous NaOH solution (1 cm^3, 0.1 mmol) was added (1 min) with stirring to a solution of diene **25***a* (17.7 mg, 0.05 mmol) in THF (0.5 cm^3). The solution turned yellow. The solution was stirred a further 30 min and worked up as described in the previous reaction to give 3,5-di-*tert*-butyl-2,4-dinitrophenol (**19**) (12 mg); ^1H nmr ($CDCl_3$) δ: 1.35 (s, 9, 5-$C(CH_3)_3$), 1.44 (s, 9, 3-$C(CH_3)_3$), 7.15 (s, 1, 6-*H*) ppm. The dinitrophenol **19** obtained from **25***a* is identical to the one obtained earlier in the nitration of **14**, after the nitration mixture had been reacted with ammonia in methanol.

*Nitration of α-(3,5-di-*tert*-butylphenoxy)isobutyric acid (**20**b) in acetic anhydride*

A solution of **20***b* (1.46 g, 5 mmol) in acetic anhydride (3 cm^3) at −60°C was added to a nitrating mixture prepared from nitric acid (0.95 g, 15 mmol) and acetic anhydride (1.72 cm^3), also at −60°C. The ^1H nmr spectrum taken a few minutes after mixing, 6.97 (br s, 1) and 7.29 (br s, 1) ppm, showed no change on warming the sample to ambient temperature. The reaction mixture was poured into a mixture of 30% aqueous ammonia (15 cm^3) and ether (50 cm^3) at 0°C. The ether layer was separated and dried and the ether evaporated to an oil which on crystallization from ether–pentane gave colourless crystals of α-(3,5-di-*tert*-butyl-2-nitrophenoxy)isobutyramide (325 mg), mp 146–148°C; ^1H nmr ($CDCl_3$) δ: 1.28 (s, 9, $C(CH_3)_3$), 1.36 (s, 9, $C(CH_3)_3$), 1.54 (s, 6, $(CH_3)_2$), 6.00 (br s, 1, NH_2), 6.54 (br s, 1, NH_2), 6.98 (d, 1, J = 2 Hz, 6-*H*), 7.21 (d, 1, J = 2 Hz, 4-*H*) ppm; ms (methane CI) *m/e* (relative intensity): 377 (8, M + 41), 365 (24, M + 29), 337 (100, M + 1).

*Nitration of **20**b in trifluoroacetic anhydride/[^2H]chloroform*

A solution of **20***b* (1.46 g, 5 mmol) in [^2H]chloroform (4 cm^3) at −60°C was added to a mixture of nitric acid (473 mg, 7.5 mmol) in trifluoroacetic anhydride at −60°C. The ^1H nmr spectrum indicated the formation of α-(3,5-di-*tert*-butyl-2-nitrophenoxy)isobutyric acid (**23***b*, δ 6.87 (s, 1) and 7.25 (s, 1) ppm) and 7,9-di-*tert*-butyl-3,3-dimethyl6,10-dinitro-1,4-dioxaspiro[4,5]deca-6,8-dien-2-one (**24***b*, δ 5.17 (s, 1) and 6.50 (s, 1) ppm). The ratio of **24***b* to **23***b* increased with time. Evaporation of the solvent from the reaction mixture gave an oil which was dissolved in ether and washed with aqueous sodium bicarbonate. The ether layer was separated, dried, and evaporated and the residue recrystallized from chloroform–pentane to give **24***b*, mp 154–158°C (dec.); uv (MeOH) λ_{max} (ε): 215 (645), 274 (524 m^2 mol^{-1}) nm; ^1H nmr ($CDCl_3$) δ: 1.15 (s, 9, $C(CH_3)_3$), 1.27 (s, 9, $C(CH_3)_3$), 1.44 (s, 3, 3-CH_3), 1.64 (s, 3, 3-CH_3), 5.16 (s, 1, 10-*H*), 6.44 (s, 1, 8-*H*) ppm; ^{13}C nmr ($CDCl_3$) δ_C: 24.63 (3-CH_3), 25.78 (3-CH_3), 27.95 (7- and 9-$C(CH_3)_3$), 36.31 ($C(CH_3)_3$), 36.44 ($C(CH_3)_3$), 79.32 (*C*-3), 86.56 (*C*-10), 102.03 (*C*-5), 123.88 (*C*-8), 137.70 (*C*-6), 141.58 and 141.64 (*C*-7 and *C*-9), 172.55 (*C*-2) ppm; ms (methane CI) *m/e* (relative intensity): 411 (5, M + 29), 383 (3, M + 1), 377 (5), 366 (3), 365 (9), 337 (85), 319 (4), 318 (3), 306 (3), 291 (5), 290 (5), 280 (17), 252 (100). The ^1H nmr of the crude nitration product showed that a second diene, presumably **25***b*, was formed in the ratio **24***b*/**25***b* = 85:15. This diene was not isolated but, from the mixture, it had ^1H nmr ($CDCl_3$) δ: 1.23 (s, 9, $C(CH_3)_3$), 1.27 (s, 9, $C(CH_3)_3$), 1.43 (s, 3, CH_3), 1.60 (s, 3, CH_3), 6.10 (s, 1, 4-*H* or 6-*H*), 6.18 (s, 1, 6-*H* or 4-*H*) ppm. The structural assignment is supported by the close similarity of the ^1H nmr spectra for corresponding hydrogen atoms of **25***a* and **25***b*. The interfacial layer from the sodium bicarbonate extraction was partitioned between ether and aqueous acid. The resulting ethereal solution was dried and the ether evaporated to give a mixture of crystals and oil from which the oil was removed by washing with pentane to give the acid **23***b*, mp 130–145°C (dec.); ^1H nmr ($CDCl_3$) δ: 1.27 (s, 9, $C(CH_3)_3$), 1.36 (s, 9, $C(CH_3)_3$), 1.58 (s, 6, $C(CH_3)_2$), 6.95 (d, 1, J = 2 Hz, 6-*H*), 7.19 (d, 1, J = 2 Hz, 4-*H*), 10.70 (br s, 1, COO*H*) ppm; ^{13}C nmr (CD_3OD) δ_C: 25.22 ($C(CH_3)_2$), 31.20 and 31.43 ($C(CH_3)_3$), 36.09 and 36.81 ($C(CH_3)_3$), 81.83 ($C(CH_3)_2$), 115.38 (*C*-6), 119.14 (*C*-4), 142.01 (*C*-3), 143.44 (*C*-2), 148.41 (*C*-5), 153.97 (*C*-1), 177.17 (*C*OOH) ppm; ms (methane CI) *m/e* (relative intensity): 378 (2, M + 41), 367 (4), 366 (16, M + 29), 339 (5), 338 (26, M + 1), 337 (8), 336 (4), 332 (3), 322 (6), 294 (3), 293 (22), 292 (100), 290 (7).

*Reaction of **24**b with base*

The dinitrodiene **24***b* did not rearomatize on heating under reflux in chloroform for 24 h. It also did not react to any significant extent when treated with aqueous sodium bicarbonate.

Excess ammonia was condensed into a solution of **24***b* (1.65 g) in ether (150 cm^3) at −60°C. The mixture was warmed to ambient temperature, water (100 cm^3) was added, and the mixture was then acidified by the dropwise addition of concentrated HCl. The ether layer was separated, dried, and the ether evaporated. Recrystallization

of the residue (1.31 g, 80%) from acetone–pentane gave α-(3,5-di-*tert*-butyl-2,6-dinitrophenoxy)isobutyric acid, mp 196°C (dec.); ^{1}H nmr ($(CD_3)_2CO$) δ: 1.38 (s, 18, 3- and 5-C(CH_3)$_3$), 1.48 (s, 6, (CH_3)$_2$), 7.69 (s, 1, 4-*H*) ppm; ^{13}C nmr ($(CD_3)_2CO$)/CD_3OD) δ_C: 24.94 (C(CH_3)$_2$), 30.91 (C(CH_3)$_3$), 37.41 (C(CH_3)$_3$), 87.43 (C(CH_3)$_2$), 125.58 (*C*-4), 141.92 (*C*-2 and *C*-6), 143.58 (*C*-3 and *C*-5), 146.28 (*C*-1), 175.42 (*C*OOH) ppm; ms (methane CI) *m/e* (relative intensity): 411 (11, M + 29), 383 (15, M + 1); ms (70 eV) *m/e* (relative intensity): 382.181 (1, M_r $^{12}C_{18}{}^1H_{26}{}^{14}N_2{}^{16}O_7$ = 382.174), 364.171 (1, M_r $^{12}C_{18}{}^1H_{24}{}^{14}N_2{}^{16}O_6$ = 364.163) 337 (3), 297 (5), 296 (20), 282 (4), 281 (27), 280 (3), 279 (4), 220 (3). Titration of this solid with aqueous NaOH indicated that 97.4 ± 2% of the material was the acid.

Acknowledgements

We thank the National Sciences and Engineering Research Council of Canada and the University of Victoria for financial support.

1. C. K. INGOLD. Structure and mechanism in organic chemistry. Cornell University Press, Ithaca, NY. 1953. p. 279.
2. H. CERFONTAIN and A. TELDER. Recl. Trav. Chim. Pays-Bas, **86**, 371 (1967).
3. P. KREIENBÜHL and H. ZOLLINGER. Tetrahedron Lett. 1739 (1965).
4. G. A. OLAH and S. J. KUHN. J. Am. Chem. Soc. **80**, 6541 (1958).
5. K. SCHOFIELD. Aromatic nitration. Cambridge University Press, Cambridge. 1980. (*a*) p. 120; (*b*) Chapt. 4.
6. G. A. OLAH, H. C. LIN, and Y. K. MO. J. Am. Chem. Soc. **94**, 3667 (1972).
7. C. E. BARNES and P. C. MYHRE. J. Am. Chem. Soc. **100**, 975 (1978).
8. A. FISCHER and J. N. RAMSAY. J. Chem. Soc. Perkin Trans. 2, 237 (1973).
9. P. C. MYHRE and M. BEUG. J. Am. Chem. Soc. **88**, 1569 (1966); P. C. MYHRE, M. BEUG, and L. L. JAMES. J. Am. Chem. Soc. **90**, 2105 (1968).
10. P. C. MYHRE and M. BEUG. J. Am. Chem. Soc. **88**, 1568 (1966); P. C. MYHRE, M. BEUG, K. S. BROWN, and B. OSTMAN. J. Am. Chem. Soc. **93**, 3452 (1971).
11. V. V. ERSHOV, A. A. VOLOD'KIN, and G. N. BOGDANOV. Russ. Chem. Rev. **32**, 75 (1963); A. J. WARING. Adv. Alicyclic Chem. **1**, 172 (1966).
12. D. J. BLACKSTOCK, M. P. HARTSHORN, K. E. RICHARDS, J. VAUGHAN, and G. J. WRIGHT. J. Chem. Soc. B, 1212 (1971); A. H. CLEMENS, M. P. HARTSHORN, K. E. RICHARDS, and G. J. WRIGHT. Aust. J. Chem. **30**, 113 (1977); C. E. BARNES, K. S. FELDMAN, M. W. JOHNSON, H. W. H. LEE, and P. C. MYHRE. J. Org. Chem. **44**, 3925 (1979).
13. A. FISCHER and G. N. HENDERSON. Tetrahedron Lett. 4661 (1980).
14. G. G. CROSS, A. FISCHER, G. N. HENDERSON, and T. A. SMYTH. Can. J. Chem. **62**, 1446 (1984).
15. G. A. ZLOBINA and V. V. ERSHOV. Izv. Akad. Nauk SSSR Ser. Khim. 1666 (1964).
16. V. V. ERSHOV and G. A. ZLOBINA. Zh. Org. Khim. **2**, 299 (1966).
17. V. V. ERSHOV and G. A. ZLOBINA. Izv. Akad. Nauk SSSR Ser. Khim. 1667 (1963).
18. V. V. ERSHOV and G. A. ZLOBINA. Izv. Akad. Nauk SSSR Ser. Khim. 2235 (1963).
19. C. E. BARNES and P. C. MYHRE. J. Am. Chem. Soc. **100**, 973 (1978).
20. V. V. ERSHOV and A. A. VOLOD'KIN. Izv. Akad Nauk SSSR Otd. Khim. Nauk, 730 (1962); A. A. VOLOD'KIN and V. V. ERSHOV. Izv. Akad. Nauk SSSR Otd. Khim. Nauk, 2022 (1962).
21. V. V. ERSHOV, G. A. ZLOBINA, and G. NIKIFOROV. Izv. Akad. Nauk SSSR Ser. Khim. 1877 (1963).
22. G. A. ZLOBINA and V. V. ERSHOV. Izv. Akad. Nauk SSSR Ser. Khim. 189 (1966).
23. (*a*) G. S. BAPAT. Ph.D. Dissertation. University of Victoria, Victoria, B.C., Canada. 1983; (*b*) G. S. BAPAT, A. FISCHER, G. N. HENDERSON, and S. RAYMAHASAY. J. Chem. Soc. Chem. Commun. 119 (1982).
24. H. HART and F. A. CASSIS, JR. J. Am. Chem. Soc. **73**, 3179 (1951).
25. D. R. MUSSEL. U.S. Patent No. 2935392 (1960); Chem. Abstr. **54**, 15820i (1960).
26. J. W. ELDER and R. P. MARIELLA. Can. J. Chem. **41**, 1653 (1963).

Can. J. Chem. Downloaded from www.nrcresearchpress.com by 210.87.254.6 on 09/06/12
For personal use only.

The chemistry of thujone. XI.[1] Thujone as a chiral synthon for the preparation of sesquiterpene lactones. Synthesis of (*l*)-α-santonin

JAMES P. KUTNEY AND ASHOK K. SINGH

Department of Chemistry, University of British Columbia, 2036 Main Mall, University Campus, Vancouver, B.C., Canada V6T 1Y6

Received April 17, 1984

JAMES P. KUTNEY and ASHOK K. SINGH. Can. J. Chem. **62**, 2813 (1984).

An efficient synthesis of (*l*)-α-santonin is described. The thujone-derived trienone **1**, bearing only one chiral center, is transformed, via a controlled hydroboration process, to the isomeric triols **7** and **9** in which four new chiral centers (C-3, C-6, C-7, and C-11) are established in one step and with the correct absolute configuration. An oxidative cyclization process converts **7** and **9** into 1,2-dihydro-6α-santonin (**3**), with the latter being transformed directly to the natural product employing DDQ as a dehydrogenating agent. The overall strategy reveals an attractive synthetic entry into the family of natural sesquiterpene lactones.

JAMES P. KUTNEY et ASHOK K. SINGH. Can. J. Chem. **62**, 2813 (1984).

On décrit une synthèse efficace de la (*l*)-α-santonine. Faisant appel à une réaction d'hydroboration contrôlée, la triénone **1**, qui est dérivée de la thujone et qui ne porte qu'un centre chiral, a été transformée en triols isomères **7** et **9** dans lesquels quatre nouveaux centres chiraux (C-3, C-6, C-7 et C-11) ont été établis en une seule étape et avec la bonne configuration absolue. Une cyclisation oxydante transforme les triols **7** et **9** en dihydro-1,2 6α-santonine (**3**) qui conduit directement au produit naturel si on fait appel à la DDQ comme agent de déshydrogénation. Il appert que cette stratégie globale représente une voie d'accès attrayante à la famille des lactones sesquiterpéniques naturelles.

[Traduit par le journal]

Our previous publications in this series (1–4) have indicated that thujone[2] can serve as an effective chiral synthon for the syntheses of various sesquiterpenes. We wish now to present our results relating to the synthesis of chiral sesquiterpene lactones from the thujone-derived trienone (**1**). In this study it is to be noted that three new chiral centers are readily introduced at C-6, C-7, and C-11 in **1** through a hydroboration–oxidative cyclization process.

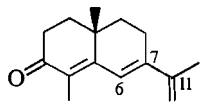

1

In developing the synthetic strategy for a versatile and efficient route to chiral sesquiterpene lactones, we considered electrophilic addition to the 6,7-double bond in **1**, a reaction which was expected to proceed from the α-face of the molecule in accord with previous findings (2). Success in this direction would therefore afford the desired absolute stereochemistry at C-6 and C-7 as known in the family of naturally occurring sesquiterpene lactones. For this purpose hydroboration of **1** seemed like an attractive alternative and we initiated our experiments with diborane under varying conditions.

Reaction of diborane with **1** can obviously occur at the three olefinic centres and the carbonyl group under varying reaction rates. In order to ascertain the course of this process and, in turn, develop the optimum reaction conditions for the required intermediates, for example, **6** (Scheme 1), we have first developed the chemistry of santonin (Scheme 1) so as to derive standard comparison samples for the hydroboration study.

The natural product, α-santonin **2**, upon hydrogenation in ethanol–benzene over Wilkinson's catalyst (5) afforded the 1,2-dihydro-6α-santonin **3** (92%). Of particular relevance to the subsequent discussion, and relating to diborane addition to **1**, are the nmr data representing the three important chiral centers (C-6, C-7, and C-11). Thus the C-6 proton (δ 4.68, dd, J = 2 and 12 Hz) is coupled to C-7 and, through long range coupling, with the vinyl methyl group at C-4 (δ 2.01, d, J = 2 Hz). The C-6 – C-7 coupling constant of 12 Hz clearly reveals the expected *trans* relationship of these two protons and this analysis was confirmed when irradiation at the C-14 methyl group resonance caused the C-6 signal to collapse into a doublet (J = 12 Hz). The C-11 proton appears as a sextet (δ 2.35, J = 6 and 12 Hz), thus indicating coupling with the proton at C-7 and the C-13 methyl group (δ 1.28, d, J = 6 Hz). Irradiation at the latter group frequency causes the sextet to collapse into a doublet (J = 12 Hz), thereby confirming the *trans* relationship of the C-7 and C-11 protons. Irradiation at the C-11 proton frequency causes the C-13 methyl signal to collapse into a singlet. This detailed nmr evaluation allows subsequent unambiguous assignments to the chiral centers in the intermediates **4**–**9** (Scheme 1) and **10** (Scheme 2).

Compound **3** reacted smoothly with ethanedithiol, *p*-toluenesulphonic acid in benzene, giving **4** in 89% yield.

Treatment of **4** with lithium aluminum hydride (LAH) in boiling ether afforded the desired hydroxy thioketal **5** in 91% yield. The β-axial configuration of the C-6 proton in **5** was deduced from the 400-MHz nmr spectrum which showed a signal at δ 4.38 (1H, dd, J = 12, 2 Hz).

Hydrolysis of **5** with $HgCl_2$ and $CdCO_3$ in aqueous acetone gave hydroxyketone **6** in 16% yield. It should be noted that optimum conditions for this reaction were not pursued since **6**, as derived from natural santonin, was merely a standard comparison sample for future studies with **1**.

Dihydrosantonin **3**, when refluxed with a suspension of LAH in ether, afforded, as a major product, the triol **7** in 75% yield and a minor product, the triol **9** in 15% yield. The α-axial configuration of the C-3 hydroxyl group in **7** was confirmed from the 400-MHz nmr spectrum which showed the C-3 proton signal at δ 3.93 (1H, t, J = 6 Hz).

With the above compounds in hand, it was now appropriate

[1]For Part X, see ref. 4.

[2]Thujone is the major component (ca. 80%) of the steam distillate from the slash (waste) of Western red cedar.

Can. J. Chem. Downloaded from www.nrcresearchpress.com by 210.87.254.6 on 09/06/12
For personal use only.

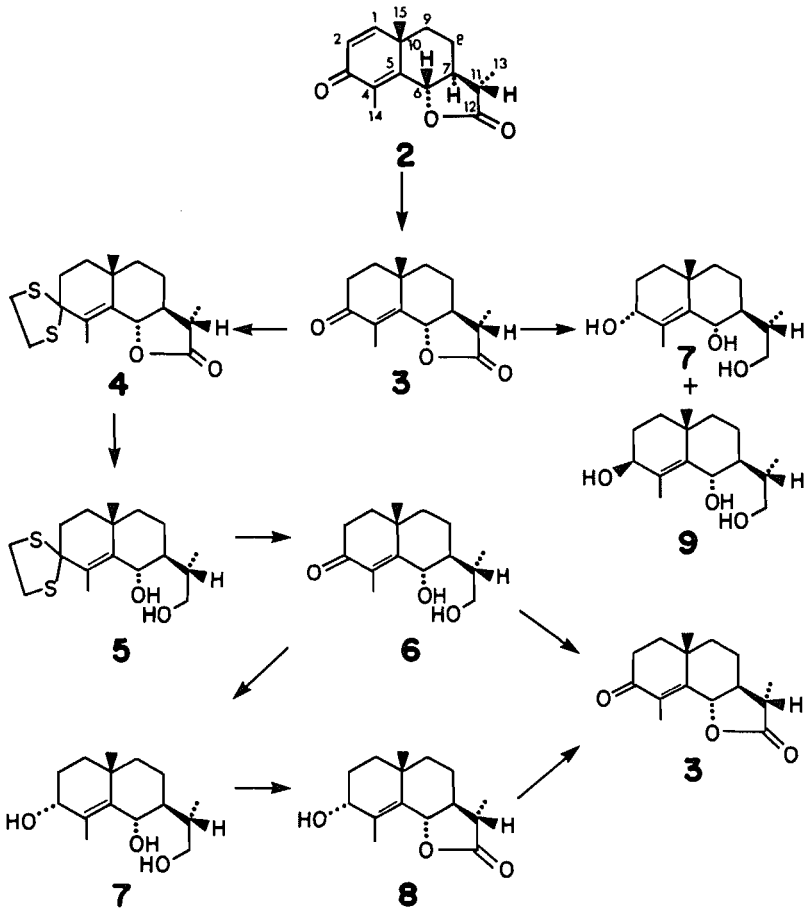

SCHEME 1

to study the elaboration of the thujone-derived intermediate **1** to sesquiterpene lactones. Hydroboration of **1** proceeded stepwise, the carbonyl being the first group attacked. Interruption of the reaction after short periods yielded mostly the hydroxy triene **10**. After a longer reaction time (5 h), two products **10** (36%) and **11** (50%) were obtained. Upon increase of reaction time (20 h), three products **10** (27%), **11** (39%), and **7** (10%) were obtained. Thus, it appears that there is a large increase in reactivity of the terminal double bond (C11—C12) and little effect on the internal double bond (C6—C7) following the hydroboration of the carbonyl group. A substantial increase in the initial amount of borane added revealed that highly reproducible results were obtained. Thus with 40 equivalents of diborane, a 62% yield of isomeric triols **7** and **9** was realized without the complicating presence of **10** and **11**. A general summary of these results is provided in Table 1.

Although the hydroxy compounds **10** and **11** are relatively unstable it was possible, nevertheless, to obtain data for complete structural assignments. The nmr spectra of **10** and **11** showed a triplet (J = 6 Hz) at δ 4.10 and 4.12 respectively. This is indicative of an equatorial proton at C-3. The nmr spectra of the products **7** and **9**, obtained from the borane reaction, were identical with those obtained from santonin.

Oxidation of a mixture of triols **7** and **9** with silver carbonate on Celite yielded a mixture of hydroxy-lactone and keto lactone **3**. The latter, without further separation, was subjected to CrO_3/pyridine oxidation to afford 1,2-dihydro-6α-santonin **3**. The physical properties were identical with **3** obtained from santonin. In summary, the overall yield in the sequence, **7**, **9**→**3** is 68% when isolation of intermediates is omitted.

TABLE 1. Summary of results obtained from hydroboration of trienone **1**

Amount of trienone (mg)	Time (h)	Amount of BH_3–THF (equivalents)	Products (%)		
			10	**11**	**7** and **9**
100	5	5	36	50	—
100	20	5	27	39	10
100	20	15	20	36	11
100	48	25	—	40	34
100	20	25	—	—	42
100	18	30	—	—	56
100	12	40	—	—	62

Oxidation of **3** with 2,3-dichloro-5,6-dicyano-1,4-benzoquinone (DDQ) in benzene, under reflux for 64 h, afforded (*l*)-α-santonin in 84% yield, based on recovered starting material. The synthetic (*l*)-α-santonin was identical with natural (*l*)-α-santonin in all respects.

In order to substantiate the arguments made earlier from nmr studies of **3**, as they relate particularly to the stereochemistry at C-7, a detailed nmr study on santonin (**2**) was also made. In this instance the spectrum is better resolved in the region of relevance. Thus the C-7 proton appears as an octet (δ 1.82, dddd, J = 4 and 12 Hz), thereby indicating a coupling with the protons at C-6, C-11, and C-8. Irradiation at the C-7 proton resonance caused the C-6 signal to collapse into a singlet, the C-11 signal into a quartet (J = 6 Hz), the C-8 axial proton

Can. J. Chem. Downloaded from www.nrcresearchpress.com by 210.87.254.6 on 09/06/12
For personal use only.

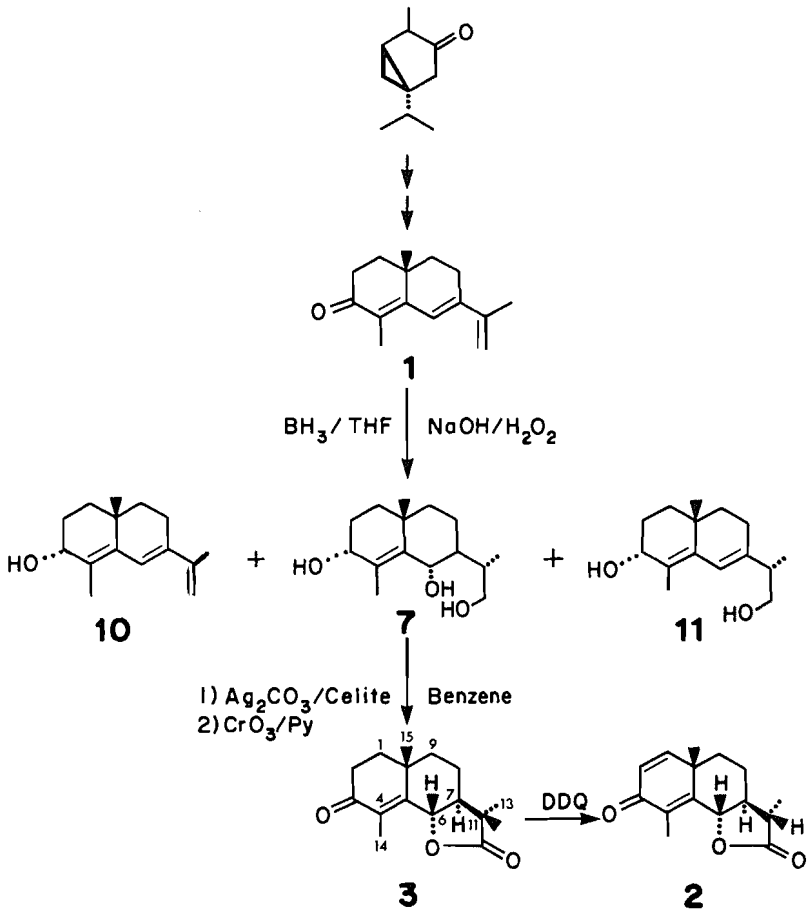

SCHEME 2

signal into a sextet (J = 4 and 12 Hz), and the C-8 equatorial proton signal into a sextet (J = 4 and 12 Hz). Hence it is clear that the C-7 proton is *trans* to protons at C-6 and C-11. The data for C-6 and C-11 are identical with those discussed earlier for **3**.

In conclusion, trienone **1**, with only one chiral center, is transformed efficiently via the hydroboration approach into the triols **7** and **9**, bearing four chiral centers of correct absolute stereochemistry, for efficient syntheses of optically active sesquiterpene lactones. This procedure affords the best overall approach to the synthesis of these natural products. Further studies with such intermediates are underway.

Experimental

Melting points were determined on a Büchi melting point apparatus and are uncorrected. Ultraviolet spectra were recorded on a Cary 15 spectrophotometer in methanol solution. Infrared spectra were measured on a Perkin–Elmer-710 spectrophotometer using chloroform as solvent. The ^{1}Hmr spectra were recorded on Bruker WH-400, Bruker WP-80, Varian XL-100, or Nicolet–Oxford H-270 instruments. Deuteriochloroform was used as the solvent with TMS as internal standard. Low resolution mass spectra were determined on either an AEI-MS-902 or an Atlas-CH-4B spectrometer. High resolution mass measurements were made on an AEI-MS-50 spectrometer. Optical rotations were recorded on a Perkin–Elmer 141 polarimeter using a cell with a path length of 10 cm. Microanalyses were performed by Mr. P. Borda, Microanalytical Laboratory, University of British Columbia. Column chromatography utilized Merck silica gel 60 (70–230 mesh). Preparative and thin layer chromatography utilized Merck silica gel GF_{254}. Petroleum ether refers to the fraction with boiling range 30–60°C.

1,2-Dihydro-6α-santonin 3

A modified procedure of Sims *et al.* (6) was used for the preparation of **3**. To a solution of (*l*)-α-santonin **2** (1 g) in benzene–ethanol (220 mL, 1:1 v/v) was added tris(triphenylphosphine)rhodium(I)chloride (1.0157 g). The mixture was flushed with hydrogen and stirred under hydrogen for 24 h. The solvents were evaporated and the residue chromatographed on silica gel (70 g), eluted with ethyl acetate – petroleum ether (1:4, v/v) to give 1,2-dihyro-6α-santonin **3** (0.930 g, 92%). The latter was recrystallized from petroleum ether – carbon tetrachloride, mp 98–99°C (lit. (7) mp 101–102°C); $[\alpha]_D$ +71.29° (*c* 0.519, EtOH) (lit. (7) $[\alpha]_D$ +79° (*c* 1.42, $CHCl_3$)); ir ν_{max}: 1780, 1670, 1625 cm^{-1}; uv λ_{max}: 244 (ε 15 113) nm (lit. (7) λ_{max}: 244 (ε 14 700) nm); ^{1}Hmr δ: 1.28 (3H, d, J = 6 Hz), 1.34 (3H, s), 1.50–2.00 (7H, m), 2.01 (3H, d, J = 2 Hz), 2.35 (1H, sextet, J = 12, 6 Hz), 2.44 (1H, dt, J = 16, 4 Hz), 2.53 (1H, ddd, J = 16, 4 Hz), 4.68 (1H, dd, J = 12, 2 Hz), ms *m/e*: 248 (M^+), 233, 220, 205, 192. High resolution molecular weight determination, calcd. for $C_{15}H_{20}O_3$: 248.1412; found: 248.1413. *Anal.* calcd. for $C_{15}H_{20}O_3$: C 72.58, H 8.06; found: 72.10, H 8.01.

Thioketal lactone 4

The Ourisson (8) modified procedure was used in the preparation of **4**. A solution of 1,2-dihydro-6α-santonin **3** (500 mg) in anhydrous benzene (45 mL), ethanedithiol (1.5 mL), and *p*-toluenesulphonic acid (40 mg) was heated at reflux under nitrogen for 3 h. The cooled solution was diluted with water (50 mL) and extracted with chloroform (50 mL). The organic layer was washed with a saturated solution of sodium bicarbonate (50 mL), water (50 mL), saturated brine (50 mL), and dried ($MgSO_4$). Evaporation of the solvent left crystalline thioketal lactone **4** (579 mg, 89%). The analytical sample was obtained by recrystallization from ether – petroleum ether, mp 167–168°C (lit. (8) mp 166–168°C); $[\alpha]_D$ +41° (*c* 0.4098, $CHCl_3$); ir ν_{max}: 1766 cm^{-1}; ^{1}Hmr δ: 1.17 (3H, s), 1.23 (3H, d, J = 6 Hz), 1.35–1.93 (7H,

Can. J. Chem. Downloaded from www.nrcresearchpress.com by 210.87.254.6 on 09/06/12
For personal use only.

Can. J. Chem. Downloaded from www.nrcresearchpress.com by 210.87.254.6 on 09/06/12
For personal use only.

m), 2.11 (3H, d, J = 2 Hz), 2.18–2.31 (3H, m), 3.24 (1H, m), 3.31–3.42 (3H, m), 4.56 (1H, dd, J = 12, 2 Hz); ms m/e: 324 (M^+), 309, 296, 264. High resolution molecular weight determination, calcd. for $C_{17}H_{24}O_2S_2$: 324.1218; found: 324.1218. *Anal.* calcd. for $C_{17}H_{24}O_2S_2$: C 62.96, H 7.41, O 9.88; found: C 62.84, H 7.36, O 9.70.

Hydroxy thioketal **5**

To a suspension of lithium aluminum hydride (300 mg) in anhydrous ether (50 mL) was added a solution of thioketal lactone **4** (500 mg) in ether (25 mL). The mixture was refluxed for 1 h under nitrogen, then excess hydride was destroyed by the careful addition of cold water and extracted with ethyl acetate (2 × 75 mL). The organic extracts were dried ($MgSO_4$) and evaporated to afford hydroxy thioketal **5** (458 mg, 91%), which was recrystallized with ether – petroleum ether, mp 159–160°C; $[\alpha]_D$ +65.49° (c 0.284, $CHCl_3$); ir ν_{max}: 3250 cm^{-1}; ^{1}Hmr δ: 0.95 (3H, d, J = 6 Hz), 1.12 (3H, s), 1.25 (1H, m), 1.40–1.59 (5H, m), 1.69 (1H, m), 1.78–1.93 (3H, m, including 1.88 (2H, bs, D_2O exchangeable)), 2.08 (1H, m), 2.18–2.24 (4H, m, including 2.19 (3H, d, J = 2 Hz)), 3.25 (1H, m), 3.33–3.43 (3H, m), 3.54 (1H, dd, J = 12, 6 Hz), 3.65 (1H, dd, J = 12, 6 Hz), 4.38 (1H, dd, J = 12, 2 Hz); ms m/e: 328 (M^+), 310, 295, 268, 251, 236. High resolution molecular weight determination, calcd. for $C_{17}H_{28}O_2S_2$: 328.1531; found: 328.1535. *Anal.* calcd. for $C_{17}H_{28}O_2S_2$: C 62.19, H 8.54, O 9.76; found: C 62.00, H 8.27, O 9.56.

Hydroxyketone **6**

A solution of the hydroxy thioketal **5** (208.6 mg) in aqueous 95% acetone (20 mL) was added to an efficiently stirring solution of mercuric chloride (250 mg) and cadmium carbonate (250 mg) in the same solvent mixture (10 mL). The mixture was stirred for 26 h at ambient temperature and filtered through a sintered funnel. The filter cake was washed with CH_2Cl_2 – petroleum ether (50 mL, 1:1 v/v) and the organic solution evaporated to dryness. The residue was diluted with CH_2Cl_2 (75 mL) and washed successively with 5 M aqueous ammonium acetate (20 mL), water (25 mL), brine (25 mL), and dried ($MgSO_4$). The crude residue, after evaporation of the solvent *in vacuo*, was chromatographed on silica gel (4 g). Elution with ethyl acetate – petroleum ether (1:1, v/v) afforded hydroxyketone **6** (25 mg, 16%), which was recrystallized from ethyl acetate – petroleum ether, mp 142–143°C; $[\alpha]_D$ +92.11° (c 0.5103, $CHCl_3$); ir ν_{max}: 3400, 1600 cm^{-1}; uv λ_{max}: 252 (ε 12 618) nm; ^{1}Hmr δ: 1.02 (3H, d, J = 6 Hz), 1.26 (3H, s), 1.36–1.78 (6H, m), 1.70–2.02 (4H, m, including 1.94 (2H, bs, D_2O exchangeable)), 2.10 (3H, d, J = 2 Hz), 2.39–2.64 (2H, m), 3.60 (1H, dd, J = 12, 6 Hz), 3.75 (1H, dd, J = 12, 6 Hz), 4.54 (1H, dd, J = 10, 2 Hz); ms m/e: 252 (M^+), 234, 221, 219, 193. High resolution molecular weight determination, calcd. for $C_{15}H_{24}O_3$: 252.1725; found: 252.1724. *Anal.* calcd. for $C_{15}H_{24}O_3$: C 71.43, H 9.52, O 19.05; found: C 71.41, H 9.60, O 19.10.

Triols **7** *and* **9**

A solution of 1,2-dihydro-6α-santonin **3** (291 mg) in anhydrous ether (25 mL) was added to a suspension of lithium aluminum hydride (291 mg) in ether (50 mL) and the mixture refluxed for 2 h under nitrogen. It was cooled, excess LAH decomposed with cold water, extracted with ethyl acetate (150 mL), dried ($MgSO_4$), and concentrated *in vacuo*. The crude material was chromatographed on silica gel (20 g), and eluted with methanol – ethyl acetate (0.1:9.9, v/v) to give the less polar product **7** (0.229 g, 77%), mp 125–126°C; $[\alpha]_D$ −14.11° (c 0.5245, EtOH); ir ν_{max}: 3425 cm^{-1}; ^{1}Hmr δ: 0.93 (3H, d, J = 6 Hz), 1.10 (3H, s), 1.19–1.59 (7H, m), 1.63–1.78 (2H, m), 1.81–1.96 (2H, m), 2.02 (3H, s), 2.22–2.55 (2H, bs, D_2O exchangeable), 3.51 (1H, dd, J = 12, 6 Hz), 3.63 (1H, dd, J = 12, 6 Hz), 3.93 (1H, t, J = 6 Hz), 4.37 (1H, d, J = 10 Hz); ms m/e: 254 (M^+), 239, 236, 177. High resolution molecular weight determination, calcd. for $C_{15}H_{26}O_3$: 254.1882; found: 254.1886. *Anal.* calcd. for $C_{15}H_{26}O_3$: C 70.87, H 10.24; found: C 71.05, H 10.23. The more polar product was **9** (0.0458 g, 15%), mp 165–166°C; $[a]_D$ +61.83° (c 0.4205, EtOH); ir ν_{max} (Nujol): 3375 cm^{-1}; ^{1}Hmr (DMSO) δ: 0.85 (3H, d, J = 6 Hz), 0.97 (3H, s), 1.08–1.20 (2H, m), 1.28–1.36 (2H, m), 1.38–1.63 (5H, m), 1.97 (3H, s), 2.17 (1H, m), 3.23–3.30 (2H, m), 3.57 (1H, m, $\frac{1}{2}w$ = 12 Hz), 4.13 (1H, dd, J = 12, 4 Hz), 4.27 (1H, m, D_2O exchangeable), 4.36 (1H, m, D_2O exchangeable), 4.44 (1H, m, D_2O exchangeable); ms m/e: 254 (M^+), 236, 221, 218, 205. High resolution molecular weight determination, calcd. for $C_{15}H_{26}O_3-H_2O$: 236.1776; found: 236.1785. *Anal.* calcd. for $C_{15}H_{26}O_3$: C 70.87, H 10.24; found: C 70.58, H 10.28.

Hydroxy triene ***10*** *and hydroxy diene* ***11***

An aliquot of diborane (9.3 mL) (1 M BH_3 in tetrahydrofuran solution), was added to a stirring, ice-cold solution of triene **1** (400 mg) in THF (2 mL) kept under argon. The cooling bath was removed and the solution stirred at room temperature for 5 h. The reaction flask was cooled in an ice bath and excess diborane was destroyed by a careful addition of water (0.3 mL), followed immediately by 3 N NaOH solution (9.3 mL) and 30% aqueous hydrogen peroxide (9.3 mL). After stirring for 1 h at room temperature the mixture was saturated with NaCl and extracted with ethyl acetate (100 mL). The organic layer was washed with saturated brine (50 mL), dried ($MgSO_4$), and evaporated. The residual viscous oil was chromatographed over silica gel (30 g) and eluted with a mixture of ether and petroleum ether (4:6, v/v) to provide pure hydroxy triene **10** (144.9 mg, 36%) and hydroxy diene **11** (218.2 mg, 50%) as viscous oils. The physical properties are as follows: **10**: ir ν_{max}: 3338, 1646, 1616, 1590 cm^{-1}; ^{1}Hmr δ: 1.02 (3H, s), 1.10–1.70 (7H, m), 1.80 (3H, s), 1.97 (3H, s), 2.05–2.40 (2H, m), 4.10 (1H, t, J = 6 Hz), 4.90 (1H, s), 5.05 (1H, s), 6.42 (1H, s); ms m/e: 218 (M^+), 203; **11**: ir ν_{max}: 3288, 1640, 1616 cm^{-1}; ^{1}Hmr δ: 1.00 (3H, s), 1.02 (3H, d, J = 6 Hz), 1.22–1.62 (8H, m), 1.80 (3H, s), 1.94–2.52 (3H, m), 3.42–3.62 (2H, m), 4.12 (1H, t, J = 6 Hz), 6.20 (1H, s); ms m/e: 236 (M^+), 221, 218, 205, 187, 177. High resolution molecular weight determination, calcd. for $C_{15}H_{24}O_2$: 236.1776; found: 236.1783.

(l)-α-*Santonin* **2**

A solution of **1** (100 mg) in THF (2 mL) was hydroborated with an aliquot of diborane (18.5 mL) (1 M diborane in THF) at 0°C by dropwise addition of the diborane solution. The reaction mixture was stirred for 12 h at room temperature, cooled, and then treated with water (0.6 mL), 3 N NaOH solution (18.5 mL), and 30% H_2O_2 (18.5 mL). Work-up as above provided the crude product, which was then chromatographed over silica gel (20 g). Elution with methanol – ethyl acetate (0.1:9.9, v/v) gave an analytical sample of triol **7** (58 mg, 49%) and triol **9** (15 mg, 13%). The ir, ms, and ^{1}Hmr spectra of these products were identical with those obtained from naturally occurring santonin **2** as shown in Scheme 1.

To a round bottomed flask equipped with a magnetic stirring bar, a Dean–Stark trap, and a condenser, was added a mixture of triols **7** and **9** (100 mg), silver carbonate on Celite (3.4 g), and benzene (30 mL). The resulting mixture was refluxed for 3 h, cooled to ambient temperature, and filtered. The solvent was removed to provide a mixture of hydroxy-lactone and keto lactone (100 mg) as a viscous material. The latter was used for the subsequent reaction without further separation.

Chromic anhydride (225 mg) was added into pyridine (3 mL) and stirred for 10 min. The above crude mixture dissolved in pyridine (2 mL) was added, and the mixture was stirred at room temperature for 1 h. The reaction mixture was diluted with water (15 mL), extracted with ether (3 × 50 mL), dried ($MgSO_4$), and evaporated. The residue was chromatographed on silica gel (20 g) with ethyl acetate – petroleum ether (1:4, v/v) as eluting solvent to afford 1,2-dihydro-6α-santonin **3** (66 mg, 68%) as a crystalline solid. An analytical sample was obtained by recrystallization from CCl_4 – petroleum ether, mp 98–99°C. This material was identical by ^{1}Hmr, ir, and optical rotation with **3** prepared from (*l*)-α-santonin **2** (Scheme 1).

To a solution of **3** (32 mg) in dry benzene (10 mL), was added DDQ (87.8 mg) and the mixture was refluxed for 64 h under argon. The reaction mixture was cooled, filtered, and the solvent was removed under reduced pressure. Column chromatography of the residue on silica gel (10 g) with ethyl acetate – petroleum ether (1:4, v/v) as eluting solvent afforded (*l*)-α-santonin **2** (14.1 mg, 44%) and starting

material **3** (15 mg, 47%). Recrystallization from ethyl acetate – petroleum ether yielded material of analytical purity, mp 172–173°C (lit. (9) mp 170–173°C; $[\alpha]_D$ −172.8° (*c* 0.5535, EtOH) (lit. (9) $[\alpha]_D$ −172° (EtOH)); ir ν_{max}: 1886, 1666, 1641, 1616 cm^{-1}; uv λ_{max}: 240 (ε 13 000), 260 (8700) nm (lit. (10) λ_{max}: 240 (ε 13 182), 260 (8511) nm); ^{1}Hmr δ: 1.28 (3H, d, J = 6 Hz), 1.34 (3H, s), 1.52 (1H, dddd, J = 12, 4 Hz), 1.70 (1H, ddd, J = 12, 4 Hz), 1.82 (1H, dddd, J = 12, 4 Hz), 1.91 (1H, dddd, J = 12, 4 Hz), 2.03 (1H, ddd, J = 12, 4 Hz), 2.14 (3H, d, J = 2 Hz), 2.42 (1H, sextet, J = 12, 6 Hz), 4.80 (1H, dd, J = 12, 2 Hz), 6.25 (1H, d, J = 10 Hz), 6.70 (1H, d, J = 10 Hz); ms *m/e*: 246 (M^+), 231, 218, 203. High resolution molecular weight determination, calcd. for $C_{15}H_{18}O_3$: 246.1256; found: 246.1262. *Anal.* calcd. for $C_{15}H_{18}O_3$: C 73.17, H 7.32; found: C 73.06, H 7.42.

Acknowledgements

Financial aid from the Natural Sciences and Engineering Research Council of Canada is gratefully acknowledged. The authors would also like to thank Mr. Alan Moss and Associates for generous samples of cedar leaf oil. We are grateful to Dr. Lewis S. L. Choi for helpful discussions and assistance.

1. J. P. KUTNEY, J. BALSEVICH, and P. GRICE. Can. J. Chem. **58**, 2641 (1980).
2. J. P. KUTNEY and A. K. SINGH. Can. J. Chem. **60**, 1842 (1982).
3. J. P. KUTNEY and A. K. SINGH. Can. J. Chem. **61**, 1111 (1983).
4. J. P. KUTNEY and A. K. SINGH. Can. J. Chem. **62**, 1407 (1984).
5. J. F. YOUNG, J. A. OSBORN, F. H. JARDINE, and G. WILKINSON. Chem. Commun. 131 (1965); F. H. JARDINE, J. A. OSBORN, G. WILKINSON, and J. F. YOUNG. Chem. Ind. (London), 560 (1965); J. A. OSBORN, F. H. JARDINE, J. F. YOUNG, and G. WILKINSON. J. Chem. Soc. (A), 1711 (1966).
6. J. J. SIMS, V. K. HONWAD, and L. H. SELMAN. Tetrahedron Lett. 87 (1969).
7. J. C. BANERJI, D. H. R. BARTON, and R. C. COOKSON. J. Chem. Soc. 5041 (1957), and earlier papers cited therein.
8. A. E. GREENE, J. C. MULLER, and G. OURISSON. J. Org. Chem. **39**, 186 (1974).
9. N. H. FISCHER, E. J. OLIVER, and H. D. FISCHER. Prog. Chem. Org. Nat. Prod. **38**, 47 (1979).
10. J. B. HENDRICKSON and T. L. BOGARD. J. Chem. Soc. 1678 (1962).

Can. J. Chem. Downloaded from www.nrcresearchpress.com by 210.87.254.6 on 09/06/12
For personal use only.

Novel benzo[*a*]naphthacene quinones from an actinomycete, *Frankia* G-2 (ORS 020604)

NANCY N. GERBER AND MARY P. LECHEVALIER

Waksman Institute of Microbiology, P.O. Box 759, Rutgers, The State University of New Jersey, Piscataway, NJ 08854, U.S.A.

Received November 7, 1983[1]

NANCY N. GERBER and MARY P. LECHEVALIER. Can. J. Chem. **62**, 2818 (1984).

Frankia sp. G2 (ORS 020604), grown for one month without shaking, produced a mixture of 2 quinonoid pigments. The structure of one, G-2N, was shown by chemical and physical methods to be 2-methyl-4,7,9,12-tetrahydroxy-5,6-dihydro benzo[*a*]naphthacene-8,13-dione. The other, G-2A, has the same structure with the addition of a carboxyl group at position 10 or 11. Natural quinones with this ring system have not been reported previously.

NANCY N. GERBER et MARY P. LECHEVALIER. Can. J. Chem. **62**, 2818 (1984).

Si l'on fait croître du *Frankia* sp. G2 (ORS 020604) pendant un mois sans agitation, il se forme un mélange de deux pigments de nature quinonoïde. Faisant appel à des méthodes chimiques et physiques, on a démontré que l'un de ces produits, le G-2N, est la méthyl-2 tétrahydroxy-4,7,9,12 dihydro-5,6 benzo[*a*]naphthacènedione-8,13. L'autre composé, le G-2A, possède la même structure de base, mais il porte en plus un groupement carboxyle dans les positions 10 ou 11. Aucune quinone naturelle comportant ce système cyclique n'avait été signalée antérieurement.

[Traduit par le journal]

Can. J. Chem. Downloaded from www.nrcresearchpress.com by 210.87.254.5 on 09/06/12
For personal use only.

Actinomycetes of the genus *Frankia* fix nitrogen in symbiosis with angiospermous higher plants. Although the existence of these microorganisms had been known for more than one hundred years, they have been isolated and maintained in pure culture only recently (1–3). Several of the Frankiae under investigation in these laboratories produce pigments (4). *Frankia* sp. G2 (ORS 020604) isolated by Gautier *et al.* (5) from the nodules of a *Casuarina equisetifolia* plant in Guadeloupe was chosen for study because of its relatively rapid growth and simple pigment mixture.

As described in the experimental section, two red-orange crystalline quinonoid pigments G-2N and G-2A were obtained. The absorption spectrum of G-2N showed maxima at 265, 311, and 470 nm; the ir spectrum had bands at 3380(OH), 1620, and 1595 cm^{-1}. The pigment did not melt below 350°C, gave a positive ferric chloride test for phenolic hydroxyls, was decolorized by sodium borohydride, and reoxidized in air to the original compound. In the mass spectrum the molecular ion at 388 was the base peak and, except for $M + 1$, $M - 1$, and $M - 18$, all other peaks were less than 20% of the base peak. This indicated a very stable, cyclic structure.

G-2N has the molecular formula $C_{23}H_{16}O_6$; the four oxygens are accounted for by a quinone function and four hydroxyls, as the pigment forms a tetraacetate. Zinc dust distillation furnished a small amount of hydrocarbon which, after column chromatographic purification, had a uv spectrum virtually identical with that of 1,2-benzo[*a*]naphthacene (6) but whose molecular ion at 292, 14 more than that of benzonapthacene, suggested a methylbenzonaphthacene. The aromatic methyl subsitutent was seen at 2.25 ppm in the nmr of G-2N and at 2.35 ppm in the spectrum of the acetate derivative.

A fully aromatic methylbenzo[*a*]naphthacene with 7 substituents (4 hydroxy, 1 methyl, and 2 quinone carbonyls) could have only 14 hydrogens ($C_{23}H_{14}O_6$; mol. wt. = 386) and 7 of these would be in the aromatic region of the nmr spectrum. However, G-2N had 5 aromatic hydrogens and a slightly broadened singlet at 2.8 ppm equivalent to 4 hydrogens. This suggested that one of the unsubstituted double bonds in the benzo[*a*]naphthacene framework had been replaced by a single bond. The placement of the single bond in ring D as shown in Fig. 1 is the only location consistent with the magnetic equivalence of the four hydrogens shown by the 4H singlet band. Furthermore, the uv–visible absorption spectrum resembles the combined spectra of a hydroxy anthraquinone (267 and 470 nm) and an alkylated phenol (311 nm).

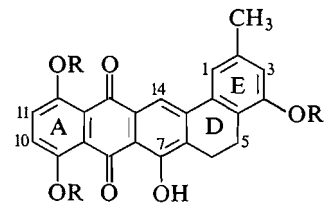

FIG. 1. The structures of G-2N, G-2N trimethylether, and G-2A. G-2N: R = H; G-2N trimethylether: R = methyl; G-2A: R = H, COOH at 10 or 11.

The arrangement of substituents on rings A through D follows in part from the nmr chemical shift (in DMSO-d_6) of H-14 at 8.8 ppm. Hydrogens *peri* to carbonyls are always deshielded (7); the range of values for this kind of H in some naturally occurring anthraquinones is 7.3 to 8.3 ppm (8) and in some anthracyclinones is 7.7 to 8.2 ppm (9). Thus H-14 is somewhat more deshielded than these examples; it may also be influenced by *peri* interactions with H-1. The nmr spectrum also shows two slightly broadened singlets at 6.70 and 6.68 ppm, each equivalent to one hydrogen, which are attributed to H-10 and 11. This is the normal appearance for an AB quartet where the difference between the chemical shifts is the same order of magnitude as the coupling constant (7). In addition, the shift of the visible absorption maximum from 470 nm in neutral solution to 553 nm in basic solution suggests an anthraquinone with three α hydroxyl substituents (8).

The problem of the location of the substituents on ring E is partially solved by the obviously *meta*-coupled aromatic protons at 6.61 and 7.16 ppm in the nmr of G-2N and at 7.2 and 7.9 ppm in the tetraacetate derivative. Since the hydrogens at positions 5 and 6 are magnetically equivalent in both spectra, they must be in an identical environment in both molecules. This leads to the arrangement of substituents on ring E shown

[1] Revision received June 20, 1984.

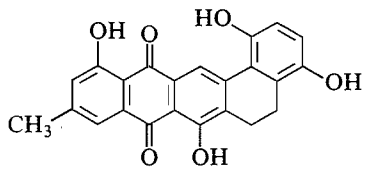

FIG. 2. A possible alternate structure for G-2N ruled out by nmr solvent shifts.

in Fig. 1 rather than alternative structures with substituents at positions 1 and 3 or one with the hydroxy at 2 and the methyl at 4. The possible alternate structure shown in Fig. 2, which retains the magnetic equivalence of H-5 and 6, is excluded by the chemical shift values of the *meta* coupled aromatic protons. In 3-methyl-1,6,8-trihydroxyanthraquinone the protons analogous to H-9 and 11 are observed at 7.10 and 7.64 ppm (8).

Although G-2N readily formed a tetraacetate derivative, it was difficult to methylate with dimethyl sulfate. A poor yield was obtained of a mixture of two monomethyl ethers, one di, one tri, and the tetramethyl ether. After preparative tlc separation the triether was used for nmr studies since the markedly different electronic absorption spectrum of the tetramethyl ether suggested molecular distortion due to steric strain.

The possible alternate structure shown in Fig. 2 is also excluded by the solvent shifts shown by G-2N trimethyl ether when the nmr solvent is changed from deuterochloroform to deuterobenzene. The upfield shift for the methyl band is small (0.26 ppm), not large (0.52–0.60 ppm) as would be expected for a C-2 or C-3 methyl substituent of an anthraquinone (10). The other solvent shifts, 0.6–0.7 ppm upfield for the three methoxyl methyls and 0.3 ppm downfield for H-14, are in accordance with published values (10).

The location of the methoxyl groups at positions 4, 9, and 12 in the trimethyl ether was shown by the appearance of the methylene band. No longer in a magnetically equivalent environment, the hydrogens at positions 5 and 6 are seen as a multiplet (2.75–2.89 ppm) with 2 small peaks at 2.82 and 2.86 ppm. In deuterobenzene the signals are completely separated and the two multiplets (2.40–2.59 and 2.84–3.03 ppm) resemble the A_2B_2 system pictured on p. 136 of ref. 7.

The electronic absorption spectrum of G-2A showed maxima at 300, and 460 nm; the ir spectrum had bands at 3360, 3110, 3030, 1720, 1620, and 1595 cm^{-1}; both spectra were very similar to those of G-2N. The pigment was sufficiently soluble in 5% aqueous sodium bicarbonate to impart a strong red coloration; the mass spectrum was virtually identical with that of G-2N except for a strong (100%) peak at $m/e = 44$ amu. This suggested that the structure of G-2A was identical to that of G-2N with the addition of a carboxyl group. However, when the room temperature acetylation procedure which furnished the tetraacetate derivative of G-2N was used for G-2A, a triacetate was obtained. This implied that the carboxyl group was adjacent and strongly hydrogen bonded to one of the four hydroxyl groups.

The G-2A tetraacetate was prepared by acetylation at 70°C. Although it was not sufficiently volatile for a satisfactory mass spectrum, the nmr spectrum clearly showed the four acetate groups and the other features associated with the G-2N structure: the aromatic methyl at 2.35 ppm, H-14 at 8.9 ppm, the 4H methylene singlet at 2.84 ppm, and the *meta* coupled hydrogens of ring E. Only the AB quartet was missing and replaced by a one-H singlet at 7.3 ppm. Thus the carboxyl group of G-2A was placed at C-10 or 11.

It is reasonable to assume that G-2N and G-2A are products of polyketide biosynthesis as are most other hydroxyquinones (8). There is circumstantial evidence that G-2A is transformed to G-2N, since production flasks incubated for 5 months yielded G-2N only. The location of the methyl and carboxyl groups (irrespective of whether the carboxyl is at 10 or 11) suggests that two polyketide chains are involved. Considering the methyl and carboxyl as chain terminals and using obvious and straightforward ways to visualize the assembly of G-2A from two polyketide chains, position 10 is favored over 11 as the location of the carboxyl group.

In a search of Chemical Abstracts we found no previous natural products from plants or microorganisms with the benzo[*a*]naphthacene ring system. Surprisingly, benzo[*a*]naphthacene has not been found carcinogenic although benzo[*a*]anthracene has (11). Free and glycosylated hydroxybenzo[*a*]anthraquinones are known as microbial products (12). They are biosynthesized from a single polyketide chain. We have also found one or both of these benzo[*a*]naphthacene compounds in other *Frankia* held in our collection, including D11 (ORS 020602), DBB-Eu11b, ULQ-EuN1$_f$, ULQ-EAN1$_{pcc}$, DBB-53001, and ULF-Hipp.

Experimental

Melting points were taken on a Kofler hot stage apparatus and are uncorrected. For column chromatography, neutral silica was HI-FLOSIL, 60/200 mesh, Applied Science Laboratories, State College, Pennsylvania; acidic silica was silicAR CC-4 from Mallinkrodt. The pH 8 silica was prepared from HI-FLOSIL by shaking it on a shaking machine with excess distilled water and adjusting, with NaOH, the pH to 8 initially and then intermittently until there was no change. The aqueous layer was decanted and the silica air-dried in a shallow pan. Polygram sil G/UV$_{254}$ 0.25-mm layer precoated plastic sheets, 5 × 10 cm, from Macherey–Nagel, were used for all analytical tlc. For preparative tlc, glass plates covered with Macherey–Nagel Kieselgel G were used. Ultraviolet–visible absorption spectra were recorded on a Beckman UV 5270 spectrophotometer; ir spectra were obtained using the Perkin–Elmer Model 283 spectrophotometer. Low resolution mass spectra were obtained with the Hewlett–Packard 5983 using the direct inlet, electron-impact mode with 70 eV; the high resolution instrument was the AEI-Kratos MS 50. The nmr spectra were taken on a Varian XL 100-15 or Varian FT-80 with tetramethyl silane as internal standard.

Production, isolation, and purification of G-2N and G-2A

Frankia sp. G2 was obtained through the kindness of Dr. Y. Dommergues of Dakar, Senegal. It is now referred to as ORS 020604 (Y. Dommergues, personal communication). It was maintained as a still culture in yeast-Czapeks (YCz) broth (13) at 27°C, transferring every 3 months. For pigment production, 3–4 week old cells, still-grown at 27°C in a medium containing 0.5% NZ Amine A (Sheffield Products, Memphis, Tennessee) and 0.1% potato starch in tap water, pH 7.0 before autoclaving, were used to inoculate fresh flasks of the same medium (5% inoculum). After 3–4 weeks of incubation, cells and the pigment, which had crystallized out of solution during growth, were harvested by centrifugation and extracted with 95% ethanol using overnight shaking. Three extractions were usually necessary to remove all of the color. Typical yields were 115 mg of red, partially crystalline, residue extracted from 4.3 g of moist cells which had been obtained from 75 Erlenmeyer flasks, each of which originally contained 50 mL of growth medium. The residue from the ethanol extracts was dissolved in methanol/concentrated ammonia 98:2 and added to 7 g of neutral silica. When dry, this was layered onto the top of a 100-g column of neutral silica which had been made up in chloroform/ethanol/concentrated ammonia 25:25:2. Elution with the same solvent mixture brought down the main red band, G-2N. With the solvent mixture in the ratio 25:50:3, the second major red

Can. J. Chem. Downloaded from www.nrcresearchpress.com by 210.87.254.5 on 09/06/12
For personal use only.

band, G-2A, was eluted. Combined fractions of each component were allowed to evaporate to dryness. Typical yields were 25 and 35 mg respectively from 120 mg of residue. The two pigments were well separated by tlc using chloroform/ethanol/concentrated ammonia 10:10:1 (R_f 0.6 and 0.2) or chloroform/ethyl acetate 1:1 (R_f 0.8 and 0.1).

Crude G-2N (30 mg) was dissolved in about 50 mL of refluxing acetone containing 0.15 mL concentrated HCl. After hot filtration, the solution was concentrated to 20 mL and 20 mL of benzene added. The concentration and addition of benzene were repeated twice; toward the end a gel appeared. After standing overnight, the gel had changed to dark red crystals which were filtered by suction, yield 10 mg. G-2N could also be purified using a column of acidic silica and eluting with a chloroform/acetone gradient; uv (EtOH) λ_{max} nm(ϵ): 265 (8200), 311 (15 000), 470 (6900); (EtOH/NH_3) λ_{max} nm: 292, 328, 515; (EtOH/aq. NaOH) λ_{max} nm: 255, 293–306 (shoulder), 318, 348, 550; ir (KBr) ν_{max}: 3380 (O—H), 2920 (C—H), 1620 (C=O), 1595 (aryl), 1490, 1445, 1400, 1335, 1265, 1185, 1165, 1100, 760, 745, 600; ^{1}H nmr (DMSO-d_6) δ_{TMS}: 2.25 (s, 3H, Me), 2.76 (s, 4H, H-5 and 6), 6.61 (d, 1H, J = 2.5, H-3), 7.16 (d, 1H, J = 2.5, H-1), 6.70 (br s, 1H, H-10 or 11), 6.68 (br s, 1H, H-10 or 11), 8.81 (s, 1H, H-14); ms m/e: 389 (25.4%), 388 (100%), 387 (35%), 373 (12%), 371 (20%), 370 (28%), 69, 57, and 55 (all 20%); high resolution M^+ calcd.: 388.0945; found: 388.0951.

G-2A was not sufficiently soluble in any neutral organic solvent for recrystallization or column chromatography. It was obtained from the residue of the combined eluate fractions by trituration with 1% HCl in ethanol; it could be precipitated from solution in dry dimethylformamide by the addition of methanol; uv (EtOH) λ_{max} nm: 301, 463; (EtOH/ammonia), λ_{max} nm: 332, 400 (small), 515; (EtOH/NaOH) λ_{max} nm: 297, 345, 540; ir (KBr) ν_{max}: 3360, 3110, 3030, 2920, 2840, 1720, 1620, 1595, 1400, 1335, 1285, 1250, 1190, 1165, 1105, 760, 745 cm^{-1}; ms m/e: 389 (17.9%), 388 (70.7%), 387 (25.2%), 373 (12.1%), 371 (18.5%), 370 (25.3%), 194 (14.4%) 69 (13.6%), 57 (9.3%), 55 (11.0%), 44 (100%); high resolution M^+ − 44 calcd.: 388.0945; found: 388.0948.

G-2N tetraacetate

The acetyl derivative of G-2N (20 mg) was prepared using acetic anhydride (10 mL) and 3 drops of concentrated sulfuric acid at room temperature for 3–5 days. It was purified by column chromatography on neutral silica eluting with chloroform and recrystallized from chloroform/heptane; R_f 0.7 in chloroform/ethyl acetate 18:2, mp 248–253°C; uv (EtOH) λ_{max} nm (ϵ): 300 (21 700), 382 (1500); ir (KBr) ν_{max}: 2930, 1770 (aryl acetate), 1670 (C=O), 1590 (aryl), 1365, 1320, 1250, 1185, 1137, 1113, 1085, 1028 cm^{-1}; ^{1}H nmr ($CDCl_3$) δ_{TMS}: 8.86 (s, 1H, H-14), 7.95 (d, 1H, J = 2.5, H-1 or H-3), 7.23 (d, 1H, J = 2.5, H-1 or H-3), 7.0 (br s, 1H, H-10 or H-11), 6.92 (br s, 1H, H-10 or H-11), 2.18 (s, 4H, H-5 and 6), 2.49 (s, 3H, OAc), 2.44 (s, 3H, OAc), 2.36 (s, 6H, OAc × 2), 2.35 (s, 3H, Me); ms m/e: 556 (M^+), 514 (M − 42), 472 (M − 42 × 2), 430 (M − 42 × 3), 388 (M − 42 × 4), 373 (388 − 15), 371 (388 − 17), 370 (388 − 18).

Zinc dust distillation of G-2N

This was carried out in the usual way in a 5-mm id Pyrex glass tube using a mixture of 10 mg G-2N and 200 mg Zn dust over which was layered an additional 1 g of Zn dust. When the tube and contents were heated with a small flame to dull red heat, yellow sublimate appeared in the upper portion of the tube. This was washed out with heptane and purified on a small silica column eluting with heptane. The absorption maxima of the purified material were: 448, 421, 397, 375, 316, 303, 291, 258 nm in heptane, 454, 426, 401, 379, 321, 307 nm in benzene, and the relative intensities of the various bands matched those of benzo[*a*]naphthacene. The literature values (6) for benzo[*a*]-naphthacene in benzene are, λ_{max} (log ϵ): 453 (4.0), 425 (3.97), 402 (3.8), 385 (3.5), 361 (3.16), 320 (4.98), 306 (5.01). The mass spectrum showed peaks at 278 (23%, $C_{22}H_{14}$), 292 (39%, $C_{23}H_{16}$), and 306 (12%, $C_{24}H_{18}$).

Methylation of G-2N

A mixture of G-2N, 26 mg, 3 g anhydrous potassium carbonate, 3 mL dimethyl sulfate, 10 mL dry acetone, and 5 mL dry dimethylformamide was refluxed 24 h. The mixture was poured into water, acidified with glacial HOAc, extracted twice with chloroform, and then extracted with EtOAc, which removed unreacted G-2N, 3 mg. Column chromatography of the chloroform extracts on acidic silica using a benzene/acetone gradient gave components A and B well separated, C, D, and E not well resolved, and 10 mg of recovered G-2N. From further chromatography of mixed fractions it could be seen that C and D cochromatographed on acidic silica but were well separated from E. On pH 8 silica, D and E cochromatographed but were well separated from C, which was the major product, 6.1 mg.

The properties of the 5 components are given in this order: R_f in benzene/acetone 19:1, color on tlc plate, fluorescence on tlc plate, λ_{max} nm (EtOH), λ_{max} nm (EtOH/aq. NaOH), mp (if obtained), ms m/e. A: 0.87, orange, red, 305 and 463, 280 and 515, 416 (M^+ 100%), 401 (M − 15), 398 (M − 18), a dimethylether, very minor amounts. B: 0.78, pale yellow, faint yellow, 304 and 445, 275 and 493, least amount, mass spectrum not obtained. C: 0.47, orange, dark red, 302 and 453, in base maxima flatten but do not shift, mp 261–263°C with sublimation and no dec., 430 (M^+ 100%), 415 (M − 15), 412 (M −18), a trimethyl ether, the major product; High resolution M^+ calcd.: 430.1417; found: 430.1404. D: 0.33, red-orange, none, 311 and 467, 515–535, crystal change at 305°C, sublimed away by 340°C with no melting, 402 (M^+ 100%), 387 (M − 15), 384 (M − 18), 385 (M − 17), a monomethyl ether. E: 0.22, yellow, orange, 302, and 415 (small), no shift in base, mp 245–249°C with sublimation and no dec., 444 (M^+ 52%), 429 (M − 15, 100%), 427 (M − 17), 426 (M − 18), 425 (M − 19), the tetramethyl ether.

The second methylation reaction used 27 mg of G-2N, methyl ethyl ketone instead of acetone; additional potassium carbonate (3 g) and dimethylsulfate (3 mL) were added after 4 h of refluxing. Nevertheless, half of the G-2N was recovered unchanged. Thin-layer chromatography disclosed components A, C, D, and E described above plus an additional component, F. All were obtained by preparative tlc on laboratory-made silica gel G plates run in benzene/acetone 95:5. Yields were (in mg): A, 0.6; D, 0.8; C, 1.5; E, 1.2; F, 0.6. Component F had uv (EtOH) λ_{max} nm: 308, 465; (EtOH/aq. NaOH) λ_{max} nm: 538 (broad); ms m/e: 402 (M^+ 100%), 387 (M − 15), 386 (M − 16), 315 (M − 87), a monomethyl ether which was clearly distinguished from monomethyl ether D by tlc on normal or NaOAc buffered plates, R_f for D, 0.6 and 0.6 respectively; for F, 0.4 and 0.5.

The λ_{max} and the ratio of optical density at 302–311 to the optical density at the visible maxima are given below in order to show the discontinuity between the values for the tetramethyl ether E and the others. G-2N: 311, 470, ratio 2.2; monomethyl ether D: 311, 467, ratio 2.0; monomethyl ether F: 309, 465, ratio 2.1; dimethyl ether A: 305, 463, ratio 2.7; trimethyl ether C: 302, 453, ratio 2.7; tetramethyl ether E, 302, 415, ratio 4.7.

Trimethyl ether C, ^{1}H nmr ($CDCl_3$) δ_{TMS}: 2.37 (s, 3H, Me), 2.75–2.89 (m, 4H, H-5 and 6), 4.03, 3.98, 3.94 (each s, 3H, 3 OMe) 7.50 (d, 1H, J = 2.5, H-1), 6.78 (d, 1H, J = 2.5, H-3), 6.73 (br s, 2H, H-10 and 11), 8.72 (s, 1H, H-14), 13.52 (s, 1H, O—H at C-7); (C_6D_6) δ_{TMS}: 2.11 (s, 3H Me), 2.45–2.59 (m, 2H, H-5 or 6) 2.84–2.99 (m, 2H, H-5 or 6), 3.24, 3.32, 3.40 (each s, 3H, 3 OMe), 6.36 (d, 1H, J = 3, H-3), 7.54 (d, 1H, J = 3, H-1), 6.40 (br s, 1H, H-10 or 11), 6.46 (br s, 1H, H-10 or 11), 9.2 (s, 1H, H-14).

G-2A tetraacetate

A mixture of 10 mg G-2A, 10 mL acetic anhydride, and 2 drops of sulfuric acid was heated for 1 h at 70°C. The reaction mixture was poured into 200 mL water and, after standing overnight, the crude product was obtained by centrifugation and washed. Dried crude product was dissolved in acetone and purified by preparative tlc on 20 laboratory-made silica gel G plates run in benzene/acetone/acetic acid 80:20:1. The desired tetraacetate shows a weak fluroescence on the plate, the R_f in analytical tlc is 0.3 in benzene/acetone/acetic acid

Can. J. Chem. Downloaded from www.nrcresearchpress.com by 210.87.254.5 on 09/06/12
For personal use only.

18:2:0.2. Incompletely acetylated (or deacetylated) material appeared as slower moving spots with strong yellow fluorescence. Faster moving, red fluorescent spots, presumably impurities, were also present. The separation could not be accomplished using columns of neutral silica; with acidic silica deacetylation occurred. To minimize deacetylation during tlc, plates should be run right after material has been applied; solvent and eluant acetone should be stored over anhydrous potassium carbonate; the band of tetraacetate should be eluted within 1/2 h of removal from the tlc tank.

The yield of G-2A tetraacetate was 5.9 mg after precipitation from benzene with heptane; uv ($CHCl_3$) λ_{max} nm: 295, 370; (EtOH, difficultly soluble) λ_{max} nm: 300, 387; ir (KBr) ν_{max}: 3350, 3240, 2960, 1775 (OAc), 1750, 1720 (COOH), 1660 (C=O), 1585 (aryl), 1500, 1145, 920, 740; ^1H nmr ($CDCl_3$) δ_{TMS}: 2.35 (s, 6H, aryl Me and OAc), 2.84 (s, 4H, H-5 and 6), 7.96 (d, 1H, J = 2.5, H-1), 8.90 (s, 1H, H-14), 2.45 (s, 3H, OAc), 2.49 (s, 6H, 2 × OAc), bands for H-3 and H-10 or 11 obscured by solvent; (DMSO-d_6) δ_{TMS}: 2.23 (s, 3H, Me), 2.79 (br s, 4H, H-5 and 6), 7.90 (d, 1H, J = 2.5, H-1), 7.50 (d, 1H, J = 2.5, H-3), 7.3 (s, 1H, H-10 or 11), 8.67 (s, 1H, H-14), 2.34, 2.37, 2.40 (m, 4 × OAc, too close to solvent for accurate integration).

Methylation of G-2A

This was carried out as for the second methylation of G-2N using 36 mg of G-2A. Thin-layer chromatography of the combined chloroform extracts disclosed four components which were separated by suitable combinations of preparative tlc and column chromatography on neutral silica, as for the methyl ethers of G-2N. It was noted that component E runs ahead of F in tlc but behind F on columns. The recovered G-2A from ethyl acetate extracts was 27 mg. The properties of the 4 components are given in this order: R_f in benzene/acetone 18:2, color on tlc plate, fluorescence on tlc plate, λ_{max} nm (EtOH), λ_{max} nm (EtOH/ aq.NaOH), mp, yield, ms m/e. A: 0.87, yellow, yellow, 298 and 460, 283 and 515, 330–345°C dec., 0.8 mg, 474 (M^+ 72%), 473 (24%), 472 (39%), 442 (5.2%), 44 (100%), a dimethylether monomethyl ester or a trimethylether acid. B: 0.7, yellow, very bright yellow, 228, 298 and 458, 292 and 460, 240–245°C, 0.6 mg, 488 (M^+ 100%), 44 (100%), a trimethylether monomethylester or a tetramethylether acid. C: 0.6, orange, orange, 233, 298 and 475, 525, no melting under 350°C, 0.5 mg, not sufficiently volatile for ms, insoluble in benzene when pure. D: 0.42, yellow, weak dull yellow, 234, 299 and 405, 234, 299 and 390–405, mp 204–206°C, 0.6 mg, 502 (M^+ 94%), 487 (100%), 485 (67%), 484 (72%), 483 (79%), 471 (21%), 470 (14%), 455 (35%), 44 (0%), the tetramethylether methylester. High resolution M^+ calcd.: 502.1627; found: 502.1653.

Acknowledgments

This work was partially supported by the Charles and Johanna Busch bequest and by Grant No. 80-CRCR-1-0439 from the U.S. Department of Agriculture. The able assistance of Magda Gagliardi is gratefully acknowledged. We are indebted to Dorothy Denney for some of the nmr spectra, Harry L. Yale for valuable suggestions, and Raghvendra Sahai for analyzing some of the other *Frankia* strains for the presence of these compounds. We also wish to thank J. Theilleux and Rhone–Poulenc Recherches, Vitry, France, as well as L. R. Schronk and Wyeth Laboratories, Philadelphia, Pennsylvania, for the high-resolution mass spectra.

1. D. CALLAHAM, P. DELTREDICI, and J. G. TORREY. Science, **199**, 899 (1978).
2. M. P. LECHEVALIER and H. A. LECHEVALIER. *In* Symbiotic nitrogen fixation in the management of temperate forests. *Edited by* J. C. Gordon, C. T. Wheeler, and D. A. Perry. Forest Research Laboratory, Oregon State Univ., Corvallis. 1979. pp. 111–122.
3. D. BAKER. Actinomycetes Relat. Org. **17**, 35 (1982).
4. M. P. LECHEVALIER, F. HORRIERE, and H. LECHEVALIER. Dev. Ind. Microbiol. **23**, 51 (1982).
5. D. GAUTIER, H. G. DIEM, and Y. DOMMERGUES. Appl. Environ. Microbiol. **41**, 306 (1981).
6. M. ZANDER und W. H. FRANKE. Chem. Ber. **97**, 212 (1964).
7. L. M. JACKMAN and S. STERNHELL. Applications of nuclear magnetic resonance spectroscopy in organic chemistry. 2nd ed. Pergamon Press, Oxford. 1969. pp. 130, 136, 206–207.
8. R. H. THOMSON. Naturally occurring quinones. 2nd ed. Academic Press, London. 1971. pp. 41, 62, 74, 513.
9. H. BROCKMANN. Fortschr. Chem. Org. Naturst. **21**, 121 (1963).
10. J. H. BOWIE, D. W. CAMERON, P. E. SCHUTZ, and D. H. WILLIAMS. Tetrahedron, **22**, 1771 (1966).
11. I. A. SMITH, P. G. SEYBOLD, and M. P. SERVE. Cancer Res. **38**, 2968 (1968).
12. N. IMAMURA, K. KAKINUMA, and N. IKEKAWA. J. Antibiot. **35**, 602 (1982).
13. M. L. HIGGINS and M. P. LECHEVALIER. J. Virol. **3**, 210 (1969).

Can. J. Chem. Downloaded from www.nrcresearchpress.com by 210.87.254.5 on 09/06/12
For personal use only.

The structures of the nellionols. Synthesis of model abieta-8,11,13-trien-7-ones. Synthesis of 5-dehydronellionol trimethyl ether

ROBERT H. BURNELL, MICHEL JEAN, DONALD POIRIER, AND SYLVAIN SAVARD
Département de chimie, Université Laval, Québec (Qué.), Canada G1K 7P4

Received May 7, 1984

ROBERT H. BURNELL, MICHEL JEAN, DONALD POIRIER and SYLVAIN SAVARD. Can. J. Chem. **62**, 2822 (1984).

The synthesis of model ketones derived from podocarpic and dehydroabietic acids prompted us to question the published structures for the nellionols to accommodate more adequately their reported spectral characteristics. Both the originally proposed structure for 5-dehydronellionol and our suggested modification have been synthesized (as the methyl ethers). The nellionols must have the 11,12-dioxy structures rather than the isomeric 11,14-dioxy substitution pattern.

ROBERT H. BURNELL, MICHEL JEAN, DONALD POIRIER et SYLVAIN SAVARD. Can. J. Chem. **62**, 2822 (1984).

Les données spectrales recueillies lors de la synthèse de cétones dérivées des acides podocarpique et déshydroabietique nous ont amené à douter des structures proposées pour les nellionols. Deux synthèses de dérivés méthylés du déshydro-5-nellionol ont été effectuées: celle de la structure qui avait été proposée et celle de la structure que nous avons modifiée. Les structures des nellionols correspondent donc à celles de produits oxygénés aux positions 11 et 12 plutôt qu'aux positions 11 et 14.

Can. J. Chem. Downloaded from www.nrcresearchpress.com by 210.87.254.40 on 09/06/12
For personal use only.

Among the diterpenoid constituents isolated from *Premna latifolia* and described in structural detail by Rao *et al.* (1) were three "nellionols" for which the structures **1**, **2**, and **3** were advanced. Obviously the general features of these compounds could not be in doubt but we found the position of the nmr signals for the aromatic protons in all three cases reminiscent of a C.14 proton in close proximity to a C.7 carbonyl rather than of the C.12 type proposed. Many examples could be quoted to underline our suspicion, for instance ketones **8** and **15** which we have prepared in unambiguous fashion in unpublished model studies concerning the syntheses of coleon U (2) and taxodione (3).

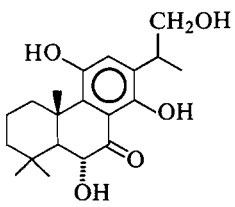

1

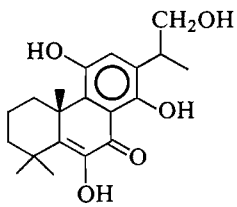

2

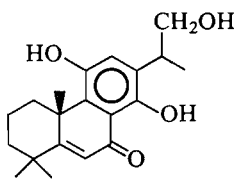

3

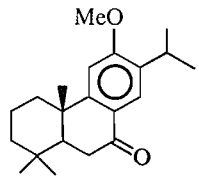

4

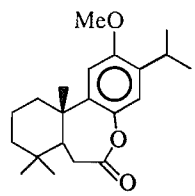

7

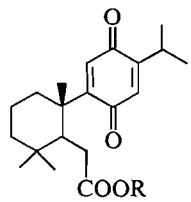

5*a* R = H
5*b* R = Me

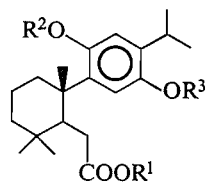

6*a* R^1 = Me R^2 = Me R^3 = Me
6*b* R^1 = Me R^2 = Me R^3 = H
6*c* R^1 = Me R^2 = H R^3 = Me
6*d* R^1 = H R^2 = Me R^3 = Me

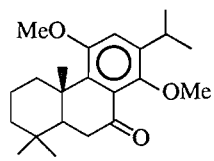

8

The 11,14-dimethoxy compound **8** was prepared from sugiol methyl ether **4** (prepared from podocarpic acid (4)) via the quinone **5***a*. The latter was catalytically reduced and methylated *in situ* to give mostly the ester **6***a*, much smaller quantities of the incompletely methylated compounds **6***b* and **6***c*, and acidification of the aqueous phase afforded varying amounts of the dimethoxy acid **6***d*. All of these products could be used since both **6***b* and **6***c* gave the dimethoxy ester on further methylation. Ester **6***a* was also prepared from **4** by Baeyer–Villiger oxidation, which gave mostly the lactone **7**, and this on methanolysis afforded the previously mentioned phenol ester **6***c* and lesser amounts of the quinone ester **5***b*. Even though both of these products could be integrated into the synthesis (the former by methylation and the latter by reduction and methylation), the yields remained poor. Hydrolysis of the ester **6***a* was affected in aqueous base and the resulting acid **6***d* cyclized readily ($(CF_3CO)_2O$, room temperature) to the ketone **8**. The nmr spectrum of the latter shows a single aromatic proton at δ 6.97.

The abietatrien-7-one **9** was prepared from commercial dehydroabietic acid by known methods (5). Baeyer–Villiger oxidation of this aromatic ketone afforded the seven-membered lactone **10** which was (not isolated but rather) converted directly to the phenol ester **11** by methanolysis. Further oxidation of the phenol with benzene seleninic anhydride following Barton's procedure (6) gave two quinones of which the minor product was the previously described *para*-quinone ester **5***b* and the major product was the *ortho*-quinone **12**. The latter was catalytically reduced and the intermediate catechol was imme-

Can. J. Chem. Downloaded from www.nrcresearchpress.com by 210.87.254.40 on 09/06/12
For personal use only.

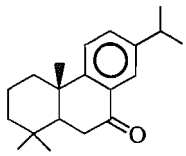

9

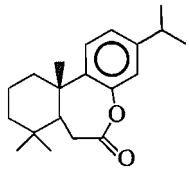

10

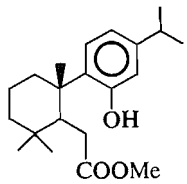

11

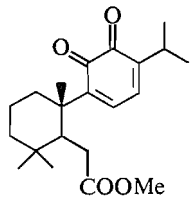

12

diately methylated, while still under hydrogen, to give the dimethoxy ester **14***a*. Hydrolysis to the acid **14***c* and trifluoroacetic anhydride-promoted cyclization gave the ketone **15**. The aromatic proton in the nmr spectrum of this isomer was at δ 7.70.

The published nmr figures for the nellionols and their derivatives show aromatic protons in the range δ 7.34 to 8.17 depending on the substituents, and the closest analogy to our two models (5-dehydronellionol dimethyl ether) shows the aromatic proton at δ 7.61. This compares favorably with our second model and can only mean that the structures proposed by Rao *et al.* (1) must be modified to **16**, **17**, and **18** respectively. It must be noted that the introduction of the enolic ketone at C.6 has virtually no effect on the chemical shift of the aromatic protons. Re-examining the evidence for the original structures suggests that undue importance was credited to the Gibbs test for free *para* positions in phenols, but this useful colour reaction is well known to be misleading (7). The "*para*-quinone" obtained by oxidation during the structure elucidation must have been an *ortho*-quinone and, while no uv/vis spectrum was quoted, the colour of the crystals is quite suggestive.

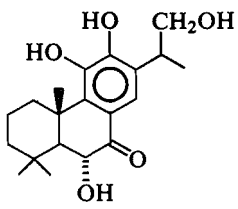

16

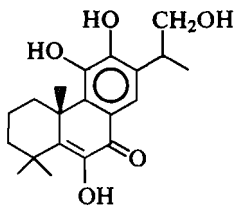

17

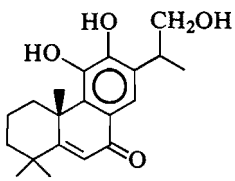

18

Having on hand a small quantity of the quinone **19** (from our synthesis of coleon C (8)) we saw that a rapid synthesis of Rao's 5-dehydronellionol was possible. As originally intended (9), the following sequence was carried through without formally isolating the intermediates and, while our reason was more the fear of insufficient material in this case, the reliability of the scheme has been well demonstrated (see refs. 2, 8, and 9). The product of each reaction was purified by dry column chromatography, the necessary spectral evidence was secured to identify both the nature and the homogeneity of the material, and this "clean" product was subjected to the next reaction in the scheme. Catalytic reduction of the quinone **19** and methylation *in situ* (under hydrogen) afforded the ester **20***a* which was readily hydrolysed to the acid **20***b*, some of which we had previously isolated from the methylation step (above). In trifluoroacetic anhydride the acid **20***b* cyclized in modest yield to the aromatic ketone **21** in which, due to the imposed rotation of the aromatic ring, the methoxyl residues are necessarily at C.11 and C.14. The C.6 position was oxidized by oxygen in *tert*-butanol containing potassium *tert*-butoxide to give the enolic α-diketone **22***a*, which could be O-methylated to the tri-O-methyl derivative **22***b*. As predicted, the synthetic compound, unambiguously corresponding to structure **22***b*, was not identical with the 5-dehydronellionol trimethyl ether described by Rao. The real structures for the nellionols must therefore contain the 11,12-dioxy substitution pattern.

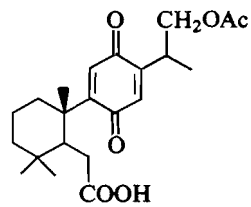

19

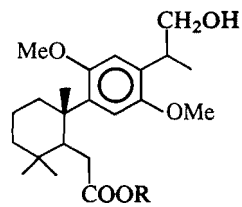

20*a* R = Me
20*b* R = H

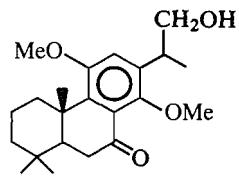

21

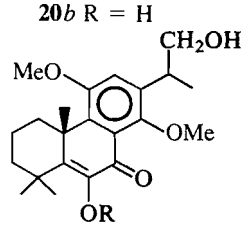

22*a* R = H
22*b* R = Me

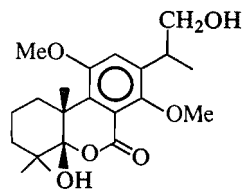

23

In searching for a relatively simple but convincing synthesis of a nellionol, the ester **14***a*, which we had already prepared in earlier model studies, attracted our interest because the introduction of the sidechain hydroxyl would be straightforward in the absence of a competing benzylic position found in compounds containing the normal B ring. At first, attempted functionalization in the isopropyl group using *N*-bromosuccinimide gave discouraging results in that several compounds were formed. After some experimentation we returned to the normal reaction conditions which led to three major products: the isopropenyl derivative **25** (ca. 25%), the tertiary alcohol **24** (31%), and the bromohydrin **26** (41%), and all three could be transformed to the primary alcohol **28***a*. Obviously the alcohol

Can. J. Chem. Downloaded from www.nrcresearchpress.com by 210.87.254.40 on 09/06/12
For personal use only.

TABLE 1. ^{13}C nuclear

Carbon	4	8	9	15	21	29	7	5*a*	5*b*	19	12	6*a*	6*c*	6*d*
1	38.2	37.4	38.2	37.3	37.3	37.3	41.5	36.7	36.9	37.0	37.0	41.5	41.3	41.4
2	19.0	19.3	19.0	19.3	19.2	19.2	19.0	18.7	18.9	18.8	19.7	19.4	19.5	19.4
3	41.6	41.3	41.6	41.3	41.3	41.3	32.0	40.8	40.9	40.9	41.1	36.6	36.4	36.4
4	33.4	33.1	36.4	35.7	33.5	33.2	39.3	34.2	34.2	33.7	34.2	34.4	42.6	34.6
5	49.9	49.6	49.6	50.3	49.5	50.3	40.2	44.3	44.8	44.7	44.7	44.6	44.6	44.7
6	36.1	37.0	36.4	33.3	36.9	35.7	56.6	32.6	32.6	31.9	32.7	33.0	32.8	33.0
7	198.4	199.5	199.8	199.0	199.5	198.7	173.4	180.8	174.5	177.1	174.8	175.1	176.0	180.7
8	124.5	127.0	131.0	128.3	127.2	128.6	138.6	188.1	188.1	187.4	135.4	113.0	113.1	113.1
9	156.5	142.0	154.0	146.2	143.0	146.9	145.4	154.5	154.8	154.8	148.8	135.3	136.3	135.2
10	38.4	40.8	38.0	40.8	40.9	40.9	36.2	43.3	43.4	43.0	43.2	42.6	34.5	42.8
11	104.8	152.1	123.8	151.5	153.8	151.7	107.6	134.7	134.6	134.6	181.2	153.1	149.3	150.6
12	161.9	116.1	132.5	156.7	116.8	157.3	154.4	187.9	188.1	187.2	180.8	111.4	116.1	111.5
13	135.5	141.4	146.9	141.4	136.5	136.6	135.5	152.7	152.5	146.4	148.5	135.6	133.1	136.2
14	125.9	153.8	125.1	121.1	152.8	121.9	118.8	133.5	133.8	135.9	133.1	150.4	151.3	153.1
15	26.8	33.5	33.7	27.1	34.9 34.8	35.3	26.8	26.3	26.4	31.8	27.2	29.6	26.6	26.9
16	22.5	23.6	23.9	23.4	68.2	68.1	22.5	21.6	21.4	66.7	21.4	22.8	22.8	22.6
17	22.5	23.3	23.9	23.1	17.3	17.4 17.2	22.5	21.0	21.4	14.7	21.4	22.8	22.8	22.6
18	32.6	26.3	33.7	33.7	33.1	33.7	33.3	33.4	33.5	33.7	33.5	33.9	33.6	33.8
19	21.4	21.7	21.4	21.7	21.7	21.7	21.5	22.8	22.8	22.8	22.5	22.8	23.1	22.6
20	23.3	22.7	23.4	19.9	18.1	19.9	20.5	20.1	20.1	19.8	18.9	21.1	21.1	21.2
COO*Me*	—	—	—	—	—	—	—	—	51.4	—	51.6	51.0	51.3	—
OMe (11)	—	56.0	—	60.2	56.0	60.2	—	—	—	—	—	55.8	—	55.9
OMe (12)	55.5	—	—	60.0	—	60.0	55.6	—	—	—	—	—	—	—
OMe (14)	—	62.7	—	—	62.8	—	—	—	—	—	—	56.6	56.9	56.9

[a]In ppm from TMS.
[b]Comparison spectrum recorded on a Bruker WH-400 (400 MHz).

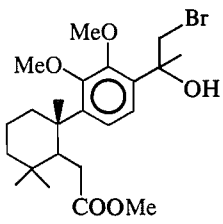

26

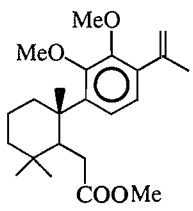

25

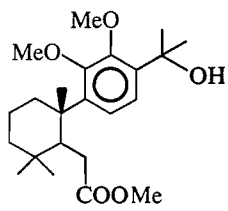

24

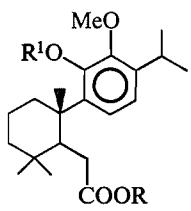

14*a* R = R' = Me
14*b* R = Me R' = H
14*c* R = H R' = Me

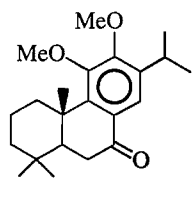

15

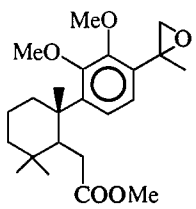

27

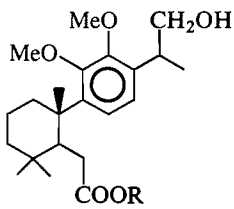

28*a* R = Me
28*b* R = H

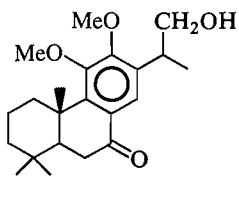

29

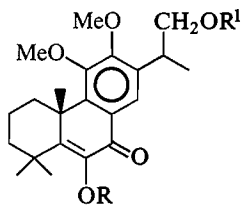

30*a* R = R' = H
30*b* R = Me R' = H
30*c* R = R' = Me

24 was readily dehydrated to the olefin **25** and the latter, on treatment with diborane and subsequent oxidation, afforded the required **28***a*. The bromohydrin **26** was quantitatively converted to the epoxide **27** (both epimers) which was reductively cleaved (diborane – BF_3·etherate) to the primary alcohol **28***a*. The overall yield for the transformation isopropyl **14***a* to the

magnetic resonance data[a]

Compound															
11	**14***a*	**14***c*	**20***a*	**20***b*	**25**	**26**	**26***M*	**27**	**27***M*	**28***a*	**28***aM*	**28***b*	**30***a*	**30***b*	**30***b*[b]
35.8	37.3	37.0	36.4	36.1	37.2	37.2	—	37.1	—	37.2	—	36.9	28.0	29.8	29.1
19.5	19.5	19.4	19.4	19.3	19.4	19.5	—	19.4	—	19.4	—	19.4	18.1	18.1	17.9
41.1	41.7	41.5	41.4	41.4	41.6	41.6	—	41.6	—	41.6	—	41.5	36.7	37.2	37.2
34.3	34.6	34.8	34.4	34.5	34.5	34.7	—	34.5	—	34.5	—	34.7	36.7	37.2	37.2
44.0	46.1	46.0	44.7	44.9	46.0	46.0	—	45.9	—	46.0	—	46.4 46.2	143.3	—	—
32.6	32.9	32.9	33.0	32.9	33.0	32.9	—	32.9	—	33.0	—	32.9	144.1	144.1	144.3
176.6	175.0	180.7	175.0	179.7 179.0	175.0	175.0	—	175.0	—	175.0	—	180.1 179.2	179.9	180.8	180.5
128.5	119.6	119.7	113.1	113.4	122.4	120.6	121.2	120.6	120.7	120.4	121.0	120.8 120.4	124.0	126.8	126.6
132.0	141.1	139.8	136.3	136.0	143.6	143.6	127.7	142.5	127.5	140.9	127.6	140.8 140.6	146.1	151.7 151.5	149.2
42.1	43.0	43.0	42.7	42.7	43.0	43.2	—	43.2	—	43.0	—	43.0	41.5	42.3	42.2
155.6	153.0	152.9	153.2	153.4	153.3	153.3	111.6	153.0	110.6	153.1	111.0	153.1	151.3	150.8	150.5
115.3	151.5	151.5	112.5	112.0	151.5	151.5	156.7	151.8	157.3	152.3	157.7	152.2	157.3	158.3 156.1	158.2 155.7
148.0	140.0	141.4	130.5	130.7	136.7	135.7	132.0	134.3	130.5	136.2	132.2	136.2	137.6	137.4	137.1
117.4	123.4	123.2	151.1	151.2	123.2	123.2	129.0	123.4	128.9	123.7	127.6	123.9 123.7	120.6	120.3	120.4
33.6	26.8	26.8	35.8 35.6	36.3 36.1	141.8	73.9	73.8	56.6	56.6	35.3	35.5	35.6	35.3	35.3	35.1
23.9	23.6	23.4	68.0	67.6	23.4	26.8	25.8	23.6	23.0	17.3	16.7	17.3	17.5 17.3	17.3	17.4
23.7	23.6	23.4	16.5	16.5	115.0	44.9	44.0	54.8	55.2	68.5	67.9	68.3	68.0	68.1	68.1
33.3	33.9	33.7	33.8	33.8	33.8	33.8	—	33.8	—	33.8	—	33.7	31.6	31.5	31.4
23.0	21.6	21.7	22.7	22.7	21.7	21.7	—	21.7	—	21.5	—	21.6	29.3	29.3	29.7
21.0	22.9	23.0	21.1	21.1	22.9	23.1	—	22.9	—	22.9	—	22.8	27.3		
51.3	50.9	—	51.0	—	50.9	51.2	—	50.9	—	51.0	—	—	—	—	—
—	59.9	59.9	56.6	56.8	59.9	60.0	—	59.6	—	60.0	—	59.9	60.3	60.2	60.2
—	59.6	59.7	—	—	59.9	59.4	55.5	59.6	55.4	59.6	55.5	59.7	59.9	59.9	59.9
—	—	—	55.8	55.7	—	—	—						OMe (6)	59.4	59.5

2-hydroxyisopropyl **28***a* was superior to 65%. Hydrolysis of the ester function in **28***a* gave the acid **28***b* which cyclized readily to the ketone **29**. The final oxidation was achieved in the normal manner with oxygen and strong base, and the enolic α-diketone was O-methylated for comparison with this same derivative (**30***b*) in the literature. The identity of the spectral results shows that this is indeed 5-dehydronellionol trimethyl ether. Our synthesis is not decisive as to the configuration at C.15; the original authors are not specific on this point either, and for this reason direct comparison would be of limited value since in the present synthesis (other than the selectivity induced by the asymmetry already present) no effort was made to direct the configuration at C.15. The diastereomers were in fact not readily separable.

After our preliminary reports (10*a*, *b*), Matsumoto's group also published convincing evidence (11) to correct the Rao structures. Their syntheses are quite different from those described here but the conclusions are the same. More recently (12), they have synthesized structure **18** (as the triacetate) only to find that their sample was not identical with the 5-anhydronellionol triacetate described in the literature. In fact the latter turned out to be the acetate of 5-dehydronellionol **17**.

The ^{13}Cmr spectra of many of the compounds described in these syntheses are listed in Table 1. The assignments are based on values given by Enzell and co-workers (13*a*), Wehrli and Nishida (13*b*) and Wenkert *et al.* (13*c*) and by comparing with many spectra of similar molecules which our recent syntheses

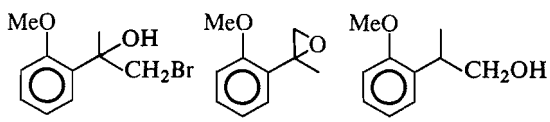

26*M* **27***M* **28***aM*

have engendered. The spectra of three very simple model compounds **26***M*, **27***M*, and **28***aM* are also included in the table in partial support for attributions of particular resonances where we had no previous experience.

Experimental

Unless otherwise stated, the conditions and instruments used to characterize the products were: melting points, Electrothermal, uncorrected; ultraviolet spectra, ethanol solutions (ε in parentheses), Hewlett Packard 8450A; infrared spectra, solids as KBr pellets and others as carbon tetrachloride solutions, Beckman 4250 and Perkin Elmer 457; proton magnetic resonance spectra, deuteriochloroform solutions, TMS internal standard, (multiplicity, integrated peak areas, coupling constants, and assignments in parentheses), Bruker HX 90; carbon-13 magnetic resonance spectra, deuteriochloroform solutions, TMS internal standard, Bruker WP 80; mass spectra, Hewlett Packard 5992. Elemental analyses were by Galbraith Laboratories, Knoxville, Tenn. The high resolution mass spectra were recorded on an AEI MS30.

Dry column chromatography (abbreviated dry col chrom) implies the use of Merck Kieselgel 60F (70–230 mesh) in nylon foil tubing and development with either hexane – ethyl acetate or carbon tetra-

Can. J. Chem. Downloaded from www.nrcresearchpress.com by 210.87.254.40 on 09/06/12
For personal use only.

Can. J. Chem. Downloaded from www.nrcresearchpress.com by 210.87.254.40 on 09/06/12
For personal use only.

chloride – ethyl acetate (proportions determined by prior thin layer chromatography using Machery–Nagel precoated plastic sheets).

Baeyer–Villiger oxidation of sugiol methyl ether **4** *and methanolysis of lactone* **7**

Sugiol methyl ether **4** (8.8 g) in $CHCl_3$ (100 mL) was added drop by drop to a stirred solution of *m*-chloroperbenzoic acid (9.8 g) in $CHCl_3$ (150 mL). Stirring was continued at room temperature for 4 days when another equivalent of *m*-CPBA was added and the reaction continued for 4 more days. The solution was well washed, dried, and evaporated, and a small portion of the product was purified by dry col chrom. With difficulty a small quantity of the pure lactone **7** was obtained, mp 145°C (needles from hexane); uv: 238(6300) and 279(4200) nm; ir: 1745 cm^{-1}; H nmr δ: 0.91, 1.16, and 1.51 (3s, Me at C.4 and C.10), 1.20 (d, 6H, J = 7 Hz, iPr Me), 2.60 (d, J = 5.5 Hz, C.6-H), 2.61 (d, J = 6.5 Hz, C.6-H), 1.83 (m, C.5-H), 3.27 (m, iPr CH), 3.86 (s, Ar-OMe), 6.82 and 6.96 (2s, arom H); ^{13}Cmr, see table; ms *m/e*: 330 (M^+, $C_{21}H_{30}O_3$) and 315.

The crude lactone (8.9 g) was dissolved in MeOH (160 mL) and, after adding concentrated H_2SO_4 (2.0 mL), the mixture was refluxed for 2 h. Ether extraction (after removing much of the MeOH under vacuum) gave a yellow oil (5.1 g) which was purified by column chromatography (SiO_2, hexane – ethyl acetate) to afford the phenol ester **6***c* (2.62 g; 27%; *methyl 2-(5-methoxy-2-hydroxy-4-isopropylphenyl)-2,6,6-trimethylcyclohexylethanoate)*, mp 171–172°C (needles, hexane); uv: 228(7000) and 290(6800) nm; ir: 3390 and 1710 cm^{-1}; H nmr δ: 0.97, 1.00, and 1.39 (3s, three Me-C), 1.12 (d, J = 7 Hz, iPr Me), 2.20 (d, J = 6.5 Hz, C.6-H), 2.21 (d, J = 4.5 Hz, C.6-H), 3.27 (s, COOMe – falls on m, C.5-H and iPr CH), 3.77 (s, Ar-OMe), 6.63 (s, C.11-H), and 6.76 (s, 2H, C.14-H and OH (D_2O)); ^{13}Cmr, see table; ms *m/e*: 362 (M^+) and 330. *Anal.* calcd. for $C_{22}H_{34}O_4$: C 72.89, H 9.45; found: C 72.69, H 9.56.

A second product from the chromatogram was the *p*-benzoquinone ester **5***b* (1.05 g; 11%; yellow oil); ir: 1735 and 1655 cm^{-1}; H nmr δ: 0.93 (s, 6H, *gem* diMe), 1.13 (d, J = 7 Hz, iPr Me), 1.18 (s, C.10-Me), 3.42 (s, COOMe), 6.45 and 6.53 (2s, olefinic H); ^{13}Cmr, see table; ms *m/e*: 346 (M^+).

Methylation of the phenol ester **6**c

The phenol (1.7 g), K_2CO_3 (24 g), and excess dimethyl sulfate were taken up in dry acetone (250 mL). After 24 h at reflux, the cooled mixture was diluted with water, most of the acetone was removed in vacuum, and the product was obtained by ether extraction. The yellow oil (1.7 g) was chromatographed to give unctuous yellow crystals of the ester **6***a*, *methyl 2-(2,5-dimethoxy-4-isopropylphenyl)-2,6,6,-trimethylcyclohexylethanoate*, mp 51–54°C (from CCl_4, 610 mg; 33%); ir: 1730 cm^{-1}; H nmr δ: 0.94 and 0.99 (2s, *gem* diMe), 1.22 (d, J = 7 Hz, iPr Me), 1.43 (s, C.10-Me), 2.13 (d, J = 5 Hz, C.6-H), 2.20 (d, J = 4.5 Hz, C.6-H), 3.25 (m, iPr CH), 3.28 (s, COOMe), 3.82 and 3.89 (2s, Ar-OMe), 6.76 and 6.84 (2s, arom H); ^{13}Cmr, see table; ms *m/e*: 376 (M^+). *Anal.* calcd. for $C_{23}H_{36}O_4$: C 73.36, H 9.64; found: C 73.13, H 9.90.

Reduction and methylation of the p-*quinone* **5**a

The *p*-quinone **5***a* (0.5 g) in MeOH (70 mL) was introduced into a hydrogenation flask containing prehydrogenated Adams' catalyst (40 mg) and MeOH (15 mL). The mixture was stirred under hydrogen until the yellow colour had disappeared (ca. 45 min) and then every hour, for 12 h, aqueous NaOH (2.0 mL of 30%) and dimethyl sulfate (1.5 mL) were added while the mixture was stirred under hydrogen. The catalyst was removed by filtration, most of the MeOH was removed at the pump, and the crude product (yellow oil, 0.46 g) obtained by ether extraction was purified by dry col chrom to give three products: dimethoxy ester **6***a* (362 mg; 64%), identical with that described above; phenol ester **6***c* (27 mg; 5%), also described above; the isomeric phenol ester **6***b* (16 mg; 3%), *methyl 2-(2-methoxy-5-hydroxy-4-isopropylphenyl)-2,6,6-trimethylcyclohexylethanoate*,white needles, mp 161–162°C (from hexane); ir: 3595, 3400 and 1715 cm^{-1}; H nmr δ: 0.96 (s, 6H, *gem* diMe), 1.12 (d, J = 7 Hz, iPr Me), 1.37 (s, C.10-Me), 2.12 (d, J = 3.5 Hz, C.6-H), 2.20 (d, J = 2.5 Hz, C.6-H), 3.18 (m, iPr CH), 3.24 (s, COOMe), 3.74 (s, Ar-OMe), 6.00 (s, OH (D_2O)), 6.53 and 6.70 (2s, arom H); ms *m/e*: 362 (M^+), 347 and 331. *Anal.* calcd. for $C_{22}H_{34}O_4$: C 72.89, H 9.45; found: C 72.81, H 9.49.

Further methylation of the phenol esters **6***b* and **6***c* (Me_2SO_4, NaOH) afforded the dimethoxy compound **6***a*.

Hydrolysis of ester **6**a

To the dimethoxy ester (0.5 g) in MeOH (25 mL) was added aqueous KOH (25 mL of 10%) and the mixture was refluxed for 4 h. After evaporation of most of the MeOH, the aqueous phase was washed with ether and then acidified to permit the extraction of the acid **6***d* with ether. The product, *2-(2,5-dimethoxy-4-isopropylphenyl)-2,6,6,-trimethylcyclohexylethanoic acid*, recrystallized from hexane, mp 148°C (white needles); ir: 1705 cm^{-1}; H nmr δ: 0.87 and 0.95 (2s, *gem* diMe), 1.13 and 1.15 (2d, J = 7 Hz, iPr Me), 1.30 (s, C.10-Me), 3.03 (m, iPr CH), 3.70 and 3.76 (2s, Ar-OMe at C.11 and C.14 resp), 6.66 and 6.76 (2s, arom H); ^{13}Cmr, see table; ms *m/e*: 362 (M^+) and 347. *Anal.* calcd. for $C_{22}H_{34}O_4$: C 72.89, H 9.45; found: C 73.00, H 9.48.

Cyclization to ketone **8**

A solution of the dimethoxy acid **6***d* (70 mg) in trifluoroacetic anhydride (1.0 mL) was stirred at room temperature for 24 h. The reaction mixture was poured into ice-water and the crude cyclized product (the enol trifluoroacetate) was taken up in MeOH (25 mL) and hydrolysed immediately by adding aqueous KOH (4 mL of 10%). After 1 h, the MeOH was evaporated and the product obtained by ether extraction. Dry col chrom afforded the ketone **8** (25 mg; 39%; *7-oxo-11,14-dimethoxyabieta-8,11,13-triene*), mp 98–99°C (from hexane) uv: 228(7800), 261(3200), and 331(7800) nm; ir: 1680 cm^{-1}; H nmr δ: 0.95 and 0.98 (2s, *gem* diMe), 1.22 (2d, J = 7 Hz, iPr Me), 1.34 (s, C.10-Me), 1.81 (dd, J = 10.5 and 7.5 Hz, C.5-H), 2.62 (d, J = 10.5 Hz, C.6-H), 2.64 (d, J = 7.5 Hz, C.6-H), 3.41 (sept, iPr CH), 3.78 and 3.82 (2s, Ar-OMe at C.11 and C.14 resp), and 6.97 (s, arom H); ^{13}Cmr, see table; ms *m/e*: 344 (M^+) and 328. *Anal.* calcd. for $C_{22}H_{32}O_3$: C 76.70, H 9.36; found: C 76.83, H 9.66.

7-Oxo-abieta-8,11,13-triene **9**

To a solution of abietatriene (prepared from dehydroabietic acid, 10 g) in glacial HOAc (75 mL) was added chromium trioxide (15.0 g) in 80% HOAc (115 mL). After 4 h at room temperature, the reaction mixture was poured into ice-water and the crude ketone (9.1 g; 86%), which was obtained by ether extraction, could be used as such for the next step. A small sample was purified by dry col chrom to give the pure ketone **9**, mp 89–90°C (from hexane); uv: 254(12 000) and 302(2300) nm; ir: 1690 cm^{-1}; H nmr δ: 0.94 and 1.01 (2s, *gem* diMe), 1.25 (d, J = 7 Hz, iPr Me), 1.24 (s, C.10-Me), 2.80 (sept, J = 7 Hz, iPr CH), 7.40 (m, 2H, arom H at C.11 and C.12), and 7.90 (d, J = 2 Hz, arom H at C.14); ms *m/e*: 284 (M^+), 269, 227, and 201. *Anal.* calcd. for $C_{20}H_{28}O$: C 84.45, H 9.92; found: C 84.47, H 10.02.

Baeyer–Villiger oxidation of ketone **9** *and methanolysis of lactone* **10**

A solution of *m*-chloroperbenzoic acid (13.0 g, 2 equiv.) in $CHCl_3$ (180 mL) was added dropwise to the ketone **9** (9.1 g) dissolved in $CHCl_3$ (55 mL). Stirring was continued at room temperature for 8 days but further equivalents of *m*-CPBA (6.5 g) in $CHCl_3$ (90 mL) were added after the second, fourth, and fifth days. After rigorous washing, the solution was filtered through a short column of silica gel and evaporated to give the lactone **10** as an oil (7.4 g); ir: 1760 cm^{-1} and ms *m/e*: 300 (M^+).

Without purification the lactone (7.2 g) was taken up in MeOH (75 mL) to which concentrated H_2SO_4 (3.0 mL) was added and the solution refluxed for 45 min. After evaporating most of the MeOH, the product was obtained by ether extraction. Crystallization from hexane gave the phenol ester **11** (1.5 g) and further quantities (2.07 g) were obtained by chromatography of the mother liquors. The yield of **11** was only 34% (from the ketone **9**, some of which (0.36 g) was recovered from the reaction). The ester **11** (*methyl 2-(2-hydroxy-4-isopropylphenyl)-2,6,6-trimethylcyclohexylethanoate*) showed mp

Can. J. Chem. Downloaded from www.nrcresearchpress.com by 210.87.254.40 on 09/06/12
For personal use only.

141–143°C (from hexane–ether); ir: 3500–3200 (br, OH), 1710, and 1620 cm^{-1}; H nmr δ: 0.98, 1.01, and 1.39 (3s, Me-C), 1.18 (d, J = 7 Hz, iPr Me), 2.77 (sept, J = 7 Hz, iPr CH), 3.29 (s, COOMe), 3.40 (dd, J = 7 and 5 Hz, C.5-H), 6.60 (m, arom H at C.12 and C.14), 7.00 (s, OH (D_2O)), and 7.10 (d, J = 8 Hz, C.11-H); ^{13}Cmr, see table; ms m/e: 332 (M^+), 300, and 257. *Anal.* calcd. for $C_{21}H_{32}O_3$: C 75.86, H 9.70; found: C 76.08, H 9.84.

*Oxidation of the phenol ester **11** (to give quinones **12** and **5**b)*

The phenol ester **11** (0.48 g) was dissolved in THF (18 mL) and added dropwise to a stirred suspension of benzene seleninic anhydride (1.05 g; 2.5 equiv.) in THF (50 mL) heated to 50–55°C. The reaction was followed by tlc and was complete in ca. 3 h. After pouring the reaction mixture into ice-water, the organic layer was well washed and then evaporated to afford an orange oil (890 mg). Dry col chrom gave diphenyl diselenide (160 mg), the *p*-quinone **5***b* (160 mg; 32%), and the *o*-quinone **12** (296 mg; 59%; *methyl 2-(4-isopropylbenzoquinone-2,3)yl-2,6,6-trimethylcyclohexylethanoate*), mp 100–101°C (from hexane); uv: 274(700), 418(1600), and 586 (weak !) nm; ir: 1725, 1680, 1660, and 1650(sh) cm^{-1}; H nmr δ: 0.92 (s, 6H, *gem* diMe), 1.10 (d, J = 7 Hz, iPr Me), 1.19 (s, C.10-Me), 2.93 (sept, J = 7 Hz, iPr CH), 3.47 (s, COOMe), and 6.70 (ABq, J = 7 Hz, arom H at C.8 and C.14); ^{13}Cmr, see table; ms m/e: 348.2290 (M^+ + 2), 346.2119 (M^+, $C_{21}H_{30}O_4$ requires 346.2144), 318 and 316. *Anal.* calcd. for $C_{21}H_{30}O_4$: C 72.80, H 8.73; found: C 73.12, H 8.70.

*Reduction and methylation of quinone **12***

A solution of the *o*-quinone **12** (296 mg) in MeOH (10 mL) was added to prehydrogenated Adams' catalyst (20 mg) in MeOH (5 mL) in an atmospheric pressure hydrogenation apparatus. When the red color had disappeared, NaOH solution (total of 8 mL of 30%) and dimethyl sulfate (total 5 mL) were added over a period of 10 h with continuous stirring. After filtering, most of the MeOH was removed under vacuum and the product (270 mg) was obtained by ether extraction. Dry col chrom gave a small quantity of the starting quinone (30 mg; 10%), the 11-hydroxy-12-methoxy compound **14***b* (50 mg; 16%), and **14***a* (*methyl 2-(2,3-dimethoxy-4-isopropylphenyl)-2,6,6-trimethylcyclohexylethanoate*), 160 mg; 50%; yellow oil); ir: 1730 cm^{-1}; H nmr δ: 0.91, 0.97, and 1.31 (3s, Me-C), 1.19 (2d, J = 7 Hz, iPr Me), 3.24 (s, COOMe), 3.74 and 3.96 (2s, Ar-OMe), and 6.90 (ABq, J = 8 Hz, arom H); ^{13}Cmr, see table; ms m/e: 376 (M^+) and 345. *Anal.* calcd. for $C_{23}H_{36}O_4$: C 73.36, H 9.64; found: C 73.46, H 9.80.

*Hydrolysis to acid **14**c*

To the ester **14***a* (160 mg) in MeOH (20 mL) was added NaOH solution (10 mL of 10% aqueous) and the mixture was refluxed for 5 h. Most of the MeOH was removed at the pump and the aqueous residue was extracted with ether to remove unchanged starting material (40 mg). After acidification, the acid **14***c* (114 mg; 74%; *2-(2,3-dimethoxy-4-isopropylphenyl)-2,6,6-trimethylcyclohexylethanoic acid*) was obtained by ether extraction; ir: 1700 cm^{-1}; H nmr δ: 0.84, 0.94, and 1.24 (3s, Me-C), 1.13 (2d, J = 7 Hz, iPr Me), 3.18 (sept, J = 7 Hz, iPr CH), 3.66 and 3.87 (2s, Ar-OMe), 6.87 (ABq, J = 8 Hz, arom H), and 10.07 (s, COOH (D_2O)); ^{13}Cmr, see table; ms m/e: 362 (M^+), 347, and 332. *Anal.* calcd. for $C_{22}H_{34}O_4$: C 72.89, H 9.45; found: C 72.71, H 9.65.

*Cyclization to the ketone **15***

The acid **14***c* (94 mg) was dissolved in trifluoroacetic anhydride (3.0 mL) and the solution stirred for 6 h at room temperature. The mixture was decomposed by pouring onto ice and the crude enol trifluoroacetate, secured by ether extraction, was hydrolysed by taking up in MeOH containing aqueous KOH (5 mL of 10%). After 1 h, the neutral product was once more obtained by extraction. Dry col chrom gave the oily ketone **15** (70 mg; 78%; *7-oxo-11,12-dimethoxyabieta-8,11,13-triene*); $[\alpha]_D^{25}$ +52° (*c* 1.23, $CHCl_3$); uv: 273 (23 600) nm; ir: 1670 cm^{-1}; H nmr δ: 0.94, 0.99, and 1.39 (3s, Me-C), 1.21 and 1.24 (2d, J = 7 Hz, iPr Me), 3.20 (sept, J = 7 Hz, iPr CH), 3.85 (s, 6H, Ar-OMe), and 7.70 (s, arom H at C.14); ^{13}Cmr, see table; ms m/e: 344 (M^+) and 329. *Anal.* calcd. for $C_{22}H_{32}O_3$: C 76.70, H 9.36; found: C 76.91, H 9.49.

*Reduction and methylation of quinone **19***

The quinone **19** (300 mg: prepared from podocarpic acid by previously described methods (9)) in MeOH (10 mL) was added to prehydrogenated Adams' catalyst (50 mg) in MeOH (10 mL) in an atmospheric pressure hydrogenation apparatus. After the yellow solution had lost all color (ca. 1 h), portions of aqueous NaOH (2.0 mL of 30%) and dimethyl sulfate (1.0 mL) were added every 2 h (total, 12 mL NaOH and 6 mL Me_2SO_4) and the mixture stirred for a total of 72 h. The usual work-up gave a crude oil (300 mg) which was purified by dry col chrom to give the dimethoxy ester **20***a*, which was used as such for the next step (180 mg; 60%; *methyl 2-(4-(2-hydroxyisopropyl)-2,5-dimethoxyphenyl)-2,6,6-trimethylcyclohexylethanoate*); uv: 227(5600) and 290(3200) nm; ir: 3440 and 1730 cm^{-1}; H nmr δ: 0.92, 0.97 and 1.37 (3s, Me-C), 1.26 (d, J = 7 Hz, iPr Me), 2.01 (dd, J = 16 and 6 Hz, C.6-H), 3.08 (dd, J = 7 and 6 Hz, C.5-H), 3.28 (s, COOMe), 3.41 (m, C.15-H), 3.70 (d, 2H, J = 6 Hz, CH_2OH), 3.82 and 3.88 (2s, Ar-OMe), 6.73, and 6.87 (2s, arom H at C.8 and C.12 resp); ^{13}Cmr, see table; ms m/e: 392 (M^+).

A smaller quantity of the more polar acid **20***b* (80 mg; 28%) was also obtained from the column; for properties see later.

*Hydrolysis to acid **20**b*

The ester **20***a* (170 mg) was hydrolysed by refluxing in MeOH (20 mL) containing 10% aqueous NaOH (20 mL). The crude extract (161 mg) was chromatographed (dry col) to give the glassy acid **20***b* (150 mg; 92%; *2-(4-(2-hydroxyisopropyl)-2,5-dimethoxyphenyl)-2,6,6-trimethylcyclohexylethanoic acid*); uv: 232(sh, 4600) and 289(2700) nm; ir: 3600–2500 (br, COOH) and 1700 cm^{-1}; H nmr δ: 0.95 (s, 6H, *gem* diMe), 1.37 (s, C.10-H), 1.18 and 1.21 (3d, J = 7 Hz, iPr Me – two isomers), 1.97 (dd, J = 16 and 7 Hz, C.6-H), 3.05 (dd, J = 7 and 5 Hz, C.5-H), 3.73 and 3.80 (2s, Ar-OMe), 6.31 (br, 2H, COO*H* and OH (D_2O)), 6.63 and 6.65 (2s, total 1H, C.8-H – two isomers), and 6.84 (s, C.14-H); ^{13}Cmr, see table; ms m/e: 378 (M^+).

*Formation of ketone **21***

The acid **20***b* (160 mg) was stirred in trifluoroacetic anhydride (6 mL) for 12 h at room temperature. After isolation by ether extraction, the crude enol trifluoroacetate was hydrolysed by stirring for 1 h at room temperature in MeOH (20 mL) containing 10% aqueous NaOH (15 mL). Dry col chrom of the yellowish oil gave the cyclized ketone **21** (75 mg; 48%; *7-oxo-11,14-dimethoxy-16-hydroxyabieta-8,11,13-triene*), mp 92–95°C; uv: 231(10 200), 261(4200), and 330(2500) nm; ir: 3440 and 1680 cm^{-1}; H nmr δ: 0.96, 0.99, and 1.36 (3s, Me-C), 1.28 (d, J = 7 Hz, Me-CH), 1.82 (dd, J = 10 and 7 Hz, C.5-H), 1.99 (m, OH (D_2O)), 2.52 (dd, J = 10 and 17 Hz, C.6-H), 2.72 (dd, J = 17 and 7 Hz, C.6-H), 3.40 (sex, J = 7 Hz, Me-C*H*), 3.72 (d, 2H, J = 7 Hz, CH_2OH), 3.78 and 3.81 (2s, Ar-OMe), and 6.95 (s, arom H); ^{13}Cmr, see table; ms m/e: 360 (M^+).

*Oxidation to the enolic α-diketone **22**a*

The ketone **21** (72 mg) in *t*-BuOH (10 mL) was added to a solution prepared by dissolving potassium (1.6 g) in *t*-BuOH (40 mL). The mixture was vigorously stirred under oxygen for 1 h and then the crude product, obtained by extraction, was purified by dry col chrom to give the enol **22***a* (45 mg; 60%; *7-oxo-11,14-dimethoxy-6,16-dihydroxyabieta-5,8,11,13-tetraene*); uv: 245(10 200), 273(5900), and 340(6800) nm; ir: 3430, 3340, and 1620 cm^{-1}; H nmr δ: 1.28 and 1.31 (2d, 3H total, J = 7 Hz, Me-CH), 1.46 (s, 6H, *gem* diMe), 1.64 (s, C.10-Me), 3.36 and 3.83 (m, 3H, CH_2OH and C.15-H), 3.76 and 3.86, (2s, Ar-OMe), 7.04 (s, arom H), and 7.40 (s, OH (D_2O)); *Exact Mass* (m/e) calcd. for $C_{22}H_{30}O_5$: 374.2093; found: 374.2109.

A second, much more polar product was also obtained from the dry col. From the following characteristics and analogy with similar products, this minor component must be the lactol **23** (21 mg; 26%); uv: 212(7200), 233(3900), 264(1700), and 326(1100) nm; ir: 3400 and 1685 cm^{-1}; H nmr δ: 1.11, 1.21, and 1.46 (3s, Me-C), 1.29 (d, J = 6.5 Hz, Me-CH), 3.26–3.89 (m, 3H, CH_2OH and C.15-H), 3.80 and 3.83 (2s, Ar-OMe), and 6.99 (s, arom H).

Can. J. Chem. Downloaded from www.nrcresearchpress.com by 210.87.254.40 on 09/06/12
For personal use only.

Methylation to the trimethyl ether ***22b***

To the enolic α-diketone ***22a*** (40 mg) in MeOH (7 mL) was added 30% aqueous NaOH (5 mL). After stirring for 20 min, dimethyl sulfate (3 mL) was added and the mixture stirred at room temperature for 36 h. The extracted material was purified by dry col chrom affording the trimethyl ether ***22b*** (35 mg; 84%; *7-oxo-6,11,14-trimethoxy-16-hydroxyabieta-5,8,11,13-tetraene*), mp 99−100°C (from ether−hexane); uv: 226(sh, 17 400), 249(11 000), 271(sh, 8900), 296(7200), and 338(6300) nm; ir: 3420 and 1650 cm^{-1}; H nmr δ: 1.29 (d, J = 7 Hz, Me-CH), 1.43 (s, 6H, *gem* diMe), 1.63 (s, C.10-Me), 3.27−3.84 (m, CH_2OH and C.15-H), 3.72 (s, 6H, MeO at C.14 and C.6), 3.85 (s, MeO at C.11), and 6.78 (s, arom H); *Exact Mass* (*m/e*) calcd. for $C_{23}H_{32}O_5$: 388.2250; found: 388.2268.

Reaction of the dimethoxy ester ***14a*** *with* N-*bromosuccinimide*

N-Bromosuccinimide (92 mg) was introduced to a solution of dimethoxy ester ***14a*** in CCl_4 (10 mL). The mixture was heated to reflux and then illuminated (Photoflood DXC) for 50 min, the lamp acting as a source of both light and heat. The cooled solution was filtered and then evaporated in the presence of silica gel (1 g) and then chromatographed (dry col, hexane−EtOAc 9:1). Three products were obtained (in order of increasing polarity).

(*i*) *Olefin* ***25*** (32 mg; 25%; oil; *methyl 2-(4-isopropenyl-2,3-dimethoxyphenyl)-2,6,6-trimethylcyclohexylethanoate*); ir(film): 1738 cm^{-1}; H nmr δ: 0.93, 1.00, and 1.35 (3s, Me-C), 2.13 (m, J = 1 Hz, CH_3—C=CH_2), 2.92 (t, J = 6 Hz, C.5-H), 3.32 (s, COOMe), 3.76 and 4.04 (2s, Ar-OMe), 5.10 (m, H_2C=C), and 6.90 (ABq, J = 8 Hz, 2 arom H); ^{13}Cmr, see table.

(*ii*) *Bromohydrin* ***26*** (66 mg; 41%; oil; *methyl 2-(4-(2-bromo-1-hydroxyisopropyl)-2,3-dimethoxyphenyl)-2,6,6-trimethylcyclohexylethanoate*); ir(film): 3500 and 1740 cm^{-1}; H nmr δ: 0.92, 0.99, 1.34, and 1.69 (4s, Me-C), 3.33 (s, COOMe), 3.85 (m, CH_2Br), 3.91 and 3.96 (2s, Ar-OMe), and 7.02 (s, 2H, arom H); ^{13}Cmr, see table.

(*iii*) *Alcohol* ***24*** (42 mg; 31%; oil; *methyl 2-(4-(1-hydroxyisopropyl)-2,3-dimethoxyphenyl)-2,6,6-trimethylcyclohexylethanoate*); ir(film): 3520, 3440, and 1735 cm^{-1}; H nmr δ: 0.91, 1.00, 1.45, and 1.70 (6H, 4s, Me-C), 3.96 and 3.97 (2s, Ar-OMe), 4.40 (br s, OH (D_2O)), and 6.94 (ABq, J = 8 Hz, arom H).

Alcohol ***28a*** *from bromohydrin* ***26***

To the bromohydrin ***26*** (118 mg) in MeOH (25 mL) was added K_2CO_3 (55 mg) and the mixture was stirred at room temperature for 90 min. The MeOH was evaporated and the residue triturated with CCl_4 which was filtered and evaporated to give the epoxide(s) as a yellow oil (106 mg; ir: 1734 cm^{-1}; H nmr δ: 0.91, 0.99, 1.33, and 1.64 (4s, Me-C), 3.28 and 3.30 (2s, 3H, COOMe − two isomers), 4.01 (s, Ar-OMe), and 6.93 (s, 2H, arom H)).

Without further purification the epoxide(s) ***27*** (90 mg) in THF was added to a solution of diborane (0.23 mL of 1.0 *M* in THF) and BF_3·etherate (0.25 mL) in THF (2 mL), and cooled to 0°C. After stirring for 30 min, water was added to stop the reaction, the solution was saturated with K_2CO_3, and the product obtained by ether extraction. The crude oily material was purified by dry col chrom, affording the alcohol ***28a*** as a pale yellow oil (74 mg; 75% from the bromohydrin; *methyl 2-(4-(2-hydroxyisopropyl)-2,3-dimethoxyphenyl)-2,6,6-trimethylcyclohexylethanoate*); ir: 3440 and 1730 cm^{-1}; H nmr δ: 0.91, 0.98, and 1.33 (3s, Me-C), 1.22 and 1.23 (2d, J = 7 Hz, iPr Me), 3.28 (s, COOMe), 3.40 (m, iPr CH), 3.66 and 3.67 (2d, J = 7 Hz, CH_2OH), 3.79 (s, Ar-OMe), 3.98 and 3.99 (2s, 3H, Ar-OMe − two isomers), and 6.92 (ABq, J = 8 Hz, arom H); ^{13}Cmr, see table; *Exact Mass* (*m/e*) calcd. for $C_{23}H_{36}O_5$: 392.2563; found: 392.2562.

Alcohol ***28a*** *from olefin* ***25*** *and from alcohol* ***24***

The tertiary alcohol ***24*** (40 mg) was refluxed in glacial HOAc (10 mL) for 2.5 h and the solution then evaporated under vacuum. The residue was taken up in hexane−EtOAc (9:1) and filtered through a short column of silica gel. Two products were obtained, the more polar starting material (6 mg) and a pale yellow oil (21 mg; 65%), identical with the olefin ***25*** described above.

The olefin ***25*** (60 mg) in THF (4 mL), cooled in an ice bath, was treated with borane − methyl sulfide (0.05 mL of 10.2 *M*). After stirring for 10 h, aqueous NaOH (0.3 mL of 10%) was added, followed by H_2O_2 (30 wt.%, 0.12 mL). The mixture was heated to reflux for 1 h and then the crude product (57 mg) was obtained by ether extraction. Dry col chrom afforded the alcohol ***28a*** (49 mg; 78%; identical with that obtained earlier).

Hydrolysis of ester ***28a*** *and cyclization to the ketone* ***29***

To the ester ***28a*** (120 mg) in MeOH (10 mL) was added aqueous KOH (10 mL of 10%) and the mixture was refluxed for 4 h. Most of the MeOH was removed at the pump and the aqueous residue was washed with ether, acidified with concentrated HCl, and then extracted with ether to give the acid ***28b*** (110 mg; *2-(4-(2-hydroxyisopropyl)-2,3-dimethoxyphenyl)-2,6,6,-trimethylcyclohexylethanoic acid*); ir: 1700 cm^{-1}; H nmr δ: 0.89, 0.96, and 0.94, 0.97 (two × 2s, 2 Me-C, two isomers), 1.19 (d, J = 7 Hz, iPr Me), 1.32 (br s, Me-C), 3.30 (sex, C.15-H), 3.65 (d, J = 7 Hz, CH_2OH), 3.73 (s, Ar-OMe), 3.94 and 3.95 (2s, Ar-OMe − two isomers), 6.10 (br s, COOH and OH), and 6.90, 6.91 (2 × ABq, J = 8 Hz, 2 arom H − two isomers); ^{13}Cmr, see table; ms *m/e*: 378 (M^+).

The acid ***28b*** (100 mg − without further purification) was stirred in trifluoroacetic anhydride (4 mL) for 6 h at room temperature. The reaction mixture was poured onto ice and the product obtained by ether extraction (the enol trifluoroacetate) was hydrolysed by standing in aqueous KOH (5 mL of 10%). Ether extraction gave a yellowish neutral oil which was chromatographed (dry col) to afford the ketone ***29*** (oil, 73 mg; 72%; *7-oxo-11,12-dimethoxy-16-hydroxyabieta-8,11,13-triene*); ir: 3430 and 1680 cm^{-1}; H nmr δ: 0.96, 1.00, and 1.40 (3s, Me-C), 1.24 and 1.29 (2d, J = 7 Hz, iPr Me), 3.38 (sex, J = 7 Hz, iPr CH), 3.70 and 3.73 (2d, J = 7 Hz, CH_2OH), 3.86 (s, 6H, Ar-OMe), and 7.76 (s, arom H); ^{13}Cmr, see table; *Exact Mass* (*m/e*) calcd. for $C_{22}H_{32}O_4$: 360.2301; found: 360.2291.

Enolic α-diketone ***30a***

The ketone ***29*** (70 mg) in *t*-BuOH (10 mL) was added to the solution prepared by dissolving potassium (0.5 g) in *t*-BuOH (12 mL). A stream of oxygen was passed through the solution which became increasingly yellow. After 75 min the mixture was poured into ice-water, acidified with concentrated HCl, and extracted with ether. Evaporation gave a yellow oil which on dry col chrom gave the diosphenol ***30a***, mp 129−130°C (colorless needles from hexane/EtOAc; 46 mg; 65%; *7-oxo-11,12-dimethoxy-6,16-dihydroxyabieta-5,8,11,13-tetraene*); uv: 243(15 000), 279(16 000), and 321(17 000) nm; ir: 3580, 3480, 3360, 1625 and 1590 cm^{-1}; H nmr δ: 1.28 and 1.31 (2d, J = 7 Hz, iPr Me), 1.48 (6H) and 1.66 (2s, 3 Me-C), 3.40 (m, iPr CH), 3.72 and 3.80 (2d, J = 7 Hz, CH_2OH), 3.86 and 3.93 (2s, 2 Ar-OMe), 7.09 (s, OH (D_2O)), and 7.87 (s, arom H); ^{13}Cmr, see table; ms *m/e*: 374 (M^+) and 289. *Anal.* calcd. for $C_{22}H_{30}O_5$: C 70.56, H 8.08; found: C 70.30, H 8.21.

O-*Methylation of the enolic α-diketone* ***30a***

The enol ***30a*** (36 mg) in 50% aqueous EtOH (6 mL) was treated first with aqueous NaOH (2 mL of 30%) and then (slowly) with dimethyl sulfate (1.0 mL). After stirring for 24 h at room temperature, more water was added, the solution was acidified with dilute HCl, and the product was then obtained by ether extraction. Dry col chrom of the yellowish oil afforded first a tetra-O-methyl ether ***30c*** (8 mg; 21%) and then the tri-O-methyl ether ***30b*** (17.2 mg; 46%; *7-oxo-6,11,12-trimethoxy-16-hydroxyabieta-5,8,11,13-tetraene*), mp 159−160°C (from hexane−EtOAc; lit. (1) mp 153−154°C); uv: 240(7000), 275(9000), and 302(9500) nm; ir: 3500, 1638, and 1590 cm^{-1}; H nmr δ: 1.26 and 1.29 (2d, J = 7 Hz, iPr Me; lit. 1.29), 1.42 and 1.65 (2s, Me-C; lit. 1.44 and 1.64), 3.45 (m, C.15-H; lit. 3.43), 3.70 (m, CH_2OH; lit. 3.73), 3.80, 3.83, and 3.90 (3s, Ar-OMe), and 7.81 (s, arom H; lit. 7.80); ^{13}Cmr, see table; ms *m/e*: 402 (M^+), 387, 359, and 333 (base). *Anal.* calcd. for $C_{23}H_{32}O_5$: C 71.10, H 8.30; found: C 70.81, H 8.08.

Acknowledgments

We thank the Natural Sciences and Engineering Research

Council of Canada and the Ministère de l'Education du Québec for operating and equipment grants. Graduate bursaries are gratefully acknowledged by S.S. (N.S.E.R.C.) and D.P. (Ministère de l'Education, Québec).

1. C. B. RAO, T. N. RAO, and E. K. S. VIJAYAKUMAR. Indian J. Chem. **18B**, 513 (1979).
2. S. SAVARD, M.NERON-DESBIENS, and R. H. BURNELL. Synth. Commun. **11**, 399 (1981).
3. D. POIRIER, M. JEAN, and R. H. BURNELL. Synth. Commun. **13**, 201 (1983).
4. M. JEAN. Mémoire pour la Maîtrise, Université Laval, Québec. 1982.
5. D. POIRIER. Mémoire pour la Maîtrise. Université Laval, Québec. 1982.
6. D. H. R. BARTON, A. C. BREWSTER, S. V. LEY, C. M. READ, and M. N. ROSENFELD. J. Chem. Soc. Perkin Trans. 1, 1473 (1981).
7. J. C. DACRE. Anal. Chem. **43**, 589 (1971).
8. R. H. BURNELL, M. NERON-DESBIENS, and S. SAVARD. Synth. Commun. **12**, 11 (1982).
9. R. H. BURNELL, A. ANDERSEN, M. NERON-DESBIENS, and S. SAVARD. Can. J. Chem. **59**, 2820 (1981).
10. (*a*) R. H. BURNELL, M. JEAN, D. POIRIER, and S. SAVARD. Synth. Commun. **13**, 63 (1983); (*b*) D. POIRIER and R. H. BURNELL. Synth. Commun. **13**, 357 (1983).
11. T. MATSUMOTO, S. IMAI, S. TAKEDA, and M. MITSUKI. Bull. Chem. Soc. Jpn. **56**, 2013 (1983).
12. T. MATSUMOTO, S. IMAI, M. MITSUKI, and S. MAETA. Bull. Chem. Soc. Jpn. **56**, 2981 (1983).
13. (*a*) T. NISHIDA, I. WAHLBERG, and C. R. ENZELL. Org. Magn. Reson. **9**, 203 (1977); (*b*) F. W. WEHRLI and T. NISHIDA. Fortschr. Chem. Org. Naturst. **36**, 1 (1979); (*c*) E. WENKERT, B. L. BUCKWALTER, I. R. BURFITT, M. J. GAŠIĆ, H. E. GOTTLIEB, E. W. HAGAMAN, F. M. SCHELL, and P. M. WOVKULICH. Carbon-13 NMR spectroscopy of naturally occurring substances. *In* topics in carbon-13 NMR spectroscopy. Vol. 2. *Edited by* G. C. Levy. Wiley–Interscience, New York. 1976.

Can. J. Chem. Downloaded from www.nrcresearchpress.com by 210.87.254.40 on 09/06/12
For personal use only.

Conformational consequence of stereoelectronic effects in seven-membered cyclic acetals: nuclear magnetic resonance investigation of 1,3-benzodioxepin and its 2-substituted derivatives

ROBERT ST-AMOUR, M. T. PHAN VIET, AND MAURICE ST-JACQUES

Département de Chimie, Université de Montréal, C.P. 6210, Succ. A, Montreal (Qué.), Canada H3C 3V1

Received March 28, 1984

ROBERT ST-AMOUR, M. T. PHAN VIET, and MAURICE ST-JACQUES. Can. J. Chem. **62**, 2830 (1984).

The conformational and dynamic properties of 1,3-dioxa-4,5-benzocycloheptene (**8**) and several 2-substituted derivatives were investigated by ^1H and ^{13}C low temperature nmr methods. The results are strikingly different from those reported for the analogous symmetrical dioxepin isomers derived from **2**. The unexpectedly large preference of the 2-methoxy derivative (**8***c*) for the C_e conformation is explained in terms of deformed torsional angles in the seven-membered ring relative to those in the analogous six-membered one. These results therefore help delineate the limitations to the conformational biasing normally associated with the anomeric effect.

ROBERT ST-AMOUR, M. T. PHAN VIET et MAURICE ST-JACQUES. Can. J. Chem. **62**, 2830 (1984).

Les propriétés conformationnelles et dynamiques du dioxa-1,3 benzo-4,5 cycloheptene (**8**) et de quelques dérivés en position 2 ont été étudiées par les techniques de rmn ^1H et ^{13}C à basse température. Les résultats obtenus sont très différents de ceux précédemment rapportés pour les isomères analogues de la benzodioxépine symmétrique dérivés de **2**. La grande préférence du dérivé méthoxy-2 (**8***c*) pour la forme C_e est expliquée par une déformation des angles de torsion du cycle à sept chaînons comparativement aux dérivés analogues cycliques à six chaînons. Ces résultats permettent de mieux circonscrire les conséquences conformationnelles associées à l'effet anomère.

Stereoelectronic effects (1) in acetals and related functions have recently brought into focus the important relationship between conformation and reactivity for several classes of molecules. Studies on the simplest acetal, dimethoxymethane (2), indicate that the g^+g^+ arrangement is most stable in conformity with observations made on carbohydrates (3) and 2-substituted tetrahydropyrans (4). This preference constitutes the basis of the anomeric and the *exo*-anomeric effects extensively investigated for these molecules (5). The relative stabilities of the various arrangements possible for a $—CH_2—O—CH_2—O—CH_2—$ fragment have been difficult to assess (1) and the need for a quantitative evaluation based on experimental measurements led to the recent investigation (6) of a broader range of stereochemical arrangements as exist in bicyclic acetals such as **1**. By comparison, studies of the cyclic acetal 1,3-dioxane are limited because of the relatively high conformational energy of the twist-boat (*TB*) conformation (7) and the fact that only highly substituted derivatives have been found to exist in this form.

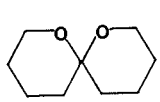

1

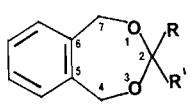

2

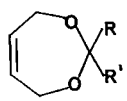

3

The two possible *TB* forms of 1,3-dioxane (**4** and **5**) are characterized by $—CH_2—O—CH_2—O—CH_2—$ fragments in the g^+g^+ disposition and slightly deformed g^+g^- disposition respectively. Previous studies (7) could not clearly distinguish experimentally between these forms because they interconvert easily as a result of the low energy barrier for the pseudorotation motion involved, although calculations suggest that **5** is more stable than **4** (7). In contrast, the dioxepins **2** and **3** provided an opportunity (8, 9) to investigate experimentally the stabilizing effect associated with the g^+g^+ acetal arrangement in a ring system because the only *TB* form possible for these molecules has the appropriate bond disposition as shown by **6**. On the other hand, the features of **5** can be found in a benzocycloheptene derivative only if a change in the position of the

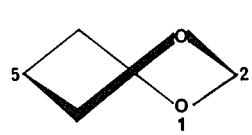

4

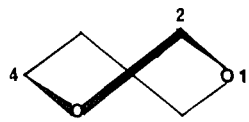

5

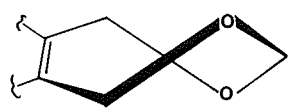

6

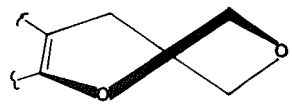

7

oxygen atoms takes place as in **7**, which represents the *TB* form of 1,3-benzodioxepin (**8**).

In addition, previous nmr observations on the 2-methoxy derivative of **2** (R = H, R' = OCH_3) have provided unique insight into the conformational change caused by the polar substituent. Whereas, for the analogous six-membered orthoformate 2-methoxy-1,3-dioxane, both axial and equatorial chair conformations (i.e. C_a and C_e respectively) are observed (10), the 2-methoxy derivative of **2** was found to exist only in the *TB* form (8). Presumably, repulsive steric interactions destabilize the C_a form while electronic factors destabilize the C_e form and stabilize the *TB* form.

Consequently, we sought to identify and quantify the various factors governing the conformational properties of seven-membered rings containing the acetal and related functions through a dynamic ^1H and ^{13}C nmr investigation of compounds **8** to **8***e*. The results show a behavior strikingly different from that of the symmetrical series **2** and provide a better appreciation of factors affecting the generalized anomeric effect.

Results

Variable temperature ^1H and ^{13}C nmr studies of compounds **8** to **8***e* revealed spectral modifications for all compounds except **8***a*. Table 1 contains a summary of the ^1H nmr parameters

Can. J. Chem. Downloaded from www.nrcresearchpress.com by 210.87.254.6 on 09/06/12
For personal use only.

TABLE 1. ^{1}H nuclear magnetic resonance parameters for compound **8** and its 2-substituted derivatives at high and low temperatures[a]

	R	R^1	Temperature (°C)	Solvent	H_{4e}	H_{4a}	H_{5a}	H_{5e}	$^2J_{5a-5e}$	$^2J_{4a-4e}$	$^3J_{5e-4a}$	$^3J_{5a-4a}$	$^3J_{5e-4e}$	$^3J_{5a-4e}$
8	H	H	−5	CHF_2Cl	3.81	3.81	3.00	3.00	[b]	[b]	[b]	[b]	[b]	[b]
			−125	CHF_2Cl	4.25	3.49	3.30	2.79	−15.4	−11.9	[c]	11.9	3.4	3.3
8*a*	H	CH_3	25	$CDCl_3$	4.14	3.48	3.26	2.63	−15.1	−11.8	0.9	11.8	3.7	3.1
			−125	CHF_2Cl	4.20	3.56	3.27	2.77	−15.4	−12.0	[c]	12.0	3.4	3.3
8*b*	H	$(CH_3)_3$	25	$CDCl_3$	4.17	3.41	3.24	2.59	−15.0	−11.7	1.0	11.8	3.6	3.1
			−125	CHF_2Cl	4.23	3.51	3.25	2.75	−15.3	−12.1	[c]	12.1	3.2	3.3
8*c*	H	OCH_3	25	$CDCl_3$	4.21	3.72	3.16	2.84	−15.4	−11.9	2.0	9.8	5.7	3.0
			25	CCl_4	4.16	3.72	3.05	2.95	−15.2	−11.7	2.5	8.2	7.0	2.7
			−135	CHF_2Cl	4.24	3.68	3.26	2.74	−15.4	−12.1	[c]	12.1	3.1	3.2
8*d*	CH_3	CH_3	25	$CDCl_3$	3.91	3.91	2.97	2.97	[b]	[b]	[b]	[b]	[b]	[b]
			−125	CHF_2Cl	3.91	3.91	3.27	2.67	−15.4	−12.0[d]	~1[d]	12.0[d]	3.4[d]	3.2[d]
8*e*	CH_3	OCH_3	25	$CDCl_3$	3.82	4.11	3.15	2.85	−15.3	−12.1	2.8	10.0	5.1	4.1
			−90	CHF_2Cl	3.82	3.90	3.27	2.73	−15.4	−12.0	[c]	11.5	3.2	3.7

[a] Determined from spectra at 400.1 MHz.
[b] Because of the extensive averaging existing for these compounds, averaged coupling constants were not determined.
[c] This coupling constant is small and was not determined under the conditions used.
[d] The various coupling constants were determined by spectral simulation using the PANIC program included with the Bruker Aspect 2000 software package.

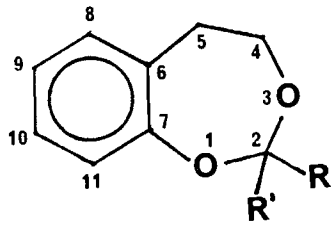

8 R = R' = H
8*a* R = H, R' = CH_3
8*b* R = H, R' = t-Bu
8*c* R = H, R' = OCH_3
8*d* R = CH_3, R' = CH_3
8*e* R = CH_3, R' = OCH_3

obtained at high and low temperatures for all six compounds, while Table 2 contains corresponding ^{13}C chemical shifts. The characteristic spectral changes observed are described next.

For compound **8** in CHF_2Cl only the ^{1}H nmr spectrum, recorded at 400.1 MHz, was found to undergo a change, as illustrated in Fig. 1. The singlet of the methylene protons at position 2 (H-2) splits into an AX pattern, whereas the signals of the H-4 and H-5 methylene protons also broaden and split, so that a 4-spin first-order pattern is observed at −137°C. Spectral analysis gave the parameters reported in Table 1, except for $^3J_{5e4e}$, which is too small to be observed in the low temperature spectrum. The various signals at −137°C are labelled in accordance with conformational assignments made in the next section. Finally, a free energy of activation of 8.4 kcal/mol is calculated at −77°C (the coalescence temperature T_c) from the splitting of the H-2 signal using the two-site approximation and a transmission coefficient of one-half (8).

Only the *tert*-butyl methyl signal of **8***b* showed a change at low temperature. At 20.15 MHz, the methyl ^{13}C nmr singlet was observed to split into a doublet with component intensity 2:1 at 157°C. A free energy of activation of 6.1 kcal/mol was estimated at −149°C (T_c) using the two-site approximation and a transmission coefficient of one.

Compound **8***c* (R = H, R^1 = OCH_3) showed a more complex behavior. Whereas both high field ^{1}H and ^{13}C nmr spectra for CHF_2Cl solutions were found not to change at low temperature, a change of solvent to dimethyl ether enabled a spectral change to be observed. Figure 2 illustrates the 100.6 MHz ^{13}C nmr spectral modification detected for the sp^3 carbon atoms. It is seen that C-2 and C-4 have broadened appreciably at −92°C and then split into doublets whose unequally intense components are identified by C_e and C_a in accordance with conformational arguments presented in the next section. Whereas the C_a lines of the C-2 signal and C-5 are readily observed, that of C-4 is most probably under the large solvent signal. The slight broadening of C-5 at −92°C is compatible with the closely spaced lines at −132°C. The OCH_3 signal is also very narrow at −92°C; if it does split, the minor component would be at lower field under the solvent peaks. Integration of the C-2 signals at −132°C yields 88% for the C_e line and 12% for the C_a line. Furthermore, an estimate of 7.8 kcal/mol is obtained for the free energy of activation at −88°C using the two-site approximation and a transmission coefficient of one. The free energy difference (ΔG^0) at −132°C is 0.56 kcal/mol.

The 400.1 MHz ^{1}H spectrum of **8***c* was recorded in CHF_2Cl and two other solvents. First-order analysis at high temperature provided the parameters in Table 1. The low temperature ^{1}H spectrum of **8***c* in CHF_2Cl is found much less useful than the ^{13}C spectra to identify the small signals arising from the minor conformation and was not studied in this work.

Both ^{1}H and ^{13}C high field nmr spectra of compound **8***d* (R = R^1 = CH_3), exhibited spectral changes at low temperatures. Figure 3 shows the effect of temperature on the ^{13}C spectra at 100.6 MHz in CHF_2Cl. It is seen that both the C-4 and C-5 signals split into doublets of unequal intensities labelled *C* and *TB* in accordance with conformational conclusions drawn in the next section. The methyl signal, on the other hand, shows a more complex behavior whereby it broadens and splits ($T_c \approx$ −73°C) into a broad doublet (−103°C in Fig. 3) which eventually becomes a four-line signal at −123°C; two lines are equally tall (88%), and the two other equally small (12%). Furthermore, the ^{13}C spectra of **8***d* in dimethyl ether showed a similar pattern with signals at −128°C in a ratio of 95:5; chemical shifts are very similar to those determined in CHF_2Cl and reported in Table 2. The free energy differences between

Can. J. Chem. Downloaded from www.nrcresearchpress.com by 210.87.254.6 on 09/06/12
For personal use only.

Can. J. Chem. Downloaded from www.nrcresearchpress.com by 210.87.254.6 on 09/06/12
For personal use only.

TABLE 2. ^{13}C nuclear magnetic resonance chemical shifts for compound **8** and its 2-substituted derivatives at high and low temperatures[a]

Compounds (R, R[1])	Solvent	T(°C)	C-7	C-6	C-8	C-10	C-9	C-11	C-2	C-4	C-5	Other signals
8 (H, H)	CHF_2Cl	−20	160.90	134.24	131.87	128.87	125.17	122.23	99.00	70.30	38.94	
		−115	160.41	134.30	132.12	128.96	125.35	122.31	98.83	69.95	38.46	
8*a* (H, CH_3)	CHF_2Cl	−20	159.99	134.51	131.69	118.84	125.05	122.32	105.67	69.64	38.43	22.90 (CH_3)
		−115	159.49	134.61	131.94	128.92	125.25	122.45	105.59	69.37	37.98	22.80 (CH_3)
8*b* (H, *t*-Bu)	CHF_2Cl	−20	160.66	134.60	131.66	128.78	124.75	121.86	114.37	69.82	38.46	37.25 (C) 25.45 (CH_3)
		−115	160.20	134.49	131.98	128.87	124.97	121.94	114.38	69.52	38.01	37.14 (C) 27.13 21.22 (CH_3)[b]
8*c* (H, OCH_3)	CHF_2Cl	−20	155.17	134.72	131.63	129.27	125.87	122.77	117.10	66.18	37.18	54.78 (OCH_3)
		−115	154.76	134.94	131.95	129.37	126.06	122.74	118.01	67.33	36.74	55.52 (OCH_3)
	CH_3OCH_3	−20	155.27	134.39	130.96	128.60	124.90	122.62	115.31	64.60	37.18	53.14 (OCH_3)
		−128 (C_e)	155.31	134.67	131.37	128.85	125.21	122.35	117.45	66.53	36.57	53.62 (OCH_3)
		(C_a)	[c]	[c]	130.61	[d]	[d]	123.21	110.23	[e]	37.29	53.62 (OCH_3)
8*d* (CH_3CH_3)	CHF_2Cl	−20	155.74	134.72	130.96	128.69	125.23	123.71	103.91	61.57	36.91	25.90 (CH_3)
		−125 (*C*)	156.11	135.16	131.33	128.94	125.17	123.47	103.42	61.99	37.65	30.50, 21.01 (CH_3)
		(*TB*)	153.21	133.95	130.33	[d]	126.04	123.70	104.67	60.02	32.48	26,98, 23.72 (CH_3)
	CH_3OCH_3	−20	155.83	134.42	130.57	128.20	124.59	123.44	103.03	61.21	37.03	25.78 (CH_3)
		−128 (*C*)	156.49	134.84	130.82	128.56	124.62	123.13	102.28	61.53	37.50	30.51, 20.67 (CH_3)
		(*TB*)	[d]	[d]	[d]	128.03	125.17	123.84	[d]	[e]	33.43	26.36, 24.14 (CH_3)
8*e* (CH_3OCH_3)	CHF_2Cl	−20	154.38	134.57	130.87	128.69	125.41	123.62	116.13	61.08	36.64	51.89 (OCH_3) 23.32 (CH_3)
		−130	153.89	135.09	131.07	129.02	125.75	123.22	[c]	60.80	36.91	52.31 (OCH_3) 23.97 (CH_3)

[a] Data obtained for solutions containing TMS and CD_2Cl_2 (15%) for field lock at 100.62 MHz unless otherwise noted.
[b] Chemical shifts determined at −155°C at 20.15 MHz.
[c] Sample signal under CHF_2Cl solvent signal.
[d] Not observed clearly, either because of overlap with other signals or because of small S/N under the recording conditions.
[e] Sample signals under CH_3OCH_3 solvent signals.

Can. J. Chem. Downloaded from www.nrcresearchpress.com by 210.87.254.6 on 09/06/12
For personal use only.

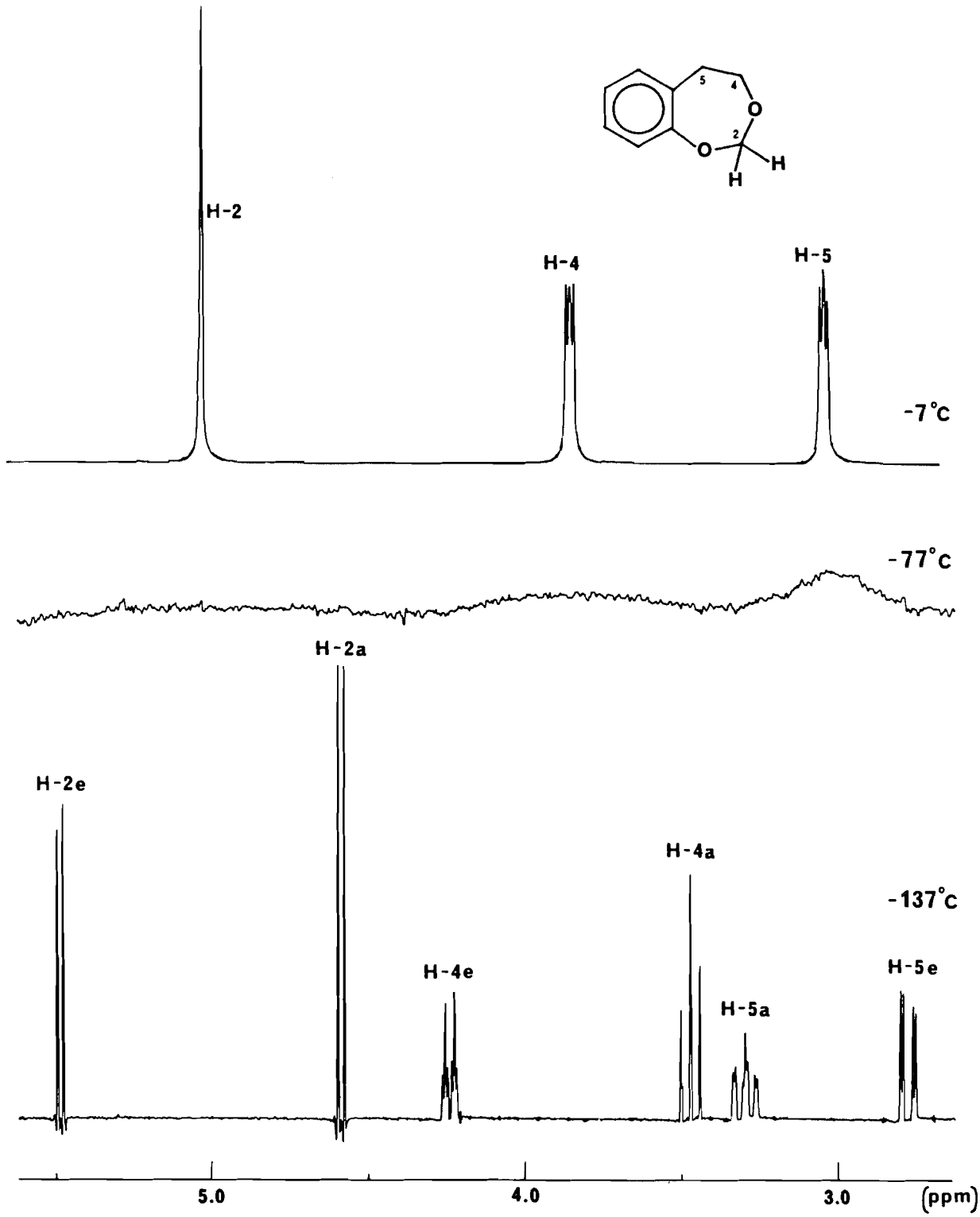

FIG. 1. Partial 400.1 MHz ^{1}H nmr spectra of the methylene protons of **8** in CHF_2Cl at several temperatures.

C and *TB* are 0.60 kcal/mol for CHF_2Cl at −123°C and 0.85 kcal/mol for CH_3OCH_3 at −128°C.

The two-site approximation yields a free energy of activation of about 7.8 kcal/mol at −93°C (T_c) from the splitting of the C-4 line in CHF_2Cl using a transmission coefficient of one. In addition, a complete lineshape analysis of the methyl signal changes (described in the next section) using the DNMR-2 program (ref. 11; a copy of the program was obtained from QCPE) gave two free energy values: 8.3 kcal/mol at −68°C and 7.5 kcal/mol at −101°C.

The 400.1 MHz ^{1}H nmr spectrum of **8***d* shows important changes for the H-4, H-5 and CH_3 signals. Firstly, the methyl singlet at room temperature splits at −90°C into an intense doublet and a weak one, centered at 1.47 ppm (separation = 148 Hz) and 1.53 ppm (separation = 112 Hz), respectively, at −130°C. Secondly, the room temperature triplet of the H-5

Can. J. Chem. Downloaded from www.nrcresearchpress.com by 210.87.254.6 on 09/06/12
For personal use only.

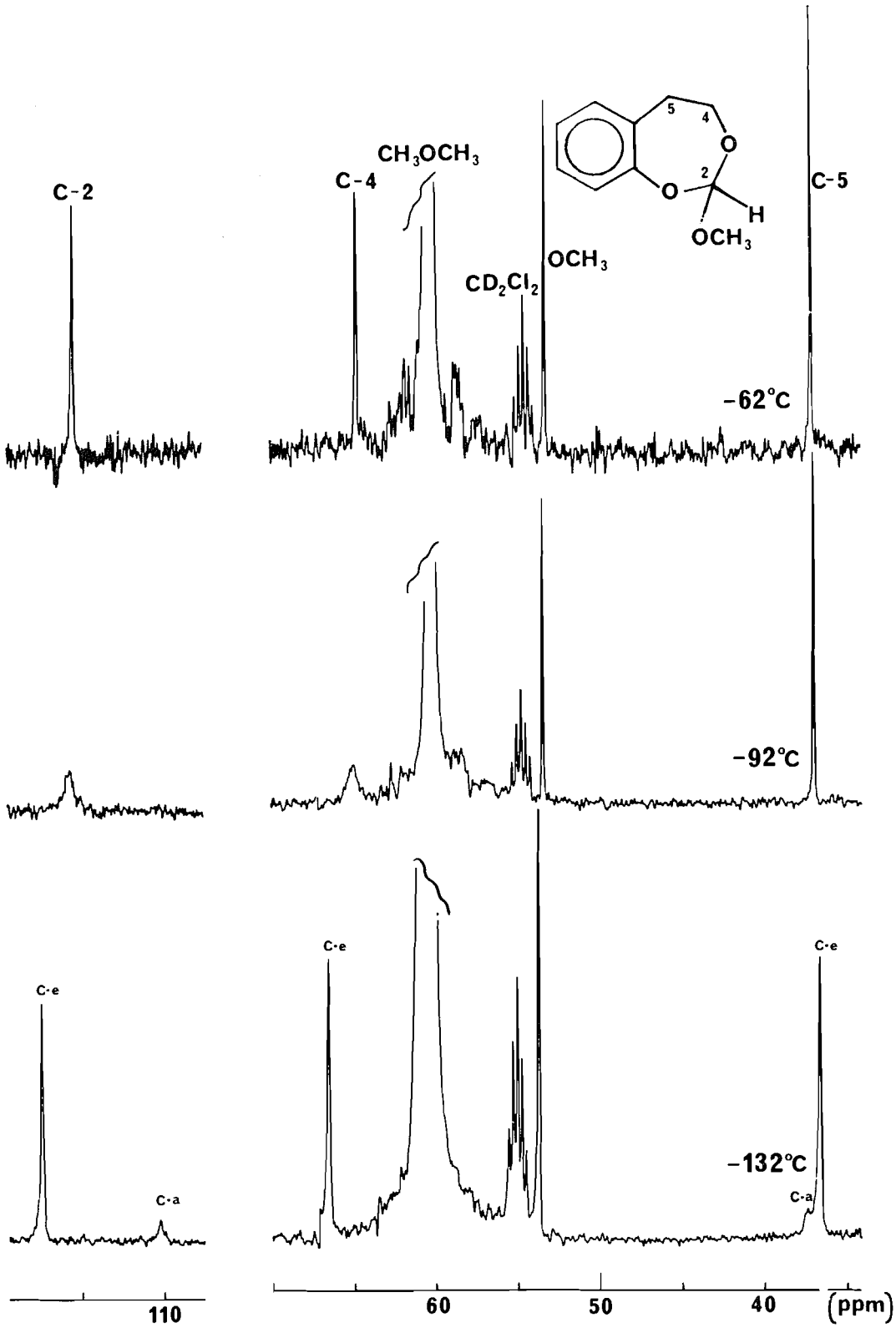

FIG. 2. Partial 100.6 MHz ^{13}C nmr spectra of the aliphatic carbons of **8***c* in CH_3OCH_3 at several temperatures.

methylene group changes below −90°C into a doublet and a quintet, in the ratio 1:1 for the major species and two broad unresolved signals for the minor one (~3.4 and ~2.9 ppm). Finally, the triplet of the H-4 methylene group becomes a doublet for the major conformer and two unresolved signals for the minor one (~4.2 and ~3.7 ppm). The spectrum of the major conformer of **8***d* at −130°C shows a pattern containing elements of deceptively simple spectra arising from the accidental equivalence of the H-4a and H-4e chemical shifts. The ^1H parameters were determined by a simulation using the

Can. J. Chem. Downloaded from www.nrcresearchpress.com by 210.87.254.6 on 09/06/12
For personal use only.

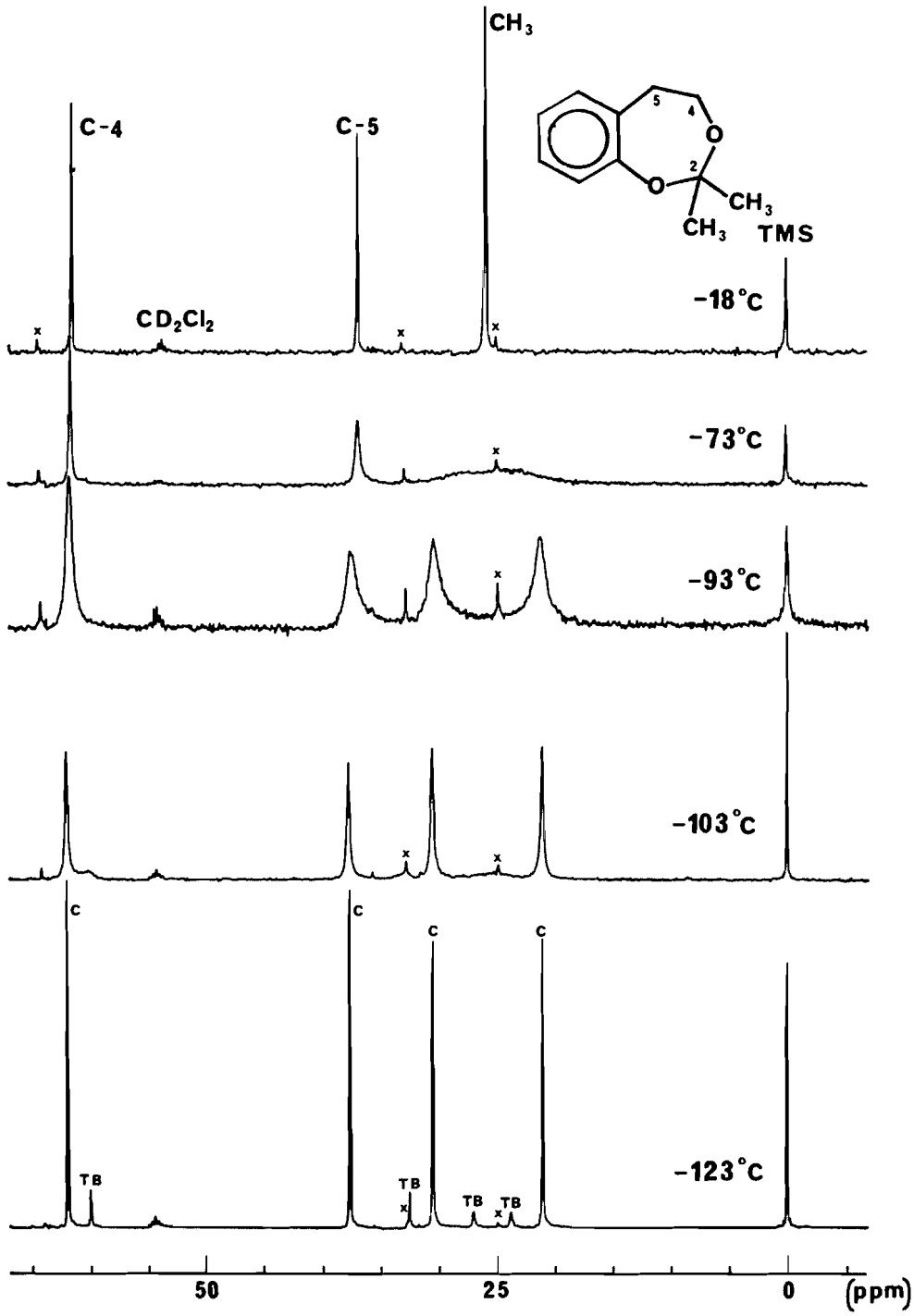

FIG. 3. Partial 100.6 MHz ^{13}C nmr spectra of the methylene and methyl carbons of **8***d* in CHF_2Cl at several temperatures (× denotes impurities).

PANIC program and are reported in Table 1.

Although the ^1H nmr spectrum of **8***e* (R = CH_3, R^1 = OCH_3) does not show a spectral modification of conformational dynamic origin, it shows, on lowering the temperature, large changes in chemical shifts which lead eventually to the merging of the signals of H-4e and H-4a, so that at −125°C only one signal is observed for the two H-4 protons. All other signals remain unchanged and the ^1H parameters at −90°C are reported in Table 1. The ^{13}C nmr spectra do not change on lowering the temperature and the ^{13}C parameters are reported in Table 2.

Discussion

Identification of the stable conformations

The absence of change in the ^{13}C nmr spectra of **8** down to −135°C indicates that it exists in only one conformation capable of an inversion process detected by the ^1H spectral modification shown in Fig. 1. The geometry of the stable conformation of **8** can be deduced from the following evidence, which points to a chair form.

One argument is based on the fact that the $^2J_{HH}$ coupling between the benzylic methylene protons is dependent on the

proton orientations with respect to the benzene ring (12). Assuming that the second oxygen at position 1 in **8** should not affect $^2J_{5a,5c}$ significantly, the value of −15.4 Hz (Table 1), being similar to the corresponding (13) value of −15.3 Hz for the chair form of 5-oxabenzocycloheptene (**9**), suggests that **8** and **9** should have a similar angular relationship about the C(5)—C(6) bond. This constraint is respected only if **8** also exists in the chair form. Confirming evidence is provided by a comparison of the vicinal coupling constants characterizing the C(4)—C(5) bond of **8** (given in Table 1), which are found to be similar to those reported earlier for the chair form of **9** ($^3J_{aa}$ = 11.2, $^3J_{ee}$ = 5.0, $^3J_{ae}$ = 2.0, and $^3J_{ea}$ = 0.6 Hz).

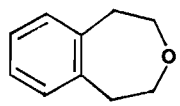

9

The interpretation of the data obtained for the methyl derivative (**8***a*) clearly shows that it exists exclusively in the C_e conformation. Firstly, Table 1 shows that ^{1}H chemical shifts and coupling constants of H-4 and H-5 are very similar to those characterizing the chair form of **8**. Secondly, the equatorial orientation of the methyl group is indicated by the comparison of the ^{13}C α, γ, and δ parameters characterizing C-2, C-4, and C-5 (namely 6.8, −0.7, and −0.6 ppm), with corresponding values (14) reported for the equatorial form of 2-methyl-1,3-dioxane (5.0, −0.1, and −0.8 ppm). Furthermore, analogous values for the C_e form of the 2-methyl derivative of **2** (i.e. **2***b*) are 6.22, −1.54, and −0.21 ppm (8). Thus the methyl group in **8***a* is equatorial and the larger γ parameter for **2***a* (−1.54 vs. −0.7 ppm) suggests that the dihedral angles about the C(2)—O(3) bond differ slightly in each seven-membered chair (15). Similarly, both ^{1}H and ^{13}C nmr data indicate that the *tert*-butyl derivative **8***b* also exists solely in the C_e form.

Before proceeding to the conformational analysis of compound **8***c* substituted with a polar methoxy group, it is useful to characterize the dimethyl derivative **8***d*. In contrast to the previous three compounds, the ^{13}C nmr spectra of **8***d* (Fig. 3) reveal the existence of two ring conformations in the ratio of 88:12 in CHF_2Cl. The assignment of the signals to the respective conformers is possible through a consideration of the ^{13}C parameters α, γ and δ relative to the chemical shifts of **8**. These values are 4.6, −8.0, and −0.8 ppm for the more intense signals and 5.8, −9.9, and −6.0 ppm for the weaker lines. The parameters determined for the intense signals are similar to those reported (14) for the chair form of 2,2-dimethyl-1,3dioxane (3.6, −7.0, and −0.9 ppm). It is therefore clear that the *C* conformation is dominant for **8***d*.

Possible conformations for the minor form of **8***d* are the boat (*B*) and twist-boat (*TB*) forms. Examination of structures **10** (*B*) and **11** (*TB*) shows that **10** contains a repulsive 1,3-*syn*-methyl-hydrogen interaction, whereas only a 1,4-methyl-hydrogen interaction is possible for **11**. The carbon-13 chemical shifts in Table 2 show that $\delta_{C\text{-}5}$ of the minor form is 5.17 ppm upfield from the signal of the major *C* form, whereas $\delta_{C\text{-}4}$ is only 1.97 ppm upfield. The upfield displacement for $\delta_{C\text{-}4}$ (γ effect) appears too small for *B* and the difference in chemical shifts observed for $\delta_{C\text{-}5}$ is similar to the difference observed (8) between the chemical shifts of the benzylic methylene carbons of the *C* and *TB* forms of **2**. These arguments therefore strongly indicate that the minor conformation of **8***d* has the *TB* geometry.

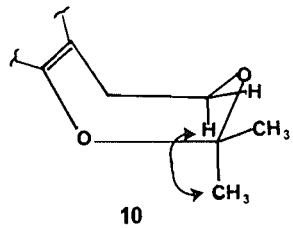

10

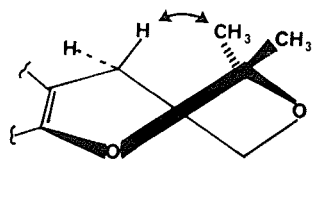

11

Additional support for the identity of the major conformation comes from the ^{1}H nmr parameters given in Table 1 for the most intense signals in the spectrum at −125°C, as determined by calculations using the PANIC program. The similar coupling constants for **8***d* and those for **8**, **8***a*, and **8***b* confirm that *C* is the predominant form for **8***d*.

It is interesting to draw attention to the near equivalence of the chemical shifts of H-4a and H-4e (~1 Hz difference) for the *C* form of **8***d*, while a difference of about 200–250 Hz characterizes the *C* form of the monosubstituted derivatives **8** to **8***b*. Anisotropic effects of the axial methyl group, whereby H-4a is deshielded by ~0.35 ppm and H-4e is shielded by ~0.3 ppm, are undoubtedly responsible in large part, as suggested by the report that, in 1,3-dioxanes, a 2-axial methyl group shifts H-4e upfield by about 0.16 ppm and H-4a downfield by about 0.2 ppm (16).

The presence of a single polar substituent in methoxy derivative **8***c* raises the interesting question of assessing the relative importance of stereoelectronic interactions involving the methoxy substituent on the relative stability of the possible conformations. The ^{13}C spectra in Fig. 2 show the existence of two conformations easily detected at −132°C in CH_3OCH_3 (88:12). Information on the geometry of the major form is derived in part from the proton–proton coupling constants reported in Table 1, where it is seen that all couplings are similar to those for the chair forms of **8**, **8***a*, **8***b*, and **8***d*. In addition, the ^{13}C parameters offer an equally valuable conformational probe because of the sensitivity of $\delta_{C\text{-}5}$ to ring conformation as was shown earlier (8, 15) for **2** and **3**, and in this work for **8***d*. Considering that a *TB* form should be characterized by a $\delta_{C\text{-}5}$ value about 5–6 ppm upfield from that observed for **8**, the observation that the C-5 chemical shifts of both lines of **8***c* are within 2 ppm of that of **8** suggests strongly that both conformations of **8***c* have a chair geometry.

The orientation of the OCH_3 substituent on the *C* form can now be determined from the analysis of α and γ substituent effects, which are known to be stereodependent. The corresponding substituent effects reported for 2-methoxy-1,3-dioxane are used as reference parameters (10); in CHF_2Cl at −144°C, the values are 19.1 and −1.3 ppm for C_e compared to 14.0 and −8.6 for C_a. As a consequence, the major conformer of **8***c*, being characterized by values of 19.2 and −2.6 ppm, is clearly the C_e form. Because the C-4 signal of the minor form was not located, only the α parameter can be used; its value of ~11.4 ppm (obtained using the data in CH_3OCH_3) is in reasonable agreement with the C_a form.

Furthermore, additional information on the relative populations of the C_e and C_a forms of **8***c* can be obtained at room temperature through the analysis of the weighted averaging of vicinal coupling constants for the $C(4)H_2$—$C(5)H_2$ fragment. Reference values for $^3J_{aa}$ and $^3J_{ee}$ are taken as those observed for **8***a* and **8***b* in $CDCl_3$, namely 11.8 and 3.7 Hz respectively. Thus the room temperature C_e/C_a ratio is found to be approximately 75:25 in $CDCl_3$ and 55:45 in CCl_4.

Can. J. Chem. Downloaded from www.nrcresearchpress.com by 210.87.254.6 on 09/06/12
For personal use only.

Can. J. Chem. Downloaded from www.nrcresearchpress.com by 210.87.254.6 on 09/06/12
For personal use only.

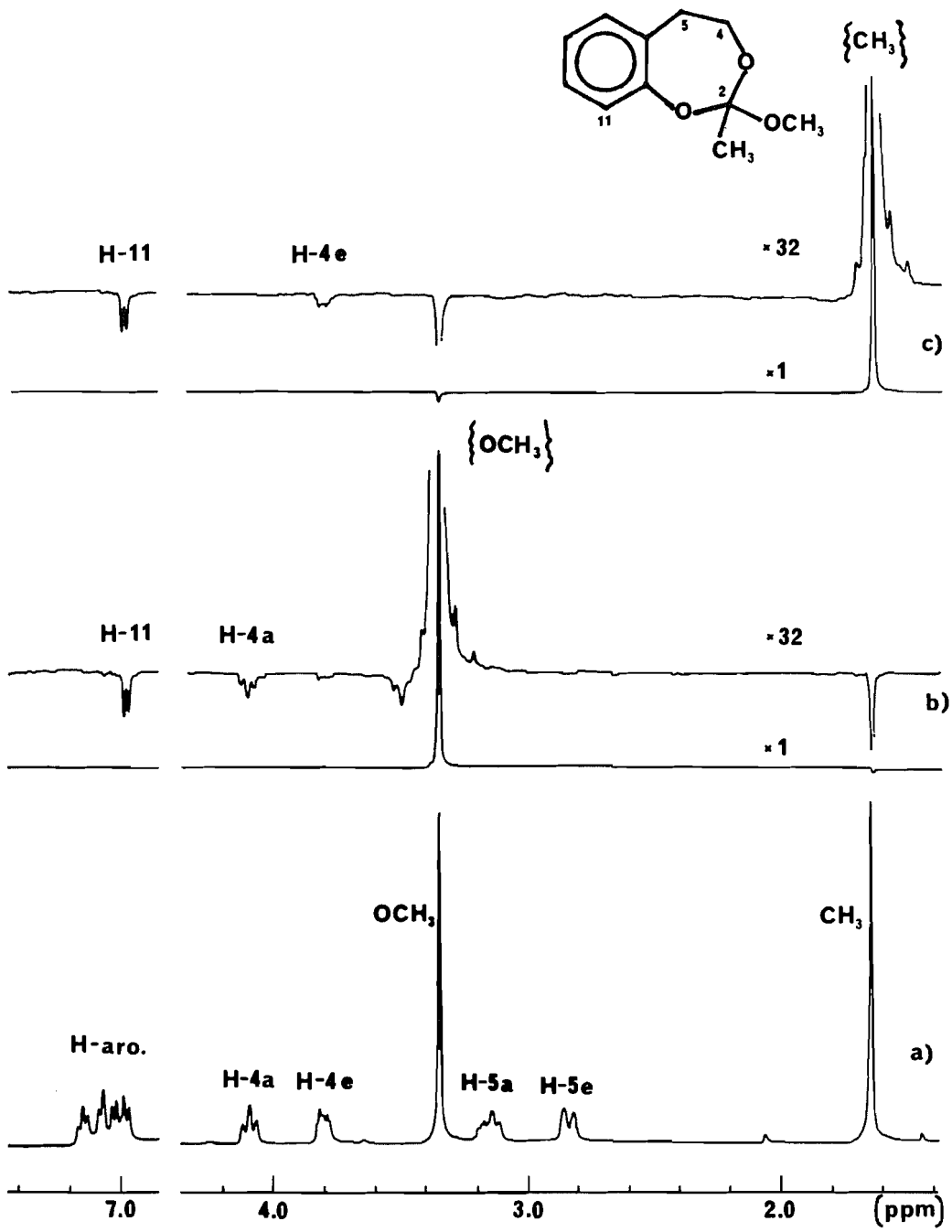

FIG. 4. The 400.1 MHz ^1H nmr spectra of **8***e* at room temperature. (a) Normal spectrum; (b) differential nOe spectrum produced by irradiation of the methoxy signal; and (c) effect produced by irradiation of the methyl signal. The effects of double irradiation are visible in the amplified (×32) spectra in (b) and (c).

Finally, compound **8***e* (OCH_3, CH_3) adopts only one stable conformation, as indicated by the absence of conformationally significant spectral change at low temperature. Coupling constants given in Table 1 indicate a chair form. Because the use of ^1H and ^{13}C nmr parameters does not lead to a clear-cut decision on the orientation of the methyl and methoxy groups, an nOe difference experiment on **8***e* was carried out at +20°C for a solution in $CDCl_3$ (see experimental section for details).

Figure 4 shows that irradiation of the methoxy protons produces a significant effect on the signal at δ_H 4.11, whereas irradiation of the methyl singlet produces an effect on the signal at δ_H 3.82. It is therefore possible to conclude that the signal at 4.11 ppm is *syn* to OCH_3 while the signal at 3.82 ppm is *syn* to the methyl group. The information that H-4a absorbs at 4.11 ppm, gained from the spectral analysis of the CH_2CH_2 pattern, indicates clearly that **8***e* exists in the chair form with the methoxy group in the axial position.

Features of the conformational equilibria

Table 3 shows that the families of compounds derived from **2** and **8** have different conformational properties, the most striking differences being manifested by **8***c*, **8***d*, and **8***e*.

At the outset it is useful to recall that the *TB* form of **2** is stabilized by the generalized anomeric effect (8). Consequently the conformational difference between **2** and **8** suggests significantly less stabilization of the acetal function in the *TB* form of

TABLE 3. Conformational equilibria[a] and activation energies[b] for the analogous series of compounds derived from **8** and **2**

Compounds	Conformation (%)	$\Delta G^{\ddagger}$	Compounds	Conformation (%)	$\Delta G^{\ddagger}$
8	*C* (100%)	8.4[c]	**2**	$C \leftrightharpoons TB$ (20%)	7.9[d]
8*a*	C_e (~100%)	[e]	**2***a*	$C_e \leftrightharpoons TB$ (4%)	7.8[d]
8*b*	C_e (~100%)	[e]	**2***b*	C_e (~100%)	[e]
8*c*	$C_e \leftrightharpoons C_a$ (12%)[f]	7.8	**2***c*	*TB* (~100%)	6.7[g]
8*d*	$C \leftrightharpoons TB$ (12%)	8.3[g]	**2***d*	*TB* (~100%)	10.0[g]
	$TB \leftrightharpoons TB^*$	7.5[g]			
8*e*	*C* (~100%)	[e]	**2***e*	*TB* (~100%)	8.5[g]

[a] For solutions in CHF_2Cl (unless otherwise noted) at low temperatures.
[b] In kcal/mol at the coalescence temperature.
[c] For the chair inversion process.
[d] For the $C \rightarrow TB$ transformation (transmission coefficient of 1/2; *vide infra*).
[e] No spectral change detected for this compound. Unpublished results by R. St-Amour.
[f] For a solution in dimethyl ether. The quantity of the second of the two conformers is given in brackets whenever an equilibrium exists.
[g] For the pseudorotation process involved in *TB* inversion where the * indicates an inverted *TB* conformation.

8. Indeed the C—O—C—O—C moiety has the most favorable g^+g^+ disposition in the *TB* conformation of **2** relative to the g^+g^- arrangement in *C*, while both the *TB* and *C* forms of **8** have the g^+g^- arrangement. It should be noted, however, that the g^+g^- bond arrangements are characterized by slightly different dihedral angles in the various forms.

In contrast to **2***c* for which only the *TB* form has been detected, the equilibrium $C_e \leftrightharpoons C_a$ has been identified for **8***c* in CH_3OCH_3. Surprisingly, the C_e form is found to be highly predominant at low temperature (88% at −132°C in CH_3OCH_3), contrary to straightforward expectation from the anomeric effect and steric interactions involving the axial OCH_3 group. In fact, previous studies (17) of 4-methoxybenzocycloheptene (**12**) have revealed that the C_a population at −100°C in CHF_2Cl is 37%, suggesting the absence of severe steric interactions.

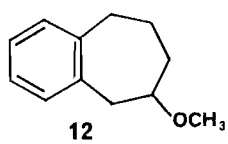

12

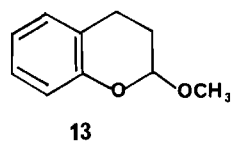

13

The effect of successive incorporation of oxygen atoms in six-membered rings is revealed by low temperature nmr results (10), which have shown that the C_a amount in CHF_2Cl is 6% for methoxycyclohexane (at −128°C), 60% for 2-methoxytetrahydropyran (−130°C), and 30% for 2-methoxy-1,3-dioxane (−148°C), while the change of solvent to dimethyl ether increases these quantities to 13%, 84%, and 65% respectively. Finally, the oxygen atom at the benzylic position of **8***c* might also favor the C_a form, as a previous study of 2-methoxychromane (**13**) suggests (18). Why then is the axial form so weakly favored for **8***c* at low temperature? Obviously several factors must be examined in an attempt to rationalize this observation. The large equatorial preference for **8***c* may result from geometrical factors such as torsional angles specific to the seven-membered ring and (or) entropy effects, recently suggested as important for 2-methoxytetrahydropyran (19).

The fact that the $C_a \leftrightharpoons C_e$ equilibrium constant varies with temperature in comparably nonpolar solvents (from 1.2 in CCl_4 at +25°C to 7.3 in CH_3OCH_3 at −132°C) suggests that entropic factors are not as prevalent for **8***c* as may be the case for 2-methoxytetrahydropyran (19). Furthermore, the data summarized above suggest that the axial form should not be disfavored unduly by repulsive non-bonding interactions, so that it appears that torsional angles in **8***c* may play an important role as suggested by Pople and co-workers (2*a*) and Gorenstein and Kar (2*b*) from studies on dimethoxymethane.

Methods of calculation (2) to evaluate the relative stabilization from the anomeric effect have been developed for acetals; it is doubtful that they can be applied to orthoformates such as **8***c* without adaptation. In addition, the presence of a benzylic oxygen is specific to **8** and its derivatives. Nevertheless, the accepted models (2) reveal the nature of the relationship with the CH_3O—C(2)—O—C torsional angles and suggest that changes ought to modify the relative stability of the C_e and C_a forms.

Torsional angles involving the OCH_3 substituent about the C(2)—O(3) and C(2)—O(1) bonds are estimated from Dreiding models to be in the range 25–40° for the C_a form of **8***c* compared to 55–60° for the C_a form of 2-methoxy-1,3-dioxane. On the other hand, values in the range of 145–160° are observed for the C_e form of **8***c* compared to about 175–180° for the analogous 2-methoxy-1,3-dioxane. Such changes in angles are expected to modify the stabilization associated with factors contributing to the anomeric effect. This is particularly clear from the data reported by Jeffrey *et al.* (2*a*) for the C_a form, from which a decrease from 60° is predicted to lead to strong destabilization. Similarly, for the C_e form, a reduction in the C(2)—O torsional angles from 180° should lead to some destabilization, but the calculations suggest that the effect is stronger for the C_a form. The effect of the angular differences present in the seven-membered ring coupled with accompanying changes in dipolar interactions (20) could well account for the large equatorial preference of the methoxy group of **8***c*.

Table 3 shows that compound **8***d* (2,2-dimethyl) presents another interesting equilibrating conformational mixture. Whereas **2***d* exists only in the *TB* form, **8***d* is found to exist as a $C \leftrightharpoons TB$ equilibrium for which *C* is the predominant form.

The *TB* preference of **2***d* has been explained (8) in terms of stabilizing stereoelectronic and electrostatic interactions involving the ring oxygen atoms and favoring the *TB* form, together with a destabilization of the *C* form by significant repulsive non-bonded interactions between the axial methyl group and the two axial benzylic protons. In contrast, only one

Can. J. Chem. Downloaded from www.nrcresearchpress.com by 210.87.254.6 on 09/06/12
For personal use only.

Can. J. Chem. Downloaded from www.nrcresearchpress.com by 210.87.254.6 on 09/06/12
For personal use only.

such 1,3-axial interaction exists in the *C* form of **8***d*, suggesting less destabilization, whereas the *TB* form is not appreciably stabilized by the generalized anomeric effect. As a consequence, the *C* form predominates in the equilibrium mixture detected.

Finally, Table 3 shows that compound **8***e* also exhibits important conformational specificity, strikingly different from observations made for **2***e*. The greater stability of the *C* form for **8***e* follows from the arguments given above for **8***d* and the position of the substituents can be rationalized in terms of a greater equatorial preference by the methyl group for steric reasons.

In conclusion, the results for compounds **8** to **8***e* illustrate the consequence of lesser stabilization of the acetal function in the *TB* form **7** compared to **6**, contrary to extrapolations from studies on 1,3-dioxane where the opposite has been suggested (7). This result also suggests that more complete calculations for all possible conformations of 1,3-dioxane ought to be carried out using an approach which includes explicitly the stabilizing effect resulting from the anomeric effect (21).

Dynamic properties

Table 3 indicates that compounds **8**, **8***c*, and **8***d* undergo conformational averaging processes which can be characterized by the analysis of the ^1H and (or) ^{13}C nmr spectral changes observed at low temperatures.

As reference value, it is useful to recall that the inversion of the chair form of benzocycloheptene is characterized by a free energy value of 10.9 kcal/mol (22), which is associated with the flipping motion of the saturated end of the molecule involved in the $C \rightarrow B$ step of the inversion itinerary (23). The substitution of C-5 by an oxygen atom in 5-oxabenzocycloheptene (**9**) lowers the energy barrier to 9.5 kcal/mol (13). Furthermore, the presence of two oxygen atoms in the ring reduces the value to 7.9 kcal/mol for **2** and to 6.5 kcal/mol for 1,5-dioxa-6,7-benzocycloheptene (**14**) (8, 24). The free energy barrier determined for **8** (8.4 kcal/mol) is therefore higher than that of both **2** and **14**, whereas an intermediate value might have been expected if the effect of each oxygen atom were independent and additive.

The $\Delta G^{\neq}$ value for the $C_e \rightarrow C_a$ transformation of **8***c* is 7.6 kcal/mol, about 1 kcal/mol lower than the value noted for **8**. A similarly lowered energy barrier, by about 2 kcal/mol (from ~9.5 to 7.5 kcal/mol), has also been observed for the 2-methoxy derivative of 1,3-dioxane (10).

Finally, compound **8***d* exhibits spectral changes arising from the slowing down on the nmr time scale of two independent processes: the $C \leftrightharpoons TB$ interconversion (8.3 kcal/mol) and the *TB* inversion (7.5 kcal/mol). By comparison, the $\Delta G^{\neq}$ value for the pseudorotation motion of the *TB* inversion of **2***d* is about 2.5 kcal/mol higher (8), probably resulting in significant part from greater stereoelectronic stabilization in the *TB* form of **2***d* than of **8***d*, together with reduced steric interaction in the transition state of the *TB* inversion of **8***d*.

Experimental

The vpc analysis and separations were carried out on a Varian–Aerograph Model 920 instrument using helium as carrier gas. High resolution mass spectra at 70 eV were recorded using an Associated Electrical Industries Model MS-902 spectrometer.

The variable temperature ^1H nmr spectra were recorded at 400.13 MHz on a Bruker WH-400 spectrometer, located at the "Laboratoire régional de RMN à haut champ" in Montreal. Temperatures were determined directly using the B-VT-100 unit. Verification using a calibrated copper–constantan thermocouple inside a solvent-containing nmr tube indicates that the low temperatures reported are known within ±3°. The samples were studied as solutions in chlorodifluoromethane (5–25 mg in 0.55 mL of solution) containing ~15% of CD_2Cl_2 (for locking purpose) and a small quantity of TMS in 5-mm tubes which had been degassed and sealed. The ^1H nmr spectra at room temperature were recorded in $CDCl_3$ and CCl_4 (10–20 mg in 0.55 mL). The following instrumental parameters were used: flip angle = 25°; SW = 4500 Hz; data size = 16 K data points and zero filled to 32 K; acquisition time = 0.9 s. Gaussian multiplication was applied with LB values of −2 and −5 and GB = 0.4 to 0.9. The number of scans varied from 200 to 500.

The variable temperature ^{13}C nmr spectra were recorded at 100.6 MHz on the same Bruker WH-400. The samples were studied as solutions in chlorodifluoromethane and in dimethyl ether (80–150 mg in 2.2 mL of solution) containing ~15% of CD_2Cl_2 (for locking purpose) and a small quantity of TMS in 10-mm tubes which had been degassed and sealed. The following instrumental parameters were used: flip angle = 75°; SW = 1700–20 000 Hz; data size = 16 K or 8 K data points and zero filled to 16 K; acquisition time = 0.2–0.4 s; number of scans = 500–2000. The nmr data were treated by an exponential multiplication with LB varying from 1 to 6. A delay of 0.1 to 0.2 s was added between pulses for the spectra used for integration; this magnitude was found to be sufficient, as indicated by results published previously (25).

The complete ^{13}C nmr variable temperature study of **8***c* was done at 20.15 MHz on a Bruker WP-80 equipped with the Bruker variable temperature accessory. The parameters used were: flip angle = 75°; SW = 6000 Hz; data size = 8 K data points; acquisition time = 0.7 s; number of scans = 1000; RD = 0.1 s. The FID obtained was treated by exponential multiplication (LB = 4).

The rate constants were determined at the coalescence temperature using the equation $k = \pi \Delta\nu/\sqrt{2}$ for singlet to doublet splitting in ^{13}C nmr spectra; this equation is known to give acceptable approximation even in the case of lines of unequal intensities (26). The equation $k = \pi (\Delta\nu^2 + 6J^2)^{1/2}/\sqrt{2}$ was used for singlet to AB ^1H nmr spectral change. The free-energy barriers ($\Delta G^{\neq}$) were calculated from standard equations (27) using a transmission coefficient of one-half or one (*vide infra*).

Determinations of activation parameters of **8***d* ($\Delta G^{\neq}_{C \rightarrow TB}$ and $\Delta G^{\neq}_{TB \rightarrow TB'}$) were done by calculation of spectra at low temperature using a slightly modified version of the DNMR-2 program on a CDC Cyber 173 computer (24). The simulations were done by a visual comparison of the calculated and experimental spectra. Free energies of activation were calculated from a ln k/T vs. $1/T$ plot using the Eyring equation (28). Calculations of $\Delta S^{\neq}$ and $\Delta H^{\neq}$ were not expected to be sufficiently reliable because of the uncertainty in temperature (±3°), uncertainties in T_2 arising from possible small long-range coupling, as well as the fact that the conformational populations and chemical shifts were kept constant through the whole temperature interval. The complete treatment was done as reported previously (24).

The steady state nOe difference (29) measurements on **8***e* were done in a $CDCl_3$ solution which had been degassed and the nmr tube sealed. The FID were accumulated with 16 K data points. The difference spectra were obtained by subtraction of the transformed spectra; transients were collected after preirradiation (10–12 s) at selective frequencies and recycled to average the drift effect.

The ^1H nmr chemical shifts and coupling constants of **8***d* reported in Table 1 were determined from simulated spectra using the PANIC program, a Bruker version of the LAOCOON program.

1,3-Dioxa-4,5-benzocycloheptene (8) and its methyl (8a) and tert-butyl (8b) derivatives

These three compounds were prepared according to a published general procedure (30) from *o*-hydroxyphenethyl alcohol (Aldrich 99%, distilled before used), the corresponding aldehyde (formaldehyde, acetaldehyde, and trimethyl acetaldehyde), and *p*-toluenesulfonic acid (catalylic quality) in benzene. The benzene solvent was removed by flash evaporator and each compound was obtained pure

by reduced pressure distillation. Compound **8** was obtained in a 50% yield, **8***a* in a yield of 74% (bp 44°C at 0.1 Torr; 1 Torr = 133.3 Pa), and **8***b* in a yield of 76% (bp 60–62°C at 0.09 Torr). Their ^1H and ^{13}C nmr spectra (Tables 1 and 2) and the high resolution mass spectra are characteristic of the compounds. Compound **8**, *Mol. Wt.* calcd. for $C_9H_{10}O_2$: 150.0681; found (mass spectrum at 70 eV): 150.0691. Compound **8***a*, *Mol. Wt.* calcd. for $C_{10}H_{12}O_2$: 164.0838; found (mass spectrum at 70 eV): 164.0890. Compound **8***b*, *Mol. Wt.* calcd. for $C_{13}H_{18}O_2$: 206.1307; found (mass spectrum at 70 eV): 206.1305.

*2,2-Dimethyl-1,3-dioxa-4,5-benzocycloheptene (8*d)

Compound **8***d* was prepared by a procedure already published (8) from *o*-hydroxyphenethyl alcohol, dimethoxypropane, acetone, and *p*-toluene sulfonic acid (catalytic quantity) in benzene. The product was distilled under vacuum to give a colourless liquid (bp 38–40°C at 1.15 Torr) in a 50% yield. Its ^1H and ^{13}C nmr spectra (Tables 1 and 2) and its high resolution mass spectrum confirmed its identity as **8***d*. *Mol. Wt.* calcd. for $C_{11}H_{13}O_2$: 178.0894; found (mass spectrum at 70 eV): 178.0999.

*2-Methoxy-1,3-dioxa-4,5-benzocycloheptene (8*c*) and 2-methoxy-2-methyl-1,3-dioxa-4,5-benzocycloheptene (8*e*)*

A mixture of *o*-hydroxyphenethyl alcohol (1 equiv.) and trimethyl orthoformate (1.2 equiv.) with a catalytic amount of *p*-toluenesulfonic acid in benzene was stirred and refluxed to allow benzene and methanol to distill off. Dry benzene was added periodically to the reaction flask. The evolution of the reaction was followed by vpc (OV 101 at 1.5%, 4 ft at 80°C with a flow of 1 mL/s). After 8 h, most of the starting material had disappeared (less ~30%); compounds **8***c* and **8***e* were then isolated and purified from the crude mixture by vpc under the conditions given above. Each product was characterized by ^1H and ^{13}C spectra (Tables 1 and 2) and its high resolution mass spectra. Compound **8***c*, *Mol. Wt.* calcd. for $C_{10}H_{12}O_3$: 180.0787; found (mass spectrum at 70 eV): 180.0845. Compound **8***e*, *Mol. Wt.* calcd. for $C_{11}H_{14}O_3$: 194.2314; found (mass spectrum at 70 eV): 194.0782.

Acknowledgements

We wish to acknowledge the valuable contribution of the "Laboratoire Régional de RMN à Haut Champ" in Montreal. We thank the Natural Sciences and Engineering Research Council of Canada and the Ministère de l'Education du Québec for their financial assistance.

1. P. DESLONGCHAMPS. Stereoelectronic effects in organic chemistry. Pergamon Press, Willowdale, Ontario. 1983.
2. (*a*) G. A. JEFFREY, J. A. POPLE, J. S. BINKLEY, and S. VISHVESHWARA. J. Am. Chem. Soc. **100**, 373 (1978); (*b*) D. G. GORENSTEIN and D. KAR. J. Am. Chem. Soc. **99**, 672 (1977); (*c*) I. TVAROSKA and T. BLEHA. Collect. Czech. Chem. Commun. **45**, 1883 (1980); (*d*) I. TVAROSKA and T. BLEHA. Can. J. Chem. **57**, 424 (1979); (*e*) I. TVAROSKA and T. BLEHA. J. Mol. Struct. **24**, 249 (1975); (*f*) E. E. ASTRUP. Acta Chem. Scand. **27**, 3271 (1973).
3. G. A. JEFFREY. *In* Anomeric effect; origin and consequences. *Edited by* Walter A. Szarek and Derek Horton. ACS Symposium Series. Vol. 87. Washington, DC. 1979. Chapt. 4.
4. (*a*) A. ABE. J. Am. Chem. Soc. **98**, 6477 (1976); (*b*) R. U. LEMIEUX, A. A. PAVIA, J. C. MARTIN, and K. A. WATANABE. Can. J. Chem. **47**, 4427 (1969).
5. (*a*) R. U. LEMIEUX, S. KOTO, and D. VOISIN. *In* Anomeric effect; origin and consequences. *Edited by* Walter A. Szarek and Derek Horton. ACS Symposium Series. Vol. 87. Washington, DC. 1979. Chapt. 2; (*b*) R. U. LEMIEUX and S. KOTO. Tetrahedron, **30**, 1933 (1974).
6. (*a*) P. DESLONGCHAMPS, D. D. ROWAN, N. POTHIER, G. SAUVÉ, and J. K. SAUNDERS. Can. J. Chem. **59**, 1105 (1971); (*b*) N. POTHIER, D. D. ROWAN, P. DESLONGCHAMPS, and J. K. SAUNDERS. Can. J. Chem. **59**, 1132 (1981).
7. (*a*) M. J. O. ANTEUNIS, D. TAVERNIER, and F. BORREMANS. Heterocycles, **4**, 293 (1976), and references therein; (*b*) U. BURKERT. Tetrahedron, **35**, 691 (1979), and references therein; (*c*) N. L. ALLINGER and D. Y. CHUNG. J. Am. Chem. Soc. **98**, 6798 (1976).
8. A. BLANCHETTE, F. SAURIOL-LORD, and M. ST-JACQUES. J. Am. Chem. Soc. **100**, 4055 (1978).
9. R. ST-AMOUR and M. ST-JACQUES. Can. J. Chem. **59**, 2283 (1981).
10. F. SAURIOL. Ph.D. Thesis, Université de Montréal, 1980.
11. G. BINSCH. J. Am. Chem. Soc. **91**, 1304 (1969).
12. M. BARFIELD and D. M. GRANT. J. Am. Chem. Soc. **85**, 1899 (1963).
13. L. CANUEL and M. ST-JACQUES. Can. J. Chem. **52**, 3581 (1974).
14. K. PIHLAJA and T. NURMI. Isr. J. Chem. **20**, 160 (1980).
15. R. ST-AMOUR and M. ST-JACQUES. Can. J. Chem. **61**, 109 (1983).
16. P. MARONI, L. CAZAUX, J.-P. GORRICHON, P. TISNES, and J. G. WOLF. Org. Magn. Reson. **5**, 517 (1973).
17. D. MÉNARD and M. ST-JACQUES. Tetrahedron, **39**, 1041 (1983).
18. (*a*) J. BADIN and G. DESCOTES. Bull. Soc. Chim. Fr. 1949 (1970); (*b*) G. DESCÒTES, J. C. MARTIN, and N. MATHICOLONIS. Bull. Soc. Chim. Fr. 1077 (1972).
19. H. BOOTH, T. B. GRINDLEY, and K. A. KHEDHAIR. J. Chem. Soc. Chem. Commun. 1047 (1982).
20. M. K. KALOUSTIAN. J. Chem. Educ. **51**, 777 (1974).
21. H. THOGERSEN, R. U. LEMIEUX, K. BOCK, and B. MEYER. Can. J. Chem. **60**, 44 (1982).
22. H. FRIEBOLIN, R. MECKE, S. KABUSS, and A. LÜTTRIN-GHAUS. Tetrahedron Lett. 1929 (1964).
23. (*a*) N. L. ALLINGER and J. T. SPRAGUE. J. Am. Chem. Soc. **94**, 5734 (1972); (*b*) G. FAVINI and A. NAVA. Gazz. Chim. Ital. **104**, 621 (1974).
24. D. MÉNARD and M. ST-JACQUES. Can. J. Chem. **59**, 1160 (1981).
25. H. BOOTH and M. L. JOZEFOWICZ. J. Chem. Soc. Perkin Trans. 2, 895 (1976).
26. F. A. L. ANET, P. J. DEGEN, and J. KRANE. J. Am. Chem. Soc. **98**, 2059 (1976).
27. J. SANDSTRÖM. Dynamic NMR spectroscopy. Academic Press, Toronto. 1982. Chapt. 7.
28. G. BINSCH. Top. Stereochem. **3**, 87 (1968).
29. J. K. SANDERS and J. D. MERSH. Prog. Nucl. Magn. Reson. Spectrosc. **15**, 353 (1982).
30. K. C. BRANNOCK and G. R. LAPPIN. J. Org. Chem. **21**, 1366 (1956).

Can. J. Chem. Downloaded from www.nrcresearchpress.com by 210.87.254.6 on 09/06/12
For personal use only.

Synthesis, electronic spectra, and solvatochromic behaviour of 4-arylidene-1-(2,4-dinitrophenyl)-3-methyl-2-pyrazolin-5-ones

SAID A. IBRAHIM AND M. S. K. YOUSSEF

Department of Chemistry, Faculty of Science, Assiut University, Assuit, Egypt

Received July 19, 1983[1]

SAID A. IBRAHIM and M. S. K. YOUSSEF. Can. J. Chem. **62**, 2841 (1984).

The uv–visible electronic spectra of 4-arylidene-1-(2,4-dinitrophenyl)-3-methyl-2-pyrazolin-5-ones have been studied. The different bands observed have been assigned to the proper electronic transition. Solvatochromic behaviour of these compounds is investigated by studying their visible spectra in organic solvents of different polarities. The longer wavelength band displayed by *para*-hydroxy derivative is assigned to an intermolecular CT transition. The solvated H-bond complexes formed between ethanol or DMF and the *para*-hydroxy derivative are investigated. Transition moment (μ_{CTL}), ΔG, and K_f values of these complexes have been determined.

SAID A. IBRAHIM et M. S. K. YOUSSEF. Can. J. Chem. **62**, 2841 (1984).

On a étudié les spectres électroniques uv-visible des arylidène-4 (dinitro-2,4 phényl)-1 méthyl-3 pyrazoline-2 ones-5. On a attribué les diverses bandes observées aux transitions électroniques appropriées. On a étudié le comportement solvatochromique de ces composés en déterminant leurs spectres visibles dans des solvants organiques de polarités diverses. On a attribué la bande apparaissant à la plus grande longueur d'onde du spectre du dérivé *para*-hydroxy à une transition CT intermoléculaire. On a étudié les complexes dus aux liaisons hydrogènes solvatées qui se forment entre l'éthanol ou la DMF et le dérivé *para*-hydroxy. On a déterminé les valeurs des moments de transition (μ_{CT}) des ΔG et des K_f de ces complexes.

[Traduit par le journal]

Can. J. Chem. Downloaded from www.nrcresearchpress.com by 210.87.254.42 on 09/06/12
For personal use only.

Introduction

It is of interest to note that 2-pyrazolin-5-ones have wide applications in industry as purple and blue–green photographic colour couplers (1). This class of compounds is also known as filter dyes and electron acceptors (2). As these compounds are used in the preparation of cyanine dyes, they may be used as photosensitizers (3, 4). Some literature concerning the synthesis (5, 6) and electronic spectra (7) of pyrazolines is reported. However, data on the synthesis and electronic spectra of the title compounds are yet scarce in the literature. In view of these findings, 4-arylidene-1-(2,4-dinitrophenyl)3-methyl-2-pyrazolin-5-ones are prepared by reaction of 1-(2,4-dinitrophenyl)-3-methyl-2-pyrazolin-5-ones with aromatic aldehydes. Their electronic spectra and solvatochromic behaviour are studied. The solvated H-bond complexes formed in solution have been investigated.

Experimental

Preparation of the 4-arylidene-5-pyrazolones

A mixture of 1-(2,4-dinitrophenyl)-3-methyl-2-pyrazolin-5-ones (0.01 mol) and the appropriate aldehyde (0.015 mol) in absolute ethanol was refluxed on a water bath for 6 h. The solid that separated was filtered off and recrystallized from the proper solvent (cf. Table 1). The structure and purity of these compounds were checked by elemental analysis and ir spectra. The results are listed in Table 1.

The following compounds were prepared:

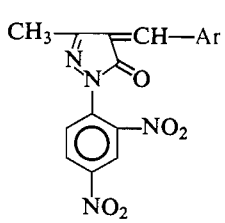

I, Ar = C_6H_5; **II**, Ar = $C_6H_4OH(o)$; **III**, Ar = $C_6H_4OH(p)$; **IV**, Ar = $C_6H_4NO_2(p)$; **V**, Ar = $C_6H_4Cl(p)$; **VI**, Ar = C_4H_3S(thienyl)

[1]Revision May 24, 1984.

Solutions

The organic solvents used (ethanol, ether, cyclohexane, DMF, DMSO) were all spectrograde BDH or Merck products.

Stock solutions (10^{-3} *M*) of the pyrazolone derivatives were prepared by dissolving the accurate amount of the recrystallized product in the required solvent. Solutions of lower molarities, used in spectral measurements, were obtained by accurate dilution.

Apparatus

The absorption spectra at 25°C were recorded on a Cary 219 spectrophotometer in the wavelength range 200–600 nm using 1-cm matched silica cells. Infrared spectra of the solids were recorded on a Perkin-Elmer 599 B spectrophotometer as KBr discs.

Results and discussion

Effect of molecular structure on the eletronic spectra

The electronic absorption spectral features (λ_{max} and ϵ_{max} values) of the arylidene pyrazolones under investigation in ethanolic solutions are cited in Table 2. The data given in this table reveal that spectra of these compounds comprise mainly three absorption bands. The one of shortest wavelength appearing in the range 212–224 nm can be assigned to a $\pi-\pi^*$ transition of the benzenoid system of the compounds. This assignment is substantiated from the observation that the λ_{max} of this band is slightly altered by the change of the substituent (Ar). The second uv band observed in the spectra of compounds **III**, **IV**, and **VI** within the wavelength range 275–320 nm may be attributed to the $n-\pi^*$ transition involving the non-bonding electrons of the pyrazolone carbonyl oxygen. The disappearance of this band in case of compound **II** (*o*-OH derivative) confirms its $n-\pi^*$ nature since the carbonyl oxygen is involved in an intramolecular H-bonding. The involvement of the OH group in H-bonding in compound **II** is substantiated by the lower frequency of the carbonyl stretching relative to that of compound **III**, that has its OH group in *para* position (Table 1). A further support for this $n-\pi^*$ assignment is achieved by the disappearance of this band in acidic solutions in which the n-electrons are expected to be blocked by H^+ ions.

The longer wavelength band observed in the spectra of these compounds in the wavelength range 338–385 nm can be as-

TABLE 1. Elemental analysis data, colour, melting point, and some ir frequencies of 4-arylidene-1-(2,4-dinitrophenyl)-3-methyl-2-pyrazolin-5-ones (**I**–**VI**)

Compound	Ar	Colour	Solvent of crystn[a]	Melting point (°C)	Yield (%)	Mol. formula (mol. wt.)	Calcd. (found)% C	H	N	ν_{ir} (cm^{-1}) OH	C=O	C=N
I	C_6H_5	Yellow	A	157–159	70	$C_{17}H_{12}N_4O_5$ (352.3)	57.95 (58.09)	3.40 (3.56)	15.90 (15.72)	—	1625	1595
II	$C_6H_4OH(o)$	Yellow	E	202–204	70	$C_{17}H_{12}N_4O_6$ (368.3)	55.43 (55.34)	3.26 (3.40)	15.21 (15.11)	3100 *b*[d]	1600	1570
III	$C_6H_4OH(p)$	Red	A	244–245	75	$C_{17}H_{12}N_4O_6$ (368.3)	55.43 (55.50)	3.26 (3.23)	15.21 (15.26)	3200 *b*[d]	1660	1595
IV	$C_6H_4NO_2(p)$	Orange	DA	164–166	76	$C_{17}H_{11}N_5O_7$ (397.3)	51.38 (51.30)	2.77 (2.79)	17.63 (17.55)	—	1690	1625
V	$C_6H_4Cl(p)$	Yellow	E	182–184	71	$C_{17}H_{11}N_4O_5Cl$[b] (386.7)	52.78 (52.88)	2.84 (2.91)	14.48 (14.53)	—	1620	1595
VI	C_4H_3S (thienyl)	Brown	A	230–231	78	$C_{15}H_{10}N_4O_5S$[c] (358.3)	50.27	2.79	15.64 (50.34)	— (2.65)	1685 (15.58)	1585

[a]A = acetic acid, DA = dilute acetic acid, E = ethanol.
[b]Cl: calcd. 9.18, found 9.07.
[c]S: calcd. 8.39, found 9.13.
[d]*b* = broad band.

TABLE 2. Electronic spectral bands of compounds **I**–**VI** in ethanol[a]

Compound	$\pi \rightarrow \pi^*$ λ_{max}	$\epsilon_{max}\times10^{-3}$	$n \rightarrow \pi^*$ λ_{max}	$\epsilon_{max}\times10^{-3}$	Intramolecular CT λ_{max}	$\epsilon_{max}\times10^{-3}$	Intermolecular CT λ_{max}	$\epsilon_{max}\times10^{-3}$
I	212	25.75	—	—	338	11.00	—	—
II	218	23.75	—	—	334 355*sh*	12.00 11.25	—	—
III	215 255*sh*	9.25 5.50	315*sh*	3.50	385	14.00	492	9.00
IV	218	23.75	275	14.25	335*sh*	10.00	—	—
V	218	23.75	—	—	344	11.00	—	—
VI	224	1.50	320	0.75	374	2.75	—	—

[a]λ in nm, ϵ in mol^{-1} cm^2.

signed to a $\pi-\pi^*$ transition with considerable charge transfer character. The charge transfer character of this band is substantiated by the effect of the substituent (Ar) on its location and intensity. In general, this band exhibits a marked red shift, when the substituent is an electron-releasing one, relative to the unsubstituted or electron-withdrawing substituted derivatives. Also, the broadness of this band can be considered as an evidence for its CT nature (8). Such a charge transfer may take place from the aryl moiety as the donor to the pyrazolone carbonyl group as the acceptor center, and it can be represented schematically as follows:

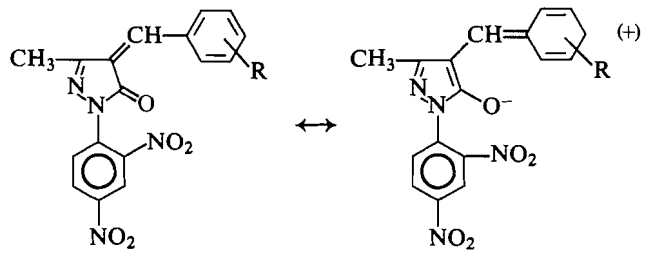

The charge transfer character of this band is further confirmed by the solvatochromic behaviour observed on studying the effect of solvent, in the visible region, on the electronic spectra of these compounds as explained hereafter. Moreover, good evidence for the CT nature of this band is attained from ir spectra where the carbonyl stretching appears at lower frequencies characteristic for polarized C=O groups (cf. Table 1).

An extra new band with lower intensity is observed in the electronic spectra of compound **III** (Ar = $C_6H_4OH(p)$) at 490 nm. This band may be assigned to an intermolecular charge transfer transition (7, 9, 10–12). Such an assignment is supported by the non-linear relationship obtained on plotting the absorbance of this band against the molar concentration of the compound.

Effect of solvent

The electronic absorption spectra of the title pyrazolone derivatives, in the wavelength range 300–600 nm, are studied in different organic solvents, viz. cyclohexane, ether, DMF, and DMSO. This is made with the intention to investigate the solvatochromic behaviour of these compounds. λ_{max} and ϵ_{max} values of the intramolecular and intermolecular CT bands are given in Table 3. It is clear from these data that λ_{max} of the intramolecular CT band exhibits a marked red shift on transfer from nonpolar to polar solvent (Fig. 2). The observed shifts run according to the following order.

cyclohexane < ether < ethanol < DMF < DMSO

This order is in harmony with the increase in solvent polarity

Can. J. Chem. Downloaded from www.nrcresearchpress.com by 210.87.254.42 on 09/06/12
For personal use only.

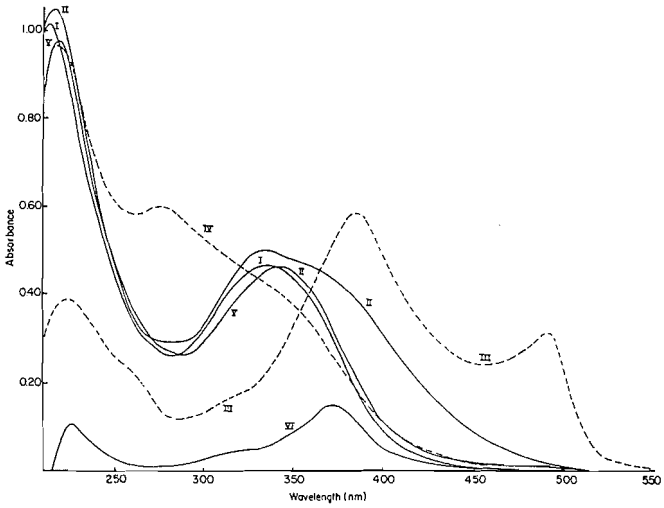

FIG. 1. Electronic absorption spectra of 2.0×10^{-5} *M* ethanolic solutions of the arylidene pyrazolones **I**–**VI**.

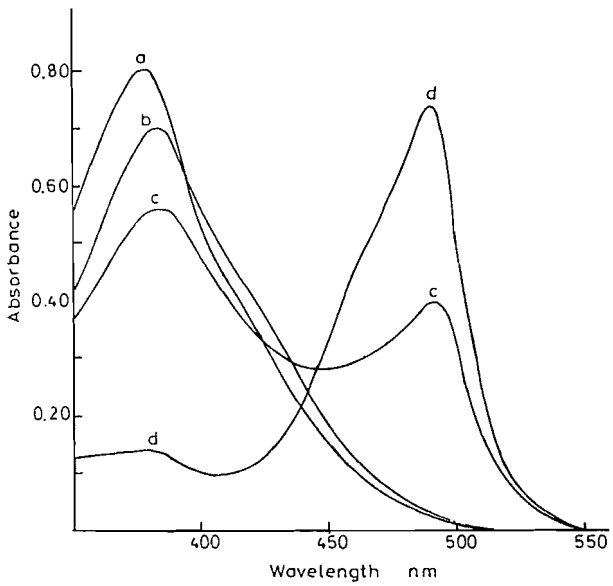

FIG. 2. Spectra of 4.0×10^{-5} *M* solutions of compound **III** (*p*-OH) in different organic solvents.

in the same direction. This behaviour indicates that the polar excited states of these compounds are stabilized as the polarizability of the solvent is increased, i.e., lower excitation energy is required.

It is noteworthy that the intramolecular CT band appears at a longer wavelength in the case of compound **III** (*p*-OH) than that of compound **II** (*o*-OH) in all the solvents used (cf. Table 3). This behaviour reflects the role played by the intramolecular hydrogen bond established in molecules of compound **II** which hinders the charge transfer process. Such an intramolecular H-bond can be represented as follows

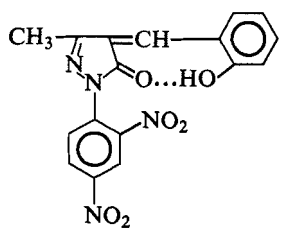

TABLE 3. Intramolecular charge transfer bands of compounds **I**–**VI** in various organic solvents

Compound	λ_{max} ($\epsilon_{max} \times 10^{-3}$)[b] when solvent =			
	Cyclohexane	Ether	DMF	DMSO
I	320(11.0)	335(17.5)	360(19.0)	355(19.7)
II	325(12.5)	335(13.5)	368(15.5)	365(15.5)
III	383(18.2)	378(20.7)	380(8.6)	384(14.7)
			[a]492(18.0)	[a]492(10.0)
IV	335(19.20)	336(21.0)	355(26.6)	350(27.0)
V	334(18.70)	335(21.20)	356(13.8)	352(13.8)
VI (thienyl)	365(6.0)	365(7.0)	370(6.2)	374(6.10)

[a]Intermolecular CT bands.
[b]λ in nm, ϵ in mol^{-1} cm^2.

Furthermore, a longer wavelength band having λ_{max} similar to that observed in ethanol (~490 nm) is observed in DMF and DMSO solutions of compound **III** (Fig. 2).

Spectra in mixed organic solvents

The visible spectra of compound **III** (*p*-OH) are investigated in cyclohexane–ETOH, ETOH–DMF, and cyclohexane–DMF mixtures. This is performed in order to study the solvated H-bond complexes liable to be formed between the solute molecules and H-bond acceptor solvents. The visible spectrum of this compound in pure cyclohexane displays only one band with λ_{max} = 384 nm (cf. Fig. 2). On adding ethanol or DMF, a new band at ~490 nm appears where its absorbance increases as the molarity of ethanol or DMF is increased; meanwhile the absorbance of the 384 nm band decreases. A fine isosbestic point is obtained in each case indicating the existence of an equilibrium between the solvated complex and the free solute molecules (Fig. 3). In the case of ethanol–DMF mixed solvent, the absorbance of the longer wavelength band (492 nm) increases, with a slight red shift, as the molarity of DMF is increased. At the same time, the absorbance of the shorter wavelength band decreases and a fine isosbestic point is obtained. This behaviour indicates that DMF molecules have greater tendency to form solvated complexes with the solute molecules relative to ethanol. This is due to the low ionization potential of DMF as well as its high H-bond accepting character.

A plot of absorbance of the longer wavelength band against the molarity of DMF or EtOH, gave a sigmoidal curve typical for an association process (Fig. 4). This can be considered as convincing evidence for the formation of solvated H-bond complexes.

A support for H-bond formation between solute and DMF molecules can be obtained from the value of the free energy of formation (ΔG) of the solvated complexes obtained from the relation

$$-\Delta G = RT \ln K_f$$

K_f values are calculated utilizing the reported relation for behaviour in mixed organic solvents (13). Values of K_f and ΔG are reported in Table 4.

The transition moment μ_{CT} of the solvated complexes formed are calculated using the folllowing equation (14):

$$\mu_{CT} = 0.0958 \left\{ \epsilon_{max} \frac{\Delta \bar{\nu}^{1/2}}{\bar{\nu}_{max}} \right\}^{1/2}$$

where ϵ_{max} is the molar extinction coefficient; $\Delta \bar{\nu}^{1/2}$ is the band

Can. J. Chem. Downloaded from www.nrcresearchpress.com by 210.87.254.42 on 09/06/12
For personal use only.

Can. J. Chem. Downloaded from www.nrcresearchpress.com by 210.87.254.42 on 09/06/12
For personal use only.

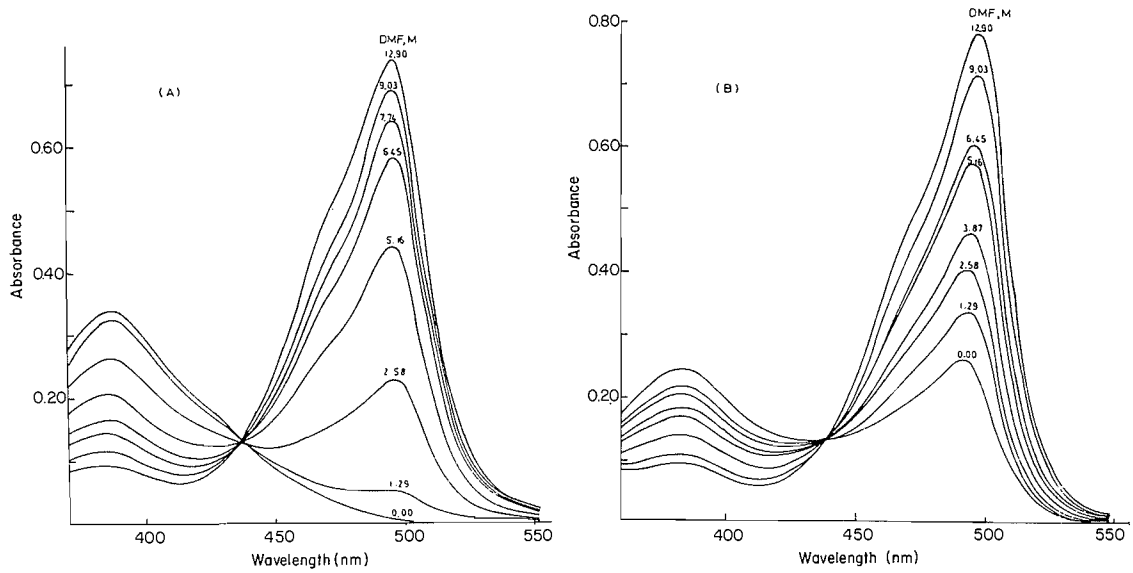

FIG. 3. Absorption spectra of 4.0×10^{-5} *M* solutions of compound **III** (*p*-OH) in mixed organic solvents. *A*, cyclohexane–DMF mixtures; *B*, EtOH–DMF mixtures.

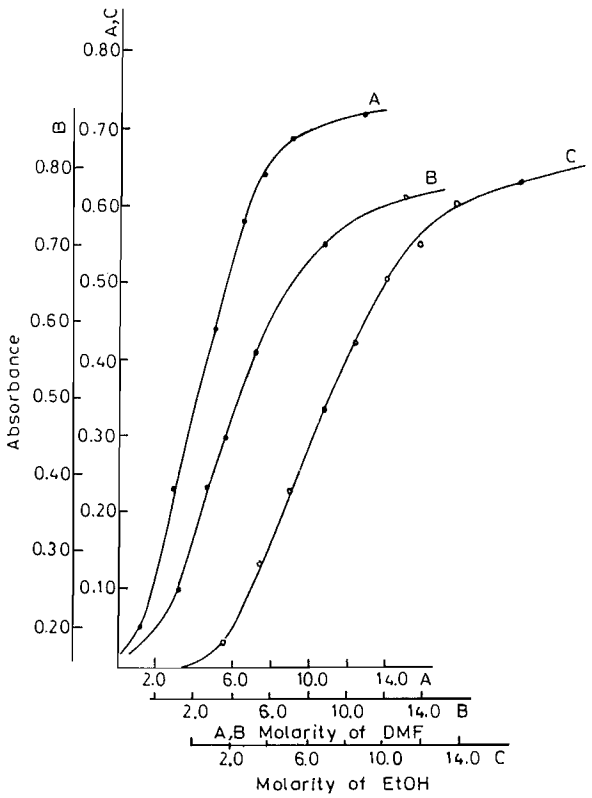

FIG. 4. Relation between absorbance of the intermolecular CT band and molarity of the more polar solvent. *A*, cyclohexane–DMF mixtures; *B*, EtOH–DMF mixtures; *C*, cyclohexane–EtOH mixtures.

half-width in cm^{-1}. The obtained μ_{CT} values for the investigated solvated H-bond complexes together with ϵ_{max} values are assembled in Table 4. These values are quite high, indicating a strong CT interaction since it is reported that the stronger the CT interaction is, the longer the intensity of the CT absorption band (15).

TABLE 4. Values of K_f, ΔG, ϵ_{max} (mol^{-1} cm^2) and μ_{CT} for the H-bonding solvated complexes of compound **III**

System	K_f	$-\Delta G$ (K J mol^{-1})	$\epsilon_{max} \times 10^{-3}$	μ_{CT}[a]
Cyclohexane–DMF	4.26	3.59	6.30	7.20
Cyclohexane–EtOH	6.45	4.68	7.30	8.07
EtOH–DMF	5.49	4.22	7.70	8.73

[a]in Debye units.

1. EASTMAN KODAK CO., Ger, Pat. 1, 181, 057 (C1 Go 3C), Nov. 5, 1964; Chem. Abstr. **26**, 2865 (1965).
2. VAN LARE and J. EARL. (EASTMAN KODAK CO.), U.S. Pat. 3, 615, 608 (1971); Chem. Abstr. **76**, 114853 (1972).
3. A. M. OSMAN, M. S. K. YOUSSEF, and KH. M. HASSAN. J. Prakt. Chem. **320**, 857 (1978).
4. P. K. JESTHI, M. BOY, and S. K. MOHAPATRA. J. Indian Chem. Soc. **Lv**, 712 (1978).
5. H. AMAL and A. H. COOK. Pharm. Acta. Helv. **26**, 379 (1951).
6. A. SAMMOUR, A. ABDEL RAOUF, M. ELKASABY, and M. A. HASSAN. Egypt. J. Chem. **15**, 429 (1972).
7. M. R. HAMMOUD, H. S. EL-KASHEF, and R. ABDEL-HAMIDE. Spectrochim. Acta, **37**, 519 (1981).
8. G. BRIEGLEB. Elektron Donator-Acceptor Komplex. Springer Verlag, Berlin. 1961.
9. E. M. KOSOWER. J. Am. Chem. Soc. **82**, 2188 (1958).
10. J. F. COETZOE and C. O. RITCHIE. Solute–solvent interaction. Marcel Dekker, New York-London. 1969. pp. 226–231.
11. N. MATAGA and T. KUBOTA. Molecular interactions and electronic spectra. Marcel Dekker, New York. 1970. p. 293.
12. M. R. MAHMOUD, P. M. HAMMAM, and S. A. IBRAHIM. Z. Phys. Chem. Leipzig, **265**, 302 (1984) .
13. R. M. ISSA, M. M. GHONEIM, K. A. IDRISS, and A. A. HARFOUSH. Z. Phys. Chem. (N.F.B.) **945**, 135 (1975).
14. N. MATAGA and T. KUBOTA. Molecular interactions and electronic spectra. Marcel Dekker, New York. 1970. p. 212.
15. P. A. D. DE MAINE. J. Chem. Phys. **26**, 1199 (1957).

Electrochemical deglycosidation of anthracyclines: stereoelectronic requirements

VINCENZO MALATESTA, SERGIO PENCO, NEREO SACCHI, LUIGI VALENTINI, ARISTIDE VIGEVANI, AND FEDERICO ARCAMONE

Farmitalia Carlo Erba S.p.A., Ricerca & Sviluppo Chimico Via dei Gracchi, 35 – 20146 Milano (Italy)

Received February 10, 1984

VINCENZO MALATESTA, SERGIO PENCO, NEREO SACCHI, LUIGI VALENTINI, ARISTIDE VIGEVANI, and FEDERICO ARCAMONE. Can. J. Chem. **62**, 2845 (1984).

The redox behavior of daunorubicin and its analogues has been studied by differential pulse polarography (DPP) in phosphate-buffered (pH 7.1) solutions at 37.5°C. The reductive deglycosidation reaction has been found to be under stereoelectronic control as the conformation of the alicyclic ring strongly affects the kinetics of the sugar moiety detachment. The substitution pattern of the anthraquinone system and/or the cyclohexene ring may determine the shape of the latter and in turn the stability of the glycosidic bond. We observe that while daunorubicin, 4-demethoxy-11-deoxydaunorubicin, and 10(*R*)-methoxydaunorubicin easily eliminate L-daunosamine upon polarographic reduction yielding the corresponding 7-deoxyaglycones, 4-demethoxy-6-deoxydaunorubicin and 10(*S*)-methoxydaunorubicin are stable towards deglycosidation. There is a pronounced stereoelectronic effect which results in a faster cleavage of those glycosidic bonds which have a relatively small dihedral angle with respect to the π-type orbital(s) of the anthraquinone system. Among the aglycones, the 10(*S*)-acetoxy and 10(*R*)-azidodaunomycinones are reductively converted to daunomycinone whereas the 10(*R*)- and 10(*S*)-methoxydaunomycinones do not undergo splitting of either the benzylic C10—OCH_3 or the C7—OH bond.

VINCENZO MALATESTA, SERGIO PENCO, NEREO SACCHI, LUIGI VALENTINI, ARISTIDE VIGEVANI, et FEDERICO ARCAMONE. Can. J. Chem. **62**, 2845 (1984).

Faisant appel à la polarographie pulsée différentielle (PPD) et opérant à 37,5°C, dans des solutions tampons de phosphate (pH 7,1), on a étudié le comportement redox de la daunorubicine et de ses analogues. On a trouvé que la réaction de déglycosidation réductrice se produit sous contrôle stéréoélectronique puisque la conformation du cycle alicyclique influence fortement la cinétique de la dissociation du sucre. Les divers types de substitution sur le système anthraquinone et/ou sur le cyclohexène peuvent éventuellement déterminer la forme de ce dernier et, par voie de conséquence, la stabilité du lien glycosidique. Alors que la réduction polarographique de la daunorubicine, de la déméthoxy-4 déoxy-11 daunorubicine et de la méthoxy-10(*R*) daunorubicine provoque une élimination facile de la L-daunosamine conduisant aux déoxy-7 aglycones correspondantes, la déméthoxy-4 déoxy-6 daunorubicine et la méthoxy-10(*S*) daunorubicine sont stables vis à vis de la déglycosidation. Il existe un effet stéréoélectronique prononcé qui provoque un clivage plus rapide des liaisons glycosidiques qui ont un angle dièdre relativement petit par rapport à (aux) l'orbitale(s) du système anthraquinone. Parmi les aglycones, les acétoxy-10(*S*) et azido-10(*R*) daunomycinones sont réduites en daunomycinones tandis que les méthoxy-10(*R*) et -10(*S*) daunomycinones ne subissent aucune rupture soit du lien benzylique C10—OCH_3 ou de la liaison C7—OH.

[Traduit par le journal]

Can. J. Chem. Downloaded from www.nrcresearchpress.com by 210.87.254.42 on 09/06/12
For personal use only.

The investigation of the electrochemical behaviour of anthracyclines, a class of widely used antitumor antibiotics (1–3) has attracted a great deal of interest. It is anticipated that because of the quinone–hydroquinone character of the chromophore the redox states properties should relate to the expression of the biological anti-neoplastic activity of the anthracyclines.

Although the intercalation of anthracyclines within the base pairs of the DNA (3–8) has been proposed as a prerequisite in the mechanism of biological action of this class of antibiotics, the real possibility exists for covalent binding to other parts of the cell besides the intercalative region of stacked base-pairs. The same electronic features that render the anthracyclines molecules particularly suited for intercalation with DNA bases allow them to act as very efficient electron acceptors. Thus the anthracyclines can be activated in biochemical systems via enzyme mediated redox processes to free radical state (9–11). Their ability to generate active oxygen in the form of high energy oxygen centered radicals ($O_2^{\cdot-}$, OH·) that are claimed to be linked to the cardiotoxicity of these drugs (7, 12–14) is a result of this reductive activation.

There is a growing body of evidence suggesting that the single electron reduction product of the anthracyclines, the semiquinone, besides functioning as electron shuttle between the enzyme(s) and the molecular oxygen can undergo an intramolecular electron transfer and rearrange to give a sugar residue anion and a carbon centered radical (8, 12, 15–17) which could subsequently engage in the alkylation of biomolecules (bioalkylation).

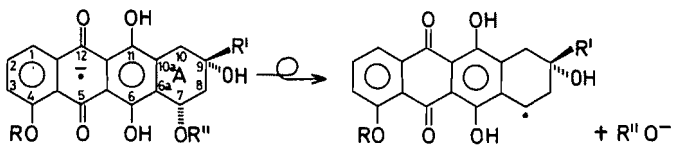

R" = sugar residue

Furthermore, the involvement of a free radical intermediate in the metabolism by mammalian microsomes of the anthracyclines has been substantiated (13, 18–20), but its chemistry has not as yet been defined. It is within this perspective that an integrated understanding of the factors affecting the reductive splitting is of importance.

The work of Rao *et al.* (21) has shown that both daunorubicin and doxorubicin undergo, upon polarographic reduction, a loss of the amino sugar (*reductive deglycosidation*) to give the corresponding 7-deoxyaglycone through a consecutive two-steps electrochemical–chemical–electrochemical (E.C.E.) process (Scheme 1).

The differential pulse polarography (DPP) is a technique particularly suited for the study of systems characterized by two or more consecutive electron transfer steps, e.g., E.C.E. processes, especially when the half-wave potentials of the individual steps are so closely similar that the conventional direct current polarography (DCP) would not allow a clear-cut resolution. During the course of our DPP investigation of the electrochemical properties of new synthetic anthracycline analogues

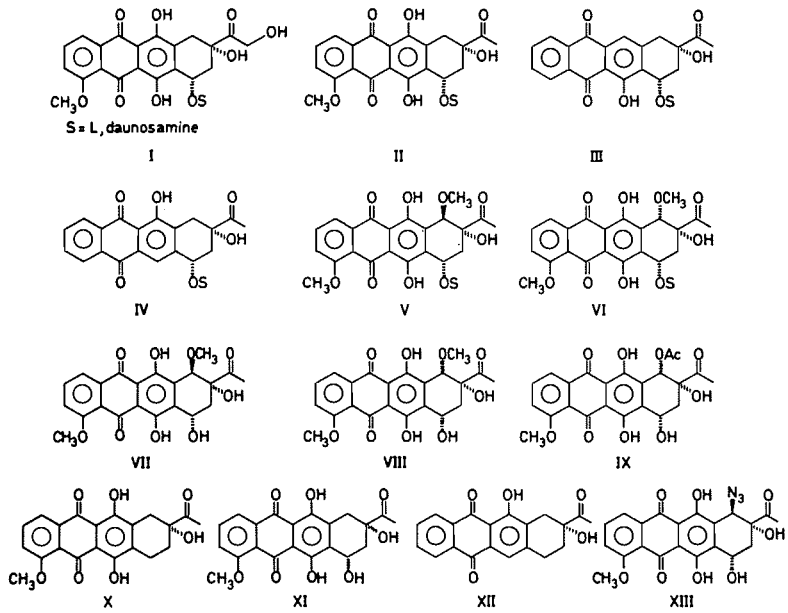

CHART 1

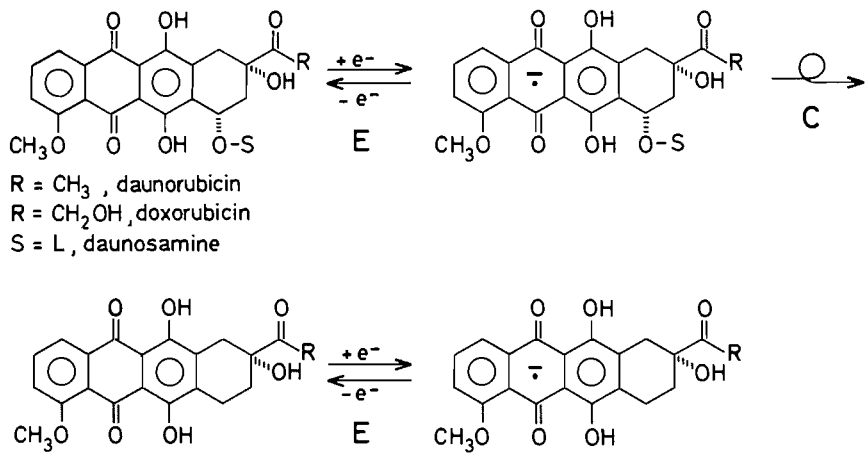

SCHEME 1

we were surprised to find out that the stability of the glycosidic bond was markedly different in two anthracycline derivatives differing by only the stereochemistry at C10. We found that while the 10(*R*)-methoxydaunorubicin (**V**, Chart 1) underwent a reductive deglycosidation to the corresponding 10(*R*)-methoxy-7-deoxydaunomycinone, the glycosidic bond of the enantiomeric 10(*S*)-methoxydaunorubicin (**VI**) was stable.

Previous nmr studies (22) on the 10(*R*)-and 10(*S*)-methoxydaunomycinone in $CDCl_3$ had shown that the two enantiomers differ by the conformation of the A ring with the 10(*S*) enantiomer preferring the distorted boat conformation to the more common half-chair form. The same two compounds adopt two different half-chair conformations in more polar solvents like DMSO-d_6 and D_2O (see infra). We have then sought other examples of anthracycline derivatives (Chart 1) characterized by such a conformational bias with the aim of ascertaining the generality of our observation. We found that the results of our polarographic studies require, in order to be rationalized, a conformation-dependent reactivity of the glycosidic linkage.

Results

Single peak differential pulse polarograms were obtained for the aglycones: 10(*R*)- and 10(*S*)-methoxydaunomycinones (**VII, VIII**), 7-deoxydaunomycinone (**X**), daunomycinone (**XI**), 4-demethoxy-6,7-bisdeoxydaunomycinone (**XII**), and the two glycosides 4-demethoxy-6-deoxydaunorubicin (**IV**) and 10(*S*)-methoxydaunorubicin (**VI**). The remaining glycosides of Chart 1 (**1, II, III, V**) and the two aglycones 10(*S*)-acetoxydaunomycinone (**IX**) and 10(*R*)-azidodaunonomycinone (**XIII**) all underwent an E.C.E. process, giving rise to two peaks polarograms.

E.C.E. and E. processes exemplified

*10(*R*)-Methoxydaunorubicin (V)*

The differential pulse polarography (0.0−1.0 V vs. Ag/AgCl electrode) of a 3.2×10^{-5} *M* solution of (**V**) gave two cathodic peaks (−0.536 and −0.596 V), Table 1, whose relative intensities depended on the drop time (Fig. 1*a*). At a drop time of 6 s the two peaks are clearly defined and at shorter

Can. J. Chem. Downloaded from www.nrcresearchpress.com by 210.87.254.42 on 09/06/12
For personal use only.

TABLE 1.

	Anthracycline	E_p[a]	Reductive cleavage product	E_p[a]
I	Doxorubicin	−0.560	7-Deoxyadriamycinone	−0.612
II	Daunorubicin	−0.572	7-Deoxydaunomycinone	−0.624
III	4-Demethoxy-11-deoxydaunorubicin	−0.468	4-Demethoxy-7, 11-bisdeoxydaunomycinone	−0.540
IV	4-Demethoxy-6-deoxydaunorubicin	−0.524	None	—
V	10(*R*)-Methoxydaunorubicin	−0.536	10(*R*)-Methoxy-7-deoxydaunomycinone	−0.596
VI	10(*S*)-Methoxydaunorubicin	−0.532	None	—
VII	10(*R*)-Methoxydaunomycinone	−0.544	None	—
VIII	10(*S*)-Methoxydaunomycinone	−0.536	None	—
IX	10(*S*)-Acetoxydaunomycinone	−0.468	Daunomycinone	−0.592
X	7-Deoxydaunomycinone	−0.624	None	—
XI	Daunomycinone	−0.588	None	—
XII	4-Demethoxy-6, 7-bisdeoxydaunomycinone	−0.580	None	—
XIII	10(*R*)-Azidodaunomycinone	−0.424	Daunomycinone	−0.592

[a]Peak potentials (V) vs. Ag/AgCl at 37.5°C in phosphate buffer, pH 7.1.

drop times, e.g., 1.4 s, the second peak becomes less prominent. The HPLC analysis (see Materials and methods) of the coulometric reduction at fixed potential (−0.500 V) allowed us to identify the product of the first reduction step as the 10(*R*)-methoxy-7-deoxydaunomycinone.

10(S)-Methoxydaunorubicin (VI)

Only one peak (−0.532 V) was detectable at each of the drop times used in the present study (Fig. 1*b*). The fact that the shoulder noticeable at 1.4 s drop time does not show a (drop) time dependence does indicate that this is a peak due to some impurity. Cyclic voltammetry experiments confirmed the reversibility of the process and the absence of a chemical reaction following the electrochemical reduction. The ^{1}H-nmr spectrum (DMSO-d_6) of **VI** is similar to that of **V** ($J_{H10c-H8c}$ = 1.5 and 1.1 Hz, respectively) although one would expect that because of the opposite configuration at the C10 chiral center if the same ring A α-conformation (23) were retained, the 1,3-diequatorial coupling, i.e., $J_{H10c-H8c}$ should be observed only in the case of **V**. For **VI** the A ring boat conformation is also ruled out on the same grounds. The nmr data seem to be in keeping with a half-chair conformation having the C10—OCH_3 bond pseudoaxial and the glycosidic bond pseudoequatorial.[1] This assignment is supported also by the rather different values of the H7 J_{vic} which are 4.4 and 8 Hz for the 10(*R*)- and the 10(*S*)-methoxydaunorubicin, respectively.

4-Demethoxy-11-deoxydaunorubicin (III)

The alicyclic ring has the more common α half-chair form and the electrochemical behaviour of **III** stands in sharp contrast with that of **IV** in that the former compound undergoes an E.C.E process (first peak, −0.468 V; second peak, −0.540 V), whereas the latter is engaged in a simple, reversible, electrochemical process without concomitant splitting.

10(S)-Acetoxydaunomycinone (IX)

The differential pulse polarogram reveals two peaks attributable, the first (−0.468 V) to the reduction of the starting material and the second (−0.592 V) to the reversible reduction of the deacetylation product, daunomycinone. The most relevant resonances in the ^{1}H-nmr spectrum (DMSO-d_6) are: H10, 6.32 ppm (s, W_H = 3.0 Hz); H7, 4.90 ppm (dt, J_{vic} = 8.2, 6.2 Hz; J_{lr} = 1.6 Hz); H8eq, 2.31 ppm (ddd, J_{gem} = 14.0 Hz; J_{vic} = 6.2 Hz; $J_{H8e-H10e}$ = 1.6 Hz); H8ax, 2.08 ppm (dd, J_{gem} = 14.0 Hz; J_{vic} = 8.2 Hz). The presence of the long range coupling between H10 and H8 and the *S* configuration require a β half-chair conformation for the A ring.

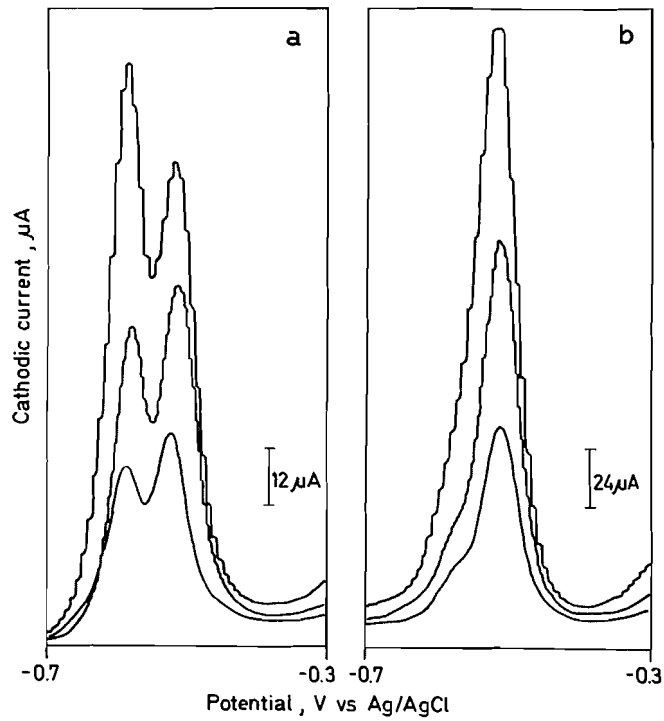

FIG. 1. Differential pulse polarograms of (*a*) 10(*R*)-methoxydaunorubicin (**V**) (3.3 × 10^{-5}*M*) and (*b*) 10(*S*)-methoxydaunorubicin (**VI**) (3.2 × 10^{-5} *M*), pH 7.1 in phosphate buffer at 37.5°C, ν = 1.33 mV/s. The drop time values are 1.4, 3, and 6 s for the lower, middle, and top curve, respectively.

10(R)-Azidodaunomycinone (XIII)

The loss of the azido group upon reductive activation of **XIII** is fast and even at the fastest drop time, 1.4 s, used in the present study the first peak of the polarogram is small. The prominent second peak is attributed to the reversible reduction of the reaction product, the daunomycinone.

Discussion

The reactivity towards reductive cleavage of a glycosidic bond and a benzylic bond in general on ring A of the anthracyclines could in principle depend, when all other electronic factors are the same, upon the configuration of neighbouring chiral centers and/or the conformation of the ring itself. We

[1]The nmr data are in agreement with those obtained in ref. 24, from University of Milan.

Can. J. Chem. Downloaded from www.nrcresearchpress.com by 210.87.254.42 on 09/06/12
For personal use only.

Can. J. Chem. Downloaded from www.nrcresearchpress.com by 210.87.254.42 on 09/06/12
For personal use only.

must note that the most stable conformation could also be determined by existing configurational features. We know for instance that the enantiomeric 10(*R*)- and 10(*S*)-methoxydaunorubicins adopt two different half-chair conformations for the A ring and that the reductive splitting of the glycosidic bond is observed only in the case of the 10(*R*) enantiomer. Thus the conformational features of the alicyclic ring must be determining the fate of the intermediate free radical or ion formed upon reduction of the antibiotics, assuming that the same conformation is retained in the reduced intermediate. It is well documented (25–29) that the heterolytic and/or homolytic fission is favoured when the bond undergoing cleavage can assume near *coplanarity* with the *adjacent semioccupied* p *orbital*, an *unoccupied non-bonding orbital* or *an occupied* π *orbital*. We have shown (30) that the theoretical rationalization of such an effect, the *stereoelectronic effect*, is based on the concept of conjugative delocalization. The extent of the delocalization is a function of the dihedral angle θ between the C—X bond being broken or formed and the orbital of π symmetry on the atom adjacent to the reaction center.

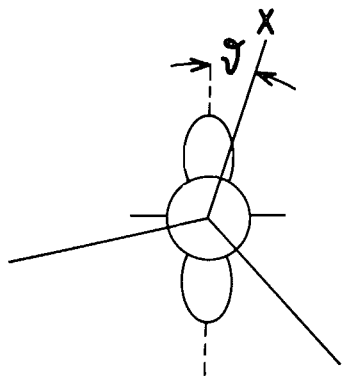

The interaction deemed to be important in determining the reactivity of the glycosidic linkage(s) (benzylic in general) in the anthracyclines radical anion is a conjugative delocalization between the doubly-occupied *p* orbital on C6a or C10a and the antibonding orbital of the C—X bond (p-σ^*_{C-X}) of the reaction center(s) C7 and/or C10. Resonance forms of the semiquinone for the C7 and C10 reaction centers can be represented as

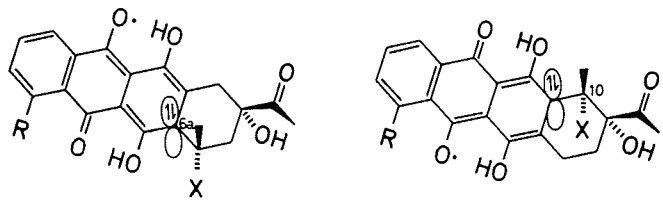

As we have anticipated the p-σ^*_{C-X} interaction will be dihedral angle dependent with the value of θ being determined by the conformation of the alicyclic cyclohexenic A ring. In most of the anthracyclines so far reported the A ring has a half-chair form. It should, however, be emphasized that in the cyclohexene derivatives the conformational energy difference between the half-chair and the (skew) boat form is relatively small (ca. 2–4 kcal/mol) (31) and that small structural changes can easily alter the ring shape. Furthermore a β half-chair conformation is possible as seen in the case of the 10(*S*)-methoxydaunorubicin.

The different conformations adopted by the enantiomeric 10(*R*) (**V**) and 10(*S*)-methoxydaunorubicin (**VI**) serve to illustrate this point.

The Newman projections along the C7—C6a bond help to visualize the extent of the interaction responsible for the different reactivity.

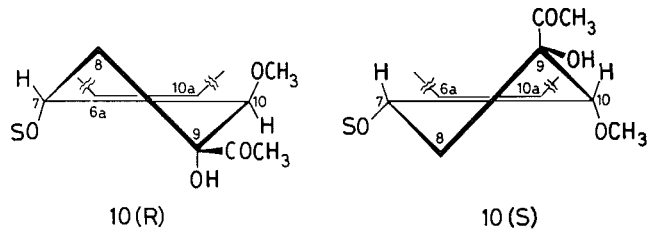

In 10(*R*) because of the small dihedral angle ($\theta \leq 15°$) the conjugative delocalization (partial developing overlap) is expected to be effective and substantially contribute to the driving force of the reaction. On the other hand, because of the larger value of θ ($\geq 45°$) in 10(*S*), it is anticipated that the interaction is much less effective and the glycosidic bond more stable.

It is worth pointing out that the same rationale would apply whether the reductive deglycosidation mechanism is ionic (two-electron reduction) or free radical (one electron) in nature.[2]

Admittedly the extent of the interaction is expected to be energetically different for the free radical and the ionic intermediate but the magnitude of the interaction in 10(*R*) would still be sufficiently different from that in 10(*S*) to cause the observed reactivity pattern.

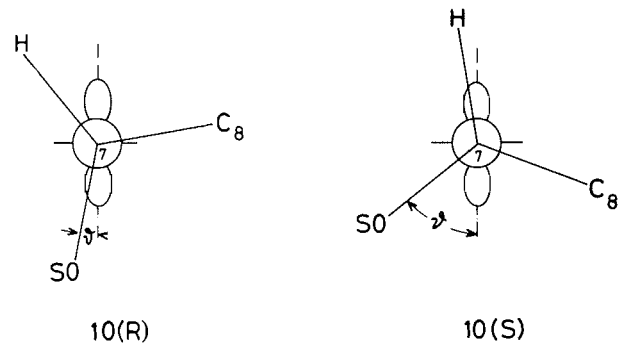

Another point deserves further comments. The C10—OMe bond in 10(*R*) is *trans*-diaxial with respect to the labile glycosidic bond and forms the same dihedral angle ($\theta \leq 15°$) with the π-type orbital(s) of the B ring. However, the stability of the CH_3O—C bond is not completely surprising in view of the fact that the methoxyl is not a good leaving group when compared to the sugar moiety. This is also confirmed by the stability towards reductive elimination of the OH and CH_3O groups in the aglycones. Indeed the differential pulse polarograms (see results) of the 10(*R*)-methoxydaunomycinone (**VII**) and daunomycinone (**XI**) show only one peak, corresponding to a reversible electrochemical reduction of the chromophore not followed by elimination of CH_3O^- or OH^-.

[2]It is a matter of current debate whether the electrochemical reduction intermediate is a radical ion, i.e., semiquinone or the dianion dihydroquinone. While the pH dependence of the half-wave potentials seems to indicate that two electrons – two protons are involved in each step of the E.C.E. process (21), the fact that the semiquinone is reported to form easily in multiple enzymatic and esr experiments (32) suggests that the first peak in the cyclic voltammograms of Rao *et al.* (21) is actually the one electron reduction to semiquinone (33).

Can. J. Chem. Downloaded from www.nrcresearchpress.com by 210.87.254.42 on 09/06/12
For personal use only.

*4-Demethoxy-6-deoxydaunorubicin (**IV**) and 4-demethoxy-11-deoxydaunorubicin (**III**)*

The stability of the glycosidic linkage in the 6-deoxy derivative **IV** further illustrates the reactivity dependence on the conformation. As we have noted the removal of the OH on C6 profoundly affects the conformation of the A ring which changes from the more common α half-chair to the β form. The 11-deoxy analogue **III**, on the other hand, maintains the α half-chair form and easily undergoes reductive splitting of the glycosidic bond. The same arguments we have used before nicely rationalize the observed results.

*10(S)-Acetoxydaunomycinone (**VIII**) vs. 10(S)-methoxydaunomycinone (**IX**)*

Although these two compounds are characterized by the same chirality at C10 their reactivity towards reductive elimination is strikingly different as the former compound, in contrast with the 10(*S*)-methoxydaunomycinone, easily eliminates the acetoxy group yielding the daunomycinone. In both compounds the A ring has a β half-chair conformation and therefore the dihedral angle θ has the same value. However, as the elimination occurs only in the case of the 10-acetoxydaunomycinone and as the resonance stabilized acetoxy is a better leaving group than the methoxy, we must conclude that the leaving group properties are also important in the deglycosidation reaction.

*10(R)-Azidodaunomycinone (**XIII**) vs. 10(R)-methoxydaunomycinone (**VII**)*

This is a particularly nice example of how the nature of the leaving group and *not* necessarily the configuration determines the reactivity of the bond on the benzylic position(s). Indeed, although both the conformation and configuration are the same in the two compounds, only the azido group is easily eliminated because of its better leaving group properties.

Kinetic considerations

Accurate values for the rate constants of the irreversible chemical reaction of deglycosidation in the E.C.E. process are difficult to obtain because of the heterogeneous nature of the reaction and the complicating absorption phenomena at the electrode. A qualitative comparison can, however, be made based on the values of the relative ratio of the first to the second peak at the same drop time. As the drop time increases the time available for the chemical reaction increases and the two peaks are more easily distinguishable (Fig. 1*a*). Then if we take the longest drop time, i.e. 6 s, we note that the ratio increases (0.84; 1.2; 2.2) along the series 10(*R*)-methoxydaunorubicin (**V**), daunorubicin (**I**), 4-demethoxy-11-deoxydaunorubicin (**III**) and that must correspond to an increase in the stability of the glycosidic bond. We can not invoke conformational effects to rationalize the trend as the three above compounds adopt the same half-chair conformation for the A ring. Rather, electronic effects must be determining the stability of the intermediate glycoside semiquinone. The removal of electron-donating groups such as OCH_3 and OH results in an increased stability of the radical anion and this in turn translates into a lower reactivity of the glycosidic bond. For this series the results seem to indicate that the deglycosidation reaction is under thermodynamic control. An extension of this rationalization would require that the reactivity of the 4-demethoxy-6-deoxydaunorubicin should be comparable with that of the 11-deoxy analogue. We have already seen that the two daunorubicins differ by the conformation of ring A and that unfavourable stereoelectronic effects reduce even further the reactivity of **IV**.

Conclusion

The compounds reported in Chart 1 can be divided into two classes. For **I**, **II**, **III**, **V**, **IX**, and **XIII**, a combination of small dihedral angle (**I**, **II**, **III**, **V**) and good leaving group properties (**IX**, **XIII**) contribute to the lability of the benzylic bond(s). On the other hand, **IV**, **VI**, **VII**, **VIII**, and **XI**, because of either a large dihedral angle (**IV**, **VI**) or the nature of the leaving group (CH_3O; HO), are stable towards reductive splitting. The evidence presented so far seems to establish that the reactivity of the groups on the benzylic C7 and C10 centers of the anthracyclines is under stereoelectronic control. It is therefore not possible to predict the reactivities of such centers by referring only to their configuration as the conformational requirements are clearly a key factor. As the bond-making and bond-breaking processes in enzyme catalyzed reactions are generally fast, we may expect that even small energy barriers of conformational origin can become significant and often rate determining and the stereoelectronic effects would also play an important role for the anthracyclines *in vivo* enzyme mediated reactions.

Finally, we would like to emphasize that although the understanding of the electrochemical behavior of the anthracyclines is *per se* important, their redox properties should not be dissociated from conformational considerations when trying to predict the reactivities of their intermediates.

Experimental

Materials and methods

All the compounds used in the present study were synthesised in our laboratories. They were purified by crystallization and/or semi-preparative HPLC on reverse phase Micro Pack MCH-10 column (250 × 8 mm) eluted (8 mL/min) with a H_2O–ACN mixture (69:21) buffered at pH 2.

The differential pulse polarograms were recorded on a Metrohom E 506 polarograph equipped with a dropping mercury electrode (DME). A three electrode system was used with the reference electrode being an Ag/AgCl electrode and the auxiliary electrode a platinum wire. The measurements were carried out in a 20 ml thermostated cell (37.5°C) flushed with prepurified N_2 (10 min) and kept during the experiments under a positive pressure of nitrogen. The concentrations of the solutions were in the range $3-5 \times 10^{-5}$ *M* depending on the solubility of the individual compounds. The solutions were buffered at pH 7.1 with 0.01 *M* phosphate buffer, 0.1 *M* KCl, and 0.004% triton X-100. In the case of the aglycones, because of their lower solubility it was necessary to add up to 33% of acetonitrile. The identification of the reduction products was made on the basis of the peak potential (E_p) and HPLC retention time values which were compared to those of authentic samples. For the E.C.E. processes the product identification was performed in two steps. For the product corresponding to the first E.C.E. stage a small scale reduction was carried out at a fixed potential ca. 50 mV less cathodic than the peak maximum in order to avoid a further reduction to hydroquinone. The solutions were then extracted with methylene chloride, the organic layer separated, and after drying (Na_2SO_4) the solvent was removed under vacuum. The residue was taken up in the proper solvent and an aliquot was analyzed by HPLC on a Brownlee RP8C column (250 × 4 mm) using the same above mentioned eluent. The remainder of the solution was evaporated to dryness and used for the second step of the reduction at a fixed potential corresponding to the second peak maximum. When the current dropped to ca. 5% of the starting value the hydroquinone formed was reoxidized to the quinone by sweeping the potential back to 0 V. The solution was extracted and analyzed as described above. The structure assignments were also confirmed by mass spectrometry and ^{1}H-nmr spectroscopy. The cyclic voltammetry was performed on a BAS CV-1B apparatus. The ^{1}H-nmr spectra were recorded on a Varian XL-200 spectrometer in the appropriate solvent (D_2O, $CDCl_3$,

DMSO-d_6) having TMS as internal standard. A Varian MAT 311A mass spectrometer operating on F.D. mode was used to obtain the mass spectra.

1. A. DI MARCO, F. ARCAMONE, and F. ZUNINO. *In* Antibiotics III. Mechanism and action of antimicrobial and antitumor agents *Edited by* J. W. Corcoran and F. E. Manh. Springer, New York. 1975 pp. 101–128.
2. F. ARCAMONE. *In* Topics in antibiotic chemistry. *Edited by* P. Sammes. Wiley, New York. 1978. pp. 102–239.
3. F. ARCAMONE. *In* Doxorubicin. Anticancer antibiotics. Academic Press. 1981.
4. S. NEIDLE. *In* Topics in antibiotic chemistry Vol. 2. Part D. *Edited by* P. Sammes. Ellis Horwood, Chichester, England. 1978. p. 240.
5. S. NEIDLE. Prog. Med. Chem. **16**, 196 (1979).
6. H. BERG and K. ECKARDT. Z. Naturforsch. B**25**, 362 (1970).
7. J. W. LOWN, S. SIM, K. C. MAJUMDAR, and R. CHANG. Biochem. Biophys. Res. Commun. **76**, 705 (1977).
8. B. K. SINHA. Chem. Biol. Interact. **30**, 67 (1980).
9. R. GOLDMAN, T. FACCHINETTI, D. BACH, A. RAZ, and M. SHINITZKY. Biochem. Biophys. Acta, **512**, 254 (1978).
10. W. S. THAYER. Chem. Biol. Interact. **19**, 265 (1977).
11. C. E. MYERS, W. P. MCGUIRE, R. H. LISS, I. IFRIM, K. GROTZINGER, and R. C. YOUNG. Science, **197**, 165 (1977).
12. N. R. BACHUR, S. L. GORDON, and M. V. GEE. Cancer Res. **38**, 1745 (1978).
13. S. PAN and N. R. BACHUR. Mol. Pharmacol. **17**, 95 (1980).
14. H. H. DOROSHOW and J. REEVES. Biochem. Pharm. **30**, 259 (1980).
15. B. K. SINHA and R. H. SIK. Biochem. Pharmacol. **29**, 1867 (1980).
16. B. K. SINHA and J. L. GREGORY. Biochem. Pharmacol. **30**, 2626 (1981).
17. H. W. MOORE and R. CZERNIAK. Medicinal Res. Rev. **1**, 249 (1981).
18. T. T. OKI, T. KOMIYAMA, H. TONE, and T. INUI. J. Antiobiot. **30**, 613 (1977).
19. N. R. BACHUR and M. V. GEE. J. Pharmacol. Exp. Ther. **197**, 681 (1976).
20. N. R. BACHUR, S. L. GORDON, and M. V. GEE. Mol. Pharmacol. **13**, 901 (1977).
21. G. M. RAO, J. W. LOWN, and J. A. PLAMBECK. J. Electrochem. Soc. **125**, 534 (1978).
22. S. PENCO, F. GOZZI, A. VIGEVANI, M. BALLABIO, and F. ARCAMONE. Heterocycles, **13**, 281 (1979).
23. S. C. BROWN, P. A. KOLLMAN, and P. K. WEINER. Biochem. Biophys. Acta, **717**, 49 (1982).
24. R. MONDELLI. Private communication.
25. V. MALATESTA, R. D. MCKELVEY, B. W. BABCOCK, and K. U. INGOLD. J. Org. Chem. **44**, 1872 (1979).
26. V. MALATESTA and K. U. INGOLD. J. Am. Chem. Soc. **103**, 609 (1981).
27. V. MALATESTA and J. C. SCAIANO. J. Org. Chem. **47**, 1455 (1982).
28. D. GRILLER, J. A. HOWARD, P. R. MARIOTT, and J. C. SCAIANO. J. Am. Chem. Soc. **103**, 619 (1981).
29. P. DESLONGCHAMPS. Heterocycles, **7**, 1271 (1977).
30. A. R. GREGORY and V. MALATESTA. J. Org. Chem. **45**, 122 (1980).
31. E. L. ELIEL, N. L. ALLINGER, S. J. ANGYAL, and G. A. MORRISON. *In* Conformational analysis. Interscience Publ., New York. 1965. p. 484.
32. J. W. LOWN and H. H. CHEN. Can. J. Chem. **59**, 3212 (1981).
33. D. L. KLEYER and T. H. KOCH. J. Am. Chem. Soc. **105**, 2504 (1983); **105**, 5911 (1983).

Can. J. Chem. Downloaded from www.nrcresearchpress.com by 210.87.254.42 on 09/06/12
For personal use only.

Viscosity data of binary mixtures: ethyl acetate + cyclohexane, + benzene, + toluene, + ethylbenzene + carbon tetrachloride, and + chloroform at 303.15 K

SHANTILAL OSWAL[1] AND MANAPRAGADA V. RATHNAM
Department of Chemistry, South Gujarat University, Surat-395007, India

Received November 11, 1982[2]

SHANTILAL OSWAL and MANAPRAGADA V. RATHNAM. Can. J. Chem. **62**, 2851 (1984).

Viscosities have been determined for six binary mixtures of ethyl acetate with cyclohexane, benzene, toluene, ethylbenzene, carbon tetrachloride, and chloroform at 303.15 K. Excess viscosities, η^E, and excess free energies of activation of flow, ΔG^{*E}, were calculated from these experimental data. Excess free energies of activation of flow, ΔG^{*E}, are large negative values for the mixture ethyl acetate + cyclohexane. The negative values of ΔG^{*E} are reduced when benzene, toluene, ethylbenzene, and carbon tetrachloride is used instead of cyclohexane in the binary mixture. High positive values of ΔG^{*E} are found for the mixture ethyl acetate + chloroform.

SHANTILAL OSWAL et MANAPRAGADA V. RATHNAM. Can. J. Chem. **62**, 2851 (1984).

On a mesuré les viscosités de six mélanges binaires de l'acétate d'éthyle avec le cyclohexane, le benzène, le toluène, l'éthylbenzène, le tétrachlorure de carbone et le chloroforme, à 303,15 K. A partir de ces données, on a calculé les viscosités en excès, η^E, et les énergies libres d'activation d'écoulement en excès, ΔG^{*E}. Les valeurs de ΔG^{*E} sont élevés et négatives pour le mélange acétate d'éthyle + cyclohexane. Si on remplace le cyclohexane par du benzène, du toluène, de l'éthylbenzène ou du tétrachlorure de carbone, les valeurs négatives du ΔG^{*E} sont réduites. Dans le cas du mélange d'acétate d'éthyle avec le chloroforme, les valeurs du ΔG^{*E} sont positives et élevées.

[Traduit par le journal]

Introduction

Excess thermodynamic functions have been used as a qualitative and quantitative guide to predict the extent of complex formation in binary liquid mixtures of nonelectrolytes (1–4). If the viscosity data for the mixtures could be obtained as a function of composition the existence or nonexistence of the specific interactions in them could be indicated by estimating the strength of interactions (5–7). A number of workers (8–11) have utilised the direct approach developed by Grunberg and Nissan (6) and Katti and Chaudri (7) to estimate the strength of interactions in binary mixtures of nonelectrolytes from viscosity data. In continuation of our work (12–15) on solution properties we report in this paper the viscosity measurements for the study of molecular interactions of six binary mixtures of cyclohexane, benzene, toluene, ethylbenzene, carbon tetrachloride, and chloroform in ethyl acetate at 303.15 K.

Experimental

Viscosity was measured with a modified Ubbelohde viscometer (16). The time of efflux of a constant volume of liquid through the capillary was measured with the help of a precalibrated RACER stopwatch correct to ±0.1 s. The viscometer was always kept in a vertical position in a water thermostat at 303.15 ± 0.02 K. The efflux time for water at 303.15 K was about 215 s. Viscosity was calculated from the measured efflux time (t) using the relation [1].

$$[1] \quad \eta = \rho(At - B/t)$$

where ρ is the density and A and B are characteristic constants of the viscometer, which were determined by taking water and benzene as the calibrating liquids. The correctness of these constants was checked by comparing the experimentally determined viscosities for cyclohexane, ethyl acetate, toluene, carbon tetrachloride, ethylbenzene, chloroform with corresponding literature values (17, 18) (Table 1). The agreement was within ±0.2%. Densities of mixtures needed to calculate viscosities of mixtures were taken from earlier reported data (15, 19).

Materials and solutions

Ethyl acetate (BDH Analar), cyclohexane (BDH Analar), benzene (BDH Analar), toluene (Analar), ethylbenzene (Fluka AG), carbon tetrachloride (BDH Spectroscopic), and chloroform (BDH Spectroscopic) were purified by standard procedure given by Riddick and Bunger (18). Ethyl acetate was fractionally distilled, stored over potassium carbonate for 15 days, and redistilled over phosphorous pentoxide before use. Cyclohexane was vigorously shaken with a mixture of concentrated nitric and sulphuric acids for 8 h at temperatures below 10°C, then washed repeatedly with distilled water, dried over calcium chloride, and fractionally distilled over sodium. Benzene and toluene were freed from thiophene by shaking with sulphuric acid, the samples so obtained were washed with water, followed by subsequent washings with sodium hydroxide and distilled water, dried thoroughly over anhydrous calcium chloride, and fractionally distilled thrice. Carbon tetrachloride was refluxed over alcoholic potassium hydroxide, washed with distilled water several times, dried over anhydrous calcium chloride, and fractionally distilled twice. Chloroform was shaken with concentrated sulphuric acid, then washed with dilute sodium hydroxide and with ice water, dried over potassium carbonate, and fractionally distilled twice. Ethylbenzene (Fluka AG) of purity greater than 99% was used as received. Purity of all these liquids was checked by measuring their densities and refractive indices at 303.15 K, which compared well with the literature data (17, 18) (Table 1).

Results and discussion

Viscosity (η) data at 303.15 K over the entire range of composition from 0.0 to 1.0 mole fractions were measured for binary mixtures ethyl acetate + cyclohexane, + benzene, + toluene, + ethylbenzene, + carbon tetrachloride, and + chloroform.[3] The excess viscosities η^E calculated from the relation [2]

$$[2] \quad \eta^E = \eta_{12} - [X_1\eta_1 + X_2\eta_2]$$

over the entire range of composition were fitted to the following empirical equation [3]

[1]To whom all correspondence should be addressed.
[2]Revision received April 3, 1984.

[3]All numerical results are available, at a nominal charge, from the Depository of Unpublished Data, CISTI, National Research Council of Canada, Ottawa, Ont., Canada K1A 0S2.

Can. J. Chem. Downloaded from www.nrcresearchpress.com by 210.87.254.105 on 09/06/12
For personal use only.

TABLE 1. Physical properties of components in present work and in the literature at 303.15 K

Components	Density, ρ (g cm^{-3})		Refractive index n_D		Viscosity η (cp)	
	Experimental	Literature[a]	Experimental	Literature[a]	Experimental	Literature[a]
Ethylacetate	0.8885	0.8885	1.3680	1.3672	0.403	0.400
Cyclohexane	0.7693	0.7693	1.4207	1.4208	0.819	0.819
Benzene	0.8684	0.8685	1.4945	1.4947	0.560	0.562
Toluene	0.8577	0.8577	1.4911	1.4913	0.517	0.520
Ethylbenzene	0.8583	0.8583	1.4910	1.4905	0.593	0.590
Carbon tetrachloride	1.5748	1.5748	1.4550	1.4547	0.845	0.845
Chloroform	1.4706	1.4706	1.4400	1.4400	0.519	0.514

[a]References 17, 18.

TABLE 2. Parameters for least-squares fit of results by eq. [3] and standard deviation σ for excess viscosity data

System	A_0	A_1	A_2	$\sigma\times10^3$
Ethyl acetate + cyclohexane	−0.5757	0.3605	−0.2178	4.16
Ethyl acetate + benzene	−0.1214	0.0443	−0.0080	2.16
Ethyl acetate + toluene	−0.0211	0.0154	0.0233	1.57
Ethyl acetate + ethylbenzene	−0.0193	−0.0199	0.0238	1.77
Ethyl acetate + carbon tetrachloride	−0.2400	0.1188	−0.0631	3.40
Ethyl acetate + chloroform	0.2405	−0.1386	−0.0929	2.47

$$[3]\quad \eta^E = X_1X_2[A_0 + A_1(X_1 - X_2) + A_2(X_1 - X_2)^2]$$

where 1, 2 represent the pure components, 12 their mixture, and A_0, A_1, and A_2 are constants. The method of least-squares was used to determine the values of the constants. The values of these constants along with the standard deviation σ defined by

$$\sigma^2 = \Sigma\{\eta^E_{exp} - \eta^E_{cal}\}/(n - 3)$$

are given in Table 2, where n is the total number of measurements. Excess free energies of activation of flow, ΔG^{*E}, are used to estimate the strength of interactions in the present study, using the relation [4]:

$$[4]\quad \Delta G^{*E} = RT[\ln \eta_{12}V_{12} - (X_1 \ln \eta_1V_1 + X_2 \ln \eta_2V_2)]$$

where V_{12}, V_1, and V_2 are the molar volumes of the mixture and of the pure components, R is the gas constant, and T is the absolute temperature. The results of ΔG^{*E} are represented graphically in Fig. 1. Memmi and Piekarski (11) have measured viscosity for ethyl acetate + cyclohexane mixtures at 298 K. Their value of Grunberg and Nissan (6) parameter $d = -0.82$ at $X = 0.5$ estimated from graph is in quite good agreement with ours (−0.83). It is observed that there is a large negative deviation from rectilinear dependence of viscosity on mole fraction for the mixture ethyl acetate + cyclohexane. The negative deviation is sufficiently reduced when cyclohexane is replaced either by benzene, toluene, ethylbenzene, or carbon tetrachloride. The large positive deviation is observed for the ethyl acetate + chloroform mixture.

It is instructive to compare the present ΔG^{*E} data with the few selected binary mixtures already reported in literature.

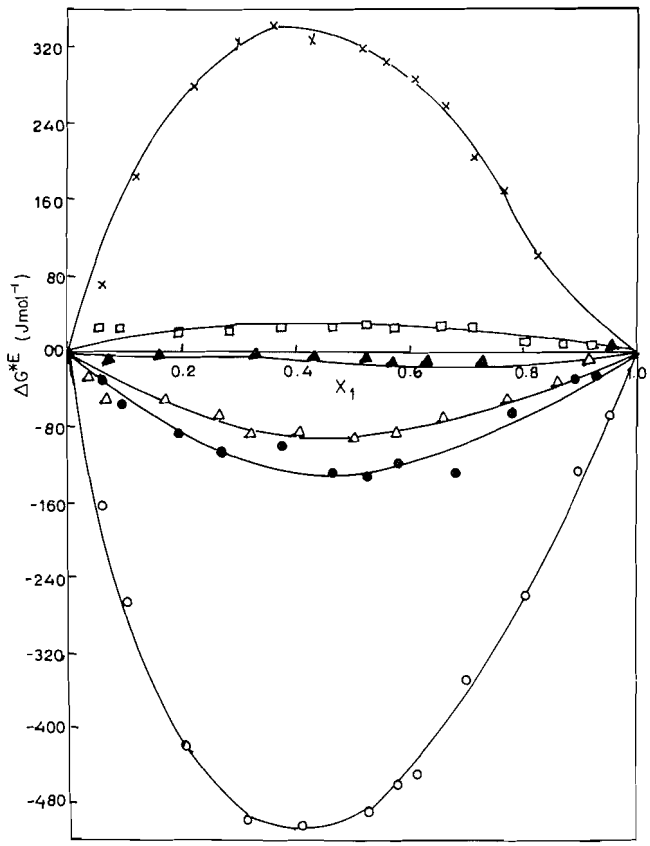

FIG. 1. Excess free energy of activation of flow ΔG^{*E} for ethyl acetate + cyclohexane ○; + benzene ●; + toluene △; + ethylbenzene △; + carbon tetrachloride □; + chloroform ×.

These are summarised in Table 3. Ethyl acetate + cyclohexane mixture has large negative ΔG^{*E} values. This behaviour is characteristic of mixtures in which dispersion forces are dominant, e.g., benzene + cyclohexane (20), cyclohexane + *n*-pentane (8), benzene + *n*-hexane (8), acetone + cyclohexane (9), methylethylketone + cyclohexane (9) and benzene + ethylene dichloride (5).

For mixtures ethyl acetate + benzene + toluene, + ethyl benzene, we observe less negative ΔG^{*E} values than that of ethyl acetate + cyclohexane. This behaviour is similar to that observed for the mixtures acetone + benzene (9), methylethylketone + benzene (9), methylethylketone + *p*-xylene (9), and acetone + *p*-xylene (9).

We observe large positive ΔG^{*E} values for the ethyl acetate + chloroform mixture, similar to those of chloroform + acetone (5), chloroform + dioxane (5, 8), and chloroform +

Can. J. Chem. Downloaded from www.nrcresearchpress.com by 210.87.254.105 on 09/06/12
For personal use only.

TABLE 3. Comparison of excess free energy of activation of flow (ΔG^{*E}) of several binary mixtures, X_1 is the mole fraction of first component

System	Temperature (K)	X_1	ΔG^{*E} (J mol^{-1})	Reference
Benzene + cyclohexane	298	0.5490	−408.9	20
Cyclohexane + *n*-pentane	298	0.6163	−397	8
Benzene + *n*-hexane	293	0.5799	−367	8
Acetone + cyclohexane	307.2	0.5299	−242	9
EMK + cyclohexane	307.2	0.4975	−320.8	9
Benzene + ethylene dichloride	298	0.4	−236	5
Acetone + benzene	307.2	0.4938	−66.6	9
Benzene + chloroform	298	0.4	7.3	5
EMK + benzene	307.2	0.5084	−115.3	9
EMK + *p*-xylene	307.2	0.5326	64.0	9
Acetone + *p*-xylene	307.2	0.5768	231.2	9
Chloroform + dioxane	298	0.4	367.7	5
Chloroform + dioxane	303	0.5194	438.7	8
Chloroform + acetone	298	0.4	337.2	5
Chloroform + acetone	303	0.5487	499	8
Chloroform + diethyl ether	303	0.5582	529.5	8
Ethyl acetate + cyclohexane	303	0.5224	−485.5	This work
Ethyl acetate + benzene	303	0.5281	−123.9	This work
Ethyl acetate + toluene	303	0.5183	−3.4	This work
Ethyl acetate + ethylbenzene	303	0.5354	33.4	This work
Ethyl acetate + carbon tetrachloride	303	0.5007	−97	This work
Ethyl acetate + chloroform	303	0.5145	320.8	This work

diethyl ether (8), indicating hydrogen bonding between unlike molecules.

Acknowledgement

The authors thank the Head, Department of Chemistry, South Gujarat University, for providing necessary facilities.

1. R. BATTINO. Chem. Rev. **71**, 5 (1971).
2. J. S. ROWLINSON. Liquid and liquid mixtures. Butterworths, London. 1969.
3. I. PRIGOGINE. The molecular theory of solutions. North Holland Publ. Co. 1957.
4. K. N. MARSH. Ann. Rep. C. Chem. Soc. London, 101 (1980).
5. R. J. FORT and W. R. MOORE. Trans. Faraday Soc. **62**, 1112 (1966).
6. L. GRUNBERG and A. H. NISSAN. Nature, London, **164**, 799 (1949).
7. P. K. KATTI and M. CHAUDRI. J. Chem. Eng. Data, **9**, 442 (1964).
8. R. K. NIGAM and B. S. MAHL. Indian J. Chem. **9**, 1255 (1971).
9. R. R. YADAVA and S. S. YADAVA. Indian J. Chem. **20**A, 221 (1981).
10. R. RIGGIO, J. F. RAMOS, M. H. UBELA, and J. A. ESPINDOLA. Can. J. Chem. **59**, 3305 (1981).
11. A. MEMMI and S. PIEKARSKI. J. Chem. Res. **5**, 98 (1982).
12. D. D. DESHPANDE and S. L. OSWAL. J. Chem. Thermodyn. **7**, 155 (1975).
13. S. L. OSWAL and D. D. DESHPANDE. Indian J. Chem. **16**A, 798 (1978).
14. S. L. OSWAL. Indian J. Chem. **18**A, 353 (1979).
15. S. L. OSWAL and M. V. RATHNAM. J. Indian Chem. Soc. **61**, 269 (1984).
16. L. UBBELOHDE. Ind. Eng. Chem. Anal. Ed. **9**, 85 (1937).
17. R. C. WEAST. Handbook of chemistry and physics. The Chemical Rubber Co., OH. 1971.
18. J. R. RIDDICK and W. B. BUNGER. Organic solvents physical properties and methods of purification. Wiley Interscience, New York. 1970.
19. S. L. OSWAL and K. G. PATHAK. Indian J. Chem. **21**A, 712 (1982).
20. L. GRUNBERG. Trans. Faraday Soc. **50**, 1293 (1954).

Can. J. Chem. Downloaded from www.nrcresearchpress.com by 210.87.254.105 on 09/06/12
For personal use only.

Excess free energies of the Lennard–Jones (6:12) fluid

YOSHINORI ADACHI AND BENJAMIN C.-Y. LU
Department of Chemical Engineering, University of Ottawa, Ottawa, Ont., Canada K1N 9B4
AND
HIDEZUMI SUGIE
Center of Information Processing Education, Nagoya Institute of Technology, Nagoya, Japan

Received June 23, 1983[1]

YOSHINORI ADACHI, BENJAMIN C.-Y. LU, and HIDEZUMI SUGIE. Can. J. Chem. **62**, 2854 (1984).

The umbrella sampling technique advanced by Torrie and Valleau for estimating free energies was followed in this work for calculating the excess Helmholtz free energy for the Lennard–Jones (6:12) fluid at 48 points. These values were combined with data available in the literature for the establishment of tables of excess Helmholtz and Gibbs free energies over wide ranges of T^* (0.50 to 2.75) and ρ^* (0.05 to 0.80). The values of excess Helmholtz free energy were used to develop a correction function for modifying the second-order perturbation term of the Barker–Henderson perturbation treatment with its subsequent application to the calculation of compressibility factor, vapor–liquid coexistence curve of the Lennard–Jones (6:12) fluid, and Henry's constants for 26 systems.

YOSHINORI ADACHI, BENJAMIN C.-Y. LU et HIDEZUMI SUGIE. Can. J. Chem. **62**, 2854 (1984).

Dans le présent travail, on a fait appel à la technique de l'échantillonnage en ombrelle proposée par Torrie et Valleau pour évaluer les énergies libres en excès de Helmholtz pour le fluide de Lennard–Jones (6:12) à 48 points. On a combiné ces valeurs avec les données disponibles dans la littérature pour établir des tables d'énergie libre en excès de Helmholtz et de Gibbs pour des valeurs de T^* allant de 0,50 à 2,75 et pour des valeurs de ρ^* s'étalant de 0,05 à 0,80. On a utilisé les valeurs d'énergie libres en excès de Helmholtz pour développer une fonction de correction en vue de modifier le terme de perturbation de second ordre du calcul de perturbation de Barker–Henderson; on a éventuellement appliqué cette expression modifiée au calcul du facteur de compressibilité, à la courbe de coexistence vapeur–liquide du fluide de Lennard–Jones (6:12) et aux constantes d'Henry de 26 systèmes.

[Traduit par le journal]

Can. J. Chem. Downloaded from www.nrcresearchpress.com by 210.87.254.6 on 09/06/12
For personal use only.

Introduction

Torrie and Valleau (1, 2) have proposed the umbrella sampling method for estimating free energy of a fluid. This Monte Carlo technique involves the use of arbitrary sampling distribution chosen to facilitate the estimate instead of using the Boltzmann-weighted sampling distribution. It has been successfully applied by these authors to the Lennard–Jones (6:12) fluid in a wide range of temperature including part of the vapor–liquid coexistence region, using a small number of particles. Nevertheless, the free energy values reported by these authors as well as those from other Monte Carlo methods are still very fragmentary for the fluid. Extrapolation to the regions of low temperature and high density presents a serious problem due to the sensitivity of the numerical values to the variation of the density.

In this work, the excess Helmholtz free energy (ΔF^E) values for the Lennard–Jones (LJ) fluid were selectively calculated by means of the umbrella sampling method at six reduced temperature T^* ($= kT/\epsilon$) conditions and eight reduced density ρ^* ($N\sigma^3/v$) conditions for a total of 48 points. In our calculation, a slight modification was made in the umbrella sampling method on the weighting function. These values together with the values reported in the literature were correlated by the Lagrange interpolation method, resulting in a comprehensive table of 416 values of $\Delta F^E/NkT$. The LJ fluid was selected because it resembles the properties of the real fluid argon. Furthermore, the calculated results are useful to the extension of the calculation using the Kihara potential. In addition, the excess Gibbs free energy (ΔG^E) values were calculated over the same ranges of T^* and ρ^*.

The Barker–Henderson perturbation theory has been frequently used in chemical engineering calculations. In the calculation of vapor–liquid equilibrium values, Rogers and Prausnitz in 1971 (3) applied the theory to binary mixtures of spherical-type molecules at pressures up to the critical; Uno *et al.* (4) in 1976 applied the theory to normal fluid mixtures; and Masuoka *et al.* (5, 6) in 1977 applied the theory to systems containing a non-polar substance and a polar substance including ammonia. Other applications include the calculation of Henry's constant for normal fluids (7) and the calculation of *PVT* relations for non-polar and polar substances (8). All these applications involved the second-order term in the perturbation expansion. As an application of the excess Helmholtz free energy table, an effort was made to improve the second-order perturbation term of the Barker–Henderson treatment (9, 10) obtained from the macroscopic compressibility approximation (9). This modification was made by multiplying the term with a correction function in terms of ρ^*. The values of $\Delta F^E/NkT$ and compressibility factor Z calculated by means of the modified expression were compared with those obtained from other methods to verify the modification. An attempt was made to establish the limitations of the applicability of the LJ fluid by comparing the calculated Z values with those correlated by Lee and Kesler (11). The modified expression was also used to calculate the coexisting vapor–liquid curve for the LJ fluid and Henry's constants for 26 systems.

Calculation of excess free energies

According to the umbrella sampling method advanced by Torrie and Valleau (1, 2), the Helmholtz free-energy difference between the system of interest with internal energy of $U(q_N)$ at temperature T and a reference system with internal energy $U_0(q_N)$ at temperature T_0 is given by:

$$[1] \quad \frac{F}{kT} - \frac{F_0}{kT_0} = -\ln \int_{-\infty}^{\infty} f_0(\Delta U^*) \exp(-\Delta U^*)\, d\Delta U^*$$

[1] Revision received May 1, 1984.

Can. J. Chem. Downloaded from www.nrcresearchpress.com by 210.87.254.6 on 09/06/12
For personal use only.

where U^* is the reduced energy U/kT, $\Delta U^* = (U/kT - U_0/kT_0)$, and $f_0(\Delta U^*)$ is the probability density of ΔU^* in the reference fluid. Because of the difficulty encountered in estimating $f_0(\Delta U^*)$ exp $(-\Delta U^*)$ by means of the conventional Boltzmann sampling, a suitable weighting function $w(q_N) = W(\Delta U^*)$ is chosen by Torrie and Valleau to favor those configurations with values of ΔU^* important to the integral in eq. [1]. The Boltzmann distribution exp $(-\beta U)$ is therefore replaced by a new distribution, $W(\Delta U^*)$ exp $(-\beta U)$. The probability density $f_0(\Delta U^*)$ can be recovered from the probability density of ΔU^* in the biased Monte Carlo experiment, $f_w(\Delta U^*)$, by reweighting:

$$[2] \quad f_0(\Delta U^*) = \frac{f_w(\Delta U^*)/W(\Delta U^*)}{\langle 1/W \rangle_w}$$

The expression $\langle\rangle_w$ denotes an ensemble average over the weighted chain of configuration. Torrie and Valleau (2) adjusted $W(\Delta U^*)$ by trial and error until $f_w(\Delta U^*)$ is as wide and uniform as possible, and named their technique "umbrella sampling" because of the requirement that the sampling distribution specified by W should cover the regions of configuration space relevant to two or more physical systems simultaneously.

In this work, a simpler method was found to obtain the weighting function. An exponential expression, C_1 exp $\{C_2(\Delta U^* - C_3)C_4\}$, was used to fit the quantity $f_0(\Delta U^*)$ and the weighting function was expressed by eq. [3].

$$[3] \quad W(\Delta U^*) = \exp\{-C_2(\Delta U^* - C_3)^{C_4}\}$$

Other than the selection of the weighting function, the umbrella sampling technique was followed for the determination of the difference of Helmholtz free energy of eq. [1] for the LJ fluid.

The calculation procedure for determining the parameters of the weighting function may be briefly outlined as follows:

(*1*) Obtain the unweighted distribution of ΔU^* by means of the Monte Carlo sampling method of Metropolis *et al.* (12) for 100 000 steps.

(*2*) Determine the four parameters by fitting the distribution obtained from step 1 using the expression of C_1 exp $\{C_2(\Delta U^* - C_3)^{C_4}\}$. The initial values of $C_1 = 0.2$, $C_2 = 0.2$ were used in the fitting procedure. The value of $C_4 = 2$ was fixed at this stage. The value of C_3 depends on the location of the peak of the distribution.

(*3*) Choose a value of ΔU_1^* to "cover" the exp $(-\Delta U^*)$ distribution which is estimated in step 2 by calculating C_1 exp $\{C_2(\Delta U^* - C_3)^{C_4}\}$ exp $(-\Delta U^*)$, and let $\Delta U_2^* = C_3$. The weighting function $W(\Delta U^*)$ is obtained as follows:

$$W(\Delta U^*) = \begin{cases} \exp\{-C_2(\Delta U^* - C_3)^{C_4}\} & \text{if } \Delta U_1^* < \Delta U^* < \Delta U_2^* \\ \exp\{-C_2(\Delta U_1^* - C_3)^{C_4}\} & \text{if } \Delta U^* < \Delta U_1^* \\ \exp\{-C_2(\Delta U_2^* - C_3)^{C_4}\} & \text{if } \Delta U_2^* < \Delta U^* \end{cases}$$

(*4*) Do 500 000 steps of umbrella sampling (Run I), and check the shape of the weighted distribution. If the shape of the weighted distribution is not sufficiently flat and not adequate to cover the range of the exp $(-\Delta U^*)$ distribution, modify the value of C_4 empirically. The value of C_4 is usually around 1.7 to 2.0.

(*5*) Repeat step 4 and do Run II etc.

Typical distribution functions for (U_6/kT) are depicted in Fig. 1 (top) in which $\rho^* = 0.85$, $T^* = 2.74$, and $N = 32$. These values are identical to those used in the illustration of Torrie and Valleau (ref. 2, Fig. 1). They were selected in this work to facilitate comparison. The values of the parameters C_2, C_3, and C_4 of the weighting function (eq [4]) are 0.1518, −147, and 1.7, respectively. In the calculation (Run I), $\Delta U_1^* = -161$ and

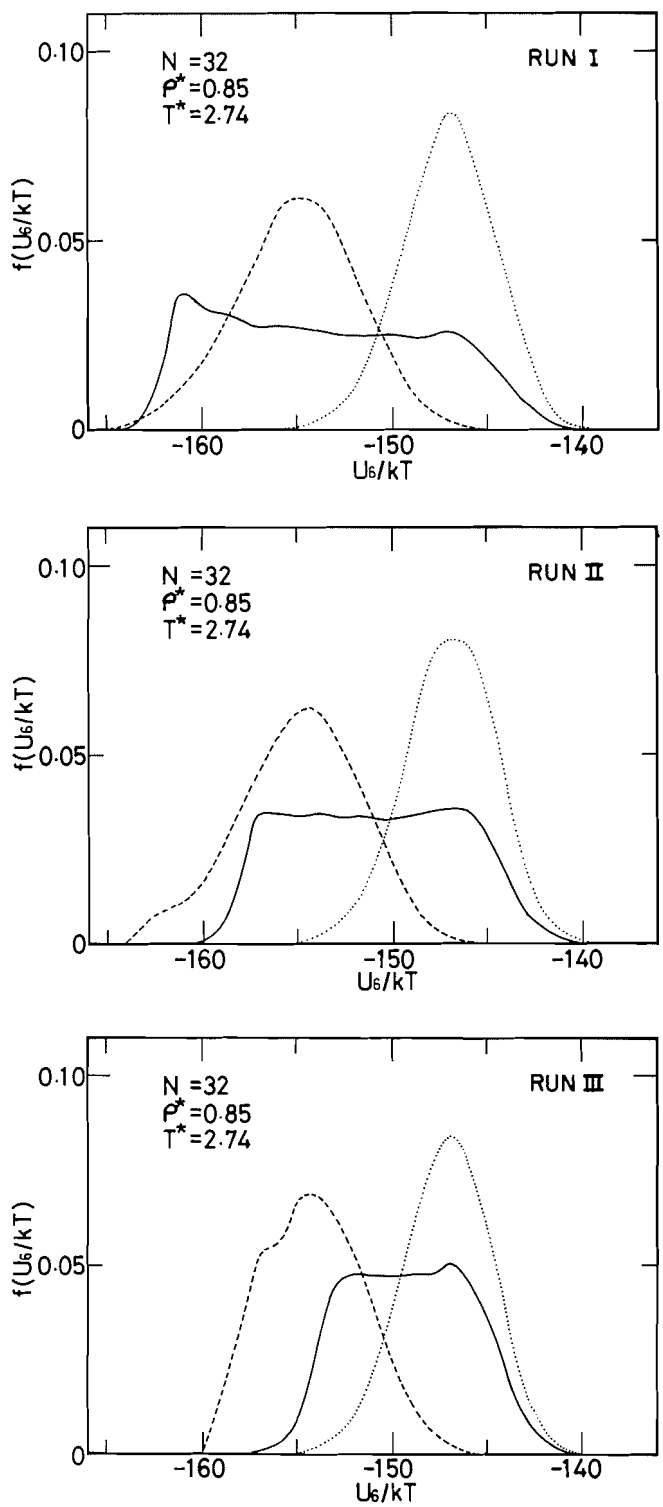

FIG. 1. Probability density distributions. Solid line (f_w): the biased probability density. Dotted line (f_0): the unbiased probability density obtained by reweighting f_w. Broken line: relative values of $f_0(U_6/kT)$ exp $(-U_6/kT)$ normalized to unity.

TABLE 1. Excess Helmholtz free energy, $\Delta F^E/NkT$, obtained from the umbrella sampling method for the Lennard–Jones fluid

	$\Delta F^E/NkT$ for $\rho^* =$							
T^*	0.1	0.2	0.3	0.4	0.5	0.6	0.7	0.8
0.501	−1.38	−2.37	−3.46	−4.50	−5.59	−6.65	−7.40	−7.86
0.7	−0.88	−1.56	−2.25	−2.92	−3.56	−4.14	−4.66	−4.82
0.885	−0.62	−1.09	−1.58	−2.02	−2.46	−2.85	−3.14	−3.18
1.002	−0.48	−0.88	−1.25	−1.67	−1.96	−2.24	−2.47	−2.46
1.261	−0.32	−0.61	−0.93	−1.12	−1.32	−1.48	−1.52	−1.46
1.511	−0.22	−0.43	−0.61	−0.76	−0.90	−0.95	−0.92	−0.76

$\Delta U_2^* = -147$ ($=C_3$).

In order to illustrate the effect of the proposed weighting function on the determination of $\Delta F/N\epsilon$ values, we have used the above system ($\rho^* = 0.85$, $T^* = 2.74$, and $N = 32$) and altered the value of ΔU_1^* from −161 to −157 and −153 for two additional runs (Run II and Run III of step 5) without changing the parameter values of the weighting function. The resulting weighted distributions are depicted in Fig. 1 (middle and lower boxes). The values of $\Delta F/N\epsilon$ obtained from these three runs are as follows:

Run	$\Delta F/N\epsilon$
I	−12.855
II	−12.848
III	−12.835

All three values are in good agreement with the value reported by Torrie and Valleau ($\Delta F/N\epsilon = -12.85 \pm 0.015$, ref. 2, Table II). In other words, the equilibrium value of $\Delta F/N\epsilon$ has not been significantly affected by the significant variation in the weighted distribution. This may come as a result of sufficient number of configurations, i.e., 500 000. It was observed that the $\Delta F/N\epsilon$ values obtained from Run I and Run II are usually very close to each other, and the weighted distributions of Run II appear to be adequate. In this work, the average values of the first two runs are reported.

The $\Delta F/NkT$ values were determined in this work at six T^* conditions in the range of 0.5 to 1.5 and eight ρ^* conditions in the range of 0.1 to 0.8 for a total of 48 points. For the Lennard–Jones fluid, the reference system used in the calculation is the "soft sphere" fluid with internal energy $U_0 = U_{12}$ at the same density and temperature. This reference system was used by Hoover *et al.* (13) and was also adopted by Torrie and Valleau (1) in their calculations. Complete thermodynamic information on the reference system is available in the work of Hoover *et al.* (13), and was used in the calculation of excess Helmoltz free energy at the 48 conditions. The results are reported in Table 1. It should be mentioned that all runs were for 32-particle samples. Some 64- and 108-particle samples were carried out for checking purpose in this work, but the calculated equilibrium values are not significantly dependent on the number of particles of the samples.

The values of Table 1 were correlated together with other values reported in the literature (ref. 14, column 5 of Table 1; ref. 15, columns 3 and 5 of Table 1; ref. 16, column 7 of Table 4 for $T^* = 2.74$; and ref. 17, column 6 of Table 1) by means of the Lagrange interpolation method for establishing a set of ΔF^E values for the LJ fluid over wide ranges of temperature and density at specified intervals of T^* and ρ^*. These values in the form of $\Delta F^E/NkT$ are presented in Table 2, in which the ranges of T^* and ρ^* covered are 0.50 to 2.75 and 0.05 to 0.80, respectively. In terms of the properties of argon, the temperature range of the table extends from the temperature lower than the triple point to that twice above the critical temperature, and the density range extends from about twice the critical density to that of a large volume gas.

It should be mentioned that the Lagrange interpolation method was used twice in this work, one in the direction of ρ^* and the other, T^*. For each interpolated point, only four properly selected data points were used for its determination.

In addition, these excess Helmholtz free energy values were combined with *PVT* data (18, 19) for establishing a set of excess Gibbs free energy values for the LJ fluid over the same ranges of temperature and density with the same intervals of T^* and ρ^* as those listed in Table 2. The calculated $\Delta G^E/NkT$ values are presented in Table 3.

Modification of the second order perturbation term of the Barker–Henderson treatment

Perturbation theory is a very successful integral-equation extension of hard-sphere theory to real fluids. One of the approaches was developed by Barker and Henderson (BH). The BH expression for the Helmholtz free energy of a pure fluid is:

$$[4] \quad F = F_{hs} + 2N\pi\rho \int_\sigma^\infty u(r) g_{hs}(r) r^2 \, dr - N\pi\rho \left(\frac{\partial\rho}{\partial p}\right)_{hs} \int_\sigma^\infty u^2(r) g_{hs}(r) r^2 \, dr = F_{hs} + F_1 - F_2$$

when the so-called "macroscopic compressibility" approximation (9) is used in the derivation. In eq. [4], F_{hs}, g_{hs}, and $(\partial\rho/\partial p)_{hs}$ are the Helmholtz free energy, radial distribution function, and compressibility, respectively, of a reference hard-sphere system of effective diameter d; the quantities F_1 and F_2 are the first-order and the second-order perturbation terms, respectively. The quantity d is defined by:

$$[5] \quad d = \int_0^\sigma \left\{1 - \exp\left[-\frac{u(r)}{kT}\right]\right\} dr$$

It is dependent on the potential function $u(r)$ and temperature. The quantity σ is the value of molecular separation at $u(r) = 0$. The reason for using the macroscopic compressibility, instead of the local compressibility approximation, is because the former one is simpler to use computationally. Both of these approximations were suggested by Barker and Henderson (9) yielding similar results.

Can. J. Chem. Downloaded from www.nrcresearchpress.com by 210.87.254.6 on 09/06/12
For personal use only.

TABLE 2. Values of excess Helmholtz free energy, $\Delta F^E/NkT$, for the Lennard–Jones fluid

	$\Delta F^E/NkT$ for $\rho^* =$							
T^*	0.05	0.10	0.15	0.20	0.25	0.30	0.35	0.40
0.50	−0.77	−1.38	−1.90	−2.38	−2.92	−3.47	−3.99	−4.51
0.55	−0.68	−1.21	−1.64	−2.03	−2.50	−2.99	−3.48	−3.97
0.60	−0.60	−1.07	−1.45	−1.80	−2.22	−2.65	−3.10	−3.54
0.65	−0.54	−0.96	−1.32	−1.66	−2.03	−2.42	−2.81	−3.20
0.70	−0.48	−0.88	−1.23	−1.56	−1.91	−2.25	−2.59	−2.92
0.75	−0.43	−0.81	−1.16	−1.48	−1.80	−2.11	−2.40	−2.68
0.80	−0.39	−0.74	−1.05	−1.35	−1.64	−1.92	−2.18	−2.43
0.85	−0.36	−0.67	−0.94	−1.20	−1.46	−1.72	−1.95	−2.18
0.90	−0.33	−0.60	−0.84	−1.06	−1.30	−1.53	−1.75	−1.97
0.95	−0.29	−0.54	−0.76	−0.96	−1.17	−1.38	−1.60	−1.81
1.00	−0.25	−0.48	−0.69	−0.88	−1.07	−1.25	−1.47	−1.67
1.05	−0.23	−0.45	−0.64	−0.82	−1.00	−1.17	−1.36	−1.55
1.10	−0.22	−0.42	−0.60	−0.78	−0.94	−1.10	−1.27	−1.43
1.15	−0.20	−0.39	−0.56	−0.73	−0.89	−1.05	−1.19	−1.33
1.20	−0.19	−0.36	−0.52	−0.67	−0.84	−1.00	−1.12	−1.23
1.25	−0.17	−0.33	−0.47	−0.62	−0.79	−0.94	−1.05	−1.14
1.30	−0.16	−0.31	−0.45	−0.59	−0.74	−0.87	−0.98	−1.06
1.35	−0.16	−0.30	−0.43	−0.58	−0.68	−0.80	−0.90	−1.00
1.40	−0.15	−0.28	−0.41	−0.52	−0.63	−0.74	−0.84	−0.93
1.45	−0.13	−0.26	−0.37	−0.48	−0.58	−0.68	−0.77	−0.85
1.50	−0.11	−0.23	−0.34	−0.44	−0.53	−0.62	−0.70	−0.78
1.75	−0.09	−0.18	−0.27	−0.36	−0.43	−0.50	−0.56	−0.61
2.00	−0.07	−0.14	−0.21	−0.28	−0.34	−0.39	−0.43	−0.46
2.25	−0.05	−0.11	−0.16	−0.20	−0.24	−0.27	−0.29	−0.31
2.50	−0.03	−0.07	−0.10	−0.12	−0.15	−0.16	−0.16	−0.16
2.75	−0.01	−0.03	−0.04	−0.05	−0.05	−0.05	−0.03	−0.00

	$\Delta F^E/NkT$ for $\rho^* =$							
T^*	0.45	0.50	0.55	0.60	0.65	0.70	0.75	0.80
0.50	−5.06	−5.60	−6.16	−6.67	−7.08	−7.42	−7.69	−7.89
0.55	−4.46	−4.95	−5.42	−5.85	−6.27	−6.59	−6.75	−6.69
0.60	−3.98	−4.40	−4.80	−5.18	−5.57	−5.86	−5.98	−5.84
0.65	−3.58	−3.94	−4.29	−4.61	−4.96	−5.22	−5.34	−5.24
0.70	−3.25	−3.56	−3.86	−4.14	−4.43	−4.66	−4.80	−4.82
0.75	−2.96	−3.23	−3.49	−3.74	−3.97	−4.17	−4.34	−4.47
0.80	−2.68	−2.92	−3.16	−3.38	−3.57	−3.74	−3.89	−4.01
0.85	−2.41	−2.64	−2.86	−3.06	−3.23	−3.37	−3.47	−3.52
0.90	−2.18	−2.39	−2.58	−2.76	−2.92	−3.04	−3.10	−3.07
0.95	−1.99	−2.16	−2.33	−2.49	−2.64	−2.74	−2.79	−2.74
1.00	−1.83	−1.97	−2.11	−2.25	−2.38	−2.48	−2.52	−2.47
1.05	−1.69	−1.82	−1.95	−2.07	−2.18	−2.25	−2.28	−2.24
1.10	−1.58	−1.70	−1.81	−1.92	−2.00	−2.05	−2.07	−2.04
1.15	−1.47	−1.59	−1.69	−1.79	−1.84	−1.87	−1.88	−1.86
1.20	−1.35	−1.46	−1.56	−1.65	−1.69	−1.70	−1.70	−1.67
1.25	−1.24	−1.34	−1.44	−1.51	−1.54	−1.55	−1.54	−1.50
1.30	−1.16	−1.25	−1.32	−1.38	−1.41	−1.41	−1.39	−1.34
1.35	−1.09	−1.16	−1.22	−1.26	−1.29	−1.29	−1.26	−1.19
1.40	−1.01	−1.08	−1.12	−1.15	−1.17	−1.17	−1.13	−1.05
1.45	−0.93	−0.99	−1.04	−1.06	−1.07	−1.05	−1.01	−0.92
1.50	−0.85	−0.92	−0.95	−0.97	−0.97	−0.94	−0.89	−0.81
1.75	−0.67	−0.71	−0.73	−0.73	−0.71	−0.67	−0.60	−0.50
2.00	−0.50	−0.52	−0.52	−0.50	−0.46	−0.41	−0.32	−0.21
2.25	−0.32	−0.32	−0.31	−0.27	−0.22	−0.14	−0.05	0.08
2.50	−0.15	−0.13	−0.09	−0.04	0.03	0.12	0.23	0.37
2.75	0.03	0.07	0.12	0.19	0.27	0.38	0.51	0.66

Correction function for F_2

The evaluation of Helmholtz free energy by means of eq. [4] is not exact. Because the exact second-order perturbation term cannot be easily calculated, the macroscopic compressibility approximation was used. In addition to this approximation, the truncation of higher-order perturbation terms and the solution of the Percus–Yevick (PY) approximation used for the hard-sphere radial-distribution function also caused errors in the evaluation. An attempt was made in this work to reduce these errors by introducing a correction function to F_2 of eq. [4]. The

Can. J. Chem. Downloaded from www.nrcresearchpress.com by 210.87.254.6 on 09/06/12
For personal use only.

TABLE 3. Values of excess Gibbs free energy, $\Delta G^E/NkT$, for the Lennard–Jones fluid

	$\Delta G^E/NkT$ for ρ^* =							
T^*	0.05	0.10	0.15	0.20	0.25	0.30	0.35	0.40
0.50	−1.61	−2.89	−3.94	−4.72	−5.33	−5.86	−6.50	−7.50
0.55	−1.38	−2.51	−3.44	−4.16	−4.78	−5.33	−5.95	−6.81
0.60	−1.20	−2.20	−3.03	−3.72	−4.33	−4.87	−5.46	−6.20
0.65	−1.06	−1.95	−2.72	−3.39	−3.96	−4.48	−5.02	−5.67
0.70	−0.94	−1.75	−2.48	−3.11	−3.67	−4.16	−4.65	−5.20
0.75	−0.83	−1.59	−2.28	−2.88	−3.41	−3.86	−4.30	−4.78
0.80	−0.75	−1.44	−2.05	−2.62	−3.10	−3.53	−3.93	−4.36
0.85	−0.69	−1.30	−1.85	−2.35	−2.80	−3.20	−3.56	−3.95
0.90	−0.63	−1.17	−1.67	−2.11	−2.52	−2.89	−3.23	−3.60
0.95	−0.56	−1.06	−1.51	−1.92	−2.29	−2.63	−2.97	−3.30
1.00	−0.50	−0.95	−1.38	−1.76	−2.10	−2.40	−2.73	−3.04
1.05	−0.46	−0.89	−1.27	−1.62	−1.95	−2.23	−2.52	−2.81
1.10	−0.43	−0.82	−1.18	−1.52	−1.81	−2.07	−2.33	−2.58
1.15	−0.39	−0.76	−1.10	−1.41	−1.69	−1.95	−2.17	−2.38
1.20	−0.37	−0.70	−1.02	−1.30	−1.58	−1.83	−2.02	−2.20
1.25	−0.34	−0.65	−0.93	−1.20	−1.48	−1.70	−1.88	−2.02
1.30	−0.32	−0.61	−0.88	−1.13	−1.37	−1.58	−1.74	−1.87
1.35	−0.31	−0.58	−0.83	−1.06	−1.27	−1.45	−1.60	−1.74
1.40	−0.29	−0.54	−0.78	−0.98	−1.17	−1.34	−1.48	−1.60
1.45	−0.26	−0.50	−0.71	−0.91	−1.08	−1.23	−1.36	−1.46
1.50	−0.23	−0.45	−0.66	−0.84	−0.99	−1.13	−1.24	−1.33
1.75	−0.17	−0.33	−0.48	−0.61	−0.71	−0.79	−0.84	−0.86
2.00	−0.13	−0.25	−0.35	−0.45	−0.52	−0.56	−0.57	−0.56
2.25	−0.09	−0.18	−0.25	−0.30	−0.33	−0.34	−0.32	−0.28
2.50	−0.06	−0.11	−0.15	−0.17	−0.18	−0.15	−0.10	−0.01
2.75	−0.03	−0.05	−0.06	−0.06	−0.03	0.02	0.10	0.23

	$\Delta G^E/NkT$ for ρ^* =							
T^*	0.45	0.50	0.55	0.60	0.65	0.70	0.75	0.80
0.50	−8.93	−10.55	−12.09	−13.20	−13.71	−13.75	−13.50	−12.99
0.55	−7.93	−9.19	−10.35	−11.19	−11.67	−11.75	−11.46	−10.77
0.60	−7.12	−8.12	−9.02	−9.69	−10.09	−10.14	−9.84	−9.06
0.65	−6.43	−7.24	−7.97	−8.49	−8.81	−8.81	−8.50	−7.75
0.70	−5.85	−6.51	−7.10	−7.52	−7.73	−7.69	−7.38	−6.73
0.75	−5.33	−5.88	−6.37	−6.70	−6.82	−6.73	−6.44	−5.88
0.80	−4.84	−5.31	−5.72	−5.98	−6.04	−5.90	−5.57	−4.99
0.85	−4.38	−4.80	−5.14	−5.35	−5.36	−5.18	−4.79	−4.13
0.90	−3.97	−4.34	−4.62	−4.77	−4.76	−4.55	−4.10	−3.35
0.95	−3.62	−3.92	−4.15	−4.26	−4.22	−3.97	−3.51	−2.74
1.00	−3.32	−3.56	−3.73	−3.80	−3.73	−3.46	−2.99	−2.22
1.05	−3.05	−3.25	−3.39	−3.43	−3.32	−3.03	−2.53	−1.76
1.10	−2.81	−2.99	−3.09	−3.10	−2.95	−2.63	−2.12	−1.37
1.15	−2.59	−2.75	−2.83	−2.81	−2.62	−2.27	−1.75	−1.01
1.20	−2.37	−2.50	−2.56	−2.52	−2.31	−1.94	−1.41	−0.66
1.25	−2.16	−2.27	−2.32	−2.25	−2.02	−1.65	−1.10	−0.35
1.30	−2.00	−2.08	−2.09	−2.00	−1.76	−1.37	−0.82	−0.06
1.35	−1.85	−1.90	−1.88	−1.76	−1.52	−1.13	−0.56	0.21
1.40	−1.69	−1.73	−1.69	−1.55	−1.29	−0.90	−0.32	0.46
1.45	−1.54	−1.56	−1.52	−1.36	−1.09	−0.68	−0.10	0.69
1.50	−1.39	−1.42	−1.35	−1.18	−0.90	−0.47	0.11	0.89
1.75	−0.86	−0.83	−0.74	−0.58	−0.38	−0.03	0.60	1.50
2.00	−0.53	−0.44	−0.31	−0.15	0.12	0.57	1.24	2.06
2.25	−0.20	−0.07	0.10	0.33	0.63	1.09	1.73	2.53
2.50	0.11	0.27	0.48	0.75	1.07	1.53	2.13	3.06
2.75	0.36	0.55	0.78	1.06	1.42	1.85	2.53	3.60

correction function was obtained by: (*i*) calculating the differences of Helmholtz free energies between the values of Table 2 and the corresponding values calculated from eq. [4] but limited to the first-order perturbation term, (*ii*) obtaining correction factors by dividing these differences with the F_2 values obtained from eq. [4] at the corresponding conditions, and (*iii*) correlating these ratios in terms of T^* and ρ^*. In the calculation, the hard-sphere model of Carnahan and Starling (20) was used as the reference. The correlation results as shown in Fig. 2 indicate that the correction factors are not strongly de-

Can. J. Chem. Downloaded from www.nrcresearchpress.com by 210.87.254.6 on 09/06/12
For personal use only.

Can. J. Chem. Downloaded from www.nrcresearchpress.com by 210.87.254.6 on 09/06/12
For personal use only.

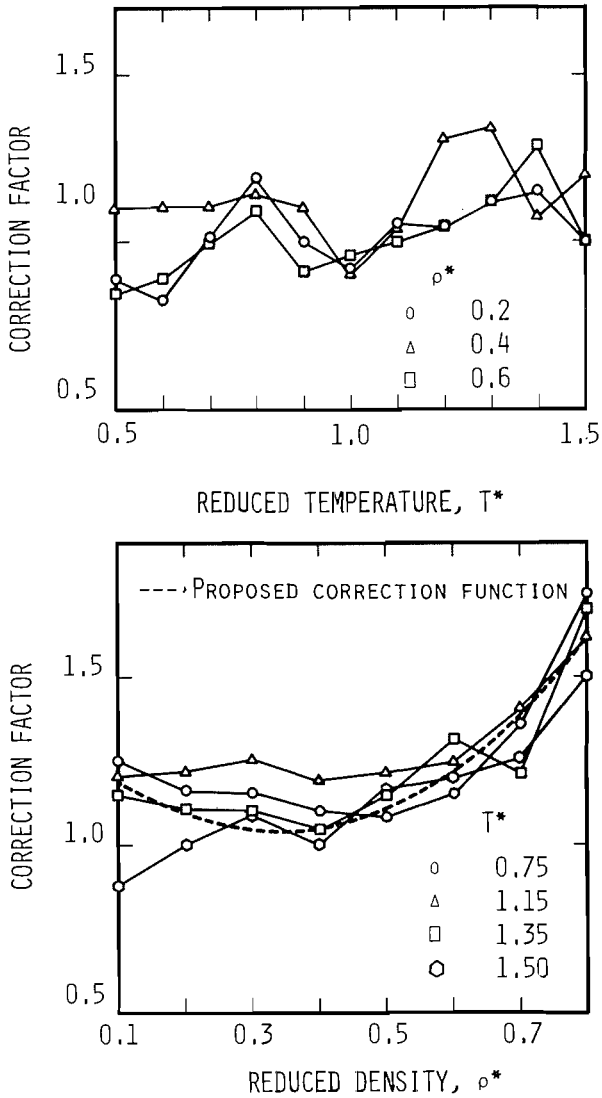

FIG. 2. The effect of T^* and ρ^* on correction factors.

pendent on temperature but more dependent on density. The need of a density correction function in the high density region can also be shown from the study of the radial distribution function of the hard-sphere fluid. The calculated radial distribution functions at three $\eta\,(=(\pi/6)\,\rho d^3)$ values, using the PY approximation and the Monte Carlo method, are depicted in Fig. 3. The deviations between the two methods increase with the increase of η. In this work, the correction function was simply expressed in terms of ρ^* by means of a quadratic equation,

$$[6] \quad C(\rho^*) = 1.6736 - 3.5710\rho^* + 5.3665\rho^{*2}$$

The approximate representation of the correction factors by means of eq. [6] is depicted in Fig. 2, and eq. [4] was modified to

$$[7] \quad F = F_{hs} + F_1 - C(\rho^*)F_2$$

Applicability of the proposed modification

The applicability of eq. [7] was first tested by calculating the excess Helmholtz free energy and the compressibility factor,

$$[8] \quad \left(\frac{P}{\rho kT}\right) = \left(\frac{P}{\rho kT}\right)_{hs} + \rho\frac{\partial}{\partial\rho}\left(\frac{F - F_{hs}}{NkT}\right)$$

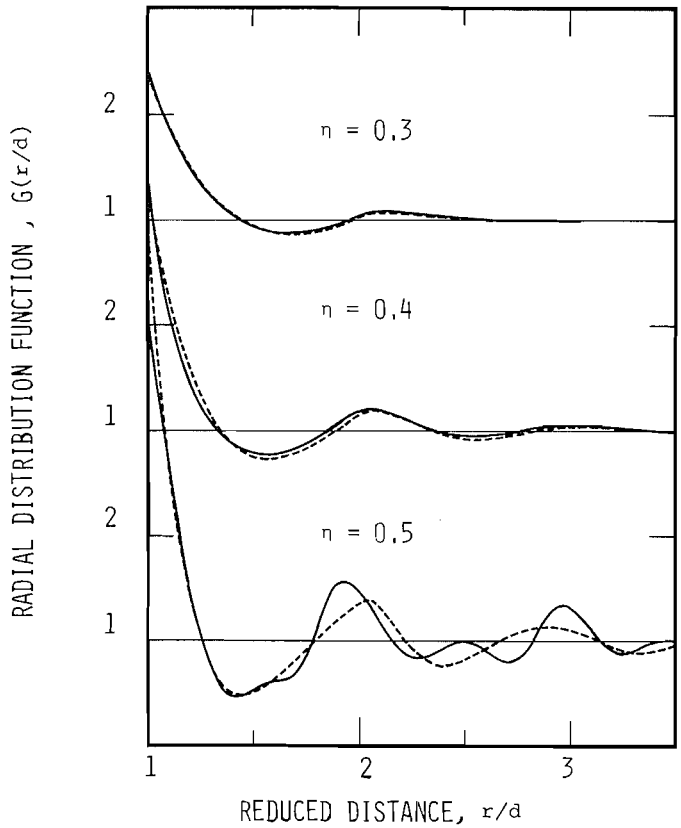

FIG. 3. Radial distribution function of the hard-sphere fluid ($\eta = (\pi/6)\,\rho d^3$): — Monte Carlo method, --- PY approximation.

for the LJ fluid at 20 selected conditions. In eq. [8], the subscript hs refers to the hard sphere. The calculated results were then compared in Table 4 with the values obtained from the Monte Carlo (MC) method, the perturbation theory advanced by Weeks, Chandler, and Andersen (WCA) (21) as well as those obtained from eq. [4]. The comparison indicates that the calculated values are as accurate as those obtained from the WCA method, which yields results closer to those obtained from the MC method than does the original second-order perturbation expression of Barker and Henderson. The proposed modification is, however, much simpler to use computationally than is the WCA method.

For the purpose of determining the limitations of the applicability of the LJ fluid, Z values were calculated at four values of acentric factor ω, in the ranges of reduced temperature $T_r(=T/T_c)$ from 0.8 to 2.0 and reduced pressure $P_r(=P/P_c)$ from 0 to 10. These values are compared with those correlated by Lee and Kesler (11) in Fig. 4.

At lower values of ω and at moderate pressures, the Z values obtained from eq. [7] are acceptable. However, at $\omega \geq 0.2$, the deviations become very noticeable even when the temperature is high. At $\omega = 0$, the calculated Z values are acceptable at $T_r \geq 1.0$, but the agreement is poor at $T_r < 1.0$, indicating the need of higher-order perturbation terms for the prediction of Z values at low temperatures.

The densities and pressures of the coexisting vapor and liquid phases for the LJ fluid were also calculated. The calculated reduced densities ρ^* are compared in Fig. 5 with the MC results of Adams (22) and the values obtained from the equation of state of Nicolas *et al.* (23) for the LJ fluid, and those from eq. [4], the original second-order perturbation expression of Barker

Can. J. Chem. Downloaded from www.nrcresearchpress.com by 210.87.254.6 on 09/06/12
For personal use only.

TABLE 4. Comparison of calculated values of excess Helmholtz free energy and compressibility factor for the Lennard–Jones fluid

		$-\Delta F^E/NkT$				Z			
T^*	ρ^*	MC	WCA	BH	This work	MC	WCA	BH	This work
0.75	0.1	0.80	0.75	0.73	0.79	0.23	0.25	0.31	0.31
	0.6	3.74	3.73	3.68	3.77	—	—	−1.67	−1.90
	0.7	4.16	4.19	4.06	4.19	−1.71	−1.69	−1.22	−1.44
	0.8	4.46	4.48	4.29	4.44	−0.53	−0.45	−0.01	−0.15
1.15	0.1	0.39	0.37	0.37	0.40	0.61	0.64	0.65	0.65
	0.2	0.73	0.73	0.71	0.73	0.35	0.33	0.34	0.36
	0.3	1.06	1.03	1.03	1.04	0.12	0.09	0.09	0.10
	0.4	1.33	1.32	1.32	1.33	−0.09	−0.09	−0.08	−0.10
	0.5	1.57	1.57	1.56	1.59	−0.13	−0.17	−0.09	−0.16
	0.6	1.79	1.77	1.75	1.78	0.07	−0.02	0.14	0.04
	0.65	1.85	1.85	1.81	1.85	0.31	0.22	0.39	0.29
	0.75	1.87	1.90	1.84	1.90	1.17	1.12	1.28	1.20
1.35	0.1	0.29	0.28	0.28	0.30	0.72	0.73	0.73	0.73
	0.2	0.54	0.53	0.53	0.55	0.50	0.51	0.51	0.53
	0.3	0.80	0.77	0.77	0.77	0.35	0.34	0.34	0.35
	0.4	0.98	0.97	0.97	0.98	0.27	0.24	0.26	0.24
	0.5	1.16	1.14	1.13	1.15	0.30	0.27	0.33	0.27
	0.55	1.22	1.20	1.19	1.21	0.41	0.35	0.44	0.37
	0.7	1.30	1.28	1.25	1.29	1.17	1.17	1.28	1.21
	0.8	1.21	1.19	1.14	1.19	2.42	2.43	2.48	2.43

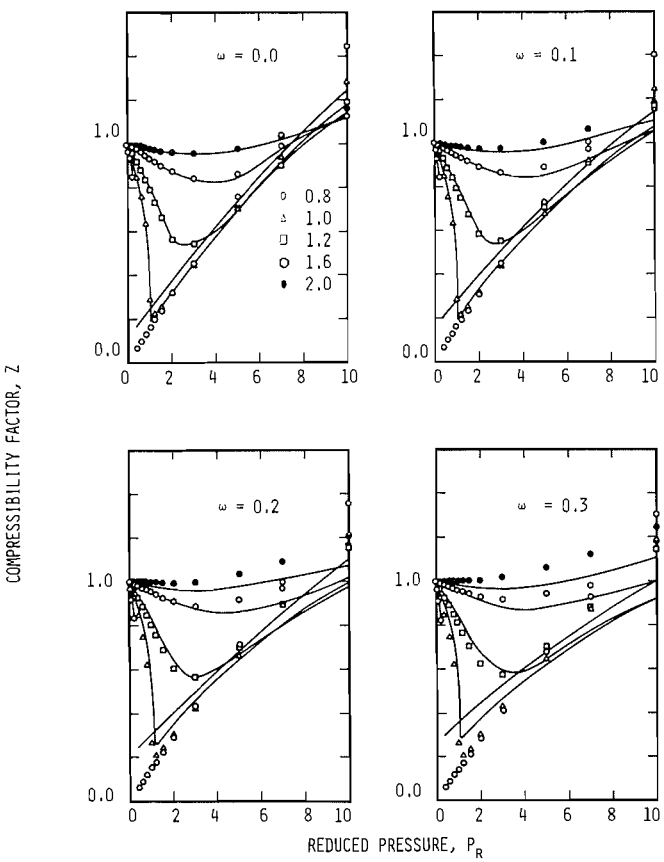

FIG. 4. Comparison of compressibility factors Z with the correlation of Lee and Kesler (11).

and Henderson. The data for argon reported by Gosman *et al.* (24) were converted into the reduced form by using $\sigma = 3.405$ Å and $\epsilon/k = 119.76$ K and are included in Fig. 5 for comparison. These parameter values were determined from the second virial coefficient of argon (18). Also included in the comparison is the locus of the mid-points (rectilinear diameters). The large cross included in the figure indicates the estimated location of the critical point of the LJ fluid (15).

TABLE 5. Comparison of calculated Henry's constants using parameters derived from different properties for the binary nitrogen–methane system

	Average absolute percentage deviations			
Temperature range (K)	Second virial coefficient	Viscosity	Saturation property	*PVT* data
120–160	26.1	24.9	15.5	10.6

The comparison indicates that much improved density prediction in the liquid phase was obtained with the proposed modification (eq. [7]) than the original BH expression. The calculated results agree well with the MC results of Adams and, with the exception of the critical region, the data of argon and the results from the analytical equation of Nicolas *et al.* The equation of Nicolas *et al.* is of the Strobridge type with its coefficient obtained from fitting the data of the LJ fluid.

The modified equation was further applied to the calculation of Henry's constants for 26 binary systems containing nitrogen, carbon dioxide, hydrogen sulfide, and normal alkanes up to heptane. In the calculation, a binary characteristic constant k_{12} was introduced in the mixing rule for the cross energy parameter ϵ_{12} as follows:

$$[9] \quad \epsilon_{12} = (\epsilon_{11}\epsilon_{22})^{1/2}\,(1 - k_{12})$$

with its value determined by minimizing the differences between the calculated values and those reported by Prausnitz and Chueh (25). The effect of the parameter values on the calculated results was evaluated. In addition to those values obtained from viscosity data and from second virial coefficients as reported by Hirschfelder *et al.* (26) for the LJ potential, the parameter values determined in this work from saturation properties and from *PVT* data were also used. The values obtained

Can. J. Chem. Downloaded from www.nrcresearchpress.com by 210.87.254.6 on 09/06/12
For personal use only.

TABLE 6. Comparison of the calculated Henry's constants with those reported by Prausnitz and Chueh

System	Temperature range (K)	N.P.	k_{ii}	AAD* (atm)	AAD* (%)
Nitrogen – methane	125–160	8	0.022	6.8	10.6
Nitrogen – ethane	125–260	10	0.065	5.4	2.4
Nitrogen – butane	315–375	13	0.340	10.6	1.8
Nitrogen – hexane	345–440	20	0.372	31.8	5.7
Nitrogen – heptane	310–405	20	0.391	37.8	6.2
Methane – ethane	205–270	14	0.0	5.6	6.4
Methane – propane	195–290	20	0.040	4.7	4.7
Methane – butane	315–375	13	0.090	7.7	3.8
Methane – pentane	315–410	20	0.121	4.7	2.2
Methane – hexane	315–410	20	0.144	7.7	3.4
Methane – heptane	205–395	20	0.171	5.7	2.7
Methane – heptane	445–485	9	0.220	4.6	1.9
Methane – carbon dioxide	210–265	12	0.060	12.5	6.0
Ethane – benzene	325–465	15	0.012	5.1	3.6
Ethane – propane	315–330	4	−0.003	2.2	5.9
Ethane – butane	315–375	13	−0.001	3.2	6.1
Ethane – pentane	315–410	20	0.001	3.6	5.0
Ethane – heptane	315–410	20	0.058	3.9	5.6
Propane – butane	345–375	7	−0.014	1.8	6.9
Propane – pentane	345–410	14	−0.026	2.3	7.6
Propane – benzene	380–475	20	−0.022	3.7	4.7
Butane – heptane	425–485	13	−0.041	1.1	3.6
Carbon dioxide – propane	295–330	8	0.107	2.2	2.8
Carbon dioxide – butane	315–375	13	0.137	2.8	2.6
Carbon dioxide – pentane	315–365	11	−0.013	3.4	6.9
Hydrogen sulfide – butane	355–380	6	0.097	0.2	0.3
Hydrogen sulfide – pentane	380–410	7	0.035	12.2	24.4

* AAD = average absolute deviation.

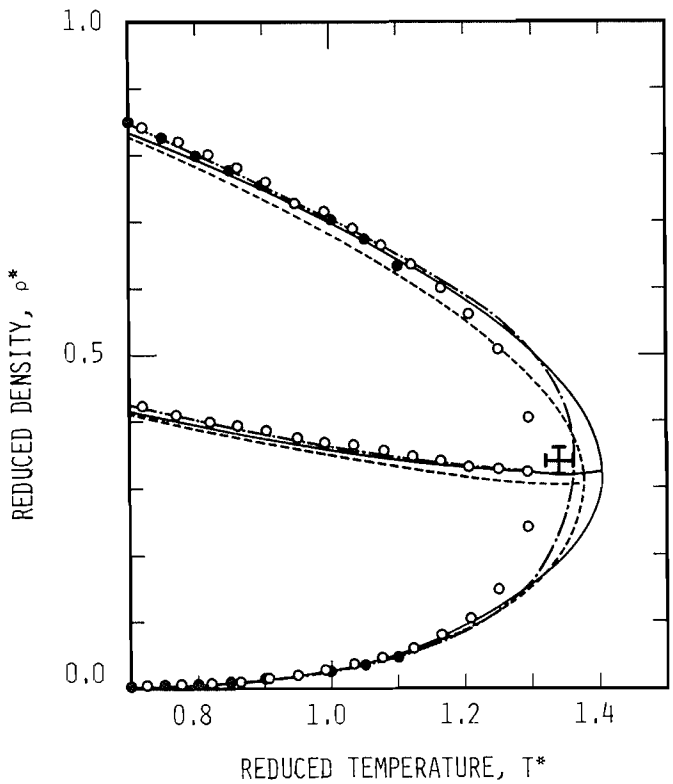

FIG. 5. Comparison of calculated saturation curves for the LJ fluid: ○, date of argon (24); ●, MC results of Adams (22); -·-·-; equation of Nicholas *et al.* (23); ---, eq. [4]; —, this work; +, estimated critical point (15).

in this work were generalized in terms of ω and critical properties. Hence from saturation properties (27–29),

$$[10]\quad \epsilon/kT_c = 0.7687$$

$$[11]\quad \sigma(NZ_c/V_c)^{1/3} = 0.4524 - 0.0766\omega$$

and from *PVT* data (11)

$$[12]\quad \epsilon/kT_c = 0.7700 - 0.1400\omega \quad (0 \le \omega \le 0.3)$$

$$[13]\quad = 0.7510 - 0.0745\omega \quad (0.3 \le \omega \le 0.5)$$

$$[14]\quad \sigma(NZ_c/V_c)^{1/3} = 0.4482 - 0.0723\omega$$

Henry's constants of nitrogen in methane were determined using these parameter values and compared with the values of Prausnitz and Chueh (25). As the values of Prausnitz and Chueh were reported at zero pressure, their values were adjusted to the saturation pressure by the Ponting correction. A comparison of the calculated results is shown in Fig. 6. The deviations between the calculated values and the adjusted Henry's constants are summarized in Table 5. It appears that the potential parameters determined from *PVT* data yielded the best results. Consequently, Henry's constants for all the binary systems tested were determined using the parameter values given by eqs. [12]–[14]. The values obtained from nitrogen in ethane and methane in heptane are depicted in Fig. 7. A summary of the calculated results is presented in Table 6. It is generally accepted that at high pressure (e.g. $P_r > 3$), the second-order BH perturbation expression cannot yield satisfactory Henry's constants. Nevertheless, with the introduction of the proposed correction function, the average absolute deviations obtained for most systems are less than 8%.

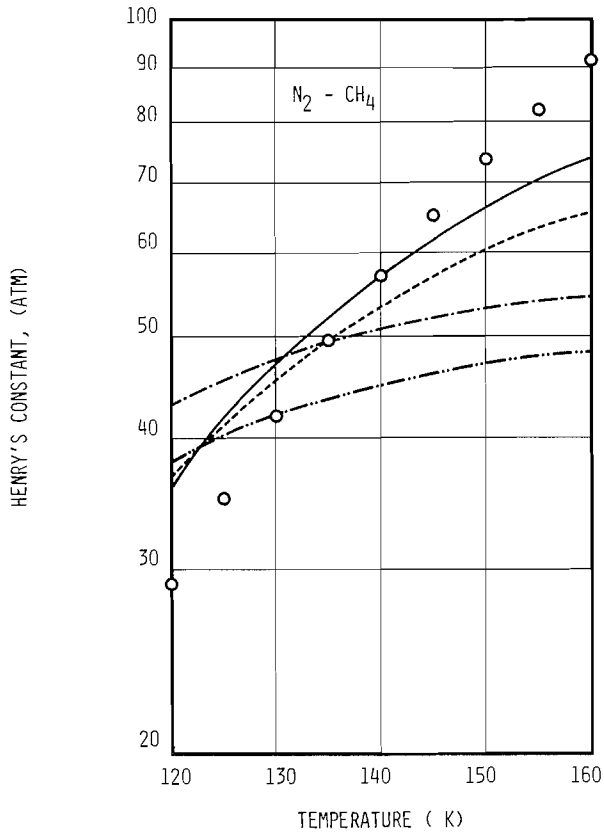

FIG. 6. The effect of parameter values on the calculation of Henry's constant: ◯, Prausnitz and Chueh (25); -·-·-, parameters from viscosity; ····, parameters from second virial coefficients; ---- parameters from saturation properties; —, parameters from *PVT* data.

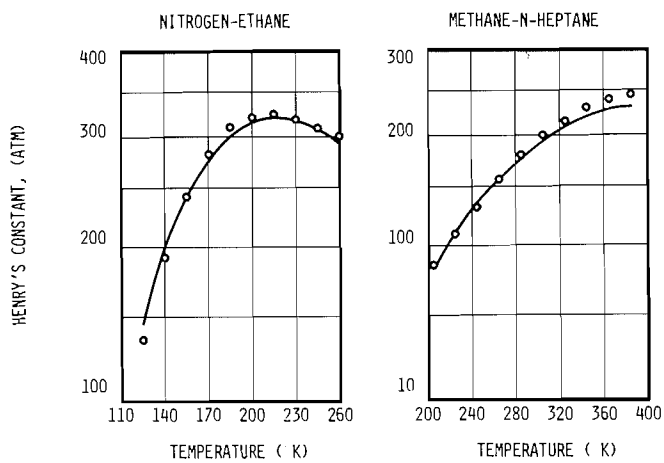

FIG. 7. Henry's constant from nitrogen in ethane and methane in *n*-heptane: ◯, Prausnitz–Chueh (25); —, this work.

Can. J. Chem. Downloaded from www.nrcresearchpress.com by 210.87.254.6 on 09/06/12
For personal use only.

Acknowledgement

The authors are indebted to the Natural Sciences and Engineering Research Council of Canada for financial support.

1. G. M. TORRIE and J. P. VALLEAU. Chem. Phys. Lett. **28**, 578 (1974).
2. G. M. TORRIE and J. P. VALLEAU. J. Comp. Phys. **23**, 187 (1977).
3. B. L. ROGERS and J. M. PRAUSNITZ. Trans. Faraday Soc. **67**, 3474 (1971).
4. K. UNO, Y. ARAI, and S. SAITO. J. Chem. Eng. Jpn. **9**, 182 (1976).
5. H. MASUOKA, Y. ARAI, and S. SAITO. J. Chem. Eng. Jpn. **10**, 171 (1977).
6. H. MASUOKA, C. YOKOYAMA, Y. ARAI, and S. SAITO. J. Chem. Eng. Jpn. **10**, 482 (1977).
7. K. UNO, E. SARASHINA, Y. ARAI, and S. SAITO. J. Chem. Eng. Jpn. **8**, 201 (1975).
8. M. YORIZANE and Y. MIYANO. J. Chem. Eng. Jpn. **13**, 433 (1980).
9. J. A. BARKER and D. HENDERSON. J. Chem. Phys. **47**, 2856 (1967).
10. J. A. BARKER and D. HENDERSON. J. Chem. Phys. **47**, 4714 (1967).
11. B. I. LEE and M. G. KESLER. AIChE J. **21**, 510 (1975).
12. N. A. METROPOLIS, A. W. ROSENBLUTH, M. N. ROSENBLUTH, A. H. TELLER, and E. TELLER. J. Chem. Phys. **21**, 1087 (1953).
13. W. G. HOOVER, M. ROSS, K. W. JOHNSON, D. HENDERSON, J. A. BARKER, and B. C. BROWN. J. Chem. Phys. **52**, 4931 (1970).
14. D. LEVESQUE and L. VERLET. Phys. Rev. **182**, 307 (1969).
15. J.-P. HANSEN and L. VERLET. Phys. Rev. **184**, 151 (1969).
16. J.-P. HANSEN. Phys. Rev. A, **2**, 221 (1970).
17. H. C. ANDERSEN, D. CHANDLER, and J. D. WEEKS. J. Chem. Phys. **56**, 3812 (1972).
18. Y. ADACHI and H. SUGIE. Intern. Chem. Eng. **21**, 604 (1981).
19. F. DIN. Thermodynamic functions of gases. Vol. 2. Butterworths, London. 1962. pp. 190–193.
20. N. F. CARNAHAN and K. E. STARLING. J. Chem. Phys. **51**, 635 (1969).
21. J. D. WEEKS, D. CHANDLER, and H. C. ANDERSEN. J. Chem. Phys. **54**, 5237 (1971).
22. D. J. ADAMS. Mol Phys. **32**, 647 (1976).
23. J. J. NICOLAS, K. E. GUBBINS, W. B. STREET, and D. J. TILDESLEY. Mol. Phys. **37**, 1429 (1979).
24. A. L. GOSMAN, R. D. MCCARTY, and J. G. HUST. Natl. Stand. Ref. Data Ser. Natl. Bur. Stand. RSRDS-NBS 27, 1969.
25. J. M. PRAUSNITZ and P. L. CHUEH. Computer calculations for high-pressure vapor–liquid equilibria. Prentice-Hall, Englewood Cliff, NJ. 1969.
26. J. O. HIRSCHFELDER, C. F. CURTISS, and R. B. BIRD. Molecular theory of gases and liquids. John Wiley, New York. 1954. pp. 1110–1112.
27. M. GOMEZ-NIETO and G. THODOS. Ind. Eng. Chem. Fundam. **17**, 45 (1978).
28. C. F. SPENCER and S. B. ADLER. J. Chem. Eng. Data, **23**, 82 (1978).
29. R. G. BARILE and G. THODOS. Can. J. Chem. Eng. **43**, 137 (1965).

Structure, spectra, and stability of solid bismuth carbonates[1]

PETER TAYLOR, S. SUNDER, AND VINCENT J. LOPATA

Research Chemistry Branch, Whiteshell Nuclear Research Establishment, Atomic Energy of Canada Limited, Pinawa, Man., Canada R0E 1L0

Received April 16, 1984

PETER TAYLOR, S. SUNDER, and VINCENT J. LOPATA. Can. J. Chem. **62**, 2863 (1984).

A previously unreported basic bismuth carbonate, $(BiO)_4(OH)_2CO_3$, has been identified as an intermediate product in the interconversion of α-Bi_2O_3 and synthetic bismutite, $(BiO)_2CO_3$, in aqueous carbonate solutions. It has a narrow stability field, between CO_2 partial pressures of $10^{-5.5\pm1.0}$ Pa and $10^{-4.4\pm1.0}$ Pa, in the presence of dilute aqueous solution at 25°C. Gibbs energies of formation, calculated from these partial pressures, are $\Delta_fG^0((BiO)_4(OH)_2CO_3, s, 298.15\ K) = -1678 \pm 9$ kJ mol^{-1} and $\Delta_fG^0((BiO)_2CO_3, s, 298.15\ K) = -945 \pm 7$ kJ mol^{-1}. The two carbonates have been compared by thermogravimetric analysis, X-ray powder diffractometry, and infrared and Raman spectroscopy. The unit cell of $(BiO)_4(OH)_2CO_3$ is dimensionally orthorhombic, with $a = 10.772(1)$, $b = 5.4898(5)$, $c = 14.757(1)$ Å, $Z = 4$, but its true symmetry is probably triclinic. A structural model for $(BiO)_4(OH)_2CO_3$, and two modified models for $(BiO)_2CO_3$, are proposed. The possible natural occurrence of $(BiO)_4(OH)_2CO_3$ is discussed.

PETER TAYLOR, S. SUNDER, et VINCENT J. LOPATA. Can. J. Chem. **62**, 2863 (1984).

Un carbonate basique du bismuth qui n'avait pas été rapporté antérieurement, le $(BiO)_4(OH)_2CO_3$, a été identifié comme intermédiaire dans l'interconversion, en solutions aqueuses de carbonate, du α-Bi_2O_3 et de la bismutite synthétique $(BiO)_2CO_3$. Son domaine de stabilité est étroit; à 25°C et en solutions aqueuses diluées, il est défini par des pressions partielles minimales et maximales de CO_2 de $10^{-5.5\pm1.0}$ Pa et $10^{-4.4\pm1.0}$ Pa. Les énergies de formation de Gibbs, calculées à partir de ces pressions partielles, sont: $\Delta_fG^0((BiO)_4(OH)_2CO_3, s, 298{,}15\ K) = -1678 \pm 9$ kJ mol^{-1} et $\Delta_fG^0((BiO)_2CO_3, s, 298{,}15\ K) = -945 \pm 7$ kJ mol^{-1}. On a comparé les deux carbonates en faisant appel à l'analyse thermogravimétrique, à la diffraction des poudres par rayon-X et aux spectroscopies infrarouge et Raman. Du point de vue des dimensions, la maille élémentaire du $(BiO)_4(OH)_2CO_3$ est orthorhombique avec $a = 10{,}772(1)$, $b = 5{,}4898(5)$, $c = 14{,}757(1)$ Å, $Z = 4$; toutefois, sa symétrie réelle est probablement triclinique. On propose un modèle de structure pour le $(BiO)_4(OH)_2CO_3$ et deux modèles modifiés pour le $(BiO)_2CO_3$. On discute de l'existence possible du $(BiO)_4(OH)_2CO_3$ à l'état naturel.

[Traduit par le journal]

I. Introduction

Frondel (1), in his critical review of the mineralogy of bismuth oxides and carbonates in 1943, concluded that bismutite (Bi_2CO_5 or $(BiO)_2CO_3$) is the only well-established solid carbonate in the system $Bi_2O_3-CO_2-H_2O$. He determined that most prior reports of ill-defined natural and synthetic bismuth carbonates of other compositions are referable to bismutite, and that the water content of these materials is crystallographically non-essential. However, Sahama and Lehtinen (2) cautiously stated: "It seems that not all the water in bismutite can be considered entirely non-essential, but that the deficiency in CO_2 found in some bismutite samples is balanced by a certain water content."

Our interest in bismuth carbonates arose from possible applications to the immobilization of ^{14}C that is formed in nuclear power reactors (3). During an investigation of the interconversion of α-Bi_2O_3 and $(BiO)_2CO_3$ in aqueous carbonate solutions, we isolated and identified an additional solid, $(BiO)_4(OH)_2CO_3$; we report here its preparation and characterization.

II. Experimental

"Precipitated" bismutite (~5 g) was prepared by mixing solutions of $Bi(NO_3)_3 \cdot 5H_2O$ and excess Na_2CO_3 or K_2CO_3. "Autoclaved" bismutite was prepared by heating α-Bi_2O_3 (~5 g) with excess CO_2 in water for 3–5 days at 200°C in a Teflon-lined stainless-steel autoclave. The solid product was pulverized, then allowed to react further with aqueous CO_2, and the process was repeated until no Bi_2O_3 remained, as indicated by X-ray diffraction, and by the absence of yellow colour; usually three cycles sufficed.

A second basic bismuth carbonate, $(BiO)_4(OH)_2CO_3$, was first observed in overnight reactions between various proportions of M_2CO_3 (M = Na or K) and Bi_2O_3 (1 to 7 mmol of each, in 40 cm^3 of water), at room temperature. Bismutite was the major product at M_2CO_3:Bi_2O_3 ratios greater than one. The new phase occurred, admixed with bismutite and/or unreacted Bi_2O_3, at lower ratios. It was obtained as a pure phase when Bi_2O_3 (1 mmol) was allowed to react with a solution having MOH and M_2CO_3 concentrations both near 0.1 mol dm^{-3}. Products obtained with either Na_2CO_3 or K_2CO_3 were indistinguishable by X-ray diffraction, showing that the alkali ions are not essential components. Thermogravimetric experiments, described in section III.1, below, indicated the stoichiometry $2Bi_2O_3 \cdot CO_2 \cdot H_2O$ [$(BiO)_4(OH)_2CO_3$].

Experiments on solid interconversions were performed using suspensions of the solids in aqueous solutions of M_2CO_3 and MOH, contained in screw-topped plastic bottles and continuously agitated, at room temperature unless otherwise stated. These experiments followed a strategy similar to that previously used to determine stability limits between lead oxides and carbonates (4). Solids were isolated by filtration, washed with deionized water, air-dried, and identified by X-ray powder diffractometry (XRD), using a Philips PW-1150 diffractometer with CuKα radiation and a diffracted-beam monochromator. Further characterization was done on samples shown by XRD to be at least 95% phase-pure. Thermogravimetric analyses were obtained using a Perkin-Elmer TGS-1 thermobalance, with scanning rates of 5–20°C min^{-1}, in either a CO_2 or N_2 atmosphere.

Raman spectra were recorded using a SPEX-1403 double monochromator, equipped with an RCA C31034 photomultiplier tube and controlled by a SPEX-DATAMATE microprocessor. The spectra were excited using the 488.0 or 514.5 nm lines of a Spectra-Physics 165-09 Ar^+ laser, or the 647.1 nm line of a Coherent Radiation Innova 90-K Kr^+ laser. The incident laser beam was filtered using an interference filter. Samples were polycrystalline solids, contained in Pyrex melting-point capillaries. A 90° scattering geometry was used. Spectral resolution was ~1 cm^{-1}, unless otherwise stated. The spectrometer was calibrated using the emission lines of a mercury lamp, and the plasma lines of the Ar^+ laser.

Infrared spectra were obtained from polycrystalline samples dispersed in CsI and KBr discs, using a Nicolet MX-1 FT-IR spec-

[1]AECL No. 8309.

Can. J. Chem. Downloaded from www.nrcresearchpress.com by 210.87.254.40 on 09/06/12
For personal use only.

Can. J. Chem. Downloaded from www.nrcresearchpress.com by 210.87.254.40 on 09/06/12
For personal use only.

trometer, and also a Perkin-Elmer PE-457 spectrophotometer. The spectrum of $(BiO)_2CO_3$ was also recorded on a PE-225 instrument at the Memorial University of St. John's, Newfoundland. Excellent agreement was observed between the spectra obtained using the different spectrometers. The FT-IR spectra were recorded using the standard settings of the MX-1 instrument, i.e. an effective resolution of ~2 cm^{-1} and an average of 27 scans.

III. Results and discussion

1. Thermogravimetry

Samples from three different preparations of both $(BiO)_4(OH)_2CO_3$ and $(BiO)_2CO_3$ were examined by thermogravimetric analysis (TGA), between 25°C and 550–700°C. One half of the experiments were run in an N_2 atmosphere, and the remainder in CO_2. Some additional runs were terminated before decomposition was complete.

All the TGA runs showed a slow, continuous weight loss of 0.1 to 0.4% below 200°C, which we attribute to sorbed water. The decomposition of $(BiO)_4(OH)_2CO_3$ then occurred in two principal stages. The first stage occurred on average between 230 and 325°C (extreme onset temperatures 200, 260°C; extreme termination temperatures 300, 350°C; there was no systematic variation with atmosphere). The weight loss, which we attribute to loss of water, ranged between 1.6 and 2.3%, with an average of 1.9%. Products removed at 350°C were shown by XRD to consist of Bi_2O_3 and $(BiO)_2CO_3$. Additional diffuse diffraction features may have arisen from an intermediate anhydrous phase, such as $Bi_4O_5CO_3$.

The second stage of decomposition was a prolonged weight loss in the temperature range 330–670°C, totalling 4.6 to 5.9% (average 5.0%) of the sample weight. The average onset temperature in a CO_2 atmosphere was about 50°C higher than in N_2, consistent with a process involving the evolution of CO_2. Some runs showed fine structure in the TGA trace, suggestive of intermediate compound formation, but only $(BiO)_2CO_3$ and α-Bi_2O_3 could be detected by XRD in products removed at 425 and 550°C. The final product of decomposition was phase-pure α-Bi_2O_3.

The TGA data yielded empirical formulae in the range $Bi_2O_3 \cdot 0.46-0.66H_2O \cdot 0.52-0.68CO_2$, with an average of $Bi_2O_3 \cdot 0.53H_2O \cdot 0.57CO_2$. On this basis, we assigned the stoichiometry $Bi_2O_3 \cdot 0.5H_2O \cdot 0.5CO_2$ ($\equiv (BiO)_4(OH)_2CO_3$). We recognize that a more complex formulation is possible, bearing in mind the unusual stoichiometries of many other basic bismuth salts, as exemplified by the nitrates (5–7). However, the assigned stoichiometry is completely compatible with the XRD data, discussed at length in section III.4, below. The thermal decomposition route is summarized in the following reaction sequence [1]:

$$[1a]\quad (BiO)_4(OH)_2CO_3 \xrightarrow{230-325°C} Bi_4O_5CO_3(?) + H_2O$$

$$[1b]\quad Bi_4O_5CO_3 \rightarrow (BiO)_2CO_3 + Bi_2O_3$$

$$[1c]\quad (BiO)_2CO_3 \xrightarrow{330-670°C} Bi_2O_3 + CO_2$$

Our TGA experiments on $(BiO)_2CO_3$ showed that it decomposed to Bi_2O_3 in a single prolonged process. In N_2 atmosphere, CO_2 evolution commenced at 350–390°C, and continued until 530–650°C. The onset temperature was consistently higher, 400–430°C, in a CO_2 atmosphere, as expected. These results are consistent with Beck's differential thermal analyses of three specimens of natural bismutite (8), which showed decomposition in air to occur between about 400 and 530°C. They also parallel the second stage in the decomposition of $(BiO)_4(OH)_2CO_3$, described above. There was no indication of any solid intermediate in the decomposition of $(BiO)_2CO_3$. The six TGA runs (two on each of three samples) yielded empirical compositions in the range $Bi_2O_3 \cdot 0.95-1.03CO_2$, with an average of $Bi_2O_3 \cdot 1.00CO_2$ $[(BiO)_2(CO_3)_{1.00}]$. The less reproducible data for $(BiO)_4(OH)_2CO_3$ than $(BiO)_2CO_3$ reflect the difficulty of preparing pure $(BiO)_4(OH)_2CO_3$.

2. Determination of stability limits

Interconversions between the bismuth compounds may be expressed in terms of anion exchange (reactions [2*a*], [3*a*], [4*a*] below), or of reactions involving CO_2 and water ([2*b*], [3*b*], [4*b*]):

$$[2a]\quad 2Bi_2O_3(s) + CO_3^{2-}(aq) + 2H_2O(l) \rightleftharpoons (BiO)_4(OH)_2CO_3(s) + 2OH^-(aq)$$

$$[2b]\quad 2Bi_2O_3(s) + CO_2(g) + H_2O(l) \rightleftharpoons (BiO)_4(OH)_2CO_3(s)$$

$$[3a]\quad (BiO)_4(OH)_2CO_3(s) + CO_3^{2-}(aq) \rightleftharpoons 2(BiO)_2CO_3(s) + 2OH^-(aq)$$

$$[3b]\quad (BiO)_4(OH)_2CO_3(s) + CO_2(g) \rightleftharpoons 2(BiO)_2CO_3(s) + H_2O(l)$$

$$[4a]\quad Bi_2O_3(s) + CO_3^{2-}(aq) + H_2O(l) \rightleftharpoons (BiO)_2CO_3(s) + 2OH^-(aq)$$

$$[4b]\quad Bi_2O_3(s) + CO_2(g) \rightleftharpoons (BiO)_2CO_3(s)$$

The anion-exchange equations give a more realistic description of the net reactions in alkaline solution, and equilibrium constants of the form $K_{eq} = \{OH^-\}^2/\{CO_3^{2-}\}$ define the boundaries of adjoining solid stability fields. The alternative equations involving $CO_2(g)$ are more convenient for general discussion of stability relationships, as described in ref. 4, and lead to an alternative expression of the equilibrium constants[2] as $1/p(CO_2)$. Hereafter, p_1 and p_2 refer to the equilibrium CO_2 partial pressures for reactions [2*b*] and [3*b*], respectively.

Reactions of bismuth oxide, α-Bi_2O_3

Bismuth oxide was converted to $(BiO)_4(OH)_2CO_3$ by reaction in solutions with $[K_2CO_3] = 0.25$ mol dm^{-3} and $[KOH] = 0.05$ to 0.4 mol dm^{-3}, or with $[K_2CO_3] = 0.1$ mol dm^{-3} and $[KOH] = 0.1$ to 0.3 mol dm^{-3}. When no KOH was added to the K_2CO_3 solutions, the reaction proceeded through to $(BiO)_2CO_3$. The final pH in such runs was only about 0.3 units less than in those with 0.1 mol dm^{-3} of KOH added, due to OH^- release according to reaction [4*a*]. No solid carbonates were formed when Bi_2O_3 was exposed to solutions with $[K_2CO_3] = 0.25$ mol dm^{-3} and $[KOH] \geq 0.5$ mol dm^{-3}.

Reactions of the basic bismuth carbonate, $(BiO)_4(OH)_2CO_3$

This solid was converted to $(BiO)_2CO_3$ by a 0.1 mol dm^{-3} solution of K_2CO_3. It was converted to Bi_2O_3 by solutions with $[K_2CO_3] \leq 0.1$ mol dm^{-3} and $[KOH] \geq 1.0$ mol dm^{-3}. It survived unchanged for 67 days when contacted with solutions having $[K_2CO_3] = 0.1$ mol dm^{-3} and $[KOH] = 0.1$ to 0.3 mol dm^{-3}.

Reactions of synthetic bismutite, $(BiO)_2CO_3$

"Precipitated" bismutite was converted to $(BiO)_4(OH)_2CO_3$

[2]The two equilibrium constants are interrelated by the carbonate ionization equilibrium: $CO_2(g) + 2OH^-(aq) \rightleftharpoons H_2O(l) + CO_3^{2-}(aq)$. For the forward reaction, $\Delta_r G^0 = -56.01$ kJ mol^{-1}, based on the Gibbs energy data of ref. 10, at 298.15 K and 1 bar. Hence, for any carbonate solution, the equilibrium CO_2 partial pressure, in pascals, is equal to $10^{-4.81} \times \{CO_3^{2-}\}/\{OH^-\}^2 = 10^{-4.81}/K_{eq}$.

Can. J. Chem. Downloaded from www.nrcresearchpress.com by 210.87.254.40 on 09/06/12
For personal use only.

by solutions with $[K_2CO_3] = 0.25$ mol dm^{-3} and $[KOH] = 0.4$ to 1.0 mol dm^{-3}. Further decarbonation to α-Bi_2O_3 occurred with solutions having $[K_2CO_3] \leq 0.25$ mol dm^{-3} and $[KOH] \geq 1.0$ mol dm^{-3}. We did not observe $(BiO)_4(OH)_2CO_3$ in a similar series of reactions with "autoclaved" bismutite, probably because it was more crystalline, and hence less reactive, than the "precipitated" material.

Thermochemical deductions

We conclude from the above observations that $(BiO)_4(OH)_2CO_3$ has a narrow stability field in the system $Bi_2O_3-CO_2-H_2O-(KOH)$ at 25°C. The boundary for its conversion to $(BiO)_2CO_3$ lies within the range $0.05 < [KOH] < 0.3$ mol dm^{-3}, at $[K_2CO_3] = 0.1$ mol dm^{-3}. Using Davies' approximation (9) to estimate ionic activity coefficients — this approximation is at the very limit of its applicability at such high ionic strengths — these concentrations yield the following equilibrium relationship for reaction [3*a*]:

$$\log [\{OH^-\}^2/\{CO_3^{2-}\}] = -0.4 \pm 1.0$$

This corresponds to an equilibrium CO_2 partial pressure, $p_2 = 10^{-4.4\pm1.0}$ Pa (see footnote 2).

The boundary for the conversion of $(BiO)_4(OH)_2CO_3$ to α-Bi_2O_3 lies within the limits $0.3 < [KOH] < 1.0$ mol dm^{-3} at $[K_2CO_3] = 0.1$ mol dm^{-3}. These concentrations are too high for Davies' approximation to be applied. We could not measure the limits in more dilute carbonate solutions (10^{-2} and 10^{-3} mol dm^{-3}) due to slow kinetics and the difficulty of measuring small changes in carbonate concentration in strongly alkaline solutions. However, we can estimate p_1 by comparing our results for this system with those for the conversion of PbO to plumbonacrite, $Pb_{10}O(OH)_6(CO_3)_6$, reported in ref. 4. The limits for the PbO-plumbonacrite equilibrium (reaction [5])

$$[5] \quad \frac{5}{3}PbO(s) + CO_3^{2-}(aq) + \frac{3}{2}H_2O(l) \rightleftharpoons \frac{1}{6}Pb_{10}O(OH)_6(CO_3)_6(s) + 2OH^-(aq)$$

are $0.1 < [KOH] < 0.5$ mol dm^{-3} at $[K_2CO_3] = 0.1$ mol dm^{-3}. For reaction [5], measurements could be made at lower carbonate concentrations, and yielded a CO_2 partial pressure of $10^{-4.9\pm0.6}$ Pa for equilibrium [6] at 25°C:

$$[6] \quad \frac{5}{3}PbO(s) + CO_2(g) + \frac{1}{2}H_2O(l) \rightleftharpoons \frac{1}{6}Pb_{10}O(OH)_6(CO_3)_6(s)$$

Since the limiting solution conditions for the α-Bi_2O_3/$(BiO)_4(OH)_2CO_3$ interconversion at $[CO_3^{2-}] = 0.1$ mol dm^{-3} are slightly more alkaline than for the $PbO/Pb_{10}O(OH)_6(CO_3)_6$ case, we deduce that p_1 is slightly lower than $10^{-4.9\pm0.6}$ Pa, so we assign an estimated value of $10^{-5.5\pm1.0}$ Pa.

These estimated equilibrium partial pressures can be combined with literature values of the Gibbs energies of formation of the component oxides, to calculate the Gibbs energies of the solid carbonates. Reference 10 gives $\Delta_f G^0$(298.15 K, 1 bar) = -493.5 ± 1.5, -394.38 ± 0.17, and -237.14 ± 0.08 kJ mol^{-1}, for α-Bi_2O_3(s), CO_2(g), and H_2O(l), respectively. Applying these data to reaction [2*b*], with $p_1 = 10^{-5.5\pm1.0}$ Pa ($10^{-10.5\pm1.0}$ bar), we obtain:

$$\Delta_f G^0((BiO)_4(OH)_2CO_3, s, 298.15\ K) = 2\Delta_f G^0(\alpha\text{-}Bi_2O_3, s) + \Delta_f G^0(CO_2, g) + \Delta_f G^0(H_2O, l) + RT \ln (p_1/\text{bar}) = -1678 \pm 9\ \text{kJ mol}^{-1}$$

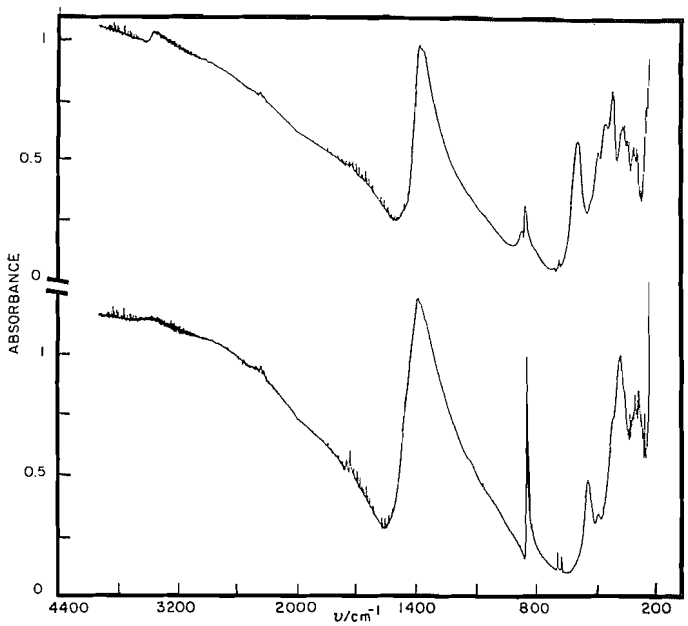

FIG. 1. Inrared spectra of $(BiO)_4(OH)_2CO_3$ (top spectrum) and $(BiO)_2CO_3$ (bottom spectrum), as polycrystalline solids dispersed in KBr pellets (about 1 mg in 200 mg of KBr).

Similarly, using reaction [3*b*], with $p_2 = 10^{-4.4\pm1.0}$ Pa ($10^{-9.4\pm1.0}$ bar), we obtain

$$\Delta_f G^0((BiO)_2CO_3, s, 298.15\ K) = \frac{1}{2}\{\Delta_f G^0((BiO)_4(OH)_2CO_3, s) + \Delta_f G^0(CO_2, g) - \Delta_f G^0(H_2O, l) + RT \ln(p_2/\text{bar})\} = -945 \pm 7\ \text{kJ mol}^{-1}$$

Note that the limits of stability of $(BiO)_4(OH)_2CO_3$, $10^{-5.5}$ Pa $\leq p(CO_2) \leq 10^{-4.4}$ Pa, apply in dilute aqueous solution. The stability field becomes narrower at lower water activities, and $(BiO)_4(OH)_2CO_3$ becomes unstable with respect to disproportionation, according to reaction [7], at relative humidities below $\simeq$ 10%:

$$[7] \quad (BiO)_4(OH)_2CO_3(s) \rightleftharpoons (BiO)_2CO_3(s) + Bi_2O_3(s) + H_2O(g)$$

This disproportionation is probably very slow at room temperature, but it is the first step in the dry thermal decomposition of $(BiO)_4(OH)_2CO_3$, as discussed in section III.1, above.

The narrowness of the stability field of $(BiO)_4(OH)_2CO_3$, and the low solubilities of all the solids ($<10^{-5}$ mol dm^{-3}), make it difficult to prepare pure $(BiO)_4(OH)_2CO_3$ in quantities greater than ~1 g. The stability field of $(BiO)_4(OH)_2CO_3$ is probably still narrower at higher temperatures, based on our previous observations on the lead carbonate system (4).

3. Vibrational spectroscopy

The infrared spectra of $(BiO)_4(OH)_2CO_3$ and $(BiO)_2CO_3$ are shown in Fig. 1, while Figs. 2, 3, and 4 show the 20–320, 200–1800, and 2800–3800 cm^{-1} regions, respectively, of the Raman spectra. These spectra confirm the distinct identities of the two solids. Frequencies (±1 cm^{-1} for sharp peaks), relative intensities (uncorrected for spectral response), and assignments of the observed spectral features are given in Table 1.

The infrared spectrum of $(BiO)_2CO_3$ in Fig. 1 is in general agreement with four earlier reports (11–14), except that ref. 13 shows an absorption near 723 cm^{-1}, which presumably arose

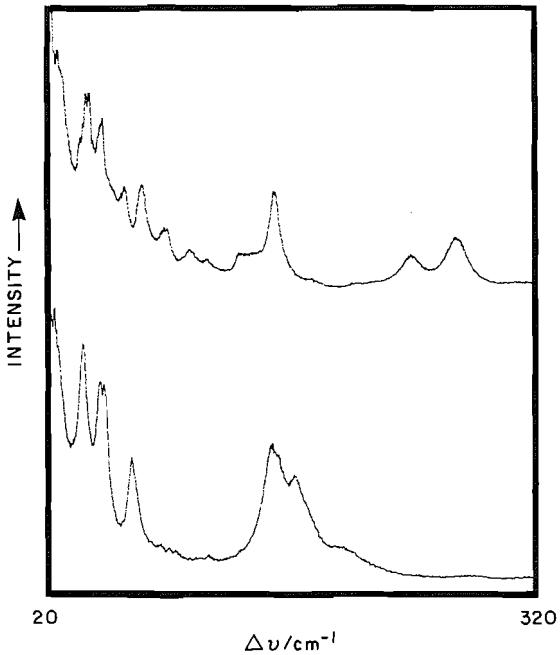

FIG. 2. Raman spectra of $(BiO)_4(OH)_2CO_3$ (top spectrum) and $(BiO)_2CO_3$ (bottom spectrum), as polycrystalline solids, for the 20–320 cm^{-1} region. Spectral band pass ~1 cm^{-1}, 647.1 nm excitation.

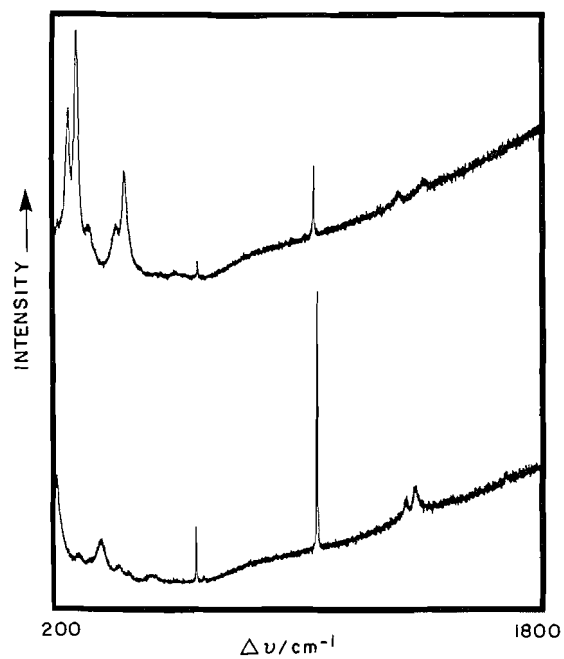

FIG. 3. Raman spectra of $(BiO)_4(OH)_2CO_3$ (top spectrum) and $(BiO)_2CO_3$ (bottom spectrum), as polycrystalline solids, for the 200–1800 cm^{-1} region. Spectral band pass ~1 cm^{-1}, 647.1 nm excitation.

from an impurity. We are also in essential agreement with Rulmont's report (14) of the Raman spectrum of $(BiO)_2CO_3$. However, we observed additional Raman bands closer to the exciting line, resolved some bands previously reported as single peaks into two or more features, and detected some additional low intensity features.

We have followed Herzberg's notation (15) in assigning the "internal vibrations" of hydroxyl and carbonate moieties in

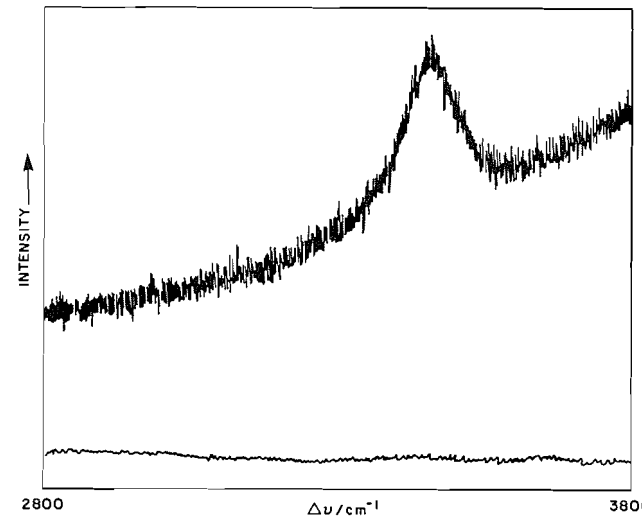

FIG. 4. Raman spectra $(BiO)_4(OH)_2CO_3$ (top spectrum) and $(BiO)_2CO_3$ (bottom spectrum), as polycrystalline solids, for the hydroxyl stretching region. Spectral band pass ~2 cm^{-1}, 514.5 nm excitation. These spectra are averages of four scans each.

Table 1. The fundamental vibrations of the carbonate ion are well established (15–19), and require no discussion. The assignment of some weak features to isotopically substituted species and overtone/combination bands is based on our earlier discussion in ref. 20.

The strong bands below 600 cm^{-1} are mainly due to "lattice vibrations". Those between 350 and 600 cm^{-1} probably arise from the motion of oxygen atoms in the polymeric $(BiO)_n^{n+}$ cation. This assignment is based on those suggested for the bismuth oxyhalides (BiOCl, BiOBr, BiOI, see refs. 14, and 21–25). These compounds have layered structures that are closely related to those of the carbonates, as discussed in the following section. There is an approximate correspondence between most of the lattice vibrations for $(BiO)_2CO_3$ and $(BiO)_4(OH)_2CO_3$, although the spectra of the latter compound are more complex, presumably reflecting its lower symmetry. Two strong bands at 244 and 272 cm^{-1} in the Raman spectrum of $(BiO)_4(OH)_2CO_3$ have no counterparts in the $(BiO)_2CO_3$ spectrum, so we tentatively assign them to concerted motions of the OH moieties.

The spectral features due to the internal vibrations of CO_3^{2-} are weaker for $(BiO)_4(OH)_2CO_3$ than for $(BiO)_2CO_3$, consistent with the former's lower carbonate content. The high symmetry structure (space group $I4/mmm$ (No. 139, D_{4h}^{17}), $z = 2$) suggested by Lagercrantz and Sillén (26) for $(BiO)_2CO_3$ requires carbonate ions to occupy sites with point symmetry D_{4h}. To reconcile this with the lower molecular symmetry, D_{3h}, of the ion, these authors postulated disorder or free rotation of the anions. Although a temperature-dependent study would be needed to rule out the possibility of freely rotating carbonate ions, the narrow profiles of the Raman bands assigned to carbonate vibrations do not seem consistent with a freely rotating anion, or a disordered structure (27–30). The sharp, narrow profiles of the bands assigned to the ν_1, ν_2, and ν_4 modes of CO_3^{2-} indicate orientational order in the carbonate sublattices of both solids. There is no observable splitting of the ν_1 mode of the carbonate ion in either compound, indicating that all the carbonate ions in each crystal structure occupy crystallographically equivalent sites. Turcotte *et al.* (12) made a similar observation for $(BiO)_2CO_3$, and for the "Type I" form of the

Can. J. Chem. Downloaded from www.nrcresearchpress.com by 210.87.254.40 on 09/06/12
For personal use only.

TABLE 1. Vibrational spectra of the two bismuth carbonates at room temperature[a]

$(BiO)_2CO_3$		$(BiO)_4(OH)_2CO_3$		
Infrared	Raman	Infrared	Raman	Assignment[b]
	23 m		25 m	
	40.5 vs		42 vs	
			44 vs	
	51 vs		52 vs	
	53 vs			
			66 m	
	70 vs		77 s	
	91 vw		92 m	
	94 vw		106 w	
	97 vw			
	118 vw		117 w	
			139 sh	
160[c]	158 vs		160 vs	
	162 sh			
	172 s			
			182 w, sh	
220[c]	203 m		210 w, br	
			244 s	
	277 vw	289 m	272 s	
303 m	312 vvw	305 m	313 w	
		339 sh		
376 s	351 mw	362 m		
	410 vw		403 w	
		414 s	430 s	
	445 vw	450 ms		
488 w		485 m		
	519 vw, br			
536 ms		525 w, sh		
		586 s		
			600 vw, br	
671 w	667 m	676 w	671 w	ν_4
691 w	688 vw	700 vw		ν_4
819 vw				$\nu_2[^{13}CO_3^{2-}]$
845 vs		853 ms		ν_2
		867 m		
			1037 vvw	$\nu_1[(C^{18}O^{16}O_2)^{2-}]$
1065 vvw	1067 vs		1056 s	ν_1
1351 sh	1360 w		1337 w	ν_3
1389 vs	1392 mw	1384 vs	1415 w	ν_3
	1690 vw		1705 vvw, br	$2\nu_2$
1734 vw		1727 vw		$\nu_1 + \nu_4$
1755 vvw				
		3430 w	3455 w	ν_{OH}

[a]All frequencies are in cm^{-1}; s, m, w, v, br and sh stand for strong, medium, weak, very, broad, and shoulder, respectively.
[b]See text for the assignment of some of the lattice modes.
[c]Bands observed in AgI matrix by Rulmont (14).

lanthanide oxycarbonates, $(LnO)_2CO_3$. This contrasts with the situation in the basic lead carbonates, hydrocerussite and plumbonacrite, and in the "Type IA" lanthanide oxycarbonates, all of which appear to contain more than one crystallographically distinct carbonate site (12, 20). The ν_2 mode is absent in our Raman spectra of the bismuth carbonates, and the ν_1 mode is a very weak feature of the infrared spectra, indicating that the carbonate ions are only slightly distorted from C_{3h} or D_3 symmetry. The reduction of molecular point symmetry from D_{3h} to either C_{3h} or D_3 does not change the selection rule for the ν_1 and ν_2 modes of the carbonate ion, as shown in the correlation table of the D_{3h} point group (31). Any further lowering of the carbonate site symmetry should make the ν_1 mode infrared-active and the ν_2 mode Raman-active.

The ν_1 mode frequency of CO_3^{2-} is about 10 cm^{-1} lower, and the splitting of the ν_3 mode is about 50 cm^{-1} greater, in $(BiO)_4(OH)_2CO_3$ than in $(BiO)_2CO_3$ (Table 1), suggesting weak hydrogen bonding between the OH^- and CO_3^{2-} ions. The OH stretching frequency is ~3455 cm^{-1}, confirming that hydrogen bonding is not strong. The sharp, well-defined shape of this band suggests that all hydrogen bonds are of approximately equal strength. Using the Lippincott–Schroeder curve, we estimate a hydrogen-bonded O(H) . . . . O distance of about 2.9Å (18, 32).

A calculation of lattice modes (33) for $(BiO)_2CO_3$, based on the primitive cell of the body-centred lattice reported by

Can. J. Chem. Downloaded from www.nrcresearchpress.com by 210.87.254.40 on 09/06/12
For personal use only.

Can. J. Chem. Downloaded from www.nrcresearchpress.com by 210.87.254.40 on 09/06/12
For personal use only.

Lagercrantz and Sillén (26), gives ten translational and two rotational modes ($A_{1g} + 3A_{2u} + B_{2g} + 2E_g + 3E_u$ and $A_2g + E_g$, respectively). Two of the translational lattice modes, one A_{2u} and one E_u, correspond to the acoustic branch, and will be optically inactive. The total numbers of infrared- and Raman-active lattice modes will thus be only four ($2A_{2u} + 2E_u$) and six ($A_{1g} + A_{2g} + B_{2g} + 3E_g$), respectively. The numbers of observed features in the lattice-vibration regions of the $(BiO)_2CO_3$ spectra are much greater (Table 1), indicating a larger unit cell and/or lower symmetry than in the reported structure (26). This is consistent with reports of a superlattice, in refs. 2 and 34. This combination of spectroscopic and crystallographic evidence prompted us to develop an alternative structural model for $(BiO)_2CO_3$, as described below.

4. *Crystallography*

The crystal structure of $(BiO)_2CO_3$

Lagercrantz and Sillén (26) showed that $(BiO)_2CO_3$ contains polymeric cations, $(BiO)_n^{n+}$, with a layer structure in which Bi atoms lie alternately above and below the interstices in a square lattice of O atoms, which is parallel to the (001) plane. These cations are stacked in a centred manner, such that the Bi atoms on the lower side of one layer lie directly above those on the upper side of the layer below. The stacking is body-centred with respect to the tetragonal sublattice, and face-centred with respect to the orthorhombic superlattice, as discussed below. The carbonate anions occupy two-dimensional tesselated arrays of tetragonal cavities, 3.87 Å × 3.87 Å × 4.38 Å, which are defined by the Bi atoms, as shown in Fig. 5. Many other oxysalts of Bi, Pb, and the lanthanides contain similar cations, with different stacking arrangements that are determined by their stoichiometries (14, 26, 35, 36). Bismutite is isostructural with the Type I lanthanide oxycarbonates, $(LnO)_2CO_3$ (12, 37).

Lagercrantz and Sillén (26) deduced that the tetragonal lattice of $(BiO)_2CO_3$, as indicated by X-ray diffraction (a = 3.867 Å, c = 13.686 Å), could only accommodate the carbonate ions in orientations parallel to the {110} planes, since other arrangements result in exceedingly close inter-anionic contacts. They favoured a disordered structure, but did not rule out an ordered arrangement. However, they reported Bi . . . . OCO_2 distances as low as 2.19 Å, which seems improbably short when compared with the Bi—O bond-length of 2.29 Å within the cation layers. Such a strong bond would cause much greater distortion of the carbonate anion than the spectroscopic data indicate (see section III.3).

Sahama and Lehtinen (2) and Nefedov (34) independently reported an orthorhombic, diagonal superlattice ($a' = b' = \sqrt{2}a$) for $(BiO)_2CO_3$. This superlattice removes the constraint for all carbonate ions to lie in identical orientations; indeed, it probably arises from an ordered alternation of anion orientations.[3] This is consistent with the conclusions in section III.3, that the structure is ordered, and has a larger unit cell and/or lower symmetry than is indicated by X-ray diffraction. (X-ray diffraction intensities are dominated by the Bi sublattice.)

Given the high symmetry of the anion cavity (Fig. 5), we expect one of the C_2 axes of the carbonate ion to coincide with one of the symmetry elements of the cavity. We considered two

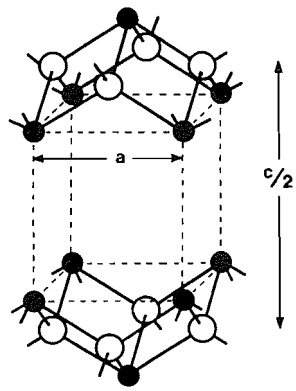

FIG. 5. Sections of two polymeric cations, $(BiO)_n^{n+}$, in the crystal structure of $(BiO)_2CO_3$. The broken lines outline an anion cavity. The dimensions a and c refer to the tetragonal unit cell of Lagercrantz and Sillén (26). Small filled circles and large open circles represent Bi and O atoms, respectively.

models, with a C_2 axis of the anion parallel and perpendicular to the crystallographic c-axis, respectively.[4] Each model could accommodate tolerable O . . . . O and Bi . . . . O contact distances (≥ 2.8 Å and 2.4 Å, respectively). Two possible arrangements, which are compatible with a $\sqrt{2}a$, $\sqrt{2}a$ superlattice, are shown in Fig. 6. In each case, the carbonate groups have been rotated from the diagonal of the pseudotetragonal cell, to optimize Bi . . . . O and O . . . . O contacts. There is no clear-cut choice between these models; both arrangements depart from tetragonal symmetry, the departure being greater in Fig. 6(*b*).

The crystal structure of $(BiO)_4(OH)_2CO_3$

The diffraction patterns of $(BiO)_4(OH)_2CO_3$ and $(BiO)_2CO_3$, which are compared in Table 2, are similar, but many $(BiO)_4(OH)_2CO_3$ peaks occur at d-values higher than the corresponding peaks for $(BiO)_2CO_3$. Also, some peaks are split into doublets, and many additional weak features are present. The two crystal structures thus appear related, but $(BiO)_4(OH)_2CO_3$ has a larger unit cell, and lower symmetry, than $(BiO)_2CO_3$.

We indexed all 23 strong diffraction peaks ($I/I_o > 5$) of $(BiO)_4(OH)_2CO_3$ on the basis of a monoclinic subcell, derived from the tetragonal pseudo-cell of $(BiO)_2CO_3$. The cell dimensions were refined, using the least-squares computer program of Appleman and Evans,[5] and constraining a and b to be equal by including *hkl* and *khl* reflections with equal d in the input data. This yielded the dimensions and standard deviations $a = b = 3.8451(3)$ Å, $c = 14.7574(11)$ Å, $\gamma = 91° 5.7(0.4)'$, with a maximum 2θ discrepancy of 0.020°. Systematic instrumental errors were not estimated, so the computed standard deviations reflect the precision, but not the accuracy, of the diffraction data. The excellent agreement between observed and calculated 2θ, with a and b held equal, indicates that the true symmetry is orthorhombic, with the monoclinic cell edges lying on diagonals of the orthorhombic lattice.

Most of the remaining weak diffraction peaks were indexed on the basis of a $2\sqrt{2}a$, $\sqrt{2}a$ orthorhombic superlattice derived from the monoclinic subcell, as shown in Table 2. The

[3]Sahama and Lehtinen (2) also observed electron diffraction features corresponding to a still larger superlattice, $a'' = 5a'$, for one sample of natural bismutite. We suspect that this arises from deviations from the ideal stoichiometry, $(BiO)_2CO_3$, rather than from purely structural/geometrical origins.

[4]In their discussion of $(LnO)_2CO_3$ structures, Turcotte *et al.* (12) only considered the perpendicular orientation, and only with the anion lying parallel to {100} or {110} planes.

[5]D. E. Appleman and H. T. Evans, Jr. U.S. Geological Survey, Geological Division, Washington, D.C. 20244.

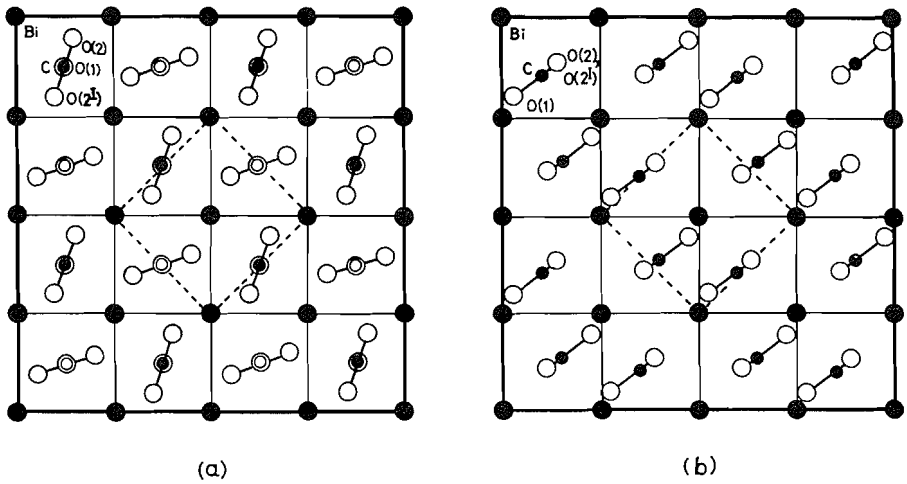

FIG. 6. Two possible arrangements of anion layers in $(BiO)_2CO_3$, viewed in projection down in the c-axis: (a) with a C_2 axis of the carbonate group, C—O(1), vertical, parallel to the crystallographic c-axis; (b) with C—O(1) horizontal. The arrangements are chosen to comply with the $\sqrt{2}a$, $\sqrt{2}a$ superlattice (broken lines), and to optimize Bi . . . . O and O . . . . O contact distances. Oxygen atoms in the polymeric cations have been omitted for clarity.

only unaccountable features with $d > 1.5$ Å were at 3.186, 2.777, 1.934, and 1.675 Å, all with $I/I_o \simeq 1$. Since these lie close to the major diffraction peaks of δ-Bi_2O_3 (3.187, 2.755, 1.953, 1.666 Å, ref. 38), we ascribe them to a δ-Bi_2O_3-like phase. The superlattice dimensions, calculated from the monoclinic subcell without further refinement, are a = 10.772(1), b = 5.4898(5), and c = 14.757(1) Å.

The related unit-cell dimensions of $(BiO)_2CO_3$ and $(BiO)_4(OH)_2CO_3$ indicate that the two structures contain similar cationic moieties. By analogy with other MOX salts (36), we assume that the longer c-axis in $(BiO)_4(OH)_2CO_3$ compared to $(BiO)_2CO_3$ reflects a greater inter-cation spacing. The inter-layer Bi . . . Bi distance in $(BiO)_2CO_3$, i.e., the depth of the anion cavity (Fig. 5), is $0.32c$ = 4.38 Å (2). The c-axis expansion, from 13.69 Å in $(BiO)_2CO_3$ to 14.76 Å in $(BiO)_4(OH)_2CO_3$, implies an inter-layer Bi . . . Bi spacing of 4.38 + 0.5(14.76 − 13.69) = 4.92 Å in the latter material (the factor of 0.5 arises because there are two layers per unit cell). It is noteworthy that $(BiO)_4(OH)_2CO_3$ has a higher volume per BiO^+ unit than $(BiO)_2CO_3$ (54.5 $Å^3$ vs. 51.3 $Å^3$). This contrasts, for example, with the relative crystallographic volumes per Pb atom for hydrocerussite and cerussite:

$\frac{1}{3}[Pb_3(OH)_2(CO_3)_2]$, 62.5 $Å^3$; $PbCO_3$, 67.5 $Å^3$ (39, 40).

Hydroxide ions might replace carbonate ions in $(BiO)_2CO_3$ to give $(BiO)_4(OH)_2CO_3$ in two ways: (i) complete substitution of alternate anion layers, or (ii) substitution of alternate anions within each layer. The first possibility can be ruled out, since alternation of $(BiO)_2CO_3$-type and BiOX-type (X = OH) layers would give a complex cation-stacking sequence, and hence a much longer c-axis than is observed (see Fig. 2 of ref. 2). Also, the anion layers would be too far apart, and too efficiently shielded by the cations, to permit the hydroxide-to-carbonate hydrogen-bonding, OH . . . . OCO_2, which was discussed in section III.3. The second possibility is compatible with both the spectroscopic and diffractometric data. The observed diagonal superlattice is consistent with the removal of alternate carbonate ions; the further doubling of a suggests a further alternation in the manner of their replacement by hydroxide ions.

Since there is only one type of cavity in the $(BiO)_2CO_3$ structure that can accommodate anions, each substituted cavity in $(BiO)_4(OH)_2CO_3$ must contain two hydroxide ions. These are expected to occupy diametrically opposed sites within the cavity. We believe that the observed c-axis expansion is caused by this "crowding" of anions; expansion in the ab plane is severely constrained by the rigidity of the cation (36).

We have developed a structural model for $(BiO)_4(OH)_2CO_3$ by placing pairs of hydroxide ions in alternate sites, and then adjusting anion positions to avoid unrealistically close contacts, and to achieve an efficient anion packing arrangement. This procedure was greatly assisted by assuming a rigid geometry for the $(BiO)_n^{n+}$ cations. (The departure from tetragonal dimensions necessitates a slight distortion of the cation.) The structural model was refined to meet six criteria: (i) No inter-anionic O . . . . O contacts should be less than 3.0 Å, except the slightly shorter hydrogen-bonded contacts. (ii) Weak bonding interactions between the anions and bismuth were accepted, with a minimum Bi . . . . O contact of 2.5 Å. (iii) The carbonate ion retains D_{3h} symmetry, with C—O = 1.29 Å (41). (iv) All CO_3^{2-} ions are crystallographically equivalent. (v) All OH^- ions have similar environments. (vi) There is no obvious "wasted space" in the anion packing.

The final structural model for the anion layer in $(BiO)_4(OH)_2CO_3$ is shown in Fig. 7. Atomic positional parameters and interatomic distances are listed in Tables 3 and 4, respectively. This model corresponds to the triclinic system, space group $P\bar{1}$ (No. 2, C_i^1). Higher dimensional symmetry is retained within experimental error, i.e., the triclinicity is very slight, because the anions are only slightly displaced from positions of higher symmetry. We emphasize that this is not a refined crystal structure in the usual sense, but is a realistic model based on limited structural data and reasonable crystal-chemical constraints.

This structure can accommodate several hydrogen-bonding arrangements, since the hydroxide ions are approximately equidistant from oxygen atoms on three different carbonate groups (e.g., O(1) has close contacts to O(4), O(5), $O(3^I)$ and $O(3^{II})$). We favour the arrangement shown in Fig. 7, because each hydroxide group is antiparallel to its three closest neighbour hydroxides. However, the atomic displacement required to achieve other hydrogen-bonding configurations are slight

Can. J. Chem. Downloaded from www.nrcresearchpress.com by 210.87.254.40 on 09/06/12
For personal use only.

TABLE 2. Comparison of X-ray powder diffraction data for $(BiO)_4(OH)_2CO_3$ and $(BiO)_2CO_3$

$(BiO)_4(OH)_2CO_3$				$(BiO)_2CO_3$[a]		
hkl[b]	d_{calcd}[b]	d_{obs}	I/I_o[c]	hkl	d_{obs}	I/I_o
002	7.3790	7.3740	~30[d]	002	6.85	15
011	5.1453	5.1437	2			
202	4.3503	4.3498	1			
112	4.0769	4.0750	3			
211	3.7204	3.7201	35	101	3.724	30
004	3.6895	3.6885	~15[d]	004	3.422	14
113	3.4685	3.4679	3			
213	3.0292	3.0296	100	103	2.953	100
114	2.9455	2.9450	2			
311	2.9445					
020	2.7449	2.7438	20	110	2.737	41
400	2.6929	2.6929	~20[d]			
121	2.6177	2.6178	1			
015	2.5997	2.5994	2			
304	2.5732	2.5740	4			
022	2.5727			112	2.542	6
402	2.5297	2.5295	6			
006	2.4597	2.4597	~10[d]	006	2.280	13
023	2.3970	2.3963	1			
215	2.3412	2.3418	6			
024	2.2023	2.2025	8	114	2.137	25
404	2.1751	2.1745	10			
124	2.1576	2.1576	1			
321	2.1572					
322	2.0913	2.0901	1			
502	2.0680	2.0674	1			
224	2.0384	2.0383	1			
306	2.0292	2.0295	2			
405	1.9894	1.9884	1			
511	1.9872					
017	1.9681	1.9683	3			
420	1.9223	1.9220	15	200	1.9354	20
415	1.8703	1.8700	2			
504	1.8604	1.8601	6	202	1.8620	6
422	1.8602					
217	1.8486	1.8489	10			
026	1.8318	1.8323	8			
406	1.8161	1.8163	9	116	1.7502	22
031	1.8160					
126	1.8059	1.805 sh	1			
130	1.8041					
132	1.7525	1.7521	1			
208	1.7452	1.7456	3			
231	1.7208	1.7207	5			
424	1.7048	1.7042	4	211[e]	1.7178	11
611	1.6951	1.6954	4	204	1.6843	9
520	1.6947					
407	1.6600	1.6591	1			
515	1.6588					
233	1.6342	1.6342	12			
109	1.6211	1.6212	1	213[e]	1.6184	30
134	1.6207					
506	1.6206					
331	1.6205					
613	1.6121	1.6119	11			
332	1.5920	1.593 sh	1			
417	1.5890	1.5890	2			
035	1.5553	1.5546	2			
119	1.5547					
516	1.5543					
426	1.5146	1.5148	6	206	1.4760	9

Can. J. Chem. Downloaded from www.nrcresearchpress.com by 210.87.254.40 on 09/06/12
For personal use only.

TABLE 2. (*Concluded*)

$(BiO)_4(OH)_2CO_3$				$(BiO)_2CO_3$[a]		
hkl[b]	d_{calcd}[b]	d_{obs}	I/I_o[c]	*hkl*	d_{obs}	I/I_o
219	1.5083	1.5081	8	109	1.4166	9
621	1.4947	1.4946	1			
235	1.4942					
0010	1.4758	1.4758	3[d]	0010	1.3688	7
228	1.4727	1.4728	3			
622	1.4722					

[a]Data of Sahama and Lehtinen (2); indexed on pseudo-tetragonal cell, $a_0 = 3.870 \pm 0.002$ Å, $c_0 = 13.697 \pm 0.005$ Å, $Z = 2$, $\rho_{calcd} = 8.25$. Our results for synthetic $(BiO)_2CO_3$ are in good agreement with these data.

[b]Based on orthorhombic unit cell with $a_0 = 10.7716 \pm 0.0015$ Å, $b_0 = 5.4898 \pm 0.0008$ Å, $c_0 = 14.7574 \pm 0.0022$ Å (2σ), $Z = 4$, $\rho_{calcd} = 7.56$.

[c]Based on peak height measurements from diffractogram.

[d]These reflections are subject to slight preferred orientation effects.

[e]The 211 and 213 reflections for $(BiO)_2CO_3$ correspond to (231 + 611) and (233 + 613), respectively, for $(BiO)_4(OH)_2CO_3$.

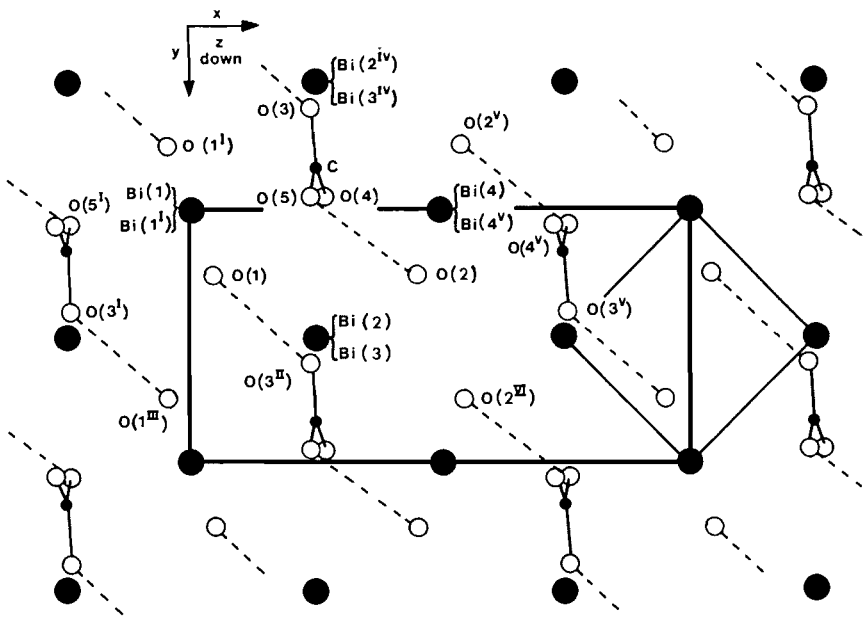

FIG. 7. Structural model for $(BiO)_4(OH)_2CO_3$, viewed in projection down the *c*-axis. The notation corresponds to that in Tables 3 and 4. The unit cell is outlined; the monoclinic (pseudo-tetragonal) sublattice is delineated by the Bi atoms. The oxygen atoms in the cation, and the second layer of Bi atoms, are omitted for clarity.

(<0.3 Å).

We can say little about the anion-layer stacking sequence in either $(BiO)_2CO_3$ or $(BiO)_4(OH)_2CO_3$, except that polytypic or disordered sequences seem likely, because of the high symmetry of the cations, and the effective shielding of the anion layers by the cations, in each structure. Any conclusions based on X-ray diffraction intensities would be tenuous, because of the dominance of Bi. However, the diffraction pattern of $(BiO)_4(OH)_2CO_3$ (Table 2) does include weak reflections that disobey both face-centring and body-centring conditions. A complete structural analysis of either compound would probably require high quality neutron-diffraction data.

5. Comments on natural occurrence

We have identified a previously undescribed basic bismuth carbonate, $(BiO)_4(OH)_2CO_3$, which is not identical with either of the unidentified solids observed by Lagercrantz and Sillén (26) in their hydrothermal synthesis of $(BiO)_2CO_3$ crystals, although they may well be structurally related. The narrow stability field of $(BiO)_4(OH)_2CO_3$ precludes its widespread occurrence in oxidized bismuth ore deposits. However, its presence could account for the water-rich, carbonate-deficient analyses reported by Sahama and Lehtinen for some natural bismutite specimens (2). Nearly all the analyses of natural bismutite, shown in Fig. 2 of ref. 2, lie within the composition triangle $(BiO)_2CO_3-(BiO)_4(OH)_2CO_3-H_2O$. This suggests that much of the water is indeed non-essential, as asserted by Frondel, but that some is chemically incorporated in $(BiO)_4(OH)_2CO_3$. It is interesting that this empirical formula corresponds to that of "Basobismutite", which was reported by Nenadkevitch (42), but was discredited by Frondel (1). We have observed minor quantities of both $(BiO)_4(OH)_2CO_3$ and $(BiO)_2CO_3$ on the surface of α-Bi_2O_3 powders that had been exposed to moist air. Therefore, it may well be worth exam-

Can. J. Chem. Downloaded from www.nrcresearchpress.com by 210.87.254.40 on 09/06/12
For personal use only.

Can. J. Chem. Downloaded from www.nrcresearchpress.com by 210.87.254.40 on 09/06/12
For personal use only.

TABLE 3. Atomic positional parameters describing one anion layer in the model structure for $(BiO)_4(OH)_2CO_3$[a]

Atom	x/a_0	y/b_0	z/c_0
Bi(1)[b]	0	0	0.1667[c]
Bi(2)	1/4	1/2	0.1667
Bi(3)	1/4	1/2	−0.1667
Bi(4)	1/2	0	0.1667
C	0.2526	−0.1676	−0.0007
O(1)	0.0427	0.2495	0.0271
O(2)	0.4568	0.2495	−0.0271
O(3)	0.2434	−0.4026	0.0000
O(4)	0.2690	−0.0510	0.0740
O(5)	0.2452	−0.0510	−0.0760

[a]Space group $P\bar{1}$ (C_i^1); cell dimensions are given in Table 2.
[b]Only those Bi atoms that delineate the anion cavities are listed. They do not occupy special positions, but they have not been displaced from sites (0,0,z), referred to the monoclinic sublattice. Additional Bi atoms are present at the positions (±1/4, 0, 1/3), (0,1/2, 1/3) and (1/2, 1/2, 1/3). The oxygen atoms in the $(BiO)_n^{n+}$ cations are situated at approximately (±1/8, ±1/4, 1/4) and (±3/8, ±1/4, 1/4). An additional anion layer is situated at $z/c \simeq 1/2$. The x and y coordinates of the atoms in this layer depend on the stacking sequence, as discussed in the text.
[c]The four-figure precision of the coordinates does not reflect the accuracy of the model, but was necessary to demonstrate that the model could meet the constraints on interatomic distances, within limits of ±0.01 Å.

TABLE 4. Interatomic distances in the structural model for $(BiO)_4(OH)_2CO_3$[a]

O(1) contacts		O(2) contacts	
Bi(1)	2.52	Bi(4^{V})	2.52
O(3^{II})	2.91	O(5)	2.91
O(1^{I})	3.00	O(2^{V})	3.00
O(1^{III})	3.01	O(2^{VI})	3.01
O(4)	3.03	O(4)	3.02
O(5)	3.14	O(3^{II})	3.01
O(3^{I})	3.21	O(3^{V})	3.36
O(5^{I})	3.36	O(4^{V})	3.22
O(cat)[b]	3.41	O(cat)[b]	3.41

O(3) contacts		O(4) contacts		O(5) contacts	
Bi(2^{IV})	2.52	Bi(4)	2.85	Bi(3^{IV})	2.81
Bi(3^{IV})	2.52	Bi(2^{IV})	2.83	Bi(1^{I})	2.96
O(4)	2.23	O(3)	2.23	O(3)	2.23
O(5)	2.23	O(5)	2.23	O(4)	2.23
O(1^{IV})	2.91	O(1)	3.03	O(2)	2.91
O(2^{IV})	3.01	O(2)	3.02	O(1)	3.14
O(1^{I})	3.21	O(2^{V})	3.22	O(1^{I})	3.36
O(2^{V})	3.36	O(cat)[b]	3.04	O(cat)[b]	3.07
O(cat)[b]	4.00				
C	1.29	C	1.29	C	1.29

[a]Roman numeral superscripts refer to the following symmetry operations on the parameters given in Table 3: I, ($\bar{x}$, $\bar{y}$, $\bar{z}$); II, (x, 1+y, z); III, ($\bar{x}$, 1−y, $\bar{z}$); IV, (x, y−1, z); V, (1−x, $\bar{y}$, $\bar{z}$); VI, (1−x, 1−y, $\bar{z}$). The numbering of atoms corresponds to that in Fig. 7.
[b]O(cat) refers to the closest contact of each oxygen to an oxygen atom in the cationic moiety.

ining samples of bismite (natural α-Bi_2O_3) and bismutite for possible minor natural occurrences of $(BiO)_4(OH)_2CO_3$.

NOTE ADDED IN PROOF: We have just learned that Levin and Roth (43) reported an unidentified compound, formed by aging Bi_2O_3 in air. They reported X-ray diffraction features at d = 3.71, 3.68, 3.02, 2.74, and 2.45 Å. These correspond to major peaks in the diffraction pattern of $(BiO)_4(OH)_2CO_3$ in Table 2.

Acknowledgements

We are grateful to A. M. Duclos and J. M. Snider for obtaining the X-ray diffraction data, to N. J. Flemming and B. L. Sanipelli for the thermogravimetric measurements, to M. H. Brooker for the infrared spectrum (PE-225 instrument) of $(BiO)_2CO_3$, and to R. I. Haines for the FT-IR spectra. Part of this work was jointly funded by AECL and Ontario Hydro under the CANDEV agreement.

1. C. FRONDEL. Am. Miner. **28**, 521 (1943).
2. T. G. SAHAMA and M. LEHTINEN. Bull. Geol. Soc. Finland, **40**, 145 (1968).
3. R. R. STASKO and G. A. VIVIAN. An overview of the Ontario Hydro Carbon-14 Control Program. in: Proc. Int. Conf. Radioactive Waste Management, Winnipeg, September 1982. Canadian Nuclear Society, Toronto. pp. 547−553.
4. P. TAYLOR and V. J. LOPATA. Can. J. Chem. **62**, 395 (1984).
5. F. LAZARINI. Acta Crystallogr. B**35**, 448 (1979).
6. F. LAZARINI. Acta Crystallogr. B**34**, 3169 (1978).
7. F. LAZARINI. Cryst. Struct. Commun. **8**, 69 (1979).
8. C. W. BECK. Am. Miner. **35**, 985 (1950).
9. C. W. DAVIES. *In* Ion association. Butterworths, London. 1962. Chapt. 3.
10. R. A. ROBIE, B. S. HEMINGWAY, and J. R. FISHER. U. S. Geol. Surv. Bull. 1452 (reprinted with corrections, 1979).
11. J. M. HUNT, M. P. WISHERD, and L. C. BONHAM. Anal. Chem. **22**, 1478 (1950).
12. R. P. TURCOTTE, J. O. SAWYER, and L. EYRING. Inorg. Chem. **8**, 238 (1969).
13. R. A. NYQUIST and R. O. KAGEL. Infrared spectra of inorganic compounds. Academic Press, New York. 1971. p. 82.
14. A. RULMONT. Mem. Cl. Sci. Acad. R. Belg. Collect. 8°, **42** (87 pp.) (1976).
15. G. HERZBERG. Molecular spectra and molecular structure. II. Infrared and Raman spectra of polyatomic molecules. Van Nostrand, New York. 1962. pp. 177−179.
16. L. COUTURE. Ann. Phys. **12**, 5 (1947).
17. S. D. ROSS. Inorganic infrared and Raman spectra. European Chemistry Series. McGraw Hill, London. 1972. pp. 141−160.
18. W. B. WHITE in Monograph 4: The infrared spectra of minerals. *Edited by* V. C. Farmer. Mineralogical Society, London. 1974. pp. 227−284.
19. K. NAKAMOTO. Infrared and Raman spectra of inorganic and coordination compounds. 3rd ed. Wiley, New York. 1978. p. 129.
20. M. H. BROOKER, S. SUNDER, P. TAYLOR, and V. J. LOPATA. Can. J. Chem. **61**, 494 (1983).
21. R. BONNAIRE. C. R. Acad. Sci. Ser. B, **268**, 1415 (1968).
22. A. RULMONT. C. R. Acad. Sci. Ser. B, **272**, 1364 (1971).
23. A. RULMONT. Spectrochim. Acta Part A, **28**, 1287 (1972).
24. J. E. D. DAVIES. J. Inorg. Nucl. Chem. **35**, 1531 (1973).
25. A. RULMONT. Spectrochim. Acta Part A, **30**, 311 (1974).
26. Å. LAGERCRANTZ and L. G. SILLÉN. Arkiv f. Kemi, Miner. o. Geol. **25**A, No. 20 (1947).
27. E. WHALLEY. J. Chem. Phys. **51**, 4040 (1969).
28. J. E. BERTIE and S. SUNDER. J. Chem. Phys. **59**, 3853 (1973).
29. W. B. WHITE. *In* Monograph 4: The infrared spectra of minerals. *Edited by* V. C. Farmer. Mineralogical Society, London. 1974. pp. 87−110.

30. S. SUNDER. Can. J. Chem. **57**, 846 (1979).
31. E. B. WILSON, JR., J. C. DECIUS, and P. C. CROSS. Molecular vibrations. McGraw-Hill, New York. 1955. p. 388.
32. E. R. LIPPINCOTT and R. SCHROEDER. J. Chem. Phys. **23**, 1099 (1955).
33. D. L. ROUSSEAU, R. P. BAUMAN, and S. P. S. PORTO. J. Raman Spectrosc. **10**, 253 (1981).
34. E. I. NEFEDOV. Inform. Sbornik Vsesoyuz. Nauch.-Issledovatel. Geol. Inst. No. 3, 80 (1956); abstract only seen.
35. P. E. CARO. J. Less-Common Metals, **16**, 367 (1968).
36. A. F. WELLS. Structural inorganic chemistry. 4th ed. Clarendon Press, Oxford. 1975. pp. 408–409.
37. J. O. SAWYER, P. CARO, and L. EYRING. Monatsh. Chem. **102**, 333 (1971).
38. J. W. MEDERNACH and R. L. SNYDER. J. Am. Ceram. Soc. **61**, 494 (1978).
39. J. K. OLBY. J. Inorg. Nucl. Chem. **28**, 2507 (1966).
40. K. SAHL. Z. Krist. **139**, 215 (1974).
41. J. P. R. DEVILLIERS. Am. Miner. **56**, 758 (1971).
42. K. A. NENADKEVITCH. Bull. Acad. Sci. Petrograd, **7**, 447 (1917); abstract only seen.
43. E. M. LEVIN and R. S. ROTH. J. Res. NBS, **68**A, 189 (1964).

Can. J. Chem. Downloaded from www.nrcresearchpress.com by 210.87.254.40 on 09/06/12
For personal use only.

Glycosides from *Muscari comosum*. 6[1]. Use of homo- and heteronuclear two-dimensional nuclear magnetic resonance spectroscopy for the structure determination of the novel glycoside muscaroside C

R. LANZETTA, G. LAONIGRO, AND M. PARRILLI[2]

Dipartimento di Chimica Organica e Biologica della Università di Napoli, Via Mezzocannone 16, 80134 Napoli, Italy

AND

E. BREITMAIER

Institut für Organische Chemie und Biochemie der Universität Bonn, Gerhard-Domagk-Str. 1,D-5300 Bonn 1, Federal Republic of Germany

Received May 23, 1984

R. LANZETTA, G. LAONIGRO, M. PARRILLI, and E. BREITMAIER. Can. J. Chem. **62**, 2874 (1984).

A combined use of homo- and heteronuclear nmr spectroscopy in the structure elucidation of a minor glycoside extracted from the bulbs of *Muscari comosum* is described. This glycoside **1**, termed muscaroside C, posseses a β-D-apio-D-furanosyl-(1→2)-β-D-glucopyranosyl(1→2)-α-L-arabinopyranosyl(1→6)-β-D-glucopyranosyl chain linked at the 3-position of (23*S*)-17,23-epoxy-3β,30,31,-trihydroxy-27-nor-5α-lanost-8-ene **2**.

R. LANZETTA, G. LAONIGRO, M. PARRILLI et E. BREITMAIER. Can. J. Chem. **62**, 2874 (1984).

On décrit une utilisation combinée des spectroscopies rmn homo- et hétéronucléaires permettant l'élucidation de la structure d'un glycoside mineur extrait des bulbes du *Muscari comosum*. Ce glycoside (**1**), que l'on a appelé muscaroside C, possède une chaîne β-D-apiofurannosyl (1→2) β-D-glucopyrannosyl (1→2) α-L-arabinopyrannosyl (1→6) β-D-glucopyrannosyle qui est reliée à la position 3 du (23*S*)-époxy-17,23 trihydroxy-3β,30,31 nor-27 5α-lanostène-8 (**2**).

[Traduit par le journal]

In connection with our studies (1–5) on the glycoside fraction of *Muscari comosum* we recently reported the isolation and structure determination of muscarosides A (4) and B (5). In this paper we describe the structure elucidation of a minor glycoside, muscaroside C, **1**, which possesses a β-D-apio-D-furanosyl(1→2)-β-D-glucopyranosyl-(1→2)-α-L-arabinopyranosyl(1→6)-β-D-glucopyranosyl chain linked at the 3-position of (23*S*)-17,23-epoxy-3β,30,31-trihydroxy-27-nor-5α-lanost-8-ene **2** (2).

Muscaroside C was obtained by column chromatography and hplc purification (C-18 reverse phase column) of the crude glycoside extracted from bulbs as a homogeneous (tlc, ^{1}H and ^{13}C nmr spectroscopy) amorphous solid.

The FAB-ms spectrum of **1** showed a pseudomolecular ion peak at m/z 1085 ($M + Na^+$) which, together with ^{13}C data, suggested the molecular formula $C_{51}H_{82}O_{23}$.

Acid hydrolysis (7% H_2SO_4) of muscaroside C, which caused decomposition of the aglycone (3), afforded glucose, arabinose, and apiose as identified by tlc and hplc comparison with equilibrated authentic samples of the monosaccharides. A 2:1:1 molar ratio of glucose, arabinose, and apiose was established on integration of hplc peak areas and confirmed by fragmentation of **1** in the FAB-ms spectrum which showed the loss of two hexose units (see below).

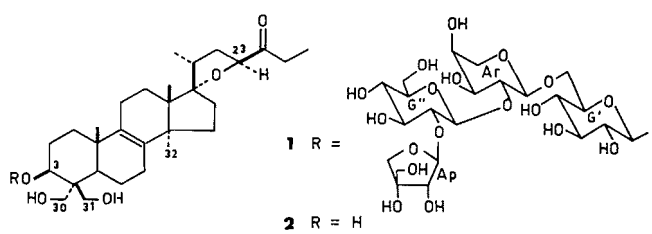

Owing to the small amount of **1** available, structure determination was essentially based on nmr spectroscopy rather than chemical degradative methods. The results of the spectroscopic investigation are presented in Table 1.

The ^{1}H spectrum of **1** in Py-d_5 at 500 MHz shows, in the downfield part, four anomeric proton signals as doublets at δ 6.40 (2.0 Hz), 5.18 (4.1 Hz), 5.14 (7.8 Hz), and 5.07 (7.3 Hz); in the 4.8–3.6 ppm region, overlapping resonances of oligosaccharide rings; and, in the upfield part, signals of the aglycone moiety. In this zone the signals of five methyl groups are clearly recognized; three of them are tertiary (δ 0.92 s, 1.04 s, 1.47 s), one is secondary (δ 1.02 d), and one is primary (δ 1.04 t). In addition, a methylene signal appears at δ 2.52 as a quartet, correlated by scalar coupling with the primary methyl group. In combination with the general appearance of the ^{1}H nmr spectrum, these findings suggested **2** to be the aglycone moiety of **1**.

The ^{13}C nmr data were obtained from a proton noise-decoupled spectrum and from DEPT (6) experiments that allowed us to recognize the number of CH, CH_2, and CH_3 carbons unequivocally. The striking similarity between ^{13}C data of **1** in Py-d_5 and those of **2** in $CDCl_3$[3] (see Table 1) definitively confirmed the identification of the aglycone moiety. In this respect it is also important to emphasize that **2** had been isolated previously (2) on enzymatic hydrolysis of the entire *Muscari comosum* glycoside fraction.

The ^{13}C nmr permits identification of monosaccharide ring size by comparison with ^{13}C signal values of reference methyl-glycosides and, on the basis of the glycosylation shift (7–10), the positions of interglycosidic linkages. However, the identification of ^{13}C signals belonging to each single monosaccharide residue is often a serious problem when more units of the same

[1]Part 5: ref. 5.

[2]Author to whom correspondence should be addressed.

[3]The different solvents can be assumed not to affect the validity of this comparison as a closely related compound, eucosterol, displays very similar ^{13}C chemical shifts in both Py-d_5 and $CDCl_3$ (1, 4); see also ref. 7.

Can. J. Chem. Downloaded from www.nrcresearchpress.com by 210.87.254.6 on 09/06/12
For personal use only.

TABLE 1. ^{1}H and ^{13}C data of muscaroside C from one- and two-dimensional experiments, and ^{13}C chemical shifts of reference substances (glycosylation shift)

Carbon	Reference substance[a]	DEPT[b]	Muscaroside C[b]	Proton	2D-COSY[b,c]	$J_{Z,Y}$[d] Hz	Z	Y
1	A[b] 105.4	CH	G′ 105.5	1	5.14	7.8	1	2
2	74.8	CH	75.5	2	4.00	9.1	2	3
3	78.1	CH	78.3	3	4.07	8.7	3	4
4	71.4	CH	72.6	4	4.20	9.5	4	5
5	78.1	CH	75.5 (−2.6)	5	3.82	4.0	5	6a
6	62.5	CH_2	68.8 (+6.3)	6a, 6b	4.41, 4.17	4.5	5	6b
						10.4	6a	6b
1	B[b] 105.9	CH	Ar 101.3 (−4.6)	1	5.18	4.1	1	2
2	72.2	CH	79.6 (+7.4)	2	4.52	[e]	2	3
3	74.4	CH	72.1 (−2.3)	3	4.55	[e]	3	4
4	69.1	CH	66.9	4	4.54	[e]	4	5
5	66.6	CH_2	63.2	5a, 5b	4.35, 3.82	11.2	5a	5b
1	A[b] 105.4	CH	G″ 103.7 (−1.7)	1	5.07	7.3	1	2
2	74.8	CH	79.8 (+5.0)	2	4.16	8.3	2	3
3	78.1	CH	77.6 (−0.5)	3	4.14	[e]	3	4
4	71.4	CH	71.2	4	4.22	[e]	4	5
5	78.1	CH	78.2	5	3.68	2.3	5	6a
6	62.5	CH_2	63.2	6a, 6b	4.33, 4.26	4.6	5	6b
						12.0	6a	6b
1	C[b] 111.2	CH	Ap 111.2	1	6.40	2.0	1	2
2	78.1	CH	77.9	2	4.79	2.0	2	1
3	80.4	C	80.4	—	—	—	—	—
4	75.3	CH_2	75.4	4a, 4b	4.80, 4.38	9.3	4a	4b
5	65.5	CH_2	66.0	5a, 5b	4.26	11.3	5a	5b
1	D[f] 35.5	CH_2	35.8	1a, 1b	1.70	[e]		
2	27.5	CH_2	27.3	2a, 2b	[2.38, 2.10]	[e]		
3	77.9	CH	82.2 (+4.3)	3	[4.49]	16.5[g]	3	2a, 2b
4	46.0	C	48.2[h]	—	—	—	—	—
5	47.3	CH	43.6 (−3.7)	5	2.20	[e]		
6	18.7	CH_2	18.8	6a, 6b	2.18	[e]		
7	26.2	CH_2	26.6	7a, 7b	1.40	[e]		
8	134.1	C	134.8	—	—	—		
9	135.5	C	135.8	—	—	—		
10	36.5	C	36.8	—	—	—		
11	20.8	CH_2	21.2	11a, 11b				
12	24.9	CH_2	25.4	12a, 12b	1.42	[e]		
13	48.7	C	49.0[h]	—	—	—		
14	50.6	C	50.9	—	—	—		
15	31.7	CH_2	32.2	15a, 15b	1.65, 1.35	[e]		
16	39.7	CH_2	39.8	16a, 16b	2.14	[e]		
17	97.2	C	97.2	—	—	—		
18	19.5	CH_3	19.4	18-H_3	0.92	—		
19	19.2	CH_3	19.7	19-H_3	1.04	—		
20	43.6	CH	43.8	20	[2.05]	[e]		
21	17.2	CH_3	17.3	21-H_3	[1.02]	6.6	20	21
22	36.8	CH_2	36.9	22a, 22b	[1.92, 1.78]	[e]		
23	81.5	CH	81.7	23	[4.61]	17.7[g]	22	23
24	213.6	C	212.5	—	—	—		
25	32.3	CH_2	32.4	25-H_2	2.52]	7.3	25	26
26	7.4	CH_3	7.7	26-H_3	1.04]	7.3	25	26
30	71.3	CH_2	61.2[i] (−10.1)	30a, 30b	4.92, 4.35	11.6	30a	30b

Can. J. Chem. Downloaded from www.nrcresearchpress.com by 210.87.254.6 on 09/06/12
For personal use only.

TABLE 1. (*concluded*)

Carbon	Reference substance[a]	DEPT[b]	Muscaroside C[b]	Proton	2D-COSY[b,c]	$J_{Z,Y}$[d] Hz	Z	Y
31	63.8	CH_2	62.7[i]	31a, 31b	4.58, 3.93	11.6	31a	31b
32	25.9	CH_3	26.3	32-H_3	1.47	—		

[a]Reference substances: A, methyl β-D-glucopyranoside (ref. 19); B, methyl α-L-arabinopyranosyl (ref. 19); C, methyl β-D-apio-D-furanoside (ref. 20); D, **2** (ref. 2).
[b]Measured in pyridine-d_5.
[c]Proton chemical shifts of the aglycone moiety were assigned mainly from two-dimensional carbon–proton shift correlation, except for some protons linked at carbons shifted by glycosylation (see text). Proton correlations clearly recognizable in the 2D-COSY are indicated by solid lines in the table.
[d]Absolute values of apparent coupling constants between protons Z and Y.
[e]Obscured by other resonances.
[f]Measured in $CDCl_3$.
[g]Value of $J_{AX} + J_{BX}$ of an X quartet of an ABX system.
[h]Interchangeable values.
[i]30-CH_2 and 31-CH_2 protons were assigned on the basis of nOe enhancements measured for the proton signals at δ 4.58 and at δ 4.35 upon irradiation of 19-H_3 and 3-H_α protons respectively.

monosaccharide are present in the sugar chain. This can now be facilitated by two-dimensional nmr experiments (11, 12) using nuclear proton shift correlation (COSY) (13) to establish the scalar connectivity of the proton resonances of each monosaccharide unit, starting from anomeric signals, and heteronuclear carbon–proton shift correlation (14) to trace out all one-bond carbon–proton connectivities. Substructures can be derived by combining the information of both shift correlation experiments.

Figure 1 displays the 2D-COSY spectrum of the 3.6–5.0 ppm and anomeric regions of **1** together with the corresponding segment of its one-dimensional spectrum. The analysis of 2D-COSY for one monosaccharide unit serves to illustrate the approach described above.

The anomeric proton at δ 5.14, indicated by G′-1 in Fig. 1, is coupled to the G′-2 signal at δ 4.00 and this to G′-3 at δ 4.07. Continuing this *J*-connectivity path (see figure, dotted lines), it was possible to identify G′-4 at δ 4.20, G′-5 at δ 3.82, G′-6a at δ 4.41, and G′-6b at δ 4.17. In this way the chemical shifts of all protons belonging to the G′ unit had been identified; they were subsequently assigned by two-dimensional carbon–proton shift correlation to the attached carbon chemical shifts at δ 105.5 (G′-1), 75.5 (G′-2), 78.3 (G′-3), 72.6 (G′-4), 75.5 (G′-5) and at δ 68.8 (G′-6) (see Table 1). When these ^{13}C data were compared with those of methyl β-D-glucopyranoside as reference, deshielding of G′-6 (+6.3) and shielding of G′-5 (−2.6) were observed, while the other chemical shifts were very similar. From these data a β-D-glucopyranosyl structure linked at its 6-position was inferred for the G′ residue.

Using a similar procedure, the ^{13}C data of other saccharide units of the sugar chain were assigned (see Table 1).

The downfield shifts observed for the Ar-2 (+7.2) and G″-2 (+5.0) signals, in addition to the upfield shifts of the Ar-1, Ar-3 and of the G″-1, G″-3 signals, compared with the ^{13}C data of methyl α-L-arabinopyranoside and methyl β-D-glucopyranoside, respectively, established that both of these units were linked at the 2-position. As for the apiose unit, a close similarity of its ^{13}C signals and those of methyl β-D-apio-D-furanoside indicated that this residue was the terminal one in the saccharide chain. This was confirmed by T_1 measurements: the apiose carbon atoms displayed the largest NT_1 values due to their segmental mobility at the end of the glycoside chain.

Analysis of the 2D-COSY spectrum also allowed assignment of those proton signals of the aglycone moiety which overlap saccharide resonances. Thus, the methine signals of 3-H_α and 23-H were identified at δ 4.49 and 4.61, respectively, while the protons of the AB systems of the 30- and 31-oxymethylene groups resonate at δ 4.92 and 4.35, and at δ 4.58 and 3.93, respectively. The carbons directly attached to these protons were identified by the heteronuclear-2D spectrum.

The glycosylation shift (+4.3) observed for C-3 of the aglycone moiety revealed (7–10) that the sugar chain is linked at this carbon. The upfield shifts of C-30 and C-5 signals were in agreement with this conclusion (9).

The proton assignments of **1** were also confirmed by the general appearance of the splitting patterns and, when it was possible, by $J_{H,H}$ values (see Table 1).

The sugar sequence was established by negative-ion FAB-ms on the basis of the following signals. The spectrum displayed a pseudomolecular ion at *m/z* 1061 $(M - H)^-$ and fragments at *m/z* 929 $((M - H) - 132)^-$, 767 $((M - H) - 132 - 162)^-$, 635 $((M - H) - 132 - 162 - 132)^-$, and 473 $((M - H) - 132 - 162 - 132 - 162)^-$, respectively, corresponding to the consecutive losses of the apiosyl, glucosyl, arabinosyl, and glucosyl units.

The significant Overhauser effect measured for the signal at δ 5.14 of the anomeric proton of the β-D-glucopyranosyl unit, linked at its 6-position upon irradiation of the 3-H_α proton, safely indicated that this glucose residue is directly attached to the aglycone moiety.

The relative configuration at the anomeric centres was inferred to be β for both glucopyranosyl units and for the apiosyl unit on the basis of the value of $^3J_{H\text{-}1,H\text{-}2}$ (7 Hz) (15) and the value of the anomeric carbon chemical shift (δ 111.2) (16), respectively.

No direct evidence for the α-configuration of the L-arabinopyranosyl unit was found, owing to its high conformational mobility (4, 5, 17). However, an α-configuration was inferred from the striking similarity between the ^{13}C data of the L-arabinopyranosyl unit of **1** and those found for the α-L-arabinopyranosyl residues identically located in muscarosides A and B (4, 5).

Can. J. Chem. Downloaded from www.nrcresearchpress.com by 210.87.254.6 on 09/06/12
For personal use only.

Can. J. Chem. Downloaded from www.nrcresearchpress.com by 210.87.254.6 on 09/06/12
For personal use only.

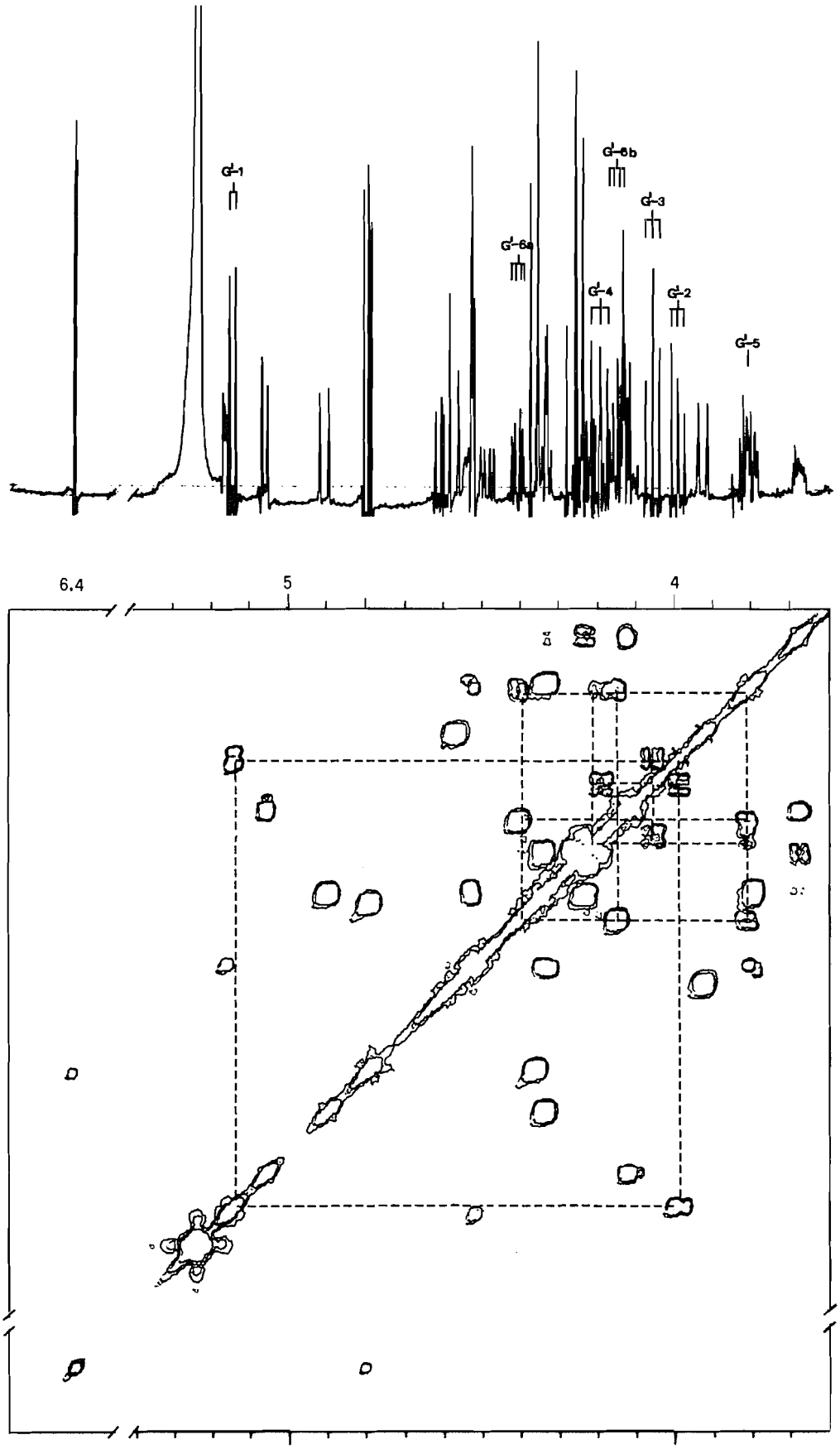

FIG. 1. One-dimensional proton nmr spectrum and two-dimensional proton correlated (COSY-45°) spectrum of **1** between 3.6 and 6.6 ppm. *J*-connectivities are indicated for residue G'.

Can. J. Chem. Downloaded from www.nrcresearchpress.com by 210.87.254.6 on 09/06/12
For personal use only.

Experimental

Mass spectra were recorded with a VG ZAB HF instrument equipped with a FAB source. The hplc analysis was performed with a Varian 5020 instrument using a Waters R 401 differential refractometer as the detector. Thin-layer chromatography was carried out on precoated silica gel layers (0.25 mm, Merck F_{254}). Silica gel 0.05–0.20 (Merck) was used for column chromatography. Sugars were detected with aniline phthalate or *p*-anisaldehyde, glycosides with chromium oxide/sulphuric acid.

Isolation of muscaroside C

Fraction b (ref. 4) gave by hplc (Lichrosorb RP-18 (7 μm), 70:30 methanol–water, 5 mL min^{-1}), besides muscaroside B (5), a minor impure product (20 mg). This was subjected twice, successively, to analytical hplc (Lichrosorb RP-18 (5 μm), 80:20 methanol–water, 0.5 mL min^{-1}) to give pure muscaroside C (6 mg); FAB-ms: 1085 $(M + Na)^+$ m/z. The ^1H and ^{13}C data are given in Table 1.

Acidic hydrolysis of muscaroside C

Acidic hydrolysis of muscaroside C was performed as for muscaroside A (4). The water-soluble fraction of the hydrolysate was analyzed by tlc (silica gel layers, 14:6:1 chloroform–methanol–water) and by hplc (Lichrosorb NH_2 (10 μm), 4:1 acetonitrile–water, 0.5 mL min^{-1}); the presence of apiose, glucose, and arabinose was established by comparison with authentic samples. The hplc peak areas of the monosaccharides occurring in the hydrolysate were in the same ratio as a 2:1:1 mixture of equilibrated authentic glucose, arabinose, and apiose. The latter was obtained by hydrolysis of apiin, a flavanoid glycoside, purchased from ICN-K&K (New York).

Proton and carbon nuclear magnetic resonance spectra

Proton spectra were obtained on a Bruker WM-500 spectrometer equipped with an Aspect 2000 computer, operating in the Fourier transform mode with quadrature detection. One-dimensional spectra were typically obtained with 5000-Hz spectral width (0–10 ppm), using TMS as internal reference. For removal of exchangeable protons, the sample (6 mg) was solubilized three successive times in CH_3OD (0.5 mL) and the solvent evaporated at low pressure. The residue was dissolved in 0.4 mL of Py-d_5 and placed in a 20 cm × 5 mm diameter nmr tube.

Nuclear Overhauser enhancements were obtained in the difference mode as reported in ref. 2.

Two-dimensional correlated spectroscopy (COSY-45) (18) was executed with 90°–45° pulses separated by an incrementable evolution time t_1. Each spectrum required a total of 32 pulses in a 512 × 2048 data set, which took approximately 10 h to acquire. Quadrature detection was applied in both directions using a 16-step phase cycling for N-type peak selection. Data were multiplied with a sine-bell shaping function, zero filled, Fourier transformed, and symmetrized. Processing and plotting time for the spectrum was approximately 2h.

Carbon spectra were taken at 100.576 MHz on a Fourier transform Bruker instrument WM-400, equipped with dual probe, using the same sample (6 mg of **1** dissolved in 0.4 mL of Py-d_5 in a 5-mm diameter nmr tube) utilized for proton studies.

Two DEPT experiments were performed using polarization transfer pulses of 90° and 135°, respectively, obtaining in the first case only CH groups and in the other case positive signals for CH and CH_3 and negative ones for CH_2 groups. Polarization transfer delays were adjusted to an average CH coupling of 145 Hz. These delays were also applied for two-dimensional carbon–proton shift correlation in a 256 × 1024 data matrix. Each FID required a total of 600 scans. Total acquisition time was 36 h. An eight-step pulse cycle was used for P-type selection. Processing time (exponential multiplication in both dimensions, zero filling, Fourier transform) was 25 min.

Acknowledgments

We thank Professor H. Egge, Institut für Physiologische Chemie, Universität Bonn, for the FAB-ms spectrum, MPI (Ministero della Pubblica Istruzione, Roma) and CNR (Consiglio Nazionale delle Ricerche, Roma) for financial support, and DAAD (Deutscher Akademischer Austauschdienst, Bonn) for the award of a fellowship to R.L. The ^1H nmr spectra at 500 MHz were performed at IMIB-CNR, Arco Felice (Napoli).

1. M. PARRILLI, M. ADINOLFI, and L. MANGONI. Gazz. Chim. Ital. **109**, 611 (1979).
2. M. PARRILLI, R. LANZETTA, M. ADINOLFI, and L. MANGONI. Tetrahedron, **36**, 3591 (1980).
3. M. PARRILLI, R. LANZETTA, V. DOVINOLA, M. ADINOLFI, and L. MANGONI. Can. J. Chem. **59**, 2261 (1981).
4. M. ADINOLFI, G. BARONE, R. LANZETTA, G. LAONIGRO, L. MANGONI, and M. PARRILLI. Can. J. Chem. **61**, 2633 (1983).
5. M. ADINOLFI, G. BARONE, R. LANZETTA, G. LAONIGRO, L. MANGONI, and M. PARRILLI. Can. J. Chem. **62**, 1223 (1984).
6. D. M. DODDRELL, D. T. PEGG, and M. R. BENDALL. J. Magn. Reson. **48**, 323 (1982); M. R. BENDALL, D. M. DODDRELL, D. T. PEGG, and W. E. HULL. "DEPT" Brochure with experimental details, Bruker Inc., Karlsruhe. 1982.
7. K. YAMASAKY, H. KOHDA, T. KOBAYASHI, R. KASAI, and O. TANAKA. Tetrahedron Lett. 1005 (1976).
8. R. KASAI, M. SUZUO, J. T. ARAKAWA, and O. TANAKA. Tetrahedron Lett. 175 (1977).
9. K. TORI, Y. YOSHIMURA, S. SEO, K. SAKURWI, Y. TOMITA, and H. ISHII. Tetrahedron Lett. 4167 (1976).
10. K. TORI, S. SEO, Y. YOSHIMURA, H. ARITA, and Y. TOMITA. Tetrahedron Lett. 179 (1977).
11. L. D. HALL, G. A. MORRIS, and S. SUKUMAR. J. Am. Chem. Soc. **102**, 1745 (1980).
12. G. A. MORRIS and L. D. HALL. J. Am. Chem. Soc. **103**, 4703 (1981).
13. W. P. AUE, E. BARTHOLDI, and R. R. ERNST. J. Chem. Phys. **64**, 2229 (1976).
14. R. FREEMAN and G. A. MORRIS. J. Chem. Soc. Chem. Commun. 684 (1978).
15. T. D. INCH. Nuclear magnetic resonance spectroscopy in the study of carbohydrates and related compounds. *In* Annual Reports on NMR Spectroscopy. *Edited by* E. F. Mooney, Academic Press, London. 1972. p. 305, and references therein.
16. T. KONISHI, A. TADA, J. SHOJI, R. KASAI, and O. TANAKA. Chem. Pharm. Bull. **26**, 668 (1978).
17. H. ISHII, I. KITAGAWA, K. MATSUSHITA, K. SHIRAKAWA, K. TORI, T. TOZYO, M. YOSHIKAWA, and Y. YOSHIMURA. Tetrahedron Lett. 1529 (1981).
18. A. BAX and R. FREEMAN. J. Magn. Reson. **44**, 542 (1981).
19. S. SEO, Y. TOMITA, K. TORI, and Y. YOSHIMURA. J. Am. Chem. Soc. **100**, 3331 (1978).
20. H. ISHII, K. TORI, T. TOZYO, and Y. YOSHIMURA. Chem. Pharm. Bull. **26**, 674 (1978).

Improved formulae for thermal unimolecular reaction rates with randomisation failure

S. R. VATSYA AND H. O. PRITCHARD
Centre for Research in Experimental Space Science, York University, Downsview, Ont., Canada M3J 1P3

Received January 19, 1984

S. R. VATSYA and H. O. PRITCHARD. Can. J. Chem. **62**, 2879 (1984).

Simpler and more general expressions are presented for the rate constants of thermal unimolecular reactions, for all randomisation rates $0 \leq \mu_r < \infty$, and for any number of reaction channels.

S. R. VATSYA et H. O. PRITCHARD. Can. J. Chem. **62**, 2879 (1984).

On a développé des expressions simples et plus générales pour les constantes de vitesse de réactions thermiques unimoléculaires, pour tous les taux de distribution au hasard $0 \leq \mu_r < \infty$ et quel que soit le nombre de canaux réactionnels.

[Traduit par le journal]

Can. J. Chem. Downloaded from www.nrcresearchpress.com by 210.87.254.105 on 09/06/12
For personal use only.

Introduction

In an earlier paper, we provided a solution to the problem of the fall-off of a thermal unimolecular reaction in which the collisional excitation process is exponential, with rate μ, and the randomisation within grain r has rate μ_r, also exponential; numerical illustrations were provided for the case where μ_r was considered to be the same for all r (1).

This solution followed fairly closely the lines of a previous approximate treatment of the problem, in which it was assumed that the relaxations with rates μ and μ_r were separable, leading to the calculation of an effective rate constant $d_r\,[\equiv k(E)]$ with which the population of each grain would decay for the given randomisation rate μ_r (2). This approach to the coupled μ, μ_r problem led to formulae which were not always easy to use numerically because of cancellation; now, we develop a much more direct derivation of the rate constant (γ_0) for the coupled problem, resulting in a final expression which is relatively impervious to cancellation difficulties. It also avoids the necessity of calculating the eigenvalue spectrum for each grain, not a trivial problem when there are several decay channels to be taken into account.

Mathematical preliminaries

I. We begin with eq. [9] of ref. 1, i.e.

$$[1]\quad \gamma_0 = \mu(S_0, [\mu + \mathbf{V} + \mathbf{D} - \gamma_0]^{-1}\,[\mathbf{V} + \mathbf{D}]S_0)$$

where all the symbols are as defined before. Since $\mathbf{V}S_0 = 0$,

$$[2]\quad \gamma_0 = \mu(S_0, [\mu + \mathbf{V} + \mathbf{D} - \gamma_0]^{-1}\,\mathbf{D}S_0)$$

The first task is to derive a useful form for the matrix

$$[3]\quad [\mu + \mathbf{V} + \mathbf{D} - x]^{-1} = \left[\mu + \mathbf{D} - x + \sum_{r=1}^{M} \mu_r(I_r - \rho_{r0})\right]^{-1} = \sum_{r=1}^{M} [\mu + \mu_r - x + \mathbf{D}_r - \mu_r\rho_{r0}]^{-1}$$

Let $\mathbf{B} = \mathbf{A} - \nu\rho_0$ with $\rho_0 = \boldsymbol{u}_0(\boldsymbol{u}_0, \;)$ and $(\boldsymbol{u}_0, \boldsymbol{u}_0) = 1$: then

$$\mathbf{B}^{-1} = (\mathbf{A} - \nu\rho_0)^{-1} = \mathbf{A}^{-1} + \frac{\nu\mathbf{A}^{-1}\boldsymbol{u}_0(\mathbf{A}^{-1}\boldsymbol{u}_0, \;)}{1 - \nu(\boldsymbol{u}_0, \mathbf{A}^{-1}\boldsymbol{u}_0)}$$

whenever the right-hand side is defined (3); expression [3] now becomes

$$\sum_{r=1}^{M} \{[\mu + \mu_r - x + \mathbf{D}_r]^{-1} + \frac{\mu_r}{1 - \mu_r\lambda_r}[\mu + \mu_r - x + \mathbf{D}_r]^{-1}\,\rho_{r0}[\mu + \mu_r - x + \mathbf{D}_r]^{-1}\}I_r$$

where

$$[4]\quad \lambda_r = (I_rS_0, [\mu + \mu_r - x + \mathbf{D}_r]^{-1}I_rS_0)/(S_0, I_rS_0)$$

Also,

$$\rho_{r0} = I_rS_0(I_rS_0, \;)/(I_rS_0, I_rS_0)$$

and $(S_0, I_rS_0) = \beta_r$, the equilibrium population of grain r. Consequently,

$$[5]\quad [\mu + \mathbf{V} + \mathbf{D} - x]^{-1}f = \sum_{r=1}^{M} \left\{[\mu + \mu_r - x + \mathbf{D}_r]^{-1}\,I_rf + \frac{\mu_r}{\beta_r(1 - \mu_r\lambda_r)}[\mu + \mu_r - x + \mathbf{D}_r]^{-1} \times I_rS_0(I_rS_0, [\mu + \mu_r - x + \mathbf{D}_r]^{-1}I_rf)\right\}$$

where f is any arbitrary vector.

II. Let $\mathbf{A} = \mu(1 - p_0) + \mathbf{V} = \mu(1 - p_0) + \sum_{r=1}^{M} \mu_r(I_r - \rho_{r0})$; we have that $\mathbf{A}S_0 = 0$, i.e., the lowest eigenvalue $\sigma_0(\mathbf{A}) = 0$. For the next eigenvalue,

$$\sigma_1(\mathbf{A}) = \inf\,(\phi, \mathbf{A}\phi) \text{ where } \|\phi\| = 1 \text{ and } (S_0, \phi) = 0$$
$$= \inf\left(\phi, \left[\mu(1 - p_0) + \sum_{r=1}^{M} \mu_r(I_r - \rho_{r0})\right]\phi\right)$$
$$= \inf\left[\mu + \sum_{r=1}^{M} \mu_r(\phi, [I_r - \rho_{r0}]\phi)\right]$$

Since $\mu_r \geq 0$ and $(\phi, \rho_{r0}\phi) \leq (\phi, I_r\phi)$, $\sigma_1(\mathbf{A}) \geq \mu$.

III. We define two functions:

$$\bar{\phi}(x) = \alpha(S_0, [\mathbf{A} + \mathbf{D} + \alpha p_0 - x]^{-1}\,\mathbf{D}S_0)$$
$$\phi(x) = \alpha(S_0, [\mathbf{A} + \mathbf{D} + \alpha p_0 - x]^{-1}\,S_0)$$

As we have shown previously (4), for all $\alpha > 0$, $\bar{\phi}(\gamma_0) = \gamma_0$; moreover, if $\alpha \leq \sigma_1(\mathbf{A})$ and $x \leq \gamma_0$, then $\bar{\phi}(x) \leq \gamma_0$. Also $\chi(\gamma_0) = \gamma_0$ where $\chi(x) = \bar{\phi}(x)/\phi(x)$, and if $x \leq \gamma_0$, $\chi(x) \geq \gamma_0$. Thus, we have two independent procedures which can be used to form converging bounds to γ_0; however, it will not usually be necessary to resort to these successive approximation procedures. We have (4)

$$[6]\quad \chi(0) = \bar{\phi}(0)/\phi(0) \geq \gamma_0 \geq \bar{\phi}(0)$$

Also, since $\bar{\phi}(x) = \alpha - (\alpha - x)\phi(x)$, this inequality reads

$$\frac{\alpha\bar{\phi}(0)}{\alpha - \bar{\phi}(0)} \geq \gamma_0 \geq \bar{\phi}(0)$$

We may then choose $\alpha = \mu$ as a convenient and permissible value, giving

$$\chi(0) = \frac{\mu\bar{\phi}(0)}{\mu - \bar{\phi}(0)} \geq \gamma_0 \geq \bar{\phi}(0)$$

Now, if $\mu \gg \gamma_0$, as is often the case, then $\chi(0) \simeq \bar{\phi}(0)$, but since $\chi(0)$ and $\bar{\phi}(0)$ bracket γ_0, $\bar{\phi}(0)$ itself may be taken as the required solution.

IV. With $\alpha = \mu$, the inverse operator required in calculating both $\phi(x)$ and $\bar{\phi}(x)$ is

$$[\mathbf{A} + \mathbf{D} + \mu p_0 - x]^{-1} = [\mu + \mathbf{V} + \mathbf{D} - x]^{-1}$$

which was given above, eq. [5]. Consequently, after some straightforward manipulation

$$[7] \quad \bar{\phi}(x) = \mu \sum_{r=1}^{M} \frac{1}{1 - \mu_r\lambda_r} (I_r S_0, [\mu + \mu_r + \mathbf{D}_r - x]^{-1} \mathbf{D} S_0)$$

$$[8] \quad \phi(x) = \mu \sum_{r=1}^{M} \frac{1}{1 - \mu_r\lambda_r} (I_r S_0, [\mu + \mu_r + \mathbf{D}_r - x]^{-1} I_r S_0)$$

$$= \mu \sum_{r=1}^{M} \frac{\beta_r\lambda_r}{1 - \mu_r\lambda_r}.$$

Expressions for γ_0

Let each grain r be composed of $\dim(I_r)$ types of states, numbered $j = 0$ to $N = [\dim(I_r) - 1]$, with equilibrium populations as follows: β_{r0} states having zero decay rate; β_{r1} states having decay rate constant d_1; β_{r2} states having decay rate constant d_2, and so on, with

$$\beta_{rj} = (I_r S_0, I_{rj} I_r S_0) = (S_0, I_{rj} S_0)$$

$$\sum_{j=0}^{N} \beta_{rj} = \beta_r \text{ and } \sum_{j=0}^{N} d_j I_{rj} = \mathbf{D}_r$$

Then, from eq. [4]

$$\lambda_r(0) = \frac{1}{\beta_r} \sum_{j=0}^{N} \frac{\beta_{rj}}{\mu + \mu_r + d_j}$$

whence

$$[9] \quad \gamma_0 \simeq \bar{\phi}(0) = \mu \sum_{r=1}^{M} \frac{\sum_{j=0}^{N} \frac{\beta_{rj} d_j}{\mu + \mu_r + d_j}}{1 - \frac{\mu_r}{\beta_r} \sum_{j=0}^{N} \frac{\beta_{rj}}{\mu + \mu_r + d_j}}$$

Discussion

In both of our previous papers (1, 2), we provided *approximate* solutions for the rate constant when the randomisation process was not transparent; here, however, we present rigorous bounds to the exact eigenvalue γ_0. Inspection of eq. [6] shows that the quantity $\phi(0)$ defines the spread within which γ_0 must lie. Expanding eq. [8] in detail yields an expression almost identical to that for $\bar{\phi}(0)$ in eq. [9], but with two minor differences: (*i*) that we have just β_{rj} rather than $\beta_{rj} d_j$ in the numerator, and (*ii*) that the summation has to be taken, as well, over all the unreactive states below threshold, which simply adds a term $(1 - \Sigma'\beta_r)$ to the revised expression (Σ' is used here, as usual, to denote summation over states above threshold only). Thus, $\phi(0) \rightarrow (1 - \Sigma'\beta_r)$ as $\mu \rightarrow 0$, $\phi(0) \rightarrow 1$ as $\mu \rightarrow \infty$, and since the total equilibrium population above threshold is often miniscule, eq. [6] provides very tight bounds on γ_0 for all pressures. When compared with our earlier results, differences occurred in the fourth decimal place, or later, confirming the general quality of those earlier approximate solutions (and in which the computational effort was an order of magnitude greater). Thus, the use of eq. [9] should facilitate the examination of the problem of what values are required for the randomisation rate μ_r to reproduce the observed strong-collision behaviour in various thermal reactions, and of the effects of interference which can occur between competing reaction channels. Also, since we have defined weak-collision behaviour as the occurrence of departures from strong-collision properties (5), eq. [9] provides a vehicle for exploring such behaviour.

Notice that eq. [9] becomes inaccurate when $\mu_r \gg$ all d_j, but since the d_j are of the order of vibration frequencies, i.e. $\sim 10^{13}$ s^{-1}, this can be overcome very easily by performing the calculations in double-length arithmetic if exceedingly large values of μ_r are needed.

Determination of the limits of γ_0 with μ, μ_r is much simpler than before, by direct expansion of [8] and/or [9], but the results are the same as those given previously (1).

1. H. O. PRITCHARD and S. R. VATSYA. Can. J. Chem. **59**, 2575 (1981).
2. H. O. PRITCHARD. Can. J. Chem. **58**, 2236 (1980).
3. H. O. PRITCHARD and S. R. VATSYA. J. Chem. Phys. **76**, 1024 (1982).
4. H. O. PRITCHARD and S. R. VATSYA. J. Comp. Phys. **49**, 173 (1983).
5. H. O. PRITCHARD. Quantum theory of unimolecular reactions. Cambridge University Press. 1984.

Can. J. Chem. Downloaded from www.nrcresearchpress.com by 210.87.254.105 on 09/06/12
For personal use only.

Molecular orbital treatment of substituent effects. II. Structures of some carboxylic acids and their conjugate bases

KENNETH E. EDGECOMBE AND RUSSELL J. BOYD[1]
Department of Chemistry, Dalhousie University, Halifax, N.S., Canada B3H 4J3

Received January 24, 1984

KENNETH E. EDGECOMBE and RUSSELL J. BOYD. Can. J. Chem. **62**, 2881 (1984).

Theoretical structures of the *cis* and *trans* conformations of acetic, fluoroacetic, difluoroacetic, trifluoroacetic, chloroacetic, dichloroacetic, and trichloroacetic acids and their carboxylate anions are compared with the available experimental structures. In every case the *cis* conformation, in which one of the atoms bonded to the α carbon lies in the carboxylate plane and is eclipsed with the carbonyl group, is predicted to have a lower energy than any other conformation of the acetic acids. The preferred conformation of the *trans* form of the haloacetic acids is characterized by a planar X—C—C—O—H ring which is interpreted in terms of an internal hydrogen bond. The long C—C bonds of the acetates at the minimal basis set level are corrected by partial geometry optimizations with split-valence basis sets. The partially optimized structures are very similar to the fully optimized structures and are sufficient for the elucidation of chemical trends. For more accurate acetate structures the 3-21 + G basis set introduced recently by von R. Schleyer and co-workers is recommended.

KENNET E. EDGECOMBE et RUSSEL J. BOYD. Can. J. Chem. **62**, 2881 (1984).

On compare les structures théoriques des conformations *cis* et *trans* des acides acétique, fluoroacétique, difluoroacétique, trifluoroacétique, chloroacétique, dichloroacétique et trichloroacétique ainsi que de leurs anions carboxylates avec les structures disponibles expérimentalement. Dans chaque cas, on prédit que l'énergie de la conformation *cis*, dans laquelle un des atomes liés au carbone α se trouve dans le plan du carboxylate et est éclipsé par le groupement carbonyle, sera plus faible que celle de n'importe quelle autre conformation des acides acétiques. La conformation privilégiée de la forme *trans* des acides haloacétiques est caractérisée par un cycle plan X—C—C—O—H que l'on interprète en rapport avec une liaison hydrogène interne. Les calculs effectués au niveau d'ensembles de base minimale prédisent que les liaisons C—C sont longues; on corrige ces prédictions en effectuant des optimisations partielles de la géométrie à l'aide d'ensembles de base du type valence dédoublée. Les structures partiellement optimisées sont très semblables aux structures complètement optimisées et elles sont appropriées pour l'élucidation des tendances chimiques. Si on veut obtenir des structures plus précises des acétates, il est recommandé d'utiliser l'ensemble de base 3-21+G introduit récemment par von R. Schleyer et ses collaborateurs.

[Traduit par le journal]

Can. J. Chem. Downloaded from www.nrcresearchpress.com by 210.87.254.40 on 09/06/12
For personal use only.

Introduction

The first paper (1) in this series dealt with an *ab initio* molecular orbital (MO) study of multiple substituent effects in three series of carbon acids and their corresponding conjugate bases. The calculations were carried out to provide theoretical estimates of the proton affinities of some carbanions (CH_3^-, CH_2X^-, CHX_2^-, and CX_3^-, where X = F, CN, or NO_2) or equivalently the intrinsic acidities of the parent molecules. Within the series of methane acids, substitution takes place at the carbon atom to which the acidic proton is bonded. This may be contrasted with carboxylic acids in which substitution takes place at a carbon atom which is at least one bond removed from the oxygen to which the acidic proton is bonded. The observed dissociation constants in aqueous solution suggest that the acidity of acetic acid is much less enhanced by electronegative substituents than that of methane. Thus successive nitro substituents lower the pK_a of methane from 48[2] through 11 and 4 to 0 for trinitromethane (3). The corresponding values for the nitrile series are 31, 12, and 0, whereas the pK_a of acetic acid is only reduced from 4.75 to 2.85, 1.48, and 0.70 with one, two, and three chlorine substituents, respectively (4). In view of these marked differences and in order to complement our earlier study of multiple substituent effects in carbon acids, we have completed extensive *ab initio* MO calculations for the fluoro- and chloroacetic acids and their carboxylate anions.

Method

Standard single determinant *ab initio* MO theory, according to which closed-shell molecules and ions are treated by the spin-restricted Hartree–Fock (RHF) procedure (5), has been used throughout. The majority of the calculations were carried out using the GAUSSIAN 76 program (6*a*), or an expanded version (6*b*), on a CDC CYBER 170–720 computer. A few supplemental calculations were performed on a Perkin-Elmer 3230 computer using the GAUSSIAN 80 series of programs (7). Complete geometry optimizations, subject only to a planar carboxylate group, were performed at the STO-3G level (8). The assumption of a planar carboxylate group is supported by experiment and previous theoretical work (9, 10). In the case of the trichloroacetate anion the structure could not be optimized at the STO-3G level. Starting with a typical C—C bond length, the C—C bond lengthened and the OCO angle opened until a minimum corresponding to isolated CCl_3^- and CO_2 was obtained. The dissociative behaviour of $CCl_3CO_2^-$ was corrected by optimizing the C—C bond at the 4-31G level (11). The C—C bond was then fixed and the remainder of the molecule was optimized at the STO-3G level. The C—C bond was re-optimized at the 4-31G level and the cyclic procedure was repeated until the structure converged to an equilibrium geometry.

For each molecule, two conformations of the carboxylic acid group were optimized. In the *cis* (or *syn*) conformation, the acidic hydrogen forms a dihedral angle of 0° with the carbonyl oxygen, as shown in structure **I** of Fig. 1. In the *trans* (or *anti*) conformation the acidic hydrogen is at a dihedral angle of 180° with respect to the carbonyl oxygen. The *trans* conformation is

[1]To whom all correspondence should be addressed.

[2]Electrochemical measurements by Breslow and Grant (ref. 2) yield a pK_a for methane in the range 68 to 70.

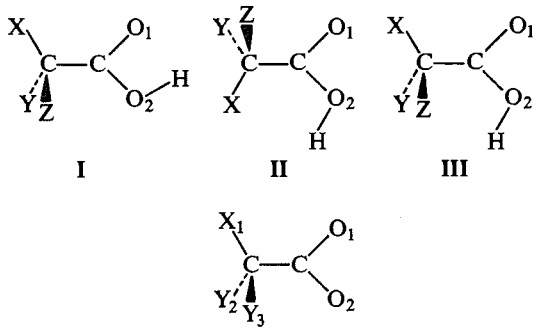

FIG. 1. The STO-3G equilibrium conformations of carboxylic acids and their conjugate bases. In the *trans* forms, structure **II** is favoured in all cases except acetic and trichloroacetic acids, for which structure **III** is favoured.

illustrated by structures **II** and **III** of Fig. 1. The STO-3G equilibrium geometries of the *cis* and *trans* conformations of some carboxylic acid molecules are compared with the available experimental data in Table 1. The corresponding results for the formates and acetates are listed in Table 2. For each species the point group of the equilibrium geometry is listed in the appropriate table, while the types of equilibrium conformations are illustrated in Fig. 1. The structures of *cis* and *trans* formic acid and *cis* acetic acid (10) are included for completeness.

Table 3 lists the STO-3G//STO-3G, K-LMG//STO-3G and K-LMG//"K-LMG" total energies, where "K-LMG" refers to the partial geometry optimizations described herein. The 4-31G basis set (11) has been used for molecules containing chlorine, while calculations with a split-valence basis set for the other species have been carried out at the 3-21G level (12). A few 4-31G single point calculations for some of the molecules are included for comparison with the STO-3G and 3-21G results.

Results and discussion

In this section we discuss the types of equilibrium conformations of the acetic acids and the extent to which the theoretical results are corroborated by experiment. Following a brief discussion of the barriers to interconversion of the conformations we compare the theoretical geometrical parameters with the experimental data. Particular attention is paid to the inadequate description of C—C bonds in acetates at the minimal basis set level and several methods for improving the results. We conclude by summarizing the experimental data which supports the interpretation of the preferred conformations of the haloacetic acids in terms of an internal hydrogen bond between a halogen and the carboxylic proton.

In the *cis* conformation of the carboxylic acid group, all acetic acid molecules are predicted to have equilibrium conformations corresponding to type I in Fig. 1, with the unique atom of the mono- and di-substituted species occupying position X. The *cis* conformation of the acetic acids is found to have a lower energy than any other conformation. These conclusions are consistent with the available gas-phase structures (9).

Optimization of the geometries of the *trans* acetic acids leads to two types of preferred conformations. In all but two cases, the lowest energy conformation is the type **II** structure shown in Fig. 1. The two exceptions occur for CH_3CO_2H and CCl_3CO_2H for which the type **III** structure is lower in energy. In molecules for which the type **II** structure is preferred, position X is occupied by a halogen. These observations are readily interpreted in terms of a competition between steric effects which favour **III** and intramolecular or internal hydrogen bonding which favours **II**. In *trans* acetic acid, where there is no hydrogen bonding, the lowest energy is obtained with conformer **III**. Among the substituted acetic acid molecules included in this work, steric effects would be at a maximum in the trichloro compound. Moreover, the long O—Cl distance, and the nonlinear arrangement, implies weak hydrogen bonding. The theoretical equilibrium conformation of *trans* trichloroacetic acid is, therefore, not surprising. Even in the preferred conformation **III**, there may be some hydrogen bonding. This suggestion is supported by recent microwave spectroscopic results (19) which indicate that the most stable conformation of glycine may be interpreted in terms of an internal bifurcated hydrogen bond between the carbonyl oxygen of the carboxylic group and two hydrogens of the amine group. Similarly, a weak bifurcated hydrogen bond between the hydroxyl group and two chlorine atoms of *trans* trichloroacetic acid may contribute to the stability of **III**.

With reference to the equilibrium conformations, it should be noted that the barriers to internal rotation about the C—C bond are much smaller than the barriers for the interconversion of the *cis* and *trans* acetic acids. The barriers for rigid rotation about the C—O bond at the STO-3G level are about 10 to 11 kcal/mol and are not strongly affected by the number of halogen substituents. This may be compared with the C—C barriers in the fluoroacetic acid series. For rigid rotation at the STO-3G level we obtain 5.5, 6.3, and 2.2 kcal/mol with one, two, and three fluorines, respectively, in the *trans* conformations and 1.0, 0.5, and 0.3 kcal/mol, respectively, in the *cis* conformations. The larger barriers for the *trans* conformations support the interpretation of the *trans* conformations in terms of internal hydrogen bonding. Furthermore, the lower value for trifluoroacetic acid suggests the presence of a bifurcated hydrogen bond in the type **III** conformation. Indeed, the rigid barriers of 0.5 and 1.7 kcal/mol at the STO-3G level in the *cis* and *trans* forms of trichloroacetic acid are consistent with the bifurcated hydrogen bond interpretation.

Lack of experimental data precludes a detailed analysis of the accuracy of the theoretical equilibrium structures. A few comparisons can be made, however, for the carboxylic acids. At the STO-3G level, the C=O bond length is insensitive to substituents, and where comparison with experiment is possible, the agreement is much better than average. Here we note that the STO-3G basis set usually gives bond lengths within 0.03 Å and bond angles within 4° of the experimental values for neutral molecules in their ground states (20). For the C=O bonds the agreement is about 0.01 Å or better. There is insufficient experimental data to confirm the STO-3G prediction that the C=O bond length is insensitive to the number of halogens on the carbon. In view of the underestimation of the effect of substituents on bond lengths in the carbon acids (1) at the minimal basis set level, the near constancy of the C=O bond lengths may be an anomaly of the STO-3G basis set. The STO-3G results for the C—OH bond show only slightly greater variation than the C=O values and are consistently too long relative to the experimental values. With the exception of the C—C bond lengths, the agreement between the STO-3G and experimental results for the other bond lengths and angles is quite typical (20).

The tendency of the C—C bond length to increase about 0.01 to 0.02 Å per fluoro and chloro substituent at the STO-3G level as the number of halogens on the α carbon increases is one

Can. J. Chem. Downloaded from www.nrcresearchpress.com by 210.87.254.40 on 09/06/12
For personal use only.

TABLE 1. Equilibrium geometries[a] of some carboxylic acids

Molecule[b]	Parameter[c]	*cis*	*trans*	Experimental
HCO_2H	r(C—O_1)	1.214	1.211	1.213[d]
(C_s)	r(C—O_2)	1.386	1.393	1.368
	r(O_2—H)	0.990	0.988	0.97
	r(C—H)	1.104	1.108	1.09
	∠(OCO)	123.7	121.3	123.5
	∠(HO_2C)	104.7	105.7	
	∠(HCO_1)	126.0	124.1	
FCO_2H	r(C—O_1)	1.213	1.209	
(C_s)	r(C—O_2)	1.387	1.388	
	r(O_2—H)	0.989	0.990	
	r(C—F)	1.346	1.356	
	∠(OCO)	126.4	124.9	
	∠(HO_2C)	104.5	105.1	
	∠(FCO_1)	124.5	123.8	
CH_3CO_2H	r(C—O_1)	1.216	1.214	1.214[e]
(C_s)	r(C—O_2)	1.392	1.398	1.364
	r(O_2—H)	0.990	0.988	0.97
	r(C—C)	1.537	1.546	1.520
		(1.494)[f]	(1.506)[f]	
	∠(OCO)	121.8	119.3	122.8
	∠(HO_2C)	104.6	106.2	107.0
	∠(CCO_1)	126.8	124.8	126.6
CH_2FCO_2H	r(C—O_1)	1.215	1.213	1.202[g]
(C_s)	r(C—O_2)	1.390	1.388	1.344
	r(O_2—H)	0.990	0.990	0.971
	r(C—C)	1.555	1.569	1.534
		(1.494)[f]	(1.521)[f]	
	r(C—F)	1.385	1.386	1.387
	∠(OCO)	122.9	122.3	125.1
	∠(HO_2C)	104.7	103.8	105.9
	∠(CCO_1)	126.1	124.7	126.1
	∠(FCC)	109.7	108.1	109.2
CHF_2CO_2H	r(C—O_1)	1.215	1.213	1.212[h]
(C_s, C_1)	r(C—O_2)	1.386	1.386	1.345
	r(O_2—H)	0.991	0.991	0.96
	r(C—C)	1.577	1.588	1.517
		(1.504)[f]	(1.528)[f]	
	r((C—F)	1.378	1.380	1.354
			1.377	
	∠(OCO)	123.1	122.8	123.9
	∠(HO_2C)	104.9	104.1	107
	∠(CCO_1)	125.5	123.9	110.6
	∠(FCC)	110.2	107.5	108.7
			111.0	
CF_3CO_2H	r(C—O_1)	1.214	1.212	
(C_s)	r(C—O_2)	1.385	1.385	
	r(O_2—H)	0.990	0.990	
	r(C—C)	1.592	1.603	
		(1.498)[f]	(1.528)[f]	
	r(C—F)	1.370	1.377	
		1.372	1.370	
	∠(OCO)	124.2	123.3	
	∠(HO_2C)	105.0	104.5	
	∠(CCO_1)	125.2	123.4	
	∠(FCC)	110.0	107.9	
		110.6	111.6	
CH_2ClCO_2H	r(C—O_1)	1.213	1.215	1.223[i]
(C_s)	r(C—O_2)	1.390	1.386	1.352
	r(O_2—H)	0.990	0.988	0.97
	r(C—C)	1.549	1.567	1.508
		(1.493)[f]	(1.514)[f]	
	r(C—Cl)	1.803	1.812	1.778
	∠(OCO)	123.4	120.4	123.3
	∠(HO_2C)	104.7	106.8	105.8
	∠(CCO_1)	127.3	120.5	126.1
	∠(ClCC)	111.3	113.4	112.5
$CHCl_2CO_2H$	r(C—O_1)	1.215	1.214	
(C_s, C_1)	r(C—O_2)	1.383	1.383	
	r(O_2—H)	0.990	0.987	
	r(C—C)	1.558	1.584	
		(1.494)[f]	(1.527)[f]	
	r(C—Cl)	1.810	1.816	
			1.810	
	∠(OCO)	123.9	121.2	
	∠(HO_2C)	104.9	107.1	
	∠(CCO_1)	124.1	120.4	
	∠(ClCC)	110.4	112.6	
			109.7	
CCl_3CO_2H	r(C—O_1)	1.211	1.211	
(C_s)	r(C—O_2)	1.382	1.385	
	r(O_2—H)	0.990	0.989	
	r(C—C)	1.576	1.592	
		(1.514)[f]	(1.526)[f]	
	r(C—Cl)	1.813	1.806	
		1.818	1.823	
	∠(OCO)	125.6	122.6	
	∠(HO_2C)	104.9	107.3	
	∠(CCO_1)	124.5	121.6	
	∠(ClCC)	109.2	109.7	
		109.0	108.7	

[a]Bond lengths in angstroms and bond angles in degrees. Bond lengths and angles involving C—H bonds have been omitted to save space. The complete structures have been compiled (ref. 13) and are available from the authors.

[b]The point group of the equilibrium conformation is shown in parentheses. Where there are two, one is for *cis* and the following one is for the *trans* conformation.

[c]The numbering of the atoms is shown in Fig. 1. Where more than one bond length or angle involving F or Cl is listed, the first data entry refers to the halogen in the carboxylate plane.

[d]Reference 14.

[e]Reference 9*a*.

[f]Carbon—carbon bond lengths listed in parentheses are the "K-LMG" values described in the text.

[g]Reference 9*b*. Assuming that some of the molecular parameters are the same as those observed in *cis*-fluoroacetic acid, the following experimental parameters were obtained for *trans*-fluoroacetic acid: r(O—H) = 0.928 A, ∠(OCO) = 122.3°, ∠(CCO_1) = 119.8° and ∠(FCC) = 111.7°.

[h]Reference 9*c*.

[i]Reference 9*d*.

of the most apparent features of Table 1. Furthermore, the C—C bond length of the acetate anion is of the order of 0.1 Å too long and each successive fluoro substituent stretches the C—C bond by about 0.02 Å, while the effect of chloro substituents is even greater. The effect is so great in the case of the trichloroacetate anion that dissociation to CCl_3^- and CO_2 is predicted. In the haloacetate anions the minimal basis set provides only a small number of basis functions for a relatively

Can. J. Chem. Downloaded from www.nrcresearchpress.com by 210.87.254.40 on 09/06/12
For personal use only.

TABLE 2. Equilibrium geometries[a] of some carboxylate anions

Anion[b]	Parameter[c]	Theoretical	Experimental	Anion[b]	Parameter[c]	Theoretical	Parameter
HCO_2^-	r(C—O)	1.267		$CF_3CO_2^-$	r(C—O)	1.252	1.269[h]
(C_{2v})	r(C—H)	1.151		(C_s)	r(C—C)	1.703	1.542
	∠(OCO)	130.3				(1.562)[e]	
	∠(HCO)	114.9			r(C—F_1)	1.382	1.346
					r(C—F_2)	1.385	
FCO_2^-	r(C—O)	1.258			∠(OCO)	134.5	128.3
(C_{2v})	r(C—F)	1.419			∠(CCO_1)	112.8	115.8
	∠(OCO)	133.5			∠(F_1CC)	113.3	111.5
	∠(FCO)	113.3			∠(F_2CC)	113.5	
$CH_3CO_2^-$	r(C—O_1)	1.263	1.240[d]	$CH_2ClCO_2^-$	r(C—O_1)	1.249	
(C_s)	r(C—O_2)	1.265	1.261	(C_s)	r(C—O_2)	1.258	
	r(C—C)	1.629	1.514		r(C—C)	1.670	
		(1.566)[e]				(1.553)[e]	
	∠(OCO)	130.0	123.3		r(C—Cl)	1.847	
	∠(CCO_1)	115.3	119.6		∠(OCO)	134.0	
					∠(CCO_1)	116.7	
$CH_2FCO_2^-$	r(C—O)	1.259	1.242[f]		∠(ClCC)	117.4	
(C_s)	r(C—C)	1.650	1.495				
		(1.553)[e]		$CHCl_2CO_2^-$	r(C—O_1)	1.245	
	r(C—F)	1.392	1.391	(C_s)	r(C—O_2)	1.238	
	∠(OCO)	132.1	127.0		r(C—C)	1.759	
	∠(CCO_1)	114.6	115.0			(1.579)[e]	
	∠(FCC)	113.5	113.0		r(C—Cl)	1.850	
					∠(OCO)	137.4	
$CHF_2CO_2^-$	r(C—O)	1.257	1.241[g]		∠(CCO_1)	108.9	
(C_s)	r(C—C)	1.670	1.533		∠(ClCC)	113.9	
		(1.553)[e]					
	r(C—F)	1.389	1.353	$CCl_3CO_2^-$	r(C—O_1)	1.249	1.20[i]
	∠(OCO)	132.8	128.3	(C_s)	r(C—O_2)	1.252	1.27
	∠(CCO_1)	113.1	115.8		r(C—C)	1.596	1.54
	∠(FCC)	112.8	111.2		r(C—Cl_1)	1.845	
					r(C—Cl_2)	1.849	
					∠(OCO)	134.8	127
					∠(CCO_1)	113.6	
					∠(Cl_1CC)	114.2	
					∠(Cl_2CC)	111.5	

[a]Bond lengths in angstroms and angles in degrees.
[b]Point group of the equilibrium conformation is shown in parentheses.
[c]The numbering of the atoms is shown in Fig. 1. Where more than one bond length or angle involving F or Cl is listed, the first data entry refers to the halogen in the carboxylate plane.
[d]Reference 15.
[e]Carbon—carbon bond lengths listed in parentheses are the "K-LMG" values described in the text.
[f]Reference 16.
[g]Reference 16.
[h]Reference 17.
[i]Reference 18.

large number of electrons. The number of basis functions varies stepwise from 23 in acetate to 47 in trichloroacetate. The corresponding number of electrons varies from 32 to 80, while the number of virtual orbitals remains constant at 7. Thus a large fraction (0.85) of the molecular orbitals are occupied in $CCl_3CO_2^-$ at the STO-3G level. The fraction is lower for the other ions (0.70 in the acetate ion), but still high relative to the range encountered in hydrocarbons (0.56 and 0.58 for ethane and benzene, respectively). After accounting for the many lone-pairs and inner pairs of electrons, the STO-3G basis is insufficiently flexible to provide a reasonable description of the C—C bond of the acetates. It is not surprising that the inadequacy of the STO-3G basis set is greater in the anions than in the parent acids, since it is well known that extended basis sets are necessary to obtain an accuracy comparable to the minimal basis set geometries of neutral molecules and cations (21–26). In the haloacetates the well-known difficulties associated with MO calculations on anions are compounded by the electron-rich character of the ions.

In order to improve upon the STO-3G results, split-valence basis sets were used. The size of the molecules and anions included in this work precludes complete geometry optimizations for all species and, therefore, we carried out partial geometry optimizations. A few full optimizations provide a check on the partial optimizations. With the remainder of the geometry constrained to the STO-3G structure, the C—C bond of each species was optimized at the 3-21G or 4-31G level. The latter was used for molecules containing chlorine since the 3-21G basis set for second-row atoms was not available at the time when these calculations were completed. For convenience we denote the partially optimized structures by "K-LMG" to distinguish them from the fully optimized K-LMG structures.

Can. J. Chem. Downloaded from www.nrcresearchpress.com by 210.87.254.40 on 09/06/12
For personal use only.

Can. J. Chem. Downloaded from www.nrcresearchpress.com by 210.87.254.40 on 09/06/12
For personal use only.

TABLE 3. Total energies[a] of some carboxylic acids and their conjugate bases

Species	STO-3G//STO-3G[b]	K-LMG//STO-3G	K-LMG//"K-LMG"
c-HCO_2H	−186.21788	−187.69638	
t-HCO_2H	−186.21081	−187.68403	
HCO_2^-	−185.45627	−187.10333	
c-FCO_2H	−283.69317	−286.03119	
t-FCO_2H	−283.69070	−286.02675	
FCO_2^-	−282.96284	−285.48167	
c-CH_3CO_2H	−224.81020	−226.53043	−226.53139
t-CH_3CO_2H	−224.80205	−226.51645	−226.51723
CH_3CO^-	−224.04830	−225.93066	−225.93202
c-CH_2FCO_2H	−322.25177	−324.83281	−324.83462
t-CH_2FCO_2H	−322.24909	−324.82875	−324.82988
$CH_2FCO_2^-$	−321.50455	−324.25089	−324.25401
c-CHF_2CO_2H	−419.70881	−423.14967	−423.15218
t-CHF_2CO_2H	−419.70570	−423.14428	−423.14595
$CHF_2CO_2^-$	−418.97597	−422.58543	−422.58939
c-CF_3CO_2H	−517.17994	−521.48405	−521.48808
t-CF_3CO_2H	−517.17611	−521.47469	−521.47723
$CF_3CO_2^-$	−516.46206	−520.93644	−520.94148
c-CH_2ClCO_2H	−678.80246	−685.85779	−685.85958
t-CH_2ClCO_2H	−678.79615	−685.84805	−685.84952
$CH_2ClCO_2^-$	−678.07422	−685.30154	−685.30639
c-$CHCl_2CO_2H$	−1132.79033	−1144.24505	−1144.24726
t-$CHCl_2CO_2H$	−1132.78218	−1144.23225	−1144.23393
$CHCl_2CO_2^-$	−1132.08962	−1143.70070	−1143.70892
c-CCl_3CO_2H	−1586.77311	−1602.62644	−1602.62849 (−1602.62855)[c]
t-CCl_3CO_2H	−1586.76614	−1602.61570	−1602.61786 (−1602.61794)[c]
$CCl_3CO_2^-$	Dissociates		(−1602.10252)

[a]All energies are in atomic units: 1 au = 27.2116 eV.

[b]Notation A//B indicates that the energy has been calculated at level A using a geometry which is optimum for level B.

[c]Values in parentheses were obtained by the cyclic method described in the text for trichloroacetate.

The "K-LMG" carbon—carbon bond lengths listed in parentheses in Tables 1 and 2 are closer to the observed range of C—C bond lengths. In the case of the parent acids there is a tendency for the partial optimizations to over-correct the minimal basis set values. This appears to be due to the choice of a split-valence basis set rather than to the optimization procedure since full 4-31G optimizations yield 1.533, 1.536, 1.494, and 1.506 Å for the C—C bonds of fluoroacetate, difluoroacetate, and *cis* and *trans* fluoroacetic acid, respectively. As a further test of the ability of the partial optimizations to yield good approximations to the full optimizations, we optimized the C—C bonds of formamide and *cis* acetic acid at the 3-21G level while constraining the remainder of the molecule to the STO-3G structure (10). This leads to 1.515 and 1.494 Å for the C—C bonds of CH_3CONH_2 and *c*-CH_3CO_2H, respectively, in excellent agreement with the fully optimized values (10) of 1.510 and 1.497 Å, respectively. The discrepancies between the partially and fully optimized values of the other geometrical parameters are small and well within the range of error associated with small basis set calculations (20).

We conclude that the partial optimizations yield C—C bond lengths within 0.01 Å of the true theoretical values and that the "K-LMG" structures form a useful set for the elucidation of chemical trends, such as the proton affinities discussed in the following paper (27). Here we would like to mention that von R. Schleyer and co-workers (23) have recently shown that diffuse function — augmented split-valence basis sets yield excellent geometries for anions. The 3-21+G value (23*c*) of 1.546 Å for the C—C bond length of acetate may be compared with the 3-21G value of 1.576 Å and the "3-21G" value of 1.566 Å listed in Table 2. The 3-21+G calculations make even greater demands on computer memory and time than the 3-21G calculations and are not practical for the large species considered in this paper. For example, a 3-21+G calculation on CCl_3CO_2H involves 105 basis functions. Since our objective is to study chemical trends, we treat all species at a uniform theoretical level. Furthermore, the errors associated with the "K-LMG" calculations appear to be largely systematic, as observed in K-LMG calculations on small anions (23), and, therefore, it is not unreasonable to expect chemically useful information from the present approach.

Some insight into the inadequacy of the STO-3G basis set for the prediction of the equilibrium structures of electron-rich species can be gained by use of mixed basis sets. With a 4-31G basis set on O, STO-3G on C and Cl, and the geometry constrained to the structure given in Table 2, optimization of the C—C bond of $CCl_3CO_2^-$ leads to 1.603 Å. Repeating the procedure with a 4-31G basis on C and STO-3G on the other centres leads to 1.638 Å for the C—C bond, while a 44-31G basis set on Cl and STO-3G elsewhere leads to a C—C bond length of 1.761 Å. This shows that the inadequacy of the STO-3G basis for the electron-rich acetates is primarily associated with the lone pairs on the oxygen atoms and not with the lone pairs on the halogen atoms. This is not surprising in view of the fact that the Mulliken atomic charges, as well as the formal charges associated with the Lewis structures, place the majority of the negative charge of the acetates on the oxygen atoms.

The total energies of the *cis* and *trans* conformations of the carboxylic acids and their conjugate bases are listed in Table 3. A detailed analysis will not be given in this paper but rather the energies will be used in the following paper (27) on the effect of multiple substituents on the proton affinities of the carboxylate anions. Analysis of the data in Table 3 reveals that the total energies are non-additive with respect to the number of substituents. Here we would like to emphasize that recent studies of multiple substitution at the same carbon by highly electronegative substituents exhibit similar nonadditive energetic and geometric effects (28−30).

To conclude our discussion we consider the extent to which experimental evidence corroborates the interpretation of the preferred conformations of the haloacetic acids in terms of internal hydrogen bonding of the type

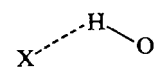

where X may be either F or Cl. The most direct evidence is provided by a microwave spectroscopic and electron diffraction study of monofluoroacetic acid (9*b*). In the *cis* conformation the chain of atoms F—C—C—O—H is zig-zag, whereas the *trans* conformation is cyclic. Both conformations have a plane of symmetry. Thus the results summarized in Table 1 and

Fig. 1 are in complete agreement with the experimental studies on monofluoroacetic acid in the gas phase. Molecules in which the internal hydrogen bond involves five atoms in a ring include 2-fluoroethanol (31), 1,2-propanediol (32), β-hydroxyacrolein (33), and 2-fluoropropanol (34). Similarly there is much evidence for internal hydrogen bonding in rings involving six atoms in molecules such as malonaldehyde (33), triformylmethane (35), 2-nitrophenol (36), and the hydrogen maleate ion (37).

Acknowledgements

We gratefully acknowledge the constructive criticism of the referees, helpful correspondence from Dr. W. Caminati (Bologna), a generous allocation of computing time from the Dalhousie University Computer Centre, financial support in the form of an Operating Grant (to R.J.B.) from the Natural Sciences and Engineering Research Council of Canada, and a Fellowship (to K.E.E.) from the Walter C. Sumner Foundation.

1. K. E. EDGECOMBE and R. J. BOYD. Can. J. Chem. **61**, 45 (1983).
2. R. BRESLOW and J. L. GRANT. J. Am. Chem. Soc. **99**, 7745 (1977).
3. T. H. LOWRY and K. S. RICHARDSON. Mechanism and theory in organic chemistry. Harper and Row, New York. 1981.
4. CRC Handbook of Chemistry and Physics. CRC Press, Inc., Boca Raton, FL. 1981.
5. C. C. J. ROOTHAAN. Rev. Mod. Phys. **23**, 69 (1951).
6. (*a*) J. S. BINKLEY, R. A. WHITESIDE, P. C. HARIHARAN, R. SEEGER, J. A. POPLE, W. J. HEHRE, and M. D. NEWTON. QCPE **11**, 368 (1978); (*b*) R. J. BOYD and K. E. EDGECOMBE. QCPE Bulletin, **2**, 10 (1982).
7. J. S. BINKLEY, R. A. WHITESIDE, R. KRISHNAN, R. SEEGER, D. J. DEFREES, H. B. SCHLEGEL, S. TOPIOL, L. R. KAHN, and J. A. POPLE. Department of Chemistry, Carnegie-Mellon University, Pittsburgh, PA 15213.
8. W. J. HEHRE, R. F. STEWART, and J. A. POPLE. J. Chem. Phys. **51**, 2657 (1969).
9. (*a*) J. L. DERISSEN. J. Mol. Struct. **7**, 67 (1971); (*b*) B. P. VAN EIJCK, G. VAN DER PLAATS, and P. H. VAN ROON. J. Mol. Struct. **11**, 67 (1972); (*c*) J. M. J. M. BIJEN and J. L. DERISSEN. J. Mol. Struct. **27**, 233 (1975); (*d*) J. L. DERISSEN and J. M. J. M. BIJEN. J. Mol. Struct. **29**, 153 (1975).
10. R. A. WHITESIDE, M. J. FIRSCH, J. S. BINKLEY, D. J. DEFREES, H. B. SCHLEGEL, K. RAGHAVACHARI, and J. A. POPLE. Carnegie-Mellon Quantum Chemistry Archive. 2nd ed. July 1981.
11. (*a*) R. DITCHFIELD, W. J. HEHRE, and J. A. POPLE. J. Chem. Phys. **54**, 724 (1971); (*b*) W. J. HEHRE and W. A. LATHAN. J. Chem. Phys. **56**, 5255 (1971).
12. J. S. BINKLEY, J. A. POPLE, and W. J. HEHRE. J. Am. Chem. Soc. **102**, 939 (1980).
13. K. E. EDGECOMBE. M.Sc. thesis. Dalhousie University, Halifax. 1982.
14. V. SCHOMAKER and J. M. O'GORMAN. J. Am. Chem. Soc. **69**, 2638 (1947).
15. A. ITAI and Y. IITAKA. Acta Crytstallogr. B**34**, 3420 (1978).
16. K.-T. WEI and D. L. WARD. Acta Crystallogr. B**32**, 2768 (1975).
17. D. W. J. CRUICKSHANK, D. W. JONES, and G. WALKER. J. Chem. Soc. 1303 (1964).
18. L. GOLIC and F. LAZARINI. Cryst. Struct. Commun. **3**, 645 (1974).
19. W. CAMINATI and R. CERVELLATI. J. Am. Chem. Soc. **104**, 4748 (1982).
20. J. A. POPLE. Modern theoretical chemistry. Vol. 3. *Edited by* H. F. Schaeffer, III. Plenum Press, New York. 1977.
21. P. CARSKY and M. URBAN. Lecture notes in chemistry. No. 16. Springer-Verlag, Berlin. 1980.
22. A. J. DUKE. Chem. Phys. Lett. **21**, 275 (1973).
23. (*a*) J. CHANDRASEKHAR, J. G. ANDRADE, and P. VON R. SCHLEYER. J. Am. Chem. Soc. **103**, 5609 (1981); (*b*) G. W. SPITZNAGEL, T. CLARK, J. CHANDRASEKHAR, and P. VON R. SCHLEYER. J. Comput. Chem. **3**, 363 (1982); (*c*) T. CLARK, J. CHANDRASEKHAR, G. W. SPITZNAGEL, and P. VON R. SCHLEYER. J. Comput. Chem. **4**, 294 (1983).
24. L. RADOM. Modern theoretical chemistry. Vol. 4. *Edited by* H. F. Schaeffer III. Plenum Press, New York. 1977.
25. R. AHLRICHS. Chem. Phys. Lett. **34**, 570 (1975).
26. A. C. HOPKINSON and M. H. LIEN. Int. J. Quantum Chem. **18**, 1371 (1980).
27. K. E. EDGECOMBE and R. J. BOYD. Can. J. Chem. **62**, 2887 (1984).
28. N. C. BAIRD. Can. J. Chem. **61**, 1567 (1983).
29. L. RADOM, W. J. HEHRE, and J. A. POPLE. J. Am. Chem. Soc. **93**, 289 (1981).
30. A. PROSS and L. RADOM. J. Comput. Chem. **1**, 295 (1980).
31. K. HAGEN and K. HEDBERG. J. Am. Chem. Soc. **95**, 8263 (1973).
32. W. CAMINATI. J. Mol. Spectrosc. **86**, 193 (1981).
33. S. L. BAUGHCUM, R. W. DUERST, W. F. ROWE, Z. SMITH, and E. B. WILSON. J. Am. Chem. Soc. **103**, 6296 (1981).
34. O.-A. BRAATHEN, K.-M. MARSTOKK, and H. MOLLENDAL. Acta Chem. Scand. A**36**, 173 (1982).
35. P. H. TURNER. J. Chem. Soc. Faraday II, **76**, 383 (1980).
36. S. LEAVELL and R. F. CURL, JR. J. Mol. Spectrosc. **45**, 428 (1973).
37. (*a*) W. F. ROWE, JR., R. W. DUERST, and E. B. WILSON. J. Am. Chem. Soc. **98**, 4021 (1976); (*b*) P. GEORGE, C. W. BOCK, and M. TRACHTMAN. J. Phys. Chem. **87**, 1839 (1983).

Can. J. Chem. Downloaded from www.nrcresearchpress.com by 210.87.254.40 on 09/06/12
For personal use only.

Molecular orbital treatment of substituent effects. III. Proton affinities of some methyl and carboxylate anions

KENNETH E. EDGECOMBE AND RUSSELL J. BOYD[1]

Department of Chemistry, Dalhousie University, Halifax, N.S., Canada B3H 4J3

Received February 13, 1984

KENNETH E. EDGECOMBE and RUSSELL J. BOYD. Can. J. Chem. **62**, 2887 (1984).

Extensive *ab initio* molecular orbital calculations for the proton affinities of $CH_{n-1}X_{4-n}^-$, where n = 1, 2, 3, or 4 and X = F, CN or NO_2, formate, fluoroformate, and a number of acetates, $CH_{n-1}X_{4-n}CO_2^-$, where n = 1, 2, 3, or 4 and X = F or Cl are presented. Comparison of the theoretical and experimental gas-phase data indicates that the general chemical trends are well described by small basis sets of the split-valence type, but that better quantitative agreement is obtained by use of the diffuse function-augmented basis set (3-21+G) recommended by von R. Schleyer and co-workers (J. Comput. Chem. **4**, 294 (1983)) for anion calculations. Large basis sets and post Hartree–Fock calculations are included for CH_3^-, CH_2F^-, and CH_2CN^-.

KENNETH E. EDGECOMBE et RUSSELL J. BOYD. Can. J. Chem. **62**, 2887 (1984).

On rapporte des calculs poussés *ab initio* d'orbitales moléculaires relatifs à l'affinité pour les protons des anions $CH_{n-1}X_{4-n}^-$ où n = 1, 2, 3 ou 4 et X = F, CN, NO_2, formiate ou fluoroformiate et d'un certain nombre d'acétates, $CH_{n-1}X_{4-n}CO_2^-$, où n = 1, 2, 3 ou 4 et X = F ou Cl. Une comparaison des données théoriques et expérimentales indique que les tendances chimiques générales sont bien décrites par des ensembles de type valence-dédoublée tirées de bases restreintes; toutefois, on obtient un meilleur accord quantitatif si on utilise l'ensemble tiré d'une base rehaussée par une fonction diffuse (3-21+G) recommandé par von R. Schleyer et ses collaborateurs (J. Comput. Chem. **4**, 294 (1983)) pour des calculs relatifs aux anions. Dans le cas des anions CH_3^-, CH_2F^- et CH_2CN^-, on a aussi inclus des calculs obtenus à l'aide de bases élargies et de calculs post Hartree–Fock.

[Traduit par le journal]

Introduction

The proton affinity of an anion A^-, or equivalently the standard enthalpy change ΔH for the deprotonation reaction

[1] $AH \rightarrow A^- + H^+$

is determined experimentally by measurement of the equilibrium constant of the proton transfer reaction

[2] $A_1^- + A_2H \underset{k_{-1}}{\overset{k_1}{\rightleftharpoons}} A_1H + A_2^-$

in the gas-phase (1). Recent measurements of the equilibrium constant for reaction [2] by high-pressure mass spectrometry (2), flowing afterglow (3), and ion cyclotron resonance spectrometry (4) have provided reliable gas-phase data on the acidities of a variety of carbon acids and a few carboxylic acids (1, 5). The gas-phase studies have yielded valuable information on the effect of substituents on the intrinsic properties of carbanions, whereas until recently our knowledge has been based on thermodynamic and kinetic studies in solution. The solution-phase results are often more a reflection of the effects of solvation than an accurate indication of the inherent properties of the anions. In fact, solvation energies, which are of the order of 50–90 kcal/mol (6) are often sufficient to obscure intrinsic acidity differences. For example, acetophenone is six orders of magnitude more acidic than fluorene in benzene (7), but in dimethyl sulfoxide, fluorene is 10^2 times stronger. In view of the complexity of the treatment of solute–solvent interactions (8), it is not practical to determine indirectly intrinsic acidity differences from solution-phase results.

An alternative method for obtaining data appropriate to molecules in the gas phase is provided by *ab initio* molecular orbital theory. Theoretical calculations have been shown to reproduce intrinsic acidity differences for a variety of systems, including those in which gas-phase and solution-phase results are in conflict. Several extensive studies on cations (9), anions (10, 11), and radicals (12) have been reported.

The purpose of this paper is to report an extensive *ab initio* MO study of the relative proton affinities of $CH_{n-1}X_{4-n}$, where n = 1, 2, 3, or 4 and X = F, CN or NO_2, formate, fluoroformate and a number of acetates, $CH_{n-1}X_{4-n}CO_2^-$, where n = 1, 2, 3, or 4 and X = F or Cl. Calculations with diffuse-function augmented basis sets and post Hartree–Fock calculations with extended basis sets are included for comparison with the results obtained with minimal and split-valence basis sets.

Method and results

The optimized structures and the total energies have been described elsewhere for the carbon acids and their conjugate bases (13) and the carboxylic acids and their conjugate bases (14). The proton affinities of the methyl anions are listed in Table 1 where the notation A//B indicates that the proton affinity has been calculated at the level of basis set A with the equilibrium geometry obtained at the level of basis set B. The available high-pressure mass spectroscopic values (5) are included for comparison. The corresponding data for some carboxylate anions are compiled in Table 2.

The theoretical proton affinities have been calculated as the difference between the total energies of the anion and its parent acid at their respective equilibrium geometries. Thus, for a chosen basis set the proton affinity of A^- is given by

[3] $PA(A^-) = E(A^-) - E(AH)$

In order to correct the relative proton affinities given by eq. [3] to absolute proton affinities several corrections must be made. These include a thermodynamic term, $(5/2)RT$, which arises from the change in the number of molecules and a change from absolute zero to the temperature of interest. In principle, a correction should also be made for the difference in the zero-

[1]To whom all correspondence should be addressed.

Can. J. Chem. Downloaded from www.nrcresearchpress.com by 210.87.254.42 on 09/06/12
For personal use only.

TABLE 1. Proton affinities of some methyl anions[a]

Anion	STO-3G//STO-3G[b]	3-21G//STO-3G[b]	3-21+G//3-21+G[c]	Expt.[d]
CH_3^-	559.8	463.4	431.7	416
CH_2F^-	538.1	444.1	414.5	
CHF_2^-	515.6	423.2		
CF_3^-	491.7	396.6	361.6	375.6
CH_2CN^-	496.7	406.7	384.1	372.2
$CH(CN)_2^-$	441.1	355.7	341.4	336.0
$C(CN)_3^-$	396.8	316.7		
$CH_2NO_2^-$	475.3	371.2	342.3	358.7
$CH(NO_2)_2^-$	424.6	333.3		
$C(NO_2)_3^-$	392.5	314.7		

[a]In kcal/mol.

[b]Calculated from the total energies of the anions and their conjugate acids. The equilibrium geometries and total energies are reported in ref. 13.

[c]The value for $CH_2NO_2^-$ is from ref. 11. The 3-21+G optimized structures are: CH_4 (T_d) r(CH) = 1.083; CH_3^- (C_{3v}) r(CH) = 1.091, ∠(HCH) = 113.0°; CH_3F (C_{3v}) r(CF) = 1.434, r(CH) = 1.077, ∠(HCF) = 107.4°; CH_2F^- (C_s) r(CF) = 1.571, r(CH) = 1.102, ∠(HCF) = 99.4, ∠(HCH) = 105.8°; CHF_3 (C_{3v}) r(CF) = 1.364, r(CH) = 1.067, ∠(HCF) = 111.1°; CF_3^- (C_{3v}) r(CF) = 1.461, ∠(FCF) = 98.6°; CH_3CN (C_{3v}) r(CC) = 1.460, r(CN) = 1.141, r(CH) = 1.083, ∠(HCC) = 110.0°; CH_2CN^- (C_{2v}) r(CC) = 1.375, r(CN) = 1.171, r(CH) = 1.074, ∠(HCC) = 120.4; $CH_2(CN)_2$ (C_{2v}) r(CC) = 1.463, r(CN) = 1.139, r(CH) = 1.085, ∠(CCC) = 111.4°, ∠(HCH) = 108.0°, ∠(CCN) = 180.0°; $CH(CN)_2^-$ (C_{2v}) r(CC) = 1.389, r(CN) = 1.159, r(CH) = 1.072, ∠(CCC) = 122.4°, ∠(HCC) = 118.8°, ∠(CCN) = 180.0°.

[d]All data from ref. 5.

TABLE 2. Proton affinities of some carboxylate anions[a]

Anion[b]	STO-3G//STO-3G	K-LMG//STO-3G[c]	K-LMG//"K-LMG"[c]	Expt.[d]
c-HCO_2^-	477.9	372.1 (357.3)		345.2
t-HCO_2^-	473.5	364.4		
c-FCO_2^-	458.3	344.8		
t-FCO_2^-	456.7	342.0		
c-$CH_3CO_2^-$	478.1	376.4 (363.6)	376.1 (362.5)	348.5
t-$CH_3CO_2^-$	473.0	367.6 (354.6)	367.2 (353.4)	
c-$CH_2FCO_2^-$	468.9	365.2 (351.5)	364.3	337.6
t-$CH_2FCO_2^-$	467.2	362.6	361.4	
c-$CHF_2CO_2^-$	459.9	354.1 (339.9)	353.2	330.0
t-$CHF_2CO_2^-$	457.9	351.7	349.3	
c-$CF_3CO_2^-$	450.5	343.6 (329.2)	343.0	322.7
t-$CF_3CO_2^-$	448.1	337.8	336.2	
c-$CH_2ClCO_2^-$	457.0	349.1	347.1	335.4
t-$CH_2ClCO_2^-$	453.0	342.9	340.8	
c-$CHCl_2CO_2^-$	439.7	341.6	337.8	328.4
t-$CHCl_2CO_2^-$	434.6	333.6	329.5	
c-$CCl_3CO_2^-$			330.0	
t-$CCl_3CO_2^-$			323.4	

[a]In kcal/mol.

[b]The prefixes refer to the *cis* and *trans* forms of the corresponding carboxylic acids.

[c]All values were calculated by use of the 3-21G basis set, except in the chloro series for which the 4-31G basis set was used. The values in parentheses are the 4-31G//STO-3G results. The partial K-LMG optimizations, denoted by "K-LMG", are described in ref. 14.

[d]All data from ref. 5.

point energies of A^- and AH. The change in zero-point energy is readily calculated if all the vibrational frequencies of the normal modes are known. There is, however, insufficient data for the anions. A rough estimate of the magnitude of the zero-point correction and its dependence on the number and type of substituents can be obtained by noting that deprotonation of AH leads to a loss of three degrees of freedom, the most important of which is associated with a A—H stretching mode. If we assume that the structure of the anion is not significantly different from that of the parent acid, and that the fundamental frequencies are not appreciably affected, then the force constant of the A—H bond may be expected to yield a fairly good approximation to the change in the zero-point energy. For the methyl anions listed in Table 1 we obtain 5.31, 5.09, 4.93, 4.90, 5.15, 5.06, 4.97, 5.16, 5.02, and 5.01 kcal/mol, respectively, for the zero-point energy correction. These estimates are based on STO-3G force constants which are known to overestimate the force constants of most bonds (15). However, this overestimation is offset by neglecting two lower frequencies associated with bending modes. The STO-3G values for the O—H force constant yield 5.98, 6.02, 6.05, 6.03, 5.97, 5.97, 5.95, 5.95, 5.90, 5.95, 5.96, 5.93, 5.98, 5.98, 5.88, 6.21, 5.89, and 5.72 kcal/mol, respectively, for the zero-point correction of the anions listed in Table 2. The near constancy of the approximations to the zero-point energy correction is a reflection of the insensitivity of the C—H and O—H bonds to substituents (13, 14). In view of the larger changes in some of the other geometrical parameters associated with deprotonation of AH, it is quite likely that the simple force constant method may underestimate the zero-point energy correction. Even if the variation in the zero-point energy correction is an order of magnitude greater than the above estimate, differences of the order of 2 to 3 kcal/mol within a given series will not have a substantial effect on the general trends. Furthermore the thermodynamic correction term, which is about 1.5 kcal/mol for typical experimental conditions, and the zero-point energy correction contribute to the proton affinity with opposite signs (16). Neglecting the zero-point and thermodynamic correction terms leads to errors of about 5–8 kcal/mol. These errors are small, however, relative to the basis set error. The size of the larger members of the series of molecules dictates the use of small basis sets. In principle, we require a mathematically complete basis set for the calculation of the absolute acidities. The use of a finite basis set leads to a substantial error. Even with a complete basis we can do no better than attain the Hartree–Fock (HF) limit. The energies will still be in error due to neglect of electron correlation. To eliminate or even estimate the correlation error we must go beyond the Hartree–Fock limit by using configuration interaction (CI) or other techniques such as Møller–Plesset perturbation theory (17). Large basis sets and post Hartree–Fock calculations are impractical for all but the smallest members of the series included in this work. Consequently we have concentrated our study on basis sets and methods which can be applied to all members of the series. A few calculations with larger basis sets and post Hartree–Fock methods are included as a check on the small basis set calculations. The 3-21+G optimizations (11) and post Hartree–Fock calculations were carried out on a Perkin–Elmer 3230 computer using the GAUSSIAN 80 series of programs (18).

Discussion

Gas-phase proton affinities are available for only 5 of the 10

Can. J. Chem. Downloaded from www.nrcresearchpress.com by 210.87.254.42 on 09/06/12
For personal use only.

Can. J. Chem. Downloaded from www.nrcresearchpress.com by 210.87.254.42 on 09/06/12
For personal use only.

methyl anions included in this study. To make matters worse, a complete set of values is not available for any of the three series. Nevertheless, it is immediately apparent that the minimal basis set grossly overestimates the proton affinities, due to a larger basis set error for the energy of the anions than their corresponding conjugate acids. The 3-21G proton affinities are about 80 to 100 kcal/mol lower than the STO-3G values and are closer to the magnitude of the experimental values. Further improvement requires the addition of diffuse basis functions which provide a better description of the anion (19–21). Recent calculations by von R. Schleyer and co-workers (11, 21) have shown that diffuse function-augmented split-valence basis sets describe the proton affinities of anions better than minimal and standard split-valence basis sets. The mean deviation between theory and experiment for 21 anions is only 3.1 kcal/mol at the 3-21+G level (11), whereas the 3-21G and 4-31G mean deviations are 42 and 30.5 kcal/mol, respectively, for smaller subsets. From Table 1, it is apparent that the effect of adding a set of diffuse functions to the 3-21G basis set is to lower the proton affinities by amounts ranging from 14 to 35 kcal/mol, only a small fraction (0.6 kcal/mol in CH_3^-) of which is due to optimizing the structures at a higher level. Although the improvement is significant, the mean deviation of 12.7 kcal/mol between experiment and theory indicates that the 3-21+G basis set is much less successful for the present set of methyl anions than the ones studied by von R. Schleyer and co-workers (11). Furthermore, there is some indication that the 3-21+G basis set underestimates the proton affinities of the methyl anions containing two or three electronegative substituents, the largest of which are impractical to treat at the 3-21+G level. For example, a 3-21+G calculation on $CH(NO_2)_3$ involves 132 basis functions. For a discussion of general trends, we refer to the 3-21G values in Table 1 in order that all anions may be treated uniformly. Although the 3-21+G values are substantially lower than the 3-21G values, and on average closer to the experimental values, the two sets of data lead to the same chemical trends.

On the basis of the 3-21G results we may predict that within the fluoro series each successive fluorine substituent lowers the proton affinity more than the previous one, whereas in the cyano and nitro series there is an opposite effect associated with multiple substituents. Unfortunately, there is insufficient experimental data to corroborate the 3-21G predictions. We may note, however, that the data for the cyano series is consistent with this observation: the first cyano group lowers the PA by 44 kcal/mol and the second one by 36 kcal/mol in fair agreement with the 3-21G lowerings of 57 and 51 kcal/mol, respectively. The 3-21+G lowerings due to the first and second cyano groups are 48 and 43 kcal/mol, respectively. Also the 3-21G, the 3-21+G and experimental values show a larger decrease in PA for one nitro group than one cyano group. In general the tendency of the 3-21G calculations to underestimate the acidity of the C—H bond appears to diminish as the number of substituents increases.

From eq. [3] it is apparent that in order for small basis set calculations to yield proton affinities in good agreement with gas-phase data, there must be substantial cancellation of errors. Optimizing the structures with extended basis sets may be expected to lead to greater changes in the equilibrium geometries of the anions than the protonated species since larger basis sets are required to obtain the same accuracy for anions as obtained for neutral molecules and cations with smaller basis sets (10*b*, 11, 20–22). In order to provide an indication of the magnitude of the basis set and correlation energy errors we have carried out a few higher-level calculations for the proton affinities of CH_3^-, CH_2F^-, and CH_2CN^- (see Table 3). The data for CH_3^- illustrate a very large basis set dependence. Optimization of the CH_3^- and CH_4 structures at the 6-31G* level reduces the relative PA to 457.0 kcal/mol from the 3-21G//STO-3G value of 463.4 kcal/mol. Including the effects of electron correlation by means of Møller–Plesset perturbation theory (17) terminated at second (MP2) and third (MP3) order has little effect at the 6-31G* level, and actually leads to a small increase in the theoretical values. With a triple-split valence, polarized basis set, 6-311G** (23), substantial improvement is obtained at the HF, MP2, and MP3 levels, while maintaining the structures at their 6-31G* values. Repeating the calculations at the 6-311G** geometries leads to changes of about 0.1 kcal/mol. Configuration interaction (CI) with all single and double substitutions (CIDS) at the 6-311G** level leads to very similar results as the MP2 and MP3 methods. We note that inclusion of the size-consistency correction (SCC) and freezing the core electrons in the carbon 1*s* Hartree–Fock MO have little effect on the results. Optimizing the geometries at the MP2 level with the 6-311G** basis set lowers the energy of CH_3^- by only 7×10^{-5} au but has no effect on the computed proton affinity. None of the extended basis sets mentioned above is as effective, however, as the 3-21+G basis set recommended by von R. Schleyer. Even at the Hartree–Fock level the 3-21+G results are distinctly better. At the MP2/3-21+G//HF/3-21+G level the agreement with experiment is improved for CH_3^- by 7.0 kcal/mol (cf. Tables 1 and 3).

In view of the results presented in Table 3 for CH_3^-, the structures of CH_2F^- and CH_2CN^- were optimized at the HF/6-31G* level, and the proton affinities were calculated by the HF and MP2 methods at the 6-311G** level. The larger basis set lowers the proton affinities by 8 and 10 kcal/mol, respectively, relative to the 3-21G values. The correlation corrections for CH_2F^- and CH_2CN^- are smaller and larger, respectively, than in CH_3^- at the same level. The range of correlation corrections is, however, small. As in the case of CH_3^-, the addition of diffuse functions to the 3-21G basis set at the HF level has a much greater effect than any of the larger basis sets or post Hartree–Fock methods. Including electron correlation at the MP2/3-21+G//HF/3-21+G level further improves the result for CH_2CN^- by 2.0 kcal/mol.

As in the case of the methyl anions, the STO-3G basis set overestimates the relative proton affinities of the carboxylate anions. In fact the K-LMG values are of the order of 100 kcal/mol lower and closer to the range of experimental data. Both the minimal and split-valence basis set calculations are consistent with the observed trend: the proton affinity of the acetate ion decreases as the number of halogen substituents increases. This is also consistent with the increase in acidity in solution phase as the number of halogens increases. It is significant that despite the poor description of the C—C bonds at the STO-3G level (14) in the haloacetate anions, the K-LMG proton affinities at the partially optimized K-LMG geometries do not differ substantially from the K-LMG//STO-3G results. Furthermore full geometry optimizations at the 4-31G level on *c*-CH_2FCO_2H and $CH_2FCO_2^-$ raise the PA by only 0.6 kcal/mol. Comparing the 4-31G PA's in Table 2 with the seven experimental values indicates that the theoretical values are systematically too large by amounts ranging from 6.5 to 14 kcal/mol. The mean deviation of 11 kcal/mol and the fairly

TABLE 3. Post Hartree–Fock total energies and relative proton affinities of selected anions

Anion	Method		Total energy[a]	Proton affinity[b]
	Energy	Geometry[c]		
CH_3^-	HF/6-31G*	HF/6-31G*	−39.46684	457.0
	MP2/6-31G*		−39.60272	457.9
	MP3/6-31G*		−39.61729	458.8
	HF/6-311G**		−39.49704	446.8
	MP2/6-311G**		−39.67028	444.8
	MP3/6-311G**		−39.68668	446.5
	HF/6-311G**	HF/6-311G**	−39.49709	446.7
	MP2/6-311G**		−39.67022	444.9
	MP3/6-311G**		−39.68661	446.5
	CIDS/6-311G**		−39.68024	447.2
	CIDS/6-311G** (SCC)		−39.69065	446.6
	CIDS(Full)/6-311G**		−39.69817	447.5
	CIDS(Full)/6-311G** (SCC)		−39.71031	446.9
	MP2/6-311G**	MP2/6-311G**	−39.67029	444.9
	MP2/3-21+G	HF/3-21+G	−39.40200	424.7
CH_2F^-	HF/6-311G**	HF/6-31G*	−138.38340	436.0
	MP2/6-311G**		−138.74405	435.2
	MP2/3-21+G	HF/3-21+G	−137.89373	409.7
CH_2CN^-	HF/6-311G**	HF/6-31G*	−131.32846	396.8
	MP2/6-311G**		−131.77487	394.8
	MP2/3-21+G	HF/3-21+G	−131.50622	382.1

[a]In atomic units. 1 au = 627.5095 kcal/mol.

[b]In kcal/mol.

[c]The equilibrium C—H bond lengths (Å) of CH_4 and CH_3^- and the HCH angle (deg) of CH_3^- are 1.084, 1.119, 101.7; 1.084, 1.117, 102.7; and 1.090, 1.122, 101.6 at the HF/6-31G*, HF/6-311G** and MP2/6-311G** levels, respectively. The 6-31G* equilibrium (C_s) structural parameters of CH_2F^- are r(CF) = 1.495, r(CH) = 1.117, ∠(HCF) = 100.2 and ∠(HCH) = 100.5°. The 6-31G* equilibrium (C_{2v}) structural parameters of CH_2CN^- are r(CN) = 1.165, r(CC) = 1.376, r(CH) = 1.075 and ∠(HCC) = 120.5. The 3-21+G equilibrium structures are given in footnote *c* of Table 1.

small range of mean deviations indicates that the PA's of the haloacetic acids are moderately well described at the 4-31G level. The 3-21G values for the fluoroacetic acids are about 13–14 kcal/mol higher than the 4-31G values. Adding diffuse basis functions would improve the agreement between theory and experiment. In fact, at the 3-21+G level the relative PA's of formate and acetate are calculated (11) to be 344.4 and 349.5 kcal/mol, respectively, in remarkable agreement with the experimental values of 345.2 and 348.5 kcal/mol.

Acknowledgements

We thank the referees for several helpful suggestions. A generous allocation of computing time from the Dalhousie University Computer Centre, the financial support of the Natural Sciences and Engineering Research Council of Canada, and a Fellowship (to K.E.E.) from the Walter C. Sumner Foundation are gratefully acknowledged.

1. M. J. PELLERITE and J. I. BRAUMAN. *In* Comprehensive carbanion chemistry. *Edited by* E. Buncel and T. Durst. Elsevier, Amsterdam. 1980.
2. (*a*) J. B. CUMMING and P. KEBARLE. Can. J. Chem. **56**, 1 (1978); (*b*) P. KEBARLE. Ann. Rev. Phys. Chem. **28**, 445 (1978).
3. (*a*) J. H. STEWART, R. H. SHAPIRO, C. H. DEPUY, and N. M. BIERBAUM. J. Am. Chem. Soc. **99**, 7650 (1977); (*b*) G. I. MACKAY, R. S. HEMSWORTH, and D. K. BOHME. Can. J. Chem. **54**, 1624 (1976).
4. (*a*) J. E. BARTMESS, J. A. SCOTT, and R. T. MCIVER, JR. J. Am. Chem. Soc. **101**, 6046 (1979); (*b*) R. GYGAX, H. L. MCPETERS, and J. I. BRAUMAN. J. Am. Chem. Soc. **101**, 2657 (1979); (*c*) R. FARID and T. B. MCMAHON. Can. J. Chem. **58**, 2307 (1980).
5. J. E. BARTMESS and R. T. MCIVER. *In* Gas phase ion chemistry. *Edited by* M. T. Bowers. Academic Press, New York. 1979.
6. F. G. BORDWELL, J. E. BARTMESS, G. E. DRUCKER, Z. MARGOLIN, and W. S. MATTHEWS. J. Am. Chem. Soc. **97**, 3226 (1975).
7. W. K. MCEWEN. J. Am. Chem. Soc. **58**, 1124 (1936).
8. J. F. COETZEE and C. D. RITCHIE. *In* Solute–solvent interactions. Marcel Dekker, New York. 1969.
9. (*a*) J. A. POPLE. Int. J. Mass Spectrom. Ion Phys. **19**, 89 (1976); (*b*) W. J. HEHRE. Acc. Chem. Res. **8**, 369 (1975); (*c*) L. RADOM, D. POPPINGER, and R. C. HADDON. *In* Carbonium ions. Vol. V. *Edited by* G. A. Olah and P. von R. Schleyer. Wiley-Interscience, New York. 1976; (*d*) W. J. HEHRE. *In* Modern theoretical chemistry. Vol. 4. *Edited by* H. F. Schaeffer. Plenum Press, New York. 1977.
10. (*a*) L. RADOM. *In* Modern theoretical chemistry. Vol. 4. *Edited by* H. F. Schaeffer. Plenum Press, New York. 1977; (*b*) A. PROSS, D. J. DEFREES, B. A. LEVI, S. K. POLLACK, L. RADOM, and W. J. HEHRE. J. Org. Chem. **46**, 1693 (1981) and references therein.
11. T. CLARK, J. CHANDRASEKHAR, G. W. SPITZNAGEL, and P. VON R. SCHLEYER. J. Comput. Chem. **4**, 294 (1983).
12. (*a*) F. BERNARDI, N. D. EPIOTIS, W. CHERRY, H. B. SCHLEGEL, M. H. WHANGBO, and S. WOLFE. J. Am. Chem. Soc. **98**, 469 (1976); (*b*) A. M. DE P. NICHOLAS, R. J. BOYD, and D. R. ARNOLD. Can. J. Chem. **60**, 3011 (1982).
13. K. E. EDGECOMBE and R. J. BOYD. Can. J. Chem. **61**, 45 (1983).

Can. J. Chem. Downloaded from www.nrcresearchpress.com by 210.87.254.42 on 09/06/12
For personal use only.

14. K. E. EDGECOMBE and R. J. BOYD. Can. J. Chem. **62**, 000 (1984).
15. M. D. NEWTON, W. A. LATHAN, W. J. HEHRE, and J. A. POPLE. J. Chem. Phys. **52**, 4064 (1970).
16. (*a*) R. A. EADES, K. SCANLON, M. R. ELLENBERGER, D. A. DIXON, and D. S. MARYNICK. J. Phys. Chem. **84**, 2840 (1980); (*b*) D. S. MARYNICK, K. SCANLON, R. A. EADES, and D. A. DIXON. J. Phys. Chem. **85**, 3364 (1981).
17. C. MØLLER and M. S. PLESSET. Phys. Rev. **46**, 618 (1934).
18. J. S. BINKLEY, R. A. WHITESIDE, R. KRISHNAN, R. SEEGER, D. J. DEFREES, H. B. SCHLEGEL, S. TOPIOL, L. R. KAHN, and J. A. POPLE. Department of Chemistry, Carnegie–Mellon University, Pittsburgh, PA 15213.
19. A. J. DUKE. Chem. Phys. Lett. **21**, 275 (1973).
20. P. CARSKY and M. URBAN. Lecture notes in chemistry. No. 16. Springer-Verlag, Berlin. 1980 and references therein.
21. (*a*) J. CHANDRASEKHAR, J. G. ANDRADE, and P. VON R. SCHLEYER. J. Am. Chem. Soc. **103**, 5609 (1981); (*b*) G. W. SPITZNAGEL, T. CLARK, J. CHANDRASEKHAR, and P. VON R. SCHLEYER. J. Comput. Chem. **3**, 363 (1982).
22. Previous *ab initio* calculations on substituted methyl anions include: (*a*) J. N. MURRELL, B. VIDAL, and M. F. GUEST. J. Chem. Soc. Faraday Trans. II, **71**, 1577 (1975); (*b*) S. WOLFE, H. B. SCHLEGEL, I. G. CSIZMADIA, and F. BERNARDI. Can. J. Chem. **53**, 3365 (1975); (*c*) F. BERNARDI, I. G. CSIZMADIA, A. MANGINI, H. B. SCHLEGEL, M. H. WHANGBO, and S. WOLFE. J. Am. Chem. Soc. **97**, 2209 (1975); (*d*) A. STREITWIESER and J. E. WILLIAMS. J. Am. Chem. Soc. **97**, 2634 (1975); (*e*) P. G. MEZEY, A. J. KRESGE, and I. G. CSIZMADIA. Can. J. Chem. **54**, 2526 (1976); (*f*) J.-M. LEHN and G. WIPFF. J. Am. Chem. Soc. **98**, 7498 (1976); (*g*) A. C. HOPKINSON, M. H. LIEN, K. YATES, P. G. MEZEY, and I. G. CSIZMADIA. J. Chem. Phys. **67**, 517 (1977); (*h*) D. W. BOERTH and A. STREITWIESER. J. Am. Chem. Soc. **100**, 750 (1978); (*i*) P. G. MEZEY, M. A. ROBB, K. YATES, and I. G. CSIZMADIA. Theoret. Chim. Acta, **49**, 277 (1978); (*j*) G. I. MACKAY, M. H. LIEN, A. C. HOPKINSON, and D. K. BOHME. Can. J. Chem. **56**, 131 (1978); (*k*) T. CLARK, H. KORNER and P. VON R. SCHLEYER. Tetrahedron Lett. 743 (1980); (*l*) J. K. WILMSHURST and C. E. DYKSTRA. J. Am. Chem. Soc. **102**, 4668 (1980).
23. R. KRISHNAN, J. S. BINKLEY, R. SEEGER, and J. A. POPLE. J. Chem. Phys. **72**, 650 (1980).

Can. J. Chem. Downloaded from www.nrcresearchpress.com by 210.87.254.42 on 09/06/12
For personal use only.

Fluorosulfates of the noble metals. Part 6.[1] Synthesis and magnetic properties of fluorosulfato compounds of ruthenium

PATRICK C. LEUNG AND FRIEDHELM AUBKE

Department of Chemistry, The University of British Columbia, 2036 Main Mall, University Campus, Vancouver, B.C., Canada V6T 1Y6

Received December 12, 1983[2]

PATRICK C. LEUNG and FRIEDHELM AUBKE. Can. J. Chem. **62**, 2892 (1984).

Oxidation of ruthenium by bis(fluorosulfuryl)peroxide in HSO_3F solution results in the formation of ruthenium(III) fluorosulfate, $Ru(SO_3F)_3$. Complexation reactions afford $ClO_2[Ru(SO_3F)_4]$ and $Cs[Ru(SO_3F)_4]$. The presence of alkali metal fluorosulfate allows oxidation of ruthenium to the 4+ oxidation state and the complexes $K_2[Ru(SO_3F)_6]$, $Cs_2[Ru(SO_3F)_6]$, and $Cs[Ru(SO_3F)_5]$ are obtained.

Vibrational spectra and the results of magnetic susceptibility measurements down to 80 K are reported and discussed.

PATRICK C. LEUNG et FRIEDHELM AUBKE. Can. J. Chem. **62**, 2892 (1984).

L'oxydation du ruthénium, par le peroxyde de bis(fluorosulfuryl) en solution dans le HSO_3F, conduit à la formation du fluorosulfate de ruthénium, $Ru(SO_3F)_3$. Des réactions de complexation fournissent le $ClO_2[Ru(SO_3F)_4]$ et le $Cs[Ru(SO_3F)_4]$. La présence d'un fluorosulfate d'un métal alcalin permet d'oxyder le ruthénium à son niveau d'oxydation 4+ et on a obtenu les complexes $K_2[Ru(SO_3F)_6]$, $Cs_2[Ru(SO_3F)_6]$ et $Cs[Ru(SO_3F)_5]$.

Opérant à des températures allant jusqu'à 80 K, on a déterminé les spectres vibrationnels et les susceptibilités magnétiques de ces composés et on discute des résultats obtenus.

[Traduit par le journal]

Introduction

Metal oxidation by bis(fluorosulfuryl)peroxide, $S_2O_6F_2$, in the presence of fluorosulfuric acid, HSO_3F, as a reaction medium, had proven in the past a simple and quantitative route to metal fluorosulfates, according to:

$$[1]\quad 2M + nS_2O_6F_2 \xrightarrow{HSO_3F} 2M(SO_3F)_n$$

as well as to metal fluorosulfato complexes as illustrated by a recent example (1):

$$[2]\quad 2CsCl + 2HSO_3F + Pd + 2S_2O_6F_2 \xrightarrow[120°C,\ 30\,h]{HSO_3F} Cs_2[Pd(SO_3F)_6] + 2HCl$$

While of general applicability, our interest had primarily focussed on reactions involving electron-rich 4*d*- and 5*d*-block elements, such as Pd(1), Ag(2), Au(3), Ir(4), and Pt(5) for the following reasons:

(*i*) The fluorosulfates obtained by reactions involving these elements were thermally stable up to 200°C and above, and decomposition to oxy- or fluorofluorosulfates did not occur.

(*ii*) All metals were found to be capable of forming a variety of anionic complexes, allowing more extensive studies.

(*iii*) Detailed studies had revealed unusual magnetic properties in some cases, such as Pd(II) with a $^3A_{2g}$ ground state (1) and Ag(II) in both a magnetically dilute and concentrated system (2). Interesting reactivity patterns were found in other instances, e.g. solutions of $Au(SO_3F)_3$ (3) and $Pt(SO_3F)_4$ (5) in fluorosulfuric acid had exhibited super acidity.

(*iv*) The metals studied had displayed a wide range of reactivity towards $S_2O_6F_2$, with the oxidation of gold complete within a few hours at 25°C (3) while the oxidation of iridium to the Ir^{4+} oxidation state required several days with a reaction temperature of 120°C (4).

We became interested in extending our study to ruthenium in search of similar features as had been discovered previously.

Experimental

Chemicals

Ruthenium metal powder, −80 mesh of 99.9% purity was obtained from the Ventron Corporation. Technical grade fluorosulfuric acid (Allied Chemicals) was double distilled at atmospheric pressure as described previously (6). Bis(fluorosulfuryl)peroxide (7) and chloryl fluorosulfate (8) were synthesized according to published methods. All other chemicals used in this study were obtained from commercial sources in the highest degree of purity available.

Instrumentation and analysis

Details on our instrumentation and the techniques employed in manipulating volatile and moisture-sensitive substances, the recording of infrared, Raman, epr, and electronic spectra and the calibration of magnetic susceptibility measurements have been published previously (2). The Gouy apparatus used in this study has been described earlier (9). Diamagnetic corrections were calculated from Pascals constants (10). Magnetic data on other ruthenium compounds were obtained from reference compilations (10).

All reactions were performed in Pyrex reaction vials of about 40 mL volume fitted with Kontes Teflon stem valves and Teflon coated magnetic stirring bars. The course of reaction was monitored by recording weight changes of the nonvolatile products. Microanalyses were performed by Analytische Laboratorien, Gummersbach, West Germany.

Synthetic reactions

(a) $Ru(SO_3F)_3$

In a typical reaction 0.253 g (2.503 mmol) of ruthenium powder were allowed to react at 60°C for 24 h with a mixture approximately 2.5 mL of $S_2O_6F_2$ and 5 mL of HSO_3F. Completion of the reaction was indicated by the consumption of all metal powder and the formation of a dark red–brown solution. After removal of all volatiles *in vacuo* at 60°C, 1.050 g of an almost black, dark red–brown solid remained, which analysed as $Ru(SO_3F)_3$. *Anal.* calcd.: Ru 25.38, S 24.15, F 14.31; found: Ru 25.15, S 24.02, F 14.46. $Ru(SO_3F)_3$ is hygroscopic, very soluble in HSO_3F, and thermally stable up to 140°C. Above this point decomposition is noted and a red–brown liquid is formed.

[1] For Part 4, see ref. 4; for Part 5, see ref. 5.

[2] Revision received June 26, 1984.

Can. J. Chem. Downloaded from www.nrcresearchpress.com by 210.87.254.6 on 09/06/12
For personal use only.

Can. J. Chem. Downloaded from www.nrcresearchpress.com by 210.87.254.6 on 09/06/12
For personal use only.

(b) $ClO_2[Ru(SO_3F)_4]$

Excess dark red ClO_2SO_3F (~5.6 g) was added to a one-piece Pyrex reactor containing 0.925 g (2.32 mmol) of $Ru(SO_3F)_3$ inside the drybox. After stirring the mixture at ~70°C for one day, complete dissolution of $Ru(SO_3F)_3$ was observed. Excess ClO_2SO_3F was then removed *in vacuo* with the reactor and content kept at 70°C. Due to the low volatility of ClO_2SO_3F, the residual amount was pumped off with the reactor kept at 100°C, leaving 1.334 g of black solid behind. The expected weight for $ClO_2Ru(SO_3F)_4$ was 1.312 g. Elemental analysis of the material suggests the composition $ClO_2Ru(SO_3F)_4$. *Anal.* calcd.: Ru 17.90, Cl 6.28, F 13.46; found: Ru 17.68, Cl 6.38, F 13.58. Infrared bands (cm^{-1}) are listed with estimated intensities in parentheses and bands attributed to ClO_2^+ denoted with an asterik: 1360 (s, b), 1295* (m), 1190 (vs), 1140 (s, sh), ~1040* (m, sh), 940 (s, vb), 810 (s, b), 630 (w), 575 (m), 545 (m), 515* (w), 475 (vw), 435 (vw).

(c) $Cs[Ru(SO_3F)_4]$

A 1:1 stoichiometric mixture of $Ru(SO_3F)_3$ (1.739 g, 4.366 mmol) and $CsSO_3F$ (1.013 g) was loaded into a one-part Pyrex reactor under an inert atmosphere. Excess HSO_3F (~10 mL) was directly distilled into the mixture. Subsequent stirring at ~60°C for one day resulted in complete dissolution. The HSO_3F was then removed *in vacuo* at ~60°C. The homogeneous, very dark brown–black solid obtained was identified by its elemental analysis to have the composition $Cs[Ru(SO_3F)_4]$. *Anal.* calcd.: Cs 21.09, Ru 16.04, F 12.06; found: Cs 20.97, Ru 15.90, F 11.96.

(d) $K_2[Ru(SO_3F)_6]$ and $Cs_2[Ru(SO_3F)_6]$

A 2:1 mole ratio mixture of KSO_3F (0.776 g) and ruthenium powder (0.284 g, 2.81 mmol) was loaded into a one-part Pyrex reactor inside the drybox. Approximately 5 mL of HSO_3F and an equal volume of $S_2O_6F_2$ were distilled successively onto the mixture. Subsequent stirring at ~60°C overnight resulted in a red solution. The excess $S_2O_6F_2$ and HSO_3F were removed *in vacuo* with the reactor and the content kept at ~50°C. Removal of all volatiles from the viscous red–orange solution yielded 2.188 g of a bright orange solid as compared to 2.174 g expected for $K_2[Ru(SO_3F)_6]$. An identical procedure was used to synthesize $Cs_2[Ru(SO_3F)_6]$. Elemental analyses gave the following.

(*i*) *Anal.* calcd. for $K_2[Ru(SO_3F)_6]$: K 10.11, Ru 13.06, F 14.73; found: K 9.99, Ru 13.06, F 14.77.

(*ii*) *Anal.* calcd. for $Cs_2[Ru(SO_3F)_6]$: Cs 27.65, Ru 10.51, F 11.86; found: Cs 27.78, Ru 10.57, F 11.97.

Electronic spectra (mull and diffuse reflectance) with λ_{max} in cm^{-1}, $K_2[Ru(SO_3F)_6]$: 22 200 cm^{-1}, $Cs_2[Ru(SO_3F)_6]$: 20 400 cm^{-1}.

(e) $Cs[Ru(SO_3F)_5]$

In a typical reaction, an approximately equimolar mixture of ruthenium powder, 0.232 g (2.296 mmol) and 0.534 g (2.302 mmol) of $CsSO_3F$ were allowed to react with ~10 mL of a 1:1 mixture (by volume) of HSO_3F and $S_2O_6F_2$ at about 60°C overnight. Removal of all impurities resulted in the formation of a slightly inhomogeneous looking mixture of a red–brown solid with dark brown impurities. An additional 3 mL of $S_2O_6F_2$ afforded 1.686 g (2.312 mmol) of a homogeneous looking red–brown powder that analysed as $Cs[Ru(SO_3F)_5]$. *Anal.* calcd.: Cs 18.22, Ru 13.86, S 21.98, F 13.03; found: Cs 18.38, Ru 13.68, S 22.12, F 13.17.

Results and discussion

Synthesis

Ruthenium is found to be moderately reactive in the oxidation reactions described above. Generally a reaction temperature of 60°C and reaction times of 24 h are sufficient for a complete conversion. If the metal alone is reacted, analytically pure $Ru(SO_3F)_3$ results, even though oxidation to the 4+ state is possible under very similar condition and illustrated by the isolation of $Cs_2[Ru(SO_3F)_6]$ and $Cs[Ru(SO_3F)_5]$. It may be argued that any $Ru(SO_3F)_4$ initially formed does subsequently decompose reversibly when the temperature is raised to 60°C, to allow complete removal of HSO_3F *in vacuo*. A number of unsuccessful attempts were made to achieve further oxidations of ruthenium: reaction of $Ru(SO_3F)_3$ with a large excess of $S_2O_6F_2$, was attempted initially at 60°C and later at 90°C. After 24 h the weight remains unchanged. Ruthenium metal, when reacted with bromine(I) fluorosulfate, $BrSO_3F$ at 85°C gives a red, viscous liquid. Complete reactant removal *in vacuo* requires a temperature of 100°C, before a dry product results. This product appears to be rather impure $Ru(SO_3F)_3$. Attempts to obtain either $Ru(SO_3F)_4$ or possibly an oxyfluorosulfate of ruthenium by the reaction of RuO_2 with either $S_2O_6F_2$, a $S_2O_6F_2/HSO_3F$ mixture or $BrSO_3F$ at elevated temperature result in only very minimal weight increases after reaction times of several days. It seems the noted lack of reactivity makes RuO_2 unsuitable as a starting material in oxidation reactions.

Complex formation of $Ru(SO_3F)_3$ is easily accomplished. Chloronium fluorosulfate, ClO_2SO_3F, is a viscous, very slightly volatile liquid (8), which offers some advantages in preliminary complexation reactions. No solvent is needed, the ClO_2^+ cation is well established (11) and many ClO_2^+ salts of noble metal fluorosulfates have been obtained by us (1, 3*a*, 4, 5). Furthermore, any excess of ClO_2SO_3F can be removed *in vacuo*. In our example the composition $ClO_2[Ru(SO_3F)_4]$ is confirmed by chemical analysis. Initial formation of $(ClO_2)_3[Ru(SO_3F)_6]$ can not be ruled out since temperatures of ~100°C are required before a dry material is obtained.

The corresponding salt $Cs[Ru(SO_3F)_4]$ forms again easily according to:

$$[3]\quad CsSO_3F + Ru(SO_3F)_3 \xrightarrow{HSO_3F} Cs[Ru(SO_3F)_4]$$

When a 3:1 molar ratio of $CsSO_3F$ and $Ru(SO_3F)_3$ is used instead, an inhomogeneous product results and the infrared spectrum reveals a mixture of $CsSO_3F$ (11) and $Cs[Ru(SO_3F)_4]$. While precedents like the ions $[RuCl_6]^{3-}$ (12) are found in solid complexes as well as in solutions, isolation attempts of analogous $[Ru(SO_3F)_6]^{3-}$ containing salts starting with $Ru(SO_3F)_3$ appear to be unsuccessful due to preferential $[Ru(SO_3F)_4]^-$ salt formation.

Where synthetic reactions, aimed at complex formation, involve ruthenium powder as starting material the metal oxidation leads to Ru(IV) complexes instead. The ease with which this oxidation occurs lends credence to the view, that the previously noted isolation of $Ru(SO_3F)_3$ may be due to the isolation method rather than to the limitations of the oxidizing agent. A close parallel is found in reactions of palladium (1). While all attempts to isolate $Pd(SO_3F)_4$ have failed and $Pd(SO_3F)_3$, formulated as $Pd^{(II)}Pd^{(IV)}(SO_3F)_6$, forms instead, salts like $K_2[Pd(SO_3F)_6]$ are very easily obtained (1).

The synthetic route to $Cs[Ru(SO_3F)_5]$, the first example of a pentakis(fluorosulfato)metallate (the tin (13) and platinum (5) analogues have been obtained since), is found by accident. A 1:1 molar ratio of $CsSO_3F$ and ruthenium was employed in an attempt to oxidize ruthenium to the 5+ oxidation state according to:

$$[4]\quad 2CsSO_3F + 2Ru + 5S_2O_6F_2 \xrightarrow{HSO_3F} 2Cs[Ru(SO_3F)_6]$$

however, $Cs[Ru(SO_3F)_5]$ forms instead. The solid is heated at 100°C in the presence of a large excess of $S_2O_6F_2$ for several days, however, no weight increase is noted and further oxidation of ruthenium does not seem to be possible under the

TABLE 1. Infrared frequencies of $Ru(SO_3F)_3$ and related compounds

$Ru(SO_3F)_3$		$Fe(SO_3F)_3$[a]		$Sn(SO_3F)_4$[b]		
ν (cm^{-1})	Int.[c]	ν (cm^{-1})	Int.	ν (cm^{-1})	Int.	Assignment
1430	s,sh			1438 1411	s s	$\nu_{asym}SO_2$ (mono)
1390	vs,b	1360	m	1395	w,sh	ν SO_3 (bi)
1220	s			1232	s	ν_{sym} SO_2 (mono)
1110	sh	1137	s	1130	s	ν SO_3 (bi)
1025	vs,b	1090	s	1085	s	ν SO_3 (bi)
920	w			980 920	w,sh m	ν S—O (mono)
860 820	s sh	850	m	850 832	m s	ν S—F (mono + bi)
645 605	mw,b w	630	m	657 628	m,sh m	M—O stretch δ SO_3 (bi)
585 550	m ms	579 551	w m	585 550	m s	SO_3 bend (mono + bi)
474 450	vw,sh w	442	w	460 438	w m	δ SO_3F (mono) δ SO_3F rock
300	w,b	318	m	328 294	m w	deformation modes

[a] Reference 14.
[b] Reference 15.
[c] Int = intensity, s = strong, m = medium, w = weak, v = very, b = broad, sh = shoulder, asy = asymmetric, sym = symmetric, mono = monodentate, bi = bidentate, stretch = stretching vibration, bend = bending, rock = rocking.

conditions stated. Our previously discussed failure to obtain $Ru(SO_3F)_4$ precludes the possibility of viewing $Cs[Ru(SO_3F)_5]$ as an equimolar mixture of $Cs_2[Ru(SO_3F)_6]$ and $Ru(SO_3F)_4$. It seems common to compounds of the general type $M'[M(SO_3F)_5]$ where M' = K or Cs and M = Ru, Pt, or Sn, that acid salts of the type $M'H[M(SO_3F)_6]$ are thermally not sufficiently stable to allow isolation.

Participation of HSO_3F in the formation of anionic fluorosulfato complexes is generally a definite possibility since the preparations are undertaken in HSO_3F as reaction medium. However, neither here nor in any previous study on similar complexes (refs. 1 to 5, 13) has there been any evidence for their presence as stable species. Microanalysis with a detection limit well below 0.1% and the absence of OH stretching vibrations, recognizing that H-bridge bonding may well cause shifts down to 2500 to 2000 cm^{-1}, are taken as criteria to probe into their presence. The absence of HSO_3F allows us to deduce the oxidation state of ruthenium from the chemical analysis data with additional support coming from magnetic susceptibility data (see below).

Vibrational spectra

The rather intense color of the ruthenium(III) compounds studied by us here prevents the use of Raman spectroscopy. This limits the use of vibrational spectroscopy severely, since the infrared bands are broad and only poorly resolved. This is particularly true for the spectra obtained for $Cs[Ru(SO_3F)_4]$ and $(ClO_2)[Ru(SO_3F)_4]$ listed in the experimental section. Only cautious comments in regard to these two compounds may be made. The three fundamentals attributed to ClO_2^+ are easily recognized and assigned by comparison (14). The remaining bands of $(ClO_2)[Ru(SO_3F)_4]$ agree well with those of $Cs[Ru(SO_3F)_4]$ in band position and intensity. The band positions in the SO_3 stretching region are not consistent with the sole presence of monodentate —OSO_2F or bidentate SO_3F groups. A tetrahedrally coordinated, mononuclear anion is also inconsistent with the magnetic data (*vide infra*), as is a regular octahedral environment. The broadness of many vibrational bands precludes any meaningful interpretation.

The infrared spectra obtained for $Ru(SO_3F)_3$ are of better quality. The data are listed in Table 1 and compared to published ir data of $Fe(SO_3F)_3$ (14) and $Sn(SO_3F)_4$ (15). For the latter compound infrared, Raman, and ^{119}Sn Mössbauer data are most consistent with a polymeric structure, with hexacoordination for tin and the presence of mono- and bidentate bridging SO_3F groups (15). Vibrational data and magnetic moments suggest a regular octahedral environment for Fe^{3+}, a $^6A_{1g}$ ground state for iron and hence bidentate bridging fluorosulfate groups, for $Fe(SO_3F)_3$ (14). For $Ru(SO_3F)_3$ the vibrational band pattern show a better agreement with those of $Sn(SO_3F)_4$ rather than with $Fe(SO_3F)_3$. The assignment presented in Table 1 is rather tentative without Raman data.

The value of Raman data becomes evident, when turning to a discussion of ruthenium(IV) fluorosulfato complexes. For $K_2[Ru(SO_3F)_6]$ and its cesium analogue, well-resolved Raman spectra are obtained, while the ir bands are again rather broad and poorly resolved, particularly in the stretching frequency range. The poor quality of the infrared spectra is due to the high reactivity of the complexes, which prohibits the use of mulling agents. The darker color of $Cs[Ru(SO_3F)_5]$ affects the quality of the Raman spectrum adversely, and only a limited number of bands in the stretching frequency range are observed. However, here a combination of ir and Raman data allows some structural conclusions. The vibrational frequencies for all three complexes are listed in Table 2 together with estimated intensities and a tentative assignment. The Raman spectrum of

Can. J. Chem. Downloaded from www.nrcresearchpress.com by 210.87.254.6 on 09/06/12
For personal use only.

TABLE 2. Vibrational frequencies of anionic fluorosulfato complexes of ruthenium(IV)

$K_2[Ru(SO_3F)_6]$				$Cs_2[Ru(SO_3F)_6]$				$Cs[Ru(SO_3F)_5]$				
Infrared		Raman		Infrared		Raman		Infrared		Raman		
ν (cm^{-1})	Int.	$\Delta\nu$ (cm^{-1})	Int.	ν (cm^{-1})	Int.	$\Delta\nu$ (cm^{-1})	Int.	ν (cm^{-1})	Int.	$\Delta\nu$ (cm^{-1})	Int.	Assignment
1450	vs,b	1398	vw	1400	vs,b	1405	w	1405	vs,b	1400	vw	ν_{asy} SO_2 (mono) and ν SO_3 (bi, A'')
		1261	vs			1252	vs			1252 1241	s s	ν_{sym} SO_3 (mono)
1205	vs	1216	w	1210	vs			1215	vs			ν_{sym} SO_2 (mono)
								1140	m			ν SO_3 (bi, A′)
		1052	vs			1055	s	1040	m	1057	s	ν SO_3 (bi,A) or ν S—O—Ru (mono)
		~970	w,b			~960	w			995	mw	ν_s—O—Ru (mono)
925	vs,b	~910	vw	930	vs,b			925	vs,b			
		852	m			~845	vw			~865	vw	
825	s,b	800	vw	810	s,b	~820	vw	810	s,b			ν S—F (mono, bi)
650	m	620	mw	650	mw	633	m	660	m			ν Ru—O skeletal vibration
580	ms	589	w	580	m			580	ms			ν SO_3F def. modes
550	ms	568	w	550	m			550	ms			
460	w			450	mw							Ru—O skeletal vibration
440	m	442	mw			440	mw	440	mw			SO_3F rock. modes
310	ms	280	m			277	m			269	ms	Ru—O skeletal vibration
		270	w									

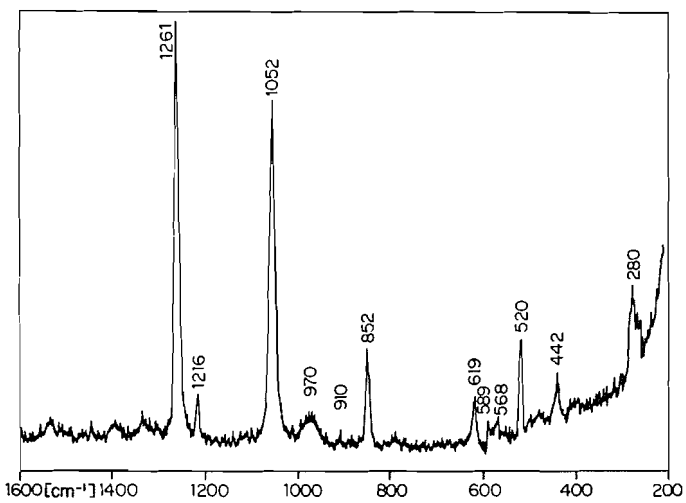

FIG. 1. The Raman spectrum of $K_2[Ru(SO_3F)_6]$.

$K_2[Ru(SO_3F)_6]$ is shown in Fig. 1.

The observed band pattern found for the two $[Ru(SO_3F)_6]^{2-}$ complexes with SO_3 stretching vibrations at ~1400, 1210, and 1050 to 970 cm^{-1} is characteristic for monodentate —OSO_2F groups in anionic complexes with vibrational interaction causing band proliferation. Very similar spectra have previously been obtained by us on other complexes containing the $[M(SO_3F)_6]^{2-}$ ion with M = Sn (16), Ge (13), Pd (1), Pt (1, 2, 5), and Ir (4), and identification by spectral comparison is readily accomplished. Bands at ~640, ~440, and 280 cm^{-1} are characteristic for hexakis(fluorosulfato)metallate(IV) complexes, and are seen to be, at least in part, due to M—O skeletal vibrations, mixed with —OSO_2F deformation modes. Not unexpectedly, these bands do show some dependency on the type of central atom present in the complex.

The more complex situation for $Cs[Ru(SO_3F)_5]$, which results in a greater number of bands, is best seen in the infrared spectrum. Two additional bands, not found for the two hexakis(fluorosulfato)ruthenate(IV) complexes, at 1140 and 1045 cm^{-1}, are indicative of SO_3 stretches in bidentate, possibly bridging fluorosulfate groups in anionic complexes. Bands in a very similar position are found for $Cs[Pt(SO_3F)_5]$ (6) as well as for $Cs[Sn(SO_3F)_5]$ (13) and a common structure involving an oligomeric, polynuclear anion is suggested. Additional evidence had come from the ^{119}Sn spectrum for $Cs[Sn(SO_3F)_5]$ (13). In our case, the electronic mull spectrum has two broad bands at 22 200 and 28 600 cm^{-1} rather than only one for $Cs_2[Ru(SO_3F)_6]$, suggesting a lower symmetry. The magnetic data, to be discussed below, suggest for $Cs[Ru(SO_3F)_5]$ weak antiferromagnetic interaction which is again consistent with the presence of a polynuclear anion.

Magnetic properties

In salts of the type $M_2[Ru(SO_3F)_6]$ with M = K or Cs and in $Cs[Ru(SO_3F)_5]$ a d^4 electron configuration is encountered. With spin pairing, a $^3T_{1g}$ ground term is anticipated in an octahedral ligand environment. As many precedents indicate (10), the magnetic moments should decrease with decreasing temperature from ~3.0 μ_B at room temperature to ~1.7 μ_B at 80 K. For example, K_2RuF_6 shows a magnetic moment of 2.86 μ_B at 300 K (16) with similar values found for other hexahalogeno complexes.

The hexakis(fluorosulfato)ruthenate(IV) complexes show a similar trend, as seen in Table 3. The gradual decrease is consistent with an octahedral environment, and differences in the magnitude may be due to a different packing mode in the crystal lattices of the two salts. Similar differences are encoun-

Can. J. Chem. Downloaded from www.nrcresearchpress.com by 210.87.254.6 on 09/06/12
For personal use only.

TABLE 3. Susceptibility data of $K_2[Ru(SO_3F)_6]$, $Cs_2[Ru(SO_3F)_6]$, and $Cs[Ru(SO_3F)_5]$

$K_2[Ru(SO_3F)_6]$			$Cs_2[Ru(SO_3F)_6]$			$Cs[Ru(SO_3F)_5]$		
χ_M^{corr} ($\times 10^{-6}$ cm^3 mol^{-1})	μ_{eff} (μ_B)	T (K)	χ_M^{corr} ($\times 10^{-6}$ cm^3 mol^{-1})	μ_{eff} (μ_B)	T (K)	χ_M^{corr} ($\times 10^{-6}$ cm^3 mol^{-1})	μ_{eff} (μ_B)	T (K)
3401	2.85	298	3238	2.78	298	2607	2.49	297
3654	2.83	273	3490	2.75	271	2812	2.47	271
3957	2.81	250	3740	2.73	249	3033	2.46	249
4336	2.79	224	4083	2.70	223	3268	2.42	224
4753	2.75	200	4442	2.66	200	3600	2.39	199
5217	2.70	175	4856	2.61	175	3938	2.35	175
5761	2.64	152	5302	2.54	153	4343	2.29	150
6352	2.54	127	5800	2.44	128	4717	2.20	128
7190	2.49	108	6246	2.33	109	5149	2.12	109
7625	2.16	76	6652	2.02	77	5682	1.87	77

tered for hexahalogeno complexes of Ru(III) (10, 16). In any event the data suggest magnetically dilute complexes in both cases.

Noticeably lower magnetic moments are found for $Cs[Ru(SO_3F)_5]$ where the values range from 2.49 to 1.87 μ_B. It is likely that slight anti-ferromagnetic coupling is brought about by either bridging SO_3F groups in a superexchange process or weak direct metal–metal interaction. The data shown in Table 3 are consistent with the presence of a polynuclear complex anion, as suggested by the ir data.

A more complicated situation is found for the two ruthenium(III) compounds, where magnetic studies were undertaken, $Ru(SO_3F)_3$ and $Cs[Ru(SO_3F)_4]$. For Ru^{3+} a d^5 electron configuration is present and with spin pairing in an octahedral complex a $^2T_{2g}$ ground state should give rise to magnetic moments of about 2 μ_B at room temperature. Indeed all reported magnetic moments fall into this range with very few exceptions (10). The magnetic moments obtained for $Ru(SO_3F)_3$ shown in Table 4 are all below 1 μ_B. Furthermore, entirely inconsistent with the expected $^2T_{2g}$ ground state, the data follow the Curie–Weiss law with $C = 0.1291 \pm 0.0036$ and a Weiss constant $\theta = -43.4 \pm 6.7$ K. The resulting magnetic moments $\mu_{eff}^{C.W.}$ are 1.02 ± 0.02 μ_B invariant of temperature. However, this applied correction must be viewed with some caution because θ is fairly large here.

Electron paramagnetic resonance data obtained are tabulated in Table 5 and found to be consistent with the magnetic results. The variation in g_0 values between 295 and 80 K appears to be slight. The lack of fine structure, neither ^{99}Ru or ^{101}Ru hyperfine coupling, nor any resolution into parallel or perpendicular compounds of the g-tensor, suggests a low symmetry site for the paramagnetic species. A frozen solution of $Ru(SO_3F)_3$ in HSO_3F gives at 80 K an anisotropic spectrum with three distinct principle g-values; however, the solution process may have caused some structural changes.

While both a single, magnetically dilute environment for Ru^{3+} and a regular octahedral site for the cation are ruled out, three other structural proposals may also be dismissed: a mixed valency compound $Ru^{II}Ru^{IV}(SO_3F)_6$, reminiscent of the $Pd^{II}Pd^{IV}(SO_3F)_6$ structure (1, 17), with diamagnetic Ru^{II} and magnetically dilute Ru^{IV}, would have substantially higher magnetic susceptibilities and would not show Curie–Weiss law behavior. Likewise a binuclear structure, similar to the structure of $Ru_2(O_2CCH_3)_4Cl$ (18), with a $Ru_2(SO_3F)_4$ core and two terminally bonded —OSO_2F groups would either be more strongly paramagnetic, assuming a triplet ground state, or show

TABLE 4. Magnetic susceptibility data of $Ru(SO_3F)_3$[a]

χ_M^{corr} (10^6 cm^3 mol^{-1})	μ_{eff} (μ_B)	T (K)	$\mu_{eff}^{C.W.}$ (μ_B)
391	0.966	298	1.03
410	0.946	273	1.02
437	0.934	250	1.01
477	0.922	223	1.01
524	0.909	197	1.00
576	0.897	175	1.00
656	0.890	151	1.01
745	0.871	127	1.01
884	0.876	108	1.04
1120	0.830	77	1.04

[a] $C = 0.1291 \pm 0.0036$, $\theta = -43.4 \pm 6.7$ K.

TABLE 5. Electron paramagnetic resonance data of $Ru(SO_3F)_3$

Sample	T (K)	g values
$Ru(SO_3F)_2$ powder	295	$g_0 = 1.804$
$Ru(SO_3F)_3$ powder	80	$g_0 = 1.777$
$Ru(SO_3F)_3$ in HSO_3F	80	$g_1 = 1.515 = g_\parallel$
		$g_2 = 1.831$
		$g_3 = 1.956$
		($g_0 = 1.777$)

a more pronounced temperature dependence of χ_M^{corr}, if a singlet–triplet equilibrium is encountered. For the very same reason, the lack of temperature dependence rules out a possible phase equilibrium between a diamagnetic and a paramagnetic form.

The existence of two, or perhaps even more structurally different phases for $Ru(SO_3F)_3$ remains a distinct possibility and ruthenium(III) chloride, $RuCl_3$, provides an example for such polymorphism. Depending on the method of preparation two structurally different forms are obtained (12). A black α-form has Ru^{3+} in a significantly distorted octahedron (19) resulting in paramagnetism with Curie–Weiss law behavior between 300 and 80 K (10) and a more complicated magnetic behavior at lower temperatures (19). The dark brown β-form is antiferromagnetic below 600 K on account of rather short Ru—Ru bonds (2.83 Å) (19); however, the presence of α-$RuCl_3$ as contaminant has obscurred the situation somewhat.

Can. J. Chem. Downloaded from www.nrcresearchpress.com by 210.87.254.6 on 09/06/12
For personal use only.

The $\beta-\alpha$ transition occurs at 450°C and is irreversible (20).

In summary the color, the magnetic behavior, the existence of mixed phases and the rather high transition temperature of $RuCl_3$ provide intriguing points of comparison and the previously mentioned unusual complexity in the vibrational spectrum of $Ru(SO_3F)_3$ is not inconsistent with the presence of a similar mixture. Furthermore, it is noteworthy that two different forms for $Os(SO_3F)_3$ have been detected and identified by differences in color and vibrational band positions (21).

Whether we are dealing with a mixture of two contrasting forms or an unusually complicated structure with both magnetically dilute paramagnetic and antiferromagnetic components remains an unanswered question. Interestingly magnetic measurement over the temperature range from 300 to 80 K on different preparations of $Ru(SO_3F)_3$ were virtually identical over the whole temperature range in spite of slight variations in the preparative procedure. This reproducibility might suggest a well defined albeit complicated structure. The experimental value of χ_M^{corr} at 298 K allows an approximate estimate of "paramagnetic Ru^{3+}" in the compound. Assuming the antiferromagnetic compound to be essentially diamagnetic at this temperature and a "normal" average μ_{eff} value of 2.0 to 2.1 μ_B would imply χ_M^{corr} between 1680 to 1850 $\times$ 10^{-6} cm^3 mol^{-1}, with approximately only 21 to 23% of Ru^{3+} in a magnetically dilute environment. This admittedly rough estimate does not readily suggest a simple, well-defined structure and further discussions do not appear to be warranted in the absence of a detailed structure.

For $Cs[Ru(SO_3F)_4]$ the situation appears to be even more complicated. The magnetic moments, measured between 300 and 77 K decrease from 0.54 to 0.31 μ_B. The χ_M^{corr} value at 300 K suggests magnetically dilute Ru^{3+} concentration of about 7%. The Curie–Weiss law does not appear to be followed. An epr signal at room temperature is barely detectable. At 80 K two overlapping lines with g_0 values of 1.979 and 1.846, respectively, suggest two slightly different sites for the paramagnetic centers. Again the bulk of the substance appears to be antiferromagnetic or diamagnetic, and it is significant that complexation of $Ru(SO_3F)_3$ with $CsSO_3F$ in HSO_3F solution has resulted in such a significant reduction in paramagnetic ruthenium(III).

One alternative interpretation still remaining is that ruthenium(IV), present as an impurity, may be the cause of the observed paramagnetism. However, the previously discussed reduction in χ_M^{corr} on complexation of $Ru(SO_3F)_3$, the Curie–Weiss law behavior found for this compound and the epr spectra, which are reportedly very rarely observable for d^4 ion, in particular for Ru^{4+} (22) and which compare well to previous reports for Ru^{3+} complexes (22), all argue strongly against the presence of significant amounts of ruthenium(IV), which would also affect the overall composition and the chemical analysis.

It appears then that $Ru(SO_3F)_3$ and $Ru(SO_3F)_4^-$ complexes are readily and cleanly obtainable, the occurrence of polymorphism appears to affect the vibrational spectra and even more noticeably the magnetic behavior, with ruthenium(III) chloride providing a reasonable precedent. Further oxidation to the 4+ state, only possible in the presence of SO_3F^- ions, results in more regular systems.

Acknowledgement

Financial support by the Natural Sciences and Engineering Research Council of Canada is gratefully acknowledged.

1. K. C. LEE and F. AUBKE. Can. J. Chem. **57**, 2058 (1979).
2. P. C. LEUNG and F. AUBKE. Inorg. Chem. **17**, 1765 (1978).
3. K. C. LEE and F. AUBKE. Inorg. Chem. (*a*) **18**, 389 (1979); (*b*) **19**, 119 (1980).
4. K. C. LEE and F. AUBKE. J. Fluorine Chem. **19**, 501 (1982).
5. K. C. LEE and F. AUBKE. Inorg. Chem. **23**, 2124 (1984).
6. J. BARR, R. J. GILLESPIE, and R. C. THOMPSON. Inorg. Chem. **3**, 1149 (1964).
7. G. H. CADY and J. M. SHREEVE. Inorg. Synth. **7**, 124 (1963).
8. H. A. CARTER, A. M. QURESHI, and F. AUBKE. Chem. Commun. 1461 (1968).
9. H. C. CLARK and R. J. O'BRIEN. Can. J. Chem. **39**, 1030 (1961).
10. LANDOLT-BORNSTEIN. Numerical data and functional relationships in science and technology. Vol. 2. Magnetic properties of coordination and organometallic transition metal compounds. Springer Verlag, Berlin. 1966.
11. A. RUOFF, J. B. MILNE, G. KAUFMANN, and M. LEROY. Z. Anorg. Allg. Chem. **372**, 119 (1970).
12. W. P. GRIFFITH. Chemistry of the rarer platinum metals (Os, Ru, Ir, and Rh). Interscience, London. 1967.
13. S. P. MALLELA, K. C. LEE, and F. AUBKE. Inorg. Chem. **23**, 653 (1984).
14. J. GOUBEAU and J. B. MILNE. Can. J. Chem. **45**, 2321 (1967).
15. P. A. YEATS, B. L. POH, B. F. E. FORD, J. R. SAMS, and F. AUBKE. J. Chem. Soc. A, 2188 (1970).
16. A. EARNSHAW, B. N. FIGGIS, J. LEWIS, and R. D. PEACOCK. J. Chem. Soc. 3132 (1961).
17. K. C. LEE and F. AUBKE. Can. J. Chem. **55**, 2473 (1977).
18. M. J. BENNETT, K. G. CAULTON, and F. A. COTTON. Inorg. Chem. **8**, 1 (1969).
19. J. M. FLETCHER, W. E. GARDNER, A. C. FOX, and G. TOPPING. J. Chem. Soc. A, 1038 (1967).
20. E. V. STROGANOV and K. V. ORCHINNIKOV. Vestn. Leningr. Ser. Fiz. ikim. No. 4, **12**, 152 (1957); Chem. Abstr. **52**, 13356 (1958).
21. P. C. LEUNG and F. AUBKE. To be published.
22. B. A. GOODMAN and J. B. RAYNOR. Adv. Inorg. Radiochem. **13**, 136 (1970).

Can. J. Chem. Downloaded from www.nrcresearchpress.com by 210.87.254.6 on 09/06/12
For personal use only.

Solute–solute–solvent interactions in aqueous solutions of triethanolamine and dimethylsulfoxide. Microcalorimetric study

GIANNA BORGHESANI AND FERNANDO PULIDORI

Department of Chemistry, University of Ferrara, Via L. Borsari 46, 44100 Ferrara, Italy

Received October 19, 1983[1]

GIANNA BORGHESANI and FERNANDO PULIDORI. Can. J. Chem. **62**, 2898 (1984).

The heats of dilution of aqueous solutions of triethanolamine (TELA) and dimethylsulfoxide (DMSO) were determined up to ~3 mol kg^{-1}, at 25°C.

The various enthalpic pair and triplet interaction coefficients, h_{xx}, h_{xxx}, have been evaluated from the data.

The h_{xx} for both TELA and DMSO are positive and indicate a prevailing hydrophobic character of TELA and DMSO interactions in highly dilute aqueous solutions.

The triplet coefficients are small and negative for both compounds. Dipolar interactions and normal solvation through H-bonding seem to be more important than the size or the solvophobic effect in determining the triplet enthalpic coefficients.

GIANNA BORGHESANI et FERNANDO PULIDORI. Can. J. Chem. **62**, 2898 (1984).

Opérant à 25°C et à des concentrations allant jusqu'à environ 3 mol/kg, on a déterminé les chaleurs de dilution de solutions aqueuses de triéthanolamine (TELA) et de diméthylsulfoxyde (DMSO).

Utilisant ces données, on a évalué les divers coefficients, h_{xx} et h_{xxx}, d'interaction enthalpique.

Les valeurs de h_{xx} tant pour la TELA que pour le DMSO sont positives; ces résultats indiquent que, en solutions aqueuses très diluées, les interactions de la TELA et du DMSO ont un caractère prédominant qui est hydrophobe.

Pour chacun des composés, les coefficients triplets sont petits et négatifs. Les interactions dipolaires et la solvatation normale par le biais de liaisons hydrogènes semblent donc des facteurs plus importants que la taille ou l'effet solvophobe dans la détermination des coefficients enthalpiques triplets.

[Traduit par le journal]

Can. J. Chem. Downloaded from www.nrcresearchpress.com by 210.87.254.105 on 09/06/12
For personal use only.

Triethanolamine (TELA) and dimethylsulfoxide (DMSO) belong to different classes of polar organic compounds which are miscible with water in any proportion. Whereas TELA, often defined as a highly hydrophilic substance, is polyfunctional in its interactions with water, DMSO is controversially defined (1, 2) and is only capable of acting as an H-acceptor in H-bonding with water.

The physicochemical properties, thermochemical ones in particular, of TELA and related compounds in aqueous solutions have not been extensively studied (3–7).

On the contrary, extensive studies have been performed on the thermochemical properties (1, 8–13) as well as other thermodynamic properties (14, 15) of DMSO-H_2O mixtures. Some of the works quoted, together with spectroscopic evidence of various nature (6, 8, 12, 16–19), underline the formation of H-bonded DMSO–H_2O complexes. Cautious and more in depth analysis (11, 19) points out the possibility of different kinds of interactions between DMSO and water in different concentration regions.

However, although some peculiarities of the above mentioned systems can be deduced from the analysis of the physicochemical properties over the whole composition range, the relationships between these properties, excess ones in particular, and composition are rather complicated, especially for sufficiently high organic concentrations. Thus from these relationships it is difficult to draw detailed information as to the nature and entity of solute–solute and solute–solvent pair and multiplet interactions.

This information is more easily obtained from direct measurements of excess thermodynamic properties of the system in the water-rich region, by considering the organic component as the solute.

Since, to our knowledge, no systematic work on this point has been done for either TELA or DMSO and since these substances are important in different biological and chemical application, the present work is devoted to the determination of the enthalpic properties of TELA and DMSO dilute aqueous solutions.

Particular attention is paid to the role hydrophobicity plays in defining the interactions of these "hydrophilic" compounds.

Experimental

Reagents and instrumentation

Pure TELA from Fluka Chemicals was further purified by fractional distillation under reduced pressure in a N_2 atmosphere. The fraction used had the following characteristics: bp (15 mm Hg) = 206°C; mp = 21.2°C; n_D^{25} = 1.4835; d^{25} = 1.1281 g mL^{-1}. Pure DMSO is hard to obtain, unless due care is taken (20). The pure reagent from Carlo Erba Chemicals was accordingly refluxed over CaH_2 in a N_2 atmosphere under reduced pressure, then fractionally distilled. The fraction boiling at 40–41°C (2–3 mm Hg) was collected and kept frozen in the dark until use. All solutions were prepared by weight with deionized and tridistilled water.

The integral heats of dilution were measured employing an LKB model 2701 flow microcalorimeter equipped with a pair of peristaltic pumps LKB-10200, each working at a preset flow rate. The flow rate of each pump was controlled after each dilution experiment by weighing the liquids pumped through the calorimeter over a defined time interval. The reproducibility of the heats of dilution was of about ±1%, i.e., consistent with this kind of measurement (21).

The flow calorimeter standardization was performed by titrating a 0.01 *N* HCl aqueous solution with NaOH and by comparing the water ionization enthalpy thus obtained with reference literature data (ΔH = 55.7 vs. 55.9 kJ mol^{-1} (22)). The agreement was always better than ±0.5%. The reliability of the calorimeter was also checked by measuring the dilution heats of urea (23) and sucrose (24) aqueous solutions for which good reference data are available and by calculating the related enthalpic pair coefficients, h_{xx}, of the excess enthalpy. The data obtained ($h_{xx,\,urea}$ = −345 ± 10 J mol^{-2} kg; $h_{xx,\,sucrose}$ = +580 ± 16 J mol^{-2} kg) were in good agreement with the values reported in the literature ($h_{xx,\,urea}$ = −350 ± 11 J mol^{-2} kg; $h_{xx,\,sucrose}$ = +577 J mol^{-2} kg (25, 26)).

All measurements were performed at 25 ± 0.02°C.

[1]Revision received March 16, 1984.

TABLE 1. Calorimetric data of TELA aqueous solutions

m_i (mol kg^{-1})	m_f (mol kg^{-1})	$-\Delta H$ ($m_i \rightarrow m_f$) J kg^{-1}	$\Delta H(m_i \rightarrow m_f)/m_i(m_f - m_i)$ (J kg mol^{-2})
3.660	1.736	2570	769
3.660	1.593	2586	785
3.660	1.578	2563	780
3.660	1.559	2739	836
3.660	1.411	2521	795
3.660	0.593	1610	885
2.807	1.245	1637	842
2.807	0.474	1029	932
1.678	0.797	642	914
1.678	0.784	673	960
1.678	0.360	502	1058
1.471	0.711	555	1028
1.471	0.279	340	1023
1.287	0.245	280	1097
0.948	0.467	234	1042
0.948	0.176	147	1082
0.743	0.375	156	1130
0.743	0.372	148	1073
0.743	0.150	101	1135
0.743	0.149	97.1	1098
0.633	0.317	105	1047
0.633	0.129	73.2	1125
0.387	0.197	40.6	1084
0.387	0.080	27.3	1111
0.200	0.103	11.3	1134
0.145	0.075	6.1	1161

Results and discussion

The integral heats of dilution $\Delta H(m_i \rightarrow m_f)$ from the initial m_i to the final molality m_f are obtained by using the equation:

$$[1] \quad \Delta H(m_i \rightarrow m_f) = -(dQ/dt)/P_1$$

where dQ/dt is the stationary thermal flux and P_1 is the total mass flow rate of the solvent. The heats of dilution are expressed in J kg^{-1} of water in the final solution. The enthalpy change per kg of solvent, associated with the integral dilution process,also represents the corresponding excess enthalpy variation, ΔH^E.

The McMillan–Mayer theory of aqueous solutions (27) has long been considered particularly attractive and useful (28) in giving direct information on the interaction between solute molecules.

Accordingly, the excess enthalpy, H^E, of a solution containing 1 kg of solvent may be written as

$$[2] \quad H^E = h_{xx}m^2 + h_{xxx}m^3 + \ldots\ldots$$

where h_{xx}, h_{xxx}, ... are the pairwise, triplet, ... enthalpic interaction coefficients between solute molecules.

When working in suitably diluted solutions, the coefficients of eq. [2] can be obtained from the heats of dilution (21, 29) which can be fitted according to the following equation:

$$[3] \quad \frac{\Delta H(m_i \rightarrow m_f)}{m_f(m_f - m_i)} = h_{xx} + h_{xxx}(m_f + m_i)$$

The results of dilution experiments obtained with TELA and DMSO are collected in Tables 1 and 2, respectively.

Keeping in mind the suggestions of Monk and Wadsö (30) and in particular with the more viscous TELA solutions, separate runs were carried out by varying both the dilution ratios and the total flow rate between 40 and 4 mL h^{-1}. The results in terms of pair and triplet coefficients proved to be independent of the flow rate, thus demonstrating the completeness of the mixing process.

The h_{xx} and h_{xxx} values and their 95% confidence limits are reported in Table 3 together with those of some other aliphatic compounds for the sake of comparison and discussion.

As is well known, the theoretical expression of h_{xx} is

$$[4] \quad h_{xx} = \frac{1}{2}\int_0^\infty \frac{\partial(W(r)/kT)}{\partial(1/kT)}\, g(r)4\pi r^2 \cdot dr$$

where $W(r)$ is the potential of mean force and $g(r)$ the radial distribution function.

Since it is quite difficult to reproduce the experimental data through an adequate model representation of $W(r)$ and to attribute a reliable value to $g(r)$, it is worthwhile assigning a semiquantitative meaning to the h_{xx} coefficients in order to reasonably rationalize and foresee the behaviour of classes of solutes. This may be tried through the Savage and Wood additivity rule (26), which states that each functional group on molecule A interacts with every functional group on molecule B, independent of the mutual position of the interacting groups.

This is summarized by the equation:

$$[5] \quad h_{AB} = \sum_{i,j} n_i^A \cdot n_j^B \cdot H_{i,j}$$

where n_i^A, n_j^B are the number of i-type groups in the molecule A and of j-type groups in the molecule B respectively; $h_{i,j}$ is the characteristic contribution to the enthalpic coefficient from the i,j-th interaction. When A = B, $h_{AB} = h_{xx}$.

The limits of eq. [5] have been repeatedly discussed (29, 31–35). The group additivity principle seems to work correctly within classes of compounds which are of related structure. Instead its predictive ability appears strongly reduced or

Can. J. Chem. Downloaded from www.nrcresearchpress.com by 210.87.254.105 on 09/06/12
For personal use only.

Can. J. Chem. Downloaded from www.nrcresearchpress.com by 210.87.254.105 on 09/06/12
For personal use only.

TABLE 2. Calorimetric data of DMSO aqueous solutions

m_i (mol kg^{-1})	m_f (mol kg^{-1})	$-\Delta H$ ($m_i \rightarrow m_f$) (J kg^{-1})	$\Delta H(m_i \rightarrow m_f)/m_f(m_f - m_i)$ (J kg mol^{-2})
0.1498	0.0757	3.0	534
0.2284	0.1149	7.0	534
0.2284	0.1155	7.0	535
0.5612	0.2760	40.1	509
0.8472	0.4164	91.9	512
0.8472	0.4191	91.0	507
1.0097	0.4933	128	502
1.0097	0.4939	129	506
1.0097	0.4948	129	507
1.0097	0.4964	128	503
1.0097	0.4957	129	506
1.2771	0.6209	204	501
1.5666	0.7536	299	488
1.5666	0.7736	301	491
1.5666	1.0343	269	488
1.6191	0.7779	319	487
1.7938	0.8551	393	490
1.7938	0.8772	392	488
1.9327	0.9156	449	482
1.9327	0.9276	451	484
2.0650	0.9724	511	480
2.3378	1.1265	646	473
2.4180	1.1721	688	471
2.5464	1.1893	766	475

TABLE 3. Pairwise and triplet enthalpic interaction parameters of various aliphatic compounds at 25°C

Compound	$h_{xx,exp.}$ (J mol^{-2} kg)	$h_{xxx,\ exp.}$ (J mol^{-3} kg^2)	Reference
Urea	−350±11	+22	25
Monomethylurea	−85±1	+21±1	45
1,3-Dimethylurea	+35	+78	46
1,3-Diethylurea	+1011	+139	25
Dimethylsulfoxide	+533±3	−18±3	This work
Acetone	+770±6	−6	32
Ethylmethyl ketone	+1188±20	+5	32
Ethanol	+242.9±9.6	+64.8±5.4	43
Propane-1-ol	+558.9±14.2	+158.4±7.9	43
Butane -2-ol	+1003±15	+646±56	43
Triethanolamine	+1151±22	−64±16	This work
Ethane-1,2-diol	+415±30	−21±16	31
Ethane-1,2-diol	+362	−6	33
Glycerol	+251±10	—	33

fails when steric, inductive, or specific orientation-dependent solvation effects cannot be neglected.

The problem of the general applicability of $H_{i,j}$ values has been discussed particularly in connection with the contribution of polar groups in polyols and sugars (29, 31, 35). The peculiar behaviour of these classes of compounds has been explained in terms of their different conformational effects on the solute–water interactions (36, 37). In this context, the amount of useful h_{xx} data available on molecules containing —N< or SO groups are at present too limited (38, 39) to make an acceptably precise estimate of the corresponding $H_{i,j}$ contributions by means of eq. [5].

Nevertheless, h_{xx} of TELA, calculated as a first approximation by neglecting the group contributions bound to —N< and by using tabulated data for the interaction $CH_2 \ldots CH_2$, $OH \ldots OH$, $CH_2 \ldots OH$ (29, 35) and $CHOH \ldots CHOH$, $CH_2 \ldots CHOH$ (33, 34), varies between 1665 and 1899 J kg mol^{-2}. The low energy barrier of the nitrogen pyramidal inversion as well as the low TELA basicity ($pK_a^{25} = 7.76$ (40)), due both to inductive and steric factors (41), could justify some masking of the aminic nitrogen. However, only the sign and the order of magnitude of the calculated coefficient appear reasonable.

Neither value is in accordance with the experimental one (Table 3).

It may be noted that the calculated pair coefficient proved to be practically independent of the choice of characteristic polar groups. It seems rather to depend on the homogeneous (29, 33, 35) or non-homogeneous (34) character of the set of solutes from which the $H_{i,j}$ contributions were derived.

A further approach was tried by considering that h_{xx} is not only the resultant of hydrophobic and hydrophilic interactions but it also depends on the size of the solute itself. It was, therefore, assumed that it may be reasonable to consider one $N(CH_2CH_2OH)_3$ molecule equivalent in size and interaction to three (NCH_2CH_2OH) groups, even by analogy with the reported equivalence $NH_3 = 3NH$ (38). In this way, the enthalpic pair contribution associated with the moiety NCH_2CH_2OH, drawn from the expermental h_{xx} of TELA (Table 3) amounts to 384 J kg mol^{-2}.

This value is comparable to that reported for ethane-1,2-diol (Table 3) a molecule of size and hydrophilic/hydrophobic group ratio like those of the moiety considered. This allows one to assume that the various group contributions bound to tertiary nitrogen cannot be neglected. These should be not too different from those bound to OH groups.

Qualitatively, the h_{xx} value and sign point to a prevailing hydrophobic character of TELA interactions in highly dilute aqueous solutions. This agrees with the hydrophobic character

Can. J. Chem. Downloaded from www.nrcresearchpress.com by 210.87.254.105 on 09/06/12
For personal use only.

of dilute solutions of 2-aminoethanol, which steadily increases with the introduction of methyl groups into the molecule, as shown by the trend of partial molar volumes and enthalpies of these compounds (7).

Again in the case of DMSO, the group contribution principle cannot be correctly applied to calculate h_{xx}, due to the lack of experimental data. An evaluation of its reliability was made, as for TELA, by considering the h_{xx} value of a molecule of comparable size and hydrophilic/hydrophobic group ratio as, for example, acetone and with the aid of other h_{xx} experimental data, reported in Table 3.

When going from urea to acetone, the enthalpic pair coefficients of Table 3 vary from a very negative to a high positive value. Urea, a known "water structure breaker" participates in H-bond formation by interacting with the solvent and with itself in many ways. Acetone, a typical "hydrophobic solute" (32, 42), only acts as a weak acceptor for water hydrogens in H-bond formation. DMSO has a less pronounced hydrophobic character than acetone owing to the stronger $SO \ldots H_2O$ interactions, as indicated by ir and nmr measurements (8).

Furthermore, the data collected in Table 3 show that h_{xx} shifts towards more positive values when the hydrocarbon part of the molecule is increased. When identical hydrocarbon groups are present in different molecules, a decrease in the hydrophobic character is to be expected with an increase in the polar group hydrophilicity, as observed for DMSO in respect to acetone ($h_{xx,\mathrm{DMSO}} < h_{xx,\mathrm{acetone}}$, Table 3). The same trend is observed as the number of polar groups in the same aliphatic skeleton increases (e.g., butane-1-ol/butane-1,4-diol; propane-1-ol/glycerol, Table 3).

Regarding the triplet interaction coefficients of TELA and DMSO, h_{xxx}, the greater complexity of the related interactions is all the more reason why their evaluation is hardly possible by means of the additivity rule. From Table 3 it can be seen that, except in a few cases, the triplet interactions exert a negligible influence on the properties of the solutes, particularly for small and very soluble molecules at high dilutions. Triplet terms are generally one order of magnitude lower than the corresponding pair terms and can bear either positive or negative signs. Only when large hydrocarbon groups are present in a molecule may the triplet interaction coefficient become positive and higher than normal (e.g., alkylated ureas and alkanols, Table 3). This behaviour was ascribed to some cooperativity in the interactions of hydrocarbon groups and was defined as peculiar of the hydrophobic interaction (43).

Instead, for a great variety of molecules and, in particular, for simple highly polar solutes and most sugars, polyols and related compounds (32, 44), h_{xxx} coefficients are very small and often negative. It has been claimed (32, 44) that the scattering of dilution heats at high dilutions makes the triplet coefficients ambiguous or meaningless in these cases. However, the accuracy of TELA and DMSO experimental data is good enough for the following remarks. The negative sign of h_{xxx} observed for both TELA and DMSO (Table 3) should mean that dipolar interactions and normal solvation through H-bonding are more important than size or solvophobic effect in determining the triplet enthalpic coefficients. Therefore, what observed ($h_{xxx,\mathrm{DMSO}} < h_{xxx,\mathrm{acetone}}$) seems to be reasonable in view of the higher DMSO dipole moment ($\mu_{\mathrm{DMSO}} = 3.96$ D; μ_{acetone} 2.88 D).

Also the h_{xxx} coefficient found for TELA, nearly equal to $3h_{xxx}$ of ethane-1,2-diol (Table 3), may be qualitatively justified in terms of the greater polarity of TELA and the increased number of hydrophilic sites as well. This parallels the trend also observed for h_{xx} and h_{xxx} coefficients of more complex solutes, such as disaccharides, which are nearly equivalent to the sum of the corresponding coefficients of the monose subunits (44).

In conclusion, sign and entity of the enthalpic interaction coefficients of both TELA and DMSO point to the existence and prevalence of hydrophobic interactions in very dilute aqueous solutions. The measurement of other thermodynamic quantities as free energy and volumes (to be published) shows that the disturbances produced in water at high dilutions are limited, particularly for DMSO. With increasing concentration, other kinds of interactions, particularly H-bonding, will increasingly prevail, thus giving these compounds the typical "aqueous" or "hydrophilic" character.

Acknowledgements

The purchase of LKB 2107 flow microcalorimeter was possible by a special grant from the University of Ferrara for interdisciplinary research. This work was supported by the Italian Ministry of Education (M.P.I.).

1. M. E. Fox and K. Whittingham. J. Chem. Soc. Faraday Trans. 1, **75**, 1407 (1975).
2. F. Rallo, F. Rodanti, and P. G. Silvestroni. Termochimica Acta, **1**, 311 (1970).
3. S. Cabani, P. Gianni, V. Mollica, and L. Lepori. J. Solution Chem. **10**, 8 (1981).
4. Y. M. Tseng and A. P. Thompson. J. Chem. Eng. Data, **9**, 264 (1964).
5. I. Duldner, A. Weidenbacher, S. Serban and F. Oancea. Rev. Chim. Bucharest, **20**, 649 (1969).
6. W. A. De Oliveira, A. F. Marconsin, A. P. Chagas, and P. L. Volpe. Thermochim. Acta, **42**, 387 (1980).
7. H. Touhara, S. Okazaki, F. Okino, H. Tanaka, K. Ikari, and K. Nakanishi. J. Chem. Thermodyn. **14**, 145 (1982).
8. W. Drinkard and D. Kivelson. J. Phys. Chem. **62**, 1494 (1958).
9. H. L. Clever and S. P. Pigott. J. Chem. Thermodyn. **3**, 221 (1971).
10. R. Philippe and C. Jambon. J. Chim. Phys. **71**, 1041 (1974).
11. M. I. Davis. Thermochim. Acta, **63**, 67 (1983).
12. J. M. G. Cowie and P. M. Toporowski. Can. J. Chem. **39**, 2240 (1961).
13. J. Kentamä and J. J. Lindberg. Suomen Kem. B, **33**, 32 (1960).
14. C. De Visser, L. A. Dunn, and G. Somsen. J. Chem. Soc. Faraday Trans. I, **74**, 1159 (1978).
15. O. Kiyohara, G. Perron, and J. E. Desnoyers. Can. J. Chem. **53**, 3263 (1975).
16. I. Bulla, P. Tormäla, and J. J. Lindberg. Acta Chem. Scand. A**29**, 89 (1975).
17. G. Dawber. J. Chem. Soc. Faraday Trans. I, **78**, 1127 (1982).
18. J. R. Scherer, M. K. Go, and S. Kint. J. Phys. Chem. **77**, 2108 (1973).
19. G. J. Safford, P. C. Schaffer, P. S. Lenny, G. F. Doebler, G. W. Brady, and E. F. X. Lyden. J. Chem. Phys. **50**, 2140 (1969).
20. D. R. Burfield and R. H. Smithers. J. Org. Chem. **43**, 3966 (1978).
21. G. Barone, P. Cacace, G. Castronuovo, and V. Elia. Gazz. Chim. Ital. **110**, 215 (1980).
22. C. E. Vanderzee and J. A. Swanson. J. Phys. Chem. **67**, 2608 (1963).
23. F. T. Gucker and H. B. Pickard. J. Am. Chem. Soc. **61**, 1464 (1939).
24. F. T. Gucker, H. B. Pickard, and R. W. Plank. J. Am. Chem. Soc. **61**, 459 (1939).

25. V. ABATE, G. BARONE, G. CASTRONUOVO, V. ELIA, and P. MASTURZO. Gazz. Chim. Ital. **111**, 85 (1981).
26. J. J. SAVAGE and R. H. WOOD. J. Solution Chem. **5**, 733 (1976).
27. W. MCMILLAN and J. MAYER. J. Chem. Phys. **13**, 276 (1945).
28. J. J. KOZAK, W. S. KNIGHT, and W. KAUZMANN. J. Chem. Phys. **48**, 675 (1968).
29. G. BARONE, G. CASTRONUOVO, D. DOUCAS, V. ELIA, and C. A. MATTIA. J. Phys. Chem. **87**, 1931 (1983).
30. P. MONK and I. WADSÖ. Acta Chem. Scand. **22**, 1942 (1968).
31. F. FRANKS and M. D. PEDLEY. J. Chem. Soc. Faraday Trans. I, **79**, 2249 (1983).
32. F. FRANKS and M. D. PEDLEY. J. Chem. Soc. Faraday Trans. I, **77**, 1341 (1981).
33. R. TASKER and R. H. WOOD. J. Phys. Chem. **86**, 4040 (1982).
34. B. Y. OKAMOTO, R. H. WOOD, J. E. DESNOYERS, G. PERRON, and L. DELORME. J. Solution Chem. **10**, 139 (1981).
35. G. BARONE, P. CACACE, G. CASTRONUOVO, and V. ELIA. Carbohydr. Res. **119**, 1 (1983).
36. N. N. SKÖLD, R. SPINK, C. J. SUURKUUSK, and I. WADSÖ. J. Chem. Thermodyn. **8**, 1081 (1976).
37. Y. N. LIAN, A. T. CHEN, J. SUURKUUSK, and I. WADSÖ. Acta Chem. Scand. A**36**, 735 (1982).
38. W. J. M. HEUVESLAND, C. DE VISSER, and G. SOMSEN. J. Chem. Soc. Faraday Trans. I, **77**, 1191 (1981).
39. R. BURY, A. MAYAFFRE, and C. TREINER. J. Chem. Soc. Faraday Trans. I, **79**, 2517 (1983).
40. R. A. ROBINSON, R. H. STOKES, and E. H. STOKES. Electrolyte solutions. Butterworth, London. 1968. p. 517.
41. M. EIGEN, G. MAASS, and G. SCHWARZ. Z. Phys. Chem. **74**, 319 (1971).
42. A. V. BENEDETTI, M. CILENSE, D. R. VOLLET, and R. C. MONTONE. Thermochim. Acta, **66**, 219 (1983).
43. F. FRANKS, M. D. PEDLEY, and D. S. REID. J. Chem. Soc. Faraday Trans. I, **72**, 359 (1976).
44. G. BARONE, P. CACACE, G. CASTRONUOVO, and V. ELIA. Gazz. Chim. Ital. **112**, 153 (1982).
45. G. BARONE, G. CASTRONUOVO, V. ELIA, and A. MENNA. J. Solution Chem. **8**, 157 (1979).
46. G. BARONE, G. CASTRONUOVO, V. CRESCENZI, V. ELIA, and G. RIZZO. J. Solution Chem. **7**, 179 (1978).

Can. J. Chem. Downloaded from www.nrcresearchpress.com by 210.87.254.105 on 09/06/12
For personal use only.

Comments on the structure of alkylammonium hexachlorostannates

M. H. BEN GHOZLEN AND Y. MLIK

École Nationale D'ingenieurs SFAX, Ministère de l'Enseignement supérieur et de la recherche scientifique, Route de Soukra 3038 SFAX, Tunisia

Received January 22, 1984

M. H. BEN GHOZLEN and Y. MLIK. Can. J. Chem. **62**, 2903 (1984).

Both dimethyl and trimethylammonium hexachlorostannates crystallise in space groups which are subgroups of the antifluorite structure ($Fm3m$, $Z = 1$). These two symmetry changes are described on the basis of Landau theory for continuous phase transitions. The involved irreducible representation is E_g at the X high symmetry point of the cubic face centred Brillouin zone.

M. H. BEN GHOZLEN et Y. MLIK. Can. J. Chem. **62**, 2903 (1984).

Les hexachlorostannates de diméthyl- et de triméthylammonium cristallisent tous les deux dans des groupes d'espace qui sont des sous-groupes de la structure de l'antifluorine ($Fm3m$, $Z = 1$). On décrit ces deux changements de transition en faisant appel à la théorie de Landau pour des transitions de phase continues. La représentation irréductible impliquée est E_g au point de plus haute symétrie de X de la zone de Brillouin du cube à face centrée.

[Traduit par le journal]

Knop *et al.* (1) have recently reported an important experimental study on the alkylammonium hexachlorostannates (crystal structures and infrared spectroscopy). The solved cristalline structures at room temperature are compared to the antifluorite parent structure. Likewise, the authors try to relate all the obtained space groups to $Fm3m$ ($Z = 1$). In Table 15, they state that di- (2MHS) and trimethylammonium hexachlorostannate (3MHS) space group are not subgroups of $Fm3m$.

In fact, the analysis of the structures of these two compounds, which had been solved previously (2, 3), on the basis of a recent work on the $Fm3m$ subgroups (4) reveals that the symmetry changes from $Fm3m$ ($Z = 1$) to $Pnnm$ ($Z = 2$) and to $Pa3$ ($Z = 4$), the structures of 2MHS and 3MHS, respectively, are realized at the high symmetry point X of the cubic face centred Brillouin zone. The associated order parameters of these symmetry changes are, respectively (q, q, 0, 0, 0, 0) and (0, q, 0, q, 0, q); they transform as the irreducible representation E_g at the X point of $Fm3m$ (4).

For $Pnnm$ space group only one arm of the star is involved in the symmetry change (5). The corresponding order parameter is left invariant by the following $Fm3m$ symmetry operations (in the notation of Bradley and Cracknell (5)):

$$(C_{2c}|0),\ (C_{2y}|t_1),\ (C_{2e}|t_1),\ \text{and}\ (I|0)$$

The new Bravais battice can be described by

$$A = \frac{t_1 - t_2 + t_3}{2}$$

$$B = \frac{t_1 - t_3}{2}$$

$$C = t_2$$

The obtained primitive cell being pseudo-quadratic, agrees very well with the experimental values (7.220 (1) Å; 7.340 (2) Å; 14.446 (3) Å) of the crystal parameters.

For the distorted cubic structure of 3MHS all the arms of the star are involved in the symmetry change. The generator symmetry operations which lead to $Pa3$ space group are (again in the notation of Bradley and Cracknell):

$$(C_{2x}|t_3),\ (C_{2z}|t_2),\ (I|0),\ (C_{31}^{+}|0)$$

The translational part of the induced irreducible representation lead to the following cubic primitive cell:

$$A = -t_1 + t_2 - t_3$$

$$B = t_1 - t_2 + t_3$$

$$C = t_1 + t_2 - t_3$$

On the other hand, a study of the external vibrations for the two compounds shows that these symmetry changes are obtained from $Fm3m$ structure by slight distorsions which can be described as translations of the organic groups and rotations of the $SnCl_6^{2-}$ octahedra (6).

1. O. KNOP, T. S. CAMERON, M. A. JAMES, and M. FALK. Can. J. Chem. **61**, 1620 (1983).
2. M. H. BEN GHOZLEN, A. DAOUD, and J. W. BATS. Acta Crystallogr. B**37**, 1415 (1981).
3. M. H. BEN GHOZLEN and J. W. BATS. Acta Crystallogr. B**38**, 1308 (1982).
4. M. H. BEN GHOZLEN and Y. MLIK. J. Phys. C. Solid State Phys. **16**, 4365 (1983).
5. C. J. BRADLEY and A. P. CRACKNELL. The mathematical theory of symmetry in solids. Clarendon Press, Oxford. 1969.
6. Y. MLIK. Unpublished work.

The electrochemical behaviour of some 1-ethylmercapto-3-(4*H*)isoquinolones derivatives. Part I. Electroreduction of 4-arylazo-1-ethylmercapto-3 (4*H*)isoquinolones derivatives in alcoholic aqueous media

H. M. FAHMY, H. A. DABOUN, AND M. ABDEL AZZEM

Department of Chemistry, Faculty of Science, Cairo University; and Faculty of Electronic Engineering, El-Menoufia University (Egypt)

AND

G. CAUQUIS AND G. PIERRE

Laboratoire de Chimie (LA CNRS 321), Departement de Recherche Fondamentale, Centre d'Etudes Nucleaires de Grenoble, 85 X, 38041 Grenoble-Cedex, France, et Laboratoire de Chimie Organique Analytique (LA CNRS 321), Université Scientifique et Medicale de Grenoble, Bp 68, 38402 Saint-Martin-Heres-Cedex

Received March 2, 1983[1]

H. M. FAHMY, H. A. DABOUN, M. ABDEL-AZZEM, G. CAUQUIS, and G. PIERRE. Can. J. Chem. **62**, 2904 (1984).

The polarographic reduction data of 4-arylazo-1-ethylmercapto-3-(4*H*)isoquinolone derivatives in 50% by volume ethanolic aqueous buffered media are reported and discussed. These compounds exist in several tautomeric forms so their structures have been investigated using ir and polarographic analyses. The data obtained indicated that these compounds in aqueous media and in solid state exist predominantly in the azo form. A mechanism interpreting the electrode process is proposed and confirmed via the identification of CPE products and Hammett's $\sigma-E$ relations.

H. M. FAHMY, H. A. DABOUN, M. ABDEL-AZZEM, G. CAUQUIS, and G. PIERRE. Can. J. Chem. **62**, 2904 (1984).

On rapporte et on discute de données relatives aux réductions polarographiques, effectuées dans des milieux aqueux tamponnés contenant 50% par volume d'éthanol, d'arylazo-4 éthylmercapto-1 (4*H*)-isoquinolones-3. Ces composés existant sous plusieurs formes tautomères, on a étudié leurs structures en se basant sur des analyses des données ir et polarographiques. Les données obtenues indiquent que, en solution dans des milieux aqueux ainsi qu'à l'état solide, ces composés existent d'une façon prédominante sous la forme azo. On propose un mécanisme interprétant le processus au niveau de l'électrode et ce mécanisme est confirmé d'une part l'identification des produits CPE et d'autre part par les relations $\sigma-E$ de Hammett.

[Traduit par le journal]

Introduction

We have been dealing for sometime with the electroreduction of five-membered heterocyclic systems of biological interest. These systems contain the sequence —S—C=N—CO—C—N=N— (1, 2) in their structure. It also seemed worthwhile to investigate this sequence in six-membered heterocyclic systems. 4-Arylazo-1-ethylmercapto-3-(4*H*)isoquinolones (**I***a*–*f*) attracted our attention since they met our requirement. These compounds may exist in one of the three potentially tautomeric structures **I**α–γ.

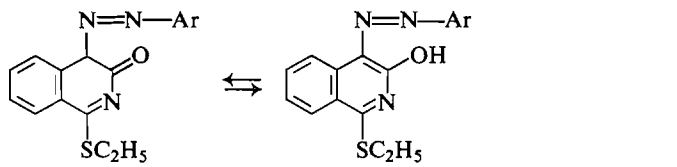

Iα

Iβ

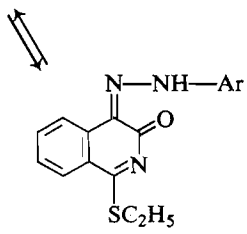

Iγ

I*a* Ar = C_6H_5 — **I***d* Ar = p-OCH_3—C_6H_4
I*b* Ar = p-CH_3—C_6H_4 — **I***e* Ar = p-Cl—C_6H_4
I*c* Ar = m-CH_3—C_6H_4 — **I***f* Ar = p-NO_2—C_6H_4

[1]Revision received June 7, 1984.

Recently it has been shown that the polarographic data of azo–hydrazo tautomeric compounds can be used for their structural identification (3–6). In the present work the electrochemical reduction of **I***a*–*f* in 50% ethanolic aqueous buffers was studied to elucidate the mechanism of electroreduction and to determine the most predominant tautomeric structure of these molecules in aqueous media.

Experimental

1. Organic synthesis

To a cooled solution of 1-ethylmercapto-3-(4*H*)isonolone (7) (6.7 g) in 20 mL of ethanol containing 10 g of sodium acetate was added dropwise the diazonium chloride solution from 3.7 g of aniline. After addition was complete, the red product of **I***a* was collected by filtration, washed with water, and crystallized from ethanol. The above experiment was repeated using the appropriate diazotized amine to give arylazo derivatives **I***b*–*f*. Compounds **I***e* and **I***f* were recrystallized from acetic acid. Melting points (°C) of **I***a*–*f* are 155, 167, 161, 173, 198, and 283, respectively.

2. Polarographic investigations

(a) Apparatus

Voltammograms were obtained using a Tacussel instrumentation: PRT 40 as potentiostat, EPL 1 as recorder, and PRG 3 as pilot. The cell was a Tacussel RMO4 cell which can hold 20 mL of solution. The capillary was a Tacussel CMT 5/24, m = 0.33 mg s^{-1} for h = 50 cm and was controlled by a hammer with a frequency of 1 Hz. Infrared spectra were recorded in KBr pellets on a Perkin-Elmer 397.

(b) Measurements

All experiments were carried out at 20 ± 2°C. The half-wave potentials were measured graphically and expressed versus the saturated calomel electrode (SCE).

(c) Procedure

Ethanol and the appropriate Britton–Robinson modified universal

Can. J. Chem. Downloaded from www.nrcresearchpress.com by 210.87.254.42 on 09/06/12
For personal use only.

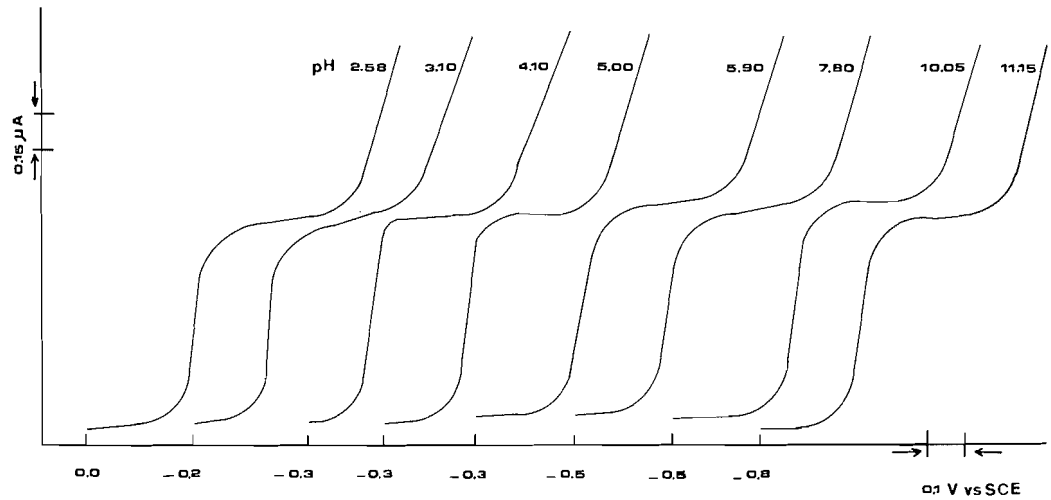

FIG. 1. Schematic representation of the polarograms of 10^{-4} *M* I*a* in 50% by volume ethanolic Britton–Robinson buffers.

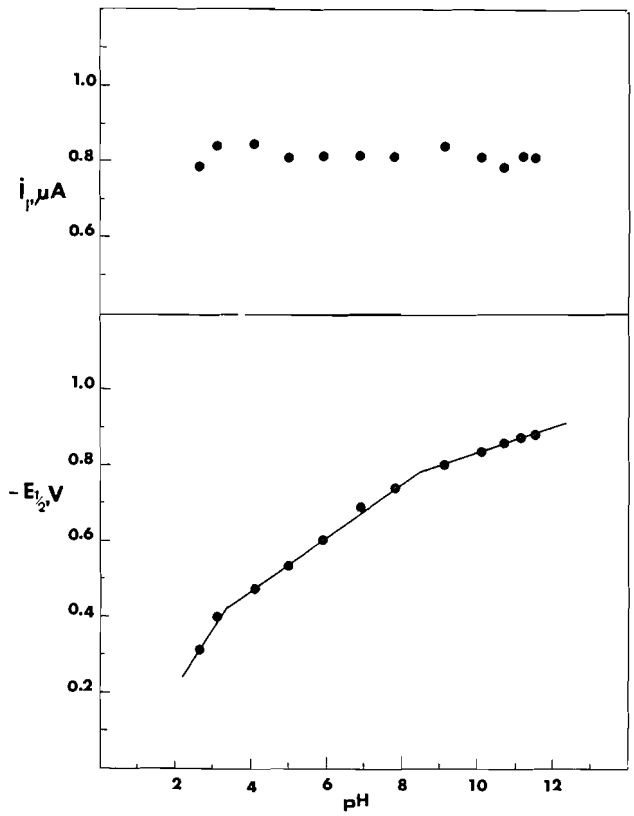

FIG. 2. $E_{1/2}$–pH and i_l–pH plots of the polarographic wave of 10^{-4} *M* I*a* in 50% by volume ethanolic Britton–Robinson buffers.

buffer (8) solutions were introduced into the polarographic cell. The solution was then deaerated by bubbling a stream of nitrogen for 10 min. The calculated amount of stock solution was then introduced into the cell so that the final concentration was 10^{-4} *M*.

3. Controlled potential electrolysis (CPE) and the identification of the resulting products

CPE was carried out on a mercury pool with 100 mg of I*a* taken as a typical example in 200 mL of 50% by volume ethanol – 10^{-2} *M* HCl solution, using the same apparatus as described in a former paper (9). The applied potential was −0.3 V, i.e., on the limiting current plateau of the wave. The number of electrons was found to be 4 mol of electrons per mol of product. After complete electrolysis, the solution was evaporated *in vacuo*. The obtained mixture was treated with water. The insoluble part was isolated by filtration and identified as 4-aminohomophthalimide hydrochloride (**V**) (by mp and mmp determination (10) and ir spectra). The soluble part was concentrated by evaporation to half its volume and the presence of aniline in the solution was revealed by a standard spot test (11).

Results and discussion

Polarographic behaviour of I*a–f*

Compounds I*a–e* exhibit one well-defined polarographic wave (cf. Fig. 1). The half-wave potential is pH-dependent, shifting to more negative values with the increase of pH as indicated by Fig. 2. The shift of $E_{1/2}$ with pH for compounds I*a–f* are compiled in Table 1 in the form of linear equations. On the other hand, the limiting current is practically independent of pH as shown in Fig. 2. The shift of $E_{1/2}$ with increase of pH by an average of 0.068 in the pH range 3–9 for the second segment together with the independency of i_l on pH is a direct indication that the rate-determining step is the preprotonation of the molecule. This is confirmed by applying the equation (12) $dE_{1/2}/dpH = (-2.3RT/\alpha n)\ p$ which gives a value of $1H^+$ per molecule. On the other hand, the abnormal increase in the value of $dE_{1/2}/dpH$ (0.153–0.204) for the first segment can be explained by the following: (*a*) that such basic molecules are most probably involved in other acid–base equilibria at their basic sites or with the buffer constituents of solution; (*b*) that a diprotonated species is the reduced form in pH values below 3.

At pH > 9 the $E_{1/2}$ values are practically pH-independent ($dE_{1/2}/dpH \sim 0.035$), this can be taken as an indication that at these pH values both the protonated (IH^+) and unprotonated (**I**) species are reduced at compatible potentials and that the unprotonated form is the predominant one. Cyclic voltammetry using a hanging mercury drop together with logarithmic analyses of the waves indicated that the process is irreversible in nature. Routine analyses of this wave through the effect of concentration and height of mercury column showed that this wave is diffusion controlled. In addition to the well-defined polarographic wave A exhibited by compounds I*a–e*, the polarograms of compound I*f* displayed another wave B at a more negative potential. Comparison of the polarograms of I*f* with those of I*a–e* indicates that this wave is due to the nitro group occupying the *para* position. Also, a wave-height ratio comparison with wave A indicates that B is a four-electron wave

Can. J. Chem. Downloaded from www.nrcresearchpress.com by 210.87.254.42 on 09/06/12
For personal use only.

and $E_{1/2}$–pH plot of B seemed to be compatible with the one reported for the reduction of aromatic nitro compounds into the hydroxylamine derivatives (13, 14), following the equation

$$E_{1/2} = -0.139 - 0.086\text{pH}$$

In the pH range 3–6 and pH > 10, another wave appeared with a limiting current equal to ~ 2 e with a pH-independent $E_{1/2}$. This wave can be suggested for the further reduction of the —NHOH group into the amino group as previously described in detail (15).

From the foregoing results it is not unreasonable to conclude that wave A is due to the reduction of an azo (—N=N—) moiety. This assignment is based on the following facts: (*1*) The comparison of $E_{1/2}$ position and shift is within good limits with those of similar heterocyclic azo and not hydrazono compounds (16–18). (*2*) The appearance of the reduction of nitro group after the wave A is a direct indication that the reduced species is an azo and not a hydrazono linkage (15, 19).

Thus one can assume that structures **I**α and **I**β are the most probable ones in 50% ethanolic aqueous media. Theoretically, the conjugation in system **I**β can be considered the most stable since the double single bond sequence is not interrupted. In addition, structure **I**β can be further stabilized through hydrogen bonding between OH group and the N attached to the aryl group. Furthermore, ir spectra indicate no sharp carbonyl CO band between 1700–1800 cm^{-1}.

Based on the above findings the following overall mechanism is suggested and is confirmed via the isolation and identification of both products of electrolysis: 4-aminohomophthalimide hydrochloride (**V**) and aniline.

Mechanism

That the polarograms displayed only one four-electron wave is rationalized by the fact that the values of E_1^a and E_2^a are too close and therefore merge to form a single well-defined wave. The fact that this wave predominates over the whole pH range indicates that these molecules are highly basic in nature. Furthermore, the ir spectra of compound **V** (cf. CPE) as main electrolysis product suggested that compound **IV** hydrolyses in highly acidic media (HCl) to give **V** (16).

[1] 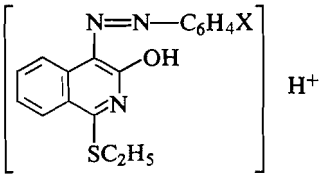

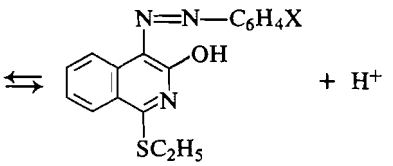

I

[2] 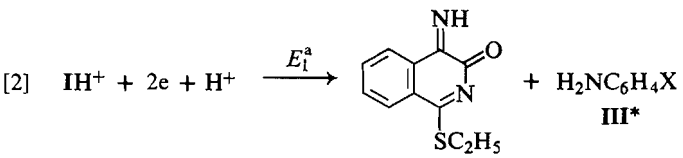

II

[3] 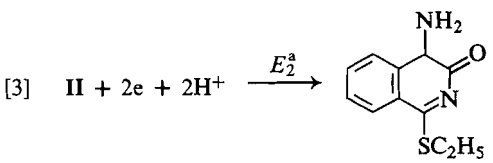

IV

[4] 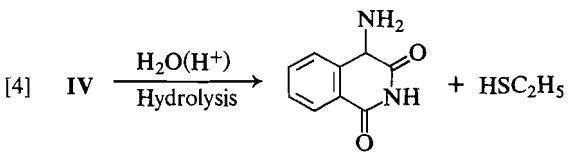

V*

*isolated products

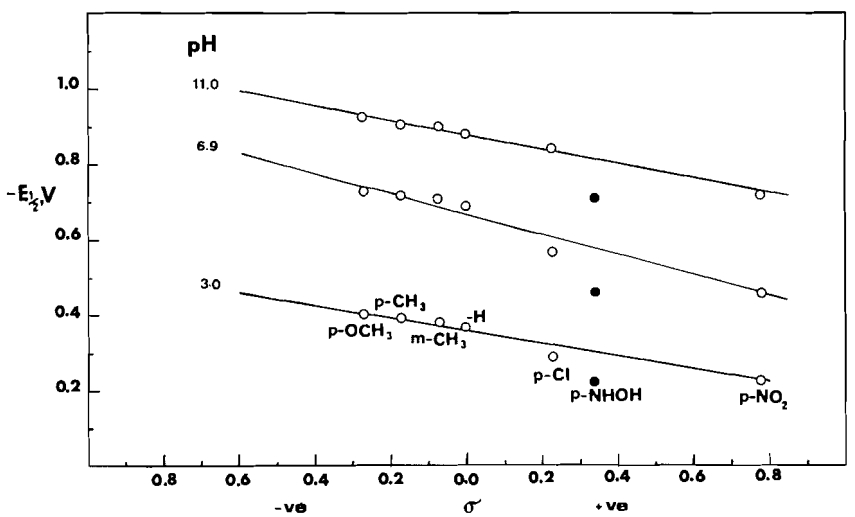

FIG. 3. $E_{1/2}$–σ relation for 4-arylazo-1-ethylmercapto3-(4*H*)isoquinolones derivatives at different pH values.

Can. J. Chem. Downloaded from www.nrcresearchpress.com by 210.87.254.42 on 09/06/12
For personal use only.

TABLE 1. Linear representation of $E_{1/2}$–pH dependence of 4-arylazo-1-ethylmercapto-3-(4*H*)isoquinolones derivatives (**I***a–f*)

Compd No.	$E_{1/2}$–pH equation of the first segment	$E_{1/2}$–pH equation of the second segment
I*a*	$E_{1/2} = 0.137 - 0.173$pH	$E_{1/2} = -0.195 - 0.069$pH
I*b*	$E_{1/2} = 0.177 - 0.185$pH	$E_{1/2} = -0.192 - 0.073$pH
I*c*	$E_{1/2} = 0.231 - 0.204$pH	$E_{1/2} = -0.189 - 0.071$pH
I*d*	$E_{1/2} = 0.454 - 0.261$pH	$E_{1/2} = -0.183 - 0.074$pH
I*e*	$E_{1/2} = 0.489 - 0.256$pH	$E_{1/2} = -0.140 - 0.075$pH
I*f*	$E_{1/2} = 0.268 - 0.163$pH	$E_{1/2} = -0.176 - 0.048$pH

The most reliable $E_{1/2}$ values at selected pH have been correlated with different Hammett's constants (20). Statistical treatment of the data was carried using Jaffé calculations (21) (Table 2). Representative $E_{1/2}$–σ plots are illustrated in Fig. 3. As is clear the plots have reasonable linearity with $+\rho$ values varying between 0.186 and 0.298 for σ and σ^0 constants. These values are in good agreement with those reported for arylazo derivatives (22–24) and not hydrazones (25). That *r* and *s* values are better correlated with σ and σ^0 constants is an indication that substituents can affect the reaction center mainly by their inductive effects. The fact that the point for *p*-NO_2 derivative lies on the $E_{1/2}$–σ plots when using $\sigma_{p\text{-}NO_2}$ and deviates with $\sigma_{p\text{-}NHOH}$ or $\sigma_{p\text{-}NH_2}$ is another confirmation that the compound is in the azo and not in the hydrazono form; since it is well known that the N=N moiety is reduced prior to the NO_2 group. On the other hand, the NO_2 group will be reduced prior to C=N—NH in the case of hydrazones (15, 25).

TABLE 2. Results of statistical treatment of $E_{1/2}$–σ data for 4-arylazo-1-ethylmercapto-3-(4*H*)isoquinolones derivatives (**I***a–f*)

	σ			σ^0			σ^+		
pH	*p*[a]	*r*[b]	sd[c]	*p*	*r*	sd	*p*	*r*	sd
3.0	0.186	0.972	0.053	0.195	0.975	0.600	0.133	0.867	0.026
6.9	0.282	0.971	0.080	0.298	0.983	0.089	0.196	0.842	0.047
11.0	0.201	0.998	0.055	0.209	0.994	0.063	0.145	0.899	0.023

[a]Slope.
[b]Correlation coefficient.
[c]Standard deviation.

1. H. M. FAHMY, M. A. ABDEL AZIZ, A. H. BADRAN, and M. ABDEL AZZEM. J. Electroanal Chem. **127**, 103 (1981).
2. H. M. FAHMY, H. A. DABOUN, K. AZZIZ, and M. ABDEL AZZEM. J. Chem. Soc. Perkin II, 425 (1983).
3. M. H. ELNAGDI, M. M. M. SALLAM, H. M. FAHMY, S. A. IBRAHIM, and M. A. M. ELLAS. Helv. Chim. Acta, **59**, 551 (1976).
4. M. H. ELNAGDI, H. M. FAHMY, and M. A. MORSI. J. Electroanal. Chem. **68**, 737 (1976).
5. H. M. FAHMY and M. H. ELNAGDI. Electrochim. Acta, **23**, 255 (1978).
6. H. M. SAMOUR, H. M. FAHMY, and M. H. ELNAGDI. J. Prakt. Chem. **317**, 257 (1975).
7. A. F. A. SHALABY, A. A. EL SAYED, and H. A. DABOUN. J. Prakt. Chem. **313**(6), 1039 (1971).
8. H. T. S. BRITTON. Hydrogen ions. Vol. 1. 4th ed. Chapman and Hall, London. 1955. p. 365.
9. H. M. FAHMY, H. A. DABOUN, M. ABDEL AZZEM, and G. PIERRE. Electrochim. Acta. **28**, 605 (1983).
10. J. DECOME AND C. FOURNIER. Compt. Rend. Acad. Sci. Paris, **256**, 1545 (1963).
11. F. FEIGL. Spot tests. Vol. 2. 4th ed. Elsevier. 1954. p. 109.
12. S. G. MAIRANOVSKU. J. Electroanal. Chem. **4**, 166 (1962).
13. H. M. FAHMY, M. H. ELNAGDI, Z. E. KANDEL, and G. PIERRE. J. Chem. Tech. Biotechnol. **31**, 688 (1981).
14. H. LUND. *In* Organic electrochemistry. *Edited by* M. M. Baizer. Dekker, New York. 1973. Chapt. VII. p. 315.
15. A. B. SAKLA, H. M. FAHMY, and M. A. ABOUTABL. J. Electroanal. Chem. **90**, 261 (1978).
16. S. DARWISH, H. M. FAHMY, M. A. ABDEL AZIZ, and A. A. EL MAGHRABY. J. Chem. Soc. Perkin II. 344 (1981).
17. W. U. MALIK and R. N. GOYAL. Indian Acad. Sci. **84**A(1), 35 (1976).
18. W. U. MALIK and R. JAIN. J. Indian Chem. Soc. **LIX**, 191 (1982).
19. L. HOLLECK and G. HOLLECK. Monatsh. Chem. **95**, 990 (1964).
20. C. D. RICHIE and W. F. SAGAR. Prog. Phys. Org. Chem. 334 (1964).
21. H. H. JAFEE. Chem. Rev. 53 (1953).
22. M. KOZENY and V. VELICH. Collect. Czech. Chem. Commun. **25**, 3271 (1960).
23. A. B. SAKLA, H. M. FAHMY, and M. A. ABOUTABL. Electrochim. Acta, **25**, 1333 (1980).
24. P. ZUMAN. Substituent effects in organic polarography. Plenum Press, New York. 1967. p. 63.
25. M. H. ELNAGDI and H M. FAHMY. J. Electroanal. Chem. **84**, 149 (1977).

Can. J. Chem. Downloaded from www.nrcresearchpress.com by 210.87.254.42 on 09/06/12
For personal use only.

The effect of *d* electron configuration on a mononuclear transition metal species of a Schiff-base ligand with a N_2S_2 donor set (sacacen)

RENZO CINI[1] AND ARNALDO CINQUANTINI
Dipartimento di Chimica, Universitá di Siena, 53100 Siena, Italy

PIER LUIGI ORIOLI
Dipartimento di Chimica, Universitá di Firenze, 50100 Florence, Italy

AND

CARLO MEALLI[1] AND MICHAL SABAT
Istituto di Stereochimica ed Energetica dei Composti di Coordinazione, C.N.R., Via Guerrazzi 27, 50132 Florence, Italy

Received March 5, 1984

RENZO CINI, ARNALDO CINQUANTINI, PIER LUIGI ORIOLI, CARLO MEALLI, and MICHAL SABAT. Can. J. Chem. **62**, 2908 (1984).

The X-ray crystal structure of Co(sacacen), sacacen = *N*,*N*′-ethylenebis(thioacetylacetoneiminato), has been determined to add a new member to the series of mononuclear complexes M(sacacen), M = Ni, Cu, Zn, whose structures were previously reported. The number of *d* electrons within the series is systematically varied from 7 to 10. The four structures are compared in detail to find the parameters that govern the deformation trends. An extended Hückel MO treatment has been applied to determine the relationships between the geometry and the number of *d* electrons at the metal. The results are compared with the esr and electrochemical experimental data that have been previously reported for these compounds.

RENZO CINI, ARNALDO CINQUANTINI, PIER LUIGI ORIOLI, CARLO MEALLI et MICHAL SABAT. Can. J. Chem. **62**, 2908 (1984).

Dans le but d'ajouter un nouveau terme à la série de complexes mononucléaires M(sacacen) dont les structures ont été publiées antérieurement (M = Ni, Cu, Zn) et faisant appel à la diffraction des rayons-X, on a déterminé la structure cristalline du complexe Co(sacacen) dans lequel sacacen = *N*,*N*′-éthylènebis(thioacétylacétoneiminato). Dans cette série, on a fait varier systématiquement de 7 à 10 le nombre d'électrons *d*. On a comparé en détail les quatre structures pour déterminer quels sont les paramètres qui gouvernent les tendances observées dans les déformations. On a appliqué un traitement élargie des OM de Hückel pour déterminer les relations existant entre la géométrie et le nombre d'électrons *d* du métal. On a comparé les résultats obtenus avec les valeurs expérimentales de la rpe et de l'électrochimie rapportées antérieurement pour ces composés.
[Traduit par le journal]

Can. J. Chem. Downloaded from www.nrcresearchpress.com by 210.87.254.105 on 09/06/12
For personal use only.

Introduction

The thio-iminato analog, sacacen, of *N*,*N*′-ethylenebis(acetylacetoneiminato), acacen (see **a**), represents an interesting alternative for the synthesis of new complexes that may be used as substrates for the activation of molecular oxygen or other small molecules (1).

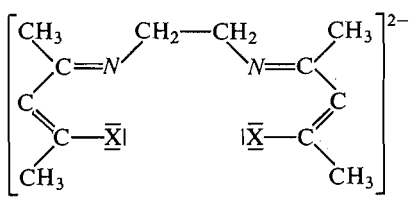

a

X = S, sacacen
X = O, acacen

The bonding capabilities of sacacen toward transition metal atoms may be properly evaluated from a comparative examination of the crystal structures of a series of complexes where the number of *d* electrons is systematically varied. For this purpose we have now performed the crystal structure analysis of the compound Co(sacacen), **1**, which is the fourth member in the series of structures of M(sacacen) complexes. Structural details have been previously reported for the Ni, Cu, and Zn derivatives, **2**, **3**, and **4**, respectively (2). The *d* electrons at these bivalent metal centers span the numbers between seven and ten. It is obvious that the different electronic requirements of the metals may not be always compatible with the stericity of this particularly rigid ligand. In fact, the two lateral five-membered chelate fragments of the dianionic sacacen are normally forced to be planar on account of operative π-type conjugation and, at the same time, are held together by an ethylenic chain. The first goal of this study is that of individuating the geometrical parameters which govern both the coordination at the metal and the deformation inside the tetradentate ligand. The second step is that of gaining a deeper insight into the electronic structure of these compounds. With the aid of the extended Hückel method (3), the principal metal–ligand interactions are evaluated both in terms of the ligand's deformation parameters identified from the detailed analysis of the structures. Finally, the results will be checked against the findings of other experimental techniques already performed on these compounds. In particular esr data are available for some paramagnetic species of the series (1*d*–2*a*). These data contain precious information about the nature of the orbital having the unpaired electron and provide a good test for the reliability of the calculations. Electrochemistry of these compounds has been studied (4) with some interesting results that will be kept in mind during the discussion.

Comparison between the structures

Figure 1 shows views of the structures **1**–**4** down the bisector of the N—M—N angle. By examining Table 1, which reports some selected geometrical magnitudes of the compounds, a few conclusions can be drawn about the deformation trends within the series. Whereas the N_2M fragment is, in a first approximation, almost unchanged (the N—M—N angles vary

[1] To whom correspondence should be addressed.

TABLE 1. Selected geometrical parameters for the structures **1** to **4**[a]

Parameter	Distance (Å)			
	Co(sacacen), **1**	Ni(sacacen), **2**	Cu(sacacen), **3**	Zn(sacacen), **4**
M—S(1)	2.155(1)	2.163(2)	2.226(3)	2.293(1)
M—S(2)	2.142(2)	2.139(2)	2.239(3)	2.293(1)
M—N(1)	1.905(4)	1.923(5)	1.992(8)	2.027(2)
M—N(2)	1.910(4)	1.917(5)	1.983(7)	2.027(2)
S(1)—C(1)	1.70(1)	1.70(1)	1.73(1)	1.73(1)
S(2)—C(11)	1.67(1)	1.67(1)	1.73(1)	1.73(1)
C(1)—C(2)	1.37(1)	1.33(1)	1.34(1)	1.35(1)
C(11)—C(21)	1.35(1)	1.37(1)	1.37(1)	1.35(1)
C(2)—C(3)	1.41(1)	1.45(1)	1.42(1)	1.43(1)
C(21)—C(31)	1.43(1)	1.42(1)	1.39(1)	1.43(1)
C(3)—N(1)	1.33(1)	1.31(1)	1.28(1)	1.30(1)
C(31)—N(2)	1.29(1)	1.31(1)	1.31(1)	1.30(1)
	Angle (deg)			
Parameter	Co(sacacen), **1**	Ni(sacacen), **2**	Cu(sacacen), **3**	Zn(sacacen), **4**
S(1)—M—S(2)	81.7(1)	80.5(1)	88.0(1)	113.6(1)
N(1)—M—N(2)	87.8(2)	87.5(2)	86.3(3)	83.2(1)
S(1)—M—N(1)	95.9(2)	95.6(2)	96.9(3)	96.0(1)
S(2)—M—N(2)	95.4(1)	96.4(2)	96.2(2)	96.0(1)
S(1)—M—N(2)	172.1(1)	176.3(2)	160.0(2)	135.6(1)
S(2)—M—N(1)	173.7(2)	176.1(2)	158.7(2)	135.6(1)
M—S(1)—C(1)	112.4(2)	110.9(2)	108.6(4)	102.8(1)
M—S(2)—C(11)	113.1(2)	112.9(3)	108.2(4)	102.8(1)
S(1)—C(1)—C(2)	125.4(5)	126.9(6)	125.8(8)	129.3(2)
S(2)—C(11)—C(21)	125.9(5)	125.4(6)	125.7(8)	129.3(2)
C(1)—C(2)—C(3)	128.1(6)	128.4(4)	133.1(5)	131.4(2)
C(11)—C(21)—C(31)	127.6(6)	128.6(4)	134.1(5)	131.4(2)
C(2)—C(3)—N(1)	124.9(5)	123.3(4)	124.0(5)	122.4(2)
C(21)—C(31)—N(2)	124.5(5)	124.9(4)	122.1(5)	122.4(2)
M—N(1)—C(3)	132.4(4)	133.0(4)	130.5(5)	128.0(2)
M—N(2)—C(31)	132.9(4)	131.3(4)	130.4(5)	128.0(2)
N_2M/NC_3S[b]	10.5 5.0	11.0 4.2	14.7 14.9	29.2
N(1)—C(3)—C(2)—C(1)	−8.6	−8.9	0.0	15.3
N(2)—C(31)—C(21)—C(11)	−2.7	−7.4	1.1	15.3
C(3)—C(2)—C(1)—S(1)	−1.4	−2.0	0.0	−7.2
C(31)—C(21)—C(11)—S(2)	0.7	0.6	2.15	−7.2

[a]The labelling of the atoms is not always consistent with that previously reported in refs. 2*a*–2*c*.

[b]N_2M/NC_3S is the dihedral angle between the planes defined by the N_2M fragment and the least-squares plane of the chelate fragment of the ligand (NC_3S).

in the narrow range 88.0(2)–83.2(1)°), the S—M—S angles change remarkably in going from cobalt to zinc (limiting values 80.5(1)° in **2** and 113.6(1)° in **4**). At the same time the M—N and M—S distances vary almost consistently with the sum of their covalent radii (5). Noteworthy, but not unexpected in view of the rigidity of the chelating bite, the N—M—S angles are practically equal in all cases (96.0 ± 1.0°). All these mean that the coordination geometry which is approximately square planar with C_{2v} symmetry in **1** and **2** becomes progressively distorted in **3** and **4**, where only C_2 symmetry is preserved. Since the two chelating arms of sacacen like to be as planar as possible to satisfy the π conjugation and since these arms are connected by an ethylenic chain, the whole ligand is highly constrained. Consequently it is hard for the metals richer in electrons to adopt the tetrahedral coordination which is the most favourable one for them.

A certain degree of flexibility is attained through torsions about the M—N bonds. Indeed the dihedral angles between the N_2M plane and the least-squares plane through the NC_3S atoms of the chelating fragments increase within the series up to a 30° value in **4**. The latter seems the largest torsion tolerated by the complexing ligand; on the other hand full coplanarity of the system seems also unobtainable: both in **1** and **2** one chelate ring is almost coplanar with the N_2M plane (dihedral angle <4°) whereas the other is biased of about 10°. Thus the ligand seems to have a minimum strain in **3**, as indirectly shown by the planarity of the NC_3S groupings (the largest deviation from the least-squares plane is ca. 0.004 Å); in all of the other complexes there is also some torsion about the C—C bonds of the chelating ring which in some cases can be as large as 15°. For this reason the deviation of the atoms from the NC_3S plane can be also an order of magnitude larger than in **3**. It is also noteworthy that in **1** and **2**, which are isostructural, one of the six-membered chelate rings is more distorted than the other.

In summary it seems evident that the different modes of coordination at the metal atoms are mainly obtained through

Can. J. Chem. Downloaded from www.nrcresearchpress.com by 210.87.254.105 on 09/06/12
For personal use only.

Can. J. Chem. Downloaded from www.nrcresearchpress.com by 210.87.254.105 on 09/06/12
For personal use only.

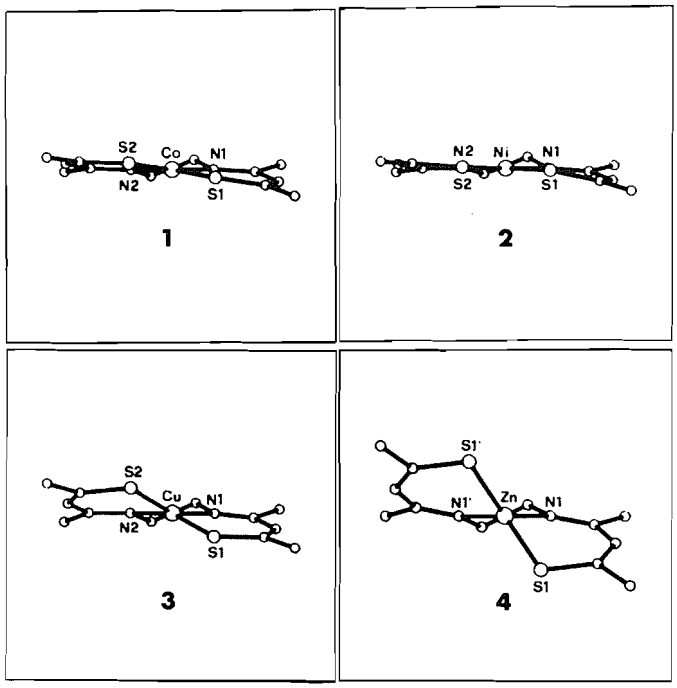

FIG. 1. Views of Co(sacacen) (**1**), Ni(sacacen) (**2**), Cu(sacacen) (**3**), and Zn(sacacen) (**4**) down the bisector of the N—M—N angle.

simultaneous clockwise (or anticlockwise) torsions at the M—N bonds. Since the two chelating fragments of the ligand are held together by the ethylenic chain and the nitrogen atoms maintain an sp^2 hybridization, the range of values for the torsion angles at the M—N bonds is restricted and not always suitable to fully cope with the stereochemical requirements of the different metals. Hence some other geometrical rearrangements are sought by the ligand to accommodate the different metal atoms. In effect, besides the mentioned distortions from planarity of the NC_3S groupings,some other minor variations in bond distances and angles are observed.

MO calculations

In order to simplify the MO analysis of these molecules, it is important to fix a model where the number of geometrical parameters that define the deformation pathway from d^7 to d^{10} species is as small as possible. Our starting model is the C_{2v} molecule shown in **b**. The ethylenic chain was purposely excluded. We fixed bond distances and angles to the values reported in the experimental section and we simulated the passage from one compound to another only through variations of the torsion angle θ and by artificially changing the number of d electrons at the metal.[2]

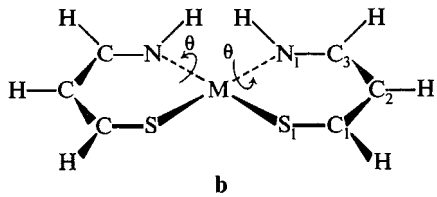

b

Unless specifically stated, the atomic parameters of nickel were invariably used for the calculations. The NC_3S groupings were kept planar and rigid; as a result the fit to the real structures becomes poorer in those cases where other magnitudes also change significantly: e.g., the metal–donor distances and degree of planarity of NC_3S. Whereas a simple torsion of 15° in θ reproduces the S—Cu—S angles of ca. 88° in **3**, a 30° torsion is insufficient to reproduce the S—Zn—S angle of 113.6(1)° in **4**. Nonetheless, we have found that significant pieces of information may be obtained by the evolution of the MO's in terms of the θ angle at least for structures **1**–**3** and these may be extrapolated to the zinc derivative. Figure 2 shows an interaction diagram of Ni(sacacen) having rigorous C_{2v} symmetry. The d_{xy} orbital is highly destablized on account of the antibonding interaction with the b_2 combination of lone pairs at nitrogen and sulfur atoms; the remaining four d orbitals are more closely compacted, a situation typical for square planar complexes. However, the relative order of these lower d orbitals is not the standard one for complexes having four exclusively σ donor ligands (6). The conjugation in the five-membered chelate arms places some ligand π* orbitals at comparable energies with those of the metal d orbitals. This new situation affects the yz orbital which is most destabilized and it is the HOMO in the cobalt and nickel complexes. The xz and $x^2 - y^2$ orbitals also suffer some destabilizing interaction with ligand orbitals mainly centered at the sulfur atoms, as seen in Fig. 2. The z^2 orbital remains at lower energy as an almost pure d orbital (85%). The different electron population of the HOMO in **1** and **2** should affect the distances between metal and donor atoms because of their π-type antibonding. However, it is hard to detect any such trend from the structural comparison. The fact that all the M—S distances are practically equal does not exclude that the Ni—S linkage is weaker than the Co—S linkage; bond lengths are not properly related to bond strengths when dealing with different pairs of atoms.

Very similar results have been obtained for the complex Co(acacen) by using different theoretical methods (1*b*, 1*d*, 7, 8). Remarkably only an *ab initio* calculation (9) assigned the HOMO as z^2, a result in clear disagreement with experimental epr data (1*d*). In our case the presence of sulfur in place of oxygen ensures a larger metal–ligand overlap and hence a larger splitting of yz with respect to the other d-orbitals (ca. 0.6 vs. 0.1 eV). The correct assignment of the HOMO also relies on recent epr results, reported for Co(sacacen) (1*d*, 2*a*). In fact, it has been ascertained that when Co(sacacen) is doped in a host Ni(sacacen) crystal, the unpaired electron unambiguously resides on the yz orbital. Conversely, the z^2 orbital becomes the HOMO of Co(sacacen) in a host crystal of Zn(sacacen). Also for this reason the evolution of the MO's as a function of θ, the parameter that macroscopically governs the deformation along the series, seems particularly interesting. A Walsh diagram is shown in Fig. 3. The most remarkable trend is the drop in energy of the xy (b_2) orbital (becomes 4*b* in C_2 symmetry) on account of the decreasing σ* character when the S atoms are displaced out of the main plane. The $2b_1$ and $2a_2$ levels are unaffected because of their π* ligand nature. The crossing between the latter and xy is unimportant when all the levels are empty as in **1** and **2**. The four low lying d orbitals are not shuffled; however, there are important changes in their composition. Notice that on account of the descent in symmetry three of them belong to the same species (**a**), and are allowed to mix with each other. In particular, whereas the $x^2 - y^2$ orbital is little engaged in mixing and remains substantially unchanged (2*a*), the orbitals 1*a* and 3*a* mix more and more with each other and eventually reverse their composition. This

[2] The torsion angle θ can be envisaged as the dihedral angle between the N_2M and NC_3S planes.

Can. J. Chem. Downloaded from www.nrcresearchpress.com by 210.87.254.105 on 09/06/12
For personal use only.

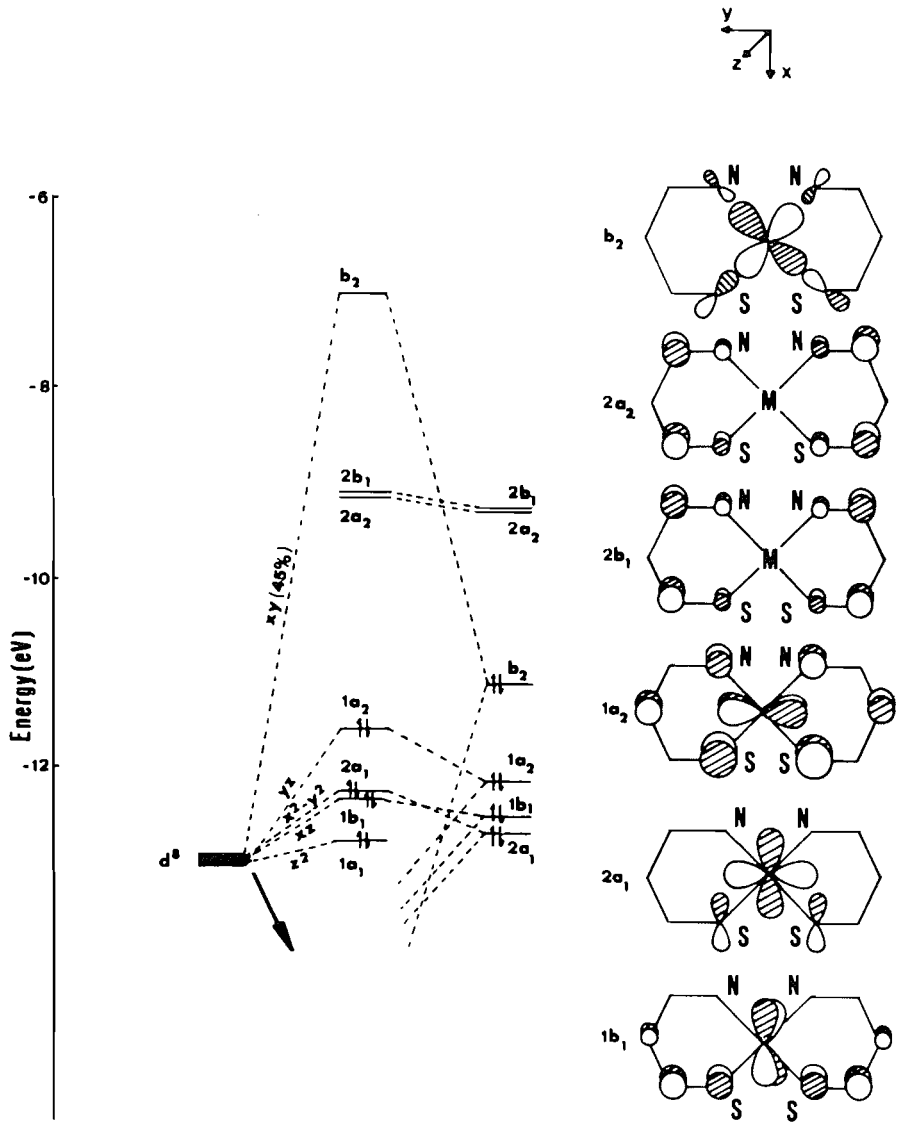

FIG. 2. Interaction diagram of Ni(sacacen) having rigorous C_{2v} symmetry.

is intuitively understood since the reorientation of the NC_3S planes progressively reduces the overlap between *yz* and the combination of the sulfur p_π orbitals in the ligand's $1a_2$ level. At the same time these p_π orbitals become more involved in a π^* interaction with z^2, as shown in **c**. In order to avoid a crossing between orbitals of the same symmetry, the descending $3a$ and the ascending $1a$ levels mix into each other.

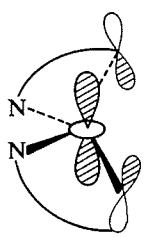

c

At $\theta \sim 40°$ the orbital $3a$, HOMO, has mainly z^2 character, having lost most of its initial *yz* character. The result is most interesting and fully matches the epr data for the cobalt doped zinc complex ($2a$). It is also worthwhile to point out that the deformation pathway is symmetry-allowed for **1** and **2** as no crossing of the HOMO with any other level is encountered.

In the copper complex, **3**, the unpaired electron lies almost certainly on the level $4b$, metallic *xy* in character and metal–ligand σ antibonding. The Walsh diagram of Fig. 3 was calculated by using the parameters of nickel. Were the copper parameters used, the general trends would not change dramatically: $4b$ crosses the ligand π orbitals at an earlier stage ($\theta \sim 15°$). The total energy continues to lower for larger θ values, but the experimental θ in **3** (ca. 15°) seems a good compromise between the energy gained on stabilizing the HOMO and that which would be lost on deforming excessively the tetradentate ligand.

In the zinc complex, **4**, there are two electrons which drop steeply in energy on increasing θ. More properly one can say that only at sufficiently large θ values the repulsion between the filled *xy* metal orbital and the σ lone pairs of the donor atoms is sufficiently relieved. The large torsion is hardly tolerated by sacacen and the complex undergoes other deformations as described in the previous paragraph.

The above qualitative MO picture is helpful in rationalizing some electrochemical results previously reported for com-

Can. J. Chem. Downloaded from www.nrcresearchpress.com by 210.87.254.105 on 09/06/12
For personal use only.

pounds **2** and **3** (4). It has been ascertained that **2** undergoes a reversible oxidation with a maximum loss of four electrons. If the geometry is assumed to remain unchanged, the oxidized species must be guaranteed a formal 16-electron count that ensures stability to square planar complexes. The level which is first oxidized is $1a_2$ (see Fig. 2) which has ca. 60% ligand character; as a result the electron population at the metal is not excessively affected. From another point of view one can say that the interaction between *yz* and the ligand $1a_2$ orbital is 4-electron destabilizing and the depopulation of their antibonding combination triggers a stabilizing metal–ligand π bonding. In a sense $1a_2$ is equivalent to a fifth lone pair donated from the ligand to ensure a total 16-electron count anyway. Those illustrated above are two extreme points of view which frame the actual situation of the system, still stable upon oxidation. Similar arguments may be invoked for the second pair of electrons removed from the system. In this case, since the metal–ligand antibonding combinations involving *xz* and $x^2 - y^2$ orbitals are almost degenerate, it is difficult to predict which one is going to be depopulated. In a sense *xz* establishes with a ligand π^* orbital an interaction which is analogous to that involving *yz*: for this reason $1b_1$ seems a better candidate to oxidation than $2a_1$.

The nickel species may also be electrochemically reduced. However, the process is not easy as shown by the very negative value (−1.8 V vs. sce) of the peak potential. Some information on the location of the extra electron is provided by an esr spectrum in solution (4*a*). A *g* value of 2.13 in fact can occur only for an electron not localized over the ligand. This would be the case if either the $2a_2$ or $2b_1$ orbital of Figs. 2 and 3 were occupied. Since also for the d^8 case a θ torsion is a quite feasible process, it is likely that the electron is taken by the system after the *xy* orbital has crossed the two ligand orbitals. On the other hand, the copper(II) complex and the reduced nickel(I) species are not very dissimilar (4*a*).

In conclusion the present study has confirmed that the Schiff-base sacacen has π^* orbitals at comparable energies with metal *d* orbitals. When the stereochemistry is square planar, the ligand and metal orbitals interact well and the typical level ordering found in common square planar complexes is greatly altered. The π-type interactions are 4-electron destabilizing, thus an oxidation process, which transforms some of these into stabilizing bonding interactions, is not difficult. Distortion from planarity also lessens the destabilizing interactions, but the polydentate ligand, from a certain point on, is not easily deformed.

Experimental

Preparation of the crystals

Both ligand and metal complexes were prepared as previously described (10). Crystal of Co(sacacen) suitable for X-ray analysis were obtained by dissolving about 100 mg of the cobalt complex in 50 mL of toluene. The solution was filtered and then allowed to evaporate under a slow stream of nitrogen at room temperature. Well-shaped red crystals formed in about 24 h.

Crystallography

Crystal data are as follows:

$C_{12}H_{18}CoN_2S_2$ mw = 312.9

Orthorhombic, $P2_12_12_1$, a = 15.840(4), b = 12.010(4), c = 7.339(3) Å, U = 1396.2(8) Å^3, Z = 4, D_c = 1.49 Mg m^{-3}, $F(000)$ = 652, Mo-K$_\alpha$ radiation, λ = 0.7107 Å, μ(Mo-K$_\alpha$) = 3.13 cm^{-1}.

Intensity measurements

A total of 2614 reflections were collected on a Philips PW1100 diffractometer with θ–2θ scan techniques, in the range $5° < 2\theta < 40°$, on a crystal of dimension 0.10 × 0.17 × 0.60 mm. The scan width was 1.40°, and the scan speed was 0.03 (deg/s). Lattice constants were obtained by the least-squares method applied to the setting angles of 25 reflections. The crystal was confirmed to be isostructural with the compound Ni(sacacen). The intensity of three standard reflections ($\bar{7}\,\bar{1}\,1$, $7\,1\,1$, $7\,\bar{1}\,\bar{1}$) measured every 180 min showed no appreciable variation during data collection. A total of 1199 unique reflections with $I > 2.5\,\sigma(I)$ were observed and used for the crystallographic calculations. The intensities were corrected for Lorentz-polarization effects. No absorption correction was applied as a ψ scan on a few reflections showed a maximum deviation of 6%.

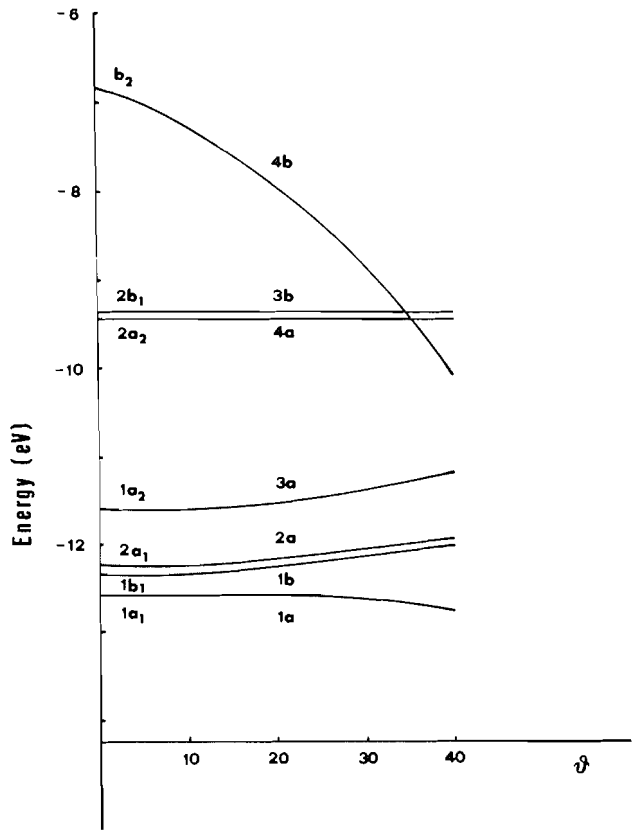

FIG. 3. A Walsh diagram.

Solution and refinement of the structure

The atomic parameters of the nickel derivative were used as starting values for the crystallographic refinement. A series of full-matrix least-squares cycles with anisotropic temperature factors for all the non-hydrogen atoms were performed. A total of 16 hydrogen atoms were included in the final refinement with fixed coordinates and fixed temperature factors U of 0.06 Å^2. The agreement index $R = \Sigma(|F_o| - |F_c|)$ reached the value of 0.0297. The index $R_w = \Sigma[w(|F_o| - |F_c|)^2/wF_o^2]^{1/2}$ was 0.0317. The function minimized was $\Sigma w(|F_o| - |F_c|)^2$ with weights $w = 1/(\sigma^2(F) + 0.0005F^2)$. The atomic scattering factors of C, N, H, and S were taken from SHELX 76 (11) package; those of Co were taken from ref. 12. No unusual features were shown by a final ΔF map. The Hamilton test was applied to establish the absolute configuration of the molecule.

Table 2 lists the atomic coordinates for all the non-hydrogen atoms. The thermal parameters as well as the observed and calculated structure factors are available as supplementary material.[3]

[3] Complete set of data is available, at a nominal charge, from the Depository of Unpublished Data, CISTI, National Research Council of Canada, Ottawa, Ont., Canada K1A 0S2.

Can. J. Chem. Downloaded from www.nrcresearchpress.com by 210.87.254.105 on 09/06/12
For personal use only.

TABLE 2. Positional parameters ($\times 10^4$) with the estimated standard deviations in parenthesis

Atom	x/a	y/b	z/c
Co	2701(0)	6437(1)	2045(1)
S(1)	4056(1)	6547(1)	2220(2)
S(2)	2827(1)	8195(1)	1636(3)
N(1)	2649(3)	4854(4)	2157(6)
N(2)	1497(3)	6450(4)	2196(6)
C(1)	5425(4)	5335(6)	2943(12)
C(4)	4516(4)	5289(6)	2585(8)
C(2)	4108(4)	4282(6)	2549(8)
C(3)	3244(4)	4074(5)	2253(8)
C(5)	3043(5)	2873(5)	2050(10)
C(6)	1779(4)	4466(5)	1866(9)
C(11)	1983(4)	1.0145(5)	1372(11)
C(41)	1904(4)	8864(5)	1640(9)
C(21)	1136(4)	8392(6)	1873(11)
C(31)	947(4)	7238(6)	2170(10)
C(51)	20(4)	7044(6)	2488(12)
C(61)	1175(4)	5309(5)	2580(8)

TABLE 3. Parameters used in EH calculations

Orbital		H_{ii} (eV)	ξ_1	ξ_2	C_1^a	C_1^a
Ni	3*d*	−12.99	5.75	2.0	0.5683	0.6292
	4*s*	−8.86	2.10			
	4*p*	−4.90	2.10			
Cu	3*d*	−14.00	5.95	2.3	0.5933	0.5744
	4*s*	−11.40	2.20			
	4*p*	−6.06	2.20			
S	3*s*	−20.00	1.817			
	3*p*	−13.30	1.817			
N	2*s*	−26.00	1.95			
	2*p*	−13.40	1.95			
C	2*s*	−21.40	1.625			
	2*p*	−11.40	1.62			
H	1*s*	−13.60	1.3			

[a] Coefficients in double ξ expansion.

Computational method

The program used to perform extended Hückel calculations was ICON8 (3) implemented on a SEL 32/70 computer. The parameters[4] used were those of Table 3 with the modified Wolfsberg–Helmholz approximation (14). In all the calculations, the M—N, N—C(3), C(3)—C(2), C(2)—C(1), and C(1)—S(1) distances were kept fixed at the values 1.92, 1.32, 1.46, 1.33, 1.70 Å, respectively. The angles N(1)—M—N(2), M—N(1)—C(3), N(1)—C(3)—C(2), C(3)—C(2)—C(1) were fixed at 87, 123, 128, 127, 133°, respectively. All the C—H or N—H distances were taken as 1.05 Å.

[4] The parameters for Cu were taken from ref. 13(*a*), those for Ni and other atoms (except S) were taken from ref. 13(*b*), and those for the sulphur atoms were taken from ref. 13(*c*).

1. (*a*) R. S. DRAGO, B. B. CORDEN, and A. ZOMBECK. Comments Inorg. Chem. **1**, 53 (1981); (*b*) R. BOČA. Coord. Chem. Rev. **50**, 1 (1983); (*c*) R. D. JONES, D. A. SUMMERVILLE, and F. BASOLO. Chem. Rev. **79**, 139 (1979); (*d*) C. DAUL, C. W. SCHLÄPTER, and A. VON ZELEWSKY. Struct. Bonding, **36**, 129 (1979).
2. (*a*) D. ATTANASIO, G. DESSY, V. FARES, and G. PENNESI. Mol. Phys. **40**, 269 (1980); (*b*) R. CINI, A. CINQUANTINI, P. L. ORIOLI, and M. SABAT. Cryst. Struct. Commun. **9**, 865 (1980); (*c*) R. CINI, A. CINQUANTINI, P. L. ORIOLI, and M. SABAT. Inorg. Chim. Acta, **41**, 151 (1980).
3. (*a*) R. J. HOFFMANN. J. Chem. Phys. **39**, 1937 (1963); (*b*) R. HOFFMANN and W. N. LIPSCOMB. J. Chem. Phys. **36**, 2872 (1962).
4. (*a*) A. CINQUANTINI, R. CINI, R. SEEBER, and P. ZANELLO. J. Electroanal. Chem. **111**, 309 (1980); (*b*) A. CINQUANTINI, R. CINI, R. SEEBER, and P. ZANELLO. J. Electroanal. Chem. **121**, 301 (1981).
5. J. E. HUHEEY. Inorganic chemistry. Harper Row Publishers, New York. 1975.
6. T. A. ALBRIGHT. Tetrahedron, **38**, 1339 (1982).
7. P. FANTUCCI and V. VALENTI. J. Am. Chem. Soc. **98**, 3832 (1976).
8. M. A. HITCHMAN. Inorg. Chem. **16**, 1985 (1977).
9. (*a*) M. M. ROHMER, A. DEDIEU, and A. VEILLARD. Theoret. Chim. Acta, **39**, 189 (1975); (*b*) A. DEDIEU and A. VEILLARD. Theoret. Chim. Acta, **36**, 231 (1975).
10. P. R. BLUM, R. M. C. WEI, and S. C. CUMMINGS. Inorg. Chem. **13**, 450 (1974).
11. G. M. SHELDRICK. SHELX76. Program for crystal structure determination. Cambridge University. 1976.
12. International tables of crystallography. Vol. 4. 1974. Kynoch Press, Birmingham.
13. (*a*) P. K. MEHROTRA and R. HOFFMANN. Inorg. Chem. **17**, 2187 (1978); (*b*) T. A. ALBRIGHT, R. HOFFMANN, J. C. THIBEAULT, and D. L. THORN. J. Am. Chem. Soc. **101**, 3801 (1979); (*c*) P. KUBACEK and R. HOFFMANN. J. Am. Chem. Soc. **103**, 4320 (1981).
14. J. H. AMMETER, H. B. BÜRGI, J. C. THIBEAULT, and R. HOFFMANN. J. Am. Chem. Soc. **100**, 3686 (1978).

Isomer enumeration of nonradical strictly *peri*-condensed polycyclic aromatic hydrocarbons

JERRY RAY DIAS

Department of Chemistry, University of Missouri, Kansas City, MO 64110, U.S.A.

Received January 16, 1984

JERRY RAY DIAS. Can. J. Chem. **62**, 2914 (1984).

A new concept for isomer enumeration of *peri*-condensed benzenoid hydrocarbons (PAH6) based on the enumeration of their excised internal structures is presented. Formulas corresponding only to strictly *peri*-condensed benzenoid hydrocarbons can be identified from a previously derived Formula Periodic Table for PAH6. The number of benzenoid PAH6 isomers having formulas $C_{38}H_{16}$, $C_{40}H_{16}$, $C_{42}H_{16}$, $C_{48}H_{18}$, $C_{50}H_{18}$, $C_{52}H_{18}$, $C_{60}H_{20}$, $C_{62}H_{20}$, and $C_{64}H_{20}$ are 10, 3, 1, 22, 7, 2, 20, 12, and 3, respectively (Fig. 1). A nomenclature for these PAH6s based on an already established nomenclature for their corresponding small-molecule, excised internal structures is proposed. The structure counts of these PAHs, being related to their resonance energy, have been determined, and this will permit researchers to estimate the most probable structures of the macromolecular benzenoid hydrocarbons of this class formed via pyrolytic processes.

JERRY RAY DIAS. Can. J. Chem. **62**, 2914 (1984).

On présente un nouveau concept qui permet de faire l'énumération des isomères d'hydrocarbures benzènoïdes *péri*-condensés (HAP6); ce nouveau concept est basé sur l'énumération des structures internes simplifiées de ces hydrocarbures. Faisant appel à un tableau périodique des formules de HAP6 qui a été dérivé antérieurement, on peut identifier des formules qui correspondent spécifiquement à des hydrocarbures benzènoïdes strictement *péri*-condensés. Parmi les produits benzènoïdes de formules $C_{38}H_{16}$, $C_{40}H_{16}$, $C_{42}H_{16}$, $C_{48}H_{18}$, $C_{50}H_{18}$, $C_{52}H_{18}$, $C_{60}H_{20}$, $C_{62}H_{20}$ et $C_{64}H_{20}$, les nombres d'isomères de HAP6 sont respectivement 10, 3, 1, 22, 7, 2, 20, 12 et 3 (Fig. 1). On propose un système de nomenclature de ces HAP6 isomères qui est basé sur un système de nomenclature des petites molécules correspondantes et de leurs structures internes simplifiées. On a déterminé que le compte de structure de ces HAP est relié à leur énergie de résonance et ceci permettra aux chercheurs d'évaluer les structures les plus probables des hydrocarbures benzènoïdes macromoléculaires de cette classe qui se forment par le biais de processus pyrolytiques.

[Traduit par le journal]

Can. J. Chem. Downloaded from www.nrcresearchpress.com by 210.87.254.40 on 09/06/12
For personal use only.

Introduction

The enumeration of *cata*-condensed benzenoid hydrocarbons has been completely successful and was accomplished by use of a dualistic graph (1). Recent computer algorithms have been reported for enumerating geometrically planar hexagonal graphs having the same number of rings (2). However, options for inclusion of circulenes and nonplanar helicenes in the isomer enumeration need to be developed. For example, a nonplanar isomer of $C_{50}H_{28}$ and up to tetradecahelicene have been synthesized and would be excluded by restricting enumeration to planar hexagonal graphs (3, 4). Note that these computer results emphasized the *cata*-condensed benzenoids and have not yet been fully tested on totally *peri*-condensed benzenoids. Herein is reported a conceptually new approach for enumerating *peri*-condensed benzenoids without *cata*-condensed appendages. For a brief history of the related hexagonal animal and cell growth problems, the reader is referred to previous work and references therein (2).

Results and discussion

Enumeration of strictly peri*-condensed benzenoid hydrocarbons*

Our previous research resulted in the development of a Formula Periodic Table for PAH6 (benzenoid polycyclic aromatic hydrocarbons comprised of exclusively fused hexagonal rings, Table 1) which for the first time unified the formula–structure relationships of PAH6s into an overall systematic framework (5, 6). The basis for this formula periodic table is $d_s + N_{iC} = (1/2)(N_C - N_H) - 1 =$ constant for all isomeric PAH structures corresponding to a particular formula; a glossary of terms used in this paper appears at the end in an appendix (further details on these terms are to be found in ref. 6). Throughout this paper only the C—C σ-bonds are shown for all the structures. Since circulene or helicene structures are not possible for strictly *peri*-condensed PAH6s (7), the ambiguity associated with other benzenoid enumerations (2) is absent in this work.

Strictly *peri*-condensed benzenoid hydrocarbons have all their internal edges mutually connected. The formulas consisting of only isomers corresponding to strictly *peri*-condensed PAH6 without *cata*-condensed appendages appear in Table 1 along the extreme left-hand diagonal formula boundary, and the corresponding number of nonradical isomers are itemized by the number in parentheses adjacent to these formulas; the number of isomers for formulas ($C_{58}H_{20}$ and $C_{46}H_{18}$) adjacent to a boundary formula should be regarded as tentative since they possess isomers having a single *cata*-condensed benzo appendage (*vide infra*). The number of isomers given for the *cata*-condensed PAH6s in the $N_C = 2N_H - 6$ row series were obtained from previous work (1). Previously, it was shown that coronene-7 ($C_{24}H_{12}$) and coronene-19 (synonymous to circumcoronene and dodecabenzocoronene, $C_{54}H_{18}$) both have no other PAH6 isomers (7). Also, $C_{30}H_{14}$ was shown to have only 3 nonradical isomers (7). Ovalene ($C_{32}H_{14}$) is known to have no other PAH6 isomer. There are 10 nonradical PAH6 isomers (**1**–**10**) with the formula of $C_{38}H_{16}$, and circumanthracene ($C_{40}H_{16}$) is one of 3 possible isomers (**11**–**13**). Circumpyrene (**14**) ($C_{42}H_{16}$) has only one PAH6 isomeric form. There are 7 PAH6 isomers (**37**–**43**) of the formula $C_{50}H_{18}$, 2 PAH6 isomers (**44**, **45**) of the formula $C_{52}H_{18}$, 22 isomers (**15**–**36**) for $C_{48}H_{18}$, and 20 isomers for $C_{60}H_{20}$ (**46**–**65**). Figure 1 presents all these isomers (**1**–**65**).

All PAH6 formulas having the same number of hydrogens are found in a linear diagonal array of formulas (Table 1) and have the same perimeter length ($q_p = 2N_H - 6 =$ constant for $N_H =$ constant). The formulas in the $N_C = 2N_H - 6$ row series

Can. J. Chem. Downloaded from www.nrcresearchpress.com by 210.87.254.40 on 09/06/12
For personal use only.

have no internal third-degree carbon vertices ($N_{iC} = 0$ and $N_C = q_p$). Thus the two isomers of $C_{14}H_{10}$ both have a perimeter length of 14 carbon atoms, and pyrene ($C_{16}H_{10}$) has two internal third-degree carbon vertices ($N_{iC} = 2$) with a perimeter length of 14 carbon atoms, giving a total of 16 carbon atoms in its formula. Similarly, all five PAH6 isomers of $C_{18}H_{12}$ have a perimeter length of 18 carbon atoms, and the three isomers of $C_{20}H_{12}$ have $N_{iC} = 2$, the two nonradical PAH6 isomers of $C_{22}H_{12}$ have $N_{iC} = 4$, and coronene ($C_{24}H_{12}$) has $N_{iC} = 6$, all with a perimeter length of 18 carbon atoms. In hexagonal graphs the maximum number of internal third-degree carbon vertices that can be contained in a 10-carbon-atom peripheral cycle is zero (naphthalene), in a 14-carbon-atom peripheral cycle it is two (pyrene), and in an 18-carbon-atom peripheral cycle it is six (coronene). Polycircumnaphthalene, polycircumpyrene, and polycircumcoronene are three series of formulas appearing on the left-hand diagonal boundary of Table 1. Each formula of these series has only one corresponding PAH6 structure. These terminal formulas have PAH6 structures containing the maximum number of internal third-degree carbon vertices ($N_{iC(max)}$) that each corresponding peripheral $q_p = 4\tau + 2$ ($\tau = 2, 3, 4, \ldots$) carbon atom can contain. Table 2 summarizes the relevant information for these one-isomer series.

From the narration presented in the last paragraph, it is evident that PAH6s have an even number of perimeter carbon vertices, since $q_p = N_{pC} + N_H = 2N_H - 6$ must be an even number. From this it follows that N_{iC} is even for even PAH6 formulas and odd for odd radical PAH6 formulas (5). For *peri*-condensed PAH6s with N_{iC} internal third-degree vertices, the number of PAH6 isomers is equal to the number of nonradical isomeric excised internal structures having N_{iC} carbon atoms obtained by clipping N_{pC} internal edges (bonds) to perimeter carbons and attaching hydrogen to N_{pC} dangling bonds thus formed on the separated structures. It is important to note that all isomeric internal structures must have the same number of rings and carbon vertices (N_{iC} of parent), i.e., d_s = constant. This process is illustrated by the structures in Fig. 2. Ethene, having two carbons, is the excised internal structure of pyrene ($C_{16}H_{10}$), and $C_{16}H_{10}$ ($N_{iC} = 2$) can only have one possible PAH6 isomer. *s-trans*-1,3-Butadiene, having four carbons, is the excised internal structure of anthanthrene ($C_{22}H_{12}$, $N_{iC} = 4$), and *s-cis*-1,3-butadiene is the excised internal structure of benzo(*ghi*)perylene ($C_{22}H_{12}$, $N_{iC} = 4$); since triangulene and its excised structure, trimethylenemethane, (which are not shown) are diradicals, the formula of $C_{22}H_{12}$ can be represented only by the above two nonradical PAH6 isomeric structures. The excised internal structure of coronene ($C_{24}H_{12}$, $N_{iC} = 6$) is benzene, and $C_{24}H_{12}$ has only one PAH6 structure. The excised internal structure of circumcoronene ($C_{54}H_{18}$) is coronene ($C_{24}H_{12}$), and circumcoronene is the excised internal structure of dicircumcoronene ($C_{96}H_{24}$). Thus dicircumcoronene and circumcoronene have no other PAH6 isomers (7). Previously, it was shown that there were only three nonradical PAH6 isomers of the formula $C_{30}H_{14}$ (7). In Fig. 2, four PAH6 structures having the formula of $C_{30}H_{14}$ are shown, along with their corresponding excised internal structures. Styrene is the excised internal structure of naphtho(*abc*)coronene, 1,2-benzoquinodimethane of dibenzo(*bc*,*ef*)coronene, 1,3-benzoquinodimethane of the third $C_{30}H_{14}$ structure, and 1,4-benzoquinodimethane of dibenzo(*bc*,*kl*)coronene (dibenzoperopyrene). However, since 1,3-benzoquinodimethane is a diradical and the [22]annulene perimeter is an even alternant hydrocarbon, the third $C_{30}H_{14}$ structure shown in Fig. 2 must be a diradical

TABLE 1. Formula periodic table for benzenoid polycyclic aromatic hydrocarbons (PAH6)[a,b,c]

$d_s=-9$	$d_s=-8$	$d_s=-7$	$d_s=-6$	$d_s=-5$	$d_s=-4$	$d_s=-3$	$d_s=-2$	$d_s=-1$	$d_s=0$	$d_s=1$	$d_s=2$	$d_s=3$	N_{iC}
Forbidden region		$C_{60}H_{60}$					Most reactive		$C_{10}H_8$ (1)	$C_{14}H_{10}$ (2)	$C_{18}H_{12}$ (5)	$C_{22}H_{14}$ (12)	0
					$N_C/N_H<2$				$C_{16}H_{10}$ (1)	$C_{20}H_{12}$ (3)	$C_{24}H_{14}$ (13)	$C_{28}H_{16}$ (62)	2
								$C_{24}H_{12}$ (1)	$C_{22}H_{12}$ (2)	$C_{26}H_{14}$ (9)	$C_{30}H_{16}$ (58)	$C_{34}H_{18}$ (>333)	4
							$C_{32}H_{14}$ (1)	$C_{30}H_{14}$ (3)	$C_{28}H_{14}$ (8)	$C_{32}H_{16}$ (46)	$C_{36}H_{18}$	$C_{40}H_{20}$	6
					$2<N_C/N_H<3$		$C_{38}H_{16}$ (10)	$C_{36}H_{16}$ (21)	$C_{34}H_{16}$ (37)	$C_{38}H_{18}$	$C_{42}H_{20}$	$C_{46}H_{22}$	8
						$C_{40}H_{16}$ (3)	$C_{44}H_{18}$	$C_{42}H_{18}$	$C_{40}H_{18}$	$C_{44}H_{20}$	$C_{48}H_{22}$	$C_{52}H_{24}$	10
					$C_{42}H_{16}$ (1)	$C_{46}H_{18}$ (56)	$C_{50}H_{20}$	$C_{48}H_{20}$	$C_{46}H_{20}$	$C_{50}H_{22}$	$C_{54}H_{24}$	$C_{58}H_{26}$	12
					$C_{48}H_{18}$ (22)	$C_{52}H_{20}$	$C_{56}H_{22}$	$C_{54}H_{22}$	$C_{52}H_{22}$	$C_{56}H_{24}$	$C_{60}H_{26}$	$C_{64}H_{28}$	14
			$C_{50}H_{18}$ (7)	$C_{54}H_{20}$	$C_{58}H_{22}$			$C_{60}H_{24}$	$C_{64}H_{26}$	$C_{68}H_{28}$			
			$C_{52}H_{18}$ (2)	$C_{56}H_{20}$	$C_{64}H_{22}$								
		$C_{54}H_{18}$ (1)	$C_{58}H_{20}$ (102)	$C_{62}H_{22}$									
Least reactive		$C_{60}H_{20}$ (20)	$C_{64}H_{22}$					Intermediate reactive					
	$C_{62}H_{20}$ (12)	$C_{66}H_{22}$											
$C_{64}H_{20}$ (3)	$C_{68}H_{22}$												
$C_{70}H_{22}$													

[a]Number of nonradical isomers in parentheses.
[b]Number of rings, $r = 1/2(N_C + 2 - N_H)$.
[c]For the row series $N_C = 2N_H - 6 + N_{iC}$, and for the column series $N_C = 3N_H - 14 - 2d_s$.

Can. J. Chem. Downloaded from www.nrcresearchpress.com by 210.87.254.40 on 09/06/12
For personal use only.

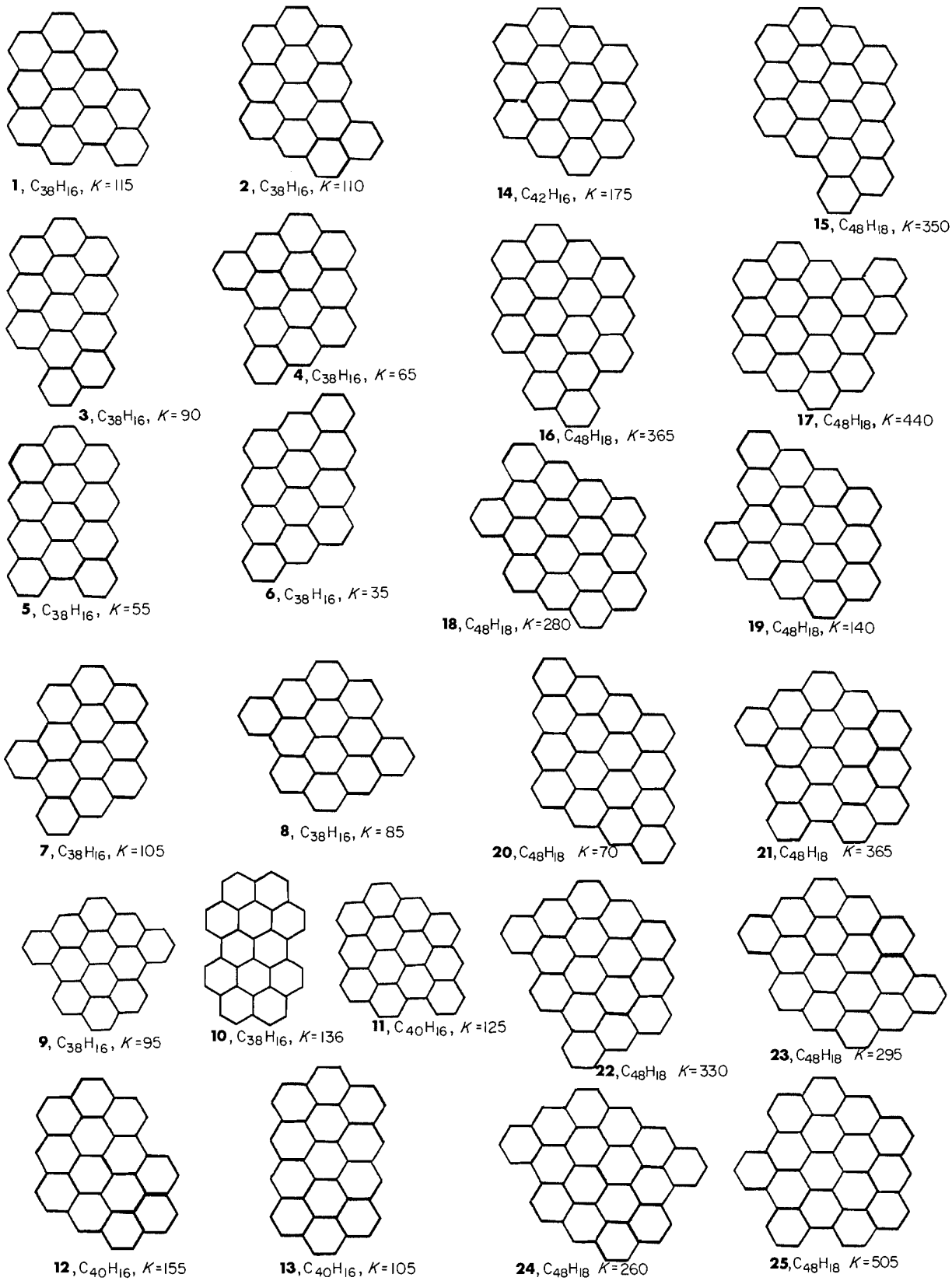

FIG. 1. All the isomers of formulas on the left-hand diagonal of Table 1.

and is not counted. In general, if the excised internal structure is a diradical which can be formed by connecting a non-starred position of a monoradical with a starred position of a second monoradical, its parent PAH6 structure will also be a diradical. Note that a strictly *peri*-condensed polycyclic aromatic hydrocarbon cannot have a disconnected excised internal structure. Thus perylene is not a strictly *peri*-condensed PAH6, nor is dibenzo(*de*,*hi*)naphthacene diradical.

Can. J. Chem. Downloaded from www.nrcresearchpress.com by 210.87.254.40 on 09/06/12
For personal use only.

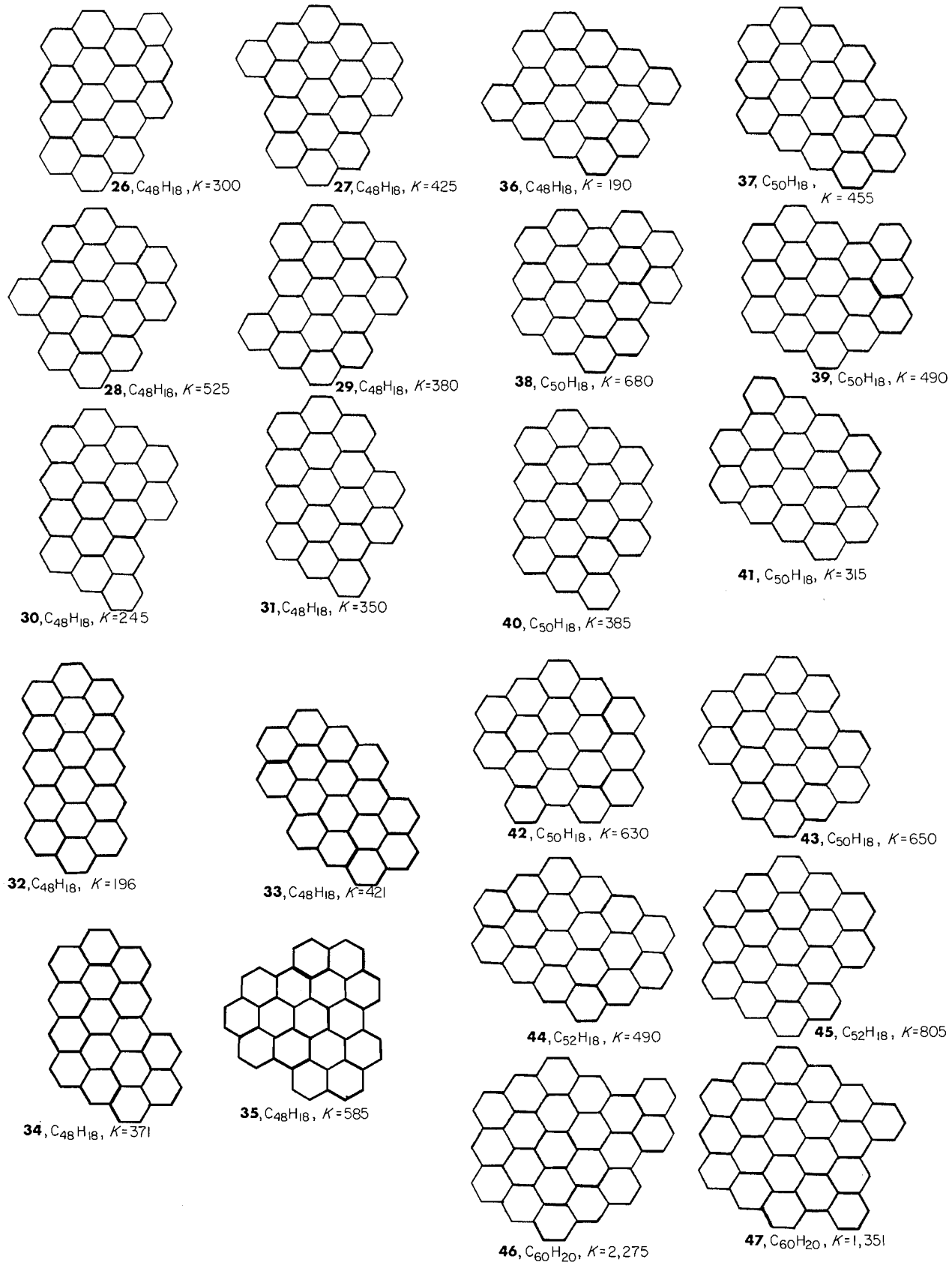

FIG. 1. (*continued*)

Enumeration of excised internal structures

Figure 3 presents all the corresponding (primed) excised internal structures of all the parent PAH6 isomers shown in Fig. 1. The first nine substituted naphthalene structures (**1′**−**9′**) and biphenyl (**10′**), all having twelve carbon atoms in Fig. 3, correspond in order and orientation to the ten $C_{38}H_{16}$ (N_{iC} = 12) isomers in Fig. 1. Only one of two possible conformers of 1-ethenylnaphthalene (**1′**) is presented, while both

Can. J. Chem. Downloaded from www.nrcresearchpress.com by 210.87.254.40 on 09/06/12
For personal use only.

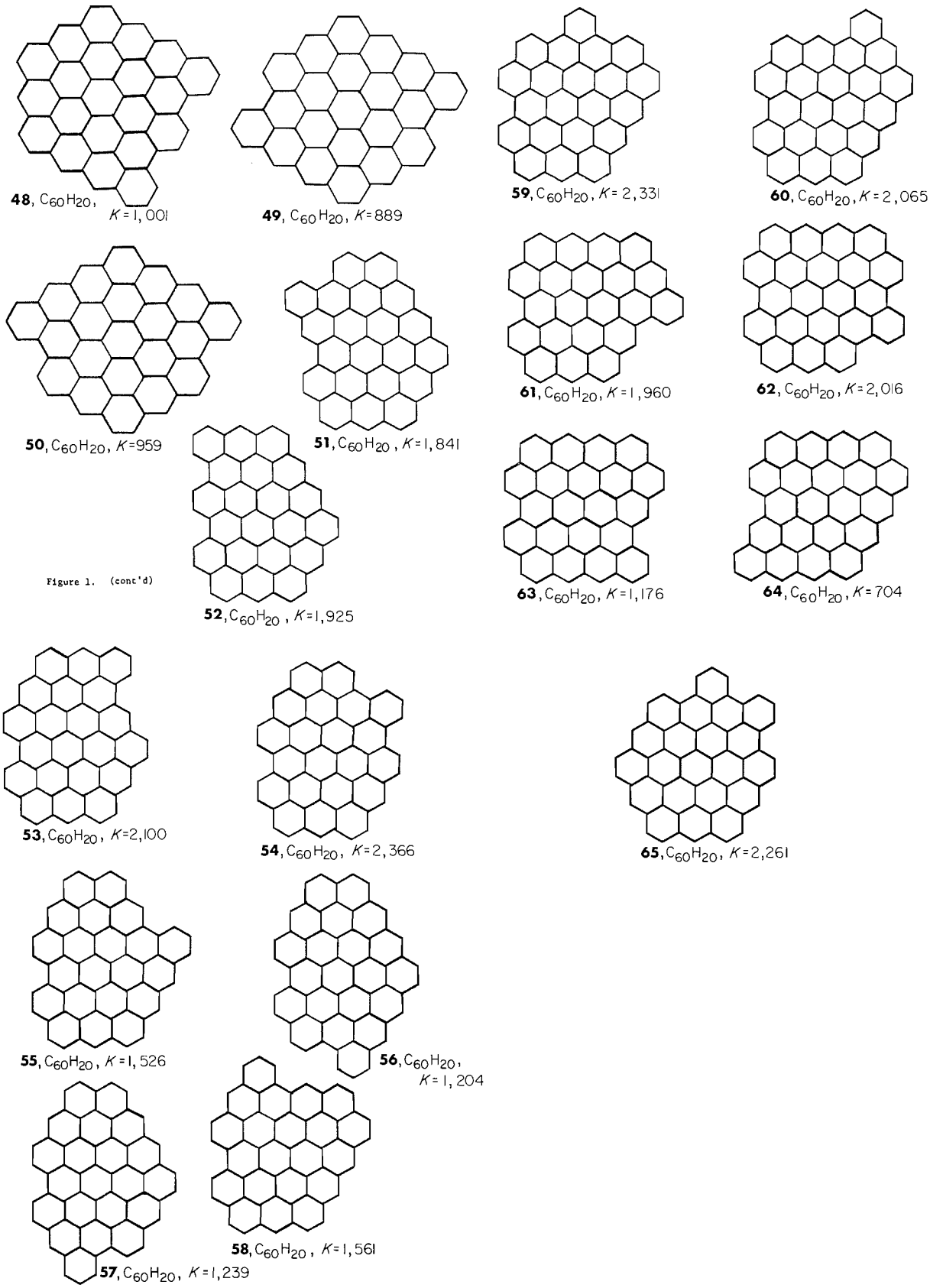

Figure 1. (cont'd)

FIG. 1. (*concluded*)

possible conformers (**2′**, **3′**) of 2-ethenylnaphthalene appear. This is because a two-carbon-atom gap needs to exist between the *s-cis*-1,3-butadiene system of any excised internal structure of a PAH6 parent. Thus the other conformer of 1-ethenylnaphthalene has a one-carbon-atom gap and is therefore excluded. Only six of ten possible naphthoquinodimethanes (**4′**−**9′**) are present in Fig. 3 because the other four are diradicals. There are only three nonradical isomeric conjugated

TABLE 2. One-isomer series of polycircumnaphthalene, polycircumpyrene, and polycircumcoronene

Formula	No. of carbon atoms around periphery $(4\tau+2)$	τ	$N_{iC(max)}$	Nomenclature	K = SC[a]
$C_{10}H_8$	10	2	0	Naphthalene	3
$C_{16}H_{10}$	14	3	2	Pyrene	6
$C_{24}H_{12}$	18	4	6	Coronene (coronene-7)	20
$C_{32}H_{14}$	22	5	10	Ovalene (circumnaphthalene)	50
$C_{42}H_{16}$	26	6	16	Circumpyrene	175
$C_{54}H_{18}$	30	7	24	Circumcoronene (coronene-19)	980
$C_{66}H_{20}$	34	8	32	Circumovalene (dicircumnaphthalene)	4,116
$C_{80}H_{22}$	38	9	42	Dicircumpyrene	24,696
$C_{96}H_{24}$	42	10	54	Dicircumcoronene (coronene-37)	232,848
$C_{112}H_{26}$	46	11	66	Tricircumnaphthalene	1,646,568
$C_{130}H_{28}$	50	12	80	Tricircumpyrene	16,818,516
$C_{150}H_{30}$	54	13	96	Tricircumcoronene (coronene-61)	267,227,530
$C_{170}H_{32}$	58	14	112	Tetracircumnaphthalene	3,184,461,400

[a]Reference 17.

Can. J. Chem. Downloaded from www.nrcresearchpress.com by 210.87.254.40 on 09/06/12
For personal use only.

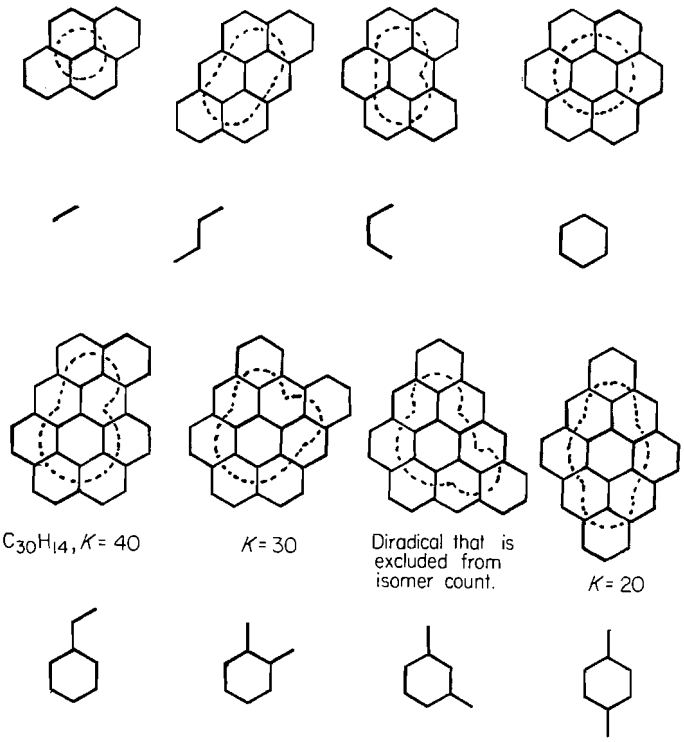

FIG. 2. Excised internal structures from strictly *peri*-condensed PAH6s.

three-ring structures of fourteen carbon vertices (**11′**−**13′**) and, therefore, only three corresponding benzenoid PAH6 structures of the formula $C_{40}H_{16}$ with N_{iC} = 14 exist. The Fig. 1 formula of $C_{42}H_{16}$ (N_{iC} = 16) has only one possible structure, circumpyrene, since the excised internal structure corresponds to pyrene (**14′**), which is the only arrangement possible for sixteen carbon vertices of four hexagonal rings.

All benzenoid PAH6 structures of the formula of $C_{48}H_{18}$ have N_{iC} = 18 and excision of their internal structures leads to three ethenylpyrene, (**15′**−**17′**), nine nonradical pyrenylquinodimethane (**18′**−**25′** and **36′**), six perianthracenylmethylene (**26′**−**31′**), naphthacene (**32′**), chrysene (**33′**), benzo(*a*)anthracene (**34′**), and triphenylene (**35′**) isomers of four rings and eighteen carbon vertices. The excised internal structures (Fig. 3) corresponding to PAH6s of the formula $C_{50}H_{18}$ (N_{iC} = 20) lead to benzo(*a*)pyrene, (**37′**), benzo(*e*)pyrene (**38′**), four methylene-substituted isomers of naphtho[2,1,8,7-*defg*]anthracene (**39′**−**42′**), and perylene (**43′**) ($C_{20}H_{12}$). The formula $C_{52}H_{18}$ (N_{iC} = 22) has only two excised internal isomeric structures, anthanthrene (**44′**) and benzo(*ghi*)perylene (**45′**) ($C_{22}H_{12}$), and therefore the benzenoid formula of $C_{52}H_{18}$ has only two corresponding PAH6 isomers. Finally, the formula of $C_{60}H_{20}$ (N_{iC} = 26) has 20 nonradical excised internal isomeric structures of twenty-six carbon vertices and seven rings (**46′**−**65′**) which correspond to 20 PAH6s.

Usually all isomers of *peri*-condensed benzenoid PAH6 isomers without *cata*-condensed appendages can be enumerated by finding all excised nonradical isomeric internal structures of N_{iC} (parent) carbon vertices. The limitations associated with this method can be illustrated by the enumeration of all eight non-radical isomers of $C_{28}H_{14}$. All the PAH6 isomers of $C_{28}H_{14}$ (N_{iC} = 6) and their corresponding excised internal structures are presented in Fig. 4. The first isomer, benzocoronene, has the same excised internal structure, benzene, as coronene and illustrates that *cata*-condensed appendages are not revealed by the excised internal structure method; this first $C_{28}H_{14}$ isomer has the only excised internal structure which is a ring, suggesting an implicit disconnection elsewhere. The next four isomers have excised internal structures corresponding to all possible conformations of 1,3,5-hexatriene that do not have less than two-carbon-atom gaps. Immediately following are the two isomers having the two conformations of 3-methylene-1,4-pentadiene as excised internal structures. Finally, the last two $C_{28}H_{14}$ benzenoid isomers have diradical excised internal structures. The first diradical can be constructed by the union of two allyl radicals through their nonstarred positions and the latter one by attaching the nonstarred position of one to the starred position of the other. Since the first diradical has two mutually exclusive $p\pi$-electron systems and the latter one does not, the corresponding PAH6 structure of the first diradical internal structure is nonradical (closed shell) and the corresponding PAH6 structure of the latter one is also a diradical (open shell) and is not included in the isomer count.

Above it was shown that the formula $C_{22}H_{12}$ had only two nonradical isomers, anthanthrene and benzo(*ghi*)perylene, with the corresponding internal excised structures of *s-trans*-1,3-butadiene and *s-cis*-1,3-butadiene (Fig. 2), respectively.

Can. J. Chem. Downloaded from www.nrcresearchpress.com by 210.87.254.40 on 09/06/12
For personal use only.

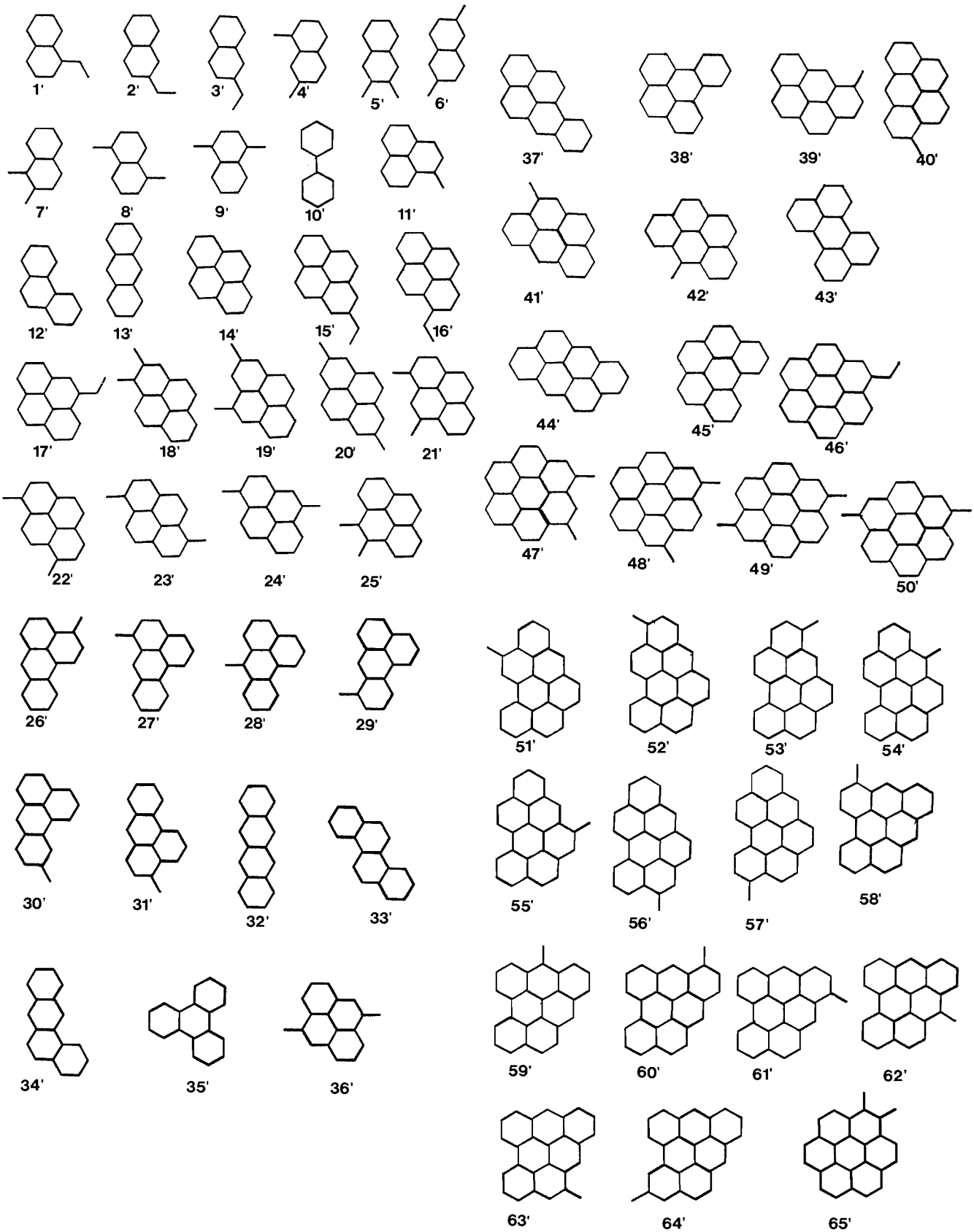

FIG. 3. Excised internal structures corresponding to the benzenoid PAH6 compounds in Fig. 2.

Anthanthrene and benzo(*ghi*)perylene are the excised internal structures of the two isomeric benzenoid hydrocarbons having the formula of $C_{52}H_{18}$ (Fig. 1); similarly, these isomeric $C_{52}H_{18}$ structures are the excised internal structures of the two benzenoid structures of the formula of $C_{94}H_{24}$, which in turn are the internal excised structures of the two benzenoid structures of the formula $C_{148}H_{30}$ (Fig. 5). There are three nonradical isomers of the formula $C_{30}H_{14}$, and these are the excised internal struc-

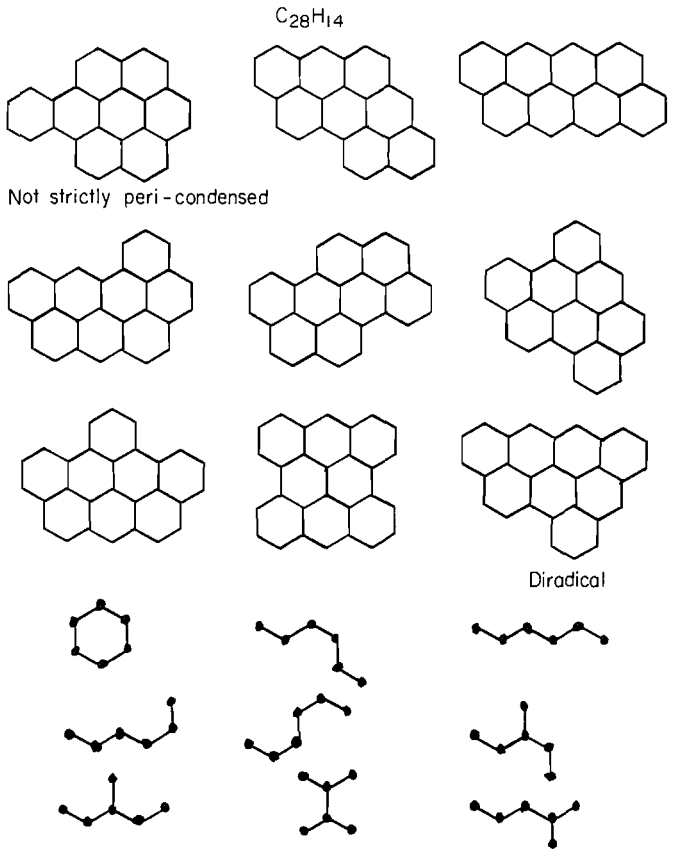

FIG. 4. All the benzenoid isomers of $C_{28}H_{14}$ and their corresponding excised internal structures.

tures of the benzenoid hydrocarbons having a formula of $C_{64}H_{20}$ (Fig. 6), which in turn are the excised internal structures associated with benzenoid hydrocarbons of the formula $C_{110}H_{26}$. Table 3 presents a summary of these polycircum two- and three-isomer series. Other polycircum isomeric series include $C_{40}H_{16}$, $C_{78}H_{22}$, $C_{128}H_{28}$ – where each of these formulas have 3 corresponding nonradical PAH6 isomers, and $C_{50}H_{18}$, $C_{92}H_{24}$, $C_{146}H_{30}$, – each having 7 corresponding nonradical PAH6 isomers.

Recognition of peri-*condensed diradical benzenoids*

Inspection of the diradical excised internal structures of triangulene, $C_{28}H_{14}$, and $C_{30}H_{14}$ reveals the following general principle for recognizing when even-carbon *peri*-condensed benzenoid hydrocarbons will be diradicals. If trimethylenemethane diradical is ultimately obtained upon successive excision and pruning of a specified benzenoid hydrocarbon having a formula below the $N_C = 2N_H - 4$ row series in Table 1, then that original benzenoid hydrocarbon is also a diradical. The trimethylenemethane diradical is the excised internal structure of triangulene and is also obtained by pruning off the even-carbon fragments of ethene from 2-methylenepentadienyl diradical (Fig. 4) and *s-trans*-butadiene from 1,3-benzoquinodimethane (Fig. 2). This recognition generalization is equivalent to taking the difference in opposing triangles generated by the corresponding dualist graph where a line is drawn from every point located at the center of all hexagons (8).

A simplified nomenclature for strictly peri-*condensed benzenoid hydrocarbons*

Successive excision of all strictly *peri*-condensed PAH6s

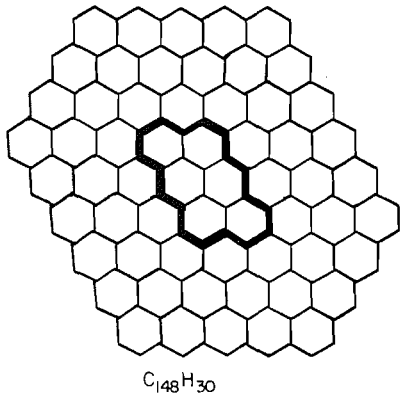

FIG. 5. Three successive excisions of $C_{148}H_{30}$ lead to isomers of anthanthrene.

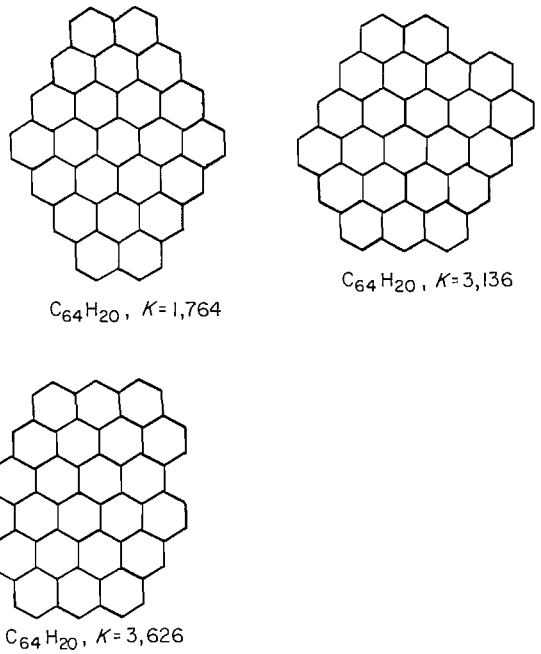

FIG. 6. The three nonradical isomers of $C_{64}H_{20}$.

usually leads to a simpler molecule which already has a standard nomenclature. Thus a straightforward nomenclature of complicated *peri*-condensed benzenoid hydrocarbons can be developed by using the corresponding excised internal structure for the parent name. Consider structure **60** in Fig. 1, which has structure **60′** in Fig. 3 as its corresponding excised internal structure. One name for this excised internal structure could be 9-methylenylbenzo(*fg*)anthanthrene, and the name of the corresponding $C_{60}H_{20}$ structure could be circum(34)[9-methylenylbenzo(*fg*)anthanthrene] where the number in parentheses after the "circum" prefix represents the number of peripheral carbon vertices circumscribed to the parent. This nomenclature would be deductively more obvious than the perifusene/dualist graph/three-digit coding nomenclature and its graphite lattice model variant previously proposed (9–11).

Computation of the number of Kekulé structures associated with strictly peri-*condensed benzenoids*

Since the logarithm of the structure count (number of Kekulé structures or 1-factor subgraphs) of benzenoid PAHs has been shown to be proportional to resonance energy, the structure count (SC = K) of the isomers shown in Fig. 1 was determined

Can. J. Chem. Downloaded from www.nrcresearchpress.com by 210.87.254.40 on 09/06/12
For personal use only.

TABLE 3. The polycircum isomeric series of anthanthrene/benzo(*ghi*)perylene and naphtho(*abc*)coronene/dibenzo(*bc,ef*)coronene/dibenzo(*bc,kl*)coronene

Formula	r	N_{iC}	Peripheral no. of carbons	No. of nonradical isomers	No. of radical isomers	K = SC[a]
$C_{22}H_{12}$	6	4	18	2	1	10,14
$C_{52}H_{18}$	18	22	30	2	1	490,805
$C_{94}H_{24}$	36	52	42	2	1	—
$C_{148}H_{30}$	60	94	54	2	1	
—	—	—	—	—	—	
$C_{30}H_{14}$	9	8	22	3	1	20,30,40
$C_{64}H_{20}$	23	30	34	3	1	1784,3136,3626
$C_{110}H_{26}$	43	64	46	3	1	—
$C_{168}H_{32}$	69	110	58	3	1	

[a]Reference 17.

(12). The computational procedure used consisted of the reduction of a given PAH6 into smaller PAH6 fragments of known structure count (13). A number of generalizations are made evident by comparison of the structure counts of the PAHs shown in Figs. 1, 2, and 6. The numerical order of the number of Kekulé structures associated with a set of isomers of strictly *peri*-condensed PAH6s parallels the numerical order of their corresponding excised internal PAH6 structures. For example, the two benzenoid isomers of $C_{52}H_{18}$ have K = 490 and 805 and their excised internal structures of anthanthrene and benzo(*ghi*)perylene have K = 10 and 14, respectively. Other things being equal, the more concave bay regions contained by a PAH6 structure, the larger the structure count. A strictly *peri*-condensed PAH6 has the same number of concave bay regions as its internal excised PAH6 structure; if its internal excised structure is not a PAH6, then its number of concave bay regions is determined by the number of distinct *s-cis*-1,3-butadiene substructures (subgraphs) present in its excised internal structure. For example, benzo(*ghi*)perylene has one bay region and its circumscribing $C_{52}H_{18}$ structure has one bay region, and anthanthrene has no bay region and its circumscribing $C_{52}H_{18}$ has no bay region (Fig. 5); the internal excised structure of benzo(*ghi*)perylene is *s-cis*-butadiene, and the excised internal structure of anthanthrene is *s-trans*-butadiene.

Conclusion

Isomer enumeration of strictly *peri*-condensed benzenoid hydrocarbons can be more easily achieved via enumeration of their excised internal structures. The formulas corresponding to strictly *peri*-condensed benzenoids can be easily identified as the left-hand diagonal boundary formulas found in the Formula Periodic Table for PAH6; these boundary formulas cannot have corresponding structures with benzo *cata*-condensed appendages, whereas the formulas immediately adjacent have some corresponding isomeric structures with benzo *cata*-condensed appendages not explicitly revealed by the excised internal structure. The (successive) excised internal structures of strictly *peri*-condensed PAH6 hydrocarbons result in simpler structures with existing standard nomenclature which can be utilized as parent names for the more complicated PAH6 derived by circumscribing them with peripheral carbon rings in a successive fashion. This need for research on very large benzenoid hydrocarbons has been pointed out by a definitive prior paper on this subject (14). Since the logarithm of the number of Kekulé structures is proportional to resonance energy and many PAH6 benzenoid compounds are produced via pyrolytic and combustion processes, the structures of the most probable macromolecular benzenoid isomers of this class formed via pyrolytic processes can be estimated from the listing of compounds in Fig. 1 (15). Strictly *peri*-condensed benzenoid hydrocarbons have totally connected internal edges and become more predominant as one moves from right to left in Table 1.

Acknowledgements

The author would like to express his gratitude to Professor Milan Randić, Drake University, and Dr. Robert L. Brown, National Bureau of Standards (cf. ref. 16 for a relevant computer program), for checking some of his Kekulé numbers and making other useful comments.

1. A. T. BALABAN and F. HARARY. Tetrahedron, **24**, 2505 (1968).
2. N. TRINAJSTIĆ, Z. JERICEVIĆ, J. V. KNOP, W. R. MÜLLER, and K. SZYMANSKI. Pure Appl. Chem. **55**, 379 (1983); J. V. KNOP, K.SZYMANSKI, Z. JERICEVIĆ, and N. TRINAJSTIĆ. J. Comput. Chem. **4**, 23 (1983), and references therein; K. SZYMANSKY. Polyhexagons der Ordnungen 1–10 Klassifiziert nach der Anzahl der inneren Knoten. Univ. Düsseldorf, Rechenzentrum. 1982.
3. R. H. MARTIN, C. EYNDELS, and N. DEFAY. Tetrahedron, **30**, 3339 (1974).
4. R. H. MARTIN and M. BAES. Tetrahedron, **31**, 2135 (1975).
5. J. R. DIAS. J. Chem. Inf. Comput. Sci. **22**, 139 (1982).
6. J. R. DIAS. MATCH (Math. Chem.), **14**, 83 (1983).
7. J. R. DIAS. J. Chem. Inf. Comput. Sci. **22**, 15 (1982).
8. A. T. BALABAN. Rev. Roum. Chem. **26**, 407 (1981).
9. A. T. BALABAN. Tetrahedron, **25**, 2949 (1969).
10. D. BONCHEV. Pure Appl. Chem. **55**, 221 (1983).
11. D. BONCHEV and A. T. BALABAN. J. Chem. Inf. Comput. Sci. **21**, 2 (1981).
12. W. C. HERNDON. Tetrahedron, **29**, 3 (1973).
13. M. RANDIĆ. J. Chem. Soc. Faraday Trans. 2, 232 (1976).
14. M. RANDIĆ. Int. J. Quantum Chem. **17**, 549 (1980).
15. W. E. MAY and S. WISE. Anal. Chem. **56**, 225 (1984); P. A. PEADEN, M. L. LEE, Y. HIRATA, and M. NOVOTNY. Anal. Chem. **52**, 2268 (1980).
16. R. L. BROWN. J. Comput. Chem. **4**, 556 (1983).
17. T. F. YEN. Theor. Chim. Acta (Berlin) **20**, 399 (1971).

Appendix: Glossary of terms

d_s:	net tree disconnections of internal graph edges (positive values) or connections (negative values − called negative disconnection)
N_C:	total number of carbon atoms in a PAH
N_H:	total number of hydrogen atoms in a PAH
N_{iC}:	number of internal carbon atoms in a PAH having a degree of 3
N_{pC}:	number of peripheral carbon atoms in a PAH having a degree of 3
PAH6:	polycyclic aromatic hydrocarbon containing exclusively fused hexagonal rings
$\|P\|=p=N_C$:	total number of graph points
p_3:	number of graph points (vertices) having a degree of 3
$\|Q\|=q$:	number of graph edges (lines or C—C bonds)
q_i:	number of internal graph edges
q_p:	number of peripheral graph edges
r:	number of rings
τ:	number of rings obtained upon deletion of all internal third-degree vertices from a PAH6 σ-bond graph

Can. J. Chem. Downloaded from www.nrcresearchpress.com by 210.87.254.40 on 09/06/12
For personal use only.

Kinetics and mechanism of the reaction of iodine with isonicotinoylhydrazide

IRENE A. FUNAI AND MIGUEL A. BLESA[1]

Departamento Química de Reactores, Comisión Nacional de Energía Atómica, Avenida del Libertador 8250, 1429 Buenos Aires, Argentina

Received December 7, 1983[2]

IRENE A. FUNAI and MIGUEL A. BLESA. Can. J. Chem. **62**, 2923 (1984).

The title reaction proceeds through two parallel pathways involving attack by IOH (k_{14} = (5.69 ± 0.97) × 10^8 mol^{-1} dm^3 s^{-1}) and by I_2 (k_{13} = 0.31 ± 0.11) mol^{-1} dm^3 s^{-1}) on $^+HNC_5H_4C(O)NHNH_2$ (INAH). These results are similar to those of Hasty on the system N_2H_4 + I_2, but differ from the mechanisms proposed by Cooper and Bah and Yew for similar systems. Because k_{14} is close enough to (though significantly less than) the diffusion limit, our data permit us to estimate the first-order rate constant for I_2 hydrolysis, obtaining in reasonable agreement with previous data k_5 = 0.33 s^{-1} at pH = 1.66. The general kinetic law is shown to give rise to an [R-NH-NH_2] independent pathway of oxidation at sufficiently high pH. A mechanism is proposed to explain the much higher reactivity of IOH (as compared to I_2) towards R-NH-NH_2.

IRENE A. FUNAI et MIGUEL A. BLESA. Can. J. Chem. **62**, 2923 (1984).

La réaction mentionnée dans le titre peut se produire par le biais de deux voies parallèles impliquant des attaques soit du IOH (k_{14} = (5,69 ± 0.97) × 10^8 mol^{-1} dm^3 s^{-1}) ou du I_2 (k_{13} = 0.31 ± 0.11) mol^{-1} dm^3 s^{-1}) sur la $^+HNC_5H_4C(O)NHNH_2$ (INAH). Ces résultats sont semblables à ceux obtenus par Hasty sur le système N_2H_4 + I_2; ils diffèrent toutefois des mécanismes proposés par Cooper et Bah et Yew pour des systèmes similaires. La valeur de k_{14} étant proche (quoique plus basse d'une façon significative) de la limite de diffusion, nos données nous permettent d'évaluer la constante de vitesse du premier ordre pour l'hydrolyse du I_2 et d'obtenir une valeur en bon accord avec la constante k_5 = 0,33 s^{-1} (à un pH de 1,66) rapportée antérieurement. On montre que la loi cinétique générale donne lieu, à des pH suffisamment élevés, à des voies d'oxydation qui ne dépendent pas de la concentration en R-NH-NH_2. On propose un mécanisme pour expliquer la réactivité beaucoup plus grande du IOH (comparée à celle du I_2) vis-à-vis le R-NH-NH_2.

[Traduit par le journal]

Introduction

It is well known that iodine quantitatively oxidizes substances containing the —NH—NH_2 group. This reaction is the basis of one of the standard analytical procedures to titrate hydrazine and related substances, in particular isonicotinoylhydrazide (isoniazid, INAH),

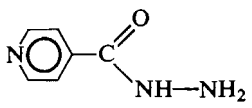

which is widely used in the pharmaceutical industry because of its bacteriostatic properties against *Mycobacterium tuberculosis*. The rate of the oxidation reaction is very sensitive to all variables which affect the speciation of both reagents in solution, and thus the rate may vary widely according to the chemistry of the solution. In the present paper we report the results of a kinetic study of the oxidation of INAH by iodine, which is important per se and also helps to shed light on the general mechanisms of oxidation of the —NH—NH_2 function by iodine.

The mechanism of oxidation of hydrazine itself by iodine has been the subject of several studies, among which no complete agreement is found. Thus, Hasty (1) reports the rate law

$$[1] \quad R = k_a [N_2H_5^+][I_2] + k_b [N_2H_5^+][HIO]$$

the second term accounting for the largest fraction of reaction under experimental conditions (large excess of iodide and pH values in the range 1–2). The values for k_a and k_b are found to be ca. 1.0 dm^3 mol^{-1} s^{-1} and 2 × 10^9 dm^3 mol^{-1} s^{-1} which are interpreted as indicative of IOH being the most active among the various oxidized iodine species (HIO, I_2, I_3^-, I_5^-). According to this study, iodine itself also reacts with $N_2H_5^+$, and because $[I_2] \gg [IOH]$, the contribution to the overall rate of the first term in eq. [1] is not negligible.

On the other hand, Cooper and co-workers (2) propose a different mechanism, involving only I^+ and N_2H_4 in the activated state. This is reached from a pre-equilibrated $N_2H_4I^+$ species, the concentration of which is sensitive to I^-:

$$[2] \quad N_2H_4 + I_2 \rightleftarrows N_2H_4I^+ + I^-$$

$$[3] \quad N_2H_4I^+ \rightarrow \text{products}$$

$$[4] \quad R = \frac{k_3k_2 [N_2H_4] [I_2]}{k_{-2} [I^-] + k_3}$$

Because of the relationship between [IOH] and $[I_2]$ (eq. [5], $Q_5 = 4.83 \times 10^{-13}$) (ref. 3),

$$[5] \quad I_2 + H_2O \rightleftarrows IOH + I^- + H^+$$

and between $[N_2H_4]$ and $[N_2H_5^+]$ (eq. [6], $K_6 = 10^{-7.98}$) (ref. 4),

$$[6] \quad N_2H_5^+ \rightleftarrows N_2H_4 + H^+$$

both mechanisms are in fact compatible with the same set of experimental data; part of the difficulty is due to the similar pH dependency of [5] and [6] in the pH range of the kinetic studies, where $[IOH] \propto [H^+]^{-1}$ and $[N_2H_4] \propto [H^+]^{-1}$ (furthermore, the proportionality constants are not very different). Kinetic data indicate only a deprotonation equilibrium generating a reactive species at high pH values.

References 1 and 2 both agree in the existence of pathways which at high enough $[I^-]$ become proportional to $[I^-]^{-2}$, although the origin of this dependency is variously attributed to equilibrium [2] (2) or to equilibrium [5] (1), which together with

$$[7] \quad I_3^- \rightleftarrows I_2 + I^- \qquad Q_7 = (736)^{-1}$$

explains the observed partial order. Other authors (5) in turn

[1]Author to whom correspondence may be addressed.

[2]Revision received June 27, 1984.

Can. J. Chem. Downloaded from www.nrcresearchpress.com by 210.87.254.105 on 09/06/12
For personal use only.

find a dependence on $[I^-]^{-1}$, giving rise to a third proposed rate law

[8] $R = k_8 [N_2H_4][I_2]$

attributed to the direct attack of I_2 on N_2H_4 as the rate-determining step. According to Hasty (1), the overall mechanism includes both the attack by IOH and by I_2 on hydrazine, although the $[H^+]$ dependency of this latter pathway is diversely reported to be of order −1 (5) or zero (1); the difference can be traced back to different assumptions as to the relative reactivities of $N_2H_5^+$ and N_2H_4.

Experimental

Analytical reagents were employed without further purification. INAH was a gift from G. Ramón Laboratories, Buenos Aires, and was recrystallized several times from doubly distilled ethanol in the presence of activated charcoal. All solutions were prepared with doubly distilled water. Iodine solutions were standardized with sodium thiosulfate.

Spectrophotometric measurements were carried out in a Hitachi–Perkin–Elmer 139 spectrophotometer fitted with thermostated cell compartments.

The kinetics of the reaction were followed by measuring the decrease in absorbance at 390 nm, 24.9°C, and I = 1 mol dm^{-3} (NaCl). The measurements were not made at 352 nm (λ_{max} of I_3^-) because, at this wavelength, background absorbance was inconveniently high.

A typical kinetic experiment was performed as follows: HCl and NaCl solution (Reagent A) and KI, I_2, and NaCl solution (Reagent B) were prepared. Solid INAH was dissolved in Reagent A and Reagent B was poured over it. The initial (analytical) concentration of iodine ($F^0_{I_2}$) was ca. 1.1×10^{-4} mol dm^{-3}. INAH and KI were in high excess over I_2. F_{INAH} and F_{I^-} were in the ranges $5 \times 10^{-3} - 5 \times 10^{-2}$ mol dm^{-3} and $1 \times 10^{-2} - 4 \times 10^{-2}$ mol dm^{-3} respectively, and were constant during each experiment. The pH was also constant during those runs without need of buffers because of the high acidities. In different experiments, pH varied in the range 1.3–2.0.

From the absorbance–time data, very good pseudo-first-order plots were obtained: $\log [(A_0 - A)/(A - A_\infty)]$ was a linear function of time for up to 5 half-lives. The reported k_{obsd} values were obtained from the slopes of the plots of duplicate experiments. No complications due to the formation of $^+HNC_5H_4C(O)HNNH(O)CC_5H_4NH^+$ were detected because, in the presence of a large excess of INAH, I_2 reacts quantitatively with the original reagent.

Results

The experimental rate constants k_{obsd} (eq. [9])

[9] $k_{obsd} = [I_3^-]^{-1} (-d[I_3^-]/dt) = F_{I_2}^{-1} (-d[I_3^-]/dt)$

are shown in Tables 1–3. Because of the large excess of I^-, the total analytical iodine concentration is identical to the actual I_3^- concentration in all the experiments.

The data in Table 1 show that the reaction is first order in INAH at pH = 1.66; similar results are found at other pH values, the rate increasing with increasing pH in the pH range 1.3–2.0 (see Table 2). The high sensitivity to pH is similar to that observed for N_2H_4. Table 3 gives the relationship between rate and F_{I^-}.

TABLE 1. Dependency of k_{obsd} on F_{INAH}; $F_{I^-} = 2 \times 10^{-2}$ mol dm^{-3}; pH = 1.66; t = 24.9°C; I = 1 mol dm^{-3} (NaCl). The data fit the equation $k_{obsd} = 4.52 \times 10^{-2}$ mol^{-1} dm^3 s^{-1} F_{INAH} with ρ = 0.9868

$k_{obsd} \times 10^4$ (s^{-1})	F_{INAH} (mol dm^{-3})
2.33	0.005
5.36	0.010
7.36	0.015
8.69	0.020
12.0	0.030
16.8	0.040
24.5	0.050

TABLE 2. Dependency of k_{obsd} on $[H^+]$; $F_{INAH} = 2 \times 10^{-2}$ mol dm^{-3}; $F_{I^-} = 3.5 \times 10^{-2}$ mol dm^{-3}; t = 24.9°C; I = 1 mol dm^{-3} (NaCl)

$k_{obsd} \times 10^4$ (s^{-1})	pH
1.03	1.297
1.31	1.418
2.47	1.531
2.96	1.591
4.33	1.713
8.61	1.954

Discussion

In the presence of large excess of INAH, I_2 is quantitatively reduced according to eq. [10] (6).

[10] R—C(O)NH—NH$_2$ + $2I_3^-$ + H_2O → R—C(O)OH + N_2 + $6I^-$ + $4H^+$

Benzoic acid may further react with excess isoniazid, eq. [11] (6).

[11] R—C(O)NH—NH$_2$ + HO(O)C—R → R—C(O)NH—NH(O)C—R + H_2O

but this reaction is irrelevant for our study. The stoichiometry of the reaction is therefore similar to that of $I_2 + N_2H_4$.

In view of the proposed mechanisms for the $I_2 + N_2H_4$ reaction, our data will be analyzed in terms of a general set of elementary equations, involving attack by both I_2 and IOH. I_3^- and I_5^- can safely be disregarded because of the inhibitory effect of iodide (Table 3).

[5a] $I_2 + H_2O \xrightarrow{k_5} IOH + I^- + H^+$

[5b] $IOH + I^- + H^+ \xrightarrow{k_{-5}} I_2 + H_2O$

[7] $I_3^- \rightleftarrows I_2 + I^-$ $\quad Q_7 = (736)^{-1}$ (ref. 3)

[12] 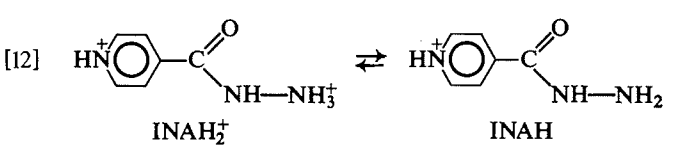

pK_a (INAH) = 1.85 (ref. 7)

[13] INAH + $I_2 \xrightarrow{k_{13}}$ products

[14] INAH + IOH $\xrightarrow{k_{14}}$ products

Thus,

[15] $-1/2 dF_{I_2}/dt = -1/2\ d\ [I_3^-]/dt = -d\ [INAH]/dt = \{k_{13}\ [I_2]\ [INAH] + k_{14}\ [IOH][INAH]\}$

The general expression for k_{obsd} under this mechanism is [16]

Can. J. Chem. Downloaded from www.nrcresearchpress.com by 210.87.254.105 on 09/06/12
For personal use only.

$$[16]\quad k_{obsd} = 2\left\{k_{13} + \frac{k_{14}}{\left(\frac{F_{I^-}\,[H^+]}{Q_5} + \frac{k_{14}\,[INAH]}{k_5}\right)}\right\} \frac{[INAH]}{\left\{F_{I^-}Q_7^{-1} + 1 + \frac{1}{\left[\frac{F_{I^-}\,[H^+]}{Q_5} + \frac{k_{14}\,[INAH]}{k_5}\right)}\right\}}$$

where

$$[17]\quad [INAH] = F_{INAH}\,K_a\,(K_a + [H^+])^{-1}$$

Two limiting assumptions can be identified by inspection of the terms in eq. [16]:

$$[18]\quad k_{13} \ll k_{14}\,k_5\,(k_{-5}\,F_{I^-}\,[H^+] + k_{14}\,[INAH])^{-1}$$

$$[19]\quad k_{14}\,[INAH] \ll k_{-5}\,F_{I^-}\,[H^+]$$

Previous work on $I_2 + N_2H_4$ has accepted [19] as a general assumption, while the ratio of the I_2 to the IOH-pathway is a matter of controversy. It must be noted, however, that the second assumption is incorrect at high pH values, and even in the pH range 1–2 the error involved may be significant if k_{14} approaches diffusion control.

Our set of data was fitted to eq. [16] by a nonlinear least-squares fitting method. According to ref. 8, for the hydrolysis of I_2 the following scheme and rate constants apply:

$$[20]\quad I_2 + H_2O \underset{1.6 \times 10^{10}\ mol^{-1}\ dm^3\ s^{-1}}{\overset{2.1\ s^{-1}}{\rightleftharpoons}} I_2OH^- + H^+$$

$$[21]\quad I_2OH^- \underset{5 \times 10^{9}\ mol^{-1}\ dm^3\ s^{-1}}{\overset{3 \times 10^{7}\ s^{-1}}{\rightleftharpoons}} IOH + H^+$$

whence

$$[22]\quad k_5^{lit} = \frac{2.1 \times 3 \times 10^7}{(1.6 \times 10^{10}\,[H^+] + 3 \times 10^7)}\ s^{-1}$$

Rather than using this expression for k_5, taken from the work of Eigen and Kustin (8), k_5 was left as another adjustable parameter and the obtained values used as a check of the procedure by comparison with literature data. Our result agrees within a factor of 2 with the Eigen and Kustin data. These in fact refer to 20°C, and kinetic $Q_5 = k_5/k_{-5}$ does not agree with equilibrium measurements at 25°C. In terms containing (k_5/k_{-5}) we have used the equilibrium value; otherwise, kinetic k_5 values were used. These results are summarized in Table 4, which gives the values of k_{13} and k_{14} obtained for various $n = (k_5^{fitted}/k_5^{lit})$, together with the corresponding standard deviations. The best fit is achieved with large n values; improvement by increasing n beyond 2 is only marginal, and therefore we have selected from our data: $k_5 = 0.33\ s^{-1}$ at pH = 1.66 (cf. $k_5^{lit} = 0.17\ s^{-1}$ as calculated from eq. [22]); $k_{13} = (0.31 \pm 0.11)\ mol^{-1}\ dm^3\ s^{-1}$; $k_{14} = (5.69 \pm 0.97) \times 10^8\ mol^{-1}\ dm^3\ s^{-1}$. The calculated standard deviations for k_{13} and k_{14} demonstrate that the rate is not overly sensitive to k_{13}, so that this parameter is affected by rather large error brackets.

In order to demonstrate that deviations from the assumed dependency on a given variable (F_{INAH}, F_{I^-}, or pH) are not blurred by the fitting to the given reaction scheme, we have taken advantage of the approximate validity of assumption [18] to plot k_{obsd}^{-1} vs. F_{INAH}^{-1} (at constant F_{I^-} and pH), $k_{obsd}^{-1}\,(Q_7^{-1}F_{I^-} + 1)^{-1}$ vs. F_{I^-} (at constant F_{INAH} and pH), and k_{obsd}^{-1} vs. $[H^+]\,(K_a + [H^+])$ (at constant F_{INAH} and F_{I^-}) to show the validity of eq. [23]–[25] which are obtained from [16], [17], and [18] by appropriate rearrangements, see Figs. 1–3.

$$[23]\quad \frac{1}{k_{obsd}} = \frac{1}{F_{INAH}}\left\{\frac{[H^+]\,\{K_a + [H^+]\}F_{I^-}\,(Q_7^{-1}F_{I^-} + 1)}{2k_{14}\,K_a\,Q_5}\right\} + \frac{(Q_7^{-1}F_{I^-} + 1)}{2k_5}$$

$$[24]\quad \frac{1}{k_{obsd}(Q_7^{-1}F_{I^-} + 1)} = F_{I^-}\left\{\frac{[H^+]\,\{K_a + [H^+]\}}{2k_{14}\,K_a\,Q_5\,F_{INAH}}\right\} + \frac{1}{2k_5}$$

$$[25]\quad \frac{1}{k_{obsd}} = [H^+]\,\{K_a + [H^+]\}\left\{\frac{F_{I^-}\,(Q_7^{-1}F_{I^-} + 1)}{2k_{14}\,K_a\,Q_5\,F_{INAH}}\right\} + \frac{(Q_7^{-1}F_{I^-} + 1)}{2k_5}$$

Values of k_{14} and k_5 from the slopes and intercepts are given in Table 5 as a check for internal consistency. The differences are related to the use of approximation [18]. Note in [25] that k_5 should in fact be pH dependent; however, a good straight line is found for a limited range in $[H^+]$ (Fig. 3).

Conversely, accepting [19], eq. [16] leads to [26] and [27]. From the intercepts and slopes of the corresponding linear plots, values of k_{14} and k_{13} are obtained (Table 6), which illustrate the errors involved in [19].

$$[26]\quad k_{obsd}\,(Q_7^{-1}F_{I^-} + 1) = \frac{1}{F_{I^-}}\left\{\frac{2k_{14}\,K_a\,Q_5\,F_{INAH}}{[H^+]\{K_a + [H^+]\}}\right\} + \frac{2k_{13}\,K_a\,F_{INAH}}{\{K_a + [H^+]\}}$$

$$[27]\quad k_{obsd}\,\{K_a + [H^+]\} = \frac{1}{[H^+]}\left\{\frac{2k_{14}\,K_a\,Q_5\,F_{INAH}}{F_{I^-}\,(Q_7^{-1}F_{I^-} + 1)}\right\} + \frac{2k_{13}\,K_a\,F_{INAH}}{(Q_7^{-1}F_{I^-} + 1)}$$

Our data indicate that both IOH and I_2 are capable of oxidizing INAH. The relative importance of both reagents is essentially dominated by the low concentrations of IOH in the pH range studied, as k_{14} approaches the diffusion controlled limit. The ratio $[k_{13}/(k_{13} + k_{14}k_5\,(k_{-5}\,F_{I^-}\,[H^+] + k_{14}\,[INAH])^{-1})]$ gives the fractions of INAH which is oxidized by I_2; this value is in the range 0.22–0.67, the highest value corresponding to the highest $[H^+][I^-]$ value used in this study.

Can. J. Chem. Downloaded from www.nrcresearchpress.com by 210.87.254.105 on 09/06/12
For personal use only.

Can. J. Chem. Downloaded from www.nrcresearchpress.com by 210.87.254.105 on 09/06/12
For personal use only.

TABLE 3. Dependency of k_{obsd} on F_{I^-}; $F_{INAH} = 2 \times 10^{-2}$ mol dm^{-3}; pH = 1.61; t = 24.9°C; I = 1 mol dm^{-3} (NaCl)

$k_{obsd} \times 10^4$ (s^{-1})	F_{I^-} (mol dm^{-3})
23.7	0.010
7.77	0.020
3.80	0.030
2.96	0.035
2.34	0.040

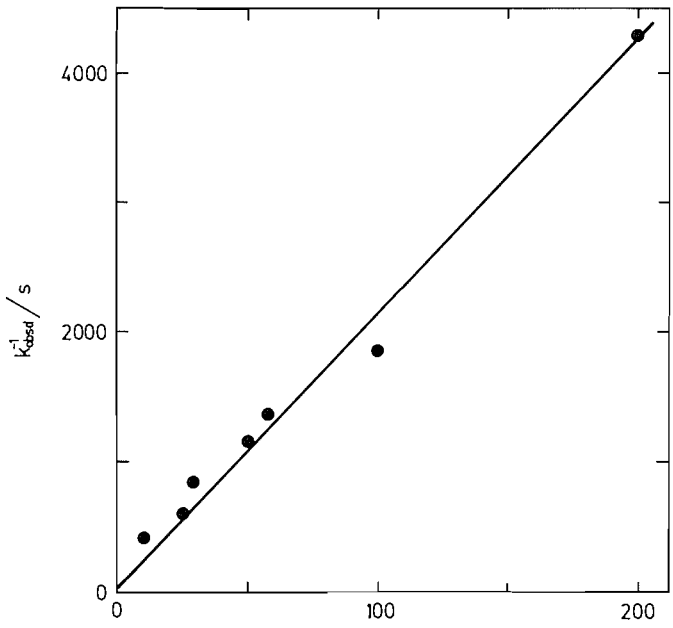

FIG. 1. k_{obsd}^{-1} as function of F_{INAH}^{-1}; $F_{I^-} = 2 \times 10^{-2}$ mol dm^{-3}; pH = 1.66; t = 24.9°C; I = 1 mol dm^{-3} (NaCl).

The value obtained for k_{14} is of the same order of magnitude as that calculated from Hasty's data (1) for:[3]

[28] $IOH + N_2H_4 \rightarrow$ products

This is reasonable in view of the high reactivity; it should be noted, however, that k_{14}, although close to the diffusion limit, is significantly below it. IOH discriminates between reacting with I^- ($+H^+$) and with R—NH—NH_2 in favour of the former for all our experimental conditions, where $[k_{-5} F_{I^-} [H^+]/k_{14} \times [INAH]] > 1$. On the other hand, it is interesting to note that under the conditions of the usual INAH titration procedure $k_{14}[INAH] > k_{-5} F_{I^-} [H^+]$, and thus the value of k_{obsd} (eq. [16]) would reduce to

$$[29] \quad k_{obsd} = 2[k_5 + k_{13} K_a F_{INAH} (K_a + [H^+])] (Q_7^{-1} F_{I^-} + 1)^{-1}$$

the IOH pathway being thus controlled by the hydrolysis of I_2 (eq. [5a]), and becoming zero order in INAH. It should also be noted that the values of the equilibrium quotients $Q_7 = (736)^{-1}$ and $Q_5 = 4.83 \times 10^{-13}$ are obtained from ref. 3, while $(k_7/k_{-7}) = (539)^{-1}$ and $(k_5/k_{-5}) = 6.82 \times 10^{-13}$ result from the

[3]From the data in Table 4 of ref. 1, the value $k_{28} = 2 \times 10^9$ mol dm^{-3} s^{-1} is obtained; this seems to be the correct value rather than that of 7×10^7 mol dm^{-3} s^{-1} later quoted in the same paper for $2k_{28}$.

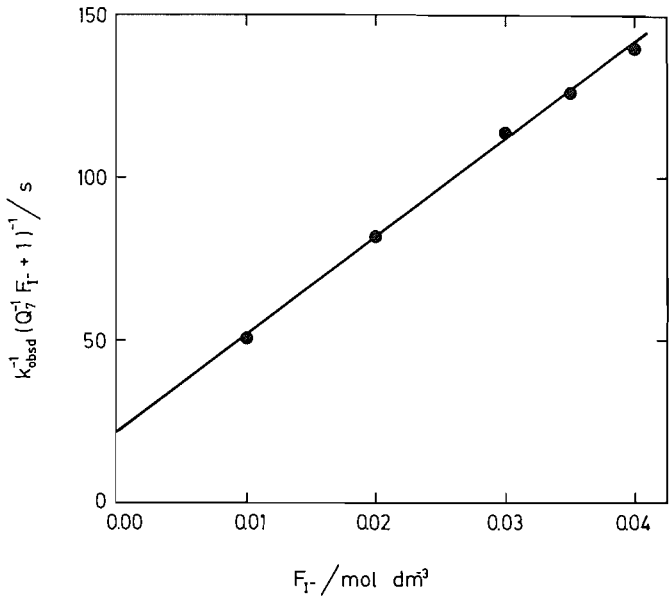

FIG. 2. $k_{obsd}^{-1} (Q_7^{-1} F_{I^-} + 1)^{-1}$ as function of F_{I^-}; $F_{INAH} = 2 \times 10^{-2}$ mol dm^{-3}; pH = 1.61; t = 24.9°C; I = 1 mol dm^{-3} (NaCl).

kinetic study of these reactions (8, 9). Furthermore, it has been suggested (3) that k_5 (and consequently k_5/k_{-5}) may be substantially larger. These errors are reflected directly in the value of k_{14}; we have chosen to use equilibrium data for Q_7 and Q_5 which are perhaps less uncertain, although sensitive to medium effects.

In part, the ambiguities in the interpretation of the data of the $I_2 + N_2H_4$ reaction arise from the pH dependency, which is consistent with either equilibrium [5] or [6].

In our system, replacement of one H by a nicotinoyl group allows us to avoid equilibrium [6] as a possible source of rate change with pH (protonation of the pyridine end is not likely to be of much influence); once the relevance of the R—NH—HN_3^+/R—NH—NH_2 equilibrium has been taken into account, it is still necessary to resort to a second pH-dependent equilibrium to explain our data, thus confirming the importance of IOH as oxidizer.

All the studies discussed thus far (including ours) yield information only on the composition of the activated state, in contrast with the information available for the oxidation of hydrazine with one-electron oxidants (known to take place via $N_2H_3^{\bullet}$ radicals or their organic analogs (10)). The nature of the species leading from R—NH—NH_2 to N_2 by reaction with I_2 is not known, but the very high ratios k_{14}/k_{13} (1.84×10^9 in our system, 2×10^9 in ref. 1) can be rationalized in terms of the following mechanism:

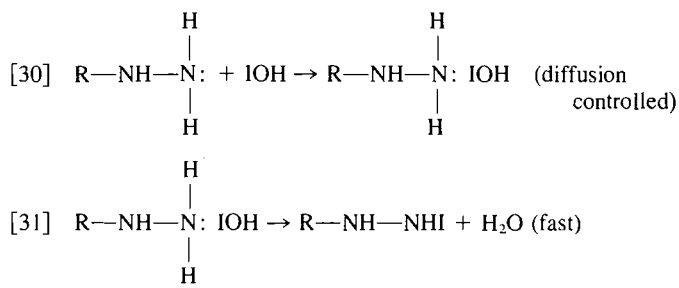

TABLE 4. Values of k_5, k_{13}, and k_{14} and their standard deviations from our experimental data

n*	$\sigma \times 10^4$ s^{-1}	k_{13} $mol^{-1}\ dm^3\ s^{-1}$	$\sigma_{k_{13}}$ $mol^{-1}\ dm^3\ s^{-1}$	$k_{14} \times 10^{-8}$ $mol^{-1}\ dm^3\ s^{-1}$	$\sigma_{k_{14}} \times 10^{-8}$ $mol^{-1}\ dm^3\ s^{-1}$
0.1	0.941	0.517	0.134	5.64	2.44
0.25	0.807	0.383	0.124	6.00	1.52
0.5	0.754	0.338	0.117	5.90	1.19
1	0.729	0.320	0.113	5.77	1.04
1.5	0.721	0.315	0.111	5.72	0.99
2	0.717	0.313	0.110	5.69	0.97

*$n = (k_5^{\text{fitted}}/k_5^{\text{lit}})$.

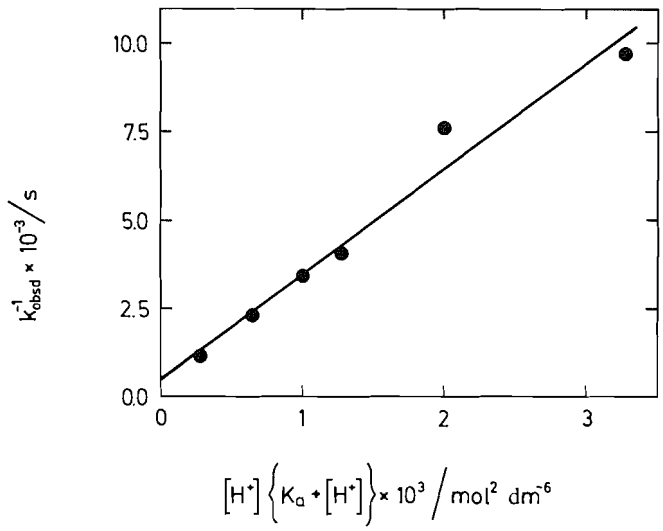

FIG. 3. k_{obsd}^{-1} as function of $[H^+]$ $(K_a + [H^+])$; $F_{INAH} = 2 \times 10^{-2}$ mol dm^3; $F_{I^-} = 3.5 \times 10^{-2}$ mol dm^3; $t = 24.9$°C; $I = 1$ mol dm^{-3} (NaCl).

TABLE 5. Estimations of k_{14} and k_5 from different sets of data, accepting approximation [18]

Equation	Variable	ρ	$k_{14} \times 10^{-8}$ $mol^{-1}\ dm^3\ s^{-1}$	k_5 s^{-1}
[23]	F_{INAH}	0.9954	8.75	0.25
[24]	F_{I^-}	0.9991	11.6	0.025
[25]	$[H^+]$	0.9835	11.5	0.025*

*See text. The nonlinear least-squares fitting method gives $k_{14} = (5.69 \pm 0.97) \times 10^8$ $mol^{-1}\ dm^3\ s^{-1}$.

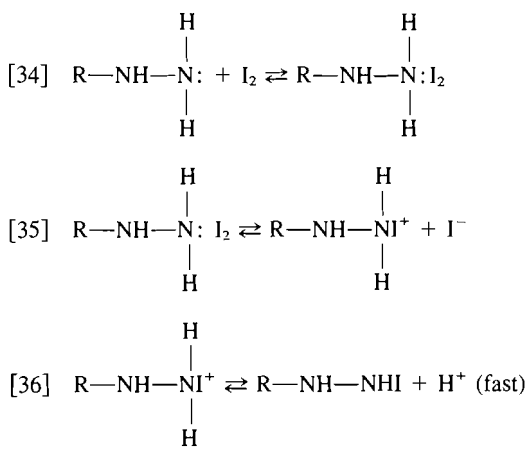

TABLE 6. Estimation of k_{14} and k_{13} from different sets of data, accepting approximation [19]*

Equation	Variable	ρ	$k_{14} \times 10^{-8}$ $mol^{-1}\ dm^3\ s^{-1}$	k_{13} $mol^{-1}\ dm^3\ s^{-1}$
[26]	F_{I^-}	0.9977	5.85	0.22
[27]	$[H^+]$	0.9879	7.50	0.12

*The nonlinear least-squares fitting method gives $k_{14} = (5.69 \pm 0.97) \times 10^8$ $mol^{-1}\ dm^3\ s^{-1}$ and $k_{13} = (0.31 \pm 0.11)$ $mol^{-1}\ dm^3\ s^{-1}$.

The slower rate of I_2 could be due either to (*a*) the lower electrophilicity of I_2 as compared to IOH, which would make [34] reversible, as compared to irreversible [30]; or (*b*) the more difficult evolution of the possible

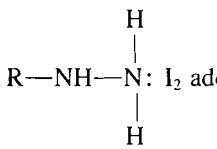

adduct (eq. [35]) as compared to

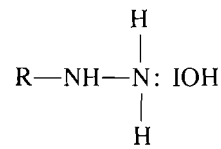

making more likely the reverse reaction [35].

In conditions of excess iodine, the stoichiometry of the initial reaction is described by eqs. [10] and [11]; thus, the analytical procedure for dosing INAH by I_2 according to ref. 6 prescribes a stoichiometry ratio $[I_2]/[INAH] = 1:1$ at 15-min reaction. By waiting longer, reaction [37] takes place:

[37] R-C(O)NH-NH(O)C-R + $2I_2$ + $2H_2O$ → 2R-C(O)OH + N_2 + $4I^-$ + $4H^+$

and therefore the ratio $[I_2]/[INAH] = 2:1$, as indicated for 90-min reaction in the U.S. Pharmacopaea (11). The kinetics of reaction [37] are currently being studied in our laboratories.

Acknowledgments

To CICPBA for partial support. M.A.B. is a member of CONICET.

1. R. A. HASTY. Z. Phys. Chem. Neue Folge (Frankfurt) **94**, 53 (1975).
2. S. E. KING, J. N. COOPER, and R. D. CRAWFORD. Inorg. Chem. **17**, 3306 (1978).
3. D. A. PALMER and M. H. LIETZKE. Radiochim. Acta, **31**, 37 (1982).

Can. J. Chem. Downloaded from www.nrcresearchpress.com by 210.87.254.105 on 09/06/12
For personal use only.

4. R. M. SMITH and A. E. MARTELL. Critical stability constants. Vol. 4. Plenum Press, New York. 1976. p. 43.
5. T. A. BAH and M. C. YEW. J. Singapore Natl. Acad. Sci. **6**, 24 (1977).
6. I. M. KOLTHOFF and R. BELCHER. Volumetric analysis. Vol. III. Interscience Publishers, Inc., New York. 1957. p. 401.
7. A. ALBERT. Nature, **177**, 525 (1956).
8. M. EIGEN and K. KUSTIN. J. Am. Chem. Soc. **84**, 1355 (1962).
9. O. E. MEYERS. J. Chem. Phys. **28**, 1027 (1958).
10. S. F. NELSEN. Acc. Chem. Res. **14**, 131 (1981).
11. THE UNITED STATES PHARMACOPAEA. 17th revision. 1965. p. 327.

Can. J. Chem. Downloaded from www.nrcresearchpress.com by 210.87.254.105 on 09/06/12
For personal use only.

Stereocontrolled synthesis of the C-1 to C-7 fragment of erythronolide A. A model study using the 1,7-dioxaspiro[5.5]undecane system

GILLES SAUVÉ,[1] DAVID A. SCHWARTZ, LUC RUEST, AND PIERRE DESLONGCHAMPS

Laboratoire de Synthèse Organique, Département de Chimie, Faculté des Sciences, Université de Sherbrooke, Sherbrooke (Qué.), Canada J1K 2R1

Received June 15, 1984

GILLES SAUVÉ, DAVID A. SCHWARTZ, LUC RUEST, and PIERRE DESLONGCHAMPS. Can. J. Chem. **62**, 2929 (1984).

Propionate spiroketal **6** has been prepared by two different methods. This compound was then converted into the substituted spiro[5.5]undecane **9** which contains five contiguous chiral centers which are found in the seco acid of erythronolide A.

GILLES SAUVÉ, DAVID A. SCHWARTZ, LUC RUEST et PIERRE DESLONGCHAMPS. Can. J. Chem. **62**, 2929 (1984).

On rapporte la synthèse du propionate spirocétalique **6** par deux méthodes différentes. Ce composé est par la suite transformé en dioxaspiro[5.5]undécane substitué **9** possédant cinq centres chiraux contigus que l'on retrouve dans l'acide seco de l'érythronolide A.

Can. J. Chem. Downloaded from www.nrcresearchpress.com by 210.87.254.5 on 09/06/12
For personal use only.

The macrolide antibiotics represent very appropriate target molecules to develop new strategies for the stereocontrolled synthesis of aliphatic chains containing several substituents and chiral centers. For instance, the total synthesis of erythromycin A has been reported by Woodward *et al.* (1) and several synthesis of the seco acid derivatives of erythronolide A (**1**) and B (**2**) have appeared in the literature (2) (Scheme 1).

A new strategy for the synthesis of erythromycin A and closely related macrolides has been developed in our laboratory.[2] This new approach to synthesis is based on the knowledge that the 1,7-dioxaspiro[5.5]undecane system is conformationally rigid, existing solely in conformation **4** (4, 5). In this conformation, steric effects are at their minimum and the acetal function has the maximum stabilizing stereoelectronic effects (3), i.e. two anomeric effects (6, 7). Consequently, the spiro system **4** can be viewed as an aliphatic chain (1,9-dihydroxyketone **5**) of nine carbon atoms that is locked rigidly in space by the acetal function; it can therefore be used as a template to introduce several chiral centers with a high degree of stereochemical control.

Erythromycin A was selected as a target molecule because its structure fits admirably well with the above strategy. Indeed, the seco acid **1** of erythronolide A can be viewed as an appropriately substituted "1,9-dihydroxyketone" which can be converted into the substituted 1,7-dioxaspiro[5.5]undecane **3** ($R^1 = R^2 = R^3 = H$) by internal acetalization. Compound **3** ($R^1 = R^2 = R^3 = H$) exists in the stereoelectronically preferred conformation **4** and most of the substituents are equatorially oriented. Thus, the spiro compound **3** ($R^1 = R^2 = R^3 = H$) has no undesirable strong steric interactions and it should be readily made from both erythromycin A and by total synthesis. The reconversion of **3** ($R^1 = R^2 = R^3 = H$) into erythromycin A would then complete the synthesis.[2]

The present work deals with the synthesis of the model compound **9** (Scheme 2), in which ring A is unsubstituted and ring B possesses the appropriate side chain at C-5 and the tertiary hydroxyl group at C-6 protected in the form of a benzyl ether.

The retrosynthetic analysis of compound **9** which contains five contiguous chiral centers is shown in Scheme 2; the main steps being (a) Claisen rearrangement of the allylic propionate (**6** → **7**), (b) hydration of the exomethylene double bond (iodolactonization followed by hydrogenolysis) (**7** → **8**), and (c) aldol condensation with methyl propionate (**8** → **9**). The preparation of spiro allylic propionate **6** and its successful conversion into compound **9** is reported in this article.

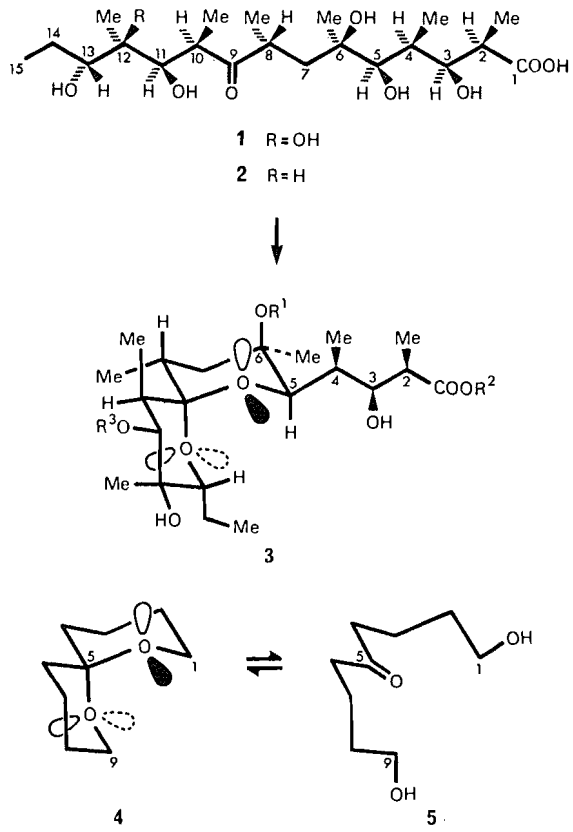

SCHEME 1

Results and discussion

Syntheses of spiroketal ester 6

The allylic propionate spiroketal **6** was synthesized by two different methods.[3] The first synthesis is shown in Scheme 3.

[1] Taken in part from the Ph.D. thesis of G. Sauvé, Université de Sherbrooke, 1981.

[2] For a previous discussion of this new synthetic approach, see pp. 330–333 in ref. 3.

[3] Several syntheses of spiro[5.5]undecane acetals have been reported in the literature; for examples, see ref. 8.

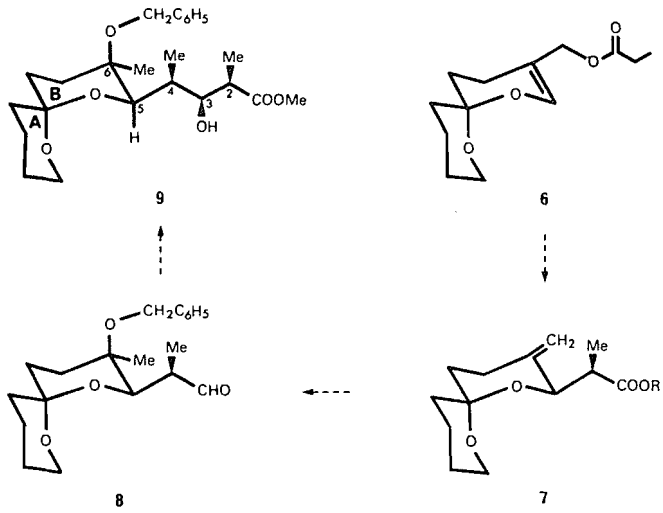

SCHEME 2

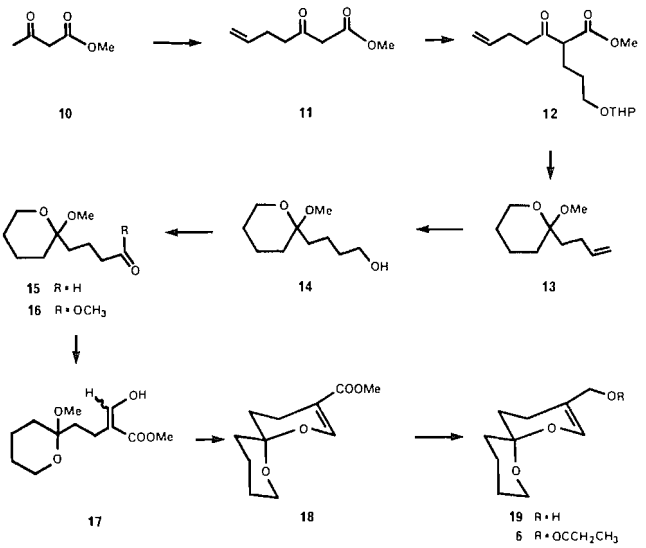

SCHEME 3

The disubstituted β-ketoester **12** was obtained by γ-alkylation of the dianion of methyl acetoacetate (**10**) with allyl bromide according to the method of Huckin and Weiler (9), followed by α-alkylation (10) of the monoanion of allyl-ketoester **11** with the tetrahydropyranyl derivative of 3-bromo-1-propanol. Decarboxylation of **12** in refluxing aqueous sodium hydroxide (11) and treatment of the crude ketone with *p*-toluenesulfonic acid in methanol containing methyl orthoformate gave the olefin cyclic acetal **13**. Hydroboration of **13** with borane – dimethyl sulfide complex (12) gave the hydroxy-acetal **14**, which was first converted into the aldehyde-acetal **15** by oxidation with Collins reagent (13) and then to the ester-acetal **16** by the reaction of ozone in basic methanolic solution (14). Hydroxymethylenation of ester-acetal **16** with methylformate (LDA) gave the crude hydroxymethylene ester **17**, which was cyclized with silica gel in methylene chloride to give the spiroketal unsaturated ester **18**. Finally, reduction of **18** with lithium aluminium hydride gave **19**, which was esterified with propionic anhydride ($(C_2H_5)_3N$ in CH_2Cl_2) to yield the allylic propionate spiroketal **6**. There are eleven steps in this synthesis and the overall yield is approximately 1%. A shorter route was therefore developed.

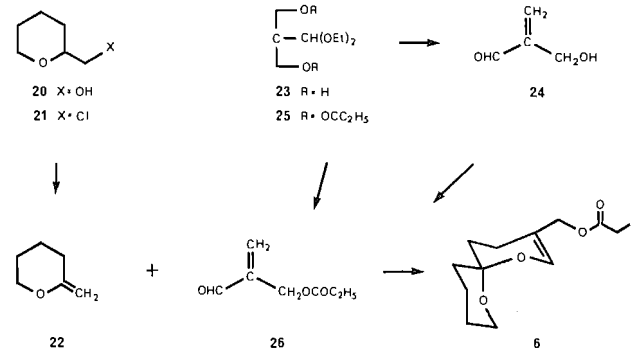

SCHEME 4

In the second synthesis, compound **6** was obtained via the Diels–Alder condensation of 2-methylenetetrahydropyran (**22**) with propenal-propionate **26** (Scheme 4). A similar cycloaddition has been previously reported between **22** and acrolein (15).

2-Methylenetetrahydropyran (**22**) was prepared by the method described by Taskinen (16): the readily available tetrahydropyranyl alcohol **20** was transformed ($SOCl_2$) into the chloride **21** (17), which was then treated with potassium hydroxide to give **22**. Propenal-propionate **26** was first produced by esterification with propionic anhydride of 2-hydroxymethyl-2-propenal (**24**), a known compound which is prepared from diol **23** (18). Diol **23** is readily available in three steps starting with dimethyl malonate (18). This sequence of operations was, however, not satisfactory due to the poor yield (~20%) in the conversion of **23** to **24**, the instability of the intermediate **24**, and the volatility of product **26**. The following modifications proved to be more satisfactory: (a) the diol **23** was acylated with propionic anhydride to give **25**, (b) the acetal function of **25** was then hydrolysed with formic acid (19) to give the corresponding aldehyde, which underwent an elimination of propionic acid on passing through a column of silica gel, yielding **26**.

The Diels–Alder reaction was carried out at room temperature by mixing 2-methylenetetrahydropyran (**22**) with the diene **26**, yielding the allylic propionate spiroketal **6** in 85% yield after distillation. This Diels–Alder route enabled us to prepare **6** in large scale and in only six steps from dimethyl malonate in 23% total yield.

Claisen rearrangement and lactonization

The allylic propionate spiroketal **6** was subjected to the Claisen rearrangement conditions developed by Ireland *et al.* (20) ((a) LDA, HMPA–THF, −78°C; (b) *t*-Bu$(CH_3)_2$SiCl, −78°C → 25°C; (c) NaOH–H_2O) to give a mixture of carboxylic acid **7** (R = H) and **27** (R = H) (Scheme 5) which on treatment with diazomethane yielded a 3:1 mixture of the two isomeric methyl esters **7** (R = CH_3) and **27** (R = CH_3). The mixture was used for the next operation. Saponification of **7** (R = CH_3) and **27** (R = CH_3) gave back the corresponding carboxylic acids which were transformed in high yield into a mixture of iodolactones **28** (X = I) and **29** (X = I) using standard experimental conditions (I_2, NaI, $NaHCO_3$, CH_3OH, H_2O, (21)). Hydrogenolysis of the iodolactone mixture with Raney nickel under a hydrogen atmosphere gave the two lactones **28** (X = H) and **29** (X = H) which were separated by chromatography on silica gel. The ^1H nmr spectrum of the major lactone **28** (X = H) shows a doublet (J = 1.0 Hz) at 3.79 ppm for the hydrogen at C-3. This small coupling is consistent with a dihedral angle close to 90° be-

Can. J. Chem. Downloaded from www.nrcresearchpress.com by 210.87.254.5 on 09/06/12
For personal use only.

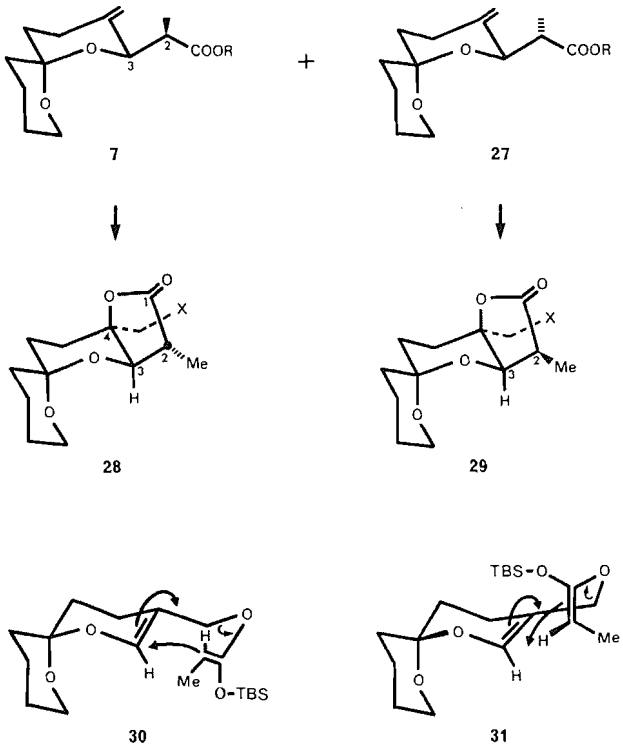

SCHEME 5

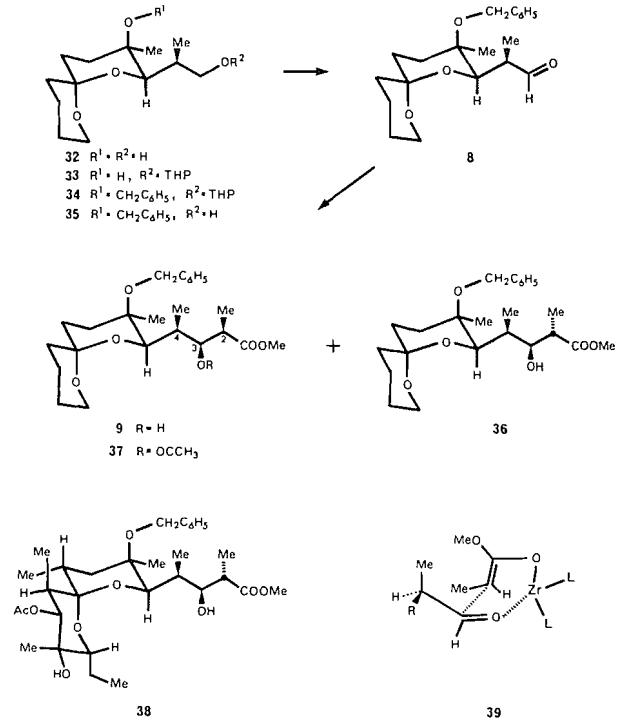

SCHEME 6

tween the hydrogens at C-3 and C-2. The ^{1}H nmr spectrum of the minor lactone **29** (X = H) shows a doublet (J = 4.4 Hz) at 3.93 ppm for the hydrogen at C-3. The magnitude of the coupling constant is in accord with the assigned stereochemistry.

The major lactone **28** (X = H) possesses the desired stereochemistry at the three contiguous chiral centers. The control of stereochemistry at C-4 is due to an internal process in which the formation of a *cis* five-membered lactone (**7** (R = H) → **28** (X = I)) is more favorable than that leading to a *trans* fused lactone. The internal Claisen rearrangement which must take place on the least hindered face of the cyclic enol ether double bond (**6** → **7**) controls the chiral center at C-3. Stereochemical control at C-2 is either due to the reaction of an *E*-enolate ion of the propionate ester via a chair-like transition state (cf. **30**) or by a *Z*-enolate reaction via a boat-like transition state (cf. **31**). Ireland *et al.* (22) have provided evidence that when a mixture of HMPA–THF is used, an *E*-enolate is preferentially formed. Consequently, the preferential formation of compound **7** (R = H) must have taken place through a transition state which has the stereochemistry illustrated by drawing **30**. In accord with this finding, when HMPA was omitted, a ~1:1 mixture of carboxylic acid **7** (R = H) and **27** (R = H) was observed.

Aldol condensation

The major lactone **28** (X = H) was first transformed into the required spiroaldehyde **8** (Scheme 6): reduction of lactone **28** (X = H) with lithium aluminium hydride gave the expected spirodiol **32** which on reaction with dihydropyran catalyzed by pyridinium *p*-toluenesulfonate (23) yielded the tetrahydropyranyl ether **33**. Treatment of **33** with sodium hydride and benzyl chloride in dimethylformamide gave the benzyl ether **34**, which was then hydrolysed to the corresponding spiroalcohol **35**. Finally, oxidation of **35** with pyridinium chlorochromate furnished the spiroaldehyde **8**.

The aldol condensation on spiroaldehyde **8** was carried out by utilizing the methodology originally developed by Evans and McGee (24). The zirconium enolate of methyl propionate was first prepared by the reaction of the lithium enolate of methyl propionate (LDA, THF) with bis(cyclopentadienyl) zirconium dichloride. The resulting solution was then added to the spiroaldehyde **8** to produce in a 8:1 ratio (62% yield) a mixture of the *erythro* and the *threo* products **9** and **36** respectively. Compounds **9** and **36** were separated by chromatography and the major *erythro* diastereoisomer **9** was converted into the corresponding acetate derivative **37**. The assignment of configuration at C-2 and C-3 in compounds **9** and **36** was made by high resolution ^{1}H nmr spectroscopic analysis, by comparison with compound **3** (R^1 = $CH_2C_6H_5$, R^2 = Me, R^3 = Ac) and its C-2 epimer **38** produced by degradation of erythromycin A.[2] Thus, following Evans' publication (24), the formation of the major *erythro* isomer **9** must be the result of a *pseudo*-boat transition state represented by drawing **39**.

The results obtained in this model study were then successfully applied for the total synthesis of erythromycin which is in progress in our laboratory.

Experimental

The ir spectra were taken on a Perkin–Elmer 257 spectrophotometer. The ultraviolet (uv) spectra were registered on a Varian Techtron 635 spectrophotometer. Proton nmr spectra were recorded on a Bruker WP-60 or Bruker WM-250 instrument. The following abbreviations have been used: s, singlet; d, doublet; d of d, doublet of doublet; t, triplet; m, multiplet; and br, broad. Chemical shifts are reported in δ values relative to tetramethylsilane as internal standard. The mass spectra (ms) were taken on a Hitachi–Perkin–Elmer RMU-6 and a Vg Micromass ZAB-2F mass spectrometer. Solutions were evaporated below 40°C under diminished pressure. Eastman chromagram plates of silica gel were used for thin-layer chromatography. Anhydrous sodium sulfate was used as the drying agent in working up reactions.

Can. J. Chem. Downloaded from www.nrcresearchpress.com by 210.87.254.5 on 09/06/12
For personal use only.

Can. J. Chem. Downloaded from www.nrcresearchpress.com by 210.87.254.5 on 09/06/12
For personal use only.

Disubstituted ketoester ***12***

A solution of sodium methoxide in methanol was prepared by adding sodium (900 mg, 39.1 mmol) to anhydrous methanol (50 mL). The allyl-ketoester **11** (5.0 g, 32 mmol), dissolved in dry methanol (15 mL), was added to the above solution. The solution was heated to gentle boiling during 10 min, then the tetrahydropyranyl 3-bromo-1-propanol derivative (prepared from 3-bromo-1-propanol and dihydropyran with acid catalyst) (8.24 g, 36.9 mmol) dissolved in dry methanol (15 mL) was added over a period of about 1 h and was refluxed for 18 h under an atmosphere of nitrogen. The mixture was cooled, filtered, and the filtrate was concentrated under reduced pressure to give an oil. This product was directly used for subsequent reactions. A small amount of the product was purified by preparative thin-layer chromatography on silica gel with hexane – ethyl acetate (9:1); ir ($CHCl_3$): 1740, 1710, and 1640 cm^{-1}; nmr ($CDCl_3$) δ: 5.60 (1H, m, olefinic proton), 4.90 (2H, m, olefinic protons), 4.55 (1H, br, OCHO), and 3.71 (3H, s, OCH_3); ms *m/e*: 198 ($M^+ - C_5H_8O_2$).

Olefin cyclic acetal ***13***

The crude disubstituted ketoester **12** was added to a solution of sodium hydroxide (1 *N*, 80 mL) and was refluxed for 20 h. After cooling, the reaction mixture was extracted with ether (5 × 40 mL). The organic phase was washed with saturated sodium chloride, dried, and evaporated. The residue, dissolved in anhydrous methanol (75 mL), was treated with *p*-toluenesulfonic acid (3 crystals) and methyl orthoformate (7.0 g, 66 mmol). The mixture was stirred at room temperature for 15 h under a nitrogen atmosphere. A saturated sodium bicarbonate solution (150 mL) was added and extracted with ether (5 × 75 mL). The organic extracts were dried over solid potassium carbonate and evaporated to an oil which was distilled under reduced pressure to yield pure olefin cyclic acetal **13** (1.5 g, 34% from **11**); bp 55°C, 0.5 Torr (1 Torr = 133.3 Pa); ir ($CHCl_3$): 1640 and 890 cm^{-1}; nmr ($CDCl_3$) δ: 5.90 (1H, m, olefinic proton), 4.90 (2H, m, olefinic protons), 3.15 (3H, s, OCH_3); ms *m/e*: 138 ($M^+ - HOCH_3$). *Mol. Wt.* (high resolution ms) calcd. for $C_{10}H_{18}O_2$: *m/e* 138.1044 ($M^+ - HOCH_3$); found: *m/e* 138.1042 ($M^+ - HOCH_3$).

Hydroxy-acetal ***14***

A solution of olefin cyclic acetal **13** (12.5 g, 73.5 mmol) in anhydrous tetrahydrofuran (300 mL) was cooled to 0°C and treated with borane – dimethylsulfide complex (5.60 g, 73.7 mmol) under a nitrogen atmosphere. The mixture was stirred for 1 h at 0°C and 1 h at room temperature. Then, after cooling to 0°C, sodium hydroxide solution (3 *N*, 100 mL) and hydrogen peroxide solution (30%, 100 mL) were added. The reaction mixture was stirred for 3 h at room temperature and extracted with ether (6 × 100 mL). The organic phase was dried with solid potassium carbonate, filtered, and evaporated to give crude hydroxy-acetal **14** (12.7 g), which was used without further purification; ir ($CHCl_3$): 3600 and 3450 cm^{-1}; nmr ($CDCl_3$) δ: 3.60 (4H, br, 2 × OCH_2), and 3.16 (3H, s, OCH_3).

Aldehyde-acetal ***15***

The hydroxy-acetal **14** (13.56 g, 72.0 mmol), dissolved in dichloromethane (10 mL), was added to a solution of chromium trioxide pyridine complex (13) (prepared from chromium trioxide (68.0 g, 0.68 mol) and pyridine (110 mL, 1.36 mol)) in the same solvent (700 mL) at 0°C. The reaction mixture was then stirred at room temperature for 30 min, decanted, and the salts were washed with ether (3 × 150 mL). The organic phase was washed with a sodium bicarbonate solution (5%, 150 mL) and saturated sodium chloride solution (400 mL). The organic extract was dried and evaporated. Distillation of the residue gave pure aldehyde-acetal **15** (6.90 g, 50% from olefin acetal **13**); bp 68°C, 0.15 Torr; ir ($CHCl_3$): 2820, 2720, and 1720 cm^{-1}; nmr ($CDCl_3$) δ: 9.60 (1H, t, J = 1.5 Hz, CHO), 3.10 (3H, s, OCH_3), and 2.40 (2H, br, CH_2CHO).

Ester-acetal ***16***

The aldehyde-acetal **15** (508 mg, 2.73 mmol) was dissolved in methanolic potassium hydroxide solution (0.5 *N*, 80 mL) and cooled to −78°C. Ozone was passed through the solution for 90 min and it was allowed to warm up to room temperature, then poured into water (75 mL), and extracted with ether (3 × 75 mL). The ether extract was washed with saturated sodium chloride solution (2 × 75 mL), dried over sodium carbonate, filtered, and evaporated to give ester-acetal **16** (325 mg, 55%) which was purified by distillation *in vacuo*; bp 75–78°C, 0.10 Torr; ir ($CHCl_3$): 1735 cm^{-1}; nmr ($CDCl_3$) δ: 3.67 (3H, s, CO_2CH_3), 3.18 (3H, s, OCH_3), and 2.40 (2H, m, $CH_2CO_2CH_3$); ms *m/e*: 184 ($M^+ - HOCH_3$).

Spiroketal unsaturated ester ***18***

n-Butyllithium (1.13 mL, 1.81 mmol, 1.6 *M* in hexane) was added dropwise to a solution of diisopropylamine (275 μL, 1.96 mmol) in tetrahydrofuran (10 mL) at 0°C under an atmosphere of nitrogen. After 15 min, the solution was cooled to −78°C and a solution of ester-acetal **16** (200 mg, 1.25 mmol) in tetrahydrofuran (10 mL) was added dropwise. After 30 min, methyl formate (225 mg, 3.73 mmol) was added and the reaction mixture was left at −78°C for 1 h, then at −20°C for 1 h, and finally at room temperature for 30 min. A saturated solution (20 mL) of ammonium chloride was added and the mixture was then extracted with ether (5 × 20 mL). The organic extract was washed with brine (25 mL), dried with sodium sulfate, filtered, and evaporated. The residue was added to a silica gel suspension in methylene chloride and stirred for 12 h. The silica gel was filtered, washed with ether, and the solvent was evaporated *in vacuo*. The residue was purified by preparative thin-layer chromatography on silica gel using ether–hexane (3.5:6.5) as eluant to yield pure spiroketal ester **18** (50 mg, 25%); uv (EtOH, 95%) λ_{max}: 237 nm (ε 11 500); ir ($CHCl_3$): 1700 and 1635 cm^{-1}; nmr (CD_2Cl_2) δ: 7.33 (1H, br s, olefinic proton), 3.54 (3H, s, OCH_3), and 2.15 (2H, m, allylic CH_2); ms *m/e*: 212 (M^+). *Mol. Wt.* (high resolution ms) calcd. for $C_{11}H_{16}O_4$: *m/e* 212.1048; found: *m/e* 212.1042.

Allylic alcohol ***19***

Lithium aluminium hydride (80.5 mg, 2.12 mmol) was added to a solution of spiroketal ester **18** (225 mg, 1.06 mmol) in anhydrous ether (10 mL) at 0°C. The mixture was stirred at 0°C for 2 h, then a saturated solution of sodium sulfate (10 mL) was added and extracted with ether (4 × 5 mL). Drying and evaporation of the organic phase gave crude allylic alcohol **19** (190 mg): ir ($CHCl_3$): 3600, 3420, and 1680 cm^{-1}; nmr ($CDCl_3$) δ: 6.36 (1H, s, olefinic proton), 3.99 (2H, s, CH_2OH), and 2.20 (2H, m, allylic CH_2).

Allylic propionate spiroketal ***6***

A solution of allylic alcohol **19** (194 mg, 1.05 mmol) in dry methylene chloride (25 mL) was treated at 0°C, under a nitrogen atmosphere, with propionic anhydride (1.60 mL, 12.6 mmol) and anhydrous triethylamine (4.5 mL, 32.3 mmol). The reaction mixture was stirred for 16 h and evaporated to give an oil (233 mg). An analytical sample of **6** was prepared by microdistillation *in vacuo*; ir ($CHCl_3$): 1740 and 1680 cm^{-1}; nmr ($CDCl_3$) δ: 6.39 (1H, s, olefinic proton), 4.46 (2H, s, CH_2OCOEt), 2.32 (2H, q, J = 7.5 Hz, $OCOCH_2CH_3$), 2.10 (2H, allylic CH_2), and 1.13 (3H, t, J = 7.3 Hz, $CO_2CH_2CH_3$); ms *m/e*: 240 (M^+).

2-Methylenetetrahydropyran (22)

The 2-chloromethyltetrahydropyran (**21**) (17) (60 g, 0.448 mol) was treated with potassium hydroxide powder (60 g, 1.07 mol) in a flask with Vigreux column and distillation head which was prewashed with potassium hydroxide solution and dried. The suspension was vigorously stirred and gradually heated to 190°C (the temperature of the distillation head must not exceed 110°C). The upper phase of the distillate containing the product **22** was redistilled under light vacuum and the distillate was collected at −78°C. Yield: 28.5 g (65%) of **21**; bp 62°C, 155 Torr; ir (neat): 3080 and 1655 cm^{-1}; nmr ($CDCl_3$) δ: 4.30 (1H, s, olefinic proton, *cis*), 4.03 (1H, s, olefinic proton, *trans*), 3.89 (2H, m, OCH_2), and 2.23 (2H, m, allylic CH_2).

Dipropionate ***25***

A solution of diol **23** (4.35 g, 24.4 mmol) in methylene chloride (25 mL) was treated with propionic anhydride (19 mL, 0.148 mol) and triethylamine (35 mL, 0.251 mol). The mixture was stirred for 15 h at room temperature under an atmosphere of nitrogen. It was then

Can. J. Chem. Downloaded from www.nrcresearchpress.com by 210.87.254.5 on 09/06/12
For personal use only.

diluted with ether (100 mL) and washed successively with sodium bicarbonate solution (5%, 2 × 50 mL) and with brine (2 × 50 mL). The organic phase was dried, filtered, and evaporated to an oil which was distilled under reduced pressure to yield pure dipropionate **25** (6.92 g, 98%); bp 126–128°C, 1 Torr; ir ($CHCl_3$): 1740 cm^{-1}; nmr ($CDCl_3$) δ: 4.52 (1H, d, J = 6.8 Hz, acetal CH), 4.38 and 4.15 (4H, AB part of ABX system, J_{AB} = 11 Hz, J_{AX} = 5.0 Hz, J_{BX} = 6.8 Hz, 2 × CH_2OCOEt), 3.64 and 3.55 (4H, 2q, J = 7.0 Hz, 2 × OCH_2CH_3), 2.33 (4H, q, J = 7.0 Hz, 2 × $O_2CCH_2CH_3$), 1.20 (6H, t, J = 7.0 Hz, 2 × OCH_2CH_3), and 1.13 (6H, t, J = 7.0 Hz, 2 × $O_2CCH_2CH_3$); ms m/e: 245 ($M^+ - OC_2H_5$).

Propenal-propionate ***26***

(a) *From 2-hydroxymethyl-2-propenal (**24**)*

A solution of 2-hydroxymethyl-2-propenal (**24**) (18) (75.0 mg, 0.872 mmol) in methylene chloride (4 mL) was treated, under a nitrogen atmosphere, at 0°C, with propionic anhydride (580 μL, 6.15 mmol) and dry triethylamine (1.22 mL, 8.75 mmol); the reaction mixture was stirred for 12 h at 0°C, and the solvent was evaporated. The residue was purified by thin-layer chromatography on silica gel with ether–hexane (4.5:5.5) to give pure propionate-propenal **26** (68.0 mg, 61%) as an oil; ir ($CHCl_3$): 3010, 2810, 2700, 1735, and 1695 cm^{-1}; nmr ($CDCl_3$) δ: 9.58 (1H, s, CHO), 6.44 (1H, s, olefinic proton, *cis*), 6.19 (1H, s, olefinic proton, *trans*), 4.82 (2H, s, allylic CH_2), 2.38 (2H, q, J = 7.2 Hz, $OCOCH_2CH_3$), and 1.14 (3H, t, J = 7.2 Hz, $CO_2CH_2CH_3$); ms m/e: 113 (M^+ − CHO).

(b) *From dipropionate **25***

Dipropionate **25** (2.95 g, 10.2 mmol) was dissolved in formic acid (30 mL) and stirred for 14 h at room temperature. Solvent was evaporated under reduced pressure and the product was purified by column chromatography on silica gel using hexane–ether (6:4) to give propionate-propenal **26** (1.20 g, 83%), identical with the material obtained from 2-hydroxymethyl-2-propenal (**24**).

Allylic propionate spiroketal ***6*** *from 2-methylenetetrahydropyran* ***22*** *and propenal-propionate* ***26***

A mixture of propenal-propionate **26** (2.30 g, 16.2 mmol) and 2-methylenetetrahydropyran (**22**) (6.5 g, 66.3 mmol) was heated for 5 h at 65°C. Evaporation of the excess **22** gave an oil which was distilled under reduced pressure to yield pure allylic propionate spiroketal **6** (3.30 g, 85%); bp 140°C, 0.2 Torr; identical with the material obtained from allylic alcohol **19**.

Claisen rearrangement of allylic propionate spiroketal ***6***

To a stirred solution of LDA (2.5 mmol) in hexamethylphosphoramide (1.0 mL) and tetrahydrofuran (2 mL) maintained at −70°C was added dropwise a solution of allylic propionate **6** (0.30 g, 1.25 mmol) in tetrahydrofuran (2 mL). The reaction mixture was stirred at −78°C for 0.5 h and a solution of *tert*-butyldimethylsilyl chloride (0.190 mg, 1.26 mmol) in tetrahydrofuran (1.5 mL) was added dropwise. Stirring was continued at −78°C for 3 h and at −30°C for 2 h. Water (20 mL) was added and the solution was extracted with ether (2 × 30 mL). The combined ethereal extracts were extracted back with sodium hydroxide solution (5%, 2 × 25 mL). The combined aqueous, basic extracts were acidified at 0°C with concentrated hydrochloric acid and extracted with ether (2 × 25 mL). The combined ethereal extracts were washed with dilute hydrochloric acid solution (0.5 N, 15 mL), dried over magnesium sulfate, filtered, and concentrated to yield 175 mg of a base-soluble product. The residue was dissolved in ether (20 mL) and treated with ethereal diazomethane. Evaporation of the ether gave an isomeric methyl ester mixture, **7** (R = CH_3) and **27** (R = CH_3) (159 mg, 50%; in a 3:1 ratio as determined from their 250-MHz ^1H nmr spectra), as a colourless oil after purification by chromatography on silica gel with hexane–ether (9:1) as the solvent; ir ($CHCl_3$): 3080, 1730 and 1655 cm^{-1}; nmr ($CDCl_3$) δ (2 isomers): 4.90, 4.75 and 4.83, 4.72 (2 × 2H, s, olefinic protons), 4.44 and 4.15 (2 × 1H, d, $J \simeq 7$ Hz, OCHR), 3.72 and 3.69 (2 × 3H, s, OCH_3), 3.65 (2 × 2H, m, OCH_2), 2.80 (2 × 1H, m, $CHCO_2R$), 2.20 (2 × 2H, m, allylic CH_2), and 1.31 and 1.25 (2 × 3H, d, $J \simeq 7$ Hz, $COOCH_3$); ms m/e: 254 (M^+). *Mol. Wt.* (high resolution ms) calcd. for $C_{14}H_{22}O_4$: m/e 254.1517; found: m/e 254.1514.

Hydrolysis of methyl esters ***7*** *(R = CH_3) and* ***27*** *(R = CH_3)*

The mixture of esters **7** (R = CH_3) and **27** (R = CH_3) (102 mg, 0.401 mmol) in dioxane (5 mL) was treated with a solution of sodium hydroxide (1 N, 2 mL) and stirred at room temperature for 12 h. Concentrated hydrochloric acid was added cautiously until a pH of 4 and then extracted with methylene chloride (6 × 15 mL). The organic phase was dried, filtered, and evaporated to give a mixture of acids, **7** (R = H) and **27** (R = H), as an oil (86 mg); ir ($CHCl_3$): 3300, 1715 and 1655 cm^{-1}; nmr ($CDCl_3$) δ (2 isomers): 10.5 (2 × 1H, br, CO_2H), 4.87 and 4.79 (2 × 2H, br s, olefinic protons), 2.91 (2 × 1H, q, J = 6.5 Hz, $CHCO_2$), 2.40 (2 × 2H, m, allylic CH_2), and 1.40 and 1.35 (2 × 3H, d, J = 7.0 Hz, $CH(CH_3)COOH$).

Iodolactonization of acids mixture ***7*** *(R = H) and* ***27*** *(R = H)*

To a solution of a mixture of acids **7** (R = H) and **27** (R = H) (95 mg, 0.396 mmol) and potassium bicarbonate (200 mg, 2.0 mmol) in methanol (7 mL) and water (3 mL) at 0°C were added potassium iodide (460 mg, 2.77 mmol) and iodine (240 mg, 0.945 mmol). The reaction mixture was stirred at 0°C for 2 h, then at room temperature for 12 h in darkness. Methylene chloride (50 mL) was added and the organic phase was washed successively with saturated sodium thiosulfate solution (20 mL) and brine (2 × 15 mL), then dried, filtered, and the solvent evaporated to give the crude iodolactones **28** (X = I) and **29** (X = I) as a mixture (135 mg); ir ($CHCl_3$): 1780 cm^{-1}; nmr ($CDCl_3$) δ (2 isomers): 4.25 and 4.04 (2 × 1H, d, J = 4.6 Hz and J = 2.7 Hz, OCH), 3.65 (2 × 2H, m, OCH_2), 3.45, 3.22, and 3.28 (2 × 2H, AB system, $J_{AB} \simeq 10$ Hz and s, CH_2I), and 1.45 and 1.27 (2 × 3H, d, J = 7.8 Hz and J = 7.0 Hz, CH_3).

Hydrogenolysis of iodolactones mixture ***28*** *(X = I) and* ***29*** *(X = I)*

To a solution of an epimeric mixture of iodolactones **28** (X = I) and **29** (X = I) (135 mg, 0.369 mmol) in ethanol (100 mL) was added Raney nickel (700 mg) and sodium bicarbonate (150 mg, 1.78 mmol). The reaction mixture was kept under an atmosphere of hydrogen (50 psi; 1 psi = 6.89 kPa) for 12 h with strong agitation. The suspension was filtered on silica gel and washed thoroughly with ethyl acetate, and the solvent was evaporated under reduced pressure to give a crude mixture of lactones **28** (X = H) and **29** (X = H) in a 3:1 ratio (determined from their 250-MHz ^1H nmr spectra). The crude product was purified by column chromatography with silica gel (hexane–ether, 9:1) to yield pure lactones **28** (X = H) (48.0 mg, 54%) and **29** (X = H) (16.0 mg, 18%).

Epimer ***28*** *(X = H)*: mp 52–54°C (ether–hexane); ir ($CHCl_3$): 1760 cm^{-1}; nmr ($CDCl_3$) δ: 3.79 (1H, d, J = 1.0 Hz, OCH), 3.66 (2H, m, OCH_2), 2.73 (1H, q, J = 8.0 Hz, $CHCO_2$), 1.43 (3H, d, J = 8.0 Hz, CH_3CHCO_2), and 1.41 (3H, s, CH_3); ms m/e: 240 (M^+). *Mol. Wt.* (high resolution ms) calcd. for $C_{13}H_{20}H_4$: m/e 240.1361; found: m/e 240.1346.

Epimer ***29*** *(X = H)*: mp 82–84°C (ether–hexane); ir ($CHCl_3$): 1760 cm^{-1}; nmr ($CDCl_3$) δ: 3.93 (1H, d, J = 4.4 Hz, OCH), 3.65 (2H, m, OCH_2), 2.97 (1H, d of q, J = 4.5 Hz, J = 7.0 Hz, $CHCO_2$), 1.33 (3H, s, CH_3), and 1.26 (3H, d, J = 7.5 Hz, CH_3CHCO_2); ms m/e: 240 (M^+). *Mol. Wt.* (high resolution ms) calcd. for $C_{13}H_{20}H_4$: m/e 240.1361; found: m/e 240.1359.

Spirodiol ***32***

Lactone **28** (X = H) (215 mg, 0.90 mmol), dissolved in anhydrous ether (6 mL), was added to a suspension of lithium aluminium hydride (53 mg, 1.39 mmol) in ether (10 mL) at 0°C under an atmosphere of nitrogen. The reaction mixture was stirred for 30 min at 0°C and then added to a saturated sodium sulfate solution (20 mL) and extracted with methylene chloride (4 × 25 mL). The organic phase was dried, the solvent evaporated, and the residue was purified by chromatography on silica gel. Spirodiol **32** (160 mg, 73%) was obtained by elution with hexane – ethyl acetate (7:3); mp 73–75°C; ir ($CHCl_3$): 3580 and 3440 cm^{-1}; nmr ($CDCl_3$) δ: 3.75 (1H, d, J = 2.5 Hz, OCH), 3.68 (2H, d, J = 5.3 Hz, CH_2OH), 1.18 (3H, s, CH_3 tertiary), and 1.13 (3H, d, J = 6.3 Hz, $CHCH_3$); ms m/e: 245. *Mol. Wt.* (high

Can. J. Chem. Downloaded from www.nrcresearchpress.com by 210.87.254.5 on 09/06/12
For personal use only.

resolution ms) calcd. for $C_{13}H_{24}O_4$: *m/e* 245.1753; found: *m/e* 245.1753.

Tetrahydropyranyl ether 33

A solution of spirodiol **32** (35.0 mg, 0.134 mmol) in methylene chloride (5 mL) was treated under an atmosphere of nitrogen with dihydropyran (46 mg, 0.55 mmol) and pyridinium *p*-toluenesulfonate (5 mg). After 4 h, additional dihydropyran (46 mg, 0.55 mmol) and pyridinium *p*-toluenesulfonate (5 mg) were added. The reaction was left for 30 min. Saturated sodium bicarbonate solution (15 mL) was added and the mixture was extracted with methylene chloride (4 × 15 mL). The dried organic phase was evaporated and the crude product was purified by column chromatography on silica gel using ether–hexane (5:5) as eluant to give pure tetrahydropyranyl ether **33** (32 mg, 69%); ir ($CHCl_3$): 3580 and 3450 cm^{-1}; nmr ($CDCl_3$) δ: 4.57 (1H, br, acetal proton), 1.16 (3H, s, $C(OH)CH_3$), and 1.06 (3H, d, J = 6.8 Hz, $CHCH_3$); ms *m/e*: 311 ($M^+ - OH$).

Benzyl ether 34

A solution of tetrahydropyranyl ether **33** (22 mg, 0.067 mmol) in dry *N,N*-dimethylformamide (4 mL) was treated with benzyl bromide (144 mg, 0.841 mmol) and sodium hydride (50% in oil, 55 mg, 1.14 mmol). The reaction mixture was stirred at 55°C for 2 h under an atmosphere of nitrogen, then cooled to 0°C, poured into a saturated sodium bicarbonate solution (15 mL), and extracted with methylene chloride (4 × 20 mL). The organic extracts were dried and evaporated. The residue was purified by preparative thin-layer chromatography on silica gel using ether–hexane (3.5:6.5) as eluent to yield pure benzyl ether **34** (19 mg, 68%); ir ($CHCl_3$): 1600, 1490, 1450, and 710 cm^{-1}; nmr ($CDCl_3$) δ: 7.32 (5H, br, aromatic), 4.63 (1H, br, acetal proton), 4.43 (2H, s, $OCH_2C_6H_5$), 1.19 (3H, s, CH_3 tertiary), and 1.10 (3H, d, J = 6.8 Hz, $CHCH_3$); ms *m/e*: 333 ($M^+ - C_5H_9O$).

Spiroalcohol 35

To a solution of benzyl ether **34** (16 mg, 0.038 mmol) in 1,2-dimethoxy ethane (2.5 mL) was added water (5 drops) and hydrochloric acid (1 *N*, 10 drops). The reaction mixture was stirred at room temperature for 1 h and at 50°C for 45 min. After cooling, saturated sodium bicarbonate solution (15 mL) was added and extracted with methylene chloride (4 × 25 mL). The organic extracts were dried and evaporated to leave an oily residue which was purified by thin-layer chromatography on silica gel using ether–hexane (3.5:6.5) as an eluent; after 5 elutions the pure spiroalcohol **35** was obtained in 63% yield (8.0 mg); ir ($CHCl_3$): 3520, 3480, 1600 and 1450 cm^{-1}; nmr ($CDCl_3$) δ: 7.27 (5H, br, aromatic), 4.37 (2H, s, $OCH_2C_6H_5$), 1.16 (3H, s, CH_3 tertiary), and 1.10 (3H, d, J = 7.2 Hz, $CHCH_3$); ms *m/e*: 334 (M^+). *Mol. Wt.* (high resolution ms) calcd. for $C_{20}H_{30}O_4$: *m/e* 334.2144; found: *m/e* 334.2144.

Spiroaldehyde 8

Pyridinium chlorochromate (25 mg, 0.116 mmol) and pulverized molecular sieves 3 Å (~20 mg) were added to a solution of spiroalcohol **35** (8.0 mg, 0.024 mmol) in methylene chloride (5 mL). The reaction mixture was stirred at room temperature for 1 h, then the suspension was filtered through a column of silica gel and washed thoroughly with ether. Evaporation of the solvent gave pure spiroaldehyde **8** (7.5 mg, 94%); ir ($CHCl_3$): 2870, 2720, 1720, 1600, 1495, and 1450 cm^{-1}; nmr ($CDCl_3$) δ: 9.72 (1H, d, J = 1.5 Hz, CHO), 7.26 (5H, br, aromatic), 4.36 (2H, s, $OCH_2C_6H_5$), 3.94 (1H, d, J = 4.0 Hz, OCH), 2.70 (1H, m, *CH*CHO), 1.26 (3H, d, J = 7.2 Hz, $CHCH_3$), and 1.13 (3H, s, CH_3 tertiary); ms *m/e* 331 ($M^+ - H$).

Aldol condensation of spiroaldehyde 8

(a) *Preparation of zirconium enolate reagent solution*

n-Butyllithium (620 μL, 1.6 *M* in hexane, 0.992 mmol) was added dropwise to a solution of diisopropylamine (115 mg, 1.14 mmol) in tetrahydrofuran (10 mL) at 0°C under an atmosphere of nitrogen. After 15 min at 0°C, the solution was cooled to −78°C and methyl propionate (79 mg, 0.894 mmol) was added dropwise. After 30 min, a solution of bis(cyclopentadienyl) zirconium dichloride (290 mg, 0.992 mmol) in tetrahydrofuran (6 mL) was added and the reaction mixture was left at −78°C for 10 min, at −40°C for 10 min, and at room temperature for 30 min. This zirconied reagent (0.0558 *M*), used in the following aldol condensation, has a light yellow color.

(b) *Aldol condensation conditions*

A solution of spiroaldehyde **8** (18.0 mg, 0.054 mmol) in tetrahydrofuran (2 mL) at −78°C under an atmosphere of nitrogen was treated dropwise with a freshly prepared zirconied enolate solution (2.4 mL, 0.0558 *M* in tetrahydrofuran, 0.13 mmol; see above). The reaction mixture was stirred for 2 h at −78°C, then for 1 h at −50°C, and quenched with saturated ammonium chloride solution (10 mL). The mixture was extracted with methylene chloride (4 × 10 mL). The dried organic phase was evaporated and the crude product was purified by thin-layer chromatography on silica gel using hexane – ethyl acetate (7:3) to give *erythro* **9** (12.5 mg, 55%), *threo* **36** (1.5 mg, 7%), and starting material **8** (5 mg).

Erythro 9; ir ($CHCl_3$): 3500, 1735, 1500, and 1450 cm^{-1}; nmr ($CDCl_3$) δ: 7.32 (5H, m, aromatic), 4.43 and 4.37 (2H, AB system, J_{AB} = 11.5 Hz, $OCH_2C_6H_5$), 3.89 (1H, d of d, $J_{3,4}$ = 1.3 Hz, $J_{2,3}$ = 9.3 Hz, H-C3), 3.71 (1H, d, $J_{4,5}$ = 1.8 Hz, H-C5), 3.67 (3H, s, OCH_3), 2.69 (1H, d of q, J = 7.0 Hz, $J_{2,3}$ = 9.3 Hz, H-C2), 1.90 (1H, m, H-C4), 1.28 (3H, d, J = 7.0 Hz, CH_3-C2), 1.18 (3H, s, CH_3 tertiary), and 1.15 (3H, d, J = 7.0 Hz, CH_3-C4); ms *m/e*: 389 ($M^+ - OCH_3$). *Mol. Wt.* (high resolution ms) calcd. for $C_{24}H_{36}O_6$: *m/e* 389.2328 ($M^+ - OCH_3$); found: *m/e* 389.2333 ($M^+ - OCH_3$).

Threo 36; ir ($CHCl_3$): 3500, 1735, 1600, 1500, and 1450 cm^{-1}; nmr ($CDCl_3$) δ: 7.26 (5H, m, aromatic), 4.44 and 4.39 (2H, AB system, J_{AB} = 11.6 Hz, $OCH_2C_6H_5$), 4.08 (1H, d, $J_{4,5}$ = 1.3 Hz, H-C5), 3.80 (1H, m, $J_{2,3}$ = 7.2 Hz, $J_{3,4}$ = 6.5 Hz, H-C3), 3.70 (3H, s, OCH_3), 2.73 (1H, m, H-C2), 1.95 (1H, m, H-C4), 1.22 (3H, d, J = 7.1 Hz, CH_3-C2), 1.19 (3H, s, CH_3 tertiary), and 1.14 (3H, d, J = 7.0 Hz, CH_3-C4); ms *m/e*: 389 ($M^+ - OCH_3$). *Mol. Wt.* (high resolution ms) calcd. for $C_{24}H_{36}O_6$: *m/e* 389.2328 ($M^+ - OCH_3$); found: *m/e* 389.2333 ($M^+ - OCH_3$).

Acetate 37

A solution of *erythro* **9** (13.0 mg, 0.039 mmol) in anhydrous triethylamine (2 mL) was treated with acetic anhydride (108 mg, 1.06 mmol) and 4-dimethylamino pyridine (1 crystal). The reaction mixture was stirred for 3 h at room temperature under an atmosphere of nitrogen, then the solvent was evaporated under reduced pressure. The residue was purified by thin-layer chromatography on silica gel using benzene–ether (8:2) to give acetate **37** (11 mg; 77%); ir ($CHCl_3$): 1740, 1600, 1500, and 1450 cm^{-1}; nmr ($CDCl_3$) δ: 7.31 (5H, m, aromatic), 5.38 (1H, d of d, $J_{3,4}$ = 6.9 Hz, $J_{2,3}$ = 5.4 Hz, H-C3), 4.44 and 4.39 (2H, AB system, J_{AB} = 11.7 Hz, $OCH_2C_6H_5$), 3.62 (3H, s, CO_2CH_3), 3.44 (1H, d, $J_{4,5}$ = 2.4 Hz, H-C5), 2.90 (1H, d of q, $J_{2,3}$ = 5.4 Hz, J = 7.0 Hz, H-C2), 2.34 (1H, m, H-C4), 2.06 (3H, s, CH_3CO_2), 1.20 (3H, s, CH_3 tertiary), 1.14 (3H, d, J = 7.0 Hz, CH_3-C2), and 1.09 (3H, d, J = 7.0 Hz, CH_3-C4); ms *m/e*: 431 ($M^+ - OCH_3$).

Acknowledgements

Support for this work by the Natural Sciences and Engineering Research Council of Canada (NSERCC) and by the Ministère de l'Éducation, Québec, is gratefully acknowledged.

1. R. B. WOODWARD, E. LOGUSCH, K. P. NAMBIAR, K. SAKAN, D. E. WARD, B.-W. AU-YEUNG, P. BALARAM, L. J. BROWNE, P. J. CARD, C. H. CHEN, R. B. CHÊNEVERT, A. FLIRI, K. FROBEL, H.-J. GAIS, D. G. GARRATT, K. HAYAKAWA, W. HEGGIE, D. P. HENSSON, D. HOPPE, I. HOPPE, J. A. HYATT, D. IKEDA, P. A. JACOBI, K. S. KIM, Y. KOBUKE, K. KOJIMA, K. KROWICKI, V. J. LEE, T. LEUTERT, S. MALCHENKO, J. MARTENS, R. S. MATTHEWS, B. S. ONG, J. B. PRESS, T. V. RAJAN BABU, G. ROUSSEAU, H. M. SAUTER, M. SUZUKI, K. TATSUTA, L. M. TOLBERT, E. A. TRUESDALE, I. UCHIDA, Y. UEDA, T. UYEHARA, A. T. VASELLA, W. C. VLADUCHICK, P. A. WADE,

R. M. WILLIAMS, and H. N.-C. WONG. J. Am. Chem. Soc. **103**, 3210 (1981); **103**, 3213 (1981); **103**, 3215 (1981).
2. E. J. COREY, P. B. HOPKINS, S. KIM, S.-E. YOO, K. P. NAMBIAR, and J. R. FALCK. J. Am. Chem. Soc. **101**, 7131 (1979); E. J. COREY, S. KIM, S.-E., YOO, K. C. NICOLAOU, L. S. MELVIN, JR., D. J. BRUNELLE, J. R. FALCK, E. J. TRYBULSKI, R. LETT, and P. W. SHELDRAKE. J. Am. Chem. Soc. **101**, 4618 (1978); **101**, 4620 (1978); S. MASAMUNE, M. HIRAMA, S. MORI, S. ASROF ALI, and D. S. GARVEY. J. Am. Chem. Soc. **103**, 1568 (1981); G. STORK, I. PATERSON, and F. K. C. LEE. J. Am. Chem. Soc. **104**, 4686 (1982).
3. P. DESLONGCHAMPS. Stereoelectronic effects in organic chemistry. Organic Chemistry Series. Vol. 1. Pergamon Press, Oxford, England. 1983.
4. P. DESLONGCHAMPS, D. D. ROWAN, N. POTHIER, G. SAUVÉ, and J. K. SAUNDERS. Can. J. Chem. **59**, 1105 (1981).
5. N. POTHIER, D. D. ROWAN, P. DESLONGCHAMPS, and J. K. SAUNDERS. Can. J. Chem. **59**, 1132 (1981).
6. R. U. LEMIEUX. Tetrahedron, **30**, 1933 (1974), and references quoted therein.
7. A. J. KIRBY. The anomeric effect and related stereoelectronic effects at oxygen. Springer Verlag, Berlin. 1983.
8. S. V. LEY and B. LYGO. Tetrahedron Lett. **25**, 113 (1984); A. P. KOZIKOWSKI and J. G. SCRIPKO. J. Am. Chem. Soc. **106**, 353 (1984); I. T. KAY and E. G. WILLIAMS. Tetrahedron Lett. **24**, 5915 (1983); M. T. CRIMMINS and D. M. BANKAITIS. Tetrahedron Lett. **24**, 4551 (1983); P. KOCIENSKI and C. YEATES. Tetrahedron Lett. **24**, 3905 (1983); D. R. WILLIAMS and B. A. BARNER. Tetrahedron Lett. **24**, 427 (1983); R. BAKER, R. H. O. BOYES, D. M. P. BROOM, J. A. DEVLIN, and C. M. SWAIN. J. Chem. Soc. Chem. Commun. 829 (1983); S. J. DANISHEFSKY and W. H. PEARSON. J. Org. Chem. **48**, 3865 (1983); R. E. IRELAND and J. P. DAUB. J. Org. Chem. **48**, 1303 (1983); R. E. IRELAND, J. P. DAUB, G. S. MANDEL, and N. S. MANDEL. J. Org. Chem. **48**, 1312 (1983); H. REDLICH and B. SCHNEIDER. Justus Liebigs Ann. Chem. 412 (1983); D. R. WILLIAMS, B. A. BARNER, K. NISHITANI, and J. G. PHILLIPS. J. Am. Chem. Soc. **104**, 4708 (1982); A. B. SMITH III, S. R. SCHOW, J. D. BLOOM, A. S. THOMPSON, and K. N. WINZENBERG. J. Am. Chem. Soc. **104**, 4015 (1982); S. V. ATTWOOD, A. G. M. BARRETT, and J.-C. FLORENT. J. Chem. Soc. Chem. Commun. 556 (1981); T. R. HOYE, D. R. PECK, and P. K. TRUMPER. J. Am. Chem. Soc. **103**, 5618 (1981); R. BAKER, R. HERBERT, P. E. HOWSE, and O. T. JONES. J. Chem. Soc. Chem. Commun. 52 (1980); C. PHILLIPS, R. JACOBSON, B. ABRAHAMS, H. J. WILLIAMS, and L. R. SMITH. J. Org. Chem. **45**, 1920 (1980); E. HUNGERBUNLER, R. NAEF, D. WASMUTH, D. SEEBACH, H.-R. LOOSLI, and A. WEHRLI. Helv. Chim. Acta, **63**, 1960 (1980); D. A. EVANS, C. E. SACKS, W. A. KLESCHICK, and T. R. TABER. J. Am. Chem. Soc. **101**, 6789 (1979); T. M. CRESP, C. L. PROBERT, and F. SONDHEIMER. Tetrahedron Lett. 3955 (1978); J. C. CHABALA and J. E. VINCENT. Tetrahedron Lett., 937 (1978).
9. S. N. HUCKIN and L. WEILER. J. Am. Chem. Soc. **96**, 1082 (1974).
10. C. S. MARVEL and F. D. HAGER. Org. Synth. Coll. Vol. I. John Wiley and Sons, New York. 1958. p. 248.
11. U. JOSS and H. SCHALTEGGER. Helv. Chim. Acta, **52**, 2465 (1969).
12. H. C. BROWN, A. K. MANDAL, and S. U. KULKARNI. J. Org. Chem. **42**, 1392 (1977).
13. J. C. COLLINS. Tetrahedron Lett. 3363 (1968).
14. P. SUNDARARAMAN, E. C. WALKER, and C. DJERASSI. Tetrahedron Lett. 1627 (1978).
15. R. PAUL and S. TCHELITCHEFF. Bull. Soc. Chim. Fr. 672 (1954); R. E. IRELAND and D. HABICH. Tetrahedron Lett. **21**, 1389 (1980).
16. E. TASKINEN. Ann. Acad. Sci. Fenn. Ser. A, **163**, 3 (1972).
17. J. J. TUFARIELLO and E. J. TRYBULSKI. J. Org. Chem. **39**, 3378 (1974).
18. J.-E. VIK. Acta Chem. Scand. **27**, 239 (1973).
19. A. GORGUES. Bull. Soc. Chim. Fr. 529 (1974).
20. R. E. IRELAND and J.-P. VEVERT. J. Org. Chem. **45**, 4259 (1980); R. E. IRELAND and J. P. DAUB. J. Org. Chem. **46**, 479 (1981).
21. C. S. RONDESTVEDT and C. D. VER NOOY. J. Am. Chem. Soc. **77**, 4878 (1955).
22. R. E. IRELAND, R. H. MUELLER, and A. K. WILLARD. J. Am. Chem. Soc. **98**, 2868 (1976).
23. M. MIYASHITA, A. YOSHIKOSHI, and P. A. GRICO. J. Org. Chem. **42**, 3772 (1977).
24. D. A. EVANS and L. R. MCGEE. Tetrahedron Lett. **21**, 3975 (1980); J. Am. Chem. Soc. **103**, 2876 (1981).

Can. J. Chem. Downloaded from www.nrcresearchpress.com by 210.87.254.5 on 09/06/12
For personal use only.

A simple method of preparing trimethylsilyl- and *tert*-butyldimethylsilyl-enol ethers of α-diazoacetoacetates and their use in the synthesis of a chiral precursor to thienamycin analogs

YASUTSUGU UEDA,[1] GUY ROBERGE,[2] AND VIVIANE VINET

Bristol Laboratories of Canada, 100 Industrial Boulevard, Candiac, P.Q., Canada J5R 1J1

Received June 1, 1984

YASUTSUGU UEDA, GUY ROBERGE, and VIVIANE VINET. Can. J. Chem. **62**, 2936 (1984).

A simple method of preparing trimethylsilyl- and *tert*-butyldimethylsilyl-enol ethers of various esters of α-diazoacetoacetic acid is described. Displacement reaction of 4-acetoxyazetidinone **8** with *tert*-butyldimethylsilylenol ethers **7***a*, followed by desilylation, afforded the key chiral precursor **2***a* for the synthesis of thienamycin analogs.

YASUTSUGU UEDA, GUY ROBERGE et VIVIANE VINET. Can. J. Chem. **62**, 2936 (1984).

On décrit une méthode simple de préparer des éthers énoliques triméthylsilylés et *tert*-diméthylsilylés de divers esters de l'acide α-diazoacétoacétique. La réaction de substitution de l'acétoxyazétidinone (**8**) par les éthers énoliques *tert*-butyldiméthylsilyles (**7***a*), suivie d'une réaction de désilylation, conduit au précurseur chiral **2***a* qui est un produit clé dans la synthèse d'analogues de la thiènamycine.

[Traduit par le journal]

Since the discovery of thienamycin **1** (R = $CH_2CH_2NH_2$), intense efforts have been directed toward the synthesis of thienamycin analogs **1** (1). While many methods are available for carbapenem synthesis, the most widely used process goes through a common intermediate, diazoazetidinone **2** (2, 3).

Recently two groups of scientists reported (3*a*, *b*) elegant ways of constructing this type of intermediate by direct introduction of the α-diazoacetoacetate moiety into the 4-position of 2-azetidinones. Karady *et al.* (3*a*) described the preparation of a chiral diazo intermediate **2** (R = CH_2Ph) by the displacement reaction of an optically active 4-chloroazetidinone **3** (R = Si*t*BuMe$_2$, X = Cl) with trimethylsilylenol ether of benzyl α-diazoacetoacetate (**4**) in the presence of silver tetrafluoroborate followed by desilylation. Similarly Reider and Grabowski (3*b*) employed a displacement reaction (4) of a chiral 4-acetoxyazetidinone **3** (R = H, X = OAc) with **4** in the presence of Lewis acid (zinc iodide) for their synthesis of an optically active diazoazetidinone **2** (R = CH_2Ph).

In both cases, the α-diazoacetoacetate unit they employed carried a benzyl group to protect the carboxylic acid. Although the benzyl ester is reported (3*a*) to be useful as a carboxyl protecting group, it has been recognized (2) and recently demonstrated (2*e*) that the *p*-nitrobenzyl ester is far superior to the benzyl ester in the synthesis of thienamycin analogs.

Karady *et al.* prepared trimethylsilylenol ether of benzyl α-diazoacetoacetate (**4**) from benzyl α-diazoacetoacetate (**5**, R = CH_2Ph) by generating the enolate with a strong base such as lithium hexamethyldisilazide, followed by trapping with trimethylsilyl chloride. While successful for the benzyl ester, unfortunately this method, which required a strong base, was not compatible with the *p*-nitrobenzyl ester, producing an intractable mixture with only a little of the desired material **6***a* (Scheme 1).

Here we wish to report (1) a facile preparation of trimethylsilylenol ether and *tert*-butyldimethylsilylenol ether of *p*-nitrobenzyl α-diazoacetoacetate (**6***a* and **7***a*) as well as some other corresponding esters (**6***b*−**6***d* and **7***b*−**7***d*), and (2) subsequent synthesis of a chiral carbapenem intermediate **2** (R = $-CH_2-C_6H_4-NO_2$) as shown in Scheme 1.

Thus, the trimethylsilylenol ether of *p*-nitrobenzyl α-diazoacetoacetate (**6***a*) was prepared in good yield from *p*-nitrobenzyl α-diazoacetoacetate (**5***a*)[3] by using trimethylsilyl trifluoromethanesulfonate as a silylating agent (5*a*) and triethylamine as a base. The reaction was complete within a few minutes in CH_2Cl_2 at 0−5°C. Although several other methods are available for the preparation of silylenol ethers (5*b*, *c*), we find this method simplest and most successful for the preparation of **6***a*. The structural assignment of this silylenol ether was made by means of its ^{1}Hmr spectrum, which showed disappearance of the acetyl group at 2.50 ppm (in compound **5***a*) and appearance of two sharp doublets at 4.23 and 4.93 ppm with a coupling constant of 2 Hz for the vinyl protons.

Although readily prepared, the trimethylsilylenol ether was somewhat labile and easily hydrolyzed to *p*-nitrobenzyl α-diazoacetoacetate (**5***a*) on contact with water or simply atmospheric moisture, thereby creating difficulty in handling. To overcome this problem, we prepared the corresponding *tert*-butyldimethylsilylenol ether **7***a* by the method described above using *tert*-butyldimethylsilyl trifluoromethanesulfonate (7) in place of trimethylsilyl trifluoromethanesulfonate (see Scheme 1). In contrast to the trimethylsilylenol ether **6***a*, the *tert*-butyldimethylsilylenol ether **7***a* was more stable towards neutral water, permitting aqueous work-up. The *tert*-butyldi-

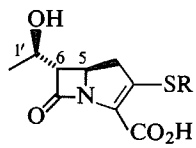

1

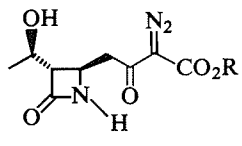

2

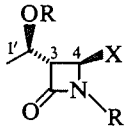

3

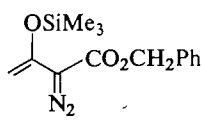

4

[1]Author to whom all correspondence should be addressed, c/o Pharmaceutical Research and Development Division, Bristol−Myers Company, Syracuse, NY 13221, U.S.A.

[2]Holder of NSERC Industrial Fellowship (1981−1986).

[3]All esters of α-diazoacetoacetic acid described here were prepared from the corresponding acetoacetate esters by the method of Regitz (6) (see Experimental).

Can. J. Chem. Downloaded from www.nrcresearchpress.com by 210.87.254.42 on 09/06/12
For personal use only.

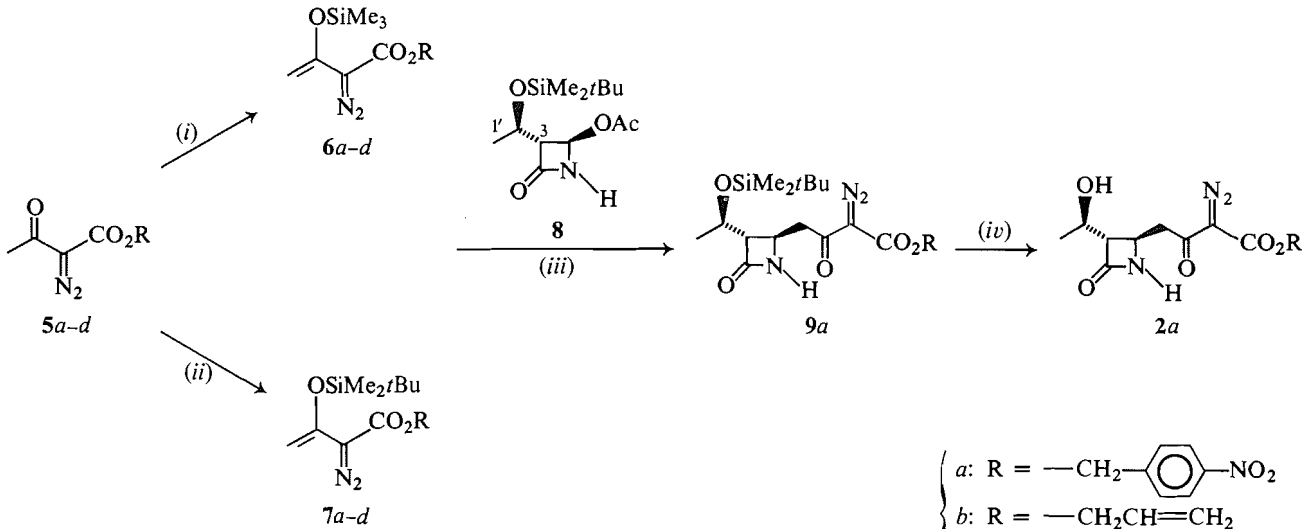

(*i*) $Me_3SiSO_2CF_3/Et_3N$, CH_2Cl_2, 0–5°C
(*ii*) $tBuMe_2SiOSO_2CF_3/Et_3N$, CH_2Cl_2, 0–5°C
(*iii*) $ZnCl_2$, CH_2Cl_2, room temperature
(*iv*) 1 *N* HCl, MeOH, room temperature

SCHEME 1.

methylsilylenol ether **7***a* (a yellow solid) has been stored in a capped bottle in a refrigerator (0–5°C) for more than 1 year without any hydrolysis to diazoacetoacetate **5***a*.

This method was found to be quite general. Thus, we prepared trimethylsilylenol ethers and *tert*-butyldimethylsilylenol ethers of allyl (**6***b* and **7***b*), trimethylsilylethyl (**6***c* and **7***c*), and ethyl (**6***d* and **7***d*) esters of α-diazoacetoacetic acid from α-diazoacetoacetates,[3] **5***b*–**5***d*. Some of these esters (e.g. allyl (8) and trimethylsilylethyl (9)) have been demonstrated to be useful carboxyl protecting groups in the synthesis of labile molecules such as penems and carbapenems.

The facile preparation of the *tert*-butyldimethylsilylenol ethers (**7***a*–**7***b*) is of particular interest, because generally the *tert*-butyldimethylsilylenol ether of α-diazoacetoacetates **7** could not be prepared, in our hands, by the method of Karady *et al.* (3*a*) which was successful for the preparation of the corresponding trimethylsilylenol ethers **6**. For example, the enolate generated from allyl α-diazoacetoacetate by lithium hexamethyldisilazide in the presence of tetramethylethylenediamine did not react with *tert*-butyldimethylsilyl chloride at −78°C. The reaction at 0°C produced diallyl terephthalate **10**[4], not silylenol ether **7***b*. The compound **10** was formed,[4] presumably by dimerization of the enolate of α-diazoacetoacetate followed by oxidation.

We investigated a direct introduction of the α-diazoacetoacetate moiety into the 4-position of 2-azetidinone by

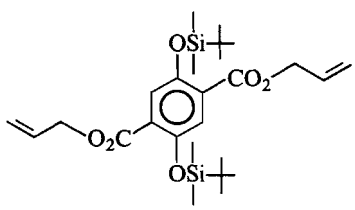

10

displacement reaction of azetidinone **3** with these silylenol ethers under the conditions of Reider *et al.* (4). An optically active 4-acetoxyazetidinone **8** was chosen as an azetidinone counterpart, for it was available from 6-aminopenicillanic acid (11) and it had the correct stereoconfigurations at the 3- and 1′-positions, for the synthesis of thienamycin analogs **1**.

As expected, the trimethylsilylenol ether **6***a* gave, stereospecifically, *trans*-azetidinone **9***a* in 54% yield. Interestingly, the *tert*-butyldimethylsilylenol ether **7***a* also reacted smoothly with 4-acetoxyazetidinone **8** in the presence of zinc chloride to produce, stereospecifically, *trans*-diazoazetidinone **9***a* in 84% yield. The assignment of the *trans*-stereochemistry was readily achieved on the basis of a small coupling constant between H3 and H4 (J_{3-4} = 1.5 Hz).

This stereospecific formation of *trans*-azetidinone, combined with the fact that the starting 4-acetoxyazetidinone has the *tert*-butyldimethylsiloxyethyl group at the 3-position with the *S*-configuration, establishes the stereochemistry at the 4-position of the product as the one found in the natural series such as thienamycin.

Finally, desilylation of this diazoazetidinone **9***a* with 1 *N* aqueous HCl in MeOH afforded key thienamycin precursor **2***a* in 84% yield. The key intermediate, **2***a*, has spectroscopic properties (^{1}Hmr, ir) consistent with data reported by Christensen *et al.* (2*b*). This compound was previously converted to thienamycin **1** (R = $CH_2CH_2NH_2$) and its analogs (2).

This whole sequence, starting from *p*-nitrobenzyl α-diazoacetoacetate (**5***a*) via the *tert*-butyldimethylsilylenol ether **7***a* constitutes an improved and practical method for the synthesis of thienamycin analogs **1**.

In summary, the trimethylsilyl- and *tert*-butyldimethylsilylenol ethers of various esters (including *p*-nitrobenzyl ester) of α-diazoacetoacetic acid were prepared by use of trimethylsilyl trifluoromethanesulfonate and *tert*-butyldimethylsilyl trifluoromethanesulfonate respectively, and they were found to be useful synthons for the synthesis of key carbapenem precursors **2**.

Experimental

Melting points were determined on a Gallenkamp melting point

[4]The structure **10** was tentatively assigned, based on the mechanistic considerations and its spectroscopic data. Ethyl γ-chloroacetoacetate was also reported to produce diethyl 2,5-dihydroxyterephthalate by base treatment.

Can. J. Chem. Downloaded from www.nrcresearchpress.com by 210.87.254.42 on 09/06/12
For personal use only.

Can. J. Chem. Downloaded from www.nrcresearchpress.com by 210.87.254.42 on 09/06/12
For personal use only.

apparatus and are not corrected. The infrared spectra were recorded on a Perkin-Elmer 267 grating infrared spectrometer. The ^{1}H nuclear magnetic resonance spectra were taken with either the Varian EM-360 (60 MHz), unless specified, or a Varian CFT-20 (80 MHz) nmr spectrometer. Tetramethylsilane was used as an internal standard and chemical shifts are reported in parts per million (δ) relative to the internal standard. The ultraviolet spectra were recorded on a Unicam SP8-100 uv spectrometer. Optical rotations were measured with a Perkin–Elmer Model 141 polarimeter. Tetrahydrofuran was freshly distilled from lithium aluminum hydride. Anhydrous diethyl ether (Fisher) was used without further treatment. All other solvents were reagent grade and had been stored over molecular sieves before use. Triethylamine and tetramethylethylenediamine were distilled from CaH_2 and stored over NaOH. Anhydrous zinc chloride was fused under reduced pressure and pulverized prior to use. Allyl diazoacetoacetate (**5***b*) (12) and ethyl diazoacetate (**5***d*) (6*a*) were prepared by the general procedure of Regitz (6). Analytical thin layer chromatography (tlc) was conducted on precoated plates (Silica Gel 60F-254, E. Merck). Visualization was effected by uv light, and iodine or ammonium molybdate (VI). Preparative layer chromatography (plc) was performed on silica gel plates prepared from Silica Gel 60 GF-254 (E. Merck). For column chromatography, 70–230 mesh Silica Gel (E. Merck) was used. The analyses were performed by Micro-Tech Laboratories, Skokie, Illinois, U.S.A.

p-*Nitrobenzyl acetoacetate*

A mixture of ethyl acetoacetate (140 g, 1.08 mol; Aldrich) and *p*-nitrobenzyl alcohol (153 g, 1.00 mol; Aldrich) in toluene (1 L) was heated and slowly distilled, removing 900 mL of the distillate over a period of 15 h. After cooling, any insoluble material was removed by filtration over Celite, washed with toluene. The filtrate and washings were combined and evaporated *in vacuo* to obtain 280 g of a crude oil. This oil was crystallized at 5°C from diethyl ether (280 mL) to yield 181.55 g (0.766 mol, yield 76.6%) of the title compound as off-white crystals, mp 40–42°C; R_f 0.45 (Et_2O); ir (film) ν_{max}: 1740 (ester), 1715 (ketone), 1515 and 1345 (NO_2) cm^{-1}; ^{1}Hmr ($CDCl_3$) δ: 1.98 (0.3H, s, *Me*(OH)═), 2.32 (2.7H, s, CH_3), 3.62 (1.8H, s, —CO*CH*$_2$CO$_2$—), 5.08 (0.1H, s, vinyl proton of the enol form), 5.28 (2H, s, —CO$_2$*CH*$_2$Ar), 7.53 (2H, 'd', *J* = 9 Hz, ArH's), and 8.23 (2H, 'd', *J* = 9 Hz, ArH's) ppm. An analytical sample was obtained by recrystallization from toluene–hexanes, mp 44–45°C; uv (CH_2Cl_2)λ_{max}: 267 nm (ε 10 800), *Anal.* calcd. for $C_{11}H_{11}NO_5$: C 55.70, H 4.67, N 5.91; found: C 55.59, H 4.62, N 5.85.

Trimethylsilylethyl acetoacetate

A solution of ethyl acetoacetate (2.60 g, 20 mmol; Aldrich) and trimethylsilylethanol (2.51 g, 21.1 mmol; Fluka) in toluene (100 mL) was heated and slowly distilled at 80–100°C with a Vigreux column (1.7 cm × 7 cm), removing most of the solvent over a period of 10 h. The residue was distilled under reduced pressure with a Vigreux column (1.7 cm × 7 cm) to obtain 3.34 g (16.5 mmol, yield 82.7%) of the title compound as a colourless oil; R_f 0.32 (20% EtOAc/hex); bp 85–88°C (0.3 Torr; 1 Torr = 133.3 Pa) (lit. (13) bp 77–80°C (1 Torr)); ir (neat) ν_{max}: 1740 (ketone) and 1720 (ester) cm^{-1}; ^{1}Hmr ($CDCl_3$) δ: 0.07 (9H, s, $SiMe_3$), 1.00 (2H, 't' *J* = 8 Hz, $SiCH_2$), 1.93 (0.45H, s, *Me*C(OH)═), 2.28 (2.55H, s, MeCO), 3.12 (0.15H, s, OH of the enol form), 3.43 (1.7H, s, $COCH_2$), 4.2 (2H, 't', *J* = 8 Hz, CO_2CH_2), and 4.95 (0.15H, s, vinyl proton of the enol form) ppm; *Anal.* calcd. for $C_9H_{18}O_3Si$: C 53.43, H 8.97; found: C 53.19, H 8.82.

p-*Nitrobenzyl α-diazoacetoacetate* (*5*a)

To a solution of *p*-nitrobenzyl acetoacetate (134.6 g, 0.568 mol) and triethylamine (79.0 nL, 0.568 mol) in CH_3CN (340 mL) was added at 0–5°C under a nitrogen atmosphere *p*-toluenesulfonyl azide[5] (14) (130 g, 0.568 mol, estimated purity 86%) over a period of 15 min. During this period the title compound started precipitating. The cooling bath was removed and the mixture stirred at room temperature for 3 h. The mixture was cooled again in an ice bath for 30 min and the precipitate was filtered, washed with cold CH_3CN (75 mL), and then cold Et_2O (200 mL) to yield 135.06 g (0.514 mol, yield 90.4%) of the title compound as pale yellow powder; R_f 0.65 (EtOAc); ir (CH_2Cl_2) ν_{max}: 2130 (N_2), 1720 (ester), 1655 (ketone), 1520 and 1350 (NO_2) cm^{-1}; uv (CH_2Cl_2) λ_{max}: 260 nm (ε 17 400); ^{1}Hmr ($CDCl_3$) δ: 2.50 (3H, s, CH_3), 5.38 (2H, s, CO_2CH_2Ar), 7.53 (2H, 'd', *J* = 9 Hz, ArH's), and 8.27 (2H, 'd', *J* = 9 Hz, ArH's) ppm.

2-Trimethylsilylethyl α-diazoacetoacetate (*5*c)

To a solution of trimethylsilylethyl acetoacetate (10.6 g, 50.0 mmol) and triethylamine (7.10 mL, 51.5 mmol) in acetonitrile (85 mL) was added in an ice bath *p*-toluenesulfonyl azide[5] (14) (10.0 g, 50.7 mmol) and the reaction mixture stirred at room temperature for 20 h. After evaporation of the solvent *in vacuo*, the residue was extracted with Et_2O (90 mL) and this extract was washed with a solution of KOH (3.0 g) in H_2O (83 mL) and again a solution of KOH (0.9 g) in H_2O (30 mL), then brine, and dried (Na_2SO_4). Evaporation of the solvent *in vacuo* gave 11.6 g of a crude oil which was purified by column chromatography (SiO_2, 150 g) eluting with 20% EtOAc/hexanes, to obtain 9.65 g (42.3 mmol, yield 84.5%) of the title compound as yellowish oil; R_f 0.44 (20% EtOAc/hex); ir (neat) ν_{max}: 2130 (C═N_2), 1715 (ester), and 1660 (ketone) cm^{-1}; uv (CH_2Cl_2) λ_{max}: 257 nm (ε 7200); ^{1}Hmr ($CDCl_3$) δ: 0.07 (9H, s, $SiMe_3$), 1.03 (2H, 't' *J* = 8 Hz, CH_2Si), 2.47 (3H, s, $COCH_3$), and 4.30 (2H, 't' *J* = 8 Hz, CO_2CH_2) ppm.

2-Diazo-3-trimethylsilyloxy-3-butenoic acid esters (**6**a–**6**d) *(general procedure)*

To a stirred solution (or suspension for the *p*-nitrobenzyl ester) of α-diazoacetoacetic acid esters, **5***a*–**5***d*, (1 mmol) and triethylamine (0.20 mL, 1.4 mmol) in dry CH_2Cl_2 or CCl_4 (2 mL) was added at 0–5°C trimethylsilyl trifluoromethanesulfonate (0.22 mL, 1.1 mmol; Aldrich) under a dry nitrogen atmosphere and the mixture stirred (0–5°C, N_2) for 30 min. To this clear yellow solution was added anhydrous hexanes (30 mL for the *p*-nitrobenzyl ester or 5 mL for the other esters) and stirred for 10 min under a nitrogen atmosphere. After removing the oily deposit by gravity filtration, the hexanes solution was evaporated *in vacuo* and the residue was re-dissolved in anhydrous hexanes (50 mL for the *p*-nitrobenzyl ester or 10 mL for the other esters). The insoluble material was again removed by gravity filtration and the filtrate was evaporated *in vacuo* to obtain **6***a* as yellow crystals or **6***b*–**6***d* as orangish oil in 77–97% yield. The whole operation should be performed under an anhydrous atmosphere since the products are sensitive to moisture.

Compound **6**a: 90% yield: ir (film) ν_{max}: 2100 (C═N_2), 1705 (ester), 1520 and 1345 (NO_2) cm^{-1}; ^{1}Hmr (CCl_4) δ: 0.28 (9H, s, $SiMe_3$), 4.17 (1H, d, *J* = 2 Hz, vinyl proton), 4.93 (1H, d, *J* = 2 Hz, vinyl proton), 5.29 (2H, s, CO_2CH_2Ar), 7.50 (2H, 'd' *J* = 9 Hz, ArH's), and 8.20 (2H, 'd', *J* = 9 Hz, ArH's) ppm.

Compound **6**b: 77% yield: ir (neat) ν_{max}: 2100 (C═N_2), 1710 (ester), and 1605 (C═C) cm^{-1}; ^{1}Hmr (CCl_4) δ: 0.20 (9H, s, $SiMe_3$), 4.15 (1H, d, *J* = 2 Hz, vinyl proton), 4.63 (2H, d, *J* = 5 Hz, CO_2CH_2), 4.95 (1H, d, *J* = 2 Hz, vinyl proton), and 5–6.2 (3H, m, vinyl protons) ppm.

Compound **6**c: 97% yield; ir (neat) ν_{max}: 2090 (C═N_2), 1705 (ester), and 1605 (C═C) cm^{-1}; ^{1}Hmr (CCl_4) δ: 0.07 (9H, s, $SiMe_3$), 0.25 (9H, s, $OSiMe_3$), 1.00 (2H, 't', *J* = 8 Hz, CH_2Si), 4.15 (1H, d, *J* = 2 Hz, vinyl proton), 4.23 (2H, 't' *J* = 8 Hz, CO_2CH_2), and 4.98 (1H, d, *J* = 2 Hz, vinyl proton) ppm.

Compound **6**d: 78% yield; ir (neat) ν_{max}: 2090 (C═N_2), 1710 (ester), and 1605 (C═C) cm^{-1}; ^{1}Hmr (CCl_4) δ: 0.25 (9H, s, $SiMe_3$), 1.32 (3H, t, *J* = 7 Hz, CH_3), 4.17 (1H, d, *J* = 2 Hz, vinyl proton), 4.23 (2h, q, *J* = 7 Hz, CO_2CH_2), and 4.97 (1H, d, *J* = 2 Hz, vinyl proton) ppm.

[5]*p*-Toluenesulfonyl azide, when prepared from unpurified *p*-toluenesulfonyl chloride by warming (ca. 50°C) to dissolve in EtOH, was contaminated by ethyl *p*-toluenesulfonate (ca. 15%). *p*-Toluenesulfonyl azide, free from ethyl *p*-toluenesulfonate, can also be prepared in aqueous acetone.

Can. J. Chem. Downloaded from www.nrcresearchpress.com by 210.87.254.42 on 09/06/12
For personal use only.

p-*Nitrobenzyl 2-diazo-3-(*tert-*butyldimethylsiloxy)-3-butenoate (7a)*

To a stirred suspension of *p*-nitrobenzyl α-diazoacetoacetate (26.30 g, 0.100 mol) and triethylamine (20.0 mL, 0.140 mol) in CH_2Cl_2 (200 mL) was added at 2°C *tert*-butyldimethylsilyl trifluoromethanesulfonate (27.5 mL, 0.12 mol; Fluka), in 30 min, under a nitrogen atmosphere and the mixture stirred at 2°C for 1 h. The clear orange solution was diluted with CH_2Cl_2 (50 mL) and washed with water (3 × 200 mL) and then brine (100 mL), dried (Na_2SO_4), and evaporated, yielding 37.40 g (0.0991 mol, yield 99.1%) of the title compound as a yellow solid; R_f 0.44 (20% EtOAc/hex: partially decomposed to *p*-nitrobenzyl α-diazoacetoacetate on the plate); ir (film) ν_{max}: 2090 (br, C=N_2), 1694 (ester), 1600 (C=C), and 1344 (NO_2) cm^{-1}; uv (CH_2Cl_2) λ_{max}: 271 nm (ε 14 500); ^{1}Hmr ($CDCl_3$) δ: 0.26 (6H, s, $SiMe_2$), 0.96 (9H, s, Si-*t*Bu), 4.25 (1H, d, J = 2.5 Hz, vinyl proton), 4.97 (1H, d, J = 2.5 Hz, vinyl proton), 5.32 (2H, s, CO_2H_2), 7.48 (2H, 'd' J = 9 Hz, ArH's), and 8.22 (2H, 'd', J = 9 Hz, ArH's) ppm. This material was purified by crystallization from hexanes to obtain an analytical sample: uv (CH_2Cl_2) λ_{max} 270 nm (ε 15 500).

*2-Diazo-3-(*tert-*butyldimethylsiloxy)-3-butenoic acid esters (7b–7d) (general procedure)*

To a stirred solution of α-diazoacetoacetic acid esters, **5b–5d**, (1 mmol) and triethylamine (0.20 mL, 1.4 mmol) in dry CH_2Cl_2 (2 mL) was added, at 0–5°C, *tert*-butyldimethylsilyl trifluoromethanesulfonate (0.28 mL, 1.2 mmol; Fluka) under a nitrogen atmosphere and the yellow mixture stirred at 0–5°C for 15 min. This was diluted with hexanes (20 mL), washed with a diluted $NaHCO_3$ solution and then brine, dried (Na_2SO_4), and evaporated to obtain **7b–7d** as orangish oil in 93–99% yield.

Compound **7b**: 96% yield; R_f 0.6 (20% EtOAc/hex; partially decomposed to α-diazoacetoacetate on the plate); ir (film) ν_{max}: 2100 (C=N_2), 1715 (ester), and 1610 (C=C) cm^{-1}; uv (CH_2Cl_2) λ_{max}: 280 nm (ε 6000); ^{1}Hmr ($CDCl_3$) δ: 0.23 (6H, s, $SiMe_2$), 0.93 (9H, s, Si-*t*Bu), 4.20 (1H, d, J = 5 Hz, J = 2 Hz, vinyl proton), 4.63 (2H, br d, J = 5 Hz, CO_2CH_2), 4.95 (1H, d, J = 2 Hz, vinyl proton), and 5–6.3 (3H, m, vinyl protons) ppm.

Compound **7c**: 94% yield; R_f 0.7 (20% EtOAc/hex; partially decomposed to α-diazoacetoacetate on the plate); ir (film) ν_{max}: 2100 (C=N_2), 1710 (ester), and 1610 (C=C) cm^{-1}; uv (CH_2Cl_2) λ_{max}: 280 nm (ε 7600); ^{1}Hmr (acetone-d_6; CFT-20) δ: 0.06 (9H, s, $SiMe_3$), 0.25 (6H, s, $SiMe_2$), 0.94 (9H, s, Si-*t*Bu), 1.05 (2H, t, J = 8.3 Hz, $CO_2CH_2CH_2SiMe_3$), 4.31 (1H, d, J = 1.8 Hz, vinyl proton), 4.32 (2H, t, J = 8.3 Hz, $CO_2CH_2CH_2SiMe_3$), and 5.03 (1H, d, J = 1.8 Hz, vinyl proton) ppm.

Compound **7d**: 99% yield; R_f 0.66 (20% EtOAc/hex; partially decomposed to α-diazoacetoacetate on the plate); ir (film) ν_{max}: 2090 (C=N_2), 1710 (ester), and 1610 (C=C) cm^{-1}; uv (CH_2Cl_2) λ_{max}: 282 nm (ε 7950); ^{1}Hmr (acetone-d_6; CFT-20) δ: 0.25 (6H, s, $SiMe_2$), 0.94 (9H, s, Si-*t*Bu), 1.26 (3H, t, J = 7.1 Hz, $CO_2CH_2CH_3$), 4.25 (2H, q, J = 7.1 Hz, $CO_2CH_2CH_3$), 4.28 (1H, d, J = 2 Hz, vinyl proton), and 5.02 (1H, d, J = 1.9 Hz, vinyl proton) ppm.

*Attempted preparation of allyl 3-*tert-*butyldimethylsiloxy-2-diazo-3-butenoate 7b through the enolate (formation of diallyl terephthalate **10***

To a stirred solution of lithium hexamethyldisilazide in THF (1 *M* solution, 1.2 mL, 1.2 mmol; Aldrich) and tetramethylethylenediamine (0.16 mL, 1.1 mmol) in THF (4 mL) was added slowly at −78°C, under a nitrogen atmosphere, allyl α-diazoacetoacetate (**5b**) (12) (168 mg, 1.00 mmol) and the mixture stirred (−78°C, N_2) for 1 h. To this solution was added a solution of *tert*-butyldimethylsilyl chloride (237 mg, 1,57 mmol; Aldrich) in THF (0.8 mL) and this was stirred at −78°C for 20 min. The mixture (1.2 ml) was partitioned between H_2O and hexanes. The hexanes phase was dried (Na_2SO_4) and evaporated to obtain 52 mg of a crude oil, the ^{1}Hmr ($CDCl_3$) spectrum of which indicated this to be mainly the starting diazoacetoacetate **5b**. The rest of the reaction mixture was warmed gradually to 0°C by replacing the Dry Ice − acetone bath with an ice bath over a period of 2 h. This was diluted with hexanes, washed with H_2O, dried (Na_2SO_4), and evaporated, yielding 241 mg of an oily solid. Purification of this material by plc (SiO_2, Et_2O/hex 1:1) gave 101 mg of diallyl 2,5-bis (*tert*-butyldimethylsiloxy)terephthalate (**10**) as a white solid; R_f 0.19 (Et_2O/hex 1:1); ir (film) ν_{max}: 1720 (ester) cm^{-1}: ^{1}Hmr ($CDCl_3$) δ: 0.15 (6H, s, $SiMe_2$), 0.95 (9H, s, Si-*t*Bu), 4.75 (2H, br d, J = 6 Hz, CO_2CH_2), 5–6.4 (2H, m, vinyl protons), and 7.27 (1H, s, ArH) ppm.

This material in EtOH was treated with 1 *N* aqueous HCl at room temperature to obtain diallyl 2,5-dihydroxyterephthalate, mp 85–87°C; R_f 0.47 (EtOAc); ir (film) ν_{max}: 3400 (OH) and 1700 (ester) cm^{-1}; ^{1}Hmr ($CDCl_3$, CFT-20) δ: 4.89 (2H, 'd', J = 5.81 Hz, CO_2CH_2), 5–6.4 (2H, m, vinyl protons), 7.34 (1H, s, ArH), and 8.20 (br, OH) ppm. This compound gave intense purple colour when treated with an aqueous solution of ferric chloride, indicating the presence of a phenolic hydroxy group (10).

*(3S)-{(1R)-(*tert-*butyldimethylsiloxy)ethyl}-(4R)-{3-(*p-*nitrobenzyloxy) carbonyl-2-oxo-3-diazopropan-1-yl}azetidin-2-one (9a)*

To a stirred mixture of (3*R*)-{(1*R*)-(*tert*-butyldimethylsiloxy)-ethyl)-(4*R*)-acetoxy-2-azetidinone (**8**) (144 mg, 0.50 mmol, mp 101–103°C) (11) and anhydrous $ZnCl_2$ (34 mg, 0.25 mmol) in CH_2Cl_2 (3 mL) was added at room temperature, under a nitrogen atmosphere, a solution of *p*-nitrobenzyl 2-diazo-3-trimethylsiloxy-3-butenoate (**6a**) (308 mg, 1.00 mmol) or *p*-nitrobenzyl 3-(*tert*-butyldimethylsiloxy)-2-diazo-3-butenoate (**7a**) (226 mg, 0.60 mmol) over a period of 2–3 h. The mixture was stirred another 1–2 h under the same conditions. This was diluted with EtOAc (20 mL), washed with H_2O and then brine, dried (Na_2SO_4), and evaporated, yielding a crude oil. This was purified by column chromatography (SiO_2, 20 g) eluting with 20% EtOAc in CH_2Cl_2 to obtain 132 mg (0.269 mmol, yield 53.8%) from the reaction with **6a**, or 207 mg (0.422 mmol, yield 84.4%) from the reaction with **7a**, of the title compound as a colourless oil; R_f 0.39 (20% EtOAc/CH_2Cl_2); ir (neat) ν_{max}: 3000 (br, NH), 2140 (C=N_2), 1755 (β-lactam), 1720 (ester), 1655 (C=O), 1525 and 1350 (NO_2) cm^{-1}; $[\alpha]_D^{20}$ +44.3° (*c* 1.0, CH_2Cl_2); ^{1}Hmr ($CDCl_3$, CFT-20) δ: 0.06 (6H, s, $SiMe_2$), 0.86 (9H, s, Si-*t*Bu), 1.21 (3H, d, J = 6.3 Hz, 1′-Me), 2.85 (1H, dd, $J_{3-1'}$ = 5Hz, J_{3-4} = 2.5 Hz, 3-H), 2.96 (1H, dd, J_{gem} = 18 Hz, $J_{1''-4}$ = 9.5 Hz, 1″–Ha), 3.41 (1H, dd, J_{gem} = 18 Hz, $J_{1''-4}$ = 3.5 Hz, 1″–Hb), 3.8–4.3 (2H, m, 4–H and 1′–H), 5.35 (2H, s, CO_2CH_2Ar), 5.95 (br, s, NH), 7.53 (2H, 'd', J = 8.8 Hz, ArH's), and 8.26 (2H, 'd', J = 8.8 Hz, ArH's) ppm.

The reaction with **7a** was also carried out on a large scale (0.25 mol of **8**) without lowering the yield.

*(3S)-{(1R)-Hydroxyethyl}-(4R)-{3-(*p-*nitrobenzyloxy)carbonyl-2-oxo-3-diazopropan-1-yl}azetidin-2-one (2a)*

To a stirred solution of **9a** (39.25 g, 80.0 mmol) in MeOH (240 mL) was added 1 *N* aqueous HCl (80 mL) and the mixture stirred at room temperature for 6 h. During this period the title compound was precipitated. This was cooled, filtered, and washed with cold MeOH–H_2O (9:1) and then cold Et_2O to obtain 25.26 g (67.2 mmol, yield 84.0%) of the title compound as white solid, mp 151–152°C (CH_3CN); $[\alpha]_D^{22}$ +21.8° (*c* 0.23, CH_3CN); R_f 0.19 (EtOAc); ir (Nujol) ν_{max}: 3390 (OH), 2130 (C=N_2), 1730 (β-lactam), 1705 (ester), 1660 (ketone), 1605 (Ar), 1520 and 1350 (NO_2) cm^{-1}; ^{1}Hmr ($CDCl_3$, CFT-20) δ: 1.33 (3H, d, J = 6.3 Hz, 1′–Me), 1.91 (br, OH), 2.88 (1H, dd, $J_{3-1'}$ = 7.3 Hz, J_{3-4} = 2.2 Hz, 3–H), 3.25 (2H, m, 1′–H's), 3.8–4.2 (1H, m, 4–H), 4.17 (1H, 'q', J = 6.7 Hz, 1′–H), 5.36 (2H, s, CO_2CH_2), 5.96 (1H, br, NH), 7.54 (2H, 'd', J = 8.6 Hz, ArH's), and 8.27 (2H, 'd', J = 8.7 Hz, ArH's) ppm.

Acknowledgements

We would like to thank Professor B. Belleau of McGill University and Dr. M. Ménard for their interest in this work. One of us (G.R.) acknowledges the award of an Industrial Fellowship from the Natural Sciences and Engineering Research Council of Canada.

1. (*a*) R. W. RATCLIFFE and G. ALBERS-SCHÖNBERG. *In* Chemistry and biology of β-lactam antibiotics. Vol. 2. *Edited by* R. B. Morin and M. Gorman. Academic Press, New York, NY 1982. pp. 227–313; (*b*) T. KAMETANI. Heterocycles, **17**, 463 (1982).
2. (a) T. N. SALZMANN, R. W. RATCLIFFE, B. G. CHRISTENSEN, and F. A. BOUFFARD. J. Am. Chem. Soc. **102**, 6161 (1980); (*b*) B. G. CHRISTENSEN, T. N. SALZMANN, and R. W. RATCLIFFE. European Patent Application 0007973 (1980); (*c*) D. G. MELILLO, I. SHINKAI, T. LIU, K. RYAN, and M. SLETZINGER. Tetrahedron Lett. **21**, 2783 (1980); (*d*) D. G. MELILLO, T. LIU, K. RYAN, and I. SHINKAI. Tetrahedron Lett. **22**, 913 (1981); (*e*) T. MIYADERA, Y. SUGIMURA, T. HASHIMOTO, T. TANAKA, K. IINO, and S. SUGAWARA. J. Antiobiot. **36**, 1034 (1983).
3. (*a*) S. KARADY, J. S. AMATO, R. A. REAMER, and L. M. WEINSTOCK. J. Am. Chem. Soc. **103**, 6765 (1981); (*b*) P. J. REIDER and E. J. J. GRABOWSKI. Tetrahedron Lett. **23**, 2293 (1982).
4. P. J. REIDER, R. RAYFORD, and E. J. J. GRABOWSKI. Tetrahedron Lett. **23**, 379 (1982).
5. (*a*) G. SIMCHEN and W. KOBER. Synthesis, 259 (1976); (*b*) J. K. RASMUSSEN. Synthesis, 91 (1977); (*c*) P. BROWNBRIDGE. Synthesis, 1 (1983); 85 (1983).
6. (*a*) M. REGITZ and A. LIEDHEGENER. Chem. Ber. **99**, 3128 (1966); (*b*) M. REGITZ. Angew. Chem. **79**, 786 (1967); (*c*) M. REGITZ. Synthesis, 351 (1972).
7. (*a*) H. EMDE. Dissertation, Universitat Stuttgart, 1979; H. EMDE *et al.* Synthesis, 1 (1982); (*b*) E. J. COREY, H. CHO, C. RUCHER, and D. H. HUA. Tetrahedron Lett. **22**, 3455 (1981).
8. P. D. JEFFREY and S. W. MCCOMBIE. J. Org. Chem. **47**, 587 (1982).
9. (*a*) A. MARTEL *et al.* Can. J. Chem. **60**, 942 (1982); (*b*) D. T. W. CHU, J. E. HENGEVELD, and D. LESTER. Tetrahedron Lett. **24**, 139 (1983).
10. T. P. PILLAI, K. RAJAGOPALAN, B. GOPALAN, and S. SWAMINATHAN. Indian J. Chem. **16*B***, 235 (1978).
11. A. YOSHIDA, T. HAYASHI, N. TAKEDA, S. OIDA, and E. OHKI. Chem. Pharm. Bull. **29**, 2899 (1981).
12. G. CANNIC, G. LINSTRUMELLE, and S. JULIA. Bull. Soc. Chim. Fr. 4913 (1968).
13. V. F. MIRONOV, V. P. KOZYUKOV, and V. D. SHELYUDYAKOV. Zh. Obshch. Khim. **37**, 1915 (1967); Chem. Abstr. **68**, 29768w (1968).
14. (*a*) W. VON E. DOERING and C. H. DUPUY. J. Am. Chem. Soc. **75**, 5955 (1953); (*b*) M. REGITZ, J. HOCKER, and A. LIEDHEGENER. Org. Synth. Coll. Vol. **V**, 179 (1973).

Can. J. Chem. Downloaded from www.nrcresearchpress.com by 210.87.254.42 on 09/06/12
For personal use only.

Reagents and synthetic methods 41: oxidations with chromium trioxide under the influence of crown ethers

M. JUARISTI, J. M. AIZPURUA, B. LECEA, AND C. PALOMO[1]

Kimika Organikako Departamentua, Kimika Fakultatea, Euskal Herriko Unibertsitatea, Altza, Donostia, Spain

Received May 16, 1984

M. JUARISTI, J. M. AIZPURUA, B. LECEA, and C. PALOMO. Can. J. Chem. **62**, 2941 (1984).

An unusual new application of crown ethers in organic synthesis is described. Chromium trioxide, in the presence of a crown ether as catalyst, in dichloromethane as solvent, was found an efficient oxidizing system for the chemoselective oxidation of mercaptans to disulfides. It is also highly efficient for the oxidation of hydroquinones to the corresponding benzoquinones in almost quantitative yield. A high conversion of polynuclear hydrocarbons into quinones in acetic acid media is also briefly described.

M. JUARISTI, J. M. AIZPURUA, B. LECEA et C. PALOMO. Can. J. Chem. **62**, 2941 (1984).

On décrit une utilisation nouvelle et exceptionnelle des éthers couronnes en synthèse organique. On a trouvé que le trioxyde de chrome dans le dichlorométhane, en présence d'un éther couronne comme catalyseur, permet d'oxyder les mercaptans en disulfures d'une manière efficace et chimiosélective. Ce système est également très efficace pour oxyder les hydroquinones en benzoquinones correspondantes avec un rendement presque quantitatif. On décrit brièvement une transformation, qui se fait avec des taux élevés de conversion, d'hydrocarbures polynucléaires en quinones en milieu acétique.

[Traduit par le journal]

Can. J. Chem. Downloaded from www.nrcresearchpress.com by 210.87.254.40 on 09/06/12
For personal use only.

The use of crown ethers in organic synthesis has become significant during recent years. Concerning oxidation reactions, they have been used in phase transfer catalyzed permanganate, chromate, dichromate, and potassium superoxide promoted oxidation reactions (1); however, no report related to oxidation reactions achieved by means of chromium trioxide/crown ether systems has been described. We have recently reported the first application of crown ethers in the oxidation of alcohols to carbonyl compounds promoted by chromium trioxide (2). This communication describes a preparative application of this new oxidizing system.

Oxidation of mercaptans

Selective oxidation of mercaptans to disulfides without overoxidation is well investigated, and several reagents have been used for this purpose (3). However, selective oxidation between mercaptans is rare. We wish to report here the first evidence of the oxidation of mercaptans to disulfides promoted by powdered chromium trioxide under the influence of crown ethers. Moreover, our major finding is that arenethiols are chemoselectively oxidized to the corresponding arenedisulfides in the presence of alkanethiols by means of this oxidation system.

In order to find the optimum reaction conditions, we have tested this method for 4-chlorothiophenol using different molar ratios of thiol to chromium trioxide. The results are summarized in Table 1, and show that the molar ratio of thiol to chromium trioxide necessary for a total oxidation is 1:4. The role of the crown ether as phase transfer agent is not clear at present, but in its absence no oxidation takes place, and the starting thiol is recovered unchanged.

Figure 1 shows the chemoselective oxidation of an equimolecular mixture of benzenethiol and benzylmercaptan by means of this oxidizing system. Thus, equimolecular mixtures of the respective thiols were treated with chromium trioxide

[1]Author to whom correspondence should be addressed.

TABLE 1. Oxidation of 4-chlorothiophenol

		Material balance (%)[b]	
CrO_3[a]	Time (h)	4-ClC_6H_4SH	$(4\text{-}ClC_6H_4S)_2$
2	5	24	76
2	24	[c]	84
3	24	[c]	85
4	2	—	84[d]
5	2	—	85[d]

[a]Equivalents.
[b]Determined by ^1H nmr analysis of the crude reaction mixture.
[c]Starting thiol was detected by tlc analysis.
[d]A single spot was detected by tlc analysis.

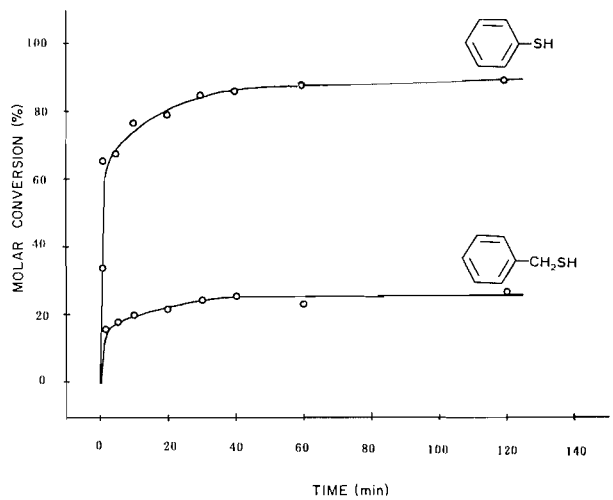

FIG. 1. Oxidation of an equimolecular mixture of benzenethiol and benzyl mercaptan (0.33 *M*) with CrO_3/18-crown-6 (4 equiv./0.1 equiv.) in CH_2Cl_2 at 10°C.

Can. J. Chem. Downloaded from www.nrcresearchpress.com by 210.87.254.40 on 09/06/12
For personal use only.

TABLE 2. Selective oxidation of thiols to disulfides with chromium trioxide/18-crown-6 system

Run	Substrate(s)	Molar ratio[a]	Time (h)	Product(s)	Yield[b] (%)
1	C_6H_5SH $C_6H_5CH_2SH$	1:1:4	2.5	$(C_6H_5S)_2$ $C_6H_5CH_2SH$	77 75
2	$4\text{-}ClC_6H_4SH$ $C_6H_5CH_2SH$	1:1:4	2.0	$(4\text{-}ClC_6H_4S)_2$ $C_6H_5CH_2SH$	65 87
3	$4\text{-}CH_3C_6H_4SH$ $CH_3(CH_2)_6SH$	1:1:4	2.0	$(4\text{-}CH_3C_6H_4S)_2$ $CH_3(CH_2)_6SH$	71 66
4	$C_6H_5CH_2SH$	1:4	5.0	$(C_6H_5CH_2S)_2$ $C_6H_5CH_2SH$	51[c] 49[c]
5	$C_6H_5CH_2SH$	1:4	24.0	$(C_6H_5CH_2S)_2$ $C_6H_5CH_2SH$	92[c,d] 8[c]
6	$4\text{-}ClC_6H_4SH$	1:4	2.0	$(4\text{-}ClC_6H_4S)_2$	84
7	$4\text{-}CH_3OC_6H_4SH$	1:4	2.25	$(4\text{-}CH_3OC_6H_4S)_2$	76
8	$4\text{-}CH_3C_6H_4SH$	1:4	2.0	$(4\text{-}CH_3C_6H_4S)_2$	81

[a]Molar ratio substrate(s)/chromium trioxide.
[b]Yield (referred to each starting substrate) of pure products isolated by distillation and (or) recrystallization; purity ≥ 98% by glc, tlc, and nmr analysis.
[c]Conversion determined by nmr analysis from the crude reaction mixture.
[d]81% yield of isolated pure product (only a single spot detected by tlc analysis).

TABLE 3. Oxidation of polynuclear aromatic hydrocarbons

Entry	Substrate[a]	Time (min)	Product	Yield (%)[b]
1	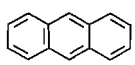	30	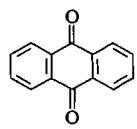	98
2	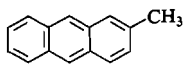	30	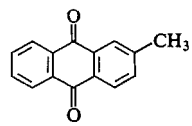	95
3		120	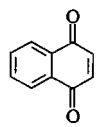	50
4	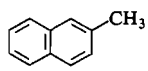	120	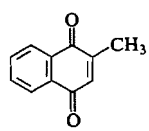	62
5	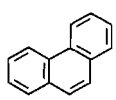	60	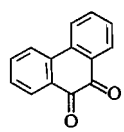	80

[a]Molar ratio (substrate/chromium trioxide, 1:4).
[b]Yield of isolated pure products isolated by recrystallization.

and a catalytic amount of 18-crown-6 in dichloromethane for different reaction times. The reaction mixture was analyzed from its ^1H nmr spectrum, mainly by observing the change of the relative intensities of the corresponding mercapto groups. The chemoselectivity of this oxidation system is further demonstrated by the representative examples listed in Table 2. As shown in runs 4 and 5, benzylmercaptan alone is slowly oxidized to the corresponding disulfide, but this oxidation is minimized when an arenethiol is present. To our knowledge, this is an unusual oxidation reaction.

TABLE 4. Oxidation of hydroquinones

Substrate[a]	Solvent/catalyst	Time (min)	Product	Yield[b,c] (%)
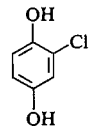	CH_2Cl_2/18-crown-6	45	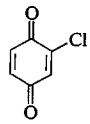	85
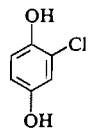	CH_2Cl_2/—	360	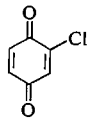	79[d]
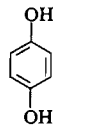	CH_2Cl_2/Et_2O	5	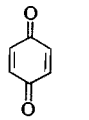	98
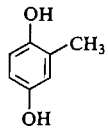	CH_2Cl_2/Et_2O	10	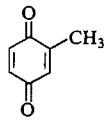	97
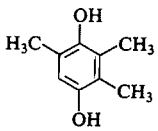	CH_2Cl_2/Et_2O	5	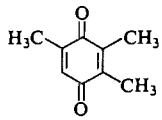	97
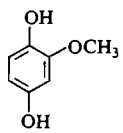	$CH_2Cl_2-Et_2O$/18-crown-6	10	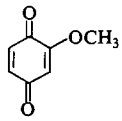	85

[a]Molar ratio (substrate/chromium trioxide, 1:5).
[b]Yield of pure products isolated by recrystallization.
[c]Physical properties were in agreement with those reported for authentic samples (from Aldrich).
[d]Starting hydroquinone was detected by tlc analysis.

Preparation of quinones

Conversion of polynuclear aromatic hydrocarbons and hydroquinones into their corresponding quinones is of great preparative value in organic synthesis, because their structure is observed in some synthetic dyes and in many naturally occurring substances. Various oxidizing agents have been developed for the synthesis of quinones (4). Recently, Chaudhuri and co-workers (4*c*) have reported that pyridium fluorochromate oxidizes anthracene and phenanthrene to their corresponding quinones in good to excellent yields, but this method seems to be not very convenient for a large preparative scale. Pletcher *et al.* (4*d*) have described the oxidation of polynuclear hydrocarbons by dichromate anions in aqueous sulfuric acid under phase transfer conditions, even if low yields are obtained in the oxidation of naphthalenes.

In a first experiment, we have found that under the same conditions as those used in the oxidation of mercaptans, polynuclear aromatic hydrocarbons are oxidized into quinones in poor yields. However, when the reaction was carried out in glacial acetic acid, anthracenes were rapidly transformed into anthraquinones in nearly quantitative yield, and the reaction proceeded more smoothly than in the conventional procedure (4*c*). Although in the case of anthracenes the yields are comparable to those obtained from chromium trioxide/acetic acid alone (4*e*), the oxidation of naphthalenes into naphthoquinones in yields of the range 50–60% (Table 3) when crown ethers are used as catalysts is of special significance.

The wide utility of this oxidation system is further exemplified by the fast and mild oxidation of hydroquinones in almost quantitative yields. In a preliminary observation, we have found that 2-chlorohydroquinone was slowly oxidized to 2-chlorobenzoquinone by chromium trioxide in dichloromethane as solvent, but in the presence of a catalytic amount of 18-crown-6 the reaction takes place much more rapidly. When the hydroquinone was not soluble in dichloromethane, the reaction was carried out by adding a diethyl ether/dichloromethane (50% v) solution of the substrates to a suspension of powdered chromium trioxide in dichloromethane. In such cases, addition of crown ethers is not necessary and the reaction proceeds very quickly. We suppose that diethyl ether and crown ethers can act in a similar manner with chromium trioxide to form some active soluble species which are able to oxidize hydroquinones into benzoquinones under mild conditions and nearly quantitative yields. The results are summarized in Table 4. The synthetic utility of this procedure is shown by the conversion of trimethyl-*p*-hydroquinone to the

Can. J. Chem. Downloaded from www.nrcresearchpress.com by 210.87.254.40 on 09/06/12
For personal use only.

corresponding *p*-benzoquinone, which is a key intermediate in the synthesis of tocopherol (Vitamin E) (5).

Conclusions

The results obtained show the versatility of the present method and the advantages of the use of readily accessible and inexpensive chromium trioxide instead of other reagents employed in oxidation reactions, especially when used on a molar preparative scale.

Experimental

Chemoselective oxidation of thiophenol

To a suspension of finely powdered chromium trioxide (4.0 g, 40 mmol) in dichloromethane (30 mL), 18-crown-6 (0.3 g, 1.1 mmol) was added and the suspension was stirred at room temperature for 10 min to form a red-brown heterogeneous mixture. Then, thiophenol (1.02 mL, 10 mmol) and benzyl mercaptan (1.18 mL, 10 mmol) were added consecutively and the mixture was stirred at room temperature until the arenethiol could no longer be detected by tlc analysis (silica gel plates; n-hexane/ethyl acetate 1:3). On completion (2.5 h), the reaction mixture was worked up by filtration through silica gel. Removal of the solvent left a mixture of products which was analyzed from its nmr spectrum and then purified by distillation and crystallization, to give phenyldisulfide (0.84 g, 77%), mp 60–61°C (lit. (*4c*) mp 61–62°C) and unchanged benzyl mercaptan (0.93 g, 75% recovered), bp 140–145°C/20 Torr (1 Torr = 133.3 Pa).

Naphthoquinone. Typical procedure

A solution of naphthalene (1.28 g, 10 mmol) in glacial acetic acid (10 mL) was added dropwise to a suspension of finely powdered chromium trioxide (4 g, 40 mmol) and a catalytic amount of 18-crown-6 (0.4 g) in the same solvent (30 mL), at room temperature. The reaction mixture was heated in a steam bath at 50–55°C during 30 min. Then the reaction was allowed to reach room temperature, filtered off through a pad of silica gel, and washed with dichloromethane (100 mL). The organic layer was washed with water (3 × 50 mL) and then with saturated sodium hydrogen carbonate solution (3 × 50 mL). The solvent was dried with sodium sulfate and evaporated under reduced pressure to give a crude product which was crystallized from hexane to afford naphthoquinone (0.79 g, 50%), mp 115–116°C (lit. (6) mp 117–118°C).

Oxidation of hydroquinones

2,3,5-Trimethylhydroquinone (1.52 g, 10 mmol) in dichloromethane (25 mL)/diethyl ether (30 mL) was added dropwise to a suspension of powdered chromium trioxide (5 g, 50 mmol) in dichloromethane (10 mL) at 0–5°C over 10–15 min, and the mixture was stirred at room temperature for 5 min. The resulting dark-brown suspension was filtered off through a pad of silica gel and washed with dichloromethane (100 mL). Removal of the solvent gave 1.43 g (97%) of pure 2,3,5-trimethylbenzoquinone, mp 32–35°C (lit. (6) mp 32°C).

Acknowledgement

We thank the Hezkuntza Saila of Eusko Jaurlaritza (Basque Government) for financial support of this work.

1. (*a*) W. P. WEBER and G. W. GOKEL. Phase transfer catalysis in organic synthesis. Springer Verlag, Berlin. 1977; (*b*) CH. M. STARKS and CH. LIOTTA. Phase transfer catalysis. Academic Press, New York. 1978; (*c*) W. E. KELLER. Compendium of phase transfer reactions and related synthetic methods. Fluka AG, Switzerland. 1979.
2. I. GANBOA, J. M. AIZPURUA, and C. PALOMO. J. Chem. Res.(S), 92 (1984).
3. G. CAPOZZI and G. MODENA. *In* The chemistry of the thiol group. Part 2. *Edited by* S. Patai. John Wiley, New York. 1974. pp. 785–839.
4. (*a*) C. A. BUEHLER and D. E. PEARSON. Survey of organic synthesis. Vol. 1. Wiley–Interscience, New York. 1970. p. 724; (*b*) Vol. 2. 1977. p. 635; (*c*) M. N. BHATTACHARGEE, M. K. CHAUDHURI, H. S. DASGUPTA, and N. ROY. Synthesis, 588 (1982); (*d*) D. PLETCHER and S. J. D. TAIT. J. Chem. Soc. Perkin Trans. 2, 788 (1979). (*e*) L. F. FIESER. J. Biol. Chem. **133**, 391 (1940).
5. P. SCHUDEL, H. MAYER, and O. ISLER. *In* The vitamins. Vol. 5. 2nd ed. *Edited by* W. H. Sebrell, Jr. and R. S. Harris. Academic Press, New York. 1972. p. 165.
6. Z. RAPPOPORT. Organic compounds identification. 3rd ed. C. R. C. Press, Cleveland, Ohio 1977.

Can. J. Chem. Downloaded from www.nrcresearchpress.com by 210.87.254.40 on 09/06/12
For personal use only.

Total regiospecific synthesis of the selagine tricyclic ring system[1]

D. GRAVEL,[2] L. BORDELEAU, G. LADOUCEUR, J. RANCOURT,[3] AND D. THORAVAL[4]

Département de Chimie, Université de Montréal, C.P. 6210, Succ. A, Montreal (Que.), Canada H3C 3V1

Received July 30, 1984

D. GRAVEL, L. BORDELEAU, G. LADOUCEUR, J. RANCOURT, and D. THORAVAL. Can. J. Chem. **62**, 2945 (1984).

Starting from 4-methylcyclohexanone, a total synthesis of the selagine tricyclic ring system is described in which complete control of regiospecificity is achieved in the elaboration of functionality.

D. GRAVEL, L. BORDELEAU, G. LADOUCEUR, J. RANCOURT et D. THORAVAL. Can. J. Chem. **62**, 2945 (1984).

A partir de la méthyl-4 cyclohexanone, une synthèse totale du squelette tricyclique de la sélagine est rapportée dans laquelle un contrôle complet de la régiospécificité a été atteint dans l'élaboration de toutes les fonctions.

Can. J. Chem. Downloaded from www.nrcresearchpress.com by 210.87.254.5 on 09/06/12
For personal use only.

The total synthesis of selagine (**1**), a Lycopodium alkaloid whose structure was determined over twenty years ago by Wiesner, Valenta, and co-workers (1), still remains an open challenge in the literature and recent publications which have appeared (2–5) attest to the interesting problems of regiochemistry posed by this molecule.

In the present communication we report the first total synthesis of the selagine tricyclic ring system **2** which is constructed in a regiospecific sequence starting from 4-methylcyclohexanone (**3**). In a first stage, rapid and efficient access is gained to the key bicyclic precursor **4** which has all of the necessary functionality properly positioned to complete the AB ring portion of the target compound **1**.

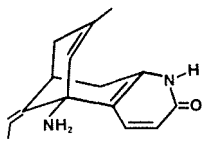

1

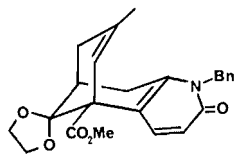

2

Carbomethoxylation of 4-methylcyclohexanone (**3**) by the Ruest–Blouin–Deslongchamps procedure (6) (NaH, KH cat., THF, Me_2CO_3, reflux) gave a 94% yield of the desired 2-carbomethoxy-4-methylcyclohexanone (**5**), bp 90–92°C/10 Torr (1 Torr = 133.3 Pa); ir ($CHCl_3$) ν_{max}: 1735, 1705, 1650, 1610 cm^{-1}; ^1H nmr[5] ($CDCl_3$) δ: 1.00 (d, J = 5.6 Hz, 3H), 1.0–2.5 (m, 7H), 3.75 (s, 3H), 12 (approx.) (s, 1H); ms, CI, *m/e*: 171 (MH^+), 140 ($MH^+ - OCH_3$). Introduction of unsaturation at the α,β-position also proceeded in essentially quantitative yield by the phenylselenenylation–oxidation method of Reich *et al.* (7). In a first step, phenylselenenylation of β-ketoester **5** (NaH, THF, PhSeCl, −78°C → rt) took place in a 96–100% yield to give **6** as a mixture of two isomers: orange oil; ir (film) ν_{max}: 1750–1705 cm^{-1}; ^1H nmr ($CDCl_3$) δ: 0.93 and 0.99 (2d, J = 6.5 Hz and 7.0 Hz, 3H), 1.2–3.3 (m, 7H), 3.68 and 3.70 (2s, 3H), 7.2–7.8 (m, 5H); ms, CI, *m/e*: 324 (M^+), 326 ($M^+ + 2$). In a second step, oxidation of **6** (H_2O_2 30%, CH_2Cl_2, 0°C → rt) gave the expected α,β-unsaturated β-ketoester **7** in an 83–90% yield (crude): yellow oil, unstable, used as such for the next step; ir (film)

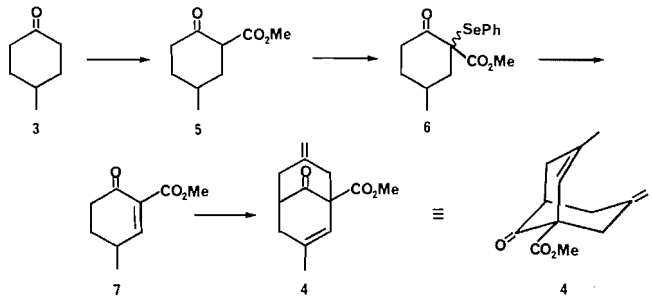

3 5 6 7 4 4

ν_{max}: 1735, 1685 cm^{-1}; ^1H nmr ($CDCl_3$) δ: 1.24 (d, J = 7.0 Hz, 1H), 1.5–2.9 (m, 5H), 3.80 (s, 3H), 7.52 (m, 1H); ms, CI, *m/e*: 169 (MH^+). *Exact Mass* calcd. for $C_9H_{12}O_3$: 168.0787; found (ms): 168.0767. The crucial one-step annelation reaction (8) was then carried out on the α,β-unsaturated β-ketoester **7** using methallyl dichloride (NaH, DMF, $CH_2{=}C(CH_2Cl_2)$, 95°C) to yield the desired bicyclo[3.3.1] precursor **4** in a 35–42% yield: mp 102–103°C; ir (film) ν_{max}: 1740, 1718 cm^{-1}; ^1H nmr ($CDCl_3$) δ: 1.74 (s, 3H), 2.1–3.3 (m, 7H), 3.79 (s, 3H), 4.8 (br s, 1H), 5.0 (br s, 1H), 5.3 (br s, 1H). *Anal.* calcd. for $C_{13}H_{16}O_3$: C 70.89, H 7.32; found: C 70.95, H 7.34.

Before coming to the second stage of the synthesis, i.e. the regiospecific introduction of a three-carbon side chain, precursor of the fused α-pyridone ring, some slight functional group adjustments were necessary. In the first instance, protection of the ketone in the usual manner was carried out prior to liberation of the latent carbonyl group by ozonolysis of the exocyclic methylene. Thus, ketalization of **4** (ethylene glycol, *p*-TsOH, C_6H_6, reflux) gave 70–80% of the corresponding ketal **8**: colorless oil; ir (film) ν_{max}: 1720 cm^{-1}; ^1H nmr ($CDCl_3$) δ: 1.71 (s, 3H), 1.9–3.2 (m, 7H), 3.74 (s, 3H), 3.9 (m, 4H), 4.57 and 4.78 (2d, J = 2 Hz, 1H and J = 2 Hz, 1H), 5.28 (br s, 1H). *Exact Mass* calcd. for $C_{15}H_{20}O_4$: 264.1361; found (ms): 264.1360. Ozonolysis of the ketal **8** (O_3, CH_2Cl_2, −78°C, followed by Zn, AcOH, rt) yielded 70% of the desired ethylenedioxyketoester **9**: mp 77–78°C; ir ($CHCl_3$) ν_{max}: 1720 (br) cm^{-1}; ^1H nmr (400 MHz) ($CDCl_3$) δ: 1.72 (s, 3H), 1.94 (d, J = 17.8 Hz, 1H), 2.22 (ddd, J = 15.8, 2.7, and 1.8 Hz, 1H), 2.32 (m, 1H), 2.38 (dd, J = 14.9 and 2.8 Hz, 1H), 2.72 (dd broadened, $J \simeq 18$ and 6 Hz, 1H), 2.89 (dd, J = 15.7 and 6.6 Hz, 1H), 3.39 (d, J = 14.9 Hz, 1H), 3.76 (s, 3H), 3.93–4.14 (m, 4H), 5.45 (br s, 1H). *Exact Mass* calcd. for $C_{14}H_{18}O_5$: 266.1154; found (ms): 266.1154. This important intermediate in our synthetic plan was also synthesized by Kende *et al.* (5) using a totally different sequence and the reported spectroscopic data correspond to ours with minor discrepancies.

Having thus manipulated the functional groups to obtain

[1] Presented in part at the 67th Annual CIC Conference, June 3–6, 1984, Montreal, Canada.

[2] Author to whom correspondence should be addressed.

[3] Holder of an NSERC scholarship (1983–1985).

[4] Holder of a Université de Montréal scholarship (1982–1983).

[5] The ^1H nmr spectra were recorded on a 90-MHz apparatus unless otherwise indicated.

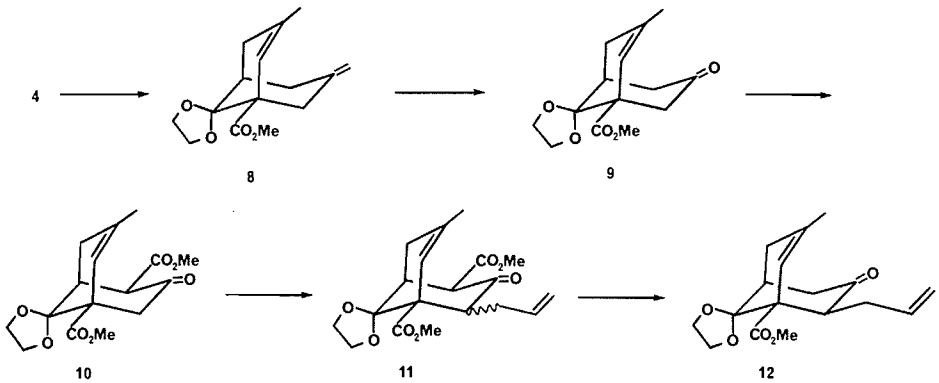

intermediate **9** we were in a position, as stated above, to envisage the second stage of the synthesis, namely: the regiospecific introduction of a three-carbon side chain α to the ketone, precursor of the fused α-pyridone ring. This objective, it appeared, could possibly be attained in a number of ways, one of which readily achieved the desired regiospecific alkylation. Thus, a sequence of carbomethoxylation, alkylation, and decarbomethoxylation was employed. Application with slight modification of the procedure (6) used for compound **3** to the conversion of **9** (NaH, KH, MeONa, THF, Me_2CO_3, reflux), gave regiospecific α-carbomethoxylation at the methylene opposite to the angular carbomethoxy group to yield 65–70% of the bicyclic β-ketoester **10** (sole regioisomer found): mp 138–139°C; ir ($CHCl_3$) ν_{max}: 1730, 1660, 1620 cm^{-1}; ^1H nmr (400 MHz) ($CDCl_3$) δ: 1.72 (s, 3H), 1.95 (broadened d, J = 17.3 Hz, 1H), 2.37 (d, J = 18.1 Hz, 1H), 2.66 (broadened d, J = 17.4 Hz, 1H), 2.78 (dd, J = 5.1 and 1.4 Hz, 1H), 3.38 (d, J = 18 Hz, 1H), 3.76 (s, 3H), 3.77 (s, 3H), 3.89–4.08 (m, 4H), 5.47 (br s, 1H), 12.19 (br s, 1H). *Exact Mass* calcd. for $C_{16}H_{20}O_7$: 324.1209; found (ms): 324.1212. *Anal.* calcd. for $C_{16}H_{20}O_7$: C 59.25, H 6.22; found: C 59.42, H 6.46. Alkylation of **10** by the Weiler method (9) (LDA, THF, −78°C → 0°C, CH_2=CH—CH_2Br, HMPA, −78°C → rt) yielded 74–80% of the desired ketodiester **11** as a mixture of stereoisomers; more polar isomer (tlc, ethyl acetate – hexanes 2:3): yellowish oil; ir (film) ν_{max}: 1720, 1640, 1605 cm^{-1}; ^1H nmr ($CDCl_3$) δ: 1.75 (br s, 3H), 1.7–2.9 (m, 5H), 3.69 (s, 3H), 3.77 (s, 3H), 4.0 (m, 4H), 4.9–6.1 (m, 4H), 5.59 (m, vinylic CH), 12 (approx.) (s, 1H). *Exact Mass* calcd. for $C_{19}H_{24}O_7$: 364.1522; found (ms): 364.1514; less polar isomer (tlc, ethyl acetate – hexanes 2:3): mp 104–105°C; ir (film) ν_{max}: 1740, 1650, 1610 cm^{-1}; ^1H nmr ($CDCl_3$) δ: 1.66 (s, 3H), 1.7–2.9 (m, 6H), 3.66 (s, 3H), 3.77 (s, 3H), 4.1 (m, 4H), 4.7–6.1 (m, 4H), 5.67 (m, vinylic CH), 12 (approx.) (s, 1H). *Exact Mass* calcd. for $C_{19}H_{24}O_7$: 364.1522; found (ms): 364.1538. Finally, saponification and decarboxylation (10) of the β-ketoester moiety in **11** (10% aqueous KOH, dioxane, reflux) gave in a 54–74% yield the all-important precursor **12** regiospecifically alkylated in the desired position and ready for further elaboration to the selagine ring system **2**: colorless oil; ir ($CHCl_3$) ν_{max}: 1720, 1710 cm^{-1}; ^1H nmr ($CDCl_3$) δ: 1.72 (s, 3H), 1.8–3.1 (m, 7H), 3.49 (dd, J = 7.6 and 4.1 Hz, 1H), 3.75 (s, 3H), 4.0 (m, 4H), 4.9–5.1 (m, 2H), 5.5–6.0 (m, 2H), 5.58 (m, vinylic CH). *Exact Mass* calcd. for $C_{17}H_{22}O_5$: 306.1467; found (ms): 306.1481.

Transformation of the allyl side chain to a methyl propionate chain took place smoothly by a hydroboration (Sia_2BH, THF, 0°C), oxidation (H_2O_2 30%, aqueous NaOH 5%, rt, followed by Jones), esterification (CH_2N_2, AcOEt) sequence to give the required ketodiester **13** in a 45% yield: colorless oil; ir ($CHCl_3$) ν_{max}: 1720 cm^{-1}; ^1H nmr ($CDCl_3$) δ: 1.70 (s, 3H), 1.8–3.4 (m, 10H), 3.65 (s, 3H), 3.77 (s, 3H), 3.9–4.2 (m, 4H), 5.6 (s, 1H). *Exact Mass* calcd. for $C_{18}H_{24}O_7$: 352.1522; found (ms): 352.1542. Attempted formation of the corresponding dihydropyridone ($PhCH_2NH_2 \cdot AcOH$, n-butanol, reflux, 20 h) gave instead the piperidone **14** in a 48–58% yield: colorless gum; ir ($CHCl_3$) ν_{max}: 1720, 1660, 1630 cm^{-1}; ^1H nmr (400 MHz) ($CDCl_3$) δ: 1.59 (d, J = 17.2 Hz, 1H), 1.68 (s, 3H), 1.72 (dd, J = 12.7 and 4.7 Hz, 1H), 2.33 (dd, J = 5.4 and 5.4 Hz, 1H), 2.51 (m, 1H), 2.65 (dd, J = 13.0 and 5.8 Hz, 1H), 2.74 (ddd, J = 17.5, 4.7, and 2.3 Hz, 1H), 3.52 (d broadened, J = 12.6 Hz, 1H), 3.77 (s, 3H), 3.8–4.0 (m, 4H), 4.56 (d, J = 16.4 Hz, 1H), 4.80 (dd, J = 5.9 and 2.2 Hz, 1H), 5.38 (d, J = 16.4 Hz, 1H), 5.50 (s, 1H), 7.1–7.3 (m, 5H). *Exact Mass* calcd. for $C_{24}H_{27}NO_5$: 409.1889; found (ms): 409.1863.

Although the attempted isomerization of **14** in acid failed to

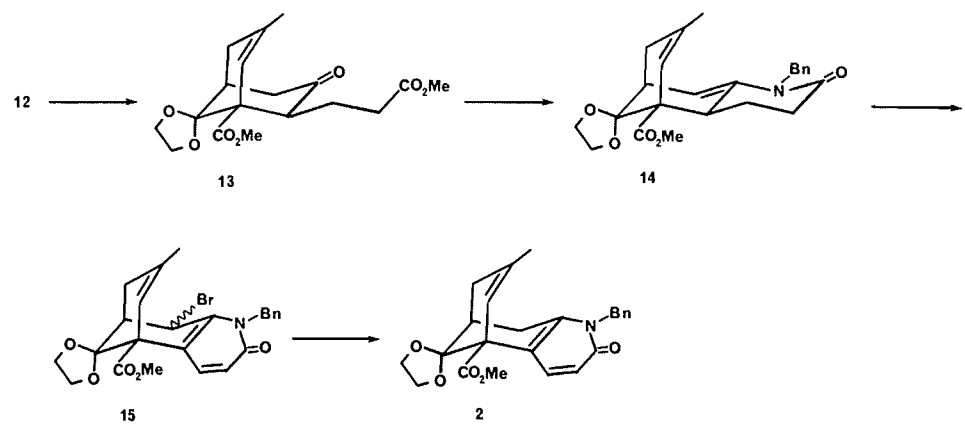

Can. J. Chem. Downloaded from www.nrcresearchpress.com by 210.87.254.5 on 09/06/12
For personal use only.

produce the corresponding dihydropyridone, treatment with bromine (Br_2, CH_2Cl_2, rt) gave bromopyridone **15** in a 58% yield: mp 203–204°C dec.; ir ($CHCl_3$) ν_{max}: 1720, 1650, 1580 cm^{-1}; ^1H nmr ($CDCl_3$) δ: 1.52 (s, 3H), 2.3–2.9 (m, 2H), 3.89 (s, 3H), 4.0–4.2 (m, 4H), 4.83 (br s, 1H), 5.23 (d, J = 17.2 Hz, 1H), 5.85 (br s, 1H), 6.38 (d, J = 17.0 Hz, 1H), 6.74 (d, J = 9.8 Hz, 1H), 6.94 (d, J = 9.7 Hz, 1H), 6.8–7.4 (m, 5H). *Exact Mass* calcd. for $C_{24}H_{24}NO_5Br$: 485.0839; found (ms): 485.0833. Finally, reduction of bromopyridone **15** (Bu_3SnH, AIBN cat., C_6H_6, reflux) was achieved in an 80% yield to give the desired selagine tricyclic ring system **2**: mp 229°C; ir ($CHCl_3$) ν_{max}: 1720, 1650, 1580 cm^{-1}; ^1H nmr (400 MHz) ($CDCl_3$) δ: 1.64 (s, 3H), 1.72 (d, J = 18.6 Hz, 1H), 2.32 (dd, J = 7.1 and 7.1 Hz, 1H), 2.53 (d, J = 18.0 Hz, 1H), 2.58 (dd, J = 18.3 and 6.8 Hz, 1H), 3.28 (dd, J = 17.9 and 7.2 Hz, 1H), 3.85 (s, 3H), 3.9–4.0 (m, 4H), 5.06 (d, J = 16.4 Hz, 1H), 5.58 (d, J = 16.4 Hz, 1H), 5.87 (s, 1H), 6.52 (d, J = 9.4 Hz, 1H), 6.90 (d, J = 9.4 Hz, 1H), 7.1–7.3 (m, 5H). *Exact Mass* calcd. for $C_{24}H_{25}NO_5$: 407.1733; found (ms): 407.1760.

Further work is currently in progress in our laboratories to complete the total synthesis of selagine (**1**).

Acknowledgements

We wish to thank the Natural Sciences and Engineering Research Council of Canada and le Ministère de l'Education du Québec for financial support to D.G. and a scholarship (NSERC) to J.R. We also wish to thank l'Université de Montréal for a scholarship to D.T. and Miss Suzanne Milette for her important contribution as a summer research participant in this project.

1. Z. VALENTA, H. YOSHIMURA, E. F. ROGERS, M. TERNBAH, and K. WIESNER. Tetrahedron Lett. No. 10, 26 (1960); H. YOSHIMURA, Z. VALENTA, and K. WIESNER. Tetrahedron Lett. No. 12, 14 (1960); M. SHAMMA, C. D. JONES, and J. A. WEISS. Tetrahedron, **25**, 4347 (1969).
2. A. S. KENDE and J. A. SCHNEIDER. Synth. Commun. **9**, 419 (1979).
3. D. GRAVEL, R. DÉZIEL, and L. BORDELEAU. Tetrahedron Lett. **24**, 699 (1983).
4. A. S. KENDE, F. H. EBETINO, R. BATTISTA, R. J. BOATMAN, D. P. LORAH, and E. LODGE. Heterocycles, **21**, 91 (1984).
5. A. S. KENDE, R. A. BATTISTA, and S. B. SANDOVAL. Tetrahedron Lett. **25**, 1341 (1984).
6. L. RUEST, G. BLOUIN, and P. DESLONCHAMPS. Synth. Commun. **6**, 169 (1976).
7. H. J. REICH, J. M. RENGA, and I. L. REICH. J. Am. Chem. Soc. **97**, 5434 (1975).
8. N. NOZAKI. H. YAMAMOTO, and T. MORI. Can. J. Chem. **47**, 1107 (1969); T. MORI, K. KIMOTO, M. KAWANISI, and H. NOZAKI. Tetrahedron Lett. 3653 (1969).
9. S. N. HUCKIN and L. WEILER. J. Am. Chem. Soc. **96**, 1082 (1974).
10. R. H. KAYSER, M. BRAULT, R. M. POLLACK, S. BANTIA, and S. F. SADOFF. J. Org. Chem. **48**, 4497 (1983).

Can. J. Chem. Downloaded from www.nrcresearchpress.com by 210.87.254.5 on 09/06/12
For personal use only.

ADDITIONS AND CORRECTIONS / AJOUTS ET CORRECTIONS

Vol. 61, 1983

Peter Yates, Patrick Hugh Helferty, and Paul Mahler. Nucleophilic and acid-catalyzed cleavage of the cyclopropane rings of β,γ-unsaturated α-spirocyclopropyl ketones.

Page 78. In the first line of the English abstract 1,2-dibromomethane should read 1,2-dibromoethane.

Page 81. Structure **23** should appear as below.

Page 82. Structure **33** should appear as below.

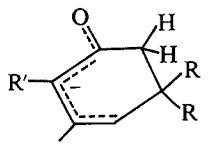

23

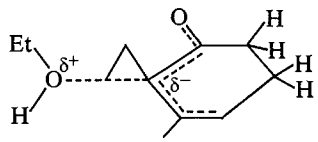

33

H. Rüeger and M. H. Benn. The alkaloids of *Senecio triangularis* Hook.

Page 2527. Table 1. Carbon 4 should be carbon 5. The entries for **5** need to be corrected. The chemical shifts for C-5 and C-7 were 53.8 and 73.7, respectively. As well, the assignments given for C-4′ and C-5′ in the entries for compounds **3**–**5** should be interchanged.

We thank Dr. James N. Roitman for drawing these matters to our attention.

Vol. 62, 1984

Robin A. Cox and Keith Yates. Hydrolysis mechanisms for acylhydrazines in aqueous sulfuric acid, determined using the excess acidity method.

Page 1613. Left-hand column: line 6 from bottom, *read* Mashima *instead of* Mashim.

Page 1613. Right-hand column: line 17 of Kinetic analysis, *read* carboxylic acid product *instead of* benzoic acid product.

Page 1613. Right-hand column: line 10 from bottom, *read* k_0 *instead of* k_0.

Page 1613. Equation [2] should read:

$$[2] \quad k_\psi C_{SH^+} = k_0 a_{SH^+} a_{H^+}/f_\ddagger = k_0 C_{SH^+} C_{H^+} (f_{SH^+} f_{H^+}/f_\ddagger)$$

Page 1614. Right-hand column: line 11 from bottom, *read* k_0' *instead of* k_0'.

Can. J. Chem. Downloaded from www.nrcresearchpress.com by 210.87.254.105 on 09/06/12
For personal use only.